

Annual Cumulated Index

ACCESSION NOS. A69-10001 to A69-43818

INTERNATIONAL AEROSPACE ABSTRACTS

U. of ILL. LIBRARY

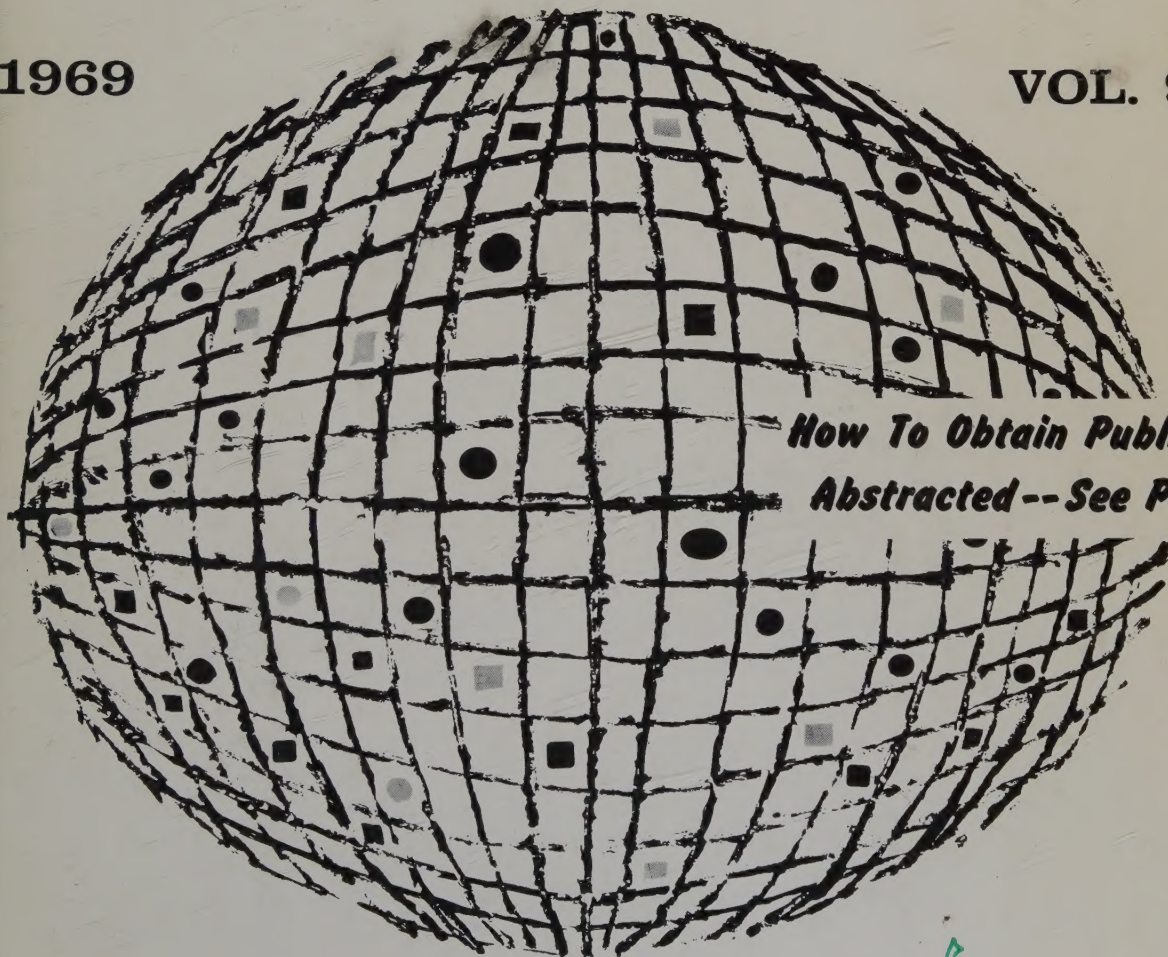
JAN 9 1970

PART 2, SUBJECT INDEX, M - Z

CHICAGO CIRCLE

1969

VOL. 9



*How To Obtain Publications
Abstracted -- See Page V*

PUBLISHED BY THE TECHNICAL INFORMATION SERVICE
AMERICAN INSTITUTE OF AERONAUTICS AND ASTRONAUTICS

INTERNATIONAL AEROSPACE ABSTRACTS

TL
500
I57
vol. 9
1969
index
pt. 2
N/c

ANNUAL

CUMULATED

INDEX

PART 2

SUBJECT INDEX, M - Z

VOLUME 9

JANUARY-DECEMBER

1969

ACCESSION NUMBERS A69-10001 to A69-43818

INTERNATIONAL AEROSPACE ABSTRACTS is prepared and published semimonthly (except March, June, September, and December, which have three issues) by the Technical Information Service, American Institute of Aeronautics and Astronautics, Inc., for the Institute and the National Aeronautics and Space Administration under Contract No. NSR 33-003-009. Editorial and Subscription Offices: 750 Third Avenue, New York, N. Y. 10017. Copyright © 1969 by the American Institute of Aeronautics and Astronautics, Inc.
Telephone: 212 TN-7-8300 TWX: 212 867-7265

SUBSCRIPTION INFORMATION. Semimonthly issues: United States and Possessions, 1 year, \$54 postpaid; Foreign Countries, 1 year, \$68.25 postpaid. Cumulated Index Volumes: United States and Possessions, 1 year, \$30 postpaid; Foreign Countries, 1 year, \$35 postpaid. Second-class postage paid at Phillipsburg, N.J.

STAFF, AIAA Administrator—Technical Information Programs, Robert R. Dexter

STAFF, TECHNICAL INFORMATION SERVICE Director, John J. Glennon • Associate Director—Administrative, Thomas J. Meskel • Associate Director—Technical, Irene W. Bogolubsky • Manager—Information Systems, William T. Morris, Jr. • Chief Librarian, Patricia M. Marshall

Sheridan Printing Company, Inc.
Phillipsburg, N. J.

CONTENTS

Pages

PART 1

LIST OF PERIODICALS SCANNED

SUBJECT INDEX, A - L

PART 2

INTRODUCTION iv

HOW TO OBTAIN PUBLICATIONS ABSTRACTED v

CROSS REFERENCES v

SUBJECT INDEX, M - Z A1058 - A2177

PART 3

PERSONAL AUTHOR INDEX

CONTRACT NUMBER INDEX

MEETING PAPER AND REPORT NO. INDEX

ACCESSION NUMBER INDEX

INTRODUCTION

INTERNATIONAL AEROSPACE ABSTRACTS (IAA) is an abstracting and indexing service covering the world's published literature in the field of aeronautics and space science and technology. IAA is issued semimonthly, on the 1st and 15th of each month (except March, June, September, and December, which have three issues).

Coverage of Published Literature

The following types of publications are covered in IAA:

- Periodicals (including government-sponsored journals) and books.
- Meeting papers and conference proceedings issued by professional societies and academic organizations.
- Translations of journals and journal articles.

Coverage of Reports ("Unpublished" Literature)

Abstracts and indexes of report literature are issued in SCIENTIFIC AND TECHNICAL AEROSPACE REPORTS (STAR), which is published by the Scientific and Technical Information Division, National Aeronautics and Space Administration.

By special arrangement between NASA and the American Institute of Aeronautics and Astronautics, IAA is issued in coordination with the twice-monthly schedule of STAR, which appears on the 8th and 23rd of each month.

IAA and STAR both utilize identical subject categories and indexes, which are described below.

Thus the two services provide comprehensive access to the national and international unclassified report and published literature of current significance to aerospace science and technology.

Arrangement of the Semimonthly Issues

IAA is arranged in two major sections:

- (1) Abstracts Section. This section contains complete bibliographic citations with informative abstracts, arranged by appropriate subject categories to facilitate scanning. The subject categories are numbered from 01 to 34, and the scope of each category is outlined in the Table of Contents and again at the beginning of each category in the Abstracts Section. Each abstract is prefixed by the IAA accession number.
- (2) Index Section. Five indexes are contained in this section: Subject, Personal Author, Contract Number, Meeting Paper and Report Number, and Accession Number. Each index is prefaced by explanatory notes to guide the user to the desired abstract.

Cumulated Indexes

Cumulated indexes are prepared and issued promptly at the end of each quarter year, with the 4th quarterly being the Annual Index.

Each cumulated index contains the following sections: A—Subject Index, B—Personal Author Index, C—Contract Number Index, D—Meeting Paper and Report Number Index, and E—Accession Number Index.

Indexing Vocabulary

The Preliminary Edition of the NASA THESAURUS (December 1967) (NASA SP-7030) is the authority for the indexing vocabulary that appears in the subject indexes to STAR and IAA. The NASA Thesaurus should be consulted for a total picture of the current indexing vocabulary and associated cross-reference structure. Copies of the NASA Thesaurus may be obtained from the Clearinghouse for Federal Scientific and Technical Information or the U.S. Government Printing Office at a price of \$8.50 for the three-volume set.

Information regarding SCIENTIFIC AND TECHNICAL AEROSPACE REPORTS and the availability of INTERNATIONAL AEROSPACE ABSTRACTS to organizations having contractual arrangements with NASA may be obtained from the following address:

National Aeronautics and Space Administration
Scientific and Technical Information Division
Attention: Code USI
Washington, D.C. 20546

how to obtain publications abstracted

All documents abstracted are available from the AIAA Technical Information Service as follows:

- Paper copies of accessions announced in IAA and of other published articles in the TIS library are available at \$3.00 per document up to a maximum of 20 pages. The charge for each additional page is \$0.25.
- Paper copies of accessions announced in *Scientific and Technical Aerospace Reports* (STAR) and of similar unpublished reports in the TIS library are available at the rate of \$0.25 per page, minimum order \$3.00.
- Microfiche of documents announced in IAA are available at the rate of \$0.50 per microfiche on demand. Documents available in this manner are identified by the symbol # following the accession number in the Abstracts Section and in the Meeting Paper and Report Number and the Accession Number Indexes.
- Minimum air-mail postage to foreign countries is \$1.00.
- A number of publications, because of their special characteristics, are available only for reference in the library.

PLEASE REFER TO THE ACCESSION NUMBER WHEN REQUESTING PUBLICATIONS

Address all inquiries and requests to:

Technical Information Service
American Institute of Aeronautics
and Astronautics, Inc.
750 Third Avenue, New York, N. Y. 10017

Telephone: 212 TN-7-8300
TWX: 212 867-7265

CROSS REFERENCES

The subject index includes two types of cross references to aid the user of the index in locating the material being sought:

1. "USE" references (U) direct the user to alternate headings under which material on the subject will be found, for example

COLUMBIUM
U NIOBIUM

2. "NARROWER TERM" references (NT) refer the user to more specific headings in the same subject area, for example

LUMINESCENCE
NT ELECTROLUMINESCENCE

VOLUME 9

A Notation of Content, rather than the title of the publication, appears under each subject heading; it is listed under several subject headings which provide multiple access to the subject content of each accession. The IAA accession number is located under and to the right of the Notation of Content. It is preceded by numbers identifying the issue and page of *International Aerospace Abstracts* where the abstract is located.

To illustrate:

Issue Number	Page Number	Accession Number
01	p0006	A69-11016
M		

M WINGS

U VARIABLE SWEEP WINGS

M-1 ENGINE

Scale models of M-1 rocket engine oxygen and hydrogen pump driven two stage turbines used to determine performance and compact inlet manifolds problems
[AIAA PAPER 69-553] 16 p2840 A69-32678

M-2 LIFTING BODY

Lifting body type M2-F1 and M2-F2 aircraft enabling astronauts to make own landings at choice airport
03 p0366 A69-13367

M-2F2 LIFTING BODY

Lifting Body Test Program at Edwards AFB compared with flight testing standards of high performance aircraft, discussing testing philosophy
06 p1017 A69-17671

MACH CONES

Conical flow past cruciform wing-body and tail-body systems, considering various positions of leading edges with respect to Mach cone
15 p2548 A69-31002

Supersonic combustible gas mixture flow around circular cone, discussing ignition by shock wave and flow modification by conical flame front
15 p2548 A69-31007

Mach disk and Riemann wave location, size and strength in underexpanded jet flows, proposing model for conservation equation satisfaction
[AIAA PAPER 69-665] 17 p2954 A69-33460

MACH INERTIA PRINCIPLE

Mach principle in scalar-tensor gravitation theory, discussing self energy calculations in canonical formalism for solitary neutral and charged point particles
01 p0120 A69-10858

Cosmological model based on inertia and relativity principles, considering scalar gravitational and electrostatic potential, light velocity, gravitational interaction and observed galactic red shift
18 p3206 A69-35470

MACH NUMBER

Reynolds and Mach numbers influence on loss coefficient magnitude at straight airfoil lattice
03 p0364 A69-13788

Axially symmetric bodies shape for static pressure at location independent of Mach number
04 p0542 A69-14738

Wall temperature and Mach number effect on heat

flux distribution at spreading line of flow for supersonic gas on ellipsoid of revolution
06 p0858 A69-17331

Mach number effects on pattern of vortex flow past delta wing and circular cones at various Reynolds numbers
06 p0858 A69-17339

High enthalpy, Mach and Reynolds number flight studies on ballistic ranges, describing launchers, flight simulation, measuring and recording techniques
06 p0860 A69-17632

MHD shock discontinuities above critical Alfvén-Mach numbers in two fluid plasma
06 p0970 A69-17954

Mixture Mach number defined for collisionless plasma flow about solid body by extending cold-ion theory
[AIAA PAPER 69-78] 06 p0971 A69-18128

Air intakes for fixed exhaust throat hypersonic ramjet engines, discussing configuration dependence on Mach number at beginning of combustion
[ONERA-TP-658] 07 p1203 A69-18418

Pressure distribution on star-shaped bodies in wind tunnel at Mach 4 and Reynolds number .000006
07 p1050 A69-18703

Mach number distribution along axes of underexpanded supersonic jets measured in wind tunnel experiments
07 p1050 A69-18922

Mach number values and propagation rates of wear disturbances in interplanetary medium obtained from Mariner 2 data during low solar activity
09 p1575 A69-21523

Compressor inlet Mach number choice to control high performance variable stator compressors geometry
[ASME PAPER 69-GT-14] 09 p1571 A69-22502

Oblique shock wave properties with free stream Mach number and flow deflection angle as independent variables, noting explicit solution
11 p1819 A69-25378

Mach numbers effect on pressure distribution and friction moment in nonisothermal layer of gas lubricant, using power series
15 p2629 A69-31021

Mach reflection shock-shock locus in shock tube implosions generation by area change
16 p2766 A69-31919

Hydrodynamic parameters of annular Couette flow in longitudinal magnetic field for variable Reynolds and Mach numbers
16 p2821 A69-31953

Gas ducted flow at subsonic inlet velocity and critical outlet Reynolds numbers, proposing surface friction relation to Mach number
16 p2771 A69-31956

Shock polar equation in polar coordinates, showing shock polar shape dependence on Mach number
16 p2772 A69-32178

Mach number values and propagation rates of weak disturbances in interplanetary medium obtained from Mariner 2 data during low solar activity
16 p2851 A69-32518

Supersonic blowdown wind tunnel noting cylindrical diffusers efficiency in starting supersonic nozzles increased in proportion to Mach number
17 p2890 A69-33125

Mach number, cone angle, bluntness and wall to recovery temperature ratio effects on slender cones boundary layer transition measurements at hypersonic speeds
17 p2890 A69-33250

Plane shock wave interaction with plane rigid net-like wall, obtaining Mach numbers for reflected and penetrating shock waves
17 p2957 A69-33719

Large scale axisymmetric inlet systems performance capabilities, reviewing theoretical and experimental programs
[AIAA PAPER 68-580] 17 p3022 A69-34018

Flow viscosity and heat conduction effects on shock wave propagation in bent channel with weak Mach reflection
18 p3124 A69-35326

Flow velocity, flow Mach number and weak

disturbance velocity behind shock wave measured for nitrogen, oxygen and carbon dioxide
19 p3298 A69-36362

Global properties of solution of inverse detached shock problem analyzed by characteristic coordinates at low Mach number
19 p3301 A69-36788

Low density free jet properties, discussing velocity distribution perpendicular to axis and correlation of all terminal parallel Mach numbers for monatomic gases
20 p3514 A69-37206

Aerodynamic skin heating at high Mach numbers affecting structural design, noting use of high temperature materials, insulation systems and shell construction method
21 p3646 A69-38460

Detonation driven shocks of high Mach number obtained in improved membrane shock tube by heating and compressing driver gas
23 p4198 A69-41545

MACH-ZEHNDER INTERFEROMETERS

Mach-Zehnder interferometer for studying temperature distribution and heat transfer in turbulent jets, noting temperature dependence on jet thickness at different angles of attack
01 p0005 A69-10101

Electron density measurement in rapidly varying plasma, using improved Mach-Zehnder interferometer
05 p0760 A69-15613

Plane shock wave propagation around cylinders of various radii recorded with shadowgrams and Mach-Zehnder interferograms, discussing wave diffraction mechanics
18 p3120 A69-34472

High electron density in transient mercury vapor plasma determined using He-Ne laser interferometer measurements
18 p3153 A69-35307

Mach-Zehnder laser interferometer for measurements of electron density in transient Hg vapor plasma, noting agreement with microwave measurements
22 p3965 A69-40924

MACHINE LEARNING

U LEARNING MACHINES

MACHINE LIFE

U SERVICE LIFE

MACHINE ORIENTED LANGUAGES

NT FORTRAN

NT LANGUAGE PROGRAMMING

NT ON-LINE PROGRAMMING

NT SYMBOLIC PROGRAMMING

CASSANDRE language in computer simulation
03 p0401 A69-14178

CASSANDRE programming language for digital systems, noting application to logic systems
03 p0401 A69-14179

ASTRE programming language applicability to maximum memory information treatment in aerial navigation
03 p0401 A69-14180

NASA-Ames hybrid simulation software systems, subsystems and implementation
04 p0567 A69-15353

Interpretive Checkout Test Language /CTL/ designed in near English form for aerospace checkout tasks
04 p0569 A69-15364

Hardware and software as single entity in small scale programs, describing English language oriented program code of Controller /Programmer/ Evaluator
11 p1864 A69-25062

Abbreviated Test Language for Avionics Systems /ATLAS/ as standard compiler input language for commercial airline automatic test equipment /ATE/
11 p1842 A69-25064

Soviet book on automated information retrieval systems covering computer languages, search in complex ordered codes, translation from Russian into computer language, etc
13 p2225 A69-27933

Checking automation languages defined as one way stack languages subfamily forming full AFL closed under substitution
16 p2755 A69-32078

Problem-oriented languages in man-computer inter-communication

18 p3106 A69-34658

Interactive experimenter computer system software and hardware design considerations based on astronaut-machine/experimenter question-answer interactions

[AIAA PAPER 69-953] 22 p3904 A69-40335

SIMUPOL /Simulation Procedure Oriented Language/ system for hardware description and architecture and interface requirements of digital processor

[AIAA PAPER 69-960] 22 p3905 A69-40341

MACHINE RECOGNITION

U ARTIFICIAL INTELLIGENCE

MACHINE STORAGE

U COMPUTER STORAGE DEVICES

MACHINE TOOLS

NT BORING MACHINES

Laser application to machine tool accuracy and alignment

[ASTME PAPER MR68-407] 02 p0252 A69-11797

Thin film lubricant effect on machine dynamic performance, proposing inclusion with machine structure for reducing vibration effect

03 p0435 A69-13948

Laser interferometer gauges for machine tool accuracy, discussing operation, application, manufacture, cost and closed loop numerical control systems

04 p0606 A69-14880

Electron beam process application to welding, machining and assembling in automobile mass production

04 p0608 A69-15484

Clearing and blocking control over frequently overadjusted automatic equipment in precision machine and device construction

06 p0931 A69-17692

Book on machinability and producibility of metals, plastics, nonmetallic materials and composites, emphasizing machine tools and tool holders

06 p0931 A69-17782

Machine cutting tool for cutting and splicing endless magnetic tape 30 microns thick, noting film safety feature and nonmagnetic steel scissors

08 p1321 A69-20876

Tape placement machines to fabricate composite high modulus filamentary tape reinforced aerospace structures, anticipating future generations evolution into automatic control

19 p3323 A69-35584

Machine tools design for performing cutting operations within acceptable vibration limits

22 p3928 A69-40672

Electrochemical dimensional machining of metals and alloys with rotating cathode in parts manufacture from mechanically intractable materials

23 p4168 A69-41309

Holo-diagram device for making and evaluating holograms for small deformations measurement in large machine tool parts

24 p4317 A69-43760

MACHINE TRANSLATION

Soviet book on automated information retrieval systems covering computer languages, search in complex ordered codes, translation from Russian into computer language, etc

13 p2225 A69-27933

Algorithm for programming language grammars conversion into pushdown store automata translators

21 p3679 A69-39607

MACHINERY

Matrix-harmonic method for vibration study of mechanisms and machines

03 p0468 A69-13860

Matrix-harmonic method of vibration study extended to include autonomous vibrations of single degree of freedom machines

03 p0468 A69-13861

Soviet collection of papers on dynamics and strength of machines

06 p1026 A69-18013

Lubrication systems for high speed machinery, discussing wet and dry sump arrangements, gearbox heat rejection, oil flow requirements, X-22A aircraft, etc

[ASME PAPER 69-DE-65] 14 p2454 A69-28845

Collection of soviet articles on vibrations and stability of devices, machines and control system elements

14 p2536 A69-29741

Independent operations optimum performing sequence determined for parallel machines differing in

technological characteristics and with assigned time using algorithm

16 p2763 A69-31626

Rotating machinery fracture and design approach based on effect of detailed stress and strain duty on imperfect materials metallurgical behavior

17 p3060 A69-33561

Soviet papers on dynamics and strength of machines covering oscillations of shells and impeller blades, stress concentration at shallow shell holes, thermoclasticity, etc

19 p3435 A69-35841

MACHINING

NT CHEMICAL MACHINING

NT ELECTROCHEMICAL MACHINING

NT HOT MACHINING

NT MILLING [MACHINING]

NT SPARK MACHINING

Laser applications in metal working including dissimilar metal welding, hole drilling, material removal and dynamic balancing

[ASTME PAPER MR68-406] 02 p0252 A69-11796

Surface smoothness of laser beam holes, discussing possible damage and technology recommendations

04 p0606 A69-14607

Plastic deformation, aging, heat treatment and machining effect on structure of thin films of AMg11 alloy

05 p0783 A69-16814

Book on machinability and producibility of metals, plastics, nonmetallic materials and composites, emphasizing machine tools and tool holders

06 p0931 A69-17782

Micromachining with laser beam, choosing mirrors and lenses of optical system to provide uniform energy distribution for microwelding or hole boring

08 p1324 A69-19980

Pulsed ruby laser of small output for hole drilling, studying correlation of vaporization, hole diameter and depth with laser output

09 p1504 A69-22247

Oxide ceramics finishing processes, discussing leaching, machining, surface finishing, strengthening by compressive surface layers and joining

09 p1510 A69-22350

Fiber reinforced materials shear and tensile strength effect on stress-strain state of composite materials machine parts, considering design requirements

11 p1907 A69-25680

Electrical discharge machining effect on heat resistant alloys surface finish, noting volt-ampere characteristics

18 p3147 A69-34547

Machining processes effect on surface integrity of machine parts and effects on product quality

18 p3149 A69-35129

Precision of gas turbine compressor blade positioning devices during machining, analyzing causes of inaccuracies

21 p3731 A69-38880

Two machining processes for eliminating unbalanced state of machine parts, using eccentric cutting and adjustment of part CG for coincidence with spindle axis

21 p3732 A69-39097

He-Nc laser system for micromachining thin film photolithographic masks, describing computer controlled coordinate table and product quality

22 p3954 A69-40236

Digital computer systems for automating machine parts design main metal cutting operations, emphasizing optimal instrument usage, reliability, digital algorithm language and economics

23 p4169 A69-41952

MACROCLIMATE

U CLIMATE

MACROSCOPIC EQUATIONS

Macroscopic quasi-linear theory of HF radiation in cold electron-proton plasma allowing direct use of plasma and Maxwell equations

16 p2819 A69-31684

Earth bow shock electrical conductivity estimation from macroscopic equations without knowing microscopic dissipation processes

18 p3131 A69-35191

MACULAR VISION

U VISION

MAGIC TEES

Tunable ferrimagnetic bandpass filter using magic T configuration to permit low magnetic field strength and retain nonstacked configuration advantages

04 p0573 A69-14343

MAGMA

Lunar relief mechanism based on experimental cratering by pasty projectiles, proposing terrestrial magma genesis

15 p2698 A69-31373

MAGNESIUM

Shear accommodation kinking at second order twin bands in critically deformed magnesium investigated for dislocation mechanism

01 p0093 A69-10063

Radiation, Stark and van der Waals level broadening constants for Mg I and Si I calculated to interpret solar and stellar spectral line widths

02 p0310 A69-11454

Migration and penetration of vacancies in quenched magnesium analyzed by electrical resistivity measurements and electron microscopy

02 p0267 A69-12187

Interaction between point defects and magnesium atoms in aluminum irradiated by neutrons, analyzing magnesium concentration effect on recovery

05 p0781 A69-16613

Temperature distribution in low pressure magnesium vapor-oxygen diffusion flames, discussing environmental conditions and visible radiation

07 p1241 A69-18367

Titanium tetrachloride reduction to titanium by magnesium, showing autocatalytic process

07 p1163 A69-18784

Magnesium boron composite fabrication by diffusion bonding and liquid metal infiltration, obtaining minimized property variations and high strength to density ratios

09 p1507 A69-22332

Vegetable diet including 210 g of dry Chlorella biomass decreases effect on calcium and magnesium assimilation to produce insignificant negative balance of K and Mn

10 p1647 A69-23590

Solar spectra of Mg II doublet lines during September 22, 1968 eclipse, considering chromospheric activity effects on emission peaks

11 p1958 A69-24591

Spectral line formation in nonlinear multilevel atom line transfer problems, considering radiation transfer through plane parallel atmospheres of H and Mg atoms

12 p2133 A69-26967

Stannate immersion process for reduction of magnesium-steel couples galvanic corrosion, discussing bath operating limits

14 p2466 A69-29933

MAGNESIUM ALLOYS

Aluminum-Zn-Mg alloys weldability, discussing base metal composition and heat treatment influence during gas-shielded arc welding

01 p0086 A69-10536

Long term atmospheric corrosion test program for aluminum and magnesium base alloys, comparing tensile strength of exposed and control specimens

01 p0100 A69-11353

Al-Mg-Si alloy strain aging, noting effect of deformation stresses on kinetics and aging mechanism for prior and concurrent deformation

04 p0614 A69-14575

Effective slip systems in hexagonal close packed magnesium alloy under static and hydroexplosive loading, examining flow mechanism for fine structure formation

04 p0615 A69-14639

Aging and recovery effect on structure and hardness of Ag and Be doped Al-Mg alloys

05 p0783 A69-16811

Plastic deformation, aging, heat treatment and machining effect on structure of thin films of AMg11 alloy

05 p0783 A69-16814

Microstructure of diffusion zone during contact fusion in magnesium-nickel system at high temperatures

06 p0945 A69-17895

Plastic deformation of internally oxidized dispersion strengthened silver magnesium alloys, noting hardening effect dependence on oxidation temperature

07 p1159 A69-18627

Polycrystalline Mg-Ti-Zr alloy precipitation hardening investigated by tensile and hardness tests and transmission electron microscopy

07 p1167 A69-19265

Low temperature low cost dip brazing technique for light weight magnesium alloy electronic packaging structures, noting distortion

09 p1509 A69-22346

Transgranular stress corrosion crack propagation in thin sheet single phase magnesium-aluminum alloy

10 p1710 A69-23086

- Thermal and microstructural analyses to determine phase interactions nature in Mg alloys of Mg-Nd-Al system
11 p1902 A69-24271
- Solid solution decomposition effect on binary Mg alloys recrystallization temperature containing Al and Nd, using X ray and microstructural analysis
11 p1902 A69-24272
- Al-Mg-Si alloy strain aging, noting effect of deformation stresses on kinetics and aging mechanism for prior and concurrent deformation
15 p2638 A69-30276
- Lattice components of heat conductivity and chemical composition relations of magnesium alloy solid solutions
16 p2824 A69-31567
- Creep rate and temperature effect on creep resistance shown in direct correlation with Al-Mg alloys strength by long term high temperature tests
16 p2801 A69-31782
- Mg alloys applications to construction, discussing strength-to-weight ratio of cast and wrought alloys
16 p2801 A69-31787
- Creep experiments on Mg alloys, discussing dispersed phases influence on creep cavitation and grain boundaries mobility
17 p2985 A69-32907
- Crystal twinning directional effect on Mg alloys tensile yield strength degradation, investigating recovery methods
19 p3341 A69-35583
- Aluminum 7 percent Mg alloys stress corrosion cracking, presenting aging kinetics and depletion zone dislocations at grain boundaries
19 p3350 A69-36896
- Shrinkage cavity volume formulas for alloy castings with wide liquidus to solidus range, considering effects of diffused porosity and clustering for Mg alloy
20 p3548 A69-37329
- Al and Mg alloys as ultrasonic wave acoustic lines, considering sound velocity, damping factor, grain size, chemical composition, etc
20 p3564 A69-38290
- Age hardening response of Mg-Th-Zr alloy at 60-450 C, discussing peak strengthening, superlattice formation, precipitation processes, etc
21 p3743 A69-38735
- Seam welding processes and power supply effects on control efficacy based on electrode displacement for Al-Mg alloys
24 p4319 A69-42919
- Stored energy of cold work and electrical resistivity of Ag-Mg solid solution alloys measured as functions of strain, Mg concentration and initial state of order
24 p4332 A69-43029
- Lap-shear strengths of Mg-Al alloy bonded with nylon-epoxy adhesive, including anodized coating rolling schedule and honeycomb core fabrication
24 p4323 A69-43417
- MAGNESIUM CHLORIDES**
Metallographic analysis of stress corrosion cracking of Ti alloys of Al and Sn in aqueous magnesium chloride solutions, noting cleavage process
19 p3352 A69-36903
- MAGNESIUM COMPOUNDS**
NT CHLOROPHYLLS
NT CORDIERITE
NT DOLOMITE [MINERAL]
NT ENSTATITE
NT HEXAHEDRITE
Spectra of hydrides of Mg 25 and Mg 26 in photosphere, searching for weak lines on basis of isotope shifts
03 p0515 A69-14035
Magnesium silicate crystal structure, discussing transformations under high pressure, crystallochemistry and implications for physics of earth mantle
08 p1267 A69-19904
Low temperature specific heat of praseodymium magnesium nitrate
12 p2026 A69-25784
Structural formula of slowly cooled Mg and Al-Mg microvapor ferrites, noting ion mobility during cooling
15 p2670 A69-31184
- MAGNESIUM ISOTOPES**
Threshold photonuclear cross section for Mg 26, discussing resonances as primary production mechanism for stellar neutrons
21 p3788 A69-38599
- MAGNESIUM OXIDES**
Reflection indicatrices of aluminum oxide, MgO, Au and Pt surfaces for normal irradiation noting temperature and surface treatment effects
03 p0534 A69-14161
- Surface UV irradiated MgO powder catalytic activity for hydrogen-deuterium exchange reaction
07 p1073 A69-18374
- Vaporizer temperature and collision efficiency correlation data for magnesium oxide-argon dilute diffusion flames studied for determining inverse temperature dependence
13 p2380 A69-28461
- CaO and MgO reflectance spectra measurements at high resolution and at low temperature including exciton spectra at 25 K, obtaining fine structure
18 p3181 A69-34274
- Chromium composites mechanical properties, studying effects of alloying with spinel and magnesium oxides
23 p4177 A69-41672
- MAGNESIUM PERCHLORATES**
Ammonium and magnesium perchlorate mixture thermal stability study with differential scanning calorimetry, noting exothermic decomposition of AP [AIAA PAPER 69-500]
16 p2833 A69-32661
- MAGNESIUM SULFATES**
U HEXAHEDRITE
MAGNESYN [TRADEMARK]
U SERVOMOTORS
- MAGNET COILS**
NT FIELD COILS
Min B magnetic trap, discussing induction coils, ponderomotive forces and mechanical stresses sustained by coils
04 p0634 A69-14299
Active magnetic coils for attitude control of synchronous satellites by computer simulation and laboratory tests
06 p1017 A69-17944
Electromagnetic vibration exciters based on permanent magnet and AC coil interaction
16 p2790 A69-32077
- MAGNETIC ABSORPTION**
U ELECTROMAGNETIC ABSORPTION
MAGNETIC ANNULAR SHOCK TUBES
Flow analysis in magnetic annular shock tube in magnetic field varying with time
08 p1366 A69-20787
Shock and current sheet separation in magnetic shock tubes, determining electron temperature behind shock and within current layer
20 p3511 A69-38241
- MAGNETIC ANOMALIES**
NT GEOMAGNETIC HOLLOW
F 2 layer equatorial anomaly at local noon, discussing position of trough center in latitudinal distribution of ionization
03 p0422 A69-13515
Aeromagnetic profiles across Reykjanes ridge southwest of Iceland, noting magnetic anomalies symmetry and ocean floor spreading since Mesozoic
04 p0592 A69-14660
Global geomagnetic anomalies influence on longitudinal pattern of solar quiet day variations and in phases of second harmonics of components
06 p0920 A69-17734
Spatial structure of residual anomalous magnetic field, determining parameters of eccentric horizontal dipole as main source of geomagnetic field
06 p0922 A69-17755
Anomalous magnetic field energy spectrum obtained from aeromagnetic survey and approximation valid for earth crust and upper mantle
09 p1487 A69-21554
Quasi-integral operator applicability to analytical continuation of potential field into complex region arising during gravitational and magnetic anomalies interpretation
10 p1689 A69-24082
Magnetic anomalies off Cape Hatteras explained as possible edge effect, discussing ocean and continental magnetic crusts and igneous and magnetic rocks
11 p1879 A69-25405
Statistical method for calculating upper bound heights of sources responsible for magnetic anomalies
12 p2071 A69-26696
Onboard magnetic anomaly detection system for Canadian helicopter, discussing magnetometer location, boom design and testing and equipment installation
[AIAA PAPER 68-487]
12 p2094 A69-26771
Sea tides and ionospheric effects on lunar variation of geomagnetic field vertical component
12 p2161 A69-26957
Anomalous magnetic field energy spectrum obtained from aeromagnetic survey and approximation valid for earth crust and upper mantle
16 p2784 A69-32549
- Lower ionospheric electron concentration and collision frequency measurements by Nike-Apache rockets suggesting geomagnetic anomaly in D region
18 p3127 A69-34799
- Solar wind plasma effects on lunar wake umbral and penumbral interplanetary magnetic field anomalies, evaluating roles of electrons and ions
20 p3609 A69-38095
- Ionospheric F region equatorial anomaly in electron density showing high correlation with equatorial electrojet range and poor correlation with Fugue range
23 p4160 A69-42432
- Equatorial anomaly during declining solar activity, treating seasonal and daily variations, longitude dependence and geomagnetic storm-time distortions
23 p4161 A69-42436
- MAGNETIC CIRCUITS**
Circuits with magnetic coupling, describing digital computer algorithms for assembly of loop circuit equations
01 p0036 A69-10745
Magnetic core logic circuit system for bidirectional stepping motor drive voltage power supply control in proper phase and time sequence
01 p0047 A69-11000
Square loop magnetic core model for computer aided circuit transient analysis
06 p0899 A69-16888
O shaped magnetic systems using unsaturated steel magnetic circuit to produce strong uniform magnetic fields for MHD machines
10 p1636 A69-23102
Time dependences of retardation effect, reversible magnetic permeability and magnetic viscosity during pulse magnetization of ferrite cores
13 p2319 A69-27993
Ferrite parameters measurement in alternating fields based on continuous analysis of magnetic, magnetizing and measuring circuits for assessing errors
13 p2320 A69-27996
Lumped element circuit producing directional coupling by electric and magnetic coupling of reactance quadrupoles, discussing insufficient coverage of calculated frequency range
16 p2763 A69-32581
Book on digital magnetic logic, considering digital magnetic core circuits consisting of magnetic components and interconnecting conductors
20 p3498 A69-37144
Ultrasonic oscillations effects on magnetic permeability of ferrite circuit components
23 p4138 A69-41873
- MAGNETIC COILS**
NT FIELD COILS
Proton spin maser oscillator with emission coils coupled by prepolarized liquid, discussing tuning and detuning
08 p1324 A69-20231
High homogeneity sixth order superconducting solenoids with coil inner surface notch correction, describing graphical design techniques
10 p1665 A69-23857
Cryogenic solenoids with pure Al conductor for production of strong magnetic fields, discussing softness and strain resistivity problems
12 p2016 A69-26497
Horseshoe electromagnet sensors above ferromagnetic plate, analyzing electromagnetic properties of plate and coil impedance
12 p2094 A69-26719
Sealed and unsealed relay coils temperature rise at simulated outer space air pressure levels
13 p2231 A69-28048
Shield facility and Helmholtz coil system used to investigate chronic effects on man of zero magnetic field regulated to cancel geomagnetic field variations
15 p2586 A69-30382
Book on solenoid magnet design covering magnetic and mechanical aspects of resistive and superconducting systems
20 p3464 A69-37145
Choke coil magnetoelastic sensors thermal stability found decreasing proportionally to measurement range decrease /below 100 newtons/
23 p4166 A69-41995
- MAGNETIC COMPASSES**
Book on magnetic compasses and magnetometers covering pivoted needle instruments, surveying, transmitting and gyromagnetic compasses, inductor instruments and compass testing
08 p1315 A69-20444
Quartz compasses designed for orientation of electronic devices with respect to magnetic meridians at low horizontal component values
23 p4166 A69-41869

MAGNETIC CONTROL

Magnetic orientation and attitude control of spin stabilized satellites, synthesizing control circuits and calculating power requirements

03 p0521 A69-13644

Book on Hall generators /magnetically controllable semiconductor elements/, discussing principles of operation, design, manufacture and applications

03 p0406 A69-13954

Automatic closed loop distortionless control of magnetic field modulation using light sensitive resistor as one leg of attenuator

06 p0897 A69-17708

Magnetic attitude detection and control system for Radio Astronomy Explorer satellite [AIAA PAPER 68-855]

12 p2174 A69-26779

Spatial harmonics of harmonic frequency instabilities of cyclotron half frequency in system of two symmetrical electron beams confined by magnetic field

13 p2314 A69-28364

Permanent magnets optimal design and properties for attitude control of German research satellite Azur, considering environmental influences

16 p2868 A69-31936

Diademe satellites stabilization system to measure station-to-satellite distance by laser pulse, discussing reflector, magnet for attitude control, damping device, etc

17 p3046 A69-33224

MAGNETIC CORES

Delayed response in threshold switching from reset state in ferrite memory cores consisting of magnesium compounds [IEEE PAPER 16.4]

01 p0045 A69-10719

Ferrite core temporary storage unit with 500 nsec cycle time

04 p0564 A69-15222

Square loop magnetic core model for computer aided circuit transient analysis

06 p0899 A69-16888

Transformer inrush transients control by selection of core material, primary turn number and trigger circuitry

06 p0894 A69-17221

Neutron irradiation and temperature effects on ferrite and Permalloy memory cores hysteresis loops

12 p2142 A69-26259

Model for perturbations in earth rotation and geomagnetic core-mantle coupling, discussing electromagnetic restoring torque

12 p2077 A69-27110

E shaped cores for miniaturized transformers and inductors from high permeability plastic bonded materials

13 p2237 A69-28586

Time logarithmic switching to explain anomalous delay in threshold response of MgMnZn ferrite memory cores

15 p2668 A69-30688

Magnetic core material and process technologies for space power electronic applications noting pulse transformers, nonlinear reactors and tapes

19 p3319 A69-35543

Computer memory with digit wire magnetic circuit /torus/, discussing capacity, access and output

20 p3503 A69-37402

Stored program decommutation techniques involving small core storage elements insertion into data path between decommutator equipment and computer

23 p4133 A69-41749

MAGNETIC DIFFUSION

Liquid copper electrical conductivity temperature dependence at very high temperatures from magnetic diffusion and flux penetration measurements, noting exploding wires role

01 p0119 A69-10673

Gas dynamic shock wave entry into magnetic field, discussing field distribution behind shock front and diffusion and medium motion effects on penetration depths

07 p1192 A69-19022

Diffusion times for saturated region in Hipernorm tubes measured for various exciting magnetic fields and pulse duration

23 p4141 A69-42222

MAGNETIC DIPOLES

Effect of steady flow of incompressible conducting fluid on magnetic dipole at center of sphere

01 p0128 A69-10363

Planetary magnetic field measurements near Venus, Mars, and moon, noting magnetic dipole comparison with earth and solar wind interactions [AAS PAPER 68-186]

02 p0311 A69-11471

Magnetosphere boundary determined in two dipole model approximation, taking into account current layer in tail

02 p0236 A69-11655

Dipole models of geomagnetism at earth surface used to calculate magnetic field in outer space

02 p0238 A69-11673

Magnetotopometer for measuring torque /proportional to magnetic dipole moment/ exerted on object by earth magnetic field

02 p0248 A69-11768

Algorithm computing spherical harmonic coefficients for eccentric geomagnetic dipole potential

02 p0245 A69-12735

Plasma slab acceleration along magnetic dipole guard field null, noting lack of equilibrium and no decrease of plasma losses

03 p0475 A69-13157

Mathematical dipole model for geomagnetic field to provide main magnetic field source distribution within earth

03 p0424 A69-13543

Dipole model of geomagnetic field in terms of spatial distribution of vertical component, discussing computer program for calculating rectangular components

03 p0424 A69-13544

Flow development around impulsively rotating dipole magnetized sphere in viscous incompressible conducting fluid, noting diffusing Alfvén waves and induced field

03 p0477 A69-13793

Outer magnetosphere average magnetic field configuration between 5 and 18 earth radii, noting various maps in equatorial plane

03 p0425 A69-14012

Stormer problem of charged particle motion in magnetic dipole field, discussing analytical method for high and low energy particles

03 p0504 A69-14127

Capture of electrically charged micrometeorites and corpuscles in magnetic field of gravitating dipole, noting necessary condition on particle motion

04 p0659 A69-14962

Supersonic plasma flow interaction with two dimensional magnetic dipole

06 p0967 A69-17738

Spatial structure of residual anomalous magnetic field, determining parameters of eccentric horizontal dipole as main source of geomagnetic field

06 p0922 A69-17755

Damping boom flutter and magnetic dipoles effects on attitude stability of gravity gradient satellites with three axis stabilization

07 p1227 A69-18332

Charged particle motion in electromagnetic field from basic equation of motion for magnetosphere, discussing dipolar magnetic field, Stormer trapped particle theory, etc

07 p1208 A69-19355

Magnetic energy relationships in magnetosphere, discussing confinement energy of magnetic dipole field, energy of transient compression and zero order energy of trapped particles

07 p1128 A69-19359

Magnetohydrostatic cavity formed round magnetic field of line dipole-line current combination by infinitely conducting plasma at uniform pressure

08 p1369 A69-20998

Power radiated by oscillating magnetic and electric dipoles in cold streaming plasma calculated by Poynting vector method

09 p1544 A69-21329

Pulsars rotating neutron star model analyzed on basis of magnetic dipole rotating in vacuum

09 p1592 A69-21463

Captured particles magnetic drift envelopes in magnetosphere calculated by model considering perpendicular geomagnetic dipole to solar wind

09 p1574 A69-21521

Charged particles motion in geomagnetic field from analyzing spatial distribution within framework of two dipole magnetosphere model

10 p1756 A69-22818

Dipole magnetosphere model with cylindrical or spherical forbidden band for studying plasma motion in quasi-hydrodynamic approximation

10 p1769 A69-23901

Magnetosphere boundary configuration calculated with allowance for geomagnetic dipole inclination to geographic axis and nondipole section of geomagnetic field

10 p1686 A69-23902

Plasma distribution and Alfvén wave velocity field in magnetosphere, discussing distortion of dipole magnetic field, ring current and wave propagation

10 p1742 A69-24205

Reflection and absorption characteristics of two dimensional array of magnetic dipoles for microwaves, considering element orientation and distribution

12 p2035 A69-25901

Geomagnetic field dipole model by extrapolating vertical Z component for 1955 to heights between 500 and 25,000 km

12 p2071 A69-26695

Model for self consistent time independent ring current of charged particle distribution under combined field of earth dipole and particle motion current

12 p2151 A69-26948

Radiation pattern of electric and magnetic dipole on flat semiinfinite impedance system edge found similar

13 p2236 A69-28546

Magnetosphere boundary determined in two dipole model approximation, taking into account current layer in tail

13 p2256 A69-28686

Dipole models of geomagnetism at earth surface used to calculate magnetic field in outer space

13 p2257 A69-28704

Boundary conditions for equilibrium diamagnetic plasma in magnetic dipole having constant and isotropic pressure in system

14 p2489 A69-28910

Geomagnetic field secular variations relation to variations of magnetic field of optimum dipoles, noting earth core role

14 p2436 A69-29061

Geomagnetic ring current study, giving exact kinetic description based on Vlasov equation of plasma ring current in dipolar field

15 p2598 A69-31218

Self consistent ring current of radiation belt under combined influence of earth dipole field and field due to currents of particle motions

16 p2776 A69-32096

Captured particles magnetic drift envelopes in magnetosphere calculated by model, considering perpendicular geomagnetic dipole to solar wind

16 p2851 A69-32516

Capture of electrically charged micrometeorites and corpuscles in magnetic field of gravitating dipole, noting necessary condition on particle motion

18 p3197 A69-34725

Chapman-Ferraro approximation for magnetic interior field line configuration in plasma flow around two dimensional dipole, allowing for tail formation and neutral sheet

18 p3129 A69-34955

Spectral lines due to magnetic dipole transitions in fine structure levels in collisionally excited neutral H clouds, discussing theoretical difficulties in interpretation

19 p3379 A69-36225

Geomagnetic field model /POGO/ to confirm eccentric dipole westward velocity secular decrease predicted by day length changes

20 p3523 A69-37490

Electromagnetic radiation in moving uniaxially anisotropic medium, obtaining time dependent solutions for oriented magnetic dipole current distribution density

20 p3576 A69-37578

Equilibrium plasma configurations in magnetic field of two dimensional dipole analyzed under similar conditions to magnetospheric tail formation with neutral hot plasma layer

23 p4205 A69-41835

Successive approximations convergence analyzed in solving supersonic collisionless plasma flow past magnetic dipole

23 p4156 A69-41853

Single dipole field approximation of geomagnetic field, minimizing sum of squares of differences between dipole field and geomagnetic field

23 p4158 A69-42173

Two and three dipole approximation of main geomagnetic field based on minimization of sum of squares of differences between dipole and geomagnetic fields

23 p4158 A69-42174

MHD disturbances in earth core produced by sudden introduction of magnetic dipole with axis positioned perpendicular to earth mantle and toroidal excitation fields

23 p4158 A69-42176

Pulsar model with seat as rotating neutron star having dipolar magnetic field not parallel to rotation axis

24 p4377 A69-42666

MAGNETIC DISPERSION

Hydromagnetic radiation characteristics of electric and magnetic dipoles in homogeneous anisotropic cold plasma, obtaining field components and wave propagation modes

24 p4307 A69-42905

Magnetic dipole field variations effects on planetary atmosphere erosion by solar wind, discussing Mars and Venus atmospheres above ionosphere

24 p4385 A69-43224

MAGNETIC DISPERSION

Dispersion measurements and spectrum variations analysis to study pearl micropulsations frequency variation during sudden deformation of magnetosphere by magnetic storms

02 p0240 A69-11697

Solar flares and plagues free energy origin in magnetic field dissipation

06 p0996 A69-17446

Dispersion measurements and spectrum variations analysis to study pearl micropulsations frequency variation during sudden deformation of magnetosphere by magnetic storms

13 p2258 A69-28728

Dispersoids and temperature effect on coercive force of 19 Co base and 10 Fe plus 27 percent Co base

15 p2669 A69-30689

Polycrystalline ferroelectrics dielectric dispersion region in decimeter-centimeter wavelength range using waveguide resonance method employing wideband strip line

22 p3997 A69-41167

MAGNETIC DISTURBANCES

Differential Faraday technique to determine electron content latitude dependence in Northern Hemisphere during magnetically disturbed periods in March 1966

01 p0146 A69-11128

Sudden magnetic field increase associated with July 8, 1966 sudden commencement observed by OGO 3 satellite in magnetotail

01 p0075 A69-11226

Whistler dynamic spectra variation studies, emphasizing distorted magnetospheric geomagnetic field structure effect

02 p0238 A69-11671

Polar geomagnetic disturbance development and decay during solar quiet and moderately disturbed periods

02 p0240 A69-11724

Electron concentration profile change in ionospheric F region in auroral zone during negative magnetic bay disturbances

03 p0423 A69-13530

Helicon waves in nonresistive cylindrical and spherical plasmas

03 p0479 A69-13961

Equatorial semiaxis of magnetospheric tail at distances between 10 and 80 earth radii for various intensities of polar magnetic disturbances

05 p0753 A69-16050

Magnetic disturbance vector distribution during polar magnetic substorm

05 p0755 A69-16271

Cut-off boundary latitude and electron flux changes in midnight sector of outer radiation belt during magnetic bay periods from Injun 4 satellite data

07 p1204 A69-18836

Hourly N/h/ profiles of F region calculated from nomograms by normal integral method during magnetic disturbance, measuring region temperature

10 p1687 A69-23928

Polar geomagnetic disturbances global current systems representation by prototypes of equivalent current systems

10 p1688 A69-23937

Ionospheric irregularities drift and anisotropy parameters variation with true reflection height during magnetically disturbed conditions

10 p1659 A69-24062

Recurrent geophysical disturbances associated with solar active regions and low latitude background field pattern on solar surface magnetic fields

11 p1964 A69-25415

Auroral cosmic noise absorption relationship to auroral geomagnetic disturbances, investigating absorption diurnal distribution

12 p2071 A69-26706

Solar control of day-to-day variability in phase of solar diurnal variation of horizontal magnetic intensity on quiet days

12 p2073 A69-26954

Magnetospheric ring current model from ground stations data to interpret observed magnetic field disturbances

13 p2253 A69-27699

Whistler dynamic spectra variation studies, emphasizing distorted magnetospheric geomagnetic field structure effect

13 p2257 A69-28702

High latitude ionization spikes observed by POGO spacecraft, noting frequency correlation with magnetic disturbances and development by high energy electron injections

14 p2511 A69-28950

Tangential solar wind discontinuity observed by Vela 2A satellite, producing ground magnetic disturbances conjunctively with magnetospheric, ground and ionospheric currents

14 p2512 A69-29041

Radio waves propagation along polar auroras region, obtaining ionospheric parameters for magnetic disturbances based on penetration probability

14 p2436 A69-29058

Polar auroral region displacement ascribed to distant magnetic field disturbances, proposing calculation method

14 p2436 A69-29059

Sporadic electron flux contribution to high latitude geomagnetic disturbances at outer radiation belt boundary estimated from Elektron 1 and 2 observations

14 p2438 A69-29079

Rocket measured electron densities of nighttime auroral E region over Canada at different magnetic activity levels, noting frequency and plasma density relations

14 p2439 A69-29117

Magnetic field variations in magnetosphere and interplanetary space correlated with polar magnetic disturbances from dynamic morphology data

14 p2441 A69-29387

Corpuscular radiation intensity during geomagnetic disturbances measured during rocket flights at 50-100 km, discussing effects on lower ionospheric radio absorption

15 p2677 A69-31327

Ion-neutral air motion in F region under time dependent electric and constant magnetic field effect, using partial differential equations

16 p2777 A69-32181

Equatorial electrojet north-south cross sections in Pacific observed by airborne equipment during magnetically quiet day, moderately disturbed day and solar eclipse

16 p2777 A69-32182

Latitude variations of delays between spread F and magnetic activity shown to be different at various parts of solar cycle

16 p2779 A69-32194

Synoptic observations of F 2 region in magnetically conjugate regions of Kerguelen and Archangel, comparing critical frequencies during magnetic and ionospheric disturbances

16 p2784 A69-32612

Polar auroral zone boundaries from C-180 camera photographs related to magnetic disturbance level, noting evening-morning asymmetry

17 p2963 A69-33951

High latitude geomagnetic disturbances, incoming electron fluxes and riometric absorption relationship in lower ionosphere studied by X ray bremsstrahlung with sounding balloons

17 p2964 A69-33961

Daytime magnetoionospheric disturbances in auroral zone, discussing time lag of perturbations for absorption and geomagnetic field bays

17 p2964 A69-33962

Geomagnetic disturbances intensity spatiotemporal distribution at Northern Hemisphere high latitudes during IGY and IQSY

17 p2965 A69-33966

Auroral absorption maximum frequency correlation with years of solar activity reduction and magnetic activity from riometric data long term variations

17 p2968 A69-33991

Correlation between disturbances in troposphere and in geomagnetic field observed after widespread high winds and magnetic storms, using superposed epoch method

18 p3127 A69-34648

Antarctic VLF emissions observations at 12 kHz, showing dependence on geomagnetic disturbances, auroras and radio absorption in ionosphere

18 p3102 A69-34964

Earth ionosphere and magnetosphere electrodynamic state analyzed as function of neutral gas small scale motions, considering magnetic disturbances and ionospheric discontinuities

20 p3519 A69-37026

Ionospheric and magnetic disturbances at midlatitudes related, noting individual and simultaneous disturbances

20 p3527 A69-37673

Equatorial semiaxis of magnetospheric tail at distances between 10 and 80 earth radii for various intensities of polar magnetic disturbances

20 p3532 A69-37959

High latitude magnetospheric convection patterns determined from ionospheric current distribution using magnetic disturbance plots

21 p3709 A69-38503

Auroral electric current system model to explain magnetic disturbances associated with auroral breakups

21 p3710 A69-38505

Long time scale magnetodynamic noise in geomagnetic tail, discussing hourly ranges of fluctuations measured by IMP 1 satellite and planetary K index correlation

22 p3935 A69-39967

Distinction between faint and bright sources of slowly varying solar microwave emission components applied to geomagnetic activity statistics

22 p4020 A69-40306

Short lived Forbush decreases, discussing phase differences between stations due to asymptotic directions changed by geomagnetic field and spatial anisotropy

23 p4204 A69-41480

Geomagnetic disturbances relations to cosmic ray diurnal variation phase and amplitude, including Forbush decreases

23 p4204 A69-41483

MAGNETIC DOMAINS

Domain structure of barium titanate single crystals during polarization reversal by sinusoidal AC field

06 p0981 A69-17893

Magnetic domain structure in supercritical ferromagnetic films with perpendicular anisotropy

12 p2143 A69-26458

Flux grown magnetic garnet crystal internal defects analyzed by etching and Lang X ray transmission topography, revealing tubular structural deviations

16 p2825 A69-31692

MAGNETIC EFFECTS

Light scattering from plasmas embedded in homogeneous magnetic field, discussing solid state and high temperature gas plasmas

01 p0125 A69-10015

Density gradient measurement method for plasma column with propagation and electric field perpendicular to external magnetic field

01 p0128 A69-10390

Axial magnetic field effect on exploding wire phenomenon, studying direct interaction

01 p0118 A69-10660

Current/field characteristic of n-type GaAs, using high power microwave techniques in presence and absence of transverse magnetic field

01 p0139 A69-10819

Electromagnetic wave path emitted by artificial satellites across anisotropic ionosphere due to geomagnetic field determined by computer program

01 p0068 A69-11115

Laminar natural convection of electrically conducting fluid under magnetic field, noting temperature profiles

01 p0134 A69-11407

Solar eclipse effect on geomagnetic field at and near dip equator observed at Huancayo Observatory, Peru

02 p0241 A69-11727

Solar eclipse effects on ionospheric conductivity and geomagnetic field at and near dip equator observed at Huancayo, Peru

02 p0241 A69-11728

Laser produced sparks in 200 kG magnetic field in air, butane and helium at atmospheric pressure

02 p0260 A69-12659

Magnetic field effect on amplitude, frequency and form of LF oscillations in Gunn diodes

02 p0222 A69-12684

Magnetic shear effect on stability of electron-neutral collision dominated plasma, noting helical perturbations onset

03 p0473 A69-12925

Galactic cosmic ray modulation by interplanetary magnetic fields, discussing compatibility of several models with experimental data

03 p0498 A69-12933

Existence and stability of periodic waves in cold collisionless plasma in magnetic field

03 p0474 A69-13143

Diurnal, magnetic and solar cycle dependences of auroral emission variations and auroral occurrence

03 p0420 A69-13325

Magnetic retuning of resonator with helical electron flux /gyromonotron/ in starting and prestarting modes

03 p0407 A69-13979

Midlatitude nighttime total ionospheric electron content during magnetically disturbed periods from geostationary satellites Canary Bird and ATS 3

03 p0426 A69-14030

Nonlinear mechanism for solar surge involving rapid acceleration of high electrical conductivity and macroscopic dimension plasma regions

03 p0516 A69-14044

Uniform external magnetic field effect on electric potential distribution within ion-electron beams near planar emitting surface

03 p0482 A69-14214

Cosmic ray time variation and anisotropies near earth, discussing galactic and solar cosmic rays, trajectories in geomagnetic field, etc

03 p0504 A69-14236

Magnetic field dependences of Josephson critical current in high and low current Josephson junctions, discussing influence of induced self field

04 p0640 A69-14437

Magnetic field effects on heat transfer between Ar plasma flow and channel wall, noting effects of temperature and Reynolds number

04 p0636 A69-14989

Transverse magnetic field effect on three dimensional nonisothermal lubrication layer of conducting gas at small magnetic Reynolds number

04 p0607 A69-14990

Dispersion of solute in electrically conducting fluid flowing between two parallel plates in magnetic field

04 p0638 A69-15194

Spherical shock wave propagation in polytrope with poloidal magnetic field, noting application to shock waves in magnetic stars

04 p0664 A69-15438

Stabilizing influence of axial magnetic field on confined vortex flow of aqueous electrolytic conductor generated by two dimensional wall jets

05 p0798 A69-15611

Electron cyclotron instability and HF ionization in beam-plasma experiment using electron beam guided by magnetic field through He gas

05 p0798 A69-15612

Charged particle motion in constant direction magnetic field varying exponentially with time, discussing electric field effect on particle motion

05 p0801 A69-15744

Polar aurora incident energetic particles spectroscopic analysis, showing system of lines and bands intensity dependence on particle energy spectrum and magnetic activity

05 p0752 A69-15799

Linc broadening possibility for Q switched iodine laser with aid of magnetic effect/Zecman effect/, noting energy storage capability increase

05 p0773 A69-16288

Time independent solar wind equations applied to spherical symmetry and radial magnetic field at solar surface, noting thermal conductivity anisotropy

05 p0817 A69-16703

Magnetoplasticity induced in metal by high magnetic fields, examining stationary flow in two dimensional deformation

05 p0844 A69-16804

High Q magnetically tunable microwave filters using magnetodynamic modes in ferrite spheres

06 p0892 A69-16831

Transverse magnetic field effect on ohmic plasma heating in Tuman apparatus

06 p0963 A69-16906

Solar flare eruptions due to current disruption, leading to magnetic energy transfer from whole current circuit to very small volume

06 p0995 A69-17444

Alternated magnetic field effects on lasing in ionized Ar

06 p0934 A69-17467

Plasma flute instability in magnetic trap with wall/plasma interface, using system of sensors and amplifiers

06 p0966 A69-17544

Ion laser emission cessation with increasing pressure, magnetic field and current strength due to lower transition level lifetime increase

06 p0934 A69-17682

VLF radiation bursts /July-October 1966/ in U.S.S.R., noting detection probability increase with increasing magnetic activity

06 p0920 A69-17731

Magnetic activity dependence of VLF emission properties at magnetically conjugate points

06 p0920 A69-17735

Damping boom flutter and magnetic dipoles effects on attitude stability of gravity gradient satellites with three axis stabilization

07 p1227 A69-18332

Output polarization rotation sensitivity to axial magnetic field varied by variable angle quartz flat inside He-Ne laser resonator

07 p1198 A69-18646

Equatorial hourly storm time part of disturbances field for 1958, discussing magnetic storm effects

07 p1124 A69-18822

Hot plasma containment by magnetic field, presenting results from stellarator for toroidal sheared magnetic field properties

07 p1190 A69-18929

Axisymmetric turbulent conducting fluid jet propagation in longitudinal magnetic field without induction

07 p1192 A69-19019

Kelvin-Helmholtz instability for interface between two uniform superposed fluids with constant densities and velocities in horizontal motion in oblique magnetic field

07 p1182 A69-19274

Rayleigh-Taylor instability for interface between two uniform superposed fluids under combined effect of horizontal and vertical magnetic fields

07 p1182 A69-19275

Electron plasma and magnetic field effects on polaritons in semiconducting GaAs studied by Raman scattering of light at small angles

07 p1200 A69-19401

Gas breakdown in HF uniform electric field with/without steady transverse magnetic field

07 p1194 A69-19415

Unsteady MHD convective flow with suction of viscous incompressible electrically conducting fluid above vertical porous wall, noting horizontal magnetic field effect

07 p1195 A69-19477

Turbulent incompressible MHD flow between two parallel smooth plates in transverse magnetic field, determining magnetic Reynolds number

07 p1195 A69-19736

Electron anomalous magnetic moment effect on nonlinear Lagrangian of electromagnetic field, deriving additional nonlinear corrective term

08 p1353 A69-19781

Stability of plane vortex sheet in magnetic fields, noting stabilization effect of compressibility for nonmagnetic case

08 p1358 A69-19797

Primordial magnetic field effects on spatially homogeneous cosmological models with anisotropic Euclidean metric

08 p1383 A69-20049

Earth internal magnetic field effects on cosmic ray measurements, dipole approximation and effect of external sources

08 p1378 A69-20219

Behavior of bounded and free arc discharges under action of transverse magnetic fields and gas flows

08 p1366 A69-20767

Impurity elimination from hydrogen plasma jets injected from coaxial source normal to octupole magnetic field

08 p1370 A69-21016

Longitudinal polarization behind front of plasma flow interacting with transverse magnetic field, showing electric potential and magnetic field exhibit structural fluctuations

08 p1370 A69-21018

Ion-acoustic wave excitation in plasma layer affected by incident p-polarized magnetic wave, deriving expressions for reflection, transmission and energy absorption coefficients

08 p1370 A69-21025

MGD stagnation point flow, discussing relaxation region influenced by magnetic field

09 p1543 A69-21300

Eleven year cyclicity of geomagnetic activity from Sverdlovsk Observatory data, noting possible relation with structural features of solar activity cycles

09 p1486 A69-21552

Antiferromagnetic semiconductor transformation into metal in magnetic field

09 p1556 A69-21672

Stark broadening of Balmer H alpha, H beta, H gamma and H delta lines in plasma region in strong magnetic fields

09 p1542 A69-22248

Plasma cavity shape formed by magnetic field effect due to several parallel line currents

09 p1553 A69-22569

HF magnetic field effect on oscillations and instabilities of plasma confined by fixed magnetic field

10 p1739 A69-23623

Fe-Fe interactions influence on increase in thermoelectric power with applied magnetic field at low temperatures for dilute alloys of Fe in Au

10 p1639 A69-23861

Coupling coefficients for integral charged component of cosmic rays determined from measuring azimuthal geomagnetic effect on rays observed in crossed telescopes

10 p1770 A69-23925

Velocity profiles of turbulent plasma flow in circular tube during application of longitudinal homogeneous magnetic field

11 p1922 A69-24234

He-Ne laser radiation frequency spectrum as function of transverse magnetic field determined by photoheterodyne method

11 p1894 A69-24622

Auroral infrasonic waves morphology related to temporal and spatial distributions of supersonic auroral motions during polar magnetic storms

11 p1878 A69-25152

MHD free convection from horizontal isothermal plate in vertical uniform magnetic field, considering boundary layer thickness

11 p1930 A69-25277

Magnetic field effects on rotational MHD flow in container, noting Taylor-Proudman theorem, Ekman layers and vertical Stewartson boundary layers

11 p1930 A69-25279

Magnetic anomalies off Cape Hatteras explained as possible edge effect, discussing ocean and continental magnetic crusts and igneous and magnetic rocks

11 p1879 A69-25405

Magnetically selective microwave filters using magnetodynamic natural oscillations in premagnetized ferrite sphere at cavity center

11 p1855 A69-25626

Electromagnetic wave propagation cut-off in slightly noncompensated electron hole plasma, discussing wave evanescence above critical magnetic field value

12 p2133 A69-25926

Power output of He-Ne laser as function of transverse magnetic field strength

12 p2104 A69-26023

Laser diode output efficiency increased in presence of transverse magnetic field suppressing higher order TE and TM modes

12 p2039 A69-26353

Ion cloud ambipolar diffusion and motion dependence on initial configuration and close magnetic field alignment above 95 km, discussing observations of meteor trains

12 p2074 A69-26961

Coherent radio emission mechanism in quasars and supernova remnants, discussing magnetic effects

12 p2168 A69-27050

MHD Stokes flow for rotating disk in parallel magnetic field, showing Lorentz force inhibiting effect on fluid motion

13 p2305 A69-27325

Magnetic curvature effect on collisionless plasma density gradient drift instabilities, covering mean ion larmor radius and Alfvén modes

13 p2305 A69-27375

Stationary magnetic field effect on sum and difference frequency generation due to nonuniform RF electric fields applied externally to plasma

13 p2305 A69-27376

Electron gas behavior in nondegenerate envelope of magnetic white dwarf, discussing increased opacity due to magnetic fields

13 p2343 A69-27624

Applied magnetic field effects on longitudinally magnetized reciprocal ferrite phase shifters, showing shift type dependence on guide electrical thickness

13 p2229 A69-27673

Local stability of rotating stars in toroidal and poloidal magnetic fields, using linear stability analysis

13 p2346 A69-27707

Cadmium arsenide carriers effective mass under strong transverse magnetic field, noting restricted role of thermal EMF and Hall coefficients

13 p2318 A69-27897

Soviet monograph on design and theory of linear induction pumps for liquid metals covering electromagnetic phenomena, optimized dimensions, etc

13 p2209 A69-27926

Fluctuations in electric field induced by plasma flow in constant magnetic field, performing spectral analysis of voltage and current fluctuations in plasma

13 p2310 A69-28029

Deuterium plasma jets passage through pulsed magnetic field by means of thermal and diamagnetic probes, noting magnetic field strength effect
13 p2311 A69-28107

Plasma jets tangential injection into toroidal magnetic field, discussing polarization interaction and depolarization effect
13 p2311 A69-28108

High pressure AC arc heater system design criteria, discussing magnetic field, chamber gas flow, stabilizing elements, etc
[AIAA PAPER 69-348] 13 p2243 A69-28283

Magnetized plasma waveguide dispersion characteristics using Maxwell equations, stressing interaction of electron beam with wave modes
13 p2315 A69-28571

Magnetic and electric field effects on undamped electron-hole LF frequency plasma oscillations in spatially homogeneous nonpolar semiconductor
13 p2323 A69-28581

Biological effects of low magnetic field environments studied by physiological, visual and psychological tests on animal, plant and human subjects
13 p2211 A69-28596

Superconductivity methods to neutralize ambient magnetic field by free electrons motion for nonmagnetic environments
13 p2244 A69-28604

Magnetic damping of homogeneous cylindrical satellite rotation about transverse axis
14 p2530 A69-29065

Potential distribution between point in interelectrode gap and thermionic converter cathode in collisionless mode under transverse magnetic field
14 p2401 A69-29235

Peltier measurements below 4 K capable of measuring low Seebeck coefficient on high resistivity alloys and in presence of magnetic field
14 p2449 A69-29563

Longitudinal electric field penetration into plasma slab in constant magnetic field
14 p2493 A69-29665

Magnetic field effect on heat and mass transfer in incompressible fluid MHD flow
14 p2500 A69-29901

Pressure drop fluctuations amplitude and frequency effect on channel resistance and magnetic field effect on fluctuations intensity in laminar conducting fluid flow
14 p2501 A69-29909

Longitudinal pressure distribution in MHD channel with electrodes parallel to applied transverse magnetic field
14 p2501 A69-29918

Conductivity tensor of collisional plasma in magnetic field, basing method on iterative procedure
14 p2503 A69-29999

Electrical conductivity tensor of many component collisional relativistic plasma in magnetic field and near equilibrium, expressing collisional part as momentum integral
14 p2503 A69-30000

Ambipolar to free diffusion transition in magnetized slab plasmas, discussing basic equations, iterative numerical procedure, characteristic parameters and H plasma
15 p2657 A69-30023

Electron densities measurement in plasmas in magnetic fields from profiles of spectral lines, noting Stark and Zeeman effect
15 p2657 A69-30027

Disaccommodation component of magnetic aftereffect causing dynamic absorption of HF magnetic energy in ferrites
15 p2665 A69-30038

Shield facility and Helmholtz coil system used to investigate chromic effects on man of zero magnetic field regulated to cancel geomagnetic field variations
15 p2586 A69-30382

Stagnation flow of viscous fluid against rotating magnetized disk, determining effects on magnetic and velocity fields, currents and shear stresses
15 p2659 A69-30674

X pocket Fermi surface of ferromagnetic Ni, considering magnetic breakdown effects
15 p2668 A69-30687

Magnetic field effect on neutron beta decay rate, considering calculations applicability to elementary particle production
15 p2690 A69-30694

Temperature and density models for coronal green line enhancements with and without magnetic field effects, using graded height spectrograms
15 p2693 A69-30782

MHD stability and equilibrium of toroidal high beta configurations achieved by superimposing oscillating magnetic field on linear plasma column
15 p2660 A69-30877

Atmospheric density dependence on solar and geomagnetic activity at low latitudes, discussing atmospheric expansion
15 p2605 A69-31441

Lattice component of heat conductivity in n-type cadmium arsenide at low temperatures by suppressing electron component of conductivity with strong transverse magnetic field
16 p2824 A69-31568

Magnetic field effect on thermal convection onset in compressible polytropic atmosphere compared with results from thin layer approximation
16 p2855 A69-31658

Radar Thomson scatter from nonthermal steady state level of plasma waves in ionosphere measured, studying role of angle between wave vector and magnetic field
16 p2818 A69-31678

Physics of solids in intense magnetic fields - Conference, Chania, Crete, July 1967
16 p2826 A69-31819

Magnetoquantum-electric effect, analyzing center motion of cyclotron orbit during photon and phonon absorption and current quantity
16 p2826 A69-31823

External magnetic force and internal Coulomb force influence on carriers in conduction or valence band of semiconductor, considering H atom spectra
16 p2826 A69-31824

Magnetic field effects on ultrasonic propagation in high field superconductors
16 p2826 A69-31825

Hydrodynamic parameters of annular Couette flow in longitudinal magnetic field for variable Reynolds and Mach numbers
16 p2821 A69-31953

Auroral absorption occurrence patterns mappable onto magnetotail developed as function of magnetic activity, discussing magnetotail neutral sheet source width changes
16 p2848 A69-31968

Self consistent ring current of radiation belt under combined influence of earth dipole field and field due to currents of particle motions
16 p2776 A69-32096

Plasma cluster interaction with axially symmetric magnetic field, deriving plasma diamagnetic current, inductance and resistance from measured coil flux dependence on distance
16 p2823 A69-32365

Eleven year cyclicity of geomagnetic activity from Sverdlovsk Observatory data, noting possible relation with structural features of solar activity cycles
16 p2784 A69-32547

Nonequilibrium ionized gas flow past insulated wall with corners under magnetic field, discussing flow characteristics
17 p3010 A69-32865

Geomagnetic field effects on microwave noise spectrum in earth-ionosphere resonator, calculating field energy spectrum near resonance maximum, discussing excitation by lightning
17 p2918 A69-33034

Splintering loop prominences, noting 7 October 1967 prominence interpretable as ejected prominence streamer capture by transverse magnetic fields of loop
17 p3029 A69-33052

Earth quadrupole moment effects on precession of gyroscope in satellite in equatorial orbit
17 p2972 A69-33072

Flywheels desaturated by magnetic action for optimizing stabilization system of satellite in circular orbit [ONERA-TP-732] 17 p3049 A69-33241

Magnetic field effects on rotating cone compressible boundary layer at zero angle of attack, describing changes in drag coefficient, torque and velocity profiles [AIAA PAPER 69-721] 17 p2892 A69-33484

Transverse magnetic field effect on shear turbulence structure of magneto-fluid-mechanic pipe flow with and without heat transfer [AIAA PAPER 69-723] 17 p3012 A69-33497

Ta type I and II wire resistance in transverse magnetic field during superconducting to normal transition, discussing strain and impurity effects
17 p3016 A69-33791

Collisionless plasma heating mechanisms from current layer turbulence in theta pinch experiment and shock wave front structure as function of initial magnetic field
17 p3013 A69-33824

Wave propagation in plasma filled cylindrical waveguide in axial magnetic field, approximating plasma density profile by WKB method
17 p2926 A69-33848

Magnetic activity influence on polar auroras height
17 p2963 A69-33953

Diurnal sporadic E layer height variations analyzed for singularities in height peak behavior as function of geography, season and magnetic activity
17 p2968 A69-33996

Geomagnetic field latitudinal variation effect on cutoff frequencies of proton whistlers, discussing LF electromagnetic wave propagation in cold multicomponent plasma
18 p3100 A69-34253

Magnetic declination effect on F 2 layer critical frequency diurnal variations attributed to vertical ionospheric drift due to neutral air winds
18 p3126 A69-34256

Quiet solar wind model with magnetic field numerically calculated, obtaining coronal electron densities and angular momentum near earth
18 p3186 A69-34301

Elastic beam-plate vibration natural frequency and dynamic instability in transverse static or oscillating magnetic field [ASME PAPER 69-APM-B] 18 p3215 A69-34400

Microwave reflection and noise emission from cylindrical rare gas afterglow plasmas in axial magnetic field measured near electron cyclotron resonance
18 p3127 A69-34436

Trapped particle acceleration by random bimodal diffusion in inhomogeneous magnetic field accounting for high energy particles trapped in earth radiation belts
18 p3186 A69-34808

Whistler vertical propagation downwards through inhomogeneous ionosphere in vertical magnetic field, deriving wave equation, calculating transmission and reflection coefficients
18 p3130 A69-34972

Magnetic field effect on Gunn diode vibrations and LF oscillations, noting increase in threshold field and decrease in threshold current
18 p3183 A69-35267

Equilibrium state of diamagnetic plasma configuration in inhomogeneous magnetic fields with complex potential near neutral point, noting solar flares and magnetic traps
19 p3380 A69-36467

Gravitational stability of infinite conducting fluid cylinder in axial magnetic field and surrounded by fluid of different density
19 p3380 A69-36483

Magnetic field effects on emission line shift, threshold current and power output of GaAs injection laser, discussing spontaneous radiation in magnetic field
19 p3387 A69-36529

GaSb p-n injection laser output at 4.2 K in strong transverse magnetic field, deducing effective mass and g-factor from stimulated emission peak shift
19 p3387 A69-36530

Anomalous phenomenon in resistance and magnetoresistance of cleaved InAs surface, plotting temperature and magnetic field variation effects, proposing explanation of anomaly
19 p3388 A69-36543

Hot electron behavior in n-type InSb under magnetic fields at 4.2 and 1.7 K, plotting current-voltage and current-Hall voltage characteristics, etc
19 p3388 A69-36544

Unsteady laminar MHD flow of electrically conducting viscous fluid between porous coaxial circular cylinders under radial magnetic field
20 p3581 A69-36912

Structure of isolated MHD shock wave in viscous heat-conducting radiating gas finite electrical conductivity and transverse magnetic field
20 p3581 A69-37189

He-Ne laser output intensity saturations in presence of axial magnetic field, noting moving and fixed minima
20 p3553 A69-37433

Plasma ion and electron concentration perturbations in wake of body moving at high velocity in collisionless plasma under steady magnetic field
20 p3459 A69-37659

F zero layer occurrence relation to solar, magnetic and ionospheric activity levels variations from Ashkhabad observations /1958- 1964/ 20 p3527 A69-37671

Alternated magnetic field effects on lasing in ionized Ar
20 p3555 A69-37950

Flares and fast processes interrelation with active region stationary filaments, filament field magnetic envelope explosion stimulation of surges, plasma stream ascents, etc

20 p3591 A69-38042

Radial diffusion coefficient calculation in presence of magnetic shell splitting in magnetosphere

20 p3534 A69-38094

Polarized radiation resonance scattering in weak uniform magnetic field, using Monte Carlo method to trace and count photons

20 p3577 A69-38157

Incompressible electrically conducting fluid in presence of magnetic field and Coriolis forces, analyzing Rayleigh-Taylor instability by variational principles

20 p3577 A69-38195

Luminous tenuous collimated electron beam from plume of MPD arc in fiberglass vacuum tank, examining beam trajectory in geomagnetic fields

20 p3582 A69-38236

Normal ionizing shock waves in H, analyzing shock velocities as function of drive magnetic field using Chapman-Jouguet hypothesis

21 p3691 A69-38332

Momentum and energy equations for fluctuating flow of viscous incompressible conducting fluid past flat plate with time dependent suction under transverse magnetic field

21 p3691 A69-38445

Magnetic activity effects on horizontal drifts, anisotropy and random change characteristics of E region ionization irregularities

21 p3715 A69-38561

Parameters of DC discharge between concentric cylinders calculated for plasma probes by pressure theory, noting ion neutral collisions and magnetic field effects

21 p3776 A69-38712

Electromagnetic wave reflection and transmission from boundary between semiinfinite plasma and air by applying static magnetic field

21 p3672 A69-38743

Current carrier concentration and magnetic field as factors influencing laser frequency resonance mixing in semiconductors with narrow forbidden bands

21 p3737 A69-38998

Plane electromagnetic waves penetration into ferromagnetic medium with permeability increasing with magnetic field, showing nonlinearity effect

21 p3771 A69-39109

Multimode He-Ne laser radiation polarization modulation as function of magnetic field, cavity anisotropy and frequency, using Macaluso-Corbino effect

21 p3739 A69-39447

Uniformly and differentially rotating stars taking into account magnetic fields effects, discussing radiative and hydrostatic equilibrium in nonspherical configurations, stellar atmospheres, etc

21 p3812 A69-39519

Microwave absorption by Ar plasma of positive column discharge in waveguide under inhomogeneous magnetic field

21 p3778 A69-39547

Magnetic declination effect on altitude of top of F 2 ionospheric layer at midlatitudes using M/3000/F 2 transmission factor

21 p3717 A69-39577

MHD pivoted slider bearing with convex pad surface under azimuthal magnetic field

21 p3733 A69-39744

Geomagnetic field and aerodynamic perturbation effects on satellite motion about center of mass, using asymptotic methods of nonlinear oscillation theory

21 p3830 A69-39835

Manned relativistic space flight limitations dependence on biomagnetic levitation of human body in inhomogeneous magnetic field to compensate inertial forces during acceleration

22 p3889 A69-39906

Magnetoplasma with Maxwellian velocity distribution, investigating quantitatively longitudinal dielectric function

22 p3988 A69-40066

Turbulent Hartmann flow between rough walls in transverse magnetic field, determining field influence on resistance coefficient

22 p3989 A69-40255

Laminar MHD flow in porous walled channel in transverse magnetic field, determining velocity distributions, induced fields and current over channel cross section

22 p3989 A69-40256

Magnetic field inhomogeneities effect on line contours and magnetographic measurements, constructing

two stream models using Unno solution of transfer equations

22 p4019 A69-40288

Variable magnetic field effect on rotation of solar outer layers, applying to spectroscopic observations of rotation velocity at solar limb

22 p4019 A69-40293

Hypersonic flow for low Reynolds number, including magnetic field and wall temperature effects on heat transfer and skin friction for blunt shapes

22 p3860 A69-40540

Pitch angle distribution of cosmic ray electrons in decreasing magnetic field for waves in ionized plasma, noting anisotropy due to synchrotron radiation

22 p4006 A69-40642

Aligned uniform magnetic field effect on hydromagnetic stability of two dimensional incompressible electrically conducting jet flow with large Reynolds number

22 p3931 A69-40687

Pulsar magnetic models, coherent radio emission mechanisms, radiation polarization, data summary and astrophysical nature

22 p4030 A69-40905

Primordial He 3 and deuterium production from magnetic effects during nucleosynthesis epoch of big bang cosmologies

22 p4035 A69-41210

Hydrodynamic stability of conducting fluid in external magnetic field subject to attraction of external spherically symmetric gravitational field

23 p4213 A69-41717

Equilibrium plasma configurations in magnetic field of two dimensional dipole analyzed under similar conditions to magnetospheric tail formation with neutral hot plasma layer

23 p4205 A69-41835

Magnetic activity effect on electron density in topside ionospheres determined from Alouette 1 data statistical analysis

23 p4156 A69-41856

Day-to-day changes of cosmic ray diurnal variation measured on meson and neutron components, showing relationship with interplanetary magnetic field

23 p4206 A69-42012

Homogeneous axisymmetric anisotropic cosmological models, analyzing magnetic fields and initial anisotropies effect on 3K radiation and primordial He production

23 p4222 A69-42402

Time dependent unsteady flow of incompressible and electrically conducting fluid between two infinite disks rotating in uniform axial magnetic field

23 p4153 A69-42410

Parallel magnetic field effect on free boundary layer type flows stability of low Reynolds number between parallel streams of viscous incompressible conducting fluid

24 p4298 A69-42596

Magnetic dipole field variations effects on planetary atmosphere erosion by solar wind, discussing Mars and Venus atmospheres above ionosphere

24 p4385 A69-43224

Magnetic and electron temperature interaction effects in fast MHD shock waves in slightly ionized plasma

24 p4356 A69-43361

Self induced magnetic field influence on plasma positive column stability in longitudinal magnetic field

24 p4356 A69-43366

Moving plasma partial capture in transverse magnetic field in experimental plasma source, noting influence of repulsion effect of plasma polarization volume charge

24 p4357 A69-43469

Drift characteristics of hydrogen plasma partially captured by transverse magnetic field, finding drift rate dependence on magnetic field level

24 p4357 A69-43470

Polarization induced oscillations in forward portion of plasma flux crossing magnetic field, showing variations in maximum longitudinal potential of plasmoid

24 p4358 A69-43471

Hydrogen plasmoids in axisymmetric magnetic field with acute angle geometry produced by opposing coils, measuring induction current field and plasmoid density distribution

24 p4358 A69-43473

Time-variable pulsed transverse magnetic field used to cut off tails of plasmoids ejected from conical Plexiglas plasma gun into curvilinear magnetic field

24 p4358 A69-43476

Magnetic field energy supply to solar flares from consideration of energies in solar active regions

24 p4370 A69-43606

MAGNETIC EQUATOR

North-south ionospheric drift velocities near magnetic equator, noting marked seasonal characteristics and diurnal variations

01 p0062 A69-10138

Explorer 26 observations of solar proton penetration inside trapped radiation near geomagnetic equator

01 p0146 A69-11122

Solar eclipse effects on ionospheric conductivity and geomagnetic field at and near dip equator observed at Huancayo, Peru

02 p0241 A69-11728

F 2 layer equatorial anomaly at local noon, discussing position of trough center in latitudinal distribution of ionization

03 p0422 A69-13515

Diurnal variations of neutral and charged particle temperatures in equatorial F region

05 p0755 A69-16270

Vertical ionospheric motions near magnetic equator measured by Doppler shifts of incoherent scatter frequency spectra

09 p1489 A69-21704

Nighttime electric fields and vertical ionospheric drifts near magnetic equator concurrent measurements

09 p1489 A69-21705

Geomagnetic pulsations recorded in equatorial regions of Africa found continuous and not pearl modulated

09 p1491 A69-22051

Equatorial electrojet role in electromagnetic induction at magnetic dip equator, applying Price theory for space gradients

13 p2252 A69-27519

Diurnal variation of cosmic ray muon intensity near geomagnetic equator and primary anisotropy monitored by cubical counter telescope

14 p2512 A69-28966

Lunar tidal variations of electron concentration in F 2 region near magnetic equator showing large latitudinal dependence

16 p2776 A69-32090

Lower ionosphere electric fields and currents vertical profiles above geomagnetic equator under quiet geomagnetic conditions from rocket data

20 p3521 A69-37053

Lower ionosphere over geomagnetic equator during evening twilight characterized by solar disturbances, using rocket-borne Langmuir and plasma noise probes

21 p3702 A69-38353

Primary H nuclei flux and spectrum near geomagnetic equator, discussing emulsion stack exposure

22 p4005 A69-40520

Equatorial E sub sq and daytime blanketing sporadic E occurrence frequencies compared in magnetic equatorial zone, considering diurnal, seasonal, latitudinal and vertical variations

23 p4160 A69-42426

Magnetic dip equator position at E layer and gradient with time and altitude, using geomagnetic field models

23 p4160 A69-42428

VHF radio propagation over transequatorial circuit related to equatorial anomaly in F layer, suggesting F2/F2 propagation mode role

23 p4127 A69-42431

Ionospheric heating and velocity dependence of collision cross sections on transversely propagated equatorial hydromagnetic waves, discussing ordinary and extraordinary modes

23 p4161 A69-42437

MAGNETIC FIELD COILS

U FIELD COILS

MAGNETIC FIELDS

NT FORCE-FREE MAGNETIC FIELDS

NT GEOMAGNETISM

NT INTERPLANETARY MAGNETIC FIELDS

NT INTERSTELLAR MAGNETIC FIELDS

NT LUNAR MAGNETIC FIELDS

NT MAGNETOSTATIC FIELDS

NT NONUNIFORM MAGNETIC FIELDS

NT PALEOMAGNETISM

NT PLANETARY MAGNETIC FIELDS

NT SOLAR MAGNETIC FIELD

NT STELLAR MAGNETIC FIELDS

NT TRAPPED MAGNETIC FIELDS

Gas laser amplifier nonlinear behavior in axial magnetic fields and operating with two polarized light signals of strong or weak intensities

01 p0088 A69-10010

Megagauss magnetic field generation methods, discussing high explosives, initial field, flux compression, capacitor discharges and applications

01 p0115 A69-10049

Viscous electrically conducting fluid with aligned magnetic field flowing past flat plate at nonzero angle of attack

01 p0126 A69-10163

Electromagnetic wave propagation in superconductors, noting transmission line structure variation with magnetic fields and current and suitability for parametric amplifiers

01 p0135 A69-10176

Couette flow stability in axial magnetic field, considering time bounded perturbation energy during increasing angular velocity in radial direction

01 p0059 A69-10233

Nonlinear hydromagnetic solitary wave propagation at angle to magnetic field in fully ionized quasi-neutral collisionless warm plasma, noting isotropic pressure effect

01 p0127 A69-10336

Symmetrically truncated right angle E-plane corner, placing electric and magnetic walls in symmetry plane, solving resulting boundary value problems

01 p0044 A69-10624

Axial magnetic field effect on exploding wire phenomenon, studying direct interaction

01 p0118 A69-10660

MHD equations describing interactions between gases and magnetic fields solved by finite difference method

01 p0129 A69-10722

Particle moving in circular orbit perpendicular to axis of cylindrically symmetric magnetic field

01 p0120 A69-10816

Magnetic field data from OGO-2 spacecraft and surface magnetic observatories, noting magnetic storm occurrence and magnetospheric inflation and detection of polar ionospheric currents

01 p0069 A69-11125

MHD flow through circular, elliptic and rectangular straight channels with external magnetic field transverse to flow direction

01 p0132 A69-11209

Resistive spherical plasma expansion into external magnetic field noting magnetic stream function

01 p0132 A69-11211

Ion acoustic wave dispersion in highly ionized Ar plasma in longitudinal magnetic field, noting effects of several phenomena

01 p0133 A69-11216

Ring current particle energy density distribution for symmetric portion of magnetic storm derived from current magnetic field profile measurements

01 p0147 A69-11227

Electromagnetic wave propagation across magnetic field under relative streaming motion, noting plasma frequency cut-off

01 p0134 A69-11247

Transverse plasma velocity component effect on boundary layer structure between cold plasma and confined magnetic field

02 p0235 A69-11424

Electric discharge in gas flow with magnetic field, showing varying charged particle density as function of argon-caesium pressure

02 p0285 A69-11570

Charged particle motion caused by ELF electromagnetic waves in presence of constant magnetic field, noting earth ionosphere application

02 p0240 A69-11712

Instability of longitudinal plasma waves propagating across magnetic field in plasma with electrons and ions drifting with different velocities across field

02 p0286 A69-11830

Hydromagnetic stability of free boundary layer between two uniform streams in presence of aligned uniform magnetic field at large Reynolds number

02 p0287 A69-11832

General structure of magnetic surfaces of 3-turn helical magnetic field with axial current flow, noting closed magnetic trap production

02 p0288 A69-12168

Equations for studying plasma stability in sheared magnetic field examined for normal mode and wave packet perturbations

02 p0289 A69-12173

Electromagnetic wave scattering by turbulent plasma pulsations in external magnetic field

02 p0289 A69-12174

Current carrying curved plasma column flute instability analysis, noting effect of increasing divergence from axial symmetry on Q values

02 p0289 A69-12175

Wave measurements of normal electric field and tangential magnetic field over microwave disk antenna surfaces

02 p0219 A69-12342

Criterion for magnetic plasma stability near magnetic axis, noting parameters for deriving criterion integrand

02 p0290 A69-12355

Characteristic time on motion of magnetic lines of force in medium with Hall effect

02 p0290 A69-12399

Plasma stability under anisotropic pressure in axisymmetric magnetic fields determined by quasi-hydrodynamic approximation

02 p0291 A69-12552

Plasma diagnostics in magnetic field with thin cylindrical probe based on Langmuir method

02 p0292 A69-12556

Plasma jet motion in time constant and time variable magnetic fields noting particle deflection, polarization loss, capture and cut-off

02 p0292 A69-12558

Electromagnetic wave propagation in metals in magnetic field, noting helicon waves, magnetoplasma waves, waves with discrete spectrum or near cyclotron resonance and quantum phenomena

02 p0299 A69-12565

Magnetic field effect on amplitude, frequency and form of LF oscillations in Gunn diodes

02 p0222 A69-12684

Transverse magnetic field influence on power and polarization of helium-neon laser emission

02 p0260 A69-12844

Magnetic shear effect on stability of electron-neutral collision dominated plasma, noting helical perturbations onset

03 p0473 A69-12925

Transport phenomena in crossed electric and strong magnetic fields, developing semiclassical and quantum treatments

03 p0473 A69-12926

Axial magnetic field effect on steady linear Ekman boundary layer

03 p0474 A69-13141

Cylindrical jet stability of perfectly conducting, incompressible and inviscid fluid in presence of axial magnetic field

03 p0474 A69-13142

Ion-ion velocity space instability due to difference between ion temperatures perpendicular and parallel to magnetic field

03 p0475 A69-13154

Electric effect in ruby, discussing resonance magnetic field and transition

03 p0485 A69-13320

Nonlinear interaction of steady state circularly polarized electromagnetic wave with cold plasma in constant longitudinal magnetic field

03 p0476 A69-13381

Electromagnetic wave propagation in nonlinear media with permittivity dependent on modulus of magnetic field

03 p0396 A69-13707

Two band model for determining linear and nonlinear electromagnetic responses of small band gap semiconductors in magnetic field

03 p0487 A69-13753

Space charge plasma acceleration in axially nonuniform magnetic field

03 p0477 A69-13760

Boundary layer equations for uniform motion of semiinfinite flat plate through incompressible conducting fluid at rest and in magnetic field, using numerical method

03 p0477 A69-13794

Plasma transverse injection into toroidal magnetic field created by linear current leads to plasma confinement along magnetic force lines

03 p0478 A69-13837

Diffusion across magnetic field of unstable plasma with highly inhomogeneous density

03 p0478 A69-13840

Magnetoelastic vibrations of fluid filled cylindrical cavity in infinite solid medium in presence of uniform axial magnetic field

03 p0528 A69-13927

Upper bound for free energy of nonlocal superconductor in magnetic field, using variational method and perturbation theory

03 p0491 A69-13971

Acceleration of charged particles in strong DC magnetic field by electrostatic waves with spatially varying phase velocities integrated numerically on IBM 360/65

03 p0479 A69-14028

Electron viscosity coefficient in weakly turbulent plasma in strong magnetic field, noting electrical and thermal conductivity

03 p0480 A69-14136

Uniform external magnetic field effect on electric potential distribution within ion-electron beams near planar emitting surface

03 p0482 A69-14214

Charged particles motion in spatially modulated magnetic field solved using modification of Krylov-Bogoliubov asymptotic method

04 p0633 A69-14297

Asymptotic method for studying charged particle motion in spatially modulated magnetic field

04 p0634 A69-14298

Discontinuities in plasma situated in magnetic field, noting drift of quasi-neutral inhomogeneities of electron and ion density

04 p0634 A69-14431

MHD instability in current discharges in magnetic field stabilized by current frequency modulation higher than perturbation increment of plasma column

04 p0635 A69-14549

Magnetic field effects on heat transfer between Ar plasma flow and channel wall, noting effects of temperature and Reynolds number

04 p0636 A69-14989

Transverse magnetic field effect on three dimensional nonisothermal lubrication layer of conducting gas at small magnetic Reynolds number

04 p0607 A69-14990

Electromagnetic wave propagation in uniform anisotropic plasma, considering wave vectors perpendicular to magnetic field

04 p0637 A69-15048

Collapsing cylindrical ionizing shock in axial magnetic field, solving governing equations numerically

04 p0637 A69-15049

Transverse ionizing MHD shock waves, discussing jump conditions with magnetic field in shock plane

04 p0637 A69-15052

Magnetic lines curvature behind pseudostationary hydromagnetic shock determined, assuming parallel magnetic field and velocity vectors

04 p0638 A69-15092

Local hydromagnetic mechanism to increase magnetic fields and shape into bipolar sunspot group configuration, discussing applicability to solar atmosphere

04 p0662 A69-15243

Longitudinal and transverse magnetoresistance in n-type InSb single crystals in magnetic fields, noting preparation effect on existence magnetophonon oscillations

04 p0643 A69-15262

Vector potentials for Dirac equation derived assuming time independent external magnetic field without scalar potential

04 p0638 A69-15273

Space-time function for joint probability distribution of velocity and magnetic fields from hydromagnetic turbulence equations

04 p0638 A69-15277

Spherical shock wave propagation in polytrope with poloidal magnetic field, noting application to shock waves in magnetic stars

04 p0664 A69-15438

Magnetic field confinement of plasma produced by focusing Q switched laser output on solid deuterium pellet

05 p0798 A69-15585

Flow of two conducting immiscible liquids between parallel porous moving plates under transverse magnetic field

05 p0743 A69-15600

Boltzmann equation for weakly ionized gas electron component, solved by transformation to integral equation, applied to Lorentz gas in alternating electric field

05 p0795 A69-15619

Weak magnetic fields effect on molecular oscillator frequency taking into account Zeeman sublevels

05 p0727 A69-15643

MHD flow in square cross sectional channel in transverse magnetic field with conducting walls parallel to magnetic field

05 p0799 A69-15697

Fermi surface topology effects on Nernst-Ettingshausen coefficient from measurements in magnetic fields to 3.3 tesla and 1.2-4.2 K temperatures in metallic tin

05 p0808 A69-16357

Collision induced instability of partially ionized gases having large Ramsauer effect in external magnetic field, analyzing nonlinear characteristics

05 p0804 A69-16441

Effective collision frequency deduced from ratio of microwave conductivity to electron density in PIG discharge plasma

05 p0804 A69-16442

RF electron heating by beam-plasma interaction in uniform magnetic field

05 p0804 A69-16458

Viscous electrically conducting liquid flow through insulating porous medium in presence of transverse magnetic field in region of validity of Darcy law

05 p0805 A69-16603

Magnetic fields role in neuropsychiatric and physiological experiments, noting effect on phagocyte activity

05 p0715 A69-16627

Critical electron drift velocity threshold in surface wave amplification in semiconductor in magnetic field, noting partial effect of diffusion

05 p0810 A69-16648

Optimum magnetic field axial component and plasma gun discharge voltage for high velocity plasma injection into symmetrical cusp field

05 p0805 A69-16655

Electron plasma interaction with transverse EM wave propagating along magnetic field, calculating permittivity, density, field strength and applied frequency

05 p0805 A69-16699

Coaxial Hall plasma accelerator, noting interaction between radial applied magnetic field and axial applied electric field

05 p0806 A69-16734

Relationship between microhardness of niobium and other variables characterizing superconductivity

05 p0810 A69-16805

Spatial dispersion of electromagnetic waves reflection from moving plasma layer in magnetic field, determining transmission and energy absorption coefficients

06 p0886 A69-16895

Hydrodynamic and lattice vibrations equations for coupled waves in ion semiconductors in external electric and magnetic fields, observing sound amplification

06 p0978 A69-16897

Bounded and spatially separated plasmas wave oscillations stability in magnetic field, observing hydrodynamic slipping and drift instability

06 p0963 A69-16903

Transverse magnetic field effect on ohmic plasma heating in Tuman apparatus

06 p0963 A69-16906

Plasma confined in transverse magnetic field analyzed for drift rates, noting role of injection direction

06 p0963 A69-16907

Zeman effect in He-Ne lasers during simultaneous emissions at various gas pressures and currents in magnetic fields

06 p0932 A69-16912

Molecular and atomic beam focusing in electric and magnetic fields with helical symmetry of specified type

06 p0959 A69-16917

Hall effect and magnetoresistance for compensated n-InP samples, discussing dependence on magnetic field

06 p0978 A69-16987

Soviet satellite exploration of space magnetic fields and charged particles, noting Proton satellites and protons and carbon nuclei inelastic interactions

[UN PAPER 68-95768] 06 p0986 A69-17031

Magnetobremstrahlung /synchrotron/ and Cerenkov radiation of ultrarelativistic particles, radiation reabsorption and magnetic field measurement

06 p0962 A69-17245

Radio spectrum and cosmic ray electron data evaluated concerning conditions in Galaxy, deducing mean magnetic fields

06 p0991 A69-17309

Particle radiations and magnetic fields in metagalaxy, discussing galactic injection spectrum problems

06 p0991 A69-17310

Ionized plasma electrical conductivity in magnetic field calculated by supplementing BGK collision terms with Vlasov equation

06 p0965 A69-17482

Cusp magnetic field stabilizing superimposition on toroidal plasma discharge in polytron machine, noting role of Hall acceleration mechanism

06 p0965 A69-17514

Resonance particle effects on flute oscillation kinetic stability when resonance particles drift under influence of magnetic field inhomogeneity

06 p0965 A69-17516

Closed analytic expressions for vector potential and magnetic field generated by axisymmetric multipole line currents

06 p0965 A69-17518

Department of Defense Gravity Experiment /DODGE/ attitude stabilization simulation with time-lag magnetic damping

06 p1014 A69-17584

Ion laser emission cessation with increasing pressure, magnetic field and current strength due to lower transition level lifetime increase

06 p0934 A69-17682

Automatic closed loop distortionless control of magnetic field modulation using light sensitive resistor as one leg of attenuator

06 p0897 A69-17708

Enhanced microwave scattering by plasma instability in magnetic field, using microwave interferometer with horn antenna system

06 p0967 A69-17717

Laminar constant pressure gradient flow of viscous incompressible conducting fluid through rotating straight circular pipe with perpendicular magnetic field

06 p0967 A69-17718

Resonance in fundamental harmonic identified with Pc4 and in second harmonic with Pc3 geomagnetic pulsations

06 p0921 A69-17737

Supersonic plasma flow interaction with two dimensional magnetic dipole

06 p0967 A69-17738

Oscillating electric dipole in cold plasma with ideal conductivity along lines of force of external magnetic field

06 p0921 A69-17743

Trapped mode wave propagation for cold uniform magnetoplasma cylinder in free space, studying dipole modes and one-wave approximation

06 p0967 A69-17756

Electrostatic waves in inhomogeneous plasma in finite magnetic field, noting dispersion relation for cold plasma and stabilization of instability

06 p0967 A69-17761

Resonant frequencies and fields in circular cylindrical microwave cavity containing cold uniform magnetoplasma dielectric

06 p0968 A69-17763

Nonlinear interaction between cyclotron harmonic waves propagating perpendicular to static magnetic field in warm magnetoplasma, noting parametric amplification and mode conversion

06 p0968 A69-17766

Magnetic field generation in nonuniformly rotating plasma by current density from electron drift relative to positive ion gases due to viscous forces

06 p1009 A69-17966

Retrograde motion of electric arcs in transverse magnetic fields, using multifluid equation to predict inclination and properties

[AIAA PAPER 69-45] 06 p0971 A69-18091

Electromagnetic ion acceleration in steady electric and magnetic fields chosen to match fields of Alkali Plasma Hall Accelerator /ALPHA/

[AIAA PAPER 69-111] 06 p0985 A69-18175

Electromagnetic thrust equations for coaxial MPD accelerator, noting role of externally applied magnetic field

[AIAA PAPER 69-108] 06 p0972 A69-18197

High efficiency ion lasers without additional axial magnetic field

06 p0938 A69-18221

Axisymmetric poloidal vacuum magnetic fields in low pressure plasmas in MHD equilibrium

06 p0972 A69-18230

Three axis gravity gradient stabilization system to minimize stray magnetic fields

07 p1226 A69-18329

Magnetic field at synchronous equatorial orbit by analyzing magnetometer data recorded by ATS 1 satellite during magnetic storms, geomagnetic substorms and quiet times

07 p1123 A69-18343

Structure of plane shock wave of arbitrary force propagating across magnetic field in hot rarefied plasma

07 p1190 A69-18692

Steady rotation of insulating body of revolution in unbounded electrically conducting fluid permeated by applied axial magnetic field

07 p1190 A69-18814

Hot plasma containment by magnetic field, presenting results from stellarator for toroidal sheared magnetic field properties

07 p1190 A69-18929

Monocenergetic relativistic electrons stream gyrating along cold magnetoactive plasma with pitch angle radiatively unstable with respect to synchrotron radiation

07 p1191 A69-18958

Solar type 4 bursts characteristics accounted for by cyclotron mechanism, assuming models of spot magnetic field configuration and electron density distribution

07 p1205 A69-18959

Stabilization of plasma filament with alternating current by quadrupole magnetic field

07 p1191 A69-18987

Interaction between shock wave and magnetic field of current carrying grid for ideal gas with constant coefficients, discussing dissipation, ionization and Joule heat

07 p1120 A69-18998

Laminar conducting wall jet injected in transverse magnetic field, analyzing partial differential equations obtained

07 p1192 A69-19020

Pulsation energy balance of turbulent jet of conducting fluid expanding in longitudinal magnetic field

07 p1192 A69-19021

Gas dynamic shock wave entry into magnetic field, discussing field distribution behind shock front and diffusion and medium motion effects on penetration depths

07 p1192 A69-19022

Longitudinal and transverse conductivities and anisotropy tangent for noncharged plasma in magnetic field

07 p1193 A69-19025

Maxwell equations solution for linear induction MHD machine coil area field components, allowing for finiteness of magnetic permeability of iron

07 p1059 A69-19028

He-Ne and He-Xe laser lines in IR tuned by axial magnetic field, observing Stark patterns of organic molecules

[IEEE PAPER C-5] 07 p1150 A69-19050

Statistical theory of ionization for magnetoactive plasma with nonequilibrium concentration level and nonequilibrium energy distribution

07 p1193 A69-19142

Kelvin-Helmholtz instability for interface between two uniform superposed fluids with constant densities and velocities in horizontal motion in oblique magnetic field

07 p1182 A69-19274

Rayleigh-Taylor instability for interface between two uniform superposed fluids under combined effect of horizontal and vertical magnetic fields

07 p1182 A69-19275

Hydromagnetic wave propagation and generation in magnetosphere, discussing hydromagnetic waves in uniform and axisymmetric magnetic fields

07 p1208 A69-19356

Electron plasma and magnetic field effects on polaritons in semiconducting GaAs studied by Raman scattering of light at small angles

07 p1200 A69-19401

Plasma heating dynamics by straight turbulent discharge current influenced by initial plasma parameters

07 p1195 A69-19592

High energy particles obtained by accelerating plasma with frozen-in magnetic field to relativistic velocities during scattering of fast electron beam

08 p1358 A69-19805

Plasma instability with isotropic ion or electron velocity distribution function /nonMaxwellian/, discussing magnetic field and particle energy distribution functions

08 p1359 A69-19949

Steady shock discontinuity in perfectly conducting gas flow in arbitrarily oriented magnetic field for various Mach numbers

08 p1360 A69-19988

Antenna impedances in cold plasma with perpendicular static magnetic field

08 p1281 A69-20029

Nuclear fusion reactor development, discussing magnetic field confinement of hot dense plasmas and electric power production economic possibilities

08 p1361 A69-20124

Magnetic field distribution and resistance of homogeneous type 2 superconductor cylinder at transition under effect of axial current

08 p1371 A69-20202

Positive column in longitudinal magnetic field in helium and neon, noting agreement with collision diffusion theory and Kadomtsev perturbation theory

08 p1361 A69-20212

Solution of equations of motion of charged particles in constant magnetic field and variable electric field

08 p1361 A69-20213

Ambipolar diffusion in electron concentration inhomogeneities of weakly ionized plasma in magnetic field analyzed by linearized quasi-hydrodynamic equations

08 p1362 A69-20426

HF electromagnetic wave scattering at small scale plasma turbulence in magnetic fields, discussing interactions in frequent collisions region
08 p1275 A69-20435

Spatial distribution and temporal variation measurements of magnetic fields in plasma, emphasizing pulsed discharges
08 p1364 A69-20472

Viscous stress tensor for collisionless plasma with anisotropic pressure in magnetic field
08 p1365 A69-20522

Inhomogeneous collision plasma drift instabilities in strong magnetic field analyzed by solving nonlinear equations
08 p1365 A69-20549

Slow distribution function of magnetoactive plasma, deriving kinetic equation in quasi-linear approximation for analyzing particle-HF electromagnetic wave interactions
08 p1365 A69-20550

Analog study of periodic permanent magnet focusing, considering ray equation, beam radius dependence on distance, amplitude variations, etc
08 p1285 A69-20555

Wave behavior in warm inhomogeneous plasma with magnetic field perpendicular to density gradients of unperturbed plasma, solving Maxwell-Vlasov equations by perturbation methods
08 p1365 A69-20744

Nondispersive LF mode in magnetized plasma with frequencies lower than ion cyclotron frequency, discussing plasma stability in presence of electron drift
08 p1366 A69-20750

Magnetophonon oscillations of transverse magnetoresistance of n-type epitaxial GaAs in pulsed magnetic field
08 p1373 A69-20760

Behavior of bounded and free arc discharges under action of transverse magnetic fields and gas flows
08 p1366 A69-20767

Flow analysis in magnetic annular shock tube in magnetic field varying with time
08 p1366 A69-20787

Vorticity behind shock waves in conducting gases when magnetic field is tangential or normal to shock surface using momentum equation
08 p1367 A69-20789

Plasma oscillation modes perpendicular to magnetic field used to study energy conversion by wave coupling across density discontinuity
08 p1367 A69-20795

Electromagnetic microinstabilities of plasmas associated with transverse waves propagating perpendicular to external uniform magnetic induction, noting allowable frequencies
08 p1368 A69-20804

Fast electron diffusion in stochastic magnetic field, obtaining diffusion coefficient as function of ratio of correlation time to Larmor period
08 p1368 A69-20807

Plasma stream behavior emerging from magnetic field, noting transverse velocity imparted to electrons by field
08 p1368 A69-20808

Double adiabatic MHD fluid equations for electrons and ions with pressure gradients for collisionless plasma in magnetic field
08 p1369 A69-20815

Loss cones effect of anisotropic Maxwellian velocity distribution on EM waves propagating perpendicular to magnetic field in infinite plasma
08 p1369 A69-20820

Flute instabilities in rarefied plasma with intrinsic electric field, discussing plasma density profile and uncompensation degree effects on plasma magnetic field stability
08 p1370 A69-21013

Plasma flow motion and polarizing interaction in multipole magnetic field
08 p1370 A69-21015

Hall current influence on plasma jet interaction with space periodic magnetic field created by system of coaxial coils with alternating current directions
08 p1370 A69-21017

Plasma flow from hot cathode discharge in magnetic field increases ion flux intensity and prevents flow divergence in vacuum
08 p1370 A69-21075

Electromagnetic wave attenuation propagating along external magnetic field ascribed to cyclotron wave energy absorption by resonant plasma particles
08 p1277 A69-21077

Cyclotron waves interaction when propagating in solid state plasma in magnetic field, determining amplification zones and factors
08 p1374 A69-21078

Lithium vapor fueled applied field MPD arc jet performance using open end heat pipe vaporizer and hollow cathode
08 p1561 A69-21222

Rotating plasma disturbances onset in MPD arc, determining magnetic field dependence on mass flow, background pressure and propellant
08 p1562 A69-21225

Coaxial electrodes with electric and magnetic fields to study instability in MPD arcs
08 p1563 A69-21231

Background pressure and magnetic field shape effect on MPD thruster performance, testing radiation cooled thrusters
08 p1564 A69-21239

Electron multiplication during ionized H plasma exposure to annular electric field and magnetic field, including microwave diagnostics
08 p1543 A69-21299

Amplitude modulated radio wave interaction with rarefied plasma in magnetic field, considering possible ionospheric heating by mechanism
08 p1543 A69-21543

Zero reference field for quiet day solar variations, considering magnetic field levels and errors
08 p1575 A69-21551

Ferroelectric Li niobate single crystals internal magnetic field analysis by acoustic EPF, establishing field induced hypersound resonance absorption in spin systems
08 p1556 A69-21563

Inhomogeneous collisionless plasma drift-oscillation stability in magnetic field augmented by E wave HF field
08 p1546 A69-21564

Plasma conductivity tensor components in crossed fields calculated by Boltzmann kinetic equation, noting influence of magnetic field presence
08 p1546 A69-21565

Magnetoactive plasma containing fast monoenergetic ions noting stability at drift frequencies and in terms of Alfvén wave buildup
08 p1546 A69-21566

Electromagnetic wave fluctuations and scattering in plasma in strong electric and magnetic fields at magnetoacoustic frequencies
08 p1543 A69-21569

Self focusing of plasma whistler wave along magnetic field at small threshold power
08 p1546 A69-21577

Discharge plasmas produced from solid materials at low pressures and temperatures and compressed against wall by magnetic field
08 p1547 A69-21594

Steady state currents effect on hydrodynamic waves propagated normal to magnetic field
08 p1547 A69-21662

Nonlinearity of Hall voltage induced in plasma by external magnetic field under various assumptions
08 p1548 A69-21683

Irregular regions in Antarctic ionosphere from Polar Ionosphere Beacon Satellite S-66 recordings, obtaining irregularities density from nulls clarity
08 p1490 A69-21716

Near cathode magnetic field effect on instability in linear Hall current accelerators, using geometry of field extending from anode to cathode region
08 p1568 A69-21731

Kaufman thruster performance dependence on transmission of ion extraction optics and magnetic field shape
08 p1569 A69-21878

Electrothermal instabilities of ionization region of nonequilibrium MHD generator in presence of magnetic field
08 p1548 A69-21919

Kinetic theory of electromagnetic wave passage through magnetoactive plasma, discussing dispersion and specular and diffuse reflection
08 p1550 A69-22022

Resonant interaction between traveling charge with superimposed magnetic field and Alfvén wave in plasma cylinder, showing cyclotron orbit variations
08 p1551 A69-22035

Phase characteristics and magnetic mirrors effect on charge motion in spatially periodic magnetic field
08 p1551 A69-22036

Magnetic masses of differentiating or integrating floating gyroscope effect on gyro moment sensor per-

formance, examining utilization of multipole permanent magnet
09 p1497 A69-22102

Centering force and initial rigidity of magnetically suspended bearings of integrating floating gyroscope with allowance for mutual inductance of exciting coils
09 p1497 A69-22104

Cometary magnetic fields by measuring depolarization of molecular resonance fluorescence
09 p1603 A69-22234

Plasma ion heating by external stochastic HF field, noting avoidance of special thermalization processes
09 p1553 A69-22527

Weak discontinuities in wave propagation, studying ionized gas nonsteady flow having electrical conductivity in magnetic field
10 p1727 A69-22916

Three dimensional MHD flow near forward stagnation point magnetic fields with large induction values described by differential equations, showing tendency towards two dimensional flow
10 p1727 A69-23100

Busbar effect on interaction between conducting fluid flow and traveling wave magnetic field created by long line with concentrated inductance and capacitance, deriving line gain
10 p1727 A69-23101

MHD flow and heat transfer between coaxial rotating disks under axial magnetic field, using powers expansion of Reynolds number
10 p1728 A69-23234

Transverse magnetic field and shock strength effects on curvature ratio of attached shock waves and wedge
10 p1728 A69-23238

Induced magnetic fields determination in linear DC MHD generators with ferromagnetic and nonmagnetic walls, using Fredholm equation
10 p1636 A69-23454

Conductivity and electron temperature in coaxial MHD generator plasma with magnetic field, studying Joule heating effect on performance
10 p1735 A69-23463

Closed cycle MPD experiments with applied electric and magnetic fields emphasizing current leakage, segmentation, relaxation and aerodynamic effects
10 p1738 A69-23479

Dynamic mode electromagnetic surface waves on axially magnetized single crystalline YIG and polycrystalline ferrite rods
10 p1746 A69-23513

Earth currents and magnetic field variations recording in period range 10-200 sec, computing power density spectra on analog computer
10 p1682 A69-23593

HF magnetic field effect on oscillations and instabilities of plasma confined by fixed magnetic field
10 p1739 A69-23623

Boundary conditions for nonlinear equations of MHD for vicinity of zero magnetic field line, considering plasma pinch and current density
10 p1739 A69-23626

Slow electromagnetic wave propagation along cold collisionless cylindrical plasma in axial magnetic field, noting surface wave metamorphosis into bulk waves
10 p1739 A69-23659

Spontaneous magnetic field excitation in turbulent plasma noting possible instability
10 p1740 A69-23715

Beam displacement at plasma under magnetic field connected with polarized electromagnetic wave reflections
10 p1740 A69-23724

High homogeneity sixth order superconducting solenoids with coil inner surface notch correction, describing graphical design techniques
10 p1665 A69-23857

Electromagnetic wave propagation along longitudinally magnetized plasma column surrounded by isotropic dielectric medium, without making quasi-static assumption
10 p1658 A69-24061

Linear MHD generator power characteristics at large magnetic Reynolds numbers, analyzing magnetic field distribution for sectioned and solid electrodes
11 p1824 A69-24224

Weak magnetic field dynamics in bounded conducting medium having turbulent motion induced under zero boundary conditions
11 p1922 A69-24240

Plasma wave conversion into electromagnetic waves in strong magnetic field, studying nonlinear coalescence and scattering on thermal and epithermal ions
11 p1922 A69-24245

Rotational discontinuity in plasma, noting behavior for particle reflection off front side or back side of MHD wave

11 p1923 A69-24293

Electric shock tube for measurement of plasma magnetic fields induced by shock plasma moving through DC magnetic field transverse to flow

11 p1925 A69-24311

Pfirsch-Schluter factor calculation for stationary toroidal plasma diffusion enhancement due to current along magnetic field over diffusion over that associated with diamagnetic current

11 p1925 A69-24312

Turbulence formation in conducting liquid at increasing Reynolds numbers, discussing cause of spontaneous magnetic field appearance

11 p1955 A69-24392

Dispersion relation for internal gravity wave propagation across exponentially decreasing magnetic field in conducting fluid, noting atmospheric wave propagation in ionosphere

11 p1877 A69-24564

Hydromagnetic instability onset in dissipative flow of electrically conducting fluid between rotating permeable perfectly conducting cylinders, noting oscillatory axisymmetric critical modes

11 p1926 A69-24895

HF instability of low pressure discharge in magnetic field, discussing plasma diffusion and oscillations

11 p1927 A69-24912

Excitation of plane plasma layer in magnetic field perpendicular to wave vector of excitation wave in gyrotropic waveguide

11 p1927 A69-24916

Plasma confinement experiments with Tokamak type magnetic configuration device, giving schematics for thermonuclear reactor

11 p1927 A69-25099

Thermodynamic approach to equation of state of magnetized Fermi gas, deriving energy eigenvalues of free electron in magnetic field

11 p1961 A69-25107

Hall type electromagnetic plasma accelerator, with thrust affected only by Lorentz forces in external magnetic field, compared to pure Hall accelerator

11 p1866 A69-25214

Linear interaction of electron beam and plasma in magnetic field noting convective wave instability, wave dispersion and properties behavior

11 p1929 A69-25267

Magnetic field effects on rotational MHD flow in container, noting Taylor-Proudman theorem, Ekman layers and vertical Stewartson boundary layers

11 p1930 A69-25279

Nonlinear DC magnetic fields for nonhomogeneous isotropic current free regions in presence of ferromagnetic materials, discussing analytic solutions of boundary value problems

11 p1888 A69-25311

HF electrostatic waves propagation in nonuniform plasma in uniform magnetic field, obtaining solutions of dispersion relation

11 p1931 A69-25360

Synchrotron radiation amplification by monoenergetic electron stream helically gyrating in static magnetic field of cold plasma, discussing amplification rate frequency dependence

11 p1931 A69-25361

HF electrostatic waves propagation excited by electron beam in hot inhomogeneous plasma in magnetic field, studying wave transformation and absorption

11 p1931 A69-25364

Faraday type MHD energy converters in nonequilibrium conduction mode, analyzing two dimensional current and potential distributions in plane normal to magnetic field

11 p1826 A69-25397

Constant and traveling magnetic fields MHD converters induction and finite dimensions influence analyzed by conformal mapping, separation, Fourier and finite difference methods

11 p1827 A69-25399

Motion equations for conducting paramagnetic fluid in magnetic field derived, including MHD equations and equation determining magnetic moment variation rates

11 p1932 A69-25465

Natural oscillations excitation in magnetoactive plasma by modulated electron beam ascribed to Doppler or Cerenkov effects

11 p1932 A69-25535

Natural oscillations excitation instabilities by modulated ion beams in magnetoactive plasma ascribed to anomalous Doppler effect

11 p1932 A69-25536

Low power gradient uniform electric arc column in cross flow and transverse magnetic field, analyzing temperature, velocity, pressure and magnetic field distribution

11 p1933 A69-25556

Thermal conductivity of hydrogen plasma in transverse magnetic field at high temperatures

12 p2133 A69-25765

Angle-to-code converter designed on basis of quantum magnetometers frequency sensors, transforming vector sum of bias magnetic fields into pulse repetition rates

12 p2016 A69-25963

Dynamic characteristics of plasma fluxes across magnetic field of diverter inside plasma cylinder formed during injection

12 p2134 A69-25977

Double focalization in atomic hydrogen maser by hexapolar magnets selecting hyperfine energy transitions

12 p2105 A69-26050

Hydromagnetic fluid flow between flat plates oscillating with phase difference, same frequency and different amplitudes

12 p2135 A69-26273

Viscous incompressible conducting fluid flow through porous coaxial nonconducting cylinders under radial magnetic field with pressure gradients functions of time

12 p2062 A69-26275

Hydromagnetic flow of viscous conducting fluids through porous coaxial cylinders in radial magnetic field solved by Laplace transform

12 p2135 A69-26276

Plasma instability in magnetic and HF electric fields, observing aperiodic short wave and oscillatory instabilities

12 p2136 A69-26526

Low pressure arc discharge plasma, studying ion-acoustic oscillations development in magnetic field

12 p2136 A69-26527

Quantitative magnetic field models of magnetosphere for analyzing field configuration variations and adiabatic particle motion

12 p2072 A69-26738

Boundary layer between cold plasma and vacuum magnetic field, considering transverse velocity component perpendicular to field

12 p2139 A69-26944

Polarization and structure of magnetic fields of quasars, E galaxies, normal galaxies and other extragalactic radio sources

12 p2165 A69-27034

Inhomogeneous and anisotropic cold plasma filled plane capacitor resonance in steady magnetic field applied to plasma diagnostics, using calculus of variations

13 p2304 A69-27240

Infinitely long journal bearing using ionized gas lubricant with magnetic field applied axially and electric field applied transversely to fluid film [ASME PAPER 68-LUBS-30]

13 p2267 A69-27287

Magnetic and electric fields influence on gas lubrication of bearings [ASME PAPER 68-LUBS-26]

13 p2267 A69-27288

Nonlinear periodic wave propagation at angle to magnetic field in collisionless plasma studied by two fluid plasma equations

13 p2304 A69-27297

Current, magnetic field, flow velocity and plasmatron dimensions effects on arc voltage in coaxial plasmatron

13 p2306 A69-27388

Zeeman laser with one end mirror exhibiting x-y-type loss anisotropy, considering resonance condition for round trip pass and self consistent field equations

13 p2271 A69-27398

Incompressible conducting fluid turbulent flow velocity distribution in transverse magnetic field at small magnetic Reynolds numbers and constant MHD interaction frequency

13 p2246 A69-27498

MHD channel mercury flow with hydraulic shock in transverse magnetic field, determining characteristic values distribution over range of principal parameters

13 p2307 A69-27499

Variable fluid and field velocity HF induction generator, determining interaction between fluid dynamic forces and magnetic field and kinetic energy

13 p2207 A69-27502

Transient response in liquid-metal conduction MHD generators, analyzing constant magnetic field using differential equation

13 p2207 A69-27506

Sodium liquid-metal jet MHD generators tested under constant and rising magnetic fields and off and on loads

13 p2208 A69-27511

Cosmic ray propagation theory for steady streaming along magnetic field and down cosmic ray density gradient, noting MHD wave generation by anisotropy

13 p2326 A69-27569

Surface resistivity oscillatory dependence on magnetic field in single crystal metals, examining electron trajectories, energy levels and wave functions

13 p2316 A69-27641

Dispersion relations in semiconductors in magnetic field indicating current anisotropic instability association with excessive noise

13 p2317 A69-27876

Ferrites dynamic characteristics in alternating magnetization pulse with variable amplitude indicating linearity loss in strong fields

13 p2320 A69-27994

Electric relays requirements for spacecraft with magnetic field constraints

13 p2231 A69-28046

Deuterium plasma jets passage through pulsed magnetic field by means of thermal and diamagnetic probes, noting magnetic field strength effect

13 p2311 A69-28107

Plasma jets tangential injection into toroidal magnetic field, discussing polarization interaction and depolarization effect

13 p2311 A69-28108

Tensor analysis of four photon interaction in rarefied plasma in magnetic field, determining cubic current of plasma wave self action

13 p2314 A69-28444

Transverse particle and energy fluxes in toroidal magnetic traps magnetic fields with ionized plasmas, discussing particle diffusion coefficient and thermal conductivity

13 p2314 A69-28446

Screw instability in glowing discharge plasma column in longitudinal magnetic field generalized to instabilities in low pressure arc, Penning and high current discharges

13 p2315 A69-28526

Biological effects of low magnetic field environments studied by physiological, visual and psychological tests on animal, plant and human subjects

13 p2211 A69-28596

Large amplitude pulsations in magnetic field magnitude and proton fluxes observed by satellite during magnetic storm compared with various models

14 p2434 A69-28947

Reflection and absorption coefficients analyzed for obliquely incident electromagnetic wave from magnetoactive plasma in constant parallel magnetic field

14 p2411 A69-28997

Magnetic field intensity, plasma pressure and energy density relations for macroscopic plasma motion inside neutral sheet from two dimensional model

14 p2440 A69-29119

Kelvin-Helmholtz instability noting effects of oblique magnetic field and rotation, deriving dispersion relation

14 p2491 A69-29335

Linear polarization achieved in He-Ne laser by applying external transverse magnetic field to plasma discharge

14 p2459 A69-29569

Amplitude modulation of electromagnetic waves by modulated magnetic fields for communications through rocket exhausts and reentry plasma sheaths during blackout

14 p2417 A69-29591

Three level He-Ne laser, showing nonlinear interference effects on gain line shape and use in magnetic field and frequency stabilization

14 p2460 A69-29671

Low beta fusion research in open end magnetic mirrors covering scope, end losses, fusion economics, flute instability, stabilization, etc

14 p2498 A69-29843

Electron and ion mobility in multiple cusp magnetic fields related to Polytron experiment

14 p2499 A69-29852

Two piston flow stability separated by thin wall in traveling magnetic field, finding piston inertia centers velocity equal to field velocity

14 p2500 A69-29903

Compressible gas MHD steady one dimensional flow in electric and magnetic fields

14 p2500 A69-29905

MHD mercury flow in rotating torus with little friction investigated for Reynolds numbers, considering induction pump forces and magnetic field influences
14 p2500 A69-29907

Turbulent Hartmann flow between planes in perpendicular magnetic field including flow velocity profile measurements
14 p2500 A69-29908

One dimensional approximation for free jet nozzle flow in perpendicular magnetic field, calculating velocity distributions
14 p2501 A69-29910

Plane linear induction pump design optimization without short circuiting bus bars, allowing for MHD effects induced by traveling magnetic field
14 p2405 A69-29913

MHD interaction between plasma and transverse magnetic field in shock tube, noting unsteady shock wave propagation in interaction zone
14 p2501 A69-29919

Detached MHD shock wave formation in front of magnetic field acting as piston moving collisionless plasma, discussing time dependence, Alfvén speed and plasma parameters
14 p2502 A69-29958

Vector magnetograph to measure magnetic field vector components, obtaining field direction azimuth by servo circuit
14 p2453 A69-29972

Josephson current density distribution in thin film superconductors, determining relation between tunneling density and magnetic field for films with/without current
15 p2667 A69-30196

Hydromagnetic fast shock strength and direction in inhomogeneous gravitational atmosphere with uniform magnetic field, discussing heating in solar corona
15 p2680 A69-30202

Plasma stability under anisotropic pressure in axisymmetric magnetic fields determined by quasi-hydrodynamic approximation
15 p2658 A69-30249

Plasma diagnostics in magnetic field with thin cylindrical probe based on Langmuir method
15 p2658 A69-30253

Plasma jet motion in time constant and time variable magnetic fields noting particle deflection, polarization loss, capture and cut-off
15 p2658 A69-30255

Criterion for magnetic plasma stability near magnetic axis, noting parameters for deriving criterion integrand
15 p2658 A69-30265

Electron energy distribution determination from electron synchrotron radiation spectrum for various magnetic field configurations within radio source
15 p2655 A69-30546

Particle drift velocity distribution of fully ionized plasma in magnetic field calculated by integration of Boltzmann equation
15 p2659 A69-30707

Continuous supersonic plasma wind tunnel obtained using magnetic Laval nozzle made by modification of Q device normal magnetic field configuration
15 p2589 A69-30909

Nonlinear effects and turbulent behavior in beam plasma instability, studying interactions in magnetic field
15 p2660 A69-30917

Self consistent solutions for collisionless plasma penetration across magnetic field, showing electrons ability to accompany ions across field
15 p2661 A69-30923

Nonlinear boundary value problems for isotropic plasma with known magnetic field, examining electromagnetic waves scattering at magnetic fluctuations
15 p2569 A69-30938

Molecular beam behavior in constant electric and magnetic fields, applying laser frequency dependence on magnetic field orientation to resonator
15 p2655 A69-30943

Regulating setup for controlling AC voltage surrounding polarization of magnetic electrode in plasma
15 p2664 A69-31094

Atomic beam for H maser operation prepared by using nonadiabatically changing magnetic field in transition region
15 p2635 A69-31103

Inversion coefficient for two orientations of ruby crystal with respect to external magnetic field perpendicular and push-pull orientations
16 p2795 A69-31570

Magnetic field lines curvature effect on plasma instabilities due to ion temperature gradient, noting frictional gravitation field simulation
16 p2816 A69-31636

Nonlinear interaction between three monochromatic waves propagating parallel to magnetic field in plasma, considering relativistic drift motions of particles
16 p2816 A69-31640

Charged particle motion in superposed Heliotron and biconical cusp magnetic fields, considering particle confinement
16 p2817 A69-31643

Transverse instabilities in collisionless electron plasma in absence of permanent magnetic field with spheroidal velocity distribution, noting application to shock theory
16 p2817 A69-31645

Exact solution for motion of conducting solid of revolution rotating in infinite conducting viscous fluid, describing magnetic field
16 p2817 A69-31666

Wide argon plasma column by axial current density measurements, confirming existence of instability and determining critical magnetic field
16 p2819 A69-31680

High beta theta pinch stability against tearing modes, determining necessary magnetic field conditions for slab and cylindrical cases
16 p2819 A69-31681

Nonlinear theory of $E \times B$ instability for weakly ionized plasma in presence of density gradient and parallel electric field perpendicular to magnetic field
16 p2819 A69-31682

Traveling wave tube amplifier for wideband radio in SHF range containing periodically integrated magnetized system, discussing output power variation range
16 p2759 A69-31863

Screw pinch stability explained by strong force free current carried by magnetic field around central plasma column
16 p2821 A69-32037

Plasma magnetic field and electron density measured by Faraday rotation using resonant gas laser radiation
16 p2822 A69-32041

Plasma wave echoes concept extended to transverse electromagnetic wave excitation propagating parallel to external magnetic field
16 p2823 A69-32467

Weak magnetic fields effect on molecular oscillator frequency taking into account Zeeman sublevels
16 p2762 A69-32500

Amplitude modulated radio wave interaction with rarefied plasma in magnetic field, considering possible ionospheric heating by mechanism
16 p2754 A69-32538

Zero reference field for quiet day solar variations, considering magnetic field levels and errors
16 p2851 A69-32546

MHD of interstellar gas-dust medium, analyzing gas-dust flow and gas-dust shock waves in magnetic fields
16 p2823 A69-32590

Cavity linear phase anisotropy and axial magnetic field effect on single mode Zeeman gas laser
16 p2798 A69-32606

Boltzmann equation for Lorentzian plasma in elliptic magnetic field solved by expanding distribution function in Legendre polynomials
17 p3009 A69-32827

Linearized motion equations for conducting gas in magnetic and electric field solved for coaxial channel and free jet, assuming small Reynolds number and parallel flow
17 p3010 A69-33016

Steady state flux jumping for thin walled tubular superconducting NbTi subjected to coaxial superimposed AC and DC magnetic fields, discussing effective resistivity
17 p3016 A69-33787

Magnetized solar wind model to evaluate temperature, density, velocity and magnetic field for various boundary conditions
17 p3041 A69-33812

Electromagnetic fields theory simultaneously determining vector electric and magnetic field aspects in terms of operator Green functions
17 p2924 A69-33833

Magnetic field susceptibility testing method as defined in DOD Electromagnetic Compatibility Control documents MIL-STD-461 and MIL-STD-462
17 p2947 A69-34133

Level crossing signal obtained by magnetic/electric field modulation, tabulating corrections to widths and centers for distortions
17 p3009 A69-34155

Electromagnetic wave propagation in unbounded compressible plasma under drift velocity and magnetic field, obtaining dispersion equation for current density
18 p3179 A69-34261

Whistlers propagation in cold plasma in uniform magnetic field, considering amplitude dispersion effect
18 p3179 A69-34437

Drift waves parametric excitation in resistive plasma derived from fluid equations, assuming plane geometry with periodic boundary conditions in magnetic field and azimuthal directions
18 p3179 A69-34440

Severe magnetosphere distortions in north-south direction with parallel/antiparallel magnetosheath to magnetospheric field ascribed to solar wind property changes from Explorer 12 observations
18 p3128 A69-34947

Chapman-Ferraro approximation for magnetic interior field line configuration in plasma flow around two dimensional dipole, allowing for tail formation and neutral sheet
18 p3129 A69-34955

Microfluctuations frequency and wavelength of electromagnetic, electric and magnetic field distributions in plasma shock wave front found consistent with ion-acoustic origin hypothesis
18 p3180 A69-35017

Electromagnetic and cyclotron waves interaction across opaque boundary in moving plasma in one dimensional approximation
18 p3181 A69-35027

Magnetic field effect on Gunn diode vibrations and LF oscillations, noting increase in threshold field and decrease in threshold current
18 p3183 A69-35267

Electromagnetic shaping of metallic parts using equations describing magnetic and electric field intensity as function of blank profile and cylindrical blank wall thickness
18 p3151 A69-35456

Self excited vibration of flowing medium and infinite cylindrical duct wall in primary magnetic field, discussing vibration stability and critical speeds
18 p3226 A69-35462

Electromagnetic wave effect on electron in homogeneous magnetic field, noting relativistic momenta of dragged electrons
18 p3181 A69-35497

Gas ionizing shock waves structure in arbitrary magnetic field, considering greater magnetic viscosity than dissipative coefficients
19 p3381 A69-36773

Turbulent boundary layer of conducting fluids on dielectric plate in transverse magnetic field in presence and absence of pressure gradient
20 p3513 A69-37092

Electric field correlation to magnetic fields in quantum theory of coherence, deriving dynamical equations governing space-time development of correlation matrix
20 p3575 A69-37304

VLF electric and magnetic fields observed in auroral zone with Javelin 8.46 sounding rocket, noting HF electrostatic noise bursts
20 p3533 A69-38080

Twenty year wave in diurnal anisotropy component of galactic cosmic rays arriving at earth from asymptotic direction east of sun interpreted as magnetic reconnection
20 p3592 A69-38098

Equilibrium and stability of axisymmetric gaseous polytropes in toroidal magnetic fields, calculating harmonic oscillations by virial tensor method
21 p3797 A69-38534

Ferromagnetism stable state in degenerate electron gas and magnetic fields in gravitationally collapsed bodies based on total microscopic magnetic moments associated with Landau level electrons
21 p3798 A69-38600

Two dimensional numerical solution for Faraday DC MHD generators with variable conductivity, velocity and magnetic field
21 p3649 A69-39027

Dispersion relations in semiconductors in magnetic field indicating current anisotropic instability association with excessive noise
21 p3782 A69-39142

Jupiter magnetospheric radio emissions, discussing magnetic field and plasma-magnetic interactions
21 p3812 A69-39517

Extragalactic radio sources linear polarized radiation distribution at 1418 MHz indicating ordered magnetic fields often oriented differently
22 p4015 A69-40155

Kinematic dynamo waves, discussing excitation and maintenance of magnetic field by assumed motion of uniformly conducting fluid using small parameter and numerical methods

22 p3989 A69-40195

Injun 5 satellite VLF electric and magnetic fields observations, discussing antenna operation, Poynting flux and noise band measurements

22 p3938 A69-40503

Differential rotation of incompressible inviscid fluid of infinite electrical conductivity in spherical shell, noting toroidal magnetic field for sun

22 p4027 A69-40658

Diffuse reflection of electromagnetic longitudinal wave from magnetoactive plasma in oblique incidence

22 p3990 A69-40788

Theory for current magnetic field characteristics of Penning discharge valid to extinction point

22 p3991 A69-40865

Supercritical frequencies horizontal gradient ducting effects on backscatter sounding of F region magnetic field aligned irregularities

22 p3941 A69-40913

Conductor material thermal conductivity contribution to self similar explosion in strong magnetic field, determining critical field strength

22 p3982 A69-41019

Ionizing shock wave propagation and reflection in transverse magnetic field based on MHD theory, assuming gas thermal equilibrium

22 p3992 A69-41176

Multiple strip H guide field distribution and low loss wave mode analysis, obtaining approximate thin layer equations

22 p3917 A69-41254

Dirac equation in external electromagnetic fields, deriving solution for constant orthogonal electric and magnetic fields encountered in plasma transport

23 p4190 A69-41357

Nonlinear interaction between extraordinary waves propagating perpendicular to static magnetic field in cold homogeneous magnetoplasma

23 p4195 A69-41538

Conducting fluid flow in spherical container in rotating magnetic field, calculating induced field velocity and inside and outside components

23 p4196 A69-41609

Eddy current plasmoids formation in potential magnetokinematic plasma flux found economical in terms of energy requirements

23 p4214 A69-41834

Force acting on multipole in external magnetic field, noting dependence on multipole axes

23 p4158 A69-42172

Boundary layer separating collisionless plasma from one dimensional magnetic field for anisotropic particle velocity distribution functions, preserving charge neutrality in boundary layer

23 p4197 A69-42415

Transverse plasma waves propagating along parallel static electric and magnetic fields may lead to instabilities regardless of carriers sign

24 p4355 A69-42923

Sounding rocket measurements of electric and magnetic fields near auroral electrojet

24 p4310 A69-43188

Self induced magnetic field influence on plasma positive column stability in longitudinal magnetic field

24 p4356 A69-43366

Hydrogen plasma-axisymmetric magnetic field interaction, studying plasmoid motions during exit from field

24 p4358 A69-43472

Electric arc stabilization in crossed convective and magnetic fields, discussing column slanting relationship to widening near downstream electrode

[AIAA PAPER 68-709] 24 p4359 A69-43572

Low pressure arc discharge motion between concentric electrodes in transverse magnetic field, noting Lorentz, stationary and retrograde modes due to temperature nonequilibrium

[AIAA PAPER 68-708] 24 p4359 A69-43644

Steady state interaction between collisionless plasma flow and immersed stationary magnetized or unmagnetized objects by inserting Cs ion accelerator into plasma wind tunnel

24 p4359 A69-43646

Turbulence formation in conducting liquid at increasing Reynolds numbers, discussing cause of spontaneous magnetic field appearance

24 p4390 A69-43782

MAGNETIC FILMS

Kerr magneto-optic camera for 10 nsec exposures of dynamic magnetization configuration in magnetic thin film during high speed flux reversal

17 p2970 A69-32853

MAGNETIC FLUX

Megagauss magnetic field generation methods, discussing high explosives, initial field, flux compression, capacitor discharges and applications

01 p0115 A69-10049

Stable fluxgate magnetometer sensor for exploration of space magnetic fields, discussing equipment specifications and performance tests

[IEEE PAPER 10.2] 01 p0081 A69-10715

Quasi-static Kerr magneto-optic observation and procedure to predict results of dynamic flux reversal in thin Ni-Fe films

[IEEE PAPER 11.7] 01 p0138 A69-10716

Electromagnetic waves parametric interactions during unsteady Josephson effect as function of wavelength ratio, magnetic field penetration and contact dimensions

02 p0293 A69-11464

Magnetic paleointensity studies in basalts from Flagstaff, Arizona, noting oxidation effect on magnetic strength after heating

02 p0244 A69-12018

Critical state model of type 2 superconductor taking account of critical current on magnetic field and surface sheath currents, evaluating flux penetration, hysteresis, AC losses, etc

02 p0298 A69-12030

Dipole model of geomagnetic field in terms of spatial distribution of vertical component, discussing computer program for calculating rectangular components

03 p0424 A69-13544

Thermal EMF in indium phosphide crystals as function of temperature, electron concentration and magnetic field strength, determining effective mass of electrons

03 p0489 A69-13889

Interplanetary magnetic field fluctuations obtained by IMP 2

05 p0824 A69-16264

Magnetoplasticity induced in metal by high magnetic fields, examining stationary flow in two dimensional deformation

05 p0844 A69-16804

Plasma column radial density profile measurement by electron plasma waves propagation in presence of strong magnetic field

07 p1194 A69-19323

Geomagnetic field strength in early Precambrian, discussing thermoremanent normal remnant and saturation inverse remnant magnetization studies of Botswana Modipe gabbro

08 p1309 A69-20580

Magnetic field decay modes due to nonuniform rotation having angular velocity as increasing function of distance from axis in infinite circular conducting fluid cylinder

08 p1369 A69-20999

Type two superconductors physical properties, discussing magnetic flux lines interaction with structural defects

09 p1555 A69-21490

Anomalous magnetic field energy spectrum obtained from aeromagnetic survey and approximation valid for earth crust and upper mantle

09 p1487 A69-21554

Static ferromagnetic frequency doubler graphic design, considering magnetic field strength and flux density, energy cycle and energy transfer

10 p1663 A69-23566

Auroral oval and ring current in magnetosphere, analyzing boundaries of lines of force on night side of earth

10 p1689 A69-24203

Thermal EMF in indium phosphide crystals as function of temperature, electron concentration and magnetic field strength, determining effective mass of electrons

11 p1939 A69-25690

Power output of He-Ne laser as function of transverse magnetic field strength

12 p2104 A69-26023

Solar photosphere and sunspot magnetic fields structure and strength dependence on sunspot area

14 p2528 A69-29965

Type 3 radio bursts time profile for estimating magnetic field strength in solar corona

15 p2675 A69-30554

Galactic magnetic field structure and strength, considering cosmic ray flux, continuum radio emission, starlight polarization, star formation, etc

15 p2694 A69-30857

Similarity concepts extended to shock initiated flux compression devices for magnetic flux concentration

16 p2768 A69-31665

Plasma cluster interaction with axially symmetric magnetic field, deriving plasma diamagnetic current, inductance and resistance from measured coil flux dependence on distance

16 p2823 A69-32365

Anomalous magnetic field energy spectrum obtained from aeromagnetic survey and approximation valid for earth crust and upper mantle

16 p2784 A69-32549

Magnetic analysis by successive double heat treatment of miocene lava cooled during geomagnetic polarity reversal for determining field intensity

16 p2788 A69-32646

Kerr magneto-optic camera for 10 nsec exposures of dynamic magnetization configuration in magnetic thin film during high speed flux reversal

17 p2970 A69-32853

Pulsar emission and magnetic field in Crab Nebula, discussing magnetic flux amplification, gravitational to magnetic energy conversion and pulsars as pulsed signals

17 p3026 A69-32859

Steady state flux jumping for thin wall tubular superconducting NbTi subjected to coaxial superimposed AC and DC magnetic fields, discussing effective resistivity

17 p3016 A69-33787

Dynamic Kerr observations of high speed flux reversal and relaxation process in permalloy thin films by magneto-optical camera with Q switched ruby laser

19 p3383 A69-36446

Proton concentrations, magnetic field strength and temperatures distribution in interplanetary plasma flows as function of latitudinal distance from center of active region

20 p3594 A69-37020

Time-invariant magnetic fields at planetary surfaces resulting from permanent magnetic bodies or distorting effect of inhomogeneous permeability on main field, computing components

20 p3609 A69-38105

Radiation sources fields and propagation in homogeneous lossy magnetoplasma, deducing wave equations for electric and magnetic current electron flux and mechanical body force sources

21 p3775 A69-38434

Galactic radio emission and magnetic field strength and structure, using radio surveys to obtain information on cosmic rays

21 p3790 A69-38820

Analyzing conditions for variable magnetic and electric noise occurrence at input of nuclear precession magnetometer used in field strengths measurements

23 p4165 A69-41852

Weak magnetic field amplification in turbulent flow with velocity field as random function of space and time

24 p4375 A69-42657

MAGNETIC FORMING

Electromagnetic forming principles and applications describing large capacitor bank facility design for multipurpose research

[ASTME PAPER MR68-418] 02 p0252 A69-11798

Decoupling force exerted by magnetic forming Be coil assembly on metallic plate during forming

11 p1888 A69-25310

MAGNETIC INDUCTION

Vacuum deposited n-type InAs films magnetoresistance coefficient dependences on length-to-width ratio, homogeneity moving carriers size and magnetic inductance

01 p0136 A69-10254

Small metallic sphere detection by electromagnetic induction method, emphasizing masking effect of resistive half space below scatterer

01 p0047 A69-10974

Electromagnetic induction theory for spherical earth model involving conducting core with radial conductivity variation and concentric nonconducting mantle

03 p0423 A69-13523

Mathematical theory of electromagnetic induction for spherical model of earth with conductivity distribution given by sine function

06 p0921 A69-17739

Matched asymptotic expansions method applied to magnetic field induction in thin toroidal wire and flow past circular cylinder at small Reynolds number
07 p1180 A69-18811

Electromagnetic microinstabilities of plasmas associated with transverse waves propagating perpendicular to external uniform magnetic induction, noting allowable frequencies
08 p1368 A69-20804

Magnetic pinch effect in thermal RF induction plasma in argon, developing theory for calculating excess magnetic pressure
09 p1544 A69-21341

Vacuum deposited n-type InAs films magnetoresistance coefficient dependences on length-to-width ratio, homogeneity, moving carriers size and magnetic inductance
09 p1559 A69-22647

Striated flow induction synchronous MHD generator, producing striated flow by nonthermal ionization of inert seeded gas in electric field
10 p1638 A69-23487

Static ferromagnetic frequency doubler graphic design, considering magnetic field strength and flux density, energy cycle and energy transfer
10 p1663 A69-23566

Magnetic field induced nonequilibrium argon plasma ionization relaxation processes obtained with allowance for flow parameters change in relaxation zone
11 p1922 A69-24225

External modulated currents induced electromagnetic field effect on density distribution of bounded plasma, discussing fluctuations in various configurations
11 p1927 A69-24910

Induced EMF method for calculation of antenna impedance, discussing effects of approximations in calculation
11 p1851 A69-24997

Transient processes in conduction type MHD generators due to external circuits induction distribution
12 p2017 A69-26545

One dimensional calculations of finite length MHD uniform traveling wave induction generator, discussing magnetic field distribution, electrical impedance and conversion efficiency
13 p2206 A69-27494

Three phase high temperature liquid metal induction MHD generator performance, noting velocity profile nonuniformity influence
13 p2208 A69-27513

Equatorial electrojet role in electromagnetic induction at magnetic dip equator, applying Price theory for space gradients
13 p2252 A69-27519

Ideal MHD induction converter pressure and generator cycles compared for calculating maximum output and pressure, considering current-conducting walls effects
14 p2393 A69-28887

Time dependent magnetic field induced inside rotating spherical conductor by external sources applied to moon
14 p2518 A69-29121

MHD mercury flow in rotating torus with little friction investigated for Reynolds numbers, considering induction pump forces and magnetic field influences
14 p2500 A69-29907

Free surface in supercritical regime downstream of valve submerged in MHD flow, noting effects of horizontal and vertical magnetic induction fields
15 p2659 A69-30299

Space charge formation in MHD generator channels ascribed to gas parameters nonuniformity and magnetic induction vector presence, assuming steady flow
15 p2659 A69-30635

Entrainment of viscous electrically conducting liquid in long duct with narrow rectangular cross section and movable walls in magnetic induction field
16 p2816 A69-31606

Electromagnetic induction in concentric thin shell-enclosed solid conducting sphere immersed in varying electromagnetic field
[AFRL-69-0082]
18 p3101 A69-34803

Self induction of conical electrode type plasma accelerator with and without allowance for magnetic scattering field, investigating acceleration process
19 p3379 A69-35821

Inductively coupled RF excited toroidal Ar ion laser, confining current discharge by strong axial magnetic field to reduce wall losses
19 p3338 A69-36690

Herzenberg geomagnetic dynamo model extensions including rigid rotors calculus, laminated rotors, induction problem and fluid rotors in rigid conductor
22 p3989 A69-40193

Conducting fluid flow in spherical container in rotating magnetic field, calculating induced field velocity and inside and outside components
23 p4196 A69-41609

Conical induction plasma accelerator design for studying acceleration process characteristics
24 p4357 A69-43468

MAGNETIC MATERIALS

NT FERRIMAGNETIC MATERIALS

NT FERROMAGNETIC FILMS

NT FERROMAGNETIC MATERIALS

NT MAGNETITE

NT PERMALLOYS [TRADEMARK]

Magnetic experiment on Surveyor 5 revealing magnetic material presence in Mare Tranquillitatis, discussing analogy to powdered basalt
02 p3231 A69-12226

Ground state energy for single magnetic impurity dissolved in nonmagnetic metal, applying cluster variation method to s-d interaction Hamiltonian
03 p0485 A69-13298

Soft magnetic materials, ferrites and magnetic particle composites as two layer laminates for shielding in audio and microwave frequencies
09 p1500 A69-22310

Magnetism and magnetic materials - IEEE and AIP Conference, New York, November 1968
15 p2668 A69-30683

Time dependent Green function method for premature saturation due to parametric amplification of nonuniform spin wave modes by one and two magnon processes
15 p2668 A69-30685

Magnetic materials simulation for satellite stabilization device based on magnetic hysteresis, using mathematical models and direct magnetic measurements
17 p2945 A69-33235

Diffusion times for saturated region in Hipernom tubes measured for various exciting magnetic fields and pulse duration
23 p4141 A69-42222

MAGNETIC MEASUREMENT

Vector helium magnetometer for Mariner 4 /Mars 1964/ and Mariner 5 /Venus 1967/, discussing efforts to reduce spacecraft stray fields
[IEEE PAPER 10.1]
01 p0081 A69-10714

Planetary magnetic field measurements near Venus, Mars, and moon, noting magnetic dipole comparison with earth and solar wind interactions
[AAS PAPER 68-186]
02 p0311 A69-11471

Geomagnetic field components measurements from moving object, investigating astronomical orientation applicability for three component geomagnetometer
02 p0277 A69-11674

Magnetotropometer for measuring torque /proportional to magnetic dipole moment/ exerted on object by earth magnetic field
02 p0248 A69-11768

Surveyor 6 magnet experiment following lunar landing, noting presence of magnetic material in Sinus Medii indicating basaltic composition
02 p0317 A69-12015

Surveyor 5 alpha particle backscattering instrument measurement, TV pictures of lunar surface elemental composition and magnetic and mechanical measurements
02 p0317 A69-12023

Elektron 2 satellite magnetic measurement of high latitude nocturnal magnetosphere, discussing variations, antisolar effect and elongation of magnetic field
03 p0422 A69-13505

Earth magnetic field measurements, attributing field origin to random mechanism
03 p0426 A69-14061

Error distribution maps for measurements of parameters epsilon, F and E of geomagnetic potential in Northern and Southern Hemispheres
04 p0627 A69-15031

Neutral sheet structure and orientation in geomagnetic tail, computing field lines on basis of Explorer 14 magnetic field measurements
05 p0753 A69-16256

Geomagnetic field strength in early Precambrian, discussing thermomagnetic normal remnant and saturation inverse remnant magnetization studies of Botswana Modipe gabbro
08 p1309 A69-20580

Atmospheric humidity effect on efficiency of geomagnetic field scales with taut-strip suspension and temperature fluctuation
09 p1494 A69-21518

Geomagnetic secular variations calculated by comparison of satellite, oceanic and aeromagnetic surveys
09 p1485 A69-21534

Separation of normal geomagnetic field component from limited length measurements by moving averages, considering error and inhomogeneity of anomalous field
09 p1486 A69-21537

Magnetic declination from moving objects measured by geomagnetic vector projection in solar direction
09 p1486 A69-21538

Solar flare energetic electron access to polar zones from measurements made by nine channel magnetic spectrometer on polar orbiting vehicle
09 p1577 A69-21709

InAs thin film sensors using Hall effect to measure magnetic fields at cryogenic temperatures
10 p1696 A69-23717

Stationary Babinet compensator for measuring longitudinal solar magnetic fields by means of fringes introduced in spectroheliograms
11 p1880 A69-24433

Geomagnetic field vertical and horizontal intensities measured using proton magnetometer with coil theodolite
11 p1889 A69-25435

Solar and lunar/solar harmonics determination, noting effects of moon on values of horizontal magnetic component
11 p1965 A69-25555

Airborne magnetometer application for remote measurement of ocean wave spectra, obtaining wave noise power spectra and wave height profile
12 p2075 A69-26998

Geomagnetic field components measurements from moving object, investigating astronomical orientation applicability for three component geomagnetometer
13 p2257 A69-28705

Magnetosensitive quartz element with suspended magnet and two mirrors for recording magnetic variations
14 p2446 A69-29084

Crystallographic classes of ferrites for microwave devices, discussing magnetic properties, applications and work on polycrystalline yttrium-calcium iron-vanadium-indium garnet
15 p2670 A69-31208

Magnetic anisotropy and porosity from approach to saturation of polycrystalline ferrites based on magnetization measurement
16 p2825 A69-31700

Plasma magnetic field and electron density measured by Faraday rotation using resonant gas laser radiation
16 p2822 A69-32041

Geomagnetic secular variations calculated by comparison of satellite, oceanic and aeromagnetic surveys
16 p2783 A69-32529

Separation of normal geomagnetic field component from limited length measurements by moving averages, considering error and inhomogeneity of anomalous field
16 p2783 A69-32532

Magnetic declination from moving objects measured by geomagnetic vector projection in solar direction
16 p2783 A69-32533

Magnetic materials simulation for satellite stabilization device based on magnetic hysteresis, using mathematical models and direct magnetic measurements
17 p2945 A69-33235

Zeeman effect measurement revealing magnetic fields in interstellar neutral H clouds
18 p3190 A69-34291

AC technique using lock-in power amplifier SNR for measuring galvanomagnetic and Shubnikov-de Haas effects, noting error reduction
19 p3312 A69-36375

Geomagnetic field total vector modulus secular variations from airborne measurements
20 p3522 A69-37061

Magnetic measurements of active regions at various levels of solar atmosphere, discussing chromospheric cold and hot region, faculae magnetic fields, etc
22 p4010 A69-39991

Shock discontinuities in solar wind measured by magnetic field and plasma instruments on Explorer 34, applying Rankine-Hugoniot relations
22 p4020 A69-40304

Impedance of inhomogeneous earth from magnetic and electric fields and geomagnetic potential measurements
23 p4157 A69-41867

Performance test of German MPD plasma rocket engine with augmented magnetic field and 5-10 kw output, describing integral measurement procedure and observed phenomena
[DGLR-69-024D]
23 p4202 A69-41927

Error sources in magnetic field measurements using magnetic probes in high temperature plasmas, discussing detection, correction and elimination [AIAA PAPER 68-727] 24 p4316 A69-43571

MAGNETIC METALS

U METALS

MAGNETIC MIRRORS

Penning discharge in inhomogeneous magnetic mirror field, observing high burning voltage at low current in rarefied hydrogen plasma 01 p0133 A69-11218

Thermalization of kinetic energy of plasma flow by shock phenomena produced by magnetic mirror field 02 p0289 A69-12176

Ion cyclotron wave generation in RF self sustained mode improved by installing grid structures in plasma near magnetic mirrors 03 p0474 A69-13113

Two dimensional equilibria for high beta mirror devices found by solving Vlasov equation and Ampere law, including particle loss 03 p0475 A69-13152

Polynomial representations of mirror cusp fields produced by combination of mirror coils and loffe /multipole/ bars 06 p0966 A69-17522

Longitudinal electrostatic oscillations in plasma with Fermi distribution of energies, noting oscillation frequency dependence on electron density 08 p1359 A69-19985

Nonadiabatic and stochastic mechanisms for cyclotron resonance trapping and heating in magnetic mirror geometries 08 p1364 A69-20518

Electron cyclotron resonance absorption of injected radiation magnetic mirror, noting effect of RF heating on plasma electron distribution 08 p1364 A69-20519

Heating of collisionless plasma in magnetic mirror by random electric field transverse to magnetic field 08 p1368 A69-20805

Phase characteristics and magnetic mirrors effect on charge motion in spatially periodic magnetic field 09 p1551 A69-22036

Stochastic model of electron cyclotron heating, calculating energy gain during transit of magnetic mirror field in presence of microwave electric field 09 p1551 A69-22038

Rotating plasma behavior in magnetic mirror trap, using radial electric field 10 p1740 A69-23716

Longitudinal electric field distribution and charged particle density in magnetic mirror under potential difference between magnetic equator and plane 10 p1689 A69-24204

Electron confinement in magnetic mirror geometry supplemented with RF quasi-potential barriers, considering gas scattering 11 p1924 A69-24306

Centrifugal instability of plasma column generated by cyclotron absorption of microwave power in magnetic mirror field 11 p1931 A69-25366

Low beta fusion research in open end magnetic mirrors covering scope, end losses, fusion economics, flute instability, stabilization, etc 14 p2498 A69-29843

Magnetic mirrors, Doppler and relativistic effects, wave attenuation and radiation pressure during gyroresonant particle acceleration in nonuniform magnetostatic and HF fields 14 p2499 A69-29845

Charged particle motion in magnetic mirror trap, observing time dependence with respect to orbital magnetic moment conservation 15 p2659 A69-30724

Axially symmetric magnetic fields for constant radius annular electron beams reflection, applying results to design of reflex klystron millimeter oscillator 19 p3267 A69-35930

MAGNETIC MOMENTS

Lunar magnetic moment and surface field, discussing Explorer 35 field measurements 03 p0514 A69-14005

Electron anomalous magnetic moment effect on nonlinear Lagrangian of electromagnetic field, deriving additional nonlinear corrective term 08 p1353 A69-19781

Quantum theory of electron gas with anomalous magnetic moments in intense magnetic fields, noting pair creation from thermodynamic energy in system 08 p1353 A69-19782

Magnetic sublattices interactions in gadolinium ferrite garnet, estimating magnetization level temperature dependence 08 p1374 A69-21186

Motion equations for conducting paramagnetic fluid in magnetic field derived, including MHD equations and equation determining magnetic moment variation rates 11 p1932 A69-25465

Magnetic sublattices interactions in gadolinium ferrite garnet, estimating magnetization level temperature dependence 18 p3183 A69-35155

Plasma acceleration away from rotating magnetized astrophysical objects analyzed and applied to pulsar NP 0532 for magnetic moment and mass loss rate calculations 20 p3598 A69-37419

Contactless correcting devices based on magnetic moments for automatic control 21 p3685 A69-38453

Ferromagnetism stable state in degenerate electron gas and magnetic fields in gravitationally collapsed bodies based on total microscopic magnetic moments associated with Landau level electrons 21 p3798 A69-38600

Satellite stabilization by earth magnetic field through conservative magnetic moments application 21 p3830 A69-39834

Spin compensated state of localized magnetic impurity moment in space, calculating size range of magnetic impurity spin/conduction electron spin correlation function 22 p3983 A69-40061

MAGNETIC PERMEABILITY

Second order susceptibilities of III-V and II-VI compounds using Phillips model, discussing second optical harmonic in III-V compounds with tetrahedral bonds 01 p0138 A69-10365

Vanadium-gallide alloys critical temperature of transition into superconducting state determined by measuring cast alloy samples magnetic permeability 03 p0483 A69-13023

Room temperature lattice spacings of PdIn, PtIn and PtSn alloys including magnetic susceptibility 05 p0779 A69-15832

Magnetic susceptibility of InP-GaAs solid solutions at various temperatures and for varying GaP content 07 p1200 A69-19013

Maxwell equations solution for linear induction MHD machine coil area field components, allowing for finiteness of magnetic permeability of iron 07 p1059 A69-19028

Lunar depth profiles of conductivity, dielectric constant and magnetic permeability from radar, radiothermic and magnetic measurements, discussing lunar models 07 p1216 A69-19221

Steady state operation of atomic hydrogen maser by analogy with electronic circuits, calculating atomic magnetic susceptibility using density matrix and deriving equivalent circuits 09 p1517 A69-22093

Input admittance response characteristics and input susceptance and input conductance of resonant reactive modulator with varactors and nonlinear losses 10 p1665 A69-24066

Field equations for plane-parallel induction MHD machines with allowance for winding zone thickness and magnetic permeability of iron 14 p2405 A69-29914

Magnetic field susceptibility testing method as defined in DOD Electromagnetic Compatibility Control documents MIL-STD-461 and MIL-STD-462 17 p2947 A69-34133

High field susceptibility in Fe and Ni and high field Mossbauer study in Fe relating results to band structure and models of ferromagnetism 19 p3383 A69-36050

Magnetic properties of stone, stony-iron and iron meteorites, discussing natural remanent magnetization origin in parent bodies and magnetic susceptibility 19 p3415 A69-36122

Melting points, electrical conductivity, Hall constants, magnetic susceptibility, density, bending strength, microhardness and elastic modulus of zirconium nitride in homogeneity range 20 p3558 A69-37014

Time-invariant magnetic fields at planetary surfaces resulting from permanent magnetic bodies or distorting effect of inhomogeneous permeability on main field, computing components 20 p3609 A69-38105

Ultrasonic oscillations effects on magnetic permeability of ferrite circuit components 23 p4138 A69-41873

MAGNETIC PISTONS

Detached MHD shock wave formation in front of magnetic field acting as piston moving collisionless plasma, discussing time dependence, Alfvén speed and plasma parameters 14 p2502 A69-29958

MAGNETIC POLES

Micropulsations at magnetoconjugate points in Arctic and Antarctic, noting diurnal and seasonal variations and latitude dependence 01 p0068 A69-11112

Earth pole coordinates calculated from latitude variations at Pulkovo, Greenwich and Washington, giving components of earth motion 03 p0420 A69-13094

High energy pure photon showers in cosmic ray emulsions in relation to production of magnetic pole-antipole pairs 06 p0996 A69-17883

Earth dipole magnetic field effect on bearing deviation in HF transionospheric propagation analyzed by computer ray tracing 07 p1086 A69-19224

Earth pole coordinates calculated from latitude variations at Pulkovo, Greenwich and Washington, giving components of earth motion 14 p2433 A69-28776

Remanent magnetization properties in alkalic igneous complexes at Magnet Cove and Potash Suphur Spring, Ark., calculating paleomagnetic pole during Cretaceous 14 p2445 A69-29884

Altitude asymmetry of instantaneous auroral oval plotted for geomagnetic pole and earth surface 20 p3522 A69-37056

Cosmic X ray background spectral measurement from rocket flight near geomagnetic pole 21 p3787 A69-38351

Magnetic monopole search using synchrotrons and cosmic radiation to destroy ferromagnetic materials binding in rocks, meteorites and deep sea sediments 22 p3981 A69-40197

MAGNETIC PROBES

Small metallic sphere detection by electromagnetic induction method, emphasizing masking effect of resistive half space below scatterer 01 p0047 A69-10974

Magnetic probes characteristics measurement for frequency range from 10 kc to 50 mc, using quenching resistors 08 p1313 A69-20120

Analytic investigation of spectrum of electrical signals induced by spherical defects in ferroprobe sensors 10 p1675 A69-24072

Magnetovariational sounding procedure for determining vertical distribution of earth mean electrical conductivity using geomagnetic field spatial derivatives for spherical earth 14 p2438 A69-29081

Magnetic monopole search using synchrotrons and cosmic radiation to destroy ferromagnetic materials binding in rocks, meteorites and deep sea sediments 22 p3981 A69-40197

MAGNETIC PROPERTIES

NT ANTIFERROMAGNETISM

NT CURIE TEMPERATURE

NT DIAMAGNETISM

NT FERRIMAGNETISM

NT FERROMAGNETISM

NT GEOMAGNETISM

NT GYROFREQUENCY

NT GYROMAGNETISM

NT MAGNETOACOUSTICS

NT MAGNETOACTIVITY

NT MAGNETORESISTIVITY

NT MAGNETOSTRICTION

NT PALEOMAGNETISM

NT PARAMAGNETISM

NT POLARIZATION CHARACTERISTICS

NT RELUCTANCE

NT REMANENCE

NT SPIN-LATTICE RELAXATION

NT THERMOMAGNETIC EFFECTS

High temperature magnetic analysis of metallurgical structure of high strength steels and composites, including phase transformation and matrix grain structure 01 p0093 A69-10111

Applied magnetics - IEEE Conference, Washington, D.C., April 1968 01 p0045 A69-10712

Wall streaming, creeping and parade motion in Ni-Fe films excited by hard axis pulses
[IEEE PAPER 11.8] 01 p0138 A69-10717

Electrical, optical, magnetic and structural properties of titanium oxide, stressing transition difference with vanadium oxide 03 p0490 A69-13923

Ferrite materials characteristics related to choice for use in waveguide devices, noting importance of low HF magnetic losses and thermal stability 05 p0810 A69-16792

Magnetic and semiconducting properties of samarium boride, noting effect of decreasing temperature 07 p1200 A69-19403

Warm plasma magnetic interactions, discussing density waves, pair correlation function and transport coefficients 08 p1366 A69-20749

Meteoritic materials structure, composition and magnetic properties, supporting theory for solar system formation from supernova outbursts 09 p1593 A69-21581

High temperature magnetic testing and analysis of structure sensitive hysteresis properties 09 p1512 A69-22375

Stochastic and ergodic aspects of magnetic lines of force, discussing cosmic ray diffusion in interplanetary magnetic field 10 p1770 A69-24111

Force-free magnetic field integral properties, obtaining rate of decrease limitation via virial theorem 11 p1951 A69-24239

Electrical resistivity and magnetization saturation in cobalt alloys during formation of modulated structures 11 p1904 A69-24707

Magnetic crystallographic anisotropy of Li-Ga ferrite single crystals at temperature range measured by ferromagnetic resonance techniques 12 p2144 A69-26721

Magnetic models of pulsars and rotating neutron stars to explain narrowness of radiation beam in polar diagram 12 p2172 A69-27168

Phase composition and Co content effect in WC-Co and WC-TiC-Co alloys on magnetic properties behavior 13 p2275 A69-27343

Exchange interactions in lithium ferrite aluminates, measuring spontaneous magnetization by ballistic technique from 77 K to Curie point 13 p2320 A69-27995

Polycrystalline Ca-V garnets and Mg-Cr ferrites magnetic properties after adding rare earth elements 13 p2320 A69-27999

Substituted lithium ferrites analyzed to obtain materials with small initial magnetic losses at different microwave ranges 13 p2320 A69-28000

Magnetic properties of ferrites with garnet structure, discussing temperature effect on magnetic states of Gd, Li, Y and Lu sublattices 13 p2323 A69-28564

Equation system for asynchronous MHD generator operating in self oscillating mode derived and solved 14 p2405 A69-29457

Solar corona magnetic field and polar rays, emphasizing field topology and local magnetic structure 14 p2525 A69-29718

Rare earth niobates magnetic properties measured in pulsed magnetic fields 15 p2667 A69-30195

Magnetism and magnetic materials - IEEE and AIP Conference, New York, November 1968 15 p2668 A69-30683

Faraday effect for magnetic properties of chromium tribromide along various isotherms near critical point, confirming scaling laws 15 p2668 A69-30686

Crystallographic classes of ferrites for microwave devices, discussing magnetic properties, applications and work on polycrystalline yttrium-calcium iron-vanadium-indium garnet 15 p2670 A69-31208

Double shock method for detecting pressure limits in magnetic phase transition of solids 16 p2825 A69-31696

Gravity gradient satellite stabilization and magnetic hysteresis damping systems, outlining energy dissipation device involving torques 17 p3047 A69-33231

Directionally solidified Co-Nb eutectic alloys mechanical properties and magnetic performance for elevated temperature space applications 19 p3341 A69-35542

Transverse electromagnetic wave propagation in cylindrically stratified axially magnetized plasma, obtaining plasma properties profiles from method for isotropic media 19 p3266 A69-35619

Magnetic test facilities at ESTEC consisting of system for geomagnetic field compensation and facility for magnetization and demagnetization, testing ERSO satellite models 20 p3512 A69-38279

Magnetic ordering in dysprosium phosphate observed by high resolution spectral line intensity measurements, finding Neel temperature 21 p3773 A69-38331

Magnetic crystallographic anisotropy of Li-Ga ferrite single crystals measured by ferromagnetic resonance techniques 21 p3781 A69-39134

Magnetic hysteresis dynamic model suitable for digital computer simulation of near-earth satellite attitude motions damping compared with experimentally generated loops [AIAA PAPER 69-833] 21 p3821 A69-39364

Phase diagram, dielectric and magnetic properties of Bi manganate/Pb titanate solid solutions of perovskite structure, showing dependence on composition and temperature 22 p3996 A69-41163

Al-Ni-Co alloys precipitation mechanism effect on magnetic properties, including heat treatment and Ti alloying effects 23 p4175 A69-41298

MAGNETIC PUMPING

Heating of nonuniform plasma cylinder in constant magnetic field by magnetic pumping with oscillating magnetic field, determining energy absorption 02 p0288 A69-12167

Quantum paramagnetic amplifier using natural andalusite single crystal and operating with four level pumping 04 p0577 A69-14781

Plasma ion heating by external stochastic HF field, noting avoidance of special thermalization processes 09 p1553 A69-22527

Parametric excitation of spin waves during parallel pumping of rubidium nickel fluoride ferrite, relating relaxation time and temperature 21 p3781 A69-39069

MAGNETIC RECORDING

Rotary head units used in telemetry magnetic recorders, explaining concepts and advantages of rotary scanning 07 p1077 A69-18826

Effects, measurement and analysis of flutter in instrumentation recorders 07 p1133 A69-19118

Computer simulation of unbiased digital recording composed of sequential computations intended for various bit densities [IEEE PAPER 3.3] 09 p1461 A69-22562

Dual inertia magnetic tape recorder/reproducer combining low wideband flutter and low time base errors 10 p1693 A69-23289

Signal to noise ratio in spectral composition of FM signals in magnetic recorder channels, taking into account parasitic FM and AM 11 p1834 A69-24612

Thermistor instrument for remote sensing, magnetic synchronous recording and linear display of temperature 14 p2449 A69-29562

Recording technique for measuring short period variations of radio signal reflections altitudes from ionosphere applicable to fast ionospheric processes 20 p3521 A69-37054

Wideband telemetry recording error compensator for reducing flutter and interchannel time-base error in magnetic tape instrumentation 23 p4137 A69-41775

MAGNETIC RELAXATION

U SPIN-LATTICE RELAXATION

MAGNETIC RESONANCE

NT ELECTRON PARAMAGNETIC RESONANCE
NT FERROMAGNETIC RESONANCE
NT NUCLEAR MAGNETIC RESONANCE
NT PARAMAGNETIC RESONANCE
NT PROTON MAGNETIC RESONANCE

Standing Alfvén wave resonances in liquid sodium 01 p0131 A69-10820

Cold plasma magnetoacoustic resonance, showing nonlinear exciting magnetic field dependence on polarity and energy 09 p1548 A69-21668

Geomagnetic field Pc 3 and Pc 4 pulsation generation mechanism explained by resonance of MHD waves in force tubes adjoining radiation belt maximum 10 p1689 A69-24206

Magnetoelastic resonant interaction of microwave longitudinal phonons propagating at right angles to magnetic bias applied to YIG rod axis 15 p2565 A69-30184

MAGNETIC RIGIDITY

Oriented nuclear emulsion stack for determining differential rigidity spectrum of primary He nuclei between 12 and 35 bv 06 p0988 A69-17276

Permanent magnet and nuclear emulsion for measuring He nuclei momentum spectra up to 100 gv rigidity 06 p0989 A69-17277

Rigidity spectra of total primary cosmic radiation by ascending or descending balloon-borne detectors in atmosphere, with changing mean response energy 06 p0989 A69-17279

Proton and alpha particle fluxes above specified vertical geomagnetic cut-off rigidity measured by balloon-borne Cerenkov scintillation counter telescope 14 p2511 A69-28951

MAGNETIC SHIELDING

Soft magnetic materials, ferrites and magnetic particle composites as two layer laminates for shielding in audio and microwave frequencies 09 p1500 A69-22310

Superconductivity methods to neutralize ambient magnetic field by free electrons motion for nonmagnetic environments 13 p2244 A69-28604

Residual field in inner airspace of magnetostatic shielding thin walled stretched ellipsoids of revolution 13 p2237 A69-28610

Earth core conductivity effects on ionospheric shielding against geomagnetic changes from external sources, noting earth-ionosphere coupling 17 p2959 A69-32925

MAGNETIC SIGNATURES

Flares and chromospheric absorption features locations compared with H alpha magnetograms, noting double emission ribbons development 09 p1579 A69-22179

F region during earth passage through solar corpuscular stream, analyzing critical frequencies, virtual height, magnetogram H component and ionospheric storm effects attributed to downward drift 17 p2967 A69-33989

MAGNETIC SPECTROSCOPY

Magnetic electron multiplier used as particle detector in time-of-flight (TOF) mass spectrometers can introduce mass discrimination effects 04 p0599 A69-15014

Permanent magnet and nuclear emulsion for measuring He nuclei momentum spectra up to 100 gv rigidity 06 p0989 A69-17277

Gas laser application to magnetospectroscopy of graphite, Bi, As and pyrolytic graphite single crystals 16 p2796 A69-31822

Spectroscopic azimuthal and axial measurement of jet velocity in MPD X9 rocket engine by spectrograph and Fabry-Perot interferometer [DGLR-69-024B] 23 p4202 A69-41925

MAGNETIC STARS

Plasma acceleration away from rotating magnetized astrophysical objects analyzed and applied to pulsar NP 0532 for magnetic moment and mass loss rate calculations 20 p3598 A69-37419

MAGNETIC STORAGE

Reading amplifier for thin magnetic film memory stores permitting tunnel diode register positioning 04 p0579 A69-15319

Magnetic reversible phase holograms on thin film Mn-Bi by Curie-point writing technique 10 p1706 A69-24007

Time logarithmic switching to explain anomalous delay in threshold response of MgMnZn ferrite memory cores 15 p2668 A69-30688

Computer memory with digit wire magnetic circuit /torus/, discussing capacity, access and output 20 p3503 A69-37402

CRT display system coupling interface with magnetic storage determined from algorithms and time diagrams, describing character storage and system logic design 22 p3908 A69-40936

MAGNETIC STORMS

- Low latitude m arcs in 6300 angstrom emission during intense geomagnetic storm related to auroral red oxygen emission peak
01 p0062 A69-10136
- Geomagnetic disturbance activity forecasting method using solar coronal streams, noting reliability of test forecasts
01 p0150 A69-10372
- Magnetic storm principal phase explained by interaction between quasi-trapped particles stream and magnetosphere
01 p0144 A69-10573
- Equatorial enhancement of storm sudden commencements and sudden impulses in horizontal component in American Zone during IGY/IGC
01 p0068 A69-11116
- Solar and geophysical activity during February 1965 and March 1966 indicating geomagnetic activity on 27-day recurrence diagram
01 p0068 A69-11118
- Solar X-ray high activity level during spring 1966 connected with gamma type magnetic solar regions and correlated with ionospheric effects
01 p0146 A69-11119
- Solar, interplanetary and magnetospheric electromagnetic events before and during magnetic storm from ground observatory and earth satellite data
01 p0156 A69-11120
- Solar proton event generating sudden commencement magnetic storm, discussing effects on outer belt electrons as observed by Explorer 26 and time delay
01 p0146 A69-11124
- Magnetic field data from OGO-2 spacecraft and surface magnetic observatories, noting magnetic storm occurrence and magnetospheric inflation and detection of polar ionospheric currents
01 p0069 A69-11125
- Latitudinal variations in auroral and subauroral region F layer diurnal and magnetic storm pattern shown by scintillation measurements
01 p0069 A69-11127
- Magnetic field behavior at synchronous orbit during magnetospheric substorms, interpreting satellite observed data in terms of partial ring currents
01 p0075 A69-11225
- Ring current particle energy density distribution for symmetric portion of magnetic storm derived from current magnetic field profile measurements
01 p0147 A69-11227
- Solar plasma observations during magnetic storms, discussing shocks and tangential discontinuities, geomagnetic variations and He
01 p0076 A69-11234
- Upper atmosphere oxygen emission and heating during geomagnetic disturbances
02 p0235 A69-11421
- Polar ionosphere heating by spill-over electron energy during strong geomagnetic disturbances, giving mathematical representation
02 p0237 A69-11664
- Perturbed geomagnetic field structure during magnetic storm recovery phase calculated by magnetosphere magnetic field model, accounting for various external field sources
02 p0237 A69-11666
- Relationship between polar geomagnetic disturbances and DR variations value of geomagnetic field
02 p0238 A69-11672
- Dispersion measurements and spectrum variations analysis to study pearl micropulsations frequency variation during sudden deformation of magnetosphere by magnetic storms
02 p0240 A69-11697
- Vertical and horizontal components of geomagnetic storm main phase magnetic variations applied to vertical electromagnetic soundings of earth
02 p0240 A69-11700
- Characteristics of electrovortices and auroral electrojets of polar disturbance field, discussing dynamics during geomagnetic storms
02 p0240 A69-11723
- Parameters of solar wind responsible for geomagnetic activity, relating magnetic storm features to physical structure of interplanetary space and solar wind bubbles
02 p0240 A69-11725
- Hydromagnetic emissions observed at Antarctic auroral zone, discussing relation to sudden storm commencement
02 p0241 A69-11726
- Geomagnetic and interplanetary field variation measurements from Mariners 2, 4 and 5, noting correlation between solar phenomena and geomagnetic storms
02 p0241 A69-11737
- Magnetic storm of January 1967 due to 3B solar flare noting spacecraft observations, intensity, magnetospheric distortions and solar wind dynamics
03 p0500 A69-13430
- Ionospheric F 2 layer following SSC magnetic storm, noting similarity with polar aurora region
03 p0423 A69-13531
- Ionospheric parameters variation during SC effect as function of solar and magnetic activities
03 p0423 A69-13534
- Sudden acceleration of electrons in magnetosphere and magnetic tail related to magnetic bays, noting acceleration occurrence first in magnetosphere during polar substorm
04 p0594 A69-15122
- East-West aligned fast auroral waves, suggesting origin in hydromagnetic processes occurring near equatorial plane
04 p0594 A69-15123
- Charged particles injection into captured radiation zone of Van Allen belts during main phase of magnetic storm indicated by proton data analysis
05 p0815 A69-16057
- Elektron satellite recorded sporadic radio emission noting relationship to geomagnetic disturbances and dependence on satellite position
05 p0824 A69-16059
- F region seasonal and magnetic storm behavior from region daily behavior showing global upper atmospheric circulation
05 p0757 A69-16404
- Ionospheric electron content and slab thickness changes during magnetic storm in June 1965 using Faraday rotation and critical frequencies
05 p0759 A69-16420
- Book on polar and magnetospheric substorms including daily variation data, satellite observations, etc
06 p0915 A69-16832
- Vertically moving ionized formations relation to solar and magnetic activity
06 p0920 A69-17730
- Magnetospheric ring current effect on main phase of geomagnetic storms, calculating diurnal storm-time portion of perturbation field
07 p1122 A69-18296
- Equatorial hourly storm time part of disturbances field for 1958, discussing magnetic storm effects
07 p1124 A69-18822
- Magnetospheric magnetic field ring current asymmetry during different phases of geomagnetic storm observed by Explorer 26 and Vela 2 satellites
07 p1129 A69-19611
- Trapped electron belts formation and storm time behavior assuming presence of bimodal diffusion from low energy source at magnetosphere outer edge
08 p1307 A69-20184
- Midday enhancement of sudden commencements and sudden impulses in H and Z at equatorial stations in Indian zone during IGY
08 p1307 A69-20187
- Geomagnetic storms, substorms and auroral displays as functions of processes in solar wind and upper atmosphere
08 p1307 A69-20188
- Auroral zone X ray measurements emphasizing temporal intensity variations, energy spectra changes and source region movements during magnetospheric substorms
08 p1379 A69-20534
- Auroral oval boundary and median line variations with increasing magnetic storm time intensity, noting ring current effect on polar aurora location
09 p1485 A69-21532
- Charged particles equations of motion in earth magnetosphere in polar storms, considering auroral zone, diurnal variations and electron and proton velocities
09 p1485 A69-21535
- Aeronomical parameters effect on ionospheric effect of SC magnetic storm, calculating maximum ionization levels, F layer ionization and vertical ionization profile parameters
09 p1486 A69-21546
- Upper atmospheric density relation to AE indices sum and solar radio flux during geomagnetic disturbances
09 p1488 A69-21657
- Low energy solar cosmic ray proton flux characteristics observed by Injun 1 satellite after July 1961 sudden commencement magnetic storm
09 p1576 A69-21707
- Average geomagnetic storm ranges as function of latitude, noting disturbances caused by ring and ionospheric currents
09 p1489 A69-21715
- Sudden commencement associated discontinuities in interplanetary magnetic field observed by IMP 3 satellite, stressing shocks and tangential and rotational discontinuities
09 p1598 A69-22183
- Auroral electrojet precursors and geomagnetic variations before onset of bays, noting satellite observations
10 p1681 A69-22804
- Simultaneous interplanetary magnetic field measurements by geocentric satellites Explorer 33 and IMP 3 of MHD shock wave associated with July 8, 1966 sudden storm commencement
10 p1783 A69-23773
- Topside ionospheric electron density profiles compared for magnetically quiet and disturbed periods surrounding December 17, 1962 magnetic storm
10 p1685 A69-23835
- Magnetic lines of force penetration into magnetosphere accompanied by plasma insertion generating ring current responsible for main phase of magnetic storm
10 p1687 A69-23923
- Midlatitude ionospheric disturbances accompanied by auroral type radio absorption observed by radio astronomy and probes during May 26, 1967 storm
10 p1688 A69-23935
- Harmonic analysis of magnetic storms initial phases having steep leading edges and distinct steady portions, showing homogeneity in first approximation
10 p1688 A69-23938
- Outer radiation zone electron intensities during magnetic storms for morphology of zone electron acceleration mechanisms
11 p1950 A69-25147
- Auroral infrasonic waves morphology related to temporal and spatial distributions of supersonic auroral motions during polar magnetic storms
11 p1878 A69-25152
- Solar flare and magnetic storm signals from ATS 1 geostationary satellite on May 28, 1967, deriving total electron content
11 p1951 A69-25161
- Magnetospheric substorm as discharge process of associated electric current system, discussing relaxation processes, explosive release of energy, etc
11 p1879 A69-25249
- Auroral arcs drift as function of polar storm initial phase, noting agreement with satellite data on plasma motion in magnetosphere
12 p2071 A69-26694
- Auroras and polar magnetic substorm observations limited comparison due to magnetospheric models inability to interpret daytime precipitation zones and particle energy spectra
12 p2072 A69-26740
- Solar wind induced magnetospheric convection for interpretation of geomagnetic storms, aurora and trapped particle belts, noting electric fields
12 p2073 A69-26749
- Solar-terrestrial environment, discussing mathematical development of solar wind, satellite measurement, magnetic storms, aurora and cosmic rays
12 p2161 A69-26941
- Satellite observation of intensity and distribution of VLF emission at medium latitude during magnetic storm interpreted by transverse resonance plasma instability
12 p2073 A69-26947
- Polar ionosphere heating by spill-over electron energy during strong geomagnetic disturbances, giving mathematical representation
13 p2257 A69-28695
- Perturbed geomagnetic field structure during magnetic storm recovery phase calculated by magnetosphere magnetic field model, accounting for various external field sources
13 p2257 A69-28697
- Relationship between polar geomagnetic disturbances and DR variations value of geomagnetic field
13 p2257 A69-28703
- Dispersion measurements and spectrum variations analysis to study pearl micropulsations frequency variation during sudden deformation of magnetosphere by magnetic storms
13 p2258 A69-28728
- Vertical and horizontal components of geomagnetic storm main phase magnetic variations applied to vertical electromagnetic soundings of earth
13 p2258 A69-28731
- Magnetic storm time variations of electron concentrations in upper ionosphere near north geomagnetic pole, discussing magnetic time, altitude and latitude dependence
14 p2510 A69-28939

MAGNETIC SURVEYS

Large amplitude pulsations in magnetic field magnitude and proton fluxes observed by satellite during magnetic storm compared with various models
14 p2434 A69-28947

Auroral electrojet index in relation to magnetic storm sudden commencements, ring current main phase and energetic solar protons
14 p2511 A69-28954

Ionospheric effect sudden commencement parameters of magnetic storm related to distance from origin in polar regions
14 p2435 A69-29051

Oscillations intervals with diminishing period observed during magnetic storms, noting relationship to midlatitude disturbances in F region
14 p2436 A69-29060

September 14, 1966 magnetic storm observation by Explorer 33 in geomagnetic tail and by polar stations, studying relation in magnetosphere and on earth
14 p2438 A69-29078

Nonuniform ring current belt growth, discussing associated magnetospheric substorms
14 p2513 A69-29123

Frequency time dispersion of storm sudden commencement micropulsations, noting polarization effects
14 p2440 A69-29129

Geomagnetic storm induced temporary radiation zones located by determining Explorer 30 attitude and spin axis orientation
14 p2514 A69-29384

Geomagnetic storms caused by plasma streams impinging on earth related to preceding cosmic flares, discussing polar cap absorption and ground level effects
14 p2514 A69-29416

Amplitude and frequency spectra for Ipc pulsations during geomagnetic storms
14 p2441 A69-29417

Statistical analysis of data for 18-19 June 1936, estimating expressions involving external and internal components of geomagnetic field at storm time disturbances
14 p2444 A69-29883

Auroral substorms concept extended to include associated effects at all local times throughout magnetosphere, considering particle precipitation influence on substorms in midnight sector
15 p2593 A69-30008

Auroral substorm westward traveling surge and poleward, eastward and equatorward motion analyzed from all sky photographs
15 p2595 A69-30214

Auroral displays observed in combined field of view of polar all sky camera networks, considering simultaneous geomagnetic disturbances over Alaska
15 p2595 A69-30215

Magnetic storm principal phase explained by interaction between quasi-trapped particles stream and magnetosphere
15 p2675 A69-30743

Magnetic storm effects on electrons and protons in outer belt, using satellite data for intensity and differential energy spectra
15 p2676 A69-31314

Gravity waves in thermospheric heating during magnetic storm, discussing electron density and temperature and ion velocity variations
15 p2605 A69-31435

Worldwide changes in geomagnetic field, determining causes by examining magnetic field and plasma data from solar wind and classifying as SSC or SI
16 p2847 A69-31963

Simultaneous solution of continuity and heat conduction equations for ionospheric electrons, ions and neutral species for studying F region magnetic storm behavior
16 p2775 A69-32083

Radio wave emission bursts at 28 MHz at onset of nighttime absorption dip and close to auroral zone from riometer recordings, noting relation to geomagnetic storms
16 p2775 A69-32085

Geomagnetic storms generation interpreted using solar coronal arrangements above central meridian
16 p2777 A69-32100

Low latitude asymmetric disturbance field analyzed using equivalent current vectors during magnetic storms, allowing for solar quiet day variation and declination
16 p2778 A69-32184

Low latitude sporadic E layer associated with geomagnetic activity studied in Hong Kong using proton precession magnetometer and standard ionosonde
16 p2779 A69-32195

Infrasonic waves identified with supersonic auroral electrojets crossing zenith from northwest during substorm activity
16 p2780 A69-32303

Interplanetary magnetic fields from Explorer 33 magnetometer relationship to surface geomagnetic variations emphasizing unified view
16 p2862 A69-32309

Auroral oval boundary and median line variations with increasing magnetic storm time intensity, noting ring current effect on polar aurora location
16 p2783 A69-32527

Charged particles equations of motion in earth magnetosphere in polar storms, considering auroral zone diurnal variations and electron and proton velocities
16 p2783 A69-32530

Aeronomical parameter effect on ionospheric effect of SC magnetic storm, calculating maximum ionization levels, F layer ionization and vertical ionization profile parameters
16 p2783 A69-32541

Polar substorms resulting from interaction between magnetized plasma stream and geomagnetic field in magnetosphere
16 p2852 A69-32620

Electromagnetic /ULF, VLF/ and light emissions development during magnetic substorms, discussing varied pulsations present in development phases
16 p2788 A69-32648

Magnetic storm energy balance, assessing solar corpuscular flux energy consumption in and beyond magnetosphere
17 p2964 A69-33959

Planetary ionospheric effect of 15 July 1959 sudden commencement magnetic storm based on N/h profiles of earth day and night sides
17 p2967 A69-33987

Initial phases of ionospheric and magnetic storms compared from data, noting good correlation due to ionospheric fields influence
17 p2967 A69-33988

Geomagnetic storms and Forbush decreases accounted for by interplanetary solar corpuscular streams effects described by interplanetary magnetic field structure, noting independence of flares
18 p3187 A69-34937

Electron temperature, density and magnetic disturbances measurements at 1000 km compared with visual observations during 25-26 May 1967 magnetic storm and aurora
18 p3129 A69-34954

Whistlers occurrence and dispersion rate variations from data obtained at lower latitudes during magnetic storms
18 p3102 A69-34967

Ionospheric electric current systems dynamics in polar latitude in relation to 1966 geomagnetic storms
18 p3130 A69-35188

Geomagnetic storms data compilation /1957-1964/, showing solar activity effect on solar corpuscular stream velocity
20 p3587 A69-37036

Magnetic field variation rates characteristics during magnetic storms investigated for longitudinal dependence and influence of equatorial electric current
20 p3520 A69-37037

Gokhberg magnetovariational sounding method for single location analysis of magnetic storms early phases, comparing ground station network observations
20 p3521 A69-37040

Upper ionosphere Thomson scatter, electron number density measurements and topside sounding results during geomagnetic storms using electrodynamic drift theory
20 p3530 A69-37872

Charged particles injection into captured radiation zone of Van Allen belts during main phase of magnetic storm indicated by proton data analysis
20 p3591 A69-37967

Elektron satellite recorded sporadic radio emission noting relationship to geomagnetic disturbances and dependence on satellite position
20 p3606 A69-37969

Three dimensional current systems constructed semiquantitatively for polar magnetic substorms based on magnetic field distribution on earth surface
20 p3533 A69-38085

Doppler broadened atomic O emission line measurement providing indication of exospheric temperature storm-time variations
20 p3546 A69-38099

Auroral zone geomagnetic pulsations on nightside and dayside of earth related to magnetospheric substorm and particle precipitation
21 p3708 A69-38497

Polar upper atmospheric phenomena interpreted as magnetospheric substorm manifestations, discussing role of asymmetric ring current formation
21 p3710 A69-38504

Charged particle acceleration in interplanetary plasma from analysis of cosmic ray intensity increases accompanied by SC magnetic storms and Forbush effects
21 p3788 A69-38587

Explorer 34 observations of hydrogen and He ions in solar wind, noting number density variations and tentative association with geomagnetic storms
22 p4004 A69-40305

Geomagnetic disturbances and cosmic ray storm of 25-26 May 1967 caused by McMath plage region 8818, noting Forbush decreases and ring current effect
22 p4004 A69-40307

Cosmic ray proton cut-off increase at high latitudes during magnetospheric substorms, using balloon time observations of nuclear gamma ray flux
22 p4005 A69-40509

Corpuscular radiation intensity measurements in upper atmosphere at midlatitudes by meteorological probe during geomagnetic storm, noting radio wave absorption
22 p4008 A69-41104

Sudden and gradually developing geomagnetic storms with 27 day recurrence period and relation to 11 year solar activity cycle
23 p4156 A69-41849

Geomagnetic ring current effect on position of auroral absorption zone in northern polar region, noting storm time part of disturbance
23 p4157 A69-41859

Topside ionosphere response to magnetic storms, using Explorer 22 satellite electron concentration and temperature measurements
23 p4161 A69-42438

Electron intensities and substorm drift effects in outer radiation belt using two satellite technique
24 p4309 A69-43172

Magnetospheric electron sudden intensity increases correlated with magnetic substorms occurrence at midnight meridian from ATS 1 observation
24 p4367 A69-43173

Thermosphere dynamic response to low altitude geomagnetic disturbances, showing time lag dependence on perturbation intensity
24 p4310 A69-43180

MAGNETIC SURVEYS

Aeromagnetic profiles across Reykjanes ridge southwest of Iceland, noting magnetic anomalies symmetry and ocean floor spreading since Mesozoic
04 p0592 A69-14660

Structure, temporal behavior, shape and length of earth magnetic tail via satellite mapping
07 p1208 A69-19363

Secular variations distribution on earth surface, plotting isopore charts from mean annual values of magnetic elements /1960-1965/
10 p1687 A69-23920

Interplanetary magnetic fields from Explorer 33 magnetometer relationship to surface geomagnetic variations emphasizing unified view
16 p2862 A69-32309

MAGNETIC SUSPENSION

Multichannel telemetering device for magnetically suspended or free flight wind tunnel models noting strain gage pickups, switching and auxiliary circuits [ONERA-TP-643]
02 p0226 A69-11623

Low g accelerometers including air-film, electrically suspended, vibrating string, semiconductor and ONERA [ONERA-TP-449]
05 p0766 A69-16749

Atmospheric humidity effect on efficiency of geomagnetic field scales with taut-strip suspension and temperature fluctuation
09 p1494 A69-21518

Centering force and initial rigidity of magnetically suspended bearings of integrating floating gyroscope with allowance for mutual inductance of exciting coils
09 p1497 A69-22104

Rational shape selection for magnetoelectroconductors of centering elements of magnetically suspended bearings, studying effects on initial rigidity
09 p1497 A69-22105

Magnetic suspension device replacing mechanical bearings of inertial guidance systems gyro rotors, evaluating device strength and stability
14 p2479 A69-29492

Rocket sled incorporating magnetic suspension system
15 p2585 A69-30361

Lift and drag determination for moving rectangular coils over infinite plane sheet for magnetic suspension and guidance for rocket sleds

17 p2946 A69-33789

Magnetic suspension system used as dynamic balance for wind tunnel models, discussing delta wing test results

19 p3292 A69-35738

Wind tunnel model one component magnetic support and balance system for sphere drag investigation at subsonic Mach numbers
[AIAA PAPER 68-401]

24 p4298 A69-43714

MAGNETIC SWITCHING

Time logarithmic switching to explain anomalous delay in threshold response of MgMnZn ferrite memory cores

15 p2668 A69-30688

Dynamic Kerr observations of high speed flux reversal and relaxation process in permalloy thin films by magnetooptical camera with Q switched ruby laser

19 p3383 A69-36446

MAGNETIC TAPE RECORDERS

U TAPE RECORDERS

MAGNETIC TAPES

Time coding system for recording balloon measurements on magnetic tape

05 p0762 A69-15825

Root mean square time delay error with respect to playback time and autocorrelation function of tape recorded sine wave for studying jitter spectra

07 p1132 A69-18827

High reliability magnetic tape recorders for satellite, aircraft and drone applications

07 p1133 A69-19104

Magnetic tape recording of ultrasonic test information with oscilloscope used for playback

07 p1117 A69-19697

Machine cutting tool for cutting and splicing endless magnetic tape 30 microns thick, noting film safety feature and nonmagnetic steel scissors

08 p1321 A69-20876

Magnetic tape recorder/reproducer for FM analog test data

10 p1691 A69-23233

Stiction friction on magnetic tape and contact surfaces noting effect of binders, plasticizers, humidity and temperature

19 p3312 A69-36285

MAGNETIC TRANSDUCERS

Pressure transducers with variable reluctance and magnetic signal transmission techniques

10 p1690 A69-23226

Signal conditioning for transducers covering piezoelectric devices, thermocouples, resistance transducers, reluctance and differential transformer sensors

10 p1691 A69-23228

MAGNETIC TRAPS

U PLASMA CONTROL

MAGNETIC VARIATIONS

NT GEOMAGNETIC MICROPULSATIONS

NT GEOMAGNETIC PULSATIONS

26-month periodicity in quiet day range of geomagnetic field horizontal force, noting similar periodicity in sunspot number and 16-month oscillation in both phenomena

01 p0063 A69-10427

Microstructure analysis and relationship between microvariations and macroscopic events, using magnetic variations recordings of IGY network

01 p0069 A69-11126

Solar plasma observations during magnetic storms, discussing shocks and tangential discontinuities, geomagnetic variations and He

01 p0076 A69-11234

Secular change examination in cislunar geomagnetic tail field gradient during summers of 1966 and 1967, using Explorer 33 and 35 results

01 p0077 A69-11237

Relationship between polar geomagnetic disturbances and DR variations value of geomagnetic field

02 p0238 A69-11672

Vertical and horizontal components of geomagnetic storm main phase magnetic variations applied to vertical electromagnetic soundings of earth

02 p0240 A69-11700

Numerical calculations for oscillatory solutions of system of nonlinear differential equations, noting circularly polarized magnetic oscillations observed near earth bow shock front

02 p0241 A69-11729

Charts summarizing daily solar phenomena, cosmic rays, geomagnetic variation, ionosphere, radiowave propagation and airglow observations in Japan

02 p0315 A69-11732

Geomagnetic and interplanetary field variation measurements from Mariners 2, 4 and 5, noting correlation between solar phenomena and geomagnetic storms

02 p0241 A69-11737

World maps highlighting differences in geomagnetic field at conjugate localities

02 p0245 A69-12737

Earth magnetic field variations, discussing source of field, dynamo theory and paleomagnetic evidence for polarity reversals

03 p0420 A69-12935

Elektron 2 satellite magnetic measurement of high latitude nocturnal magnetosphere, discussing variations, antisolar effect and elongation of magnetic field

03 p0422 A69-13505

Geomagnetic field quiet day solar variations current system calculated, using 2000 LT as zero level basis

03 p0424 A69-13541

Time dependent variations in magnetic fields of active sunspot clusters in photosphere observed by magnetograph

04 p0651 A69-14369

Dissipation time of sunspot magnetic field determined as function of minimum spot value

04 p0660 A69-15039

Interplanetary magnetic field fluctuations obtained by IMP 2

05 p0824 A69-16264

Global geomagnetic anomalies influence on longitudinal pattern of solar quiet day variations and in phases of second harmonics of components

06 p0920 A69-17734

Lunar core electrical conductivity determination based on induced magnetic field arising from time varying interplanetary magnetic field associated with solar wind plasma

07 p1215 A69-18832

Equatorial counter-electrojet and inverse quiet day solar diurnal variation current layers, noting regular diurnal variation horizontal component and latitude effect

08 p1306 A69-19884

Midday enhancement of sudden commencements and sudden impulses in H and Z at equatorial stations in Indian zone during IGY

08 p1307 A69-20187

Geomagnetic secular variations calculated by comparison of satellite, oceanic and aeromagnetic surveys

09 p1485 A69-21534

Mariner 2 data on large scale variations in magnetic field, solar wind density and temperature in interplanetary plasma

09 p1592 A69-21540

Geomagnetic field mean hourly values continuous smoothing from recordings at drifting arctic stations for determining time variations

09 p1487 A69-21553

Radial velocity, light and magnetic variations of HD 10783 from concurrent UVB photometric and Zeeman spectroscopic observations

09 p1600 A69-22197

VLF polar chorus emission and geomagnetic variations caused by compressions or expansions of magnetosphere

10 p1681 A69-22803

Auroral electrojet precursors and geomagnetic variations before onset of bays, noting satellite observations

10 p1681 A69-22804

Asymmetrical solar wind volume variations of magnetic inhomogeneities and cosmic ray absorption in earth atmosphere, including barometric coefficients of neutron component

10 p1760 A69-22844

Magnetic field decay in sunspot group 21034 during July 7, 1966 proton flare

10 p1766 A69-23759

Geomagnetic field variations in middle and high latitudes during proton flare event, discussing UV radiation and period and energy spectra

10 p1683 A69-23780

Lunar diurnal variation parameters at Irkutsk determined from IGY data concerning geomagnetic field components

10 p1687 A69-23918

Secular variations distribution on earth surface, plotting isopor charts from mean annual values of magnetic elements /1960-1965/

10 p1687 A69-23920

Microscale fluctuations in interplanetary magnetic field, considering proton thermal energy and magnetic field energy densities

10 p1785 A69-24100

Quantitative magnetic field models of magnetosphere for analyzing field configuration variations and adiabatic particle motion

12 p2072 A69-26738

Drift velocity of earth magnetic field based on spherical harmonic analysis of geomagnetic secular variation

12 p2077 A69-27111

Geomagnetic field daily variations, discussing observational techniques, observation analysis, S-field seasonal changes, equatorial electrojet, solar wind effects, dynamo theory, etc

12 p2077 A69-27143

Relationship between polar geomagnetic disturbances and DR variations value of geomagnetic field

13 p2257 A69-28703

Vertical and horizontal components of geomagnetic storm main phase magnetic variations applied to vertical electromagnetic soundings of earth

13 p2258 A69-28731

Electron concentration enhancement in upper atmosphere at polar latitudes, noting three independent zones and relation to magnetic local time

14 p2510 A69-28938

Power spectrum analysis and linear filtering for 27 day variation amplitude of geomagnetic disturbance subject to semiannual amplitude modulation

14 p2434 A69-28955

Magnetic field fluctuations of interplanetary plasma, considering anisotropic temperature instabilities

14 p2517 A69-29064

Magnetosensitive quartz element with suspended magnet and two mirrors for recording magnetic variations

14 p2446 A69-29084

Magnetic field variations in magnetosphere and interplanetary space correlated with polar magnetic disturbances from dynamic morphology data

14 p2441 A69-29387

Short period pulsations in solar magnetic fields and chromosphere, determining optimum conditions for formation of standing oscillations

15 p2688 A69-30556

Zeeman spectroscopy and UVB photometry of 17 Com and kappa Cnc, observing periodic magnetic and light variations

15 p2692 A69-30774

Nonlinear boundary value problems for isotropic plasma with known magnetic field, examining electromagnetic waves scattering at magnetic fluctuations

15 p2569 A69-30938

Solar cycle effect on high latitude magnetic activity, discussing annual variations and Lassen auroral zone model confirmation

15 p2598 A69-31207

ESRO 2 satellite observations of solar proton event of 9 June 1968, comparing flux profile variations across polar cap with magnetic changes at earth surface

15 p2677 A69-31347

Interplanetary magnetic field radial dependence from Mariner 4 measurements between earth and Mars, indicating fluctuations produced by dynamic processes in solar wind

16 p2856 A69-31964

Horizontal magnetic variation peak at eight degree dip latitude, noting F region contribution to magnetic tubes of force integrated transverse conductance

16 p2778 A69-32189

Satellite radio signal scintillation variations association with sporadic E and spread F and dependence on magnetic activity in Southern Hemisphere during sunspot minimum

16 p2780 A69-32307

Solar quiet day geomagnetic variations harmonic analysis with respect to time intervals centered around noon, defining parameters responsible for modulated Sq

16 p2781 A69-32452

Equations of transformation for hourly data harmonic terms used in computation and representation of solar and lunar daily magnetic variations

16 p2782 A69-32457

Semiannual variation in amplitude of solar daily quiet geomagnetic variation, discussing sunspot dependence of seasonal secondary minimum and maxima

16 p2782 A69-32459

Upper atmospheric winds to produce solar quiet day magnetic variations based on dynamo theory, illustrating solenoidal, irrotational and mixed winds

16 p2782 A69-32460

Geomagnetic secular variations calculated by comparison of satellite, oceanic and aeromagnetic surveys

16 p2783 A69-32529

Mariner 2 data on large scale variations in magnetic field, solar wind density and temperature in interplanetary plasma

16 p2864 A69-32535

- Geomagnetic field mean hourly values continuous smoothing from recordings at drifting arctic stations for determining time variations 16 p2784 A69-32548
- Solar magnetic field strength distribution in active region during proton flares, using statistical analysis 17 p3025 A69-34225
- Attitude stabilized rocket-released magnetometer for detection of earth field magnitude and direction changes 19 p3309 A69-35994
- OGO triaxial search coil magnetometer for measuring earth magnetic fluctuations, discussing design rationale and observation results 19 p3284 A69-36675
- Reversal rate of earth magnetic field deduced from observed and theoretical polarity interval length using hydrolic transmission line theory 19 p3304 A69-36869
- Magnetic field variation rates characteristics during magnetic storms investigated for longitudinal dependence and influence of equatorial electric current 20 p3520 A69-37037
- Geomagnetic field total vector modulus secular variations from airborne measurements 20 p3522 A69-37061
- Geomagnetic field model (POGO) to confirm eccentric dipole westward velocity secular decrease predicted by day length changes 20 p3523 A69-37490
- HD 188041 magnetic field variations from Zeeman measurements correlated to spectral variations 20 p3611 A69-38156
- Morphology of discrete polar cap and polar glow auroras, noting diurnal variations correlation with magnetic activity changes at low latitude 21 p3707 A69-38487
- Geomagnetic field horizontal component daily variations in relation to solar wind, noting effects of ambient field night side decrease 21 p3714 A69-38549
- Spatial gradient and amount of auroral radio absorption measured by riometers at magnetically conjugate and closely spaced stations 22 p3934 A69-39966
- Homogeneous conducting moon-solar wind interactions, describing time dependent lunar magnetic and electric fields induced by interplanetary magnetic field variations 22 p4023 A69-40518
- Disagreement between Mariner 2 and IMP 1 data concerning interrelation between solar wind velocity and geomagnetism ascribed to instrumental errors and changes in magnetospheric properties 23 p4205 A69-41848
- Magnetic activity effect on electron density in topside ionospheres determined from Alouette 1 data statistical analysis 23 p4156 A69-41856
- Noncyclic daily solar quiet variation in mean hourly geomagnetic field by including noncyclic variation term in regression model 23 p4158 A69-42170
- Geomagnetic activity hourly and daily variations during solar cycle at Huancayo 23 p4162 A69-42442
- Pulsating aurora diurnal variations and dependence on latitude and magnetic activity, photometric observations 24 p4308 A69-43004
- Saturn F-1 rocket engine as generator of infrasonic waves and magnetic fluctuations, noting ignition and cut-off signal characteristics 24 p4365 A69-43415
- MAGNETICALLY TRAPPED PARTICLES**
- NT ARTIFICIAL RADIATION BELTS
- NT INNER RADIATION BELT
- NT OUTER RADIATION BELT
- NT PROTON BELTS
- NT RADIATION BELTS
- Trapped particles drift velocity in time dependent meridional magnetic and perpendicular electric field 08 p1368 A69-20809
- Magnetohydrostatic cavity formed round magnetic field of line dipole-line current combination by infinitely conducting plasma at uniform pressure 08 p1369 A69-20998
- Captured particles magnetic drift envelopes in magnetosphere calculated by model considering perpendicular geomagnetic dipole to solar wind 09 p1574 A69-21521
- Increased energy losses and microwave emission at cyclotron frequency harmonics during plasma electron heating at cut-off plasma concentrations in magnetic trap 10 p1728 A69-23130
- Energy loss during turbulent plasma heating by current in open magnetic trap, attributing heating to ion-acoustic instability in plasma 11 p1935 A69-25753
- Trapping of plasmoids injected from two coaxial plasma sources through magnetic gaps of diverter, discussing alternate and simultaneous injection 12 p2133 A69-25976
- Charged particles influx from cusp shaped regions of stagnant plasma trapped in vicinity of two magnetic cusps on polar magnetopause 12 p2151 A69-26945
- RF synchrotron radiation emitted by electrons from geomagnetic fields above auroral zones, discussing electron flux and cosmic background 12 p2151 A69-26949
- ESRO 1 satellite measuring proton intensities and energy spectra of precipitated and magnetically trapped electrons 13 p2327 A69-27754
- Transverse particle and energy fluxes in toroidal magnetic traps magnetic fields with ionized plasmas, discussing particle diffusion coefficient and thermal conductivity 13 p2314 A69-28446
- Time dependent convection electric fields as agents for diffusing trapped magnetospheric radiation inward toward earth, discussing one dimensional diffusion equation 14 p2510 A69-28936
- Electron and ion mobility in multiple cusp magnetic fields related to Polytron experiment 14 p2499 A69-29852
- Fermi acceleration of energetic electrons trapped within dipole magnetic field analyzed to obtain quantitative results for wave-particle interaction within complex magnetospheric configuration 15 p2594 A69-30095
- Captured particles magnetic drift envelopes in magnetosphere calculated by model, considering perpendicular geomagnetic dipole to solar wind 16 p2851 A69-32516
- Corpuscular radiation distribution function with trapped particles maximum density fixed in equatorial plane and reflection points vicinity of magnetic force line 19 p3396 A69-36630
- Radial motion of trapped electrons caused by pitch angle scattering in distorted geomagnetic field, noting diffusion coefficient 20 p3593 A69-38104
- Solar flare energy source derived from energetic protons trapped in sunspot magnetic field prior to flare occurrence 24 p4374 A69-43623
- MAGNETITE**
- Magnetite content of type I carbonaceous meteorite from quantitative X ray diffractometry of Orgueil meteorite 02 p0328 A69-12729
- Magnetite morphological variations of type I carbonaceous meteorites, discussing isometric crystals, spheres, spherulites, platelets and filaments 08 p1406 A69-20932
- Black magnetite spherules electromagnetically separated from residue of Permian rock salt, determining content and properties of extraterrestrial material 12 p2154 A69-25821
- Black magnetite bearing spherules extracted from tektites, and magnetic fractions of impact glasses, determined by reflecting microscope and electron microprobe 23 p4210 A69-41349
- MAGNETIZATION**
- Pressure and magnetostriction effects on magnetization curves of type 2 superconducting In-Tl alloy, noting Ginzburg-Landau parameter stress dependence 02 p0294 A69-11776
- Yttrium iron garnet sublattice magnetization calculation using Oguchi method 03 p0485 A69-13297
- Dispersive properties of axial and annular longitudinally magnetized plasma waveguides 05 p0802 A69-15925
- Quantum oscillations of magnetization, undamped magnetoplasma waves development and sound amplification by electron drift in crossed fields observed in semimetals 09 p1556 A69-21615
- Dislocations effect on magnetization process in YIG crystals, using polarization optical method 09 p1559 A69-22532
- Polycrystalline Fe-Ni, Fe-Ni-Co ferrites structure, magnetostriction, magnetization curves and hysteresis prior and after thermomagnetic treatment 13 p2319 A69-27992
- Ferrites dynamic characteristics in alternating magnetization pulse with variable amplitude indicating linearity loss in strong fields 13 p2320 A69-27994
- Exchange interactions in lithium ferrite aluminates, measuring spontaneous magnetization by ballistic technique from 77 K to Curie point 13 p2320 A69-27995
- Remanent magnetization properties in alkalic igneous complexes at Magnet Cove and Potash Suphur Spring, Ark., calculating paleomagnetic pole during Cretaceous 14 p2445 A69-29884
- Rare earth niobates magnetic properties measured in pulsed magnetic fields 15 p2667 A69-30195
- Nuclear magnetic resonance flowmeter operating from outside pipe walls, discussing operating principles and applications 15 p2616 A69-31290
- Magnetized minerals studied to investigate space-time structure and reversal of main geomagnetic field 16 p2782 A69-32462
- Kerr magneto-optic camera for 10 nsec exposures of dynamic magnetization configuration in magnetic thin film during high speed flux reversal 17 p2970 A69-32853
- MAGNETO-OPTICS**
- Electro-optical and magneto-optical effects in solids, noting high sensitivity and resolution in application to spectroscopic investigation of absolute spectra 08 p1371 A69-20217
- Free carrier magnetoplasma effect used for far IR phase matched difference frequency generation in semiconductors, discussing carbon dioxide laser transitions 09 p1556 A69-21578
- Magnetic reversible phase holograms on thin film Mn-Bi by Curie-point writing technique 10 p1706 A69-24007
- Coulomb interaction during optical transitions between Landau subbands of Ge semiconductor valence and conduction bands in magnetic field, observing diamagnetic excitons 11 p1936 A69-24640
- Near IR radiation magneto-optic light modulators using Faraday effect in yttrium-iron garnet and in related compounds 11 p1886 A69-25057
- RLC integrated low inductance circuit for magneto-optical high speed camera shutters, Q switched ruby laser and short light pulses in spark gap 12 p2084 A69-26149
- Magneto-optical oscillation of absorption coefficient in semiconductors during direct electron transitions 16 p2824 A69-31574
- Normal modes of electrons-electromagnetic field coupled system for many valley semiconductors, calculating dielectric constant for electron gas for ellipsoidal energy surfaces 16 p2826 A69-31821
- Optical mixing and harmonic generation in semiconductors, discussing magnetoconductivity tensors and magneto-optical phenomena due to free carriers 19 p3385 A69-36519
- Electroreflection study of inversion asymmetry and warping induced interband magneto-optical transitions in InSb, employing low temperature electric field modulation technique 19 p3386 A69-36521
- Magneto-optical constants and conduction band parameters of GaAs by coherent radiation at high temperatures, measuring Faraday rotation 19 p3386 A69-36522
- Optical pumping and selective population applications, considering double magneto-optic resonance and inelastic interatomic collisions 21 p3735 A69-38454
- MAGNETOACOUSTIC WAVES**
- Alfven and magnetoacoustic waves propagation in inhomogeneous stable plasma situated in field with helical lines of forces 01 p0130 A69-10742
- Stationary and nonstationary weak discontinuity surfaces propagation for ideal and viscous compressible conductive atmosphere with regard to heat flux, using Hadamard method 03 p0422 A69-13511
- Magnetosonic wave propagation across magnetic field in warm collisionless Maxwellian multicomponent

plasma studied for small electron cyclotron and ion cyclotron radii

03 p0479 A69-14020

MHD waves, Landau damping and magnetosonic waves in homogeneous relativistic Vlasov plasma

04 p0636 A69-15043

Plasma instability in inhomogeneous magnetic field noting wavefront structure role

09 p1546 A69-21571

MHD first order partial differential equations used to investigate wave front between perturbed and unperturbed flow regions in magnetosonic propagation through homogeneous medium

10 p1727 A69-23090

Conical refraction of magnetosonic waves occurring when Alfvén waves propagate at speed of sound in conducting fluid in presence of constant uniform magnetic field

10 p1727 A69-23091

Unstabilizing effect of inhomogeneities on magnetosonic waves in slightly ionized gases with current perpendicular to magnetic field

10 p1734 A69-23459

Magnetoacoustic waves generated by Cerenkov radiation from corpuscular fluxes due to star interaction with stellar wind, determining deceleration forces on star

11 p1955 A69-24385

Plasma properties when carrying periodic magnetoacoustic wave expressed in terms of periodic functions, discussing small perturbation propagation

12 p2138 A69-26708

Alfvén and slow and fast magnetoacoustic waves excited during decay instability of initial Alfvén wave, noting dissipation effect on stability

14 p2489 A69-28735

Coupled magnetoacoustic waves in conducting paramagnetic fluid in resonance region due to mechanical and magnetic motions, considering dissipation

14 p2492 A69-29609

Hydrogen plasma heating by fast large amplitude magnetoacoustic wave, measuring resonance excitation and absorption of wave

14 p2493 A69-29643

Magnetoacoustic waves generated by Cerenkov radiation from corpuscular fluxes due to star interaction with stellar wind, determining deceleration forces on star

24 p4390 A69-43775

MAGNETOACOUSTICS

Cold plasma magnetoacoustic resonance, showing nonlinear exciting magnetic field dependence on polarity and energy

09 p1548 A69-21668

Single particle and collective excitations of plasmas in solids and interactions with acoustic and electromagnetic waves in magnetic field

16 p2821 A69-31820

Amplitude equations for magnetoacoustic and entropy waves diverging from normal MHD shock, obtaining energy flux ratios associated with incident and transmitted waves

20 p3582 A69-38242

MAGNETOACTIVITY

NT MAGNETORESISTIVITY

Polarization tensor variation due to Faraday effect and differential absorption of ordinary and extraordinary waves for radiation propagating in magnetoactive cosmic plasma

05 p0805 A69-16650

Quasi-static theory of antenna in magnetoactive plasma subjected to resonance, solving boundary value problem

07 p1099 A69-18522

Penfield-Haus solution to magnetodynamic effect problem as inertial effect of orbital angular momentum, deriving Bohr magneton formula from Einstein equivalence principle

11 p1919 A69-25098

Propagation and linear transformation of HF electrostatic waves in hot magnetoactive radially inhomogeneous plasma, noting wavelength shortening

16 p2816 A69-31638

Radiation fields from energetic electron moving in helical orbit in magnetoactive plasma, using Maxwell equations

22 p4008 A69-39965

MAGNETOELASTIC WAVES

NT MAGNETOACOUSTIC WAVES

Dispersive two port components for application to microwave pulse compression, coupling YIG crystal magnetoelastic spin wave mode to acoustic transducer

02 p0217 A69-12149

Magnetoelastic coupling constant b measured by propagating microwave signals in pure and substituted YIG

02 p0299 A69-12243

Magnetoelastic vibrations of fluid filled cylindrical cavity in infinite solid medium in presence of uniform axial magnetic field

03 p0528 A69-13927

Magnetosonic waves absorption in plasmas, studying collisions leading to HF energy resonant absorption at lower hybrid frequency

06 p0963 A69-16904

Magnetosonic wave evolution in inhomogeneous dispersive plasma created by magnetic piston, discussing equation solution

07 p1181 A69-19001

Stresses and waves in highly conducting magnetoplastic metals as analogy of MHD processes in plasma

09 p1551 A69-22033

Microwave magnetoelastic wave propagation in ferromagnet subjected to pulsed magnetic field using coupled mode approach

10 p1746 A69-23655

Heat propagation in discharge plasma heated by magnetosonic wave, constructing transverse temperature profile

10 p1741 A69-23896

Saturation and distortion effects on magnetoelastic wave excitation in yttrium garnet single crystals by large amplitude microwave frequency field

12 p2145 A69-26725

Plasma turbulence effect on magnetosonic wave attenuation, noting increased electron and ion collision frequency and appearance of anomalous resistance

16 p2820 A69-31794

Stochastic heating of protons by random magnetosonic wave propagating normal to magnetic field to explain proton energy excess in magnetotail plasma sheet

16 p2848 A69-31969

Saturation and distortion effects on magnetoelastic wave excitation in yttrium garnet single crystals by large amplitude microwave frequency field

21 p3782 A69-39138

MAGNETOELASTICITY

U MAGNETOSTRICTION

MAGNETOELECTRIC MEDIA

Magnetolectric characteristics of inversion layers below gate region in transistors, noting Hall mobility

08 p1372 A69-20460

Electrostatic electron bombardment ion thruster with magneto-electrostatically contained plasma

[AIAA PAPER 69-260] 09 p1567 A69-21262

MOS transistor Hall voltage, mobility and constant verified by magnetolectric measurements of Si p-inversion layer

13 p3232 A69-28331

Electromagnetic wave propagation through magnetolectric media in circular waveguide

14 p2416 A69-29540

Reflection and transmission coefficient matrices for stratified magnetoionic medium determined by thin film optical technique and iteration procedure

17 p2927 A69-33863

MAGNETOGASDYNAMICS

U MAGNETOHYDRODYNAMICS

MAGNETOGRAMS

U MAGNETIC SIGNATURES

MAGNETOGRAPHS

U MAGNETOMETERS

U RECORDING INSTRUMENTS

U MAGNETOHYDRODYNAMIC ACCELERATION

U PLASMA ACCELERATION

MAGNETOHYDRODYNAMIC FLOW

Viscous electrically conducting fluid with aligned magnetic field flowing past flat plate at nonzero angle of attack

01 p0126 A69-10163

Boundary value problems for steady, three dimensional MHD flow of viscous incompressible conducting fluid past various bodies, proving existence of solutions

01 p0126 A69-10164

Dense plasma with plasma frequency greater than cyclotron frequency, discussing flow past slender bodies

01 p0126 A69-10226

Heat transfer situations in plasma flow indicates very high heat fluxes per unit area on surfaces with electric current

[ASME PAPER 68-HT-38] 01 p0175 A69-10314

MHD boundary layer equations in Blasius problem reduced to differential equations and solved by Laplace transform

01 p0127 A69-10337

Effect of steady flow of incompressible conducting fluid on magnetic dipole at center of sphere

01 p0128 A69-10363

High temperature plasmas generation by exploding gold wires in vacuum, using time of flight technique for plasma densities and flow velocities

01 p0129 A69-10667

Two dimensional ionized plasma flow in coaxial channels calculated using differential equations

01 p0130 A69-10723

Semiempirical theory of turbulent MHD tube flow at small Reynolds numbers taking into account magnetic field presence

01 p0130 A69-10769

Stabilization of plane parallel MHD flow at inlet and outlet of flat rectangular tube with transverse magnetic field

01 p0130 A69-10770

Boundary layer of MHD flow past semifinite plate, using Navier-Stokes equations

01 p0130 A69-10771

Axisymmetric MHD flow in turbulence chamber at large Hartmann numbers studied for flow boundary layer effects

01 p0130 A69-10772

Steady state three dimensional MHD flow in variable profile channels calculated by reducing problem to two dimensional approximation using curvilinear coordinate system

01 p0131 A69-10776

Electromagnetic fields effect on turbulent boundary layer characteristics of compressible fluid on insulating wall of MGD channel

01 p0131 A69-10777

Hall effect in unperturbed flow of fluids near thin profiles at infinity

01 p0132 A69-11133

MHD flow through circular, elliptic and rectangular straight channels with external magnetic field transverse to flow direction

01 p0132 A69-11209

Resistive spherical plasma expansion into external magnetic field noting magnetic stream function

01 p0132 A69-11211

Polar wind, describing upward plasma expansion of topside polar ionosphere and acceleration of positive H and He ions

01 p0077 A69-11239

Helium isotopes escape mechanism from earth atmosphere related to polar wind ionospheric plasma flow from earth

01 p0077 A69-11240

Rarefied plasma flow interactions with conductors having cross sections equal to Debye radius, noting production of self consistent electrostatic potential

01 p0134 A69-11307

Wake structure behind spherical bodies in rarefied plasma flow by measuring plasma parameters and disturbances with probes

01 p0134 A69-11308

Laminar natural convection of electrically conducting fluid under magnetic field, noting temperature profiles

01 p0134 A69-11407

Thermal radiation effects on two dimensional steady MHD jet of conducting ionized gas confined by magnetic field

02 p0287 A69-11831

Plate temperature oscillation effects on forced convection laminar viscous incompressible MHD boundary layer flow from semiinfinite flat plate

02 p0288 A69-12143

Two dimensional unsteady Rayleigh flow velocity of conducting and nonconducting viscous fluid past porous plate, analyzing suction and magnetic field effects

02 p0232 A69-12156

Thermalization of kinetic energy of plasma flow by shock phenomena produced by magnetic mirror field

02 p0289 A69-12176

Heat transfer of steady laminar flow of incompressible, viscous and electrically conducting fluid between parallel porous plates

02 p0289 A69-12235

Accelerated plate motion effect on flow of electrically conducting viscous incompressible fluid past infinite flat plate in uniform magnetic field

02 p0289 A69-12237

Electric field, current density and magnetic induction of plasma flow measured, obtaining plasma con-

MAGNETOHYDRODYNAMIC FLOW

- ductivity and flow velocity for electron temperature and density
[ONERA-TP-649] 03 p0473 A69-12877
- Axial magnetic field effect on steady linear Ekman boundary layer
03 p0474 A69-13141
- Heat transfer in crossed field MHD Couette flow for incompressible fluid, assuming linear wall temperature in flow direction
03 p0476 A69-13306
- Cold plasma motion caused by electromagnetic wave pressure propagating along uniform magnetic field
03 p0477 A69-13413
- Plasma drift global distribution due to neutral gas motion in F 2 region, noting effect on electron concentration distributions
03 p0422 A69-13513
- Flow development around impulsively rotating dipole magnetized sphere in viscous incompressible conducting fluid, noting diffusing Alfvén waves and induced field
03 p0477 A69-13793
- Boundary layer equations for uniform motion of semiinfinite flat plate through incompressible conducting fluid at rest and in magnetic field, using numerical method
03 p0477 A69-13794
- Coefficient of friction variations for MHD flow of electrically conducting liquid across porous medium under transverse magnetic field
03 p0480 A69-14112
- Nozzle geometry influence on argon plasma flow parameters in shock tube, discussing measurement data behind shock wave front
03 p0481 A69-14160
- Wave number frequency dependent spectral function and space-time correlation function in turbulent plasma, noting utility for probes and scattering analysis
03 p0483 A69-14255
- Electromotive force along magnetic field induced by liquid metal flow /alpha effect/, giving foundation for self excitation of electromagnetic field
04 p0635 A69-14547
- Steady state plasma flows stability equations, using variational principle for analyzing toroidal plasmas
04 p0635 A69-14556
- Series solutions for compressible and incompressible flows at low Reynolds number, including axisymmetric and MHD Stokes flow
04 p0587 A69-14609
- Average energy dissipation in MHD duct flow of arbitrary cross sectional shape, evaluating bulk temperature, net wall heat flux and pressure gradient
04 p0635 A69-14724
- MHD channel flow temperature distributions with Hall effect, using formulation for momentum and energy equations
04 p0635 A69-14746
- Magnetic field effects on heat transfer between Ar plasma flow and channel wall, noting effects of temperature and Reynolds number
04 p0636 A69-14989
- Perfect magnetofluid model to study laminar flow stability along magnetic field, considering time dependences and rigid and free boundaries
04 p0637 A69-15045
- Unsteady hydromagnetic flow of viscous electrically conducting incompressible liquid over infinite conducting harmonically oscillating plate
04 p0638 A69-15093
- LF electrical resonance oscillations in nonisothermal plasma jet flow, noting pressure and magnetic field effects on amplitude and frequency
04 p0638 A69-15174
- Dispersion of solute in electrically conducting fluid flowing between two parallel plates in magnetic field
04 p0638 A69-15194
- MHD flow in square cross sectional channel in transverse magnetic field with conducting walls parallel to magnetic field
05 p0799 A69-15697
- Deceleration of conducting plasmas moving in channels in nonuniform magnetic field
05 p0801 A69-15781
- Evolutionarity of equations of MHD with Hall effect allowance for nondissipative plasma two dimensional flow
05 p0801 A69-15788
- Unsteady motion of ideally conducting gas flow in transverse magnetic field with allowance for gravitational forces
05 p0802 A69-15789
- Perturbed wake behind spherical models in rarefied plasma flow, noting effects of electron temperature and electric potential of models
05 p0803 A69-16048
- Mathematical problem of MHD thermal entrance regions for parallel plate channel solved by Galerkin method
[ASME PAPER 68-WA/HT-10] 05 p0803 A69-16118
- Detached lunar compression wave, noting positive evidence from solar wind flux and direction measurements near lunar wake
05 p0824 A69-16251
- Field aligned Birkeland currents generation at auroral latitudes
05 p0755 A69-16266
- Viscous electrically conducting liquid flow through insulating porous medium in presence of transverse magnetic field in region of validity of Darcy law
05 p0805 A69-16603
- Two dimensional aligned field MGD flows analyzed using corresponding basic equations
05 p0806 A69-16735
- Steady two dimensional MHD flow of perfectly conducting fluid past nonconducting wedge with magnetic field orthogonal to flow velocity
06 p0964 A69-17244
- Viscous MGD channel flow in boundary layer approximation with heat conduction, transforming resultant partial differential equations set to system of ordinary differential equations
06 p0966 A69-17523
- Shock formation in supersonic plasma flow guided by magnetic channel up to magnetic barrier
06 p0966 A69-17524
- Three dimensional steady/unsteady flows of conducting inviscid gas in magnetic field, in absence of electric field, solving related Cauchy problem
06 p0966 A69-17541
- Finite conductivity or ohmic resistance effect on stationary axisymmetric self constricting MHD flow
06 p0966 A69-17548
- Laminar heat transfer in electrically conducting fluids flowing in parallel plate channels
[JPL-TR-32-1335] 06 p1033 A69-17555
- Plasma impedance effect on time variation of inverse pinch
06 p0967 A69-17716
- Laminar constant pressure gradient flow of viscous incompressible conducting fluid through rotating straight circular pipe with perpendicular magnetic field
06 p0967 A69-17718
- MHD aligned flow of compressible fluid past slender body in wind tunnel
06 p0861 A69-17719
- Supersonic plasma flow interaction with two dimensional magnetic dipole
06 p0967 A69-17738
- Plasma flow in electromagnetic shock tube with various pressures and speeds, noting turbulence onset in shock layer
06 p0968 A69-17764
- Surface wave propagation on circular plasma column moving in axial direction in free space region
06 p0968 A69-17775
- MHD flows in channels of MHD devices, emphasizing two and three dimensional problems
06 p0969 A69-17913
- Approximate solution of equations for boundary layer flow of conducting medium on insulating and electrode walls of MHD generator channel
06 p0871 A69-17914
- Unsteady flow of viscous incompressible conducting fluid in MHD generator channel, discussing external circuit inductance and flow velocity during start-up
06 p0969 A69-17915
- Optimal flow conditions in linear conduction type MHD generators for obtaining maximum power per unit channel length or volume
06 p0871 A69-17916
- Channel parameters, magnetic field level, electrical potential and channel output pressure for optimal integral characteristic of MHD system selected by variational method
06 p0969 A69-17917
- Electromagnetic field induced energy and momentum changes effects on pressure, temperature and particle velocity of flows behind propagating gaseous detonation waves
[AIAA PAPER 69-44] 06 p0970 A69-18084
- Velocities of neutral and ionic species in MPD flow determined from Doppler shift of selected spectral lines
[AIAA PAPER 69-109] 06 p0971 A69-18116
- Mixture Mach number defined for collisionless plasma flow about solid body by extending cold-ion theory
[AIAA PAPER 69-78] 06 p0971 A69-18128
- Steady two dimensional MHD flow in finite region of aligned fields
07 p1188 A69-18274
- Two fluid approximation of one dimensional steady state flow of inviscid plasma with thermal gradients, considering ionization and recombination processes
07 p1189 A69-18691
- Plasma diagnostics by spectroscopic techniques, measuring polarity dependences of temperature and charged particle concentration for flows with shock wave and periodic structure
07 p1190 A69-18695
- Uniqueness theorem for laminar MHD duct flows
07 p1190 A69-18813
- Model experiment on plasma flow about obstacle to simulate solar wind interaction with moon
07 p1205 A69-18851
- Pulse broadening in MHD copper vapor laser
07 p1149 A69-18904
- Comparative models of magnetoplasma, discussing wave propagation in cold plasma, warm plasma and microscopic model
07 p1190 A69-18919
- Conducting gas acceleration in strong unsteady electromagnetic field, discussing channel flow in relation to time and pressure gradient
07 p1191 A69-18988
- One dimensional flow of conducting inviscid compressible fluid in channel in presence of transverse fields, discussing steady velocity flows
07 p1191 A69-19014
- Two dimensional flow of conducting fluid in channels with longitudinal transverse magnetic field and Hall effect, discussing gas motion equations linearization
07 p1192 A69-19015
- MHD flow in channels with abruptly widening sections and finned walls under transverse magnetic field, discussing effects on drag
07 p1192 A69-19016
- Hydraulic drag coefficient in MHD fluid flows in traveling magnetic field from motion equations for turbulent flows, considering velocity profiles
07 p1192 A69-19017
- Laminar flow of viscous conducting fluid between parallel walls in traveling magnetic field, using Hartmann number expansion
07 p1192 A69-19023
- MHD flow of compressible conducting fluid around cylindrical body with quasi-aligned magnetic field and velocity
07 p1194 A69-19350
- Periodic pulling mechanism for explaining transition to turbulence in bounded plasma with weakly unstable drift modes
07 p1194 A69-19400
- Periodic asymptotically stable MHD motions, proving uniqueness and existence theorems
07 p1194 A69-19437
- Unsteady MHD convective flow with suction of viscous incompressible electrically conducting fluid above vertical porous wall, noting horizontal magnetic field effect
07 p1195 A69-19477
- Turbulent incompressible MHD flow between two parallel smooth plates in transverse magnetic field, determining magnetic Reynolds number
07 p1195 A69-19736
- Steady shock discontinuity in perfectly conducting gas flow in arbitrarily oriented magnetic field for various Mach numbers
08 p1360 A69-19988
- Free surface of electrically conducting liquid in gradually varied supercritical regime in horizontal rectangular channel
08 p1362 A69-20273
- Analytical model for compressible MHD boundary layers formulated by transport equations for turbulent fluctuations of species mass density, velocity and temperature
08 p1366 A69-20786
- Plasma stream behavior emerging from magnetic field, noting transverse velocity imparted to electrons by field
08 p1368 A69-20808
- Partially ionized argon plasma stagnation flow past blunt body using multifluid theory, obtaining flow profiles
08 p1369 A69-20817

Hydromagnetic steady forced flow against porous rotating disk, integrating equations of motion by Karman-Pohlhausen and series methods

08 p1370 A69-21005

Longitudinal polarization behind front of plasma flow interacting with transverse magnetic field, showing electric potential and magnetic field exhibit structural fluctuations

08 p1370 A69-21018

Plasma flow from hot cathode discharge in magnetic field increases ion flux intensity and prevents flow divergence in vacuum

08 p1370 A69-21075

Hall effect and mass flow influence on MPD arc jet radial pressure profile calculated as function of pressure and magnetic field

[AIAA PAPER 69-246] 09 p1562 A69-21226

MPD engine plasma flow investigated by Langmuir probe measurement of ion saturation current

[AIAA PAPER 69-233] 09 p1567 A69-21266

MGD stagnation point flow, discussing relaxation region influenced by magnetic field

09 p1543 A69-21300

Magnetospheric gusts of streaming positive ions in equatorial plane detected by ATS 1 synchronous satellite

09 p1574 A69-21309

Power radiated by oscillating magnetic and electric dipoles in cold streaming plasma calculated by Poynting vector method

09 p1544 A69-21329

Transverse density nonuniformity effect on electromagnetic wave propagation in cylindrical plasma waveguide immersed in magnetic field, noting frequency increase

09 p1545 A69-21348

Convective MHD channel flow in vertical channel subjected to temperature and pressure gradients, discussing wall conductance effects on flow rate and heat transfer

09 p1545 A69-21441

High time resolution electrical conductivity measurement of ionized plasma gas flow, using changes in Q of circuit

09 p1546 A69-21585

MHD oscillatory flow along infinite plane porous wall with variable suction velocity, obtaining expressions for velocity and magnetic fields in boundary layer

09 p1547 A69-21607

Electron drainage currents from dilute streaming plasmas to positively biased silicon and cadmium sulfide solar cell arrays

[AIAA PAPER 69-262] 09 p1436 A69-21726

Interplanetary plasma flow simulation around earth magnetosphere and planets not considering initial conditions influence

09 p1577 A69-21768

Lagrangian evolution criterion for electromagnetohydrodynamic fluid and MHD flow, defining generalized fluxes and forces

10 p1727 A69-22904

Magnetically aligned flows between sunspots, considering Evershed effect on umbrae and penumbrae

10 p1772 A69-22907

Numerical solution of MHD equations for boundary layer electrically conducting gas flow near flat plate when velocity distribution of external flow obeys power law

10 p1727 A69-23093

General solutions of MHD equations for linear nonsteady and plane steady motions of ideally conducting gas

10 p1727 A69-23096

Laminar turbulent transition conditions in MHD channel flow

10 p1727 A69-23097

MHD fluid flow in rectangular duct with allowance for finite wall conductivity

10 p1727 A69-23098

Rotating disk induced viscous conducting fluid motion in axial magnetic field

10 p1727 A69-23099

Three dimensional MHD flow near forward stagnation point magnetic fields with large induction values described by differential equations, showing tendency towards two dimensional flow

10 p1727 A69-23100

MHD flow and heat transfer between coaxial rotating disks under axial magnetic field, using powers expansion of Reynolds number

10 p1728 A69-23234

Hydromagnetic laminar natural convection flow and heat transfer of nonNewtonian fluid between parallel electrically conducting walls

10 p1728 A69-23237

Transverse magnetic field and shock strength effects on curvature ratio of attached shock waves and wedge

10 p1728 A69-23238

Moving conducting media velocity measurement using Reynolds number and electrical conductivity values, based on magnetic field distortion

10 p1731 A69-23435

Velocity and temperature influence on discharge characteristics of K seeded argon plasma flow at 1 atm pressure

10 p1733 A69-23449

MHD flows in MHD generator channel under magnetic field, analyzing steady laminar flow during entry and Hall effect on conductivity temperature dependence

10 p1734 A69-23455

Current-voltage characteristics of combustion driven shock tube generated argon plasma

10 p1737 A69-23466

Quasi-neutral plasma formation in hydrodynamic channel flow, discussing ignition and breakdown processes in preionized gaseous flow

10 p1737 A69-23467

Shock front propagation in argon with electrode-drawn induced EMF, using shock tube with induced transverse magnetic field

10 p1737 A69-23469

Toshiba blowdown MHD test facility experiments on nonequilibrium ionization, using K seeded He for working gas

10 p1673 A69-23477

Boundary conditions for nonlinear equations of MHD for vicinity of zero magnetic field line, considering plasma pinch and current density

10 p1739 A69-23626

Dipole magnetosphere model with cylindrical or spherical forbidden band for studying plasma motion in quasi-hydrodynamic approximation

10 p1769 A69-23901

Velocity profiles of turbulent plasma flow in circular tube during application of longitudinal homogeneous magnetic field

11 p1922 A69-24234

Heat transfer in MHD parallel plate channel flow in entrance regions analyzed by Galerkin method, noting Hall current effect

11 p1923 A69-24290

Electric shock tube for measurement of plasma magnetic fields induced by shock plasma moving through DC magnetic field transverse to flow

11 p1925 A69-24311

Hartmann problem for motion of electroconductive fluid in homogeneous porous medium, modifying classical MHD equations by introduction of velocity of filtration

11 p1925 A69-24324

Hydromagnetic instability onset in dissipative flow of electrically conducting fluid between rotating permeable perfectly conducting cylinders, noting oscillatory axisymmetric critical modes

11 p1926 A69-24895

Hot wire and hot film anemometers for measuring turbulence in MHD flow noting applications in flowing mercury

11 p1886 A69-25087

Pressure distribution measurement over sphere with cylindrical afterbody in magnetofluid dynamic flow, showing drag decrease at large magnetic field

11 p1873 A69-25136

Small scale oscillations stability in quasi one dimensional conducting gas flow with longitudinal superimposed magnetic field, noting radiation role in transverse oscillations development

11 p1928 A69-25222

MHD free convection from horizontal isothermal plate in vertical uniform magnetic field, considering boundary layer thickness

11 p1930 A69-25277

Steady linearized aligned fields flow of collisionless plasma past slender body, noting effect of tensor conductivity

11 p1930 A69-25278

Magnetic field effects on rotational MHD flow in container, noting Taylor-Proudman theorem, Ekman layers and vertical Stewartson boundary layers

11 p1930 A69-25279

Boundary layer calculation during laminar MHD channel flow under crossed magnetic and electric fields using successive approximation method

11 p1932 A69-25491

Plasma flow from Penning discharge with incandescent cathode in vacuum controllable by varying voltage, pressure and magnetic field strength

11 p1933 A69-25543

Correlation functions and spectral density of current fluctuations in weakly ionized plasma flows

11 p1934 A69-25715

Flow in linear MHD channel with two permeable electrodes, solving Riemann boundary value problem for electric field in channel

11 p1934 A69-25727

Electrical breakdown between cold electrodes in contact with flowing plasma produced by electromagnetic shock tube

12 p2134 A69-26098

Hydromagnetic fluid flow between flat plates oscillating with phase difference, same frequency and different amplitudes

12 p2135 A69-26273

Hydromagnetic flow of viscous conducting fluids through porous coaxial cylinders in radial magnetic field solved by Laplace transform

12 p2135 A69-26276

Dense plasma flow across transverse inhomogeneous magnetic field, proving adiabatic nature of motion

12 p2137 A69-26528

Rarefied Ar plasma flow current-voltage characteristics in discharge tube, noting plasma boundary layer thickness influence on saturation current

12 p2137 A69-26532

Steady state flow of viscous conducting liquid in inlet of channel with or without transverse magnetic field, emphasizing approach to Hartmann-Poiseuille patterns downstream

12 p2138 A69-26626

Neutral gas motions causing plasma motions in F region, obtaining vertical plasma velocity component pronounced diurnal variations

12 p2070 A69-26684

Interplanetary plasma flow directional velocity distribution from solar atmosphere active regions found inhomogeneous

12 p2149 A69-26698

Solar plasma flow around magnetosphere, discussing plasma velocity, density and temperature and magnetic field space and time variations

12 p2150 A69-26736

MHD Stokes flow for rotating disk in parallel magnetic field, showing Lorentz force inhibiting effect on fluid motion

13 p2305 A69-27325

Two dimensional flow of conducting gas dynamic and electrical parameters in MGD generator channel, considering magnetic field and plasma conductivity

13 p2305 A69-27386

Nonconducting vanes end effects on electrical characteristics of MHD channels, analyzing current density, Joule losses and finite length vanes

13 p2306 A69-27497

Laminar-turbulent transition in MHD channel in transverse and longitudinal magnetic fields, discussing Reynolds equation for large Hartmann numbers

13 p2307 A69-27500

Velocity profiles of MHD flow through electrically insulated circular channel in transverse magnetic field

13 p2307 A69-27501

Transient heat transfer in formation of steady crossed fields MHD plane Couette flow for walls, giving momentum, induction and energy equations

13 p2375 A69-27791

Radiative thermal losses of K in gases for MHD flow

13 p2308 A69-28022

Temperature measurement of plasma consisting of combustion products in MHD duct, measuring spectral line contours by Fabry-Perot interferometer for accuracies

13 p2309 A69-28023

Shear stress and velocity profile in MHD duct, examining turbulence damping by electromagnetic coupling

13 p2309 A69-28024

Boundary value problem for one dimensional unsteady equations for inviscid conducting gas during transition processes in MHD duct

13 p2309 A69-28027

Fluctuations in electric field induced by plasma flow in constant magnetic field, performing spectral analysis of voltage and current fluctuations in plasma

13 p2310 A69-28029

Current distribution in MHD duct with permeable electrodes with tensor conductivity, obtaining Riemann-Hilbert heterogeneous boundary value problem solution by finding electric field

13 p2310 A69-28030

Geomagnetic storms caused by plasma streams impinging on earth related to preceding cosmic flares, discussing polar cap absorption and ground level effects

14 p2514 A69-29416

MAGNETOHYDRODYNAMIC FLOW

MHD equations system in intrinsic form, establishing conditions of integrability 14 p2492 A69-29593

Convective and nonconvective two stream instability for hot plasmas, approximating equilibrium distribution function for given temperature by resonance functions 14 p2499 A69-29844

Ionospheric models for motion of slightly ionized homogeneous cold plasma influenced by electrostatic field and neutral particles flow, considering geomagnetic effects 14 p2499 A69-29863

Ionospheric inhomogeneity model for motion of infinite elliptical cylinder of cold plasma in neutral particle flow and ambient electrostatic and magnetostatic fields 14 p2500 A69-29864

Ionospheric inhomogeneities models for plasma motions, considering electron-ion collisions 14 p2443 A69-29865

Magnetic field effect on heat and mass transfer in incompressible fluid MHD flow 14 p2500 A69-29901

MHD quantities in linear wave and small intensity shock wave dissipation and structure determinable by right and left eigenvectors of matrix MHD flow equation 14 p2500 A69-29902

MHD channel flow calculations by quasi one dimensional approximation, considering potential drops at electrodes 14 p2500 A69-29904

Compressible gas MHD steady one dimensional flow in electric and magnetic fields 14 p2500 A69-29905

MHD mercury flow in rotating torus with little friction investigated for Reynolds numbers, considering induction pump forces and magnetic field influences 14 p2500 A69-29907

Shunting effect of conducting channel walls in induction MHD machines, discussing wall effects on pressures during pumping and generating operation modes 14 p2405 A69-29912

Velocity distribution effect on electric field at walls for axisymmetric flow of electrolyte in circular channel in magnetic field of E shaped inductor 14 p2501 A69-29915

Flow phenomena associated with electrically conducting boundary layer jet injection through slot into uniform slipstream in presence of transverse magnetic field 14 p2501 A69-29917

Longitudinal pressure distribution in MHD channel with electrodes parallel to applied transverse magnetic field 14 p2501 A69-29918

Free surface in supercritical regime downstream of valve submerged in MHD flow, noting effects of horizontal and vertical magnetic induction fields 15 p2659 A69-30299

Space charge formation in MHD generator channels ascribed to gas parameters nonuniformity and magnetic induction vector presence, assuming steady flow 15 p2659 A69-30635

Stagnation flow of viscous fluid against rotating magnetized disk, determining effects on magnetic and velocity fields, currents and shear stresses 15 p2659 A69-30674

Continuous supersonic plasma wind tunnel obtained using magnetic Laval nozzle made by modification of Q device normal magnetic field configuration 15 p2589 A69-30909

Hamiltonian variational principle for stationary bounded MHD flows, choosing suitable functions and rigid conducting boundary location 15 p2660 A69-30910

Self consistent solutions for collisionless plasma penetration across magnetic field, showing electrons ability to accompany ions across field 15 p2661 A69-30923

Hydrogen plasmas motions in multipole magnetic fields, discussing plasma polarization, double vortex flow patterns and field line configurations 15 p2661 A69-30924

Steady incompressible MHD laminar flow between parallel porous disks solved for large Reynolds and Hartmann numbers 15 p2662 A69-30968

Single and two phase subsonic plasma jets temperature and velocity distribution, noting reduction by condensed phase and use of Schlichting curves 15 p2663 A69-30989

Plasma parameters, except ion temperature, obtained from current-voltage characteristics of flowing

plasma measured by electrostatic probes in low density wind tunnel 16 p2816 A69-31637

High temperature ionized turbulent argon jet gasdynamics noting electron density 16 p2770 A69-31889

Plasma flow pattern in twilight regions of earth magnetosheath from positive ion observations of twin Vela 3 satellites 16 p2773 A69-31961

Micropulsation records for full moon effect on hydromagnetic emission activity of magnetosphere, noting W and Kp indices 16 p2774 A69-31979

Diagonal conducting wall /DCW/ MHD generator channel flows in formulation including Hall effect, electrode drop and electrode wall angle 16 p2736 A69-32172

MHD of interstellar gas-dust medium, analyzing gas-dust flow and gas-dust shock waves in magnetic fields 16 p2823 A69-32590

Polar substorms resulting from interaction between magnetized plasma stream and geomagnetic field in magnetosphere 16 p2852 A69-32620

Linearized motion equations for conducting gas in magnetic and electric field solved for coaxial channel and free jet, assuming small Reynolds number and parallel flow 17 p3010 A69-33016

Conducting fluid and plasma rotation between concentric cylinders due to crossed fields, determining velocity distribution, induced magnetic field and kinetic energy [AIAA PAPER 69-726] 17 p3011 A69-33472

Fluid dynamic simulation of gas core nuclear rocket chamber for separating light and heavy gas via centrifugal force produced by MHD-driven rotational flow [AIAA PAPER 69-727] 17 p3004 A69-33483

One dimensional viscous magnetofluidynamic flow in annulus formed by concentric cylindrical electrodes, reducing problem to linear partial differential equation set [AIAA PAPER 69-725] 17 p3012 A69-33493

MGD hypersonic shock layer at spherically blunted body analyzed by utilizing induction equation including Hall effect [AIAA PAPER 69-722] 17 p3012 A69-33494

Transverse magnetic field effect on shear turbulence structure of magneto-fluid-mechanic pipe flow with and without heat transfer [AIAA PAPER 69-723] 17 p3012 A69-33497

LF electrical resonance oscillations in nonisothermal plasma jet flow, noting pressure and magnetic field effects on amplitude and frequency 18 p3180 A69-34716

Chapman-Ferraro approximation for magnetic interior field line configuration in plasma flow around two dimensional dipole, allowing for tail formation and neutral sheet 18 p3129 A69-34955

Deceleration of conducting plasmoids moving in channels in nonuniform magnetic field 18 p3181 A69-35033

Evolutionarity of equations of MHD with Hall effect allowance for nondissipative plasma two dimensional flow 18 p3181 A69-35039

Unsteady motion of ideally conducting gas flow in transverse magnetic field with allowance for gravitational forces 18 p3181 A69-35040

MHD flow, deriving equation system and boundary conditions for gas dynamic process 18 p3181 A69-35054

Small continuum electrostatic probes calibration and operation in ionized plasma flow with sheath dimensions larger than boundary layer dimensions 19 p3304 A69-35719

Magnetic fields and electrically conducting fluids interaction with emphasis on magnetodynamics equations, investigating rectilinear flows in pipes and nozzles, shock waves, etc 19 p3379 A69-35804

Combined free and forced convection hydromagnetic flow and heat transfer of electrically conducting fluid subjected to temperature variations in vertical channel 19 p3380 A69-36304

Multiple electrode probe characteristics in rarefied plasma flow created by ion source, noting electrode potential role 19 p3314 A69-36622

Conducting gas flow parameters in coaxial duct, considering magnetic nonuniformity, Hall currents and fields distortion near electrodes 19 p3381 A69-36772

Unsteady laminar MHD flow of electrically conducting viscous fluid between porous coaxial circular cylinders under radial magnetic field 20 p3581 A69-36912

Plasma flow structure near frontal point in earth magnetosphere, using quasi-hydrodynamic two dimensional model to obtain power series solution 20 p3594 A69-37019

Proton concentrations, magnetic field strength and temperatures distribution in interplanetary plasma flows as function of latitudinal distance from center of active region 20 p3594 A69-37020

Turbulent boundary layer of conducting fluids on dielectric plate in transverse magnetic field in presence and absence of pressure gradient 20 p3513 A69-37092

Homogeneous compressible fluid sphere with axisymmetric magnetic field, analyzing oscillations and stability using variational principle 20 p3605 A69-37822

Perturbed wake behind spherical models in rarefied plasma flow, noting effects of electron temperature and electric potential of models 20 p3581 A69-37957

Low energy plasma escape flow from polar region /polar wind/, examining H, He and O ions participation in expansion 21 p3713 A69-38528

Boundary layer equations solved for MHD version of Falkner-Skan problem, using Laplace transform and steepest descent technique 21 p3693 A69-38750

MHD energy converters electric fields and current distributions, analyzing MHD flow problems 21 p3777 A69-39480

Shock waves in closed cycle MHD with gaseous working fluids, investigating MHD channel flow 21 p3778 A69-39482

MHD losses in liquid metal converters due to nonideal magnetic field profile and to flow hydraulics 21 p3649 A69-39483

Drag effect on plasma motion in high current pulsed plasma accelerators of Marshall type, calculating current variations, voltage, particle velocity, efficiency and impulse 21 p3778 A69-39548

Turbulent Hartmann flow between rough walls in transverse magnetic field, determining field influence on resistance coefficient 22 p3989 A69-40255

Laminar MHD flow in porous walled channel in transverse magnetic field, determining velocity distributions, induced fields and current over channel cross section 22 p3989 A69-40256

Homogeneous, viscous and electrically conducting fluid bounded at one end by infinite plane surface of rigid body vibrating relative to fluid body 22 p3991 A69-41036

Plasma pause form in equatorial plane in presence of magnetospheric tail subsonic potential convective flow 22 p3942 A69-41103

Dirac equation in external electromagnetic fields, deriving solution for constant orthogonal electric and magnetic fields encountered in plasma transport 23 p4190 A69-41357

Distribution function of output energies of polycrystalline metal surface used as plasma probe, considering homogeneous plasma flow and isotropic particle velocity distribution 23 p4196 A69-41696

Eddy current plasmoids formation in potential magnetokinematic plasma flux found economical in terms of energy requirements 23 p4214 A69-41834

Successive approximations convergence analyzed in solving supersonic collisionless plasma flow past magnetic dipole 23 p4156 A69-41853

Rotational arc motion in MPD accelerators with strong axial fields predicted by plasma physics equations 23 p4201 A69-41909

Time dependent unsteady flow of incompressible and electrically conducting fluid between two infinite disks rotating in uniform axial magnetic field 23 p4153 A69-42410

MHD flow of incompressible viscous fluid between rotating electrical insulator disks 24 p4354 A69-42599

Electromagnetic scattering by small plasma ellipsoid moving in vacuum through external steady magnetic field, analyzing resonance phenomena

24 p4282 A69-42979

Moving plasma partial capture in transverse magnetic field in experimental plasma source, noting influence of repulsion effect of plasma polarization volume charge

24 p4357 A69-43469

Crossed inhomogeneous electric and magnetic fields effect on H plasma fluxes dynamic behavior, deriving plasma motion formula

24 p4358 A69-43475

Actuator disk model for study of azimuthally nonuniform MPD arc plasma dynamics [AIAA PAPER 68-714]

24 p4359 A69-43570

Steady state interaction between collisionless plasma flow and immersed stationary magnetized or unmagnetized objects by inserting Cs ion accelerator into plasma wind tunnel

24 p4359 A69-43646

MAGNETOHYDRODYNAMIC GENERATORS

MHD technology applications to industry and cost and performance of MHD generators

01 p0013 A69-11394

Condensing injector cycles internal efficiency for high velocity liquid metal flows in closed cycle MHD power plants

02 p0194 A69-11582

Inert gas nonequilibrium MHD power generation in shock tube

02 p0196 A69-12425

MHD generator two dimensional analysis for studying edge effect, taking into account Hall effect

03 p0480 A69-14099

MHD generator and compressor Joule losses effect on thermoelectric energy conversion closed cycle efficiency with electrical conductivity maintained by nonequilibrium ionization

03 p0369 A69-14152

Thermodynamic comparison of MHD generators using Brayton and Rankine cycles, showing Rankine cycle conversion at higher channel Mach numbers for nonequilibrium ionization

03 p0369 A69-14154

Temperature drop in combustion chamber of open cycle MHD power plant due to added potassium carbonate as function of various parameters

03 p0369 A69-14162

Soviet collection of papers on MHD method of obtaining electrical energy, noting plasma properties in MHD generators

06 p0870 A69-17905

Potassium seeded argon plasma conductivity in induced electric field at static gas temperature for MHD generator model

06 p0871 A69-17909

MHD generators with nonequilibrium conductivity, taking into account ionization instability of plasma

06 p0871 A69-17912

Optimal flow conditions in linear conduction type MHD generators for obtaining maximum power per unit channel length or volume

06 p0871 A69-17916

Channel parameters, magnetic field level, electrical potential and channel output pressure for optimal integral characteristic of MHD system selected by variational method

06 p0969 A69-17917

Doppler shift measurements of axial and rotational velocities in MPD arc, using reference lines from iron arc [AIAA PAPER 69-110]

06 p0972 A69-18171

Current load distribution for optimizing MHD generator efficiency determined by variational method, noting dependence on relative length

07 p1058 A69-19012

Transfer coefficients for inhomogeneous systems characterized by constant density, mean free path and activation energy of carriers at each point

07 p1193 A69-19024

Linear induction MHD generator using Rankine cycle with K-Na working fluid noting longitudinal edge effect compensation

07 p1058 A69-19026

Longitudinal edge effect in primary circuit of open loop linear MHD induction machines, determining forward, reverse and zero sequence currents and voltages

07 p1058 A69-19027

Maxwell equations solution for linear induction MHD machine coil area field components, allowing for finiteness of magnetic permeability of iron

07 p1059 A69-19028

Electrical characteristics of linear Faraday generator using binary mixture of noble gases with nonequilibrium ionization

08 p1359 A69-19880

Rotating spoke in unstable pulsed MPD arc, noting rotation frequency and resemblance to plasma rotation [AIAA PAPER 69-234]

09 p1561 A69-21219

Thermodynamic cycle and optimum conditions of electric power source of MHD generator in combination with thermocompressor

09 p1435 A69-21592

Electrothermal instabilities of ionization region of nonequilibrium MHD generator in presence of magnetic field

09 p1548 A69-21919

Optimum operation modes of MHD converter

10 p1636 A69-23095

O shaped magnetic systems using unsaturated steel magnetic circuit to produce strong uniform magnetic fields for MHD machines

10 p1636 A69-23102

Effect of degree of expansion of ionized gas in nozzle on specific power of MHD generator

10 p1636 A69-23103

MHD electrical power generation - Conference, Warsaw, July 1968, Volume 1, Closed cycle MHD with gaseous working fluids

10 p1729 A69-23433

Low temperature optically thick boundary layers influence on spectroscopic temperature measurements in plasma MHD channels

10 p1731 A69-23434

Two temperature plasma model applicability in analyzing nonequilibrium MHD generator

10 p1731 A69-23438

Ar-K plasma studied as possible MHD generator working fluid by investigating influence of emission and external magnetic field on nonequilibrium electrical conductivity

10 p1732 A69-23441

Momentum transfer cross sections, recombination coefficients and ionization coefficients of working gases for MHD energy converter

10 p1733 A69-23446

Argon discharges in metal capillary cathodes noting effects of electron density, flow velocity, electrode phenomena and gas temperature

10 p1733 A69-23450

Rare gas-alkali plasma electrical conductivity dependence on gas temperature and preionization to determine optimum operating conditions for MHD generator

10 p1733 A69-23451

Electron temperature distributions in Ar-K plasma of simulated Faraday type MHD generator for current distributions, determining current density distribution experimentally

10 p1734 A69-23453

Induced magnetic fields determination in linear DC MHD generators with ferromagnetic and nonmagnetic walls, using Fredholm equation

10 p1636 A69-23454

MHD flows in MHD generator channel under magnetic field, analyzing steady laminar flow during entry and Hall effect on conductivity temperature dependence

10 p1734 A69-23455

Electrothermal instabilities in small magnetic Reynolds number limit and ionization equilibrium at electron temperature using quasi-linear plane wave analysis

10 p1734 A69-23456

Instabilities in K seeded Ar plasma in crossed electric and magnetic fields and with nonequilibrium ionization, noting effects on MHD generator characteristics

10 p1734 A69-23457

Mercury cesium plasma in crossed electric and magnetic fields as working fluid of MHD generators based on Rankine cycle

10 p1636 A69-23458

Unstabilizing effect of inhomogeneities on magnetoacoustic waves in slightly ionized gases with current perpendicular to magnetic field

10 p1734 A69-23459

Turbulent plasma near stability limit in MHD generator with constant load coefficients, noting effective conductivity and effects of gas temperature

10 p1735 A69-23460

Effective Ohm law for inhomogeneous weakly ionized gas and Hartmann flow analysis, noting electron density fluctuation effect on conductivity

10 p1735 A69-23462

Conductivity and electron temperature in coaxial MHD generator plasma with magnetic field, studying Joule heating effect on performance

10 p1735 A69-23463

MHD electrical power generation - Conference, Warsaw, July 1968, Volume 2, Closed cycle MHD with gaseous working fluid

10 p1735 A69-23464

Linear nonequilibrium MHD generator operating at Mach 2 and Hall parameter of 3 using cesium seeded helium as working fluid

10 p1636 A69-23471

Power conversion efficiency of diverging channel nonequilibrium MHD generator with small electrode losses, examining influence of channel design

10 p1637 A69-23472

Large disk MHD generator operating at high Hall coefficient and driven by cesium seeded argon or molecular gases

10 p1637 A69-23473

Blowdown wind tunnel designed for studying closed cycle MHD converters, describing subsystems

10 p1673 A69-23474

MHD conversion experiments using rare gas, considering Typhee loop, electron heating and correction effects

10 p1738 A69-23475

MHD generators with segmented electrodes at high Hall parameters, noting electron density, conductivity and Hall field reduction factor

10 p1637 A69-23476

Argas test loop as model for MHD power plant study, discussing component testing including channel preionization and relaxation experiments

10 p1673 A69-23478

Closed cycle MPD experiments with applied electric and magnetic fields emphasizing current leakage, segmentation, relaxation and aerodynamic effects

10 p1738 A69-23479

MHD generator performance operating on nonequilibrium Ar plasma with K additions in presence of electric fields

10 p1637 A69-23480

Nonequilibrium ionization effects on performance of subsonic constant area MHD generator, using closed cycle blowdown loop facility

10 p1637 A69-23481

MHD blowdown loop facility for alkali seeded noble gas MHD energy conversion, noting performance and plasma insulation from ground

10 p1674 A69-23482

Closed loop magnetoplasmadynamic energy conversion system design, operation and duct section

10 p1638 A69-23483

Impulse induction MHD generator with cylindrical channel, finding differential equations for velocity and current

10 p1638 A69-23484

Engineering and reactor parameters associated with ionization of gas passing through nuclear reactor used as closed cycle MHD system working fluid

10 p1723 A69-23485

Two dimensional flow of unipolar medium in electrodynamic power generation channel, discussing stationary model, electric field and ion density distributions

10 p1638 A69-23486

Striated flow induction synchronous MHD generator, producing striated flow by nonthermal ionization of inert seeded gas in electric field

10 p1638 A69-23487

Power generating equipment operating with high temperature plasma as working medium requiring reactors with plasmized nuclear fuel coupled to MPD generators

10 p1738 A69-23489

Experimental arrangement consisting of closed cycle system, ionization duct and inductive MPD converter with traveling wave component, using Hg as working medium

10 p1638 A69-23490

Gaseous suspensions of thermionic emitting particles assessed as MHD working fluids in large scale MHD electric power generators

10 p1738 A69-23491

Properties of superdense NaCl plasmas as model working substance for MHD generator, discussing ion concentration and collisions, charge reversal and conductivities

10 p1739 A69-23493

Boundary layers influence on external electrical characteristics of MHD generator

11 p1824 A69-24221

MAGNETOHYDRODYNAMIC GENERATORS

Throttling effect on thermodynamic efficiency of MHD generator Rankine cycle with various working fluids
11 p1824 A69-24222

Closed loop cycle converter, composed of MHD generator and compressor consuming thermal energy, exhibiting moderate cycle efficiency decreases
11 p1824 A69-24223

Linear MHD generator power characteristics at large magnetic Reynolds numbers, analyzing magnetic field distribution for sectioned and solid electrodes
11 p1824 A69-24224

Magnetic field induced nonequilibrium argon plasma ionization relaxation processes obtained with allowance for flow parameters change in relaxation zone
11 p1922 A69-24225

MHD generator plasma anisotropic instability caused by amplified magnetosonic waves propagating normal to current
11 p1922 A69-24227

MHD power plant research and development, discussing shock wave electric power generators and modulated systems
11 p1925 A69-24469

Supersonic nozzle cross section and diffuser throat in MHD generator calculated by continuity equation
11 p1826 A69-25348

Current and voltage distribution around normal shock in MHD duct using conformal transformation, considering continuous and segmented electrode boundary conditions
11 p1931 A69-25359

Faraday type MHD energy converters in nonequilibrium conduction mode, analyzing two dimensional current and potential distributions in plane normal to magnetic field
11 p1826 A69-25397

Constant and traveling magnetic fields MHD converters induction and finite dimensions influence analyzed by conformal mapping, separation, Fourier and finite difference methods
11 p1827 A69-25399

Transient processes in conduction type MHD generators due to external circuits induction distribution
12 p2017 A69-26545

Voltage characteristics in MHD generator with water cooled segmented electrodes using potential probes, considering forced convection heat transfer
12 p2017 A69-27178

Two dimensional flow of conducting gas dynamic and electrical parameters in MGD generator channel, considering magnetic field and plasma conductivity
13 p2305 A69-27386

Electricity from MHD - Conference, Warsaw, July 1968, Volume 5, Open-cycle MHD
13 p2284 A69-27468

Chemical corrosion of zirconia-based refractories in MHD generators, considering thermal cycling and shock, seed migration and prevention
13 p2284 A69-27469

Oxide and carbide high-melting-point materials for MHD generator electrode walls
13 p2284 A69-27471

MHD generators semihot wall duct, discussing structural design, ceramic insulation elements brazing, temperature control, electrodes, working fluid, etc
13 p2372 A69-27473

Electricity from MHD - Conference, Warsaw, July 1968, Volume 3, Closed cycle MHD with liquid-metal working fluids
13 p2203 A69-27474

Speed of sound and shock waves in two phase flows of liquid metal MHD generators, considering droplets uniformly dispersed in gaseous phase
13 p2245 A69-27475

Laser Doppler method for measuring local particle velocities in two phase flows of liquid-metal MHD generators
13 p2260 A69-27476

High velocity liquid lithium effect on structural materials for MHD power generators, discussing material loss
13 p2278 A69-27478

Two phase MHD generator with gas in liquid metal emulsions, discussing loops efficiency
13 p2306 A69-27479

Energy conversion with liquid metal working fluids in MHD generators, discussing single stage fully Carnotized process
13 p2372 A69-27482

Thermal efficiencies of liquid-metal MHD generator cycles, analyzing optimum parameters, working fluid and partial irreversibilities
13 p2205 A69-27484

Liquid metal two phase flow MHD generators efficiency prediction, discussing end losses and flow velocity
13 p2205 A69-27485

Thermodynamic efficiency of MHD cycles for liquid Na with multistage injection and injection condensation
13 p2205 A69-27487

Optimal cycle parameters for liquid metal single component MHD cycle, employing condensing ejector in front of generator
13 p2205 A69-27488

Liquid metal MHD generator cycles thermodynamic analysis, considering multicycle operation improvement with heat regeneration
13 p2372 A69-27489

Piston-like laminar liquid metal flow in MHD generator to increase thermodynamic efficiency of cycle and to generate electricity by synchronous principle
13 p2206 A69-27491

Liquid-metal MHD space power generation system using intermittent vaporization slugs shooting at 2700 R peak temperature
13 p2206 A69-27492

Electrical end losses in liquid-metal MHD generators with variable conductivity, noting working fluids and aspect ratios
13 p2206 A69-27493

One dimensional calculations of finite length MHD uniform traveling wave induction generator, discussing magnetic field distribution, electrical impedance and conversion efficiency
13 p2206 A69-27494

Liquid flow MHD alternating current generator design, considering induced current in rotor and resulting magnetic field in pole gap
13 p2206 A69-27495

MHD induction converters operational characteristics calculations with simultaneous considerations for finite length and channel width
13 p2207 A69-27496

MHD channel mercury flow with hydraulic shock in transverse magnetic field, determining characteristic values distribution over range of principal parameters
13 p2307 A69-27499

Variable fluid and field velocity HF induction generator, determining interaction between fluid dynamic forces and magnetic field and kinetic energy
13 p2207 A69-27502

Liquid metal MHD induction generators design and performance, considering effect of geometry, operating conditions, fluid properties and power level on efficiency
13 p2207 A69-27503

Single wavelength design with compensation compared to multiwavelength design without compensation for liquid metal MHD induction converter, discussing optimization
13 p2207 A69-27504

Linear inductive MHD converters, reducing effects of losses due to finite length of converter by cylindrical construction
13 p2207 A69-27505

Transient response in liquid-metal conduction MHD generators, analyzing constant magnetic field using differential equation
13 p2207 A69-27506

Optimal mean radius and half height of channel of liquid metal coaxial linear induction MHD generator with unilateral and bilateral excitation
13 p2207 A69-27507

Rayleigh-Taylor instability in synchronous liquid metal MHD generators, showing stabilization by channel positioning and threshold power rating
13 p2307 A69-27508

Liquid metal induction MHD generator I-V characteristics at no load permitting self excitation with capacitors
13 p2208 A69-27509

Liquid metal MHD power plant system tested under open and closed loop conditions for liquid circulation
13 p2208 A69-27510

Sodium liquid-metal jet MHD generators tested under constant and rising magnetic fields and off and on loads
13 p2208 A69-27511

Induction, helical and straight through liquid metal MHD generators tested under independent and self excitation conditions
13 p2208 A69-27512

Three phase high temperature liquid metal induction MHD generator performance, noting velocity profile nonuniformity influence
13 p2208 A69-27513

MHD generator analysis, formulating boundary value problem for ion diffusion and Fourier series solution for end effect of electrodes pair
13 p2208 A69-27613

Electricity from MHD - Conference, Warsaw, July 1968, Volume 4, Open cycle MHD
13 p2308 A69-28021

Tensor conductivity measured and analyzed for MHD generator duct with electric and magnetic fields
13 p2309 A69-28026

Conducting liquid boundary layer flow and heat flux on electrodes of MHD generator, including one dimensional flow outside boundary layer
13 p2309 A69-28028

Segmented-electrode and Hall ducts tested on supersonic magnetoaerodynamic conversion rig, defining electrical model for boundary layer losses at electrode surfaces
13 p2311 A69-28034

Ideal MHD induction converter pressure and generator cycles compared for calculating maximum output and pressure, considering current-conducting walls effects
14 p2393 A69-28887

MHD generator design using shock wave kinetic energy produced by explosion in shock tube with superconducting magnetic system
14 p2393 A69-28911

Equation system for asynchronous MHD generator operating in self oscillating mode derived and solved
14 p2405 A69-29457

Boundary problems solution for electromagnetic field two dimensional distributions in MHD channels at arbitrary magnetic Reynolds numbers, considering longitudinal terminal effects
14 p2500 A69-29906

MHD generator design with electric conductivity waveform at small magnetic Reynolds numbers
14 p2405 A69-29911

Shunting effect of conducting channel walls in induction MHD machines, discussing wall effects on pressures during pumping and generating operation modes
14 p2405 A69-29912

Field equations for plane-parallel induction MHD machines with allowance for winding zone thickness and magnetic permeability of iron
14 p2405 A69-29914

Space charge formation in MHD generator channels ascribed to gas parameters nonuniformity and magnetic induction vector presence, assuming steady flow
15 p2659 A69-30635

Integral charge neutrality effect on local space charge density of MHD generator channel, examining electrode couple for Faraday generators
15 p2664 A69-31055

Nuclear energy conversion for long space missions, comparing dynamic Brayton, liquid metal MHD gas, dynamic Rankine and LMMHD Rankine cycles
16 p2810 A69-31748

Thermodynamic parameters of MHD cycle employing supercritical Hg, indicating need for more suitable fluids
16 p2736 A69-31914

Fringing effects on electric efficiency variation with slip for cylindrical induction MHD device operable as accelerator, generator or Joule heater [AIAA PAPER 67-714]
16 p2736 A69-32152

Diagonal conducting wall /DCW/ MHD generator channel flows in formulation including Hall effect, electrode drop and electrode wall angle
16 p2736 A69-32172

Conducting fluid incompressible flow in entrance of MHD channel by momentum integral method, permitting edge stress existence at boundary layer free stream interface [AIAA PAPER 69-724]
17 p2952 A69-33436

Thermal cycle for direct flow supersonic compressorless MHD generator without heat regeneration and high temperature exchange
18 p3093 A69-34714

High temperature combustion chamber as high velocity gas generator, noting application to MHD power generator research
18 p3184 A69-34931

Conducting and insulating construction materials at high temperatures for MHD conversion nozzles, noting lifetimes
21 p3751 A69-38456

Two dimensional numerical solution for Faraday DC MHD generators with variable conductivity, velocity and magnetic field
21 p3649 A69-39027

DC MHD generator using gas plasma as working fluid, discussing fundamental principle, components interactions and energy conversion

21 p3777 A69-39165

Superconducting magnets for MHD generators, discussing design, construction and operation problems

21 p3782 A69-39478

MHD energy converters electric fields and current distributions, analyzing MHD flow problems

21 p3777 A69-39480

Plasma instabilities in closed cycle MHD generator with gaseous working fluids, discussing effective Hall parameters

21 p3777 A69-39481

MPD converters in pulsed and continuous modes, discussing inductive propulsion system

22 p3999 A69-39905

Interaction between two temperature plasma flux and electrodes in MHD channel with crossed electric and magnetic fields, studying boundary layer dynamics

22 p3991 A69-41022

Optimization of Faraday MHD generators with nonequilibrium ionization and plasma turbulence, assuming electrons at Saha equilibrium at elevated temperatures

24 p4256 A69-43682

MAGNETOHYDRODYNAMIC STABILITY

Collection of papers on physics, Volume 31, Part 1, covering stellar evolution, electron transport in semiconductors, plasma microstability, etc

01 p0115 A69-10045

Microinstabilities of plasma confined by magnetic trap, discussing stabilization, drift waves and anomalous diffusion of plasma by turbulence

01 p0125 A69-10048

Inhomogeneous magnetically confined plasma stability, examining dissipative effects on spectra of drift oscillations with kinetic theory

01 p0126 A69-10187

Plasma stability criterion for universal mode, discussing cusp curvature stability

01 p0127 A69-10279

Stability of gravitating fluid layer of infinite extent but finite thickness including Hall effect

01 p0128 A69-10342

Asymptotic method for analyzing small long wave perturbations in plasma, showing instability with respect to perturbations propagating at angles to ion-acoustic wave

01 p0131 A69-10788

Thermonuclear fusion program, discussing plasma instabilities suppression, toroidal installations, magnetic trap systems, plasma heating and dynamic stabilization

01 p0156 A69-11065

Cross field plasma instability resulting in charge density irregularities shown to meet requirements for ionospheric irregularities model

01 p0073 A69-11178

Ionospheric irregularities and cross field plasma instability, analyzing nonlinear behavior of latter with two dimensional model

01 p0073 A69-11179

Stability of weakly inhomogeneous plasmas with free energy available for nonlinear resonant three wave interactions

01 p0133 A69-11212

Garden hose instability quasi-linear stabilization employing macroscopic viewpoint, discussing fluid model

01 p0133 A69-11217

Steady one dimensional motion of current sheets in plasma accelerators, noting condition of zero initial conductivity

01 p0133 A69-11220

Electrostatic plasma wave instabilities in ionosphere along auroral field lines, noting critical electron flux and subsequent acceleration of electrons

01 p0075 A69-11222

Formation mechanism for heterogeneous structure of interplanetary plasma based on plasma instability from temperature anisotropy

02 p0314 A69-11638

Polar auroral fine scale structure interpretation based on plasma instabilities characteristics

02 p0239 A69-11693

Instability of longitudinal plasma waves propagating across magnetic field in plasma with electrons and ions drifting with different velocities across field

02 p0286 A69-11830

Hydromagnetic stability of free boundary layer between two uniform streams in presence of aligned uniform magnetic field at large Reynolds number

02 p0287 A69-11832

Overheated semiconductor plasma instability in crossed electric and magnetic fields, deriving condition for occurrence

02 p0298 A69-12099

Ion cyclotron drift loss cone instability for cases of steep particle density gradients, magnetic field gradients and finite plasma dimensions

02 p0288 A69-12169

Equations for studying plasma stability in sheared magnetic field examined for normal mode and wave packet perturbations

02 p0289 A69-12173

Current carrying curved plasma column flute instability analysis, noting effect of increasing divergence from axial symmetry on Q values

02 p0289 A69-12175

Shear instability in unbounded collisionless cold plasma in external uniform magnetic field in current free case, noting dispersion relations

02 p0289 A69-12177

Criterion for magnetic plasma stability near magnetic axis, noting parameters for deriving criterion integrand

02 p0290 A69-12355

Plasma stability under anisotropic pressure in axisymmetric magnetic fields determined by quasi-hydrodynamic approximation

02 p0291 A69-12552

Free fluid hydrodynamics equations applied to weakly ionized plasma stability, considering drift oscillations excitation

02 p0291 A69-12553

Anisotropic plasma cyclotron instability in magnetic trap with cold ion background and isotropic Maxwellian velocity distribution

02 p0292 A69-12554

Thermodynamic stability of plasma with strong interaction, discussing relationship to simultaneous oscillation forms

02 p0292 A69-12635

Wave analysis for energy propagation in plasma, discussing excitation spectrum and stability properties

02 p0293 A69-12782

Plasma instabilities covering astrophysical phenomena, Rayleigh-Taylor instability, anisotropic and LF MHD, electrostatic and electromagnetics, warm plasmas, etc

02 p0293 A69-12783

Magnetic shear effect on stability of electron-neutral collision dominated plasma, noting helical perturbations onset

03 p0473 A69-12925

Relationship between instabilities and turbulence in plasma, using spectrum of plasma fluctuations

03 p0474 A69-13115

Existence and stability of periodic waves in cold collisionless plasma in magnetic field

03 p0474 A69-13143

Scattering of energetic charged particles in weakly unstable plasma for integrated spectrum of plasma electric field autocorrelation function

03 p0475 A69-13151

Two dimensional equilibria for high beta mirror devices found by solving Vlasov equation and Ampere law, including particle loss

03 p0475 A69-13152

Ion-ion velocity space instability due to difference between ion temperatures perpendicular and parallel to magnetic field

03 p0475 A69-13154

Critical pressure in mean magnetic well with closed lines, noting longitudinal resistivity annihilation of stabilizing effect of toroidal shear

03 p0476 A69-13382

Cone instability role in auroral electron and proton dynamics, discussing plasma instability control of maximum captured particle densities in various magnetosphere regions

03 p0501 A69-13526

Plasma gravitational stability problem with Hall effect, noting relevance to astrophysical systems

03 p0478 A69-13803

Hall effect destabilization influence in Kelvin-Helmholtz problem for ideal plasma, noting instability growth rate

03 p0478 A69-13804

Cyclotron drift instabilities of low pressure plasma containing charged impurities

03 p0478 A69-13834

Diffusion across magnetic field of unstable plasma with highly inhomogeneous density

03 p0478 A69-13840

Transverse perturbation influence on helical instability in oscillator

03 p0488 A69-13886

Langmuir wave disintegration, analyzing instability criterion and growth rate

03 p0480 A69-14057

Aperiodic hydrodynamic beam instability development and energy losses, discussing plasma oscillation enhancement and nonlinearities

03 p0480 A69-14137

Ion beam interaction with plasma in presence of charge exchange and zero external magnetic field, studying stability of system

03 p0481 A69-14200

MHD instability in current discharges in magnetic field stabilized by current frequency modulation higher than perturbation increment of plasma column

04 p0635 A69-14549

Nonlinear electron oscillations in plasma, deriving asymptotic expression for plasma perturbation

04 p0635 A69-14552

Steady state plasma flows stability equations, using variational principle for analyzing toroidal plasmas

04 p0635 A69-14556

Equilibrium and stability of strong current discharge in dense optically transparent plasma, determining cause of instability

04 p0636 A69-14983

Perfect magnetofluid model to study laminar flow stability along magnetic field, considering time dependences and rigid and free boundaries

04 p0637 A69-15045

Hydromagnetic analogs calculated for Rayleigh-Taylor problem with Hall effect, confirming introduction of plasma instabilities

04 p0637 A69-15050

Stabilizing influence of axial magnetic field on confined vortex flow of aqueous electrolytic conductor generated by two dimensional wall jets

05 p0798 A69-15611

Tearing mode instability in Bessel function model preliminary to study of tearing mode in diffuse pinches

05 p0799 A69-15615

Nondegenerate dense plasma thermodynamic stability by nonclassical methods, discussing atomic concentration dependence on ionic concentration

05 p0802 A69-15892

Plasma instabilities produced by beam plasma discharge in mirror magnetic trap

05 p0803 A69-16212

Gravitational instability of rotating anisotropic plasma for longitudinal wave propagation mode, obtaining dispersion by using modified Chew-Goldberger-Low equation

05 p0827 A69-16596

Bounded and spatially separated plasmas wave oscillations stability in magnetic field, observing hydrodynamic slipping and drift instability

06 p0963 A69-16903

Plasma confined in transverse magnetic field analyzed for drift rates, noting role of injection direction

06 p0963 A69-16907

Temperature distribution for static stellar corona in presence of magnetic field, noting energy flow process

06 p1002 A69-17316

Cusp magnetic field stabilizing superimposition on toroidal plasma discharge in polytron machine, noting role of Hall acceleration mechanism

06 p0965 A69-17514

Moment equations of Vlasov plasma used for pressure effects on gravitational flute instability of nonuniform plasma

06 p0965 A69-17515

Resonance particle effects on flute oscillation kinetic stability when resonance particles drift under influence of magnetic field inhomogeneity

06 p0965 A69-17516

Hydromagnetic plasma stability in infinite electrical conductivity approximation applied to smooth closed systems, discussing ballooning instability mode

06 p0965 A69-17519

Integrodifferential equation for plasma oscillations solved for effect of ion Larmor radius size and intrinsic electric field on flute instability of axially symmetric plasma

06 p0966 A69-17520

Plasma flute instability in magnetic trap with wall/plasma interface, using system of sensors and amplifiers

06 p0966 A69-17544

Enhanced microwave scattering by plasma instability in magnetic field, using microwave interferometer with horn antenna system

06 p0967 A69-17717

Linear approximation of ionization instability in disk channel of nonequilibrium MHD generator, calculating

MAGNETOHYDRODYNAMIC STABILITY

interatomic collisions frequency as function of temperature
06 p0871 A69-17911

MHD generators with nonequilibrium conductivity, taking into account ionization instability of plasma
06 p0871 A69-17912

Ion-cyclotron instabilities in hot-ion cold-electron plasma resulting from left-hand circularly polarized wave propagating parallel to magnetic field
06 p0969 A69-17951

Plasma instability role in radiant energy release from astronomical objects, noting plasma instabilities in solar system, cosmic rays, galactic and extragalactic objects
06 p1009 A69-17967

Electromagnetic waves excitation during interaction between density modulated beam and plasma in magnetic field, analyzing instabilities
07 p1189 A69-18508

Kinetic model describing collisions in nonequilibrium multicomponent plasma, studying pair collisions effect on stability of plasma-beam system
07 p1189 A69-18539

MHD models for analysis of nonhomogeneous magnetized plasma stability with regard to perturbations having electrical field as potential field
07 p1190 A69-18694

Stabilization of plasma filament with alternating current by quadrupole magnetic field
07 p1191 A69-18987

Transverse waves instability in relativistic plasma, noting condition of isotropy and existence of electromagnetic waves
07 p1193 A69-19032

Wave propagation and instabilities in rotating anisotropic collisionless plasma, analyzing plane and cylindrical perturbations
07 p1195 A69-19438

Cold plasma stability during traversing by electron beams in presence of external magnetic field, obtaining dispersion relations for longitudinal and transverse modes
07 p1195 A69-19465

Nonlinear interactions of positive and negative energy electrostatic modes of plasma immersed in magnetic field, discussing instability criterion and Landau damping
[IAEA PAPER CN-24/E-13]
07 p1196 A69-19768

Plasma instability with isotropic ion or electron velocity distribution function /nonMaxwellian/, discussing magnetic field and particle energy distribution functions
08 p1359 A69-19949

High density plasma dynamic stability in magnetic containment using variational calculations
08 p1359 A69-19984

Ionospheric plasma flute instability considered as possible cause of occurrence of elongated small scale inhomogeneities in F2 layer
08 p1309 A69-20425

Inhomogeneous collision plasma drift instabilities in strong magnetic field analyzed by solving nonlinear equations
08 p1365 A69-20549

Nondispersive LF mode in magnetized plasma with frequencies lower than ion cyclotron frequency, discussing plasma stability in presence of electron drift
08 p1366 A69-20750

Discharge structure and stability of nonequilibrium plasma undergoing supersonic flow through linear MHD channel
08 p1366 A69-20788

Fluid equations for collisionless plasma including finite ion Larmor radius and finite beta effects
08 p1368 A69-20802

Electromagnetic microinstabilities of plasmas associated with transverse waves propagating perpendicular to external uniform magnetic induction, noting allowable frequencies
08 p1368 A69-20804

Time rates for growth and damping of resistive instability in gaseous plasma in crossed electric and magnetic fields
08 p1369 A69-20886

Flute instabilities in rarefied plasma with intrinsic electric field, discussing plasma density profile and uncompensation degree effects on plasma magnetic field stability
08 p1370 A69-21013

LF electric potential oscillation of discharge plasma, describing oscillation behavior by theory of dissipative drift instability of weakly ionized plasma
08 p1370 A69-21020

Rotating plasma disturbances onset in MPD arc, determining magnetic field dependence on mass flow, background pressure and propellant
[AIAA PAPER 69-232]
09 p1562 A69-21225

Coaxial electrodes with electric and magnetic fields to study instability in MPD arcs
[AIAA PAPER 69-230]
09 p1563 A69-21231

Inhomogeneous collisionless plasma drift-oscillation stability in magnetic field augmented by E wave HF field
09 p1546 A69-21564

Magnetoactive plasma containing fast monoenergetic ions noting stability at drift frequencies and in terms of Alfvén wave buildup
09 p1546 A69-21566

Plasma instability in inhomogeneous magnetic field noting wavefront structure role
09 p1546 A69-21571

MHD stability of straight multipoles with shear, considering scalar-pressure perfectly conducting two dimensional MHD equilibria
09 p1546 A69-21576

Plasma mixed ion heating by small scale HF turbulent electron sound pulsations
09 p1548 A69-21673

Near cathode magnetic field effect on instability in linear Hall current accelerators, using geometry of field extending from anode to cathode region
[AIAA PAPER 69-381]
09 p1568 A69-21731

Electrothermal instabilities of ionization region of nonequilibrium MHD generator in presence of magnetic field
09 p1548 A69-21919

Plasma dissipative drift instability and nonlinear wave interaction from discharge with oscillating electrodes, investigating LF plasma oscillations
09 p1550 A69-22019

Alfvén oscillations in inhomogeneous decaying plasma from pulsed discharge with oscillating electrons
09 p1550 A69-22020

Raman microwave scattering with low frequency oscillations caused by plasma drift instabilities
09 p1550 A69-22021

Warm plasma addition to mirror confined hot plasma stabilizing convective loss cone mode
09 p1551 A69-22040

Electrons velocity-space instability in plasma column, analyzing unstable wave and dispersion characteristics
09 p1552 A69-22041

Rotating plasma gravitational instability during discharge as function of centrifugal acceleration, noting Coriolis and Larmor effects
09 p1552 A69-22043

Asymptotic toroidal equilibrium for guiding center plasma model based on stellarator expansion, considering toroidal curvature, helical currents and plasma pressures
09 p1552 A69-22044

Current instability in H plasma in electric field of large amplitude fast magnetosonic wave, noting plasma heating
09 p1552 A69-22526

Quasi-linear relaxation of electron beam in magnetoactive plasma, noting instability of plateau in velocity distribution function
09 p1553 A69-22659

Two dimensional flat geometry for initial solar flare development stage, discussing tearing mode energy source for solar flares and plasma compressibility effects
09 p1583 A69-22757

Asymptotic method for analyzing small long wave perturbations in plasma, showing instability with respect to perturbations propagating at angles to ion-acoustic wave
09 p1653 A69-23107

Increased energy losses and microwave emission at cyclotron frequency harmonics during plasma electron heating at cut-off plasma concentrations in magnetic trap
09 p1728 A69-23130

Plasma ions turbulent heating during electron-acoustic instability in field of circularly polarized electromagnetic wave at ion cyclotron frequency
09 p1728 A69-23137

Finite Larmor radius, finite conductivity, rotation and Hall current effects on Jeans criterion for gravitational instability of plasma
09 p1729 A69-23408

Nonequilibrium ionization in central regions of low temperature plasma, describing charged particle drift by using diffusion time concept
09 p1732 A69-23440

MHD boundary layer nonlinear instability, treating laminar to turbulent flow transition as reversible process
10 p1734 A69-23452

Electrothermal instabilities in small magnetic Reynolds number limit and ionization equilibrium at electron temperature using quasi-linear plane wave analysis
10 p1734 A69-23456

Instabilities in K seeded Ar plasma in crossed electric and magnetic fields and with nonequilibrium ionization, noting effects on MHD generator characteristics
10 p1734 A69-23457

Unstabilizing effect of inhomogeneities on magnetoacoustic waves in slightly ionized gases with current perpendicular to magnetic field
10 p1734 A69-23459

Turbulent plasma near stability limit in MHD generator with constant load coefficients, noting effective conductivity and effects of gas temperature
10 p1735 A69-23460

Plasma ionization instability linear growth problem analyzed in bounded region
10 p1735 A69-23461

Equilibrium loss in closed cycle MHD generator using rare gases binary mixtures as working fluid
10 p1737 A69-23468

HF magnetic field effect on oscillations and instabilities of plasma confined by fixed magnetic field
10 p1739 A69-23623

Discharge plasma ionized waves, determining mechanism of wave propagation and instabilities
10 p1740 A69-23699

Spontaneous magnetic field excitation in turbulent plasma noting possible instability
10 p1740 A69-23715

Transport of matter in nonisothermal weakly ionized plasma due to traveling ion-acoustic wave propagation, noting plasma oscillations and instability
10 p1741 A69-23945

Density modulated charged particle beam interaction with plasma under paramagnetic resonance, analyzing longitudinal oscillations and parametric instability zone
10 p1741 A69-23947

One dimensional nonlinear model of anisotropic plasma instability with respect to Alfvén waves growth, noting applicability to solar wind processes
10 p1741 A69-23961

Ionization instability in low temperature magnetized plasma, analyzing electron concentration perturbation caused by Joule heating during electron-ion collisions
10 p1741 A69-23962

MHD generator plasma anisotropic instability caused by amplified magnetosonic waves propagating normal to current
11 p1922 A69-24227

Thermodynamic stability of dense plasma consisting of electrons and charged ions, plotting ionization potential as function of electron density and temperature
11 p1922 A69-24232

One dimensional electrostatic plasma oscillations in alternating external electric field, noting plasma stability and electron-electron two stream instability
11 p1924 A69-24298

Explosive and reversible onset of helical instability in weakly ionized discharge plasmas, noting ambient noise level role
11 p1924 A69-24299

Electric field fluctuations in inhomogeneous plasma calculated by test particle method, interpreting results in convective modes terms in plasma control and stability
11 p1924 A69-24301

Dynamics, stability and approach to equilibrium of bounded one dimensional collisionless plasma representing minimum energy states with nonlinear Vlasov equation solutions
11 p1924 A69-24305

Toroidal plasma radial drift suppression on curved theta pinch axis through introduction of transverse conducting ring inside vacuum tube
11 p1925 A69-24313

Hydromagnetic instability onset in dissipative flow of electrically conducting fluid between rotating permeable perfectly conducting cylinders, noting oscillatory axisymmetric critical modes
11 p1926 A69-24895

HF instability of low pressure discharge in magnetic field, discussing plasma diffusion and oscillations
11 p1927 A69-24912

Charge bunching approach for gravitational hydrodynamic instability of infinite uniform self

gravitating system in translational motion, using conservation laws

11 p1961 A69-25105

Spectrum space-time characteristics of electrically produced plasma discharges magnetically compressed to discharge tube wall, using spectrochromograph and spectrographs

11 p1927 A69-25217

Dense gas equilibrium plasma thermodynamic stability in case of high electrostatic interaction energy of charged particles, analyzing phase transition possibility

11 p1928 A69-25234

Linear interaction of electron beam and plasma in magnetic field noting convective wave instability, wave dispersion and properties behavior

11 p1929 A69-25267

LF waves and instabilities on positive column in axial magnetic field, noting axisymmetric and asymmetric ion acoustic and electron wave modes and current convective instability

11 p1929 A69-25268

Kink type instability of rotating linear theta pinch plasma, calculating perturbation behavior with bounce model

11 p1929 A69-25270

Unstable ion sound wave propagation across magnetic field in collisionless shock waves, noting drift instability

11 p1930 A69-25273

Asymptotic solution for Fokker-Planck equation at low collision frequency, studying electron-ion collisions effect on universal instability in inhomogeneous plasma

11 p1930 A69-25358

LF electromagnetic waves stability and propagation conditions in plasma confined in central-conductor configuration measured, noting agreement with wave equation solution

11 p1931 A69-25362

Critical condition for electromagnetic radiation generation by energetic electrons gyrating in dense magnetized plasma, proposing plasma instability mechanism

11 p1931 A69-25363

Surface instabilities at tangential discontinuity between media caused by beam-plasma interaction, deriving dispersion relation

11 p1931 A69-25365

Centrifugal instability of plasma column generated by cyclotron absorption of microwave power in magnetic mirror field

11 p1931 A69-25366

Natural oscillations excitation instabilities by modulated ion beams in magnetoactive plasma ascribed to anomalous Doppler effect

11 p1932 A69-25536

Current carrying inhomogeneous dense plasma instabilities confined in magnetic field, deriving dispersion relations in geometric optics approximation

11 p1932 A69-25537

Convective drift and flute instabilities of plasma stabilized by exerting HF forces on electrons, determining required HF field amplitudes

11 p1932 A69-25538

Convective wave instability resulting from modulated electron beam injection into plasma, noting amplitude restraint due to collisional damping effect

11 p1934 A69-25576

Electrostatic drift wave dissipative instability in framework of macroscopic theory, accounting for resistivity and viscosity using WKB method

11 p1934 A69-25655

Transverse perturbation influence on helical instability in oscillator

11 p1939 A69-25687

Flute oscillation instability of dense plasma cylinder under nonuniform electric field, analyzing oscillation spectrum properties

11 p1934 A69-25707

Energy loss during turbulent plasma heating by current in open magnetic trap, attributing heating to ion-acoustic instability in plasma

11 p1935 A69-25753

Ionization instability in plasma enclosed by two infinitely segmented and ideally emitting electrode walls and two insulator walls

12 p2134 A69-26095

Finite ion Larmor radius effect on gravitational instability of two superposed fluids in uniform rotation, analyzing interchange perturbations and vortex sheet

12 p2062 A69-26461

Plasma instability in magnetic and HF electric fields, observing aperiodic short wave and oscillatory instabilities

12 p2136 A69-26526

Transient processes in conduction type MHD generators due to external circuits induction distribution

12 p2017 A69-26545

Plasma properties when carrying periodic magnetoacoustic wave expressed in terms of periodic functions, discussing small perturbation propagation

12 p2138 A69-26708

Surface dissipation effect induced by end electrodes on drift instabilities in cold ion plasma column described by differential equation with constant coefficient

12 p2138 A69-26710

Rarefied plasma potential fluctuations when bounded by surface having complex conductivity and dispersing properties

12 p2139 A69-26712

Magnetospheric plasma instabilities, discussing pitch angle diffusion instabilities, auroral precipitation boundary location, radial diffusion and maximum dissipation limit

12 p2072 A69-26748

Satellite observation of intensity and distribution of VLF emission at medium latitude during magnetic storm interpreted by transverse resonance plasma instability

12 p2073 A69-26947

Steady helical discharges /skin effect/ in air and Ar under high pressure without gas injection, discussing discharge stability factors

12 p2140 A69-27122

Electrodynamics model applicability to HF flame discharge for case of flame discharge stabilization by axial air injection

12 p2140 A69-27126

Instabilities related to particles transit time in system of two counterstreaming electron beams of finite length, noting wave dispersion

12 p2141 A69-27179

Magnetic curvature effect on collisionless plasma density gradient drift instabilities, covering mean ion Larmor radius and Alfvén modes

13 p2305 A69-27375

Finite Larmor radius effects on gravitational instability of rotating anisotropic plasma for transverse wave propagation mode

13 p2346 A69-27704

Hydromagnetic stability of spiral arm embedded in gravitating medium from analysis of instability of self gravitating incompressible cylinder

13 p2346 A69-27705

Finite Larmor radius and collision with neutral atoms simultaneous effects on plasma gravitational instability

13 p2346 A69-27708

Dissipative drift instability due to electron density gradient and dissipative mechanism /neutral-electron and ion-electron collisions/ in plasma in constant magnetic field

13 p2308 A69-27979

Rayleigh-Taylor instabilities in two fluid hydraulic model, noting perturbation direction and Lorentz forces effects on instabilities growth time

13 p2310 A69-28033

Current carrying cylindrical plasma column oscillations surrounded by electric excitation with multiple feedback radio, discussing stabilization possibility

13 p2311 A69-28106

Unstable weakly ionized HF magnetoplasma fluctuations with no axial drift, noting phase velocity parametric dependence

13 p2312 A69-28197

Alternating current plasma arc coaxial flow stabilization [AIAA PAPER 68-706]

13 p2313 A69-28232

Variational method for time invariant states of collisionless plasma in oscillating electromagnetic field

13 p2314 A69-28365

Convective-current instability in finite length plasma column, analyzing spectrum of unstable harmonics

13 p2314 A69-28441

Langmuir HF turbulence effect on anisotropic plasma oscillation spectra, determining instability conditions

13 p2315 A69-28448

Axisymmetric instabilities by Z-pinch and reverse axial current discharges in plasmas of arbitrary conductivity

13 p2315 A69-28449

Screw instability in glowing discharge plasma column in longitudinal magnetic field generalized to instabilities in low pressure arc, Penning and high current discharges

13 p2315 A69-28526

Polar auroral fine scale structure interpretation based on plasma instabilities characteristics

13 p2258 A69-28724

Alfvén and slow and fast magnetoacoustic waves excited during decay instability of initial Alfvén wave, noting dissipation effect on stability

14 p2489 A69-28735

Potassium plasma drift instability suppression by applied external HF electric field, noting plasma diffusion decrease toward container wall

14 p2489 A69-28740

Boundary conditions for equilibrium diamagnetic plasma in magnetic dipole having constant and isotropic pressure in system

14 p2489 A69-28910

Equatorial jet stream excitation of longitudinal waves, analyzing plasma beam instability and spectrum of short wave inhomogeneities by quasi-hydrodynamic equations

14 p2437 A69-29073

Kelvin-Helmholtz instability noting effects of oblique magnetic field and rotation, deriving dispersion relation

14 p2491 A69-29335

Radiative effect on rotating gaseous magnetic mass stability in thermodynamic equilibrium, including small oscillations stability

14 p2522 A69-29596

Low beta fusion research in open end magnetic mirrors covering scope, end losses, fusion economics, flute instability, stabilization, etc

14 p2498 A69-29843

Collisionless Ce and K plasmas measurements to determine steady state parameters and LF oscillations, noting noise relationship to drift instability

14 p2499 A69-29849

General algorithm for eruptive plasma instabilities in fusion plasmas, flares and novae, yielding time behavior and dissipative effects

14 p2499 A69-29850

Collisionless plasma slab drift mode stabilization at uniform temperature by oscillating electromagnetic field

14 p2499 A69-29851

Synthesized plasma from neutralized mercury ion beam ejected from electron bombardment source, analyzing temperature, plasma sheath and stability

14 p2502 A69-29956

LF electrostatic oscillations of inhomogeneous solid state plasma with small number of current carriers in parallel external electric and magnetic fields

15 p2665 A69-30042

Drift wave instability due to particle number density gradient of plasmopause, considering velocity shear modification

15 p2595 A69-30096

Plasma stability under anisotropic pressure in axisymmetric magnetic fields determined by quasi-hydrodynamic approximation

15 p2658 A69-30249

Free fluid hydrodynamics equations applied to weakly ionized plasma stability, considering drift oscillations excitation

15 p2658 A69-30250

Anisotropic plasma cyclotron instability in magnetic trap with cold ion background and isotropic Maxwellian velocity distribution

15 p2658 A69-30251

Criterion for magnetic plasma stability near magnetic axis, noting parameters for deriving criterion integrand

15 p2658 A69-30265

Hall generator electrical characteristics, discussing plasma homogeneity, stability and shock tube priming

15 p2658 A69-30298

Hydromagnetic stability calculations applied to umbral models, showing overstable oscillations relation to thermal hydromagnetic wave generation occurrence in sunspots

15 p2693 A69-30780

MHD stability and equilibrium of toroidal high beta configurations achieved by superimposing oscillating magnetic field on linear plasma column

15 p2660 A69-30877

Nonlinear effects and turbulent behavior in beam plasma instability, studying interactions in magnetic field

15 p2660 A69-30917

Plasma instabilities due to anisotropic velocity distributions computer analyzed to study nonlinear phenomena and validity limits of linear theory

15 p2661 A69-30920

Turbulent diffusion and ion heating in plasmas in presence of current instability

15 p2662 A69-30959

Radial self focusing of low density electron beam by interaction with plasma in presence of beam plasma instability

15 p2662 A69-30964

Nonlinear wave scattering at plasma particles and weak plasma inhomogeneity effects on plasma current instability

15 p2662 A69-30965

Eigenfrequency spectrum and stability of perfectly conducting inviscid incompressible fluids in cylindrical channels and twisted magnetic fields, noting flowfields and critical wavelengths

15 p2664 A69-31063

Interchange stability and drift motion of plasma with loss from ends of axisymmetric magnetic bottle, using hydromagnetic equations

15 p2664 A69-31100

Low density cold plasma effect on stability of cylindrical layer of charged particles against electrostatic perturbations in uniform magnetic field

16 p2816 A69-31635

Magnetic field lines curvature effect on plasma instabilities due to ion temperature gradient, noting frictional gravitation field simulation

16 p2816 A69-31636

Transverse instabilities in collisionless electron plasma in absence of permanent magnetic field with spheroidal velocity distribution, noting application to shock theory

16 p2817 A69-31645

Quasi-linear theory of waves in collisionless plasma in absence of external fields, relating wave energy growth and decay to plasma stability

16 p2817 A69-31646

Wide argon plasma column by axial current density measurements, confirming existence of instability and determining critical magnetic field

16 p2819 A69-31680

High beta theta pinch stability against tearing modes, determining necessary magnetic field conditions for slab and cylindrical cases

16 p2819 A69-31681

Nonlinear theory of $E \times B$ instability for weakly ionized plasma in presence of density gradient and parallel electric field perpendicular to magnetic field

16 p2819 A69-31682

Temperature gradients effect on ion flute mode in low beta plasma having density gradients in x direction, obtaining instability condition

16 p2819 A69-31689

Collisionless drift plasma wave instability growth rate calculation noting destabilization from resonant electrons

16 p2820 A69-31691

Plasma experiments with TM-3 apparatus under stable discharge conditions in H, discussing energy loss mechanisms, transport coefficients, reciprocal lifetime, etc

16 p2820 A69-31795

Charge density irregularities of midlatitude ionospheric E region related to cross field plasma instability noting turbulence

16 p2773 A69-31972

Energy principle applied to Astron type device stability based on model with rigid E layer electrons, finding critical pressure expression for ballooning modes

16 p2821 A69-32035

Screw pinch stability explained by strong force free current carried by magnetic field around central plasma column

16 p2821 A69-32037

Electromagnetic wave propagation in plasmas and plasma instabilities due to oscillations, deriving equations for frequency distributions in various plasma compositions

16 p2823 A69-32243

Multipole configuration toroidal plasma confinement device MHD equilibrium and stability from measured data

16 p2823 A69-32563

Time resolved beam distribution functions resulting from cyclotron instability and harmonics in electron injection machine during beam-plasma experiment

17 p3014 A69-33829

Semiconductor plasma DC overheating instability in electric and magnetic fields, determining growth increments of oscillation amplitude

18 p3182 A69-35022

Waves in auroral ionosphere due to particle precipitation, indicating ionospheric plasma instabilities

18 p3130 A69-35187

Equilibrium state of diamagnetic plasma configuration in inhomogeneous magnetic fields with complex potential near neutral point, noting solar flares and magnetic traps

19 p3380 A69-36467

Gravitational stability of infinite conducting fluid cylinder in axial magnetic field and surrounded by fluid of different density

19 p3380 A69-36483

Solar wind velocity cycles from fluid MHD viewpoint, applying Kelvin theorem on circulation stability in closed fluid system

20 p3587 A69-37041

Plasma instabilities produced by beam plasma discharge in mirror magnetic trap

20 p3581 A69-37784

Homogeneous compressible fluid sphere with axisymmetric magnetic field, analyzing oscillations and stability using variational principle

20 p3605 A69-37822

Asymptotic method for analyzing small long wave perturbations in plasma, showing instability with respect to perturbations propagating at angles to ion-acoustic wave

20 p3582 A69-38005

Electron ejections from nuclei of radio galaxies and quasars explained on basis of plasma stability, discussing role of relativistic electrons and resulting unstable pinch

20 p3606 A69-38032

Lower E region field-aligned plasma instability arising from neutral wind driving ionization across magnetic field

20 p3534 A69-38091

Kinetic model describing collisions in nonequilibrium multicomponent plasma, studying pair collisions effect on stability of plasma-beam system

21 p3776 A69-38691

Scalar conductivity as governing parameter in determining current sheet diffusion and energy dissipation in MHD shock producing devices

21 p3776 A69-38708

Temperature gradient effect on plasma stability in maximum J configuration

21 p3776 A69-38711

Closed cycle MHD with gaseous working fluids and steady state nonequilibrium ionization

21 p3777 A69-39479

Plasma instabilities in closed cycle MHD generator with gaseous working fluids, discussing effective Hall parameters

21 p3777 A69-39481

Shock wave effect on ionization of detonation waves in propane-O mixtures producing stable high velocity plasma, measured by double probe method

21 p3853 A69-39745

Aligned uniform magnetic field effect on hydromagnetic stability of two dimensional incompressible electrically conducting jet flow with large Reynolds number

22 p3931 A69-40687

Homogeneous magnetoactive plasma longitudinal oscillations stability with fast monoenergetic ions addition, noting ion temperature increase stabilizing effect

22 p3990 A69-40789

Type II and type III solar radio burst relation to plasma instability associated with coherent synchrotron deceleration of electrons, discussing resonant power exchange

22 p4007 A69-40898

Electromagnetic wave propagation instabilities in semiconductor magnetoplasmas not diffusion limited to LF, using dispersion equation

22 p3902 A69-41223

Hydrodynamic stability of conducting fluid in external magnetic field subject to attraction of external spherically symmetric gravitational field

23 p4213 A69-41717

Equilibrium plasma configurations in magnetic field of two dimensional dipole analyzed under similar conditions to magnetospheric tail formation with neutral hot plasma layer

23 p4205 A69-41835

Pearl type geomagnetic micropulsation development by studying Alfvén waves cyclotron instability in plasma with hot protons anisotropic distribution

23 p4206 A69-41850

Instability theory of baroclinic vortices in incompressible and inviscid fluid, investigating symmetric meridional motions time evolution by numerical integration of hydrodynamic equations

23 p4153 A69-42346

Short term frequency fluctuations of CW HCN masers reduced to 10 kHz by improving plasma stability

24 p4327 A69-42614

Fire hose instability growth rate in relativistic plasma with anisotropic pressure, discussing importance to cosmic ray liberation and isotropization at galactic halo

24 p4376 A69-42660

Plasma instabilities in astrophysics - Conference, Monterey, October 1968

24 p4377 A69-42681

LF instability in plasmas and hydromagnetic fluids, discussing MHD equations, Rayleigh-Taylor instability, interchange mode, Kelvin-Helmholtz instability, etc

24 p4355 A69-42683

MHD tearing mode, considering most unstable wavelength, energetics and stability in two dimensional equilibria

24 p4355 A69-42684

Two stream instabilities, considering uniform infinite collisionless plasma with stream of electrons passing through ion-electron medium

24 p4355 A69-42685

Plasma microinstabilities due to ion and electron anisotropic velocity distributions, considering frequencies near harmonics of ion cyclotron frequency

24 p4355 A69-42686

Solar corona instabilities and shock waves indicated by type 3 and 2 bursts, considering electrons ejection

24 p4378 A69-42689

Transverse plasma waves propagating along parallel static electric and magnetic fields may lead to instabilities regardless of carriers sign

24 p4355 A69-42923

Two stream plasma instability in equatorial electrojet extended to nonlinear domain by nonlinear treatment of ion kinetic equation

24 p4310 A69-43182

Stationary equilibrium of two dimensional plasmas with motion perpendicular to uniform magnetic field and gravitational field, considering resistive diffusion role

24 p4356 A69-43365

Self induced magnetic field influence on plasma positive column stability in longitudinal magnetic field

24 p4356 A69-43366

Electrothermal waves in nonequilibrium electrical discharge in potassium seeded argon plasma

24 p4359 A69-43645

Unsteady MHD conducting fluid flow in arbitrary ducts under transverse magnetic field, studying effects of pressure gradient impulsive change

24 p4359 A69-43678

Plasma-dynamic forces used to suppress fuel-propellant interface turbulence in coaxial jet gas core reactors

24 p4349 A69-43679

MAGNETOHYDRODYNAMIC TURBULENCE

Space-time function for joint probability distribution of velocity and magnetic fields from hydromagnetic turbulence equations

04 p0638 A69-15277

Plasma mixed ion heating by small scale HF turbulent electron sound pulsations

09 p1548 A69-21673

Sun-like alternating field generators, discussing dynamo theory of stellar and planetary magnetic fields based on nonmirror symmetrical turbulent motion in conducting fluid

10 p1782 A69-23703

Dynamo action origin of stellar and planetary magnetic fields, considering turbulent helical motions of H convection zone of sun

22 p4011 A69-39998

MHD disturbances in earth core produced by sudden introduction of magnetic dipole with axis positioned perpendicular to earth mantle and toroidal excitation fields

23 p4158 A69-42176

MAGNETOHYDRODYNAMIC WAVES

NT ELECTROSTATIC WAVES

NT PLASMA WAVES

Electron cyclotron harmonic waves in magnetoplasma irradiated by external microwaves

01 p0127 A69-10335

Nonlinear hydromagnetic solitary wave propagation at angle to magnetic field in fully ionized quasi-neutral collisionless warm plasma, noting isotropic pressure effect

01 p0127 A69-10336

Alfvén and magnetoacoustic waves propagation in inhomogeneous stable plasma situated in field with helical lines of forces

01 p0130 A69-10742

Standing Alfvén wave resonances in liquid sodium

01 p0131 A69-10820

Hydromagnetic wave propagation in current carrying regions of ionosphere and magnetosphere using macroscopic equations, deriving dispersion relation

01 p0067 A69-10972

- MHD waves and toroidal mode existence by mathematical approximation
02 p0236 A69-11430
- Alfven wave propagation in nonhomogeneous systems for relativistic MHD, discussing magnetic and velocity perturbations
02 p0290 A69-12254
- Geomagnetic micropulsations mechanism, discussing hydromagnetic waves transmission generated by interface instability between solar wind and magnetosphere, noting transmission path role
02 p0244 A69-12395
- Geomagnetic micropulsation theory, discussing mechanisms responsible for amplitude spectrum at earth surface and power spectral density
02 p0244 A69-12396
- Alfven wave propagation designations in terms of polarization and propagation velocity, resolving contradictory aspects
02 p0290 A69-12400
- Collisionless plasma heating by hydromagnetic waves in solar wind
02 p0309 A69-12714
- Electrostatic acoustic wave mode with plasma motion in magnetic surfaces perpendicular to field in toroidal systems with geodesic curvature
03 p0475 A69-13147
- Geomagnetic field topology of nighttime magnetosphere, showing pi 2 pulsations excitation mechanism in terms of Alfven waves resonance in external cavity
03 p0423 A69-13524
- LF hydromagnetic waves propagation in ionospheric waveguide duct resulting from minimum in Alfven speed near F 2 ionization peak
03 p0399 A69-14023
- MHD waves, Landau damping and magnetosonic waves in homogeneous relativistic Vlasov plasma
04 p0636 A69-15043
- Transverse ionizing MHD shock waves, discussing jump conditions with magnetic field in shock plane
04 p0637 A69-15052
- Two fluid MHD equations in form of nonlinear ion waves with magnetic vector
04 p0662 A69-15244
- Pc 1 micropulsation and magnetosonic amplification of hydromagnetic waves
05 p0754 A69-16263
- Alfven waves observed propagating along lines of force in inhomogeneous plasma in presence of homogeneous gravitational field
05 p0805 A69-16706
- MHD shock wave decay in one dimensional unsteady flow of ideal inviscid perfectly conducting compressible fluid subjected to transverse magnetic field
05 p0806 A69-16736
- MHD shock discontinuities above critical Alfven-Mach numbers in two fluid plasma
06 p0970 A69-17954
- Thickness of resistivity controlled hydromagnetic shock wave, using classical one fluid equations and generalized Ohm law
06 p0970 A69-17956
- Transverse LF oscillations in geomagnetic field observed during January 1967, noting possibility of being second harmonic of magnetospheric standing Alfven waves
07 p1124 A69-18835
- Jump conditions across MHD shock waves, reducing relations to identities applicable to nonequilibrium situations
07 p1193 A69-19242
- Hydromagnetic wave propagation and generation in magnetosphere, discussing hydromagnetic waves in uniform and axisymmetric magnetic fields
07 p1208 A69-19356
- Fluid motion and MHD disturbances in viscous incompressible fluid of finite electrical conductivity, studying axis of oscillating dipole perpendicular to exciting field
07 p1195 A69-19451
- Steady shock discontinuity in perfectly conducting gas flow in arbitrarily oriented magnetic field for various Mach numbers
08 p1360 A69-19988
- Symmetric Alfven waves propagation in hydrogen plasma with nonuniform density distribution, deriving dispersion relations for fully ionized plasma
08 p1367 A69-20794
- Quasi-linear theory of hydromagnetic waves in non-relativistic collisionless plasma, noting resonant diffusion effect on plasma heating mode
08 p1367 A69-20797
- Steady state currents effect on hydrodynamic waves propagated normal to magnetic field
09 p1547 A69-21662
- Singular shock waves formation during pulsed forward motion of conducting piston in MHD medium
09 p1551 A69-22034
- Resonant interaction between traveling charge with superimposed magnetic field and Alfven wave in plasma cylinder, showing cyclotron orbit variations
09 p1551 A69-22035
- Switch-on ionizing shock waves structure, analyzing condition of downstream state and effect on hydromagnetic wave speed
09 p1552 A69-22045
- Collisionless plasma heating by damping hydromagnetic waves applied to solar wind qualitative model, discussing magnetoacoustic wave energy
09 p1607 A69-22426
- Conical refraction of magnetosonic waves occurring when Alfven waves propagate at speed of sound in conducting fluid in presence of constant uniform magnetic field
10 p1727 A69-23091
- Electron density and collision frequency of MHD plasma determined directly by measuring phase shift and attenuation of propagating laser microwave signal
10 p1731 A69-23436
- Simultaneous interplanetary magnetic field measurements by geocentric satellites Explorer 33 and IMP 3 of MHD shock wave associated with July 8, 1966 sudden storm commencement
10 p1783 A69-23773
- Geomagnetic field directed hydromagnetic waves propagation in lower ionosphere, noting inhomogeneous conductivity, Hall effect and lines of forces role
10 p1687 A69-23926
- Plasma concentration diagnostics in magnetosphere based on hydromagnetic whistlers/pearls/dispersion
10 p1688 A69-23934
- Plasma distribution and Alfven wave velocity field in magnetosphere, discussing distortion of dipole magnetic field, ring current and wave propagation
10 p1742 A69-24205
- Geomagnetic field Pc 3 and Pc 4 pulsation generation mechanism explained by resonance of MHD waves in force tubes adjoining radiation belt maximum
10 p1689 A69-24206
- Nonuniformity of magnetic field effect on steady flow of incompressible inviscid electrically conducting fluid in duct, considering Reynolds and Alfven numbers
11 p1923 A69-24291
- [JPL-TR-32-1376]
- Rotational discontinuity in plasma, noting behavior for particle reflection off front side or back side of MHD wave
11 p1923 A69-24293
- Geomagnetically trapped particle loss processes and equilibrium distribution resulting from MHD wave field interaction described using sandbox model
11 p1948 A69-24856
- LF waves and instabilities on positive column in axial magnetic field, noting axisymmetric and asymmetric ion acoustic and electron wave modes and current convective instability
11 p1929 A69-25268
- Cyclotron harmonic waves/CHW/ nonlinear decay instability and parametric amplification, considering applicability to practical amplifiers
12 p2135 A69-26314
- Nonuniform two dimensional hydromagnetic waves incident on idealized lower ionosphere, discussing validity of various models
12 p2074 A69-26960
- Solar chromosphere and corona heat intensity above 1000 km attributed to tongues of turbulence, considering convective zone exciting MHD waves mechanism
13 p2337 A69-27549
- Cosmic ray propagation theory for steady streaming along magnetic field and down cosmic ray density gradient, noting MHD wave generation by anisotropy
13 p2326 A69-27569
- Geomagnetic pulsations and hydromagnetic wave propagation in magnetosphere, using geometric optics approximation
13 p2254 A69-28176
- MHD waves and oscillations in cylindrical plasma column contained by longitudinal magnetic field, noting dispersion equations
14 p2489 A69-28732
- Alfven and slow and fast magnetoacoustic waves excited during decay instability of initial Alfven wave, noting dissipation effect on stability
14 p2489 A69-28735
- Correlation coefficients between radial components of interplanetary magnetic field and solar wind velocity from Mariner 5 data due to Alfven waves
14 p2510 A69-28949
- Hydromagnetic waves propagation in finitely conducting fluid mass immersed in nonuniform magnetic field, using curvilinear coordinates based on lines of force
14 p2491 A69-29336
- Magnetospheric plasma motion associated with Alfven mode time fluctuations of magnetic field in solar wind
14 p2521 A69-29382
- Detached MHD shock wave formation in front of magnetic field acting as piston moving collisionless plasma, discussing time dependence, Alfven speed and plasma parameters
14 p2502 A69-29958
- Hydromagnetic fast shock strength and direction in inhomogeneous gravitational atmosphere with uniform magnetic field, discussing heating in solar corona
15 p2680 A69-30202
- Galactic cosmic rays and Alfven waves interaction, considering gyration frequency resonance, wave growth, Fokker-Planck equation and diffusion model
15 p2675 A69-30761
- Hydromagnetic stability calculations applied to umbral models, showing overstable oscillations relation to thermal hydromagnetic wave generation occurrence in sunspots
15 p2693 A69-30780
- Interstellar hydromagnetic waves due to streaming cosmic rays indicated by pulsar scintillations studies
15 p2676 A69-30889
- Final states of density, velocity and pressure in gas, comparing states reached after transition through single oblique hydromagnetic shock and two successive shocks
15 p2664 A69-31217
- Transmission of Alfven waves through earth bow shock based on hydromagnetic shocks theory, discussing amplitude amplification
16 p2777 A69-32099
- Weak nonlinear hydromagnetic waves in cold collisionless plasma, using nonlinear perturbation method
17 p3010 A69-32866
- Active solar centers interactions above photospheric level and through corona linkages, noting MHD shock waves and magnetic field lines
17 p3040 A69-33801
- Oblique hydromagnetic shock waves in magnetized hydrogen plasma enclosed in pyrex chamber by oscillatory zeta discharge, probing for front development and structure
17 p3013 A69-33823
- Hydromagnetic whistlers propagation mechanism in magnetosphere determined by wave theory, assuming Gaussian radial density distribution and estimating duct width necessary for trapping
18 p3102 A69-34966
- Hydromagnetic wave-charged particle resonant interaction described by diffusion equation in momentum space, deriving diffusion coefficients and time evolution ultrarelativistic particle energy spectrum
19 p3424 A69-36335
- Structure of isolated MHD shock wave in viscous heat-conducting radiating gas finite electrical conductivity and transverse magnetic field
20 p3581 A69-37189
- Doppler observations of ionospheric motions associated with magnetic micropulsations, noting hydromagnetic and neutral gas waves
20 p3535 A69-38194
- Amplitude equations for magnetoacoustic and entropy waves diverging from normal MHD shock, obtaining energy flux ratios associated with incident and transmitted waves
20 p3582 A69-38242
- Hydromagnetic waves equations of motion for non-relativistic case, discussing particle and fluid flow models
20 p3616 A69-38317
- Collisional shocks in inverse pinch MHD shock producing device, discussing position in current sheet and effect on conductivity and diffusion
21 p3776 A69-38709
- Propagation, damping, power coupling and plasma heating characteristics of harmonic ion cyclotron waves, noting temperature effects
21 p3777 A69-39455
- Shock waves in closed cycle MHD with gaseous working fluids, investigating MHD channel flow
21 p3778 A69-39482
- Auroral zone Birkeland currents in magnetosphere, analyzing particle trajectories for plasma sheet energy distribution and Alfven layer position
21 p3792 A69-39567

Chromospheric heating above sunspots by analyzing MHD wave generation and propagation in sunspots and solar atmosphere

22 p4010 A69-39992

Coherent MHD waves propagation in presence of plasma density fluctuations, applying perturbation technique to solve stochastic wave equation

22 p3990 A69-40529

MHD waves attenuation in ionosphere due to gyrorelaxation, reducing analysis to determination of anomalous absorption of acoustic waves

23 p4155 A69-41841

H and He atoms escape from atmosphere under MHD waves action at exosphere boundary

23 p4156 A69-41847

Pearl type geomagnetic micropulsation development by studying Alfvén waves cyclotron instability in plasma with hot protons anisotropic distribution

23 p4206 A69-41850

LF hydromagnetic waves propagation along geomagnetic field lines in gyrotropic ionosphere model taking Hall effect into account

23 p4157 A69-41864

Guiding center Vlasov equation derived dielectric tensor of collisionless plasma, obtaining dispersion relation of Alfvén waves in warm plasma

23 p4197 A69-42416

Ionospheric heating and velocity dependence of collision cross sections on transversely propagated equatorial hydromagnetic waves, discussing ordinary and extraordinary modes

23 p4161 A69-42437

Gravitational field structure effects on Alfvén waves propagation in inhomogeneous medium

23 p4223 A69-42478

Fluctuating electric fields relations to MHD bow shock structure, using LF fluxgate magnetometer aboard OGO 5

24 p4306 A69-42693

Hydromagnetic radiation characteristics of electric and magnetic dipoles in homogeneous anisotropic cold plasma, obtaining field components and wave propagation modes

24 p4307 A69-42905

Magnetic and electron temperature interaction effects in fast MHD shock waves in slightly ionized plasma

24 p4356 A69-43361

MAGNETOHYDRODYNAMICS

MHD equations describing interactions between gases and magnetic fields solved by finite difference method

01 p0129 A69-10722

Plane MHD jets with variable conductivity, showing effective mixing length as function of distance

01 p0130 A69-10773

Structure of shock waves from MHD jet injected into zero viscosity, finite thermal and electrical conductivity medium analyzed by nonlinear differential equation system

01 p0130 A69-10774

Electrohydrodynamic analogies to known MHD effects studied by differential equations for hydrodynamic and electric field energy relations

01 p0131 A69-10775

MHD technology applications to industry and cost and performance of MHD generators

01 p0013 A69-11394

Hydromagnetic emissions observed at Antarctic auroral zone, discussing relation to sudden storm commencement

02 p0241 A69-11726

Quasi-one dimensional analysis of MPD arcs with nonequilibrium ionization taking into account finite rate processes and variable area

[AIAA PAPER 68-87]

02 p0291 A69-12505

Cosmic MHD, discussing mechanisms responsible for solar phenomena and dynamics of interstellar medium

02 p0293 A69-12789

Exact solutions with helical symmetry for hydromagnetic dynamo problem steady state equations

03 p0476 A69-13380

Plasma equation of motion in external electromagnetic field analyzed as generalization of Bernoulli equation in relativistic MHD

03 p0476 A69-13385

Electrodynamics of turbulent conducting media based on nonrelativistic MHD

03 p0479 A69-13972

Adiabatic motion of hydromagnetic fluid behind spherical fast shock wave for Parker solar wind model

04 p0660 A69-15126

Steady longitudinal motion of insulating cylinder in conducting fluid, discussing analog between steady MHD and acoustic scattering

04 p0638 A69-15192

Local hydromagnetic mechanism to increase magnetic fields and shape into bipolar sunspot group configuration, discussing applicability to solar atmosphere

04 p0662 A69-15243

MHD quasar model consisting of galaxy with supermassive plasma nucleus moving in magnetic field

05 p0822 A69-15853

Injector vaporizer performance in liquid metal MHD system, using model for total and static pressure distribution

06 p0871 A69-17918

Injector design based on MHD injector components performance, establishing minimum diffuser nozzle area

06 p0872 A69-17920

Liquid metal MHD systems efficiency when operating with pressure jump in diffuser nozzle

06 p0872 A69-17921

Nonsimilar MHD channels boundary layers on insulating walls noting influence of loading factor, wall temperature and Hall effect on separation

[AIAA PAPER 69-46]

06 p0972 A69-18192

Prigogine evolution criterion extended to MHD, considering Hartmann flow

07 p1188 A69-18267

Group analysis of MHD equations, determining group properties of motion equations of compressible fluid, obtaining invariant solutions

07 p1191 A69-18994

Current and voltage distribution in electromagnetic compressor channel with solid electrodes of finite resistance, noting error analysis

07 p1059 A69-19029

Power losses in MHD channel due to longitudinal end effects related to finite dimensions of electrodes and terminal insulators

07 p1193 A69-19030

Montardi circuit with sectioned electrodes to simulate isotropically conducting still liquid for application in MHD pump, discussing potentials distribution

07 p1059 A69-19031

Two dimensional unsteady wave motion in shallow water using MHD theory

08 p1362 A69-20354

Double adiabatic MHD fluid equations for electrons and ions with pressure gradients for collisionless plasma in magnetic field

08 p1369 A69-20815

Two dimensional steady flow of finitely conducting compressible fluid subjected to magnetic field with two zero components

08 p1369 A69-20843

Magnetic field decay modes due to nonuniform rotation having angular velocity as increasing function of distance from axis in infinite circular conducting fluid cylinder

08 p1369 A69-20999

MPD plasma acceleration in West Germany, discussing Hall acceleration, electrodeless plasma acceleration by electromagnetic waves and space charge neutralized Hall ion thruster

[AIAA PAPER 69-279]

09 p1564 A69-21238

Radiation cooled MPD arc thruster design and performance, noting specific impulse relation to arc spoke rotation frequencies

[AIAA PAPER 69-245]

09 p1566 A69-21259

Power series solutions of MHD boundary layer equations for flat plate with transverse magnetic field and arbitrary pressure gradient, discussing skin friction

09 p1545 A69-21396

Angular inertia of lubricant in MHD hydrostatic thrust bearings, obtaining critical angular speed of rotor

09 p1503 A69-21443

Lifetime and radial oscillations of magnetically confined laser produced plasma, solving hydrodynamical equations

09 p1545 A69-21493

Turbulent heat transfer in conducting fluid flow through circular tube in longitudinal magnetic field and constant wall heat flux, using Lyon relation

09 p1621 A69-21590

Singular surface theory combined with ray theory for propagation of weak discontinuities in nonlinear anisotropic media applied to MGD

09 p1547 A69-21613

Stresses and waves in highly conducting magnetoplastic metals as analogy of MHD processes in plasma

09 p1551 A69-22033

Topology of solar magnetic field differential rotation, using hydromagnetic equations

09 p1606 A69-22425

Transverse waves induced by disk oscillations about state of steady rotation in MHD, revealing circularly polarized waves with different phase velocities

10 p1728 A69-23239

Plasma and magnetic field measurements of tangential discontinuities in solar wind by Pioneer 6, considering velocity shears and rotation of sun

11 p1946 A69-24430

Degree of knottedness of tangled vortex lines, discussing vorticity distribution for inviscid flow and MHD invariants

11 p1872 A69-25126

Space-time hypersurfaces representations of shock waves of relativistic MHD, discussing compressibility role in proving consistency with relativistic theory

11 p1928 A69-25246

Motion equations for conducting paramagnetic fluid in magnetic field derived, including MHD equations and equation determining magnetic moment variation rates

11 p1932 A69-25465

Thermodynamic atomization in MHD energy conversion through convergent-divergent nozzles, noting nozzle efficiency and droplet size

13 p2245 A69-27477

Coupled magnetoacoustic waves in conducting paramagnetic fluid in resonance region due to mechanical and magnetic motions, considering dissipation

14 p2492 A69-29609

MHD properties of velocity measurement method using cylindrical glass filament probe and Pitot and Prandtl tubes

14 p2453 A69-29920

Entrainment of viscous electrically conducting liquid in long duct with narrow rectangular cross section and movable walls in magnetic induction field

16 p2816 A69-31606

Hydrodynamic parameters of annular Couette flow in longitudinal magnetic field for variable Reynolds and Mach numbers

16 p2821 A69-31953

Hydrodynamics of gas flow due to solar flares using point explosion model, determining shock wave travel time to earth orbit

18 p3189 A69-35397

Magnetospheric electromagnetic phenomena explained by equations of motion for particle acceleration, forbidden regions and MHD processes

21 p3707 A69-38485

Electricity from MHD - Conference, Warsaw, July 1968, Volume 6

21 p3777 A69-39477

MHD pivoted slider bearing with convex pad surface under azimuthal magnetic field

21 p3733 A69-39744

Solar physics and hydromagnetics - Conference, Sopot, Poland, September 1966

22 p4009 A69-39982

MHD dynamo construction with emphasis on fluid motion effect on magnetic field, considering spatially periodic dynamo derivation from kinematic considerations

22 p3989 A69-40196

MHD of ideal charged gravitating fluid by variational principle, considering Einstein general relativity theory

22 p3992 A69-41056

Ionizing shock wave propagation and reflection in transverse magnetic field based on MHD theory, assuming gas thermal equilibrium

22 p3992 A69-41176

Rumanian book on MHD covering electromagnetic field theory, motion equations, laminar flow, MHD generators, fluid motion past thin airfoils, shock waves, etc

23 p4195 A69-41363

MHD Rankine-Hugoniot equations for ion density, thermal pressure and convective velocity magnitude and orientation during Pioneer 6 traversal of earth bow shock

23 p4222 A69-42417

Circular arm with elliptical cross section used as magnetohydrodynamical model of helical magnetic field in spiral arms to demonstrate interstellar gas flow path

24 p4388 A69-43640

MAGNETOHYDROSTATICS

Magnetohydrostatic cavity formed round magnetic field of line dipole-line current combination by infinitely conducting plasma at uniform pressure

08 p1369 A69-20998

Axisymmetric solutions of magnetohydrostatic equations for large conductivity media satisfying second order partial differential equation containing two arbitrary functions
21 p3778 A69-39498

MAGNETOIONIC PLASMA
U PLASMAS [PHYSICS]

MAGNETOIONICS

Magnetoionic propagation of signals in magnetosphere using Maxwell equations and tensor quantities, linking to Hall, transverse and longitudinal conductivities
[ONERA-TP-593] 02 p0236 A69-11617

Algorithm for N/h/ ionospheric profiles calculations using both x and o magnetoionic components, taking into account interlayer and underlying ionization influence
02 p0239 A69-11687

Statistical characteristics of magnetoionic components of obliquely incident waves, obtaining envelope distribution of signal reflected from F 2 layer
02 p0314 A69-11691

Power radiated in magnetoionic mode by electron spiraling in magnetoplasma
02 p0309 A69-12720

Radiation resistance of short dipole immersed in cold magnetoionic medium, using polarized wave modes
07 p1107 A69-19226

Conjugate echoes in Alouette 2 topside sounder ionograms explained by multiple reflections between conjugate points of field line, noting magnetospheric waveguides role
08 p1274 A69-20045

Magnetoionic formulas similarity in ionospheric radio propagation and atmospheric acoustic gravity wave propagation above electron gyrofrequency
10 p1655 A69-23419

Ground wave propagation attainment of electron plasma resonance of F region, stressing need of wave vector orientation toward magnetic north
10 p1684 A69-23828

Algorithm for N/h/ ionospheric profiles calculations using both x and o magnetoionic components, taking into account interlayer and underlying ionization influence
13 p2258 A69-28718

Statistical characteristics of magnetoionic components of obliquely incidence waves, obtaining envelope distribution of signal reflected from F 2 layer
13 p2355 A69-28722

Thin film optical method generalization accounting for intermode coupling and oblique incidence in plane stratified magnetoionic medium applied to ionospheric LF and hydromagnetic propagation
16 p2753 A69-32393

Electromagnetic field eigenvalues along conductive circular cylinder in magnetoionic medium, assuming lossless medium and field frequency not equal to cyclotron frequency
16 p2754 A69-32568

Reflection and transmission coefficient matrices for stratified magnetoionic medium determined by thin film optical technique and iteration procedure
17 p2927 A69-33863

Ion and temperature effects on lower ionosphere refractive index for VLF radio wave propagation
18 p3102 A69-34971

Propagation characteristic model study of kinked Z trace observed on topside ionograms and explained by magnetoionic theory
20 p3531 A69-37893

Polarization measurement of slowly varying component of sun by pencil-beam antenna at 8.6 mm, analyzing data by magnetoionic theory
22 p4027 A69-40660

Approximate expressions derived from Appleton-Hartree magnetoionics formula tested for validity in computation of radio wave absorption in model ionospheric layers
23 p4126 A69-42354

MAGNETOMETERS
NT VARIOMETERS

Magnetometric equipment on board Luna 10 and Venera 4 space stations for studying magnetic field in interplanetary space, describing circuit and metrological characteristics
01 p0080 A69-10582

Vector helium magnetometer for Mariner 4 /Mars 1964/ and Mariner 5 /Venus 1967/, discussing efforts to reduce spacecraft stray fields
[IEEE PAPER 10.1] 01 p0081 A69-10714

Stable fluxgate magnetometer sensor for exploration of space magnetic fields, discussing equipment specifications and performance tests
[IEEE PAPER 10.2] 01 p0081 A69-10715

Three axis magnetometers to determine nonoriented satellite axial orientation in absolute coordinates
01 p0163 A69-11303

Magnetometer experiment for Apollo project to measure lunar surface magnetic field, describing mission requirements and instrumentation
[AAS PAPER 68-206] 02 p0312 A69-11481

Geomagnetic field H and Z components measured by proton magnetometer, applying supplementary field method for error correction
02 p0238 A69-11675

Rubidium self oscillating magnetometer long term stability, noting changes affecting accuracy and sensitivity
02 p0250 A69-12394

High resolution magnetograph study of solar magnetic field, showing magnetic asymmetry and fluctuations
04 p0651 A69-14367

Spatial distribution of background magnetic fields of quiet sun from photoelectric magnetograph observations, noting relation to supergranulation
04 p0663 A69-15396

Large scale pattern in solar magnetic field correlated with interplanetary magnetic field
04 p0665 A69-15532

Book on magnetic compasses and magnetometers covering pivoted needle instruments, surveying, transmitting and gyromagnetic compasses, inductor instruments and compass testing
08 p1315 A69-20444

Z magnetometer with quartz sensitive element suspended by thread in silicone oil design and operation
09 p1494 A69-21539

Magnetograph in Italian observatory for weak solar magnetic field longitudinal components avoiding differential amplifier by electronic compensation
10 p1693 A69-23311

Interplanetary magnetic field near Venus, analyzing data by magnetometer onboard Venera 4
10 p1791 A69-24199

Geomagnetic field vertical and horizontal intensities measured using proton magnetometer with coil theodolite
11 p1889 A69-25435

Angle-to-code converter designed on basis of quantum magnetometers frequency sensors, transforming vector sum of bias magnetic fields into pulse repetition rates
12 p2016 A69-25963

Onboard magnetic anomaly detection system for Canadian helicopter, discussing magnetometer location, boom design and testing and equipment installation
[AIAA PAPER 68-487] 12 p2094 A69-26771

Airborne magnetometer application for remote measurement of ocean wave spectra, obtaining wave noise power spectra and wave height profile
12 p2075 A69-26998

Soviet satellite and probe studies of earth, moon, Venus and Mars magnetic fields, noting automatic magnetometer
13 p2336 A69-27352

Geomagnetic field H and Z components measured by proton magnetometer, applying supplementary field method for error correction
13 p2257 A69-28706

Deep freezing of nuclear precession magnetometer elements for improving instrument characteristics
14 p2446 A69-29083

Vectormagnetograph to measure magnetic field vector components, obtaining field direction azimuth by servo circuit
14 p2453 A69-29972

Magnetometric equipment on board Luna 10 and Venera 4 space stations for studying magnetic field in interplanetary space, describing circuit and metrological characteristics
15 p2610 A69-30752

Magnetometers role in Aurorae satellite attitude stabilization, discussing operation principle, characteristics and performances
15 p2611 A69-31087

Z magnetometer with quartz sensitive element suspended by thread in silicone oil design and operation
16 p2792 A69-32534

Interplanetary and photospheric magnetic fields polarities observed by Mariner 4 and with solar magnetograph, noting noncorrelated data along latitudinal strip
18 p3205 A69-35399

Attitude stabilized rocket-released magnetometer for detection of earth field magnitude and direction changes
19 p3309 A69-35994

Rocket-released magnetometer probe for upper atmospheric measurements, discussing construction, flight, sensitivity and ionosphere current detection
19 p3309 A69-35995

OGO triaxial search coil magnetometer for measuring earth magnetic fluctuations, discussing design rationale and observation results
19 p3284 A69-36675

Radial velocities recording inaccuracies by solar magnetographs caused by dissimilarity between photomultipliers characteristics, describing photometer designs to eliminate errors
20 p3547 A69-38308

Magnetic field inhomogeneities effect on line contours and magnetographic measurements, constructing two stream models using Unno solution of transfer equations
22 p4019 A69-40288

Low noise nuclear precession magnetometer noise rejection optimization design specifications for measuring geomagnetic field components
23 p4165 A69-41868

MAGNETOMETRY
U MAGNETIC MEASUREMENT

MAGNETOPOUSE

Bow shock and magnetopause boundary observations with IMP 2 plasma detector
07 p1129 A69-19372

Magnetopause, magnetosheath, bow shock and adjoining interplanetary domain study by IMP-1 satellite, discussing macroscopic plasma variables and fluid model for solar wind
07 p1129 A69-19374

Boundary layer between cold plasma and vacuum magnetic field, considering transverse velocity component perpendicular to field
12 p2139 A69-26944

Charged particles influx from cusp shaped regions of stagnant plasma trapped in vicinity of two magnetic cusps on polar magnetopause
12 p2151 A69-26945

MAGNETOPLASMAS
U PLASMAS [PHYSICS]

MAGNETORESISTANCE
U MAGNETORESISTIVITY

MAGNETORESISTIVITY

Vacuum deposited n-type InAs films magnetoresistance coefficient dependences on length-to-width ratio, homogeneity moving carriers size and magnetic inductance
01 p0136 A69-10254

Magnetoconductance of nonequilibrium plasmas in indium antimonides, noting anisotropy effect of electric and magnetic field orientation
03 p0486 A69-13463

CdS Hall coefficient, Hall mobility and magnetoresistance coefficient dependence on electric field, magnetic field and scattering mechanisms
03 p0490 A69-13945

N-type GaAs single crystal magnetoresistivity, noting charge carrier scattering mechanisms
03 p0492 A69-14177

P-type GaSb crystals with various impurity concentrations noting conductivity, transverse magnetoresistance, Hall effect and acceptor band width and conductivity
04 p0643 A69-15259

Longitudinal and transverse magnetoresistance in n-type InSb single crystals in magnetic fields, noting preparation effect on existence magnetophonon oscillations
04 p0643 A69-15262

Magnetoresistance of tellurium single crystals with various current carrier concentration at liquid helium temperatures
06 p0978 A69-16986

Hall effect and magnetoresistance for compensated n-InP samples, discussing dependence on magnetic field
06 p0978 A69-16987

Magnetophonon oscillations of transverse magnetoresistance of n-type epitaxial GaAs in pulsed magnetic field
08 p1373 A69-20760

Vacuum deposited n-type InAs films magnetoresistance coefficient dependences on length-to-width ratio, homogeneity, moving carriers size and magnetic inductance
09 p1559 A69-22647

MAGNETOSONIC RESONANCE

Hall effect theory and devices, noting application to measurement of several physical quantities and sources of errors in devices
09 p1541 A69-22698

Longitudinal magnetoresistance oscillations in n-type GaSb single crystals associated with electron concentrations minima
13 p2319 A69-27900

N-type InSb single crystals with high dislocation density, investigating anisotropy of mobility, Hall effect and transverse and longitudinal magnetoresistance
14 p2503 A69-28734

Shubnikov-de Haas effect and quantum limit phenomena concerning oscillatory magnetoresistance in semiconductors
16 p2827 A69-31826

Anomalous phenomenon in resistance and magnetoresistance of cleaved InAs surface, plotting temperature and magnetic field variation effects, proposing explanation of anomaly
19 p3388 A69-36543

Nernst effect in pyrolytic graphite at low temperatures including thermal EMF, electrical conductivity, thermal conductivity and magnetoresistance coefficients
21 p3753 A69-39562

MAGNETOSONIC RESONANCE

Bounce resonant scattering of auroral zone electrons, noting contribution to microbursts and mirror point diffusion
05 p0754 A69-16260

Electromagnetic wave scattering in ferromagnetic crystals with anisotropy, discussing correlation functions of characteristics fluctuations and magnetoacoustic resonance
05 p0809 A69-16547

Magnetosonic waves absorption in plasmas, studying collisions leading to HF energy resonant absorption at lower hybrid frequency
06 p0963 A69-16904

MHD generator plasma anisotropic instability caused by amplified magnetosonic waves propagating normal to current
11 p1922 A69-24227

MAGNETOSPHERE

NT GEOMAGNETIC TAIL NT MAGNETOPAUSE

Artificial visible plasma clouds in space interacting with electric and magnetic fields around earth
01 p0151 A69-10533

Magnetic storm principal phase explained by interaction between quasi-trapped particles stream and magnetosphere
01 p0144 A69-10573

Hydromagnetic wave propagation in current carrying regions of ionosphere and magnetosphere using macroscopic equations, deriving dispersion relation
01 p0067 A69-10972

Solar, interplanetary and magnetospheric electromagnetic events before and during magnetic storm from ground observatory and earth satellite data
01 p0156 A69-11120

Magnetic field behavior at synchronous orbit during magnetospheric substorms, interpreting satellite observed data in terms of partial ring currents
01 p0075 A69-11225

Magnetospheric plasma distribution determination based on analysis of structured elements in micropulsations
01 p0076 A69-11229

Amplification process for VLF whistler mode radio signals observed in study of magnetosphere frequency shifting mechanism
01 p0077 A69-11241

Partial differential equation for distribution function in transport of charged particles in earth magnetosphere
01 p0147 A69-11320

Magnetoionic propagation of signals in magnetosphere using Maxwell equations and tensor quantities, linking to Hall, transverse and longitudinal conductivities [ONERA-TP-593]
02 p0236 A69-11617

Magnetosphere boundary determined in two dipole model approximation, taking into account current layer in tail
02 p0236 A69-11655

Whistler dynamic spectra variation studies, emphasizing distorted magnetospheric geomagnetic field structure effect
02 p0238 A69-11671

Soviet book on dynamics of radiation belts of earth covering theories concerning magnetosphere, magnetic fields and plasma and electromagnetic pulsations
02 p0307 A69-11799

Magnetosphere studies in France noting magnetosphere characteristics, wave propagation, charged particles, particle precipitation mechanisms in auroral zones and polar caps
02 p0242 A69-11904

Subsolar magnetosphere dimensions from ground observations of geomagnetic micropulsation period changes during magnetosphere deformations caused by solar wind inhomogeneities
02 p0244 A69-12356

Geomagnetic micropulsations mechanism, discussing hydromagnetic waves transmission generated by interface instability between solar wind and magnetosphere, noting transmission path role
02 p0244 A69-12395

Spatial variations in particle intensity near and inside magnetosphere during September 1966 solar cosmic ray events, noting magnetosphere screening effectiveness
02 p0309 A69-12740

Aurora displays distribution over earth, analyzing magnetosphere dependence on astronomical orientation of geomagnetic field in relation to solar wind
02 p0247 A69-12772

Magnetic storm of January 1967 due to 3B solar flare noting spacecraft observations, intensity, magnetospheric distortions and solar wind dynamics
03 p0500 A69-13430

Elektron 2 satellite magnetic measurement of high latitude nocturnal magnetosphere, discussing variations, antisolar effect and elongation of magnetic field
03 p0422 A69-13505

Polar auroral region cosmic radio noise absorption bays diurnal variations attributed to drift of electrons captured in magnetosphere
03 p0423 A69-13520

Cone instability role in auroral electron and proton dynamics, discussing plasma instability control of maximum captured particle densities in various magnetosphere regions
03 p0501 A69-13526

High latitude electrons boundary dependent on geomagnetic axis orientation, noting role of coupling between solar wind and magnetosphere
03 p0502 A69-14003

Two dimensional magnetosphere with tail and neutral sheet, using Chapman-Ferraro approximation by mapping in potential plane
03 p0425 A69-14011

Outer magnetosphere average magnetic field configuration between 5 and 18 earth radii, noting various maps in equatorial plane
03 p0425 A69-14012

Energetic electron fluxes measured at 2000 km over auroral and polar regions and at 17 earth radii in magnetotail plasma sheet
03 p0503 A69-14013

Low energy electrons on day side of magnetosphere observed with MIT electron detector onOGO 3 satellite
03 p0503 A69-14027

Sudden acceleration of electrons in magnetosphere and magnetic tail related to magnetic bays, noting acceleration occurrence first in magnetosphere during polar substorm
04 p0594 A69-15122

Small scale filament structure of current systems in earth magnetosphere, noting coherence of magnetic disturbances in conjugate regions
05 p0753 A69-16049

Equatorial semiaxis of magnetospheric tail at distances between 10 and 80 earth radii for various intensities of polar magnetic disturbances
05 p0753 A69-16050

Pc 1 micropulsation and magnetospheric amplification of hydromagnetic waves
05 p0754 A69-16263

Cross field energy transfer in collisionless plasma across earth magnetospheric boundary, using computer and one dimensional sheet model simulation [ISAS-429]
06 p0916 A69-17023

Plasma physics in space research, discussing solar wind, planetary atmosphere bow shock and convective motions of magnetosphere plasma [ISAS-431]
06 p1000 A69-17026

Packet of finite amplitude VLF whistler waves, examining cyclotron resonance interaction with high energy electrons and development in magnetosphere
06 p0917 A69-17378

Seasonal variations in auroral absorption zone position interpreted as consequence of asymmetric shape of magnetosphere
06 p0920 A69-17728

Induced and combination scattering of high HF radio waves in ionosphere and magnetosphere
07 p1076 A69-18521

Magnetospheric ELF noise, discussingOGO 3 spectrum analysis
07 p1124 A69-18834

Transverse LF oscillations in geomagnetic field observed during January 1967, noting possibility of being second harmonic of magnetospheric standing Alfvén waves
07 p1124 A69-18835

Magnetosphere - Conference, Boston College, June 1967
07 p1207 A69-19351

Magnetosphere dynamical properties, discussing atmosphere, ionosphere, magnetopause, magnetosheath, bow shock, solar wind, collisionless plasmas, etc
07 p1127 A69-19352

Solar wind and magnetosphere, discussing hydrodynamic expansion of solar corona
07 p1207 A69-19353

Charged particle motion in electromagnetic field from basic equation of motion for magnetosphere, discussing dipolar magnetic field, Stormer trapped particle theory, etc
07 p1208 A69-19355

Hydromagnetic wave propagation and generation in magnetosphere, discussing hydromagnetic waves in uniform and axisymmetric magnetic fields
07 p1208 A69-19356

Geomagnetic field line stretching outward due to energy entry in form of large number of charged particles or increase in particle temperature /inflation/
07 p1127 A69-19357

Low energy charged particles in earth magnetosphere observed byOGO satellite
07 p1208 A69-19358

Solar wind flow past earth and magnetosphere correspondence to external aerodynamics of round nosed bodies in supersonic stream
07 p1128 A69-19360

Solar wind, bow shock and magnetosheath observations by charged particle analyzers on Vela satellites
07 p1208 A69-19361

Particle measurements by Vela nuclear test detection satellites /2A and 2B/ noting plasma sheet in center of magnetotail
07 p1208 A69-19362

Structure, temporal behavior, shape and length of earth magnetic tail via satellite mapping
07 p1208 A69-19363

Magnetospheric plasma probe results with Pioneer 6 and 7, discussing plasma fluctuations and solar wind interaction with geomagnetic field
07 p1128 A69-19364

Geomagnetic tail topology, reconnection and interaction with moon from Explorer 33 satellite data
07 p1128 A69-19365

Low energy electrons in magnetosphere fromOGO-1 andOGO-3 observations, discussing plasma sheet, magnetic bay activity, electron pressure, temperature and density gradient
07 p1209 A69-19373

Magnetospheric magnetic field ring current asymmetry during different phases of geomagnetic storm observed by Explorer 26 and Vela 2 satellites
07 p1129 A69-19611

VLF wave electromagnetic properties in magnetosphere, noting whistler mode propagation and refractive index and electron density of medium
08 p1306 A69-20180

Synchrotron radiation from relativistic electrons in magnetosphere, calculating variation with frequency and height of lines of force
08 p1306 A69-20182

Bimodal diffusion mechanism for acceleration of trapped particles in earth magnetosphere, noting particle intensity profiles and energy spectra
08 p1307 A69-20183

Magnetospheric gusts of streaming positive ions in equatorial plane detected by ATS 1 synchronous satellite
09 p1574 A69-21309

Charged particles equations of motion in earth magnetosphere in polar storms, considering auroral zone, diurnal variations and electron and proton velocities
09 p1485 A69-21535

Modified first order theory of magnetosphere boundary shape incorporating effects of neutral sheet currents of extended geomagnetic tail
09 p1488 A69-21661

Solar protons in magnetospheric tail after flare of July 7, 1966 with isotropic pitch angle distribution, expressing energy spectrum as exponential in rigidity
09 p1576 A69-21699

DC electrical resistance of magnetosphere between two satellites with sheaths and current voltage relation of satellite sheath
09 p1489 A69-21710

Solar wind-magnetosphere pressure balance and proton density of solar wind
09 p1577 A69-21711

Reflected particle acceleration at magnetospheric bow shock front attributed to interplanetary electric field
09 p1577 A69-21714

Interplanetary plasma flow simulation around earth magnetosphere and planets not considering initial conditions influence
09 p1577 A69-21768

Satellite data on galactic cosmic ray variations near magnetosphere and in interplanetary space, discussing Forbush decreases
10 p1756 A69-22819

Earth thermal plasmasphere contraction subsequent to solar flare obtained from ion mass spectrometers on OGO satellites
10 p1683 A69-23777

Low energy particles during solar proton flare and effects on magnetosphere, cosmic ray intensity, ionosphere and geomagnetic activity
10 p1768 A69-23786

Dynamo action produced magnetospheric currents in ionosphere computable without knowing real horizontal ionospheric current system
10 p1685 A69-23836

Mariner 2 measurements of geomagnetic field and interplanetary plasma parameters for analyzing interaction between interplanetary medium and magnetosphere during decreased solar activity
10 p1769 A69-23900

Dipole magnetosphere model with cylindrical or spherical forbidden band for studying plasma motion in quasi-hydrodynamic approximation
10 p1769 A69-23901

Magnetosphere boundary configuration calculated with allowance for geomagnetic dipole inclination to geographic axis and nondipole section of geomagnetic field
10 p1686 A69-23902

Magnetic lines of force penetration into magnetosphere accompanied by plasma insertion generating ring current responsible for main phase of magnetic storm
10 p1687 A69-23923

Plasma concentration diagnostics in magnetosphere based on hydromagnetic whistlers/pearls/dispersion
10 p1688 A69-23934

Auroral oval and ring current in magnetosphere, analyzing boundaries of lines of force on night side of earth
10 p1689 A69-24203

Plasma distribution and Alfvén wave velocity field in magnetosphere, discussing distortion of dipole magnetic field, ring current and wave propagation
10 p1742 A69-24205

Stable particle trapping zone in magnetosphere, discussing results of adiabatic theory application to charged particle motion in earth magnetic field
11 p1948 A69-24858

Anisotropic fluxes of energetic particles in and near distant trapping region encountered by Explorer 33 satellite in outer magnetosphere
11 p1950 A69-25146

Magnetospheric plasma heating by magnetosheath generated electromagnetic waves
11 p1950 A69-25149

Plasmapause position measurements by ion mass spectrometers and broadband VLF receivers on OGO 1 and OGO 3 and by broadband recordings at Antarctica
11 p1878 A69-25153

Artificial triggering of VLF magnetospheric noise by NAA Morse code transmission during whistler duct drift across magnetic shells on 17 June 1965
11 p1878 A69-25154

Artificial magnetospheric VLF noise triggering by Morse code dots at 14.7 kHz from NAA verified at Antarctica
11 p1878 A69-25155

Transmitter frequency increase effect on production of artificial stimulated VLF emissions in magnetosphere
11 p1878 A69-25156

Light ion abundance measurements of OGO satellites and field aligned diffusive equilibrium theory with temperature and concentration latitudinal variations
11 p1879 A69-25157

Potential mechanisms of electron acceleration inside magnetosphere, measuring power spectrum of X rays by electron braking in upper atmosphere
12 p2066 A69-26295

Auroral arcs drift as function of polar storm initial phase, noting agreement with satellite data on plasma motion in magnetosphere
12 p2071 A69-26694

Physics of magnetosphere - Conference, Washington, D.C., September 1968
12 p2071 A69-26734

Solar wind interaction with geomagnetic field, considering bow shock, field confinement in magnetosphere and stretching out of lines of force
12 p2072 A69-26735

Solar plasma flow around magnetosphere, discussing plasma velocity, density and temperature and magnetic field space and time variations
12 p2150 A69-26736

Laboratory models for solar wind and magnetosphere interactions with similarity laws of Vlasov theory as reference system
12 p2150 A69-26737

Quantitative magnetic field models of magnetosphere for analyzing field configuration variations and adiabatic particle motion
12 p2072 A69-26738

Satellite observations of geomagnetic tail in magnetosphere near midnight meridian plane, discussing formation, shape, plasma sheet and models
12 p2072 A69-26739

Auroras and polar magnetic substorm observations limited comparison due to magnetospheric models inability to interpret daytime precipitation zones and particle energy spectra
12 p2072 A69-26740

Dynamics of magnetosphere, discussing auroral oval position, ring currents, plasma density and magnetic field variations in near polar region
12 p2072 A69-26741

Earth radiation belts formation as function of particle injection into trapped radiation zones or proton and electron leakage
12 p2150 A69-26742

Charged particle population dynamics in outer radiation zone of magnetosphere, discussing ring current particles, protons, electrons, alpha particles and electric field
12 p2150 A69-26743

Particle fluxes in outer radiation belt and unstable radiation zone of outer geomagnetic field, discussing electron diffusion into magnetosphere and magnetic disturbances
12 p2150 A69-26744

LF wave propagation and emission in magnetosphere, discussing steady noise and discrete emissions
12 p2072 A69-26745

Low energy plasma fluxes in magnetosphere, discussing plasmapause position dependence on geomagnetic activity
12 p2150 A69-26747

Magnetospheric plasma instabilities, discussing pitch angle diffusion instabilities, auroral precipitation boundary location, radial diffusion and maximum dissipation limit
12 p2072 A69-26748

Solar wind induced magnetospheric convection for interpretation of geomagnetic storms, aurora and trapped particle belts, noting electric fields
12 p2073 A69-26749

Solar wind plasma observations in geomagnetospheric wake compared at 1000 and 500 earth radii, considering ion energy spectra and geomagnetic tail
12 p2151 A69-26943

Energy exchange between LF waves and magnetospheric energetic particle population by bounce resonant interaction
12 p2073 A69-26946

Magnetosphere model for plasma pressure by solar wind, discussing plasma drift from neutral sheet into geomagnetic tail
12 p2076 A69-27106

Magnetospheric field configuration in midnight meridian, considering cavity boundary surface and trapping region currents and tail sheet current
13 p2252 A69-27532

Io as unipolar inductor, analyzing interaction with Jupiter magnetosphere and decimetric synchrotron radiation
13 p2337 A69-27552

Magnetospheric ring current model from ground stations data to interpret observed magnetic field disturbances
13 p2253 A69-27699

VLF morning and evening magnetosphere emission distinction by studying spectrum width as function of variations in K index
13 p2253 A69-27740

Geomagnetic pulsations and hydromagnetic wave propagation in magnetosphere, using geometric optics approximation
13 p2254 A69-28176

Magnetospheric corpuscular fluxes night ionization role in E and D region, considering precipitation from outside, trapped and dumped particles of radiation belts
13 p2254 A69-28333

Diurnal hemisphere auroras assuming origins in magnetosphere tail with pressure responsible for tail formation, discussing tentative model and implications
13 p2256 A69-28654

Magnetosphere boundary determined in two dipole model approximation, taking into account current layer in tail
13 p2256 A69-28686

Whistler dynamic spectra variation studies, emphasizing distorted magnetospheric geomagnetic field structure effect
13 p2257 A69-28702

Time dependent convection electric fields as agents for diffusing trapped magnetospheric radiation inward toward earth, discussing one dimensional diffusion equation
14 p2510 A69-28936

Low energy charged particle motion parallel with magnetic force lines analyzed in magnetosphere model with constant electric field
14 p2512 A69-29040

Pc 2-4 geomagnetic pulsations abrupt disappearance on global scale ascribed to magnetosphere boundary stabilization, noting interplanetary magnetic field role
14 p2438 A69-29080

Geomagnetic cut-off influence on charged particle dynamics in geomagnetic field, applying charged particle motion theories to magnetosphere fields
14 p2513 A69-29099

Magnetic field intensity, plasma pressure and energy density relations for macroscopic plasma motion inside neutral sheet from two dimensional model
14 p2440 A69-29119

Magnetic field variations in magnetosphere and interplanetary space correlated with polar magnetic disturbances from dynamic morphology data
14 p2441 A69-29387

Auroral substorms concept extended to include associated effects at all local times throughout magnetosphere, considering particle precipitation influence on substorms in midnight sector
15 p2593 A69-30008

Fermi acceleration of energetic electrons trapped within dipole magnetic field analyzed to obtain quantitative results for wave-particle interaction within complex magnetospheric configuration
15 p2594 A69-30095

Drift wave instability due to particle number density gradient of plasmapause, considering velocity shear modification
15 p2595 A69-30096

Magnetic storm principal phase explained by interaction between quasi-trapped particles stream and magnetosphere
15 p2675 A69-30743

Neutral point theory applied to solar wind and magnetospheric physics, discussing magnetic field reconstructions
16 p2846 A69-31596

Plasma flow pattern in twilight regions of earth magnetosheath from positive ion observations of twin Vela 3 satellites
16 p2773 A69-31961

Solar energetic proton penetration into magnetotail from proton data collected by Vela 4 energetic particle telescopes, comparing proton fluxes inside and outside magnetotail
16 p2847 A69-31966

Auroral absorption occurrence patterns mappable onto magnetotail developed as function of magnetic activity, discussing magnetotail neutral sheet source width changes
16 p2848 A69-31968

Micropulsation records for full moon effect on hydromagnetic emission activity of magnetosphere, noting W and Kp indices
16 p2774 A69-31979

Banded chorus, VLF discrete emissions in magnetosphere in single variable frequency band with frequency depending on equatorial electron gyrofrequency
16 p2774 A69-31981

Low energy solar protons entry into magnetosphere on 26 May 1967 showing diffusion control
16 p2849 A69-31984

Noise signals in earth magnetosheath interpreted as electromagnetic waves propagating in whistler mode
16 p2774 A69-31985

Charged particles equations of motion in earth magnetosphere in polar storms, considering auroral zone diurnal variations and electron and proton velocities
16 p2783 A69-32530

Trapped protons acceleration through bimodal diffusion in magnetosphere, noting spatial patterns and temporal behavior of proton and electron belts
16 p2851 A69-32618

Polar substorms resulting from interaction between magnetized plasma stream and geomagnetic field in magnetosphere
16 p2852 A69-32620

Heliosphere boundary location significance for Jovian magnetosphere configuration, considering inverse correlation between sunspot number and Jovian decametric radio emission
17 p3033 A69-33379

VLF and ULF whistler propagation in magnetosphere for remote sensing magnetospheric plasma parameters, exhibiting characteristic patterns and interaction with plasma
17 p2962 A69-33712

Physical model for IGY radio aurora data correlated with Brice magnetospheric convection model
18 p3125 A69-34231

Dawn-dusk electric field in outer radiation zone associated with magnetospheric plasma convection, comparing electron densities for magnetically quiet periods
18 p3128 A69-34942

Hydromagnetic whistlers propagation mechanism in magnetosphere determined by wave theory, assuming Gaussian radial density distribution and estimating duct width necessary for trapping
18 p3102 A69-34966

Relationship between micropulsation periods and size of magnetosphere expressed in power law form and interpreted with wave propagation
18 p3131 A69-35193

Plasma density in magnetosphere by measuring geomagnetic pi 2 micropulsations in direction related to polar aurora oval southern boundary, determining period of pi 2 oscillations
19 p3303 A69-36205

Geomagnetic field micropulsation observations by U.S.S.R. and possible applications to diagnostics of magnetosphere
19 p3304 A69-36642

Plasma flow structure near frontal point in earth magnetosphere, using quasi-hydrodynamic two dimensional model to obtain power series solution
20 p3594 A69-37019

Earth ionosphere and magnetosphere electrodynamic state analyzed as function of neutral gas small scale motions, considering magnetic disturbances and ionospheric discontinuities
20 p3519 A69-37026

Plasma concentration in nondipole magnetosphere model from pc 5 pulsations periods for high geomagnetic latitudes, noting solar winds effect
20 p3521 A69-37043

Small scale filament structure of current systems in earth magnetosphere, noting coherence of magnetic disturbances in conjugate regions
20 p3532 A69-37958

Equatorial semiaxis of magnetospheric tail at distances between 10 and 80 earth radii for various intensities of polar magnetic disturbances
20 p3532 A69-37959

Radial diffusion coefficient calculation in presence of magnetic shell splitting in magnetosphere
20 p3534 A69-38094

Venus magnetosphere induced by piling up magnetic field from solar wind due to ionospheric conductivity and collisions with planetary atmospheric particles
21 p3794 A69-38381

Magnetospheric electromagnetic phenomena explained by equations of motion for particle acceleration, forbidden regions and MHD processes
21 p3707 A69-38485

Auroral zone geomagnetic pulsations on nightside and dayside of earth related to magnetospheric substorm and particle precipitation
21 p3708 A69-38497

High latitude magnetospheric convection patterns determined from ionospheric current distribution using magnetic disturbance plots
21 p3709 A69-38503

Dungey reconnection model of magnetosphere with daytime current sheet and pseudotrapping region compared with dayside observations of precipitation regions
21 p3711 A69-38511

Jupiter magnetospheric radio emissions, discussing magnetic field and plasma-magnetic interactions
21 p3812 A69-39517

Auroral zone Birkeland currents in magnetosphere, analyzing particle trajectories for plasma sheet energy distribution and Alfvén layer position
21 p3792 A69-39567

Drift shell splitting in nondipolar distorted magnetosphere tested with data from electron spectrometer on ATS 1 and OGO 3 satellites
22 p4005 A69-40508

Cosmic ray proton cut-off increase at high latitudes during magnetospheric substorms, using balloon time observations of nuclear gamma ray flux
22 p4005 A69-40509

Daily variation of trajectory derived high latitude vertical cut-off rigidities in magnetospheric model consistent with proton and electron experiments
22 p4005 A69-40513

Horizontal and vertical magnetospheric electric fields measured by balloon, determining average field strength for quiet and active periods
22 p3939 A69-40514

Disagreement between Mariner 2 and IMP 1 data concerning interrelation between solar wind velocity and geomagnetism ascribed to instrumental errors and changes in magnetospheric properties
23 p4205 A69-41848

Magnetospheric stable charged particle beams for pearl pulsations and discrete VLF radiation in geomagnetic field, attributing synchronization to space charge
23 p4206 A69-41851

Magnetospheric natural toroidal oscillation periods solved by expression from perturbation method given by Landau and Lifshits where WKB method inapplicable
23 p4157 A69-41863

Interplanetary magnetic field role in interaction between terrestrial magnetosphere, solar plasma and solar flux energy transfer
23 p4214 A69-41865

Concurrent geomagnetic micropulsations at equatorial and high latitude stations, discussing magnetospheric sources of Pi and Pc types
23 p4161 A69-42439

Polar cap ionospheric response to solar cosmic ray events observed by Mariners 2 and 4 solar proton measurements used to test magnetosphere models
24 p4373 A69-43621

MAGNETOSPHERIC ELECTRON DENSITY

Atmospheric whistlers trajectories in magnetosphere calculated, assuming electron concentration as exponential function of altitude
08 p1309 A69-20429

Plasmapause, plasma sheet and energetic trapped electrons in earth magnetosphere, considering slot, peak intensity and trapping boundary
12 p2151 A69-26953

Van Allen radiation belts proton and electron components recorded by Soviet lunar probes and Cosmos and Elektron satellites
13 p2326 A69-27350

Diffusion of equatorial particles in outer radiation zone caused by expansions and contractions of permanently compressed magnetosphere, obtaining electric fields
14 p2510 A69-28937

Magnetospheric equatorial electron density profile estimated from midlatitude whistler observations, determining paths from dispersion data
15 p2677 A69-31357

Diurnal, seasonal and spatial variations in height and occurrence frequency of low electron density region below 3000 km
20 p3532 A69-37959

Electron intensities and substorm drift effects in outer radiation belt using two satellite technique
24 p4309 A69-43172

Magnetospheric electron sudden intensity increases correlated with magnetic substorms occurrence at midnight meridian from ATS 1 observation
24 p4367 A69-43173

Nighttime protonosphere thermal balance from Alouette 2 electrostatic probe measurements of electron temperature and concentration in magnetosphere
24 p4310 A69-43181

MAGNETOSPHERIC INSTABILITY

Plasma waves and particle interaction in nonuniform magnetic waves, considering propagation across sheets of steep density gradient and auroral precipitation
02 p0235 A69-11429

Perturbed geomagnetic field structure during magnetic storm recovery phase calculated by magnetosphere magnetic field model, accounting for various external field sources
02 p0237 A69-11666

Dispersion measurements and spectrum variations analysis to study pearl micropulsations frequency variation during sudden deformation of magnetosphere by magnetic storms
02 p0240 A69-11697

Geomagnetic field topology of nighttime magnetosphere, showing pi 2 pulsations excitation mechanism in terms of Alfvén waves resonance in external cavity
03 p0423 A69-13524

Drift periodic echoes in outer zone electron flux due to magnetospheric disturbance
05 p0815 A69-16259

Book on polar and magnetospheric substorms including daily variation data, satellite observations, etc.
06 p0915 A69-16832

Magnetospheric and high latitude ionospheric disturbances, bulk motion/convective/flow pattern and electric field distribution
07 p1128 A69-19370

VLF emissions intensity and spectra variations compared with energetic electron fluxes variations during magnetosphere storm periods
09 p1488 A69-21698

Real configuration effect of magnetic field in moderately perturbed magnetosphere on whistlers dynamic spectra, stressing geomagnetic perturbation detection
09 p1490 A69-21766

VLF polar chorus emission and geomagnetic variations caused by compressions or expansions of magnetosphere
10 p1681 A69-22803

Magnetospheric perturbations as aftermath of proton flare discovered by whistlers, noting plasmapause movement toward earth
10 p1683 A69-23776

Magnetospheric substorm as discharge process of associated electric current system, discussing relaxation processes, explosive release of energy, etc.
11 p1879 A69-25249

Perturbed geomagnetic field structure during magnetic storm recovery phase calculated by magnetosphere magnetic field model, accounting for various external field sources
13 p2257 A69-28697

Dispersion measurements and spectrum variations analysis to study pearl micropulsations frequency variation during sudden deformation of magnetosphere by magnetic storms
13 p2258 A69-28728

Magnetospheric plasma motion associated with Alfvén mode time fluctuations of magnetic field in solar wind
14 p2521 A69-29382

Severe magnetosphere distortions in north-south direction with parallel/antiparallel magnetosheath to magnetospheric field ascribed to solar wind property changes from Explorer 12 observations
18 p3128 A69-34947

Magnetospheric disturbances effect on radio wave propagation, discussing wave-particle interactions, VLF emissions and electrostatic waves
19 p3303 A69-36429

Transverse wave propagation and instabilities within magnetosphere, noting loss cone limited velocity-space distribution function
20 p3533 A69-38081

Polar upper atmospheric phenomena interpreted as magnetospheric substorm manifestations, discussing role of asymmetric ring current formation
21 p3710 A69-38504

Long time scale magnetodynamic noise in geomagnetic tail, discussing hourly ranges of fluctuations measured by IMP 1 satellite and planetary K index correlation
22 p3935 A69-39967

Magnetospheric instabilities and whistler mode turbulence relationship to loss of high energy electrons from Van Allen belts
24 p4306 A69-42692

MAGNETOSPHERIC PROTON DENSITY

Solar protons in magnetospheric tail after flare of July 7, 1966 with isotropic pitch angle distribution, expressing energy spectrum as exponential in rigidity
09 p1576 A69-21699

Pitch angle distribution function of thermal protons in magnetosphere taking into account earth gravitational field
12 p2067 A69-26354

Van Allen radiation belts proton and electron components recorded by Soviet lunar probes and Cosmos and Elektron satellites
13 p2326 A69-27350

MAGNETOSTATIC FIELDS

Electromagnetic fields and magnetic and dielectric constants in fiberglass reinforced polymers determined by treating polymers as ideal dielectrics

08 p1336 A69-20336

Unstable transverse potential oscillations in plasma with beam anisotropy and initial density modulation and analogy with known electrostatic oscillations

10 p1727 A69-23092

Cerenkov radiation from point charge uniformly moving along external magnetostatic field in warm anisotropic plasma, noting excitation modes and propagation frequencies

13 p2307 A69-27964

Plane TM surface waves supported by plane ungrounded magnetoplasma slab with magnetostatic field parallel to two parallel interfaces and perpendicular to propagation direction

13 p2308 A69-27966

Residual field in inner airspace of magnetostatic shielding thin walled stretched ellipsoids of revolution

13 p2237 A69-28610

Magnetic mirrors, Doppler and relativistic effects, wave attenuation and radiation pressure during gyroresonant particle acceleration in nonuniform magnetostatic and HF fields

14 p2499 A69-29845

Transverse wave-beam interaction propagation in fast wave structure in finite homogeneous magnetostatic field, deriving wave-beam equation for non-relativistic beams

21 p3672 A69-38435

Axisymmetric solutions of magnetohydrostatic equations for large conductivity media satisfying second order partial differential equation containing two arbitrary functions

21 p3778 A69-39498

MAGNETOSTATICS

Nonlinear DC magnetic fields for nonhomogeneous isotropic current free regions in presence of ferromagnetic materials, discussing analytic solutions of boundary value problems

11 p1888 A69-25311

YIG single crystal disk instability, noting dispersion of magnetostatic and plane spin waves from supplementary absorption and LF oscillations recording

21 p3783 A69-39561

MAGNETOSTRICTION

Pressure and magnetostriction effects on magnetization curves of type 2 superconducting In-Tl alloy, noting Ginzburg-Landau parameter stress dependence

02 p0294 A69-11776

Noncontacting torqueimeters using magnetoelastic properties of steel shafts, discussing gas turbine and industrial applications

[ASME PAPER 69-GT-64] 09 p1500 A69-22480

Flow instability of incompressible nonconducting fluid in thin cylindrical conducting elastic pipe in constant uniform magnetic field

10 p1798 A69-23094

Polycrystalline Fe-Ni, Fe-Ni-Co ferrites structure, magnetostriction, magnetization curves and hysteresis prior and after thermomagnetic treatment

13 p2319 A69-27992

Magnetothermoelasticity equations, uniqueness and reciprocity theorems and solutions emphasizing moving media

15 p2715 A69-31215

Choke coil magnetoelastic sensors thermal stability found decreasing proportionally to measurement range decrease /below 100 newtons/

23 p4166 A69-41995

MAGNETOTELLURIC PROFILING

U GEOMAGNETISM

U MAGNETIC SURVEYS

MAGNETOVARIOMETERS

U VARIOMETERS

MAGNETRONS

Magnetron ionization gauge in helium for low pressure measurement, discussing striking characteristics and time lags

01 p0012 A69-10606

Voltage tunable magnetron used in conjunction with ferrite circulator as phase locked amplifier

01 p0045 A69-10632

Permanent magnets used in conjunction with magnetrons, crossed-field amplifiers, klystrons, traveling wave tubes and microwave ferrite devices

[IEEE PAPER 2.3] 01 p0045 A69-10713

Linear analysis of operation of multistage magnetron amplifiers using injected electron flux and stepwise varying dimensions of interaction space

03 p0407 A69-13977

Output power, efficiency and gain of two stage magnetron-type cascade amplifier

03 p0407 A69-13978

Back bombardment of magnetron cathode as single surface multipactor, noting effects of cathode grooves and output loading

07 p1101 A69-18656

X band internal cavity voltage tunable magnetron operating in theta mode, solving output loading, interaction limitations and cavity dimensions

07 p1102 A69-18670

High power voltage tunable magnetron, discussing operating characteristics, life and applications

13 p2232 A69-28056

Frequency distribution and statistical characteristics of high level RF noise produced by high permeance electron beam of magnetron injection gun/MIG/

14 p2449 A69-29558

Bent beam ionization gage linearity from calibrated nude Modulated Bayard-Alpert /MBA/ gage, discussing buried collector and tabulated magnetron gages

22 p3950 A69-41216

MAGNETS

NT CRYOGENIC MAGNETS

NT ELECTROMAGNETS

NT HIGH FIELD MAGNETS

NT SUPERCONDUCTING MAGNETS

Permanent magnets used in conjunction with magnetrons, crossed-field amplifiers, klystrons, traveling wave tubes and microwave ferrite devices

[IEEE PAPER 2.3] 01 p0045 A69-10713

Permanent magnets optimal design and properties for attitude control of German research satellite Azur, considering environmental influences

16 p2868 A69-31936

Electromagnetic vibration exciters based on permanent magnet and AC coil interaction

16 p2790 A69-32077

MAGNITUDE

Radio galaxies radio luminosity function expressed by means of power dependence, assuming three absolute visual magnitudes for each galaxy

02 p0325 A69-12563

Magnitude data for Saturn satellites compiled and analyzed, noting discrepancy for Iapetus

08 p1394 A69-20619

Cepheid variable stars light curves analyzed to determine radii and absolute magnitudes

10 p1775 A69-23200

Improved extraatmospheric wideband sensor nominal S-4 magnitudes of bright stars observed with narrowband UVBRI filter-sensor combinations

11 p1960 A69-24853

Quasi-stellar objects anomalous Hubble plot, suggesting explanation for steeper plot under assumption on red shift vs apparent magnitude relation

15 p2701 A69-31536

MAGNONS

Magnon density of states of ferromagnetic gadolinium trichloride in magnetic field, using high resolution optical spectroscopy

03 p0494 A69-14257

Anisotropic Heisenberg antiferromagnetism in spin wave approximation, calculating thermodynamic quantities in terms of elliptic integrals

12 p2144 A69-26500

Electron magnon interaction in ferromagnetic and antiferromagnetic semiconductors, showing conduction band and electron effective mass and magnetic moment dependences on temperature and spin direction

14 p2504 A69-28991

Theory of temperature dependent magnon energies in antiferromagnets based on spin wave operator expansion of Hamiltonian, taking into account dynamical interaction between waves

15 p2668 A69-30684

Time dependent Green function method for pre-mature saturation due to parametric amplification of nonuniform spin wave modes by one and two magnon processes

15 p2668 A69-30685

Parametric excitation of spin waves during parallel pumping of rubidium nickel fluoride ferrite, relating relaxation time and temperature

21 p3781 A69-39069

YIG single crystal disk instability, noting dispersion of magnetostatic and plane spin waves from supplementary absorption and LF oscillations recording

21 p3783 A69-39561

MAGNUS EFFECT

Normal and negative Magnus force experienced by rotating cylinder in air flow, discussing wind tunnel tests, laminar and turbulent boundary layers separation, pressure distribution, etc

17 p2958 A69-34213

Stability conditions determination for spinning projectile based on ballistic equations, discussing role of Magnus effect

21 p3772 A69-39294

MAIN SEQUENCE STARS

Stellar evolution, discussing stellar structure, pre- and post-main sequence evolution, solar system origin, supernovae, white dwarfs, variable stars and close binaries

01 p0148 A69-10046

Late type stars, discussing main sequence for Population I and Population 2 stars and ages and chemical composition of old galactic clusters and globular clusters

01 p0158 A69-11325

Revision of RCU photometry fundamental data, noting main sequence curve position of O-B5 and distinction between zero age main sequence and class V

03 p0514 A69-13963

Empirical relation between /B-V/ color and radiation temperature by observing eclipsing variables undergoing total eclipses

03 p0469 A69-13964

Mass exchange and evolution of close binaries /Main Sequence stars/

04 p0653 A69-14614

Spectrum of accelerated particles on surface of stars revealed by observation of photospheric lithium and beryllium

05 p0817 A69-16711

Homogeneous main sequence star models with convective cores, considering core chemical composition, size and energy generation ratio mechanism

05 p0829 A69-16777

Stellar element abundance ratios determination using relative strengths of molecular lines or bands

06 p1003 A69-17320

Dynamical stability in premain sequence stars, discussing adiabatic models for pure hydrogen composition and collapse initiation by low opacity

07 p1220 A69-19388

Rapid differential rotation effect on massive main sequence O and B stars, discussing bolometric magnitude deficiencies and shifted position in Hertzsprung-Russell diagram

07 p1220 A69-19390

Curve-of-growth abundance analysis for main sequence lambda Bootis stars, suggesting type Ap star characteristics

08 p1385 A69-20062

Convection inhibition effects on premain sequence evolution of solar mass star, discussing largely radiative models

08 p1386 A69-20088

Binary stars systems with same total mass calculated for evolution from main sequence stage through mass exchange to white dwarfs

08 p1393 A69-20569

Atmospheric models for metal deficient stars of K and G spectral type, studying reduced metal abundance effect on atmospheric structure

09 p1596 A69-22055

Distance of bright stars in Cepheus OB2 region by MK spectral classification and UVB photometry, noting early main sequence and supergiant stars

09 p1599 A69-22194

Stellar models for Population II lower main sequence stars, discussing uncertainties in radii and bolometric magnitude

09 p1601 A69-22214

Absolute dimensions of 34 eclipsing variables having both components near main sequence, comparing mass luminosity and mass spectrum to homogeneous model stars

11 p1952 A69-24248

Physical structure of convective envelopes of population II main sequence stellar models by mixing length theory, emphasizing hydrogen molecule formation and pressure ionization

11 p1961 A69-25109

Statistical data for visual binary systems with known spectral classes or colors and one component near main sequence

12 p2159 A69-26666

Linear oscillation modes of premain sequence star model of pure hydrogen composition with variable specific heats ratio, discussing dynamic instability of polytropes

13 p2336 A69-27449

Line absorption effect on opacity and main sequence model stars noting luminosity, radius and mass of convective core

13 p2340 A69-27578

Flare star astrometric study to determine possible variable proper motion

13 p2348 A69-27810

Lithium depletion in main sequence stars of one solar mass, suggesting e-folding time scale indicated by Coma Cluster data

14 p2517 A69-29089

Optical depths of convection related to metal deficiency for main sequence and giant stars

14 p2527 A69-29946

Photoelectric index of main sequence stars in F5 to G2 spectral range, as indicator of atmospheric microturbulent velocities

15 p2695 A69-30999

Equilibrium models reliability for main sequence stars estimated from systematic applications of physical assumption sets and numerical methods

16 p2859 A69-32219

Microturbulent velocities of A and F stars observed for reciprocal effective temperature range

17 p3039 A69-33729

Masses of visual binaries above main sequence with published orbits determined as function of position in H-R diagram, using spectroscopic parallaxes

18 p3195 A69-34429

Balmer line spectrum formation in extended atmospheres of Be and shell stars, noting influence of angle of inclination to observer

18 p3204 A69-35349

Fluxes and luminous efficiencies tabulated for main sequence and subgiant stars within reflection effect problem in eclipsing binaries and Chandrasekhar non-gray atmospheric models

20 p3600 A69-37479

Stellar mass loss in gravitational contraction and variation of rotation law during transition to main sequence

20 p3607 A69-38041

Main sequence star models for diverse solar masses, covering hydrogen burning phase in core and conditions for dynamic instability and mass exchange

23 p4208 A69-41286

Eclipsing binaries spectroscopic and photometric data compared to Iben and Horn models of main sequence stars, noting stellar mass effects

23 p4208 A69-41287

MAINTAINABILITY

Weightless simulators effectiveness for obtaining space systems maintainability criteria, using non-parametric experimental design for performance data

06 p0882 A69-17648

Spacecraft onboard checkout systems and design of ground support equipment and software, noting adaptive dynamic analysis and maintenance /ADAM/ concept

[AIAA PAPER 69-307] • 09 p1478 A69-22382

Digital computer simulation as maintainability design and prediction tools, discussing fault localization in complex electronics systems

10 p1668 A69-22974

Probability of completing countdown in single malfunction encounters, considering development of industry and government guidelines

10 p1792 A69-22979

Saturn 5 holddown and service arm electrical system design program optimized by integrating reliability and maintainability at initial design phase

[AIAA PAPER 69-309] 10 p1670 A69-23043

Automatic support systems for advanced maintainability - IEEE Conference, St. Louis, November 1968

11 p1863 A69-25059

Military systems trouble documentation and evaluation, emphasizing computerized monitoring of reliability and maintainability

15 p2722 A69-31121

Computerized Markov effectiveness models of repairable and nonrepairable complex aerospace systems

18 p3195 A69-34527

Equipment maintainability demonstration technique, discussing simulation, repair time rates mathematical distribution, range and limits

18 p3117 A69-34530

Strapdown inertial reference unit system for inflight reliability and maintainability, discussing design and components

19 p3370 A69-35803

Reliability and maintainability - Conference, Denver, July 1969

19 p3324 A69-35999

FAA ARTS-III terminal air traffic control system reliability and maintainability, discussing module addition

19 p3370 A69-36000

Microelectronics role in maintenance and maintainability of subminiature solid state components, emphasizing functional packaging at module level

19 p3283 A69-36021

Maintainability and maintenance analysis in managing integrated logistic support /ILS/ system

19 p3455 A69-36035

System effectiveness for reliability and maintainability achievement, analyzing people, organizations, value systems and accomplishment criteria in development program

19 p3455 A69-36044

Maintainability as design requirement in system specifications and contracts, noting MIL-STD-471 program of maintainability demonstration tests

20 p3551 A69-38268

Book on maintainability principles and implementation methods covering program implementation, quantitative factors, maintenance concept, tradeoff techniques, design liaison, etc

21 p3734 A69-39815

DC-10 aircraft CF6 engine thrust reverser and spoiler design features impacting operational characteristics, maintainability, noise reduction, structural concept, control and actuation system

[SAE PAPER 690411] 23 p4200 A69-41639

Monitoring devices and modular construction features of Rolls-Royce RB.211 three shaft turbofan engine, discussing maintainability

24 p4321 A69-43112

MAINTENANCE

NT AIRCRAFT MAINTENANCE

NT SPACE MAINTENANCE

Mathematical model constructed for behavior of multicomponent system subject to cannibalization

01 p0086 A69-10651

Maintenance practices for rigid concrete pavement of runways including joint and crack sealing and patching, considering necessary surface preparation and equipment

01 p0057 A69-11277

Reliability of operational satellite systems consisting of two single purpose satellites in interchangeable orbits, discussing outage and replacement

02 p0333 A69-11805

Automatic preventive maintenance program for hybrid computer system by checking individual units

04 p0568 A69-15359

Diagnostic techniques development to test and perform preventive maintenance on hybrid system

04 p0568 A69-15360

Nonreplicative self repairing control, describing prototype computer construction for testing feasibility

04 p0569 A69-15457

Resin bonded glass cloth for large airframe structures rectification

06 p0931 A69-17713

Maintenance process simulation for engine and major components to provide routine material usage forecast and policies

09 p1503 A69-21802

Group relative values for system criteria, showing application to illustrative maintenance criteria

10 p1668 A69-22973

Maintenance van loading technique for number of spares and test equipment in Minuteman weapon system for uncommissioned launch facilities at minimum cost

10 p1669 A69-22980

Spare kit evaluation model for problems with constraints on spare parts quantities, considering optimization and simulation routines for weapon system maintenance

10 p1669 A69-22981

High speed automatic test sets and rapid repair procedures under adverse conditions for individuals of relatively low technical skill

11 p1851 A69-25063

Modular designed automatic test system consisting of central computer controlled system with multiplexed remote test stations for depot level maintenance

11 p1864 A69-25067

Single purpose, multipurpose and multistation automatic test systems for production and maintenance

11 p1864 A69-25068

USAF Logistics Command /AFLC/ Missile Fleet Status Tool /MSFT/ for monitoring and control of Minuteman guidance and control system

11 p1865 A69-25073

Reliability improvement influence on life cycle costs of high volume piece of military/commercial equipment

12 p2101 A69-25848

Models for cognitive behavior and psychomotor behavior for maintenance tasks

12 p2025 A69-27086

Value engineering proposal costs sustained by maintenance and overhaul industry in government contract negotiations, discussing reimbursement and proposed central agency

13 p3283 A69-28099

Long life repairable equipment reliability and mean time between failure with limited life components and material in normal life maintenance environment

15 p2581 A69-31134

Equipment life cycle costs computer simulation for design and changes evaluation, including maintenance analysis example

15 p2723 A69-31138

Automated patching system design for analog and hybrid computers to reduce number of switches required

16 p2756 A69-32551

Life cycle maintenance costs reduction in aerospace industry by computers, describing on-line and off-line test systems

17 p2979 A69-33649

Airborne electric power systems maintenance aids, describing design and operation of annunciator for establishment and display of system failure causes

17 p2905 A69-34112

Steady state availability of system with limited repairable spares for online units, considering statistical dependence among similar units

18 p3144 A69-34493

Mean-time-to-repair of complex systems with consideration for repair policies and number of repairmen, noting application to systems reliability engineering

18 p3144 A69-34494

Reliability measurements based on maintenance records, considering human factor and life limiting and random chance design

19 p3327 A69-36013

Microelectronics role in maintenance and maintainability of subminiature solid state components, emphasizing functional packaging at module level

19 p3283 A69-36021

Availability measure defined in terms of maintenance demand rate and mean downtime for cost prediction involving various parameters

19 p3327 A69-36036

Electron beam welding for repair and production, discussing application to Ti VHF antennas, Concorde switchgears and nuclear reactor loading tubes [SBAC PAPER 14]

20 p3550 A69-37451

Probability theory applied to age and block replacement models in preventive maintenance of parts, noting inspection cost distribution

20 p3551 A69-38267

Bayesian estimate of individual truck maintenance costs based on optimum replacement maintenance age

23 p4241 A69-41577

Gas turbine engine problem causing component failures, considering alternative replacement strategies

24 p4318 A69-42774

Damage repair techniques of polyimide honeycomb sandwich panels constructed with polyimide and T face sheets, using precured plugs, prepreg disks, sealants, etc

24 p4323 A69-43420

MAJORITY CARRIERS

Photoluminescence measurement of distribution of majority carrier concentration in GaAs

03 p0489 A69-13893

Majority and minority carrier trapping in neutron irradiated Si diodes, measuring transient junction capacitance recovery

06 p0975 A69-18869

Majority carrier concentration changes in P-doped n-type Si during fast electron bombardment, discussing relative effect of A and E centers

07 p1199 A69-18684

Photoluminescence measurement of distribution of majority carrier concentration in GaAs

11 p1939 A69-25694

Majority carrier lifetime temperature dependence obtained from photoconductivity measurements of p-type GaAs crystals doped with Ge

15 p2666 A69-30056

MALES

Space flight hypokinesia simulation experiments to study oxygen balance in man

10 p1646 A69-23507

MALFUNCTIONS

- Reliable computation in computing systems designed from unreliable components, considering two models for component malfunctions
04 p0569 A69-15456
- Jet aircraft engines condition monitoring system for detecting malfunctions without engine disassembly [ASME PAPER 69-GT-66]
09 p1501 A69-22518
- Probability of completing countdown in single malfunction encounters, considering development of industry and government guidelines
10 p1792 A69-22979
- Reliability functions and cycles number before breakdown of finite automaton with account of randomness of malfunctions, structure and input signal distribution
13 p2224 A69-27250
- Finite automaton malfunctions, discussing input sequences construction and output sequences analysis for malfunction subsets recognition
13 p2239 A69-28536
- Electronic systems packaging substitution method for optimized malfunction isolation at succeeding levels to final discard-at-failure
14 p2420 A69-29494

MALKUS THEORY

- Minimum Reynolds number and Malkus theory of turbulent channel flow, discussing stability, equilibrium flow, and stationary turbulence via variational theorem
17 p2957 A69-33764

MAMMALS

- NT BABOONS
- NT CATS
- NT CHIMPANZEES
- NT DOGS
- NT GROUND SQUIRRELS
- NT GUINEA PIGS
- NT HAMSTERS
- NT HUMAN BEINGS
- NT MICE
- NT MONKEYS
- NT POCKET MICE
- NT RABBITS
- NT RATS
- NT RODENTS
- Pharmacological tools in autonomic nervous system research, discussing norepinephrine biosynthesis, storage, release and inactivation in mammals
02 p0200 A69-12722
- Mammalian radiobiological studies of effects of heavy particles, discussing therapeutically advantageous characteristics
03 p0374 A69-13499
- Uptake, metabolism and enzymatic synthesis of adrenaline in mammalian brain
07 p1066 A69-19260
- Noble gases effect at low pressures on O consumption by mammalian tissue, noting Xe, Kr, N and nitrous oxides effect on rat liver
19 p3258 A69-36454
- Electrophysiological data for directionally sensitive units in optic tectum of mammals, indicating midbrain as site for rotating spiral motion aftereffects
20 p3480 A69-38264
- Mammalian pineal gland as neuroendocrine transducer, studying melatonin role in ovulation, gonadal growth, etc
20 p3480 A69-38284
- Mammalian brain epinephrine metabolism data after isotonic saline perfusion into cranial vasculature
21 p3650 A69-38323
- Carbon monoxide displacement rate of oxygen from combination with oxyhemoglobin solutions from human adult and fetal, horse, goat, dog, cat and rabbit
21 p3650 A69-38384
- Cytoplasmic and ciliary connections between inner and outer segments of mammalian visual receptors
22 p3881 A69-40857

MAN

U HUMAN BEINGS

MAN MACHINE SYSTEMS

- Man machine relationship in V/STOL control display, discussing inflight simulators, emphasizing NASA X-14 and CH-3C programs
01 p0010 A69-10452
- Probabilistic Information Processing System using men and machines to perform diagnostic information processing and to guide decision making
01 p0037 A69-10954
- Manual control using matched manipulator technique, noting control task complexity decrease and improved performance
02 p0202 A69-11951

- Large scale information displays for group sharing in air traffic control, military operations and organization management
02 p0250 A69-12159
- Research center for investigating man/computer interaction, discussing display systems, computers, languages and data entities
04 p0566 A69-15342
- Multilevel modeling structure for interactive computer graphic design, discussing conversational display manipulation program and interconnection with analysis program
05 p0724 A69-16381
- Computer graphics and manufacturing, discussing man computer system for transformation of blueprint to numerically controlled machine tape with no time delay
07 p1089 A69-19741
- Computer aided design methods for electronic and mechanical materials, discussing basic concepts and problems
08 p1278 A69-19971
- Human engineering program at early design phase of SST aircraft to achieve maximum human efficiency and man machine compatibility
09 p1447 A69-22546
- Roll-motion cues for man-vehicle control in compensatory tracking task with disturbance input
10 p1650 A69-23879
- VTOL aircraft flight control systems, considering computerization and automation approach with human pilot serving as monitor and emergency system
11 p1823 A69-25387
- Man machine integration, detailing sensory input and motor /or output/ systems, control loop and social structure impact
11 p1831 A69-25656
- Human operators instrument-monitoring behavior noting optimal control, information processing, physical limitations, etc
12 p2022 A69-25929
- Polarity coincidence correlation method due to random processes state characterization applied to man machine systems
12 p2022 A69-25931
- Traditional flight crew organization relevance to current and developing flight systems, discussing inadequacies, anachronisms and safety threats
12 p2023 A69-26555
- Man machine model for prediction of human control behavior, generating model from analysis of helicopter pilot tasks
12 p2025 A69-27082
- Complex piloting simulation including fatigue for optimizing man machine synergy, emphasizing human adaptability and computer precision and speed
12 p2025 A69-27083
- Mathematical models of human performance in man machine systems, discussing operations research, maintainability and real time computer simulation for command and control systems
12 p2025 A69-27085
- Computer simulation models for prediction of individual and crew performance in man machine environments
12 p2026 A69-27087
- Man machine interactive structural analysis using digital computer with CRT display, detailing design
12 p2035 A69-27098
- Ergonomics and aviation medicine, discussing biotechnological aspects of information in man machine systems and observation tasks
17 p2915 A69-33770
- Problem-oriented languages in man-computer intercommunication
18 p3106 A69-34658
- Man-computer speech communication, discussing model and aspects of acoustics, phonetics, linguistics, language training, physiology, psychology, bionics, etc
18 p3107 A69-35099
- Tremographic studies of central nervous system during supersonic flight as engineering psychology application to man machine relations in aircraft-spacecraft industries
19 p3259 A69-35834
- Man machine interface problems in C-5 equipment and system design
19 p3261 A69-36024
- Man machine modeling technique for establishing personnel performance requirements, discussing field tests
19 p3261 A69-36025

- Controlled-variable prediction display based on Taylor series computation, describing acceleration system simulator and human operator performance
19 p3313 A69-36414
- Human operator decision making in vehicle manual control, considering success likelihood and possible outcome costs based on signal detection model
20 p3482 A69-37720
- Computer aided data interpretation system converting ionograms to vertical electron density profiles
20 p3504 A69-37866
- Multistable logic circuitry with 10 stability levels based on phased pulse principle, noting efficiency and complexity in man machine interface
21 p3686 A69-39065
- Man-computer interactive Terminal Interface System /ITIS/ compatible for programming graphics, character scopes and typewriter using FORTRAN [AIAA PAPER 69-955]
22 p3905 A69-40337
- SST flight crew operational requirements to achieve maximum human efficiency and man/machine compatibility, discussing pilot role, advanced flight instrumentation, etc
23 p4107 A69-41820
- Flight indicators monitoring by pilots, describing physiological and psychotechnical criteria for dials and clocks arrangement to improve efficiency
23 p4108 A69-41827
- Head-Up Display /HUD/ incorporated with autopilot for human participation in flight control for all-weather operation
23 p4109 A69-41871
- Man-machine /semiautomatic/ control for optimal decision making, discussing automatic control disadvantages and limitations, multilevel system hierarchical structures, three level models, etc
23 p4112 A69-42443
- Man machine systems - IEEE Conference, Cambridge, England, September 1969
24 p4273 A69-43014
- Human sciences contribution to man-computer interaction based on review of relevant human factors literature
24 p4273 A69-43015
- Man-computer interaction problems for human factors research, considering conversational languages development and evaluation, use patterns and interaction modeling
24 p4274 A69-43016
- Decision process model for man-machine decision task structuring by system designers
24 p4274 A69-43018
- Basic task archetypes in man-computer problem solving including detection, planning, optimization, designing, etc
24 p4274 A69-43019
- Manual vehicle control analysis based on feedback systems analysis and mathematical models for human operators engaged in control tasks
24 p4274 A69-43021
- Adaptive manual control rapid variation determined by input, controlled element, task and programmed adaptation systems, discussing human strategy changes
24 p4274 A69-43022
- Ergonomic study of experimental tests design for comparing equipments efficiency with man
24 p4275 A69-43023

MANAGEMENT

- NT CONFIGURATION MANAGEMENT
- NT CONTRACT MANAGEMENT
- NT PROJECT MANAGEMENT
- NT WEAPON SYSTEM MANAGEMENT
- Industrial loyalty and trade secrets, discussing preservation of forms of intellectual property posed by mobile employee and management policies
01 p0180 A69-10991
- Adaptation process of management systems from point of view of control system philosophy [AIAA PAPER 68-807]
08 p1422 A69-20197
- Structure and scoring method for judging alternatives in contract selection
20 p3640 A69-38023
- Programmatic constraints on onboard processing of data collected by payload sensors [AIAA PAPER 69-942]
22 p3904 A69-40325

MANAGEMENT PLANNING

- Human factors in aircraft systems, discussing personnel selection throughout design and manufacturing phases
01 p0019 A69-10449
- National space program management, discussing NACA and NASA, lunar mission planning, procedures and program flexibility and responsibility
01 p0178 A69-10468

Cost prediction equations used in perturbed environment of learning curves subjected to design change in industry

01 p0180 A69-10652

Systematic approach to standard launch vehicle based on governmental expenditure minimization while attaining mission goals

01 p0162 A69-11096

Long range management forecasting by Delphi technique, describing expert panel selection, composite group replies and successive revisions

01 p0180 A69-11250

Survival of PERT/Cost technique without government impetus noting advantages for planning, monitoring and controlling technical performance objectives

01 p0180 A69-11251

Aerospace management technology transferability to problems of society and government

02 p0355 A69-11754

Large scale information displays for group sharing in air traffic control, military operations and organization management

02 p0250 A69-12159

Project management in complex research, discussing incentive contracting decision model and resources allocation

02 p0356 A69-12476

Aerospace research and development projects selection and planning for success in manufacturing competition

03 p0393 A69-13252

Aerospace company engineering administration criteria and functions for chief project engineer [SAE PAPER 680682]

03 p0535 A69-13447

Aerospace manufacturing contribution to engineering function in design development [SAE PAPER 680668]

03 p0433 A69-13451

Research and development project selection and planning, outlining system to identify capabilities contributing to increasing success probability

03 p0535 A69-13552

Book on economic management of research and engineering covering project plan impact, projects control and evaluation of research and engineering structure

04 p0688 A69-14530

Elasticity of demand theory applied to fare changes effect on passenger volume, noting interdependence of aircraft size and fare formulation

04 p0689 A69-14805

Cost dependent utility characteristics in mathematical model for optimum research and development resource allocation, computing optimum fund distribution with Lagrange multipliers

04 p0689 A69-14807

Predictive model for risk in technological research and development

04 p0689 A69-14980

Graphical evaluation and review technique /GERT/ in R and D project planning processes

04 p0689 A69-15100

Product development process diagram, systems engineering checklists and program plankit as devices to assist product manager [ASME PAPER 68-WA/MGT-3]

05 p0850 A69-16146

Statistical analysis of aircraft programs engineering man hours, aircraft performance and weight, avionics systems, schedules, etc, as estimating standards

05 p0769 A69-16239

Computer use evaluation, discussing standards for automatic data processing /ADP/ investment and operations

05 p0850 A69-16299

Cost and schedule planning and control /CSPC/ project progress reporting technique

05 p0850 A69-16300

Technological forecasting role in company growth planning via Delphi technique

06 p1044 A69-17871

Electromagnetic interference /EMI/ created by noise coupling through conductive paths, discussing responsibility for control within systems management

07 p1079 A69-18944

Management control systems, discussing malfunction, inefficiency and needs of human elements

07 p1244 A69-18963

Organization behavior models compared in theory of scientific and professional personnel management, noting compromise between excess restrictions and freedom [AIAA PAPER 68-805]

08 p1422 A69-20196

Transport aircraft fleet management and handling of mechanical and avionic machine defects using operations research

08 p1422 A69-20626

Defense project management and discrepancies between estimates and final costs

08 p1423 A69-20628

Cost control for project management based on detailed programming

08 p1423 A69-20629

Project control cycle, cost monitoring and reporting to management

08 p1423 A69-20630

Decision oriented automatic data processing systems design, noting quantity and quality of upward directed information to management

08 p1423 A69-20733

U.S. Army Materiel Command R and D planning structure and technical planning processes influence on decisions improvement

08 p1423 A69-21153

Organization and manpower utilization in R and D, determining criteria for organizational form selection

08 p1423 A69-21155

Statistical approach to design and management, discussing multiple regression analysis, attributes, intuition, probability, simulation and applications

08 p1344 A69-21162

NASA long range planning of primary electric propulsion for automated space program [AIAA PAPER 69-247]

09 p1565 A69-21251

Incentive provisions used by mutual agreement between purchaser and contractor for project management covering planning, control, financial, technical and personnel functions

09 p1626 A69-22777

Maintenance van loading technique for number of spares and test equipment in Minuteman weapon system for uncommissioned launch facilities at minimum cost

10 p1669 A69-22980

Federal Government budgeting, discussing systems analysis, planning-programming, etc

10 p1811 A69-23351

Federal Government policies analysis, discussing advantages of planning-programming-budgeting system /PPBS/

10 p1811 A69-23353

Potential hazards of government sponsored technology, examining SST and fluoridation projects and weather problems

10 p1811 A69-23392

Airport operation and administration, discussing supply, costs, tariffs, etc

10 p1811 A69-23602

Statistical, economic and psychological aspects of aeronautical and astronautical profitable reliability in relation to operation, using mathematical model

10 p1700 A69-23839

Design management in next century covering computer methods, market needs, etc

11 p2004 A69-24371

Operational research applications to management problems, discussing specific airlines operations cases

11 p1822 A69-24377

Management training goals and methods for executive development, comparing effective and ineffective programs

11 p2005 A69-25305

Reliability planning role in directing business functions to quality efforts integration in engineering, production and testing of electronic equipment

12 p2102 A69-25971

Research and development organizations under pressure of corporate assessment and systems management approach, suggesting core-technology structure and training

12 p2192 A69-26732

Intracompany research and development, noting separate philosophies approach

12 p2192 A69-26733

Financial, political and engineering considerations influencing space flight programs implementation, including nuclear systems examination for propulsion and power capability

13 p2334 A69-27296

Air Canada flight safety system including company philosophy, safety activities, incident and accident handling and information schemes

13 p2201 A69-27541

Value engineering ultimate objectives in industry, discussing engineering and procurement role in prorating goal to applicable departments

13 p2383 A69-28101

Management and control techniques for aircraft product engineering changes [ASME PAPER 69-DE-67]

14 p2540 A69-28850

Urban noise control over transportation systems including aircraft and highway traffic operating beyond local noise ordinance purview

14 p2541 A69-29157

Cost estimates of R and D, considering planned profit and loss following products introduction to market

14 p2541 A69-29280

Capital budgeting for R and D, discussing control of rising costs

14 p2541 A69-29281

Procurement procedures in management planning, discussing document flow charts, contract negotiation, etc

15 p2719 A69-30314

Independent testing laboratory management, outlining requirements specialized to fit continued growth conditions

15 p2720 A69-30402

Defense integrated management engineering system at California Naval Air Rework Facility

15 p2588 A69-30427

MACRO /methodology for allocating corporate resources to objectives/ for R and D, discussing program for optimal budget management

15 p2720 A69-30958

Heuristic methods to determine scientific activities planning emphasizing problem definition, purposes, possibilities of solution and difficulties

15 p2720 A69-30969

Research and development planning and control models based on subjective probability estimates for failing projects identification

15 p2721 A69-31072

Behavioral differences between engineers and scientists with reference to work environment

15 p2721 A69-31073

Characteristics, incentive and promotional patterns and work adjustment of engineering technicians

15 p2723 A69-31242

Book on space age management, considering large scale approach

16 p2881 A69-31766

Civil aircraft requirements from 1975 onward, discussing classes, categories and R and D

16 p2882 A69-32022

Motivation and performance increase in R and D by incentive plans, discussing prestige, power, responsibility, recognition, work, salary, comfort, etc

17 p3075 A69-32963

Research productivity in large organizations stressing interface problem minimization, recommending deferred bonus system

17 p3075 A69-32964

Research management differences between European and American corporate structures, discussing cultural differences, cost comparisons, social mobility, etc

17 p3075 A69-32965

Space program design, discussing NASA centers and NASA R and D life sciences, technological developments and federal action

17 p3076 A69-34042

R and D for economic growth, discussing interaction between management, planning, engineering, marketing, production, customers and competitors

17 p3077 A69-34126

Technology or Research Quantitative Utility Evaluation /TORQUE/ system genesis and operation, with implications affecting R and D

17 p3077 A69-34130

Technical and operational planning activities of airline resulting from airport restrictions in terms of congestion, performance and noise and runway strength

17 p2948 A69-34206

All-weather operations, aircraft size, air traffic and noise as airport design factors, discussing financing priorities for runway construction, facilities and personnel

17 p3004 A69-34207

Reliability tasks vs product reliability, discussing differences in effectiveness and management programming

18 p3143 A69-34484

Apollo project by-products, emphasizing NASA project management methods application to large R and D projects

18 p3233 A69-34649

Cost risk management procedure in defense industry contracting, including risk percent limits and identification in proposals, specifications relief, escalation clauses, etc

18 p3233 A69-34655

Expected occurrences mathematical model for flight system availability under uncertainty

18 p3210 A69-35083

Aerospace management technology transfer, discussing conceptual contributions, planning, administrative and evaluation methods 18 p3236 A69-35086

System approach to reliability demonstration, discussing design and impact on levels, risks, requirements, testing, cost and incentives 19 p3327 A69-36003

Optimized contracting for systems engineering management, discussing industry views, scope, application, depth, procurement and performance measurement 19 p3454 A69-36005

Systems effectiveness function from project and organization management viewpoint 19 p3454 A69-36006

R and D program risk evaluation methodology in density functions form for program goals probabilities, noting random variables as parameters 19 p3455 A69-36008

Maintainability and maintenance analysis in managing integrated logistic support /ILS/ system 19 p3455 A69-36035

System effectiveness for reliability and maintainability achievement, analyzing people, organizations, value systems and accomplishment criteria in development program 19 p3455 A69-36044

Stochastic model for estimating manufacturing costs, discussing Mellin and Laplace transforms and Gram-Charlier series approximations 20 p3633 A69-36924

Delphy technique of technological forecasting used for R and D planning 20 p3639 A69-37353

In-house research on R and D management in government agencies, discussing manning, training, center programs, case studies, etc 20 p3640 A69-38022

U.S. space program since establishment in 1958, NASA mission successes and management systems for future projects 20 p3641 A69-38116

Launch vehicle cost reduction by minimizing software, fabricating in commercial shops and avoiding sophistication, parts and acts of man 21 p3857 A69-39688

Book on maintainability principles and implementation methods covering program implementation, quantitative factors, maintenance concept, tradeoff techniques, design liaison, etc 21 p3734 A69-39815

Civil cargo aircraft characteristics and development trends, discussing cargo and passenger traffic management, communications network, etc 22 p3863 A69-40427

Complex program management emphasizing systems engineering management, noting applications to aeronautical systems [RAES PAPER 9] 22 p4053 A69-40489

Airline management service to cockpit team for safe operation providing safety information sources and transmission channels and undesirable trend detection and correction 22 p4054 A69-41149

Airline economics long term trends requiring management tools for cost control, operations simulation and monitoring, computer use and information data processing [SAE PAPER 690414] 23 p4241 A69-41641

Management activities related to economics of failure in aerospace industry 24 p4416 A69-42777

Management role in ensuring products and components quality and reliability, analyzing failure reasons 24 p4416 A69-42778

Commercial aircraft environmental compatibility planning, considering problems of airport traffic growth and restrictive air traffic control regulations [AAS PAPER 69-326] 24 p4252 A69-42808

Logistics management developed for Apollo Applications Program of NASA Manned Spacecraft Center [AAS PAPER 69-204] 24 p4417 A69-42812

Technological forecasting as aid to aerospace planner in optimizing R and D resources allocation [AAS PAPER 69-105] 24 p4417 A69-42819

Space program planning, noting market requirements, acceptability and future characteristics [AAS PAPER 69-083] 24 p4418 A69-42820

Communication in large organizations, describing internal communication model 24 p4419 A69-42930

Space flight programs management cooperation and limited competition advantages, emphasizing single

management team responsibility for effective multi-lateral activities 24 p4419 A69-43043

MANDELSTAM REPRESENTATION
 Ruby laser to study stimulated Mandelstam-Brillouin scattering in liquids and in various crystals in UV 03 p0438 A69-13053
 Laser power increase noting influence of Mandelstam-Brillouin induced backscattering 04 p0612 A69-15414

MANEUVERABILITY
 Hovercraft handling characteristics, seakeeping and maneuverability during English Channel operation 02 p0277 A69-11592
 Differential games method solving pursuit problem for pursuer with greater maneuverability than pursued 09 p1476 A69-22671
 Visual simulation for critical maneuvers of aircraft takeoff and landing, noting method based on limited corridor simulation and maneuver freedom [AIAA PAPER 68-255] 11 p1866 A69-25376
 Maneuverability domains optimization with semilinear boundaries, noting application to orbital transfer 19 p3399 A69-35668

MANEUVERABLE SATELLITES
 U SATELLITES

MANEUVERABLE SPACECRAFT
 NT AEROSPACEPLANES
 NT APOLLO SPACECRAFT
 NT FERRY SPACECRAFT
 NT HL-10 REENTRY VEHICLE
 NT LIFTING REENTRY VEHICLES
 NT RENDEZVOUS SPACECRAFT
 Rendezvous maneuver with minimum fuel in circular orbit solved without restrictive conditions for accelerations due to approach thrust 16 p2852 A69-31558
 Human operator decision making in vehicle manual control, considering success likelihood and possible outcome costs based on signal detection model 20 p3482 A69-37720
 Mission and planetary vehicles characteristics affecting design of solid propellant motors and thrust vector control systems in planetary orbiters and landers [AIAA PAPER 68-815] 21 p3819 A69-39031

MANEUVERS
 NT ORBITAL RENDEZVOUS
 NT SIDESLIP
 NT SPACECRAFT DOCKING
 NT SPACECRAFT MANEUVERS
 Situation/command system displays and maneuvers for collision avoidance systems, discussing pilot preferences 17 p3002 A69-34096
 Additional yawing by gyroscopic moment of power plant and effect on aircraft maneuver during curvilinear flight, noting compensation by automatic control 18 p3092 A69-34973
 Flight training using digital simulators, including maneuver analysis for TWA 707 program 22 p3928 A69-41137
 Unstabilized astronaut, hand-held and integrated life support EVA maneuvering units tested in gimbaled six degree of freedom servo driven moving base simulator [AAS PAPER 69-516] 24 p4272 A69-42850

MANGANESE
 Temperature dependence of Hall coefficient, conductivity and carrier mobility in manganese doped indium antimonides 04 p0643 A69-15257
 Manganese catalyst photoreactivation in photosynthetic oxygen evolution in Mn deficient alga *Anacystis nidulans* cells 13 p2210 A69-28257
 Chondritic Cr and Mn content studied by X ray fluorescence, noting positive correlation in H and L groups and negative correlation in carbonaceous chondrites 15 p2681 A69-30416
 Manganese deficiency effect on growth and chlorophyll content of algae with and without hydrogenase 15 p2558 A69-31551
 Effective temperature and gravity values for Mn Ap stars by comparing spectrum scans and H line profiles with predictions from atmospheric models 17 p3038 A69-33724
 Colorimetric method to determine small amounts of Mn in metallic Ti by potassium periodate solution 20 p3544 A69-37813

MANGANESE ALLOYS
 NT MANGANIN [TRADEMARK]

Structural stability of manganese austenitic steels at high temperatures, discussing phase transformations and carbide precipitation changes 01 p0100 A69-11294

Low carbon maraging steel, studying age hardening behavior of iron-manganese-nickel alloys with titanium additions 05 p0781 A69-16541

Heat treatment effect on Ti-Mn alloy microstructure, discussing fcc martensite transformation into alpha, beta and intermediate phases as function of aging 11 p1906 A69-25578

Al-Mn-V ternary system equilibrium diagram at various aluminum concentrations determined by magnetic and microhardness measurements, microstructural observations and X ray analysis 24 p4330 A69-42601

MANGANESE COMPOUNDS
 Chemical analysis and paragenesis of manganous ilmenite from Sierran adamellite using electron microprobe 19 p3302 A69-35977

MANGANESE ISOTOPES
 Neutron activation method for Mn 53 in meteoritic Fe by X ray and gamma counters, noting extraction of Mn 54 free reference source 20 p3601 A69-37504

MANGANESE OXIDES
 Pyrolusite samples high dielectric and ferroelectric properties value ascribed to parasitic effects occurring in commonly used contacts 05 p0809 A69-16374

MANGANIN [TRADEMARK]
 Etched manganin gauge for shock pressure measurement in high noise environments containing radiation and electromagnetic effects 04 p0603 A69-15431

MANIFOLDS
 Local cross sections method for optimal control, considering control plant with variable control range and constraints on phase coordinates 07 p1115 A69-19003
 Sobolev type boundary value problems for elliptic operators using manifold theory 08 p1344 A69-21157
 Elliptic complexes over compact manifolds without boundary, discussing general theory of elliptic operators in vector bundles 09 p1532 A69-21733
 Frequency characteristics of flexible compensated manifolds for aircraft engines, considering axial force 11 p1826 A69-25332
 Pressure and flow rate variations at any point of manifold with control units calculated using transfer functions 11 p1942 A69-25335
 Sobolev type boundary value problems for elliptic operators using manifold theory 15 p2645 A69-31250
 Scale models of M-1 rocket engine oxygen and hydrogen pump driven two stage turbines used to determine performance and compact inlet manifolds problems [AIAA PAPER 69-553] 16 p2840 A69-32678

MANIFOLDS [MATHEMATICS]
 Differential equations of steady motion construction from integral manifold 15 p2654 A69-31260
 Stability criteria for integral manifold formed by intersection of hypersurfaces in Euclidean n-dimensional space 21 p3770 A69-38850

MANIPULATION
 U MANIPULATORS

MANIPULATORS
 Remote manipulators applications in space, discussing joint configurations, master-slave systems design, control systems, etc 15 p2558 A69-30187
 Ground controlled remote manipulator spacecraft system to perform unmanned satellite orbital maintenance, discussing refurbishment, laboratory simulation, system cost effectiveness and feasibility 19 p3430 A69-36001
 Remote manipulator spacecraft system for refurbishing synchronous communication satellite, emphasizing compatibility with standard shroud Titan 3C launch vehicle 24 p4297 A69-43041

MANNED ORBITAL LABORATORIES
 Geophysical investigations on manned orbital space laboratories, discussing space photography, spectrophotometry, terrain pictures and aerosol layers 05 p0759 A69-16633

Earth-orbiting manned space station as single facility base for power, volume, logistics, experimental equipment and data communications

19 p3431 A69-36464

MANNED ORBITAL RESEARCH LABORATORIES

Bio waste propelled resistojet control systems selection criteria based on NASA Manned Orbital Research Laboratory with six man crew

[AIAA PAPER 68-121] 04 p0554 A69-15506

Orbital biomedical laboratory for in-flight measurement to assure human safety and optimize astronauts performance in extended space mission

23 p4223 A69-41801

MANNED ORBITAL SPACE STATIONS

U ORBITAL SPACE STATIONS

MANNED ORBITAL TELESCOPES

Optical space astronomy, discussing Large Space Telescope, intermediate scale telescopes and lunar systems

[AAS PAPER 68-218] 02 p0313 A69-11484

Apollo telescope mount (ATM) for solar experiments conducted from manned earth orbiting laboratory

10 p1791 A69-22871

Equations of motion computerized simulation for attitude stabilization of orbiting telescope coupled to crew compartment

13 p2261 A69-27952

Attitude control system for Apollo Telescope Mount, discussing selection features based on manned orbital space platform requirements

18 p3168 A69-34683

MANNED REENTRY

Apollo spacecraft command module aerodynamic characteristics during entry compared with wind tunnel test predictions

[AIAA PAPER 68-1008] 12 p2012 A69-26789

MANNED SPACE FLIGHT

NT APOLLO FLIGHTS

NT APOLLO 10 FLIGHT

NT APOLLO 11 FLIGHT

NT APOLLO 7 FLIGHT

NT APOLLO 8 FLIGHT

NT APOLLO 9 FLIGHT

NT GEMINI FLIGHTS

NT GEMINI 11 FLIGHT

Cardiac output during space flight based on rebreathing method for estimation of gas tension in mixed venous blood and Fick equation

[UN PAPER 68-95746] 01 p0151 A69-10527

Cosmic radiation genetic, cytological and histological changes, particularly of pathological nature, on ecological systems employed in long duration Soviet manned flights

01 p0016 A69-10948

Biological problems in prolonged space voyages including oxygen replacement, water supply and food regeneration

01 p0020 A69-11075

Soviet book on human movements coordination during space flight covering space walks, lunar surface photographs, space docking, weightlessness, etc

01 p0018 A69-11180

French applied and basic research in space biology including manned space flight, deep space problems, weightlessness and cosmic heavy ion radiation effects

02 p0199 A69-11909

Weightlessness effects research during Soviet and U.S. manned space flights

02 p0199 A69-12120

Manned Mars and Venus missions role in overall planetary exploration program

02 p0324 A69-12304

Future space programs as governed by cost limitations, suggesting development of economical launch vehicle for shuttling between earth and orbital space stations

02 p0326 A69-12680

Manned reusable space transportation systems development, discussing requirements for future space mission planning

03 p0519 A69-13395

Interplanetary transportation network involving numerous spacecraft on various planetary flyby trajectories, discussing integration of gravity thrust, braking and scramjet concept

03 p0511 A69-13402

Parametric analysis of life support systems developing scaling laws adapted to computer solutions, discussing manned orbital missions

[SAE PAPER 680746] 03 p0379 A69-13438

Microbiology of water management subsystem for manned space flight, discussing sterilization by heat and tests inside Integrated Life Support System (ILSS)

[SAE PAPER 680718] 03 p0379 A69-13441

Wet oxidation process for management of organic waste products in closed ecologies of long term multimanned space missions

[SAE PAPER 680714] 03 p0380 A69-13443

Heavy cosmic ray particles effect in manned space flight, noting results of deuteron microbeam experiment

03 p0373 A69-13494

Weightlessness effect on blood circulation system of human beings and animals during suborbital/orbital space flight

03 p0376 A69-14194

Cardiovascular system, respiratory system and metabolism of cosmonauts on three man flight of Voskhod, noting physiological and biochemical studies

03 p0377 A69-14195

Biological space research, discussing microecology and weightlessness effects on human space flight

[DVL-847] 04 p0553 A69-14811

German analysis of preparatory technology of U.S. space programs, noting effects of hardware development for manned space travel on future planning

05 p0849 A69-15576

Mars contamination with terrestrial microorganisms, considering possibility of waste materials ejection from manned orbital vehicles

05 p0714 A69-15951

Manned spacecraft systems design optimization for extended space missions replacement modules

05 p0830 A69-16380

Orthostatic intolerance, with assessment of circulatory problem of weightlessness in prolonged space flight

06 p0873 A69-17016

Biological aspects of space exploration, analyzing human response to artificial environment in prolonged space missions

[UN PAPER 68-95715] 06 p0873 A69-17035

Manned space flight programs, discussing U.S. technological, scientific and practical contributions

06 p1001 A69-17074

Ground based guidance systems for supplementing onboard guidance of manned space vehicles

06 p0955 A69-17580

Systems engineering activities in manned space flight involving design, development, manufacture, test and operation of Mercury, Gemini and Apollo flight systems

06 p1016 A69-17602

Manned space flight safety, discussing astronaut exposure to danger on ground, in training and in space mission

06 p0882 A69-17650

Manned orbital space stations design, purposes and applications, balancing costs against benefits

06 p1019 A69-18237

Rules for selecting Soviet cosmonauts and physiological studies concerning heart and respiratory reactions to accelerations and weightlessness during preparation

07 p1060 A69-18569

Physiological aspects of weightlessness

07 p1060 A69-18573

Statistical correlation between cardiovascular activity and respiration dynamics of cosmonauts during orbital flight, discussing heart beat and respiration rates

07 p1061 A69-18584

Pneumograms and EKG used to determine heart beat, respiration rates and systolic index of cosmonauts during Voskhod 2 flight

07 p1062 A69-18585

Human perception in space as function of nervous relationships involving optic, kinesthetic, vestibular and other analyzers

08 p1263 A69-19938

Resistojet control system combined with control moment gyro payload capability for long duration manned orbital spacecraft missions

[AIAA PAPER 69-255] 09 p1561 A69-21220

Space biological tests performed on lower animals and vegetables relating to higher organisms reactions during prolonged manned space flights, reviewing Nasa experiments

12 p2019 A69-26494

Human ecology in space flight - USN-NASA Conference, Princeton, October 1965, Volume 3

13 p2213 A69-27266

Hardware limitations on communications, instrumentation and data handling for manned deep space missions

13 p2219 A69-27666

Human expansion in space, discussing moon landing and exploitation

13 p2352 A69-27901

Space travel and lunar exploration medical problems

13 p2210 A69-27909

Earth orbital manned space astronomy, discussing long range program, instruments, facilities and data processing

13 p2240 A69-27947

Pharmacology for long term manned space flights

13 p2211 A69-28613

Circadian rhythms characteristics in humans, animals and plants, noting possible effects of rhythm disturbances on astronauts

13 p2211 A69-28614

Sweet potatoes productivity and nutritive value as carbohydrates source in manned spaceflights

13 p2216 A69-28619

Thermal vacuum /TV/ manned test operations related to Apollo lunar module in simulated space environment

15 p2558 A69-30394

Calcium mobilization control by adequate calcium intake and programmed exercise during space flight suggested from metabolic balance data

15 p2557 A69-31468

Design philosophy for cost reductions on future space transportation systems, exemplifying application to booster system for earth orbital logistics

[AIAA PAPER 69-439] 16 p2882 A69-32654

Visual perception of three dimensional objects under simulated solar illumination in space considered in relation to manned spaceflight maneuvers

17 p2913 A69-33174

Manned space telescope attitude stabilization using counter-rotational triaxial gyro system

18 p3206 A69-34371

AIAA view on Post-Apollo space program, considering multiple goals, unmanned application satellites and manned space flight objectives

18 p3236 A69-35136

Medical and biological laboratory ground experiments role in development of life support systems and suitable environments for prolonged manned space flights

18 p3098 A69-35165

Future combined environment space simulation tests duplicating environment interaction encountered during earth orbits, deep space probes and manned flights

19 p3288 A69-35531

Navigation, guidance and control developments for manned space missions, discussing earth orbital exploration bases

19 p3369 A69-35801

Amendments considered for international law regarding earth and space rescue services as result of contemporary U.S. manned space flight programs

20 p3637 A69-37115

Infectious diseases in space flight, considering environment role in infection transmission, occurrence and severity

20 p3479 A69-37973

Propulsion system performance relationship to manned planetary mission capability, discussing anticipated performance of advanced propulsion concepts

20 p3586 A69-38118

Communications, instrumentation and data handling for manned planetary missions, discussing data rate limitations

21 p3674 A69-39018

Somatic radiation effects on human organism related to manned space flights

21 p3660 A69-39172

Mineral dynamics during hibernation and disuse atrophy in connection with organismal homeostasis and chronic-term manned space flight, noting skeletal effect of immobility

21 p3660 A69-39175

Periodic orbits for interplanetary flight, using patched conic analysis for determining inclined elliptic free fall trajectory shuttling between earth and Venus

[AAS PAPER 68-102] 21 p3804 A69-39203

Reducing cost of space transportation - AAS Conference, Washington, D.C., March 1969

21 p3856 A69-39686

Space transportation cost factors, discussing payload characteristics, carrier utilization, program duration, government participation and control, carrier design, hardware costs, launch costs, etc

21 p3857 A69-39687

Crew and passenger transportation to and from space station orbits, discussing cost reduction possibilities with current or future technology

21 p3827 A69-39691

Reusable Crew Module, Reusable Orbital System and Reusable All Systems options for low cost space transportation system

21 p3827 A69-39693

Manned transport into orbit and manned orbital operations systems, considering systems selection factors and mission and cost influences

21 p3857 A69-39696

Manned relativistic space flight limitations dependence on biomagnetic levitation of human body in inhomogeneous magnetic field to compensate inertial forces during acceleration

22 p3889 A69-39906

Real time digital computer hardware simulation of Apollo Telescope Mount /ATM/ mission [AIAA PAPER 69-940]

22 p3919 A69-40323

Electric power system selection for long duration manned space station [AIAA PAPER 68-1034]

22 p3869 A69-40549

Photogrammetric camera system developed from NASA requirements to document lunar surface environment during manned space flight exploration

22 p3948 A69-40989

Astronaut weight loss during space flight related to mission duration, noting dehydration and catabolism roles

23 p4100 A69-41303

Manned lunar exploration programs and site evaluation concerning volcanic processes, chemical and mineralogical differentiation, atmosphere and protobiological materials

23 p4216 A69-42200

Manned flyby/orbiter of Mars providing scientific information at low incremental cost [AAS PAPER 69-180]

24 p4379 A69-42813

Space research in past and expected scientific knowledge from manned and automated earth orbital science missions [AAS PAPER 69-036]

24 p4379 A69-42825

Manned flyby and stopover missions to Mars and Venus with chemical propulsion and Saturn 5 launch vehicles, noting short duration low energy missions [AAS PAPER 69-492]

24 p4380 A69-42839

Technology flow for future manned earth orbit and lunar operations and planetary exploration [AAS PAPER 69-494]

24 p4380 A69-42840

Management system for safety in NASA Manned Space Flight Program, discussing hazard analyses and reduction precedence sequence [AAS PAPER 69-522]

24 p4418 A69-42851

Manned space flight history and spacecraft development [AAS PAPER 69-501]

24 p4380 A69-42852

Material recovery from metabolic and other wastes for long duration manned space missions, discussing carbon dioxide removal, bioregenerative food systems, etc [AAS PAPER 69-143]

24 p4272 A69-42876

MANNED SPACECRAFT

NT AEROSPACEPLANES

NT APOLLO SPACECRAFT

NT FERRY SPACECRAFT

NT GEMINI SPACECRAFT

NT LUNAR MODULE

NT MERCURY SPACECRAFT

NT ORBITAL SPACE STATIONS

NT ORBITAL WORKSHOPS

NT SOYUZ SPACECRAFT

NT SPACE STATIONS

NT VOSKHOD 1 SPACECRAFT

NT VOSKHOD 2 SPACECRAFT

NT VOSKHOD MANNED SPACECRAFT

Meteorological satellite research program, including unmanned satellite observations and possibilities with meteorologist on board manned spacecraft [UN PAPER 68-95350]

01 p0109 A69-10483

Man as main component of future spacecraft or planetary station closed ecological system, discussing spacecrew physiological monitoring for biological cycles optimization

01 p0020 A69-11076

Handheld optical range finder for manned spacecraft orbital rendezvous, discussing target shapes and range errors

02 p0250 A69-12366

Lifting body type M2-F1 and M2-F2 aircraft enabling astronauts to make own landings at choice airport

03 p0366 A69-13367

Occupant restraint systems for automobiles, aircraft and manned space vehicles, discussing cost, practicability, ease of use, acceptability and possible improvements

03 p0380 A69-13459

Photographic control system requirements for Project Apollo manned launches, considering extreme heat, vibration and sound pressure environment [SMPT PAPER 104-20]

04 p0596 A69-14360

Manned spacecraft systems design optimization for extended space missions replacement modules

05 p0830 A69-16380

Life in spacecraft - Conference, Belgrade, September 1967

06 p0881 A69-17642

System designs for manned spacecraft gravity gradient stabilization of Saturn S-4B stage at 400 km and lunar module at synchronous altitude

07 p1228 A69-18338

Communications for Apollo Applications Program, considering extended duration manned missions in low earth orbit and Gemini, Saturn and Apollo hardware

07 p1083 A69-19124

Displays and controls requirements in manned spacecraft to integrate man into vehicle system, noting man capability for task diversity

08 p1312 A69-19968

Manned spacecraft electrical power systems requirements, noting Gemini and Apollo fuel cell system design and configuration

08 p1259 A69-21035

Common nuclear propulsion modules for wide spectrum of manned planetary missions, discussing payload, mission and program flexibility [AIAA PAPER 68-590]

09 p1539 A69-21984

Manned spacecraft developments, considering Apollo Applications Program, space station establishment, space shuttle operations and payload cost

10 p1791 A69-22866

Reaction control rocket engines for manned spacecraft, discussing operating and cycle life, thrust response, specific impulse and reliability

16 p2867 A69-31746

Dim astronomical sources observability from sunlit spacecraft, considering coma of micron sized ice crystals influence on scattering by condensation model

16 p2861 A69-32301

Weight estimation and forecast in manned spacecraft design, noting size and weight relationship [SAWE PAPER 793]

18 p3208 A69-35058

Manned spacecraft earth resource sensing, discussing advantages and applications in agriculture, forestry, geography, hydrology, oceanography and geology

18 p3208 A69-35058

Kennedy Space Center Vehicle Assembly Building construction, capacity and operation for manned spacecraft

19 p3288 A69-35500

Low cost rate transportation as mandatory goal for future space program, discussing recovery and reuse, launch system costs, hardware development, etc

20 p3618 A69-38117

Cone-conical-frustum configurations meeting center of gravity requirements for higher hypersonic lift-drag ratios in axisymmetric manned spacecraft

21 p3644 A69-39237

Ground based guidance for land-landing manned spacecraft with low velocity descent systems, discussing high and low altitude glide path intercept and spiral

[AIAA PAPER 69-864]

21 p3762 A69-39390

Statistical error analysis of autonomous manned spacecraft navigation in long duration eccentric Mars orbits

[AIAA PAPER 69-880]

21 p3763 A69-39406

Seals leak testing for complex manned spacecraft structures [AIAA PAPER 69-1030]

22 p3924 A69-40399

Nuclear reactor/thermoelectric power system design for manned orbiting space station, discussing station integration and operation

23 p4187 A69-42256

Dynamic power and life support systems electrical/thermal integration for manned spacecraft using low temperature Rankine cycle generator

23 p4189 A69-42269

Adaptive control function technique to design lateral stability augmentation system for hypothetical manned, lifting body entry vehicle

24 p4394 A69-43301

Flexible parawing lifting decelerator research data from wind tunnel and flight tests, noting manned space vehicle recovery and aircraft escape systems [AIAA PAPER 68-967]

24 p4254 A69-43715

MANOMETERS

Noiseproof ionization manometer with ion current dual modulation for ultrahigh vacuum measurement in magnetic field with extraneous charged particles interference

03 p0429 A69-13263

Multichannel optical interference fluid manometer, using laser light source for fringe pattern photographic record

13 p2263 A69-28190

Monograph on investigation of rarefied gas flows by means of miniature pressure probes in transition region between molecular and continuum flows

14 p2430 A69-29289

Ionization manometer flange transducer with axial cathode and collector for high vacuum measurements, describing air resistant yttrium oxide coated cathode with Ir core

21 p3724 A69-39077

MANPOWER

NT SCIENTISTS

Organization and manpower utilization in R and D, determining criteria for organizational form selection

08 p1423 A69-21155

MANTLE [EARTH STRUCTURE]

U EARTH MANTLE

MANUAL CONTROL

NT VISUAL CONTROL

Manual control using matched manipulator technique, noting control task complexity decrease and improved performance

02 p0202 A69-11951

Manual optimal guidance schemes for space vehicles to minimize computational and display requirements for pilot task loading

02 p0279 A69-12365

Flight test evaluation of small one man lunar flying device /POGO/, discussing vehicle control, pressure suit factors and piloting differences [AIAA PAPER 68-240]

02 p0229 A69-12379

Advance indication based on extrapolation for aiding manual attitude control of VTOL aircraft in hovering flight, noting results on flight simulator

03 p0366 A69-13645

Hand operated visual signaling devices, discussing Mini Signals and cartridge load aerial signals

06 p0878 A69-16962

Manual and automatic spacecraft rendezvous and docking, discussing docking of Cosmos 186 and 188 in 1967 [UN PAPER 68-95764]

06 p1013 A69-17057

Predictive display technique for remote manual control of roving lunar and planetary surface vehicles

06 p0928 A69-17925

Manual performance of aircraft pilots under sustained acceleration using measurements of hand-writing pressure

06 p0884 A69-18030

Finger dexterity in JMG-1 pressure gloves with regard to efficiency associated with fine adjustments

06 p0884 A69-18032

Minimal angle of resolution /MAR/ between point and extended circular source and between point source and simulated horizon, studying irradiation effects on manual navigation

07 p1177 A69-19208

Human operator manual control of spacecraft under accelerations up to 18 g, noting performance and efficiency of males

08 p1265 A69-19936

Operational reliability of manual and automatic flight control systems and components and current safety standards

08 p1255 A69-20720

Manual onboard computation procedures and devices for determination of maneuvers for orbital navigation and guidance

08 p1348 A69-21184

Control operation time found dependent on gloves, physical characteristics of control and type of required operation

10 p1648 A69-23180

Glove characteristics effects on manipulability, finding operation time differences between gloved and banded operation dependent on type of required control operation

10 p1648 A69-23181

Manual control displays for instrument landing approach of large subsonic jet transport, evaluating closed loop system performance and scanning workload

10 p1650 A69-23877

Roll-motion cues for man-vehicle control in compensatory tracking task with disturbance input

10 p1650 A69-23879

Semiautomatic and automatic off-line module testing machines, comparing costs for different test populations

11 p1865 A69-25076

- Human operators instrument-monitoring behavior noting optimal control, information processing, physical limitations, etc
12 p2022 A69-25929
- Lunar visual environment effects on astronaut control manipulation task performance, discussing solar illumination simulation facility
12 p2059 A69-26554
- Analog correction method to suppress pilot maneuver effects during analysis of aircraft accelerations induced by atmospheric turbulence
[ICAS PAPER 68-39] 17 p2901 A69-33590
- Manual procedures for midcourse and terminal guidance, discussing onboard optical measurements and calculations
19 p3368 A69-35792
- Earth orbit estimation by manual stadimeter, space sextant and small data processor, discussing orbital parameter errors due to instrument and environment uncertainties
19 p3369 A69-35793
- Human operator decision making in vehicle manual control, considering success likelihood and possible outcome costs based on signal detection model
20 p3482 A69-37720
- Adaptive compensation to minimize human task in continuous manual control system using various models
20 p3482 A69-37721
- Manual guidance and control of Saturn launch vehicles, considering feasibility, reliability and hardware implementation
[AIAA PAPER 69-876] 21 p3824 A69-39402
- Manual attitude control for Lunar Module employing directional stability, coordinated turn and attitude command
[AIAA PAPER 69-892] 21 p3824 A69-39417
- Biological model describing spacecraft operator sensorimotor activity in response to various spacecraft control stimuli, outlining computer algorithm
22 p3892 A69-40281
- Manual vehicle control analysis based on feedback systems analysis and mathematical models for human operators engaged in control tasks
24 p4274 A69-43021
- Adaptive manual control rapid variation determined by input, controlled element, task and programmed adaptation systems, discussing human strategy changes
24 p4274 A69-43022
- Manual method for navigating and guiding spacecraft to rendezvous with orbiting target, using hand-held unpowered optical instruments and manual computations
[AIAA PAPER 68-859] 24 p4348 A69-43243
- Gliding cargo airdrop system including automatic homing and manual control
[AIAA PAPER 68-958] 24 p4254 A69-43723
- ### MANUALS
- Instruction manual for maintenance personnel and pilots regarding clear vision and window integrity of Convair aircraft, discussing windshield installation and replacement
14 p2391 A69-28932
- Documentation aspects of computer programs use in civil engineering, describing maintenance, users and operators manuals
22 p3904 A69-40140
- ### MANUFACTURING
- Integrated circuit manufacturing status, discussing raw materials, crystal imperfections, surface damage, epitaxy and diffusion techniques
01 p0045 A69-10650
- Aerospace research and development projects selection and planning for success in manufacturing competition
03 p0393 A69-13252
- Aerospace manufacturing contribution to engineering function in design development
[SAE PAPER 680668] 03 p0433 A69-13451
- Quality control in welding from design through experimental manufacture, product testing, large scale production and improvements
04 p0608 A69-15485
- Book on machinability and producibility of metals, plastics, nonmetallic materials and composites, emphasizing machine tools and tool holders
06 p0931 A69-17782
- Plain and rolling metal bearings manufacture and use, discussing materials structure and properties, operating conditions, lubrication, etc
11 p1903 A69-24517
- Systems design value analysis including alternate solutions to cost effectiveness for design development and production phases
13 p2383 A69-28097
- Reliability control of 1/4-W resistors of tin oxide on glass substrate manufactured in quantity
15 p2627 A69-30837
- Highly concentrated hydrogen peroxide production, handling and storage, discussing crystallization process, equilibrium diagram, decomposition reduction and stabilizers
17 p3017 A69-33353
- Development, manufacturing and logistic costs of reliability improvement in electronic equipment design
18 p3231 A69-34485
- Scientific satellites structural design problems, considering limitations imposed by weight, layout, environmental conditions, mission and manufacture
18 p3208 A69-34792
- Manufacturing in space based on nongravity and hard vacuum environment, considering crystal growth and refinement, perfectly shaped bodies, refractory metals ultrapurification, etc
18 p3234 A69-35066
- Space manufacturing operations program, discussing zero gravity effect during earth orbit flight, Apollo Applications Program Orbital Workshop Flight 2, etc
18 p3208 A69-35067
- Technological possibilities of gravity free production in space environment, discussing containerless manufacture of glass, liquid metal manipulation and defect free fibers
18 p3206 A69-35490
- Materials and products fluid state processing in space, discussing g, zero-g and induced forces effect on fluid matter and process, cost and operational effectiveness
19 p3324 A69-35588
- Materials processing in space, suggesting electronic single crystals preparation, materials melting and utilization of low g earth orbit environment
19 p3324 A69-35589
- Stochastic model for estimating manufacturing costs, discussing Mellin and Laplace transforms and Gram-Charlier series approximations
20 p3633 A69-36924
- Carbon materials manufacture, properties and applications in space technology, discussing carbon fibers, textiles, graphite, pyrolytic carbon, composites and vitreous carbon
23 p4180 A69-42160
- Space manufacturing processes for orbital low and zero gravity environment, discussing buoyancy and thermal convection sensitive and molecular forces controlled methods
[AAS PAPER 69-486] 24 p4380 A69-42844
- ### MANY BODY PROBLEM
- N-body problem in celestial mechanics, using differential equations, reduced to quadratures
[UN PAPER 68-95268] 01 p0150 A69-10476
- N body gravitational problem - Conference, Paris, August 1967
02 p0322 A69-12267
- Numerical regularization of single binary collision in n body gravitational problem
02 p0322 A69-12268
- N body systems with/without external field, noting galactic field effect on system flattening
02 p0322 A69-12270
- Computer study of collisionless self gravitating system using two dimensional model, obtaining gravitational field by solving Poisson equation
02 p0322 A69-12272
- Spacecraft trajectories computation from initial conditions by techniques involving construction of N body reference orbit
03 p0518 A69-14248
- Natural longitudinal single frequency oscillations of system of n material points connected in series by non-linear elastic threads and with energy dissipation
05 p0832 A69-15687
- Atomic Li photoionization cross sections calculated with Brueckner-Goldstone many body perturbation theory
06 p0961 A69-17134
- Approximate solution of celestial mechanics differential equations by reducing to quadratures for n body problems
06 p1006 A69-17566
- Trajectory error propagation upper bounds in many body field for impulsive initial error, relating error to mission tolerances
09 p1595 A69-21937
- Clouds-in-clouds and clouds-in-cells method /CIC/ for many body nonlinear plasma problems, calculating density and force of particles
12 p2138 A69-26625
- Three and n body problems solution by reduction of independent variables and maximum principle
15 p2652 A69-30448
- Oscillator strengths calculated for transitions in Si III using dipole length and velocity matrix elements, comparing many electron correlation problem approximations
15 p2656 A69-31158
- Ground state energy inequalities for N particle non-relativistic quantum mechanical system, showing non-saturating gravitational forces and increasing binding energy per particle
17 p3028 A69-32900
- Quasi-periodic solutions for canonical systems of differential equations in plane n-body problem
17 p3035 A69-33620
- Grobner method of Lie series applied to numerical integration of spacecraft trajectories and n-body problems
23 p4223 A69-42476
- Collective rotational motion separation from internal motion in system of n point masses based on wave mechanics, emphasizing three body problem
24 p4349 A69-42650
- Density matrices of symmetry projected single determinant wave functions for finite groups, considering many particle system
24 p4351 A69-43810
- Many body perturbation theory with time dependent perturbations applied to frequency dependent polarization of atomic oxygen
24 p4354 A69-43816
- ### MAP MATCHING GUIDANCE
- Airborne radar navigation with emphasis on semiautomatic fixing, describing beacon mode, map matching and airborne weather radar
18 p3169 A69-34851
- ### MAPPING
- Satellite photography applications to geography and cartography based on Gemini 7 photographs
[UN PAPER 68-95401] 01 p0178 A69-10489
- Error analysis of orientation methods for extraterrestrial stereophotogrammetric mapping
[JPL-TR-32-1344] 03 p0429 A69-13299
- Optimal circular satellite orbits for planetary surface mapping mission minimizing overlap
03 p0518 A69-14247
- One to one mappings of Fourier series of analytic almost periodic functions and Dirichlet series, discussing satisfaction of functional equation
05 p0786 A69-15882
- Horizontal aerotriangulation by independent models using photogrammetric extension of horizontal control for small scale superwide angle photography, horizon photography and B 8 plotter
06 p0925 A69-17468
- Mars imaging mission and astrodynamical interaction, discussing arrival geometry and orbit size effects
[AIAA PAPER 69-127] 06 p1011 A69-18169
- Low latitudes observations of 21 cm line of H I in galactic center direction, giving contours maps of brightness temperature
08 p1392 A69-20562
- Hertzian radiometric antennas and signal processing techniques for aerial mapping project for sun
08 p1290 A69-20976
- Relative heights on moon, tabulating lunar topography and comparing micrometrical measurements and map data
10 p1782 A69-23697
- B, L coordinates for mapping geomagnetically trapped particles distribution computed by perturbation method, using perfect dipole as zero order approximation
11 p1949 A69-24861
- Cartographic representation methods in climatological regional charts, discussing topographical elements, scale, screen patterns and area color
12 p2124 A69-25893
- Electro-optical scanning device and electro-optical matrix for mechanization of difference measurements in automatic photointerpretation of surveillance maps
12 p2090 A69-26302
- Radiophase mapping utilizing VLF radio signals to detect conductive sheets and surface impedance of earth
12 p2075 A69-26982
- Geographic and cartographic mapping applications of remote sensor data from orbital heights, discussing hardware, instrumentation, NASA role in data selection, etc
12 p2192 A69-26984
- Cartographic interpretation of TV cloud pictures transmitted by Molniya 1 satellite
13 p2292 A69-27730
- Side-looking radar and thermal IR photography as mapping system, discussing resolution and distortion
15 p2612 A69-31162

Visual mapping and photometric scanning of Saturn with rings from earth, noting ring brightness edgewise linear dependence on rings opening

15 p2697 A69-31256

Survey of six year period of satellite observed tropical Pacific cloud mapping

17 p2996 A69-33001

Topographic mapping by high altitude jet aircraft photography

18 p3134 A69-34339

Satellite photography for snow cover mapping and depth estimation

18 p3167 A69-35084

Solar radio emission during quiet sun years 1964-1965 mapped using Stanford spectroheliograph, attributing slowly varying component to electron density enhancement

18 p3188 A69-35395

Color coded area sensitivity maps of photomultiplier tubes by multicolor display technique, noting focus electrode voltage

19 p3305 A69-35724

Side-looking radar and IR line scanning as method for simultaneous stereo height mapping, using images produced from same vantage point

20 p3536 A69-36929

Aerial photography in geomorphological interpretations, noting advantages over conventional maps in slope microreliefs, soil erosion network and karst, glacial, aeolian and shore features

20 p3539 A69-37512

Normalized hodographic mapping for constrained trajectory families, discussing mapping concepts, information content and applications

[AIAA PAPER 69-924] 21 p3809 A69-39362

Orbit selection rules for planetary cartographic spacecraft derived from relations connecting camera angle, view field and imaging resolution

[AIAA PAPER 69-879] 21 p3763 A69-39405

Point mapping in optimal control, describing maximum principle, dynamic programming and substitution of variables

21 p3688 A69-39860

Hyperlatitude photographs for geological mapping from Gemini spacecraft, noting remote sensing imagery

22 p3935 A69-40040

Orthophoto maps production, discussing scales, aerial photography, control points, orthoprojection, cartography and printing

22 p3951 A69-41246

Spherical trajectories control by star height maintenance, analyzing resulting cycloid and cartographic representations

23 p4186 A69-42023

MAPS

NT ASTRONOMICAL MAPS
NT LUNAR MAPS
NT METEOROLOGICAL CHARTS
NT RADAR CLUTTER MAPS
NT RADAR MAPS
NT RELIEF MAPS

World maps highlighting differences in geomagnetic field at conjugate localities

02 p0245 A69-12737

Map information display methods comparison for tactical image interpreters

06 p0924 A69-17212

Numerical decile value maps of sporadic E layer ionization critical frequency for each month of solar cycle minimum and maximum year

10 p1682 A69-23418

Moving map pictorial display system for on board capability of area navigation, noting crew reaction

[SAE PAPER 690393] 23 p4186 A69-41663

MARAGING STEELS

Structural transformations of quenched Fe-Ni-Nb austenitic alloy from X ray diffraction microstructure examination and hardness measurements

01 p0095 A69-10603

Maraging steels ductile and strength characteristics with increased Co and Mo as function of Ni content, tempering method and aging

01 p0098 A69-10731

Shot peening effect on fatigue properties of maraging and Al-Zn-Mg alloy steel welds, using repeated tensile tests

02 p0253 A69-12061

Butt weld fatigue properties improvement in maraging steels, using shot peening and prestretching

03 p0434 A69-13762

Fracture toughness of Ni maraging steel weldments, using bending tests

[AIAA PAPER 68-507] 03 p0450 A69-13910

Experimental high strength maraging steel mechanical properties optimization, discussing heat treatment, quenching, aging and reducing conditions

04 p0615 A69-14645

Overheated maraging steel mechanical properties improvement by heat treatment

04 p0615 A69-14646

Brittle fracture resistance of low carbon maraging and martensitic steels with cracks established by crack growth measurements during tensile and impact tests

04 p0615 A69-14647

Alpha to gamma transformation kinetics in maraging steel during heating, studying alloying elements redistribution

04 p0616 A69-14648

Cobalt concentration reduction in maraging steels by Cr replacement and increased Mo and Ti additions

04 p0616 A69-14649

Maraging steel with reduced Co, establishing optimal temperature range for short aging

04 p0616 A69-14650

Low carbon maraging steel, studying age hardening behavior of iron-manganese-nickel alloys with titanium additions

05 p0781 A69-16541

Maraging stainless steel for manufacturing liquid rocket propellant tanks, discussing composition determination and mechanical properties

07 p1166 A69-19236

High strength 18 percent nickel maraging steel with 350 ksi yield strength

08 p1330 A69-20009

Fabrication welding with maraging steels with emphasis on minimizing heat input

08 p1320 A69-20407

Weldability of maraging steels, suggesting factors for weld toughness and reliability

08 p1320 A69-20408

Plain strain fracture toughness tests on two inch thick maraging steel plates of various strengths, using bend and compact tension tests

10 p1795 A69-23057

Molybdenum, titanium and cobalt effects on nickel maraging steel strength and ductility

11 p1904 A69-24643

Highly alloyed steels weldability, considering nickel maraging and precipitation hardening stainless steels

12 p2111 A69-25829

Plane strain fracture toughness tests on maraging steel plates for various yield strengths and large dimensions

12 p2114 A69-26496

Homogenization of martensite formation in nickel 300 grade maraging steel, analyzing anisotropic transformation strains during thermal cycling

13 p2278 A69-27410

Reversion and drawing techniques for ultrahigh strength ductile maraging steel wire without excessive deformation

13 p2278 A69-27412

Plastic deformation effects by hydrostatic fluid extrusion on mechanical properties of Ni maraging steels

13 p2278 A69-27414

Thin walled maraging steel tube toughness determined by Charpy prcrack testing of transverse and longitudinal impact properties

13 p2269 A69-28183

Nickel maraging steel polarization behavior in acidic solutions, noting corrosion potential dependence on pH

13 p2282 A69-28188

Stress corrosion in smooth and prenotched maraging steels exposed to sodium chloride solution and natural sea water

14 p2467 A69-29940

Maraging steel weldability, discussing residual stresses, hydrogen cold cracking, age hardening and hot cracking

15 p2617 A69-30098

Maraging steel tensile strength increased, plasticity and toughness properties decreased with Ti content increase

15 p2639 A69-30630

Chemical composition effect on Cr-Ni-Mo-Ti stainless maraging steels mechanical properties

15 p2640 A69-30631

Cumulative rapid thermal cycling influence on progressive disappearance martensitic transformation in 18 percent nickel maraging steel

18 p3155 A69-34650

Nickel maraging steel weld metal impact strength and fracture toughness improved by heat treatment

18 p3151 A69-35430

Ni-Ti maraging steel hardness impact strength and thermal EMF changes during quenching

19 p3345 A69-36154

Extrastrong maraging steel based on 18 percent Ni, noting alloying elements percentages, mechanical properties and applications

22 p3971 A69-40833

Forming techniques to overcome pressing behavior of maraging steels, noting tendency to thin during stretching and reluctance to stretch

23 p4170 A69-42157

Rotational bending fatigue strength of plain and notched conventional and maraging steels, evaluating gas nitriding effects

24 p4335 A69-43802

MARIA

U LUNAR MARIA

MARINE NAVIGATION

U SURFACE NAVIGATION

MARINE PROPULSION

NT UNDERWATER PROPULSION

Semiamphibious Vosper VT 1 hovercraft for passengers and cars, discussing design, water contact propulsion, peripheral skirt, supercavitating propellers, structure, performance, etc

04 p0549 A69-15187

UK hovercraft research covering internal/external dynamics, propulsion systems and full scale tests

05 p0702 A69-16393

MARINER SPACE PROBES

Vector helium magnetometer for Mariner 4 /Mars 1964/ and Mariner 5 /Venus 1967/, discussing efforts to reduce spacecraft stray fields

[IEEE PAPER 10.1] 01 p0081 A69-10714

Geomagnetic and interplanetary field variation measurements from Mariners 2, 4 and 5, noting correlation between solar phenomena and geomagnetic storms

02 p0241 A69-11737

Unmanned planetary exploration using Mariner class spacecraft for solar system and life origin

02 p0334 A69-12302

Geomagnetic variability relations to interplanetary magnetic field transverse fluctuations, discussing data from Mariner flights

14 p2510 A69-28948

Venus atmosphere physical properties and chemical composition, considering Venera 4 and Mariner 5 data

18 p3201 A69-35164

Mariner Mars 1969 flyby missions objectives, experiments, spacecraft configuration, trajectory design, sterilization, flight path control and photographic imaging

[AAS PAPER 68-134] 19 p3402 A69-35938

Orbital Experimental Capsule /OEC/ as subsatellite concept for Martian fields and particles measurements, noting Voyager exploring vehicle applications

21 p3805 A69-39215

Mariner Mars 1969 TV system environmental test and calibration program

22 p3920 A69-40372

Friction tests for Mariner Mars 1969 spacecraft mechanisms in ultrahigh vacuum molecular sink chamber, noting increased friction attributed to vacuum environment

[AIAA PAPER 69-996] 22 p3920 A69-40374

Mars atmosphere study by Mariner 6 and 7 spacecraft, discussing instrumentation on board

[AAS PAPER 69-091] 24 p4393 A69-42881

Mars thermal energy emission measurement by Mariner 1969 IR radiometer, indicating frozen carbon dioxide cap and minimum temperature

24 p4384 A69-43196

MARINER SPACECRAFT

Design of interface between Mariner Mars spacecraft and Mars planetary entry/landing capsule

[AIAA PAPER 68-1162] 03 p0521 A69-13671

Mars unmanned spacecraft mission profiles for surface imaging, noting influence of lighting requirements

[SMPT PAPER 104-21] 04 p0650 A69-14361

Mariner 1969 high rate telemetry system portions pertinent to combinatorial mathematicians, discussing coding and encoding

06 p0890 A69-17862

Mariner 1969 multimission high rate deep space telemetry system design, hardware and application

07 p1083 A69-19125

Lightweight double walled meteoroid shield for Mariner Mars 1971, considering Teflon impregnated glass fabric outer sheet and multilayer thermal insulation

[AIAA PAPER 69-377] 13 p2357 A69-28307

MARINER 1 SPACE PROBE

Comparisons and combinations of geodetic parameters from dynamic and geometric satellite solutions and Mariner flights

15 p2600 A69-31362

Two channel IR radiometer for 1969 Mariner mission measuring equivalent black body surface temperature

17 p2972 A69-33085

Acoustic spectrum averager for Mariner spacecraft environmental tests, calculating rms average 1/3 octave spectrum bands in real time

[JPL-TR-32-1442] 17 p2946 A69-33658

Mariner Mars 1969 flyby missions objectives, experiments, spacecraft configuration, trajectory design, sterilization, flight path control and photographic imaging

[AAS PAPER 68-134] 19 p3402 A69-35938

Mariner attitude control system limit cycle operation during cruise, noting variation from ideal case to single side operation

[AIAA PAPER 69-844] 21 p3822 A69-39374

Targeting technique for Atlas/Centaur Mariner Mars 1969 mission, noting suitability to flyby, orbiter or landing interplanetary missions

[AIAA PAPER 69-881] 21 p3764 A69-39407

Mariner Mars 1969 spacecraft real time test support system and recorded data analysis including routing to printers, CRT displays and incremental plotters

[AIAA PAPER 69-982] 22 p3907 A69-40362

Mars landers impactable power subsystems, considering thermoelectric generators, batteries, conversion equipment, Mars environment, etc

23 p4069 A69-42253

Manned flyby and stopover missions to Mars and Venus with chemical propulsion and Saturn 5 launch vehicles, noting short duration low energy missions

[AAS PAPER 69-492] 24 p4380 A69-42839

MARINER 1 SPACE PROBE

Computer program reliability enhancement, discussing significance of underestimation

08 p1278 A69-19845

MARINER 2 SPACE PROBE

Zodiacal dust density in interplanetary space

08 p1407 A69-20938

MARINER 4 SPACE PROBE

Martian upper atmosphere and ionosphere, considering Mariner 4 occultation results and various atmospheric models

02 p0320 A69-12112

Mariner 4 Martian ionospheric data interpreted in terms of E, F1 and F2 regions

02 p0320 A69-12113

Mariner 4 ionospheric densities to deduce Martian atmospheric modes, discussing validity of using ionospheric properties to discriminate between models

02 p0320 A69-12114

Radio amplitude and phase measurements during Mariner-Mars encounter, providing evidence for Martian atmospheric models

• 02 p0320 A69-12116

Annular and linear Martian surface formations nature and origin from analysis of Mariner 4 photographs

03 p0506 A69-13087

Mars surface features identification from comparison of Mariner 4 and ground bases telescopic photographs

07 p1213 A69-18605

Zodiacal dust density in interplanetary space

08 p1407 A69-20938

Martian crater density determined by comparison of statistical counts from Mariner 4 photographs

12 p2157 A69-26309

Martian canals nature based on high contrast photographs obtained by Mariner 4 space probe

12 p2171 A69-27133

Annular and linear Martian surface formations nature and origin from analysis of Mariner 4 photographs

14 p2515 A69-28769

Interplanetary magnetic field radial dependence from Mariner 4 measurements between earth and Mars, indicating fluctuations produced by dynamic processes in solar wind

16 p2856 A69-31964

Lunar magnetic field measurements by Mariner 4 near sun-moon line extension, discussing search for lunar wake

16 p2856 A69-31986

Mars internal structure and composition modeling, considering core, mantle and temperature via earth analogy and Mariner 4 data

17 p3037 A69-33652

Interplanetary and photospheric magnetic fields polarities observed by Mariner 4 and with solar mag-

netograph, noting noncorrelated data along latitudinal strip

18 p3205 A69-35399

MARINER 5 SPACE PROBE

Venus atmospheric structure from surface to 20,000 km radial distance from Mariner 5 radio experiments, noting large mass-2 hydrogen component in upper atmosphere

02 p0330 A69-12802

Venus radius determined by planetary radar and Mariner 5 radio tracking data

03 p0508 A69-13348

Venus and Mars atmosphere structure, comparing Venus atmosphere model with Mariner 5 observations

05 p0824 A69-16248

Lyman-alpha observations of Venus by Mariner 5 analyzed, assuming resonance scattering of flux by hydrogen or deuterium atoms in Venus atmosphere

05 p0815 A69-16255

Translational forces on Mariner 5 stemming from attitude control system studied to determine trajectory for scientific and operational purposes

[AIAA PAPER 69-114] 06 p1018 A69-18108

Venus research, discussing Mariner 5 and Venera, 4 data, radar tracking, orbit, diameter, gravity, density distribution, etc

08 p1391 A69-20456

Venus atmosphere structure determined from Mariner 5 flyby S band radio occultation measurements of ionosphere and atmosphere at illuminated and dark sides

21 p3794 A69-38380

Translational forces on Mariner 5 stemming from attitude control system, determining trajectory for scientific and operational purposes

[AIAA PAPER 69-114] 24 p4394 A69-43256

MARINER 6 SPACE PROBE

Mariner 6 and 7 Mars probes, describing mission profile, basic structure, trajectory design and scientific experiments

18 p3198 A69-34795

Mars exploration by 1969 Mariner 6 and 7 flyby, discussing mission and instrumentation

18 p3201 A69-35141

Narrow angle high resolution TV camera design and testing for Mariner 6 and 7 Mars flyby missions, noting computer drawn spot diagrams

19 p3307 A69-35808

Mariner 6 TV pictures with description of craters and south polar cap, noting moon-like crater abundance, form, arrangement and crater sizes

21 p3803 A69-38981

Mars upper atmosphere ionized carbon dioxide and CO emission spectra in 1900-4300 A region measured by Mariner 6, observing atomic hydrogen and oxygen lines

22 p4023 A69-40568

MARINER 7 SPACE PROBE

Mariner 6 and 7 Mars probes, describing mission profile, basic structure, trajectory design and scientific experiments

18 p3198 A69-34795

Mars exploration by 1969 Mariner 6 and 7 flyby, discussing mission and instrumentation

18 p3201 A69-35141

Narrow angle high resolution TV camera design and testing for Mariner 6 and 7 Mars flyby missions, noting computer drawn spot diagrams

19 p3307 A69-35808

Mars TV pictures from Mariner 7, describing prominent surface features

21 p3806 A69-39330

MARINER-MERCURY 1973

Mariner-Mercury 1973 flyby mission using Atlas-Centaur rocket and gravity-assisted maneuvers, discussing encounter geometries, spacecraft configuration and Venus probe considerations

[AAS PAPER 69-288] 24 p4381 A69-42862

MARINER PROGRAM

NT MARINER-MERCURY 1973

Deep space network system for radio navigation of Mariner mission in 1969, discussing objectives, spacecraft, tracking and data system, mission accuracy, etc

16 p2749 A69-31725

MARKETING

Air cargo transportation in 1970s, discussing Boeing 747 and Lockheed 500 super airfreighters, terminals, rates, marketing, etc

13 p2381 A69-27336

Internationalized defense marketing, suggesting formation of international consortia of industrial companies to design and produce defense systems

14 p2540 A69-28933

Ti alloys commercial applications and properties, discussing alloying elements influence, deformability, weldability, stress corrosion and market trends

16 p2801 A69-31784

R and D for economic growth, discussing interaction between management, planning, engineering, marketing, production, customers and competitors

17 p3077 A69-34126

Aerospace R and D marketing decisions, considering capability identification, business opportunities, strategies and independent program funding

17 p3077 A69-34127

Soviet efforts to market civil aviation equipment in West

18 p3232 A69-34538

Cargo handling systems for worldwide door to door service from marketing systems viewpoint

[RAES PAPER 1] 22 p4053 A69-40482

Space program planning, noting market requirements, acceptability and future characteristics

[AAS PAPER 69-083] 24 p4418 A69-42820

MARKING

NT ISOTOPIC LABELING

Electrolytic marking process for aircraft component identification without use of stamping or engraving

02 p0253 A69-12065

Cross hatching on various body surfaces due to periodic surface pressure fluctuations, discussing origin from counterrotating longitudinal vortices in boundary layer

[AIAA PAPER 69-11] 06 p0915 A69-18213

MARKOV CHAINS

Exponential distributions in Markov chain models for communication channels, considering error free runs of tropospheric systems

01 p0027 A69-10267

Monte Carlo method used to construct optimal algorithms for simulating homogeneous Markov chains whose trajectories reach absorbing state with probability of one

01 p0105 A69-10726

Noise resistance investigation of period synchronization systems described by Markov chains, determining phasing error for circuits

01 p0031 A69-10881

Optimal control problems for Markov chains solved by iterative method, using nonlinear finite difference equations to approximate degenerate elliptic functions

02 p0224 A69-11963

Delay method of finite ergodic Markov chains, analyzing first moments of state probabilities with aid of asymptotic equation

04 p0624 A69-15002

Time dependent statistical equilibrium equations solutions for describing time development of atomic populations by means of ergodic Markov chain

09 p1542 A69-22218

Iterative algorithm to determine transition probability final distribution in Markov extremal systems

11 p1861 A69-25712

Noise resistance of period synchronization systems described by Markov chains, determining phasing error for circuits

12 p2031 A69-26645

Optimal control of variational problem for Markov chain, discussing convexity and concavity of loss function

14 p2470 A69-28903

Moving targets trajectories determination from radar data, using posteriori probability distribution represented by Markov chain

15 p2566 A69-30334

Target trajectories determination based on radar data with allowance for association between neighboring readings, using statistical characteristics obtained with Markov chains

15 p2566 A69-30335

Markov chain applications to avionics weapons system reliability specifications starting with mission profile, failure rates, success probabilities, etc

15 p2581 A69-31136

Existence theorem for Markov chain finite state stochastic games applied to saddle point and optimal strategy or epsilon-optimal strategy pairs

22 p3975 A69-41010

Group interaction finite Markov chain model, analyzing changes in interpersonal relationships based on balanced dyadic states

23 p4110 A69-42017

MARKOV PROCESSES

Optimal distribution of search effort for moving target location, suggesting Markovian decision models

01 p0104 A69-10653

Sequential probability ratio test for detecting changes in Gauss-Markov process characteristics, noting application to fault detection in gyro navigational system
01 p0083 A69-11002

Ideal gas spectra and density fluctuations correlations calculated during Markovian and nonMarkovian wandering of particles
03 p0477 A69-13414

Finite state finite-action-space Markovian decision process, discussing optimal policies set in discrete dynamic programming
04 p0624 A69-14951

Markov extremum drift dual compensation in optimal systems with learning experiments
05 p0741 A69-16671

Secondary acquisition systems analysis by semi-Markov process model, defining minimum average acquisition time
08 p1270 A69-19852

Continuous variate duration estimates by Markov process, giving example of surface air temperature conditional probability distribution
08 p1346 A69-20731

Confidence limits determined for damping parameter of complex stationary Gaussian Markov process
11 p1910 A69-25700

WSEIAC /Weapon System Effectiveness Industry Advisory Committee/ formula, analyzing correctness within Markovian limitations and reward systems extension
12 p2102 A69-26570

Optimal direction finding systems based on bearing angle representation in multidimensional Markov process, considering white and interference noise
13 p2219 A69-27254

Heat transfer and temperature distribution in thin fins with stochastic root temperature due to excitation by stochastic and Markov processes [ASME PAPER 68-HT-35]
13 p2374 A69-27780

Computerized Markov effectiveness models of repairable and nonrepairable complex aerospace systems
18 p3195 A69-34527

Homogeneous Markovian sum of sequence of random quantities series, deriving limiting theorem for sum density
21 p3757 A69-39538

Random processes integration and differentiation and spectral density determination, examining Markov, Gaussian and point processes
22 p3975 A69-40777

Fokker-Planck plasma collision equation derived from Boltzmann equation, Markov process and Liouville equation
23 p4195 A69-41516

MARROW

Bone marrow cell division disturbance in rats after proton irradiation
07 p1064 A69-18973

Bone marrow cell division disturbance in rats after proton irradiation
20 p3479 A69-38221

MARS [PLANET]

Extraterrestrial life possibility in solar system, noting Martian atmosphere and terrestrial life adaption to Mars simulations
02 p0198 A69-11770

Manned Mars and Venus missions role in overall planetary exploration program
02 p0324 A69-12304

Jupiter, Venus and Mars 8.6 mm radio emission, obtaining average disk brightness temperatures
02 p0327 A69-12716

Entry and terminal deceleration systems for unmanned Martian landers, discussing parachute landing and lifting entry vehicles [AIAA PAPER 68-1147]
03 p0521 A69-13670

Mars biological exploration, discussing life detection, chemical and biological experimental strategy [AIAA PAPER 68-1122]
03 p0375 A69-13700

Microorganism viability in rocket engine combustion environments used to determine probability of biological contamination of Mars by Voyager missions
05 p0714 A69-15949

Mars contamination with terrestrial microorganisms, considering possibility of waste materials ejection from manned orbital vehicles
05 p0714 A69-15951

Meteorological observations of Mars northern polar cap and Southern Hemisphere from northern summer solstice to early autumn
05 p0825 A69-16302

Mars polar cap ice cap and dry ice theories, discussing dark wave and cloud distribution meteorological observations
07 p1212 A69-18603

Lunar opposition effect theory applied to Mars opposition effect on brightness
07 p1214 A69-18616

Martian structure theory, comparing mathematical model based on earth long term evolution and ad hoc models
08 p1387 A69-20092

Maximum capacity estimation for one way transportation systems to moon and Mars, analyzing technical and economic aspects
09 p1586 A69-21297

Spectral reflectivity curves for bright and dark areas of Mars noting seasonal crossings
09 p1587 A69-21308

Bioorganic comparative analysis of desert soils, Precambrian shales and meteorites by automated pyrolysis-gas chromatography-mass spectrometry system for future Mars soil analysis [JPL-TR-32-1368]
11 p1832 A69-25640

Limits for Martian surface materials established by comparing visible and IR spectra with laboratory spectra
12 p2156 A69-26225

Photometric and polarimetric properties of Mars, discussing powder covering, chemical composition and particle size of bright and dark areas and blue haze
12 p2171 A69-27145

Chemical composition of earth, Venus, Mars, Mercury and moon calculated from mathematical models, constructing approximate equations of state at high pressure
14 p2526 A69-29878

Fluid controlled solid rocket motors design for Mars mission with acceleration level as parameter, discussing mission specifications, system design and component considerations [AIAA PAPER 69-446]
16 p2841 A69-32687

Photographic observations of Mars position and surrounding stars, correcting coordinates for Mars phase by local desensitization of plate
17 p3027 A69-32873

Mars internal structure and composition modeling, considering core, mantle and temperature via earth analogy and Mariner 4 data
17 p3037 A69-33652

Mars 1969 opposition observations, discussing extremes in north and south hemispherical polar cap behavior, frosty deposit colorings and polar vapor/clouds
17 p3043 A69-34141

Mars autonomous entry navigation, discussing flight path angle control with onboard sensors using realistic sun, Canopus and planet line of sight tracker accuracies
19 p3368 A69-35790

Moon composition and similarities to Mars explained by silicates in solar system raw material
20 p3604 A69-37563

Abort capability mission selection criterion, evaluating energy requirements, Mars flyby and velocity contours [AAS PAPER 68-139]
21 p3805 A69-39209

Statistical error analysis of autonomous manned spacecraft navigation in long duration eccentric Mars orbits [AIAA PAPER 69-880]
21 p3763 A69-39406

Mars positions determined from photographic observations by zone astrophot, establishing rms errors and objective centering error
22 p4025 A69-40613

Spectral reflectivity curves for Mars light and dark areas and seasonal changes of dark area simulated in laboratory
23 p4209 A69-41319

Mars exploration for life by Mariner flybys and orbiters and 1973 Viking landers
23 p4212 A69-41611

Life on Mars, past and future missions, possibilities of metabolic system and analysis methods
23 p4212 A69-41612

Mars landing site topography reconstructed via stereoscopic pictures returned by surface-based imaging systems
23 p4164 A69-41618

Manned flyby/orbiter of Mars providing scientific information at low incremental cost [AAS PAPER 69-180]
24 p3379 A69-42813

Mariner 6 and 7 TV data, discussing implications for Mars present state, past history and biological status
24 p4384 A69-43195

MARS ATMOSPHERE

Ebert spectrometric experiment during Mars flyby aimed at detecting upper atmosphere atoms, ions and molecules in 1100-4300 angstrom spectral range [AAS PAPER 68-184]
02 p0311 A69-11469

S-band radio occultation for probing atmospheres of Mars and Venus [AAS PAPER 68-185]
02 p0311 A69-11470

Direct planetary atmosphere measurement by vehicles entering atmosphere, using Mars and Venus model atmospheres for accuracy expectation [AAS PAPER 68-187]
02 p0311 A69-11472

Active control system augmentation of inherent aerodynamic damping assuring acceptable limits on oscillatory rotational motion during hypersonic Martian atmospheric entry
02 p0333 A69-11742

Ablative heat shield materials for Mars and Venus atmospheric entries
02 p0333 A69-11750

Extraterrestrial life possibility in solar system, noting Martian atmosphere and terrestrial life adaption to Mars simulations
02 p0198 A69-11770

Collection of papers on atmospheres of Venus and Mars covering atmospheric models, light scattering, radio occultation experiments, etc
02 p0318 A69-12101

Mars and Venus atmospheres, Martian atmosphere dynamics, Mars ionosphere and use of space probes
02 p0318 A69-12102

Mars lower atmospheric pressure, temperature and composition, noting consistency between photometric, spectroscopic and occultation techniques
02 p0319 A69-12104

Atmospheric circulation on rotating and nonrotating planets with shallow atmospheres applied to Mars and Venus atmospheres
02 p0320 A69-12110

Martian upper atmosphere and ionosphere, considering Mariner 4 occultation results and various atmospheric models
02 p0320 A69-12112

Mariner 4 Martian ionospheric data interpreted in terms of E, F1 and F2 regions
02 p0320 A69-12113

Mariner 4 ionospheric densities to deduce Martian atmospheric modes, discussing validity of using ionospheric properties to discriminate between models
02 p0320 A69-12114

Radio occultation measurements of Venus and Mars atmospheres using Mariner spacecraft
02 p0320 A69-12115

Radio amplitude and phase measurements during Mariner-Mars encounter, providing evidence for Martian atmospheric models
02 p0320 A69-12116

Martian upper atmospheric ionization process analogous to cometary material ionization in solar wind
02 p0320 A69-12117

Photoelectron energy loss mechanisms in planetary atmospheres, considering possible constituents in Mars and Venus upper atmospheres
02 p0321 A69-12118

Planetary atmosphere determination error analysis using Kalman filter, noting results of simulated Martian atmosphere entry
02 p0331 A69-12806

Deceleration control system for aerobraking and skipout to orbit at Mars [AIAA PAPER 68-1146]
03 p0520 A69-13564

Aeroshell structural development for Mars flyby and entry landing mission compatible with Atlas/Centaur launch vehicle [AIAA PAPER 68-1159]
03 p0521 A69-13667

Venus and Mars atmosphere structure, comparing Venus atmosphere model with Mariner 5 observations
05 p0824 A69-16248

Terrestrial and Martian aerosols estimation based on carbon dioxide spectral and Mariner 4 RF occultation measurements [AIAA PAPER 69-52]
06 p1011 A69-18199

Dynamic stability derivatives of large angle blunted conical spacecraft near transonic speed in simulated Mars environment for various angles of attack [AIAA PAPER 69-104]
06 p1019 A69-18210

Mars polar cap ice cap and dry ice theories, discussing dark wave and cloud distribution meteorological observations
07 p1212 A69-18603

Mars lower ionosphere ionization from spectroscopic and Mariner 4 occultation data, discussing various ionization sources
07 p1213 A69-18607

MARS ENVIRONMENT

Recombination mechanism between CO and O produced by photodissociation of carbon dioxide in upper atmosphere of Venus and Mars
07 p1214 A69-18615

Monte Carlo method for calculating atomic hydrogen escape rate from carbon dioxide atmosphere, considering Mars and Venus atmospheres
08 p1386 A69-20076

Mars and Earth atmospheric carbon dioxide simulation and spectroscopic measurement for developing planetary surface pressure estimating procedures from IR transmission measurements
08 p1354 A69-20151

Mars and Venus atmospheric properties, noting influence of biosphere and human activity on earth atmosphere
08 p1408 A69-21160

Gamma ray scattering gauge design optimum parameters to measure Mars atmospheric density
09 p1495 A69-21842

Aerothermoelasticity problems for Mars entry vehicles, discussing deceleration loads, separated hot gas flow, shield thermal gradients and oscillatory body motion
[AIAA PAPER 68-283] 09 p1610 A69-21991

Carbon dioxide abundance in Mars atmosphere measured with three etalon Fabry-Perot spectrometer
09 p1607 A69-22427

Optical characteristics of Martian atmosphere from photometric data for continent-mare contrasts, discussing transmittance and optical thickness
11 p1959 A69-24727

Venus and Mars atmospheric braking entry and associated equipment, discussing potential cost savings
11 p1968 A69-25722

Mars higher atmospheric transparency and changes in surface colors
12 p2154 A69-25823

Atmospheric models for exospheric temperatures of Mars and Venus based on photoionization heating efficiency
12 p2155 A69-26020

Planet Mars stellar magnitude found dependent on processes occurring in atmosphere and at surface
15 p2689 A69-30565

Radio wave absorption by water vapor in Venusian and Martian atmospheres, constructing model from Venera 4 data
15 p2569 A69-30952

Mars surface and atmospheric properties from polarization degree measurements, discussing optical properties of soil and detection of veils, mists and clouds
16 p2854 A69-31655

Martian surface features and climate with emphasis on atmospheric surface layers, assessing Mariner 4 data
17 p3029 A69-33040

Shock layer properties, radiative and convective heat transfer about two hypersonic blunt bodies at zero angle of attack in assumed Martian atmosphere
[AIAA PAPER 69-634] 17 p2891 A69-33281

Earth ecosystem chemical composition compared with Mars and Venus ecosystems to determine presence of life
18 p3193 A69-34361

UV solar radiation variation effects on Mars and Venus upper atmosphere temperatures
20 p3595 A69-37136

Adaptive control for Mars entry based on sensitivity analysis
[AIAA PAPER 68-8355] 20 p3573 A69-37193

Colpoda maupasis resistance to Martian atmospheric pressure and oxygen partial pressure noting adaptation, reproduction and existence
20 p3478 A69-37627

Mayeda flare observed on Mars on 4 June 1937, suggesting oriented reflection of solar rays from ice crystals cloud or Martian surface feature
20 p3608 A69-38049

Martian surface and atmosphere interpretation through polarimetric and photometric simulation
20 p3614 A69-38253

Venus, Mars and Jupiter lower atmospheric motions, considering atmospheres thermal and chemical composition
21 p3811 A69-39511

Martian atmosphere circulation compared to terrestrial, considering absence of oceans, radiative coupling and planetary scale motions
21 p3814 A69-39569

Deceleration control system for aerobraking and skipout to orbit at Mars
[AIAA PAPER 68-1146] 21 p3828 A69-39761

Water vapor abundance in Mars atmosphere determined from spectrograms, noting restricted existence on surface
22 p4018 A69-40268

Dynamic stability derivatives of large angle blunted conical spacecraft near transonic speed in simulated Mars environment for various angles of attack
22 p4036 A69-40550

Mars upper atmosphere ionized carbon dioxide and CO emission spectra in 1900-4300 A region measured by Mariner 6, observing atomic hydrogen and oxygen lines
22 p4023 A69-40568

Mars atmosphere response to surface temperature changes by radiative and convective heating, noting strong solar control of mean wind distribution
23 p4212 A69-41614

Mars light polarization observations noting unsatisfactory surface pressure determinations
23 p4212 A69-41615

Mars atmospheric features from measurements during entry and after landing, discussing atmospheric state properties, diurnal variability, clouds and winds
23 p4212 A69-41617

Carbon monoxide presence in Martian atmosphere from Mars line spectra, giving content, surface pressure and concentration
23 p4220 A69-42379

Mars atmosphere study by Mariner 6 and 7 spacecraft, discussing instrumentation on board
[AAS PAPER 69-091] 24 p4393 A69-42881

Vector matrix second order sensitivity equation application to Mars entry guidance, performing numerical simulation of second order sensitivity guidance and tabulating results
24 p4388 A69-43690

MARS ENVIRONMENT

Soil, moisture and other requirements for microorganism survival in simulated Martian environment
01 p0018 A69-11091

Enzymes in simulated Martian environment exhibit higher resistance than in earth atmosphere at 4 C
07 p1065 A69-18974

Martian entry test facility for real size entry systems, discussing design, fabrication and operation
15 p2587 A69-30390

Mars lander thermal control system design parameters including environment, power duty cycle and lander size and weight
[AIAA PAPER 69-610] 17 p3072 A69-33274

Mars exploration by 1969 Mariner 6 and 7 flybys, discussing mission and instrumentation
18 p3201 A69-35141

Enzymes in simulated Martian environment exhibit higher resistance than in earth atmosphere at 4 C
20 p3479 A69-38222

Physical and life supporting properties of hypothetical Martian biosphere, considering organism adaptation theories
22 p3876 A69-40271

Mars thermal energy emission measurement by Mariner 1969 IR radiometer, indicating frozen carbon dioxide cap and minimum temperature
24 p4384 A69-43196

MARS EXCURSION MODULE

Impact limiter system design for Mars landing vehicle noting balsa wood or phenolic honeycomb construction
[AIAA PAPER 68-161] 21 p3820 A69-39228

MARS PROBES

NT MARINER 4 SPACE PROBE

NT VIKING LANDER SPACECRAFT

Soviet lunar and planetary probes, reviewing payload characteristics, principal mission features and photographs associated with Luna, Mars, Venera and Zond series
01 p0162 A69-10938

Multieengine Martian soft lander guidance and control system design with single engine failure accommodation based on six degrees of freedom computer simulation
02 p0277 A69-11740

Mars planetary entry and landing model tests, demonstrating technological feasibility of mission
02 p0333 A69-11746

Mars capsule feasibility model terminal dry heat thermal sterilization cycle determined from microbial data
02 p1201 A69-11772

Longitudinal range dispersion of unmanned Mars landers using VM-8 and VM-9 atmospheric models, discussing Syrtis Major as possible landing site
02 p0324 A69-12390

Mars and Venus probes antenna problems in environments of near earth space, deep space and nonearth planetary atmospheres
02 p0223 A69-12811

Mission capability differences between direct and orbital Mars missions as to launch period selection, targeting capability and error analysis
02 p0331 A69-12821

Mission mode and delivery method influence on payload maximization for Mars capsule system
02 p0335 A69-12822

Mars unmanned spacecraft mission profiles for surface imaging, noting influence of lighting requirements
[SMPT PAPER 104-21] 04 p0650 A69-14361

Suboptimal guidance corrections for continuous thrust vehicle disturbances during minimum fuel rendezvous in Martian orbit, discussing physical and modified cost functional
[AIAA PAPER 69-76] 06 p0956 A69-18081

Mars imaging mission and astrodynamic interaction, discussing arrival geometry and orbit size effects
[AIAA PAPER 69-127] 06 p1011 A69-18169

NERVA rocket engine with 200,000-250,000 lb thrust to replace Saturn 5 upper stage for manned interplanetary flights, discussing Mars flight
08 p1410 A69-21029

Mars planetary landing program schedule, COSPAR quarantine policy and biological losses from failures to collect data and from contamination
11 p1828 A69-25459

Reliability and maintainability analysis of two year spacecraft mission combining earth orbits and Mars program, using computerized mathematical model
[AIAA PAPER 68-1059] 12 p2174 A69-26797

Exploding bridgwire /EBW/ systems compared to hot-wire initiators for Mars space probe
17 p2905 A69-34108

Scientific space research program /1968-1978/ outlining advanced lunar orbiter and Mars, Venus and Mercury probes
18 p3193 A69-34360

Mariner Mars 1969 flyby missions objectives, experiments, spacecraft configuration, trajectory design, sterilization, flight path control and photographic imaging
[AAS PAPER 68-134] 19 p3402 A69-35938

Friction tests for Mariner Mars 1969 spacecraft mechanisms in ultrahigh vacuum molecular sink chamber, noting increased friction attributed to vacuum environment
[AIAA PAPER 69-996] 22 p3920 A69-40374

Mars exploration for life by Mariner flybys and orbiters and 1973 Viking landers
23 p4212 A69-41611

Mars atmospheric features from measurements during entry and after landing, discussing atmospheric state properties, diurnal variability, clouds and winds
23 p4212 A69-41617

MARS SPACECRAFT

U MARINER SPACECRAFT

MARS SURFACE

Wolf Trap life detector design to sample and culture Martian surface dirt for microorganism growth
02 p0201 A69-11769

Annular and linear Martian surface formations nature and origin from analysis of Mariner 4 photographs
03 p0506 A69-13087

Martian surface properties, discussing limonites prevalence and dust layer evidence as causes for reddish color
03 p0509 A69-13357

Mars unmanned spacecraft mission profiles for surface imaging, noting influence of lighting requirements
[SMPT PAPER 104-21] 04 p0650 A69-14361

Lunar and Martian annular formations and structures, discussing classification, morphological characteristics, incidence frequencies and area sizes
04 p0658 A69-14959

Mars surface photometric and spectrophotometric measurements, relating opposition effect details with corresponding laboratory sample measurements
07 p1212 A69-18601

Mars surface features identification from comparison of Mariner 4 and ground bases telescopic photographs
07 p1213 A69-18605

Spectral reflectivity curves for bright and dark areas of Mars noting seasonal crossings
09 p1587 A69-21308

Martian polar caps dimensions as function of planet heliocentric longitude examined from photographic observations, noting compatibility with spectroscopic data
11 p1959 A69-24728

Mars photographic and radar data correlation indicating smoothness of dark areas and roughness of desert areas
11 p1964 A69-25406

Mars higher atmospheric transparency and changes in surface colors
12 p2154 A69-25823

Martian crater density determined by comparison of statistical counts from Mariner 4 photographs
12 p2157 A69-26309

Martian canals nature based on high contrast photographs obtained by Mariner 4 space probe
12 p2171 A69-27133

Martian diagonal and longitudinal-meridional canals mapped into grid systems, noting differences between Martian and lunar crusts tectonic activity
13 p2337 A69-27533

Spectral reflectivity differences of selected dark and bright regions of Mars observed with double beam photometer
13 p2338 A69-27553

Annular and linear Martian surface formations nature and origin from analysis of Mariner 4 photographs
14 p2515 A69-28769

Planet Mars stellar magnitude found dependent on processes occurring in atmosphere and at surface
15 p2689 A69-30565

Mars surface and atmospheric properties from polarization degree measurements, discussing optical properties of soil and detection of veils, mists and clouds
16 p2854 A69-31655

Martian bright surface areas identified as homogeneous powder having opaque grains, discussing hydrated iron oxides contributions to observed optical properties
16 p2855 A69-31660

Martian topography during rotation observed using radar round trip echo delay at 7840 MHz, discussing dark areas relation to elevation
16 p2860 A69-32238

Martian surface features and climate with emphasis on atmospheric surface layers, assessing Mariner 4 data
17 p3029 A69-33040

Thermal design of landed vehicle on Mars surface, discussing instrument package covering inside surface coating and battery insulation
[AIAA PAPER 69-611] 17 p3049 A69-33295

Mars surface temperature calculated by applying Humphrey formula for planetary radiation energy, finding mean annual values of temperature for different albedo
17 p3034 A69-33412

Subsurface Martian temperature from sinusoidal temperature variation theory for semiinfinite homogeneous medium, plotting amplitude, mean surface and diurnal soil temperature curves
17 p3034 A69-33413

Lunar and Martian annular formations and structures, discussing classification, morphological characteristics, incidence frequencies and area sizes
18 p3197 A69-34722

Mars photographs from various observatories taken during 1969
20 p3598 A69-37424

Adenosine triphosphate /ATP/ content of terrestrial soils, based on firefly bioluminescent reaction, for Mars soil problems
20 p3473 A69-37567

Mayeda flare observed on Mars on 4 June 1937, suggesting oriented reflection of solar rays from ice crystals cloud or Martian surface feature
20 p3608 A69-38049

Optical parameters of Martian surface and temperature, discussing brightness distribution along diameter in red spectral region, based on photoelectric cross sections
20 p3608 A69-38050

Martian surface and atmosphere interpretation through polarimetric and photometric simulation
20 p3614 A69-38253

Mariner 6 TV pictures with description of craters and south polar cap, noting moon-like crater abundance, form, arrangement and crater sizes
21 p3803 A69-38981

Mars TV pictures from Mariner 7, describing prominent surface features
21 p3806 A69-39330

Computer system functional requirements for autonomous Martian surface roving vehicle, emphasizing vehicle motion control system
[AIAA PAPER 69-980] 22 p3907 A69-40360

Mars atmosphere response to surface temperature changes by radiative and convective heating, noting strong solar control of mean wind distribution
23 p4212 A69-41614

Mars light polarization observations noting unsatisfactory surface pressure determinations
23 p4212 A69-41615

Martian surface mineralogical study of present state and past processes from rock analyses by unmanned spacecraft instruments to test planetary models
23 p4212 A69-41619

Solar array configurations and performance on Martian surface, including hard lander design and surviving shock levels
23 p4073 A69-42289

Mariner 6 and 7 TV data, discussing implications for Mars present state, past history and biological status
24 p4384 A69-43195

Design criteria for antenna control equipment for earth tracking from landing site on Martian surface
[AIAA PAPER 68-868] 24 p4348 A69-43246

Average meteorite flux at Martian surface estimated by generating flux distribution for Martian atmosphere top and adjusting for mass loss and deceleration
24 p4387 A69-43351

Martian seasonal darkening attributed to windblown dust
24 p4389 A69-43742

MARS 69 PROJECT

Targeting technique for Atlas/Centaur Mariner Mars 1969 mission, noting suitability to flyby, orbiter or landing interplanetary missions
[AIAA PAPER 69-881] 21 p3764 A69-39407

Mariner Mars 1969 TV system environmental test and calibration program
22 p3920 A69-40372

MARTENSITE

Martensite transformation by simple shear in equiatomic Ni-Ti alloy, using transmission electron microscopy
02 p0265 A69-12024

Metal/alumina interfaces strength, examining correlation with wetting and bonding and martensitic transformations
03 p0447 A69-13612

Martensitic transformation in Ti-Al-Mo alloys, noting specific features and effects of Mo content
04 p0617 A69-14940

Electron microscopic study of structural changes occurring during aging of martensite in Fe-Ni-Ti alloy
05 p0783 A69-16813

Titanium vanadium martensite decomposition kinetics during heating, showing shearing process and dependence on temperature during quenching
07 p1163 A69-18778

Spontaneous martensite phase transformation in Ti-Cr alloy thin foils formed electrolytically
10 p1708 A69-22994

Monograph on effect of boron, zirconium and titanium on austenite transformation of CrMo steels bainite and martensite covering carbides, nitrides, mechanical properties, etc
11 p1903 A69-24634

Lattice defects in annealed and plastically deformed cobalt, showing increase with increasing martensite transformations
12 p2113 A69-26042

Martensite transformation in Ti-Cr binary alloys by thin foil electron microscopy, noting crystallographic theory
13 p2276 A69-27369

Structural features of Fe-Ni massive martensite observed by light, electron and hot stage microscopies showing parallel block packet
13 p2276 A69-27401

Homogenization of martensite formation in nickel 300 grade maraging steel, analyzing anisotropic transformation strains during thermal cycling
13 p2278 A69-27410

Precipitation influence on martensite formation kinetics and structure of Fe-Ni-Ti alloys
13 p2279 A69-27765

Tishomingo iron meteorite metallography, noting nickel content and martensitic microstructure evolution
13 p2353 A69-28159

Nital etchant and sodium bisulfite stain for morphology of quenched dilute alloy Fe-Ni martensite
13 p2282 A69-28166

Martensite transformation with fcc lattice in Ti alloys containing 5.9 percent Fe analyzed as function of cooling rate using X ray analysis
15 p2636 A69-30105

Titanium alloy martensites crystallography by electron microscope, discussing lattice parameters and spontaneous transformation
18 p3154 A69-34245

Cumulative rapid thermal cycling influence on progressive disappearance martensitic transformation in 18 percent nickel maraging steel
18 p3155 A69-34650

Martensite transformation, C content and work hardening relations in stainless steels studied for magnetic detection of embrittlement during deformation
18 p3138 A69-35117

Phase shape deformation and austenite stabilization in Fe-Ni and Fe-Ni-Ti alloys following secondary alpha phase of reversed martensite-austenite transformation
18 p3159 A69-35448

Isothermal and thermal martensite transformations on polished surfaces of Fe-Ni-Mo alloys
19 p3344 A69-35983

Quench rate effect on martensite start temperature and fine structure of Fe-C and Fe-C-Ni steel, using transmission electron microscopy
20 p3557 A69-36956

Crystallographic relations between mother gamma phase and bulk martensitic structure of Fe-Ni alloys with less than 20 percent Ni, using radioisotopes
20 p3562 A69-37781

Ti-V martensite decay during heating, noting temperature dependence of elastic moduli and electrical conductivity
21 p3746 A69-39160

MARTENSITIC STAINLESS STEELS

High pressure hydrogen environment on tensile properties of stainless steel with and without strain induced martensite
01 p0093 A69-10062

Kinetic features of martensitic transformation of nickel steels dependent on plastic deformation degree at 525 C
02 p0267 A69-12190

Aging of iron-nickel-titanium alloys during heating in reverse martensitic alpha to gamma transformation process, investigating phase parameter changes
04 p0613 A69-14558

High strength martensitic aging steels alloying effects, phase transformation and aging
04 p0615 A69-14644

Brittle fracture resistance of low carbon maraging and martensitic steels with cracks established by crack growth measurements during tensile and impact tests
04 p0615 A69-14647

Retained austenite content control, strain aging and ausforming to improve toughness of high strength martensitic stainless steel without strength loss
08 p1330 A69-20010

Austenite to martensite strain induced transformation effect on energy absorption during crack propagation
10 p1709 A69-23074

Thermal fatigue testing system for martensitic steels using fluidized bed heating and cooling, specimen manipulation means, cycle control, data evaluation, etc
10 p1714 A69-23979

Stainless steels stress corrosion susceptibility, detecting chromium carbide in martensitic matrix by galvanic nondestructive test method
14 p2466 A69-29935

Alloying elements effect on low temperature notch-bend fracture toughness of martensitic high strength steels, noting transition temperature
20 p3556 A69-36952

Precipitation hardening stainless steels applications in aerospace industry, discussing steel selection and heat treatment
20 p3563 A69-37931

MARTIN MILITARY AIRCRAFT
U MILITARY AIRCRAFT

MASCONS

Lunar geophysical features origin, noting mascons influence and surface rigidity
13 p2352 A69-27903

Convection within moon as explanation of maria on near side, presence of mascons, etc
20 p3603 A69-37561

Lunar mascons and maria isostasy, discussing time requirements
20 p3604 A69-37564

Lunar Orbiter data for existence of unequal mass distributions in lunar interior confirmed by manned Apollo 8 and 10 flights, discussing origin
20 p3606 A69-37933

Figure and inhomogeneities relationship for moon, Mercury, Venus, Mars and earth, discussing circular basins and mascons
21 p3803 A69-38980

Variations in gravity, plotting results for U.S., with tables for Alaska, Mexico, India, Africa, etc
21 p3718 A69-39735

Lunar gravitational field data from Lunar Orbiter spacecraft reprocessed, discussing mascon effects on moon structure and evolution theories
24 p4379 A69-42785

MASER OUTPUTS

Hydrogen maser oscillations with external gain, noting frequency stability
04 p0611 A69-14443

Molecular interactions in ammonia maser beam, discussing influence on oscillation extinction beyond given flow rate
07 p1145 A69-18478

Rate equation analysis for internally optically pumped millimeter wave maser operating in laser crystal
07 p1146 A69-18480

Trivalent iron doped andalusite crystals dielectric and maser properties, investigating spin-lattice relaxation, cross relaxation times and inversion ratio [IEEE PAPER C-2]
07 p1150 A69-19049

Upper and lower frequency stability bounds using hydrogen masers, studying signal power and relaxation rate as function of resonator effective field
08 p1327 A69-20715

Transition probabilities in repetitively Q modulated HCN maser radiation dependent on gas discharge current
09 p1516 A69-21626

Cavity system for constructing paramagnetic masers with different active materials
09 p1519 A69-22288

Electron density and collision frequency of MHD plasma determined directly by measuring phase shift and attenuation of propagating laser microwave signal
10 p1731 A69-23436

Condensation sources of maser radiation observed in W3 hydroxyl lines, discussing polarization and designation as protostars
11 p1954 A69-24379

Maser emission in interstellar OH ground state produced by IR pumping, noting population inversion mechanism
15 p2691 A69-30762

Maser amplification of 9.5 GHz longitudinal elastic waves in divalent nickel impurity ions doped sapphire by stimulated emission from inverted spin population
16 p2795 A69-31554

Quantum mechanical microwave frequency doubling in ruby, discussing output power variation with orientation
17 p3015 A69-33024

Q switching of CW 337 mu maser, gain factor measurements for pulse discharges and data on saturation and time dependence
17 p2981 A69-33088

Lambda doublet maser emission from excited OH rotational level, discussing conditions necessary for microwave radiation
18 p3185 A69-34292

Maser submillimeter emission lines used to determine atmospheric and water vapor absorption, noting role of pressure
20 p3553 A69-37296

Protostar chemical processes responsibility for population inversion and properties in OH and water masers
22 p4018 A69-40267

Condensation sources of maser radiation observed in W3 hydroxyl lines, discussing polarization and designation as protostars
24 p4389 A69-43769

MASER RESONATORS

U MASERS

MASERS

NT GAS MASERS

NT PROTON MASERS

NT TRAVELING WAVE MASERS

Partial maser effect in recombination lines of hydrogen atoms in nebular plasma due to overpopulation of energy levels at thermodynamic equilibrium
01 p0148 A69-10042

Parallel and coplanar Brewster angle grinding of maser tube ends
03 p0440 A69-13302

Radiation intensity from system of monoenergetic relativistic electrons in plasma, discussing maser effect in coherent synchrotron radiation
03 p0500 A69-13407

Interstellar gas masers account for properties of 18 cm emission lines from OH molecules
03 p0511 A69-13465

Maser model of single mode field coupled to N identical two level atoms, deriving threshold, stable and unstable steady states, relaxation oscillations, etc
03 p0441 A69-14108

Quantum paramagnetic amplifier using andalusite single crystal and operating with three level pumping system
04 p0577 A69-14780

Pulsed radar quantum paramagnetic amplifier protection from driving pulse leakage power by transient processes
05 p0728 A69-15644

Cyclotron resonance measurements of quantum effects in Ge valence bands by CW molecular gas laser, developing tunable submillimeter maser [IEEE PAPER C-6]
07 p1150 A69-19051

Amplitude modulation of radiation pulses of two level paramagnetic maser as affected by inhomogeneous broadening and spinning of resonance line
07 p1158 A69-19751

Molecule reorientation and transition probability in molecular beam maser using formaldehyde
07 p1158 A69-19760

Quantum paramagnetic amplifier saturating power dependence on input pulses length and frequency determined by kinetic equations solution
08 p1325 A69-20436

Cavity system for constructing paramagnetic masers with different active materials
09 p1519 A69-22288

Atomic clocks frequency standards, discussing masers, atomic beam resonators and gas cells and various applications
09 p1501 A69-22598

Cyclotron harmonic waves /CHW/ nonlinear decay instability and parametric amplification, considering applicability to practical amplifiers
12 p2135 A69-26314

Pulse radar quantum paramagnetic amplifier protection from saturation by transmitter power, using linear electrical bias of EPR line
15 p2579 A69-30956

Pulsed radar quantum paramagnetic amplifier protection from driving pulse leakage power by transient processes
16 p2762 A69-32501

Wide tuning range S band low noise maser amplifier system, discussing bandwidth, gain and packaging for antenna mounting
17 p2979 A69-32914

Quantum electronics, Volume 2, Maser amplifiers and oscillators
17 p2982 A69-33687

Gas and solid state microwave quantum generators and amplifiers, discussing radiation characteristics
18 p3153 A69-35407

Andalusite crystals as active media in paramagnetic quantum amplifiers, discussing design and performance
19 p3333 A69-35881

Lasers and maser devices in radio quantum electronics, discussing optical parametric and microwave devices including transistors, diodes, magnetrons, etc
19 p3284 A69-36433

Accuracy and frequency stability of H masers in terms of wall collision effect and cavity resonator tuning
21 p3741 A69-39685

MASKING

Refractory metal silicon device technology noting high temperature diffusion masking properties for possible use in MOSFET technology
06 p0930 A69-17152

Auditory temporal masking of tonal signal by narrow band noise and perception of temporal order noting effects of intensity, frequency and time
11 p1830 A69-24795

Visual retroactive perceptual masking effect in monkeys pretrained in visual discrimination task, interpreting electrical potentials recorded along optic pathways
22 p3876 A69-40265

Visual backward masking experiment for studying overlapping and nonoverlapping contours of target and masking stimuli straight line
22 p3879 A69-40843

MASKS

NT OXYGEN MASKS

Radio telemetry system for evaluating protective masks dynamic performance by remote simultaneous monitoring of respiration, acceleration and temperature data generated by human subjects
23 p4121 A69-41765

MASS

NT CRITICAL MASS

NT ELECTRON MASS

NT MASCONS

NT PARTICLE MASS

NT PLANETARY MASS

NT STELLAR MASS

Meteor masses and atmospheric density calculation inaccuracy by use of effective stellar magnitudes of meteors
02 p0314 A69-11695

Mass effect on frequency tested during approach of pulsar to sun
02 p0323 A69-12298

Instability phenomena encountered in galaxies determined based on classification of galaxies according to mass and brightness
12 p2163 A69-27019

Meteor masses and atmospheric density calculation inaccuracy by use of effective stellar magnitudes of meteors
13 p2355 A69-28726

Nuclear level density and mass shell corrections relationship for deformed and undeformed nuclei
14 p2488 A69-29337

Inertial and gravitational mass equality reexamined, considering Galileo, Newton and Eotvos experiments
14 p2486 A69-29647

Optical and radio estimations of galactic masses, analyzing radius of rotation curve inflection point
15 p2687 A69-30547

Rotation curve, mass and M/L ratio of Sc galaxy NGC 6574, discussing nucleus and systemic velocity
15 p2691 A69-30764

Radio galaxy Messier 87 mass determined using virial theorem for nucleus velocity dispersion
15 p2695 A69-30883

Line widths of 48 galaxies at 21 cm and spectroscopic data, estimating masses and angular momenta, finding mass-angular momentum relation
16 p2866 A69-32818

Partially conserved axial vector currents and current algebra to obtain vertex functions at point having zero mass by extrapolations
17 p3008 A69-33004

Meteor dynamical and photometrical analyses compared quantitatively, determining mass loss value from fragmentation model
17 p3045 A69-34223

MASS BALANCE

Laminar flow stream containing periodic fluctuation of mass fraction of chemical species over flat plate with reactive surface
11 p1831 A69-24284

Satellite attitude control mass properties, showing weight tradeoff analyses role in selecting control system
18 p3208 A69-34885

PDP8 digital computer and Trebel vertical balancing machine combined for real time presentation of trim weights and positions, noting noise in force components
18 p3220 A69-34888

Moment of inertia measurements facility for spacecraft dynamic balancing operations at low angular rates
18 p3118 A69-34889

Aircraft on board weight and balance system, discussing operations and economics programs [SAWE PAPER 805]
18 p3091 A69-34901

MASS DISTRIBUTION

Gas combustion hydrodynamic stability using feedback equation and theorems for variations in mass and momentum vector
01 p0173 A69-10087

Open cosmological model containing radiation and matter, noting matter density relationship to visible matter average
01 p0150 A69-10371

Mass functions of real earth derived from satellite orbital perturbations [UN PAPER 68-95385]
01 p0064 A69-10460

Einstein equations obtained for axisymmetric distribution of masses in approximation of square of stellar rotation angular velocity in empty space
02 p0317 A69-11956

Mass points substitution for mass of earth, giving gravitational effect equal to observed gravity values corrected for centrifugal acceleration
02 p0243 A69-12008

Mass distributions of meteoroids obtained from underdense radio meteor echoes
03 p0518 A69-14254

Lunar mascons size and depth calculated in terms of mare formed by low velocity iron meteorites impact
04 p0654 A69-14629

Lunar mascons, interpreting lunar gravitational field anomalies over maria in terms of near-surface slab-like model for maria structure
04 p0654 A69-14630

- Lunar crater formation studied to explain distortion in large craters or maria, discussing mass concentrations indicated by positive residuals of gravimetric map
04 p0654 A69-14632
- Lunar surface formation, emphasizing density variations and mass concentrations
04 p0654 A69-14633
- Lunar high density mass concentrations effect on Lunar Orbiters accelerations, discussing lunar gravity field determination
04 p0661 A69-15145
- Vibration analysis of plates with discrete mass distribution based on Galerkin approach
04 p0682 A69-15293
- Self balancing single degree of freedom free fall space environment simulator, discussing coincidence of mass and rotation centers
04 p0586 A69-15468
- Hydrothermal investigation of Ge trace quantity distribution between metal, silicate and sulfide phases at controlled oxygen partial pressure by oxygen buffer techniques
05 p0819 A69-15624
- Large mass concentrations /mascons/ effect on moon dynamical figure, considering production of asymmetries
05 p0820 A69-15762
- Radar determination of exponent s for describing mass distribution of Geminid and Quadrantid meteoric bodies
05 p0823 A69-16033
- Meteoroid mass distribution determined by radar observations of underdense meteor trails at Springhill Meteor Observatory
06 p1003 A69-17493
- Rolling ballistic vehicles mass and aerodynamic characteristics determined from dynamic motion data by performing Fourier analysis on roll axis equation of motion
[AIAA PAPER 69-102] 06 p0862 A69-18039
- Mass distribution and inertia characteristics influence on spin susceptibility and spin recovery characteristics for eight current fighter aircraft
[AIAA PAPER 69-188] 06 p0868 A69-18057
- Lunar mass concentrations /mascons/ origin and nature, postulating primordial lunar atmosphere and hydrosphere and carbon derived from primordial organic compounds
08 p1397 A69-20697
- Symmetrical body rotational motion with asymmetrical mass distribution about center of mass, determining minimum initial value of angular velocity
09 p1595 A69-21762
- Euler rotational equations for bodies with variable inertia tensor subjected to extreme variations of mass distribution and mass loss
09 p1616 A69-21956
- Increasing rotation of axisymmetric body about velocity vector ascribed to asymmetry in mass distribution, defining conditions for occurrence
09 p1431 A69-22077
- Neutral hydrogen content and distribution of late type spiral galaxy NGC 6946 from 21 cm line measurements
09 p1598 A69-22187
- Rotation and mass of Sb galaxy NGC 1832, giving central and mean densities
09 p1599 A69-22188
- Interstellar reddening material distribution within 2500 parsecs of sun, noting concentration in galactic plane, spiral arms and cloud complexes
10 p1773 A69-22961
- Mass and velocity distribution of interstellar clouds from Oort model simulated by Monte Carlo method on computer, predicting rogue cloud existence
10 p1779 A69-23608
- Dynamical model for spherical inhomogeneity in mean mass density of universe to predict velocity dispersion observed for Coma Cluster
10 p1789 A69-24133
- Variational equations for rotation of heavy solid body with fixed point about horizontal axis, noting mass distribution
11 p1917 A69-24778
- Vector equation for correction masses for dynamic balancing of rotor supported on n points derived from bearing structure vibrations amplitude and phase
12 p2180 A69-26243
- Nonrelativistic theory of rotating configurations in terms of gravitational potential, center mass density and variable angular velocity
12 p2159 A69-26662
- Galactic descriptive functions and empirical model construction methods for determining mass distribution
12 p2160 A69-26852
- Moon internal structure, discussing aggregation origin of Moon parallel to earth and three layer model of nife core, sima mantle and porous sheath
12 p2160 A69-26896
- Mass distribution for bodies fallen on planets during formation estimated from present inclination of planetary axes of rotation, using limit theorems of probability theory
13 p2345 A69-27652
- Photometric data and law of rotation in symmetry plane for constructing mathematical model of mass and luminosity distribution in M 31
13 p2351 A69-27870
- Moon-earth system origin emphasizing mass distribution
13 p2352 A69-27902
- Integral equation solved by successive approximation procedure for determining mass distribution in galaxies on radial velocity basis, applying to NGC 7331
13 p2353 A69-28325
- Finite difference method for motion stability of periodic bipolar vibrational systems, considering perturbations
14 p2534 A69-29039
- Classical and relativistic gravitation theories using harmonic coordinate system, interpreting Einstein equations for insular distribution of masses and applications in geodesy
15 p2596 A69-30573
- Interplanetary dust and distribution study by micrometeorite analyzer and by zodiacal light observations using solar probe
15 p2694 A69-30879
- Lunar mascon origin from collisions of large masses with lunar surface
15 p2698 A69-31328
- Lunar mass and gravitational field determined from lunar satellite dynamics, using potential function in terms of spherical harmonics
15 p2699 A69-31405
- Fuel injector-induced mass flux and mixture ratio distributions effects on combustion performance, chamber volume and stability, discussing combustion oscillation avoidance
16 p2877 A69-31731
- Einstein field equations solutions generated via static spherically symmetric mass and charge distributions
16 p2812 A69-32053
- Fixed mass of monatomic gas unsteady spherically symmetric expansion into vacuum by asymptotic Boltzmann equation expansion
16 p2772 A69-32168
- Bending vibratory motion instability of rotor on elastic shaft with uniform mass distribution along axis, using variational methods
16 p2875 A69-32249
- Frequency distribution of star masses formed from solid H grains clouds, noting agreement with Salpeter initial mass function
16 p2862 A69-32372
- Mass of Jupiter system from motion of Doris, using variational equations for initial rectangular coordinates and velocities with respect to mass of Jupiter
16 p2863 A69-32403
- Lunar localized subsurface mass concentration association with circular maria, noting two large mascon basins from gravity data and orbital photography
16 p2864 A69-32446
- Mascons implications in selenodetic data analysis conducted at U.S. space centers
17 p3028 A69-32922
- Interferometric study of electron concentration and mass density profiles through ionized argon thermal end-wall layer formed in shock tube
[AIAA PAPER 69-694] 17 p3074 A69-33477
- Stars kinetic energy and escape rates from isolated cluster with arbitrary stellar mass distributions, assuming spherical symmetry and velocity distribution isotropy
17 p3038 A69-33721
- Forced oscillations of resonance machine elements represented by truss of concentrated masses and external forces, taking into account aerodynamic energy dissipation
17 p3064 A69-33916
- Tail tip-evacuation limits, calculating aircraft balance effect of passenger relocations by graphical method
[SAWE PAPER 765] 18 p3091 A69-34877
- Aerospace balancing system with hydrostatic spindle, describing component construction and functions
[SAWE PAPER 737] 18 p3118 A69-34890
- Dynamic balancing mechanics covering graphical representation, mass asymmetries corrections or adjustment calculations and ballasting equations
[SAWE PAPER 736] 18 p3220 A69-34891
- Bjerhammer gravity reduction method applied to gravity in space, analyzing two test models with mass focused between topographical and reference surface
18 p3173 A69-35197
- Leonid meteoroids mass distribution law exponent evaluation based on unstable meteoric radio echo durations integral distribution
18 p3203 A69-35334
- Free oscillations of rigidly clamped circular plate carrying concentrated masses, deriving frequency equation and value of lower roots
18 p3226 A69-35377
- Newton gravitational constant determination from measured acceleration and known magnitude of masses, describing control system
20 p3537 A69-37140
- Photographic photometry investigation of Light distribution in spiral galaxies NGC 681, 972 and 1084, discussing mass distribution
20 p3599 A69-37476
- Galactic mass relativistic distribution calculated, considering spherically symmetric model differential rotation near sun
20 p3600 A69-37484
- Satellite representations of earth gravity field portraying consistent pattern of mass anomalies due to density differences in layers
20 p3523 A69-37566
- Galaxy NGC 3593 with large amounts of interstellar dust, calculating galactic mass and central density
20 p3610 A69-38143
- Data on mass distribution of terrestrial fragmented rocks to interpret lunar rock samples, noting origin of asteroids and meteorites
20 p3613 A69-38250
- Book on mathematical model for heat and material exchange in bubbles covering bubble formation, transition period and quasi-stationary bubble rise
21 p3847 A69-38448
- Lunar surface, asteroids and meteorites properties by mass distributions of fragmented rocks
21 p3800 A69-38677
- Spherically symmetrical T models of dust matter yielding method for obtaining maximum total mass effect in general relativity theory different from Friedman closed model
21 p3803 A69-38994
- Meteoroid penetration damage to spacecraft system, showing particle mass density distribution as protection criterion
21 p3805 A69-39229
- Earth shape and areas of anomalous gravity from satellite orbital perturbations, tabulating results from various experimenters
21 p3718 A69-39734
- Variations in gravity, plotting results for U.S., with tables for Alaska, Mexico, India, Africa, etc
21 p3718 A69-39735
- Bok globules in Orion nebula, deriving temperature and density data
22 p4022 A69-40465
- Matter surface distribution in general relativity, deriving matching conditions
22 p3982 A69-40753
- Gyroscopic motion with center of mass displaced along suspension axes and kinetic moment varying as power law under linear accelerations
23 p4163 A69-41552
- Increasing rotation of axisymmetric body about velocity vector ascribed to asymmetry in mass distribution, defining conditions for occurrence
23 p4060 A69-41968

MASS FILTERS
U FLUID FILTERS
MASS FLOW

- Sonic nozzle mass flow measurement errors at high supply pressures and moderate temperatures due to real gas effects
[ASME PAPER 68-WA/FM-4] 05 p0699 A69-16114
- Mass motions in solar flares - Conference, Anacapri, Italy, June 1968
06 p0992 A69-17426
- Mass motions in solar flares using line profiles and filtergrams
06 p0993 A69-17427

- Optical evidence for mass motions in solar flares [1937-1967] 06 p0993 A69-17428
- Mass motion in solar flares, discussing loop flares from emission line profile characteristics 06 p0993 A69-17429
- Small scale mass motions in chromospheric structures surrounding solar flare indicating changes in magnetic field 06 p0993 A69-17431
- Mass motions in flares and moustaches indicated by spectral features, discussing red asymmetry of line emission 06 p0994 A69-17432
- Spectrographic H alpha observations indicating effects of rotary mass motion in flares and prominences 06 p0994 A69-17434
- Solar moustaches H alpha profiles spectroscopic studies indicating near symmetry 06 p0994 A69-17435
- Hall effect and mass flow influence on MPD arc jet radial pressure profile calculated as function of pressure and magnetic field [AIAA PAPER 69-246] 09 p1562 A69-21226
- Fluid injection into flowfield from porous forward portion of blunt body in stagnation region flow, determining reservoir pressure and mass flow rate 09 p1430 A69-21973
- Mechanical properties of glass, discussing volume flow, hardness, strength and scratchability 12 p2119 A69-26831
- NGC 4038-9 velocity field from spectrum obtained at McDonald Observatory, suggesting existence of two centers of matter ejection 12 p2169 A69-27060
- Diffusion and mass flow in steady state magnetically stabilized helium arc plasma effects on spectroscopic determinations of electron temperature, discussing degree of ionization 12 p2141 A69-27146
- Numerical solutions of equations for high Prandtl number boundary layers in two dimensional flat plate incompressible flow with mass injection 13 p2249 A69-28238
- Mixing regimes for flows with different stagnation enthalpies subject to mass flow limitation due to thermal choking 13 p2251 A69-28499
- Perturbation technique application to stability criterion for rectilinear missile flight with arbitrary inclination, noting mass reduction and flow and gravity effect 19 p3429 A69-35779
- Supersonic air to air ejectors performance for low secondary-to-primary mass flow ratios, deriving correction factor for Fabry-Paulon theory 21 p3644 A69-38654
- Viscoelastic fluid steady flow in porous walled channel, examining mass flow solution continuity 22 p3930 A69-40118
- Quasi-one dimensional analysis for nonequilibrium flow of dissociated diatomic gas through converging-diverging nozzle, discussing critical mass flow rate 22 p3927 A69-40583
- Optimum functions for mass and energy flow during spacecraft orbital transfer, emphasizing time behavior of propulsion variables 24 p4382 A69-42921
- Mass injection by strong blowing across Couette-Poiseuille shear flow 24 p4301 A69-43354
- Stagnation temperature determined in transition and free molecule region of rarefied gas flows from critical mass flow dependence on temperature and stagnation pressure 24 p4408 A69-43492
- MASS FLOW RATE**
- Local mass transfer from wall with homogeneous or heterogeneous chemical reactions in uniform velocity flow, Couette flow and boundary layer flow 02 p0232 A69-12234
- Quasi-one dimensional analysis of MPD arcs with nonequilibrium ionization taking into account finite rate processes and variable area [AIAA PAPER 68-87] 02 p0291 A69-12505
- Controllable sonic flow orifice, discussing mass flow rate, area and upstream stagnation pressure 10 p1693 A69-23343
- Mass flow rates for nearly free molecular flow through two dimensional slit for several tank pressure ratios 11 p1874 A69-25357
- Steady deflagration of homogeneous monopropellant in condensed phase, considering nonequilibrium surface condition for mass decomposition rate [WSCI PAPER 69-6] 16 p2830 A69-32347
- Rarefied gas flow between parallel plates using linearized Boltzmann transport equation, deriving integral equation for mass flow velocity 19 p3296 A69-35621
- Temperature measurement in and near opposed-jet diffusion flame subjected to electric field, discussing flame behavior at low mass flow rate 21 p3852 A69-39597
- Operational characteristics of multiple arcjet wind tunnel for time varying mass flow rate programs, calculating isentropic core densities and velocities [AIAA PAPER 68-229] 22 p3927 A69-40541
- Radial pressure distribution in steady state rotationally symmetrical plasma jet subjected to axial magnetic field, emphasizing mass entrainment effect [DGLR-69-024A] 23 p4202 A69-41924
- Mass injection effects on viscous hypersonic low Reynolds number shock layer downstream and at stagnation point in blunt forebody region analyzed for non-reacting gas 24 p4249 A69-43663
- MASS RATIOS**
- NT PAYLOAD MASS RATIO
- NT PROPELLANT MASS RATIO
- Autonomous two degrees of freedom Hamiltonian system triangular libration points found stable for all mass ratios in circular restricted three body problem 12 p2155 A69-25883
- Resonant long-period orbits around Lagrange equilateral points for critical mass ratio of main bodies 13 p2346 A69-27706
- Restricted three body problem of conservative Hamiltonian systems with two degrees of freedom and mass ratio parameter, considering phase space around L sub 4 13 p2346 A69-27711
- Parallax and mass ratio of visual type K6 dwarf binary system, ADS 1865, BD plus 30339 13 p2349 A69-27811
- Lunar origin theories, considering moon/earth mass ratio, earth-moon system angular momentum deficiency and differential volatilization in earth 14 p2527 A69-29882
- Carbonaceous meteorites specimen petrographic observations, noting genetic interrelations with urelites regarding S-C and reduced Fe oxidized Fe ratios 19 p3413 A69-36112
- Mean velocity and pressure fields in turbulent boundary layer on flat plate at Mach 2 investigated for ratios of mass flow [AIAA PAPER 68-129] 24 p4304 A69-43581
- MASS SPECTRA**
- Plasma jet mass structure investigated for decomposition during passage through vacuum by spectrometer and probe techniques 03 p0478 A69-13841
- Mass spectrometric studies of plasmas produced by laser beam interaction with solid materials 06 p0932 A69-16921
- Mass spectra of quinoline and isoquinoline N-oxides, discussing diagnostic values of fragmentation reactions for heteroaromatic N-oxide function presence 07 p1075 A69-19496
- Mass spectral fragmentation of substituted aliphatic glycols and hydroxylated carbon-carbon bond 09 p1448 A69-22551
- Absolute dimensions of 34 eclipsing variables having both components near main sequence, comparing mass luminosity and mass spectrum to homogeneous model stars 11 p1952 A69-24248
- Mass spectra peaks of N-Acyl-2-indolinols fragmentation processes upon electron impact, noting compounds predominance in open chain tautomer gas phase 15 p2561 A69-30407
- Electron impact field ionization source for mass measurement of molecular ions, noting organic geochemistry applications 15 p2608 A69-30428
- Qualitative interpolation formula for phonon frequency spectrum of mass disordered alloys three dimensional systems at high concentrations 20 p3583 A69-37279
- MASS SPECTROMETERS**
- NT TIME OF FLIGHT SPECTROMETERS
- Electrode geometry for mass spectrometer ion source to measure electron ionization cross section of low vapor pressure materials 01 p0080 A69-10605
- Mass spectrometer helium leak testing of cryogenic storage vessels, noting procedures and insulation and evacuation of jacket space 02 p0252 A69-11811
- Lower thermosphere composition over New Mexico, discussing rocket flight mass spectrometer measurements during summer 1967 03 p0425 A69-14009
- Mass spectrometer leak testing by calibrated enclosure method for quantification of gaseous leaks in large complex systems 04 p0598 A69-14974
- Magnetic electron multiplier used as particle detector in time-of-flight (TOF) mass spectrometers can introduce mass discrimination effects 04 p0599 A69-15014
- Oil lubricant vapors under frictional working conditions in vacuum analyzed by mass spectrometer and gas-liquid chromatography concerning molecular weight and composition [IME PAPER 11] 07 p1137 A69-18558
- Electron impact induced fragmentation of ring D steroids involving loss of carbon atoms analyzed by mass spectrometry 07 p1069 A69-19497
- Nose cone ejecting system with pyrotechnic devices for two stage Centaur rockets /Sud-Aviation/ with RF mass spectrometer 10 p1635 A69-23034
- Spectral baseline instability correction for time of flight mass spectrometer operating at source pressures up to one torr 10 p1693 A69-23345
- Ethylene oxide and ethane low pressure fuel-rich flames mass spectrometry, analyzing composition and temperature profiles and OH radical role 11 p1831 A69-24478
- Drift velocity and longitudinal and transverse diffusion coefficient for low energy N ions in N gas in mass spectrometer at room temperature 13 p2302 A69-27458
- Metastable ions formation and detection in double focusing mass spectrometer, calculating location of decomposition in electrostatic analyzer and doubly charged ions transition 15 p2561 A69-30021
- Ion-molecular reactions measurements in ionosphere by VV type device and RF mass spectrometer 15 p2603 A69-31407
- Gas chromatograph-mass spectrometer combination for in situ analysis of lunar organic matter, describing instrument design and operation 18 p3113 A69-34238
- Shock wave studies of gaseous NO thermal ionization in Kr as function of temperature, using time-of-flight mass spectrometer 18 p3099 A69-34464
- Ar 39-Ar 40 method using neutron activation and inert gas mass spectrometry to investigate meteoritic thermal histories 19 p3412 A69-36105
- Earth satellite sweeping mass spectrometer for measuring atmospheric neutral particle and positive ion concentration 19 p3314 A69-36681
- Explorer 31 ion mass spectrometer calibrated in flight and compared with Alouette 2 topside electron concentration data 20 p3545 A69-37879
- Meteoritic organic matter origin, discussing time-of-flight mass spectrometer combined with gas chromatographic capillary column 22 p4012 A69-40085
- Digital processing of rocket-borne mass spectrometers for measurements in upper atmosphere, discussing calibration 22 p3904 A69-40232
- Computerized mass spectrometer for monitoring atmosphere in astronaut suits and cabin [AIAA PAPER 69-1016] 22 p3922 A69-40388
- Laser produced Sb and Te vaporization near critical point, using time of flight mass spectrometer 22 p3993 A69-40719
- MASS SPECTROSCOPY**
- Leak flow rates of nitrogen and helium at various pressure gradients measured by gas chromatography and mass spectroscopy 01 p0079 A69-10297
- Automatic heteroatomic plotting of high resolution mass spectral data, presenting relative intensity vs elemental composition in bar form 01 p0024 A69-10905
- Planetary atmosphere composition determination using mass spectrometry for neutral components, ion

spectrometry for ionic components and data system optimization
[AAS PAPER 68-183] 02 p0247 A69-11468

Automatic equipment for sampling and preparing gases by dual column gas chromatography for subsequent mass spectral analysis of carbon isotopes during methane metabolism
02 p0205 A69-12603

Mass spectrometric technique applied to positive column of hydrogen glow discharge for plasma properties, including relative densities of various hydrogen ions
05 p0802 A69-15913

Mass spectrometric measurements to determine energy distributions of ions produced in dissociative photoionization of O molecules
06 p0960 A69-17110

Supersonic molecular beam sampling system for coupling mass spectrometer to alkali metal-air reacting flow system in kinetics study, noting gas dynamic effects
[AIAA PAPER 69-94] 06 p0930 A69-18099

Ammonium perchlorate high temperature decomposition by using carbon dioxide laser pyrolysis/mass spectrometry
[AIAA PAPER 69-143] 06 p0885 A69-18111

Mass spectrometer application to plasma diagnostics, discussing mass spectra, particle extraction, low and high pressure discharges, supersonic flow, ion detection methods, etc
08 p1316 A69-20475

Partition coefficients between natural melts and plagioclase phenocrysts determined for rare earth elements and barium by mass spectrometry
08 p1310 A69-20944

Dominant ionic species in cesium plasma through mass spectrometer analysis, measuring total ion and electron currents
09 p1544 A69-21335

Quadrupole mass filter for rocket-borne measurements of thermospheric helium content, discussing turbopause level and winter helium bulge
09 p1489 A69-21712

Mass spectrometric analysis of silicon carbide for inhomogeneity in sample, noting metallic impurities
09 p1448 A69-22313

Mass spectrometric determination of pyrolysis products generated from heated polymer samples
09 p1448 A69-22314

Lunar surface chemical composition using RF mass spectrometer
10 p1698 A69-24207

Pyrimidine and purine bases analysis by time of flight mass spectrometry and paper chromatography
11 p1832 A69-24738

Semiconductor thin films analysis using mass spectrometer with spark source
13 p2316 A69-27293

Borane carbonyl pyrolysis in low pressure tubular flow reactor measured by mass spectrometry, noting wall collision role in diborane bond dissociation
14 p2410 A69-29282

Mass spectroscopic structural analysis of organic compounds, discussing computer application to data recording, processing and evaluation
18 p3099 A69-34553

Spark source mass spectroscopy for determining trace elements in Ti and Ti alloys used in aeronautical and aerospace technology
[ONERA-TP-723] 18 p3155 A69-34638

Leak tests for sealed electronic circuits using helium mass spectrometer
18 p3138 A69-35271

Mass spectrometric investigation of thermosphere at high latitudes, measuring number densities for nitrogen, Ar and molecular and atomic oxygen
20 p3533 A69-38086

Acid fraction extraction of Green River shale identified by gas chromatography-mass spectrometry-computer system, noting trimethyl pentadecanoic acid
21 p3669 A69-38983

Aromatic and nonaromatic hydrocarbon fractions in terrestrial graphite, discussing classification and analysis by chromatography and mass spectrometry
22 p3934 A69-39890

Lunar rocks types determination by mass spectrometry, describing results of terrestrial rocks tests
22 p4034 A69-41106

Mass spectrometric analysis of lunar material from soil vaporization products ion component by electron beam
22 p4034 A69-41107

Pb isotopic analysis using double spike mass spectrometric method to achieve reproducibility and accuracy, discussing principles and performance
24 p4280 A69-42733

MASS TRANSFER

Mass or energy transfer in reinforced media, discussing components characteristics and role of diffusion processes
01 p0173 A69-10079

Simple and shock waves in nonlinear unsteady heat and mass transfer, discussing conditions for transforming simple waves into shock waves
01 p0174 A69-10096

Linear partial differential equations for nonlinear intensive heat and mass transfer, discussing analogy between transfer processes and electromagnetic waves distribution
01 p0174 A69-10104

Heat and mass transfer coefficients derived for reacting gas mixtures by applying variational principle
01 p0006 A69-10400

Turbulent heat and mass transfer in rotating incompressible fluid flow analyzed by kinetic energy and shear stress equations
01 p0060 A69-10402

Mathematical models of energy and mass transfer processes in closed loop multicomponent life support systems
01 p0021 A69-11316

Turbulent fluid transport properties predicted by simple model for fluid behavior, obtaining mass, momentum and energy diffusivities
01 p0177 A69-11402

Dynamics of moving gas bubble injected in quiescent liquid, considering velocity, heat flow and mass transfer [ASME PAPER 67-WA/HT-30]
02 p0351 A69-12201

Local mass transfer from wall with homogeneous or heterogeneous chemical reactions in uniform velocity flow, Couette flow and boundary layer flow
02 p0232 A69-12234

Determining influence of blowing various gases into boundary layer on friction and heat and mass transfer when external flow velocity varies according to power law
02 p0234 A69-12581

Transpiration cooling of porous flat plate by injection of carbon dioxide or air into carbon dioxide and air free streams
03 p0413 A69-12996

Conservation equations for steady incompressible flow in variable area duct with mass transfer at walls simplified by linearizing inertial and convective terms
03 p0413 A69-13011

Dynamic processes of heat and mass transfer in transpiration cooling of gas flow
04 p0684 A69-14355

Confined jet mixing region at entrance of tubular reactor, discussing mass and momentum transfer, chemical conversion and effect of Reynolds number
[AIChE PAPER 25A] 04 p0586 A69-14508

Mass exchange and evolution of close binaries/Main Sequence stars/
04 p0653 A69-14614

Turbulent flow transfers from applications point of view, noting example of cooling of heated wall
05 p0743 A69-15558

Injection or suction at disk surface, noting effects on heat and mass transfer in laminar flow about rotating disk
06 p1029 A69-17002

Heat and mass transfer by catalytic effect at wall, noting interaction of laminar boundary layer on flat plate
06 p1030 A69-17115

Laminar near wake flow field of two dimensional adiabatic circular cylinder with surface mass transfer
[AIAA PAPER 69-67] 06 p0862 A69-18044

Compressibility transformation theory extended for turbulent boundary layer, involving mass transfer with/without chemical reactions
[AIAA PAPER 69-161] 06 p0912 A69-18045

Chemical nonequilibrium, mass transfer and viscous interaction effects on spherically blunted cones at hypersonic conditions, emphasizing stagnation point
[AIAA PAPER 69-168] 06 p0862 A69-18047

Effects of multidimensional flow through porous matrices in mass transfer cooling, analyzing one dimensional model for blunt axisymmetric surfaces
[AIAA PAPER 69-149] 06 p1038 A69-18179

Heat and mass transfer - Conference, Minsk, May 1968
07 p1243 A69-19732

Electrochemical kinetic and mass transport model for studying stress corrosion crack propagation in Ti [ECS PAPER 147] 08 p1332 A69-20359

Binary stars systems with same total mass calculated for evolution from main sequence stage through mass exchange to white dwarfs
08 p1393 A69-20569

Bounds on mass and momentum transport by turbulent flow between parallel plates derived for Couette and Poiseuille flows
08 p1305 A69-20840

Hot air open circuit wind tunnel for testing vaporized fuel films heat and mass transfer over flat plates
08 p1302 A69-20878

Mass transfer during interfacial turbulence induced by Marangoni effect in physical model
09 p1621 A69-21903

Local creation of mass in steady state universe as source of static field energy propagating away at speed of light
09 p1601 A69-22212

Thin wall flow of circular jets in bounded transverse flow, showing hydrodynamical parameter of mixture effect on jets dimensionless path
10 p1679 A69-23567

Heat and mass transfer between cryogenic fluid and superheated wall, analyzing experimental data
11 p1996 A69-24228

Dynamical effects of mass exchange in close binary systems ejection modes from point of view of orbital elements evolution
11 p1962 A69-25113

Three dimensional laminar boundary layer near windward generator of cone subjected to uniform mass transfer by suction or injection
11 p1874 A69-25281

Close binaries evolution and mass exchange for stars of 5 solar masses with very short periods, using modified Henyey method
11 p1964 A69-25414

Heat and mass transfer in laminar boundary layer on porous flat plate with variable suction or injection velocity and constant wall temperature
12 p2061 A69-25947

Heat and mass transfer coefficients derived for reacting gas mixtures by applying variational principle
12 p2062 A69-26668

High velocity liquid lithium effect on structural materials for MHD power generators, discussing material loss
13 p2278 A69-27478

Heat and mass transfer conditions in ablation of shear thinning and thickening fluids at stagnation point [ASME PAPER 67-HT-78] 13 p2374 A69-27778

Heat and mass transfer in two dimensional turbulent free shear flows including separated and reattached flows
13 p2377 A69-28145

Mass transfer cooling of high velocity surfaces in gaseous environment noting applications to atmospheric entry
13 p2377 A69-28146

Mass transfer cooling data correlation for estimating mass injection effect on slender cone drag
13 p2199 A69-28224

Convective heat and mass transfer in binary turbulent vertical boundary layer
13 p2378 A69-28311

Heat and mass transfer coefficients in binary laminar boundary layer during natural convection, taking into account enthalpy and thermal diffusion effects
13 p2378 A69-28312

Mass transfer due to plasma recombination, ambipolar diffusion and electrode erosion and resistance forces effects on electrodynamic accelerated plasma
13 p2315 A69-28555

Similarity theory similar to Nusselt and Stanton numbers obtained by triple analogy for heat, mass and momentum transfer
13 p2380 A69-28560

Coupled heat and mass transfer with zero order reactions in two phase systems consisting of drops, bubbles or solid particles
14 p2537 A69-29012

Partially ionized multicomponent gas mixture kinetics in strong electromagnetic field, determining magnetic field, stress tensors and transfer coefficients
14 p2492 A69-29610

Halley comet abrupt daily motion variation ascribed to solid particles ejection from ice nucleus stimulated by gas outflow
14 p2524 A69-29712

Bibliography of Soviet books and articles on heat and mass transfer covering thermodynamics, heat conduction, convection and radiation, etc

14 p2540 A69-29900

Magnetic field effect on heat and mass transfer in incompressible fluid MHD flow

14 p2500 A69-29901

Convective heat and mass transfer coupling in laminar hydrodynamic duct flow, obtaining values for bulk and wall temperatures, transfer coefficients and rates, etc

15 p2716 A69-30004

Heat and mass transfer interaction at wall for laminar boundary layer on flat plate, considering catalytic effect of wall in atomic nitrogen recombination

15 p2716 A69-30415

Mass transfer during Cs condensation from moving vapor mixture containing Ar in water-cooled tube

15 p2718 A69-30998

Heat and mass transfer in porous medium with bulk flow in thin adjacent channel, applying Green function analysis to hydrogen-oxygen fuel cell

15 p2552 A69-31115

Energy relations and conversion for electrodynamic plasma acceleration with allowance for mass transfer processes resulting from recombination, diffusion and electrode erosion

15 p2664 A69-31176

Plane Cauchy problem solution for differential equations in heat and mass transfer theory, applying contour integral method in matrix construction

15 p2719 A69-31262

Flow field around sharp slender cones with surface mass transfer at zero angle of attack in low density supersonic and hypersonic flow [AIAA PAPER 68-66]

16 p2732 A69-31887

Soviet bibliography of heat and mass transfer covering thermodynamics, aerohydrodynamics, MHD, transfer processes in various media, etc

16 p2878 A69-31960

Hybrid rockets combustion mechanism, discussing turbulent boundary layer with heat and mass transfer, chemical reactions, etc

16 p2879 A69-32002

Monograph on engineering calculations of momentum, heat and mass transfer through laminar boundaries having arbitrary pressure distribution and constant physical properties

16 p2879 A69-32203

Mean patterns of meridional interhemispheric flow for 40 degree equatorial sector, calculating mean air mass transport in lower troposphere over western Indian Ocean

18 p3166 A69-34420

Heat and mass transfer on vertical surface under combined free and forced convection, solving laminar boundary layer equations by stream function

19 p3453 A69-36844

Book on heat and mass transfer in recirculating flows, presenting elliptic differential equations and numerical solutions by computer

21 p3691 A69-38333

Heat and mass transfer coefficients in binary laminar boundary layer during natural convection obtained with integral equations and Karman-Pohlhausen method

21 p3848 A69-38633

Heat flow in belt-type heat transport device allowing for conductive and mass transport effects, deriving expression for heat transfer capability

22 p4050 A69-40554

Finite-difference grid procedure for predicting friction heat and mass transfer in two dimensional boundary layers

22 p3932 A69-40939

Momentum, heat and mass transfer in turbulent channel flow emphasizing phenomena close to wall, using boundary layer growth-breakdown model

24 p4407 A69-42914

Heat transfer to highly accelerated turbulent boundary layer with and without mass addition, presenting data in terms of Stanton number vs Reynolds number [ASME PAPER 69-HT-53]

24 p4409 A69-43518

Heat and mass transfer in gas suspension, studying suspended particles effects on heat transfer by irreversible thermodynamics

24 p4410 A69-43528

Turbulent pipe flow with wall suction, calculating friction factor, pressure gradient, heat and mass transfer coefficients, velocity and temperature profiles [ASME PAPER 69-HT-4]

24 p4414 A69-43562

Oxygen and carbon dioxide transfer in membrane oxygenators, considering liquid dispersion and membrane diffusion limitations

24 p4279 A69-43799

MAST SHOCK TUBES

U MAGNETIC ANNULAR SHOCK TUBES

MATCHING

Matched asymptotic expansions for establishing relationship between inner and outer expansions of unknown function, discussing classes of singular perturbation

07 p1180 A69-18809

Visual backward masking experiment for studying overlapping and nonoverlapping contours of target and masking stimuli straight line

22 p3879 A69-40843

MATERIAL ABSORPTION

Purines, pyrimidines and nucleosides absorption by Li-, Na-, Mg- and Ca-montmorillonite in aqueous solutions over range pH 2-12 by cation exchange

05 p0716 A69-15973

Absorption of nucleosides, purine and pyrimidine derivatives by Co-, Cu- and Ni-montmorillonite taking place by cation exchange process

05 p0716 A69-15974

MATERIAL BALANCE

U WATER BALANCE

MATERIAL REMOVAL (MACHINING)

U MACHINING

MATERIALS

Materials research - Conference, Tokyo, September 1967

06 p0941 A69-17120

Structures, structural dynamics, materials and aeroelasticity - ASME-AIAA Conference, New Orleans, April 1969

11 p1988 A69-25492

Book on mathematical model for heat and material exchange in bubbles covering bubble formation, transition period and quasi-stationary bubble rise

21 p3847 A69-38448

MATERIALS EROSION

U EROSION

MATERIALS HANDLING

NT GROUND HANDLING

NT PROPELLANT TRANSFER

Air cargo traffic increase, discussing technical and economical prospects, use of intermodal containers and transportation automation tendency

01 p0008 A69-10030

Remotely controlled explosives processing facility for handling unfamiliar sensitive materials, noting safety aspects and inspection, testing, transporting and destroying techniques

02 p0226 A69-11523

Air cargo terminal materials handling, discussing computer control, off-airport consolidation, packaging, etc

13 p2239 A69-27337

Highly concentrated hydrogen peroxide production, handling and storage, discussing crystallization process, equilibrium diagram, decomposition reduction and stabilizers

17 p3017 A69-33353

Materials processing in space, suggesting electronic single crystals preparation, materials melting and utilization of low g earth orbit environment

19 p3324 A69-35589

Air cargo traffic, discussing payload lots, aircraft types suitable for freight transport, difficulties and solution

22 p4052 A69-40426

Cargo handling systems for worldwide door to door service from marketing systems viewpoint [RAES PAPER I]

22 p4053 A69-40482

Handling and processing function in air freight transportation, discussing system design approaches, cargo terminals, materials handling systems and containerization

22 p4053 A69-40483

MATERIALS RECOVERY

NT WATER RECLAMATION

Second phase hardened materials recovery creep rate model, showing dependence on stress level

03 p0447 A69-13615

Point defects in body centered cubic transition metals, discussing thermal equilibrium, irradiation cold work, high and low temperature recovery, etc

03 p0447 A69-13817

Aging and recovery effect on structure and hardness of Ag and Be doped Al-Mg alloys

05 p0783 A69-16811

Deformation dependence on strain hardening and recovery rate during transient and steady state creep

06 p0943 A69-17236

Soft fiber reinforced plastics creep and recovery properties, discussing test equipment, rheological properties, polishing effects, etc

23 p4179 A69-42006

Material recovery from metabolic and other wastes for long duration manned space missions, discussing carbon dioxide removal, bioregenerative food systems, etc [AAS PAPER 69-143]

24 p4272 A69-42876

MATERIALS SCIENCE

Corrosion control, discussing corrosive concentration cells, coatings and sacrificial systems of protection, deep corrosion, corrosion augmented stress, forgings and titanium corrosion testing

01 p0093 A69-10148

Mechanical and thermodynamic theories of material behavior based on rate independence concept, discussing equivalence of various theories

01 p0166 A69-10227

Handbook on fatigue properties for product design covering metals stress conditions, machine parts load and stress determination, cyclic stress, etc

01 p0170 A69-10918

Cumulative damage theories application to fatigue data for high strength materials, discussing stress levels

04 p0668 A69-14379

Book on modern materials covering radiation processed wood plastic materials, industrial jewels, solid propellants, superconductors and beryllium

04 p0619 A69-14581

Method of finding new nonlinear optical materials using anharmonic oscillator model [IEEE PAPER F-5]

05 p0808 A69-16312

Cryogenic properties of polymers - NASA/Case Conference, Cleveland, April 1967

05 p0784 A69-16485

Manufacture and properties of carbonaceous materials for nuclear and aerospace technologies, discussing pyrolytic graphite, vitreous carbon and carbon fiber

05 p0786 A69-16657

Papers on materials research advances, Volume 3, covering continuum theory, fatigue hardening, crystal lattices, etc

06 p0944 A69-17501

Materials compatibility for space requirements, discussing shape retention, ductility, tensile strength, dissimilar materials stability, etc

06 p0945 A69-17872

Aerospace material investigation and fabrication techniques - Conference, Cocoa Beach, November 1968

09 p1504 A69-22301

Dielectric relaxation for analysis of defect structure, microstructure, surface behavior, structural changes kinetics and environmental effects in insulators and semiconductors

09 p1559 A69-22307

Thermodynamic properties of materials in critical region, discussing inhomogeneity

11 p2003 A69-25440

Astronautics - Conference, Braunschweig, West Germany, October 1968, Volume 3, Strength, material, methods of construction

12 p2176 A69-25850

Structures, structural dynamics and materials - AIAA-ASME Conference, New Orleans, April 1969

12 p2183 A69-26807

Spacecraft construction materials and strength problems including stress-strain determination, thin shell structural stability, dynamic loads, heat resistance, fiber-reinforced composites, ablation materials, etc

13 p2362 A69-27920

Sliding behavior of nonmetallic bearing materials /plastics, ceramics and cermets/, discussing non-lubricated bearing application

14 p2454 A69-28851

Civil aircraft projected development regarding materials and structures, discussing new components and fuel contribution to weight and metals and composites for replacing Al

16 p2872 A69-32024

Book on superconducting materials physical metallurgy covering fundamental theory, material properties, behavior regularities, applications, etc

16 p2802 A69-32051

Kim-Anderson flux flow theory for materials with kappa nearly equal to 1, discussing pinning forces and sites

17 p3016 A69-33754

Materials and processes for aerospace applications in 70s - Conference, Los Angeles, April-May 1969

19 p3315 A69-35501

Materials research - Conference, Kyoto, September 1968

Crack density effects on stress-dependent creep rate in isotropic and anisotropic materials undergoing high temperature creep deformation

Viscoelastic materials gradual resilience loss under tensile stress, discussing mathematical relations between stress, loading time, elastic deformation and experimental verification

Acoustic emission signals for nondestructive testing and material evaluation, determining critical stress intensity factor for stress corrosion cracking

Radio telescope structure material selection criteria, developing deformability criteria for structures under various stresses

Three dimensional X ray pictures of flaws shape and location in various materials

Carbon fiber reinforced materials applications in aerospace industry, discussing long term potential and applications in F-5 aircraft

Linear elastic isotropic materials for model tests, describing properties of material composed of Araldite B and air

Temperature, applied stress and pressurization effects on materials corrosion by liquid F and F containing oxidizers

Vacuum exposure nephelometer system for materials contamination screening in space applications

Materials research structural design cycle, discussing simultaneous optimization, constituent materials, fabrication process, load environment and mission constraints

Materials in space technology - Conference, Bristol, England, April 1969

Metallic and nonmetallic materials for space applications with launch and orbit condition requirements, examining finishes and lubricants

Aerospace pressure vessel materials selection and construction, applying Apollo program experience to future programs

MATERIALS TESTING REACTORS
U NUCLEAR RESEARCH AND TEST REACTORS

MATERIALS TESTS

Trailing camera technique to photograph impact and projectile penetration into earth materials from above and behind test vehicle

Technique for compressive mechanical behavior of viscoplastic nonlinear composites, discussing rate dependence and one dimensional stress-strain time properties

Evaporographic converter to test for striations /schlieren/ in materials used in IR

Optimization of plane smooth rectangular panels of constant cross section subjected to loading and heating conditions

Refractory metal, precious metal and ceramic material compatibility tested by metallography and by microprobing for protective coatings possibilities

Materials, processing and testing variables effects on mechanical properties determined for metal matrix composites [ASME PAPER 69-GT-23]

Tests and quality control equipment used in German aeronautical and astronautical industries

Material selection for structures under vibration loads, analyzing fatigue strength on basis of stress susceptibility and relationship with tensile strength

Structural reliability tests using photoelasticity and associated techniques, discussing computer methods, materials research, etc

Tires tested for road hazards, noting correlation to population density and rainfall

Impact hardness of materials determined by Drozd method of static hardness determination, noting tests on steel

Metal surface distribution of electromagnetic field from striding transducer in eddy current flow detection, calculating magnetic field component

Microcracking susceptibility studies of Inconel 718 weld heat affected zones, noting hot ductility, weld circle patch and fillerless fusion welding tests

Dielectric properties of high loss nonmagnetic microwave materials used for waveguide absorbers and anechoic chamber linings

Ablation characteristics of heat shield materials measured in arc heated wind tunnels, considering influence of model scale, heating rate and pressure level

Book on ultrasonic methods in solid state physics covering stress wave propagation in solids, pulse methods of velocity change and attenuation measurements and causes of losses

Epoxy adhesives physical chemistry, curing processes, formulation, surface application methods, testing and health hazards

Impact testing machine with dropping load, noting provision for sample fastening to reduce reflected tensile wave effect

IR techniques for nondestructive testing, discussing applications to heat injection and generation and IR test equipment capabilities

High temperature ultrasonic testing to measure and control solid materials early in processing

Book on ultrasonic testing of materials covering ultrasonics application to nondestructive testing, flaw detection and quality control

Blast response of model structures fabricated from material differing from prototype structures, testing in dynamic, impulsive and quasi-static loading realms

Ablative materials in hydrogen/oxygen thrust chamber using expansion nozzle to substitute regenerative thrust chamber assembly [AIAA PAPER 69-442]

Betatrions for nondestructive quality control for materials and products under special conditions

Thermoelectrical leg product specification /TELPS/ apparatus and data reduction technique for determining temperature dependent thermoelectric properties of material

Full circle Be brake disks in C-5 aircraft, discussing properties at elevated temperature and fastening of friction lining

Syntactic foam prepreg for low density laminate construction, presenting design and mechanical test data

Unfilled Pyrrone prepared from powder into molded parts for flexural tests at elevated temperatures observed for stability to electron irradiation in air

Materials evaluation for devices with long term underground exposure, including field tests at tropical locations

Nondestructive testing for aerospace corrosion, discussing light, penetrants, X rays, sound, ultrasounds, electrical conductivity, magnetic reaction and radiation backscatter methods

Sand crosion behavior of metals and plastics in air blast rig under varying exposure time, angles of impact and tensile stress

Soviet book on resistance of materials to deformation and fracture in complex stress states covering elasticity, mechanical theories of limiting stress state, experimental verification, etc

Structural ceramics and testing of brittle materials - U.S. Army Conference, Chicago, March 1967

Structural analysis and statistical fracture approach to design and testing for polycrystalline ceramic materials, including combined stress testing and load redistribution models

Mechanical testing procedures for brittle materials, discussing test philosophy, tabular data, laboratory tests correlation, etc

Parametric influence on strength of brittle materials, considering volume, surface, notch, strain rate, modulus variations and material variability effects

Brittle materials mechanical properties test programs design based on nature of material, use of data and available techniques

Elastomers for SST aircraft applications, discussing properties evaluation, material selection, scantal requirements, etc

Anaerobic adhesives for aircraft bonding tested for mechanical properties, noting advantages over epoxy adhesives

MATHEMATICAL ANALYSIS
U APPLICATIONS OF MATHEMATICS

MATHEMATICAL LOGIC
NT ALGORITHMS
NT BOOLEAN ALGEBRA
NT BOOLEAN FUNCTIONS
NT BOREL SETS
NT EQUIVALENCE
NT FORMULAS [MATHEMATICS]
NT LATTICES [MATHEMATICS]
NT SET THEORY
NT THRESHOLD LOGIC

Axiomatic explanation of complete self reproduction, noting logical mathematical biological reasoning and evolution theories

GO/NO/GO logic synthesis for probability functions development for systems operational readiness tests

MATHEMATICAL MODELS
NT DIGITAL SIMULATION
NT THOMAS-FERMI MODEL

Modified admittance yielding Kubo admittance at nonzero frequencies, discussing transformation of correlations of Ising model

Generalized plane stress concept extended for mathematical model to study out of plane displacement restraint in thin plates

Output p-channel MOS transistor selection tree for display and information storage systems

Exponential distributions in Markov chain models for communication channels, considering error free runs of tropospheric systems

Equation of characteristic functional for Burgers one dimensional model fluid turbulence using logarithmic expansion method, discussing change in time of energy spectrum

Mathematically stylized simple systems representing systems with functional law varying as function of acquired experience

Difference methods in solution of incorrect Cauchy problem simulating ideal gas flow in nozzle

Spiral structure of cloudiness in occluded cyclones studied by mathematical model based on meteorological satellite photographs [UN PAPER 68-95429]

CRT method of processing contoured data from hemispheric and global numerical models simulating general atmospheric circulation

Radiation models using discrete radiator ensembles having applications to analysis of forward and backscatter from rough surfaces, clutter and chaff models, etc

Optimal predictor design by comparison of statistical input models, measuring signal filter performance by root-mean-squared errors

Multiple configuration analysis of structures systematically predicting static and dynamic response of structures of single configuration class

MATHEMATICAL MODELS

Mathematical model constructed for behavior of multicomponent system subject to cannibalization
01 p0086 A69-10651

Digital simulation models for continuous systems determined by direct search minimization
01 p0036 A69-10706

Two dimensional structural model of micropolar continuum involving orientable points joined by extensible and flexible rods
01 p0169 A69-10810

Simultaneous estimation of parameters in multiple equation regression model arising from radioactive tracer experiments using compartmental models
01 p0106 A69-10926

Nonlinear buckling analyzed by mathematical models and computational procedures using organized matrix approach to structural analysis based upon finite element
01 p0171 A69-10964

Tracking radar glint analysis model using diffraction theory to evaluate parameters of fields received from scattering centers on target aircraft
01 p0033 A69-11007

Model describing outflow of cryogenic propellant tank pressurized by pressurizing gas, predicting pressurant mass, gas and wall temperature distribution, inlet flow rate, etc
01 p0163 A69-11147

Mathematical models of energy and mass transfer processes in closed loop multicomponent life support systems
01 p0021 A69-11316

MHD waves and toroidal mode existence by mathematical approximation
02 p0236 A69-11430

Lunar electrical parameters range determination using models [AAS PAPER 68-199]
02 p0312 A69-11477

Mathematical simulation of temperature and humidity changes in compartments of hermetically sealed space vehicle cabins
02 p0200 A69-11489

Mathematical models for Chlorella cell and biomass growth under illumination during space flight, noting ionizing radiation presence
02 p0198 A69-11508

Bayesian method for optimizing controlled plant characteristics using self adaptive model
02 p0223 A69-11566

Magnetosphere boundary determined in two dipole model approximation, taking into account current layer in tail
02 p0236 A69-11655

Data acquisition program for Apollo crew motion disturbances experiment consisting of ground simulations and orbital experiment establishing mathematical model of human body
02 p0201 A69-11759

Singular perturbation method for reducing order of mathematical models in optimal sensitivity control problems
02 p0224 A69-11967

Model for asymptotic separated flow in wake behind broadside of bluff body, discussing separation point, interaction, reattachment, base flow and near wake
02 p0188 A69-11986

Seismic wave generation, propagation, dispersion and attenuation in gravitating sphere having homogeneous elastic mantle and liquid core, giving theoretical seismograms
02 p0243 A69-12010

Metal fatigue crack propagation mechanism, deriving basic laws for failure in high and low stress regions, determining material parameters
02 p0340 A69-12025

Model for fast randomization of electron gas by trapped electroacoustical waves
02 p0289 A69-12236

Numerical solution on UNIVAC 1107 for model describing symmetrical gravitational collision of two four body systems
02 p0322 A69-12269

Collisionless computer model performing gravitational experiments with two dimensional galaxy
02 p0322 A69-12271

Computer study of collisionless self gravitating system using two dimensional model, obtaining gravitational field by solving Poisson equation
02 p0322 A69-12272

Space-station-centrifuge configuration dynamic stability exhibiting instabilities at lower and higher centrifuge rotational speeds [AIAA PAPER 68-142]
02 p0334 A69-12373

Probabilistic model for scattering function to solve radiative transfer problems in externally illuminated spherical shell atmosphere with perfectly absorbing core
02 p0328 A69-12751

Ultrahigh energy interactions working model, suggesting interpretation of cosmic ray experimental data on basis of Aleph plus Pionization model
03 p0499 A69-12945

Semiconductor nonlinear electron polarizability, using model to obtain correct order of magnitudes
03 p0483 A69-13035

Mathematical modeling of gyro drift rate in inertial navigation based on stationary and nonstationary time series analysis
03 p0463 A69-13213

Mathematical dipole model for geomagnetic field to provide main magnetic field source distribution within earth
03 p0424 A69-13543

Mathematical models to investigate transient plane bending wave propagation in elastic plates, using elasticity and plate theories
03 p0525 A69-13606

Long period variations in zonally symmetric circulations of tropical stratosphere, using zonally averaged momentum, continuity and heat and heat energy equations for numerical model
03 p0461 A69-13681

Two band model for determining linear and nonlinear electromagnetic responses of small band gap semiconductors in magnetic field
03 p0487 A69-13753

Lenz-Ising model of ferromagnetism noting mathematical methods used to investigate model properties
03 p0488 A69-13785

Tactical aspects of pursuit and evasion, emphasizing analysis of conceptual framework and construction of analytic models
03 p0457 A69-13898

Mathematical model derivation for observed atmospheric tide phenomena, taking into account thermal and other effects
03 p0426 A69-14098

Air traffic prediction based on mathematical econometric methods
03 p0536 A69-14105

Book on nonlinear programming covering models for weapon systems assignment, alkylation process optimization, chemical equilibrium, launch vehicle design, etc
04 p0621 A69-14362

Model for predicting characteristics of short duration intense microwave pulse propagating in heated high temperature air
04 p0634 A69-14453

Optimal control of linear stochastic systems using noise measurement data mathematical model
04 p0581 A69-14569

Thin shells deformations described by finite element model accounting for transverse shear deformations
04 p0674 A69-14588

Mathematical density-depth model proposed for lunar outermost layer compared to Matveev model, noting Surveyor estimates
04 p0655 A69-14659

Mathematical modeling of Gaussian and non-Gaussian processes obtained by linear and nonlinear transformations of white Gaussian noise, noting Markov processes
04 p0623 A69-14694

Perturbation behavior of solid propellant combustion, discussing relevance of analytical models and use of qualitative models
04 p0685 A69-14726

Predictive model for risk in technological research and development
04 p0689 A69-14980

Gaussian channels capacity, studying supremum of information transmission rates with small error probability
04 p0558 A69-15006

Interaction of gas atoms with solid surface, giving mathematical model assumptions
04 p0632 A69-15008

Kinetic model equation for electron plasma incorporating collision terms for model scattering
04 p0636 A69-15042

Properties and methods of generation of pseudorandom binary signals, developing linear modeling for multivariable systems
04 p0583 A69-15113

Flux equivalences of reflected and transmitted radiation among Rayleigh, isotropic and other scattering models
04 p0687 A69-15281

Domestic satellite communication system model for greatest possible amount of traffic using Saturn 5 propulsion systems, multibeam antennas, synchronous repeater platforms, etc
04 p0561 A69-15447

Mathematical models relating gain, cost, diameter, frequency and rms surface tolerance of ground antennas for exposed and radome enclosed parabolic reflectors
04 p0561 A69-15449

Laminar flow of nonNewtonian fluids described via rheological three parameter model
05 p0744 A69-15678

Mathematical theory for describing mechanical behavior of continuous media based on principle of determinism for stress
05 p0833 A69-15729

Mathematical theory for describing geometric structure of simple bodies, discussing dislocation distribution and exact field equations for elastic bodies motion
05 p0834 A69-15731

Models of continuous media with internal degrees of freedom based on Lagrangian variational principle
05 p0793 A69-15775

Factor analysis applied to identifying extremal plants, presenting regression analysis based on least squares techniques to calculate mathematical model coefficients
05 p0737 A69-15888

Collection of papers on computerized simulation covering dynamic modeling of ideas and systems
05 p0724 A69-16467

Mathematical model simulation of structures using building block approach
05 p0842 A69-16471

Ionizing radiation effects in microcircuits, using lumped model technique to derive mathematical model from electronic characteristics and boundary values of each semiconductor
06 p0977 A69-16886

Models to predict transient radiation responses in microcircuits, discussing model accuracy for junction and dielectrically isolated circuits
06 p0977 A69-16887

Laser Doppler meter model interpreting output frequency in terms of particle crossing set of fringes
06 p0932 A69-16927

Intervalley scattering model for Gunn domain dynamics, noting effects comparable to diffusion
06 p0893 A69-16937

Cosmic ray propagation model, considering determination of He interstellar spectrum and amount of matter traversed at low energies
06 p0988 A69-17270

Adaptive modeler to estimate state and future trajectory of unknown plant having automatically synthesized control
06 p0900 A69-17353

On-line optimization of stochastic control systems based on learning controller model, discussing computer simulation results
06 p0900 A69-17354

Mathematical description of electromagnetic field containing plasma, discussing energy transfer modes between plasma and containing field
06 p0965 A69-17517

Mathematical theory of electromagnetic induction for spherical model of earth with conductivity distribution given by sine function
06 p0921 A69-17739

Dermal injury predictability for exposure to thermal radiation based on mathematical model using temperature-time histories
06 p0875 A69-17840

Nonsteady combustion models for gases, liquid fuels and solid propellants, reviewing errors in physics and mathematics [AIAA PAPER 69-178]
06 p1037 A69-18100

Mathematical model for flow within external target type thrust reverser, assuming inviscid incompressible two dimensional flow [AIAA PAPER 69-3]
06 p0985 A69-18124

Model for spectral bidirectional reflectance of rough surface producing good agreement with experimental data [AIAA PAPER 69-64]
06 p0959 A69-18125

Analytical model developed from turbulent shear flow study, discussing Reynolds number effect [AIAA PAPER 69-163]
06 p0914 A69-18139

Computer model for n-p-n transistor in integrated circuit using substrate p-n junction isolation
07 p1114 A69-18246

Explorer 40 satellite mathematical model and verification testing for close spacecraft flight temperature predictions
[SAE PAPER 690202] 07 p1239 A69-18305

Thermally excited oscillation experienced by OGO 4 boom antenna demonstrated by mathematical model, showing nonplanar coupled bending-torsion oscillation by solar radiation
07 p1227 A69-18333

Ignition pressure transient for solid propellant rockets predicted by computer program
[WSCI PAPER 68-35] 07 p1203 A69-18352

Empirical and analytic modeling of propellant role in ignition, discussing ignition transient prediction to describe propellant ignitability characteristics
[WSCI PAPER 68-34] 07 p1202 A69-18364

Analytical model for thrust-time curve during ignition transient of solid propellant rocket engines, discussing flame spreading
[WSCI PAPER 68-33] 07 p1203 A69-18365

Nondemographic model predicting market shares of V/STOL aircraft in competition with automobiles and conventional airliners for short haul intercity business travel markets
07 p1244 A69-18967

Spatially nonuniform laser model allowing for photon density and inversion variations, noting self Q switching mechanisms from stimulated scattering processes
[IEEE PAPER Q-6] 07 p1154 A69-19078

Statistical analysis of cascade of bandpass limiter, ideal phase detector and video filter for mathematical modeling of coherent communication systems
07 p1084 A69-19147

Analytical model of spoiler generated sound in jet pipe, presenting data on level, spectrum and directivity of sound
07 p1183 A69-19462

Mathematical model of radar display, considering radar construction tube resolution, environment and eye perception parameters
07 p1136 A69-19504

Lifting rotor blades flapping response to atmospheric turbulence, discussing time averaging and perturbation schemes
[AIAA PAPER 69-206] 07 p1057 A69-19577

Mathematical models of crack propagation in solids noting similarity for equilibrium crack length
07 p1238 A69-19692

Viscoelastic rod model of human spine subjected to accelerations
07 p1072 A69-19725

Interaction between atom and plane monochromatic traveling wave taking into account pressure effect occurring in strong collision model
08 p1354 A69-19954

Linville model for describing elementary phenomena of electronic equipment in terms of physical data applied to irradiated semiconductor diode and transistor
08 p1280 A69-19974

Controlled charge models for computer calculation of electronic circuits, discussing tunnel diode static characteristics and equivalent transistor circuits
08 p1280 A69-19975

Distributed type bipolar transistor model construction, considering methods of development and computer tests for transient conditions
08 p1280 A69-19976

Vector equation of transfer for planetary atmosphere describing light scattering by anisotropic particles and analysis of resonance line scattering
08 p1385 A69-20063

Organization behavior models compared in theory of scientific and professional personnel management, noting compromise between excess restrictions and freedom
[AIAA PAPER 68-805] 08 p1422 A69-20196

Adaptation process of management systems from point of view of control system philosophy
[AIAA PAPER 68-807] 08 p1422 A69-20197

Iterative methods for composite layer slabs transport models, using invariant imbedding approach to transport theory
08 p1343 A69-20353

Electrochemical kinetic and mass transport model for studying stress corrosion crack propagation in Ti
[ECS PAPER 147] 08 p1332 A69-20359

Tuning design optimization of single circuit LF automatic control systems, using transfer functions and phase amplitude graphs
08 p1297 A69-20418

Dynamics and instability of multilayered systems models in field of gravity, noting isostatic adjustment of layered globe
08 p1309 A69-20578

Monograph on mathematical model for aircraft separation in air traffic safety control, analyzing aircraft motions and collision avoidance
08 p1347 A69-20712

Vortex valves and amplifiers small signal analysis using mathematical model to describe quantitative effects of vortex parameter changes
[AGARDOGRAPH-118] 08 p1257 A69-20953

Mission model construction for power limited systems, discussing flight concepts, propulsion mixes and electric propulsion
09 p1584 A69-21205

Mathematical models for outgoing traffic flow in airport terminal used for determining service requirements
09 p1476 A69-21439

Theoretical models describing quasi-stellar objects and radio galaxies, noting objects locality, semilocality and cosmological distances
09 p1594 A69-21693

Local axial voltage variation from one dimensional model applied to solve thermionic boundary conditions in two dimensional thermal analysis of converter
09 p1440 A69-21834

Mathematical model for improving statistical approximation convergence and accuracy in estimating structural components parameters
09 p1461 A69-21857

Bayesian reliability growth model with random variable parameters, discussing multimode failures
09 p1504 A69-21912

Computer study of analytical model of boundary layer transition from laminar to turbulent flow
[AIAA PAPER 68-38] 09 p1482 A69-21945

Single sideband modulation theory explained by sum representation of sampling theorem, comparing different signal generating methods
09 p1456 A69-22290

Deterministic model for cost effectiveness of avionics support programs based on subsystems support ability, test philosophy and test equipment design and manufacture
[AIAA PAPER 69-305] 09 p1478 A69-22377

Kalman filter with delayed states as observables, discussing extra computer effort and modeling technique
09 p1473 A69-22438

Mathematical model, analog computer simulation and information comparison of closed Brayton cycle systems for power conversion
[ASME PAPER 69-GT-50] 09 p1442 A69-22479

Mathematical, physical and physiological modeling for analysis of functional changes during varying gravity conditions
09 p1444 A69-22541

Radio signal reflection from objects of complex configurations by statistical model
09 p1460 A69-22662

Nonlinear control plants model with pure delay effect identified by harmonic balance method
09 p1475 A69-22669

Elasticity theory upper and lower bounds for two and three dimensional inhomogeneous problems and applications to plates
10 p1794 A69-22889

Turbulent transport processes mathematical model, determining upper and lower bounds
10 p1677 A69-22895

Model explaining intergranular crack initiation parallel to pulling axis in samples of spun beryllium broken under pressure
10 p1708 A69-22996

Electrical conductivity, electron density and population temperature as functions of current density in Cs-Hc thermal plasma studied with nonequilibrium ionization model
10 p1732 A69-23443

Mathematical model of closed biological cycle regenerating part of life support products, incorporating astronaut, storage and regenerating waste disposal units
10 p1649 A69-23580

Book on rocket propellants covering propulsion fundamentals, liquid, solid and hybrid propellants properties, performance calculations, rocket technology, etc
10 p1752 A69-23806

Human pilot adaptation in simulated multiloop VTOL hovering task with series loop closure model
10 p1650 A69-23878

Programmed search and gradient search methods for determination of sampling intervals in synthesis of sampled data models of human operators
10 p1650 A69-23881

Probability models used in statistical approach to fracture mechanics, noting role of weakest link model in representing brittle fracture
11 p1975 A69-24673

Constraint theory for analysis of mathematical models to alleviate software problems associated with simulation of complex large scale systems
11 p1858 A69-24936

Einstein field equations solutions for homogeneous cosmological models, assuming perfect fluid gravitation source and existence of simply transitive surface motions
11 p1919 A69-25245

Optimal control theory for systems modeled by ordinary differential equations, considering delay in control action
11 p1860 A69-25447

Modeling errors in linear discrete stochastic system effects on Kalman filter state estimates
11 p1860 A69-25448

Mathematical model for initial conditions of asymptotically stable nonlinear control system to estimate region of acceptable motions
11 p1861 A69-25453

Mathematical model with straight wake airfoil to determine aerodynamic forces on oscillating rotor blades in hovering flight
11 p1821 A69-25514

Aircraft stability derivatives determined by adaptive method, emphasizing physical and mathematical characteristics of learning model
11 p1824 A69-25671

Streamer based on model of perfectly conducting plasma produced on boundaries by entering and departing electrons, discussing streamer thickness and propagation velocity
11 p1935 A69-25759

Optimum nonstationary Gaussian signals estimation in presence of noise, generalizing Wiener stationary processes filtering theory
12 p2029 A69-26202

Detection of known signals in general noise, describing sufficient conditions for singular detection and estimation
12 p2029 A69-26203

Gallium arsenide junction laser resonant modes from theoretical model, calculating frequency separation
12 p2108 A69-26637

Mathematically stylized simple systems representing systems with functional law varying as function of acquired experience
12 p2054 A69-26670

Difference methods in solution of incorrect Cauchy problem simulating ideal gas flow in nozzle
12 p2012 A69-26671

Model, assuming electron thermal conductivity contribution, applied to studying solar plasma discharge characteristics in presence of three dimensional thermal sources in solar corona
12 p2149 A69-26680

Geomagnetic field dipole model by extrapolating vertical Z component for 1955 to heights between 500 and 25,000 km
12 p2071 A69-26695

Adaptive pattern recognition system simulated and tested with agricultural radar images, describing predictive environmental model mathematically
12 p2097 A69-26990

Human operator as servo system element of subassemblies in tracking and equilibrium tasks, stressing results of electromyographic analysis
12 p2025 A69-27081

Man machine model for prediction of human control behavior, generating model from analysis of helicopter pilot tasks
12 p2025 A69-27082

Model for temporal structure of human behavior from analysis of temporal information treatment in subjective synchronization task
12 p2025 A69-27084

Mathematical models of human performance in man machine systems, discussing operations research, maintainability and real time computer simulation for command and control systems
12 p2025 A69-27085

Models for cognitive behavior and psychomotor behavior for maintenance tasks
12 p2025 A69-27086

Abrasive wear model leading to abrasive wear equation and empirical findings on relative abrasive wear resistances 13 p2265 A69-27233

Mathematical relations presented for parameters of technological, transport and information systems reliability and life expectancy 13 p2268 A69-27436

Photometric data and law of rotation in symmetry plane for constructing mathematical model of mass and luminosity distribution in M 31 13 p2351 A69-28770

Theoretical model of homogeneous solid propellant ignition in neutral nonflow environment, discussing ignition time 13 p2324 A69-28218

Maxwellian velocity distributions simulated in one, two and three dimensions by superposition of N monoenergetic isotropic distributions, noting application to kinetic theory computation 13 p2313 A69-28222

Mathematical models for ballistic limit of single and double wall structures, yielding equations for relation to projectile and target characteristics [AIAA PAPER 69-370] 13 p2367 A69-28302

Nuclear emulsion high energy nucleon-nuclei interaction model accounting for two maxima track formation 13 p2303 A69-28371

Four dimensional momenta transfer during high energy cosmic ray particle collisions, comparing various collision models 13 p2330 A69-28375

Stable homogeneous combustion of condensed substances (CS), systematizing and analyzing elementary CS combustion models 13 p2379 A69-28454

Phenomenological macrorheology, discussing mechanical models designed for studying relation between stresses and strains in materials 13 p2369 A69-28562

Magnetosphere boundary determined in two dipole model approximation, taking into account current layer in tail 13 p2256 A69-28686

Model equation for Reynolds stress in turbulent two dimensional shear flow 14 p2428 A69-29000

Deterministic economic mathematical models for optimum airline networks, considering transportation cost 14 p2540 A69-29141

Thermionic converter components reliability under mechanical load and failure models, showing probabilistic nature of failures 14 p2400 A69-29227

Mathematical model of mechanical wear in surface friction based on approximation of cross section profiles, using Fokker-Planck equation for distribution function 14 p2455 A69-29331

Machine vibration effects on human operator performance using locomotor model 14 p2409 A69-29742

Binary encounter model for ionization by charged particle impact modified to evaluate cross section for ionization of positive ions by electron impact 14 p2489 A69-29996

PCM oscillator synchronization system stability, considering sampled model by digital nature of equipment 15 p2565 A69-30171

Electronic analog model for differential equations of equilibrium of gaseous combustion products based on asymptotic stability 15 p2717 A69-30862

Dynamic characteristics of model of spacecraft-astronaut-tether system during approach, deriving kinetic potential 15 p2696 A69-31064

Mathematical model for money expenditure on product oriented research programs, based on accumulated profits 15 p2721 A69-31068

Unknown channels classes epsilon capacity applied to estimating capacity of channels with additive noise, discussing models and upper and lower bounds 15 p2570 A69-31142

Metal oxide semiconductor structural model usefulness in understanding behavior near transition region, discussing surface inversion layer properties, surface mobility theory, etc 16 p2757 A69-31612

Time and space on-line simulation of analog, digital and hybrid block diagram systems 16 p2755 A69-31709

Mechanical systems modeling modification to include mobile coordinates, introducing gyroscopic and pseudogyroscopic terms into motion equations 16 p2875 A69-32246

Soviet book on nervous mechanisms of vestibular reactions emphasizing mathematical description of operation, neurohythmic changes in cerebellar cortex and oculomotor activity modeling 16 p2746 A69-32605

Hazards model for probabilistic prediction of casualties by exploding solid propellant rockets, deriving casualty expectation equation [AIAA PAPER 69-461] 16 p2869 A69-32749

Finite resolution effect on solar granulation simulated by numerical experiments using two dimensional smeared pattern 17 p3029 A69-33046

Planetary zonal flows hydrodynamic instability characteristics analysis, using quasi-geostrophic numerical model to study earth atmospheric cyclone wave role 17 p2960 A69-33149

Satellites and space vehicles attitude control mathematical model accounting for nonrigidity, sloshing and energy dissipation in vehicle interior 17 p3048 A69-33239

Radiant heat transfer predictions between isothermal plates based on diffuse plus specular directional property model 17 p3070 A69-33259

Mathematical model for determining time dependent terrain surface temperatures and radiances, considering radiative transfer convection, evaporation, ground vegetation temperature, etc [AIAA PAPER 69-592] 17 p3071 A69-33263

Rotary wing aircraft height-velocity testing, analyzing engine-out landing by combining flight tests with mathematical simulation model [AHS PAPER 353] 17 p2900 A69-33524

Finite difference schemes for barotropic fluid free surface model primitive equations tested for numerical integration stability and accuracy 17 p2997 A69-33691

Closed compartment fire mathematical model to analyze combustion parameter effects, atmosphere pressure and temperature during fire [AIAA PAPER 69-618] 17 p3074 A69-33704

Model calculations for movement of barotropic and initially symmetric vortices in rotating fluids with Coriolis parameter or fluid depth varying horizontally 17 p3000 A69-33761

Mathematical model of fields reradiated by Huygen sources in front of array for glide path site analysis 17 p3003 A69-34107

Mathematical model for aircraft antenna to antenna electromagnetic interference analysis, emphasizing techniques for propagation paths and shading factors 17 p2943 A69-34134

Torkington progressive rigidity model with successive minimum requirements relation to diagonal matrix elements of molecular force constants 17 p3068 A69-34230

Saturn 5 system simulation showing feasibility, efficiency and economy of real time simulation using large mathematical model and general purpose digital computer 18 p3113 A69-34268

Structural members stability mathematical models using lumped bars and springs simulating postbuckling behavior 18 p3211 A69-34342

High speed ball bearing skidding, proposing analytic model as design tool, discussing effects of thrust load, speed, oil temperature and flow rate [ASME PAPER 69-LUBS-20] 18 p3140 A69-34377

Mathematical model for operational readiness of dormant systems /periodically checked missiles/, discussing time distribution to failure detection, occurrence and between tests 18 p3142 A69-34477

Human performance reliability, testing mathematical model application and implications of time to first error concept by vigilance task 18 p3097 A69-34478

Mathematical index model based on weighted factor analysis to facilitate management and technical decisions concerning achievement of numerous tasks with fixed funds 18 p3232 A69-34504

Mathematical model of yielding of adhesive bonds in form of viscous threads between elastic bodies, obtaining solution to two dimensional problem 18 p3215 A69-34569

Rarefied gases transfer coefficients stochastic process calculation models, comparing results with correlation functions derived from transport equation 18 p3121 A69-34710

Local radiation characteristics calculation method, consisting of reducing integral equations to linear algebraic equations, applied to solve radiative heat exchange problems 18 p3229 A69-34713

Statistical model for coherent functions obtained from laser equation, showing amplitude and frequency coupling of radiation fluctuations 18 p3152 A69-34820

Stochastic meteorological models based upon presence of weather regimes, illustrating association with statistical inference problems 18 p3166 A69-34822

Models of continuous media with internal degrees of freedom based on Lagrangian variational principle 18 p3173 A69-35028

Stochastic failure models based on stress peak distributions, including randomly deteriorating strength model and increasing hazard reliability functions 18 p3148 A69-35079

Expected occurrences mathematical model for flight system availability under uncertainty 18 p3210 A69-35083

Four terminal silicon planar p-n-p-n model operating as semiconductor small signal linear tetrode amplifier, discussing properties and mathematical models 18 p3109 A69-35293

Hydrodynamics of gas flow due to solar flares using point explosion model, determining shock wave travel time to earth orbit 18 p3189 A69-35397

Parameters distinguishing analytic queuing models of time sharing algorithms, emphasizing techniques used for analyzing round-robin and multiple level queuing models 19 p3279 A69-35600

Shadow effects on current-voltage characteristics of solar cell array circuits, developing mathematical models 19 p3254 A69-35709

Mathematical basis for human operators purposeful behavior in complex systems control situation requiring decision reaching 19 p3260 A69-35895

Kinetic model and steepest descent method to optimize one dimensional combustor [AIAA PAPER 68-644] 19 p3448 A69-35943

Cost model to trade off competing systems designs for space communications, navigation, operational availability and ballistic missile defense 19 p3454 A69-36007

Partial prior information utilization via confidence intervals for mean time to failure of exponential reliability model 19 p3360 A69-36038

Mathematical model of CW ring laser mode coupling in limits of low excitation 19 p3334 A69-36047

Modified Monte Carlo model applied to computerized meteoric orbit evolution, simulating secular perturbations by imposing sinusoidal variation on orbital elements 19 p3414 A69-36117

Wall boundary condition model modification applied to molecular beam-solid surface scattering, noting qualitative agreement with observed distributions 19 p3377 A69-36179

Geometrical model for surface contact area, noting influence of nonlimitations on friction coefficient in elastic deformation 19 p3329 A69-36494

Numerical simulation of macrophysical and microphysical processes in convective cloud, including cloud geometry and equations describing dry and moist phases 19 p3362 A69-36497

Finite difference scheme for primitive equation model, emphasizing two grid internal noise suppression to improve gradient force expression accuracy 19 p3364 A69-36507

Adaptive predicting filter mathematical model based on information probability, using adaptive systems latent memory 19 p3287 A69-36665

Electric models optimization for heat exchange systems based on mathematical similarity between equations describing temperature and electrical potential fields 19 p3256 A69-36717

Graphical representation of friction stresses produced on mechanical parts surface layers, using mathematical model based on Poisson ratio and friction coefficient

19 p3329 A69-36723

Linearized wave propagation digital simulation models to predict arterial blood flow characteristics and impedance, comparing phase velocity and transmission per wavelength

19 p3264 A69-36868

Stochastic model for estimating manufacturing costs, discussing Mellin and Laplace transforms and Gram-Charlier series approximations

20 p3633 A69-36924

Multilevel mathematical model of oculomotor apparatus using neuron networks and complex activators, including computer analysis

20 p3470 A69-37245

Mechanical loss factors calculated by approximation formula from resonance curves of Voigt-Kelvin and Maxwell models

20 p3623 A69-37435

Mathematical model of nonlinear microwave breakdown for overdense and underdense plasma outside reentry vehicle, predicting nonlinear pulse transmission through high temperature plasma

20 p3495 A69-37853

Model predicting steady state input-output characteristics of vortex amplifiers operating in incompressible flow regime, correlating model with experimental data [ASME PAPER 69-FLCS-20]

20 p3465 A69-37980

Mathematical models and solution techniques for calculating optimal elastoplastic structures by computer, discussing methods for displacements preceding plastic failure

21 p3831 A69-38414

Book on mathematical model for heat and material exchange in bubbles covering bubble formation, transition period and quasi-stationary bubble rise

21 p3847 A69-38448

Book on mathematical foundations of systems analysis covering calculus, linear algebra, linear and nonlinear programming and major applications

21 p3754 A69-38576

Random variable used as model for unknown parameter in linear system, describing orthonormal expansion for evaluating mean-integral-squared error

21 p3685 A69-38727

Mathematical models of human vestibular system for dynamic space orientation, using control theory

21 p3662 A69-38728

One dimensional model and equation of energy spectrum function solved in studying turbulent diffusion in fluid at rest

21 p3693 A69-38749

Mathematical model of probability of errorless human performance for time continuous tasks for use in systems reliability analysis

21 p3664 A69-38971

Model of isotropic polycrystal generalized to composite materials including mechanical mixtures, calculating macroscopic constants in heat conduction, diffusion and elasticity

21 p3752 A69-39193

Mathematical model for determining trusted interplanetary spacecraft orbit, considering time history of position, velocity and thrust acceleration [AIAA PAPER 69-901]

21 p3806 A69-39335

Gyro drift rate mathematical modeling based on stationary and nonstationary time series analysis techniques with random process reduction to white noise residuals [AIAA PAPER 69-838]

21 p3761 A69-39369

Model performance index /PI/ providing criterion for approximating one dynamic flight control system by another based on geometrical representation of linear autonomous systems [AIAA PAPER 69-885]

21 p3764 A69-39410

Soviet monograph on mathematical methods of optimal control, discussing models and synthesis of optimal quick response systems by Pontryagin principle

21 p3757 A69-39524

Condensation dynamics of atom by solid body model consisting of one dimensional chain of harmonic oscillators

21 p3775 A69-39557

Mathematical model of astronaut motion and spacecraft angular control during tethered reentry, discussing conditions preventing spinning and collisions

21 p3667 A69-39630

Mathematical modeling techniques applied to thermoclastic cooling for plate without clamping and

mechanical loads, examining integrator schematic diagram

21 p3680 A69-39851

Homogeneous dynamo in cylindrically symmetric volume with symmetrically moving fluid and large magnetic Reynolds number, demonstrating first and second approximations using Braginskii method

22 p3989 A69-40192

Steady state mathematical modeling of light field structure for narrow collimated light beams propagating in artificial dispersive media

22 p3981 A69-40245

Algorithm for numerical modeling by Monte Carlo method of diffusion bounded light beams in dispersive media, applying to light pulse in cloudlike medium

22 p3981 A69-40248

Mathematical model of optimal partially closed life support system consisting of man, recycling unit, storage unit and waste disposal outlet

22 p3892 A69-40272

Mathematical models for describing visual perception of distance to ground during VTOL landing and takeoff

22 p3892 A69-40282

Natural torsional-flexural vibrations of bars with single symmetry, using matrix equations of equilibrium, displacements and natural coupled vibrations

22 p4043 A69-40456

Time dependent mathematical double acceptor model including heat effects for analyzing Q switching and stimulated emission time delays in pulsed junction lasers

22 p3962 A69-40560

Reliability engineering application to aircraft safety, considering mathematical models involving safety, human errors and accident causes

22 p3867 A69-41129

Human vision mathematical simulation, relating optical input signal parameters to corresponding visual impression

23 p4109 A69-41978

Human hearing and vision mathematical simulation, relating signal perception parameters to corresponding adaptation processes

23 p4109 A69-41979

Mathematical model for information processing of biological memory as cybernetic system

23 p4110 A69-41982

Dynamic reactions of mathematical model representing vision and hearing process adaptation

23 p4110 A69-41984

Mathematical model construction to simulate light adaptation in human vision based on Maxwell disk experimental results

23 p4110 A69-41985

Teleological systems behavior modeling based on input, output, goals, operation duration, etc

23 p4134 A69-42059

ASTRA /advanced structural analyzer/ based on stiffness approach to finite element method, generating mathematical model for stresses and deflections

23 p4232 A69-42144

Interference prediction models of equipment emissions and susceptibility thresholds based on limited spectrum signature data

23 p4126 A69-42223

Controlled plant in n dimensional Euclidean space, analyzing optimal trajectory using integral equations

23 p4183 A69-42472

Compartmental models for radioactive tracer experiments with known tracer material amount, using generalized Spearman simultaneous estimation procedure

24 p4339 A69-42765

Air traffic growth forecasting, describing various mathematical econometric models [AAS PAPER 69-329]

24 p4417 A69-42807

Decision process model for man-machine decision task structuring by system designers

24 p4274 A69-43018

Solar wind collisionless hydromagnetic flow interaction with planetary atmosphere, using mathematical model to determine bow shock position limits in atmosphere

24 p4368 A69-43178

Mathematical input-output model for vestibular system, relating linear and angular motions to non-visual perception of orientation, motion and nystagmus for physiological characteristics

24 p4276 A69-43274

Time-invariant multivariable linear systems, discussing structure theorem for controllable systems and application to decoupling problem

24 p4294 A69-43314

Geomagnetic zenith calculation at given point based on geomagnetic field model, using polynomial development

24 p4311 A69-43505

Stagnation region heat transfer with nongray gas subjected to external radiation using two step continuum absorption coefficient model

24 p4415 A69-43590

Shock formation mechanism in simple shock tube using multistage modification of White model, deriving variation of shock Mach number

24 p4305 A69-43631

MATHEMATICAL STATISTICS

U STATISTICAL ANALYSIS

MATHEMATICAL TABLES

Tabulation of high accuracy gamma function values for some rational arguments, noting applications to Gaussian quadrature formulas, fractional Bessel functions and Airy functions

03 p0455 A69-13375

Soviet book of statistical and mathematical tables for calculation, analysis and control of reliability

04 p0608 A69-15540

Stability derivative estimation at subsonic speeds for preliminary design engineer

05 p0700 A69-15545

Mathematical formulation of Noy tables, noting more efficient programming and minimal disagreement with original tables

08 p1266 A69-20403

Data interpretation, discussing correlation describing effectiveness of independent variable and table giving values directly from sample size, t, z, F and chi square values

10 p1669 A69-23040

Table of definite and indefinite integrals of products of exponential integrals with elementary or transcendental functions

24 p4341 A69-43324

MATHEMATICS

Latvian yearbook on mathematics covering rectangular thermal problems, second order systems, metric theory and nonlinear oscillatory systems

03 p0468 A69-13862

Physics, mathematics, mechanics - Conference Moscow, December 1964

13 p2300 A69-28430

MATHIEU FUNCTION

Mathieu equation with square law damping effect on first order instability range

10 p1724 A69-22920

Differential equations application to electrical circuit problems, solving voltage for series LCR networks and transforming Mathieu into Hill equation

12 p2052 A69-26351

Nonlinear time varying feedback control system stability applied to damped Mathieu equation

23 p4146 A69-42473

MATRICES [CIRCUITS]

Wideband hybrid junctions synthesis from given parameters, suggesting matrix representation of ring circuits

01 p0043 A69-10593

Electronic beam-rotation systems operation using matrix network to feed circular arrays, noting applicability to direction finding or radar systems

08 p1288 A69-20964

Algorithms in electronic circuit analysis, establishing algebraic and topological analogs based on generation of fundamental relations

09 p1472 A69-21777

Thermionic converters with matrix circuit connections, considering current flow patterns in matrices to evaluate electrical failure spreading

14 p2400 A69-29225

Algorithm for enumerating all circuits of linear graph, noting suitability for computerization without large computer memory

14 p2421 A69-29541

Topological circuit analysis by digital computer, using conductivity matrix determinant in form of sum of trees

15 p2582 A69-30112

Lumped and distributed parameter systems, discussing transfer matrix elements, connecting lines, etc

15 p2582 A69-30319

Memory matrices sensitivity to laser beams with various emission power densities, considering matrices of thin metal layers on transparent base

19 p3335 A69-36198

- Quadrupole network transfer matrix calculation from known octupole matrix, describing frequency response determination of coupled transmission lines 22 p3912 A69-40257
- MATRICES [MATHEMATICS]**
- NT ADJOINTS
- NT CANONICAL FORMS
- NT EIGENVALUES
- NT EIGENVECTORS
- NT JORDAN FORM
- Oblique matrix pseudoinverse concept extended, discussing elementary properties and applications 01 p0104 A69-10315
- Matrix procedures for stability of nonlinear control with nonlinearities, discussing system with three actuating elements 01 p0050 A69-10355
- Book on advanced linear programming computing techniques covering algebraic theory and construction of computer programs 01 p0035 A69-10701
- Matrix technique for transformation of equation of motion into first order equation in analyzing perturbation forces producing mechanical oscillations 01 p0170 A69-10827
- Coulomb approximation for dipole and quadrupole transitions, calculating tables for radial matrix elements 01 p0124 A69-10901
- Integral operators on space of Borel measurable functions bounded considering weight function, giving condition for infinite complex matrices, mapping analytic sequence spaces 01 p0107 A69-11244
- Keplerian motion parameters second derivatives determined from initial conditions by deriving differential equations 01 p0107 A69-11305
- Stable high order implicit methods to solve numerically differential equation systems with matrix coefficients used for heat conduction equation 01 p0107 A69-11364
- Structure oriented parallel algorithms for matrix operations, noting applicability to real time calculations for discrete Kalman filter and control problems 02 p0224 A69-11743
- Matrix transformation applications in dynamic system theory and stability test 02 p0281 A69-11943
- Matrix representation of linear active two port noise figures and charts in terms of power wave variables 02 p0211 A69-12444
- Fast Fourier-Hadamard transform for digitized signal representation, classification, discrimination and efficiency 03 p0392 A69-13249
- Eigenvector approximation of complex matrix by inverse iteration, giving Algol 60 program 03 p0455 A69-13371
- Matrizants construction for Keplerian motions, discussing Hamiltonian character of variational equations for planar two body problem 03 p0513 A69-13779
- Planar array multiple beam generation and position determination using N-port Butler matrices 04 p0570 A69-14309
- Invariance of stabilized coordinates in power gyro stabilizers, using matrix equivalent of gyroscopic moments acting on platform 04 p0597 A69-14602
- Matrix elements calculation for one dimensional quantum-mechanical problems using transformation theory 04 p0632 A69-14866
- Two dimensional elementary transformation for obtaining eigenvalues, considering programming aspects for computing characteristic roots of matrix 04 p0624 A69-14967
- Green matrix of periodic boundary value problem for system of linear differential equations 04 p0624 A69-15098
- Instrumental Stokes vector calculating method involving light flow transformation matrix elements determination 04 p0601 A69-15248
- Higher dimensional Dirac Hamiltonians from L-matrix hierarchy using dimensional eigenvector 04 p0625 A69-15275
- Approximate expressions for displacement state of orthotropically reinforced conical thin walled shell, finding stiffness matrix by numerical integration 05 p0835 A69-15829
- Stiffness matrices for buckling or vibration analysis of long thin flat plate structures connected at longitudinal edges 05 p0836 A69-16029

- Dynamic equations for offset unsymmetric gyroscope with obliquely placed rotor, using dual transformation matrices [ASME PAPER 68-WA/DE-5] 05 p0764 A69-16170
- Sensitivity matrix in multivariable feedback control systems, discussing loop gain matrix design to achieve desired insensitivity to system error sources [ASME PAPER 68-WA/AUT-9] 05 p0738 A69-16179
- Matrix Riccati and matrix quadratic equations in problems of stochastic control and filtering 05 p0740 A69-16601
- Optimal approximation of functional matrix, giving upper bounds for deviations of general matrices from closest special matrices 06 p0948 A69-17495
- Spin-other-orbit matrix elements for F super 3 electron configurations 06 p0962 A69-17819
- Linear equivalent gain matrix of multivariable non-linearity evaluated with equivalent gain concept for monovariable nonlinear stochastic process 07 p1114 A69-18286
- Fourier transform algorithm introduction leading to image coding technique with image transformed by Hadamard matrix operator 07 p1078 A69-18859
- Sparse matrix scheme for computer analysis of structures, introducing term searching factor as efficiency guide for matrix routines 07 p1089 A69-19723
- Separable expansion for off shell two body t matrix with Coulomb potential to solve nonrelativistic three body problem with two body interactions 08 p1354 A69-20205
- Multiloop control plant described by Jacobian transfer matrix to control spectral characteristics of random processes 08 p1296 A69-20233
- Synthesis method for UHF transistor oscillators tunable in wideband using Y-matrices 08 p1285 A69-20380
- Explicit transverse bending stiffness and mass matrices for triangular finite plate element with linear thickness variation, using matrices for natural frequencies of vibration 08 p1414 A69-20526
- Linear systems analysis by generalized numbers method, discussing algorithms for manual or computer analysis 09 p1472 A69-21778
- Specialized mathematical machine for expanding matrix determinants and solving combinatorial problems, discussing symbolic circuit 09 p1460 A69-21782
- Circuit function determination from Laplace transforms without calculating transient state matrix, using numerical method 09 p1472 A69-21785
- Digital computer algorithm for analyzing circuits represented as autonomous multiport networks 09 p1472 A69-21786
- Matrix elements for asymmetric rotors using rigid rotor reduced energies, describing computations method 09 p1614 A69-21913
- Error bounds for estimation error covariance matrix of fixed point smoothing and fixed interval smoothing algorithms for optimum linear estimation 09 p1533 A69-22436
- Quasi-static modified field distributions in inhomogeneously filled cavities and waveguide tubes, comparing with homogeneously filled cavities and obtaining matrix eigenvalues 09 p1467 A69-22561
- Signal flow graphs based on matrix methods, discussing loop currents, systems orientation and transfer functions 09 p1475 A69-22600
- Variational approximation of probability measures and products of random matrices, discussing point distribution on Lobachevskii plane 10 p1719 A69-23399
- Multiple loop feedback systems synthesis utilizing extended node introduction synthesis theory, considering filter response functions characteristics 10 p1667 A69-24037
- Matrix Computer for solution of algebraic and integrodifferential equations in linear and nonlinear statics and dynamics, considering mechanical vibration problems [ASME PAPER 69-VIBR-12] 10 p1806 A69-24167

- Order of finite order linear continuous completely controllable completely observable system, using impulse response matrix and order of corresponding differential equations 11 p1858 A69-24567
- Radiant power flow, transmittance and absorptance of absorbing thin film multilayer in terms of characteristic matrix and admittance of surrounding media 11 p1896 A69-24850
- Matrix Riccati equation duality and bounds, discussing duality in context of optimal control 11 p1909 A69-24885
- Matrix computation operations devoid of sense and relevancy arising in interdisciplinary problems 11 p1910 A69-25522
- Transient response of linear time invariant system from state transition matrix, eliminating evaluation of eigenvalues 12 p2120 A69-25913
- Matrix transfer functions factorization to obtain irreducible representations of multivariable control systems used for studying invariant linear multidimensional processes 12 p2047 A69-26072
- Liapunov matrix equation solution, discussing restriction removal 12 p2121 A69-26377
- Inverse iteration method insensitive to small eigenvalue errors for finding eigenvectors 12 p2121 A69-26510
- Rational transfer function matrix realization into irreducible Jordan canonical form state equation by nonsingular transformations 12 p2122 A69-26511
- Negative exponential solution of matrix Riccati equation associated with linear optimal regulator and filter problems for time invariant plants 12 p2122 A69-26513
- Radiation diffusion in medium of finite optical thickness, computation of source function and tabulation of matrices 12 p2131 A69-26661
- Nonsingular matrices inversion method by group partitioning applied to noise covariance matrix used in optimal prediction and control 12 p2123 A69-26754
- Asymptotically stable discrete time closed loop linear systems synthesis, presenting feedback matrix as illustration 13 p2287 A69-27238
- Square matrices decomposition into orthogonal and triangular matrices products for computer storage applications 13 p2290 A69-28485
- Homogeneous finite automaton asymptotic analysis, calculating series terms for matrix transition probability function 13 p2239 A69-28535
- Group code decoding, discussing equivalent transformations of reference matrix and reduction of equipment losses 13 p2225 A69-28537
- Electro-optical Q switched lasers with prismatic reflectors and phase shifter studied using Johns matrices for polarizer, Kerr cell and Porro prism elements 14 p2459 A69-29390
- Eigenvalues of finite matrix Hamiltonian, considering convergence radius of perturbation series, limits and renormalization 14 p2470 A69-29451
- MHD quantities in linear wave and small intensity shock wave dissipation and structure determinable by right and left eigenvectors of matrix MHD flow equation 14 p2500 A69-29902
- Coupled equations for heavy particle motion expressed by introducing generalized matrix operator for effective momentum in atomic collision problems 14 p2489 A69-29997
- Moving targets trajectories determination from radar data, using posteriori probability distribution represented by Markov chain 15 p2566 A69-30334
- Optimum order for column orthonormalization of sparse matrices, applying results to Gram-Schmidt and Householder methods 15 p2644 A69-30425
- Economical computer techniques for numerically integrated finite elements, creating 96 element square matrix 15 p2711 A69-30873

Probabilistic automata stochastic matrices algebraic properties of definite, quasi-definite, periodic and quasi-periodic sets

15 p2645 A69-31141

Plane Cauchy problem solution for differential equations in heat and mass transfer theory, applying contour integral method in matrix construction

15 p2719 A69-31262

Approximation of vector linear differential equations with slowly varying matrix coefficients on time sharing computers, noting modeling possibilities

17 p2996 A69-33879

Reduction of partitioned submatrices functions for expediting calculations of hypercirculant and hyper-hyper Jacobi analytic functions

18 p3163 A69-34330

Matrix formulation for discrete element method applied to linear static and eigenvalue problems of thin walled segments, using homogeneous differential equations

19 p3445 A69-36831

Ensembles of random Hermitian cyclic matrices in statistical theory of complex systems energy level spectra, noting Gaussian density function of eigenvalues

20 p3567 A69-36988

Generalized Clifford matrix algebra applications, noting relation to generators of special unity group

20 p3568 A69-37072

Perturbation matrix derivation in rectangular coordinates using Sitarsky two body variational equation for all motions

20 p3568 A69-37200

Mathematical properties of involutorial matrix solutions to simple quadratic equation, obtaining symmetry properties, eigenvalues and recursion formulas

20 p3568 A69-37579

Physical networks with lumped components and hydraulic, pneumatic, electric, thermal and elastic lines of transfer matrices

[ASME PAPER 69-FE-15] 20 p3568 A69-37999

First order linear differential equations subject to linear constraints, discussing solution uniqueness dependence on matrix nonsingularity

21 p3754 A69-38744

Unitary matrix representing generalized inverses, proving weak method of steepest descent for least squares solution of equations

21 p3755 A69-38926

Transfer matrix symmetry about secondary diagonal in vibration analysis useful for computer programming

22 p4040 A69-39938

Natural torsional-flexural vibrations of bars with single symmetry, using matrix equations of equilibrium, displacements and natural coupled vibrations

22 p4043 A69-40456

Matrix identity associated with linear digital filtering and recursive estimating determined using matrix projection operators and properties

22 p3975 A69-41014

Frequency response of control systems analyzed by digital computer using operational arrays, noting extensions to time response and root locus computation

22 p3909 A69-41255

Green matrix for operator M governing steady state wave propagation in inhomogeneous anisotropic media obtained as solution of integral equations system

23 p4180 A69-41368

Fast Fourier Transform connection with circulant and permutation matrices for case with discrete time sample number equal to discrete frequency samples

23 p4182 A69-41761

Three dimensional pin-jointed trusses calculation method by state vector incorporating force and displacement matrices

23 p4236 A69-42485

Iterative and vectorial methods for correcting computed direction cosine matrix errors

23 p4134 A69-42543

Sequential vector estimation of matrix of second partial derivatives, suggesting alternative least squares method

24 p4340 A69-42958

Triangular plate bending element using Herrmann variational method, deriving matrices for finite elements

24 p4404 A69-43591

Vector matrix second order sensitivity equation application to Mars entry guidance, performing numerical simulation of second order sensitivity guidance and tabulating results

24 p4388 A69-43690

P-Q norms generalized inverse concept of matrix derived from extension of Penrose best approximate solution of linear equations

24 p4342 A69-43703

Density matrices of symmetry projected single determinant wave functions for finite groups, considering many particle system

24 p4351 A69-43810

MATRIX ALGEBRA **U MATRICES [MATHEMATICS]**

MATRIX ANALYSIS **U MATRICES [MATHEMATICS]**

MATRIX METHODS

Sheba family of shell elements for matrix displacement method applied to problems of thin shells under membrane and bending action

01 p0170 A69-10865

Nonlinear buckling analyzed by mathematical models and computational procedures using organized matrix approach to structural analysis based upon finite element

01 p0171 A69-10964

Physical interpretation for Choleski decomposition method applied to structural analysis, discussing stiffness and flexibility methods

01 p0173 A69-11417

Computer stress analysis may result in automated designs, emphasizing finite element technique

02 p0341 A69-12153

Matrix displacement method for nonlinear elastic analysis of shells of revolution under symmetrical and asymmetrical loadings

02 p0346 A69-12511

Compatibility equations in plane micropolar thermoelasticity theory obtained by associated matrix method

03 p0525 A69-13607

Matrix-harmonic method for vibration study of mechanisms and machines

03 p0468 A69-13860

Matrix-harmonic method of vibration study extended to include autonomous vibrations of single degree of freedom machines

03 p0468 A69-13861

TUBA family of plate elements, discussing kinematically equivalent load matrices, initial loads due to initial strains, geometrical stiffness and square plates

03 p0530 A69-14090

Matrix perturbation method for hyperstatic structure modification by combining original solution elements with data on modification

04 p0668 A69-14380

Panel flutter in supersonic flow, using finite element approach in matrix displacement methods to derive aerodynamic influence coefficient matrices

04 p0676 A69-14707

Stiffness matrices for sector elements under membrane stress, considering alternative displacement distributions within element

04 p0676 A69-14728

Laminated plates vibrational characteristics calculations by transition matrices, relating stresses and displacements under load

04 p0679 A69-14907

Matrix displacement and force methods of stability analysis, deriving method of determining geometrical stiffnesses for complex structures

05 p0841 A69-16399

Unsymmetrically laminated simply supported plates approximate solutions, considering potential energy and reduced stiffness matrix

07 p1232 A69-18725

Book on computer calculation of structures covering programming, computer language, mathematical aspects of structural analysis, matrix computation, etc

07 p1233 A69-19349

Matrix method for structural analysis using force and rigidity methods

07 p1239 A69-19776

Explicit transverse bending stiffness and mass matrices for triangular finite plate element with linear thickness variation, using matrices for natural frequencies of vibration

08 p1414 A69-20526

Curved tetrahedral and triangular elements in matrix displacement method covering linear and nonlinear cases

08 p1415 A69-20631

Matrix displacement method for nonlinear elastoplastic two or three dimensional structures or continua, discussing strain distribution

08 p1416 A69-20705

Wave interaction in magnetically confined plasma taking into account body and surface waves

08 p1370 A69-21014

Stiffness matrix for doubly curved shallow shell element with rectangular plane projection applied to circular cantilevered cylinder and barrel vault

10 p1802 A69-23892

Natural mode structural analysis matrix methods for small displacements, discussing curved local subbeam in space and circular arch

11 p1969 A69-24374

Dynamic unified structural analysis method in computer program, calculating stiffness matrix to obtain natural frequencies and mode shapes

11 p1987 A69-25367

Strip method for prediction of subcritical frequency and damping characteristics for subsonic wind tunnel and flight flutter tests

11 p1987 A69-25368

Discrete linear optimal control system with quadratic performance index synthesized by dynamic programming method, obtaining matrix equations

12 p2050 A69-26091

Linear, quadratic, optimal control problems solved by sweep method, discussing time role, feedback control law and use of matrix equations

12 p2053 A69-26512

Laminated plates vibrational characteristics calculations by transition matrices, relating stresses and displacements under load

12 p2182 A69-26660

Automated Structural Analysis Procedure employing Displacement Method of Matrix analysis applied to validation studies of various finite elements for wing structures

12 p2184 A69-26809

Shallow hyperbolic paraboloidal shell with large deflections, analyzing nonlinear behavior with numerical method based on integral equations

12 p2185 A69-26820

Load deflection equation solution based on row operations, involving three passes of coefficient matrix, using wavefront processing and modified Gauss algorithm

13 p2358 A69-27208

Stiffness matrix derived for skewed curved shallow shell element with reference to oblique coordinate system

13 p2358 A69-27210

Discrete element plastic analysis of long prismatic bars under transverse loading in longitudinal direction, based on matrix displacement method

13 p2365 A69-28237

Power gyrostatic kinematic structure synthesis, applying matrix methods to design variables

14 p2446 A69-28924

Elastoplastic matrix for stress increments for yield surfaces with associated flow rule, considering initial stress computation

15 p2706 A69-30433

Stiffness matrix for refined triangular plate bending finite element, considering Kirchhoff theory

15 p2706 A69-30434

Stiffness matrix of polygonal finite plate bending element derived using assumed stress distribution

15 p2710 A69-30867

Nondeformable closed contour spatial gear kinematics using matrix tensor method suitable for computer programming

15 p2713 A69-31020

Statistical calculation of three dimensional frames of thin walled rods, using method of initial parameters in matrix form

15 p2714 A69-31199

Triangular shell element SHEBA for arbitrary curvature variation as means of performing large displacement matrix analyses, discussing local subelement, natural modes, cross sectional results, etc

16 p2872 A69-32025

Aerodynamic control surface/trim tab coupling coefficients in subsonic two dimensional unsteady flow using matrix method valid for motion involving harmonic oscillations

17 p2895 A69-33597

Complete spherical shells nonsymmetric vibrations frequencies and mode shapes calculated by matrix method

17 p3061 A69-33706

Torkington progressive rigidity model with successive minimum requirements relation to diagonal matrix elements of molecular force constants

17 p3068 A69-34230

Finite element analysis of nonlinear elastoplastic material-geometric behavior problems, describing computer program and incremental stiffness matrices

18 p3219 A69-34664

Elastic stiffness, kinematically equivalent loads and initial loads due to initial strains of FUGA 6 element, describing program for matrices generation

19 p3447 A69-36852

Rectangular plate bending element corresponding to finite difference method use, deriving stiffness matrix from strain energy approximation
20 p3619 A69-36949

Stiffness matrices in plane elasticity problems by Galerkin method, leading to simultaneous expressions related to finite element method
20 p3619 A69-36951

Matrix displacement method of structural analysis applied to dynamic buckling of clamped shallow spherical caps under step pressure loading
20 p3622 A69-37229

Airframe stability of VAK 191 examined by displacement method, using matrix calculations within Automatic System of Kinematic Analysis
20 p3462 A69-37515

Parallel wire antenna array design for specified pattern using matrix methods and method of moments for self and mutual impedances and required excitations
20 p3507 A69-37847

Automatic structural analysis by matrix force method, giving diagrams of load paths, equilibrium sequence and flow chart
21 p3843 A69-39311

Strain anisotropy matrix construction for various strain trajectories from elastic properties of expression relating stress and elastic strain deviators
22 p4039 A69-39915

Thin walled rods for girder and frame systems designed by matrix method, solving differential equations for tension, compression, bending and torsion
23 p4230 A69-42005

ASTRA /advanced structural analyzer/ based on stiffness approach to finite element method, generating mathematical model for stresses and deflections
23 p4232 A69-42144

Field transfer matrices for simultaneous treatment of free and forced vibrations and buckling through axially loaded Timoshenko beam
23 p4234 A69-42400

Matrix method for free and forced oscillations of complex linear damping system with known linear vectors
23 p4236 A69-42484

Matrix method for analyzing elastic structures linear transient response to time dependent loads and temperature change
24 p4399 A69-42988

MATRIX THEORY

Oblique matrix pseudoinverse concept extended, discussing elementary properties and applications
01 p0104 A69-10315

Exchange rule to solve system of linear matrix equations in sense of Chebyshev, giving various algorithms
01 p0105 A69-10705

Physical interpretation for Choleski decomposition method applied to structural analysis, discussing stiffness and flexibility methods
01 p0173 A69-11417

Matrix theorem giving necessary and sufficient conditions for leaving cone invariant, considering finite dimensional spaces
04 p0624 A69-15003

Theorems and lemmas formulated pertaining to Volterra equations stability
05 p0787 A69-16449

Optimal approximation of functional matrix, giving upper bounds for deviations of general matrices from closest special matrices
06 p0948 A69-17495

Asymptotic solution to problem of finding time optimal transformation for controlled plant with motion in phase space described by matrix differential equation
10 p1666 A69-23883

Matrix formulation of electromagnetic field equations and nonlinear conservation laws for measurable quantities
10 p1725 A69-24049

Oscillation theorems for linear self adjoint elliptic equations of even order $2m$, discussing proofs dependence on Swanson comparison theorem
11 p1909 A69-24882

Matrix Riccati equation duality and bounds, discussing duality in context of optimal control
11 p1909 A69-24885

Numerical computation method for evaluating transition matrix of linear time invariant system, estimating error propagated in transient response
11 p1910 A69-25660

Matrix eigenvalue problems with statistical properties, applying to dynamic structural systems and verifying solutions by Monte Carlo simulation
16 p2871 A69-31878

Algorithm minimizing nonzero elements during Crout reduction of sparse matrices
20 p3497 A69-36946

Asymptotic stability of null solution of matrix differential equation, considering linearized equations of rotational motion for hinged two body gravity gradient satellite orbit
20 p3575 A69-37212

N symmetric matrices orthogonal integrity basis, considering product traces, polynomial invariants, tensor groups, etc
20 p3624 A69-37587

Matrix pseudoinverses producing necessary and sufficient conditions for positive and nonnegative definiteness
21 p3756 A69-39497

Fast Fourier Transform connection with circulant and permutation matrices for case with discrete time sample number equal to discrete frequency samples
23 p4182 A69-41761

Book on matrix-computer methods in engineering covering matrix algebra and calculus, computer programming, Fourier transforms, etc
23 p4234 A69-42421

Generalized inverse of matrix computation method, using elementary orthogonal matrices and Gaussian elimination
24 p4339 A69-42762

MATTER (PHYSICS)

Open cosmological model containing radiation and matter, noting matter density relationship to visible matter average
01 p0150 A69-10371

Superdense matter possibly present in neutron stars, discussing relation with Einstein theory and nuclear physics
06 p1012 A69-18240

Relativistic cosmological models with radiation and matter, analyzing conversion from radiation-like models to dust-like models
07 p1222 A69-19587

General theory of relativity and tensor field equations relating space time characteristics to local properties of matter and vacuum, using Palatini Lagrangian method
09 p1593 A69-21572

Equilibrium state of matter at high temperatures and densities with respect to nuclear reactions, determining neutron-proton ratio
11 p1957 A69-24403

Neutrons overloaded nuclei role studied for neutronization of matter at high densities in statistical equilibrium with respect to nuclear reactions
11 p1957 A69-24404

Extragalactic gamma ray fluxes predicted, discussing collisions, matter-antimatter annihilation and cosmological implications
11 p1946 A69-24466

Mathematical methods for quantum mechanical problems caused by electromagnetic field interaction with matter
18 p3175 A69-35402

Coherent radiation generation using gas lasers, analyzing interaction between EM radiation and matter
19 p3335 A69-36067

Meteorite and primordial matter composition related to possible fractionation processes influence, discussing nuclear species abundance
19 p3406 A69-36073

Solar system matter evolutionary beginning traced to chemical elements synthesis by considering radioactive decay irreversible processes
19 p3406 A69-36076

Cosmic matter density and velocity in expanding universe with negative curvature within Einstein-Friedman theory
20 p3599 A69-37472

Matter and radiation interaction in hot model universe, investigating residual radiation spectrum deviation from Planck curve
21 p3797 A69-38536

Universal dependence of density fluctuations on specific entropy derived from equation describing material composed of neutral particles and equal number of charged and antiparticles
21 p3771 A69-38995

Matter surface distribution in general relativity, deriving matching conditions
22 p3982 A69-40753

Equilibrium state of matter at high temperatures and densities with respect to nuclear reactions, determining neutron-proton ratio
24 p4391 A69-43793

Neutrons overloaded nuclei role studied for neutronization of matter at high densities in statistical equilibrium with respect to nuclear reactions
24 p4391 A69-43794

MATURING U GROWTH

MAXIMUM PRINCIPLE

Dynamic programming to demonstrate sufficient conditions of optimality in maximum principle when regular control synthesis is realized
02 p0225 A69-11975

Quantitative form of maximum principle for elliptic partial differential equations
03 p0457 A69-13826

Trajectory optimization, obtaining sequence of control functions by iterative application of maximum principle /min H/ to nonoptimal functions [DVL-852]
04 p0548 A69-14827

Pontryagin maximum principle used to solve optimal control problems on analog computer
05 p0739 A69-16473

Maximum principle application to stochastic systems, developing set of stochastic partial differential equations
05 p0788 A69-16482

Maximum principle in integral form for optimal control problems with delay differential system equations, using vector matrix notation
10 p1718 A69-23038

Dynamic programming to demonstrate sufficient conditions of optimality in maximum principle when regular control synthesis is realized
10 p1666 A69-23884

Successive approximation techniques for problems in optimum control theory, considering maximum principle and Banach space
11 p1908 A69-24771

Feedback control of linear systems subject to sudden changes in parameter values
12 p2052 A69-26502

Maximum principle for infinitesimal deformations of convex surface with nonnegative Gaussian curvature, noting application to rotation and displacement diagrams
13 p2361 A69-27741

Optimal control conditions for systems described by differential equations with deviating neutral type argument formulated in maximum principle form
14 p2426 A69-29419

Three and n body problems solution by reduction of independent variables and maximum principle
15 p2652 A69-30448

Pontryagin maximum principle applied to time optimal control of autonomous second order system with constant coefficients and differentiation in transfer function numerator
15 p2583 A69-31059

Suboptimal closed loop control of nonlinear systems subject to quadratic performance indices by invariant imbedding concepts and maximum principle
18 p3111 A69-34678

Coplanar impulsive transfers and second variation test, using maximum principle and Lagrangian multiplier technique for propellant expenditure minimization
19 p3400 A69-35676

Linear optimal control problem for system with variable terminals, proving maximum principle and transversality conditions under minimum constraints
19 p3285 A69-35859

Variational or optimal control for delayed systems, involving integrated maximum principle for problems with nonlinear functional differential systems
21 p3754 A69-38429

Point mapping in optimal control, describing maximum principle, dynamic programming and substitution of variables
21 p3688 A69-39860

MAXIMUM USABLE FREQUENCY

Gain from communications operation at maximum usable frequency estimated on basis of long range ionospheric prediction technique adapted to computer
03 p0421 A69-13377

Ionospheric beam deflection maximum and minimum levels, deriving equations for maximum usable frequency at given ionization conditions and radiation angles
03 p0424 A69-13540

IC selection for minimum thermal effects, discussing speed, power dissipation, maximum operating frequency and noise threshold
06 p0894 A69-17219

Maximum horizontally radiated power of earth stations in any 4-kHz band for multichannel telephony and TV using satellites
09 p1450 A69-21278

Gain from communications operation at maximum usable frequency estimated on basis of long range ionospheric prediction technique adapted to computer
14 p2433 A69-28827

MAXWELL BODIES

Correlation between temperature and stress field in thermal buckling of square viscoelastic Maxwell plates under random temperature
12 p2188 A69-27113

MAXWELL-BOLTZMANN DENSITY FUNCTION

Statistical description of nonelastic processes in nonequilibrium plasma in transverse magnetic field, using kinetic equations for distribution functions
03 p0476 A69-13412

Qualitative mechanisms to explain Langmuir paradox, discussing wall mechanism for Maxwellian distribution formation in low pressure discharges
06 p0960 A69-16922

Noncoherent scattering of atoms with Maxwellian distribution in moving atmosphere, discussing Doppler broadening expansion in Legendre polynomials
07 p1219 A69-19286

Complex microwave incremental conductivity of InSb at 77 K in steady electric field using displaced Maxwellian distribution function
07 p1200 A69-19447

Nonlinear longitudinal oscillations in nonisothermal electron plasma with Maxwellian distribution in velocity space and different temperatures of electrons and ions
09 p1550 A69-22025

Fast electron energy distribution function and atom concentration in first excited level in weakly ionized plasma, considering transitions between excited levels
10 p1739 A69-23628

Maxwellian velocity distributions simulated in one, two and three dimensions by superposition of N monoenergetic isotropic distributions, noting application to kinetic theory computation
13 p2313 A69-28222

Gain and loss collision integrals in Boltzmann equation for rigid sphere gas evaluated for distribution expressed as linear combination of Maxwellians
14 p2431 A69-29578

Lorentz gas approximation to Boltzmann collision operator generalized for heavy molecule nonMaxwellian gas distribution function, obtaining equilibrium distribution applicable to ionized gas
18 p3179 A69-34438

Solar wind temperature, using distribution function for solar wind ions in anisotropic Maxwell distribution form
19 p3396 A69-36631

MAXWELL EQUATION

Einstein-Maxwell equations corresponding to superposed electric and magnetic fields stationary solutions, noting singularities in metric tensor
01 p0115 A69-10020

Optical pulse generator consisting of solid state laser with saturable absorber at cavity end using perturbation theory and Maxwell equations
01 p0089 A69-10179

Plasma stability criterion for universal mode, discussing cusp curvature stability
01 p0127 A69-10279

Symmetric tensor of time averaged stresses for collisionless plasma in oscillating field derived by Maxwell equations
02 p0286 A69-11588

Magnetoionic propagation of signals in magnetosphere using Maxwell equations and tensor quantities, linking to Hall, transverse and longitudinal conductivities [ONERA-TP-593]
02 p0236 A69-11617

Godel type solution of Einstein-Maxwell equation for dust filled universe, using Rainich equations
02 p0280 A69-11814

Kerr family of solutions of Einstein and Einstein-Maxwell equations for gravitational field of rotating body, noting global structure and causality
03 p0466 A69-13473

MHD generator two dimensional analysis for studying edge effect, taking into account Hall effect
03 p0480 A69-14099

Monograph on classical electromagnetism via relativity, developing Maxwell equations from Coulomb law
07 p1180 A69-18404

Geometrical optics approximation of Maxwell equations for electrodynamics of inhomogeneous anisotropic media
07 p1076 A69-18519

Maxwellian field and second order invariant system in vacuum in three dimensional Riemannian space with positive-definite metric, discussing Lorentz invariant equations
09 p1541 A69-22392

Coherence theory of electromagnetic field from classical/wave/ or quantum /particle/ standpoint, stressing information theory
11 p1915 A69-24455

Maxwell theory basis of special theory of relativity, discussing universal length constant
11 p1920 A69-25562

Limiting frequencies of inhomogeneously filled lossless rectangular waveguides and field states, using Maxwell equations
11 p1855 A69-25620

Guided waves in circular cylindrical radially inhomogeneous medium, using vector theory based on Maxwell equations
13 p2221 A69-28062

Magnetized plasma waveguide dispersion characteristics using Maxwell equations, stressing interaction of electron beam with wave modes
13 p2315 A69-28571

Macroscopic quasi-linear theory of HF radiation in cold electron-proton plasma allowing direct use of plasma and Maxwell equations
16 p2819 A69-31684

Nonlinear Maxwell equations applied to non-monochromatic emission for nonlinear crystal situated in resonator, examining generation of second optical harmonic
19 p3332 A69-35869

Radiation fields from energetic electron moving in helical orbit in magnetoactive plasma, using Maxwell equations
22 p4008 A69-39965

Mode conversion in nonuniform multimode waveguides and transitions using Maxwell equations, considering tapered and circular waveguides
23 p4135 A69-41354

MAXWELL FLUIDS

Idealized slider bearings with Maxwell liquid as lubricant, analyzing elasticity effects on pressure, load capacity and friction
02 p0253 A69-12413

Class of uniform motions of continuous media and rarefied gases
05 p0751 A69-16677

Asymptotic solutions of Grad system of kinetic moments
05 p0752 A69-16678

State variables of ideal gas in two phase region, discussing determination from equations of state and equation for internal energy and Maxwell criterion inapplicability
06 p1030 A69-17170

One dimensional unsteady monotonic Maxwellian gas flow at small Knudsen numbers using Hilbert method, noting validity for shear flows
14 p2432 A69-29611

Plane shock layer structure in pseudoMaxwellian monatomic gas, integrating Krook equation for gas molecule velocity
14 p2432 A69-29613

Pressure gradient produced steady plane flow of Maxwellian gas between infinite parallel planes, describing linearized Boltzmann equation solution
19 p3379 A69-36604

MAXWELLIAN DISTRIBUTION [DENSITY]
U MAXWELL-BOLTZMANN DENSITY FUNCTION

MCDONNELL AIRCRAFT
U DC 10 AIRCRAFT
U F-4 AIRCRAFT

MCDONNELL MILITARY AIRCRAFT
U MILITARY AIRCRAFT

MEAN

Lunar components in mean values of geomagnetic field daily variations, discussing lunar phase during selected quiet days
16 p2782 A69-32458

MEAN FREE PATH

Radio telescope measurements of total vertical atmospheric absorption to determine effective mean free path of oxygen and water vapor for absorption
02 p0206 A69-11450

Transfer coefficients for inhomogeneous systems characterized by constant density, mean free path and activation energy of carriers at each point
07 p1193 A69-19024

Enskog method for Boltzmann equation, analyzing asymptotic nature of integral kinetic equation for molecular mean free paths and Laplace probabilities
09 p1481 A69-21889

Electromagnetic field penetration into plasma cylinder having electron mean free path comparable with plasma diameter, noting anomalous skin effect
12 p2133 A69-25833

Gas molecular mean free path effect on performance of spiral grooved thrust bearing, discussing slip flow factor and He Knudsen number [ASME PAPER 68-LUBS-17]
13 p2266 A69-27273

Mean free path of interaction of nuclear active particles in Fe with energies greater than 530 gev
13 p2303 A69-28385

Neutron star atmosphere and X ray emission spectrum, computing incident protons mean free path for two assumptions
15 p2686 A69-30535

High energy cosmic ray proton, electron and photon propagation through cosmic microwave background, discussing mean free paths
16 p2852 A69-32819

Gas dynamics of material slab under radiation impact assuming thermal equilibrium reemission, discussing equations of motion and mean free path as function of frequency
19 p3449 A69-36355

Absorption mean free path for radiation absorbed by given medium, using zenith angle distribution from particle counter telescope
21 p3723 A69-38841

Varying ratio between mean free path and spherical particle radius at 0-10 km, discussing free molecular flow effects in cloud physics
24 p4345 A69-43145

MEASURANDS
U MEASUREMENT

MEASURE AND INTEGRATION
NT BINARY INTEGRATION
NT BOREL SETS
NT FUNCTIONAL INTEGRATION
NT INTEGRAL CALCULUS
NT NUMERICAL INTEGRATION
NT RUNGE-KUTTA METHOD
NT STIELTJES INTEGRAL
NT WEIGHTING FUNCTIONS

Multidimensional nonlinear plants adaptive control by direct integration, identifying differential equations coefficients
01 p0053 A69-10875

Integration for equations governing linearized thermoelastic transformations of incompressible solids
02 p0340 A69-12033

Integration method for equations of plastic two dimensional stressed state with Mises yield condition, noting stress concentration at hole with pressure on contour
04 p0679 A69-14924

Analytical expressions for integrals involving Euler and Bernoulli numbers
04 p0624 A69-14969

Integrability of equations for problem of motion of heavy solid body about fixed point
05 p0794 A69-16206

Integration forms suitable for fabrication of hybrid and monolithic microwave integrated circuits
07 p1096 A69-18441

Riemann sum definition and development of bounds for error in approximating integral, showing quadrature formulas as Riemann sums
10 p1719 A69-23521

Hamilton-Jacobi equation integrated for Hamiltonians, extending method to more than two variables case
11 p1910 A69-25747

Navigational equations solution by airborne analog computer techniques, describing electronic, electromechanical, digital reset and mechanical integrations with respect to time
18 p3107 A69-34847

Asymptotic evaluation of complex frequency integrals in theory of radiation from transient sources in dispersive media, interpreting results in terms of space-time rays
20 p3494 A69-37841

Motion equations of quasi-linear nonautonomous systems with many degrees of freedom, obtaining periodic solutions by asymptotic integration
23 p4183 A69-42477

MEASUREMENT

SNR variation with PCM using quantization distortion equations applied to coding-decoding facilities not exactly matched with respect to amplitude

10 p1656 A69-23692

MEASURING

U MEASUREMENT

MEASURING INSTRUMENTS

NT ACCELEROMETERS
NT ACTINOMETERS
NT ALTIMETERS
NT ANALYZERS
NT ANEMOMETERS
NT APPROACH INDICATORS
NT ATOMIC CLOCKS
NT ATTITUDE INDICATORS
NT BATHYMETERS
NT BAYARD-ALPERT IONIZATION GAGES
NT BOLOMETERS
NT CALORIMETERS
NT CATHETOMETERS
NT CERENKOV COUNTERS
NT CHRONOMETERS
NT CINETHODOLITES
NT CLOCK PARADOX
NT CLOCKS
NT CLOUD HEIGHT INDICATORS
NT COMPARATORS
NT CONDUCTIVITY METERS
NT CORONAGRAPHS
NT COUNTERS
NT DEFORMETERS
NT DENSITOMETERS
NT DICKE RADIOMETERS
NT DIFFRACTOMETERS
NT DISTANCE MEASURING EQUIPMENT
NT DOSIMETERS
NT DROPSONDES
NT DYNAMOMETERS
NT ELECTRICAL CONDUCTIVITY METERS
NT ELECTROMETERS
NT ELECTRON COUNTERS
NT ELECTRON PROBES
NT ELECTROPHOTOMETERS
NT ELECTROSTATIC PROBES
NT ELLIPSOMETERS
NT ENGINE ANALYZERS
NT ENGINE MONITORING INSTRUMENTS
NT ERGOMETERS
NT EXTENSOMETERS
NT FABRY-PEROT INTERFEROMETERS
NT FABRY-PEROT SPECTROMETERS
NT FIELD INTENSITY METERS
NT FLAME PROBES
NT FLIGHT LOAD RECORDERS
NT FLIGHT RECORDERS
NT FLOW DIRECTION INDICATORS
NT FLOWMETERS
NT FUEL GAGES
NT GALVANOMETERS
NT GEIGER COUNTERS
NT GERDIEN CONDENSERS
NT GONIOMETERS
NT GRAVIMETERS
NT GYROCOMPASSES
NT HELIOMETERS
NT HOT-WIRE ANEMOMETERS
NT HOT-WIRE FLOWMETERS
NT HYGROMETERS
NT HYPSONOMETERS
NT IMPEDANCE PROBES
NT INDICATING INSTRUMENTS
NT INFRARED DETECTORS
NT INFRARED INSTRUMENTS
NT INFRARED SCANNERS
NT INFRARED SPECTROMETERS
NT INFRARED SPECTROPHOTOMETERS
NT INTERFEROMETERS
NT ION PROBES
NT ION TRAPS [INSTRUMENTATION]
NT IONIZATION GAGES
NT IONOSONDES
NT KNUDSEN GAGES
NT LIGHT SCATTERING METERS
NT LUNAR SEISMOGRAPHS
NT MACH-ZEHNDER INTERFEROMETERS
NT MAGNETIC PROBES
NT MAGNETOMETERS
NT MANOMETERS
NT MICHELSON INTERFEROMETERS
NT MICROBALANCES
NT MICROMETERS
NT MICROWAVE INTERFEROMETERS
NT MICROWAVE PLASMA PROBES
NT MICROWAVE PROBES
NT MICROWAVE RADIOMETERS
NT MICROWAVE REFLECTOMETERS
NT MOISTURE METERS
NT MONOCHROMATORS
NT NEPHELOMETERS
NT NEUTRON COUNTERS

NT NOISE METERS
NT OPTICAL MEASURING INSTRUMENTS
NT OPTICAL PYROMETERS
NT OPTICAL RANGE FINDERS
NT OPTICAL SCANNERS
NT OPTOMETRY
NT OSCILLOGRAPHS
NT OSMOMETERS
NT OXYGEN ANALYZERS
NT PARTICLE TELESCOPES
NT PENETROMETERS
NT PHOTOMETERS
NT PIEZOELECTRIC GAGES
NT PIRANI GAGES
NT PLAN POSITION INDICATORS
NT PLASMA PROBES
NT POLARIMETERS
NT POLARISCOPES
NT POSITION INDICATORS
NT POTENTIOMETERS [INSTRUMENTS]
NT PRESSURE GAGES
NT PROFILOMETERS
NT PROPORTIONAL COUNTERS
NT PSYCHROMETERS
NT PYRANOMETERS
NT PYROMETERS
NT QUANTUM COUNTERS
NT RADIATION COUNTERS
NT RADIATION DETECTORS
NT RADIATION MEASURING INSTRUMENTS
NT RADIATION PYROMETERS
NT RADIO ALTIMETERS
NT RADIO FREQUENCY IMPEDANCE PROBES
NT RADIO INTERFEROMETERS
NT RADIOMETEOROLOGRAPHY
NT RADIOMETERS
NT RADIOSONDES
NT RANGE FINDERS
NT RAWINSONDES
NT REFLECTOMETERS
NT REFRACTOMETERS
NT RESISTANCE THERMOMETERS
NT RESONANCE PROBES
NT RHEOMETERS
NT RIOMETERS
NT SCINTILLATION COUNTERS
NT SEISMOGRAPHS
NT SHOCK MEASURING INSTRUMENTS
NT SIGNAL ANALYZERS
NT SILICON RADIATION DETECTORS
NT SOLAR SPECTROMETERS
NT SONDES
NT SONIC ANEMOMETERS
NT SPACECRAFT POSITION INDICATORS
NT SPARK CHAMBERS
NT SPECTROHELIOGRAPHS
NT SPECTROPHOTOMETERS
NT SPECTRORADIOMETERS
NT SPEED INDICATORS
NT STRAIN GAGE BALANCES
NT STRAIN GAGES
NT TACHOMETERS
NT TEMPERATURE MEASURING INSTRUMENTS
NT TEMPERATURE PROBES
NT TENSIMETERS
NT THEODOLITES
NT THERMAL CONDUCTIVITY GAGES
NT THERMOCOUPLE PYROMETERS
NT THERMOMETERS
NT THRESHOLD DETECTORS [DOSIMETERS]
NT TIME MEASURING INSTRUMENTS
NT TIMING DEVICES
NT TORQUEMETERS
NT TRANSITS
NT TURBULENCE METERS
NT ULTRAVIOLET SPECTROMETERS
NT ULTRAVIOLET SPECTROPHOTOMETERS
NT VACUUM GAGES
NT VARIOMETERS
NT VIBRATION METERS
NT VISCOMETERS
NT VOLTMETERS
NT WEATHER DATA RECORDERS
NT WEIGHT INDICATORS
NT WIND VANES

Direct reading device for minority carriers lifetimes measurement in semiconductor single crystals
01 p0078 A69-10073

Human systolic and diastolic blood pressure measuring apparatus and method
01 p0079 A69-10296

Electrode geometry for mass spectrometer ion source to measure electron ionization cross section of low vapor pressure materials
01 p0080 A69-10605

Jet fuel lubricity evaluation by ball-on-cylinder device
[ASLE PREPRINT 68AM 4A-2]
01 p0083 A69-10914

Spadoryc slide rule for damping determination from vibration decay traces, noting use in flight flutter tests
01 p0087 A69-11029

Vibrating rod automatic ice detection and control system for fixed and rotary wing aircraft
01 p0083 A69-11046

Simultaneous measurement of gain and noise of linear two port device using noise generators as signal sources
02 p0210 A69-12430

Microwave oscillator AM and FM noise measurement using Schottky barrier diode detector, discriminator, storage oscilloscope and wave analyzer
02 p0220 A69-12453

Surface temperature thermal fluxmeters used in measurements of shock tubes [ONERA-TP-648]
03 p0427 A69-12876

Stark effect meter for electric field measurement in space, discussing absorption cell development
03 p0429 A69-13222

Nondestructive measurement of thin transparent film thickness by interference method, noting diffusion profiles
03 p0430 A69-13634

Absolute rotation in space measured with microwave rotation sensor using polarization of electromagnetic wave
04 p0573 A69-14342

Standing wave methods for measuring permittivities of liquids having attenuation coefficients over considerable range
04 p0599 A69-15015

Direct reading instrument using four point probe and two analog computing circuits for Si and Ge resistivity measurements
04 p0599 A69-15019

Make wire, light pipe and spring wire ablation sensors development for measuring parameters of heat shield materials for reentry vehicles
04 p0602 A69-15428

Transient method for measuring thermal properties of biological materials, concerning thermal conductivity, inertia and blood flow rate
06 p0879 A69-17086

Device for measurement of time to failure of brittle materials in thermal-endurance testing, noting shock wave
06 p0927 A69-17690

Nose cone reentry simulation under low temperature subliming ablators, discussing dry ice, camphor and steel calibrations models fabrication, instrumentation and boundary layer measurements [AIAA PAPER 69-152]
06 p0929 A69-18098

Book on fundamentals of temperature, pressure and flow measurements covering standards, calibration, moving fluid effects, transient effects and installations in fluids and solids
07 p1131 A69-18410

Nonstationary aerodynamic load for harmonically oscillating body in fluid flow with constant mean velocity measured, determining errors as functions of system parameters
07 p1050 A69-18752

Hypoxia warning system based on dry electrolyte oxygen sensor with millisecond response time
07 p1071 A69-19430

Adapter circuits for MOSFET electrical properties measurement
07 p1113 A69-19780

Atmospheric turbidity and visibility measuring instrument /videograph/ using light backscattering, noting shipboard, coast guard service, large cities and weather stations applications
08 p1314 A69-20376

Linearization unit for compensating hyperbolic characteristic of capacitive displacement sensor used for contactless displacement measurement
08 p1317 A69-20879

Three dimensional laser Doppler velocity instrument for mean velocity and turbulence measurements in subsonic jet shear layer [SAE PAPER 690266]
09 p1494 A69-21555

Vibration measurements on rotating machinery, using diode switching potentiometric strain gage circuit and multiple common rings
09 p1496 A69-22014

Self oscillations in angular velocity sensor using electric spring and potentiometric pickup, examining friction moment and inductance coil effects
09 p1497 A69-22106

High sensitivity gyroscopic HF angular acceleration sensor using special differentiator, obtaining motion equations and dynamic response
09 p1498 A69-22109

Radial inflow gas turbine engine performance testing, discussing instrumentation, recording systems and calibration techniques
[ASME PAPER 69-GT-104]

09 p1501 A69-22522

Automatic level measuring system, consisting of decade control oscillator, digital level generator and selective level meter for 200Hz-2MHz range

09 p1501 A69-22577

Complex admittances and impedances of various networks determined by impedance bridge, describing frequency dependent limits of measurement parameters

09 p1501 A69-22578

Hall effect theory and devices, noting application to measurement of several physical quantities and sources of errors in devices

09 p1541 A69-22698

Lasers industrial manufacturing applications, discussing processing operations and measurement and inspection techniques

09 p1521 A69-22783

Noise in instrumentation systems, considering coupling and current noise source and reduction by isolation and filtering

10 p1691 A69-23231

Gage for measurement of density variation between expansion chamber and driver gas of valve driven shock tube

10 p1673 A69-23342

Relative heights on moon, tabulating lunar topography and comparing micrometrical measurements and map data

10 p1782 A69-23697

Digital design techniques for electronic equipment including measuring instruments, generators, synthesizers, etc

10 p1664 A69-23796

Tunnel diode test circuit, measuring differential resistances and bias voltages on loss resistance and of socket capacitance

10 p1665 A69-24215

Direct measurement device for metallic material response to mechanical stresses from stress force and global displacement/including material deformation/

11 p1884 A69-24757

Dynamometer based on electrical capacitance change in sensor element, discussing working range, circuit diagram and mechanical design

11 p1887 A69-25207

Second tacite sounding rocket test for measuring UV radiation in transition zone between upper ionosphere and space

11 p1887 A69-25213

Integral normal emissivity of electrically conducting materials heated to high temperatures by HF field of inductor, discussing measurement procedure and equipment

11 p1888 A69-25230

Nonorientable five channel adapter with spherical measuring head for three dimensional gas flow measurement, noting sensitivity to mechanical disturbances in calibration

11 p1888 A69-25340

Sweep frequency measuring setup for adjusting equalizers in carrier transmission systems

11 p1841 A69-25639

Computer controlled network analyzer performing automatic microwave measurements of passive and active networks, based on signal splitting and detecting

12 p2037 A69-26048

Precision measuring instrument for negative conductance of active element at microwave region

12 p2038 A69-26054

Dielectric loss tangents measurements combining coherent optical resonator with microwave techniques, noting application at mm wavelengths

12 p2080 A69-26057

Calibration and accuracy check of measuring instruments at National Center of Space Studies in France, emphasizing reference instruments

12 p2080 A69-26123

High sensitivity LF and HF frequency deviation meter with resonant RC amplifiers for frequency discrimination and filtering

12 p2038 A69-26337

Inelastic interactions between Tev cosmic particles and light element nuclei, describing design and operation of measuring apparatus and derivable data

12 p2093 A69-26583

Horseshoe electromagnet sensors above ferromagnetic plate, analyzing electromagnetic properties of plate and coil impedance

12 p2094 A69-26719

Lasers application to measurement techniques including alignment, direction, distance, elongation, interferometric, holographic, etc

12 p2094 A69-26903

Microminiature five point measuring head with linear point design for resistivity measurement of semiconductor films, noting four point head capabilities

12 p2099 A69-27104

Pulse frequency integral estimate devices with integrating chemotron tetrodes for automatic systems metering applications

13 p2227 A69-27522

Instrumental investigation of submillimeter astronomy, noting advancements in semiconductor physics, quantum electronics and space astronomy

13 p2342 A69-27602

Earth orbital manned space astronomy, discussing long range program, instruments, facilities and data processing

13 p2240 A69-27947

Cosmic ray muons angular distribution measuring device for determining pion/kaon ratio

13 p2332 A69-28421

Dynamic instrumental errors of quasi-steady state mechanical meters approximated by graph analytical method

14 p2451 A69-29747

MHD properties of velocity measurement method using cylindrical glass filament probe and Pitot and Prandtl tubes

14 p2453 A69-29920

Surveyor lunar landing procedures and results including instrumentation, lunar topography, selenology, chemical and physical properties, solar corona and earth laser output observations

15 p2681 A69-30324

Saturn 5 boost phase environment simulation on Apollo stages, discussing fixtures, load devices, instrumentation and ground test

15 p2588 A69-30405

Hypersonic wakes interference effects induced by facility instrumentation, discussing results of wind/shock tunnel investigations

15 p2588 A69-30475

Crack growth monitoring and recording techniques during fracture testing, using foil gauge, potential flow and acoustic pickup methods

15 p2713 A69-31109

Test measurement - Conference, New York, October 1968

15 p2612 A69-31267

Fatigue life gage on operational aircraft providing in situ monitoring of fatigue damage prior to and during propagation of running fatigue cracks

15 p2613 A69-31271

Ceramic heat transfer gage for supersonic wind tunnel investigation of blunt swept wing leading edges aerodynamic heating

15 p2613 A69-31272

Water cooled split-flow probe measuring enthalpy of high temperature subsonic streams

15 p2614 A69-31275

Laser Doppler heterodyning for monitoring motion noting solid surfaces vibration, liquid and solid surfaces linear velocity and turbulence in liquids and gases

15 p2614 A69-31276

Maximum likelihood methods applied to device performing ion swarm experiments, measuring positive ion mobility in hydrogen

16 p2788 A69-31670

Multiple function combination probe design for compressor and turbine air flow research

16 p2766 A69-31917

Polish electronic measurement devices operating principles and specifications including vibration, frequency and pressure meters, fatigue testing machines, etc

16 p2790 A69-32076

Instrument azimuth determination, discussing observations and theory

16 p2791 A69-32227

Inertial navigation system theory that uses increased numbers of newtonometers/force measuring devices/in place of gyroscopic sensitive elements

16 p2791 A69-32283

Hall generator for measuring mechanical displacements and vibrations of 10 A, describing operating principles and arrangements

17 p2971 A69-33022

Column method of measuring thermal conductivity of CO and oxygen in 350-1500 degrees K temperature range, discussing error sources and data reliability

17 p3073 A69-33298

Instrumentation for rotorcraft aerodynamics, considering boundary layer measurements, hot-wire anemometer and schlieren system for rotors and propellers

17 p2895 A69-33539

Metrological measuring instrument scales selection principles for ensuring constant sensitivity and Q factor

17 p2975 A69-33614

Measurement errors and geometry effects on navigational accuracy, determining maximum allowable error for measuring devices employed

17 p3002 A69-34098

Gyroscopic apparent rate meters generating steering moments in inertial navigation systems for determining moving object position and course

18 p3134 A69-34556

Self contained hand held battery operated aerosol particle analyzer, measuring aerosol concentration and size distribution for laboratory and space flight applications

18 p3136 A69-34691

Ultrasonic spectrometry application to thickness measurement of thin and thick welded articles

18 p3137 A69-35110

Skin friction balance in Mach 5 wind tunnel with high heat transfer, measuring shear forces

19 p3292 A69-35734

Skin friction balance for shear stress measurements in presence of ablation, describing balance construction, calibration, flexure range, etc

19 p3292 A69-35735

Radio measurement methods and standards including measurements of attenuation, phase shift, time delay, impedance, field strength, antenna characteristics, RF properties of materials, etc

19 p3276 A69-36426

S/N fatigue life gage response to constant frequency random amplitude input strain

20 p3537 A69-37007

Dynamic cathode ray tube spot size measurement by two slit technique, noting relationship to beam current and luminance

21 p3719 A69-38329

Automated rebound resilience apparatus for polymer dynamic mechanical properties studies over wide temperature range, using photoelectric device

21 p3689 A69-38593

Fluidic angular rate sensor, obtaining rate information by sensing laminar jet flow deflection from nozzle, discussing advantages over mechanical rate sensors

21 p3722 A69-38766

Device determining dynamic mechanical properties of tissues and various transducers, evaluating elastic properties of polyurethane, Hevea rubber and descending thoracic aorta

22 p3890 A69-40204

Photoelectric methods for pulsed and CW lasers output power and energy measurements

22 p3961 A69-40239

Phase equilibrium apparatus for measurement of thermodynamic properties of cryogenic fluid mixtures, including argon-methane data

22 p3947 A69-40630

Absolute thermal conductivity measurements on fluid normal H and fluid parahydrogen, noting apparatus and data graphical presentation along isotherms, isochors and isobars

22 p3998 A69-40631

Electronic measurement and control in industry - Conference, Budapest, 1969

22 p3915 A69-40934

Choke coil magnetoelastic sensors thermal stability found decreasing proportionally to measurement range decrease/below 100 newtons/

23 p4166 A69-41995

Balloon-borne instrument for auroral X ray measurements at Antarctic station, discussing design requirements, circuit characteristics and improvement recommendations

23 p4166 A69-42011

Instrumentation and data interpretation method for particle size determination by low-angle light scattering

24 p4313 A69-42764

Separation theorem for arbitrary nonlinear measurements to find optimal stochastic control without dynamic programming

24 p4291 A69-43269

MECHANICAL DEVICES

Thermal IR imaging devices for shape recognition and target position, emphasizing optical mechanical image or object plane scanners using point detectors

19 p3310 A69-36064

Ordinary coherence functions for computing frequency response in mechanical systems under random excitation

20 p3537 A69-37162

Rigid and flexible coupling devices for spacecraft rendezvous, describing general operating conditions

22 p4036 A69-40008

MECHANICAL DRAWINGS

U ENGINEERING DRAWINGS

MECHANICAL DRIVES

NT HELICOPTER PROPELLER DRIVE

NT PROPELLER DRIVE

Intermittent traversing gear with stepping motor for small hypersonic helium wind tunnels

01 p0054 A69-10219

Hydrostatic bearings, hydraulic drive system and hydraulic braking system for radio telescope with 2550 tons moving weight

[ASME PAPER 68-WA/PEM-2]

05 p0743 A69-16147

Mechanically and electronically despun spacecraft antennas, comparing designs and projected performances for spin stabilized Intelsat 3 satellite

06 p0897 A69-17590

Rotary engines, discussing scissor, eccentric rotor, multiple rotor and revolving block types

07 p1203 A69-18910

Mechanical systems modeling modification to include mobile coordinates, introducing gyroscopic and pseudogyroscopic terms into motion equations

16 p2875 A69-32246

Aircraft auxiliary power systems, discussing weight and power requirements, component design, driving methods and influence on power plant design

17 p3018 A69-33217

Mechanical drives effectiveness for large antenna tracking/communications systems evaluated in terms of reliability and availability

18 p3100 A69-34522

Minimum radius of three dimensional cam gears calculated from driven element motion and pressure angle

23 p4168 A69-41413

Structural features and performance of 300 ft steerable receiving antenna, discussing aiming error, aperture efficiency, azimuth and altitude drive

23 p4148 A69-42121

MECHANICAL ENGINEERING

Book on stability criteria for linear mechanical engineering systems covering response characteristics, encirclement theorem, Routh and Hurwitz criterions, root loci, D partition, etc

02 p0281 A69-12276

Metal strip angled profile shaping by sliding application of forces with draw plate, analyzing friction effect with thin plastic shell engineering theory

03 p0432 A69-12962

Applied mechanics yearbook covering shell theory, elastic stability and other problems

05 p0831 A69-15685

Program to study interactive graphic display console systems use for solving mechanical design problems involving plate cam and follower mechanisms

05 p0724 A69-16384

Clearing and blocking control over frequently overadjusted automatic equipment in precision machine and device construction

06 p0931 A69-17692

Microminiature system mechanical design for aerospace environment, considering guidelines for implementation of requirements

[AGARDOGRAPH-114]

08 p1291 A69-20986

Stress analysis, Volume 12, Theoretical and experimental studies of strength of machine structures

11 p1980 A69-24940

Mechanical engineering applications to aerospace flight, discussing stability and piloting problems and experimental methods

11 p1824 A69-25672

Soviet collection of articles on theoretical and experimental investigations of strength of mechanical engineering structures

17 p3056 A69-33190

Guide for establishing harmonious relationships with design engineers within typical mechanical engineering department

17 p3077 A69-34198

Mechanical failure technology, describing programs of government coordinated Mechanical Failure Working Group/MFWG/

18 p3144 A69-34492

Extreme disturbance analysis and optimum performance and design problems for structural and

mechanical dynamic systems, basing solutions on linear, nonlinear and dynamic programming

18 p3106 A69-34663

Stress corrosion cracking research, history, engineering and education, incorporating stress corrosion data in mechanical design, terminology and nomenclature

19 p3348 A69-36884

Lasers and mechanical engineering - Conference, London, November 1968

22 p3960 A69-40234

Machine tools design for performing cutting operations within acceptable vibration limits

22 p3928 A69-40672

MECHANICAL IMPEDANCE

Human body dynamic response to vibration combined with linear acceleration, noting changes in body mechanical impedance and resonance

01 p0022 A69-11335

Holographic mode shapes used in conjunction with mechanical impedance approach for vibration analysis of turbine blades

[ASME PAPER 69-VIBR-32]

10 p1806 A69-24174

Fluidic feedback oscillator performance from fluid density effects analysis including supply jet, feedback line dynamics and load and control port impedances

[ASME PAPER 69-FLCS-39]

20 p3465 A69-37984

MECHANICAL MEASUREMENT

NT DISPLACEMENT MEASUREMENT

NT DRAG MEASUREMENT

NT FLOW MEASUREMENT

NT FRICTION MEASUREMENT

NT PRESSURE MEASUREMENTS

NT STRESS MEASUREMENT

NT THRUST MEASUREMENT

NT VELOCITY MEASUREMENT

NT VIBRATION MEASUREMENT

NT WIND MEASUREMENT

NT WIND VELOCITY MEASUREMENT

NT X RAY STRESS MEASUREMENT

Surveyor 5 alpha particle backscattering instrument measurement, TV pictures of lunar surface elemental composition and magnetic and mechanical measurements

02 p0317 A69-12023

In-flight measurement of shear, bending moment and torque on lifting or control surfaces and loads on nose and main landing gear

04 p0677 A69-14842

Plane shear strain measurement by means of properly oriented strain gages on surface and proper disposition of gages in Wheatstone bridge circuit

04 p0603 A69-15498

Fracture toughness measurements by means of dimensionless fracture toughness parameters, noting results for materials with very different elastic moduli

05 p0780 A69-16080

Cylindrically orthotropic hollow cylinder elastic properties determination using experimental test for production of stress and strain states and end effects

07 p1232 A69-18718

Four point flexure, ring flexure and NOL ring tension tests for evaluation of composite material mechanical properties

09 p1499 A69-22308

Capacitance methods for measuring adhesives mechanical properties in thin film bonded joints, noting results for tension, compression and shear loading

09 p1500 A69-22309

Fiber glass reinforced plastic backing phase of composite armor, noting test method for evaluation of performance

09 p1507 A69-22319

Silica fabric reinforced phenolic composites mechanical properties at temperatures above cure level

09 p1530 A69-22321

Plain strain fracture toughness tests on two inch thick maraging steel plates of various strengths, using bend and compact tension tests

10 p1795 A69-23057

Tensile strength and failure loading evaluation for structure, discussing stresses in neighborhood of crack, crack toughness measurement and fracture mechanics

12 p2176 A69-25861

Plane strain fracture toughness tests on maraging steel plates for various yield strengths and large dimensions

12 p2114 A69-26496

Wing section of high lift/drag test vehicle for 2500 F reentry, describing design, manufacture and testing

12 p2103 A69-26837

Error analysis in efficiency measurement of gas turbines, considering thermodynamics and power output

14 p2509 A69-29509

Dynamic instrumental errors of quasi-steady state mechanical meters approximated by graph analytical method

14 p2451 A69-29747

Complex mechanical vibrations causes determined by sensor signals analysis

16 p2876 A69-32434

Polyethylene stainless steel lap joints and polyethylene samples yield strengths measurements at high temperature, suggesting yield mechanism based on dislocation loops

16 p2794 A69-32572

Hall generator for measuring mechanical displacements and vibrations of 10 A, describing operating principles and arrangements

17 p2971 A69-33022

Mechanical and resistance type fatigue life indicator, comparing operating and performance characteristics [AHS PAPER 378]

17 p3059 A69-33511

Measuring elastic modulus and tensile strength of high modulus graphite fibers including comparative data, error sources and full strand test

19 p3355 A69-35520

Test stand for measurement of forces and moments from thrust vector controlled rocket, analyzing dynamic characteristics of hydrostatic supports

21 p3691 A69-39631

MECHANICAL OSCILLATORS

NT GYROSCOPIC PENDULUMS

NT PENDULUMS

Wagon rolling toward piston executing HF oscillations, discussing periodic solutions of equations of motion corresponding to piston phase at collision

04 p0630 A69-14893

Linear mechanical systems idealized by single degree of freedom system with viscous damping subjected to combined deterministic and random excitation

04 p0680 A69-14968

Impacting oscillatory devices for use as mechanical frequency dividers

07 p1136 A69-19458

Vibration machine as vibration environment simulation for product reliability testing, analyzing spectrum of acceleration waveforms

12 p2060 A69-26940

Pressure distribution in viscous flow between parallel disks with sinusoidal oscillation, noting effects of oscillation amplitude and vibrating disk velocity

[ASME PAPER 68-LUBS-1]

13 p2244 A69-27278

Viscous friction damping effect on impact vibrator stability, analyzing boundary region of multiply periodic single impact motion by point mapping

18 p3172 A69-34588

Machine parts vibration attenuation, discussing input vibration reduction, resonance avoidance, damping, vibrating parts strengthening and shakers

18 p3148 A69-34619

Monograph on frequency response characteristics of mechanical oscillator chains, calculating forced vibrations in linear systems

20 p3577 A69-37920

MECHANICAL PROPERTIES

NT ABRASION RESISTANCE

NT AEROELASTICITY

NT AEROTHERMOELASTICITY

NT ANELASTICITY

NT BRITTLENESS

NT BULK MODULUS

NT COLD STRENGTH

NT COMPRESSIBILITY

NT COMPRESSIVE STRENGTH

NT CREEP PROPERTIES

NT CREEP RUPTURE STRENGTH

NT CREEP STRENGTH

NT DIMENSIONAL STABILITY

NT DUCTILITY

NT DYNAMIC MODULUS OF ELASTICITY

NT ELASTIC PROPERTIES

NT ELASTOPLASTICITY

NT ELECTROSTRICTION

NT FATIGUE LIFE

NT FIBER STRENGTH

NT FLEXIBILITY

NT FRACTURE STRENGTH

NT HARDNESS

NT HIGH STRENGTH

NT HYDROELASTICITY

NT IMPACT STRENGTH

NT MAGNETOSTRICTION

NT MICROHARDNESS

NT MODULUS OF ELASTICITY

NT NOTCH SENSITIVITY

NT NOTCH STRENGTH

NT PHOTOELASTICITY

NT PHOTOVISCOELASTICITY

NT PIEZOELECTRICITY

NT PLASTIC PROPERTIES

NT POISSON RATIO
 NT RESILIENCE
 NT SHEAR PROPERTIES
 NT SHEAR STRENGTH
 NT SHELL STABILITY
 NT STEADY STATE CREEP
 NT STIFFNESS
 NT STRESS CYCLES
 NT STRESS RATIO
 NT STRESS RELAXATION
 NT STRUCTURAL STABILITY
 NT TENSILE CREEP
 NT TENSILE PROPERTIES
 NT TENSILE STRENGTH
 NT THERMAL RESISTANCE
 NT THERMOELASTICITY
 NT THERMOPLASTICITY
 NT THERMOVISCOELASTICITY
 NT TOUGHNESS
 NT VISCOELASTICITY
 NT VISCOPLASTICITY
 NT WELD STRENGTH
 NT YIELD POINT
 NT YIELD STRENGTH

Hydrostatic pressure effects on mechanical properties of hot pressed, extruded and rolled polycrystalline beryllium sheet
 01 p0092 A69-10059

Beta titanium alloys mechanical properties improvement, discussing effects of alloying elements, heat treatment and high temperature deformation
 01 p0093 A69-10213

Mechanical properties of lithium fluoride single crystals, taking into account equilibrium lattice defect structures
 01 p0138 A69-10602

Interstitial impurity effects on mechanical properties of molybdenum single crystals, considering temperature dependence of flow stress in bcc metals
 01 p0095 A69-10609

Chemical vapor deposited W and W-Re alloys for structural applications, discussing fabrication methods and effects on mechanical properties
 01 p0096 A69-10641

Silicon carbide filament fabrication by chemical vapor deposition, noting physical and mechanical properties and application to other refractories
 01 p0097 A69-10645

Chemical vapor deposited W and W-Re alloys investigated for deposition variables and heat treatment effects on mechanical properties
 01 p0097 A69-10648

Collection of Soviet papers on problems of dynamics and strength, Number 15
 01 p0086 A69-10826

Mechanical properties of AZ5G-Zr-Cr alloy welded sheet subjected to biaxial stress at low temperature
 01 p0088 A69-11152

Strain measurements in pure polycrystalline Ti at constant temperature and strain, considering creep and elastic aftereffects
 01 p0101 A69-11363

Steel selection for heat treated parts, discussing strength and hardness, service conditions, carbon content, quenching, cost, etc
 01 p0101 A69-11397

High strength steel welding with physical properties equal to parent metal, discussing gas tungsten-arc, electron beam and plasma arc techniques
 01 p0088 A69-11399

Homogenous mechanical stresses in amorphous and crystalline gallium films during vacuum deposition and annealing
 01 p0141 A69-11420

Alloying additions effect on mechanical properties of Zr-V-Nb system
 02 p0263 A69-11849

Fe, Ni and Cr influence on corrosion resistance and mechanical properties of Zr-Cu-Mo system alloys
 02 p0263 A69-11853

Silicide coatings effect on Mo mechanical properties subjected to tensile tests in vacuum and air at various temperatures
 02 p0264 A69-11883

Polymeric film properties related to metal substrate interface corrosion, considering effects of stress concentration, surface cleanliness and adsorbed gases
 02 p0265 A69-11896

Metal fatigue crack propagation mechanism, deriving basic laws for failure in high and low stress regions, determining material parameters
 02 p0340 A69-12025

Vacuum heating and thermal cycling influence on mechanical and structural properties of aluminum sheets fabricated from sintered powder
 02 p0266 A69-12126

Hydroextrusion effect on Mo structure and mechanical properties, noting improved ductility after high temperature annealing
 02 p0267 A69-12189

Molybdenum elasticity limit and rupturing stress dependence on structure for high temperature annealing, noting changes in solid solution interstitial impurity concentration
 02 p0268 A69-12191

Ni-Cr-Ti-Al /Nimonic/ alloy single crystal mechanical properties at room temperature, determining importance of structure
 02 p0268 A69-12192

Lunar surface mechanical properties at Surveyor 5 site
 02 p0321 A69-12225

Mechanical behavior of materials under dynamic loads - Conference, San Antonio, September 1967
 02 p0342 A69-12277

Free surface motion and stress measuring instrumentation, describing plate impact one dimensional strain configuration for determining mechanical properties under stress wave propagation
 02 p0344 A69-12290

Kinetic theory of fracture initiation, discussing changes in relative orientation distribution of network chains
 02 p0345 A69-12401

Aluminum alloy with lithium and magnesium noting mechanical properties and electrical and corrosion resistance
 03 p0443 A69-13026

Fatigue and corrosion fatigue properties of aluminum alloys, noting elastic modulus, cyclic loading strength, corrosion resistance, etc
 03 p0443 A69-13027

Grooved commercial Ti and Ti alloys mechanical properties under uniaxial static tension at low temperatures
 03 p0443 A69-13028

Mechanical and optical viscoelastic characterization of Hysol 4290 epoxy polymer as function of time and temperature, using creep test data
 03 p0524 A69-13064

Physical and mechanical properties of surfaces and interfaces - Conference, Raquette Lake, New York, August 1967
 03 p0448 A69-13867

Surface and interface phenomena in engineering technology, determining mechanical or electronic properties
 03 p0434 A69-13868

Surface effects on metals mechanical properties, discussing dislocation dynamics and resulting effects on macroscopic plastic behavior
 03 p0448 A69-13869

Surface effects on mechanical properties of crystalline and vitreous materials, considering environmental effects on dislocation mobility
 03 p0454 A69-13870

Directional solidification and composite structures, discussing structure changes effect on mechanical properties
 03 p0449 A69-13877

Fiber-matrix interfacial bond function and bond strength role in fiber composites mechanical behavior
 03 p0450 A69-13881

Grain boundary sliding influence on gross mechanical behavior and stress distributions, emphasizing creep behavior
 03 p0450 A69-13882

Mechanical properties of thermally diffused layers obtained by vacuum chromizing of steel, establishing need to decarburize substrate material
 03 p0450 A69-13913

Chemical treatment effects on mechanical properties of titanium alloy tubes
 03 p0434 A69-13914

Powdering temperature effect on mesh size, structure and mechanical properties of pressed semifinished sintered Al-Cr and Al-Fe alloys
 03 p0452 A69-14119

Si and iron impurities effects on duraluminum alloy structure and mechanical and plastic properties for fabrication from granules and rolling from ingots
 03 p0452 A69-14120

Cold rolling and annealing effects on tensile strength, heat resistance and ductility of sintered Al powder sheets
 03 p0452 A69-14121

Alloying elements effect on mechanical and refractory properties and structure of forging of age hardenable Ni base alloys
 03 p0452 A69-14122

Machine for simultaneous creep and long term strength evaluation of multiple metallic specimens
 04 p0584 A69-14537

Prolonged loading effect on mechanical properties of 18Kh2N4VA steel at low temperature, discussing notched and unnotched specimens
 04 p0614 A69-14573

Mechanical properties and stress concentration sensitivity of structural alloys at low temperature
 04 p0614 A69-14574

Nb and Cr additions effects on Hadfield type steel mechanical properties, noting improvement especially at low temperatures
 04 p0614 A69-14579

Low temperature aging prior to higher temperature artificial aging increases Al alloys strength
 04 p0614 A69-14634

Thermal strengthening effect in aluminum due to temperature fluctuations
 04 p0615 A69-14638

Experimental high strength maraging steel mechanical properties optimization, discussing heat treatment, quenching, aging and reducing conditions
 04 p0615 A69-14645

Overheated maraging steel mechanical properties improvement by heat treatment
 04 p0615 A69-14646

Whisker research history, discussing characteristic morphology, mechanical and physical properties and future applications as reinforcing components in reinforced metals
 04 p0616 A69-14843

Strain hardening and softening characteristics of maraging steels, Ni-Co and other steels and Ti-Al-Mo alloy
 04 p0618 A69-15156

Plastic deformation effect on structure, yield point and tensile strength of aged austenitic alloy containing Ni, Cr and Ti
 04 p0618 A69-15177

Mathematical theory for describing mechanical behavior of continuous media based on principle of determinism for stress
 05 p0833 A69-15729

Mechanical and physical properties and cryogenic wear tests performed on composite materials, considering NERVA cryogenic turbopump bearing retainer development
 [ASME PAPER 68-WA/LUB-10]
 05 p0768 A69-16133

Hot working temperature effects on Rene 63 mechanical properties and microstructures, using tensile and stress rupture tests, electron microscopy and X ray diffraction analysis
 05 p0781 A69-16446

Cryogenic behavior of adhesive materials used in fabrication of liquid hydrogen/liquid oxygen powered Saturn S-4B stage
 05 p0784 A69-16487

Film processing effects on cryogenic mechanical properties of polyethylene terephthalate
 05 p0785 A69-16490

Cryogenic mechanical properties of epoxy resins and glass/epoxy composites
 05 p0785 A69-16491

Mechanical behavior of polyethylene terephthalate at cryogenic temperatures
 05 p0785 A69-16494

Vulcanizable elastomers suitable for contact with liquid oxygen, discussing preparation, mechanical properties, transition temperature and structure
 05 p0717 A69-16497

Transition temperature from brittle to plastic state of W-Mo alloys in recrystallized state, noting increased Mo content effect
 05 p0783 A69-16809

Diffusion bonded aluminum-boron composite material, discussing mechanical, metallographic and radiographic properties
 06 p0939 A69-16946

Micromechanics of boron filament reinforced aluminum composites
 06 p0940 A69-16948

Aluminum-silica fiber reinforced metal composite, discussing mechanical behavior and effect upon engineering applications
 06 p0940 A69-16949

Strain rate effect on structure and mechanical properties of rapidly stretched metals
 06 p0941 A69-17122

Stress-strain relations for laminar anisotropic medium from known mechanical properties of layers for application to fiber reinforced plastics
 06 p1021 A69-17176

Sigma formation effects on cast nickel-based superalloys properties, discussing sigma occurrence prevention for longer service life of gas turbines
06 p0942 A69-17223

Materials compatibility for space requirements, discussing shape retention, ductility, tensile strength, dissimilar materials stability, etc
06 p0945 A69-17872

Precipitation hardening stainless steels, discussing corrosion resistance, high strength, weldability, fabricability, heat treatment, etc
06 p0932 A69-17874

Ti alloys chemical composition, fatigue life, stress rupture strength, crack susceptibility and nature of stress-strain rate
07 p1161 A69-18763

Corrosion resistance and mechanical properties of Ti-Mo alloy, developing processing methods for forgings, bars and sheets
07 p1163 A69-18781

Powder metallurgy, fusion and chemical vapor deposition techniques in manufacturing tungsten base alloys
07 p1165 A69-18792

Alumina radomes fabrication and control techniques to assure reproducibility of electrical and mechanical properties, detailing finished product inspection methods
07 p1142 A69-19529

Strength increase in steel components of aircraft, missiles and subsurfaces in relation to chronological application sequence, discussing ultimate strength [ASM PAPER GG8-9.4]
07 p1169 A69-19675

Elevated temperature mechanical properties data for commercially produced super-strength alloys supplemented by product description tables
08 p1328 A69-19913

Weld mechanical properties of Ti-6Al-2Sn-4Zr-2Mo titanium alloy as function of cooling rate changes or transformation rate shifts resulting in wide range of hardnesses
08 p1318 A69-19965

Roll planishing and thermal treatments effects on gas tungsten arc welded Ti-6Al-4V alloy on residual stresses, tensile, formability and fracture toughness properties
08 p1319 A69-19966

Structural parameters influence on fiberglass reinforced plastics strength studied for optimal structure selection
08 p1335 A69-20332

Structural residual stresses determination in oriented fiberglass reinforced plastics by models taking into account mutual influence of fibers
08 p1335 A69-20333

High modulus and high strength carbon fibers and composites, discussing mechanical properties and interlaminar shear strength
08 p1338 A69-20488

Filament winding process variables effect on carbon or fiberglass reinforced composites, determining mechanical properties
08 p1338 A69-20489

Mechanical properties of cast epoxy resins correlation with corresponding composites strength under static and dynamic fatigue stressing
08 p1340 A69-20510

Direct chemical bonding effect on flexural strength and flexural modulus of glass fiber reinforced plastics, noting degradation reactions
08 p1341 A69-20514

Mechanical properties of ceramic material consisting of pure silica matrix reinforced by carbon fibers
08 p1341 A69-20700

Monograph on precipitation hardening and mechanical properties of various heat resistant alloys with Co contents to 35 percent
08 p1334 A69-20763

Viscoelastic properties of heterogeneous media of composite sphere model type obtained from shear modulus formula
08 p1417 A69-20825

Thermal stress field under uniform heat flow due to elliptical elastic inclusion for anisotropic case
08 p1418 A69-21003

Glass science and technology noting optical, electrical and mechanical properties, forming techniques, structure, ionic properties, high pressure effects and glass ceramics
08 p1341 A69-21126

Al alloys application to Concorde project and other aircraft structures, noting mechanical properties
08 p1335 A69-21141

Shell theories for polymer and reinforced plastic shells, giving revised temperature and creep problem solutions due to mechanical behavior
09 p1611 A69-21481

Dynamic tests of mechanical properties of polyamide Tarlon X-A using free and resonant vibrations methods
09 p1528 A69-21496

Spinodal decomposition effect on Al-Zn alloy mechanical properties noting strengthening, brittleness and work hardening capacity
09 p1522 A69-21501

Deformation processing of superalloy gas turbine components, studying inert characteristics, alloy segregation effect and thermomechanical properties [SAE PAPER 690101]
09 p1503 A69-21557

Heat resistant nickel alloys for castings, tabulating chemical composition, mechanical properties, heat treatment, weldability, etc
09 p1522 A69-21608

Metals structure and mechanical properties after hydroexplosive forming analyzed by X ray diffraction
09 p1503 A69-21851

In situ vacuum testing requirement for valid measurement of vacuum induced changes in mechanical and thermal properties of various filled elastomers
09 p1477 A69-22008

Boron-epoxy composites applications and properties, comparing strength to weight and stiffness to weight ratios with aluminum, titanium and beryllium
09 p1529 A69-22068

Temperature dependence of high melting point metals mechanical properties
09 p1525 A69-22138

Structure and properties of high heat resistant alloys based on high melting point metals with bcc lattice explained by electron theory
09 p1525 A69-22139

Metallic and nonmetallic matrices reinforcement by ceramic whiskers, describing mechanical properties
09 p1525 A69-22142

Alloying elements effects on structure, mechanical properties, aging and composition of precipitation hardening intermetallic phases in Ni and Fe based alloys
09 p1525 A69-22143

Mechanical properties of welds of niobium and Ni based heat resistant alloys and susceptibility to crack formation at high temperatures
09 p1504 A69-22146

Four point flexure, ring flexure and NOL ring tension tests for evaluation of composite material mechanical properties
09 p1499 A69-22308

Adhesive bonded lap joint strength dependence on adherend mechanical properties under conditions of homogeneous adherend and cohesive failure
09 p1530 A69-22317

Silica fabric reinforced phenolic composites mechanical properties at temperatures above cure level
09 p1530 A69-22321

Magnesium boron composite fabrication by diffusion bonding and liquid metal infiltration, obtaining minimized property variations and high strength to density ratios
09 p1507 A69-22332

Pyrolytic carbon felt composite development and properties, measuring and tabulating mechanical, thermal and ablation properties
09 p1530 A69-22364

Materials, processing and testing variables effects on mechanical properties determined for metal matrix composites [ASME PAPER 69-GT-23]
09 p1527 A69-22496

Titanium-boron composites for gas turbines, mechanical properties and service life in high temperature environment [ASME PAPER 69-GT-1]
09 p1527 A69-22510

Static and dynamic strength tests and modulus data for graphite fiber/epoxy composite yarn, noting ply winding and dimensions [ASME PAPER 69-GT-114]
09 p1531 A69-22520

Stress graphitizing and boron codeposition effect on dynamic mechanical properties of pyrolytic carbon, noting increase in internal friction and dynamic modulus
10 p1716 A69-23036

Ductile to brittle transition shown in tensile stress-strain curves of polycrystalline body centered cubic and hexagonal close packed materials
10 p1795 A69-23063

Austenite to martensite strain induced transformation effect on energy absorption during crack propagation
10 p1709 A69-23074

Aluminum plates bending fatigue tests, discussing mechanical properties, structural failure, grain size, strain hardening, stress-strain-time relations, heat treatment, etc
10 p1711 A69-23356

Intermolecular potential function relation to individual macroscopic properties extended to simultaneous fit of all possible pair combinations
10 p1652 A69-23391

Rubber modified thermoplastics structure and mechanical properties, emphasizing stress concentration around composite particles and crazing role in creep and fracture
10 p1716 A69-23985

Metals with combined high damping and good mechanical properties for solving fatigue, noise and vibration problems
10 p1715 A69-24044

Book on strength and failure of viscoelastic materials covering linear and three dimensional polymers or polymer-based materials, flexibility and temperature effects
11 p1970 A69-24610

Beryllium properties and processing including magnesian thermal reduction, powder purity, oxygen content, grain size and temperature effects on mechanical properties
11 p1904 A69-24897

Preliminary natural aging effects on maximum strength properties obtained at various artificial aging temperatures for aluminum ternary alloy
11 p1905 A69-24921

Aging effects on hardness and tensile strength of nickel-chromium steels at various high temperatures and time periods
11 p1906 A69-25439

Polyurethane foam high velocity deformation properties, discussing results of dynamic uniaxial stress tension and compression tests
11 p1907 A69-25648

Fiber reinforced materials shear and tensile strength effect on stress-strain state of composite materials machine parts, considering design requirements
11 p1907 A69-25680

Glass fiber reinforced plastics shells stability under external hydrostatic pressure, discussing compression and axial tests for normal elastic modulus, shear modulus and Poisson coefficient
11 p1995 A69-25681

Metal adhesive bonding strength behavior in satellite and space vehicle applications, noting effects of various space environment factors
12 p2101 A69-25858

Book on hard alloy properties, discussing bending and compression properties, tensile, torsional and impact strength, wear resistance and thermal shock resistance
12 p2111 A69-25902

Surface wave patterns of truncated conical shells with free edges attributed to mechanical properties
12 p2178 A69-26002

Nimonic alloy single crystals strengthening during plastic deformation, analyzing jump phenomenon at high and low temperatures
12 p2112 A69-26038

Plasticizer mechanical properties and content in paste, considering effects on texture of coagulation structure during die extrusion of compacts
12 p2118 A69-26257

Soviet monograph on nuclear radiation effect on structure and properties of metals and alloys covering electron, gamma and neutron radiation
12 p2114 A69-26469

Hydrogen embrittlement of stainless steel and effects on mechanical properties, discussing martensitic phase role
12 p2115 A69-26616

Soviet book on strength, stability and vibrations covering stability of rods, plates and shells subjected to plastic and elastic deformations, etc
12 p2182 A69-26755

Composite materials consisting of brittle inorganic glass matrix with metallic or inorganic crystal microspheres, noting strength and elasticity
12 p2115 A69-26830

Mechanical properties of glass, discussing volume flow, hardness, strength and scratchability
12 p2119 A69-26831

Crystal microstructure and mechanical properties of unidirectionally solidified Ni-Ni-Nb intermetallic eutectic alloy at high temperature, examining deformation and fracture modes
13 p2276 A69-27402

Temperature effects on mechanical properties and fracture behavior of lamellar Ni-nickel titanide inter-

metallic eutectic alloy showing dependence on inter-metallic constituent

13 p2277 A69-27406

Composition, gamma structure and mechanical properties of three unidirectionally solidified eutectics within Ni-Al-Cb, Ni-Al-Zr and Ni-Al-Ti systems

13 p2277 A69-27407

Plasma spray quenched Al-V alloys resulting in dispersion strengthening of material

13 p2277 A69-27409

Plastic deformation effects by hydrostatic fluid extrusion on mechanical properties of Ni maraging steels

13 p2278 A69-27414

Polymer structure relationship to thermal, mechanical and chemical properties of electrical insulating materials

13 p2285 A69-27986

Dielectric thin film electrical and mechanical properties and preparation for semiconductor devices, emphasizing Si compounds

13 p2286 A69-28004

Aluminum alloys precipitation hardening types requiring solution heat treatment, quenching and artificial aging, noting advantages in strength and weldability

13 p2282 A69-28180

Crack behavior and toughness of aluminum alloy parent metal and weldments, noting temperature effect

14 p2462 A69-29003

Ceramic and cermet materials insulating, physical and mechanical properties for use in thermionic converters

14 p2467 A69-29214

Titanium alloys for thermionic nuclear converters, discussing melting, forging, drawing and quality control of mechanical and physical properties

14 p2462 A69-29217

Beta Ti alloy initial state effect on mechanical properties and dislocation structure after cold deformation by rolling

14 p2463 A69-29313

Glass finish and glass resin chemical bond adhesion roles in filament wound structures response, failure and filament strength

14 p2468 A69-29345

Woven roving construction and fill/warp ratio effects on flexural strengths of four ply laminates

14 p2469 A69-29414

Casting variables of Co base superalloys, discussing variables effects on ultimate mechanical properties, investment casting, etc

14 p2456 A69-29893

Tungsten vacuum-arc melted samples in deformed and recrystallized conditions, studying mechanical properties at temperatures near ductile to brittle transition

15 p2637 A69-30267

Beta titanium alloys mechanical properties improvement, discussing effects of alloying elements heat treatment and high temperature deformation

15 p2637 A69-30269

Prolonged loading effect on mechanical properties of 18Kh2N4VA steel at low temperature, discussing notched and unnotched specimens

15 p2638 A69-30274

Mechanical properties and stress concentration sensitivity of structural alloys at low temperature

15 p2638 A69-30275

Metaloceramic materials strength as function of porosity calculated for tension, shear, bending and torsion deformations

15 p2638 A69-30283

VM-1 alloy investigated for creep mechanisms and ultimate strength for applications in reactors, rockets and aircraft construction

15 p2638 A69-30284

Structural strength calculations, considering micro and macro stress distributions

15 p2706 A69-30447

Concorde aircraft and engine materials selection factors including mechanical properties of metals and nonmetals, corrosion resistance, service life, sealants, weight analysis, etc

15 p2639 A69-30464

Chemical composition effect on Cr-Ni-Mo-Ti stainless maraging steels mechanical properties

15 p2640 A69-30631

Titanium effect on structural steels mechanical properties noting anisotropy ascribed to sulfides, nitrides and borides

15 p2640 A69-30633

Tensile, bending and impact strengths of materials produced by metal porous blank impregnation with molten glass, noting metal density and sintering effects

15 p2643 A69-31188

Refractory materials based on BN and silicon nitride, studying effect of sintering conditions and chemical composition on mechanical properties

15 p2643 A69-31244

Trace elements influence on precipitation process and properties of Al-Cu, Al-Zn-Mg and Al-Mg alloys, using X ray diffraction

16 p2801 A69-31783

Ti alloy forgings production for optimal mechanical properties by cross section and structural condition selection and avoidance of oxygen, nitrogen and hydrogen pickup

16 p2801 A69-31785

Slow forming forging and extrusion required for Ti alloys, discussing mechanical properties as function of beta transformation temperature

16 p2793 A69-31786

Optical measuring methods of cross sections and mechanical properties of heat resistant fiber reinforced materials

16 p2803 A69-31804

Hydroextrusion influence on mechanical properties of powder compacts of sintered Mo rods

16 p2803 A69-32491

Precipitation processes and effect on properties of Cr-Ni-W-Ti heat resistant austenitic steel, using electron diffraction and transmission electron microscopy

17 p2984 A69-32833

Dimensioning and strength calculations - Conference, Budapest, October-November 1968

17 p3051 A69-32975

Binder polymer network and microstructure effects on solid rocket propellant properties, emphasizing choice of polymer ingredients

17 p3017 A69-33668

Surface layer role in strengthening of iron determined from examining temperature dependence of internal friction during thermomechanical treatments

17 p2991 A69-33939

Lunar surface uppermost layer physical and mechanical properties investigated by soilmeter-penetrometer and radiation densimeter on Luna 13

18 p3113 A69-34239

Metallurgy, properties and applications of Co-Ni-Mo-Cr ultrahigh strength alloy, discussing corrosion

18 p3154 A69-34307

Polymer molecular structure influence on physical and mechanical properties, considering regularity, chain flexibility, crosslinking and intermolecular forces

18 p3099 A69-34606

Composite materials behavior studies for structural applications, using macroscopic and microscopic phenomenological approach

18 p3154 A69-34607

Omega phase formation in Ti and Zr alloys with transition metals, discussing effects on mechanical and superconducting properties

18 p3155 A69-34634

Hydraulically extruded Mo properties after annealing, showing reduction in stability and hardness and varying nature of change in plasticity

18 p3156 A69-34719

Silicide coatings effect on Mo mechanical properties subjected to tensile tests in vacuum and air at various temperatures

18 p3156 A69-35043

Thin brittle plastic shells mechanical properties differing under tension and compression described by solving differential equations in successive approximation

18 p3224 A69-35327

Optimal structure model of fiberglass reinforced materials with polymer matrix, obtaining strength utilization coefficient dependence on length/ diameter ratio

18 p3162 A69-35356

Metal alloys mechanical properties summary for cryogenic applications, considering fracture and thermal behavior, cryogenic structures fabrication and composites applicability

18 p3158 A69-35416

Mechanical properties and weldability of austenitic steel for cryogenic applications

18 p3158 A69-35417

Soviet collection of papers on strength and plasticity of Ni and Ti and alloys covering high temperature internal friction, deformation and creep characteristics

18 p3158 A69-35442

Group 7A and group 8 elements alloying effect on Cr dislocation structure and mechanical properties, discussing ductile-brittle transition temperature and electronic theory

18 p3160 A69-35452

B-epoxy and B-Al composites compared for strength/weight and modulus/weight ratios, moisture absorption, corrosion resistance, projected costs, etc

19 p3340 A69-35506

Syntactic foam prepreg for low density laminate construction, presenting design and mechanical test data

19 p3353 A69-35512

Mechanical properties and thermal aging of laminated specimens of collimated B monofilament reinforced composites preimpregnated with polyimide resin

19 p3354 A69-35514

Mechanical properties associated with 55-Nitinol memory effect, presenting stress-strain and electrical resistivity as function of temperature

19 p3340 A69-35523

Be/Al cast duplex alloy with Be embedded as discrete particles in Al matrix, detailing fabrication techniques and mechanical properties

19 p3340 A69-35524

Directionally solidified Co-Nb eutectic alloys mechanical properties and magnetic performance for elevated temperature space applications

19 p3341 A69-35542

Military storage and environment effects on strength of filament wound glass reinforced epoxy structures, tested on plastic motor case and pressure vessels

19 p3321 A69-35567

Elastomeric and coating materials for aerospace systems, considering temperature, rain, sand erosion, propellant and radiation resistant properties

19 p3357 A69-35586

Bonded solderless solar cell panel prototype withstanding high annealing temperature and thermal shock without electrical or mechanical degradation

19 p3251 A69-35688

Strength analysis of three layer rectangular plates under complex load and support distributions

19 p3434 A69-35827

Glass fiber with epoxy resins compared to polyester resins, discussing chemical reactions, bonding and strength relations

19 p3358 A69-35902

Morphologies and mechanical properties for identification of phosphides /schreibersite/ and carbides /cohenite/ in iron meteorites, noting nucleation and growth

19 p3417 A69-36133

Heat treatment effects on mechanical properties of Ti-Fe and Ti-Fe-Al alloys

19 p3344 A69-36151

Quenching temperature and deformation conditions for Ti alloy bars optimal mechanical properties, emphasizing effect of primary structure

19 p3328 A69-36152

Fabrication effects on high strength Al alloy plate properties, comparing texture, plane strain fracture toughness, yield stress, ultimate tensile stress and elongation

19 p3346 A69-36437

Static theory of fibrous surface media based on continuum mechanics, neighboring fibers noninteraction principle and additivity of mechanical properties

19 p3447 A69-36858

Transverse stiffness and strength of unidirectional fiber-reinforced composites determined as function of fiber volume content, using finite element method and stress functions

20 p3623 A69-37354

Inorganic heat resistant coatings high temperature mechanical tests noting corrosion, safety factors and rigidity after heating and temperature gradients

20 p3538 A69-37360

Monograph on solid rocket propellants covering composition, combustion characteristics and energetic, mechanical and operational properties

20 p3585 A69-37441

Rheology application to description, explanation and measurement of materials properties during deformation

20 p3561 A69-37599

Storage and loss moduli measurement for laminated glass fiber reinforced epoxy composite beams, discussing moduli prediction

20 p3627 A69-37763

Beta working effect on Ti alloy mechanical and fatigue properties

20 p3564 A69-38136

Carbon fiber reinforced plastics application to aircraft metal components for weight reduction, low cost and high mechanical properties

21 p3750 A69-38428

Ti-Al-V fasteners heat treated in beta field, showing superior mechanical properties to samples treated in alpha plus beta field

21 p3729 A69-38661

Ti-Al-V sheets quenched from alpha plus beta field into salt bath at various high temperatures, studying effects of bath temperature and holding time on aging and mechanical properties

21 p3730 A69-38667

Al alloys properties evaluated to determine tensile and static fracture behavior

21 p3743 A69-38668

Statistical mechanics applied to mechanical properties and thermodynamics studies of rapidly expanding or collapsing self gravitating systems

21 p3801 A69-38702

Fiber reinforced plastics mechanical behavior including thermosetting and thermoplastic polymers reinforcement mechanism

21 p3752 A69-38933

Plastic deformation combined effect with aging on mechanical properties of phase-hardened austenitic Fe-Ni-Ti alloys

21 p3746 A69-38956

High temperature electronic tensile testing device utilizing SCR to study strain rate effect on metals properties

21 p3727 A69-39811

Trace elements role in precision metallurgy for obtaining certain steel properties

21 p3750 A69-39870

Cu, Ni, Co, Cr and Ti effect on high temperature mechanical properties and stability after prolonged annealing of Al-Si alloy with added 1 percent Mg

22 p3968 A69-40063

Device determining dynamic mechanical properties of tissues and various transducers, evaluating elastic properties of polyurethane, Hevea rubber and descending thoracic aorta

22 p3890 A69-40204

Carbon monoxide effect on dog lung volume, mechanical properties and diffusing capacity

22 p3874 A69-40224

Mission sequential environment effects on Dacron parachute material mechanical properties

[AIAA PAPER 69-1018] 22 p3923 A69-40390

Preferential welding oxidation emphasized as element transfer mechanism in weld metal composition control

22 p3955 A69-40460

Dual filler metals for increasing joint efficiency by changing fusion zone composition, discussing mechanical properties in Ti and Al plates welding

22 p3956 A69-40462

Anodic Al oxide films mechanical and fracture properties, studying roles of environmental water vapor and film thickness

[ECS PAPER 81] 22 p3973 A69-40736

Residual stress effect on strength of oriented glass fiber reinforced plastics under transverse and longitudinal tension

22 p3973 A69-40745

Alloy Inconel 625 precipitation behavior and effect on short and long term properties, discussing tetragonal phase segregate and creep strength

22 p3971 A69-40802

Mechanical properties of aircraft fasteners high temperature materials

22 p3956 A69-40823

Extrastrong maraging steel based on 18 percent Ni, noting alloying elements percentages, mechanical properties and applications

22 p3971 A69-40833

Mechanical and thermal properties of vanadium alloys and austenitic stainless steels compared to determine applicability in high temperature reactor fuel jackets

22 p3971 A69-40973

Glass fibers strength in relation to surface defects, comparing behavior of flawless and commercial fibers

22 p3974 A69-41039

Nonmetallic inclusions effect on steels cyclic strength dependence on inclusion composition and metallic matrix properties, derived from fatigue tests

22 p4047 A69-41064

V contents influence on high temperature strength and fine structure interrelation in low alloy CrMoWV steels

22 p3972 A69-41083

Physicomechanical properties of tuff rock based on similarity to lunar surface rock, determining natural density, porosity and compression strength

22 p4034 A69-41105

Mechanical properties of welded joints in Kh 18N9T steel at very low temperatures using austenitic-ferritic and austenitic welds

22 p3958 A69-41204

Bright chromium electrodeposition principles and properties of coatings

22 p3958 A69-41263

Metallurgy and properties of quenched and tempered high strength Ni-Co steels, discussing welding and aerospace applications

23 p4175 A69-41299

Ingot dendrite arm spacing and thermomechanical treatment effects on fracture behavior and mechanical properties of Al alloy, finding ultimate and yield strengths

23 p4176 A69-41506

Ni based superalloy mechanical properties, determining chromium carbide discontinuous precipitation effects at various temperatures

23 p4176 A69-41507

Chromium composites mechanical properties, studying effects of alloying with spinel and magnesium oxides

23 p4177 A69-41672

Exposure rate influence on mechanical properties of polymer binder cross-linked by gamma radiation exposure from cobalt isotope source

23 p4179 A69-41711

Temperature influence on mechanical properties and creep curves of fiberglass reinforced textolites compared with data from elasticity theory

23 p4179 A69-41993

Mechanical properties of fiberglass reinforced textolite at normal temperature, noting applicability of elasticity formulas

23 p4179 A69-41994

B, silicon carbide, C and Be reinforcing fibers technology, thermal and physicomechanical properties, noting coating, surface defects and improvement over glass fibers

23 p4179 A69-42154

Low temperature mechanical properties of structural materials for high energy propulsion systems, using low boiling point propellants as liquid hydrogen, fluorine and oxygen

23 p4177 A69-42159

Cold working and aging effects on mechanical properties of TiAl-V including creep and temperature effects

[DGLR-69-002] 23 p4177 A69-42163

Lunar surface material mechanical properties from Surveyor observations, analyzing grain size, rock density, internal friction, cohesion and bulk density compared to Luna observations

24 p4383 A69-42962

Mechanical properties and dislocation configurations and densities of Nb single crystals measured at various strain rates

24 p4332 A69-43030

Mechanical properties of glass and glass-ceramics products improvement through prestressing

24 p4335 A69-43034

Shear load, cohesion and internal friction measurements of low bulk density particulate silicates of complex shape, noting significance for lunar comparison

24 p4383 A69-43040

Static mechanical strength of syntactic foam tested by generating failure conditions based on combined biaxial and triaxial stress

[ASME PAPER 69-APMW-24] 24 p4336 A69-43095

Mechanical testing procedures for brittle materials, discussing test philosophy, tabular data, laboratory tests correlation, etc

24 p4333 A69-43340

Ti and Ti alloys investment castings mechanical properties, dimensional control and corrosion resistance in aircraft and aerospace structural application

24 p4324 A69-43433

Postcured low void content graphite fiber reinforced polyimide resin composites fabrication including shear, flexural and tensile strength data

24 p4337 A69-43446

Anaerobic adhesives for aircraft bonding tested for mechanical properties, noting advantages over epoxy adhesives

24 p4338 A69-43464

MECHANICAL RESONANCE U RESONANT VIBRATION

MECHANICAL SHOCK NT HYDRAULIC SHOCK

Channel wall effect on gain of apparent mass of cylindrical and elliptical bodies floating in channel and subject to vertical impact

11 p1875 A69-25487

Shock waves in solids, discussing gas gun firing and explosive detonating at specimen, transformations measurement and materials processing applications

13 p2360 A69-27341

Shock spectra practical applicabilities to simulated and real shock equivalence, including spectra definitions and determinations

13 p2369 A69-28600

Shock development in electrothermal shock tube with performance simulation of mechanical shock tube with hot driver but turbulent or unstable driver-shock interface

14 p2427 A69-29768

Optimal active shock isolation by nonlinear elements for system subjected to shock type loadings, discussing impulse shapes

15 p2713 A69-31019

Micropropulsion system with sublimable solid fuel for satellite attitude control, satisfying mechanical and thermal environmental conditions during launch and in space

17 p3021 A69-33359

Mechanical linear accelerator simulating acceleration, shock and weightlessness, noting data acquisition and interpretation

17 p2945 A69-33423

Laplace-Carson integral transforms for analyzing surface waves generated by central impact of two elastic bodies

23 p4226 A69-41702

MECHANICAL TWINNING

Mechanical finishing abrasion induced plastic deformation microtwinning observed in thin stainless steel films by transmission electron microscopy

02 p0251 A69-11542

Ferroelectric domain structure to explain microcracks nucleated at twinband intersections in mechanically deformed lithium niobate

03 p0486 A69-13618

Crystal twinning directional effect on Mg alloys tensile yield strength degradation, investigating recovery methods

19 p3341 A69-35583

Iron meteorites microscopic and macroscopic features due to preterrestrial mechanical deformation, stressing local displacements encountered in normal or acicular kamacites

19 p3418 A69-36134

MECHANICS [PHYSICS]

Mechanical and thermodynamical theories of material behavior based on rate independence concept, discussing equivalence of various theories

01 p0166 A69-10227

Applied mechanics - Conference, Laval University, Quebec, May 1967

02 p0339 A69-11984

Higher order differential operators description and derivation of analytical mechanics for holonomic and nonholonomic systems and impact phenomena

02 p0281 A69-12199

Applied mathematics and mechanics - Conference, Prague, April 1968

10 p1675 A69-22874

Fundamental concepts of nonholonomic coupling and coordinates in nonholonomic mechanics

12 p2129 A69-25990

Physics, mathematics, mechanics - Conference, Moscow, December 1964

13 p2300 A69-28430

Computational approaches in applied mechanics - ASME Conference, Chicago, June 1969

18 p3105 A69-34657

Applied mechanics - Conference, Waterloo, Ontario, Canada, May 1969

19 p3374 A69-36655

Averaging methods applied to nonlinear equations in mechanics, discussing solution convergence estimation

20 p3576 A69-37440

Collection of papers on mechanics including quantum theory, mechanics of micropolar continua, elasticity and plasticity, rheology, etc

20 p3623 A69-37580

MECHANISM

Equations of motion of holonomic and non-holonomic mechanical systems obtained by displacement operators

22 p3980 A69-40106

MECHANIZATION

Software remechanization of conventional hyperbolic LORAN for totally passive closed loop one way direct range measurements to individual LORAN transmitters

17 p3002 A69-34079

MEDIA

NT ANISOTROPIC FLUIDS

NT ANISOTROPIC MEDIA
 NT ELASTIC MEDIA
 NT INTERGALACTIC MEDIA
 NT INTERPLANETARY DUST
 NT INTERPLANETARY GAS
 NT INTERPLANETARY MEDIUM
 NT ZODIACAL DUST

Motion of medium at ultrarelativistic velocities in general theory of relativity, noting velocity minimum at radius limit

15 p2653 A69-31067

Circular antenna arrays radiation pattern synthesis in moving medium relative to main beam, noting medium motion influence on pattern changes

22 p3915 A69-40706

MEDICAL ELECTRONICS

Linear passive electrical analog model of human systemic arterial tree, discussing artery segment modeling, vessels input impedance, wave travel, etc

17 p2908 A69-33007

Diathermy instrument using solid state circuits to provide square wave pulses, discussing operating parameters for bipolar coagulation and advantages over spark gap instruments

18 p3134 A69-34537

Variable time lapse videoscintiscopes in medical applications, discussing implementation of TV camera, signal tape recording and audio activation

18 p3134 A69-34541

Wireless telemetry system design for physiological signals in human diagnosis, discouraging casual use of wireless transmission

19 p3261 A69-36269

Electronic stethoscopes for use in high background noise environments for patients on air evacuation flights

21 p3667 A69-39444

Algorithmic approach to nonlinear signal estimation problem useful in fetal electrocardiography

21 p3668 A69-39866

Collection of papers on biomedical engineering and medical physics covering cardiac pumps, neural models, control theory, telemetry and laser applications, etc

22 p3893 A69-40784

Telemetry in medicine and biology, describing applications and operation of various systems

22 p3893 A69-40787

MEDICAL EQUIPMENT

NT RESPIRATORS
 NT STETHOSCOPES
 NT SURGICAL INSTRUMENTS

White rat physiological processes while maintained on hypothermic cardiopulmonary bypass with small membrane type heart-lung machines

05 p0708 A69-15971

Pulmonary mouth pressure and heart rate in Flack test for flight personnel by simultaneous double recordings

05 p0710 A69-16626

Cardiopulmonary bypass developed for studies of long term weightlessness on cardiovascular system of mice, white rats and squirrel monkeys

24 p4278 A69-43394

MEDICAL PERSONNEL

NT FLIGHT SURGEONS
 NT PHYSICIANS

Aircraft pilots medical disabilities as potential flight safety hazard, discussing aerospace medical specialist role and pilot education in symptoms evaluation

22 p3894 A69-41146

Private one doctor one nurse clinic at Sydney airport, discussing history, operating conditions, medical record and statistics

23 p4105 A69-41786

Interplanetary space travel medical problems during long duration missions, noting earth diagnostic and therapeutic methods adaptation, drugs selection, astronaut medical training, etc

24 p4278 A69-43396

MEDICAL PHENOMENA

NT PHENOMENOLOGY

In-flight medical disorders sustained by crew members of various aircraft in French Air Force correlated with aircraft accidents, flight experience and age

24 p4277 A69-43383

MEDICAL SCIENCE

NT DENTISTRY
 NT EPIDEMIOLOGY
 NT GYNECOLOGY
 NT HISTOLOGY
 NT IMMUNOLOGY
 NT NEUROLOGY
 NT NEUROPSYCHIATRY
 NT OTOTOLOGY
 NT PHENOMENOLOGY

NT RADIOBIOLOGY
 NT RADIOLOGY
 NT RADIOPATHOLOGY
 NT SOCIAL PSYCHIATRY

Space technology contributions to medical problems, discussing organization and achievements of biochemical application program of NASA [UN PAPER 68-95417] 01 p0020 A69-10471

Book on space clinical medicine covering hypoxia, ebullism, decompression, aerotitis, dehydration, hypothermia, cabin atmosphere contamination, urinary calculus, etc

05 p0711 A69-16801

Medical investigation of aviation accidents - Conference, Washington, D.C., September 1966

12 p2021 A69-25837

Aeromedical developments by NASA biomedical applications program applied to general medical equipment including cardiac sensors, surgical sterilization, ballistocardiograph, etc

16 p2882 A69-32430

Book on simulation in biology and medicine covering mathematical models, blood circulation, pulmonary ventilation, etc

19 p3260 A69-35894

Centrifugation for removal of bullet fragment floating freely in ventricular system of human brain to fixed safe position in left lateral ventricle wall

24 p4265 A69-43372

MEDICAL SERVICES

Aeronautical health service problems relating to efficiency of military and civil aviation personnel of all nations

12 p2023 A69-26490

Electrophysiological /electrosplanchnogram/ medical data transmission via satellite from France to U.S. for real time computer processing

16 p2746 A69-32070

Helicopter evacuation role in mortality rate among wounded in battle in Korea and Vietnam, discussing air ambulance unit organization

23 p4107 A69-41809

Medical aid organization after aircraft accidents at airports, examining injury probability by statistical methods

23 p4107 A69-41812

Medical aid, equipment and organization for injured passengers in large aircraft accidents at airports and immediate neighborhood

24 p4270 A69-42602

Algorithm for aeromedical airlift system stop selection and sequencing, minimizing patient in-system time and aircraft flight distance [AAS PAPER 69-385] 24 p4251 A69-42804

MEDIUM SCALE INTEGRATION

MSI 12 bit digital to analog converter in integrated circuit form using MOS switching circuit [AIAA PAPER 69-968] 22 p3906 A69-40349

Spacecraft onboard data handling system with MSI complementary MOS arrays, describing various components

23 p4133 A69-41739

MEETINGS

U CONFERENCES

MEISSNER EFFECT

U DIAMAGNETISM
 U SUPERCONDUCTIVITY

MELLIN TRANSFORMS

Wave scattering from nonplanar periodic structures using periodicity method, including Green function and Mellin transform

17 p2929 A69-33880

MELTING

NT ARC MELTING
 NT FUSION [MELTING]
 NT VACUUM MELTING

Gas content and impurities in aluminum melts, analyzing oxides and hydrogen interactions

01 p0098 A69-10958

Wires electric... explosion applications used to study equilibrium characteristics of metals and alloys at high temperatures

02 p0280 A69-11581

Microscopic time lapse movies in solid/liquid interface profile during melting and freezing of materials for spacecraft thermal control as reversible heat sink [AIAA PAPER 69-95] 06 p1038 A69-18126

Mathematical model for melting of finite paraffin slab based on method on numerical computer solution of heat conduction equations for thermal control devices

12 p2190 A69-26785

Particles maximum diameter numerical values for melting during injection into plasma jet calculated for various metals and refractory dielectrics

17 p3009 A69-32825

Molten iron plane melt flow duration and mass in bimetallic castings production determined using nomogram

18 p3149 A69-35289

Ramsdorf meteorite chondrules and metal particles formation attributed to shock-induced partial melting and rapid cooling

19 p3409 A69-36088

Unsteady heat transfer between gas flow and solid surface during melting

20 p3631 A69-37088

MELTING POINTS

Superconductivity and melting point of metals, discussing cause of anomalies

02 p0283 A69-11785

Melting points of tetrahedral phases with stoichiometric vacancies found proportional to covalent bonds number in semiconductors

02 p0297 A69-11881

Relative heats of formation and reduced melting temperatures of lanthanide compounds correlated to lanthanide contraction

07 p1168 A69-19597

Refractory compounds static strength temperature dependence at high temperatures measured in reference to melting temperature

09 p1523 A69-21873

Heat resistant alloying of niobium with group 4A, 5A and 6A elements, studying elements diffusion mobility dependence on melting point

09 p1525 A69-22144

Hydrogen solubility in solid and liquid Ti close to melting point, showing no effect on welds and castings porosity

11 p1905 A69-24963

Melting points of tetrahedral phases with stoichiometric vacancies found proportional to covalent bonds number in semiconductors

18 p3182 A69-35041

Melting points, electrical conductivity, Hall constants, magnetic susceptibility, density, bending strength, microhardness and elastic modulus of zirconium nitride in homogeneity range

20 p3558 A69-37014

Ammonium perchlorate melting point estimate taking into account theory of corresponding states encompassing two sets of experimental independent data

20 p3585 A69-37217

Enthalpy and heat capacity of high melting point homogeneous Ti, Zr and Nb carbides, analyzing influence of Me-Me bonds and carbon sublattice defects

21 p3742 A69-38614

Low melting point material selected model melt simulating shrinking process in castings of melt with broad liquidus-solidus interval

21 p3733 A69-39720

Fusibility diagrams for Ti-Ta-Cr by determining specimens melting points after homogenization at various temperatures in argon

22 p3969 A69-40075

MEM [EXCURSION MODULE]

U MARS EXCURSION MODULE

MEMBRANE ANALOGY

U STRUCTURAL ANALYSIS

MEMBRANE STRUCTURES

NT SKIN [STRUCTURAL MEMBER]

Hysteresis properties of membrane structures with soldered or rolled edges noting superiority of added elastic element in clamped area

01 p0087 A69-10828

Sheba family of shell elements for matrix displacement method applied to problems of thin shells under membrane and bending action

01 p0170 A69-10865

Critical internal pressure induced plastic instability in membrane shells of revolution determined by graphical numerical method

02 p0338 A69-11719

Flutter vibration in subsonic flows, analyzing critical velocity for membrane and damping destabilizing effects in nonconservative system

02 p0192 A69-12825

Stiffness matrices for sector elements under membrane stress, considering alternative displacement distributions within element

04 p0676 A69-14728

Elastic-plastic analysis of flat plates in membrane stretching and flexure, using method of initial strains [ASME PAPER 68-WA/PVP-10]

05 p0840 A69-16191

MEMBRANE THEORY

Natural frequencies and modes of skew membranes obtained by Rayleigh-Ritz method

06 p1021 A69-17146

Existence and uniqueness theorems for boundary value problems of axisymmetric deformation of circular membrane at normal pressure, using membrane theory and shooting method

07 p1233 A69-19299

Capacitance and lowest eigenvalue bounds for two dimensional anisotropic media as exemplified by transverse vibrations of stretched membrane

08 p1418 A69-20848

Finite inelastic deformations under transverse impulsive loading of clamped thin rectangular planform shells idealized as membranes, using incremental plasticity theory

09 p1616 A69-21939

Axisymmetric vibration modes of cylindrical-hemispherical membrane tank partly filled with liquid [AIAA PAPER 67-75]

09 p1482 A69-21940

Acceleration effects on cellular and subcellular structures enzyme activity in humans and animals, noting changes resulting from changed permeability of membranes

10 p1645 A69-23496

Finite deformation equations for flat annular membranes deduced from equations for thin shells of revolution, discussing displacement equations and fixed edge forces

11 p1979 A69-24813

Deformation processes of geometrically nonlinear rotational membrane shells under internal pressure

11 p1980 A69-24821

Buckling loads for anisotropic fiber reinforced composite plates with strong bending membrane coupling terms

12 p2186 A69-26840

Creep stresses and displacements in conical membrane shells at small angle of attack to supersonic flow field, discussing temperature distributions

13 p2364 A69-28205

Membrane flutter and panel stability in supersonic flow, considering infinite aspect ratio equation solution through Galerkin method

13 p2365 A69-28236

Circular membranes vibrational and stability characteristics under simultaneous constant spin and precessional motions, obtaining Hill equation for motion amplitude coefficients

13 p2370 A69-28665

Semifree elastic membranes standing waves fundamental frequency, developing variational principle for first eigenvalue

14 p2535 A69-29365

Perturbation analysis for error estimates in algebraic eigenvalues and eigenvectors problems for solving skewed membrane vibrations

15 p2703 A69-30211

Membrane analogy for flexure of prismatical beams with square cross section and longitudinal cavities, employing Saint-Venant solution

15 p2704 A69-30288

Uncoupled field equations for free large amplitude axisymmetric transverse vibrations of spinning membrane disks

15 p2704 A69-30303

Local buckling of infinite continuous plane elastic membrane under longitudinal load in form of concentrated forces

16 p2875 A69-32293

Hydrogen-oxygen ion exchange membrane fuel cells for sounding balloons, discussing flight duration and power requirements, gas supply pressure effects, etc

16 p2738 A69-32413

Eigenvalue problems in partial differential equations solved by extended Kantorovich method, considering vibration of rectangular membrane and stability of elastic rectangular plate

16 p2876 A69-32783

Nonlinear equations for elastic strain of circular toroidal membrane shell under uniform pressure, computing stress and displacement fields

18 p3216 A69-34575

Transverse vibration and wave solutions for nonlinear equations governing transverse motions of spinning circular membrane disks

19 p3440 A69-36637

Nonlinear rotational viscoelastic membranes creep rupture and failure found dependent on function of accumulated energy and power dissipation during deformation

19 p3444 A69-36806

Equilibrium equations reduced to single partial differential equation for membrane theory of shells having

coefficients of first quadratic form and specified curvature radius

20 p3622 A69-37220

Plane membranes finite deformation, deriving energy theorems for potential U bounds estimation

20 p3624 A69-37588

Complex representation of strain and displacement state in spherical shell using membrane theory, deriving shear forces resulting from single moment loading

21 p3831 A69-38416

Stiffness matrix for curved membrane shell, outlining discrete element representation of cylinders with widely spaced circumferential stiffeners

21 p3842 A69-39305

Wrinkling of pressurized cylindrical and conical fixed free membrane column under lateral load, considering membrane sheets elastic properties

22 p4045 A69-40814

High pressure hydrogen-oxygen reversible fuel cells using calcia stabilized porous zirconia as membrane and aqueous KOH as electrolyte

23 p4076 A69-42308

Asymmetric dynamic response to free and forced vibrations of thin membrane shells at given stress state due to previous loads

24 p4399 A69-42990

Finite deformation of circular elastic membrane spinning with constant angular velocity, solving nonlinear differential equations by Runge-Kutta method for three boundary conditions

24 p4404 A69-43651

Large deflections of circular air mat plates consisting of inflatable structures of two membranes connected by inextensible cords network

24 p4405 A69-43688

Oxygen and carbon dioxide transfer in membrane oxygenators, considering liquid dispersion and membrane diffusion limitations

24 p4279 A69-43799

MEMBRANE THEORY

U STRUCTURAL ANALYSIS

MEMBRANES

NT CHOROID MEMBRANES

NT ION EXCHANGE MEMBRANE ELECTROLYTES

NT MEMBRANE STRUCTURES

NT PLEURAE

NT SKIN [STRUCTURAL MEMBER]

Gyroscopically induced vibrational response of rectangular plates and membranes, determining spin and precession effects on natural frequencies

02 p0347 A69-12519

Membrane vapor diffusion for water reclamation from urine and wash water on space missions

03 p0379 A69-12992

Natural frequencies controllability by induced thermal membrane stresses examined for thin disk

04 p0682 A69-15494

Cylindrical elastic membranes with finite axisymmetric deformation, discussing exact solution by strain energy method

08 p1418 A69-21001

Abiogenic synthesis of prebiological membranes under assumed primitive earth conditions by UV radiation of alkanes on phosphate and Mg ions aqueous solutions

11 p1828 A69-25462

Molecular flow network theory extended to pulsed operation with gases mixtures having various molecular weights

13 p2247 A69-28085

Natural oscillations of loaded strings, membranes and geometric bodies with distributed loads treated as material discontinuities

20 p3578 A69-38292

Nonlinear theory of elastic membranes accounting for thickness effects, obtaining field equations and constitutive relations for various cases

21 p3832 A69-38465

Membrane vibration problems for combined free and forced laminar convection through vertical ducts, obtaining expressions for velocity, temperature and Nusselt numbers

21 p3851 A69-38974

MEMORY

Holographic theory of visual memory behavior, discussing human tests in situation of prompted visual recall

01 p0083 A69-10985

Mathematical model for information processing of biological memory as cybernetic system

23 p4110 A69-41982

Cybernetic approach to memory, proposing model characterized by hierarchical structural order and sequence to study physiological rhythms

23 p4110 A69-41983

Human body responses to microwave irradiation, discussing thermal and nonthermal effects and damage to eyes and to information storage in living systems

23 p4111 A69-42216

MEMORY STORAGE UNITS

U COMPUTER STORAGE DEVICES

MENTRUSTUATION

Jet flying effects on air hostess menstrual function, considering cycle length, duration, regularity, dysmenorrhea and flow severity

23 p4103 A69-41685

MENTAL HEALTH

Cardiovascular system, neuromuscular activity and mental fitness of subjects performing physical and mental assignments with prescribed work-rest schedule during confinement

17 p2906 A69-32936

Pilots mental and physical welfare, discussing roles of mental hygiene and preventive medicine in flight surgeons programs

18 p3097 A69-35301

MENTAL PERFORMANCE

Reduced sensory input states psychobiology, discussing brain-mind relationship and dynamic information transfer loop for normal brain-mental operations

06 p0873 A69-17020

Cybernetic structural model for learning and mental operation comprehending symbol systems, languages, homeostatic mechanisms, etc

07 p1070 A69-18385

Mental and physical human performance characteristics under thermal loads noting admissible temperatures and endurance limits

08 p1263 A69-19940

EEG electrode stimulated simian mental activity in problem solving during simulated space flight, discussing skull implantation and EEG recordings of hippocampus activity

17 p2910 A69-33749

Human radar operator effectiveness at night noting vigilance level lowering, discussing possible logic mechanism perturbation

21 p3666 A69-39268

Human mental performance impairment at simulated 8000 ft altitude indicated in increasingly difficult tests

23 p4102 A69-41680

Mental patient performance in detecting and identifying visual signals under fixed interval schedule, noting nonuniform performance and comparing to normal subjects

23 p4091 A69-42014

Psychological stress effect on human convergent and divergent thinking after presentation of disturbing or benign control films

24 p4269 A69-42555

MENTAL STRESS

U STRESS [PSYCHOLOGY]

MERCAPTAN

U THIOLS

MERCAPTO COMPOUNDS

U THIOLS

MERCATOR PROJECTION

Lunar gravimetric data reprocessed to present in usable and readable form, plotting acceleration on Mercator projection of lunar surface

18 p3194 A69-34413

MERCURY [METAL]

Exploding wire self healing fuse feasibility demonstrated with Hg, noting dynamics of conversion of electric to mechanical energy

01 p0120 A69-10677

Interferometric laser beam scanner using hollow cathode mercury ion laser output

04 p0609 A69-14288

Heated liquid mercury rotation rate and direction counter to rotating bunsen flame related to Venus cloud formations high velocities

04 p0664 A69-15466

Antimony bromine and mercury abundances in meteoritic materials determined by neutron activation analysis

08 p1404 A69-20919

Mercury concentration relation to thermal history of chondritic meteorites, using activation analysis

08 p1404 A69-20920

Liquid mercury cathode thrusters characteristics satisfying constraints imposed by solar flux variations with distance from sun [AIAA PAPER 69-237] 09 p1565 A69-21246

Liquid mercury cathode electron bombardment thrusters applicability to electric propulsion missions [AIAA PAPER 69-302] 09 p1569 A69-21876

Viscosity and electrical conductivity effects on axisymmetric instabilities of current carrying annular cylinder of mercury 11 p1923 A69-24292

Dynamic growth of positive ion sheath on plane electrode in mercury plasma, measuring sheath thickness and current 12 p2134 A69-26099

Argon ion laser with water cooled mercury pool cathode shielded by U-bent section trap, considering advantages as compared to oxide cathodes 12 p2107 A69-26326

Shift of certain Hg spectral line by high power pulse from Nd laser through perturbation of atomic energy levels 13 p2270 A69-27202

MHD channel mercury flow with hydraulic shock in transverse magnetic field, determining characteristic values distribution over range of principal parameters 13 p2307 A69-27499

MHD mercury flow in rotating torus with little friction investigated for Reynolds numbers, considering induction pump forces and magnetic field influences 14 p2500 A69-29907

Smooth and notched tensile properties of Fe-Ni alloys in liquid Hg, discussing ductility and toughness 20 p3563 A69-38025

Liquid mercury flow turbulent intensity measured by quartz insulated Pt hot-film sensors, discussing calibration equation and measurement techniques 21 p3722 A69-38769

Pitot probe measurements of Hg drop growth rates and diameters, allowing for thermal and diffusion effects 24 p4316 A69-43583

MERCURY (PLANET)

Mercury radio emission phase dependence, discussing brightness temperature value approximation and surface layer properties 02 p0314 A69-11640

Planet Mercury rotation, showing reminiscence of apparent path of sun to Ptolemaic concept of planetary system 03 p0509 A69-13368

Mercury radio emission theory, calculating Mercurian brightness temperature as function of solar illumination and distance from sun 03 p0512 A69-13688

Mercury rotation period determination by surface photography, correcting earlier interpretation 03 p0517 A69-14233

Mercury atmospheric models for preliminary environmental criteria to be used in spacecraft design and engineering trade-off studies [AIAA PAPER 69-54] 06 p1010 A69-18042

Mercury transits in 1970 and 1973 to resolve prominence threads and spicules, sunspot fine structures, etc 11 p1958 A69-24434

Icarus radar and optical observations analyzed to verify general relativity predictions using Schwarzschild metrics and to estimate solar oblateness, Mercury mass, etc 13 p2350 A69-27823

Chemical composition of earth, Venus, Mars, Mercury and moon calculated from mathematical models, constructing approximate equations of state at high pressure 14 p2526 A69-29878

Cassini laws applied to moon and Mercury, determining relations between moment differences for spin vector, orbital angular-momentum vector and precessional velocity 16 p2861 A69-32239

Suspected phase anomaly and Mercury atmosphere 17 p3034 A69-33414

Particulate thermophysical lunar soil model for measuring lunation nighttime and eclipse cooling, noting applicability to IR surface brightness temperature of Mercury hot pole 18 p3191 A69-34303

Mercury internal constitution and chemical composition, discussing models with iron cores and iron admixtures in mantle 20 p3597 A69-37331

Mercury and Venus thermal histories based on analogy to earth models 20 p3597 A69-37333

Resonant spin and anomalous rotation of Mercury, analyzing influence of tidal degradation and permanent deformation of planet 21 p3814 A69-39568

Venus and Mercury diurnal period commensurability associated with Venus spin-orbit resonance with earth orbit 22 p4018 A69-40270

Venus swingby and direct Mercury trajectories analysis for optical imaging from flyby missions [AAS PAPER 69-258] 24 p4380 A69-42860

MERCURY ARCS

Mercury ion thrusters and facilities automatic controls durability testing, discussing vacuum chamber systems, unattended operation and control [AIAA PAPER 68-576] 02 p0229 A69-12385

MERCURY COMPOUNDS

Effective masses of electrons and holes in HgSe and HgTe characterized by narrow forbidden bands and high charge carrier mobility 11 p1937 A69-24920

MERCURY LAMPS

Long lived low level chemiluminescence due to gaseous reactions at low concentrations induced by mercury lamp irradiation or Tesla coil discharge 01 p0024 A69-10618

Pulse ruby lasers with mercury lamps for pumping noting improved efficiency, power and temperature regime due to reduced IR radiation 19 p3336 A69-36347

Hg injection lamp with high power and variable spectral energy distribution as light source for testing solar radiation effects 20 p3510 A69-37630

MERCURY PROJECT

Gemini and Mercury space flights medical results, summarizing physiological effects noted on body systems 01 p0017 A69-11074

Systems engineering activities in manned space flight involving design, development, manufacture, test and operation of Mercury, Gemini and Apollo flight systems 06 p1016 A69-17602

MERCURY SPACECRAFT

Guidance and control concepts and hardware for atmospheric entry of Mercury, Gemini and Apollo spacecraft 11 p1914 A69-25724

MERCURY TELLURIDES

HgTe-CdTe single crystals homogeneity and Cd distribution obtained by Bridgman and/or zone melting studied for carrier concentration and electron mobility 09 p1557 A69-21737

Photovoltaic effects in cadmium mercury tellurides, considering band-gap variations, effective masses, mobilities, majority carrier concentration and pair lifetime 19 p3381 A69-35680

HgTe-CdTe single crystals homogeneity and Cd distribution obtained by Bridgman and/or zone melting studied for carrier concentration and electron mobility 20 p3584 A69-38215

HgCdTe as IR satellite detector for terrestrial, atmospheric and ocean mapping, IR astronomy and optical communication 24 p4362 A69-43666

MERCURY VAPOR

High sensitivity mercury vapor analysis automated to provide continuous monitoring of Hg in atmosphere, discussing winter and summer concentrations 02 p0244 A69-12019

Contact phenomena theory in decaying plasma applied to deionizing mercury vapor diode gas discharge plasma diagnostics 03 p0404 A69-13547

Equivalent pressure concept verification for arc discharge with incandescent cathode in mercury vapor 03 p0478 A69-13843

Free fall theory for afterglow decay of average electron density and temperature in pulsed cylindrical mercury vapor discharge plasma 08 p1358 A69-19811

Hollow cathode mercury electron bombardment thruster design, emphasizing low specific impulse operation and discharge chamber improvements [AIAA PAPER 69-300] 09 p1569 A69-21880

Mercury cesium plasma in crossed electric and magnetic fields as working fluid of MHD generators based on Rankine cycle 10 p1636 A69-23458

Thermal accommodation coefficient and critical supersaturation for nucleation of mercury vapor on pyrex glass 13 p2321 A69-28005

Balance equations for axial separation in anisothermal plasma columns with radial variation of neutral gas temperature applied to argon discharge with mercury vapor addition 14 p2493 A69-29690

Synthesized plasma from neutralized mercury ion beam ejected from electron bombardment source, analyzing temperature, plasma sheath and stability 14 p2502 A69-29956

Thermodynamic parameters of MHD cycle employing supercritical Hg, indicating need for more suitable fluids 16 p2736 A69-31914

I-V characteristics of caloroelectric plasma converter with concentric electrodes measured for various hot electrode temperatures and mercury vapor flow rates 16 p2822 A69-32065

RF ion thrusters using electrodeless self sustaining mercury discharge, describing basic theory, component design, performance optimization and test results 17 p3018 A69-33326

Heated Hg shock tube construction and operation, application to high electron density plasmas and problem of shock bifurcation in Hg monatomic gas 18 p3116 A69-34453

High electron density in transient mercury vapor plasma determined using He-Ne laser interferometer measurements 18 p3153 A69-35307

Mach-Zehnder laser interferometer for measurements of electron density in transient Hg vapor plasma, noting agreement with microwave measurements 22 p3965 A69-40924

MERIDIANAL FLOW

Mean meridional circulation models in tropics based on vorticity equation 03 p0460 A69-13334

Sensible and latent heat meridional transport associated with standing eddies computed from climatic mean data 04 p0627 A69-15085

Time dependent model of photochemical, advective and turbulent effects on meridional ozone distribution 07 p1122 A69-18253

Geostrophic trajectories of horizontal diffusivity estimated in midlatitude troposphere and lower stratosphere 08 p1308 A69-20310

Meridional flow, angular momentum and energy flux in atmosphere calculated from IGY data 08 p1346 A69-20312

Two level quasi-geostrophic model to probe atmospheric general circulation, noting functional dependence of zonal momentum meridional flux 08 p1346 A69-20314

Oscillation cycle of atmospheric circulation, analyzing solar activity effects on lunar and solar semidiurnal tides and transition from zonal to meridional circulation 12 p2070 A69-26692

Expansion of stream function of steady meridional flow of viscous fluid at small Reynolds numbers, giving expansion in spherical coordinates 13 p2247 A69-27737

Secular instability of steadily rotating stars, analyzing meridional motions in radiation zones by linear perturbation theory 13 p2354 A69-28566

Ozone concentration changes in polar regions and tropical zone due to meridional atmospheric circulation 14 p2442 A69-29830

Regional distribution of relative angular momentum transport over equator, noting advective and turbulent transfer 16 p2773 A69-31793

Atmospheric ozone distribution in meridional plane including time effects of photochemistry, advection and turbulence assuming zonal symmetry 16 p2785 A69-32624

Mean patterns of meridional interhemispheric flow for 40 degree equatorial sector, calculating mean air mass transport in lower troposphere over western Indian Ocean 18 p3166 A69-34420

Turbomachine blade thickness effect on meridional flow disturbances analyzed through blade geometry using differential equations 20 p3457 A69-37084

Meridional circulations in kinetic energy budget of Northern Hemisphere troposphere based on winter and summer climatic mean data, noting Hadley circulation 20 p3523 A69-37505

Model equatorial electrojet with meridional current system constructed by spherical harmonic expansion for geomagnetic field, noting current loops
20 p3533 A69-38084

WE and SN wind components models from 60 to 130 km for different months and latitudes, discussing meridional and interhemispheric circulations
23 p4154 A69-41306

Instability theory of baroclinic vortices in incompressible and inviscid fluid, investigating symmetric meridional motions time evolution by numerical integration of hydrodynamic equations
23 p4153 A69-42346

Hadley and equatorial cell models for mean meridional circulation in terms of vorticity equation
24 p4345 A69-43152

MEROMORPHIC FUNCTIONS

U ELLIPTIC FUNCTIONS

U RATIONAL FUNCTIONS

MESH

Image tube storage target mesh electrode structure and transmission data for electron beams of various velocities, noting secondary electron redistribution control
11 p1848 A69-24749

Erectable metal booms and meshes structural analysis, design and mounting and deployment techniques for space applications
19 p3433 A69-35544

MESITYLENE

Isopentane and mesitylene index of refraction variations with pressure, determining average molecular radii and polarizabilities
01 p0123 A69-10685

MESON-NUCLEON INTERACTIONS

Electromagnetic muon-nucleon interaction explanation for observed horizontal air showers, reexamining shower data in view of triplet particles
15 p2678 A69-31498

Approximations for meson-nucleus scattering length from energy level measurements on mesonic atoms, emphasizing formula for negative pi mesonic atoms
22 p3987 A69-41004

High energy negative kappa meson-nucleon interactions with respect to multiplicity distribution of charged pions in nucleon-antinucleon annihilation, showing binomial distribution
24 p4351 A69-42791

MESON RESONANCES

Fireball events, isobars and meson resonances in very high energy nuclear interactions, discussing dispersion and four momenta transfer methods
13 p2303 A69-28380

MESONS

NT K-MESONS

NT MESON RESONANCES

NT MUONS

NT PIONS

Cosmic ray meson diurnal anisotropies direction calculated on basis of subtracted diurnal vectors
02 p0306 A69-11730

Atmospheric temperature and water vapor variations and seasonal environmental changes effects on cosmic ray neutron and meson monitor counting rates
03 p0498 A69-12936

Cosmic ray meson component solar diurnal variation calculations noting amplitude, average deflection angle and dependence on zenith angle of arrival
03 p0501 A69-13752

Electromagnetic theory of gravitational forces unifying electromagnetic, meson and gravitational fields
03 p0469 A69-14096

Amplitude and phase of cosmic ray meson diurnal variation, noting less variation in neutron diurnal variation
04 p0648 A69-14374

Primary cosmic ray intensity variation with cut-off energy of particular secondary component, using ground based monitors
06 p0925 A69-17295

Geomagnetic activity correlation to cosmic ray solar daily variation underground, observing primary cosmic ray flux with meson telescopes
09 p1583 A69-22755

Low momentum muon directional coupling coefficients based on latitude survey of directional meson intensity
09 p1583 A69-22759

Nonmesonic to mesonic decay ratio estimated for delta hydrogen hyperfragments
12 p2133 A69-26298

High energy mu-mesons component of atmospheric cosmic ray showers by particle impact penetration using multiple underground ionization chambers
13 p2332 A69-28409

Meteorological corrections of meson megatelescope data based on hourly ground-level pressures and temperatures, considering vector and regression analyses
19 p3308 A69-35991

MESOPAUSE

Reversed thermal conditions in mesopause, examining atomic oxygen IR radiation effect
01 p0062 A69-10129

Near mesopause atmospheric layer energy balance, noting atomic oxygen diffusion role in redistributing absorbed solar energy among atmospheric layers
03 p0422 A69-13408

Mesopause wind measurements at high latitude locations by sounding rockets noting relation to noctilucent clouds
13 p2294 A69-28466

Ionospheric winter anomaly duration in height range of mesopause region based on zenith angle dependence of absorption at LF
16 p2782 A69-32456

MESOPHILES

Ferredoxin from thermophilic and mesophilic Clostridia, noting difference in heat stability due to iron and sulfide environments
22 p3897 A69-41068

MESOSPHERE

Rocket and radiosondes data from measurements over Northern Hemisphere used to study stratospheric and mesospheric circulation during three midwinter periods
05 p0753 A69-15800

Wind data from Arctic upper mesosphere showing easterly winds increasing with height, resolving diurnal and semidiurnal oscillations
06 p0949 A69-17005

Midwinter warmings in upper stratosphere for differences between various stratospheric and mesospheric levels, noting need for additional upper air data
08 p1345 A69-20134

Carbon dioxide absorption and emission in mesosphere, discussing vibrational relaxation time and radiative heating rate
08 p1308 A69-20308

Air movement component of winter anomaly effect on radio wave absorption in mesosphere directly detected by rocket sounding
11 p1913 A69-25436

Zonal and meridional wind components monthly global cross sections for stratosphere and mesosphere from sounding and radar data
12 p2070 A69-26577

Satellite and rocket probe measurements of water vapor in mesosphere
13 p2253 A69-27694

Cloud drift radar measurements for determining wind velocity profiles in mesosphere, using rocket released dipole reflectors
13 p2253 A69-27848

Latitudinal and vertical variations in six-month zonal wind cycles in equatorial and tropical stratosphere and lower mesosphere, utilizing rocket observations
13 p2294 A69-27854

Thermally excited diurnal wind oscillations in lower mesosphere using model atmosphere in CIRA 1965, discussing daytime ozone density profiles
14 p2441 A69-29379

Two year cyclic monsoon type variations in zonal wind distribution in tropical stratosphere and mesosphere obtained by rocket measurements
14 p2478 A69-29834

Aerosol content of mesosphere with noctilucent clouds measured with optical radar in Norway
14 p2444 A69-29877

Internal gravity waves suggested as possible cause for anomalous mesospheric temperatures
15 p2601 A69-31376

Longitudinal variations of density, temperature and pressure distributions in stratosphere and mesosphere based on rocket observations, emphasizing arctic and subarctic regions
15 p2602 A69-31379

Mesospheric fine winds structure, discussing data obtained by Skua II rocket with chaff payload
15 p2604 A69-31415

Rocket and radiosondes data from measurements over Northern Hemisphere used to study stratospheric and mesospheric circulation during three midwinter periods
17 p2962 A69-33779

Physical process providing EMF for maintaining electrical structure of stratosphere and mesosphere shown to center in lower ionospheric thermally driven tidal motions
18 p3130 A69-35103

Atmospheric flow with respect to mesoscale disturbances, examining conditions for hydrodynamic stability
18 p3167 A69-35343

Convective momentum exchange in mesoscale gravity wave
20 p3522 A69-37350

Mesosphere and lower thermosphere molecular O density from solar radiation atmospheric absorption, using satellite measurements
20 p3523 A69-37413

Solar activity effect on short term meteorological processes and dynamic state of mesosphere and ionosphere, emphasizing relationship to entire atmosphere dynamics
20 p3590 A69-37684

Mesospheric wind measurement by meteorological rockets based on radar determination of drift trajectories of chaff clouds
20 p3529 A69-37797

Distributions, seasonal variations and ionospheric implications of mesospheric nitric oxide concentration
21 p3703 A69-38364

Altitude variation of mesospheric daytime sky brightness from earth based measurements of twilight sky brightness, noting inconsistency in calculations based on standard atmospheres
21 p3716 A69-39116

Rocket optical experiment for determining water, methane, nitric oxide and ozone vertical profiles in stratosphere and mesosphere
22 p4035 A69-39910

Upper stratosphere warming and associated structure of mesosphere from rocket sounding, discussing high winds related to pressure gradient, upward vertical motion, etc
22 p3977 A69-39928

Mesospheric circulation related to noctilucent cloud data, discussing seasonal variations
24 p4307 A69-42965

MESSAGES

NT SYMBOLS

Probabilistic analysis of code message distortion due to pulse noise in modulation systems and comparison between linear and quadratic detections
17 p2919 A69-33145

METABOLIC WASTES

NT FECEs

NT HUMAN WASTES

NT URINE

Discharge rates of metabolic products in men confined in pressure chamber wearing airtight suits and gas masks
10 p1646 A69-23508

Mineralizing metabolic wastes by catalytic oxidation of pyrolysis products, noting nutritive value of ash solutions for *Chlorella* cultivation
10 p1649 A69-23579

METABOLISM

NT ADRENAL METABOLISM

NT CALCIUM METABOLISM

NT CARBOHYDRATE METABOLISM

NT ENZYME ACTIVITY

NT HORMONE METABOLISMS

NT HYPERGLYCEMIA

NT HYPOGLYCEMIA

NT LIPID METABOLISM

NT OXYGEN METABOLISM

NT PHOSPHORUS METABOLISM

NT PROTEIN METABOLISM

Basal metabolism in humans restricted to prolonged bed rest, noting decreased oxygen consumption rates
02 p0197 A69-11497

P32 distribution in protein of blood serum, liver and brains of rats bombarded with high energy protons
02 p0198 A69-11507

Handbook on metabolism and nutrition containing tables, charts and diagrams on food composition, material incorporation into organism, energy exchange and end products
04 p0553 A69-14908

Energy metabolism changes during weightlessness, considering effects on basal and nonbasal requirements connected with added increments for activity
06 p0872 A69-17014

Radiative, convective and evaporative heat losses and thermal comfort conditions for human beings, describing theoretically and empirically based equation
06 p0880 A69-17087

Objective evaluation of metabolic reactivity of organism based on biophysical model compared with experimental individual
06 p0874 A69-17595

Oxygen intake and body temperature of basal and sleeping Andean natives at high altitude
06 p0874 A69-17835

Human body cold tolerance and relation to BMR seasonal variation
06 p0876 A69-18024

Depressed metabolism - Conference, Washington, August 1968
10 p1641 A69-23116

High temperature acclimation, climates with heat dissipation problems and hibernation or torpor effects on metabolic depression in homeotherms
10 p1642 A69-23121

Electrocardiograms of homeothermic animal, hibernator, warm and cool climate poikilothermic animals compared for hypothermia, considering metabolic changes contributing to EKG changes
10 p1643 A69-23123

Physiologic and metabolic effects in humans undergoing therapeutic hypothermia
10 p1643 A69-23125

Radiation resistance of animals in hibernation and hypothermia, noting temperature dependence of protective effect
10 p1643 A69-23126

Hypokinesia effect on dynamics of metabolic processes in athletes muscular system by comparison of diuresis, creatinine excretion and cutaneous fat layer indices
10 p1646 A69-23582

Heart rate and bodily fluid changes in aestivating desert anurans, discussing weight loss and metabolism reduction
11 p1827 A69-24923

F-102 pilot anticipatory and flight stress, noting endocrine-metabolic hyperactivity
12 p2023 A69-26552

Prolonged dehydrated food diet effect on metabolism of humans, noting complete adaptation after three or four months
13 p2212 A69-28624

Preferential shifts in consumption of metabolic fuels following exposure to hydrazine or monomethylhydrazine, considering biochemical and physiological responses
14 p2407 A69-29303

Glycolysis control by respiration in human leukocytes with and without Pasteur effect conditions
15 p2555 A69-30413

Human locomotion analysis, measuring metabolic expenditure and mechanical energy levels of principal body segments during walking
15 p2558 A69-30587

Experiments integrated into single automated laboratory to detect extraterrestrial life through measuring metabolism and growth in planetary surface material
17 p2912 A69-32969

Extraterrestrial life detection experiments integrated into single multipurpose space laboratory, including chemical analyses, metabolism identification, observation for molecular and/or cellular growth and replication
17 p2912 A69-32970

Glutamic acid metabolism compartmentation in brain cortex demonstrated in vitro, using isotopic labeling
18 p3096 A69-35172

Urinalysis of crew members of first transatlantic helicopter flight indicating interindividual endocrine-metabolic variability and circadian trends modification
19 p3263 A69-36452

Mammalian brain epinephrine metabolism data after isotonic saline perfusion into cranial vasculature
21 p3650 A69-38323

Human metabolic response to hypothermia measured over wide range of work intensities and durations
22 p3891 A69-40215

Real time metabolic rate analysis of suited astronaut using heart rate and O methods during thermal vacuum and extravehicular mobility tests
[AIAA PAPER 69-993] 22 p3893 A69-40371

GABA shunt contribution to total metabolism of alpha ketoglutarate to succinate and high pressure O effect on system under in vitro conditions
22 p3877 A69-40776

Receptor and adrenergic blockade effects on blood loss, tolerated period and metabolic sequels of hypotension in dogs
23 p4098 A69-42102

X band pulsed microwaves effect on skin metabolism including respiratory activity, biochemistry and biosynthesis of intercellular materials, etc
24 p4270 A69-42575

METAGALAXY
U UNIVERSE

METAL ALLOYS
U ALLOYS

METAL BONDING
NT METAL-METAL BONDING

Electrode indentation in resistance spot welds related to weld strength for titanium, steel and aluminum alloy
01 p0086 A69-10538

Fusion, resistance and pressure welding of titanium, discussing shielding, brazing, diffusion and adhesive bonding
02 p0253 A69-12064

Metal/alumina interfaces strength, examining correlation with wetting and bonding and martensitic transformations
03 p0447 A69-13612

Braze bonds of refractory electrical contacts using induction heating
04 p0607 A69-15218

Phosphate cements for bonding mica ceramic to titanium in jet engine equipment
05 p0786 A69-16799

Diffusion bonding of whisker reinforced aluminum in closed steel die in argon atmosphere
06 p0943 A69-17238

Aluminum and aluminum alloys surface treatment prior to adhesive bonding, discussing degreasing, anodization, shear and bond strengths
07 p1141 A69-19312

Methyl 2-cyanoacrylate adhesive bonding characteristics, noting importance of film thickness
09 p1529 A69-22316

Adhesive bonded lap joint strength dependence on adherend mechanical properties under conditions of homogeneous adherend and cohesive failure
09 p1530 A69-22317

Fracture toughness of laminated adhesive bonded structures and monolithic aluminum, considering fracture stresses and ductile and brittle failure
09 p1526 A69-22318

Metallic systems microbonding and joining reliability, noting electron and laser beam welding and deposited film connections
09 p1510 A69-22348

Pulse echo ultrasonic nondestructive testing of C-5 adhesive bonded aluminum composites with multiple bond lines
10 p1698 A69-23047

Aluminum bonded structures corrosion resistance through adhesive primers and surface treatments
10 p1700 A69-24088

Diffusion processes in metal welding noting role of recovery, polygonization, recrystallization, polymorphic transformations, etc
11 p1890 A69-24799

Diffusion bonding as solid state metal joining process for nuclear and aerospace hardware, discussing tooling and nondestructive tests
[ASME PAPER 69-DE-7] 14 p2454 A69-28840

Metal joints mechanisms in soldering, brazing and welding
14 p2455 A69-29344

Bonding strength of plasma coatings with substrate, testing aluminum oxide on steel
15 p2630 A69-31189

Solar furnace for metal soldering, brazing and welding, using Pb-Sn solder for various joint types, twisted wires and rod-flange joining
16 p2793 A69-31818

Quartz fiber adhesion to Re measured in LEED /low energy electron diffraction/ apparatus for clean and O layer surfaces, noting brittle fracture
18 p3156 A69-35182

Room temperature vulcanizing silicone rubber adhesive sealants strength and self bonding, describing primerless adhesion to Ti and Al alloys, Al, Ni and stainless steels
19 p3356 A69-35532

Resistance spot welds in Al, Ti and stainless steel in air and hard vacuum, showing feasibility for space assembly
19 p3310 A69-35554

High temperature structural adhesives developed from thermoplastic aromatic-heterocyclic polymers
19 p3357 A69-35560

Beryllium bonding, evaluating various surface preparations and adhesives
19 p3320 A69-35561

Spray cleaning and deoxidizing of Al surfaces for structural bonding using sulfuric acid-sodium dichromate deoxidizer, noting tests with proprietary solutions
19 p3321 A69-35564

Diffusion welding and soldering of metallic wire with graphite and graphitized viscose applied to chromel, copel, chromel-alumel, Mo, W and W-Re
21 p3728 A69-38617

Bonding mechanisms in Mo-Mn-Ti metallizing and Cu brazing in metal to ceramic seals by strength test, microscopy and electron probe microanalysis
21 p3733 A69-39599

Load transfer to sheet metal plate from bonded strip axially loaded by single force, assuming linear viscoelastic adhesive layer
22 p4038 A69-39896

METAL CARBIDES
U CARBIDES

METAL COATINGS
NT ALUMINUM COATINGS
NT GOLD COATINGS

Chemical vapor deposition of beryllium metal coatings noting thickness, purity and processing effects on surface properties
01 p0097 A69-10644

Electroless deposition of various metals with emphasis on nickel, discussing mechanism, plating solutions, substrates, deposit properties and applications
01 p0099 A69-11060

Silicon carbide deposition from liquid organic compounds using film boiling applied on heated tungsten wire substrate
02 p0252 A69-11804

Color and appearance properties of paint films and relations to amounts and properties of colorants, noting translucent plastics and metallized paint films
04 p0620 A69-14886

Tungsten coatings applied on stainless steel and titanium alloy surfaces by plasma jet
07 p1165 A69-18931

X ray and photomicrographic study of metal layer-ceramic seal interface reaction products, discussing phase transformations, temperature effects and time dependence
08 p1320 A69-20375

Oxidation influence on molybdenum disilicide coatings emissivity, determining degree of blackness over thermal stability range
09 p1522 A69-21588

Graphite fiber electroplating with nickel on continuous basis for ribbon like continuous flexible twist free yarn
09 p1512 A69-22362

Vacuum deposition of Cr-Al film on Ni-Mo alloys, describing operating pressure, temperature and film thickness
10 p1715 A69-24013

Bulk weld filler metals, discussing granular compositions, electrodes and iron, nickel and cobalt base deposits
11 p1891 A69-24931

Deposition and interdiffusion of W layers on Mo emitter of in-core thermionic reactor, investigating microstructure of transition zone
14 p2462 A69-29210

Thermionic emission from bare and Cs-covered metal surfaces, calculating current and work function by employing localized electron orbital model
14 p2505 A69-29264

Alkaline metal adsorption on high work function metals with charge transfer, measuring polycrystalline Mo photoelectric emission as function of Cs coverage
14 p2507 A69-29275

Stannate immersion process for reduction of magnesium-steel couples galvanic corrosion, discussing bath operating limits
14 p2466 A69-29933

Electrodeposits on molybdenum alloys in high temperature oxidizing environments, noting performance of Cr-Ni-Cr composite coating
14 p2466 A69-29934

Plating wear resistant electrodeposits of Ag, Cu, Ni and Cr on Ti, noting adhesion tests
18 p3148 A69-34654

Molybdenum coatings electrodeposition from fused salt system
18 p3156 A69-35001

Reflection reduction properties of symmetrical, light transmitting three layer coating consisting of zinc sulfide-magnesium fluoride-zinc sulfide films
18 p3173 A69-35147

Thermogravimetric study of oxidation protection of refractory metals by fused LiF coating, noting oxidation retardation of Ta, Nb and W
19 p3341 A69-35573

Controllable process for forming Ti-Ni intermetallic wear resistant coating on Ti alloys, discussing techniques, weight saving advantage, gear tests, etc
19 p3323 A69-35582

- Collection of papers on protective coatings of metals
19 p3328 A69-36155
- Steels chromized by vacuum diffusion, studying depth, microstructure and properties of chromized layer
19 p3329 A69-36572
- Coating deposition theory on high temperature materials, discussing interfacial energy and wetting properties of molten metal drop on solid base material surface
20 p3560 A69-37358
- Temperature fields and stresses in heat resistant ceramic coatings, illustrating alumina coating on Mo to calculate heating rate
20 p3565 A69-37359
- Temperature effect on grain size, crystal orientation, microhardness and heat resistance of diffusion Si coatings on Mo
20 p3560 A69-37361
- Zr and Nb carbide coatings on Nb, Ta Mo and W, investigating methods for coating and base metal combinations
20 p3560 A69-37362
- Diffusion processes during formation of coatings by condensation
20 p3549 A69-37365
- Diffusion processes, composition and structure of vapor deposited Ni coatings on Nb substrate, plotting intermetallic compounds growth against temperature
20 p3560 A69-37366
- Niobium carbide deposition from gaseous halogen compounds on graphite particles in pseudoliquefied state, noting stoichiometric coatings
20 p3566 A69-37369
- Carbide coatings formation on graphite in molten media, determining diffusion coefficient of carbon in molten Zr
20 p3566 A69-37372
- Tungsten carbide erosion resistant coatings, discussing optimum plasma deposition process and coating characteristics
20 p3561 A69-37373
- Re and Re alloy powder metallurgy, noting fabrication of Re coated W particles
20 p3562 A69-37749
- Large aperture Al alloy telescope mirrors consisting of Tenzallay Al coated with Ni alloy, presenting performance data
20 p3546 A69-38193
- Plasma metal spray coating for Al and Mg alloy aircraft components adhesive bonding repair technique compared to welding and electroplating
21 p3728 A69-38462
- Metal matrix compatibility of metal coated graphitized, silicon carbide and boron fibers, discussing fiber weakening processes
[ASM PAPER W9-20.1] 21 p3751 A69-38670
- Metal or ceramic layers application to substrate by flame spraying process
21 p3731 A69-38938
- Tungsten coatings applied on stainless steel and titanium alloy surfaces by plasma jet
21 p3746 A69-39152
- Titanium diboride electrodeposition on Inconel from molten salt electrolyte at high temperatures noting electrolyte metabolates and coating thickness range
22 p3970 A69-40735
- Galvanic corrosion prevention measures for airframe fasteners, discussing crevice sealants, primers, zinc chromate, cadmium and aluminum coatings
22 p3957 A69-40825
- Wear protection of pressure loaded Ti-Mn alloy by heat diffused lubricated electrodeless Ni coatings
24 p4331 A69-42786
- METAL COMBUSTION**
- Burning ability and inflammability of mixtures of powdered Mg, Al, Mg alloys or Al alloys and C-H-O organic compounds
02 p0355 A69-12669
- Temperature distribution and vaporization rate boundary conditions on metal particle surface during preignition heating in oxygen containing medium
02 p0355 A69-12670
- Tungsten delay powders combustion mechanism and intermediate stages of burning process, noting burning rate
[WSCI PAPER 68-19] 07 p1202 A69-18370
- Metallic particle ignition in oxygen containing media, obtaining temperature curves and vaporization rates
08 p1375 A69-20343
- UV, visible and near IR spectral characteristics of hydrocarbon-air flames with particulate Al, Mg and B, noting hot metal continuum and oxide emissions
11 p1940 A69-24483
- Boron combustion for air augmented rocket applications, discussing single boron particle ignition and combustion characteristics
16 p2828 A69-31737
- Laser ignited Zr droplet free fall combustion in oxygen, analyzing metal conservation and luminosity correlation assuming reflux action from fog layer
[WSCI PAPER 69-1] 16 p2830 A69-32342
- Combustion of pulse heated single Al and Be particles in various oxidizers
[WSCI PAPER 69-2] 16 p2830 A69-32343
- Combustion of isolated aluminum particles ignited by laser and burning in controlled gas mixture observed by cinephotomicrography
[WSCI PAPER 69-3] 16 p2830 A69-32344
- Combustion of pure crystalline boron single particles injected into hot oxidizing gases streams at atmospheric pressure
[AIAA PAPER 69-562] 16 p2880 A69-32741
- Interaction between two phase dynamical and combustion parameters in one dimensional gas-metal combustion system
[AIAA PAPER 69-540] 16 p2880 A69-32742
- Aluminum oxide droplets condensation from atmosphere of metal vapor and oxygen, studying temperature and time effects on particle nucleation, growth and distribution
21 p3783 A69-38799
- Beryllium fluoride heat of formation from heat of combustion of Be-polytetrafluoroethylene mixture in fluorine
21 p3853 A69-39703
- Combustion considerations in fuel rich solid and hybrid propellant systems in air breathing propulsion for comparison with metal ignition requirements
23 p4199 A69-41894
- METAL CORROSION**
- U CORROSION**
- METAL CRYSTALS**
- Yield condition of polycrystalline hcp metal, considering slip characteristics of hcp crystals
01 p0094 A69-10304
- Theory of fatigue crack growth crystal in metals in terms of coplanar dislocation arrays extended to oblique slip planes, discussing orientation
01 p0168 A69-10344
- Soviet book on structure of thin metal films covering electron microscopic and electronographic studies, crystallization and heat treatment effects
01 p0140 A69-11106
- Vacancies and interstitials in metals - Conference, Jülich, West Germany, September 1968
02 p0267 A69-12185
- Migration and penetration of vacancies in quenched magnesium analyzed by electrical resistivity measurements and electron microscopy
02 p0267 A69-12187
- Strain rate effect on dislocation substructure in deformed niobium single crystals, investigating relationship between mechanical properties and dislocation substructure
02 p0268 A69-12287
- Free flight impact tests showing deformation curve for aluminum and copper single crystals representable as 1/4 power law
02 p0344 A69-12288
- Model of creep in solids based on Markov process, discussing dislocation movement by means of thermal activation
03 p0529 A69-13942
- Orientation dependence of pitting and blistering in proton irradiated Al polycrystal surfaces
04 p0640 A69-14451
- Unified theory of stress-strain curve of fcc metal crystals in Stages II and III of work hardening
05 p0778 A69-15755
- Cross slip model for work hardening of nickel aluminate crystals, discussing temperature dependence
05 p0779 A69-15760
- Book on plastic deformation of metals in terms of dislocation theory covering single crystals, alloying solid solutions, aggregates, annealing, etc
05 p0841 A69-16369
- Electromagnetic wave scattering in ferromagnetic crystals with anisotropy, discussing correlation functions of characteristics fluctuations and magnetoacoustic resonance
05 p0809 A69-16547
- Magnetoresistance of tellurium single crystals with various current carrier concentration at liquid helium temperatures
06 p0978 A69-16986
- Deformation and fracture of Be bicrystals grown by seeding and floating zone melting method from Be single crystal
06 p0942 A69-17225
- Diamond pyramid hardness dependence on grain size of recrystallized alpha titanium
06 p0943 A69-17235
- Unified methods based on dislocation theory for direct solution of problems pertaining to physical properties of metals
06 p0944 A69-17502
- Fatigue hardening in fcc metals, discussing dislocation distribution in unidirectionally deformed single crystals
06 p0944 A69-17503
- Chemisorption of H onto Nb (110) surface, measuring low energy electron diffraction and inelastic electron scattering from clean and H-covered surfaces
06 p0980 A69-17758
- Anomalous size effects in galvanomagnetic properties of zinc crystal samples caused by compensation
06 p0981 A69-18232
- Dislocation redistribution during annealing and shock deformation in liquid nitrogen of chromium, molybdenum and tungsten single crystals
07 p1159 A69-18534
- Ti alloy beta phase variations in quantity, composition and dispersion during quenching, thermomechanical treatment and aging
07 p1163 A69-18777
- Plastic deformation in bcc, fcc and hcp metals as function of initial impact load energy, noting strain hardening effects
07 p1166 A69-19144
- Polycrystalline Mg-Th-Zr alloy precipitation hardening investigated by tensile and hardness tests and transmission electron microscopy
07 p1167 A69-19265
- Crystal growth and deformation induced recrystallization in pure aluminum
[ONERA-TP-671] 07 p1167 A69-19340
- Polycrystalline beryllium specimens fabricated from powders, discussing initial powder particle size and distribution effects on microyield strength
07 p1168 A69-19598
- Structural defects in annealed niobium crystals observed by optical microscopy, discussing etch pits
07 p1169 A69-19603
- Subgrain diameter relation to misorientation in melt-grown aluminum single crystals from etch pitting and X ray techniques, discussing critical shear stress
08 p1330 A69-20011
- Fiber-metal matrix composites fabrication, applications, mechanical properties and powder metallurgy
08 p1332 A69-20204
- Binary vanadium alloys property change regularities using alloying elements
08 p1333 A69-20439
- Thermally activated processes influence on dislocation interaction and on temperature dependence of flow stress in niobium single crystals
08 p1333 A69-20446
- Tensile deformation properties of copper single crystals strengthened by fine dispersions of BeO particles
08 p1334 A69-20575
- Dislocation damping measurements made on Fe-18Cr-Ni alloys, noting damping relation to nickel content and stacking fault
08 p1334 A69-20576
- Alkali halide crystals destruction by laser radiation for estimating optical strength, discussing impact ionization hypothesis
08 p1328 A69-21188
- Work function change of tungsten single crystal (100) surface measured as time function during surface molecular gas adsorption
09 p1521 A69-21338
- Effective work function of Re and Mo electrode samples determined from Schottky plots and emission measurements from grains
09 p1557 A69-21807
- Surface characterization on chemical vapor deposited tungsten, evaluating grain size effect
09 p1558 A69-21810
- Partial pole figures in vapor deposited and wrought cylindrical tungsten specimens, noting random surface produced by orientation
09 p1558 A69-21811
- Omega phase transformation in binary and ternary Zr alloys after water quenching from within alpha plus beta phase region
10 p1707 A69-22988

Impurities effect on plastic flow stress and activation volume as functions of strain, strain rate and temperature in molybdenum crystals
10 p1710 A69-23089

Recrystallization diagrams of commercially pure Mo and Mo alloyed with Fe, Co or Fe plus Ni, noting additions effect on recrystallized grain size
10 p1715 A69-24012

Chromium-rhenium-boron ternary system using X ray diffraction and microstructure analysis, establishing phase equilibria at high temperatures
10 p1715 A69-24054

Zirconium-rhenium-carbon ternary system, determining resistivity of melted alloys, discussing eutectic quasi-binary compounds
10 p1715 A69-24055

Diffusion constant of Ni in Ti alloys with Al, Mo and Nb, considering beta phase
11 p1902 A69-24274

Acicular crystals growth and dendrites orientation in Mo ingots prepared by electron beam and arc melting analyzed by X rays
11 p1903 A69-24538

Gadolinium-cobalt system investigation by X ray diffraction thermoanalysis and metallography for inter-metallic compounds, noting structure transformation and homogeneity
11 p1903 A69-24574

Microsectioning technique applied to measurement of diffusion coefficients of Cr 51 in polycrystalline Nb at 1220-1766 K temperature range
11 p1903 A69-24577

Stress-strain relation in crystalline media for pure tension and elongation epsilon several times conventional elastic limit, verifying by testing Al alloy [ONERA-TP-695]
11 p1975 A69-24754

Temperature and stress dependence of microstrain and microyielding in polycrystalline W for range of impurities and dislocations, considering transition to macrostrain
11 p1905 A69-25183

Dislocation structure and surface deformation markings correlation analyzed on fatigued Al electron microscope foils
11 p1905 A69-25184

Molybdenum additive role in deformed carbonylic nickel recrystallization process
12 p2114 A69-26454

Temperature effect on tensile brittle fracture stress of polycrystalline tungsten
12 p2116 A69-27135

Molybdenum dislocation velocity and macrodeformation, noting thermal double kink mechanism inconsistencies and strain role in strain-rate relationship
13 p2276 A69-27392

Surface resistivity oscillatory dependence on magnetic field in single crystal metals, examining electron trajectories, energy levels and wave functions
13 p2316 A69-27641

Beryllium single crystals c axis compression behavior at three purity levels under hydrostatic pressures
13 p2279 A69-27760

Grain size effect on room temperature tensile strength of alpha-titanium analyzed by tensile testing and electron transmission
13 p2280 A69-27766

Polycrystalline Re high temperature plastic deformation during tensile creep, including activation energy and substructure dislocation study
13 p2280 A69-27767

Grain size and deformation velocities effects on plasticity of dispersion hardened alloy
13 p2283 A69-28489

Internal friction, Young modulus and resistivity measurements for stage I interstitials in electron irradiated tungsten
13 p2284 A69-28682

Book on defects and radiation damage in metals covering collision cascades, point defects clustering and impurities behavior
14 p2503 A69-28889

Electron work function profile determined for polycrystalline Mo and W single crystals with and without Cs vapors by emission microscope and photomultiplier
14 p2507 A69-29276

Monograph on mechanical behavior of crystalline solids at elevated temperatures, discussing creep properties of metals, solid solutions and two phase alloys
14 p2465 A69-29749

Macrostructure of steel, zinc and aluminum ingots using electromagnetic vibrations during crystallization, for stress relieving of welded structures
14 p2456 A69-29916

CoO complex defects indicated by negative enthalpy of formation, considering isobaric electrical conductivity measurements at various temperatures and oxygen pressures
14 p2508 A69-29925

Strain aging of polycrystalline Nb containing interstitial impurities as function of temperature, discussing interstitials role in recovery substages
15 p2636 A69-30194

W single crystals cleavage cracks by spark discharge, showing effective surface energy dependence on crack initiation and propagation temperatures
15 p2637 A69-30226

Heat resistant fiber composites produced by oriented eutectic crystallization in Co and Ni quaternary alloys [ONERA-TP-710]
16 p2799 A69-31765

Oxygen adsorption on Mo single crystals /100/ surface as function of temperature using low energy electron diffraction
16 p2748 A69-32795

Creep behavior of oriented Al bicrystals, emphasizing intergranular creep types and crystal orientation
17 p2985 A69-32906

Creep tests on polycrystalline Be and Be alloy at various temperatures and stresses
17 p2986 A69-32912

Thermionic emission parameters for faces of W-Re, Mo-Re and Ta-Mo single crystals determined by Richardson method of straight lines
17 p3015 A69-33630

Alkali halide crystals destruction by laser radiation for estimating optical strength, discussing impact ionization hypothesis
18 p3152 A69-35157

Group 7A and group 8 elements alloying effect on Cr dislocation structure and mechanical properties, discussing ductile-brittle transition temperature and electronic theory
18 p3160 A69-35452

Recrystallization limit effects on coarse grain growth in aluminum alloys extruded sections, studying roles of additives, extruding temperature and heat treatment duration
18 p3160 A69-35472

Crystal twinning directional effect on Mg alloys tensile yield strength degradation, investigating recovery methods
19 p3341 A69-35583

Molybdenum single crystals deformation in direct shear, determining stress temperature dependence and critical regions for various slip systems
19 p3342 A69-35811

Surface grains orientation effect on fatigue behavior in polycrystalline Al, noting strain hardening role in failure
20 p3561 A69-37597

Fe crystals dislocations dynamic behavior during plastic flow development, describing stress and temperature effects on dislocations propagation and interactions
21 p3833 A69-38569

Structural changes during annealing of W and Mo single crystals deformed by rolling, using X ray diffraction topography methods with two crystal spectrometer
21 p3742 A69-38583

Dislocations multiplication and rearrangement structure in thermal fatigue of Mo single crystals produced by electron beam zone melting
21 p3746 A69-39162

Dislocation structures in Nb-Ti alloys formed after annealing
21 p3747 A69-39163

Field emission and field-ion microscopic adsorption studies, discerning major states in chemisorption for metal-crystal surfaces
22 p3895 A69-39898

Bcc metals strengthening and alloy softening mechanisms, studying temperature and additives effects
22 p3970 A69-40166

Electron spin resonance /ESR/ of polycrystalline Mo/V/ complexes with diprydil and phenanthroline, observing hyperfine interaction due to odd numbered isotopes
22 p3897 A69-40971

Thermal isolation characteristics of low conductance interstitial materials determined, using test apparatus of axially loaded radiation shielded cylindrical column in vacuum [AIAA PAPER 68-31]
23 p4239 A69-41889

Fcc metals higher order elastic constants calculated by Morse potential function, considering atomic interactions truncation and pressure derivatives
23 p4233 A69-42337

Linear elastic theory for calculating monovacancies entropy and energy of formation in metals
24 p4360 A69-42649

Mechanical properties and dislocation configurations and densities of Nb single crystals measured at various strain rates
24 p4332 A69-43030

High temperature anelastic effect in Mo single crystals ascribed to internal friction peak due to electronic interactions between dislocations and C interstitials
24 p4332 A69-43031

METAL CUTTING

Electrochemical grinding application to metal cutting of refractory alloys in aircraft jet engine overhaul [SAE PAPER 680662]
03 p0433 A69-13453

Pressure properties of fluorides and silicofluorides as cutting and grinding lubricants for titanium [ASLE PAPER 68-LC-20]
07 p1141 A69-19311

Finish turning cutting speed effects on titanium alloy surface layers
18 p3148 A69-34548

Cutting loads measured as function of cutting rate and cutting tool geometry during boring of Cr-Ni steel pipe blanks
21 p3731 A69-38878

Machine tools design for performing cutting operations within acceptable vibration limits
22 p3928 A69-40672

Automation of single pass electric spark machining of high alloy steels and hard alloys, including anodic-mechanical profiling, cutting and drilling
23 p4168 A69-41308

Digital computer systems for automating machine parts design main metal cutting operations, emphasizing optimal instrument usage, reliability, digital algorithm language and economics
23 p4169 A69-41952

METAL DRAWING

Metal strip angled profile shaping by sliding application of forces with draw plate, analyzing friction effect with thin plastic shell engineering theory
03 p0432 A69-12962

Cold drawing workability of Nb, Mo and Ta using dies with lubrication for metal sheets
03 p0452 A69-14124

Strain rate effect on structure and mechanical properties of rapidly stretched metals
06 p0941 A69-17122

Reversion and drawing techniques for ultrahigh strength ductile maraging steel wire without excessive deformation
13 p2278 A69-27412

Unstable metal deformation, discussing volume displacement in necking leading to fracture, homogeneous total deformation and torsion
17 p3053 A69-32987

METAL FATIGUE

Low cycle fatigue life of aluminum alloy in reversed biaxial bending
01 p0093 A69-10116

Cycle dependent fatigue hardening and softening of metals in terms of crystal structure and stress amplitude
01 p0165 A69-10133

Theory of fatigue crack growth crystal in metals in terms of coplanar dislocation arrays extended to oblique slip planes, discussing orientation
01 p0168 A69-10344

Surface fatigue significance in sliding wear studied from damage on copper single crystal using electron microscope techniques
01 p0085 A69-10368

Moisture effects on crack propagation in high strength aluminum alloys studied by fatigue tests
01 p0098 A69-10766

Low stress fracture criteria for large elastic structures and small brittle laboratory specimens below transition temperature
01 p0169 A69-10768

Substructures around fatigue cracks in fcc metals and alloys, noting relation between structural formation and crack propagation
02 p0260 A69-11826

Metal fatigue crack propagation mechanism, deriving basic laws for failure in high and low stress regions, determining material parameters
02 p0340 A69-12025

Ductile crack propagation speed relation to dynamic flow properties of metals analyzed using Dugdale crack model
02 p0343 A69-12283

Plastic fatigue life of steel under rotary bending, proposing fracture criterion based on strain amplitude for low cycle stress levels

02 p0346 A69-12421

Damping capacity and resistance to resonance fatigue of titanium and aluminum based steels and alloys

03 p0443 A69-13025

Fatigue and corrosion fatigue properties of aluminum alloys, noting elastic modulus, cyclic loading strength, corrosion resistance, etc

03 p0443 A69-13027

Spin tests to determine brittle fracture under plane strain, using cyclic thermal stress or hydrostatic pressure to generate fatigue crack in rotor blank

03 p0524 A69-13060

Dynamic tensile stress-strain curves for annealed Al, Cu and Fe at constant strain rates, describing experimental method

03 p0524 A69-13065

Dispersed hard particles effect on high strain fatigue behavior of nickel at room temperature

03 p0443 A69-13121

Heavy titanium carbide precipitation on fatigue slip zones of stainless steel, noting rupture produced crystallographic facets

03 p0447 A69-13605

Stability of ductility and fatigue strength of stainless steel under long time static loads in vacuum and in liquid lithium

03 p0450 A69-13912

Fatigue strength reduction of structural steels fatigued in rotating bending after tensile deformation

03 p0450 A69-13916

Torsion bar with two inertia masses attached used to determine damping capacity and torsional fatigue strength

03 p0431 A69-13917

Fatigue mechanism in fcc metals at ultrasonic frequencies, comparing microstructural changes in copper and alpha-brass

04 p0613 A69-14448

Inelastic strain measurement in metals during cyclic loads by impact tester

04 p0674 A69-14539

Delayed rupture strength of metals and welded joints at fixed stress level

04 p0674 A69-14541

Heat treatment and shot peening effects on Al alloy fatigue strength and fine crystallographic structure

04 p0614 A69-14576

Residual gas effect on fatigue behavior of pure iron subjected to alternating bending load in ultrahigh vacuum

04 p0616 A69-14846

Random cumulative damage theory for fatigue failure of steel under sinusoidal loading taking into account randomness of time to failure and possession of memory

04 p0680 A69-15154

Cold working considered for decreasing fatigue crack propagation rate in thin duraluminum sheets with various plastic deformations

04 p0681 A69-15170

Thermal stress in fiber reinforced metals, assuming Young modulus variable when thermal stress is applied during heating and cooling

04 p0682 A69-15393

Linear cumulative damage theory defining low cycle fatigue region of classic S-N curve, providing biaxial strain mode by centrifugally loading rotors [ASME PAPER 68-WA/MET-8]

05 p0838 A69-16151

Fatigue crack growth in notched samples of aluminum alloy subjected to cyclic compressive loading, noting residual tensile strength at notch root [ASME PAPER 68-WA/MET-16]

05 p0838 A69-16154

Crack formation and propagation in metallic materials under dynamic fatigue loading, noting dislocation during work hardening

05 p0781 A69-16542

Fatigue crack propagation in machine parts under cyclic loading

05 p0842 A69-16543

Fatigue life reduction in Al alloy specimens with stress concentrations due to notches

05 p0843 A69-16696

Fatigue performance of composites consisting of W or Mo helical coils embedded in Cu matrix, discussing evaluation from microstructural behavior

06 p0940 A69-16951

Strain near fatigue crack tip in notched steel plates measured by copper electroplating method

06 p1022 A69-17198

Semiconductor device failure modes temperature dependence, discussing bonds, metallization and packaging

06 p0894 A69-17218

Fatigue hardening in fcc metals, discussing dislocation distribution in unidirectionally deformed single crystals

06 p0944 A69-17503

Collection of papers on metal fatigue theory and design

06 p1024 A69-17525

GP zones study in aluminum alloys during fatigue process by electrical measurement, discussing resistivity, cyclic deformation, loading and unloading

07 p1166 A69-18962

Fatigue damage of metals under cyclic stressing, noting deformation modes dependence on stress amplitude and material type

07 p1166 A69-19215

Metal fatigue simulation by Monte Carlo method, showing programmed fatigue tests in form of life distribution functions

07 p1233 A69-19314

Fatigue tests on steel of various diameters using standard and accelerated methods

07 p1233 A69-19315

Forging and heat treatment parameters effect on Ti-Al-V alloy low cycle fatigue properties, relating crack initiation and propagation rates to microstructures [ASME PAPER D8-24.4]

07 p1169 A69-19669

Breakdown regularity of metals having different crystal structure, considering metal lifetime dependence on stress magnitude and test temperature

08 p1328 A69-19793

Fatigue characteristics of unidirectionally solidified Al-intermetallic aluminum nickel eutectic alloy consisting of discontinuous Al-Ni intermetallic whiskers in Al matrix

08 p1329 A69-20006

Vibration characteristics of rectangular plate with fatigue crack and subject to tensile load, applying results to crack propagation in fuselage panels

08 p1413 A69-20399

Ductile fracture behavior of two phase stainless steel examined by straining smoothed and notched tensile and Charpy impact specimens

08 p1333 A69-20574

Sample changer for metal fatigue studies under ultrahigh vacuum conditions, noting successive testing in same vacuum

08 p1302 A69-20877

Aircraft structural aluminum alloy fatigue life, considering atmospheric relative and absolute humidity

09 p1521 A69-21390

Methanol-water-chloride solutions effect on titanium alloys failure time, noting effect of changing water volume on cracking

09 p1521 A69-21400

Heat resistant nickel alloys static and dynamic properties at high temperature, creep-fatigue interaction, etc

09 p1523 A69-21609

Fretting fatigue prevention in Al alloys, noting strength reduction due to fretting

09 p1526 A69-22148

Titanium alloy castings fatigue behavior at room and elevated temperatures in annealed and heat treated conditions [ASME PAPER 69-GT-22]

09 p1619 A69-22497

Oxidation effects on creep and fatigue properties of metals noting time and temperature roles

10 p1708 A69-22998

Aluminum alloy thin sheets with central transverse fatigue cracks subjected to increasing static loads to fracture, investigating crack tip deformation

10 p1709 A69-23056

Strain fatigue mechanism of crack propagation in ductile metals, considering distribution of plastic cohesive stresses at crack tip

10 p1795 A69-23059

Substructural changes during fatigue due to stacking fault energy variations related to morphology of fracture surface in solid solution Ni-Co alloys

10 p1795 A69-23060

Geometry at tip of growing fatigue crack, measuring crack propagation rate and fitting data to nucleation theory

10 p1795 A69-23062

Electron fractography of aluminum alloy fatigue for intermetallic particles and inclusions effects on crack growth

10 p1795 A69-23065

Fatigue crack propagation in cylindrical shells under fluctuating internal pressure, considering stress intensity factor

10 p1795 A69-23066

Existing predictive methods for determining high temperature low cycle fatigue life reexamination based on experiments on nickel

10 p1796 A69-23068

Mechanical model for investigating macrobehavior of cyclic fatigue crack propagation in plates of several metal alloys

10 p1796 A69-23072

High temperature effect on fatigue deformation and fracture of nickel base superalloy in single crystal and columnar grained forms

10 p1709 A69-23073

Debonding mechanism role in fatigue crack development in notched aluminum alloy samples using optical and electron microscopy

10 p1710 A69-23076

Plastic crack propagation near fatigue fracture surface during tensile mode crack growth in copper single crystals by transmission electron microscopy

10 p1797 A69-23077

Fatigue crack propagation and crack tip stresses measurements in tensioned cracked panels subjected to acoustic loading

10 p1797 A69-23078

Dislocation substructure near fatigue fracture surface during tensile mode crack growth in copper single crystals by transmission electron microscopy

10 p1797 A69-23079

Low cycle fatigue fracture behavior at high temperatures, noting fatigue crack behavior and crack density concept

10 p1797 A69-23081

Mechanical model for fatigue crack propagation assuming propagation as function of material strain cycling at crack tip

10 p1797 A69-23082

Low cycle fatigue of metals under biaxial strain, considering specimen life and strain amplitude correlation

10 p1797 A69-23083

Environment influence on fatigue crack propagation mechanisms in aluminum alloys in vacuum, ambient air and distilled and sea water

10 p1710 A69-23084

Aluminum plates bending fatigue tests, discussing mechanical properties, structural failure, grain size, strain hardening, stress-strain-time relations, heat treatment, etc

10 p1711 A69-23356

Cyclic stress-strain and fatigue behavior in aircraft structural metals, discussing hardening and softening in aluminum alloys, steels and titanium alloys

10 p1714 A69-23981

Cyclic stress-strain curve of metals determined using companion specimens, step strain tests, monotonic tension and hysteresis loop analysis

10 p1715 A69-23982

Cyclic deformation resistance and fatigue damage accumulation in aluminum alloys, aircraft steels and titanium alloys

10 p1715 A69-23983

Metal fatigue at elevated temperatures concerning viscosity, energy loss and stress, strain and temperature cycling

10 p1803 A69-24043

Macroscopic states of stress criteria for plastic flow initial yielding, plastic flow and brittle fracture of ductile and brittle metals

11 p1975 A69-24671

Tresca shear stress fatigue failure criterion and experimental data for combined bending and torsion acting out of phase

11 p1984 A69-25140

Dislocation structure and surface deformation markings correlation analyzed on fatigued Al electron microscope foils

11 p1905 A69-25184

Aircraft structures fatigue life determination based on Kordonskii method, comparing steel tests result with linear summation theory

11 p1987 A69-25345

Fcc metals cyclic deformation and fatigue dependence on cross slip of screw dislocations, considering strain hardening and crack propagation

11 p1906 A69-25389

Compressive and tensile creep of metals, discussing compressive stress, void nucleation, barreling specimen shape and platen lubrication

12 p2175 A69-25836

High speed deformation of metals under pulse loading, noting role of maximum stress magnitude and deformation characteristics

12 p2113 A69-26043

Fatigue life of Al alloy thin laminated sheets, considering cyclic frequency and temperature effects

12 p2180 A69-26359

Energy dissipation and fatigue in metals under cyclic static loads, determining logarithmic decrements of vibrations and Bauschinger effect

12 p2181 A69-26612

Fatigue crack propagation and fail-safe design for stiffened large Al alloy panels with crack stoppers, using residual strength analysis method

12 p2186 A69-26835

Metal fatigue mechanisms - Conference, Brno, Czechoslovakia, June 1968

12 p2116 A69-26911

Tension-compression fatigued alpha Ti twin formation contribution to fatigue damage during cyclic loading

12 p2116 A69-26913

Fatigue crack initiation and propagation correlation with substructure formation by static and alternating stresses in Al

12 p2188 A69-26915

Fatigue fracture surfaces in cast steel and Al alloys, studying fracture morphology, crack propagation rate and striation spacing with microfractographic methods

12 p2116 A69-26916

Oxygen content effect on tension-compression fatigue of alpha Ti alloys, discussing internal damage associated with twin formation

12 p2116 A69-27134

Microscopic mechanisms in fracture surface markings, using electron fractography cleavage, fatigue, stress corrosion cracking, microvoid coalescence and tear ridge formation

13 p2274 A69-27224

Structural modes of fracture, analyzing brittle, ductile, fatigue and stress corrosion fractures using fractography

13 p2274 A69-27226

Metal fatigue in Al alloys subjected to stress cycles, determining macrocracks propagation stages

13 p2359 A69-27291

Ambient air pressure effects on fatigue crack growth rate in strain hardened aluminum

13 p2276 A69-27393

Low cycle fatigue crack initiation in Ti-6Al-4V at room and high temperatures and in aqueous salt environment

13 p2278 A69-27413

Aluminum alloys ductile fatigue striations, considering dependence on grains crystallographic orientation and vacuum effect

13 p2278 A69-27415

Fatigue crack propagation in aged aluminum alloy sheets, studying specimen geometry and stress level variations effects

13 p2280 A69-27835

Copper and aluminum fatigue in vacuum and ultrahigh vacuum, discussing effects of hydrogen, nitrogen and oxygen pressures

13 p2280 A69-28088

Sinusoidal or random excitations equivalence from point of view of rupture risks, considering industrial applications

13 p2370 A69-28602

Physical limit model of fatigue in metals and alloys to determine stress producing plastic flow in surface layer

14 p2461 A69-28913

Linear cumulative damage theory defining low cycle fatigue region of classic S-N curve, providing biaxial strain mode by centrifugally loading rotors [ASME PAPER 68-WA/MET-8]

14 p2535 A69-29438

Titanium alloys fatigue properties at various temperatures using notched and unnotched specimens, considering vibrational fatigue strength and notch sensitivity

15 p2637 A69-30227

Heat treatment and shot peening effects on Al alloy fatigue strength and fine crystallographic structure

15 p2638 A69-30278

Structural fatigue-inducing random load spectrum analyzed and computed for laboratory simulation

15 p2705 A69-30363

Room temperature fatigue crack propagation rates for high strength aluminum alloy in heavy water environment compared with argon and distilled water

15 p2640 A69-30815

Plastic expansion in metals due to alternating torsional and static tensile loading

16 p2875 A69-32291

Short life fatigue data for metals, noting applications in design

17 p3052 A69-32978

Rotating bending fatigue tests on aluminum alloys based on statistical analysis for material strength

17 p3052 A69-32979

Load carrying capacity of thin steel plates fatigued by cyclic shear buckling

17 p3052 A69-32980

Fatigue cracks initiation and propagation studied by surface plastic replication method, noting metallographical and continuum mechanical factors influence on low carbon steel

17 p3052 A69-32981

Cumulative metal fatigue damage gauges, analyzing resistance change properties by using strain amplitude tests

17 p3053 A69-32989

Fatigue crack growth rates in stainless steel at elevated temperature measured as function of oxygen pressure in resonant fatigue machine

17 p2987 A69-33074

Low cycle fatigue behavior prediction for 304 and 306 stainless steels based on temperature and strain rate ratio to tensile ductility

17 p2987 A69-33079

Fatigue crack propagation in thin aluminum alloy plates under plane bending using microscopic surface observation and electron fractography, noting role of aging conditions

17 p3061 A69-33677

Damping, fatigue and optimal heat treatment of Cr-Ni steel for compressor blades operating at temperatures up to 500 K

17 p2990 A69-33933

Mean stresses effect on fatigue strength by specimens vibratory/tensile mean stress diagram combining Goodman line and Gerber parabola merits with increased accuracy

17 p3067 A69-34197

Testing machine for in vacuo tensile testing of tubular metallic specimens at high temperatures and low pressures

18 p3117 A69-34604

Nondestructive eddy current testing of chromium steel for early stage fatigue damage of aircraft components

18 p3136 A69-34777

Low cycle fatigue leading to failure on AISI 321 stainless steel as function of elevated temperature and straining frequency

18 p3219 A69-34834

Thermal stress in fiber reinforced metals, assuming Young modulus variable when thermal stress is applied during heating and cooling

18 p3223 A69-35021

Ti-6Al-4V alloy general and stress corrosion behavior in Freon environments, discussing fracture mechanics

18 p3150 A69-35411

Collection of articles on physical nature of plastic deformation and failure of metals

18 p3159 A69-35451

Fatigue characteristics of Al alloys by fatigue tests with complex stress patterns, finding secondary stress wave effects

19 p3342 A69-35772

Nickel base superalloy high temperature fatigue properties, comparing crack initiation and propagation in directionally solidified and conventionally cast forms

19 p3342 A69-35919

Titanium alloys wear and fatigue resistance as functions of time and temperature of nitriding by purified nitrogen

19 p3347 A69-36743

Electroplating method for local stress concentrations determination, discussing measurement techniques, metal fatigue failure prediction, etc

19 p3441 A69-36751

Stress corrosion cracking of metals related to surface phenomena involving surface reaction layer ruptures or selective electrochemical dissolution along defects

19 p3349 A69-36885

Dislocation effects on stress corrosion of metals, discussing behavior of porous structure and metal/corrosion film interface under applied stress

19 p3349 A69-36886

Stress corrosion cracking in stainless steel foils correlated with stacking fault energy and ordering, emphasizing environmental forming tendencies

19 p3350 A69-36892

Aluminum 7 percent Mg alloys stress corrosion cracking, presenting aging kinetics and depletion zone dislocations at grain boundaries

19 p3350 A69-36896

Titanium alloys stress corrosion cracking (SCC) from metallurgical-mechanical viewpoint, discussing phase transformations, dislocation arrangements, crack propagation, etc

19 p3352 A69-36902

Metallographic analysis of stress corrosion cracking of Ti alloys of Al and Sn in aqueous magnesium chloride solutions, noting cleavage process

19 p3352 A69-36903

Oxygen environment influence on Inconel X-750 surface deformation and cracking during fatigue related to chemisorption and oxidation

20 p3558 A69-36966

Apparent dynamic modulus and damping under multilevel loading during fatigue cycling to estimate stainless steel specimens cumulation fatigue lives

20 p3620 A69-36997

Soviet monograph on metal fatigue in aircraft structures, discussing effects of temperature, loading, residual stresses, surface finish and contact corrosion

20 p3622 A69-37231

Weld defect data analysis in relation to aerospace structure performance, emphasizing effect on fatigue behavior and acceptance standard [SBAC PAPER 17]

20 p3550 A69-37450

Electron beam welding for fabrication of aircraft structures, discussing fatigue strength of Ti and Al alloys and marking and low alloy steels [SBAC PAPER 12]

20 p3550 A69-37456

Surface grains orientation effect on fatigue behavior in polycrystalline Al, noting strain hardening role in failure

20 p3561 A69-37597

Fatigue crack initiation in relation to contact stresses due to fretting, studying causes of strength reduction and crack inclination to surface

20 p3563 A69-38110

Mean stresses effects on fatigue crack initiation and propagation under controlled fretting slip amplitude

20 p3563 A69-38111

Beta working effect on Ti alloy mechanical and fatigue properties [ASM PAPER D8-24.3]

20 p3564 A69-38136

B fiber reinforced Ni failure characteristics at high temperature, discussing plastic deformation and matrix role in crack inhibition

21 p3743 A69-38616

Stress concentration and surface strain hardening effects on fatigue strength of refractory alloy specimens with and without cut

21 p3745 A69-38875

Ti-Al-V forgings macro /prior beta/ grain size and in-process thermal treatment effects on fatigue life [AIME PAPER S69-2]

21 p3732 A69-39470

Thermal fatigue combined with mean stress, reversed mechanical stress, low cycle fatigue and static creep in stainless steel

21 p3847 A69-39813

Impact effects on metallic materials deformation and wear, considering impact force, time and coefficients, penetration depth, deformation energy, etc

22 p3966 A69-39876

Metal fatigue crack nucleation at stresses below static fracture strength, determining local plastic strain under cyclic loading

22 p4041 A69-40053

Uniaxial tensile testing machine to operate under combined creep and fatigue conditions for studying dislocation structure changes in metals and alloys at high temperature

22 p3926 A69-40441

Titanium stress pin with headed straight-shank pin and collar for reducing fatigue stress around holes

22 p3957 A69-40832

Partial differential equation for creep process in plane stressed metals, interrelating strain, rate, stress tensors, temperature and time

22 p4048 A69-41268

Alpha Ti fatigue properties, studying internal precracking effects in alloys of various tensile strength

23 p4178 A69-42360

Stress corrosion cracks propagation from fatigue precrack in Al alloy exposed to organic liquid environments

23 p4178 A69-42452

Cylindrical steel specimens high strain rate tensile tests, using Malvern theory for ideal elastoplastic and work hardened materials

23 p4236 A69-42529

Notch effect on corrosion fatigue behavior of high strength Al alloy under bending and direct stresses

24 p4330 A69-42553

Structural changes in subsurface layer and surface microgeometry factors of metal fatigue failure, explaining crack formation and propagation

24 p4395 A69-42559

Room temperature tensile tests determining failure modes and defect influence on diffusion welds of unalloyed Ti, using electron microscopy and fractography

24 p4331 A69-42939

Porosity and inclusions effects on Al arc weld fatigue properties at ambient and cryogenic temperatures
24 p4331 A69-42940

Low cycle fatigue strength tested on notched and unnotched round steel bars, distinguishing between fatigue lives for crack initiation and propagation
24 p4404 A69-43627

Rotational bending fatigue strength of plain and notched conventional and maraging steels, evaluating gas nitriding effects
24 p4335 A69-43802

METAL FILMS

Vortices coupling between superposed superconducting tin films as function of perpendicular magnetic field, primary current and temperature
01 p0135 A69-10014

Quasi-static Kerr magneto-optic observation and procedure to predict results of dynamic flux reversal in thin Ni-Fe films
[IEEE PAPER 11.7] 01 p0138 A69-10716

Wall streaming, creeping and parade motion in Ni-Fe films excited by hard axis pulses
[IEEE PAPER 11.8] 01 p0138 A69-10717

Soviet book on structure of thin metal films covering electron microscopic and electronographic studies, crystallization and heat treatment effects
01 p0140 A69-11106

Homogenous mechanical stresses in amorphous and crystalline gallium films during vacuum deposition and annealing
01 p0141 A69-11420

Electrical properties of vacuum deposited Bi, noting association of negative temperature coefficient of resistance in Bi thin films with grain-boundary effects
02 p0296 A69-11878

Photoelectric effect of thin gold films on silver and quartz substrates, analyzing work function dependence on thickness of deposited metal
02 p0300 A69-12630

Photoelectric effect of thin gold film under electric field, noting work function dependence on film thickness exhibits extremum
02 p0300 A69-12631

Spectrum and yield of emitted electrons resulting from passage of heavy ions through metal films
03 p0471 A69-13164

Electrical resistance temperature dependence below room temperature for polycrystalline epitaxially grown Au and Ag films, noting effects of alpha irradiation
03 p0486 A69-13582

Brittle surface films role in stress-corrosion phenomena in various environments
03 p0448 A69-13873

Superconductivity of electron beam evaporated tungsten films by X ray and electron diffraction techniques, discussing temperature dependence of energy gap
04 p0640 A69-14447

Selective etching process for microminiaturization of special circuits for aerospace
05 p0736 A69-16753

Barium, oxygen and BaO adsorption influence on Mo and Ti thin films conductivity and work functions
06 p0978 A69-16900

Passivated metal semiconductor IMPATT diode for microwave CW oscillation
08 p1286 A69-20862

Ag-GaAs Schottky barrier photodiodes, describing fabrication and use as UV radiation detectors
09 p1462 A69-21334

Presprayed metal films influence on visibility and contact resistance of GaAs prior to fusing in Sn, In and lead contacts
10 p1748 A69-24214

Electrodeposition of Te-containing Permalloy films with uniaxial magnetic anisotropy, noting electrolyte composition and film structure
11 p1935 A69-24332

Hetero-epitaxial germanium films on GaAs by germanium condensation from molecular beams in vacuum, obtaining p-type conductivity
11 p1938 A69-25033

Absorption characteristics of thin metallic films in standing light wave for mode selection and conversion in lasers
12 p2104 A69-26024

Physics of metal films - Conference, Kiev, October 1966
12 p2143 A69-26456

Vacuum evaporation effects on internal macrostresses in deposited metal films based on X ray analysis, showing substrate temperature contribution
12 p2143 A69-26457

Scale effect on gold films electrical conductivity, analyzing film thickness and electron parameters of mean free path, concentration and surface reflection
12 p2143 A69-26459

Gases effect on electrical conductivity of vacuum deposited thin films of Cr, Be, Ni, Au and Ge at different thickness and low pressure
12 p2143 A69-26460

Avalanche Schottky barrier photodiodes fabricated by plating GaAs with thin Pt layer and forming proton radiation guard ring, discussing gain bandwidth and SNR
13 p2226 A69-27195

Gold-underlayer film combinations adhesion to oxide substrates, describing adhesion changes as function of Au and underlayer film thickness, time, environment, etc
13 p2321 A69-28007

Electrical properties of electron beam evaporated Ti, Zr and Hf films as function of substrate temperature, material and film thickness
13 p2321 A69-28010

Resistivity, capacitance and dielectric loss measurements for diode reactive sputtering grown AlN films and film sandwich structures of Ta, Au and Al films
13 p2322 A69-28013

Adsorption of N, H, O and CO on thick vapor deposited Be films at room temperature
13 p2322 A69-28017

Effects of cold electron and light emission centers from dispersed Au films in electric field, as universal qualities characterizing dispersed metal films
14 p2504 A69-28992

Metal layers deposition, structure and properties obtained by H reduction of metal halides in vapor phase
14 p2462 A69-29209

Dry lubricant films of soft metals, self lubricating plastics and crystalline powders, noting design and tests
15 p2642 A69-30328

Metal film resistor reliability for conventional and space use, outlining guidelines for fabrication and quality control
15 p2628 A69-30847

Gas laser cutting of thin carbon films on thick pyrex glass and ceramic substrates
15 p2635 A69-31037

Electromigration role in material accumulation and depletion forming regions in Au film conductors, discussing regions origin from and correlation with thermal gradients along conductor
17 p2936 A69-32896

Single frequency lasers using thin metal film mode selection filters, discussing film properties and experiments with Ar ion and Nd-YAG lasers
17 p2982 A69-33399

He-Ne laser emission tuning with thin absorbing metallic film situated near reflecting mirror
20 p3555 A69-37730

Bloch wall motion along hard direction of Permalloy films due to fast rising hard-axis pulses
20 p3584 A69-38191

Metal semiconductor contact resistance determination from measuring voltage drop in current passing through contact and second metallic contact
21 p3780 A69-39046

Impurities effects on single crystal film formation of fcc metals on alkali-halide cleavage planes, stressing stacking fault energy importance
22 p3992 A69-39899

Dispersion relations for surface plasma oscillations in normal metals for single and multiple films taking into account retardation effects, noting dielectric function
22 p3992 A69-40419

Josephson currents interaction with LF surface plasmons in superposed thin dielectric and superconducting metal films, noting I-V characteristics
22 p3992 A69-40420

Physicochemical principles of electrolysis and electrodeposition of metals for obtaining bright galvanic coatings
22 p3958 A69-41262

Si integrated circuits single and composite layered metallization systems, comparing characteristics of various refractory and noble metals
24 p4286 A69-42761

Ge films formation by evaporation technique, discussing background O pressure effect
24 p4361 A69-43345

METAL FINISHING

NT ELECTROPOLISHING

NT SHOT PEENING

Metal electrolyte system for electrochemical machining in sodium chloride solution for achieving dimensional control
13 p2268 A69-27521

Military specifications validity with reference to reliability and metal finishing industry
15 p2722 A69-31120

METAL FOILS

Fatigue-damage evaluation system for transport aircraft, noting use of cumulative strain gauge that stores strain history
01 p0165 A69-10118

Photoelectric effect of thin gold films on silver and quartz substrates, analyzing work function dependence on thickness of deposited metal
02 p0300 A69-12630

Electron emission from metal foils used to study lifetime, concentration and mean ion energy of hot plasma
03 p0481 A69-14211

Smear out electron beam generation for experiments on weak plasma turbulence by passing beam through aluminum foils
04 p0636 A69-15020

Electron microscopic and microdiffraction study of structure of quenched and annealed titanium alloy foils at high temperatures
05 p0783 A69-16810

Fresnel formulas for surface plasma waves excitation by light in thin metal foil embedded between dielectric layers, discussing transmissive and absorptive resonances
08 p1372 A69-20290

Glass reinforced polyimide laminate fabrication, discussing metal foil laminates
09 p1530 A69-22363

Spontaneous martensite phase transformation in Ti-Cr alloy thin foils formed electrolytically
10 p1708 A69-22994

Dislocation structure and surface deformation markings correlation analyzed on fatigued Al electron microscope foils
11 p1905 A69-25184

Multifoil thermal insulation using oxide particle layer separation, discussing insulation heat transfer characteristics as function of source temperature and oxide particle size
14 p2539 A69-29213

Dislocation pattern in thin Mo foils deformed by hydroextrusion observed by transmission electron microscope
14 p2463 A69-29311

Thin foil penetration measurements for Fe microparticle impacts on metal and Mylar foils in space
15 p2641 A69-31339

Electron beam welding method for very thin foils, discussing welding of pinhole free Ni, Cu and stainless steel foils
17 p2977 A69-32854

Secondary recrystallization in cold rolled molybdenum foil as function of temperature using electron microscopy and diffraction
18 p3157 A69-35253

Multifoil thermal insulation for radiation shields from cryogenic temperatures to 3500 F, noting thermal conductivity
19 p3341 A69-35540

Manufacturing ultrahigh purity aluminum strip for cryogenic magnets, discussing ingot preparation, rolling, chemical milling and cleaning, arc welding, annealing and sampling
19 p3318 A69-35541

Polycrystalline nickel foil microstructure after explosive shock loading and heat treatments, using transmission electron microscopy
20 p3563 A69-38126

Solar wind sample collection, describing experiment to determine ion flux capture efficiency for various metal foils
23 p4205 A69-41539

Temperature dependence of equilibrium solid solubility of C in Au, Cu and Ag foils with respect to graphite
24 p4334 A69-43413

METAL FORGING

U FORGING

METAL FORMING

U FORMING TECHNIQUES

METAL FUELS

Composite modified cast-double-base rocket propellants with large proportions of metallic fuel and oxidizer, discussing application rocket propulsion
17 p3017 A69-33349

METAL-GAS SYSTEMS

Concentration changes in binary metal-gas solutions during simultaneous degassing kinetics and metal evaporation
09 p1528 A69-22732

Dissolved gases and carbon effect on transition temperature from plastic to brittle state of high melting metals including niobium and vanadium
10 p1715 A69-24011

Desorption of hydrogen and methane from Al, Mg and Mb under room temperature tensile deformation in ultrahigh vacuum
23 p4176 A69-41541

METAL GRINDING

Pressure properties of fluorides and silicofluorides as cutting and grinding lubricants for titanium
[ASLE PAPER 68-LC-20] 07 p1141 A69-19311

METAL HALIDES

NT ALKALI HALIDES
NT ALUMINUM CHLORIDES
NT BERYLLIUM FLUORIDES
NT CALCIUM FLUORIDES
NT CESIUM IODIDES
NT CHROMIUM BROMIDES
NT IRON CHLORIDES
NT LANTHANUM FLUORIDES
NT LITHIUM FLUORIDES
NT MAGNESIUM CHLORIDES
NT NICKEL FLUORIDES
NT POTASSIUM BROMIDES
NT POTASSIUM CHLORIDES
NT SILVER HALIDES
NT SILVER IODIDES
NT SODIUM CHLORIDES
NT TITANIUM CHLORIDES
NT URANIUM FLUORIDES

Metal fluoride compounds as cathodes for use with mixed fluoride electrolyte /LiF-NaF-KF eutectic/ in thermal batteries
10 p1640 A69-23997

Metal layers deposition, structure and properties obtained by H reduction of metal halides in vapor phase
14 p2462 A69-29209

METAL HARDENING

U HARDENING [MATERIALS]

METAL HYDRIDES

NT BERYLLIUM HYDRIDES
NT LITHIUM ALUMINUM HYDRIDES
NT LITHIUM HYDRIDES

Spectra of hydrides of Mg 25 and Mg 26 in photo-sphere, searching for weak lines on basis of isotope shifts
03 p0515 A69-14035

Nondestructive detection of titanium hydride formation in threaded joints of Ti alloy pressurization tanks by neutron radiography
24 p4320 A69-42998

METAL IONS

Metal ionic reactions with weak chemical bond breaking and three body reactions forming molecular ions without bond breaking, discussing sporadic E deionization
01 p0071 A69-11168

Midlatitude sporadic E layer, examining hypothesis of wind action on metallic ions and metallic ion accumulation caused by gravity waves
01 p0072 A69-11173

Ionized metals emission lines intensity in chromosphere observed with coronagraph, determining hydrogen concentration
02 p0314 A69-11635

Coronagraphic determination of hydrogen concentration in luminescence regions of ionized metals in lower chromosphere
03 p0420 A69-13086

Alkali metal ion sources noting cesium ion engine development for space propulsion
[ECS PAPER 170B] 03 p0478 A69-13859

Collisional ionization cross section for Fe ions evaluated to estimate solar corona temperature
04 p0651 A69-14365

Coherent emission from rare earth ions in electro-optic crystals, noting oscillations and electric field modulation occurrence
09 p1514 A69-21339

Cs and K ions drift velocity calculations in vapors of own atoms under various electric field strengths effect
11 p1922 A69-24226

Stimulated emission cross section measurement of Nd ions in calcium tungstate using Edwards method
11 p1938 A69-25049

Microwave analysis of plasmas produced by laser beam on aluminum spheres, noting expansion velocity and electron density
11 p1930 A69-25287

Uranyl ions interaction with phospholipid and cholesterol monolayers, using surface pressure and potential measurements
11 p1832 A69-25641

Oscillator strengths and wavelengths of X ray and EUV transitions in highly ionized iron line spectra
13 p2326 A69-27554

Fe III line profiles and equivalent widths from spectrograms of zeta Cas and gamma Peg for Fe abundance, using model atmospheres
13 p2347 A69-27715

Coronagraphic determination of hydrogen concentration in luminescence regions of ionized metals in lower chromosphere
14 p2433 A69-28768

Fe and Ti line growth in 12 July 1961 solar flare spectrum, finding ionized titanium, neutral and ionized iron excitation temperatures
14 p2514 A69-29720

Fe II forbidden lines profiles and equivalent widths prediction for solar photospheric spectrum, deducing photospheric Fe abundance
16 p2854 A69-31652

Center limb observations of Ca II emission core interpretations, discussing chromospheric thickness effects on Doppler width
16 p2854 A69-31653

Coronal Fe ionization lines X, XIII and XIV photographed by UV coronagraph
16 p2847 A69-31661

Charge transfer cross section between mercury ion and Cs assessed, considering ion engine positive ion beam neutralization
16 p2835 A69-31895

Meteoritic elements ionization and loss mechanisms in E region, discussing roles of atomic oxygen and metal ions chemical reactions
16 p2780 A69-32313

MH alpha 328116 /Cygnus/ spectrum noting three Fe IV lines
16 p2866 A69-32815

Catalytic activity enhancement of complex Co/III/ compounds on standing explained by hydrated Co/II/ ions appearance
17 p2988 A69-33433

Tau-luminescence in thin gamma-colored and uncolored ruby crystals containing Cr ions measured, discussing ions absorption spectrum changes
19 p3335 A69-36166

Ammonium perchlorate experimental heat capacity data significance for rotational freedom of ammonium ion
20 p3484 A69-37344

Ultrasonic paramagnetic resonance investigations of Pr ions ground state energy levels in calcium fluoride
24 p4360 A69-42790

Elastic differential Li ion scattering cross sections on helium, nitrogen and oxygen
24 p4354 A69-43817

METAL JOINTS

NT SOLDERED JOINTS
NT SPOT WELDS
NT WELDED JOINTS

Fusion, resistance and pressure welding of titanium, discussing shielding, brazing, diffusion and adhesive bonding
02 p0253 A69-12064

Beryllium assemblies for aerospace and nuclear requirements, emphasizing braze joining structural components and effective manufacturing methods
[SAE PAPER 680651] 03 p0433 A69-13454

Glued metal joints under cyclic loading evaluated by change in short term strength as function of time at stress levels
04 p0605 A69-14540

Metal welding procedures for aircraft assembly, discussing weight, specific alloys and airframe components
04 p0608 A69-15483

Reliable fluid transmission systems by brazed joints, noting base and filler metals, fitting designs and various processes
09 p1507 A69-22333

Joining methods for fabricating thoria dispersion strengthened nickel and nickel chromium materials
09 p1509 A69-22342

Vacuum brazing technique for joining dissimilar metals without oxide and nitride film contamination
09 p1509 A69-22343

Metallic systems microbonding and joining reliability, noting electron and laser beam welding and deposited film connections
09 p1510 A69-22348

Thermal resistance of bolted or screwed sheet metal joints in vacuum, using method applicable to different materials and surface finishes
12 p2191 A69-26803

Adhesive metal bonding methods including continuous surface bonds, core to face bonds, lap joints and structural adhesive materials
14 p2454 A69-28847

Metal joints mechanisms in soldering, brazing and welding
14 p2455 A69-29344

Solar furnace for metal soldering, brazing and welding, using Pb-Sn solder for various joint types, twisted wires and rod-flange joining
16 p2793 A69-31818

Thermal silicone grease type filler materials for heat transfer across bolted or clamped sheet metal surfaces in electronic equipment for space applications
16 p2794 A69-32560

Wire-wrap solderless joints production technology in electronic equipment
16 p2763 A69-32579

Dielectric overcoating effects on electromigration Al interconnections, showing dependence on thickness and surface passivation
17 p2935 A69-32889

Vacuum and thermal environment long term influence on thermal resistance for Mg to aluminum and Mg to Mg bolted joints
[AIAA PAPER 69-628] 17 p3073 A69-33309

Diffusion bonding of metals, discussing interface joining processes and application to fluoric devices, jet engine servovalves and porous woven structures
17 p2978 A69-33374

Machined fastened joints for airframe structural parts, discussing fatigue life, strength and fastener hole preparation
19 p3319 A69-35553

Outdoor aging effects on unstressed Al-Al lap shear joints bonded by various polymeric adhesives
19 p3320 A69-35562

Various fasteners influence on fatigue life of bolted joints, noting high clamping force beneficial effect
24 p4325 A69-43438

F-111 sandwich structure adhesive joints glue-lines, describing thickness measurement techniques and acceptance criteria
24 p4403 A69-43461

METAL MATRIX COMPOSITES

Bonded Al-B metal matrix composite materials hot press fabrication and design, discussing temperature pressure time cycles and honeycomb sandwich structures
09 p1510 A69-22351

Materials, processing and testing variables effects on mechanical properties determined for metal matrix composites
[ASME PAPER 69-GT-23] 09 p1527 A69-22496

Aluminum-boron metal matrix composite joining methods including electron beam, resistance spot, plasma arc and fusion welding
[ASM PAPER W9-23.4] 14 p2455 A69-29449

Tensile and creep deformation of fiber reinforced composites consisting of Mg-Li alloy matrix with high strength precipitation hardening stainless steel wire
17 p2986 A69-33073

B-epoxy and B-Al composites compared for strength/weight and modulus/weight ratios, moisture absorption, corrosion resistance, projected costs, etc.
19 p3340 A69-35506

Forming, machining and joining characteristics of B-Al composite sheet metal material for space structures
19 p3318 A69-35507

Beryllium wire reinforced Al composites, discussing layup techniques and coated filament advantages
19 p3340 A69-35508

Silicon carbide coated boron fibers in aluminum alloy matrix, discussing tensile and structural properties of braze bonded specimens
19 p3340 A69-35509

Electroforming of Al matrix composites by codeposition of short graphite fibers, obtaining increased strength and elastic modulus
19 p3318 A69-35510

Filament reinforced metal matrix composites made by continuous casting process, discussing tensile tests results and production costs
19 p3318 A69-35511

Silicon carbide coated boron fiber reinforced /Bor-sic/ Al composites tensile strength and elastic properties
19 p3344 A69-35926

Metal fiber reinforced thermoplastic composites, analyzing unidirectional, crossed and random orientation cases taking into account adhesion efficiency between fiber and matrix
20 p3559 A69-37083

High porosity W-Ta matrix to thin solid Ta support structure joining technique involving vapor-deposited coating process

20 p3548 A69-37216

Boron fiber reinforced Al alloys spall failure and shock induced filament damage, using flyer plate technique

20 p3562 A69-37772

Diffusion bonding of Al and boron filament layers into continuous structural material, studying process variables including heat treatment and cross rolling effects

[AIME PAPER S69-6] 20 p3564 A69-38197

B fiber reinforced Ni failure characteristics at high temperature, discussing plastic deformation and matrix role in crack inhibition

21 p3743 A69-38616

Metal matrix compatibility of metal coated graphitized, silicon carbide and boron fibers, discussing fiber weakening processes

[ASM PAPER W9-20.1] 21 p3751 A69-38670

Al-B composite aircraft structure fabrication, discussing wingspan segment, resistance spot welding, hot forming of joggles, etc

[AIME PAPER S69-1] 21 p3732 A69-39471

BORSIC Al composites for propeller blades, discussing designs, fabrication methods and tensile test results

[AIME PAPER S69-4] 21 p3733 A69-39473

Stress-strain curves of W wires and of aligned composites of same wires in Cu matrix

21 p3845 A69-39709

Metal matrix fiber-reinforced composite materials joining by welding and brazing techniques

22 p3956 A69-40480

Cyclic stress tests of stainless steel fiber Al alloy matrix composite, including strain hardening and stiffness characteristics

24 p4331 A69-42925

Tensile strength improvement in Al-B composites by heat treatment to T6 condition and subsequent cold rolling

24 p4334 A69-43449

Al-B composites fracture toughness obtained by comparing notched tensile data with unnotched specimens

24 p4335 A69-43451

Tensile data and photomicrographs of explosively bonded metal matrix composites interfaces

24 p4326 A69-43452

METAL-METAL BONDING

Diffusion welding of AMS 4921 titanium, discussing premature pressure removal before completion of first joining stage

01 p0086 A69-10535

Phenolic and epoxy adhesives for metal-metal and honeycomb bonding, discussing cold cure adhesives for aircraft structures and aircraft floor sandwich design optimization

04 p0606 A69-14845

Explosive welding application to dissimilar metals and tube to tube plate welding, noting influence of detonation and sound bulk velocity

04 p0608 A69-15481

Helicopter rotor blades in metal sandwich bonding, discussing component parts assembly by adhesive films

07 p1143 A69-19731

Metal adhesive bonding strength behavior in satellite and space vehicle applications, noting effects of various space environment factors

12 p2101 A69-25858

Metal bonded and sandwich structures application to space vehicles, launch vehicles, rocket motors, ground equipment and balloon gondolas, noting inspection methods

12 p2101 A69-25859

Vacuum effects on resistance spot welds in aluminum, stainless steel and titanium alloys, noting X ray and tensile shear test results

12 p2103 A69-26622

Metallographic analysis techniques for high aluminum activity pack cementation coating on nickel-base alloy

13 p2282 A69-28163

Adhesive metal bonding methods including continuous surface bonds, core to face bonds, lap joints and structural adhesive materials

14 p2454 A69-28847

Explosive bonding technique, discussing choice of explosive and geometrical parameters to match material parameters

[ASME PAPER 69-DE-47] 14 p2454 A69-28849

Aluminum-boron metal matrix composite joining methods including electron beam, resistance spot, plasma arc and fusion welding

14 p2455 A69-29449

Diffusion bonding for leaktight joints in connectors using intermediate metal system of Au-Cu-Au

15 p2617 A69-30100

Outdoor aging effects on unstressed Al-Al lap shear joints bonded by various polymeric adhesives

19 p3320 A69-35562

Adhesive bonding of Al sheets for honeycomb sandwich material, using electrical conductivity to measure sheets age hardening progress during high temperature curing

19 p3321 A69-35565

High porosity W-Ta matrix to thin solid Ta support structure joining technique involving vapor-deposited coating process

20 p3548 A69-37216

Plasma metal spray coating for Al and Mg alloy aircraft components adhesive bonding repair technique compared to welding and electroplating

21 p3728 A69-38462

Aluminum alloy laminates composed of two metallogically bonded Al alloys of different composition

21 p3745 A69-38937

Stainless steel cladding of metals to combine desirable properties into composite, describing bonding, product types and treatment

21 p3745 A69-38937

Outdoor aging effects on unstressed adhesive-bonded Al to Al lap shear joints

24 p4319 A69-42932

Corrosion resistant bonding materials, discussing metal-to-metal adhesive primers, Al honeycomb core and foil finish

24 p4334 A69-43421

Polycarbonate and polysulfone thermoplastic bonding of Al and Ti in aircraft structures, discussing peel strength and stress crazing tests

24 p4326 A69-43459

METAL OXIDE SEMICONDUCTORS

MOSFET drivers for low current memory fabricated in 64 unit monolithic strips, discussing driver performance data

01 p0039 A69-10172

Output p-channel MOS transistor selection tree for display and information storage systems

01 p0039 A69-10173

Electron transfer through metal/semiconductor contact surfaces, measuring electrical conductivity on sintered cylinders with or without silver addition

02 p0296 A69-11790

Semiconductor center traps effect on characteristics of metal oxide semiconductor transistors

02 p0299 A69-12183

Silicon nitride gate insulator in metal-insulator-silicon /MIS/ devices, noting sandwich structures with thermally grown oxides removes limitations

02 p0299 A69-12244

Radiation resistance of MOS transistors noting relationship with thermal stability, gate oxidation and metals used

02 p0221 A69-12468

Wafer chip assembling technique for high density interconnection of silicon devices in large monolithic electronic systems, noting application to MOS shift register

02 p0222 A69-12472

MOST devices characteristics at cryogenic temperatures, studying variation in gain over audio frequency range

03 p0405 A69-13642

Relaxation effect in epitaxial silicon MOS structures, formulating differential equation for doping distribution in epitaxial layer

03 p0490 A69-13947

Substrate terminal current anomalous enhancement observed in n-channel Si MOS transistors beyond pinch-off

04 p0574 A69-14348

Voltage variable resistor MOST, noting channel resistance controllability

04 p0574 A69-14351

Device and logic/system designers and design aids interaction, emphasizing engineering trends in large scale integration area using MOS arrays

04 p0568 A69-15356

MOS GP computer suitable for navigation applications

04 p0568 A69-15357

Semiconductor memory units, considering bipolar, p channel MOS and complimentary MOS chip technologies

04 p0569 A69-15362

Freeze-out characteristics of MOS varactor, noting impurity effects and compensation

05 p0806 A69-15809

Electric field effects on thermal annealing of electron irradiation damage in p-channel MOSFET device

05 p0733 A69-16562

MOSFET fabrication by ion implantation using gate metal as mask, noting source and drain alignment with gate and low feedback capacitance

05 p0734 A69-16563

Physical and physicochemical properties of anodic silica obtained by silicon oxidation in organic bath, discussing possible applications

05 p0810 A69-16589

Neutron radiation effects on MOSFET, presenting model for neutron produced ionization in oxide layer

06 p0976 A69-16875

Gamma radiation effects on gate threshold voltages in modified oxide insulators in MOS structures

06 p0976 A69-16876

Electron radiation damage in MOSFET devices using bias temperature treatments

06 p0976 A69-16877

Interface states effects on characteristics of p-channel MOS transistors

06 p0979 A69-17117

Audio frequency noise in p channel MOST at cryogenic temperatures, noting trap contribution

06 p0979 A69-17151

Refractory metal silicon device technology noting high temperature diffusion masking properties for possible use in MOSFET technology

06 p0930 A69-17152

Immobile space charge in MOS semiconductors as function of external voltage

06 p0979 A69-17153

Two section model of saturation drain conductance of MOS transistors

06 p0893 A69-17155

Metal oxide semiconductor random-access memories, discussing large scale integration and static and dynamic circuits chip size

06 p0894 A69-17203

MOS technique applied to fabrication of integrated monolithic miniature circuits

07 p1099 A69-18494

P-n channel MOS triode fabricated by doped-stepped-oxide method, obtaining p-channel enhancement

07 p1100 A69-18622

Substrate bias influence on AC characteristics of MOS transistors used in variable resistor region

07 p1102 A69-18860

Metal oxide semiconductor circuits with higher orders of complementarity for performing multiple electronic functions, noting I-V characteristics and effects of bias

07 p1104 A69-18887

MOS technology developments for higher speeds in logic circuits

07 p1113 A69-19765

Flip-flops built with complementary symmetry MOS, discussing power, noise and load stability due to n and p channel series transistors

07 p1113 A69-19766

Adapter circuits for MOSFET electrical properties measurement

07 p1113 A69-19780

MOS transistor logic circuit performance optimization through component geometry and feed voltage

08 p1280 A69-19977

MOS transistor equivalent circuit for computer aided calculations with IMAG I program, noting versatility of model

08 p1280 A69-19978

Magnetoelectric characteristics of inversion layers below gate region in transistors, noting Hall mobility

08 p1372 A69-20460

Metal oxide semiconductor technology and applications, discussing gates, analog computers, switching circuits and inverters

08 p1286 A69-20833

Ionizing radiation effects on space charge of MOS devices, showing electron-hole pairs within oxide and electron injection from cathode

08 p1373 A69-20864

HF excess noise and equivalent circuit representation of MOSFET with n-type channel, noting local mobility fluctuations effect

09 p1463 A69-22094

- Electronic systems partitioning in preparation for MOS large scale integration for system performance and cost improvement
09 p1466 A69-22451
- Supplementary bibliography of papers on metal insulator semiconductor theory and technology
10 p1743 A69-23169
- Positive space charge buildup produced in silicon dioxide by low energy electrons as function of beam energy and oxide thickness
10 p1743 A69-23172
- N enhancement silicon MOST saturation current as function of temperature
10 p1743 A69-23175
- Transient response of MOS capacitance caused by mechanisms dependent on electric field distribution between silicon and oxide
10 p1744 A69-23176
- Interfacial stress between thermally grown silicon dioxide and single crystal silicon correlated with oxide compressive strength
10 p1744 A69-23177
- Interfacial charges in MOS transistors determined as function of surface potential by measuring channel conductance as function of temperature
10 p1744 A69-23178
- Surface charge exchange in metal oxide silicon capacitors generated at low temperatures by surface state free carrier trapping
10 p1744 A69-23179
- Silicon single crystal substrate, preoxidation, oxidation and low temperature heat treatment effects on MOS transistor compared with Silicon-Silicon dioxide interface characteristics
10 p1665 A69-24051
- Drift and tunnel effect of MOS transistors under ionizing electron and X ray irradiation, considering fabrication, electrical characteristics and D-2 satellite tests
11 p1848 A69-24873
- Silicon nitride as ambient alkali barrier liner analogous to silicon carbide in MIS devices for thermal growth of silicon oxide
12 p2142 A69-25935
- Beryllium oxide semiconductor thermistor for temperatures to 2500 K, discussing construction materials and test results
12 p2092 A69-26478
- LF generation-recombination noise in MOS transistors with depletion region impurity centers, analyzing noise resistance saturation and drain-voltage dependence
12 p2041 A69-26627
- MOS and junction transistors damage due to radiation, noting decrease in collector current under fast neutron dose
13 p2227 A69-27514
- MOS transistor Hall voltage, mobility and constant verified by magnetoelectric measurements of Si p-inversion layer
13 p2323 A69-28331
- Small signal, HF equivalent circuit for intrinsic metal oxide semiconductor field effect transistor, considering nonpinchoff and pinchoff modes
13 p2238 A69-28429
- MOS unitoron switching circuit operation subjected to nonlinear load, using analytic approximations of current-voltage characteristics
13 p2234 A69-28507
- Large signal transit time effects in MOS transistor, noting drain current response
14 p2418 A69-28891
- Charge flow injection into MOS substrate attributed to gate pulses, correlating charge magnitude with pulse frequency
15 p2573 A69-30033
- MOSFET/unitoron/ switching circuits classification in terms of load curve shapes obtained with different output connections of load elements
15 p2574 A69-30122
- Frequency response of MIS capacitance beyond inversion voltage, discussing recombination rate and generation-recombination current in space charge region
15 p2565 A69-30179
- Linear metal oxide semiconductor integrated circuits, discussing advantages, disadvantages and use of current source load device to improve voltage gain and swing
15 p2577 A69-30594
- MOS devices for radiation environments utilizing aluminum oxide as gate insulator for developing resistance to radiation damage
15 p2577 A69-30595
- VHF and uHF MOS tetrode minimum noise factor computed as function of frequency by adding thermal noise sources to resistive parts of equivalent circuit
15 p2577 A69-30603
- High temperature effects on electron and X ray irradiated MOS transistors for space charge analysis and defects in silica films
15 p2625 A69-30828
- MIS devices with dielectric properties avoiding positive space charge formation, discussing radiation effect
15 p2625 A69-30829
- Production line requirements for MOS and IC, considering high reliability at minimum cost for space applications
15 p2627 A69-30841
- Large scale integrated MOS devices tests for space applications, establishing quality specifications
15 p2580 A69-31131
- Metal oxide semiconductor structural model usefulness in understanding behavior near transition region, discussing surface inversion layer properties, surface mobility theory, etc
16 p2757 A69-31612
- Metal oxide semiconductor integrated circuits, showing failure rates and degradation causes
16 p2759 A69-31851
- Surface state density determination as function of surface potential in MIS capacitors, discussing MIS capacitance method theory and computer programs
16 p2827 A69-32556
- Neutron bombardment and ionizing radiation resistance of aluminum oxide MOS devices using gate insulator fabricated by plasma anodization
17 p2935 A69-32888
- Computer aided design of machines with custom LSI arrays, describing error detection procedures and MOS logic circuits
17 p2942 A69-34121
- Silicon MOS transistor characteristics, discussing stability, temperature effects and inherent noise, noting applications to amplifier circuits
18 p3109 A69-35161
- Failure mechanisms and analyses of large scale integrated circuits based on bipolar and MOS transistors, describing measurement and probing techniques
19 p3282 A69-35787
- Electron-plasmon interaction in degenerate semiconductors, using mathematical model for rectifying metal contacts tunneling characteristics
19 p3382 A69-36049
- Current-voltage characteristics of unitoron with metal-dielectric-semiconductor structure /MOSFET/ taking into account substrate potential effect
19 p3284 A69-36592
- MOS threshold voltages calculations, considering fixed bulk and oxide charges and difference in work function between metal and semiconductor, considering MOS-FET devices
20 p3506 A69-37779
- Silicon dioxide film doped with Al to increase MOS structure radiation resistance
20 p3584 A69-38070
- Metal insulator semiconductor volt-capacitance changes due to light flux, introducing surface recombination rate to improve model
20 p3585 A69-38273
- MOS arrays failure mechanisms, discussing oxide defects, contamination and metal migration due to mode of operation and fabrication techniques
21 p3684 A69-39605
- MSI 12 bit digital to analog converter in integrated circuit form using MOS switching circuit
22 p3906 A69-40349
- Critical transition temperature of vanadium oxide semiconductors as function of doping element content and lattice constant, using X ray diffraction
23 p4198 A69-41564
- Spacecraft onboard data handling system with MSI complementary MOS arrays, describing various components
23 p4133 A69-41739
- METAL OXIDES**
NT ALUMINUM OXIDES
NT ANATASE
NT BARIUM OXIDES
NT BERYLLIUM OXIDES
NT BISMUTH OXIDES
NT CALCIUM OXIDES
NT CESIUM OXIDES
NT CHROMITES
NT CHROMIUM OXIDES
NT COBALT OXIDES
NT COPPER OXIDES
NT ILMENITE
NT IRON OXIDES
NT LEAD OXIDES
- NT LITHIUM OXIDES
NT MAGNESIUM OXIDES
NT MAGNETITE
NT MANGANESE OXIDES
NT MOLYBDENUM OXIDES
NT NICKEL OXIDES
NT NIOBIUM OXIDES
NT RUTILE
NT SAPPHIRE
NT THORIUM OXIDES
NT TIN OXIDES
NT TITANIUM OXIDES
NT TUNGSTEN OXIDES
NT URANIUM OXIDES
NT VANADIUM OXIDES
NT ZINC OXIDES
NT ZIRCONIUM OXIDES
- Gas content and impurities in aluminum melts, analyzing oxides and hydrogen interactions
01 p0098 A69-10958
- Metal oxides catalytic and inhibitory effects on photolysis of alanine by UV light
01 p0025 A69-11095
- Stone meteorite chemical composition, analyzing chondrites Borodino, Lavrentevka, Alfianello and Nardoo II
01 p0026 A69-11382
- Liquid oxides wetting and spreading capabilities on refractory metal surfaces, noting chemical reaction oxide reducing effect
02 p0265 A69-11884
- Impurities effect on defects in oxygen deficient niobium, tantalum and zirconium oxide scales at high oxygen pressures, noting relationship to metal oxidation
03 p0444 A69-13312
- Thermodynamic and kinetic interactions of high melting point metal oxides reduction by carbon
03 p0445 A69-13568
- Metal oxide and carbon interaction during spatial separation of reagents, noting influence of reducing agent activity on metal vapors
03 p0445 A69-13569
- Thermodynamic evaluation of interaction between solid metals and dispersed high melting point oxides, stressing isobaric potentials
03 p0446 A69-13571
- Insensitive explosive trigger or initiator consisting of metal/metal oxide powder with low shock sensitivity and high thermal stability
04 p0646 A69-15300
- Aluminum, Cu, Ni and titanium oxides injection into axis of Ar thermal induction plasma, observing decomposition as function of distance traveled within plasma
13 p2315 A69-28458
- Thin film metallic oxide catalysts for oxidation in low temperature cells using hydrogen and hydrocarbons and for oxygen reduction in acid electrolyte
16 p2738 A69-32408
- Electrochemical couples of zinc-metallic oxides or O used in battery with water electrolyte
16 p2740 A69-32421
- Metal oxide particle growth processes in rocket chambers and nozzles, using generalized kinetic-coagulation equation
16 p2844 A69-32724
- Liquid oxides wetting and spreading capabilities on refractory metal surfaces, noting chemical reaction oxide reducing effect
18 p3156 A69-35044
- H release, pressure and oxide layer formed by reaction during ball milling Cr in water
21 p3728 A69-38567
- Semiconducting properties of lanthanum-cobalt oxide measured, using Seebeck coefficient for analysis as function of resistivity
21 p3780 A69-38612
- Solid metal oxide particles temperature in premixed flames determined from intensity/ wavelength plots of continua
21 p3852 A69-39592
- METAL PARTICLES**
NT POWDERED ALUMINUM
- Temperature rise of micron sized silver particles on carbon film due to electron beam heating, setting up heat balance equation
04 p0640 A69-14449
- Metallic particle ignition in oxygen containing media, obtaining temperature curves and vaporization rates
08 p1375 A69-20343
- UV, visible and near IR spectral characteristics of hydrocarbon-air flames with particulate Al, Mg and B, noting hot metal continuum and oxide emissions
11 p1940 A69-24483

Aerodynamic field around symmetric profile two dimensional plates, visualizing velocity fields with Al particles

12 p2011 A69-26288

Monograph on interstellar extinction computations covering theoretical curves for spherical metal and graphite particles, albedo, optical constants, normalization, temperature dependence, etc

14 p2516 A69-28901

Metal particles evaporation kinetics in plasma arc, determining total and unsteady evaporation time by spectroscopy and absorption radiography

15 p2663 A69-30990

Effective heat transfer coefficient lambda for microscopic Fe particles traversing rarefied air, oxygen and Ar target gases

16 p2769 A69-31870

Particles maximum diameter numerical values for melting during injection into plasma jet calculated for various metals and refractory dielectrics

17 p3009 A69-32825

Metallic aerosol generator application in shock tube spectrometric measurements of radiation by molecules occurring as solids before decomposition to vapor phase

18 p3099 A69-34461

Ramsdorf meteorite chondrules and metal particles formation attributed to shock-induced partial melting and rapid cooling

19 p3409 A69-36088

METAL PLATES

Displacement function selection in calculating rubber-metal valve design, considering boundary conditions of material deformation

01 p0087 A69-10829

Symmetric and asymmetric metal flanges effects on radiation patterns of H plane sectoral horns, noting theoretical explanation and applications

02 p0216 A69-12027

Subsequent yield surfaces in cross shaped brass plates determined after prestraining or cold rolling

04 p0682 A69-15302

Strain near fatigue crack tip in notched steel plates measured by copper electroplating method

06 p1022 A69-17198

Histogram approximation of plastic deformation of metals, analyzing tube under internal load and sandwiched layer compression

10 p1793 A69-22850

Plain strain fracture toughness tests on two inch thick maraging steel plates of various strengths, using bend and compact tension tests

10 p1795 A69-23057

Very low temperature dependence of thin single crystal Al plates electrical resistance, noting Umklapp processes contribution

10 p1711 A69-23620

Decoupling force exerted by magnetic forming Be coil assembly on metallic plate during forming

11 p1888 A69-25310

Plane strain fracture toughness tests on maraging steel plates for various yield strengths and large dimensions

12 p2114 A69-26496

Crack opening displacements of stationary and running cracks and of inclined stationary cracks in centrally notched plates, noting normal strain fields

12 p2189 A69-27163

Pyrex spheres accelerated to 15 km/sec by plasma rail gun to study hypervelocity impact in thin stainless steel and Al targets

[AIAA PAPER 69-378]

13 p2368 A69-28308

Two plate meteoroid shields effectiveness determined by analyzing debris cloud ejected behind front plate after hypervelocity impact

[AIAA PAPER 69-380]

13 p2368 A69-28310

Initial comparisons between theory and experiment of strain fields in cracked copper plate

15 p2640 A69-30810

Air resistance effect on transverse vibration damping of flat specimens of heat resistant alloy, duraluminum, Ti, Mo and Nb

17 p2991 A69-33947

Fabrication effects on high strength Al alloy plate properties, comparing texture, plane strain fracture toughness, yield stress, ultimate tensile stress and elongation

19 p3346 A69-36437

Dual filler metals for increasing joint efficiency by changing fusion zone composition, discussing mechanical properties in Ti and Al plates welding

22 p3956 A69-40462

Thickness direction tensile properties, ultrasonic attenuation and mild steel plate lamellar tearing in multipass fillet joints measured by weld cracking test

24 p4320 A69-42942

METAL POLISHING

NT ELECTROPOLISHING

Radiation emission factors determination of polished metallic surfaces

07 p1242 A69-18952

Electrolytic and mechanical polishing techniques for metallographic specimens of beryllium

13 p2281 A69-28161

METAL POWDER

NT POWDERED ALUMINUM

Burning ability and inflammability of mixtures of powdered Mg, Al, Mg alloys or Al alloys and C-H-O organic compounds

02 p0355 A69-12669

Temperature distribution and vaporization rate boundary conditions on metal particle surface during preignition heating in oxygen containing medium

02 p0355 A69-12670

Exothermal effects during sintering of nickel-aluminum powder mixture

02 p0269 A69-12838

Exothermal effects during sintering of nickel-aluminum powder mixture, showing role of liquid phase decomposition and intermetallics

02 p0269 A69-12843

Electrical resistivity of sintered high melting point metal oxides, noting width of semiconductor forbidden band

03 p0445 A69-13570

Insensitive explosive trigger or initiator consisting of metal/metal oxide powder with low shock sensitivity and high thermal stability

04 p0646 A69-15300

Compaction kinetics in continuous quasi-viscous medium having plastic flow material under applied load, discussing hot pressing of nichrome powders

04 p0618 A69-15389

Two stage thermal treatment inhibiting influence on swelling and porosity linked to Kirkendall effect during sintering of Fe-Ni powder mixtures

05 p0782 A69-16616

Properties of electrolytic and reduced titanium powders and sinterability of porous compacts

05 p0782 A69-16795

Tungsten delay powders combustion mechanism and intermediate stages of burning process, noting burning rate

[WSCI PAPER 68-19]

07 p1202 A69-18370

Electroslag welding using plasma jets with powdered material, discussing various parameters

08 p1321 A69-20766

Physical properties control in nickel powders obtained by hydrogen reduction of nickel diamine sulphate solutions

08 p1334 A69-21057

Bulk weld filler metals, discussing granular compositions, electrodes and iron, nickel and cobalt base deposits

11 p1891 A69-24931

Ductile metal powder chemical reactions during comminution in pure or oxygenated water

13 p2216 A69-27762

Sintered mixtures of Ni-Mo powder noting electrical resistance, alloy and shear strength and impact viscosity

15 p2638 A69-30280

Mathematical analysis of compaction process for powder mixtures of different metals assuming known characteristics of components

15 p2641 A69-31182

Powder properties effect on rolled strip thickness and compactness, angles, pressure at roll and torsion during rolling, analyzing Fe, Ni and Cu powders

15 p2630 A69-31183

Thermal EMF, electrical conductivity and Peltier effect in sintered refractory oxides at high temperature in air and in Ar

17 p3068 A69-32990

Optical characteristics at 2-25 micron spectral interval for various metal blacks vaporized in vacuum on KBr, Ni foils and nitrocellulose substrates

17 p3075 A69-33976

Carburizing spherical powders of Nb, Mo and W to obtain carbides, noting agreement between theoretical and experimental data

19 p3345 A69-36162

X ray analysis of rolled and compressed Ti powder produced by calcium hydride reduction, noting coexistence of screw dislocations

21 p3745 A69-38952

Compactibility dependence of Fe, Co and Ni powders with Zr, Nb and Mo carbide additives on pressure, carbide content and lubricant

22 p3970 A69-40634

Optimal conditions for extrusion compacting of hard alloy mixtures plasticized with paraffin, determining plasticizer content, upsetting, pressure and temperature

22 p3956 A69-40635

METAL PROPELLANTS

Beryllium propellants for space applications, considering composite solid propellant with powdered Be as fuel

02 p0303 A69-11763

Liquid alumina particles agglomeration in convergent and throat region of nozzle leading to performance decrease by increasing velocity and temperature difference between phases

22 p4001 A69-40929

METAL SHEETS

Elastic anisotropy and polycrystalline orientations in cold rolled titanium sheets investigated by Fourier series method, discussing Young modulus values

01 p0094 A69-10431

Prestraining of stainless steel En58b sheet at room and cryogenic temperature, noting effect on tensile properties

01 p0099 A69-11151

Mechanical properties of AZ5G-Zr-Cr alloy welded sheet subjected to biaxial stress at low temperature

01 p0088 A69-11152

Vacuum heating and thermal cycling influence on mechanical and structural properties of aluminum sheets fabricated from sintered powder

02 p0266 A69-12126

Fabrication of large arched bottoms for pressure vessels from aluminum alloys, discussing sheet cutting and welding, annealing, machining, etc

02 p0254 A69-12678

Aluminum plastic sandwich products production costs compatibility with conventional materials

02 p0348 A69-12749

Cold rolling and annealing effects on tensile strength, heat resistance and ductility of sintered Al powder sheets

03 p0452 A69-14121

Sheet steel composition effect on gas-tungsten arc welds porosity

04 p0607 A69-15219

Anisotropic plasticity in sheet metals under uniaxial and balanced biaxial tension

05 p0837 A69-16030

Air cushion effect on dimensional accuracy in explosive forming of metal sheet

06 p0930 A69-17001

Air cushion effect in explosive forming of metal sheets, considering simple geometrical shape

06 p0931 A69-17526

Surface edge preparation of titanium alloy sheets for argon shielded arc welding

06 p0932 A69-17898

TIG welding introduced residual stresses amplitude and distribution in Ti sheets, studying effects on mechanical properties

[ASM PAPER GG8-6.2]

07 p1169 A69-19674

Elastic springback and residual stress distribution in sheet metal formed by bending determined as function of radius sheet thickness and stress-strain characteristics

08 p1319 A69-20005

Electron fractographic study of fatigue cracks in wrought beryllium sheet, noting transgranular and intergranular modes on fracture surface

09 p1500 A69-22324

FM Lamb wave system for flaws and defects detection in thin metal sheets

10 p1699 A69-23048

Aluminum alloy thin sheets with central transverse fatigue cracks subjected to increasing static loads to fracture, investigating crack tip deformation

10 p1709 A69-23056

Buckling deformation and stress fields around central slits in photoelastic models and metal sheets under tensile load

10 p1796 A69-23069

Mechanical model for investigating macrobehavior of cyclic fatigue crack propagation in plates of several metal alloys

10 p1796 A69-23072

Testing system stiffness effect on sheet fracture, discussing notch strength dependence on stiffness

10 p1796 A69-23075

Transgranular stress corrosion crack propagation in thin sheet single phase magnesium-aluminum alloy

10 p1710 A69-23086

Structural inhomogeneity of Ti alloys cause increased susceptibility to production of sheets, forgings and drop forgings
11 p1902 A69-24276

Annealing effects on cold rolled titanium sheets, noting changes in Young modulus and characteristics of recrystallized titanium
11 p1904 A69-24899

Fatigue life of Al alloy thin laminated sheets, considering cyclic frequency and temperature effects
12 p2180 A69-26359

Thermal resistance of bolted or screwed sheet metal joints in vacuum, using method applicable to different materials and surface finishes
12 p2191 A69-26803

Rolled sheets from beryllium scrap converted into vacuum cast ingots, discussing preparation techniques
13 p2281 A69-28160

Aluminum double sheet target penetration resistance determined by studying high velocity pyrex glass impact effects on front/rear sheets and spacing [AIAA PAPER 69-375]
13 p2367 A69-28305

Strain rate and temperature effects on sintered molybdenum sheets strength and elongation characteristics
14 p2464 A69-29322

Adhesive pressure welded joints tightness and fabrication stability analyzed on duraluminum sheet samples
17 p2978 A69-32949

Plastic energy dissipation rate during stable crack growth in sheet under uniaxial tension
18 p3212 A69-34345

Optimum conditions for producing Ti-V alloy sheet plated on one side with Nb by hot rolling
18 p3155 A69-34652

Explosives parameters effect on metal sheet velocity during explosive welding, considering load density and explosive force
18 p3149 A69-35279

Forming, machining and joining characteristics of B-Al composite sheet metal material for space structures
19 p3318 A69-35507

Axial load fatigue crack propagation tests on Al alloy sheets for stress ratio effects
19 p3346 A69-36435

Anisotropy coefficients obtained during annealed Al sheet tests based on stress-strain characteristics, noting fading memory effects
19 p3447 A69-36857

Recrystallization in thoria dispersed Ni sheet as function of strain-anneal cycles, using electron transmission technique quantitative determination
20 p3557 A69-36958

Sheet metals deformation behavior during punch stretching and hydraulic bulging, noting effects of lubrication, stress-strain relation, anisotropy and microcracks
20 p3551 A69-38115

Al alloys sheet, plate and weldments crack behavior and fracture toughness at cryogenic temperatures, using notched and surface flawed plane strain specimens [ASM PAPER W9-19.3]
21 p3743 A69-38669

Fatigue resistance of bimetallic sheets of steel and Al alloys by fatigue resonant machine, analyzing lifetime distribution and failure probability
21 p3835 A69-38773

Galvanostatic anodic and cathodic currents effect on stress corrosion of Be sheet in aerated synthetic sea water at 72 F
21 p3747 A69-39436

Load transfer to sheet metal plate from bonded strip axially loaded by single force, assuming linear viscoelastic adhesive layer
22 p4038 A69-39896

Creep at 400 degree C in Ti alloy sheets in short period plastic deformation due to work hardening by stepwise drawing in extensometric device
22 p3971 A69-41032

High temperature vacuum treatment of thick stainless steel sheets reducing hydrogen content and outgassing
22 p3958 A69-41217

METAL SHELLS

Fragmentation behavior of small thin walled metal cylinders during explosions as function of expansion velocity and material parameters
09 p1611 A69-21352

Permanent displacement relationship to shell thickness following snap-through of loaded rigid boss in spherical metal shell
11 p1980 A69-24822

Plane monochromatic and pulsed electromagnetic waves penetration into metal cylindrical shells, deriving equations for electromagnetic field in interior
15 p2569 A69-30950

Cylindrical reinforced steel shells stability under external pressure
18 p3225 A69-35371

METAL STRIPS

Metal strip angled profile shaping by sliding application of forces with draw plate, analyzing friction effect with thin plastic shell engineering theory
03 p0432 A69-12962

Stress distribution in infinite strip with equally spaced identical semicircular notches on one edge and subject to transverse bending
05 p0842 A69-16643

Stresses in finite width infinite elastic isotropic strip with equally spaced identical semicircular notches under uniform tension or pure bending
05 p0843 A69-16644

Power law taperings for minimizing peak to trough deflection of cross section of strip bent longitudinally into cylindrical surface
06 p1023 A69-17374

Minimal interference thin metal strap support system for dynamic stability tests of high fineness ratio wind tunnel models [AIAA PAPER 69-350]
13 p2243 A69-28284

Oxygen influence on low pressure ethylene decomposition on high temperature tungsten and Re ribbons surface
19 p3266 A69-36732

Electromagnetic wave diffraction normally incident on symmetrical five element metallic array
23 p4123 A69-42029

Plane electromagnetic wave diffraction by screened periodic metallic strips array with real ferrite transversely magnetized to saturation
23 p4124 A69-42032

Electromagnetic wave diffraction by multielement periodic metallic strips arrays positioned transversely in rectangular waveguide
23 p4124 A69-42035

Rectangular waveguide with periodic array of infinitely thin metallic strips, studying intrinsic oscillations critical frequencies and amplitude spectrum
23 p4124 A69-42036

Dispersion and resonant properties of electromagnetic waves propagating along plane metallic strip array with shield and dielectric
23 p4124 A69-42038

Plane polarized electromagnetic wave diffraction incident on skewed metal ribbons array
23 p4125 A69-42043

METAL SURFACES

Streak interferometry method for measuring transient deformation data on metallic solid surfaces
01 p0078 A69-10117

Corrosion of steel surfaces in contact with molybdenum disulphide noting influence of high humidity, milling and inhibitors
01 p0094 A69-10367

Microfacets of metal surface cracks studied for plastic deformation and atomic separation mechanisms by electron diffraction
01 p0098 A69-10763

Heat transfer dependence on direction of heat flow in stainless steel/aluminum interfaces, showing surface roughness and flatness influence
01 p0177 A69-11406

Kinetics of vaporization of metals with surface subjected to incident radiation flux noting pulse duration
02 p0350 A69-11577

Monocarbide phases high temperature vaporization from open metal surfaces into vacuum, obtaining temperature dependence
02 p0260 A69-11583

Force law determining impact processes of pyramidal and conical body penetration into smooth surface of rigid plastic metals
02 p0337 A69-11615

Electron plasmas near plane metallic surfaces, determining transmittance and reflectance of incident light waves and surface waves dispersion characteristics
02 p0286 A69-11788

Electron transfer through metal/semiconductor contact surfaces, measuring electrical conductivity on sintered cylinders with or without silver addition
02 p0296 A69-11790

Substructures around fatigue cracks in fcc metals and alloys, noting relation between structural formation and crack propagation
02 p0260 A69-11826

Liquid oxides wetting and spreading capabilities on refractory metal surfaces, noting chemical reaction oxide reducing effect
02 p0265 A69-11884

Polymeric film properties related to metal substrate interface corrosion, considering effects of stress concentration, surface cleanliness and adsorbed gases
02 p0265 A69-11896

Surface preparation effect on stress corrosion cracking of type 310 stainless steel wires in boiling aqueous magnesium chloride solutions
03 p0444 A69-13311

Surface effects on metals mechanical properties, discussing dislocation dynamics and resulting effects on macroscopic plastic behavior
03 p0448 A69-13869

Metal surface degradation by constant density laser radiation, computing screening effect
03 p0442 A69-14221

Emissivity of rough metallic surfaces with preserved profile similarity, showing independence to roughness height
05 p0845 A69-15894

Radiation emission factors determination of polished metallic surfaces
07 p1242 A69-18952

Field diffraction at finite metallic surface represented in eigenfunctions of discrete spectrum, considering forced oscillations of open circuit
07 p1084 A69-19151

Radome axis error due to phase /dielectrics/ and metallic obstacles
07 p1112 A69-19542

Ruby laser beam incident on steel surface in air or water measured for energies, determining reflected energy dependence on incident energy for self insulation effect
07 p1157 A69-19594

Work function and desorption energy measurements of alkali metals from metallic substrates with modulated molecular beam, noting surface contamination
09 p1558 A69-21808

Eddy current nondestructive tests of nonmagnetic thin metallic sheets and plates from single surface
10 p1698 A69-23046

Ultrasonic technique for metal surface and near surface residual stress measurement, emphasizing aluminum alloys
10 p1794 A69-23052

Screw dislocation interaction with partially bonded bimetallic interface, using isotropic elastic continuum approximation
10 p1802 A69-24027

Fractures in refractory metals surface layers due to Q switched laser pulses
11 p1899 A69-25402

Laser radiation in vacuum effects on metals and alloys
11 p1906 A69-25684

Metallic impurities effect on Ge surface charge and recombination properties, noting fast and slow electron density changes by forbidden band penetration
11 p1939 A69-25703

Reflection of moving rarefied AR plasma from surface of nickel cylinder inserted into gas discharge tube
11 p1934 A69-25710

Sr and La ionization on crystal surfaces of W and polycrystalline W, discussing temperature effect on oxidation and work function
12 p2142 A69-26113

Inelastic interactions cross sections of slow electrons with adsorbed particles on W surface as function of temperature in surface bond vibrational region
12 p2132 A69-26114

Desorption kinetics of atomic and oxide phases, analyzing composition of surface film formed from W and Mo single crystals interaction with oxygen
12 p2026 A69-26115

Back scattered electron inelastic LEED spectra of cesium plasma in W/100/-Cs system, noting strong loss peak
12 p2132 A69-26116

Fatigue strength reduction in Ti alloy in sliding friction contact with metallic materials caused by fretting corrosion
12 p2113 A69-26125

Electronic structure of clean metallic interfaces, considering electron, ion and surface interactions for metal-vacuum interface
13 p2321 A69-28008

Free electron model for electron work functions and number density distributions and surface potentials in metals
14 p2504 A69-29009

Thermionic emission from bare and Cs-covered metal surfaces, calculating current and work function by employing localized electron orbital model
14 p2505 A69-29264

Tungsten surfaces with high work functions generated by electrochemical etching, discussing effects of heat treatment in vacuum
14 p2506 A69-29267

Tungsten emitting surfaces work functions, discussing dense crystalline planes electrolytic or pyrolytic deposit growth and surface chemical or electrolytic attack
14 p2506 A69-29268

Corrosion at polymeric film-metal substrate interfaces, noting roles of film properties, bond strengths and primer coats
14 p2466 A69-29938

Oxygen adsorption on Mo single crystals /100/ surface as function of temperature using low energy electron diffraction
16 p2748 A69-32795

Field ionization at metal surfaces as rearrangement collision, considering anisotropic electron tunneling probabilities produced by Fermi surface
17 p3015 A69-32821

Secondary electron emission from gas covered metal surfaces, discussing results of neutral beam investigations
17 p3008 A69-33000

Thin surface films effect on radiative properties of metal surfaces determined by thin film optics, noting dependence on refractive index
[AIAA PAPER 69-623] 17 p3072 A69-33283

Heat transfer from cylindrical copper surface to liquid helium at 4 degrees K, discussing temperature fluctuations in nucleate boiling region
17 p3074 A69-33780

Finish turning cutting speed effects on titanium alloy surface layers
18 p3148 A69-34548

Wavelength dependence of total and depolarized backscatter laser light cross section for rough metallic surfaces
18 p3172 A69-35011

Liquid oxides wetting and spreading capabilities on refractory metal surfaces, noting chemical reaction oxide reducing effect
18 p3156 A69-35044

Low energy electron diffraction oxygen adsorption kinetics on planes of tungsten at coverages below monolayer and work function measurements
18 p3183 A69-35106

Oxygen 18 adsorption on silicon activation analysis measurements used to obtain kinetic curve for chemisorption from monolayers
18 p3183 A69-35107

Electron current flow from metal target in gas due to laser radiation, showing increased dependence on gas pressure
18 p3152 A69-35124

Friction coefficient increase caused by metal surface textures anisotropic effect on friction force
18 p3149 A69-35151

Quartz fiber adhesion to Re measured in LEED /low energy electron diffraction/ apparatus for clean and O layer surfaces, noting brittle fracture
18 p3156 A69-35182

Beryllium bonding, evaluating various surface preparations and adhesives
19 p3320 A69-35561

Microbiological corrosion and degradation of aircraft metals and organic materials in fuel tanks
19 p3341 A69-35569

Electric fields and electron work functions, surface potentials and number density distributions in selected metals surfaces determined using free electron model
19 p3382 A69-36045

Low pressure ethylene decomposition on high temperature W ribbon surface
19 p3265 A69-36729

Low pressure ethylene decomposition on high temperature Re ribbon surface
19 p3266 A69-36730

Surface structures, work function changes, Auger electron and surface plasma losses for Cs on clean W surface
19 p3392 A69-36733

Fracture surfaces of stress corrosion cracks in Fe-Cr-Ni alloys studied by electron microfractography, noting cleavage fracture
19 p3350 A69-36891

Surface cavity profiles created by pulsed laser on Ti, Al, Cu, Pb and Zn, compared with isotherms computed from heat conduction models
20 p3552 A69-36917

Plasma coating formation mechanisms and parameters, studying metal surface and deposited particles temperatures, spraying time effects, etc
20 p3549 A69-37374

Titanium surface cleaning and descaling in preparation for machining, discussing acid pickling, mechanical abrasion, conditioning cycles, etc
20 p3549 A69-37434

Dielectric response of semiinfinite metal surface to external point charge in linearized Fermi-Thomas approximation, discussing potential in metal and vacuum
20 p3583 A69-37498

C and O atoms chemisorption on Mo surface demonstrated by surface striation
20 p3562 A69-37782

Maxwell coefficient change of Cd atoms /in molecular beam/ diffusely reflected from metal surfaces related to reflector temperature, material and fabrication method
20 p3580 A69-37814

Microstructure and X ray structure compared for two and three component chromide, titanide and silicide diffusion layers on Nb, discussing phase composition
20 p3563 A69-37820

Vacuum apparatus for measuring uniaxially loaded metal surfaces interfacial adhesion, showing surface oxide removal effectiveness influence in adhesion strength
21 p3689 A69-38594

Diffuse reflection of UV radiation from rough metallic surfaces, noting irregularities
21 p3770 A69-38796

Stress concentrations in metals determined through surface properties measurements, correlating local electrochemical potentials and metal-metal oxide junction parameters
21 p3747 A69-39326

Field emission and field-ion microscopic adsorption studies, discerning major states in chemisorption for metal-crystal surfaces
22 p3895 A69-39898

DC beam experiment for determining molecule sticking coefficients of gas beams incident on Ti, Ba and Sr gettering surfaces at cryogenic temperature
23 p4151 A69-41544

Distribution function of output energies of polycrystalline metal surface used as plasma probe, considering homogeneous plasma flow and isotropic particle velocity distribution
23 p4196 A69-41696

Corrections for eliminating anomalous skin effect on IR emissivity for Ag, Cu, Au and Al
23 p4177 A69-42212

Surface texture effects, discussing metallic and elastomeric contacts, measurement, profile, model parameters, adhesion, hysteresis, lubrication, squeeze films, macroelastohydrodynamics and randomness
23 p4170 A69-42359

Solid film lubricants deposited by DC triode sputtering on Ni, Ni-Cr and Nb surfaces friction tested under ultrahigh vacuum conditions
24 p4321 A69-43126

METAL VAPORS

NT MERCURY VAPOR

Electrical equation of state of metals determination from density, conductivity, energy and metal vapor velocity measurements in wire explosions
01 p0117 A69-10659

Alkali metal vapors thermal conductivity determination by temperature difference dilatometric measurement
02 p0247 A69-11579

Magnetic confinement of electric arc in alkali metal vapor containing gas flow, considering degree of ionization
02 p0286 A69-11585

Spectroscopy of potassium vapor using laser induced fluorescence, noting laser line coincides with several molecular transitions
05 p0771 A69-15907

Gasdynamic flow shock wave phenomena during exploding wire dwell time inside metal vapor cylinder, noting effect on reignition
07 p1188 A69-18275

Temperature distribution in low pressure magnesium vapor-oxygen diffusion flames, discussing environmental conditions and visible radiation
[WSCI PAPER 68-20] 07 p1241 A69-18367

Pulse broadening in MHD copper vapor laser
07 p1149 A69-18904

Rubidium vapor laser pumping induced frequency shifts eliminated by detuning resonator without decreasing output power
09 p1520 A69-22636

Concentration changes in binary metal-gas solutions during simultaneous degassing kinetics and metal evaporation
09 p1528 A69-22732

Cs and K ions drift velocity calculations in vapors of own atoms under various electric field strengths effect
11 p1922 A69-24226

Liquid-metal MHD space power generation system using intermittent vaporization slugs shooting at 2700 R peak temperature
13 p2206 A69-27492

Metal layers deposition, structure and properties obtained by H reduction of metal halides in vapor phase
14 p2462 A69-29205

Barium vapor effect on converter materials, examining metals-ceramics compatibility at high temperatures
14 p2467 A69-29215

Saturated Li vapor pressure measured by static equilibrium technique based on use of null membrane, tabulating pressures for various temperatures
15 p2656 A69-30997

High energy electrons emission during alloy evaporation on hot metal filaments used for thin film deposition
16 p2827 A69-32016

Electric field variations in vicinity of auroral forms from motions of Ba vapor clouds released from Nike-Tomahawk rockets
18 p3128 A69-34935

Aluminum oxide droplets condensation from atmosphere of metal vapor and oxygen, studying temperature and time effects on particle nucleation, growth and distribution
21 p3783 A69-38799

Laser produced Sb and Te vaporization near critical point, using time of flight mass spectrometer
22 p3993 A69-40719

Spectrum characteristics of plasma generated by pulses of solid state laser radiation on metals and alloys in regular and quasi-stable regimes of emission
22 p3964 A69-40793

Equilibrium vapor compositions and activities over Fe-Cr-Ni alloys at 1600 C determined by collecting effusate from thoria Knudsen cells
23 p4175 A69-41503

Sonic vapor flow heat transfer limitations in heat pipes for Na, K and Cs, showing strong influence of temperature and working fluid
23 p4239 A69-41719

METAL WHISKER REINFORCEMENT

U WHISKER COMPOSITES

METAL WORKING

NT AUSFORMING

NT BULGING

NT CLADDING

NT COINING

NT EXPLOSIVE FORMING

NT FORGING

NT HYDROFORMING

NT MAGNETIC FORMING

NT SIZING [SHAPING]

Nichrome bars production dispersion hardened by alumina and zirconia inclusions, noting extrusion temperature influence
01 p0085 A69-10397

Chemical vapor deposited W and W-Re alloys for structural applications, discussing fabrication methods and effects on mechanical properties
01 p0096 A69-10641

Strain measurements in pure polycrystalline Ti at constant temperature and strain, considering creep and elastic aftereffects
01 p0101 A69-11363

Laser applications in metal working including dissimilar metal welding, hole drilling, material removal and dynamic balancing
[ASTME PAPER MR68-406] 02 p0252 A69-11796

Deformation temperature and reduction effects on structure and properties of cylindrical specimens of various titanium alloys
02 p0266 A69-12124

Shot impact shaping of parts made of monolithic panels, relating curvature of profile to parameters of process
03 p0433 A69-12963

Fabrication of Cu-W composites with discontinuous fibers based on sintering and rolling
03 p0444 A69-13349

Tubular metal parts and assemblies, discussing flaring, forming, beading, tapering and step drawing
03 p0435 A69-13918

Soviet book on press working of aviation materials, noting granulated and powdered materials and high strength and refractory materials
03 p0451 A69-14117

Tangential and normal stress distribution in deformed metals, discussing work hardening of metals and cold working without softening effect

03 p0435 A69-14118

Alloying elements effect on mechanical and refractory properties and structure of forging of age hardenable Ni base alloys

03 p0452 A69-14122

Geometrical and thermomechanical effects on pressure and forces in deformation of thin Ti alloy blanks

03 p0452 A69-14123

Closed die development for forging very large and complex parts to meet needs of high Mach aircraft

04 p0604 A69-14523

Extrusion processes used for aluminum, magnesium and titanium extrusions, presenting die configurations

04 p0604 A69-14526

Beryllium properties, metallurgy, alloys, fabrication and applications in guidance components, aerospace structures and nuclear reactors

04 p0614 A69-14586

Ti alloy sheet, plates, rods, sectional shapes, forgings, stampings, pipes and wire production from ingots and blanks

07 p1161 A69-18762

Ti alloys thermomechanical treatment effect on strength and plasticity characteristics, noting single and double phase alloys and rupture

07 p1161 A69-18766

Production technology of sheets, forgings and drop forgings from Ti and Ti alloys, discussing gas saturation prevention and plastic deformation

07 p1164 A69-18786

Technology of titanium for C-5A aircraft, discussing structural and functional components and machining, welding, forging, etc

[ASM PAPER D8-26.2] 07 p1143 A69-19672

Elastic springback and residual stress distribution in sheet metal formed by bending determined as function of radius sheet thickness and stress-strain characteristics

08 p1319 A69-20005

Microfilaments, Taylor production method, mechanical properties and comparison to whisker

08 p1320 A69-20582

Contour of axisymmetric holes in dimensional electron-beam machining calculated from density distribution of transmitted energy

08 p1321 A69-20727

Deformation processing of superalloy gas turbine components, studying ingot characteristics, alloy segregation effect and thermomechanical properties

[SAE PAPER 690101] 09 p1503 A69-21557

Whisker metal matrix composite fabrication, discussing aligned whisker distribution without degrading strength or fracturing and detailing extrusion process

09 p1511 A69-22361

Laser applications to production line metal working, discussing economics, welding, drilling, automation, thermal and atmospheric effects, etc

10 p1698 A69-22985

Superimposed tool vibration function in deep drawing, ironing and cold forging, discussing equipment instrumentation, emphasizing dynamic force measurement

[ASME PAPER 69-VIBR-8] 10 p1700 A69-24164

Slip band extrusions in hexagonal close packed Cd, Mg and Ti subject to cyclic stresses, noting microstructural changes

12 p2116 A69-26912

Rolled sheets from beryllium scrap converted into vacuum cast ingots, discussing preparation techniques

13 p2281 A69-28160

Ruby and neodymium glass lasers applicability to metal working, investigating factors affecting integral pulse power stability

13 p2273 A69-28431

Titanium alloys for thermionic nuclear converters, discussing melting, forging, drawing and quality control of mechanical and physical properties

14 p2462 A69-29217

Dislocation pattern in thin Mo foils deformed by hydroextrusion observed by transmission electron microscope

14 p2463 A69-29311

Hot extrusion process for steel and various metals in U.S. semifinished product industry, considering lubrication problems, research centers and development

15 p2618 A69-30228

Powder properties effect on rolled strip thickness and compactness, angles, pressure at roll and torsion during rolling, analyzing Fe, Ni and Cu powders

15 p2630 A69-31183

Ti alloys commercial applications and properties, discussing alloying elements influence, deformability, weldability, stress corrosion and market trends

16 p2801 A69-31784

Microstructural factors role in metal fracture toughness, considering effects of deformation processing and heat treatment, grain size, structural refinement, fibering, etc

17 p2988 A69-33552

Welding technique using pulsed current supply to achieve smooth metal transfer on thin sections in various positions

18 p3150 A69-35418

Electromagnetic shaping of metallic parts using equations describing magnetic and electric field intensity as function of blank profile and cylindrical blank wall thickness

18 p3151 A69-35456

Low temperature predeformation and disorientation of mosaic blocks to strengthen aluminum

20 p3562 A69-37819

Beta working effect on Ti alloy mechanical and fatigue properties

[ASM PAPER D8-24.3] 20 p3564 A69-38136

Shock hardening of Al alloys in annealed, solution heat treated and aged conditions compared with cold-rolled materials

[ASM PAPER W9-10.4] 21 p3729 A69-38664

Gas turbine compressor blade buckling during blade fabrication by hydraulic pellet jet technique eliminated by controlling working pressure of jet

21 p3731 A69-38879

Forming techniques to overcome pressing behavior of maraging steels, noting tendency to thin during stretching and reluctance to stretch

23 p4170 A69-42157

Explosive forming theory and experience including explosives characteristics, dimensional relations, hold-down pressure, economics and applications

24 p4320 A69-43038

METALLIC PLASMAS NT CESIUM PLASMA

Simulation experiments using artificial plasma for astrophysical rocket exploration, discussing experiments leading to barium-copper oxide mixture choice for plasma cloud

06 p0999 A69-16973

Dynamic growth of positive ion sheath on plane electrode in mercury plasma, measuring sheath thickness and current

12 p2134 A69-26099

Collisionless Ce and K plasmas measurements to determine steady state parameters and LF oscillations, noting noise relationship to drift instability

14 p2499 A69-29849

Synthesized plasma from neutralized mercury ion beam ejected from electron bombardment source, analyzing temperature, plasma sheath and stability

14 p2502 A69-29956

METALLIZING

Mechanical properties of thermally diffused layers obtained by vacuum chromizing of steel, establishing need to decarburize substrate material

03 p0450 A69-13913

Integrated circuit interconnection patterns computerized design, discussing automatic laser mask-making control

06 p0931 A69-17199

X ray and photomicrographic study of metal layer-ceramic seal interface reaction products, discussing phase transformations, temperature effects and time dependence

08 p1320 A69-20375

Narrow gap gas metal arc welding process in spray transfer range for narrow welds in thick plates, discussing equipment and applications

11 p1891 A69-24930

Sintered metal powder process for metal-to-ceramic seals for thermionic converters, giving results for tensile strength, thermal cycling and cesium corrosion

14 p2454 A69-29211

Large scale integrated circuits reliability with emphasis on multilayer metallization, designing test vehicles for failure mechanisms

17 p2935 A69-32887

Steels chromized by vacuum diffusion, studying depth, microstructure and properties of chromized layer

19 p3329 A69-36572

Bonding mechanisms in Mo-Mn-Ti metallizing and Cu brazing in metal to ceramic seals by strength test, microscopy and electron probe microanalysis

21 p3733 A69-39599

Hybrid microwave IC assembly techniques, discussing active devices connection to substrate with thick or thin film metallizations

22 p3912 A69-40068

Si integrated circuits single and composite layered metallization systems, comparing characteristics of various refractory and noble metals

24 p4286 A69-42761

METALLOGRAPHY

High temperature magnetic analysis of metallurgical structure of high strength steels and composites, including phase transformation and matrix grain structure

01 p0093 A69-10111

A15 type phase in vapor deposited W-Re alloys identified by X ray diffraction, metallography and hardness measurements

01 p0098 A69-10649

Diffusion zones in filament reinforced metal matrix composites, using metallographic technique

01 p0103 A69-11269

Structure of zirconium corner of Zr-V-Ni system phase diagram, using metallography, hardness and microhardness methods

02 p0262 A69-11847

Diamond abrasive process for preparation of microminiature devices for metallographic analysis

03 p0402 A69-13007

Stress corrosion crack initiation in aluminum alloy observed by optical microscopy

06 p0944 A69-17855

Carbon influence on cast Waspaloy, discussing chemical segregation, chemical gradients and tensile ductility

[SAE PAPER 690100] 07 p1158 A69-18307

Structure and critical superconductivity current of titanium niobium alloy as function of heat treatment and deformation

07 p1158 A69-18532

Time and temperature dependence of Mo and W deformation structure variation and primary recrystallization from metallographic investigations using electron microscopy

08 p1334 A69-21058

Structure of spinodal decomposition in Al-Zn alloys by X ray diffraction noting anisotropy, periodicity and stability

09 p1522 A69-21502

Metals structure and mechanical properties after hydroexplosive forming analyzed by X ray diffraction

09 p1503 A69-21851

Polarized light microscope for application to metallic crystallographic studies noting grain orientation, hep grain basal pole orientation and etched fcc metals

09 p1499 A69-22302

Molybdenum, titanium and cobalt effects on nickel maraging steel strength and ductility

11 p1904 A69-24643

Soviet collection of articles on atomic ordering effects on alloy properties

11 p1936 A69-24701

Metallographic aspects of fracture, analyzing very brittle solids, Griffith cracks, ductile solids and ductile to brittle transition

13 p2274 A69-27225

Metallography - Conference, Denver, November 1968

13 p2280 A69-28154

Metallographic study of microstructure recrystallization of 50 Ni-50 Fe alloy during annealing using special etchants and methods

13 p2281 A69-28155

Electrolytic and mechanical polishing techniques for metallographic specimens of beryllium

13 p2281 A69-28161

Metallographic analysis techniques for high aluminum activity pack cementation coating on nickel-base alloy

13 p2282 A69-28163

Dispersion-strengthened alloys from extraction replicas, determining volume fraction and spacing of dispersed phase particles

13 p2282 A69-28167

Metallography of iron meteorites emphasizing Canyon Diablo anomaly

13 p2353 A69-28169

Structural modifications of metals and alloys accompanying various stages of creep, interpreting equations describing time-deformation relation

17 p2985 A69-32904

Iron distribution inconsistency indicated in Group H and L chondrites through Ni and Co analysis of frac-

tionated samples, plotting atomic ratios on Prior diagram
19 p3407 A69-36078

Meteorites Ni-Fe metal structures analysis as part of petrology study of mesosiderites
20 p3602 A69-37536

La-Rh system study by powder X ray diffraction, metallographic and differential thermal analysis, constructing equilibrium diagram and determining crystal structure data
21 p3744 A69-38739

Dislocation structure of Al, Ni, Cu and Ag during creep, noting dependence of creep rate on stacking-fault energy
22 p3972 A69-41080

Metallographic techniques for meteorite studies, determining etching topography and orientational difference within each phase
24 p4382 A69-42934

METALLOIDS

NT ANTIMONY

NT ARSENIC

NT BORON

NT BORON ISOTOPES

NT BORON 10

NT GERMANIUM

NT POLONIUM ISOTOPES

NT SILICON

NT TELLURIUM

Electron vs phonon superconductivity mechanism conditions for semiconductors, semimetals and molecular crystals
03 p0492 A69-14176

Quantum oscillations of magnetization, undamped magnetoplasma waves development and sound amplification by electron drift in crossed fields observed in semimetals
09 p1556 A69-21615

METALLOID ORGANIC COMPOUNDS

U ORGANOMETALLIC COMPOUNDS

METALLURGY

Meteoritic extraterrestrial materials sampling for chemical, petrographic and metallurgical analyses, discussing microstructure and optimum specimen weight for representative analysis
[UN PAPER 68-95381] 01 p0150 A69-10480

Dendrite formation and solidification relationship in highly alloyed materials from quantitative determination of controlling factors for segregation
01 p0098 A69-10899

Hydraulic press large closed die forging of various alloys and refractory materials, evaluating mechanical and metallurgical problems
[ASM PAPER C7-5.4] 04 p0604 A69-14522

Beryllium properties, metallurgy, alloys, fabrication and applications in guidance components, aerospace structures and nuclear reactors
04 p0614 A69-14586

Metals study using field ion microscope for detecting dislocations, crystal boundaries and growth surfaces and surface diffusion energies
06 p0943 A69-17376

Refractory metal alloys metallurgy and technology - Conference, Washington, D.C., April 1968
07 p1164 A69-18790

Metals hydrogen embrittlement theory, discussing role of dynamic strain aging hypothesis in overcoming theory defects
09 p1523 A69-21849

Aluminum alloys role in aerospace technology, discussing temperature characteristics, gas absorption, weldability, purity, etc
11 p1903 A69-24518

Cast and forged steel mechanical properties noting starting materials and production methods roles in cast steel improvement
11 p1904 A69-24644

Beryllium properties and processing including magnesian reduction, powder purity, oxygen content, grain size and temperature effects on mechanical properties
11 p1904 A69-24897

Steels classification for welded construction according to heat treatment and metallurgical structures
12 p2111 A69-25826

Beryllium production, properties and technology, discussing ductility, welding and soldering problems, temperature effects, etc
16 p2793 A69-31788

Metallurgy, properties and applications of Co-Ni-Mo-Cr ultrahigh strength alloy, discussing corrosion
18 p3154 A69-34307

Z-micron sections removed from metal specimens by microtome for radiotracer study of mass dependence of self diffusion
19 p3313 A69-36490

METALS

NT ACTINIDE SERIES

NT ALKALI METALS

NT ALUMINUM

NT ALUMINUM COATINGS

NT ALUMINUM 26

NT BARIUM

NT BERYLLIUM

NT BERYLLIUM 7

NT BERYLLIUM 10

NT BERYLLIUM ISOTOPES

NT BISMUTH

NT CADMIUM

NT CADMIUM ISOTOPES

NT CALCIUM

NT CALCIUM ISOTOPES

NT CERIUM

NT CESIUM

NT CESIUM VAPOR

NT CESIUM 133

NT CHROMIUM

NT CHROMIUM ISOTOPES

NT COBALT

NT COBALT ISOTOPES

NT COBALT 60

NT COPPER

NT DYSPROSIUM

NT ERBIUM

NT EUROPIUM

NT GADOLINIUM

NT GALLIUM

NT GOLD

NT GOLD COATINGS

NT HAFNIUM

NT INDIUM

NT IRIIDIUM

NT IRON

NT IRON ISOTOPES

NT LANTHANUM

NT LANTHANUM ISOTOPES

NT LEAD [METAL]

NT LEAD ISOTOPES

NT LIQUID METALS

NT LIQUID POTASSIUM

NT LIQUID SODIUM

NT LITHIUM

NT LITHIUM ISOTOPES

NT MAGNESIUM

NT MAGNESIUM ISOTOPES

NT MANGANESE

NT MANGANESE ISOTOPES

NT MERCURY [METAL]

NT MERCURY VAPOR

NT METAL COATINGS

NT METAL CRYSTALS

NT METAL FILMS

NT METAL FOILS

NT METAL MATRIX COMPOSITES

NT METAL POWDER

NT METAL VAPORS

NT MOLYBDENUM

NT NEODYMIUM

NT NICKEL

NT NIOBIUM

NT OSMIUM

NT PALLADIUM

NT PLATINUM

NT PLUTONIUM ISOTOPES

NT PLUTONIUM 238

NT POTASSIUM

NT POTASSIUM ISOTOPES

NT POTASSIUM 40

NT POWDERED ALUMINUM

NT PRASEODYMIUM

NT RADIUM 226

NT RARE EARTH ELEMENTS

NT REFRACTORY METALS

NT RHENIUM

NT RHODIUM

NT RUBIDIUM

NT RUBIDIUM ISOTOPES

NT RUBIDIUM 86

NT RUTHENIUM

NT SAMARIUM

NT SCANDIUM

NT SCANDIUM ISOTOPES

NT SILVER

NT SINTERED ALUMINUM POWDER

NT SODIUM

NT SODIUM ISOTOPES

NT SODIUM VAPOR

NT SODIUM 22

NT STRONTIUM

NT STRONTIUM ISOTOPES

NT STRONTIUM 90

NT TANTALUM

NT TERBIUM

NT THALLIUM

NT THORIUM

NT THORIUM ISOTOPES

NT THULIUM ISOTOPES

NT TIN

NT TITANIUM

NT TRANSITION METALS

NT TUNGSTEN

NT ULTRAPURE METALS

NT URANIUM

NT URANIUM ISOTOPES

NT URANIUM 235

NT VANADIUM

NT YTTRIUM

NT ZINC

NT ZIRCONIUM

NT ZIRCONIUM ISOTOPES

NT ZIRCONIUM 95

Solar absorptance, total hemispherical emittance and absorptance/emittance ratio for metals at cryogenic temperatures measured simultaneously with sinusoidally perturbed incident radiation
01 p0176 A69-10847

Superconductivity and melting point of metals, discussing cause of anomalies
02 p0283 A69-11785

Tabular reduction of crystal structure chemical information for metals and semiconductors for material selection use
02 p0295 A69-11786

Dynamic mechanical behavior of metal at tip of plain strain crack, discussing fracture strength relation to triaxial plastic stability
02 p0343 A69-12284

Electromagnetic wave propagation in metals in magnetic field, noting helicon waves, magnetoplasma waves, waves with discrete spectrum or near cyclotron resonance and quantum phenomena
02 p0299 A69-12565

Metal composite materials, discussing strengthening mechanism for inclusion of high elastic coefficient and creep limit fibers in weak ductile matrices
02 p0268 A69-12750

Ground state energy for single magnetic impurity dissolved in nonmagnetic metal, applying cluster variation method to s-d interaction Hamiltonian
03 p0485 A69-13298

Metal-insulator transition, observability and transition in ionic lattices and polar liquids
03 p0489 A69-13922

Analytical determination of traces of metals caused by wear in aircraft liquid fuels, hydraulic fluids and lubricants, noting polarography and coulometry
03 p0435 A69-14101

Localized umklapp scattering effect on galvanomagnetic properties of nearly free electron bcc metal with spherical Fermi surface
03 p0493 A69-14240

Plasticity of metals under isothermal conditions at elevated temperatures
04 p0671 A69-14454

Metal heating by laser, noting heating rates exponential increase with time due to optical characteristics changes
06 p0932 A69-16915

Metal matrix composites - ASTM Conference, Boston, June 1967
06 p0938 A69-16940

Metal matrix composites highest potential for future use and development of filament-matrix compatibility in relation to high temperatures
06 p0939 A69-16941

Metal atom production by bombarding metal with positive ions from microwave discharge, obtaining isolation in inert gas matrix and UV spectra
06 p0957 A69-17113

Galvanic corrosion couples of metals and alloys tested in liquid fluorine, determining corrosion rates for possible missile components application
06 p0944 A69-17854

Solar absorptance and hemispherical emittance of metals at space conditions determined with cyclic incident radiation technique
[AIAA PAPER 69-60] 06 p0945 A69-18154

Direct bead sampling by aspiration of molten metal in open hearth furnaces and converters
07 p1141 A69-19341

Stellar atmospheres radiative opacity, computing metal absorption coefficients
07 p1220 A69-19392

Filler metals for HY steels, discussing tensile and yield strength, elongation and area reduction of butt welds deposited
08 p1320 A69-20406

Stresses and waves in highly conducting magnetoplastic metals as analogy of MHD processes in plasma
09 p1551 A69-22033

Atmospheric models for metal deficient stars of K and G spectral type, studying reduced metal abundance effect on atmospheric structure

09 p1596 A69-22055

Boron carbide filaments as reinforcements for metal structures, noting vapor deposition use of silica

09 p1529 A69-22070

Ceramic whiskers and metallic matrix chemical reactions during composite formation, analyzing coated and uncoated SiC whiskers in titanium matrix

09 p1527 A69-22359

Materials, processing and testing variables effects on mechanical properties determined for metal matrix composites

[ASME PAPER 69-GT-23] 09 p1527 A69-22496

Carbidothemic production of metals and binary and ternary alloys, discussing eutectic properties

09 p1514 A69-22731

Metallicity index Q value difference between cluster and noncluster galaxies determined from UV, blue and violet observation data

10 p1774 A69-22964

Metals with combined high damping and good mechanical properties for solving fatigue, noise and vibration problems

10 p1715 A69-24044

Electroplating solutions test for filament winding and electroforming process used in fabricating fiber reinforced metal composites

11 p1890 A69-24337

Direct measurement device for metallic material response to mechanical stresses from stress force and global displacement /including material deformation/

11 p1884 A69-24757

Soviet collection of papers on diffusion processes in metals covering welding, annealing, anisotropic crystals, metal condensation layer, cast iron decarboxization, etc

11 p1890 A69-24798

Diffusion processes during annealing of metals irradiated by electrons and neutrons, discussing crystal damage, recovery and recrystallization

11 p1891 A69-24800

Testing machines for metallic materials, discussing design criteria and application to tensile strength, vibration and durability test machines

[DVL-865] 11 p1889 A69-25682

Soviet monograph on nuclear radiation effect on structure and properties of metals and alloys covering electron, gamma and neutron radiation

12 p2114 A69-26469

Thermal emission from metal in contact with dielectric for cryogenic insulation applications

13 p2374 A69-27783

Optical depths of convection related to metal deficiency for main sequence and giant stars

14 p2527 A69-29946

Metallo ceramic materials strength as function of porosity calculated for tension, shear, bending and torsion deformations

15 p2638 A69-30283

Thermal stresses in fiber reinforced metals as function of volumetric content of fiber phase

15 p2638 A69-30285

Tensile, bending and impact strengths of materials produced by metal porous blank impregnation with molten glass, noting metal density and sintering effects

15 p2643 A69-31188

Solar chromosphere metal abundance determined taking into account local thermodynamic equilibrium departures

16 p2855 A69-31657

Light metals - Conference, Leoben, Austria, June 1968

16 p2799 A69-31774

Ceramic phase reinforcement of metals and alloys, discussing interfacial energies, binding forces and elastic stress fields

[ONERA-TP-661] 16 p2802 A69-32204

Structural modifications of metals and alloys accompanying various stages of creep, interpreting equations describing time-deformation relation

17 p2985 A69-32904

Sliding friction and wear properties of metal ceramic composites applied to aircraft brakes

17 p2987 A69-33375

Collection of papers on fracture, Volume 6, Fracture of metals

17 p2988 A69-33550

Temperature dependence of metal elastic properties including thermal strains effect on stress field, yield stress changes and elastic modulus variations

18 p3212 A69-34353

Electrode potential measurements for corrosion study of metals and alloys in aqueous solutions, molten salts and gaseous atmospheres

18 p3150 A69-35412

Optical frequencies mixing based on photoelectric effect in metals and semiconductors, noting internal photoconductivity

19 p3332 A69-35871

Atmospheric models for specified effective temperatures, hydrogen-to-metal ratios and surface gravities in studying metal deficiency effect on stellar atmosphere

19 p3425 A69-36338

Space age metals supply and demand relationships, discussing system engineering criteria for maximum efficiency

19 p3346 A69-36635

Low strain rate effects on metals yield and tensile strength

20 p3563 A69-38063

Vacuum heat treating and joining process for various ferrous and nonferrous metals and alloys, discussing advantages, applications and economics

[ASM PAPER D8-22.3] 20 p3551 A69-38132

Metals plastic behavior including strain hardening and Bauschinger effect

21 p3832 A69-38466

Metal deformation dynamics at elevated temperatures, discussing closed loop electrohydraulic testing machine for stress relaxation and strain rate sensitivity

21 p3689 A69-38595

Metal-polymer-metal and metal-polymer-silicon thin film structures analysis for polymers bulk properties and insulator-silicon interface, noting dipole-like relaxation

21 p3782 A69-39464

Molybdenum disulfide influence on electrochemical corrosion of metals

21 p3733 A69-39804

Metals conductivity under high pressure, giving theories for electrons scattering cross sections on ions and for Debye temperature

22 p3980 A69-40187

Multiquantum photoemissive effect in metals, semiconductors and dielectrics emphasizing laser application for studying electromagnetic field

22 p3964 A69-40690

Seizing characteristics of metals using electrical resistance as measure of lattice imperfection density due to friction

22 p3957 A69-41111

Galactic evolution using concept of stellar populations and correlation with metal and He abundances

23 p4218 A69-42323

Metallic and nonmetallic materials for space applications with launch and orbit condition requirements, examining finishes and lubricants

24 p4332 A69-43207

METAMORPHISM [GEOLOGY]

Textural variation relation to mineralogical and chemical characteristics of chondrites from review of published data

08 p1391 A69-20516

METASTABILITY

U METASTABLE STATE

METASTABLE ATOMS

Elastic scattering cross section for low energy electrons on metastable He atoms, using polarized orbital method

03 p0469 A69-12922

Time dependence of laser output in C and N atoms following dissociative excitation transfer explained in terms of measured populations of excited states

05 p0795 A69-15663

Noble gas atom simultaneous ionization and excitation by removal of metastable electron in fast collision

06 p0961 A69-17137

Forward scattering of metastable and ground state argon atoms after argon ion-atom charge transferring collisions, discussing excitation resonances

08 p1354 A69-19809

Continuous polarized electron beam produced from spin conversion in ionizing reactions involving optically pumped metastable atoms in He discharge

12 p2130 A69-26312

Laser interferometer determining spatial distribution of neon metastable state in He-Ne active discharge, discussing lens effects

12 p2108 A69-26636

Residual gas analyzer and leak detector by time of flight measurements on neutral metastable atoms and molecules between pulsed electron gun and auger surface detector

13 p2262 A69-28006

Photoinduced shock processes involving metastable hydrogen atoms and molecules, discussing vibrational and rotational levels

16 p2813 A69-31754

Monograph on ionization of Ar-CH mixtures during Townsend discharge, covering metastable Ar atoms lifetime in various pressure ranges

16 p2814 A69-31841

Forbidden atomic transitions involving metastable species in upper atmosphere, tabulating permitted and forbidden molecular band systems

19 p3421 A69-36214

Spectroscopic measurements of weakly ionized Ar plasma premixed with diatomic N in plenum chamber, demonstrating role of competitive reactions for metastable Ar atom

21 p3779 A69-39794

Metastable atom detection system for ground state atom beams, measuring Ar beam density five orders lower than background gas density

22 p3950 A69-41230

Detection of metastable He, H, Ne, Ar, Kr, Xe and molecular nitrogen with continuous channel electron multipliers

22 p3917 A69-41235

He-Ne laser heterodyne system for measuring dispersion at 6328 and 6401 A due to Ne metastable atoms in gas discharge

23 p4172 A69-41397

METASTABLE STATE

Metastable positive He molecules and He atoms decay in afterglow, taking into account simultaneous emission at 4650 angstroms during absorption studies

02 p0287 A69-11932

Metastability of 1D state of negative N ion, instability of 3P state and energies of both states

02 p0284 A69-12598

Q switched Ruby laser metastable state population kinetics and resonator losses, discussing internal energy redistribution with subsequent absorption spectrum changes

04 p0610 A69-14381

Metastable phases of binary zirconium-niobium system, defining decomposition of solid solution in cooling

05 p0781 A69-16614

Metastable level population measurement in laser crystal based on luminescence changes under influence of stimulated emission

06 p0934 A69-17457

Metastable helium abundance in interstellar and intergalactic space, inferring low energy cosmic ray concentration

06 p1010 A69-17973

Metastable phases in titanium alloys with beta alloying elements

07 p1162 A69-18773

Temperature profile and power density distribution in metastable level of ruby laser rod during pumping in air

07 p1150 A69-18937

Metastable molecules and fragments produced by electron excitation of nitrogen, hydrogen, carbon dioxide and nitrous oxide, noting excitation functions, kinetic energy, etc

13 p2301 A69-27362

Combined free and forced convection flows in parallel channel systems and in single channels, discussing metastable flow regimes, single phase laminar flows, etc

13 p2377 A69-28152

Q switched ruby laser metastable state population kinetics and resonator losses, discussing internal energy redistribution with subsequent absorption spectrum changes

14 p2456 A69-28754

Metastable ions formation and detection in double focusing mass spectrometer, calculating location of decomposition in electrostatic analyzer and doubly charged ions transition

15 p2561 A69-30021

Two photon decay of metastable levels of hydrogenic and He-like ions in solar corona, depopulating via proton collisional excitation to 2p level

19 p3396 A69-36218

Metastable level population measurement in laser crystal based on luminescence changes under influence of stimulated emission

20 p3555 A69-37940

Spectral distribution of two photon emission from metastable state of singly ionized He by broadband spectroscopic coincidence counting technique

23 p4220 A69-42378

- Elastic electron scattering by metastable states of rare gases, using effective potential matching experimental binding energy of negative ions
24 p4354 A69-43818
- METAZOA**
U ANIMALS
- METEOR BURSTS**
U METEOROID SHOWERS
- METEOR HAZARDS**
U METEOROID HAZARDS
- METEOR TRAILS**
Mechanism responsible for luminosity of long duration meteor trains, discussing color changes, band emission and train spectra as function of height and duration
01 p0154 A69-10874
- Wind profile harmonic analysis based on meteor trail observations, noting wind power spectra and propagating waves in atmosphere
01 p0072 A69-11170
- Particles behavior after separation from meteor, considering deceleration for separation altitudes and initial velocities
02 p0314 A69-11645
- Envelope distribution of echo signal during reflection scattering by extended turbulent meteor trails
02 p0207 A69-11690
- Meteor masses and atmospheric density calculation inaccuracy by use of effective stellar magnitudes of meteors
02 p0314 A69-11695
- Wind measurements by radio observation of meteor trails compared with fading drift results
02 p0275 A69-12042
- Electron concentration in lower ionosphere based on measurement of Faraday rotation of polarization plane of radio waves scattered by meteor trail
03 p0423 A69-13535
- Bolide fireball radiation maximum efficiency from observed spectra, using monochromatic radiation efficiency data for rarefied atoms and ions in meteor comas
03 p0512 A69-13692
- Diffuse meteor stream separation from sporadic background, using orbital elements of individual meteors
04 p0659 A69-15034
- Soviet book on meteor trail scatter communications covering civil and military advantages over troposcatter systems, meteor trail scatter properties, etc
04 p0562 A69-15488
- Meteoroid mass distribution determined by radar observations of underdense meteor trails at Springfield Meteor Observatory
06 p1003 A69-17493
- Receiving system of CENFAM multistation radar project for meteoric and upper atmosphere studies composed of antennas connected to form product-interferometer pairs
07 p1077 A69-18674
- Duty cycle increase on meteor forward scatter radio communication paths by use of wide-beam transmitting antenna along great circle
08 p1394 A69-20609
- 11 Canis Minor meteor stream orbit computed, noting retrograde orbit and 4.2 million km perihelion
08 p1394 A69-20621
- Ionized meteor trails initial radii statistical characteristics determined for two models
10 p1783 A69-23917
- Spectral measurement of luminous trails produced by injecting high velocity submicron diameter iron particles into gaseous targets compared with meteor spectra
10 p1790 A69-24142
- Artificial noctilucent clouds or meteor trails positions determined by transforming photogrammetric coordinates
12 p2154 A69-25822
- Color photograph of group of meteor trails with red glow beneath by automatic camera from balloon at 30.6 km
12 p2157 A69-26231
- Reflection coefficient of polarized radio waves at ionized meteoric trails obtained by numerical integration of differential equations
12 p2031 A69-26691
- Wind structure in atmosphere meteor region from persistent meteor trail radio echoes amplitude fluctuations, noting horizontal wind velocity profiles
12 p2074 A69-26962

- Visual and photographic observations of Perseids meteor trails velocity noting discrepancy
13 p2353 A69-28035
- Envelope distribution of echo signal during reflection scattering by extended turbulent meteor trails
13 p2224 A69-28721
- Meteor masses and atmospheric density calculation inaccuracy by use of effective stellar magnitudes of meteors
13 p2355 A69-28726
- 17 November 1966 Leonids return, tabulating data from previous returns starting with October 899
14 p2525 A69-29715
- Lyrid and Perseid meteor spectra for spectral line identifications in 3100-4000 Å UV range, listing lines from six neutral atoms and five ions
15 p2700 A69-31500
- Meteorite entering earth atmosphere on 25 April 1969 over England, describing path, size and recovered fragments
15 p2701 A69-31528
- Meteoric elements ionization and loss mechanisms in E region, discussing roles of atomic oxygen and metal ions chemical reactions
16 p2780 A69-32313
- Meteoric trails radar observations to measure zonal wind profiles between 80-110 km, noting short period oscillations
16 p2865 A69-32609
- Meteor trail drift radar observations in Kharkov, giving wind velocity diurnal and seasonal variations
17 p3041 A69-33897
- Radar unit for network component (wind patrol) in statistical observations of wind drift conditions in meteor trails
17 p2939 A69-33901
- Automatic radar station for meteor observations, discussing separate transmitting and receiving antennas directive gain and radio echo power
17 p2939 A69-33902
- Photographic networks for meteors orbits and trajectories and meteorites impact points during nighttime, discussing fireball occurrence
19 p3415 A69-36120
- Network for fireball trajectories rapid analysis to recover meteorites and obtain orbital elements data, noting role of planetariums
19 p3295 A69-36121
- Wind shear effects on radar echo decay constant for finite meteor trail, considering roles of trail length and electron density variations
19 p3276 A69-36482
- Meteor radio electronics principles, methods and equipment, discussing ionized meteor trail formation, radar tracking and utilization of trails for communications
19 p3277 A69-36591
- Meteor winds analysis method used on tidal period wind measurement data obtained by chemical release from rocket in 95-135 km region
20 p3574 A69-38092
- Radio wave reflection from irregularly ionized meteor trains, discussing decay time scatter and electron line density
22 p3899 A69-39969
- Visual observation of meteor and train microstructure obtained by refractor
22 p4033 A69-41058
- Radio echoes diffraction patterns determination from reflection coefficients of polarized radio waves reflected from ionized meteor trails
23 p4214 A69-41846
- Qualitative model of atmospheric mass circulation constructed from radar meteor trail drifts observations, considering solar thermal radiation and zonal wind direction
23 p4214 A69-41862
- Ionized meteor trails reflection zone altitudes determination by interferometric measurements of phase differences
24 p4311 A69-43508
- METEORITE COLLISIONS**
Barrier penetration depth by meteorite particles at prethreshold impact velocities, taking into account energy dissipation on shock wave front
01 p0152 A69-10579
- Ching iron meteorite discovery site, noting no crater or impact traces
01 p0160 A69-11380
- Meteoroid hazard, discussing possible future collisional dangers for space traffic
01 p0160 A69-11412

- Barrier penetration depth by meteorite particles at prethreshold impact velocities, taking into account energy dissipation on shock wave front
15 p2709 A69-30749
- Lunar mascon origin from collisions of large masses with lunar surface
15 p2698 A69-31328
- Meteorite impact hypothesis supported by autochthonous and mixed breccias, shattercones and microscopic shock deformation evidence in central uplift rocks at La Malbaie structure
22 p4021 A69-40410
- METEORITE COMPRESSION TESTS**
U COMPRESSION TESTS
U MECHANICAL PROPERTIES
U METEORITES
- METEORITE CRATERS**
Meteorite structure and origin, discussing cosmic dust analysis and collection, Tungusk silicate-magnetite spherules, asteroid collisions and meteorite ages
01 p0159 A69-11367
- Thermoluminescence intensity of dolomite specimens from Kaali meteorite craters, discussing meteorite impact thermomechanical effect and crystal lattice defects
01 p0159 A69-11371
- Lunar mascons size and depth calculated in terms of mare formed by low velocity iron meteorites impact
04 p0654 A69-14629
- Nature and origin of lunar far side Tsiolkovsky crater
06 p1003 A69-17386
- Structure transitions in iron meteorites from Widmanstätten to granular pattern to study Barringer crater and Canon Diablo meteorites formation
09 p1597 A69-22154
- Meteor explosion theory of origin of lunar craters and round maria, suggesting endogenic origin
10 p1784 A69-23960
- Moldavites and Ries crater material, studying Rb-Sr isochronal relationship
23 p4154 A69-41341
- Impact origin of Ivory Coast tektites and Bosumtwi Crater indicated by gamma ray spectrometric study of U, Th and K abundance patterns
23 p4210 A69-41347
- METEORITES**
NT ACHONDrites
NT AUSTRALITES
NT CARBONACEOUS METEORITES
NT CHONDRITES
NT IRON METEORITES
NT KAPOETA ACHONDRITE
NT MURRAY METEORITE
NT ORGUEIL METEORITE
NT PANTAR CHONDRITES
NT SIKHOTE-LIN METEORITE
NT STONY METEORITES
NT TEKTITES
NT TUNGUSK METEORITE
- Preatmospheric meteorite size determination from distribution of radioactive isotopes resulting from nuclear reactions produced by cosmic rays, discussing core sources
01 p0159 A69-11375
- Meteorite collections in museums of Lvov, U.S.S.R., noting specimens from Pultusk shower, Kansas, Mexico, Czechoslovakia and U.S.S.R.
01 p0160 A69-11388
- Etching techniques for revelation and viewing of fossil charged particle tracks in meteoritic and terrestrial minerals
02 p0245 A69-12569
- Chemical composition of nuclear cosmic rays with Z greater than 22, noting etching techniques for utilizing meteoritic minerals as detectors
05 p0816 A69-16355
- Meteorites radiogenic and cosmic ray exposure ages, orbits and parent bodies, discussing H and L group chondrites
08 p1405 A69-20928
- Asteroidal and cometary orbits and origin of meteorites, discussing eccentricities, exposure ages and mass yield
08 p1406 A69-20929
- Stratospheric dust, discussing terrestrial and meteoritic origins, volatility of particles smaller than few microns, and light scattering and direct sampling measurements
09 p1608 A69-22689
- Possible sources of meteoritic material from Hopewell Indian burial mounds
11 p1963 A69-25401
- Vilna meteorite bolide observation with all-sky camera noting seismic and analytic records
13 p2334 A69-27189

Meteorite entering earth atmosphere on 25 April 1969 over England, describing path, size and recovered fragments

15 p2701 A69-31528

X ray detectable preferred disorder in solids by shock loading studied in Ainsworth meteorite and in hexagonal alpha silicon dioxide

15 p2671 A69-31538

Meteorite origin theory limitations from microscopic examination and microprobe analyses of chondrules in unequilibrated meteorites

17 p3034 A69-33585

Meteorite research - Conference, Vienna, August 1968

19 p3403 A69-36072

Meteorites data in planetary cosmogony, discussing iron meteorite ages, Xe retention in chondrites and synchronism of sun and protoplanetary cloud forming

19 p3406 A69-36075

Densities and angular distributions of fossil tracks in meteorites produced by slowing down heavy primary cosmic ray nuclei

19 p3410 A69-36096

Meteorite orbits analysis with emphasis on recovered meteorites, noting fireballs and hyperbolic orbits

19 p3414 A69-36115

Modified Monte Carlo model applied to computerized meteorite orbit evolution, simulating secular perturbations by imposing sinusoidal variation on orbital elements

19 p3414 A69-36117

Photographic networks for meteorites orbits and trajectories and meteorites impact points during nighttime, discussing fireball occurrence

19 p3415 A69-36120

Saint-Severin amphoterite geometrically reconstructed from fragments in form prior to atmospheric breakup, noting agreement with track densities of iron ions

19 p3416 A69-36128

Shock histories of hexahedrites and Ga-Ge group III octahedrites based on metallographic and X ray diffraction analysis, noting meteorites shocked preterrestrially

19 p3418 A69-36136

Shock wave parameters from meteoric body moving at high supersonic speeds through atmosphere, calculating specific heat ratio

19 p3428 A69-36841

Soviet book on shock waves propagated by meteorite intrusion into earth atmosphere, covering interaction with earth surface, Tungusk meteorite, etc

20 p3613 A69-38205

Average meteorite flux at Martian surface estimated by generating flux distribution for Martian atmosphere top and adjusting for mass loss and deceleration

24 p4387 A69-43351

METEORITIC COMPOSITION

Meteoritic extraterrestrial materials sampling for chemical, petrographic and metallurgical analyses, discussing microstructure and optimum specimen weight for representative analysis

[UN PAPER 68-95381] 01 p0150 A69-10480

Monograph on nature of planets and solar system origin covering meteorite observations and age determination, chondrite composition, metallic elements, etc

01 p0152 A69-10702

Replicate neutron activation determinations of Ga, Ge, In and Ir in L group chondrites, proposing model which accounts for observations

01 p0155 A69-10976

Chondrules in Sharps /H-3/ chondrite show evidence of recrystallization and homogeneous olivines and pyroxenes

01 p0156 A69-10977

Carbonaceous, enstatite and stony meteorite classification on basis of siderophyllic, chalcophyllic and lithophilic element proportions or isotope composition, discussing thermodynamic equilibrium

01 p0025 A69-11368

Uranium in meteorites, discussing U content and isotope composition, Pb isotope ratios, radiogenic Pb, origin of matter and meteorite ages

01 p0025 A69-11369

Mineralogy of iron fragments from impact craters near Lake Kaali, Estonia, discussing structure and type of meteorite

01 p0159 A69-11370

Nerft and Kaande stony meteorites mineralogical composition from microscopy, noting olivine hypersthene chondrite classification

01 p0159 A69-11374

Meteoritic materials investigated for Sc, Ce and Eu content and distribution in various phases, using neutron activation analysis

01 p0026 A69-11376

Tungusk meteorite preceding and succeeding atmospheric events, explosion and origin

01 p0159 A69-11378

Chemical composition of various types of chondrites, determining quantitative proportions soluble and insoluble in acids

01 p0026 A69-11381

Stone meteorite chemical composition, analyzing chondrites Borodino, Lavrentevka, Alfianello and Nardoo II

01 p0026 A69-11382

Minerals in ablated crust of Saratov meteorite using X ray analysis

01 p0160 A69-11385

Meteorite dust composition of Tungusk meteorite noting angular and spherical particles

01 p0160 A69-11386

Enstatite chondrites structure and mineral content and composition using microscopic and X ray analysis, grouping parameters in distinguishing types

02 p0317 A69-12016

Rubidium, Sr and Sr isotopic composition of normal gray hypersthene chondrite falls, noting Rb/Sr and Sr87/Sr86 ratio determination of Bath Furnace L chondrite isochron

02 p0317 A69-12020

Magnetite content of type I carbonaceous meteorite from quantitative X ray diffractometry of Orgueil meteorite

02 p0328 A69-12729

Meteorite fragments fall and distribution at Bur-Ghelui, Somalia, discussing crust morphology, mineralogical composition and structure

03 p0507 A69-13095

Australites from Port Campbell and Princetown region of Western Australia

03 p0507 A69-13096

South African octahedrite containing inclusions of troilite and graphite veined with kamacite

03 p0507 A69-13097

Oxygen partial pressure, temperature and olivine composition related, determining distribution coefficient of Fe and Mg between olivine and pyroxene

03 p0516 A69-14082

Electron microprobe analysis of potassium feldspar in Weekeroo Station meteorite

04 p0659 A69-14979

Nepheline occurrence in unequilibrated chondrites, discussing crystallographic evidence from X ray powder patterns

04 p0659 A69-15010

Boron determination in type I carbonaceous chondrites by nonaqueous colorimetry, comparing results with ordinary chondrites

04 p0661 A69-15147

Hydrothermal investigation of Ge trace quantity distribution between metal, silicate and sulfide phases at controlled oxygen partial pressure by oxygen buffer techniques

05 p0819 A69-15624

Heavy xenon isotopic anomalies in carbonaceous chondrites, rejecting plutonium 244 spontaneous fission decay mechanism

05 p0819 A69-15625

Chemical compositions and structural states of feldspar in recrystallized /Type 6/ chondrite meteorites, using electron microprobe analysis and X ray diffraction techniques

05 p0819 A69-15626

Nitrogen abundances in chondritic meteorites determined by carrier gas fusion extraction

05 p0825 A69-16301

Stony meteorite Krahenberg, determining isotopic composition, rubidium and strontium age of dark and light portions by neutron activation analysis

05 p0826 A69-16439

Rare gases in stony meteorites, noting premordial inheritance and complex Xe anomalies

05 p0826 A69-16440

Isotopic composition in near-surface regions of meteorites due to nuclear processes with low energy solar particles

06 p0989 A69-17282

Electron microprobe analysis of vanadium in presence of titanium by compositional measurement of chromite in chondritic meteorites

07 p1073 A69-18419

Chemical composition and morphological, structural, textural and mineralogical characteristics of chondrules and chondrites

07 p1212 A69-18548

Chemical analysis, isotopic composition, structure and mineralogy of meteorites for classification into iron and stones, discussing time variation of temperature, pressure, etc

07 p1224 A69-19710

Alternative explanation of garnet composition in Coorara meteorite, giving probable formula

08 p1382 A69-19819

Chondrite meteorite fall /1969/ in Mexico, noting opaque and microcrystalline matrices and gamma rays from short lived isotopes

08 p1396 A69-20686

Plutonium-244 existence in early solar system concluded from relative abundance ratios of excess meteoritic heavy Xe isotopes

08 p1401 A69-20900

Primitive elemental abundances in solar system, discussing composition of sun, meteorites and lunar maria

08 p1403 A69-20914

Fractionation of abundant lithophile element ratios in chondrites emphasizing Si-Mg ratio

08 p1403 A69-20915

Rare earth elements and yttrium in meteoritic chondrules determined by radiochemical neutron activation analysis

08 p1403 A69-20916

Indium abundances in chondritic and achondritic meteorites and terrestrial rocks determined by radiochemical neutron activation analysis

08 p1404 A69-20917

Gold and iridium concentrations in meteoritic and terrestrial materials by neutron activation, discussing chondrules, meteoritic troilite and metallic spherules

08 p1404 A69-20918

Antimony bromine and mercury abundances in meteoritic materials determined by neutron activation analysis

08 p1404 A69-20919

Mercury concentration relation to thermal history of chondritic meteorites, using activation analysis

08 p1404 A69-20920

Trace element distribution in metal phase of chondrites and iron meteorites, using neutron activation analysis with radiochemical separation

08 p1404 A69-20921

Trace elements distribution in Smithonia iron meteorite by spark source mass spectrometry, noting terrestrial weathering effects

08 p1404 A69-20922

Chlorine as indicator of terrestrial contamination in iron meteorites, using neutron activation analysis and metallographic observation

08 p1405 A69-20923

Radioactive decay products concentration from extinct radioisotopes in meteorites with estimation of formation interval, discussing fissiogenic xenon and solar system nucleosynthesis

08 p1405 A69-20924

Ne and Xe in carbonaceous chondrites, noting large amounts of fission Xe and implications for galactic nucleosynthesis models

08 p1405 A69-20925

Redistribution of potassium and argon in meteorites and rock samples, discussing thermal diffusion and grain size

08 p1405 A69-20926

Electron probe analysis of olivine and pyroxene in LL-group chondrites, discussing iron and fayalite composition and unequilibrated stones

08 p1406 A69-20931

Magnetite morphological variations of type I carbonaceous meteorites, discussing isometric crystals, spheres, spherulites, platelets and filaments

08 p1406 A69-20932

Boron in tektites determined by calorimetric technique for analysis of boron in silicates, comparing results with values from igneous and sedimentary parents

08 p1407 A69-20936

Geochemistry and element abundances for Henbury impact glass, Darwin glass and australites, noting evidence for meteorite impact on sandstone

08 p1407 A69-20937

Statistical distribution of chemical elements average abundances in earth crust and meteorites and nucleosynthesis of elements under specific astral conditions

08 p1310 A69-20941

Rare earths relative and absolute terrestrial abundances in shales, basalts, rhyolites and granites

08 p1310 A69-20942

Meteoritic materials structure, composition and magnetic properties, supporting theory for solar system formation from supernova outbursts

09 p1593 A69-21581

Kodaikanal iron meteorite measurements for cosmogenic rare gases and K-Ar isotopes ages for glass inclusions

09 p1596 A69-22047

Thin sections of ringwoodite natural spinel in Tenham meteorite shower, observing various rounded purple isotropic grains

09 p1597 A69-22155

Tritium and argon 39 measurements of stone and iron meteorites, discussing decay and production rates and cosmic ray intensity

09 p1604 A69-22398

Cosmic ray induced radioactivity in lunar surface and meteorites calculated together with cosmic ray intensity variations

10 p1756 A69-22817

Water content of tektites, impactites and artificial glass of tektite composition using IR absorption measurements

10 p1778 A69-23413

Aluminum abundances in stony meteorites measured using nondestructive instrumental neutron activation analysis

11 p1952 A69-24334

Chemical and mineralogical study of Kodaikanal meteorite silicate and metal phases, using optical, X ray and electron microprobe techniques

11 p1953 A69-24335

Chemical composition analysis of one mesosiderite and seven chondrites, with notes on mineralogy and chemical procedures

11 p1953 A69-24336

Organic matter signals in carbonaceous meteorites, discussing possible relation to extraterrestrial life and origin

11 p1953 A69-24342

Chemical composition of stony meteorites by analytical methods, discussing sample preparation and X ray fluorescence

11 p1953 A69-24358

Quality assessment of quantitative data on chemical composition of stony meteorites, considering precision and accuracy

11 p1953 A69-24359

Lithophile elements relationship in chondrites and basaltic achondrites, tabulating Ca-Al ratios and Ca, Al, Ti, Zr, Sr, Ba and Sc percentages

11 p1954 A69-24360

Possible sources of meteoritic material from Hopewell Indian burial mounds

11 p1963 A69-25401

Freshly fallen meteorites from Portugal and Mexico, determining exposure age and classifying into iron meteorite and carbonaceous chondrite types

12 p2160 A69-26935

Organic analysis of Pueblito de Allende meteorite using thin layer chromatography or combined gas chromatography and mass spectrometry

13 p2337 A69-27520

Chondritic meteorites arsenic, tin and antimony content determined by anion-exchange chromatography and neutron activation analysis

13 p2344 A69-27630

Tishomingo iron meteorite metallography, noting nickel content and martensitic microstructure evolution

13 p2353 A69-28159

Oxide composition of silicate spherules from forest area devastated by Tunguka meteorite explosion using electron microprobe analysis

14 p2516 A69-28869

Rb 87-Sr 87 age of bronzite chondrites, analyzing olivine bronzite chondrite falls for K, Rb and Sr elemental concentrations

14 p2526 A69-29881

Geochemistry of fission Xe component in chondrites, suggesting Xe derivation from superheavy elements with Z 112 to 119

15 p2681 A69-30325

Chondritic Cr and Mn content studied by X ray fluorescence, noting positive correlation in H and L groups and negative correlation in carbonaceous chondrites

15 p2681 A69-30416

Chlorapatite and whitlockite compositions of phosphate minerals from chondrites determined by electron microprobe

15 p2690 A69-30706

Silicon in iron meteorites and earth core determined by activation analysis on octahedrites, hexahedrites and ataxites

16 p2865 A69-32807

Volatiles percentage at 1000 C in nitrogen atmosphere for chondrites, considering cosmo-petrological significance of microchondrule coalescence

17 p3030 A69-33067

Cosmogenic Al 26 in achondrites and chondrites measured by nondestructive gamma-gamma coincidence counting

17 p3034 A69-33584

Uranium abundances in several eucrites measured by fission track method, discussing Pu-Xe decay interval question

17 p3044 A69-34167

Heavy nuclei origin based on empirical abundance distribution, discussing stellar, galactic and cosmic events for nuclear genesis

17 p3009 A69-34190

Percorait phase in nickel analog of clinohyrosite formed under hydrothermal conditions in Wolf Creek meteorite cracks

18 p3199 A69-34824

Bovey Chondrite fall in Northern Ireland, describing fragments trajectory and metal, sulphide and silicate presence

18 p3200 A69-34993

Barringerite as Fe-Ni phosphide occurring in meteorite Ollague pallasite, indicating troilite and schreibersite crystallization at high temperatures

18 p3205 A69-35433

Meteorite and primordial matter composition related to possible fractionation processes influence, discussing nuclear species abundance

19 p3406 A69-36073

Pu/U ratio from fossil track studies bearing on extinct Pu 244 in Campo del Cielo and Kodaikanal meteorites

19 p3407 A69-36077

Iron distribution inconsistency indicated in Group H and L chondrites through Ni and Co analysis of fractionated samples, plotting atomic ratios on Prior diagram

19 p3407 A69-36078

Terrestrial planets high temperature evolution from solar system genesis theory, discussing meteorite chemical composition, petrography, mineralogy and age determination

19 p3407 A69-36079

Meteoritic trace elements with varying chemical and physical properties investigated for abundance by neutron activation technique

19 p3407 A69-36080

Carbon content and isotopic composition in light and dark portions of gas-rich chondrites Breitscheid and Pantar

19 p3408 A69-36081

Mossbauer spectra of Fe minerals in unequilibrated ordinary chondrites, noting ratios of olivine to pyroxene iron

19 p3408 A69-36082

Meteorite Li isotopic composition variations to determine neutron role in nucleosynthesis of solar system light elements

19 p3408 A69-36084

Boron, Li and Cl contents in iron and stone meteorites by fluorometric, thermal-neutron activation and pyrohydrolytic separation methods, tabulating results

19 p3408 A69-36085

Sharps chondrite chemical, petrographic and mineralogical studies suggesting formation from complex and repetitious high temperature events and agglomeration processes

19 p3408 A69-36086

Fractionation of abundant lithophile element ratios of Si, Mg, Ca, Al and Ti in carbonaceous, common and enstatite chondrites

19 p3409 A69-36087

Ramsdorf meteorite chondrules and metal particles formation attributed to shock-induced partial melting and rapid cooling

19 p3409 A69-36088

Tieschitz and Mezo-Madaras chondrites and chondrules formation from considerations of coexisting minerals and interstitial ground mass

19 p3409 A69-36089

Bjurböle chondrules composition and density, discussing formation of homogeneous olivines and pyroxenes

19 p3409 A69-36090

Ca-rich achondrites genesis implied from rare earth and Ba absolute and relative concentrations

19 p3409 A69-36091

Cosmic ray produced radionuclides and rare gas isotopes from Saint-Severin meteorite surface, showing relative Kr spallation mass yields dependence on cosmic ray energy spectra

19 p3410 A69-36093

Cosmic ray produced radionuclides P 32, Cl 36, Ar 37 and Ar 39 determined in separate mineral phases of meteorites, emphasizing ratios in metals

19 p3410 A69-36094

Energy spectrum of Fe group heavy nuclei from fossil track densities depth variation in hypersthene and oligoclase crystals from meteorite Saint-Severin, noting ablation

19 p3410 A69-36095

Heat generation in meteorites by radioactive isotopes generated by early solar proton irradiation prior to solar system solidification

19 p3411 A69-36098

Cosmic-ray-produced stable and long-lived nuclides in iron meteorites, considering shielding effect on spallation production

19 p3411 A69-36099

Ar 39 and Cl 36 production rates and ratios in stone and stony-iron meteorites metal phases, discussing terrestrial age calculation

19 p3411 A69-36100

Ar 39 content in chondrites interpreted for meteorite size, exposure age and orbital elements

19 p3411 A69-36101

Meteoritic trace elements and radionuclides measured by gamma coincidence techniques, emphasizing Mn 53 and Al 26

19 p3412 A69-36103

K and Ar 40 determination in iron meteorites by neutron activation for K/Ar dating

19 p3412 A69-36106

Lance chondrite C III, studying mineral composition of chondrules and heterogeneous crystalline fragments

19 p3413 A69-36110

Carbonaceous meteorites mineralogically identified by selected-area electron diffraction, suggesting formation from minerals mixtures

19 p3311 A69-36111

Carbonaceous meteorites specimen petrographic observations, noting genetic interrelations with ureilites regarding S-C and reduced Fe oxidized Fe ratios

19 p3413 A69-36112

Isoprenoids and isomeric alkanes identification in carbonaceous chondrites by gas-chromatographic mass-spectrometric analyses, including results from troilite nodules

19 p3414 A69-36113

Proton and deuteron energy used to study solid state chemical reactions effects on meteorites composition and properties, obtaining hydroxyl ions and hydrocarbons

19 p3414 A69-36114

Cr-S and Cr-Fe-S systems phase relations, using silica tube and collapsible tube experiments, correlating formation conditions of meteoritic sulfide assemblages

19 p3359 A69-36123

Reflectivity and chemical composition of metallic phase minerals in stone meteorites, showing optical characteristics sensitivity to composition

19 p3415 A69-36124

Phosphate mineralogy of meteorites using X ray, electron-microprobe and chemical analyses, noting predominance of whitlockite

19 p3416 A69-36126

Black chondrite inclusions in Cumberland Falls meteorite, discussing inclusion chemical, mineralogical and electron probe data

19 p3416 A69-36127

Iron meteorites genetic classification based on parent body cooling rate and Ga-Ge trace element content

19 p3416 A69-36129

Iron meteorites analysis for Ni, Co, P, C, S and Cu elements by milling technique, noting superiority degree based on Co-Ni correlation

19 p3417 A69-36130

Kamacite analysis for P and Ni in chondrites, palasite and iron meteorites, considering cooling rate and rhadbite

19 p3417 A69-36131

Morphologies and mechanical properties for identification of phosphides /schreibersite/ and carbides /cohenite/ in iron meteorites, noting nucleation and growth

19 p3417 A69-36133

Dynamically deformed structures in chondrites and hexahedrites observed to discriminate among theories about origin of chondrules and meteorites

19 p3418 A69-36135

K 40-Ar 40 age measurements in separated mineral phases of chondrites, including production rates of spallation isotopes

19 p3418 A69-36137

Spallogenic rare gas concentrations and isotopic ratios in taenite of iron meteorites measured mass spectrometrically and compared with kamacite values

19 p3419 A69-36139

Trapped rare gases in Fe phase and silicate inclusions of Campo del Cielo Meteorite, El Taco

19 p3419 A69-36140

Thermal rare gas release from mineral separates of Mocs meteorite, using method giving activation energies as function of temperature

19 p3419 A69-36141

Distribution and origin of primordial He, Ne and Ar in Fayetteville and Kapoeta meteorites extracted and analyzed by laser-microprobe mass spectrometer

19 p3419 A69-36142

Stony meteorite barium isotopes and iron meteorite and terrestrial silicate inclusions analyzed using double spike method for laboratory fractionation correction

19 p3425 A69-36422

Alpha-scattering experiments by Surveyor missions, studying hypothesis regarding lunar origin of eucrites and howardites

20 p3597 A69-37341

V 50/V 51 abundance ratios in chondrite, terrestrial diabase standard W-1 and reagent V

20 p3601 A69-37501

Spontaneous symmetric fission of superheavy elements near doubly magic nucleus as explanation for Xe and Kr isotopic composition anomalies in meteorites

20 p3601 A69-37503

Petrology, mineralogy and phase composition of Siena chondrite, interpreting meteorite as ignimbritic rock or welded tuff

20 p3602 A69-37534

Calcium rich achondrites radiation ages determined from measuring He, Ne and Ar in howardites, nakhlites and angrite

20 p3602 A69-37535

Meteorites Ni-Fe metal structures analysis as part of petrology study of mesosiderites

20 p3602 A69-37536

Chemical classification of iron meteorites with Ge concentrations between 80 and 200 ppm, reporting concentrations of Ge, Ni, Ga and Ir

20 p3602 A69-37537

Meteorite minerals as detectors for studying fossil record of cosmic ray nuclei, emphasizing feldspars and pyroxenes

20 p3590 A69-37568

Gamma ray emission of meteorite of 25 April 1969 measured by scintillation spectrometry, attributing peaks to annihilation radiation, Cs 137, Mn 54, etc

20 p3590 A69-37571

Fe-Ni unmelted and unablated micrometeorites number at earth surface calculated, using space density of interplanetary particles and micrometeoritic theory

20 p3614 A69-38251

Abundance compilations of elements due to nuclear processes, discussing carbonaceous chondrites character

21 p3789 A69-38812

Meteoritic compositions used to determine prehistoric cosmic rays composition and energy spectrum

21 p3789 A69-38815

Amphoterite /LL/ chondrites Rb-Sr age determination, noting high brecciation

21 p3814 A69-39583

Sporopollenin content of Orgueil and Murray meteorites as evidence for extraterrestrial life

21 p3662 A69-39617

Morphological, chemical and X ray analysis of urelite meteorite, identifying diamonds with kamacite and troilite admixtures from carbonaceous material

21 p3816 A69-39626

Stony meteorite composition and structure studied for conditions of preplanetary stage of solar system

22 p4012 A69-40084

Meteoritic organic matter origin, discussing time-of-flight mass spectrometer combined with gas chromatographic capillary column

22 p4012 A69-40085

Tektite origin theories, discussing Surveyor experiments effects on lunar geology and Tektite origin

22 p4012 A69-40086

Hoba meteorite surface radioactive isotope composition measured, finding terrestrial age from Ni-59 activity

22 p4021 A69-40411

Meteorite chemical and mineralogical composition and classification

22 p4032 A69-40981

Extraterrestrial objects composition in defining cosmic abundance curve, including solar and meteoritic data

22 p4032 A69-40982

Bogou iron meteorite Ni-Cu-Zn contents determined by radiochemical methods

23 p4209 A69-41321

Moldavites and Ries crater material, studying Rb-Sr isochronal relationship

23 p4154 A69-41341

Rb-Sr isotope patterns in tektites from Southeast Australian strewn field, studying Rb volatilization role in Rb-Sr isochron production

23 p4154 A69-41342

Tektites chemical composition showing minor concentration changes during melting used for parent material identification

23 p4210 A69-41346

Impact origin of Ivory Coast tektites and Bosumtwi Crater indicated by gamma ray spectrometric study of U, Th and K abundance patterns

23 p4210 A69-41347

Chemical composition and lechatelierite size frequency influence on moldavites bulk density, using data to elucidate origin

23 p4210 A69-41348

Ivory Coast microtektites chemical composition from electron microprobe analysis

23 p4211 A69-41351

Ilmenite composition in equilibrated ordinary chondrites, analyzing Fe, Mg, Ti and Cr content

24 p4382 A69-42890

Chemical composition of carbonaceous chondrites /Orgueil, Nogoya and Ormans/ and LL group chondrite /Ngawi/, confirming Ca/Al ratio

24 p4382 A69-42927

Chemical composition of basaltic achondrites /eucrites and howardites/, indicating dominant role of physical process over magmatic differentiation

24 p4382 A69-42928

Halogen concentrations in basaltic achondritic meteorites, discussing applications to rare gas and lunar surface studies

24 p4382 A69-42929

Metallographic techniques for meteorite studies, determining etching topography and orientational difference within each phase

24 p4382 A69-42934

Primordial hydrogen and helium concentration in Pesyanoe meteorite measured by gas chromatography, indicating solar wind injection source

24 p4384 A69-43213

Rb-Sr isotopic determinations for Olivenza olivine-hypersthene chondrite, noting isotopic ratio vs age

24 p4385 A69-43214

Trapped Ne in carbonaceous chondrites and gas-rich meteorites, observing Ne 20/Ne 22 ratio variance

24 p4385 A69-43217

Fe abundance in sun and carbonaceous chondrites, noting agreement between solar and meteorite abundances of Ni, Mg, Si and Li

24 p4385 A69-43223

METEORITIC DAMAGE

Meteoroid flux measured by Explorer 16 and Lunar Orbiter, analyzing penetration rate, average velocity and consistency with photographic meteors

13 p2349 A69-27820

Lunar surface environmental factors including molecular gas behavior under weak gravity and low atmospheric density, radiation and temperature effects, meteorite bombardment, etc

13 p2352 A69-27904

Lunar surface characteristics, discussing light polarization, lunar radiation, solar radiation and meteorite impact effects, etc

16 p2856 A69-32069

Hypervelocity micrometeor impact sites identification on aluminized glass, using conchoidal pattern as criterion in analysis

18 p3199 A69-34952

Pressure and temperature effects on reversal transitions of stishovite, noting meteoritic impact formation at Meteor Crater, Arizona

22 p4021 A69-40412

METEORITIC DIAMONDS

Morphological, chemical and X ray analysis of urelite meteorite, identifying diamonds with kamacite and troilite admixtures from carbonaceous material

21 p3816 A69-39626

METEORITIC DUST

U MICROMETEORITIDS

METEORITIC IONIZATION

U ATMOSPHERIC IONIZATION

U METEOR TRAILS

METEORITIC MICROSTRUCTURES

Mineralogy of iron fragments from impact craters near Lake Kaali, Estonia, discussing structure and type of meteorite

01 p0159 A69-11370

Enstatite chondrites structure and mineral content and composition using microscopic and X ray analysis, grouping parameters in distinguishing types

02 p0317 A69-12016

Meteorite fragments fall and distribution at Bur-Gheluai, Somalia, discussing crust morphology, mineralogical composition and structure

03 p0507 A69-13095

Disordered chondritic pyroxenes, analyzing X ray patterns of meteoritic and synthetic crystals

03 p0516 A69-14083

Deformation microstructures in shock loaded olivine, discussing planar features

05 p0818 A69-15607

Specific gravity data for olivine-pyroxene and enstatite chondrites, aerolites, siderites, amphoterites, pallasites and Butler meteorites

08 p1389 A69-20262

Chondrite meteorite fall /1969/ in Mexico, noting opaque and microcrystalline matrices and gamma rays from short lived isotopes

08 p1396 A69-20686

Magnetite morphological variations of type 1 carbonaceous meteorites, discussing isometric crystals, spheres, spherulites, platelets and filaments

08 p1406 A69-20932

Meteoritic materials structure, composition and magnetic properties, supporting theory for solar system formation from supernova outbursts

09 p1593 A69-21581

Structure transitions in iron meteorites from Widmanstatten to granular pattern to study Barringer crater and Canon diablo meteorites formation

09 p1597 A69-22154

Meteorite fragment from Arizona Meteor Crater, establishing probable history from shock loading experiments on iron alloys

12 p2158 A69-26344

Structure of meteorite Gibeon section containing taenite grains and annealing twins indicating plastic deformation of taenite followed by recrystallization and grain growth

17 p3034 A69-33586

Ar 39-Ar 40 method using neutron activation and inert gas mass spectrometry to investigate meteoritic thermal histories

19 p3412 A69-36105

Isotopic age determinations on iron and stone meteorites, discussing Rb-Sr and K-Ar results, internal isochrones, Kodaikanal data and planetary formation

19 p3413 A69-36108

Lance chondrite C III, studying mineral composition of chondrules and heterogeneous crystalline fragments

19 p3413 A69-36110

Fe-Ni-P phase diagram studies applied to schreibersite and rhodite formation in iron meteorites

19 p3417 A69-36132

Iron meteorites microscopic and macroscopic features due to preterrestrial mechanical deformation, stressing local displacements encountered in normal or acicular kamacites

19 p3418 A69-36134

Dynamically deformed structures in chondrites and hexahedrites observed to discriminate among theories about origin of chondrules and meteorites

19 p3418 A69-36135

Meteoritic cosmic ray exposure time from method based on spallogenic Ar 36/Ar 38 ratio, noting impracticality for exposures longer than 5 million years

19 p3418 A69-36138

Primitive low energy Fe-group nuclei irradiation of meteoritic crystals from studies of pyroxene and feldspar from meteorites, discussing astrophysical implications

20 p3590 A69-37569

Stony meteorite composition and structure studied for conditions of preplanetary stage of solar system

22 p4012 A69-40084

Black magnetite bearing spherules extracted from tektites, and magnetic fractions of impact glasses, determined by reflecting microscope and electron microprobe

23 p4210 A69-41349

Metallographic techniques for meteorite studies, determining etching topography and orientational difference within each phase

24 p4382 A69-42934

METEOROID CONCENTRATION

Meteorite scattering in geogravitational field and influence on lunar meteorite precipitation distribution

01 p0153 A69-10756

Mass distributions of meteoroids obtained from underdense radio meteor echoes

03 p0518 A69-14254

Lunar influences on meteoroid influx to earth, tabulating binomial distributions and probabilities of meteorite falls according to different lunar angles

04 p0655 A69-14663

- Mass influx and penetration rate of meteor streams
06 p1000 A69-17007
- Meteoroid mass distribution determined by radar observations of underside meteor trails at Springhill Meteor Observatory
06 p1003 A69-17493
- Region of transition from laminar to turbulent flow in meteor trains, suggesting electron attachment processes to molecular oxygen in presence of third body
08 p1393 A69-20608
- 11 Canis Minor meteor stream orbit computed, noting retrograde orbit and 4.2 million km perihelion
08 p1394 A69-20621
- Meteoric matter distribution by calculating orbital elements of 12,500 meteors from radar data, using diversity reception for radio waves scattered at meteor trails
17 p3041 A69-33894

METEOROID CRATERS

U METEORITE CRATERS

METEOROID DUST CLOUDS

U ZODIACAL DUST

METEOROID HAZARDS

- Meteoroid hazard, discussing possible future collisional dangers for space traffic
01 p0160 A69-11412
- Meteoroid perforation effects on space cabin design, discussing simulated destructive environmental tests [AIAA PAPER 69-365]
13 p2357 A69-28297
- Meteoroid penetration damage to spacecraft system, showing particle mass density distribution as protection criterion
21 p3805 A69-39229
- Spacecraft probes design for mapping meteoroid environment and penetration hazard through asteroid belt [AAS PAPER 69-321]
24 p4392 A69-42867
- Meteoroid shower model for interplanetary flight hazard evaluation, suggesting shower zone defining on ecliptic plane
24 p4385 A69-43258

METEOROID PROTECTION

- Barrier penetration depth by meteorite particles at prethreshold impact velocities, taking into account energy dissipation on shock wave front
01 p0152 A69-10579
- Meteoroid penetration detector development program for spacecraft construction, discussing design, materials and environmental tests
02 p0338 A69-11749
- Super insulation blankets comprised of dacron sailcloth, silk net or aluminized mylar, describing crinkling, cutting, sewing and hole drilling techniques
09 p1507 A69-22330
- Space suit meteoroid protection for extravehicular activity, discussing Gemini and lunar surface EVA suits and bumper concept [AIAA-PAPER-69-366]
13 p2213 A69-28298
- Fracture of bumper protected fuel tanks subjected to hypervelocity meteoroid impact, applying method of characteristics to stress wave propagation in tank walls [AIAA PAPER 69-369]
13 p2367 A69-28301
- Mathematical models for ballistic limit of single and double wall structures, yielding equations for relation to projectile and target characteristics [AIAA PAPER 69-370]
13 p2367 A69-28302
- Penetration mechanics of multisheet structures based on discrete particle modeling of impact debris [AIAA PAPER 69-371]
13 p2367 A69-28303
- Multisheet meteoroid protection design in Apollo program, discussing bumper, backup sheet and honeycomb cells insulation [AIAA PAPER 69-372]
13 p2367 A69-28304
- Hypervelocity projectile size and density effect on ballistic limit of dual sheet spacecraft meteoroid protection structures, considering penetration of low and high density particles [AIAA PAPER 69-376]
13 p2367 A69-28306
- Lightweight double walled meteoroid shield for Mariner Mars 1971, considering Teflon impregnated glass fabric outer sheet and multilayer thermal insulation [AIAA PAPER 69-377]
13 p2357 A69-28307
- Two plate meteoroid shields effectiveness determined by analyzing debris cloud ejected behind front plate after hypervelocity impact [AIAA PAPER 69-380]
13 p2368 A69-28310
- Barrier penetration depth by meteorite particles at prethreshold impact velocities, taking into account energy dissipation on shock wave front
15 p2709 A69-30749

- Meteoroid penetration damage to spacecraft system, showing particle mass density distribution as protection criterion
21 p3805 A69-39229
- Meteoroid shower model for interplanetary flight hazard evaluation, suggesting shower zone defining on ecliptic plane
24 p4385 A69-43258

METEOROID SHOWERS

- NT LEONID METEORIODS
NT ORIONID METEORIODS
NT PERSEID METEORIODS
- Frequency occurrence of small particles in meteor showers, discussing fragmentation and cosmic erosion as primary effects in small particle development
01 p0154 A69-10872
- Meteor grouping in meteor streams analyzed using radar records of meteor showers
01 p0154 A69-10873
- Origin and mineralogical composition of stones associated with 1824 stone hail near Sterlitamak
01 p0160 A69-11387
- Cosmic rays intensity increase due to meteor showers noting maximum solar activity effects
03 p0500 A69-13509
- Diurnal variations of visual meteoric activity mean hourly rates compared with earlier observations
04 p0658 A69-14879
- Diffuse meteor stream separation from sporadic background, using orbital elements of individual meteors
04 p0659 A69-15034
- Sporadic background separation from radar observations of meteor showers, using echo range distribution, head echoes and antenna direction change
04 p0659 A69-15035
- Radar determination of exponent s for describing mass distribution of Geminid and Quadrantid meteoric bodies
05 p0823 A69-16033
- Mass influx and penetration rate of meteor streams
06 p1000 A69-17007
- Meteor angular velocities distribution over sky in showers, considering effect of altitude, night hour, season and azimuth
08 p1393 A69-20607
- Thin sections of ringwoodite natural spinel in Tenham meteorite shower, observing various rounded purple isotropic grains
09 p1597 A69-22155
- Statistical analysis of photometric curves for meteors undergoing fragmentation at onset of vaporization
12 p2154 A69-25819
- Efficiency parameter beta for ion and electron production by meteoritic processes, noting importance to nighttime sporadic E ionization
14 p2520 A69-29372
- Micrometeoroid showers proximity to epsilon Leonid showers in earth orbit, analyzing Helfenzreider comet role from satellite data
14 p2522 A69-29588
- Meteor showers contribution to interplanetary dust flux based on relative number of particles of various size
15 p2697 A69-31308

- Picogram dust particle flux in selenocentric space measurement by Lunar Explorer 35, showing enhancement during meteor showers
15 p2699 A69-31396
- Noctilucent clouds seasonal frequency, considering meteor shower effects and temperature dependence role
16 p2781 A69-32453
- Meteor station photorecorder of reflected radio signals, discussing design and performance during meteor shower
17 p2976 A69-33898
- Meteor burst communication channel parameters for low data rate telemetry, considering signal amplitudes, decay, duty cycle, multipath, phase stability, trail location and variations
19 p3271 A69-36250
- Meteor shower effects on rainfall, noting anomalous radar meteor influx increase and subsequent subnormal precipitation
20 p3609 A69-38062
- Meteoroid shower model for interplanetary flight hazard evaluation, suggesting shower zone defining on ecliptic plane
24 p4385 A69-43258

METEORIODS

- NT BOLIDES
NT LEONID METEORIODS
NT MICROMETEORIODS
NT ORIONID METEORIODS

- NT PERSEID METEORIODS
NT RADIO METEORS
NT SPORADIC METEORIODS
NT ZODIACAL DUST

- Meteor photographic observation noting initial mass, motion, position and duration, disintegration in process of flaring, spectra and meteor flare classification scheme
01 p0159 A69-11372
- Monograph on orbit computation of doubly photographed meteors employing method of least squares, giving computer programs and tables of data printout
02 p0324 A69-12495
- Cometary origin of meteorites, discussing and rejecting origin from recent asteroidal collisions
05 p0818 A69-15588
- Simultaneous photographic and radar observations of meteors, determining absolute stellar magnitude of meteor as function of parameters
08 p1390 A69-20337
- Cometary origin of meteors and element abundance in primitive solar nebula, discussing neutron capture products in chondrites
08 p1406 A69-20930
- Ablation rate of Saint-Severin amphoterite based on heavy primary cosmic ray track densities in surface samples
08 p1406 A69-20933
- Atmospheric density analyzed on basis of photographic observations of meteors, comparing vertical profile with CIRA profile
10 p1688 A69-23936
- Cometary, lunar and solar effects on precipitation, considering joint influence of meteoric streams and moon
11 p1965 A69-25420
- Photometric standardization and calibration of meteor spectrograms for real meteor masses determination using spectrosensitometer
12 p2154 A69-25820
- Meteoroid flux measured by Explorer 16 and Lunar Orbiter, analyzing penetration rate, average velocity and consistency with photographic meteors
13 p2349 A69-27820
- CENFAM radar receiving system for meteoric and upper atmospheric data on amplitude, range and direction of meteor echoes through interferometer pairs
13 p2354 A69-28649
- Photographically observed meteor orbits 1937-1963, noting overestimation of hyperbolic orbits due to observation errors
15 p2697 A69-31253
- Antimatter meteors detectability, considering annihilation and vaporization in earth atmosphere
17 p3034 A69-33579
- Directional transmitting and receiving antenna arrays for short wave meteor studies in Kharkov
17 p2939 A69-33903
- Angular velocity effects on meteors apparent brightness
17 p3045 A69-34222
- Meteor dynamical and photometrical analyses compared quantitatively, determining mass loss value from fragmentation model
17 p3045 A69-34223
- Meteor flakes nature and statistics from studying 318 meteors characterized by irregular brightness curve
18 p3203 A69-35333
- Meteorite orbits and radiant calculated, noting asteroidal belt origin
19 p3414 A69-36116
- Transmitting antenna design of multistation radar system for meteors and upper atmosphere investigation, discussing amplitude and phase of electromagnetic field
19 p3278 A69-36661
- Visual observation of meteor and train microstructure obtained by refractor
22 p4033 A69-41058
- Cometary and asteroidal orbital differences and similarities, emphasizing limiting cases to study orbital evolution of meteors
23 p4208 A69-41284
- Spacecraft probes design for mapping meteoroid environment and penetration hazard through asteroid belt [AAS PAPER 69-321]
24 p4392 A69-42867

METEOROLOGICAL BALLOONS

- Inner and outer meteorological balloon assembly for fast rising and high altitude sounding
01 p0010 A69-10541

Ghost project for gathering weather data by balloons and transmission of data to central data processing stations by satellite
03 p0520 A69-13621

All weather wind profile monitoring system using FPS-16 radar/Jimsphere system and flight simulation for protection of space vehicle and missile launches
03 p0462 A69-13852

Tetroon flight observations of eddy velocities in planetary boundary layer, noting effects of height and seasonal variations
04 p0626 A69-14912

Eole satellite and meteorological balloons telecommunications used to study wind distribution in Southern Hemisphere and other atmospheric parameters
07 p1084 A69-19134

Error analysis of high resolution balloon-borne temperature sensor and comparison of temperature data with simultaneous rawinsonde measurements
09 p1494 A69-21642

Power supplies for balloon-borne instruments, describing light flexible NiCd batteries and solar cells used in EOLE project
16 p2736 A69-31745

Wind profile data measured by AN/FPS-16 radar/superpressure balloon system, noting error sources
18 p3139 A69-35428

METEOROLOGICAL CHARTS

Numerical maps of sporadic E critical frequency for solar cycle maximum and minimum to estimate propagation
01 p0070 A69-11160

Numerical radar information charts, plotting radio echo reflection boundaries from cloud and precipitation observations by weather radars
03 p0459 A69-13287

Temperature change and fog forecasting diagram modified by Swinbank relation in place of Brunt formula
03 p0462 A69-13965

Tiros and ESSA weather satellites meteorological contributions, discussing photographic interpretation for weather predictions
04 p0626 A69-14690

Synoptic density maps for postreentry altitudes derived from constant pressure charts and horizontal gradients
04 p0626 A69-14909

Meteorological satellites in weather forecasting, contrasting satellite data continuity to discreteness of synoptic charts
[UN PAPER 68-95760] 06 p0949 A69-17037

Computerized objective analysis of meteorological variables based on weight determination involving autocovariances
08 p1345 A69-20309

Zonal and meridional wind components monthly global cross sections for stratosphere and mesosphere from sounding and radar data
12 p2070 A69-26577

Complex climatological cloud profiles structural characteristics along given air traffic routes prepared for practical aviation problems
12 p2127 A69-26899

Height and temperature vertical variability in mid and upper stratosphere determined from constant pressure charts /1964-1966/
13 p2290 A69-27637

Radiation fields and large scale atmospheric disturbances analyzed, using radiation maps from Cosmos satellites
13 p2291 A69-27727

Satellite radiation maps for synoptic analysis regarding world weather maps, discussing front, intertropical convergence zones and typhoon location
14 p2473 A69-29729

Jet stream vertical wind shear chart construction for aircraft with gas turbine propulsion
14 p2473 A69-29730

Irregular data obtained by radiosondes in winter for charts of high isobaric levels, noting stratospheric temperature effects on radiosonde ascent height
14 p2473 A69-29731

Secular fluctuations of atmospheric circulation over Northern Hemisphere analyzed using isobaric and composite-kinematic surface maps, discussing analogies with Southern Hemisphere
14 p2478 A69-29836

Global mean monthly charts for IR radiation temperature, based on Cosmos 144 satellite data
15 p2596 A69-30643

Meteorological satellite data application to weather analyses and forecasts, discussing sea-ice boundaries and snow fields location
15 p2650 A69-31364

Daily European weather surveys based on meteorological satellite pictures transmitted during third quarter 1967
17 p3000 A69-33769

Climatological patterns of atmospheric kinetic energy dissipation in free atmosphere derived from upper wind statistics of Northern Hemisphere, using Kolmogoroff functions
18 p3166 A69-34825

Diurnal wind variations below 30 km plotted on constant pressure charts, showing topographical influence on tidal fluctuations
18 p3166 A69-34828

Precipitation zone-cloud mass correlation based on Tiros cloud photographs, synoptic charts and weather maps for European U.S.S.R.
19 p3366 A69-36671

Meteorological data real time processing for automatic weather analysis and prognosis, program used and computer output charts
22 p3977 A69-40732

Amplitude and phase maps for annual global variations in atmospheric pressure based on harmonic data analysis, suggesting standing wave type distributions
23 p4185 A69-42493

Multiple exposure averaging technique summarizing satellite cloud photographs for various periods, presenting entire earth cloud cover atlas
24 p4343 A69-42897

METEOROLOGICAL FLIGHT

Meteorological rocket soundings and global synoptic observations, noting influence of atmospheric middle region
[UN PAPER 68-95405] 01 p0109 A69-10484

Destructible low cost meteorological sounding rocket Dart for global observation of upper atmosphere
[UN PAPER 68-95467] 01 p0161 A69-10510

Meteorological and sounding British rockets Skylark, Petrel and Skua, showing capabilities, payloads and experiments
[UN PAPER 68-95785] 01 p0161 A69-10530

Selective chopper radiometer for remote atmospheric temperature sounding, discussing satellite versions for Nimbus D and Nimbus E
[UN PAPER 68-95797] 01 p0080 A69-10531

Aircraft instrumentation system for cloud nucleation studies measures and records ice nucleus and aerosol concentration/distribution, temperature, etc
01 p0080 A69-10542

Meteorological rockets for space meteorology, aeronomy and weather forecasting, noting international programs involving U.S.S.R.
06 p1043 A69-17056

Interamerican Experimental Network of Meteorological Investigation with Rockets /EXAMETNET/, discussing atmospheric parameters measurement at high altitude
[UN PAPER 68-95903] 06 p0950 A69-17062

Rocket transportation for upper atmospheric measurements, discussing sensors and cost effectiveness
[AIAA PAPER 69-159] 06 p1018 A69-18066

Remote sensing platform requirements for oceanographic and meteorologic observations, discussing orbital and aircraft platforms
[AIAA PAPER 69-154] 06 p1044 A69-18122

Aerial chronophotography of Southern Hemisphere conducted on around world polar flight analyzed for meteorological and geographical aspects and compared with satellite data
09 p1534 A69-21405

Meteorological rocket probes in Spain for wind and temperature measurements, including stratospheric circulation data
11 p1877 A69-24519

Nimbus D meteorological satellite construction, control system, orbit, etc
13 p2356 A69-27832

Meteorological analysis of stratospheric clear air turbulence flights, discussing vertical temperature structure in terms of wave motion and turbulence intensity
17 p2999 A69-33736

METEOROLOGICAL INSTRUMENTS

NT CLOUD HEIGHT INDICATORS

NT DROPSONDES

NT IONOSONDES

NT RADIOMETEOROGRAPHS

NT RADIOSONDES

NT RAWINSONDES

NT SONDERS

NT WEATHER DATA RECORDERS

NT WIND VANES

Satellite meteorological research in U.S.S.R., discussing Cosmos satellites instrumentation, earth thermal radiation distribution, IR and UV spectra and cloud photography
01 p0111 A69-10950

Cloud instrumentation for measurement of icing conditions of airplane flight tests
01 p0055 A69-11044

Meteorological instrumentation in India for surface and upper air observation
02 p0248 A69-11817

Atmospheric measurements and experiments using aircraft as platforms, noting aircraft operation in severe weather, electrical supply problem and aircraft wake problem
[AIAA PAPER 69-157] 06 p0869 A69-18153

Dew /or frost/ point determination method for low temperature humidity measurement
09 p1502 A69-22691

Anemometer based on neon helium ring laser with four mirror resonator
13 p2260 A69-27857

Cloud distribution effect on global coverage of remote radiometric sounding of atmosphere, considering Nimbus 1 and 2 data
15 p2650 A69-31335

Amplitude and intensity distributions of plane periodic Fresnel diffraction grating calculated by Fraunhofer theory, noting applicability to spectrometric and meteorological instruments
19 p3372 A69-35906

A scope laser radar to measure atmospheric particles spatial distribution through echo pattern and beam attenuation
20 p3487 A69-37284

METEOROLOGICAL PARAMETERS

Soviet book on methods of calculating characteristics of solar radiation covering short wave radiation, relationship to meteorological factors, applications, etc
20 p3570 A69-37233

Electronic data collection for climatological stations, describing acquisition and processing of various identification signals and meteorological parameters
20 p3538 A69-37428

Cumulus and cumulonimbus clouds electrical and microphysical properties measured by instrumented aircraft
20 p3572 A69-37907

Meteorological parameters-radio propagation characteristics correlation, studying feasibility of data acquisition by occultation satellite system
21 p3705 A69-38374

Daily simultaneous solar measurements of microwave atmospheric absorption and emission to determine frequency correlation between meteorological phenomena and atmospheric parameters
21 p3718 A69-39747

Uniform random field model development by taking moments in linear transformation form of certain initial field
23 p4183 A69-41523

Mars atmospheric features from measurements during entry and after landing, discussing atmospheric state properties, diurnal variability, clouds and winds
23 p4212 A69-41617

Nighttime F region time-altitude variations in aeronomic parameters calculated under conditions close to solar activity maximum
23 p4156 A69-41844

METEOROLOGICAL PROBES

U SONDERS

METEOROLOGICAL RADAR

Fluctuating radar echoes from cloud targets with vibrating drops, noting amplitude modulation effect of changing cross section on backscattered signals
02 p0208 A69-12021

Numerical radar information charts, plotting radio echo reflection boundaries from cloud and precipitation observations by weather radars
03 p0459 A69-13287

All weather wind profile monitoring system using FPS-16 radar/Jimsphere system and flight simulation for protection of space vehicle and missile launches
03 p0462 A69-13852

Quantitative estimations of cloud and precipitation by radar meteorology, assuming homogeneous reflectivity distribution of clouds
04 p0626 A69-14507

Level crossing rate meter correction for boxcar width and receiver noise readings in incoherent weather radars
04 p0557 A69-14915

- Upper wind observation and computation accuracy, comparing radar and slide rule instrument errors
06 p0950 A69-17788
- Power relations to fit radar meteorology parameters including rainfall, reflectivity function and attenuation rate
09 p1536 A69-21643
- CENFAM radar receiving system for meteoric and upper atmospheric data on amplitude, range and direction of meteor echoes through interferometer pairs
13 p2354 A69-28649
- Radar backscatter analysis for Arctic ice identification, deriving ice surface roughness factors from Kirchhoff-Huygens principle
14 p2416 A69-29530
- Radar meteorology - Conference, Dolgo-Prudnaya, U.S.S.R., April 1966
16 p2805 A69-32263
- Precipitation intensity measurements, obtaining distribution parameters from radar reflectivity at two wavelengths and microwave attenuation factor at third wavelength
16 p2806 A69-32265
- Turbulence dissipation rate in clouds and precipitations determined from rms width of vertical sounding radar signal fluctuation spectra, distinguishing gravity and turbulence effects
16 p2807 A69-32273
- Meteorological effects on anomalous radio echo determined from simultaneous aerological and radar observations, noting maximum signal amplitude during high humidity and low wind speeds
16 p2808 A69-32277
- MRL-1 meteorological radar station detection of cloud types under steady rain, showers and storm conditions, describing radar data analysis procedure
16 p2808 A69-32278
- Automatic meteorological radar data processing system incorporating MRL-1 radar and low speed digital computer
16 p2791 A69-32279
- Automatic conversion receiver of meteorological radar data, examining reception amplitude sensitivity and frequency characteristics
16 p2791 A69-32280
- Meteorological radar dead zone diminished by using hybrid electronic waveguide suppression system to eliminate antenna sidelobe reflections
16 p2791 A69-32281
- Airborne radar navigation with emphasis on semiautomatic fixing, describing beacon mode, map matching and airborne weather radar
18 p3169 A69-34851
- Meteorological Doppler radar information display for real time identification of hazardous winds and turbulence in storms
18 p3139 A69-35427
- Wind profile data measured by AN/FPS-16 radar/superpressure balloon system, noting error sources
18 p3139 A69-35428
- Microwave application in determining atmosphere meteorological characteristics compared with visual and IR wavelength measurements
20 p3569 A69-36984
- Millimeter wave pseudorandom coded CW meteorological radar for precipitation drop size spectrum analysis and cloud studies, discussing overall system design
23 p4115 A69-41531
- Radar signal reflectivity and precipitation relationship revised on basis of radio signal damping for improved measurement accuracy
23 p4185 A69-42494
- Simultaneous lower atmosphere clear air turbulence analysis by multiwavelength radar, jet aircraft and special rawinsondes
24 p4342 A69-42894
- Thunderstorm turbulence relationship to weather radar echoes from storm penetrations in Oklahoma by instrumented aircraft
24 p4347 A69-43720
- Satellite automatic picture transmission application to meteorological and hydrological problems including wind estimates, atmospheric stability and cloud distributions
[UN PAPER 68-95300] 01 p0108 A69-10462
- Atmospheric model development relating temperature, density, moisture and energy measurements from satellite observations for long term weather forecasting
[UN PAPER 68-95397] 01 p0108 A69-10463
- Space applications program including communications and navigation meteorology, earth resources survey and geodesy
[UN PAPER 68-95437] 01 p0178 A69-10472
- World Weather Watch /WWW/ system and meteorological satellites, discussing observational networks, data centers, telecommunication facilities, research, education and training program
[UN PAPER 68-95209] 01 p0178 A69-10478
- Utility of satellite cloud pictures to meteorological work, discussing weather observation in Israel
[UN PAPER 68-95571] 01 p0109 A69-10482
- Meteorological satellite research program, including unmanned satellite observations and possibilities with meteorologist on board manned spacecraft
[UN PAPER 68-95350] 01 p0109 A69-10483
- Passive and active transmitters and receivers of electromagnetic radiation in earth orbital satellites to collect pictorial or numerical data to study hydrology
[UN PAPER 68-95333] 01 p0064 A69-10487
- Satellites use in meteorology, noting monsoon rain forecasting through mesoscale sea surface temperatures of Indian Ocean
[UN PAPER 68-95555] 01 p0109 A69-10502
- Meteorological satellite observations value to Southern Hemisphere
[UN PAPER 68-95213] 01 p0109 A69-10513
- Automated layered-nephelanalysis and numerical total cloud cover prediction program using moisture data from Tiros 7 photographs
01 p0110 A69-10691
- Satellite meteorological research in U.S.S.R., discussing Cosmos satellites instrumentation, earth thermal radiation distribution, IR and UV spectra and cloud photography
01 p0111 A69-10950
- Satellites use in French space meteorology, discussing evolution, achievements, Eole project, etc
02 p0275 A69-11911
- Meteorological satellites for atmospheric data collection applicable to weather forecasting and synoptic analysis
02 p0277 A69-12778
- Application satellites for air traffic control, meteorology and earth resources, considering European participation
03 p0520 A69-13587
- Tiros and ESSA weather satellites meteorological contributions, discussing photographic interpretation for weather predictions
04 p0626 A69-14690
- Soviet book on attitude control of meteorological satellites noting reference systems, sensing units and control algorithms
04 p0666 A69-15012
- Outgoing radiation field based on interpretation of broad sector radiometer measurements made from meteorological earth satellites
04 p0627 A69-15032
- Interpretation technique for weather satellite photographs of spatially coherent cloud distributions
04 p0628 A69-15090
- Satellites role in observing and forecasting global atmospheric behavior, discussing World Weather Watch and Global Atmospheric Research Program
06 p0916 A69-16854
- Meteorological satellites data for safe navigation of ships, discussing techniques to overcome difficulties in interpreting ice and cloud photographs
[UN PAPER 68-95776] 06 p0916 A69-17028
- Atmospheric processes interpretation from cloud cover pictures televised by orbiting satellite, examining indirect weather forecasting
[UN PAPER 68-95713] 06 p0949 A69-17029
- Meteorological satellites data for quantitative weather forecasts, discussing error effects due to data treatment in adiabatic approximation
06 p0949 A69-17032
- Meteorological satellites in weather forecasting, contrasting satellite data continuity to discreteness of synoptic charts
[UN PAPER 68-95760] 06 p0949 A69-17037
- Meteorological satellite TV data of earth cloud cover for determining atmosphere pressure field
[UN PAPER 68-95654] 06 p0949 A69-17052
- U.S.S.R. system Meteor consisting of four Cosmos satellites in polar orbits to observe cloud distribution, snow and ice field boundaries, etc
06 p1013 A69-17053
- Eole meteorological satellite secondary use, discussing cosmic rays monitoring, navigation purposes and oceanographic research
[UN PAPER 68-95833] 06 p1013 A69-17077
- Dynamic stability tests of tilt winged V/STOL aircraft model in ultralow speed range, discussing apparatus for stability derivatives
06 p0866 A69-17091
- Cloud features produced by European tropospheric low pressure areas observed by meteorological satellite photographs, noting cyclonic systems development
06 p0950 A69-17619
- Soviet papers on satellite meteorology covering equipment onboard meteorological satellites, data processing, photograph interpretation, etc
06 p0951 A69-17976
- Calibrating long wave actinometric instruments designed for Soviet meteorological satellites
06 p0929 A69-17978
- Informative properties of IR scanning equipment of meteorological satellites, discussing radiative flux measurements and thermal mapping
06 p0929 A69-17979
- Lower atmosphere pressure field determination based on meteorological satellite observations of amount and types of clouds and upper boundary altitude
06 p0952 A69-17987
- Radiating surface temperature and total atmospheric moisture content determinations based on meteorological earth satellite measurements of outgoing radiation in IR
06 p0952 A69-17988
- Atmospheric measurements from satellites, discussing ATS-1 cloud images for definition of wind and use of WEFAX through ATS 2 satellites for data transmission
[AIAA PAPER 69-158] 06 p0954 A69-18038
- Eole satellite and meteorological balloons telecommunications used to study wind distribution in Southern Hemisphere and other atmospheric parameters
07 p1084 A69-19134
- Meteorological satellites observation of energy exchange between earth and space, discussing planetary albedo, energy absorption and source and sink regions
07 p1127 A69-19261
- Radiocommunications from Tiros and Nimbus meteorological satellites, noting weather data communications and hydrological experiments
09 p1451 A69-21289
- Meteorological observation problems from satellites, considering lower atmosphere measurements and accuracies
09 p1537 A69-22690
- Apollo 7 and weather satellite observation photographs of hurricane Gladys and typhoon Gloria
10 p1722 A69-22944
- ATS satellite distorted photographs conversion into normal and Mercator projections, using computer programs
10 p1689 A69-22945
- Soviet meteorological and geophysical rockets, satellites and techniques in cloud studies and weather forecasting, noting Cosmos results
13 p2290 A69-27348
- Collection of articles on satellite meteorology including vertical air motions, clouds and radiation fields
13 p2291 A69-27723
- Satellite and aerological ground station data combined to determine geopotential fields and wind velocity fields for inadequately serviced areas
13 p2292 A69-27732
- High and low latitude cellular cloud patterns observed by meteorological satellites, noting frequent occurrence over oceans
14 p2473 A69-29727
- Air density at various heights determined from analysis of satellite low perigee orbits, discussing periodic density variations and correlation with daily geomagnetic index
15 p2599 A69-31348
- Air densities from satellite obtained orbital data, comparing accuracy of values and methods of analysis
15 p2600 A69-31349
- Meteorological satellite data application to weather analyses and forecasts, discussing sea-ice boundaries and snow fields location
15 p2650 A69-31364

European geostationary satellite orbit inclination and eccentricity modification for maximum observation time of Northern Hemisphere by high resolution IR radiometer

15 p2650 A69-31389

Antenna array construction for reception of weather satellite transmissions, noting automatic picture transmission systems /APT/

17 p2946 A69-33767

Daily European weather surveys based on meteorological satellite pictures transmitted during third quarter 1967

17 p3000 A69-33769

Meteorological satellite research, ATS-3 program earth color picture from oceanographic and geomorphological viewpoints and U.S.S.R. research

17 p3000 A69-33777

Daily European weather surveys based on pictures transmitted by satellite during fourth quarter 1967

17 p3000 A69-33778

Satellite photography for snow cover mapping and depth estimation

18 p3167 A69-35084

Image dissector meteorological cameras, discussing ATS-III and Nimbus systems, high resolution camera and multispectral cameras

18 p3137 A69-35101

Soviet collection of papers on satellite meteorology problems covering cloud physics, jet streams, cyclones, satellite photography, etc

19 p3365 A69-36667

Meteorological parameters-radio propagation characteristics correlation, studying feasibility of data acquisition by occultation satellite system

21 p3705 A69-38374

Satellite synoptic meteorological data collection systems, discussing configurations, global location requirements and digital code platforms position determination

[AIAA PAPER 68-1095] 21 p3819 A69-39029

Satellite-based meteorological observation system for global atmospheric research program, discussing wind measurement, IR and microwave sounding possibilities, etc

[AAS PAPER 69-120] 24 p4307 A69-42817

METEOROLOGICAL SERVICES

Utility of satellite cloud pictures to meteorological work, discussing weather observation in Israel Meteorological Service

[UN PAPER 68-95571] 01 p0109 A69-10482

WEFAX /Weather Facsimile/ experiment to explore operational feasibility of direct meteorological data transmission via satellite relay from central station to remote stations

03 p0411 A69-13240

Soviet papers on satellite meteorology covering equipment onboard meteorological satellites, data processing, photograph interpretation, etc

06 p0951 A69-17976

Ground, aircraft and spacecraft actinometric data compared for clear sky

06 p0951 A69-17982

Constant level sounding balloon systems providing global data on atmospheric circulation, discussing icing problems and average life improvement

07 p1053 A69-18955

Satellites in meteorological service, describing TOS, ESSA and Nimbus satellites operation methods

08 p1409 A69-19960

Satellite and aerological ground station data combined to determine geopotential fields and wind velocity fields for inadequately serviced areas

13 p2292 A69-27732

Wind velocity, geopotential and atmospheric layer temperature fields constructed from Tiros 9 satellite cloud data using least squares method and trigonometric polynomials

13 p2292 A69-27733

Automatic processing and error analysis of horizontal, vertical, static and geostrophic wind data by U.S.S.R. Hydrometeorological Service

13 p2292 A69-27839

Statistical analysis of radiation temperature structure for automatic recognition of meteorological situations from actinometric satellite observations

13 p2293 A69-27842

Meteorological problems in Italy analyzed by digital computer program through numerical integration of atmospheric models to provide weather forecasts

13 p2295 A69-28651

Jet stream vertical wind shear chart construction for aircraft with gas turbine propulsion

14 p2473 A69-29730

Soviet collection of articles on aviation forecasting of cloud cover, high altitude wind and turbulence

14 p2473 A69-29734

Probabilistic forecasts in meteorological support of aviation, comparing economic implications of squall forecasting

14 p2474 A69-29739

Clear air turbulence computerized analysis and forecast over U.S. using upper air rawinsonde measurements

22 p3976 A69-39927

Atmospheric variability at proposed flight levels, analyzing meteorological requirements of SST operations, discussing annual cycles in stratospheric circulation

24 p4251 A69-42711

Short range aviation terminal weather predictions concerning runway visual range, cloud-base height and wind, using FAA mesometeorological network

24 p4342 A69-42892

METEOROLOGICAL STATIONS

U WEATHER STATIONS

METEOROLOGY

NT AEROLOGY

NT HURRICANES

NT HYDROMETEOROLOGY

NT LONG RANGE WEATHER FORECASTING

NT MICROMETEOROLOGY

NT NUMERICAL WEATHER FORECASTING

NT POLAR METEOROLOGY

NT RADIO METEOROLOGY

NT STATISTICAL WEATHER FORECASTING

NT SYNOPTIC METEOROLOGY

NT TROPICAL METEOROLOGY

NT TROPICAL STORMS

NT TYPHOONS

NT WEATHER FORECASTING

Meteorological satellite research program, including unmanned satellite observations and possibilities with meteorologist on board manned spacecraft

[UN PAPER 68-95350] 01 p0109 A69-10483

Japanese space research organizations, sounding rockets, meteorology, satellite communications, geodesy, etc

[UN PAPER 68-95563] 01 p0151 A69-10501

Automatic picture transmission station equipment including antenna, cavity filters, tape recorder, oscilloscope, facsimile system and kinescope

[UN PAPER 68-95450] 01 p0054 A69-10522

Australian sounding rocket programs carried out in conjunction with U.S. satellite experiments

[UN PAPER 68-95214] 06 p1013 A69-17076

Soviet papers on satellite meteorology covering equipment onboard meteorological satellites, data processing, photograph interpretation, etc

06 p0951 A69-17976

Automation of meteorological fields analysis using computer

07 p1175 A69-18677

Meteorology - Conference, Berlin, September 1968

09 p1534 A69-21512

Meteorological data for flight path climatologies, analyzing annual frequency distribution of maximum wind velocities

09 p1535 A69-21519

One and two dimensional frequency distributions for probability estimates of climatological quantities, discussing temperature and interdiurnal changes

09 p1535 A69-21520

Electron production rates variations in lower ionosphere cosmic layer related to meteorological, geomagnetic and cosmic conditions

10 p1759 A69-22839

Soviet collection of articles on satellite data interpretation and use for meteorological services

11 p1911 A69-24824

Buoyancy in turbulent shear flow, rotation or streamline curvature effects and meteorological parameters, drawing formal exact algebraic analogy

11 p1870 A69-24894

Meteorology and space vehicle capabilities noting earth, outer space and earth atmosphere observations and measurements, relaying telecommunication signals, etc

12 p2126 A69-26126

Optimum coordination between homogeneous isotropic geopotential field and derivatives, estimating efficiency of geopotential and wind fields simultaneous analysis

12 p2126 A69-26580

Radar application to meteorology, entomology and ornithology, discussing clear air turbulence detection and flight tracking of birds and insects

12 p2034 A69-27004

Vertical refraction effect on gas laser beam propagation near earth surface under various meteorological conditions, comparing index for diffuse light

13 p2220 A69-27827

Blocking processes synchronous development involving atmospheric circulation disturbances in Northern and Southern Hemispheres, noting localization in Pacific and Atlantic oceans

13 p2292 A69-27840

Anomalous meteorological field distribution as observed by correlated stations, determining independent stations number observing same data

13 p2293 A69-27851

Time correlation functions for wind vectors and components at various altitudes over Moscow in winter and summer

13 p2294 A69-27856

Passive remote sensing at microwave frequencies for meteorology, oceanography and geology, reviewing physics of wave interactions, mathematics of data interpretation, etc

14 p2414 A69-29514

Collection of Soviet papers on planetary atmospheric circulation covering tropospheric and stratospheric temperature distribution, cloud patterns, wind fluctuations, etc

14 p2472 A69-29723

Soviet collection of papers on general circulation of atmosphere

14 p2475 A69-29818

Dynamic meteorology quasi-stable problems solved using sequential approximations solution for barotropic model of Euler equations

14 p2476 A69-29821

Meteorological elements variation from measuring earth radiation in different spectral regions by satellites, determining temperature and humidity profiles

14 p2477 A69-29828

Stellar scintillation spectra for different zenith distances, correlating data with meteorological conditions at time of observation

15 p2647 A69-30165

Monograph on large scale cloud distribution in extratropical low pressure regions, using classical meteorological observations and Tiros weather satellites data

15 p2650 A69-31212

Israel research on space data for meteorological purposes, describing automatic picture transmission data and errors in surface temperature determination by satellite radiometry

15 p2650 A69-31422

Book on operational meteorological information processing by computers, discussing synoptic and aerological data, automatic data processing in operational numerical forecasting, etc

18 p3105 A69-34332

Advanced Meteorological Sounding System /AMSS/ for measurements up to 150,000 ft, discussing configuration, characteristics, radiosonde, ranging, telemetry data ground equipment and test

18 p3108 A69-35102

Meteorological corrections of meson megatelescope data based on hourly ground-level pressures and temperatures, considering vector and regression analyses

19 p3308 A69-35991

Large atmospheric motions analyzed by elliptic partial differential equation and hydrostatic and quasi-geostrophic approximations

19 p3364 A69-36504

Soviet collection of papers on satellite meteorology problems covering cloud physics, jet streams, cyclones, satellite photography, etc

19 p3365 A69-36667

Mesometeorology in central Europe, discussing applications of numerical techniques to forecasting

20 p3570 A69-37427

Solar activity effect on short term meteorological processes and dynamic state of mesosphere and ionosphere, emphasizing relationship to entire atmosphere dynamics

20 p3590 A69-37684

Lidar technology application to atmospheric and meteorological problems in clouds and cloud structures, air motion and inhomogeneity in clear air

22 p3977 A69-40535

Meteorology and geophysics - Conference, Hamburg, April 1968

24 p4344 A69-43144

IR measurements applications to meteorology, discussing IR radiation characteristics, atmospheric effects, thermal radiation detection and differences between real and black bodies

24 p4316 A69-43507

METEORS

METEORS

U METEOROIDS

METERS

U MEASURING INSTRUMENTS

METHACRYLATE RESINS

U ACRYLIC RESINS

METHANE

Methane IR absorption band centered near wavenumber 9050, noting R branch features and fine structure
01 p0023 A69-10289

Thermal model for interaction of exploding wires with methane atmosphere, discussing energy transfer efficiency in high temperature pyrolyses near explosion
01 p0119 A69-10674

Jovian atmospheric rotational temperature from rotational lines in methane band
01 p0153 A69-10856

Gas chromatographic determination of hydrocarbon quantity in methane in parts per billion range
03 p0382 A69-14115

Trace analysis /parts per billion/ of methane in helium, hydrogen and neon
03 p0382 A69-14116

Methane broadening and anomalously small pressure shift of 3.39 micron rotation-vibration line, using laser saturated molecular absorption
04 p0633 A69-15424

Charge exchange cross sections in methane and ammonia, noting dissociative charge exchange role
06 p0884 A69-17114

NASA atlas of IR solar spectrum, reporting B and 4 meter spectrometer recordings over band containing methane telluric absorptions
06 p1008 A69-17810

Deuterated diazomethane prepared by base catalyzed reaction of hydrazine with chloroform
06 p0885 A69-17885

Chemiluminescence in high temperature oxidation of methane studied in shock tube
06 p0885 A69-17937

Ignition time of methane and acetylene, considering concentration and thermodynamic properties during reaction
[WSCIPAPER 68-41] 07 p1240 A69-18356

Radiogenic theory of origin of He in natural gas and absence of Ar from K 40 decay, discussing primordial earth atmosphere composition
08 p1311 A69-20947

Vibrational relaxation times in pure O and in O with methane impurity determined with acoustic absorption measurements
09 p1542 A69-21721

Molar heat and entropy of adsorption and activity coefficient of adsorbed phase for methane-ethane-silica gel system
10 p1652 A69-23370

Methane absorption distribution in 6190 A band over Jupiter disk based on spectrograms, noting center to limb variations
11 p1960 A69-24730

Methane absorption distribution in 6190 A band over Saturn disk at center and polar latitudes based on spectrograms
11 p1960 A69-24731

Thermal ignition of methane-oxygen mixture, observing flame propagation
13 p2380 A69-28459

Leak rate measurement accuracy of rate-of-rise technique for nitrogen, methane and He between millionth and thousandth torr
16 p2791 A69-32326

Space storable regenerative cooling with FLOX/methane under conditions for small pump fed engine, describing injector and chamber design
[AIAA PAPER 69-509] 16 p2844 A69-32718

Flox/methane pump fed engine, discussing RL-10-1-A engine tests and optimized 5000 lb thrust engine design
[AIAA PAPER 69-510] 16 p2741 A69-32720

Jupiter photochemistry above 1000 A, noting methane and ammonia photolysis zones, atmospheric pressures and hydrogen recombinations
17 p3032 A69-33165

Primitive earth upper atmosphere thermal models, considering roles of exospheric temperature and free hydrogen availability in methane dominated environment
20 p3608 A69-38056

Methane abundance and rotational temperature of Jupiter, considering effects of line saturation
20 p3613 A69-38174

Methane rotational temperature in Jovian atmosphere deduced from equivalent widths of lines at 1.1 micron band
22 p4028 A69-40663

Formation mechanism of positive ethyl ion and hydrogen molecule during interaction between positive methyl ion and methane molecule
24 p4280 A69-43814

METHIONINE

Chlorella seaweed hybrid strains containing larger amounts of amino acids than original parent species
13 p2216 A69-28620

METHOD OF CHARACTERISTICS

Two dimensional compressible inviscid laminar gas flows unsteady processes studied by extending method of characteristics
01 p0008 A69-11360

Survey of papers on computer calculation of two and three dimensional gas flows, emphasizing method of characteristics and finite difference techniques
03 p0363 A69-13657

Induced flow determination in pulsejet ejector, solving momentum and continuity equations by method of characteristics and mathematical model
[ASME PAPER 68-WA/FE-33] 05 p0812 A69-16106

Quasi-method of characteristics with application to fluid lines with frequency dependent wall shear and heat transfer
[ASME PAPER 68-WA/AUT-7] 05 p0750 A69-16181

Method of characteristics for nonequilibrium internal flow fields in propulsion systems, discussing focusing, shock wave and accuracy
[AIAA PAPER 69-6] 06 p0915 A69-18170

Three dimensional hypersonic steady flow around blunt and pointed cones at nonzero angles of attack calculated by method of characteristics
[AIAA PAPER 69-187] 06 p0865 A69-18176

Unstationary characteristics method applied to numerical computation of steady compressible flow around airfoil
[ONERA-TP-630] 07 p1049 A69-18413

Large amplitude longitudinal wave propagation in elastic rod solved by method of characteristics, prescribing end velocity as step function of time
07 p1233 A69-19176

Characteristics method for solution of differential equations representing time changes of wind and pressure fields in divergent barotropic channel flow
11 p1911 A69-24585

Delta wing in three dimensional supersonic flow analyzed by method of characteristics, discussing leading edge problems
11 p1820 A69-25425

Relaxing gas nonequilibrium flow in plane expansion, comparing partial differential equations with method of characteristics
13 p2244 A69-27322

Transport equation numerical solution for unsteady radiation field by straight lines method, allowing for scattering indicatrix forms with passage of time
13 p2350 A69-27858

Characteristics method for stress waves from hypervelocity impact of circular cylinder on half space, discussing numerical diffusion effect on pressure and flow fields
[AIAA PAPER 69-355] 13 p2365 A69-28287

Three dimensional supersonic nozzle flow field calculations using second order numerical method of characteristics and computer programmed for internal flows
[AIAA PAPER 69-463] 16 p2734 A69-32766

Method of characteristics for computing supersonic jets and wakes with given boundary pressure distribution
[ONERA-TP-721] 18 p3121 A69-34636

Monograph on method of characteristics for three dimensional supersonic flows, covering numerical calculations of steady gas flow past bodies at angle of attack
19 p3238 A69-36170

Flowfield properties of two dimensional supersonic jet near sonic nozzle exit by numerical method of characteristics
22 p3860 A69-40920

Shock wave transient motion during passage through ducts in inviscid gas containing convergences, using characteristics method
23 p4153 A69-42398

METHODOLOGY

Nonlinear transport equations solution methodology covering transformations, invariants, boundary value problems, numerical methods, etc
21 p3697 A69-39729

Top-down initiating technique for forecasting future decade major systems requirements based on information progression
[AAS PAPER 69-409] 24 p4417 A69-42803

METHODS

U METHODOLOGY

METHYL ALCOHOLS

Hydrogen peroxide electrode cathodic polarization studied for liquid oxidant use in methanol fuel cells
11 p1825 A69-24523

Stress corrosion cracking of Ti-6Al-4V alloy tensile tested in anhydrous methanol by electron fractography and diffraction, noting hydrogen embrittlement
11 p1903 A69-24576

Titanium alloy tensile specimens tests in liquid methanol and anhydrous methanol environments at known stress-strain-time relations examined by fractography and high resolution electron diffraction
16 p2799 A69-31718

Stress corrosion cracking of alpha Ti in liquid nitrogen tetroxide and various methanol environments, considering failure mechanisms
19 p3352 A69-36906

Methyl alcohol, ether and acetone vapors decomposition in microwave discharge, obtaining H and CO in addition to solid polymeric films
22 p3895 A69-40103

METHYL COMPOUNDS

IR and Raman spectra of solid and matrix isolated methylamine and deuterium derivatives, locating amine twisting vibration in solid phase IR spectra
01 p0023 A69-10287

Photoionization curves and threshold energies for fluorocarbon and trifluoromethyl halide molecules and ions, calculating ionic heats of formation and bond dissociation energies
02 p0205 A69-12464

Methyl 2-cyanoacrylate adhesive bonding characteristics, noting importance of film thickness
09 p1529 A69-22316

Electron spin resonance spectra of gamma irradiated single crystals of 9-methyladenine, analyzing H abstraction radical and temperature effects
19 p3264 A69-35974

Chromatographic analysis of products formed during induction period of 2-methylbutane gaseous oxidation in flow system at low temperatures and long residence times
21 p3669 A69-38798

Rotational microwave spectrum of 2-methylfuran, using fourth order perturbation method for internal rotation A-E doublet splittings
24 p4280 A69-43811

METHYLHYDRAZINE

Macaque monkey behavior after injection of monomethylhydrazine with and without pyridoxine HCl, noting effects of aversively and appetitively rewarded training
03 p0375 A69-14068

Renal pathology of acute methylhydrazine intoxication in dogs, noting hemolytic anemia and hemoglobinuric nephropathy
06 p0883 A69-17847

Monomethylhydrazine /MMH/ toxic effects on cornea and blood aqueous barrier studied in vivo on dogs
09 p1447 A69-22547

IR and Raman spectra of gas and liquid phase methylhydrazine and deuterated methylhydrazines, discussing vibrational motions, H bonding and thermodynamic functions
10 p1752 A69-23528

Preferential shifts in consumption of metabolic fuels following exposure to hydrazine or monomethylhydrazine, considering biochemical and physiological responses
14 p2407 A69-29303

Monomethylhydrazine absorption through canine skin noting metabolic aftereffects and methemoglobinemia
22 p3887 A69-41191

METROLOGY

Operational principles and characteristics of pulse width modulator designed on basis of autooscillator amplifier, giving circuit diagrams
10 p1664 A69-23817

Metrological measuring instrument scales selection principles for ensuring constant sensitivity and Q factor
17 p2975 A69-33614

Technical and metrological characteristics of short base strain gages and bonding to specimen, investigating sensitivity and creep
20 p3544 A69-37817

- Holography for engineering metrology, discussing interferometry, pattern interpretation, inspection techniques, etc
22 p3945 A69-40235
- MICA**
Phosphate cements for bonding mica ceramic to titanium in jet engine equipment
05 p0786 A69-16799
Heat resistance and strength properties of porous Ni-base cermet materials with mica additions under high temperature oxidation
21 p3751 A69-38615
- MICE**
NT POCKET MICE
Vertical vibration stimulation of growth of onion bulbs and mice body weights
01 p0014 A69-10584
Renal effects of moderate hypoxia exposure in mice as reflected in urine volume and electrolyte excretion patterns during four days at simulated altitude
01 p0015 A69-10921
Deuteron microbeam for simulating biological effects of ionization by heavy cosmic ray particles
03 p0373 A69-13493
Histological investigation of internal organs of mice exposed to atmosphere with high oxygen content
05 p0709 A69-16513
Immunological and histochemical methods for studying mice reactivity after long term exposure to hyperoxic atmosphere
07 p1065 A69-18975
In vivo hemolytic susceptibility to hyperoxia in mice deficient in tocopherol
07 p1066 A69-19422
Microwave radiation effects on body weight and peripheral blood hemograms of mice, discussing maximum safe exposure related to generator output
08 p1266 A69-20678
Barbamyl effect with and without somatotropic hormone injection in mice during prolonged isolation and hypokinesia, noting sleep duration
10 p1646 A69-23576
Sublethal ionizing radiation doses effect on hemolytic immunocompetent spleen cells in mice upon using chemical radiation protectors
13 p2210 A69-28334
Hypokinesia effects on transversostriated muscle fibers of mice, noting changes in myofibrillar apparatus, mitochondria and sarcoplasm
13 p2212 A69-28616
Vertical vibration stimulation of growth of onion bulbs and mice body weights
15 p2555 A69-30754
Diurnal variations in radiation sensitivity of mice and rats to irradiation with median lethal doses, noting sine curve survival function
15 p2557 A69-31458
Antihypoxic preparations protective effect on white mice and rats subjected to gravitational accelerations
17 p2906 A69-32931
Oxygen consumption and rectal temperature in male mice confined in nitrogen and helium diluted hyperoxic atmosphere at specific temperature and humidity ranges
17 p2906 A69-32932
Corneal epithelium chromosome rearrangements in gamma irradiated white adult mice, noting radiation dosage and duration
17 p2907 A69-32944
Transverse acceleration overstrain effect on mice sensitivity to cystamine
17 p2909 A69-33386
Centrifugation effects on body composition and growth of mice
17 p2910 A69-33746
Histological investigation of internal organs of mice exposed to atmosphere with high oxygen content
18 p3096 A69-34732
Mice convulsions at varying hyperbaric oxygen pressures and carbon dioxide content correlated with decreasing brain alpha aminobutyric acid levels
19 p3257 A69-35972
Immunological and histochemical methods for studying mice reactivity after long term exposure to hyperoxic atmosphere
20 p3479 A69-38223
Retarded immunological recovery in sublethally X-irradiated mice by additional thymic exposure reversal with injected marrow cells
22 p3887 A69-41194
X ray radiation damage to white mice blood serum proteins disappearing following intraperitoneal administration of imidazole or benzimidazole
23 p4077 A69-41300
White mice gastrocnemius muscle wet mass, dry mass and noncollagen-nitrogen /NCN/ content, noting /NCN/ content dependence on body mass
23 p4080 A69-41406
Radioprotective effects of 5-azacytidine on bone marrow and blood leukocytes of X ray irradiated AKR mice
23 p4080 A69-41429
Whole body X irradiation effect on protein degradation in mice, using radioactive I labeled albumin
23 p4099 A69-42151
Altered gaseous environments effect /parabiosis/ on interferon production in mice injected with Newcastle disease virus, noting hypoxia role
24 p4262 A69-42888
White mice survival rates and blood morphology and sedimentation rates in low ambient pressure confinement following infectious bacteria injection
24 p4267 A69-43397
- MICHELL THEOREM**
Michell type optimum fiber arrangement for transferring torque across annulus, considering single straight, double and multiple annular arrays under single load system
19 p3447 A69-36851
- MICHELSON INTERFEROMETERS**
Elastic and inelastic collisions between deformable bodies, using Michelson interferometer with He-Ne laser as source
02 p0282 A69-12607
Stellar spectra taken with rapid scanning Michelson interferometer, noting IR excess due to radiation from clouds surrounding stars
04 p0655 A69-14667
Helium-neon gas laser as coherent light source for holograms of vaporizing fuel films and for Michelson interferometer
08 p1327 A69-20874
Optical diagnostics methods for fast processes in rarefied plasma, using Michelson interferometers with ruby and Nd lasers as light sources
12 p2089 A69-26186
Contrast interference patterns obtained in Michelson interferometer at various path differences, using He-Ne laser as light source
12 p2108 A69-26593
Signal strength of two beam interferometers with laser illumination, considering modulation depth of interference pattern
13 p2259 A69-27450
Dynamic Michelson interferometer equipped with Ge detector to obtain spectra of airglow from 1.2-1.6 microns
13 p2252 A69-27587
Michelson interferometers with large interference fields for plasma diagnostics emphasizing structural rigidity, monochromatic light pulse power, instruments vibrations resistance, etc
14 p2496 A69-29776
Long path difference vacuum Michelson interferometer application to far IR and IR laser wavelength measurements compared with 6328 A He-Ne wavelength
17 p3006 A69-33405
Modular Michelson interferometer used as IR spectrometer for absorption and dispersion studies, describing instrument construction, range and accuracy
20 p3538 A69-37297
Vibrational displacement phase measurement by Michelson interferometer with laser source
20 p3538 A69-37320
Transverse and longitudinal laser modes in holography, noting Michelson interferometer interference pattern role
21 p3734 A69-38398
Intensity interferometer applications comparison with Michelson interferometer, discussing sensitivities, radio and optical wavelength astronomy, space plane waves, etc
21 p3722 A69-38794
Single mode high power He-Ne laser with Michelson interferometer in cavity, describing performance determination method
22 p3962 A69-40473
- MICROANALYSIS**
Magnified image of Al-Mg specimen microanalyzed during examination by electron microscope, studying segregation and initial precipitation at grain boundaries
03 p0442 A69-12894
Microchemical analysis for diffusion measurement of laser produced lithium plasma in uniform magnetic field
05 p0762 A69-15960
- Carbon influence on cast Waspaloy, discussing chemical segregation, chemical gradients and tensile ductility
[SAE PAPER 690100]
07 p1158 A69-18307
X ray microanalyzer maximum sensitivity obtained using flow type proportional and scintillation counters with proper tuning and eliminating scattered electrons
12 p2093 A69-26596
Radioactivity induced in solid materials for components microautoradiography and radiograph information quantitative evaluation
13 p2297 A69-28157
Chlorapatite and whitlockite compositions of phosphate minerals from chondrites determined by electron microprobe
15 p2690 A69-30706
- MICROBALANCES**
Oscillating fiber microbalance for direct mass determinations in .1 mg to .0001 microgram range
21 p3720 A69-38592
- MICROBE**
U MICROORGANISMS
MICROBIOLOGY
NT BACTERIOLOGY
Space controlled microbiology, discussing telemetry control of waste material conversion in air and water pollution
[UN PAPER 68-95861]
01 p0014 A69-10456
Biological life support system for regenerating closed atmosphere by photosynthesis, using gas exchange between man and microalgae
01 p0021 A69-11078
Terrestrial microorganism survival in space aboard Gemini satellite, discussing lethal effects of solar radiation
01 p0018 A69-11087
Ionospheric and stratospheric UV radiation effects on survival of microorganisms
01 p0018 A69-11088
Pedoscope use in soil microbiological studies including ecology, infection susceptibility, etc
01 p0021 A69-11092
Biological monitoring during assembly of Technological Feasibility Spacecraft /Mars lander/ to evaluate thermal control techniques and microbiological burden prior to sterilization
02 p1201 A69-11774
Microbiology of water management subsystem for manned space flight, discussing sterilization by heat and tests inside Integrated Life Support System /ILSS/ [SAE PAPER 680718]
03 p0379 A69-13441
Microbial contaminants on space hardware, discussing detection and enumeration techniques
05 p0714 A69-15954
Microbiological surface sampling methods, noting role in detecting contamination on eating utensils, blankets, sheets, etc
05 p0715 A69-15982
Microbiology quality assurance program for planetary mission, considering spacecraft sterilization during fabrication, test and launch site activities
15 p2559 A69-31124
Manganese deficiency effect on growth and chlorophyll content of algae with and without hydrogenase
15 p2558 A69-31551
Microbiological influence on astronauts efficiency during and after long space flights, stressing simulated microclimates and confinement effects on flora
18 p3097 A69-35304
Microbiological corrosion and degradation of aircraft metals and organic materials in fuel tanks
19 p3341 A69-35569
Microbial protein extraction from Chlorella algae and Torulla yeasts using urea soaking method
21 p3662 A69-39712
Prokaryotic and eucaryotic microfossils localized in pre-Paleozoic microfiora, noting radiometric age and association with stromatolites
22 p3935 A69-40052
Open cell ester-base polyurethane foam effect on fuel-utilizing microorganisms growth in jet fuel- water systems
24 p4271 A69-42700
- MICROCALORIMETERS**
U CALORIMETERS
MICROCIRCUITS
U MICROELECTRONICS
MICROCLIMATOLOGY
Microbiological influence on astronauts efficiency during and after long space flights, stressing simulated microclimates and confinement effects on flora
18 p3097 A69-35304

MICROCRACKS

MICROCRACKS

Dead-end microcracks stress fields, studying positive /tensile/ and negative /compressive/ nature dependence on crack size

04 p0674 A69-14548

Surface environment effects on mode of microcrack formation during fatigue of Al single crystals, noting surface void formation mechanism

07 p1235 A69-19387

Micromechanism of crack propagation in brittle fracture, considering kinematics for steady state crack in plane strain and energy dissipation

10 p1796 A69-23070

Fracture mechanics of polymers and fiberglass reinforced plastics, indicating microcracking under static and cyclic loading due to resin phase brittleness and low strength

12 p2120 A69-26849

Microcrack detection by holographic interferometry, describing experimental apparatus and test procedure and results

24 p4317 A69-43763

MICROELECTRONICS

Performance characteristics of microstrip ferrite devices for hybrid microwave integrated circuit systems, including meander line phasers and YIG elements

01 p0040 A69-10191

Thin ferrite use in microwave integrated circuits including phase shifters, latching circulators, isolators and phase and amplitude modulators

01 p0040 A69-10192

Hybrid integrated parametric amplifier design considerations for fabrication in microstrip transmission line

01 p0040 A69-10193

Hybrid microstrip integrated microwave circuits, discussing substrate and conductor materials and fabrication processes

01 p0040 A69-10199

Microstrip-like transmission lines analyzed by method based on line capacitance variational calculation and charge density distribution

01 p0044 A69-10625

Planar technology application to germanium electronic components and integrated circuits

02 p0214 A69-11597

Neutral buoyancy microelectrode for prolonged recording from single nerve units

02 p0202 A69-11865

Air gap isolated microcircuit beam-lead devices fabrication, operation, electrical performance and radiation resistance

02 p0221 A69-12469

Microelectronic components joining technique by compliant bonding, utilizing deformable medium between tool and beam leads to eliminate intricate tool shapes and alignments

02 p0254 A69-12473

Analysis and design of synchronous filter compatible with microelectronics requirements, switching N monolithic RC thin film devices to signal source of resistance

03 p0403 A69-13206

RF sputter etching of microcircuits and components

04 p0606 A69-14874

Medium scale integration for packaging hybrid electronic monolithic systems

05 p0735 A69-16752

Temperature effects on primary photocurrent of base collector and collector substrate junctions of isolated transistors from microcircuits

06 p0977 A69-16881

Models to predict transient radiation responses in microcircuits, discussing model accuracy for junction and dielectrically isolated circuits

06 p0977 A69-16887

Microelectronics in astronautics, discussing properties of thick and thin film electronic devices, integrated semiconductor circuits and hybrid circuits

07 p1089 A69-18256

Collection of papers on applications of microelectronics to aerospace equipment, noting design and reliability of circuits and computers

[AGARDOGRAPH-114] 08 p1291 A69-20981

Microelectronics technology and economics, discussing semiconductor integrated, discrete component and thin film hybrid circuits and MOSFET devices

[AGARDOGRAPH-114] 08 p1291 A69-20983

Microcircuit components and microelectronic systems reliability assessment including short term testing, noting digital systems, packaging, production controls, etc

[AGARDOGRAPH-114] 08 p1291 A69-20984

Microminiature system mechanical design for aerospace environment, considering guidelines for implementation of requirements

[AGARDOGRAPH-114] 08 p1291 A69-20986

Microcircuits, integrated circuits and other monolithic solid state circuits failure mechanisms examined and applied to reliability methodology

[AGARDOGRAPH-114] 08 p1292 A69-20987

Microelectronic studies in France noting semiconductor integrated circuits, thin film devices and application to airborne apparatus and small computer

[AGARDOGRAPH-114] 08 p1292 A69-20993

Conventional electronic and microelectronic circuits reliability, discussing external stress effects on improvement in avionics and rocket applications

08 p1293 A69-21112

Integrated semiconductor circuits reliability in electronics and microelectronics, discussing hybrid and monolithic circuits in thin/thick film design and on Si monocrystals

08 p1294 A69-21118

Reliability in microelectronics estimated from failures expected during lifetime, describing various test methods

08 p1294 A69-21121

Precision trimmed RC active networks for high selectivity microelectronic filter fabrication for frequency division multiplex applications

09 p1466 A69-22452

Microelectronics for digital adaptive controls, discussing digital filter design and chips required in fabrication

09 p1474 A69-22453

Microelectronic data and remote control function transmission system for wind tunnel testing of aircraft dynamic response to gusts and turbulence

10 p1672 A69-23283

Laser application to welding, drilling and other processes involving material removal for microelectronic circuits and components fabrication

11 p1846 A69-24600

Radioisotope fueled miniature thermionic converter for fractional watt level operation, defining optimum interaction of variables

14 p2399 A69-29193

Microelectronic technology for mass production of high reliability hybrid thin film circuits

15 p2628 A69-30845

Quality control of high volume microelectronic circuit assembly of military computer emphasizing preventive action

15 p2580 A69-31129

Microelectronic S band upconverter designed and fabricated in microstrip on alumina substrate

16 p2762 A69-32562

Functional signal conversion operations in microelectronic radio equipment, examining components in analog and pulsed devices synthesis

18 p3109 A69-35162

Intermediate level mathematical reliability model relating failure mechanism, part strength and interaction of application stresses to parts failure rates, with emphasis on microcircuits

19 p3283 A69-36019

Microelectronics and IC process and quality control check list including conductor screening, resistor abradings and discrete part attachment

19 p3283 A69-36020

Microelectronics role in maintenance and maintainability of subminiature solid state components, emphasizing functional packaging at module level

19 p3283 A69-36021

Book on field effect and bipolar junction transistors and microcircuits, covering ideal and practical amplifiers, circuit characteristics, etc

20 p3505 A69-37147

Lasers as tools for integrated circuits fabrication, noting roles of various laser operating parameters

21 p3742 A69-39705

Hybrid microelectronic circuit failure mechanisms for thick and thin film resistors, conductors and capacitors, noting packaging contributions

22 p3910 A69-39954

Wire, flip-chip and beam-lead bonding processes effects on hybrid microcircuits reliability

22 p3911 A69-39956

He-Ne laser system for micromachining thin film photolithographic masks, describing computer controlled coordinate table and product quality

22 p3954 A69-40236

Radiation hardened microcircuits and transistors for protection against transient radiation released by nuclear weapons

23 p4135 A69-41528

Hybrid techniques to produce thin and thick film microcircuits and logic system parameters

24 p4286 A69-42906

Hybrid and monolithic integrated microcircuits application to electronic digital computer structures

24 p4284 A69-42907

Thin film field effect transistors and integrated microcircuits, investigating active and passive elements fabrication

24 p4419 A69-42908

Microcircuit phased array electronic countermeasures system design and hardware techniques for aerospace applications, analyzing adaptive, retrodirective and combination array systems

24 p4287 A69-43111

Microelectronics test program consisting of four reliability screening levels based on Mil-Std 883

24 p4287 A69-43205

Materials problems in microelectronic circuits, discussing multilayer interconnection arrays production by thick film or print-and-fire process

24 p4333 A69-43212

MICROFIBERS

Microfilaments, Taylor production method, mechanical properties and comparison to whisker

08 p1320 A69-20582

Microfibrous boehmite as binder for molybdenum disulfide in formation of ductile water resistant dry lubricant films

[ASLE PAPER 68-LC-14] 15 p2642 A69-30606

MICROFILMS

Micromation and micrographics, discussing nonimpact printing in computer avoiding output imbalance by high speed microfilm recorder

18 p3234 A69-35059

MICROGRAPHY

U PHOTOMICROGRAPHY

MICROHARDNESS

N- and p-type InSb and GaSb single crystals microhardness, noting decrease after doping is limited to thin surface layer

01 p0139 A69-10832

Zirconium corner of Zr-Cu-Mo phase diagram, using microstructure analysis of hardness and microhardness measurements, discussing plasticity variations and corrosion resistance

02 p0263 A69-11852

Relationship between microhardness of niobium and other variables characterizing superconductivity

05 p0810 A69-16805

Ion nitrided binary iron alloys and steels electron microscopic studies reveal particle formation during hardenings

06 p0942 A69-17224

N and p type InSb and GaSb single crystals microhardness, noting decrease after doping is limited to thin surface layer

11 p1936 A69-24699

Book on hard alloy properties, discussing bending and compression properties, tensile, torsional and impact strength, wear resistance and thermal shock resistance

12 p2111 A69-25902

Nb and Ti carbides investigated for lattice parameters, microhardness and resistivity in homogeneity domain

15 p2638 A69-30282

Photomechanical and electromechanical effects in semiconductors, considering indentation microhardness decrease caused by light irradiation or electric field

19 p3386 A69-36526

MICROINDENTATION

U MICROHARDNESS

MICROMANOMETERS

U MANOMETERS

MICROMETEORITES

U MICROMETEOROIDS

MICROMETEOROID EXPLORER SATELLITES

NT EXPLORER 16 SATELLITE

Micrometeoroid showers proximity to epsilon Leonid showers in earth orbit, analyzing Helfenzreider comet role from satellite data

14 p2522 A69-29588

MICROMETEOROIDS

NT ZODIACAL DUST

Micrometeorites acoustic recordings on Cosmos 135, investigating data reliability influenced by appearance of thermal noise

01 p0152 A69-10578

Meteorite particles recording by piezoelectric transducers, comparing data collected by Soviet and American scientists
01 p0152 A69-10587

Micrometeorite and meteoric dust data obtained in Soviet space flights
01 p0155 A69-10939

Meteorite dust spherules at Tungusk and Sikhote-Alin falls investigated for mineral composition using X ray analysis
01 p0160 A69-11383

Meteoritic dust composition of Tungusk meteorite noting angular and spherical particles
01 p0160 A69-11386

Particles behavior after separation from meteor, considering deceleration for separation altitudes and initial velocities
02 p0314 A69-11645

Micron and submicron particle cumulative flux upper limits in satellite micrometeoroid environment of Gemini 12
07 p2125 A69-18845

Stony meteoric particles size and velocity during passage through atmosphere
12 p2157 A69-26341

Meteoritic dust particles collections prediction in atmosphere for low and high entry fluxes
12 p2158 A69-26342

Micrometeoroid showers proximity to epsilon Leonid showers in earth orbit, analyzing Helfenzreider comet role from satellite data
14 p2522 A69-29588

Micrometeorites acoustic recordings on Cosmos 135, investigating data reliability influences by appearance of thermal noise
15 p2691 A69-30748

Meteorite particles recording by piezoelectric transducers, comparing data collected by Soviet and American scientists
15 p2691 A69-30757

Interplanetary dust and distribution study by micrometeorite analyzer and by zodiacal light observations using solar probe
15 p2694 A69-30879

Micrometeoroid collections, describing Gemini satellite and Aerobee rocket-borne equipment and experimental results
15 p2700 A69-31440

Micrometeorite simulation by wire explosion plasma, discussing energy requirements and simulator performance
16 p2821 A69-31839

Hypervelocity micrometeor impact sites identification on aluminized glass, using conchoidal pattern as criterion in analysis
18 p3199 A69-34952

Fe-Ni unmelted and unablated micrometeorites number at earth surface calculated, using space density of interplanetary particles and micrometeoritic theory
20 p3614 A69-38251

Rocket and satellite particle collection experiment to confirm reduced micrometeoroid flux near earth, noting inconclusive size frequency distributions of exposed flight samples
21 p3793 A69-38343

Piezoelectric microphone sensor flown on rocket for recording micrometeoritic impacts during noctilucent cloud display, determining cosmic dust particles flux
21 p3793 A69-38348

MICROMETEOROLOGY

Horizontal wind velocity energy spectra, attributing free atmosphere meso and microscale turbulence to meso and micrometeorological processes
12 p2070 A69-26575

Objective analysis of pressure trend fields and surface pressure retaining field with scale of 100 km, using filtering procedure
18 p3166 A69-34816

MICROMETEORS

U MICROMETEORIDS

MICROMETERS

Pitch determination of micrometer screw by scalar star pairs derived from FK3 and Washington zenith catalog noting temperature and dampness effects
16 p2859 A69-32218

MICROMINIATURIZATION

Integrated circuits technology, discussing thin film, monolithic compatible and hybrid circuit techniques
02 p0216 A69-12050

Selective etching process for microminiaturization of special circuits for aerospace
05 p0736 A69-16753

Semiconductor standard memory circuits, discussing arrays and density
06 p0894 A69-17202

Microfilaments, Taylor production method, mechanical properties and comparison to whisker
08 p1320 A69-20582

Microsoldering techniques for thin and thick film hybrid circuits and microminiature printed circuit boards
09 p1510 A69-22349

Engineering problems in IC microminiaturization, dividing devices according to suitability for microminiaturization
15 p2576 A69-30352

Unoccupied space utilization in aircraft compartments due to microminiaturization, considering reliability enhancement of electronic equipment
15 p2576 A69-30353

MICROMINIATURIZED ELECTRONIC DEVICES

NT MICROMODULES

Diamond abrasive process for preparation of microminiature devices for metallographic analysis
03 p0402 A69-13007

Microminiature system mechanical design for aerospace environment, considering guidelines for implementation of requirements [AGARDOGRAPH-114]
08 p1291 A69-20986

Micromin alumina substrates design data, determining dielectric constant, impedance vs line width and wavelength vs frequency
09 p1460 A69-22792

Microminiature latching relay design and manufacturing cost
13 p2232 A69-28049

Visual inspection, thermal and mechanical shock, burn-in and hermeticity tests of microelectronic equipment, reviewing test methods and procedures of MIL-STD-883 program
19 p3284 A69-36043

Microminiature Elliott MCS 920 M digital computer for inertial guidance of CECLES-ELDO launcher, discussing construction, code, interrupt, guidance system and functions
20 p3501 A69-37391

Microminiaturized digital computers for missiles and aircraft, discussing characteristics, environmental conditions and transformation possibility for use in satellites
20 p3502 A69-37392

Miniature floated ball gimballess inertial platform construction, functions, readout, digital computer coupling, etc [AIAA PAPER 69-835]
21 p3761 A69-39366

Hybrid microelectronic modules, using basic thermal design guidelines
22 p3910 A69-39952

MICROMODULES

Micromodule unsteady thermal behavior reduced to calculating linear heat flux for boundary conditions containing temporal and spatial derivatives
23 p4136 A69-41558

MICROORGANISMS

NT AEROBES

NT ANAEROBES

NT AZOTOBACTER

NT BACILLUS

NT BACTERIA

NT BACTERIOPHAGES

NT ESCHERICHIA

NT FLAGELLATA

NT HYDROGENOMONAS

NT MESOPHILES

NT MICROSPORES

NT NITROBACTER

NT PARAMECIA

NT PROTOZOA

NT PSEUDOMONAS

NT SPORES

NT STEAROTHERMOPHILUS

NT VIRUSES

Lethal effect of solar UV radiations on dried Coliphage T-1 exposed to space at sounding rocket altitudes
01 p0017 A69-11086

Terrestrial microorganism survival in space aboard Gemini satellite, discussing lethal effects of solar radiation
01 p0018 A69-11087

Ionospheric and stratospheric UV radiation effects on survival of microorganisms
01 p0018 A69-11088

Soil, moisture and other requirements for microorganism survival in simulated Martian environment
01 p0018 A69-11091

Wolf Trap life detector design to sample and culture Martian surface dirt for microorganism growth
02 p0201 A69-11769

Spacecraft sterilization techniques for space exploration, discussing mathematical models for planetary quarantine and contamination by nonlanding vehicles
05 p0712 A69-15935

Modeling requirements and methods for monitoring microbial contamination, discussing vacuum probe sampler to recover microorganisms from large surface areas
05 p0713 A69-15948

Microorganism viability in rocket engine combustion environments used to determine probability of biological contamination of Mars by Voyager missions
05 p0714 A69-15949

Split-seam process for inserting sterile objects into isolated sterile environment without contamination as method for sterile spacecraft repair
05 p0714 A69-15950

Mars contamination with terrestrial microorganisms, considering possibility of waste materials ejection from manned orbital vehicles
05 p0714 A69-15951

Protein free diets effects on rat intestinal microflora, noting decrease in lactic acid bacteria and increase in spore forming bacteria
05 p0709 A69-16516

Amino acid biosynthesis control in microorganisms by end product/feedback/ inhibition of enzyme action
06 p0876 A69-18238

Vacuum, radiation and freeze drying effects on survival rate of microorganisms, noting influence of protective materials on extent of damage
07 p1064 A69-18943

Axial units with basal plates in spermatozoa of Chlidia groenlandica negatively stained with phosphotungstic acid, showing doublet microtubules
07 p1066 A69-19263

Aircraft design, fabrication and finish techniques taking into account aircraft integral fuel tank corrosion due to contaminants associated with microbiological debris [NACE PAPER 49]
08 p1320 A69-20599

Microorganism survival in space for exposure to solar UV radiation on balloons, rockets and satellites
11 p1828 A69-25457

Spacecraft sterilization requirements, evaluating viable organisms release probability from spacecraft as function of equipment fracturing
11 p1828 A69-25460

Microbial contamination release probability from solids fractured by impact, considering spacecraft sterilization requirements
11 p1828 A69-25461

Unicellular microorganisms size and concentration estimates based on light scattering measurements of suspensions in spectrophotometer cuvette compartment
11 p1829 A69-25643

Biochemiluminescent luminol-peroxide reaction to detect iron porphyrin proteins in microorganisms for extraterrestrial life search, discussing reaction kinetics
15 p2556 A69-31325

Dry heat destruction rates for microorganisms encapsulated in and on spacecraft hardware, concluding temperature and water conditions in spore as major factors
15 p2560 A69-31444

Gas environment effect on catabolic activities and enzymatic reactions of trachoma and meningopneumonitis agents of genus Chlamydia
16 p2747 A69-31865

Origin of microbial life on earth and implications for extraterrestrial forms
17 p2907 A69-32972

Protein free diets effects on rat intestinal microflora, noting decrease in lactic acid bacteria and increase in spore forming bacteria
18 p3096 A69-34735

Soviet book on cosmos and microorganism utilization for creating regenerative life support in spacecraft
20 p3467 A69-37230

Microorganisms death by exposure to high intensity visible and UV light, discussing effect of endogenous photosensitized oxidation on caratoid- containing Rhodoturla glutinus
20 p3475 A69-37613

Microbial contamination release from impact- fractured solids, examining bacterial spores growth in fractured methyl methacrylate plastic for application to space exploration
20 p3475 A69-37614

Space contamination by spacecraft-borne terrestrial microorganisms, testing vacuum effect on water desorption rate using mass spectrometry on various cells

20 p3475 A69-37615

Radiation effects on microorganisms and plants during space flight on Biosatellite 2 and Gemini 11 missions

20 p3476 A69-37617

Regenerative life support system development, considering synthesized organic compounds and microorganisms as foods for long duration space missions

20 p3477 A69-37623

Cell-like structures containing biochemicals as inevitable event under various hypothetical primitive earth conditions

23 p4085 A69-41479

MICROPARTICLES

Submicron particles spatial location in three dimensional volume detected by Fraunhofer holography

04 p0596 A69-14292

Satellite data for reevaluating extraterrestrial particles origin found in polar ice, atmosphere and terrestrial surface collections

04 p0654 A69-14655

Acidic, neutral and basic proteinoids thermal synthesis, discussing characterization and tendency to form microparticles

07 p1074 A69-18633

Micron and submicron particle cumulative flux upper limits in satellite micrometeoroid environment of Gemini 12

07 p1215 A69-18845

Thermochemically synthesized high melting micropowders grinding by vibrational method and classification for polishing and finishing applications

12 p2113 A69-26256

Composite materials consisting of brittle inorganic glass matrix with metallic or inorganic crystal microspheres, noting strength and elasticity

12 p2115 A69-26830

Thin foil penetration measurements for Fe microparticle impacts on metal and Mylar foils in space

15 p2641 A69-31339

Time dependent diffusion of light particles of Lorentz fluid approximated by Boltzmann equation leading to microscopic telegrapher equation

22 p3984 A69-40530

MICROPHOTOGRAPHS

Microholographic system for nonpseudoscopic stereoscopic image reconstruction of transparent and nontransparent microobjects

21 p3726 A69-39702

MICROPHOTOMETERS

U PHOTOMETERS

MICROPULSATIONS

NT GEOMAGNETIC MICROPULSATIONS

Acoustic waves pressure field micropulsations in turbulent fluid, analyzing space-time spectrum

09 p1492 A69-22710

Frequency time dispersion of storm sudden commencement micropulsations, noting polarization effects

14 p2440 A69-29129

Acoustic waves pressure field micropulsations in turbulent fluid, analyzing space-time spectrum

16 p2782 A69-32489

MICROROCKET ENGINES

Cesium electron bombardment microthruster system, discussing ion engine, feed, discharge neutralizer, power conditioning and control electronics

[AIAA PAPER 69-293] 09 p1561 A69-21223

Pulsed plasma microthruster propulsion system for synchronous orbit LES 6 satellite

[AIAA PAPER 69-298] 09 p1562 A69-21227

RF ion thrusters using self sustaining electrodeless discharge

[AIAA PAPER 69-285] 09 p1565 A69-21247

Cesium microthruster system using beam deflection for satellite control, describing ion engine subsystem and control logic/power conditioner subsystem

[AIAA PAPER 69-292] 09 p1569 A69-21875

Hollow cathode mercury electron bombardment thruster design, emphasizing low specific impulse operation and discharge chamber improvements

[AIAA PAPER 69-300] 09 p1569 A69-21880

Simulator for testing colloid microthruster, discussing spacecraft interfaces and time of flight thrust data

[AIAA PAPER 69-314] 09 p1478 A69-22380

Reaction control rocket engines for manned spacecraft, discussing operating and cycle life, thrust response, specific impulse and reliability

16 p2867 A69-31746

Microthrusters thrust requirements for attitude control and orbital transfer of gravity gradient geostationary satellite

17 p3019 A69-33336

Micropropulsion system with sublimable solid fuel for satellite attitude control, satisfying mechanical and thermal environmental conditions during launch and in space

17 p3021 A69-33359

Boundary layer formed in miniature nozzle studied for effect on jet spreading discharged into space at high Mach numbers

19 p3395 A69-36760

Valving concepts and functional approaches for inert gas attitude control thruster systems providing redundancy safeguards at minimum weight, volume and power costs

[AIAA PAPER 69-843] 21 p3786 A69-39373

MICROSCALES

U MICROBALANCES

MICROSCOPES

NT ELECTRON MICROSCOPES

NT ION MICROSCOPES

NT OPTICAL MICROSCOPES

Rapid recording microspectrophotometer for IR to UV absorption spectra of living cells, cell organelles and half micron diameter particles

03 p0428 A69-13109

Polarized light microscope for application to metallic crystallographic studies noting grain orientation, hcp grain basal pole orientation and etched fcc metals

09 p1499 A69-22302

Polishing-etching cell permitting continuous sample surface observation for use with inverted stage microscopes

13 p2281 A69-28156

MICROSCOPY

Electrical properties of edge and screw type dislocations in germanium, using bilateral microscopy

03 p0488 A69-13761

Lasers application to measurement techniques including alignment, direction, distance, elongation, interferometric, holographic, etc

12 p2094 A69-26903

MICROSPORES

Cytological analysis of *Tradescantia paludosa* microspores for space flight influence onboard Cosmos 110

01 p0018 A69-11317

MICROSTRUCTURE

NT METEORITIC MICROSTRUCTURES

NT WIDMANSTATTEN STRUCTURE

Structural transformations of quenched Fe-Ni-Nb austenitic alloy from X ray diffraction microstructure examination and hardness measurements

01 p0095 A69-10603

Microfacets of metal surface cracks studied for plastic deformation and atomic separation mechanisms by electron diffraction

01 p0098 A69-10763

Microstructure analysis and relationship between microvariations and macroscopic events, using magnetic variations recordings of IGY network

01 p0069 A69-11126

Mechanical finishing abrasion induced plastic deformation microwinning observed in thin stainless steel films by transmission electron microscopy

02 p0251 A69-11542

Isothermal sections construction of zirconium corner of ternary phase diagram of Zr-Mo-V system from microstructure of cast and quenched alloy specimens

02 p0262 A69-11846

Structure of zirconium corner of Zr-V-Ni system phase diagram, using metallography, hardness and microhardness methods

02 p0262 A69-11847

Zirconium corner of Zr-Cu-Mo phase diagram, using microstructure analysis of hardness and microhardness measurements, discussing plasticity variations and corrosion resistance

02 p0263 A69-11852

Solid solutions microstructure and electrical conductivity in InAs-CdS and InAs-CdS and InAs-CdSe systems

02 p0297 A69-11882

Hydroextrusion effect on Mo structure and mechanical properties, noting improved ductility after high temperature annealing

02 p0267 A69-12189

Molybdenum elasticity limit and rupturing stress dependence on structure for high temperature annealing, noting changes in solid solution interstitial impurity concentration

02 p0268 A69-12191

Ni-Cr-Ti-Al /Nimonic/ alloy single crystal mechanical properties at room temperature, determining importance of structure

02 p0268 A69-12192

Structural influence on superconductivity of niobium-titanium alloys, using electron microscopy and measurements of current density vs magnetic field strength

02 p0269 A69-12763

Fatigue mechanism in fcc metals at ultrasonic frequencies, comparing microstructural changes in copper and alpha-brass

04 p0613 A69-14448

Heat treatment and shot peening effects on Al alloy fatigue strength and fine crystallographic structure

04 p0614 A69-14576

Ferrite-austenitic stainless steels with Ti analyzed during aging at 450-600 C for steel phase nature

04 p0615 A69-14641

Structural microheterogeneities in monophase Ti alpha alloys, using complex phase analysis method

04 p0617 A69-14939

Alloying elements and cold rolling deformation effects on formation of texture in Ti alloys, noting inhomogeneity

04 p0617 A69-15077

Plastic deformation effect on structure, yield point and tensile strength of aged austenitic alloy containing Ni, Cr and Ti

04 p0618 A69-15177

Superconductors and living matter behavior, studying conditional parallelism via microstructure, cryogenic and electronic fundamentals

04 p0644 A69-15321

Molybdenum oxide crystals growth and microstructure, using X ray and electron diffraction analyses

05 p0779 A69-15831

Nickel structure alterations during interaction with high speed air flow at elevated temperatures

05 p0783 A69-16812

Metal matrix composites compression microstrain behavior, analyzing continuous fiber composites of magnesium-boron and copper-tungsten

06 p0939 A69-16945

Fatigue performance of composites consisting of W or Mo helical coils embedded in Cu matrix, discussing evaluation from microstructural behavior

06 p0940 A69-16951

Strain rate effect on structure and mechanical properties of rapidly stretched metals

06 p0941 A69-17122

Controlled microstructures of eutectic aluminum-copper aluminides produced for mechanical properties studies

06 p0942 A69-17227

Localized microstructural changes and fatigue crack propagation in cantilever type notched specimens of austenitic stainless steel under cyclic bending at constant load

06 p0943 A69-17237

Microstructure of diffusion zone during contact fusion in magnesium-nickel system at high temperatures

06 p0945 A69-17895

Microstructural changes during liquid phase sintering of alloys, considering temperature effect on carbide grain growth and activation energies

07 p1168 A69-19599

Microstructure relationship to tensile strength and creep resistance in Zn-Ni-Ti alloy extrusions, discussing role of finely dispersed intermetallic particles

08 p1329 A69-20002

Microstructural changes in 52100 steel bearing inner rings during cyclic stressing, obtaining thickening rate data on white-etching regions and lenticular carbides

08 p1319 A69-20004

Phase identification and microstructural effects of gaseous nitrogen reaction with binary Nb-Ti alloys at 1000 C

08 p1331 A69-20195

Binary vanadium alloys property change regularities using alloying elements

08 p1333 A69-20439

Microstructure for spinodal decomposition in Al-Zn alloys noting Zn precipitation, fracture mechanics, dislocations and transmission electron microscopy results

09 p1522 A69-21503

Brittleness and physical causes of cold shortness in Cr, discussing high purity metal formation and fine and superfine grain structures synthesis

09 p1526 A69-22147

Primary silicon crystals content and grain size effect on wear of high silicon aluminum alloys

09 p1526 A69-22281

Unidirectional filamentary composites thermoelastic properties relation to constituent materials properties, using semiempirical micromechanics theory

09 p1530 A69-22320

Gas turbine blade materials after long term service, analyzing tensile, impact and stress rupture properties and microstructure

[ASME PAPER 69-GT-12] 09 p1527 A69-22503

Microstructure and crystallography of lamellar eutectic alloy of Ni and intermetallic Ni-Ti compound

10 p1707 A69-22986

Microstructural analysis, determining junction orientation polarity effect on draw junction structure in GaSb crystals at room temperature

10 p1745 A69-23330

Nickel base wrought and cast superalloys examined to determine minor phases and microstructure thermal stability in high temperature heat treated condition

10 p1714 A69-23977

Chromium-rhenium-boron ternary system using X ray diffraction and microstructure analysis, establishing phase equilibria at high temperatures

10 p1715 A69-24054

Thermal and microstructural analyses to determine phase interactions nature in Mg alloys of Mg-Nd-Al system

11 p1902 A69-24271

Solid solution decomposition effect on binary Mg alloys recrystallization temperature containing Al and Nd, using X ray and microstructural analysis

11 p1902 A69-24272

Micropolar elasticity theory for materials exhibiting granular structure and microstructure, discussing deformation geometry and measurement, strain kinematics, microstrains, thermodynamics, etc

11 p1975 A69-24674

Electrical resistivity and magnetization saturation in cobalt alloys during formation of modulated structures

11 p1904 A69-24707

Temperature and stress dependence of microstrain and microyielding in polycrystalline W for range of impurities and dislocations, considering transition to macrostrain

11 p1905 A69-25183

Heat treatment effect on Ti-Mn alloy microstructure, discussing fcc martensite transformation into alpha, beta and intermediate phases as function of aging

11 p1906 A69-25578

Microscopic mechanisms in fracture surface markings, using electron fractography cleavage, fatigue, stress corrosion cracking, microvoid coalescence and tear ridge formation

13 p2274 A69-27224

Macroscopic crack extension force, critical flaw size and minimum fracture strength calculated from microscopic quantities

13 p2275 A69-27227

Microstructured mixtures theory including energy balance, mass and momentum equations and entropy production inequality for structured fluids in motion

13 p2371 A69-27318

Structural features of Fe-Ni massive martensite observed by light, electron and hot stage microscopies showing parallel block packet

13 p2276 A69-27401

Matrix grain size relation to dispersed particle size distribution and Zener-McLean equation description of microduplex structure in superplastic Ni-Fe-Cr alloy

13 p2278 A69-27411

Microstructural stability Fe-Ni base heat resistant alloy Pyromet 860 during long time creep-rupture testing

13 p2279 A69-27764

Polycrystalline Fe-Ni, Fe-Ni-Co ferrites structure, magnetostriction, magnetization curves and hysteresis prior and after thermomagnetic treatment

13 p2319 A69-27992

Metallographic study of microstructure recrystallization of 50 Ni-50 Fe alloy during annealing using special etchants and methods

13 p2281 A69-28155

Microstructure of light scattering media consisting of large size spherical particles

14 p2481 A69-28737

Double notch creep rupture tests of Cr-Mo steels, investigating changes in notch profile, dimensions and structure

[ASME PAPER 68-WA-MET-7] 14 p2464 A69-29441

Co base high temperature binary alloys microstructure, investigating diffusion coefficients, stacking faults, vacancies, etc

14 p2465 A69-29890

High temperature properties relationship to microstructure of Co base superalloys and strengthening methods

14 p2465 A69-29891

Time and temperature effects on corrosion and structure of Hastelloy alloy C-276

14 p2466 A69-29930

Shock hardening in Ni at high pressure observed by electron microscopy showing dominating thermal effects on microstructure

15 p2637 A69-30225

Heat treatment and shot peening effects on Al alloy fatigue strength and fine crystallographic structure

15 p2638 A69-30278

Friction effects on friction couples made of two different nonferrous alloys, discussing temperature regime difference effects on microgeometry and structure

15 p2629 A69-31027

Austenitic alloy structure and stress rupture after boron addition

17 p2985 A69-32908

Microstructural factors role in metal fracture toughness, considering effects of deformation processing and heat treatment, grain size, structural refinement, fibering, etc

17 p2988 A69-33552

Dynamic model of bodies with microstructure and nondissipative energy motion, discussing action steadiness, invariance conditions and Galilean relativity

17 p3067 A69-34149

Composite materials behavior studies for structural applications, using macroscopic and microscopic phenomenological approach

18 p3154 A69-34607

Micropolar liquid basic flows, considering case with coupling constant relating microstructure to macroscopic flow greater than viscosity coefficient

18 p3121 A69-34786

Solid solutions microstructure and electrical conductivity in InAs-CdS, InAs-CdSe systems

18 p3182 A69-35042

WC-Co alloys structural changes under loads near yield limit, noting formation of slip bands

18 p3158 A69-35261

Statistical description of microstructural elements /fibers and fillers/ in unidirectional fiberglass reinforced plastics determined in lattice nodes

18 p3163 A69-35363

Tempering time and temperature effect on microstructure, superconductivity, tensile strength and electrical conductivity of recrystallized Nb-Ti alloy

19 p3345 A69-36302

Continuous particle media on basis of microstructure, discussing granular media deformation, elastic media dilatation, turbulent flow and dilute suspensions

19 p3446 A69-36833

Processing variables influence on microstructure of extruded Ti-Al-Sn alloy, noting deformation by slip over temperature range

20 p3557 A69-36955

Alpha and alpha plus beta Ti alloys analyzed to relate phase composition and microstructure to stress corrosion cracking in NaCl solution

20 p3557 A69-36961

Microstructure and X ray structure compared for two and three component chromide, titanide and silicide diffusion layers on Nb, discussing phase composition

20 p3563 A69-37820

C content and microstructure effect on electrochemical parameters of Fe and steels in dilute sulfuric acid, discussing Tafel constants and current density

20 p3563 A69-38002

Polycrystalline nickel foil microstructure after explosive shock loading and heat treatments, using transmission electron microscopy

20 p3563 A69-38126

WC-Co alloys microstructure and microproperties, considering individual phase behavior and grain-solid solution interactions

20 p3564 A69-38246

Extrusion variables influence on microstructure and hardness level of Ti-Al-Sn compared with recrystallization behavior after cold swaging

[ASM PAPER W9-8.2] 21 p3729 A69-38660

Structural defects of neutron irradiated W wire noting microstress relaxation using atomionic microscope

21 p3749 A69-39623

Mn, S and rare earth additions influence on Inconel alloy weld microfissuring including material, hot ductility and tensile strength data

22 p3967 A69-39883

Photoelastic behavior in amorphous solids, proposing microstructural mechanism for deformation birefringence

22 p3972 A69-40081

Visual observation of meteor and train microstructure obtained by refractor

22 p4033 A69-41058

Hafnium microstructure and impurity concentrations before and after electron beam melting

23 p4178 A69-42361

Early Precambrian Onverwacht microstructures studied in petrographic thin sections and powdered preparations for possibility of oldest terrestrial fossils

24 p4263 A69-43221

Polycrystalline ceramics chemical and microstructural control through thermomechanical and thermochemical hot forming techniques, discussing pressure sintering, hot extrusion, strain annealing, etc

24 p4321 A69-43338

MICROTHRUST

Cesium contact ion microthruster experiment on-board ATS 4, measuring emission currents and spacecraft potentials

[AIAA PAPER 69-297] 09 p1561 A69-21218

Spacecraft trajectory using microthrust and lunar gravitational attraction for acceleration into heliocentric orbit

09 p1593 A69-21620

Geodetic satellites transfer between low ellipticity orbits by microthrust

21 p3793 A69-38338

Cs contact ion microthruster system design, fabrication and flight qualification, noting control logic/power conditioning unit and electronic packaging

[AIAA PAPER 68-552] 21 p3783 A69-39212

Cesium contact ion microthruster experiment on-board ATS 4, measuring emission currents and spacecraft potentials

[AIAA PAPER 69-297] 24 p4365 A69-43238

MICROTOMY

Z-micron sections removed from metal specimens by microtome for radiotracer study of mass dependence of self diffusion

19 p3313 A69-36490

MICROTOPOGRAPHY

U TERRAIN

MICROTRONS

Electron acceleration in microtron through injection from low pressure gas discharge plasma

08 p1279 A69-19803

MICROWAVE AMPLIFIERS

Microwave amplifier design with hybrid integrated circuits of thin film lumped elements, noting gain and efficiency of transistor circuits

01 p0039 A69-10190

Microwave transistor amplifier computerized design, discussing wide bandwidth and flat in-band gain response optimization on high dielectric substrates

01 p0404 A69-10194

Energy source specifications and control techniques evaluated for microwave amplifier arrays, discussing use of common power supply and energy storage bank

01 p0447 A69-10998

Punch-through microwave negative resistance diode explained and contrasted with similar Read and Shockley structures

02 p0215 A69-11938

Additive noise measurement in microwave power amplifiers under continuous wave and pulsed conditions

02 p0221 A69-12454

Low noise microwave amplifiers for radio astronomy and satellite communications receiving system preamplification

03 p0402 A69-13017

Electroacoustic amplifier based phonon devices, using surface waves on piezoelectric materials to speed radar data real time processing

03 p0394 A69-13353

Microwave generation and amplification, noting microwave transit time tubes, semiconductor devices and methods utilizing quantum electronic effects to generate and amplify EHF oscillations

03 p0395 A69-13611

Maser model of single mode field coupled to N identical two level atoms, deriving threshold, stable and unstable steady states, relaxation oscillations, etc

03 p0441 A69-14108

SNR analysis at amplifier output with AGC, noting increase with signal strength

05 p0729 A69-16085

Log-periodic circuits for application to microwave amplifiers in antenna design, noting bandwidth

05 p0739 A69-16554

- Microwave and optical generation and amplification - Conference, Hamburg, September 1968
07 p1090 A69-18420
- High power microwave oscillator/carpitron/ for pure or FM signal amplification, noting low output noise level
07 p1096 A69-18437
- Microwave oscillation and amplification in long bulk GaAs with barium titanate sheets on surface due to differential negative resistance across terminals
07 p1197 A69-18452
- High efficiency punch-through avalanche transit time diode for generating microwaves over three octaves
07 p1098 A69-18457
- Tunnel diode amplifiers for amplifying weak microwave signals, discussing low noise wideband preamplifier for communication satellites
07 p1099 A69-18464
- Sideband amplification via saturated gas resonance in 258 GHz reflection amplifier with hydrogen cyanide, gas filled cylindrical cavity
07 p1145 A69-18479
- Microwave amplification using silicon diodes in avalanche resonance pumped modes
08 p1279 A69-19909
- Multichannel microwave amplifier at L band frequencies, using several amplifiers in parallel
09 p1466 A69-22446
- Transmit-receive device noise contribution effect on receiving system noise factor for device insertion immediately before low noise microwave amplifier
09 p1469 A69-22605
- Microwave avalanche diode oscillators performance estimates, discussing operation modes and transit time
10 p1665 A69-23873
- Computerized design techniques for microwave components using diodes, detailing X band parametric amplifier
10 p1661 A69-23874
- Microwave amplifiers and receivers noise performance factors measurement noting thermal noise, definitions of noise temperatures and noise figure, noise generators, etc
11 p1840 A69-25301
- Integrated tunnel diode amplifiers, discussing low noise, bandwidth, reliability, miniaturization and applications
11 p1854 A69-25611
- Ultrawideband DC transistor amplifier for pulsed switching circuits with subnanosecond risetimes, discussing multistages with feedback dipoles, transient response and drift problems
11 p1854 A69-25612
- Thin film lumped passive elements for microwave power amplifier integrated circuits, discussing distributed reactances, element size and fabrication, etc
11 p1856 A69-25654
- Transmission type E saki diode amplifier with stabilizing dielectric loaded rectangular waveguide
13 p2233 A69-28067
- Negative resistance amplifier with stabilizing resistor in compensating circuit for operation in microwave duct mismatched beyond amplifier passband range
15 p2573 A69-30118
- Traveling wave tube amplifier for wideband radio in SHF range containing periodically integrated magnetized system, discussing output power variation range
16 p2759 A69-31863
- Gunn effect applied to digital electronics, discussing diode characteristics, microwave amplifier design, pattern recognition, analog- numerical conversion, etc
19 p3285 A69-36708
- Microwave oscillations amplification in bulk GaAs, discussing experimental verification of small signal theory
21 p3781 A69-39127
- Solid state SHF transmission amplifiers design using rectangular waveguides and biased bulk GaAs
21 p3683 A69-39452
- Amplifrons use as broadband microwave amplifiers in high power radar systems with frequency agility, involving modified high vacuum tube modulator and modulator circuit
23 p4135 A69-41384
- Constant beamwidth antenna consisting of parabolic reflector and ridge loaded horn, noting conical scan tracking antenna application
02 p0218 A69-12325
- Wave measurements of normal electric field and tangential magnetic field over microwave disk antenna surfaces
02 p0219 A69-12342
- Dual band shunt slot linear array for S and X band radiation patterns generated from single aperture
02 p0219 A69-12344
- Cosmic microwave background radiation measurement, discussing measurement techniques for antenna temperature at microwave frequencies
02 p0210 A69-12431
- High gain self steering repeater for multibeam microwave array system for earth-satellite communications
04 p0573 A69-14330
- Earth effect on signal correlation in space diversity microwave reception antennas, analyzing vertical separation and out of phase signals
05 p0720 A69-16530
- Antennas with any mean surface, prescribed feeder and radiation pattern synthesized by microwave holography
05 p0734 A69-16574
- Microwave antennas simulation by optical systems based on Huygens-Kirchhoff approximation, noting application to antenna analysis, synthesis and radiation patterns
05 p0736 A69-16780
- Optical simulation of microwave antennas with variable profile reflectors, investigating radiation patterns by photometric scanning of photographs obtained with He-Ne laser
05 p0736 A69-16781
- Bounds on electric field outside radiating system determined for application to UHF and VHF systems design, considering microwave breakdown
08 p1273 A69-20026
- Pressure formed parabolic reflectors for millimeter waves, discussing electrical measurements at 30 GHz
08 p1282 A69-20039
- Microwave antennas optical simulation, discussing given phase amplitude distribution problems
09 p1469 A69-22625
- Small microwave antenna calibration by method of two black bodies exposed to different temperatures, reducing influence of cloudiness and humidity
11 p1844 A69-24450
- Vertical parabolic antenna array and receiving system for S band transhorizon signal phase and amplitude measurement
11 p1851 A69-24987
- Complete electric field of idealized infinite slot antenna with uniform excitation in infinite conducting plane
11 p1851 A69-24994
- High gain self steering microwave repeater for earth-satellite communications noting design, performance and results of color TV transmissions
11 p1839 A69-25294
- Microwave antenna testing on small indoor ranges, discussing reflectors and feeds for generation of approximately uniform plane waves for antenna illumination
11 p1852 A69-25314
- Electronically scanned and fixed multiple beam phased arrays for spaceborne microwave radiometric sensors
12 p2044 A69-26977
- Input impedance measurement of radiating symmetrical HF and microwave antennas, using solid state oscillator for feeding
14 p2420 A69-29394
- Wideband frequency switch to connect narrow band auxiliary to wideband radio system antenna, describing components
16 p2759 A69-31861
- Earth effect on signal correlation in space diversity microwave reception antennas, analyzing vertical separation and out of phase signals
16 p2753 A69-32472
- Horn antenna with parabolic reflector for 30 cm wavelength, calculating field distribution, main and side lobe radiation patterns and aperture efficiency
17 p2937 A69-33147
- Double aperture problem with partially coherent incident field, noting application to microwave antenna-reflector combination
17 p2929 A69-33877
- Monopulse parabolic antenna radiator design for decimeter and meter wavelengths, discussing characteristic properties at optimal dimensions
17 p2939 A69-33905
- Radio interferometry for suppressing background variance between microwave radiometer antenna and random terrestrial background
20 p3506 A69-37712
- Space erectable microwave truss antenna automatically deploying rigid parabolic reflector
22 p3913 A69-40696
- Omnidirectional microwave parallel plate waveguide fed antenna design for flush mounted broadband spacecraft, noting equatorial and polar patterns
22 p3913 A69-40697
- Focus broadening by astigmatism of large microwave parabolic antennas, discussing large span surface deformations caused by astigmatic aberration
23 p4140 A69-42188

MICROWAVE ATTENUATION

- Microwave absorption and series resistance of silicon mesa parametric amplifier diodes, discussing p-n junction and dielectric loss mechanism
05 p0732 A69-16347
- Collisionally induced microwave absorption by non-polar gases, discussing dimer absorption
06 p0962 A69-17816
- Microwave absorption and scattering by atmospheric precipitation as function of temperature and water droplet size
06 p0954 A69-17997
- Radio emission and microwave absorption spectrum dependence on physical properties of clouds in millimeter and centimeter wavelength range
06 p0954 A69-17998
- Pulsar distance estimates based on evaluation of galactic H absorption of 21 cm radiation
06 p1012 A69-18225
- Microwave absorption by free carriers in c domain barium titanate crystals inserted in waveguide during polarization reversal
08 p1374 A69-21189
- Ferromagnetic composite materials for microwave absorption and shielding over frequency band 0.3 to 10.0 GHz
09 p1510 A69-22352
- Spatial density distribution and local values of attenuation of pulsed reflex discharge plasma determined from measured attenuation of microwave beam
13 p2312 A69-28112
- Microwave propagation in Venusian atmosphere, analyzing refraction angles, attenuation and field strength fluctuations
13 p2223 A69-28567
- Magnetoelastic resonant interaction of microwave longitudinal phonons propagating at right angles to magnetic bias applied to YIG rod axis
15 p2565 A69-30184
- Nonresonant absorption and dispersion of microwaves by gases, studying gaseous mixtures, relaxation parameters, anomalous dispersion and temperature effects
15 p2654 A69-31219
- Waveguide capacitive screw tuners effects on dissipative loss, discussing microwave measurements with copper screw tuners
16 p2757 A69-31586
- Microwave power loss and semiconductor conductivity relationship measured for carrier lifetime and mobility, noting nonlinearity and accuracy
16 p2825 A69-31617
- Solid fuel propulsion systems for tactical rockets design, discussing microwave attenuation, acceleration-combustion interactions and performance optimization
16 p2836 A69-31998
- Precipitation intensity measurements, obtaining distribution parameters from radar reflectivity at two wavelengths and microwave attenuation factor at third wavelength
16 p2806 A69-32265
- Attenuation statistics due to rain measured on earth-space path at 16 and 30 GHz, using sun as signal source
17 p2920 A69-33398
- Microwave absorption by free carriers in c domain barium titanate crystals inserted in waveguide during polarization reversal
18 p3183 A69-35158
- Mathematical model of nonlinear microwave breakdown for overdense and underdense plasma outside reentry vehicle, predicting nonlinear pulse transmission through high temperature plasma
20 p3495 A69-37853

MICROWAVE ANTENNAS
NT HORN ANTENNAS
NT LENS ANTENNAS
NT SLOT ANTENNAS

Phase, frequency and amplitude scanning, noting array design and applications

01 p0049 A69-11348

Microwave absorption by Ar plasma of positive column discharge in waveguide under inhomogeneous magnetic field

21 p3778 A69-39547

Microwave absorption by biological materials, noting energy distribution between reflected, transmitted and absorbed radiation as function of medium physical properties

24 p4270 A69-42574

Air density determination using transit time method involving microwave phase measurements

24 p4313 A69-42898

MICROWAVE CIRCUITS

Performance characteristics of microstrip ferrite devices for hybrid microwave integrated circuit systems, including meander line phasers and YIG elements

01 p0040 A69-10191

Thin ferrite use in microwave integrated circuits including phase shifters, latching circulators, isolators and phase and amplitude modulators

01 p0040 A69-10192

Diode structure optimization for monolithic integrated circuit for Ku-band reflective phase shifter

01 p0040 A69-10195

Gallium arsenide single crystal epitaxy with doping/concentrations into semiinsulating microwave circuits

01 p0040 A69-10196

Hybrid microstrip integrated microwave circuits, discussing substrate and conductor materials and fabrication processes

01 p0040 A69-10199

Energy source specifications and control techniques evaluated for microwave amplifier arrays, discussing use of common power supply and energy storage bank

01 p0047 A69-10998

Fundamental microwave oscillations at high frequencies in GaAs epitaxial sandwich layers, using space charge growth control

02 p0297 A69-11941

Thermal noise from passive linear multiports, noting influence of temperature and absorption coefficients

02 p0211 A69-12443

Matrix representation of linear active two port noise figures and charts in terms of power wave variables

02 p0211 A69-12444

Circulator power splitting and isolating function in integrated microwave network

02 p0222 A69-12475

Circuit properties of microwave dielectric resonators, discussing mode identification, resonant frequencies, coupling control, loaded Q, frequency tuning and periodic arrays

04 p0575 A69-14750

Equivalent generator approach to facilitate scattering matrix analysis of complicated microwave circuit

04 p0582 A69-14755

Equivalent circuit for parallel conductor array based on array capacitance matrix

04 p0576 A69-14756

Hybrid loop properties determination using quadrupole algebra, noting frequency dependence of input impedance and voltage transmission

04 p0582 A69-15072

Equipment for minimum cost laboratory for thin and thick film hybrid circuits

04 p0559 A69-15198

Loss factors effects on substrate choice in production of microwave printed circuit components

04 p0578 A69-15199

General theorem of isotropic microwave waveguide junction ports imposed by reflection symmetry

06 p0893 A69-16935

Beam modulation resynchronization at large signal levels by TWT circuit wave to enhance efficiency

07 p1094 A69-18423

Traveling wave amplifiers beam defocusing by RF circuits and space charge fields under large signal operating conditions, discussing magnetic field strength

07 p1094 A69-18424

Integration forms suitable for fabrication of hybrid and monolithic microwave integrated circuits

07 p1096 A69-18441

Monolithic HF circuits stability in TV and HF devices noting need for appropriate amplifiers

07 p1103 A69-18883

Y-circulators specified, measured and calculated values correlated as function of leakage matrix elements and terminating dipoles reflection

09 p1473 A69-22114

Microwave techniques for bondline defects and thickness of reentry elastomeric heat shield material bonded to titanium alloy

09 p1499 A69-22306

Frequency conversion in microwave crystal mixer with EMF amplitude fluctuations in heterodyne

09 p1469 A69-22644

Computer program for analysis of linear microwave multiport circuit by means scattering matrix equivalent

11 p1858 A69-24572

Fabrication procedure for microwave epitaxial GaAs diodes applicable for switching purposes

12 p2035 A69-25831

Microstripline circuit for stabilizing oscillating frequency of Gunn diodes prepared with GaAs slices

12 p2036 A69-25924

Tunnel diode nonlinear p-n junction capacitance influence on characteristics of diode microwave self excited oscillator

12 p2043 A69-26889

Microstrip circulator size reduction attained by tight inductive ferrite coupling for incorporation with microwave integrated circuits

13 p2230 A69-27679

Solid state radar feasibility, discussing circuit components, circuit design problems involving striplines and monoblocks, phase controlled antenna, solid state computers, etc

13 p2230 A69-27928

TEM mode networks design for producing phase coherent pulse modulated microwave signals through spectrum S band

13 p2234 A69-28073

Spatial harmonic spectrum and tangential field distributions in microwave devices showing separation of higher harmonics through delay structure

13 p2236 A69-28576

Microwave dispersion systems, using waveguide loaded with dielectric material to obtain group linear frequency delay characteristic

14 p2412 A69-29395

SHF solid state phased array radar with Gunn effect modular microwave IC design, discussing air and ground applications

14 p2420 A69-29435

Waveguide below cut-off resonators for active microwave circuits, describing experiments with avalanche and Gunn diodes

15 p2577 A69-30613

Stripline microwave integrated circuits in terms of building blocks and components, discussing hybrids, backward wave coupler, balanced modulators and mixers, etc

15 p2579 A69-31075

Hybrid coupled low power digital microwave phase shifters design, discussing lumped element L-C and variable C shifter theories, power limitations and construction techniques

15 p2580 A69-31076

Broadband microwave double balanced mixer/modulators, discussing bandwidth, conversion loss, noise figure, intermodulation and power dissipation

15 p2580 A69-31077

Crystallographic classes of ferrites for microwave devices, discussing magnetic properties, applications and work on polycrystalline yttrium-calcium iron-vanadium-indium garnet

15 p2670 A69-31208

Disk and transmission line microstrip resonators radiation, measuring fractional amount of radiated power

16 p2760 A69-31946

Book on physics of microwave semiconductor diodes covering p-n junction theory and device characteristics and applications

21 p3682 A69-38990

Hybrid microwave IC assembly techniques, discussing active devices connection to substrate with thick or thin film metallizations

22 p3912 A69-40068

Microwave integrated circuit applications to reflective and transmissive phased arrays, discussing radar system elements

24 p4286 A69-43109

MICROWAVE COUPLING

NT COUPLING CIRCUITS

Plasma waveguide properties during high intensity electromagnetic wave propagation, discussing microwave waveguide coupling

03 p0482 A69-14228

Toroidal gas discharge in waveguide by coupling of microwave power into gas to heat gas, noting plasma confinement

[IMPI PAPER A4]

04 p0636 A69-14999

Coupled cavity short slit delay lines in high power traveling wave tubes

07 p1095 A69-18428

Design of coupled cavity extended interaction output resonators for klystron amplifiers

07 p1095 A69-18431

Microwave directional filter using ring resonator and couplers to obtain low transmission loss and center frequency tuning

13 p2226 A69-27187

Microwave propagation in coupled pairs of microstrip transmission lines for integrated circuit design, discussing dielectric Green function

13 p2229 A69-27672

Power coupling among modes in semiconductor lasers in presence of spontaneous or forced microwave modulation of population inversion

15 p2634 A69-30875

Approximate solution for coupled microstrip transmission lines in integrated circuits, discussing impedance, capacitance and testing

15 p2580 A69-31078

MICROWAVE EQUIPMENT

NT BACKWARD WAVE TUBES

NT CARCINOTRONS

NT CATHODE RAY TUBES

NT COLD CATHODE TUBES

NT GAS DISCHARGE TUBES

NT GYRATORS

NT HELITRONS

NT HORN ANTENNAS

NT IMAGE ORTHICONS

NT IMAGE TUBES

NT KLYSTRONS

NT LENS ANTENNAS

NT MAGNETRONS

NT PHOTOMULTIPLIER TUBES

NT PHOTOTUBES

NT PICTURE TUBES

NT PLANOTRONS

NT SLOT ANTENNAS

NT THERMIONIC DIODES

NT THYRATRONS

NT TRAVELING WAVE TUBES

NT VIDICONS

Microwave applications of monolithic and hybrid semiconductor circuit technologies, considering cost and performance

01 p0039 A69-10188

X band mixer with reactively terminated image, using gallium arsenide barrier diodes and microwave integrated circuit techniques

01 p0039 A69-10189

Digital loaded-line phase shift networks for microwave thin film applications, emphasizing design equations

01 p0040 A69-10198

Bulk effect germanium hot-carrier microwave modulator for Q band, reducing required applied voltages by using short length semiconductor ships

01 p0043 A69-10563

Microwave carrier graycode analog to digital converter capable of 1200 megabits per second

01 p0044 A69-10627

Output power of Gunn effect microwave diode using equal area analysis and Fourier transforms

01 p0049 A69-11195

Microwave frequency multipliers for radio relay systems based on VHF transistors and varactor diodes

02 p0216 A69-12097

Miniaturized X band IMPATT microstrip power sources based on Si avalanche transit time diodes integrated with microstrip oscillator circuits

02 p0216 A69-12146

Dispersive two port components for application to microwave pulse compression, coupling YIG crystal magnetoelastic spin wave mode to acoustic transducer

02 p0217 A69-12149

Weak signal interaction between electron beam and microwave resonators, obtaining electron conductance, gain and transfer admittance

02 p0208 A69-12265

Microwave transistor noise figure, power gain and noise measure as function of source admittance and source reflection coefficient in L and S bands

02 p0219 A69-12427

Microwave thermal noise standards, discussing construction, calibration and errors for field operational liquid nitrogen cooled waveguide noise standard

02 p0210 A69-12438

Noise generation and propagation in linear N cascaded mismatched two port networks, noting application to microwave measurements in low noise technology

02 p0211 A69-12445

Low temperature microwave thermal noise standard, discussing waveguide termination, cryogenic cooling and temperature and pressure controls
02 p0211 A69-12446

Cavity stabilization of microwave oscillator for noise reduction
02 p0220 A69-12451

Microwave oscillator AM and FM noise measurement using Schottky barrier diode detector, discriminator, storage oscilloscope and wave analyzer
02 p0220 A69-12453

Microwave measurements of AM and FM noise spectra with video frequency and RF coverage flexibility and high sensitivity
02 p0221 A69-12455

Amplitude noise spectra of X band microwave oscillators with Si avalanche diodes, noting various contributions and dependence on circuit and operating parameters
02 p0221 A69-12456

Probability density function measurement for microwave noise generator
02 p0221 A69-12459

Voltage probability density of wideband microwave noise, discussing measurement technique of dividing spectrum down by noise bandwidth
02 p0211 A69-12460

AM/PM noise conversion in solid state FM microwave signal sources, relating baseband noise power contribution to PM baseband noise power
02 p0212 A69-12462

Gunn effect in bulk GaAs, noting microwave oscillator applications
03 p0484 A69-13292

Holographic and microwave technology relationship, noting side-looking radar photos and X band radiation
03 p0430 A69-13354

Electrically controlled broadband microwave phase shifter consisting of coaxial line with varactors or ferroelectrics
03 p0408 A69-13987

Bandpass characteristic for wide instantaneous bandwidth microwave components for phased arrays, noting error effect on compressed signal and time delay design
04 p0571 A69-14318

Semiconductor microwave phase shifters for electronic steering of phased array radar antennas noting cost, reliability and properties of steerable antennas
04 p0572 A69-14319

Absolute rotation in space measured with microwave rotation sensor using polarization of electromagnetic wave
04 p0573 A69-14342

Waveguide arc location by sound ranging to determine RF breakdown onset in high power microwave system, describing experiment determining feasibility
04 p0576 A69-14762

Microwave power applications to propulsion, noting spacecraft launching, aircraft takeoff thrust assistance and power transmission in space
[IMPI PAPER D2] 04 p0647 A69-15000

Microwave diodes on GaAs base, determining basic parameters and effects on crystal formation and device construction
05 p0730 A69-16222

Equivalent circuit for microwave point diode noting waveform calculations, frequency dependent elements and recovery phenomena
05 p0735 A69-16605

Measurement methods at IF and baseband sections of microwave links, calculating noise superimposed on each swept measurement curve
05 p0722 A69-16728

Microwave generator of FM oscillations using two reflex klystrons and modified by wideband regenerative amplifier to minimize intrinsic AM
05 p0736 A69-16791

Radar detector for survivors, using inexpensive microwave mixer detector crystal
06 p0878 A69-16964

Noise generation mechanism of Read microwave avalanche diode under large signal conditions
06 p0895 A69-17472

High accuracy microwave phase standard for calibration laboratories, discussing broadband differential phase shifter
06 p0896 A69-17487

Automatic compensation of unwanted signal level fluctuation in measuring setups including microwave generators and detectors
06 p0903 A69-17489

Acoustical and microwave holography obviating need for real or simulated reference wave, using recording time for reference
06 p0928 A69-17902

Microwave and optical generation and amplification - Conference, Hamburg, September 1968
07 p1090 A69-18420

Microwave semiconductor devices, discussing performance trends in detectors, tunnel diodes, mixers, varactors, transistors and Gunn effect devices
07 p1096 A69-18440

IMPATT diode microwave oscillator, discussing large signal characterization and model for efficiency dependence on load conductance and admittance plane characteristics
07 p1101 A69-18650

Quenched multiple domain mode oscillations in GaAs microwave diodes noting relationships between efficiency, power output, negative resistance and bias voltage
08 p1282 A69-20107

Microwave converters structural characteristics, calculating noise figure
08 p1285 A69-20594

Microwave power and low noise transistors, noting continuous wave output and circuit design
09 p1462 A69-21407

Microwave silicon technology applied to fabrication of high gain high efficiency transistor
09 p1462 A69-21410

Microwave solid state power sources including transistors, varactor harmonic generator chains, tunnel diodes, avalanche transit time devices, etc
10 p1662 A69-23144

Computerized design techniques for microwave components using diodes, detailing X band parametric amplifier
10 p1661 A69-23874

Microwave amplifiers and receivers noise performance factors measurement noting thermal noise, definitions of noise temperatures and noise figure, noise generators, etc
11 p1840 A69-25301

P-n-p planar epitaxial germanium microwave transistor used as amplifier in 1-4 GHz range and as high speed switch, summarizing design, fabrication and characterization
12 p2037 A69-25940

Dielectric properties of high loss nonmagnetic microwave materials used for waveguide absorbers and anechoic chamber linings
12 p2079 A69-26047

Transmission and reflection scattering coefficient measurements of microwave networks by Fourier analysis of transient response to impulsive or steplike waveforms
12 p2038 A69-26056

Varactor diode parameters measurements by microwave power reflection method
13 p2327 A69-28645

Avalanche diodes as high power pulsed microwave sources, noting power yields and efficiencies
14 p2418 A69-28890

Noise reduction techniques using injection phase locking and high-Q cavities for HF oscillator high order multiplier and avalanche diode oscillator microwave sources
14 p2420 A69-29458

Communication satellite frequency and time divisions multiple access problem, detailing microwave multiplexers design
14 p2417 A69-29688

Design and electrical features of microwave measurement system for solid state spectroscopy, discussing waveguides, signal source, detector, etc
15 p2610 A69-30709

Microwave hologram construction and image reconstruction by laser beam, analyzing results by matrix expression
15 p2610 A69-30802

Linearly tapered transmission line equation and transfer matrix parameters, considering input impedances and microwave application
16 p2749 A69-31582

Dual channel waveguide insertion loss test set for calibrations at 90 GHz in radio astronomy and communication systems, using sprayed thermistor mount
16 p2760 A69-31945

Microwave scanning beam landing guidance system for Swedish tactical aircraft Saab 37 Viggen, reviewing ground station and onboard equipment
16 p2735 A69-32057

Soviet book on avalanche transit time diodes and applications in microwave technology, describing p-n

junction model, negative resistance, dynamic characteristics, synchronized oscillators, etc
16 p2761 A69-32109

Solar radio bursts polarization measured with microwave correlation polarimeter, noting output recording rate
18 p3188 A69-35213

Gunn effect and devices effective use for specific purposes and as components of microwave systems
18 p3183 A69-35263

Microwave equipment reliability considered in terms of various subsystems and components, showing carefully formulated and executed test program as essential
19 p3282 A69-35785

Lasers and maser devices in radio quantum electronics, discussing optical parametric and microwave devices including transistors, diodes, magnetrons, etc
19 p3284 A69-36433

Low noise microwave devices performance and price, discussing transistor and tunnel diode amplifiers, traveling wave tubes and price reductions via manufacturing methods
20 p3504 A69-36913

Equivalent circuit for microwave cavity containing active GaAs device applied to waveguide and radial mode cavity design
20 p3508 A69-37900

X ray emission from high voltage microwave devices during high velocity electron braking measured using X ray sensitive film with superimposed aluminum scale
21 p3664 A69-39059

Germanium microwave backward diodes optimum design and performance prediction through computer calculation for important parameters
22 p3916 A69-41224

Collection of papers on microwaves covering phasers and time delay elements, mm waveguides application to railroad communications and mode conversions
23 p4135 A69-41352

Electronically controlled microwave phasers and time delay elements design and operation, discussing beam width, steering and effects, directivity and planar arrays
23 p4135 A69-41353

Transient processes in microwave quadrupoles with ferrite resonators
23 p4139 A69-41948

Helicopter powering and positioning by CW microwave beam, describing antenna and sensor arrays, feasibility experiments, system applications, etc
23 p4063 A69-42534

High intensity electromagnetic fields generation equipment for calibrating field intensity monitors, discussing anechoic chamber, transmitting antenna, etc
24 p4312 A69-42577

MICROWAVE FILTERS

Microwave selective filter using resonant cavity with single coupling component in feedback circuit of amplifier traveling wave tube or klystron
01 p0042 A69-10384

Tunable ferrimagnetic bandpass filter using magic T configuration to permit low magnetic field strength and retain nonstacked configuration advantages
04 p0573 A69-14343

High Q magnetically tunable microwave filters using magnetodynamic modes in ferrite spheres
06 p0892 A69-16831

Cut-off coupled microwave bandpass filters for use in dielectric filled waveguide systems
09 p1466 A69-22447

Filter circuits for stabilization of solid state microwave devices, noting input matching characteristics
11 p1849 A69-24961

Magnetically selective microwave filters using magnetodynamic natural oscillations in premagnetized ferrite sphere at cavity center
11 p1855 A69-25626

Microwave filters with lumped capacitances and coupled waveguides derived by frequency conversion from lumped filters circuits
11 p1855 A69-25628

Transmission characteristics of narrow band microwave bandpass filters with power cascade and Chebyshev behavior
11 p1857 A69-25677

Synchronized microwave harmonic energy generation by filtering using DC step source feeding modified pulse forming network
12 p2041 A69-26630

Microwave directional filter using ring resonator and couplers to obtain low transmission loss and center frequency tuning
13 p2226 A69-27187

Microwave filters for canonical realization of non-minimum phase transfer functions, combining magic-T or hybrid junction with ladder structure network
13 p2228 A69-27668

Tunable band stop filter realization from characteristic equation solution for propagation modes by magnetized ferrite slab placed in rectangular waveguide
14 p2422 A69-29751

Microwave filter tailored for frequency response in L through S band regions for high range resolution radar receiver
14 p2423 A69-29759

Stepped digital narrow band bandpass microwave elliptic function filters design and construction
16 p2759 A69-31939

Microwave bandpass linear phase filters design and synthesis for simultaneous flat amplitude and delay response
16 p2759 A69-31941

Mode filters for oversized rectangular waveguides, considering resistive sheet with complex surface impedance
16 p2760 A69-31948

Waveguide band filter with reflecting ferrite resonators and frequency matched loads for improved microwave SNR
23 p4139 A69-41945

Microwave bandpass step filters, listing structural dimensions and design parameters
23 p4139 A69-41947

Noise elimination by filtering in high power microwave transmitters, noting practical design tradeoffs
23 p4142 A69-42235

MICROWAVE FREQUENCIES

NT C BAND

NT EXTREMELY HIGH FREQUENCIES

NT SUPERHIGH FREQUENCIES

Microwave second harmonic, sum and difference frequencies generation for two different microwaves normally incident on low temperature semiconductor slab in DC field
01 p0137 A69-10334

Multifrequency three layer sandwich radomes design for reflectionless sandwich at second frequency
01 p0034 A69-11037

Fundamental microwave oscillations at high frequencies in GaAs epitaxial sandwich layers, using space charge growth control
02 p0297 A69-11941

Tunnel breakdown in p-n junctions used to generate microwave oscillations, discussing Si and Ge properties
03 p0492 A69-14163

Free carrier Faraday effect in piezoelectric semiconductors investigated for microwave frequencies, low temperatures, mixed deformation potential and piezoelectric scattering
04 p0643 A69-15201

Wideband microwave KDP light modulator for amplitude and phase modulation, using ring-plane traveling wave circuit
05 p0732 A69-16553

Microwave oscillations during interaction between electron beam and plasma in electron tube
07 p1189 A69-18504

Harmonic generation in microwave gas discharge in pure and air mixed gases, noting rare gases failure in power source applications
08 p1283 A69-20177

Mode designation and propagation characteristics of dielectric tube waveguide, noting practicability at higher microwave frequencies
08 p1284 A69-20296

Galactic and intergalactic ionic fine structure transitions effect on background microwave radiation intensity
09 p1590 A69-21445

Theta pinch plasma microwave emission from electrodeless inductive discharge at low pressures recorded at near plasma frequencies
09 p1549 A69-22017

Nonthermal plasma emission from cold cathode PIG discharge plasma, noting wide spectrum of electron cyclotron frequency harmonics
09 p1549 A69-22018

Stochastic model of electron cyclotron heating, calculating energy gain during transit of magnetic mirror field in presence of microwave electric field
09 p1551 A69-22038

Phase synchronized oscillators in microwave frequency multipliers with improved SNR
09 p1464 A69-22113

Slowly varying component height for microwave radio emission during IQSY, noting magnetic field changing strength effect
09 p1598 A69-22176

Soft magnetic materials, ferrites and magnetic particle composites as two layer laminates for shielding in audio and microwave frequencies
09 p1500 A69-22310

Microwave frequency room temperature acoustic surface wave propagation losses in lithium niobate measured by laser light deflection, discussing propagation and insertion losses
10 p1703 A69-23511

Microwave magnetoelastic wave propagation in ferromagnet subjected to pulsed magnetic field using coupled mode approach
10 p1746 A69-23655

Error analysis in conversion of two port scattering parameters used in microwave transistor characterization
11 p1852 A69-25200

Microwave oscillations amplitude spatial distribution in gas discharge plasma excited by electron beam
11 p1933 A69-25542

Storage varactors and frequency dependent diode input power for multiplier cascades control, discussing series connections and limitations by thermal noise
11 p1841 A69-25607

Varactor diodes for microwave frequency tuning of resonators used for oscillators of avalanche transit time and Gunn diodes, discussing Q factors
11 p1854 A69-25610

Resonators made of YIG single crystals exhibiting lowest linewidth in ferromagnetic resonance at microwave frequencies
11 p1855 A69-25627

Upconverter with gain and stabilized frequency, using sideband locking of IMPATT diode oscillator
12 p2036 A69-25909

Microwave modulation of GaAs injection laser radiation, using Zaleskii recording method and liquid nitrogen to cool laser diode
12 p2105 A69-26031

Precision measuring instrument for negative conductance of active element at microwave region
12 p2038 A69-26054

Microwave frequency synthesizer for digitally tuned UHF and microwave superheterodyne receivers, considering phase locking voltage-tuned transistor oscillator
12 p2030 A69-26390

Substituted lithium ferrites analyzed to obtain materials with small initial magnetic losses at different microwave ranges
13 p2320 A69-28000

Microwave measurement methods, discussing uses of digital computers and sampling techniques
13 p2223 A69-28605

Microwave oscillations in low pressure arc noting long gas discharge in small transverse dimensions
14 p2489 A69-28739

Passive remote sensing at microwave frequencies for meteorology, oceanography and geology, reviewing physics of wave interactions, mathematics of data interpretation, etc
14 p2414 A69-29514

Microwave brightness temperatures for downward viewing over open seas from above atmosphere, using tropospheric model containing homogeneous layer clouds
14 p2415 A69-29515

Plasma surface HF harmonic oscillations amplitude determined by comparing side frequencies intensities of reflected microwave signal
14 p2497 A69-29794

Shields frequency ranges analysis to determine frequencies and parameters for electrostatic and magnetostatic modes transition to electromagnetic and microwave modes
15 p2562 A69-30120

CdS films vacuum deposited on optically polished single crystals used for converting microwave radio signals into hypersonic waves
15 p2575 A69-30236

Frequency effects on Gunn oscillator modulation sensitivity, discussing microwave-frequency deviation and diode impedance
15 p2577 A69-30614

Complex refractive index profiles and wave polarizations calculated for electromagnetic waves transmission through ionosphere at micropulsation frequencies
17 p2927 A69-33864

MICROWAVE INTERFEROMETERS

Artificial plasma properties at microwave frequencies, determining plasma electron density and effects on horn antenna radiation characteristics
18 p3100 A69-34271

Occurrence frequency distributions at microwave frequencies as function of peak intensity and directivities of solar bursts
18 p3187 A69-34969

Electro-optical crystals resonance modulator for coherent light beams and microwave frequencies, describing application to multichannel TV transmission system
19 p3266 A69-35763

Microwave holograms generated by spinning dipole field perturbation technique, showing zone plates and moire fringe resolution
19 p3315 A69-36824

Josephson frequency-voltage relation at microwave and far IR frequencies compared, using radiation induced steps
20 p3583 A69-37418

Sensitivity improvement for inertialess microwave signal scanning and readout by applying pulse compression concepts, discussing application to real time microwave imaging and holography
20 p3545 A69-37901

Microwave frequency measuring instruments design solutions for electric measurements reduction to length measurement
21 p3720 A69-38563

Daily simultaneous solar measurements of microwave atmospheric absorption and emission to determine frequency correlation between meteorological phenomena and atmospheric parameters
21 p3718 A69-39747

Solar microwave flux density during solar activity cycle tabulated, noting discrepancies in absolute flux levels
22 p4001 A69-39987

Molecular collision pumping mechanism for anomalous microwave absorption by formaldehyde rotational transition in Galaxy dust cloud
22 p4029 A69-40768

Parametric losses in nonlinear centrosymmetrical ferroelectric ceramic in strong microwave field at temperatures above Curie point
22 p3996 A69-41164

Human body responses to microwave irradiation, discussing thermal and nonthermal effects and damage to eyes and to information storage in living systems
23 p4111 A69-42216

Space vehicle multibeam Cassegrain antenna system design meeting radiometric mapping requirements in microwave frequency range, discussing mounting, degrees of freedom, etc
23 p4143 A69-42527

RF and microwave signal variable delay and processing using laser-acoustic interactions, photodetector and electrical-to-acoustical transducer
24 p4283 A69-43027

MICROWAVE INTERFEROMETERS

Electron density measurement technique for dense thick steady state plasmas using swept microwave interferometer
02 p0290 A69-12349

Flight inspection positioning system, discussing microwave interferometer angle calibration for instrument landing
03 p0430 A69-13680

Microwave Fabry-Perot resonator for anisotropic plasma diagnostics in presence of static magnetic field
04 p0635 A69-14757

Double microwave interferometer for measuring hydrogen plasma decay
04 p0600 A69-15024

Argon plasma characteristics calculated from 8 mm interferometer data, interpreting transmission coefficients of dielectric film with permittivity gradient
07 p1194 A69-19324

Fast response microwave interferometers classification and construction principles
09 p1496 A69-22028

Microwave interferometer circuits errors, considering interferometers with phase detector, logic counting circuits, frequency conversion and amplitude modulation
09 p1496 A69-22029

Time dependent plasma density variations studies by microwave interferometer having reflector for modulated or nonmodulated microwaves
09 p1496 A69-22030

Refraction errors in plasma density measurement by microwave interferometry
09 p1496 A69-22031

Radio sources angular dimensions determined by microwave interferometry, discussing distinctions between quasars, galaxies and unidentified sources
12 p2166 A69-27039

Plasma microwave interferometry error due to refraction and beam displacement at receiving antenna aperture
13 p2312 A69-28113

Microwave interferometer with digital-logic elements for phase shift measurements in pulsed plasmas without frequency range limitations
14 p2452 A69-29802

Earth based microwave data revealed isothermal layer in extrapolating Venus atmospheric profile below region probed by Mariner 5 and Venera 4
16 p2852 A69-31553

Venus brightness and polarization distributions measurement at centimeter wavelengths using two element interferometer, suggesting Venus atmosphere as main source of radiation
18 p3191 A69-34302

MICROWAVE OSCILLATORS

Microwave oscillations amplification in bulk GaAs, discussing experimental verification of small signal theory
21 p3781 A69-39127

Superconducting cavity X band oscillator designed for study of stability and spectral purity dependence on temperature
21 p3683 A69-39453

Design and performance of microwave open resonators with diffraction grating in mirror, describing Q factor calculation
23 p4139 A69-42045

MICROWAVE PLASMA PROBES

Plasma density dynamic measurements by Fabry-Perot microwave resonator, discussing resonator and coupling problems
01 p0080 A69-10318

Electron radial distribution determination in positive Hg plasma column using simultaneous measurements with two different microwave cavities
02 p0290 A69-12404

Procedure and apparatus for integral microwave and X ray and spectral measurements of quasi-steady plasma radiation
03 p0473 A69-12897

Electron distribution function effect on microwave emission and HF conductivity of weakly ionized discharge plasma
05 p0799 A69-15734

Time resolved measurements, microwave interferometer and pulsed double probe for studying collision dominated plasma expansion in inductive HF He discharge
05 p0804 A69-16535

Microwave spectrum of n-InSb avalanche plasmas under magnetic field, considering dynamic current-voltage characteristics, hole wave instabilities and microwave emission processes
07 p1197 A69-18466

Epithelial microwave radiation from plasma produced by PIG Reflex in magnetic field with mirror geometry, discussing radiation at harmonics of electron cyclotron frequency
08 p1370 A69-21019

Microwave interferometer circuits errors, considering interferometers with phase detector, logic counting circuits, frequency conversion and amplitude modulation
09 p1496 A69-22029

Time dependent plasma density variations studies by microwave interferometer having reflector for modulated or nonmodulated microwaves
09 p1496 A69-22030

Plasma microwave diagnostics by multifrequency probes in geometric optics approximation, assuming inhomogeneous and semiinfinite plasmas with sharp boundaries and nonunity permittivities
11 p1926 A69-24602

Microwave analysis of plasmas produced by laser beam on aluminum spheres, noting expansion velocity and electron density
11 p1930 A69-25287

Soviet book on microwave methods of plasma investigation based on electromagnetic wave interaction, covering microwave probes and plasma radiation
12 p2139 A69-27073

Spatial density distribution and local values of attenuation of pulsed reflex discharge plasma determined from measured attenuation of microwave beam
13 p2312 A69-28112

Plasma microwave interferometry error due to refraction and beam displacement at receiving antenna aperture
13 p2312 A69-28113

Spatial distribution of plasma density from phase shift measurement in millimeter waves based on microwave multichannel probes
14 p2497 A69-29792

Optical image diffraction method for analyzing radiation patterns of horn antenna sounding beams used in microwave measurement of expanding plasmoids
14 p2497 A69-29793

Three channel microwave FM phase meter for studying plasma electron concentrations directional distribution without interferences between channels
14 p2497 A69-29799

FM homodyne phase meter with klystron oscillator for measuring plasma electron concentration, giving block diagrams of meter, detector and oscillator
14 p2451 A69-29800

Direct phase measuring and measured phase compensating microwave devices designed for plasma diagnostics applications
14 p2452 A69-29804

Phase measurements at IF in microwave plasma diagnostics, examining phase stabilization processes
14 p2452 A69-29805

Plasma microwave measurement error allowance for multiple reflection of waves from vacuum chambers dielectric walls
14 p2498 A69-29806

Passive electric microwave probe with balancing capacitance for studying waveguide fields at high microwave power levels in radiative plasma accelerators
14 p2498 A69-29807

Electronic density of collisional cesium plasma, comparing measurements made by Langmuir and HF spherical probes
15 p2659 A69-30300

Microwave-plasma interaction instrumentation for supersonic channel constructed to investigate turbulent boundary layers formed over ablating heat shield materials
19 p3294 A69-35754

Laser radiation power and electron concentration in He-Ne plasma measured by microwave diagnostics
22 p3964 A69-40794

MICROWAVE PROBES

Barium plasma density measurements by Langmuir, microwave probes and resonance fluorescence scattering compared in Q device
02 p0288 A69-12172

Microwave holographic reconstruction of metal objects inside purse by nonscanning method, visualizing microwave field by polaroid and liquid-crystal techniques
07 p1135 A69-19449

Frequency shift and Q change of microwave cavity caused by lossy dielectrics and plasmas, examining perturbing volume requirements for conductor behavior
09 p1544 A69-21323

Hyperbolic EM microwave field used for contactless measurements of parabolic antenna surfaces
19 p3281 A69-35766

Microwave refraction method for satellite horizontal probing of earth atmosphere, discussing phase delay data inversion, air density and intersatellite relative velocity
21 p3671 A69-38376

MICROWAVE RADIATION U MICROWAVES

MICROWAVE RADIOMETERS

3.3 mm radiometer long integration time performance and output noise spectral distribution
02 p0220 A69-12433

Radome material insertion loss measurement by radiometric method noting error analysis
02 p0251 A69-12434

Microwave radiometer with two reference temperatures, discussing overall stability of design, sensitivity and airborne design for operation in X band [DVL-895]
02 p0220 A69-12435

X band radiometer to minimize errors in calibration of microwave noise sources
02 p0220 A69-12440

Broadband null balancing microwave scanning radiometer using diode in feedback loop as reference noise source
02 p0221 A69-12457

Two dimensional electronically scanned k-band phased array antenna design and performance, discussing radiometric system
04 p0572 A69-14328

Microwave radiometer for measuring mesosphere and stratosphere temperature as function of altitude using atmospheric oxygen line
06 p0924 A69-17247

Atmospheric water vapor content determination from microwave radiation measurements and satellite aircraft
06 p0953 A69-17996

Atmospheric microwave radiation and sensitivity of airborne radiometric sounding in water and moisture contents determination
06 p0954 A69-18001

Shock layer microwave radiation measurements during reentry flight of spherical nose cone, determining effective plasma temperature [AIAA PAPER 69-183]
06 p0865 A69-18201

Satellite and aircraft radiation measurements in cm and mm wavelength range to provide information on underlying surfaces
07 p1130 A69-18257

Cutaneous receptor response to microwave irradiation, measuring warmth sensory effects in human forehead with radiometer [AGARDOGRAPH-111]
08 p1266 A69-20677

Hertzian radiometric antennas and signal processing techniques for aerial mapping project for sun
08 p1290 A69-20976

Microwave radiometric sensor operational principles and capabilities, discussing antennas and radiometric receivers
12 p2033 A69-26976

Electronically scanned and fixed multiple beam phased arrays for spaceborne microwave radiometric sensors
12 p2044 A69-26977

Microwave radiometric brightness temperature relationship to soil moisture content for estimating bearing strength
12 p2099 A69-27008

Radar radiometer by adding radar to scanning microwave radiometer, discussing applications to spacecraft measurement of oceanic winds, waves and precipitation
14 p2421 A69-29528

Periodic stellar radiation at 3.5 mm from pulsar CP1919 measured by paraboloid antenna and radiometer
14 p2529 A69-29978

Directional couplers design considerations for use in microwave power meters, analyzing directivity and mismatch effect on system error
19 p3282 A69-35826

Radiometer for 4 cm wavelength range with receiver circuit incorporating tunnel and parametric HF amplifiers, describing design and operation including subunits
21 p3724 A69-39076

Airborne microwave radiometric measurements of simulated ocean surface under various conditions, suggesting possible wind velocity measurement by satellite
21 p3726 A69-39750

Clear air turbulence detection in troposphere by multifrequency radiometric sensor, noting multibeam system for supersonic aircraft
23 p4144 A69-42536

Electron energy measurement accuracy in carbon dioxide laser plasma by S band radiometer
24 p4327 A69-42613

MICROWAVE REFLECTOMETERS

Elastic scattering of electrons from argon atoms in argon air plasmas by shock tube microwave reflection method, measuring power reflection coefficient [AIAA PAPER 68-138]
04 p0632 A69-14701

Swept frequency microwave measurements in simulated reentry environments using dielectric layers, glow discharge plasma and aperture antenna-plasma layer model [AIAA PAPER 69-701]
17 p2920 A69-33461

Microwave reflection technique for transient and quiescent electrical conductivity of Si, noting nonohmic contacts
22 p3997 A69-41226

Swept frequency X band reflectometer for measuring antenna properties in simulated reentry environments [AAS PAPER 69-282]
24 p4313 A69-42861

MICROWAVE RESONANCE

Electron cyclotron harmonic waves in magnetoplasma irradiated by external microwaves
01 p0127 A69-10335

Resonant frequencies and fields in circular cylindrical microwave cavity containing cold uniform magnetoplasma dielectric

06 p0968 A69-17763

Traveling wave microwave and optical resonators synthesis, determining design conditions for resonant frequencies

07 p1145 A69-18477

Microwave resonator characteristics, deriving expressions for Q for pure or coupled electric or magnetic modes

09 p1464 A69-22096

Varactor diodes for microwave frequency tuning of resonators used for oscillators of avalanche transit time and Gunn diodes, discussing Q factors

11 p1854 A69-25610

Electromagnetic fields in cylindrically symmetrical microwave resonator filled with premagnetized ferrite along cylinder axis

11 p1855 A69-25625

Resonance method determining spurious modes excitation in natural mode converter, discussing construction, application and mathematical correlation

11 p1856 A69-25630

Lumped element construction technique involving crossed coils to reduce ferrite produced heat in resonance isolators, using substituted YIG

11 p1856 A69-25632

Dielectric loss tangents measurements combining coherent optical resonator with microwave techniques, noting application at mm wavelengths

12 p2080 A69-26057

Microwave and LF oscillations interactions in plasma beam system, showing oscillation amplitude dependence on frequency relationships

13 p2312 A69-28111

Microwave cavity bandwidth determined from reflection coefficient measurements, considering reflection magnitude and phase

13 p2223 A69-28606

IR radiation detection by photoconductor in microwave resonator noting electric field influence

13 p2223 A69-28639

X band open resonator terminated by step-rimmed flat mirrors, discussing rim effect on Fabry-Perot diffraction loss

14 p2424 A69-29765

Helicon wave dimensional resonance in n-InSb plasma waveguides at different wavelengths relative to wall thickness

19 p3383 A69-36479

MICROWAVE SCATTERING

Enhanced microwave scattering by plasma instability in magnetic field, using microwave interferometer with horn antenna system

06 p0967 A69-17717

Collection of Soviet papers on microwave radiation transport in atmosphere covering radiation field, water vapor content determination, absorption and scattering by precipitation, etc

06 p0953 A69-17994

Microwave absorption and scattering by atmospheric precipitation as function of temperature and water droplet size

06 p0954 A69-17997

Microwave scattering by turbulent plasma column noting effects of plasma density

07 p1194 A69-19411

Microwave scattering from longitudinal plasma waves propagating in collisionless plasma column

08 p1276 A69-20798

Active microwave scattering antenna arrays at super-high frequencies, noting low bias power requirement

08 p1290 A69-20975

Raman microwave scattering with low frequency oscillations caused by plasma drift instabilities

09 p1550 A69-22021

Electron concentration at front of anisotropic plasma expanding in axial direction in electrodeless induction discharge from measurements of reflected microwaves

09 p1550 A69-22027

Limits in applicability of earth equivalent radius to measuring microwave diffraction field in atmosphere

09 p1456 A69-22284

Troposphere effects on millimeter wave radio astronomy measurements, discussing solar noise fluctuations due to clouds and precipitation

13 p2223 A69-28607

Nonresonant absorption and dispersion of microwaves by gases, studying gaseous mixtures, relaxation parameters, anomalous dispersion and temperature effects

15 p2654 A69-31219

Microwave reflection and noise emission from cylindrical rare gas afterglow plasmas in axial magnetic field measured near electron cyclotron resonance

18 p3127 A69-34436

Microwave background angular fluctuations investigated for relationship between whirl motion velocity and temperature dispersion, noting role of scattering by moving plasma

18 p3188 A69-35208

Numerical procedure obtaining scattering matrix of passive reciprocal two port from standing wave measurements, using image circle in Smith chart

24 p4281 A69-42617

MICROWAVE SPECTRA

Microwave and far IR molecular rotational absorption spectra investigated for measuring concentrations of reacting molecular and atomic species in hypersonic projectile wakes

01 p0006 A69-10961

Microwave spectra of peak flux of solar radio bursts of March and July 1966, relating plage regions to spectral characteristics

01 p0069 A69-11121

Water molecules radio spectral lines from microwave emission sources in Galaxy studied for variability, size and polarization

09 p1587 A69-21307

Surface dielectric constant and microwave opacity of Venus atmosphere as function of wavelength determined by radar observations

12 p2153 A69-25805

Venus brightness temperatures vs phase angle to define spectra of day and night face at short wavelengths, using model atmosphere

12 p2153 A69-25806

Frequency spectra of radio galaxies, supernova remnants and quasars observed by radio telescope operating in decimeter wave range

12 p2167 A69-27041

Quasar spectra changes observed from 1962 to 1966 including flux density and antenna temperature for 3C 279 at cm wavelengths

12 p2167 A69-27043

Lambda-doublet radiation from excited state of interstellar OH detected at 5 cm wavelength

13 p2335 A69-27312

Millimeter and submillimeter microwave spectrometric studies of high temperature plasmas and noise emission, discussing instrumentation and absolute measurements

14 p2451 A69-29786

Unsuccessful attempt to observe high charge ion lines generated by dielectronic recombination in solar corona at 5-cm wavelength

15 p2689 A69-30568

Design and electrical features of microwave measurement system for solid state spectroscopy, discussing waveguides, signal source, detector, etc

15 p2610 A69-30709

Absorption coefficient in three microwave lines of O with different rotational quantum numbers calculated, examining Zeeman effect in geomagnetic field

15 p2597 A69-30941

Venus microwave spectrum analyzed by comparing various thermal and nonthermal emission models, discussing surface temperature and atmospheric composition

16 p2853 A69-31597

Lambda doublet maser emission from excited OH rotational level, discussing conditions necessary for microwave radiation

18 p3185 A69-34292

Microwave thermal emission by water measured from aircraft, studying radiation dependence on surface roughness

18 p3127 A69-34421

Solar microwave emission heliographic distribution during pronounced geomagnetic recurrence, noting brightness temperature nonuniformity due to coronal depression through polytrope models for solar wind

18 p3188 A69-35396

Quantum transitions between molecular or atomic energy levels noting microwave spectroscopy utilization

18 p3099 A69-35405

Water vapor microwave emission measurement from galactic hydroxyl sources

18 p3205 A69-35435

Solar microwave emission relationship to geomagnetic activity, analyzing statistically source intensity and model of coronal condensation associated with sunspots based on electron densities

20 p3589 A69-37557

Coupled Fabry-Perot interferometer for microwave spectra with improved selectivity of interference filter

22 p3947 A69-40800

Rotational spectra of methylchlorodiazirine at room and dry ice temperature, using K band and Stark effect spectrometers

23 p4194 A69-42207

Observational cosmology developments with radio and X ray astronomy emphasizing existence, origin, effects and anisotropy of excess microwave background

23 p4219 A69-42327

Single frequency microwave solar bursts correlation with flares and associated active regions based on spectral grouping

24 p4372 A69-43616

Rotational microwave spectrum of 2-methylfuran, using fourth order perturbation method for internal rotation A-E doublet splittings

24 p4280 A69-43811

MICROWAVE SWITCHING

S band thyatron waveguide switch as pretriggered megawatt balanced duplexer

01 p0048 A69-11035

Control signal correction in microwave ferrite modulators, eliminating losses due to screening effect of feeder

13 p2226 A69-27216

Ultrahigh speed microwave diode switch used as transmitter-modulator in PCM systems, utilizing varactor diode avalanche breakdown

13 p2229 A69-27671

High power ferrite latching switch with forced air cooling, discussing nonreciprocal phase shifter materials and configurations

13 p2229 A69-27674

Microwave tunnel diode switch design noting applications to information storage

15 p2574 A69-30132

Wideband frequency switch to connect narrow band auxiliary to wideband radio system antenna, describing components

16 p2759 A69-31861

Distributed communications for earth orbiting global satellite network defined parametrically, describing relay/switching and terminal station satellites

23 p4130 A69-42515

S-band pin-diode switch for high CW power satellite and deep space probe communication, using multiple quarter-wave transformers to stepdown diode impedance

23 p4143 A69-42518

MICROWAVE TRANSMISSION

NT MANDELSTAM REPRESENTATION

Dielectric surface coatings effect on transmission and loss properties of silicon-microstrip microwave transmission lines

01 p0041 A69-10201

Microwave signal nonlinear interaction in isotropic positive column

01 p0127 A69-10282

Microwave second harmonic, sum and difference frequencies generation for two different microwaves normally incident on low temperature semiconductor slab in DC field

01 p0137 A69-10334

Worldwide navigation system consisting of synchronous satellites equipped with pulse modulated microwave transmitters [UN PAPER 68-95205]

01 p0113 A69-10514

Influence of winds aloft on fading rate of microwaves propagated beyond horizon

01 p0030 A69-10566

First normal modes characteristics and lateral wave in weak dielectric layer applicable to microwave propagation

01 p0033 A69-10975

Mean error rates in microwave PCM systems with wave distortion due to multipath propagation

02 p0208 A69-12307

Mismatched errors associated with Y factor power ratio measurement effect on microwave noise-temperature calibrations [JPL-TR-32-1345]

02 p0211 A69-12442

Mutual RF interference between satellite and terrestrial telecommunications microwave relay system at shared frequencies

03 p0392 A69-13242

Wavelength dependence of microwave propagation beyond radio horizon

03 p0395 A69-13626

Relation between satellite data concerning thermal microwave radiation and meteorological conditions in

lower atmosphere for possible use in weather forecasting
06 p0953 A69-17995

Complex microwave incremental conductivity of InSb at 77 K in steady electric field using displaced Maxwellian distribution function
07 p1200 A69-19447

Thermal noise and other disturbances from mismatched two port isolator in low power microwave transmission antenna noise between generators and leads
07 p1108 A69-19486

Plasma waveguide parameter changes due to additional gas ionization from microwave field
07 p1196 A69-19750

Ionospheric and tropospheric effects on microwave propagation including Faraday rotation, atmospheric refraction, attenuation and noise
08 p1272 A69-19958

Complex microwave transmission coefficient of nominal cut-off plasma for several different types of electron distribution, noting discharge characteristics for cut-off
08 p1366 A69-20759

Nonohmic microwave conductivity in semiconductor posts in rectangular waveguide, measuring incident, transmitted and reflected microwave powers
08 p1373 A69-20859

Sensitivity of microwave earth stations for analog and digital communications
09 p1453 A69-21409

Multipath fading reduction on line of sight microwave radio relay links by dual space diversity, noting effects of vertical antenna separation, frequency, etc
[IEEE PAPER 68-TP-350-COM]
10 p1656 A69-23535

Space and carrier frequency diversity determination for mutually interfering microwave radio equipments
11 p1835 A69-24952

Wave propagation in 11.7-12.7 GHz range studied for application to TV transmission, describing emitter, omnidirectional antenna and receiving station
11 p1841 A69-25637

Fresnel dragging effect on 3 cm microwaves by electron gas drift in low pressure glow discharge, noting electron density and excitation modes
12 p2133 A69-25766

Transmission and reflection scattering coefficient measurements of microwave networks by Fourier analysis of transient response to impulsive or steplike waveforms
12 p2038 A69-26056

Internal guiding of microwaves by elevated tropospheric layer noting refractive index, radius of curvature and attenuation
12 p2032 A69-26856

Circular polarization of solar microwave radio emission in Southern and Northern Hemispheres due to solar magnetic field
13 p2326 A69-27550

Microwave propagation in coupled pairs of microstrip transmission lines for integrated circuit design, discussing dielectric Green function
13 p2229 A69-27672

Applied magnetic field effects on longitudinally magnetized reciprocal ferrite phase shifters, showing shift type dependence on guide electrical thickness
13 p2229 A69-27673

Microwave propagation in Venusian atmosphere, analyzing refraction angles, attenuation and field strength fluctuations
13 p2223 A69-28567

Multipath resolution of tropospheric scatter medium by incorporating Rake instrumentation into tropospheric transhorizon microwave experiments
14 p2448 A69-29524

Elastic microwaves propagation attenuation along lithium niobate crystals trigonal axis at various temperatures
15 p2665 A69-30040

Microwave strip transmission line, discussing evolutionary improvements, computerized design, materials, semiconductors, packaging, reliability, etc
15 p2721 A69-31074

Broadband low VSWR transitions between rectangular waveguides and coaxial transmission lines, discussing asymmetrical probe and ridge types
16 p2757 A69-31584

Noise levels due to long range tropospheric transmission calculated for microwave radio systems
17 p2919 A69-33146

Microwave propagation inside hollow cylinder using model plasma as dielectric, deriving relationship between phase shift and free electron density
17 p2932 A69-34218

Microwave application in determining atmosphere meteorological characteristics compared with visual and IR wavelength measurements
20 p3569 A69-36984

Microwave power transmission to high or low altitude balloon systems for stationkeeping, describing flexible diode array rectifier antenna
22 p3870 A69-40809

Carpitron locked oscillator with wide electronic tuning range, describing CW operation characteristics and application to ground station microwave transmitters
23 p4135 A69-41302

Periodic ladder type design delay equalizer for linear delay characteristics in millimeter waveguide systems
23 p4135 A69-41361

Intersatellite microwave laser communication system for ATS-F and ATS-G, discussing experiment, functional design and parameters
23 p4120 A69-41758

MICROWAVE TUBES

NT BACKWARD WAVE TUBES

NT CARCINOTRONS

NT CATHODE RAY TUBES

NT COLD CATHODE TUBES

NT GAS DISCHARGE TUBES

NT HELITRONS

NT IMAGE ORTHICONS

NT IMAGE TUBES

NT KLYSTRONS

NT MAGNETRONS

NT PHOTOMULTIPLIER TUBES

NT PHOTOTUBES

NT PICTURE TUBES

NT PLANOTRONS

NT THERMIONIC DIODES

NT THYRATRONS

NT TRAVELING WAVE TUBES

NT VIDICONS

Transit time and anomalous modes of oscillation in high pulsed power punch-through Si avalanche diode microwave oscillators
02 p0216 A69-12145

High power microwave interactions in pulsed electron beam plasma klystron
07 p1095 A69-18433

C band waveguide window for average power transmission featuring relatively small biconcave dielectric disk
07 p1096 A69-18435

High power microwave oscillator/carpitron/ for pure or FM signal amplification, noting low output noise level
07 p1096 A69-18437

Convergent high-perveance electron gun design for use in microwave tubes, reducing anode aperture effect on current density
07 p1101 A69-18658

Periodic electrostatic focusing structures in microwave tubes, evaluating properties by action function method
07 p1102 A69-18659

Microwave oscillator design employing avalanche transit time diodes
07 p1107 A69-19155

Barkhausen oscillator for LF domain by substituting Cs and K positive ions for electrons, giving oscillation curves and spectral analysis
08 p1280 A69-19981

Microwave tube development, discussing cold cathodes, ferrite and semiconductor integration into tubes, tube failure physics, etc
11 p1847 A69-24745

Microwave breakdown dependence on elevated gas temperature in electric arc shock tube, considering air, nitrogen and argon
16 p2749 A69-31693

Pulse-to-pulse carrier frequency stability of microwave radar transmitter tube for fixed target suppression
20 p3485 A69-36943

Triode with emitter controlled negative resistance of GaAs as oscillator for microwave applications
22 p3911 A69-40010

MICROWAVES

NT MILLIMETER WAVES

Roughness effect on microwave emissivity according to geometric optics with application to moon and Venus
02 p0207 A69-12017

Venus microwave phase effect analyzed assuming dry massive Venus atmospheric model, discussing heat transfer processes
02 p0319 A69-12108

Magnetoclastic coupling constant b measured by propagating microwave signals in pure and substituted YIG
02 p0299 A69-12243

Compact high-gain chromium doped rutile traveling wave masers for Onsala radio telescope for galactic and extragalactic microwave emission studies
02 p0257 A69-12463

Natural microwave radiation generation and propagation and wideband signal detection in problems connected with radio wave propagation, geophysics, radiometeorology and plasma physics
03 p0420 A69-12919

Microwave energy generation with solid state equipment, noting Gunn effect diodes, avalanche diodes and limited space charge accumulation/LSA/ devices
03 p0402 A69-12971

Generation of UHF space charge waves by nonlinear interaction of two microwave signals in magnetoplasma, predicting optical mixing
03 p0475 A69-13146

Pressure induced microwave absorption in molecular N for various temperatures, determining dielectric loss, absorptivity and quadrupole moment
03 p0472 A69-13317

Reduction of optical breakdown threshold in laser focus by superimposed microwave field
03 p0441 A69-13997

Single punch through silicon avalanche diode structure and two distinct modes of oscillation making possible pulsed generation of microwaves
04 p0573 A69-14334

Microwave excited argon discharge emission spectrum analysis, suggesting possible laser action in microwave discharges
04 p0609 A69-14346

Power and time characteristics of He-Ne laser pumped by microwave pulses
04 p0610 A69-14423

Model for predicting characteristics of short duration intense microwave pulse propagating in heated high temperature air
04 p0634 A69-14453

Microwave power applications to propulsion, noting spacecraft launching, aircraft takeoff thrust assistance and power transmission in space
[IMPI PAPER D2]
04 p0647 A69-15000

High efficiency microwave oscillations in Si p-n and p-n-p positive avalanche diodes under pulsed conditions
04 p0580 A69-15491

Polarization enhancements in solar microwave radiation, noting correlation with other solar events and geophysical effects
05 p0813 A69-15761

Nonlinear optics, discussing frequency mixing, induced changes in dielectric constant and parametric amplification in microwave region of spectrum
05 p0772 A69-16229

Jupiter microwave radiation flux density at 81 MHz, noting spectrum of microwave emission
05 p0827 A69-16506

Antennas with any mean surface, prescribed feeder and radiation pattern synthesized by microwave holography
05 p0734 A69-16574

Domain oscillations removal in n-type gallium arsenides by externally applied microwave field, noting doping effect on LSA conversion efficiency
07 p1196 A69-18446

Dependence of microwave emission from n-InSb on crystalline orientations, noting anisotropy in case of rotation in perpendicular plane
07 p1198 A69-18647

Dynamics of pulsed microwave breakdown in nonuniform field at waveguide fed mica aperture, noting electric field distribution change due to initial plasma configuration
07 p1107 A69-19448

Water in interstellar regions detected by microwave emission from 6 sub 16 to 5 sub 23 rotational transition
08 p1383 A69-19896

Microwave plasma diagnostics, discussing electromagnetic radiation and wave propagation measurements
08 p1316 A69-20470

Microwave radiation effects on body weight and peripheral blood hemograms of mice, discussing maximum safe exposure related to generator output
08 p1266 A69-20678

Cosmic microwave background variations produced by nonthermal gravitational radiation, imposing limits on equivalent mass density

08 p1398 A69-20773

Passivated metal semiconductor IMPATT diode for microwave CW oscillation

08 p1286 A69-20862

Microwaves from celestial objects noting radio emission from sun, moon and Jupiter, cosmic fireball and pulsars

08 p1407 A69-21125

Correlated microwave and energetic X ray emission from solar flare with 16-sec periodic pulsations, discussing energy during modulation peaks

09 p1574 A69-21457

Anomalous mode avalanche diodes for pulse power generation noting output, efficiency, mode of operation, microwave oscillations and IMPATT diodes

09 p1466 A69-22455

Increased energy losses and microwave emission at cyclotron frequency harmonics during plasma electron heating at cut-off plasma concentrations in magnetic trap

10 p1728 A69-23130

Pulsed and CW microwave power effects on rabbit eyes, noting lens opacities produced

10 p1648 A69-23185

Limitations of N-port concept in microwave technology, proposing definitions to avoid contradictions

11 p1841 A69-25624

Reflection and absorption characteristics of two dimensional array of magnetic dipoles for microwaves, considering element orientation and distribution

12 p2035 A69-25901

Liquid crystals for photographically recording microwave holograms, noting impossibility of three dimensional image reconstruction with side-looking radar zone plates

12 p2079 A69-25917

Microwave harmonic generation in plasma capacitor, considering power resonances dependence on electron temperature and density

12 p2037 A69-25939

Mismatch correction in microwave power measurements based on directional coupler techniques

12 p2038 A69-26055

Microwave background radiation by intense sources studied by homogeneous and isotropic Friedmann and steady state models

13 p2339 A69-27574

Microwaves - IEEE Conference, Detroit, May 1968

13 p2228 A69-27667

Nonlinear generation of sum and difference frequencies in ionized plasma current densities by nonuniform microwave fields noting electron scattering

14 p2507 A69-29350

Periodic stellar radiation at 3.5 mm from pulsar CP1919 measured by paraboloid antenna and radiometer

14 p2529 A69-29978

Electron temperature relaxation in shock heated Ar plasma, measuring plasma microwave radiation

15 p2663 A69-30995

Microwave field-plasma slab nonlinear interaction in rectangular waveguide, analyzing current and electron density and second harmonic TE and TM power

16 p2749 A69-31703

Solar microwave radiation burst of 29 October 1968 from active region behind west limb

16 p2865 A69-32811

Microwave holography for antenna synthesis, radiation patterns and visible images reconstruction

17 p2976 A69-33891

Microwave background anisotropy induced by gravitational effects interpreted using spatially flat Friedmann model for substratum

18 p3190 A69-34286

Remote sensing by electromagnetic waves in microwave region, describing differences between microwave and optical sensing

20 p3493 A69-37741

Microwave elastic propagation in single crystal specimen of yttrium-iron-garnet ferrite, discussing attenuation

21 p3780 A69-38774

Temperature fluctuations in microwave background radiation from primeval perturbations compared with perturbations from discrete radio sources

21 p3815 A69-39611

Microwave power coupling to high density plasmas for electrons heating, using dielectric plates

21 p3779 A69-39746

Methyl alcohol, ether and acetone vapors decomposition in microwave discharge, obtaining H and CO in addition to solid polymeric films

22 p3895 A69-40103

Microwave radiation hazard data from experimental animals and surveys on humans, considering nonthermal effects, genetic and neurological effects, etc [MPI PAPER DA-6]

22 p3889 A69-40104

Microwave background radiation in steady state cosmological model, attempting interpretation as discrete extragalactic radio sources population

22 p4029 A69-40765

Radio and microwaves biological effects, discussing differences between U.S. and Soviet assessments of radiation hazards

23 p4099 A69-42516

Microwave radiation effects on biological systems, discussing categories according to radiation protection guide /RPG/ numbers, tissue properties and interactions

24 p4270 A69-42579

Microwave holography by two beam interference method, discussing operating principles, equipment, image reconstruction, etc

24 p4314 A69-42976

MICROWEIGHING

U WEIGHT MEASUREMENT

MICTURITION

U URINATION

MIDCOURSE GUIDANCE

Optimization procedure developed and applied to minimum fuel midcourse guidance of spacecraft, discussing optimal closed loop control of linear stochastic systems

06 p0955 A69-17576

Linearized theory for minimum fuel guidance in neighborhood of minimum fuel space trajectory, unrestricted thrust magnitude and allowances for midcourse impulses [AIAA PAPER 69-74]

06 p0956 A69-18183

Midcourse maneuvers in interplanetary guidance, considering spin stabilized spacecraft flyby for Jupiter mission

13 p2354 A69-28504

Filtering and optimal control problems for discrete stochastic dynamical systems, describing various feedback controls and midcourse guidance optimization

18 p3109 A69-34660

Manual procedures for midcourse and terminal guidance, discussing onboard optical measurements and calculations

19 p3368 A69-35792

Optimum midcourse impulses effects on heliocentric launch window, comparing two and three impulse delta 5 performance for two and three dimensional solar system models [AAS PAPER 68-095]

21 p3804 A69-39201

Interplanetary midcourse velocity correction schedules optimization, discussing timing equations modifications, mission simulation and role of earth based radar

21 p3766 A69-39646

Variable time of arrival /VTA/ guidance generalized, developing computational algorithms to supplement linear guidance method

22 p3979 A69-41186

MIDCOURSE TRAJECTORIES

Optimality criterion and equations of motion determined for fixed time impulsive trajectory to minimize total characteristic velocity

06 p1007 A69-17575

MIDDLE EAR

Rapid decompression and recompression in stapectomized cat, noting fibrous tissue response in middle ear at reconstructions utilizing polyethylene struts on gelfoam

14 p2406 A69-29292

MIDLATITUDE ATMOSPHERE

Sporadic E layer boundary frequencies disturbances at midlatitudes, noting solar activity effects, diurnal variations and effect of meteor fluxes

01 p0066 A69-10600

Cause and structure of temperate latitude sporadic E - Conference, Vail, Colorado, June 1968, Volume 2

01 p0072 A69-11169

Midlatitude ionospheric wind profiles noting seasonal and time differences in circulation patterns, speed, shear, wavelength, energy content and dissipation

01 p0072 A69-11171

Midlatitude sporadic E layer, examining hypothesis of wind action on metallic ions and metallic ion accumulation caused by gravity waves

01 p0072 A69-11173

Midlatitude sporadic E layer vertical and horizontal structure and statistical properties, discussing theory of ion concentration by wind shear

01 p0073 A69-11177

Fast neutron fluxes at various atmospheric levels and geomagnetic northern midlatitudes measured by proportional counters using boron trifluoride

03 p0501 A69-13528

Midlatitude nighttime total ionospheric electron content during magnetically disturbed periods from geostationary satellites Canary Bird and ATS 3

03 p0426 A69-14030

Mechanism for noon electron concentration maximum in F region at midlatitudes found to be recombination process

05 p0753 A69-16031

Electron cooling rates in midlatitude and auroral zone thermosphere measured by probe rockets

05 p0755 A69-16267

Midlatitude neutral thermosphere density and temperature measurements, noting effect of atomic oxygen adsorption by instruments

05 p0755 A69-16268

Stratospheric critical clear atmospheric turbulence at midlatitudes, noting applications to supersonic aircraft design

06 p0950 A69-17789

Simultaneous solution of time-dependent momentum and continuity equations for ions and neutral air in midlatitude F2 region conditions

07 p1123 A69-18818

Cosmic ray absorption and modulation in lower ionosphere at midlatitudes, considering 11 year variations, Forbush effects and solar radiation on electron concentration

10 p1759 A69-22840

Low energy particle effects on midlatitude lower ionosphere conditions after July 7, 1966 proton flare, using ground based measurement

10 p1684 A69-23782

Rocket sounding data on ionospheric currents at mid and low latitudes, showing absence in D and above E region

10 p1686 A69-23909

Midlatitude ionospheric disturbances accompanied by auroral type radio absorption observed by radio astronomy and probes during May 26, 1967 storm

10 p1688 A69-23935

Nighttime maxima anomaly in electron concentration of ionospheric F layer at midlatitudes, considering diffusion and recombination

12 p2064 A69-26007

Monochromatic midlatitude auroral arc /M arc/ observation on 28-29 September 1967 at Moscow, Idaho

12 p2065 A69-26105

Mean vertical moisture profile for summer and winter midlatitude stratosphere from Soviet radiosonde data

12 p2070 A69-26582

Oscillations intervals with diminishing period observed during magnetic storms, noting relationship to midlatitude disturbances in F region

14 p2436 A69-29060

Noon electron densities between 65-90 km from measurements of differential absorption of partial reflections, discussing seasonal variations at midlatitudes

14 p2439 A69-29110

Ozone soundings data obtained over Australia and Colorado to obtain vertical picture of synoptic climatology of ozone at midlatitudes

15 p2649 A69-30898

Morning, daytime and nighttime rocket measurements of electron flux in upper atmosphere at 80-165 km altitudes, noting energy flux

15 p2677 A69-31413

Simultaneous middle and low latitude Thomson scatter measurements, comparing electron density, temperature and exospheric temperature data on quiet and disturbed days

15 p2604 A69-31418

Combined midlatitude neutral air wind and equatorial electrodynamic drift effect on F2 layer diurnal variations

16 p2781 A69-32316

Solar corpuscular and UV radiation variation relationship to midlatitude airglow intensity in O I line

16 p2850 A69-32322

Ionospheric and magnetic disturbances at midlatitudes related, noting individual and simultaneous disturbances

20 p3527 A69-37673

Alouette topside ionograms of ionospheric storms at midlatitudes indicating critical frequencies difference between F1 and F2 layers

20 p3532 A69-37894

Auroral midlatitude red arcs ground and satellite data, noting field aligned electron density depression, plasma temperature increase and O plus-H plus transition altitude

20 p3532 A69-37897

Midlatitude thermosphere vertical air motions to balance divergence and convergence caused by large scale horizontal wind systems

21 p3714 A69-38553

Magnetic declination effect on altitude of top of F 2 ionospheric layer at midlatitudes using M/3000/F 2 transmission factor

21 p3717 A69-39577

Midlatitude F region continuity equation solutions, including east-west electric field effects on electron density

22 p3941 A69-40917

Midlatitude ionospheric electron density rocket data survey, including nighttime and daytime N/h profiles for specific solar activities

23 p4155 A69-41563

Radiative cooling models for various midlatitude synoptic features, including stationary front and cyclones

24 p4343 A69-43064

Midlatitude sporadic E model, discussing overdense ionization layers spatial distribution, wind shear effects, periodic variations, etc

24 p4311 A69-43743

MIDLATITUDES

U TEMPERATURE REGIONS

MIE SCATTERING

NT RAYLEIGH SCATTERING

Mie total and differential backscattering cross sections at laser wavelengths for Junge size distribution aerosol models

04 p0609 A69-14290

Stratospheric aerosol investigation by IR and lidar, applying Mie theory to model aerosol size distribution

04 p0592 A69-14654

Atmospheric droplets diameter, number density and scattering cross sections determined from laser radar return equation and Mie theory

06 p0888 A69-17483

Radiation scattering changes due to droplet size distribution change during stratus cloud formation calculated, using development model and Mie theory

08 p1346 A69-21093

Interstellar extinction models of classical Mie particles and quantum mechanical polycyclic aromatic molecules

10 p1781 A69-23679

Optical constants of bulk diamonds compared with interstellar extinction, calculating extinction curves for diamond particles from Mie theory

12 p2157 A69-26230

Optical radar studies of lower atmosphere, giving Mie theory calculations of clear atmosphere volume backscattering cross sections for four laser wavelengths

• 12 p2033 A69-27001

Subroutines for computing characteristics of electromagnetic radiation scattered by absorbing and homogeneous sphere employing logarithmic derivative method

14 p2412 A69-29283

Zodiacal light brightness and polarization measurements from space probes approximated by Mie scattering of interplanetary dust particles

16 p2857 A69-32092

Particle albedos and extinction cross sections computed by Mie theory showing dependence on refractivity, considering thermal radiation from cloudy planetary atmospheres

20 p3614 A69-38255

MIGRATION

Migration and penetration of vacancies in quenched magnesium analyzed by electrical resistivity measurements and electron microscopy

02 p0267 A69-12187

Charge and degree of ionization of nickel alloyed with molybdenum analyzed by electrolytic ion migration method

07 p1159 A69-18535

MILITARY AIR FACILITIES

Tactical airfield/aircraft system effectiveness in terms of ground support resources, aircraft reliability and maximum potential sorties

05 p0743 A69-16238

MILITARY AIRCRAFT

VTOL or V/STOL Light Intratheater Transport /LIT/ for future tactical airlift situations, comparing tiltwing, liftjet, stowed rotor and fan-in-wing concepts

01 p0008 A69-10146

Military aircraft procurement trends examined to forecast military aircraft market

01 p0009 A69-10147

Hydraulic powered flight control system for Jaguar supersonic military training aircraft

01 p0012 A69-10634

Cost factors in choosing single or twin-engine layout for tactical aircraft

02 p0193 A69-12066

Aeronautics - Conference, Beverly Hills, September 1968

06 p0866 A69-17658

T-53 engine operation in U.S. Army helicopters noting design problems from compressor blade failure, sand and dust erosion and bearing and lubrication malfunctions

[AHS PAPER 215] 07 p1203 A69-18867

Military applications of VTOL aircraft, discussing role in battle area with restricted surface transportation

[AIAA PAPER 69-326] 07 p1055 A69-19556

Compound rotary wing aircraft research, discussing XH-51A maneuverability program and UH-1 high Mach and high advance ratio program

[AIAA PAPER 69-218] 07 p1056 A69-19568

Satellite navigation system feasibility for accurate and continuous navigation capability for Army tactical aircraft

08 p1349 A69-21193

Flight testing and preflight simulated testing of Lockheed C-5 Galaxy transport aircraft

10 p1634 A69-23599

Military forward air control aircraft conversion from lightweight commercial tandem engine aircraft noting visibility, communication and navigation equipment

[SAE PAPER 690313] 11 p1822 A69-24511

Military aircraft operating in various environments with low support costs emphasizing improved design, development and manufacturing standards

14 p2392 A69-29503

Automatic navigation and sighting system for French specified Jaguar combat aircraft development

16 p2809 A69-31760

Military V/STOL aircraft flying qualities specification, considering structure, hover and low speed requirements, forward flight, transition maneuverability and control

[AHS PAPER 363] 17 p2900 A69-33520

Turboshaft engines for military aircraft, discussing size, technology and environmental factors with respect to anticipated market

[AHS PAPER 331] 17 p3022 A69-33530

Canadair CL-84 two propeller V/STOL utility tilt wing vehicle development program and flight tests to assess military potential of aircraft

17 p3077 A69-34065

Parametric approach for weight estimation of surface control systems of transonic and supersonic combat and subsonic transport aircraft

[SAWE PAPER 812] 18 p3221 A69-34898

Military aircraft design, discussing reduction of specialization bias and timely application of technical advances

18 p3092 A69-35137

U.S. military aircraft technology, flight environments, trends toward larger aircraft and R and D

18 p3092 A69-35138

Avionics and electronic countermeasures equipment design, development, installation and application problems for high performance military aircraft to meet hostile electronic environment

[AIAA PAPER 69-822] 19 p3243 A69-35599

Quiet military aircraft design factors, considering human hearing characteristics, noise suppression methods, propeller noise-performance relationships and jet engine noise nature

[AIAA PAPER 69-792] 19 p3243 A69-35637

YF-12A interceptor aircraft development and testing, discussing titanium alloys application, aerodynamics and thermodynamics, escape systems for high speed and altitude tests

[AIAA PAPER 69-757] 19 p3245 A69-35652

Flight control systems influence on military aircraft design and performance, discussing static stability, ride quality, flutter margin and maneuver load controls

[AIAA PAPER 69-767] 19 p3245 A69-35656

Cost comparison of single and twin engine layouts for tactical strike/close support aircraft

19 p3248 A69-36855

Wakkel engine development in Poland for powered military gliders at 18 hp and 5500 rpm

22 p3999 A69-40006

Beriev Be-12 cranked wing seaplane design including technical and operational data

24 p4251 A69-42796

Aero L-39 low wing cantilever monoplane jet trainer developed in Czechoslovakia

24 p4251 A69-42797

Engine design program for TF34-GE2 high bypass ratio turbofan military aircraft engine, outlining estimating procedures for thrust, fuel consumption and weight requirements

24 p4364 A69-43042

Aerodynamics, transonic performance, airframe/propulsion, compatibility, structures and materials, flight controls, takeoff and landing capabilities and combat survivability of next generation military aircraft

24 p4252 A69-43046

Military aircraft service life problems solved by alternative replacement policies comparative present value analysis

24 p4253 A69-43058

F-5 cockpit fogging during low flights and dive bombing in South Vietnam attributed to hot humid weather, recommending cockpit temperature control and pilot diet

24 p4277 A69-43376

MILITARY AVIATION

Automatic air traffic control systems design, development and application to civil and military aviation

06 p0955 A69-17858

Helicopters and fixed wing STOL and VTOL aircraft for intertheater military logistics transportation, discussing C-5A role in 1970s

07 p1053 A69-19177

Interim revision of military flying qualities specifications according to experimental data and characteristics of existing aircraft

[AIAA PAPER 68-245] 17 p2902 A69-34026

Aircraft avionics subsystems and weapon system functional integration reflecting aircraft mission, operational, natural and enemy environments

18 p3109 A69-35140

In-flight medical disorders sustained by crew members of various aircraft in French Air Force correlated with aircraft accidents, flight experience and age

24 p4277 A69-43383

MILITARY HELICOPTERS

NT CH-34 HELICOPTER

NT CH-46 HELICOPTER

NT CH-47 HELICOPTER

NT CH-54 HELICOPTER

NT OH-6 HELICOPTER

NT SA-330 HELICOPTER

Helicopter self defense armament for fire support of British Army operations, discussing vulnerability, weapons selection and tactics, logistics, etc

01 p0010 A69-10869

Helicopter use in military activities noting role in overcoming combined enemy, weather and terrain conditions

[AIAA PAPER 69-190] 07 p1244 A69-19547

Helicopters operation from small ships, describing underside harpoon mooring technique for Alouette 2 and 3

08 p1255 A69-20654

Skorsky HH-3F helicopters electronic equipment, discussing communication and navigation aids, search and recovery missions, etc

10 p1662 A69-23222

Optimized automated system for direct support maintenance of AH-56A subsystem equipment

11 p1865 A69-25075

AH-56A Cheyenne armed compound helicopter designed to operate from unimproved bases with minimum support equipment, noting on-board fueling capacity

[AIAA PAPER 68-560] 12 p2017 A69-26770

NASA flight test of hingeless rotor compound helicopter to determine lift sharing characteristics, showing rotor lift dependence on airspeed

14 p2393 A69-29702

Helicopter fire control systems evaluation by computer model for hit probability and impact point sensitivity to various parameters

[AHS PAPER 316] 17 p2933 A69-33540

Helicopter flight loads spectra data compared on statistical basis to establish component service lives

[AHS PAPER 301] 17 p2901 A69-33548

Helicopter evacuation role in mortality rate among wounded in battle in Korea and Vietnam, discussing air ambulance unit organization

23 p4107 A69-41809

Twin engine five seater BO-105 military helicopter design and subsystems and shipboard compatibility evaluation

24 p4252 A69-42937

MILITARY PSYCHOLOGY

Psychiatric study of master attack carrier aviators in ability to fly, considering adult situational reaction diagnosis 03 p0369 A69-12883

Aviation combat performance criterion by analyzing questionnaires sent to combat deployed flight surgeons, noting possible value of peer rating 09 p1447 A69-22549

Military flying career choice as neurotic compensation for personality defects, stressing personality screening during interview 12 p0203 A69-26492

In-flight illnesses in French Air Force, emphasizing psychological failures in etiology 21 p3666 A69-39270

MILITARY SPACECRAFT
NT VELA SATELLITES

Electron measurements at 18 earth radii in Vela satellite program 02 p0307 A69-11735

TRANSIT /Navy Navigation Satellite System/ military and commercial applications 02 p0278 A69-12359

Error correcting coding on DCSP satellite channels, discussing single access communication through wide-band SHF repeaters in synchronous earth orbit 03 p0387 A69-13177

Solar thermal vacuum test for space flight qualification of military spin stabilized synchronous orbit communications satellite 15 p2587 A69-30391

Research satellite, commercial satellite, lunar spacecraft and military satellite missions, discussing Intelsat, Comsat, Early Bird, MOL and ESRO space program 19 p3432 A69-36750

Interpretation of peaceful uses of outer space in Space Treaty, emphasizing provision forbidding individual military space activities whether aggressive or nonaggressive 20 p3635 A69-37106

MILITARY TECHNOLOGY

Operational research in RAF, discussing weapons tactics and research, strike aircraft speed and height effect on target-finding, VTOL and STOL dispersion value, etc 01 p0180 A69-10863

Helicopter self defense armament for fire support of British Army operations, discussing vulnerability, weapons selection and tactics, logistics, etc 01 p0010 A69-10869

Aircraft squadron performance effectiveness model 03 p0367 A69-13911

Military rotor blade radar antennas for all-weather low level flight and fire control 04 p0559 A69-15197

Tactical support aircraft size, economy and flexibility requirements based on Vietnam experience 04 p0549 A69-15486

Satellite communication requirements for UK defense establishment, describing SKYNET system 08 p1272 A69-19957

Boron carbide body armor fabrication by hot pressing in graphite molds 08 p1320 A69-20411

Space boosters, performance of launch vehicles and requirements for future U.S. space launch capability from USAF vantage point 08 p1410 A69-20882

U.S. Army Materiel Command R and D planning structure and technical planning processes influence on decisions improvement 08 p1423 A69-21153

USAF Logistics Command /AFLC/ Missile Fleet Status Tool /MSFT/ for monitoring and control of Minuteman guidance and control system 11 p1865 A69-25073

Store separation from high speed aircraft via wind tunnel test techniques, discussing drop model, flowfield survey and captive trajectory testing [AIAA PAPER 68-361] 11 p1819 A69-25373

Inertial guidance system synthesis for infantry missile with 1 n mile range against small hardened targets requiring 3 ft maximum miss distance 12 p2129 A69-26791

Value engineering and component/products improvement incentive contract clauses role in defense product quality improvement 13 p2383 A69-28100

VHF to UHF telemetry bands transition implemented by Naval Weapons Center 14 p2411 A69-28880

A-New avionics system for carrier based VSX aircraft used in U.S. Navy aerial submarine hunting, discussing TV, lasers, sonobuoy system, radar, etc 14 p2392 A69-29430

Ground military equipment hardening against nuclear environment, selecting worst case levels from isodamage curves 15 p2651 A69-30380

Integrated circuit failure analysis in military and space applications utilizing type-test programs 15 p2624 A69-30820

Military specifications validity with reference to reliability and metal finishing industry 15 p2722 A69-31120

Military systems trouble documentation and evaluation, emphasizing computerized monitoring of reliability and maintainability 15 p2722 A69-31121

Cost effectiveness of DOD/military systems, discussing principles and analytical model with case study 15 p2722 A69-31125

Avionics systems with integration and federation applied to integrated light attack avionics system /ILAAS/ design to provide navigation, weapon delivery and flight control 17 p2976 A69-34057

TC-2 general purpose digital avionics computer in A-7D/E avionics system performing tasks in weapon delivery, navigation and guidance, display updating, self testing, etc 17 p2933 A69-34059

Airborne radomes reliability and high temperature environments, discussing missile nose cones, light weight ceramic techniques, circular polarization, etc 17 p2942 A69-34084

Failure analyses of semiconductor devices for military use, suggesting modifications to MIL-STD reliability screen tests 18 p3108 A69-34499

Reliability demonstration by MIL-STD-781 for equipment failure and success, proposing useful alternatives 18 p3145 A69-34507

U.S. military aircraft technology, flight environments, trends toward larger aircraft and R and D 18 p3092 A69-35138

Visual inspection, thermal and mechanical shock, burn-in and hermeticity tests of microelectronic equipment, reviewing test methods and procedures of MIL-STD-883 program 19 p3284 A69-36043

High density environment-resistant circular connectors, discussing design, applications, test and performance data compliance with MIL-C-81511 specifications 22 p3910 A69-39947

Implementation of MIL-STD-781 reliability test specification from contractor viewpoint, detailing test procedures /procedural, decision, reporting and corrective action rules/ 22 p3952 A69-40025

Reliability test program based on MIL-STD-781 B specification, noting test environments with AGREE chamber 22 p3953 A69-40027

MIL-STD-781A vibration requirements, using mechanical shakers for AGREE vibration testing 22 p3954 A69-40036

Low light level TV systems for military uses, describing design and operation of various image intensifier tubes 22 p3945 A69-40141

Training missions and military exercises to field test weapons system models [AAS PAPER 69-478] 24 p4296 A69-42884

Aerodynamics, transonic performance, airframe/propulsion, compatibility, structures and materials, flight controls, takeoff and landing capabilities and combat survivability of next generation military aircraft 24 p4252 A69-43046

All-equipments reliability test improved by removing usual truncation and extending accept-reject lines of test plan MIL-STD-781 24 p4321 A69-43203

Microelectronics test program consisting of four reliability screening levels based on Mil-Std 883 24 p4287 A69-43205

Gliding cargo airdrop system including automatic homing and manual control [AIAA PAPER 68-958] 24 p4254 A69-43723

MILITARY VEHICLES

Computer program /TACTICS/ for simulating three vehicles simultaneous motion in space, considering interceptor-target guidance and intercept trajectories [AIAA PAPER 69-890] 21 p3678 A69-39415

Handbook of electronic packaging including rigid and flexible printed wiring, soldering and mechanical interconnections, bonding, computer and military applications, etc 22 p3911 A69-40046

MILKY WAY GALAXY

Galactic H II regions morphology from high resolution radio observations, noting variation of electron density with region size 01 p0151 A69-10552

Metagalactic cosmic rays, galactic halo and sources of cosmic rays in Galaxy, noting models, electron component of cosmic rays and evolutionary cosmology 03 p0497 A69-12929

Galactic cosmic rays energy modulation spectrum in interplanetary space, showing influence of solar wind velocity and diffusion coefficient dependence 03 p0501 A69-13527

Cosmic X ray sources resolved against diffuse background radiation lying close to galactic plane 03 p0501 A69-13767

Life probability and origin on Milky Way planets with emphasis on solar system, discussing molecular biology role 05 p0707 A69-15966

Pulsars, noting clusters associated with spiral arm tangential points, anomalous distribution and possible association with galactic disk or spiral arms 05 p0825 A69-16356

Galactic magnetic field estimation obtained from cosmic ray electron spectrum and radio data 05 p0828 A69-16612

Lunar occultations of galactic center region observed at 1667 MHz indicating OH absorption origin in uniform rotating cloud 06 p1009 A69-17961

Galactic rotation constant calculated from radial velocities of O, B and A stars in Cassiopeia constellation, using Fehrenbach objective prism 07 p1214 A69-18664

Contour map of southern Milky Way at 1410 MHz obtained using 210 ft radio telescope at Parkes, Australia 07 p1214 A69-18667

Interstellar light absorption in Milky Way region of Cepheus analyzed by excess color technique 07 p1216 A69-18855

Galactic Wolf-Rayet star distances and distribution on galactic plane, noting concentration difference toward galactic center 07 p1223 A69-19636

Gas remnant of large scale explosive event in galactic plane at 60 degree longitude, discussing resultant extension on line profile 07 p1225 A69-19717

Milky Way local spiral arm 10 MHz absorption, noting interstellar absorption effect and evidence for cool electron gas 08 p1383 A69-19900

Three color RGU system photometry in Milky Way field in direction of anticenter, determining absolute brightness, luminosity and density of stars 08 p1387 A69-20119

Interlocking systems within Galaxy, deducing gravitational theory accounting for galactic spiral patterns 08 p1387 A69-20136

Spatial distribution of stars and obscuring matter in Milky Way field in Kapteyn Selected Area 195 in Circinus, cataloging UBv photometry of stars 08 p1389 A69-20246

Photoelectric UBv photometry of stars in Puppis-Vela border region for associations of intermediate type stars 08 p1389 A69-20248

Helium production in Galaxy, assuming homogeneous evolution of some massive stars due to external factors 08 p1401 A69-20895

Galactic dust layer spatial structure and relation to brightness of Milky Way based on analysis of photoelectric color excesses in Aql and Cyg stars 09 p1590 A69-21381

Further microwave emission lines and ammonia clouds in Sagittarius region, tabulating relevant transitions in ammonia and water 09 p1597 A69-22150

Far IR source in galactic center detected at 100 microns, noting thermal emission of interstellar dust grains as possible mechanism
09 p1603 A69-22264

Galactic structure and space distribution of known Classical Cepheids, noting interstellar absorption and variation of period with distance to galaxy center
10 p1773 A69-22962

Error analysis of Hubble galaxies count to resolve contradiction of values for average optical half thickness tau of galactic absorbing layer
10 p1779 A69-23609

Infinitesimal bending oscillations and/or responses of thin rotating disks applied to thin disk galaxies, discussing Magellanic Cloud passage near galactic center
10 p1786 A69-24110

Temporal variation of metal content in galaxy, discussing stellar radiation pressure effects on heavy element abundance of interstellar gas
12 p2160 A69-26854

Statistical analysis of UVB characteristics of blue objects located near galactic north pole by scintillation techniques
12 p2168 A69-27054

Ionized gas cloud eruption from galactic nucleus deduced from observed hydrogen line at 5.1 cm
12 p2171 A69-27068

IR objective-prism survey along southern Milky Way for identifying high luminosity stars
13 p2335 A69-27314

Emission line fluxes of southern planetary nebulae in Magellanic Clouds and Galaxy measured photoelectrically, giving upper limit to H beta emission of Magellanic planetary
14 p2520 A69-29376

Radial velocities of planetary nebulae in Magellanic Clouds and Galaxy, discussing Population I and II kinematics
14 p2520 A69-29377

Planetary nebulae nuclei magnitudes in Magellanic Clouds and Galaxy measured photoelectrically, discussing early evolution
14 p2520 A69-29378

Contour maps of Milky Way continuum radiation at 1410 and 2650 MHz from low latitude survey, listing sources with estimates of flux density
14 p2526 A69-29772

Milky Way structure, discussing dust bridge and density of absorbing matter between spiral arms of Sagittarius and Carina Cygnus
15 p2683 A69-30514

Galactic magnetic field structure and strength, considering cosmic ray flux, continuum radio emission, starlight polarization, star formation, etc
15 p2694 A69-30857

Carbon stars in south galactic pole region detected in objective prism survey, including variable R Scl and early R stars
16 p2860 A69-32232

Southern Milky Way spectral survey for selection, classification and photometry of interesting objects
17 p3031 A69-33101

Extragalactic radiation depolarization through Milky Way transit determined from linear polarization and flux density measurements of discrete radio sources at 21.2 cm
18 p3190 A69-34287

Dwarf elliptical galaxies of local group, discussing star distribution and orbits, formation process, origin and distribution about Milky Way
18 p3194 A69-34424

Galactic dust layer spatial structure and relation to brightness of Milky Way based on analysis of photoelectric color excess in Aql and Cyg stars
18 p3198 A69-34769

Milky Way continuum radiation at 4170 MHz using parabolic antenna, mapping discrete sources concentration at galactic equator
18 p3200 A69-34996

Stellar populations in Milky Way galaxy, considering stellar motions, spectroscopy, spatial distribution and galactic dynamics
18 p3202 A69-35284

Unresolved background radiation at 2695 MHz surveyed for galactic wing extent determination
20 p3606 A69-37830

NonJeans gravitational instability of stars and interstellar gas in Galaxy due to wave interaction with stars having velocity near wave phase velocity
20 p3607 A69-38037

Galactic radio sources high resolution observations at 178 MHz, determining flux densities and angular structures, noting supernovae remnants
21 p3801 A69-38701

Interstellar matter, considering objects size, solar wind structure, galactic parameters, magnetic fields and cosmic ray heating
21 p3802 A69-38819

Galactic radio emission and magnetic field strength and structure, using radio surveys to obtain information on cosmic rays
21 p3790 A69-38820

Radio background radiation produced by Galaxy, considering energy, isotropy of radiation and black body character
21 p3790 A69-38821

Galactic gaseous disk dynamics, considering interstellar gas behavior and cosmic ray-magnetic field instability
21 p3802 A69-38824

Ariel 3 satellite attempted background radiation measurement between 2-4 MHz to show absorption onset in Galaxy
21 p3806 A69-39258

Galactic hydrogen distribution, discussing velocity field, spiral structure, symmetry, layer shape, ionization, spectra, etc
21 p3810 A69-39503

Milky Way galactic diffuse radiation photometric study using Schmidt camera, stressing Northern Coal-sack commencement region
21 p3817 A69-39725

Space density of giant M stars as function of distance at galactic anticenter
22 p4014 A69-40125

Book on radial velocities and distances in southern Milky Way stellar fields, covering statistical study of star motions in Galaxy, instrumentation, procedures, etc
22 p4020 A69-40317

Possible star formation regions in Milky Way galaxy searched for compact H II regions, tabulating results
22 p4024 A69-40576

Cold neutral H cloud existence in Galaxy from measurements of 21 cm line spectra
22 p4025 A69-40644

Interstellar reddening in solar vicinity, analyzing roles of galactic latitude and longitude and heliocentric distance
22 p4026 A69-40648

Galactic center observations over various wavelengths including polarization, diameter, flux measurements and power output
22 p4029 A69-40767

Radial velocities for O and B stars in Milky Way field in Scorpius determined from prism spectrograms with specific dispersion at H gamma line
23 p4211 A69-41489

X ray spectra of four high energy sources near galactic center
23 p4206 A69-42114

Radio studies of galactic structure, discussing Milky Way origin and formation
23 p4217 A69-42320

Mean and variance of Faraday rotation and pulsar signal dispersion in galactic turbulent structure, applying to statistically homogeneous disk model of Galaxy
24 p4375 A69-42659

Milky Way hydrogen line survey with Parkes telescope, giving velocity-longitude control maps and tabulated data covering galactic equator
24 p4383 A69-42961

MILLIMETER WAVES

Microstrip transmission line integrated circuits on semiinsulating GaAs substrates, showing feasibility at millimeter wave frequencies
01 p0040 A69-10197

Atmospheric noise at millimeter wavelengths, discussing solar radiation and antenna near and far field patterns
01 p0028 A69-10420

Millimeter wave oscillator AFC system utilizing inherent stability of molecular rotational transition applied to reflex klystron stabilization
01 p0044 A69-10628

Figures of merit for polycrystalline uniaxial antiferromagnetic materials, for nonreciprocal devices at millimeter and submillimeter wavelengths, calculated from perturbation theory
01 p0045 A69-10720

Electromagnetic wave generation in 0.2-3mm range, noting applications to physics, biology and technology
02 p0250 A69-12247

Digital transmission at 35 GHz, noting atmospheric and rainfall effect on terrestrial millimeter wave propagation
03 p0389 A69-13192

Short wave bands for earth-space communications, considering propagation anomalies compensated systems and frequency bands availability
03 p0397 A69-13721

Millimeter waves in communication navigation and research, discussing radar range resolution and remote sensing
03 p0397 A69-13722

Point to point millimeter wave communication system design, discussing propagation and data transmission
03 p0405 A69-13723

Millimeter wave lunar radar system component specifications and design with paraboloidal antenna, emphasizing reflectivity of moon
03 p0397 A69-13725

Low and high power pi-mode Ladderton oscillator design operation and performance characteristics
03 p0405 A69-13726

Spectrum and diameter of source of slowly varying component of solar radio emission between 3.3 mm and 21 cm
03 p0516 A69-14045

Single band millimeter wave amplitude modulator for phase meters with homodyne frequency conversion
04 p0577 A69-14850

Diffraction effects on periodic structures in millimeter wavelength range, discussing apparatus for measurements of Fraunhofer zone field, polarization and phase characteristics
04 p0598 A69-14852

Photographs of intensity of radio emission in millimeter band, using luminophor based on ZnS and CdS
04 p0560 A69-15272

Second order nonlinear coefficient measurement for optical generation of millimeter wave difference frequencies in GaAs waveguide, using carbon dioxide laser
06 p0928 A69-17903

Sideband amplification via saturated gas resonance in 258 GHz reflection amplifier with hydrogen cyanide gas filled cylindrical cavity
07 p1145 A69-18479

Rate equation analysis for internally optically pumped millimeter wave maser operating in laser crystal
07 p1146 A69-18480

Wideband superheterodyne tunable radiometers of millimeter wave range using input mixer and high intermediate frequency
07 p1131 A69-18517

Solar intensity measurements at 1.2 mm during partial solar eclipse, noting solar limb brightening and intense solar outburst near end of eclipse
07 p1217 A69-19243

Background radiation intensity upper limits for mm and submillimeter wavelengths in interstellar medium, noting intense flux in far IR
07 p1221 A69-19404

Radome materials with superior dielectric and temperature characteristics for constructing high tolerance microwave multiband radome
07 p1109 A69-19514

Dielectric constant and loss angles measurement in Ku band used for onboard radars
07 p1112 A69-19544

Pressure formed parabolic reflectors for millimeter waves, discussing electrical measurements at 30 GHz
08 p1282 A69-20039

Galactic H 56 alpha recombination radio line observation in Omega Nebula in millimeter band with radio telescope, obtaining electron temperature
08 p1397 A69-20771

Taurus A flux density measurement at 4.3 mm with 36-ft antenna at National Radio Astronomy Observatory to determine spectrum unambiguously
09 p1591 A69-21450

Large steerable mm wave radio telescope of Simcik observatory in U.S.S.R. noting computer aided pointing system
10 p1674 A69-23805

Millimeter and submillimeter radio waves attenuation in rain, showing effective loss cross section as function of raindrop diameter and wavelength
10 p1657 A69-23943

Venus and Jupiter brightness temperature and radio emission at 2.25 and 8 mm wavelengths observed with radio telescope
11 p1956 A69-24396

Millimeter wave propagation over water, discussing fading characteristics and atmosphere absorption effects
11 p1836 A69-24989

Feed shift beam switch for radiometric measurements of astronomical objects emission at millimeter wavelengths
11 p1836 A69-24996

Dielectric loss tangents measurements combining coherent optical resonator with microwave techniques, noting application at mm wavelengths
12 p2080 A69-26057

Barrier capacitance measurement in mm wavelength parametric and multiplication diodes eliminating socket capacitance influence, describing oscilloscope and indicator methods
12 p2043 A69-26885

Far IR and millimeter solar continuum, analyzing flatness of limb darkening curves and brightness temperature near minimum
13 p2341 A69-27591

Millimeter and submillimeter astronomy, discussing lunar poleward darkening function, solar eclipse measurements, observations of Jupiter, Fourier transform and filter spectroscopy uses, etc
13 p2343 A69-27603

Orotron electron beam excited oscillator-generator of millimeter and submillimeter wave bands with wide frequency tuning range
14 p2421 A69-29546

Millimeter and submillimeter microwave spectrometric studies of high temperature plasmas and noise emission, discussing instrumentation and absolute measurements
14 p2451 A69-29786

Single band millimeter wave amplitude modulator for phase meters with homodyne frequency conversion
15 p2575 A69-30242

Diffraction effects on periodic structures in millimeter wavelength measurements of Fraunhofer zone field, polarization and phase characteristics
15 p2607 A69-30244

Superheterodyne millimeter and submillimeter wave detection, allowing harmonics separation
15 p2570 A69-31093

Channel dropping filter for millimeter wave in low loss circular waveguide for overland telecommunications in bandwith over 10 GHz
17 p2936 A69-33032

Fourier transform laboratory spectroscopy for absorption near earth atmosphere millimeter wave spectrum, discussing integrated absorption strength and dimeric effect
18 p3177 A69-35240

Communication satellites equipment and techniques, considering global network, satellite design, millimeter wave systems, etc
19 p3275 A69-36314

Radio measurements of nonionized media and planetary atmospheres, discussing uses of millimeter waves, line of sight propagation, scattering, etc
19 p3276 A69-36427

Free space to dielectric waveguide millimeter wavelength ratio as function of frequency, discussing equipment and procedure
21 p3674 A69-39130

Strong IR millimeter wave emission from galactic center due to interstellar dust grains resembling semiconductor structure
23 p4215 A69-42115

Measurement technique using dielectric waveguides for studying microwave fields influence on and energy imparted to body tissue
24 p4279 A69-43705

Venus and Jupiter brightness temperature and radio emission at 2.25 and 8 mm wavelengths observed with radio telescope
24 p4390 A69-43786

MILLING [MACHINING]

Beryllium chemical and mechanical machining in quantity production, examining salvage and safety precautions
[SAE PAPER 680649] 03 p0434 A69-13455

Torsional moments and forces during Ti alloy and refractory alloy milling with cylindrical cutter
21 p3731 A69-38877

Metal removal mechanisms during electrochemical milling for moving electrodes, noting equations of motion of point for nonmoving electrodes
23 p4168 A69-41310

MINE DETECTORS

Small metallic sphere detection by electromagnetic induction method, emphasizing masking effect of resistive half space below scatterer
01 p0047 A69-10974

MINERAL OILS

Lubrication properties of mineral oils for power hydraulics using Stanhope-Shell four ball test machine
17 p2991 A69-32948

MINERALOGY

Mineralogy of iron fragments from impact craters near Lake Kaali, Estonia, discussing structure and type of meteorite
01 p0159 A69-11370

Nerft and Kaande stony meteorites mineralogical composition from microscopy, noting olivine hypersthene chondrite classification
01 p0159 A69-11374

Origin and mineralogical composition of stones associated with 1824 stone hail near Sterlitamak
01 p0160 A69-11387

Enstatite chondrites structure and mineral content and composition using microscopic and X ray analysis, grouping parameters in distinguishing types
02 p0317 A69-12016

Chemical analysis, isotopic composition, structure and mineralogy of meteorites for classification into iron and stones, discussing time variation of temperature, pressure, etc
07 p1224 A69-19710

Textural variation relation to mineralogical and chemical characteristics of chondrites from review of published data
08 p1391 A69-20516

Chemical and mineralogical study of Kodaikanal meteorite silicate and metal phases, using optical, X ray and electron microprobe techniques
11 p1953 A69-24335

Magnetized minerals studied to investigate space-time structure and reversal of main geomagnetic field
16 p2782 A69-32462

Terrestrial planets high temperature evolution from solar system genesis theory, discussing meteorite chemical composition, petrography, mineralogy and age determination
19 p3407 A69-36079

Sharps chondrite chemical, petrographic and mineralogical studies suggesting formation from complex and repetitious high temperature events and agglomeration processes
19 p3408 A69-36086

C3 and C4 carbonaceous chondrites origin, evolution and classification based on mineralogic and petrologic data
19 p3413 A69-36109

Lance chondrite C III, studying mineral composition of chondrules and heterogeneous crystalline fragments
19 p3413 A69-36110

Carbonaceous meteorites mineralogically identified by selected-area electron diffraction, suggesting formation from minerals mixtures
19 p3311 A69-36111

Carbonaceous meteorites specimen petrographic observations, noting genetic interrelations with ureilites regarding S-C and reduced Fe oxidized Fe ratios
19 p3413 A69-36112

Quantitative mineralogical characterization of chondrites by modal analysis using electron microprobe
19 p3416 A69-36125

Phosphate mineralogy of meteorites using X ray, electron-microprobe and chemical analyses, noting predominancy of whitlockite
19 p3416 A69-36126

Petrology, mineralogy and phase composition of Siena chondrite, interpreting meteorite as ignimbritic rock or welded tuff
20 p3602 A69-37534

Lunar surface, asteroids and meteorites properties by mass distributions of fragmented rocks
21 p3800 A69-38677

Meteorite chemical and mineralogical composition and classification
22 p4032 A69-40981

Martian surface mineralogical study of present state and past processes from rock analyses by unmanned spacecraft instruments to test planetary models
23 p4212 A69-41619

Thermal conductivities /K/ of rock forming minerals reveals K as linear function of density for constant mean atomic weight
24 p4310 A69-43216

MINERALS

NT ALUMINUM SILICATES

NT ANDESITE

NT ASBESTOS

NT BERYL

NT CALCITE

NT CHROMITES

NT COHENITE

NT CORDIERITE

NT CRYOLITE

NT DOLOMITE [MINERAL]

NT ENSTATITE

NT FAYALITE

NT FELDSPARS

NT FLUORITE

NT GARNETS

NT HEXAHEDRITE

NT ILMENITE

NT KAMACITE

NT MAGNETITE

NT MICA

NT MONTMORILLONITE

NT NEPHELINE

NT OLIVINE

NT PEROVSKITES

NT PYROXENES

NT SCHREIBERSITE

NT SILICATES

NT SPINEL

NT TROILITE

NT WURTZITE

NT YTTRIUM-ALUMINUM GARNET

NT YTTRIUM-IRON GARNET

Meteorite dust spherules at Tungusk and Sikhote-Alin falls investigated for mineral composition using X ray analysis
01 p0160 A69-11383

Etching techniques for revelation and viewing of fossilized particle tracks in meteoritic and terrestrial minerals
02 p0245 A69-12569

South African octahedrite containing inclusions of troilite and graphite veined with kamacite
03 p0507 A69-13097

Ionic and nonionic mineral oxide powder fillers influence on stereopolymers lattices formed from phenolformaldehyde oligomers, discussing mechanical properties
08 p1335 A69-20331

Mineralizing metabolic wastes by catalytic oxidation of pyrolysis products, noting nutritive value of ash solutions for Chlorella cultivation
10 p1649 A69-23579

Complex index of refraction of naturally occurring rock and mineral as function of wavelength of incident radiation
17 p2973 A69-33093

Percorite phase in nickel analog of clinohysotile formed under hydrothermal conditions in Wolf Creek meteorite cracks
18 p3199 A69-34824

Cosmic ray produced radionuclides P 32, Cl 36, Ar 37 and Ar 39 determined in separate mineral phases of meteorites, emphasizing ratios in metals
19 p3410 A69-36094

Shock histories of hexahedrites and Ga-Ge group III octahedrites based on metallographic and X ray diffraction analysis, noting meteorites shocked preterrestrially
19 p3418 A69-36136

Mineral dynamics during hibernation and disuse atrophy in connection with organismal homeostasis and chronic-term manned space flight, noting skeletal effect of immobility
21 p3660 A69-39175

MINIATURE ELECTRONIC EQUIPMENT

Shockley theory of field effect transistors, calculating characteristics in miniaturization problems by removing geometric constraints with aid of electric analog
02 p0215 A69-11781

Miniaturized X band IMPATT microstrip power sources based on Si avalanche transit time diodes integrated with microstrip oscillator circuits
02 p0216 A69-12146

MOS technique applied to fabrication of integrated monolithic miniature circuits
07 p1099 A69-18494

Miniature microwave tuners with solid state reliability and reduced power consumption, using YIG, mixer circuits and integrated control circuitry
07 p1102 A69-18672

Miniature current discontinuity antennas for VHF and UHF, describing airborne electronically steerable array exhibiting efficiency and minimum structural disturbance
07 p1105 A69-19111

Miniature power amplifier stage for telemetry transmitters, discussing equipment size and weight reduction methods and hermetic envelope
07 p1106 A69-19115

Miniaturized E-Tee three port circulator with wide bandwidth, noting negligible effect of static field small variations on performance
08 p1291 A69-20980

Microelectronic multimode airborne radar system with modular construction, discussing system design, development, flight testing and operational results [AGARDOGRAPH-114] 08 p1277 A69-20989

Airborne ILS marker beacon receivers and secondary surveillance radar transponder using microelectronic equipment, noting thermal dissipation problems [AGARDOGRAPH-114] 08 p1292 A69-20991

Microelectronic equipment for aerospace application and integrated circuit production in UK [AGARDOGRAPH-114] 08 p1292 A69-20992

Microelectronic studies in France noting semiconductor integrated circuits, thin film devices and application to airborne apparatus and small computer [AGARDOGRAPH-114] 08 p1292 A69-20993

Automatic plasma needle arc fusion welding for computer memory arrays and miniature electronic devices 09 p1511 A69-22355

Multichannel miniature telemetry for vibration, strain and temperature measurements in high speed machinery by solid state encapsulated devices 10 p1654 A69-23251

Miniature telemetry systems for gun launched projectile instrumentation and ejection payloads, noting voltage controlled oscillators, commutators and VHF FM transmitters 10 p1654 A69-23280

Integrated tunnel diode amplifiers, discussing low noise, bandwidth, reliability, miniaturization and applications 11 p1854 A69-25611

Logarithmic response electrometer for upper atmosphere satellite measurements using subminiature vacuum tube 12 p2092 A69-26476

Microstrip circulator size reduction attained by tight inductive ferrite coupling for incorporation with microwave integrated circuits 13 p2230 A69-27679

Temperature measurement miniature telemetry transmitter 15 p2607 A69-30156

Unoccupied space utilization in aircraft compartments due to microminiaturization, considering reliability enhancement of electronic equipment 15 p2576 A69-30353

Seam and stitch welding in miniaturized semiconductor package fabrication, including leak rate tables 18 p3149 A69-35272

EEG monitoring during decompression illness/bends/treatment by hyperbaric procedure using small multichannel telemetry pack 19 p3261 A69-36268

Miniaturized FM telemeter for transmitting electrical activity of single nerve cells in brain of awake and unrestrained animal 19 p3261 A69-36270

Miniature transducer to measure low transient pressures on models in rarefied shock tunnel flows, emphasizing mechanical vibration, convective heating and miniaturization 22 p3950 A69-41227

MINIATURIZATION

NT MICROMINIATURIZATION

Fluidic display systems, discussing thermochromic modules and decoder with miniature components 01 p0078 A69-10155

Fluid logic circuits miniaturization for flow in straight and curved channels of various cross sections 02 p0196 A69-12084

Mini trend hookup copper wire insulation performance evaluation 05 p0730 A69-16242

Miniaturized transmitter for single channel biotelemetric system to transmit electromyograms incorporating thin film components 08 p1265 A69-19836

E shaped cores for miniaturized transformers and inductors from high permeability plastic bonded materials 13 p2237 A69-28586

Microelectronics role in maintenance and maintainability of subminiature solid state components, emphasizing functional packaging at module level 19 p3283 A69-36021

Miniature hydraulic controls with emphasis on four-way directional control valve for space and cost problems 22 p3870 A69-41243

Laser beam circuitry miniaturization facilitating laser circuit assembly isolation from thermal, mechanical and ambient changes 24 p4328 A69-43327

MINIMA

Minimum theorems in elastoplastic theory extended to continua for plastic strains governed by holonomic and nonholonomic stress-strain laws 07 p1235 A69-19442

Reliability of individual components of multicomponent systems under variable loads, using asymptotic distribution of minimal values 08 p1322 A69-21103

MINIMAX TECHNIQUE

Algorithm minimaxing performance index and sensitivity of controller design with and without saddle point 02 p0224 A69-11966

Algorithm with iterative technique for nonlinear minimax approximations 08 p1344 A69-20829

Nondifferential function minimization on entire vector space or bounded subset for application to minimax problems in function spaces, time optimal control, etc 10 p1721 A69-23863

Minimax error technique used with finite difference methods to estimate error in approximations to functions defined by nonlinear differential equations 20 p3568 A69-37832

Discrete problems of optimal control solved by general minimum principle, proposing several algorithms for optimality problems 20 p3509 A69-38295

Minimax sensitivity criteria used to synthesize filters for estimating state of first order plant subject to dynamic and/or statistical parameters uncertainties 22 p3918 A69-41016

MINIMIZATION

U OPTIMIZATION

MINIMUM DRAG

Supersonic gas dynamics variational problems concerning determination of axisymmetric minimum drag 05 p0699 A69-16675

Axisymmetric bodies longitudinal contours for hypersonic flow minimum drag, considering Newtonian pressure distribution and skin friction 10 p1632 A69-23886

Surface of minimum drag symmetrical trapezoidal wing in supersonic flow solved by variational method 15 p2548 A69-31022

Optimum form for hypersonic profile with minimum drag for given bending strength solved by variational method 21 p3644 A69-39099

MINORITY CARRIERS

Direct reading device for minority carriers lifetimes measurement in semiconductor single crystals 01 p0078 A69-10073

P-n-p junctions photoconductivity decay observation, determining signal bulk minority carrier lifetime in thin n regions 01 p0136 A69-10242

Transistor parameters for operation as minority carrier charge controlled device, developing equivalent circuit for computer calculation of transient response 01 p0046 A69-10748

Minority carrier density and diode current obtained as Laplace transforms from analyzing differential equations, describing charge carriers in semiconductor 01 p0049 A69-11361

Base transit time of minority carriers in double diffused Si transistors with small emitter area, discussing cut-off frequency 02 p0297 A69-11995

Minority carriers lifetime measurement in degenerate GaAs, showing dependence on current density and operating temperature 03 p0483 A69-12917

Majority and minority carrier trapping in neutron irradiated Si diodes, measuring transient junction capacitance recovery 06 p0975 A69-16869

Growth induced dislocation effect on lifetime of minority charge carriers in silicon single crystals 06 p0980 A69-17551

Minority carrier distribution in doped semiconductor space-charge layer assuming relation between diffusion and Debye length 07 p1198 A69-18506

Diffusion and minority carriers drift effect on current-voltage characteristics of p-n-p-n structure in high density current 10 p1742 A69-22997

Surface charge exchange in metal oxide silicon capacitors generated at low temperatures by surface state free carrier trapping 10 p1744 A69-23179

Electronic states and minority carrier transport in mixed semiconductors with graded composition, noting position dependent band gaps and effective masses 10 p1745 A69-23360

Minority carrier density in base region of uniform base transistor at arbitrary injection level, using two dimensional model 11 p1845 A69-24569

Single crystal solar cell degradations in space, duplicating radiation effect on minority carriers lifetime by laboratory tests 11 p1826 A69-24876

Cyclotron resonance of minority carriers measured in p-type InSb, giving temperature dependences of absorption derivative and field ratio to line half width 15 p2667 A69-30068

Double diffused transistor with Gaussian impurity distribution analyzed by power series for carrier density distribution and frequency response 16 p2758 A69-31616

Injection level effects on minority carrier lifetimes in lithium-doped devices and solar cells irradiated by electrons and reactor neutrons 19 p3252 A69-35698

Minority carriers penetration depth in solid aluminum gallium arsenide solutions with variable forbidden bandwidth determined from recombination radiation spectra 19 p3391 A69-36606

Active Ni centers properties in Si with emphasis on increasing and reducing minority carrier lifetime in silicon integrated circuits, discussing energy levels 24 p4360 A69-42759

MINUTEMAN ICBM

On job training of logistic publications engineers, emphasizing technical publications and system engineering and development for Minuteman program 10 p1811 A69-22977

Maintenance van loading technique for number of spares and test equipment in Minuteman weapon system for uncommissioned launch facilities at minimum cost 10 p1669 A69-22980

USAF Logistics Command /AFLC/ Missile Fleet Status Tool /MSFT/ for monitoring and control of Minuteman guidance and control system 11 p1865 A69-25073

MIRROR POINT

Bounce resonant scattering of auroral zone electrons, noting contribution to microbursts and mirror point diffusion 05 p0754 A69-16260

MIRRORS

NT MAGNETIC MIRRORS

NT PARABOLOID MIRRORS

NT ROTATING MIRRORS

Mirror photogrammetry geometric principles, studying photo pairs, mirror reflection and reduction methods 01 p0077 A69-10025

Positive feedback of spring mass system for mirror control on spectroheliometer of Apollo Telescope Mount flight 02 p0248 A69-11738

Errors of wavemeter employing open resonator with spherical mirrors 03 p0407 A69-13983

Electromagnetic theory of surface radiation properties, analyzing specular reflectance of optically smooth surfaces 04 p0684 A69-14357

Optical performance of coupled Fabry-Perot resonators with additional mirrors, determining frequency separation parameters due to third mirror 04 p0612 A69-15372

Standing waves effect on spectral and power characteristics of laser with plane mirrors, determining dependence on pumping power 07 p1148 A69-18800

Fabry-Perot laser operation having third mirror inserted on optical axis, analyzing equations solution stability according to Liapunov 07 p1148 A69-18802

Periodic model variations in ruby and neodymium lasers with tilted mirrors, discussing factors in resonator misalignment 09 p1520 A69-22663

Laser frequency drift effect on operation of three mirror interferometer, noting wave reflection by two compounded mirrors 11 p1895 A69-24720

Single and double mirror systems geometrical optical image aberrations noting focal number, angle of field,

secondary magnification and mutual position tolerances
11 p1918 A69-24836

Single mirror scanning geometry and kinematics, analyzing spatial motion of objects plane mirror image
12 p2091 A69-26367

Single mirror image scanning mechanism vector analysis and formulas for vector rotation
12 p2091 A69-26368

Large astronomical mirrors support and testing - Conference, Tucson, December 1966
12 p2055 A69-26406

Elastic mirror flexure and distortion patterns, considering periodic nature of load in polar coordinates, second flexure mode avoidance and friction elimination
12 p2056 A69-26407

Thermal effects in large mirrors, considering temperature gradients parallel to reflecting surface or to optical axis
12 p2056 A69-26408

Antiflexure cylinder for large astronomical mirror, noting support by astatic counterpoint levers and simple flanges
12 p2056 A69-26409

Lever support systems for telescopes noting tilt compensation, acceleration balance and problems of friction, pivot viscosity, thermal effects and weight
12 p2057 A69-26410

Optical tests of Hale telescope mirror and support system at Palomar, noting various maladjustments and malfunctions
12 p2057 A69-26411

Axial support systems for large astronomical mirrors, considering gas support system for flat mirror submerged and floating in isostatic liquid
12 p2057 A69-26412

Sinusoidal tension and compression radial support system for large solid disk primary mirror, noting pivot design and pad bonding adhesive
12 p2057 A69-26413

Large mirror support systems definition in terms of axial location and radial position
12 p2057 A69-26414

Lick telescope support system for 120 inch mirror, noting use of levers and counterweights concept
12 p2058 A69-26415

Isaac Newton telescope, describing support of 98 inch mirror, structure between fabricated cell steel surface and mirror and tests with air bag support
12 p2058 A69-26416

Support system for McDonald 107 inch telescope mirror, adopting Couder design using lily pad single lever supports for axial thrust
12 p2058 A69-26417

Axial support system for Canadian 150 inch telescope mirror, discussing flexural and shear analyses and ring supports repositioning for balancing shear
12 p2058 A69-26418

Construction techniques for lightweight mirrors for secondaries, considering optical finishing and thermal expansion
12 p2058 A69-26420

Axial support system for controlling thermal distortion of 82 inch heliostat mirror for Kitt Peak solar telescope
12 p2058 A69-26422

Dynamic relaxation method for elastic deformation in mirrors, using tensor equations of elasticity in nonorthogonal curvilinear coordinates
12 p2187 A69-26890

Test methods for telescope mirror, discussing polishing, monitoring by Hartmann test and visual null test
13 p2259 A69-27205

Zeeman laser with one end mirror exhibiting x-y-type loss anisotropy, considering resonance condition for round trip pass and self consistent field equations
13 p2271 A69-27398

Light scattering from high reflectivity dielectric mirrors, measuring angular power distribution from beam axis by scanning with narrow slit
13 p2298 A69-27663

Segmented active mirror optics design concept for lightweight optically stable primary reflector used in large orbiting astronomical telescopes
13 p2261 A69-27950

Control system for thin diffraction limited orbiting astronomical telescope mirror based on structural analysis of static deflections
13 p2261 A69-27951

Ultralightweight mirror blanks for astronomical telescopes, discussing weight saving low thermal expansion and fused monolithic core technology
13 p2261 A69-27953

Thermal and mechanical stability of fused silica lightweight mirror structures, examining impact and shear strengths of fused joints
13 p2261 A69-27954

Outgassed condensation effects in vacuum on magnesium difluoride overcoated UV irradiated Al mirrors, including temperature effects, Lyman alpha reflectance and IR analysis of deposits
13 p2299 A69-28015

Photogrammetric calibration of Surveyor 7 stereo mirror based on vector analysis
[JPL-TR-32-1390]
13 p2263 A69-28199

Gas laser design utilizing internal window mirrors deposited with dielectric coating outside resonator
14 p2457 A69-29160

X band open resonator terminated by step-rimmed flat mirrors, discussing rim effect on Fabry-Perot diffraction loss
14 p2424 A69-29765

Pulsed IR laser optimal Q switching mode by using semiconductor mirror with nonparabolic dispersion law and changing mirror opening moment delay time
15 p2633 A69-30064

Spatial and energy characteristics of laser with nonuniform transmittance across resonator mirrors, analyzing transverse modes interaction
15 p2634 A69-30962

Optical performance of coupled Fabry-Perot resonators with additional mirrors, determining frequency separation parameters due to third mirror
16 p2797 A69-32119

Optical computerized design procedure for Ritchey-Chretien corrector, combining ray deviation error function and third order aberration design techniques
17 p2972 A69-33087

Mosaic mirror and lens camera system for multiple image high resolution photography
17 p2972 A69-33089

Ruby laser resonator losses resulting from changes in mirror transmittance or inclination, or introduction of bleachable absorbers
19 p3331 A69-35863

Wave equation of electromagnetic field of optical resonator with arbitrary mirrors, utilizing Schroedinger equation and equivalent mechanical system
19 p3333 A69-35880

Second surface mirror used as coating for spacecraft thermal control
20 p3632 A69-37290

Large aperture Al alloy telescope mirrors consisting of Tenzalloy Al coated with Ni alloy, presenting performance data
20 p3546 A69-38193

Standing waves effect on spectral and power characteristics of laser with plane mirrors, determining dependence on pumping power
21 p3736 A69-38945

Fabry-Perot laser operation having third mirror inserted on optical axis, analyzing equations solution stability according to Liapunov
21 p3736 A69-38947

Annular gas laser cavity designs with additional mirrors for longitudinal oscillation mode selection, noting positive results for He-Ne laser
21 p3740 A69-39553

Thermal control coatings, windows and mirrors for 1973 Mars Viking Lander vehicles under simulated Martian surface conditions
[AIAA PAPER 69-1023]
22 p3923 A69-40393

Ruby laser resonator mirror mechanical vibrations effects on emission temporal behavior, spectral output and far field pattern, describing conditions for spiking
22 p3962 A69-40562

Axial mode frequencies, loss coefficients and optimal parameters of three and four mirror resonators of gas lasers, including designs with maximum selectivity
22 p3964 A69-40796

Mirror mount for shock tube laser cavity with alignment capability, noting seal against internal pressures
22 p3951 A69-41233

Ni plated 40-cm lightweight Al alloy telescope mirror, noting weldment stress relief by annealing
23 p4164 A69-41624

Radial velocity errors in high dispersion astronomical spectrographs in terms of variable spectral shifts along plate produced by mirror surface irregularities
23 p4167 A69-42189

MISALIGNMENT

Misalignment and eccentricity effect on face seal, discussing leakage dependence on phase angle
[ASLE FICFS PREPRINT 15A]
15 p2620 A69-30483

Dynamic balancing mechanics covering graphical representation, mass asymmetries corrections or adjustment calculations and ballasting equations
[SAWE PAPER 736]
18 p3220 A69-34891

MISSIBILITY
U SOLUBILITY

MISFIRES
U FAILURE
U FIRING [IGNITING]

MISMATCH
U IMPEDANCE MATCHING

MISORIENTATION
U MISALIGNMENT

MISS DISTANCE
Virtual or projected miss distance for assessment of missile homing impairment effects, deriving expression based on kinematics
04 p0629 A69-15517

Fixed-tuned telemetry receiver as miss distance indicator /MDI/ to provide information in missile performance program
23 p4138 A69-41781

MISSILE ANTENNAS
Boresight error in missile radome-antenna combination due to reflection and surface wave effects
07 p1111 A69-19536

S band antenna systems for missiles, designed in various types to obtain RF telemetry links reliability by sharing effort between airborne and ground station equipment
23 p4137 A69-41753

MISSILE COMPONENTS
High strength room temperature vulcanizing silicone rubber for tooling and fabrication of aircraft and missile components
09 p1507 A69-22331

Monograph on calculation of linearized supersonic flow on rocket configurations at zero angle of attack, particularly at interfaces between components, covering applications
11 p1817 A69-24637

Detonation system for exploding missile warheads, discussing trigger detonation and safety release elements
17 p3050 A69-33698

Thermal protection for air-launched missile electronics during carry and free flight, considering active, passive and combination systems and weight penalties
22 p4049 A69-39943

MISSILE CONFIGURATIONS
Monograph on calculation of linearized supersonic flow on rocket configurations at zero angle of attack, particularly at interfaces between components, covering applications
11 p1817 A69-24637

Computer programs determining gaseous properties and aerodynamic characteristics for missiles, reentry vehicles and spacecraft at angles of attack
18 p3107 A69-35068

MISSILE CONTROL
Soviet book on inertial control of ballistic rockets covering rocket flight deviations measured by onboard sensors and computer
01 p0113 A69-10994

Missile control during propulsion period, emphasizing vane deflection required for lateral wind compensation
01 p0163 A69-11297

Proportional navigation guidance systems for interceptor missiles optimized by adding biased term to guidance equation
02 p0278 A69-11973

Digital simulation based on guided missile experience, discussing numerical methods for ordinary differential equations, literature, choice of method and simulation languages
03 p0401 A69-13763

Computer programs and analysis methods for digitalization of continuous feedback network in missile control systems
05 p0725 A69-16470

Digital simulation of vehicle motion and control for six degree of freedom simulations of Gemini reentry and aircraft, missile control, etc
05 p0725 A69-16477

Hydraulic control valves for guidance of rockets by secondary liquid injection into nozzle skirt, discussing structure, single nozzle missile and mass gain
07 p1230 A69-19293

Optimal lift and thrust control programs to maximize range of missile in horizontal flight
09 p1610 A69-22086

Flat flexible printed circuitry in AWG-10 missile control system on F-4J, regarding wire harness packaging 09 p1511 A69-22356

Guidance law for autoguided system trajectory to impact target, noting kinematic study 10 p1723 A69-23701

USAF Logistics Command /AFLC/ Missile Fleet Status Tool /MSFT/ for monitoring and control of Minuteman guidance and control system 11 p1865 A69-25073

Inertial guidance system synthesis for infantry missile with 1 n mile range against small hardened targets requiring 3 ft maximum miss distance 12 p2129 A69-26791

Stability analysis of missile lateral supersonic flutter based on Lagrange equations, considering conservative thrust, control deviation and aerodynamic forces 17 p3045 A69-32946

Book on flight mechanics of aircraft and missiles covering mass, propulsion and aerodynamic forces, TOL problems, optimization problems, etc 17 p2898 A69-33319

Perturbation technique application to stability criterion for rectilinear missile flight with arbitrary inclination, noting mass reduction and flow and gravity effect 19 p3429 A69-35779

Missile and spacecraft guidance navigation and control, discussing fluidics, self adaptive and digital control and Kalman filtering 19 p3370 A69-36316

Soviet book on radio control of rocket missiles and space vehicles covering control principles, systems analysis and synthesis, vehicle characteristics, etc 20 p3574 A69-37232

Missile-borne and satellite-borne computers analogies, comparing design, operational conditions and functional requirements 20 p3500 A69-37380

Microminiaturized digital computers for missiles and aircraft, discussing characteristics, environmental conditions and transformation possibility for use in satellites 20 p3502 A69-37392

Single stage rocket control and trajectories for maximum target strike probability within given range 21 p3818 A69-38857

Integrated sensor controllers for missile directional control, discussing test results for two different systems [AIAA PAPER 69-837] 21 p3761 A69-39368

Controllers design for reaction jet controlled aerospace vehicles, studying second order pitch-plane representation with actuator modeled as pure delay [AIAA PAPER 69-854] 21 p3822 A69-39382

Strapped down phased array radar tracker mechanization with digital loop closure electronics for homing missiles, noting cost advantages [AIAA PAPER 69-873] 21 p3763 A69-39399

Reliability assessment of ballistic missile inertial guidance system, discussing objectives and requisites 22 p3953 A69-40028

Monograph on selection of radar echoes from nearly colocated reflection centers, discussing guided missile multiple target resolution 22 p3899 A69-40533

High temperature pneumatic systems for missile and space vehicle control, describing pressure regulators, flow controls, thrusters and analog valves 22 p3870 A69-41240

Antitank missile guidance system with tracker using two optical paths and pyrotechnic flare noting transmission ratios, visibility coefficients and improvement factors 23 p4164 A69-41625

UHF down-converter design used in various Navy missiles UHF telemetry/miss-distance information system 23 p4137 A69-41778

Fixed-tuned telemetry receiver as miss distance indicator /MDI/ to provide information in missile performance program 23 p4138 A69-41781

Rendezvous, intercept and injection optimal control laws derived from inhomogeneous linear differential equations with quadratic performance index 23 p4224 A69-41921

All-electric nonlinear actuator steering advanced tactical missiles, noting 99.29 percent delivered unit reliability during mass production 23 p4225 A69-42458

Controlled plant in n dimensional Euclidean space, analyzing optimal trajectory using integral equations 23 p4183 A69-42472

Extreme value statistics used to determine minimum acceptable tensile strength of wire command links in TOW antitank missiles 24 p4318 A69-42642

Space and missile guidance performance analysis through automatic generation of mission performance sensitivity with respect to error sources from Monte Carlo simulation [AAS PAPER 69-404] 24 p4347 A69-42836

Missile response-PDM guidance and control system parameters relationship, using phase plane representation [AIAA PAPER 68-820] 24 p4283 A69-43252

Quasi-optimum proportional navigation for interceptor missiles, discussing feedback guidance law and attack geometry 24 p4348 A69-43292

Policies and controller design for pursuing vehicle based in terms of pursuit-evasion differential games 24 p4341 A69-43295

MISSILE DESIGN

Liquid hydrogen and LOX boost pump design for Centaur missile and liquid hydrogen and LOX chill-down pump design for Saturn 4B missile 01 p0087 A69-11149

Galvanic corrosion couples of metals and alloys tested in liquid fluorine, determining corrosion rates for possible missile components application 06 p0944 A69-17854

Solid fuel propulsion systems for tactical rockets design, discussing microwave attenuation, acceleration-combustion interactions and performance optimization 16 p2836 A69-31998

Missile and space support planning, objectives, technology development, functions, maintenance and in-flight maintainability 19 p3295 A69-36327

MISSILE ENGINE CASES

U ROCKET ENGINE CASES

MISSILE LAUNCHERS

U MOBILE MISSILE LAUNCHERS

MISSILE RANGES

White Sands Missile Range space and missile test facilities and support facilities for space exploration 02 p0227 A69-11761

Kwajalein Missile Range UHF telemetry conversion program using S band antennas with three channel monopulse autotrack systems 07 p1077 A69-18829

UHF telemetry conversion program at Pacific Missile Range, describing antenna, receive-record and separation display systems 09 p1454 A69-21800

Active interferometer controlled telemetry tracking system for missile range, discussing automatic target acquisition, dish feed, costs and optimized data-channel antenna patterns 19 p3271 A69-36253

MISSILE ROLL CONTROL

U LATERAL CONTROL

MISSILE SILOS

Air pressure wave forces on missile from silo wall motion resulting from close nuclear blast, using acoustic wave equation for concentric cylinder flow 21 p3691 A69-39765

MISSILE SIMULATION [MATH MODELS]

U MATHEMATICAL MODELS

U MISSILES

MISSILE SIMULATORS [TRAINING]

U MISSILES

U TRAINING SIMULATORS

MISSILE STABILIZATION

U STABILIZATION

MISSILE STAGING

U MISSILES

U STAGE SEPARATION

MISSILE STRUCTURES

Book on material and design problems encountered in construction of high performance missiles, rockets and spacecraft, considering influence of space environment 01 p0084 A69-10021

Active feedback control of distributed parameter systems including elastic airplane and missile structures, noting feedback loop coupling problem [ASME PAPER 69-VIBR-61] 10 p1668 A69-24145

Dynamic IR inspection to detect fatigue cracks in aircraft and missile structure from distance 11 p1861 A69-24262

Large plastic deformation of two metallic cylindrical flat ended missiles in mutual longitudinal impact 12 p2179 A69-26217

Finite element techniques of structural analysis for missile and space structures, including Apollo computerized analysis and structural optimization 19 p3438 A69-36324

Composite-to-metal joints design and fabrication, using carbon yarn in epoxy matrix for missile interstage application 24 p4323 A69-43426

High modulus carbon filament composite structural elements for missile interstage application, showing weight savings 24 p4325 A69-43444

MISSILE SYSTEMS

NT GROUND OPERATIONAL SUPPORT SYSTEM

Radome materials design and performance for guided weapons systems, describing research conducted in UK 07 p1112 A69-19540

USAF Logistics Command /AFLC/ Missile Fleet Status Tool /MSFT/ for monitoring and control of Minuteman guidance and control system 11 p1865 A69-25073

Tactical rocket propulsion - Conference, La Jolla, California, April 1965 16 p2836 A69-31991

Liquid expulsion by direct pressurization of propellant tank in spinning missile system, demonstrating feasibility with subscale hardware [AIAA PAPER 69-527] 16 p2838 A69-32651

Kormoran airborne missile weapon system for attacking seagoing targets, discussing navigation guidance, radar tracking and homing system 17 p3050 A69-33697

Polaris and Poseidon nuclear missile systems, considering efficiency and launching depth from nuclear submarine 19 p3432 A69-36687

IRIG /Inter-Range Instrumentation Group/ telemetry standards for U.S. Department of Defense missile and weapons systems, reviewing evolution, content, scope, philosophy, revisions, etc 23 p4121 A69-41770

MISSILE TEST LABORATORIES

U LABORATORIES

MISSILE TESTS

Wind tunnel rain erosion testing of components of aircraft or missiles flying at high speed 07 p1117 A69-19534

Hypersonic flight test data of Berenice missile compared to wind tunnel test data, discussing in-flight flow separation, Mach-Reynolds torque, etc 10 p1632 A69-23842

Mathematical model for operational readiness of dormant systems /periodically checked missiles/, discussing time distribution to failure detection, occurrence and between tests 18 p3142 A69-34477

Computerized prediction of RF instrumentation system signal margins for missile flight tests based on trajectory and range balance equation 18 p3103 A69-35097

Portable UHF telemetry receiving station for medium range surface-to-air missiles testing, analyzing antenna coverage over water and system prediction allowing variable parameters 23 p4122 A69-41780

MISSILE TRACKING

Missile radar cross section based on modeling from simple forms, noting computer program 03 p0384 A69-12910

Radar cross section of missile and aircraft configurations, comparing theoretical and experimental results for Convair 990 static test model 03 p0384 A69-12911

Shipborne self pointing antenna for reception of telemetry signals from maneuverable missile, discussing tracking and compensation for ship platform motion 10 p1664 A69-23803

Phased array radar system for UHF detection, identification and tracking of orbiting objects and ballistic missiles, noting system design and hardware 12 p2028 A69-25906

Antitank missile guidance system with tracker using two optical paths and pyrotechnic flare noting transmission ratios, visibility coefficients and improvement factors 23 p4164 A69-41625

MISSILE TRAJECTORIES

- Virtual or projected miss distance for assessment of missile homing impairment effects, deriving expression based on kinematics 04 p0629 A69-15517
- Trajectories minimizing missile velocity losses due to gravity by setting boundary conditions and trend of thrust in time 08 p1409 A69-20587
- Mechanics of missile dispersion due to dynamic unbalance and rocket spin stabilization problems [SAWE PAPER 741] 18 p3208 A69-34886
- Flight times compared for intercept and pure pursuit missile trajectories 20 p3618 A69-37716
- Single stage rocket control and trajectories for maximum target strike probability within given range 21 p3818 A69-38857

MISSILE VIBRATION

- Close coupled accumulators for suppressing missile longitudinal oscillations /POGO/ developed for Gemini and Titan 3, including pump interaction [AIAA PAPER 69-547] 16 p2869 A69-32729
- Aircraft and missile dynamic characteristics for heavy loads and large heat flux, noting small harmonic vibrations of heated structures in plastic domain [ICAS PAPER 68-38] 17 p3061 A69-33589

MISSILE WINGS

U LOW ASPECT RATIO WINGS

MISSILES

- NT AIR TO AIR MISSILES
- NT AIR TO SURFACE MISSILES
- NT ANTIAIRCRAFT MISSILES
- NT ANTIMISSILE MISSILES
- NT ANTITANK MISSILES
- NT BALLISTIC MISSILES
- NT INTERCONTINENTAL BALLISTIC MISSILES
- NT MINUTEMAN ICBM
- NT POLARIS MISSILES
- NT SURFACE TO AIR MISSILES
- NT V-2 MISSILE

- Secondary explosives ignition by primers and other explosive wire devices on missiles, discussing circuitry and resistance to severe climatic and electrical environments 10 p1751 A69-23021

- Guidance law for autoguided system trajectory to impact target, noting kinematic study 10 p1723 A69-23701

- Main tank injection for packaged liquid missiles, discussing propulsion system design, pressurization, packaging and screen reservoir [AIAA PAPER 68-627] 19 p3429 A69-35947

MISSILERY

U MISSILES

MISSION PLANNING

NT COUNTDOWN

- National space program management, discussing NACA and NASA, lunar mission planning, procedures and program flexibility and responsibility 01 p0178 A69-10468

- Solar system origin and evolution by future space mission experiments, discussing theories and mission objectives [AAS PAPER 68-191] 01 p0153 A69-10823

- Planetary quarantine and biological search strategy, discussing Voyager-Mars mission configuration, sterilization, back contamination and decisions 01 p0021 A69-11090

- Systematic approach to standard launch vehicle based on governmental expenditure minimization while attaining mission goals 01 p0162 A69-11096

- Scientists involvement in planetary spacecraft missions, considering organization for particular instruments and more complex payloads [AAS PAPER 68-192] 02 p0311 A69-11473

- U.S. space program projections, discussing earth orbit operations, lunar and planetary explorations, costs and timetable 02 p0355 A69-11744

- Planetary exploration strategy for form and origin of universe, unified field theory and abiogenesis, discussing mission planning group 02 p0324 A69-12305

- Planetary swingby theory mechanics and applications for optimization of interplanetary trajectories 02 p0331 A69-12818

- Mission capability differences between direct and orbital Mars missions as to launch period selection, targeting capability and error analysis 02 p0331 A69-12821

- Lunar geoscience role in lunar mission planning, discussing costs, reduced gravity effects, sample mass limits and seismology 03 p0510 A69-13391

- Manned reusable space transportation systems development, discussing requirements for future space mission planning 03 p0519 A69-13395

- Mission analysis for applications satellites, discussing tradeoffs among mission objectives, launch vehicles, spacecraft and geopolitical considerations 03 p0511 A69-13428

- Aeroshell structural development for Mars flyby and entry landing mission compatible with Atlas/Centaur launch vehicle [AIAA PAPER 68-1159] 03 p0521 A69-13667

- Mars unmanned spacecraft mission profiles for surface imaging, noting influence of lighting requirements [SMPT PAPER 104-21] 04 p0650 A69-14361

- Iterative guidance mode /IGM/ applied to effective gravity vector prediction, acceleration measurement of noise sensitivity and energy limitations [AIAA PAPER 67-620] 04 p0629 A69-15501

- German analysis of preparatory technology of U.S. space programs, noting effects of hardware development for manned space travel on future planning 05 p0849 A69-15576

- Technological base for planning space flight missions to obtain data on earth resources, detailing earth resources technology satellites /ERTS/ 05 p0830 A69-15921

- Jupiter unmanned flyby probes trajectory and mission analysis, considering planetary gravitational field role for trajectory shaping and flight times 06 p1007 A69-17598

- Analytical technique for unmanned spacecraft sizing for planetary missions, considering scientific objectives, characteristics and requirements [AIAA PAPER 69-125] 06 p1018 A69-18076

- Astrodynamical data compilation for use by system engineer for mission planning [AIAA PAPER 69-124] 06 p1011 A69-18090

- Sun-orbit plane relationship effects on mission planning [AIAA PAPER 69-129] 06 p1011 A69-18093

- Eole satellite and meteorological balloons telecommunications used to study wind distribution in Southern Hemisphere and other atmospheric parameters 07 p1084 A69-19134

- Electric propulsion missions analysis for spacecraft design engineer, discussing out-of-ecliptic and Jupiter flyby probes 09 p1584 A69-21203

- Low thrust mission simulation dependence on hardware definition, discussing power plant characteristics, jet velocity and thruster efficiency 09 p1584 A69-21204

- Mission model construction for power limited systems, discussing flight concepts, propulsion mixes and electric propulsion 09 p1584 A69-21205

- Interplanetary low thrust mission analysis model, discussing major elements interactions 09 p1585 A69-21206

- Space flight trajectory analysis of aerospace systems, discussing Analytical Trajectory Optimization Model 09 p1585 A69-21207

- Low thrust mission analysis techniques and computer programs, discussing electric propulsion 09 p1585 A69-21208

- Predesign and mission analysis software capability for sizing, design, fabrication and developmental testing of flight hardware for electrically propelled interplanetary spacecraft 09 p1585 A69-21210

- Automated parameter search techniques applied to low thrust mission design, stressing trajectories and mission optimization 09 p1585 A69-21211

- West German activity in field of electrostatic propulsion, discussing ion thrusters, colloid thruster development and mission analysis [AIAA PAPER 69-288] 09 p1565 A69-21248

- Ion thrusters and various microthrusters /electron bombardment ion and pulsed plasma/ for proposed European missions [AIAA PAPER 69-274] 09 p1565 A69-21250

- Reactor and mission requirements interaction for unmanned thermionic nuclear electric propulsion, discussing lifetime, payload, power levels, etc [AIAA PAPER 69-250] 09 p1539 A69-21253

- SERT 2 thruster system performance over expected mission parameters, noting operational lifetime excess over mission requirements [AIAA PAPER 69-235] 09 p1566 A69-21255

- Common nuclear propulsion modules for wide spectrum of manned planetary missions, discussing payload, mission and program flexibility [AIAA PAPER 68-590] 09 p1539 A69-21984

- Space exploration plans adaptation, considering spacecraft design, programs, costs and schedules flexibility 10 p1811 A69-22863

- Low thrust space probe mission to Halley comet, utilizing nuclear electric propulsion 10 p1772 A69-22864

- Model simulation in program planning for space station with emphasis on accommodation of logistics 10 p1669 A69-22976

- Spacecraft propulsion systems comparison and evaluation, discussing quality, schedules and costs in relation to mission requirements 11 p1965 A69-25600

- Space experiments analysis involving standardization for economy and mission thesis compromise, detailing aeronomic satellite project with integrated utilization 12 p1713 A69-26128

- Problem areas within cryogenic chemical and nuclear propulsion systems for space missions, noting available technology and limitations [AIAA PAPER 67-454] 12 p2174 A69-26782

- Reliability and maintainability analysis of two year spacecraft mission combining earth orbits and Mars program, using computerized mathematical model [AIAA PAPER 68-1059] 12 p2174 A69-26797

- Large power systems integration in manned space stations, discussing design, selection and application criteria 13 p2209 A69-27939

- Markov chain applications to avionics weapons system reliability specifications starting with mission profile, failure rates, success probabilities, etc 15 p2581 A69-31136

- Manned space stations role in future space plans, discussing prototypes and conceptual design 16 p2866 A69-31736

- Project Symphonie German-French communication satellite mission and technical data 16 p2868 A69-32055

- Fluid controlled solid rocket motors design for Mars mission with acceleration level as parameter, discussing mission specifications, system design and component considerations [AIAA PAPER 69-446] 16 p2841 A69-32687

- Lunar orbital mission plans intended to optimize spacecraft procurement, flight schedules, science objectives and available funds 18 p3193 A69-34362

- Market analysis program to evaluate relationship between launch vehicle jettison weight and total cost based on all projected missions [SAWE PAPER 776] 18 p3208 A69-34872

- General aviation missions in national transportation system /1968, 1975, 1980/, considering fuel taxes, overall system economics, ground facilities, etc [AIAA PAPER 69-818] 19 p3453 A69-35624

- Mission windows for single and multiple planet swingbys past Jupiter to outer planets [AAS PAPER 68-115] 19 p3402 A69-35936

- Approach navigation accuracy for planetary atmosphere braking to orbit about Mars and Venus [AAS PAPER 68-122] 19 p3402 A69-35937

- Mariner Mars 1969 flyby missions objectives, experiments, spacecraft configuration, trajectory design, sterilization, flight path control and photographic imaging [AAS PAPER 68-134] 19 p3402 A69-35938

- Operational missile flight program validation plan noting mission analysis, computer programming, program preparation and performance prediction 19 p3279 A69-35955

- Earth orbital space program mission effectiveness increased through utilization of standby launch vehicles, spacecraft and space station systems 19 p3430 A69-36010

- Worldwide cloud cover simulation procedure providing data for computer simulation of earth oriented space missions, describing computer program using Monte Carlo mission simulation 20 p3573 A69-38120

- Earth resources technology satellite /ERTS/ choice regarding local time of ascending node based on cloud cover and IR measurement considerations 21 p3798 A69-38628

Orbital images for earth resources satellite mission planning using Mercury, Gemini and Apollo synoptic terrain photographs

21 p3721 A69-38632

Two dimensional gravity assisted trajectories for solar probe missions in ecliptic plane, discussing Venus and Jupiter assist missions

21 p3804 A69-39022

Mission and planetary vehicles characteristics affecting design of solid propellant motors and thrust vector control systems in planetary orbiters and landers [AIAA PAPER 68-815]

21 p3819 A69-39031

Spacecraft guidance analysis of multiple outer planet mission utilizing gravity assist swingbys to achieve planetary flybys with single spacecraft [AAS PAPER 68-109]

21 p3761 A69-39205

Triple planet ballistic flybys, discussing mission opportunities and launch windows [AAS PAPER 68-114]

21 p3805 A69-39206

Mission analysis for 1972 Venus launch opportunity, discussing launch period selection and trajectory constraints for Atlas/Centaur vehicle [AAS PAPER 68-135]

21 p3805 A69-39208

Abort capability mission selection criterion, evaluating energy requirements, Mars flyby and velocity contours [AAS PAPER 68-139]

21 p3805 A69-39209

Secondary or abort mission maximized subject to primary mission constraints by variational treatment of optimal branched trajectories [AAS PAPER 68-138]

21 p3819 A69-39210

Lunar Orbiter missions pre- and postflight error analyses compared to estimate dispersions from reference trajectory [AAS PAPER 68-108]

21 p3805 A69-39220

Direct flight and Jupiter swingby heliocentric trajectory modes of elliptic capture orbits compared for unmanned missions to outer planets [AAS PAPER 68-105]

21 p3805 A69-39221

Analytical technique for unmanned spacecraft sizing for planetary missions, considering scientific objectives, characteristics and requirements [AIAA PAPER 69-125]

21 p3828 A69-39770

Mission analysis and trajectory simulation (MATS)/program, discussing computer controls, modular design, integration evaluation [AIAA PAPER 69-939]

22 p3904 A69-40322

Operational reliability verification of Apollo real time mission program and testing structure, discussing environment, processing, controls, response criteria, etc [AIAA PAPER 69-981]

22 p3907 A69-40361

Trajectory analysis of multiplanet Grand Tour mission to four large outer planets on single flight, discussing mission planning [AIAA PAPER 68-1055]

22 p4023 A69-40544

Spatial region accessible to earth launched probes determined for mission planning for exploration of aperiodic comets, discussing orbit parameters

23 p4212 A69-41536

Space power systems analysis, using computer program to correlate systems characteristics with mission parameters for automated satellite repair vehicle and space stations

23 p4068 A69-42240

Adaptive cost equations in computer programs supporting launch vehicle long range planning, based on launch vehicle anticipated usage [AAS PAPER 69-164]

24 p4392 A69-42815

Space program planning, noting market requirements, acceptability and future characteristics [AAS PAPER 69-083]

24 p4418 A69-42820

Navigation systems analysis for space missions planning, discussing onboard equipment and lunar landing accuracies [AAS PAPER 69-406]

24 p4347 A69-42833

Mariner-Mercury 1973 flyby mission using Atlas-Centaur rocket and gravity-assisted maneuvers, discussing encounter geometries, spacecraft configuration and Venus probe considerations [AAS PAPER 69-288]

24 p4381 A69-42862

Space mission opportunities selection from analysis of short period comet perihelia, discussing flyby and rendezvous mission payloads [AAS PAPER 69-320]

24 p4381 A69-42866

Planning lunar surface experiments in nets or at selected sites for optimum scientific return [AAS PAPER 69-207]

24 p4381 A69-42874

Economic aspects of future space activities noting systems analysis, operations research, manned and unmanned space capabilities, etc [AAS PAPER 69-113]

24 p4418 A69-42878

Cape Kennedy space research and national priorities, indicating performance and progress of future space operations [AAS PAPER 69-110]

24 p4419 A69-42879

Space flight programs management cooperation and limited competition advantages, emphasizing single management team responsibility for effective multi-lateral activities

24 p4419 A69-43043

Mars and Venus flyby missions and Mercury planetary exploration plans, discussing future conditions permitting Jupiter, Saturn, Uranus, Neptune, Pluto flybys

24 p4384 A69-43137

Sun-orbit plane relationship effects on mission planning [AIAA PAPER 69-164]

24 p4386 A69-43261

MIST

Vaporization of mist of small droplets by intense light beam for droplet extinction rate proportional to absorbed radiant energy

09 p1539 A69-21346

MITOCHONDRIA

Mitochondrion-endoplasmic reticulum connection in hepatocytes, discussing possible protein molecule transfer

23 p4083 A69-41455

Rodent swimming and treadmill training effect on capacity of mitochondrial fraction from hind limb muscles to oxidize pyruvate triples

23 p4095 A69-42084

MITOSIS

Bone marrow cell division disturbance in rats after proton irradiation

07 p1064 A69-18973

Bone marrow cell division disturbance in rats after proton irradiation

20 p3479 A69-38221

Hyperoxia and hypoxia effects on mitotic activity in regenerating and normal rat liver exposed to environmental conditions

24 p4269 A69-43565

MIXED FLOW

U MULTIPHASE FLOW

MIXERS

Optimal layout of turbofan jet engines, discussing experimental rig for high thrust measurement [AIAA PAPER 67-416]

01 p0143 A69-11015

MIXING

NT DISSOLVING
NT LAMINAR MIXING
NT SIGNAL MIXING
NT SUSPENDING [MIXING]
NT TURBULENT MIXING

Deflection effect on flow and mixing process in flames covering enclosed turbulent diffusion flames in combustion chamber

17 p3068 A69-32966

MIXING CIRCUITS

X band mixer with reactively terminated image, using gallium arsenide barrier diodes and microwave integrated circuit techniques

01 p0039 A69-10189

Voltage controlled oscillator with fixed frequency crystal oscillator, noting double mixing scheme and rejection of all discrete sidebands

01 p0042 A69-10418

Wideband electronically scanned receiver, using varactor diode upper sideband parametric frequency upconverter for frequency mixing

01 p0048 A69-11036

Space charge limited square law diodes as HF mixers, noting low conversion loss of asymmetrical type

03 p0404 A69-13580

Diode mixer power series coefficients for spurious response prediction in superheterodyne receiver

03 p0399 A69-13905

Difference frequency generation by multiple quantum transition from laser medium considered as resonant optical frequency mixing device

07 p1144 A69-18470

Miniature microwave tuners with solid state reliability and reduced power consumption, using YIG, mixer circuits and integrated control circuitry

07 p1102 A69-18672

Frequency conversion in microwave crystal mixer with EMF amplitude fluctuations in heterodyne

09 p1469 A69-22644

Broadband double balanced mixer/modulators compared with single balanced and unbalanced mixer/modulators

10 p1665 A69-23876

Minimum conversion loss in general mixer circuit configuration, noting dependence on time varying resistance and equal terminating impedances

11 p1845 A69-24550

Parametric frequency converter consisting of mixer head in bridge circuit with varactors for 12 GHz TV transmitters

11 p1854 A69-25614

Critical review of statements concerning previous paper on noise in transistor mixers at HF

11 p1857 A69-25662

Tunnel diode harmonic mode mixer having IF receiver, studying combination and cross noise rejection efficiency

14 p2424 A69-29763

Ferrite frequency mixers used with heterodyne receiver, studying combination and cross noise rejection efficiency

15 p2574 A69-30129

Broadband microwave double balanced mixer/modulators, discussing bandwidth, conversion loss, noise figure, intermodulation and power dissipation

15 p2580 A69-31077

Noise during frequency combination and conversion in mixer

17 p2931 A69-33911

MIXING LENGTH FLOW THEORY

Coaxial jet mixing regimes in jet engines, determining requirements for compatibility by applying aerodynamic theory of ejectors [ONERA-TP-599]

02 p0187 A69-11619

Hydrodynamic analysis for determining steady flow region with closed separation area for Reynolds numbers to describe viscous mixing by Prandtl equations

02 p0190 A69-12570

Equilibrium turbulent boundary layer prediction for proposed Prandtl mixing length distribution

03 p0419 A69-13992

Amount of flux carried by convection in late type stars, reevaluating drag role in mixing length theory

06 p1003 A69-17321

Wind velocity and shear stress profiles above surface with changed roughness, using mixing length theory

08 p1346 A69-20311

Temperature gradient in semiconvective region, examining molecular weight distribution in mixing due to overstability

09 p1596 A69-22057

Carbon dioxide laser combining gas flow with fluid mixing to achieve high gain

10 p1701 A69-22954

Physical structure of convective envelopes of population II main sequence stellar models by mixing length theory, emphasizing hydrogen molecule formation and pressure ionization

11 p1961 A69-25109

Mixing regimes for flows with different stagnation enthalpies subject to mass flow limitation due to thermal choking

13 p2251 A69-28499

Viscous incompressible fluid self similar mixing problems, performing group analysis for complete boundary value problem

14 p2428 A69-28803

Outer convection zone of cool white dwarf by atmospheric models, using mixing length theory and abundances

14 p2529 A69-29982

Velocity field in turbulent flow based on momentum transfer, determining velocity distribution for flow near solid surface

16 p2772 A69-32128

Flow over uniformly rough surface in planetary boundary layer from mixing length wind spiral model, using surface shear stress and wind direction data

17 p2997 A69-33153

Mixing length model to relate turbulent shear stress to mean velocity field within planetary boundary layer above surface roughness change

17 p2997 A69-33154

Compressible hypersonic turbulent boundary layers solution by finite difference method, relating mixing length to velocity profile shape factor [AIAA PAPER 69-684]

17 p2955 A69-33474

Turbulent kinetic energy equation for determining turbulent flow fields applied to free mixing problem of constant density streams [AIAA PAPER 69-683]

17 p2956 A69-33492

Prandtl mixing length theory for flow in pipes and channels described by spatial exponential form, developing velocity profile and friction factor [ASME PAPER 69-FE-48]

20 p3516 A69-37978

Diffusion parameters for fluid stream flowing from round hole with given radius and velocity into wake flow

21 p3696 A69-39091

Mixing length theory including eddies axial motion, discussing turbulent field of temperature or concentration

24 p4407 A69-42917

Separation flows in flat channel with step recess, analyzing dynamic characteristics in mixing region, in wake of rarefaction waves and in attachment zone

24 p4247 A69-43498

Outer solar convection zone structure dependence on change of parameters in mixing length theory examined to construct model

24 p4387 A69-43634

MIXTURES

NT ADMIXTURES
NT AEROSOLS
NT BINARY FLUIDS
NT BINARY MIXTURES
NT COLLOIDAL PROPELLANTS
NT COLLOIDS
NT DETONABLE GAS MIXTURES
NT DISPERSIONS
NT EMULSIONS
NT EUTECTIC ALLOYS
NT EUTECTICS
NT FOG
NT GAS MIXTURES
NT LIQUID-GAS MIXTURES
NT METAL MATRIX COMPOSITES
NT NUCLEAR EMULSIONS
NT PHOTOGRAPHIC EMULSIONS
NT SMOKE
NT SOLID SOLUTIONS
NT SOLID SUSPENSIONS
NT SOLUTIONS

Microstructured mixtures theory including energy balance, mass and momentum equations and entropy production inequality for structured fluids in motion

13 p2371 A69-27318

Thermal conductivity prediction technique for two and three phase solid heterogeneous mixtures

13 p2378 A69-28337

Sintered mixtures of Ni-Mo powder noting electrical resistance, alloy and shear strength and impact viscosity

15 p2638 A69-30280

Absorption spectroscopy using resonance broadened atomic lines for two phase mixtures study

21 p3774 A69-39239

MOBILE MISSILE LAUNCHERS

Temporary launching sites for rocket probes, discussing CNES activity, Dragon and Titus programs and mobile launching units

02 p0228 A69-11921

MOBILITY

U ELECTRON MOBILITY
U HOLE MOBILITY
U IONIC MOBILITY

MODAL RESPONSE

Natural frequencies and mode shapes of coupled bending vibrations of pretwisted rectangular cross section beams determined by Rayleigh-Ritz energy method

03 p0529 A69-13989

Dynamic instability of solid bodies, using modal vibration method to establish criteria on basis of equivalent energy conditions

05 p0844 A69-16742

Modal response analysis of servomechanisms as deduced from vibration test, for possible application to aircraft [ONERA-TP-668]

06 p0869 A69-17100

Vibration natural frequencies and mode shapes in cylindrical shells clamped at both ends, using fundamental differential equation under dynamic surface loading

09 p1618 A69-22274

Aircraft modal control systems synthesis to improve response characteristics by altering pairs of complex conjugate and real eigenvalues simultaneously

09 p1435 A69-22779

Damping of response of integrally stiffened skin structures to random acoustic pressures, reducing rms stress in case of broad band excitation [ASME PAPER 69-VIBR-26]

10 p1806 A69-24172

Holographic mode shapes used in conjunction with mechanical impedance approach for vibration analysis of turbine blades [ASME PAPER 69-VIBR-32]

10 p1806 A69-24174

Aerospace structures modal vibration tests data acquisition including multishake excitation methods

15 p2585 A69-30358

Nondivergent oscillations in solar atmosphere forming normal modes or free oscillations, assuming free surface of chromosphere coronal interface and large density in convective zone

17 p3029 A69-33048

Natural frequencies and vibration modal shapes of asymmetrical airfoil blades analyzed by differential equations of motion, noting flexure coordinates center variations effect

17 p3067 A69-34053

Rectangular cross section pretwisted beams modal curves for turbine and compressor blading vibrational studies

20 p3621 A69-37080

Lasing properties of Ni-doped GaAs diodes evaluated by plotting resonance, mode amplitudes and frequencies for various bias currents and external capacitance

22 p3912 A69-40606

Transverse acoustic wave excitation of elastic circular cylindrical sandwich shell submerged in infinite fluid medium, describing simultaneous equations development for modal response [ASME PAPER 69-APMW-17]

24 p4401 A69-43100

MODE OF VIBRATION

U VIBRATION MODE

MODE SHAPES

U MODAL RESPONSE

MODE TRANSFORMERS

Resonance method determining spurious modes excitation in natural mode converter, discussing construction, application and mathematical correlation

11 p1856 A69-25630

Mode filters for oversized rectangular waveguides, considering resistive sheet with complex surface impedance

16 p2760 A69-31948

Mode conversion in nonuniform multimode waveguides and transitions using Maxwell equations, considering tapered and circular waveguides

23 p4135 A69-41354

MODELS

NT AIRCRAFT MODELS
NT ASTRONOMICAL MODELS
NT ATMOSPHERIC MODELS
NT BREADBOARD MODELS
NT DIGITAL SIMULATION
NT DYNAMIC MODELS
NT ENVIRONMENT MODELS
NT LIGHTHILL GAS MODEL
NT MATHEMATICAL MODELS
NT REFERENCE ATMOSPHERES
NT SCALE MODELS
NT SPACECRAFT MODELS
NT THOMAS-FERMI MODEL
NT WIND TUNNEL MODELS

Technological forecasting by intuitive forecasts, consensus methods, analogy, trend extrapolation and structural models

13 p2382 A69-28040

Equivalent dielectric tensor for warm drifting electron plasma using model

16 p2820 A69-31701

Vaporization interaction liquid rocket performance model, discussing performance loss evaluation and test data

[AIAA PAPER 69-470]

16 p2838 A69-32663

Hydraulic tank for visualizing flows around stationary models, noting absence of wall effects [ONERA-TP-708]

17 p2956 A69-33588

Linear elastic isotropic materials for model tests, describing properties of material composed of Araldite B and air

21 p3844 A69-39319

Step recovery diode principle and operation mode as frequency multiplier explained by models

21 p3684 A69-39736

Linear models with self excitation for brightness and contrast perception studies in human visual system

22 p3881 A69-40862

Intercity travel demands simulation by linear graph model applied to Windsor-Montreal corridor [AAS PAPER 69-382]

24 p4417 A69-42805

Training missions and military exercises to field test weapons system models [AAS PAPER 69-478]

24 p4296 A69-42884

MODERATION [ENERGY ABSORPTION]

U NEUTRON THERMALIZATION
U THERMALIZATION [ENERGY ABSORPTION]

MODES

U COUPLED MODES
U LASER MODES
U PROPAGATION MODES
U UNCOUPLED MODES
U VIBRATION MODE

MODIFIERS

U ADDITIVES

MODULATED CONTINUOUS RADIATION

Solar modulating function form changes resulting in hysteresis near solar minimum

05 p0815 A69-16249

Discrete continuous signals transmission with minimum noise along synchronous and asynchronous channels

11 p1835 A69-24953

MODULATION

NT AMPLITUDE MODULATION
NT DELTA MODULATION
NT FEEDBACK FREQUENCY MODULATION
NT FREQUENCY MODULATION
NT FREQUENCY SHIFT KEYING
NT INTERMODULATION
NT IONOSPHERIC CROSS MODULATION
NT LIGHT MODULATION
NT PHASE MODULATION
NT PHASE SHIFT KEYING
NT PULSE AMPLITUDE MODULATION
NT PULSE CODE MODULATION
NT PULSE DURATION MODULATION
NT PULSE FREQUENCY MODULATION
NT PULSE FREQUENCY MODULATION
NT TELEMETRY
NT PULSE MODULATION
NT PULSE TIME MODULATION
NT TRAVELING WAVE MODULATION
NT ULTRASONIC LIGHT MODULATION
NT VELOCITY MODULATION

Ground state population modulation in trivalent rare earth doped single crystals by means of optical double resonance, noting applications

01 p0134 A69-10013

Optimum modulation technique determination for single channel voice communication under severe noise conditions [UN PAPER 68-95851]

01 p0029 A69-10526

Communication satellites systems, discussing Intelsat satellite specifications and modulation methods for multiple access

03 p0383 A69-12870

Galactic cosmic rays energy modulation spectrum in interplanetary space, showing influence of solar wind velocity and diffusion coefficient dependence

03 p0501 A69-13527

Modulation of galactic cosmic rays due to electromagnetic conditions of interplanetary space, considering time variations and Parkers model

06 p0989 A69-17287

Drag force measurement in low density flows using modulation techniques

06 p0861 A69-17638

Image averaging time effects on modulation transfer function /MTF/ of system comprising telescope objective and horizontal propagation path in turbulent atmosphere

06 p0890 A69-17806

Cosmic ray modulation by solar wind, discussing anisotropic diffusion during propagation through interstellar magnetic field

10 p1759 A69-22842

MHD power plant research and development, discussing shock wave electric power generators and modulated systems

11 p1925 A69-24469

Ruby laser performance with perturbing effect of standing wave field on homogeneity of deexcitation of level populations eliminated by HF modulation

11 p1900 A69-25569

Hologram recording by offsetting reference beam temporal frequency instead of using reference beam spatial offset

13 p2258 A69-27201

Reference oscillator synchronization inaccuracy influence on SNR at output of correlation receiver during reception of signals with pseudonoise modulation

15 p2563 A69-30141

Discharge parameters modulation caused by acoustic wave propagating in partially ionized plasma, deriving perturbation current density and irradiated light intensity

16 p2752 A69-32364

Modulation transfer function based on Fourier techniques, discussing nonlinear film development process

17 p3005 A69-33080

Holography of intensities, discussing recording of self luminous body by modulation of scattered radiation using optical Q switch

17 p2973 A69-33113

Probabilistic analysis of code message distortion due to pulse noise in modulation systems and comparison between linear and quadratic detections

17 p2919 A69-33145

MODULATORS

- Deformation of amplitude and frequency envelopes of plane modulated electromagnetic waves with dispersion in isotropic dielectric with cubic nonlinearity
17 p2928 A69-33869
- Rocket measurements indicating auroral electrons modulation near equatorial plane, noting intensity changes as function of rocket flight time and altitude
21 p3709 A69-38499
- Modulation envelopes, tables of profiles and harmonic components for modulated waves in electrical and communications problems
21 p3673 A69-38778

MODULATORS

- Bulk effect germanium hot-carrier microwave modulator for Q band, reducing required applied voltages by using short length semiconductor ships
01 p0043 A69-10563
- Working equivalent circuits for fluidic transverse impact modulator in LF and IF range
02 p0196 A69-12082
- High power pulse generators with four layer p-n-p-n structure, discussing design, principles and applications of semiconductor elements as modulators and switches
03 p0402 A69-12978
- Intermodulation and cross modulation distortions in double balanced modulator
04 p0573 A69-14341
- Single band millimeter wave amplitude modulator for phase meters with homodyne frequency conversion
04 p0577 A69-14850
- Modems for high data transmission rates on available voice bandwidth channels, noting point to point and multipoint polled networks and signal to noise ratio
04 p0564 A69-15208
- Broadband hybrid junction of parallel transmission lines application to four diode star mixer/modulator
06 p0896 A69-17485
- Vortex valve pure fluid modulators steady state characteristics, analyzing geometry of exit, control and supply areas and chamber
09 p1443 A69-22738
- Radar signal cross correlation function calculation with reference function, applying acousto-optical modulator
10 p1694 A69-23539
- Broadband double balanced mixer/modulators compared with single balanced and unbalanced mixer/modulators
10 p1665 A69-23876
- Input admittance response characteristics and input susceptance and input conductance of resonant reactive modulator with varactors and nonlinear losses
10 p1665 A69-24066
- Electro-optic broadband laser light modulator designs and modulation characteristics, computing curve set for evaluation of various materials
11 p1897 A69-25039
- Near IR radiation magnetooptical light modulators using Faraday effect in yttrium-iron garnet and in related compounds
11 p1886 A69-25057
- AM-FM calibration modulator for microwave oscillator noise measurement
11 p1856 A69-25631
- Control signal correction in microwave ferrite modulators, eliminating losses due to screening effect of feeder
13 p2226 A69-27216
- Electrooptical ADP modulator design for use with helium-neon laser, considering temperature stability and crystal faces parallelism
13 p2272 A69-28191
- Operation mode of modulator with p-n diode, determining modulus and phase of reflection factor
13 p2235 A69-28518
- Numerical solution of differential equations for two channel PFM with pulse element, applying Dirac pulse sequence to input
14 p2426 A69-29148
- Capacitive parametric modulator transient processes and second harmonic effect analysis, obtaining transient response and recovery time
15 p2574 A69-30125
- Single band millimeter wave amplitude modulator for phase meters with homodyne frequency conversion
15 p2575 A69-30242
- Broadband microwave double balanced mixer/modulators, discussing bandwidth, conversion loss, noise figure, intermodulation and power dissipation
15 p2580 A69-31077
- 360 degree varactor linear phase modulator, analyzing impedance matching, insertion loss, tuning design and serrodyne application
16 p2756 A69-31577

- Single balanced modulators using square law resistors /space charge limited diodes/, discussing noise properties, conversion losses and terminating conductance
16 p2758 A69-31756
- Popov type graphic criterion for determining absolute stability of modulation systems
16 p2764 A69-32440
- Fluidic direct impact modulator design, studying effects of pressure levels and nozzle geometries [ASME PAPER 69-FLCS-38]
20 p3465 A69-37983

MODULES

- NT COMMAND MODULES
NT COMMAND SERVICE MODULES
NT ELECTRONIC MODULES
NT LANDING MODULES
NT LUNAR LANDING MODULES
NT LUNAR MODULE
NT MARS EXCURSION MODULE
NT MICROMODULES
NT SERVICE MODULES
NT SPACECRAFT MODULES
- Pneumatic elements, discussing development from process control via modules systems to logic elements and fluid sensors
02 p0197 A69-12795
- Common nuclear propulsion modules for wide spectrum of manned planetary missions, discussing payload, mission and program flexibility [AIAA PAPER 68-590]
09 p1539 A69-21984
- OMNITRAC general purpose airborne digital computer with permanent memory of 4096 words of 23 bits, noting modular construction
10 p1659 A69-22845
- Modular hydraulic power source systems for general aviation aircraft, discussing design selection, phase in and customer acceptance problems [SAE PAPER 690329]
11 p1825 A69-24505
- Torsion theory for modules over integral domain, giving definition of injective sums
13 p2287 A69-27339
- Primary isotope thermionic electric power module design, considering various assemblies
14 p2398 A69-29190
- MERA /Molecular Electronics for Radar Applications/ modules testing in planar array simulator, measuring far field amplitude patterns in transmitting and receiving modes
22 p3912 A69-40067
- Design, fabrication and evaluation of lunar base solar array power modules, emphasizing structural/ dynamic, thermal vacuum and acoustic tests
23 p4072 A69-42288

MODULI

U RATIOS

MODULUS OF ELASTICITY

- NT DYNAMIC MODULUS OF ELASTICITY
- Kinetic theory of fracture initiation, discussing changes in relative orientation distribution of network chains
02 p0345 A69-12401
- Pressure and temperature dependence of isotropic elastic moduli of polycrystalline alumina, noting Grueneisen parameter, equation of state and Debye temperature
02 p0268 A69-12407
- Fatigue and corrosion fatigue properties of aluminum alloys, noting elastic modulus, cyclic loading strength, corrosion resistance, etc
03 p0443 A69-13027
- Niobium based alloys modulus of elasticity temperature stability, investigating admixture effects
04 p0615 A69-14642
- Hydrogen effect on interatomic bonds of Ti beta alloy and Young modulus, noting measurements at various temperatures
04 p0618 A69-15178
- Thermal stress in fiber reinforced metals, assuming Young modulus variable when thermal stress is applied during heating and cooling
04 p0682 A69-15393
- Young modulus of sintered nonporous titanium, zirconium and chromium nitrides, computing characteristic temperature and root mean square atomic displacements in lattices
06 p0938 A69-16830
- Dynamic measurements of modulus of elasticity for polycrystalline nickel-tungsten alloys at elevated temperatures
06 p0943 A69-17232
- Statistical computations of elastic moduli of macroscopically isotropic particulate composites, discussing porosity and elastic properties of materials made by sintering
07 p1159 A69-18722

- Fiberglass reinforced plastics modulus of elasticity and Poisson ratio determined by strain gauges and frequency and resistivity measurements
08 p1335 A69-20330

- Multidirectional boron-epoxy laminates shear strengths and elastic moduli, calculating in-plane tension and compression
08 p1337 A69-20484

- Thermoelastic properties of particulate, filamentary and layered composites, summarizing Soviet theoretical and experimental work
08 p1339 A69-20500

- Shop-ready high modulus carbon and fiberglass composite reinforcement system, stressing effect of modulus fibers amount in laminate
08 p1340 A69-20508

- Transversely isotropic elastic solid approximation for oriented fibers of polyethylene, nylon, polyethylene terephthalate and polypropylene, measuring elastic compliances
09 p1528 A69-21504

- Tensile strengths and elasticity moduli of graphite fibers produced from textile organic thread, discussing application to composites, ablative and fiber reinforced materials
09 p1529 A69-22071

- Forced vibrations in semibounded elastic bar with various moduli of elasticity, discussing reversing longitudinal force and elastic waves propagation
10 p1799 A69-23155

- Ultrasonics for automatic measurements of temperature and elastic moduli above 5000 F
10 p1694 A69-23373

- Young modulus temperature dependence and order-disorder transformations in ternary nickel alloys
11 p1904 A69-24705

- Symmetrically loaded weak moment shells of revolution made of materials with different moduli of elasticity
11 p1980 A69-24819

- Annealing effects on cold rolled titanium sheets, noting changes in Young modulus and characteristics of recrystallized titanium
11 p1904 A69-24899

- Reduced modulus of elasticity dependence on form of plane stressed state, assuming initially anisotropic body with transversely isotropic elastic properties
11 p1986 A69-25182

- Modulus of elasticity changes and stress relaxation spectra of viscoelastic liquids measured by acoustic methods
11 p1887 A69-25206

- Comparison of errors obtained by using linearly gliding and rotating strengthening moduli in stress-strain state on basis of linear stepwise approximation
11 p1986 A69-25342

- Characteristic temperature, Young modulus and rms atomic displacement in metal borides of various porosities, using dynamic method based on ultrasonic oscillations measurement
12 p2115 A69-26615

- Effective tensors of elastic moduli and yielding of composite materials, considering multiparticle interactions and use of equilibrium and incompatibility equations
13 p2360 A69-27382

- Theoretical compression strength of reinforced materials determined assuming material components differing elasticity moduli
14 p2532 A69-28973

- Thermoelastic stress-strain state of infinite circular cylindrical shell with elasticity modulus temperature dependence expressed by exponential function
14 p2532 A69-28980

- Beam deflection equations having different rigidity moduli on each half span
15 p2705 A69-30417

- Bending theory of orthotropic plates with variable elastic modulus under transverse loads, utilizing stress-strain relations and Kirchhoff-Love hypothesis
15 p2708 A69-30661

- Uniaxial stress effects on molecular breakage rate, relating structure-sensitive parameter to elastic modulus
15 p2709 A69-30807

- Extensional vibration of thin inhomogeneous circular plate with variable modulus of elasticity and central hole, calculating periods of vibration
15 p2713 A69-31026

- Thermal stress in fiber reinforced metals, assuming Young modulus variable when thermal stress is applied during heating and cooling
18 p3223 A69-35021

- Oriented glassfiber reinforced plastics elastic moduli and tensile strength along anisotropic axes determined

- nondestructively, considering component content and material porosity
18 p3162 A69-35359
- Weak moment shells made from materials with different elastic moduli, developing theory based on undeformable normals
18 p3225 A69-35367
- Measuring elastic modulus and tensile strength of high modulus graphite fibers including comparative data, error sources and full strand test
19 p3355 A69-35520
- Hollow cylinder plane stress-strain state analyzed for effect of variable modulus of elasticity of cylinder material
19 p3436 A69-35858
- Two dimensional stress analyzed near crack in infinite elastic sheet, considering crack shape and Young modulus
19 p3440 A69-36638
- Melting points, electrical conductivity, Hall constants, magnetic susceptibility, density, bending strength, microhardness and elastic modulus of zirconium nitride in homogeneity range
20 p3558 A69-37014
- Ti-V martensite decay during heating, noting temperature dependence of elastic moduli and electrical conductivity
21 p3746 A69-39160
- High E modulus, structure, strength and temperature characteristics of reinforcement fibers, considering B, silicon carbide, C and Be
22 p3951 A69-39907
- Elastic modulus of beta Ti alloy containing Mo, Cr, Fe and Al measured under vibrations and shear modulus determined under torsion
22 p3969 A69-40072
- Sandwich beams interlaminar shear stress calculations, considering roles of moduli of elasticity and layers thickness relative to beam
22 p4041 A69-40080
- Young modulus for wire or strip shaped specimens determined from unloaded cantilever vibration considerations
22 p4042 A69-40443
- Reinforcement effect on stress relaxation and creep in hereditary elastic materials, assuming integral shear modulus operator with exponential kernel
22 p4045 A69-40744
- Static pressure-diameter measurements on small pulmonary blood vessels of frogs, analyzing capillary septal area as function of intravascular pressures noting high compliance
22 p3885 A69-40974
- Stress-strain relations for materials with variable modulus of elasticity applied to internal work, obtaining potential strain energy
22 p4047 A69-41171
- Positive phase shift relation to elastic modulus enhancement of smooth muscles of rabbit, cat and dog bladder, pulmonary artery and large veins
23 p4083 A69-41459
- Overall elastic moduli evaluation for solid composite materials comprising matrix of homogeneous elastic materials embedded with cylindrical shape inclusions
24 p4396 A69-42731
- Composite media elastic moduli upper and lower bounds determination using variational principles to characterize displacement and stress in time harmonic deformation
24 p4406 A69-43701
- MOHR CIRCLES**
U FRACTURE MECHANICS
- MOIRE EFFECTS**
Moire fringe interpolation and multiplication by shifting master interference grating, noting increased measurement sensitivity
03 p0524 A69-13063
- Mirror image and oblique shadow method forming moire patterns to measure surface topography
08 p1312 A69-20103
- Moire patterns for photoelastic strain analysis noting applications to elasticity, plasticity and creep problems
11 p1982 A69-24944
- Holographic in-focus projection of images on three dimensional focal planes of arbitrary shape, noting moire pattern strain analysis
11 p1889 A69-25653
- Moire fringes, discussing fringe multiplication by filtering to obtain small strain measurement sensitivity and engraving technique for wave front reconstruction
12 p2099 A69-27164
- Moire and gridwork methods of plastic strain analysis with application to plane strain and axisymmetric extrusion
13 p2359 A69-27256
- Optical refraction effects from refractive index gradients in stressed models as limitation on moire interferometry usefulness in Boussinesq problem and expanding pulse studies
14 p2531 A69-28883
- Stress and strain fields for circular rubber ring under diametrical compression between flat plates, using moire, large strain analysis and photoelastic verification
14 p2531 A69-28884
- Optophotoclectric pickup design for angular displacement measurements, considering application of moire pattern produced by radial diffraction gratings
14 p2447 A69-29327
- Bending surface of shells under crosswise load analyzed by moire method, considering rotating cylindrical surfaces
15 p2713 A69-31056
- Rotatory cylindrical shells supported at corners under symmetric load, determining deformation in arbitrary locations by moire method
15 p2715 A69-31546
- Moire reflection technique applied to study of stress-strain state of partially clamped rectangular cantilever plates under various loads
17 p3058 A69-33203
- Strains in solids of any form, using moire method combined with holographic interferometry
18 p3139 A69-35280
- Book on moire fringes in strain analysis, discussing methods for strain measurement in deformed bodies and engineering structures
19 p3435 A69-35835
- Microwave holograms generated by spinning dipole field perturbation technique, showing zone plates and moire fringe resolution
19 p3315 A69-36824
- Vibrating circular plate standing wave lateral displacements visualization by photographically recorded moire patterns
20 p3537 A69-37067
- Telecentric lens principle for accurate optical strain measurements, using moire grids
21 p3844 A69-39322
- Fringe multiplication techniques for moire fringe arrays of inhomogeneous strain fields
21 p3845 A69-39328
- Moire technique for gaging surface deformations or surface configuration differences by optical interference patterns
21 p3726 A69-39775
- Grids applied to plastic samples for strain measurement using moire fringe method, comparing tensile test results with Linley extensometer
22 p4042 A69-40312
- Moire effect applications to stress analysis, enumerating advantages over conventional grid techniques
22 p4042 A69-40315
- MOISTURE**
Moisture effects on crack propagation in high strength aluminum alloys studied by fatigue tests
01 p0098 A69-10766
- Soil, moisture and other requirements for microorganism survival in simulated Martian environment
01 p0018 A69-11091
- Moisture and hydrogen role in hot chloride salt stress corrosion cracking of Ti alloys by radiotracer technique and mass spectrography
19 p3352 A69-36904
- MOISTURE CONTENT**
NT ATMOSPHERIC MOISTURE
Total atmospheric moisture content by measuring radio wave absorption at water vapor molecule rotational spectrum absorption line
02 p0274 A69-11438
- Atmospheric water vapor content from summer-fall 1966 measurements of atmospheric radio wave absorption of thermal radio emission, describing experimental apparatus
02 p0274 A69-11439
- Hot pressed boron nitride properties and fabrication, noting low moisture absorptivity and aerospace applications
02 p0270 A69-11802
- Dry heat sterilization of spacecraft, microorganism water content and recommendations for fabrication conditions for spacecraft
05 p0712 A69-15939
- Atmospheric noise at 33.5 GHz observed most on days of cumulus clouds probably due to local convective activity
05 p0721 A69-16661
- Flow velocity, density, temperature, dryness and pressure in mixing chamber of MHD vaporizer
06 p0871 A69-17919
- Radiating surface temperature and total atmospheric moisture content determinations based on meteorological earth satellite measurements of outgoing radiation in IR
06 p0952 A69-17988
- Water content of tektites, impactites and artificial glass of tektite composition using IR absorption measurements
10 p1778 A69-23413
- Lunar surface pore water /or ice/ detection by active orbital or surface electromagnetic experiments, noting water effect on reflection coefficient
11 p1958 A69-24693
- Mean vertical moisture profile for summer and winter midlatitude stratosphere from Soviet radiosonde data
12 p2070 A69-26582
- Thunderstorm thermal noise emission determined by radiometer and steerable parabolic antenna in preparing water content contours along radio rays
12 p2127 A69-27002
- Microwave radiometric brightness temperature relationship to soil moisture content for estimating bearing strength
12 p2099 A69-27008
- Radio wave single scattering at particles randomly grouped in space, showing correlation function of water content fluctuations in scattered field in clouds
16 p2807 A69-32267
- Dimensions, concentration and spectrum of large precipitation particles in clouds and cloud water content by measuring reflectivity and absorptivity at different wavelength
16 p2807 A69-32268
- He-Ne laser emission attenuation coefficient relation to water content of artificial fogs for 0.63, 1.15 and 3.39 microns
21 p3738 A69-39118
- Rocket optical experiment for determining water, methane, nitric oxide and ozone vertical profiles in stratosphere and mesosphere
22 p4035 A69-39910
- Environmental neutron flux measured by various techniques, studying effects of soil and moisture on density
22 p4002 A69-40094
- Subjective feeling of dampness correlation with relative humidity of air at zero and below zero C temperatures
23 p4109 A69-41870
- Radiative transfer theory applied to layer cloud with normal liquid moisture content, discussing volume extinction, scattering and absorption coefficients, etc
23 p4184 A69-42177
- Solid cloud cover moisture content relation to outgoing thermal radiation, obtaining correlation coefficient and regression equations
23 p4184 A69-42488
- MOISTURE METERS**
NT HYGROMETERS
NT PSYCHROMETERS
Cloud instrumentation for measurement of icing conditions of airplane flight tests
01 p0055 A69-11044
- Moisture detector for evaluating trapped water effects in thermal insulation, describing equipment and test procedure
24 p4312 A69-42755
- MOL [ORBITAL LABORATORIES]**
U MANNED ORBITAL LABORATORIES
- MOLABS**
U LUNAR MOBILE LABORATORIES
- MOLDAVITE**
Moldavites and Ries crater material, studying Rb-Sr isochronal relationship
23 p4154 A69-41341
- Chemical composition and lechatelierite size frequency influence on moldavites bulk density, using data to elucidate origin
23 p4210 A69-41348
- Petrology of Czechoslovak moldavites, tabulating properties, mapping locations and distribution
23 p4210 A69-41350
- MOLDING MATERIALS**
Epoxy molding compounds characterization and classification for development and evaluation of raw materials
04 p0620 A69-14954
- Electric components encapsulation by combining liquid resin techniques and transfer molding
04 p0607 A69-14955
- Matched metal molding of short graphite fiber composites
08 p1339 A69-20502

Potential usage of titanium in cast parts for gas turbine engines, emphasizing alloys development
[ASME PAPER 69-GT-24] 09 p1513 A69-22494

Glass reinforced plastic molding compounds for OV-10A airplane structural components, noting cost savings
[SAE PAPER 690342] 11 p1890 A69-24497

Compression molding of molecular salt-like intermediate Pyrrone powders by two pressure method, noting volatiles elimination 14 p2469 A69-29415

Injection holding for ceramic parts from nonplastic materials, presenting time-temperature schedules for low temperature removal of molding material without damage 17 p2978 A69-33376

Epoxy molding compounds performance on DIP integrated circuits, determining comparative moisture protection provided by encapsulants 19 p3280 A69-35546

Transfer molded epoxy dielectrics, comparing encapsulation rate, pressure and cure times to compression molding 19 p3281 A69-35548

Moldable plastic shim material for structural airframe components, discussing application requirements 19 p3319 A69-35551

Molded fiber composites in aerospace components applications, considering weight, stiffness, production and cost 24 p4326 A69-43448

MOLDS

Rigid PVC, urethanes and thermosets processing for high performance, noting injection molding and machine developments role 18 p3148 A69-34611

MOLECULAR ABSORPTION

Oscillator strength determination for Schumann-Runge band system in molecular oxygen 02 p0284 A69-12832

Pressure induced microwave absorption in molecular N for various temperatures, determining dielectric loss, absorptivity and quadrupole moment 03 p0472 A69-13317

Dark equatorial belt of Jupiter atmosphere in 1962 and 1963, noting photometric contrasts, molecular absorption and possible structure 04 p0658 A69-14961

Methane broadening and anomalously small pressure shift of 3.39 micron rotation-vibration line, using laser saturated molecular absorption 04 p0633 A69-15424

Absolute wavelength standard using saturated molecular absorption in methane inside He-Ne laser cavity [IEEE PAPER P-1] 05 p0775 A69-16323

Collisionally induced microwave absorption by non-polar gases, discussing dimer absorption 06 p0962 A69-17816

Atmosphere effects on solar IR spectra, discussing role of absorbing molecule distribution in transmittance calculations 13 p2341 A69-27589

Neodymium laser emission of organic molecules in UV region noting molecular absorptivity and fluorescence 13 p2271 A69-27657

CO absorption lines in solar spectrum analyzed theoretically and experimentally indicating random distribution of molecules 15 p2688 A69-30552

Dark equatorial belt of Jupiter atmosphere in 1962 and 1963, noting photometric contrasts, molecular absorption and possible structure 18 p3197 A69-34724

Atmospheric slant path molecular absorption and emission from band model methods, discussing computer program prediction capabilities 19 p3375 A69-36052

DC beam experiment for determining molecule sticking coefficients of gas beams incident on Ti, Ba and Sr gettering surfaces at cryogenic temperature 23 p4151 A69-41544

MOLECULAR BEAMS

Intensity of visible and UV light from beam of positive deuterium molecular ions excited by passage through thin C foil 03 p0471 A69-13166

Crossed beam studies of ion-molecule reaction mechanisms, crossing approximately monoenergetic ion beam with thermal molecular beam 03 p0382 A69-13460

Molecular jets obtained by charge exchange of triatomic ion beams consisting of hydrogen, deuterium and nitrogen, noting formation, energy level, etc 05 p0797 A69-16339

Molecular and atomic beam focusing in electric and magnetic fields with helical symmetry of specified type 06 p0959 A69-16917

Dissociation of hydrogen on tantalum using modulated molecular beam mass spectrometry 06 p0960 A69-17107

Supersonic molecular beam sampling system for coupling mass spectrometer to alkali metal-air reacting flow system in kinetics study, noting gas dynamic effects [AIAA PAPER 69-94] 06 p0930 A69-18099

Collimated nozzle beam for probing low density gas flows, discussing transition from free molecular to isentropic flow and Knudsen numbers 07 p1136 A69-19467

Molecule reorientation and transition probability in molecular beam maser using formaldehyde 07 p1158 A69-19760

Molecular beam gas laser operating at transitions between ground state and resonance excited state of inert gas atom, obtaining population inversion 08 p1325 A69-20325

Speed distribution and density of molecular beam from time domain measurements of propagated beam perturbations, discussing gate functions 10 p1652 A69-23340

Hetero-epitaxial germanium films on GaAs by germanium condensation from molecular beams in vacuum, obtaining p-type conductivity 11 p1938 A69-25033

Crossed beam apparatus with mass selected variable energy primary beam for study of angular and velocity spectra of ion-molecule reactions 12 p2092 A69-26477

Molecular beam scattering analysis by four parameter B-C intermolecular potential, plotting expansion coefficients against reduced curvature 13 p2301 A69-27206

Metastable molecules and fragments produced by electron excitation of nitrogen, hydrogen, carbon dioxide and nitrous oxide, noting excitation functions, kinetic energy, etc 13 p2301 A69-27362

Molecular beam behavior in constant electric and magnetic fields, applying laser frequency dependence on magnetic field orientation to resonator 15 p2655 A69-30943

Hyperfine spectrum analysis of NaCl at low field using molecular beam electric resonance method, discussing Hamiltonian function representation 16 p2815 A69-32794

Molecular beam gas laser operating at transitions between ground state and resonance excited state of inert gas atom, obtaining population inversion 17 p2981 A69-33315

Molecular beam experiments on moon, noting lunar environmental advantages for studies of beam-beam scattering, beam-surface interactions, beam-field deflection, etc 18 p3113 A69-34240

Strong shock wave structural model, considering near molecular beam, upstream hypersonic and downstream subsonic flows and beam-continuum conversion by collision 18 p3120 A69-34457

Velocity and angular distributions of KBr formed in reactive collisions between crossed molecular beams of K and thermal HBr/DBr/ 18 p3178 A69-35476

High and medium energy molecular beams - Conference, Cannes, July 1969 19 p3375 A69-36171

Skimmer interaction influences on nozzle beam production explaining intensity maxima, proposing model assuming normal shock across skimmer mouth 19 p3238 A69-36172

Single junction vacuum thermocouple measuring thermal beam effect with reference to velocity distribution perturbation in molecular beam scattering 19 p3376 A69-36173

Thermal molecular beam sources fabricated from multichannel arrays, describing molecular flux leak rates and angular distributions 19 p3376 A69-36175

High energy neutral molecule beam for gas-surface interaction studies generated in electron bombardment ion source 19 p3376 A69-36176

Low and moderate energy gas molecule-solid surface interactions, using molecular beams 19 p3376 A69-36177

Wall boundary condition model modification applied to molecular beam-solid surface scattering, noting qualitative agreement with observed distributions 19 p3377 A69-36179

Solid surface roughness influence on reflection of thermal energy molecular jets, showing shock determined by incidence angle 19 p3377 A69-36180

Gas molecules scattering by solid surface for monoenergetic and Maxwellian beams, discussing model with different values for magnitude and velocity direction 19 p3377 A69-36181

Satellite-borne experiments of neutral molecular beam-solid surface interactions, describing Molsink chamber, densitometer, sphere and paddlewheel satellites 19 p3377 A69-36182

Heated supersonic beam study of He-Ar intermolecular potential, determining total elastic collision cross section as function of velocity in scattering chamber 19 p3377 A69-36183

Energy dependence of elastic total collision cross section of identical He molecules, using velocity selected primary beams at low target temperature 19 p3378 A69-36186

Supersonic molecular beam relative intensity represented as function of nozzle to collimator distance and gas admission pressure 20 p3579 A69-37432

Maxwell coefficient change of Cd atoms in molecular beam/ diffusely reflected from metal surfaces related to reflector temperature, material and fabrication method 20 p3580 A69-37814

Aerodynamic forces under space-like conditions measured by swing balance, using large scale molecular beams for rarefied hypersonic gas flow simulation [AIAA PAPER 69-1032] 22 p3924 A69-40400

Molecular beams for simulating orbital flight through planetary atmospheres, considering various nozzle beam systems [AIAA PAPER 69-1031] 22 p3926 A69-40437

Crossed beam apparatus (evatron) for studying energy spectra of crossed positive ethylene ion beams and neutral ethylene molecule beams 24 p4280 A69-43813

MOLECULAR BONDS
U CHEMICAL BONDS

MOLECULAR CHAINS

Cross-links effect on char yields of azomethine polymers produced by aryl diamines with aryl diketones 08 p1269 A69-21060

Schiff base cross-links effect on synthesis of polymeric azomethines produced by bis exchange reactions, carbonyl and amine 08 p1269 A69-21061

Molecular rearrangements of nitrene intermediates, suggesting role in bond formation and breaking at nitrogen 20 p3484 A69-37485

Amino acid sequence of dogfish lactic dehydrogenase, isolating acylated amino-terminal peptide and arginine residues, indicating four polypeptide chain composition 24 p4280 A69-43051

Helix to coil transition for triple stranded macromolecule in solution, calculating ring weighting and partition functions and intact bonds 24 p4353 A69-43812

MOLECULAR COLLISIONS

Spatial and kinetic distributions of molecules reflected by surface in rarefied atmosphere, discussing mathematical model 01 p0122 A69-10041

Analytical mechanics of chemical reactions, discussing natural collision coordinates for three dimensional reactions and exchange collisions for molecule and atom 01 p0123 A69-10681

Intermolecular collision induced vibration to vibration energy transfer in nitrous oxide in various gas mixtures, measuring fluorescence and relaxation rates 01 p0123 A69-10684

HI and DI reaction into HD and 2I, noting need for rotational or vibrational excitation in addition to translational energy of collision 01 p0123 A69-10686

Collision integrals for high temperature gases calculated for high order potentials 01 p0124 A69-10929

Preionization of gases by laser beam using theory based on molecular equilibrium concentration and collision excitation

02 p0283 A69-11703

Numerical solution for excitation of oscillations in diatomic molecules during atom-molecule collisions at high temperatures, determining intermolecular interaction forces

02 p0284 A69-12485

Energy distribution among products of reactive collision of atomic H with Br molecule yielding HBr and Br atom, using perturbed Morse oscillator approximation

03 p0472 A69-13316

Frictional forces and collision frequencies for ions moving in neutral gases

03 p0421 A69-13328

Electron backscattering from cathode to cathode due to collisions with molecules, assuming isotropy of scattering

05 p0800 A69-15738

Uranium hexafluoride-hydrogen hydrogen fluoride chemical laser, discussing conditions for negligible collisional deactivation and defined rotational temperature determination

05 p0771 A69-15906

Ion-molecule collisions of Ar-Co and N-No pairs, discussing charge exchange reaction rates and spiraling nature

05 p0797 A69-16428

Population inversion of vibrational levels due to molecular collisions in carbon dioxide lasers, calculating transition probabilities, laser parameters and gain profile [IEEE PAPER G-15]

07 p1151 A69-19061

Optical potentials for rotational and vibrational transitions in inelastic molecular collisions, considering adiabatic and sudden approximations

08 p1358 A69-21008

Near resonant transfer of vibrational energy from carbon dioxide nu 3 mode to N 14 and N 15 molecules in collisions

08 p1358 A69-21011

Hydrodynamic equations and Grad transport coefficients for nonequilibrium rarefied monatomic gases developed for molecular collisions

09 p1481 A69-21888

Enskog method for Boltzmann equation, analyzing asymptotic nature of integral kinetic equation for molecular mean free paths and Laplace probabilities

09 p1481 A69-21889

Nonadiabatic collision broadening theory for IR spectral lines applied to carbon dioxide-carbon dioxide and carbon dioxide-nitrogen collisions, estimating rotational line widths

09 p1543 A69-22250

Molecular reaction rates and ion/electron vertical profile and concentrations in equatorial ionosphere, applying computer simulation to numerical solution of continuity equations

10 p1688 A69-23929

Exact solutions for two state potential curve crossing in subexcitation molecular collisions in terms of various decoupling schemes

12 p2131 A69-25983

Translational-vibrational energy transfer value between atom and diatomic molecule determined using steric factor with repulsive interaction potential

12 p2134 A69-25988

Shapes of extreme wings of collision-broadened carbon dioxide lines, noting absorption deviation from Lorentz-shaped lines

12 p2132 A69-26248

Vibrational energy exchange between diatomic molecules by IR emission of CO fundamental behind shock waves

13 p2301 A69-27361

Oscillations and decomposition of diatomic gas molecules at high temperatures during atom/molecule collisions, deriving kinetic equations for energy level changes

13 p2302 A69-27797

Carbon dioxide band vibration-rotation transitions saturation characteristics, stressing role of collisions in molecular gas lasers

14 p2457 A69-28928

Plane shock layer structure in pseudoMaxwellian monatomic gas, integrating Krook equation for gas molecule velocity

14 p2432 A69-29613

Perturbed molecular distribution in translational and internal degrees of freedom in dilute chemically reacting gases with low ion concentrations

14 p2410 A69-29988

Kinetic theory of gases collision cross section definition compared to usual definition, discussing time reversed collisions

14 p2488 A69-29993

Gasdynamic model of comet nucleus region, discussing molecular collisions, surface brightness distribution and dust particle motion

15 p2684 A69-30520

Nonlinear rarefied gas flow problems with thermal nonequilibrium solved by numerical methods, considering intermolecular collisions effect

17 p2952 A69-33325

Long lived highly excited atoms production in electron collisions with CO, O and N molecules

18 p3177 A69-35125

Velocity and angular distributions of KBr formed in reactive collisions between crossed molecular beams of K and thermal HBr/DBr/

18 p3178 A69-35476

Ion cyclotron double resonance technique to identify collision-induced ion fragmentation pathways illustrated with p-chloroethylbenzene

19 p3265 A69-36292

Deactivation rate constants of carbon dioxide vibrationally excited by high temperature collision with carbon dioxide or nitrogen molecules, describing laser apparatus and reaction cells

20 p3578 A69-36937

Gas molecule collision influence on photon echo intensity produced by two linearly polarized laser pulses incident on sulfur hexafluoride

21 p3774 A69-38589

Collision processes in gaseous nitrogen leading to production of positive triatomic, diatomic and monatomic nitrogen ions

22 p3986 A69-40722

Molecular collision pumping mechanism for anomalous microwave absorption by formaldehyde rotational transition in Galaxy dust cloud

22 p4029 A69-40768

Lyman alpha radiation from electron collisions with simple H-containing molecules, finding dissociative excitation cross section role

24 p4351 A69-43033

Computer made movies and time history plots for ion-dipole collisions involving polar molecules /CO, HCL and acetonitrile/

24 p4352 A69-43124

Monte Carlo calculation of free molecular flow over concave spherical surface, considering partial diffuse reflection and imperfect energy accommodation

24 p4248 A69-43592

MOLECULAR DIFFUSION

High speed automatic osmometer applied to measurements of diffusible branched polyethylene samples, discussing apparent molecular weight observations

01 p0024 A69-10933

Radiative transfer equation for pure molecular scattering inverted for estimating vertical ozone distribution

07 p1126 A69-19042

Temperature variability data for 120-km altitude from observations of grenade glow clouds, calculating molecular diffusion coefficients and atmospheric temperature and density

07 p1127 A69-19277

Laser diodes p-n junctions obtained by Zn diffusion into Ga arsenide, stressing junction flatness problem and arsenic vapor pressure effect

13 p2323 A69-28640

Atomic nitrogen and nitric oxide density in upper atmosphere during nighttime calculated, allowing for atomic and molecular diffusion

16 p2785 A69-32622

Rotational-vibrational relaxation and molecular diffusion effect on saturation parameter of carbon dioxide laser, measuring gain as function of input power

19 p3338 A69-36692

Diffusion parameters for fluid stream flowing from round hole with given radius and velocity into wake flow

21 p3696 A69-39091

Free stream dispersion without permeation using nonporous glass beads and solutes, examining flow rate, particle size distribution, solute diffusivity, etc

22 p3894 A69-39873

MOLECULAR DISSOCIATION

U DISSOCIATION

MOLECULAR ELECTRONICS

MERA /Molecular Electronics for Radar Applications/ modules testing in planar array simulator, measuring far field amplitude patterns in transmitting and receiving modes

22 p3912 A69-40067

MOLECULAR ENERGY LEVELS NT INTERMOLECULAR FORCES

Ground state energies of HeH divalent ion, comparing perturbation calculation values with variation-perturbation technique

01 p0123 A69-10547

Preionization of gases by laser beam using theory based on molecular equilibrium concentration and collision excitation

02 p0283 A69-11703

Doublet electronic states of benzyl radical, discussing configuration-interaction calculations and transition predictions

03 p0472 A69-13321

Thermodynamic approach to calculation of molecular lasers, determining various population levels of carbon dioxide molecule by measuring amplification factors for rotational vibrational transitions

06 p0934 A69-17465

Population inversion of vibrational levels due to molecular collisions in carbon dioxide lasers, calculating transition probabilities, laser parameters and gain profile [IEEE PAPER G-15]

07 p1151 A69-19061

Perturbation methods for exchange and Coulomb energy of hydrogen molecule, calculating Hamiltonian by wave function

07 p1186 A69-19446

Heat transfer effect on population inversion time variation in pulsed carbon dioxide laser and molecules excitation rates dependence on gas mixture composition

09 p1519 A69-22289

Carbon dioxide laser upper level rotational relaxation rate constant measurement, observing CW gain

10 p1701 A69-22948

Rotational excitation and scattering cross sections for rigid diatomic molecules reduced to yield distorted wave approximation, resulting in inelastic transition probabilities

10 p1726 A69-23524

Oscillations and decomposition of diatomic gas molecules at high temperatures during atom/molecule collisions, deriving kinetic equations for energy level changes

13 p2302 A69-27797

Lifetime of vibrational levels of carbon dioxide molecules as function of discharge current and power dissipation, noting gas heating

13 p2273 A69-28579

Energy level population of carbon dioxide molecules, noting intensity of spontaneous emission

13 p2274 A69-28580

Radiative decay of polyatomic molecules, applying Green function form for transition probability to decay of manifold of closely spaced coupled levels

14 p2488 A69-29924

Lambda doublet maser emission from excited OH rotational level, discussing conditions necessary for microwave radiation

18 p3185 A69-34292

Quantum transitions between molecular or atomic energy levels noting microwave spectroscopy utilization

18 p3099 A69-35405

Rate coefficient for primary process in removing molecular nitrogen in high vibrational levels from active nitrogen by N atoms

19 p3379 A69-36424

Electron reactivity of one equivalent oxidizing agents at ZnO surface by electrochemical reduction

19 p3392 A69-36731

Thermodynamic approach to calculation of molecular lasers, determining various population levels of carbon dioxide molecule by measuring amplification factors for rotational vibrational transitions

20 p3555 A69-37948

Photochromic panel for flash blindness protection using epoxy plastic plates containing aromatic hydrocarbon compounds excited to triplet states

21 p3668 A69-39783

Excited states lifetime of carbon dioxide and nitrous oxide ions deduced from spontaneous radiative deexcitation in vacuum after passage through gaseous target

22 p3985 A69-40715

Herzberg bands synthetic spectra matched to various spectrograms to determine vibrational populations of molecular O state in nightglow

24 p4310 A69-43186

MOLECULAR FLOW

NT SLIP FLOW

NT TRANSITION FLOW

Book on mathematical and physical fundamentals of molecular gasdynamics based on statistical mechanics, discussing free molecular flow

01 p0060 A69-10711

Molecular flow in space simulation chambers with cryowalls, noting nonuniform flux density distribution
01 p0057 A69-11153

Crystals and molecules diffraction in supersonic molecular jets
02 p0284 A69-12629

Continuum flow boundary in freely expanding jet estimated from molecular mean free path and modulus of random motion mean velocity
10 p1679 A69-23425

Gas molecular mean free path effect on performance of spiral grooved thrust bearing, discussing slip flow factor and He Knudsen number
[ASME PAPER 68-LUBS-17]
13 p2266 A69-27273

Molecular gas flows in containers for space environment simulation, discussing flux distribution
13 p2241 A69-28081

Molecular flow network theory extended to pulsed operation with gases mixtures having various molecular weights
13 p2247 A69-28085

Molecular flow network theory applicable to volumes interconnected by small orifices or porous membranes for transient pressure measurements
16 p2813 A69-32325

Supersonic leading edge problem using nonlinear Boltzmann equation with ellipsoidal model, calculating molecular distribution functions for flow field
[AIAA PAPER 69-652]
17 p2892 A69-33464

Pure gas suction through free jet shock structure, analyzing aerodynamic effect of molecular separation
19 p3240 A69-36650

Rarefied molecular gas flow past permeable surface, determining reflection law and flow parameters
20 p3459 A69-37438

MOLECULAR GASES

NT DIATOMIC GASES

NT POLAR GASES

NT POLYATOMIC GASES

Multiphoton ionization of molecular hydrogen and rare gases using Q switched Nd laser apparatus
02 p0283 A69-11701

Equilibrium of rotational degrees of freedom in gases undergoing relaxation, noting excitation, relaxation time, kinetics, transfer effects and measurements for hydrogen
02 p0284 A69-12667

Trimodal solutions for strong shock structure in gas of spherocylindrical molecules
03 p0414 A69-13136

Energy transfer and viscosity coefficients during gas molecular interactions, using spherical monatomic gas molecules model
03 p0415 A69-13419

Ammonia gas molecules in interstellar medium, discussing detection in direction of galactic center by means of microwave emission
03 p0518 A69-14258

Gases optical pumping by self radiation laser action, discussing high intensity oscillatory transitional wide bands of molecular gases
04 p0610 A69-14382

Activation energies of bimolecular multivalent transfer reactions of gaseous compounds, considering bond dissociation energy, length and order
[WSCI PAPER 68-48]
07 p1239 A69-18321

Variational solution of linearized molecular chemical-kinetic Boltzmann equation, discussing perturbation of Maxwell distribution, nonequilibrium correction to reaction rate and activation energy
07 p1185 A69-19301

Dissociation-ionization fronts in interstellar molecular hydrogen clouds, analyzing effects of UV radiation from early stars
07 p1221 A69-19584

Wavelike photodissociation of gas molecules under quasi-monochromatic pulsed radiation, investigating associated supersonic disturbances
08 p1354 A69-19950

Gas adsorption of molecular oxygen and hydrogen on molybdenum surface using collector section of field emission retarding potential analyzer
08 p1268 A69-20179

Region of transition from laminar to turbulent flow in meteor trains, suggesting electron attachment processes to molecular oxygen in presence of third body
08 p1393 A69-20608

Luminescence spectra of molecular gases excited by fast electrons in infrared spectral region, noting H alpha line
09 p1590 A69-21382

Effective cross sections of UV radiation absorption by molecular oxygen in Schumann-Runge bands at high temperatures
11 p1921 A69-24617

Molecular carbon dioxide laser radiation emission in tube containing low pressure atmospheric air, using C cathode and Al cold cathode
11 p1895 A69-24625

Slip flow problem for general specular-diffuse boundary condition in kinetic theory of gases, noting molecular distribution function
11 p1869 A69-24893

Slow charged products of charge exchange collisions by ions in molecular gases, comparing kinetic energies during various reactions
13 p2301 A69-27455

Molecular gas flows in containers for space environment simulation, discussing flux distribution
13 p2241 A69-28081

Charge transfer and vibrational excitations in hydrogen molecular ion-hydrogen gas collisions
13 p2302 A69-28196

Fluorescence stimulated by high energy electron and ion beams, determining vibrational temperature and concentration of molecular oxygen in high enthalpy wind tunnel flows
13 p2302 A69-28265

Gases optical pumping by self radiation laser action, discussing high intensity oscillatory transitional wide bands of molecular gases
14 p2456 A69-28755

Molecular hydrogen electron scattering, optical refractivity and molecular anisotropy used to construct model dipole spectrum consistent with oscillator strength rules
14 p2488 A69-29094

Ion-molecular reactions measurements in ionosphere by VV type device and RF mass spectrometer
15 p2603 A69-31407

Molecular gas absorption coefficient dependence on laser emission energy density, considering disturbed equilibrium distribution of molecules
17 p2983 A69-33973

Luminescence spectra of molecular gases excited by fast electrons in IR spectral region, noting H alpha line
18 p3176 A69-34770

Thermal energy rate constants of ion-molecule reactions in gaseous hydrogen, deuterium and HD, using ion cyclotron resonance method
20 p3578 A69-36934

Electron band forces probable values of Meinel system positive N molecules and first positive system of nitrogen molecules at high temperatures
20 p3579 A69-37307

Ambient atmospheric temperature and molecular nitrogen density measured simultaneously by rocket-borne electron beam luminescence method
20 p3543 A69-37799

Gas molecule collision influence on photon echo intensity produced by two linearly polarized laser pulses incident on sulfur hexafluoride
21 p3774 A69-38589

Molecular hydrogen, oxygen and deuterium additions effect on CW laser operation with ordinary and heavy water as active medium
21 p3738 A69-39131

Rocket measurements of diurnal variations of F region concentrations and temperature of molecular N and O, showing disagreement with satellite drag data
22 p3939 A69-40515

DC beam experiment for determining molecule sticking coefficients of gas beams incident on Ti, Ba and Sr gettering surfaces at cryogenic temperature
23 p4151 A69-41544

MOLECULAR INTERACTIONS

Ion reactions with neutral molecules, discussing analogies with conventional chemical systems
01 p0124 A69-10859

Intermolecular interaction potentials for dissociating air components determined by calculating collision integrals for very high temperature gases
02 p0283 A69-11586

Electro-optical measurements to determine intermolecular interaction temperatures in organic liquids compressed by shock waves
02 p0230 A69-11979

Energy transfer and viscosity coefficients during gas molecular interactions, using spherical monatomic gas molecules model
03 p0415 A69-13419

Crossed beam studies of ion-molecule reaction mechanisms, crossing approximately monoenergetic ion beam with thermal molecular beam
03 p0382 A69-13460

Negative ion-molecule reactions in nitrous oxide using mass spectrometer, noting negative ion concentration pressure dependence
06 p0960 A69-17106

Reaction rates coefficients of oxygen ions with molecular oxygen and nitrogen in nighttime F region over Moscow based on loss coefficient estimate
06 p0919 A69-17724

Molecular interactions in ammonia maser beam, discussing influence on oscillation extinction beyond given flow rate
07 p1145 A69-18478

Statistical theory of fluids in equilibrium based on correlation functions for pair interactions between constituent molecules, invoking superposition closure approximation
08 p1350 A69-19868

Ion-molecule reactions constants studied directly in ionosphere, using air injection from geophysical probe and airborne RF mass spectrometer
08 p1311 A69-21159

Electrons resonance scattering by diatomic molecules from elastic and inelastic channel measurements in transmission
11 p1921 A69-24418

Superstructures in multicomponent alloys, transition mode and temperature, ordered state and atomic interactions
11 p1937 A69-24703

Crossed beam apparatus with mass selected variable energy primary beam for study of angular and velocity spectra of ion-molecule reactions
12 p2092 A69-26477

London-van der Waals interaction energy of symmetric molecular pair calculated in perturbation theory second order as infinite series in negative powers of separation
12 p2131 A69-26606

Exchange interactions in lithium ferrite aluminates, measuring spontaneous magnetization by ballistic technique from 77 K to Curie point
13 p2320 A69-27995

Two center Coulomb integrals expressed in terms of center separation, noting applications to molecular calculations
14 p2471 A69-29926

Electro-optical measurements to determine intermolecular interaction temperatures in organic liquids compressed by shock waves
15 p2561 A69-30264

Elementary processes cross sections in charged states changes during proton-hydrogen molecule interactions
15 p2655 A69-30963

Temperature dependence of intermolecular interaction averaged potentials with respect to vibrational states
15 p2655 A69-30982

Langevin equation for interacting molecule system derived by Fourier transformation of Hamiltonian, noting physical correspondence to equation for shear viscosity in monatomic liquids
16 p2815 A69-32370

Nitrous oxide-CO bimolecular reaction and O-CO recombination in single pulse shock tube
16 p2748 A69-32793

Free jet shock wave structure penetrated by surrounding pure gas molecules
18 p3086 A69-34819

Low and moderate energy gas molecule-solid surface interactions, using molecular beams
19 p3376 A69-36177

Gas molecules scattering by solid surface for monoenergetic and Maxwellian beams, discussing model with different values for magnitude and velocity direction
19 p3377 A69-36181

Acetonitrile ion-molecule chemistry using ion cyclotron resonance, discussing reaction of vibrationally excited methyl ions from electron impact
19 p3265 A69-36290

Gas phase ion-molecule chemistry of HCN by ion-cyclotron resonance spectroscopy identifying individual reactions by double resonance
20 p3485 A69-38262

Singlet-singlet energy transfer kinetics dependence on emission and absorption spectra overlap via dipole-dipole interaction
22 p3895 A69-40056

Quantum-mechanical theory of unimolecular kinetics and predissociation developed from generalized Fano theory of resonant scattering
22 p3986 A69-40724

Chemical high pressure laser action produced by stimulated phototransition of electrons at contact mo-

ment between pair of reacting nonexcited gas molecules
22 p3965 A69-41117

Formation mechanism of positive ethyl ion and hydrogen molecule during interaction between positive methyl ion and methane molecule
24 p4280 A69-43814

MOLECULAR IONS

Ground state energies of HeH divalent ion, comparing perturbation calculation values with variation-perturbation technique
01 p0123 A69-10547

Alpha recombination coefficient of molecular helium ions measured in helium afterglow plasmas as function of electron density and gas temperature
02 p0283 A69-11834

Metastable positive He molecules and He atoms decay in afterglow, taking into account simultaneous emission at 4650 angstroms during absorption studies
02 p0287 A69-11932

Charge transfer cross sections for slow ion production in nitrogen molecular ion beams incident on hydrogen and deuterium
05 p0796 A69-15914

Hydrogen ions collision-induced dissociation cross section angular dependence measured, showing qualitative agreement with theoretical predictions
05 p0798 A69-16698

Nitrogen ion number density time dependence by mass spectrometric probing of decaying nitrogen plasmas, noting molecular ion production by colliding metastable nitrogen molecules
07 p1184 A69-19141

Two body rate coefficients for charge transfer reactions of nitrogen, oxygen and NO positive ions to Na atoms measured using flowing afterglow system
07 p1185 A69-19303

Drift measurements of rate constants for charge transfer in ion-molecule processes
08 p1355 A69-20210

Temperature dependence of dissociative recombination and molecular ion formation in decaying He, Ne and Ar plasmas in discharge tube energized with capacitor bank
08 p1356 A69-20741

Molecular ion C13H line found in zeta Oph at 4232.08 A, measuring equivalent width and finding C12/C13 ratio
09 p1603 A69-22266

Ratio of volume emission rates of 5577 A band and of positive N molecular ion first negative system for use in auroral observations
09 p1491 A69-22607

Direct nonresonance excitation of rotational and vibrational states of diatomic molecular ions by electrons in Born-Coulomb approximation
10 p1726 A69-23627

Nitrogen dioxide molecular ions formation in air, discussing absence at lower pressures and early afterglow dominance in air ionized and dissociated by microwave pulses
11 p1879 A69-25158

Charge transfer and vibrational excitations in hydrogen molecular ion-hydrogen gas collisions
13 p2302 A69-28196

Spectrometric characteristics of He, H and molecular H ion recording counters as function of temperature
14 p2452 A69-29811

Electron impact field ionization source for mass measurement of molecular ions, noting organic geochemistry applications
15 p2608 A69-30428

RF spectra for hyperfine structure of ortho-hydrogen molecular ion, calculating doubling constant for vibrational effects
15 p2693 A69-30784

Lifetime of ground state oxygen molecular ions in sunlight from photodetachment rate by free electron production measurement from ions in buffer gas
16 p2848 A69-31973

Molecular ion concentrations determined using flat probe collector trap on Cosmos 5 satellite at 200-300 km
20 p3519 A69-37021

Photodetachment of electrons from nitrogen dioxide ions by light in violet portion of visible spectrum, noting wavelength dependence
22 p3985 A69-40575

Excited states lifetime of carbon dioxide and nitrous oxide ions deduced from spontaneous radiative deexcitation in vacuum after passage through gaseous target
22 p3985 A69-40715

Collision processes in gaseous nitrogen leading to production of positive triatomic, diatomic and monatomic nitrogen ions
22 p3986 A69-40722

Formation mechanism of positive ethyl ion and hydrogen molecule during interaction between positive methyl ion and methane molecule
24 p4280 A69-43814

MOLECULAR ORBITALS

Benzene anion radical in solid solution ESR spectrum, noting removal of orbital degeneracy at 4.2 degrees K
03 p0382 A69-13379

Linear combination of atomic orbitals-molecular orbitals self consistent fields calculation on beryllium dihydride, using Gaussian basis functions
05 p0811 A69-15910

Natural orbitals calculated from spin free one density matrix of open shell limited configuration-interaction wave function constructed from nonorthogonal basis
23 p4194 A69-42206

MOLECULAR OSCILLATIONS

Raman spectra and temperature dependent nuclear quadrupole resonance frequencies of p-dichlorobenzene and p-dichlorobenzene-D, calculating librational amplitudes
01 p0122 A69-10286

Numerical solution for excitation of oscillations in diatomic molecules during atom-molecule collisions at high temperatures, determining intermolecular interaction forces
02 p0284 A69-12485

Electron impact excitation cross sections for emission from first negative bands of positive N molecule ion
06 p0961 A69-17135

Absorption oscillator strengths for rotational lines in Lyman transition vibrational bands of molecular hydrogen from equivalent widths measured photoelectrically
06 p0962 A69-17818

Laser excited vibrational fluorescence for determining vibrational energy transfer rates in HCl-carbon dioxide, HCL-HI and HI-carbon dioxide
07 p1144 A69-18289

Sideband amplification via saturated gas resonance in 258 GHz reflection amplifier with hydrogen cyanide gas filled cylindrical cavity
07 p1145 A69-18479

Competition effects between rotational levels of carbon dioxide rotation-vibration band in traveling and standing wave lasers
[IEEE PAPER G-6] 07 p1151 A69-19055

Single mode carbon dioxide laser Lamb dip and vibration rotation lines absorption coefficients
[IEEE PAPER P-6] 07 p1153 A69-19075

Population inversion mechanism based on electron collisional excitation cross sections for molecular vibrational levels in carbon dioxide lasers
07 p1157 A69-19655

Optical potentials for rotational and vibrational transitions in inelastic molecular collisions, considering adiabatic and sudden approximations
08 p1358 A69-21008

Carbon dioxide bending mode deactivation by orthohydrogen, parahydrogen and deuterium through rotational transitions
08 p1358 A69-21010

Near resonant transfer of vibrational energy from carbon dioxide nu 3 mode to N 14 and N 15 molecules in collisions
08 p1358 A69-21011

Vibrational relaxation times in pure O and in O with methane impurity determined with acoustic absorption measurements
09 p1542 A69-21721

IR and Raman spectra of gas and liquid phase methylhydrazine and deuterated methylhydrazines, discussing vibrational motions, H bonding and thermodynamic functions
10 p1752 A69-23528

Direct nonresonance excitation of rotational and vibrational states of diatomic molecular ions by electrons in Born-Coulomb approximation
10 p1726 A69-23627

Vibrational energy transfer computed for processes in carbon dioxide-nitrogen laser based on vibrational relaxation data
10 p1706 A69-24083

Vibrationally excited nitrous oxide formation in reaction of N atoms with nitrogen dioxide, noting IR emission and vibrationally excited nitric oxide
11 p1832 A69-24880

Quantum oscillators interaction with two level molecules system in circular laser
11 p1899 A69-25325

Molecular vibration absorption spectra from variation of field emitted electron energy distribution due to inelastic electron-molecule interaction at metal-vacuum interface
12 p2132 A69-26097

Charge transfer and vibrational excitations in hydrogen molecular ion-hydrogen gas collisions
13 p2302 A69-28196

Electron cooling rates due to vibrational excitation of molecular oxygen calculated as function of electron temperature in E region
16 p2774 A69-31982

Torkington progressive rigidity model with successive minimum requirements relation to diagonal matrix elements of molecular force constants
17 p3068 A69-34230

Raman scattering during external and internal motion of oxygen molecules condensed phases, observing gamma and liquid phase bandwidths during stretching vibrations
24 p4353 A69-43808

MOLECULAR OSCILLATORS

Oscillator strength determination for Schumann-Runge band system in molecular oxygen
02 p0284 A69-12832

Weak magnetic fields effect on molecular oscillator frequency taking into account Zeeman sublevels
05 p0727 A69-15643

Oscillatory relaxation of multiatomic gases and gas mixtures with quantum exchange between oscillators, noting gasdynamic applications
15 p2654 A69-30109

Weak magnetic fields effect on molecular oscillator frequency taking into account Zeeman sublevels
16 p2762 A69-32500

Transient oscillations in ammonia maser oscillator observation based on switching achieved by signal injection into cavity at molecular resonance frequency
19 p3339 A69-36825

Hydrogen high level transition probabilities formula, giving two tables of oscillator strengths [AFCRL-69-0301]
22 p3983 A69-40149

MOLECULAR PHYSICS

Atomic and molecular excitation mechanisms in nonequilibrium gases up to 20000 K
08 p1354 A69-20146

Molecular state of hydrogen gas in high density condensations in H II regions, discussing effects of nearby stars
11 p1963 A69-25258

MOLECULAR RELAXATION

Molecular velocity distribution function in nonequilibrium flows, detailing asymptotic expansions in different velocity domains for weak shock
01 p0059 A69-10330

Relaxation processes and radiation stimulation in dense low temperature ionized plasma can lead to population inversion of several levels
01 p0131 A69-10789

Vibrational relaxation of diatomic gases behind shock waves, with variable heat bath temperature extended to constant enthalpy and constant total enthalpy conditions
01 p0061 A69-11204

Numerical solution for excitation of oscillations in diatomic molecules during atom-molecule collisions at high temperatures, determining intermolecular interaction forces
02 p0284 A69-12485

Krook kinetic relaxation equation generalized to include approximate kinetic equations with velocity independent collision frequency
02 p0234 A69-12582

Inverse population of vibrational levels generation in polyatomic molecules
02 p0259 A69-12647

Equilibrium of rotational degrees of freedom in gases undergoing relaxation, noting excitation, relaxation time, kinetics, transfer effects and measurements for hydrogen
02 p0284 A69-12667

Parameter changes of diatomic gas behind direct shock wave with simultaneous oscillatory and dissociative relaxation
03 p0418 A69-13835

Transitions in glasses at low temperatures, noting molecular relaxation dependence on copolymer composition
04 p0621 A69-15308

Equations describing chemical kinetics and conservation law derived for ionization relaxation processes behind shock wave front in air

05 p0746 A69-15891

Mechanical relaxation of poly 4 methyl pentene 1 at cryogenic temperatures, discussing temperature dispersion curve and secondary absorption associated with thermal motion of side chains

05 p0785 A69-16492

Chemical kinetic numerical integration techniques applied to equations for chemical relaxation [WSCI PAPER 68-45]

07 p1073 A69-18315

Relaxation equations for oscillatory degrees of freedom of molecular supersonic binary gas flow in Laval nozzle, obtaining population inversion

07 p1118 A69-18540

Thermal disturbance radiative decay time in carbon dioxide at low pressures and for nonzero vibrational relaxation times

07 p1215 A69-18843

Carbon dioxide bending mode deactivation by orthohydrogen, parahydrogen and deuterium through rotational transitions

08 p1358 A69-21010

Vibrational relaxation times in pure O and in O with methane impurity determined with acoustic absorption measurements

09 p1542 A69-21721

Atmospheric molecular oxygen temperatures from photoelectric recordings of absorption bands, analyzing relaxation process and photoeffects in oxygen molecules

09 p1490 A69-21863

Steady compression waves properties in relaxing gases found independent of thermodynamic behavior and relaxation process

10 p1631 A69-22893

Steady three dimensional flow of gases with thermodynamic relaxation, noting flow field weak discontinuities and effect of discontinuities in wall curvature

10 p1677 A69-22894

Carbon dioxide laser upper level rotational relaxation rate constant measurement, observing CW gain

10 p1701 A69-22948

Vibrational energy transfer computed for processes in carbon dioxide-nitrogen laser based on vibrational relaxation data

10 p1706 A69-24083

Carbon dioxide-N-He laser amplifier, noting gain time dependence and thermal relaxation rate after gas heating

11 p1899 A69-25054

Vibrational relaxation frequency of asymmetric stretching mode of carbon dioxide determined by measuring rate of thermal emission in shock waves near 4.3 microns

11 p1922 A69-25128

Vibrational energy exchange between diatomic molecules by IR emission of CO fundamental behind shock waves

• 13 p2301 A69-27361

Fluids structural relaxation analyzed by nonequilibrium thermodynamics and molecular kinetic theory, considering Brownian motion

13 p2299 A69-28037

Radiative decay of polyatomic molecules, applying Green function form for transition probability to decay of manifold of closely spaced coupled levels

14 p2488 A69-29924

Oscillatory relaxation of multiatomic gases and gas mixtures with quantum exchange between oscillators, noting gasdynamic applications

15 p2654 A69-30109

Radiative and conductive heat transfer in heated finite gaseous body with emphasis on collisional and radiative relaxation, noting cooling as two stage process [AIAA PAPER 69-638]

17 p3073 A69-33311

Chemical relaxation, optimum propellant mixture ratio, combustion chamber pressure, gas jet impulse, mass flow and drive capacity of space propulsion systems

18 p3229 A69-34773

Radiation emission by molecules in electromagnetic field, considering cavity resonators and waveguide excitation

18 p3178 A69-35404

Gaseous and solid phase properties of atomic and molecular systems, treating statistical energy distribution, kinetics, excited states and relaxation

18 p3178 A69-35406

Flow velocity, flow Mach number and weak disturbance velocity behind shock wave measured for nitrogen, oxygen and carbon dioxide

19 p3298 A69-36362

Rotational-vibrational relaxation and molecular diffusion effect on saturation parameter of carbon dioxide laser, measuring gain as function of input power

19 p3338 A69-36692

Relaxing polyatomic gases transport properties from Boltzmann equations obtained without knowing excitation probabilities of internal molecular degrees of freedom

19 p3300 A69-36787

Relaxation processes and radiation stimulation in dense low temperature ionized plasma leading to population inversion of several levels

20 p3582 A69-38006

Relaxation time for rotational transitions of linear polyatomic carbon dioxide calculated by using Brout theory for diatomic H rotational relaxation calculations

20 p3581 A69-38121

Relaxation equations for oscillatory degrees of freedom of molecular supersonic binary gas flow in Laval nozzle, obtaining population inversion

21 p3693 A69-38692

Carbon dioxide laser amplifiers gain saturation time dependence characteristics by theoretical model taking rotational relaxation into account

21 p3736 A69-38941

Vibration relaxation time and dissociation rate constant of carbon dioxide in high temperature shock waves, using IR emission

21 p3775 A69-39801

Molecular vibrational relaxation effect on dissociating airflow behind shock wavefront, giving relations to chemical reaction rates in diffusion approximation

24 p4302 A69-43486

Viscous shock wave chemical relaxation for diatomic nonequilibrium dissociating gas flow, using Navier-Stokes and chemical kinetics equations

24 p4302 A69-43487

MOLECULAR ROTATION

Millimeter wave oscillator AFC system utilizing inherent stability of molecular rotational transition applied to reflex klystron stabilization

01 p0044 A69-10628

High resolution spectroscopic study of stimulated rotational transitions of nitrogen molecules using crossed grating Echelle spectrograph

02 p0284 A69-12621

Equilibrium of rotational degrees of freedom in gases undergoing relaxation, noting excitation, relaxation time, kinetics, transfer effects and measurements for hydrogen

02 p0284 A69-12667

Far IR and Raman spectra of ethylene carbonate, gamma butyrolactone and cyclopentanone, noting consistency with hindered pseudorotation

02 p0206 A69-12723

Trimodal solutions for strong shock structure in gas of spherocylindrical molecules

03 p0414 A69-13136

Photosphere models comparison based on theoretical rotational temperatures of various diatomic molecular free radicals, using faint lines method

03 p0512 A69-13694

Separation of center of mass and rotational coordinates from N electron diatomic Schrodinger equation

04 p0554 A69-14861

Molecular motion in polytetrafluoroethylene crystals at cryogenic temperatures, noting crystal defect permitting angular displacements of chain segments

05 p0797 A69-16495

Polar molecule rotational excitation diffusion cross sections for electron scattering

06 p0961 A69-17139

Spontaneous Raman band shapes and depolarization ratios in liquid nitrogen and oxygen measured and compared to gas, discussing time dependence of rotational motion

06 p0962 A69-17817

Absorption oscillator strengths for rotational lines in Lyman transition vibrational bands of molecular hydrogen from equivalent widths measured photoelectrically

06 p0962 A69-17818

Competition effects between rotational levels of carbon dioxide rotation-vibration band in traveling and standing wave lasers [IEEE PAPER G-6]

07 p1151 A69-19055

Single mode carbon dioxide laser Lamb dip and vibration rotation lines absorption coefficients [IEEE PAPER P-6]

07 p1153 A69-19075

Franck-Condon factors for high rotational levels of nitrogen calculated in Morse potential approximation for application to plasma diagnostics

07 p1185 A69-19169

Water in interstellar regions detected by microwave emission from 6 sub 16 to 5 sub 23 rotational transition

08 p1383 A69-19896

Optical potentials for rotational and vibrational transitions in inelastic molecular collisions, considering adiabatic and sudden approximations

08 p1358 A69-21008

Emission-absorption intensity ratio temperature measurements of diatomic molecules under thermal nonequilibrium conditions, considering rotational population distribution during vibration temperature measurement

09 p1623 A69-22255

Hydroxyl luminescence spectrographic observations at twilight in vibrational-rotational band from 10600 to 11200 A

10 p1681 A69-22847

Carbon dioxide laser upper level rotational relaxation rate constant measurement, observing CW gain

10 p1701 A69-22948

Direct nonresonance excitation of rotational and vibrational states of diatomic molecular ions by electrons in Born-Coulomb approximation

10 p1726 A69-23627

Vertical atmospheric absorption of radio waves by water vapor and oxygen molecules near rotational resonance based on radio emission measurements

10 p1658 A69-23944

Barrier to internal rotation from PMR spectrum for 1, 2-disubstituted ethanes, studying vicinal coupling parameters dependence

12 p2132 A69-25987

Carbon dioxide rotational constants from CW beat measurement in bulk GaAs mixer between carbon dioxide vibrational-rotational laser lines

12 p2105 A69-26311

Relative intensities of lines in vibration and rotation bands of isotopic carbon dioxide in planet Venus, tabulating partition functions

15 p2656 A69-31154

Photoinduced shock processes involving metastable hydrogen atoms and molecules, discussing vibrational and rotational levels

16 p2813 A69-31754

Lambda doublet maser emission from excited OH rotational level, discussing conditions necessary for microwave radiation

18 p3185 A69-34292

Molecular N rotational temperature effect on rare gases scattering cross section

19 p3377 A69-36184

Central tuning dip on rotation-vibration transitions of nitrous oxide and carbon dioxide laser with nitrogen, noting frequency discriminator generation

19 p3339 A69-36698

Ammonium perchlorate experimental heat capacity data significance for rotational freedom of ammonium ion

20 p3484 A69-37344

Rotational analysis of O_2/O_2 band of gamma-prime system of TiO molecule, considering transition to ground state

20 p3577 A69-38170

Coupled equations for determining cross sections for rotational transitions in CN induced by low energy electron impact

21 p3773 A69-38476

Upper atmospheric temperature by spectroscopy, considering rotational, OH nightglow, nitrogen cation dayglow and twilight temperatures

21 p3712 A69-38516

Ammonia inversion radiation in Sgr B2 region, observing distribution of density, velocity and rotational excitation

21 p3799 A69-38647

Diatomic molecules rotational excitation calculated from electron molecule elastic scattering parameters in fixed nuclei approximation

21 p3775 A69-39665

Molecular collision pumping mechanism for anomalous microwave absorption by formaldehyde rotational transition in Galaxy dust cloud

22 p4029 A69-40768

Rotational spectra of methylchlorodiazirine at room and dry ice temperature, using K band and Stark effect spectrometers

23 p4194 A69-42207

Order-disorder transitions in solid hydrogen, discussing model to explain molecular rotation angular momentum operator fluctuations

24 p4350 A69-43119

Raman scattering during external and internal motion of oxygen molecules condensed phases, observing

gamma and liquid phase bandwidths during stretching vibrations

24 p4353 A69-43808

Rotational microwave spectrum of 2-methylfuran, using fourth order perturbation method for internal rotation A-E doublet splittings

24 p4280 A69-43811

MOLECULAR SPECTRA

NT ELECTRONIC SPECTRA

NT RAMAN SPECTRA

NT VIBRATIONAL SPECTRA

Methane IR absorption band centered near wavenumber 9050, noting R branch features and fine structure

01 p0023 A69-10289

Carbon dioxide spectral line broadening and self broadening coefficients, using carbon dioxide laser radiant energy

01 p0091 A69-10844

Microwave and far IR molecular rotational absorption spectra investigated for measuring concentrations of reacting molecular and atomic species in hypersonic projectile wakes

01 p0006 A69-10961

Absorption coefficients of molecular oxygen at Lyman alpha line and vicinity measured by vacuum spectroscopy

01 p0076 A69-11230

High resolution spectroscopic study of stimulated rotational transitions of nitrogen molecules using crossed grating Echelle spectrograph

02 p0284 A69-12621

Electronic transition moment for C /Swan/ bands measured in shock tube in carbon dioxide and argon mixtures

02 p0285 A69-12833

Molecular O 0.7620 micron absorption band in pure O and air, noting rotational lines mean half width and lower atmosphere transmission function

03 p0458 A69-13272

Benzene anion radical in solid solution ESR spectrum, noting removal of orbital degeneracy at 4.2 degrees K

03 p0382 A69-13379

Spectra of hydrides of Mg 25 and Mg 26 in photosphere, searching for weak lines on basis of isotope shifts

03 p0515 A69-14035

Night airglow spectrum between four and four microns, noting sequence of hydroxyl bands

03 p0426 A69-14251

Protostars as sources of anomalous OH emission, discussing densities, masses and temperatures of OH condensations

04 p0661 A69-15143

Far IR observations of atmospheric molecular lines, using high altitude aircraft platforms

04 p0628 A69-15146

Nanosecond range flash photolysis technique and application to absorption spectra of excited singlet states

05 p0760 A69-15608

Hydrogen, helium and electron flux measurements by differential detectors at Fort Churchill in 1967

05 p0756 A69-16277

Stellar element abundance ratios determination using relative strengths of molecular lines or bands

06 p1003 A69-17320

Absorption oscillator strengths for rotational lines in Lyman transition vibrational bands of molecular hydrogen from equivalent widths measured photoelectrically

06 p0962 A69-17818

Shock tube study of ammonia oxidation at high temperature, detecting molecular species in reaction zone by IR emission

06 p0885 A69-17936

Water in interstellar regions detected by microwave emission from 6 sub 16 to 5 sub 23 rotational transition

08 p1383 A69-19896

IR zero one band of molecular O observed in day airglow with ground based scanning grating spectrometer

08 p1306 A69-20096

Radio wavelength range observations of NO molecule lines in interstellar space

09 p1590 A69-21377

Luminescence spectra of molecular gases excited by fast electrons in infrared spectral region, noting H alpha line

09 p1590 A69-21382

Molecular line intensity requirement in line of sight for detecting interstellar water vapor cloud, assuming transparent atmosphere and ideal radio telescope

09 p1591 A69-21446

Cometary magnetic fields by measuring depolarization of molecular resonance fluorescence

09 p1603 A69-22234

Emission-absorption intensity ratio temperature measurements of diatomic molecules under thermal nonequilibrium conditions, considering rotational population distribution during vibration temperature measurement

09 p1623 A69-22255

Relative band intensities of atmospheric and IR atmospheric systems of molecular oxygen compared with Franck-Condon factor calculations

10 p1681 A69-23163

Barrier to internal rotation from PMR spectrum for 1, 2-disubstituted ethanes, studying vicinal coupling parameters dependence

12 p2132 A69-25987

IR spectroscopic observations of moon to interpret molecular vibration spectra in terms of molecular composition, discussing rock surface roughness effects

13 p2341 A69-27582

Molecular O 0.7620 micron absorption band in pure O and air, noting rotational lines mean half width and lower atmosphere transmission function

14 p2487 A69-28780

Excited cyanide molecules concentration in arc discharge determined from spectral bands absolute intensities during electron transition

15 p2654 A69-30080

Molecular benzene emission spectra excited by electron beams in RF modulated source, tabulating lifetime measurements

15 p2562 A69-30468

Cyanogen molecules increase attributed to nova shell compression from analyzing absorption spectrum of DQ Herculis 1934 after brightness maximum

15 p2688 A69-30558

Transition probabilities for radiative lifetime of Swan and Mulliken diatomic C bands calculated from lifetime data using Franck-Condon factors

15 p2694 A69-30789

Pressure and wavelength dependence of molecular O absorption coefficient near 1215 A, utilizing UV emission from crossed beam atomic collision

15 p2656 A69-31031

Franck-Condon factors for band systems of molecular hydrogen, computing wave functions for vibrational levels using potential energy function, Part I

15 p2656 A69-31156

Cross sections threshold behavior for Cs II resonance lines excitation due to Cs ion-H collision

17 p3008 A69-33388

Radio wavelength range observations of NO molecule lines in interstellar space

18 p3198 A69-34765

Luminescence spectra of molecular gases excited by fast electrons in IR spectral region, noting H alpha line

18 p3176 A69-34770

Computer program to predict spectra from electronic transitions of diatomic molecules and atoms, noting line intensity distribution by Voigt profile

18 p3177 A69-35239

Forbidden atomic transitions involving metastable species in upper atmosphere, tabulating permitted and forbidden molecular band systems

19 p3421 A69-36214

Rotational analysis of /O,O/ band of gamma-prime system of TiO molecule, considering transition to ground state

20 p3577 A69-38170

Franck-Condon factors for band systems of molecular hydrogen, computing wave functions for each electronic state by numerical solutions of radial Schroedinger equation

21 p3774 A69-38758

IR molecular radiation spectra of upper atmosphere in 3-8 micron range investigated by rockets and satellites, discussing radiation energy density during magnetic storms

21 p3792 A69-39772

Absorption spectrum of NO molecule, analyzing f complexes electron structure, ionization potential and quadrupole moment

22 p3984 A69-40477

Hydrogen fluoride chemical laser emission spectrum, studying rotational-vibrational transition of molecules triggered optically or electrically

23 p4172 A69-41493

Rotational spectra of methylchlorodiazirine at room and dry ice temperature, using K band and Stark effect spectrometers

23 p4194 A69-42207

MOLECULAR SPECTROSCOPY

Fluorescence spectroscopy of proteins, analyzing polarity, distances between groups, flexibility and conformational transitions

01 p0023 A69-10291

Far IR and Raman spectra of ethylene carbonate, gamma butyrolactone and cyclopentanone, noting consistency with hindered pseudorotation

02 p0206 A69-12723

Atomic physics of lasers and active materials, noting multiplet spectra of atoms, molecular spectroscopy, energy level population distribution and amplification

06 p0937 A69-18004

Hydrogen molecule spectroscopy in vicinity of ionization limit, determining absorption and ionization cross sections and fluorescence

07 p1184 A69-18490

Speed distribution and density of molecular beam from time domain measurements of propagated beam perturbations, discussing gate functions

10 p1652 A69-23340

MOLECULAR STRUCTURE

Sliding surface tracks from hardened steel sliders on flat PTFE examined for molecular orientation with electron microscope

01 p0085 A69-10369

Crystal and molecular structure of mu-oxo-bis(chlorobis/2, 4-pentanedionato/titanium/IV/-chloroform solved by symbolic sign determination method and Patterson map interpretation

01 p0023 A69-10411

Perhydroxyl radical electron spin resonance spectrum in solution of hydrogen peroxide and water at 77 K, noting g factor, hyperfine splitting and molecular structure

01 p0024 A69-10683

Europium complexes high resolution emission spectra in relation to molecular configuration

01 p0024 A69-10893

Automatic heteroatomic plotting of high resolution mass spectral data, presenting relative intensity vs elemental composition in bar form

01 p0024 A69-10905

Radiation structural and transcription damage to deoxyribonucleic acid /DNA/, noting postirradiation repair on molecular level

03 p0372 A69-13489

Mechanical anisotropy of polyethylene terephthalate and relation to molecular structure and cold drawing

05 p0785 A69-16489

Rotational spectrum of ethylene episulfide to determine molecular structure, particularly orientation of C sub 2 S ring

08 p1268 A69-20535

Network rupture hypothesis and molecular structure considerations used in obtaining constitutive equations for flow of polymer melts and solutions

10 p1800 A69-23369

Monograph on molecular structure and polymer properties, covering coherent adhesive layer of polymeric material for paint film in protective coatings

10 p1717 A69-24187

Order-disorder in alloys with several phase transition temperatures, discussing crystal lattices, interstitial alloys, atomic and magnetic ordering

11 p1936 A69-24702

Thermally stable polymers for high stress aerospace applications, noting chemical stability and structure of high polymers

12 p2117 A69-25853

Water vapor laser, discussing water vapor molecular structure, population inversion mechanism, perturbation model, etc

12 p2106 A69-26325

Synthesis of N-/trimethylsilylalkyl/ diamines and N-/trimethylsilylalkyl/-N-/2-mercaptoethyl/ diamines, determining structure by IR spectra

15 p2561 A69-30414

Constitutive equation variation effect on near wall flow pattern of dilute polymer solutions

17 p2951 A69-33257

Molecular structure and uses of heat resistant plastics, discussing aromatic polyamides

18 p3161 A69-34279

Polymer molecular structure influence on physical and mechanical properties, considering regularity, chain flexibility, crosslinking and intermolecular forces

18 p3099 A69-34606

Spherulite boundaries and interspherulite breakdown in polyethylene, considering structure control by varying macromolecular microstructure

22 p3973 A69-40740

DNA polymerase from *Escherichia coli*, discussing physical and chemical properties of enzyme and polypeptide chain consistency

22 p3898 A69-41070

MOLECULAR THEORY

Franck-Condon factors in radiative, excitation and ionization molecular transitions of oxygen, carbon monoxide, nitric oxide, etc

05 p0795 A69-15664

Molecular radiobiology, discussing physicochemical processes caused by energy absorption in targets, leading to inactivation under various circumambient conditions

23 p4090 A69-41963

MOLECULAR WEIGHT

High speed automatic osmometer applied to measurements of diffusible branched polyethylene samples, discussing apparent molecular weight observations

01 p0024 A69-10933

Low temperature effects on calf thymus deoxynucleoprotein, crystalline egg albumin and fibrillar actin, noting molecular weight and viscosity changes

01 p0018 A69-11089

Structure and mean molecular weight measurement of unknown atmosphere assessed from high altitude tests in earth atmosphere

[AIAA PAPER 68-1054] 03 p0512 A69-13699

Ultrahigh molecular weight polyethylene terephthalate synthesis from commercial solid state materials, noting effects of several parameters

05 p0797 A69-16496

Injectant stagnation temperature and molecular weight variation effect on flow field generated from secondary injection into supersonic stream

[AIAA PAPER 69-1] 06 p1039 A69-18196

Crack propagation in crosslinked glassy polymers, noting effects of added elastomers molecular weight

08 p1338 A69-20492

Temperature gradient in semiconvective region, examining molecular weight distribution in mixing due to overstability

09 p1596 A69-22057

Two temperature gasdynamics for binary gas mixtures of differing molecular weight components, analyzing ultrasound and shock wave propagation

13 p2250 A69-28447

Molecular engineering of high organic polymers, discussing molecular weight, crystallization, elastomers, fiber formers and building construction materials

20 p3566 A69-37598

Hemoglobin O reaction model explaining molecular weight and oxygen dissociation curve dependence on hemoglobin concentration

23 p4097 A69-42097

MOLECULES

- U DIATOMIC MOLECULES
- U MONATOMIC MOLECULES
- U POLYATOMIC MOLECULES
- U TRIATOMIC MOLECULES

MOLIERE FORMULA

- U COSMIC RAY SHOWERS
- U SECONDARY COSMIC RAYS
- U SPATIAL DISTRIBUTION

MOLNIYA SATELLITES

Communication satellites development in U.S.S.R., discussing Molniya 1 satellite design and objectives and Echo 2 satellite transmission experiments

01 p0032 A69-10949

Molniya 1 communication satellite using elliptical orbit to provide radio, telephone and TV service

[UN PAPER 68-95771] 06 p1013 A69-17044

MOLTEN SALT ELECTROLYTES

Electrolytic deposits of titanium, vanadium and alloys from molten salts, discussing formation conditions, velocity and properties

03 p0446 A69-13574

Secondary cells with liquid lithium anodes and immobilized fused salt electrolytes

04 p0552 A69-15330

Dual gas reference electrode system for molten carbonate cells with immobilized electrolyte

05 p0706 A69-16237

MOLTEN SALT NUCLEAR REACTORS

Shock tunnel hypersonic flow effect on critical Weber number for zirconium drop breakup in partially and fully molten states

12 p2063 A69-26802

MOLYBDENUM

Interstitial impurity effects on mechanical properties of molybdenum single crystals, considering temperature dependence of flow stress in bcc metals

01 p0095 A69-10609

Silicide coatings effect on Mo mechanical properties subjected to tensile tests in vacuum and air at various temperatures

02 p0264 A69-11883

Sintered molybdenum deoxidation effect with C, B and Si, analyzing hardness, tensile strength and ductility

02 p0265 A69-12002

Formation energy of heat vacancies in molybdenum and temperature dependence of concentration determined on basis of enthalpy data

02 p0266 A69-12184

Heat of solution and diffusivity of nitrogen in molybdenum analyzed by quenching technique and resistivity measurements at liquid helium temperature

02 p0267 A69-12188

Hydroextrusion effect on Mo structure and mechanical properties, noting improved ductility after high temperature annealing

02 p0267 A69-12189

Molybdenum elasticity limit and rupturing stress dependence on structure for high temperature annealing, noting changes in solid solution interstitial impurity concentration

02 p0268 A69-12191

Molybdenum interband transitions noting low energy optical property anomalies and origin of two absorption bands

03 p0442 A69-12986

Temperature dependence of internal friction in molybdenum wire in moderate and high temperatures

03 p0446 A69-13576

Internal friction temperature effects on amplitude dependence in niobium and molybdenum

04 p0614 A69-14635

Structural changes and cold shortness of molybdenum in deformation

04 p0615 A69-14637

Complex form internal friction maximum composed of interstitial atoms in molybdenum solid solution

04 p0615 A69-14640

Cobalt concentration reduction in maraging steels by Cr replacement and increased Mo and Ti additions

04 p0616 A69-14649

Carburization structure on surface of Mo and Nb castings cast in graphite molds showing changes in plastic properties of metals

04 p0619 A69-15391

Microplastic properties of arc-cast and Ti-Zr-Mo molybdenum sheet in tension at room temperature, measuring plastic strains with resistance strain gages

05 p0778 A69-15759

Si diffusion rate in single crystal and polycrystalline Mo, using various donor materials

05 p0780 A69-15990

Pitting corrosion resistance improvement in austenitic stainless steels with added molybdenum through electroslog resmelting

05 p0781 A69-16499

Molybdenum disilicide allotropy influence on coating growth rate and morphology

[ONERA-TP-642] 08 p1335 A69-19967

Time and temperature dependence of Mo and W deformation structure variation and primary recrystallization from metallographic investigations using electron microscopy

08 p1334 A69-21058

Effective work function of Re and Mo electrode samples determined from Schottky plots and emission measurements from grains

09 p1557 A69-21807

Metal composites of Ni or Mo fibers in Be matrix, discussing chemical compatibility in terms of reactions, solid solubility and diffusion at various temperatures

10 p1707 A69-22991

Impurities effect on plastic flow stress and activation volume as functions of strain, strain rate and temperature in molybdenum crystals

10 p1710 A69-23089

Molybdenum fiber sintering activation by adding nickel, noting decrease in impact viscosity

10 p1711 A69-23336

Recrystallization diagrams of commercially pure Mo and Mo alloyed with Fe, Co or Fe plus Ni, noting additions effect on recrystallized grain size

10 p1715 A69-24012

Acicular crystals growth and dendrites orientation in Mo ingots prepared by electron beam and arc melting analyzed by X rays

11 p1903 A69-24538

Molybdenum additive role in deformed carbonylic nickel recrystallization process

12 p2114 A69-26454

Surface free energy of solid Mo measured by Udin zero-creep method at high temperatures, noting low value due to residual impurity adsorption

12 p2117 A69-27137

Molybdenum dislocation velocity and macrodeformation, noting thermal double kink mechanism inconsistencies and strain rate relationship

13 p2276 A69-27392

Sensitivity decrease of reversible temper brittleness of low alloy steels due to Mo inhibiting effect on phosphorus diffusion

13 p2283 A69-28491

Micrographic reagent coloring grains of Mo in relation to crystalline orientation applied to refractory metal welding and diffusion studies

14 p2505 A69-29221

Alkaline metal adsorption on high work function metals with charge transfer, measuring polycrystalline Mo photoelectric emission as function of Cs coverage

14 p2507 A69-29275

Electron work function profile determined for polycrystalline Mo and W single crystals with and without Cs vapors by emission microscope and photomultiplier

14 p2507 A69-29276

Vacuum thermal decomposition of molybdenum sesquisulfide into metallic Mo, discussing reaction kinetics, mass transfer, diffusivity of sulfur gas, etc

14 p2467 A69-29287

Strain rate and temperature effects on sintered molybdenum sheets strength and elongation characteristics

14 p2464 A69-29322

Double notch creep rupture tests of Cr-Mo steels, investigating changes in notch profile, dimensions and structure

[ASME PAPER 68-WA/MET-7] 14 p2464 A69-29441

Cold worked high purity Mo wire recovery after plastic deformation at room temperature, considering electrical resistivity decrease as function of annealing temperature

15 p2636 A69-30082

Hydroextrusion influence on mechanical properties of powder compacts of sintered Mo rods

16 p2803 A69-32491

Oxygen adsorption on Mo single crystals /100/ surface as function of temperature using low energy electron diffraction

16 p2748 A69-32795

German monograph on yttrium addition effects on tension and compression behavior of Nb and Mo at high temperature in vacuum

17 p2990 A69-33570

Molybdenum coatings electrodeposition from fused salt system

18 p3156 A69-35001

Carburization structure on surface of Mo and Nb castings cast in graphite molds showing changes in plastic properties of metals

18 p3156 A69-35019

Silicide coatings effect on Mo mechanical properties subjected to tensile tests in vacuum and air at various temperatures

18 p3156 A69-35043

Secondary recrystallization in cold rolled molybdenum foil as function of temperature using electron microscopy and diffraction

18 p3157 A69-35253

Diffusion saturation of Mo and Mo alloys by nitrogen in ammonia with formation of nitride films, noting surface hardness

18 p3158 A69-35288

Molybdenum single crystals deformation in direct shear, determining stress temperature dependence and critical regions for various slip systems

19 p3342 A69-35811

Diffusion during high temperature exposure of protective coatings on Mo, noting compact layers and carbide forming elements effect on thermal stability

19 p3345 A69-36156

Boron thermal diffusion effects on plastic properties of pure Mo subjected to recrystallization

19 p3328 A69-36160

Wear and friction of fiber-metal Mo bodies impregnated with molybdenum disulfide, noting coating-endurance life

20 p3547 A69-36953

Negative electric potential effect on deposition rate of Mo from molybdenum carbonyl and on deposit chemical composition during pyrolysis

20 p3559 A69-37016

- Temperature effect on grain size, crystal orientation, microhardness and heat resistance of diffusion Si coatings on Mo
20 p3560 A69-37361
- C and O atoms chemisorption on Mo surface demonstrated by surface striation
20 p3562 A69-37782
- Structural changes during annealing of W and Mo single crystals deformed by rolling, using X ray diffraction topography methods with two crystal spectrometer
21 p3742 A69-38583
- Grain boundary grooving kinetics for Cr, W and Mo in Ar and vacuum, determining interface free energies and surface self diffusion coefficients
21 p3744 A69-38740
- Abnormal grain growth during secondary recrystallization of hydraulically extruded molybdenum as function of annealing
21 p3745 A69-38953
- Dislocations multiplication and rearrangement structure in thermal fatigue of Mo single crystals produced by electron beam zone melting
21 p3746 A69-39162
- Structural changes in Mo single crystal under action of laser radiation of various power densities
21 p3750 A69-39842
- Electron spin resonance /ESR/ of polycrystalline Mo/V/ complexes with dipyrityl and phenanthroline, observing hyperfine interaction due to odd numbered isotopes
22 p3897 A69-40971
- High temperature anelastic effect in Mo single crystals ascribed to internal friction peak due to electronic interactions between dislocations and C interstitials
24 p4332 A69-43031
- MOLYBDENUM ALLOYS**
- Nitriding effect on heat resistance and transition temperature of molybdenum alloys
01 p0093 A69-10212
- Zirconium corner of Zr-Mo-Ni phase diagram using metallographic analysis, hardness and microhardness methods, constructing isothermal sections for high temperatures
02 p0264 A69-11855
- Zirconium corner of Zr-Nb-Mo system phase diagram, using microstructure, microhardness, hardness and radiographic methods
02 p0264 A69-11856
- Adiabatic elastic constants of molybdenum-rich rhenium alloys, studying concentration effects on bulk modulus, Debye temperatures and interatomic forces
04 p0613 A69-14455
- Martensitic transformation in Ti-Al-Mo alloys, noting specific features and effects of Mo content
04 p0617 A69-14940
- Phase equilibria, phase transformation temperatures and relation between resistivity and chemical composition for alloys of Ti-Al-Mo-Zr system
04 p0618 A69-15079
- Quasi-ternary titanium dichromide-V-Mo system composition at high temperatures, physical properties and phase diagrams
04 p0618 A69-15080
- Be, Ce, V and Ti additions effect on oxidizability of cast, forged and cold worked Nb-Cr-Mo alloys
04 p0618 A69-15081
- Microplastic properties of arc-cast and Ti-Zr- Mo molybdenum sheet in tension at room temperature, measuring plastic strains with resistance strain gages
05 p0778 A69-15759
- Long term creep behavior of nickel-chromium-molybdenum alloy, noting temperature effect on grain boundaries
05 p0781 A69-16500
- Transition temperature from brittle to plastic state of W-Mo alloys in recrystallized state, noting increased Mo content effect
05 p0783 A69-16809
- Isochronic annealing effect on coercive force of Mo Permalloy samples bombarded with neutrons in nuclear reactor
05 p0783 A69-16815
- Creep of high purity Nb-Mo alloys in 800-1300 C range and at 1500-13000 lb/square inch stresses, giving activation energy for creep
10 p1711 A69-23375
- Recrystallization diagrams of commercially pure Mo and Mo alloyed with Fe, Co or Fe plus Ni, noting additions effect on recrystallized grain size
10 p1715 A69-24012
- Plasticity increase of molybdenum alloys during precipitation of second phase at high temperatures due to lattice defects redistribution and plastic deformation
11 p1906 A69-25685
- Heat treatment effects on molybdenum-rhenium alloy field emission and surface structure in alpha and sigma phase regions
12 p2113 A69-26041
- Intermetallic compound precipitation effects on mechanical properties of Fe-Mo alloy at high temperatures
12 p2116 A69-26925
- W, Mo and heat treatment effects on phase composition and heat resistance of ferrite and austenitic steels
13 p2283 A69-28487
- Temperature dependent aging mechanisms in deformed Mo alloys during annealing, using transmission electron microscope
14 p2463 A69-29312
- Electrodeposits on molybdenum alloys in high temperature oxidizing environments, noting performance of Cr-Ni-Cr composite coating
14 p2466 A69-29934
- Ion nitride hardening of Mo-Ti alloy at 1300 degrees C in cathode glow discharge tube
15 p2637 A69-30212
- Nitriding effect on heat resistance and transition temperature of molybdenum alloys
15 p2637 A69-30268
- Sintered mixtures of Ni-Mo powder noting electrical resistance, alloy and shear strength and impact viscosity
15 p2638 A69-30280
- In-process annealing and warm working temperature effects on long time creep rupture properties of Mo alloys tested in vacuum furnace
17 p2987 A69-33076
- Optical constants of Ta-W and Nb-Mo measured in IR and visible ranges as function of incandescent temperatures
17 p2990 A69-33574
- Carbide phase growth rate in Mo-TZC alloy with particle size distribution maintained over time-temperature spectrum, noting diffusion and interface controlled processes
18 p3155 A69-34632
- Hydraulically extruded Mo properties after annealing, showing reduction in stability and hardness and varying nature of change in plasticity
18 p3156 A69-34719
- Diffusion saturation of Mo and Mo alloys by nitrogen in ammonia with formation of nitride films, noting surface hardness
18 p3158 A69-35288
- Metal purity effect of nickel and Ni-Mo alloy on nucleation and recrystallization nuclei growth following 80 percent plastic deformation
18 p3159 A69-35449
- Silicide and B-modified coatings on Mo, noting improved high temperature oxidation resistance under thermocycling
22 p3957 A69-40972
- Ce, Zr, Nb and B effect on heat resistance and structure of low alloy CrMoWV steels /type CSN 41 5335/
22 p3972 A69-41079
- MOLYBDENUM CARBIDES**
- Surface precipitation of carbides in solution treated and cooled molybdenum and tungsten
03 p0451 A69-14000
- Group 4A carbides and nitrides formation in Mo by arc melting, determining threshold solute metal-interstitial atom ratios
12 p2117 A69-27136
- Carburizing spherical powders of Nb, Mo and W to obtain carbides, noting agreement between theoretical and experimental data
19 p3345 A69-36162
- MOLYBDENUM COMPOUNDS**
- Thermal decomposition of molybdenum carbonyl, deriving general equations, noting agreement with experimental data
20 p3558 A69-37015
- Negative electric potential effect on deposition rate of Mo from molybdenum carbonyl and on deposit chemical composition during pyrolysis
20 p3559 A69-37016
- Molybdenum disilicide oxidation kinetics at various temperatures by thermal conductivity method, determining oxidation rates and activation energy
20 p3567 A69-37780
- MOLYBDENUM DISULFIDES**
- Physical sputtering deposition of molybdenum disulfide films as solid lubricant on rotating and sliding components, discussing lubrication properties in vacuum [ASLE PAPER 68-LC-15]
07 p1140 A69-19308
- Hot pressed molybdenum disulphide-nickel composite film friction and wear tests in air and face seal configuration [ASLE FICFS PREPRINT 23]
15 p2620 A69-30491
- Microfibrinous boehmite as binder for molybdenum disulfide in formation of ductile wear resistant dry lubricant films [ASLE PAPER 68-LC-14]
15 p2642 A69-30606
- Solid lubricants on molybdenum disulfide base at various temperatures and low pressures, noting film mass losses and possible use with organic materials under high vacuum
16 p2793 A69-31561
- Wear and friction of fiber-metal Mo bodies impregnated with molybdenum disulfide, noting coating-endurance life
20 p3547 A69-36953
- Molybdenum disulfide influence on electrochemical corrosion of metals
21 p3733 A69-39804
- Wear resistance of briquetted lubricants from fluoroplast and molybdenum disulfide under pressure
21 p3733 A69-39805
- Lamellar solids abrasiveness, effects of particle share in graphite and molybdenite samples
22 p3966 A69-39877
- MOLYBDENUM OXIDES**
- Molybdenum oxide crystals growth and microstructure, using X ray and electron diffraction analyses
05 p0779 A69-15831
- Oxidation influence on molybdenum disilicide coatings emissivity, determining degree of blackness over thermal stability range
09 p1522 A69-21588
- MOLYBDENUM SULFIDES**
- Vacuum thermal decomposition of molybdenum sesquisulfide into metallic Mo, discussing reaction kinetics, mass transfer, diffusivity of sulfur gas, etc
14 p2467 A69-29287
- MOMENT DISTRIBUTION**
- Structural analysis by direct moment distribution, Volume 1, covering statistically indeterminate structures formed of prismatic members
01 p0165 A69-10156
- Distribution of moment of first passage through positive level for homogeneous process with independent increments and exponential characteristic function, constructing integral equation
01 p0104 A69-10265
- Moment method used to determine pulsed radiation instability propagating in luminescent scattering medium
04 p0610 A69-14425
- Phase method of photoelectric registration of stellar transition moments
04 p0601 A69-15252
- Moment equations for general gas mixture from Boltzmann-like equations, evaluating collision integrals
04 p0633 A69-15436
- Moment curvature models under reverse cyclic straining developed from stress-strain curves for rectangular beams
04 p0683 A69-15497
- Effect of small periodic moment applied to axis of inner gimbal on gyro drift when gyro is mounted on base fluctuating about two mutually perpendicular axes
06 p0924 A69-17183
- Helicopter instability on ground with propulsion system operating and inoperative, discussing overturning, restoring moments and pilot training
09 p1433 A69-21385
- Optimal additional loading at zero moment stress-strain state in simply connected shell of complex design under external loads, using successive approximation
12 p2181 A69-26610
- Motion of slender axisymmetric bodies in rotating fluid, relating Long hypotheses to flow reversal and dipole distribution effects on lee waves
13 p2248 A69-28170
- Boundary layer equation of viscous incompressible fluid with moment stresses, noting flow around thin plate and submerged jet problems
14 p2428 A69-28815
- Distribution of moment of first passage through positive level for homogeneous process with independent increments and exponential characteristic function, constructing integral equation
19 p3360 A69-36200
- Circular cylindrical freely supported shell moment state stability, solving critical parameters by infinite matrix eigenvalues determination
21 p3835 A69-38724
- Control function ensuring minimal response time of controlled plant with motion described by integral equations system, using method of distributed moments
21 p3685 A69-38847

Dynamic behavior of infinitely long cylindrical shells of ideally rigid plastic materials strengthened with ring ribs, determining distribution of moments and displacements

21 p3837 A69-39156

MOMENTS

NT BENDING MOMENTS
NT DIPOLE MOMENTS
NT DISTRIBUTION MOMENTS
NT ELECTRIC MOMENTS
NT LOADING MOMENTS
NT MAGNETIC MOMENTS
NT MEAN
NT PITCHING MOMENTS
NT ROLLING MOMENTS
NT STABILITY DERIVATIVES
NT STANDARD DEVIATION
NT TORQUE
NT VARIANCE [STATISTICS]

Aerodynamic lift and moment fluctuations of sphere at supercritical Reynolds numbers measured by hot-wire anemometers, noting dependence on time

14 p2390 A69-29573

Moment and discrete ordinate methods in radiative transfer problems in planar, radiating and nonscattering media, noting conical transformation of moment equations

18 p3174 A69-35237

MOMENTS OF INERTIA

Large mass concentrations / mascons / effect on moon dynamical figure, considering production of asymmetries

05 p0820 A69-15762

Integrability of equations of motion of gyrostat about fixed point inertial moments varying identically in time

05 p0764 A69-16504

Nutational stability of multibody spin stabilized satellites, discussing moment of inertia ratios role with energy dissipative damper on despun platform

06 p1015 A69-17585

Mass distribution and inertia characteristics influence on spin susceptibility and spin recovery characteristics for eight current fighter aircraft

[AIAA PAPER 69-188] 06 p0868 A69-18057

Circular cylindrical spinning shells vibrations by gyroscopically induced inertia loads, formulating equations of motion based on shallow shell theory

07 p1236 A69-19459

Ground and air resonance measured with gimbaled whirl tower stand for soft inplane matched stiffness rotor, discussing body inertia and speed limits

[AIAA PAPER 69-205] 07 p1055 A69-19559

Rotatory inertia and shear deformation effects on natural frequency and bending mode shape in equations of motion of rotating turbomachine blade

[ASME PAPER 69-VIBR-50] 10 p1804 A69-24148

Numerical method for coupled moments of inertia and integral equations of boundary value problems for fluid in moving cavities

11 p1868 A69-24774

Inplane and rotary inertia effects on free vibration frequencies of circular cylindrical shells eccentrically stiffened by orthogonal set of stringers and/or rings

11 p1992 A69-25520

Magnetic desaturation of inertia flywheels of satellite in equatorial or slightly inclined orbit, discussing satellite stabilization

13 p2357 A69-28476

Natural oscillation frequency of gyrocompass mounted in torsional suspension, taking into account moments of inertia of sensitive element

16 p2791 A69-32282

Transverse shear deformation and rotatory inertia effects on large amplitude lateral free vibrations of transversely isotropic plates

[ASME PAPER 69-APM-10] 18 p3213 A69-34386

Pulsar PSR 0833-45 period decrease resulting from mass addition leading to radius and inertia moment decreases

18 p3196 A69-34646

Calculator for obtaining moments of inertia data to determine control power for vehicle orientation and to avoid control systems over design

[SAWE PAPER 792] 18 p3118 A69-34865

Moment of inertia measurements facility for spacecraft dynamic balancing operations at low angular rates

[SAWE PAPER 739] 18 p3118 A69-34889

Triaxial static gyro stabilizer drifts, assuming perturbing moment steady centered random force applied along stabilizing gimbal axis

19 p3311 A69-36195

Slow rotation of relativistic polytropes with linear corrections, showing inertia moment distribution and metric component

19 p3426 A69-36576

Inertial motion of body produced by revolving uniformly deformed configuration, showing constant semiaxes without kinetic energy losses

21 p3772 A69-39620

Normal frequencies, force constants and moment of inertia of carbon dioxide isotope molecules from spectroscopic data, calculating atmospheric transmission of carbon dioxide laser radiation

21 p3742 A69-39780

Spherical motion of solid body about fixed point with nonholonomic coupling, deriving equations for centrifugal moments of inertia effects on motion

21 p3773 A69-39840

Moments of inertia and gravity field of moon, noting application to earth tides

22 p4030 A69-40902

Gyroscopic motion with center of mass displaced along suspension axes and kinetic moment varying as power law under linear accelerations

23 p4163 A69-41552

MOMENTUM

NT ANGULAR MOMENTUM

S matrix theory without restriction to asymptotic particle momentum measurements, introducing main nondynamical features

03 p0467 A69-13754

Cosmic ray magnetic spectrograph for measurement of momentum spectrum, charge ratio and specific ionization of muons, discussing magnetic and scattering displacement

06 p0925 A69-17302

Equations for gradually changing motion by differentiating momentum and energy equations with respect to abscissa noting wall resistance, viscosity, turbulence and Coriolis coefficients

15 p2593 A69-31489

Accelerated boundary layers classified in terms of integral balance of pressure, inertia, wall friction forces and entrainment momenta

[AIAA PAPER 69-666] 17 p2955 A69-33462

Momentum control system for satellite maneuvering and pointing in pitch and roll developed by modifying existing libration damping gyrostabilizer

18 p3207 A69-34684

Transverse momentum of fireball particles emitted in high energy inelastic collision related to emission angle and energy in accelerators

19 p3396 A69-36644

Gas flow past bodies, deriving solution method without partial differential equations for flows with momentum potential

24 p4244 A69-43071

MOMENTUM ENERGY

U KINETIC ENERGY

MOMENTUM PRECESSION

U PRECESSION

MOMENTUM THEORY

Representation for real functions of quantum mechanical momentum operator obtained by functional integration in phase space

01 p0106 A69-10930

Continuity and momentum equations for cosmic ray gas particles in interplanetary region

06 p0992 A69-17379

Computer programmed momentum theory for induced flow field of helicopter rotor in forward flight

[AIAA PAPER 69-224] 07 p1052 A69-19562

Photon momentum distribution role and relation to thermal radiation spectrum in fully ionized gases

08 p1357 A69-20747

Semiempirical parameters in streamline division and momentum integral analyses for separated flows, using error function velocity profile and spreading parameter sigma

14 p2389 A69-29028

Coupled equations for heavy particle motion expressed by introducing generalized matrix operator for effective momentum in atomic collision problems

14 p2489 A69-29997

Numerical estimates of momentum integral error in applying locally similar solutions to nonsimilar problems, assuming two dimensional or axisymmetric flow

16 p2772 A69-32174

Rotor static performance calculation with near wake interference effects on rotor inflow distribution, considering strip momentum theory

18 p3088 A69-35221

MOMENTUM TRANSFER

Relationships derived by dimensional arguments connecting vertical heat fluxes and horizontal momentum in constant flux layer with other relevant variables

02 p0275 A69-12692

Confined jet mixing region at entrance of tubular reactor, discussing mass and momentum transfer, chemical conversion and effect of Reynolds number

[AIChE PAPER 25A] 04 p0586 A69-14508

Laminar flow stability parameter presenting coupling ratio between angular momentum change and loss rate by frictional drag

05 p0750 A69-16187

Simultaneous solution of time-dependent momentum and continuity equations for ions and neutral air in midlatitude F2 region conditions

07 p1123 A69-18818

Interhemispheric transfer of atmospheric angular momentum, noting hemispheric angular momentum contents and annual variations

07 p1127 A69-19258

Bounds on mass and momentum transport by turbulent flow between parallel plates derived for Couette and Poiseuille flows

08 p1305 A69-20840

Momentum and energy transfers analogy in turbulent convection fluid flow emphasizing difficulties in case of liquid metals

09 p1480 A69-21687

Zonal momentum vertical transport due to large scale moving disturbances in westerlies of equatorial lower stratosphere

09 p1537 A69-22299

Vibrating momentum exchange device /VMED/ in single axis configuration as competitor for inertia wheel or twin gyro

09 p1538 A69-22435

Control moment gyro /CMG/ and use in space vehicle attitude control system, emphasizing control laws

[AIAA PAPER 67-589] 12 p1219 A69-26777

Wave damping in plasma, developing Boltzmann analysis of electron mode dispersion relations involving momentum transfer and relaxations of electron-ion temperature and anisotropy

13 p2305 A69-27377

Four dimensional momenta transfer during high energy cosmic ray particle collisions, comparing various collision models

13 p2330 A69-28375

Similarity theory similar to Nusselt and Stanton numbers obtained by triple analogy for heat, mass and momentum transfer

13 p2380 A69-28560

Unignited mode converter and emitter work function patches, calculating electron-cesium momentum transfer cross sections from saturation current measurements

14 p2490 A69-29240

Regional distribution of relative angular momentum transport over equator, noting advective and turbulent transfer

16 p2773 A69-31793

Ion momentum transfer through charge exchange in mixture of ion gases and parent neutral gases under thermal nonequilibrium, noting role of Boltzmann equation

16 p2822 A69-32108

Velocity field in turbulent flow based on momentum transfer, determining velocity distribution for flow near solid surface

16 p2772 A69-32128

Monograph on engineering calculations of momentum, heat and mass transfer through laminar boundaries having arbitrary pressure distribution and constant physical properties

16 p2879 A69-32203

Direct wind measurement and momentum transport estimates obtained from cyclones and anticyclones daily displacements over Northern Hemisphere, applying results to planetary atmospheres

16 p2780 A69-32306

Solar wind phenomenon, discussing angular momentum loss to sun, fluctuations at earth orbit and wind conditions at terminus and regions unvisited by spacecraft

17 p3023 A69-33370

Clear air turbulence uninfluenced by mesoscale disturbances or terrain, discussing relationship between density profile curvature and heat and momentum transfer

17 p2998 A69-33733

Lateral mixing of air masses in jet stream by water fluid model experiments, discussing steady and non-steady state turbulent momentum exchange

17 p3000 A69-33759

Tropical circulation long term mean values of wind and temperature fields, momentum and heat fluxes from weather stations data, noting consistent pattern and energy source

18 p3165 A69-34418

Source requirements for cosmic radiation origin model, noting fluctuations in momentum changing process

18 p3188 A69-35005

Airborne astatic vertical gyro motion found dependent on aircraft motion along trajectory

19 p3311 A69-36194

Time scale of diffusion of angular momentum estimated by model for disturbances occurring in star with secularly unstable angular velocity distribution

20 p3605 A69-37826

Electron momentum transfer cross sections by numerically solving electron energy distribution function from Boltzmann equation in Lorentz approximation

21 p3773 A69-38396

Axial and angular momentum flux, flow force and circulation to determine strength and structure of narrow rotating axisymmetric vortex and swirling core flows

24 p4298 A69-42598

Momentum, heat and mass transfer in turbulent channel flow emphasizing phenomena close to wall, using boundary layer growth-breakdown model

24 p4407 A69-42914

Interphase momentum transfer during propagation of infinitesimal pressure pulse through bubbly flow two phase mixture

24 p4409 A69-43511

MONATOMIC GASES

Radiation attenuation cross sections of monatomic and diatomic xenon gas from UV absorption measurements near resonance line

02 p0284 A69-12551

Hydrodynamic theory of light scattering by dilute monatomic gases generalized by using linearized Burnett equations instead of Navier-Stokes equations

03 p0466 A69-13135

Ionizing shock front structure in monatomic gas, considering atom-atom and electron-atom collisional ionization rates

03 p0414 A69-13138

Stagnation point electrostatic probe measurements of flowing partially ionized high density monatomic gases

06 p0964 A69-17196

Shock waves internal structure in perfect monatomic gases, discussing density distribution in shock layer experimental measurement

07 p1120 A69-18930

Collision cross sections between monatomic gas impurities and metastable atoms in He-Ne laser from output curve and impurity partial pressure

08 p1325 A69-20278

Two fluid kinetic model for analyzing shock wave structure in binary mixtures of monatomic inert gases, noting no overshoot in velocity profiles

08 p1304 A69-20813

Hydrodynamic equations and Grad transport coefficients for nonequilibrium rarefied monatomic gases developed for molecular collisions

09 p1481 A69-21888

Shock wave structure determination in simple monatomic gas, using statistical counting and successive approximation algorithm

10 p1680 A69-23894

Kinetic theories applied to shock wave structure study of monatomic gas

11 p1870 A69-25007

Winter polar mesosphere atomic-oxygen distribution by analyzing data concerning intensity and energy of corpuscular fluxes in auroras

12 p2070 A69-26690

Plane shock layer structure in pseudo-Maxwellian monatomic gas, integrating Krook equation for gas molecule velocity

14 p2432 A69-29613

Fluctuation spectra of monatomic gases, using two time probability distributions for distribution function autocorrelations

16 p2817 A69-31669

Fixed mass of monatomic gas unsteady spherically symmetric expansion into vacuum by asymptotic Boltzmann equation expansion

16 p2772 A69-32168

Shock wave structure in single component monatomic gas by expanding Boltzmann equation distribution function in terms of Hermite polynomial

18 p3124 A69-35170

Low density free jet properties, discussing velocity distribution perpendicular to axis and correlation of all terminal parallel Mach numbers for monatomic gases

20 p3514 A69-37206

Rocket probe devices based on thermometrical body principle for measuring upper atmosphere water vapor and atomic oxygen

20 p3543 A69-37798

Diatomic-monatomic oxygen collision cross section determined from rotational line width in diatomic oxygen Schumann-Runge emission spectra

22 p3983 A69-40099

MONATOMIC MOLECULES

Langvin equation for interacting molecule system derived by Fourier transformation of Hamiltonian, noting physical correspondence to equation for shear viscosity in monatomic liquids

16 p2815 A69-32370

MONAURAL SIGNALS

Probability density distributions for monaural detection of tonal signal in continuous background of Gaussian noise as modified noncentral chi distribution

02 p1201 A69-11821

MONITORS

Resistance welding monitoring systems including thermal expansion slow scan ultrasonic and electric energy monitor/limiter systems

02 p0253 A69-11864

Atmospheric temperature and water vapor variations and seasonal environmental changes effects on cosmic ray neutron and meson monitor counting rates

03 p0498 A69-12936

Multiplicity of secondary neutrons counted by IGY neutron monitor detecting cosmic radiation

06 p0925 A69-17297

Rechargeable nickel cadmium batteries state of charge determination by monitoring capacitance

09 p1435 A69-21425

Jet aircraft engines condition monitoring system for detecting malfunctions without engine disassembly [ASME PAPER 69-GT-66]

09 p1501 A69-22518

Telemetry monitor systems for high speed rotating equipment, discussing data recording, transmission, decoding, thin-thick film microtechniques, etc

10 p1692 A69-23249

Monitors to detect incipient failure during turbine engine development, describing servocontrol

10 p1692 A69-23253

Sonic boom simulation methods using shock tube, booth type simulators, ballistic ranges and explosives, discussing unmanned data recorder as monitoring device

15 p2585 A69-30371

On-course monitoring for instrument landing system glide path operating with far field samples

17 p3003 A69-34105

Automatic ultrasonic instrument monitoring on-line welding conditions of RF longitudinally seamwelded tubes

18 p3136 A69-34778

Carrier frequency monitoring amplifier with automatic bridge tuning for coupling to passive sensors including strain gages, inductive transmitters, etc

22 p3915 A69-40937

Thin film bolometer for monitoring RF radiation of arbitrary polarization and direction of propagation

24 p4311 A69-42572

High intensity electromagnetic fields generation equipment for calibrating field intensity monitors, discussing anechoic chamber, transmitting antenna, etc

24 p4312 A69-42577

MONKEYS

Monkey psychomotor reactions during ballistic flight, noting alertness reduction during weightlessness

01 p0017 A69-11082

Acute somatic effects in monkeys irradiated with protons of various discrete energies representing significant portions of space proton spectrum

03 p0374 A69-13497

Biological effects on rhesus monkeys of high energy protons compared to effects of cobalt 60 gamma radiation

03 p0374 A69-13498

Steroid hormones effect on nervous system and behavior from data on gonadectomized rats and monkeys treated with testosterone propionate

03 p0375 A69-13551

Macaque monkey behavior after injection of monomethylhydrazine with and without pyridoxine HCl, noting effects of aversively and appetitively rewarded training

03 p0375 A69-14068

High energy X ray irradiation of head of Macaca mulatta, determining effect on cerebral blood flow and blood pressure

03 p0376 A69-14075

Increased gravitational stress effects on esophageal sphincter pressures and gastroesophageal reflux in rhesus monkeys, noting cardia competence

06 p0874 A69-17838

Abrupt deceleration effects on monkey heart rate, noting occurrence of relative bradycardia

06 p0876 A69-18031

Monkey behavior in high atmosphere under weightless conditions, discussing problems connected with biological measurements, logic systems and vibration protection

09 p1447 A69-22722

Macaque monkeys in weightless state on sounding rocket, noting vigilance level and characteristics

09 p1445 A69-22724

Microvillar bleb formation in proton irradiated primate hepatocytes with electron microscope, noting sinusoidal lumen

10 p1641 A69-23045

Psychomotor reaction time and motions, myogenic tonus at rest and precision of monkeys during rocket flights along ballistic curve, noting weightlessness effect

10 p1646 A69-23575

Oxidative and dephosphorylating enzymes and esterases in rat and squirrel monkey cerebral cortexes, noting neuron activity

12 p2018 A69-25773

Histochemical studies on nucleus basalis of Meynert of squirrel monkey

12 p2018 A69-25774

Penile erection electrically evoked from Macaca mulatta forebrain, measuring density and distribution of responding points

12 p2018 A69-25775

Histochemical tests on enzymes distribution in rhesus and squirrel monkeys intrafusal and extrafusal muscle fibers

12 p2018 A69-25777

Lactate dehydrogenase and monoamine oxidase distribution in medulla oblongata and cerebellum of squirrel monkey

12 p2018 A69-25778

Light effects on circadian rhythms in monkeys, describing changes in deep body temperature and locomotor activity phase relationships

15 p2556 A69-31336

EEG electrode stimulated simian mental activity in problem solving during simulated space flight, discussing skull implantation and EEG recordings of hippocampus activity

17 p2910 A69-33749

Enzymes distribution in subfornical organ in squirrel monkey

20 p3478 A69-37934

Squirrel monkeys escape behavior under centrifuge simulated gravity in excess of earth gravity

21 p3665 A69-39174

Normobaric oxygen toxicity pathology in baboons and Macaca, irus and squirrel monkeys during 14 day exposure

21 p3660 A69-39179

Rhesus monkeys visual responses recorded before and after unilateral striate lesions, optic tract section and inferotemporal lesions

22 p3876 A69-40263

Visual retroactive perceptual masking effect in monkeys pretrained in visual discrimination task, interpreting electrical potentials recorded along optic pathways

22 p3876 A69-40265

Squirrel monkey retinas spectral stimulation, determining differential color responses reaching striate and prestriate cortex

22 p3879 A69-40844

Visual field meridians in circumstriate visual cortex of monkey determined by tracing degenerating axons stained by Nauta method

22 p3881 A69-40858

Nocturnal and diurnal monkeys spectral sensitivity functions determined from simultaneous recordings of light-evoked cortical and retinal responses

22 p3882 A69-40867

Squirrel monkeys exposed to centrifugally generated artificial gravity trained to respond for food reinforcement at selected gravity levels

23 p4081 A69-41434

Cerebrospinal fluid /CSF/ formation in male monkeys as function of fluid pressure at third ventricle level following temperature stress and feeding

23 p4084 A69-41469

Central nervous, cardiovascular and metabolic data of Macaca nemestrina during simulated Biosatellite flight, testing data acquisitions systems
24 p4260 A69-42703

Social entrainment of feeding rhythms in Rhesus monkeys with light, temperature and sound held constant
24 p4260 A69-42704

Circadian rhythm phase relationships between photoperiodism and heart rate, locomotor activity and deep body temperature (DBT) in unrestrained monkeys
24 p4260 A69-42706

Physiological circadian rhythms in isolated and nonisolated Macaca Nemestrina living under varied light intensities, noting telemetered deep body temperature, urine volume and sodium, etc
24 p4261 A69-42707

Abnormal biologic rhythm in rhesus monkeys associated with behavioral stress, noting brain temperature periodicities sensed with implanted extradural thermistor
24 p4261 A69-42708

Nonhuman primate circadian rhythms as functions of phase shift carried out in advance or delay
24 p4261 A69-42709

MONOCHROMATIC RADIATION

Organic dye lasers energy characteristics excited by monochromatic radiation, investigating radiation absorption during transitions from lower to higher electron-vibrational levels
01 p0090 A69-10381

Solar corona electron density, polarization, temperature and monochromatic emission during November 1966 eclipse
02 p0310 A69-11457

Quadratic and cubic response in photoelectric emission in potassium antimonide under laser irradiation observed with measurement of energy distribution of excited electrons
05 p0771 A69-15813

Differential cross section frequency dependence for resonant scattering of monochromatic light by dilute gas atoms
[IEEE PAPER T-8]
05 p0776 A69-16328

Submillimeter plane monochromatic wave amplitude and phase fluctuations during propagation in turbulent atmosphere surface layer, considering absorption by water vapor
05 p0722 A69-16778

Surface UV irradiated MgO powder catalytic activity for hydrogen-deuterium exchange reaction
07 p1073 A69-18374

Electromagnetic field strength of narrow polarized monochromatic light beam, noting spatial curvature and twisting in beam current line
07 p1147 A69-18524

Nonpolarized single frequency gas laser radiation produced by interferential effects in complex resonator
07 p1149 A69-18936

Wavelike photodissociation of gas molecules under quasi-monochromatic pulsed radiation, investigating associated supersonic disturbances
08 p1354 A69-19950

Optical systems with quasi-monochromatic partially coherent illumination, discussing energy distribution computation program
08 p1353 A69-21096

Far IR radiation from water vapor laser, noting monochromaticity and strong linear polarization
10 p1702 A69-23160

Diffuse reflection of monochromatic radiation by semiinfinite plane layer in case of isotropic scattering, reducing problem to power series
11 p1960 A69-24732

Monochromatic midlatitude auroral arc /M arc/ observation on 28-29 September 1967 at Moscow, Idaho
12 p2065 A69-26105

Organic dye lasers energy characteristics excited by monochromatic radiation, investigating radiation absorption during transitions from lower to higher electron-vibrational levels
12 p2109 A69-26676

Gas lasers, including stimulated emission in monochromatic field of traveling and standing plane waves, spontaneous emission with stimulated transitions, etc
12 p2109 A69-26906

Minimum height of monochromatic radiation ionization in atmosphere assuming spherical earth for space science applications
13 p2256 A69-28653

Plane monochromatic and pulsed electromagnetic waves penetration into metal cylindrical shells, deriving equations for electromagnetic field in interior
15 p2569 A69-30950

Frequency selector for gas laser, considering monochromatic emission and multimode oscillation
16 p2795 A69-31608

Thick gas model for monochromatic one dimensional radiant flux near diffusely emitting and reflecting boundaries, discussing gray gas and exponential kernel approximations
16 p2769 A69-31871

Atmospheric extinction determined by monochromatic photometry in Chile in 3000 to 6000 Å range, discussing components
17 p3031 A69-33100

Monochromatic undulating light vertical refraction path curvature radii calculation based on refractive index
18 p3174 A69-35201

Dual beam white or nearly monochromatic light source providing programmed repetitive sample illumination with variable intensity, pulse duration and sequence for photosynthesis research
19 p3312 A69-36378

Monochromatic electromagnetic field in resonant medium, examining linear, incoherent and coherent nonlinear propagations and resonant scattering
21 p3769 A69-38382

Monochromatic radiation diffusion in one dimensional bounded medium, deriving equations for probability density of quantum yield and intensity of light fluxes
21 p3769 A69-38586

Cross correlation coefficient for submillimeter monochromatic wave amplitude and phase fluctuations in turbulent atmospheric boundary layer
21 p3674 A69-39129

Absorption spectrum of CS atoms excited by electrical discharge and irradiated by monochromatic light and ionized by electron collisions
22 p3984 A69-40418

Temperature distribution on surfaces of close binary stars as basis for predicting variation of monochromatic reflection effect
24 p4387 A69-43350

MONOCHROMATIZATION

Fabry-Perot etalon for obtaining monochromatic weak solar prominences
02 p0248 A69-11634

Optimal thickness of inhomogeneous absorption layer subjected to normally incident plane monochromatic wave treated as Mayer-Boltz variational problem
13 p2297 A69-27381

Michelson interferometers with large interference fields for plasma diagnostics emphasizing structural rigidity, monochromatic light pulse power, instruments vibrations resistance, etc
14 p2496 A69-29776

Accuracy standards for diffraction measurements of electromagnetic waves incident on periodic arrays, using monochromatic field and plane phase wavefront
23 p4139 A69-42042

MONOCHROMATORS

Absorption coefficient of hydrazine and hydrogen peroxide determined with 2.5 angstrom bandwidth monochromator, giving results in graphical form
02 p0205 A69-11873

Ion and electron temperature and density measurement by Thomson scattering with low resolution monochromator for Salpeter parameter near unity
11 p1925 A69-24310

Automatic recording of spectral distribution of high resistance semiconductors photoconductivity using spectrograph monochromator
14 p2447 A69-29409

Solar spectral irradiance measured by airborne instruments, discussing construction, calibration, etc, of photoelectric filter radiometer and Leiss monochromator
16 p2861 A69-32261

Monochromatic linearly polarized electromagnetic beam generator for submillimeter band, discussing applications
17 p2932 A69-34162

CaO and MgO reflectance spectra measurements at high resolution and at low temperature including exciton spectra at 25 K, obtaining fine structure
18 p3181 A69-34274

Optical design of double monochromator for use in EUV, describing astigmatism and transmission properties
24 p4351 A69-43758

MONOCOQUE CYLINDERS

U CYLINDRICAL SHELLS

MONOCOQUE STRUCTURES

Titanium monocoque fuselage reinforced by composite boron filaments in polyimide resin matrix tested

for SST applications, noting weight savings over all titanium structure
[AIAA PAPER 69-763]
19 p3329 A69-36298

MONOCRYSTALS

U SINGLE CRYSTALS

MONOCULAR VISION

Holographic photogrammetry compared with conventional holography in monocular and binocular parallax reconstruction and stationary stability of objects
22 p3944 A69-40044

Target distance and direction monocular estimates with stabilized and nonstabilized retinal images, finding eye movements not improving spatial judgment accuracy
22 p3878 A69-40838

Landing performance in T-33A aircraft with loss of binocular vision compared to performance with both eyes
23 p4102 A69-41675

MONOLITHIC CIRCUITS

U INTEGRATED CIRCUITS

MONOMERS

Monograph on crystallization during polymerization, discussing categories, monomers capable of step reaction, chain reaction, nucleation crystal growth and perfection
05 p0783 A69-15967

Polymerization of monomers considered for direct synthesis of iminobenzylidene
10 p1651 A69-23308

Luminescence spectra of aromatic polymers, monomers and dimers under high energy electron excitation using molecular resonance model
16 p2828 A69-32792

MONOMOLECULAR FILMS

Uranyl ions interaction with phospholipid and cholesterol monolayers, using surface pressure and potential measurements
11 p1832 A69-25641

MONOPLANES

U A-6 AIRCRAFT
U A-7 AIRCRAFT
U AN-24 AIRCRAFT
U B-52 AIRCRAFT
U BAC 111 AIRCRAFT
U BOEING 707 AIRCRAFT
U BUCCANEER AIRCRAFT
U C-130 AIRCRAFT
U C-141 AIRCRAFT
U CV-990 AIRCRAFT
U DC 3 AIRCRAFT
U DC 8 AIRCRAFT
U DH 121 AIRCRAFT
U DO-31 AIRCRAFT
U E-2 AIRCRAFT
U F-2 AIRCRAFT
U F-4 AIRCRAFT
U F-5 AIRCRAFT
U F-104 AIRCRAFT
U F-106 AIRCRAFT
U G-91 AIRCRAFT
U OV-10 AIRCRAFT
U P-1127 AIRCRAFT
U SC-7 AIRCRAFT
U SE-210 AIRCRAFT
U TU-104 AIRCRAFT
U TU-134 AIRCRAFT
U VC-10 AIRCRAFT
U XC-142 AIRCRAFT
U XV-4 AIRCRAFT

MONOPOLE ANTENNAS

Radiation pattern, gain and polarization of omnidirectional antenna consisting of dipoles or monopoles arranged along circular cone
01 p0046 A69-10738

End correction for input admittance of electrically thick monopole antenna with arbitrary radius driven from coaxial line
02 p0219 A69-12346

Monopole antenna behavior over grounded metal hemisphere, noting application to spacecraft and broadcasting antennas erected on hill
08 p1282 A69-20040

Capacitance and effective height for VLF umbrella antennas using multiple wire structural members to increase effective antenna surface area
08 p1282 A69-20041

Space frequency filter antennas, using multiple terminals for signal processing as function of frequency and angle
08 p1290 A69-20977

Multiple beam HF receiving antenna system for directivity, azimuthal coverage and noise limitation
13 p2228 A69-27631

Vertically polarized log periodic antenna consisting of unipole vertical radiators with side radiators for achieving minimum size

16 p2763 A69-32580

Radiation and impedance characteristics of spherically capped conical and monopole antennas protruding from spherical vehicle related to cone height, angle and vehicle diameter

22 p3908 A69-40699

MONOPOLES

Magnetic monopole search using synchrotrons and cosmic radiation to destroy ferromagnetic materials binding in rocks, meteorites and deep sea sediments

22 p3981 A69-40197

MONOPROPELLANTS NT AEROZINE

Flame zone development of monopropellant droplets during heat-up period

02 p0352 A69-12310

Spherical monopropellant droplet radially symmetric burning during adiabatic vaporization and direct decomposition, examining near-equilibrium limit by asymptotic analysis

12 p2190 A69-25948

Extinction kinetics of monopropellant droplet burning in inert gas reservoir with atmospheric temperature lower than adiabatic combustion temperature

13 p2378 A69-28250

Semiempirical correlation of characteristic velocity for Otto Fuel II during monopropellant combustion, assuming droplet vaporization as rate controlling process [AIAA PAPER 69-419]

16 p2877 A69-31843

Steady deflagration of homogeneous monopropellant in condensed phase, considering nonequilibrium surface condition for mass decomposition rate [WSCI PAPER 69-6]

16 p2830 A69-32347

Pilot chamber initiated thermal decomposition reactor concept for monopropellant thruster, discussing thrust levels and throttling ratios [AIAA PAPER 69-420]

16 p2841 A69-32685

Pure monopropellant steady droplet burning rate theory for determining heat-up and convection transport rates in droplet combustion products of flat flame burner [AIAA PAPER 69-563]

16 p2834 A69-32722

Rocket motors using hydrazine as monopropellant, considering doping as means of using anhydrous hydrazine mixed with other products

17 p3019 A69-33340

Titan 3 transtage attitude control system hydrazine rocket engine design and performance, emphasizing problems associated with monopropellant [AIAA PAPER 69-422]

19 p3394 A69-36300

Adiabatic model deflagration limits for steady linear monopropellant burning at Lewis number of unity and one step gas phase reaction

24 p4415 A69-43670

MONOPULSE ANTENNAS

Monopulse ground station antenna configuration for improvement of sidelobe level in satellite transmission [DVL-856]

02 p0214 A69-11599

Contour pattern analysis of AN/FPQ-6 monopulse radar Casscgrainian antenna, giving three dimensional drawings

04 p0576 A69-14769

Kwajalein Missile Range UHF telemetry conversion program using S band antennas with three channel monopulse autotrack systems

07 p1077 A69-18829

Axis deviation and refraction errors to correct design in radome of monopulse antenna, comparing various RF radome performances

07 p1110 A69-19520

Radioelectric axis deviation of radome in front of monopulse radar antenna

07 p1111 A69-19524

Stepped scanned ring monopulse array, discussing pattern analysis, directivity, co-phased and quasi-phased model

14 p2419 A69-28894

Monopulse parabolic antenna radiator design for decimeter and meter wavelengths, discussing characteristic properties at optimal dimensions

17 p2939 A69-33905

Multiplicative feed system for monopulse angle tracking antennas, discussing influence of sidelobe and backlobe responses on control function slope determining antenna bearing angle

20 p3510 A69-37704

Phase error in monopulse antenna system attributed to far field background noise sources during passive or active objects tracking

20 p3492 A69-37707

Monopulse telemetry tracking system, describing equipment and mobile operation

22 p3900 A69-40681

Monopulse, high power, three channel antenna feed system design for communication satellites, noting orthogonal polarization of transmit and receive functions

23 p4120 A69-41750

Parabolic antenna properties generated by dual band circularly polarized focused two channel monopulse feed system, discussing tracking data from helicopter, Apollo 8 and Cassiopeia A

23 p4120 A69-41752

MONOPULSE RADAR

Multiple target monopulse radar signal processing technique

04 p0562 A69-15470

Signal processors for implementation of monopulse tracking radar with three instead of four beams, investigating accuracy

08 p1270 A69-19855

Radar target detection and angular location estimation in amplitude comparison monopulse radar by simultaneous observation with group of antennas

09 p1452 A69-21312

Angle of arrival in amplitude comparison monopulse radars in presence of internally generated thermal noise

13 p2220 A69-27942

Electronic boresight shift in space-borne monopulse radar system, expressing antenna and signal parameters in terms of equivalent branch and channel asymmetries

14 p2411 A69-28895

MONOSACCHARIDES

Physicochemical synthesis of monosaccharides from human waste products at atmospheric and elevated pressures, considering methane oxidation by nitrogen oxides and ozone

07 p1071 A69-18971

Monosaccharide production from carbon dioxide from respiration or human waste incineration, evaluating toxicological effects of synthetic monosaccharides

15 p2557 A69-31471

Physicochemical synthesis of monosaccharides from human waste products at atmospheric and elevated pressures, considering methane oxidation by nitrogen oxides and ozone

20 p3483 A69-38219

Carbohydrate analyses of upper carboniferous plant fossils in England, noting monosaccharides separation

21 p3661 A69-39534

MONOSTABLE MULTIVIBRATORS

Circuit for linear voltage amplitude to pulse width conversion using controlled unijunction monostable multivibrator

02 p0217 A69-12151

MONOTONE FUNCTIONS

Brightness curves of eclipsing systems under monotonicity of unknown functions, using stable algorithm

09 p1588 A69-21363

Optimal control problem involving approximation by monotone functions

09 p1531 A69-21412

Tricomi theorem extension concerning intermediate value property of continuous real valued functions of real variable

09 p1533 A69-22797

Monte Carlo method for integral of monotonic continuously differentiable function

13 p2288 A69-27735

Brightness curves of eclipsing systems under monotonicity of unknown functions, using stable algorithm

18 p3197 A69-34753

Monotonic minimization algorithm for nonsmooth extremal problems of mathematical programming, game theory, approximations and optimal control in arbitrary Banach space

23 p4181 A69-41524

MONSOONS

Satellites use in meteorology, noting monsoon rain forecasting through mesoscale sea surface temperatures of Indian Ocean [UN PAPER 68-95555]

01 p0109 A69-10502

Steady state solution of quasi-geostrophic perturbation equations for atmospheric forced response to parametrized heating as global monsoon theory

19 p3362 A69-36405

MONTE CARLO METHOD

Ionization cross sections of excited states of hydrogen atoms and hydrogenoids calculated by Monte Carlo method

01 p0122 A69-10040

Monte Carlo simulation procedure synthesizing probability distributions of reliability parameters with individually exponential components

01 p0036 A69-10707

Monte Carlo method used to construct optimal algorithms for simulating homogeneous Markov chains whose trajectories reach absorbing state with probability of one

01 p0105 A69-10726

Monte Carlo method accuracy improvement for calculating probability characteristics of nonlinear ordinary differential equations, describing nonlinear automatic control

01 p0105 A69-10730

Monte Carlo method to calculate distributions describing particle behavior in Knudsen cell, clarifying relationship between gaseous collisions and Knudsen number

06 p0908 A69-17111

Random search and multiple integral based Monte Carlo method for computer solution of nonlinear aerodynamic problems

06 p0858 A69-17334

Monte Carlo solution of linearized Boltzmann equation in rarefied gas dynamics, noting Knudsen layer and Couette flow applications

06 p0910 A69-17345

Flow near leading edge of sharp insulated and cooled flat plates, using Monte Carlo direct molecular simulation [AIAA PAPER 69-141]

06 p0866 A69-18208

Metal fatigue simulation by Monte Carlo method, showing programmed fatigue tests in form of life distribution functions

07 p1233 A69-19314

Arrival time distribution and energy content of extensive air shower at large core distances, discussing photon energy spectra and Monte Carlo calculation

07 p1186 A69-19410

Monte Carlo method applied to calculation of radiation transmission and dosage behind space vehicle shields during passage through earth radiation belt

08 p1377 A69-19843

Complex bodies aerodynamic characteristics in free molecular gas flow by applying Monte Carlo method

09 p1430 A69-21793

Spatial distribution of residual nuclei produced in thick Fe targets by one and three Gev protons, noting total production and longitudinal variation of production

10 p1760 A69-23411

Mass and velocity distribution of interstellar clouds from Oort model simulated by Monte Carlo method on computer, predicting rogue cloud existence

10 p1779 A69-23608

Interstellar dust alignment mechanisms investigated by Monte Carlo model, discussing grain velocity maintenance by radiation pressure and effects of magnetic constraint on charged grain trajectory

10 p1781 A69-23675

Monte Carlo digital computer simulations, considering sample sizes and confidence intervals in multinomial output

10 p1661 A69-23853

Optimal estimation of conditional mean of posterior probability density function in multistage nonlinear filters, using Monte Carlo techniques and Bayes theorem

10 p1667 A69-24039

Monte Carlo method application to heat transfer analysis including radiation, rarefied gas energy transfer and conduction

11 p1997 A69-24457

Model for radiative transfer in atmosphere-ocean system by Monte Carlo method, considering Rayleigh and Mie scattering

11 p1877 A69-24851

Monte Carlo method for integral of monotonic continuously differentiable function

13 p2288 A69-27735

Proton initiated nuclear cascade in atmosphere calculated using Monte Carlo method, relating electron number to primary proton energy

13 p2331 A69-28397

COHORT-II Monte Carlo computer program written in Fortran IV to model radiation shielding problems

14 p2417 A69-29004

Direct simulation Monte Carlo method for hypersonic rarefied gas flow past solids, modeling on digital computer

14 p2390 A69-29580

Quasi-uniform pseudorandom numbers program transmitter statistical characteristics suited for solving problems by Monte Carlo method

15 p2572 A69-30336

MONTH

Vapor-liquid transition in inert gases based on Monte Carlo method, including comparison with van der Waal equation and plasma ionization equilibrium
15 p2655 A69-30981

Three dimensional Monte Carlo calculations for hadronic component of extensive air showers using semiempirical model high energy nuclear interactions
15 p2678 A69-31482

Normal and directional emittance for two dimensional emitting, absorbing and scattering semiinfinite plane slab based on Monte Carlo method compared with Bobco approximation
[AIAA PAPER 69-625]
17 p3005 A69-33301

Data inaccuracy used for calculating forecasts of reliability analyzed by Monte Carlo simulation
17 p2937 A69-33389

Monte Carlo inversion of seismic body waves for transposing uncertainties of observations to velocity models
17 p2962 A69-33654

Atomic excitation and ionization by thermal electrons, using Monte Carlo trajectories to determine adiabatic collisions effects on energy transfer near dissociation limit
18 p3176 A69-34790

Monte Carlo method application to neutron streaming in hemispherical air-filled ducts in water tank to determine leakage through nuclear reactor shields
18 p3171 A69-35178

Modified Monte Carlo model applied to computerized meteorite orbit evolution, simulating secular perturbations by imposing sinusoidal variation on orbital elements
19 p3414 A69-36117

Chondritic meteorites initial orbits evolution to earth impact calculated by Monte Carlo method, considering relationships to meteorite sources
19 p3415 A69-36118

Monte Carlo relaxation method for physically self consistent model stellar atmospheres, discussing stability, accuracy and convergence of solution
19 p3425 A69-36337

Monte Carlo method for constructing catalogs of stellar positions, distances and velocities
20 p3605 A69-37829

Space mission sensitivity to parameters of interest determined by Monte Carlo simulation samples
21 p3804 A69-39036

Algorithm for numerical modeling by Monte Carlo method of diffusion bounded light beams in dispersive media, applying to light pulse in cloudlike medium
22 p3981 A69-40248

Circular and spherical antenna arrays elements random distribution in three dimensional space using Monte Carlo method, considering arbitrary excitation and nonisotropic elements
22 p3914 A69-40704

Monte Carlo methods for electromagnetic showers simulation, noting electron track length distribution in Pb glass absorber
22 p4007 A69-41057

Monte Carlo method for energy transfer efficiency of ruby laser pumping cavities by helical flash lamps, noting dependence on ruby parameters
23 p4173 A69-41630

Space and missile guidance performance analysis through automatic generation of mission performance sensitivity with respect to error sources from Monte Carlo simulation
[AAS PAPER 69-404]
24 p4347 A69-42836

Monte Carlo calculation of free molecular flow over concave spherical surface, considering partial diffuse reflection and imperfect energy accommodation
24 p4248 A69-43592

MONTH

Synodic month length variations since late Cambrian, noting paleontological evidence in mollusks and stromatolites and associated geological changes
02 p0241 A69-11807

MONTMORILLONITE

Purines, pyrimidines and nucleosides absorption by Li-, Na-, Mg- and Ca-montmorillonite in aqueous solutions over range pH 2-12 by cation exchange
05 p0716 A69-15973

Absorption of nucleosides, purine and pyrimidine derivatives by Co-, Cu- and Ni-montmorillonite taking place by cation exchange process
05 p0716 A69-15974

MOON

Meteorite scattering in geogravitational field and influence on lunar meteorite precipitation distribution
01 p0153 A69-10756

Roughness effect on microwave emissivity according to geometric optics with application to moon and Venus
02 p0207 A69-12017

Moon figure from meridional measurements of visible diameters at different angles of libration, deriving equation for polar and equatorial compression of lunar ellipsoid
03 p0512 A69-13690

Selenographic and celestial selenocentric coordinate systems, noting precession and nutation of lunar rotation axis
04 p0662 A69-15250

Large mass concentrations/mascons/ effect on moon dynamical figure, considering production of asymmetries
05 p0820 A69-15762

Detached lunar compression wave, noting positive evidence from solar wind flux and direction measurements near lunar wake
05 p0824 A69-16251

Origin of moon indicating pristine structure on basis of mascons, alpha scattering and crater formation
06 p1001 A69-17160

Lunar opposition effect theory applied to Mars opposition effect on brightness
07 p1214 A69-18616

Lunar core electrical conductivity determination based on induced magnetic field arising from time varying interplanetary magnetic field associated with solar wind plasma
07 p1215 A69-18832

Model experiment on plasma flow about obstacle to simulate solar wind interaction with moon
07 p1205 A69-18851

Lunar depth profiles of conductivity, dielectric constant and magnetic permeability from radar, radiothermic and magnetic measurements, discussing lunar models
07 p1216 A69-19221

Geomagnetic tail topology, reconnection and interaction with moon from Explorer 33 satellite data
07 p1128 A69-19365

Models for lunar density distribution consistent with available data on lunar physical properties
08 p1393 A69-20579

Low energy proton flux in neighborhood of Moon measured by Luna 12 satellite indicating magnetized plasma region effect on burst
09 p1577 A69-21773

Radiometric observations of moon during total lunar eclipse at 3.33 mm, noting decrease in equivalent black body disk temperature
10 p1789 A69-24132

Solar and lunar/solar harmonics determination, noting effects of moon on values of horizontal magnetic component
11 p1965 A69-25555

Moon internal structure, discussing aggregation origin of Moon parallel to earth and three layer model of nife core, sima mantle and porous sheath
12 p2160 A69-26896

Lunar dynamic response to discontinuities in interplanetary magnetic field to determine electrical conductivity and internal temperature
15 p2700 A69-31442

Cassini laws applied to moon and Mercury, determining relations between moment differences for spin vector, orbital angular-momentum vector and precessional velocity
16 p2861 A69-32239

Moon density and nucleation of planets, explaining low density and absence of heavy core by late aggregation from nonmetallic particles
16 p2865 A69-32808

Lunar rotation parameters determined from photographs and visual observations independent of moon profile
17 p3027 A69-32874

Numerical integration of lunar motion equations to investigate lunar theory for high precision applications and to examine motion departures from gravitational theory
20 p3603 A69-37560

Hypothetical planet captured by earth, becoming earth satellite/moon/, discussing Mercury orbits peculiarities
20 p3603 A69-37562

Spherical lunar coordinates for arbitrary moment of time calculated by digital computer using Brown lunar motion theory
22 p4024 A69-40611

MOON-EARTH TRAJECTORIES

Reentry trajectories from lunar surface and orbit obtained by computer with allowance for initial data spread
09 p1594 A69-21756

Earth-moon and moon-earth trajectory parameters related to lunar orbit conditions for synthesizing lunar orbit trajectory
18 p3196 A69-34704

Moon to earth trajectories analyzed numerically to determine effect of specified earth entry conditions on hyperbolic elements near moon for abort
[AAS PAPER 68-089]
20 p3595 A69-37174

MOONMOBILES

U LUNAR SURFACE VEHICLES

MOREHOUSE COMET

Solar wind directional fluctuation derived from wavy structure of comet Morehouse ionic tail rays, noting solar wind bulk velocity
02 p0311 A69-11459

Motion of condensations within tail of comet Morehouse 1908 III from photographs
08 p1382 A69-19870

MORL

U MANNED ORBITAL RESEARCH LABORATORIES

MORNING

Irregular pulsations in morning sky brightness using all-sky photographic airborne auroral observations along auroral oval
09 p1594 A69-21666

MORPHOLOGICAL INDEXES

Morphological properties and history of Zabrode stony meteorite, discussing storage, disappearance and recovery
01 p0160 A69-11384

MORPHOLOGY

NT GEOMORPHOLOGY
NT ISOMORPHISM
NT LUNG MORPHOLOGY
NT POLYMORPHISM

Pathomorphological aspects of radiation sickness in animals irradiated by high energy protons, showing changes in lymph node, stellate ganglion and spleen
05 p0708 A69-16509

Morphology of E and SO galaxies in terms of equilibrium isopleths within general relativity
08 p1395 A69-20636

Magnetite morphological variations of type 1 carbonaceous meteorites, discussing isometric crystals, spheres, spherulites, platelets and filaments
08 p1406 A69-20932

Grain morphology and preferred orientation effects on direction and propagation of stress corrosion cracking of aluminum alloy plate
09 p1521 A69-21399

Morphological microchanges in solar plexus ganglia of white rats after X irradiation
12 p2019 A69-26347

Spiral galaxies with connectors observed in Southern Hemisphere, noting galactic nuclei differences and nucleus relation to galaxy morphological type
12 p2165 A69-27030

Coding of morphological evolution in time of auroral displays as genericization of existing IUGG code
13 p2256 A69-28655

Pathomorphological aspects of radiation sickness in animals irradiated by high energy protons, showing channels in lymph node, stellate ganglion and spleen
18 p3095 A69-34728

Three dimensional morphology of systems engineering, using model for applications in taxonomy, new activities sets discovery and systems science curriculum design
18 p3236 A69-35235

Noctilucent clouds morphological and kinematic characteristics based on photographs
18 p3132 A69-35335

Tungsten influence on morphology and lattice parameter of fcc gamma prime phase in Ni-Cr-Ti-Al alloys
20 p3558 A69-36962

Lunar morphology evolution by dust transport on surface, discussing possibility of fluidization
23 p4221 A69-42392

MORPHOTROPISM

U ISOMORPHISM

MORSE CODE

Artificial magnetospheric VLF noise triggering by Morse code dots at 14.7 kHz from NAA verified at Antarctica
11 p1878 A69-25155

MORSE POTENTIAL

- Franck-Condon factors for high rotational levels of nitrogen calculated in Morse potential approximation for application to plasma diagnostics
07 p1185 A69-19169
- Fcc metals higher order elastic constants calculated by Morse potential function, considering atomic interactions truncation and pressure derivatives
23 p4233 A69-42337

MORTALITY

- Risk factors in coronary diseases modified to provide base for estimating achievable mortality magnitude reduction
24 p4262 A69-43059
- Stillbirth and neonatal death in stressed rats exposed to mild and acute gravitational loads in automobile ride and aircraft flight
24 p4266 A69-43381

MOS [SEMICONDUCTORS]

U METAL OXIDE SEMICONDUCTORS

MOSAICS

- Solid state IR imaging using monolithic Ge mosaics of isolated sensor elements, discussing design, structure, fabrication, system readout and operation
11 p1938 A69-25307
- Mosaic mirror and lens camera system for multiple image high resolution photography
17 p2972 A69-33089

MOSS [SPACE STATIONS]

U ORBITAL SPACE STATIONS

MOSSBAUER EFFECT

- Temperature dependent isomer shift and anharmonic binding of Sn 119 in niobium stannide, measuring Mossbauer recoil free fraction
01 p0134 A69-10009
- Mossbauer spectra of shocked and unshocked iron meteorite and fayalite
03 p0517 A69-14231
- Stainless steel sensitization analyzed using Mossbauer spectroscopy and X ray diffraction, noting ferromagnetic phase
06 p0944 A69-17852
- Phonon interactions with recoilless gamma rays, considering usability of Mossbauer effect as probe for VHF acoustic experiments
10 p1724 A69-23088
- Mossbauer spectroscopy, discussing nuclear resonance fluorescence and equipment
18 p3099 A69-34622
- High field susceptibility in Fe and Ni and high field Mossbauer study in Fe relating results to band structure and models of ferromagnetism
19 p3383 A69-36050
- Quantitative analysis and classification of stony meteorites, including carbonaceous chondrites, by Mossbauer characteristics, discussing Prior plot and weather influence role in finds and falls
19 p3408 A69-36083

MOT [ORBITAL TELESCOPES]

U MANNED ORBITAL TELESCOPES

MOTILITY

U LOCOMOTION

MOTION

- Motion measurement using Doppler shift of scattered laser light, noting high resolution
09 p1492 A69-21398
- Laser Doppler heterodyning for monitoring motion noting solid surfaces vibration, liquid and solid surfaces linear velocity and turbulence in liquids and gases
15 p2614 A69-31276
- Deterministic and statistical prediction techniques for aircraft carrier motions at sea for application to aircraft landing operations [AIAA PAPER 68-123]
17 p2902 A69-34014
- Band movement phenomenon model for temporal and spatial interactions
22 p3880 A69-40854

MOTION AFTEREFFECTS

- Strain releasing method for reduction of small local movements of recording holographic emulsions resulting in degradation of holographically reconstructed wavefronts
06 p0923 A69-16930
- Motion coordination capacity of persons subjected to 40 days bed rest studied by dynamographic technique, discussing nature of slackening
17 p2906 A69-32937
- Human motion coordination under acceleration followed by weightlessness during jet flights along Keplerian orbits, discussing initial disturbance and subsequent subsiding
17 p2907 A69-32938

Electrophysiological data for directionally sensitive units in optic tectum of mammals, indicating midbrain as site for rotating spiral motion aftereffects
20 p3480 A69-38264

Visual long term storage capability demonstration, describing negative aftereffect of motion perceived after fixation of moving spiral pattern
21 p3661 A69-39332

MOTION EQUATIONS

U EQUATIONS OF MOTION

MOTION PERCEPTION

U SPACE PERCEPTION

MOTION PICTURES

- Systems analysis in aerospace engineering by adding motion pictures and TV techniques [SMPTE PAPER 104-17]
04 p0596 A69-14359
- Digital computer motion pictures generation for ground controlled intercept simulation
06 p0906 A69-17397
- Holographic motion picture recorded using CW Q switched laser and conventional camera
10 p1697 A69-24002
- Photography role in experimental research with applications to flight analysis and comparison with human visual accuracy
11 p1881 A69-24573
- Cineradiography based on repetitive flashes drawn from single field emission X ray tube energized by high voltage pulse generator
12 p2086 A69-26163
- Cinematic holography as continuous motion uninterrupted viewing system compared with standard cinematography, noting flicker-free shutterless reproduction
12 p2087 A69-26173
- Holographic cine-interferometry, using live fringe method with Q switched pulsed ruby lasers to obtain consecutive submicrosecond interferograms
18 p3133 A69-34265
- Nanosecond photography with superradiant light source, X rays or electrons using multipurpose electron accelerator, obtaining stop motion pictures
19 p3305 A69-35721

MOTION SICKNESS

- Physiological causes and prevention of motion sickness during space flight, emphasizing conditioned reflex, different analysts interactions and vestibular-vegetative changes during weightlessness
02 p2000 A69-12122
- Overt motion sickness prevention by incremental exposure to Coriolis accelerations
07 p1067 A69-19425
- Motion sickness inhibitive effect on stomach motor activity, measuring biopotential of stomach wall, pyloric sphincter and ganglions
08 p1263 A69-19935
- Motion sickness studied with slow rotation room having controlled Coriolis accelerations, discussing oculogyral illusion, nystagmus, dizziness and neuromuscular incoordination
12 p2019 A69-26547
- Head movements controlled for rapid vestibular adaptation in slow rotation room /SRR/, preventing motion sickness
17 p2908 A69-33178
- Motion cues simulation system with seat of six differentially inflatable sections, discussing DYNASEAT
17 p2947 A69-34007
- Motion sickness forms in human subjects subjected to induced rocking, noting impaired performance and sensorimotor reactions to visual stimuli
20 p3472 A69-37263
- Vestibular analyzer function relation to arterial pressure during otolith stimulation experiments on subjects susceptible and nonsusceptible to motion sickness
20 p3472 A69-37264
- Motion sickness as sensory rearrangement phenomenon, proposing neural mismatch hypothesis to account for symptom pattern
20 p3483 A69-38266
- Human susceptibility to motion sickness under Coriolis acceleration during parabolic flight weightlessness
21 p3659 A69-39168
- Motion sickness susceptibility during parabolic flight, comparing weightlessness and hypergravity effects on normal and labyrinthine-defective subjects
21 p3660 A69-39176

MOTION SICKNESS DRUGS

- Antimotion sickness drugs tested in slow rotation room with controlled Coriolis accelerations, noting summation effect of dextroamphetamine sulfate and scopolamine hydrobromide
03 p0381 A69-14079

Motion sickness treatment with bethanecol chloride, noting negative results with 12 airsick student naval aviators
12 p2024 A69-26561

Diphenidol and prochlorperazine effect on human semicircular canal function, noting failure of drug to alter vestibular responses
17 p2913 A69-33168

Motion sickness prophylaxis for rabbits subjected to rotation, investigating effects of adrenalin, ephedrine, sympatholitin, piperoxane and pyridoxophene on nystagmus and respiration
20 p3472 A69-37265

Motion sickness prophylactic action of sodium hydrocarbonate in dogs subjected to vertical accelerations, using intravenous administration
20 p3473 A69-37269

MOTION STABILITY

- NT AERODYNAMIC STABILITY
- NT AIRCRAFT STABILITY
- NT ATTITUDE STABILITY
- NT BOUNDARY LAYER STABILITY
- NT DIRECTIONAL STABILITY
- NT FLAME STABILITY
- NT FLOW STABILITY
- NT GYROSCOPIC STABILITY
- NT HOVERING STABILITY
- NT LATERAL STABILITY
- NT LONGITUDINAL STABILITY
- NT LOW SPEED STABILITY
- NT MAGNETOHYDRODYNAMIC STABILITY
- NT ROTARY STABILITY
- NT SPACECRAFT STABILITY

Spacecraft periodic motion near center of mass determined by point transformation combined with bifurcation theory, studying stability and parametric dependence
01 p0161 A69-10205

Theory for stability of steady motions of system with cyclic coordinates applicable to total damping
01 p0151 A69-10567

Dynamically symmetric gyrostat steady motion stability in relation to satellite motion
01 p0163 A69-11301

Stability characteristics of small and moderately sized short period Trojan librations in sun-Jupiter restricted three body problem
01 p0158 A69-11329

Rotating bodies stability conditions relative to radial disturbances found to be field strength dependence on internal mass at any point
02 p0317 A69-11978

Mathematical aspects of stability of equilibrium configurations
02 p0340 A69-11991

Motion stability of two tethered unsymmetrical earth pointing bodies in circular orbit, presenting nine degrees of freedom differential equations of motions
02 p0324 A69-12507

Finite length cylindrical shell dynamic response to uniform radial impulse, noting simple harmonic motion and flexural mode excitation instability [AIAA PAPER 68-144]
02 p0347 A69-12517

Self oscillations of dynamic systems representing space vehicles, considering periodic motions stability, bifurcation curves and energy consumption requirement limit
03 p0519 A69-13068

Role of second order internal resonance in problem of stability of equilibrium of system neutral in linear approximation
03 p0466 A69-13404

Stability of steady motion of body with cavity containing one or several nonmixing liquids as problem of bounded oscillations about motion
03 p0418 A69-13815

Idealized point mass motion in axisymmetric gravitational field, discussing orbital stability about oblate planet
04 p0658 A69-14887

Perturbed nonlinear systems with many degrees of freedom, analyzing resonant oscillatory and rotary motions
04 p0631 A69-15536

Asymptotic stability of gyroscopic systems equilibria with partial dissipation used for motion stability analysis
04 p0631 A69-15537

Stabilization of steady motions of nonlinear controlled systems with two purely imaginary roots, using Liapunov stability theory
05 p0794 A69-15790

Stability of unsteady motion of nonlinear systems during limited time interval, applying differential inequalities method to Liapunov function
05 p0794 A69-16209

Motion stability analysis of system represented by differential equation having continuously differentiable functions as continuously acting disturbances
05 p0794 A69-16450

Satellite relative equilibrium stability under action of gravitational and aerodynamic moments
05 p0830 A69-16503

Motion of gyroscopic integrator of linear accelerations, analyzing nutational vibrations imposed on precession
06 p0927 A69-17688

Rolling ballistic vehicles mass and aerodynamic characteristics determined from dynamic motion data by performing Fourier analysis on roll axis equation of motion
[AIAA PAPER 69-102] 06 p0862 A69-18039

Semipassive three axis stabilization for dumbbell type satellites, considering pitch, roll and yaw motions damping
07 p1226 A69-18324

Stability of motion of spherically symmetric mass of compressible gas with constant space density in absence of gravitational field
07 p1215 A69-18706

Periodic asymptotically stable MHD motions, proving uniqueness and existence theorems
07 p1194 A69-19437

Damping flywheel to stabilize permanent rotation of weightless solid body moving by inertia, obtaining differential equations of motion
07 p1183 A69-19678

Steady state motions stability of gyroscope mounted on satellite in gravitational orbit
07 p1137 A69-19679

Motion of condensations within tail of comet Morehouse 1908 III from photographs
08 p1382 A69-19870

Stability and instability conditions derived for undisturbed motion of system over finite period of time
08 p1351 A69-20321

Ponderomotive forces and irregularities in earth rotation, considering core and lower mantle as closed system with respect to periodic electromagnetic and mechanical effects
09 p1487 A69-21636

Periodic motion of satellite with magnetic damper along circular orbit, assuming small value of damping coefficient
09 p1609 A69-21761

Motion stability over finite interval of time for perturbed mechanical systems
09 p1539 A69-21881

Incompressible fluid unsteady motion between journal and bearing solved in form of Reynolds number power series from stream functions
09 p1514 A69-22712

Gravitational potential of circular rings used to investigate motion stability of Saturn rings
10 p1771 A69-22855

Holonomous and scleronomic dynamic systems steady state motion stability under effect of generalized forces derived on basis of Liapunov theory
10 p1724 A69-22929

Planar motion of satellite containing damping mechanism, considering small dampers case
10 p1791 A69-22935

Harmonic balance procedure to study periodic motions in nonlinear stabilization system of nonrigid satellite
10 p1792 A69-24195

Atmospheric influence on plane oscillations of space vehicle moving at 100-150 km heights
10 p1792 A69-24208

Dynamics of gyroscopic synchronous servo system intended for remote measurement of spatial orientation coordinates of sensor moving element
11 p1881 A69-24558

Motion of body with cavity containing liquid based on Kharlamov solution, noting gyrostatic moment and liquid sloshing effect
11 p1868 A69-24775

Control sets corresponding to desired stability behavior of controlled motion, giving theorem concerning differential inequality
11 p1910 A69-25412

Stability of stationary motion, analyzing gyroscopically uninstabilizable systems and extension to continuous spectrum case
11 p1919 A69-25437

Stability of steady state motions of nonholonomic mechanical systems, noting Chetaev method for construction of Liapunov functions
11 p1920 A69-25742

Gyrostabilized satellite steady state motions in Newtonian force field having displaced satellite center of mass orbital plane relative to center of attraction
12 p2173 A69-25885

Jet flows instabilities with vertical and horizontal velocity drifts from numerical integration of atmospheric motion equations linearized with respect to small perturbations
12 p2125 A69-25950

Boussinesq approximation for compressible fluids, discussing perturbation pressure and velocities and vertical scale motions
12 p2061 A69-26013

Helicoidal precession stability in sense of Liapunov, Poincare and Lagrange
12 p2130 A69-26286

Flat disk squeeze film air bearing, determining motion of supported mass by computer program
[ASME PAPER 68-LUBS-38] 13 p2266 A69-27272

Flat disk squeeze film air bearing, determining motion of supported mass by computer program
[ASME PAPER 68-LUBS-35] 13 p2266 A69-27280

Gyroscope motion with unbalanced rotor in run-down mode, integrating equations for small oscillations
13 p2259 A69-27429

Stratified rotating fluid time dependent motion characterized by stability frequency ratio and Coriolis parameter within quasi-geostrophic approximation
13 p2248 A69-28171

Spacecraft periodic motion near center of mass determined by point transformation combined with bifurcation theory, studying stability and parametric dependence
14 p2530 A69-28741

Self oscillations of dynamic systems representing space vehicles, considering periodic motions stability, bifurcation curves and energy consumption requirement limit
14 p2530 A69-28750

Rotary oscillatory solution of parameterized system with stable unexcited motion using successive approximations
14 p2482 A69-28812

Dynamic process during rms deviation of nonlinear system from prescribed trajectory described by nonlinear differential equations
14 p2425 A69-28822

Unsteady pressure on oscillating slender cone in hypersonic flow derived by expanding flow equations in powers of shock density parameter
14 p2389 A69-29020

Finite difference method for motion stability of periodic bipolar vibrational systems, considering perturbations
14 p2534 A69-29039

Rigid obstacle unsteady motion in compressible fluid with load applied to surface layer, deriving numerical solution of pressure expansion
14 p2430 A69-29480

Incompressible viscous fluid steady motion caused by rotating ellipsoid, determining drag moments for circular disk and sphere
14 p2432 A69-29627

Halley comet abrupt daily motion variation ascribed to solid particles ejection from ice nucleus stimulated by gas outflow
14 p2524 A69-29712

Two piston flow stability separated by thin wall in traveling magnetic field, finding piston inertia centers velocity equal to field velocity
14 p2500 A69-29903

Rotating bodies stability conditions relative to radial disturbances found to be field strength dependence on internal mass at any point
15 p2680 A69-30260

Sufficient conditions for asymptotic stability of motion in finite and whole of nonlinear systems by Liapunov second method
15 p2652 A69-30660

Theory for stability of steady motions of system with cyclic coordinates applicable to total damping
15 p2690 A69-30737

Collisionless stability of relativistic, spherically symmetric star clusters against radial perturbations, considering one dimensional sufficient criteria
15 p2691 A69-30765

Steady state motion of multiple unit impact damper attached to sinusoidally excited primary system, determining asymptotically stable regions
15 p2714 A69-31144

Differential equations of steady motion construction from integral manifold
15 p2654 A69-31260

Satellite motion about center of mass, discussing satellite stabilization and libratory motion in gravitational force field, planet resonances, etc
15 p2703 A69-31411

Stability of steady circular motions in systems with hidden variables analyzed by using Lejeune-Dirichlet theorem
16 p2804 A69-31621

Conditional trajectory stability associated with first integral compared with orbital stability on base of topological method
16 p2853 A69-31622

Liapunov functions applications in motion stability theory problems, considering dynamic systems, periodic orbits, optimum damping and control
16 p2804 A69-32248

Bending vibratory motion instability of rotor on elastic shaft with uniform mass distribution along axis, using variational methods
16 p2875 A69-32249

Energy method determining sufficient conditions for fluid motion stability described by infinitesimal theory of viscoelasticity, restricting analysis to confined fluids or periodic velocity field
17 p2949 A69-33015

Rotating cylinder or vortex motion in shear flow with friction, noting drag and rotor force combined influence
17 p2950 A69-33151

Stable motions determination of solid bodies with liquid filled cavities and satellites motions stability in central Newtonian force field
17 p3005 A69-33228

Stability and instability conditions derived for undisturbed motion of system over finite period of time
17 p3005 A69-33314

Isolated symmetric doubly asymptotic solutions existence in neighborhood of symmetric periodic solutions of nonautonomous canonical system with one degree of freedom near resonance
17 p2996 A69-33619

Tire test machine for tire parameter determination in aircraft landing gear shimmy stability studies
[AIAA PAPER 68-311] 17 p2902 A69-34029

Soviet monograph on liquid rocket as controlled plant covering rocket bodies, liquids motion stabilization and gyrosystem positioning
18 p3206 A69-34333

Pendulum motion about stationary axis of solid body containing damper, ascribing instability to center of gravity shift with respect to cavity
18 p3135 A69-34557

Rotary motion stability of axisymmetric solid body or gyroscope suspended on string and containing ellipsoidal cavity filled with liquid
18 p3135 A69-34558

Steady motion stability of satellite gyroscope in Cardan suspension traveling along circular orbit in Newtonian central force field
18 p3135 A69-34585

Nonlinear systems of differential equations to free oscillations about equilibrium, obtaining periodic solutions
18 p3172 A69-34591

Exponential boundedness of system motion for Lure type forced systems, using quadratic Liapunov functions
18 p3164 A69-34674

Spiral disk galaxies stability analysis assuming centrifugal force balancing self gravitation, transforming linearized equations of motion into eigenvalue equations
18 p3200 A69-35131

Instability criterion for motion differing from criteria of Liapunov and Chetaev
18 p3174 A69-35317

Autonomous system steady motion with rotating phase and deviating argument solved by successive approximation over infinite time interval
18 p3175 A69-35323

Liquid filled rigid bodies motion stability defined and solved for system with infinite number of degrees of freedom
19 p3301 A69-36810

Stability of motions about triangular libration points in elliptic restricted three body problem
[AAS PAPER 68-090] 20 p3595 A69-37175

Liapunov stability theory for motion of spacecraft with flexible and moving parts in force free space
[AAS PAPER 68-125] 20 p3617 A69-37180

Jacobi integral and Hill criterion for analyzing motion stability of natural satellites and large planets inside gravitational sphere
20 p3596 A69-37314

Airborne imaging radar motion compensation and sensing problems concerning perturbed signal correction, discussing spatial sensitivity measures and constraints

20 p3490 A69-37645

Positive pitch-flap coupling for controlling helicopter rotor blade motion stability involving blade in-plane deflections

20 p3463 A69-37808

Motion stability in nonresonant case of four pairs of imaginary roots in characteristic equation

21 p3770 A69-38883

Time-independent feedback attitude control system for high accuracy earth pointing motion of stable and unstable satellites in elliptic orbits

21 p3804 A69-39020

Critical case of stable motion for differential equations having two zero roots

21 p3771 A69-39108

Steady motion of frictionless indenters along surface of elastic layer in plane strain, using Fourier transform and Fredholm equations for numerical solution

21 p3837 A69-39155

Motion and stability characteristics of dual spin satellite system with pendulous type nutation dampers, noting mass unbalance effect
[AIAA PAPER 69-857]

21 p3823 A69-39385

Motion stability of hydraulic actuators with open loop control system in presence of nonlinear negative resistance damping

21 p3650 A69-39716

Randomly moving objects holography and reduction of stability requirement during exposure period due to automatic phase modulation

21 p3726 A69-39741

Closed form solution to stability of coupled libration motion of slender axisymmetric satellite in circular orbit limited to small amplitude vibrations

22 p4008 A69-39936

Minimization of motion deviation from prescribed motion analyzed as differential game of converging motions using equations of motion

22 p3980 A69-40105

Representative data of actual forces and moments applicable to large spacecraft attitude control system for typical crew activities obtained through simulation programs
[AIAA PAPER 69-1006]

22 p3921 A69-40380

Motion stability of rapidly spinning satellite, discussing elastic booms effect

22 p4037 A69-41091

Entropy definition for nonequilibrium states, using mathematical theory of stability of motion applied to kinetic equations of irreversible processes

23 p4238 A69-41366

System asymptotic motion stability for given parameter values using algorithms with aid of R functions

23 p4191 A69-41704

Magnetospheric stable charged particle beams for pearl pulsations and discrete VLF radiation in geomagnetic field, attributing synchronization to space charge

23 p4206 A69-41851

Book on interaction between oscillatory systems and energy source of limited capacity, examining stability and resonance phenomena

23 p4170 A69-42166

MOTIVATION

Science education and training, discussing student motivation
[UN PAPER 68-95809]

01 p0179 A69-10515

Lateral hypothalamic stimulation bound eating motivation in animals, comparing electrical stimulation and hunger elicited eating

17 p2910 A69-33752

Electrical stimulation effect on drive specificity in lateral hypothalamus area of sated rat, suggesting fallacy in previous conclusion concerning appetite

22 p3876 A69-40269

Group leadership attempting behavior dependence on situational and perceptual variables

23 p4110 A69-42015

MOTOR SYSTEMS (BIOLOGY)

U EFFERENT NERVOUS SYSTEMS

MOTORS

NT ELECTRIC MOTORS

NT SERVOMOTORS

NT SYNCHRONOUS MOTORS

NT TORQUE MOTORS

Fluidic numerical controls of linear or rotating motors, discussing pneumatic, hydraulic, hybrid logic components and amplifiers

04 p0550 A69-15082

Compact hydraulic power transfer units in aircraft with common connecting shaft for pump/motor elements, discussing integrated power package

06 p0930 A69-17168

Optical motor system to efficiently convert laser energy into mechanical rotational energy, giving equations for controlling motor speed

09 p1442 A69-22457

MOUNTAIN INHABITANTS

Oxygen intake and body temperature of basal and sleeping Andean natives at high altitude

06 p0874 A69-17835

Irreversible blunted respiratory response to ventilation in high altitude natives, considering hypoxic and hypercapnic stimuli

12 p2018 A69-26130

Transient ventilatory response to breaths of nitrogen at rest and during exercise in high altitude and sea level natives

12 p2019 A69-26131

MOUNTAINS

Mountain structures surrounding lunar craters, discussing possible origin by impacting planetesimals shock waves

04 p0661 A69-15142

Clear air turbulence in upper atmosphere and in mountain waves, discussing density variations

24 p4343 A69-42913

MOUNTING

NT RIGID MOUNTING

Compact antivibration mounting for carrying instruments, using bicycle tire inner tube around heavy slab to provide elasticity and damping

09 p1502 A69-22692

Linear analysis of damped flexibly mounted rolling element bearings influence on dynamic rotor unbalance response, including optimum support characteristics
[ASME PAPER 69-LUBS-8]

18 p3212 A69-34382

Mirror mount for shock tube laser cavity with alignment capability, noting seal against internal pressures

22 p3951 A69-41233

External load distribution in bracket between bolts and joint, verifying Reshetov mounting bolt formulas

23 p4168 A69-41417

Mounting elements alloys relaxation characteristics at various temperatures, considering effects of scale factor and stress concentrations

23 p4169 A69-41419

MOUNTS

U SUPPORTS

MOVEMENT

U MOTION

MOVING TARGET INDICATORS

Automatic sequential detector for noncoherent moving target indicator radar, describing noise and clutter residue control

03 p0389 A69-13197

Moving target indicator (MTI) performance degradation by limiting clutter analyzed for various pulse cancellers and verified by time-domain Monte Carlo simulation

03 p0390 A69-13198

Coherent moving target indicator radar receiver behavior as function of input situation, using improvement factor

04 p0556 A69-14338

Line filter compression and positioning of bipolar video pulse trains for conjunctive use with moving target indicator in echo elimination

04 p0558 A69-15071

Moving window radar detector design for moving targets, giving chart for SNR derivation to obtain given detection probability

04 p0558 A69-15073

Digital filters for moving target indicator radars compared with analog filter systems

04 p0580 A69-15463

Statistical analysis of Radicord/radar digitizing and recording/clutter and signal spectra and moving target detection by pulse radar

05 p0721 A69-16619

Input signal history analysis in recognition of moving or changing objects based on classification definition and Wald sequential analysis

08 p1297 A69-20419

Clutter residues of coherent MTI radar receiver, emphasizing IF stages saturation nonlinearity affecting cancelling circuits performance

13 p2220 A69-27941

MULTICHANNEL COMMUNICATION

Input signal history analysis in recognition of moving or changing objects based on classification definition and Wald sequential analysis

14 p2427 A69-29657

Moving targets trajectories determination from radar data, using posteriori probability distribution represented by Markov chain

15 p2566 A69-30334

Moving target selector radars subsystems amplitude and phase instability effects on interference signal suppression

15 p2576 A69-30339

Position sensitive sensors design of optical tracking systems with emphasis on amplitude, phase, frequency and pulse-time sensors

16 p2790 A69-32111

SNR changes loss factor effect during passage through MTI coherent receiver followed by video integrator

16 p2753 A69-32438

Gyroscopic apparent rate meters generating steering moments in inertial navigation systems for determining moving object position and course

18 p3134 A69-34556

Moving target indication, discussing target motion effects dependence on Doppler imaging radar scan rate and compression ratio

20 p3490 A69-37644

Moving model target for laboratory measurements of radar cross section to simulate satellite or reentry vehicle precession motion, noting signature data analysis

20 p3511 A69-37850

Delay line MTI receivers performance calculation accuracy, discussing error for general and restricted number of pulses from single and double cancellation at IF

23 p4117 A69-41605

MRKOS COMET

Sodium atoms and NO molecules role in atomic O 6300 and 5577 A emissions in comet Mrkos 1957d due to charge exchanges and dissociative recombination

14 p2523 A69-29707

MSRE REACTORS

U MOLTEN SALT NUCLEAR REACTORS

MTI RADAR

U MOVING TARGET INDICATORS

MUBIS [SCANNERS]

U MULTIPLE BEAM INTERVAL SCANNERS

MULLITES

Nickel reinforced with mullite whiskers produced by hot pressing

05 p0782 A69-16794

MULTICHANNEL COMMUNICATION

Multichannel amplitude analyzer for space applications, noting use as gamma-spectrometer component in Lunik 10 and 4096 bit/channel traffic capacity

01 p0084 A69-11315

Multichannel telemetering device for magnetically suspended or free flight wind tunnel models noting strain gage pickups, switching and auxiliary circuits
[ONERA-TP-643]

02 p0226 A69-11623

Multichannel digital data compression simulation, discussing algorithms, buffer queue control, identification coding and system performance measurements

02 p0213 A69-12814

Multichannel communication received signals irregular components, discussing signal phase and amplitude fluctuations correlation coefficients

03 p0394 A69-13519

High gain self steering repeater for multibeam microwave array system for earth-satellite communications

04 p0573 A69-14330

Soviet book on multichannel and TV signals transmission over radio relay links using microwave tropospheric scatter propagation

04 p0558 A69-14919

Wideband multichannel optical signals nonlinear distortions during transmission by electrooptical modulators using Pockels effect

05 p0718 A69-15655

Digital adaptive recording system (DARS) 12 channel flight recorder

05 p0766 A69-16754

Diffractional crosstalk in optical beam waveguide during simultaneous multibeam transmission arising from beam coupling by aperture diffraction

07 p1100 A69-18648

Frequency modulation methods and multiple access for communication satellite systems, considering bandwidth for space station transponder

09 p1449 A69-21274

Multiple access in communication satellite systems for achieving maximum flexibility of interconnection between earth stations

09 p1450 A69-21276

Maximum horizontally radiated power of earth stations in any 4-kHz band for multichannel telephony and TV using satellites

09 p1450 A69-21278

Signal processing regenerative technique used for multichannel predetection combining, including carrier suppressed signals

09 p1458 A69-22472

Noise rejection in multichannel telephone signal reception with FM and multiplexing, determining SNR dependence on SNR at receiver input

09 p1459 A69-22640

Multichannel bit error probability for FSK and DPSK obtained for slow nonselective-fading multipath as function of multipath parameters and diversity order

10 p1656 A69-23533

Discrete continuous signals transmission with minimum noise along synchronous and asynchronous channels

11 p1835 A69-24953

Sampled data multichannel telemetry using pseudorandom sequences generated by linear shift registers

12 p2028 A69-25925

Time domain method for hybrid simulation to compute interchannel distortions due to linear transducers in FM systems

14 p2417 A69-29556

Multichannel telemetry system for chronic implantation in animals to monitor physiological parameters

15 p2559 A69-31044

Wideband multichannel optical signals nonlinear distortions during transmission by electro-optical modulators using Pockels effect

16 p2754 A69-32512

Multibeam transmission in optical beam waveguides by simulation, discussing intensity profiles phase fronts and cross scattering

17 p2974 A69-33400

Shifted pulse multichannel generator producing pulses and pulse sequences time delayed with respect to reference channel

17 p2938 A69-33899

Information storage of multichannel analyzer of continuous and pulsed processes

17 p2939 A69-33900

Electro-optical crystals resonance modulator for coherent light beams and microwave frequencies, describing application to multichannel TV transmission system

19 p3266 A69-35763

Demultiplexing of high speed multichannel optical pulse code transmission systems, based on coincidence detection using locally generated reference pulses

19 p3279 A69-36764

Multiple access techniques of SSB-PM and PCM-PM frequency translation for satellite communication system, comparing performance characteristics

21 p3678 A69-39807

Three channel inertial ship or aircraft navigator for determining gravity vector, using earth gravity field model

23 p4162 A69-41320

Equal bandwidth multichannel FM/FM EEG telemetry system using subcarrier frequencies and HF modulation via varactor diodes

23 p4106 A69-41802

Multichannel time division multiple access system for communication satellite networks, considering PSK modems, PCM codes and channel capacity

23 p4129 A69-42511

Multichannel spectral line receiver for 210 ft Australian radio telescope with front ends covering wide frequency range

24 p4283 A69-43115

MULTICHANNEL RECEIVERS

U RECEIVERS

MULTICHANNEL TRANSMITTERS

U TRANSMITTERS

MULTIENGINE VEHICLES

Multieengine helicopter scheduled passenger service operations in Europe

11 p2004 A69-24378

MULTILAYER INSULATION

Scale modeling of multilayer insulated spacecraft for thermal design, considering solar probe and two meter telescope models

[AIAA PAPER 69-613]

17 p3049 A69-33267

Gas pressure differential across multilayer insulation blanket during rapid evacuation predicted, using one dimensional flow theory

[AIAA PAPER 69-608]

17 p3072 A69-33275

Planetary lander model thermal design, analysis and testing, emphasizing lightweight multilayer insulation, discussing thermal/vacuum testing

[AIAA PAPER 69-612]

17 p3049 A69-33296

Heat transfer in evacuated multilayer insulation by radiation and conduction, considering optically thin media separating reflective layers

[AIAA PAPER 69-607]

17 p3073 A69-33300

Damping properties of multilayer coatings for aircraft structures analyzed on duralumin samples subjected to bending at room, elevated and low temperatures

17 p2993 A69-33941

Multifoil thermal insulation for radiation shields from cryogenic temperatures to 3500 F, noting thermal conductivity

19 p3341 A69-35540

MULTILAYER STRUCTURES

U LAMINATES

MULTILOOP SYSTEMS

U CASCADE CONTROL

MULTIMODE RESONATORS

Normal multimode laser action with and without phase locking, using exact steady state solution of Fokker-Planck equation

08 p1325 A69-20291

Microwave resonator characteristics, deriving expressions for Q for pure or coupled electric or magnetic modes

09 p1464 A69-22096

Intensity interferometry by two photon excitation of fluorescence trace for three mode laser under phase locking, free running and FM-like conditions

10 p1705 A69-23811

Singly resonant optical parametric oscillator, noting single mode and multimode oscillation for various pump powers, pump wave depletion and mode competition

11 p1897 A69-25038

Frequency memory in cavity controlled Gunn oscillators, discussing loop gain and bandwidth dependence on oscillation mode and bias voltage

13 p2229 A69-27677

RF band multimode parametric pulsed oscillations in distributed system using one dimensional resonators

16 p2758 A69-31796

Laser multimode emission kinetic theory, discussing quasi-equilibrium disturbance effects and nature of inhomogeneity

19 p3333 A69-35875

Frequency stabilization in He-Ne three mode laser by stabilizing LF oscillations via automatic adjustment of laser resonator length

21 p3738 A69-39078

MULTIPACTOR DISCHARGES

Back bombardment of magnetron cathode as single surface multipactor, noting effects of cathode grooves and output loading

07 p1101 A69-18656

MULTIPATH TRANSMISSION

Multiple transmission principles, examining linear systems, synchronous and asynchronous codes and channel interference

01 p0026 A69-10068

Optimal coherent reception of frequency diversity signals in multipath channels investigated for noise immunity

01 p0028 A69-10375

Mean error rates in microwave PCM systems with wave distortion due to multipath propagation

02 p0208 A69-12307

Digital simulation of demodulator/tracking phase locked loop of navigation/traffic control satellite system in thermal noise diffuse multipath fading environment

03 p0390 A69-13204

VOR path course errors, emphasizing effects of propagation and receiver processing

03 p0392 A69-13245

Coherent PSK system in multipath environment/Rician fading and additive Gaussian white noise/ with phase locked loop for coherent reference extraction

03 p0393 A69-13255

Path length and path length rate variations in synchronous satellite communications link

04 p0561 A69-15448

Nonlinear distortion of FM signal during passage through multipath medium, using analysis of linear passive four terminal network

05 p0721 A69-16531

UHF telemetry flight tests at White Sands Missile Range, discussing multipath and target scintillation problems

07 p1082 A69-19116

Optical communications applications with emphasis on large capacity transmission

09 p1456 A69-22131

Multipath fading reduction on line of sight microwave radio relay links by dual space diversity, noting effects of vertical antenna separation, frequency, etc

[IEEE PAPER 68-TP-350-COM]

10 p1656 A69-23535

Analog signal transmission through randomly fading channels, proposing pseudorandom phase reversals method for slowly varying multipath communication channels

11 p1834 A69-24552

Digital simulation of phase locked receiver in diffuse multipath fading environment with band limited thermal noise

11 p1839 A69-25298

Binary error investigation in noncoherent FSK communication link with nonselective fading, noting Doppler shift

14 p2414 A69-29498

Multipath resolution of tropospheric scatter medium by incorporating Rake instrumentation into tropospheric transhorizon microwave experiments

14 p2448 A69-29524

Nonlinear distortion of FM signal during passage through multipath medium, using analysis of linear passive four terminal network

16 p2753 A69-32473

Optimal ratio predetection combiner used with diversity signals and various modulations, showing significant improvement in telemetry systems performance

19 p3270 A69-36241

Field strength determination at reception point for long range short wave paths, taking into account multiple ray paths and antenna radiation patterns

20 p3520 A69-37035

MULTIPHASE FLOW

NT TWO PHASE FLOW

Gray radiation and conductive heat transfer in Oseen-like free mixing flow, computing temperature distribution by inversion integral

02 p0354 A69-12504

Environmental temperature and water vapor increases associated with ascending thermals estimated by penetrative convection

03 p0460 A69-13340

Viscid-inviscid equations solution, describing flows with coupled mixing, combustion and lateral pressure gradients

[AIAA PAPER 69-83]

06 p1037 A69-18109

Shock wave in two dimensional mixed transonic airfoil flows, discussing initial value problem for flow downstream of shock

[AIAA PAPER 69-43]

06 p0915 A69-18180

Mixed sub- and supersonic gas flow in plane pressure nozzle free of vortex and neglecting viscosity and heat conduction

07 p1050 A69-18739

MULTIPLE BEAM INTERVAL SCANNERS

Multiple beam electronically steerable retrodirective antenna array with automatic inertialess compensation for altitude or beacon location

02 p0212 A69-12816

Broadband multibeam antenna array with frequency independent beam directions, noting aperture gain limitation

08 p1288 A69-20965

Maxson multibeam antenna design for noninteracting beams, considering beam shapes and positions and applications

09 p1463 A69-21676

Electronically scanned and fixed multiple beam phased arrays for spaceborne microwave radiometric sensors

12 p2044 A69-26977

Electroacoustic transducers interaction effects in multibeam acoustical reflector type receiving antennas

13 p2227 A69-27536

MULTIPLE DEGREES OF FREEDOM

U DEGREES OF FREEDOM

MULTIPLETS

U FINE STRUCTURE

MULTIPLEX TRANSMISSION

U MULTIPLEXING

MULTIPLEXERS

U MULTIPLEXING

MULTIPLEXING

NT FREQUENCY DIVISION MULTIPLEXING

NT TIME DIVISION MULTIPLEXING

Adaptive multiplex telemetry use in scientific satellite data management

02 p0212 A69-12817

Space and immersion suits physiological evaluation by pulse duration multiplexing telemetry, using commercial FM receiver

06 p0883 A69-17845

Tape flutter and additive noise time base errors in coherent demodulation of suppressed carrier AM multiplex

07 p1082 A69-19119

Analog to digital conversion for data sampling systems including scanning, distributors, multiplexing, automatic ranging, noise reduction and data storage techniques

10 p1660 A69-23232

Design of 126 channel PCM telemetry unit for C-5 aircraft flight test, discussing FET analog multiplexing

10 p1693 A69-23275

Holographic multiplexing for producing three dimensional reconstruction of nonlaboratory objects in horizontal direction, noting TV and X ray pictures applications

11 p1883 A69-24684

Multiple information storage in sampled hologram in space division multiplexing holography, constructing hologram with sound waves and reconstructing images with laser light

12 p2079 A69-25921

Time function multiplex system for simultaneous communication via satellite between number of stations, considering transmission capacity decrease due to hard limiting amplifier

17 p2919 A69-33320

Phase locked loop design of desensitized monolithic integrated circuits for FM multiplex signal filtering and demodulation, describing external tuning

19 p3273 A69-36274

Computer program designing multiplex taper to minimize FM/FM telemetry system carrier threshold SNR, examining noise behavior of multiplex system stages for system performance

19 p3273 A69-36275

Addressable remote multiplexed PCM data system used on Titan III launch vehicles

19 p3274 A69-36279

Demultiplexing of high speed multichannel optical pulse code transmission systems, based on coincidence detection using locally generated reference pulses

19 p3279 A69-36764

MULTIPLICATION

Multiplication effects on noise in Si avalanche diodes, noting high resolution apparatus for measurement of spatial variations

04 p0573 A69-14332

Multiplication of solutions of homogeneous linear differential systems

08 p1342 A69-20349

Lower bound for time required for group multiplication by logic circuits, using modified Winograd model for Abelian group

12 p2034 A69-26752

MULTIPLIER PHOTOTUBES

U PHOTOMULTIPLIER TUBES

MULTIPLIERS

Full multiplier design based on stable iterative array cells interconnected to provide logical functions, noting capabilities for binary numbers

01 p0048 A69-11138

Time averaged products and squares of fluid turbulence signals at LF, using Hall effect multiplier device and integrating voltmeter

04 p0601 A69-15116

Stability of time varying systems by construction of multipliers with prescribed phase characteristics

05 p0740 A69-16598

Collection efficiency of continuous dynode electron multiplier arrays, discussing incident electron current

06 p0897 A69-17699

Analog multiplier with controlled current splitting devices and feedback technique for stabilization of transfer characteristics, noting implementation in bipolar transistor

09 p1475 A69-22584

Noise reduction techniques using injection phase locking and high-Q cavities for HF oscillator high order multiplier and avalanche diode oscillator microwave sources

14 p2420 A69-29458

Pulse height distributions, gain and counting rate characteristics of two magnetic strip multipliers and two channel multipliers in 1.5 to 44 A region of soft solar X-rays

17 p2972 A69-33082

Vector integral extension to optimal trajectory coordinate multiplier systems with constant of motion demonstrated for coast-arc problem

[AIAA PAPER 69-907] 21 p3807 A69-39339

MULTIPOLAR FIELDS

Coulomb approximation for dipole and quadrupole transitions, calculating tables for radial matrix elements

01 p0124 A69-10901

Closed analytic expressions for vector potential and magnetic field generated by axisymmetric multipole line currents

06 p0965 A69-17518

Polynomial representations of mirror cusp fields produced by combination of mirror coils and loffe /multipole/ bars

06 p0966 A69-17522

Axially symmetric static solutions of Einstein equations with singularities on z axis allowing for higher multipole moments in general relativity

08 p1350 A69-19783

Electromagnetic multipole left- and right-hand circularly polarized modal fields for multiarm log spiral antennas, discussing current distributions, multipole coefficients and field patterns

08 p1281 A69-20018

Plasma flow motion and polarizing interaction in multipole magnetic field

08 p1370 A69-21015

Impurity elimination from hydrogen plasma jets injected from coaxial source normal to octupole magnetic field

08 p1370 A69-21016

Elastic materials with particle interactions of finite range, establishing continuum field and constitutive equations from particle mechanics

13 p2371 A69-28674

Hydrogen plasmas motions in multipole magnetic fields, discussing plasma polarization, double vortex flow patterns and field line configurations

15 p2661 A69-30924

Multipole configuration toroidal plasma confinement device MHD equilibrium and stability from measured data

16 p2823 A69-32563

Spherical aberration effect on atomic beam focusing in six pole magnetic system

19 p3380 A69-36602

Atomic sources local multipolar field in anisotropic dielectrics determined from magnetic dipole radiation spatial distribution measurements

21 p3779 A69-38531

Geomagnetic multipole parameters changes using spherical harmonic coefficients of geomagnetic potential, relating to secular variation field

23 p4158 A69-42171

Force acting on multipole in external magnetic field, noting dependence on multipole axes

23 p4158 A69-42172

H plasmoid tail cut-off eliminating plasma impurities during injection across octupole magnetic field from coaxial source

24 p4358 A69-43474

MULTIPOLES

Simple dipolar stresses, noting effect of antisymmetry on equations of motion and energy equation

06 p1022 A69-17239

MHD stability of straight multipoles with shear, considering scalar-pressure perfectly conducting two dimensional MHD equilibria

09 p1546 A69-21576

Relativistic behavior of electromagnetic multipolar nongravitating particle, discussing integrability of field equations

14 p2486 A69-29594

MULTIPROGRAMMING

Multiprocessing system simulation using GPSS /General Purpose Simulation System/ model

02 p0213 A69-12492

Parameters distinguishing analytic queueing models of time sharing algorithms, emphasizing techniques used for analyzing round-robin and multiple level queueing models

19 p3279 A69-35600

Real time multiprocessing telemetry ground support integrated system design with expanded definition of hardware/software decision tradeoffs

[AIAA PAPER 69-971] 22 p3907 A69-40351

MULTIPROPELLANTS

U ROCKET PROPELLANTS

MULTISTAGE COMPRESSORS

U TURBOCOMPRESSORS

MULTISTAGE ROCKET VEHICLES

NT ATLAS CENTAUR LAUNCH VEHICLE

NT ATLAS SLV-3 LAUNCH VEHICLE

NT BERNICE ROCKET VEHICLE

NT BLACK KNIGHT ROCKET VEHICLE

NT DIAMANT LAUNCH VEHICLE

NT ELDO LAUNCH VEHICLE

NT KAPPA ROCKET VEHICLES

NT SATURN LAUNCH VEHICLES

NT SATURN 5 LAUNCH VEHICLES

NT SCOUT LAUNCH VEHICLE

NT SKYLARK ROCKET VEHICLE

NT TITAN LAUNCH VEHICLES

NT TITAN 3 LAUNCH VEHICLE

Turquoise satellite booster, using stages of SSBS and MSBS ballistic missiles

02 p0334 A69-12232

Atmospheric entry testing in terms of velocity-altitude duplication, suggesting multistage rocket propelled aeroballistic range type testing

[AIAA PAPER 69-166] 06 p0907 A69-18189

Optimum attitude program for multistage satellite launch vehicle with impact restrictions

07 p1229 A69-18492

Feasibility of nuclear stage for space missions, discussing Saturn 5 third stage replacement, payload gain, reactor and engine size

08 p1409 A69-20158

Variation in spinning velocity around axis of last stage of solid propellant rocket in flight

08 p1409 A69-20160

Dynamic programming computational approach to optimization with state variable discontinuities, treating problems as multistage optimization with continuous subarc stages

09 p1474 A69-22440

Space stage separation qualification of ONERA rocket vehicles based on angular perturbation measurements during variable roll speeds

10 p1669 A69-23005

Multistage rocket trajectories optimized by second order numerical technique and digital computer program, considering coasting, vacuum flight and transition times

16 p2857 A69-32154

Two stage vehicle gross weight minimization determined by slide rule computation using formula based on specific impulse differences between stages

19 p3429 A69-35918

Rapid Targeting Procedures computer program for optimized orbital payload and associated launch vehicle targeting data with one submittal and minimum user intervention

[AAS PAPER 68-148] 19 p3402 A69-35951

MULTIVIBRATORS

NT FLIP-FLOPS

NT MONOSTABLE MULTIVIBRATORS

Soviet book on impulse generators in transistors covering multivibrators and pulse generators with timer circuits, crystal controlled frequency and delayed feedback

04 p0578 A69-15053

Multivibrator with two widely different zones of discontinuous oscillation

06 p0896 A69-17474

Multivibrator circuit for generation of oscillations with frequency stability against transistor ambient temperature changes

12 p2036 A69-25919

Resonant fixtures used for mechanical amplification of vibrator output to desired test levels

15 p2588 A69-30404

MUONS

Pionic 2p-1s X ray transition energy and natural linewidth and muonic 2p-1s X ray transition energy measurements for Na 23

01 p0122 A69-10035

Energetic cosmic radiation in deep mines, giving hypothesis of new particles more effective than muons

01 p0144 A69-10444

Extensive air showers at sea level, presenting experimental data for muon and electron numbers spectra

03 p0498 A69-12937

Muons in EAS, single unaccompanied muons, underground muons and experiments involving neutrinos

03 p0499 A69-12946

Upper limit estimated for anomalous interaction between cosmic muons with greater than 100 Bev energy

06 p0986 A69-17246

Data on muons indicating temperature effect diurnal maximum and pressure corrected daily variation

06 p0924 A69-17294

Low energy muons and nuclear active particles measured with extensive air showers array composed of scintillation detectors, spectrometer and Geiger counters

06 p0990 A69-17299

Extensive air shower high energy muons measurements noting energy spectrum, lateral spread and dependence on shower size

06 p0990 A69-17300

Cosmic ray magnetic spectrograph for measurement of momentum spectrum, charge ratio and specific ionization of muons, discussing magnetic and scattering displacement

06 p0925 A69-17302

Cloud chamber for measuring specific ionization in relativistic region by muons in gases, using drop counting method

06 p0925 A69-17303

Simultaneous parallel penetrating muons observed in multiplate cloud chambers, obtaining information about sea level muons interactions and EAS

06 p0991 A69-17304

Energy spectra of muons determined from knock-on electrons projected angles of emission in C, Al and Cu

06 p0991 A69-17305

High energy muons Cerenkov radiation, using water filled counter as function of muon momentum, noting no intensity decrease

06 p0991 A69-17306

Muon component of extensive cosmic ray showers, discussing effect of multiplicity of secondary particles created by high energy nuclear interactions

07 p1207 A69-19325

Direct muon production, discussing range vs energy relation for favorable experiment and difficulties with observed muon flux isotropy

07 p1209 A69-19406

Renormalizable weak interaction mechanism for generation of high energy muons from TeV cosmic rays in upper atmosphere

09 p1581 A69-22530

Weak interaction theory modifications needed for high energy cosmic ray muons to not violate conservation of probability

09 p1583 A69-22758

Low momentum muon directional coupling coefficients based on latitude survey of directional meson intensity

09 p1583 A69-22759

Secondary muon flux from primary cosmic ray particles monitored during minimum solar activity by telescopes at 60 mwe underground

10 p1769 A69-23827

Charged primary cosmic rays responsible for relative intensities of muon-poor extensive air showers at mountain and sea levels

12 p2152 A69-27099

High energy nuclear active particles and muons studied with calorimeters, noting cascades muon origin and muon energy spectra

13 p2331 A69-28395

High energy muons energy spectrum in extensive cosmic ray showers from spectrum study of ionization bursts due to penetrating component

13 p2332 A69-28403

Sea level fluctuations of electron-photon, muon and active nuclear components of extensive cosmic ray showers determined, obtaining shower parameters

13 p2332 A69-28406

Cosmic ray muons energy and angular distribution measurements, obtaining curve with respect to projection angles

13 p2332 A69-28420

Cosmic ray muons angular distribution measuring device for determining pion/kaon ratio

13 p2332 A69-28421

Form factor of nucleus effect on high energy muons bremsstrahlung cross section

13 p2333 A69-28422

Muon energy losses due to pair formation taking into account nucleus screening by electrons

13 p2304 A69-28423

Monte Carlo method used to calculate probability of muon penetration to deep underground levels with sea level energies

13 p2333 A69-28424

Muonic component diurnal wave trains at 70 mwe during cosmic ray decreases, discussing Forbush decay as result of shock front advance

14 p2511 A69-28962

Diurnal variation of cosmic ray muon intensity near geomagnetic equator and primary anisotropy monitored by cubical counter telescope

14 p2512 A69-28966

Lateral density distribution of muon component in central region of extensive air showers, using Lodz analyzer

15 p2677 A69-31481

Ground level muon density of extensive air showers related to threshold energy and zenith angle for primary particles

15 p2678 A69-31483

Frequency of multiple muons from extensive air showers as function of zenith angle, noting mean transverse momentum and density spectrum

15 p2678 A69-31484

Multiple muon showers penetrating deep underground, discussing radial extent and occurrence frequency against multiplicity spectrum

15 p2678 A69-31485

Electromagnetic muon-nucleon interaction explanation for observed horizontal air showers, reexamining shower data in view of triplet particles

15 p2678 A69-31498

Near horizontal air showers relationship to direct muon production and heavy triplet particles of unit charge, discussing nuclear interactions and muon bremsstrahlung

15 p2678 A69-31499

High energy cosmic ray muon charge ratios at large zenith angles measured as function of momentum by using spectrometer

17 p3023 A69-33321

Cosmic ray shower axis mean distance from apparatus determined by measuring muon to charged particles densities ratio

17 p3024 A69-33580

Cosmic ray muons for calibrating dE/dx counter used in particle identification by determining cosmic particles distribution as function of energy losses due to ionization

21 p3724 A69-39075

Air showers muon threshold energies deep underground as function of zenith angle, discussing nucleon-air-nucleus collision parameters variation effect

23 p4207 A69-42497

Diurnal variations in solar cosmic ray muon component near sea level, using scintillation counters assembled in muon telescope array

23 p4207 A69-42498

Cosmic ray pions and muons anomalous measurements above 1000 Gev explained by medium-strong contact interaction between protons

24 p4353 A69-43194

MURRAY METEORITE

Sporopollenin content of Orgueil and Murray meteorites as evidence for extraterrestrial life

21 p3662 A69-39617

MUSCLES

NT MYOCARDIUM

Increased gravitational stress effects on esophageal sphincter pressures and gastroesophageal reflux in rhesus monkeys, noting cardia competence

06 p0874 A69-17838

Structural and functional changes in cells as result of freezing of muscular tissue or suspension of erythrocytes

10 p1642 A69-23117

Histochemical tests on enzymes distribution in rhesus and squirrel monkeys intrafusal and extrafusal muscle fibers

12 p2018 A69-25777

Hypokinesia effects on transversostriated muscle fibers of mice, noting changes in myofibrillar apparatus, mitochondria and sarcoplasm

13 p2212 A69-28616

Histological and histochemical studies of dephosphorylating enzyme distribution in muscle spindle capsule of guinea pig thigh muscles and cat calf muscles

15 p2554 A69-30406

Surface electromyography /EMG/ frequency analysis of normal and pathological muscle or nerve contraction as diagnostic tool for industrial physician

21 p3664 A69-38920

Critical closing phenomenon in dog gracilis muscle, using pressure flow measurements and tissue staining techniques, detecting sudden vessel closure in microcirculation

22 p3873 A69-40202

Catalytic, physical and chemical properties of enzyme lactate dehydrogenase isolated from lobster tail muscle

22 p3897 A69-41069

White mice gastrocnemius muscle wet mass, dry mass and noncollagen-nitrogen /NCN/ content, noting /NCN/ content dependence on body mass

23 p4080 A69-41406

Tension effects on amino acid incorporation rate into proteins of cross-striated muscles of rats

23 p4083 A69-41458

Isometric recording device for tensile stresses on muscle preparations in vitro, based on differential transformer

23 p4111 A69-42056

Electric potential measuring device for frog isolated skeletal muscle fiber mounted on micromanipulator

23 p4111 A69-42058

Energy cost of muscular exercise in gastrocnemius muscle of dogs anesthetized with morphine, chloralose and urethane

23 p4093 A69-42065

Fibrosis histological patterns of left ventricular papillary muscles from comparison of hearts with myocardial infarction, noting acute and healed mural lesions

24 p4261 A69-42724

Radioisotopic determination of haemodynamic and bioelectric disturbances of rat striated muscles subjected to acceleration and hypokinesia

24 p4268 A69-43409

MUSCULAR FATIGUE

Hypokinesia effect on dynamics of metabolic processes in athletes muscular system by comparison of diuresis, creatinine excretion and cutaneous fat layer indices

10 p1646 A69-23582

Exhaustion time extension in rats by altitude acclimation, noting adaptation loss resulting from physical exercise discontinuation

23 p4086 A69-41787

MUSCULAR FUNCTION

Musculoskeletal system and weightlessness state, concerning muscular disuse atrophy possibility during prolonged space flights

06 p0873 A69-17018

Hypokinesia muscular activity deficit in males confined to bed rest compensated for by physical exercise, noting orthostatic resistance, acceleration endurance, immunity, etc

08 p1263 A69-19932

Arterial tone and human muscular activity limitations, analyzing hypodynamic effects on aorta, arm and leg vessels constriction

10 p1647 A69-23586

Posture role in physiological effects of acceleration on motor activity, discussing gravitational importance to vital processes

13 p2211 A69-28593

Hand movements in water environment, weightlessness and normal gravity conditions, discussing inner coordinative structure and muscular efforts

17 p2915 A69-33385

Muscle motor performance under continuous practice conditions, analyzing individual differences, intraindividual variability and remoteness

17 p2911 A69-34003

Muscle power output relation to imposed load modified to accommodate inverse relationship between generated force and contraction speed for determining maximum strength

17 p2916 A69-34011

Nervous system relations to insect flight musculature of lift and thrust mechanism

21 p3651 A69-38780

Positive phase shift relation to elastic modulus enhancement of smooth muscles of rabbit, cat and dog bladder, pulmonary artery and large veins

23 p4083 A69-41459

Cat papillary muscle length-tension curves before and after inotropic intervention, noting optimal length changes

23 p4084 A69-41461

Muscle function measurement in astronauts using electromyogram, electrocardiogram and isometric tension at fixed percentage of maximum voluntary contraction

23 p4103 A69-41684

Exercise prescription for hypokinetic airline pilots to prevent physiological deterioration and maintain performance, discussing predictive tests, tolerance evaluation, training regimens, etc

23 p4106 A69-41800

Spinal cord temperature effect on stretch responses of muscle spindle endings of triceps surae, anterior tibialis and extensor digitorum longus in anesthetized cats

23 p4093 A69-42067

Rodent swimming and treadmill training effect on capacity of mitochondrial fraction from hind limb muscles to oxidize pyruvate triples

23 p4095 A69-42084

Primary muscle spindle afferents from gastrocnemius muscle of cat before, during and after cold shivering, utilizing ramp stretches of same muscle

23 p4096 A69-42091

- Training effect on fast muscle isometric contraction in rats, discussing mechanical characteristics
23 p4097 A69-42095
- Spinal cord temperature influence on stretch response of tonic and phasic alpha-motoneurons by filament recordings from ventral roots in anesthetized cats
23 p4098 A69-42099
- Isometric contraction tension after sudden isotonic to isometric contraction mode change in cat papillary muscle, discussing temperature effects, tension development changes, etc
24 p4258 A69-42631

MUSCULAR STRENGTH

- Isolation effects on higher nervous activity, motor and vegetative reactions, muscular strength and emotional state
03 p0377 A69-14202
- Hypohydration effects on isometric muscular strength, noting decreasing trends in maximal strength
05 p0708 A69-15983
- Muscle power output relation to imposed load modified to accommodate inverse relationship between generated force and contraction speed for determining maximum strength
17 p2916 A69-34011
- Muscular strength dynamometric measurements in subjects during prolonged inactivity with restricted caloric and protein intake, showing decrease in strength
21 p3653 A69-38901
- Isometric tensions of detached lateral rectus muscles measured during strabismus surgery for mechanical components of human eye movements, giving muscle tone range
22 p3872 A69-40200
- Maximum voluntary isometric muscle strength relation to endurance time in static work during partial curarization
22 p3890 A69-40213

MUSCULAR TONUS

- NT HYPOTONIA**
- Oculomotor muscular tonus of rabbit during rocket flight acceleration and weightlessness
07 p1062 A69-18590
- Psychomotor reaction time and motions, myogenic tonus at rest and precision of monkeys during rocket flights along ballistic curve, noting weightlessness effect
10 p1646 A69-23575
- Prolonged bed rest effect on human myogenic tonus and proprioceptive reflexes, comparing test subjects with and without physical exercises
10 p1646 A69-23583
- Phase and tonic activity of oculomotor apparatus of rabbits during vestibular reflexes and postrotational nystagmus
20 p3469 A69-37243
- Motor and tonic reactions in animals during weightlessness, discussing interaction between gravity receptors and visual analysis
20 p3470 A69-37247
- Whole body LF mechanical vibration effects on anesthetized dogs peripheral circulation and vascular smooth muscle
22 p3875 A69-40228
- Spontaneous rhythmical activity and mean vascular tone dependence in isolated helical rat aorta strips on extracellular concentration of noradrenalin
23 p4093 A69-42069
- Venous tone, peripheral venous pressure, skin and muscle blood flow, alterations of heart rate and respiration in men during leg exercise
23 p4096 A69-42090

MUSCULOSKELETAL SYSTEM

- NT BONES**
- NT CARTILAGE**
- NT CEREBRUM**
- NT COLLAGENS**
- NT CRANIUM**
- NT MARROW**
- NT SCIATIC REGION**
- NT SKULL**
- NT VERTEBRAL COLUMN**
- Thyroid gland role in resistance and myoglobin content of skeletal muscles of flat land and high altitude acclimatized white rats
05 p0709 A69-16517
- Musculoskeletal system and weightlessness state, concerning muscular disuse atrophy possibility during prolonged space flights
06 p0873 A69-17018

- Physiological response of human skeleton to hypogravity and hypodynamics studied by bed rest experiments, suggesting disuse atrophy of bone
06 p0873 A69-17019
- Decrease in bioelectric activity of skeletal muscles in animals and man during intermittent acceleration and weightlessness
07 p1062 A69-18591
- Thyroid gland role in resistance and myoglobin content of skeletal muscles of flat land and high altitude acclimatized white rats
18 p3096 A69-34736

MUSEUMS

- Meteorite collections in museums of Lvov, U.S.S.R., noting specimens from Pultusk shower, Kansas, Mexico, Czechoslovakia and U.S.S.R.
01 p0160 A69-11388

MUTATIONS

- Accelerated helium and carbon ions effects on mutation-induction and nuclear inactivation in *Neurospora crassa* compared with X rays, discussing relative biological effectiveness /RBE/
03 p0373 A69-13490
- Recessive lethal mutations frequency in gametes of male and female *Drosophila melanogaster* onboard Vostok spacecraft
07 p1063 A69-18598
- Amber suppressors conversion to ochre suppressors in RNA of bacterium or bacteriophage using uracil mutagen
07 p1068 A69-19493
- Escherichia coli* WWU multiautotrophic revertants with nonsense suppression, noting role in aberrant morphology and in catabolizing thymidine for energy and carbon
07 p1069 A69-19503
- Radiobiology of *Tradescantia* clone orbited in Biosatellite 2, analyzing space effects on spontaneous and radiation induced mutation and cytological changes
15 p2556 A69-31321
- Insects mutational responses to space flight and associated radiation on biosatellite 2 compared with ground based controls
20 p3476 A69-37618
- Adenosine triphosphate /ATP/ production in normal cells and sporulation mutants of *Bacillus subtilis*, discussing applications of ATP synthesis response to C sources
22 p3886 A69-41076

MYOCARDIUM

- Electrocardiographic tests to study changes in electropotentials of heart in flying personnel after flight, noting changes in myocardium
03 p0378 A69-14207
- Myocardial repolarization changes in healthy persons with restricted motor activity
07 p1066 A69-18984
- Glycolysis rate and lactic acid content in rats myocardium during adaptation to hypoxia, using pressure chamber
10 p1645 A69-23501
- Bed rest effect on orthostatic tolerance of patients with acute myocardial infarction and without heart failure
10 p1648 A69-24189
- Myocardial changes in rabbits after general chronic ionizing irradiation attributed to lower cardiac activity, hypotrophy and dystrophy
17 p2906 A69-32929
- Myocardial repolarization changes in healthy persons with restricted motor activity
20 p3480 A69-38232
- Heart muscle ultrastructure during general hypoxia in dogs, noting development of compensatory-adaptational and dystrophic changes in myocardial intracellular components
21 p3651 A69-38412
- Temperature dependence of action potential, isometric tension development and relaxation rate of mammalian myocardium at low temperature, considering Ca ions role
23 p4092 A69-42060
- Myocardial muscle fibers transient inward current components during sheep ventricle voltage clamp analysis
23 p4095 A69-42080
- Refractory period adaptation to sudden heart rate changes in dogs
24 p4257 A69-42628
- Contraction frequency increment effects on myocardial oxygen consumption in dogs determined for various heart rate levels, using isovolumic left ventricular preparation
24 p4258 A69-42634

- Experimental myocardial infarction in dogs, examining lysosomal enzymes activity changes in soluble and particle-bound fraction
24 p4259 A69-42636
- Myocardium protein metabolism and heart physiology and pathophysiology, examining contractile function and energy transformation in hyperfunction, hypertrophy and heart failure
24 p4259 A69-42637
- Fibrosis histological patterns of left ventricular papillary muscles from comparison of hearts with myocardial infarction, noting acute and healed mural lesions
24 p4261 A69-42724
- Supraventricular arrhythmias after acute myocardial infarction, noting benefit of early DC shock
24 p4262 A69-42729

MYOELECTRICITY

- Myocardial repolarization changes in healthy persons with restricted motor activity
07 p1066 A69-18984
- Myocardial repolarization changes in healthy persons with restricted motor activity
20 p3480 A69-38232
- Myocardial muscle fibers transient inward current components during sheep ventricle voltage clamp analysis
23 p4095 A69-42080

MYOPIA

- Plots myopia incidence statistical study after initiate medical examination, emphasizing skiagram value in prognosis
24 p4267 A69-43400

N

N-N JUNCTIONS

- Photoelectric properties of n-n junction interfaces in gallium phosphide and arsenide semiconductors
02 p0294 A69-11630
- Differential capacitance of n-n heterojunction calculated by metal semiconductor contact method
09 p1555 A69-21476
- Emission and diffusion theories of metal-semiconductor contacts for describing current characteristics of abrupt isotype nGe-nGaAs heterojunction
11 p1938 A69-25115
- Differential capacitance of n-n heterojunction calculated by metal semiconductor contact method
15 p2669 A69-30721

N-P JUNCTIONS

U P-N JUNCTIONS

N-P-N JUNCTIONS

- Double diffused planar Ge n-p-n and p-n-p transistors with high switching speed, noting fabrication and performance
05 p0809 A69-16557
- Recovery and long term reliability of Si n-p-n transistors subject to gamma radiation, using military specifications for failure
06 p0976 A69-16878
- Monolithic operational amplifier design combining junction FET with n-p-n transistor
07 p1103 A69-18876
- Nondrifting n-p-n semiconductor current gain dependence on surface recombination rate
13 p2236 A69-28547

N-TYPE SEMICONDUCTORS

- Vacuum deposited n-type InAs films magnetoresistance coefficient dependences on length-to-width ratio, homogeneity moving carriers size and magnetic inductance
01 p0136 A69-10254
- Electrical properties of gold-gallium arsenide n-type junctions investigated for influence of crystallographic orientation of surface and charge carrier density
01 p0138 A69-10432
- Negative differential resistance effect producing relaxation type oscillations in n-type gallium arsenide
01 p0138 A69-10557
- Current/field characteristic of n-type GaAs, using high power microwave techniques in presence and absence of transverse magnetic field
01 p0139 A69-10819
- N- and p-type InSb and GaSb single crystals microhardness, noting decrease after doping is limited to thin surface layer
01 p0139 A69-10832
- Impurity concentration in n-type indium antimonide semiconductors at liquid nitrogen temperatures estimated by current-voltage measurements
02 p0294 A69-11631

Low field helicon wave transmission through n-type Ge at liquid He temperature, noting cyclotron resonance damping

02 p0295 A69-11787

Faraday effect of free carriers on n-type GaSb at 20 K, determining mass and mobility of electrons from Hall effect and conductivity

02 p0298 A69-12039

Many valley n-type Ge and Si semiconductors dissipative current breakdown effects, noting dependence on symmetry of valleys and phonon scattering pattern

02 p0298 A69-12098

Conduction band anisotropy in n-type cadmium tin arsenides, analyzing galvanomagnetic tensor and distribution of isoenergetic surfaces for electrons

03 p0488 A69-13888

Transport phenomena analysis in n-InSb semiconductors during elastic/inelastic current carrier scattering

03 p0492 A69-14171

IR absorption and reflection in doped n-GaSb, obtaining absorption coefficient for various impurity concentrations

03 p0492 A69-14174

N-type GaAs single crystal magnetoresistivity, noting charge carrier scattering mechanisms

03 p0492 A69-14177

Cathodoluminescence of n-type GaAs with various carrier concentration bombarded with 24-kv electrons, studying emission spectrum for radiative transition

04 p0639 A69-14436

Fermi level in n- and p-type Ge after irradiation by 50 Mev electrons determined by temperature dependence of carrier concentration

04 p0640 A69-14444

N-type Si surface photopotential, conductivity and capacitance during anodic oxidation in absolute ethylene glycol

04 p0643 A69-15260

Longitudinal and transverse magnetoresistance in n-type InSb single crystals in magnetic fields, noting preparation effect on existence magnetophonon oscillations

04 p0643 A69-15262

Homogeneous electroluminescence at 77 K in n-type GaAs single crystals without artificial p-n junctions, noting effects of electric field strength and Zn doping

04 p0644 A69-15271

Bridge circuit n-type conductivity converter with internal compensation of parasitic effects

05 p0727 A69-15641

Multiple high field domain nucleation in GaAs, discussing dependence on contact inhomogeneities

05 p0807 A69-15959

Incremental conductance of heavily doped n-type Si semiconductor barrier tunneling as function of bias voltage, indicating Fermi level dependence on dopants

05 p0808 A69-16285

Electrical properties of n-type Cd tin arsenide single crystals with impurity concentrations at various temperatures

05 p0809 A69-16375

Diffused Si and GaAs diodes electroluminescence and current-voltage characteristics

06 p0893 A69-16898

Gunn effect verification using n-type semiconductor single crystals in DC field, noting microwave field polarization plane rotation

06 p0978 A69-16902

Hall effect and magnetoresistance for compensated n-InP samples, discussing dependence on magnetic field

06 p0978 A69-16987

Hall effect and resistivity of n-type gallium arsenide phosphides doped with Te and Se

06 p0978 A69-16988

Temperature dependence of n-InSb Hall coefficient and resistivity, noting increase in conductivity with degree of compensation associated with electrical breakdown

06 p0978 A69-16990

Quantum oscillations of Maggi-Righi-Leduc (MRL) effect in n-InSb and n-InAs samples from single crystals at liquid helium temperature

06 p0979 A69-16992

Injection characteristics of n-aluminum gallium arsenides p-GaAs heterojunctions from recombination radiation spectra

06 p0979 A69-16993

Domain oscillations removal in n-type gallium arsenides by externally applied microwave field, noting doping effect on LSA conversion efficiency

07 p1196 A69-18446

Stable negative RF conductance and oscillation conditions for n-GaAs crystals of low $n \times L$ product

07 p1197 A69-18448

Absorption edge broadening by electric field in Gunn domain of N-GaAs crystals

07 p1197 A69-18454

Nonisothermal wave propagation in n-type indium antimonide in orthogonal static and magnetic fields, considering instabilities and acoustic and polar optical phonon scattering

07 p1197 A69-18467

Dependence of microwave emission from n-InSb on crystalline orientations, noting anisotropy in case of rotation in perpendicular plane

07 p1198 A69-18647

Equations for electron scattering by sound in n-type semiconductors, giving corrections to sound propagation velocity during interactions

07 p1199 A69-18680

Temperature dependence of conversion coefficients and sensitivity of n-type InSb detectors in millimeter and submillimeter ranges

07 p1199 A69-18683

Majority carrier concentration changes in P-doped n-type Si during fast electron bombardment, discussing relative effect of A and E centers

07 p1199 A69-18684

Magnetophonon oscillations of transverse magnetoresistance of n-type epitaxial GaAs in pulsed magnetic field

08 p1373 A69-20760

Vapor deposition of high purity epitaxial layers of n-type gallium arsenide, noting resistivity and Hall coefficient measurements

08 p1373 A69-21067

Copper diffusion coefficient in undoped n-type gallium arsenide measured by ultrasonic method

09 p1555 A69-21471

N type surface layer in p type sample noting effect on Hall constant and relationship to temperature

09 p1555 A69-21472

Diffusion method for fabricating negative resistance diodes consisting of Cd doped silicon, introducing Cd into n-type silicon plates in evacuated vials

09 p1462 A69-21477

Vacuum deposited n-type InAs films magnetoresistance coefficient dependences on length-to-width ratio, homogeneity, moving carriers size and magnetic inductance

09 p1559 A69-22647

N enhancement silicon MOST saturation current as function of temperature

10 p1743 A69-23175

Voltage dependence of red and green electroluminescence in GaP diodes prepared by growing n-type liquid epitaxial layer on p-type solution grown substrate

10 p1663 A69-23664

N and p type InSb and GaSb single crystals microhardness, noting decrease after doping is limited to thin surface layer

11 p1936 A69-24699

Forward and reverse current-voltage characteristics and reverse biased capacitance for $n\text{-ZnSe-pGe}$ emitter base diodes of heterojunction transistors

11 p1851 A69-25114

Conduction band anisotropy in n-type cadmium tin arsenides, analyzing galvanomagnetic tensor and distribution of isoenergetic surfaces for electrons

11 p1939 A69-25689

IR absorption spectrum of Br-doped n-CdTe specimen, considering donor level transfer mechanism

12 p2142 A69-25979

Etched surfaces inhomogeneity of n-type GaAs single crystals, noting oxide layers formation

12 p2142 A69-25980

Electron cyclotron resonance measurement in n-type indium antimonide using far IR emission from HCN and water vapor lasers, noting magnetic field strength effects

13 p2270 A69-27200

Relaxation oscillations in field ionized epitaxial n-GaAs Gunn oscillators on semiinsulating substrates, discussing recombination of excess electrons and holes

13 p2227 A69-27236

Conduction band structure in GaSb noting temperature dependence

13 p2319 A69-27899

Longitudinal magnetoresistance oscillations in n-type GaSb single crystals associated with electron concentrations minima

13 p2319 A69-27900

N-type InSb single crystals with high dislocation density, investigating anisotropy of mobility, Hall effect and transverse and longitudinal magnetoresistance

14 p2503 A69-28734

Galvanomagnetic characteristics of n-type semiconductor subjected to perpendicular electric and magnetic fields, noting electron temperature

14 p2505 A69-29037

Plasma screening effect on energy spectra of electrons localized at surface charges in weakly doped unipolar n-type semiconductor

14 p2505 A69-29170

Dislocations effect on carrier mobility and concentration in p-type and n-type InSb crystals

14 p2507 A69-29646

Semiconductor materials and fabrication methods for surface barrier junction n-type and p-type silicon counters used in hydrogen ion flux recording

14 p2452 A69-29810

Burstein-Moss effect observed in studying n-GaAs crystals electrical reflection spectra with large free carrier concentration at two temperatures and low energy levels

15 p2666 A69-30060

Secondary effects role in n-GaAs crystals electrical reflection spectra with low free carrier concentration at room temperature in external electric field

15 p2666 A69-30061

Current and electroluminescence brightness dependence on reverse voltage in n-SiC diodes including tunnel and avalanche processes

15 p2573 A69-30062

Copper diffusion coefficient in undoped n-type gallium arsenide measured by ultrasonic method

15 p2669 A69-30716

N type surface layer in p type sample noting effect on Hall constant and relationship to temperature

15 p2669 A69-30717

Diffusion method for fabricating negative resistance diodes consisting of Cd doped silicon, introducing Cd into n-type silicon plates in evacuated vials

15 p2578 A69-30722

Lattice component of heat conductivity in n-type cadmium arsenide at low temperatures by suppressing electron component of conductivity with strong transverse magnetic field

16 p2824 A69-31568

Two donor levels and conduction properties of n-type semiconductors demonstrated by capacitance measurements of single crystal tungsten oxide in presence of electrolyte

16 p2825 A69-31609

N-type In-doped ZnSb with melt under H-gas preparation and properties

18 p3183 A69-35268

Schottky barrier diodes for high temperature operation prepared on n-type GaP single crystals, studying I-V and C-V characteristics

19 p3381 A69-35681

Photocurrents and recombination luminescence in n-type diamonds subjected to UV, TI 204 and X ray irradiation indicating local electron centers formation

19 p3383 A69-36167

Transient recombination lifetimes in n-type float zone Si from 4.2 K to room temperature, obtaining electrical and photoconductivity values

19 p3383 A69-36447

Helicon wave dimensional resonance in n-InSb plasma waveguides at different wavelengths relative to wall thickness

19 p3383 A69-36479

IR absorption in n-type gallium phosphide doped with telluride or Si in 1.5-2.0 micron range, analyzing wavelength dependence

19 p3385 A69-36518

Combined resonance transition in n-type InSb by IR radiation, plotting intensity against magnetic field for different carrier concentrations to infer band structure

19 p3385 A69-36520

Hot electron behavior in n-type InSb under magnetic fields at 4.2 and 1.7 K, plotting current-voltage and current-Hall voltage characteristics, etc

19 p3388 A69-36544

InSb instabilities and time dependence of transverse breakdown, performing Hall effect measurements on n-type InSb at 77 K

19 p3389 A69-36546

Temperature dependence of g-value in spin resonance in partially degenerate region in pure n-type InSb and InAs

19 p3389 A69-36549

Low temperature energy band gap in n-type single semiconductor crystals of In-Sb-Bi alloys analyzed by measuring Hall constant and optical absorption coefficient

19 p3390 A69-36552

Charge transport in n and p type samples of beta phase semiconducting iron disilicide, noting effect of room temperature doping

19 p3390 A69-36556

Undoped n-type gallium arsenide single crystals edge emission spectral band shape dependence on crystal type and ambient temperature

19 p3392 A69-36610

- N-type GaAs optical properties after proton irradiation, noting transmission spectra dependence on initial electron concentration and irradiation dose
20 p3582 A69-36969
- Crystallization front topography and stratified structure of melt extracted n-type GaAs single crystals from anodic etching method
20 p3582 A69-37013
- Tunnel p-n junctions preparation by diffusing Zn into degenerate Te doped n-type GaSb between 580-600 C, measuring volt-ampere and capacitance characteristics
21 p3780 A69-39043
- Electron irradiation-temperature dependence of introduction rate and room temperature annealing of carrier-removal defects in Li-doped Si
24 p4360 A69-42647
- NA-300 AIRCRAFT**
U OV-10 AIRCRAFT
- NACELLES**
C-5 engine inlet development, presenting two phase nacelle forebody and five phase model tests, scale corrections inlet/cowl optimization and prototype tests [ASME PAPER 69-GT-52] 09 p1570 A69-22481
- Stratospheric balloons launching and nacelles for measurement of cosmic rays, at atmosphere high altitude characteristics, discussing French launching center
16 p2734 A69-31759
- Power plant installation on swept winged transport aircraft, discussing interference drag sources, high lift problems, unorthodox installations, nacelle effects, etc
17 p2898 A69-33214
- Aerodynamic characteristics of power plant installation, discussing nacelle design from viewpoint of aircraft performance and economic efficiency
17 p2898 A69-33215
- NAMING**
U NORMS
- NAPHTHALENE**
Q switched laser excitation flash spectroscopic analysis of naphthalene, describing equipment arrangement and experimental results
02 p0254 A69-11544
- NARCOSIS**
Auditory evoked response /AER/ as measure of narcosis induced at depth in diving personnel, discussing hyperbaric nitrogen and oxygen effects
14 p2407 A69-29302
- Physiological and psychological measurements of high pressure effects on man and animals, discussing decompression sickness, respiratory embarrassment, inert gas narcosis, helium tremble, etc
21 p3655 A69-38912
- NARCOTICS**
Mandrax and barbiturates effects on aircrew reaction time, response time and tracking ability
21 p3661 A69-39274
- NASA PROGRAMS**
NT APOLLO APPLICATIONS PROGRAM
NT APOLLO PROJECT
NT ECHO PROJECT
NT GEMINI PROJECT
NT MARINER PROGRAM
NT MARS 69 PROJECT
NT MERCURY PROJECT
NT NIMBUS PROJECT
NT ROVER PROJECT
NT SATURN PROJECT
NT SURVEYOR PROJECT
- Man machine relationship in V/STOL control display, discussing inflight simulators, emphasizing NASA X-14 and CH-3C programs
01 p0010 A69-10452
- National space program management, discussing NASA and NASA, lunar mission planning, procedures and program flexibility and responsibility
01 p0178 A69-10468
- Space technology contributions to medical problems, discussing organization and achievements of biochemical application program of NASA [UN PAPER 68-95417] 01 p0020 A69-10471
- Space biology, discussing U.S. research program, emphasizing gravity/organism reactions, biochronology and exobiology [UN PAPER 68-95345] 01 p0014 A69-10486
- Scientific advances from space research in communications astronomy, electronics, transportation, etc
01 p0151 A69-10498
- NASA university program, discussing participation in space and aeronautics development based on project oriented research grants and Sustaining University grants [UN PAPER 68-95413] 01 p0179 A69-10506
- NASA Technology Utilization Program, discussing information dissemination [UN PAPER 68-95131] 01 p0179 A69-10512
- NASA programs and opportunities for international cooperation in space [UN PAPER 68-95367] 01 p0179 A69-10516
- San Marco project, discussing Italian Space Commission and NASA cooperation, equatorial range concept and development [UN PAPER 68-95862] 01 p0180 A69-10518
- NASA programs impact on U.S. education [UN PAPER 68-95291] 01 p0180 A69-10519
- Aerospace management technology transferability to problems of society and government
02 p0355 A69-11754
- Weightlessness effects research during Soviet and U.S. manned space flights
02 p0199 A69-12120
- NASA Planetary Exploration Program to gather data on origin of solar system and life, discussing planetary evolution and extraterrestrial life
02 p0200 A69-12804
- NASA Plum Brook Reactor Facility /PBRF/ for determining radiation tolerance to support nuclear power application in space for propulsion and power
03 p0465 A69-13128
- NASA Space Application Program strategy, discussing research and development trend toward complexity, versatility and multidisciplinary use of larger spacecraft
03 p0511 A69-13427
- Cooperation between U.S. and Europe in space programs, discussing contracts and conditions
03 p0535 A69-13590
- Cooperation between U.S. and Europe in communication satellite programs
03 p0535 A69-13591
- NASA-Ames hybrid simulation software systems, subsystems and implementation
04 p0567 A69-15353
- NASA research on flexible and stiffened flexible wings, discussing range of applicability, aerodynamic characteristics and wind tunnel results
05 p0701 A69-15568
- Federal government contracting, discussing legality of NASA service contracts
05 p0850 A69-15987
- Proton beams uniformity available at NASA synchrocyclotron designed for radiation biology research by simulating space radiation environment
05 p0742 A69-15992
- NASA civil aviation electronics research program, discussing feasibility of V/STOL aircraft all-weather operations
05 p0850 A69-16718
- NASA scientific and technical information program for building technical data and literature repository for scientists, engineers and technical managers, describing IAA and STAR [UN PAPER 68-95317] 06 p1043 A69-17068
- Manned space flight programs, discussing U.S. technological, scientific and practical contributions
06 p1001 A69-17074
- U.S. space research program and achievements, describing practical aspects
06 p1005 A69-17562
- Arizona-NASA atlas of IR solar spectrum, reproducing photometric tracings obtained from CV-990 aircraft flights
06 p1008 A69-17808
- NASA atlas of IR solar spectrum, reporting B and 4 meter spectrometer recordings over band containing methane telluric absorptions
06 p1008 A69-17810
- Life raft thermal protection against exposure of aircrews to cold, noting chemically fueled heaters and IR reflective liners
06 p0883 A69-17841
- Multifunction Receiver System rationale, concepts, background requirements and technical justifications for tracking, telemetry and ranging data acquisition by Goddard Center
07 p1081 A69-19101
- Small Scientific Satellite program, discussing payload for investigating magnetosphere and near interplanetary space [IEEE PAPER 3C-1] 07 p1230 A69-19195
- NASA flight safety research, discussing size effects on aircraft handling and built-in response to failure modes
07 p1057 A69-19764
- Space boosters, performance of launch vehicles and requirements for future U.S. space launch capability from USAF vantage point
08 p1410 A69-20882
- NASA program in electric propulsion, noting applications for spacecraft position control and for small automated interplanetary spacecraft [AIAA PAPER 69-248] 09 p1561 A69-21216
- NASA long range planning of primary electric propulsion for automated space program [AIAA PAPER 69-247] 09 p1565 A69-21251
- Saturn 5 holddown and service arm electrical system design program optimized by integrating reliability and maintainability at initial design phase [AIAA PAPER 69-309] 10 p1670 A69-23043
- Integrated management information system /IMIS/, discussing logistics, reliability and quality assurance disciplines
11 p2005 A69-25304
- Ablation characteristics of heat shield materials measured in arc heated wind tunnels, considering influence of model scale, heating rate and pressure level
12 p2119 A69-26813
- NASA manned aerospace simulation techniques and equipment as used at Ames Research Center, noting applications to various types of manned vehicles [ASME PAPER 69-DE-56] 14 p2427 A69-28844
- NASA flight test of hingeless rotor compound helicopter to determine lift sharing characteristics, showing rotor lift dependence on airspeed
14 p2393 A69-29702
- Outer space law principle sources including divine law, UN and NASA contractors regulations
15 p2720 A69-31052
- NASA laser systems for satellite tracking, determining ranging accuracy by comparing laser and computed reference orbital data
15 p2571 A69-31312
- NASA planetary program, discussing Mars, Jupiter, Mercury, Venus and Saturn missions
15 p2723 A69-31318
- Report on U.S. space science program to COSPAR on stellar and solar astronomy, lunar and planetary research, upper atmospheric physics, etc
15 p2723 A69-31430
- Aeromedical developments by NASA biomedical applications program applied to general medical equipment including cardiac sensors, surgical sterilization, ballistocardiograph, etc
16 p2882 A69-32430
- Planetary quarantine constraints by NASA insuring low contamination probability from extraterrestrial biological exploration, giving contamination probability equations and sterilization procedures
16 p2746 A69-32435
- Space program design, discussing NASA centers and NASA R and D life sciences, technological developments and federal action
17 p3076 A69-34042
- Commercial utilization of space technology, discussing cost reduction and role of NASA Apollo Program
17 p3043 A69-34044
- NASA photogrammetric lunar activities, discussing imagery and control data by Lunar Orbiter and photogrammetric data reduction for preparing manned lunar landing
18 p3133 A69-34336
- Orbital astronomy support facility research requirements analysis, discussing objectives and measurement needs, instrumentation, spacecraft and facilities, etc
18 p3206 A69-34369
- Professional programs for aeronautics, rocketry and astronautics development
18 p3233 A69-34552
- Space exploration influence on science education, showing NASA instructional materials for teachers in biology, chemistry, physics, mathematics, industrial arts, etc
18 p3235 A69-35077
- NASA Pilot Program in instructional monographs to provide up-to-date material from current research for engineering education
18 p3236 A69-35078
- NASA technology utilization program for civilian economy benefit, discussing scientific and technical documentation and transfer across industrial, disciplinary and regional boundaries
18 p3236 A69-35105
- AIAA view on Post-Apollo space program, considering multiple goals, unmanned application satellites and manned space flight objectives
18 p3236 A69-35136
- NASA planetary entry parachute program for rocket launched and balloon deployment tests [AIAA PAPER 68-934] 19 p3247 A69-35952
- Industrial, scientific and commercial applications of NASA developed telemetry technology
19 p3455 A69-36258

NASA Earth Resources Survey Aircraft Program, describing aircraft and remote sensors characteristics
19 p3312 A69-36259

U.S. space program since establishment in 1958, NASA mission successes and management systems for future projects
20 p3641 A69-38116

Universities and public service education noting NASA requirements and programs
20 p3641 A69-38282

NASA Lunar Orbiter Program of lunar photography from orbiting spacecraft
21 p3794 A69-38377

Planetary atmosphere structure and mean molecular weight determination from onboard measurements tested at high altitude in earth atmosphere, based on NASA Program
[AIAA PAPER 68-1054] 21 p3715 A69-39023

PostApollo space goals based on manned and unmanned planetary exploration and space science programs, considering human factors and propulsion problems
21 p3856 A69-39167

NASA current awareness service SCAN/selected current aerospace notices/, promoting selectivity in information transfer to abstract journals, accession lists and bibliographies
21 p3856 A69-39581

Telemetry data processing, describing designation, tasks and possibilities of data reduction laboratory attached to NASA Goddard Space Flight Center
22 p3919 A69-40352

NASA structural analysis (NASTRAN) program applied to large radio telescopes, discussing static and dynamic analysis, problem formulation, finite element method, etc
23 p4232 A69-42145

NASA programs for space stations and base development, discussing housing and equipment capacity, manned and unmanned stations and shuttlecraft for interstation travel
23 p4224 A69-42456

NASA program for radio spectrum utilization in aerospace communication systems
23 p4128 A69-42502

Planetary exploration and NASA program objectives
[AAS PAPER 69-286] 24 p4379 A69-42810

Logistics management developed for Apollo Applications Program of NASA Manned Spacecraft Center
[AAS PAPER 69-204] 24 p4417 A69-42812

Earth resources surveys by space flights and plans for future satellites, describing results of EROS and ERTS programs
[AAS PAPER 69-058] 24 p4307 A69-42824

Launch vehicle upper stage requirements in space missions, discussing space engine for lunar, planetary and interplanetary exploration
[AAS PAPER 69-359] 24 p4418 A69-42828

Management system for safety in NASA Manned Space Flight Program, discussing hazard analyses and reduction precedence sequence
[AAS PAPER 69-522] 24 p4418 A69-42851

Pioneer F/G mission to Jupiter by NASA for exploring interplanetary medium, asteroid belt, planet and environment
[AAS PAPER 69-290] 24 p4381 A69-42863

Cape Kennedy space research and national priorities, indicating performance and progress of future space operations
[AAS PAPER 69-110] 24 p4419 A69-42879

NASA programs for development of high temperature alloys for advanced air breathing engines emphasizing cast Ni-base alloy
[ICAS PAPER 68-26] 24 p4335 A69-43718

NATIONAL AIRSPACE UTILIZATION SYSTEM

Government role in air transportation policy, considering growing demands on air traffic control
06 p1040 A69-16835

NATIONAL SEVERE STORMS PROJECT

Atmospheric turbulence in cloudless region above thunderstorms and relation between turbulence and radar pictures of storms
15 p2649 A69-31211

NATURAL FREQUENCIES

U RESONANT FREQUENCIES

NATURAL SATELLITES

NT DEIMOS
NT IAPETUS
NT MOON
NT PHOBOS

Jupiter outer satellites orbits determination with computer program based on modified Cowell/Moulton methods for adjusting initial conditions
01 p0158 A69-11330

Surface temperatures for Galilean satellites of Jupiter calculated through corresponding lunations, assuming synchronous orbits with respect to Jupiter
03 p0513 A69-13776

Europa control of decametric emission from Jupiter
05 p0813 A69-15605

Commensurability among pairs of mean motions of natural satellites of major planets and hypothesis of tidal evolution of satellite systems
07 p1223 A69-19638

Commensurability among pairs of mean motions of satellites of major planets and power law relation for orbital periods of satellites
07 p1224 A69-19639

Magnitude data for Saturn satellites compiled and analyzed, noting discrepancy for Iapetus
08 p1394 A69-20619

Intermediate orbits to construct motion theory of natural satellites of all planets
11 p1952 A69-24253

Io as unipolar inductor, analyzing interaction with Jupiter magnetosphere and decimetric synchrotron radiation
13 p2337 A69-27552

Jupiter decametric radio emission periodicity attributed to undiscovered satellite in unstable orbit, discussing application to satellite discovery
13 p2343 A69-27622

Natural terrestrial satellites existence suggested by telescopic and photographic observations and artificial satellites orbital perturbations
13 p2344 A69-27642

Photographic observations of fifth satellite and disk of Jupiter against stars background for mean motion and regression of nodes
13 p2345 A69-27653

Lunar surface and earth early satellite system, discussing maria distribution, satellite impacts and close passage collisions
13 p2345 A69-27654

Zonal harmonics of Legendre polynomial series of Jupiter attractive force function effects on motion of fifth satellite
14 p2521 A69-29463

Mimas-Tethys commensurability of motions and inclinations, calculating libration amplitude variation by numerical integration
16 p2861 A69-32241

Relativistic effect in pericenter motion of comets and natural satellites from major semiaxes and eccentricities of natural bodies
17 p3044 A69-34174

Catastrophic and noncatastrophic alternatives for earth capture of moon, discussing tidal action and spin-orbit resonance
18 p3198 A69-34823

Polar flattening influence of Jupiter on artificial satellite motion around Callisto noting orbital perturbations
18 p3199 A69-34913

Jupiter tenth satellite reobserved, discussing calculations and computer techniques for determining orbit
[AAS PAPER 68-140] 20 p3595 A69-37194

Jacobi integral and Hill criterion for analyzing motion stability of natural satellites and large planets inside gravitational sphere
20 p3596 A69-37314

Janus discovery, discussing solar distance, rotation period, diameter, opposition brightness and planetary parameters derived from pictures
20 p3597 A69-37337

Hansen method applied to Jupiter tenth satellite orbit correction and perturbations, describing computer program and formulas used
20 p3602 A69-37529

Optical properties and thickness of Saturn rings from observations during ring plane crossing of earth or sun, determining Tethys diameter and albedo
20 p3605 A69-37821

Jupiter mass determined by applying Cowell numerical integration to equations of motion for ninth satellite
21 p3795 A69-38468

Spacecraft-based navigation instruments for outer planet missions using celestial directions to outer planet natural satellites
[AIAA PAPER 69-902] 21 p3761 A69-39348

Perturbative effects of Jupiter moons on spacecraft flyby and postencounter heliocentric trajectories, noting precision targeting
[AIAA PAPER 69-932] 21 p3809 A69-39361

Light pressure induced secular effect contributing to planetary satellites and lunar orbits evolution calculated by numerical integration
22 p4033 A69-41084

Galilean satellites perturbing effect on motion of fifth Jupiter satellite
23 p4214 A69-41730

NAVIER-STOKES EQUATION

Asymptotic forms of Navier-Stokes equations for laminar motions of incompressible viscous fluid, discussing validity and applications
[ONERA-TP-651] 01 p0059 A69-10383

Boundary layer of MHD flow past semifinite plate, using Navier-Stokes equations
01 p0130 A69-10771

Two dimensional Navier-Stokes equations of axisymmetric motion of viscous incompressible fluid, giving integral and solutions for stream function
02 p0231 A69-12133

Mixed boundary value problem for system of Navier-Stokes equations for viscous incompressible fluid in stationary motion in vessel, noting rotating fluid
02 p0272 A69-12223

Exact solutions for Navier-Stokes equations for non-steady incompressible viscous flow near two dimensional or axisymmetrical stagnation point
02 p0233 A69-12527

Finite difference solution of time dependent Navier-Stokes equation for incompressible fluids, using velocities and pressure as variables
03 p0415 A69-13369

Difference schemes to solve Navier-Stokes equations for viscous incompressible fluid by substituting fourth order partial differential equation
03 p0415 A69-13650

Analysis of solution of Navier-Stokes equations describing two dimensional flow of viscous incompressible fluid by finite difference techniques and introduction of curl
03 p0416 A69-13652

Problem of viscous supersonic flow past blunt bodies based on Navier-Stokes equations formulated and solved numerically with explicit difference scheme
03 p0363 A69-13653

Navier-Stokes equations for self gravitating viscous fluid, discussing generalization based on irreversible thermodynamics
04 p0588 A69-14699

Algorithm for Navier-Stokes and continuity equations used to derive curvilinear coordinate system
04 p0564 A69-14858

Viscous incompressible fluid motion in two or more dimensions and with zero fluid velocity on domain boundary, determining lower bounds and uniqueness for solutions
04 p0626 A69-15311

Self similar solution for Navier-Stokes equations describing steady motion of submerged eddy jet of incompressible viscous fluid injected into half space
06 p0908 A69-16825

Cauchy problem for nonstationary linearized Navier-Stokes equations for fixed container partially filled with liquid
06 p0959 A69-17888

Computer solution of incompressible two dimensional time dependent Navier-Stokes equations for oscillating body with rectangular boundaries
[AIAA PAPER 69-185] 06 p0914 A69-18135

Time dependent technique for inviscid blunt body flows to analyze viscous rarefied shock layer regime using Navier-Stokes equations
[AIAA PAPER 69-139] 06 p0865 A69-18173

Motion of viscous incompressible fluid in interspace between rotating and parallel fixed permeable plane having supplementary fluid injection solved by Navier-Stokes equations
07 p1119 A69-18743

Navier-Stokes equations solved for viscous incompressible fluid flow due to laminar jet flow into channel in presence of magnetic field
07 p1120 A69-18997

Clebsch transformation application to equations describing viscous fluid, deducing canonical equations equivalent to Navier-Stokes equations
08 p1303 A69-20125

Integral of Navier-Stokes equations for steady three dimensional motion of incompressible viscous fluid, giving angular velocity vector projections
08 p1342 A69-20320

Statistical dynamics of turbulent incompressible fluid, discussing harmonic function in Navier-Stokes equation
08 p1303 A69-20323

Digital computer method for Navier-Stokes equation in prototype cavity flow problems, noting applications to biharmonic problems
08 p1305 A69-20831

Boundary value problem for linearized system of Navier-Stokes equations in three dimensional space, determining velocity vector and pressure
08 p1344 A69-21156

Navier-Stokes equations solution applicable to source type low Reynolds number flow through conical nozzles
09 p1482 A69-21976

Approximate solution method for Navier-Stokes equations for incompressible viscous fluids
10 p1718 A69-22861

Viscous fluids rotational flow in cylindrically symmetrical vessels, circumventing Navier-Stokes equations of motion by Wedemeyer approximation
10 p1677 A69-22896

Navier-Stokes boundary value problem bifurcation solution analysis, determining stability ranges
10 p1677 A69-22901

Requirements for numerical solution of Navier-Stokes equations by finite difference method found limited to Re values with no turbulence
10 p1678 A69-22917

Laminar boundary steady two dimensional constant velocity flow over curved surface equation derived from Navier-Stokes equation
11 p1867 A69-24375

Navier-Stokes equations for compressible gas, generalizing viscous channel flow of heat conducting gas to slip flow of rarefied gas
12 p2061 A69-25887

Smooth solutions to Navier-Stokes equation obtained by imposing bound on associated pressure pertaining to weak solution
12 p2124 A69-26971

Navier-Stokes equations of slow viscous fluid laminar flow near pipe inlet and exit with negligible mass forces, discussing velocity and pressure distribution
13 p2244 A69-27258

Turbulent fluid flow analysis described by Navier-Stokes equations, introducing asymmetric tensors for anisotropic cases
13 p2297 A69-27289

Incompressible uniform shear flows merging behind trailing edge of semiinfinite flat plate, using inner-outer expansion method based on Navier-Stokes equation
13 p2248 A69-28223

Numerical method for time dependent compressible Navier-Stokes equations applied to axisymmetric flow field produced by hypervelocity impact, examining viscous effects
[AIAA PAPER 69-354] 13 p2366 A69-28288

Flat plate turbulent boundary layer, noting Navier-Stokes equations solutions and formation of rotations to determine velocity field
13 p2251 A69-28632

Nonuniqueness in Hopf weak solutions for Navier-Stokes equations using solutions with rotational symmetry
14 p2428 A69-28900

Boundary value problem for linearized system of Navier-Stokes equations in three dimensional space, determining velocity vector and pressure
15 p2645 A69-31249

Monograph on Navier-Stokes equations with integral relations approximate solution and application to flow around flat plate of finite length
17 p2949 A69-32993

Statistical dynamics of turbulent incompressible fluid, discussing harmonic function in Navier-Stokes equation
17 p2952 A69-33313

Taylor vortices calculated as branching solutions of nonlinear Navier-Stokes boundary value problem
17 p2958 A69-34152

Transient uniform flow over sphere at intermediate Reynolds numbers with recirculatory wakes, utilizing difference approximation to time dependent Navier-Stokes equations
18 p3120 A69-34434

Shock wave profiles in molecular N-H gas mixtures in shock tube measured by optical electron beam method, noting disagreement with Navier-Stokes calculations
18 p3134 A69-34458

Convergence of discrete approximations of Navier-Stokes equations to solutions of corresponding differential equations
18 p3121 A69-34613

Transformed Navier-Stokes equations for incompressible fluids flow, deriving forces acting on surface of bounded region
18 p3122 A69-34830

Higher order boundary layer theory development from Prandtl simplification of Navier-Stokes equations to successive approximations for incompressible and compressible flows
18 p3123 A69-34923

Discrete fractional steps method for approximate solution to Navier-Stokes equations, noting perturbation
18 p3165 A69-35278

Laminar flow of viscous compressible fluid with density dependent on temperature, calculating steady state Navier-Stokes equations using vector function
19 p3297 A69-35852

Asymptotic form of axisymmetric solution with Dirichlet integral for Navier-Stokes equations applied to flow past bodies of revolution with smooth surfaces
19 p3298 A69-36143

Boundary conditions of incompressible fluid viscous flow on semiinfinite plate edge defined using difference methods for Navier-Stokes equations
19 p3299 A69-36394

Coupling conditions by distinct equations for two laminar flow regions, studying near wake and considering Euler, Navier-Stokes and Prandtl correlations [ONERA-TP-738]
19 p3299 A69-36649

Navier-stokes equation numerical integration for three dimensional incompressible flow, discussing annulus thermal convection and trigonometric transforms algorithm
21 p3694 A69-38770

Spheres impulsive starting in incompressible viscous fluid, including Reynolds number and investigation time parameters in Navier-Stokes equation
21 p3696 A69-39296

Laminar corner boundary layer flow with suction, discussing Navier-Stokes equations and steady state heat conduction problems
21 p3696 A69-39578

Oscillations of highly viscous incompressible fluid in partially filled cavity of body moving about fixed point, solving Navier-Stokes equations by asymptotic method
22 p3929 A69-40117

Navier-Stokes equations exact solutions for two dimensional steady flow of compressible viscous heat conducting perfect gas
22 p3929 A69-40117

Dynamics of viscous electrically charged gas using Navier-Stokes equation
22 p3931 A69-40686

Navier-Stokes equations numerical integration based on biharmonic operator inversion by alternating direction method of Douglas-Rachford type
22 p3932 A69-40928

Ionized plasma motion under plane piston action by self similar solution of Navier-Stokes equations
22 p3991 A69-41021

Mixed boundary value problem for system of Navier-Stokes equations for viscous incompressible fluid in stationary motion in vessel, noting rotating fluid
23 p4183 A69-41974

Turbulent flow, discussing light scattering techniques, correlation functions, statistical theory, modified Navier-Stokes equation, etc
23 p4153 A69-42314

Stokes stream function and forces acting on two spheres moving in contact along line of centers through viscous fluid
24 p4299 A69-42747

NAVIGATION

NT AIR NAVIGATION

NT ALL-WEATHER AIR NAVIGATION

NT ASTRONAVIGATION

NT CELESTIAL NAVIGATION

NT DEAD RECKONING

NT DECCA NAVIGATION

NT DIGITAL NAVIGATION

NT DOPPLER NAVIGATION

NT GIMBALLESS INERTIAL NAVIGATION

NT HYPERBOLIC NAVIGATION

NT INERTIAL NAVIGATION

NT INTERPLANETARY NAVIGATION

NT LORAN

NT LORAN C

NT OMEGA NAVIGATION SYSTEM

NT RADAR NAVIGATION

NT RADIO NAVIGATION

NT SPACE NAVIGATION

NT SURFACE NAVIGATION

NT TACAN

NT VHF OMNIRANGE NAVIGATION

Minimal angle of resolution (MAR/ between point and extended circular source and between point source and simulated horizon, studying irradiation effects on manual navigation
07 p1177 A69-19208

Future navigation systems and ATC, discussing traffic flow factors and approach and landing systems
17 p3004 A69-34201

Polynomial approximations in perturbational navigation and guidance schemes including Chebyshev and least square approximations
19 p3368 A69-35664

NAVIGATION AIDS

NT BEACONS

NT GYROCOMPASSES

NT MAGNETIC COMPASSES

NT RADAR BEACONS

NT RADIO BEACONS

NT RADIO DIRECTION FINDERS

Navigation instruments developments during past fifty years emphasizing land, marine and air navigation aids
01 p0112 A69-10311

Airline area navigation system functions for developing map type pictorial display system including digital computer, cockpit control unit and microfilm charts
01 p0112 A69-10453

Nonmilitary marine uses of navigation satellites [UN PAPER 68-95305]
01 p0112 A69-10469

Navigation Service Satellite System for aiding aircraft and ships at sea in Pacific Ocean, noting equipment and functions [UN PAPER 68-95251]
01 p0112 A69-10470

Sequential probability ratio test for detecting changes in Gauss-Markov process characteristics, noting application to fault detection in gyro navigational system
01 p0083 A69-11002

Laser gyro applications including guidance, navigation and control problems
02 p0248 A69-11741

TRANSIT /Navy Navigation Satellite System/ military and commercial applications
02 p0278 A69-12359

Navigation techniques for emergency helicopter services in medical evacuation and air/sea rescue missions, discussing displays and search patterns
02 p0279 A69-12363

Celestial navigation, discussing position fixing on rotating earth, time input, navigation aids and sextant angle
03 p0463 A69-13207

Short baseline radiating satellite interferometer concept for reducing satellite navigation systematic errors for aircraft and ships
03 p0463 A69-13208

OMEGA radio navigation system optimization, emphasizing implementation of phase modulation to ensure lane identification
03 p0463 A69-13212

SPOT /Speed, Position and Track/ transoceanic traffic surveillance and navigation system for aircraft and marine users
03 p0463 A69-13234

Transatlantic aircraft cross-track air navigation error reducible by augmenting Doppler system with satellite ranging system
03 p0464 A69-13237

Navigation computer utilizing current integrators and step motors to record flight path
03 p0404 A69-13431

MOS GP computer suitable for navigation applications
04 p0568 A69-15357

Meteorological satellites data for safe navigation of ships, discussing techniques to overcome difficulties in interpreting icc and cloud photographs [UN PAPER 68-95776]
06 p0916 A69-17028

SGN-10 inertial navigation system evaluation by Pan American World Airways
06 p0955 A69-17663

Doppler radar inertial navigation, discussing developments in sensors and digital computers
06 p0956 A69-17859

Sight reduction tables for orbital plane determination checked out by sextant sightings onboard Gemini 7
07 p1177 A69-19206

Aircraft traffic control with cockpit self sufficiency for accurate and reliable navigation capability, discussing radar vector navigation and communication
07 p1177 A69-19210

Airborne area navigational capability achieved by course line computer processing VOR information
07 p1178 A69-19763

OMEGA airborne navigational computers, discussing earth ellipticity and phase variations problems for signal conversion into latitude and longitude coordinates
08 p1347 A69-20778

Control and recording device for parameters and information relating to takeoff and landing, using detection elements and cross wire on runway
08 p1347 A69-20780

Long range subsonic transport navigation systems accounting for reductions in horizontal separation on high density oceanic routes
08 p1348 A69-21062

Velocity meter for precision adjustment of orbits of vehicles in space for long periods using digital integrating accelerometer
08 p1348 A69-21063

Flight test performance of airborne Omega radio navigation system capable of worldwide coverage, discussing diurnal variations effects in phase velocity
08 p1348 A69-21191

National plan for air navigation covering R and D and operational aspects
08 p1348 A69-21192

Satellite navigation system feasibility for accurate and continuous navigation capability for Army tactical aircraft
08 p1349 A69-21193

Vector analog computer functions and applications in air traffic control, discussing area navigation equipped aircraft
08 p1349 A69-21195

Integrated inertial aircraft navigation with velocity and position aids, discussing in-flight calibration capabilities, performance under quick-reaction constraints and digital simulation results
08 p1349 A69-21196

Marine and aircraft satellite navigation techniques, discussing equipment requirements, related performance characteristics and limitations
08 p1349 A69-21198

Skorsky HH-3F helicopters electronic equipment, discussing communication and navigation aids, search and recovery missions, etc
10 p1662 A69-23222

Cockpit TV-radar for providing pilots with navigation, weather and traffic data, discussing safety factors and radar picture transmission quality
[SAE PAPER 690327] 11 p1833 A69-24506

Navy Navigational Satellite System for position location accuracy in marine and oceanographic exploration applications
[AIAA PAPER 68-471] 13 p2295 A69-27247

Litton LTN-51E inertial navigation system accuracy and reliability evaluated on basis of transpacific flights
[SAE PAPER 680299] 13 p2296 A69-28103

National plan for air navigation covering R and D and operational aspects
14 p2480 A69-29858

Dioscures project for telecommunication, ATC and navigation by satellites to provide continuous position determination
15 p2651 A69-30691

Navigational information display in aircraft, discussing moving map technique and mechanization
15 p2558 A69-30692

Terminal area navigation and landing guidance systems for V/STOL intercity transport aircraft, considering radio guidance, aircraft control and system interaction
17 p2897 A69-33210

Integrated trajectory error display /ITED/ for flight path control of helicopters and VTOL, describing principles governing display synthesis
[AHS PAPER 314] 17 p3001 A69-33541

AH-56A Cheyenne integrated avionics, armament and fire control system for precise weapons delivery and navigation
[AHS PAPER 312] 17 p2903 A69-33542

General purpose /GP/, differential digital analyzer /DDA/ and CORDIC /coordinate rotation digital computer/ computers for navigation system computations
17 p3003 A69-34100

Navigation equations, discussing earth geometry, coordinates, gravity, dead reckoning and radio computations with regard to LORAN
18 p3169 A69-34845

Navigational equations solution by airborne analog computer techniques, describing electronic, electromechanical, digital reset and mechanical integrations with respect to time
18 p3107 A69-34847

Artificial satellites as navigation aids, describing angle, range and range-angle systems, discussing orbital mechanics and communications difficulties
18 p3169 A69-34855

Automatic flight control, discussing equipment, components and relationship between autopilot and navigation system
18 p3170 A69-34856

Pictorial display area navigation system for air traffic control in terms of cockpit utilization, interface with ground navigation aids, parallel multiple routes, etc
[AIAA PAPER 69-798] 19 p3367 A69-35632

Earth orbit estimation by manual stadimeter, space sextant and small data processor, discussing orbital parameter errors due to instrument and environment uncertainties
19 p3369 A69-35793

Masking and standby redundancy approach to fault tolerance in space navigation computers with illustrations, discussing automatic maintenance
19 p3279 A69-35798

Star/horizon measurements for onboard spacecraft navigation without cloud cover obscuration, discussing sightings, data processing and evaluation
19 p3369 A69-35800

Computerized clock sequenced ATC system, area navigation /R Nav/ systems and STOL flight control
19 p3370 A69-36317

Optimal timing of measurements to minimize dispersion of navigational observation parameters by least squares method with application to Keplerian orbit elements
19 p3370 A69-36614

Inertial navigation systems technology, discussing man machine dialog, alignment, etc
19 p3371 A69-36703

IR equipment to aid air navigation, discussing detection cells, temperature direction finding, mobile source tracking, etc
19 p3371 A69-36705

Onboard navigation digital computer simulation to verify calculation principle and logic units during design and construction
20 p3502 A69-37398

Imaging radar applications noting military surveillance, navigation assistance, iceberg detection, sea rescue operations, all-weather traffic surveys, terrain mapping, etc
20 p3491 A69-37649

Balloon location by low orbit meteorological satellites, discussing balloon movement due to wind and geometric and nongeometric effects on errors
21 p3760 A69-38618

Guidance and navigation flight tests, demonstrating system performance improvements by onboard inertial system communicating with external navigation aid
[AIAA PAPER 69-842] 21 p3765 A69-39429

Moving map pictorial display system for on board capability of area navigation, noting crew reaction
[SAE PAPER 690393] 23 p4186 A69-41663

Spherical trajectories control by star height maintenance, analyzing resulting cycloid and cartographic representations
23 p4186 A69-42023

Maritime navigation hyperbolic charts for aircraft position determination
23 p4186 A69-42026

Surface and aerospace navigation by VLF radio network, discussing Omega transmitting station location, operational modes and daytime-nighttime accuracies
[AAS PAPER 69-405] 24 p4347 A69-42834

NAVIGATION INSTRUMENTS

NT BEACONS
NT GYROCOMPASSES
NT MAGNETIC COMPASSES
NT RADAR BEACONS
NT RADIO BEACONS
NT RADIO DIRECTION FINDERS

Gyroscope with rotational symmetry subjected to random input torques analyzed by Euler equation of motion
01 p0079 A69-10236

FAA coded broadcasting to transponder equipped aircraft for air traffic control, navigation, collision avoidance and airfield approach
04 p0629 A69-15478

Mechanical calculators for solving spherical triangle problem of navigation
07 p1135 A69-19207

Analytic platform or strapdown systems application, discussing closed and open loop leveling techniques
08 p1347 A69-19862

Polar flight navigation charts showing feasibility of three dimensional celestial positioning
09 p1538 A69-21406

Systematic errors caused by planet asphericity in measurements of orientation and motion parameters of orbiting object compensated by scanning navigation system
10 p1693 A69-23320

Differential equation for dynamic behavior of acrobatic flight navigation instruments in steep flight,

considering vertical gyroscopes, gimbal platforms and time optimal control
11 p1880 A69-24328

Optimal navigation system for supersonic Concorde aircraft, discussing in-flight and terminal navigation methods
14 p2480 A69-29859

Automatic navigation and sighting system for French specified Jaguar combat aircraft development
16 p2809 A69-31760

Measurement errors and geometry effects on navigational accuracy, determining maximum allowable error for measuring devices employed
17 p3002 A69-34098

Attitude and heading reference devices for aircraft navigation, describing instruments, gyroscopes and gravity sensors
18 p3169 A69-34853

Induced-emission oscillator navigation sensor with performance limitations, noting ring laser and nuclear maser gyro and laser accelerometer
19 p3369 A69-35795

Kalman recursive filtering method applied to inertial navigation systems resetting
19 p3286 A69-36645

Spacecraft-based navigation instruments for outer planet missions using celestial directions to outer planet natural satellites
[AIAA PAPER 69-902] 21 p3761 A69-39348

Aircraft navigation system requiring computer and display for approach guidance to circular orbit over fixed ground area
[AIAA PAPER 69-986] 22 p3978 A69-40366

Apollo 11 guidance and navigation systems involved in lunar landing, describing command and service modules design
24 p4295 A69-42550

NAVIGATION SATELLITES

NT EXPLORER 22 SATELLITE
NT TRANSIT 4A SATELLITE
NT TRANSIT SATELLITES

Nonmilitary marine uses of navigation satellites
[UN PAPER 68-95305] 01 p0112 A69-10469

Navigation Service Satellite System for aiding aircraft and ships at sea in Pacific Ocean, noting equipment and functions
[UN PAPER 68-95251] 01 p0112 A69-10470

Space applications program including communications and navigation meteorology, earth resources survey and geodesy
[UN PAPER 68-95437] 01 p0178 A69-10472

Navigation services satellite systems including position determination, communication and telemetry for ships and aircraft
[UN PAPER 68-95363] 01 p0113 A69-10479

Worldwide navigation system consisting of synchronous satellites equipped with pulse modulated microwave transmitters
[UN PAPER 68-95205] 01 p0113 A69-10514

Ship and aircraft traffic conditions in Japan and neighboring areas and requirements for navigation satellite system
[UN PAPER 68-95226] 01 p0113 A69-10520

Navigation by satellite systems, discussing vehicle position determination and communications link for traffic control with comment on French space program
02 p0278 A69-11912

Short baseline radiating satellite interferometer concept for reducing satellite navigation systematic errors for aircraft and ships
03 p0463 A69-13208

Transatlantic aircraft cross-track air navigation error reducible by augmenting Doppler system with satellite ranging system
03 p0464 A69-13237

Acronautical service satellites, considering communications, surveillance for navigation, traffic control, collision avoidance and search and rescue, weather and border control functions
04 p0666 A69-15295

Dioscures system for international air traffic control and navigation over North Atlantic by means of two geostationary satellites
[UN PAPER 68-95832] 06 p0954 A69-17063

Eole meteorological satellite secondary use, discussing cosmic rays monitoring, navigation purposes and oceanographic research
[UN PAPER 68-95833] 06 p1013 A69-17077

Navigation satellites system designed for ATC without requirement for onboard transmitter, discussing spectrum occupancy, satellite power, lane ambiguities and computational procedures
07 p1177 A69-19212

- Marine and aircraft satellite navigation techniques, discussing equipment requirements, related performance characteristics and limitations
08 p1349 A69-21198
- Radio location system based on measuring distance between object and two stationary satellites, noting application to air traffic over North Atlantic
09 p1537 A69-21269
- Satellite-borne terrestrial radiodetermination systems, noting VLF transmissions usage to overcome coverage problem
09 p1537 A69-21287
- Space vehicles and marine navigation using navigation satellites, radar, Doppler navigation, etc
13 p2296 A69-27918
- Dioscures project for telecommunication, ATC and navigation by satellites to provide continuous position determination
15 p2651 A69-30691
- Dioscures project for worldwide telecommunications, air traffic control and navigation by satellites, discussing technical, operational and economic characteristics
16 p2749 A69-31601
- North Atlantic aircraft navigation and traffic control system using satellites
16 p2809 A69-32054
- Artificial satellites as navigation aids, describing angle, range and range-angle systems, discussing orbital mechanics and communications difficulties
18 p3169 A69-34855
- Satellites and ground stations system providing transoceanic civil, air and marine traffic control in North Atlantic, discussing position determination, communication and navigation, etc
18 p3170 A69-35065
- Satellite systems for air traffic control, navigation, communications and telemetry in view of regulations of frequency allocations
18 p3103 A69-35089
- Sun-moon short term disturbances effect on synchronous equatorial navigation satellite orbits, noting fuel expenditure
[AIAA PAPER 69-927] 21 p3761 A69-39356
- Air traffic control transoceanic satellite system for minimizing navigation errors forcing wide separations, providing VHF voice communication and position surveillance
22 p3901 A69-41147
- Aircraft navigation by geostationary satellites, discussing Dioscures project
24 p4280 A69-42568
- NAVY**
- VFX fighter aircraft, discussing U.S. Navy requirements influence in VFX-1 and VFX-2 design
03 p0367 A69-13675
- U.S. Navy Numerical Value Rating System computing method of selecting lowest cost design approach to accomplish specific function
13 p2383 A69-28098
- Navy Navigation Satellite System (NAVSAT) applications, considering nonmilitary marine and air all-weather navigation and positioning
14 p2479 A69-29856
- Defense integrated management engineering system at California Naval Air Rework Facility
15 p2588 A69-30427
- Plastics applications in naval air systems command, discussing polymer families, nonstructural glass fiber-based products, radomes, electromagnetically transparent bodies, advanced composites, etc
21 p3751 A69-38532
- NC-130 AIRCRAFT**
U C-130 AIRCRAFT
- NEAR INFRARED RADIATION**
- Angular and spectral distribution of earth IR radiation near horizon from satellite observation and spectrograms
03 p0422 A69-13506
- Angular distribution measurements of visible and near IR radiation reflected from carbon dioxide cryodeposits formed on liquid nitrogen cooled surface in vacuum
[AIAA PAPER 69-63] 06 p0959 A69-18131
- Laser modulation at optical and near IR frequencies, discussing beam characteristics changes and information transmission
07 p1158 A69-19742
- Oscillator strengths of transitions in shock tube between nitric oxide Rydberg states in near IR
08 p1354 A69-20150
- Near IR transparent aluminocalcium glasses with improved spectral properties
08 p1336 A69-20386
- Quasi-stellar objects photometric selection in near IR
09 p1604 A69-22272
- Near field repeatable stimulator of infrared earth horizon sensors in variable environments and test levels, noting orbital conditions
[AIAA PAPER 69-322] 09 p1478 A69-22376
- Near IR radiation magnetooptic light modulators using Faraday effect in yttrium-iron garnet and in related compounds
11 p1886 A69-25057
- Night sky background observation by near IR radiation flux, using rocket-borne telescope and ground based equipment
13 p2342 A69-27600
- Weak emissions in near IR daytime airglow using rocket-borne spectrometers
16 p2776 A69-32094
- Spectral variations of red variable stars analyzed by objective-prism spectra in near IR
16 p2860 A69-32235
- Ice clouds near IR spectral reflectivity dependence on particle size, noting application to planetary atmospheres
18 p3126 A69-34283
- Carbon dioxide lasers near IR spontaneous emission spectra
19 p3339 A69-36697
- Pulsed Hg ion-He laser operation, revealing transition in near IR
23 p4171 A69-41393
- NEAR ULTRAVIOLET RADIATION**
- Astronomical wide field cameras of large aperture ratio to detect extended near UV light sources outside atmosphere
12 p2080 A69-26127
- Spectral transmission curves in near UV for optical glasses
12 p2130 A69-26599
- Atmospheric optical density vertical distribution curves in near UV from spectrophotometer data of Echo type satellites entry into earth shadow
16 p2787 A69-32638
- NEBULAE**
NT CASSIOPEIA A
NT CRAB NEBULA
NT PLANETARY NEBULAE
- Partial maser effect in recombination lines of hydrogen atoms in nebular plasma due to overpopulation of energy levels at thermodynamic equilibrium
01 p0148 A69-10042
- High velocity motions in diffuse nebulas connected with stellar wind, noting wind formation of 2-layer shell between two shocks
01 p0148 A69-10050
- IR emission in NGC 7027 spectrum and role of discrete line emissions, discussing magnetic dipole transitions, temperature and density
01 p0148 A69-10051
- Fe II lines relative intensities in eta Carinae spectrum, discussing possible intrinsic reddening of object and representation of visible and near IR continuum
07 p1217 A69-19253
- Rosette Nebula structure from high resolution observations at 178 MHz of galactic plane, deriving 8600 K electron temperature for Nebula, discussing Monoceros Nebulosity
07 p1223 A69-19625
- Electron-ion collisions during forbidden lines excitation in gaseous nebulae, using Hartree-Fock functions and variational principles
08 p1391 A69-20530
- Galactic H 56 alpha recombination radio line observation in Omega Nebula in millimeter band with radio telescope, obtaining electron temperature
08 p1397 A69-20771
- Electron temperature of Orion Nebula at 6750 K from intensities of hydrogen n alpha lines, discussing Stark broadening
08 p1398 A69-20776
- Chemical composition of diffuse Orion Nebula and stars compared for lighter elements, considering solar system formation from interstellar medium
08 p1402 A69-20908
- Hydrogen alpha emission nebulae catalog in western half of Cygnus X region, obtaining interstellar absorption from nebular distances determination
09 p1596 A69-22053
- High level hydrogen populations in gaseous nebulae, noting electron density range and temperature effect
09 p1604 A69-22406
- Radio spectra and structure of H II regions in emission nebula NGC 281 and unnamed nebula near NGC 2264
10 p1773 A69-22957
- Bright emission nebula components and electron temperature determined by radio telescope observation
10 p1778 A69-23603
- Double structure in IR near Trapezium region of M42 in Orion Nebula center
10 p1786 A69-24105
- IR spectral distribution from region between stars of Trapezium in Orion Nebula
10 p1786 A69-24106
- Nebular abundances allowing for temperature variations in nebula along line of sight, correcting changes in electron temperature along path of observation
10 p1787 A69-24116
- Hydrogenic recombination decrements in gaseous nebulae, discussing effects of Lyman line leakage, Balmer line self absorption, internal dust, optical depth, etc
10 p1787 A69-24118
- Radio nebula NRAO 591/593, discussing thermal and nonthermal source and models based on electron density distribution
10 p1790 A69-24136
- Expected IR line spectra of gaseous nebulae based on physical conditions, listing line intensities
13 p2342 A69-27595
- Dielectronic recombination influence on radio recombination lines of carbon under typical nebular conditions
13 p2346 A69-27703
- Excited hydrogen RF spectral lines from nebula NGC 6618, calculating frequency for transitions by Balmer formula
13 p2353 A69-28433
- H II alpha and beta radio recombination lines strengths predicted, noting role of calculations of hydrogen energy levels non-LTE populations
14 p2517 A69-29088
- Radio observations of emission nebulae for flux densities, deriving electron temperatures
[ASME PAPER 69-DE-46] 14 p2527 A69-29941
- Amplitude and scale of microscopic fluctuations of electron density within M8 from brightness ratios of O II lines, using multiple shell model
14 p2514 A69-29949
- Emissivity of two photons decay from metastable 2s level of pure hydrogen gaseous nebula, noting radiative and collisional excitation
14 p2529 A69-29975
- Filamentary nebula IC 443 observation by Fabry-Perot etalon with image converter, determining radial, expansion velocities and H alpha line half width
15 p2686 A69-30538
- RF spectral line detection from ortho hydrogen ions in Omega Nebula and NML Cygnus
16 p2864 A69-32571
- Photoelectric method to measure galactic reflection nebulae brightness, color and polarization used to explore interstellar grains physical nature
17 p3032 A69-33104
- Radio map of Orion A region, resolving M 42 and M 43 nebulae at 1.94 cm wavelength, noting optical photographs comparison
17 p3035 A69-33609
- RF recombination lines measurement of helium for abundance in nebulas, comparing optical and radio values for H II regions
18 p3190 A69-34293
- Book on Messier nebulae and star clusters covering current astronomical ideas, star maps, identification diagrams, telescope illustrations and astronomical data
18 p3206 A69-35471
- Magellanic clouds positions, associated gases, evolution, etc
19 p3401 A69-35757
- Forbidden lines emitted by gaseous nebulae, emphasizing relative intensities of O II and O III lines
19 p3422 A69-36220
- M8 electron temperature and internal kinematics from photoelectric Fabry-Perot spectrometric recording of H alpha line profiles and N II
19 p3424 A69-36334
- M 31 nebula radio continuum survey, describing discrete sources catalog and Andromeda nebula radiation distribution
20 p3601 A69-37493
- Star counts in Ophiuchus nebula darkened region /Scorpius-Ophiuchus/ and in comparison fields Corona Australis and Sagittarius
20 p3604 A69-37788
- H alpha line for emission nebulae analyzed by Fabry-Perot etalon, noting Doppler profile
20 p3607 A69-38039

Gas in H II regions and associated stars radial velocities correlation and systematic difference suggesting relationship between nebulae and stars

20 p3611 A69-38150

N I nebular doublet and auroral and nebular lines of O I obtained with multifilter scanning photometer in France, Norway and at magnetic equator

21 p3712 A69-38519

Evolution of diffuse nebulae, considering gas dynamic equations, shock and ionization fronts, models and numerical methods, radiation pressure, interstellar magnetic field, etc

21 p3810 A69-39504

Soviet collection of papers on nebulae and interstellar medium covering computer simulation, photometric observation results, etc

21 p3816 A69-39721

Catalog of reflection nebulae with known dimensions and flux characteristics noting spectrum characteristics

21 p3816 A69-39722

Computer simulation of radiation scattering of spherical nebula with central isotropic star, discussing proposed program and parameters

21 p3816 A69-39723

NGC 7023 nebula physical characteristics observation based on flux and brightness measurement, noting spectral energy distribution and causes

21 p3816 A69-39724

IC 2118 nebula luminosity study by polarimetry and photometry, showing role of light scattering and color properties

21 p3817 A69-39726

IC 349 nebula in Pleiades investigated with diffraction spectrograph, observing spectral energy distribution relationship to illuminating star

21 p3817 A69-39728

Spectroscopic analysis of nebula NGC 6302 for identification as highly excited gaseous nebula, noting He-H ratio

22 p4026 A69-40647

High radial velocity matter of bright region near Trapezium in Orion Nebula, determining electron density lower limit and mean velocity

22 p4029 A69-40769

Orion nebula isophotal contours optical observation for three continuum colors/blue, yellow and IR/ and H alpha

22 p4031 A69-40942

Galactic mass model and interstellar dust scattering data used to examine high latitude nebulae illumination possibility by integrated galactic light

22 p4033 A69-41059

OB stars near emission nebula RCW 103, describing galactic structure in Norma

23 p4220 A69-42384

NEGATIVE CONDUCTANCE

Negative differential resistance effect producing relaxation type oscillations in n-type gallium arsenide

01 p0138 A69-10557

Quantum devices operation analyzed by introducing quasi-linear negative conductance into system by active substance, deriving equations to characterize saturation effects

05 p0719 A69-16223

Stability of negative differential conductivity state with respect to small disturbances, based on hydrodynamic equations for two valley GaAs semiconductors

06 p0981 A69-17879

Stable negative RF conductance and oscillation conditions for n-GaAs crystals of low $n \times L$ product

07 p1197 A69-18448

Thin semiconductor plates negative differential resistance associated with captures at surface, describing electron gas by electron temperature

08 p1374 A69-21081

Precision measuring instrument for negative conductance of active element at microwave region

12 p2038 A69-26054

Stability of negative differential conductivity state with respect to small disturbances, based on hydrodynamic equations for two valley GaAs semiconductors

14 p2503 A69-28788

Injection phase-locking characteristics of LSA/limited space charge accumulation/ mode transferred-electron diode oscillators, employing negative conductance and equivalent circuit

14 p2421 A69-29544

Nonlinear voltage dependence on current in p-type indium selenide single crystals, detecting negative resistance under pulsed electric field

22 p3992 A69-40602

NEGATIVE FEEDBACK

NT SENSORY FEEDBACK

Integrated operational amplifiers for control systems, noting high stability and linearity through negative feedback

01 p0039 A69-10169

Phase-pulse multistable circuit reliability improvement by additional negative feedback increasing parametric variation tolerance, feeding voltages and temperature

23 p4143 A69-42338

Paradoxical inhibition negative feedback principle in oscillatory systems, using mathematical model of nerve membrane

23 p4112 A69-42444

NEGATIVE RESISTANCE CIRCUITS

Stability limits of regenerative echo amplifier during simultaneous variation of network capacitance and negative resistance

04 p0577 A69-14778

Bridge circuit n-type conductivity converter with internal compensation of parasitic effects

05 p0727 A69-15641

Cascaded avalanche diodes in negative resistance amplifying mode for increased output power and extended dynamic range

09 p1462 A69-21408

Equivalence and stability for negative impedance converter of bridge circuits by symmetrical amplifier design

09 p1467 A69-22559

Negative resistance effects computed for HF operation of SCL diodes, based on quantitative analysis of small signal response

12 p2038 A69-26349

LF negative resistance of X band Gunn diodes with lumped components, using coaxial circuit

12 p2039 A69-26387

Triode with emitter controlled negative resistance of GaAs as oscillator for microwave applications

22 p3911 A69-40010

NEGATIVE RESISTANCE DEVICES

Negative resistance behavior of InSb diodes at 77 K, extending double injection theory for insulators to extrinsic semiconductors

02 p0294 A69-11722

Punch-through microwave negative resistance diode explained and contrasted with similar Read and Shockley structures

02 p0215 A69-11938

Traveling high electric field domains in bulk semiconductors use in high speed integrated electronics, noting domain properties of GaAs and CdS

02 p0216 A69-12144

Nonisothermal space charge wave analysis of transit time mode oscillations in bulk GaAs, studying device reactance at given negative resistance

02 p0299 A69-12240

Epitaxial GaAs transferred electron oscillators pulsed operation at bias voltage ten times threshold voltage, noting power output and efficiency

03 p0402 A69-12854

Noise measure formula for negative resistance amplifiers imbedded in lossy passive network

05 p0735 A69-16731

Gallium arsenide double injection diode using vacuum deposited film electrode on single crystal substrate, noting current controlled negative resistance

06 p0893 A69-17156

Stability of negative differential conductivity state with respect to small disturbances, based on hydrodynamic equations for two valley GaAs semiconductors

06 p0981 A69-17879

External impedance controlled nucleation of Gunn effect domains studied theoretically by Nyquist criterion

06 p0981 A69-18217

Gunn effect pulse devices with resistive loading, discussing logic, circuits and low power consumption

07 p1097 A69-18453

Diffusion method for fabricating negative resistance diodes consisting of Cd doped silicon, introducing Cd into n-type silicon plates in evacuated vials

09 p1462 A69-21477

Series operation of Gunn devices with differing threshold currents at SHF

09 p1463 A69-21684

Current controlled negative differential resistivity observed during current-voltage measurements made with p-type Te at 77 K

09 p1557 A69-21747

Gunn diode field distribution with distributed capacitance electrode analyzed with one dimensional computer simulation

09 p1470 A69-22789

Transient characteristics of negative resistance zinc alloy diodes, investigating temperature effects

10 p1662 A69-23157

Semiconductors with negative differential conductivity, investigating decreasing current-voltage characteristics, S or N shaped curves, perturbation parameters, instability, etc

10 p1744 A69-23300

Current voltage characteristics in silicon carbide diodes having negative differential resistance

10 p1663 A69-23571

High current density filaments formation in silicon p-n-n avalanche diodes caused by incremental negative resistance in static current-voltage characteristics

12 p2036 A69-25916

Negative resistance parametric amplifier used as tracking filter, noting resonant frequency dependence on pumping frequency and input and idler circuits

13 p2225 A69-27183

Negative resistance in GaP electroluminescent diodes with p-i-n structure at low temperatures, noting oxygen role

13 p2226 A69-27194

Negative resistance formation in impurity compensated semiconductor diodes ascribed to injected carrier drift path increment with increasing current, deriving I-V characteristics

13 p2230 A69-27877

Capture centers effect on current-voltage characteristic of p-i-n diodes during injection, noting negative resistance appearance

13 p2236 A69-28525

Stability of negative differential conductivity state with respect to small disturbances, based on hydrodynamic equations for two valley GaAs semiconductors

14 p2503 A69-28788

Negative resistance amplifier with stabilizing resistor in compensating circuit for operation in microwave duct mismatched beyond amplifier passband range

15 p2573 A69-30118

Bulk negative resistance material stability, discussing amplifier skin effect limitation and instability beyond critical length

15 p2575 A69-30172

Diffusion method for fabricating negative resistance diodes consisting of Cd doped silicon, introducing Cd into n-type silicon plates in evacuated vials

15 p2578 A69-30722

Negative resistance converter with single differential input operational amplifier, discussing input and output signal

15 p2580 A69-31091

Negative resistance section of current-voltage curve for long diodes of p-type indium antimonide, noting magnetic field effects on electrical breakdown

15 p2581 A69-31149

Gunn device performance for various oscillator types, discussing cavity oscillator characteristics variation

21 p3681 A69-38394

Frequency and phase instability characteristics of negative resistance amplifier due to changes in circuit parameters

22 p3916 A69-40962

NEGATRONS

Cosmic ray negatron and positron spectra using balloon-borne magnetic spectrometer, obtaining absolute solar modulation of positron flux

08 p1380 A69-20728

NEODYMIUM

Selection of transverse oscillations of unstable Nd laser resonator modes with system of two mirrors and two variable focal length convex lenses

03 p0440 A69-13426

Neodymium glass properties degradation during laser operation due to short wave pumping radiation and stimulated emission

03 p0442 A69-14219

Refractive index and expansion thermal coefficients along axis of oriented Nd-YAG laser rod

04 p0609 A69-14293

Output characteristics of slowly Q switched neodymium in calcium tungstate laser

04 p0612 A69-15206

Glass lasers, discussing neodymium properties in glass, flexibility of glass in size, shape and optical excellence, temperature coefficient of index of refraction, etc

05 p0772 A69-16227

Laser emission of neodymium salt dissolved in polonium-chlorine, discussing fluorescence intensity

06 p0936 A69-17778

- Induced emission cross section of neodymium glass laser in quasi-steady mode measured as function of rod section, mirror reflectivity and output
07 p1156 A69-19161
- Stimulated emission of laser employing crystal and glass lasers doped with neodymium ions, using high temperature spectroscopy
08 p1323 A69-19944
- Stimulated emission of water cooled CW Nd doped lanthanum fluoride at room temperature
08 p1323 A69-19945
- Stimulated emission of trivalent Nd ions in glass base, explaining connection between efficiency and emission polarization by interaction of laser modes with ions
10 p1703 A69-23618
- Nd glass laser for emission of high radiance diffraction limited pulses, noting long path air breakdown and second harmonic generation
10 p1704 A69-23654
- Stimulated emission cross section measurement of Nd ions in calcium tungstate using Edwards method
11 p1938 A69-25049
- Transverse passive mode locking by dye technique for neodymium glass laser with confocal cavity
12 p2107 A69-26327
- Far IR electronic and vibronic transitions in single crystals of Nd ions in tysonite lanthanide fluorides
13 p2316 A69-27628
- Negative dispersion of light in neodymium activated calcium tungstate single crystal using neodymium glass laser source, analyzing interferential bands in spectral diagrams
15 p2632 A69-30051
- Passive mode locking of pulsed Nd-YAG laser using saturable absorber, noting two photon fluorescence contrast ratio
16 p2797 A69-32019
- Laser effect in neodymium glass, estimating efficiency of light energy output vs electric energy input
17 p2979 A69-32828
- Kr and Ar flash lamps pumping efficiencies compared for Nd-doped YAG and glass lasers
17 p2980 A69-32958
- Polymethine dyes in passive Q switches of neodymium lasers, noting effects of absorption band intensity, width and position on single pulse laser energy yield
17 p2983 A69-33968
- Stable passive Q-switch of neodymium laser, presenting single pulses energy, time and spectral characteristics
17 p2983 A69-33969
- Polarized emission from Nd activated glass, establishing S and P polarization component energy dependence on pumping energy
17 p2984 A69-33974
- Neodymium activated glass laser efficiency as function of absorption of pumping and emission energy by glass
22 p3964 A69-40797
- NEODYMIUM COMPOUNDS**
- Phonon states effective density in neodymium trichloride from vibronic spectra accompanying electronic transitions in trivalent Pr and Nd ions
03 p0473 A69-13907
- NEON**
- Rodents exposure to neon enriched atmosphere for three weeks in sealed recycling system, discussing body weight pregnancies and litter
01 p0019 A69-11342
- He/Ne ratio effect on performance of He-Ne laser in annular cavity
04 p0612 A69-15176
- Fluorescent light polarization of neon atoms subjected to gas discharge, static magnetic field and laser beam
[IEEE PAPER T-9]
07 p1155 A69-19084
- Total ionization cross section for symmetric collisions measured as function of energy by using neutral atomic beams of neon and krypton
08 p1356 A69-20740
- Nc and Xe in carbonaceous chondrites, noting large amounts of fission Xe and implications for galactic nucleosynthesis models
08 p1405 A69-20925
- Detection of micron Ne emission line from planetary nebula IC 418 using IR spectrometer
09 p1591 A69-21452
- O, Ne, Si and Fe ionization equilibria in low density plasma, including dielectronic recombination and autoionization processes in calculations
09 p1543 A69-22404
- Linear dependence of saturation parameter on active medium density of He-Ne laser explained by considering exchange collisions of neon atoms
09 p1521 A69-22687
- Neon discharges, discussing similarities in type p plasma ionization waves generated by pulsing
10 p1740 A69-23721
- Transport and balance coefficients in ionized neon and helium plasmas in homogeneous electric field, calculating electron mobility, diffusion coefficient, energy and collision parameters
10 p1740 A69-23722
- Neon discharge positive column at medium gas pressures, discussing calculated and experimental data concerning diffusion theory to interpret parameters
10 p1740 A69-23723
- Optical depth at under 110 A due to continuous absorption by N, O and Ne ions estimated in high excitation planetary nebulae
10 p1790 A69-24140
- Disaligning and velocity changing collisions influence on laser light induced saturation peaks or holes in velocity distribution of Ne atoms
12 p2105 A69-26317
- Laser interferometer determining spatial distribution of neon metastable state in He-Ne active discharge, discussing lens effects
12 p2108 A69-26636
- He/Ne ratio effect on performance of He-Ne laser in annular cavity
18 p3152 A69-34718
- NEON ISOTOPES**
- Saturated absorption by Ne inside 6328 A He-Ne laser, discussing selection of Ne isotopes in gain and loss tubes
07 p1149 A69-18898
- Upper bounds for electromagnetic transition rates for Ne 20 determined using Hartree-Fock wave functions
18 p3177 A69-35166
- Trapped Ne in carbonaceous chondrites and gas-rich meteorites, observing Ne 20/Ne 22 ratio variance
24 p3855 A69-43217
- NEOPLASMS**
- U CANCER**
- NEPHANALYSIS**
- Automated layered-nephanalysis and numerical total cloud cover prediction program using moisture data from Tiros 7 photographs
01 p0110 A69-10691
- NEPHELINE**
- Nepheline occurrence in unequilibrated chondrites, discussing crystallographic evidence from X ray powder patterns
04 p0659 A69-15010
- NEPHELOMETERS**
- Photoelectric equipment for nephelometric simulation studies of light scattering by cloud particles
06 p0953 A69-17993
- Vacuum exposure nephelometer system for materials contamination screening in space applications
24 p4297 A69-42931
- NEPHRITIS**
- Renal pathology of acute methylhydrazine intoxication in dogs, noting hemolytic anemia and hemoglobinuric nephropathy
06 p0883 A69-17847
- NEPTUNE [PLANET]**
- Two element interferometer observing Saturn, Uranus and Neptune at 3.12 cm, determining equivalent black body disk temperature
01 p0148 A69-10052
- Neptune mean diameter determination by photometric observations of stellar occultation by planet
01 p0150 A69-10386
- Pluto mass from observations of perturbation on motion of Neptune
02 p0315 A69-11808
- Neptune atmosphere height scale and density from photometric observation of star occultation
04 p0660 A69-15061
- Pluto mass from Neptune orbital longitude, comparing observations and theory
04 p0663 A69-15385
- Photoelectric observation of star occultation by Neptune for mean radius determination
06 p1007 A69-17693
- Photoelectric observation of star occultation by Neptune for scale height determination
06 p1008 A69-17694
- Radio telescope observations at 11.13 cm for polarized E vector intensities of Saturn and disk temperature of Uranus and Neptune
17 p3039 A69-33731
- Relative positions of Neptune and BD minus 17 degrees 4388 star determined by Yale-Columbia refractor and double star camera, noting ephemerides correction from stellar occultation
17 p3041 A69-33814
- Photoelectric observations of BD minus 17 degrees 4388 occultation by Neptune on 7 April 1968, studying light curves during immersion and emersion of star
17 p3041 A69-33815
- Neptune radius, density and atmosphere deduced from observations during occultation of BD minus 17 degrees 4388 by Neptune
17 p3041 A69-33816
- Diameter density and atmosphere of Neptune revised based on star eclipse, noting altitude and temperature
18 p3205 A69-35438
- Pluto mass and density accuracy, questioning values derived from Neptune observations
19 p3403 A69-35969
- Neptune equatorial radius, diameter, flattening and upper atmosphere optical properties determined from photometric curves of star BD-17 occultation
21 p3796 A69-38471
- Photographic observations of Neptune occultation of BD-17 degree 4388, Zodiac Catalog number 2232 in April 1968, noting geocentric separation and planet radius
23 p4221 A69-42388
- NERNST-ETTINGSHAUSEN EFFECT**
- Fermi surface topology effects on Nernst-Ettingshausen coefficient from measurements in magnetic fields to 3.3 tesla and 1.2-4.2 K temperatures in metallic tin
05 p0808 A69-16357
- Kinetic coefficients of carrier motion in semiconductor obtained by Boltzmann equation, considering impacts between carriers
09 p1554 A69-21468
- Indium arsenide electrical parameters analyzed by kinetic effects, considering conductivity, thermal and magnetothermal EMF and transverse Nernst-Ettingshausen effect
15 p2666 A69-30066
- Kinetic coefficients of carrier motion in semiconductor obtained by Boltzmann equation, considering impacts between carriers
15 p2669 A69-30713
- Transverse thermomagnetic EMF and Nernst-Ettingshausen coefficient in GaSb semiconductor with double conduction band and strong degeneracy of current carriers
21 p3783 A69-39558
- Nernst effect in pyrolytic graphite at low temperatures including thermal EMF, electrical conductivity, thermal conductivity and magnetoresistance coefficients
21 p3753 A69-39562
- NERNST HEAT THEOREM**
- U NERNST-ETTINGSHAUSEN EFFECT**
- NERVA [ENGINE]**
- U NUCLEAR ENGINE FOR ROCKET VEHICLES**
- NERVES**
- Neural buoyancy microelectrode for prolonged recording from single nerve units
02 p0202 A69-11865
- Morphological microchanges in solar plexus ganglia of white rats after X irradiation
12 p2019 A69-26347
- Optic nerve spikes elicited by acetylcholine application on isolated perfused retina of frog, varying response by prostigmine and atropine
23 p4084 A69-41465
- NERVOUS SYSTEM**
- NT AFFERENT NERVOUS SYSTEMS**
- NT AUTONOMIC NERVOUS SYSTEM**
- NT AXONS**
- NT BRAIN**
- NT BRAIN STEM**
- NT CENTRAL NERVOUS SYSTEM**
- NT CEREBELLUM**
- NT CEREBRAL CORTEX**
- NT CEREBRUM**
- NT DIENCEPHALON**
- NT EFFERENT NERVOUS SYSTEMS**
- NT GANGLIA**
- NT HIPPOCAMPUS**
- NT NERVES**
- NT NEURONS**
- NT PERIPHERAL NERVOUS SYSTEM**
- NT SPINAL CORD**
- NT SPINE**

NT SYMPATHETIC NERVOUS SYSTEM

NT SYNAPSES

NT THALAMUS

Human nervous system and vestibular and auditory
analyses functional changes under combined
hypokinesia and radial accelerations effects
02 p0197 A69-11496

Hypoxia effects on vestibular analyzer function of
rats in pressure chambers at simulated altitudes from
11,000 to 12,000 m
02 p0198 A69-11506

External observer effect on human behavior during
sensory deprivation tests conducted in isolation cham-
bers as factor in estimating personality
02 p0200 A69-11516

Steroid hormones effect on nervous system and
behavior from data on gonadectomized rats and mon-
keys treated with testosterone propionate
03 p0375 A69-13551

Human perception in space as function of nervous
relationships involving optic, kinesthetic, vestibular
and other analysors
08 p1263 A69-19938

Nervous system relations to insect flight musculature
of lift and thrust mechanism
21 p3651 A69-38780

Nervous system reactions and resistance to ionizing
radiation noting role of functional, morphological and
physicochemical changes in nerve tissues
21 p3659 A69-39061

Robot command and control by computer assembly,
describing engineering analog of vertebrate nervous
system
21 p3679 A69-39603

Model of nerve elements, discussing subthreshold
processes parameter system and analog investigation of
transient processes for various stimuli at model input
23 p4110 A69-41981

Respiration effects on heart rhythm emphasizing
direct mechanical influences
23 p4097 A69-42093

Paradoxical inhibition negative feedback principle in
oscillatory systems, using mathematical model of nerve
membrane
23 p4112 A69-42444

Sensory information processing model for tactile
perception using array of airjet and piezoelectric stimu-
lators applicable to display design and nervous system
investigation
24 p4276 A69-43273

NETHERLANDS

Netherlands space research covering solar and stellar
research, cosmic radiation, photometry and satellite
geodesy
15 p2725 A69-31464

NETS

U NEURAL NETS

NETWORK ANALYSIS

NT CRITICAL PATH METHOD

Passive circuit to transform voltage of indefinitely re-
peated positive or negative pulses using transistors,
diodes and magnetic cores
01 p0043 A69-10564

Electronic device networks periodic structures accu-
racy estimated by automatic measurement of complete
error spectrum of network spacings
01 p0045 A69-10732

Variable impedance matching device employing
lumped and homogeneous circuit elements and stub
line technique
01 p0046 A69-10740

Soviet collection of papers on electric circuits and
electromagnetic systems
01 p0046 A69-10744

Circuits with magnetic coupling, describing digital
computer algorithms for assembly of loop current
equations
01 p0036 A69-10745

Universal NOR element design with resistors, deter-
mining permissible combinations for static mode of
operation by computer method
01 p0037 A69-10746

Semiconductor switching diode, evaluating opera-
tion with nonlinear time delay equivalent circuit
01 p0046 A69-10747

Equivalent circuits for transient characteristics ap-
proximation of distributed RC circuits
01 p0046 A69-10779

Self adaptive control circuit diagram examination,
considering phase shift measurement reliability by
eliminating distortion caused by system nonlinearities
and noise
01 p0052 A69-10796

Spatial filtering effectiveness determination by
equivalent spatial operations, deriving expression for
SNR
01 p0052 A69-10799

Computer analysis of linear active nontime varying
circuits by two graph topological approach based on
Binet-Cauchy theorem
01 p0037 A69-11349

Shockley theory of field effect transistors, calculat-
ing characteristics in miniaturization problems by
removing geometric constraints with aid of electric
analog
02 p0215 A69-11781

Inverse Laplace transform determination method for
periodic functions applied to rectangular pulse train
and rectified sine wave
02 p0271 A69-11983

Noise generation and propagation in linear N
cascaded mismatched two port networks, noting appli-
cation to microwave measurements in low noise
technology
02 p0211 A69-12445

Analysis and design of synchronous filter compatible
with microelectronics requirements, switching N
monolithic RC thin film devices to signal source of re-
sistance
03 p0403 A69-13206

Direct and indirect synchronization of pulsed oscilla-
tor with interrupted synchronizing signal for spectral
purity of output waveform and locking range of system
03 p0404 A69-13301

Topological principles of gate and contact self cor-
recting circuits not using self correcting codes
03 p0410 A69-13421

Open and closed path orthogonal analysis for struc-
tural network
03 p0526 A69-13735

Active circuit analysis by state variable method,
defining state vector as set of voltages between nodes
and reference node
03 p0410 A69-13831

Plane of symmetry determination for generalized
junction gate field effect transistors extended to in-
clude impurity profiles and bias voltage conditions
04 p0574 A69-14344

Transistor circuits analysis with aid of signal flow
graphs
04 p0575 A69-14461

Varactor Q calculation from impedance vs bias mea-
surements, circumventing circuit loss problem by
procedure based on Weissfloch equivalent circuit of
lossy two port network
04 p0575 A69-14753

Lossless multiple beam forming device operational
principles, noting parallel plate radial transmission line
network construction
04 p0576 A69-14768

Hybrid loop properties determination using quadru-
pole algebra, noting frequency dependence of input im-
pedance and voltage transmission
04 p0582 A69-15072

Equipment for minimum cost laboratory for thin and
thick film hybrid circuits
04 p0559 A69-15198

Electric quadrupole parameters, discussing relation-
ship between voltages at terminals
04 p0579 A69-15228

Electrical circuits time domain analysis, describing
method for computer solution of circuit equations
05 p0737 A69-15766

Passive four terminal elements series connection
transmission characteristics, considering line losses
05 p0729 A69-16081

Engineering solution for integrodifferential equa-
tions of physical systems with electronic circuits
05 p0724 A69-16468

Nonlinear distortion of FM signal during passage
through multipath medium, using analysis of linear pas-
sive four terminal network
05 p0721 A69-16531

Book on electric elements and circuits for automatic
control, discussing electric machines as control loop
elements, stability criteria and synthesis, electric
drives, etc
05 p0739 A69-16545

Frequency and noise characteristics of gyrator cir-
cuits, analyzing Q factor, stability and oscillation sen-
sitivity
05 p0735 A69-16621

Ionizing radiation effects in microcircuits, using
lumped model technique to derive mathematical model
from electronic characteristics and boundary values of
each semiconductor
06 p0977 A69-16886

Square loop magnetic core model for computer
aided circuit transient analysis
06 p0899 A69-16888

Combined neutron degradation and gamma induced
effects on closed loop system simulated by SECURE
program
06 p0899 A69-16889

Soviet Orbita communication satellite system net-
work operation, design and technical and economic
aspects
06 p0886 A69-17043

Circuit and system theory - Conference, University
of Illinois, October 1968
06 p0901 A69-17391

Deterministic pattern classification algorithms
discussing abstraction problem, stochastic algorithms,
minimum error scheme and modified least squares
scheme
06 p0892 A69-17395

Requirements for analysis and synthesis of diagnostic
tests for detecting faults in combinational logic circuit
06 p0892 A69-17408

Linear network analysis by topological formulas for
derivation of k-tree terms without generation of k-trees
of graph
06 p0903 A69-17409

Self dual graphs and diagraphs enumeration and prop-
erties
06 p0947 A69-17410

Multivibrator with two widely different zones of
discontinuous oscillation
06 p0896 A69-17474

Voltage divider network board composed of compo-
site carbon resistors for measurement of terminal
voltage of 3 Mev Dynamitron electron accelerator re-
calibration
06 p0907 A69-17705

Harmonic oscillations in tunnel diode circuits for
three intersection points of loadline with characteristic
curve, discussing larger total positive circuit resistance
case
06 p0898 A69-17801

Automatic control textbook covering theoretical and
practical principles of control engineering, analysis,
design, servomechanisms and instrumentation
06 p0904 A69-17856

Energy transfer from pulse network to mass as-
sociated with propagating current sheet in linear pinch
discharge, discussing pulsed plasma accelerator effi-
ciency
[AIAA PAPER 69-113]
06 p0971 A69-18123

Microelectronics in astronautics, discussing prop-
erties of thick and thin film electronic devices, integrated
semiconductor circuits and hybrid circuits
07 p1089 A69-18256

Response curves of frequency changer circuits /mul-
tipliers and dividers/ using reactive nonlinearity calcu-
lated as function of filter mismatch
07 p1114 A69-18279

Control system analysis and synthesis by means of
generalized root-locus method on digital computer
07 p1114 A69-18291

Self organizing trainable logical networks /TLN/ as
stable controllers in multiaxis vehicle control problem,
reviewing TLN concepts and training theory
07 p1070 A69-18388

Circuit producing electrical and optical oscillations
simultaneously constructed by combining semiconduc-
tor laser diode with photodiode
07 p1148 A69-18688

Unified theory of normal mode analysis of RLC net-
works based on Tellegen theorem of Kirchhoff law,
discussing coupled networks
07 p1115 A69-18858

Linear noisy two port preceded by nonreciprocal
lossless network analyzed, showing existence of as-
sociated quantity invariant under lossless transforma-
tion
07 p1104 A69-18891

Diode pump type circuit without diodes in signal
path providing accurate transfer function analysis con-
sidered for spacecraft use
[IEEE PAPER 3A-3]
07 p1134 A69-19191

Algorithm for calculating Moore automaton or con-
nected network channel capacity and source of input
symbols for full capacity utilization
07 p1088 A69-19707

Feedback systems analysis, considering single phase
and polyphase coupled and uncoupled commutation
networks in forward loop and linear transfer function
feedback loop
08 p1295 A69-19853

Differentiating network with nonlinear resistance and capacitance elements, noting improvement in pulse shaping properties
08 p1295 A69-19910

Computer aided design program for testing equivalent circuits of bipolar transistors in static regime under various polarization conditions
08 p1280 A69-19972

Controlled charge models for computer calculation of electronic circuits, discussing tunnel diode static characteristics and equivalent transistor circuits
08 p1280 A69-19975

Computer aided automatic drawing of printed circuits, including design and manufacture of films for engraving
08 p1296 A69-19979

Parasitic reactance disturbing attenuation and return loss of reactance filters, discussing correction of numerator polynomial of characteristic function
08 p1283 A69-20128

Passive circuit components electrical properties at HF using equivalent circuit
08 p1283 A69-20135

Final stage of three phase DC/AC converter, noting three phase control circuit for power stages with germanium transistors
08 p1285 A69-20381

Book on analysis and synthesis of linear active networks covering filter design, negative resistance, network theorems and stability, amplifier role, etc
08 p1298 A69-20885

Vortex valves and amplifiers small signal analysis using mathematical model to describe quantitative effects of vortex parameter changes [AGARDOGRAPH-118]
08 p1257 A69-20953

Variable phase shifters and delay lines, discussing mechanical and electronic adjustments
08 p1290 A69-20978

Nonlinear capacitive parallel frequency converter circuit stability, using filtered circuit method
08 p1299 A69-21148

Delta functions spectrum in reciprocal time domain for LC and RC structures due to impulse response in distributed parameters
09 p1471 A69-21327

Transient analysis for uniform RC structures using impulse excitations in open and short circuit configurations
09 p1471 A69-21328

Nonlinear analysis of transistor networks using Kron mesh method, developing quasi-linear equations characterizing common emitter transistor
09 p1471 A69-21632

Decoupling by state variable feedback and determination of inverse extended to linear time varying multivariable system
09 p1472 A69-21680

Algorithms in electronic circuit analysis, establishing algebraic and topological analogs based on generation of fundamental relations
09 p1472 A69-21777

Linearized radio circuits frequency characteristics calculations using digital computers, noting system nodes number influence on computer rate
09 p1472 A69-21783

Circuit function determination from Laplace transforms without calculating transient state matrix, using numerical method
09 p1472 A69-21785

Digital computer algorithm for analyzing circuits represented as autonomous multiport networks
09 p1472 A69-21786

Noise factor of two port in terms of various sets of noise parameters and source immittances, giving table for conversion formulas
09 p1455 A69-21897

Soviet book on statistical theory of discrete signal demodulation, covering demodulator analysis and synthesis methods
09 p1455 A69-21933

Microwave interferometer circuits errors, considering interferometers with phase detector, logic counting circuits, frequency conversion and amplitude modulation
09 p1496 A69-22029

Ultimate state periodic analysis of nonlinear electric systems by approximation methods in calculus of variations, discussing functional concept
09 p1474 A69-22448

Density functions analytic solution for Fokker-Planck equation representing cascaded phase locked loops
09 p1474 A69-22450

Complex admittances and impedances of various networks determined by impedance bridge, describing frequency dependent limits of measurement parameters
09 p1501 A69-22578

Vortex amplifiers small signal analysis based on mathematical model and network theory
09 p1443 A69-22739

Simulation to correlate integrated logistic support recommendations for dynamic analysis of planned logistic network
10 p1668 A69-22975

Electronic circuit analysis by computer programming including system and program commands, network data, output control, discussing steady state circuit programming
10 p1659 A69-23143

Vortex amplifier as active element in analog circuits
10 p1639 A69-23556

Single circuit parametric oscillator excitation by small external narrow band signal, using method of slowly varying amplitudes
11 p1845 A69-24453

Passive structural units in fluidic circuits, discussing tesla diode and proportional amplifier
11 p1825 A69-24542

Minimum conversion loss in general mixer circuit configuration, noting dependence on time varying resistance and equal terminating impedances
11 p1845 A69-24550

Computer program for analysis of linear microwave multiport circuit by means scattering matrix equivalent
11 p1858 A69-24572

Estimation system distinction from adaptive system, discussing network of adaptive estimation systems
11 p1858 A69-24937

Rectangular RC distributed circuits with shaped electrodes, analyzing short circuit admittance parameters
11 p1858 A69-24938

Load admittance effect on low pass voltage transfer characteristics of RC lines, analyzing shaped lines at open circuit under terminated conditions
11 p1859 A69-24939

Hybrid matrix algorithm for electronic circuits analysis, showing applications to transistorized circuits
11 p1859 A69-24954

Log periodic dipole array antennas simulated with simple RLC circuit loading uniform transmission line
11 p1850 A69-24977

Transient behavior of transistor UHF oscillator, discussing network analysis for oscillation amplitude calculation by nonlinear transistor equivalent circuit diagram
11 p1854 A69-25613

Fluidic quantities analogous to electrical properties of lumped circuit elements in DC networks, noting validity of Kirchhoff node and mesh theorems
11 p1861 A69-25676

Narrow band LC 70 MHz IF filter design method
12 p2036 A69-25915

Steady state solution of periodically excited circuit, constructing Green function for use in convolution integral
12 p2036 A69-25918

Computer controlled network analyzer performing automatic microwave measurements of passive and active networks, based on signal splitting and detecting
12 p2037 A69-26048

Digital computer analysis of multivariable control system in frequency domain, using operational array technique programming method
12 p2046 A69-26064

Book on random signal analysis covering Fourier analysis, circuit analysis, Fourier transform theory, operators, probability, random variables, stochastic processes
12 p2031 A69-26632

Network method for Dirichlet problem of Laplace equation in regions with rounded corners, noting polar and composite errors
12 p2123 A69-26730

Transient response of transistor in common emitter circuit using charge method taking into account base current switching pulse parameters
12 p2043 A69-26884

Current driven AGC effectiveness in selective amplifiers, including conductance variation effect on pass-band instability and frequency response
12 p2043 A69-26887

Power losses of varactor frequency multipliers with series connected circuits including open circuit tuned to second harmonic
12 p2043 A69-26888

Computer determination of symbolic state equations for nonlinear circuits using FORTRAN notation
12 p2055 A69-27097

Power gain in TWT attenuators with linear tapered ends, considering conversion loss due to tapering
12 p2044 A69-27102

Ground station network and facilities for control of and acquisition and processing data from ESO 1 satellite
13 p2220 A69-27751

Ferrite parameters measurement in alternating fields based on continuous analysis of magnetic, magnetizing and measuring circuits for assessing errors
13 p2230 A69-27996

Molecular flow network theory extended to pulsed operation with gases mixtures having various molecular weights
13 p2247 A69-28085

MOS unitoron switching circuit operation subjected to nonlinear load, using analytic approximations of current-voltage characteristics
13 p2234 A69-28507

Transistorized DC amplifier circuit with reversible and controllable transfer constant based on voltage conversion principle
13 p2235 A69-28511

Transistor circuits analysis with aid of signal flow graphs
14 p2418 A69-28832

Small signal transient characteristics of semiconductor diodes analyzed by charge method, studying processes during p-n junction diode switching at low currents
14 p2419 A69-28918

Two stage amplifier with two differential feedbacks, investigating tuning sensitivity
14 p2426 A69-29147

Numerical solution of differential equations for two channel PFM with pulse element, applying Dirac pulse sequence to input
14 p2426 A69-29148

Pull-in performance of phase locked loops with phase comparator having asymmetric triangular characteristic
14 p2413 A69-29482

Performance of oscillating limiter driven by noise corrupted FM signals covering frequency deviations, carrier to noise ratio, etc
14 p2413 A69-29497

Algorithm for enumerating all circuits of linear graph, noting suitability for computerization without large computer memory
14 p2421 A69-29541

Topological circuit analysis by digital computer, using conductivity matrix determinant in form of sum of trees
15 p2582 A69-30112

Wideband transistorized amplifier frequency response analysis by simplified approximations, subdividing operational frequency range
15 p2573 A69-30113

Transistorized circuit operation with nonlinear feedback through tunnel diode analyzed by piecewise-linear approximation of I-V characteristics
15 p2573 A69-30114

Different parametric converters amplitude characteristics analysis for determining necessary pumping power, allowing for saturation
15 p2574 A69-30119

MOSFET/unitoron/ switching circuits classification in terms of load curve shapes obtained with different output connections of load elements
15 p2574 A69-30122

Push-pull circuit configurations for GaAs transferred electron oscillators, discussing CW X band and pulsed L band devices operation
15 p2574 A69-30168

Lumped and distributed parameter systems, discussing transfer matrix elements, connecting lines, etc
15 p2582 A69-30319

False alarm stabilization circuits efficiencies compared in unsteady Gaussian noise, considering phase autocorrelator performance
15 p2567 A69-30342

Equivalent circuit of single winding transformer, using distributed constant theory
15 p2578 A69-30793

Varactors for frequency conversion circuits, discussing efficiency and output power
15 p2578 A69-30797

Disturbances simulation in instrumentation utilizing digital integrated circuits for reliability computation in complex circuits
15 p2628 A69-30848

Hydraulic resistance, capacitance and inductance of fluidic element derived by analogy with electric circuits 15 p2552 A69-31060

Broadband microwave double balanced mixer/modulators, discussing bandwidth, conversion loss, noise figure, intermodulation and power dissipation 15 p2580 A69-31077

Approximate solution for coupled microstrip transmission lines in integrated circuits, discussing impedance, capacitance and testing 15 p2580 A69-31078

Similarity between semiconductor discrete devices and integrated circuits, considering materials, processing and failure modes 15 p2580 A69-31128

Linear high resolution gate function in blocking out analog signals or reproducing signal amplitudes at output, noting semiconductor elements utilization 15 p2581 A69-31523

Computerized finite element waveguide analysis for determining propagating modes and cut-off frequencies 16 p2760 A69-31942

Molecular flow network theory applicable to volumes interconnected by small orifices or porous membranes for transient pressure measurements 16 p2813 A69-32325

Nonlinear distortion of FM signal during passage through multipath medium, using analysis of linear passive four terminal network 16 p2753 A69-32473

Amplitude-frequency characteristic and noise bandwidth of electron tube reflex autodyne operating in over or under voltage mode and including IR feedback 16 p2761 A69-32477

Spacecraft antennas properties, structure and problems including frequency ranges, external influences, omnidirectional radiation, input impedance, etc 16 p2763 A69-32584

Scanning electron mirror microscope advantages over electron mirror and scanning electron microscopes for examining integrated circuits 17 p2971 A69-32891

German monograph on theoretical and experimental investigations of tubes and lumped fluidic elements covering equivalent circuit 17 p2903 A69-33573

Superconducting antenna factors and matching circuit equivalents developed for predicting efficiency and Q increase on basis of Pb surface resistance 17 p2937 A69-33784

Computer program and component part models for nonlinear DC circuit simulation at various temperatures 18 p3108 A69-34525

Circuits and systems - Conference, Pacific Grove, California, October-November 1968 18 p3109 A69-34671

Computerized analysis and design of nonlinear servomechanisms, using describing functions technique 18 p3110 A69-34672

Parameter sensitivity analysis of discrete suboptimal filters from optimal rmse estimate of actual system performance measure 18 p3110 A69-34675

Multiloop feedback in active distributed RC networks for low parameter sensitivity with low amplifier gain compared to single loop circuits 18 p3111 A69-34679

Network Analysis for Systems Application Program development for batch and on-line solution of circuit problems 18 p3111 A69-34680

Networks of ideal inductors, capacitors and periodically operated switches with no energy loss, deriving frequency-power formulas from response functions 18 p3111 A69-34682

Shadow effects on current-voltage characteristics of solar cell array circuits, developing mathematical models 19 p3254 A69-35709

Integrating filter analysis for effect of phase detector sawtooth characteristics on locking range of phase locked oscillator 20 p3486 A69-37011

Physical networks with lumped components and hydraulic, pneumatic, electric, thermal and elastic lines of transfer matrices [ASME PAPER 69-FE-15] 20 p3568 A69-37999

Data transmission of variables in deterministic networks 21 p3673 A69-38775

Electrical properties of passive line elements of hybrid integrated circuits on insulating substrates for radio systems 21 p3684 A69-39563

Analysis and synthesis of distributed transmission line networks with open or short circuited shunts or series stubs, describing composite transfer matrices 21 p3687 A69-39660

Network analysis for systems application program /NASAP/ in FORTRAN for batch and on-line analysis of electronic circuits 21 p3856 A69-39662

Correction to circuit theory textbooks concerning observable but not controllable modes and stability 22 p3917 A69-40135

Real time network support simulation allowing network configuration for nominal or perturbed trajectory for Saturn vehicles, applicable to any flight azimuth 22 p4020 A69-40319

Book on Smith chart electronic applications in waveguide, circuit and component analysis and synthesis 22 p3915 A69-40780

Spatiotemporal patterns learning among sensory and motor organs with linearly ordered components by nonlinear networks in terms of embedding fields theory 22 p3887 A69-41196

Frequency response of control systems analyzed by digital computer using operational arrays, noting extensions to time response and root locus computation 22 p3909 A69-41255

Periodic ladder type design delay equalizer for linear delay characteristics in millimeter waveguide systems 23 p4135 A69-41361

Recursion formula for multilayer interferometer derived, with allowance for multiwave interference, to calculate resonant circuit maxima and minima 23 p4165 A69-41729

Power combining network for high power UHF solid state satellite transmitters with low loss, compact size and input port selection capability 23 p4137 A69-41743

N-terminal parent networks with symmetry constraints derived for nonredundant one port configurations through combinatorial functions test patterns, using computer algorithm 23 p4134 A69-42524

Electromagnetic processes analysis in autonomous inverters simplified by linear graph method to derive characteristic equation 24 p4255 A69-42571

Logic networks of Boolean analogs analyzed by algebraic signal flow theory, introducing variational derivative for test detection in combinational and sequential networks [AAS PAPER 69-236] 24 p4288 A69-42811

On-off limit cycle controllers for reaction-jet controlled systems, investigating delay effects 24 p4291 A69-43271

Liapunov functionals for time delay systems by path integrals in state space, using convolution equations involving distributions with compact support 24 p4295 A69-43317

NETWORK SYNTHESIS

Nonlinear programming for optimal circuits design, discussing search method of ACOP/Automatic Circuit Optimization Program/ 01 p0035 A69-10067

Sensitivity of voltage transfer function relative to variation in value of components of resistance terminated reciprocal reactive network 01 p0049 A69-10069

Integrated circuit digital filters design characterized by weight coefficients containing Lanczos factor for application to processing of signal transmitted from space vehicles 01 p0038 A69-10071

Microstrip transmission line integrated circuits on seminsulating GaAs substrates, showing feasibility at millimeter wave frequencies 01 p0040 A69-10197

Digital loaded-line phase shift networks for microwave thin film applications, emphasizing design equations 01 p0040 A69-10198

Synthesis of infinite and finite Wiener optimal networks or equalizers using delay lines with feedforward and/or feedback taps 01 p0029 A69-10554

Wideband hybrid junctions synthesis from given parameters, suggesting matrix representation of ring circuits 01 p0043 A69-10593

Algorithms for linear system of first order differential equations, emphasizing equations associated with computer oriented circuit design 01 p0036 A69-10708

Data compression methods noting block and circuit diagrams 01 p0031 A69-10735

Dynamic system for self adaptive control of inertial plant described by differential equations, noting synthesis method eliminates distortion 01 p0052 A69-10797

Analytical expressions for transfer function matrices of four terminal signal shaping networks, assuming rational matrix spectral density of randomly polarized signal 01 p0031 A69-10880

Soviet book on design of multidimensional automatic control systems, covering structural circuit synthesis and individual element characteristics 01 p0053 A69-10995

Full multiplier design based on stable iterative array cells interconnected to provide logical functions, noting capabilities for binary numbers 01 p0048 A69-11138

Dynamic programming to demonstrate sufficient conditions of optimality in maximum principle when regular control synthesis is realized 02 p0225 A69-11975

Variation method for optimal solution of antenna synthesis problem for given radiation pattern 02 p0217 A69-12260

P-i-n structure isolation method for fabricating monolithic integrated circuits 02 p0222 A69-12471

Breadboard chip for use in computer aided design and analysis of integrated circuits, describing components and application to differential amplifiers 03 p0402 A69-13008

Generalized digital low pass filter synthesis by recursion technique, noting coefficient sensitivity simplification 03 p0403 A69-13227

Linear transistor models synthesis based on measured characteristics of four terminal admittance parameters 03 p0404 A69-13596

Self adaptive circuit parameters synthesis of systems using amplitude-frequency characteristic by Chaplygin theorem 03 p0410 A69-13685

Equivalent circuit for parallel conductor array based on array capacitance matrix 04 p0576 A69-14756

Optimal linear controller synthesis with minimized trajectory sensitivity achieved by using quadratic cost function 04 p0582 A69-14941

Reliability system design, emphasizing circuit design analysis, failure drifts and component failure modes by use of computer programs /ECAP, CIRC and IMAG/ 04 p0608 A69-15224

Digital nth order phase locked loop for FM demodulation 04 p0561 A69-15452

Unified lunar control photogrammetric network produced by mapping satellite in 28 day polar orbit, using recurrent partitioning 05 p0819 A69-15628

Time domain synthesis of multivariable automatic control with predetermined output signal shape, allowing for internal cross coupling effects 05 p0737 A69-15887

Synthesis of simulated aircraft cabin pure fluidic temperature control system [ASME PAPER 68-WA/FE-30] 05 p0705 A69-16103

Broadband LC filters having prescribed amplitude response and constant group delay, emphasizing IF filters for radio relays 05 p0732 A69-16343

Continuous parameter identification methods for parameter optimization in automatic control system analysis and synthesis, using modified steepest descent optimization 05 p0725 A69-16474

Controllable gyrator use in nonlinear network synthesis 05 p0735 A69-16620

Spherical gyroscope servosystem probabilistic synthesis ensuring minimum dispersion of random drift 05 p0764 A69-16669

Markov extremum drift dual compensation in optimal systems with learning experiments 05 p0741 A69-16671

3-terminal gyrator circuits using operational amplifiers, noting exact cancellation of negative by positive resistance and unattainability of LF unstable modes

06 p0893 A69-16936

Integrated circuit interconnection patterns computerized design, discussing automatic laser mask-making control

06 p0931 A69-17199

Metal oxide semiconductor random-access memories, discussing large scale integration and static and dynamic circuits chip size

06 p0894 A69-17203

Thermal management of integrated circuits design, noting dependence on circuit and component configurations and parameter variations

06 p0894 A69-17217

Multivariable self adaptive control system design using sensitivity methods, obtaining adaptation stability by Liapunov synthesis

06 p0900 A69-17352

Adaptive modeler to estimate state and future trajectory of unknown plant having automatically synthesized control

06 p0900 A69-17353

Learning control system design, using a priori information in subgoal selection, control situation grid extensions and controller initialization

06 p0900 A69-17355

Requirements for analysis and synthesis of diagnostic tests for detecting faults in combinational logic circuit

06 p0892 A69-17408

Radio channel circuit outlined for tracking interplanetary spacecraft and probes with signal delay time prediction

06 p0888 A69-17623

Automatic control textbook covering theoretical and practical principles of control engineering, analysis, design, servomechanisms and instrumentation

06 p0904 A69-17856

Digital computer circuit design book covering requirements of circuit for digital logic and memory functions and physical properties of components

06 p0892 A69-17869

Control system analysis and synthesis by means of generalized root-locus method on digital computer

07 p1114 A69-18291

Integration forms suitable for fabrication of hybrid and monolithic microwave integrated circuits

07 p1096 A69-18441

Coupled and uncoupled terminals series connection for reactive multiport network determined by transforming scattering matrix columns into coordinate vectors

07 p1100 A69-18529

Transversal equalizer circuit consisting of delay line and variable sampler and reinsertion coupler for microwave frequencies

07 p1102 A69-18671

Two signal four quadrant multiplier design having subnanosecond response

07 p1103 A69-18879

All-diffused process to build monolithic high power series voltage regulator with separately optimized DC and AC characteristics

07 p1103 A69-18881

Monolithic HF circuits stability in TV and HF devices noting need for appropriate amplifiers

07 p1103 A69-18883

Integrated frequency selective amplifier design for radio frequencies based on feedback configuration with positive real zero in loop transmission function

07 p1104 A69-18886

Montardi circuit with sectioned electrodes to simulate isotropically conducting still liquid for application in MHD pump, discussing potentials distribution

07 p1059 A69-19031

High data rate coherent telemetry systems synthesis, discussing multiphase modulation and demodulation to achieve bandwidth requirements

07 p1083 A69-19123

Computer aided circuit design by singular imbedding, beginning with prespecified topology and undetermined elements

07 p1115 A69-19148

DC servo system with torque feedback, discussing bang-bang system comparison, analog simulation, damping and quasi-optimum behavior

07 p1059 A69-19229

Frequency transformation allowing comb-line filters of narrow and wide bandwidth, using resonance type filters with lumped elements

07 p1108 A69-19487

RC converter filters and delay lines by expanding transfer function into series of components

07 p1113 A69-19677

Computer aided design methods for electronics and logic systems, noting linear circuits and one dimensional transistors

08 p1278 A69-19970

Computer aided design methods for electronic and mechanical materials, discussing basic concepts and problems

08 p1278 A69-19971

Sawtooth generators production based on equivalent circuit theory, calculating linearity errors in voltages

08 p1296 A69-20105

Pseudoexact Chebyshev response curves for bandpass filter design, discussing phase response and time delay characteristics

08 p1283 A69-20227

Nonlinearities identification in closed loop systems using harmonic balance principle for transforming measured block diagram into diagram of simple form

08 p1297 A69-20302

Design and construction of linear digital filters for signal processing, discussing digital filtering of various signals for space research

08 p1297 A69-20303

Transfer function and frequency response of notch filters used to achieve notch filter dimensioning and design

08 p1284 A69-20379

Synthesis method for UHF transistor oscillators tunable in wideband using Y-matrices

08 p1285 A69-20380

Pulse transformer design relationships and definitions, discussing core and winding structure choice

08 p1285 A69-20382

Tuning design optimization of single circuit LF automatic control systems, using transfer functions and phase amplitude graphs

08 p1297 A69-20418

Analog video processor in omnidirectional radar system for flight safety, discussing construction, transistorization and circuitry

08 p1276 A69-20605

Metal oxide semiconductor technology and applications, discussing gates, analog computers, switching circuits and inverters

08 p1286 A69-20833

Composite transistor simulation of circuit inductor effect for synthesizing frequency selective circuits

08 p1286 A69-20834

Nonlinear feedback shift register circuit design by logical sequences

08 p1298 A69-20835

Book on analysis and synthesis of linear active networks covering filter design, negative resistance, network theorems and stability, amplifier role, etc

08 p1298 A69-20885

Fluidics in UK, discussing digital control elements and systems and transmission lines in alternating flow hydraulics

[AGARDOGRAPH-118] 08 p1257 A69-20952

Ultrahigh speed systems and logic circuits specifications implementation into electrical design, discussing circuit selection, line propagation delays, noise margins and temperature effects

[AGARDOGRAPH-114] 08 p1298 A69-20985

Electrical design of low cost, highly maintainable general purpose computer optimized with respect to product of power and speed

[AGARDOGRAPH-114] 08 p1278 A69-20988

Spherical electronically tunable multiresonator YIG filters design using filter tables and coupling bandwidth charts

08 p1292 A69-21006

Equivalent circuit synthesis with six reactances- two terminal network bridges

08 p1295 A69-21166

All-pass transfer functions of new class type for design of quadrature filter networks, using Chebyshev approximation

08 p1277 A69-21167

Chebyshev filter with flat group delay obtaining transfer function, noting cascade synthesis and extended bisection theorem

08 p1299 A69-21169

Iterative Chebyshev approximation for computerized network design by linearizing original nonlinear programming

08 p1299 A69-21170

Transfer function of low pass filters with Chebyshev attenuation characteristic in stopband and predetermined phase or delay time realized by ladder network

08 p1300 A69-21171

Filter design using transformed frequency variables suitable for computer programs

08 p1300 A69-21172

Insertion-loss synthesis of narrow band crystal band-elimination filters, using narrow band approximation and pseudoreactance theory

08 p1300 A69-21173

Zero sensitivity integrated RC filter circuits design, exploiting capacitors and resistors property of having same temperature coefficient

08 p1300 A69-21174

Airborne digital computers for optimization of aircraft control and monitoring functions, discussing avionics and circuit technology

08 p1349 A69-21194

Linear shift register synthesis algorithm found to coincide with Berlekamp iterative algorithm for decoding BCH codes

09 p1470 A69-21317

Microwave power and low noise transistors, noting continuous wave output and circuit design

09 p1462 A69-21407

Equations adaptable to computer for RLC circuits containing linear and nonlinear n-terminal networks derived by nodal method

09 p1472 A69-21779

Low sensitivity electric circuits synthesis based on analytical and numerical analysis of sensitivity function characteristics of selective polynomial circuits

09 p1472 A69-21780

Linear electronic circuit canonical synthesis by computer, using algorithm based on linear and nonlinear programming

09 p1472 A69-21781

Soviet book on statistical theory of discrete signal demodulation, covering demodulator analysis and synthesis methods

09 p1455 A69-21933

Optimum timing extraction /bit synchronization/ in pulse code transmission, analyzing probabilistic structure by statistical parameter estimation and deriving system

09 p1455 A69-22115

Optimal receiving circuit determined for elliptically polarized signals in randomly polarized noise by deriving integral equation

09 p1456 A69-22285

RLC two terminal bridge network synthesis, considering two reactances, three resistances and constraints

09 p1464 A69-22291

Hybrid circuit technology application to packaging electronic systems

09 p1508 A69-22336

Thick film hybrid circuit technology and equipment reviewing conductors, resistors, and insulator inks

09 p1508 A69-22337

Wire, lead frame, direct bonding and beam lead techniques for interconnecting active elements into hybrid circuits

09 p1508 A69-22338

Precision trimmed RC active networks for high selectivity microelectronic filter fabrication for frequency division multiplex applications

09 p1466 A69-22452

Microelectronics for digital adaptive controls, discussing digital filter design and chips required in fabrication

09 p1474 A69-22453

Frequency modulation feedback demodulator design procedure for satellite communications, noting importance of nonideal implementation

09 p1457 A69-22464

Adaptive logic trees with two input gates for mechanization of any desired function of variable set, deriving multilevel representations of functions

09 p1475 A69-22583

Control system controllability under discontinuous control constraints, presenting optimal response rate linear system synthesis with continuous restriction on control function

09 p1475 A69-22670

Statistical theory and dynamic programming to synthesize optimal pulsed control systems having restrictions on control device storage capacity

09 p1476 A69-22673

Aircraft modal control systems synthesis to improve response characteristics by altering pairs of complex conjugate and real eigenvalues simultaneously

09 p1435 A69-22779

Pseudoexact bandpass filter response curves and electrical characteristics based on ripple Chebyshev responses

09 p1470 A69-22794

DC to DC converters design using HF transistors to achieve high switching speeds while reducing size and weight

10 p1635 A69-22983

Computer aided circuit design programs combining technical engineering skills with building block programs

10 p1659 A69-23141

Dynamic programming to demonstrate sufficient conditions of optimality in maximum principle when regular control synthesis is realized

10 p1666 A69-23884

Multiple loop feedback systems synthesis utilizing extended node introduction synthesis theory, considering filter response functions characteristics

10 p1667 A69-24037

Filter network synthesis for realization of rational functions, discussing numerator polynomial inclusion by choice of divisor polynomial and branch introduction and parallel systems

10 p1667 A69-24038

RC circuit with variable time constant using variable resistor

10 p1667 A69-24046

Antenna array statistical synthesis, investigating signal detection capacity for large phase fluctuations

11 p1833 A69-24439

Laser application to welding, drilling and other processes involving material removal for microelectronic circuits and components fabrication

11 p1846 A69-24600

Polyharmonic predictive and self tunable filters synthesis based on signal periodic components detection, noting role in information transmission and processing systems

11 p1849 A69-24966

Low pass filters synthesis based on Chebyshev polynomials properties noting requirements of critical frequency, frequency response decline rate and tolerance range

11 p1887 A69-25210

Linear active adjustable VLF filters for polynomial transfer functions

11 p1859 A69-25392

Microwave filters with lumped capacitances and coupled waveguides derived by frequency conversion from lumped filters circuits

11 p1855 A69-25628

Lumped element construction technique involving crossed coils to reduce ferrite produced heat in resonance isolators, using substituted YIG

11 p1856 A69-25632

Circuit designs using differential amplifier devices or operational amplifier integrated circuits

11 p1857 A69-25664

Narrow band LC 70 MHz IF filter design method

12 p2036 A69-25915

Feedback design for monotonically stabilized linear sampled data control system

12 p2045 A69-25961

Linear bridge circuits design having proportional output signal to first or second derivative of input signal envelope

12 p2037 A69-25962

Synthesis of multivariable control systems at minimal integral square quality functional

12 p2046 A69-26061

Multivariable control system decoupling by appropriate choice of decoupling network structure and location in system

12 p2048 A69-26074

Nonlinear multivariable control systems synthesis, considering synthesis expressibility in known linear formulation

12 p2048 A69-26077

Shutter drive circuits for image converter camera noting focusing, deflection system, applications in plasma research, etc

12 p2082 A69-26138

Equivalent subsystems for designing multivariable linear automatic control system

12 p2052 A69-26280

Multiinput sine comparators graphical analysis and design considerations, emphasizing semiconductor circuit providing quadrilateral polar characteristic on impedance plane

12 p2039 A69-26350

Ultra lowpass filter circuit with two point contact Ge diodes and capacitor

12 p2039 A69-26379

Analytical expressions for transfer function matrices of four terminal signal shaping networks, assuming rational matrix spectral density of randomly polarized signal

12 p2031 A69-26644

Asymptotically stable discrete time closed loop linear systems synthesis, presenting feedback matrix as illustration

13 p2287 A69-27238

Pulse frequency integral estimate devices with integrating chemotron tetrodes for automatic systems metering applications

13 p2227 A69-27522

Microwave filters for canonical realization of non-minimum phase transfer functions, combining magic-T or hybrid junction with ladder structure network

13 p2228 A69-27668

Multiaperture waveguide directional couplers analyzed by four port equivalent circuits, discussing synthesis method for optimizing coupling directivity

13 p2228 A69-27669

Microstrip circulator size reduction attained by tight inductive ferrite coupling for incorporation with microwave integrated circuits

13 p2230 A69-27679

Solid state radar feasibility, discussing circuit components, circuit design problems involving striplines and monoblocks, phase controlled antenna, solid state computers, etc

13 p2230 A69-27928

Transmission line all pass equalizers theory and design for operation in TEM, TE or TM modes

13 p2233 A69-28065

Two idler parametric amplifiers bandwidth properties investigated using equivalent circuit, noting role of idler circuit design

13 p2233 A69-28066

Chebyshev polynomial of even order used in synthesis of equally terminated low pass lumped and distributed filters of even order

13 p2233 A69-28068

Synthesis for asymmetrical branch guide directional coupler-impedance transformers, noting application in antenna design

13 p2233 A69-28069

TEM mode networks design for producing phase coherent pulse modulated microwave signals through spectrum S band

13 p2234 A69-28073

Asynchronous finite state sequential nonlinear controller synthesis with few flip-flops for dynamic space vehicle systems [AIAA PAPER 67-988]

13 p2225 A69-28201

Tunnel diode slideback sampling gate circuits, discussing response characteristics and operational specifications

13 p2236 A69-28538

Two stage tunnel diode amplifier synthesis with gain stabilization circuit widening passband, discussing operating frequency and maximally flat amplitude frequency response

13 p2236 A69-28575

Optimization criterion for synthesizing discrete nonlinear control system subjected to random controlling and perturbing effects

14 p2425 A69-28825

Trigger demodulator theory, design and circuits

14 p2419 A69-28907

Compensating /feedback/ loops determination method for linear two dimensional control system, achieving self regulation

14 p2425 A69-28908

Statistical synthesis of optimal control for quasi-harmonic systems by extending asymptotic method to include unremovable measurement error in output value

14 p2426 A69-29420

Optimum nonlinear digital filter synthesis for smoothing, predicting and differentiating measured quantity having uniform probability distribution over finite number of discrete values

14 p2426 A69-29421

SHF solid state phased array radar with Gunn effect modular microwave IC design, discussing air and ground applications

14 p2420 A69-29435

Optimized receivers synthesized for narrow band radio signal filtration, comparing noise rejection properties of various pulse modulation types during speech transmission

14 p2413 A69-29464

Notch filter construction by single operational amplifier, adjusting notch bandwidth by varying ratio of resistors and capacitors

14 p2421 A69-29550

Capacitors pi network representation of series gap in center conductor of matched coaxial transmission line

14 p2424 A69-29766

Digital notch filters synthesis based on bilinear transformation method

15 p2575 A69-30182

Nanosecond pulse generator for powering semiconductor lasers, examining circuit diagram and elements design

15 p2633 A69-30234

Thermistor thermometer with low energy dissipation for flow measurements, discussing design considerations

15 p2608 A69-30296

Differential equations for optimum reception to synthesize detectors of deterministic signals against nonGaussian background noise using Markov process

15 p2567 A69-30340

Electron beam exposure system to photoetch integrated circuit patterns without photomasks, using electronic computer for automatic pattern generation and registration

15 p2579 A69-31039

Stripline microwave integrated circuits in terms of building blocks and components, discussing hybrids, backward wave coupler, balanced modulators and mixers, etc

15 p2579 A69-31075

Hybrid coupled low power digital microwave phase shifters design, discussing lumped element L-C and variable C shifter theories, power limitations and construction techniques

15 p2580 A69-31076

Pseudoexact bandpass filter design, presenting graphs for passband loss, voltage standing wave ratio and time delay as function of frequency

15 p2581 A69-31526

Mathematical optimization to achieve near equal-ripple response in passband for coaxial low pass filters having unequal line lengths

16 p2757 A69-31583

Demand assigned frequency division multiple access-PCM system designed by COMSAT for satellite communication

16 p2749 A69-31602

High voltage thin film transistor, discussing design criteria, fabrication, I-V characteristics and switching speed

16 p2757 A69-31614

Logic circuits abstract synthesis for detecting signals against noise background using known conditional quantized signal distributions

16 p2749 A69-31627

Microwave bandpass linear phase filters design and synthesis for simultaneous flat amplitude and delay response

16 p2759 A69-31941

Equal ripple nonuniform tapered line coupler design and computed performance by evaluating cascade matrix as function of frequency

16 p2760 A69-31944

Autooscillatory process in n-circuit tunnel diode LC oscillators acted upon by external sinusoidal voltages

16 p2764 A69-32256

Wideband selective amplifier design methods proposed by Martini and Schiaffino

16 p2761 A69-32442

Microelectronic S band upconverter designed and fabricated in microstrip on alumina substrate

16 p2762 A69-32562

Lumped element circuit producing directional coupling by electric and magnetic coupling of reactance quadrupoles, discussing insufficient coverage of calculated frequency range

16 p2763 A69-32581

Broadband continuously variable phase shifter with microstrip construction, describing phase rotation via stripline connected directional couplers

16 p2763 A69-32582

Short backfire antenna based on yagi type equipped with end reflector, noting fewer elements and low sidelobe advantages

16 p2763 A69-32586

Network synthesis technique applied to structural dynamics design, using topological formulas to express systems response transfer functions

17 p2933 A69-33709

Active antenna impedance matching network constituting low noise device for electromagnetic interference measurements useful for automatic or manual scanning

17 p2943 A69-34131

Airborne communication receiver solid state interference blanker circuitry comprising black box insertable between antenna and RF input

17 p2943 A69-34132

Vibration-proof devices obtained by relating variance determination errors in selective filter response, modulating process bandwidth and spectral analyzer passband

18 p3109 A69-34584

Circuits and systems - Conference, Pacific Grove, California, October-November 1968

18 p3109 A69-34671

Analytical, graphical and graph-analytical methods for synthesis of passive circuits ensuring air removal from chambers of pneumatic logic control and servomechanisms

18 p3093 A69-34831

Functional signal conversion operations in microelectronic radio equipment, examining components in analog and pulsed devices synthesis

18 p3109 A69-35162

Current generator circuit designed for semiconductor laser excitation with pulses modulated by sinusoidal signals at 4.75 MHz

18 p3153 A69-35256

Nanosecond pulse generator circuits based on four layer Si diodes designed for semiconductor laser excitation

18 p3153 A69-35257

Solid state S band to VHF converter design to obtain optimum system noise for radio telemetry, discussing cost effectiveness and system performance

19 p3270 A69-36238

High bit rate signal conditioning, bit and group synchronization of NRZ PCM, considering gain and power bandwidth limitations and delays

19 p3271 A69-36247

Phase locked loop design of desensitized monolithic integrated circuits for FM multiplex signal filtering and demodulation, describing external tuning

19 p3273 A69-36274

Information theory, circuit optimization and computer aided design in radio wave information transmission

19 p3286 A69-36432

Single loop directional stripline filters synthesis, including general expression for frequency characteristics based on wave matrices

19 p3284 A69-36570

Pneumatic control circuits design based on logic functions and truth tables, noting fluid logic application

19 p3256 A69-36714

Dispersive quadrupole network design using algorithm method

19 p3287 A69-36740

Quasi-optimal synthesis for reception indicator used in radio interferometers for measuring signal amplitudes in presence of normal noise

20 p3504 A69-37009

Voltage variation frequency analysis for narrow-band sweep oscillators circuit design

20 p3486 A69-37010

Time division multiplexing of asynchronous digital signals from independent sources in continuous or bit stuffing mode, evaluating reliability and efficiencies

20 p3493 A69-37715

Equivalent circuit for microwave cavity containing active GaAs device applied to waveguide and radial mode cavity design

20 p3508 A69-37900

Near constant phase variable attenuator for RF signal containing Doppler information, centering design around p-i-n diode as control element

21 p3681 A69-38410

Multiplexer network synthesis based on arbitrary divisibility of frequency range and obtainability of input impedance at all frequencies

21 p3681 A69-38530

Radiometer for 4 cm wavelength range with receiver circuit incorporating tunnel and parametric HF amplifiers, describing design and operation including sub-units

21 p3724 A69-39076

Ionization manometer flange transducer with axial cathode and collector for high vacuum measurements, describing air resistant yttrium oxide coated cathode with Ir core

21 p3724 A69-39077

Automatic frequency control circuit for stabilizing beat emissions of coupled multifrequency gas lasers

21 p3738 A69-39079

Antenna synthesis problems in mathematical physics, discussing radiation pattern, shape and source and optimal solution via operators spectral theory

21 p3682 A69-39124

Synthesis by differential equation technique for linear antenna arrays of identical radiators radiation patterns

21 p3682 A69-39125

Computer program for generation of test patterns for multiterminal devices and networks

21 p3679 A69-39604

Analysis and synthesis of distributed transmission line networks with open or short circuited shunts or series stubs, describing composite transfer matrices

21 p3687 A69-39660

Stable linear system /shaping filter/ synthesis transforming stationary white noise into random process having given covariance function

21 p3688 A69-39661

Optimal control synthesis by determining conditions for absolute minimum in quick response having no regular constraints on phase coordinates

21 p3689 A69-39863

Computerized algorithm facilitating automatic synthesis of time invariant linear compensation for highly complex multiloop control systems [AIAA PAPER 69-941]

22 p3917 A69-40324

Linear flight control system synthesis by using optimal control theory associated with quadratic performance index

22 p3864 A69-40588

Book on Smith chart electronic applications in waveguide, circuit and component analysis and synthesis

22 p3915 A69-40780

Time varying resistance wire to arrest oscillations in pulsed capacitor discharge circuit, deriving over, under and critical damping conditions

22 p3917 A69-41228

Distributed RC networks combined with lumped passive and active elements to produce distributed-lumped-active /DLA/ networks for filter requirements

23 p4144 A69-41401

Electromagnetic compatibility /EMC/ filter design and test methods to achieve effectiveness and reliability, emphasizing transfer impedance characteristics

23 p4142 A69-42233

High efficiency boost regulator design and tests for planetary spacecraft, considering input and output voltages

23 p4075 A69-42302

Phase-pulse multistable circuit reliability improvement by additional negative feedback increasing parametric variation tolerance, feeding voltages and temperature

23 p4143 A69-42338

Electrical power system synthesis for manned lunar base for surface explorations of increasing energy requirements and duration, discussing thermal control, reliability, etc

23 p4076 A69-42541

Hybrid techniques to produce thin and thick film microcircuits and logic system parameters

24 p4286 A69-42906

Optimum control synthesis for nonlinear plant subject to white noise perturbation, using integral estimates of phase coordinate functions

24 p4289 A69-42949

Nonblocking switching networks operating in ordinary and in simultaneous switching regime, including control algorithms for optimal space communication

24 p4289 A69-43138

Materials problems in microelectronic circuits, discussing multilayer interconnection arrays production by thick film or print-and-fire process

24 p4333 A69-43212

On-off limit cycle controllers for reaction-jet controlled systems, investigating delay effects

24 p4291 A69-43271

Fluid logic feedback control circuit synthesis using synthesis table, describing procedure to assign memory valves and switching signals

24 p4292 A69-43290

General purpose computer program for synthesis of multivariable systems decoupled by state feedback

24 p4294 A69-43307

Laser beam circuitry miniaturization facilitating laser circuit assembly isolation from thermal, mechanical and ambient changes

24 p4328 A69-43327

On-board digital filtering applied to spectral estimation and data compression, discussing theory, techniques, computerized implementation and prototype design [AIAA PAPER 69-969]

24 p4285 A69-43510

NEUMANN PROBLEM

Dirichlet and Neumann problems solvability using potential theory methods, limiting study to three dimensional domains

07 p1173 A69-18496

Electric analogy technique for torsion and flexure functions of uniform beams with terminal loads, considering Neumann boundary value problem

11 p1995 A69-25649

Simultaneous Wiener-Hopf equations for electromagnetic wave diffraction, giving cyclic matrix solutions for Dirichlet and Neumann mixed boundary value problems

13 p2287 A69-27299

NEURAL NETS

Mathematical model of spike activity of auditory neurons constructed from functional point of view

07 p1070 A69-18384

Hypothalamic motivational systems and stimulation, discussing behavior patterns and plasticity

09 p1444 A69-21310

NEUROLOGY

Head injury clinical and laboratory long term follow-up data, discussing conscious state alterations, focal neurological deficit, EEG abnormalities, etc

01 p0022 A69-11346

Radiological properties of high energy proton beams from synchrocyclotron in tumor treatment and neurosurgery

03 p0373 A69-13495

Neurological impairment in baboons exposed to prolonged decompression simulating high altitude aircraft cabin structural failure, noting neuropathological examination results

07 p1067 A69-19426

Jet fighter pilot spatial disorientation during flight and on ground, emphasizing vestibular neuronitis diagnosis

10 p1649 A69-23382

Hypokinesia effects on human neurology on extended space flights simulated by 72-day bed rest

10 p1646 A69-23506

Neurological changes in men due to hypokinesia, analyzing tremor data, EEG recordings and stabilography fluctuations

10 p1647 A69-23585

Soviet book on nervous mechanisms of vestibular reactions emphasizing mathematical description of operation, neurophysiologic changes in cerebral cortex and oculomotor activity modeling

16 p2746 A69-32605

Valsalva maneuver produced abrupt onset of ptosis and proptosis caused by ethmoidal air cell rupture, discussing oticlogies

17 p2909 A69-33186

Book on neurocybernetics and neurobiology covering mathematical and physiological models, artificial neurons, image recognition theories, biological control systems, etc

19 p3263 A69-36747

Motion sickness as sensory rearrangement phenomenon, proposing neural mismatch hypothesis to account for symptom pattern

20 p3483 A69-38266

NEUROMUSCULAR TRANSMISSION

Neuromuscular actuation system model, noting compatibility with human physiological and anatomical data in tracking tasks

02 p0202 A69-11952

Man machine integration, detailing sensory input and motor /or output/ systems, control loop and social structure impact

11 p1831 A69-25656

Nerve and muscle tissues subthreshold reactions on analog model, discussing transient characteristics under various excitations

23 p4109 A69-41980

Training effect on fast muscle isometric contraction in rats, discussing mechanical characteristics

23 p4097 A69-42095

NEURON TRANSMISSION

U BIOELECTRICITY

NEURONS

Neutral buoyancy microelectrode for prolonged recording from single nerve units

02 p0202 A69-11865

Cerebral cortical neurons response to visual stimuli during stationary and rapid eye movement

03 p0369 A69-13360

Mathematical model of spike activity of auditory neurons constructed from functional point of view

07 p1070 A69-18384

Oxidative and dephosphorylating enzymes and esterase in rat and squirrel monkey cerebral cortexes, noting neuron activity

12 p2018 A69-25773

Histochemical studies on nucleus basalis of Meynert of squirrel monkey

12 p2018 A69-25774

High altitude environmental effects on adrenal glands and hypothalamic neurosecretion in rats

13 p2211 A69-28615

Miniaturized FM telemeter for transmitting electrical activity of single nerve cells in brain of awake and unrestrained animal

19 p3261 A69-36270

- Electrical response of frog and human visual cortex neurons to thermal vestibular and light flash stimulation
20 p3469 A69-37242
- Labyrinth polarization effect on stimulation and neuron activity in visual cortex of cats, using electroencephalograph
20 p3469 A69-37244
- Multilevel mathematical model of oculomotor apparatus using neuron networks and complex activators, including computer analysis
20 p3470 A69-37245
- Vestibular neurons activity in decerebrized cats under ipsilateral and contralateral labyrinth polarization combined with acoustic and caloric stimulation
20 p3471 A69-37254
- Cats vestibular neurons reactions to labyrinths mon- and binaural polarization and caloric stimulation
20 p3471 A69-37255
- Neuron activity simulation applied to vestibular neurons electrical activity analysis, discussing feedback circuitry and cathodic depression
20 p3471 A69-37256
- Neuronal organization of initial afferent inflow in thalamic visual center /lateral geniculate body /LGB/ of unanesthetized cats/, noting unit activity
22 p3879 A69-40845
- Psychopharmacological drug effects on retinal neuron activity in cats measured by microelectrodes, noting spontaneous activity decrease
22 p3879 A69-40846
- Statistical critique of Polyak values for tangential dendritic spread of primate retinal neurons
22 p3880 A69-40848
- Retinal topography relation to blue arcs phenomenon, assessing disparity in photoreceptor location and associated neurones for analysis of critically sited plots
22 p3882 A69-40872
- Functional relation between primary response individual phases and neurons activity in cats cerebral cortex
22 p3886 A69-41067
- D-amphetamine effect on single tectal neurons activity of cat opticum recorded by steel microelectrodes before and after intravenous injection
23 p4084 A69-41466
- Stimulus correlated with neuronal discharge periodicities in colliculus inferior, deriving structure models, discussing acoustic channel below geniculatum mediale
23 p4096 A69-42089
- NEUROPHYSIOLOGY**
- Surgical radiolesion in human brain by high energy protons
03 p0374 A69-13501
- Analytical model for frog retinal bug detector cell to make possible signal measurement in frog optic fibers
07 p1070 A69-13833
- Central adrenergic mechanisms role in neurosecretory function of hypothalamo-hypophyseal system of rabbits under transverse accelerations in centrifuge
15 p2554 A69-30055
- Book on neurocybernetics and neurobionics covering mathematical and physiological models, artificial neurons, image recognition theories, biological control systems, etc
19 p3263 A69-36747
- Cerebral subcortical structures controlling effect on central and peripheral nervous systems, discussing motion coordination, space orientation, search reflexes and physiological sleep
22 p3889 A69-41275
- NEUROPSYCHIATRY**
- Steroid hormones effect on nervous system and behavior from data on gonadectomized rats and monkeys treated with testosterone propionate
03 p0375 A69-13551
- Magnetic fields role in neuropsychiatric and physiological experiments, noting effect on phagocyte activity
05 p0715 A69-16627
- Man psychic activity interference resistance, discussing stress effects characterized by theta and delta rhythms
08 p1262 A69-19839
- Human adaptation to various environments, emphasizing experimental space psychoneurology role in human behavior examinations during space missions
10 p1647 A69-23587
- NEUROSCIENCE**
- U NEUROLOGY**
- NEUROSES**
- NT NEUROTIC DEPRESSION**
- Military flying career choice as neurotic compensation for personality defects, stressing personality screening during interview
12 p2023 A69-26492
- Psychiatric morbidity as absenteeism cause among ground and flight personnel in civil aviation, recommending psychotherapy and chemotherapy
24 p4266 A69-43378
- NEUROSPORA**
- Accelerated helium and carbon ions effects on mutation-induction and nuclear inactivation in *Neurospora crassa* compared with X rays, discussing relative biological effectiveness /RBE/
03 p0373 A69-13490
- Structural phospholipoprotein isolated from *hydrogenomonas facilis* and *neurospora crassa*
22 p3871 A69-40049
- NEUROTIC DEPRESSION**
- Psychological study of stewardesses for depressive, neurotic and psychosomatic episodes, discussing psychopathological structures corresponding to biological sequences
07 p1067 A69-19434
- Psychotherapeutic treatment of depressions and neuroses in flight crews, noting face to face method effectiveness
23 p4086 A69-41690
- NEUTRAL BEAMS**
- NT MOLECULAR BEAMS**
- Average ionization cross sections of atomic and molecular H and He beams ionized by plasma electrons with Maxwellian velocity distribution
12 p2138 A69-26542
- Three component fast neutral beam for hydrogen plasma ion density and electron temperature determination, improving accuracy and reliability
14 p2452 A69-29812
- Secondary electron emission from gas covered metal surfaces, discussing results of neutral beam investigations
17 p3008 A69-33000
- NEUTRAL PARTICLES**
- NT COLD NEUTRONS**
- NT FAST NEUTRONS**
- NT NEUTRONS**
- NT PHOTONEUTRONS**
- NT THERMAL NEUTRONS**
- Radioactive decay of neutral pions generated in metagalactic cosmic ray interactions as source of high energy isotropic gamma rays observed by OSO-3
02 p0308 A69-12092
- Screening of high density plasma from penetration by neutral gas, discussing prevention of high energy losses by charge exchange collisions
02 p0288 A69-12170
- Automatic recording of neutral atom temperature and free electron density of partially ionized gas by Fabry-Perot interferometer
03 p0428 A69-13111
- Electron scattering by neutral acceptors in semiconductors, noting relaxation time for Ge at very low temperatures
03 p0484 A69-13280
- Electron, ion and neutral particle temperatures of upper atmosphere
04 p0592 A69-14975
- F 2 layer formation and fast neutral particles ionization source due to charge exchange between solar wind protons and moving interstellar hydrogen
04 p0592 A69-15009
- Pumping requirements for nozzle skimmer region of neutral particle nozzle beam source, using two stage mechanical pump
04 p0600 A69-15026
- Diurnal variations of neutral and charged particle temperatures in equatorial F region
05 p0755 A69-16270
- Neutral interstellar matter particle fluxes and densities for earth, noting effects on upper atmosphere gas densities
05 p0828 A69-16653
- Energy flux into earth thermosphere due to fast corpuscular neutrals arising from charge transfer collisions between solar protons and neutral interstellar H
05 p0817 A69-16654
- Neutral hydrogen distribution and dynamics in galaxies, discussing observations by spectrographic transit telescope, data processing and profiles
07 p1224 A69-19711
- Chain mechanism of arc discharge development in crossed electric and magnetic fields explained by direct ionization of neutral particles by ions
11 p1932 A69-25540
- Electrohydrodynamic flows at large electric Reynolds numbers, obtaining Bernoulli and Cauchy-Lagrange integrals
13 p2305 A69-27379
- Finite Larmor radius and collision with neutral atoms simultaneous effects on plasma gravitational instability
13 p2346 A69-27708
- Neutral hydrogen cloud observed at high galactic latitude, discussing top intensity velocity, peak intensity dispersion, age, hydrogen mass and density
13 p2347 A69-27719
- Residual gas analyzer and leak detector by time of flight measurements on neutral metastable atoms and molecules between pulsed electron gun and auger surface detector
13 p2262 A69-28006
- Oscillating electron ion discharge in magnetic field in system of alternating positive and negative electrodes to obtain fast neutral particle fluxes
13 p2311 A69-28109
- Neutral gas pressure in positive column plasma between two coaxial insulated cylinders as function of cylinders radii
14 p2490 A69-29036
- 21 cm line emission surveyed for spatial distribution of random velocities of neutral hydrogen in solar neighborhood
14 p2520 A69-29371
- Electron scattering by neutral acceptors in semiconductors, noting relaxation time for Ge at very low temperatures
14 p2508 A69-29653
- Ionospheric models for motion of slightly ionized homogeneous cold plasma influenced by electrostatic field and neutral particles flow, considering geomagnetic effects
14 p2499 A69-29863
- Neutral hydrogen in dark dust clouds in 21 cm line, showing hydrogen excesses and deficiencies
15 p2691 A69-30763
- Neutral hydrogen high velocity clouds as possible extragalactic objects in Local Group not contracted to galactic dimensions or densities
15 p2694 A69-30785
- Low energy neutral bremsstrahlung cross sections for Ne, Ar and Xe, using rapid scanning spectrometer
15 p2657 A69-31159
- Radiative scattering cross sections of electrons from neutral O and atomic and molecular N using rapid scanning spectrometer for bremsstrahlung intensity
15 p2657 A69-31160
- Interstellar particle penetration into solar system, discussing impact ionization of earth ionosphere by interstellar neutral hydrogen and helium
15 p2699 A69-31390
- Xenon atom and ion densities downstream from coaxial plasma gun measured using vacuum UV emission, absorption spectroscopy and Langmuir probe
16 p2819 A69-31690
- Perturbation theory for nonlinear oscillations in ionized plasma, treating electron-neutral collisions effect by Boltzmann-Vlasov equation relaxation term, noting distribution function
16 p2820 A69-31702
- Ion momentum transfer through charge exchange in mixture of ion gases and parent neutral gases under thermal nonequilibrium, noting role of Boltzmann equation
16 p2822 A69-32108
- Combined midlatitude neutral air wind and equatorial electrodynamic drift effect on F 2 layer diurnal variations
16 p2781 A69-32316
- Electron impact broadening of isolated spectral lines emitted by neutral atoms in plasma
16 p2823 A69-32468
- High energy neutral molecule beam for gas-surface interaction studies generated in electron bombardment ion source
19 p3376 A69-36176
- Earth satellite sweeping mass spectrometer for measuring atmospheric neutral particle and positive ion concentration
19 p3314 A69-36681
- Lower thermosphere ion and neutral minor constituent concentrations in nighttime auroral zone, considering ionization due to electron precipitation and bremsstrahlung
21 p3704 A69-38365
- Neutral components of arctic thermosphere measured with rocket-borne RF mass spectrometers, discussing origin of atomic hydrogen and water lines
21 p3704 A69-38367

Neutral particle density ratios in thermosphere by rocket-borne monopole mass spectrometers

21 p3704 A69-38368

Universal dependence of density fluctuations on specific entropy derived from equation describing material composed of neutral particles and equal number of charged and antiparticles

21 p3771 A69-38995

NEUTRALIZERS

Plasma generator for maintenance of space vehicle electrical neutrality during ejection of high velocity electron pulses

[AIAA PAPER 69-273]

09 p1567 A69-21263

DNA denaturation without variance from pH 7.0 by adding NaOH observed with viscosity measurements, obtaining similar results with hydrochloric acid

24 p4263 A69-43225

NEUTRINOS

Viscous effects of neutrinos in anisotropic cosmological models examined using Boltzmann equation with simple collision term

01 p0148 A69-10053

Weakly interacting neutrinos in anisotropic cosmological models with emphasis on equilibrium period, noting energy increment

01 p0123 A69-10348

Neutrino radiation in universe with emphasis on stellar neutrino radiation, analyzing emission during nuclear fusion of C-N, He and Ne-Na cycles

01 p0145 A69-10754

Solar neutrino flux dependence on rotation rate of solar core and fractional mass involved in interior mixing

02 p0325 A69-12600

Muons in EAS, single unaccompanied muons, underground muons and experiments involving neutrinos

03 p0499 A69-12946

Mixing effect on solar neutrino fluxes, assuming solar convective core with rapid thorough mixing

06 p1001 A69-17192

Null solar neutrino flux possible relation to 2 year solar cycle, discussing energetic disturbances at solar core and sunspots

08 p1377 A69-19902

Neutrino emission and carbon burning onset in 1.45 solar mass stellar models with pure He envelope, He burning shell and degenerate C-O core

08 p1384 A69-20059

Star collapse under energy losses due to neutrino emission, analyzing self similar asymptotic solutions

09 p1587 A69-21359

Solar neutrinos and convective core mixing on short time scale resulting in flux reduction

09 p1574 A69-21453

Brans-Dicke gravitation theory effects on solar evolution and neutrino flux, discussing solar luminosity

09 p1605 A69-22415

Neutrino loss effects on evolution of pure iron stars, considering white dwarf, presupernova models and iron-helium transition

09 p1606 A69-22420

Neutron proton plasma properties in massive stars and supernovae, discussing neutrino emission

10 p1756 A69-22814

Superhigh energy cosmic ray interaction with neutrinos in universe, shape of cosmic ray spectrum and universe development

10 p1757 A69-22826

Neutrino groups generation in internal regions of sun, analyzing flux ambiguities due to error of cross section parameter of nuclear reactions

10 p1757 A69-22827

Red supergiants as old derivatives of main sequence O and B stars, discussing neutrino emissions and carbon core contraction

10 p1788 A69-24125

Superdense stars energy yield from neutrino emission, assuming incomplete degeneration of elementary particle Fermi gas

13 p2336 A69-27435

Structure and thermometry of solar interior from measuring neutrino fluxes intensities emitted by unit mass

13 p2333 A69-28434

Neutrino and antineutrino emission by URCA process calculated, assuming nuclear reactions in static and beta processes in kinetic equilibrium

15 p2674 A69-30542

Solar neutrino fluxes sensitivity to localized changes in opacity and equation of state, discussing solar models

15 p2675 A69-30768

Turbulent diffusion inside sun as explanation of solar spindown, Li depletion at surface and neutrino discrepancy, discussing diffusion coefficient and stellar evolution

16 p2866 A69-32814

Solar thermonuclear reactions studied by emitted neutrinos detection, plotting energy spectra for sensitivity of CI 37 detection system

18 p3185 A69-34278

Solar energy release by quark fusion catalysis of alpha reaction without production of neutrinos, noting temperature dependent reaction rate

18 p3186 A69-34643

Star collapse under energy losses due to neutrino emission, analyzing self similar asymptotic solutions

18 p3197 A69-34749

Neutrino-pair bremsstrahlung for hot degenerate electron gas during Coulomb scattering on imbedded nuclei in stellar regimes including lattice structure effects

18 p3176 A69-35004

Solar neutrinos capture rate estimation by using Li 7 as detector

20 p3588 A69-37420

Solar He abundance limits and discrepancies of CI 37 solar neutrino count experiment

20 p3592 A69-38068

Solar neutrinos emission mechanism for information on central region of sun, discussing detection and flux density

21 p3790 A69-38827

Lepton nonconservation implications for experiments involving solar neutrinos, showing effect on capture rate at earth for pep neutrinos

23 p4194 A69-41596

Complex phenomena in theoretical astronomy including neutrino pair emission in stellar interiors, molecular H in interstellar gas, neutron stars, etc

23 p4217 A69-42316

Stellar neutrino energy loss due to electron-electron neutrino bremsstrahlung in nondegenerate gas determined from transition probability for charged baryons or leptons interaction

24 p4351 A69-42794

NEUTRON ACTIVATION ANALYSIS

Replicate neutron activation determinations of Ga, Ge, In and Ir in L group chondrites, proposing model which accounts for observations

01 p0155 A69-10976

Meteoritic materials investigated for Sc, Ce and Eu content and distribution in various phases, using neutron activation analysis

01 p0026 A69-11376

Stony meteorite Krahenberg, determining isotopic composition, rubidium and strontium age of dark and light portions by neutron activation analysis

05 p0826 A69-16439

Rare earth elements and yttrium in meteoritic chondrites determined by radiochemical neutron activation analysis

08 p1403 A69-20916

Antimony bromine and mercury abundances in meteoritic materials determined by neutron activation analysis

08 p1404 A69-20919

Chlorine as indicator of terrestrial contamination in iron meteorites, using neutron activation analysis and metallographic observation

08 p1405 A69-20923

Aluminum abundances in stony meteorites measured using nondestructive instrumental neutron activation analysis

11 p1952 A69-24334

Meteoritic trace elements with varying chemical and physical properties investigated for abundance by neutron activation technique

19 p3407 A69-36080

Ar 39-Ar 40 method using neutron activation and inert gas mass spectrometry to investigate meteoritic thermal histories

19 p3412 A69-36105

K and Ar 40 determination in iron meteorites by neutron activation for K/Ar dating

19 p3412 A69-36106

Neutron activation method for Mn 53 in meteoritic Fe by X ray and gamma counters, noting extraction of Mn 54 free reference source

20 p3601 A69-37504

Neutron activation analysis for oxygen determination in Be by gamma emission intensity from nitrogen 16, noting bound oxygen

20 p3544 A69-37811

NEUTRON COUNTERS

Cosmic ray neutron integrated flux measurements up to 350 km for energies to 15 Mev, determining neutron leakage flux

01 p0146 A69-11223

Atmospheric temperature and water vapor variations and seasonal environmental changes effects on cosmic ray neutron and meson monitor counting rates

03 p0498 A69-12936

Barometric coefficients of multiplicities calculated using cosmic ray interactions model and neutron monitors response to secondary nucleons

03 p0425 A69-14025

Neutron counter for measurements of atmospheric and earth leakage flux of secondary cosmic ray neutrons, discussing design and calibration

07 p1209 A69-19454

Ground level solar proton event recorded by neutron monitors

10 p1766 A69-23761

Forbush decrease associated with July 7 1966 proton event from cosmic ray intensity variation measurements by neutron monitors

10 p1768 A69-23774

Scintillation counter to determine neutrons number and distribution in time in pulses generated in hot plasma

14 p2452 A69-29809

Solar neutrons upper limits measured for 28 July 1967 importance 1 flares

18 p3187 A69-34959

OGO-F neutron monitor for measuring cosmic ray neutron flux near earth, locating sensor on boom to minimize spacecraft produced neutrons

19 p3314 A69-36678

Radiocarbon natural production by cosmic ray neutrons, utilizing proportional counters filled with N atmospheres

22 p4003 A69-40095

Errors due to neutron counter radioactivity in cosmic rays nucleon measurements analyzed in reducing readings to barometric pressure

23 p4206 A69-41855

NEUTRON CROSS SECTIONS

S-process nucleosynthesis and temperature averaged neutron capture cross sections studied in relation to solar system, considering elemental and specific isotopic abundances

08 p1357 A69-20896

Resonances and doublets observation by neutron radiative capture and transmission of W and Zr isotopes in kev region, noting partial wave strength functions

18 p3175 A69-34314

Group cross section generating techniques to calculate neutron capture rates and spatial capture distribution in depleted thick U slab, using GAROL program

18 p3177 A69-35179

Threshold photoneutron cross section for Mg 26, discussing resonances as primary production mechanism for stellar neutrons

21 p3788 A69-38599

Thermal neutron capture cross section at high temperature irradiations determined for W 184, describing radiochemical separation and flux counting techniques

24 p4315 A69-43192

NEUTRON DECAY

Magnetic field effect on neutron beta decay rate, considering calculations applicability to elementary particle production

15 p2690 A69-30694

Cosmic ray albedo neutron decay /CRAND/ source for trapped protons, showing disagreement with intensities in inner zone measured on OVI 2 spacecraft

22 p4005 A69-40512

NEUTRON DIFFRACTION

Long range order formation in Ni-Cr alloys analyzed by direct neutron diffraction, considering disorder-order transition temperature and chemical composition

10 p1714 A69-23964

Nondestructive detection of titanium hydride formation in threaded joints of Ti alloy pressurization tanks by neutron radiography

24 p4320 A69-42998

NEUTRON DISTRIBUTION

Fast and slow neutron latitude variation at aircraft altitudes during solar minimum, noting environment effects on measurement

09 p1574 A69-21402

Kinetic equation solved for radiation propagation in atmosphere, considering neutron density variations and spatial distribution

12 p2149 A69-26683

Scintillation counter to determine neutrons number and distribution in time in pulses generated in hot plasma

14 p2452 A69-29809

Fissioning plasma generated in shock tube with 235 uranium hexafluoride gas, selecting tube diameter, reflector depth and initial gas density for specific neutron multiplication

18 p3180 A69-34455

Group cross section generating techniques to calculate neutron capture rates and spatial capture distribution in depleted thick U slab, using GAROL program

18 p3177 A69-35179

Franco-Soviet rocket probe launchings for measuring daytime/nighttime ions and neutrons

18 p3210 A69-35282

Sayan Sun Observatory experimental equipment, discussing instruments for solar observation, earth currents measurement and cosmic ray neutron components recording

22 p3943 A69-39997

NEUTRON EMISSION

Thermonuclear neutron emission from high temperature deuterium plasma produced by focusing high power laser radiation on lithium deuteride surface [IEEE PAPER O-11]

07 p1153 A69-19072

Neutron emission anisotropies in capacitor discharge produced plasma focus, detailing coaxial plasma gun energy spectrum and flux measurement

11 p1930 A69-25321

Solar cosmic ray flare of 28 January 1967 observed by neutron monitors, determining emission and particle spectrum at atmosphere boundary

14 p2513 A69-29066

Plasma ion temperature measurement based on integral neutron yield, noting density determination

14 p2498 A69-29808

Monte Carlo method application to neutron streaming in hemispherical air-filled ducts in water tank to determine leakage through nuclear reactor shields

18 p3171 A69-35178

Threshold photoneutron cross section for Mg 26, discussing resonances as primary production mechanism for stellar neutrons

21 p3788 A69-38599

Solar flare optical, neutron and gamma emission, discussing ionization losses and nuclear interaction of accelerated particles in flares

22 p4003 A69-40296

NEUTRON FLUX

U FLUX [RATE]

NEUTRON FLUX DENSITY

Cosmic ray neutron integrated flux measurements up to 350 km for energies to 15 Mev, determining neutron leakage flux

01 p0146 A69-11223

Fast neutron fluxes at various atmospheric levels and geomagnetic northern midlatitudes measured by proportional counters using boron trifluoride

03 p0501 A69-13528

High energy proton and neutron fluxes and spectra from nuclear emulsion stacks on Cosmos satellites, calculating cosmic radiation doses

05 p0814 A69-16051

Neutron counter for measurements of atmospheric and earth leakage flux of secondary cosmic ray neutrons, discussing design and calibration

07 p1209 A69-19454

Energy density of neutron star matter from Brueckner theory calculations of nuclear matter and pure neutron gas, determining proton relative density

08 p1381 A69-19785

Fast and slow neutron latitude variation at aircraft altitudes during solar minimum, noting environment effects on measurement

09 p1574 A69-21402

Solar neutron flux measurement at earth in energy region 20-120 Mev by detector in balloon flight

11 p1945 A69-24421

Postirradiation investigation of uranium dioxide fuelled thermionic emitters by evaluating released fission gases, noting different neutron fluxes metallurgical effects

14 p2481 A69-29200

Fast atmospheric neutrons flux and spectrum measurement during two balloon flights, tabulating results and evaluating albedo flux during quiet sun period

16 p2851 A69-32616

Boron 10 absorption cross sections from counting rates measurements of boron trifluoride proportional counter used to monitor neutron fluxes

17 p3008 A69-33753

Solar neutrons upper limits measured for 28 July 1967 importance I flares

18 p3187 A69-34959

OGO-F neutron monitor for measuring cosmic ray neutron flux near earth, locating sensor on boom to minimize spacecraft produced neutrons

19 p3314 A69-36678

High energy proton and neutron fluxes and spectra from nuclear emulsion stacks on Cosmos satellites, calculating cosmic radiation doses

20 p3591 A69-37961

Thermal neutron flux perturbations in cylinders in test reactors, using regression analysis to obtain polynomials for flux perturbation, depression, self shielding factors, etc

20 p3575 A69-38274

Diurnal variations of cosmic ray neutrons corrected for barometric and temperature effects by harmonic analysis

21 p3791 A69-38840

Cosmic ray neutron studies of atmospheric nucleon component equilibrium and flux fluctuations at atmosphere top

22 p4002 A69-40092

Environmental neutron flux measured by various techniques, studying effects of soil and moisture on density

22 p4002 A69-40094

Neutron flux measurements on Cosmos 53, discussing equipment and calculation of secondary neutrons due to bombardment of satellite components

22 p4003 A69-40274

Thermal neutron capture cross section at high temperature irradiations determined for W 184, describing radiochemical separation and flux counting techniques

24 p4315 A69-43192

NEUTRON IRRADIATION

Irradiation influence on chromium transition temperature explained by defect clusters and embrittling impurity redistribution

01 p0095 A69-10604

Neutron and gamma irradiation effects on CdS crystals structure and properties, outlining electron energy level scheme

02 p0298 A69-12119

Isochronic annealing effect on coercive force of Mo Permalloy samples bombarded with neutrons in nuclear reactor

05 p0783 A69-16815

Carrier scattering from defects in neutron irradiated semiconductors, noting mobility and relaxation time

06 p0974 A69-16864

Neutron irradiation produced defects in p-type Si at 76 K, measuring Hall effect and electrical conductivity

06 p0975 A69-16868

Majority and minority carrier trapping in neutron irradiated Si diodes, measuring transient junction capacitance recovery

06 p0975 A69-16869

Rapid annealing data for silicon transistors after reactor neutron pulse, deriving equation for defect recombination in cluster and subsequent diffusion outside cluster

06 p0975 A69-16870

Recombination statistical model for neutron irradiated Si transistors, considering diffusion potential, junction voltage, temperature, activation energy and capture ratio for holes and electrons

06 p0975 A69-16871

Neutron irradiated Si transistors radiation and annealing characteristics determined for inverse configuration

06 p0975 A69-16872

Thermal time constant in Si diffused transistors decreases with increased neutron dosage

06 p0975 A69-16873

Nearly abrupt X band Si avalanche IMPATT diodes irradiated by fast neutrons, noting effects on DC and microwave characteristics

06 p0976 A69-16874

Neutron radiation effects on MOSFET, presenting model for neutron produced ionization in oxide layer

06 p0976 A69-16875

Combined neutron degradation and gamma induced effects on closed loop system simulated by SECURE program

06 p0899 A69-16889

Neutron and X ray radiation effects upon gallium arsenide devices including Gunn oscillators, transistors, Schottky barrier diodes and optoelectronic pulse amplifiers

06 p0978 A69-16890

Instrumentation design problems connected with NERVA, considering high gamma and neutron radiations and temperature environments [IEEE PAPER 2D-5]

07 p1134 A69-19189

Dislocation channeling process in polycrystalline Nb subject to tensile deformation after neutron irradiation

09 p1521 A69-21345

Ionization and recombination processes in He 3 plasmas produced by neutron irradiation of H 3

10 p1738 A69-23488

Diffusion processes during annealing of metals irradiated by electrons and neutrons, discussing crystal damage, recovery and recrystallization

11 p1891 A69-24800

Compact device for low temperature neutron irradiation of deformed specimens under tensile stress, emphasizing specimen carrier

11 p1862 A69-24901

Neutron irradiation and temperature effects on ferrite and Permalloy memory cores hysteresis loops

12 p2142 A69-26259

Neutron irradiated Nb single crystals tensile tested over temperature range, discussing athermal radiation hardening

13 p2275 A69-27368

Critical parameters of isothermal quasi-degenerate white dwarfs calculated by energy method, allowing for relativity theory error and neutron irradiation effect

13 p2351 A69-27871

Forward current decrease in Si mesa diodes under fast neutron irradiation ascribed to increase in base resistance

13 p2236 A69-28549

Neutron irradiation effect on efficiency and other parameters of IMPATT diode

14 p2423 A69-29761

Slow neutrons irradiation compensated high resistivity p-InSb current instability

15 p2666 A69-30058

Neutron bombardment and ionizing radiation resistance of aluminum oxide MOS devices using gate insulator fabricated by plasma anodization

17 p2935 A69-32888

Fast neutron irradiation effect on niobium nitride current carrying capacity, showing enhancement

17 p3008 A69-33765

Radiation resistant devices for minimizing neutron and gamma radiation effects on military electronic components, discussing selection features and sampling lot sizes

18 p3144 A69-34491

Solar cells designed to survive exposure to fission/fusion neutrons and electromagnetic spectrum products of nuclear weapon detonation

19 p3251 A69-35689

Photoresponse and minority carrier diffusion length long term stability of Li doped solar cells after proton, neutron and electron irradiation

19 p3252 A69-35697

Injection level effects on minority carrier lifetimes in lithium-doped devices and solar cells irradiated by electrons and reactor neutrons

19 p3252 A69-35698

Meteorite Li isotopic composition variations to determine neutron role in nucleosynthesis of solar system light elements

19 p3408 A69-36084

Supralethal doses of pulsed mixed gamma-neutron radiations from TRIGA reactor administered to unshielded, head shielded and trunk shielded beagles

19 p3259 A69-36459

RBE of fast neutrons on mice, rats and guinea pigs, discussing suppression of mitosis in isolated cells

20 p3478 A69-37629

Fast neutron irradiation effect in Ge crystals, using X ray diffraction and volumetric measurements

20 p3584 A69-38125

Structural defects of neutron irradiated W wire noting microstress relaxation using autoionic microscope

21 p3749 A69-39623

Radioactive decay and conductivity changes with time in high and low resistivity CdS single crystals after irradiation with 14 Mev and reactor fast neutrons

22 p3993 A69-40728

Hemoglobin inhomogeneity in rats irradiated with lethal doses of X rays and fast neutrons, using fractions prepared by column chromatography

22 p3888 A69-41274

Radiation hardened microcircuits and transistors for protection against transient radiation released by nuclear weapons

23 p4135 A69-41528

Fast neutron irradiation effect on IR absorption in single crystal GaAs for various fluences
23 p4198 A69-41540

Plane strain fracture toughness of S-200 grade Be for 77-533 K temperature range, noting effects of loading, heat treatment and neutron irradiation
23 p4178 A69-42450

NEUTRON SCATTERING

High energy neutron transport calculated using one dimensional discrete ordinates code with anisotropic scattering, comparing results with nucleon transport code calculations
14 p2481 A69-29592

Computer codes describing nuclear weapons effects associated with X ray transport, neutron transport and X ray interactions with material, fireball, blast environments, etc
15 p2652 A69-30381

NEUTRON SOURCES

Whirling liquid hydrogen layer thermal and hydrodynamical conditions, noting application to cold neutrons source in high flux beam reactor
05 p0849 A69-16818

NEUTRON SPECTRA

Slow atmospheric neutron energy spectrum determined by resonance detectors and λ/ν detectors, measuring cadmium ratio dependence on longitude and latitude
10 p1758 A69-22831

Solar neutron flux measurement at earth in energy region 20-120 Mev by detector in balloon flight
11 p1945 A69-24421

Solar cosmic rays diffusion enclosure in interplanetary space magnetic boundary suggested from balloon, satellite and ground observations of solar flare neutron component
14 p2513 A69-29067

Fast atmospheric neutrons flux and spectrum measurement during two balloon flights, tabulating results and evaluating albedo flux during quiet sun period
16 p2851 A69-32616

Fast neutron spectrum for subcritical section of homogeneous U 235-polyethylene thermionic critical assembly measured by pulsed source time-of-flight method
18 p3170 A69-34313

Neutrons energy spectrum at sea level calculated and proved consistent with satellite cosmic ray data
23 p4205 A69-41701

NEUTRON STARS

Pulsar discovery at position of suspected supernova remnant, suggesting pulsars as rotating neutron stars formed in stellar explosion
01 p0149 A69-10268

Pulsars features explained by model based on binary system of neutron stars, discussing associated stellar plasmas as directional HF radio wave source
01 p0156 A69-10981

Gas accretion on neutron star surface as energy source for X ray radiation
05 p0814 A69-15847

Spinning neutron star model for pulsars based on slowing down of pulse rate, proposing emission mechanism for radio energy and relativistic gas
05 p0825 A69-16351

Pulsar model based on rapidly rotating neutron star with radiating attached plasma, discussing test of radiation mechanism by means of coherence of emission
06 p1012 A69-18226

Superdense matter possibly present in neutron stars, discussing relation with Einstein theory and nuclear physics
06 p1012 A69-18240

Energy density of neutron star matter from Brueckner theory calculations of nuclear matter and pure neutron gas, determining proton relative density
08 p1381 A69-19785

Pulsar emission possible connection with rotating neutron stars, discussing rotational energy transfer to circumstellar plasma and production of periodic shock waves
08 p1383 A69-19895

Rotating and oscillating magnetic neutron stars causing pulsars radio and optical signals, stressing UV line emissions theory
08 p1394 A69-20624

Radio emission from magnetic neutron stars as possible model for pulsars, noting optical and IR emission bands
08 p1397 A69-20729

Instability of stellar structures intermediate between white dwarfs and neutron stars shown by stellar models, discussing pulsar signals periodicities
08 p1397 A69-20770

Rotational energy conversion of neutron star into relativistic electrons energy suggested by increasing period of pulsating radio source in Crab Nebula
09 p1591 A69-21454

Pulsars rotating neutron star model analyzed on basis of magnetic dipole rotating in vacuo
09 p1592 A69-21463

X ray universe, considering contribution of X ray astronomy to phenomena of big bang, supernovae, neutron stars, exploding galaxies, etc
10 p1760 A69-22869

Ferromagnetic transition in superdense nuclear matter and neutron stars, developing relativistic equation of state
11 p1965 A69-25564

Magnetic models of pulsars and rotating neutron stars to explain narrowness of radiation beam in polar diagram
12 p2172 A69-27168

Gravitational parameters of highly condensed objects, considering white dwarf evolutionary stages, density and upper mass limit
13 p2334 A69-27190

Superdense stars energy yield from neutrino emission, assuming incomplete degeneration of elementary particle Fermi gas
13 p2336 A69-27435

Pulsars and neutron star formation based on stellar evolution theory, suggesting massive O stars as origin
13 p2337 A69-27517

Pulsars suggested as magnetic rotating neutron stars with unstable oscillations
13 p2352 A69-27912

Neutron star atmosphere and X ray emission spectrum, computing incident protons mean free path for two assumptions
15 p2686 A69-30535

Pulsar clock mechanisms on basis of relativistic gravitational effects, considering white dwarfs and neutron stars
15 p2694 A69-30855

Energy release efficiency in gravitational collapse, estimating rest energy fraction from energy conservation, neutron star stability and spherically symmetrical systems collapse considerations
16 p2853 A69-31594

Superfluidity and superconductivity under cosmic conditions, discussing Bose-Einstein condensation, Fermi particles, boson systems, neutron stars, etc
16 p2853 A69-31595

Pulsars properties, nature and utilization for interstellar medium study including radiation mechanisms, white dwarf stars and neutron star development
16 p2855 A69-31762

Superfluidity and superconductivity under cosmic conditions, discussing Bose-Einstein condensation, neutron stars, white dwarfs, etc
16 p2856 A69-31950

Spin down effects on neutron stars, discussing decrease of period of PSR 0833-45 as result of differential rotation instability
16 p2865 A69-32803

Superdense stars torsional oscillations and crystallization among nuclei from comparison with melting temperature and transverse shear wave velocities of dense conventional matter
17 p3037 A69-33643

Pulsars properties and distribution in galactic coordinates, deriving interstellar medium properties and physical nature of objects based on neutron star rotation
17 p3040 A69-33800

Models for pulsars periodicity and period range due to nonradial gravity wave in almost adiabatic matter of degenerate neutron stars
18 p3196 A69-34645

Pulsars cosmic ray mass and charge spectra analyzed for evidence of neutron star origin
20 p3588 A69-37487

Radial pulsations of neutron star losing mass, interpreting Crab Nebula pulsar observed period and secular increase of period
20 p3604 A69-37573

Rotating neutron star model to fit pulsar data, considering star crust formation and properties, angular velocity changes and starquake effects
21 p3798 A69-38544

Normal radial vibrations in Newtonian and general relativistic stellar objects and dynamic instability, determining modes and natural frequencies
22 p4014 A69-40142

Rotating neutron stars with magnetic fields symmetric about rotation axis considered for pulsar model
22 p4027 A69-40657

Complex phenomena in theoretical astronomy including neutrino pair emission in stellar interiors, molecular H in interstellar gas, neutron stars, etc
23 p4217 A69-42316

Pulsars models and radiation mechanism, noting neutron stars with rotating magnetospheres
23 p4218 A69-42326

Neutron star formation, discussing influence of supernova explosions and need of pulsar study
23 p4222 A69-42393

Crab Nebula pulsars radio properties, possible neutron star origin, interstellar gas and magnetic fields, etc
24 p4375 A69-42556

Pulsar model with seat as rotating neutron star having dipolar magnetic field not parallel to rotation axis
24 p4377 A69-42666

Rotating neutron stars, pulsars and cosmic X ray sources, accounting for large and small diameter sources by rotating neutron star losing mass in magnetic field
24 p4369 A69-43222

NEUTRON THERMALIZATION

Thermal-neutron flux generated by high energy protons in water moderator surrounding thick targets calculated as function of position
02 p0279 A69-11837

NEUTRON TRANSMUTATION

U NUCLEAR REACTIONS

NEUTRONS

NT COLD NEUTRONS
NT FAST NEUTRONS
NT PHOTONEUTRONS
NT THERMAL NEUTRONS

Amplitude and phase of cosmic ray meson diurnal variation, noting less variation in neutron diurnal variation
04 p0648 A69-14374

Solar neutron production and propagation to earth, discussing particle detectors
06 p0989 A69-17281

Multiplicity of secondary neutrons counted by IGY neutron monitor detecting cosmic radiation
06 p0925 A69-17297

Lunar photon leakage spectrum due to photons from capture and inelastic scattering of neutrons by galactic cosmic rays
09 p1597 A69-22088

Asymmetrical solar wind volume variations of magnetic inhomogeneities and cosmic ray absorption in earth atmosphere, including barometric coefficients of neutron component
10 p1760 A69-22844

Neutron radiography facility for production non-destructive testing inspection of aerospace components, noting collimation, neutron/gamma ray ratio optimization and neutron source
[AGN-TP-229] 10 p1699 A69-23051

Neutrons overloaded nuclei role studied for neutronization of matter at high densities in statistical equilibrium with respect to nuclear reactions
11 p1957 A69-24404

Neutron production cross sections prediction at proton bombarding energies below 50 Mev and above threshold for multiple nucleon emission
12 p2192 A69-26299

Tritium contamination reduction in small ion accelerators for neutron production, discussing pumping problems and vacuum systems
12 p2059 A69-26499

Similarity method applied to linear integrodifferential equations of neutron transport in homogeneous space
19 p3361 A69-36774

Neutrons overloaded nuclei role studied for neutronization of matter at high densities in statistical equilibrium with respect to nuclear reactions
24 p4391 A69-43794

NEW JERSEY

Redevelopment program for Newark airport noting runway construction, underground fuel system and passenger terminal complex
01 p0057 A69-11275

NEW MEXICO

White Sands Missile Range space and missile test facilities and support facilities for space exploration
02 p0227 A69-11761

Lower thermosphere composition over New Mexico, discussing rocket flight mass spectrometer measurements during summer 1967
03 p0425 A69-14009

NEW YORK

Shuttle VTOL airport access system analysis for New York area
[AIAA PAPER 69-804] 19 p3288 A69-35592

STOLport policy for New York City including travel time analysis, ground transport systems, political and community acceptance, aircraft noise, etc.
[RAES PAPER 3] 22 p3927 A69-40484

NEWTON PRESSURE LAW

Axisymmetric bodies longitudinal contours for hypersonic flow minimum drag, considering Newtonian pressure distribution and skin friction
10 p1632 A69-23886

NEWTON-RAPHSON METHOD

Multilevel optimization techniques for dynamic systems control evaluated, developing second level Newton-Raphson controller
01 p0051 A69-10440

Convergence theorems for perturbed Newton methods for solution of nonlinear equation systems, suggesting algorithm holding Jacobian matrix elements constant during iterations
01 p0106 A69-10988

Lambert problem of fitting conic to two position vectors with specified time interval solved numerically by Newton-Raphson iteration
03 p0518 A69-14250

Shallow shell deformations based on nonlinear equations solved by Newton-Raphson iteration
04 p0674 A69-14591

Newton-Raphson technique development for determining stability derivatives from flight data, noting use of a priori wind tunnel information
[AIAA PAPER 69-315] 09 p1434 A69-22379

One parameter operator imbedding to modify Newton method for solution of nonlinear equations
10 p1719 A69-23519

Finite difference Newton-Raphson algorithm extension to solve variational equations for simultaneous optimization of trajectories and associated parameters
[AIAA PAPER 68-115] 13 p2353 A69-28203

Modified Newton-Raphson methods for preliminary orbit determination, showing fast convergence and short computation times
19 p3397 A69-35613

Newton-Raphson function space algorithm for optimizing control systems with discontinuities and terminal constraints, discussing spacecraft examples
22 p3918 A69-41009

Newton method providing continuing solutions of nonlinear differential equations through limit or bifurcation points, discussing elastic stability applications
[ASME PAPER 69-APMW-14] 24 p4401 A69-43102

Optimal control for systems with discontinuities and terminal constraints using Newton-Raphson algorithm/successive sweep method/
24 p4294 A69-43306

NEWTON THEORY

Gravitation theory similar to special relativity and Newtonian theories, noting gravitational potential, metric and Newtonian charts
01 p0115 A69-10340

Newtonian theory of rotating configurations, noting use of algebraic equations
05 p0826 A69-16427

Special and general relativity theories following Newtonian mechanics and gravitation theories, discussing metric tensor, sun oblateness and experiments with gyroscope spin axis precession
07 p1181 A69-18928

Isotropic Newtonian cosmological models symmetry shown to have velocity distribution obtainable from solution of Vlasov equation
08 p1386 A69-20073

Hydrodynamic equations and conservation laws for nonviscous fluid in postNewtonian approximation of Brans-Dicke theory applied to gaseous mass dynamic instability
10 p1789 A69-24130

Test particle classical dynamics in closed expanding universe, discussing Newtonian inertial mass decrease and canonical methods for determining momentum, velocity and energy
11 p1920 A69-25561

Linear automatic control optimization by modified Newton method for determining real function zero value of real argument
13 p2239 A69-28436

Increases of Newtonian potential, gradient and second derivative on gravitating body, considering positive and negative masses
13 p2300 A69-28545

Electrodynamic law between current elements consistent with Newtonian dynamics, noting consequences in discharge and plasma control
14 p2485 A69-29320

Galactic formation in Lemaitre universe from statistically probable density fluctuations, using perturbation theory and Newtonian cosmology
14 p2520 A69-29373

Inertial and gravitational mass equality reexamined, considering Galileo, Newton and Eotvos experiments
14 p2486 A69-29647

Small perturbations propagation in plasma at Newtonian acoustic velocity, determining temperature, pressure and current densities
15 p2663 A69-30993

Discrepancy between Kepler first two laws and corresponding Newton propositions, noting necessary substitution of ovals for elliptical orbits
15 p2695 A69-31011

Newtonian invariant mechanics, giving inertial interpretation of gravitation and Hubble expansion of universe
15 p2654 A69-31214

Generalized Newtonian theory of gravitation, stressing internal solutions of gravitational field equations and incompressible fluid configuration in state of equilibrium
16 p2865 A69-32599

Steady motion stability of satellite gyroscope in Cardan suspension traveling along circular orbit in Newtonian central force field
18 p3135 A69-34585

Hard cosmic radiation hypothesis for Newton gravitation law for neighboring bodies, obtaining gravitational energy quanta and propagation velocity relationship
18 p3172 A69-34627

Hydrogen atom excess charge creating universal repulsive force in analyzing cosmological gravitational contraction in terms of Newtonian mechanics
18 p3206 A69-35469

Translating Tolman problem of cosmic dust motion into centrally symmetrical reading system, showing relativistic and Newtonian motion laws coincidence
20 p3594 A69-37079

Newtonian and general relativistic orbits of point mass in inverse square law force field, noting radar determination of spacecraft orbits
[AAS PAPER 68-098] 20 p3595 A69-37176

Hydrostatic instability in high temperature stars in postNewtonian approximation
20 p3580 A69-37926

Five dimensional theory applied to Einstein generalized gravity equations for spherically symmetrical gravitational waves, yielding gravity constant variation from Newton approximation
21 p3802 A69-38842

Statistical analysis of galactic structures subject to Newton gravitation covering globular clusters and spiral disk and rotating bar galaxies
21 p3803 A69-38924

Normal radial vibrations in Newtonian and general relativistic stellar objects and dynamic instability, determining modes and natural frequencies
22 p4014 A69-40142

NEWTONIAN FLUIDS

Laminar flow of anisotropic Ericksen fluid near wall at large Reynolds numbers, discussing Newtonian behavior, viscosity coefficient and particle orientation
02 p0231 A69-12141

Lift and drag parameters of axisymmetric bodies in Newtonian flow at random incidence by summation of appropriate portions
04 p0542 A69-14745

Velocity and temperature fields in Newtonian fluid in motion past stationary obstacle in gravitational field, noting similarity parameters reduction
09 p1429 A69-21686

Incompressible Newtonian flow between two parallel planes, noting marginal stability condition, mean velocity profile and turbulence
10 p1678 A69-22909

Numerical solutions for incompressible Newtonian flow around circular cylinder for various Reynolds numbers
11 p1867 A69-24279

Laminar Newtonian flow heat transfer to fluids with variable physical properties in vertical tubes with constant wall heat flux, considering viscosity and density
11 p2000 A69-25164

Analog problem solution for semiinfinite medium with Newtonian cooling at boundary, noting first term of asymptotic expansion in heat conduction equation
22 p4052 A69-41126

NICHROME [TRADEMARK]

Nichrome bars production dispersion hardened by alumina and zirconia inclusions, noting extrusion temperature influence
01 p0085 A69-10397

NICKEL

Saturation solubility of carbon in cobalt and nickel with respect to graphite determined by vapor transport experiments over large temperature range
01 p0092 A69-10066

Electroless deposition of various metals with emphasis on nickel, discussing mechanism, plating solutions, substrates, deposit properties and applications
01 p0099 A69-11066

Angular correlation between inelastically scattered 42 Mev alpha particles and emitted gammas from 2-plus Ni 58
03 p0470 A69-13100

Dispersed hard particles effect on high strain fatigue behavior of nickel at room temperature
03 p0443 A69-13121

Recovery behavior of nickel strain hardened by impact loading by aluminum projectiles, showing microstructure correlation with stress levels
03 p0447 A69-13620

Nickel reinforced with mullite whiskers produced by hot pressing
05 p0782 A69-16794

Nickel structure alterations during interaction with high speed air flow at elevated temperatures
05 p0783 A69-16812

Interaction of nitrogen oxides and carbon dioxide on nickel crystal surface using low energy electron diffraction and mass spectrometer, discussing work function
08 p1268 A69-20138

Nodal precipitation and cellular solidification substructure in commercial purity nickel, discussing supercooling, NiO and eutectic composition
08 p1332 A69-20289

Tensile and creep behavior of nickel at 600 C after oxidation at 1200 C, correlating results with structural differences caused by oxidation
08 p1333 A69-20556

Physical properties control in nickel powders obtained by hydrogen reduction of nickel diamine sulphate solutions
08 p1334 A69-21057

Temperature dependence of conductivity and Hall constant of GaAs single crystals with nickel impurity, noting diode structure and I-V curve shapes
09 p1555 A69-21475

Metal composites of Ni or Mo fibers in Be matrix, discussing chemical compatibility in terms of reactions, solid solubility and diffusion at various temperatures
10 p1707 A69-22991

Existing predictive methods for determining high temperature low cycle fatigue life reexamination based on experiments on nickel
10 p1796 A69-23068

Molybdenum fiber sintering activation by adding nickel, noting decrease in impact viscosity
10 p1711 A69-23336

Peaked electron emission from nickel surface with large work function under laser radiation, discussing emission pulses, electron currents and surface temperature time variations
10 p1703 A69-23572

Diffusion constant of Ni in Ti alloys with Al, Mo and Nb, considering beta phase
11 p1902 A69-24274

Molybdenum additive role in deformed carbonylic nickel recrystallization process
12 p2114 A69-26454

Tishomingo iron metcorite metallography, noting nickel content and martensitic microstructure evolution
13 p2353 A69-28159

Shock hardening in Ni at high pressure observed by electron microscopy showing dominating thermal effects on microstructure
15 p2637 A69-30225

Temperature effects on magnetomechanical damping in Fe, Ni and mumetal, noting behavior difference due to domain structures
15 p2639 A69-30586

X pocket Fermi surface of ferromagnetic Ni, considering magnetic breakdown effects
15 p2668 A69-30687

Temperature dependence of conductivity and Hall constant of GaAs single crystals with nickel impurity, noting diode structure and I-V curve shapes
15 p2669 A69-30720

Boron effect on sintered porous Ni friction at high sliding velocities and temperatures, analyzing oxide film destruction restraint by decreased Ni plasticity
15 p2641 A69-31187

Materials integral hemispheric radiative capacity determination based on cooling rate of thin walled specimen in vacuum, considering stainless steel, Ni and Cu
18 p3156 A69-34698

Dislocation structure of pure polycrystalline nickel subjected to high temperature creep, using electron microscopy following cold working and room temperature annealing
18 p3157 A69-35254

Preprogrammed deformation temperature influence on Ni creep strength, emphasizing smoothly changing loads effects
18 p3160 A69-35455

High field susceptibility in Fe and Ni and high field Mossbauer study in Fe relating results to band structure and models of ferromagnetism
19 p3383 A69-36050

Dynamic recrystallization in Ni and Ni-Fe alloys during torsional high temperature deformation
19 p3344 A69-36147

Recrystallization in thoria dispersed Ni sheet as function of strain-anneal cycles, using electron transmission technique quantitative determination
20 p3557 A69-36958

Polycrystalline nickel foil microstructure after explosive shock loading and heat treatments, using transmission electron microscopy
20 p3563 A69-38126

Bright nickel plating, examining brighteners and antipitting additions effect on deposition mechanism
22 p3959 A69-41264

Creep strength as function of oxygen pressure for Ni at 510 and 600 C, dropping creep rupture life to plateau of nearly constant life
23 p4176 A69-41504

Active Ni centers properties in Si with emphasis on increasing and reducing minority carrier lifetime in silicon integrated circuits, discussing energy levels
24 p4360 A69-42759

Wear protection of pressure loaded Ti-Mn alloy by heat diffused lubricated electrodeless Ni coatings
24 p4331 A69-42786

NICKEL ALLOYS

NT HASTELLOY [TRADEMARK]
NT INCONEL [TRADEMARK]
NT KAMACITE
NT MANGANIN [TRADEMARK]
NT NICHROME [TRADEMARK]
NT WASPALOY

Irradiation influence on yield stress of Ni-Al intermetallics noting temperature dependence and electron dosage
01 p0095 A69-10608

Zirconium corner of Zr-Mo-Ni phase diagram using metallographic analysis, hardness and microhardness methods, constructing isothermal sections for high temperatures
02 p0264 A69-11855

Nickel-rich region of Al-Ni-Y ternary system, emphasizing identification of solid phase equilibria through analysis of equilibrated alloy specimens
02 p0265 A69-12004

Martensite transformation by simple shear in equiatomic Ni-Ti alloy, using transmission electron microscopy
02 p0265 A69-12024

Cooling rate effect during aging on heat resistance of forged blanks of nickel based chromium alloy
02 p0266 A69-12125

Structural influence on superconductivity of niobium-titanium alloys, using electron microscopy and measurements of current density vs magnetic field strength
02 p0269 A69-12763

Electron band structure of copper-nickel alloys, discussing thermoelectric properties, energy ranges and effect of alloying additions
02 p0301 A69-12765

Creep relaxation and kinking of aluminum-nickel whiskers at elevated temperature, noting permanent plastic deformation after heat treatment
03 p0443 A69-13119

Interfaces role in Ni-base superalloy, discussing grain boundaries and coherent/incoherent phase boundaries
03 p0449 A69-13878

Alloying elements effect on mechanical and refractory properties and structure of forging of age hardenable Ni base alloys
03 p0452 A69-14122

Nickel-cobalt fcc alloys rolling and recrystallization textures established with filtered Aco K-alpha radiation, considering stacking fault energy effects
04 p0615 A69-14643

Solid phase equilibria in nickel-aluminum-scandium system at 1000 C
05 p0779 A69-15833

Hot working temperature effects on Rene 63 mechanical properties and microstructures, using tensile and stress rupture tests, electron microscopy and X ray diffraction analysis
05 p0781 A69-16446

Long term creep behavior of nickel-chromium-molybdenum alloy, noting temperature effect on grain boundaries
05 p0781 A69-16500

Low carbon maraging steel, studying age hardening behavior of iron-manganese-nickel alloys with titanium additions
05 p0781 A69-16541

Sintered W-Ni-Fe alloys strength and precipitation hardening characteristics for various compositions and cooling conditions
05 p0782 A69-16798

Structural characteristics of Ni-Mo alloys analyzed using electron microscopy and X ray diffusion scattering
05 p0782 A69-16808

Dynamic measurements of modulus of elasticity for polycrystalline nickel-tungsten alloys at elevated temperatures
06 p0943 A69-17232

Microstructure of diffusion zone during contact fusion in magnesium-nickel system at high temperatures
06 p0945 A69-17895

Charge and degree of ionization of nickel alloyed with molybdenum analyzed by electrolytic ion migration method
07 p1159 A69-18535

Ductility as principal cause of postweld heat treated stress relaxation cracking in nickel based Waspaloy and alloy 718
08 p1318 A69-19964

Statistical techniques to develop nickel base superalloy with high temperature capabilities for jet engine turbine bucket applications
08 p1329 A69-20001

Electrical resistivity of commercial nickel base alloys containing iron, chromium and molybdenum, noting anomaly in 20 percent chromium alloy
08 p1329 A69-20003

Temperature dependence of single crystal elastic constants of nickel aluminide determined by ultrasonic wave propagation measurement
08 p1332 A69-20288

Hydrogen solubility in solid and liquid phases of nickel-molybdenum and nickel-tungsten alloys at high temperatures
08 p1333 A69-20448

Self diffusion coefficients measurements for cobalt in nickel-cobalt alloys, using cobalt radioisotope 60
08 p1334 A69-20577

Monograph on precipitation hardening and mechanical properties of various heat resistant alloys with Co contents to 35 percent
08 p1334 A69-20763

Crystal lattice and orientation of precipitate responsible for hardening water quenched Ni-Cr-Nb alloy
08 p1334 A69-20852

Heat resistant nickel alloys for castings, tabulating chemical composition, mechanical properties, heat treatment, weldability, etc
09 p1522 A69-21608

Heat resistant nickel alloys static and dynamic properties at high temperature, creep-fatigue interaction, etc
09 p1523 A69-21609

Alloying elements effects on structure, mechanical properties, aging and composition of precipitation hardening intermetallic phases in Ni and Fe based alloys
09 p1525 A69-22143

Joining methods for fabricating thoria dispersion strengthened nickel and nickel chromium materials
09 p1509 A69-22342

Nickel base superalloys for aircraft gas turbines, considering strengthening mechanisms for creep resistance [ASME PAPER 69-GT-7]
09 p1527 A69-22506

Nickel alloy high temperature tests, noting coagulation of precipitated gamma prime phase, vacancies and creep rate increase
09 p1528 A69-22733

Microstructure and crystallography of lamellar eutectic alloy of Ni and intermetallic Ni-Ti compound
10 p1707 A69-22986

Supersaturation of dissolved B in splat quenched Fe-Ni-B alloys, noting interstitial and substitutional B in martensitic and austenitic phases
10 p1707 A69-22987

Intermediate Ni-Nb intermetallic formation as decomposition product from supersaturated Ni rich Ni-Nb solid solution aged above room temperature
10 p1708 A69-22993

Substructural changes during fatigue due to stacking fault energy variations related to morphology of fracture surface in solid solution Ni-Co alloys
10 p1795 A69-23060

High temperature effect on fatigue deformation and fracture of nickel base superalloy in single crystal and columnar grained forms
10 p1709 A69-23073

Composition and sintering temperature cooling effects on fracture properties of W-Ni-Fe alloys, using electron microscope fractography
10 p1711 A69-23333

High temperature metallic material strengthening methods, noting metallurgical factors and temperature effects on mechanical properties
10 p1712 A69-23630

Initial aging stage in Fe-Ni-Ti alloys using diffuse X ray scattering with electron microscopy of thin foils
10 p1712 A69-23720

Long range order formation in Ni-Cr alloys analyzed by direct neutron diffraction, considering disorder-order transition temperature and chemical composition
10 p1714 A69-23964

Nickel base wrought and cast superalloys examined to determine minor phases and microstructure thermal stability in high temperature heat treated condition
10 p1714 A69-23977

Vacuum deposition of Cr-Al film on Ni-Mo alloys, describing operating pressure, temperature and film thickness
10 p1715 A69-24013

Vanadium side of V-Ni phase diagram, using X ray analysis, differential dilatometry, thermal analysis and metallographic methods
11 p1903 A69-24579

Molybdenum, titanium and cobalt effects on nickel maraging steel strength and ductility
11 p1904 A69-24643

Young modulus temperature dependence and order-disorder transformations in ternary nickel alloys
11 p1904 A69-24705

Order-disorder transformations in nickel alloys under loading operations
11 p1904 A69-24706

Weld cracking sensitivity of Inconel 713C investigated for determining aluminum content effect on weldability of nickel base heat resistant alloys
11 p1906 A69-25577

Ni-Ti alloy intergranular deformation at constant tension within wide temperature range
12 p2113 A69-26044

Reaction between nickel-base alloy and hydrogen sulphide at high temperatures under atmospheric pressure, discussing activation energy
12 p2115 A69-26617

Gamma prime phase coherent equilibrium solubilities in Ni alloys of Al, Si and Ti from magnetic studies of particle coarsening and electron metallographic observations
13 p2276 A69-27370

Structural features of Fe-Ni massive martensite observed by light, electron and hot stage microscopies showing parallel block packet
13 p2276 A69-27401

Crystal microstructure and mechanical properties of unidirectionally solidified Ni-Ni-Nb intermetallic eutectic alloy at high temperature, examining deformation and fracture modes
13 p2276 A69-27402

Nickel base superalloys long time carbide and intermetallic phases stability at high temperatures
13 p2277 A69-27405

Temperature effects on mechanical properties and fracture behavior of lamellar Ni-nickel titanide intermetallic eutectic alloy showing dependence on intermetallic constituent
13 p2277 A69-27406

Composition, gamma structure and mechanical properties of three unidirectionally solidified eutectics within Ni-Al-Cb, Ni-Al-Zr and Ni-Al-Ti systems
13 p2277 A69-27407

Quantitative separation of elements in gamma prime from precipitation hardened high temperature nickel-base alloys by anodic dissolution
13 p2277 A69-27408

Matrix grain size relation to dispersed particle size distribution and Zener-McLean equation description of microduplex structure in superplastic Ni-Fe-Cr alloy
13 p2278 A69-27411

Small strain plasticity theory for planar slip in specific nickel base alloy deformation
13 p2362 A69-28120

Metallographic study of microstructure recrystallization of 50 Ni-50 Fe alloy during annealing using special etchants and methods
13 p2281 A69-28155

Metallographic analysis techniques for high aluminum activity pack cementation coating on nickel-base alloy
13 p2282 A69-28163

Nital etchant and sodium bisulfite stain for morphology of quenched dilute alloy Fe-Ni martensite
13 p2282 A69-28166

Ni alloys phase precipitation and Fe substitution effects on heat resistant alloys
13 p2283 A69-28488

Tungsten alloy fiber reinforced nickel base alloy composites stress-rupture strength, oxidation and impact resistance for high temperature turbojet engine buckets
14 p2462 A69-29010

Thoria strengthened Ni-Cr alloys high temperature stability, noting thoria particle size influence
14 p2465 A69-29682

Crystal structures of Ni-rich rare earth/Ni phases, including high temperature forms
15 p2637 A69-30213

Sintered mixtures of Ni-Mo powder noting electrical resistance, alloy and shear strength and impact viscosity
15 p2638 A69-30280

Temperature effects on magnetomechanical damping in Fe, Ni and mumetal, noting behavior difference due to domain structures
15 p2639 A69-30586

Electrode potentials of pure metals, Ni-Cr and Ni base alloys in molten salts applied to corrosion studies
17 p2990 A69-33650

Polygonization and strengthening effects simultaneous action at grain boundaries increased thermal stability of thermomechanically treated Ni-Cr alloy
17 p2991 A69-33940

Cumulative rapid thermal cycling influence on progressive disappearance martensitic transformation in 18 percent nickel maraging steel
18 p3155 A69-34650

Nickel solid solutions strengthening under cold deformation studied by X ray, noting screw and edge dislocations role
18 p3157 A69-35246

Soviet collection of papers on strength and plasticity of Ni and Ti and alloys covering high temperature internal friction, deformation and creep characteristics
18 p3158 A69-35442

Annealing temperature effect on Ni-Ti alloys internal friction, noting peak connected with solid solution grain boundaries
18 p3158 A69-35443

Annealing time effects on creep properties of Ni at various temperatures after work hardening
18 p3159 A69-35445

Phase shape deformation and austenite stabilization in Fe-Ni and Fe-Ni-Ti alloys following secondary alpha phase of reversed martensite-austenite transformation
18 p3159 A69-35448

Metal purity effect of nickel and Ni-Mo alloy on nucleation and recrystallization nuclei growth following 80 percent plastic deformation
18 p3159 A69-35449

Mechanical properties associated with 55-Nitinol memory effect, presenting stress-strain and electrical resistivity as function of temperature
19 p3340 A69-35523

Tensile and stress rupture strengths of diffusion bonded Ni superalloys, using spin tests of simulated hollow turbine disks
19 p3320 A69-35559

Nickel base superalloy high temperature fatigue properties, comparing crack initiation and propagation in directionally solidified and conventionally cast forms
19 p3342 A69-35919

Ni-Cr alloy unidirectionally solidified, grain and eutectic structure and alloy strength
19 p3343 A69-35921

Stoichiometric NiAl slip line and dislocation structures during creep at high temperatures, considering possible creep mechanisms
19 p3343 A69-35923

Ni base superalloy stacking fault energy, studying effects of various solute additions
19 p3343 A69-35925

Dynamic recrystallization in Ni and Ni-Fe alloys during torsional high temperature deformation
19 p3344 A69-36147

Stress corrosion cracking of stainless steels and Inconel and Inconel alloys in chloride, caustic, oxygenated and miscellaneous environments
19 p3349 A69-36890

Tungsten influence on morphology and lattice parameter of fcc gamma prime phase in Ni-Cr-Ti-Al alloys
20 p3558 A69-36962

Elements substitution for Al in gamma prime of Ni-Al alloy to change aged hardness by gamma prime mismatch and coherency strains
20 p3558 A69-36963

Supersaturated solid solution decomposition in Ni-Cr-Ti system, discussing precipitation mechanism of eta phase
20 p3558 A69-36968

Smooth and notched tensile properties of Fe-Ni alloys in liquid Hg, discussing ductility and toughness
20 p3563 A69-38025

Repair welding methods for trailing edge cracks in nickel base superalloy used in turbine vanes, emphasizing plasma arc fusion welding
20 p3551 A69-38137

B fiber reinforced Ni failure characteristics at high temperature, discussing plastic deformation and matrix role in crack inhibition
21 p3743 A69-38616

Flow stress temperature dependence of Ni-Cr-Al alloys consisting of gamma prime dispersion in Ni base solid solution
21 p3744 A69-38738

Slip band etching procedure revealing Ni-base superalloy plastic deformation, accentuating slip bands and subgrain boundaries by electropolishing
21 p3744 A69-38741

Creep resistance increase of Ni refractory alloy by thermovibrational treatment under stress relaxation conditions
21 p3744 A69-38869

Powder metallurgy all inert processing method for producing nickel base superalloys forgings, discussing microstructure, reproducibility, mechanical properties, etc
21 p3745 A69-38929

Minor element effects on Ni alloy weldability - Conference, Houston, October 1967
22 p3966 A69-39878

Minor element influence on high temperature weldability of high Ni alloys and weld quality
22 p3967 A69-39879

C and B influence on heat affected zone hot cracking and postweld heat treatment on Ni base superalloys
22 p3967 A69-39880

Minor elements effect on weld-metal cracking resistance of wrought Ni-base heat resistant alloy by Circular Patch Test
22 p3967 A69-39882

Ti, Al, S and P influence on Ni alloys weldability, discussing chemical composition, susceptibility to hot cracking and ductility temperatures
22 p3967 A69-39884

Composition and thermal treatment effects on weldability of precipitation hardened Ni base alloy, analyzing heat affected zone cracking sensitivity
22 p3968 A69-39885

Burner rig hot corrosion test facility for evaluating Ni-Co alloys used in gas turbine engines operating in marine environment
22 p3928 A69-40673

Extrastrong maraging steel based on 18 percent Ni, noting alloying elements percentages, mechanical properties and applications
22 p3971 A69-40833

Al-Ni-Co alloys precipitation mechanism effect on magnetic properties, including heat treatment and Ti alloying effects
23 p4175 A69-41298

Ternary diffusion at high temperature in Fe-Co-Ni alloy system covering entire ternary phase diagram, including computed interdiffusion coefficients
23 p4176 A69-41505

Ni based superalloy mechanical properties, determining chromium carbide discontinuous precipitation effects at various temperatures
23 p4176 A69-41507

Ni-Nb alloys precipitates tetragonal structure as function of time and temperature using electron and X ray diffraction
24 p4331 A69-42903

NASA programs for development of high temperature alloys for advanced air breathing engines emphasizing cast Ni-base alloy
24 p4335 A69-43718

NICKEL CADMIUM BATTERIES

ESRO satellites power supply design, operation and characteristics
05 p0829 A69-15919

Nickel-cadmium and Ag-Cd storage batteries performance, discussing methods to lengthen battery life and improvement of characteristics
08 p1261 A69-21051

Rechargeable nickel cadmium batteries state of charge determination by monitoring capacitance
09 p1435 A69-21425

Design aspects and relation to optimum operation on overcharge in Ni-Cd cells
10 p1639 A69-23991

Sealed nickel-cadmium cell design optimization, evaluating effects of various electrochemical treatments on energy density of nickel oxide positive electrode
10 p1639 A69-23992

Signal electrode charge control of sealed Ni-Cd batteries, discussing signal voltage for overcharge control
10 p1640 A69-23993

Maintenance free high rate sealed Ni-Cd battery power system compatible with existing aircraft electrical systems
10 p1640 A69-23994

Power supplies for balloon-borne instruments, describing light flexible NiCd batteries and solar cells used in EOLE project
16 p2736 A69-31745

Ni-Cd and Ag-Cd storage batteries for space applications, discussing performance, life and reliability
16 p2740 A69-32422

Gamma radiation effects on behavior of nickel and cadmium electrodes in alkaline solution
20 p3466 A69-38072

Ceramic-sealed Ni-Cd secondary batteries space environmental behavior testing to determine heat dissipation during spaceborne operation
22 p3869 A69-40591

Aerospace NiCd batteries charge control, discussing depth of discharge, limiting voltage and environmental temperature interrelationship
23 p4071 A69-42282

Scaled Ni-Cd battery with bipolar construction to reduce internal resistance and increase power bursts capacity, emphasizing electrical characteristics and economic considerations
23 p4072 A69-42283

Space vehicle flight performance of Ni-Cd batteries noting reliability, consistency and predictability
23 p4072 A69-42285

NICKEL COMPOUNDS

NT COHENITE

NT SCHREIBERSITE

Cross slip model for work hardening of nickel aluminate crystals, discussing temperature dependence
05 p0779 A69-15760

Microstructure and crystallography of lamellar eutectic alloy of Ni and intermetallic Ni-Ti compound
10 p1707 A69-22986

Intermediate Ni-Nb intermetallic formation as decomposition product from supersaturated Ni rich Ni-Nb solid solution aged above room temperature
10 p1708 A69-22993

Monograph on vanadium selenides and tellurides with NiAs structure covering existence regions, superstructures and equiatomic compounds from viewpoint of thermodynamics
15 p2667 A69-30602

Synthetic ferrites and sulfides of Ni and Co sulfated in presence of molten sodium pyrosulfate and sodium bisulfate
16 p2747 A69-32567

Percorite phase in nickel analog of clinohrosyllite formed under hydrothermal conditions in Wolf Creek meteorite cracks
18 p3199 A69-34824

TiNi compound alloying with Al and Fe, considering effect on hot hardness at various temperatures
18 p3157 A69-35249

NICKEL FLUORIDES

Parametric excitation of spin waves during parallel pumping of rubidium nickel fluoride ferrite, relating relaxation time and temperature
21 p3781 A69-39069

NICKEL OXIDES

Aluminothermic reduction of Ti and Ni oxides for obtaining Ti-Ni-Al system
22 p3969 A69-40070

NICKEL PLATE

Ni plated 40-cm lightweight Al alloy telescope mirror, noting weldment stress relief by annealing
23 p4164 A69-41624

NICKEL STEELS

Kinetic features of martensitic transformation of nickel steels dependent on plastic deformation degree at 525 C
02 p0267 A69-12190

Fracture toughness of Ni maraging steel weldments, using bending tests
[AIAA PAPER 68-507]
03 p0450 A69-13910

Properties of Ni-Mo-Al age hardening steels, discussing data confirming validity of low carbon low aluminum approach
04 p0613 A69-14527

Nitrogen solubility measured in liquid Fe-Cr-Ni-Al alloys, noting solubility increase with increasing Al content
06 p0942 A69-17228

High strength 18 percent nickel maraging steel with 350 ksi yield strength
08 p1330 A69-20009

Monograph on effect of nitrogen on precipitation behavior of austenitic chromium-nickel steel covering carbides, intermetallics, phase transportations, corrosion resistance, etc
11 p1902 A69-24369

Molybdenum and vanadium effects on nickel steel properties, stressing brittleness avoidance and quenchability
11 p1904 A69-24642

Aging effects on hardness and tensile strength of nickel-chromium steels at various high temperatures and time periods
11 p1906 A69-25439

Highly alloyed steels weldability, considering nickel maraging and precipitation hardening stainless steels
12 p2111 A69-25829

Homogenization of martensite formation in nickel 300 grade maraging steel, analyzing anisotropic transformation strains during thermal cycling
13 p2278 A69-27410

Plastic deformation effects by hydrostatic fluid extrusion on mechanical properties of Ni maraging steels
13 p2278 A69-27414

Nickel maraging steel polarization behavior in acidic solutions, noting corrosion potential dependence on pH
13 p2282 A69-28188

Rolling direction tensile tests of alloy steel plate displaying various fracture configurations over distinct temperature ranges, noting stress state, void formation and anisotropy
[ASME PAPER 68-WA/MET-1]
14 p2464 A69-29440

Damping, fatigue and optimal heat treatment of Cr-Ni steel for compressor blades operating at temperatures up to 500 K
17 p2990 A69-33933

Nickel maraging steel weld metal impact strength and fracture toughness improved by heat treatment
18 p3151 A69-35430

Ni-Ti maraging steel hardness impact strength and thermal EMF changes during quenching
19 p3345 A69-36154

Cutting loads measured as function of cutting rate and cutting tool geometry during boring of Cr-Ni steel pipe blanks
21 p3731 A69-38878

Metallurgy and properties of quenched and tempered high strength Ni-Co steels, discussing welding and aerospace applications
23 p4175 A69-41299

NIGHT

Nighttime equatorial Pi 2 micropulsations, noting seasonal and diurnal distributions and dependence on three hour index of magnetic activity
07 p1125 A69-18841

Nighttime latitude variations in Danjon astrolabe observations at Poltava, noting decrease from early evening to midnight
17 p2959 A69-32870

Limb darkening on earth night side observed by Aerobee rocket, with explanation based on atmospheric opacity in water vapor and carbon dioxide bands
17 p2960 A69-33167

NIGHT AIRGLOW

U AIRGLOW

NIGHT E LAYER

U E REGION

U NIGHTGLOW

NIGHT F LAYER

U F REGION

NIGHT SKY

H alpha emission symmetrical spatial distribution of night airglow observed with high transmission diffraction spectrographs
01 p0062 A69-10128

Night ionosphere electron content changes in Southern Hemisphere, discussing diffusion from exosphere and corpuscular radiation as sources of ionization
01 p0063 A69-10423

Soviet rocket and satellite night, twilight, airglow and auroral studies, discussing day sky brightness, night airglow and atmospheric stratification
01 p0066 A69-10941

Nighttime sporadic E rocket measurements, discussing descending layer thickness and electron density and lower boundary
01 p0071 A69-11165

Ionic composition and temperature of nighttime topside ionosphere from analysis of incoherent backscatter spectra, discussing solar activity effects
01 p0076 A69-11233

Far IR rocket observations of night sky background radiation
01 p0121 A69-11249

Ion concentrations and temperature measurements by magnetic trap on Cosmos 5 between 1000-1200 km
02 p0306 A69-11656

Lower ionosphere vertical motions found responsible for nighttime variation of radio waves total field strength
02 p0207 A69-11689

Tropical night F layer maintenance mechanism, noting airglow enhancement and ionization source association with plasma drifts
02 p0242 A69-11825

Electron and positive ion density measurements during nighttime auroral absorption event
03 p0421 A69-13327

Geomagnetic field topology of nighttime magnetosphere, showing pi 2 pulsations excitation mechanism in terms of Alfvén waves resonance in external cavity
03 p0423 A69-13524

Midlatitude nighttime total ionospheric electron content during magnetically disturbed periods from geostationary satellites Canary Bird and ATS 3
03 p0426 A69-14030

Light polarization of night sky components scattered by troposphere
04 p0595 A69-15247

Reaction rates coefficients of oxygen ions with molecular oxygen and nitrogen in nighttime F region over Moscow based on loss coefficient estimate
06 p0919 A69-17724

Night sky surface brightness and polarization measurements as basis for zodiacal dust cloud particle density distribution normal to ecliptic plane
07 p1222 A69-19588

Cosmos 92 satellite observation of night airglow flare, discussing NO bands emission and origin
09 p1485 A69-21533

Regular disturbance in topside ionosphere on summer nights from continuous records of ionospheric electron content, discussing magnetic activity and sunspot number effects
09 p1489 A69-21703

Nighttime electric fields and vertical ionospheric drifts near magnetic equator concurrent measurements
09 p1489 A69-21705

Quasi-trapped particle currents having discontinuities on daytime and nighttime sides of earth
09 p1577 A69-21767

Nighttime ionospheric recombination studies by model reference heights varying diurnally, seasonally and with solar flux and geographic location
10 p1685 A69-23834

VHF radar observations of electron density irregularity in nighttime equatorial electrojet, comparing day and night time electron drift rates and directions
10 p1769 A69-23837

Aeronomical phenomena observed near Altair and theta Aquila ascribed to Apollo 8 lunar flight
11 p1957 A69-24411

Aerobee rocket-borne liquid helium cooled telescope for IR night sky observations
11 p1885 A69-24852

Nighttime distribution of nitrogen ion and lambda 5755 emission in ionosphere with incidence of aurora
12 p2066 A69-26110

H beta emission line in night sky spectrum measured with gas pressure scanned Fabry-Perot interferometer in Italian alps
12 p2074 A69-26963

NIGHT VISION

Night sky background observation by near IR radiation flux, using rocket-borne telescope and ground based equipment
13 p2342 A69-27600

Magnetospheric corpuscular fluxes night ionization role in E and D region, considering precipitation from outside, trapped and dumped particles of radiation belts
13 p2254 A69-28333

Ion concentrations and temperature measurements by magnetic trap on Cosmos 5 between 1000-1200 km
13 p2333 A69-28687

Lower ionosphere vertical motions found responsible for nighttime variation of radio waves total field strength
13 p2224 A69-28720

Night airglow variations observed during Cosmos 92 satellite orbits, determining atmospheric albedo wavelength dependence for solid and medium cloudiness and clear skies
14 p2435 A69-29042

Forbidden NI transitions in nighttime upper atmosphere observed with Fabry-Perot spectrometer
14 p2440 A69-29120

Nocturnal development of air mass stratus clouds in Texas and mechanism of formation, discussing turbulent mixing theory
15 p2649 A69-30893

Hydroxyl band contamination of emission and background radiation from night sky
16 p2774 A69-31987

Thermosphere neutral wind speed measured from observing Doppler shift in O I 6300 night airglow line with Fabry-perot interferometer
16 p2776 A69-32093

Portable photometer with red-sensitive photocathode and high SNR for O I 6300 airglow experiments
16 p2777 A69-32107

Night sky far IR observation by rocket-borne telescope, discussing minimum signal detection and origin
16 p2781 A69-32445

Cosmos 92 satellite observation of night airglow flare, discussing NO bands emission and origin
16 p2783 A69-32528

Atomic nitrogen and nitric oxide density in upper atmosphere during nighttime calculated, allowing for atomic and molecular diffusion
16 p2785 A69-32622

Faraday rotation measurements in ionosphere by geostationary satellite ATS-3 as evidence of considerable nighttime electron transport
17 p2959 A69-32926

Day sky brightness at altitude above 100 km obtained during rocket flight compared to night sky viewed from ground
17 p3037 A69-33664

Metagalactic light measurements by lunar based night sky photography
18 p3189 A69-34242

Radiative recombination of atomic oxygen ions in nighttime F region UV radiation detected by polar-orbiting OGO 4 satellite
18 p3129 A69-34957

Nighttime ionospheric F region velocity component and recombination coefficient computer calculation
20 p3521 A69-37049

Spectral intensity distribution of night airglow, noting visual spectra distribution difference from G2 stars
20 p3522 A69-37057

Residual nighttime radio wave absorption in ionosphere, noting absorption-magnetic activity relation existence
20 p3528 A69-37678

Nighttime F region nonlinear recombination and variable drift effects, suggesting empirical model
21 p3715 A69-38559

Nighttime atmospheric shape analysis created by lightning and propagating in earth lower ionosphere waveguide
22 p3941 A69-40961

Nighttime F region time-altitude variations in aeronomical parameters calculated under conditions close to solar activity maximum
23 p4156 A69-41844

NIGHT VISION

Xenon plasma continuous illumination sources design and operation for night and color aerial photography covering photogrammetric resource surveys, ground traffic, flight paths, etc
22 p3950 A69-41000

B-747 safety assurance program, discussing organization, management, hazard sources, accident statistics, night visual approach and maintainability
22 p3867 A69-41135

Night vision requirements of Vietnam combat pilots investigated for relationship to Skyraider fatal crash during target strafing and H-34 helicopter crash landing
23 p4107 A69-41807

NIGHTGLOW

Tropical 6300 angstrom red oxygen nightglow enhancements related to variations in height of nighttime F 2 layer, noting implications for layer structure and physics
01 p0068 A69-11113

Polarization of nightglow, line vs continuum
02 p0235 A69-11428

Rocket sounding for studying positive ions nighttime composition in E layer after magnetic storm at midlatitudes
02 p0239 A69-11686

Nighttime E layer mean variations noting critical frequencies, electron density and seasonal and solar activity effects at sunset, midnight and sunrise
03 p0398 A69-13899

Night airglow spectrum between four and four microns, noting sequence of hydroxyl bands
03 p0426 A69-14251

Attitude stabilized balloon telescope for measuring interplanetary scattered light and nightglow
06 p0999 A69-16972

Nightglow intensities correlated with atmospheric ozone concentration and stratospheric temperatures
07 p1123 A69-18675

Differential brightness of night airglow spectrum, obtaining rotational temperature by comparison with synthetic spectra
09 p1488 A69-21656

Nighttime Venus ionosphere models compared with Mariner 5 observations, discussing implications with regard to He and H abundance consequences and nightglow
09 p1594 A69-21695

Photoelectric measurements of nightglow intensities during sunspot minima by zenith photometer, considering background continuum
11 p1877 A69-24584

Nightglow intensity variations at sunspot minimum from measurements in South West Africa, considering relationship to ionospheric vertical movements and density variations
12 p2066 A69-26133

Magnetospheric corpuscular fluxes night ionization role in E and D region, considering precipitation from outside, trapped and dumped particles of radiation belts
13 p2254 A69-28333

Rocket sounding for studying positive ions nighttime composition in E layer after magnetic storm at midlatitudes
13 p2258 A69-28717

IQSY night airglow photometric observations, summarizing zenith intensity and north/south intensity ratio data
15 p2594 A69-30019

Hydrogen Lyman alpha nightglow models, discussing solar photon scattering in geocorona and hydrogen vertical distribution
15 p2595 A69-30191

Photometric observations of zodiacal light, noting dust in earth-moon environment
15 p2599 A69-31334

Sporadic E layer nighttime electron density profiles obtained by Langmuir probe equipped sounding rockets
15 p2603 A69-31398

Photoionizing effect of hydrogen and helium UV glow in nighttime ionosphere compared with ground based IF ionosonde and sounding rocket observations
15 p2605 A69-31436

Vertical wind effects in atmosphere on 5577 A radiance, showing dependence on atomic oxygen density
16 p2778 A69-32185

Relationship between sporadic E and 5577 A nightglow emission attributable to ionization redistribution in E region due to dynamic processes
16 p2788 A69-32782

Rocket photometer observations of midnight atomic oxygen glow at 6300 A during ascending and descending flights
21 p3703 A69-38360

Spectrum, latitude dependence and diurnal variation of night airglow emission, noting space and time correlation and magnetic activity relationship to luminous intensity
21 p3711 A69-38514

Nocturnal electron/ion density balance in F region ionosphere from examining 6300 A emission
21 p3712 A69-38518

N I nebular doublet and auroral and nebular lines of O I obtained with multifilter scanning photometer in France, Norway and at magnetic equator
21 p3712 A69-38519

Intensity changes of OI nightglow emission at 100 km by transport associated with tides, gravity waves and turbulent mixing
21 p3713 A69-38526

Far IR nightglow emission from atomic oxygen observed by rocket-borne liquid He-cooled telescope
22 p3940 A69-40521

Herzberg bands synthetic spectra matched to various spectrograms to determine vibrational populations of molecular O state in nightglow
24 p4310 A69-43186

NIMBUS PROJECT

NIMBUS program individual missions characteristics emphasizing NIMBUS 3 results and weather forecasting improvements
[AAS PAPER 69-421] 24 p4392 A69-42835

NIMBUS SATELLITES

Selective chopper radiometer for remote atmospheric temperature sounding, discussing satellite versions for Nimbus D and Nimbus E
[UN PAPER 68-95797] 01 p0080 A69-10531

IR spectrometer for Nimbus meteorological satellite for terrestrial spectral radiance data for atmospheric temperature profiles
06 p0926 A69-17621

Satellites in meteorological service, describing TOS, ESSA and Nimbus satellites operation methods
08 p1409 A69-19960

Nimbus D meteorological satellite construction, control system, orbit, etc
13 p2356 A69-27832

Regression generated radiometric and contour height fields of North American Continent using Nimbus 2 IR equivalent black body temperature and geopotential data
24 p4343 A69-42896

NIMBUS 3 SATELLITE

NIMBUS program individual missions characteristics emphasizing NIMBUS 3 results and weather forecasting improvements
[AAS PAPER 69-421] 24 p4392 A69-42835

NIMONIC ALLOYS

Ni-Cr-Ti-Al /Nimonic/ alloy single crystal mechanical properties at room temperature, determining importance of structure
02 p0268 A69-12192

Nimonic alloys high temperature annealing effect on dislocation structure stability created by thermochemical treatment, using transmission microscopy
04 p0615 A69-14636

Nimonic alloys recovery analyzed by X rays and electrolytic phase separation, showing precipitated gamma phase effect
07 p1159 A69-18533

Nimonic alloy single crystals strengthening during plastic deformation, analyzing jump phenomenon at high and low temperatures
12 p2112 A69-26038

Growth kinetics, lattice constant changes and hardness during aging of nimonic alloy from X ray diffraction diagrams
14 p2463 A69-29310

Preliminary plastic deformations effect on dispersion hardened nimonic-80 alloy creep properties
18 p3159 A69-35446

NIMPHE (ENGINE)

U HYDRAZINE ENGINES

NIOBATES

Ferroelectric strontium barium niobate as sensitive detector of single pulse IR radiation, noting application to Q switched carbon dioxide laser output
02 p0300 A69-12623

Ferroelectric domain structure to explain microcracks nucleated at twinband intersections in mechanically deformed lithium niobate
03 p0486 A69-13618

Longitudinal elastic wave damping, excitation and propagation in lithium niobate crystals at frequencies from 200 to 2000 MHz
03 p0487 A69-13729

Lithium niobate single crystals for holographic storage, noting use for optical information storage, processing and display devices
03 p0432 A69-14184

Electro-optic properties of tungsten-bronze niobate ferroelectric crystals
[IEEE PAPER F-7] 05 p0808 A69-16313

Emission of Nd giant pulse laser with high repetition rate and peak power to generate second harmonic radiation in lithium niobate single crystals
07 p1144 A69-18469

Li niobate crystal emission excited by Ar laser beam, deriving laser action formulas
08 p1323 A69-19941

Second harmonic generation conversion efficiencies at 5300 A with KDP and lithium niobate crystals, using Nd-glass laser of high radiance and narrow bandwidth
09 p1514 A69-21333

Nonlinear optical properties of barium sodium niobate in ferroelectric tetragonal phase above room temperature, noting spontaneous parametric emission
09 p1515 A69-21354

Ferroelectric Li niobate single crystals internal magnetic field analysis by acoustic EPR, establishing field induced hypersound resonance absorption in spin systems
09 p1556 A69-21563

Microwave frequency room temperature acoustic surface wave propagation losses in lithium niobate measured by laser light deflection, discussing propagation and insertion losses
10 p1703 A69-23511

Optical rectification effect in lithium metaniobate crystals under neodymium laser radiation, comparing results with data for potassium dihydrophosphate crystals
14 p2458 A69-29168

Noncollinear single cavity optical parametric oscillation with specified energy conversion using ruby laser-pumped lithium niobate, discussing tuning
14 p2460 A69-29605

Elastic microwaves propagation attenuation along lithium niobate crystals trigonal axis at various temperatures
15 p2665 A69-30040

Rare earth niobates magnetic properties measured in pulsed magnetic fields
15 p2667 A69-30195

NIOBIUM

Surface structure effect on flux penetration and AC losses in superconductive niobium
02 p0298 A69-12031

Strain rate effect on dislocation substructure in deformed niobium single crystals, investigating relationship between mechanical properties and dislocation substructure
02 p0268 A69-12287

Rhenium-niobium cylindrical thermionic converters with mechanically polished or electroetched emitters, comparing performance
03 p0368 A69-13126

Relaxation mechanism of low temperature internal friction peaks in niobium quenched to room temperature
03 p0447 A69-13617

Internal friction temperature effects on amplitude dependence in niobium and molybdenum
04 p0614 A69-14635

Carburization structure on surface of Mo and Nb castings cast in graphite molds showing changes in plastic properties of metals
04 p0619 A69-15391

Relationship between microhardness of niobium and other variables characterizing superconductivity
05 p0810 A69-16805

Chemisorption of H onto Nb (110) surface, measuring low energy electron diffraction and inelastic electron scattering from clean and H-covered surfaces
06 p0980 A69-17758

Structural defects in annealed niobium crystals observed by optical microscopy, discussing etch pits
07 p1169 A69-19603

Thermally activated processes influence on dislocation interaction and on temperature dependence of flow stress in niobium single crystals
08 p1333 A69-20446

Dislocation channeling process in polycrystalline Nb subject to tensile deformation after neutron irradiation
09 p1521 A69-21345

Comparative performance of niobium cylindrical thermionic converters with vapor deposited rhenium, stressing emitters surface preparation
09 p1438 A69-21816

Cylindrical thermionic converter with vapor deposited rhenium emitter and niobium collector, measuring efficiency and power density
09 p1438 A69-21817

Microsectioning technique applied to measurement of diffusion coefficients of Cr 51 in polycrystalline Nb at 1220-1766 K temperature range
11 p1903 A69-24577

Diffusion coefficients of carbon in tantalum, niobium and vanadium by sectioning method, using carbon 14 as tracer
11 p1906 A69-25575

Neutron irradiated Nb single crystals tensile tested over temperature range, discussing athermal radiation hardening
13 p2275 A69-27368

X ray investigation of niobium, aluminum and niobium-aluminum systems to obtain K-spectra and L-spectra
14 p2508 A69-29664

Strain aging of polycrystalline Nb containing interstitial impurities as function of temperature, discussing interstitial role in recovery substages
15 p2636 A69-30194

N precipitation kinetics in deformed Nb, finding constant in rate equation dependent on temperature and correlated to precipitates nature
15 p2639 A69-30585

Flexure of Ta and Nb thin rectangular specimens during high temperature oxidation, showing stress generation due to O dissolution into metal surface [ECS PAPER 87]
15 p2641 A69-31541

German monograph on yttrium addition effects on tension and compression behavior of Nb and Mo at high temperature in vacuum
17 p2990 A69-33570

Tunnel junctions with low background currents made by reacting active gas layer adsorbed on Nb film surface with Pb upper film to form barrier
17 p3016 A69-33788

Optimum conditions for producing Ti-V alloy sheet plated on one side with Nb by hot rolling
18 p3155 A69-34652

Carburization structure on surface of Mo and Nb castings cast in graphite molds showing changes in plastic properties of metals
18 p3156 A69-35019

Nb single crystals plastic deformation influencing tensile strength, noting rolling directions
18 p3160 A69-35454

Depth dependent variations in texture in Nb due to inhomogeneous plastic deformation during cold rolling
21 p3744 A69-38737

Nb supersaturated solid solution in Co precipitation mechanism analyzed by X rays and electron microscope, noting diffusive scattering effects
21 p3750 A69-39788

Nb single crystals oxidation in dry oxygen at high pressure and temperature indicating suboxide platelets existence as function of temperature
23 p4177 A69-42357

Mechanical properties and dislocation configurations and densities of Nb single crystals measured at various strain rates
24 p4332 A69-43030

NIOBIUM ALLOYS

Nb-W alloy solution hardening and deformation, noting flow stress dependence on strain rate and temperature plus activation energy of deformation
01 p0095 A69-10488

Metallographic and radiographic analysis of zirconium corner in Zr-Bc-Nb system, discussing phase transformation during quenching
02 p0262 A69-11843

Zirconium corner of Zr-Nb-Mo system phase diagram, using microstructure, microhardness, hardness and radiographic methods
02 p0264 A69-11856

Superconductivity of niobium-titanium-oxygen alloy wires containing 40 percent minimum niobium weight, noting thermomechanical aging effect on critical current density
03 p0484 A69-13118

Nb and Cr additions effects on Hadfield type steel mechanical properties, noting improvement especially at low temperatures
04 p0614 A69-14579

Niobium based alloys modulus of elasticity temperature stability, investigating admixture effects
04 p0615 A69-14642

Be, Ce, V and Ti additions effect on oxidizability of cast, forged and cold worked Nb-Cr-Mo alloys
04 p0618 A69-15081

X ray diffraction studies of deformation effects on bcc niobium alloys in terms of particle size, strain, faulting probability and dislocation density
04 p0618 A69-15202

Metastable phases of binary zirconium-niobium system, defining decomposition of solid solution in cooling
05 p0781 A69-16614

Structure and critical superconductivity current of titanium niobium alloy as function of heat treatment and deformation
07 p1158 A69-18532

Columbium alloys properties, discussing creep strength, oxidation resistance, costs, production, etc
07 p1164 A69-18791

Zirconium niobium alloys thermodynamic properties measured by Knudsen effusion method using zirconium
07 p1165 A69-18940

Metallographic and X ray study of cellular decomposition and precipitation in superconducting niobium zirconium alloy, noting heat treatment effect on current carrying properties
08 p1331 A69-20192

Oxidation kinetics of niobium titanium alloy in air and oxygen at 1000 C, analyzing nitrogen and pressure effects
08 p1331 A69-20193

Oxidation kinetics of niobium titanium alloy in air and oxygen between 650 and 1000 C, analyzing activation energies and nitrogen effects
08 p1331 A69-20194

Phase identification and microstructural effects of gaseous nitrogen reaction with binary Nb-Ti alloys at 1000 C
08 p1331 A69-20195

Heat resistant alloying of niobium with group 4A, 5A and 6A elements, studying elements diffusion mobility dependence on melting point
09 p1525 A69-22144

Nb H alloys embrittlement, discussing hydride formation and resistance variation with temperature
10 p1707 A69-22989

Intermediate Ni-Nb intermetallic formation as decomposition product from supersaturated Ni rich Ni-Nb solid solution aged above room temperature
10 p1708 A69-22993

Creep of high purity Nb-Mo alloys in 800-1300 C range and at 1500-13000 lb/square inch stresses, giving activation energy for creep
10 p1711 A69-23375

Ti-Nb alloy structure in heat treatment states analyzed by diffuse scattering of X ray lines and by electron microscope
12 p2112 A69-26036

Quenched titanium-niobium alloy structure effect on superconductivity properties, using electron microscope and X rays
12 p2112 A69-26040

Anodic stain etching technique for carbide precipitates of niobium-base alloy Cb 132, noting X ray diffraction
13 p2282 A69-28162

Electrical resistivity decrease in niobium-hydrogen alloys during isothermal aging at low temperature attributed to hydride precipitation, noting reaction rate and activation energy
14 p2463 A69-29288

Hard metals and materials containing NbC and HfC, noting X ray studies of pseudoternary and pseudoquaternary systems
14 p2464 A69-29323

Nb-Ta alloys oxidation kinetics at high temperature and structure and composition of oxide films and scale layers, discussing anomaly in oxidation rate temperature dependence
14 p2464 A69-29650

Mu phase lattice constants and cell volume in Nb-Zn system
15 p2636 A69-30086

Maximum strengthening due to second phase precipitation within operating temperatures maintainable to 20 hr during aging of Nb-Hf-O and Nb-Zr-O alloys
15 p2640 A69-30632

Phase equilibria in ternary systems Nb-Fe-B and Nb-Co-B, determining structural types and lattice constants by using X ray and microstructural analysis
15 p2641 A69-31246

Hall effect and transverse voltages in type II superconductors in mixed state, considering cold rolled Nb-Zr alloys
16 p2827 A69-31827

Optical constants of Ta-W and Nb-Mo measured in IR and visible ranges as function of incandescent temperatures
17 p2990 A69-33574

Steady state flux jumping for thin walled tubular superconducting NbTi subjected to coaxial superimposed AC and DC magnetic fields, discussing effective resistivity
17 p3016 A69-33787

Binary Nb-Hf system phase diagram below solidus line noting lattice parameters and oxygen and nitrogen effects on phase equilibrium boundaries
18 p3157 A69-35247

Nb corner of Nb-Mo-Cr alloy phase diagram and oxidizability in air at high temperature
18 p3157 A69-35248

Carbon diffusion parameters in alloys of Nb with Ti, Zr, W and Mo, using radioactive carbon 14
18 p3157 A69-35250

Creep behavior of dispersion strengthened Nb base bcc alloy, studying temperature and stress effects on steady state creep rate
19 p3343 A69-35924

Tempering time and temperature effect on microstructure, superconductivity, tensile strength and electrical conductivity of recrystallized Nb-Ti alloy
19 p3345 A69-36302

Heat treatment effect on superconducting properties of deformed Nb-Ta alloys, noting critical current density
19 p3345 A69-36303

Oxidation resistant coating methods and systems for Cb base materials protection for aerospace vehicles and aircraft propulsion systems structures
21 p3730 A69-38672

Dislocation structures in Nb-Ti alloys formed after annealing
21 p3747 A69-39163

Multicomponent Nb alloy creep and rupture strength under loads after heat treatment, determining creep rates dependence on temperature
22 p3969 A69-40073

Niobium solution hardening by nitrogen and oxygen, noting grain size effects in electron beam refining
23 p4178 A69-42362

Ni-Nb alloys precipitates tetragonal structure as function of time and temperature using electron and X ray diffraction
24 p4331 A69-42903

NIOBIUM CARBIDES

Monocarbide phases high temperature vaporization from open metal surfaces into vacuum, obtaining temperature dependence
02 p0260 A69-11583

Vanadium-carbon and niobium-carbon binary systems revised phase diagrams, noting effect of sublattice order transformations
05 p0779 A69-15988

Preparation and properties of NbC-WC and TaC-WC carbides, analyzing hardness, resistivity, thermal expansion and dihedral angle
05 p0782 A69-16796

Zirconium and niobium carbide behavior during plasma spray coating, noting optimum oxygen content and mean carbide particle diameter in spray
07 p1165 A69-18933

Temperature vs compactness relationship in NbC compacts having nonstoichiometric composition and approximately equal specific surface, determining self diffusion coefficients
10 p1711 A69-23337

Homogeneous NbC and TiC specimens physical properties, discussing current carrier density and mobility dependence on composition
14 p2462 A69-28976

Hard metals and materials containing NbC and HfC, noting X ray studies of pseudoternary and pseudoquaternary systems
14 p2464 A69-29323

Nb and Ti carbides investigated for lattice parameters, microhardness and resistivity in homogeneity domain
15 p2638 A69-30282

Electrical resistance and temperature coefficient dependence on phase composition of Ti, Zr and Nb carbides
15 p2641 A69-31047

Carburizing spherical powders of Nb, Mo and W to obtain carbides, noting agreement between theoretical and experimental data
19 p3345 A69-36162

Nb-Ti-C alloys electrical resistivity and thermal EMF noting nearly linear variations with temperature
20 p3558 A69-36976

Zr and Nb carbide coatings on Nb, Ta Mo and W, investigating methods for coating and base metal combinations 20 p3560 A69-37362

Niobium carbide formation on graphite from gaseous niobium pentachloride and Ar mixtures, discussing parameters affecting layer growth rate 20 p3566 A69-37367

Niobium carbide deposition from gaseous halogen compounds on graphite particles in pseudoliquidified state, noting stoichiometric coatings 20 p3566 A69-37369

Recrystallization during sintering of free flowing Nb and Ti carbide powders, determining grain growth dependence on temperature and activation energy 22 p3970 A69-40636

NIOBIUM COMPOUNDS NT NIOBATES

Niobium hydride and tantalum hydride formation using metal powders, noting solid phases during dehydrogenation 09 p1448 A69-21599

Intermediate Ni-Nb intermetallic formation as decomposition product from supersaturated Ni rich Ni-Nb solid solution aged above room temperature 10 p1708 A69-22993

Analytical, IR absorption and polarographic analysis of cyclic niobium (V) and tantalum (V) esters 11 p1832 A69-24575

Niobium aluminide-niobium germanide alloys superconductivity and heat treatment influence on critical temperature 13 p3216 A69-27659

Transition metal interstitial compounds thin film preparation and superconducting properties, emphasizing high critical temperature, rock salt structure and NbN base 13 p3221 A69-28009

Niobium deposition on graphite from vapor-gas phase assuming heterogeneous process 15 p2629 A69-30992

Fast neutron irradiation effect on niobium nitride current carrying capacity, showing enhancement 17 p3008 A69-33765

NbN thin film production by refined reactive sputtering technique, discussing Pauli spin paramagnetism and spin orbit scattering in high field superconductivity 17 p3016 A69-33790

Nuclear magnetic resonance of epsilon and delta phases in NbN system with nitrogen mole fractions 19 p3383 A69-36445

Nb-gaseous Nb chlorides equilibrium from transpiration measurements at 800-1400 C, confirming importance of Nb pentachloride, Nb tetrachloride and Nb trichloride 23 p4112 A69-41339

NIOBIUM OXIDES

Thin films of niobium oxide vapor-deposited on silicon and quartz substrates, discussing optical and dielectric measurements, dispersion and absorption coefficient [ECS PAPER 17] 08 p1372 A69-20365

NbO presence uncertainty in S type stars due to close coincidences with ZrO bandheads, noting 6484 and 6591 lines in R Cygni spectrogram 19 p3403 A69-35964

NIOBIUM STANNIDES

Temperature dependent isomer shift and anharmonic binding of Sn 119 in niobium stannide, measuring Mossbauer recoil free fraction 01 p0134 A69-10009

NITRATES

NT AMMONIUM NITRATES
NT CELLULOSE NITRATE
NT NITROGLYCERIN
NT PETN
NT SILVER NITRATES

Chlorella enzymes activity in reducing nitrate to nitrite and nitrite to ammonia 24 p4263 A69-43136

NITRIC ACID

Balloon-borne IR spectrometry to study atmospheric nitric acid vapor compared with absorption by ozone and methane 11 p1879 A69-25407

Ignition delay of paraphenylenediamine associated with nitric acid, showing relation between grain diameter and hypergolic ignition mechanism, noting oxidizer concentration effects 15 p2561 A69-30185

Valence force constants for nitric acid evaluated from fundamental mode vibration spectra by matrix method 15 p2561 A69-30467

Nitric acid vapor in atmosphere as function of altitude from spectrograph, predicting downward diffusion 23 p4155 A69-41634

Absorption observation of solar radiation at sunset by nitric acid in three wavelength intervals on different balloon flights 24 p4308 A69-42969

Solid fuel ablation by nitric acid, controlling reaction interface displacement rate by mass and heat transfer phenomena 24 p4363 A69-43568

Intermediate hydrazine-RFNA reaction product formed on injector nozzle and combustion chamber surfaces after fuel injection without ignition analyzed by various methods 24 p4365 A69-43669

NITRIC OXIDE

Electron paramagnetic resonance study of interaction between adsorbed nitric oxide and NaY and deca-tionized Y zeolites surfaces, considering catalytic activity 02 p0205 A69-11900

Enhanced light emission rate in adiabatically expanded NO-O reaction ascribed to molecular clusters 04 p0555 A69-14864

Evening twilight nitric oxide density profile in gamma bands deduced from rocket measurements 07 p1125 A69-18842

Oscillator strengths of transitions in shock tube between nitric oxide Rydberg states in near IR 08 p1354 A69-20150

Atomic N and NO daytime upper atmosphere density profiles, discussing production and loss mechanisms 08 p1307 A69-20185

Recombination rate of nitrogen atoms using NO titration method, tabulating reactions and emissions during various stages of titration 08 p1309 A69-20454

Radio wavelength range observations of NO molecule lines in interstellar space 09 p1590 A69-21377

HNO role in hydrogen-NO reaction rate data reexamined by numerical integration of governing differential equations 13 p2218 A69-28457

Sodium atoms and NO molecules role in atomic O 6300 and 5577 A emissions in comet Mrkos 1957d due to charge exchanges and dissociative recombination 14 p2523 A69-29707

Electron pulse radiolysis of NO, determining absolute yields and rates of formation of nitrogen dioxide and nitrogen trioxide 14 p2410 A69-29928

D region ionizable constituent density /presumably nitric oxide/ measured, using blunt probe to detect changes in conductivity produced by Lyman alpha ionizing radiation 15 p2598 A69-31316

Atomic nitrogen and nitric oxide density in upper atmosphere during nighttime calculated, allowing for atomic and molecular diffusion 16 p2785 A69-32622

Radio wavelength range observations of NO molecule lines in interstellar space 18 p3198 A69-34765

Distributions, seasonal variations and ionospheric implications of mesospheric nitric oxide concentration 21 p3703 A69-38364

Absorption spectrum of NO molecule, analyzing f complexes electron structure, ionization potential and quadrupole moment 22 p3984 A69-40477

NITRIDES

NT ALUMINUM NITRIDES
NT BORON NITRIDES
NT SILICON NITRIDES
NT TANTALUM NITRIDES
NT TITANIUM NITRIDES
NT ZIRCONIUM NITRIDES

Vacuum melting effect on O concentration in heat resistant alloys, outlining conditions for nitrides formation in equilibrium with melt 09 p1524 A69-22136

Group 4A carbides and nitrides formation in Mo by arc melting, determining threshold solute metal-interstitial atom ratios 12 p2117 A69-27136

Fast neutron irradiation effect on niobium nitride current carrying capacity, showing enhancement 17 p3008 A69-33765

NbN thin film production by refined reactive sputtering technique, discussing Pauli spin paramagnetism and spin orbit scattering in high field superconductivity 17 p3016 A69-33790

Nuclear magnetic resonance of epsilon and delta phases in NbN system with nitrogen mole fractions 19 p3383 A69-36445

K-alpha band characteristics of N spectra stimulated in nitrides of transition metals by X rays 22 p3974 A69-41118

NITRIDING

Nitriding effect on heat resistance and transition temperature of molybdenum alloys 01 p0093 A69-10212

Ion nitrided binary iron alloys and steels electron microscopic studies reveal particle formation during hardenings 06 p0942 A69-17224

Ion nitride hardening of Mo-Ti alloy at 1300 degrees C in cathode glow discharge tube 15 p2637 A69-30212

Nitriding effect on heat resistance and transition temperature of molybdenum alloys 15 p2637 A69-30268

Diffusion saturation of Mo and Mo alloys by nitrogen in ammonia with formation of nitride films, noting surface hardness 18 p3158 A69-35288

Titanium alloys wear and fatigue resistance as functions of time and temperature of nitriding by purified nitrogen 19 p3347 A69-36743

Silicon nitride ceramics fabrication technology and dimensional stability during nitridation, discussing applicability to aerospace precision or joined ceramic shapes 24 p4336 A69-43211

Rotational bending fatigue strength of plain and notched conventional and maraging steels, evaluating gas nitriding effects 24 p4335 A69-43802

NITRILES

NT ACRYLONITRILES

Photolytic cleavage of vic-triazole ring when unsubstituted at N, finding phenylacetonitrile production mechanism 19 p3264 A69-35971

Acetonitrile ion-molecule chemistry using ion cyclotron resonance, discussing reaction of vibrationally excited methyl ions from electron impact 19 p3265 A69-36290

NITRITES

Amyl nitrite inhalation effects on cardiovascular system, discussing tachycardia and carotidograms 21 p3661 A69-39278

Chlorella enzymes activity in reducing nitrate to nitrite and nitrite to ammonia 24 p4263 A69-43136

NITRO COMPOUNDS

NT NITROGLYCERIN
NT NITROMETHANE
NT TETRYL
NT TRINITRO COMPOUNDS

Gas chromatography used to determine residual solid propellant stabilizers content and nitro derivatives, including thin film chromatography 02 p0303 A69-11528

Heat resistant DIPAM and HNS explosives in aerospace applications, considering mild detonating fuse and core loading 10 p1750 A69-23014

NITROBACTER

Consecutive reaction equations for idealized soil column solved for nitrifying metabolite concentrations as functions of time and depth 19 p3264 A69-35606

NITROCELLULOSE

U CELLULOSE NITRATE

NITROGEN

NT LIQUID NITROGEN

Nitrogen compressibility and thermodynamic functions up to 10,000 atm pressure and 400 C 01 p0175 A69-10366

Pulsed nitrogen laser design involving gas discharge tube fed by low impedance parallel plate transmission line 01 p0091 A69-10842

Nitrogen and helium as factors affecting human decompression stress severity, using urinary measurements reflecting various endocrine and metabolic changes 01 p0018 A69-11338

Intensity ratio of first negative nitrogen band and oxygen line varies in auroral displays 02 p0235 A69-11425

Radiative lifetimes for four N II excited states emitting UV during transition to lower level 02 p0280 A69-11928

Heat of solution and diffusivity of nitrogen in molybdenum analyzed by quenching technique and resistivity measurements at liquid helium temperature
02 p0267 A69-12188

High resolution spectroscopic study of stimulated rotational transitions of nitrogen molecules using crossed grating Echelle spectrograph
02 p0284 A69-12621

Pressure induced microwave absorption in molecular N for various temperatures, determining dielectric loss, absorptivity and quadrupole moment
03 p0472 A69-13317

Reentry plasma sheath simulation in wind tunnel by injection of nitrogen plasma from model vehicle nose
03 p0412 A69-13679

Chemical nitrogen fixation methods for life support systems, discussing organometallic chlorides and bromides
03 p0382 A69-14198

Superradiant and laser spectroscopy in second positive system of molecular nitrogen
04 p0609 A69-14285

Emission cross sections of first negative band system of nitrogen under electron impact excitation
05 p0795 A69-15617

Low collision energy charge transfer and dissociative charge transfer between rare gas ions and molecular nitrogen, measuring nitrogen ion kinetic energy distributions
05 p0796 A69-15909

Nitrogen abundances in chondritic meteorites determined by carrier gas fusion extraction
05 p0825 A69-16301

Nitrogen solubility in liquid Fe-Cr-Ni alloys increases with increased Cr concentration between 1550-1700 C and at one atm N pressure
06 p0942 A69-17229

Alloying elements effect on nitrogen solubility in liquid Fe-Cr-Ni alloys, defining quantitatively changes in solubility
06 p0943 A69-17234

Depolarized Rayleigh line widths measured for carbon dioxide, nitrogen and hydrogen, using measurements to calculate reorientation cross sections [IEEE PAPER B-11]
07 p1157 A69-19485

Pressure-temperature dependence of nitrogen solubility in tungsten at 2400-3000 C
07 p1168 A69-19602

Phase identification and microstructural effects of gaseous nitrogen reaction with binary Nb-Ti alloys at 1000 C
08 p1331 A69-20195

Absolute excitation cross sections for emission of second positive bands of nitrogen under electron impact
08 p1355 A69-20208

Near resonant transfer of vibrational energy from carbon dioxide nu 3 mode to N 14 and N 15 molecules in collisions
08 p1358 A69-21011

Light polarization from stimulated Brillouin effect in compressed gaseous nitrogen, presenting depolarization variations as function of gas density and laser power
09 p1516 A69-21691

Nitrogen diffusion coefficients in TiN and alpha-Ti determined by metallographic and roentgenographic analyses, establishing linear equations for temperature dependence
09 p1523 A69-21736

Lowest valence and Rydberg states assigned to ungerade singlet states in dipole allowed absorption spectrum of molecular nitrogen
09 p1542 A69-21916

Nonadiabatic collision broadening theory for IR spectral lines applied to carbon dioxide-carbon dioxide and carbon dioxide-nitrogen collisions, estimating rotational line widths
09 p1543 A69-22250

Nitrogen solubility in molten niobium and molybdenum at high temperatures in argon flow
10 p1710 A69-23213

Nitrogen impurities effect on electron energy balance in DC arc burning in inert gas
10 p1732 A69-23442

Monograph on effect of nitrogen on precipitation behavior of austenitic chromium-nickel steel covering carbides, intermetallics, phase transportations, corrosion resistance, etc
11 p1902 A69-24369

Optical cross section measurements for electron excitation from ground state of nitrogen
12 p2132 A69-26246

IR absorptance data for atmospheres of ammonia and ammonia nitrogen mixtures at various wavelengths

indicating absorption in strong line region for gas pressures used
12 p2132 A69-26247

Electromagnetic field induced plasma oscillation amplitude dependence on field frequency as function of field amplitude and discharge current at low N pressures
13 p2313 A69-28332

Ionization of rare gases /H and N/ by nitrogen ions, determining cross sections of formation of slow ions and electrons
13 p2304 A69-28440

Diffuser performance in hypersonic shock wind tunnel for nitrogen flow, discussing steady shock wave and separation zone formation time
14 p2391 A69-29622

N precipitation kinetics in deformed Nb, finding constant in rate equation dependent on temperature and correlated to precipitates nature
15 p2639 A69-30585

Temperature profiles in laminar boundary layer with endothermal reaction investigated using nitrogen plasma jet in rarefied gas wind tunnel
16 p2821 A69-31833

Leak rate measurement accuracy of rate-of-rise technique for nitrogen, methane and He between millionth and thousandth torr
16 p2791 A69-32326

Nitrogen reaction with excess fuel in ramjet engines, noting kinetic limitations in applications [WSCI PAPER 69-12]
16 p2831 A69-32351

Continuum radiation measurements for bremsstrahlung and recombination of neutral and ionized nitrogen
16 p2823 A69-32466

Prebreakdown currents measurement in H and N for deducing ionization coefficients via Townsend and Lucas equations respectively, noting validity by digital computer technique
16 p2815 A69-32574

Nitrogen density measurements up to 4000 atm and 1000 C, examining possible error sources
17 p3073 A69-33393

Emission intensity ratio change as function of polar auroral height compared to variation in atmospheric concentration ratio of oxygen to nitrogen
17 p2963 A69-33956

Electric quadrupole coupling for N 14 in aminedisulfonate studied by observation of second order transitions in electron spin resonance spectra
18 p3178 A69-35474

Molecular N rotational temperature effect on rare gases scattering cross section
19 p3377 A69-36184

IR spectra of Eta Carinae, confirming nitrogen and sulfur abundance
19 p3423 A69-36229

Deactivation rate constants of carbon dioxide vibrationally excited by high temperature collision with carbon dioxide or nitrogen molecules, describing laser apparatus and reaction cells
20 p3578 A69-36937

Nondissociating vibrationally excited dense N, analyzing compressibility factor, internal energy, enthalpy, entropy, sound speed and specific heat by state equations
20 p3631 A69-37214

Vibrational temperature of low density nitrogen measured by electron beam method, discussing relationship to ratio of integrated vibrational band intensities
20 p3579 A69-37222

Electron band forces probable values of Meinel system positive N molecules and first positive system of nitrogen molecules at high temperatures
20 p3579 A69-37307

Molecular rearrangements of nitrene intermediates, suggesting role in bond formation and breaking at nitrogen
20 p3484 A69-37485

Ambient atmospheric temperature and molecular nitrogen density measured simultaneously by rocket-borne electron beam luminescence method
20 p3543 A69-37799

Nitrogen gas breakdown threshold dependence on pressure during picosecond ruby laser pulse, discussing photoionization leading to breakdown in electromagnetic wave field
20 p3555 A69-38067

Nitrogen diffusion coefficients in TiN and alpha-Ti determined by metallographic and roentgenographic analyses, establishing linear equations for temperature dependence
20 p3564 A69-38214

N I nebular doublet and auroral and nebular lines of O I obtained with multfilter scanning photometer in France, Norway and at magnetic equator
21 p3712 A69-38519

Luminous efficiency for electron induced molecular nitrogen bands, discussing thick- and thin-target measurements of fluorescent efficiencies
21 p3774 A69-38521

Decompression research on inert gas transport in body, discussing solubility factors in decompression damage
21 p3655 A69-38913

Electron energy loss spectrum of nitrogen, suggesting atmospheric auroral nitrogen emissions compatibility with low energy electron impact excitation mechanisms
22 p3935 A69-39970

Rocket measurements of diurnal variations of F region concentrations and temperature of molecular N and O, showing disagreement with satellite drag data
22 p3939 A69-40515

Vapor pressure equation for oxygen and nitrogen derived by adding nonanalytic term, correlating equation with observed data [NAS-NRC PAPER H-1]
22 p4051 A69-40628

Collision processes in gaseous nitrogen leading to production of positive triatomic, diatomic and monatomic nitrogen ions
22 p3986 A69-40722

Molecular N UV spectrum at various pressures, showing absorption band dependence on pressure induced dipole transitions
22 p3986 A69-40723

K-alpha band characteristics of N spectra stimulated in nitrides of transition metals by X rays
22 p3974 A69-41118

Hypoxia reaction elimination in human beings by repeated exposure to hypoxia, discussing nitrogen inhalation experiments and adaptive behavior of respiratory system
23 p4214 A69-41789

Raman spectrum of solid alpha-nitrogen at low temperatures, calculating scattering intensities and Raman active librational lattice vibrations
23 p4194 A69-42204

Raman spectra analysis of solid carbon dioxide, nitrous oxide, nitrogen and CO, determining lattice mode intensities from oriented gas model
23 p4194 A69-42205

Niobium solution hardening by nitrogen and oxygen, noting grain size effects in electron beam refining
23 p4178 A69-42362

N or He additions effects on carbon dioxide laser design and power output
24 p4327 A69-42640

Ionization and light emission cross sections for collisions of protons and hydrogen atoms with atmospheric nitrogen used to analyze auroral events
24 p4368 A69-43177

Gradually decreasing N concentration effects on composition, tissue production and oxygen yield of unicellular algae in continuous culture
24 p4263 A69-43201

Ionization rate limiting processes behind strong shock waves in pure N, plotting electron density profile diagrams
24 p4302 A69-43367

Mechanism for pink afterglow accompanying microwave discharge in pure nitrogen, emphasizing gas kinetic temperature role
24 p4353 A69-43749

NITROGEN ATOMS

Solar emission line absorption by oxygen and nitrogen atomic lines, discussing effect on upper atmosphere composition measurements
03 p0425 A69-14019

Second virial coefficient of atomic nitrogen and oxygen, discussing thermodynamic properties of dissociating mixtures
03 p0473 A69-14158

Photoelectric absorption studies on molecular nitrogen indicate predissociation contributing to atomic nitrogen production in upper atmosphere
05 p0756 A69-16282

Pulsed laser emission of atomic N in mixture of molecular N and He, noting effects of pressure and frequency and duration of excitation pulses
06 p0933 A69-17258

Atomic N and NO daytime upper atmosphere density profiles, discussing production and loss mechanisms
08 p1307 A69-20185

Recombination rate of nitrogen atoms using NO titration method, tabulating reactions and emissions during various stages of titration
08 p1309 A69-20454

Vibrationally excited nitrous oxide formation in reaction of N atoms with nitrogen dioxide, noting IR emission and vibrationally excited nitric oxide
11 p1832 A69-24880

Forbidden NI transitions in nighttime upper atmosphere observed with Fabry-Perot spectrometer
14 p2440 A69-29120

Atomic nitrogen and nitric oxide density in upper atmosphere during nighttime calculated, allowing for atomic and molecular diffusion
16 p2785 A69-32622

Rate coefficient for primary process in removing molecular nitrogen in high vibrational levels from active nitrogen by N atoms
19 p3379 A69-36424

Atomic nitrogen collisional ionization and recombination rates under assumed quasi-steady nonequilibrium distribution of electron state populations
24 p4353 A69-43700

NITROGEN COMPOUNDS

U ALUMINUM NITRIDES
U AMIDES
U AMMONIA
U AMMONIUM NITRATES
U AZIDES [INORGANIC]
U AZIDES [ORGANIC]
U AZO COMPOUNDS
U BORON NITRIDES
U CELLULOSE NITRATE
U CYANO COMPOUNDS
U HYDROGEN CYANIDES
U IMIDES
U IMINES
U ISOCYANATES
U LIQUID AMMONIA
U NITRATES
U NITRIC ACID
U NITRIC OXIDE
U NITRIDES
U NITRITES
U NITRO COMPOUNDS
U NITROGLYCERIN
U NITROMETHANE
U NITROSO COMPOUNDS
U NITROUS OXIDES
U PETN
U PILOCARPINE
U POLYIMIDES
U RDX
U SILICON NITRIDES
U SILVER NITRATES
U SODIUM AZIDES
U TANTALUM NITRIDES
U TETRYL
U TITANIUM NITRIDES
U TRINITRO COMPOUNDS
U TRYPTOPHAN
U UREAS
U URIC ACID
U ZIRCONIUM NITRIDES

NITROGEN DIOXIDE

LCAO-MO-SCF wave functions determined for ground and excited states of nitrogen dioxide at five different ONO angles
06 p0960 A69-17109

Vibrationally excited nitrous oxide formation in reaction of N atoms with nitrogen dioxide, noting IR emission and vibrationally excited nitric oxide
11 p1832 A69-24880

Nitrogen dioxide molecular ions formation in air, discussing absence at lower pressures and early afterglow dominance in air ionized and dissociated by microwave pulses
11 p1879 A69-25158

Photodetachment of electrons from nitrogen dioxide ions by light in violet portion of visible spectrum, noting wavelength dependence
22 p3985 A69-40575

NITROGEN FLUORIDES

Monograph on kinetic study of fast gas reactions with shock waves covering thermal decomposition of nitrous oxide, hydrazine tetrafluoride and nitrogen tetrafluoride
08 p1304 A69-20707

NITROGEN IONS

Metastability of 1D state of negative N ion, instability of 3P state and energies of both states
02 p0284 A69-12598

Emission continuum intensity of negative nitrogen ion in nitrogen and air plasmas
04 p0639 A69-15370

Radiation intensity distribution from first negative and positive nitrogen system in equilibrium gas flow behind propagating shock front, discussing kinetics mechanism and electronic states
05 p0745 A69-15890

Molecular jets obtained by charge exchange of triatomic ion beams consisting of hydrogen, deuterium and nitrogen, noting formation, energy level, etc
05 p0797 A69-16339

Ratio of volume emission rate of 5577 A photons to volume emission rate of one band of positive nitrogen molecule first negative system in aurora
05 p0756 A69-16360

Electron impact excitation cross sections for emission from first negative bands of positive N molecule ion
06 p0961 A69-17135

Nitrogen ion number density time dependence by mass spectrometric probing of decaying nitrogen plasmas, noting molecular ion production by colliding metastable nitrogen molecules
07 p1184 A69-19141

Ion number densities time dependence in pink afterglow of N measured with quadrupole mass spectrometer
08 p1308 A69-20292

Vibrational excitation in He, H and N ion-molecule collisions on nitrogen first negative system, studying relative band intensities
08 p1356 A69-20739

Ratio of volume emission rates of 5577 A and band of positive N molecular ion first negative system for use in auroral observations
09 p1491 A69-22607

Auroral spectrum observations for absolute brightness of nitrogen Meinel and 1NG systems, considering background night airglow and atmospheric extinction
10 p1681 A69-23161

Optical depth at under 110 A due to continuous absorption by N, O and Ne ions estimated in high excitation planetary nebulae
10 p1790 A69-24140

Nighttime distribution of nitrogen ion and lambda 5755 emission in ionosphere with incidence of aurora
12 p2066 A69-26110

Nonequilibrium radiation from first negative band of molecular nitrogen ion excited by shock wave electron impact
13 p2245 A69-27380

Drift velocity and longitudinal and transverse diffusion coefficient for low energy N ions in N gas in mass spectrometer at room temperature
13 p2302 A69-27458

Ionization of rare gases /H and N/ by nitrogen ions, determining cross sections of formation of slow ions and electrons
13 p2304 A69-28440

Emission continuum intensity of negative nitrogen ion in nitrogen and air plasmas
16 p2822 A69-32117

Energy spectrum of secondary electrons and fluorescent efficiency in 3914 A band, obtaining ionization cross section
16 p2850 A69-32315

Beam foil technique to measure energy transition levels radiative lifetime for nitrogen ions
17 p3009 A69-34154

Mean life of D energy level in N IV, discussing Be I isoelectronic sequence
17 p3009 A69-34187

Recombination coefficients of oxygen and nitrogen ions with electrons related to electron temperature, using microwave afterglow/mass spectrometer
18 p3176 A69-34789

Transition probabilities of N I far UV multiplets, comparing experimental and theoretical results
18 p3178 A69-35413

M8 electron temperature and internal kinematics from photoelectric Fabry-Perot spectrometric recording of H alpha line profiles and N II
19 p3424 A69-36334

Upper atmospheric temperature by spectroscopy, considering rotational, OH nightglow, nitrogen cation dayglow and twilight temperatures
21 p3712 A69-38516

Exponential decay and mean lives of lowest P levels in N V measured with beam foil source, noting agreement with theories taking configuration interaction into account
21 p3774 A69-38760

N II 4176 A emission line occurrence in connection with type B auroras, studying secondary electrons energy spectra
24 p4309 A69-43012

NITROGEN OXIDES

NT NITRIC OXIDE
NT NITROUS OXIDES

Monograph on kinetic study of fast gas reactions with shock waves covering thermal decomposition of nitrous oxide, hydrazine tetrafluoride and nitrogen tetrafluoride
08 p1304 A69-20707

Oxygen and NO ions yields produced by dissociative attachment of electrons to nitrogen dioxide as function of electron energy, considering electron affinities lower limits
13 p2301 A69-27363

Quantitative IR spectral emissivity measurements of NO between 300-800 K made in absorption, correlating observed absorbance with optical path length and gas pressure
17 p3009 A69-34156

NITROGEN PLASMA

Nonequilibrium nitrogen plasma spectral line intensities calculated assuming optically thin plasma
01 p0124 A69-10960

Nitrogen plasma thermal radiation in spectral region from 0.5 to 1.1 micron, noting plasma state near local thermodynamic equilibrium
07 p1189 A69-18283

Franck-Condon factors for high rotational levels of nitrogen calculated in Morse potential approximation for application to plasma diagnostics
07 p1185 A69-19169

Nitrogen plasma total radiation intensity under pressure and at high temperatures calculated from radiation spectrum
11 p1922 A69-24231

N and H plasmas and N-H plasma mixtures thermodynamic properties calculation, discussing numerical methods and corrections for electrostatic interactions
21 p3847 A69-38421

Emissivity of nitrogen, oxygen and air plasmas in vacuum UV region of spectrum by photographic measurement, using He recombination radiation as brightness standard
21 p3774 A69-38944

Ionization formula linking nitrogen ion charge density ratio to plasma temperature
22 p3990 A69-40714

NITROGEN TETROXIDE

Bipropellant propulsion systems using Aerozine 50 and nitrogen tetroxide for Symphonie telecommunications satellite
16 p2828 A69-31733

Stress corrosion cracking of alpha Ti in liquid nitrogen tetroxide and various methanol environments, considering failure mechanisms
19 p3352 A69-36906

Impurities effect on corrosivity of nitrogen tetroxide with tank construction metals, Al, stainless steel and Ti-Al-V alloy, noting temperature aging and concentration
21 p3748 A69-39488

Heat transfer during nitrogen tetroxide nucleate boiling at various pressures and heat fluxes [ASME PAPER 69-HT-58]
24 p4411 A69-43536

NITROGEN 16

Neutron activation analysis for oxygen determination in Be by gamma emission intensity from nitrogen 16, noting bound oxygen
20 p3544 A69-37811

NITROGLYCERIN

Heat production rate equivalence to heat removal rate during ignition of ballistite powder by incandescent wires
02 p0354 A69-12668

NITROMETHANE

Detonation velocity variation in nitromethane with initial pressure, discussing relationships
22 p4051 A69-40713

NITRONIUM PERCHLORATE

Nitronium perchlorate thermal decomposition under overpressure of He and O between 80 and 170 degrees noting weight loss processes and crystal phase change
02 p0303 A69-11897

Intentional impurities effects on nitronium perchlorate thermal stability explained by change in cation and anion vacancies
02 p0304 A69-11899

NITROSO COMPOUNDS

Nitrosoazomethine derivatives deoxygenation for generation of azomethine nitrenes, discussing preparation by oxidation and dehydrogenation of secondary amidoximes
10 p1651 A69-23305

C-nitroso compounds chemistry covering various nitrosation reactions connected with reduction and deoxygenation
20 p3484 A69-37486

NITROUS OXIDES

- Intermolecular collision induced vibration to vibration energy transfer in nitrous oxide in various gas mixtures, measuring fluorescence and relaxation rates
01 p0123 A69-10684
- Nitrous oxide absorbance, deriving analytical expressions for transmission spectra
02 p0236 A69-11452
- Negative ion-molecule reactions in nitrous oxide using mass spectrometer, noting negative ion concentration pressure dependence
06 p0960 A69-17106
- Radiative lifetime for nitrous oxide 001-100 transition, laser level absolute population densities and saturation parameter measured in nitrous oxide-nitrogen-He laser
[IEEE PAPER G-10] 07 p1151 A69-19057
- Vibrationally excited nitrous oxide formation in reaction of N atoms with nitrogen dioxide, noting IR emission and vibrationally excited nitric oxide
11 p1832 A69-24880
- Nitrous oxide-CO bimolecular reaction and O-CO recombination in single pulse shock tube
16 p2748 A69-32793
- Shock wave studies of gaseous NO thermal ionization in Kr as function of temperature, using time-of-flight mass spectrometer
18 p3099 A69-34464
- Central tuning dip on rotation-vibration transitions of nitrous oxide and carbon dioxide laser with nitrogen, noting frequency discriminator generation
19 p3339 A69-36698
- Excited states lifetime of carbon dioxide and nitrous oxide ions deduced from spontaneous radiative deexcitation in vacuum after passage through gaseous target
22 p3985 A69-40715
- Raman spectra analysis of solid carbon dioxide, nitrous oxide, nitrogen and CO, determining lattice mode intensities from oriented gas model
23 p4194 A69-42205

NOBLE GASES

U RARE GASES

NOBLE METALS

NT COPPER
NT GOLD
NT SILVER

Less common refractory metals /rhenium, technetium, hafnium, noble metals/ properties, phase equilibria, etc
07 p1165 A69-18793

NOCTILUCENCE

U LUMINESCENCE

NOCTILUCENT CLOUDS

- Visual observations data on noctilucent clouds /1963-1967/
04 p0595 A69-15307
- Artificial noctilucent clouds or meteor trails positions determined by transforming photogrammetric coordinates
12 p2154 A69-25822
- Mesopause wind measurements at high latitude locations by sounding rockets noting relation to noctilucent clouds
13 p2294 A69-28466
- Aerosol content of mesosphere with noctilucent clouds measured with optical radar in Norway
14 p2444 A69-29877
- Noctilucent clouds thickness determinable from angular dimensions of visible edge
15 p2598 A69-31254
- Statistical data concerning noctilucent clouds formation during IQSY, noting tendency to form along geographic longitudes and day and night existence
15 p2598 A69-31255
- Inflight shadowing device incorporated into dust particle collection devices borne in Aerobee rocket sampling noctilucent cloud display over Fort Churchill
15 p2602 A69-31386
- Noctilucent clouds seasonal frequency, considering meteor shower effects and temperature dependence role
16 p2781 A69-32453
- Noctilucent cloud layer spectral brightness and transparency in E region determined from transhorizon rocket observations
18 p3130 A69-35148
- Noctilucent clouds morphological and kinematic characteristics based on photographs
18 p3132 A69-35335
- Visibility degree of noctilucent cloud determined from ratio of brightness contrast against sky to eye contrast threshold
19 p3362 A69-36410

Noctilucent clouds formation relation to ice sublimation, discussing rocket soundings
21 p3701 A69-38345

Noctilucent cloud particles nucleation and growth, noting time dependence and water vapor mixing ratio
21 p3702 A69-38346

Noctilucent clouds total or partial extraterrestrial origin, deriving minimum particulate influx from satellite and rocket data
21 p3702 A69-38347

Piezoelectric microphone sensor flown on rocket for recording micrometeoritic impacts during noctilucent cloud display, determining cosmic dust particles flux
21 p3793 A69-38348

Mesospheric circulation related to noctilucent cloud data, discussing seasonal variations
24 p4307 A69-42965

NODES [STANDING WAVES]

Cluster star color indices determination by measuring intensities at nodes of extrafocal star spectra
08 p1387 A69-20122

Deformation functions for finite beam analysis allowing continuity at nodes and accurate eigenvalues
15 p2710 A69-30869

NOISE

Nonlinear estimation with noisy data, considering least squares fit, sequential /Kalman/ estimate and iterated sequential scheme
21 p3686 A69-39370

NOISE [SOUND]

NT AERODYNAMIC NOISE
NT AIRCRAFT NOISE
NT ENGINE NOISE
NT JET AIRCRAFT NOISE
NT SONIC BOOMS
NT THERMAL NOISE

Noise and relations between environment and man, discussing sound perception, measurement and judgment of noise annoyance and harm
01 p0020 A69-10741

Impulse noise damage risk criteria, discussing maximum tolerable exposure, hazardous exposure and methods of impulse noise measurement
07 p1066 A69-19171

Turbomachinery multiple pure tone noise associated with acoustic resonance of inlet cavities examined by narrow band filter tracking integer multiples of rotative speed
[ASME PAPER 69-GT-2] 09 p1572 A69-22509

Auditory temporal masking of tonal signal by narrow band noise and perception of temporal order noting effects of intensity, frequency and time
11 p1830 A69-24795

Physiopathological reactions of humans exposed to infrasonic vibrations applied via auricular canal, observing cardiac and circulatory hemodynamic troubles
13 p2215 A69-28590

Noise as public health hazard - Conference, Washington, D.C., June 1968
14 p2541 A69-29149

Noise measurement and scales in studying psychological and nonauditory physiological effects on human functioning
14 p2485 A69-29150

Heart murmurs frequency analysis on patients to improve detection of aortic insufficiency in presence of mitral stenosis
24 p4279 A69-43800

NOISE HAZARDS

U HAZARDS

NOISE INJURIES

Impulse noise damage risk criteria, discussing maximum tolerable exposure, hazardous exposure and methods of impulse noise measurement
07 p1066 A69-19171

Mechanical vibrations and noise effects on acetylcholine concentration, esterase activity and synthesis ability in rat brain
23 p4079 A69-41381

Noise levels in twin engine general aviation light aircraft cockpits, discussing protection against possible hearing damage
24 p4252 A69-42902

NOISE INTENSITY

Aircraft noise suppression, discussing community aspects of jet and fan noise and physical mechanisms of jet noise
01 p0009 A69-10349

Atmospheric noise at millimeter wavelengths, discussing solar radiation and antenna near and far field patterns
01 p0028 A69-10420

Matrix representation of linear active two port noise figures and charts in terms of power wave variables
02 p0211 A69-12444

Noise emitted by gas filled cavity perturbed by strong coherent signal computed by Nyquist equation
02 p0211 A69-12448

Microwave oscillator AM and FM noise measurement using Schottky barrier diode detector, discriminator, storage oscilloscope and wave analyzer
02 p0220 A69-12453

Human reaction to aircraft engine noise, evaluating effective perceived noise level and constraints on engine design
02 p0204 A69-12766

Frequency dependence of atmospheric noise intensity from 1 to 1000 kHz at low and medium latitudes
05 p0758 A69-16410

High power microwave oscillator /carpenter/ for pure or FM signal amplification, noting low output noise level
07 p1096 A69-18437

Cosmic radio noise intensity measurements by ATS 2 satellite-borne radiometer
07 p1224 A69-19715

Error in receiver sensitivity calculation using approximate equation for noise power at input
08 p1275 A69-20226

Mathematical formulation of Noy tables, noting more efficient programming and minimal disagreement with original tables
08 p1266 A69-20403

Noise power ratio at output of wideband amplifier with angle modulated multicarrier input, obtaining intermodulation products from Bessel functions expansion
08 p1285 A69-20595

Interference capability of noise of different frequency bandwidths, comparing weighted sound pressure to loudness level
08 p1276 A69-20857

Antenna noise temperature at earth station due to rain on radomes, solar and cosmic noise, noting SNR degradation
09 p1461 A69-21283

Propagation and noise effects on frequency choice for communication satellite service to aircraft and ships, noting tropospheric and ionospheric attenuation considerations
09 p1451 A69-21288

VLF emissions intensity and spectra variations compared with energetic electron fluxes variations during magnetosphere storm periods
09 p1488 A69-21698

Transistorized amplifier stage noise factor dependence on parameters and modes of operation of transistors
09 p1463 A69-21724

HF excess noise and equivalent circuit representation of MOSFET with n-type channel, noting local mobility fluctuations effect
09 p1463 A69-22094

Transmit-receive device noise contribution effect on receiving system noise factor for device insertion immediately before low noise microwave amplifier
09 p1469 A69-22605

Tunnel diode amplifier operation in presence of noise
09 p1469 A69-22630

Autodyne frequency converters minimum noise and conversion factor calculation and optimal mode determination
09 p1469 A69-22631

Jet airliners noise characteristics, calculating spectral content and duration of perceived noise level and total noise level
09 p1435 A69-22637

Noise level perception and subjective judgments for broadband noise with single, modulated and multiple tones, considering tone correction procedures
11 p1830 A69-24796

Noise level criteria for acceptable voice communications in office environment, noting acclimatization
11 p1830 A69-24797

Microwave amplifiers and receivers noise performance factors measurement noting thermal noise, definitions of noise temperatures and noise figure, noise generators, etc
11 p1840 A69-25301

Annoyance caused by noise near airports, discussing PNdB /perceived noise dB/, evaluation criteria, and French, British, American and German methods
13 p2214 A69-28588

Aircraft noisiness estimation methods
13 p2216 A69-28660

Noise duration and spectral complexity effect on subjective rating of disturbance level

14 p2408 A69-29152

Mean-minute thermal noise intensity distribution in telephony channels of tropospheric radio relay systems

14 p2412 A69-29425

Optimum thermal and nonlinear noise intensities distributions in frequency division multiplex satellite communications systems, relating relay station power, frequency band and channels

14 p2412 A69-29426

Potential noise stability of reception in binary communications system with active pause in channel for unknown signal arrival time

15 p2563 A69-30134

Pulsed noise sensitivity in radar receivers having noise limiter for simple and complex signals

15 p2563 A69-30137

Fast visual task performance indoors found dependent on sound pressure level

15 p2550 A69-30305

Near field flow noise generated in boundary layer of water vehicle measured for rotating cylinder, ship and buoyant unit using hydrophone

17 p3004 A69-32953

Noise levels due to long range tropospheric transmission calculated for microwave radio systems

17 p2919 A69-33146

Noise intensity measurements in far field of circular nozzle for jet noise composition

17 p2957 A69-33602

VHF band surface incidental radio noise levels over metropolitan areas compared with airborne data

17 p2921 A69-33672

Noise during frequency combination and conversion in mixer

17 p2931 A69-33911

Intermittent noise effects on human target detection to test neutral ratio dependence on noise intensity level, noting attention flexibility

17 p2911 A69-34008

Aircraft noise acceptability tests based on listening in absence and presence of speech

18 p3097 A69-34325

Daily solar radio noise intensity at 10.7 cm with slowly varying components and quiet sun emission, revealing rise only and absorption bursts

19 p3401 A69-35758

False signals formation during random pulse noise in single command channels with PTM coding, noting code value and redundancy

19 p3278 A69-36595

Transistorized amplifier stage noise factor dependence on parameters and modes of operation of transistors

20 p3505 A69-37460

STOL aircraft characteristics emphasizing ground and air space operations requirements and noise levels

22 p3863 A69-40430

Commercial aircraft peak cockpit noise level during cruise and high speed descent, discussing damage risk criteria and inter-pilot speech interference

23 p4102 A69-41682

Supersonic aircraft sonic bang loudness level calculations by model waveforms with allowance for interaction between incident and ground reflected shock waves

23 p4063 A69-42454

Noise level effects on pharmacological effectiveness of centrally acting drugs in rats

24 p4262 A69-42947

Continuous noise level effects on stabilized escape conditioning in male albino rats

24 p4262 A69-42948

Negative surface potential effect on noise and photoconductivity in Ge doped p-type InSb single crystals at low temperature in vacuum

24 p4362 A69-43738

NOISE MEASUREMENT

U ACOUSTIC MEASUREMENTS

NOISE METERS

Transistor HF noise factor measurement by semiautomatic device with saturated diode comparison noise source heater current automatically controlled

07 p1090 A69-18292

AM-FM calibration modulator for microwave oscillator noise measurement

11 p1856 A69-25631

NOISE PROPAGATION

Measured noise temperature in argon tubes vs theoretical electron temperature for gas discharge noise sources

02 p0210 A69-12437

Noise generation and propagation in linear N cascaded mismatched two port networks, noting application to microwave measurements in low noise technology

02 p0211 A69-12445

Noise sources representation in pumped nonlinear systems simplifies noise analysis and noise propagation

05 p0720 A69-16345

Noise rejection in multichannel telephone signal reception with FM and multiplexing, determining SNR dependence on SNR at receiver input

09 p1459 A69-22640

Simultaneous transmission of information signals and pseudonoise synchronization waveforms in common bandwidth

[IEEE PAPER 67-TP-1173-COM]

10 p1655 A69-23532

Radio signals and concentrated noise amplitudes probability distributions reflected from ionosphere and scattered in troposphere calculated for Rayleigh and log-normal fading

11 p1833 A69-24440

Artificial triggering of VLF magnetospheric noise by NAA Morse code transmission during whistler duct drift across magnetic shells on 17 June 1965

11 p1878 A69-25154

Artificial magnetospheric VLF noise triggering by Morse code dots at 14.7 kHz from NAA verified at Antarctica

11 p1878 A69-25155

Soviet monograph on intrinsic noise emission in radio channels covering noise temperature at receiver input, thermal microwave radiation, etc

13 p2219 A69-27304

Equipment and test installations for turbojet noise studies, discussing noise from rotating parts, pure jet noise and air propagation of noise

13 p2325 A69-28589

Noise emission and Landau damping of plasma resonances related by network theory including Nyquist formula, discussing noise temperature in free fall region

16 p2822 A69-32038

Noise transmission from turbulent boundary layer through flexible plate into closed cavity, emphasizing nonlinear plate stiffness and mutual interaction between plate and airflow

17 p3006 A69-33409

Far field helicopter rotor noise radiation, analyzing blade slap, rotation noise, vortex noise effects and loading harmonics utilizing computer program

18 p3090 A69-34322

Microwave reflection and noise emission from cylindrical rare gas afterglow plasmas in axial magnetic field measured near electron cyclotron resonance

18 p3127 A69-34436

Terrestrial radio noise source aspects including atmospheric, propagation influence, lightning-generated noise and whistlers, radio interference, etc

19 p3276 A69-36434

ELF atmospheric propagation, determining slow-tail atmospheric group velocity, relating characteristics to spectral characteristics of lightning

23 p4114 A69-41362

NOISE REDUCTION

Aircraft engine noise reduction in test runs by sound insulating hangar

01 p0054 A69-10033

Aircraft noise suppression, discussing community aspects of jet and fan noise and physical mechanisms of jet noise

01 p0009 A69-10349

Optimal coherent reception of frequency diversity signals in multipath channels investigated for noise immunity

01 p0028 A69-10375

Coherent diversity reception of discrete signals in presence of concentrated noise investigated for use of optimal solution circuits for noise elimination

01 p0028 A69-10376

Mechanical behavior of synthetic layer coatings for damping instrumental vibration and noise

01 p0168 A69-10399

VTOL aircraft design for noise reduction, discussing localities tolerance, noise sources, operating cost, etc

01 p0009 A69-10421

Aerodynamic configurations to reduce sonic boom at supersonic speeds

01 p0007 A69-11028

RF feedback amplifier analytical design, deriving open and closed loop feedback noise figure expressions by use of equivalent noise model

02 p0217 A69-12150

Large amplitude Pc 1 events at College, Alaska, noting more ionospheric cosmic noise absorption accompanying large events

[AFCL-69-0059] 02 p0244 A69-12397

Ultra cone system for ultralow noise reception of RF space communication from Mariner 5 during occultation by Venus

[JPL-TR-32-1340] 02 p0220 A69-12429

Gas discharge tubes and waveguide mounts as reference noise accuracy standards for S, C and X bands in WR284, WR137 and WR90 waveguides

02 p0210 A69-12439

Injection phase locking for synchronizing oscillators and reducing FM noise

02 p0220 A69-12450

Cavity stabilization of microwave oscillator for noise reduction

02 p0220 A69-12451

Low noise high power transistor oscillator using directional coupler, noting isolated port for injection phase locking

02 p0220 A69-12452

Gradual memory system for noise reduction in adaptive control system

02 p0212 A69-12606

Low noise microwave amplifiers for radio astronomy and satellite communications receiving system preamplification

03 p0402 A69-13017

Noise reduction techniques in digital and analog data transmission over space program distances, emphasizing deep space missions

03 p0394 A69-13398

Soviet MI-8 and MI-4 passenger helicopters noise characteristics with turboprop and piston engines and during landing takeoff and horizontal flight

03 p0366 A69-13417

Weak periodic signal separation from noise using single and multichannel analog adders

04 p0597 A69-14848

Telemetry technique utilizing thermocouple sensors for base heating determinations on free flight blunt cone in shock tunnels, noting electrical noise reduction

[AIAA PAPER 68-407] 04 p0604 A69-15514

Jet engine inlet noise control by modification of inlet guide vanes

05 p0811 A69-15622

Noise reduction in parametric electron beam amplifier by cooling two frequency resonator noise to liquid nitrogen temperature

05 p0728 A69-15654

Frequency stabilization and noise suppression in argon FM laser

[IEEE PAPER P-7] 05 p0775 A69-16325

Sonic boom reduction devices, discussing supersonic electroaerodynamic flow with shock waves, gas discharge one dimensional continuum analysis, power expenditure and aerodynamic interaction

[AIAA PAPER 69-38] 06 p0869 A69-18150

FM noise in two and three chamber klystron oscillators, discussing tubes to reduce noise and relative merits of active or passive stabilization circuits

07 p1096 A69-18438

Injection locking method for reducing FM noise in Gunn effect oscillators

07 p1102 A69-18862

Helicopter rotor noise generation, propagation reception and reduction, discussing design charts for rotational noise spectra as function of design and flight variables

[AIAA PAPER 69-195] 07 p1055 A69-19563

Peak acoustic attenuation frequency shifts and peak power insertion losses in air flow ducts related to air specific weight changes

07 p1117 A69-19700

Acoustical measurements on MD-12 passenger aircraft before and after application of insulation for noise suppression

07 p1057 A69-19704

Anti-interference TV circuit using delay lines applied to radar systems, discussing false alarm probability and detection probabilities

08 p1271 A69-19919

Field noise reduction frequency spectra afforded by spacecraft shroud, basing estimating criterion on flight test data

09 p1609 A69-21892

Sonic boom reduction by azimuthal redistribution of supersonic aircraft pressure field variation

[AIAA PAPER 68-159] 09 p1434 A69-21948

Fan compressor noise reduction indicating effects of design, number of blades, vane/blade ratio, aerodynamic parameters and blade spacing

[ASME PAPER 69-GT-9] 09 p1571 A69-22505

Noise rejection in linear amplitude detector during weak harmonic signal reception improved by limiting threshold voltage
09 p1460 A69-22645

Noise in instrumentation systems, considering coupling and current noise source and reduction by isolation and filtering
10 p1691 A69-23231

Solar cosmic ray event of July 7 1966, noting sudden cosmic noise absorption reduction and particle absorption domination start at 0120 UT
10 p1768 A69-23771

Metals with combined high damping and good mechanical properties for solving fatigue, noise and vibration problems
10 p1715 A69-24044

DC conversion amplifier commutation induced noise and signal ratio as function of shunt capacitance across vibrator load investigated for increased noise stability
11 p1845 A69-24555

Frequency noises suppression in Gunn diode oscillators by frequency stabilization, using high Q external cavity
11 p1853 A69-25608

Concorde jet engine silencer concept and characteristics
[AIAA PAPER 67-391] 12 p2148 A69-26759

Rolls Royce noise and compressor test facility for continual lowering of engine sound pressure levels, considering sound generating mechanisms
13 p2240 A69-27616

Matched diodes in monolithic balanced mixer by diode array fabrication for noise suppression
13 p2233 A69-28071

Phase distortion, conversion of delay coefficients into channel noise and determination of waveguide delay coefficients for FM satellite communication systems
[IEEE PAPER 68-TP-382-COM] 13 p2222 A69-28153

Reduction of noise from underexpanded axisymmetric jet flows using radial jet flow impingement
[AIAA PAPER 68-81] 13 p2248 A69-28212

Input signal random amplitude fluctuations suppression by parametric power limiter, discussing limiting frequency determination and dependence on signal amplitude
13 p2236 A69-28573

L-band parametric amplifier operated in liquid N for noise reduction, discussing measurement circuit for gain, bandwidth and noise figure
13 p2237 A69-28644

Aircraft noise alleviation through flight procedures improvement, home building modification and noise standards legislation
14 p2392 A69-29154

Aircraft noise control at source through high bypass ratio engine modification, FAA decibel standards and higher capacity aircraft for increased traffic density
14 p2509 A69-29156

Urban noise control over transportation systems including aircraft and highway traffic operating beyond local noise ordinance purview
14 p2541 A69-29157

Noise reduction techniques using injection phase locking and high-Q cavities for HF oscillator high order multiplier and avalanche diode oscillator microwave sources
14 p2420 A69-29458

Optimized receivers synthesized for narrow band radio signal filtration, comparing noise rejection properties of various pulse modulation types during speech transmission
14 p2413 A69-29464

Airport noise control responsibility for airport and community planners using perceived noise level, noise and number index and community annoyance index as planning criteria
14 p2541 A69-29506

TR tubes spurious harmonic power generation investigated for intersystem interference reduction and investigation criteria, discussing effects of incident power, gas pressure and tube geometry
15 p2573 A69-30032

Ferrite frequency mixers used with heterodyne receiver, studying combination and cross noise rejection efficiency
15 p2574 A69-30129

Weak periodic signal separation from noise using single and multichannel analog adders
15 p2607 A69-30241

Jet noise causes and suppression, discussing nozzle exit area geometry
15 p2671 A69-30372

Aircraft noise environmental problem, discussing improvement through source, transmission and receiver control options
15 p2585 A69-30373

Noise sources in S band parametric amplifier with GaAs varactor diode measured at liquid nitrogen temperature, considering noise reduction
15 p2578 A69-30636

Three dimensional effects of potential minimum near cathode emitting axisymmetric beam, relating electric fields distribution to noise reduction coefficient
15 p2568 A69-30794

Slender body aerodynamics combined with wave propagation theory for sonic booms of aircraft configurations, propeller and helicopter noise, sonic boom alleviation, etc
16 p2732 A69-31867

Aircraft noise assessment, discussing computer programmed formula, noise contours and duration calculation, with appendices presenting engine noise characteristics, air and ground attenuation, etc
16 p2735 A69-32021

Unsuccessful space charge noise suppression measurements on field emission tubes, obtaining diffusion and shot noise measurements at high currents
16 p2752 A69-32384

Noise reduction in parametric electron beam amplifier by cooling two frequency resonator noise to liquid nitrogen temperature
16 p2762 A69-32511

Test rig vehicle design for noise research on single stage high bypass ratio fans for quieter turbofan powerplants
[AIAA PAPER 69-492] 16 p2767 A69-32727

Noise abatement and smoke emission reduction from aircraft engines
[AIAA PAPER 69-489] 16 p2746 A69-32764

Helicopter noise characteristics, discussing effects of noise reduction measures on design and operations
[AHS PAPER 352] 17 p2915 A69-33525

Microphonic noise measuring systems for airborne radar system design for noise reduction
17 p2937 A69-33628

Cryogenic applications to low noise reception development in radio astronomy, planetary radar and communication with deep space probes
17 p2921 A69-33685

Sonic boom theory for steady flight in atmosphere without winds, discussing sonic boom reduction by aerodynamic means
17 p2902 A69-34017

Jet and compressor noise, discussing noise suppression techniques and engineering applications
[AIAA PAPER 68-550] 17 p3022 A69-34019

Helicopter rotor vortex noise data analyzed for noise suppression, obtaining sound power equations
17 p2896 A69-34034

Airborne communication receiver solid state interference blanker circuitry comprising blank box insertable between antenna and RF input
17 p2943 A69-34132

All-weather operations, aircraft size, air traffic and noise as airport design factors, discussing financing priorities for runway construction, facilities and personnel
17 p3004 A69-34207

Aircraft noise abatement oriented toward compatibility between airports and adjacent metropolitan environs, analyzing results for theoretical and actual airports
[AIAA PAPER 69-800] 19 p3453 A69-35593

Quiet military aircraft design factors, considering human hearing characteristics, noise suppression methods, propeller noise-performance relationships and jet engine noise nature
[AIAA PAPER 69-792] 19 p3243 A69-35637

Technology trends in airbreathing propulsion, discussing noise control for subsonic jet transports, turbine blade cooling, etc
[AIAA PAPER 69-774] 19 p3244 A69-35648

Equivalent circuit demonstrating noise reduction through input transistor integration into passive receiving antenna, stressing circuit loss control and preamplification role
19 p3281 A69-35764

Finite difference scheme for primitive equation model, emphasizing two grid internal noise suppression to improve gradient force expression accuracy
19 p3364 A69-36507

Low noise microwave devices performance and price, discussing transistor and tunnel diode amplifiers, traveling wave tubes and price reductions via manufacturing methods
20 p3504 A69-36913

Photon actuated switch consisting of 10 input binary logic gate and solid state relay to reduce aerospace vehicles self generated noise
20 p3505 A69-37289

Transistorized low noise reception antennas with built-in amplifying elements, discussing radiation patterns and noise problems
21 p3683 A69-39264

Dornier Do 31 VTOL jet aircraft noise alleviation in far field, discussing shielding, interference, ground attenuation and reflection
22 p3862 A69-39932

Airport design for noise reduction, considering aircraft noise, runway orientation and flight paths
22 p3926 A69-40433

Noise reduction research for hydraulic machines, examining piston pumps noise generating mechanism
22 p3870 A69-41238

Commercial jet aircraft thrust reversers and noise suppressors developed by Rolls-Royce, discussing compatibility, reliability and applications
[SAE PAPER 690410] 23 p4200 A69-41638

Low noise nuclear precession magnetometer noise rejection optimization design specifications for measuring geomagnetic field components
23 p4165 A69-41868

Noise elimination by filtering in high power microwave transmitters, noting practical design tradeoffs
23 p4142 A69-42235

Wideband vertical electric field noise reduction in ELF/VLF atmospheric receiving systems using bucking, delayed feedback and frequency rejection units
23 p4128 A69-42504

NOISE SPECTRA

Noise resistance investigation of period synchronization systems described by Markov chains, determining phasing error for circuits
01 p0031 A69-10881

Ruby laser limiting gain, stimulated emission loss, noise loss and spectral distribution determined by radiation intensity, pumping power and mirror reflection
02 p0256 A69-12000

3.3 mm radiometer long integration time performance and output noise spectral distribution
02 p0220 A69-12433

Calibration of coaxial line noise sources in terms of rectangular waveguide standard, discussing use of adapter for comparison
02 p0210 A69-12436

Mismatched errors associated with Y factor power ratio measurement effect on microwave noise-temperature calibrations
[JPL-TR-32-1345] 02 p0211 A69-12442

Thermal noise from passive linear multiports, noting influence of temperature and absorption coefficients
02 p0211 A69-12443

Microwave measurements of AM and FM noise spectra with video frequency and RF coverage flexibility and high sensitivity
02 p0221 A69-12455

Amplitude noise spectra of X band microwave oscillators with Si avalanche diodes, noting various contributions and dependence on circuit and operating parameters
02 p0221 A69-12456

Probability density function measurement for microwave noise generator
02 p0221 A69-12459

Voltage probability density of wideband microwave noise, discussing measurement technique of dividing spectrum down by noise bandwidth
02 p0211 A69-12460

Pseudonoise generator producing controllable repetitive random signal patterns used to evaluate instrumentation system
03 p0403 A69-13188

Ariel 3 receiver for measuring galactic noise spectrum, discussing loop antenna use with swept receiver, false terrestrial signals, etc
03 p0404 A69-13581

Propagation of long electromagnetic waves in ionosphere and exosphere, discussing thunderstorm noise spectrum
03 p0396 A69-13702

Noise correlation effect on noise stability of diversity reception receiver with weighted coherent summation of signals
04 p0557 A69-14789

Equivalent noise circuit for resonant transistor amplifier, deriving expression for noise factor
05 p0729 A69-16084

Continuous and triggered audio frequency noise bands associated with ionospheric lower hybrid resonance frequency observed on OGO 2
05 p0754 A69-16257

Audio frequency noise in p channel MOST at cryogenic temperatures, noting trap contribution
06 p0979 A69-17151

Linear regression and related procedures in identifying dynamic processes
06 p0901 A69-17360

Noise characteristics of transistorized feedback amplifier stages for application in amplifier design
07 p1090 A69-18284

Magnetospheric ELF noise, discussing OGO 3 spectrum analysis
07 p1124 A69-18834

Noise generator design employing diffused Ge avalanche transit time diode
07 p1107 A69-19156

Semiconductor diode noise experimental measurements indicating fluctuation-dissipation theorem /FDT/ inapplicability to all quasi-equilibrium systems
07 p1113 A69-19596

Spectral distribution of intermodulation noise of AM and FM transmission systems calculated by probability theory
08 p1271 A69-19916

Noise properties of junction diodes and bipolar transistors as basis for low noise amplifiers design
08 p1286 A69-20839

Turbomachinery multiple pure tone noise associated with acoustic resonance of inlet cavities examined by narrow band filter tracking integer multiples of rotative speed
[ASME PAPER 69-GT-2] 09 p1572 A69-22509

Intrinsic amplitude and frequency fluctuations in transistor autooscillator, examining natural additive noise influence
09 p1469 A69-22632

Jet airliners noise characteristics, calculating spectral content and duration of perceived noise level and total noise level
09 p1435 A69-22637

Quantum phase noise in He-Ne laser, considering amplitude fluctuation, spontaneous emission and oscillator linewidth
10 p1704 A69-23669

Temperature effects on noise levels in field effect transistors, discussing Lorentz spectrum
11 p1853 A69-25391

Coaxial radiator as feed for low noise paraboloid antennas, presenting pattern synthesis
11 p1856 A69-25635

Critical review of statements concerning previous paper on noise in transistor mixers at HF
11 p1857 A69-25662

Amplitude spectra of periodic pulse sequences or pseudonoise sequences calculated using weighting and shape functions
12 p2030 A69-26389

LF generation-recombination noise in MOS transistors with depletion region impurity centers, analyzing noise resistance saturation and drain-voltage dependence
12 p2041 A69-26627

Noise resistance of period synchronization systems described by Markov chains, determining phasing error for circuits
12 p2031 A69-26645

Noise rejection and carrying capacity of wideband and narrowband discrete systems transmitting complex signals in concentrated noise spectrum
13 p2218 A69-27213

Common source and common gate FET connections showing equivalent noise figures
13 p2227 A69-27237

Noise duration and spectral complexity effect on subjective rating of disturbance level
14 p2408 A69-29152

Aircraft noise alleviation through flight procedures improvement, home building modification and noise standards legislation
14 p2392 A69-29154

Millimeter and submillimeter microwave spectrometric studies of high temperature plasmas and noise emission, discussing instrumentation and absolute measurements
14 p2451 A69-29786

Collisionless Ce and K plasmas measurements to determine steady state parameters and LF oscillations, noting noise relationship to drift instability
14 p2499 A69-29849

Potential noise stability of reception in binary communications system with active pause in channel for unknown signal arrival time
15 p2563 A69-30134

Wideband PM communication system with synchronous reception and automatic control of reception bandwidth, providing improvement in noise stability
15 p2564 A69-30147

Spectral correlation characteristics of amplitude modulated signal with background noise at envelope detector output
15 p2576 A69-30348

Vibration/acoustics digitally controlled environmental testing, describing configuration and operation of control system and statistical requirements for noise generation
15 p2587 A69-30388

Simultaneous particle flux and VLF noise spectrum measurements by rocket sounding, discussing equipment, telemetry and calibration systems and experimental data
15 p2605 A69-31423

Spectrum of clipped noise in optical spectroscopy, considering double clipping at zero photon number
15 p2571 A69-31486

Photon bunching effect in spatially coherent noise field enhanced by superposing monochromatic coherent signal and/or shaping incident noise spectra
16 p2749 A69-31694

Fluorescence noise in Q switched ruby laser atmospheric backscattering experiments, noting relation to optical radar spurious and enhanced returns
16 p2777 A69-32183

Gaussian amplitude distribution of 1/f noise by oscilloscope display and scanning with movable slit
16 p2752 A69-32383

Amplitude-frequency characteristic and noise bandwidth of electron tube reflex autodyne operating in over or under voltage mode and including IR feedback
16 p2761 A69-32477

Geomagnetic field effects on microwave noise spectrum in earth-ionosphere resonator, calculating field energy spectrum near resonance maximum, discussing excitation by lightning
17 p2918 A69-33034

Acoustic spectrum averager for Mariner spacecraft environmental tests, calculating rms average 1/3 octave spectrum bands in real time
[JPL-TR-32-1442] 17 p2946 A69-33658

Beat frequency measurements in far IR due to harmonic mixing of klystrons, discussing noise role
17 p3006 A69-33674

Earth-ionosphere waveguide excitation by lightning discharges and geomagnetic field influence on ELF noise spectrum
17 p2928 A69-33865

Spectral analyzer for structural noise spectrum of scanning ray TV transmitter
17 p2939 A69-33909

He-Ne laser light noises due to discharge current fluctuations and random mode beat
19 p3330 A69-35760

IR detector limiting noise voltage /photon noise/ due to photon arrival fluctuations at responsive element determined using Planck radiation law
19 p3309 A69-36059

Alouette satellite VLF observations data of ionosphere ion composition determined from ion whistlers and noise bands with LF cut-off
20 p3530 A69-37873

Ionospheric background noise levels and sources determined from Alouette data
20 p3495 A69-37874

ELF noise band observed by Alouette 2 receiver interpreted in terms of electrostatic proton cyclotron harmonic waves, using digital power spectrum techniques
20 p3497 A69-38079

VLF and LF emission characteristic features and origin mechanism in auroral regions of ionosphere, discussing satellite observation of noise spectrum in space
21 p3708 A69-38495

Noise influence on heart rate and oxygen consumption of young male subjects under simultaneous physical stress
21 p3654 A69-38908

Antenna noise spectrum in collisionless isotropic plasma, considering plasma fluctuation theory and reciprocity theorem
21 p3683 A69-39284

Generation-recombination noise due to trapped charge fluctuation at impurity centers in Si junction
15 p2719 A69-30374

gate field effect transistors transition regions, using lumped equivalent circuit
22 p3911 A69-40009

Quadrupole self and cross correlations of directional jet noise patterns, including frequency spectra and correlations
22 p3931 A69-40891

Nonlinearity effect on spectral shape and bandwidth in connection with frequency modulation by noise
22 p3900 A69-40923

Speech interference aspects of noise measured as function of level and spectrum of speech and noise at listener ear, using simplifying nomogram
23 p4101 A69-41495

Natural and man-made radio noise measurements, including formula for calculating signal strength of coherent interference
23 p4126 A69-42217

Digital data transition tracking loop mean square phase noise computed as function of input SNR by Fokker-Planck technique
23 p4130 A69-42514

NOISE STORMS

Solar noise storms structure and movement, discussing localization of type 1 burst emission into zones in solar corona
02 p0315 A69-11824

Structure of sources of noise storm enhancements and stationary type 4 bursts, discussing head and tail components
02 p0328 A69-12753

Solar atmosphere physical properties tabulated to interpret radio bursts and noise storms
02 p0329 A69-12786

Solar flare flux density and dynamic spectrum on 30 October 1968 at 80 MHz, showing noise storm positions and type II-III burst sources
17 p3025 A69-33807

NOISE THRESHOLD

Human auditory function during exposure to prolonged low barometric pressure unaffected with normal oxygen partial pressure
03 p0378 A69-14206

Phase locked loop discriminator in threshold region, discussing effects of loop parameters, detuning error and modulation
04 p0580 A69-15471

Phase error mean square value in phase lock loop determined from linear differential equations to determine output SNR and noise threshold
05 p0720 A69-16342

IC selection for minimum thermal effects, discussing speed, power dissipation, maximum operating frequency and noise threshold
06 p0894 A69-17219

Pure tone threshold determination based on pulse tone technique with modified audiometer
06 p0882 A69-17836

Hearing at LF, comparing noise and tone thresholds
21 p3664 A69-38986

Tradeoffs between measurement accuracy, false alarm and detection probability in practical setting of thresholds for Neyman-Pearson criterion, analyzing noise samples
22 p3902 A69-41221

Envelope detection threshold levels definition for low input SNR based on apparent modulation depth reduction
22 p3902 A69-41225

NOISE TOLERANCE

Noise and relations between environment and man, discussing sound perception, measurement and judgment of noise annoyance and harm
01 p0020 A69-10741

Impulse noise damage risk criteria, discussing maximum tolerable exposure, hazardous exposure and methods of impulse noise measurement
07 p1066 A69-19171

Interference capability of noise of different frequency bandwidths, comparing weighted sound pressure to loudness level
08 p1276 A69-20857

Noise level criteria for acceptable voice communications in office environment, noting acclimatization
11 p1830 A69-24797

Airport noise control responsibility for airport and community planners using perceived noise level, noise and number index and community annoyance index as planning criteria
14 p2541 A69-29506

Human noise tolerance laboratory and community studies, discussing proposed tone corrections for aircraft noise
15 p2719 A69-30374

Continuous and intermittent noise effects on audiovisual checking task performing subjects, considering omission errors
17 p2911 A69-34009

Jet engine noise technology evaluation, noting effects on airport neighbor
[RAES PAPER 13]
22 p3999 A69-40492

Optimum linear adaptive design of dominant-type systems with large parameter variations assuring system response within prescribed bounds by reducing internal noise sensitivity
22 p3918 A69-41011

Regression process in acetylcholine level in rats after mechanical vibrations and noise exposure
23 p4079 A69-41382

Acoustic analyzer response of man during prolonged noise effect of varying pitch and intensity
24 p4278 A69-43408

NOMENCLATURES

Differences concerning utilization of IR detectors, discussing nomenclature, fluctuations and definitions of detection, translation and readout
19 p3308 A69-35905

NOMINAL VALUES
U APPROXIMATION

NOMOGRAMS
U NOMOGRAMS
NOMOGRAPHS

Nomograph for planning circular planar aperture antenna arrays, discussing element totalling and spacing, layout geometry, sidelobe suppression and scan loss from broadside
01 p0037 A69-10017

Nomogram for nozzle thrust coefficient evaluation
03 p0365 A69-14102

Range measurement accuracy of radar automatic equipment, discussing nomograms for split-gate tracker, cyclic and pulse length errors and multipath reflections
08 p1275 A69-20228

Approximate nomography problem solution based on application of graph theory
08 p1343 A69-20663

Nomogram for aircraft rudder pedals design and construction, considering thigh and knee angles
10 p1649 A69-23377

Molten iron plane melt flow duration and mass in bimetallic castings production determined using nomogram
18 p3149 A69-35289

Solar activity effect on F 2 layer geometrical parameters, plotting prognostic maps using nomographic methods
20 p3526 A69-37663

Nomograph for rapid estimation of pressure drops across orifices in pneumatic systems using real gas data with illustration for nitrogen
20 p3467 A69-38186

Nomograms for spectral transparency of atmosphere at 2.8-5.6 microns
21 p3759 A69-39117

NONADIABATIC CONDITIONS
U ADIABATIC CONDITIONS

NONADIABATIC THEORY

Nonadiabatic reacting homogeneous system undergoing density changes, predicting chemical reaction rates and intermediate combustion products from chain reaction kinetics
[AIAA PAPER 69-87]
06 p1036 A69-18054

Nonadiabatic and stochastic mechanisms for cyclotron resonance trapping and heating in magnetic mirror geometries
08 p1364 A69-20518

Unsteady nonadiabatic shock waves in stellar gas dynamics, analyzing energy losses due to ionization at shock fronts by extended Chiznell-Wisem method
15 p2682 A69-30508

NONAXISYMMETRY
U ASYMMETRY

NONCONDUCTORS
U ELECTRICAL INSULATION

NONCONSERVATIVE FORCES

Energy transfer in circulatory force fields, noting mechanism changes for simultaneously operative original field and adjoint field energy sources
04 p0671 A69-14415

Damping effects on elastic systems stability under nonconservative forces, correlating stability and quasi-stability regions
22 p4040 A69-39981

Lepton nonconvergence implications for experiments involving solar neutrinos, showing effect on capture rate at earth for pep neutrinos
23 p4194 A69-41596

NONDESTRUCTIVE TESTS
NT PRELAUNCH TESTS
NT STATIC FIRING

Ultrasonic holography applications in nondestructive testing, describing conversion of ultrasonic field into optical field
01 p0078 A69-10132

Nondestructive testing of brazed liquid propellant rocket engine components and assemblies, describing radiographic, ultrasonic, thermographic, and leak test methods
01 p0085 A69-10534

Mass spectrometer helium leak testing of cryogenic storage vessels, noting procedures and insulation and evacuation of jacket space
02 p0252 A69-11811

X ray spectrographic camera for nondestructive spectrum analysis of small samples
03 p0427 A69-13101

Beryllium nondestructive tests, discussing eddy current inspection, ultrasonics, film radiography and scintillation
[SAE PAPER 680652]
03 p0444 A69-13546

Nondestructive measurement of thin transparent film thickness by interference method, noting diffusion profiles
03 p0430 A69-13634

High temperature eddy current crack detection technique for atomic reactor components under high thermal gradients
04 p0607 A69-14972

Nondestructive testing of quality of electroexplosive devices based on determination of heat flow between bridge wire and surroundings
04 p0607 A69-14973

HF inductive analyzer of concentrations of electrically conducting solutions and nonconducting mixtures
05 p0763 A69-15994

Nondestructive technique to measure residual and working stresses in machine parts, using specially designed circuit
06 p0926 A69-17497

Holography for display devices, nondestructive testing, quality control, high speed, microscopy, acoustic testing, sonar, data storage, etc
06 p0928 A69-17873

Nondestructive testing of welds - Conference, Chicago, January-February 1967
07 p1139 A69-18794

Ultrasonic search units in nondestructive tests, discussing piezoelectric materials and contact and immersion services
07 p1139 A69-18795

Nondestructive tests for determining braze bond quality of open face honeycomb seal rings, using low viscosity liquids with fluorescent additives
07 p1140 A69-18797

Nondestructive weld tests of propellant tanks in Saturn V-S-1C stage
07 p1140 A69-18798

Chromium steel /E1961/ susceptibility to structural damage under cyclic loads by nondestructive inspection of magnetic hysteresis and eddy current losses
07 p1141 A69-19316

Weld defects, discussing criteria for rejection, harmful and harmless defects, welding process and procedures and weld vs base metal defects
07 p1143 A69-19696

Magnetic tape recording of ultrasonic test information with oscilloscope used for playback
07 p1117 A69-19697

IR evaluation of multilayer etched circuit boards, discussing testing of circuit distributive properties and individual layers
07 p1117 A69-19698

Integrated nondestructive testing systems to ensure welded assemblies reliability for Saturn 5 program, including surface defect detection
07 p1117 A69-19699

Nondestructive testing methods for civilian transport aircraft production, overhaul and maintenance
07 p1143 A69-19702

Holography combined with laser interferometry for nondestructive testing in materials, components and assemblies
07 p1137 A69-19777

Acoustic emission from welds in stainless steel plates used for detecting defects in single and multiple pass machine welds
08 p1318 A69-19963

Nondestructive testing methods application to fiber-bonded composites, noting X ray diffraction, radiography and ultrasonics
08 p1339 A69-20498

Microwave techniques for bondline defects and thickness of reentry elastomeric heat shield material bonded to titanium alloy
09 p1499 A69-22306

IR nondestructive, in-process microweld evaluator, discussing energy correlations and tensile strength
09 p1510 A69-22347

Tumbling motion for testing gyroscopic devices quality
10 p1689 A69-22927

Pulse echo ultrasonic nondestructive testing of C-5 adhesive bonded aluminum composites with multiple bond lines
10 p1698 A69-23047

FM Lamb wave system for flaws and defects detection in thin metal sheets
10 p1699 A69-23048

Nondestructive testing methods for Saturn 5 space vehicle with emphasis on NDT equipment for Apollo program
10 p1699 A69-23050

Neutron radiography facility for production nondestructive testing inspection of aerospace components, noting collimation, neutron/gamma ray ratio optimization and neutron source
[AGN-TP-229]
10 p1699 A69-23051

Liquid crystal coatings for determining fracture initiation flaws in material structures, considering stress concentration and hysteresis heating
10 p1699 A69-23053

Radiographic, ultrasonic, thermographic and leak test quality control for brazed liquid propellant rocket engine components
10 p1699 A69-23054

Two fold congruency method for statistical evaluation of fluorescent flaw detection penetrant sensitivity and reproducibility
10 p1700 A69-23374

Holographic techniques for acoustical imaging to obtain three dimensional images of opaque objects encountered in nondestructive testing
10 p1695 A69-23544

Nondestructive thermal tests using liquid crystals thermal sensitivity for measurement of temperature changes and visualization of temperature gradients
11 p1892 A69-25293

Coherent optical flaw detection and surface microstrain measurement techniques including holographic interferometry, optical correlation and diffraction
12 p2180 A69-26305

Electrical conductivity measurements combined with indentation hardness measurements for nondestructive evaluation of commercial precipitation hardenable aluminum alloys
12 p2114 A69-26307

Tempered glass plates strength nondestructive testing by scattered light photoelastic method, discussing application to aircraft windshield sandwich structures
[AIAA PAPER 68-323]
12 p2118 A69-26768

Soviet book on quality control of materials and machine parts by ionizing radiation covering radiation hazards and protection
13 p2268 A69-27935

Radioactivity induced in solid materials for components microautoradiography and radiograph information quantitative evaluation
13 p2297 A69-28157

Electron fractography used in machine parts failure analysis to detect internal and surface cracks, forging defects, stress corrosion, fluid leakage sources, etc
13 p2269 A69-28182

Ultrasonic images detection for nondestructive testing including surface-relief technique, Pohlman cell and scanning with piezoelectric transducers
13 p2269 A69-28661

Stainless steels stress corrosion susceptibility, detecting chromium carbide in martensitic matrix by galvanic nondestructive test method
14 p2466 A69-29935

High speed picture thermography in nondestructive testing, describing IR scanning frame rate and thermal image recording
15 p2618 A69-30316

Radiology and thermography in nondestructive reliability testing of electronic equipment
15 p2610 A69-30850

Nondestructive testing - Conference, Montreal, May 1967
15 p2630 A69-31502

Controlled electric field capacitance probes for nondestructive testing, discussing field projection pattern and direction effective depth of field, applications, etc
15 p2616 A69-31503

IR techniques for nondestructive testing, discussing applications to heat injection and generation and IR test equipment capabilities

15 p2630 A69-31504

Generalized parametric form of IR radiometric scan method applied to void detection problems, designing test techniques and establishing inspection procedure

15 p2631 A69-31506

Cholesteric liquid crystal film application to test surfaces for thermal mapping, giving technique for flow pattern determination

15 p2631 A69-31507

Delta technique for ultrasonic weld inspection, noting ability to detect randomly oriented weld defects

15 p2631 A69-31508

Schlieren and photoelastic methods for continuous and pulsed ultrasonic waves propagating in transparent media, discussing nondestructive testing applications

15 p2617 A69-31510

Mechanical testing of high temperature materials subjected to thermal cycling by high power pulsed laser beam

15 p2636 A69-31512

Eddy current and ultrasonic applications to aircraft engine inspection, discussing electric and magnetic methods for quality control during fabrication

15 p2632 A69-31516

Ultrasonic probe selection and standardization for nondestructive testing, discussing instrument sensitivity and probe losses

15 p2617 A69-31517

Book on ultrasonic testing of materials covering ultrasonics application to nondestructive testing, flaw detection and quality control

16 p2790 A69-32125

Nondestructive ultrasonic, spectroscopic and TV test methods reducing time for inspection and increasing reliability of turbines

17 p2978 A69-33330

Nondestructive tests for glass filament wound composites void content, considering test methods and mechanical properties prediction role

17 p2979 A69-33656

Nondestructive testing education, current programs available and future needs

18 p3232 A69-34518

Nondestructive eddy current testing of chromium steel for early stage fatigue damage of aircraft components

18 p3136 A69-34777

Betatrans for nondestructive quality control for materials and products under special conditions

18 p3136 A69-34779

Deformation detection by stress wave analysis technique /SWAT/, noting pressure vessel applications

18 p3223 A69-35080

Integral scalar equation describing signal attenuation by acoustically soft disk for mirror-shadow method of ultrasonic flaw detection

18 p3137 A69-35109

UV excitation intensity increased for improving luminescent nondestructive testing, describing UV dosimeter and irradiation standards

18 p3138 A69-35115

Oriented glassfiber reinforced plastics elastic moduli and tensile strength along anisotropic axes determined nondestructively, considering component content and material porosity

18 p3162 A69-35359

Signature analysis diagnostic methods for reliability tests involving final product checkout and early fault detection

19 p3322 A69-35574

Radioactive Kr as gaseous penetrant for nondestructive test inspections, noting high sensitivity

19 p3322 A69-35575

Holographic interferometry for nondestructive testing of aircraft materials, discussing applications to quality control

19 p3322 A69-35576

Ultrasonic nondestructive testing technique for fatigue induced damage location and criticality in filament wound fiberglass cylinders, correlating damage to residual life

19 p3322 A69-35577

Echo amplitude measurements in ultrasonic testing to estimate flaw sizes and difficulties from artificial reflecting targets

19 p3323 A69-35578

Nondestructive testing methods for Saturn 5 space vehicle with emphasis on NDT equipment for Apollo program

19 p3431 A69-36329

Fracture mechanics application to pressure vessel design and analysis, reviewing nondestructive inspection techniques

19 p3439 A69-36438

Nondestructive test method using transducer action of flow in stress field causing plastic deformation with energy release as acoustic emission

19 p3314 A69-36634

Optical devices for nondestructive testing of large piston engine equipment

20 p3547 A69-36921

Acoustic visualization for nondestructive testing, describing image formation by lenses, reflectors, holography, Bragg diffraction and phase contrast

20 p3512 A69-38269

Acoustic emission signals for nondestructive testing and material evaluation, determining critical stress intensity factor for stress corrosion cracking

20 p3512 A69-38270

Three dimensional X ray pictures of flaws shape and location in various materials

20 p3551 A69-38311

Spectrographic analysis for ferrous and nonferrous alloys as nondestructive testing

20 p3551 A69-38313

Eddy current machine /nondestructive testing device/ for aircraft structures surface cracks detection

21 p3719 A69-38391

X ray diffraction as nondestructive technique for measuring residual surface stress

21 p3845 A69-39476

Nondestructive testing for aerospace corrosion, discussing light, penetrants, X rays, sound, ultrasounds, electrical conductivity, magnetic reaction and radiation backscatter methods

21 p3733 A69-39495

Scattered light mean intensity determination in twilight aerosol atmosphere from satellite observations, formulating boundary value problem

21 p3717 A69-39656

Reliability testing as complex element of reliability engineering noting nondestructive, destructive and selective demonstration testing, stress-time correlations, risk levels optimization, etc

22 p3952 A69-40022

Nondestructive testing techniques for flaw and defect detection, discussing radiography, ultrasonics, penetrants, thermal and magnetic methods, etc

23 p4169 A69-41529

Nondestructive testing for fatigue cracks, considering X ray, magnetic particle, penetrant, ultrasonic and eddy current inspection techniques

23 p4234 A69-42451

Scattered light methods inaccuracies for nondestructive analysis of generally stressed photoelastic models, noting modified Mini-max method

24 p4396 A69-42737

Nondestructive thermal method of measuring wall thickness and channel blockage in investment castings used in aircraft parts production

24 p4312 A69-42754

IR inspection system for detecting interstitially caused alpha segregation in Ti alloy disks

24 p4318 A69-42757

NDT techniques relation to engineering design problems with failure potential, discussing management planning and cost analysis

24 p4318 A69-42769

Nondestructive detection of titanium hydride formation in threaded joints of Ti alloy pressurization tanks by neutron radiography

24 p4320 A69-42998

NONEQUILIBRIUM CONDITIONS

Nonequilibrium carriers during semiconductor depolarization, noting microwave oscillation energy absorption in silicon and zinc sulfide crystals

01 p0138 A69-10434

Algorithms for three dimensional supersonic gas flow incident on bodies applied to calculating oxygen flow in asymmetric nozzle

01 p0060 A69-10724

Free bounded continuum processes effect in nonequilibrium gases of finite continuous opacity, noting curves of growth for finite plane parallel layer emission lines

01 p0121 A69-10959

Thermodynamics of ideal multiatomic gases in local nonequilibrium, approximating real gas system by ergodic subsystems grouped by degrees of freedom

02 p0350 A69-11552

Altitude effects on radar attenuation in nonequilibrium solid propellant afterburning rocket exhaust plumes

04 p0685 A69-14730

Oxygen index test for precise flammability ratings of plastics on numerical basis, eliminating drawbacks of ignition, end point and nonequilibrium conditions operation

04 p0621 A69-14957

Nonequilibrium statistical physics for kinetic theory of gases and statistical mechanics, noting irreversibility and entropy

05 p0793 A69-15769

Nonsteady combustion models for gases, liquid fuels and solid propellants, reviewing errors in physics and mathematics [AIAA PAPER 69-178]

06 p1037 A69-18100

Nonequilibrium electron temperature, concentration and reflection in reentry boundary layers, discussing heat transfer and ionization energy diffusion [AIAA PAPER 69-82]

06 p0915 A69-18190

Phase transformations in titanium alloys under nonequilibrium conditions

07 p1162 A69-18774

Oxygen index test for precise flammability ratings of plastics on numerical basis, eliminating drawbacks of ignition, end point and nonequilibrium conditions operation

08 p1335 A69-20114

Atomic and molecular excitation mechanisms in nonequilibrium gases up to 20000 K

08 p1354 A69-20146

High enthalpy air flow in hypersonic conical nozzle, calculating chemical and thermodynamic nonequilibrium effects with computer program

09 p1433 A69-22610

Fluctuation kinetics of electron system in nonequilibrium state arising in semiconductor in strong electric field, considering lattice and interelectron scattering

16 p2824 A69-31569

Nonequilibrium initial condition combustion effects on propellant performance for hydrazine/ chlorine pentafluoride and hydrogen/fluorine with equilibrium, kinetic and frozen nozzle flow [AIAA PAPER 69-469]

16 p2832 A69-32659

Nonequilibrium inlet conditions effect on combustor performance during H and vitiated air combustion, studying ignition delays [AIAA PAPER 69-457]

16 p2881 A69-32767

Nonlinear rarefied gas flow problems with thermal nonequilibrium solved by numerical methods, considering intermolecular collisions effect

17 p2952 A69-33325

Nonequilibrium processes behind shock wave in shock tube supersonic air and nitrogen flow, using photoelectrical shadow method

21 p3695 A69-38961

Entropy definition for nonequilibrium states, using mathematical theory of stability of motion applied to kinetic equations of irreversible processes

23 p4238 A69-41366

Nonlinear plasma physics, discussing nonequilibrium effects, wave-wave coupling, wave- particle interactions, single nonlinear wave behavior, etc

23 p4197 A69-42312

Low pressure arc discharge motion between concentric electrodes in transverse magnetic field, noting Lorentz, stationary and retrograde modes due to temperature nonequilibrium [AIAA PAPER 68-708]

24 p4359 A69-43644

NONEQUILIBRIUM DRAG

U FRICTION DRAG

NONEQUILIBRIUM FLOW

Hypersonic flow of nonequilibrium diatomic gas on and near wedge, studying shock curvature variations

01 p0005 A69-10161

Molecular velocity distribution function in nonequilibrium flows, detailing asymptotic expansions in different velocity domains for weak shock

01 p0059 A69-10330

Numerical solution of chemically reacting boundary layer equations, noting loss of accuracy due to numerical cancellations

04 p0588 A69-14737

Variational methods for nonequilibrium thermodynamic processes noting fluctuation theory introduction

04 p0551 A69-15314

Linear theory of equilibrium and nonequilibrium gas flows applied to steady two dimensional nonequilibrium flow of inviscid nonheat-conducting gas

06 p0909 A69-17327

Nonequilibrium supersonic flow calculation of detonating mixture past blunt bodies applied to flow of hydrogen-oxygen mixture past sphere

06 p0859 A69-17343

Chemical nonequilibrium, mass transfer and viscous interaction effects on spherically blunted cones at hypersonic conditions, emphasizing stagnation point [AIAA PAPER 69-168] 06 p0862 A69-18047

Experimental and numerical nonequilibrium shock layer around cones in hypersonic pure oxygen flows with simultaneous rotational, vibrational and dissociation relaxation [AIAA PAPER 69-136] 06 p0864 A69-18141

Nonequilibrium chemical reaction effect on decay in spontaneous explosion for reactive expelled gas and inert expelling gas 07 p1119 A69-18705

Laminar boundary layer on axisymmetric blunt body in dissociated air taking into account nonequilibrium homogeneous chemical reactions 07 p1050 A69-18734

Optimum profile of supersonic nozzle with nonequilibrium flow 07 p1119 A69-18737

Linearized unsteady nonequilibrium flows produced by unsteady motion of thin foil or circular cylindrical shell in compressible gas 07 p1119 A69-18738

Flow diagnostics for high enthalpy nonequilibrium gas flows in shock tubes using long pulse ionized Ar gas laser 08 p1323 A69-19879

Characteristic equation obtained by considering world line vector, basic thermodynamic variables and metric tensor as functions of Lichnerowicz class 09 p1480 A69-21614

Sonic transmission of diatomic nitrogen during nozzle flow, presenting density dependence of natural oscillation energies and temperature 10 p1632 A69-22912

Chemical species and reactions determined for propellants in calculating nonequilibrium rocket engine performance 11 p1940 A69-24905

Gas dynamics for supersonic nonequilibrium flows, discussing method for determination of nozzle contours for maximum thrust 11 p1820 A69-25475

Relaxing gas nonequilibrium flow in plane expansion, comparing partial differential equations with method of characteristics 13 p2244 A69-27322

Chemically reacting flow field and solid surfaces, formulating nonequilibrium laminar boundary layer equations for two dimensional and axisymmetric flows 13 p2377 A69-28147

Diagnostic measurements in nonequilibrium nozzle flows compared to finite rate expansion calculations, measuring pressure, temperature and density [AIAA PAPER 69-328] 13 p2200 A69-28263

Gas and polydispersed condensate parameters of nonequilibrium two phase flow in Laval nozzle, considering particle collisions and coagulation, energy exchange and momentum exchange 14 p2391 A69-29621

Optimum nonequilibrium nozzle performance for hydrogen-fluorine propellant system, considering contour, engine/nozzle weights and recombination kinetics [AIAA PAPER 69-472] 16 p2733 A69-32652

Nonequilibrium ionized gas flow past insulated wall with corners under magnetic field, discussing flow characteristics 17 p3010 A69-32865

Compressible hypersonic turbulent boundary layers solution by finite difference method, relating mixing length to velocity profile shape factor [AIAA PAPER 69-684] 17 p2955 A69-33474

Adiabatic compressible turbulent equilibrium boundary layer integral method analysis extended to study nonequilibrium laminar flows, deriving dissipation integrals, presenting numerical solutions [AIAA PAPER 69-689] 17 p2955 A69-33481

Time dependent analysis for quasi one dimensional, vibrational and chemical nonequilibrium nozzle flows approaching steady state solution by finite difference technique [AIAA PAPER 69-668] 17 p2893 A69-33491

Nonequilibrium, real gas and nose bluntness effects on hypersonic slender body flows, analyzing similitudes, free stream temperature, velocity and relaxation [AIAA PAPER 69-708] 17 p2894 A69-33501

Transport processes effect in shock wave on hypersonic flow past blunt body in neighborhood of stagnant point, noting heat transfer 18 p3086 A69-34910

Nonlinear differential equations for nonequilibrium gases with internal degrees of freedom, considering

spatially homogeneous gas and oscillatory relaxation in harmonic oscillators 18 p3122 A69-34911

Nonequilibrium behavior of shock standoff distance ahead of spheres at low supersonic Mach number 18 p3089 A69-35385

Vibrational deexcitation shocks in expanding nonequilibrium nozzle flows extended to include embedded adiabatic shock 18 p3089 A69-35386

Electrostatic probes in nonequilibrium collision dominated ionized gas flow ballistic ranges 19 p3291 A69-35716

Electron concentration in hypersonic nonequilibrium shock layer flow by two wavelength laser interferometry, noting wavelength dependence of refractivity 19 p3306 A69-35742

Nonequilibrium laminar boundary layer of dissociating air on axisymmetric body determined using concentration profiles of oxygen and nitrogen components 19 p3239 A69-36395

Relaxing polyatomic gases transport properties from Boltzmann equations obtained without knowing excitation probabilities of internal molecular degrees of freedom 19 p3300 A69-36787

Ordered sets of Massieu thermodynamic characteristic speeds for reacting gas mixtures relevant to nonequilibrium flow fields compared to Laplacian and Newtonian speeds 19 p3452 A69-36802

Radiating gas flows during hypersonic planetary reentry, discussing atmospheric composition, shock layer characteristics, nonequilibrium flows, etc 20 p3513 A69-36982

Modified model for vibration-dissociation relaxation coupling phenomena in nonequilibrium high temperature gas flow, discussing parameter U variation with kinetic temperature 20 p3514 A69-37208

Quasi-one dimensional analysis for nonequilibrium flow of dissociated diatomic gas through converging-diverging nozzle, discussing critical mass flow rate 22 p3927 A69-40583

Ionized He and Ar plasmas nonequilibrium nozzle flows, noting temperature difference between electron gas and atom-ion gas, calculating flow parameters 22 p3861 A69-41047

Dissociational nonequilibrium transonic flow near nozzle throat analyzed for diatomic gas with equilibrium vibrational energy, using perturbation method 22 p3861 A69-41177

Nonequilibrium boundary layer of dissociated diatomic gas over catalytic flat plate in hot hypersonic uniform flow 22 p3934 A69-41181

Linear small perturbation approximation for supersonic nonequilibrium flows past oscillating airfoil in two dimensional wind tunnel, noting Laplace transform solution 23 p4061 A69-42349

Viscous shock wave chemical relaxation for diatomic nonequilibrium dissociating gas flow, using Navier-Stokes and chemical kinetics equations 24 p4302 A69-43487

Charring ablator char zone nonequilibrium flow and chemical reaction kinetics as function of temperature, using thermal environment simulator 24 p4409 A69-43512

NONEQUILIBRIUM IONIZATION

Inert gas nonequilibrium MHD power generation in shock tube 02 p0196 A69-12425

Quasi-one dimensional analysis of MPD arcs with nonequilibrium ionization taking into account finite rate processes and variable area [AIAA PAPER 68-87] 02 p0291 A69-12505

Thermodynamic comparison of MHD generators using Brayton and Rankine cycles, showing Rankine cycle conversion at higher channel Mach numbers for nonequilibrium ionization 03 p0369 A69-14154

Nonequilibrium ionization rate in arc discharge, studying perturbations effect in near cathode Langmuir layer 04 p0635 A69-14763

Radiation intensity distribution from first negative and positive nitrogen system in equilibrium gas flow behind propagating shock front, discussing kinetics mechanism and electronic states 05 p0745 A69-15890

Nonequilibrium low temperature plasma theory for ionization and particle distribution based on discrete

and continuous spectra states, discussing electron distribution function 06 p0969 A69-17906

Linear approximation of ionization instability in disk channel of nonequilibrium MHD generator, calculating interatomic collisions frequency as function of temperature 06 p0871 A69-17911

MHD generators with nonequilibrium conductivity, taking into account ionization instability of plasma 06 p0871 A69-17912

Nonequilibrium electron temperature, concentration and reflection in reentry boundary layers, discussing heat transfer and ionization energy diffusion [AIAA PAPER 69-82] 06 p0915 A69-18190

Statistical theory of ionization for magnetoactive plasma with nonequilibrium concentration level and nonequilibrium energy distribution 07 p1193 A69-19142

Electrical characteristics of linear Faraday generator using binary mixture of noble gases with nonequilibrium ionization 08 p1359 A69-19880

Nonequilibrium three dimensional boundary layer over slightly yawed cone analyzed for air dissociation and ionization parameters, noting binary scaling application 09 p1430 A69-21965

Nonequilibrium ionization in central regions of low temperature plasma, describing charged particle drift by using diffusion time concept 10 p1732 A69-23440

Electrical conductivity, electron density and population temperature as functions of current density in Cs-He thermal plasma studied with nonequilibrium ionization model 10 p1732 A69-23443

Excitation and ionization relaxation of cesium seeded argon gas computed for stepwise increase of electron temperature 10 p1732 A69-23444

One dimensional analysis of stationary argon flow in linear Hall generator from continuity, momentum and energy equations, discussing electron heating and nonequilibrium ionization 10 p1736 A69-23465

Toshiba blowdown MHD test facility experiments on nonequilibrium ionization, using K seeded He for working gas 10 p1673 A69-23477

Nonequilibrium ionization effects on performance of subsonic constant area MHD generator, using closed cycle blowdown loop facility 10 p1637 A69-23481

Magnetic field induced nonequilibrium argon plasma ionization relaxation processes obtained with allowance for flow parameters change in relaxation zone 11 p1922 A69-24225

Supersonic air flow past blunt body of revolution in presence of nonequilibrium chemical reactions, ionization and molecular excitation 11 p1820 A69-25474

Kinetics of air plasma formation in wake of shock wave propagating in air, taking into account nonequilibrium ionization 12 p2062 A69-26674

Load factor role in nonequilibrium ionization process in Faraday-type generator, determining relationship with conductivity 13 p2314 A69-28361

Lower ionospheric homonuclear O combinations nonequilibrium processes by simplified balance equations, determining height distributions and ozone concentration 13 p2255 A69-28542

Electron energy distribution function and nonequilibrium ionization rate in near cathode layer of thermionic converter 14 p2404 A69-29255

Nonequilibrium multicomponent ionization calculations for stagnation merged shock layer of hypersonic blunt body by successive accelerated replacement [AIAA PAPER 69-655] 17 p2892 A69-33469

Electron energy distribution for Cs plasma in emitter region of ignited mode thermionic converter, noting nonequilibrium ionization effect 19 p3380 A69-36442

Closed cycle MHD with gaseous working fluids and steady state nonequilibrium ionization 21 p3777 A69-39479

Electron temperature profile across shock wave in weakly ionized nonequilibrium argon by numerical integration of energy conservation equation, noting three body recombination 21 p3698 A69-39791

Radiation emission and ionization in precursor and nonequilibrium region behind shock wave during approach to equilibrium in argon-like gas
22 p4006 A69-40526

Optimization of Faraday MHD generators with nonequilibrium ionization and plasma turbulence, assuming electrons at Saha equilibrium at elevated temperatures
24 p4256 A69-43682

NONEQUILIBRIUM PLASMAS

Nonequilibrium nitrogen plasma spectral line intensities calculated assuming optically thin plasma
01 p0124 A69-10960

Statistical description of nonelastic processes in nonequilibrium plasma in transverse magnetic field, using kinetic equations for distribution functions
03 p0476 A69-13412

Magnetoconductance of nonequilibrium plasmas in indium antimonides, noting anisotropy effect of electric and magnetic field orientation
03 p0486 A69-13463

Electrons relaxation caused by ionization and recombination in nonequilibrium plasma, using Kerrebrock model
03 p0477 A69-13609

Relaxation method for separation of continuous electron/ion recombination spectrum from electron spectrum in nonequilibrium gas discharge plasma
04 p0639 A69-15369

Free electron kinetic equation including inelastic electron-atom collisions derived for nonequilibrium low temperature plasma, showing interrelated electronic and atomic energy distribution
05 p0802 A69-15889

Nonequilibrium low temperature plasma theory for ionization and particle distribution based on discrete and continuous spectra states, discussing electron distribution function
06 p0969 A69-17906

Nonequilibrium of electron and gas temperatures and reaction process for force-free plasma parallel beam produced in burner by expansion of argon plasma [DVL-875]
07 p1188 A69-18277

Kinetic model describing collisions in nonequilibrium multicomponent plasma, studying pair collisions effect on stability of plasma-beam system
07 p1189 A69-18539

Two fluid approximation of one dimensional steady state flow of inviscid plasma with thermal gradients, considering ionization and recombination processes
07 p1189 A69-18691

Stationary supersonic nonequilibrium plasma source in gas vacuum expansion and nozzle flows
07 p1191 A69-18986

Statistical theory of ionization for magnetoactive plasma with nonequilibrium concentration level and nonequilibrium energy distribution
07 p1193 A69-19142

Jump conditions across MHD shock waves, reducing relations to identities applicable to nonequilibrium situations
07 p1193 A69-19242

Discharge structure and stability of nonequilibrium plasma undergoing supersonic flow through linear MHD channel
08 p1366 A69-20788

Toroidal plasma nonequilibrium in multiple confinement devices with conventional magnetically shielded supports
08 p1369 A69-20819

Electrothermal instabilities of ionization region of nonequilibrium MHD generator in presence of magnetic field
09 p1548 A69-29191

Nonequilibrium distribution functions for neutral atoms excited states in optically thin low temperature singly ionized plasma containing ions, electrons and neutrals
10 p1731 A69-23437

Two temperature plasma model applicability in analyzing nonequilibrium MHD generator
10 p1731 A69-23438

Electrical conductivity, electron energy balance, ionization equilibrium time and channel parameters in pulse discharge nonequilibrium Cs plasma containing inert gas addition
10 p1731 A69-23439

Ar-K plasma studied as possible MHD generator working fluid by investigating influence of emission and external magnetic field on nonequilibrium electrical conductivity
10 p1732 A69-23441

Electrothermal instabilities in small magnetic Reynolds number limit and ionization equilibrium at

electron temperature using quasi-linear plane wave analysis
10 p1734 A69-23456

Linear nonequilibrium MHD generator operating at Mach 2 and Hall parameter of 3 using cesium seeded helium as working fluid
10 p1636 A69-23471

Power conversion efficiency of diverging channel nonequilibrium MHD generator with small electrode losses, examining influence of channel design
10 p1637 A69-23472

MHD generator performance operating on nonequilibrium Ar plasma with K additions in presence of electric fields
10 p1637 A69-23480

Faraday type MHD energy converters in nonequilibrium conduction mode, analyzing two dimensional current and potential distributions in plane normal to magnetic field
11 p1826 A69-25397

Nonlinear algebraic equation system describing populations of excited atoms of low pressure nonequilibrium cesium plasma, determining ionization coefficient and molecular ion concentration
11 p1934 A69-25567

Radiative energy losses in nonequilibrium plasmas, considering plasma geometries and distributions of Planck's function
13 p2305 A69-27374

Laminar MGD electrode boundary layer of thermal nonequilibrium plasma from collisionless Langmuir sheath and continuum theories
13 p2310 A69-28031

Correlation functions of fluctuations in electrical characteristics of nonequilibrium electron gas during scattering, determining spectral densities and populations by kinetic equation Green function
13 p2314 A69-28445

Spectral distribution of fluctuations in stable plasma in absence of external fields, emphasizing electric field fluctuations, quasi-steady states, isotropic plasmas and thermodynamic equilibrium
14 p2490 A69-29103

Electron concentration in low temperature nonequilibrium steady state plasma, including Saha equation applicability criterion
15 p2662 A69-30975

Current distribution and Hall voltage in crossed fields discharge with split electrodes in nonequilibrium Ar and Cs plasmas
15 p2663 A69-30980

Nonequilibrium plasma boundary layer along channel insulator wall, noting different electron and heavy particle temperatures [AIAA PAPER 68-134]
16 p2821 A69-31873

Relaxation method for separation of continuous electron/ion recombination spectrum from electron spectrum in nonequilibrium gas discharge plasma
16 p2822 A69-32116

Electron heat transfer and spherical probe characteristics in moving nonequilibrium plasma analyzed at stagnation region as function of solid surface potential [AIAA PAPER 69-699]
17 p3011 A69-33475

Kinetic model describing collisions in nonequilibrium multicomponent plasma, studying pair collisions effect on stability of plasma-beam system
21 p3776 A69-38691

Differential approximation for radiant energy loss in nonequilibrium plasma generated from truncated Taylor series expansion of radiation source function
22 p3988 A69-40102

Thermal nonequilibrium state and effective collision frequency between protons and electrons in solar wind plasma, explaining abnormal dissipation
24 p4368 A69-43187

NONEQUILIBRIUM RADIATION

Visible and IR nonequilibrium radiation from dilute gases of upper atmosphere, describing laboratory, ground, aircraft and rocket observations of reactions and interactions
02 p0247 A69-12810

Nonequilibrium radiation from first negative band of molecular nitrogen ion excited by shock wave electron impact
13 p2245 A69-27380

Nonequilibrium conductivity and radiation of CdS, GaAs and PbS single crystals in waveguide cell under electron beam
13 p2318 A69-27886

Radiative instability problem of stream plasma system in kinetic regime, discussing Fung letter
14 p2502 A69-29960

NONEQUILIBRIUM GEOMETRY

U DIFFERENTIAL GEOMETRY

NONFLAMMABLE MATERIALS

Bromine containing unsaturated polyesters for fire retardancy and physical strengths, noting use in reinforced plastics for laminates, molding and corrosion
08 p1340 A69-20504

Flame resistant chlorine containing polyester resins, discussing preparation, curing characteristics, physical properties and reinforced plastics application
08 p1340 A69-20505

Fire retardant brominated epoxy systems for wet filament winding process, noting viscosity, pot life and NOL ring mechanical properties
08 p1340 A69-20506

Polyimide glass fabric laminates with nonflammable characteristics for high O concentration spacecraft environments applications
09 p1531 A69-22366

NONGRAY ATMOSPHERES

Composite heat transfer by conduction and radiation in nongray medium, outlining electronic computer program for numerical solutions
03 p0533 A69-13884

Correlations of stagnation point radiative heat transfer for earth reentry, noting use of nongray absorption coefficient models
04 p0685 A69-14736

Nongray radiation absorption coefficients reformulation employing alternative angular moment averaged absorption coefficients with emission [Planck]
04 p0686 A69-14744

Radiative heat transfer between parallel plates separated by nongray gas with picket fence absorption coefficient using integral equations
06 p1033 A69-17554

IR radiative heat transfer in nongray gases for non-black bounding surfaces, considering diatomic gases with single vibration rotation band
06 p1033 A69-17559

Diurnal thermal wave form driven by harmonically oscillating ground temperature in nongray atmosphere, calculating results for terrestrial and Martian atmospheres
07 p1126 A69-19036

Nongray radiation effects on compressible turbulent free jet mixing of nonsimilar gases, using stepwise spectral absorption coefficient and Beer law
08 p1253 A69-20844

Nongray models of atmospheres of early stars, giving Avrett-Krook method of correcting temperature distribution
11 p1954 A69-24361

Dwarf and subdwarf stars limb darkening tables for unblanketed nongray radiative model atmospheres
12 p2171 A69-27153

Nonlinear limb darkening corresponding to nongray stellar atmosphere model applied to light curve for compact eclipsing binary systems
15 p2689 A69-30563

Radiative energy transfer through nongray absorbing and emitting medium generating heat with graphical presentation of temperature distribution and flux
15 p2718 A69-31153

Nongray equilibrium radiative heat transfer in viscous radiating shock layer around blunt body entering high temperature nonisothermal carbon dioxide-nitrogen atmosphere [AIAA PAPER 69-636]
17 p3070 A69-33255

Nongray absorption and radiation cooling on smooth symmetric blunt bodies included in modified Maslen flow field method for radiation and large blowing [AIAA PAPER 69-637]
17 p2891 A69-33290

Fluxes and luminous efficiencies tabulated for main sequence and subgiant stars within reflection effect problem in eclipsing binaries and Chandrasekhar non-gray atmospheric models
20 p3600 A69-37479

Atmospheric structure, greenhouse effect and convective instability in window gray and nongray planetary atmospheres
20 p3615 A69-38257

Temperature structure of nongray planetary atmospheres, discussing scattering and absorption of solar energy by gas molecules, cloud aerosols and ground
20 p3615 A69-38258

Nongray greenhouse model of Venus atmosphere possessing IR opacity due to carbon dioxide, water and diatomic N compatible with Mariner 5 and Venera 4 results
20 p3615 A69-38259

Nongray models representing atmospheres of F and G supergiants computed and tabulated for 5400-6600 K and various surface gravities
22 p4015 A69-40152

Radiative transport in nongray cylindrical medium using total band absorptance [ASME PAPER 69-HT-38] 24 p4411 A69-43534

Stagnation region heat transfer with nongray gas subjected to external radiation using two step continuum absorption coefficient model 24 p4415 A69-43590

Quasi-isotropic semigray radiative transfer prediction using nongray model in bounded plane-parallel geometries for gas with spectrum from free-free processes 24 p4415 A69-43673

NONHOLONOMIC EQUATIONS

Nonholonomic congruences of trihedrons in metric theory of straight line complex 03 p0457 A69-13865

Equations of motion of nonholonomic mechanical systems in Poincare-Chetaev variables 05 p0793 A69-15778

Stability of steady state motions of nonholonomic mechanical systems, noting Chetaev method for construction of Liapunov functions 11 p1920 A69-25742

Nonholonomic coupling effect on mechanical system stabilization characteristics in terms of generalized coordinates 14 p2482 A69-28814

NONHOMOGENEITY

U INHOMOGENEITY

NONISOTHERMAL PROCESSES

U ISOTHERMAL PROCESSES

NONISOTROPIC PLATES

U ANISOTROPIC PLATES

NONISOTROPY

U ANISOTROPY

NONLIFTING VEHICLES

U BALLISTIC VEHICLES

NONLINEAR EQUATIONS

NT CUBIC EQUATIONS

NT DUFFING DIFFERENTIAL EQUATION

NT QUADRATIC EQUATIONS

Bounds from asymptotic behavior of solutions of nonlinear integrodifferential equation arising from nonlinear oscillators in acoustics 01 p0103 A69-10001

Incompressible fluid steady motion in curved tube investigated by Fourier series, solving coupled nonlinear equations numerically 01 p0058 A69-10142

Nonlinear circuit equations describing initial phase of exploding wire, noting solution for wire resistance variation with internal energy 01 p0117 A69-10656

Transient process in n stage nonlinear amplifiers analyzed on basis of structural circuit 01 p0047 A69-10781

Power spectrum for energy transfer region in HF turbulent plasma by nonlinear equations, with results applied to subsonic ray acceleration 01 p0145 A69-10790

Convergence theorems for perturbed Newton methods for solution of nonlinear equation systems, suggesting algorithm holding Jacobian matrix elements constant during iterations 01 p0106 A69-10988

Smoothing and prediction of satellite orbit elements by stochastic approximation method, solving nonlinear equations system 01 p0158 A69-11319

Boundedness theorem for all solutions of class of nonlinear second order differential equations 02 p0271 A69-11549

Iterative process for determining periodic solutions of nonlinear nonautonomous periodic differential equations without weak nonlinearity hypothesis applied to nonlinear synchronization 02 p0271 A69-11550

Existence of smooth solution for system of equations describing nonlinear oscillations of thin plate and shallow shell 02 p0337 A69-11654

Numerical calculations for oscillatory solutions of system of nonlinear differential equations, noting circularly polarized magnetic oscillations observed near earth bow shock front 02 p0241 A69-11729

Periodic cubic differential equation of motion solved with special reference to location of fixed points and stability of solutions 02 p0280 A69-11816

Optimal control problems for Markov chains solved by iterative method, using nonlinear finite difference equations to approximate degenerate elliptic functions 02 p0224 A69-11963

Asymptotic and approximate waves constructed for system of nonlinear partial differential equations for phases corresponding to multiple characteristics 02 p0271 A69-12034

Nonlinear boundary value problems direct generalized solutions based on linearization of Bubnov-Galerkin and Ritz method 02 p0272 A69-12136

Normal derivative of solutions to Dirichlet problem for elliptic quasi-linear equation and construction of given mean curvature hyperspace in curved space 02 p0272 A69-12221

Nonlinear integrodifferential equations of parabolic type with delayed argument, discussing boundary value problems with caloric and hereditary operators 02 p0273 A69-12249

Nonlinear first order equations solution by reduction method, using nonlinear transformation of dependent variable, noting two axis gyro drift 02 p0273 A69-12541

Method of particular solutions for use with quasi-linearization in solving nonlinear boundary value problems 02 p0273 A69-12550

Independent variables reduction in nonlinear partial differential equations, detailing group theory method 03 p0456 A69-13740

Single and double resonance in system of coupled nonlinear differential equations describing vibration phenomena in mechanical and similar systems 03 p0527 A69-13748

Integrals of nonlinear equations of evolution and solitary waves, discussing double wave solutions of Korteweg-de Vries equation 03 p0468 A69-13825

Nonlinear constitutive equations for mixture of two elastic solids linearized, assuming small displacements and subsequent temperature changes 03 p0529 A69-14063

Variational principle for solving nonlinear equations in elasticity theory, theoretical mechanics and mathematical physics 04 p0668 A69-14273

Ordinary nonlinear differential equations with linear boundary conditions, discussing formulation and proof of lemma and theorems to demonstrate existence 04 p0621 A69-14416

Book on nonlinear ordinary differential equations in transport processes, noting iterative and numerical methods for diffusion, conduction, fluid mechanics and chemical kinetics 04 p0622 A69-14599

Numerical solution of nonlinear two point boundary value problems of boundary layer type, noting shock wave formation in supersonic nozzle 04 p0544 A69-14889

Asymptotic oscillation results for solutions to first order nonlinear differential-difference equations, obtaining existence-uniqueness theorems 04 p0624 A69-14950

Averaging error of system of nonlinear differential equations with time periodic right-hand sides 04 p0624 A69-15097

Method of lines for parabolic differential equations, transforming boundary value problems into initial value problem for system of ordinary differential equations 04 p0625 A69-15132

Algorithm for simultaneous nonlinear equations solution on computer, noting quadratic convergence for convex space 04 p0565 A69-15335

Hybrid assumed mode solution of nonlinear partial differential equations/initial value problems/ in time-like independent variable 04 p0566 A69-15345

Reissner nonlinear equations for nonshallow symmetrically loaded shells of revolution 04 p0684 A69-15538

Existence and uniqueness of solution to Cauchy problem for class of second order nonlinear differential equations, applying results to mixed boundary value problem 05 p0786 A69-16061

Finite plane deformation of solid body, arbitrary deformation law and arbitrary hydrostatic stresses dependence on volume change solved by nonlinear equation 06 p1021 A69-17175

Design algorithm for adaptive control of systems using nonlinear integral equations with bounded input functions, formulating optimization as conditional minimization problem 06 p0900 A69-17351

Asymptotic solutions for nonlinear differential equations with gradually varying coefficients of great resistivity 06 p0947 A69-17392

Nonlinear equations of motion for rendezvous in circular orbits, pursuer using minimum fuel and pursued having no propulsion 06 p1014 A69-17571

Variational solutions of one dimensional nonlinear Poisson-Boltzmann boundary value problems in theory of colloids and plasmas 06 p0968 A69-17784

Nonlinear equations of motion approximate solution, determining ordnance weapons aerodynamic stability coefficients from angular motion as functions of angle of attack [AIAA PAPER 69-135] 06 p0863 A69-18120

Dirichlet problem for nonuniformly second order elliptic quasi-linear equation for case of arbitrary coefficient growth 07 p1173 A69-18500

Axisymmetric jet impingement against solid plane from tube at finite distance, using nonlinear partial differential equation in finite difference form [AICHE PAPER 31F] 08 p1302 A69-19847

Mathematical methodology for nonlinear equations of transport processes, discussing group concept and similarity, boundary value conversion to initial value, etc [AICHE PAPER 31A] 08 p1302 A69-19849

Stability theorem for nonlinear mixed integral equations in boundary value problems 08 p1343 A69-20355

Supersonic flutter of circular cylindrical heterogeneous orthotropic thin panels of finite length, obtaining nonlinear flutter equation 08 p1413 A69-20404

Simultaneous nonlinear equation solving in absence of Jacobian elements 08 p1344 A69-20832

Unsteady atmospheric motions on planetary scale using Legendre polynomials 08 p1311 A69-21158

Nonlinear control theory for constant temperature hot-wire anemometers with large velocity fluctuations, noting second harmonic generation 09 p1493 A69-21421

Nonlinear analysis of transistor networks using Kron mesh method, developing quasi-linear equations characterizing common emitter transistor 09 p1471 A69-21632

Third order nonlinear ordinary differential equation solutions oscillatory and nonoscillatory behavior for conditions on variable coefficients 09 p1533 A69-22772

Two point boundary value problems solution for parameter dependent nonlinear differential equations, noting application to hinged rod bending 10 p1718 A69-22846

Nonlinear second order elliptic difference equations in associated variational problems, considering differentiable solution of Dirichlet problem 10 p1718 A69-22879

Transient process in n stage nonlinear amplifiers analyzed on basis of structural circuit 10 p1661 A69-23110

One parameter operator imbedding to modify Newton method for solution of nonlinear equations 10 p1719 A69-23519

Comparison theorem for nonlinear real vector ordinary differential equation 10 p1720 A69-23638

Nonsymmetric periodic solutions of second order nonlinear differential equations 10 p1721 A69-23641

Existence and uniqueness of solution to Cauchy problem for class of second order nonlinear differential equations, applying results to mixed boundary value problem 10 p1721 A69-23885

Periodic solutions of strongly nonlinear differential equations for behavior of automatic control systems with delayed argument, noting autonomous and nonautonomous systems 11 p1916 A69-24765

Oscillatory properties of solutions to second order nonlinear differential equations with delayed arguments 11 p1908 A69-24767

Asymptotic series solutions for initial value problem involving nonlinear ordinary differential equation with small parameter epsilon 11 p1908 A69-24881

Solution existence of nonlinear two point boundary value problems from uniqueness

11 p1909 A69-24883

Synthesis for nonlinear second order differential equations with terms satisfying Lipschitz condition, using two person games optimal strategy

11 p1910 A69-25602

Nonstiffness of nonshallow spherical dome using asymptotic method, applying nonlinear Reissner equations to finite symmetric deformation of thin shells of revolution

11 p1996 A69-25733

Nonlinear equations solvability for elastic cylindrical shells found existing for arbitrary load and clamping conditions

12 p2177 A69-25881

Nonoscillatory solutions of second order nonlinear differential equations

12 p2120 A69-26033

Nonlinear multivariable control systems synthesis, considering synthesis expressibility in known linear formulation

12 p2048 A69-26077

Cauchy problem solution for linear/nonlinear differential equations with analytic right hand sought in form of power series

12 p2120 A69-26199

Liapunov function construction with numerical algorithm, considering systems described by dx/dt equals y and dy/dt equals $f(x,y)$

12 p2122 A69-26520

Parametric variations method for solving nonlinear algebraic and transcendental equations, determining number of solutions in complex space

12 p2123 A69-26608

Nonlinear hyperbolic partial differential equations with dissipation term for periodic solutions

12 p2124 A69-26929

Analytical expressions for nonlinear partial differential equation of heat conduction in solids, giving temperature as function of time and location

13 p2372 A69-27434

Matrix eigenvalues for nonlinear simultaneous algebraic equations, discussing computer program for numerical integration

13 p2289 A69-28227

Energy transfer by simultaneous conduction and radiation between two media in intimate contact, detailing numerical solution method for resulting coupled nonlinear integrodifferential equations

13 p2378 A69-28340

Boundary value problem for nonlinear functional differential equations, discussing matrix and general operators

14 p2470 A69-28906

Two point boundary value problem converted into Cauchy problem, deriving power series solution method and algorithms for nonlinear problems

14 p2430 A69-29362

Singularity-free global solutions to nonlinear differential equations associated with variational principles, deriving necessary condition for existence from dilatation invariance considerations

14 p2470 A69-29367

Algorithm for solving Dirichlet problem of nonlinear elliptical differential equations representing atmospheric dynamics balance equation

14 p2470 A69-29401

Polynomial and nonlinear equations of state for solids and liquids analyzed using uncommon statistical and least squares methods

14 p2486 A69-29470

Beam-plasma interactions by nonlinear Vlasov equation, describing amplification of longitudinal waves

14 p2493 A69-29692

Nonoscillatory solution to nonlinear differential equation, presenting theorem describing sufficient condition for nonoscillation

14 p2471 A69-29950

Averaging procedure for solving Cauchy problem applied to two point boundary value problem for nonlinear differential equations

15 p2644 A69-30449

Numerical solution of nonlinear Volterra integral equation by Runge-Kutta-Felberg method

15 p2644 A69-30657

Taylor expansion applied to solution of nonlinear simultaneous algebraic equations in analyses of nonlinear structural systems using finite differences or elements

15 p2711 A69-30871

Singular and sliding modes /unique extremals/ in calculus of variations for optimal control problems with nonlinear equations and linear control

16 p2764 A69-31629

Starting weight increments in aircraft designs having various structural features and dimensions

16 p2735 A69-32144

Stochastic differential game theory, discussing nonlinear partial differential equations for solution, dynamic programming validity conditions, finite difference scheme, etc

17 p2994 A69-32844

Nonlinear differential equations describing one degree of freedom systems oscillations, allowing for dry friction and internal friction in elastic element

17 p3007 A69-33913

Nonlinear differential equations of mechanical systems with restoring forces approximated by odd power displacement functions and energy dissipation approximated by displacement and velocity functions

17 p3007 A69-33914

Alternating direction iteration method for nonlinear systems of equations applied to steady state heat conduction problem with nonlinear boundary conditions

18 p3163 A69-34329

Convergence of methods of tangential parabolas and hyperbolas used in nonlinear equation solution with nondifferentiable operators

18 p3164 A69-34707

Nonlinear differential equations for nonequilibrium gases with internal degrees of freedom, considering spatially homogeneous gas and oscillatory relaxation in harmonic oscillators

18 p3122 A69-34911

Nonlinear Maxwell equations applied to non-monochromatic emission for nonlinear crystal situated in resonator, examining generation of second optical harmonic

19 p3332 A69-35869

Transverse vibration and wave solutions for nonlinear equations governing transverse motions of spinning circular membrane disks

19 p3440 A69-36637

Bending of normally loaded simply supported rectangular plates in large deflection range solved by nonlinear differential equations and minimum potential energy principle

19 p3445 A69-36828

Theorem extending results of techniques for analytical solutions of nonlinear ordinary differential equations applied to terrestrial brachistochrone problem

20 p3575 A69-37205

Optimal controls for systems governed by elliptic or parabolic nonlinear equations or inequalities for differential operator, boundary conditions or unilateral constraints

20 p3568 A69-37324

Averaging methods applied to nonlinear equations in mechanics, discussing solution convergence estimation

20 p3576 A69-37440

Particular solutions and quasi-linearization combined to solve nonlinear two point boundary value problems, illustrating method with Falkner-Skan equation

20 p3515 A69-37532

Power spectrum for energy transfer region in HF turbulent plasma by nonlinear equations, with results applied to subcosmic ray acceleration

20 p3591 A69-38008

Computer solutions for nonlinear partial differential equations governing compressible flow patterns with shocks, using Lagrange coordinates

20 p3569 A69-38212

Nonlinear partial differential equations numerical solution applied to solving Cauchy problem encountered in Goursat problem

20 p3569 A69-38293

Asymptotic method applied to nonlinear equations, determining thermal conductivity coefficient for temperature distribution in moving anisotropic media

21 p3848 A69-38642

O conductance nonlinear equation solution applied to O uptake at sea level and at altitude, noting blood transport problems

21 p3654 A69-38906

Ludwig method generalized for iterative solution of nonlinear equations systems

21 p3755 A69-39002

Near resonant and nonresonant solutions of nonlinear equation describing rotating pendulum motion under periodic disturbance

21 p3771 A69-39004

Variational problem for nonlinear functionals connected with finite plasticity, extending existence and uniqueness theorems to limit analysis

21 p3837 A69-39157

Constitutive equation for nonlinear viscoelastic materials, noting validity for short times, slow motions or small deformations

21 p3840 A69-39288

Nonlinear transport equations solution methodology covering transformations, invariants, boundary value problems, numerical methods, etc

21 p3697 A69-39729

Nonlinear shallow shell theory of stress and strain formulated via shell of revolution problem

22 p4048 A69-41198

Homogeneous equilibrium equations of nonlinear shallow shell theory, obtaining six stress function solutions for strain measures

22 p4048 A69-41199

Bogoliubov method of partial averaging for nonlinear integral equations, noting application to automatic gain control theory

23 p4181 A69-41731

Normal derivative of solutions to Dirichlet problem for elliptic quasi-linear equation and construction of given mean curvature hyperspace in curved space

23 p4182 A69-41972

Nonlinear loaded integrodifferential equation analytical and formal solutions, noting role of characteristic number relation to unity

24 p4339 A69-42595

Newton method providing continuing solutions of nonlinear differential equations through limit or bifurcation points, discussing elastic stability applications [ASME PAPER 69-APMW-14]

24 p4401 A69-43102

Numerical methods for nonlinear Volterra integral equations of second kind avoiding special starting procedures, giving convergence theorem

24 p4340 A69-43228

NONLINEAR FEEDBACK

Nonlinear negative definite feedback control systems governed by parabolic partial differential equation, deriving asymptotic stability

01 p0050 A69-10239

Absolute input-output stability of time varying nonlinear feedback system established by frequency domain test similar to Popov test

01 p0054 A69-11414

Linear equivalent gain matrix of multivariable nonlinearity evaluated with equivalent gain concept for monovariable nonlinear stochastic process

07 p1114 A69-18286

Sufficient conditions for periodic motion existence of autonomous nonlinear feedback systems derived in terms of linear system frequency response

13 p2238 A69-27923

Transistorized circuit operation with nonlinear feedback through tunnel diode analyzed by piecewise-linear approximation of I-V characteristics

15 p2573 A69-30114

Stochastic saturating systems optimal control computation, considering attitude control and tracking system design by elliptical differential equation of dynamic programming

15 p2582 A69-30601

Multiple input and output nonlinear time invariant feedback system under almost constant inputs

17 p2944 A69-33743

Frequency domain and Liapunov instability criteria for attitude control system design of large booster, noting nonlinear feedback

21 p3687 A69-39381

NONLINEAR FILTERS

Ultrashort light pulses in lasers with nonlinear absorber, evaluating random intensity peak probability created by intensity fluctuations and axial modes buildup

01 p0090 A69-10791

Book on filtering for stochastic processes with applications to guidance covering asymptotic properties, nonlinear filtering, mathematical models, etc

04 p0580 A69-14386

Linear and nonlinear filtering, discussing models for signal process, linear white noise problem, optimal estimates, colored noise and finite dimensional approximation

04 p0581 A69-14696

Phase locked automatic frequency control system with additional frequency control loop and nonlinear filter in phase control loop, analyzing dynamics

04 p0559 A69-15140

Phase lock loops design with nonlinear filtering elements in low signal to noise region, considering signal demodulation, lock range and threshold

06 p0902 A69-17398

Continuous time nonlinear dynamical system states variables estimated suboptimally from discrete noisy measurements with second order nonlinear filter, deriving dynamical equations

06 p0904 A69-17939

Optimal estimation of conditional mean of posterior probability density function in multistage nonlinear filters, using Monte Carlo techniques and Bayes theorem
10 p1667 A69-24039

Optimum nonlinear digital filter synthesis for smoothing, predicting and differentiating measured quantity having uniform probability distribution over finite number of discrete values
14 p2426 A69-29421

Parameter sensitivity analysis of discrete suboptimal filters from optimal rmse estimate of actual system performance measure
18 p3110 A69-34675

Nonlinear filter theory application to PCM bit synchronization, relating bit error rates to SNR and timing jitter
19 p3270 A69-36245

Nonlinear filter theory applied to digital telemetry binary processes, using continuous time stochastic process
19 p3274 A69-36281

Lock-on band of phase locked AFC system calculated by asymptotic method, considering frequency integrating filters with nonlinear capacitances
19 p3277 A69-36569

Ultrashort light pulses in lasers with nonlinear absorber, evaluating random intensity peak probability created by intensity fluctuations and axial modes buildup
20 p3555 A69-38009

Nonlinear filter for optimal estimation of mean, covariance and third central moments of system, noting simulation tests stability for orbital navigation [AIAA PAPER 69-852]
21 p3686 A69-39380

Quadratically nonlinear filtering systems analysis and synthesis by linear methods, discussing application to partially coherent transilluminated optical systems
24 p4350 A69-42971

NONLINEAR PROGRAMMING

Nonlinear programming for optimal circuits design, discussing search method of ACOP /Automatic Circuit Optimization Program/
01 p0035 A69-10067

Optimum control with respect to minimum fuel and power consumption involving constraints based on Kuhn-Tucker conditions and saddle point theorem
02 p0223 A69-11564

Mathematical programming in optimized truss design noting reduction of components under buckling
02 p0347 A69-12536

Nonlinear programming of optimization of parameters and control functions of dynamic systems
03 p0408 A69-12974

Optimum structural design based on linear, nonlinear and dynamic programming [SAE PAPER 680752]
03 p0525 A69-13437

Book on nonlinear programming covering models for weapon systems assignment, alkylation process optimization, chemical equilibrium, launch vehicle design, etc
04 p0621 A69-14362

Book on nonlinear programming, discussing transforming of constrained minimization problem into sequence of unconstrained minimizations of appropriate auxiliary functions
04 p0563 A69-14421

Optimization of bounded feedback gains with respect to arbitrary integral performance criterion, using nonlinear programming [ASME PAPER 68-WA/AUT-8]
05 p0738 A69-16180

Nonlinear programming computational algorithm for recursive optimal estimates of constrained states of linear system
06 p0902 A69-17403

Nonlinear computer analysis of TWT small amplitude compression and small AM to PM conversion, noting coupling and circuit breaker effects
07 p1094 A69-18422

Quadratic programming and theory of elastic perfectly plastic structures under holonomic laws, proving theorems of limit analysis
07 p1235 A69-19443

Linear electronic circuit canonical synthesis by computer, using algorithm based on linear and nonlinear programming
09 p1472 A69-21781

Nonlinear programming for calculating static and kinematic failure of one dimensional structures by extending results from linear programming
14 p2418 A69-29597

Nonlinear least squares optimization program applied to atmospheric temperature sounding, solving for

temperatures at various altitudes from simulated carbon dioxide intensity measurements
17 p2960 A69-33156

NONLINEAR SYSTEMS

Gas laser amplifier nonlinear behavior in axial magnetic fields and operating with two polarized light signals of strong or weak intensities
01 p0088 A69-10010

Conditions for nonlinear control systems observability determined for use in identification procedure and in designing control unit
01 p0049 A69-10206

Geometrical existence proof of elastically coupled nonlinear systems normal mode vibrations demonstrated by existence of extremal arcs in Riemann space
01 p0166 A69-10232

Nonlinear time dependent parameters systems, analyzing governing differential equations in terms of elliptic functions
01 p0050 A69-10237

Stochastic Lurie type systems stability using Liapunov method
01 p0050 A69-10240

Time optimal control formulated for interconnected nonlinear controlled system described by fourth order differential equations
01 p0050 A69-10354

Matrix procedures for stability of nonlinear control with nonlinearities, discussing system with three actuating elements
01 p0050 A69-10355

Partial avoidance of jump resonance in nonlinear feedback system, applying procedure to feedback amplifier circuit
01 p0051 A69-10442

Controllability of dynamic systems obtained by studying vector function increments along system trajectories
01 p0051 A69-10698

Finite difference method for boundary value problem for second order differential equation, demonstrating convergence
01 p0105 A69-10721

Variational law of control elements for automatic control systems with parameters subject to random changes
01 p0052 A69-10800

Automatic control systems correction by compensating for nonlinear statistical dynamic characteristics with aid of nonlinear devices
01 p0053 A69-10801

Multidimensional nonlinear plants adaptive control by direct integration, identifying differential equations coefficients
01 p0053 A69-10875

Nonlinear buckling analyzed by mathematical models and computational procedures using organized matrix approach to structural analysis based upon finite element
01 p0171 A69-10964

Zero memory frequency independent nonlinearities response to modulated input noting FM limiter, bandpass limiter and AC carrier control systems
01 p0034 A69-11142

Stability of weakly inhomogeneous plasmas with free energy available for nonlinear resonant three wave interactions
01 p0133 A69-11212

Moderately strong electromagnetic wave propagation in fully ionized plasma, noting nonlinear effects for frequency near plasma frequency
01 p0133 A69-11213

Landau damping in plasma, noting competing effects of nonlinearities and collisions on formation of plateau in spatially homogeneous distribution function
01 p0133 A69-11215

Garden hose instability quasi-linear stabilization employing macroscopic viewpoint, discussing fluid model
01 p0133 A69-11217

Expanded describing functions used in studying nonlinear control systems with multiplication points, considering systems with/without integral response
01 p0054 A69-11359

Absolute input-output stability of time varying nonlinear feedback system established by frequency domain test similar to Popov test
01 p0054 A69-11414

Ultraspherical potential approximation in nonlinear symmetric free oscillations applied to systems with hardening and softening cubic nonlinearities
01 p0107 A69-11418

Zener diode function generators used in analog computers for solution of complex problems involving nonlinear relationship
02 p0214 A69-11595

Frequency domain stability criterion for nonlinear feedback system consisting of nonlinear amplifier, linear dynamical system and transducer with backlash
02 p0225 A69-11968

Off-axis circle criterion for frequency domain stability of feedback systems with single monotonic nonlinearity, noting relation to Popov criterion
02 p0225 A69-11969

Nonlinear boundary value problem, discussing existence and uniqueness of solutions
02 p0272 A69-12131

Book on dynamics of linear and nonlinear systems covering mathematical methods for control system design
02 p0225 A69-12228

Critical points separating stable and unstable branches of equilibrium curve of nonlinear elastic systems, discussing flexible shallow conical shell in temperature field
02 p0341 A69-12256

Optimum critical impulse for snap-through of nonlinear dissipative dynamical system of one degree of freedom [AIAA PAPER 68-143]
02 p0346 A69-12508

Frequency of periodic solutions of autonomous nonlinear systems determined by method using Duffing approximation
02 p0348 A69-12612

Noninstantaneous, nonlocal nonlinear responses of momentum and energy flows to thermodynamic forces in single component simple fluid with memory
03 p0413 A69-12921

Statistical linearization of nonlinear memory type elements with stationary Gaussian input, applying Wiener method to one class of problems
03 p0409 A69-13005

Nonlinear optics - Conference, Novosibirsk, U.S.S.R., June 1966
03 p0435 A69-13034

Tracking conditions for observability of nonlinear controlled systems with smooth characteristics
03 p0409 A69-13069

Tracking breakdown probability during unsteady operation of nonlinear automatic control system analyzed by statistical linearization techniques and Fokker-Planck equation
03 p0409 A69-13070

Statistical linearization coefficients for arbitrary nonlinearities in automatic control systems via techniques applying characteristic functions
03 p0409 A69-13071

Stability criteria for closed rigid feedback systems with stable linear part connected in series with parametric quick response nonlinear element
03 p0410 A69-13683

Self oscillating pulse relay control system investigated by approximate method for harmonic linearization of nonlinearities, noting external effects
03 p0410 A69-13684

Single and double resonance in system of coupled nonlinear differential equations describing vibration phenomena in mechanical and similar systems
03 p0527 A69-13748

Nonlinear problems in mechanics of deformable media and qualitative analysis of properties of mathematical models of physical processes involved
03 p0467 A69-13749

Nonlinear system on-line identification in presence of noise, using stochastic methods and analog equipment
03 p0401 A69-13764

Nonlinear oscillatory systems with constant delay under random forces action, noting use of stochastic difference-differential equations
03 p0468 A69-13866

Symmetric structure stability with first and second order imperfections, analyzing discrete system with n degrees of freedom
03 p0529 A69-14062

Aperiodic hydrodynamic beam instability development and energy losses, discussing plasma oscillation enhancement and nonlinearities
03 p0480 A69-14137

Supercritical damping of nonlinear mass elastic system with damping force function dependent on fractional powers of velocity, noting impact deceleration
04 p0671 A69-14413

Motion control for nonlinear system with small initial perturbation
04 p0583 A69-15096

Stability of nonlinear time varying feedback systems, using passive operator technique
04 p0583 A69-15110

Global and nonglobal stability of continuous systems with multiplicative feedback
04 p0583 A69-15112

NONLINEAR SYSTEMS

Dynamics of single loop nonlinear sampled data systems with integrator, deriving equations of periodic motions and stability conditions by means of point transformations
04 p0583 A69-15135

Synchronization problem for quasi-harmonic oscillator with nonlinearity in form of cubic parabola, discussing existence and stability of periodic solutions
04 p0578 A69-15136

Nonlinear phase locked automatic frequency control system dynamics, noting asymptotic stability of equilibrium state in whole
04 p0559 A69-15137

Creep behavior of nonlinear rigid polyurethane foam under combined stress and applicability of multiple integral and modified superposition principle
04 p0680 A69-15155

Perturbed nonlinear systems with many degrees of freedom, analyzing resonant oscillatory and rotary motions
04 p0631 A69-15536

Field distribution and potential drop in semiconducting field emitter, noting nonlinear effects in indium trisulfide, electron mobility and multiplication factor
05 p0806 A69-15630

Natural longitudinal single frequency oscillations of system of n material points connected in series by nonlinear elastic threads and with energy dissipation
05 p0832 A69-15687

Nonlinear optics noting harmonic generation of light, optical modulation, parametric oscillators, stimulated scattering, self focusing of light and resonance phenomena
05 p0770 A69-15704

Nonlinear operation of pulse control system by means of triple modulation
05 p0736 A69-15764

Nonlinear physics - Conference, Munich, June-July 1966
05 p0792 A69-15767

Nonlinear field theories for continuum mechanics noting heat, kinematics, isotropic materials, viscometric flows, elastic bodies, thermodynamics and wave motion
05 p0792 A69-15768

Nonlinear optics, noting polarization induced by electromagnetic waves, wave propagation, light wave coupling in dispersive medium and coupled laser modes
05 p0793 A69-15771

Quantum geometrodynamics in superspace, noting dynamical evolution of geometry with no real mass energy sources
05 p0793 A69-15773

Stabilization of steady motions of nonlinear controlled systems with two purely imaginary roots, using Liapunov stability theory
05 p0794 A69-15790

Nonlinear system identification by learning model, assuming discrete on-line operation and Hammerstein form
05 p0737 A69-15805

Nonlinear steady state vibration of single degree of freedom system, obtaining relationships between non-dimensional π parameters of differential equation of motion
[ASME PAPER 68-WA/DE-7]
05 p0839 A69-16172

Identification of nonlinear control systems, determining nonlinearities in differential equation by curve fit or iteration method
[ASME PAPER 68-WA/AUT-19]
05 p0738 A69-16173

Invariant imbedding and sequential interpolating filters for nonlinear processes
[ASME PAPER 68-WA/AUT-3]
05 p0738 A69-16183

Variational principles for differential equations and initial and boundary value problems in dynamic geometrically nonlinear elasticity theory
05 p0840 A69-16202

Stress-strain state for two dimensional physically nonlinear multiply connected elastic regions, noting plate with two identical circular holes
05 p0841 A69-16203

Stability of unsteady motion of nonlinear systems during limited time interval, applying differential inequalities method to Liapunov function
05 p0794 A69-16209

Method of finding new nonlinear optical materials using anharmonic oscillator model
[IEEE PAPER F-5]
05 p0808 A69-16312

Noise sources representation in pumped nonlinear systems simplifies noise analysis and noise propagation
05 p0720 A69-16345

Discrete time positive real functions defined for analyzing system stability with memoryless feedback
05 p0739 A69-16349

Monograph on nonlinear sampled data systems covering Liapunov method, discrete systems, finite difference, flow graphs, Laplace transformations, etc
05 p0739 A69-16544

Stability analysis of nonlinear and time varying discrete feedback systems
05 p0740 A69-16600

Controllable gyrator use in nonlinear network synthesis
05 p0735 A69-16620

Random search and multiple integral based Monte Carlo method for computer solution of nonlinear aerodynamic problems
06 p0858 A69-17334

Finite amplitude longitudinal wave propagation in lattices analyzed by study of compressive wave in chain of mass points with nearest neighbor interaction
06 p1022 A69-17367

Approximate optimal control of nonlinear dynamical system with state dependent variables, using stochastic linearization of system
06 p0902 A69-17404

L super P stability conditions for nonlinear time varying feedback systems derived with transformation technique and small gain theorem
06 p0903 A69-17411

Continuous time nonlinear dynamical system states variables estimated suboptimally from discrete noisy measurements with second order nonlinear filter, deriving dynamical equations
06 p0904 A69-17939

Rearrangement inequalities for positivity of nonquadratic transformations, discussing stability of nonlinear feedback loop described by difference equations
06 p0904 A69-17943

Absolute stability of dynamic control systems with single nonlinear element function of two feedback state variables, giving sufficient conditions
06 p0905 A69-17948

Circle criterion for stability of nonlinear time varying systems, considering integrator and infinite sequence of impulses in impulse response
06 p0905 A69-17949

Linear equivalent gain matrix of multivariable nonlinearity evaluated with equivalent gain concept for monovariate nonlinear stochastic process
07 p1114 A69-18286

Root-locus curve characterization of dynamic behavior of nonlinear control system, considering effects of changes in perturbing variable or reference input
07 p1114 A69-18290

Quantum electronics trends, discussing output power, mode control, stability and lifetime of CW and Q switched lasers and parametric interactions in nonlinear optics
07 p1144 A69-18468

Stress-strain response up to ultimate failure and ultimate strength of laminated composite with nonlinear orthotropic lamina
07 p1170 A69-18710

Technique for compressive mechanical behavior of viscoplastic nonlinear composites, discussing rate dependence and one dimensional stress-strain time properties
07 p1159 A69-18721

Absolute stability of distributed control system with nonlinear elements of backlash type analyzed by distributed parameters method
07 p1115 A69-19758

Differential method with invariance principle used to analyze nonlinear invariant systems, determining physical realizability conditions
08 p1296 A69-20234

Nonlinear controller design by dynamic programming method, discussing block diagram
08 p1296 A69-20236

Nonlinearities identification in closed loop systems using harmonic balance principle for transforming measured block diagram into diagram of simple form
08 p1297 A69-20302

Time response of second order nonlinear overdamped systems calculated by Krylov-Bogoliubov method of variation of parameters
08 p1297 A69-20356

Stability analysis of model reference adaptive control system with sinusoidal inputs, using reformulation of fourth order Runge-Kutta method
08 p1297 A69-20357

Stability region of second order nonlinear autonomous system determined by numerical computational method
08 p1297 A69-20358

Transient response spectrum of nonlinear cubic spring mass system subjected to step function input, discussing viscous damping effects on peak response
08 p1413 A69-20402

Dynamic programming for nonlinear suboptimal control system with minimum Q factor, developing nonlinear functional with controller motion restraint
08 p1297 A69-20416

Nonlinear optical effects in He-Ne and ruby lasers noting laser gain, frequency splitting, frequency differences in coupled lasers and frequency band narrowing
08 p1327 A69-20768

Nonlinear behavior of two stream instability between cold electron and ion streams
08 p1367 A69-20800

Nonlinear feedback shift register circuit design by logical sequences
08 p1298 A69-20835

Differential dynamic programming algorithms of second and first order for optimal control, considering nonlinear unconstrained and constrained problems
09 p1531 A69-21415

Particular solutions in nonlinear two point boundary value problems, showing convergence for uncontrolled and controlled systems
09 p1531 A69-21416

Equations adaptable to computer for RLC circuits containing linear and nonlinear n -terminal networks derived by nodal method
09 p1472 A69-21779

Perturbation theory for analyzing nonlinear boundary value problems
09 p1540 A69-21894

Transistor large signal saturation time constant dependence on injection ratio, noting nonlinear response and saturation transistor switch storage time
09 p1464 A69-22117

Nonlinear optics, discussing materials, polarization, harmonic generation, light mixing, parametric amplification and oscillation, stimulated scattering, absorption, reflection, refractivity and self focusing
09 p1518 A69-22124

Conjugate gradient and Davidson-Fletcher-Powell methods applied to nonlinear optimization problems
09 p1474 A69-22442

Van der Pol nonlinear oscillation theory adapted to microwave reflex klystrons, explaining locked and unlocked monotonic operational modes
09 p1466 A69-22444

Ultimate state periodic analysis of nonlinear electric systems by approximation methods in calculus of variations, discussing functional concept
09 p1474 A69-22448

Solutions boundedness in autonomous nonlinear systems with single nonlinearity, using Lure type Liapunov functions to prove theorems
09 p1533 A69-22449

Nonlinear one element control system design based on correlation between responses of linear systems
09 p1475 A69-22537

Frequency domain stability criteria accuracy for application to fourth order nonlinear position control system
09 p1475 A69-22591

Nonlinear control plants model with pure delay effect identified by harmonic balance method
09 p1475 A69-22669

Stability conditions for nonlinear pulse width and pulse time modulation systems, considering pulse element properties and system continuous part frequency characteristic
09 p1476 A69-22672

Stability and dissipativity conditions for nonlinear controlled systems subjected to parametric and continuously acting disturbances
09 p1476 A69-22717

Geometrical stability criterion similar to Popov criterion for single loop time varying nonlinear control systems analysis
09 p1476 A69-22784

Nonlinear Lagrange equations and iterative solutions for studying strain state of mechanical structures on basis of very small displacements
10 p1793 A69-22888

Plasma electron beam nonlinear interaction, considering equations of motion of electron distribution function, plasma wave spectrum and mode coupling effects
10 p1729 A69-23407

- Electrothermal instabilities in small magnetic Reynolds number limit and ionization equilibrium at electron temperature using quasi-linear plane wave analysis
10 p1734 A69-23456
- Gas laser with nonlinear absorbing cell in resonator, discussing effective gain dependence on squared field amplitude, hysteresis phenomena and output power
10 p1704 A69-23625
- Differential game for determining singular fuel optimal control of plant with uncertainty in dynamic equation
10 p1667 A69-24041
- Optimal controls for differential system nonlinear in state function and linear in control function
10 p1667 A69-24057
- Response and stability of self sustained two degrees of freedom system with nonlinear damping, noting harmonic oscillations
[ASME PAPER 69-VIBR-24]
10 p1806 A69-24171
- Nonlinear large amplitude vibrations of flexible beam with pinned ends supported simply on rigid base noting frequencies, modes, waveforms and stress distribution
[ASME PAPER 69-VIBR-43]
10 p1807 A69-24181
- Parametric amplifying systems with lumped reactive nonlinear elements, emphasizing UHF systems
11 p1844 A69-24448
- Second order dynamic systems stability, analyzing nonlinear and self excited oscillations by using two differential equations
11 p1915 A69-24535
- Differential equations for effect of sinusoidal force with slowly varying frequency on dynamic behavior of nonlinear vibrator, using phase surface technique
11 p1916 A69-24760
- Random periodic forces effect on single frequency oscillations of nonlinear nonautonomous system with distributed parameters, discussing perturbed boundary value problem
11 p1916 A69-24761
- Periodic solutions of strongly nonlinear differential equations for behavior of automatic control systems with delayed argument, noting autonomous and nonautonomous systems
11 p1916 A69-24765
- Asymptotic method for single and multifrequency oscillations of quasi-linear control systems with distributed parameters and delayed time coordinate
11 p1916 A69-24766
- Random oscillations of nonlinear elastic system described by nonlinear partial differential equations
11 p1918 A69-24781
- Stress concentrations in physically nonlinear multiply connected elastic media, discussing rods, thin plates and bodies with cavities
11 p1976 A69-24783
- Existence theorems for hyperbolic genuinely nonlinear systems of conservation laws, studying Cauchy problem
11 p1909 A69-25163
- Initial conditions estimation problem for nonlinear system asymptotic stability and satisfaction of output constraints on state variables
11 p1909 A69-25290
- Nonlinear DC magnetic fields for nonhomogeneous isotropic current free regions in presence of ferromagnetic materials, discussing analytic solutions of boundary value problems
11 p1888 A69-25311
- Nonlinear bang-bang optimal control problems solution based on differential dynamic programming, noting use of Pontryagin adjoint variables
11 p1860 A69-25444
- Stability of systems with sector nonlinearities determined by converting feedback equation into positive operators equation and by introducing appropriate multiplier
11 p1860 A69-25450
- Mathematical model for initial conditions of asymptotically stable nonlinear control system to estimate region of acceptable motions
11 p1861 A69-25453
- Numerical prediction for nonlinear transient response of structures, considering geometric and material nonlinearities in systems with line elements
11 p1993 A69-25526
- Periodic solutions of quasi-linear self contained system with several degrees of freedom in case of commensurate frequencies, showing coordinates functions breakdown
11 p1920 A69-25749
- Recursive estimation of noisy nonlinear multivariable systems in white noise by Kalman, second order nonlinear and iteration filters
12 p2046 A69-26062
- Perturbation theory of nonlinear control systems with periodic coefficients and small perturbation terms, exemplifying satellite attitude control
12 p2173 A69-26067
- Nonlinear multivariable control systems synthesis, considering synthesis expressibility in known linear formulation
12 p2048 A69-26077
- Uncontrollable modes effect on transient/steady behavior and limit cycles characteristics of nonlinear multivariable control system
12 p2048 A69-26078
- Liapunov functions applied to stability analysis of nonlinear multivariable direct and indirect control systems with time lags
12 p2048 A69-26079
- Dynamic behavior of nonlinear continuous multivariable systems represented by equations derived from block diagram, stressing digital computer properties
12 p2049 A69-26081
- Book on nonlinear systems analysis and design covering parameter mapping, symmetrical, transient and forced oscillations and stability analysis
12 p2129 A69-26121
- Liapunov function construction with numerical algorithm, considering systems described by dx/dt equals y and dy/dt equals $f(x,y)$
12 p2122 A69-26520
- Approximate solution of boundary value problems for Fokker-Planck equation to determine probability of exceeding limits in nonlinear automatic control systems
12 p2054 A69-26653
- Computationally stable solution of finite element analysis of elastic-plastic response of nonlinear discrete structures loaded beyond yield load
12 p2185 A69-26819
- Shallow hyperbolic paraboloidal shell with large deflections, analyzing nonlinear behavior with numerical method based on integral equations
12 p2185 A69-26820
- Linear plate theory deficiency for large plate deflections, considering approximation of nonlinear behavior permitting changes in form without additional terms
12 p2185 A69-26822
- Soviet collection of papers on nonlinear optics, discussing lasers, electromagnetic interactions, Q switching, dynamics, etc
12 p2109 A69-26905
- Monograph on nonlinear servosystems covering nonlinearity with/without inertia, self oscillations, linearization by forced oscillations, stability theorems and Liapunov function choice
12 p2054 A69-26966
- Computer determination of symbolic state equations for nonlinear circuits using FORTRAN notation
12 p2055 A69-27097
- Nonlinear systems disturbed by random white noise analyzed by Fokker-Planck equation for probability density in state space
12 p2124 A69-27141
- Nonlinear control systems error signals convergence to steady states in frequency domain, applying step or ramp functions to single feedback system
13 p2237 A69-27188
- Nonlinear control systems analysis by successive approximations, separating dominant component in transfer function of linear part
13 p2237 A69-27252
- Natural stress concept for analysis of nonhomogeneous strains fields exhibiting geometrical nonlinearity
13 p2359 A69-27259
- Nonlinear theory for whirling of heavy string under constant axial tension, considering orbitally stable modes for eigenvalues of rotation
13 p2359 A69-27264
- Relay control systems limit cycle calculations, comparing classical differential equation, Laplace transformation and state and phase space analysis methods
13 p2238 A69-27396
- Analog simulation of nonlinear functions of single independent variable compared digital to analog representation principles
13 p2224 A69-27531
- Stationary vibration modes of systems subject to nonlinearities using finite sums of Fourier series
13 p2361 A69-27615
- Observability of phase state of nonlinear control system noting Liapunov function
13 p2238 A69-27742
- Stabilization of nonlinear control systems steady motions for two pairs of imaginary roots
13 p2298 A69-27745
- Sufficient conditions for periodic motion existence of autonomous nonlinear feedback systems derived in terms of linear system frequency response
13 p2238 A69-27923
- Trajectory terminal state error analysis using adjoint-generated sensitivities in nonlinear time-varying systems
13 p2296 A69-27940
- Asynchronous finite state sequential nonlinear controller synthesis with few flip-flops for dynamic space vehicle systems
[AIAA PAPER 67-988]
13 p2225 A69-28201
- Autonomous and nonautonomous transient processes in conservative and nonconservative nonlinear systems, deriving equations describing perturbations under loads, solving by asymptotic method
13 p2300 A69-28529
- Conditions for nonlinear control systems observability determined for use in identification procedure and in designing control unit
14 p2424 A69-28742
- Tracking conditions for observability of nonlinear controlled systems with smooth characteristics
14 p2424 A69-28751
- Tracking breakdown probability during unsteady operation of nonlinear automatic control system analyzed by statistical linearization techniques and Fokker-Planck equation
14 p2424 A69-28752
- Statistical linearization coefficients for arbitrary nonlinearities in automatic control systems via techniques applying characteristic functions
14 p2424 A69-28753
- Periodic solution to equations describing nonlinear autonomous time lag system close to Liapunov systems
14 p2482 A69-28799
- Control systems synthesis for nonlinear plants with known Liapunov functions and constraints, considering stability
14 p2424 A69-28819
- Dynamic process during rms deviation of nonlinear system from prescribed trajectory described by nonlinear differential equations
14 p2425 A69-28822
- Extremal system of adaptive circuits adjusted by random search with varying random step distribution function
14 p2425 A69-28824
- Optimization criterion for synthesizing discrete nonlinear control system subjected to random controlling and perturbing effects
14 p2425 A69-28825
- Single-sideband signal nonlinear distortion and graphical methods for calculation of oscillator tube plate current pulse components
14 p2418 A69-28828
- Root locus method for nonlinear systems analysis, determining existence, stability and parameters of periodic solutions
14 p2445 A69-28919
- Statistical linearization of strong nonlinearity in series with random-gain amplifier element, deriving formulas for statistical gain parameters
14 p2425 A69-28920
- Iterative identification method for nonlinear control systems with single element, based on criterial functional
14 p2426 A69-29306
- Vibration damping and elastic bond positioning in nonlinear systems with coincident centers of gravity and rigid damping
14 p2537 A69-29746
- Digital simulation for radio systems nonlinear elements, outlining procedures to obtain algorithms
15 p2582 A69-30111
- Air masses transformation, solving nonlinear simultaneous system of equations of motion, heat influx and turbulent energy balance
15 p2649 A69-30647
- Sufficient conditions for asymptotic stability of motion in finite and whole of nonlinear systems by Liapunov second method
15 p2652 A69-30660
- Recognition systems nonlinear discriminant function for separating linear inseparable patterns, describing orthogonal representation, correlation ratio and average variance criteria
15 p2645 A69-30806
- Taylor expansion applied to solution of nonlinear simultaneous algebraic equations in analyses of non-

linear structural systems using finite differences or elements 15 p2711 A69-30871

Nonlinear boundary value problems for isotropic plasma with known magnetic field, examining electromagnetic waves scattering at magnetic fluctuations 15 p2569 A69-30938

Steady oscillations of active nonlinear system of nonisothermal plasma and charged particle flux, noting steady ion-acoustic waves 15 p2662 A69-30947

Oscillations analysis in quasi-linear autonomous system with two degrees of freedom, using point mapping for case of resonance 15 p2653 A69-31193

Hamilton modified principle applied to nonlinear control problems including time delay, servosystem with ideal relay and liquid level control 15 p2583 A69-31304

Nonlinear discrete on-off system phase plane system analysis by motion separation method 16 p2763 A69-31628

Nonlinear nonconservative systems asymptotic stability analysis, emphasizing Zubov construction procedure for Liapunov functions 16 p2873 A69-32059

Acceleration waves propagation in nonlinear conducting thermoelastic solid, treating homogeneously deformed and undeformed media 16 p2873 A69-32060

Book on correlation theory of statistically optimal systems covering linear continuous, discrete, nearly optimal, nonlinear, decision element and adaptive systems 16 p2764 A69-32114

Stability determination for nonlinear automatic control systems, describing mathematical methods based on Liapunov functions 16 p2804 A69-32242

Nonlinear mechanical systems vibrations damping emphasizing energy dissipation 16 p2874 A69-32245

System kinetics synthesis for nonlinear multiple lumped parameter system having responses in boundary region of phase-time space 16 p2812 A69-32247

Distribution function, harmonic and statistical linearization methods applied to study forced oscillations in nonlinear oscillatory system 16 p2813 A69-32284

Almost periodical oscillations of nonlinear systems containing quasi-cyclic coordinates 16 p2813 A69-32286

Stability and dissipativity conditions for nonlinear controlled systems subjected to parametric and continuously acting disturbances 16 p2765 A69-32550

Numerical absolute stability test for nonlinear discrete systems using bilinear transformation 17 p2994 A69-32848

Modulation transfer function based on Fourier techniques, discussing nonlinear film development process 17 p3005 A69-33080

Oscillations of nonlinear dissipative mechanical system with two degrees of freedom, possessing structural damping at joints between moving masses and base 17 p3064 A69-33915

Random excitations effects on vibrating nonlinear single degree of freedom system, statistically estimating resonance mode probability 18 p3171 A69-34554

Parametric variations of nonlinear system moving in medium with nonlinear drag, using Bogoliubov-Krylov asymptotic method 18 p3171 A69-34564

Nonlinear systems of differential equations to free oscillations about equilibrium, obtaining periodic solutions 18 p3172 A69-34591

Finite element analysis of nonlinear elastoplastic material-geometric behavior problems, describing computer program and incremental stiffness matrices 18 p3219 A69-34664

Computerized analysis and design of nonlinear servomechanisms, using describing functions technique 18 p3110 A69-34672

Exponential boundedness of system motion for Lure type forced systems, using quadratic Liapunov functions 18 p3164 A69-34674

Suboptimal closed loop control of nonlinear systems subject to quadratic performance indices by invariant imbedding concepts and maximum principle 18 p3111 A69-34678

One degree of freedom systems nonlinear oscillations differential equations periodic solutions by successive approximations, obtaining proof for convergence 18 p3174 A69-35311

Human ear frequency discrimination, discussing nonlinear functional modeling systems 18 p3097 A69-35440

Two dimensional thermoelasticity problem for nonlinear media, obtaining solutions for thermal stress concentration and boundary value problems 19 p3436 A69-35848

Nonlinear free motion of conservative oscillator with one degree of freedom calculated by collocation method 19 p3438 A69-36308

Free oscillation period of nonlinear oscillators with one degree of freedom, discussing approximation method 19 p3373 A69-36310

Steady resonance operation modes of nonlinear oscillatory and rotational systems described by differential equations with deviating argument, using averaging procedure 19 p3374 A69-36469

Observation space transformed from statistical synthesis of nonlinear closed systems to multiple control system subjected to statistically assigned perturbations 19 p3287 A69-36662

First harmonic approximation method reformulated to interpret nonlinear characteristic directly, discussing oscillation stability of servosystems 19 p3287 A69-36709

Nonlinear rotational viscoelastic membranes creep rupture and failure found dependent on function of accumulated energy and power dissipation during deformation 19 p3444 A69-36806

Periodic orbits in nonlinear dynamical system constructed with iterative method based on modification of generalized Newton-Raphson technique [AAS PAPER 68-085] 20 p3595 A69-37171

Nonlinear roll-yaw attitude motion of spinning symmetric satellite in elliptical orbit near internal or external resonance [AAS PAPER 68-124] 20 p3616 A69-37178

Nonlinear viscoelastic material properties evaluation from experimental data with illustration for polymers, deriving equations from thermodynamic principles 20 p3626 A69-37719

Variational or optimal control for delayed systems, involving integrated maximum principle for problems with nonlinear functional differential systems 21 p3754 A69-38429

Existence and uniqueness of optimal feedback control proved for autonomous nonlinear differential equations, allowing any finite number of variables 21 p3685 A69-38433

Nonlinear theory of elastic membranes accounting for thickness effects, obtaining field equations and constitutive relations for various cases 21 p3832 A69-38465

Nonlinearly elastic plates with reinforced edges, deriving differential equations for boundary conditions 21 p3833 A69-38574

Taylor instability nonlinear oscillations, obtaining uniform solutions for wavenumbers near and larger than cut-off 21 p3693 A69-38703

Dynamic system absolute stability and sensitivity to parameter variations in linear part of system calculated by graphical and analytical techniques 21 p3685 A69-38729

Nonlinear computing schemes examined for necessary and sufficient conditions of stability as derived from Miklin linear operators and Frechet derivatives 21 p3678 A69-38746

Continuity of optimal control of nonlinear plant, noting search time 21 p3686 A69-38884

Spring mass nonlinear systems under constant force excitation, studying step function responses of systems with various restoring force characteristics 21 p3836 A69-38985

Sequential filter equations for nonlinear system dynamics and observational model with linear estimator, comparing difference between white and colored noise filter results [AIAA PAPER 69-840] 21 p3686 A69-39371

Nonlinear filter for optimal estimation of mean, covariance and third central moments of system, noting simulation tests stability for orbital navigation [AIAA PAPER 69-852] 21 p3686 A69-39380

Stability of nonlinear systems with state variable feedback applied to fuel valve servomechanism 21 p3687 A69-39460

Nonlinear electromagnetic wave propagation by perturbation method previously employed to treat nonlinear boundary value problems involving partial differential equations 21 p3677 A69-39465

Electromagnetic wave propagation in nonlinear media, considering evolution and decay of electromagnetic shocks 21 p3697 A69-39670

Nonlinear compensator characteristics determination for modifying compensated system output signal under various disturbances with inputs subjected to white noise 21 p3688 A69-39862

Numerical method for solution of nonlinear systems applied to damped and undamped motion with symmetrical and asymmetrical elasticity under harmonic excitation 22 p4040 A69-39937

Nonlinear system oscillations analysis based on small parameter method and difference equations, including resonant case and stability criterion for periodic solutions 22 p3980 A69-40108

Ionization wavefronts nonlinear analysis including energy effects and ionization wave structure, discussing Joule heating due to transverse electric field 22 p3990 A69-40758

Stability boundaries of discrete circuits employing delay lines with forward and feedback links, deriving equations 22 p3918 A69-40957

Second harmonic influence on traveling wave amplifier operation employing distributed nonlinear active medium 22 p3916 A69-40963

Pairs existence of symmetrical equilibrium forms in nonlinear shallow shell under load made applicable to nonshallow shells equilibrium 22 p4047 A69-41062

Spatiotemporal patterns learning among sensory and motor organs with linearly ordered components by nonlinear networks in terms of embedding fields theory 22 p3887 A69-41196

Dynamic characteristics of nonlinear discrete systems by motion division method, using discontinuous Liapunov function for stability criteria 23 p4144 A69-41956

Nonlinear formulation for rigid jointed space frame comprised of prismatic linear elastic members, using Newton-Raphson and successive substitution methods 23 p4232 A69-42142

Absolute invariance of perturbations affecting dynamic plant achievable by inertial measurement of highest derivatives 23 p4145 A69-42369

Absolute invariance conditions for closed isolated subsystem of nonlinear differential equations of Cauchy normal form 23 p4183 A69-42372

Plasma resonances driven into nonlinear regime, using models of cold plasma driven by wave source and unmagnetized Vlasov plasma by two grid source 23 p4197 A69-42418

Sufficient conditions derived for absolute stability of dynamic systems containing nonlinear functions of several state variables 23 p4145 A69-42445

Recursive estimation of noisy nonlinear multivariable systems in white noise by Kalman, second order nonlinear and iteration filters 23 p4146 A69-42447

All-electric nonlinear actuator steering advanced tactical missiles, noting 99.29 percent delivered unit reliability during mass production 23 p4225 A69-42458

Motion equations of quasi-linear nonautonomous systems with many degrees of freedom, obtaining periodic solutions by asymptotic integration 23 p4183 A69-42477

Pattern classification and iterative methods of linear/nonlinear dynamic plants identification, introducing phi machine as universal plants model 24 p4284 A69-42672

Optimum control synthesis for nonlinear plant subject to white noise perturbation, using integral estimates of phase coordinate functions 24 p4289 A69-42949

Empirical determination of equivalent frequency characteristics of nonlinear system in random noise, assessing measurement errors
24 p4289 A69-42950

Time optimal control of soft spring showing switching locus changes
24 p4289 A69-42955

Digital analysis of nonlinear control systems dynamic stability under small perturbations, using linearized differential equations
[IS-ERI-71] 24 p4285 A69-42984

Separation theorem for arbitrary nonlinear measurements to find optimal stochastic control without dynamic programming
24 p4291 A69-43269

Multidimensional approximation algorithm for parameter optimization of nonlinear stochastic systems, detailing application to space vehicle attitude controller
24 p4291 A69-43275

NONLINEARITY

Stress concentration near arbitrary hole, assuming small deformations and physical nonlinearities
04 p0667 A69-14268

Book on nonlinear boundary value problems for ordinary second order differential equations, illustrating difference between linear and nonlinear problems concerning existence and uniqueness
04 p0622 A69-14600

Articles on automatic control systems stability, discussing relation between method of Lure and Popov criteria
05 p0740 A69-16667

Energy losses of clusters of charged particles moving through unbounded isotropic plasma manifesting nonlinearity in interaction of particle generated fields
07 p1189 A69-18528

Differentiating network with nonlinear resistance and capacitance elements, noting improvement in pulse shaping properties
08 p1295 A69-19910

Elastic potential for obtaining localized strain theory, describing deformation characteristics of compressible and incompressible orthotropic materials with physical nonlinearity
08 p1412 A69-20328

Convergence extensions in quasi-linearization for optimal control, showing results for brachistochrone and reentry trajectory problems
09 p1590 A69-21414

Singular surface theory combined with ray theory for propagation of weak discontinuities in nonlinear anisotropic media applied to MGD
09 p1547 A69-21613

Nonlinear A/x/ operators in reflexive Banach space Y characterized by weak closure of values, defining solvability conditions for equations having such operator
10 p1720 A69-23563

Long and short duration pulses interactions with nonlinear dielectric, calculating frequency variations and spectral transformations
10 p1658 A69-23953

Two photon and resonance parametric lasers nonlinear polarization theory, deriving equations for electromagnetic field oscillations
12 p2110 A69-26910

Nonlinear distortions in TWT for communication satellites applications, discussing relationship with efficiency
13 p2232 A69-28060

Nonlinear effects and turbulent behavior in beam plasma instability, studying interactions in magnetic field
15 p2660 A69-30917

Physical mechanisms for nonlinearities in electromagnetic wave propagation, analyzing plane wave instability, self focused beams propagation and laser oscillations
17 p2928 A69-33867

Book on nonlinear plasma theory covering nonlinear wave, wave-particle and wave-particle nonlinear interactions and weak plasma turbulence
18 p3180 A69-34930

Fourth rank tensors analysis describing nonlinear optical effects for 32 classes of crystalline substances
19 p3334 A69-35882

Telemetry transmitter-receiver RF links quality determination, emphasizing nonlinear effects measurement by notch noise tests
19 p3270 A69-36239

Heat conduction in medium with phase transitions, solving one dimensional nonlinear problem by calculation of isotherms and reduction to Cauchy problem
19 p3453 A69-36838

Signal amplitude no memory nonlinearity effect on performance of synthetic aperture terrain imaging radar systems and simulation of CRT film systems
20 p3490 A69-37643

Nonlinear optics, properties, light waves interaction, forced scattering and application in laser technology
20 p3555 A69-38014

Nonlinearity effect on spectral shape and bandwidth in connection with frequency modulation by noise
22 p3900 A69-40923

Hologram film nonlinearity effect on reconstructed image, discussing role of illumination type
23 p4165 A69-41636

NONNEWTONIAN FLOW

Elastoviscous flow in curved channels, analyzing nonNewtonian effects for case of circular and elliptic walls
02 p0234 A69-12608

Slow nonNewtonian flow in separation zone analyzed using finite difference scheme
04 p0587 A69-14594

Flow and heat transfer on nonNewtonian fluid about disk rotating with time dependent velocity, using Runge-Kutta-Gill technique for numerical integration
05 p0745 A69-15793

NonNewtonian effects in axisymmetric rotational flows of elastico-viscous liquids
07 p1180 A69-18815

Viscous incompressible nonNewtonian fluids flow with treatment for steady rotational problems and oscillatory motion, considering primary and secondary motions
20 p3519 A69-38319

NONNEWTONIAN FLUIDS

Heat transfer, suction and injection in plane Couette flow analyzed for Rivlin-Ericksen fluid, using perturbation method
04 p0589 A69-14970

Laminar flow of nonNewtonian fluids described via rheological three parameter model
05 p0744 A69-15678

NonNewtonian hydrodynamics equations for nonlinearly viscous and viscoelastic media, analyzing dependence on rheological model
05 p0745 A69-15786

Flow and heat transfer on nonNewtonian fluid about disk rotating with time dependent velocity, using Runge-Kutta-Gill technique for numerical integration
05 p0745 A69-15793

Turbulent flow of viscous nonNewtonian fluids in smooth pipes, noting effects of viscous stresses
09 p1481 A69-21929

Hydromagnetic laminar natural convection flow and heat transfer of nonNewtonian fluid between parallel electrically conducting walls
10 p1728 A69-23237

Differential equation for laminar flow of nonNewtonian fluid in annulus with porous walls of nonuniform permeability, considering inelastic and suction Reynolds numbers
10 p1680 A69-23690

Nonnewtonian solid propellant viscosity and pseudoplasticity utilizing rheological characterization for optimal casting and pot life determination
[AIAA PAPER 69-518] 16 p2833 A69-32665

Transformation of two dimensional boundary value equations for laminar power law nonNewtonian fluid flow to yield similar solutions
17 p2957 A69-34016

NonNewtonian power law fluids flow behavior in circular pipe entry region, taking into account energy loss due to viscous dissipation in boundary layer
19 p3240 A69-36472

Quasi-linear ordinary differential equations solutions for steady two dimensional stagnation point flows of nonNewtonian power law fluids
21 p3697 A69-39674

Linear stability criteria for two dimensional wave perturbations effects on nonNewtonian fluid flow between parallel plates
22 p3933 A69-41108

NONOHMIC EFFECT

Nonohmic microwave conductivity in semiconductor posts in rectangular waveguide, measuring incident, transmitted and reflected microwave powers
08 p1373 A69-20859

NONOSCILLATORY ACTION

Nonoscillatory solutions of second order nonlinear differential equations
12 p2120 A69-26033

NONPARAMETRIC STATISTICS

Nonparametric ranking procedures /based on order statistics/ guaranteeing preassigned probability for selection from random samples populations as good as control
08 p1342 A69-20172

NONPOLAR GASES

Collisionally induced microwave absorption by nonpolar gases, discussing dimer absorption
06 p0962 A69-17816

Nonpolar gases solubilities in aqueous KOH solutions in temperature range 25 to 100 C, noting activity coefficients, salting out coefficients and heats of solution
10 p1651 A69-22937

Viscosity, thermal conductivity and diffusion predicted for dilute nonpolar, polar and mixed gases, discussing methods for rotational relaxation collision numbers and resonant correction
21 p3850 A69-38951

NONREFLECTION

U ENERGY ABSORPTION

NONRELATIVISTIC MECHANICS

Isotropic Newtonian cosmological models symmetry shown to have velocity distribution obtainable from solution of Vlasov equation
08 p1386 A69-20073

Radiation spectrum in nonrelativistic fully ionized gas in thermal equilibrium, obtaining dispersion relation for transverse electromagnetic waves and dielectric constant
08 p1357 A69-20748

Ground state energy inequalities for N particle nonrelativistic quantum mechanical system, showing non-saturating gravitational forces and increasing binding energy per particle
17 p3028 A69-32900

Newtonian and general relativistic orbits of point mass in inverse square law force field, noting radar determination of spacecraft orbits
[AAS PAPER 68-098] 20 p3595 A69-37176

Hydromagnetic waves equations of motion for nonrelativistic case, discussing particle and fluid flow models
20 p3616 A69-38317

NONRESONANCE

Continuous nonresonant visible radiation from Ar ion laser by utilization of wide bore, wall stabilized gas discharges, noting long time frequency stability
01 p0091 A69-10815

Nonresonance parametric phenomena in distributed systems, discussing interaction between signal and parameter wave at supertlight velocity
17 p2928 A69-33868

NONRIGIDITY

U FLEXIBILITY

NONSTABILIZED OSCILLATION

Saturn 5 unstable longitudinal oscillation due to coupling of structure and LOX line frequencies solved by helium injection
11 p1967 A69-25497

Thermally induced oscillatory instabilities in spacecraft booms, rederiving thermal torque equation to predict finite twist response
11 p1994 A69-25531

Unsteady oscillations after rupture in thin homogeneous isotropic elastic plate, assuming deflection amplitude smaller than thickness
16 p2873 A69-32033

Natural oscillations frequency spectrum of turbomachine impeller blades subjected to random variations determined with frequency distribution function obtained by moments method
19 p3436 A69-35844

NONUNIFORM FLOW

Flow nonuniformity measured in shock tubes by determining heat transfer rate to fine wire probes
01 p0062 A69-11219

Oblique shock wave propagation through two dimensional steady nonuniform incoming flow, discussing higher order theory via irrotational or rotational disturbances of arbitrary amplitude
[AIAA PAPER 69-39] 06 p0913 A69-18103

Expansion tube modification incorporating nozzle plate at secondary diaphragm for reducing flow nonuniformity and contamination
[AIAA PAPER 68-371] 09 p1477 A69-21960

Nonuniform propagation of imploding shock waves by extending self similar solution to earlier times in implosion process when shock strength is finite
10 p1678 A69-22931

Imaging for flowfield of nonuniform parallel streams with thin airfoil represented by vorticity distribution, noting change of lift and moment
12 p2012 A69-26775

Nonuniform gas flow past axisymmetric body from supersonic source simulating jet discharging into vacuum, using power series of stream function
19 p3238 A69-35851

Nonuniform supersonic flow of ideal inviscid gas impinging on plane obstacle, discussing flowfields and shock wave production in impact
19 p3239 A69-36397

Interaction effects between mixing and pressure distribution of heterogeneous flow in channel, deriving criteria for predicting pressure variation sign
19 p3300 A69-36785

Incompressible fluid flow inhomogeneities effect on oscillations of airfoils cascade, noting occurrence of parametric resonance in turbine engine blades
24 p4245 A69-43479

NONUNIFORM MAGNETIC FIELDS

Penning discharge in inhomogeneous magnetic mirror field, observing high burning voltage at low current in rarefied hydrogen plasma
01 p0133 A69-11218

Quasi-neutral, steady, inviscid and nonheat conducting flow of conducting gas with high magnetic Reynolds number in plane channel with transverse magnetic field
04 p0636 A69-14984

Deceleration of conducting plasmoids moving in channels in nonuniform magnetic field
05 p0801 A69-15781

Ion cyclotron resonance acceleration and higher harmonic acceleration in axially nonuniformly magnetized plasma under influence of RF electric field
08 p1360 A69-20079

Magnetic field decay modes due to nonuniform rotation having angular velocity as increasing function of distance from axis in infinite circular conducting fluid cylinder
08 p1369 A69-20999

Plasma instability in inhomogeneous magnetic field noting wavefront structure role
09 p1546 A69-21571

Interplanetary magnetic fields characteristics and magnetic inhomogeneities spectra from cosmic ray variation studies used to obtain scattering mean free path
10 p1757 A69-22824

Microwave magnetoelastic wave propagation in ferromagnet subjected to pulsed magnetic field using coupled mode approach
10 p1746 A69-23655

Nonuniformity of magnetic field effect on steady flow of incompressible inviscid electrically conducting fluid in duct, considering Reynolds and Alfvén numbers [JPL-TR-32-1376]
11 p1923 A69-24291

Dense plasma flow across transverse inhomogeneous magnetic field, proving adiabatic nature of motion
12 p2137 A69-26528

Hydromagnetic waves propagation in finitely conducting fluid mass immersed in nonuniform magnetic field, using curvilinear coordinates based on lines of force
14 p2491 A69-29336

Magnetic mirrors, Doppler and relativistic effects, wave attenuation and radiation pressure during gyroresonant particle acceleration in nonuniform magnetostatic and HF fields
14 p2499 A69-29845

Deceleration of conducting plasmoids moving in channels in nonuniform magnetic field
18 p3181 A69-35033

Conducting gas flow parameters in coaxial duct, considering magnetic nonuniformity, Hall currents and fields distortion near electrodes
19 p3381 A69-36772

NONUNIFORM PLASMAS

Alfvén and magnetoacoustic waves propagation in inhomogeneous stable plasma situated in field with helical lines of forces
01 p0130 A69-10742

Anisotropic two component plasma relaxation taking into account dynamic shielding collective effects
01 p0134 A69-11419

Heating of nonuniform plasma cylinder in constant magnetic field by magnetic pumping with oscillating magnetic field, determining energy absorption
02 p0288 A69-12167

Diffusion across magnetic field of unstable plasma with highly inhomogeneous density
03 p0478 A69-13840

Microwave Fabry-Perot resonator for anisotropic plasma diagnostics in presence of static magnetic field
04 p0635 A69-14757

HF interaction of relativistic electron beam and plasma extended to include arbitrary variation of plasma density
04 p0637 A69-15046

Flow characteristics and sound velocity in two temperature plasma
05 p0802 A69-15796

Alfvén waves observed propagating along lines of force in inhomogeneous plasma in presence of homogeneous gravitational field
05 p0805 A69-16706

Spatial and temporal characteristics of two component electron-ion nonisothermal plasma and penetration of external LF electric field into plasma
05 p0806 A69-16745

Moment equations of Vlasov plasma used for pressure effects on gravitational flute instability of nonuniform plasma
06 p0965 A69-17515

Electrostatic waves in inhomogeneous plasma in finite magnetic field, noting dispersion relation for cold plasma and stabilization of instability
06 p0967 A69-17761

Kinetic description of inhomogeneous plasma in ring approximation, discussing Vlasov equation and velocity distribution function
07 p1193 A69-19034

Cylindrical and spherical waves propagation in weakly inhomogeneous plasma treated by geometrical optics, noting caustic surfaces
07 p1195 A69-19747

Inhomogeneous collision plasma drift instabilities in strong magnetic field analyzed by solving nonlinear equations
08 p1365 A69-20549

Wave behavior in warm inhomogeneous plasma with magnetic field perpendicular to density gradients of unperturbed plasma, solving Maxwell-Vlasov equations by perturbation methods
08 p1365 A69-20744

Symmetric Alfvén waves propagation in hydrogen plasma with nonuniform density distribution, deriving dispersion relations for fully ionized plasma
08 p1367 A69-20794

Alfvén oscillations in inhomogeneous decaying plasma from pulsed discharge with oscillating electrons
09 p1550 A69-22020

Boltzmann plots derived from spatially integrated spectral line intensities emitted from nonuniform gaseous plasmas, discussing Boltzmann temperature
09 p1552 A69-22251

Unstabilizing effect of inhomogeneities on magnetoacoustic waves in slightly ionized gases with current perpendicular to magnetic field
10 p1734 A69-23459

Pulse and CW breakdown criteria for plasmas subject to spatially nonuniform electric fields, using variational formulation
10 p1739 A69-23650

Radiative transfer equation in nonuniform magnetoactive medium derived from continuity equation for radiative energy density in space of coordinates and wave vectors
10 p1742 A69-24143

Nonlinear confining and deconfining forces of laser light interaction with inhomogeneous plasma, analyzing macroscopic motion based on ponderomotive force description
11 p1923 A69-24297

Electric field fluctuations in inhomogeneous plasma calculated by test particle method, interpreting results in convective modes terms in plasma control and stability
11 p1924 A69-24301

Normal mode dispersion at upper hybrid frequency propagating parallel to uniform magnetic field in spatially inhomogeneous plasma
11 p1924 A69-24302

Computer calculated phase velocities for surface wave and waveguide modes given for circular waveguide filled with inhomogeneous electron plasma
11 p1844 A69-24437

Plasma microwave diagnostics by multifrequency probes in geometric optics approximation, assuming inhomogeneous and semiinfinite plasmas with sharp boundaries and nonunity permittivities
11 p1926 A69-24602

Transient signal propagation through cold inhomogeneous plasma with electron density decreasing exponentially in direction of propagation
11 p1836 A69-24990

Normal mode representation of HF properties of inhomogeneous plasma, analyzing Vlasov equation for free oscillations under external driving field
11 p1929 A69-25269

Asymptotic solution for Fokker-Planck equation at low collision frequency, studying electron-ion collisions effect on universal instability in inhomogeneous plasma
11 p1930 A69-25358

HF electrostatic waves propagation in nonuniform plasma in uniform magnetic field, obtaining solutions of dispersion relation
11 p1931 A69-25360

HF electrostatic waves propagation excited by electron beam in hot inhomogeneous plasma in magnetic field, studying wave transformation and absorption
11 p1931 A69-25364

Current carrying inhomogeneous dense plasma instabilities confined in magnetic field, deriving dispersion relations in geometric optics approximation
11 p1932 A69-25537

Flute oscillation instability of dense plasma cylinder under nonuniform electric field, analyzing oscillation spectrum properties
11 p1934 A69-25707

Electron motion effects along magnetic field lines on axisymmetric torsional hydromagnetic oscillations in inhomogeneous low beta plasma, discussing resonance trapping
12 p2076 A69-27107

Multifrequency interferometer for inhomogeneous plasma density soundings
14 p2497 A69-29795

Longitudinal inhomogeneities in plasma of Q machines caused by ion emission from hot plate at different radial positions
14 p2502 A69-29959

LF electrostatic oscillations of inhomogeneous solid state plasma with small number of current carriers in parallel external electric and magnetic fields
15 p2665 A69-30042

Drift wave instability due to particle number density gradient of plasmopause, considering velocity shear modification
15 p2595 A69-30096

Wave regeneration by resonant particles interaction in inhomogeneous plasma of electrons confined in quadratic potential solved in WKB approximation
15 p2660 A69-30918

Energy absorption by cold nonuniform plasma from externally driven electric field, noting relation between plasma and driving frequencies
15 p2661 A69-30922

Nonlinear wave scattering at plasma particles and weak plasma inhomogeneity effects on plasma current instability
15 p2662 A69-30965

Covariant dispersion relations for relativistic plasma oscillations for many component plasma in external magnetic field
16 p2816 A69-31633

Propagation and linear transformation of HF electrostatic waves in hot magnetoactive radially inhomogeneous plasma, noting wavelength shortening
16 p2816 A69-31638

Temperature gradients effect on ion flute mode in low beta plasma having density gradients in x direction, obtaining instability condition
16 p2819 A69-31689

Polarization characteristics of electromagnetic waves obliquely reflected from inhomogeneous isotropic plane stratified plasma
16 p2752 A69-32391

Nonlinear interaction of plane electromagnetic wave with inhomogeneous plasma layer, noting concentration and electric field discontinuity
17 p2922 A69-33693

Ray methods application to partial differential equations for electromagnetic wave propagation in ionosphere, discussing strongly and weakly anisotropic inhomogeneous plasma
17 p2925 A69-33840

Inhomogeneities time buildup in lower ionosphere weakly ionized plasma during charged particle concentration perturbations and source temperature variations
20 p3525 A69-37658

Radioastronomical investigations of inhomogeneous near solar plasma structure
20 p3606 A69-38017

Distortion of electromagnetic pulse propagating through inhomogeneous plasma medium with linear electron density variation
20 p3496 A69-38030

Nonlinear oscillations of inhomogeneous cold plasma in hybrid resonance region
21 p3672 A69-38588

Thermal effects of resonant coupling hydromagnetic oscillations in inhomogeneous finite-beta plasmas, obtaining equations for coupling modes between Alfvén and magnetosonic waves
21 p3776 A69-38710

NONUNIFORMITY
Orthonormal aspect on vibration modes for nonuniform beams, evaluating normalization for end conditions by using Rayleigh technique
14 p2534 A69-29319

NONVISCIOUS FLOW
U TURBULENT FLOW

NORADRENALINE
Sympathetic nerve liberated noradrenaline increasing melatonin synthesis, using C 14 tracer for monitoring
22 p3871 A69-40051

Noradrenalin release from hearts of open chest dogs given artificial respiration upon occlusion of left descending coronary artery
23 p4092 A69-42053

Spontaneous rhythmic activity and mean vascular tone dependence in isolated helical rat aorta strips on extracellular concentration of noradrenalin
23 p4093 A69-42069

NOREPINEPHRINE
Pharmacological tools in autonomic nervous system research, discussing norepinephrine biosynthesis, storage, release and inactivation in mammals
02 p2000 A69-12722

Brain norepinephrine effect on daily rhythmic changes in activity of tyrosine transaminase in livers of starved adrenalectomized rats
05 p0707 A69-15582

Sympathetic neurohormones measurement in plasma of race car drivers
07 p1067 A69-19424

Norepinephrine, dinitrophenol and dicumaryl effect on brown adipose tissue of cold exposed rats
19 p3258 A69-36294

C 14-tryptophan incorporation into C 14-protein in cultured rat pineals, noting norepinephrine stimulation
22 p3871 A69-40054

Olfactory bulb removal effects on uptake decline of telencephalic norepinephrine, noting use for mapping adrenergic pathways
22 p3871 A69-40055

Pituitary-adrenocortical axis of rats in oxygen atmosphere at low pressure, finding depressed norepinephrine excretion
23 p4087 A69-41790

NORMAL DENSITY FUNCTIONS
Gaussian type microfield formation in plasma by placing constraints on plasma particles displacements
02 p0285 A69-11568

Gaussian summation for ion implantation profile control in semiconductors, describing computer program selecting optimum energies to fit predetermined profiles
11 p1857 A69-24546

Gaussian particle size distribution with porosity and surface irregularity corrections used to determine mean particle size of lunar surface material at Surveyor sites
12 p2158 A69-26371

Energy detection of random processes in colored Gaussian noise, discussing filtering, threshold detection, false alarm, probability distribution and density
13 p2220 A69-27937

Algorithm for calculating recognition error by applying pattern vectors having two multivariate Gaussian distribution to optimum Bayes classifier
15 p2572 A69-31113

Electronic component life test sampling plans based on lognormal distribution and instantaneous failure rate or hazard rate criterion
15 p2630 A69-31137

Double diffused transistor with Gaussian impurity distribution analyzed by power series for carrier density distribution and frequency response
16 p2758 A69-31616

Gaussian amplitude distribution of 1/f noise by oscilloscope display and scanning with movable slit
16 p2752 A69-32383

Stress-strain state of shells under concentrated loading, emphasizing positive Gaussian curvature
18 p3219 A69-34832

Ensembles of random Hermitian cyclic matrices in statistical theory of complex systems energy level spectra, noting Gaussian density function of eigenvalues
20 p3567 A69-36988

Satellite orbit determination errors attributed to Gaussian noise effect on tracking measurements, assuming known Gaussian probability error distribution [AIAA PAPER 69-911]
21 p3807 A69-39343

Gaussian type densities estimated by representing unknown density in terms of convolution expansion of Gaussian probability density and arbitrary distribution, discussing convergence rates
21 p3756 A69-39499

NORMAL FORCE DISTRIBUTION
U FORCE DISTRIBUTION

NORMAL SHOCK WAVES
Particle volume role in normal shockwave structure in gas-particle mixtures, discussing equations of motion formulation
13 p2244 A69-27327

Polychromator measurement of hydrogen plasma electron density produced by normal ionizing shock wave, using Stark broadening study of H beta line
14 p2494 A69-29767

Laboratory plasma produced by electromagnetically generated shock front propagation through unionized hydrogen
17 p2945 A69-33447

Normal and transverse ionizing shock, discussing Alfvénic regime for normal shocks and shunting effect in transverse shocks
18 p3180 A69-34454

Normal ionizing shock waves in H, analyzing shock velocities as function of drive magnetic field using Chapman-Jouguet hypothesis
21 p3691 A69-38332

Flow and thermodynamic variables of Ar-Cs mixture behind normal shock in shock tube at various temperatures and pressures
23 p4150 A69-41335

Hydrogen-air reaction kinetics analyzed using standing wave normal shock noting wall effects, ignition delay and recombination [AIAA PAPER 67-479]
23 p4239 A69-41893

NORMALITY
One dimensional distribution law of random process with arbitrary correlation function, verifying normality hypotheses by integral criterion
08 p1299 A69-21069

One dimensional distribution law of random process with arbitrary correlation function, verifying normality hypotheses by integral criterion
16 p2765 A69-32484

NORMALIZING (STATISTICS)
Renormalization of second order self energy part of photon and lowest order corrections to single photon vertex using Lagrange vector meson density
21 p3775 A69-39468

NORMS
Personality characteristics of jet pilots measured by Edwards Personal Preference Schedule, including percentile norms table
14 p2408 A69-29294

Norms for quantitative vectorcardiography derived from statistical analysis of results from healthy young subjects, emphasizing medical evaluation of flying personnel
24 p4277 A69-43390

P-Q norms generalized inverse concept of matrix derived from extension of Penrose best approximate solution of linear equations
24 p4342 A69-43703

NORTH AMERICA
Magnetic anomalies off Cape Hatteras explained as possible edge effect, discussing ocean and continental magnetic crusts and igneous and magnetic rocks
11 p1879 A69-25405

Optical observations of Geos 1 over North America in short arc reduction to improve tracking stations survey coordinates, discussing dependence on earth gravity and mass
15 p2599 A69-31342

Book on competition in North Atlantic commercial air transport covering passengers, freight and mail from supply, demand and market point of view
16 p2881 A69-31866

Regression generated radiometric and contour height fields of North American Continent using Nimbus 2 IR equivalent black body temperature and geopotential data
24 p4343 A69-42896

NORTH AMERICAN AIRCRAFT
U B- 70 AIRCRAFT
U OV-10 AIRCRAFT
U X- 15 AIRCRAFT

NORTH AMERICAN MILITARY AIRCRAFT
U MILITARY AIRCRAFT

NORTHERN HEMISPHERE
NT ARCTIC REGIONS

Objective layer of maximum wind /LRMW/ analysis technique for Northern Hemisphere jet stream, noting generation of initial guess fields
01 p0110 A69-10689

Geophysical effects observed in Northern Hemisphere during low solar activity, discussing polar auroral intensities and positions
02 p0239 A69-11694

Ionospheric current systems for various selected very quiet and slightly disturbed international quiet days based on Northern Hemisphere observatories data
03 p0423 A69-13518

Acromagnetic profiles across Reykjanas ridge southwest of Iceland, noting magnetic anomalies symmetry and ocean floor spreading since Mesozoic
04 p0592 A69-14660

Meteorological observations of Mars northern polar cap and Southern Hemisphere from northern summer solstice to early autumn
05 p0825 A69-16302

Atmospheric turbidity coefficient distribution in Northern Hemisphere from direct solar radiation measurements, noting application to IQY data
05 p0789 A69-16585

Atmospheric wind velocity in Northern and Southern Hemisphere, noting increase with height
06 p0921 A69-17747

Blocking processes synchronous development involving atmospheric circulation disturbances in Northern and Southern Hemispheres, noting localization in Pacific and Atlantic oceans
13 p2292 A69-27840

Soviet book on temperature regime of free atmosphere above Northern Hemisphere covering aerological data processing, statistical estimates, latitudinal and seasonal variations
13 p2294 A69-27934

Geophysical effects observed in Northern Hemisphere during low solar activity, discussing polar auroral intensities and positions
13 p2258 A69-28725

Low energy electron precipitation data at northern high latitudes obtained from satellite low altitude polar orbit
14 p2512 A69-28964

Temperatures and geopotentials of isobaric surfaces in Northern and Southern Hemispheres compared for summer and winter seasons
14 p2473 A69-29724

Spatial correlation function of Northern Hemisphere geopotential, using model based on random distribution of potential vortex fluctuations for atmospheric circulation
14 p2476 A69-29822

Atmospheric circulation integral characteristics, calculating kinetic energy in Northern Hemisphere
14 p2476 A69-29824

Zonal and meridional components of air circulation in troposphere and lower stratosphere for Northern Hemisphere
14 p2477 A69-29829

Secular fluctuations of atmospheric circulation over Northern Hemisphere analyzed using isobaric and composite-kinematic surface maps, discussing analogies with Southern Hemisphere
14 p2478 A69-29836

Epochs in atmospheric circulation development over Northern Hemisphere, emphasizing solar activity roles in epochs appearances
14 p2478 A69-29837

European geostationary satellite orbit inclination and eccentricity modification for maximum observation time of Northern Hemisphere by high resolution IR radiometer
15 p2650 A69-31389

Direct wind measurement and momentum transport estimates obtained from cyclones and anticyclones daily displacements over Northern Hemisphere, applying results to planetary atmospheres
16 p2780 A69-32306

Zonal flow intensity, velocity and kinetic energy of standing and traveling waves compared for Northern and Southern Hemispheres
17 p2997 A69-33392

Continuum survey at 1415-MHz between declinations of zero and 20 degrees N with radio telescope, noting flux densities and contour maps of sources
18 p3195 A69-34428

Climatological patterns of atmospheric kinetic energy dissipation in free atmosphere derived from upper wind statistics of Northern Hemisphere, using Kolmogoroff functions
18 p3166 A69-34825

Horizontal wind components over U.S.S.R., Western Europe and Northeast Atlantic obtained from satellite photographs of vortex cloud systems
19 p3365 A69-36668

F 2 critical frequency meridional cross sections latitude profiles based on global network ionospheric stations observations, confirming daytime Northern Hemisphere ionization maximum
20 p3526 A69-37661

F 2 region critical frequencies obtained during winter at Northern and Southern Hemisphere stations located in auroral and polar zones, correlating changes with ionization
20 p3526 A69-37665

F 2 layer seasonal anomaly, discussing global distribution observed by network of ionospheric stations
20 p3526 A69-37666

Northern Hemisphere 500-mb height pattern series expansion, using optimal sets of orthonormal functions, obtaining rms error
24 p4346 A69-43157

NORTHROP AIRCRAFT

U F 5 AIRCRAFT

NORTHROP MILITARY AIRCRAFT

U MILITARY AIRCRAFT

NOSE CONES

NT ABLATIVE NOSE CONES

NT ROCKET NOSE CONES

Scaling laws for nose bluntness effects on hypersonic aerodynamics of bodies of revolution
[AIAA PAPER 68-1158] 03 p3362 A69-13566

Flight tests in wide Mach number range of blunt nosed flare stabilized hypersonic reentry nose cone, deducing drag and stability coefficients
[AIAA PAPER 68-1145] 03 p0521 A69-13668

Shock layer microwave radiation measurements during reentry flight of spherical nose cone, determining effective plasma temperature
[AIAA PAPER 69-183] 06 p0865 A69-18201

Transpiration cooling of reentry vehicle nosetips, noting two dimensional aspects of porous wall coolant flow and matrix-coolant energy exchange
[AIAA PAPER 69-96] 06 p1039 A69-18212

Laminar hypersonic roll damping derivatives for 10 degree half angle cone at zero angle of attack for environmental flow conditions of hypersonic wind tunnel
09 p1430 A69-21958

Hypersonic drag and shock wave characteristics of blunt bodies including cones, spherical nose and concave nose bodies
09 p1433 A69-22568

Nose bluntness effect on hypersonic unsteady aerodynamics of flared and conical bodies of revolution
[AIAA PAPER 68-889] 12 p2012 A69-26794

ASTRID high altitude sounding rockets orientation system aligning payload cones to target outside earth atmosphere, discussing software simulation with analog and digital computers, etc
• 17 p3001 A69-33424

Cone boundary layer transition location and Reynolds number as function of nose bluntness combined effect with Ar, air and He mass injection
[AIAA PAPER 67-706] 17 p2955 A69-33476

Nonequilibrium, real gas and nose bluntness effects on hypersonic slender body flows, analyzing similitudes, free stream temperature, velocity and relaxation
[AIAA PAPER 69-708] 17 p2894 A69-33501

Drag measurements for sharp and blunt-nosed bodies shot into wind tunnel supersonic gas counterflows, discussing shock waves for different configurations
19 p3239 A69-36401

Second order differential equations of supersonic flows past bodies at small angles of attack, showing linearized characteristics method applicability for conical nose
24 p4243 A69-42581

Flight tests in wide Mach number range of blunt nosed flare stabilized hypersonic reentry nose cone, deducing drag and stability coefficients
[AIAA PAPER 68-1145] 24 p4394 A69-43250

NOSE WHEELS

Steerable landing gear system consisting of freely castoring corotating wheel nose gear, tiltable axle and main gear skids for lifting body spacecraft
[AIAA PAPER 69-790] 19 p3243 A69-35639

NOSES (FOREBODIES)

NT ABLATIVE NOSE CONES

NT NOSE CONES

NT ROCKET NOSE CONES

ELDO Europa 1 Fairings Jettisoning System and explosive devices, discussing heat shield structure and safety regulations
10 p1635 A69-23027

Nose bluntness effect on hypersonic flow for slender blunt bodies with arbitrarily shaped lateral surfaces at small attack angle
19 p3239 A69-36402

NOTATION

U CODING

NOTCH SENSITIVITY

Impact cyclic loading fatigue tests of smooth and notched duralumin, discussing increased impact strength resulting from initial underloading
07 p1167 A69-19317

Strain concentration design factors for notch effect in low cycle fatigue and crack propagation conditions
07 p1235 A69-19383

Notched members fatigue life prediction from smooth specimen fatigue data and Neuber rule application
10 p1715 A69-23984

Crack behavior and toughness of aluminum alloy parent metal and weldments, noting temperature effect
14 p2462 A69-29003

Oxygen content and grain structure influence on TS5 Ti alloy mechanical properties, notch and crack growth sensitivity at low temperature
15 p2637 A69-30266

NOTCH STRENGTH

Ultrasonic detection and measurement of fatigue cracks in notched cylinders subjected to reversed axial cyclic loading
01 p0078 A69-10113

Plane strain yielding, stresses and fracture about notches and cracks in terms of flow and fracture stresses and crack tip radii
03 p0528 A69-13876

Theoretical buckling load for single edge notched struts, discussing brittleness effects
05 p0837 A69-16064

Elastoplastic stress in notch as cause of decreased lifetime of aircraft components, analyzing stress reversal and displacement during takeoff and landing
09 p1620 A69-22576

Testing system stiffness effect on sheet fracture, discussing notch strength dependence on stiffness
10 p1796 A69-23075

Thickness and drilled holes effects on notch toughness of Charpy V notch bars over wide temperature range
10 p1798 A69-23087

Potential testing methods for corrosion induced changes in materials, discussing mechanical properties, corrosion fatigue and cracking and creep
10 p1713 A69-23822

Notched members fatigue life prediction from smooth specimen fatigue data and Neuber rule application
10 p1715 A69-23984

High strength steels, discussing ductility, austenite to martensite transformation for increased strain hardening rate and elongation and corrosion resistance
12 p2115 A69-26829

Ultrasonic detection and measurement of fatigue cracks in notched cylinders subjected to reversed axial cyclic loading
14 p2445 A69-28882

Titanium alloys fatigue properties at various temperatures using notched and unnotched specimens, considering vibrational fatigue strength and notch sensitivity
15 p2637 A69-30227

Stress conditions of anisotropic plate with soldered in circular isotropic aluminum disk in presence of notches at seam, assuming elastic symmetry of plate
18 p3218 A69-34602

Elastic bodies brittle stability weakened by cut, developing criterion for determining critical cut length
18 p3224 A69-35314

Alloying elements effect on low temperature notch-bend fracture toughness of martensitic high strength steels, noting transition temperature
20 p3556 A69-36952

Low cycle fatigue strength tested on notched and unnotched round steel bars, distinguishing between fatigue lives for crack initiation and propagation
24 p4404 A69-43627

NOTCH TESTS

NT CHARPY IMPACT TEST

Microscopic cleavage strength of high nitrogen steel notched bars determined from critical tensile stress criteria using elastoplastic analysis method
01 p0169 A69-10765

Notch stress procedure to predict low cycle fatigue life of specimens with fabrication flaws, discussing crack initiation and propagation lives effects
[ASME PAPER 68-PVP-15] 03 p0523 A69-12997

Prolonged loading effect on mechanical properties of 18Kh2N4VA steel at low temperature, discussing notched and unnotched specimens
04 p0614 A69-14573

Load carrying capacity of V notched bars under axially symmetric tensile load, verifying influence of distance between two equal notches
04 p0680 A69-15169

Generation of crack propagation data on notched rotating beam specimens by interrupted stressing techniques
[ASME PAPER 68-WA/MET-3] 05 p0838 A69-16148

Fatigue crack growth in notched samples of aluminum alloy subjected to cyclic compressive loading, noting residual tensile strength at notch root
[ASME PAPER 68-WA/MET-16] 05 p0838 A69-16154

Fatigue life reduction in Al alloy specimens with stress concentrations due to notches
05 p0843 A69-16696

Strain near fatigue crack tip in notched steel plates measured by copper electroplating method
06 p1022 A69-17198

Localized microstructural changes and fatigue crack propagation in cantilever type notched specimens of austenitic stainless steel under cyclic bending at constant load
06 p0943 A69-17237

Plastic yielding of tensile V-notched aluminum alloys elements with intermediate thickness and various shoulder ratios, studying thickness effect on yield load
09 p1612 A69-21499

Liquid surface active media /kerosene, water, castor oil/ effect on strength of V notched polymethyl methacrylate specimens
09 p1528 A69-21852

Debonding mechanism role in fatigue crack development in notched aluminum alloy samples using optical and electron microscopy
10 p1710 A69-23076

Notched members fatigue life prediction from smooth specimen fatigue data and Neuber rule application
10 p1715 A69-23984

Crack opening displacements of stationary and running cracks and of inclined stationary cracks in centrally notched plates, noting normal strain fields
12 p2189 A69-27163

Double notch creep rupture tests of Cr-Mo steels, investigating changes in notch profile, dimensions and structure
[ASME PAPER 68-WA/MET-7] 14 p2464 A69-29441

Prolonged loading effect on mechanical properties of 18Kh2N4VA steel at low temperature, discussing notched and unnotched specimens
15 p2638 A69-30274

Fracture toughness of AlZnMgCu alloys, employing sharp notch tension, tear and precracked Charpy impact tests
16 p2800 A69-31780

Brittle toughness determination method compared with Robertson and notch impact tests, evaluating steel susceptibility to brittle failure propagation
16 p2795 A69-32796

Photoelasticity testing of stress gradient factor on notched tensile specimens
17 p3052 A69-32982

Plane strain fracture toughness determined for crack notched bend specimens using standard test procedure for specific metallic material property
17 p2989 A69-33566

Stress distribution in tension specimen notched on one edge obtained photoelastically for several notch depth to specimen width ratios, noting Neuber theory agreement
19 p3447 A69-36859

Fatigue tests with cylindrical samples for observation of macrocrack formation and propagation at bottom of notches, discussing kinetics of fatigue failure
23 p4225 A69-41425

Notch effect on corrosion fatigue behavior of high strength Al alloy under bending and direct stresses
24 p4330 A69-42553

NOTCHED METALS

U NOTCH TESTS

NOTCHED STEEL

U NOTCH TESTS

U STEELS

NOTCHES

Stress distribution in infinite strip with equally spaced identical semicircular notches on one edge and subject to transverse bending
05 p0842 A69-16643

Stresses in finite width infinite elastic isotropic strip with equally spaced identical semicircular notches under uniform tension or pure bending
05 p0843 A69-16644

NOVAE

NT HERCULES NOVA

Spectrum data of Nova Vulpeculae /1968/ summarized concerning dispersion figures
07 p1220 A69-19337

Novas in M 31 on Tautenburger Schmidt photographs
08 p1382 A69-19873

Nine spectra of recurrent Nova T Pyxidis during fifth /1966/ outburst compared to previous outbursts
08 p1391 A69-20396

Photographic observations of Nova Her 1963 in 1967, showing nonreturn to prenova stage
12 p2156 A69-26223

Fine structure of absorption lines of circumstellar Ca ejected from Nova Delphini 1967, determining ejection dates and photospheric radius
13 p2346 A69-27709

General algorithm for eruptive plasma instabilities in fusion plasmas, flares and novae, yielding time behavior and dissipative effects
14 p2499 A69-29850

Nova Delphini 1967 observational data and equipment including Cassegrain spectrograph, reflector telescope and photoelectric photometer
15 p2682 A69-30439

Nova thermal explosion, analyzing hydrogen combustion after penetration from white dwarf shell into degenerate core
15 p2682 A69-30507

Nova outburst dynamics investigation by time dependent hydrodynamics computer program including energy transport by radiation and convection
15 p2692 A69-30769

Nova Vulpeculae 1968 photographic observations analyzed for magnitudes, indicating 16 July 1968 explosion
16 p2855 A69-31659

Galactic novae observational data and theoretical interpretations, considering envelope detachment from star, luminosity, motion and emission line intensities
17 p3032 A69-33103

Forbidden emission transition probabilities in high excitation symbiotic stars, novae, Cygni stars and peculiar binaries
19 p3423 A69-36227

Forbidden lines in slow nova RR Tel spectrum, comparing ionization rate with RR Pic
19 p3423 A69-36230

Photometric evolution of Nova Delphini 1967 /HR Del/ in UPXYZVS seven color intermediate waveband system, showing position on QQ diagram
19 p3425 A69-36563

Nova Delphini 1967 /HR Del/ observations in UPX-YZV photometric system, tabulating color indices
19 p3426 A69-36564

Nova luminosity sources during premaximum, considering stellar shell separation and intense ejection of matter
19 p3426 A69-36574

UBV photoelectric observations of Nova Delphini 1967 at Bologna Observatory
20 p3599 A69-37475

Cosmic ray electron role in energetics of solar flares, stellar flares and explosions, galactic eruptions and quasars
21 p3790 A69-38823

Photoelectric observation of EM Cygni eclipsing binary and old nova
22 p4015 A69-40151

Tabulated photoelectric photometer measurements of Nova Vulpeculae 1968 No. 1
23 p4208 A69-41290

NOXIOUS MATERIALS
U CONTAMINANTS

NOZZLE DESIGN

Interactions between outer and inner jets behind maximum cross section of jet engine nozzle [ONERA-TP-600]
02 p0187 A69-11620

Nozzle geometry influence on argon plasma flow parameters in shock tube, discussing measurement data behind shock wave front
03 p0481 A69-14160

Sublimation solid reaction control, discussing propellants, nozzle performance, sublimation area, power, pressure drop, response and valueless design [AIAA PAPER 68-516]
04 p0552 A69-15322

Injector design based on MHD injector components performance, establishing minimum diffuser nozzle area
06 p0872 A69-17920

Variable geometry intake and convergent-divergent nozzle design for supersonic aircraft, noting subsonic installations
08 p1253 A69-21164

Solid propellant motors nozzle design, analyzing structural and material problems, high temperature exhaust gases effects, thermal insulation, etc
10 p1716 A69-23403

Supersonic nozzle cross section and diffuser throat in MHD generator calculated by continuity equation
11 p1826 A69-25348

Nozzle erosion profile, char penetration and temperature response predicted for nozzle material for 260 SL-3 motor [AIAA PAPER 68-504]
12 p2118 A69-26784

Axisymmetric hypersonic wind tunnel nozzle design by determining inviscid contour and correcting for turbulent boundary layer growth [AIAA PAPER 69-337]
13 p2200 A69-28273

Variational problems associated with supersonic gas flows with foreign particles, considering nozzle designs
14 p2389 A69-28801

Optimum nonequilibrium nozzle performance for hydrogen-fluorine propellant system, considering contour, engine/nozzle weights and recombination kinetics [AIAA PAPER 69-472]
16 p2733 A69-32652

Nozzle throat ablative materials for controlled high regression rates in tactical rocket motors, primarily nylon reinforced thermosetting resins [AIAA PAPER 69-423]
16 p2804 A69-32710

Location effect of power plants on aft-mounted supersonic cruise exhaust nozzles at transonic speeds in flight and wind tunnel [AIAA PAPER 69-427]
16 p2734 A69-32769

Large booster nozzle reuse, discussing design, refurbishment, performance, costs and test evaluation [AIAA PAPER 68-657]
19 p3394 A69-35944

Rocket nozzle control by side forces produced by secondary gas stream injection observed for relationship with inclination angle to nozzle axis
20 p3457 A69-37065

Liquid metal sprayer design including calculation of nozzles for subsonic and supersonic gas outflow
21 p3728 A69-38613

Nitrogen and water vapor effects on hydrogen-oxygen system recombination, using shock tubes for design of exhaust nozzles for hypersonic flow vehicles
21 p3669 A69-38801

Computerized solid rocket motor nozzle design with computer program providing weight, envelope and performance values for vehicle optimization studies [AIAA PAPER 69-975]
22 p3999 A69-40355

Pressure ratio effect on supersonic turbine nozzle performance during off-design regime operation, noting effect of low specific heat gas ratio
23 p4203 A69-42250

Large contoured nozzle fabrication using liquid epoxy as casting material, presenting molding process based on experimental data
24 p4318 A69-42643

NOZZLE EFFICIENCY

Nomogram for nozzle thrust coefficient evaluation
03 p0365 A69-14102

Pumping requirements for nozzle skimmer region of neutral particle nozzle beam source, using two stage mechanical pump
04 p0600 A69-15026

Space flight fuel consumption optimization as function of acceleration of nozzle control
10 p1666 A69-22919

Chemical reaction rate data for propellant systems containing boron or aluminum and hydrogen, chlorine and fluorine, based on finite kinetics expansions [AIAA PAPER 69-182]
11 p1940 A69-24907

Local external flow variations effect on blow-in-door nozzle performance in transonic flight regime [AIAA PAPER 69-428]
16 p2733 A69-32731

Noncavitating and cavitating performance of low area ratio water jet pumps, analyzing efficiency, area ratio, throat length, nozzle spacing and diffuser geometry
18 p3095 A69-35176

Divergence losses of noncircular C-D nozzles based on approximation by spherical source flows
19 p3238 A69-35960

Liquid alumina particles agglomeration in convergent and throat region of nozzle leading to performance decrease by increasing velocity and temperature difference between phases
22 p4001 A69-40929

Pressure ratio effect on supersonic turbine nozzle performance during off-design regime operation, noting effect of low specific heat gas ratio
23 p4203 A69-42250

Tridimensional infrasonic diffuser geometry effects on operational efficiency, considering opening angle, outlet/inlet section fields ratio and diffuser length/hydraulic radius ratio
24 p4243 A69-42560

NOZZLE EXPANSION
U GAS EXPANSION

NOZZLE FLOW

Difference methods in solution of incorrect Cauchy problem simulating ideal gas flow in nozzle
01 p0006 A69-10379

Nozzle separation for thrust vector control with applications to guidance problems
01 p0161 A69-10412

Reactions kinetics contribution to nonequilibrium recombination occurring in supersonic nozzle flow of combustion products of hydrogen in air
02 p0353 A69-12488

Minimum admissible spacing between supersonic jet expelled from VTOL aircraft nozzle and plane surface near nozzle exit
03 p0361 A69-12955

Laval nozzle resistance as result of friction and under expansion of gas, noting flow and pressure recovery coefficients
03 p0361 A69-12967

Chemical rockets theory for case of chemical equilibrium and frozen nozzle expansions
03 p0495 A69-13004

Jet pump head rise deterioration parameter for prediction of cavitation
05 p0745 A69-15791

Turbulent free jet at miniature nozzle exit, analyzing wall attachment fluid amplifier and flow characteristics
05 p0746 A69-16012

Coanda nozzle entrainment and flow augmentation approximating numerical stability by finite differences
05 p0746 A69-16021

Argon flow characteristics in converging nozzle in continuum, slip and free molecular regimes [ASME PAPER 68-WA/FE-9]
05 p0698 A69-16089

Recombination constants of dissociated oxygen and nitrogen flow in supersonic nozzle at high temperatures using modified Bray method
06 p1030 A69-17349

Liquid metal MHD systems efficiency when operating with pressure jump in diffuser nozzle
06 p0872 A69-17921

Condensation and probe interference in planar expansion deflection nozzle measurements [AIAA PAPER 69-170]
06 p0863 A69-18059

Dense gas effects in free piston hypersonic wind tunnel, discussing Longshot facility, free piston cycle, reservoir conditions decay and hypersonic nozzle flow [AIAA PAPER 69-169]
06 p0907 A69-18188

Underexpanded nozzle ejected supersonic turbulent jet off-design behavior, discussing static pressure distribution, boundary layer and Mach number effect
07 p1049 A69-18397

Relaxation equations for oscillatory degrees of freedom of molecular supersonic binary gas flow in Laval nozzle, obtaining population inversion
07 p1118 A69-18540

Optimum profile of supersonic nozzle with nonequilibrium flow
07 p1119 A69-18737

Mixed sub- and supersonic gas flow in plane pressure nozzle free of vortex and neglecting viscosity and heat conduction
07 p1050 A69-18739

Stationary supersonic nonequilibrium plasma source in gas vacuum expansion and nozzle flows
07 p1191 A69-18986

Steady conical compressed flows in nonaxisymmetric ring nozzles characterized by discontinuities
07 p1120 A69-18989

Boundary layer effect on flow coefficient of fluid amplifier feed nozzle, noting flow uniformity, incompressibility, velocity and velocity distribution assumptions
07 p1059 A69-19320

Time dependent procedure for axisymmetric transonic nozzle flows, programming governing equations for high speed computer
09 p1431 A69-21974

Navier-Stokes equations solution applicable to source type low Reynolds number flow through conical nozzles

09 p1482 A69-21976

High enthalpy air flow in hypersonic conical nozzle, calculating chemical and thermodynamic nonequilibrium effects with computer program

09 p1433 A69-22610

Sonic transmission of diatomic nitrogen during nozzle flow, presenting density dependence of natural oscillation energies and temperature

10 p1632 A69-22912

Effect of degree of expansion of ionized gas in nozzle on specific power of MHD generator

10 p1636 A69-23103

Nozzle flow temperature patterns of relaxing combustion gases compared at different temperatures and pressures, using kinetic-chemical calculations [DVL-896]

10 p1809 A69-23644

Size and velocity measurements of particles suspended in gas expanding from nozzle into vacuum simulating cometary two phase flow with evaporation

10 p1674 A69-23686

Asymptotic boundary curves for two dimensional and axisymmetric incompressible irrotational flows into throat of convergent duct

10 p1680 A69-23893

Supersonic nozzle cross section and diffuser throat in MHD generator calculated by continuity equation

11 p1826 A69-25348

Trajectories of particles entrained by gas flow in nozzles for study of erosion damage during passage of gas-particle mixture

11 p1818 A69-25355

Supersonic nozzle design ensuring desirable flow field in inviscid core of viscous gas flow, using boundary layer equations

11 p1820 A69-25473

Mixing zone of plane jet in rectangular nozzle mounted at end of controlled velocity wind tunnel

12 p2062 A69-26287

Difference methods in solution of incorrect Cauchy problem simulating ideal gas flow in nozzle

12 p2012 A69-26671

Internal flows of compressible fluids with heat transfer in accelerating nozzles and constant area ducts, simplifying equations by assuming one dimensional flow

12 p2012 A69-26790

Soviet book on liquid fuel rocket engines design covering gas expansion in nozzles, mixture formation, heat transfer, injectors and supply systems

12 p2148 A69-27078

Thermodynamic atomization in MHD energy conversion through convergent-divergent nozzles, noting nozzle efficiency and droplet size

13 p2245 A69-27477

Air-water and steam-water flows in two phase Laval nozzles, measuring flow rates and temperature and pressure variation

• 13 p2245 A69-27481

Diagnostic measurements in nonequilibrium nozzle flows compared to finite rate expansion calculations, measuring pressure, temperature and density [AIAA PAPER 69-328]

13 p2200 A69-28263

Variational problems associated with supersonic gas flows with foreign particles, considering nozzle designs

14 p2389 A69-28801

Argon flow characteristics in converging nozzle in continuum, slip and free molecular regimes [ASME PAPER 68-WA/FE-9]

14 p2390 A69-29445

Radiating gray gas laminar jet in thermodynamic equilibrium ejected from plane nozzle into wake analyzed using boundary layer, divergence and transfer equations

14 p2432 A69-29612

Gas and polydispersed condensate parameters of nonequilibrium two phase flow in Laval nozzle, considering particle collisions and coagulation, energy exchange and momentum exchange

14 p2391 A69-29621

One dimensional approximation for free jet nozzle flow in perpendicular magnetic field, calculating velocity distributions

14 p2501 A69-29910

Heat release rate during gas combustion products recombination in supersonic nozzle, using graphic interpolation of flow parameters

15 p2717 A69-30987

Stagnation region dimensionless pressure effect on flow pattern, boundary conditions and oscillation mechanism in compressible flow through nozzle in circular duct

15 p2549 A69-31220

Three dimensional laminar jet mixing of incompressible viscous fluid from rectangular cross section nozzle into uniform stream

16 p2768 A69-31687

Turbulent boundary layer laminarization in conical nozzle flow, measuring velocity profiles and friction coefficient [JPL-TR-32-1407]

16 p2732 A69-31894

Maintaining of flow similarity in calibration of nozzle type water meters for study of working processes of pumps

16 p2772 A69-32145

Nonequilibrium initial condition combustion effects on propellant performance for hydrazine/ chlorine pentafluoride and hydrogen/fluorine with equilibrium, kinetic and frozen nozzle flow [AIAA PAPER 69-469]

16 p2832 A69-32659

Free flow field from underexpanded rocket motor nozzle and impingement effects of pressure and heat transfer to flat plate [AIAA PAPER 69-568]

16 p2842 A69-32693

Three dimensional supersonic nozzle flow field calculations using second order numerical method of characteristics and computer programmed for internal flows [AIAA PAPER 69-463]

16 p2734 A69-32766

Pressure and temperature surveys of Mach 27-47 nozzle boundary layer at Ames M-50 He tunnel, determining velocity profiles, wall friction coefficient, etc [AIAA PAPER 69-686]

17 p2953 A69-33441

Time dependent analysis for quasi one dimensional, vibrational and chemical nonequilibrium nozzle flows approaching steady state solution by finite difference technique [AIAA PAPER 69-668]

17 p2893 A69-33491

Preston probe measurement of friction drag on subsonic and supersonic nozzle wall including effects of heat transfer, compressibility and pressure gradient [AIAA PAPER 69-648]

17 p2893 A69-33496

Viscous convergent-divergent nozzle flow slender channel approximations, discussing roles of nozzle geometry, Reynolds number and wall temperature, calculating velocity, enthalpy, etc [AIAA PAPER 69-654]

17 p2894 A69-33502

Jet and compressor noise, discussing noise suppression techniques and engineering applications [AIAA PAPER 68-550]

17 p3022 A69-34019

Pulsating flow analysis in finite and infinite conical nozzles under sinusoidal pressure disturbances [ASME PAPER 69-APM-16]

18 p3214 A69-34392

Shock tunnel steady flow starting process in two dimensional reflection nozzle, using multiple shadowgraphs and interferograms, noting nozzle geometry influences

18 p3085 A69-34471

Vibrational deexcitation shocks in expanding nonequilibrium nozzle flows extended to include embedded adiabatic shock

18 p3089 A69-35386

Flow rate of ideal fluid ejected from swirl injector taking into account radial component of flow velocity at nozzle exit

19 p3297 A69-35820

Divergence losses of noncircular C-D nozzles based on approximation by spherical surface flows

19 p3238 A69-35960

Skimmer interaction influences on nozzle beam production explaining intensity maxima, proposing model assuming normal shock across skimmer mouth

19 p3238 A69-36172

Diverging nozzle flow of gas mixtures containing solid or liquid particles analyzed by one dimensional approximation separately averaging boundary layer and flow core

19 p3298 A69-36389

Relaxation time influence on discharge coefficient of sonic nozzle of revolution, considering expanding polyatomic gas problem

19 p3241 A69-36721

Boundary layer formed in miniature nozzle studied for effect on jet spreading discharged into space at high Mach numbers

19 p3395 A69-36760

Jet efflux from two dimensional symmetric nozzles of arbitrary shape determined using conformal mapping and Riemann-Hilbert solution to mixed boundary value problem

21 p3692 A69-38686

Relaxation equations for oscillatory degrees of freedom of molecular supersonic binary gas flow in Laval nozzle, obtaining population inversion

21 p3693 A69-38692

Fluidic angular rate sensor, obtaining rate information by sensing laminar jet flow deflection from nozzle, discussing advantages over mechanical rate sensors

21 p3722 A69-38766

Simultaneous passage of two unmixed gas flows through joint two circuit turbojet nozzle into ambient medium

21 p3785 A69-39094

Turbulent gas jet mixing in chamber with four inlet nozzles

21 p3785 A69-39102

Liquid hydrogen pumping for Phoebus reactor, discussing feed systems, nozzles, configurations, design, testing, etc [AIAA PAPER 67-478]

21 p3769 A69-39751

Condensation and probe interference in planar expansion deflection nozzle measurements [AIAA PAPER 69-170]

21 p3645 A69-39769

Quasi-one dimensional analysis for nonequilibrium flow of dissociated diatomic gas through converging-diverging nozzle, discussing critical mass flow rate

22 p3927 A69-40583

Flexible string extraction from bobbin through nozzle, solving equations of motion by neglecting bending rigidity, extensibility, drag, internal friction, etc

22 p3930 A69-40585

Carbon dioxide free jet expanding from conical nozzle into low density atmosphere, using freeze up method

22 p4000 A69-40594

Flowfield properties of two dimensional supersonic jet near sonic nozzle exit by numerical method of characteristics

22 p3860 A69-40920

Starting process in nozzle with one dimensional flow treated numerically by finite difference method using pseudoviscosity term

22 p3860 A69-40926

Ionized He and Ar plasmas nonequilibrium nozzle flows, noting temperature difference between electron gas and atom-ion gas, calculating flow parameters

22 p3861 A69-41047

Dissociational nonequilibrium transonic flow near nozzle throat analyzed for diatomic gas with equilibrium vibrational energy, using perturbation method

22 p3861 A69-41177

Swirl influence on choking constraint in transonic flow through nozzle throat [AIAA PAPER 68-693]

23 p4151 A69-41887

Transonic expansion analysis applied to flow through convergent-divergent nozzles with small throat radius of curvature, noting coordinate system selection

23 p4060 A69-41906

Rarcfaction onset along streamline from rocket nozzle with small Knudsen number at exit plane

23 p4152 A69-41920

Underexpanded plane hypersonic gas jet injection into resting medium from straight nozzle, discussing shock wave formation

24 p4246 A69-43484

Flow discharge characteristics of nozzle during swirling gas flow ejection, considering isentropic and isothermal limiting cases

24 p4247 A69-43499

Boundary layer and heat transfer measurements for turbulent boundary layer laminarizing in conical nozzle flow with wall cooling [ASME PAPER 69-HT-56]

24 p4303 A69-43538

Uniform flow and wall boundary layer growth measurement in conical nozzle of reflected shock tunnel operating at high enthalpy conditions

24 p4247 A69-43575

Electron temperature and density of inviscid free molecular nozzle flow of shock tunnel measured with thin wire Langmuir probes

24 p4317 A69-43648

High enthalpy shock tube and nozzle gas flows for incident shock Mach numbers analyzed for laminar boundary layers and boundary layer transitions

24 p4305 A69-43664

NOZZLE GEOMETRY

Sonic nozzle optimal profile determination with and without cylindrical throats, noting sonic line curvature importance on discharge coefficient

02 p0188 A69-12037

Short cylindrical diffusers efficiency in supersonic wind tunnel with exchangeable nozzles with conical supersonic section

03 p0365 A69-14226

Soviet book on gas dynamics of solid fuel rocket motors covering combustion chamber flow, nozzle and thrust characteristics, pressure relaxation and channel charge

04 p0647 A69-15493

Condensation and probe interference in planar expansion deflection nozzle measurements
[AIAA PAPER 69-170] 06 p0863 A69-18059

Aerobell extendible nozzle rocket engine design and performance, cold flow and simulated hot flow test results
[AIAA PAPER 69-4] 06 p0985 A69-18195

Optimum fixed geometry ramjet in Mach range of 3 to 7 with successively subsonic and supersonic combustion
[ONERA-TP-656E] 07 p1203 A69-18415

Variable geometry intake and convergent-divergent nozzle design for supersonic aircraft, noting subsonic installations
08 p1253 A69-21164

Asymptotic boundary curves for two dimensional and axisymmetric incompressible irrotational flows into throat of convergent duct
10 p1680 A69-23893

Venturi meter design, discussing effects of turbulent velocity fluctuations, hole size and internal geometry on differential pressure measurement
11 p1880 A69-24468

Supersonic nozzle design ensuring desirable flow field in inviscid core of viscous gas flow, using boundary layer equations
11 p1820 A69-25473

Aircraft test setup design and techniques to simultaneously measure engine thrust and engine thrust minus drag, noting nozzle configurations variations effect
[AIAA PAPER 68-395] 12 p2059 A69-26769

Wet steam injector power losses in nozzle as function of humidity, noting compensation of nozzle throat diameter and fluid flow rates
13 p2246 A69-27490

Axisymmetric hypersonic wind tunnel nozzle design by determining inviscid contour and correcting for turbulent boundary layer growth
[AIAA PAPER 69-337] 13 p2200 A69-28273

Diffuser inlet geometry, studying effects of straight section length on flow pattern and diffuser resistance
14 p2391 A69-29899

Collapse pressure of flush cylindrical nozzle axisymmetrically intersecting conical pressure vessel for rigid plastic shells
15 p2704 A69-30289

Jet noise causes and suppression, discussing nozzle exit area geometry
15 p2671 A69-30372

Solid rocket propellants tests, considering propulsion performance measurements, altitude simulation problems, internal flow patterns, nozzle geometry, etc
16 p2765 A69-31751

Compressor surge effect on mixed compression inlet flow from numerical solution of one dimensional unsteady inviscid flow equations in variable area duct
[AIAA PAPER 69-484] 16 p2841 A69-32682

Turbulent base flowfields in multinozzle configurations, considering adiabatic flow and determining base pressure distribution from reverse jet impingement
[AIAA PAPER 69-570] 16 p2733 A69-32751

Constant chamber pressure thrust throttling of expansion-deflection rocket nozzle, calculating wall static pressure and thrust by characteristics method, discussing performance
[AIAA PAPER 69-435] 16 p2846 A69-32776

Viscous convergent-divergent nozzle flow slender channel approximations, discussing roles of nozzle geometry, Reynolds number and wall temperature, calculating velocity, enthalpy, etc
[AIAA PAPER 69-654] 17 p2894 A69-33502

Shock tunnel steady flow starting process in two dimensional reflection nozzle, using multiple shadowgraphs and interferograms, noting nozzle geometry influences
18 p3085 A69-34471

Pyrolytic graphite coated composite as nozzle throat material for high energy metallized solid propellant motors
19 p3357 A69-35539

Fluidic direct impact modulator design, studying effects of pressure levels and nozzle geometries
[ASME PAPER 69-FLCS-38] 20 p3465 A69-37983

Jet efflux from two dimensional symmetric nozzles of arbitrary shape determined using conformal mapping and Riemann-Hilbert solution to mixed boundary value problem
21 p3692 A69-38686

Condensation and probe interference in planar expansion deflection nozzle measurements
[AIAA PAPER 69-170] 21 p3645 A69-39769

Swirl influence on choking constraint in transonic flow through nozzle throat
[AIAA PAPER 68-693] 23 p4151 A69-41887

Internal flow measurements in transonic region of supersonic nozzle with small throat radius of curvature compared with prediction data
23 p4060 A69-41900

Tridimensional infrasonic diffuser geometry effects on operational efficiency, considering opening angle, outlet/inlet section fields ratio and diffuser length/hydraulic radius ratio
24 p4243 A69-42560

Large contoured nozzle fabrication using liquid epoxy as casting material, presenting molding process based on experimental data
24 p4318 A69-42643

NOZZLE INSERTS

Precracked ceramic rocket nozzle throat inserts, discussing improved thermal displacement accommodation, load transmission, fracture tolerance, articulation capability, etc
02 p0334 A69-12369

Supersonic nozzle cross section and diffuser throat in MHD generator calculated by continuity equation
11 p1826 A69-25348

NOZZLE THRUST COEFFICIENTS

Nomogram for nozzle thrust coefficient evaluation
03 p0365 A69-14102

Convergent conical nozzles discharge coefficient calculated as function of operation mode and nozzle geometry
24 p4364 A69-43074

NOZZLE WALLS

Nozzle ablations based on chemical mechanism, discussing pure or reinforced phenolic resin
11 p1999 A69-24908

Boundary layers coalescence on plane convergent channel walls investigated with analytic formulas for velocity distribution, shear stress, layer thickness, etc
15 p2592 A69-31009

Density and density fluctuations in hypersonic turbulent boundary layer on shock tunnel nozzle wall measured using electron beam probe
16 p2770 A69-31907

Graphite rocket engine nozzles chemical erosion at various temperatures, comparing reaction and diffusion rates
23 p4180 A69-42156

NOZZLES

Conducting and insulating construction materials at high temperatures for MHD conversion nozzles, noting lifetimes
21 p3751 A69-38456

NRX-A REACTOR

U NRX REACTORS
U NUCLEAR ENGINE FOR ROCKET VEHICLES

NRX REACTORS

Remote disassembly and inspection methods for evaluating NRX-AG reactor components performance
[AIAA PAPER 69-511] 16 p2810 A69-32712

NUCLEAR AUXILIARY POWER UNITS

NT SNAP 8
NT SNAP 10A
NT SNAP 13
NT SNAP 21
NT SNAP 27
NT SPACE POWER UNIT REACTORS

Nuclear reactors for powering electrical engines and current supply for satellite devices, noting ROVER project and Kiwi reactors
07 p1179 A69-19739

Radioisotope energized Stirling engine for spacecraft auxiliary electric power, discussing system configurations, weight and fuel requirements
23 p4190 A69-42281

NUCLEAR BINDING ENERGY

Approximate ionization potentials for high ionization stages of elements with atomic numbers 31 to 92 obtained by binding energy calculations
14 p2488 A69-29923

NUCLEAR CAPTURE

U ELECTRON CAPTURE

NUCLEAR CHEMISTRY

Computer-analyzer system for nuclear chemistry, noting advantage of on-line data acquisition and analysis coupled with time sharing economy
05 p0725 A69-16584

NUCLEAR-ELECTRIC MOMENTS

U ELECTRIC MOMENTS

NUCLEAR ELECTRIC POWER GENERATION

NT THERMONUCLEAR POWER GENERATION
Nuclear reactors for powering electrical engines and current supply for satellite devices, noting ROVER project and Kiwi reactors
07 p1179 A69-19739

High temperature and power gas diodes and thyatrons for nuclear electrical space power systems
11 p1847 A69-24744

Nuclear energy systems, discussing U.S. reactor concepts with emphasis on thermionic systems and space applications
14 p2404 A69-29278

Nuclear energy conversion for long space missions, comparing dynamic Brayton, liquid metal MHD gas, dynamic Rankine and LMMHD Rankine cycles
16 p2810 A69-31748

Nuclear thermal and electrovoltaic batteries design and operation, discussing applications
20 p3464 A69-37288

Space nuclear electric power systems applications and development, summarizing current status and near future programs
[AAS PAPER 69-305] 24 p4364 A69-42865

NUCLEAR ELECTRIC PROPULSION

Nuclear reactors for powering electrical engines and current supply for satellite devices, noting ROVER project and Kiwi reactors
07 p1179 A69-19739

Performance boundaries of space propulsion systems containing nuclear electric stages
[AIAA PAPER 69-249] 09 p1538 A69-21249

Reactor and mission requirements interaction for unmanned thermionic nuclear electric propulsion, discussing lifetime, payload, power levels, etc
[AIAA PAPER 69-250] 09 p1539 A69-21253

Low thrust space probe mission to Halley comet, utilizing nuclear electric propulsion
10 p1772 A69-22864

Thermionic reactor systems, discussing hybrid nuclear rocket/nuclear electric Mars mission, design features, performance and electric power characteristics
14 p2480 A69-29183

Out-of-core thermionic systems with heat pipes usable in space applications, meeting advanced auxiliary power and nuclear propulsion requirements
14 p2480 A69-29188

Space nuclear electric power systems applications and development, summarizing current status and near future programs
[AAS PAPER 69-305] 24 p4364 A69-42865

NUCLEAR EMULSIONS

Permanent magnet and nuclear emulsion for measuring He nuclei momentum spectra up to 100 gv rigidity
06 p0989 A69-17277

Density measurements of particle tracks in nuclear emulsions utilizing digitized video scan, discussing operation and instrumentation
[IEEE PAPER 2A-7] 07 p1133 A69-19185

Energy spectrum of primary cosmic ray helium nuclei from nuclear emulsion stacks exposed in sounding rocket flights
08 p1378 A69-20264

Nuclear emulsion high energy nucleon-nuclei interaction model accounting for two maxima track formation
13 p2303 A69-28371

Trans-iron nuclei flux in primary cosmic radiation determined through high altitude balloon exposure of interleaved layers of nuclear photographic emulsion and plastic detectors
21 p3787 A69-38327

Primary cosmic ray nuclei studies during Gemini 2 flight by nuclear emulsion detector with time resolution capability, describing experiment design and equipment operation
21 p3787 A69-38350

NUCLEAR ENERGY LABORATORIES

U LABORATORIES

NUCLEAR ENGINE FOR ROCKET VEHICLES

Nuclear rocket engine exhaust gas cooling by injecting water jet eliminates need for secondary cooling
[AIAA PAPER 68-604] 04 p0591 A69-15516

Radiation effects on NERVA out-of-core instrumentation, discussing cryogenic temperature measurements and transducer measuring pressure at gamma heating rates
06 p0956 A69-16882

Thermal performance of pressure transducers, accelerometers, displacement transducers, resistance thermometers and control mechanisms for NERVA reactor
06 p0956 A69-16885

NERVA transfer functions evaluation by computer data processing, using Fourier algorithm
[IEEE PAPER 2B-2] 07 p1179 A69-19187

Instrumentation design problems connected with NERVA, considering high gamma and neutron radiations and temperature environments
[IEEE PAPER 2D-5] 07 p1134 A69-19189

NERVA rocket engine with 200,000-250,000 lb thrust to replace Saturn 5 upper stage for manned interplanetary flights, discussing Mars flight
08 p1410 A69-21029

Air backflow in nuclear exhaust system duct for ground testing of NERVA engines, noting overpressure effect
[AIAA PAPER 69-325] 09 p1479 A69-22390

NERVA engine cooldown system for emergency shutdowns using high pressure liquid H followed by gaseous H warmup and liquid N cooldown
[AIAA PAPER 69-512] 16 p2810 A69-31846

Water moderated beryllium reflected reactor design for testing NERVA or Rover type fuel elements in nuclear environment, noting core location
[AIAA PAPER 69-513] 16 p2810 A69-32656

First generation nuclear flight stage with 75000 lb thrust NERVA flight engine, discussing applications design and hardware options
[AIAA PAPER 69-534] 16 p2810 A69-32707

Neutron and photon transport properties in liquid hydrogen obtained from measuring radiation environment in propellant tank mockup suspended above NERVA reactor
[AIAA PAPER 69-475] 16 p2810 A69-32716

NERVA engine operational cycle and performance, discussing startup, thrust buildup and shutdown
[AIAA PAPER 69-515] 18 p3170 A69-34809

NERVA program technological developments usability in nonspace industrial community
18 p3170 A69-35075

NERVA technology development, discussing reactor technology program, downward firing and flight-like configuration engine
[AIAA PAPER 68-612] 19 p3371 A69-35942

Water injection cooling of exhaust gases during stage testing of NERVA engine, discussing exhaust duct configuration and flow characteristics, spray nozzle geometry, etc
[AIAA PAPER 69-514] 19 p3372 A69-36301

Nuclear rocket program status and plans, presenting NERVA reactor and engine system tests
[AIAA PAPER 68-610] 21 p3768 A69-39219

NUCLEAR EXPLOSION EFFECT

Nuclear explosions electromagnetic effects on electronic systems, considering signals emitted from fireball and signal attenuation by changed atmospheric propagation
13 p2234 A69-28344

Ground military equipment hardening against nuclear environment, selecting worst case levels from isodamage curves
15 p2651 A69-30380

Solar cells designed to survive exposure to fission/fusion neutrons and electromagnetic spectrum products of nuclear weapon detonation
19 p3251 A69-35689

High altitude nuclear explosions detected by distinguishing artificial from natural sudden enhancement of atmospheric (SEA) phenomena
20 p3492 A69-37701

Crater formation by gas erosion in vent of 4.3 kiloton nuclear explosion detonated at 280 ft depth in layered trachytic volcanic rocks
22 p3937 A69-40409

NUCLEAR EXPLOSIONS

NT THERMONUCLEAR EXPLOSIONS

Inner radiation zone including data on electrons, protons and heavier particles and results from high altitude nuclear tests
12 p2152 A69-27144

Computer codes describing nuclear weapons effects associated with X ray transport, neutron transport and X ray interactions with material, fireball, blast environments, etc
15 p2652 A69-30381

Radiation effects produced by high temperatures of shock waves and nuclear explosion fireballs, air cooling, laser emission-matter interaction and optical phenomena
18 p3230 A69-34926

Air pressure wave forces on missile from silo wall motion resulting from close nuclear blast, using acoustic wave equation for concentric cylinder flow
21 p3691 A69-39765

Radiation hardened microcircuits and transistors for protection against transient radiation released by nuclear weapons
23 p4135 A69-41528

NUCLEAR FISSION

Lithium 6 and 7 fission following pion capture, searching for H 4 and 5
12 p2132 A69-26296

Single cell fission powered thermionic converters design and testing
14 p2399 A69-29195

Meteorite Li isotopic composition variations to determine neutron role in nucleosynthesis of solar system light elements
19 p3408 A69-36084

Spontaneous symmetric fission of superheavy elements near doubly magic nucleus as explanation for Xc and Kr isotopic composition anomalies in meteorites
20 p3601 A69-37503

Dirac cosmological principle of nuclear decay compared to Rutherford theory with respect to radioactive ages of terrestrial rocks and meteorites
22 p4017 A69-40176

NUCLEAR FUEL ELEMENTS

In-core thermionic sodium cooled uranium oxide fueled reactor for space vehicle power plant
02 p0279 A69-12666

Thermionic converter with external fuel surrounding inner emitter annulus for use in in-core reactors
14 p2480 A69-29185

Output current and efficiency of vapor thermionic converters obtained in terms of electrodes and interelectrode gas parameters, exemplifying nuclear fuel element
14 p2400 A69-29222

Water moderated beryllium reflected reactor design for testing NERVA or Rover type fuel elements in nuclear environment, noting core location
[AIAA PAPER 69-513] 16 p2810 A69-32656

Reactor testing, fuel elements and support materials for nuclear rocket program, discussing Phoebus 2A, Pewee I and nuclear furnace
[AIAA PAPER 69-556] 16 p2811 A69-32739

Thermionic reactors for auxiliary space power and electric propulsion applications, discussing converter development regarding nuclear fuel elements
23 p4186 A69-42246

NUCLEAR FUELS

Aerothermal-structural reentry safety evaluation for SNAP-27 radioisotope Graphite Lunar Module Fuel Cask at orbital and superorbital velocities
[AIAA PAPER 68-1166] 03 p0465 A69-13561

Nuclear reactor space power system concept using thermionic diodes, heat pipes and rod control, emphasizing neutronic aspects and feasibility
04 p0630 A69-14799

Critical end-on impact velocities calculated for reentering solid and granular radioisotopic fuel rods with solid and granular earth materials
04 p0630 A69-14800

Heat exchanger type low power solid-core fast nuclear rocket design, discussing fuels, safety aspects and space propulsion applications
17 p3004 A69-33342

Acrothermal-structural reentry safety evaluation for SNAP-27 radioisotope Graphite Lunar Module Fuel Cask at orbital and superorbital velocities
[AIAA PAPER 68-1166] 22 p3979 A69-40551

NUCLEAR FUSION

NT CONTROLLED FUSION

Neutrino radiation in universe with emphasis on stellar neutrino radiation, analyzing emission during nuclear fusion of C-N, He and Ne-Na cycles
01 p0145 A69-10754

Thermonuclear fusion program, discussing plasma instabilities suppression, toroidal installations, magnetic trap systems, plasma heating and dynamic stabilization
01 p0156 A69-11065

Nuclear fusion reactor development, discussing magnetic field confinement of hot dense plasmas and electric power production economic possibilities
08 p1361 A69-20124

Pu 244 and I 129 abundances in early solar system and continuous galactic synthesis model of element formation in stars
08 p1397 A69-20695

Nucleosynthesis in stars and early stage expanding universe, considering related nuclear reactions, helium abundances and kinematics of stars in Galaxy
08 p1357 A69-20893

S-process nucleosynthesis and temperature averaged neutron capture cross sections studied in relation to solar system, considering elemental and specific isotopic abundances
08 p1357 A69-20896

Lead isotopes nucleosynthesis by three mechanisms and contribution of mechanisms to abundances, noting chronology in nucleosynthesis
08 p1357 A69-20897

Nucleosynthesis in dynamics of massive star cores, noting element synthesis by neutron capture in supernova explosions
08 p1401 A69-20898

Model for nucleosynthesis of Li, Be and B in solar system from mass spectrometric measurements of high energy proton production of light elements
08 p1401 A69-20901

Solar element abundances from nucleosynthesis standpoint, discussing measurements with high resolution spectrometer used in double pass with intermediate slit
08 p1402 A69-20906

Radioactive decay products concentration from extinct radioisotopes in meteorites with estimation of formation interval, discussing fissionogenic xenon and solar system nucleosynthesis
08 p1405 A69-20924

Book on stellar, galactic and nucleosynthetic evolution covering nuclear, Fermi, electromagnetic and gravitational interactions roles
11 p1964 A69-25413

Low beta fusion research in open end magnetic mirrors covering scope, end losses, fusion economics, flute instability, stabilization, etc
14 p2498 A69-29843

General algorithm for eruptive plasma instabilities in fusion plasmas, flares and novae, yielding time behavior and dissipative effects
14 p2499 A69-29850

Nucleosynthesis based on stellar spectra and nuclear reactions data, discussing elements in sun and stars, meteorites, solar neutrinos, etc
14 p2529 A69-29985

Plasma physics and controlled nuclear fusion research - Conference, Novosibirsk, U.S.S.R., August 1968, Volume 2
17 p3014 A69-33826

Solar energy release by quark fusion catalysis of alpha reaction without production of neutrinos, noting temperature dependent reaction rate
18 p3186 A69-34643

Synthesis of proton rich nuclei in highly evolved stars, considering p elements production in interior by isobaric transformation
19 p3428 A69-36837

Elements nucleosynthesis during thermonuclear burning of carbon at series of temperatures and for several initial compositions
20 p3612 A69-38163

Big bang and little bang nucleosynthesis, discussing electron-neutrino or electron-antineutrino excess role in He production
21 p3801 A69-38813

Neutrons, protons and alpha particles abundance resulting from nuclear evolution of nondegenerate matter exploding at very high temperatures
22 p3980 A69-40148

Primordial He 3 and deuterium production from magnetic effects during nucleosynthesis epoch of big bang cosmologies
22 p4035 A69-41210

Main sequence star models for diverse solar masses, covering hydrogen burning phase in core and conditions for dynamic instability and mass exchange
23 p4208 A69-41286

Carbon isotopes compared in interstellar formaldehyde transition for galactic nucleosynthesis, discussing spectrum analysis of radio astronomical telescope observations
23 p4220 A69-42376

Nuclear theory of elements origin, discussing nucleosynthesis to interpret abundances
24 p4386 A69-43334

NUCLEAR HEAT

Thermal-chemical rocket based on thermal heating by energy input from nuclear fission process
03 p0496 A69-13666

Plane and cylindrical thermionic converters, considering electricity generation by heating through flame, solar radiation and nuclear flux
14 p2419 A69-29178

Heat generation in meteorites by radioactive isotopes generated by early solar proton irradiation prior to solar system solidification
19 p3411 A69-36098

NUCLEAR INTERACTIONS

NT ELECTRON CAPTURE

NT SPIN-ORBIT INTERACTIONS

Cosmic rays extensive air showers from interaction of particles with nuclei of elements in atmosphere
01 p0144 A69-10752

Strong interactions at energies above 100 Gev, examining use of cosmic ray experiment for qualitative studies of interaction process
03 p0498 A69-12939

Slow proton irradiation of ribonuclease thin layers, determining differential inactivation cross section for various proton energies
03 p0371 A69-13482

Seyfert galaxies high excitation broad emission lines and quasars resemblance, discussing causes of spiral galaxies violent nuclear activity
04 p0657 A69-14689

Natural orbital expansion coefficients of LCAO-MO-SCF-CI wave functions for ground state of H molecule
06 p0960 A69-17112

Isotopic composition in near-surface regions of meteorites due to nuclear processes with low energy solar particles
06 p0989 A69-17282

Muon component of extensive cosmic ray showers, discussing effect of multiplicity of secondary particles created by high energy nuclear interactions
07 p1207 A69-19325

Cosmic ray composition and nuclear interactions at very high energies, comparing results of Monte Carlo simulations with various experimental data
12 p2149 A69-26475

Inelastic interactions between Tev cosmic particles and light element nuclei, describing design and operation of measuring apparatus and derivable data
12 p2093 A69-26583

Superdense stars energy yield from neutrino emission, assuming incomplete degeneration of elementary particle Fermi gas
13 p2336 A69-27435

Nuclear emulsion high energy nucleon-nuclei interaction model accounting for two maxima track formation
13 p2303 A69-28371

Gamma quanta produced during high energy nucleon-nuclei interaction of air atoms recorded with X ray film
13 p2303 A69-28376

High energy nuclear interactions in graphite block at high altitude, recording gamma quanta produced
13 p2330 A69-28377

Wilson chamber and ionization calorimeter determination of cosmic ray particle-carbon nuclei interaction energy characteristics
13 p2330 A69-28379

Fireball events, isobars and meson resonances in very high energy nuclear interactions, discussing dispersion and four momenta transfer methods
13 p2303 A69-28380

Angular distribution of penetrating shower particles produced in nuclear interaction of cosmic rays with C, Sn, Cu and Pb
13 p2330 A69-28381

Pionization cross sections at 100 gev for interactions of cosmic ray neutrons and pions with C and Pb nuclei
13 p2330 A69-28382

Inelastic interaction cross sections of nuclear active particles at C and Fe in 70 to 1000 gev energy range
13 p2330 A69-28383

Inelastic interaction cross sections of nuclear active cosmic ray particles with atomic Fe and Pb in 100 to 1000 gev range
13 p2330 A69-28384

Mean free path of interaction of nuclear active particles in Fe with energies greater than 530 gev
13 p2303 A69-28385

Nuclear interactions between high energy nuclear active particles and C nuclei, studying electron-photon component energy with nuclear photoemulsions
13 p2331 A69-28388

Pion and nucleon interactions with nuclei, analyzing showers for symmetry and isotropy
13 p2331 A69-28389

Asymmetrical showers in interaction of high energy nuclear active particles with atomic nuclei, estimating target particle mass
13 p2303 A69-28391

Nuclear active cosmic ray component energy spectrum determined from calorimetric ionization burst measurements, discussing nuclear particle interactions absorption coefficients
13 p2331 A69-28393

Nuclear active cosmic ray component particle energy spectrum and nuclear cascade avalanches curves, using ionization calorimeter with Pb absorber
13 p2303 A69-28399

Sea level fluctuations of electron-photon, muon and active nuclear components of extensive cosmic ray showers determined, obtaining shower parameters
13 p2332 A69-28406

Soviet book on nuclear interactions in spacecraft shielding covering proton-Al nuclei inelastic interactions, secondary radiation, solar radiation effects, radiation belts, etc
14 p2481 A69-29817

Three dimensional Monte Carlo calculations for hadronic component of extensive air showers using semiempirical model high energy nuclear interactions
15 p2678 A69-31482

Near horizontal air showers relationship to direct muon production and heavy triplet particles of unit charge, discussing nuclear interactions and muon bremsstrahlung
15 p2678 A69-31499

Cosmic ray particle Pb nucleus interaction energy transfer to electron photon cascade in first inelastic collision, noting dependence on particle energy
17 p3008 A69-33387

Black body radiation at very high temperatures, discussing pion-nucleon interaction in pion gas in thermal equilibrium
23 p4238 A69-41358

NUCLEAR ISOBARS

Photoemulsion stacks irradiated by protons in magnetic field, determining nuclear isobar generation during quasi-nucleon interactions
13 p2303 A69-28373

Fireball events, isobars and meson resonances in very high energy nuclear interactions, discussing dispersion and four momenta transfer methods
13 p2303 A69-28380

NUCLEAR MAGNETIC RESONANCE

NT PROTON MAGNETIC RESONANCE

Raman spectra and temperature dependent nuclear quadrupole resonance frequencies of p-dichlorobenzene and p-dichlorobenzene-D, calculating librational amplitudes
01 p0122 A69-10286

Cl 35 nuclear quadrupole resonance spectra of 3,6-dichloropyridazine, tetrachloropyridazine, 2,6-dichloropyrazine and chloropyrazine
01 p0123 A69-10290

Low temperature thermometer based on temperature dependence of frequency of F-19 nuclear magnetic resonance in antiferromagnetic manganese difluoride
06 p0927 A69-17703

Superconductors with overlapping energy bands studied by nuclear magnetic resonance method
07 p1198 A69-18513

Gas-liquid and thin layer chromatography and nuclear magnetic resonance techniques to steric analysis of diketopiperazines
07 p1075 A69-19498

Quadrupole splitting of Na 23 nuclear magnetic resonance /NMR/ to investigate spontaneous polarization, coercive field and domain characteristics in Rochelle salt ferroelectric phase
09 p1559 A69-22283

Multiple particle production and resonance events during high energy particle collisions
13 p2303 A69-28372

Self diffusing substance /salt/ distribution in turbulent water flow at different Reynolds numbers by NMR, obtaining diffusion function consistent with experiments
14 p2430 A69-29424

Nuclear magnetic resonance flowmeter operating from outside pipe walls, discussing operating principles and applications
15 p2616 A69-31290

Validity of Lorentz invariance, discussing nuclear magnetic resonance test on torque for spin of electrons, muons and neutrons
18 p3176 A69-35007

Nuclear magnetic resonance of epsilon and delta phases in NbN system with nitrogen mole fractions
19 p3383 A69-36445

Boron 11 nuclear quadrupole coupling constants in solid boron halides, finding fine structure on nuclear magnetic resonance in boron fluoride
20 p3483 A69-36935

Energy level NMR spectral analysis for spin systems with sets of magnetically nonequivalent chemical-shift equivalent nuclei
20 p3579 A69-37348

NT HYPERONS

NT NUCLEONS

NT PHOTOELECTRONS

NT PIONS

NT POSITRONS

Low energy muons and nuclear active particles measured with extensive air showers array composed of scintillation detectors, spectrometer and Geiger counters
06 p0990 A69-17299

Nuclear particle plastic dielectric track detectors to record distribution of fissionable and heavy elements in nature and cosmic radiation
08 p1401 A69-20899

Mean free path of interaction of nuclear active particles in Fe with energies greater than 530 gev
13 p2303 A69-28385

Nuclear active particles energy in extensive air showers measured with ionization calorimeter, noting discrepancy attributed to ionization bursts
13 p2331 A69-28387

Nuclear interactions between high energy nuclear active particles and C nuclei, studying electron-photon component energy with nuclear photoemulsions
13 p2331 A69-28388

Angular distribution of nuclear particles dispersed during motion determined from photon energy and inelasticity coefficient
13 p2303 A69-28390

Asymmetrical showers in interaction of high energy nuclear active particles with atomic nuclei, estimating target particle mass
13 p2303 A69-28391

Cosmic ray postinteraction nuclear active particle energy spectrum measurements with ionization calorimeter, noting energy underderrating
13 p2331 A69-28392

Nuclear active cosmic ray component energy spectrum determined from calorimetric ionization burst measurements, discussing nuclear particle interactions absorption coefficients
13 p2331 A69-28393

High energy nuclear active particles and muons studied with calorimeters, noting cascades muon origin and muon energy spectra
13 p2331 A69-28395

NUCLEAR PHYSICS

NT REACTOR PHYSICS

Superdense matter possibly present in neutron stars, discussing relation with Einstein theory and nuclear physics
06 p1012 A69-18240

Nuclear science - IEEE Conference, Montreal, October 1968
07 p1179 A69-19184

NUCLEAR POWER PLANTS

Electric position servosystems for 50 ton telemetry reception antenna and 1200 ton loading turntable of nuclear power plant
04 p0585 A69-15184

Dissociating gas as working fluid for space plant, noting role in radiator area reduction
04 p0551 A69-15313

Nuclear power plant licensing, discussing public safety considerations by AEC and applicant responsibility in assuring freedom from undue risk
10 p1723 A69-23398

Solar and nuclear electric power technology for electric propulsion
[AIAA PAPER 69-826] 16 p2741 A69-32709

Nuclear aircraft power plant, discussing safety, economy and obstacles
[AIAA PAPER 69-554] 16 p2811 A69-32761

STAR /Stud and Rocker Panel/ four couple section improved by incorporating bonded tungsten electrical contacts for PbTe thermoelectric elements
23 p4188 A69-42261

NUCLEAR POWER REACTORS

NT SNAP 8

NT SNAP 10A

NT SPACE POWER UNIT REACTORS

Nuclear reactor space power system concept using thermionic diodes, heat pipes and rod control, emphasizing neutronic aspects and feasibility
04 p0630 A69-14799

Polonium 210 production for radiothermal propulsion via bismuth irradiation in graphite gas power reactor
05 p0791 A69-15594

Nuclear fusion reactor development, discussing magnetic field confinement of hot dense plasmas and electric power production economic possibilities
08 p1361 A69-20124

Nuclear power supply with in-core thermionic reactor for space power source and use in satellite TV, discussing theory, design and components
08 p1350 A69-20871

Power generating equipment operating with high temperature plasma as working medium requiring reactors with plasmized nuclear fuel coupled to MPD generators
10 p1738 A69-23489

Systems analysis of Rankine cycle nuclear-electric potassium space power system using Li cooled fast reactor and high temperature turbine inlet
23 p4189 A69-42266

NUCLEAR POWERED SHIPS

Performance potential of high speed ocean-going air cushion vehicles with aircraft nuclear power plants [AIAA PAPER 69-416]
15 p2550 A69-30480

NUCLEAR PROPELLED AIRCRAFT

Performance potential of high speed ocean-going air cushion vehicles with aircraft nuclear power plants [AIAA PAPER 69-416]
15 p2550 A69-30480

Nuclear aircraft power plant, discussing safety, economy and obstacles [AIAA PAPER 69-554]
16 p2811 A69-32761

NUCLEAR PROPULSION

Thermal-chemical rocket based on thermal heating by energy input from nuclear fission process
03 p0496 A69-13666

Low thrust nuclear engine using hydrogen suitable for transfer missions
05 p0791 A69-15598

Advanced electrical and nuclear propulsion systems for European launchers, comparing performances with chemical propulsion
06 p0984 A69-17628

Fluid and thermodynamic modeling for ground test simulation of nuclear rocket vehicle liquid hydrogen propellant behavior [SAE PAPER 690201]
07 p1178 A69-18306

Monograph on requirements for high speed interplanetary flights with nuclear engines and refueling at destination
09 p1586 A69-21298

Common nuclear propulsion modules for wide spectrum of manned planetary missions, discussing payload, mission and program flexibility [AIAA PAPER 68-590]
09 p1539 A69-21984

Book on theory and design of jet, rocket, nuclear, ion and electric propulsion systems noting combustion, detonation, fluid injection and space mission applications
11 p1943 A69-25582

Nuclear rocket propulsion, discussing solid core and fluid core systems for reactors, nozzles, feed systems, control, component design and performance
11 p1914 A69-25590

Space propulsion by radioisotope energy noting thermal heating, thruster configurations, propulsion system, mission capabilities and current thruster technology
11 p1914 A69-25591

Problem areas within cryogenic chemical and nuclear propulsion systems for space missions, noting available technology and limitations [AIAA PAPER 67-454]
12 p2174 A69-26782

Electric rocket propulsion, discussing roles of plasma and gas discharge physics in development of electromagnetic, electrostatic and thermoelectric nuclear systems
13 p2325 A69-28253

Zirconium hydride thermoelectric power system for space missions, discussing compactness, shield weight, temperature capability, reliability and SNAP 10A program
16 p2809 A69-31723

Solar and nuclear electric power technology for electric propulsion [AIAA PAPER 69-826]
16 p2741 A69-32709

Heat exchanger type low power solid-core fast nuclear rocket design, discussing fuels, safety aspects and space propulsion applications
17 p3004 A69-33342

Nuclear powered surface effects machine performance estimates, calculating reactor power and payload fraction for various clearance heights, gross weights and velocities
18 p3171 A69-35180

Technology, design, development, qualification and operational elements noting effects on performance, economics and scheduling of nuclear vehicle [AIAA PAPER 68-591]
21 p3769 A69-39752

Nuclear propulsion for solar system exploration, discussing NERVA solid core nuclear fission rocket,
21 p3792 A69-39572

nuclear-electric rockets and hybrid nuclear rocket/nuclear electric rocket systems [AAS PAPER 69-330]
24 p4349 A69-42871

NUCLEAR RADIATION

NT BETA PARTICLES
NT FAST NEUTRONS
NT GAMMA RAY BEAMS
NT GAMMA RAYS
NT PHOTONEUTRONS
NT SPALLATION
NT THERMAL NEUTRONS

Nuclear radiation dose rate and atmospheric ionization from radioactive fallout and natural sources, discussing fallout effect on population
01 p0145 A69-10982

Nuclear radiation damage vs thermal decomposition of diaminitrotrinitrobenzene and hexanitrostilbene, analyzing unchanged residual compound
02 p0304 A69-12500

Iris satellite experiments in astrophysics including nuclear and solar induced electromagnetic radiation
03 p0427 A69-12849

Explosive containment capsule for nuclear reactor irradiation
04 p0629 A69-14480

Book of engineering compendium on nuclear radiative shielding, discussing radiation sources, attenuation methods, induced heat generation, ducts and voids in shielding technology and design
05 p0791 A69-15830

Nuclear radiation influence on pool boiling heat transfer to liquid helium, using irradiated copper as boiling surface [ASME PAPER 68-WA/PID-3]
05 p0791 A69-16164

Nuclear and space radiation effects - IEEE Conference, University of Montana, July 1968
06 p0973 A69-16861

Nuclear pulsed radiation dosimeter based on strain gage measurement of induced thermal expansion, noting separation of neutron and gamma ray components
06 p0922 A69-16892

Laboratory simulation methods for cosmic nuclear radiation, discussing dosimetry methods
11 p1862 A69-24875

Soviet monograph on nuclear radiation effect on structure and properties of metals and alloys covering electron, gamma and neutron radiation
12 p2114 A69-26469

Baryon passive nuclear state nonexistence indicated by above and below ground calorimetric telescope method of nuclear cascade observation
13 p2331 A69-28401

Sirene 302 thermionic converter lifetime during irradiation in Triton immersion pile, considering effects on conversion efficiency
14 p2481 A69-29198

Diurnal variations in gamma rays produced by proton bombardment ascribed to geomagnetic time dependence for low energy solar proton cut-off
16 p2850 A69-32308

Aluminum capsule used in test reactor to irradiate explosive and propellant samples, determining radiation effects
17 p3004 A69-32945

Mossbauer spectroscopy, discussing nuclear resonance fluorescence and equipment
18 p3099 A69-34622

Nuclear environment irradiation effects on materials, emphasizing radiation chemical processes affecting polyimide and copolymer of styrene and alpha-methylstyrene
19 p3356 A69-35530

Primitive low energy Fe-group nuclei irradiation of meteoritic crystals from studies of pyroxene and feldspar from meteorites, discussing astrophysical implications
20 p3590 A69-37569

Transient effects of nuclear radiation bursts on dielectric properties of refractory low loss ceramics at L, S and X bands
20 p3584 A69-38065

NUCLEAR RADIATION SPECTROSCOPY

Nuclear gamma ray astronomy utilization for stellar interior detection, showing identification of key radioactive nuclei of supernova at explosion time
21 p3792 A69-39572

NUCLEAR REACTIONS

NT ANNIHILATION REACTIONS
NT CONTROLLED FUSION
NT ELECTRON CAPTURE
NT ELECTRON SCATTERING
NT HIGH ENERGY INTERACTIONS
NT NEUTRON EMISSION
NT NEUTRON SCATTERING

NT POSITRON ANNIHILATION
NT PROTON-PROTON REACTIONS
NT PROTON SCATTERING
NT RADIOACTIVE DECAY
NT RESONANCE SCATTERING
NT SPALLATION
NT SPIN-ORBIT INTERACTIONS
NT THERMONUCLEAR REACTIONS

Preatmospheric meteorite size determination from distribution of radioactive isotopes resulting from nuclear reactions produced by cosmic rays, discussing error sources
01 p0159 A69-11375

Absorption cross section for 68 Mev positive pion absorption by $1p\ 3/2$ neutron in C^{12} nucleus followed by single proton emission at 11 degrees
02 p0282 A69-11460

Absolute cross sections for coincidence detection of deuteron breakup by 42 Mev alpha particles, showing He 5 and Li 5 final state interaction peaks
03 p0472 A69-13469

Neutrino groups generation in internal regions of sun, analyzing flux ambiguities due to error of cross section parameter of nuclear reactions
10 p1757 A69-22827

Line spectrum of flare gamma radiation due to atmosphere nuclei excitation by high energy proton acceleration
11 p1945 A69-24241

Equilibrium state of matter at high temperatures and densities with respect to nuclear reactions, determining neutron-proton ratio
11 p1957 A69-24403

Neutrons overloaded nuclei role studied for neutronization of matter at high densities in statistical equilibrium with respect to nuclear reactions
11 p1957 A69-24404

Negative pion from 600 MeV synchrocyclotron stopped in thin Li 6 target in search for excited states of triton
12 p2132 A69-26297

Nuclear energized pulsational instability of stars based on linear quasi-adiabatic theory, including models with hydrogen burning shells
13 p2340 A69-27576

Proton initiated nuclear cascade in atmosphere calculated using Monte Carlo method, relating electron number to primary proton energy
13 p2331 A69-28397

Cosmic ray chain reaction particles energy spectrum determination in heavy media, discussing cascade parameter application in showers development
13 p2303 A69-28412

Solar system light elements investigated assuming Li, Be and B abundance as nuclear reaction products of high energy particles accelerated in early sun formation
13 p2354 A69-28495

Stellar Si burning at constant temperature studied for various initial abundance compositions, noting convergence toward pure Si relaxation
14 p2529 A69-29983

Validity range of nuclear quasi-equilibrium approximation for stellar silicon burning, discussing time rates of nuclear abundance changes and temperature effect
14 p2529 A69-29984

Nucleosynthesis based on stellar spectra and nuclear reactions data, discussing elements in sun and stars, meteorites, solar neutrinos, etc
14 p2529 A69-29985

Neutrino and antineutrino emission by URCA process calculated, assuming nuclear reactions in static and beta processes in kinetic equilibrium
15 p2674 A69-30542

Na 22 and H 3 production rates determined in stone meteorites exposed to 3 Gev isotropic protons, using radionuclide distribution data of exposed thick stone target
19 p3425 A69-36423

Stellar nuclear reactions at low energies studied to provide predictions of cross sections in carbon burning
20 p3612 A69-38164

Abundance compilations of elements due to nuclear processes, discussing carbonaceous chondrites character
21 p3789 A69-38812

Angular distributions for Sc 45-Ti 46 nuclear reactions involving 41 Mev alpha particles bombardment described by Born approximation
22 p3988 A69-41044

Equilibrium state of matter at high temperatures and densities with respect to nuclear reactions, determining neutron-proton ratio
24 p4391 A69-43793

Neutrons overloaded nuclei role studied for neutronization of matter at high densities in statistical equilibrium with respect to nuclear reactions
24 p4391 A69-43794

NUCLEAR REACTOR CONTROL

Nuclear reactor space power system concept using thermionic diodes, heat pipes and rod control, emphasizing neutronic aspects and feasibility
04 p0630 A69-14799

Pneumatic instrumentation line transfer function approximated by system model for simplifying reactor control system analysis
[IEEE PAPER 2D-6] 07 p1059 A69-19190

NUCLEAR REACTOR MATERIALS

U REACTOR MATERIALS

NUCLEAR REACTORS

NT BREEDER REACTORS
NT FAST NUCLEAR REACTORS
NT GAS COOLED REACTORS
NT GASEOUS FISSION REACTORS
NT LIQUID COOLED REACTORS
NT LITHIUM COOLED REACTOR EXPERIMENT
NT MOLTEN SALT NUCLEAR REACTORS
NT NRX REACTORS
NT PHOEBUS NUCLEAR REACTOR
NT PLUM BROOK REACTOR
NT SNAP 8
NT SNAP 10A
NT SPACE POWER UNIT REACTORS
NT WATER MODERATED REACTORS

NASA Plum Brook Reactor Facility /PBRF/ for determining radiation tolerance to support nuclear power application in space for propulsion and power
03 p0463 A69-13128

Thermal-chemical rocket based on thermal heating by energy input from nuclear fission process
03 p0496 A69-13666

Explosive containment capsule for nuclear reactor irradiation
04 p0629 A69-14480

High temperature eddy current crack detection technique for atomic reactor components under high thermal gradients
04 p0607 A69-14972

Ultrasonic thermometry for nuclear reactors based on temperature dependence of sound velocity in solids, discussing simulation experiments
[IEEE PAPER 1C-4] 07 p1134 A69-19186

Control system utilizing digital and linear integrated circuits for low power testing of Pewee 1 reactor of Rover program
[IEEE PAPER 2B-6] 07 p1179 A69-19188

Nuclear reactors for powering electrical engines and current supply for satellite devices, noting ROVER project and KIWI reactors
07 p1179 A69-19739

Engineering and reactor parameters associated with ionization of gas passing through nuclear reactor used as closed cycle MHD system working fluid
10 p1723 A69-23485

Thermionic converter power from satellite nuclear reactor for TV satellites, discussing direct heat utilization and applications
12 p2016 A69-25869

Turbomachinery buffer seals, buffer gas regulation and cleanup systems for operation of closed Brayton cycle power conversion system with gas cooled nuclear reactor
13 p2268 A69-27367

All metal nuclear thermionic modular converter, discussing applications, design and material requirements or limitations
14 p2398 A69-29181

Nuclear energy systems, discussing U.S. reactor concepts with emphasis on thermionic systems and space applications
14 p2404 A69-29278

Reactor testing, fuel elements and support materials for nuclear rocket program, discussing Phoebus 2A, Pewee 1 and nuclear furnace
[AIAA PAPER 69-556] 16 p2811 A69-32739

Monte Carlo method application to neutron streaming in hemispherical air-filled ducts in water tank to determine leakage through nuclear reactor shields
18 p3171 A69-35178

Nuclear reactor/thermoelectric power system design for manned orbiting space station, discussing station integration and operation
23 p4187 A69-42256

NUCLEAR RESEARCH AND TEST REACTORS

NT NRX REACTORS
NT PLUM BROOK REACTOR

Cavity reactor consisting of dilute fuel core surrounded by moderating reflector to attain very high temperatures in gaseous cores
07 p1179 A69-18954

SNAP 8 developmental reactor vacuum system providing space environment simulation for nuclear reactor ground testing
13 p2241 A69-28086

Aluminum capsule used in test reactor to irradiate explosive and propellant samples, determining radiation effects
17 p3004 A69-32945

NUCLEAR ROCKET ENGINES

Feasibility of nuclear stage for space missions, discussing Saturn 5 third stage replacement, payload gain, reactor and engine size
08 p1409 A69-20158

Out-of-core thermionic reactor power increase by using central heat pipe in coaxial cavity
09 p1441 A69-21836

Stability analysis including delayed collector and structure coefficients, showing thermionic reactor instability with all negative reactivity coefficients
09 p1442 A69-21841

Nuclear rocket propulsion, discussing solid core and fluid core systems for reactors, nozzles, feed systems, control, component design and performance
11 p1914 A69-25590

Electric and ion propulsion with solar array or nuclear reactor energy sources, discussing thermal thrusters, electrostatic thrusters and plasma thrusters
11 p1944 A69-25592

Nuclear rocket propulsion operation, design, properties and performance of electrostatic, electrothermal and electromagnetic systems
13 p2297 A69-28254

Nuclear type cylindrical thermionic converter with porous adsorbent structure and liquid cesium tank
14 p2397 A69-29174

Fast and thermal thermionic reactor systems characteristics including fissile material, components mass, power output and flattening and design features
14 p2480 A69-29182

Thermionic reactor systems, discussing hybrid nuclear rocket/nuclear electric Mars mission, design features, performance and electric power characteristics
14 p2480 A69-29183

Thermionic reactor design for electric propulsion with emphasis on reactor power and fuel energy and fast neutron flux
14 p2509 A69-29184

Thermionic converter with external fuel surrounding inner emitter annulus for use in in-core reactors
14 p2480 A69-29185

Out-of-core thermionic reactor concept for space power supply using lithium heat pipes in crossed layers
14 p2480 A69-29187

In-core thermionic reactor space power plants stability and control criteria, comparing linear and non-linear models
14 p2481 A69-29189

Deposition and interdiffusion of W layers on Mo emitter of in-core thermionic reactor, investigating microstructure of transition zone
14 p2462 A69-29210

Thermionic reactors U.S.S.R. space and other programs, considering power output, heat exchange and losses, neutron physics and design parameters
14 p2404 A69-29277

Nuclear energy systems, discussing U.S. reactor concepts with emphasis on thermionic systems and space applications
14 p2404 A69-29278

Analog computer for design of control systems used in nonnuclear testing of nuclear rocket engine components and subsystems
15 p2589 A69-31289

Nuclear rockets as Saturn 5 third stages, emphasizing increased payload or velocity utility and resulting engine and stage requirements
[AIAA PAPER 69-555] 16 p2867 A69-31849

Nuclear solid core rocket engine performance for interplanetary orbital launch of spacecraft by multiorbit injection
[AIAA PAPER 69-535] 16 p2810 A69-32660

Gaseous reactor fluid mechanics for nuclear rocket engines, discussing experiments on geometries used in open cycle engine for acceptable uranium loss rate
[AIAA PAPER 69-477] 16 p2811 A69-32728

Reactor testing, fuel elements and support materials for nuclear rocket program, discussing Phoebus 2A, Pewee 1 and nuclear furnace
[AIAA PAPER 69-556] 16 p2811 A69-32739

Heat exchanger type low power solid-core fast nuclear rocket design, discussing fuels, safety aspects and space propulsion applications
17 p3004 A69-33342

Fluid dynamic simulation of gas core nuclear rocket chamber for separating light and heavy gas via centrifugal force produced by MHD-driven rotational flow
[AIAA PAPER 69-727] 17 p3004 A69-33483

Secondary flows in confined viscous vortex for nuclear rockets, employing rotating disk in chamber end wall for recirculation
19 p3296 A69-35756

Liquid, solid, hybrid propellant and nuclear, electric and air breathing rocket engines, discussing orbiting payload cost, controllability, operating environments, velocity, etc
19 p3395 A69-36321

Nonintegral burn of solid core nuclear rockets, discussing modular stage concepts approach to low cost space exploration
[AIAA PAPER 68-589] 21 p3768 A69-39026

Time-optimal nuclear rocket propellant start-up with thermal stress constraints based on distributed parameter model, deriving algorithm for flow rate increase
21 p3768 A69-39632

Cement materials to attach thermocouple to stainless steel tubing in nuclear rocket engine nozzle, considering thermal conductivity, bond and tensile and compressive strengths
21 p3753 A69-39699

Technology, design, development, qualification and operational elements noting effects on performance, economics and scheduling of nuclear vehicle
[AIAA PAPER 68-591] 21 p3769 A69-39752

Thermionic reactor concepts and development in U.S., comparing strengths and weaknesses
23 p4186 A69-42245

Thermionic reactors for auxiliary space power and electric propulsion applications, discussing converter development regarding nuclear fuel elements
23 p4186 A69-42246

West German research in thermionic diodes and reactors, describing terrestrial version of thermal in-core thermionic reactor project
23 p4188 A69-42258

NUCLEAR SCATTERING

NT NEUTRON SCATTERING

NT RESONANCE SCATTERING

Asymmetry of polarized protons scattered from He 4 at 540 Mev for laboratory angles between 4 and 42 degrees
04 p0632 A69-14966

Surveyor scientific instruments and operation on moon, reviewing TV camera, alpha scattering instrument and surface sampler
[JPL-TR-32-1358] 08 p1312 A69-19850

Angular distribution of nuclear particles dispersed during motion determined from photon energy and inelasticity coefficient
13 p2303 A69-28390

Inelastic scattering cross sections calculated, comparing results for various nuclear states expressed as Wood-Saxon radial and harmonic oscillator functions
14 p2504 A69-29006

Core polarization effects in inelastic scattering cross sections for several nuclei in 2s-1d shell, using Hartree-Fock wave functions and Born approximation
14 p2487 A69-29007

High energy scattering approximation valid from small to large angles, discussing errors and proton scattering by He
14 p2487 A69-29008

K meson-light nucleus scattering lengths calculated using multiple scattering theory with Kim zero range
15 p2655 A69-30309

Coulomb interference corrections in pion-He scattering, discussing three specific formalisms
18 p3176 A69-35008

Approximations for meson-nucleus scattering length from energy level measurements on mesonic atoms, emphasizing formula for negative pi mesonic atoms
22 p3987 A69-41004

Scattering of high energy Ar beams by room-temperature Ar, He and H molecules, deriving interaction energies at internuclear distances
22 p3988 A69-41187

Intermediate energy protons elastic and quasi-elastic scattering from light nuclei, correlating p-D, p-He-3, p-p and p-He-4 data with various scattering models
24 p4352 A69-43123

Positronium formation in positron-helium scattering, including polarizability in potentials appearing in final equations
24 p4353 A69-43815

NUCLEAR SHIELDING

U RADIATION SHIELDING

NUCLEAR SPIN

Proton spin-lattice relaxation time in dilute liquid and gas solutions of orthohydrogen in parahydrogen, noting dependence on temperature, density and composition

06 p0961 A69-17141

Proton spin maser oscillator with emission coils coupled by prepolarized liquid, discussing tuning and detuning

08 p1324 A69-20231

Deep freezing of nuclear precession magnetometer elements for improving instrument characteristics

14 p2446 A69-29083

Energy level NMR spectral analysis for spin systems with sets of magnetically nonequivalent chemical-shift equivalent nuclei

20 p3579 A69-37348

Low noise nuclear precession magnetometer noise rejection optimization design specifications for measuring geomagnetic field components

23 p4165 A69-41868

NUCLEAR STRUCTURE

Cosmic rays origin, measurements of energy spectrum and stellar diurnal variations

10 p1757 A69-22823

Nuclear theory of elements origin, discussing nucleosynthesis to interpret abundances

24 p4386 A69-43334

NUCLEAR SUBMARINES

U SUBMARINES

NUCLEAR WEAPONS

Air carrier liability for nuclear weapons damage, discussing international agreements

11 p2003 A69-24260

Computer codes describing nuclear weapons effects associated with X ray transport, neutron transport and X ray interactions with material, fireball, blast environments, etc

15 p2652 A69-30381

Polaris and Poseidon nuclear missile systems, considering efficiency and launching depth from nuclear submarine

19 p3432 A69-36687

NUCLEATE BOILING

NT LEIDENFROST PHENOMENON

Nucleate pool boiling heat transfer of liquid nitrogen from circular disks with different surface conditions including copper and nickel mirror finishes, roughness and coatings

02 p0352 A69-12207

Pool boiling heat transfer from stainless steel coated with Teflon to produce nonwetted surfaces [ASME PAPER 68-WA/HT-12]

05 p0847 A69-16119

Nucleate pool boiling heat transfer data extended to relate effect of heating surface characteristics [ASME PAPER 68-WA/HT-22]

05 p0847 A69-16125

Nuclear radiation influence on pool boiling heat transfer to liquid helium, using irradiated copper as boiling surface [ASME PAPER 68-WA/PID-3]

05 p0791 A69-16164

Natural convection heat transfer for incipient vapor formation in liquid H and N and for nucleate boiling of liquid H [ASME PAPER 68-WA/PID-4]

05 p0848 A69-16165

Inception of nucleate boiling with liquid nitrogen, noting surface finish effects [ASME PAPER 68-WA/PID-10]

05 p0848 A69-16167

Temperature measurement associated with bubbles leaving heat source in subcooled pool boiling carbon tetrachloride analyzed, using high speed motion pictures by schlieren optical system [ASME PAPER 68-HT-47]

13 p2374 A69-27779

Microlayer thickness in nucleate boiling, studying liquid-vapor interface motion of growing bubble near heated surface

13 p2375 A69-27789

Functionality between heat flux and imposed operating conditions during nucleate pool boiling

13 p2376 A69-28142

Nucleate boiling burnout heat flux data for ethane, ethylene and ethane-ethylene mixtures at various pressures, discussing applicability of Noyes equations

15 p2671 A69-31118

Bubble boiling onset in forced fluid flow, deriving equations for calculating minimum temperature difference between wall and fluid, discussing applicability range

16 p2878 A69-31954

Heat transfer from cylindrical copper surface to liquid helium at 4 degrees K, discussing temperature fluctuations in nucleate boiling region

17 p3074 A69-33780

Book on heat transfer from horizontal heating surfaces to stationary boiling liquids, heating surface roughness effect and bubble formation

20 p3633 A69-37917

Induced convection effect on peak pool-boiling heat flux under variable gravity, pressure and size conditions and various boiled liquids

24 p4409 A69-43516

Heat transfer during nitrogen tetroxide nucleate boiling at various pressures and heat fluxes [ASME PAPER 69-HT-58]

24 p4411 A69-43536

Film-nucleate boiling transition for liquid nitrogen in vertical forced flow in electrically heated tube, discussing conduction model and agreement with visual experiment [ASME PAPER 69-HT-26]

24 p4412 A69-43542

Nucleate boiling effect on operation of low temperature heat pipes, using everted stainless steel to permit visualization of wick structure and bubble nucleation [ASME PAPER 69-HT-24]

24 p4412 A69-43544

NUCLEATION

NT CLOUD SEEDING

Ferrite and sigma phase formation in austenitic stainless steels with nickel and chromium content

02 p0269 A69-12764

Condensation-enhanced vaporization rates in nonisothermal systems, noting fume nucleation augmentation of rates into cooler environments

03 p0532 A69-13122

Multiple high field domain nucleation in GaAs, discussing dependence on contact inhomogeneities

05 p0807 A69-15959

Kinetics of homogeneous and heterogeneous growth of centers of new phase of semiconductor during ion bombardment as function of radiation dose

06 p0978 A69-16985

Thermal accommodation coefficient and critical supersaturation for nucleation of mercury vapor on pyrex glass

13 p2321 A69-28005

Dropwise condensation, analyzing nucleation sites, growth, vapor capture, heat transfer rates and surface texture

13 p2376 A69-28143

Semiconductor films synthesis and properties, discussing single crystal films, epitaxial nucleation, nuclei surface distribution, layer kinetics, doping and film-substrate interface

15 p2670 A69-31046

Moon density and nucleation of planets, explaining low density and absence of heavy core by late aggregation from nonmetallic particles

16 p2865 A69-32808

Metal purity effect of nickel and Ni-Mo alloy on nucleation and recrystallization nuclei growth following 80 percent plastic deformation

18 p3159 A69-35449

Aluminum oxide droplets condensation from atmosphere of metal vapor and oxygen, studying temperature and time effects on particle nucleation, growth and distribution

21 p3783 A69-38799

Impurities effects on single crystal film formation of fcc metals on alkali-halide cleavage planes, stressing stacking fault energy importance

22 p3992 A69-39899

Einstein development of theory of fluctuations applied to homogeneous nucleation, calculating activation energy, liquid drop-vapor system equilibrium state peculiarity, etc

22 p3938 A69-40448

NUCLEI

Cosmogonic nature of galactic nuclei activity, emphasizing streamers ejection and new formations in galaxies

12 p2163 A69-27016

Lallemand electronic camera application for spectroscopic observations of unsteady phenomena in galactic nuclei at 4000 A, noting radial velocities

12 p2163 A69-27017

Successive explosions produced two gas systems observed in six Seyfert galaxy nuclei by spectrophotometry, using diffraction spectrographs

12 p2164 A69-27022

Galactic nuclei congeneric and coexisting peculiarities, including hot star planar formations in spiral galaxies

12 p2164 A69-27027

Spiral galaxy nuclei, relating nuclei luminosity to galactic luminosity

12 p2165 A69-27028

Photographic magnitudes of galactic nuclei, presenting plots for stellar magnitude distribution of galactic nuclei

12 p2165 A69-27029

Spiral galaxies with connectors observed in Southern Hemisphere, noting galactic nuclei differences and nucleus relation to galaxy morphological type

12 p2165 A69-27030

Radio emission correlation to nuclei shape in normal galaxies

12 p2166 A69-27040

Comet Ikeya-Seki 1965f primary nucleus splitting date and rate established from dynamic solutions

14 p2524 A69-29710

Nongravitational force dynamic effect and model for rotating cometary nucleus, including changes in orbital elements

14 p2524 A69-29713

Galactic nuclei nature, activity, evolution and classification

14 p2527 A69-29896

Gasdynamic model of comet nucleus region, discussing molecular collisions, surface brightness distribution and dust particle motion

15 p2684 A69-30520

Expression relating gas density, radial velocity and temperature at comet nucleus surface to nucleus surface temperature, applying results to unsteady sublimation process

15 p2684 A69-30521

Spectrophotometry of elliptical galaxy NGC 1052 nucleus from 3400 to 6300 A for relating radio properties and optical characteristics

16 p2853 A69-31610

Physical characteristics of young planetary nebulae and nuclei, discussing classification of objects I 4997, M 3-27 and M 1-2

19 p3423 A69-36226

Inelastic proton scattering cross sections for target nuclei in 2s-1d shell calculated in distorted wave Born approximation with projected Hartree-Fock wave functions

22 p3988 A69-41045

NUCLEI [NUCLEAR PHYSICS]

NT ALPHA PARTICLES

NT DEUTERONS

NT HEAVY NUCLEI

Iodine 123 decay via gamma ray emission, noting energies of several transitions

03 p0470 A69-13099

Lithium, Be, B and fluorine nuclei in cosmic radiation, discussing nature of spectra

06 p0988 A69-12721

Spectra analysis of proton and He nuclei having different charge-to-mass ratios to obtain information on solar modulation and injection spectra

06 p0988 A69-12722

Cosmic ray nuclei energy spectra and abundances above 20 Mev/nucleon determined by OGO-1 satellite experiment, considering He, B, C, N, O, Ne, Mg, Si, Mn, Fe, Co and Ni

08 p1378 A69-20067

Low energy multiply charged cosmic ray nuclei propagation and source characteristics, considering two component model based on OGO satellite measurements

08 p1378 A69-20068

Energy spectra of carbon and oxygen nuclei in primary cosmic radiation, comparing results to earlier measurements and satellite observation

08 p1380 A69-20632

Spatial distribution of residual nuclei produced in thick Fe targets by one and three Gev protons, noting total production and longitudinal variation of production

10 p1760 A69-23411

Neutrons overloaded nuclei role studied for neutronization of matter at high densities in statistical equilibrium with respect to nuclear reactions

11 p1957 A69-24404

Nuclear component energy flux absorption in Fe measured with ionization calorimeter

13 p2330 A69-28386

Form factor of nucleus effect on high energy muons bremsstrahlung cross section

13 p2333 A69-28422

Core polarization effects in inelastic scattering cross sections for several nuclei in 2s-1d shell, using Hartree-Fock wave functions and Born approximation

14 p2487 A69-29007

Nuclear level density and mass shell corrections relationship for deformed and undeformed nuclei

14 p2488 A69-29337

Superdense stars torsional oscillations and crystallization among nuclei from comparison with melting

temperature and transverse shear wave velocities of dense conventional matter
17 p3037 A69-33643

Cosmic ray propagation equilibrium model for rays origin and storage in galaxy, considering energy dependence of nuclei relative abundances
18 p3185 A69-34276

Elastic scattering cross sections for 21-Mev incident protons measured for nuclei differing in mass, determining optical model potential
18 p3179 A69-35489

Quarkian core substance in superstars of great masses, discussing existence as primordial state forming baryon and nuclei and origin in stellar gravitational contraction
19 p3401 A69-35912

Meteorite minerals as detectors for studying fossil record of cosmic ray nuclei, emphasizing feldspars and pyroxenes
20 p3590 A69-37568

Primary cosmic ray nuclei studies during Gemini 2 flight by nuclear emulsion detector with time resolution capability, describing experiment design and equipment operation
21 p3787 A69-38350

Primary H nuclei flux and spectrum near geomagnetic equator, discussing emulsion stack exposure
22 p4005 A69-40520

Relative abundances U-235/U-238, Th-232/U-238, Pu-244/U-238 and I-129/I-127 at solar system formation time to obtain time evolution of gamma process nuclei
22 p3986 A69-40766

Differential cross section and polarization measurements for elastic scattering of high energy protons from light nuclei
24 p4352 A69-43125

Neutrons overloaded nuclei role studied for neutronization of matter at high densities in statistical equilibrium with respect to nuclear reactions
24 p4391 A69-43794

NUCLEIC ACIDS
NT RIBONUCLEIC ACIDS
NT URIDYLIC ACID

Protein and nucleic acid building blocks sequence differences influence on evolutionary relationship of living organisms, comparing fish and mammal globins
11 p1828 A69-25456

Quantitative gas-liquid chromatographic analysis of nucleic acid components including purine and pyrimidine bases, nucleosides or nucleotides
13 p2217 A69-28260

NUCLEON-NUCLEON INTERACTIONS
Underground search for massive strongly interacting cosmic ray particles, using shower selecting extension array and interaction detecting telescope
02 p0310 A69-12831

High energy cosmic ray research facility at mountain altitudes, noting nucleon-proton interactions, particle identification and momentum analysis
03 p0499 A69-12942

High energy inelastic particle collisions observed at high altitude station, using Monte Carlo computations for nucleon-nucleon collision model
13 p2330 A69-28374

Pion and nucleon interactions with nuclei, analyzing showers for symmetry and isotropy
13 p2331 A69-28389

Frequencies of charged secondaries numbers emitted from nucleon-nucleon and pion-nucleon inelastic collisions, observing multiplicity regularity
18 p3177 A69-35009

Cosmic ray neutron studies of atmospheric nucleon component equilibrium and flux fluctuations at atmosphere top
22 p4002 A69-40092

NUCLEON POTENTIAL
Born-Mayer parameters simplifying computation of interatomic potential, tabulating numerical values for 104 mononuclear pairs of neutral ground state atoms
13 p2301 A69-27453

He II excitation spectrum for interparticle potential using pair Hamiltonian with repulsive core and attractive well
17 p3008 A69-33118

NUCLEONICS
Aircraft nucleonic fuel gauging system, using radioactive gas to emit gamma rays for fuel mass sensing
18 p3139 A69-35468

NUCLEONS
Cosmic ray solar diurnal variations for nucleonic component, discussing differential response functions
03 p0501 A69-13751

Extensive air showers characteristics based on models of high energy interactions of nucleons and pions with air nuclei
06 p0990 A69-17301

Fluorine nuclei in primary cosmic radiation identified by counter telescope measurements on Pioneer 8 spacecraft
15 p2676 A69-30886

Cosmic rays nucleonic component latitude at solar minimum activity, using IGY neutron monitor
19 p3396 A69-36411

Errors due to neutron counter radioactivity in cosmic rays nucleon measurements analyzed in reducing readings to barometric pressure
23 p4206 A69-41855

High energy nucleons and electrons accelerated in solar flares, considering interplanetary magnetic field effect on radiation properties near earth orbit
24 p4372 A69-43617

NUCLEOPHILES
Synthesis and nucleophilic reactions of stable alpha-bromoorganolithium reagent
07 p1074 A69-19479

NUCLEOSIDES
NT ADENINES
NT ADENOSINE TRIPHOSPHATE [ATP]

Purines, pyrimidines and nucleosides absorption by Li-, Na-, Mg- and Ca-montmorillonite in aqueous solutions over range pH 2-12 by cation exchange
05 p0716 A69-15973

NUCLEOSYNTHESIS
U NUCLEAR FUSION

NUCLEOTIDES
NT ADENINES
NT ADENOSINE TRIPHOSPHATE [ATP]
NT PYRIDINE NUCLEOTIDES
NT URIDYLIC ACID

Unique sequence of oligonucleotides located in tobacco mosaic virus ribonucleic acid
03 p0370 A69-13461

Binding of lysine-rich proteinoids to organismic or thermally synthesized polynucleotides, noting polyanhydroamino acid interactions with polynucleotides
07 p1074 A69-18635

DNA replication in vivo as function of temperature sensitive polynucleotide ligase mutant Th, tsA80 in strand synthesis
10 p1647 A69-24188

Cell origin in self organizing natural polymers in terms of molecular evolutionary priority of polynucleotides and poly alpha amino acids
22 p3896 A69-40781

Exonuclease function of DNA polymerase from Escherichia coli, discussing hydrolysis of polydeoxyribonucleotides and resistancy of oligonucleotides
22 p3898 A69-41073

Fluorescence properties of nucleotides, polynucleotides and phosphorylated derivatives as function of temperature, pH and ionic strength
22 p3898 A69-41078

NUCLIDES
NT ALUMINUM 26
NT ARGON ISOTOPES
NT BERYLLIUM 7
NT BERYLLIUM 10
NT BERYLLIUM ISOTOPES
NT BORON ISOTOPES
NT BORON 10
NT CADMIUM ISOTOPES
NT CALCIUM ISOTOPES
NT CARBON ISOTOPES
NT CARBON 12
NT CARBON 13
NT CARBON 14
NT CESIUM 133
NT CHROMIUM ISOTOPES
NT COBALT ISOTOPES
NT COBALT 60
NT DEUTERIUM
NT HELIUM ISOTOPES
NT HYDROGEN ISOTOPES
NT IODINE ISOTOPES
NT IRON ISOTOPES
NT ISOTOPES
NT KRYPTON ISOTOPES
NT KRYPTON 85
NT LANTHANUM ISOTOPES
NT LEAD ISOTOPES
NT LITHIUM ISOTOPES
NT MAGNESIUM ISOTOPES
NT MANGANESE ISOTOPES
NT NEON ISOTOPES
NT NITROGEN 16
NT OXYGEN ISOTOPES
NT OXYGEN 18
NT PHOSPHORUS 32
NT PLUTONIUM ISOTOPES
NT PLUTONIUM 238

NT POLONIUM ISOTOPES
NT POTASSIUM ISOTOPES
NT POTASSIUM 40
NT RADIOACTIVE ISOTOPES
NT RADIUM 226
NT RUBIDIUM ISOTOPES
NT RUBIDIUM 86
NT SCANDIUM ISOTOPES
NT SODIUM ISOTOPES
NT SODIUM 22
NT STRONTIUM ISOTOPES
NT STRONTIUM 90
NT TELLURIUM
NT THORIUM ISOTOPES
NT THULIUM ISOTOPES
NT TRITIUM
NT URANIUM ISOTOPES
NT URANIUM 235
NT XENON ISOTOPES
NT XENON 129
NT XENON 133
NT ZIRCONIUM ISOTOPES
NT ZIRCONIUM 95

Production rates of nuclides measured in stack of glass plates under proton irradiation for calculating cosmic ray production rates in stone meteorites
06 p0989 A69-17283

Meteorite and primordial matter composition related to possible fractionation processes influence, discussing nuclear species abundance
19 p3406 A69-36073

Cosmic-ray-produced stable and long-lived nuclides in iron meteorites, considering shielding effect on spallation production
19 p3411 A69-36099

NULL REFERENCE GLIDE PATH
U GLIDE PATHS

NULL ZONES
Mars entry capsule ionized wake producing circularly polarized antenna radiation null region, noting effect on communication blackout time
22 p3914 A69-40701

NUMBER THEORY
NT ADDITION THEOREM
NT ARITHMETIC
NT CONGRUENCES
NT EXPONENTS
NT INTEGERS
NT MULTIPLICATION

Linear random processes including law of large numbers, covariance estimation and linear to normal process relationship
01 p0029 A69-10555

NUMERICAL ANALYSIS
NT APPROXIMATION
NT BORN APPROXIMATION
NT CHEBYSHEV APPROXIMATION
NT DIFFERENCE EQUATIONS
NT EDDINGTON APPROXIMATION
NT ERROR ANALYSIS
NT FINITE DIFFERENCE THEORY
NT HARTREE APPROXIMATION
NT INTERPOLATION
NT ITERATION
NT ITERATIVE SOLUTION
NT LEAST SQUARES METHOD
NT MONTE CARLO METHOD
NT NEWTON-RAPHSON METHOD
NT NOMOGRAPHS
NT OSEEN APPROXIMATION
NT PADE APPROXIMATION
NT PARTICLE IN CELL TECHNIQUE
NT RAYLEIGH-RITZ METHOD
NT RELAXATION METHOD [MATHEMATICS]
NT RITZ AVERAGING METHOD
NT RUNGE-KUTTA METHOD
NT SOMMERFELD APPROXIMATION
NT TRUNCATION ERRORS

Numerical solution method for equation of electric field affected by permanent flux of identical ions
01 p0128 A69-10364

Graphical and analytical interpolation methods for representing initial compositions in equilibrium thermodynamic systems
01 p0176 A69-10403

Complex chemical equilibrium calculation, analyzing thermodynamic principles and solution to nonlinear equations
01 p0023 A69-10588

Three leveled computer program library compiled for numerical analysis
01 p0036 A69-10709

Numerical analysis of temperature variation of spherical spinning satellite with and without radiatively coupled inner shell containing heat source
01 p0162 A69-10761

General predictor-corrector method for system of m ordinary first order differential equations proved stable

if Hermitian forms with coefficients are positive definite

01 p0105 A69-10807

Numerical evaluation of curvilinear integrals and areas, using digital computer

01 p0106 A69-10867

Collection of papers on computational fluid dynamics

01 p0061 A69-10916

Eigenproblem for displacement integral equations with finite cosine transform kernels, extending Roark-Wing numerical method for eigenvalues to kernels

01 p0106 A69-10986

Numerical filtering procedures for gust spectrum analyses compared for gain and phase lag frequency response characteristics, discussing gust acceleration spectra

01 p0084 A69-11052

Numerical method for determining group velocity of waves in homogeneous anisotropic medium, using implicit function from dispersion relation

01 p0131 A69-11117

Stable high order implicit methods to solve numerically differential equation systems with matrix coefficients used for heat conduction equation

01 p0107 A69-11364

Generalized alternating-direction implicit method involving extra parameter for solving Laplace equation used for 3d model problem

01 p0107 A69-11366

Transverse plasma velocity component effect on boundary layer structure between cold plasma and confined magnetic field

02 p0235 A69-11424

Six level model for numerical geopotential forecast allowing for quasi-static and quasi-geostrophic approximations

02 p0273 A69-11434

Numerical method of solving optimum control problems through reduction to solution of simple minimization problems by constructing suitable sequence of auxiliary functionals

02 p0271 A69-11649

Numerical differentiation formulas for coefficients of given characteristic function, using tabulated Stirling numbers

02 p0271 A69-11653

Analytical model of geomagnetic field constructed from Cosmos 49 data using spherical analysis

02 p0240 A69-11698

Numerical calculations for oscillatory solutions of system of nonlinear differential equations, noting circularly polarized magnetic oscillations observed near earth bow shock front

02 p0241 A69-11729

Computer stress analysis may result in automated designs, emphasizing finite element technique

02 p0341 A69-12153

Monograph of lectures on numerical solutions of linear, singular and nonlinear differential equations for boundary value problems using finite differences

02 p0272 A69-12157

Grobner formulas for numerical analysis of differential equations, discussing applications to orbit computations in celestial mechanics

02 p0322 A69-12250

Numerical regularization of single binary collision in n body gravitational problem

02 p0322 A69-12268

Numerical solution on UNIVAC 1107 for model describing symmetrical gravitational collision of two four body systems

02 p0322 A69-12269

Numerical solutions of elastic problems by conformal mapping and finite difference method applied to circumferentially grooved shafts in torsion

02 p0346 A69-12419

Numerical solutions elastoplastic torsion of circumferentially grooved shafts based on flow and deformation type theories

02 p0346 A69-12420

Numerical solution for ambipolar diffusion and kinetic decomposition of rotating body of complex chemical composition in ionized airstream

02 p0191 A69-12580

Automatic determination of relaxation and retardation spectra for linearly viscoelastic materials from experimental data using simple numerical techniques

02 p0348 A69-12605

Numerical estimates for degenerate pinch in InSb, determining pinch parameters

02 p0300 A69-12638

Iterative transfer of boundary values to fictitious contour in numerical solution of partial differential equations [ONERA-TP-646]

03 p0454 A69-12874

Bounded solutions for systems of ordinary second order differential equations

03 p0455 A69-13257

Tabulation of high accuracy gamma function values for some rational arguments, noting applications to Gaussian quadrature formulas, fractional Bessel functions and Airy functions

03 p0455 A69-13375

Collection of Soviet articles on computer methods and programming covering fluid flow by numerical methods

03 p0362 A69-13649

Numerical computer results applied to supersonic flow of perfect gas past staggered cones

03 p0363 A69-13659

Ideal gas flow near stagnation line for blunt bodies, applying van Dyke series truncation method to numerical solution

03 p0364 A69-13660

Numerical technique using transfer matrices to solve boundary value problems in structural analysis

03 p0526 A69-13736

Two dimensional problem of elasticity by numerical solution, outlining program for computer

03 p0527 A69-13750

Digital simulation based on guided missile experience, discussing numerical methods for ordinary differential equations, literature, choice of method and simulation languages

03 p0401 A69-13763

Numerical method for explicit solution of aircraft mass problem based on linearization of equations describing individual aircraft section masses

03 p0367 A69-13790

Three dimensional boundary layers on cones at small angle of attack, presenting numerical solutions with heat transfer effects for wind tunnel model [ASME PAPER 68-WA/APM-24]

04 p0541 A69-14389

Plates yield point loads limit determination formulated as mathematical programming problem, using finite element representations for velocity and moment fields [ASME PAPER 68-WA/APM-21]

04 p0670 A69-14405

Difference approximation with second order accuracy of numerical solution for parabolic type equations

04 p0622 A69-14618

Numerical solution of chemically reacting boundary layer equations, noting loss of accuracy due to numerical cancellations

04 p0588 A69-14737

Method for solving propellant sloshing in rotationally symmetric rocket tanks with arbitrary internal boundaries

04 p0665 A69-14840

Numerical solution of nonlinear two point boundary value problems of boundary layer type, noting shock wave formation in supersonic nozzle

04 p0544 A69-14889

Cavitation stream calculation methods for ideal incompressible fluid with free boundaries, noting cavitation generators and Riabouschinsky problems

04 p0589 A69-14994

Mathematical analysis for mechanism of spherical comet nucleus division as effect of nonuniform surface heating during rotation

04 p0659 A69-14997

Numerical solution of elliptic equations by iteration result in convergence prevention and solution of Laplace and Poisson equations with singular Laplace operator

04 p0625 A69-15133

Boundary condition description effect on numerical accuracy of series solution to boundary value problem by direct method

04 p0681 A69-15283

Characteristic coefficients in method of integral relations calculated by Lagrange interpolation, noting application to numerical solution of differential equations

06 p0857 A69-17102

Numerical method for stress function of elastoplastic torsion of hollow bars during quasi-static monotonic twist compared with relaxation method solution

06 p1023 A69-17370

Optimum control problems solved numerically on computer, noting multivalence of extremal solutions and application to orbital transfer in central gravitational field

06 p0903 A69-17539

Numerical method for attacking-lifting problems of general three dimensional wing executing arbitrary motion in potential flow [AIAA PAPER 69-23]

06 p0862 A69-18040

Aerodynamic coefficients from observed motion of body in flight, eliminating need for closed form solutions by employing numerical solutions to equations of motion

[AIAA PAPER 69-134]

06 p0864 A69-18161

Digital computer methods and numerical techniques to evaluate temperature distributions in spacecraft structures, discussing thermal modeling [SAE PAPER 690199]

07 p1239 A69-18301

Shock waveforms lengthening due to propagation to high altitudes derived from computed numerical values, studying N waves from SST

07 p1054 A69-19463

Soviet book on theory of approximate methods and applications to numerical solution of singular integral equations

07 p1174 A69-19580

Numerical analysis of periodic solutions of restricted three body problem in sun-Jupiter system, noting genealogy of periodic orbits

08 p1382 A69-19874

Numerical studies of initial value problems by boundary value techniques for cases having available asymptotic estimates or periodicity of solutions

09 p1532 A69-21610

Low sensitivity electric circuits synthesis based on analytical and numerical analysis of sensitivity function characteristics of selective polynomial circuits

09 p1472 A69-21780

Finite difference numerical solutions to free streamline axisymmetric potential fluid flow, noting independent and dependent variables consideration in boundary value problem

09 p1481 A69-21920

Digital computer programs for aerodynamics of subsonic gas turbine combustion systems applicable to incompressible flow with specified flow boundaries, noting vortices distribution

09 p1573 A69-22621

Numerical analysis for stresses in finite or infinite plate with arbitrary holes, considering boundary value problems

10 p1793 A69-22882

Numerical solution for three dimensional boundary layers based on stability determinations for linearized difference equations

10 p1631 A69-22902

Numerical orthonormalized system of functions for formulating functional equations in potential and elasticity theory, considering boundary value problems

10 p1801 A69-23687

Iterative method for numerical solution of linear algebraic equations for stationary probability distributions in queueing and reliability theory

10 p1721 A69-23691

Numerical solutions for incompressible Newtonian flow around circular cylinder for various Reynolds numbers

11 p1867 A69-24279

Numerical method for coupled moments of inertia and integral equations of boundary value problems for fluid in moving cavities

11 p1868 A69-24774

Boundary value problems numerical solutions accuracy assessed as function of grid spacing size

11 p1908 A69-24789

Integral representation for Wiener Hopf factorization of functions of complex variables for numerical processing of radiation problems

11 p1851 A69-24998

Dynamic programming approach to numerical solution of elliptic boundary value problems, using Laplace equations

11 p1910 A69-25411

Numerical prediction for nonlinear transient response of structures, considering geometric and material nonlinearities in systems with line elements

11 p1993 A69-25526

Excitation coefficients of waves subjected to sudden expansion in radiating waveguide using integral relations, noting convergence

11 p1855 A69-25621

Numerical computation method for evaluating transition matrix of linear time invariant system, estimating error propagated in transient response

11 p1910 A69-25660

Analytical synthesis of dynamic plant model to insure desired output in response to cyclic action

11 p1861 A69-25714

Exact solutions for two state potential curve crossing in subexcitation molecular collisions in terms of various decoupling schemes

12 p2131 A69-25983

Dahlquist linear multistep methods of stability analysis for ordinary differential equations extended to Volterra integrodifferential equations

12 p2123 A69-26753

Externally pressurized gas lubricated bearings treated theoretically using unevenly distributed supercharging method, noting Reynolds equation numerical integration [ASME PAPER 68-LUBS-44]

13 p2267 A69-27283

U.S. Navy Numerical Value Rating System computing method of selecting lowest cost design approach to accomplish specific function

13 p2383 A69-28098

Numerical methods for solving steady state and transient heat transfer problems suitable for high speed digital computer

13 p2376 A69-28141

Numerical method for time dependent compressible Navier-Stokes equations applied to axisymmetric flow field produced by hypervelocity impact, examining viscous effects [AIAA PAPER 69-354]

13 p2366 A69-28288

Hypervelocity impact of spheres on thin targets studied with numerical solutions utilizing STEEP code two dimensional technique based on hydrodynamic elastoplastic model [AIAA PAPER 69-357]

13 p2366 A69-28290

Energy transfer by simultaneous conduction and radiation between two media in intimate contact, detailing numerical solution method for resulting coupled nonlinear integrodifferential equations

13 p2378 A69-28340

Analytical model of geomagnetic field constructed from Cosmos 49 data using spherical analysis

13 p2258 A69-28729

Numerical solution of differential equations for two channel PFM with pulse element, applying Dirac pulse sequence to input

14 p2426 A69-29148

Numerical analysis for spreading of free turbulent gas jets with arbitrary uneven initial distribution of momentum and heat and mass fluxes

15 p2590 A69-30157

Optimum order for column orthonormalization of sparse matrices, applying results to Gram-Schmidt and Householder methods

15 p2644 A69-30425

Multistage rocket trajectories optimized by second order numerical technique and digital computer program, considering coasting, vacuum flight and transition times

16 p2857 A69-32154

Numerical analysis of asymptotic solution for earth-moon particle trajectories in idealized restricted three body problem

16 p2857 A69-32155

Numerical procedure to optimize complex structures by determining relative proportions of selected elements attaining flutter speed with minimum total mass

16 p2874 A69-32163

Numerical absolute stability test for nonlinear discrete systems using bilinear transformation

17 p2994 A69-32848

Book on quasi-reversibility application to partial differential equations covering parabolic, nonparabolic, elliptic equations and boundary conditions control

17 p2994 A69-33205

Transient thermal analysis of space radiators excluding finite difference equations, noting computer adaptability and time saving [AIAA PAPER 69-615]

17 p3070 A69-33261

Nonlinear rarefied gas flow problems with thermal nonequilibrium solved by numerical methods, considering intermolecular collisions effect

17 p2952 A69-33325

Mach disk and Riemann wave location, size and strength in underexpanded jet flows, proposing model for conservation equation satisfaction [AIAA PAPER 69-665]

17 p2954 A69-33460

Numerical solution of boundary value problems, discussing spectral domain and scattering matrix formalisms

17 p2929 A69-33882

Simultaneous integral equations numerical solution for open optical resonator mode analysis, using kernel function and Fresnel approximation

17 p2983 A69-33883

Book on numerical methods in applied theory of elasticity, discussing oscillations of twisted rods for theory of steam and gas turbine blades

18 p3211 A69-34331

Earth atmospheric large scale motion simulated in laboratory and by numerical technique

18 p3127 A69-34668

Iteration process by difference scheme for numerical solution to Dirichlet problem of two dimensional Poisson equation

18 p3164 A69-34701

Parabolic differential equations solved by variational methods, constructing numerical representations for solutions of initial boundary value problems

18 p3164 A69-34841

Spectral inhomogeneity effect on spectrum of modes emitted by semiconductor p-n junction/ laser

18 p3152 A69-35023

Numerical program for gas dynamics of hydrodynamic flow and radiation transport in diffusion and grey body approximations

19 p3450 A69-36356

Numerical simulation of macrophysical and microphysical processes in convective cloud, including cloud geometry and equations describing dry and moist phases

19 p3362 A69-36497

Moon to earth trajectories analyzed numerically to determine effect of specified earth entry conditions on hyperbolic elements near moon for abort [AAS PAPER 68-089]

20 p3595 A69-37174

Numerical solution of equations of motion of rocket under thrust in inverse square force field, discussing effects of initial acceleration

20 p3595 A69-37203

Numerical evaluation of geometrical optics radar cross sections of general doubly curved convex conducting body using surface fitting method

20 p3494 A69-37848

Book on heat and mass transfer in recirculating flows, presenting elliptic differential equations and numerical solutions by computer

21 p3691 A69-38333

Nonlinear computing schemes examined for necessary and sufficient conditions of stability as derived from Mikhlin linear operators and Frechet derivatives

21 p3678 A69-38746

Reduction of boundary value problems to initial value problems through variables transformation, considering application to eigenvalue problems

21 p3754 A69-38747

Shooting method difficulties in boundary value problem numerical solutions using computer programs to integrate differential equations

21 p3755 A69-38753

Combined analytical and numerical method for thermoelastic boundary problem of unidirectional infinite strip

21 p3836 A69-38927

Stratified cloud transport and evolution, solving kinetic equations by numerical method

21 p3759 A69-39119

Vertical factor equation numerical solution for radio wave propagation in vertically inhomogeneous troposphere

21 p3674 A69-39121

Numerical procedure for structural systems analysis, discussing computer application to hydrodynamic, electric, magnetic, thermodynamic, elastostatic and elastodynamic problems [AIAA PAPER 67-955]

21 p3839 A69-39216

Natural convection in rectangular cavity with nonuniform lateral surfaces temperature, using finite difference scheme with numerical analysis

21 p3855 A69-39853

Numerical method for solution of nonlinear systems applied to damped and undamped motion with symmetrical and asymmetrical elasticity under harmonic excitation

22 p4040 A69-39937

Algorithm for numerical modeling by Monte Carlo method of diffusion bounded light beams in dispersive media, applying to light pulse in cloudlike medium

22 p3981 A69-40248

Small curvature effect on prevention of vibration in shallow shells under random loading numerically analyzed for component modes using linear theory

22 p4044 A69-40600

Numerical analysis of plane Couette flow of rarefied binary gas mixture using relaxation type kinetic model equations, discussing slip velocity, friction coefficient, etc

22 p3931 A69-40778

Liquid drop in electric field numerically analyzed for disintegration dynamics and instability through cross section computation at time intervals

23 p4151 A69-41694

Numerical methods for radiation transport for inviscid stagnation flows, detailing spectral nature of radiation emission and absorption [AIAA PAPER 68-664]

23 p4059 A69-41890

Numerical procedure obtaining scattering matrix of passive reciprocal two port from standing wave measurements, using image circle in Smith chart

24 p4281 A69-42617

Earth-Mars and earth-Venus economical transfers derived for optimal conditions with respect to characteristic velocity, obtaining exact numerical solution [ASME PAPER 69-241]

24 p4380 A69-42855

Numerical methods for nonlinear Volterra integral equations of second kind avoiding special starting procedures, giving convergence theorem

24 p4340 A69-43228

Apollo type reentry trajectory optimization numerical methods

24 p4386 A69-43281

Optimization problems solution applied to separable but bounded state variable problem, providing control over commercial errors

24 p4292 A69-43286

Numerical solutions for time dependent boundary value problems governed by heat equation applied to transient heat conduction in irregularly shaped two dimensional regions [ASME PAPER 69-HT-50]

24 p4410 A69-43521

NUMERICAL CONTROL

Fluidic numerical controls of linear or rotating motors, discussing pneumatic, hydraulic, hybrid logic components and amplifiers

04 p0550 A69-15082

Computer graphics and manufacturing, discussing man computer system for transformation of blueprint to numerically controlled machine tape with no time delay

07 p1089 A69-19741

Numerical control as manufacturing tool, with application to aircraft engine precision components

24 p4318 A69-42710

NUMERICAL INTEGRATION

NT RUNGE-KUTTA METHOD

Phase plane diagram utility in toppling stability analysis of spacecraft, emphasizing numerical integration time reduction

02 p0334 A69-12376

Numerical integration stability of differential equations, noting limiting integration step size for unsteady distillation

02 p0273 A69-12478

Finite difference numerical integration technique for large elastoplastic deformation transient and permanent deflection responses of thin shells

02 p0347 A69-12518

Optimum addition of abscissas in quadrature formulas by expansion of abscissas equation in Legendre polynomials

03 p0455 A69-13372

Integration formulas based on set of Gauss or Lobatto points

03 p0455 A69-13374

Implicit finite difference scheme to integrate unsteady boundary layer equations for compressible gas

03 p0416 A69-13656

Acceleration of charged particles in strong DC magnetic field by electrostatic waves with spatially varying phase velocities integrated numerically on IBM 360/65

03 p0479 A69-14028

Integral equations solved numerically for general nonhomogeneous elastic inclusion problem, using linear elasticity theory

03 p0530 A69-14064

Numerical integration of elliptic mixed boundary value problem in region with curved boundary programmed in FORTRAN for general linear second order partial differential equation

04 p0625 A69-15287

Continuous dynamic systems digital simulation, noting run-time program determined by numerical integration structure

04 p0565 A69-15339

Hybrid computer algorithm for numerical integration of partial differential equations, using assumed sum separation of variables

04 p0566 A69-15346

Recursive formulas for numerical evaluation of real convolution integral for simulation of control systems and electrical networks on digital computer

06 p0947 A69-17250

Chemical kinetic numerical integration techniques applied to equations for chemical relaxation [WSCI PAPER 68-45] 07 p1073 A69-18315

Parasitic eigenvalue in integration of equations governing one dimensional flow of chemically reactive gas 07 p1118 A69-18317

Numerical analysis of stabilization of one component conducting plasma in two dimensional coaxial duct 07 p1190 A69-18757

Numerical method for three dimensional boundary layer equations, applying perturbation technique and independence principle to rotating flat blade [AIAA PAPER 69-227] 07 p1051 A69-19560

Numerical double integral evaluation technique for antenna radiation patterns, discussing error data 08 p1282 A69-20042

Numerical integration of motion equations of electrons subject to electrostatic waves, considering turbulent heating 08 p1368 A69-20806

Second order system response with variable damping computed by stepwise numerical integration 08 p1418 A69-20849

Numerical and kernel expansion procedures for laser mode, discussing Gaussian quadrature numerical integration for conversion to matrix equation 08 p1328 A69-21091

Multistep integration formulas treated as transfer system to examine properties in frequency domain for selection in digital simulation programs 09 p1460 A69-21417

Integration time reduction for equations of motion of vehicle center of mass during parabolic reentry, using Runge principle 09 p1532 A69-21763

Numerical integration of equations of three dimensional laminar boundary layer in conical flow, using integral relation method 09 p1430 A69-21789

Krause numerical solution applied to normal injection in three dimensional incompressible laminar boundary layer [DVL-902] 09 p1482 A69-21971

SNODE /spectra numerical ordinary differential equations/ computer program for solving differential equations and integration with basic time sharing system 10 p1659 A69-23142

Stability and error bounds in numerical integration of ordinary differential equations, determining highest possible degree of stable finite difference form 10 p1719 A69-23518

Integration routines performance used in dynamic systems simulation by digital programs, comparing speed, accuracy and convenience 10 p1661 A69-23854

Instabilities of numerical integration of ordinary differential equations on digital computer, considering difference approximation containing extraneous solutions 10 p1721 A69-24042

Numerical methods for time integrating first order differential equations, emphasizing atmospheric oscillations in baroclinic model, evaluating errors 13 p2290 A69-27636

Isothermal H II region dynamics for moving central star, integrating equations numerically using holograph transformation and Riemann invariants 13 p2347 A69-27712

Monte Carlo method for integral of monotonic continuously differentiable function 13 p2288 A69-27735

Matrix eigenvalues for nonlinear simultaneous algebraic equations, discussing computer program for numerical integration 13 p2289 A69-28227

Equations for steady state combustion of fuel drops in oxidizing atmosphere integrated numerically, obtaining ignition and extinction conditions 13 p2379 A69-28456

HNO role in hydrogen-NO reaction rate data reexamined by numerical integration of governing differential equations 13 p2218 A69-28457

Electron flux-atmosphere interaction solved by numerical integration on computer, discussing auroral ionosphere 14 p2513 A69-29069

External wind shear influence on isolated cumulus cloud evolution based on hydrodynamic and thermodynamic equations numerical integration 15 p2648 A69-30644

Modified Chaplygin method for approximate integration of Cauchy problem for differential equations, estimating rate of convergence 15 p2644 A69-30656

Chetaev /A, lambda/ estimates of approximate integrations of system of ordinary differential equations, analyzing stability with aid of Liapunov functions 15 p2644 A69-30664

Economical computer techniques for numerically integrated finite elements, creating 96 element square matrix 15 p2711 A69-30873

Aerodynamic properties calculations of arbitrary slender supersonic wings using sum of simple integrals 15 p2548 A69-31170

Pseudo Runge-Kutta methods stability in numerically integrating two point Cauchy problems 15 p2646 A69-31261

Numerical integration of subdominant solutions of systems of ordinary differential equations, using partial Wronskians 15 p2646 A69-31519

Finite difference schemes for barotropic fluid free surface model primitive equations tested for numerical integration stability and accuracy 17 p2997 A69-33691

Plane problems of elasticity theory solved numerically using conformal mapping 18 p3219 A69-34709

Numerical methods using analog computer in linear one dimensional transient heat conduction 18 p3229 A69-34835

Cowell equations modified for exact integration of pure Keplerian orbits, considering secular effects 18 p3165 A69-34842

Satellite motion perturbations in vicinity of critical inclination, using Encke method of numerical integration 19 p3397 A69-35607

Ordinary differential equations integration method, presenting algorithm based on double constraint of maximum accuracy and stability 19 p3279 A69-35805

Elliptic system of twelfth order equations describing elastic equilibrium of plate with kinematic functions analyzed by integration procedure 19 p3438 A69-36203

Computer program for numerical integration of chemical reaction rate equations behind steady state hydrogen-oxygen shock wave 19 p3451 A69-36366

Wind and temperature profiles in Ekman boundary layer, using numerical integrations of dynamic equations including time derivative terms 19 p3363 A69-36501

Numerical integrations for modified model incorporating ozone production equation and heating from ozone radiation absorption and long wave cooling for upper atmospheric circulation 19 p3363 A69-36502

Long term integration of fluid motion equations with finite difference scheme using hexagonal grid system to avoid nonlinear computational instability 19 p3364 A69-36508

Numerical integration of atmospheric motion equations in global domain using hexagonal grid, including sphericity corrections and Coriolis term 19 p3364 A69-36509

Numerical integration of lunar motion equations to investigate lunar theory for high precision applications and to examine motion departures from gravitational theory 20 p3603 A69-37560

Nonlinear partial differential equations numerical solution applied to solving Cauchy problem encountered in Goursat problem 20 p3569 A69-38293

Jupiter mass determined by applying Cowell numerical integration to equations of motion for ninth satellite 21 p3795 A69-38468

Navier-stokes equation numerical integration for three dimensional incompressible flow, discussing annulus thermal convection and trigonometric transforms algorithm 21 p3694 A69-38770

Laplace transforms in heat conduction theory in three dimensional infinite homogeneous body 21 p3851 A69-39011

Encke type analytical-numerical integration for solving differential equations of modified set of Lagrange planetary equations, obtaining satellite ephemeris for orbit prediction [AIAA PAPER 69-908] 21 p3807 A69-39340

Numerical calculations for boundary layer flows allowing similar solutions, using iterative numerical integration of integral equation 22 p3929 A69-39925

Navier-Stokes equations numerical integration based on biharmonic operator inversion by alternating direction method of Douglas-Rachford type 22 p3932 A69-40928

Numerical integration of double integral with Cauchy type singularity for calculation of aerodynamic or hydrodynamic load on lifting body 23 p4182 A69-41913

Grobner method of Lie series applied to numerical integration of spacecraft trajectories and n-body problems 23 p4223 A69-42476

Sufficient conditions theorems for investigation of instability of numerical integration methods to solve differential equations 24 p4339 A69-42646

Iterative integration method of numerical quadrature over finite interval for analytic function, taking into account simple nonanalytic singularities in integrand 24 p4341 A69-43229

NUMERICAL WEATHER FORECASTING

Automated layered-nephanalysis and numerical total cloud cover prediction program using moisture data from Tiros 7 photographs 01 p0110 A69-10691

Optimum overrelaxation factor in diagnostic and forecast calculations 03 p0458 A69-13033

Mean meridional pressure profiles and atmospheric mass readjustment time dependence for initially at rest atmosphere with mean baroclinity, using frozen gradient model 04 p0627 A69-15086

Multilevel numerical weather forecast scheme with stable initial data 05 p0789 A69-16636

Energy integral of equations used in studying atmospheric motions in quasi-geostrophic approximation 05 p0759 A69-16641

Multilevel objective weather analysis system for stratosphere and upper troposphere over Australia, using stream function analysis 06 p0950 A69-17787

Truncation error reducing scheme for balanced forecast models 07 p1176 A69-19629

Synoptic process predictability, discussing forecasting of large and small scale processes by mathematical formulas and statistical description 12 p2126 A69-26576

Multilevel numerical weather forecast scheme with stable initial data 14 p2472 A69-28792

Energy integral of equations used in studying atmospheric motions in quasi-geostrophic approximation 14 p2433 A69-28797

Error sources in forecasts for heights of isobaric surfaces obtained by numerical integration of prognostic equations of equivalent barotropic models 19 p3361 A69-35770

Numerical weather prediction using four level primitive atmospheric model for studying frontogenetic processes in deepening cyclone 19 p3303 A69-36408

Numerical weather prediction - Conference, Tokyo, November-December 1968 19 p3362 A69-36496

Operational circulation model numerical experiment suggesting elimination of spurious divergence-on-divergence interactions from implied vorticity equations in primitive equations 19 p3363 A69-36503

Optimum aerological network design, discussing atmospheric model, numerical analysis, data acquisition, weather forecasts, rms measurement error, etc 19 p3364 A69-36505

Numerical wind field prediction based on advection equations and quasi-geostrophic wind assumption, considering equatorial belt in case of zonal pressure field 19 p3364 A69-36506

Mesometeorology in central Europe, discussing applications of numerical techniques to forecasting 20 p3570 A69-37427

Numerical prediction experiment for dynamical structure of tropical atmosphere in equatorial latitudes, constructing pressure, temperature and vertical motion distributions from wind field 20 p3573 A69-37910

Weather prediction, considering mathematical and empirical procedures, computer applications, atmospheric instability, etc

21 p3757 A69-38324

Friction and orography effects on vertical currents in planetary boundary layer and numerical forecasting of baric field

21 p3758 A69-38837

Storm location and severity prediction by pattern recognition theory, using quantized radar data, compared with statistical prediction

21 p3678 A69-39458

Meteorological data real time processing for automatic weather analysis and prognosis, program used and computer output charts

22 p3977 A69-40732

Numerical weather forecasting at high and middle latitudes, discussing geostrophic forecasting equations and barotropic models

23 p4183 A69-42024

Initialization technique for primitive forecast equations balancing Coriolis and pressure forces effects on atmospheric observations

24 p4344 A69-43065

Angular grid spacing resolution near poles effect tests in global prediction model for geophysical fluid dynamics, investigating forecast height and wind fields

24 p4344 A69-43066

NUSSLETT NUMBER

Free convective heat transfer of cylinder in rarefied gas yielding Nusselt number as function of Grashof, Prandtl and Knudsen numbers

05 p0846 A69-15904

Two term expansion for Nusselt number for laminar natural convection about isothermal horizontal cylinder in fluid with vanishingly small Prandtl number

17 p3068 A69-33014

Heat transfer in radial flow between two parallel plates, calculating Nusselt number for laminar and turbulent flows

20 p3633 A69-38176

Heat transfer in curved channel as function of inlet configurations, obtaining Nusselt number equations for thermal and mixed convection and laminar flow

21 p3850 A69-38866

Local Nusselt number beyond abrupt circular channel expansion tested for Reynolds numbers with air as working fluid

[ASME PAPER 69-HT-35] 24 p4411 A69-43532

Transition from turbulent to laminar regime as consequence of high heating rates for internal convective flow, noting roles of Nusselt numbers and friction factors

[ASME PAPER 69-HT-9] 24 p4304 A69-43559

NUTATION

Nutational stability of multibody spin stabilized satellites, discussing moment of inertia ratios role with energy dissipative damper on despun platform

06 p1015 A69-17585

Motion of gyroscopic integrator of linear accelerations, analyzing nutational vibrations imposed on precession

06 p0927 A69-17688

Diurnal nutation and periodic terms of local coordinates using OPL model of Danjon astrolabe, presenting harmonic and Fourier analysis

09 p1596 A69-22059

Instantaneous rotational impulse imparting steady motion of disk determined for coupled gyroscope

13 p2264 A69-28527

Periodic solutions for small nutation angle of quasi-linear autonomous system of equations of motion of heavy solid body moving around fixed point

14 p2445 A69-28896

Liquid filled toroidal shaped rotating damping tube containing bubble, discussing parameters variation effect on spacecraft nutation

16 p2868 A69-32561

Nutation period of 18.6 years using data from International Latitude Service

17 p3027 A69-32868

Boundary layer theory application to dynamics of gyroscope in gimbal suspension, defining nutational and precessional motion

18 p3135 A69-34559

Optimal nutation damping of spin stabilized bodies, using Pontryagin maximum principle to optimize time, consumption and linear time-consumption combination

18 p3208 A69-34774

Time and fuel optimization of angular momentum alignment and nutation elimination of spin stabilized bodies with inertial reference direction

18 p3208 A69-34775

Earth polar wanderings attributed to rotation axis angular displacements generated by density redistribution on geologic time scale

20 p3535 A69-38192

Coordinate transformation of Euler equations governing precession and nutation of self gravitating bodies of viscous fluid in inertial coordinates

21 p3797 A69-38539

Envelope plotting of nutational vibrations of astatic gyroscope under influence of dissipative forces, noting quasi-elastic model

21 p3723 A69-38889

Earth-pole wobble /1951-1966/ by spectral analysis using least square fit method

21 p3716 A69-39244

Motion and stability characteristics of dual spin satellite system with pendulous type nutation dampers, noting mass unbalance effect

[AIAA PAPER 69-857] 21 p3823 A69-39385

Wobble tolerance influence on axis deflection affecting accuracy during assembling of turbine rotors and stators

21 p3733 A69-39719

Controlled motion of space vehicle about center of mass analyzed by equation expressing nutation angle invariance

21 p3830 A69-39839

Eulerian equations for precession and nutation of self gravitating fluid globes of arbitrary structures in inertial coordinates, discussing coplanar case, tidal breathing, etc

22 p4030 A69-40904

NUTATIONAL OSCILLATION

U NUTATION

NUTRIENTS

Human requirements for nutrients under stress responses to space flight, considering synthetic food and hothouse plants

15 p2560 A69-31462

NUTRITION

Nutritive value of protein from discolored algae biomasses on groups of rats kept on algae biomass, casein and soybean diets

02 p0198 A69-11510

Handbook on metabolism and nutrition containing tables, charts and diagrams on food composition, material incorporation into organism, energy exchange and end products

04 p0553 A69-14908

Chlorella seaweed hybrid strains containing larger amounts of amino acids than original parent species

13 p2216 A69-28620

Monosaccharide production from carbon dioxide from respiration or human waste incineration, evaluating toxicological effects of synthetic monosaccharides

15 p2557 A69-31471

Nutritive value of mycelium of *Cantharellus cibarius* mushroom on rats compared with eggs and fresh and sour milk

22 p3892 A69-40273

Glider pilots fatigue attributed to nutritional habits

23 p4106 A69-41796

NUTRITIONAL REQUIREMENTS

NT CALORIC REQUIREMENTS

Biological, psychological and technological requirements in astronaut nutrition programs, examining preservation and reconstitution techniques

04 p0554 A69-15388

Mineral nutrition elements concentration stabilization by correcting solution additions during prolonged *Chlorella* cultivation with medium recycling

10 p1646 A69-23578

Hypokinesia and nutrition deficiency effect on blood coagulation, noting combination with accelerations may lead to hypocoagulation

13 p2212 A69-28625

Human requirements for nutrients under stress responses to space flight, considering synthetic food and hothouse plants

15 p2560 A69-31462

NUTS [FASTENERS]

Crimping method for preventing nuts loosening, discussing elliptical deformation and point crimp for obtaining maximum interference fits

22 p3957 A69-40828

Screw-nut feeder and adjuster systems with compensation for clearance and wear of cutting tools, determining efficiency for conversion of rotary to translational motion

23 p4168 A69-41414

NYLON RESINS

U POLYAMIDE RESINS

NYQUIST DIAGRAM

Circle criterion for stability of nonlinear time varying systems, considering integrator and infinite sequence of impulses in impulse response

06 p0905 A69-17949

Single purpose analog computer with analog and hybrid elements for calculating Nyquist diagrams for feedback circuits

08 p1278 A69-20397

Apollo-Saturn 5 propulsion and structure feedback loop, analyzing Pogo components and Nyquist plot application

[AIAA PAPER 69-877] 21 p3824 A69-39403

NYQUIST FREQUENCIES

Multivariable automatic control systems stability, discussing applicability of Nyquist theorem and alternate frequency criterion

04 p0581 A69-14601

Frequency domain stability criterion for pulse width modulated feedback

06 p0904 A69-17942

External impedance controlled nucleation of Gunn effect domains studied theoretically by Nyquist criterion

06 p0981 A69-18217

Noise emission and Landau damping of plasma resonances related by network theory including Nyquist formula, discussing noise temperature in free fall region

16 p2822 A69-32038

NYSTAGMUS

U ASTIGMATISM

O

O RING SEALS

Wear ring seals evaluation program for application to high pressure high speed liquid rocket turbopumps impeller wear rings

[ASME PAPER 68-WA/LUB-1] 05 p0768 A69-16129

Glass vacuum systems grease free assembly method using heat shrinkable polyolefin sleeve tubing connector for compression of O ring joints

08 p1320 A69-20529

Aircraft onboard weighing system, eliminating O ring seal friction to permit accurate measurement of oleo strut pressure

[SAWE PAPER 748] 18 p3137 A69-34883

O STARS

Far UV spectra of O and B stars in Orion photographed from Aerobee rocket, describing wavelength measurements and line identifications

02 p0327 A69-12712

Hydrogen alpha line strength in 951 O, B and early A stars from narrow band photoelectric measurements for stellar luminosity

03 p0511 A69-13435

Rapid differential rotation effect on massive main sequence O and B stars, discussing bolometric magnitude deficiencies and shifted position in Hertzsprung-Russell diagram

07 p1220 A69-19390

Expanding atmospheres in OB supergiants from radial velocity measurements, proposing tentative temperature and velocity fields

08 p1387 A69-20091

Mass loss observed in Of, Wolf-Rayet and OB supergiant stars from P-Cygni profiles in far UV resonance lines

08 p1395 A69-20641

Far UV spectra of zeta Puppis and gamma super two Velorum with 1.6 A resolution photographed with all reflective objective spectrograph on Aerobee rocket

10 p1788 A69-24120

Least squares iterative program, deriving orbits for O binaries HD 93403 and HD 135240

11 p1963 A69-25257

Pulsars and neutron star formation based on stellar evolution theory, suggesting massive O stars as origin

13 p2337 A69-27517

OB stars absolute magnitude and intrinsic colors in Cleveland system related to MK system

13 p2348 A69-27806

Radial velocities of southern OB stars and supergiants noting tabulation of information

14 p2519 A69-29368

Spectral classifications and UVB photometry for southern association Sco OB 1 containing cluster NGC 6231

15 p2692 A69-30771

Surface gravity and temperature model atmospheres for O-type stars with UV line blanketing
15 p2693 A69-30778

UBV photoelectric observation of OB and open cluster Tr 16 stars in Carina-Centaurus, suggesting no limit in depth distribution
18 p3200 A69-35133

Galactic rotation in Cassiopeia region, studying O, B and A stars circular velocities as function of distance from galactic center
18 p3201 A69-35142

O stars spectrograms study for luminosity and temperature criteria
20 p3598 A69-37463

Southern stars of spectral types between O5 and A3 analyzed for equivalent widths and equatorial rotation velocity from direct intensity spectrogram tracings
20 p3600 A69-37491

MK spectral types for bright southern O and B stars
20 p3612 A69-38161

Faint OB stars data tabulation between Carina and Centaurus, noting open clusters and MK classification
23 p4211 A69-41488

Radial velocities for O and B stars in Milky Way field in Scorpius determined from prism spectrograms with specific dispersion at H gamma line
23 p4211 A69-41489

O stars absolute magnitudes scales, discussing use of Balmer discontinuity in magnitude calculations
23 p4213 A69-41699

OB stars near emission nebula RCW 103, describing galactic structure in Norma
23 p4220 A69-42384

0AO

Active optics system for obtaining perfect mirror figure in orbiting astronomical telescope, using laser and white light sources, interferometers and data converter
12 p2092 A69-26423

Astronomical UV radiation observation by OAO 2 satellite, discussing solar images, corona, chromosphere and UV spectrum, stellar evolution, etc
15 p2689 A69-30597

Orbiting Astronomical Observatory thermal test and evaluation program, discussing equipment and role in experimental design
[AIAA PAPER 69-995] 22 p3920 A69-40373

Spaceborne stored program computer design for OAO-C, noting auxiliary command storage, spacecraft monitoring and malfunction reporting, etc
23 p4132 A69-41736

0AO-A

U OAO

OBESITY

Body composition of USAF flying personnel, evaluating obesity by using radioactive potassium /K-40/ method
14 p2409 A69-29295

OBULATE SPHEROIDS

Earth oblateness, discussing geometric interpretation and direct measurement
01 p0064 A69-10447

Ground coverage of oblate planets by spin stabilized satellites, determining ground areas visible to satellite by solution of quadratic equations
03 p0522 A69-14244

Solar atmosphere model calculations of solar oblateness, discussing flux difference and Dicke experiment on general relativity
08 p1383 A69-19899

Earth ellipsoid fundamental parameters for calculation of earth flattening and normal acceleration due to gravity
09 p1487 A69-21633

Free vibration frequencies and mode shapes for thin orthotropic oblate spheroidal shells, noting isotropic oblate spheroidal shell and isotropic spherical shell
09 p1613 A69-21719

Solar interior rotational angular velocity influence on solar oblateness, noting reduction by turbulent mixing
09 p1600 A69-22201

Motion of satellite of very oblate planet, investigating axisymmetric potential
10 p1774 A69-22969

Solar oblateness and differential rotation time development due to solar wind torque
12 p2157 A69-26308

Satellites trajectories under influence of earth oblateness and low radial thrust acceleration by nonlinear mechanics asymptotic method, discussing osculating orbits
16 p2856 A69-32009

Upper limit of solar oblateness determined from secular stability of differential rotation during evolution
18 p3202 A69-35214

Periodic orbits of Poincare and Schwarzschild types in motion of artificial satellite in disturbed gravitational field of axisymmetric oblate spheroid
21 p3795 A69-38441

Neptune equatorial radius, diameter, flattening and upper atmosphere optical properties determined from photometric curves of star BD-17 occultation
21 p3796 A69-38471

Satellite position perturbation due to earth oblateness using Hansen method
[AIAA PAPER 69-909] 21 p3807 A69-39341

Solar oblateness observed by Dicke and Goldenberg as interaction between slow uniform rotation and turbulent convection
22 p4017 A69-40175

OBlique COORDINATES

Equations for bending of elastic cantilever plate with parallelogram shape in oblique angle coordinate system, constructing functions satisfying Poisson conditions at contour
15 p2710 A69-30861

OBlique SHOCK WAVES

Linear wave interaction with oblique shock waves, noting dependence of transmission, reflection and generation coefficients on Mach number
03 p0414 A69-13137

Boundary conditions in oblique reaction waves in supersonic flow, adding or subtracting heat by chemical reaction
05 p0697 A69-15828

Oblique shock wave propagation through two dimensional steady nonuniform incoming flow, discussing higher order theory via irrotational or rotational disturbances of arbitrary amplitude
[AIAA PAPER 69-39] 06 p0913 A69-18103

Oblique shock wave separation conditions in supersonic gas flow past wedge
09 p1483 A69-22665

Diffraction accompanying reflection of plane shock wave obliquely impinging on walls of obtuse wedge at finite incidence, considering Lighthill method
11 p1873 A69-25135

Oblique shock wave properties with free stream Mach number and flow deflection angle as independent variables, noting explicit solution
11 p1819 A69-25378

Final states of density, velocity and pressure in gas, comparing states reached after transition through single oblique hydromagnetic shock and two successive shocks
15 p2664 A69-31217

Oblique hydromagnetic shock waves in magnetized hydrogen plasma enclosed in pyrex chamber by oscillatory zeta discharge, probing for front development and structure
17 p3013 A69-33823

Multistep axisymmetrical supersonic exit cones optimum geometry design diagram based on external oblique and normal compression shock
21 p3785 A69-39104

OBSCURATION

U OCCULTATION

OBSEVATION

NT SATELLITE OBSERVATION

NT VISUAL OBSERVATION

Observed values concept applied to general relativity theory, considering gravitational energy problem
14 p2483 A69-28858

Epochs and ephemerides of asteroid Amor for 1916, 1924 and 1972, noting unfavorable observing conditions in future
17 p3038 A69-33723

Observer theory application to hybrid inertial navigation systems, discussing error estimation and correction, real time mechanization, eigenvalues, etc
17 p3003 A69-34099

OBSERVATION AIRCRAFT

NT CL- 84 AIRCRAFT

NT F- 5 AIRCRAFT

NT G- 91 AIRCRAFT

NT OH- 6 HELICOPTER

NT OV-10 AIRCRAFT

NT P-1127 AIRCRAFT

NT RECONNAISSANCE AIRCRAFT

Atmospheric measurements and experiments using aircraft as platforms, noting aircraft operation in severe weather, electrical supply problem and aircraft wake problem
[AIAA PAPER 69-157] 06 p0869 A69-18153

NASA Earth Resources Survey Aircraft Program, describing aircraft and remote sensors characteristics
19 p3312 A69-36259

OBSERVATORIES

U ASTRONOMICAL OBSERVATORIES

U GEOPHYSICAL OBSERVATORIES

U JODRELL BANK OBSERVATORY

U LUNAR OBSERVATORIES

U OAO

U OGO

U OGO-D

U OGO-E

U OGO-F

U OSO

U OSO- 3

U OSO-C

U SOLAR OBSERVATORIES

OBSDIAN

U MOLDAVITE

OBSTACLES

U BARRIERS

OBSTRUCTING

U BLOCKING

OCCIPITAL LOBES

Resting EEG and parieto-occipital response changes evoked by slowly repeated flashes in case of severe hypothyroidism secondary to panhypopituitarism
07 p1064 A69-18634

OCCCLUSION

Arterial occlusion effects on retinal structure in cats, describing degrees of cell degeneration
22 p3884 A69-40883

OCCULTATION

NT LUNAR OCCULTATION

NT SOLAR ECLIPSES

NT STELLAR OCCULTATION

S-band radio occultation for probing atmospheres of Mars and Venus
[AAS PAPER 68-185] 02 p0311 A69-11470

Radio occultation measurements of Venus and Mars atmospheres using Mariner spacecraft
02 p0320 A69-12115

Radio amplitude and phase measurements during Mariner-Mars encounter, providing evidence for Martian atmospheric models
02 p0320 A69-12116

Stellar image and spectrum distortions during occultation observed from satellite, discussing recovery of atmospheric composition data from stellar spectra
03 p0421 A69-13346

Radio occultation measurements of planetary atmospheres and ionospheres from orbiting pair
[AIAA PAPER 69-53] 06 p1011 A69-18104

Mercury transits in 1970 and 1973 to resolve prominence threads and spicules, sunspot fine structures, etc
11 p1958 A69-24434

Pioneer 6 S band telemetry carrier Faraday rotation during corona occultation measured by deep space tracking antenna
15 p2700 A69-31419

Meteorological parameters-radio propagation characteristics correlation, studying feasibility of data acquisition by occultation satellite system
21 p3705 A69-38374

Earth atmospheric density measurement by microwave radio occultation techniques, transmitting coherent radio signal to repeater spacecraft from master station
21 p3705 A69-38375

Venus atmosphere structure determined from Mariner 5 flyby S band radio occultation measurements of ionosphere and atmosphere at illuminated and dark sides
21 p3794 A69-38380

OCCUPATION

Occupational attrition estimation methods for determining personnel separation through marriage, death, retirement and transfer applied to engineering and nursing
07 p1245 A69-19728

OCEAN BOTTOM

Aerial photography for near-shore ecology, noting biological cover on ocean floor, submarine biological communities and human activities on submarine life
22 p3894 A69-40995

OCEANOGRAPHY

Orbiting satellite global all-weather oceanographic data acquisition to complement higher resolution data from ships, buoys and aircraft remote sensors
[UN PAPER 68-95878] 01 p0064 A69-10491

NOMAD buoy telemetry system for synoptic oceanographic and meteorological data, using digital processing and dual frequency transmissions
03 p0391 A69-13223

Remote sensing platform requirements for oceanographic and meteorologic observations, discussing orbital and aircraft platforms
[AIAA PAPER 69-154] 06 p1044 A69-18122

Ocean circulation as climate regulator, discussing role in redistributing climate-changing energy input from solar radiation or lunar tidal friction into atmosphere
12 p2067 A69-26333

Remote oceanographic sensing from ships, aircraft and spaceborne platforms, using active /radar and laser/ and passive sensors in visible, IR and microwave regions
12 p2075 A69-26997

Three dimensional model of atmospheric drift currents in equatorial region of world ocean system based on nonlinear differential equations
14 p2472 A69-29405

Passive remote sensing at microwave frequencies for meteorology, oceanography and geology, reviewing physics of wave interactions, mathematics of data interpretation, etc
14 p2414 A69-29514

Satellite observation of ocean surface and subsurface features, discussing onboard equipment and proposed orbits
15 p2607 A69-30190

Sand ridge origin and dynamical setting, discussing morphology-tidal current system equilibrium indicated by theory and field measurements
15 p2596 A69-30443

Spacecraft radar altimetry applied to study of sea surface slopes, tides, tsunamis, storm surges and submarine geology
15 p2609 A69-30461

IR measuring techniques for water surface temperature remote sensing
15 p2617 A69-31543

Sea surface temperature remote sensing by Nimbus 2 satellite using TV camera and medium and high resolution IR radiometer
18 p3130 A69-35057

Oceanographic sensing satellite systems, discussing applications, data requirements, sensors, booster and earth coverage capabilities
18 p3210 A69-35091

Eclogite fractionation role in creation and spreading of suboceanic lithospheric plate, discussing density determination at 100 km depth
18 p3132 A69-35434

Angular dependence of ocean surface-cloudless atmosphere reflectance for solar radiation studied with digitized camera signals from ATS 1 satellite
21 p3704 A69-38372

Tethered polyethylene balloon carrying radio controlled camera for time lapse photographs of wave generated near shore currents
22 p3865 A69-40808

SNAP 21 radioisotope powered thermionic generator with multiple couple Pb-Sn-telluride/Bi-Sb-telluride flat plate configuration for deep sea applications
23 p4069 A69-42248

Synoptic remote sensing oceanography from ships, aircraft and spaceborne platform, discussing fisheries
[AAS PAPER 69-062] 24 p4307 A69-42822

OCEANS

NT ARCTIC OCEAN
NT ATLANTIC OCEAN
NT INDIAN OCEAN
NT PACIFIC OCEAN

Satellites and ocean platforms for civil aviation operations over North Atlantic, noting cost justification dependence on supersonic traffic increase
[UN PAPER 68-95887] 01 p0113 A69-10521

Model for radiative transfer in atmosphere-ocean system by Monte Carlo method, considering Rayleigh and Mie scattering
11 p1877 A69-24851

Airborne magnetometer application for remote measurement of ocean wave spectra, obtaining wave noise power spectra and wave height profile
12 p2075 A69-26998

Radar radiometer by adding radar to scanning microwave radiometer, discussing applications to spacecraft measurement of oceanic winds, waves and precipitation
14 p2421 A69-29528

Ocean and atmospheric interactions analyzed by using hydrodynamic equations for boundary layers
14 p2442 A69-29838

Ocean and water surface temperature measurement by IR remote sensing from aircraft and satellites, discussing accuracy and data correction
[AIAA PAPER 69-590] 17 p2973 A69-33286

Heat flow through ocean floor by measuring temperature gradient and thermal conductivity in ocean sediment
21 p3718 A69-39733

Airborne microwave radiometric measurements of simulated ocean surface under various conditions, suggesting possible wind velocity measurement by satellite
21 p3726 A69-39750

OCTAHEDRITE

U ANATASE
U MINERALS

OCTAHEDRONS

Crystal and molecular structure of mu-oxo-bis/chlorobis/2, 4-pentanedionato/titanium/IV//chloroform solved by symbolic sign determination method and Patterson map interpretation
01 p0023 A69-10411

OCTANE

Electrocatalysts for direct electrochemical oxidation on n-octane in fuel cells, discussing platinum consumption reduction
[ECS PAPER 8] 03 p0368 A69-13856

OCULOGRAVIC ILLUSIONS

Human vestibular reactions at various bodily rotation rates and planes, including counterrotation illusion and nystagmic reaction
12 p2020 A69-26564

Human angular acceleration sensitivity using rotation and oculogyral illusion perception as indicators, relating to spatial orientation and flight control task precision
23 p4101 A69-41674

OCULOMOTOR NERVES

Ocular motor failures in pilots due to convergent and divergent strabismus, discussing low pressure chamber tests and blood pressure effects on cranial nerve
03 p0370 A69-13470

Visual feedback mechanisms in simulated high altitude conditions, discussing physiology of ocular homeostasis adaptation
06 p0882 A69-17647

Oculomotor activity of cosmonauts during orbital flight, analyzing electrooculograms taken during vestibular tests
07 p1063 A69-18594

Electrooculographic method to study eye movements control system for fixation on stationary point or following discretely or continuously moving target
09 p1447 A69-22675

Circadian rhythm of optic nerve impulses in isolated eye of sea hare Aplysia californica in total darkness
14 p2406 A69-28870

Soviet book on nervous mechanisms of vestibular reactions emphasizing mathematical description of operation, neurohythmic changes in cerebral cortex and oculomotor activity modeling
16 p2746 A69-32605

Phase and tonic activity of oculomotor apparatus of rabbits during vestibular reflexes and postrotational nystagmus
20 p3469 A69-37243

Multilevel mathematical model of oculomotor apparatus using neuron networks and complex activators, including computer analysis
20 p3470 A69-37245

Electronystagmographic method of eye movement recording, noting applications to vestibular and visual analysis and study of oculomotor nuclei- vegetative centers relations
20 p3481 A69-37273

Visual suppression association with smooth following and saccadic eye movements in tracking slow moving target
22 p3879 A69-40842

Physiological experiments to investigate aerospace flight stresses effects on oculomotor equilibrium, noting cardiovascular reaction and mechanism for interpretation
23 p4087 A69-41804

Alcoholic hangover effects on human balance system from flying demands viewpoint, discussing ocular-vestibular system disturbances
23 p4089 A69-41817

OFF-ON CONTROL

Optimal control problems with discontinuities, noting jump discontinuities in state variable derivative arising in bang-bang control problems
01 p0049 A69-10003

Performance cost functions for reaction jet controlled system during on-off limit cycle for stable and unstable plant
02 p0278 A69-11965

Predictive logic control of on-off system with one position sensor
[ASME PAPER 68-WA/AUT-14] 05 p0830 A69-16134

Nonlinear bang-bang optimal control problems solution based on differential dynamic programming, noting use of Pontryagin adjoint variables
11 p1860 A69-25444

Hysteresis of on-off element with proportional feedback around element, noting autooscillations and results for electromagnetic relay
12 p2053 A69-26506

Time optimal pitch motion of satellite in circular orbit based on maximum principle, considering variable and constant controls
18 p3207 A69-34677

On-off limit cycle controllers for reaction-jet controlled systems, investigating delay effects
24 p4291 A69-43271

OGEE WINGS

U VARIABLE SWEEP WINGS

OGO

NT OGO-D
NT OGO-E
NT OGO-F

Magnetic field data from OGO-2 spacecraft and surface magnetic observatories, noting magnetic storm occurrence and magnetosphere inflation and detection of polar ionospheric currents
01 p0069 A69-11125

Deployable appendages of OGO attitude controlled spacecraft design
06 p1017 A69-17606

Magnetospheric ELF noise, discussing OGO 3 spectrum analysis
07 p1124 A69-18834

Low energy charged particles in earth magnetosphere observed by OGO satellite
07 p1208 A69-19358

Low energy electrons in magnetosphere from OGO-1 and OGO-3 observations, discussing plasma sheet, magnetic bay activity, electron pressure, temperature and density gradient
07 p1209 A69-19373

Satellite trajectory determination and expected errors for OGO 4 and Geos 1 orbits, noting geopotential, aerodynamic drag and integration contributions
15 p2698 A69-31331

UV OGO observations of atomic hydrogen and oxygen in airglow, comparing results to exospheric models of hydrogen geocorona
15 p2603 A69-31400

Geocoronal Lyman alpha short term and 27-day variations observed by OGO 4 spacecraft attributed to flux variability at solar emission line center
15 p2699 A69-31404

OGO program failure rate analysis with respect to cost, schedule and performance tradeoffs, considering component and systems design and reliability, prelaunch feedback, etc
18 p3207 A69-34519

OGO for conducting diversified measurements to study earth atmosphere, earth-sun relationship, etc
19 p3432 A69-36674

OGO triaxial search coil magnetometer for measuring earth magnetic fluctuations, discussing design rationale and observation results
19 p3284 A69-36675

OGO 4 UV airglow spectrometer consisting of Ebert-Fastie monochromator and photomultipliers with cesium telluride and cesium iodide channels
19 p3315 A69-36682

OGO 5 spacecraft detector instrumentation for measuring electrostatic and electromagnetic waves electric fields with coupled antennas, describing in-flight operation
19 p3315 A69-36683

OGO-D

Thermally excited oscillation experienced by OGO 4 boom antenna demonstrated by mathematical model, showing nonplanar coupled bending-torsion oscillation by solar radiation
07 p1227 A69-18333

OGO-E

Electron detector for OGO-E to measure flux and energy spectrum of electrons in primary cosmic rays
[IEEE PAPER 3C-4] 07 p1135 A69-19198

OGO 5 spectrometric studies of topside ionospheric ion concentrations, noting difference between nighttime and sunlit pass 15 p2599 A69-31345

OGO 5 satellite measurements of intensity and width of Lyman alpha line scattered by hydrogen geocorona 15 p2699 A69-31412

Solar X ray detector aboard OGO 5 satellite observing two components in energetic solar X ray bursts, attributing impulsive component to bremsstrahlung 22 p4007 A69-40775

OGO-F

Solid state detector for electron spatial distribution measurements on OGO-F satellite, discussing design emphasizing reliability 19 p3284 A69-36676

OGO-F electric and electromagnetic fields measurement for ionosphere using dipole antenna, emphasizing broadband observation covering whistler mode waves 19 p3284 A69-36677

OGO-F neutron monitor for measuring cosmic ray neutron flux near earth, locating sensor on boom to minimize spacecraft produced neutrons 19 p3314 A69-36678

Gas-surface energy transfer experiment on OGO-F satellite, measuring upper atmosphere kinetic energy flux to determine accommodation and drag coefficients, density, etc 19 p3255 A69-36680

OGO-6 design, research program, orbits and instrumentation, emphasizing relationship between particle activity, aurora and airglow, geomagnetic field, atmospheric and solar energy interrelations 24 p4393 A69-43132

OH- 6 HELICOPTER

Air engineering flight testing of OH-6A helicopter, presenting test program and results 06 p0867 A69-17659

OH-6A drive system design for lightweight, low cost high performance helicopter, discussing reliability from RVN combat data [AHS PAPER 374] 17 p2900 A69-33514

Air OH-6A helicopter light weight design, considering effects of WRAP /weight, radius, area, power/ factors on empty weight [SAWE PAPER 781] 18 p3091 A69-34870

OHMIC DISSIPATION

NT SHOCK HEATING

P-n junction cut-off current density and ohmic losses effect on injection laser efficiency determined by using quality parameter 01 p0091 A69-10883

Energy release by Joule magnetic field dissipation in solar atmosphere 03 p0516 A69-14041

MHD generator and compressor Joule losses effect on thermoelectric energy conversion closed cycle efficiency with electrical conductivity maintained by nonequilibrium ionization • 03 p0369 A69-14152

Conductivity and electron temperature in coaxial MHD generator plasma with magnetic field, studying Joule heating effect on performance 10 p1735 A69-23463

Avalanche transistor pulse circuits temperature increase due to power dissipation, noting effects of external resistance grounding base and pinch in 11 p1845 A69-24570

Joule heating role in generating internal gravity wave energy in auroral electrojet region, using linear model 12 p2064 A69-26010

P-n junction cut-off current density and ohmic losses effect on injection laser efficiency determined by using quality parameter 12 p2109 A69-26647

Fringing effects on electric efficiency variation with slip for cylindrical induction MHD device operable as accelerator, generator or Joule heater [AIAA PAPER 67-714] 16 p2736 A69-32152

OIL ADDITIVES

Sulfide addition agents for diester lubricating grease and organic resin solid film lubricants, noting formulation and tests for steel and molybdenum 01 p0102 A69-10907

OILS

NT CRUDE OIL
NT FUEL OILS
NT LUBRICATING OILS
NT MINERAL OILS

Diffusion pump oil reflectance and absorption coefficients measured in three thicknesses using light source, monochromator and detector 10 p1725 A69-23647

Oil quench vacuum furnace with graphite cloth heating elements 14 p2456 A69-29894

Differential capacitance transducer measuring small displacements in heated transformer oil, air, castor oil or glycerin 22 p3946 A69-40439

OLEFINS

U ALKENES

OLFACTORY PERCEPTION

Olfactory bulb removal effects on uptake decline of telencephalic norepinephrine, noting use for mapping adrenergic pathways 22 p3871 A69-40055

OLIVINE

Deformation microstructures in shock loaded olivine, discussing planar features 05 p0818 A69-15607

Mossbauer spectra of Fe minerals in unequilibrated ordinary chondrites, noting ratios of olivine to pyroxene iron 19 p3408 A69-36082

Equation of state measurements of earth materials by, shock wave techniques, applying to olivine for earth mantle constitution problem 22 p3937 A69-40188

Olivine-bronzite chondrite fragments found near Oshkosh, Wisconsin, in fall of 1961 22 p4021 A69-40413

OMEGA NAVIGATION SYSTEM

OMEGA position location equipment /OPLE/ test data to demonstrate feasibility of using OMEGA navigational system in conjunction with synchronous satellites 07 p1176 A69-19135

Hybrid OMEGA inertial system for following vehicle maneuver without lag developed by combining Schuler tuned inertial data and radio position data 07 p1177 A69-19209

OMEGA airborne navigational computers, discussing earth ellipticity and phase variations problems for signal conversion into latitude and longitude coordinates 08 p1347 A69-20778

Flight test performance of airborne Omega radio navigation system capable of worldwide coverage, discussing diurnal variations effects in phase velocity 08 p1348 A69-21191

Airborne computerized Omega Navigation set from combination of functional analysis of Airborne Omega Navigation Receiver with capabilities of current airborne computers 08 p1349 A69-21197

OMEGA VLF navigational transmission phase delay variations and field strength measurements on transatlantic propagation path, noting effect of directional change 09 p1538 A69-22595

Omega/VLF transmission range rate measurements for satellite Doppler navigation to provide velocity and location data, noting propagation error 14 p2479 A69-29857

Atomic and astronomical time and frequency measurement via Loran C and VLF/Omega phase tracking receivers 15 p2615 A69-31285

VLF wave propagation phase velocity prediction for airborne Omega computer, using scatter model based on abnormal ionosphere 17 p3002 A69-34077

Propagation effects on lane ambiguity resolution ability of Omega VLF navigational system, noting waveguide mode interference 21 p3673 A69-38756

Omega aircraft navigation, discussing digital computer applications, SNR environment, carrier interference and accuracy requirements for signal reception 23 p4186 A69-42539

Surface and aerospace navigation by VLF radio network, discussing Omega transmitting station location, operational modes and daytime-nighttime accuracies [AAS PAPER 69-405] 24 p4347 A69-42834

OMNIDIRECTIONAL ANTENNAS

NT MONOPOLE ANTENNAS

Radiation pattern, gain and polarization of omnidirectional antenna consisting of dipoles or monopoles arranged along circular cone 01 p0046 A69-10738

Balanced symmetrical four arm conical equiangular spiral antenna providing omnidirectional circularly polarized radiation pattern in azimuthal plane 03 p0404 A69-13471

Airborne S-band telemetry antennas for omnidirectional patterns of polarization component, discussing design, pattern measurements and application 07 p1106 A69-19112

Log periodic antenna with vertically polarized omnidirectional radiation constant over bandwidth 08 p1281 A69-20033

Electronic multibeam switching X band antenna system design with separate transmitting and receiving antennas for use on continuous wave surveillance radar 08 p1289 A69-20967

Self focusing aerial antenna arrays with full angular coverage for two way airborne communications 08 p1289 A69-20971

Siting two antennas for combining signals to obtain all-around coverage in aircraft communication 08 p1289 A69-20972

Frequency independent antenna far field radiation approximated for gain, polarization, field amplitude and phase, defining omnidirectional antenna with wide-band goniometry 08 p1295 A69-21149

Wave-mode converter with feed for omnidirectional antenna excitation, discussing H to E wave conversion, waveguides, emitter, etc 11 p1854 A69-25616

Wave propagation in 11.7-12.7 GHz range studied for application to TV transmission, describing emitter, omnidirectional antenna and receiving station 11 p1841 A69-25637

Spacecraft antennas properties, structure and problems including frequency ranges, external influences, omnidirectional radiation, input impedance, etc 16 p2763 A69-32584

Residue series representation of radiation fields for azimuthal leaky wave antenna on conducting cylinder, showing zeroth term correspondence to omnidirectional antenna 20 p3506 A69-37834

Multifunction lightweight antenna system package for spin stabilized near synchronous satellite having axis normal to orbital plane 22 p3913 A69-40694

Omnidirectional microwave parallel plate waveguide fed antenna design for flush mounted broadband spacecraft, noting equatorial and polar patterns 22 p3913 A69-40697

Simple antenna with good circular polarization over wide space sector, showing geometry, normalized orthogonal field distributions and beamwidth range, considering slot combinations 23 p4137 A69-41590

Frequency diversity technique simplifying airborne antennas for UHF telemetry, useful on spin stabilized vehicles requiring omnidirectional antenna coverage 23 p4122 A69-41777

OMNIRANGE NAVIGATION

U VHF OMNIRANGE NAVIGATION

ON-LINE PROGRAMMING

Error and sensitivity analysis of on-line algorithms for fixed point linear smoothing 01 p0050 A69-10238

Nonlinear system on-line identification in presence of noise, using stochastic methods and analog equipment 03 p0401 A69-13764

Artificial intelligence application to design of off-line and on-line learning control systems for controlling spacecraft attitudes 04 p0581 A69-14568

On-line ground flight test data processing system 05 p0725 A69-16757

On-line analysis with digital computer, noting system designed for vibration and random vibration analysis 05 p0726 A69-16761

On-line optimization of stochastic control systems based on learning controller model, discussing computer simulation results 06 p0900 A69-17354

Asynchronous on-line digital data acquisition system with immediate access to on-site numerical real time printout for rocket engine performance tests [AIAA PAPER 69-323] 09 p1478 A69-22381

Adaptive control algorithm operating on-line to make discrete time adjustments in controller parameters of continuous time control system 09 p1474 A69-22441

Ground station integrated flight test data system with interactive data input terminals, on-line assembly and responsive program development 10 p1633 A69-23271

Time and space on-line simulation of analog, digital and hybrid block diagram systems
16 p2755 A69-31709

On-line central data processing system connected to time shared computer for recording data from test facilities, discussing hardware configuration, software considerations and advantages
17 p2932 A69-33106

Network Analysis for Systems Application Program development for batch and on-line solution of circuit problems
18 p3111 A69-34680

Dynamic Automated Reporting Technique /DART/ system for on-line conversational information storage and retrieval for use in large programs management
18 p3107 A69-35095

Network analysis for systems application program /NASAP/ in FORTRAN for batch and on-line analysis of electronic circuits
21 p3856 A69-39662

Image disappearance or reappearance time controlled by inducing changes in alpha occurrence probability, executing on-line closed loop program detecting alpha rhythm
22 p3871 A69-40159

Closed Loop Ionogram Processor /CLIP/ on-line computer processing system for ionospheric data [AIAA PAPER 69-952]
22 p3904 A69-40334

Adaptive control systems analysis and application, noting off-line and on-line optimization, dynamic programming, linear systems, etc
24 p4289 A69-42946

ONBOARD EQUIPMENT

NT AIRBORNE EQUIPMENT
NT AIRBORNE/SPACEBORNE COMPUTERS
NT AIRCRAFT EQUIPMENT
NT SPACECRAFT ELECTRONIC EQUIPMENT

Apollo landmark sighting by astronaut using Apollo onboard navigation system, simulating cloud cover effects with Monte Carlo technique
01 p0110 A69-10692

Electron concentration in ionospheric outer regions determined from coherent frequencies recorded on-board OGO-A
01 p0147 A69-11323

Spacecraft device for photographing and transmitting TV pictures noting limitations and spatial conditions adaptations
02 p0207 A69-11829

General purpose satellite computer, discussing on-board processor /OBP/ design, memory, central unit, input/output and software
05 p0725 A69-16710

Onboard solid state neon cryostat for IR detector, noting resistance to missile vibration, acceleration and shock tests
06 p0906 A69-17103

Narrow and wide angle actinometric instruments on-board Cosmos 122, 144 and 156, describing optical and data acquisition systems
06 p0929 A69-17977

Informative properties of IR scanning equipment of meteorological satellites, discussing radiative flux measurements and thermal mapping
06 p0929 A69-17979

Onboard calibration system for gamma ray spectrometers and X ray detector in earth satellites, describing fabrication and test results for radioactive sources [IEEE PAPER 3A-6]
07 p1134 A69-19193

IMP F and G solar cosmic ray spectrometer utilizing FET analog multiplier for onboard particle identification data processing [IEEE PAPER 3C-3]
07 p1135 A69-19197

Dielectric constant and loss angles measurement in Ku band used for onboard radars
07 p1112 A69-19544

Biomedical experiment onboard Cosmos 110 concerning nonpathological changes
08 p1261 A69-19827

Spacecraft applications of Langmuir probes, obtaining data from current-voltage characteristics for electron/ion concentrations, ion mass spectra and charged particle energy distribution
08 p1316 A69-20474

Digital telemetry from spacecraft, discussing on-board processing, data compression, coding, sequence detection and receivers
08 p1276 A69-20592

Electrical energy production on board space vehicles including solar batteries, chemical reagents and possible nuclear energy utilization
08 p1259 A69-21036

Manual onboard computation procedures and devices for determination of maneuvers for orbital navigation and guidance
08 p1348 A69-21184

Airborne computerized Omega Navigation set from combination of functional analysis of Airborne Omega Navigation Receiver with capabilities of current airborne computers
08 p1349 A69-21197

Satellite-borne terrestrial radiodetermination systems, noting VLF transmissions usage to overcome coverage problem
09 p1537 A69-21287

Spacecraft onboard checkout systems and design of ground support equipment and software, noting adaptive dynamic analysis and maintenance /ADAM/ concept [AIAA PAPER 69-307]
09 p1478 A69-22382

Onboard test and fault isolation design for airborne systems considering tradeoff parameters for optimum reliability, performance and cost [AIAA PAPER 69-306]
09 p1434 A69-22389

Transpondersondes for atmospheric measurements, considering ground tracking, radiosondes, rocket-sondes and flight results
10 p1692 A69-23257

Onboard aircraft weighing system /OBAWS/ for accurate gross weight and CG measurements, describing axle shear deflection transducer system
10 p1693 A69-23276

Onboard test instrumentation for monitoring aircraft communication, navigation and identification systems, noting adaptive programming
11 p1866 A69-25080

Onboard checkout system concept, discussing philosophy, requirements, underlying considerations, system description, development and techniques of system selection
11 p1866 A69-25081

Onboard magnetic anomaly detection system for Canadian helicopter, discussing magnetometer location, boom design and testing and equipment installation [AIAA PAPER 68-487]
12 p2094 A69-26771

Radiation dosimetry and shielding onboard Cosmos 110 artificial satellite, noting earth belt proton radiation
13 p2356 A69-27702

Satellite observation of ocean surface and subsurface features, discussing onboard equipment and proposed orbits
15 p2607 A69-30190

Flight worthiness of mishandled electronic equipment, analyzing fragility and performance of shock exposed components and connections
15 p2576 A69-30362

ESRO 1 and 2 satellites onboard remote control system, discussing tone digital standard code and equipment design features
15 p2702 A69-31086

AN/ASN-24/V/ general purpose digital computer deployed in large worldwide jet transport fleet
17 p2933 A69-34061

Aircraft solid state electric system logic level tested functionally by built-in test equipment /BITE/ operated on ground during preflight tests
17 p2977 A69-34110

Aircraft onboard weighing system, eliminating o ring seal friction to permit accurate measurement of oleo strut pressure [SAWE PAPER 748]
18 p3137 A69-34883

Aircraft on board weight and balance system, discussing operations and economics programs [SAWE PAPER 805]
18 p3091 A69-34901

Manual procedures for midcourse and terminal guidance, discussing onboard optical measurements and calculations
19 p3368 A69-35792

Star/horizon measurements for onboard spacecraft navigation without cloud cover obscuration, discussing sightings, data processing and evaluation
19 p3369 A69-35800

Onboard radar for light interceptor aircraft /Aida II/, discussing navigation, low altitude penetration and air to air missile interception
19 p3278 A69-36701

Secondary radar IFF/SIF /Identification Friend or Foe-Selective Identification Feature/ system, describing ground and onboard radar and data processing equipment
19 p3278 A69-36702

Computer based onboard satellite PCM telemetry, showing improved adaptability, size and cost reduction
20 p3500 A69-37382

Wire type memory model for satellite onboard computers, discussing nondestructive readout, power requirements, marginal temperatures, material and volume
20 p3503 A69-37403

Planetary atmosphere structure and mean molecular weight determination from onboard measurements tested at high altitude in earth atmosphere, based on NASA Program [AIAA PAPER 68-1054]
21 p3715 A69-39023

Spacecraft trajectory control algorithm for hyper-sonic reentry, describing onboard equipment role and simulation results
21 p3767 A69-39649

Thermal design of missile mounted S band telemetry transmitter package based on temperature control system, using heat-of-fusion characteristics of wax material
22 p3909 A69-39945

Computer controlled TV cloud recognition equipment on meteorological satellites, discussing multistep process of automatic perspective distortion corrections by onboard computer
22 p3977 A69-40004

Programmatic constraints on onboard processing of data collected by payload sensors [AIAA PAPER 69-942]
22 p3904 A69-40325

Three channel inertial ship or aircraft navigator for determining gravity vector, using earth gravity field model
23 p4162 A69-41320

Accelerated motion influence on onboard vertical gyro with design based on free astatic gyro with electromagnetic compensation
23 p4163 A69-41553

Centrifuge on board orbiting spacecraft as research tool for biological and physical experiments relevant to prolonged missions and spacecraft design
23 p4108 A69-41833

Navigation systems analysis for space missions planning, discussing onboard equipment and lunar landing accuracies [AAS PAPER 69-406]
24 p4347 A69-42833

Mars atmosphere study by Mariner 6 and 7 spacecraft, discussing instrumentation on board [AAS PAPER 69-091]
24 p4393 A69-42881

Satellite attitude estimation from onboard telescope celestial sightings using iterative least squares method, considering measurement error noise and axes wobble
24 p4348 A69-43244

ONBOARD NAVIGATION
U NAVIGATION

ONE DIMENSIONAL FLOW

Longitudinal short wave stability in conducting quasi-one dimensional gas flow, considering regions of high thermal emission
02 p0233 A69-12487

Similarity motion of fluid particles in one dimensional gas flow, establishing limits of slip factor value change
03 p0419 A69-13920

Second order difference scheme for calculation of plane or rotational compressible flow, investigating stationary flow as asymptotic limit of unsteady flow [ONERA-TP-652]
03 p0419 A69-14111

MHD shock wave decay in one dimensional unsteady flow of ideal inviscid perfectly conducting compressible fluid subjected to transverse magnetic field
05 p0806 A69-16736

One dimensional unsteady flows of combustible gas mixture with finite chemical reaction rates, considering piston motion, igniting shock wave propagation and point explosion
06 p0909 A69-17325

Electrodynamic gas flow in one dimensional approximation for transition through speed of sound, discussing flow parameters profile and dynamic efficiency
06 p0964 A69-17326

Parasitic eigenvalue in integration of equations governing one dimensional flow of chemically reactive gas
07 p1118 A69-18317

Two fluid approximation of one dimensional steady state flow of inviscid plasma with thermal gradients, considering ionization and recombination processes
07 p1189 A69-18691

Optimum profile of supersonic nozzle with nonequilibrium flow
07 p1119 A69-18737

Theory of unsteady one dimensional motion of ideal compressible fluid, discussing equation of state
07 p1119 A69-18750

One dimensional flow of conducting inviscid compressible fluid in channel in presence of transverse fields, discussing steady velocity flows
07 p1191 A69-19014

Frozen shock in steady one dimensional compression flow of relaxing gases weaker than equilibrium shock
08 p1304 A69-20785

Flow analysis in magnetic annular shock tube in magnetic field varying with time
08 p1366 A69-20787

Generalized Riemann function obtained as solution of transformed Boltzmann-Vlasov equation, discussing one dimensional and multidimensional cases
10 p1724 A69-22908

Optimum operation modes of MHD converter
10 p1636 A69-23095

General solutions of MHD equations for linear nonsteady and plane steady motions of ideally conducting gas
10 p1727 A69-23096

One dimensional analysis of stationary argon flow in linear Hall generator from continuity, momentum and energy equations, discussing electron heating and nonequilibrium ionization
10 p1736 A69-23465

Optimal control of one dimensional fluid flows with characteristic velocity passing through zero, showing Lagrange multipliers continuous and bounded in optimal solution
11 p1934 A69-25728

One dimensional stationary flow of medium consisting of charged and neutral components within electrohydrodynamic limits in AC and DC electric fields
12 p2135 A69-26398

Internal flows of compressible fluids with heat transfer in accelerating nozzles and constant area ducts, simplifying equations by assuming one dimensional flow
12 p2012 A69-26790

Influence coefficients for compressible flow processes involving area, friction and total temperature changes
12 p2063 A69-26799

Boundary value problem for one dimensional unsteady equations for inviscid conducting gas during transition processes in MHD duct
13 p2309 A69-28027

Conducting liquid boundary layer flow and heat flux on electrodes of MHD generator, including one dimensional flow outside boundary layer
13 p2309 A69-28028

Kolmogorov-Prandtl turbulence energy hypothesis extended from turbulent region of one dimensional flow to laminar sublayer, obtaining numerical solutions for Couette flow
13 p2250 A69-28339

Turbulent burning velocity definition for one dimensional turbulent flow and average flame orientation perpendicular to flow direction, discussing transient flames in turbulent environment
13 p2379 A69-28452

Flow stability of one dimensional Cartesian and cylindrical incompressible inviscid flows with no body forces and interfaces
14 p2429 A69-29013

One dimensional unsteady monatomic Maxwellian gas flow at small Knudsen numbers using Hilbert method, noting validity for shear flows
14 p2432 A69-29611

MHD quantities in linear wave and small intensity shock wave dissipation and structure determinable by right and left eigenvectors of matrix MHD flow equation
14 p2500 A69-29902

Asymptotic behavior of one dimensional laminar flow of incompressible viscous fluid in infinite cylindrical tube, giving equations for boundary conditions and flow rate
16 p2769 A69-31831

Normal stress effects in viscoelastic fluid theories applied to one dimensional Burgers model of weak turbulence predicting drag reduction
17 p2951 A69-33256

Gas pressure differential across multilayer insulation blanket during rapid evacuation predicted, using one dimensional flow theory
[AIAA PAPER 69-608] 17 p3072 A69-33275

Time dependent analysis for quasi one dimensional, vibrational and chemical nonequilibrium nozzle flows approaching steady state solution by finite difference technique
[AIAA PAPER 69-668] 17 p2893 A69-33491

One dimensional viscous magnetofluidynamic flow in annulus formed by concentric cylindrical electrodes,

reducing problem to linear partial differential equation set
[AIAA PAPER 69-725] 17 p3012 A69-33493

Far and near field solutions for one dimensional unsteady flows in general inviscid relaxing gas, obtaining flow field structure by matching techniques
17 p2957 A69-33599

Conducting medium steady one dimensional motions determined by assuming space charge-electric field interaction, considering electrohydrodynamic behavior of medium
18 p3181 A69-35315

Kinetic model and steepest descent method to optimize one dimensional combustor
[AIAA PAPER 68-644] 19 p3448 A69-35943

One dimensional spectra of turbulent wakes behind circular cylinders, discussing isotropy, anisotropy and Reynolds number
21 p3693 A69-38705

Self similar solution to one dimensional isothermal ionized gas outflow from ionization front in half space filled with neutral gas exposed to quanta flux
21 p3771 A69-38997

Relativistic solution by Landau procedure of initial value problem for one dimensional electron plasma wave coexisting with charged immobile background
21 p3778 A69-39579

Quasi-one dimensional analysis for nonequilibrium flow of dissociated diatomic gas through converging-diverging nozzle, discussing critical mass flow rate
22 p3927 A69-40583

One dimensional flow of perfect compressible relativistic fluids, obtaining expression showing wave velocity dependence on relativistic speed of sound
22 p3931 A69-40711

Starting process in nozzle with one dimensional flow treated numerically by finite difference method using pseudoviscosity term
22 p3860 A69-40926

Class of one dimensional nonlinear waves and shock structure reduced to steady flows in radiation gas dynamics
23 p4240 A69-42466

Iterative finite difference method for initial value problems applied to hyperbolic system representing one dimensional time dependent flow of compressible polytropic gas
24 p4340 A69-43226

Symmetry properties of Cameron-Martin-Wiener kernels in isotropic velocity field, applied to one dimensional model of incompressible turbulent flow
24 p4301 A69-43358

Rarefied gas one dimensional transverse motions consistent with Boltzmann kinetic equation, solving integrodifferential equations for shock wave structure
24 p4351 A69-43491

ONISOTROPY

U ANISOTROPY

ONSAGER PHENOMENOLOGICAL COEFFICIENT

Linear irreversible thermodynamics theory as applied with conservation principles and Maxwell relations to charged particle motion in electromagnetic field, noting Onsager coefficients role
17 p3075 A69-34142

ONSAGER RELATIONSHIP

Onsager reciprocity relations applied to thermodynamics of nonlinearity and noise in diodes
04 p0574 A69-14435

Diffusion and thermal diffusion in mixture of Maxwellian gases, analyzing Onsager reciprocity relations
05 p0849 A69-16461

Thermodynamics of sinusoidal steady state energy converters governed by Onsager reciprocity relation, determining maximum conversion efficiency
11 p1826 A69-25396

OOCYTES

U GAMETOCYTES

OPACIFIERS

Thermal analysis of opacified fibrous insulation systems, discussing heat transmission, heat transfer and thermal conductivity relations to compression load and temperature
[AIAA PAPER 69-605] 17 p3072 A69-33282

OPACITY

Angular distribution of reactive elastic scattering analyzed by opacity function/reaction probability/
04 p0554 A69-14859

Stellar atmospheres radiative opacity, computing metal absorption coefficients
07 p1220 A69-19392

Radiative opacity in stellar atmospheres, discussing effect of UV continuum on photospheric radiation field
07 p1221 A69-19393

Algorithm for high speed digital computers to evaluate stellar radiative opacities
07 p1222 A69-19589

Hydrogenic approximation validity in evaluation of atomic energy levels and radiative absorption cross sections for computation of stellar opacity
07 p1223 A69-19626

Stereoradiography using holographic techniques to examine internal structure of opaque objects
08 p1313 A69-20178

Effects of opacity arising from silicon bound-free transition on emergent fluxes and hydrogen line profiles for A and late B stellar atmospheres
09 p1604 A69-22403

Lyman alpha wing opacity effect on temperature scale and helium content in F and G subdwarf atmospheres
09 p1607 A69-22431

Static envelope with no mass outflow for star static core constructed from opacity coefficient dependence on temperature and density
10 p1775 A69-23199

Surface dielectric constant and microwave opacity of Venus atmosphere as function of wavelength determined by radar observations
12 p2153 A69-25805

Line absorption effect on opacity and main sequence model stars noting luminosity, radius and mass of convective core
13 p2340 A69-27578

Limb darkening on earth night side observed by Aerobee rocket, with explanation based on atmospheric opacity in water vapor and carbon dioxide bands
17 p2960 A69-33167

Weak displacements of opaque objects and optical distortion in solid state lasers analyzed by holographic interferometry
19 p3308 A69-35909

Autoionization lines effect on stellar structure by computing contributions to Rosseland mean opacity
20 p3612 A69-38165

Thermal conduction by electrons in stellar matter, presenting opacity tables for H, He, C and red giant cores and solar composition
22 p4014 A69-40147

OPEN CHANNEL FLOW

Two dimensional unsteady wave motion in shallow water using MHD theory
08 p1362 A69-20354

OPENINGS

NT APERTURES

NT IRISES [MECHANICAL APERTURES]

Buckling of elastic cylinders with rectangular cut-outs and reinforcements under axial or lateral loading, using modified Newton method
[AIAA PAPER 69-92] 06 p1027 A69-18060

OPERATING SYSTEMS [COMPUTERS]

Real time operating system /RTOS/ 360 for spacecraft flight control, describing hardware, applications, task management and capacity, etc
21 p3679 A69-39602

OPERATING TEMPERATURE

Microwave radiometer with two reference temperatures, discussing overall stability of design, sensitivity and airborne design for operation in X band
[DVL-895] 02 p0220 A69-12435

Solar cell generator design problems for solar probes, discussing increased operational temperature
02 p0197 A69-12665

Minority carriers lifetime measurement in degenerate GaAs, showing dependence on current density and operating temperature
03 p0483 A69-12917

Avalanche transistor pulse circuits temperature increase due to power dissipation, noting effects of external resistance grounding base and pinch in
11 p1845 A69-24570

Limiting heat power transported by sodium heat pipes dependent on capillary network geometry, inclination angle and operating temperature
14 p2538 A69-29205

Maximum strengthening due to second phase precipitation within operating temperatures maintainable to 20 hr during aging of Nb-Hf-O and Nb-Zr-O alloys
15 p2640 A69-30632

Transistor temperature and power limitations and thermal resistance calculation, discussing heat sink surface optimum design for power losses
16 p2760 A69-32047

Spacecraft electronic components operating junction temperature control, considering role of thermal resistance in controlling radiative and conductive transfer
[AIAA PAPER 69-1015] 22 p3922 A69-40387

OPERATIONAL CALCULUS

Krylov functions determined by distribution theory and operational calculus, discussing deformations and statics of straight beams
15 p2715 A69-31475

Operational calculus for n-variable functions analogous to Mikusinski method for single variable functions, giving applications to linear partial differential equations with constant coefficients
21 p3756 A69-39500

OPERATIONAL HAZARDS

Safety problems of jumbo jet airbus and SST, discussing operational safety procedures and techniques
03 p0365 A69-12882

Aircraft flight safety, discussing structural and aerodynamic concepts, maintenance and operations
03 p0365 A69-12886

Spatial disorientation as factor in accidents in operational command, noting relatively high experience level of involved pilots
07 p1072 A69-19431

Operational reliability of manual and automatic flight control systems and components and current safety standards
08 p1255 A69-20720

Accidental ignition during solid propellant processing in terms of hazard to facilities and personnel, emphasizing mixing operation
16 p2829 A69-31993

Hazard plot analysis of incomplete data involving times to failure for failed units and running times on unfail units
18 p3147 A69-34515

Laser hazard probability assessment in various applications, discussing power characteristics, attenuation by absorption and scattering and radiant energy spatial distribution
24 p4327 A69-42576

OPERATIONAL PROBLEMS

HRV-1 navy research pusher amphibian aircraft, discussing hydrofoils and operational problems
10 p1633 A69-23223

Independent operations optimum performing sequence determined for parallel machines differing in technological characteristics and with assigned time using algorithm
16 p2763 A69-31626

Flight recorder program determining combat operating environments of CH-46D helicopters analyzed and compared with aircraft design criteria
[AHS PAPER 375] 17 p3059 A69-33513

Control knob optimum diameter for minimum operation time, noting frictional resistance
21 p3664 A69-38969

OPERATIONS RESEARCH

NT CRITICAL PATH METHOD
NT DYNAMIC PROGRAMMING
NT GAME THEORY
NT LINEAR PROGRAMMING
NT MINIMAX TECHNIQUE
NT NONLINEAR PROGRAMMING
NT SADDLE POINTS [GAME THEORY]

Operational research in RAF, discussing weapons tactics and research, strike aircraft speed and height effect on target-finding, VTOL and STOL dispersion value, etc
01 p0180 A69-10863

Analytical reliability ratio to operational reliability for airborne equipment taking into account electrical and thermal aspects
01 p0011 A69-11069

Research and development project selection and planning, outlining system to identify capabilities contributing to increasing success probability
03 p0535 A69-13552

Aircraft squadron performance effectiveness model
03 p0367 A69-13911

Graphical evaluation and review technique (GERT) in R and D project planning processes
04 p0689 A69-15100

Management control systems, discussing malfunction, inefficiency and needs of human elements
07 p1244 A69-18963

Transport aircraft fleet management and handling of mechanical and avionic machine defects using operations research
08 p1422 A69-20626

Defense project management and discrepancies between estimates and final costs
08 p1423 A69-20628

Operations research in terms of contractor task formulation, project simulation, material and data collection, etc
08 p1423 A69-20868

Maintenance recording systems for aircraft fleet, discussing operations objectives and research, data collection and implementation using systems engineering
10 p1671 A69-23261

Operational research applications to management problems, discussing specific airlines operations cases
11 p1822 A69-24377

Aircraft design synthesis requirement definition in hardware commitment, discussing error effects of weight, aerodynamics and propulsion
14 p2392 A69-29432

Lidar data obtained at Hamilton AFB, Calif., computer analyzed for lidar operational utility, determining cloud ceiling and visibility for aircraft landing operations
15 p2651 A69-30895

Operations research methods applied to systems effectiveness study, using key decision models with optimized alternatives
18 p3145 A69-34503

OPERATOR PERFORMANCE

Manual control using matched manipulator technique, noting control task complexity decrease and improved performance
02 p0202 A69-11951

Operator handedness effect on control display movement stereotypes
02 p0203 A69-12212

Human operator as optimal controller, proposing quadratic performance index used by operator in judgement of own performance in tracking task
06 p0903 A69-17407

Man in loop computer facility for programmers to check out flight programs in simulated space flight environment
[AIAA PAPER 69-324] 09 p1479 A69-22384

Programmed search and gradient search methods for determination of sampling intervals in synthesis of sampled data models of human operators
10 p1650 A69-23881

Machine vibration effects on human operator performance using locomotor model
14 p2409 A69-29742

Minimum dimensions of circular nondetent knobs mounted on concentric shafts in case of nontolerable frequent inadvertent operation of adjacent coaxial knobs
17 p2916 A69-34005

Optimum knob crowding, measuring reach time, turning time, inadvertent touching and influence of knob spacing, diameter and configuration
17 p2916 A69-34006

Mathematical basis for human operators purposeful behavior in complex systems control situation requiring decision reaching
19 p3260 A69-35895

Alcohol and drug intake effects on drivers control of motor vehicles, describing postrotatory nystagmus test for toxicity measurement
21 p3652 A69-38791

Pilots and automobile drivers functional impairment due to alcohol and drugs
21 p3663 A69-38792

Human radar operator effectiveness at night noting vigilance level lowering, discussing possible logic mechanism perturbation
21 p3666 A69-39268

Sleep habits of radar operators working in alternate crews in radar station on continuous watch
21 p3666 A69-39269

Adaptive model of human operator control strategy in response to sudden changes in plant dynamics and transient disturbances
24 p4276 A69-43325

OPERATORS [MATHEMATICS]

NT BERGMAN OPERATOR

Approximate solution convergence for linear operator equation in Hilbert space by least squares method
01 p0105 A69-10728

Representation for real functions of quantum mechanical momentum operator obtained by functional integration in phase space
01 p0106 A69-10930

Integral operators on space of Borel measurable functions bounded considering weight function, giving condition for infinite complex matrices, mapping analytic sequence spaces
01 p0107 A69-11244

Higher order differential operators description and derivation of analytical mechanics for holonomic and nonholonomic systems and impact phenomena
02 p0281 A69-12199

Lie groups for equations of motion in quantum mechanics or field theory determined by operator analysis
02 p0282 A69-12840

Second order elliptical operator for m-dimensional Euclidian space with open region bounded by closed surface
03 p0456 A69-13604

Operator methods in engineering sciences, discussing integral transformations, Riesz method application to Cauchy problem, etc
03 p0457 A69-13744

Variational theorems on eigenvalues of Laplace finite difference operator with first order boundary conditions
03 p0457 A69-14230

Generalized Riemann-Liouville fractional integrodifferential operator and application to representation of analytic and harmonic functions inside circle
04 p0622 A69-14512

Stability of nonlinear time varying feedback systems, using passive operator technique
04 p0583 A69-15110

Book on linear boundary value problems of mathematical physics based on Green function covering Hilbert spaces, integral equations and spectral theory of differential operators
04 p0625 A69-15232

Theorems concerning interspherical fractionally linear transformations of operators in Hilbert spaces formulated and proved, analyzing unit sphere during fractional linear transformation
05 p0787 A69-16423

Boundary value problems for unstable quasi-linear elliptic differential operator class, proving theorems on properties of quasi-linear elliptic-parabolic equations in bounded space
05 p0787 A69-16424

Riemann problem in regions, showing integral operators become bounded if closed rectifiable Jordan curve without cusps becomes curve of bounded rotation
06 p0947 A69-16893

Lehmann-Maehly procedure for lower and upper bounds to eigenvalues of Hermitian operators in Hilbert space
06 p1020 A69-17131

Solvability of third boundary value problem for Laplace operator in three dimensional domains bounded by irregular surfaces
07 p1173 A69-18497

Maximum index of exponential growth of solution of linear Hamiltonian equation with periodic operator coefficient encountered in dynamic stability of elastic systems
07 p1231 A69-18501

Fourier transform algorithm introduction leading to image coding technique with image transformed by Hadamard matrix operator
07 p1078 A69-18859

Galerkin method of moments applied to stochastic bounded linear operator equation, discussing statistically homogeneous operator case and electric field in dielectric
07 p1174 A69-19472

Delta functions use in extending domain of Laplacian operator in quantum mechanics
07 p1174 A69-19495

Book on integral operators in theory of linear partial differential equations covering analytic functions, harmonic functions, differential equations, etc
08 p1343 A69-20725

Plasma kinetic equation obtained by method similar to Chapman-Enskog method
08 p1369 A69-20816

Elliptic complexes over compact manifolds without boundary, discussing general theory of elliptic operators in vector bundles
09 p1532 A69-21733

Theorem for necessary and sufficient condition for continuity of Chebyshev operator
10 p1718 A69-22875

One parameter operator imbedding to modify Newton method for solution of nonlinear equations
10 p1719 A69-23519

Nonlinear A/x operators in reflexive Banach space Y characterized by weak closure of values, defining solvability conditions for equations having such operator
10 p1720 A69-23563

Integral equation and related optimal regularization problems, finding operator in class of operators defined on set of functions
10 p1721 A69-23882

Vibration problem of supported beam elastically restrained against rotation at both ends solved by Hermitian and linear differential operators
11 p1976 A69-24794

Stability of systems with sector nonlinearities determined by converting feedback equation into positive operators equation and by introducing appropriate multiplier
11 p1860 A69-25450

Canonical representation of multivariable control system in state space using matrix of differential operators acting on vectors of input-output quantities
12 p2051 A69-26094

General theorems derived for Noether operator applied to integral equation with automorphic kernel
12 p2122 A69-26574

Volterra operator algebra for boundary value problems involving linear viscoelasticity with continuous relaxation time and delay time spectra
12 p2182 A69-26677

Pseudodifferential operators theory application to uniqueness of solutions of Cauchy problem
12 p2124 A69-26930

Closed linear operators in topological vector space generalized for Banach space case
13 p2288 A69-27734

Book on control theory covering automatic and remote position control, diagrams, transfer functions, operators, Laplace transform use with differential equations
13 p2238 A69-28345

Stability of quasi-solutions for equations with closed and with continuous operators
13 p2289 A69-28483

Quasi-L-analytic functions for ordinary linear operator L
13 p2290 A69-28484

Quasi-integral analytic continuation operator applicability to potential field approximated by certain truncated series expansion
14 p2470 A69-29032

Searchless gradient self adaptive system for adjusting servosystem parameters to reference model characteristics, using auxiliary operator method
14 p2426 A69-29146

Coupled equations for heavy particle motion expressed by introducing generalized matrix operator for effective momentum in atomic collision problems
14 p2489 A69-29997

Elastic collision operator for relativistic Lorentz gas converted to differential form using Fokker-Planck limit for anisotropy segments
16 p2817 A69-31668

Soviet monograph on projective-iterative methods of solving operator equations in generalized metric and structurally normalized spaces
16 p2805 A69-32366

Generalized finite difference approximations of linear partial differential operators in space based on functional approximations
16 p2756 A69-32552

Algebra of quasi-homogeneous pseudodifferential operators applied to lateral boundary values of solutions of parabolic differential equations, discussing function spaces
17 p2994 A69-32842

Friedrich qualitative analysis of ordinary differential operators modified to obtain quantitative information regarding eigenvalues distribution
17 p2995 A69-33404

Spectrum of ordinary second order differential operators, correlating spectral properties with analytic function-theoretic properties of differential equation solutions
17 p2996 A69-33793

Single parameter family of two layer difference schemes with decomposing operators for general linear second order parabolic equations with mixed derivatives and variable coefficients
18 p3164 A69-34702

Convergence of methods of tangential parabolas and hyperbolas used in nonlinear equation solution with nondifferentiable operators
18 p3164 A69-34707

Algebraic formulation of electromagnetic diffraction, discussing propagation of positive and negative time frequency components by dual operators
18 p3172 A69-35010

Engineering equations for elastic thin plate oscillations of materials with properties described by linear integral Volterra-Boltzmann operators
19 p3437 A69-35989

Finite difference analogs with increasing error terms applied to simple differential Laplace operator for accuracy determination
19 p3365 A69-36510

Ordinary differential equations in linear topological space extended from Fattorini investigation, emphasizing use of linear operator
19 p3360 A69-36599

Radiation field several wavelengths from dipole above plane earth, simplifying rigorous integral expression for Hertz vector by method of operators
21 p3770 A69-38748

Matrix identity associated with linear digital filtering and recursive estimating determined using matrix projection operators and properties
22 p3975 A69-41014

Green matrix for operator M governing steady state wave propagation in inhomogeneous anisotropic media obtained as solution of integral equations system
23 p4180 A69-41368

Differential operators representing potential energy of thin shell, discussing self conjugacy of boundary value problems
23 p4229 A69-41999

OPERATORS [PERSONNEL]

NT AIRCRAFT PILOTS
NT PILOTS [PERSONNEL]
NT TEST PILOTS

Control and sampling in sterile rooms, noting worker introduction of contaminants
05 p0714 A69-15953

Human operator as optimal controller, proposing quadratic performance index used by operator in judgement of own performance in tracking task
06 p0903 A69-17407

Programmed search and gradient search methods for determination of sampling intervals in synthesis of sampled data models of human operators
10 p1650 A69-23881

Personality factors and job performance ratings relationship in radar controllers, computing Pearson correlation matrix based on age, education, motivational distortion, etc
21 p3665 A69-39169

OPHTHALMOLOGY

NT EYE EXAMINATIONS

Ophthalmic 2 percent pilocarpine effect on normal ocular dynamics of various age groups, including visual acuity, accommodation and refraction
01 p0022 A69-11347

OPTICAL ABSORPTION

U ELECTROMAGNETIC ABSORPTION
U LIGHT TRANSMISSION

OPTICAL AMPLIFIERS

U LIGHT AMPLIFIERS

OPTICAL COMMUNICATION

Induced discharge laser wave propagation in medium with active and absorbing admixtures, determining stationary wave shape and velocity range
02 p0206 A69-11609

Atmospheric limitations for laser communications, discussing scattering and absorption effects
03 p0389 A69-13193

Optical receivers for deep space optical communications link assuming PCM scheme
03 p0389 A69-13194

Broadband signal and noise performance of direct detection optical receiver consisting of solid state photodiode and baseband amplifier
04 p0556 A69-14283

Quasi-optical transmission line composed of nonideal correctors /lenses or mirrors/
05 p0717 A69-15637

Wideband multichannel optical signals nonlinear distortions during transmission by electrooptical modulators using Pockels effect
05 p0718 A69-15655

Optical heterodyne communication experiments in TV signal transmission
05 p0720 A69-16319

[IEEE PAPER J-5]
Quasi-optical transmission lines having composite correction devices with/without phasing devices
05 p0723 A69-16784

Signal conversion by multiple modulation in optical communication system, discussing electrooptic modulators and modulation spectrum
07 p1075 A69-18472

Diffractional crosstalk in optical beam waveguide during simultaneous multibeam transmission arising from beam coupling by aperture diffraction
07 p1100 A69-18648

SNR enhancement in optical receiver by amplification before detection of carrier of modulated optical signal, using quantum amplifier
07 p1154 A69-19079

Optical heterodyne detection of randomly distorted signal beam, noting time invariant scheme yielding largest average SNR in atmospheric turbulence
07 p1087 A69-19642

Book on laser communication system design covering modulation and detection methods
08 p1277 A69-20884

Optical communications applications with emphasis on large capacity transmission
09 p1456 A69-22131

Carbon dioxide laser beam deflection and thermal defocusing due to wind in absorbing medium
10 p1701 A69-22949

IR detection at sum or difference frequency by employing optically nonlinear crystal and laser in visible and photomultiplier
10 p1704 A69-23656

Light flux intensity fluctuation dispersion and averaging effect for passage through circular receiving aperture
10 p1658 A69-23950

Mean losses in quasi-optical communication lines due to random irregularities in performance of waveguide phase correctors connected in series, noting random phase aberrations effect
10 p1658 A69-23954

Induced discharge laser wave propagation in medium with active and absorbing admixtures, determining stationary shape and velocity range
11 p1895 A69-24716

Atmospheric interference effects on optical PCM signal, analyzing absorption, beam bending, scintillation and correlation with visibility and weather
11 p1888 A69-25308

Electro-optical automatic gain control system to reduce atmospheric turbulence produced fluctuations in received optical signal strength
14 p2459 A69-29491

Ideal quantum receiver to detect coherent narrow band optical signal in presence of thermal background radiation, noting error probability
14 p2414 A69-29502

Remote polarized light source photometric observation on background of polarized light scattered horizontally, considering atmosphere optical state effect on laser communications
15 p2649 A69-30655

Optical communications experiments for quantitative data at 6328 A on system fading due to scintillation and atmospheric turbulence effects on coherent propagation at 10.6 micron
16 p2748 A69-31564

Quasi-optical transmission line composed of nonideal correctors /lenses or mirrors/
16 p2754 A69-32495

Wideband multichannel optical signals nonlinear distortions during transmission by electro-optical modulators using Pockels effect
16 p2754 A69-32512

Optical heterodyne communication system with single mode and frequency carbon dioxide laser, noting coherent photon noise limit
17 p2919 A69-33086

Multibeam transmission in optical beam waveguides by simulation, discussing intensity profiles phase fronts and cross scattering
17 p2974 A69-33400

Electromagnetic field formulation of eigenvalue problem for optical coaxial dielectric waveguide, using computer root searching method
17 p2930 A69-33892

IR nonimage-forming instruments, stressing applications to communications, intrusion detection, ranging, etc
19 p3310 A69-36062

Laser and quasi-laser pulse modulation technique for global satellites telemetry system
19 p3272 A69-36257

M-ary detection for optical communication investigated for maximum likelihood detection of one of M Poisson processes in background noise
19 p3276 A69-36486

Fourier transform techniques applications in optics, converting optical signal amplitude and phase information into electrical signal information
19 p3374 A69-36737

He-Ne laser communication feasibility experiments, discussing modulation, detection, operating parameters, etc
19 p3279 A69-36756

Demultiplexing of high speed multichannel optical pulse code transmission systems, based on coincidence detection using locally generated reference pulses
19 p3279 A69-36764

Optical information rates for photoconductor detection systems based on coherent field model, considering binary channels with or without Gaussian noise
20 p3485 A69-36923

Atmospheric natural turbulence effect of degradation of laser signal phase and amplitude characteristics, noting refractive index inhomogeneities effect on optical tracking system
[AIAA PAPER 69-871] 21 p3675 A69-39397

Solid state traveling wave optical quantum amplifier for conversion of modulated signal carrier frequency, applying to frequency conversion in laser communication links
21 p3739 A69-39540

Monograph on laser communication system in IR for industrial environments
22 p3900 A69-40617

Intersatellite microwave laser communication system for ATS-F and ATS-G, discussing experiment, functional design and parameters
23 p4120 A69-41758

Optical communication through random atmospheric turbulence via heterodyne and video detection, estimating performance from optical wave propagation analysis
23 p4125 A69-42186

Log amplitude mean value for Gaussian or laser-like optical beam propagating horizontally in turbulent atmosphere
24 p4282 A69-42970

HgCdTe as IR satellite detector for terrestrial, atmospheric and ocean mapping, IR astronomy and optical communication
24 p4362 A69-43666

OPTICAL CORRECTION PROCEDURE

Hologram chromatic aberration compensation by two lens system
01 p0080 A69-10430

Helium-neon laser for optical correction and guide beam techniques
07 p1146 A69-18484

Stars astronomical positions elimination from photographic plates because of errors, discussing elimination criteria and picture taking method
10 p1784 A69-24034

Photoelectric observation of passage of stars through meridian, detailing error sources and corrective technique
14 p2521 A69-29507

Image enhancement by coherent optical system without spatial filter, noting improved defocused transparencies
14 p2450 A69-29641

Remote sensing cross-beam cross correlation methods of determining spatially resolved average thermodynamic properties
[AIAA PAPER 67-149] 16 p2789 A69-31868

Optical computerized design procedure for Ritchey-Chretien corrector, combining ray deviation error function and third order aberration design techniques
17 p2972 A69-33087

Schmidt camera image quality examined with spot diagrams, emphasizing methods of color confusion reduction over wide wavelength range
20 p3546 A69-38272

Terrain slope estimation of position errors of differential corrections in orthophoto production
22 p3951 A69-41245

Optical interpolation for GZ-1 orthoprojector in storage mode, noting electronic contour plotter
22 p3951 A69-41247

Automatic contour plotting for orthoprojector based on adjacent profiles and linear interpolation
22 p3951 A69-41248

OPTICAL COUPLING

Optimum coupling for intracavity second harmonic generation in multilevel lasers
01 p0089 A69-10181

GaAs injection laser transmission losses and threshold current density under influence of external optical coupling with spherical mirror
02 p0260 A69-12687

Simultaneous phase locking of longitudinal and transverse laser modes in He-Ne laser
03 p0441 A69-14188

Optical performance of coupled Fabry-Perot resonators with additional mirrors, determining frequency separation parameters due to third mirror
04 p0612 A69-15372

Quasi-optical oversize waveguide directional coupler with two prisms interface matched by Brewster angle effect
14 p2424 A69-29764

Efficient extinction in optically coupled GaAs injection lasers achieved by selecting quenching radiation frequency close to operating frequency
15 p2633 A69-30059

Optical performance of coupled Fabry-Perot resonators with additional mirrors, determining frequency separation parameters due to third mirror
16 p2797 A69-32119

Optical parametric oscillator output/signal/ frequency locked to absorbing atomic transition, discussing effective linewidth
18 p3133 A69-34263

He-Ne laser subnanosecond intracavity coupler consisting of coaxial krytron pulse generator and electrooptic modulator
19 p3339 A69-36823

Transmission properties and directional coupler determined for optical circuit dielectric rectangular waveguide with surrounding dielectrics of smaller refractivity
24 p4287 A69-43328

Diffraction coupling of power from carbon dioxide laser, computing angular distribution of output light
24 p4329 A69-43753

OPTICAL DENSITY

Earth atmosphere transmission coefficients determination by relation between transparency and daytime sky brightness, noting limits of applicability
01 p0074 A69-11185

Atmospheric optical properties stability determination for various optical densities, assuming horizontally homogeneous medium with properties constant during observation
01 p0074 A69-11186

Atmosphere spectral transparency and stability spectrophotometric studies based on measuring solar aureole brightness
01 p0074 A69-11188

Atmospheric IR spectral transparency measurement, describing optical system, recording devices and data processing
05 p0759 A69-16639

Continuous emission spectrum and continuous plasma absorption spectral coefficients for optically dense quasi-steady state electrical discharge plasma in sulfur capillary
06 p0964 A69-17251

Atmospheric IR spectral transparency measurement, describing optical system, recording devices and data processing
14 p2433 A69-28795

Close confinement GaAs p-n junction lasers with reduced optical loss at room temperature
14 p2457 A69-28893

Atmospheric optical density vertical distribution curves in near UV from spectrophotometer data of Echo type satellites entry into earth shadow
16 p2787 A69-32638

OPTICAL EMISSION
U LIGHT EMISSION

OPTICAL EMISSION SPECTROSCOPY

Line shape for dynamic Stark effect during optical resonance field irradiation calculated as function of relaxation constants and beam intensity
08 p1325 A69-20282

Optical spectrum of galaxy NGC 3031 nucleus, considering emission and absorption lines and continuum
17 p3034 A69-33396

YZ Canis Minoris red dwarf star flare event observation record, noting optical spectrum energy output and slow decay
17 p3043 A69-34165

Cadmium sulfide-selenide single crystals reflection coefficient polarimetric measurement, observing reflection peaks relationship to absorption spectral temperature dependence
19 p3391 A69-36607

N II 4176 A emission line occurrence in connection with type B auroras, studying secondary electrons energy spectra
24 p4309 A69-43012

Optical solar flares, discussing flare classification, proton flares, development, limb observation, spectra, line broadening, electron density, etc
24 p4370 A69-43605

OPTICAL EQUIPMENT

NT ASTRONOMICAL TELESCOPES
NT BAKER-NUNN CAMERA
NT BALLISTIC CAMERAS
NT CAMERAS
NT CATHETEROMETERS

NT CINETHEODOLITES
NT COLLIMATORS
NT CORONAGRAPHS
NT DIFFRACTOMETERS
NT ELECTROPHOTOMETERS
NT ELLIPSONETERS
NT FRAMING CAMERAS
NT HELIOMETERS
NT HIGH SPEED CAMERAS
NT IMAGE CONVERTERS
NT IMAGE TUBES
NT INFRARED SPECTROMETERS
NT INFRARED SPECTROPHOTOMETERS
NT LALLEMAND CAMERAS
NT LIGHT SCATTERING METERS
NT MICROWAVE REFLECTOMETERS
NT NEPHELOMETERS
NT PHOTOMETERS
NT POLARIMETERS
NT POLARISCOPES
NT PRISMATIC BARS
NT PRISMS
NT REFLECTOMETERS
NT REFRACTOMETERS
NT SCHMIDT CAMERAS
NT SPECTROHELIOGRAPHS
NT SPECTROPHOTOMETERS
NT SPECTROSCOPIC TELESCOPES
NT STRATOSCOPE TELESCOPES
NT STROBOSCOPES
NT TELEVISION CAMERAS
NT THEODOLITES
NT TRANSITS
NT ULTRAVIOLET SPECTROMETERS
NT ULTRAVIOLET SPECTROPHOTOMETERS
NT WIDE ANGLE LENSES
NT X RAY TELESCOPES

Gas lens distortion of Gaussian light beam in sequence of lenses with same aberration, using shuttle pulse technique
01 p0120 A69-10849

Reflection measurements in IR, investigating effect of angle of incidence and collimated beam on reflection spectra
01 p0120 A69-10891

Reflecting telescope objective for far UV and X ray regions, discussing microfinishing and optical and mechanical tolerances
01 p0121 A69-10896

Holographic laser type memory with bulk storage capacity and short readout time
03 p0428 A69-13116

Optical correlator for fast acquisition of pseudorandom ranging codes, giving code delay estimation to synchronize local code generator of delay-lock loop
03 p0389 A69-13186

Single two dimensional coherent matched filter optical processor for simultaneous synthetic radar antenna beam sharpening and pulse compression
04 p0562 A69-15475

Line profile and optical interferometry in astronomy and geophysics
05 p0760 A69-15590

Plastic virtual infinity lens system for large aperture cathode ray tube direct view simulator displays
05 p0760 A69-15592

Electronically controlled spark gap system for HF optical frame separation based on Cranz-Schardin principle
05 p0763 A69-15985

Imagery degradation by moisture condensation on thermal IR scanners optics during aircraft descent from higher to lower altitude
08 p1311 A69-19821

Electronic optical system to process time-varying signals as optical spectrum analyzer for measuring power spectral density of input time function
08 p1317 A69-21086

Near field repeatable stimulator of infrared earth horizon sensors in variable environments and test levels, noting orbital conditions
[AIAA PAPER 69-322] 09 p1478 A69-22376

Optical motor system to efficiently convert laser energy into mechanical rotational energy, giving equations for controlling motor speed
09 p1442 A69-22457

Microwave antennas optical simulation, discussing given phase amplitude distribution problems
09 p1469 A69-22625

Computer generated kinoform optical element operating on phase of incident waves and forming wave front reconstruction single image
10 p1697 A69-23867

Intracavity acoustooptic devices based on isotropic and anisotropic acoustic Bragg diffraction, discussing efficiency, bandwidth and acoustic column width
10 p1697 A69-23871

Holographic techniques application to optical systems for high resolution images of distant objects by overcoming atmospheric turbulence and light diffraction limitations

11 p1883 A69-26488

Large capacity holographic memory design based on page organization concept, considering lens parameters and hologram size

11 p1886 A69-25041

Distance vs time and velocity vs time measurements for high speed model missiles by means of laser interferometry and optical Doppler shift method

11 p1886 A69-25042

Vignetting effect on impulse response of general coherent optical Fourier processor, noting time varying character and input position sensitivity

12 p2036 A69-25912

Precision optical systems tests, using two beam interferometer and CW gas laser to examine reflected or transmitted wavefront contours

12 p2092 A69-26421

Optical absorption cell with variable path length and temperature for measuring absorption coefficients of gases at low and high temperatures

12 p2093 A69-26482

Instrument for simultaneous observation of astronomical plate pairs for detection of stars with UV color excess

16 p2791 A69-32226

Lunar based optical workshop and repair facility, using ion beam technique to polish and repair optical element surfaces

18 p3113 A69-34243

Apollo optics system ground and flight performance tests results, suggesting possible design changes for sunlit space environments

19 p3307 A69-35796

Lasers and maser devices in radio quantum electronics, discussing optical parametric and microwave devices including transistors, diodes, magnetrons, etc

19 p3284 A69-36433

Optical devices for nondestructive testing of large piston engined equipment

20 p3547 A69-36921

Radar data optical spatial-domain processor providing azimuth processing in range channels without range compression capability, reviewing coherent optical channels properties

20 p3489 A69-37636

Variable optical system with remote and continuous adjustment of beam for solar simulation, permitting maximum test facility utilization [AIAA PAPER 69-997]

22 p3920 A69-40375

Space simulator vacuum facility for optical satellite tests, construction, operation and maintenance, emphasizing noncontaminating environment and pumping systems [AIAA PAPER 69-1026]

22 p3924 A69-40396

Optical engineering and quality control of photogrammetric instruments for aerial color photography, discussing lenses, filters, projectors, plotters, electro-optical rectifier, etc

22 p3949 A69-40996

Liquid filled adjustable optical analog of human eye for aligning, calibrating and systems testing of automatic IR optometers

22 p3888 A69-41231

Incoherent object threshold light detection by quantum limited optical system in presence of radiant thermal energy

23 p4191 A69-42147

Linear electrical analogs for two dimensional optical data processing systems, discussing diffraction field model, quadratic phase filters, thin lenses, photographic film applications, etc

24 p4286 A69-42619

Quadratically nonlinear filtering systems analysis and synthesis by linear methods, discussing application to partially coherent transilluminated optical systems

24 p4350 A69-42971

Adhesive bonding of optical components, discussing material types, test methods, problem of operation at cryogenic temperature, etc

24 p4326 A69-43465

OPTICAL FILTERS

NT INFRARED FILTERS

NT ULTRAVIOLET FILTERS

Axisymmetric optical filter synthesis based on holographic technique for making Gabor zone plates, using scalar diffraction theory

02 p0249 A69-11927

Optical narrow bandpass filter designed for precision solar corona observations, utilizing interferential polarization and thermo-optical compensation

03 p0506 A69-13085

Light pulse narrowing in laser in linear mode operation with inertialess bleachable filter

03 p0440 A69-13716

Saturable dye filters used with ruby lasers, discussing relaxation time, residual absorption source and transient spectral hole burning

07 p1155 A69-19089

Filtering system for xenon arc solar simulator to provide operation at air-mass-two /average sea level/ sun-light

09 p1476 A69-21648

Rocket-borne photoelectric photometers for UV observations of Saturn, using interference filters

09 p1602 A69-22216

Neodymium doped YAG laser efficiency dependence on pump power level and spectral filtering of pump light

10 p1705 A69-23814

Electron beam addressed electrooptic light valve used as spatial filter, discussing electronic control and optical processing in real time

10 p1697 A69-23870

Traveling wave passive Q switched laser with bleachable absorber filter, analyzing unsteady processes without expanding field along natural resonator modes

10 p1705 A69-23949

Q switched carbon dioxide laser power increased by placing bleachable /boron tetrachloride/ filter in resonator

11 p1894 A69-24454

Tilting filter photometer for faint light source spectrophotometry, discussing digital approach used with photomultipliers

11 p1884 A69-24834

Optical correlator for radar signal processing based on filtering first order diffracted light and integration on photomultiplier

12 p2028 A69-25911

Flow field over plain or complex bodies with pressure density changes, using high speed schlieren apparatus with color strip filter

12 p2088 A69-26183

Low pass quasi-optical waveguide filters, using metal strips in dielectric material to obtain broad stopband and low dissipation loss

13 p2229 A69-27675

Optical narrow bandpass filter designed for precision solar corona observations utilizing interferential polarization and thermo-optical compensation

14 p2515 A69-28767

Color IR film improvement for high altitude remote sensor, using auxiliary minus-visual filters

15 p2609 A69-30457

Restoration of photographic images by optical spatial filtering with least mean square error filter in presence of random additive noise

15 p2611 A69-31033

Aberrations of Fabry-Perot interferometers with small nonuniformities in plate spacing used as spectral and optical filters

17 p2972 A69-33081

Electronically tunable lithium niobate optical filter utilizing collinear acousto-optic diffraction in anisotropic medium

17 p2943 A69-34157

Liquid filter cells design with emphasis on filters usable for inorganic and organic liquids

21 p3770 A69-38679

Thermostatic electronic control device of birefringent filter in Wrocław Observatory coronagraph during prominence observations

22 p3943 A69-40000

OPTICAL GENERATORS

U LASERS

OPTICAL HETERODYNYING

Optical heterodyne communication experiments in TV signal transmission [IEEE PAPER J-5]

05 p0720 A69-16319

Optical heterodyning with single mode carbon dioxide laser and triglycine sulfate pyroelectric detector, noting detector sensitivity threshold

07 p1156 A69-19332

Statistical properties of intensity fluctuations of light fields consisting of incoherent Gaussian component heterodyned with single frequency coherent beam

07 p1182 A69-19416

Optical heterodyne detection of randomly distorted signal beam, noting time invariant scheme yielding largest average SNR in atmospheric turbulence

07 p1087 A69-19642

Gas laser emission natural frequency fluctuations spectral density measured by auxiliary heterodyne laser

08 p1326 A69-20540

Dispersion corrected three wavelength laser heterodyne system for plasma electron density and neutral density measurements

09 p1544 A69-21331

Radar signal cross correlation function calculation with reference function, applying acousto-optical modulator

10 p1694 A69-23539

Optical modulation through Doppler frequency shift obtained by rotating radial diffraction grating [AOLR-69-1]

11 p1889 A69-25394

Remote optical heterodyne measurement of Doppler shift as method for determining vector wind velocity, noting influence of air pollution

14 p2448 A69-29523

Laser Doppler heterodyning for monitoring motion noting solid surfaces vibration, liquid and solid surfaces linear velocity and turbulence in liquids and gases

15 p2614 A69-31276

Optical heterodyne communication system with single mode and frequency carbon dioxide laser, noting coherent photon noise limit

17 p2919 A69-33086

Coherent radiation detection using laser optical sine waves, considering detection by heterodyning, laser preamplifier and parametric amplification

19 p3335 A69-36070

He-Ne laser heterodyne system for measuring dispersion at 6328 and 6401 Å due to Ne metastable atoms in gas discharge

23 p4172 A69-41397

Optical communication through random atmospheric turbulence via heterodyne and video detection, estimating performance from optical wave propagation analysis

23 p4125 A69-42186

Hologram transmission by heterodyne scanning reference beam technique

24 p4283 A69-43333

OPTICAL ILLUSION

Depth distortions in binocular visual fields from misleading size cues

21 p3653 A69-38900

Zoellner illusion in human visual system measured as function of background pattern density consisting of intersect angles and background line spacing

22 p3879 A69-40841

OPTICAL IMAGES

U IMAGES

OPTICAL MASER MODULATION

U LIGHT MODULATION

OPTICAL MASERS

U LASERS

OPTICAL MEASUREMENT

NT ASTRONOMICAL PHOTOMETRY

NT COLORIMETRY

NT ELECTROPHOTOMETRY

NT OPTOMETRY

NT PHOTOMETRY

NT POLARIMETRY

NT SPECTROPHOTOMETRY

NT STELLAR SPECTROPHOTOMETRY

NT TELEPHOTOMETRY

NT ULTRAVIOLET PHOTOMETRY

NT VISUAL PHOTOMETRY

Optical identifications for 17 Ohio survey sources with peaked or flat spectra

01 p0153 A69-10854

Optical identification of X ray source Cen XR-2 as variable star WX Cen, discussing colors and similarity to Sco X-1

01 p0145 A69-10857

Optical measurements through retrorocket plumes of landing spacecraft, investigating reduced landing site visibility and modulation transfer function

02 p0248 A69-11765

Refractive index structure constant for different atmospheric turbulence conditions, discussing possibility of improved capabilities for imaging systems

02 p0275 A69-11930

Oscilloscope display of sample of subnanosecond light pulse, using optical analog of electronic sampling oscilloscope

02 p0259 A69-12656

Scattering data for optical diagnostic measurements on two component suspensions or gases, using random distributions of spheres

04 p0555 A69-14282

Optical signal frequency method for measuring velocity of fluid flow

04 p0598 A69-14995

Shipboard standard visibility measurements by means of AEG-FFM scattered light recorder aboard Meteor in Atlantic Ocean during 1965

04 p0628 A69-15158

Optical method of sounding cosmic matter penetrating into upper atmosphere by analyzing twilight phenomena

04 p0594 A69-15246

Poincare sphere representation of polarized light used to predict rotation effect on optical observations in photoelastic shell analysis

04 p0683 A69-15495

Venus diameter determination from optical measurements, noting cloud layer height and height of suspended particles in upper atmosphere

05 p0818 A69-15621

Electro-optical tracking devices for displacement and/or dislocation measurement without physical contact

05 p0763 A69-15986

Atmospheric vertical density and pressure profiles determined from satellite measurements of light beam phase shift and refraction angle

05 p0760 A69-16694

Microwave antennas simulation by optical systems based on Huygens-Kirchhoff approximation, noting application to antenna analysis, synthesis and radiation patterns

05 p0736 A69-16780

Optical simulation of microwave antennas with variable profile reflectors, investigating radiation patterns by photometric scanning of photographs obtained with He-Ne laser

05 p0736 A69-16781

Optical mean energy distribution of quasars, discussing red shift effects, significance of physical origin of optical continuum radiation and K-term magnitude determination

06 p0999 A69-16975

Metastable level population measurement in laser crystal based on luminescence changes under influence of stimulated emission

06 p0934 A69-17457

Hot gas flows turbulence linear component intensity and frequency spectrum using optical measurement of pulse velocities

06 p0926 A69-17540

Atmospheric effects on laser beam attenuation, noting application to optical visibility measurement by ruby laser

08 p1327 A69-21089

Laser control of French rocket head guidance system, discussing gyroscopic master, stellar or solar detectors, etc

09 p1518 A69-22162

Unicellular microorganisms size and concentration estimates based on light scattering measurements of suspensions in spectrophotometer cuvette compartment

11 p1829 A69-25643

Optical diagnostics methods for fast processes in rarefied plasma, using Michelson interferometers with ruby and Nd lasers as light sources

12 p2089 A69-26186

Stellar diameter interferometric measurements, discussing double slit arrangement and illumination in focal plane

13 p2334 A69-27305

Optical measurement method for burning surface temperature of condensed systems, realizing radiation from surface of combustion by light guide of monocryalline aluminum oxide

13 p2379 A69-28453

Focused beam wave applied to atmospheric turbulence probing for spectral density of index of refraction, structure constant and wind velocity

14 p2414 A69-29512

Log amplitude variance calculation methods compared in statistics of optical scintillation by application to measurements with laser

14 p2486 A69-29642

Optical and radio estimations of galactic masses, analyzing radius of rotation curve inflection point

15 p2687 A69-30547

Zodiacal light brightness and polarization measurements from space probes approximated by Mie scattering of interplanetary dust particles

16 p2857 A69-32092

IR and optical measurement of Crab pulsar NP 0532, analyzing energy density per pulse and smoothness of visual data

18 p3191 A69-34318

Shock wave profiles in molecular N-H gas mixtures in shock tube measured by optical electron beam method, noting disagreement with Navier-Stokes calculations

18 p3134 A69-34458

Shock heated argon thermal conductivity studied by optical interferograms, deriving equation for measured mean value

18 p3228 A69-34459

Optical distance measurement using laser and atmospheric dispersion method through average refractive index determination over path

18 p3152 A69-35198

Particle size, velocity and position in moving streams measured by tilted film plane optical system with pulsed light source

19 p3306 A69-35733

Quantitative density data from schlieren measurements by photomultiplier technique for axisymmetric flow outside diffraction bands

19 p3306 A69-35741

Manual procedures for midcourse and terminal guidance, discussing onboard optical measurements and calculations

19 p3368 A69-35792

Optical flashes from PSR 0833-45 searched using 74 inch Radcliffe telescope with pulse counting photometers

20 p3604 A69-37575

Backscattering intensity measurements by optical elements at 180 degrees to beam propagation direction, using CW He-Ne laser as radiation source

20 p3554 A69-37609

Metastable level population measurement in laser crystal based on luminescence changes under influence of stimulated emission

20 p3555 A69-37940

Nonlinear optics, properties, light waves interaction, forced scattering and application in laser technology

20 p3555 A69-38014

Optical method for upper atmosphere cosmic dust detection, emphasizing twilight luminance origin from light scattering

21 p3702 A69-38349

TV-optical observations of asteroid Icarus, discussing installation, photographs and position

21 p3719 A69-38402

Optical data supporting satellite observations of soft electron precipitation on poleward side of normal auroral zone

21 p3709 A69-38501

Ariel 3 satellite spin axis direction determination by optical means from analyzing sunlight glints reflected from surfaces

21 p3820 A69-39261

Biomedical electrical signals analysis by optical data processing, discussing conversion, SNR and filtering techniques

21 p3666 A69-39440

Eye optical system spherical aberration measured by knife-edge method derived from Foucault test, investigating retinal image quality

22 p3882 A69-40873

Contact stability of hollow cylinder compressed between parallel planes measured optically, compared to approximation of elasticity theory

23 p4162 A69-41416

Optical activity measurement for exobiology applications, considering polarimetry, gas-liquid chromatography, mass spectrometry and radioactivity detection

23 p4213 A69-41622

Spiral and irregular galaxies integral properties and relations, discussing optical and 21-cm observations, hydrogen masses, statistical corrections, hydrogen line optical depths, etc

23 p4220 A69-42383

Holo-diagram device for making and evaluating holograms for small deformations measurement in large machine tool parts

24 p4317 A69-43760

OPTICAL MEASURING INSTRUMENTS

NT CATHETOMETERS
NT CINETHODOLITES
NT CORONAGRAPHS
NT DIFFRACTOMETERS
NT ELECTROPHOTOMETERS
NT ELLIPSOMETERS
NT INFRARED SPECTROMETERS
NT INFRARED SPECTROPHOTOMETERS
NT LIGHT SCATTERING METERS
NT MICROWAVE REFLECTOMETERS
NT NEPHELOMETERS
NT PHOTOMETERS
NT POLARIMETERS
NT REFLECTOMETERS
NT REFRACTOMETERS
NT SPECTROHELIOGRAPHS
NT SPECTROPHOTOMETERS
NT THEODOLITES
NT TRANSITS
NT ULTRAVIOLET SPECTROMETERS

NT ULTRAVIOLET SPECTROPHOTOMETERS

Holographic measurement of sinusoidally vibrating Al sheet, verifying results with Twyman-Green interferometer

01 p0082 A69-10853

Laser application to machine tool accuracy and alignment [ASTME PAPER MR68-407]

02 p0252 A69-11797

Optical ozone radiosonde for vertical distribution analysis, using weak absorption of Chappuis bands

02 p0251 A69-12761

Fluid flow velocity measurements by optical device having trigonal rectangular glass prisms and microscope objective

03 p0427 A69-12969

Alignment of rocket-borne instrument with sun, discussing mechanical system design, servocontrol and silicon photodiode sensors

03 p0427 A69-12980

Laminar and turbulent flow measurement in variety of tube diameters, using ring laser without insertion of mechanical probe

04 p0596 A69-14281

Vibrational characteristics of sonar transducer analyzed by optical holographic interferometry

04 p0598 A69-14871

Laser Doppler meter model interpreting output frequency in terms of particle crossing set of fringes

06 p0932 A69-16927

Glass fiber optical angular displacement noncontacting nonloading transducer suitable for measuring torsional vibrations

06 p0923 A69-16929

Optical sighting method for determining orientation of rocket on launch pad by laser collimator, noting lining up of Cassiopeia system

06 p0930 A69-17104

Laser measurement techniques for plasma diagnostics, spectroscopy, angular rotation rate, distance, velocity and alignment of tools and assemblies [ASME PAPER 68-DE-21]

06 p0933 A69-17167

Narrow and wide angle actinometric instruments on-board Cosmos 122, 144 and 156, describing optical and data acquisition systems

06 p0929 A69-17977

Optical device for measurement of temperature changes with height in upper atmosphere by rockets or satellites

07 p1132 A69-18676

Motion measurement using Doppler shift of scattered laser light, noting high resolution

09 p1492 A69-21398

Optical frequency standards, discussing lasers VHF stability, RF and optical ranges, long and short term effects, etc

10 p1702 A69-23299

Bright fundamental stars right ascensions observed in Chile, discussing instruments, declination range, systematic errors, etc

10 p1777 A69-23388

Relative proper motions of stars measured by microscope projection technique

10 p1778 A69-23570

Single and clad glass fibers radii and refractive indices measurements on basis of laser light scattering

11 p1918 A69-25044

Optical investigation of defects in crystal lattices on stress induced birefringence basis, describing stress visualization results for Si and glass

11 p1887 A69-25199

Optical sensing devices for angle measurement between celestial body and satellite axes

12 p2078 A69-25871

Monograph on schlieren-optical technique for plasma beam temperature measurements using photoelectric scanning device

12 p2134 A69-26120

Coherent optical flow detection and surface microstrain measurement techniques including holographic interferometry, optical correlation and diffraction

12 p2180 A69-26305

Laser Doppler particle sensor to measure velocities in rocket exhausts, using He-Ne laser light source and Fabry-Perot interferometer frequency filter [AIAA PAPER 68-723]

12 p2094 A69-26783

Optophotoclectric pickup design for angular displacement measurements, considering application of moire pattern produced by radial diffraction gratings

14 p2447 A69-29327

Directional properties of electro-optical goniometric system based on known design parameters

14 p2420 A69-29332

Optical carrier single channel telemetry system providing complete electrical isolation between shock tube data acquisition and data recording instrumentation 14 p2449 A69-29561

Plasma diagnostics facilities design, circuit diagrams and operation based on Q switched ruby laser and optical recording system 14 p2461 A69-29782

Inlet shape and Reynolds number effects on entrance flow development, using laser flowmeter based on Doppler effect to obtain laminar velocity profiles 15 p2589 A69-30001

Interferometer for measuring electric fields spatial correlation function at camera aperture, describing laser light coherence measurements after propagation through turbulent atmosphere 15 p2653 A69-31164

Interferometric displacement transducer for measuring linear displacements up to one and one-half inches 15 p2614 A69-31280

Balloon for in situ measurements of atmospheric optical parameters using two axis sun pointer, spectropolarimeter and airborne telemetry 15 p2615 A69-31288

Optical measuring methods of cross sections and mechanical properties of heat resistant fiber reinforced materials 16 p2803 A69-31804

Optical probe for determining ozone vertical distribution at high altitudes, discussing optical method requirements and ozonesonde construction 16 p2792 A69-32637

Computer graphics technique for reducing photographic data from optical device to replace time consuming visual methods 18 p3134 A69-34373

Electromagnetic field signatures in optical IR spectrum of satellite-borne sensors, analyzing spectral, spatial and temporal distributions, polarization and phase 19 p3309 A69-36060

Optical system for cosine-corrected radiation point to areal source measurement, discussing adaptation to spectral instruments, photocells and photoelements 20 p3538 A69-37429

Remote sensing by electromagnetic waves in microwave region, describing differences between microwave and optical sensing 20 p3493 A69-37741

Ring laser bias in angular rotation measurement using optical phase shifters 21 p3735 A69-38651

Telecentric lens principle for accurate optical strain measurements, using moire grids 21 p3844 A69-39322

Optical instruments as visual aids in scientific research including electron optical image converters detecting emissions invisible to human eye 22 p3943 A69-39974

Ring lasers basic operating principles and primary applications, discussing Fresnel drag, magneto-optical effect, etc 22 p3961 A69-40240

Device for studying stereoscopic field of vision applied to determining field of vision standards for healthy individuals 22 p3886 A69-41113

Microcrack detection by holographic interferometry, describing experimental apparatus and test procedure and results 24 p4317 A69-43763

OPTICAL METHODS

U OPTICS

OPTICAL MICROSCOPES

IR polarizing microscope with IR corrected objectives and eyepieces providing higher contrast, sharper focusing and less light scattering 12 p2093 A69-26595

Extraterrestrial optical microscopy, discussing experiment, telemetry, data interpretation and instrument characteristics concerning biological, cytochemical and petrographic microscopes 23 p4164 A69-41621

OPTICAL MODULATION

U LIGHT MODULATION

OPTICAL PATHS

Photographic image degradation resulting from wave front distortion due to atmospheric refractive density gradients over long oblique optical path 01 p0107 A69-10223

Optical path variations and angle of emergence calculation in dynamic ionosphere 01 p0068 A69-11111

Polarization-albedo relationship for selected lunar maria, highlands and mountains in five passbands suggest optical path length function of effective refractive index and particle size 05 p0829 A69-16663

Jovian limb H alpha line due to auroral emission obtained from high dispersion spectra with long light path through upper atmosphere 07 p1214 A69-18614

Strong light flashes detected from fast pulsar NP 0532 in Crab Nebula, discussing time-averaged optical flux 08 p1394 A69-20622

Light waves transmission and beam guidance, analyzing solid lens type guide and automatic light path stabilizer 09 p1518 A69-22130

Laser frequency drift effect on operation of three mirror interferometer, noting wave reflection by two compounded mirrors 11 p1895 A69-24720

Fluctuations in angle of arrival of laser and thermal radiation beams over near ground path 11 p1840 A69-25570

Distortionless propagation of light through optical two level atoms medium, considering relation to Poynting theorem, hyperbolic secant solution and pendulum analogy 12 p2130 A69-26313

Optical absorption cell with variable path length and temperature for measuring absorption coefficients of gases at low and high temperatures 12 p2093 A69-26482

Contrast interference patterns obtained in Michelson interferometer at various path differences, using He-Ne laser as light source 12 p2108 A69-26593

Optically swept glass slab laser design, discussing pulse length and peak power 14 p2457 A69-28930

Line of sight atmospheric path measurements for atmospheric inhomogeneities, using phase quadrature, microwave and near IR techniques 14 p2415 A69-29516

Scintillation magnitude related to range and turbulence strength in near earth optical propagation, using pulsed and helium-neon laser 15 p2570 A69-31030

Quantitative IR spectral emissivity measurements of NO between 300-800 K made in absorption, correlating observed absorbance with optical path length and gas pressure 17 p3009 A69-34156

Monochromatic undulating light vertical refraction path curvature radii calculation based on refractive index 18 p3174 A69-35201

Weak displacements of opaque objects and optical distortion in solid state lasers analyzed by holographic interferometry 19 p3308 A69-35909

Atmospheric slant path molecular absorption and emission from band model methods, discussing computer program prediction capabilities 19 p3375 A69-36052

Trajectory of light ray propagating through atmosphere based on known refractive index defined by function of special Cartesian coordinates 21 p3675 A69-39245

OPTICAL POLARIZATION

Polarization of laser radiation scattered forward and back in artificial fog and smoke 03 p0393 A69-13275

Mode suppression by mixed polarization in Michelson interferometer type of optical resonator 05 p0776 A69-16330

Output polarization rotation sensitivity to axial magnetic field varied by variable angle quartz flat inside He-Ne laser resonator 07 p1198 A69-18646

Transparent dielectrics destruction by laser radiation noting stress development in medium 08 p1324 A69-19947

Light polarization from stimulated Brillouin effect in compressed gaseous nitrogen, presenting depolarization variations as function of gas density and laser power 09 p1516 A69-21691

Daytime clear sky light polarization in UV and visual spectral regions calculated with considerations for aerosol components polarization effect 09 p1491 A69-22708

Quasars optical polarization data, showing variable polarization for 3C 273 10 p1790 A69-24139

Solvent effect in catalytic hydrogenation reaction of Schiff bases of alpha-keto acids with optically active alpha-alkylbenzylamine 12 p2026 A69-25779

Optically active alanine synthesis from oxaloacetic acid by hydrogenolytic asymmetric transamination, noting role of decarboxylation 12 p2026 A69-25780

Temperature effects on polarization degree, threshold current and delay of radiation from GaAs laser diodes with diffused Zn 13 p2227 A69-27328

Polarization of laser radiation scattered forward and back in artificial fog and smoke 14 p2410 A69-28783

Polarization dependent gain saturation and non-linearity induced anisotropy in He-Ne laser amplifier 14 p2457 A69-28931

Polarization and angular distribution of 6328 A He-Ne laser light scattered by latex-sphere hydrosols, comparing coherent and incoherent scattering patterns 15 p2595 A69-30223

Time behavior of output intensity and polarization of single cavity mode internal mirror Zeeman laser in axial magnetic field 16 p2798 A69-32607

Plane wave scattering by multimode corrugated structure with H mode incidence, revealing theoretically scattering resonance as P type Wood anomalies 17 p2925 A69-33844

Polarization, frequency and energy characteristics of lasers with resonators containing polarization transforming elements 17 p2983 A69-33967

Crab Nebula pulsar NP 0532 linear and circular optical polarization measurements 21 p3798 A69-38542

Quantitative analysis of light intensity dependent changes in optical rotation angle of isotropic media caused by laser beam 22 p3959 A69-40017

Optical frequencies and polarizations of IR active phonons of tysonite lanthanide fluorides based on Kramers-Kronig reflectance spectra analysis 22 p3993 A69-40729

Optical activity measurement for exobiology applications, considering polarimetry, gas-liquid chromatography, mass spectrometry and radioactivity detection 23 p4213 A69-41622

Optical rectification in crystals by excitation of nonlinear/time constant and space variable/polarization 23 p4174 A69-41874

Index of refraction turbulent fluctuations effect on beam traversing optically active medium, discussing far field diffraction pattern and incoherent scattering [AIAA PAPER 68-683] 24 p4304 A69-43578

OPTICAL PROPERTIES

NT ABSORPTANCE
NT ABSORPTIVITY
NT BIREFRINGENCE
NT BRIGHTNESS
NT COLOR
NT DICHOISM
NT LUMINOSITY
NT OPACITY
NT PHOSPHORESCENCE
NT PHOTOCONDUCTIVITY
NT PHOTOELASTICITY
NT PHOTOELECTRIC EFFECT
NT PHOTOELECTRIC EMISSION
NT PHOTOIONIZATION
NT PHOTOVISCOELASTICITY
NT PHOTOVOLTAIC EFFECT
NT RADIANCE
NT REFLECTANCE
NT REFRACTIVITY
NT SKY BRIGHTNESS
NT SPECTRAL REFLECTANCE
NT STELLAR LUMINOSITY
NT TRANSMISSIVITY
NT TRANSMITTANCE
NT TRANSPARENCE
NT TURBIDITY

Electron transport theory for pure and doped low mobility semiconductors and for impurity conduction in disordered semiconductors, noting related optical phenomena 01 p0135 A69-10047

Ruby laser crystals optical inhomogeneity and residual mechanical stresses effects on laser beam angle of divergence 01 p0139 A69-10831

Atmospheric optical data recorded by instrumented aircraft near Crater Lake, discussing surface spectral irradiance data 01 p0111 A69-10846

- Atmospheric optics - Conference, Pulkovo, U.S.S.R., November-December 1965 and December 1966
01 p0073 A69-11181
- Tropospheric inhomogeneities properties and wind conditions in relation to lunar limb image deformations
01 p0156 A69-11182
- Atmospheric optical properties stability determination for various optical densities, assuming horizontally homogeneous medium with properties constant during observation
01 p0074 A69-11186
- Light polarization properties in atmosphere noting aerosols effect
01 p0075 A69-11189
- Partially polarized light and polarization degree measured by photoelectric polarimeter, obtaining scattering indicatrices and polarization degree dependences
01 p0075 A69-11190
- Atmospheric transmission factor and optical stability determination by photometer, estimating error due to solar aureole
01 p0075 A69-11193
- Roughness effect on microwave emissivity according to geometric optics with application to moon and Venus
02 p0207 A69-12017
- DC argon arc electrical and thermal parameters and optical properties at high pressure, using spherical anode
02 p0291 A69-12482
- Molybdenum interband transitions noting low energy optical property anomalies and origin of two absorption bands
03 p0442 A69-12986
- Radiation absorption variations in KC-19 CdSe glass during ruby laser radiation, noting microcrystals and nonlinear effects role in determining optical properties
03 p0436 A69-13036
- Aperture effects in nonlinear optical processes associated with second harmonic and parametric generation of light
03 p0439 A69-13056
- Mechanical and optical viscoelastic characterization of Hysol 4290 epoxy polymer as function of time and temperature, using creep test data
03 p0524 A69-13064
- Electrical, optical, magnetic and structural properties of titanium oxide, stressing transition difference with vanadium oxide
03 p0490 A69-13923
- Optical absorption of thin film cesium between 2300 and 11000 Å
03 p0491 A69-14060
- Optical absorption of vacuum deposited thin rubidium films, noting similarity to sodium and potassium
03 p0491 A69-14114
- Optical materials behavior after irradiation by high energy electrons, gamma rays or protons
03 p0493 A69-14190
- Vapor grown GaP electrical and optical properties, considering undoped and Se or S doped samples on GaAs and GaP substrates
04 p0640 A69-14438
- Dark equatorial belt of Jupiter atmosphere in 1962 and 1963, noting photometric contrasts, molecular absorption and possible structure
04 p0658 A69-14961
- Optical variability of quasar 3C 273, suggesting radiation emission from single bodies rather than from large complex of independent sources
04 p0662 A69-15235
- Te and Zn doped p-type GaAs single crystals optical homogeneity, using interferometry
04 p0644 A69-15266
- Glass lasers, discussing neodymium properties in glass, flexibility of glass in size, shape and optical excellence, temperature coefficient of index of refraction, etc
05 p0772 A69-16227
- Method of finding new nonlinear optical materials using anharmonic oscillator model
[IEEE PAPER F-5] 05 p0808 A69-16312
- Brewster angle window degradation of high power ionized argon gas lasers
[IEEE PAPER L-4] 05 p0775 A69-16322
- Nonlinear optical coefficients in group IV and III-V semiconductors, calculating contribution from conduction and core electrons
[IEEE PAPER V-7] 05 p0776 A69-16329
- BiTeBr semiconductor band structure determined from electrical and optical properties
05 p0810 A69-16609
- Metal heating by laser, noting heating rates exponential increase with time due to optical characteristics changes
06 p0932 A69-16915
- Regularization methods in inverse problems of atmospheric optics, analyzing atmospheric thermal sounding and interpretation of radiation measurements
06 p0919 A69-17616
- Fiber optics evolution, discussing industrial and medical applications
06 p0958 A69-17675
- Fiber optics technology, discussing fabrication and applications involving light carrying /incoherent/ and image carrying /coherent/ fibers
06 p0958 A69-17676
- High transmittance long fiber optics, presenting data on special transmission as function of temperature
06 p0958 A69-17677
- Optical commutation to permit multifield monitoring and recording with one sensor by employing high resolution imaging fiber optics elements feeding common focusing lens
06 p0926 A69-17678
- Symmetrical formulation of quantum theory of three wave optical parametric interactions in crystals
06 p0958 A69-17710
- Laser light scattering with orientation saturation of microsystems by electric field, noting application to optical anisotropy of macromolecules and colloidal particles
07 p1149 A69-18900
- Hot gases optical properties based on real spectra, discussing radiative processes and cross sections calculation methods
07 p1185 A69-19166
- Optical properties of hot air used to solve radiative transfer problems, including emissivities and absorption coefficients calculations
07 p1185 A69-19167
- Saturn rings optical properties and thickness from edgewise photometric observations, noting luminance relationship to direct brightness
07 p1219 A69-19335
- Ce activated garnet crystals optical properties, noting IR and near UV absorption spectra and room and low temperature fluorescence
07 p1201 A69-19647
- Bright galaxies observed at 408 MHz with fan beam of east-west arm of cross-type radio telescope for correlations between radio and optical properties
08 p1386 A69-20087
- Thin films of niobium oxide vapor-deposited on silicon and quartz substrates, discussing optical and dielectric measurements, dispersion and absorption coefficient
[ECS PAPER 17] 08 p1372 A69-20365
- Quasars optical and electrical properties, distance, nature and role in cosmology
08 p1390 A69-20377
- Optical systems with quasi-monochromatic partially coherent illumination, discussing energy distribution computation program
08 p1353 A69-21096
- Glass science and technology noting optical, electrical and mechanical properties, forming techniques, structure, ionic properties, high pressure effects and glass ceramics
08 p1341 A69-21126
- Alkali halide crystals destruction by laser radiation for estimating optical strength, discussing impact ionization hypothesis
08 p1328 A69-21188
- Structural and optical properties of vacuum deposited GaP films at below 240-850 C
09 p1554 A69-21332
- Nonlinear optical properties of barium sodium niobate in ferroelectric tetragonal phase above room temperature, noting spontaneous parametric emission
09 p1515 A69-21354
- Optical transfer function in single scattering approximation for light scattering media consisting of large particles
09 p1536 A69-21865
- Nonlinear optics, discussing materials, polarization, harmonic generation, light mixing, parametric amplification and oscillation, stimulated scattering, absorption, reflection, refractivity and self focusing
09 p1518 A69-22124
- Three color observations of 16 magnetic stars and photometric properties of 23 stars, discussing periodicities in variations
09 p1599 A69-22196
- Pulsar NP 0532 optical pulsations period, discussing time rates of change, pulse shape, amplitude, photons, etc
10 p1774 A69-23182
- Optical features of Sco-X-1, Tau-X-1 and Cyg-X-2 X ray sources, discussing optically thin hot plasma model for X ray emitter
10 p1682 A69-23327
- Soviet book on highly doped semiconductor covering energy spectrum analysis, kinetic effects, optical properties, fabrication and applications
10 p1746 A69-23522
- Diffusion pump oil reflectance and absorption coefficients measured in three thicknesses using light source, monochromator and detector
10 p1725 A69-23647
- IR detection at sum or difference frequency by employing optically nonlinear crystal and laser in visible and photomultiplier
10 p1704 A69-23656
- Optical observations of proton flare, discussing flash phase and sunspot umbrae
10 p1765 A69-23749
- Diamond-like glassy semiconductor compound of cadmium germanium arsenide, determining optical lattice vibrations from IR reflection spectra
10 p1747 A69-23963
- Ruby laser crystals optical inhomogeneity and residual mechanical stresses effects on laser beam angle of divergence
11 p1936 A69-24698
- Gas laser materials, fabrication and performance, analyzing gas cleanup, cathode degradation, bore erosion and optical surface contamination effects
11 p1896 A69-24743
- He-Ne laser output phase fluctuations between adjacent modes during unlocked and self locked condition, noting cavity optical length short term fluctuations influence
11 p1898 A69-25048
- Atmospheric optics by spacecraft and high altitude probes concerning ozone and aerosol distributions, scattering indicatrix polarization and dust cloud inhomogeneities
12 p2055 A69-25815
- Mars higher atmospheric transparency and changes in surface colors
12 p2154 A69-25823
- Airborne Q switched ruby laser for studying upper atmosphere meteoric formations optical characteristics and kinetics against background of underlying surface
12 p2125 A69-25955
- Kerr constant verification device to study electrooptic liquids properties
12 p2084 A69-26148
- Optical constants of bulk diamonds compared with interstellar extinction, calculating extinction curves for diamond particles from Mie theory
12 p2157 A69-26230
- Ruby crystal optical homogeneity and relation to main laser emission characteristics, discussing optical and structural surface properties
[IEEE PAPER U-7] 12 p2106 A69-26322
- Optical tests of Hale telescope mirror and support system at Palomar, noting various maladjustments and malfunctions
12 p2057 A69-26411
- Optical and spectral properties of dense plasma expanding after exploding electric wire in vacuum using high speed photography
12 p2137 A69-26533
- Spectral transmission curves in near UV for optical glasses
12 p2130 A69-26599
- Quasars optical properties, hypotheses on nature, energy distribution, red shift, stellar magnitude and distance estimation on basis of absorption
12 p2167 A69-27042
- Venus atmosphere optical properties on basis of Venera 4 data, proposing models for measured rotational temperature and subcloud atmosphere radiative equilibrium
13 p2345 A69-27691
- Optical constants of soot applied to heat flux calculations, discussing soot particles concentration determination in hydrocarbon combustion products
[ASME PAPER 68-HT-13] 13 p2374 A69-27777
- Segmented active mirror optics design concept for lightweight optically stable primary reflector used in large orbiting astronomical telescopes
13 p2261 A69-27950
- Outgassed condensation effects in vacuum on magnesium difluoride overcoated UV irradiated Al mirrors,

including temperature effects, Lyman alpha reflectance and IR analysis of deposits

13 p2299 A69-28015

Monograph on optical properties and band structure of semiconductors covering absorption and reflectivity measurement, electronic states transition, deformation, etc

13 p2323 A69-28200

X ray pulsations in Crab Nebula at frequency closely matching radio and optical pulsations, noting energy distribution

13 p2354 A69-28465

Photometric discovery of new variable stars resulting from quasars observation, noting optical variability noncorrelation with observed properties

13 p2354 A69-28468

Ruby laser beam effects on CdS crystals optical properties, measuring absorption spectrum and light dispersion in crystal

14 p2457 A69-28999

Composite ruby laser optical inhomogeneity effect on spectral, temporal and angular emission characteristics

14 p2458 A69-29163

Optical rectification effect in lithium metaniobate crystals under neodymium laser radiation, comparing results with data for potassium dihydrophosphate crystals

14 p2458 A69-29168

Reversibility principle in transilluminated three dimensional photoelastic medium

14 p2535 A69-29359

Soviet collection of articles on atmospheric optics

15 p2646 A69-30159

Plasma three electrode source ion-optical characteristics, noting beam angular divergence dependence on spacing between discharge cavity and intermediate electrode

15 p2658 A69-30240

Reflected and absorbed solar radiation by planetary atmosphere and surface determined as function of atmosphere and surface optical properties

15 p2689 A69-30564

Plasma modes, critical fluctuations and optical properties electric field dependence in two valley model of Gunn instability semiconductors

15 p2581 A69-31240

Spectrophotometry of elliptic galaxy NGC 1052 nucleus from 3400 to 6300 Å for relating radio properties and optical characteristics

16 p2853 A69-31610

Martian bright surface areas identified as homogeneous powder having opaque grains, discussing hydrated iron oxides contributions to observed optical properties

16 p2855 A69-31660

Accurate optical position of quasars determined by plate overlap for radio interferometer calibration

16 p2859 A69-32229

Objective lens of AVR-2 refractor at Poltava Observatory measured for spherical aberration, astigmatism, field curvature, coma and distortion

17 p2970 A69-32883

Monograph on GaAs injection laser electrical and optical properties during crystallization out of solution covering principle, p-n junction fabrication, I-V characteristics, doping effect, etc

17 p2982 A69-33571

Optical constants of Ta-W and Nb-Mo measured in IR and visible ranges as function of incandescent temperatures

17 p2990 A69-33574

Laser emission divergence reduced by compensating optical inhomogeneity of active elements with prismatic reflector in resonator

17 p2983 A69-33970

Optical characteristics at 2-25 micron spectral interval for various metal blacks vaporized in vacuum on KBr, Ni foils and nitrocellulose substrates

17 p3075 A69-33976

Anamorphic holography, discussing optical and nonoptical wavelength processes and generation and reconstruction of holograms for radar applications

17 p2976 A69-34062

Dark equatorial belt of Jupiter atmosphere in 1962 and 1963, noting photometric contrasts, molecular absorption and possible structure

18 p3197 A69-34724

Optical constants changes in germanium determined by modulation method of measuring light reflected at different angles

18 p3173 A69-35014

Alkali halide crystals destruction by laser radiation for estimating optical strength, discussing impact ionization hypothesis

18 p3152 A69-35157

Hologram imaging characteristics expression, deriving relations characterizing localization and dimensions of images

19 p3308 A69-35868

Fourth rank tensors analysis describing nonlinear optical effects for 32 classes of crystalline substances

19 p3334 A69-35882

Optical imaging with partially coherent nonthermal light, discussing reconstruction of object from image and similarity between object and image, including detection

19 p3372 A69-35908

Band structure and optical constants of InSb, InAs and GaSb, calculating linear momentum matrix elements and state density with spin-orbit effects included

19 p3385 A69-36515

Electrons and optical phonons interaction effects on optical and photoconducting properties of semiconductors, discussing phonon cyclotron resonance and oscillatory and magneto-oscillatory photoconductivity

19 p3385 A69-36517

Optical mixing and harmonic generation in semiconductors, discussing magnetoconductivity tensors and magneto-optical phenomena due to free carriers

19 p3385 A69-36519

InSb-InAs, InSb-GaSb, InP-GaAs and InP-GaP quasi-binary systems solid solutions optical and electrical properties, determining energy gap change as function of composition

19 p3390 A69-36554

Electronic properties changes in amorphous CdGeAs caused by long range order loss studied by measuring optical and transport properties

19 p3390 A69-36557

Optical and electrical properties of thin amorphous films of glass-forming oxide, using X ray diffraction and electron microscopy for structural features

19 p3391 A69-36561

N-type GaAs optical properties after proton irradiation, noting transmission spectra dependence on initial electron concentration and irradiation dose

20 p3582 A69-36969

Rheology application to description, explanation and measurement of materials properties during deformation

20 p3561 A69-37599

Radiative transport equation solution in two flow approximation for plane layer, considering absorption and dispersion characteristics dependence on radiation density

20 p3553 A69-37608

Optical properties and thickness of Saturn rings from observations during ring plane crossing of earth or sun, determining Tethys diameter and albedo

20 p3605 A69-37821

Nonlinear optics, properties, light waves interaction, forced scattering and application in laser technology

20 p3555 A69-38014

Optical parameters of Martian surface and temperature, discussing brightness distribution along diameter in red spectral region, based on photoelectric cross sections

20 p3608 A69-38050

Optical pulsations in aurora, studying relations to pulsations in geomagnetism, telluric currents, X rays from aurora and variations in primary particles flux

21 p3708 A69-38492

Composite laminated glass structures employed to improve safety characteristics of glass or to achieve special optical properties

21 p3752 A69-38934

Optical properties of Gabor holograms with pure reference beam, discussing image reconstruction using He-Ne laser

21 p3726 A69-39624

Solar flare optical, neutron and gamma emission, discussing ionization losses and nuclear interaction of accelerated particles in flares

22 p4003 A69-40296

Lateral waves used to explain diffraction effects by light incident upon interface at critical angle of total reflection, discussing quasi-optical properties

23 p4191 A69-42148

Acoustics and optics in terms of acoustic holography, seismic signal optical processing, acoustic and electromagnetic waveguides, etc

23 p4191 A69-42179

Ellipsometric liquid immersion method for optical parameters determination of system with nonabsorbing surface film on absorbing substrate

24 p4316 A69-43321

Electrical and optical properties correlation of air in fog, discussing droplets distribution with regard to dimensions

24 p4347 A69-43506

Optical properties of neodymium-doped YAG and glass laser materials including fluorescence lifetime and conversion efficiency, absorption spectra, sensitization effects, etc

24 p4329 A69-43751

OPTICAL PUMPING

Laser CRT with beam pumped aluminized CdS crystals, discussing single spot low duty operation

01 p0039 A69-10175

Frequency and time dependent gains of dye solution lasers for pumping by lasers and flashlamps

02 p0257 A69-12616

Chain and branched halogen-hydrogen reactions kinetic analysis for developing chemical laser with radiation energy weakly dependent on pumping energy

02 p0259 A69-12645

Pumping beam width influence on optical range resonator excited coupled oscillations, deriving approximate equations

03 p0437 A69-13043

Parametric light generation in resonator with nonlinear medium, discussing continuous pumping with laser modes matched with pumping frequency

03 p0437 A69-13044

Neodymium glass properties degradation during laser operation due to short wave pumping radiation and stimulated emission

03 p0442 A69-14219

Threshold conditions for laser pumping with emission of perfect black body

03 p0442 A69-14220

Optical pumping distortion compensation in glass laser rod by changing coolant temperature, obtaining mode locked laser pulses

04 p0609 A69-14286

Gases optical pumping by self radiation laser action, discussing high intensity oscillatory transitional wide bands of molecular gases

04 p0610 A69-14382

258 GHz reflection amplifier with saturated gas resonance, analyzing amplification variation with gas pressure, pumping power, frequency, Q values and cavity tuning

04 p0557 A69-14754

Pumping light filtration conditions effect on transition frequency of rubidium atoms

04 p0611 A69-14779

Homopolar generator as energy store for large laser pumping

04 p0612 A69-15151

Optical generation in organic luminophor solutions in 400-650 nm range

04 p0612 A69-15374

Gas lasers involving gas-discharge collisions, selective pumping or chemical reactions to produce necessary inversion, giving theoretical analysis of excitation mechanisms

05 p0772 A69-16226

Conversion of emission from pulse tube using neodymium laser with luminophor solution filled active element, discussing pumping nonlinear absorption kinetics

05 p0777 A69-16373

Gas laser operation at high pressures, examining threshold pumping and power output dependence on pressure to optimize parameters

06 p0934 A69-17680

CW laser mode steady excitation and narrow bandwidth obtainable by highly stable pumping and stable temperature of active element

06 p0934 A69-17681

Mode locked Nd glass laser to pump organic dye lasers, obtaining continuously tunable picosecond pulses

06 p0935 A69-17759

Time dependent emission spectra from flashlamp pumped organic dye lasers recorded with image converter, comparing dyes characteristics

06 p0936 A69-17901

Optical pumping of solid state lasers, reviewing processes involved and properties of lasers

06 p0937 A69-18007

Q switching of continuously pumped Nd/YAG laser using variable spacing Fabry-Perot interferometer as variable output coupler

06 p0938 A69-18229

Microwave and optical generation and amplification - Conference, Hamburg, September 1968

07 p1090 A69-18420

Rate equation analysis for internally optically pumped millimeter wave maser operating in laser crystal

07 p1146 A69-18480

Giant pulse generation by switched laser rapid pumping of neodymium doped glass laser

07 p1146 A69-18486

Standing waves effect on spectral and power characteristics of laser with plane mirrors, determining dependence on pumping power

07 p1148 A69-18800

Optical pumping at high temperatures using spin exchange signals for RF spectroscopy

07 p1148 A69-18893

Pumping power effect on He-Ne laser amplification factor dependence on temperature and discharge currents

07 p1149 A69-18935

Solar end and lateral pumping apparatus for neodymium doped YAG crystal lasers, noting applicability to space communication

07 p1150 A69-18953

Giant pulse production of Nd-glass laser with aid of coherent pumping by second harmonic of Q switched laser, noting pulse duration

07 p1156 A69-19333

Orientation of diamagnetic ground state Pb 207 atoms with nonzero orbital angular momentum by means of optical pumping and determination of nuclear moment

07 p1156 A69-19399

Coherent radiation brightness increased from liquid N Raman laser, using off-axial pumping

09 p1520 A69-22533

Rubidium vapor laser pumping induced frequency shifts eliminated by detuning resonator without decreasing output power

09 p1520 A69-22636

Liquid laser gain measurement via luminescence intensity, noting optical pumping thermal effect

09 p1520 A69-22683

Q switching combined with pulsed pumping of carbon dioxide laser for observing optimal Q switching instant, noting pulse energy increase

10 p1703 A69-23619

Neodymium doped YAG laser efficiency dependence on pump power level and spectral filtering of pump light

10 p1705 A69-23814

Capture of parametrically coupled waves by pulses and beams of pumping radiation in case of different group velocities directions

10 p1705 A69-23956

Elliptic cylindrical chambers optimum design for optical pumping of solid state lasers, discussing transfer efficiency and approximation by circular cylindrical chambers

10 p1706 A69-24010

Transverse mode dependence of spiking behavior for ruby laser pumped by pulsed argon ion laser

12 p2104 A69-25928

Pulsed laser emission from carbon dioxide collisionally pumped by vibrationally excited DF produced by reacting fluorine oxide with deuterium

12 p2104 A69-25986

Temperature regime of pulsed laser with pump laser located in cylindrical rod cavity, discussing adiabatic and nonadiabatic pumping

12 p2104 A69-26025

Atomic clock with sequential optical pumping using resonance frequency of hyperfine transition of ground state Rb 87

12 p2090 A69-26291

Continuous polarized electron beam produced from spin conversion in ionizing reactions involving optically pumped metastable atoms in He discharge

12 p2130 A69-26312

Off axial mode selection in circular cross section solid state lasers due to nonuniformity of excitation by focusing of pump power

12 p2106 A69-26320

Population densities, pumping rates, lifetimes, etc., of singly ionized krypton ion laser

12 p2109 A69-26638

Optical detection signals optimization in optical pumping, discussing light beam propagation direction, spectral composition and polarization characteristics

12 p2111 A69-27180

YAG-Nd laser continuous operation using incoherent injection luminescent pumping by gallium arsenide phosphide light emitting diodes at liquid nitrogen temperature

13 p2270 A69-27192

Ruby and neodymium glass traveling wave laser free generation spectra kinetics, noting mode transitions as function of pumping levels

13 p2271 A69-27655

Semiconductor luminescent devices and laser pumping by solar radiation modulated to interact resonantly with solid state plasma oscillations and electric field in crystal

13 p2272 A69-27969

Gases optical pumping by self radiation laser action, discussing high intensity oscillatory transitional wide bands of molecular gases

14 p2456 A69-28755

Ruby laser filled with single emission mode of oscillation using uniform pumping

14 p2458 A69-29164

CdS crystals emission spectrum during two photon excitation by ruby laser, noting dependence on pump power

14 p2458 A69-29167

Continuous IR parametric signal amplification in saturable absorber caused by carbon dioxide laser pumping

14 p2459 A69-29601

Q switched ruby laser giant pulses during pumping by another Q switched laser exhibit simple shape and low duration

15 p2634 A69-30727

Maser emission in interstellar OH ground state produced by IR pumping, noting population inversion mechanism

15 p2691 A69-30762

Pumping energy absorbed by active element of neodymium glass during laser emission related to activator concentration

15 p2635 A69-31104

Monomode giant pulse generation from neodymium glass laser by coherent pumping

16 p2797 A69-32018

Optical generation in organic luminophor solutions in 400-650 nm range

16 p2797 A69-32121

Kr and Ar flash lamps pumping efficiencies compared for Nd-doped YAG and glass lasers

17 p2980 A69-32958

Carbon dioxide flowing gas laser pumped by thermally excited nitrogen, discussing power gain and absence of chemical and charged particle effects

18 p3151 A69-34264

Population inversion in carbon dioxide laser related to pumping frequency, discussing molecular dissociation effect in gas mixture

18 p3151 A69-34620

Stimulated emission characteristics of CdS-CdSe mixed crystals subjected to two photon excitation, studying pulse energy at 77 K as function of pumping power

19 p3332 A69-35867

Single and two mode laser emission dependence on pumping power distribution between four level active centers of different types

19 p3333 A69-35878

Rb 87 vapor laser pumping, output, spectral line width and emission frequency approximated in three level system

19 p3335 A69-36342

Rb 87 vapor laser output power and spectral line width dependence on optical pumping intensity and atom density in resonator

19 p3336 A69-36343

Light induced shift of Rb 87 vapor laser emission frequency during modulated optical pumping, discussing elimination by filter temperature and tuning

19 p3336 A69-36344

Frequency shift dependence in transition of Rb 87 atoms on pulsed pumping intensity, discussing continuous and pulsed indication and peak determination

19 p3336 A69-36345

Pulse ruby lasers with mercury lamps for pumping noting improved efficiency, power and temperature regime due to reduced IR radiation

19 p3336 A69-36347

Optical pumping in pure Si at 77 K, noting dichroism conditions for dipolar electric transitions in cubic crystal

19 p3389 A69-36548

Spectrum of axial modes of laser with inhomogeneous longitudinal pumping, dividing parameter space into steady emission regions

19 p3339 A69-36880

Threshold power, gain, output power and radiation energy during optical pumping of Q switched molecular laser by black body radiation

20 p3554 A69-37722

Optical pumping and selective population applications, considering double magneto-optic resonance and inelastic interatomic collisions

21 p3735 A69-38454

Standing waves effect on spectral and power characteristics of laser with plane mirrors, determining dependence on pumping power

21 p3736 A69-38945

Emission from polymethine dye solution during optical pumping with pulses from Q switched Nd glass laser, discussing emission spectral, temporal and energy characteristics

21 p3739 A69-39542

Mode locking of organic dye laser by pumping laser with mode locked pulse train from Nd-glass laser, obtaining spectral bandwidth

21 p3740 A69-39545

Pumping and excitation spectra of solid solutions of cryptocyanine in glycerine irradiated by ruby laser, discussing population inversion and scattering and vibrational transitions

21 p3740 A69-39546

Absorption spectra from excited metastable states in tunable dye laser pumped atomic Ca, using fast flashlamp continuum

21 p3775 A69-39740

Flashlamp-pumped dye laser for resonance scattering studies of upper atmospheric composition, describing laser construction and tuning

22 p3962 A69-40440

Electron beam pumped dislocation free GaAs lasers filamentary and nonuniform emission characteristics from X ray topographs before and after bombardment

22 p3963 A69-40565

Pumping model for analyzing stimulated and enhanced potassium multiphoton emission primed by ruby laser-stimulated Raman electronic radiation

23 p4171 A69-41391

Monte Carlo method for energy transfer efficiency of ruby laser pumping cavities by helical flash lamps, noting dependence on ruby parameters

23 p4173 A69-41630

Low energy ultrafast flashlamp systems as optical pumps for lasers using fast decaying fluorescent materials/organic dyes/

23 p4174 A69-42187

Electron spin memory in optical pumping cycle of potassium halides F centers, measuring relaxed excited state g factors and spin resonance line widths

23 p4198 A69-42419

Optimum design of spherical and ellipsoidal pumping chambers for solid state lasers determined from numerical calculation of radiation transfer efficiency

24 p4327 A69-42986

Amplified radiation of laser used for coherent optical pumping in two level low pressure gas laser

24 p4327 A69-43067

OPTICAL PYROMETERS

Thermistors for total optical radiation pyrometer and for temperature control system based on radiation pyrometer, noting thermistor response and control circuit

04 p0601 A69-15119

OPTICAL RADAR

Optical radar for studying atmospheric water vapor, density, temperature and aerosols

01 p0090 A69-10540

Single transverse electromagnetic mode power output for laser radar transmitter, using near hemispherical mirror resonator

04 p0609 A69-14287

Stratospheric aerosol investigation by IR and lidar, applying Mie theory to model aerosol size distribution

04 p0592 A69-14654

Laser scatter measurements in mesosphere and above for optical radar system parameters

05 p0758 A69-16414

Atmospheric droplets diameter, number density and scattering cross sections determined from laser radar return equation and Mie theory

06 p0888 A69-17483

Continuous wave and pulsed IR signals amplification on carbon dioxide laser amplifiers, discussing design, construction and performance of transmitter

07 p1152 A69-19064

Atmospheric sodium measured at night by tuned laser radar, giving average column number density

09 p1484 A69-21464

Pulsed laser radar and applications to upper atmosphere observation equipment and distance measuring devices

09 p1456 A69-22132

Laser radar atmospheric applications, noting particulate matter mapping, backscatter density profiles and use of lidar

09 p1521 A69-22795

Laser radar eye hazard for fixed and variable transmitter intensities, considering eye damage magnitude and successful detection magnitude of transmitter intensity

11 p1830 A69-24845

Optical radar studies of lower atmosphere, giving Mie theory calculations of clear atmosphere volume backscattering cross sections for four laser wavelengths

12 p2033 A69-27001

Satellite positions measurements by radar compared with radar and photographic methods, considering measurement errors

12 p2110 A69-27149

Optical wavelength backscattering functions for nebulae in Pleiades cluster, noting color differences and surface brightness

13 p2340 A69-27577

Trapped aerosols below temperature inversions causing lidar echoes in troposphere layers, discussing simultaneous balloon refractometer, thermometer and ground based lidar soundings

13 p2254 A69-28475

Q switched ruby laser designed for lidar probing of cosmic bodies and earth atmosphere

14 p2460 A69-29660

Aerosol content of mesosphere with noctilucent clouds measured with optical radar in Norway

14 p2444 A69-29877

Lidar data obtained at Hamilton AFB, Calif., computer analyzed for lidar operational utility, determining cloud ceiling and visibility for aircraft landing operations

15 p2651 A69-30895

Photography of laser echoes on satellites, tabulating results

15 p2570 A69-31311

Laser measurements for DIADEME satellites tracking to reconstruct actual trajectory in semidynamic geodesy

15 p2600 A69-31365

Fluorescence noise in Q switched ruby laser atmospheric backscattering experiments, noting relation to optical radar spurious and enhanced returns

16 p2777 A69-32183

GaAs laser diode radar system for incremental range profiles

17 p2980 A69-32921

Electrooptical distance measurement based on laser pulse traveling time and phase measurements to determine satellite range

18 p3103 A69-35199

A scope laser radar system using Q switched solid state laser pulses, discussing configuration and performance

20 p3487 A69-37283

A scope laser radar to measure atmospheric particles spatial distribution through echo pattern and beam attenuation

20 p3487 A69-37284

Alford and Gold light modulation effect expanded to include one frequency spectrum with Doppler shift, discussing applications to optical radar for range and velocity measurements

21 p3672 A69-38409

GaAs laser tracking system for space guidance, describing equipment and operations

[AIAA PAPER 69-870] 21 p3763 A69-39396

Lidar technology application to atmospheric and meteorological problems in clouds and cloud structures, air motion and inhomogeneity in clear air

22 p3977 A69-40535

OPTICAL RANGE FINDERS

Optical ranging technique for studying lunar physical libration by measuring distance between earth observatory and two fixed points on lunar surface

01 p0158 A69-11311

Handheld optical range finder for manned spacecraft orbital rendezvous, discussing target shapes and range errors

02 p0250 A69-12366

Pseudorandom radar ranger /DIOMEDE/ using optical correlator and phase loop

03 p0393 A69-13254

Lunar laser ranging for testing Einstein and Brans-Dicke gravitational theories, discussing pulse transit time and dominant nonNewtonian correction

05 p0825 A69-16362

Optimum emission wavelengths in atmospheric refractive index determination in optical range finder/refractometer system, noting laser applicability

13 p2260 A69-27826

Optical signal conversion efficiency and threshold relationships in pulsed rangefinding systems, considering effects of noise obeying Poisson distribution

14 p2412 A69-29324

NASA laser systems for satellite tracking, determining ranging accuracy by comparing laser and computed reference orbital data

15 p2571 A69-31312

Lasers for satellite range measurements, discussing power output, mount, accuracy and data

15 p2571 A69-31337

GaAs laser diode radar system for incremental range profiles

17 p2980 A69-32921

IR nonimage-forming instruments, stressing applications to communications, intrusion detection, rangefinding, etc

19 p3310 A69-36062

Laser range measurement from earth to lunar retroreflector to study earth tipping and gravitational constant secular decrease

22 p3960 A69-40190

Ground to satellite laser ranging experiments for daylight satellite range measurements

23 p4174 A69-42193

OPTICAL REFLECTION

Reflecting telescope objective for far UV and X ray regions, discussing microfinishing and optical and mechanical tolerances

01 p0121 A69-10896

Electroreflectance spectra of Ge-Si alloys, noting concentration dependence and band structure of Si and Ge

02 p0295 A69-11784

Electron plasmas near plane metallic surfaces, determining transmittance and reflectance of incident light waves and surface waves dispersion characteristics

02 p0286 A69-11788

Lunar surface composition, hardness, porosity, microstructure and transparency based on polarization of reflected light

04 p0658 A69-14958

Phase grating formation in giant pulse laser Q switching liquid by reflecting light beam from Lippman plate at Bragg angle

05 p0771 A69-15811

Nonuniform distribution and concentration of doping materials in semiconductors determined by measuring optical reflection coefficient

05 p0764 A69-16664

Equal inclination interference fringes effects on laser beam reflection from plane parallel glass plates, evaluating angular distance between adjacent fringes

11 p1896 A69-24840

Laser pulse deflection by acoustooptical system consisting of ultrasonic cell and oscillator

11 p1840 A69-25423

Fiber optics application to fiberscopes and fused fiber optic plates, noting surface coating for light scattering prevention

12 p2084 A69-26150

Light diffusive reflection from rough surface measured as function of angle of incidence in presence of specular component by goniospectrophotometer

14 p2485 A69-29171

Visual orientation near moon and at surface, considering terrestrial and lunar objects reflectivity and light reflection at various angles of incidence

14 p2525 A69-29750

Short laser pulses reflection from artificial fog and smoke, showing dependence on reflecting medium attenuation coefficient

15 p2562 A69-30077

Lunar surface composition, hardness, porosity, microstructure and transparency based on polarization of He-Ne laser

18 p3196 A69-34721

Stimulated reflection experiment for correlation between coherent photon beams from independent lasers

18 p3153 A69-35292

Time dependent collimated light diffuse reflection and transmission by finite inhomogeneous atmosphere, using principle of invariance

18 p3132 A69-35345

Reflection and transmission measurements on as grown surfaces of tetracyanoquinodimethan, obtaining optical constants by Kramer-Kronig method

18 p3183 A69-35477

Lateral waves used to explain diffraction effects by light incident upon interface at critical angle of total reflection, discussing quasi-optical properties

23 p4191 A69-42148

Photomultiplier tubes performance enhancement by light incidence on photocathode at oblique angles explained by reflection

23 p4191 A69-42194

OPTICAL RESONANCE

Tunable optical parametric oscillator using argon laser CW output as pump and lithium niobate as nonlinear crystal

02 p0260 A69-12701

Second optical harmonic generation in uniaxial negative potassium dihydrogen phosphate, noting influence of generating process on angular structure and output power

03 p0439 A69-13057

Resonant interaction of radiation from liquid nitrogen cooled ruby laser with ruby crystal in temperature range 4.2-100 K

04 p0611 A69-14439

Laser with combined active medium resulting from investigation of autoresonant energy transfer in composite crystals with optical centers

04 p0611 A69-14546

Optimal modulation shape for light emission flux as function of photoresistance detector and resonance amplifier pulse characteristics

04 p0560 A69-15376

Line shape for dynamic Stark effect during optical resonance field irradiation calculated as function of relaxation constants and beam intensity

08 p1325 A69-20282

Population densities of UV bound resonance lines of neutral helium for 41-level model atom, discussing optical thickness and electron temperature and density

08 p1390 A69-20392

Singly resonant optical parametric oscillator, noting single mode and multimode oscillation for various pump powers, pump wave depletion and mode competition

11 p1897 A69-25038

Resonance line radiation transfer in finite homogeneous cylinders of various shapes and optical thicknesses using Monte Carlo method

12 p2191 A69-26970

Optimal modulation shape for light emission flux as function of photoresistance detector and resonance amplifier pulse characteristics

16 p2752 A69-32123

OPTICAL RESONATORS

U LASERS

OPTICAL SATELLITE TRACKING PROGRAM

International cooperation results in field of optical tracking of satellites for solving problems of atmospheric physics, geophysics and geodesy

06 p1042 A69-17050

OPTICAL SCANNERS

Rapid scan spectroscopy, reviewing dispersion optical and interferometric systems and electronic image converters

01 p0082 A69-10836

Rapid scanning Fabry-Perot spectrometers, considering time resolution, wavelength resolution, wavelength interval size, aperture diameter and limitations of mechanical components

01 p0082 A69-10837

Rapid scan spectrometer design and calibration, noting application to diagnostics of high density transient Xe and H plasmas

01 p0082 A69-10838

Hologram heterodyne scanner for production from scanning coherent light beam of electrical signal corresponding to scanned hologram, noting camera tube application

03 p0431 A69-13827

Interferometric laser beam scanner using hollow cathode mercury ion laser output

04 p0609 A69-14288

Scanned laser beam display techniques based on cathode ray tube technology, noting flying spot scanner and beam deflection

04 p0600 A69-15028

Fast digitalized scan laser using Nd-YAG as active medium and containing crossed array of lithium niobate electro-optic switches for mode selection

[IEEE PAPER R-2] 05 p0775 A69-16326

Density measurements of particle tracks in nuclear emulsions utilizing digitized video scan, discussing operation and instrumentation

[IEEE PAPER 2A-7] 07 p1133 A69-19185

Photogrammetric color negative prints, slides, etc, improved by scanning beam modulation

09 p1494 A69-21634

Systematic errors caused by planet asphericity in measurements of orientation and motion parameters of orbiting object compensated by scanning navigation system

10 p1693 A69-23320

Tilting filter photometer for faint light source spectrophotometry, discussing digital approach used with photomultipliers
11 p1884 A69-24834

Holographic scanning technique for laser beam deflection, noting two and three dimensional raster scanning
11 p1885 A69-24847

Continuously operating mirror scanning system for high speed photographic cameras, emphasizing maximum scanning speeds and framing rates
12 p2085 A69-26154

Electro-optical scanning device and electro-optical matrix for mechanization of difference measurements in automatic photointerpretation of surveillance maps
12 p2090 A69-26302

Single mirror scanning geometry and kinematics, analyzing spatial motion of objects plane mirror image
12 p2091 A69-26367

Single mirror image scanning mechanism vector analysis and formulas for vector rotation
12 p2091 A69-26368

Optical/mechanical IR line scanner imagery role in remote sensing
12 p2096 A69-26979

Acoustic hologram recorded by laser flying spot scanner
13 p2265 A69-28662

Aerial multiband remote sensors for wildland resources, considering multilens photographic systems, optical mechanical scanners and radar devices
15 p2609 A69-30458

Thermal IR imaging devices for shape recognition and target position, emphasizing optical mechanical image or object plane scanners using point detectors
19 p3310 A69-36064

Optical instruments optimal design for given requirements, discussing tradeoff studies of airborne reconnaissance scanner, spaceborne rendezvous sensor and track-while-scan radiometers
19 p3310 A69-36065

Multispectral scanner with multichannel spectrometer for earth observations, describing video image generation from detector elements output signals
19 p3310 A69-36066

Multispectral imaging system to increase contrast using optical mechanical scanner, multielement dispersing spectrometer and electronic signal processing equipment
20 p3540 A69-37737

Automatic analysis and classification of images stored on 35-mm film using CRT flying spot scanner with computer control and memory
24 p4286 A69-42744

OPTICAL SPECTRUM
U LIGHT [VISIBLE RADIATION]
U SPECTRA

OPTICAL THICKNESS
Exploding wires as light source for quantitative spectroscopy, noting optically thin plasma clouds with radial symmetry
01 p0117 A69-10658

Nonequilibrium nitrogen plasma spectral line intensities calculated assuming optically thin plasma
01 p0124 A69-10960

Radiant heat transfer in optically thick gray gas situated between parallel black diffusively emitting walls, using matched asymptotic expansion method
01 p0178 A69-11411

Weighting functions for finite optically thick atmospheres, discussing emission line formation
02 p0328 A69-12755

IR radiation heat transfer in polyatomic gases in limit of large path lengths
05 p0844 A69-15579

Pressure stratification and transparency/geometrical depth expansion/ in Fricke-Elsasser and Zwaan sunspot models
06 p0999 A69-16976

Electron temperatures and optical depths for planetary nebulae outer regions derived using radio spectra and Balmer line isophotes
06 p1009 A69-17962

Saturn rings optical properties and thickness from edgewise photometric observations, noting luminance relationship to direct brightness
07 p1219 A69-19335

Radiative transfer by doubling very thin layers in problem of diffuse reflection from plane-parallel atmosphere eliminates numerically solving transfer equation
08 p1420 A69-20064

Quantitative spectroscopy methods for determining data on chemical constitution of plasmas, treating optically thin LTE plasmas
08 p1363 A69-20465

Spectroscopic diagnostics for determining temperatures, electron densities and line shapes in optically thick plasmas
08 p1363 A69-20466

Optical depth determination in absorption lines of interstellar neutral hydrogen clouds by spectral observation of variable intensity radio sources
08 p1398 A69-20774

Galactic clusters absorption, discussing optical thickness in blue and red light
09 p1587 A69-21356

Optically thick planetary atmospheres in radiative-convective equilibrium investigated by models with adiabatic temperature gradient in troposphere, discussing gray stratospheric solution
09 p1600 A69-22200

Error analysis of Hubble galaxies count to resolve contradiction of values for average optical half thickness tau of galactic absorbing layer
10 p1779 A69-23609

Optical depth at under 110 A due to continuous absorption by N, O and Ne ions estimated in high excitation planetary nebulae
10 p1790 A69-24140

Optical characteristics of Martian atmosphere from photometric data for continent-mare contrasts, discussing transmittance and optical thickness
11 p1959 A69-24727

Radiation diffusion in medium of finite optical thickness, computation of source function and tabulation of matrices
12 p2131 A69-26661

Photometric and colorimetric characteristics of hot gas optically thin in continuous spectrum with optical thickness of several units in Balmer series lines
12 p2159 A69-26667

Resonance line radiation transfer in finite homogeneous cylinders of various shapes and optical thicknesses using Monte Carlo method
12 p2191 A69-26970

Optical depths of convection related to metal deficiency for main sequence and giant stars
14 p2527 A69-29946

Noctilucent clouds thickness determinable from angular dimensions of visible edge
15 p2598 A69-31254

Approximate expression for temperature dependent radiative heat flux in optically thin gas, considering reentry body hypersonic flight
16 p2877 A69-31892

Heat transfer in evacuated multilayer insulation by radiation and conduction, considering optically thin media separating reflective layers
17 p3073 A69-33300

Optically thin gas surrounding X ray source, plotting electron temperature and ionization equilibrium of hydrogen, He, carbon, nitrogen, oxygen and neon
18 p3186 A69-34295

X ray absorption in surrounding gas sphere as function of continuous absorption, electron scattering and diffuse ionizing radiation, using radiative transfer theory
18 p3186 A69-34296

Galactic clusters absorption, discussing optical thickness in blue and red light
18 p3197 A69-34746

Molecular concentration-optical depth curves for combinations of two photospheric and two facular models, noting lines contrast dependence on dissociation energy
18 p3204 A69-35391

Boundary conditions for differential approximation to radiative transfer, noting optically thick slip conditions
20 p3633 A69-37524

Sunspot umbra observed on 21 September 1966, computing transparency in model equaling photosphere transparency at same optical depth
20 p3605 A69-37825

Excitation temperatures and OH microwave line optical depths measured for dust clouds, discussing optical absorption lines and LF radio absorption
20 p3611 A69-38147

Effective thinness approximation for spectral line formation from photon degradation processes and random walk of scattered photons, discussing optical thickness
20 p3612 A69-38159

Light field long term behavior in dispersive medium with finite optical thickness by asymptotic solution of unsteady transport equation
22 p3983 A69-41267

Radiant energy transfer in absorbing and emitting media, noting approximate equations reduced to correct optically thin and thick limits for multidimensional problems
[ASME PAPER 69-HT-E] 24 p4410 A69-43524

OPTICAL TRACKING
Optical spacecraft tracking organization in U.S.S.R., describing network of visual observation and photographic stations for satellite and space probe tracking
01 p0032 A69-10952

Electro-optical tracking devices for displacement and/or dislocation measurement without physical contact
05 p0763 A69-15986

Automatic laser tracker system for close-up photographic coverage of rocket test
[SMPTE PREPRINT 101-91] 07 p1116 A69-18949

Low latitude easterly wind measurements by optical tracking of chemicals from sounding rockets and gun probes during darkness
09 p1487 A69-21621

Small eye movements measurement and retinal image stabilization based on tracking edge of blood vessel in optic disk
09 p1446 A69-21908

Electro-optical tracking device with pyramidal reflector for field of view dissection, determining dead zones and trajectories for pointing error correction
10 p1698 A69-24219

Radio sources optical positions for independent calibration sources
11 p1958 A69-24465

Optical satellite tracking system using multicoincidence method of photon signal counting by Q switched laser
11 p1841 A69-25579

Computer program solving for station coordinates and dynamical parameters at Smithsonian Astrophysical Observatory from optical data, laser range and range rate
12 p2068 A69-26428

Soviet and foreign visual, photographic and photometric ground observations of satellites, emphasizing synchronous optical observations role in geodesy and geophysics
13 p2219 A69-27357

Pulsed laser satellite tracking system, noting tracking mount adjustment
13 p2222 A69-28192

Secor 6 satellite /1966-51A/ orbital parameters determined from optical and radar observations noting use for upper atmosphere density and rotational speed studies
14 p2522 A69-29631

Scintillation of ground based spherical wave laser source viewed from space analyzed from Geos 2 satellite laser tracking, noting stellar scintillation correspondence
15 p2570 A69-31309

Optical observations of Geos 1 over North America in short arc reduction to improve tracking stations survey coordinates, discussing dependence on earth gravity and mass
15 p2599 A69-31342

Space direction by compensation method of cosmic triangulation network, using laser and optical observations of artificial satellites
15 p2699 A69-31377

Position sensitive sensors design of optical tracking systems with emphasis on amplitude, phase, frequency and pulse-time sensors
16 p2790 A69-32111

Satellites meridian and extrameridian observations by transit instrument, examining errors in ephemerides of bulletins
16 p2858 A69-32211

GaAs laser tracking system for space guidance, describing equipment and operations
[AIAA PAPER 69-870] 21 p3763 A69-39396

Atmospheric natural turbulence effect of degradation of laser signal phase and amplitude characteristics, noting refractive index inhomogeneities effect on optical tracking system
[AIAA PAPER 69-871] 21 p3675 A69-39397

After image measuring method of eccentric fixation during autokinetic light tracking
22 p3878 A69-40837

Horizontal tracking eye movements response to unpredictable constant velocity target motions with or

without saccadic position corrections recorded by contact lens optical lever

22 p3881 A69-40856

Antitank missile guidance system with tracker using two optical paths and pyrotechnic flare noting transmission ratios, visibility coefficients and improvement factors

23 p4164 A69-41625

OPTICAL TRANSITION

Ar atom transition probabilities in 5000-6000 angstrom range, noting effect of nonuniform source temperature

01 p0125 A69-10963

Gallium arsenide injection lasers properties, analyzing band structure, optical transitions, recombination lifetimes, conduction band states, optical gain, etc

05 p0772 A69-16228

Laser stimulated gamma-optical transitions illustrated by gamma-optical absorption detection in dysprosium ethyl sulfate

08 p1328 A69-21185

Correlation effects in water and heavy water laser transitions based on cascade effects, discussing lines in resonator arms

09 p1515 A69-21349

Coulomb interaction during optical transitions between Landau subbands of Ge semiconductor valence and conduction bands in magnetic field, observing diamagnetic excitons

11 p1936 A69-24640

P-type GaAs-Ge lasing on band to band or conduction band to acceptor impurity transitions or on both transitions simultaneously

13 p2270 A69-27193

Anomalous interaction of argon and krypton ion laser lines, considering connecting radiative transitions and cross modulation

13 p2270 A69-27204

Gas lasers output power calculation based on operating transition with mixed contour due to natural and Doppler broadenings

15 p2633 A69-30079

Electron excitation and phase shift method for radiative lifetimes of Ar II UV transitions

15 p2656 A69-31034

GaAs semiconductor laser emission band homogeneity and continuous energy spectrum levels contribution to induced optical transitions

17 p2984 A69-34161

Laser stimulated gamma-optical transitions illustrated by gamma-optical absorption detection in dysprosium ethyl sulfate

18 p3152 A69-35154

Gain modification from spectral splitting of optical transition by constant light wave on higher frequency coupled transition

22 p3965 A69-41125

OPTICS

Geometric optics inverse scattering method for smooth conducting convex bodies of revolution, demonstrating bounds on size and shape

02 p0280 A69-11929

Nonlinear optics - Conference, Novosibirsk, U.S.S.R., June 1966

03 p0435 A69-13034

Geometric optics for media with spatial dispersion, describing procedures for equation solution

03 p0467 A69-13718

Damping factor automatic determination by use of second derivatives of residuals for damped least squares method of optical design

04 p0630 A69-14295

Geometrical optics approximation of Maxwell equations for electrodynamics of inhomogeneous anisotropic media

07 p1076 A69-18519

Geometrical optics method for differential equations of fourth order in applications to LF plasma oscillations

07 p1190 A69-18697

Optical processing of planetary radar data for range Doppler image generation

08 p1270 A69-19816

Plasma microwave diagnostics by multifrequency probes in geometric optics approximation, assuming inhomogeneous and semiinfinite plasmas with sharp boundaries and nonunity permittivities

11 p1926 A69-24602

Single and double mirror systems geometrical optical image aberrations noting focal number, angle of field, secondary magnification and mutual position tolerances

11 p1918 A69-24836

Optical methods in three dimensional gas flow research, noting role in density field determination and conjunctive use with gas dynamics equations

12 p2011 A69-26191

Active optics system for obtaining perfect mirror figure in orbiting astronomical telescope, using laser and white light sources, interferometers and data converter

12 p2092 A69-26423

Soviet collection of papers on nonlinear optics, discussing lasers, electromagnetic interactions, Q switching, dynamics, etc

12 p2109 A69-26905

Spiral trajectory winding rate of asymmetrical light beams in nonlinear media analyzed in geometric optics approximation, noting diffraction influence

13 p2298 A69-27662

Segmented active mirror optics design concept for lightweight optically stable primary reflector used in large orbiting astronomical telescopes

13 p2261 A69-27950

Master equation in quantum optics phase-space formulation based on Schroedinger equation of motion, noting application to Volterra integral equation and Born approximation

15 p2633 A69-30307

Electromagnetic wave propagation in anisotropic inhomogeneous media by geometric optics approximation, obtaining equations for beam trajectories in spherically symmetrical medium

15 p2569 A69-30949

N wave propagation across nonuniform medium described by cloud or front layer, using geometrical optics

16 p2812 A69-31924

Nonmetallic materials thickness measurements at SHF, describing factors affecting geometrical-optics method

18 p3138 A69-35116

Remote sensors geometrical optics, considering power flow direction, specular reflection, imaging and dihedral in case of specular reflectors, reflection and diffraction

20 p3577 A69-37744

Numerical evaluation of geometrical optics radar cross sections of general doubly curved convex conducting body using surface fitting method

20 p3494 A69-37848

Optical and mechanical systems of Wroclaw Observatory Lyot type coronagraph for prominence observations in H alpha line

22 p3943 A69-39999

Acoustics and optics in terms of acoustic holography, seismic signal optical processing, acoustic and electromagnetic waveguides, etc

23 p4191 A69-42179

Transmission properties and directional coupler determined for optical circuit dielectric rectangular waveguide with surrounding dielectrics of smaller refractivity

24 p4287 A69-43328

Optical design of double monochromator for use in EUV, describing astigmatism and transmission properties

24 p4351 A69-43758

OPTIMAL CONTROL

NT TIME OPTIMAL CONTROL

Optimal control problems with discontinuities, noting jump discontinuities in state variable derivative arising in bang-bang control problems

01 p0049 A69-10003

Optimal control of discrete and continuous stochastic linear dynamical systems, discussing algorithms for instantaneous weighted minimum mean square error performance

01 p0051 A69-10439

Multilevel optimization techniques for dynamic systems control evaluated, developing second level Newton-Raphson controller

01 p0051 A69-10440

Sensitivity reduction in specific optimal control by use of dynamical controller

01 p0051 A69-10441

Optimal control system sensitivity definitions, analysis methods and design techniques, discussing equations of motion of dynamical system satisfying vector differential equation

01 p0051 A69-10553

Optimal AM radio reception in presence of fluctuating noise and one AM interference signal with random initial phase of carrier oscillation

01 p0031 A69-10782

Book on variational methods in optimum control theory covering necessary and sufficient conditions for extremum and functional constraints

01 p0053 A69-11107

Kalman optimal filter for linear distributed parameter systems with Gaussian disturbances and measurement noise

01 p0034 A69-11143

Optimum control with respect to minimum fuel and power consumption involving constraints based on Kuhn-Tucker conditions and saddle point theorem

02 p0223 A69-11564

Optimum linear filters for signal detection against background noise using Hodges-Lehmann method

02 p0223 A69-11565

Bayesian method for optimizing controlled plant characteristics using self adaptive model

02 p0223 A69-11566

Two parameter dynamic system of fourth order optimization based on gradient method modified for discrete optimization

02 p0224 A69-11594

Numerical method of solving optimum control problems through reduction to solution of simple minimization problems by constructing suitable sequence of auxiliary functionals

02 p0271 A69-11649

Optimal adaptive control of discrete linear systems with unknown gain, considering Gaussian distribution functions and random disturbances

02 p0224 A69-11662

Optimal control problems for Markov chains solved by iterative method, using nonlinear finite difference equations to approximate degenerate elliptic functions

02 p0224 A69-11963

Computational algorithm for determining piecewise-constant feedback gains for linear system optimal control

02 p0224 A69-11964

Performance cost functions for reaction jet controlled system during on-off limit cycle for stable and unstable plant

02 p0278 A69-11965

Algorithm minimaxing performance index and sensitivity of controller design with and without saddle point

02 p0224 A69-11966

Singular perturbation method for reducing order of mathematical models in optimal sensitivity control problems

02 p0224 A69-11967

Optimal control problem for linear regulators with constant external disturbance

02 p0225 A69-11970

Dynamic programming to demonstrate sufficient conditions of optimality in maximum principle when regular control synthesis is realized

02 p0225 A69-11975

Manual optimal guidance schemes for space vehicles to minimize computational and display requirements for pilot task loading

02 p0279 A69-12365

Optimal control of open loop aperiodically modulated discrete time systems, discussing solution of associated two point boundary problem

02 p0226 A69-12372

Optimum control of fourth order digital control system

03 p0408 A69-12916

Nonlinear programming of optimization of parameters and control functions of dynamic systems

03 p0408 A69-12974

Optimal adaptive systems synthesis by statistical theory

03 p0409 A69-12977

Incorrect variational and linear programming problems in optimal control theory, emphasizing regularization technique by Tikhonov

03 p0409 A69-13067

Synthesis of statistically optimal self adaptive system for dynamic characteristics stabilization of automatic control system main loop

03 p0410 A69-13256

Reciprocal variational formulation for optimal control, estimating difference between suboptimal system response and optimum

03 p0457 A69-13766

Synthesis of optimal second order systems with linear control

03 p0410 A69-13864

Multilevel optimal control and decomposition of trajectories by studying static and dynamic systems

04 p0581 A69-14570

Optimal control theory applied to systems described by partial differential/integral equations
04 p0581 A69-14571

Optimal stochastic control of small dynamic systems described by random differential equations, noting selective bibliography on several subjects
04 p0582 A69-14697

Optimization of control functions and parameters of dynamic systems with variable structure and discontinuous phase coordinates
04 p0582 A69-14795

Optimum stabilization of uniformly rotating axisymmetric satellite, using Liapunov theorem on asymptotic stability
04 p0666 A69-14921

Optimal linear controller synthesis with minimized trajectory sensitivity achieved by using quadratic cost function
04 p0582 A69-14941

Convergence of optimal control for denumerable system of differential equations treated by functional-space decomposition
04 p0583 A69-15095

Quadratic control problem with energy constraint, discussing approximate solutions for application to optimal control
04 p0583 A69-15111

Steady state response of inertialess discrete multivariable extremal system with noise, noting stepwise search systems
04 p0583 A69-15139

Performance index sensitivity of nominally optimal controls noting initial and final target manifolds relationship to trajectory sensitivity
05 p0737 A69-15866

Dynamic programming and indeterminate Lagrange multipliers to formulate optimal control for discrete systems
05 p0737 A69-15886

Optimal flight stabilization of VTOL aircraft in hovering mode based on linear rotation dampers system
05 p0702 A69-16024

Linear optimal control problems with quadratic performance indices, developing system equivalence for matrix Riccati equation
[ASME PAPER 68-WA/AUT-17]
05 p0738 A69-16175

Analytical measure of quality of controllability for linear dynamic system and computational procedure for maximizing adjustable structural parameters
[ASME PAPER 68-WA/AUT-4]
05 p0738 A69-16182

Pontryagin maximum principle used to solve optimal control problems on analog computer
05 p0739 A69-16473

Ruby laser characteristics at 78 K, discussing emission threshold, optimum feedback, modes, etc
05 p0777 A69-16546

Optimal control of system governed by linear parabolic equation with white noise inputs, using mathematical model to generate distributed system analog
05 p0740 A69-16599

Markov extremum drift dual compensation in optimal systems with learning experiments
05 p0741 A69-16671

On-line optimization of stochastic control systems based on learning controller model, discussing computer simulation results
06 p0900 A69-17354

M measurement optimal feedback control algorithm for stochastic discrete time systems, considering nonlinear plant, constrained controls, nonquadratic cost and simulations
06 p0902 A69-17402

Approximate optimal control of nonlinear dynamical system with state dependent variables, using stochastic linearization of system
06 p0902 A69-17404

Human operator as optimal controller, proposing quadratic performance index used by operator in judgement of own performance in tracking task
06 p0903 A69-17407

Optimum control problems solved numerically on computer, noting multivalence of extremal solutions and application to orbital transfer in central gravitational field
06 p0903 A69-17539

Space vehicle trajectory optimization using computerized step by step steepest descent to minimum cost, considering cost gradient vs control
06 p1006 A69-17570

Optimization procedure developed and applied to minimum fuel midcourse guidance of spacecraft, discussing optimal closed loop control of linear stochastic systems
06 p0955 A69-17576

Minimum fuel control of spacecraft orbital elements for transfers between elliptical orbits by low variable thrust propulsion, noting interplanetary trajectory optimization
06 p0955 A69-17579

Controllability of deep space electromagnetic wave propagation in nonvacuum by calculating optimum values of control parametric functions
06 p0888 A69-17622

Gradient method solution for class of optimal control problems, minimizing root mean square value of finite state components of object in motion
06 p0904 A69-17886

Existence and uniqueness theorem for functional equation of optimal control problems, noting stability of solution
06 p0949 A69-17889

Maximum likelihood smoother using measurements containing correlated noise for application to continuous linear dynamic systems such as inertial navigation
06 p0956 A69-17938

Limited memory optimal filter theory, output and standard filter divergence due to errors
06 p0905 A69-17946

Suboptimal guidance corrections for continuous thrust vehicle disturbances during minimum fuel rendezvous in Martian orbit, discussing physical and modified cost functional
[AIAA PAPER 69-76]
06 p0956 A69-18081

Discrete time, single input, stepping extremum control system with input disturbance and output measurement noise, discussing computer simulation and dimensional analysis
07 p1114 A69-18287

Optimum attitude program for multistage satellite launch vehicle with impact restrictions
07 p1229 A69-18492

Local cross sections method for optimal control, considering control plant with variable control range and constraints on phase coordinates
07 p1115 A69-19003

Optimum and suboptimum detection of K binary symbols corrupted by white Gaussian noise, discussing searching procedure and average error probability
07 p1081 A69-19097

Book on optimal control covering servomechanism, linear system statistical design and state representation, calculus of variations, maximum principle, dynamic programming, etc
07 p1115 A69-19143

Optimizer for shaping control signal of hunting type system with plant in form of nonlinear inertialess element, examining inadequacy for system operation
07 p1115 A69-19757

Nonlinear controller design by dynamic programming method, discussing block diagram
08 p1296 A69-20236

Compromise control in system with two hierarchy levels interrelated via lower level subsystems optimality criteria found by solving global criterion problem
08 p1297 A69-20415

Dynamic programming for nonlinear suboptimal control system with minimum Q factor, developing nonlinear functional with controller motion restraint
08 p1297 A69-20416

Tuning design optimization of single circuit LF automatic control systems, using transfer functions and phase amplitude graphs
08 p1297 A69-20418

Response optimization of feedback control systems with reference to single settlement time-constant ideal determined for error evaluation
08 p1298 A69-20855

Command inputs handling by linear optimal control theory, investigating Riccati matrix differential equation convection
08 p1298 A69-20856

Optimal control approximate synthesis partial differential equation solution in form of interpolation polynomial for functions of many variables
08 p1299 A69-21068

Optimal control synthesis for linear plant operating in noise environment, applying dual control theory
08 p1299 A69-21070

Optimal control problem involving approximation by monotone functions
09 p1531 A69-21412

Convergence extensions in quasi-linearization for optimal control, showing results for brachistochrone and reentry trajectory problems
09 p1590 A69-21414

Differential dynamic programming algorithms of second and first order for optimal control, considering nonlinear unconstrained and constrained problems
09 p1531 A69-21415

Particular solutions in nonlinear two point boundary value problems, showing convergence for uncontrolled and controlled systems
09 p1531 A69-21416

Pulsed solutions with fixed, floating and distributed pulses for optimal control of systems with differential equations unbounded and discontinuous on right side
09 p1471 A69-21435

Book on optimal control of systems governed by partial differential equations, noting systems of automation, existence theorems and numerical analysis
09 p1471 A69-21580

Optimal controls for linear systems with matrix elements and vector components discrete functions of time
09 p1473 A69-21787

Optimal linear quick response problem solving by fast convergence iterative procedure
09 p1473 A69-21791

Discrete predicting filter optimal synthesis in terms of rms error by solving normal Gaussian equations
09 p1473 A69-21858

Soviet book on methods of optimal statistical solutions and problems of optimal control covering basic equations of random processes, stochastic differential equations, etc
09 p1473 A69-21932

Optimum timing extraction /bit synchronization/ in pulse code transmission, analyzing probabilistic structure by statistical parameter estimation and deriving system
09 p1455 A69-22115

Conjugate gradient and Davidon-Fletcher-Powell methods applied to nonlinear optimization problems
09 p1474 A69-22442

Optimal stochastic control, discussing dynamic mathematical models described by differential equations
09 p1475 A69-22567

Optimal control of discrete processes with bounded phase coordinates, proving optimality conditions
09 p1475 A69-22668

Control system controllability under discontinuous control constraints, presenting optimal response rate linear system synthesis with continuous restriction on control function
09 p1475 A69-22670

Statistical theory and dynamic programming to synthesize optimal pulsed control systems having restrictions on control device storage capacity
09 p1476 A69-22673

Dynamic programming method to achieve optimal control of discrete systems with lagging control variables, considering structural properties
09 p1476 A69-22674

Maximum principle in integral form for optimal control problems with delay differential system equations, using vector matrix notation
10 p1718 A69-23038

Optimal AM radio reception in presence of fluctuating noise and one AM interference signal with random initial phase of carrier oscillation
10 p1653 A69-23111

Optimum control involving plants with intermediate position between lumped and distributed parameters
10 p1666 A69-23363

General extremality for optimal controls with restricted phase coordinates and with unorthodox criterion function, discussing hypotheses for deriving necessary conditions
10 p1721 A69-23864

Dynamic programming to demonstrate sufficient conditions of optimality in maximum principle when regular control synthesis is realized
10 p1666 A69-23884

Optimal control of time invariant uncontrollable linear systems, noting asymptotic stability
10 p1666 A69-23887

Fuel optimal control for second order system determined by game theory approach
10 p1667 A69-24040

Differential game for determining singular fuel optimal control of plant with uncertainty in dynamic equation
10 p1667 A69-24041

Optimal controls for differential system nonlinear in state function and linear in control function
10 p1667 A69-24057

Differential games solution value function constructible from solutions to associated one player optimal control problems
10 p1667 A69-24059

Optimization of autonomous system parameters, exemplifying by disturbed motion of gyroscope system
11 p1858 A69-24557

Pontryagin principle application to incorporation of singular sections into optimal trajectories of controlled systems, considering conjugation of singular and nonsingular extremals
11 p1960 A69-24764

Successive approximation techniques for problems in optimum control theory, considering maximum principle and Banach space
11 p1908 A69-24771

Matrix Riccati equation duality and bounds, discussing duality in context of optimal control
11 p1909 A69-24885

Analytical method for optimum switching function of relay servosystem subjected to stationary Gaussian random noise, considering perturbation and dynamic programming
11 p1859 A69-25025

Computational method for quasi-optimal control with parameter sensitivity function, noting application to dynamical system model
11 p1859 A69-25165

Kozhevnikov optimality principle for optimum averaging of discontinuous stochastic control systems extended to include intensities of discontinuities
11 p1966 A69-25329

Optimum controller design for dynamic stability of ideal incompressible fluid in cavity of body constrained to horizontal rectilinear translational motions
11 p1966 A69-25330

Optimization of control systems with allowance for failures of elements in parallel operation, noting application to vehicle with clustered propulsion system
11 p1966 A69-25331

Dynamic programming determining optimal feedback control policies for optimal trajectories based on invariant imbedding
11 p1910 A69-25410

Feedback control law preserving optimality for systems with unknown parameters, discussing optimally adaptive performance index
11 p1860 A69-25441

Stochastic optimal control of continuous time systems with unknown gain, discussing filtering-control interaction and computer experiments
11 p1860 A69-25442

Open loop suboptimal control for linear time dependent tradeoff between energy expenditure and probability of target set entry
11 p1860 A69-25443

Nonlinear bang-bang optimal control problems solution based on differential dynamic programming, noting use of Pontryagin adjoint variables
11 p1860 A69-25444

Optimal control theory for systems modeled by ordinary differential equations, considering delay in control action
11 p1860 A69-25447

Optimal multivariable linear control system design, based on Pontryagin principle using Laplace transform method, providing good approximation to finite interval controllers
11 p1861 A69-25663

Analytical synthesis of dynamic plant model to insure desired output in response to cyclic action
11 p1861 A69-25714

Optimal control of one dimensional fluid flows with characteristic velocity passing through zero, showing Lagrange multipliers continuous and bounded in optimal solution
11 p1934 A69-25728

Observation process optimization in system described by linear differential equations of motion reducible to optimal control problem
12 p2027 A69-25882

Human operators instrument-monitoring behavior noting optimal control, information processing, physical limitations, etc
12 p2022 A69-25929

Automatic control system design for optimality in sense of nonstatistical quality criterion for disturbances of given class, considering additive noise
12 p2045 A69-25964

Terminal optimal control problem for linear system having control criterion not dependent on all phase coordinates
12 p2045 A69-25965

Optimal communication by signal feedback link between transmitter and receiver based on optimum control and dynamic programming
12 p2046 A69-26060

Optimal control of multivariable complex systems through multilevel/hierarchical/ structure, discussing coordination problems
12 p2049 A69-26082

Optimal control trajectories computation for bilinear regulator problems including neutron kinetics of nuclear reactor
12 p2049 A69-26083

Controllability of linear multivariable time invariant optimal systems with additive parameters using Kalman controllability definition, noting role of Pontryagin principle
12 p2050 A69-26086

Optimization problem with bounded state variable, noting conditions on trajectories and relations for costate vector at connecting or branching point
12 p2050 A69-26087

Control signal interconnection of subsystems at different levels of hierarchical structure systems
12 p2050 A69-26089

Discrete linear optimal control system with quadratic performance index synthesized by dynamic programming method, obtaining matrix equations
12 p2050 A69-26091

Optimum recording conditions for analog recorders with continuous recording in rectangular coordinate system
12 p2091 A69-26332

Stability of single output sinusoidal perturbation extremal control system with output lag, discussing stability boundary
12 p2052 A69-26384

Near optimum regulator design technique for high order linear systems, using singular perturbation method to reduce system order
12 p2052 A69-26503

Space vehicle angular velocities reduced to zero through linear and nonlinear optimal feedback control systems
12 p2054 A69-26516

Suboptimal control with high performance index as alternative in restricted class of optimal control problems
12 p2054 A69-26518

Nonsingular matrices inversion method by group partitioning applied to noise covariance matrix used in optimal prediction and control
12 p2123 A69-26754

Computerized design of optimal direct lift controller for aircraft and aerodynamic surfaces, using Kalman linear state regulator theory
12 p2014 A69-26765

Book on optimal control covering types of systems, practical optima, signal properties, Bellman dynamic programming and Pontryagin maximum principle
12 p2054 A69-26919

Singularities of optimal filtration for random signals given by differential equations with variable coefficients and white noise
13 p2218 A69-27251

Optimal direction finding systems based on bearing angle representation in multidimensional Markov process, considering white and interference noise
13 p2219 A69-27254

Optimal controller design and transfer functions in linear stabilization systems subjected to unknown disturbances determined by variational calculus
13 p2259 A69-27425

Optimal parameters of hydraulic sensor of angular accelerations for given dynamic and geometrical requirements
13 p2259 A69-27432

Differential approach game for unfavorable pursued motion, examining optimum control laws
13 p2288 A69-27525

Optimal control algorithm for spacecraft descent in atmosphere based on nominal trajectory and acceleration measurements
13 p2355 A69-27683

Optimum thrust control of satellite along given trajectory to rendezvous at zero velocity with orbited satellite
13 p2356 A69-27684

Optimal motion control of spacecraft refueling during flight by liquefying atmospheric gas along prescribed trajectory under constant thrust
13 p2356 A69-27686

Optimal control for minimum trajectory sensitivity of booster using algorithm and Riccati equation
13 p2261 A69-27943

Optimal control for minimization of heating and acceleration forces to reduce kinetic energy of reentry vehicle in space missions
13 p2352 A69-27960

Book on calculus of variations and optimal control theory, discussing functional analysis for use in space science
13 p2289 A69-28054

Optimal stochastic controller synthesis theory applied to stabilizing and controlling orientation of rotating bodies in central gravitational fields
13 p2300 A69-28326

Incorrect variational and linear programming problems in optimal control theory, emphasizing regularization technique by Tikhonov
14 p2424 A69-28749

Control systems synthesis for nonlinear plants with known Liapunov functions and constraints, considering stability
14 p2424 A69-28819

Optimization criterion for synthesizing discrete nonlinear control system subjected to random controlling and perturbing effects
14 p2425 A69-28825

Optimal control of variational problem for Markov chain, discussing convexity and concavity of loss function
14 p2470 A69-28903

Weighting factors relation in optimal systems integral squared error /ISE/ cost functional, characteristic coefficients and time response performance measures
14 p2534 A69-29317

Optimal control conditions for systems described by differential equations with deviating neutral type argument formulated in maximum principle form
14 p2426 A69-29419

Statistical synthesis of optimal control for quasi-harmonic systems by extending asymptotic method to include unremovable measurement error in output value
14 p2426 A69-29420

Optimal control problems solved by dynamic programming algorithm based on successive approximations of elementary control operation in space of states
14 p2426 A69-29472

Trajectory sensitivity analysis of open and closed loop optimal control systems, demonstrating previous analysis inaccuracy
14 p2427 A69-29539

Hybrid computer system for real time optimum feedback controller using iterative algorithms with rapid convergence, discussing simulation and performance
15 p2582 A69-30071

Optimal filtering of linear distributed parameter systems corrupted by boundary and/or volume stochastic disturbances
15 p2565 A69-30183

Optimal active shock isolation by nonlinear elements for system subjected to shock type loadings, discussing impulse shapes
15 p2713 A69-31019

Optimization of control system described by linear parabolic integrodifferential equation, using dynamic programming approach
15 p2645 A69-31024

Electronic hardware optimum quality assurance selected by dynamic programming in terms of failure mechanism detection efficiency per source allocation
15 p2722 A69-31127

Asymptotic solutions of optimum control for systems with constraints as linear differential equations and quadratic type functional
15 p2583 A69-31234

Optimizing control system design using fluidic digital circuitry and FM type transducers
15 p2583 A69-31296

Singular and sliding modes /unique extremals/ in calculus of variations for optimal control problems with nonlinear equations and linear control
16 p2764 A69-31629

Book on correlation theory of statistically optimal systems covering linear continuous, discrete, nearly optimal, nonlinear, decision element and adaptive systems
16 p2764 A69-32114

Liapunov functions applications in motion stability theory problems, considering dynamic systems, periodic orbits, optimum damping and control
16 p2804 A69-32248

Optimal control approximate synthesis partial differential equation solution in form of interpolation polynomial for functions of many variables
16 p2765 A69-32483

Optimal control synthesis for linear plant operating in noise environment, applying dual control theory
16 p2765 A69-32485

Nonzero-sum differential games characteristics, generalizing optimal control concepts, discussing Nash equilibrium and noninferior set solutions
17 p2943 A69-32834

Astronomical satellite direct digital attitude control using digital computer between sensor and actuator to achieve optimal filtering and stabilization
17 p3049 A69-33244

Adaptive random search algorithm utilizing boundary cost-function hypersurfaces measurement to implement Pontryagin maximum principle, discussing hybrid computer use, iterative solution and convergence properties
17 p2933 A69-33745

Wave soldering reliability and cost saving potential in miniature circuits manufacture for aerospace applications, noting process control and machine design relationship
18 p3146 A69-34512

Book on elements of optimal control covering methods for deterministic problems including calculus of variations, Pontryagin principle, dynamic programming, feedback control, etc
18 p3109 A69-34532

Optimum automatic system for controlling helicopter formation flight, stressing transient response Q factor and transmission ratios
18 p3090 A69-34656

Filtering and optimal control problems for discrete stochastic dynamical systems, describing various feedback controls and midcourse guidance optimization
18 p3109 A69-34660

Suboptimal closed loop control of nonlinear systems subject to quadratic performance indices by invariant imbedding concepts and maximum principle
18 p3111 A69-34678

Optimal control theory applications for controllers not characterized by bang bang time responses using Pontryagin maximum principle
18 p3090 A69-34681

Algorithm for minimizing expected value of quadratic performance index in closed loop optimal control of linear time varying systems
18 p3111 A69-34688

Regularization method for maximum height ascent of rocket uniformly approximating control function by gradient projection method
18 p3164 A69-34706

Optimal nutation damping of spin stabilized bodies, using Pontryagin maximum principle to optimize time, consumption and linear time-consumption combination
18 p3208 A69-34774

Learning control systems research and applications noting trainable controllers, reinforcement control, Bayesian estimation and stochastic approximation
18 p3112 A69-35093

Optimal asymptotic stabilization of gyrostat relative equilibrium, determining norm constraints for application to global gyrostat attitude control
18 p3210 A69-35145

Minimum-fuel controls in multidimensional optimum transfer problems
19 p3400 A69-35677

Linear optimal control problem for system with variable terminals, proving maximum principle and transversality conditions under minimum constraints
19 p3285 A69-35859

Search for maximum along admissible directions in optimal control systems
19 p3286 A69-35988

Existence theorem for limits of minimizing sequences in optimal control problems, applying results to systems governed by partial differential equations
19 p3287 A69-36724

Optimal linear recursive estimators for uncertain observation, considering false alarm probability
20 p3485 A69-36922

Approximation error involved in difference optimal control problem substitution for differential optimal control problem based on functional minimization
20 p3509 A69-36989

Trajectory sensitive vector introduction into closed loop linear optimal control, considering linear or nonlinear formulations
20 p3509 A69-37141

Optimal low thrust coplanar rendezvous control for thrusting vehicle and passive vehicle in elliptical orbit using linearized equations of motion and polar coordinates
20 p3617 A69-37192

Optimal controls for systems governed by elliptic or parabolic nonlinear equations or inequalities for differential operator, boundary conditions or unilateral constraints
20 p3568 A69-37324

Discrete problems of optimal control solved by general minimum principle, proposing several algorithms for optimality problems
20 p3509 A69-38295

Variational or optimal control for delayed systems, involving integrated maximum principle for problems with nonlinear functional differential systems
21 p3754 A69-38429

Discrete extremum problems solution convergence to optimal control continuous problem as functional optimal value and optimal control
21 p3684 A69-38430

Continuous optimal control problems, proving direct solutions existence for case of differential equations system linearity in control and state variables
21 p3684 A69-38431

Existence and uniqueness of optimal feedback control proved for autonomous nonlinear differential equations, allowing any finite number of variables
21 p3685 A69-38433

Optimal control of dynamic system motion described by linear differential equation, selecting vector function ensuring predetermined trajectory
21 p3685 A69-38452

Large parameter variations effect on linear feedback control systems performance, optimal or suboptimal
21 p3685 A69-38726

Optimal boundary layer control ensuring minimum heat transfer to porous plate from incompressible flow of hot gas of cooling system
21 p3849 A69-38846

Optimal transfer between coplanar elliptical orbits of spacecraft with combined small and large thrust propulsion system
21 p3803 A69-38848

Optimal control of vibrations of liquid in cylindrical container with vertical generatrix and flat bottom, using dynamic programming
21 p3694 A69-38849

Optimal control of flight vehicle consisting of long thin elastic body under torsional deformations, solving by method of successive approximations
21 p3760 A69-38852

Control system generating compensating reactions for correcting trajectory deviations due to uncontrollable random factors, discussing linear automatic control system optimization
21 p3770 A69-38853

Optimal control of liquid vibrations in rectangular container moving in horizontal direction, deriving algebraic equations system for optimal functional
21 p3694 A69-38854

Admissible controls set for discontinuous stochastic automatic control systems, deriving mean optimal averaging of controls
21 p3770 A69-38855

Optimal control of rotational and transversal motions of elastic flight vehicles, considering torsional and flexural deformations
21 p3760 A69-38890

Optimal control of ideal noncompressible fluid vibrations partially filling rectangular container moving in horizontal direction
21 p3695 A69-38892

Optimal generalized random controls using stochastic integral equation in deterministic problem
21 p3756 A69-39266

Optimal control stationkeeping for maintaining space probe stability around collinear points in three body problem
[AIAA PAPER 69-906] 21 p3807 A69-39338

Computerized optimization of flexible booster autopilot design, considering criteria for stability margins, closed loop roots and structural load relief
[AIAA PAPER 69-875] 21 p3823 A69-39401

Neighboring optimum feedback guidance to motivate min-distance lookup parameter determined by minimizing metric function of perturbed state and reference trajectory
[AIAA PAPER 69-888] 21 p3765 A69-39414

Optimum filter design for noisy analog feedback system with forward and feedback disturbances, using mean square error criterion between signal and data
21 p3687 A69-39449

Soviet monograph on mathematical methods of optimal control, discussing models and synthesis of optimal quick response systems by Pontryagin principle
21 p3757 A69-39524

Optimal pursuit control at constant moving velocity and limited angular velocities, using Pontryagin principle
21 p3825 A69-39629

Suboptimal attitude control system for Nimbus satellite using motor-driven inertia wheels as control torque source for three dimensional control
21 p3826 A69-39642

Space vehicles optimal pulsed control systems statistical synthesis, considering structural constraints on operation, memory capacity and algorithm coefficients
21 p3767 A69-39651

Optimal control system for earth satellite orbital transfer, using wandering ellipse technique to develop trajectory correction algorithm
21 p3767 A69-39652

Variational problem involving winged flight vehicles ascending and descending flight optimal program determination, considering necessary extremal conditions
21 p3767 A69-39823

Flight vehicle motion in high density medium reacting with static, vortex and dynamic forces analyzed for optimal regime via Lagrange-Euler equation
21 p3768 A69-39824

Point mapping in optimal control, describing maximum principle, dynamic programming and substitution of variables
21 p3688 A69-39860

Weighting function of statistically optimal automatic dynamic system generating stochastic loads, using Fredholm equations
21 p3688 A69-39861

Optimal control synthesis by determining conditions for absolute minimum in quick response having no regular constraints on phase coordinates
21 p3689 A69-39863

Existence theorem for linear stochastic systems optimal control described by differential equation with random coefficients, providing rms stabilization
22 p3917 A69-40116

Nonlinear adaptive reaction jet attitude control for long life space vehicles, providing optimal performance over bias acceleration disturbances
[AIAA PAPER 69-945] 22 p4036 A69-40328

Minimization of unconstrained function of several variables by gradient dependent techniques, discussing applications to boundary value problems in optimal control
[AIAA PAPER 69-951] 22 p3975 A69-40333

Linear flight control system synthesis by using optimal control theory associated with quadratic performance index
22 p3864 A69-40588

Biological systems optimal control theory, considering various control structures and energetic and informational bases of optimization
22 p3893 A69-40786

Newton-Raphson function space algorithm for optimizing control systems with discontinuities and terminal constraints, discussing spacecraft examples
22 p3918 A69-41009

Existence theorem for Markov chain finite state stochastic games applied to saddle point and optimal strategy or epsilon-optimal strategy pairs
22 p3975 A69-41010

Optimum linear adaptive design of dominant-type systems with large parameter variations assuring system response within prescribed bounds by reducing internal noise sensitivity
22 p3918 A69-41011

Suboptimal linear regulators design method yielding feedback controller for multivariable linear systems subject to parameter variations
22 p3918 A69-41012

Parameter optimization technique for aircraft control equipment design
22 p3919 A69-41051

Minimum impulse transfer of vehicle between non-coplanar Kepler orbits, applying optimal control principles to formulation
23 p4214 A69-41878

Rendezvous, intercept and injection optimal control laws derived from inhomogeneous linear differential equations with quadratic performance index
23 p4224 A69-41921

Optimal generalized controls for systems under random forces described by hyperbolic partial differential equation system
23 p4144 A69-41957

Optimal thrust control for plane curvilinear motion of variable mass point in gravitational field
23 p4192 A69-42340

Man-machine /semiautomatic/ control for optimal decision making, discussing automatic control disadvantages and limitations, multilevel system hierarchical structures, three level models, etc
23 p4112 A69-42443

Controlled plant in n dimensional Euclidean space, analyzing optimal trajectory using integral equations
23 p4183 A69-42472

Adaptive control systems analysis and application, noting off-line and on-line optimization, dynamic programming, linear systems, etc
24 p4289 A69-42946

Optimum control synthesis for nonlinear plant subject to white noise perturbation, using integral estimates of phase coordinate functions
24 p4289 A69-42949

Weight limitations effect on optimum motion parameters of variable mass body in gravitational field applied to spacecraft optimum propulsion system controls and trajectory determination
24 p4383 A69-42956

Nonblocking switching networks operating in ordinary and in simultaneous switching regime, including control algorithms for optimal space communication
24 p4289 A69-43138

Bellman equation analyzed for higher derivatives, suggesting bounded partial derivatives of optimal feedback control function
24 p4341 A69-43234

Separation theorem for arbitrary nonlinear measurements to find optimal stochastic control without dynamic programming
24 p4291 A69-43269

Slack variable to transform optimal control problem with scalar inequality constraint on state variables into unconstrained problem of higher dimension
24 p4291 A69-43270

Optimal deterministic estimation and feedback control for linear nonstationary process and measurement systems defined by Riccati equations, including Kalman-Bucy filter
24 p4291 A69-43276

Quadratic optimization applied to helicopter flight control design, assuming constant feedback gains and command step input with zero steady state error
24 p4253 A69-43279

Quasi-optimum control law for aircraft landing control system design based on Friedland technique, evaluating effectiveness by computer simulation
24 p4253 A69-43280

Singular optimal control problems theoretical and computational aspects
24 p4292 A69-43282

Stochastic fuel regulator problem investigated by optimal and self organizing techniques, emphasizing realizability of resulting controllers
24 p4292 A69-43284

Quasi-optimum proportional navigation for interceptor missiles, discussing feedback guidance law and attack geometry
24 p4348 A69-43292

Optimal deterministic inputs derived for estimating dynamic control system parameters from white observation noise
24 p4293 A69-43294

Optimal gain theory for input vector and application to regulator problem describing aircraft dynamics
24 p4293 A69-43305

Optimal control for systems with discontinuities and terminal constraints using Newton-Raphson algorithm /successive sweep method/
24 p4294 A69-43306

Optimal allocation of pulses for array radar tracking large number of targets simultaneously, using discrete time maximum algorithm
24 p4283 A69-43311

Quasi-optimum control law for minimum-time bounded acceleration rendezvous in central force field using Friedland technique, with application to lunar flight
24 p4349 A69-43313

Optimal control with computer prediction for inertial linear plants relay system containing time lag
24 p4295 A69-43706

Optimal control parameters for gyroscopic devices with constrained phase coordinates obtained on analog computer by introducing equivalent phase coordinates system
24 p4317 A69-43708

Nonlinear programming for optimal circuits design, discussing search method of ACOP /Automatic Circuit Optimization Program/
01 p0035 A69-10067

Optimal stabilization of free gyrostats using duration of transient processes and functionals of fuel and power requirements as criteria
01 p0079 A69-10261

Basic equations for optimum inhomogeneity in pressure vessels of maximum rigidity derived, using thick walled spherical shell
01 p0167 A69-10326

Spherical shell pressure vessels investigated for optimum inhomogeneity and rigidity using Lagrange polynomials
01 p0167 A69-10327

Optimal rank algorithm construction for signal detection in noise investigated for use in information transmission systems
01 p0027 A69-10374

Antenna performance optimization, considering gain dependence on diameter, feed, tolerances, noise temperature, etc
[UN PAPER 68-95813] 01 p0043 A69-10517

Optimal predictor design by comparison of statistical input models, measuring signal filter performance by root-mean-squared errors
01 p0043 A69-10558

Digital simulation models for continuous systems determined by direct search minimization
01 p0036 A69-10706

Optimal structural design since 1962
01 p0170 A69-10814

Optimal transport aircraft, considering VTOL/STOL aircraft, construction requirements and flying distances
01 p0012 A69-11293

Interactions between outer and inner jets behind maximum cross section of jet engine nozzle
[ONERA-TP-600] 02 p0187 A69-11620

Proportional navigation guidance systems for interceptor missiles optimized by adding biased term to guidance equation
02 p0278 A69-11973

Sonic nozzle optimal profile determination with and without cylindrical throats, noting sonic line curvature importance on discharge coefficient
02 p0188 A69-12037

Optimal thin walled cross section of hollow beam for pure bending, taking into account stability requirements
02 p0340 A69-12054

Variation method for optimal solution of antenna synthesis problem for given radiation pattern
02 p0217 A69-12260

Optimal detection of random signals on background of noise of unknown intensity and persistent false alarm probability
02 p0208 A69-12264

Optimum critical impulse for snap-through of nonlinear dissipative dynamical system of one degree of freedom
[AIAA PAPER 68-143] 02 p0346 A69-12508

Mathematical programming in optimized truss design noting reduction of components under buckling
02 p0347 A69-12536

Finned tube radiators optimum design for waste heat removal from space power plants
02 p0354 A69-12664

Optimum overrelaxation factor in diagnostic and forecast calculations
03 p0458 A69-13033

Frequency locked loop /FLL/ to optimize loop filter and quantization of amplitude channel
03 p0390 A69-13202

Digital computer systems design optimization based on operational experience in development of Saturn S-IC stage Automatic Test and Checkout System
03 p0400 A69-13233

Optimal design of vibration tests based on decision theory
[SAE PAPER 680753] 03 p0525 A69-13436

Optimum structural design based on linear, nonlinear and dynamic programming
[SAE PAPER 680752] 03 p0525 A69-13437

Hypersonic lifting body optimization under single and combined constraints of volumetric efficiency, heating and skin friction, using numerical search routine
[AIAA PAPER 68-1157] 03 p0362 A69-13557

Dynamic optimization problem with several decision and state variables, examining methods of solution
03 p0456 A69-13737

Optimal body shape determination by mathematical-mechanical relations derivation, discussing variational problems and variational principles applicability
03 p0526 A69-13739

Optimum proportions of gas mixture components in He-Ne laser related to field distribution in cavity
03 p0441 A69-13847

Book on nonlinear programming, discussing transformation of constrained minimization problem into sequence of unconstrained minimizations of appropriate auxiliary functions
04 p0563 A69-14421

Maximum inversion density and output power of Ne-He laser, given optimal discharge in hollow cathode
04 p0610 A69-14422

Digital computers in space flight simulation and vehicle performance optimization, examining mission analysis
04 p0652 A69-14519

Electrochemical shaping of turbine blades under symmetric cycle conditions, showing role of experimental functions for optimum regime
04 p0605 A69-14560

Optimal detection of deterministic signals with random initial phase on background of unknown intensity noise under condition of constant false alarm probability
04 p0557 A69-14788

Variational method applied to maximization of electronic efficiency of O-type TWT
04 p0577 A69-14791

Optimized formula for MacAdam color differences with modification in weighting of chromaticity and lightness, discussing Fortran IV computer programs development
04 p0564 A69-14883

Functional optimization techniques for serial hybrid computer solution of partial differential equations, emphasizing algorithms handled on digital computer
04 p0566 A69-15344

Design parameters optimization techniques for V/STOL aircraft, noting necessary cooperation between engineering and computing facilities
05 p0701 A69-15570

Minimum sensitivity deadbeat sampled data control system design by frequency domain technique, using two controllers
[ASME PAPER 68-WA/AUT-15] 05 p0738 A69-16177

Optimization of bounded feedback gains with respect to arbitrary integral performance criterion, using nonlinear programming
[ASME PAPER 68-WA/AUT-8] 05 p0738 A69-16180

Continuous parameter identification methods for parameter optimization in automatic control system analysis and synthesis, using modified steepest descent optimization
05 p0725 A69-16474

Spherical gyroscope servosystem probabilistic synthesis ensuring minimum dispersion of random drift
05 p0764 A69-16669

Satellite communication channel number and distribution optimization, obtaining malfunction probability for telephone service communication system
[UN PAPER 68-95772] 06 p0886 A69-17030

Design algorithm for adaptive control of systems using nonlinear integral equations with bounded input functions, formulating optimization as conditional minimization problem
06 p0900 A69-17351

Double stochastic approximation algorithm for minimizing mean square error in finite expansion of unknown probability distribution functions
06 p0947 A69-17361

Optimal estimation of sampled stochastic process with finite state unknown parameters
06 p0901 A69-17362

Digital computer optimization of representation of sampled data signals on orthogonal basis, using iterative method
06 p0901 A69-17363

Nonlinear constrained optimization by nonrandom complex method demonstrated by minimum weight structural analysis of elastic ring and plate
06 p1022 A69-17366

Nonlinear programming computational algorithm for recursive optimal estimates of constrained states of linear system
06 p0902 A69-17403

Slope optimization of antenna array difference radiation patterns coinciding with antenna directive gains
06 p0895 A69-17461

OPTIMIZATION

NT FLIGHT OPTIMIZATION
NT OPTIMAL CONTROL
NT TIME OPTIMAL CONTROL
NT TRAJECTORY OPTIMIZATION

Ellipsoids of revolution in viscous flow at very low Reynolds number, determining optimum shapes and minimum resistance values

06 p0911 A69-17780

Optimum efficiency of paraboloidal reflector antennas, analyzing Potter method and use of hybrid modes

06 p0899 A69-17825

Optimal flow conditions in linear conduction type MHD generators for obtaining maximum power per unit channel length or volume

06 p0871 A69-17916

Channel parameters, magnetic field level, electrical potential and channel output pressure for optimal integral characteristic of MHD system selected by variational method

06 p0969 A69-17917

Optimization of control independent cost functions in multidimensional system with linear controllers

06 p0905 A69-17945

Linear closed loop control system poorly damped response to deterministic inputs improved by stability constraint for minimization of mean squared error

06 p0905 A69-17950

Hypersonic body shaping for minimum drag and improved performance from view of flight regimes, discussing implications of pressure laws

[AIAA PAPER 69-181]

06 p0863 A69-18052

Substructure optimization in structural synthesis, minimizing number of cells for configuration parameter

[AIAA PAPER 69-121]

06 p1027 A69-18069

Differential equations for minimum variance linear filter separating signals from additive correlated noise, using discrete time optimum formulas

[AIAA PAPER 69-73]

06 p0905 A69-18121

Constant thickness fin with arbitrarily distributed heat sources optimized using approximate physical model and closed form solution of field equation

[SAE PAPER 690198]

07 p1239 A69-18302

Optimum fixed geometry ramjet in Mach range of 3 to 7 with successively subsonic and supersonic combustion

[ONERA-TP-656E]

07 p1203 A69-18415

Desired laser characteristics for space communications compared to existing lasers

07 p1146 A69-18483

Optimum physiological parameters selection criteria for medical control of crew during space flights

07 p1071 A69-18978

Current load distribution for optimizing MHD generator efficiency determined by variational method, noting dependence on relative length

07 p1058 A69-19012

Radar signal parameters measurements consisting of SNR estimation and optimum energy supply determination from SNR estimation

07 p1085 A69-19153

Optimum geometrical design of multipad externally pressurized journal bearings

07 p1141 A69-19439

Discrete signal detection providing optimum SNR for frequency and time domain differences between signal and noise

07 p1088 A69-19676

High speed stable system by combining hunting type control system without closed cycles designed for plant optimization with recycling type controller

07 p1116 A69-19759

Secondary acquisition systems analysis by semi-Markov process model, defining minimum average acquisition time

08 p1270 A69-19852

MOS transistor logic circuit performance optimization through component geometry and feed voltage

08 p1280 A69-19977

Total error of minimization of differentiable functionals based on gradient projection procedures

08 p1342 A69-20319

Structural parameters influence on fiberglass reinforced plastics strength studied for optimal structure selection

08 p1335 A69-20332

Optimal electroluminescent efficiencies for vapor grown gallium arsenide phosphide diodes, analyzing current spreading, absorption, impurity and composition effects

[ECS PAPER 103]

08 p1284 A69-20366

Optimal length conditions of liquid rocket combustion chambers, considering propellants, injection conditions, etc, noting graphs and differential equations solutions

08 p1376 A69-20606

Minimum weight plastic design of circular and annular sandwich plates with piecewise constant cross section, discussing cost reduction

08 p1417 A69-20823

Electronically phased array antenna system design optimization and testing for application to spin stabilized satellites

08 p1289 A69-20969

Optimum integration of aircraft equipment, subsystems and computer mechanizations for low cost navigation system consistent with mission requirements

08 p1348 A69-21065

Optimum aerodynamic shapes theory, considering linearized and nonlinearized supersonic flow, Newton-Busemann hypersonic flow, free molecular flow, mathematical models and variational problems

08 p1253 A69-21127

Chebyshev error norms of polynomial approximations for ideal filter minimized by emphasizing role of transfer function even and odd parts

08 p1299 A69-21168

Optimum gathering of information for linear automatic control system with distributed parameters in presence of random input disturbance

09 p1471 A69-21437

Efficiency of weather forecasts taking into account quality criteria and integrating index number, discussing optimization principle for new parameter

09 p1534 A69-21510

Optimal moments for trajectory parameters measurements determined by linear analysis to minimize error for initial conditions

09 p1495 A69-21758

Probability approach to control system optimization problem for plant with incomplete information

09 p1473 A69-21856

Electric propulsion design, considering effects of weight, impedance matching, beam voltage regulation and operating point variations in formulating system mass and reliability

[AIAA PAPER 69-254]

09 p1569 A69-21879

Communication satellite power utilization optimized by matching final amplifiers to solar cell array

[AIAA PAPER 68-437]

09 p1442 A69-21990

Optimal receiving circuit determined for elliptically polarized signals in randomly polarized noise by deriving integral equation

09 p1456 A69-22285

Weak signal optimization of multilevel quantization and corresponding detection performance, discussing asymptotic limits

09 p1456 A69-22293

Explosive forming, discussing optimum parameters for model and prototype parts and subscale forming criteria for aluminum ellipsoidal domes

09 p1512 A69-22371

Error bounds for estimation error covariance matrix of fixed point smoothing and fixed interval smoothing algorithms for optimum linear estimation

09 p1533 A69-22436

Dynamic programming computational approach to optimization with state variable discontinuities, treating problems as multistage optimization with continuous subarc stages

09 p1474 A69-22440

Optimum selection of modulation indices for multitone phase modulation by graphical method, noting tolerance insensitivity

09 p1457 A69-22463

Noniterative wideband amplifiers having single pole transfer functions overall gain bandwidth product optimization, deriving rigorous conditions for maximum

09 p1469 A69-22606

Autodyne frequency converters minimum noise and conversion factor calculation and optimal mode determination

09 p1469 A69-22631

Optimum number of terms in approximation of realizations of random process by polynomials

09 p1475 A69-22667

Space flight fuel consumption optimization as function of acceleration of nozzle control

10 p1666 A69-22919

Optimal rendezvous for two propelled spacecraft obtained by Pontryagin principle assuming small distance between vehicles compared to distances from center of gravity

10 p1791 A69-22923

Integral equation and related optimal regularization problems, finding operator in class of operators defined on set of functions

10 p1721 A69-23882

Multiparameter optimum damping for harmonically excited linear stable strictly dissipative n degrees of freedom system, locating multivariable saddle points

[ASME PAPER 69-VIBR-42]

10 p1807 A69-24180

Displacement and acceleration criterion for synthesizing optimum linear vibration isolator systems subject to random input

[ASME PAPER 69-VIBR-44]

10 p1807 A69-24182

Optimum and suboptimum shock and vibration isolators, discussing three criteria and tradeoff between relative motion and accelerative force

[ASME PAPER 69-VIBR-45]

10 p1808 A69-24183

Optimal processing parameters for producing ingots and semifinished products from corrosion resistant Ti alloys with added Mo

11 p1902 A69-24273

Conjugated gradient components of optimization criterion in automatic control determined by applying sensitivity method to computation

11 p1857 A69-24367

Optimizing two stage procedure for detecting fluctuating incoherent signal, estimating detection attempts reliability

11 p1833 A69-24444

Propulsion optimization for various vehicles, considering power plant weight, specific fuel consumption, power and thrust ratios, etc

11 p1941 A69-24462

Optimum cooling of homogeneous isotropic cylindrical body with constraints on magnitude of thermoelastic stresses

11 p1976 A69-24772

Adaptive optimal estimation of sampled stochastic process with finite state unknown parameters, using separation technique

11 p1858 A69-24935

Optimal multidimensional sequential filtration of signal on background of time correlated noise

11 p1859 A69-24967

Approximate method for calculating linear multipole antennas parameters in terms of power requirement, considering equidistant/nonequidistant element antennas

11 p1849 A69-24969

Gas dynamics for supersonic nonequilibrium flows, discussing method for determination of nozzle contours for maximum thrust

11 p1820 A69-25475

Complex structure least weight optimization for specific frequency by computerized modification of existing member cross sectional properties

11 p1989 A69-25494

Structural optimization of designs with requirements including restrictions on structure dynamic response and characteristics

11 p1989 A69-25495

Optimal design of structures with constraints on strength and natural frequency, developing steepest descent boundary value method

11 p1989 A69-25496

Iterative algorithm to determine transition probability final distribution in Markov extremal systems

11 p1861 A69-25712

Optimal scale factor selection to ensure minimum error variance in signal detection against random noise background for input limited range of measuring instrument

12 p2079 A69-25966

Group theory application to multidimensional symmetrical linear dynamic control systems optimization, considering natural vibrations of three material points

12 p2129 A69-26071

Optimization problem with bounded state variable, noting conditions on trajectories and relations for co-state vector at connecting or branching point

12 p2050 A69-26087

Thermoelectric power generators energy output efficiency, discussing thermal and electric contact resistances influence for optimizing parameters

12 p2016 A69-26364

Computer analysis on ideal step recovery diode frequency multipliers for optimum efficiencies

12 p2039 A69-26378

Linear programming algorithms for optimal structural weight design

12 p2181 A69-26566

Conjugate gradient methods for optimization problems with terminal constraints, noting minimum time paths for V/STOL aircraft climb phase

12 p2013 A69-26763

Minimum volume face sheet design of circular cylindrical sandwich shell obeying Mises yield criterion for loads transverse to lateral surface and axisymmetric
12 p2189 A69-27117

Optical detection signals optimization in optical pumping, discussing light beam propagation direction, spectral composition and polarization characteristics
12 p2111 A69-27180

Optimal design of rectangular frames for stability
13 p2358 A69-27209

Design optimization for gas lubricated spiral grooved spool bearing based on narrow groove theory, analyzing static and dynamic characteristics for motion in axial direction
[ASME PAPER 68-LUBS-12]
13 p2266 A69-27276

Optimal mean radius and half height of channel of liquid metal coaxial linear induction MHD generator with unilateral and bilateral excitation
13 p2207 A69-27507

Soviet monograph on design and theory of linear induction pumps for liquid metals covering electromagnetic phenomena, optimized dimensions, etc
13 p2209 A69-27926

Linear automatic control optimization by modified Newton method for determining real function zero value of real argument
13 p2239 A69-28436

Minimum theorems for plastic strain rates and plastic strains governed by holonomic elastoplastic theory utilizing quadratic functions
13 p2370 A69-28629

Computerized calculation of likelihood coefficients for identifying steady random processes against background noise, minimizing mean risk of erroneous solution
14 p2410 A69-28818

Automatic search-free optimization by sensitivity functions, deriving algorithms by Q factor and discrepancy extrapolation
14 p2425 A69-28823

Parameters optimization in electronic equipment design, considering parameters and efficiency criteria as additive elements functions of dimensional chain
14 p2418 A69-28835

Deterministic economic mathematical models for optimum airline networks, considering transportation cost
14 p2540 A69-29141

He-Ne laser traveling wave output power, obtaining end mirror reflection coefficient optimal value
14 p2458 A69-29165

Thermionic electrogenerating element /EGE/ design optimization, considering one dimensional linear geometry with thin walled cylindrical sheath cathode
14 p2400 A69-29224

Optimum nonlinear digital filter synthesis for smoothing, predicting and differentiating measured quantity having uniform probability distribution over finite number of discrete values
14 p2426 A69-29421

Complex electronic systems optimum redundant element content determination for ensuring adequate supply
14 p2426 A69-29422

Optimized receivers synthesized for narrow band radio signal filtration, comparing noise rejection properties of various pulse modulation types during speech transmission
14 p2413 A69-29464

Chopper modulated IR detection system error analysis through minimizing mean square error of approximating output function
14 p2450 A69-29639

Plane linear induction pump design optimization without short circuiting bus bars, allowing for MHD effects induced by traveling magnetic field
14 p2405 A69-29913

Algorithms for optimal detection of signals on background of normal noise with time varying intensity
15 p2563 A69-30133

Cantilever beam profile optimization methods using iterative analog computation to achieve minimum deflection, showing application of Pontryagin maximum principle
15 p2709 A69-30671

Optimization techniques for stellar kinetic theory problems, discussing kinematics distribution function, cosmic gas dynamics, interstellar matter, etc
15 p2695 A69-31004

Rapid convergence algorithms as second variation methods for dynamic optimization problems
15 p2645 A69-31235

Rendezvous maneuver with minimum fuel in circular orbit solved without restrictive conditions for accelerations due to approach thrust
16 p2852 A69-31558

Mathematical optimization to achieve near equal-ripple response in passband for coaxial low pass filters having unequal line lengths
16 p2757 A69-31583

Independent operations optimum performing sequence determined for parallel machines differing in technological characteristics and with assigned time using algorithm
16 p2763 A69-31626

Minimization algorithm for complex and switching functions using unique identifiers on Karnaugh map
16 p2764 A69-31710

Three antenna interferometer angle measurement accuracy dependent on antenna spacing, deriving optimal spacing value
16 p2758 A69-31730

Transistor temperature and power limitations and thermal resistance calculation, discussing heat sink surface optimum design for power losses
16 p2760 A69-32047

Numerical procedure to optimize complex structures by determining relative proportions of selected elements attaining flutter speed with minimum total mass
16 p2874 A69-32163

Parameter selection for optimum characteristics of machine part shock absorbers subject to orthogonal impact pulses
16 p2794 A69-32297

Optimum nonequilibrium nozzle performance for hydrogen-fluorine propellant system, considering contour, engine/nozzle weights and recombination kinetics
[AIAA PAPER 69-472]
16 p2733 A69-32652

Flywheels desaturated by magnetic action for optimizing stabilization system of satellite in circular orbit
[ONERA-TP-732]
17 p3049 A69-33241

Carrying cables shape optimization for suspended structures under load, using minimum weight criterion
18 p3212 A69-34354

Optimum pressure distribution and airfoil profiles for maximum lift without separation in incompressible flow determined by second order theory
[AIAA PAPER 69-739]
18 p3083 A69-34401

Failure rate data role in reliability analysis and design optimization
18 p3147 A69-34516

Optimal overlapping theory to select nonthrottled low thrust spacecraft engines power, noting spacecraft mass invariability
18 p3184 A69-34583

Sandwich beams optimal design determined for case of constraint on elastic deflection and for load factor at plastic collapse
18 p3218 A69-34623

Cost and weight optimization for solid rocket motors using various steel casings
[SAWE PAPER 777]
18 p3208 A69-34871

Aerospace structures optimization, discussing weight considerations and finite element techniques
[SAWE PAPER 814]
18 p3221 A69-34896

Optimum efficiency of turbines with small volumetric flow rate, determining height of air-gas flow, partial admittance and flow angle in clearance
18 p3184 A69-34983

Preamphasis analysis for FM system optimization to maintain constant output signal to noise ratio throughout baseband
18 p3103 A69-35088

Parameter optimization of launch vehicle attitude control system of fixed structure for various computation techniques
18 p3210 A69-35092

Optimal structure model of fiberglass reinforced materials with polymer matrix, obtaining strength utilization coefficient dependence on length/diameter ratio
18 p3162 A69-35356

Two stage vehicle gross weight minimization determined by slide rule computation using formula based on specific impulse differences between stages
19 p3429 A69-35918

Rapid Targeting Procedures computer program for optimized orbital payload and associated launch vehicle targeting data with one submittal and minimum user intervention
[AAS PAPER 68-148]
19 p3402 A69-35951

Optimized contracting for systems engineering management, discussing industry views, scope, application, depth, procurement and performance measurement
19 p3454 A69-36005

Critical signal assignments optimization in electrical/electronic connectors, considering bent pins, signal cross talk, adjacency requirements and corona
19 p3284 A69-36030

Structural design optimization based on reliability analysis stressing proof-load test and weight savings consideration under cost constraint
19 p3437 A69-36033

Solid state S band to VHF converter design to obtain optimum system noise for radio telemetry, discussing cost effectiveness and system performance
19 p3270 A69-36238

Optimal ratio predetection combiner used with diversity signals and various modulations, showing significant improvement in telemetry systems performance
19 p3270 A69-36241

Huffman minimum redundancy coding extension to run-length information based on Poisson distribution, including optimization and data compression applications
19 p3272 A69-36262

Optimum receiver design for binary coded data detection in two channel space communication system, discussing phase error distribution and optimum decision function
19 p3275 A69-36286

Stochastic models for calculating optimal elastoplastic one dimensional systems
19 p3438 A69-36313

Representation theory of signal detection in non-Gaussian noise environments applied for improved near optimum system performance
[IEEE PAPER 69-TP-10-COM]
19 p3277 A69-36488

Optimum aerological network design, discussing atmospheric model, numerical analysis, data acquisition, weather forecasts, rms measurement error, etc
19 p3364 A69-36505

Electric models optimization for heat exchange systems based on mathematical similarity between equations describing temperature and electrical potential fields
19 p3256 A69-36717

He-Ne laser temperature condition optimization based on calculation and experiment
20 p3553 A69-37356

Discrete signal detection providing optimum SNR for frequency and time domain differences between signal and noise
20 p3488 A69-37458

Optimal plastic design of circular sandwich ring assuming symmetric loading, minimum plastic resistance and cost justification of stronger cross section
20 p3625 A69-37590

Slope optimization of antenna array difference radiation patterns coinciding with antenna directive gains
20 p3508 A69-37944

Optimum physiological parameters selection criteria for medical control of crew during space flights
20 p3483 A69-38226

Psychology and physiology of vision in relation to large screen display design, discussing effects of symbol size and spacing, color usage, etc
21 p3662 A69-38330

Optimization for processes expressed in differential equations, stressing use of calculus of variations and limitation
21 p3795 A69-38400

Mathematical models and solution techniques for calculating optimal elastoplastic structures by computer, discussing methods for displacements preceding plastic failure
21 p3831 A69-38414

All-plastic light passenger aircraft with inflated tube construction for shell, discussing design and performance
21 p3728 A69-38461

Earth resources technology satellite /ERTS/ choice regarding local time of ascending node based on cloud cover and IR measurement considerations
21 p3798 A69-38628

Optimum and suboptimum synchronizers for extracting bit synchronization from binary data, showing performance dependence on pertinent system parameters
21 p3673 A69-38923

Unknown parameter experimental estimation based on signal direct observations with solution by stochastic approximations method
21 p3756 A69-39265

Nonlinear filter for optimal estimation of mean, covariance and third central moments of system, noting simulation tests stability for orbital navigation
[AIAA PAPER 69-852]
21 p3686 A69-39380

Analytical and graphical methods for characteristics of optima produced by quadratic performance index for VTOL prefilter model reference attitude control system
[AIAA PAPER 69-884] 21 p3764 A69-39411

Filtering optimization prior to limiting digital signals in strong noise, detailing bandwidth choice of single pole low pass filter
21 p3676 A69-39450

Discrete filters for optimal processing of down-linked satellite data, considering inverse filter development by Kalman filtering techniques
21 p3677 A69-39462

Iterative method for reducing filters required for optimal Kalman filter design maintaining parameter estimation accuracy
21 p3687 A69-39463

Direction finding characteristics of nonlinear antenna, including current determination and optimal angle for sidelobe level
21 p3684 A69-39619

Book on optimal aerodynamic shapes by means of variational method, covering conventional and triangular thick wing lift systems in supersonic flow
21 p3644 A69-39667

Thermistor radiation detectors bias condition defined from equations and optimized in terms of responsivity, time constant and noise
21 p3727 A69-39782

Euler equation in variational problems for optimized process described by ordinary differential equations, deriving final extremal relationship
21 p3829 A69-39825

Satellite attitude stabilization systems transient response optimization using combined feedback
21 p3830 A69-39833

Laboratory prototype of RF ion engines for space test, discussing components optimization
22 p3998 A69-39904

Minimization of motion deviation from prescribed motion analyzed as differential game of converging motions using equations of motion
22 p3980 A69-40105

Mathematical model of optimal partially closed life support system consisting of man, recycling unit, storage unit and waste disposal outlet
22 p3892 A69-40272

Minimum bias criteria for selecting data fitting curves, allowing for unknown true equation in improving data predictability
[AIAA PAPER 69-950] 22 p3975 A69-40332

Minimization of unconstrained function of several variables by gradient dependent techniques, discussing applications to boundary value problems in optimal control
[AIAA PAPER 69-951] 22 p3975 A69-40333

Computerized solid rocket motor nozzle design with computer program providing weight, envelope and performance values for vehicle optimization studies
[AIAA PAPER 69-975] 22 p3999 A69-40355

Computerized crewstation geometry evaluation and design optimization using 23-pin-joint man-model
[AIAA PAPER 69-977] 22 p3892 A69-40357

Computer optimization of spacecraft optical coatings for temperature control, using finite element analysis and matrix inversion
[AIAA PAPER 69-979] 22 p4050 A69-40359

Payload optimization factors for orbital storage of liquid hydrogen, considering payload cost of agitation, tank pressure, pressurant weight, etc
[AIAA PAPER 69-1007] 22 p4021 A69-40381

Systems approach to avionics optimization, discussing instruments, devices, display and automation techniques
[RAES PAPER 6] 22 p3946 A69-40487

Axial mode frequencies, loss coefficients and optimal parameters of three and four mirror resonators of gas lasers, including designs with maximum selectivity
22 p3964 A69-40796

Antenna array synthesis optimization for limited deviations of source distribution function from prescribed function
22 p3916 A69-40952

Minimax sensitivity criteria used to synthesize filters for estimating state of first order plant subject to dynamic and/or statistical parameters uncertainties
22 p3918 A69-41016

Algorithm for optimal solution to secondary optimization problem in nonserial dynamic programming
22 p3976 A69-41037

Germanium microwave backward diodes optimum design and performance prediction through computer calculation for important parameters
22 p3916 A69-41224

Fittings stress distribution determined for optimization of material utilization
23 p4169 A69-41418

Minimum weight and optimal cross sections design for statically determinate and indeterminate shell and H beams, using variational method
23 p4225 A69-41424

Monotonic minimization algorithm for nonsmooth extremal problems of mathematical programming, game theory, approximations and optimal control in arbitrary Banach space
23 p4181 A69-41524

Resistance thermometer for measuring rapidly varying gas temperatures, optimizing length to eliminate heat transfer to mounting
23 p4163 A69-41557

Bayesian estimate of individual truck maintenance costs based on optimum replacement maintenance age
23 p4241 A69-41577

Feasibility studies to optimized design for 440 ft steerable filled-aperture radio and radar telescope, discussing parabolic configuration, radome selection, etc
23 p4148 A69-42123

Battery subsystems optimization for earth satellite lifetimes greater than 5 years, analyzing flexibility, weight and reliability
23 p4068 A69-42243

Spacecraft solar cell near-maximum power operation by tracking optimum value with array temperature sensor
23 p4075 A69-42303

Optimum integration of aircraft equipment, subsystems and computer mechanizations for low cost navigation system consistent with mission requirements
23 p4186 A69-42538

Quantization optimization of continuous signals with known probability distribution, using quantizers with limited output values
24 p4288 A69-42671

Public policy for urban transportation system, using calculus of variations to determine optimal introduction curve
[AAS PAPER 69-292] 24 p4417 A69-42809

Algorithm minimizing personnel number and training costs to meet uncertain skill requirements, applying to army aviation contingency force training composition
[AAS PAPER 69-116] 24 p4271 A69-42818

Differential games derived for conjugate-point necessary conditions and definitions for minimum and maximum problems
24 p4340 A69-42959

Materials research structural design cycle, discussing simultaneous optimization, constituent materials, fabrication process, load environment and mission constraints
24 p4399 A69-42991

Optimum thickness of dynamically stable composite superconducting tapes determined for substrate thickness as function of current density
24 p4361 A69-43121

SNR improvement by antenna array optimization
24 p4287 A69-43140

Optimal rule for decision to stop or continue observation of random variables after observing sequence of variables with continuous distribution function
24 p4341 A69-43235

Optimal hinged two body satellite configurations in circular and elliptical orbits, discussing need for adaptive attitude control for transient and steady state operation
24 p4393 A69-43247

Optimization problems solution applied to separable but bounded state variable problem, providing control over commercial errors
24 p4292 A69-43286

Optimization of Faraday MHD generators with nonequilibrium ionization and plasma turbulence, assuming electrons at Saha equilibrium at elevated temperatures
24 p4256 A69-43682

Optimal scheme of combining motion estimators set derived for computational simplicity and asymptotic efficiency
24 p4342 A69-43704

OPTIMUM CONTROL

U OPTIMAL CONTROL

OPTIMUM THRUST PROGRAMMING

U THRUST PROGRAMMING

OPTOMETRY

Horizontal tracking eye movements response to unpredictable constant velocity target motions with or

without saccadic position corrections recorded by contact lens optical lever

22 p3881 A69-40856

Viscoelastic properties of lenses extracted from cats and dogs analyzed as function of displacement using computer simulation

22 p3883 A69-40875

Liquid filled adjustable optical analog of human eye for aligning, calibrating and systems testing of automatic IR optometers

22 p3888 A69-41231

OR-GATES

U GATES [CIRCUITS]

ORBIS CAL SATELLITE

ORBIS-CAL designed to achieve three axis orientation to local vertical and velocity vector in eccentric orbit by gravity gradient stabilization

07 p1226 A69-18323

ORBIT CALCULATION

Satellite trajectories calculated in form of parameters derived from processing measured functions, considering optimum mathematical description selection

01 p0151 A69-10570

Theory of generalized multistep methods, using off-grid point extended to special second order differential equation, applied to unperturbed orbit trajectory

01 p0153 A69-10808

Autonomous solution to orbital navigation problem yielding direct measure of orbital parameters

01 p0114 A69-11005

Smoothing and prediction of satellite orbit elements by stochastic approximation method, solving nonlinear equations system

01 p0158 A69-11319

Comet Schwassmann-Wachmann I orbit computation, using perturbations of all planets from Venus to Neptune

01 p0158 A69-11328

Jupiter outer satellites orbits determination with computer program based on modified Cowell/Moulton methods for adjusting initial conditions

01 p0158 A69-11330

Grobner formulas for numerical analysis of differential equations, discussing applications to orbit computations in celestial mechanics

02 p0322 A69-12250

Monograph on orbit computation of doubly photographed meteors employing method of least squares, giving computer programs and tables of data printout

02 p0324 A69-12495

Short period terms elimination for problem of motion of satellite with strong inclination and eccentricity, using von Zeipel method

03 p0514 A69-13783

Spacecraft trajectories computation from initial conditions by techniques involving construction of N body reference orbit

03 p0518 A69-14248

Preliminary orbit determination, based on data collected during single pass by sensor, permitting preliminary orbital elements and data variance estimation

03 p0518 A69-14249

Kepler third law application to radar determinations of astronomical unit of length in general relativity

04 p0657 A69-14698

Artificial lunar satellite orbital motion calculated by numerical integration, including solar and lunar electromagnetic radiation pressure effects

04 p0662 A69-15251

Asymptotic solutions of restricted three body problem for one parameter periodic orbits in earth-moon synodic system, determining motion near moon

04 p0663 A69-15382

Lunar Orbiter mission objectives and orbit design

[AIAA PAPER 68-47] 04 p0664 A69-15503

Velocity increments for orbital transfer in satellite rendezvous in central Newtonian gravitational field by two impulse ballistic transfer method

05 p0789 A69-16046

Approximate solution for determining satellite motion around axisymmetric planet

06 p1905 A69-17563

Stable stationary positions for spacecraft determined by formulating variational equations for perturbing effects of earth triaxiality

06 p1006 A69-17565

Mars imaging mission and astrodynamic interaction, discussing arrival geometry and orbit size effects

[AIAA PAPER 69-127] 06 p1011 A69-18169

Transfer orbits calculation between low and high satellite orbits, determining trajectories by method with minimum use of linearization

07 p1211 A69-18503

Manual onboard computation procedures and devices for determination of maneuvers for orbital navigation and guidance
08 p1348 A69-21184

Circular satellite orbit calculation from incomplete observations of one orbital pass
09 p1589 A69-21373

Orbits with small eccentricities and inclinations in generalized problem of two fixed centers, showing osculating elements relationship to intermediate orbit elements
10 p1779 A69-23613

Secular perturbations of remote satellites within lunar gravitation field, comparing observations and analytical data
10 p1779 A69-23614

Optimal interorbital transfers between closely spaced nearly circular noncoplanar orbits, taking into account active section length for low power thrusts
10 p1783 A69-23712

Optimal transfer between coplanar orbits in Newtonian force field without intersecting circle boundaries
10 p1790 A69-24191

Equation derivation to determine optimal parameters of spacecraft orbital elements, considering constraints imposed on measured quantities
10 p1791 A69-24192

Orbital parameters changes computation in table form for binary systems with more massive component mass decrease
11 p1962 A69-25120

Least squares iterative program, deriving orbits for O binaries HD 93403 and HD 135240
11 p1963 A69-25257

Improved spheroidal method for calculation of almost polar orbit of artificial satellites, bypassing right ascension
12 p2152 A69-25799

Adaptive filtering to prevent divergence observed in application of Kalman filter to orbit determination
12 p2045 A69-26059

Satellite celestial equator intersection time calculation from visual satellite observation near equator including satellite draconic period determination, particularly for high altitude
12 p2069 A69-26438

Cosmos 17 and 44 draconic periods of rotation, discussing period variations determination from visual observations
12 p2173 A69-26439

Soviet satellites rotation periods from processing of photometric observations
12 p2069 A69-26440

Anomalous satellite periods of rotation from successive observations at same topocentric parallel
12 p2158 A69-26441

Orbit determination from satellite using linear combinations of time of flight measurements and based on expansion of satellite law of motion
12 p2159 A69-26778

Gauss method for Kepler equation ephemeris computation in nearly parabolic orbits, using expansions suitable for high speed computers
12 p2171 A69-27154

Computer method for solution of Banachiewicz graph analytic equivalent for parabolic orbits determination, noting geocentric distances variation
13 p2336 A69-27448

Resonant long-period orbits around Lagrange equilateral points for critical mass ratio of main bodies
13 p2346 A69-27706

Photoelectric yellow and blue observations of variable V502 Ophiuchi, noting influence of partial eclipses on orbital determination reliability
13 p2348 A69-27809

Periodic Trojan orbits for resonance 1/12 in restricted three body problem, noting bridge of stable and unstable orbit lanes
13 p2350 A69-27824

Provisional elliptic orbit computed for asteroid Floirac using Gauss-Encke and least squares method, tabulating residuals and ephemeris
14 p2521 A69-29585

Secor 6 satellite /1966-51A/ orbital parameters determined from optical and radar observations noting use for upper atmosphere density and rotational speed studies
14 p2522 A69-29631

Plane planetary orbits construction extended to nearly circular and quasi-plane orbits by generalizing perturbations method to problems in space
15 p2690 A69-30622

Satellite trajectories calculated in form of parameters derived from processing measured functions, considering optimum mathematical description selection
15 p2691 A69-30740

Antenna, frequency converter and automatic spectrum recorder system for closest approach times prediction and satellite identification, discussing errors
15 p2569 A69-30800

Rapid orbit prediction method for planning satellite observation programs, considering oblateness and radiation pressure effects
15 p2697 A69-31310

Generalized Fourier analysis for satellite motion deviations from arbitrarily chosen reference orbit generated analytically or numerically, determining equations for potential coefficients
15 p2697 A69-31323

Satellite trajectory determination and expected errors for OGO 4 and Geos 1 orbits, noting geopotential, aerodynamic drag and integration contributions
15 p2698 A69-31331

Average angular velocity of upper atmosphere from changes in orbital inclinations of satellites, discussing wind speeds
15 p2600 A69-31352

Satellites trajectories under influence of earth oblateness and low radial thrust acceleration by nonlinear mechanics asymptotic method, discussing osculating orbits
16 p2856 A69-32009

Tabulation of basic solar system data and formulas concerning trajectory length, escape velocity, orbits, etc
16 p2856 A69-32074

Atmospheric density at 130-160 km measured from satellite 1968-59B orbit, noting agreement with CIRA 1965
16 p2776 A69-32095

Liapunov functions applications in motion stability theory problems, considering dynamic systems, periodic orbits, optimum damping and control
16 p2804 A69-32248

Mass of Jupiter system from motion of Doris, using variational equations for initial rectangular coordinates and velocities with respect to mass of Jupiter
16 p2863 A69-32403

Equatorial moderately elliptical satellite orbit perturbations calculated in local invariants, assuming state vector dependence of acceleration
17 p3039 A69-33796

Orbit determination for short and long period comets using equations of motion including terms for radial components of nongravitational force
18 p3195 A69-34432

Cowell equations modified for exact integration of pure Keplerian orbits, considering secular effects
18 p3165 A69-34842

Geocentric orbital elements determination of lunar particles expelled into space by meteorite impact, using spheres of influence method
18 p3202 A69-35330

Orbit computation by means of predictor-corrector algorithms based on nonpolynomial functions, including numerical results for two body elliptic motion
19 p3397 A69-35611

Modified Newton-Raphson methods for preliminary orbit determination, showing fast convergence and short computation times
19 p3397 A69-35613

Orbits computation by Picard successive approximations method, discussing iterative numerical perturbation techniques
19 p3398 A69-35615

Peano-Baker method for integration of variational equations to produce partial derivatives used in satellite trajectory estimation
19 p3398 A69-35616

Optimal fuel transfers between coplanar and non-coplanar coaxial elliptical orbits determined by Pontryagin maximum principle, using digital program for Hamiltonian equations solutions
19 p3399 A69-35670

Earth orbit estimation by manual stadiometer, space sextant and small data processor, discussing orbital parameter errors due to instrument and environment uncertainties
19 p3369 A69-35793

Orbit parameters identification method based on given tracking data span applied to lunar orbiter tracking using Fourier analysis
19 p3401 A69-35916

Continuously powered deep space vehicle orbit determination, discussing state estimation accuracy and use of continuous data filtering
19 p3402 A69-35939

[AAS PAPER 68-144]

Impulsive orbit transfer optimization using accelerated gradient program based on Newtonian algorithm for digital computer method
19 p3402 A69-35956

Geometric determination of visual binary orbits, noting inadequacy of graphical method based on apparent orbit ellipse properties
19 p3403 A69-35968

Comet observations and orbit determinations, noting eccentricity of comet Thomas
19 p3403 A69-35970

Meteorite orbits analysis with emphasis on recovered meteorites, noting fireballs and hyperbolic orbits
19 p3414 A69-36115

Meteorite orbits and radiants calculated, noting asteroidal belt origin
19 p3414 A69-36116

Modified Monte Carlo model applied to computerized meteorite orbit evolution, simulating secular perturbations by imposing sinusoidal variation on orbital elements
19 p3414 A69-36117

Chondritic meteorites initial orbits evolution to earth impact calculated by Monte Carlo method, considering relationships to meteorite sources
19 p3415 A69-36118

Photographic networks for meteors orbits and trajectories and meteorites impact points during nighttime, discussing fireball occurrence
19 p3415 A69-36120

Periodic orbits in nonlinear dynamical system constructed with iterative method based on modification of generalized Newton-Raphson technique
20 p3595 A69-37171

Jupiter tenth satellite reobserved, discussing calculations and computer techniques for determining orbit
20 p3595 A69-37194

Orbital rendezvous calculation in terms of adjoint variables vector associated with vehicle velocity vector
20 p3595 A69-37202

Stationkeeping motion effect on synchronous satellite orbit determination accuracy analyzed by two dimensional model, finding position uncertainty
20 p3595 A69-37218

Minor planets osculating elements computer calculated and tabulated
20 p3596 A69-37309

Definitive orbit of comet 1943 I determined from photographic and visual observations
20 p3596 A69-37310

Initial and future orbits of comet 1959 IV Alcock determined considering Venus, Jupiter, Saturn, Uranus and Neptune perturbations, noting elliptical to hyperbolic orbit transition
20 p3597 A69-37319

Visual binary star ADS 12447 orbit elements calculated using Zwiers method
20 p3598 A69-37466

Hansen method applied to Jupiter tenth satellite orbit correction and perturbations, describing computer program and formulas used
20 p3602 A69-37529

Velocity increments for orbital transfer in satellite rendezvous in central Newtonian gravitational field by two impulse ballistic transfer method
20 p3574 A69-37955

Satellite orbit determination method allowing geogravitational field determination and correction of station coordinates
21 p3793 A69-38337

Satellite tracking and orbit determination accuracy for system of two synchronous geostationary satellites
21 p3674 A69-39019

Two dimensional gravity assisted trajectories for solar probe missions in ecliptic plane, discussing Venus and Jupiter assist missions
21 p3804 A69-39022

Periodic orbits for interplanetary flight, using patched conic analysis for determining inclined elliptic free fall trajectory shuttling between earth and Venus
21 p3804 A69-39203

Near equatorial near synchronous satellite orbits determined by supplementing spherical harmonics representation of earth gravitational field with polynomial force model representation
21 p3806 A69-39234

Mathematical model for determining thrust interplanetary spacecraft orbit, considering time history of position, velocity and thrust acceleration
21 p3806 A69-39335

Encke type analytical-numerical integration for solving differential equations of modified set of Lagrange planetary equations, obtaining satellite ephemeris for orbit prediction
21 p3807 A69-39340

[AIAA PAPER 69-908]

Satellite orbit determination errors attributed to Gaussian noise effect on tracking measurements, assuming known Gaussian probability error distribution [AIAA PAPER 69-911] 21 p3807 A69-39343

Parking orbit optimal orientation for minimal impulsive maneuvers total velocity increment in three dimensional capture-escape mission [AIAA PAPER 69-918] 21 p3808 A69-39347

Satellite orbits calculation in nonrotating atmospheres, considering atmospheric drag and zonal harmonics coupled effects [AIAA PAPER 69-925] 21 p3808 A69-39352

Computer program for eccentric geocentric satellite orbits evolution, discussing atmospheric drag, earth oblateness and solilunar effects [AIAA PAPER 69-928] 21 p3808 A69-39357

Interplanetary periodic orbits and flyby dates for multiple Earth-Venus swingby missions, describing various iterative solutions for trajectory [AIAA PAPER 69-931] 21 p3809 A69-39359

Impulsive velocity correction determination method for precise stationkeeping of stationary satellite, discussing perturbations [AIAA PAPER 68-456] 21 p3817 A69-39757

Dynamical analysis of Bernard star motion, yielding companions in co-revolving, approximately coplanar, circular orbits 22 p4013 A69-40119

Eta Cassiopeiae orbit analysis with emphasis on multiple exposure photographic observations, noting companion mass 22 p4013 A69-40120

Real time orbit determination system at NASA manned space center for Apollo missions [AIAA PAPER 69-938] 22 p4020 A69-40321

Algorithms for close earth satellite orbit calculation developed by numerical integration methods, discussing solution efficiency [AIAA PAPER 69-948] 22 p4021 A69-40331

Neglected gravity coefficients influence on computed satellite orbits and geodetic parameters 22 p4023 A69-40556

Periodic orbits obtained for special restricted three body problem in resonance using numerical integration 22 p4031 A69-40909

Light pressure induced secular effect contributing to planetary satellites and lunar orbits evolution calculated by numerical integration 22 p4033 A69-41084

Errors in determining controlled satellite rotation periods, proposing scheme for corrected trajectory calculation of small eccentricity orbits 22 p4033 A69-41086

Satellite motion initial phase vector estimation for calculating satellite motion from selection of complete or increasing volume of measurements 22 p4033 A69-41088

Spectral and orbital evidence of connection among fireballs with orbit inclination, comets and carbonaceous meteorites 23 p4208 A69-41285

Spatial region accessible to earth launched probes determined for mission planning for exploration of aperiodic comets, discussing orbit parameters 23 p4212 A69-41536

Adaptive filtering to prevent divergence observed in application of Kalman filter to orbit determination 23 p4146 A69-42446

Optimal hinged two body satellite configurations in circular and elliptical orbits, discussing need for adaptive attitude control for transient and steady state operation 24 p4393 A69-43247

Planetary gravitational fields and artificial satellite orbits determined by using earth based range rate measurements 24 p4388 A69-43650

ORBIT DECAY

Cosmos 253 rocket reentry and fragmentation over England 05 p0830 A69-16656

Orbital parameters changes computation in table form for binary systems with more massive component mass decrease 11 p1962 A69-25120

Atmospheric density measurements by triaxial accelerometer system, ionization gauges and orbital decay of OV1-15 satellite 15 p2602 A69-31384

Air density height distribution determined from satellite orbit decay analysis, noting semiannual density variations 22 p3935 A69-39971

Lifetime of artificial satellites by approximate integration method with application to Explorer 1, comparing analytical prediction 22 p4036 A69-39973

Nonlinear longitudinal dynamics of lifting orbital vehicle in near circular orbit, considering translational motion components effecting orbital decay or dilatation [AAS PAPER 69-244] 24 p4392 A69-42857

ORBIT EQUATIONS

U ORBITAL MECHANICS

ORBIT PERTURBATION

NT SATELLITE PERTURBATION

Secular perturbations produced by comet belt beyond Neptune on orbits of periodic comets of large aphelion 01 p0158 A69-11327

Comet Schwassmann-Wachmann I orbit computation, using perturbations of all planets from Venus to Neptune 01 p0158 A69-11328

Jupiter outer satellites orbits determination with computer program based on modified Cowell/Moulton methods for adjusting initial conditions 01 p0158 A69-11330

Pluto mass from observations of perturbation on motion of Neptune 02 p0315 A69-11808

Stability of elliptical Venus orbits with solar gravitational perturbations, using equation accuracy and influence on mission planning 02 p0331 A69-12819

Geopotential resonant orbital perturbations of existing satellites, noting high inclination role 03 p0521 A69-13777

Project Icarus for reduction of threat of asteroid collision with earth by deflection or disintegration, noting guidance, control and communications for rocket 04 p0652 A69-14564

Orbit corrections for lost minor planets 457, 1038, 1161, 1297, determining new ephemerides for oppositions 05 p0829 A69-16704

Stable stationary positions for spacecraft determined by formulating variational equations for perturbing effects of earth triaxiality 06 p1006 A69-17565

Suboptimal guidance corrections for continuous thrust vehicle disturbances during minimum fuel rendezvous in Martian orbit, discussing physical and modified cost functional [AIAA PAPER 69-76] 06 p0956 A69-18081

Stellar galactic orbit perturbation by irregularities in distribution of gas cloud for motion inclined to galactic plane 07 p1223 A69-19634

Air density at 470 km from orbit of satellite 1966-118 A, confirming large semiannual variation 09 p1488 A69-21659

Upper atmosphere rotation perturbation effect on satellite orbit when scale height varies with height, showing inclination reduction 09 p1594 A69-21660

Motion of satellite of very oblate planet, investigating axisymmetric potential 10 p1774 A69-22969

Earth gravitational field effect on satellite orbits, noting elliptical motion in central force field, energy criteria and rotational ratios 10 p1776 A69-23295

Perturbing body influence on motion near triangular Lagrangian solutions of restricted elliptical three body problem applied to earth-moon system under solar perturbations 10 p1779 A69-23612

Deimos and Phobos mutual secular perturbations from calculated masses and orbital elements, using canonical systems of equations 10 p1780 A69-23615

Circumpolar satellite orbits under lunar and solar perturbations based on two fixed centers problem, considering large amplitude disturbances 10 p1780 A69-23616

Intermediate orbits to construct motion theory of natural satellites of all planets 11 p1952 A69-24253

Natural terrestrial satellites existence suggested by telescopic and photographic observations and artificial satellites orbital perturbations 13 p2344 A69-27642

Solar and lunar effects on motions of polar orbiting satellites, discussing variable intermediate orbits 14 p2521 A69-29460

Zonal harmonics of Legendre polynomial series of Jupiter attractive force function effects on motion of fifth satellite 14 p2521 A69-29463

First order secular and aperiodic perturbations in Keplerian orbital elements of synchronous satellite due to earth gravitational field eccentricity 14 p2521 A69-29466

Earth reflected radiation pressure and perturbing effect on satellites 15 p2599 A69-31324

Geopotential represented in ellipsoidal harmonics, discussing Lamé functions generation and rectangular-ellipsoidal coordinates relation and orbital elements perturbations 15 p2599 A69-31333

Earth figure parameters from satellite orbit dynamics, including potential on geoidal surface and scale factor for lengths 15 p2602 A69-31387

Satellite orbit evolution data applied to refinement of geophysical parameters, including upper atmosphere parameters and zonal harmonic coefficients in gravitational potential expansion 15 p2604 A69-31417

Satellite orbital resonances due to geopotential analyzed by asymptotic expansion for nearly circular or equatorial orbits 16 p2863 A69-32401

Relativistic effect in pericenter motion of comets and natural satellites from major semiaxes and eccentricities of natural bodies 17 p3044 A69-34174

Perturbations of planet motion in planetary coordinates, noting unperturbed motion 18 p3199 A69-34912

Polar flattening influence of Jupiter on artificial satellite motion around Callisto noting orbital perturbations 18 p3199 A69-34913

Satellite motion perturbations in vicinity of critical inclination, using Encke method of numerical integration 19 p3397 A69-35607

Orbits computation by Picard successive approximations method, discussing iterative numerical perturbation techniques 19 p3398 A69-35615

Stability of motions about triangular libration points in elliptic restricted three body problem [AAS PAPER 68-090] 20 p3595 A69-37175

Minor planets osculating elements computer calculated and tabulated 20 p3596 A69-37309

Comet Arend-Roland 1957 III orbit elements computer calculated and tabulated from worldwide observations, taking into account orbital perturbations caused by major planets 20 p3596 A69-37311

Initial and future orbits of comet 1959 IV Alcock determined considering Venus, Jupiter, Saturn, Uranus and Neptune perturbations, noting elliptical to hyperbolic orbit transition 20 p3597 A69-37319

Optimal transfers in central gravitational field, using formulas for perturbations of osculating Keplerian orbital elements, applied to singular reticent solutions [ONERA-TP-729] 20 p3604 A69-37752

Satellite position perturbation due to earth oblateness using Hansen method [AIAA PAPER 69-909] 21 p3807 A69-39341

Practical stability of highly eccentric orbits quasi-normal to ecliptic, discussing parameters influence on orbital lifetime with reference to approximate stability criteria [AIAA PAPER 69-926] 21 p3808 A69-39355

Perturbative effects of Jupiter moons on spacecraft flyby and postencounter heliocentric trajectories, noting precision targeting [AIAA PAPER 69-932] 21 p3809 A69-39361

Impulsive velocity correction determination method for precise stationkeeping of stationary satellite, discussing perturbations [AIAA PAPER 68-456] 21 p3817 A69-39757

Jupiter mass determined from observations of four minor planets perturbations 22 p4013 A69-40121

Galilean satellites perturbing effect on motion of fifth Jupiter satellite 23 p4214 A69-41730

ORBITAL ASSEMBLY

Expandable D 21 airlock scheduled for testing on NASA Orbital Workshop Flight based on elastic

materials technique, noting more complex chemically rigidized concept
[IAF PAPER SD-49] 02 p0334 A69-11949

Multiple impulse orbital departure window for manned interplanetary spacecraft, discussing launch delay, space assembly, refueling and checkout, etc
[AIAA PAPER 69-126] 06 p1010 A69-18065

Soviet space stations design based on orbital docking techniques for unrestricted mass size and number of modules, describing wheel shaped station
19 p3431 A69-36465

ORBITAL ELEMENTS

Equations of motion of satellite in rotating coordinate system, noting effects of precession and nutation on transformation of orbital elements
01 p0150 A69-10445

Smoothing and prediction of satellite orbit elements by stochastic approximation method, solving nonlinear equations system
01 p0158 A69-11319

Preliminary orbit determination, based on data collected during single pass by sensor, permitting preliminary orbital elements and data variance estimation
03 p0518 A69-14249

Diffuse meteor stream separation from sporadic background, using orbital elements of individual meteors
04 p0659 A69-15034

Comet Arend-Roland orbit, deducing interstellar origin from nongravitational orbital energy increase
04 p0660 A69-15036

Nongravitational impulses on short period comets
04 p0660 A69-15037

Braking and acceleration speeds and maximum magnitude during transfer from circular orbit having earth center as focus to elliptical orbit within circular orbit
06 p1007 A69-17578

Minimum fuel control of spacecraft orbital elements for transfers between elliptical orbits by low variable thrust propulsion, noting interplanetary trajectory optimization
06 p0955 A69-17579

Commensurability among pairs of mean motions of natural satellites of major planets and hypothesis of tidal evolution of satellite systems
07 p1223 A69-19638

Commensurability among pairs of mean motions of satellites of major planets and power law relation for orbital periods of satellites
07 p1224 A69-19639

Orbital elements of visual double star and O-C residuals, noting dynamical parallax and ephemerides
08 p1393 A69-20568

Nonisotropic mass ejection from components of close binary system effects on orbital elements for small initial eccentricity case
08 p1395 A69-20634

Canonical equations of planet satellite intermediate orbits using harmonics of gravitational potential
09 p1589 A69-21374

Dimensions of 19 variable eclipsing binaries from published photometric and spectral orbital elements
09 p1590 A69-21378

Catalog of orbital elements for periodic comets during perihelion passage
10 p1777 A69-23396

Orbits with small eccentricities and inclinations in generalized problem of two fixed centers, showing osculating elements relationship to intermediate orbit elements
10 p1779 A69-23613

Deimos and Phobos mutual secular perturbations from calculated masses and orbital elements, using canonical systems of equations
10 p1780 A69-23615

Equation derivation to determine optimal parameters of spacecraft orbital elements, considering constraints imposed on measured quantities
10 p1791 A69-24192

Processing of data obtained in continuous tracking of space objects using computer algorithms
10 p1791 A69-24193

Elliptic integrals to determine orbital elements time dependence in three body problem, estimating satellite lifetime
10 p1791 A69-24196

Dynamical effects of mass exchange in close binary systems ejection modes from point of view of orbital elements evolution
11 p1962 A69-25113

Triple system p Velorum, discussing coude spectra and published visual orbital elements
11 p1963 A69-25263

Micrometric and photometric measurements of coude spectra of magnetic variable HD 125248, showing spectroscopic binary nature and computing orbital elements
11 p1963 A69-25264

Computer method for solution of Banachiewicz graph analytic equivalent for parabolic orbits determination, noting geocentric distances variation
13 p2336 A69-27448

Algorithm for solving autonomous artificial satellite orbital elements by using successive approximations
13 p2296 A69-27687

Photoelectric yellow and blue observations of variable TZ bootis light variation and orbital elements, noting maxima and secondary minimum causes
13 p2348 A69-27808

Lacerta OB 1 B spectroscopic binaries periods and orbital elements, noting limits for secular variation
14 p2519 A69-29137

Secor 6 satellite /1966-51A/ orbital parameters determined from optical and radar observations noting use for upper atmosphere density and rotational speed studies
14 p2522 A69-29631

Nongravitational force dynamic effect and model for rotating cometary nucleus, including changes in orbital elements
14 p2524 A69-29713

Cometary tails maximum lengths compared with orbit parameters and absolute magnitudes, proposing classification scheme
15 p2689 A69-30566

Mimas-Tethys commensurability of motions and inclinations, calculating libration amplitude variation by numerical integration
16 p2861 A69-32241

Meteoritic matter distribution by calculating orbital elements of 12,500 meteors from radar data, using diversity reception for radio waves scattered at meteor trails
17 p3041 A69-33894

Distributions of close planet-comet encounters for various orbital elements, calculating trajectory by conic matching
18 p3195 A69-34433

Canonical equations of planet satellite intermediate orbits using harmonics of gravitational potential
18 p3198 A69-34762

Dimensions of 19 variable eclipsing binaries from published photometric and spectral orbital elements
18 p3198 A69-34766

Geocentric orbital elements determination of lunar particles expelled into space by meteorite impact, using spheres of influence method
18 p3202 A69-35330

Orbit parameters identification method based on given tracking data span applied to lunar orbiter tracking using Fourier analysis
19 p3401 A69-35916

Geometric determination of visual binary orbits, noting inadequacy of graphical method based on apparent orbit ellipse properties
19 p3403 A69-35968

Ar 39 content in chondrites interpreted for meteorite size, exposure age and orbital elements
19 p3411 A69-36101

Interplanetary dust sources investigation based on physical and orbital parameters, noting derivation from asteroids and meteorites
19 p3415 A69-36119

Network for fireball trajectories rapid analysis to recover meteorites and obtain orbital elements data, noting role of planetariums
19 p3295 A69-36121

Balloon satellite orbital time and eccentricity correlated, investigating earth shadow and solar radiation effects
19 p3427 A69-36628

Minor planets osculating elements computer calculated and tabulated
20 p3596 A69-37309

Comet Arend-Roland 1957 III orbit elements computer calculated and tabulated from worldwide observations, taking into account orbital perturbations caused by major planets
20 p3596 A69-37311

Visual binary star ADS 12447 orbit elements calculated using Zwiers method
20 p3598 A69-37466

Orbital elements of visual binaries Don 91 and ADS 9756 derived graphically, tabulating observations with ephemerides
20 p3600 A69-37480

Optimal transfers in central gravitational field, using formulas for perturbations of osculating Keplerian orbital elements, applied to singular reticent solutions
[ONERA-TP-729] 20 p3604 A69-37752

Spectroscopic orbital elements of eclipsing binary IZ Per determined from 22 spectra using Wilsing and Russell method
21 p3795 A69-38469

Orbital parameters of short-lived low altitude earth satellites assuming no atmospheric drag, no orbital precession and flat earth condition
21 p3798 A69-38626

Earth resources technology satellite /ERTS/ choice regarding local time of ascending node based on cloud cover and IR measurement considerations
21 p3798 A69-38628

Recurrence formulas for calculating Fourier expansions in elliptic motion in terms of eccentric and mean anomaly
[AIAA PAPER 69-910] 21 p3807 A69-39342

Satellite motion orbital elements dependence on large short impulse arbitrarily directed in space, analyzing optimal orbits transfer and thrust control
21 p3818 A69-39821

Satellite motion initial phase vector estimation for calculating satellite motion from selection of complete or increasing volume of measurements
22 p4033 A69-41088

Cometary and asteroidal orbital differences and similarities, emphasizing limiting cases to study orbital evolution of meteors
23 p4208 A69-41284

ORBITAL LAUNCHING

Multiple impulse orbital departure window for manned interplanetary spacecraft, discussing launch delay, space assembly, refueling and checkout, etc
[AIAA PAPER 69-126] 06 p1010 A69-18065

Nuclear solid core rocket engine performance for interplanetary orbital launch of spacecraft by multiorbit injection
[AIAA PAPER 69-535] 16 p2810 A69-32660

ELDO/PAS rocket motor for satellite launching from elliptic orbit apogee to synchronous orbit powered by ammonium perchlorate with organic binder and Al
17 p3022 A69-33604

ORBITAL MECHANICS

NT KEPLER LAWS

Bifurcation of closed orbits from equilibrium points of autonomous differential system
02 p0281 A69-12133

Monograph on orbit computation of doubly photographed meteors employing method of least squares, giving computer programs and tables of data printout
02 p0324 A69-12495

Saturn ring gravitational field perturbations of space vehicle orbit on flyby mission solved by particle motion perturbation theory
03 p0508 A69-13260

Hansen planetary theory basic function, discussing perturbations expansion into trigonometric series
03 p0514 A69-13781

Interplanetary orbits for probe launched from earth to reencounter earth, noting relationship to three body problem
03 p0514 A69-13782

Spacecraft orbital maneuvers by means of low thrust, discussing optimization and several orbital transfer examples
03 p0522 A69-14086

Equilibrium orientations of orbiting gyrostats, giving spectrum of solutions for bodies of varied shape and internal rotor angular momentum
03 p0522 A69-14246

Spacecraft trajectories computation from initial conditions by techniques involving construction of N body reference orbit
03 p0518 A69-14248

Preliminary orbit determination, based on data collected during single pass by sensor, permitting preliminary orbital elements and data variance estimation
03 p0518 A69-14249

Lambert problem of fitting conic to two position vectors with specified time interval solved numerically by Newton-Raphson iteration
03 p0518 A69-14250

Manifold of periodic orbits, developing methods to analyze and classify families of periodic orbits in conservative dynamical system with two degrees of freedom
04 p0653 A69-14611

Space flight launches, interplanetary transfer orbits, flyby orbits and capture orbits for solar probe with 0.3 AU perihelion and Jupiter satellite probe
04 p0657 A69-14826

Idealized point mass motion in axisymmetric gravitational field, discussing orbital stability about oblate planet

04 p0658 A69-14887

Hill surfaces in triangular restricted four body problem, deriving equation of surface of zero relative velocity

04 p0660 A69-15038

Optimum spacing of communication satellites on inclined circular synchronous orbits, applying figure 8 packing schemes

04 p0562 A69-15458

Orbital trajectories about Mars or Venus, considering reentry to earth, planet perturbation effect, total mission time and orbital distance from planet

05 p0823 A69-16042

Capture and control in conservative dynamical systems, analyzing orbital mechanics of derelict and pursuit spaceships

05 p0826 A69-16462

Orbit corrections for lost minor planets 457, 1038, 1161, 1297, determining new ephemerides for oppositions

05 p0829 A69-16704

Sun-orbit plane relationship effects on mission planning [AIAA PAPER 69-129]

06 p1011 A69-18093

Transfer orbits calculation between low and high satellite orbits, determining trajectories by method with minimum use of linearization

07 p1211 A69-18503

Analytic autonomous Hamiltonian differential equations with two degrees of freedom admitting unstable equilibrium point

07 p1215 A69-18732

Resonant long period orbits around Lagrange equilateral points, discussing formal expansions method for three body problem

07 p1225 A69-19719

Stellar orbits in galactic plane represented as generalized Keplerian motion

08 p1381 A69-19792

Numerical analysis of periodic solutions of restricted three body problem in sun-Jupiter system, noting genealogy of periodic orbits

08 p1382 A69-19874

Perturbation method in rectangular coordinates based on motions of Galilean satellites of Jupiter applied to nearly circular orbits of quasi-resonant systems

08 p1390 A69-20275

Five families of simple periodic symmetrical orbits in Hill limiting case of restricted three body problem, studying asymptotic forms

08 p1393 A69-20572

Nonisotropic mass ejection from components of close binary system effects on orbital elements for small initial eccentricity case

08 p1395 A69-20634

Canonical equations of planet satellite intermediate orbits using harmonics of gravitational potential

09 p1389 A69-21374

Periodic motion of satellite with magnetic damper along circular orbit, assuming small value of damping coefficient

09 p1609 A69-21761

Resonance relations of rotational and orbital frequencies of solar system planets and satellites estimated for statistical significance

10 p1771 A69-22852

Motion of satellite of very oblate planet, investigating axisymmetric potential

10 p1774 A69-22969

Orbits of asteroids surrounding commensurabilities with Jupiter, discussing theory for origin of Kirkwood gaps

10 p1778 A69-23604

Motion problem of heavy solid body about fixed point

11 p1918 A69-24785

Spacecraft orbit control laws determined by studying influence of controlling acceleration in plane perpendicular to absolute velocity vector

11 p1965 A69-25743

Ideal resonance problem with single critical term for case of libration solved by modified Poincare method, considering 24-hr satellite

12 p2152 A69-25800

Draconic period changes of satellite 1965-11-D /Cosmos 54 rocket/ during visual observations with Interobs

12 p2174 A69-26444

Draconic periods changes of satellites 1963 53A and 1964 76A, based on observations

12 p2174 A69-26446

Gauss method for Kepler equation ephemeris computation in nearly parabolic orbits, using expansions suitable for high speed computers

12 p2171 A69-27154

Photoelectric observations of blue light minima of U Geminorum variable Ex Hydrae indicating no change in orbital period

13 p2338 A69-27558

Optimum orbital transfer of material point subjected to reactive force with minimum mass loss, discussing Kepler motion kinematics

13 p2346 A69-27698

Restricted three body problem of conservative Hamiltonian systems with two degrees of freedom and mass ratio parameter, considering phase space around L sub 4

13 p2346 A69-27711

Comet Arend-Roland type-1 tail characteristics in cluding accelerating disturbance, outward-moving waves, tail inclination, etc

13 p2349 A69-27816

Orbital elements evolution of binary or planetary system with decreasing mass by nonlinear nonautonomous differential equations

14 p2519 A69-29138

Solar and lunar effects on motions of polar orbiting satellites, discussing variable intermediate orbits

14 p2521 A69-29460

Eclipsing close binary stars orbital planes spatial position determined from stellar emission polarization

15 p2688 A69-30560

Plane planetary orbits construction extended to nearly circular and quasi-plane orbits by generalizing perturbations method to problems in space

15 p2690 A69-30622

Photographically observed meteor orbits 1937-1963, noting overestimation of hyperbolic orbits due to observation errors

15 p2697 A69-31253

Stability of steady circular motions in systems with hidden variables analyzed by using Lejeune-Dirichlet theorem

16 p2804 A69-31621

Conditional trajectory stability associated with first integral compared with orbital stability on base of topological method

16 p2853 A69-31622

Periodic solutions of variational equations near equilateral equilibria, obtaining one parameter expansion of family of long period orbits

16 p2854 A69-31654

Hill method for satellite motion with reference to rectangular rotating axes system with origin at moon center of gravity, obtaining intermediate orbits

16 p2855 A69-31656

Cassini laws applied to moon and Mercury, determining relations between moment differences for spin vector, orbital angular-momentum vector and precessional velocity

16 p2861 A69-32239

Gravitational and magnetic torque effect on rotational motion of triaxial rigid body in regressing orbit about oblate primary mass

16 p2861 A69-32240

Hansen method of partial anomalies for cometary orbits applied to comet Encke perturbed by earth and compared with perturbations by numerical integration

16 p2863 A69-32400

Long range perturbations of satellites and asteroids with arbitrary inclination and eccentricity, illustrating motion around moon, oblate and spherical planets using energy integral

17 p3031 A69-33098

Canonical equations of planet satellite intermediate orbits using harmonics of gravitational potential

18 p3198 A69-34762

Satellite motion perturbations in vicinity of critical inclination, using Encke method of numerical integration

19 p3397 A69-35607

Optimal transfers between Keplerian orbits for time free case, considering hyperbolas, ellipses external to and intersecting attracting planet

19 p3399 A69-35669

Optimal impulse rendezvous of long duration between quasi-circular, coplanar or noncoplanar close orbits

19 p3400 A69-35674

Short term motion of lunar satellite, discussing third body disturbing functions and perturbation solution of nonsingular orbit elements

19 p3402 A69-35934

Orbital trajectories about Mars or Venus, considering reentry to earth, planet perturbation effect, total mission time and orbital distance from planet

20 p3606 A69-37951

Periodic orbits of Poincare and Schwarzschild types in motion of artificial satellite in disturbed gravitational field of axisymmetric oblate spheroid

21 p3795 A69-38441

Spectroscopic orbital elements of eclipsing binary IZ Per determined from 22 spectra using Wilsing and Russell method

21 p3795 A69-38469

Orbital parameters of short-lived low altitude earth satellites assuming no atmospheric drag, no orbital precession and flat earth condition

21 p3798 A69-38626

Spacecraft and boosters for earth resources surveys, discussing design, payloads, orbits, etc

21 p3799 A69-38629

Exploration capabilities provided by Jupiter gravity assisted trajectories compared to direct ballistic flight trajectories [AAS PAPER 68-116]

21 p3805 A69-39224

Encke type analytical-numerical integration for solving differential equations of modified set of Lagrange planetary equations, obtaining satellite ephemeris for orbit prediction [AIAA PAPER 69-908]

21 p3807 A69-39340

Orbital mechanics of near earth satellite arrangements /clusters/ for satellite service vehicle /SSV/ accessibility from orbital space stations [AIAA PAPER 69-929]

21 p3809 A69-39358

Kinematic and dynamic relations analyzed by vector method for motion time and orbital flight control of point

21 p3818 A69-39820

Spherical motion of solid body about fixed point with nonholonomic coupling, deriving equations for centrifugal moments of inertia effects on motion

21 p3773 A69-39840

Satellites resonant perturbations analysis, deriving mean mean motion formulas

22 p4035 A69-39968

Symmetric periodic orbits families of restricted three body problem, using two body problem

22 p4031 A69-40908

Minimum impulse time free transfer between neighboring noncoplanar almost circular orbits with line of nodes along common latus rectum [AIAA PAPER 68-94]

23 p4215 A69-41879

Sun-orbit plane relationship effects on mission planning [AIAA PAPER 69-164]

24 p4386 A69-43261

ORBITAL MOTION

U ORBITS

ORBITAL RENDEZVOUS

Handheld optical range finder for manned spacecraft orbital rendezvous, discussing target shapes and range errors

02 p0250 A69-12366

Rendezvous maneuvers for vehicle and elliptically orbiting targets, formulating relative motion of two bodies

04 p0658 A69-14828

Minimum fuel rendezvous maneuver for two space vehicles in circular orbit, considering propelled tracking equipment nonlinear equations of motion

05 p0823 A69-16036

Velocity increments for orbital transfer in satellite rendezvous in central Newtonian gravitational field by two impulse ballistic transfer method

05 p0789 A69-16046

Nonlinear equations of motion for rendezvous in circular orbits, pursuer using minimum fuel and pursued having no propulsion

06 p1014 A69-17571

Rendezvous maneuvers for fixed elliptical target orbit, discussing numerical solution of problem and suitability of various points of target ellipse for rendezvous

09 p1538 A69-21649

Optimal rendezvous between satellite and spacecraft, determining power and time optimal coplanar rendezvous in circular orbit

09 p1538 A69-21759

Optimum thrust control of satellite along given trajectory to rendezvous at zero velocity with orbited satellite

13 p2356 A69-27684

Optimal rendezvous maneuver of pursuing vehicle with minimum fuel expenditure in approach stage on elliptic and hyperbolic orbits

15 p2701 A69-31548

Rendezvous maneuver with minimum fuel in circular orbit solved without restrictive conditions for accelerations due to approach thrust
16 p2852 A69-31558

Minimum fuel multiple impulse orbital rendezvous for fixed transfer time near circular orbits
16 p2857 A69-32161

Optimal impulse rendezvous of long duration between quasi-circular, coplanar or noncoplanar close orbits
19 p3400 A69-35674

Trajectory optimization of space vehicle with continuous thrust based on regularized equations, comparing perturbation method for earth-Jupiter rendezvous transfer
[AAS PAPER 68-099] 20 p3595 A69-37173

Orbital rendezvous calculation in terms of adjoint variables vector associated with vehicle velocity vector
20 p3595 A69-37202

Velocity increments for orbital transfer in satellite rendezvous in central Newtonian gravitational field by two impulse ballistic transfer method
20 p3574 A69-37955

Rendezvous control law for spacecraft moving in central gravitational field along trajectory representing target vehicle Keplerian orbit
22 p4036 A69-40115

Optimal minimum fuel rendezvous maneuver variational problem, generalizing circular orbit results to conical orbits
22 p4028 A69-40754

ORBITAL SIMULATORS

U SPACE SIMULATORS

ORBITAL SPACE STATIONS

Future space programs as governed by cost limitations, suggesting development of economical launch vehicle for shuttling between earth and orbital space stations
02 p0326 A69-12680

Soviet space program /1969/ objectives, Soyuz vehicle and future missions
06 p1002 A69-17265

Orbital station projects, concepts and future uses
06 p1013 A69-17266

Commercial orbital space stations economics and potential markets, considering fisheries, ocean transportation, air traffic control, resources surveys, pollution reduction, etc
06 p1007 A69-17599

Engineering designs and hardware required for low risk flight of long duration manned space stations
06 p1007 A69-17601

Manned orbital space stations design, purposes and applications, balancing costs against benefits
06 p1019 A69-18237

Apollo telescope mount /ATM/ for solar experiments conducted from manned earth orbiting laboratory
10 p1791 A69-22871

Manned space stations for future space exploration, discussing earth-like environment, artificial gravity, human factors and time dependence
11 p1965 A69-25644

Orbital astronomy support facility research requirements analysis, discussing objectives and measurement needs, instrumentation, spacecraft and facilities, etc
18 p3206 A69-34369

Attitude control system for Apollo Telescope Mount, discussing selection features based on manned orbital space platform requirements
18 p3168 A69-34683

Space manufacturing operations program, discussing zero gravity effect during earth orbit flight, Apollo Applications Program Orbital Workshop Flight 2, etc
18 p3208 A69-35067

Materials and products fluid state processing in space, discussing g, zero-g and induced forces effect on fluid matter and process, cost and operational effectiveness
19 p3324 A69-35588

Navigation, guidance and control developments for manned space missions, discussing earth orbital exploration bases
19 p3369 A69-35801

Earth-orbiting manned space station as single facility base for power, volume, logistics, experimental equipment and data communications
19 p3431 A69-36464

Soviet space stations design based on orbital docking techniques for unrestricted mass size and number of modules, describing wheel shaped station
19 p3431 A69-36465

Radiation exposure during orbital flight assessed for adverse effect on space stations and laboratories personnel, discussing shielding and dose rate tables
20 p3481 A69-37339

Motion and stability of rotating connected two body space station satellite system, developing Lagrangian equations of motion and optimizing damping system parameters
[AIAA PAPER 69-919] 21 p3820 A69-39349

Orbital mechanics of near earth satellite arrangements /clusters/ for satellite service vehicle /SSV/ accessibility from orbital space stations
[AIAA PAPER 69-929] 21 p3809 A69-39358

Mass expulsion and momentum systems for orbiting space station attitude control optimized, considering reaction jet and control moment gyro systems
[AIAA PAPER 69-846] 21 p3822 A69-39376

Manned transport into orbit and manned orbital operations systems, considering systems selection factors and mission and cost influences
21 p3857 A69-39696

Apollo 11 mission and future space exploration prospects including moon base, manned space station, reusable shuttle vehicles, etc
23 p4211 A69-41477

Solar cell power systems for manned space stations, summarizing studies of battery power system designs
23 p4068 A69-42242

Nuclear reactor/thermoelectric power system design for manned orbiting space station, discussing station integration and operation
23 p4187 A69-42256

Pu-238 isotope organic Rankine cycle system analyzed for one year manned space station, using modified H-521 Space Power computer program
23 p4188 A69-42264

Radioisotope thermal energy /RITE/ source for integrated life support systems for two man 180 day space station mission, determining optimum material selection and design details
23 p4189 A69-42268

NASA programs for space stations and base development, discussing housing and equipment capacity, manned and unmanned stations and shuttlecraft for interstation travel
23 p4224 A69-42456

Space experimental design based on manned vs unmanned spacecraft value for multipurpose low cost flexible space station in low earth orbit
23 p4223 A69-42457

Soviet space flights preliminary to formation of scientific space station
24 p4391 A69-42798

Apollo Applications Program /AAP/ spacecraft, describing contributions to space station engineering
[AAS PAPER 69-491] 24 p4392 A69-42838

ORBITAL TRANSFER

U TRANSFER ORBITS

ORBITAL VELOCITY

Icarus observation by Trepied-Metcalf method, tables show Icarus retreat and advance and velocities of eight asteroids neighboring earth
05 p0819 A69-15698

Linear multichannel spatial motion control systems for vehicles orbiting in earth atmosphere at supersonic velocities
21 p3766 A69-39645

ORBITAL WORKSHOPS

Materials processing in space, suggesting electronic single crystals preparation, materials melting and utilization of low g earth orbit environment
19 p3324 A69-35589

ORBITALS

U ELECTRON ORBITALS

U MOLECULAR ORBITALS

ORBITER PROJECT

NT LUNAR ORBITER

Crater Copernicus photograph, discussing misinterpretation of Orbiter 2 lunar surface photograph on basis of effective temperature contours analysis
01 p0154 A69-10898

NASA Lunar Orbiter Program of lunar photography from orbiting spacecraft
21 p3794 A69-38377

ORBITING ASTRONOMICAL OBSERVATORY

U OAO

ORBITING GEOPHYSICAL OBSERVATORY

U OGO

ORBITING SATELLITES

U ARTIFICIAL SATELLITES

ORBITING SOLAR OBSERVATORY

U OSO

ORBITS

NT CIRCULAR ORBITS

NT EARTH ORBITS

NT ECCENTRIC ORBITS

NT ELLIPTICAL ORBITS

NT EQUATORIAL ORBITS

NT INTERPLANETARY TRANSFER ORBITS

NT LUNAR ORBITS

NT PARKING ORBITS

NT PERIHELIONS

NT PLANETARY ORBITS

NT POLAR ORBITS

NT SATELLITE ORBITS

NT SOLAR ORBITS

NT SPACECRAFT ORBITS

NT STATIONARY ORBITS

NT TRANSFER ORBITS

NT TROJAN ORBITS

NT TWENTY-FOUR HOUR ORBITS

Parallax and orbital motion of spectroscopic binary Tau Persei determined from Sproul refractor photographs
13 p2349 A69-27812

Photographic recording of parallax, proper motion, acceleration and orbital motion of Barnards star, noting mass ratios to jupiter
13 p2349 A69-27813

ORDER-DISORDER TRANSFORMATIONS

Order-disorder in alloys with several phase transition temperatures, discussing crystal lattices, interstitial alloys, atomic and magnetic ordering
11 p1936 A69-24702

Pressure effects on hcp crystalline lattice alloys order-disorder transformations
11 p1937 A69-24704

Young modulus temperature dependence and order-disorder transformations in ternary nickel alloys
11 p1904 A69-24705

X ray detectable preferred disorder in solids by shock loading studied in Ainsworth meteorite and in hexagonal alpha silicon dioxide
15 p2671 A69-31538

Orthopyroxenes cooling history, studying order-disorder transitions between ferrous iron and magnesium
20 p3523 A69-37518

Order-disorder transitions in solid hydrogen, discussing model to explain molecular rotation angular momentum operator fluctuations
24 p4350 A69-43119

ORDINATES

U COORDINATES

ORDNANCE

Nonlinear equations of motion approximate solution, determining ordnance weapons aerodynamic stability coefficients from angular motion as functions of angle of attack
[AIAA PAPER 69-135] 06 p0863 A69-18120

ORES

U MINERALS

ORGAN WEIGHT

Body weight and organ sizes in hibernating cold and warmth adapted golden hamsters, discussing lungs, heart, kidney, pancreas and liver weight increases
23 p4084 A69-41462

ORGANIC ALUMINUM COMPOUNDS

Lewis acidity of alanes, discussing interactions of trimethylalane with amines, ethers and phosphines
07 p1074 A69-18630

ORGANIC CHEMISTRY

Heuristic Dendral program to mechanize inductive inference in organic chemistry to determine isomers in chemical compounds
07 p1075 A69-19484

C-nitroso compounds chemistry covering various nitrosation reactions connected with reduction and deoxygenation
20 p3484 A69-37486

Organic geochemical investigations of lunar rock samples based on analysis methods for carbonaceous meteorites and early Precambrian sedimentary rocks
20 p3476 A69-37616

ORGANIC COMPOUNDS

NT ACETIC ACID

NT ADENINES

NT ADENOSINE TRIPHOSPHATE [ATP]

NT ALANINE

NT AMINO ACIDS

NT CHOLINE

NT COENZYMES

NT CYSTEINE

NT FATS

NT FATTY ACIDS

NT FLUORINE ORGANIC COMPOUNDS

NT FLUOROCARBONS

NT FLUOROHYDROCARBONS

NT GLUTAMIC ACID
 NT GLYCINE
 NT LEUCINE
 NT LYSINE
 NT METHIONINE
 NT NUCLEOTIDES
 NT OXIDASE
 NT PEPTIDES
 NT PYRIDINE NUCLEOTIDES
 NT TRYPTOPHAN
 NT URIDYLIC ACID

Electric field control of growth rates of insulating organic crystals from vapor phase

01 p1035 A69-10140

Compatibility of inorganic azides with organic explosives from elevated temperature interactions using trinitrobenzene as model

02 p0304 A69-12499

Burning ability and inflammability of mixtures of powdered Mg, Al, Mg alloys or Al alloys and C-H-O organic compounds

02 p0355 A69-12669

Far IR and Raman spectra of ethylene carbonate, gamma butyrolactone and cyclopentanone, noting consistency with hindered pseudorotation

02 p0206 A69-12723

Sulfur-organic compounds association with aromatic hydrocarbons, noting oxidation inhibiting effect on petroleum oil

03 p0494 A69-13800

Photocurrent carriers recombination in organic semiconductor rhodamine B films analyzed as function of illumination

03 p0489 A69-13890

Organic plasticizers molecular vaporization process kinetics, using isothermal and nonisothermal kinetic methods

04 p0620 A69-14956

Temperature dependence of laser induced damage in plastic Q switch made of polyethylmethacrylate and vanadyl phthalocyanine for ruby laser

06 p0936 A69-17777

Organic compounds /metabolites/ extracting technique from nutrient media of *Chlorella* cultures indicate unsaturated amine and phenol composition

08 p1262 A69-19833

Inhomogeneous laser beams self focusing effects in organic liquids recorded on bases of induced stimulated scattering

08 p1326 A69-20538

Photochemical production of reduced organic compounds of C and N in primitive earth atmosphere

09 p1444 A69-21465

Polymerization of monomers considered for direct synthesis of iminobenzylidene

10 p1651 A69-23308

Abiogenic synthesis of prebiological membranes under assumed primitive earth conditions by UV radiation of alkanes on phosphate and Mg ions aqueous solutions

11 p1828 A69-25462

Photocurrent carriers recombination in organic semiconductor rhodamine B films analyzed as function of illumination

11 p1939 A69-25691

Description and automated research of correlation /DARC/ for establishing quantitative relationships between topology and properties of chemical substance

12 p2026 A69-26361

Organic analysis of Pueblito de Allende meteorite using thin layer chromatography or combined gas chromatography and mass spectrometry

13 p2337 A69-27520

Organic semiconductors physical properties and intermolecular charge transfer between donor and acceptor

13 p2317 A69-27799

Organosilicon-containing derivatives of 2-aminoethanethiols and 2-aminoethanethiosulphuric acids as radiation protective agents

13 p2210 A69-28486

Heterocyclic-aromatic organic polymer adhesives used for high temperature structural purposes, discussing processing, testing, formulating and impact on basic research

14 p2469 A69-29346

Life origin and organic-inorganic systems, emphasizing protein colloids-mineral salts interactions at protocell stage

14 p2408 A69-29632

Diperchlorates different in organic part of structure and explosive transformation heats, showing strong dependence of combustion velocity on pressure

15 p2716 A69-30108

Mass spectroscopic structural analysis of organic compounds, discussing computer application to data recording, processing and evaluation

18 p3099 A69-34553

Regenerative life support system development, considering synthesized organic compounds and microorganisms as foods for long duration space missions

20 p3477 A69-37623

Acid fraction extraction of Green River shale identified by gas chromatography-mass spectrometry-computer system, noting trimethyl pentadecanoic acid

21 p3669 A69-38983

Volatile oxygen organic compounds subjected to RF electrodeless discharge, explaining product distribution in terms of reaction sequences

21 p3670 A69-39737

Norwegian lichen species chemical investigation for aromatic compounds, hydroxy fatty acids, amino acids, soluble and bound sugars

23 p4080 A69-41428

High temperature pyrolysis of simple organic molecules in shock tube, considering diatomic C formation and decay rate

23 p4113 A69-41693

DENDRAL program used to construct all possible acyclic structural isomers of C, H, N and O

23 p4114 A69-42214

ORGANIC COOLANTS

Organic quenchant additive for distortion free heat treatment of dip-brazed aluminum parts

09 p1504 A69-22065

ORGANIC FLUORINE COMPOUNDS

U FLUORINE ORGANIC COMPOUNDS

ORGANIC LASERS

Organic dye lasers energy characteristics excited by monochromatic radiation, investigating radiation absorption during transitions from lower to higher electron-vibrational levels

01 p0090 A69-10381

Frequency and time dependent gains of dye solution lasers for pumping by lasers and flashlamps

02 p0257 A69-12616

Organic dye laser frequency variation with temperature, noting absorption and fluorescence spectra

02 p0258 A69-12617

Dye solution laser wavelength shift and simultaneous oscillations at different wavelength ranges for pumping by another dye laser

02 p0258 A69-12620

Frequency mixing of organic dye solution laser radiation with ruby laser radiation, showing broader UV spectrum

04 p0610 A69-14424

Optical generation in organic luminophor solutions in 400-650 nm range

04 p0612 A69-15374

Critical population inversion for xanthene dye solution laser, analyzing optical loss due to triplet state concentration

05 p0773 A69-16307

Laser based on xanthene series dyes and excited by neodymium laser second harmonic radiation, noting radiation spectra

06 p0932 A69-16914

Lasing threshold and spectral characteristics of organic dye solutions, using excitation of second harmonic of monopulse ruby laser

06 p0933 A69-17255

Light generation by lasing organic dye liquid solution with negative absorption on activator molecules and induced combination scattering for solvent molecules

06 p0933 A69-17256

Mode locked Nd glass laser to pump organic dye laser, obtaining continuously tunable picosecond pulses

06 p0935 A69-17759

Time dependent emission spectra from flashlamp pumped organic dye lasers recorded with image converter, comparing dye characteristics

06 p0936 A69-17901

Organic lasers, discussing coherent laser light emission induced from organic dye molecules

07 p1149 A69-18908

Organic dye lasers characteristics, describing broad continua production for nanosecond absorption spectroscopy

07 p1150 A69-19047

Triplet-triplet transitions for Q switching, examining organics for passive Q switches

09 p1520 A69-22682

Pulsed tunable lasers, emphasizing dye lasers for visible and near visible light in specialized spectroscopy

11 p1893 A69-24343

Dye lasers CW operation feasibility, showing sufficient quenching of rhodamine 6G triplet state by oxygen dissolved in methanol

11 p1893 A69-24344

Liquid lasers properties and composition including organic complex compounds, organic dyes, rare earth elements in polyphosphoric acid, etc

11 p1893 A69-24353

Organic cyanine dye solution laser pumped by Q switched ruby and another dye laser, discussing spectral distribution and modes

11 p1900 A69-25580

Organic dye lasers energy characteristics excited by monochromatic radiation, investigating radiation absorption during transitions from lower to higher electron-vibrational levels

12 p2109 A69-26676

Neodymium laser emission of organic molecules in UV region noting molecular absorptivity and fluorescence

13 p2271 A69-27657

Optical generation in organic luminophor solutions in 400-650 nm range

16 p2797 A69-32121

Frequency and time dependent gain characteristics of dye lasers, using computer program for rate equations for populations

17 p2980 A69-33025

Lasers based on organic dye solutions, discussing operation, structural formulas, absorption and luminescence spectra

20 p3555 A69-38011

Mode locking of organic dye laser by pumping laser with mode locked pulse train from Nd-glass laser, obtaining spectral bandwidth

21 p3740 A69-39545

Flashlamp-pumped dye laser for resonance scattering studies of upper atmospheric composition, describing laser construction and tuning

22 p3962 A69-40440

Flashlamp-excited organic dye lasers capable of tunable emission throughout most of visible spectrum

22 p3966 A69-41219

Low energy ultrafast flashlamp systems as optical pumps for lasers using fast decaying fluorescent materials /organic dyes/

23 p4174 A69-42187

ORGANIC LIQUIDS

Electro-optical measurements to determine intermolecular interaction temperatures in organic liquids compressed by shock waves

02 p0230 A69-11979

Q switched ruby laser nonlinear absorption in optically transparent organic liquids attributed to two quantum process with large cross section

03 p0439 A69-13055

Power generation in combat environment by tested self contained organic Rankine silent engine, discussing working fluid properties

07 p1058 A69-18309

Emission from solutions of organic luminophores excited by harmonics of Q switched neodymium laser

12 p2104 A69-26030

Kerr constant verification device to study electrooptic liquids properties

12 p2084 A69-26148

Gas chromatography based on sampling gas-vapor phase at liquid surface for determining volatile oxygen containing compounds in biological media

13 p2216 A69-28627

Electro-optical measurements to determine intermolecular interaction temperatures in organic liquids compressed by shock waves

15 p2561 A69-30264

Dielectric breakdown thresholds and cavitation in organic liquids observed during Q switched and pulsed ruby radiation

17 p2979 A69-32826

Liquid filter cells design with emphasis on filters usable for inorganic and organic liquids

21 p3770 A69-38679

Rankine cycle power systems with reciprocating engines using organic working fluids, discussing engine development, system characteristics, etc

23 p4067 A69-42237

Stress corrosion cracks propagation from fatigue precrack in Al alloy exposed to organic liquid environments

23 p4178 A69-42452

ORGANIC MATERIALS

Organic matter signals in carbonaceous meteorites, discussing possible relation to extraterrestrial life and origin

11 p1953 A69-24342

Oriented composites obtained from organic system under various directional solidification conditions
13 p2287 A69-28680

Sterile soil from Antarctica found to contain organic carbon, noting significance for biological exploration of Mars
16 p2746 A69-31552

Solid lubricants on molybdenum disulfide base at various temperatures and low pressures, noting film mass losses and possible use with organic materials under high vacuum
16 p2793 A69-31561

Gas chromatographic and mass spectrometric analyses of alicyclic hydrocarbons from Carboniferous organic materials, noting alkane distribution and evolutionary histories
17 p2917 A69-34184

Gas chromatograph-mass spectrometer combination for in situ analysis of lunar organic matter, describing instrument design and operation
18 p3113 A69-34238

Organic geochemical investigations of lunar rock samples based on analysis methods for carbonaceous meteorites and early Precambrian sedimentary rocks
20 p3476 A69-37616

Biocrystallography of organic form and structure emphasizing liquid crystals, polymers, epitaxy, inclusion compounds, electrical properties, prelife compounds, etc
21 p3656 A69-38922

Meteoritic organic matter origin, discussing time-of-flight mass spectrometer combined with gas chromatographic capillary column
22 p4012 A69-40085

Flame resistant organic fiber in cross linked polymer structure, discussing properties and aerospace applications
24 p4337 A69-43424

ORGANIC NITRATES

U CELLULOSE NITRATE
U NITROGLYCERIN
U PETN

ORGANIC PHOSPHORUS COMPOUNDS

NT URIDYLIC ACID

Structural phospholipoprotein isolated from hydrogenomonas facilis and Neurospora crassa
22 p3871 A69-40049

ORGANIC SILICON COMPOUNDS

Polymers and organic optical cements transparent in 1 to 13 micron IR region, noting organosilicon resin
08 p1336 A69-20387

Synthesis of N-/trimethylsilylalkyl/ diamines and N-/trimethylsilylalkyl/-N-/2-mercaptoethyl/ diamines, determining structure by IR spectra
15 p2561 A69-30414

Carbon fiber reinforced plastics properties improvement by applying organosilanes, discussing silanol bond formation
16 p2803 A69-31806

Gravimetric and IR absorption spectra analysis for determining heat resistance and chemical changes in organosilicon resins during heating
17 p2992 A69-33744

Glass fiber laminates based on epoxy organosilicon resins, discussing various hardeners effects on strength, etc
19 p3358 A69-35903

Silico-organic liquid water repellant coatings for increasing binder adhesion to glass fiber in glass fiber reinforced plastic materials of aircraft components
21 p3752 A69-38876

Soviet book on silicoorganic protective coatings preparation, physical, chemical and operational characteristics, with emphasis on silicates and metals
24 p4336 A69-43232

ORGANISMS

Changes in organism during sudden decompression, analyzing pressure equalization, dissolved gases transformation and body fluids vaporization
01 p0020 A69-10753

Acceleration, hypoxia and stress effects on humans and animals, noting latent functional disorders of organisms requiring special techniques for detection
02 p0197 A69-11488

Objective evaluation of metabolic reactivity of organism based on biophysical model compared with experimental individual
06 p0874 A69-17595

Electrokinetic converter of biochemical parameters for diagnosis and control of organism behavior, noting biomechanical utility
14 p2409 A69-29471

Gravity independence of life processes in terrestrial organisms concluded from zero gravity experiments with algae, hatched larvae, etc
18 p3095 A69-34692

Organism growth physiology based on decisive enzyme reactions, considering synthesis of biological proteins from DNA and molecular life processes
21 p3652 A69-38787

Biological clocks, discussing circadian rhythms of organisms using animal experiments and physical oscillator model
21 p3653 A69-38895

Microwave absorption by biological materials, noting energy distribution between reflected, transmitted and absorbed radiation as function of medium physical properties
24 p4270 A69-42574

ORGANIZATIONS

NT BUREAUS [ORGANIZATIONS]

Organizational behavior of scientists noting working environments, effectiveness of work sections, research management and organizational development
08 p1423 A69-21124

Organization and manpower utilization in R and D, determining criteria for organizational form selection
08 p1423 A69-21155

Research and development organizations under pressure of corporate assessment and systems management approach, suggesting core-technology structure and training
12 p2192 A69-26732

Aircraft accident investigation procedures in Canada for routine/major accidents and public inquiries, outlining organization
13 p2201 A69-27540

1967 Space Treaty legal aspects of consultation, suggesting international permanent body setup for resolving technical and political matters
20 p3636 A69-37111

Book on law making in International Civil Aviation Organization covering membership problems, air navigation and transport safety, settling of disputes, etc
23 p4240 A69-41297

Communication in large organizations, describing internal communication model
24 p4419 A69-42930

ORGANIZING

Engineer performance related to organizational factors, discussing colleague contact, work diversity, number of subordinates and involvement in work
15 p2721 A69-31069

Organizational identification of scientists as professional employees, exploring degree of loyalty and perceived self prestige
21 p3855 A69-38765

Safety engineering programs for aircraft design, discussing organizational relations, failure and operational safety analyses
22 p3867 A69-41132

ORGANOMETALLIC COMPOUNDS

NT CHLOROPHYLLS

NT HEMOGLOBIN

NT ORGANIC ALUMINUM COMPOUNDS

NT OXYHEMOGLOBIN

Optical absorption coefficients for triphenylmethylarsonium tetracyanoquinodimethane complex single crystal, evaluating reflectance
01 p0140 A69-10934

Chemical nitrogen fixation methods for life support systems, discussing organometallic chlorides and bromides
03 p0382 A69-14198

Absorption and emission spectra of ruthenium 2 complexes dissolved in rigid glasses, discussing crystal field theory and luminescence
07 p1200 A69-19219

Synthesis and nucleophilic reactions of stable alpha-bromoorganolithium reagent
07 p1074 A69-19479

Liquid lasers properties and composition including organic complex compounds, organic dyes, rare earth elements in polyphosphoric acid, etc
11 p1893 A69-24353

Analytical, IR absorption and polarographic analysis of cyclic niobium /V/ and tantalum /V/ esters
11 p1832 A69-24575

Additions of dialkyl and diaryldithiophosphates of Ba, Ca, Zn, Pb and Ni as antioxidants and corrosion inhibitors for hydrocarbons
12 p2027 A69-27091

Catalytic activity enhancement of complex Co/III/ compounds on standing explained by hydrated Co/II/ ions appearance
17 p2988 A69-33433

ORGANS

NT BLADDER

NT ESOPHAGUS

NT KIDNEYS

NT LIVER

NT LUNGS

NT PITUITARY GLAND

NT STOMACH

Histological investigation of internal organs of mice exposed to atmosphere with high oxygen content
05 p0709 A69-16513

Histological investigation of internal organs of mice exposed to atmosphere with high oxygen content
18 p3096 A69-34732

Histological changes in internal organs of rats after exposure to 400 r fast neutron dose, showing destructive processes followed by compensation reactions of cellular proliferation
21 p3659 A69-39062

ORGUEIL METEORITE

Magnetite content of type I carbonaceous meteorite from quantitative X ray diffractometry of Orgueil meteorite
02 p0328 A69-12729

Sporopollenin content of Orgueil and Murray meteorites as evidence for extraterrestrial life
21 p3662 A69-39617

ORIENTATION

Oriented composites obtained from organic system under various directional solidification conditions
13 p2287 A69-28680

Orientation distribution of lineal and areal elements in space, expanding density function definition of two dimensional lineal array
14 p2470 A69-29363

Fracture kinetics of biaxial oriented polymethyl methacrylate, discussing crack development and propagation as compared to unoriented polymer
18 p3162 A69-35354

Surface grains orientation effect on fatigue behavior in polycrystalline Al, noting strain hardening role in failure
20 p3561 A69-37597

Auroral arcs orientation curves for IQSY evaluated from all sky camera data, comparing results with IGY curves
24 p4308 A69-43009

ORIFICE FLOW

Gas jet interaction with supersonic flow during injection from orifice of flat body, investigating Mach number, orifice diameter and jet effects on flow pattern near injection
01 p0005 A69-10357

Discharge coefficient nondependence on Reynolds number demonstrated by measurement at orifices with sharp edges
01 p0006 A69-10362

Downstream pressure asymmetry effect on efflux angle and contraction coefficient of incompressible jet from two dimensional orifice
02 p0231 A69-12075

Flow rate effect on flow pattern of gas escaping through lateral hole of arbitrary depth
04 p0586 A69-14274

Large signal vortex amplifier analysis using load lines to evaluate series orifice and vortex flow control valve characteristics
10 p1639 A69-23558

Venturi meter design, discussing effects of turbulent velocity fluctuations, hole size and internal geometry on differential pressure measurement
11 p1880 A69-24468

Mass flow rates for nearly free molecular flow through two dimensional slit for several tank pressure ratios
11 p1874 A69-25357

Load capacity, stiffness and flow requirement of capillary and orifice compensated oil lubricated externally pressurized rectangular thrust bearings
12 p2102 A69-26239

Molecular flow network theory extended to pulsed operation with gases mixtures having various molecular weights
13 p2247 A69-28085

Exhaust plume rarefaction from sonic orifice, considering continuum to transitional behavior for perfect gas
[AIAA PAPER 69-657] 17 p2892 A69-33465

Servovalve orifice characteristics described by discharge, flow or loss coefficients for laminar and turbulent flow, noting use of Mises model
19 p3256 A69-36712

ORIFICES

- Orifice compensated hydrostatic face seal under pressure and thermal loading for aircraft gas turbine [ASME PAPER 68-WA/LUB-6]
05 p0768 A69-16131
- Controllable sonic flow orifice, discussing mass flow rate, area and upstream stagnation pressure
10 p1693 A69-23343

ORION CONSTELLATION

- Far UV spectra of O and B stars in Orion photographed from Aerobee rocket, describing wavelength measurements and line identifications
02 p0327 A69-12712
- Orion nebula flare type variable stars amplitudes, light curve sections and stability
06 p1002 A69-17264
- Three color photoelectric observations of stars near Orion Nebula, discussing gravitational contraction stars and color magnitude diagram
08 p1384 A69-20055
- Paschen line intensity measured as function of position across Orion Nebula
08 p1384 A69-20058
- Electron temperature of Orion Nebula at 6750 K from intensities of hydrogen n alpha lines, discussing Stark broadening
08 p1398 A69-20776
- Chemical composition of diffuse Orion Nebula and stars compared for lighter elements, considering solar system formation from interstellar medium
08 p1402 A69-20908
- Abundance analysis of B3 V star in Orion association, noting titanium and strontium overabundance and oxygen underabundance
08 p1407 A69-21133
- Molecular hydrogen in Orion dark cloud from observed faint emission
09 p1599 A69-22191
- Double structure in IR near Trapezium region of M42 in Orion Nebula center
10 p1786 A69-24105
- IR spectral distribution from region between stars of Trapezium in Orion Nebula
10 p1786 A69-24106
- Atomic H Lyman-alpha interstellar absorption line in theta Orionis spectrum, showing equivalent width relations to H column density and spin temperature
15 p2695 A69-30890
- Radio map of Orion A region, resolving M 42 and M 43 nebulae at 1.94 cm wavelength, noting optical photographs comparison
17 p3035 A69-33609
- Bok globules in Orion nebula, deriving temperature and density data
22 p4022 A69-40465
- High radial velocity matter of bright region near Trapezium in Orion Nebula, determining electron density lower limit and mean velocity
22 p4029 A69-40769
- Rocket measurement of far UV spectral intensity of theta Orionis for far UV interstellar extinction law in Orion nebula region
22 p4030 A69-40770
- Orion nebula isophotal contours optical observation for three continuum colors /blue, yellow and IR/ and H alpha
22 p4031 A69-40942
- Beta Orionis spectral line profiles data used to study atmospheric structure
24 p4391 A69-43804

ORIONID METEOROIDS

- Ionospheric ion composition at 130-155 km during meteor shower Orionides activity from geophysical rocket-borne RF mass spectrometer data
15 p2603 A69-31406

ORNITHOPTER AIRCRAFT
U RESEARCH AIRCRAFT

OROGRAPHY

- Three term formula for describing vertical wind velocity distribution in upper boundary layer of atmosphere, taking into account friction and orography effects
02 p0240 A69-11708
- Earth orography influence on climatological distribution of wind and geopotential fields, stressing central asiatic mountains role in atmospheric circulation
14 p2478 A69-29835
- Alpine effects on wind field at synoptic scale using potential-vorticity equation, discussing deflection angle dependence on potential temperature distribution
15 p2650 A69-31445

- Jet stream blocking process simulation using geostrophic system of equations, considering effects of orography and contrast heating due to land-sea distribution
16 p2809 A69-32602
- Lee waves and orographic wind phenomena in Rocky Mountains near Boulder, noting stratospheric standing gravity waves and turbulence sampled by HI-CAT U-2
17 p2999 A69-33738
- Friction and orography effects on vertical currents in planetary boundary layer and numerical forecasting of baric field
21 p3758 A69-38837
- Precambrian crustal geotectonic evidence of earth radius expansion based on dated orogenic fold belts distribution
22 p3936 A69-40182
- Orographic inhomogeneities of underlying surfaces for radiating atmospheric waves formation, deriving formulas for plane stable atmosphere
23 p4185 A69-42492

ORRERIES

U ASTRONOMICAL MODELS

ORTHICONS

U IMAGE ORTHICONS

ORTHO HYDROGEN

NT TRITIUM

- Proton spin-lattice relaxation time in dilute liquid and gas solutions of orthohydrogen in parahydrogen, noting dependence on temperature, density and composition
06 p0961 A69-17141
- RF spectra for hyperfine structure of orthohydrogen molecular ion, calculating doubling constant for vibrational effects
15 p2693 A69-30784

ORTHOGONAL FUNCTIONS

- Iterative method of determining orthogonalized bases for representation of sampled data signals
03 p0391 A69-13231
- Irregular Sturm-Liouville first and higher order perturbation problem in boundary layer theory providing analytical approximations to complete orthogonal set of characteristic functions
04 p0590 A69-15001
- Digital computer optimization of representation of sampled data signals on orthogonal basis, using iterative method
06 p0901 A69-17363
- Wave reflections due to rotationally symmetrical jump in circular waveguide cross section, using orthogonal expansion to solve resulting boundary value problem
11 p1855 A69-25622
- Square matrices decomposition into orthogonal and triangular matrices products for computer storage applications
13 p2290 A69-28485
- Orthogonal polynomials for solving plane elasticity theory boundary value problems without constructing mapping functions, noting applications
17 p3067 A69-34144
- Polynomial bases for orthogonal group irreducible representations, rederiving Wigner coefficients
18 p3164 A69-34807
- Data compression using orthogonal functions, design curves for given functions, signal characteristics and error avoidance
18 p3103 A69-35060
- Orthogonal functions for determining atmospheric vertical temperature profile from satellite measurement of earth outgoing radiation in carbon dioxide absorption band
19 p3303 A69-36409
- Orthogonal polynomials in three dimensional contact problems without friction, discussing construction of kernels over finite and semiinfinite intervals
22 p4041 A69-40113
- Iterative and vectoral methods for correcting computed direction cosine matrix errors
23 p4134 A69-42543

ORTHOGONAL MULTIPLEXING THEORY

- Scattering matrix for pattern forming circuit for multiple beam antenna arrays with interacting elements, noting orthogonal pattern optimization
09 p1469 A69-22627

ORTHOGONALITY

- Open and closed path orthogonal analysis for structural network
03 p0526 A69-13735

Orthogonality of natural oscillation modes of shells of arbitrary geometry, using equations of motion from Vlasov engineering moment theory
05 p0840 A69-16200

Mean number of polarization coefficient modulus zero crossings for field reduced at reception point to uncorrelated orthogonally polarized components
05 p0720 A69-16445

L-step orthogonalization of Bose-Chaudhuri-Hocquenghem codes
06 p0903 A69-17532

Generalized orthogonality principles and expansion schemes for forced response of partial differential equations, noting applicability to rodlike structures
09 p1533 A69-21975

Extremal controlled plants identification by Chebyshev orthogonal polynomials, comparing results with regression analysis
11 p1861 A69-25713

Mean number of polarization coefficient modulus zero crossings for field reduced at reception point to uncorrelated orthogonally polarized components
16 p2753 A69-32478

Asynchronous gyrostat postimpact drift direction found orthogonal with respect to initial impulse by averaging method
19 p3311 A69-36192

N symmetric matrices orthogonal integrity basis, considering product traces, polynomial invariants, tensor groups, etc
20 p3624 A69-37587

Terrain slope estimation of position errors of differential corrections in orthophoto production
22 p3951 A69-41245

Optical interpolation for GZ-1 orthoprojector in storage mode, noting electronic contour plotter
22 p3951 A69-41247

Automatic contour plotting for orthoprojector based on adjacent profiles and linear interpolation
22 p3951 A69-41248

ORTHOGRAHY

U HANDWRITING

ORTHONORMAL FUNCTIONS

- Matrix elements calculation for one dimensional quantum-mechanical problems using transformation theory
04 p0632 A69-14866
- Orthonormal aspect on vibration modes for nonuniform beams, evaluating normalization for end conditions by using Rayleigh technique
14 p2534 A69-29319
- Optimum order for column orthonormalization of sparse matrices, applying results to Gram-Schmidt and Householder methods
15 p2644 A69-30425
- Orthonormalization methods applied to heat conduction, convection and radiation problems, noting digital computer programs modifications
18 p3229 A69-34662

ORTHOSTATIC TOLERANCE

- Cardiovascular changes in male students during tilt and negative pressure tests with bed rest studied from heart rate, blood pressure and leg volume measurements
01 p0021 A69-11334
- Cardiac function changes during orthostatic tests and problems in predicting reactions of cosmonauts in flight
03 p0381 A69-14229
- Orthostatic intolerance, with assessment of circulatory problem of weightlessness in prolonged space flight
06 p0873 A69-17016
- Clinical spectrum of postural hypotension, treating vasodepressor syncope, orthostatic arterial anemia and idiopathic orthostatic hypotension
06 p0873 A69-17017
- Tilt-table and acceleration tolerance of athletes and inactive students, comparing cardiovascular responses, heart rate and blackout level [DVL-834]
09 p1444 A69-21304
- Dogs orthostatic tolerance and resistance to transverse acceleration after 14-day hypodynamia, studying tachycardia and arterial pressure
10 p1645 A69-23499
- Long term hypokinesia effect on cardiovascular system of athletes indicating human orthostatic resistance increase due to physical exercises
10 p1646 A69-23581
- Bed rest effect on orthostatic tolerance of patients with acute myocardial infarction and without heart failure
10 p1648 A69-24189

Artificial heat acclimatization effect on orthostatic tolerance in man exposed to stresses of heat, exercise and dehydration

16 p2746 A69-32810

Bedrest as analog of weightlessness, evaluating role of extravascular dehydration in postrecumbency orthostatism

17 p2909 A69-33179

Increased tolerance of orthostatic stress in heart failure patients

19 p3258 A69-36374

Diurnal rhythms of heart rate and blood pressure reactions to posture changes on tilt table, finding orthostatic lability maxima

23 p4094 A69-42072

ORTHOTROPIC CYLINDERS

Orthotropic stiffened multilayer circular cylindrical shells buckling under axial compression, lateral pressure, etc

02 p0346 A69-12510

Free vibration of thin laminated orthotropic cylindrical shells

06 p1020 A69-17145

Cylindrically orthotropic hollow cylinder elastic properties determination using experimental test for production of stress and strain states and end effects

07 p1232 A69-18718

Transient thermal stress distribution in infinite orthotropic elastic cylinder of rectangular cross section in presence of heat sources

08 p1415 A69-20664

Torsional vibrations of composite elastic orthotropic cylinders, including cylindrical shells and isotropic composite cylinder

10 p1800 A69-23243

Steady state problems of elastic orthotropic cylinder solutions applicable to boundary value problems of laminar orthotropic elliptical cylinders

13 p2369 A69-28528

Boundary conditions of orthotropic shell stability under external pressure and axial tension, analyzing critical pressure by strain energy method

18 p3222 A69-34977

Buckling strength prediction for circular cylindrical shells reinforced by circumferential and longitudinal stiffeners, solving torsional buckling of orthotropic shells under internal pressure

22 p4042 A69-40171

Nonlinear stability for closed thin walled orthotropic cylindrical shell subjected to uniform external pressure, using Bubnov-Galerkin method for approximate solution

22 p4042 A69-40454

ORTHOTROPIC PLATES

Orthotropic plates bending and thermal stress, analyzing basic equations

01 p0168 A69-10416

Deflection of orthotropic sandwich plates with unequal facing thickness with edges subjected to uniform and concentrated loading

01 p0172 A69-11270

Supersonic flutter of circular cylindrical heterogeneous orthotropic thin panels of finite length, obtaining nonlinear flutter equation

08 p1413 A69-20404

Natural vibration frequency of circular orthotropic plate with variable rigidity

09 p1618 A69-22238

Unsteady temperature field and thermal stresses for anisotropic and orthotropic plates heated by heat sources and having Newton law heat transfer

12 p2177 A69-25992

Lateral bending and two dimensional thermal stress in rectangular orthotropic plates, considering alternating direction implicit method

12 p2188 A69-27100

Sine series solution for flexural vibration of rectangular isotropic plates applied to free vibration of orthotropic plates

13 p2363 A69-28128

Bending theory of orthotropic plates with variable elastic modulus under transverse loads, utilizing stress-strain relations and Kirchhoff-Love hypothesis

15 p2708 A69-30661

Finite element analysis of flat rectangular orthotropic multilayer stiffened panels, proposing six degrees of freedom model

15 p2708 A69-30668

ORTHOTROPIC SHELLS

NT CYLINDRICAL SHELLS

Buckling equations for orthotropic cylindrical shells with eccentric spiral stiffeners derived through variation method of total potential

04 p0676 A69-14710

Exact geometrical equations and internal equilibrium for elastoplastic deflections of orthotropic shells of revolution using thin shell theory

05 p0831 A69-15680

Critical axisymmetric loads for instability in orthotropic multilayer conical shells obeying Hooke law under axial compression or external pressure

05 p0840 A69-16198

Finite elastic-plastic deflections of orthotropic shells of revolution, deriving exact geometrical relations and equilibrium equations

05 p0842 A69-16642

Stress concentration at circular hole in orthotropic cylindrical shell, using coordinates system and Bubnov-Galerkin method

06 p1021 A69-17180

Oscillations of cylindrical orthotropic three layer shell having ideal fluid flow at variable rate, establishing parametric resonance and determining limits of shell motion instability regions

06 p1022 A69-17186

Multilayer orthotropic cylindrical shells stability under distributed external load and off-center compression, analyzing subcritical deformation on critical load

09 p1613 A69-21685

Free vibration frequencies and mode shapes for thin orthotropic oblate spheroidal shells, noting isotropic oblate spheroidal shell and isotropic spherical shell

09 p1613 A69-21719

Axisymmetric free edge buckling of semiinfinite heterogeneous orthotropic cylindrical shells in axial compression, noting stability condition

10 p1802 A69-23889

Free vibrations in axisymmetrically loaded orthotropic circular conical shells with longitudinal and circumferential stiffening based on linearized theory, considering shear deformation and inertia

11 p1969 A69-24327

Axisymmetric deformation of thin orthotropic laminar spherical shells under internal loads calculated on computer using Legendre polynomials

12 p2181 A69-26611

Orthotropic cylindrical shell stability under uniform axial compression and internal pressure, taking into account subcritical state duration

14 p2532 A69-28981

Heterogeneous orthotropic circular cylindrical shell stability during axial critical compression

14 p2533 A69-29024

Laminar thin orthotropic cylindrical shells natural and forced oscillations and dynamic deflection coefficient

15 p2715 A69-31202

Eigenvalues of truncated orthotropic shells of revolution with degenerate poles and various rigidities and geometries

16 p2873 A69-32133

Long term stability of orthotropic cylindrical shells under transverse shear stresses, calculating critical stress using Kirchhoff-Love model

18 p3225 A69-35357

Elastic oscillations of inhomogeneous orthotropic ring under time-variable axisymmetric load analyzed by Fourier method

19 p3434 A69-35828

Nonlinear theory based on Euler-Bernoulli hypothesis for axisymmetric deformations of heterogeneous orthotropic shells of revolution under rotationally symmetric mechanical and thermal loads

20 p3625 A69-37592

Load carrying capacity of orthotropic circular cylindrical shell under uniformly distributed normal load, considering edge support conditions

20 p3629 A69-38075

Nonlinear problems involving large deflections of isotropic and orthotropic shallow shells of rectangular planform, deriving partial differential equations for solution

21 p3838 A69-39185

Momentless orthotropic spherical shell of variable thickness stress analyzed, assuming large deformations under uniform axisymmetric load distribution

22 p4039 A69-39916

Prebuckling deformation influence on compressive buckling load for orthotropic cylindrical shells with elasticity principal axes in axial and circumferential directions

22 p4047 A69-41182

Deformation of orthotropic layered elastic shells based on linear elasticity theory, assuming surface and stress constraints

23 p4226 A69-41535

Stability of orthotropic cylindrical shells reinforced at edges by elastic ribs, analyzing axisymmetric buckling, natural oscillations and rigidity characteristics

23 p4229 A69-41992

Algorithm for stress analysis of structurally orthotropic conical and cylindrical shells, resolving first order differential equations

23 p4229 A69-42000

Orthotropic stiffness layer models for buckling of eccentrically stiffened shells of revolution with two unbonded orthotropic layers uncracked and circumferentially cracked

24 p4405 A69-43657

ORTHOTROPISM

Off-axis test for hard orthotropic composite materials, discussing fixture design to reduce shear coupling effect

01 p0103 A69-11273

Incremental complementary energy method of stress analysis of orthotropic nonlinear materials having different behavior in tension and compression

06 p1028 A69-18159

Elastic potential for obtaining localized strain theory, describing deformation characteristics of compressible and incompressible orthotropic materials with physical nonlinearity

08 p1412 A69-20328

Orthotropic aircraft materials plasticity theory, deriving stress-strain relationships in three mutually perpendicular symmetry planes for use in engineering calculations

24 p4400 A69-43083

OSCILLATING CYLINDERS

Self gravitating pulsating cylindrical and ring shaped cosmic masses from group theory standpoint compared with oscillating stars

01 p0148 A69-10124

Linearized unsteady nonequilibrium flows produced by unsteady motion of thin foil or circular cylindrical shell in compressible gas

07 p1119 A69-18738

Liquid filled cylindrical container motion with longitudinal forces applied to base, obtaining stability conditions for natural oscillations

08 p1419 A69-21181

Torsional oscillation of cylindrical shell of non-homogeneous material under periodic shearing force

13 p2361 A69-27462

Vortex wakes behind circular cylinder subject to transverse sinusoidal oscillations in uniform water flow at specific Reynolds numbers, photographing varied frequency flow patterns

18 p3086 A69-35169

Viscous incompressible fluid flow around semi-infinite oscillating plate and skin friction on infinite cylinders oscillating parallel to length

19 p3237 A69-35620

Asymmetrical oscillations of cylindrical shell with elastic bottom containing liquid, discussing liquid level influence on natural oscillation frequencies

21 p3834 A69-38718

OSCILLATING FLOW

Relationship between cooled surface temperature and pressure self oscillation frequency during heat transfer to turbulent fluid flow, showing temperature variations

01 p0173 A69-10094

Quasi-biennial oscillation in tropical stratosphere as result of long period gravity waves interaction with zonal wind

03 p0461 A69-13342

Stokes and Rayleigh layer formation during solid body rotation of semiinfinite fluid and infinite disk

03 p0417 A69-13797

Thermal and ablative lag induced by periodic heat input to oscillating flat plate in high velocity flow, showing crossover from dynamically stabilizing to destabilizing condition as oscillation frequency increases

[AIAA PAPER 67-336] 04 p0685 A69-14720

Flow pattern induced by oscillatory point source in rotating inviscid liquid

04 p0591 A69-15279

Oscillations of cylindrical orthotropic three layer shell having ideal fluid flow at variable rate, establishing parametric resonance and determining limits of shell motion instability regions

06 p1022 A69-17186

Relaxation equations for oscillatory degrees of freedom of molecular supersonic binary gas flow in Laval nozzle, obtaining population inversion

07 p1118 A69-18540

Natural frequency of fluid oscillations in complex pipelines

07 p1119 A69-18745

Natural modes and eigenfunctions of low amplitude oscillation determined by Ritz averaging method for ideal fluid with equilibrium surface in weak force field
07 p1119 A69-18746

Liquid flow field about oscillating flat plate, comparing visualization results with numerical solution of Navier-Stokes equations
[AIAA PAPER 69-226] 07 p1121 A69-19565

MHD oscillatory flow along infinite plane porous wall with variable suction velocity, obtaining expressions for velocity and magnetic fields in boundary layer
09 p1547 A69-21607

Decrease existence at t approaching infinity solution of Sobolev linear partial differential equations describing rotating fluid small oscillations
09 p1481 A69-21899

Natural convective oscillatory three dimensional flow in cylindrical annuli, describing inception, amplitude, period and wavelength
09 p1481 A69-21902

Local heat transfer coefficients in oscillating turbulent boundary layer over flat plate
[ASME PAPER 69-GT-34] 09 p1623 A69-22490

Incompressible fluid unsteady motion between journal and bearing solved in form of Reynolds number power series from stream functions
09 p1514 A69-22712

Sonic transmission of diatomic nitrogen during nozzle flow, presenting density dependence of natural oscillation energies and temperature
10 p1632 A69-22912

Small scale oscillations stability in quasi one dimensional conducting gas flow with longitudinal superimposed magnetic field, noting radiation role in transverse oscillations development
11 p1928 A69-25222

Natural frequencies and forms of small vibrations of ideal liquid in spherical container with weak force field, considering surface tension forces
11 p1875 A69-25484

Electrohydrodynamic instability of incompressible conducting cylindrical viscous jet in external magnetic field, noting viscosity role in oscillation modes and growth rate
12 p2136 A69-26403

Oscillation in resonance tubes excited by subsonic jet, analyzing pressure and frequency for small Mach numbers by using wave diagram
13 p2370 A69-28630

Unsteady jet viscous fluid flow under pulse variations based on Prandtl equations, showing turbulent motion analogy
14 p2432 A69-29608

Drag and friction coefficients for laminar pulsating incompressible fluid flow in circular tubes obtained from Navier-Stokes equation
15 p2592 A69-30988

Stagnation region dimensionless pressure effect on flow pattern, boundary conditions and oscillation mechanism in compressible flow through nozzle in circular duct
15 p2549 A69-31220

Aerodynamic forces acting on harmonically oscillating thin profile in stalled plane parallel flow of ideal incompressible fluid
16 p2732 A69-32142

Amplified boundary layer oscillations and transition at swept flat nosed wing attachment line with/without boundary layer suction analyzed by wind tunnel tests
17 p2890 A69-33251

Time dependent analysis for quasi one dimensional, vibrational and chemical nonequilibrium nozzle flows approaching steady state solution by finite difference technique
[AIAA PAPER 69-668] 17 p2893 A69-33491

Electrohydrodynamic supersonic flow over wavy wall by oscillating piston model, calculating streamlines and density distributions
19 p3297 A69-35838

Rocket engines propellant feed systems dynamics analyzed by model using linear methods with distributed-parameter pipe representation
[ASME PAPER 69-FE-6] 20 p3586 A69-37987

Momentum and energy equations for fluctuating flow of viscous incompressible conducting fluid past flat plate with time dependent suction under transverse magnetic field
21 p3691 A69-38445

Relaxation equations for oscillatory degrees of freedom of molecular supersonic binary gas flow in Laval nozzle, obtaining population inversion
21 p3693 A69-38692

Taylor instability nonlinear oscillations, obtaining uniform solutions for wavenumbers near and larger than cut-off
21 p3693 A69-38703

Secondary losses in flat large scale turbine lattice attributed to LF pulsating flow separation on back of blade
21 p3645 A69-39717

Oscillations of highly viscous incompressible fluid in partially filled cavity of body moving about fixed point, solving Navier-Stokes equations by asymptotic method
22 p3929 A69-40111

Stroboscope method for measuring pulsating flow transient velocity based on hot-wire chronometric recording of small ion clouds emitted during pulsation
22 p3951 A69-41257

Turbomachinery periodic structures design to improve tolerance to inflow distortion and resonant oscillatory flows, considering large amplitude pressure waves propagation
[SAE PAPER 690388] 23 p4201 A69-41666

Decrease existence at approaching infinity solution of Sobolev linear partial differential equations describing rotating fluid small oscillations
23 p4152 A69-41975

Linear small perturbation approximation for supersonic nonequilibrium flows past oscillating airfoil in two dimensional wind tunnel, noting Laplace transform solution
23 p4061 A69-42349

Limit-cycle oscillations of unstable plane Poiseuille flow analyzed by nonlinear Navier-Stokes equations
24 p4298 A69-42600

Perturbation equations for oscillating wedges and caret wings with attached bow shock in hypersonic and supersonic flows
24 p4249 A69-43659

OSCILLATION DAMPERS

Active control system augmentation of inherent aerodynamic damping assuring acceptable limits on oscillatory rotational motion during hypersonic Martian atmospheric entry
02 p0333 A69-11742

Computer solution of forced torsional oscillation equations for periodic coupled machine system with viscous dampers
02 p0338 A69-11893

Acoustic absorbers for combustion stabilization, discussing analytical model based on temporal damping coefficient for oscillation modes and allowance for nonuniform distribution
03 p0532 A69-13133

Spherical and single axis passive oscillation energy dampers for gravity gradient oriented satellites, utilizing earth gravity field or solar pressure
07 p1229 A69-18347

Dielectric surface loading on GaAs for suppressing traveling high field domain mode oscillations
08 p1371 A69-19911

Time response of second order nonlinear overdamped systems calculated by Krylov-Bogoliubov method of variation of parameters
08 p1297 A69-20356

Planar motion of satellite containing damping mechanism, considering small dampers case
10 p1791 A69-22935

Steady state motion of multiple unit impact damper attached to sinusoidally excited primary system, determining asymptotically stable regions
15 p2714 A69-31144

Stationary liquid under pressure effect on energy dissipation of rectilinear pipelines under pure bending
17 p2904 A69-33930

Optimal nutation damping of spin stabilized bodies, using Pontryagin maximum principle to optimize time, consumption and linear time-consumption combination
18 p3208 A69-34774

Passive damper system for reducing precession in free symmetrical rotating space vehicle, noting linear torsional spring influence on precession decay
19 p3429 A69-35913

Vibration absorber incorporating polymer spring/damping elements for attachment to complex main system, noting butyl rubber as effective and convenient damper material
20 p3620 A69-36996

Motion and stability characteristics of dual spin satellite system with pendulous type nutation dampers, noting mass unbalance effect
[AIAA PAPER 69-857] 21 p3823 A69-39385

Artificial damping of longitudinal winged reentry vehicle motions in earth atmosphere, discussing vibration damper dynamic characteristics
21 p3829 A69-39828

Time varying resistance wire to arrest oscillations in pulsed capacitor discharge circuit, deriving over, under and critical damping conditions
22 p3917 A69-41228

OSCILLATIONS

NT ELECTRON OSCILLATIONS

NT H WAVES

NT HARMONIC OSCILLATION

NT HYDROFOIL OSCILLATIONS

NT MOLECULAR OSCILLATIONS

NT NONOSCILLATORY ACTION

NT NONSTABILIZED OSCILLATION

NT PLASMA OSCILLATIONS

NT PRESSURE OSCILLATIONS

NT SELF OSCILLATION

NT STABLE OSCILLATIONS

NT TRANSIENT OSCILLATIONS

NT TRANSVERSE OSCILLATION

NT UNDAMPED OSCILLATIONS

NT WING OSCILLATIONS

Matrix technique for transformation of equation of motion into first order equation in analyzing perturbation forces producing mechanical oscillations
01 p0170 A69-10827

Summed and differential types of higher order oscillations in vibratory systems with multiple degrees of freedom under parametric excitation
02 p0346 A69-12422

Magnetic field effect on amplitude, frequency and form of LF oscillations in Gunn diodes
02 p0222 A69-12684

Laser longitudinal oscillation modes beat frequencies measurement by grouping photoelectron velocities by HF field containing photomultiplier cathode
03 p0440 A69-13265

Comparison and oscillation theory of linear differential equations, discussing zeros of solutions and Sturm type theorems
04 p0622 A69-14598

Pulsations of relativistic and nonrelativistic narrow /paraxial/ electron beams with spatial axis curved according to various laws, deriving approximate descriptive equations
04 p0632 A69-14981

Microwave oscillation and amplification in long bulk GaAs with barium titanate sheets on surface due to differential negative resistance across terminals
07 p1197 A69-18452

Natural amplitude and phase fluctuations of originally monochromatic oscillations at output of regenerative frequency divider with thermal and shot noise
07 p1099 A69-18526

Relaxation oscillations in Si p-i-n junction diode reverse-biased into avalanche calculated by computer program
07 p1101 A69-18651

Circuit producing electrical and optical oscillations simultaneously constructed by combining semiconductor laser diode with photodiode
07 p1148 A69-18688

Viscous gravitating sphere oscillations and velocity field, noting oscillations of Maxwell sphere
07 p1123 A69-18806

Quiescent solar prominences horizontal oscillations, explaining periods, damping times and prominence shape changes by model of freely oscillating prominence in corona
07 p1205 A69-19245

Rotating stellar models oscillation and stability approximated by virial equations
07 p1220 A69-19389

Periodic solutions of autonomous system oscillations with many degrees of freedom based on Poincare method applied to Liapunov systems
07 p1183 A69-19680

Laser oscillations, discussing oscillation frequency, oscillation time, noise and spectrum width, pumping and lasing materials, line broadening and giant pulse generation
09 p1517 A69-22119

Linear elliptic partial differential equations, deriving sufficient conditions on coefficients for equations to be oscillatory in certain unbounded domains
09 p1533 A69-22771

Third order nonlinear ordinary differential equation solutions oscillatory and nonoscillatory behavior for conditions on variable coefficients
09 p1533 A69-22772

Isothermal theory of cool flames, discussing oscillations-fuel consumption relations, kinetics, etc
11 p1970 A69-24476

Oscillatory properties of solutions to second order nonlinear differential equations with delayed arguments
11 p1908 A69-24767

Unforced periodically varying systems, developing approximate solutions with Floquet theory
11 p1909 A69-25289

Quasi-stochastic nonlinear one dimensional oscillations in periodically disturbed field applied to celestial mechanics of planetoids
12 p2130 A69-26373

Bias circuit LF oscillations in short Gunn devices, analyzing sinusoidal and relaxation oscillations and stable bias in terms of terminal I-V characteristics
12 p2041 A69-26628

High efficiency LF oscillations in avalanche diodes, noting evidence for parametric generation and condition for high efficiency
13 p2227 A69-27239

Gyroscope motion with unbalanced rotor in run-down mode, integrating equations for small oscillations
13 p2259 A69-27429

Current oscillations in n-type gallium arsenide related to electroacoustic domains motions, noting oscillation period dependence on voltage
13 p2318 A69-27892

Longitudinal magnetoresistance oscillations in n-type GaSb single crystals associated with electron concentrations minima
13 p2319 A69-27900

Noncollinear single cavity optical parametric oscillation with specified energy conversion using ruby laser-pumped lithium niobate, discussing tuning
14 p2460 A69-29605

Nonoscillatory solution to nonlinear differential equation, presenting theorem describing sufficient condition for nonoscillation
14 p2471 A69-29950

Magneto-optical oscillation of absorption coefficient in semiconductors during direct electron transitions
16 p2824 A69-31574

Electromagnetic fields in closed one dimensional resonators with oscillating boundary, analyzing amplitude buildup
16 p2751 A69-32030

Dynamic systems with impact interactions and nonlinear oscillation theory
16 p2875 A69-32295

Equatorial and polar semidiurnal oscillations in earth atmospheric tides related to inertial oscillations originating in autobarotropic field
17 p2996 A69-32862

Nondivergent oscillations in solar atmosphere forming normal modes or free oscillations, assuming free surface of chromosphere coronal interface and large density in convective zone
17 p3029 A69-33048

Radial oscillation periods of Hamada-Salpeter white dwarf models graphically compared with models by Harrison-Wheeler Wakano equation of state
17 p3037 A69-33642

Nonlinear differential equations describing one degree of freedom systems oscillations, allowing for dry friction and internal friction in elastic element
17 p3007 A69-33913

Oscillations of nonlinear dissipative mechanical system with two degrees of freedom, possessing structural damping at joints between moving masses and base
17 p3064 A69-33915

Cylindrical aluminum shell dynamic stability, analyzing steady state parametric oscillations, mode shape, frequency, amplitude and damping
17 p3065 A69-33929

Thin disk galactic models small oscillations, discussing frequency spectra and types of continua
18 p3196 A69-34551

Nonlinear axisymmetric oscillations and motion stability of cylindrical wound elastic glassfiber shell under time dependent uniform internal pressure
18 p3222 A69-34975

Electroabsorption oscillations in CdTe films compared with results of interband transitions theory
19 p3386 A69-36523

He-Ne laser discharges noise and oscillations classified, investigating interaction between intrinsic oscillations
19 p3338 A69-36605

High resistivity gallium arsenide single crystal LF current oscillations at low temperature, investigating electron heating effect and mechanisms
19 p3391 A69-36609

Bubble oscillations in water filled pressure chamber with alternating pressure generated by piston, measuring temporal development
19 p3302 A69-36871

Impact mechanism in hip safety belt protection in vehicles, deriving motion for natural oscillations of upper part of human body model
20 p3482 A69-37595

Self excited oscillations in systems with one linearity symmetrical with origin determined by harmonic balance method
21 p3685 A69-38463

Gaseous rotating stars radial oscillations by perturbation method, considering angular velocity effects
21 p3795 A69-38470

Plane double front detonation wave attenuation by pursuing rarefaction waves, analyzing oscillations, onset mechanism and stability during transition to Chapman-Jouguet mode
22 p3929 A69-40112

OSCILLATORS

NT AUTODYNES
NT BACKWARD WAVE TUBES
NT CARCINOTRONS
NT CRYSTAL OSCILLATORS
NT GYROSCOPIC PENDULUMS
NT HARMONIC OSCILLATORS
NT HELITRONS
NT KLYSTRONS
NT MAGNETRONS
NT MECHANICAL OSCILLATORS
NT MICROWAVE OSCILLATORS
NT MICROWAVE TUBES
NT MOLECULAR OSCILLATIONS
NT MOLECULAR OSCILLATORS
NT PENDULUMS
NT PLANOTRONS
NT RELAXATION OSCILLATORS
NT SYNCHRONIZED OSCILLATORS
NT TRAVELING WAVE TUBES
NT UNDAMPED OSCILLATIONS
NT VACUUM TUBE OSCILLATORS

Bounds from asymptotic behavior of solutions of nonlinear integrodifferential equation arising from nonlinear oscillators in acoustics
01 p0103 A69-10001

Injection locked oscillator FM receiver consisting of linear mixer and negative resistance oscillator in phase locked configuration, solving receiver output differential equation
01 p0042 A69-10247

Voltage controlled oscillator with fixed frequency crystal oscillator, noting double mixing scheme and rejection of all discrete sidebands
01 p0042 A69-10418

Millimeter wave oscillator AFC system utilizing inherent stability of molecular rotational transition applied to reflex klystron stabilization
01 p0044 A69-10628

Narrow band normal steady state random processes applied to signal dispersion by extended oscillating body, obtaining statistical characteristics
02 p0206 A69-11602

Gunn domains reduction in sheet type GaAs oscillators by spreading of field lines out of active region
02 p0215 A69-11933

GaAs Gunn diode oscillators operating at Q band frequencies
02 p0297 A69-11944

End to end cavity oscillators, folded line type cavity oscillators and reentrant cavity oscillators for use with disk seal tubes, pencil tubes and metal-ceramic tubes
02 p0216 A69-12029

Submillimeter wave oscillator /orotron/ involving open resonator with mirror having reflection grating period less than wavelength
02 p0250 A69-12248

Cavity stabilization of microwave oscillator for noise reduction
02 p0220 A69-12451

Low noise high power transistor oscillator using directional coupler, noting isolated port for injection phase locking
02 p0220 A69-12452

Microwave oscillator AM and FM noise measurement using Schottky barrier diode detector, discriminator, storage oscilloscope and wave analyzer
02 p0220 A69-12453

Amplitude noise spectra of X band microwave oscillators with Si avalanche diodes, noting various contributions and dependence on circuit and operating parameters
02 p0221 A69-12456

Time dependent functions integration by glow discharge tube and oscillator, discussing device for voltage measurement and applications in meteorology and geophysics
02 p0251 A69-12773

Epitaxial GaAs transferred electron oscillators pulsed operation at bias voltage ten times threshold voltage, noting power output and efficiency
03 p0402 A69-12854

Pulsed subharmonic oscillation in nonlinear regenerative selective circuits with reference to graph-analytical method for explaining behavior
03 p0385 A69-12918

Gunn effect in bulk GaAs, noting microwave oscillator applications
03 p0484 A69-13292

Superconductor tunnel junction with noise, calculating frequency pulling, radiation linewidth and voltage power spectrum in AC Josephson effect
03 p0486 A69-13387

Complex Doppler effect for oscillating source moving in dispersive medium, analyzing time behavior of radiation field
03 p0396 A69-13630

Low and high power pi-mode Ladderton oscillator design operation and performance characteristics
03 p0405 A69-13726

Single punch through silicon avalanche diode structure and two distinct modes of oscillation making possible pulsed generation of microwaves
04 p0573 A69-14334

Bistable zones in series oscillator circuit consisting of inductor and nonlinear p-n junction capacitance subjected to DC and AC voltage sources
04 p0575 A69-14463

Harmonic balance method to investigate phase locked oscillator stationary modes
04 p0559 A69-15138

Transistorized LF generator, discussing tradeoff due to frequency range, harmonic distortion and output stability
04 p0579 A69-15225

Solid state precision frequency standard for L multiplex carrier equipment, using four precision quartz crystal oscillators
04 p0561 A69-15451

Phase modulator with phase locked loop oscillator as phase shifter, discussing unit cascading effect
05 p0729 A69-15965

Fluidic systems with long lines simulated by transmission lines of OR/NOR oscillator
[ASME PAPER 68-WA/AUT-12]
05 p0706 A69-16178

Frequency and polarization selection of neodymium glass laser oscillators by directing secondary radiation into laser cavity and duplicating spectral properties
[IEEE PAPER P-3]
05 p0775 A69-16324

Tube and transistor type quartz crystal FM oscillators circuitry and operating characteristics, discussing generation of three frequencies
05 p0732 A69-16532

Large signal model for analysis of RF output and efficiency of IMPATT diode oscillator, noting frequency tuning
05 p0733 A69-16555

Si IMPATT diode oscillator and amplifier for CW operation at 50 GHz noting fabrication, performance and phase locking properties
05 p0733 A69-16560

X-band swept frequency oscillator using Gunn diode and ferrite phase shifter
05 p0734 A69-16573

Microwave generator of FM oscillations using two reflex klystrons and modified by wideband regenerative amplifier to minimize intrinsic AM
05 p0736 A69-16791

Neutron and X ray radiation effects upon gallium arsenide devices including Gunn oscillators, transistors, Schottky barrier diodes and optoelectronic pulse amplifiers
06 p0978 A69-16890

Q factors dependence of IMPATT diode oscillator FM noise, noting excess noise temperature correlation with diode current
06 p0899 A69-17826

Laser amplifiers and oscillators, discussing conversion of active atom excitation energy into light energy
06 p0937 A69-18006

Oscillators and amplifiers based on intervalley electron transfer in bulk GaAs
07 p1096 A69-18442

Current and voltage waveforms of transit time, resonant domain and LSA modes of operation of transferred-electron oscillators
07 p1097 A69-18443

High peak power Gunn effect oscillators for low gigahertz frequencies in transit and nontransit time limited modes
07 p1097 A69-18447

Avalanche diode oscillators efficiency of continuous wave operation in transit time mode and high current multiresonant modes
07 p1098 A69-18456

Large signal avalanche diode oscillators parameter effect on operating characteristics at any transit angle
07 p1098 A69-18458

Swept-frequency complex return-gain response of injection locked oscillator over locking bandwidth, detecting and correcting phase errors between injection-locked diode oscillators
07 p1100 A69-18645

IMPATT diode microwave oscillator, discussing large signal characterization and model for efficiency dependence on load conductance and admittance plane characteristics
07 p1101 A69-18650

Injection locking method for reducing FM noise in Gunn effect oscillators
07 p1102 A69-18862

Frequency-stable tunnel diode oscillator loaded with transmission line
07 p1104 A69-18890

Frequency modulation of CW mm-wave IMPATT diode oscillator with wide band tunability and related harmonic generation effects
07 p1106 A69-19146

Validity of formula for oscillation frequency of nearly sinusoidal tunnel diode oscillator extended to operation in nonsinusoidal regime
08 p1279 A69-19924

Propagation induced phase fluctuations reduction in widely separated oscillators, presenting microwave and optical methods
08 p1273 A69-20022

Sine wave oscillator circuits and performance prediction for NERO thrust measurement test stand
08 p1300 A69-20155

Synthesis method for UHF transistor oscillators tunable in wideband using Y-matrices
08 p1285 A69-20380

Local oscillator for space telecommunications F9 repeater, operating principles, design calculations and test results
08 p1286 A69-20596

Large signal analysis of IMPATT oscillators with carrier velocity saturation, discussing two frequency mode of operation
09 p1463 A69-21846

Functional equations of physical systems in strong coupling solved by quantum theory model of anharmonic oscillator, discussing relativistic invariant field theories
09 p1541 A69-22393

Thermal effects on modulation sensitivity and inherent AM percentage as functions of modulation frequency in IMPATT oscillators
09 p1468 A69-22588

Pulsed J band Gunn effect oscillators performance, noting hybrid domain mode due to high bias fields
09 p1468 A69-22594

Intrinsic amplitude and frequency fluctuations in transistor autooscillator, examining natural additive noise influence
09 p1469 A69-22632

Wideband 4 GHz Esaki diode injection locked oscillator, noting locking figure of merit and locking bandwidth
09 p1470 A69-22785

Small signal and saturation characteristics for X band cyclotron resonance oscillator, discussing device design and configuration
09 p1470 A69-22786

Optimum performance from planar metal ceramic triode oscillators by pulse modulation method selection, considering plate, cathode and grid modulation
09 p1470 A69-22793

Time optimal controlled linear systems with optimally chosen parameters, considering arbitrary second order oscillator controllability
10 p1666 A69-22922

Miniature telemetry systems for gun launched projectile instrumentation and ejection payloads, noting voltage controlled oscillators, commutators and VHF FM transmitters
10 p1654 A69-23280

Quenched one dimensional bulk GaAs oscillators with linearly increasing and decreasing concave and convex doping gradients, showing profiles
10 p1663 A69-23667

Coherent detection spectroscopy with laser oscillator, emphasizing high resolution and applications in astronomical spectroscopy and IR
10 p1696 A69-23684

Microwave avalanche diode oscillators performance estimates, discussing operation modes and transit time
10 p1665 A69-23873

Frequency retuning characteristics of oscillator employing avalanche transit-time diode with complementary varactor subject to current or voltage variation
11 p1844 A69-24449

Injection locked oscillator FM demodulator, analyzing signal distortion, intermodulation noise, differential gain and differential phase
11 p1845 A69-24565

Narrow band normal steady state random processes applied to signal dispersion by extended oscillating body, obtaining statistical characteristics
11 p1835 A69-24709

Quantum oscillators interaction with two level molecules system in circular laser
11 p1899 A69-25325

Frequency noises suppression in Gunn diode oscillators by frequency stabilization, using high Q external cavity
11 p1853 A69-25608

Resonant load impedance effects on Gunn diode oscillators output fluctuations, noting maximum power conditions
11 p1853 A69-25609

Varactor diodes for microwave frequency tuning of resonators used for oscillators of avalanche transit time and Gunn diodes, discussing Q factors
11 p1854 A69-25610

Transient behavior of transistor UHF oscillator, discussing network analysis for oscillation amplitude calculation by nonlinear transistor equivalent circuit diagram
11 p1854 A69-25613

Step-up mixer converting modulated IF signal to HF level by HF high power oscillator signal, discussing efficiency
11 p1854 A69-25615

AM-FM calibration modulator for microwave oscillator noise measurement
11 p1856 A69-25631

Voltage and current waveforms of resonant domain and limited space charge accumulation modes in transferred electron oscillators, noting drift current
12 p2036 A69-25908

Multivibrator circuit for generation of oscillations with frequency stability against transistor ambient temperature changes
12 p2036 A69-25919

Current to frequency converter for astronomical photometry, discussing oscillator drift, linearity characteristics and feedback pulse counting
12 p2040 A69-26479

Standing wave theory for steady state performance of Raman laser oscillator extended for time variation of exciting laser pulse
12 p2108 A69-26634

Electrodeless plasmatron coupled with oscillator operating at 5-30 kHz, discussing parameters effect on operation mode and performance
12 p2140 A69-27123

CdS acoustoelectric oscillator steady state oscillation frequency dependence on voltage and conductivity compared with linear acoustoelectric amplification theory
13 p2227 A69-27244

Nonmagnetic quadrupole ionization gauge, discussing systems design and electron oscillations
13 p2262 A69-28020

Output power and loss analysis of 2 n injection locked oscillators combined through magic tee hybrids
13 p2232 A69-28061

Bistable zones in series oscillator circuit consisting of inductor and nonlinear p-n junction capacitance subjected to DC and AC voltage sources
14 p2418 A69-28834

Quartz oscillator with electronic temperature compensation, noting reduced size, weight and power consumption
14 p2420 A69-29398

Noise reduction techniques using injection phase locking and high-Q cavities for HF oscillator high order multiplier and avalanche diode oscillator microwave sources
14 p2420 A69-29458

Avalanche diode oscillators stacked in series for combined power output
14 p2421 A69-29543

Injection phase-locking characteristics of LSA /limited space charge accumulation/ mode transferred-electron diode oscillators, employing negative conductance and equivalent circuit
14 p2421 A69-29544

Orotron electron beam excited oscillator-generator of millimeter and submillimeter wave bands with wide frequency tuning range
14 p2421 A69-29546

Reference oscillator frequency instability effect on radio signals phase shift in ionosphere measurements, evaluating errors
14 p2444 A69-29873

Gunn effect GaAs oscillators with p-n junctions, studying electrical characteristics, threshold voltages and currents during breakdown and p-n junctions injection
15 p2666 A69-30065

Push-pull circuit configurations for GaAs transferred electron oscillators, discussing CW X band and pulsed L band devices operation
15 p2574 A69-30168

Frequency effects on Gunn oscillator modulation sensitivity, discussing microwave-frequency deviation and diode impedance
15 p2577 A69-30614

Quartz oscillator amplitude and frequency fluctuations due to elements tolerance fluctuations, examining oscillator parameters contributions to spectral line width
15 p2579 A69-30944

Semiconductor technology including radar, Gunn and limited space charge accumulation oscillators, phase locked antennas, data processing and solid state computerization
15 p2581 A69-31521

X band avalanche diode oscillator operated as super-regenerative amplifier, noting frequency response characteristics ascribed to diode susceptance modulation
16 p2757 A69-31585

FM/FM telemetry system for high altitude rocket research, using independent subcarrier oscillator for each measurement transmitted with individual frequency modulation
16 p2750 A69-31853

Autooscillatory process in n-circuit tunnel diode LC oscillators acted upon by external sinusoidal voltages
16 p2764 A69-32256

Transistorized L band oscillator tuned by Ga-doped YIG, discussing ferrimagnetic material properties and device equivalent circuit
16 p2761 A69-32450

Quantum electronics, Volume 2, Maser amplifiers and oscillators
17 p2982 A69-33687

Gunn effect theory and applications, discussing field domains in semiconductors, excited oscillations measurement, oscillators design, computer elements, etc
18 p3183 A69-35160

Parametric and forced oscillations analogy for analyzing dynamic behavior of oscillatory systems with time dependent parameters
18 p3175 A69-35322

Induced-emission oscillator navigation sensor with performance limitations, noting ring laser and nuclear maser gyro and laser accelerometer
19 p3369 A69-35795

Oscillator without reactive components for integrated circuit biotelemetry, noting transmission in AM broadcast band
19 p3261 A69-36244

Nonlinear free motion of conservative oscillator with one degree of freedom calculated by collocation method
19 p3438 A69-36308

Free oscillation period of nonlinear oscillators with one degree of freedom, discussing approximation method
19 p3373 A69-36310

Steady resonance operation modes of nonlinear oscillatory and rotational systems described by differential equations with deviating argument, using averaging procedure
19 p3374 A69-36469

Tunnel diode oscillators theory applications, investigating self resonance phenomena relating to static characteristic variations under self oscillating conditions
19 p3285 A69-36738

Voltage variation frequency analysis for narrow-band sweep oscillators circuit design
20 p3486 A69-37010

Integrating filter analysis for effect of phase detector sawtooth characteristics on locking range of phase locked oscillator
20 p3486 A69-37011

Fluidic feedback oscillator performance from fluid density effects analysis including supply jet, feedback line dynamics and load and control port impedances [ASME PAPER 69-FLCS-39]
20 p3465 A69-37984

Gunn device performance for various oscillator types, discussing cavity oscillator characteristics variation
21 p3681 A69-38394

- Gunn oscillators protection from catastrophic breakdown phenomena, using carrier velocity saturation in n-type Ge 21 p3682 A69-38777
- Periodic motions of mechanical oscillators with velocity discontinuities analyzed by differential equations 21 p3771 A69-39009
- Balloon-borne transmitter consisting of oscillator, driver and final output and connectable automatic frequency control circuit 21 p3682 A69-39251
- Laser modulation theoretical analysis based on high speed laser oscillators, discussing high energy physics research applications 22 p3959 A69-39975
- King furnace absorption source used with spectrometer in relative oscillator strength measurement, with experiments on lines of Fe I 22 p4022 A69-40466
- Oscillators frequency instability theories emphasizing difference between concepts of frequency instability and spectral purity 22 p3900 A69-40930

OSCILLOGRAMS

U OSCILLOGRAPH

OSCILLOGRAPH

- Stimulated emission properties of active fibers obtained from photomultipliers transmitting pulses to oscillograph 05 p0761 A69-15657
- Statistical processing of oscillograms of instantaneous values of wire tension during winding, determining stress characteristics 06 p0927 A69-17691
- Device to simultaneously observe integral and differential field effect curves on oscillograph screen as function of continuously varying field 10 p1698 A69-24210
- HF measurements by phase and amplification control of signal in impulse oscillography, noting accuracy in nanosecond range and signal distortion 11 p1880 A69-24541
- Stimulated emission properties of active fibers obtained from photomultipliers transmitting pulses to oscillograph 16 p2792 A69-32514

OSCILLOSCOPES

- Oscilloscope display of sample of subnanosecond light pulse, using optical analog of electronic sampling oscilloscope 02 p0259 A69-12656

OSCULATIONS

U DOUBLE CUSPS

OSCULATORY INTERPOLATION

U ORBIT CALCULATION

U ORBIT PERTURBATION

OSEEN APPROXIMATION

- Green function in closed form for energy transport equation solution in axisymmetric Oseen flow 08 p1305 A69-20850
- Leading edge conditions of obstacle exuding fuel into oxidizer stream, using Oseen equations in parabolic coordinate system 11 p1997 A69-24307

OSMIUM

- Ligand field transitions in tertiary phosphine and arsine complexes of ruthenium and osmium 07 p1075 A69-19483

OSMOMETERS

- High speed automatic osmometer applied to measurements of diffusible branched polyethylene samples, discussing apparent molecular weight observations 01 p0024 A69-10933

OSMOSIS

- Transient electro-osmosis of water in capillary tubes for pumping and generation modes, analyzing response to step change in pressure or voltage change under external loading 04 p0555 A69-14862
- Human blood viscosity measurement over wide range of shear rates, obtaining rheological data, suggesting osmotic red cell crenation role 23 p4095 A69-42078
- Respiratory effects of body temperature changes separation from blood osmolality changes in dehydrated man 23 p4097 A69-42094
- Urine osmolality of centrifuged rats compared with ad libitum or pair-fed control animals, indicating enhanced free water excretion and antidiuretic hormone involvement 24 p4262 A69-42904

OSMOTIC PRESSURE

U OSMOSIS

OSO

NT OSO-3

NT OSO-C

- OSO-4 solar UV spectrum measurements, correlating chromospheric line intensity and photospheric magnetic field strengths 02 p0313 A69-11485 [AAS PAPER 68-219]

- Space lubrication system for Orbiting Solar Observatory program, discussing theoretical high vacuum principles and flight performance and environmental test data 02 p0252 A69-11766

- OSO-B2 satellite zodiacal light observations at constant 90 degree elongation, measuring polarized component as function of time 02 p0245 A69-12718

- Proportional counter array for detection of soft X ray photons from OSO-4 observations, discussing solar event energy spectra 12 p2151 A69-26936

- OSO spacecraft thermal design modified to operate University of Minnesota zodiacal light monitor experiment [AAS PAPER 69-173] 24 p4393 A69-42873

OSO-3

- Solar X-ray events observed by scintillation counter telescope on OSO 3 satellite, discussing X ray spectra during burst initial and decay phases 20 p3593 A69-38166

OSO-C

- Solar extreme UV, soft and hard solar X rays, cosmic X rays and gamma rays, cosmic ray particles and near earth visible radiation observed by OSO-3 09 p1578 A69-22167

- Solar far UV emissions observed from OSO-C by grazing incidence grating spectrometer, noting temporal variations and atmospheric absorption characteristics 09 p1578 A69-22168

- Solar X ray and extreme UV spectra during flares, attributing intense emissions to optical transitions 09 p1578 A69-22169

- Solar and cosmic X rays observed by OSO-C, stressing galaxy M 87 upper limits and Lupus XR-1 power law spectral form 09 p1578 A69-22171

- Impulsive solar microwave bursts observed by parabolic reflector, obtaining bursts spectra and total flux density 09 p1579 A69-22178

OTOLITH ORGANS

- Otolith and cupular apparatus interaction in human vestibular analyzer during gravitational changes 07 p1062 A69-18589

- Otolith apparatus response threshold under weightlessness conditions simulated by aircraft flight, measuring galvanic current threshold for banking 08 p1263 A69-19934

- Simulated weightlessness used in determining ontogenesis of otolith organ in tadpoles and eggs as function of acceleration forces [DVL-855] 10 p1647 A69-24021

- Otolith apparatus functioning under weightlessness and accelerations in test stand experiments, discussing measuring techniques and nystagmic reaction durations 20 p3471 A69-37253

- Vestibular analyzer function relation to arterial pressure during otolith stimulation experiments on subjects susceptible and nonsusceptible to motion sickness 20 p3472 A69-37264

OTOLOGY

- Extraterrestrial vestibular research, discussing human otolithic apparatus regulation subjected to change from geocentric to heliocentric orientation [UN PAPER 68-95389] 01 p0014 A69-10508

- Structural differences effect of gyral and sulcal areas of acoustic projection cortex on primary induced acoustic responses 23 p4079 A69-41380

OUTER RADIATION BELT

- Solar proton event generating sudden commencement magnetic storm, discussing effects on outer belt electrons as observed by Explorer 26 and time delay 01 p0146 A69-11124

- High latitude outer zone electrons boundary region during geomagnetically quiet periods 03 p0502 A69-14004

- Drift periodic echoes in outer zone electron flux due to magnetospheric disturbance 05 p0815 A69-16259

- Radial diffusion of high energy electrons in outer radiation belts, determining statistically delay time between electron intensity variations 06 p0919 A69-17720

- Cyclotron instability of outer radiation belt protons, taking into account data on spatial distribution and ion composition of exospheric plasma 06 p0919 A69-17721

- Cut-off boundary latitude and electron flux changes in midnight sector of outer radiation belt during magnetic bay periods from Injun 4 satellite data 07 p1204 A69-18836

- Bimodal diffusion mechanism for acceleration of trapped electrons and protons in earth radiation belts, noting particle intensity profiles and energy spectra 09 p1576 A69-21708

- Outer radiation zone electron intensities during magnetic storms for morphology of zone electron acceleration mechanisms 11 p1950 A69-25147

- Charged particle population dynamics in outer radiation zone of magnetosphere, discussing ring current particles, protons, electrons, alpha particles and electric field 12 p2150 A69-26743

- Particle fluxes in outer radiation belt and unstable radiation zone of outer geomagnetic field, discussing electron diffusion into magnetosphere and magnetic disturbances 12 p2150 A69-26744

- High latitude capture region boundary for electrons in upper radiation belt determined relative to current electrojets in ionosphere from satellite observations 13 p2327 A69-27700

- Diffusion of equatorial particles in outer radiation zone caused by expansions and contractions of permanently compressed magnetosphere, obtaining electric fields 14 p2510 A69-28937

- Sporadic electron flux contribution to high latitude geomagnetic disturbances at outer radiation belt boundary estimated from Elektron 1 and 2 observations 14 p2438 A69-29079

- Dawn-dusk electric field in outer radiation zone associated with magnetospheric plasma convection, comparing electron densities for magnetically quiet periods 18 p3128 A69-34942

- High latitude limit of closed geomagnetic field lines indicated by high latitude electron boundary in outer radiation zone during Alouette satellite energy particle experiment 20 p3531 A69-37875

- Electron intensities and substorm drift effects in outer radiation belt using two satellite technique 24 p4309 A69-43172

- Electron intensities and substorm drift effects in outer radiation belt using two satellite technique 24 p4309 A69-43172

OUTGASSING

- Heat treatments in inert gas atmosphere improve elastic foam polyurethane by reducing capability of toxic outgassing 10 p1716 A69-23503

- Outgassed condensation effects in vacuum on magnesium difluoride overcoated UV irradiated Al mirrors, including temperature effects, Lyman alpha reflectance and IR analysis of deposits 13 p2299 A69-28015

- Outgassing rates of multifoil insulation materials for sealed vacuum systems measured over temperature range as function of pumping time 13 p2299 A69-28016

- Outgassing behavior of polymers in spacecraft by thermal-vacuum weight-loss and contamination tests 13 p2286 A69-28089

- Leak rate measurement accuracy of rate-of-rise technique for nitrogen, methane and He between millionth and thousandth torr 16 p2791 A69-32326

- Thermal rare gas release from mineral separates of Mocs meteorite, using method giving activation energies as function of temperature 19 p3419 A69-36141

- Rare gas distribution in earth atmosphere explained as outgassing from primordial solid particles, discussing stony meteorites composition 20 p3600 A69-37489

- Outgassing rates of stainless steel and Al with different surface treatments, including glass bead shot blasting, electropolishing, baking and vacuum cleaning 22 p3958 A69-41215

- High temperature vacuum treatment of thick stainless steel sheets reducing hydrogen content and outgassing 22 p3958 A69-41217

OUTLETS

U VENTS

OUTPUT

U LASER OUTPUTS

U MASER OUTPUTS

OV-10 AIRCRAFT

- Landing and takeoff demonstration tests of OV-10A aircraft through rough terrain, noting pilots excessive physiological stresses
[AIAA PAPER 69-316] 09 p1434 A69-22391
- Glass reinforced plastic molding compounds for OV-10A airplane structural components, noting cost savings
[SAE PAPER 690342] 11 p1890 A69-24497

OVERCAST

U CLOUD COVER

OVERESTIMATION

U ERRORS

U ESTIMATING

OVEREXPOSURE

U RADIATION DOSAGE

OVERPRESSURE

- Sonic boom minimum achievable shock front pressure rise and overpressure level prediction for given aircraft and flight conditions
08 p1253 A69-19903

- Sonic boom signatures produced by diverse SST configurations during cruise, indicating aircraft length as overpressure limit factor
24 p4253 A69-43661

- Sonic boom lower bounds determination in midfield based on modification of Jones results by minimizing overpressure or shock strength of boom wave positive component
24 p4254 A69-43662

OVERTONES

U HARMONICS

OVERTHROTTLE

- Failure mechanism in high-voltage semiconductor diodes explained by effect of reverse voltage pulses, considering design reliability
08 p1294 A69-21116

- Overload protection guidelines for power subsystems, discussing source and protective device characteristics emphasizing spacecraft requirements
17 p2904 A69-34088

OXIDASE

- Lactate dehydrogenase and monoamine oxidase distribution in medulla oblongata and cerebellum of squirrel monkey
12 p2018 A69-25778

OXIDATION

NT ELECTROCHEMICAL OXIDATION

NT PHOTOOXIDATION

- Titanium alloy VTZ-1 recrystallization and oxidation processes studied by heating within 700-1200 C temperature range
01 p0094 A69-10214

- Sikhote-Alin iron meteorite high temperature oxidation and ablation and simulation with Fe-Ni alloy, noting phase compositions and structure
01 p0025 A69-11373

- Olefins combustion studies, considering influence on hexane combustion at different oxidation stages leading to ignition
02 p0352 A69-12309

- Radiation resistance of MOS transistors noting relationship with thermal stability, gate oxidation and metals used
02 p0221 A69-12468

- Steel corrosion by iodine noting effects of water and oxygen
03 p0444 A69-13310

- Impurities effect on defects in oxygen deficient niobium, tantalum and zirconium oxide scales at high oxygen pressures, noting relationship to metal oxidation
03 p0444 A69-13312

- Deposit formation in empty wing tanks due to auto-oxidative degradation of hydrocarbon fuel, noting results of environment simulation tests
[SAE PAPER 680733] 03 p0366 A69-13439

- Wet oxidation process for management of organic waste products in closed ecologies of long term manned space missions
[SAE PAPER 680714] 03 p0380 A69-13443

- French collection of papers on oxidation and combustion covering reaction characteristics, thermodynamics, chain reactions, flammable gas mixtures, etc
06 p1030 A69-17412

- Phenomenological characteristics of oxidation reactions and combustion, noting nature and physical state of mixtures, localization of reaction and chain mechanisms
06 p1031 A69-17413

- Slow oxidation and self ignition in gaseous phase, discussing cold flames and interpretation of experimental data
06 p1031 A69-17416

- French collection of articles on oxidation and combustion, Volume 2
06 p1032 A69-17419

- Liquid phase radical oxidation with intermediate and end products in same phase, discussing products, hydroperoxidation and liquid systems explosiveness
06 p1032 A69-17425

- Shock tube study of ammonia oxidation at high temperature, detecting molecular species in reaction zone by IR emission
06 p0885 A69-17936

- Chemiluminescence in high temperature oxidation of methane studied in shock tube
06 p0885 A69-17937

- Plastic deformation of internally oxidized dispersion strengthened silver magnesium alloys, noting hardening effect dependence on oxidation temperature
07 p1159 A69-18627

- Tensile and creep behavior of nickel at 600 C after oxidation at 1200 C, correlating results with structural differences caused by oxidation
08 p1333 A69-20556

- Oxidation influence on molybdenum disilicide coatings emissivity, determining degree of blackness over thermal stability range
09 p1522 A69-21588

- Electron injection into ZnO from aqueous solutions of stable substances, correlating injection with oxidation potential of substance
10 p1651 A69-22940

- Oxidation effects on creep and fatigue properties of metals noting time and temperature roles
10 p1708 A69-22998

- Mineralizing metabolic wastes by catalytic oxidation of pyrolysis products, noting nutritive value of ash solutions for *Chlorella* cultivation
10 p1649 A69-23579

- Cool flames nonisothermal two-stage ignition of neopentane-oxygen mixtures, discussing chain propagation due to isomerization
11 p1940 A69-24477

- Annealing effects on titanium oxidation kinetics, indicating no relation between oxide formation and diffusion anisotropy of oxygen
12 p2112 A69-26039

- Furnace for automatic high temperature cycling in controlled oxidizing environment
12 p2093 A69-26483

- Book on oxidation and shielding of beryllium in gas media for nuclear and aircraft technology
13 p2280 A69-27927

- Nb-Ta alloys oxidation kinetics at high temperature and structure and composition of oxide films and scale layers, discussing anomaly in oxidation rate temperature dependence
14 p2464 A69-29650

- Corrosive wear due to atmospheric O in sliding metal systems, noting oxidation rate relation to wear rate and activation energy
[ASLE PAPER 68-LC-11] 15 p2622 A69-30605

- Normal, isoprenoid, dicarboxylic, keto and various aromatic acids isolated from controlled stepwise degradation of Green River kerogen by successive chromic acid oxidations
15 p2606 A69-31533

- Flexure of Ta and Nb thin rectangular specimens during high temperature oxidation, showing stress generation due to O dissolution into metal surface
[ECS PAPER 87] 15 p2641 A69-31541

- Electrochemical couples of zinc-metallic oxides or O used in battery with water electrolyte
16 p2740 A69-32421

- Flow rate effect of oxygen-argon mixture on Zr oxidation studied to determine exclusion as factor in Zr weight increase
18 p3154 A69-34272

- Low molecular weight fluorocarbons pyrolysis and oxidation in single pulse shock tubes, using vapor phase chromatography and mass spectral analyses
18 p3099 A69-34467

- Oxygen concentration effects on oxidation of synthetic paraffinic and type II ester lubricants determined from ball bearing tests at 400 and 450 degrees F
18 p3149 A69-35177

- Kinetics of titanium oxidation in transitional range at high temperatures, showing agreement with oxidation model
18 p3157 A69-35252

- Oxygen influence on low pressure ethylene decomposition on high temperature tungsten and Re ribbons surface
19 p3266 A69-36732

- Oxygen environment influence on Inconel X-750 surface deformation and cracking during fatigue related to chemisorption and oxidation
20 p3558 A69-36966

- Protective coatings for high melting point metals, discussing prevention of low temperature coating breakdown due to oxidation
20 p3561 A69-37375

- Molybdenum disilicide oxidation kinetics at various temperatures by thermal conductivity method, determining oxidation rates and activation energy
20 p3567 A69-37780

- Heat resistance and strength properties of porous Ni-base cermet materials with mica additions under high temperature oxidation
21 p3751 A69-38615

- Chromatographic analysis of products formed during induction period of 2-methylbutane gaseous oxidation in flow system at low temperatures and long residence times
21 p3669 A69-38798

- Gas phase arrest peak analogy with liquid phase oxygen cut-off during final stages of hydrocarbons gaseous oxidation reactions, noting active centers
21 p3669 A69-38805

- Oxygen pressure effect on oxide layer composition on W surface by secondary ion-ion emission
21 p3746 A69-39071

- Water purification through biological oxidation of organic wastes using controlled photosynthesis, discussing algae production and harvesting
21 p3668 A69-39711

- Preferential welding oxidation emphasized as element transfer mechanism in weld metal composition control
22 p3955 A69-40460

- Rodent swimming and treadmill training effect on capacity of mitochondrial fraction from hind limb muscles to oxidize pyruvate triples
23 p4095 A69-42084

- Nb single crystals oxidation in dry oxygen at high pressure and temperature indicating suboxide platelets existence as function of temperature
23 p4177 A69-42357

- Gamma radiation effect on AgCl-Cu redox state in AgCl activated, heat treated Na-Al-B-Si glass, using EPR method
23 p4180 A69-42471

- Oil high temperature and oxidation conditions in aircraft piston engines, including physicochemical changes
24 p4321 A69-43141

- Ellipsometer measurements for oxidation rates of binary Ti-Al alloys in vacuum and in pure and premixed gases, using in situ test cell
24 p4316 A69-43322

OXIDATION RESISTANCE

- Chemical vapor deposition of iridium coatings on graphites for high temperature oxidation protection, discussing parameters for iridium compounds and optimum depositing conditions
01 p0097 A69-10643

- Zr-Be-Nb system oxidation resistance decrease at 650 degrees C ascribed to Be and Nb additions
02 p0262 A69-11844

- Oxidation resistance of Zr-Nb-Mo alloys at high temperature in air or water
02 p0264 A69-11857

- Sulfur-organic compounds association with aromatic hydrocarbons, noting oxidation inhibiting effect on petroleum oil
03 p0494 A69-13800

- Be, Ce, V and Ti additions effect on oxidizability of cast, forged and cold worked Nb-Cr-Mo alloys
04 p0618 A69-15081

- Columbium alloys properties, discussing creep strength, oxidation resistance, costs, production, etc
07 p1164 A69-18791

- Oxidation kinetics of niobium titanium alloy in air and oxygen at 1000 C, analyzing nitrogen and pressure effects
08 p1331 A69-20193

- Oxidation kinetics of niobium titanium alloy in air and oxygen between 650 and 1000 C, analyzing activation energies and nitrogen effects
08 p1331 A69-20194

- Cobalt chromium high temperature oxidation and scale formation
[ECS PAPER 413] 08 p1332 A69-20363

Cobalt chromium alloys high temperature oxidation kinetics, discussing thermographic study of oxidation rate and oxygen pressure role [ECS PAPER 413] 08 p1332 A69-20364

Refractory metal oxidation protection by inorganic compounds at high temperatures, discussing protective mechanisms 09 p1526 A69-22322

Ductile metal clads and coatings of silicides, aluminides and noble metals to protect Cr alloys against nitrogen embrittlement and air oxidation 12 p2114 A69-26495

Chemical composition of cermet material for radial sealing of high temperature gas turbines, ensuring structural stability and oxidation resistance 13 p2275 A69-27344

Room temperature WC-Co compacts oxidation resistance in air noting increase with preliminary sintering temperature 13 p2275 A69-27345

Tungsten disilicide coated Ta-W alloy oxidation mechanisms, comparing coatings protective properties at high temperatures 13 p2280 A69-28137

Electrodeposits on molybdenum alloys in high temperature oxidizing environments, noting performance of Cr-Ni-Cr composite coating 14 p2466 A69-29934

Nb corner of Nb-Mo-Cr alloy phase diagram and oxidizability in air at high temperature 18 p3157 A69-35248

Thermoplastic polyarylsulfone thermal and electrical properties at over 500 F, noting resistance to thermal oxidative attack 19 p3355 A69-35527

Thermogravimetric study of oxidation protection of refractory metals by fused LiF coating, noting oxidation retardation of Ta, Nb and W 19 p3341 A69-35573

Boron nitride and boron nitride composite under high temperatures in air and vacuum for various time periods, discussing thermal shock and oxidation resistance 19 p3359 A69-36208

Commercial Co base superalloys oxidation and hot corrosion resistance under controlled environments, examining role of various alloying elements [ASM PAPER D8-21.5] 20 p3564 A69-38134

Oxidation resistant coating methods and systems for Cb base materials protection for aerospace vehicles and aircraft propulsion systems structures 21 p3730 A69-38672

Oxidation resistant silicide coatings for tantalum and tungsten alloys at elevated temperatures 21 p3730 A69-38673

Silicide and B-modified coatings on Mo, noting improved high temperature oxidation resistance under thermocycling 22 p3957 A69-40972

Protective coatings on Ni base superalloys for gas turbine engine blade and vane components for hot corrosion and oxidation resistance [SAE PAPER 690480] 24 p4335 A69-43515

OXIDES

NT ALUMINUM OXIDES
NT ANATASE
NT BARIUM OXIDES
NT BERYLLIUM OXIDES
NT BISMUTH OXIDES
NT CALCIUM OXIDES
NT CARBON DIOXIDE
NT CARBON MONOXIDE
NT CESIUM OXIDES
NT CHROMITES
NT CHROMIUM OXIDES
NT COBALT OXIDES
NT COPPER OXIDES
NT ENSTATITE
NT GERMANIUM OXIDES
NT HEAVY WATER
NT HYDROGEN PEROXIDE
NT ILMENITE
NT IRON OXIDES
NT LEAD OXIDES
NT LITHIUM OXIDES
NT MAGNESIUM OXIDES
NT MAGNETITE
NT MANGANESE OXIDES
NT METAL OXIDES
NT MOLYBDENUM OXIDES
NT NICKEL OXIDES
NT NIOBIUM OXIDES
NT NITRIC OXIDE
NT NITROGEN DIOXIDE
NT NITROGEN OXIDES
NT NITROGEN TETROXIDE
NT NITROUS OXIDES

NT PEROXIDES
NT PYROXENES
NT QUARTZ
NT RUTILE
NT SAPPHIRE
NT SILICON DIOXIDE
NT SILICON OXIDES
NT SULFUR OXIDES
NT THORIUM OXIDES
NT TIN OXIDES
NT TITANIUM OXIDES
NT TUNGSTEN OXIDES
NT URANIUM OXIDES
NT VANADIUM OXIDES
NT ZINC OXIDES
NT ZIRCONIUM OXIDES

Gamma radiation effects on gate threshold voltages in modified oxide insulators in MOS structures 06 p0976 A69-16876

Mass spectra of quinoline and isquinoline N-oxides, discussing diagnostic values of fragmentation reactions for heteroaromatic N-oxide function presence 07 p1075 A69-19496

Ionic and nonionic mineral oxide powder fillers influence on stereopolymers lattices formed from phenolformaldehyde oligomers, discussing mechanical properties 08 p1335 A69-20331

Oxide ceramics finishing processes, discussing leaching, machining, surface finishing, strengthening by compressive surface layers and joining 09 p1510 A69-22350

Oxide and carbide high-melting-point materials for MHD generator electrode walls 13 p2284 A69-27471

Oxide composition of silicate spherules from forest area devastated by Tungka meteorite explosion using electron microprobe analysis 14 p2516 A69-28869

Multifoil thermal insulation using oxide particle layer separation, discussing insulation heat transfer characteristics as function of source temperature and oxide particle size 14 p2539 A69-29213

Optical and electrical properties of thin amorphous films of glass-forming oxide, using X ray diffraction and electron microscopy for structural features 19 p3391 A69-36561

Thermal expansion properties of oxides and oxide solid solutions measured for improved expansion coefficient search 20 p3567 A69-38066

OXIDIZERS

NT FLOX
NT HIGH ENERGY OXIDIZERS
NT LIQUID OXIDIZERS
NT LIQUID OXYGEN
NT ROCKET OXIDIZERS

Remotely operated open-cup impact tester for studying impact initiation of reaction of various liquid fluorinating agents with metals and plastics 06 p0907 A69-17876

Oxidizer particle size and binder type effects on nonoxidative combustion instability of solid propellants [AIAA PAPER 69-175] 06 p0983 A69-18152

Ignition delay of paraphenylenediamine associated with nitric acid, showing relation between grain diameter and hypergolic ignition mechanism, noting oxidizer concentration effects 15 p2561 A69-30185

Combustion of pulse heated single Al and Be particles in various oxidizers [WSCI PAPER 69-2] 16 p2830 A69-32343

Thermal decomposition behavior of perchlorate oxidizers studied by flash mass thermal analysis for determining propellant combustion kinetics [WSCI PAPER 69-19] 16 p2832 A69-32357

Ammonium perchlorate grinding and blending facility, discussing process flow, machinery, etc [AIAA PAPER 69-516] 16 p2767 A69-32664

Loaded bipropellant liquid propulsion system sterilization studies on structural and nonmetallic materials suitability for use in oxidizer [AIAA PAPER 68-631] 21 p3785 A69-39025

OXIMETRY

Statistical relations between minute blood circulation volume, O capacity and consumption rate in tissues of men and dogs 19 p3260 A69-35896

Oxygen steady state transfer across thin layers of centrifuged erythrocytes at 37 degrees C before and after hemoglobin saturation with CO 23 p4093 A69-42064

OXYFLUORIDES

Analog simulation of chemically reacting system applied to thermal decomposition of oxygen difluoride [WSCI PAPER 68-49] 07 p1073 A69-18318

OXYGEN

NT HIGH PRESSURE OXYGEN
NT LIQUID OXYGEN
NT OZONE

Fine structure of vibrational spectra of molecular H and O, water and deuterium oxide, using molecular photoelectron spectrometer 01 p0023 A69-10141

Sulfur trioxide production in photolysis of sulfur dioxide at 1849 angstroms, noting oxygen addition effect on quantum yield 01 p0024 A69-10619

Radio telescope measurements of total vertical atmospheric absorption to determine effective mean free path of oxygen and water vapor for absorption 02 p0206 A69-11450

Oxygen addition to fuel stream effect on formation of soot and polycyclic aromatic hydrocarbons in ethane-air and ethylene-air diffusion flames 02 p0205 A69-12318

Explosion limits in hydrogen-oxygen reaction measured in diffusion regime, giving rate constant of branching step 02 p0353 A69-12319

Dissociative velocity rates of oxygen and ozone in ionosphere obtained by exponential approximation for molecular concentration distribution 02 p0246 A69-12769

Electron transition probability of oxygen molecule determined using weak bands telluric lines photoelectric recordings 03 p0420 A69-13276

Oxygen surface densities measured by method based on characteristic X ray production by 100 keV protons 04 p0631 A69-14446

Solid solutions of O in Ti and Zr, noting superstructure formation and physical properties 04 p0618 A69-15078

Mathematical analysis of oxygen diffusion to coal grains during coal dust combustion, evaluating kinetic constants by burning time 04 p0687 A69-15167

Oxygen ions motion in oxygen, measuring drift velocities in glow discharge 05 p0795 A69-15662

Similarity between characteristics of T layers in oxygen discharge positive column and Gunn instabilities in GaAs, noting role of negative O ions 05 p0800 A69-15739

Corona and breakdown voltage in helium-oxygen atmospheres, analyzing conditions for manned space flight vehicles 05 p0730 A69-16241

Continuous and pulsed lasing characteristics during discharge in pure oxygen noting ozone formation and removal at tube walls 06 p0932 A69-16923

Mass spectrometric measurements to determine energy distributions of ions produced in dissociative photoionization of O molecules 06 p0960 A69-17110

Experimental and numerical nonequilibrium shock layer around cones in hypersonic pure oxygen flows with simultaneous rotational, vibrational and dissociation relaxation [AIAA PAPER 69-136] 06 p0864 A69-18141

Oxygen diffusion parameters in beta-titanium measured by successive layer removal, noting lattice constant dependence on temperature 07 p1163 A69-18783

Chemisorbed oxygen effect on electrical conductivity of zinc doped polycrystalline tin oxides 07 p1201 A69-19478

Detonation wave propagation in H-O mixtures in supersonic flow, noting detonation front structure and velocity 08 p1420 A69-19882

Rhenium effect on lattice solid solubility of oxygen in tungsten, calculating rhenium-oxygen cluster minimum binding free energy 08 p1329 A69-20007

Ionization and attachment coefficients in oxygen at low pressures, noting Paschen curves near minimum sparking potential and secondary ionization coefficient 08 p1354 A69-20099

Oxygen index test for precise flammability ratings of plastics on numerical basis, eliminating drawbacks of ignition, end point and nonequilibrium conditions operation 08 p1335 A69-20114

Platinum electrode study of electrochemical oxygen reduction in nonaqueous media, including kinetic effects of different water concentration levels [ECS PAPER 7] 08 p1268 A69-20361

Fuel cell oxygen ionization on nickel, silver and nickel-silver disk electrodes 08 p1260 A69-21045

Li atoms and O interactions with electron radiation produced defects in Si studied by IR spectroscopy 09 p1554 A69-21337

Electron detachment cross sections for negative atomic and molecular O ions with incident energies between 3 and 100 eV 09 p1542 A69-21625

Vibrational relaxation times in pure O and in O with methane impurity determined with acoustic absorption measurements 09 p1542 A69-21721

Atmospheric molecular oxygen temperatures from photoelectric recordings of absorption bands, analyzing relaxation process and photoeffects in oxygen molecules 09 p1490 A69-21863

O, Ne, Si and Fe ionization equilibria in low density plasma, including dielectronic recombination and autoionization processes in calculations 09 p1543 A69-22404

Vertical atmospheric absorption of radio waves by water vapor and oxygen molecules near rotational resonance based on radio emission measurements 10 p1658 A69-23944

Optical depth at under 110 Å due to continuous absorption by N, O and Ne ions estimated in high excitation planetary nebulae 10 p1790 A69-24140

Resonances in cross sections for electron impact excitation of forbidden lines in oxygen molecular ion at near threshold energies for astrophysical applications 11 p1921 A69-24417

Relation between electric field strength and mean energy for electron swarms in oxygen determined, using Boltzmann transport equation 11 p1921 A69-24419

Effective cross sections of UV radiation absorption by molecular oxygen in Schumann-Runge bands at high temperatures 11 p1921 A69-24617

Molecular O and total number densities between 70 and 120 km determined with rocket measurements of atmospheric absorption of solar UV and X rays 12 p2065 A69-26106

Oxygen content effect on tension-compression fatigue of alpha Ti alloys, discussing internal damage associated with twin formation 12 p2116 A69-27134

Oxygen and NO ions yields produced by dissociative attachment of electrons to nitrogen dioxide as function of electron energy, considering electron affinities lower limits 13 p2301 A69-27363

Manganese catalyst photoreactivation in photosynthetic oxygen evolution in Mn deficient alga *Anacystis nidulans* cells 13 p2210 A69-28257

Fluorescence stimulated by high energy electron and ion beams, determining vibrational temperature and concentration of molecular oxygen in high enthalpy wind tunnel flows 13 p2302 A69-28265

Thermal ignition of methane-oxygen mixture, observing flame propagation 13 p2380 A69-28459

Electron transition probability of oxygen molecule determined using weak bands telluric lines photoelectric recordings 14 p2487 A69-28784

Nighttime molecular O densities between 100- 130 km determined from Schumann-Runge absorption data for successive far UV spectra of hot star 14 p2435 A69-28959

Spectral analysis of O and Ti based on O extraction, using Ni tank in A atmosphere with DC arc 14 p2446 A69-29158

Tungsten work function increase by oxygen in diode thermionic emission, investigating crystals and vapor deposited layers 14 p2507 A69-29273

Oxygen content and grain structure influence on TSS Ti alloy mechanical properties, notch and crack growth sensitivity at low temperature 15 p2637 A69-30266

Maximum strengthening due to second phase precipitation within operating temperatures maintainable to 20 hr during aging of Nb-Hf-O and Nb-Zr-O alloys 15 p2640 A69-30632

Pressure and wavelength dependence of molecular O absorption coefficient near 1215 Å, utilizing UV emission from crossed beam atomic collision 15 p2656 A69-31031

Oxygen physiological and biochemical effects on *Pseudomonas saccharophila*, discussing sucrose uptake, lipid synthesis and polysaccharide formation 15 p2556 A69-31045

Solid fuel ignition with gaseous oxygen in presence of copper chromate and other catalysts 16 p2829 A69-31913

Lifetime of ground state oxygen molecular ions in sunlight from photodetachment rate by free electron production measurement from ions in buffer gas 16 p2848 A69-31973

Electron cooling rates due to vibrational excitation of molecular oxygen calculated as function of electron temperature in E region 16 p2774 A69-31982

Fuel cell oxygen electrode problems, noting oxygen ionization reaction and disk electrodes role 16 p2739 A69-32416

Ozone concentration photochemistry between 30-35 km, determining parameters in Hampson theory /hydrogen-oxygen atmosphere/ 16 p2787 A69-32636

Nitrous oxide-CO bimolecular reaction and O-CO recombination in single pulse shock tube 16 p2748 A69-32793

Oxygen adsorption on Mo single crystals /100/ surface as function of temperature using low energy electron diffraction 16 p2748 A69-32795

Fatigue crack growth rates in stainless steel at elevated temperature measured as function of oxygen pressure in resonant fatigue machine 17 p2987 A69-33074

Emission intensity ratio change as function of polar auroral height compared to variation in atmospheric concentration ratio of oxygen to nitrogen 17 p2963 A69-33956

Mean lives of 1s super 2 2p super 2 super 1D level in F VI and O V measured by beam foil technique 17 p3009 A69-34188

Gladstone-Dale constants for dissociating high temperature oxygen determined for molecule and atom from density changes across shock 18 p3176 A69-34452

Recombination coefficients of oxygen and nitrogen ions with electrons related to electron temperature, using microwave afterglow/mass spectrometer 18 p3176 A69-34789

Low energy electron diffraction oxygen adsorption kinetics on planes of tungsten at coverages below monolayer and work function measurements 18 p3183 A69-35106

Oxygen concentration effects on oxidation of synthetic paraffinic and type II ester lubricants determined from ball bearing tests at 400 and 450 degrees F 18 p3149 A69-35177

OGO 5 ion spectrometer for measuring oxygen, He and hydrogen ion concentration, noting functions as energetic particle analyzer and proton energy distribution measurement capability 19 p3314 A69-36679

Mesosphere and lower thermosphere molecular O density from solar radiation atmospheric absorption, using satellite measurements 20 p3523 A69-37413

C and O atoms chemisorption on Mo surface demonstrated by surface striation 20 p3562 A69-37782

Neutron activation analysis for oxygen determination in Be by gamma emission intensity from nitrogen 16, noting bound oxygen 20 p3544 A69-37811

Molecular oxygen rate of dissociation resulting from absorption in Schumann-Runge bands, calculating effects on chemistry of lower thermosphere and upper mesosphere 20 p3534 A69-38089

Carbon monoxide displacement rate of oxygen from combination with oxyhemoglobin solutions from human adult and fetal, horse, goat, dog, cat and rabbit 21 p3650 A69-38384

Emissivity of nitrogen, oxygen and air plasmas in vacuum UV region of spectrum by photographic measurement, using He recombination radiation as brightness standard 21 p3774 A69-38944

Attachment coefficients for negative oxygen ion formation in low energy electron swarms over various voltage/pressure ratios 21 p3774 A69-39238

Molecular O distribution in thermosphere from Ariel 3 observations of solar radiation attenuation, showing large and systematic variation with longitude 21 p3717 A69-39263

P-V-T surface of fluids in critical region by dielectric measurements, presenting saturation densities of oxygen [NAS-NRC PAPER H-5] 22 p4050 A69-40623

Vapor pressure equation for oxygen and nitrogen derived by adding nonanalytic term, correlating equation with observed data [NAS-NRC PAPER H-1] 22 p4051 A69-40628

Clark oxygen electrode calibration by preparation of oxygen standard aqueous solutions, noting repair by ammonium hydroxide treatment 23 p4101 A69-41451

Creep strength as function of oxygen pressure for Ni at 510 and 600 C, dropping creep rupture life to plateau of nearly constant life 23 p4176 A69-41504

O-hemoglobin dissociation curve shape effect on O affinity of hemoglobin 23 p4095 A69-42086

Niobium solution hardening by nitrogen and oxygen, noting grain size effects in electron beam refining 23 p4178 A69-42362

Ge films formation by evaporation technique, discussing background O pressure effect 24 p4361 A69-43345

OXYGEN ANALYZERS

Lightweight sensor for telemetering oxygen partial pressure in respiration air 15 p2559 A69-31231

Vacuum distillation determination of O in Li, evaluating accuracy through O additions and recoveries, method blank and residue identification 22 p3897 A69-40932

OXYGEN ATOMS

Reversed thermal conditions in mesopause, examining atomic oxygen IR radiation effect 01 p0062 A69-10129

Enhanced 6300 angstrom emission from F region auroral latitudes in terms of reaction between oxygen ions and atoms 01 p0062 A69-10137

Oxygen electron cooling effect on ionospheric electron temperatures, noting discrepancy removal throughout day at all altitudes 02 p0245 A69-12739

Photometric measurement of atomic oxygen green line emissions and high energy electron flux using twilight sounding rocket 02 p0309 A69-12743

Near mesopause atmospheric layer energy balance, noting atomic oxygen diffusion role in redistributing absorbed solar energy among atmospheric layers 03 p0422 A69-13408

Solar emission line absorption by oxygen and nitrogen atomic lines, discussing effect on upper atmosphere composition measurements 03 p0425 A69-14019

Analysis of equivalent widths as function of disk position for six photospheric neutral atomic oxygen Fraunhofer multiplets, noting O abundance 03 p0515 A69-14034

Second virial coefficient of atomic nitrogen and oxygen, discussing thermodynamic properties of dissociating mixtures 03 p0473 A69-14158

Enhanced light emission rate in adiabatically expanded NO-O reaction ascribed to molecular clusters 04 p0555 A69-14864

Autoionizing states effects on absorption cross sections for ejection of outer subshell electron from atomic oxygen 04 p0633 A69-15127

Gas laser operating on pure O-He-Ne-Ar mixture at liquid N temperatures, noting atomic O transitions, pulsed operation and energy level populations 06 p0933 A69-17259

Diffusion coefficient of interstitial oxygen atoms in tantalum by elastic energy dissipation measurements as temperature function, discussing relaxation effect 07 p1168 A69-19452

Surface recombination efficiencies on metals measured as function of exposure time in steady Oseen flows, providing step-function increase in oxygen atom concentration 10 p1726 A69-23526

Thermosphere radiative cooling by atomic O 62 micron line, noting cooling and heating rates 12 p2064 A69-26009

Winter polar mesosphere atomic-oxygen distribution by analyzing data concerning intensity and energy of corpuscular fluxes in auroras

12 p2070 A69-26690

Beam-foil technique for measuring radiative lifetimes of excited electronic states in ionic species of O, including transition probabilities

13 p2301 A69-27452

Lower ionospheric homonuclear O combinations nonequilibrium processes by simplified balance equations, determining height distributions and ozone concentration

13 p2255 A69-28542

UV OGO observations of atomic hydrogen and oxygen in airglow, comparing results to exospheric models of hydrogen geocorona

15 p2603 A69-31400

Zenith and azimuthal photometric observations of red line atomic O airglow predawn enhancement over UK

16 p2775 A69-32086

Atomic oxygen density role in ionospheric E and F region magnetic stability, noting heat loss effect of atomic excitation

16 p2780 A69-32314

Transition probability for 5577 Å auroral green line determined from measuring number density of O atoms in oxygen-helium discharge and emitted line intensity

16 p2781 A69-32319

Laser action and spontaneous emission at atomic oxygen transition, discussing pulsed emission mode in argon-oxygen laser

17 p2982 A69-33633

Radiative recombination of atomic oxygen ions in nighttime F region UV radiation detected by polar-orbiting OGO 4 satellite

18 p3129 A69-34957

Quiet aurora atomic O red and green lines intensity ratio measured from rocket

18 p3201 A69-35192

Reactive scattering from solid surfaces, discussing atom beam reaction of O with heated Ge and Si single crystals

19 p3377 A69-36178

Rocket probe devices based on thermometrical body principle for measuring upper atmosphere water vapor and atomic oxygen

20 p3543 A69-37798

Doppler broadened atomic O emission line measurement providing indication of exospheric temperature storm-time variations

20 p3546 A69-38099

Rocket photometer observations of midnight atomic oxygen glow at 6300 Å during ascending and descending flights

21 p3703 A69-38360

Diatom-monomatomic oxygen collision cross section determined from rotational line width in diatomic oxygen Schumann-Runge emission spectra

22 p3983 A69-40099

Far IR nightglow emission from atomic oxygen observed by rocket-borne liquid He-cooled telescope

22 p3940 A69-40521

Atomic spectrophotometry to monitor O atom formation rate behind shock waves in oxygen-argon mixtures, noting dissociation over 2850-5550 K temperature range

23 p4194 A69-42209

Many body perturbation theory with time dependent perturbations applied to frequency dependent polarizability of atomic oxygen

24 p4354 A69-43816

OXYGEN BREATHING

High oxygen concentration influence on animal organisms noting respiration, pulmonary gas exchange, hypoxia, brain phosphorylation, immunological indices and morphological structure of rats and mice

05 p0709 A69-16512

Electron microscopic changes in lungs of rats after repeated exposure to pure oxygen

05 p0709 A69-16514

High oxygen concentration influence at normal pressure on evoked potential of cortical optic zone and subcortical zones

05 p0709 A69-16515

Respiratory difficulties from breathing through mask compared with changes in respiration resulting from obstruction caused by physical respiratory disorder

17 p2916 A69-33774

High oxygen concentration influence on animal organisms noting respiration, pulmonary gas exchange, hypoxia, brain phosphorylation, immunological indices and morphological structure of rats and mice

18 p3095 A69-34731

Electron microscopic changes in lungs of rats after repeated exposure to pure oxygen

18 p3096 A69-34733

High oxygen concentration influence at normal pressure on evoked potential of cortical optic zone and subcortical zones

18 p3096 A69-34734

Hyperoxia and pulmonary surfactant washout in pulmonary compliance measurements of rats subjected to 100 percent diatomic oxygen before asphyxial death

21 p3659 A69-39066

Normobaric oxygen toxicity pathology in baboons and Macaca, irus and squirrel monkeys during 14 day exposure

21 p3660 A69-39179

Pituitary-adrenocortical axis of rats in oxygen atmosphere at low pressure, finding depressed norepinephrine excretion

23 p4087 A69-41790

OXYGEN COMPOUNDS

Volatile oxygen organic compounds subjected to RF electrodeless discharge, explaining product distribution in terms of reaction sequences

21 p3670 A69-39737

OXYGEN CONSUMPTION

Basal metabolism in humans restricted to prolonged bed rest, noting decreased oxygen consumption rates

02 p0197 A69-11497

Xenon, krypton, nitrogen and nitrous oxide effect on respiration rate of rat liver slices at various oxygen partial pressures

03 p0375 A69-14069

Hemoglobin diffusion influence on oxygen uptake and release by red cells solved by calculus of finite differences

05 p0707 A69-15677

Oxygen intake and body temperature of basal and sleeping Andean natives at high altitude

06 p0874 A69-17835

Hyperoxia exposure and hemolysis in tocopherol deficient mice

06 p0874 A69-17837

Transient changes in oxygen consumption, carbon dioxide elimination and respiratory quotients during and after induced hypoxia to rabbits

06 p0876 A69-18026

Petroleum sulfides advantageous effect on oxygen consumption during combustion

07 p1202 A69-19456

Prolonged exposure of rats to oxygen concentrations studied for effects on organisms

08 p1262 A69-19831

Oxygen depletion effect in chemical reactions between pyrolysis gases and air stream on surface recession of charring ablators

09 p1622 A69-21982

Space flight hypokinesia simulation experiments to study oxygen balance in man

10 p1646 A69-23507

Euglena gracilis grown heterotrophically, investigating respiratory physiology as function of glucose, acetate or ethanol growth supporting carbon source

10 p1647 A69-24186

Altitude climates effects on human performance, discussing oxygen consumption at moderate altitudes during vigorous physical activity

11 p1827 A69-24924

High vacuum effects on oxidative processes in bacteria and physiological activities of enzymes

15 p2557 A69-31354

Oxygen consumption and rectal temperature in male mice confined in nitrogen and helium diluted hyperoxic atmosphere at specific temperature and humidity ranges

17 p2906 A69-32932

Lurain simulator for metabolic studies, using BPMU for assessing O consumption of test subjects at rest and various speeds of ambulation

17 p2914 A69-33187

Respiratory gas exchange in exercise during He-O breathing, analyzing effects on O consumption, carbon dioxide production and minute ventilation of human subjects

17 p2910 A69-33751

B Coli commune cultivated on various substrates, studying oxygen consumption under aerobic/ anaerobic conditions

18 p3097 A69-35302

Statistical relations between minute blood circulation volume, O capacity and consumption rate in tissues of men and dogs

19 p3260 A69-35896

Noble gases effect at low pressures on O consumption by mammalian tissue, noting Xe, Kr, N and nitrous oxides effect on rat liver

19 p3258 A69-36454

Oxygen replacement rate by CO from combination with oxyhemoglobin in cells at various temperatures

21 p3650 A69-38385

O conductance nonlinear equation solution applied to O uptake at sea level and at altitude, noting blood transport problems

21 p3654 A69-38906

Noise influence on heart rate and oxygen consumption of young male subjects under simultaneous physical stress

21 p3654 A69-38908

Caucasian and Bantu males oxygen consumption at different work rates, gross body weight accounted for 70 percent of differences between individuals

21 p3655 A69-38911

Atelectatic and direct toxic effects of oxygen on human subjects

22 p3873 A69-40208

Human metabolic response to hypothermia measured over wide range of work intensities and durations

22 p3891 A69-40215

Energy cost of piloting helicopters and fixed wing aircraft calculated from expired minute volume and air oxygen content measured during basal state and flight

22 p3891 A69-40218

Real time metabolic rate analysis of suited astronaut using heart rate and O methods during thermal vacuum and extravehicular mobility tests

22 p3893 A69-40371

Effects of oxygen saturation variations of blood on rates of weight gain in isolated perfused canine lung, noting pulmonary edemogenesis

22 p3887 A69-41189

Oxygen consumption, ventilation and cardiac frequency relationship to body weight during submaximal exercise in normal human beings

23 p4099 A69-42169

Contraction frequency increment effects on myocardial oxygen consumption in dogs determined for various heart rate levels, using isovolumic left ventricular preparation

24 p4258 A69-42634

OXYGEN DEFICIENCY

U HYPOXIA

OXYGEN FLUORIDES

Specific impulse deliverable performance of space storable propellant combination fluorine-oxygen/methane and oxygen difluoride/diborane

16 p2845 A69-32762

OXYGEN ISOTOPES

Formation cross sections of Li, Be and B isotopes produced from oxygen 16 spallation via high energy protons related to astrophysics and cosmic ray physics

14 p2512 A69-28968

Oxygen isotope separation magnitude in zirconia electrolytic cells found proportional to mobility difference of isotopes

15 p2552 A69-30701

Normal frequencies, force constants and moment of inertia of carbon dioxide isotopic molecules from spectroscopic data, calculating atmospheric transmission of carbon dioxide laser radiation

21 p3742 A69-39780

OXYGEN MASKS

Respiratory disturbances relationship to experience and attitudes toward gas anesthesia and response to different types of face mask

03 p0378 A69-12884

Protective filter for inspiration valve of oxygen masks in high performance aircraft, reducing respiratory volume exchange with given pressure amplitude

17 p2916 A69-33773

Respiratory difficulties from breathing through mask compared with changes in respiration resulting from obstruction caused by physical respiratory disorder

17 p2916 A69-33774

OXYGEN METABOLISM

Metabolic relationship between hypoxia and hypoglycemia in Wistar rats, noting oxygen consumption, energy expenditure under insulin and hydrogen partial pressure decrease effect

09 p1445 A69-22727

Blood oxygen metabolism, analyzing content and volume circulation in dogs under oxygen partial pressure decrease in inhaled air

12 p2019 A69-26346

Lurain simulator for metabolic studies, using BPMU for assessing O consumption of test subjects at rest and various speeds of ambulation

17 p2914 A69-33187

Pt electrode as detector of red blood cell oxygenation, attempting Fe value dependence on flow velocity determination

20 p3480 A69-38283

O uptake of middle aged men, comparing short and long term endurance running effects

21 p3654 A69-38904

Reticulocyte count comparison on trained and sedentary college male subjects before and after strenuous exercise, noting role in oxygen uptake

21 p3654 A69-38907

Blood oxygen content measured by oxygen tension after release by carbon monoxide without lysing cells

22 p3873 A69-40203

Oxygen uptake and circulatory response in human male subjects during maximal treadmill and bicycle exercise

22 p3874 A69-40226

Arterial and deep venous blood from human forearm analyzed following rest and rhythmic exercise on ergometer in hyperbaric oxygen chamber

22 p3878 A69-40834

Physical exercise effect on adolescent males, comparing oxygen uptake, heart volume and height in training and nontraining groups

23 p4077 A69-41312

Steady state and time dependent concentration gradients in and around cells due to oxygen diffusion and depletion in radiobiology

23 p4090 A69-41966

Model for human hemoglobin dissociation into subunits taking into account molecular explanation of oxygen dissociation curves

23 p4097 A69-42096

Hemoglobin O reaction model explaining molecular weight and oxygen dissociation curve dependence on hemoglobin concentration

23 p4097 A69-42097

Sinus outflow relationship to oxygen content in anterior cardiac vein blood and right ventricle systolic pressure

23 p4098 A69-42105

Oxygen exchange in Scenedesmus and Chlorella as function of carbon dioxide, compensation point, Hill activity and photorespiration, using mass spectrometry

23 p4099 A69-42528

OXYGEN PRODUCTION

Interactions between intermediate fluorescence quenching trapping center and associated electron acceptor of oxygen evolving photosynthetic spinach chloroplast photosystem

01 p0024 A69-10928

Biological problems in prolonged space voyages including oxygen replacement, water supply and food regeneration

01 p0020 A69-11075

Regenerative life support systems, discussing water reclamation, carbon dioxide removal, onboard oxygen generation and radio isotope thermal energy sources

19 p3262 A69-36318

OXYGEN RECOMBINATION

Wake temperature turbulent fluctuation decay rates deduced from atomic oxygen recombination chemiluminescence

02 p0190 A69-12525

Recombination constants of dissociated oxygen and nitrogen flow in supersonic nozzle at high temperatures using modified Bray method

06 p1030 A69-17349

Recombination mechanism between CO and O produced by photodissociation of carbon dioxide in upper atmosphere of Venus and Mars

07 p1214 A69-18615

Desorption kinetics of atomic and oxide phases, analyzing composition of surface film formed from W and Mo single crystals interaction with oxygen

12 p2026 A69-26115

OXYGEN SPECTRA

Low latitude m arcs in 6300 angstrom emission during intense geomagnetic storm related to auroral red oxygen emission peak

01 p0062 A69-10136

Enhanced 6300 angstrom emission from F region auroral latitudes in terms of reaction between oxygen ions and atoms

01 p0062 A69-10137

Tropical 6300 angstrom red oxygen nightglow enhancements related to variations in height of nighttime F 2 layer, noting implications for layer structure and physics

01 p0068 A69-11113

Absorption coefficients of molecular oxygen at Lyman alpha line and vicinity measured by vacuum spectroscopy

01 p0076 A69-11230

Upper atmosphere oxygen emission and heating during geomagnetic disturbances

02 p0235 A69-11421

Intensity ratio of first negative nitrogen band and oxygen line varies in auroral displays

02 p0235 A69-11425

Photometric measurement of atomic oxygen green line emissions and high energy electron flux using twilight sounding rocket

02 p0309 A69-12743

Oscillator strength determination for Schumann-Runge band system in molecular oxygen

02 p0284 A69-12832

Molecular O 0.7620 micron absorption band in pure O and air, noting rotational lines mean half width and lower atmosphere transmission function

03 p0458 A69-13272

Transition probability measurement of 5577 A auroral green line of oxygen used to investigate quadrupole nature of transition

03 p0424 A69-13936

Analysis of equivalent widths as function of disk position for six photospheric neutral atomic oxygen Fraunhofer multiplets, noting O abundance

03 p0515 A69-14034

Temperature dependence of O VIII Lyman alpha/Lyman beta radiation ratio in solar corona, noting coronal temperature

03 p0516 A69-14042

Latitude dependence of 6300 A/O I twilight airglow enhancement attributable to conjugate photoelectrons

05 p0756 A69-16280

Ratio of volume emission rate of 5577 A photons to volume emission rate of one band of positive nitrogen molecule first negative system in aurora

05 p0756 A69-16360

Oxygen absorption coefficients for atomic silicon in spectral range of Schumann-Runge bands

06 p0960 A69-17090

Microwave radiometer for measuring mesosphere and stratosphere temperature as function of altitude using atmospheric oxygen line

06 p0924 A69-17247

Oxygen line absorption at elevated temperatures in Schumann-Runge system, estimating line widths

06 p0962 A69-17803

IR zero one band of molecular O observed in day airglow with ground based scanning grating spectrometer

08 p1306 A69-20096

Ratio of volume emission rates of 5577 A and band of positive N molecular ion first negative system for use in auroral observations

09 p1491 A69-22607

Relative band intensities of atmospheric and IR atmospheric systems of molecular oxygen compared with Franck-Condon factor calculations

10 p1681 A69-23163

M 31 galaxy ionized gas region high resolution spectroscopy, emphasizing radial velocities in O II lines at various distances from nucleus

12 p2163 A69-27020

Molecular O 0.7620 micron absorption band in pure O and air, noting rotational lines mean half width and lower atmosphere transmission function

14 p2487 A69-28780

Sodium atoms and NO molecules role in atomic O 6300 and 5577 A emissions in comet Mrkos 1957d due to charge exchanges and dissociative recombination

14 p2523 A69-29707

Absorption coefficient in three microwave lines of O with different rotational quantum numbers calculated, examining Zeeman effect in geomagnetic field

15 p2597 A69-30941

Zenith and azimuthal photometric observations of red line atomic O airglow predawn enhancement over UK

16 p2775 A69-32086

Diurnal variations of IR atmospheric oxygen bands in airglow observed with filter photometer on balloon flights

16 p2776 A69-32091

Thermosphere neutral wind speed measured from observing Doppler shift in O I 6300 night airglow line with Fabry-perot interferometer

16 p2776 A69-32093

Portable photometer with red-sensitive photocathode and high SNR for O I 6300 airglow experiments

16 p2777 A69-32107

Vertical wind effects in atmosphere on 5577 A radiation, showing dependence on atomic oxygen density

16 p2778 A69-32185

Green line suppression in type B aurorae based on negative ion-electron chemistry below O transition region

16 p2778 A69-32191

He I/1.083 mu/ and O I/5577 A/ absolute brightness measured in sunlit aurora for various shadow heights of solar radiation, considering primary electron precipitation

16 p2780 A69-32311

Transition probability for 5577 A auroral green line determined from measuring number density of O atoms in oxygen-helium discharge and emitted line intensity

16 p2781 A69-32319

Solar corpuscular and UV radiation variation relationship to midlatitude airglow intensity in O I line

16 p2850 A69-32322

Relationship between sporadic E and 5577 A nightglow emission attributable to ionization redistribution in E region due to dynamic processes

16 p2788 A69-32782

Spectroheliograms interpretation obtained in line cores of neutral oxygen IR multiplets

18 p3204 A69-35388

Forbidden lines emitted by gaseous nebulae, emphasizing relative intensities of O II and O III lines

19 p3422 A69-36220

Absorption spectrum of diatomic oxygen excited by AC silent discharge photographed with vacuum spectrograph, associating lines with Schumann-Runge band

20 p3581 A69-38276

N I nebular doublet and auroral and nebular lines of O I obtained with multifilter scanning photometer in France, Norway and at magnetic equator

21 p3712 A69-38519

Airglow and vertical eddy transport photochemical models, analyzing O green line and OH emission distribution

21 p3713 A69-38523

Intensity changes of O I nightglow emission at 100 km by transport associated with tides, gravity waves and turbulent mixing

21 p3713 A69-38526

Instrumental profile determination for high resolution stellar spectrograph, using profiles of telluric oxygen bands obtained from emission line observations

21 p3721 A69-38696

First order profile of Utrecht Solar Atlas from second order profile and oxygen band refining procedure, deducing instrumental profile for first order spectra

21 p3722 A69-38699

Forbidden absorption bands of diatomic O in Ar continuum region, determining rotational constants of upper electronic states

22 p3896 A69-40479

Dayglow O I lambda 1304 and 1356 A radiations photoelectron excitation rates theoretical calculation and experimental data on altitude dependence characteristics

22 p3939 A69-40517

Forbidden O I 5577 A dayglow emission equatorial measurements with rocket photometer, discussing altitude profiles and excitation mechanism

24 p4314 A69-43005

Auroral short period pulsations in 6300 A O I, discussing percentage modulation, quenching rate, etc

24 p4309 A69-43171

Herzberg bands synthetic spectra matched to various spectrograms to determine vibrational populations of molecular O state in nightglow

24 p4310 A69-43186

OXYGEN SUPPLY EQUIPMENT

Emergency oxygen supply systems for aircraft, discussing simplicity, standardization, safety, reliability and maintenance

[AIAA PAPER 67-965] 01 p0013 A69-11025

Water electrolysis, discussing oxygen generators for spacecraft prototype cells and testing

03 p0379 A69-12987

Soviet papers on apparatus and machines of oxygen and cryogenic installations covering film boiling, gas vessel, thermal design, etc

04 p0686 A69-15160

Oxygen supply inert diluent impurities effect on hydrogen-oxygen fuel cell performance

04 p0551 A69-15310

Oxygen reclamation from carbon dioxide using solid oxide electrolyte, noting water vapor catalytic effect

07 p1071 A69-19423

Hypoxia warning system based on dry electrolyte oxygen sensor with millisecond response time

07 p1071 A69-19430

OXYGEN TENSION

Oxygenator for weightlessness operation, generating oxygen electrolytically and passing oxygen through membrane for animal experiments
17 p2903 A69-33039

Lithium peroxide utilization feasibility for oxygen supply and carbon dioxide control in extravehicular portable life support systems
[AIAA PAPER 69-620]
17 p2914 A69-33303

Oxygen supply and carbon dioxide absorption in long term life support systems, noting energy balances comparison of ecological systems
20 p3477 A69-37625

OXYGEN TENSION NT HYPOXEMIA

High oxygen concentration breathing effect on foveal thresholds, using sea level tests on trained observers
02 p0203 A69-12216

High oxygen tension effect on transport and incorporation of exogenous leucine and protein synthesis in *Pseudomonas saccharophila* cells
03 p0369 A69-13433

Hypoxia warning system based on dry electrolyte oxygen sensor with millisecond response time
07 p1071 A69-19430

Polyimide glass fabric laminates with nonflammable characteristics for high O concentration spacecraft environments applications
09 p1531 A69-22366

Oxygen saturation in outflowing and inflowing renal blood in dogs under normal and hypoxic conditions, assessing cannula technique
14 p2406 A69-28916

Pulmonary oxygen toxicity, analyzing reticulum and elastic tissue damage and hyaline membranes by histochemical techniques
14 p2407 A69-29298

Transfer function in pulmonary ventilation and O tension in arterial blood analyzed by automatic control
19 p3260 A69-35897

Colpoda maupasis resistance to Martian atmospheric pressure and oxygen partial pressure noting adaptation, reproduction and existence
20 p3478 A69-37627

Lobeline effect on oxygen pressure in gigantocellular nucleus of medulla oblongata and respiration rates of dogs recorded automatically
22 p3888 A69-41273

Oxygen supersaturation in unstirred blood under temperature effects, noting tension loss during stirring
23 p4077 A69-41296

Rebreathing method for determining mixed venous oxygen pressure and cardiac output during rest and exercise in trained athletes
23 p4078 A69-41316

Critical oxygen pressure dependence on buffer in diluted heart muscle sarcosome suspensions and effect of hemoglobin or myoglobin
23 p4080 A69-41427

Arterial oxygen partial pressures and heart beat rates measured in humans during acute hypoxia after altitude and ergometer training, noting sensorimotor performance
23 p4086 A69-41788

Increased oxygen tension adaptation and effects on adrenocortical and sympatho-adreno-medullary activity in rats, indicating toxic conversion of epinephrine to indoles
23 p4087 A69-41791

Coronary circulation response to hyperoxia after vagotomy and combined alpha and beta adrenergic receptors blockade in anesthetized intact dog
23 p4096 A69-42088

Digital simulation of oxygen pressure fields and supply conditions in biological tissues
23 p4097 A69-42098

Oxygen effect on X ray induced somatic crossing over frequency in *Drosophila melanogaster*, noting bristle spots number modification on abdominal tergites
23 p4099 A69-42118

OXYGEN TOXICITY U HYPEROXIA

OXYGEN 18

Oxygen 18 adsorption on silicon activation analysis measurements used to obtain kinetic curve for chemisorption from monolayers
18 p3183 A69-35107

Isotopic exchange reaction rate between O 18 and CO in shock tube coupled to time of flight spectrometer, noting rate increase with time
24 p4353 A69-43807

OXYGENATION

Diffusion coefficients for oxygen transport in whole blood, discussing effects of intact red cell concentration
02 p0200 A69-12479

Oxygen effects in Type 316 stainless steel, Nb-Zr alloy liquid potassium system, discussing thermal convection and forced circulation loops and corrosion rates
12 p2112 A69-25943

Gangrene and caisson disease due to diving accidents, discussing emergency treatment with hyperbaric oxygen
17 p2911 A69-33775

Barotrauma during hyperbaric oxygenation at flight descent or reentry into caisson, including ear trauma symptoms and use of paracetamol
17 p2911 A69-33776

Tissue pressurized oxygenation during radiation therapy emphasized for overcoming tumor radioresistance attributed to oxygen deficiency
23 p4091 A69-41967

Oxygen and carbon dioxide transfer in membrane oxygenators, considering liquid dispersion and membrane diffusion limitations
24 p4279 A69-43799

OXYHEMOGLOBIN

Hemoglobin diffusion influence on oxygen uptake and release by red cells solved by calculus of finite differences
05 p0707 A69-15677

Carbon monoxide displacement rate of oxygen from combination with oxyhemoglobin solutions from human adult and fetal, horse, goat, dog, cat and rabbit
21 p3650 A69-38384

Oxygen replacement rate by CO from combination with oxyhemoglobin in cells at various temperatures
21 p3650 A69-38385

OZONE

Photochemistry in dry atmosphere, discussing ozone density vertical distribution in upper atmosphere and influence of O and ozone reactions with H compounds
02 p0245 A69-12694

Optical ozone radiosonde for vertical distribution analysis, using weak absorption of Chappuis bands
02 p0251 A69-12761

Dissociative velocity rates of oxygen and ozone in ionosphere obtained by exponential approximation for molecular concentration distribution
02 p0246 A69-12769

Atmospheric ozone photochemistry, studying time dependence on hydrogen compounds, equilibrium concentration effects on reaction rates, latitude and season
06 p0916 A69-17004

Stratospheric temperature, wind and ozone concentration measurement during solar eclipse by sounding rocket system
06 p0916 A69-17008

Vertical ozone distribution in upper atmosphere from satellite measurements of UV solar radiation scattering by solving integral Laplace equation
06 p0996 A69-17733

Time dependent model of photochemical, advective and turbulent effects on meridional ozone distribution
07 p1122 A69-18253

Nightglow intensities correlated with atmospheric ozone concentration and stratospheric temperatures
07 p1123 A69-18675

Radiative transfer equation for pure molecular scattering inverted for estimating vertical ozone distribution
07 p1126 A69-19042

Ozone distribution in Venus atmosphere measured by Soviet space probe Venera 4
08 p1382 A69-19887

Seasonal maximum ozone concentration variations, discussing vertical ozone distribution
08 p1307 A69-20260

Horizontal ozone distribution at high cyclones and anticyclones in middle stratosphere
08 p1308 A69-20261

Ozone and carbon dioxide stratospheric and tropospheric horizontal distribution from weather data collected on polar flight
09 p1484 A69-21403

Solid state ozone generator for preparing ozone in known concentrations to 1000 ppm in air for laboratory studies
10 p1693 A69-23346

Atmospheric extinction function in Chile by using photoelectric spectrum scans, observing neutral component, Rayleigh scattering and ozone absorption variations
10 p1777 A69-23386

Atmospheric optics by spacecraft and high altitude probes concerning ozone and aerosol distributions, scattering indicatrix polarization and dust cloud inhomogeneities
12 p2055 A69-25815

Diffusion of ozone distribution tracers in stratosphere, based on photochemistry in oxygen- only and oxygen-hydrogen atmospheres
13 p2294 A69-28492

Ozone concentration changes in polar regions and tropical zone due to meridional atmospheric circulation
14 p2442 A69-29830

Ozone concentrations harmful to humans in atmosphere based on U.S. and Western European observations, emphasizing lower stratosphere
15 p2596 A69-30642

Vertical ozone profiles computed from known total ozone data based on profiles taken by Umkehr method
15 p2597 A69-30896

Ozone soundings data obtained over Australia and Colorado to obtain vertical picture of synoptic climatology of ozone at midlatitudes
15 p2649 A69-30898

Rocket observations of ozone concentration above 50 km by absorption spectroscopy, noting altitude dependence
15 p2603 A69-31397

Atmospheric ozone production by silent discharges near ground level during first stage of storm cell development
16 p2785 A69-32623

Atmospheric ozone distribution in meridional plane including time effects of photochemistry, advection and turbulence assuming zonal symmetry
16 p2785 A69-32624

Vertical ozone distribution from emission and absorption in 9.6 mu band determined during IGY in Switzerland
16 p2785 A69-32625

Ozone absorption coefficients in vicinity of Hartley band maximum verified by photographic spectrophotometry
16 p2785 A69-32626

Ozone vertical distribution variations over India observed by Brewer electrochemical ozonesonde, noting effects of dry and monsoon seasons
16 p2786 A69-32627

Horizontal and vertical ozone distributions synoptic study, comparing soundings made on both sides of Atlantic
16 p2786 A69-32628

Weather forecasting correlation between atmospheric ozone vertical profiles and post sounding ground meteorological situation, describing computer data processing
16 p2786 A69-32629

Simultaneous Umkehr observations of vertical ozone distribution in upper stratosphere using two Dobson photometers, discussing deviations due to calibration sensitivity
16 p2786 A69-32631

Statistical analysis of Brewer-Mast electrochemical soundings of vertical ozone distribution for developing computer programs of climatological behavior
16 p2786 A69-32632

Ozone and temperature profiles influence on atmospheric radiation intensities measurement by satellite in five spectral regions, noting pressure broadening effect
16 p2786 A69-32633

Ozone probe network data by Brewer-Mast electrochemical instruments, discussing vertical ozone distribution near Zurich
16 p2787 A69-32635

Ozone concentration photochemistry between 30-35 km, determining parameters in Hampson theory/hydrogen-oxygen atmosphere/
16 p2787 A69-32636

Optical probe for determining ozone vertical distribution at high altitudes, discussing optical method requirements and ozonesonde construction
16 p2792 A69-32637

Statistical characteristics of ozone measurements with Dobson spectrophotometers and filter ozonometers, determining requirements for maximum effectiveness of ozone network
16 p2787 A69-32639

Ozone soundings in upper stratosphere, discussing vertical temperature profiles relationship to vertical ozone profiles
16 p2787 A69-32640

Variations in difference between integrated ozone amount by soundings and total ozone by Dobson spectrophotometers
16 p2792 A69-32642

Atmospheric ozone distribution as function of photochemical reactions, advection and vertical motions

16 p2787 A69-32643

Ozone vertical distribution in upper stratosphere determined from OGO 4 observations, describing calibration of satellite data and onboard instrumentation

16 p2788 A69-32645

Ozone concentration worldwide anomaly above 40 km in annual variations, noting dissimilarity in seasonal maximum and minimum with lower level

17 p2960 A69-33166

Ozone vertical distribution predicted statistically, using total ozone amounts and backscattered UV spectral measurements

18 p3132 A69-35426

Numerical integrations for modified model incorporating ozone production equation and heating from ozone radiation absorption and long wave cooling for upper atmospheric circulation

19 p3363 A69-36502

Atmospheric ozone detection by three-color photometer measurements of solar UV radiation attenuation in Hartley continuum

20 p3543 A69-37802

Carbon trioxide formation during ozone photolysis in liquid carbon dioxide and sulfur hexafluoride, noting ozone disappearance quantum yield independence of oxygen/ozone ratio

23 p4112 A69-41338

Model for ozone formation, distribution and decomposition at 15-45 km assuming zonal symmetry, including time effects of photochemistry, advection and turbulence

24 p4309 A69-43147

OZONOMETRY

Ozonsonde based on modified Brewer electrochemical sonde

01 p0079 A69-10218

Air movements in lower stratosphere analyzed on basis of ozone measurements, showing correlation with north-south gradient of total ozone amount

02 p0246 A69-12762

Frequent periodic variations existence in daytime ozone content associated with solar activity

12 p2070 A69-26693

Atmospheric ozone vertical distribution and total amount determined by radiative transfer and perturbation theory, presenting error analysis

13 p2255 A69-28493

Cauchy system for reflection and transmission functions of finite isotropically scattering atmospheres with specular reflectors, noting use for ozone and cloud heights measurements

15 p2597 A69-31152

Vertical ozone distribution from emission and absorption in 9.6 mu band determined during IGY in Switzerland

16 p2785 A69-32625

Vertical ozone distribution determination discrepancies between Brewer-Mast electrochemical sonde and Umkehr methods, discussing influence of seasonal and diurnal variations

16 p2786 A69-32630

Ozone probe network data by Brewer-Mast electrochemical instruments, discussing vertical ozone distribution near Zurich

16 p2787 A69-32635

Statistical characteristics of ozone measurements with Dobson spectrophotometers and filter ozonometers, determining requirements for maximum effectiveness of ozone network

16 p2787 A69-32639

Amplifier working in conjunction with solid state phase sensitive detector replacing existing commutator in Dobson ozone spectrophotometer

16 p2792 A69-32641

Variations in difference between integrated ozone amount by soundings and total ozone by Dobson spectrophotometers

16 p2792 A69-32642

FORTTRAN computer program for quality control and calculation of total ozone measurements and lamp tests for Dobson ozone spectrophotometer

16 p2787 A69-32644

Ozone concentration worldwide anomaly above 40 km in annual variations, noting dissimilarity in seasonal maximum and minimum with lower level

17 p2960 A69-33166

Ozone measurement from satellite by direct beam and scattered light methods employing UV sunlight attenuation

21 p3721 A69-38625

OZONOSPHERE

Effective temperature values of ozone used to determine onset time and disturbance height in ionosphere

02 p0238 A69-11670

Seasonal mean vertical ozone distributions obtained with electrochemical ozone sondes over southeastern Australia

02 p0276 A69-12696

Solar flares effect on ozonosphere, calculating time necessary for solar radiation to increase ozone concentration by 50 percent

03 p0424 A69-13542

Atmospheric haze effect on Umkehr measurements, considering computation from direct sounding of vertical ozone distribution and from model atmospheres

08 p1308 A69-20316

Calculated UV spectra of solar radiation reflected from atmosphere compared with satellites photometric measurements, attributing radiation intensity distribution asymmetries to seasonal dependence of ozone content

12 p2064 A69-25952

Atmospheric ozone vertical distribution and total amount determined by radiative transfer and perturbation theory, presenting error analysis

13 p2255 A69-28493

Effective temperature values of ozone used to determine onset time and disturbance height in ionosphere

13 p2257 A69-28701

Ozonosphere inhomogeneities from UV spectra of reflected solar radiation, studying latitude dependence of seasonal behavior at different heights

15 p2597 A69-30654

P

P-I-N DIODES

U DIODES

P-I-N JUNCTIONS

P-i-n structure isolation method for fabricating monolithic integrated circuits

02 p0222 A69-12471

Fe doped Ga-as p-i-n structure electrical conductivity, Hall effect, thermally induced currents, space charge bounded currents and current instability

04 p0643 A69-15263

Negative resistance in GaP electroluminescent diodes with p-i-n structure at low temperatures, noting oxygen role

13 p2226 A69-27194

Operation mode of modulator with p-i-n diode, determining modulus and phase of reflection factor

13 p2235 A69-28518

Current-voltage characteristics for double injection processes in nonideal contact p-i-n semiconductors operating in ohmic relaxation mode

13 p2323 A69-28524

Capture centers effect on current-voltage characteristic of p-i-n diodes during injection, noting negative resistance appearance

13 p2236 A69-28525

Near constant phase variable attenuator for RF signal containing Doppler information, centering design around p-i-n diode as control element

21 p3681 A69-38410

P-N JUNCTIONS

Avalanche multiplication in abrupt silicon p-n junctions analyzed using ionization coefficient measurements for holes and electrons

01 p0135 A69-10038

Gate current measurement of p-n junction during ultralow current operation of junction field effect transistor /JFET/

01 p0038 A69-10122

Silicon p-n junction avalanche current temperature dependence calculation by considering space charge current and multiplication factor as function of temperature

01 p0136 A69-10245

GaP p-n structures creation for diode sources of green and red radiation, comparing diffusion and epitaxial methods

01 p0137 A69-10259

Optically bistable operation of continuous wave GaAs p-n junction laser at 20 K

01 p0090 A69-10565

Silicon doped p-n GaAs single crystals and epitaxial layers energy spectrum, studying shift in position of emission band maximum

01 p0139 A69-10833

P-N JUNCTIONS

Indium phosphide p-n junction current-voltage characteristics various temperatures, considering degree of doping effect

01 p0139 A69-10885

Electrical properties of p-n junctions of diffused Cd or Zn in indium phosphide

02 p0294 A69-11628

Surface charge distribution in silicon p-n junctions noting luminescence of microplasmas and inhomogeneous properties

02 p0294 A69-11629

Linearized time dependent equation for photovoltage distribution in nonuniformly illuminated p-n junction

03 p0486 A69-13636

Temperature and current distribution in avalanching silicon p-n junctions

03 p0487 A69-13637

P-n junction under arbitrary transient conditions, solving one dimensional, two carrier transport equations by numerical iterative method

03 p0487 A69-13639

Carrier generation-recombination in space charge region of asymmetrical p-n junction, noting experimental results for InSb diodes

03 p0487 A69-13641

Uniaxial pressure applied to p-n junction of GaAs injection laser, discussing effects on threshold current and wavelength

03 p0441 A69-13848

Gradual capture in p-n junctions and p-n-p transistors at AC voltage, noting diffusion capacitance and resistance

03 p0491 A69-14051

Tunnel breakdown in p-n junctions used to generate microwave oscillations, discussing Si and Ge properties

03 p0492 A69-14163

Conductivity in p-n junctions during avalanche breakdown at HF calculated, noting agreement with experiments

03 p0492 A69-14164

Radiative recombination in p-n junctions in InP at various temperatures

03 p0492 A69-14166

Hydrostatic pressure effect on recombination emission in indium phosphide p-n junctions

04 p0639 A69-14428

Bistable zones in series oscillator circuit consisting of inductor and nonlinear p-n junction capacitance subjected to DC and AC voltage sources

04 p0575 A69-14463

Equivalent circuit of varactor with open p-n junction used as frequency multiplier

04 p0575 A69-14465

Charge multiplication in crystals, analyzing ionization rate, avalanche breakdown in p-n junctions, pair production and impact of impurities

04 p0641 A69-14503

P-n junction breakdown, discussing local regions of overheating and increased current density, differential resistance frequency dependence and breakdown region temperature

04 p0577 A69-14782

Cathode ray curve tracer to record capacitance-voltage characteristics of p-n junctions

04 p0602 A69-15406

Diffusion capacitance of p-n junctions, short base semiconductor diodes and p-n-p transistor, discussing systematic error in quasi-steady state calculation

04 p0580 A69-15489

High efficiency microwave oscillations in Si p-n and p-n-p positive avalanche diodes under pulsed conditions

04 p0580 A69-15491

Approximate equations in matrix form for analyzing complex semiconductor structures with p-n junctions

05 p0806 A69-15658

Probability distribution of field strength fluctuations in p-n junctions taking into account impurities distribution

05 p0807 A69-16000

Diffusion anomaly of native acceptor defect in zinc selenide telluride p-n junctions, discussing applications in triple diffusion technique of preparing p-n junction diodes

05 p0808 A69-16286

P-n planar avalanche photodiode without guard ring noting electrical properties, uniform multiplication and fabrication

05 p0733 A69-16559

Maximum transmission coefficient of distributed p-n junction signal detector compared with concentrated detector coefficient using ordinary and tunnel diodes

05 p0736 A69-16787

P-n junctions and device structures formed by ion implantation, using Hall effect and channeling techniques to evaluate implanted layer nature
06 p0974 A69-16862

Recovery rate at room temperature in Li-doped p-n Si diodes and solar cells after 1 Mev electron irradiation, noting capacitance changes
06 p0974 A69-16867

Red light emitting p-n junctions in GaP fabricated by epitaxial growth
06 p0979 A69-16999

Electric field growth directional effect on avalanche breakdown conditions in p-n junctions
06 p0981 A69-17828

Voltage dependence of depletion layer width, maximum electric field and capacitance of Gaussian diffused plane, cylindrical and spherical p-n junctions
07 p1196 A69-18242

Computer model for n-p-n transistor in integrated circuit using substrate p-n junction isolation
07 p1114 A69-18246

P-n channel MOS triode fabricated by doped-stepped-oxide method, obtaining p-channel enhancement
07 p1100 A69-18622

Forward transient response characteristics of high resistivity, long base, low lifetime p-n silicon diodes doped with Au, noting voltage oscillations
07 p1101 A69-18652

Nonlinear coupling between background illumination and illumination signal producing lateral electrical fields in p-n junction, noting effect on sensitivity of position sensor
07 p1101 A69-18654

Diffusion current detection method applied to reverse biased volt-ampere characteristics of Ge diodes, noting surface leakage role
07 p1105 A69-19007

Digital method for quantitative study of carrier circulation phenomena in semiconductors, noting Algol program and continuously polarized p-n junction
08 p1280 A69-19973

Epitaxially grown guard rings for GaAs p-n junction and Schottky barrier avalanche diodes
08 p1284 A69-20368

Photocells with p-n heterojunctions from sintered CdS, describing spectral sensitivity and temperature dependence of no-load photo EMF
08 p1374 A69-21084

Thermal EMF in epitaxial films, analyzing potential distribution in p-n junction with temperature gradients and film thickness effects
09 p1555 A69-21473

Emission intensity and beam divergence of p-n junction GaAs laser with nonlinear passive element in resonator
09 p1515 A69-21474

Semiconductor lasers, discussing materials, oscillation wavelengths, excitation methods, operating principles, fabrication, GaAs p-n junction laser and applications
09 p1518 A69-22122

GaP p-n structures creation for diode sources of green and red radiation, comparing diffusion and epitaxial methods
09 p1559 A69-22652

Recombination parameters and depth of levels of p-n junctions in semiconductor photocells determined from position of maximum spectral sensitivity
09 p1560 A69-22718

Breakdown voltage and avalanche drift instability factors in planar passivated p-n junctions as function of oxide thickness and mobile charge
10 p1743 A69-23174

Current voltage characteristics of p-n junctions in cadmium telluride, discussing spectral sensitivity bands
10 p1744 A69-23212

Drawn n-p and p-n junctions obtained in Te and Zn doped GaSb single crystals prepared in pure Hc atmosphere by Czochralski method
10 p1745 A69-23329

Positive and negative sloped current-voltage characteristics of silicon tunnel diodes with p-n junctions
10 p1746 A69-23574

Silicon doped p-n GaAs single crystals and epitaxial layers energy spectrum, studying shift in position of emission band maximum
11 p1936 A69-24700

Silicon n-p solar cell behavior during electron radiation, describing radiation resistant solar cell
11 p1825 A69-24871

Equations for pn junction behavior valid at impurity concentrations beyond nondegenerate range, noting contact potential and carrier density
11 p1938 A69-25306

LF noise mechanism for forward biased semiconductor p-n junction, noting charge carrier capture in electron traps of carrier depleted region
11 p1857 A69-25705

Solar cells physical properties and functions, considering band structure of semiconductors, p-n junction diodes and photovoltaic effect, efficiency calculations and radiation damage
12 p2015 A69-25864

Indium phosphide p-n junction current-voltage characteristics at various temperatures, considering degree of doping effect
12 p2144 A69-26649

Tunnel diode nonlinear p-n junction capacitance influence on characteristics of diode microwave self excited oscillator
12 p2043 A69-26889

Depth and planarity of zinc diffused junctions in GaP using temperature, phosphorus overpressure and time as independent variables
13 p2322 A69-28136

Laser diodes p-n junctions obtained by Zn diffusion into Ga arsenide, stressing junction flatness problem and arsenic vapor pressure effect
13 p2323 A69-28640

Ga phosphide p-n junctions formation from GaP: Ga solution, discussing electrical and luminescence properties
13 p2323 A69-28642

Bistable zones in series oscillator circuit consisting of inductor and nonlinear p-n junction capacitance subjected to DC and AC voltage sources
14 p2418 A69-28834

Small signal transient characteristics of semiconductor diodes analyzed by charge method, studying processes during p-n junction diode switching at low currents
14 p2419 A69-28918

SiC and GaP diodes used as low power light sources, studying electroluminescence in p-n region under pulsed excitation
14 p2419 A69-29325

Strain sensor using p-n heterojunction diode fabricated by vacuum evaporation onto flexible substrate
14 p2422 A69-29555

Solar conversion efficiencies of p-n and n-p diodes calculated for specified semiconductor heterojunctions using Anderson diffusion model
15 p2552 A69-30034

Gunn effect GaAs oscillators with p-n junctions, studying electrical characteristics, threshold voltages and currents during breakdown and p-n junctions injection
15 p2666 A69-30065

Spectral distribution of photosensitivity for p-n junctions in silicon doped GaAs, showing agreement with state density model and absorption data
15 p2666 A69-30067

Thermal EMF in epitaxial films, analyzing potential distribution in p-n junction with temperature gradients and film thickness effects
15 p2669 A69-30718

Emission intensity and beam divergence of p-n junction GaAs laser with nonlinear passive element in resonator
15 p2633 A69-30719

Mesa-structure varactors /p-n junction generating harmonics by nonlinear capacity variation/ reliability, determining selection criterion and optimal test duration period
15 p2627 A69-30839

Carrier lifetime in p-nu-n diodes, discussing error of forward pulsed diode method by Wilson and alternative model
16 p2757 A69-31615

Soviet book on avalanche transit time diodes and applications in microwave technology, describing p-n junction model, negative resistance, dynamic characteristics, synchronized oscillators, etc
16 p2761 A69-32109

Approximate equations in matrix form for analyzing complex semiconductor structures with p-n junctions
16 p2827 A69-32515

Plane anisotropic dielectric p-n junction layer waveguide properties, deriving characteristic equations for refraction indices
17 p2983 A69-33971

Radiation damage and recovery of lithium-diffused silicon p-n solar cells, measuring photovoltaic parameters as function of gamma radiation fluence
19 p3251 A69-35694

GaSb p-n injection laser output at 4.2 K in strong transverse magnetic field, deducing effective mass and g-factor from stimulated emission peak shift
19 p3387 A69-36530

Voltage and temperature dependence of zero-bias anomaly in GaAs p-n junction at 0.40-60 K, investigating voltage dependence of differential resistance
19 p3388 A69-36542

Book on physics of microwave semiconductor diodes covering p-n junction theory and device characteristics and applications
21 p3682 A69-38990

Tunnel p-n junctions preparation by diffusing Zn into degenerate Te doped n-type GaSb between 580-600 C, measuring volt-ampere and capacitance characteristics
21 p3780 A69-39043

Radiative recombination in GaAs p-n structures having region with concentrations of Ge atoms
21 p3780 A69-39044

Electric field regions of p-n junctions using electron beam deflection measurement, noting application to Si specimens
22 p3994 A69-40752

P-N-P JUNCTIONS

P-n-p junctions photoconductivity decay observation, determining signal bulk minority carrier lifetime in thin n regions
01 p0136 A69-10242

Gradual capture in p-n junctions and p-n-p transistors at AC voltage, noting diffusion capacitance and resistance
03 p0491 A69-14051

DC beta falloff in transistors at large collector currents measured, discussing relation to emitter crowding
04 p0574 A69-14347

Current and voltage dependence of negative differential resistance segment of current-voltage characteristic on nature of m-p contact in germanium p-n-p-m structures
04 p0642 A69-14793

Double diffused planar Ge n-p-n and p-n-p transistors with high switching speed, noting fabrication and performance
05 p0809 A69-16557

P-n-p planar epitaxial germanium microwave transistor used as amplifier in 1-4 GHz range and as high speed switch, summarizing design, fabrication and characterization
12 p2037 A69-25940

Bipolar HF p-type Si transistors preparation by B and P ion beams and planar technology masking technique obtaining p-n-p structure
22 p3916 A69-40960

P-N-P JUNCTIONS

High power pulse generators with four layer p-n-p-n structure, discussing design, principles and applications of semiconductor elements as modulators and switches
03 p0402 A69-12978

Diffusion and minority carriers drift effect on current-voltage characteristics of p-n-p-n structure in high density current
10 p1742 A69-22997

Current-voltage characteristics of p-n-p-n diodes, discussing collector voltage effect on current carrier concentration distribution in diode base
13 p2236 A69-28531

Four terminal silicon planar p-n-p-n model operating as semiconductor small signal linear tetrode amplifier, discussing properties and mathematical models
18 p3109 A69-35293

P-TYPE SEMICONDUCTORS

Intrinsic absorption temperature dependence in doped p-InSb, discussing forbidden transitions
01 p0136 A69-10255

N- and p-type InSb and GaSb single crystals microhardness, noting decrease after doping is limited to thin surface layer
01 p0139 A69-10832

Photoluminescence measurements of p-type thermal conversion in GaAs grown from silica boats, noting compensation by copper and shallow acceptors
04 p0639 A69-14434

Fermi level in n- and p-type Ge after irradiation by 50 Mev electrons determined by temperature dependence of carrier concentration
04 p0640 A69-14444

Distribution of current carrier concentration and mobility in p-type silicon doped with phosphorus ions
04 p0643 A69-15254

P-type GaSb crystals with various impurity concentrations noting conductivity, transverse magnetoresistance, Hall effect and acceptor band width and conductivity
04 p0643 A69-15259

Te and Zn doped p-type GaAs single crystals optical homogeneity, using interferometry
04 p0644 A69-15266

Low temperature spectral distribution of impurity induced photoconductivity in p-type InSb crystals prepared by zone refining

04 p0644 A69-15270

Semiconductor memory units, considering bipolar, p channel MOS and complimentary MOS chip technologies

04 p0569 A69-15362

Diffused Si and GaAs diodes electroluminescence and current-voltage characteristics

06 p0893 A69-16898

Injection characteristics of n-aluminum gallium arsenides-p-GaAs heterojunctions from recombination radiation spectra

06 p0979 A69-16993

Interface states effects on characteristics of p-channel MOS transistors

06 p0979 A69-17117

Differential thermal EMF at room temperature in p-InSb as function of concentration for different electron and hole scattering mechanisms

06 p0981 A69-17881

P-n channel MOS triode fabricated by doped-stepped-oxide method, obtaining p-channel enhancement

07 p1100 A69-18622

Hole concentration at deep energy levels in p-type indium antimonide single crystals containing structural defects

07 p1199 A69-18687

Strong p-type conductivity of silicon doped with beryllium by thermal diffusion, giving electrical and optical measurements

09 p1556 A69-21652

Current controlled negative differential resistivity observed during current-voltage measurements made with p-type Te at 77 K

09 p1557 A69-21747

Intrinsic absorption temperature dependence in doped p-InSb, discussing forbidden transitions

09 p1559 A69-22648

Voltage dependence of red and green electroluminescence in GaP diodes prepared by growing n-type liquid epitaxial layer on p-type solution grown substrate

10 p1663 A69-23664

N and p type InSb and GaSb single crystals microhardness, noting decrease after doping is limited to thin surface layer

11 p1936 A69-24699

Forward and reverse current-voltage characteristics and reverse biased capacitance for nZnSe-pGe emitter base diodes of heterojunction transistors

11 p1851 A69-25114

P-type GaAs-Ge lasing on band to band or conduction band to acceptor impurity transitions or on both transitions simultaneously

13 p2270 A69-27193

Frenkel defects in light irradiated p-type InSb single crystals at subthreshold radiation energies

13 p2318 A69-27885

Electroluminescence of p-GaAs diodes analyzed over temperature range of linear dependence of lasing on injection current

13 p2230 A69-27887

Differential thermal EMF at room temperature in p-InSb as function of concentration for different electron and hole scattering mechanisms

14 p2503 A69-28790

Semiconductor materials and fabrication methods for surface barrier junction n-type and p-type silicon counters used in hydrogen ion flux recording

14 p2452 A69-29810

Absorption band edge position in p type indium antimonide thin films after heating, showing forbidden bandwidth function relationship to film thickness

15 p2666 A69-30044

Majority carrier lifetime temperature dependence obtained from photoconductivity measurements of p-type GaAs crystals doped with Ge

15 p2666 A69-30056

Slow neutrons irradiation compensated high resistivity p-InSb current instability

15 p2666 A69-30058

Cyclotron resonance of minority carriers measured in p-type InSb, giving temperature dependences of absorption derivative and field ratio to line half width

15 p2667 A69-30068

P-type zinc-tin-antimonide crystals electric conductivity, Hall coefficient and thermal EMF found similar to p-type diamond-like semiconductors properties

15 p2667 A69-30197

Thermoelectric parameters of polycrystalline p-type bismuth antimony telluride and bismuth antimony tellurium selenide solid solutions

15 p2668 A69-30629

Negative resistance section of current-voltage curve for long diodes of p-type indium antimonide, noting magnetic field effects on electrical breakdown

15 p2581 A69-31149

Charge transport in n and p type samples of beta phase semiconducting iron disilicide, noting effect of room temperature doping

19 p3390 A69-36556

Fe-doped p-type gallium arsenide single crystal radiative recombination emission during current carriers transition from deep acceptor level into valence band

19 p3392 A69-36611

Frenkel defects in light irradiated p-type InSb single crystals at subthreshold radiation energies

21 p3782 A69-39144

Electroluminescence of p-GaAs diodes, analyzing temperature range of linear dependence of lasing on injection current

21 p3682 A69-39145

Nonlinear voltage dependence on current in p-type indium selenide single crystals, detecting negative resistance under pulsed electric field

22 p3992 A69-40602

Bipolar HF p-type Si transistors preparation by B and P ion beams and planar technology masking technique, obtaining p-n-p structure

22 p3916 A69-40960

Negative surface potential effect on noise and photoconductivity in Ge doped p-type InSb single crystals at low temperature in vacuum

24 p4362 A69-43738

Electroluminescence in doped p-type GaAs single crystal diodes ascribed to double injection of nonequilibrium current carriers

24 p4288 A69-43739

P-1127 AIRCRAFT

Low range airspeed system (LORAS) on X-22A and P 1127 VTOL aircraft for accurate airspeed information

05 p0767 A69-16774

PACIFIC ISLANDS

U JAPAN

PACIFIC OCEAN

Telemetry capability of Air Force Western Test Range noting acquisition, tracking, data processing and display and data reduction

05 p0743 A69-16304

Pacific atmospheric circulation and Pacific equatorial sea temperature winter anomalies, noting Hadley circulations, northeast westerlies, trade winds and Walker circulation

11 p1911 A69-24322

Cloud pattern characteristics in intertropical convergence zone above Indian and Pacific oceans from meteorological satellite photographs and cloud formation maps

14 p2473 A69-29728

Survey of six year period of satellite observed tropical Pacific cloud mapping

17 p2996 A69-33001

PACKAGES

U APOLLO LUNAR SURFACE EXPERIMENTS

PACKAGE

U INSTRUMENT PACKAGES

PACKAGING

NT ELECTRONIC PACKAGING

Astronaut feeding in space and NASA criteria for space foods, eliminating foods in metal tubes and directing development efforts to dehydrated foods

15 p2560 A69-31459

PACKING DENSITY

Random arrays representing random filament packing of actual composite materials, discussing effects on transverse stiffness

20 p3626 A69-37758

PACKINGS [SEALS]

Elastomer hardness criteria ensuring maximum life and performance of rotary shaft seals

16 p2794 A69-32432

PAD

Test pad isolation characteristics mathematical model to predict pad dynamic behavior

[AIAA PAPER 69-860] 21 p3690 A69-39388

PADE APPROXIMATION

Pade method applied in aerodynamics for determining detached shock wave shapes and shock waves attached at vertex of cone

19 p3241 A69-36778

PAIN SENSITIVITY

Skin temperature and cutaneous pain during warm water immersion, refuting subcutaneous thermal gradient hypothesis for stimulation of heat pain

08 p1267 A69-20683

Limits of human tolerance to localized skin exposure to IR irradiation of various intensities from pain threshold observations, noting skin temperature role

10 p1647 A69-23589

Decreasing barometric pressure effects on abdominal gas volume in military men under simulated flight conditions, noting abdominal fullness and pain

23 p4076 A69-41291

PAINTS

Color and appearance properties of paint films and relations to amounts and properties of colorants, noting translucent plastics and metallized paint films

04 p0620 A69-14886

Stress corrosion preventative metal-pigmented paints for titanium alloys, discussing chemicals added to increase cathodic potential

14 p2469 A69-29936

Painted helicopter rotor blades ruled out as cause of flicker induced vertigo, reporting pilots psychophysiological responses to formation flying

17 p2913 A69-33175

Heat sensitive paints thermophysical characteristics determined by nonstationary heat conditions method

18 p3161 A69-34697

Computer optimization of spacecraft optical coatings for temperature control, using finite element analysis and matrix inversion

22 p4050 A69-40359

PAIR PRODUCTION

Charge multiplication in crystals, analyzing ionization rate, avalanche breakdown in p-n junctions, pair production and impact of impurities

04 p0641 A69-14503

Three energy dependent quantities examined for gases, describing relation between ionization yields, cross section and loss functions

05 p0795 A69-15660

Light absorption in semiconductors with electron hole pair formation noting conduction and valence band

06 p0978 A69-16901

Energy spectra of muons determined from knock-on electrons projected angles of emission in C, Al and Cu

06 p0991 A69-17305

Quantum theory of electron gas with anomalous magnetic moments in intense magnetic fields, noting pair creation from thermodynamic energy in system

08 p1353 A69-19782

Diffusion of ion-electron pairs produced by photoionization upstream of strong shock waves to shock tube walls based on particle flux and Poisson equations

11 p1866 A69-25275

Spatial dispersion of HF dielectric constant in semiconductor based on electron-hole pair production

12 p2145 A69-26723

Inverse problem method for reconstructing electrons differential spectral cross sections and photon pair formation in electron photon cascade

13 p2303 A69-28415

Muon energy losses due to pair formation taking into account nucleus screening by electrons

13 p2304 A69-28423

Lower auroral ionosphere rocket measurements of electrons, positive ions and energy particles, deriving height variation of ion pair production and ion-ion recombination

16 p2778 A69-32187

Spatial dispersion of HF dielectric constant in semiconductor based on electron-hole pair production

21 p3781 A69-39136

Electron-positron pair formation in electromagnetic field created by coherent laser light focused into vacuum with ideal lens

22 p3965 A69-41116

Complex phenomena in theoretical astronomy including neutrino pair emission in stellar interiors, molecular H in interstellar gas, neutron stars, etc

23 p4217 A69-42316

PAKISTAN

Pakistan space research covering meteorological rocket program, Na/K vapor experiment, satellite tracking, etc

15 p2724 A69-31455

PALEOMAGNETISM

Magnetic paleointensity studies in basalts from Flagstaff, Arizona, noting oxidation effect on magnetic strength after heating

02 p0244 A69-12018

Geomagnetic field strength in early Precambrian, discussing thermoremanent normal remnant and saturation inverse remnant magnetization studies of Botswana Modipe gabbro

08 p1309 A69-20580

Remanent magnetization properties in alkalic igneous complexes at Magnet Cove and Potash Suphur Spring, Ark., calculating paleomagnetic pole during Cretaceous

14 p2445 A69-29884

Magnetic analysis by successive double heat treatment of miocene lava cooled during geomagnetic polarity reversal for determining field intensity

16 p2788 A69-32646

Ancient and present earth radii ratios determined by triangulation using paleomagnetic sites situated on different paleomeridians

22 p3937 A69-40183

PALEONTOLOGY

Synodic month length variations since late Cambrian, noting paleontological evidence in mollusks and stromatolites and associated geological changes

02 p0241 A69-11807

Molecular mechanisms leading to mineralization of organic tissues, noting role of protein and glycoprotein matrices

04 p0555 A69-14888

Gas chromatographic and mass spectrometric analyses of alicyclic hydrocarbons from Carboniferous organic materials, noting alkane distribution and evolutionary histories

17 p2917 A69-34184

Paleozoic plant fossils carbohydrate content

21 p3669 A69-39333

Prokaryotic and eukaryotic nanofossils localized in prePaleozoic microflora, noting radiometric age and association with stromatolites

22 p3935 A69-40052

Paleontological evidence to verify varying G constant hypothesis for expanding earth theory, discussing uncertainties of geological dating

22 p4017 A69-40177

PALLADIUM

Pd-D resistivity variation with D concentration at room and liquid He temperatures, discussing structural resistivity

10 p1745 A69-23357

Book on palladium alloys covering metallography of pure metal and alloys production, physical, mechanical and chemical properties and applications

10 p1712 A69-23632

Thermal diffusivity and conductivity of rolled plane parallel spectrally pure palladium preheated in vacuum and high temperatures

15 p2636 A69-30045

Hydrogen permeability in Pd alpha phase measured, coupling with grain size measurements for grain boundary to bulk diffusivity ratio

23 p4175 A69-41502

PALLADIUM ALLOYS

Room temperature lattice spacings of PdIn, PtIn and PtSn alloys including magnetic susceptibility

05 p0779 A69-15832

Book on palladium alloys covering metallography of pure metal and alloys production, physical, mechanical and chemical properties and applications

10 p1712 A69-23632

Salt bath brazing for honeycomb structures, describing brazing techniques for thoriated dispersed Ni and NiCr, Rene 41 and Ti honeycomb panels

19 p3320 A69-35557

PAM [MODULATED]

U PULSE AMPLITUDE MODULATION

PANEL FLUTTER

Panel flutter in supersonic flow, using finite element approach in matrix displacement methods to derive aerodynamic influence coefficient matrices

04 p0676 A69-14707

Supersonic flutter of circular cylindrical heterogeneous orthotropic thin panels of finite length, obtaining nonlinear flutter equation

08 p1413 A69-20404

Supersonic flutter solutions using finite elements, analyzing rectangular plate bending elements, square simply supported and clamped panels, low aspect ratio configurations, etc

11 p1991 A69-25516

Flutter design charts for isotropic panels stressed to verge of buckling for typical values of structural damping

11 p1992 A69-25524

Perturbation method for nonlinear panel flutter at high Mach numbers, using von Karman large deflection plate theory and quasi-steady aerodynamic theory

13 p2364 A69-28204

Nonlinear Galerkin analysis of curved plate flutter, using shallow shell/von Karman equations and quasi-steady aerodynamic theory

13 p2364 A69-28207

Membrane flutter and panel stability in supersonic flow, considering infinite aspect ratio equation solution through Galerkin method

13 p2365 A69-28236

Panel flutter under loads along profile, evaluating constraints dynamic characteristics by Hamilton principle

15 p2712 A69-31001

Aeroelastic nonlinear panel stability in supersonic gas stream, defining hazardous conditions of critical flutter boundary

15 p2716 A69-31549

Supersonic flutter in square panels and cylindrical shells, measuring critical dynamic pressure

17 p3051 A69-32923

Structural damping effects on semiinfinite panel boundary aeroelastic limit by Galerkin variational method

19 p3437 A69-36148

Panel flutter testing in supersonic blowdown wind tunnels, analyzing model and test chamber layout

21 p3847 A69-39859

Supersonic panel flutter boundary of buckled and unbuckled clamped rectangular plates, discussing in-plane stress effects

22 p3930 A69-40584

Natural frequency of thin plate subject to cylindrical bending, analyzing panel flutter by three mode approximation for large buckling deflection

22 p4045 A69-40821

Buckled rectangular plates with constrained edges, analyzing natural frequencies as basis for supersonic panel flutter analysis

22 p4046 A69-41049

Shearing force and shear buckling deformation influence on supersonic panel flutter boundary of simply supported rectangular plates, basing analysis on deflection approximation

24 p4400 A69-43055

Initial deflection and internal pressure effects on supersonic panel flutter boundary of simply supported rectangular plates under diverse middle-surface stress conditions

24 p4400 A69-43056

Aeroelastic stability of thin plates exposed to supersonic flow using singular perturbation methods, obtaining flutter boundary and membrane solution

24 p4403 A69-43573

PANELS

NT CURVED PANELS

NT RECTANGULAR PANELS

Sandwich panel construction, examining design with respect to panel size, thickness and weight limit

03 p0524 A69-13124

Long term weather and radar transmission effects on three ply fabric cloth fire-retardant polyester resin radome panel

08 p1414 A69-20485

Elastic anisotropic panels mechanics analyzed using differential equations stressing transverse displacements, anisotropic thermal expansion, shape imperfections and slip deformations

15 p2711 A69-30904

Variational principles and differential equations of thin elastic panels mechanics for aerospace structures

15 p2712 A69-30974

Wide panel Ti structural extrusions with integral stiffeners, discussing material, sizes, properties and tolerances

19 p3319 A69-35552

Stiffened integrally formed panel stability evaluation based on compression structural efficiency and manufacturing costs

[AIAA PAPER 69-760] 19 p3434 A69-35660

Multilayer sandwich panels containing unequal facings with distinct orthotropic cores, calculating dynamic load and stability of triangular panels

21 p3832 A69-38418

Mathematical method of processing test data air-frame panels subjected to repeated static loads to obtain lifetime equations and statistical characteristics

24 p4400 A69-43086

PANORAMIC SCANNING

Aerial panoramic camera with instantaneous exposure using combined Bouwers concentric lens system and between lens shutter

09 p1499 A69-22246

KB-18A rotary prism moving film panoramic aerial strike camera

15 p2614 A69-31281

PANTAR CHONDRITES

Carbon content and isotopic composition in light and dark portions of gas-rich chondrites Breitscheid and Pantar

19 p3408 A69-36081

PAPER CHROMATOGRAPHY

Pyrimidine and purine bases analysis by time of flight mass spectrometry and paper chromatography

11 p1832 A69-24738

PARA HYDROGEN

Gaseous and liquid H refractive index variations with pressure and density below room temperature, noting Lorentz-Lorenz function variations

02 p0281 A69-12180

Proton spin-lattice relaxation time in dilute liquid and gas solutions of orthohydrogen in parahydrogen, noting dependence on temperature, density and composition

06 p0961 A69-17141

Ultrasonic velocity dispersion in para hydrogen and mixtures with He, Ne and Ar at 300 K, obtaining rotational relaxation times

16 p2815 A69-32791

Solid para hydrogen coated graphite particles expulsion into interstellar medium from star formation regions, considering mantles stability and particles extinction efficiency, albedo and phase function

20 p3601 A69-37492

PARABOLAS

Parabolic interpolation method for values of function given for certain values of argument and of first derivative, including numerical examples

12 p2121 A69-26434

PARABOLIC ANTENNAS

On-axis gain of parabolic reflector antennas with rough reflecting surfaces as function of surface deviation, correlation distance, area and wavelength

01 p0041 A69-10246

Spacecraft pencil beam parabolic antenna design and installation, discussing directivity factor variation with diameter and orientation accuracy effects

01 p0030 A69-10581

Constant beamwidth antenna consisting of parabolic reflector and ridge loaded horn, noting conical scan tracking antenna application

02 p0218 A69-12325

Gain factor of offset-fed paraboloidal reflector as function of angular aperture and offset angle, noting phase error effects

02 p0218 A69-12329

Testing program using electrical measurements for determining adequacy of erectable parabolic reflector for space missions

02 p0223 A69-12812

Geodesic lens radar antennas, discussing air filled devices operated in TEM mode, inclusive Luneberg lenses, double layer pillboxes and parabolic lenses

03 p0402 A69-13184

Millimeter wave lunar radar system component specifications and design with paraboloidal antenna, emphasizing reflectivity of moon

03 p0397 A69-13725

Simultaneous recording of radio emission from five sections of solar active region, using parabolic antenna and single amplification/reception channel

04 p0651 A69-14377

Feed support blockage loss in parabolic antennas evaluated by shadowgraph photography

04 p0576 A69-14771

Large paraboloid radar antennas structural setting for minimizing effects on performance due to deformation of surface by gravitational forces

06 p1023 A69-17372

Optimum efficiency of paraboloidal reflector antennas, analyzing Potter method and use of hybrid modes

06 p0899 A69-17825

Parabolic antenna beam scanning by defocusing, calculating relationship between reflector and beam tilt angles

07 p1089 A69-18248

Adaptive primary feed system for wide angle beam scanning from parabolic reflector antenna, using Fourier transformation to obtain uniform power distribution

08 p1279 A69-19908

Pointing calibration of Haystack parabolic antenna by using radiometric measurements of cosmic ray sources

08 p1281 A69-20032

Synchronous servomotor for parabolic antenna of surveillance radar, discussing motor size and optimum gear ratio determination

08 p1274 A69-20108

Galactic neutral hydrogen structure in region of Cygnus observed with parabolic antenna and frequency-switched radiometer

08 p1388 A69-20243

Earth station antennas for communication satellite service, discussing design, fabrication, main lobe gain, side and back lobe suppression and noise performance

09 p1461 A69-21281

- Construction of large parabolic antennas for radio astronomy and satellite communication, noting dimensional accuracy, directional precision and dynamical behavior
09 p1476 A69-21650
- Ground station receiving antenna design and size for indirect distribution of TV programs by geostatic satellites
10 p1654 A69-23389
- Vertical parabolic antenna array and receiving system for S band transhorizon signal phase and amplitude measurement
11 p1851 A69-24987
- Multidimensional mode shapes and frequencies of 100 ft space erectable parabolic antenna
11 p1994 A69-25532
- Coaxial radiator as feed for low noise paraboloid antennas, presenting pattern synthesis
11 p1856 A69-25635
- Thunderstorm thermal noise emission determined by radiometer and steerable parabolic antenna in preparing water content contours along radio rays
12 p2127 A69-27002
- Horn exciter with fundamental and second mode in feeding waveguide of shallow paraboloid antennas
12 p2044 A69-27093
- Periodic stellar radiation at 3.5 mm from pulsar CP1919 measured by paraboloid antenna and radiometer
14 p2529 A69-29978
- Spacecraft pencil beam parabolic antenna design and installation, discussing directivity factor variation with diameter and orientation accuracy effects
15 p2568 A69-30751
- Radio antenna consisting of truncated confocal paraboloids, discussing pencil beam pattern, antenna parameters and experimental results
17 p2939 A69-33904
- Monopulse parabolic antenna radiator design for decimeter and meter wavelengths, discussing characteristic properties at optimal dimensions
17 p2939 A69-33905
- Hyperbolic EM microwave field used for contactless measurements of parabolic antenna surfaces
19 p3281 A69-35766
- Paraboloidal reflector antennas rms phase error minimization, describing axis location and determination of focus and focal length of best fit paraboloid
19 p3283 A69-35933
- Parabolic antenna properties generated by dual band circularly polarized focused two channel monopulse feed system, discussing tracking data from helicopter, Apollo 8 and Cassiopeia A
23 p4120 A69-41752
- Feasibility studies to optimized design for 440 ft steerable filled-aperture radio and radar telescope, discussing parabolic configuration, radome selection, etc
23 p4148 A69-42123
- Multisupport suspension arrangements for reducing reflector surface weight-loading distortion in steerable parabolic radio telescope antennas
23 p4149 A69-42128
- Large reflector paraboloid antenna performance under environmental loads
23 p4231 A69-42132
- Large paraboloidal reflector antenna computerized structural design, detailing framing, steering control, support structure, etc
23 p4231 A69-42135
- RMS surface error compensation in radome-housed Cassegrain parabolic antenna including weight analysis
23 p4150 A69-42137
- Focus broadening by astigmatism of large microwave parabolic antennas, discussing large span surface deformations caused by astigmatic aberration
23 p4140 A69-42188
- Zero g deployment dynamics of erectable truss parabolic antennas, obtaining latchup loads as function of reflector mechanical energy
24 p4398 A69-42827
- PARABOLIC BODIES**
- Boundary layer approximation for steady laminar flow of viscous incompressible fluid past paraboloid of revolution, obtaining vorticity distribution
07 p1120 A69-18812
- Static axisymmetric deformation of elastic paraboloid of revolution, using integration of equilibrium equation in Lamé displacement
09 p1613 A69-21631
- Finite element displacement method extension to include geometric nonlinearity applied to arbitrary plate element, shallow cylindrical shell and shallow hyperbolic paraboloid
13 p2361 A69-27441
- Integral representation of p-analytic functions of complex variable, applying axisymmetric boundary value problems of elasticity theory for cylindrical surfaces and paraboloid of revolution
15 p2714 A69-31191
- Parabolic and cardioid plates bending under uniform load by using point matching technique
16 p2874 A69-32166
- Laminar boundary layers on slender paraboloids, analyzing skin friction formula and extension for transverse curvature ranges
23 p4152 A69-41904
- PARABOLIC DIFFERENTIAL EQUATIONS**
- Nonlinear negative definite feedback control systems governed by parabolic partial differential equation, deriving asymptotic stability
01 p0050 A69-10239
- Alternating direction implicit /ADI/ methods for solving parabolic heat conduction equation with variable coefficients in two and three space dimensions
01 p0106 A69-10987
- First boundary value problem for linear second order parabolic equation with unbounded lowest order discontinuous coefficients and free terms, discussing solvability
02 p0272 A69-12222
- Nonlinear integrodifferential equations of parabolic type with delayed argument, discussing boundary value problems with caloric and hereditary operators
02 p0273 A69-12249
- Quasi-linear parabolic partial differential equations, discussing solutions, regularity, differential geometric aspects and Dirichlet problem
02 p0273 A69-12779
- Cauchy problem and mixed boundary value problem for parabolic system solved with thermal potential theory
03 p0455 A69-13259
- Necessary conditions for stability of trivial solutions of parabolic systems of partial differential equations
03 p0456 A69-13405
- Difference approximation with second order accuracy of numerical solution for parabolic type equations
04 p0622 A69-14618
- Existence theorem for periodic solutions of parabolic boundary value problem for infinite space time cylinder
04 p0624 A69-15004
- Finite difference approximation for numerical solution of periodic parabolic problem subject to nonlinear boundary condition
04 p0625 A69-15131
- Method of lines for parabolic differential equations, transforming boundary value problems into initial value problem for system of ordinary differential equations
04 p0625 A69-15132
- Boundary value problems for unstable quasi-linear elliptic differential operator class, proving theorems on properties of quasi-linear elliptic-parabolic equations in bounded space
05 p0787 A69-16424
- Optimal control of system governed by linear parabolic equation with white noise inputs, using mathematical model to generate distributed system analog
05 p0740 A69-16599
- Methods to obtain uniqueness for partial differential /elliptic/ equations boundary problem extended to parabolic conditions, analyzing necessary conditions for existence
07 p1173 A69-18728
- Stability and perturbation theory of abstract Cauchy problem with difference scheme, showing application to parabolic differential equations
08 p1343 A69-20537
- Stabilization rate of boundary value problem for parabolic equation in n dimensional space
09 p1532 A69-21627
- Homogeneous parabolic differential equation for heat transfer of two finite bodies in thermal contact solved by power series
09 p1532 A69-21628
- Boundary value problems solutions for quasi-linear elliptic and parabolic equations of arbitrary order applied to nonlinear differential equations
10 p1717 A69-22809
- Boundary value problem for elliptic-parabolic partial differential equations in theory of random processes, obtaining analytical solution in terms of hypergeometric functions
10 p1719 A69-23516
- Uniqueness and nonuniqueness of solutions of initial value problems for second order semilinear parabolic equations
10 p1722 A69-24069
- Evolutionary hypoelliptic equations with real variable coefficients, analyzing positive solutions and application to parabolic equations
11 p1908 A69-24534
- Periodic solution to boundary value problem for quasi-linear parabolic equation with nonlinear boundary conditions obtainable by Rothe method
12 p2121 A69-26282
- Partial differential equation with stochastic characteristics reducible to parabolic equation by introducing additional variables
12 p2121 A69-26366
- Nonnegative solutions of second order linear divergence structure parabolic differential equations, discussing Cauchy problem solution, Green function, etc
13 p2290 A69-28539
- Optimization of control system described by linear parabolic integrodifferential equation, using dynamic programming approach
15 p2645 A69-31024
- Algebra of quasi-homogeneous pseudodifferential operators applied to lateral boundary values of solutions of parabolic differential equations, discussing function spaces
17 p2994 A69-32842
- Single parameter family of two layer difference schemes with decomposing operators for general linear second order parabolic equations with mixed derivatives and variable coefficients
18 p3164 A69-34702
- Parabolic differential equations solved by variational methods, constructing numerical representations for solutions of initial boundary value problems
18 p3164 A69-34841
- Difference method for parabolic differential equations solution for Rayleigh boundary layer in dissociating gas, using integral estimates to determine stability
18 p3124 A69-35295
- Asymptotic behavior of solution to parabolic equation for t approaching infinity, proposing asymptotic formula to Cauchy problem for heat conduction
18 p3231 A69-35310
- Generalized Cauchy problem solution stabilization for ultraparabolic equation by integral representation of solution in positive initial functionals
18 p3165 A69-35312
- Method of straight lines applied to two phase Stefan type problem for quasi-linear parabolic equation, obtaining existence and uniqueness of solutions
20 p3567 A69-36992
- Partial difference methods from parabolic, elliptic and hyperbolic equations solved by splittings of locally one dimensional nature
21 p3754 A69-38745
- Evolutionary hypoelliptic equations with real variable coefficients, analyzing positive solutions and application to parabolic equations
21 p3756 A69-39151
- Upper and lower bounds for growth or decay rate of solutions of parabolic differential equations for indefinitely increasing time
21 p3757 A69-39565
- Variational principles equivalent to mixed problems for parabolic equations with initial boundary conditions, noting heat conduction theory
22 p3974 A69-40231
- Positive solutions of parabolic and hyperbolic partial differential equations arising as viscoelastic media equations of motion, noting maximum principle utilization
22 p3976 A69-41035
- Parabolic equation and equation systems with relaxed assumptions involving coefficients of first derivatives and unknown function, demonstrating Pogorzelski fundamental solutions validity
23 p4180 A69-41408
- Successive approximations method applied to boundary problem for quasi-linear parabolic equation in n dimensional Euclidean space
23 p4181 A69-41411
- First boundary value problem for linear second order parabolic equation with unbounded lowest order discontinuous coefficients and free terms, discussing solvability
23 p4182 A69-41973
- PARABOLIC FLIGHT**
- Sensory and physiological reactions experienced by cosmonauts during parabolic training flights, tabulating arterial pressure, heart beat and respiration rate
07 p1061 A69-18580
- Integration time reduction for equations of motion of vehicle center of mass during parabolic reentry, using Runge principle
09 p1532 A69-21763

Orientation reflexes of animals in weightlessness, analyzing turnover, vestibular and cervix reactions using motion pictures 20 p3470 A69-37248

Weightlessness tests during parabolic flight to supplement vestibular tests in astronaut selection 20 p3481 A69-37276

Motion sickness susceptibility during parabolic flight, comparing weightlessness and hypergravity effects on normal and labyrinthine-defective subjects 21 p3660 A69-39176

PARABOLIC REFLECTORS NT PARABOLOID MIRRORS

On-axis gain of parabolic reflector antennas with rough reflecting surfaces as function of surface deviation, correlation distance, area and wavelength 01 p0041 A69-10246

Gain factor of offset-fed paraboloidal reflector as function of angular aperture and offset angle, noting phase error effects 02 p0218 A69-12329

Thermomechanical analysis of large flexible paraboloid antenna indicates RF losses due to thermal distortions significant for X band and higher transmissions [AIAA PAPER 68-333] 02 p0345 A69-12372

Testing program using electrical measurements for determining adequacy of erectable parabolic reflector for space missions 02 p0223 A69-12812

Interferometer at lambda 21 cm using fully steerable paraboloids for processing output signal with on-line digital computer 03 p0411 A69-13468

22-m parabolic reflector radio telescope with 9525 mm focal length at Crimean Astrophysical Observatory, noting high performance in mm wavelength range 04 p0584 A69-14376

Mathematical models relating gain, cost, diameter, frequency and rms surface tolerance of ground antennas for exposed and radome enclosed parabolic reflectors 04 p0561 A69-15449

High temperature directional reflectance measurements of ablative materials as function of sample temperature using paraboloid reflectometer [AIAA PAPER 68-25] 04 p0604 A69-15512

Optimum efficiency of paraboloidal reflector antennas, analyzing Potter method and use of hybrid modes 06 p0899 A69-17825

Pressure formed parabolic reflectors for millimeter waves, discussing electrical measurements at 30 GHz 08 p1282 A69-20039

Earth station antennas for communication satellite service, discussing design, fabrication, main lobe gain, side and back lobe suppression and noise performance 09 p1461 A69-21281

Impulsive solar microwave bursts observed by parabolic reflector, obtaining bursts spectra and total flux density 09 p1579 A69-22178

Dual reflector antenna design methods for obtaining necessary phase and amplitude illumination across secondary aperture in low noise applications 11 p1852 A69-25316

Number 2 ground communications antenna system on Goonhilly Downs for British Post Office earth station 12 p2044 A69-26923

Doubly curved reflectors for rotating search radar directional antenna, noting assembly of elliptical strips constituting segments of parabolic dishes and sidelobe suppression 16 p2763 A69-32790

Horn antenna with parabolic reflector for 30 cm wavelength, calculating field distribution, main and sidelobe radiation patterns and aperture efficiency 17 p2937 A69-33147

Paraboloidal reflector antennas rms phase error minimization, describing axis location and determination of focus and focal length of best fit paraboloid 19 p3283 A69-35933

Space erectable microwave truss antenna automatically deploying rigid parabolic reflector 22 p3913 A69-40696

Computerized evaluation of elastic deformations of 100 m parabolic reflector designs for Max Planck Institute radio telescope, outlining supports and dish structure 23 p4148 A69-42122

Multisupport suspension arrangements for reducing reflector surface weight-loading distortion in steerable parabolic radio telescope antennas 23 p4149 A69-42128

Parkes paraboloid radio telescope structural performance, using rapid survey instrument to measure surface deformations for optimum focusing determination 23 p4231 A69-42130

Large reflector paraboloid antenna performance under environmental loads 23 p4231 A69-42132

Canadian radio observatory 150 ft telescope antenna, discussing dish structural feature for resisting gravity, wind and thermal stresses 23 p4149 A69-42134

PARABOLIC VELOCITY U ESCAPE VELOCITY

PARABOLOID MIRRORS

Far and near fringe radiation of asymmetrical mirror and horn antennas by method of boundary waves 02 p0214 A69-11601

Radiant flux reflected by mirror and incident on receiver for paraboloidal solar devices, obtaining heat loads and radiant energy formulas 09 p1436 A69-21803

Circular central shading effect on energy distribution parameters of paraboloidal mirrors, noting reflected radiant flux power limitation 09 p1436 A69-21804

Far and near fringe radiation of asymmetrical mirror and horn antennas by method of boundary waves 11 p1846 A69-24708

Mirror correctors used with paraboloidal spaceborne telescopes in far UV, yielding enlarged photographic field 13 p2261 A69-27949

Thermionic converter matched with solar cells analyzed for parabolic mirrors, assuming heat conduction power supply to cathode and uniform temperature distribution 13 p2209 A69-27970

Electric field distribution in focal region of finite offset paraboloid reflector illuminated by linearly polarized plane wave 13 p2234 A69-28427

Rotation of antenna pattern of radio telescope parabolic mirror subjected to thermoelastic deformations due to asymmetric solar heating 20 p3497 A69-38307

PARABOLOIDS U PARABOLIC BODIES

PARACHUTE DESCENT

Mathematical formula for estimating cost and efficiency of parachuting supplies, noting shock load reduction 07 p1053 A69-19140

Coordination technique for pressure, density and temperature measurements by probes during parachute reentry into planetary atmospheres, taking into account reentry dynamics 09 p1609 A69-21775

Shock force calculation for parachute of arbitrary canopy design, illustrating simplification permitting differential equation solution in closed form 15 p2551 A69-31172

Atmospheric wind shear velocity snapping effect on yarn suspending instrument package from balloon gondola during parachute recovery 17 p2975 A69-33613

Canopy filling time for parachutes under infinite mass conditions, using continuum equation and parachute inflation concept [AIAA PAPER 68-12] 17 p2902 A69-34032

NASA planetary entry parachute program for rocket launched and balloon deployment tests [AIAA PAPER 68-934] 19 p3247 A69-35952

Distance of spacecraft descending on parachute through planetary atmosphere measured from center of planetary mass using onboard instrument data 19 p3432 A69-36633

Initial phase of parachute inflation in incompressible flow [AIAA PAPER 68-927] 20 p3461 A69-37165

Buoyant Venus Station balloon for deployment and inflation during parachute descent into Venus atmosphere tested with scale model balloons in wind tunnels [AIAA PAPER 69-1017] 22 p3922 A69-40389

PARACHUTE FABRICS

Mission sequential environment effects on Dacron parachute material mechanical properties [AIAA PAPER 69-1018] 22 p3923 A69-40390

PARACHUTES

NT DRAG CHUTES

NT RECOVERY PARACHUTES

NT RIBBON PARACHUTES

Photographic measurement of parachute exit velocity during ejection from chute, describing electronic recording and unit operation with block diagram 08 p1317 A69-20875

Parachute deployment load control by use of line ties from rocket sled tests 11 p1823 A69-25386

Hypersonic parachute structural design using nylon ribbon, glass fiber heat shield and ablative coating construction [AIAA PAPER 68-963] 21 p3647 A69-39230

Automatic, semiautomatic and manually operated parachute release systems used in Switzerland 24 p4252 A69-42911

PARACHUTING U PARACHUTE DESCENT

PARADOXES

Paradoxes associated with elastic-plastic limit load analysis of material satisfying Drucker stability postulates 02 p0337 A69-11562

Unlimited extrapolation into infinity to determine ranges of applicability of theories in relativistic cosmology noting paradoxes 14 p2516 A69-28867

Negative time interval implications for meta particle at superluminal velocity with respect to two reference frames, noting causality paradoxes 20 p3598 A69-37412

Paradox of incoming photons detection at two antennas without interference pattern disturbance explained by classical and quantum physics 20 p3538 A69-37415

PARAFFINS

Mathematical model for melting of finite paraffin slab based on method on numerical computer solution of heat conduction equations for thermal control devices 12 p2190 A69-26785

Steel ball bearing high temperature fatigue life tested with synthetic paraffinic oil, fluorocarbon and polyphenyl ether [ASME PAPER 69-LUBS-18] 18 p3140 A69-34378

Oxygen concentration effects on oxidation of synthetic paraffinic and type II ester lubricants determined from ball bearing tests at 400 and 450 degrees F 18 p3149 A69-35177

PARAGLIDERS

NT FLEXIBLE WINGS

NT PARAWINGS

Equations of motion of point restricted tethered parafoil for investigating longitudinal and lateral dynamic stability 01 p0009 A69-10415

Paraglider as recoverable sounding rocket dropped from helicopter, describing system design and flight tests [UN PAPER 68-95445] 01 p0161 A69-10465

PARALLAX

Solar gravitational field influence on annual trigonometric parallaxes within relativistic theory framework 03 p0506 A69-13091

Photographic plates based parallax determinations of nearby stars weights, relative and absolute values, probable error and observation interval 04 p0663 A69-15381

Parallax and mass ratio of visual type K6 dwarf binary system, ADS 1865, BD plus 30339 13 p2349 A69-27811

Parallax and orbital motion of spectroscopic binary Tau Persei determined from Sproul refractor photographs 13 p2349 A69-27812

Photographic recording of parallax, proper motion, acceleration and orbital motion of Barnards star, noting mass ratios to jupiter 13 p2349 A69-27813

Relative parallax, fractional mass and luminosity of visual binary 1785 determined from photographs taken with Sproul refractor 13 p2349 A69-27814

Visual binary star parallax, motions and mass ratio determined using photographic data 13 p2349 A69-27815

Solar gravitational field influence on annual trigonometric parallaxes within relativistic theory framework 14 p2516 A69-28773

Holographic photogrammetry compared with conventional holography in monocular and binocular 14 p2516 A69-28773

parallax reconstruction and stationary stability of objects
22 p3944 A69-40044

PARALLEL PLATES

Symmetrically truncated right angle E-plane corner, placing electric and magnetic walls in symmetry plane, solving resulting boundary value problems
01 p0044 A69-10624

Accommodation coefficient effect on linearized heat transfer in rarefied gas between parallel plates and concentric cylinders
01 p0177 A69-11405

Heat transfer of steady laminar flow of incompressible, viscous and electrically conducting fluid between parallel porous plates
02 p0289 A69-12235

Reflected and transmitted radiation fields for dielectric loaded infinite phased array of parallel plate waveguides as function of scan angle
02 p0218 A69-12326

Admittance of parallel plate waveguide aperture with infinite flange illuminating metal sheet, using wedge diffraction theory and integral transform method
02 p0218 A69-12328

Stationary, moving and pulsating electrohydrodynamic flow between parallel dielectric plates and Couette flow, noting reaction concentration near wall
03 p0419 A69-13919

Dispersion of solute in electrically conducting fluid flowing between two parallel plates in magnetic field
04 p0638 A69-15194

Flow of two conducting immiscible liquids between parallel porous moving plates under transverse magnetic field
05 p0743 A69-15600

Real liquid turbulent flow of two parallel eddy streams between two parallel walls with given periodic roughness
05 p0747 A69-16034

Mathematical problem of MHD thermal entrance regions for parallel plate channel solved by Galerkin method [ASME PAPER 68-WA-HT-10]
05 p0803 A69-16118

Radiative heat transfer between parallel plates separated by nongray gas with picket fence absorption coefficient using integral equations
06 p1033 A69-17554

Laminar heat transfer in electrically conducting fluids flowing in parallel plate channels [JPL-TR-32-1335]
06 p1033 A69-17555

Bounds on mass and momentum transport by turbulent flow between parallel plates derived for Couette and Poiseuille flows
08 p1305 A69-20840

Rarefied gases back diffusion between parallel plates used for studying diffusion in capillaries, deriving volume flow equation valid for any density
10 p1677 A69-22903

Hydromagnetic laminar natural convection flow and heat transfer of nonNewtonian fluid between parallel electrically conducting walls
10 p1728 A69-23237

Heat transfer in MHD parallel plate channel flow in entrance regions analyzed by Galerkin method, noting Hall current effect
11 p1923 A69-24290

Equal inclination interference fringes effects on laser beam reflection from plane parallel glass plates, evaluating angular distance between adjacent fringes
11 p1896 A69-24840

Gas jets collision flowing from parallel wall channels, applying solution to calculating geometrical characteristics of fluid jet amplifiers
12 p2016 A69-25879

Inertia effect on incompressible fluid film pressure between two oscillating parallel plates, considering Reynolds number
12 p2102 A69-26241

Hydromagnetic fluid flow between flat plates oscillating with phase difference, same frequency and different amplitudes
12 p2135 A69-26273

Pressure distribution in viscous flow between parallel disks with sinusoidal oscillation, noting effects of oscillation amplitude and vibrating disk velocity [ASME PAPER 68-LUBS-1]
13 p2244 A69-27278

Cellular convection suppression by parallel vertical thermally conducting walls inserted into bottom-heated fluid, analyzing effect on critical Rayleigh number
13 p2374 A69-27782

Turbulent flow in circular tube and parallel plate channel, considering molecular viscosity and duct shear stress variation
13 p2248 A69-28131

Radiative heat transfer calculations between parallel surfaces, applying approximations based on total emissivities to known spectral emissivities
14 p2539 A69-29223

Knudsen arcs kinetic theory with cesium/inert gas mixtures in narrow gap between parallel plate electrodes, discussing fast particle beams and electron scattering
14 p2491 A69-29245

Steady incompressible MHD laminar flow between parallel porous disks solved for large Reynolds and Hartmann numbers
15 p2662 A69-30968

Linear array composed of dual mode elements radiating into parallel plate region, obtaining scan angle compensation of element impedance
17 p2929 A69-33875

Reflection coefficient of symmetric parallel plate waveguide operating in TEM mode illuminating lossless dielectric layer, using wedge diffraction and geometrical optics methods
18 p3108 A69-34802

Rarefied gas flow between parallel plates using linearized Boltzmann transport equation, deriving integral equation for mass flow velocity
19 p3296 A69-35621

Pressure gradient produced steady plane flow of Maxwellian gas between infinite parallel planes, describing linearized Boltzmann equation solution
19 p3379 A69-36604

TEM mode reflection coefficient for symmetric parallel plate waveguide composed of adjacent conducting wedges composition and radiating into perfectly reflecting sheet
20 p3507 A69-37839

Heat transfer in radial flow between two parallel plates, calculating Nusselt number for laminar and turbulent flows
20 p3633 A69-38176

Temperature distributions and heat transfer in thermal entrance region for Hartmann liquid flows under constant pressure gradient between parallel electrically conducting walls at rest
21 p3847 A69-38442

Effective thermal conductivity parallel to laminations and total conductance for combined parallel and normal heat flow in multilayer insulation [AIAA PAPER 68-765]
21 p3853 A69-39763

Omnidirectional microwave parallel plate waveguide fed antenna design for flush mounted broadband spacecraft, noting equatorial and polar patterns
22 p3913 A69-40697

Capacitance sensor of vertical with flexible mobile electrode, describing diagram and operation
23 p4163 A69-41550

Surface integration technique used in conjunction with wedge diffraction theory to analyze TEM radiation patterns of parallel plate waveguides
23 p4136 A69-41581

Monte Carlo method applied to heat transfer in rarefied gas flow between parallel plates involving temperature jump in Knudsen layer
24 p4246 A69-43490

Lateral heat conduction and radiation along two parallel long plates separated by nonabsorbing dielectric with refractive index of unity
24 p4415 A69-43594

Gas velocity and pressure influence on electrical breakdown potential of Ar, N and He between parallel flat plate and concentric electrodes
24 p4359 A69-43693

PARALLELEPIPEDS

Unsteady three dimensional heating of finite solid rectangular parallelepiped, deducing expressions for rectangle and slab
15 p2717 A69-30790

Potential functions applications to three dimensional static elasticity problems of parallelepipeds, using general stress solution
15 p2715 A69-31216

Large elastic deformations of isotropic materials by deflection of composite parallelepiped composed of elastic incompressible materials, applying Rivlin solutions
22 p4048 A69-41277

PARALLELOGRAMS

Free vibration frequencies of simply supported parallelogrammic plates, noting skew angle splitting of degenerate frequencies and frequency crossing of modes
11 p1987 A69-25379

PARAMAGNETIC AMPLIFIERS

U MASERS

PARAMAGNETIC RESONANCE

NT ELECTRON PARAMAGNETIC RESONANCE

Acoustic paramagnetic resonance in arsenic doped germanium, measuring spin-lattice relaxation
02 p0296 A69-11835

Paramagnetic resonance of Er ion in calcium tungstate single crystal, determining spin-Hamiltonian parameters
04 p0643 A69-15141

Amplitude modulation of radiation pulses of two level paramagnetic maser as affected by inhomogeneous broadening and spinning of resonance line
07 p1158 A69-19751

Ultrasonic paramagnetic resonance investigations of Pr ions ground state energy levels in calcium fluoride
24 p4360 A69-42790

PARAMAGNETISM

Quantum paramagnetic amplifier using natural andalusite single crystal and operating with four level pumping
04 p0577 A69-14781

Radio spectrometer with paramagnetic quantum amplifier for astronomical spectral measurements in 8 mm range
04 p0597 A69-14851

Motion equations for conducting paramagnetic fluid in magnetic field derived, including MHD equations and equation determining magnetic moment variation rates
11 p1932 A69-25465

Coupled magnetoacoustic waves in conducting paramagnetic fluid in resonance region due to mechanical and magnetic motions, considering dissipation
14 p2492 A69-29609

Radio spectrometer with paramagnetic quantum amplifier for astronomical spectral measurements in 8 mm range
15 p2607 A69-30243

PARAMECIA

UV and visible light interaction effect on biological activity of Paramecia unicellular infusoria, noting cell division rates and cell deaths
01 p0017 A69-11085

PARAMETERIZATION

Monte Carlo simulation procedure synthesizing probability distributions of reliability parameters with individually exponential components
01 p0036 A69-10707

Simultaneous estimation of parameters in multiple equation regression model arising from radioactive tracer experiments using compartmental models
01 p0106 A69-10926

Nonlinear viscoelastic bodies arising in 3d rheological models with hidden parameters behaving according to law compatible with objectivity and 2nd thermodynamics principles
01 p0171 A69-11131

Equations, tables and charts for shock drag parameter in determination of shock wave drag of body in supersonic free stream of ideal gas
02 p0188 A69-11862

Parametric analysis of life support systems developing scaling laws adapted to computer solutions, discussing manned orbital missions [SAE PAPER 680746]
03 p0379 A69-13438

Electron beam welding procedure planning and production shop control parameters
04 p0605 A69-14529

Optimization of control functions and parameters of dynamic systems with variable structure and discontinuous phase coordinates
04 p0582 A69-14795

Continuous parameter identification methods for parameter optimization in automatic control system analysis and synthesis, using modified steepest descent optimization
05 p0725 A69-16474

Linear distributed parameter system identification by stochastic approximation, obtaining constant parameters sequentially
06 p0900 A69-17358

Type 2 radio burst dynamic spectra determination for finding shock wave and magnetic field parameters above active corona region
11 p1945 A69-24243

Book on nonlinear systems analysis and design covering parameter mapping, symmetrical, transient and forced oscillations and stability analysis
12 p2129 A69-26121

Parametric variations method for solving nonlinear algebraic and transcendental equations, determining number of solutions in complex space

12 p2123 A69-26608

Loitsianski method of parametric approximation extended to include flat plate with constant surface suction and flow past cylindrical cylinder

13 p2249 A69-28247

Rotary oscillatory solution of parameterized system with stable unexcited motion using successive approximations

14 p2482 A69-28812

Parameters distinguishing analytic queueing models of time sharing algorithms, emphasizing techniques used for analyzing round-robin and multiple level queueing models

19 p3279 A69-35600

Parametric differentiation applied to radiation gas dynamics equations solution, considering energy transfer by thermal radiation in high speed reentry [AIAA PAPER 68-668]

23 p4059 A69-41892

Multidimensional approximation algorithm for parameter optimization of nonlinear stochastic systems, detailing application to space vehicle attitude controller

24 p4291 A69-43275

PARAMETERS

U INDEPENDENT VARIABLES

PARAMETRIC AMPLIFIERS

Hybrid integrated parametric amplifier design considerations for fabrication in microstrip transmission line

01 p0040 A69-10193

Broadband parametric amplifier used as front amplifier in satellite communication systems ground station receiver, noting cryogenic operation capability

01 p0041 A69-10243

Forward current shot noise in parametric amplifiers using GaAs varactors, noting additional noise due to stored minority carriers current

01 p0048 A69-11137

Parametric vibrations of self excited elastic and aeroelastic systems with traveling waves, determining stable vibration boundaries

02 p0337 A69-11561

Summed and differential types of higher order oscillations in vibratory systems with multiple degrees of freedom under parametric excitation

02 p0346 A69-12422

Liquid helium cooled broadband parametric amplifier, discussing circuits and noise performance

02 p0221 A69-12458

Tunable optical parametric oscillator using argon laser CW output as pump and lithium niobate as nonlinear crystal

02 p0260 A69-12701

Low noise broadband parametric amplifier for communication satellite ground stations

03 p0406 A69-13733

Phase input power characteristics of TWT, TDA and parametric amplifiers, noting crosstalk calculations and AM-PM conversion coefficients

04 p0573 A69-14336

Noise reduction in parametric electron beam amplifier by cooling two frequency resonator noise to liquid nitrogen temperature

05 p0728 A69-15654

Traveling wave maser and cooled parametric amplifier for ultralow noise preamplification in satellite communication earth terminal installations

05 p0728 A69-15670

Nonlinear optics, discussing frequency mixing, induced changes in dielectric constant and parametric amplification in microwave region of spectrum

05 p0772 A69-16229

Microwave absorption and series resistance of silicon mesa parametric amplifier diodes, discussing p-n junction and dielectric loss mechanism

05 p0732 A69-16347

Oscillations of cylindrical orthotropic three layer shell having ideal fluid flow at variable rate, establishing parametric resonance and determining limits of shell motion instability regions

06 p1022 A69-17186

Transmission coefficient of double frequency regenerative parametric amplifier described by scattering matrices

06 p0895 A69-17456

Frequency and power stable backward wave oscillators as energy pumps for molecular and wideband parametric amplifiers used in satellite receivers

07 p1095 A69-18430

Nonlinear interaction between cyclotron harmonic waves, demonstrating synchronism conditions for

traveling wave parametric amplification and passive mode conversion

07 p1189 A69-18439

Helium cooled low noise high gain parametric preamplifier for satellite communication by stagger tuning stages

07 p1098 A69-18460

Helium closed cycle cooled very low noise high gain parametric amplifier for investigating interstellar atomic hydrogen radiation

07 p1098 A69-18461

Helium cooled low noise high gain wideband parametric amplifier for spacecraft communication

07 p1099 A69-18462

Wideband uncooled two stage reflecting parametric amplifiers with low noise temperature, noting application to space stations for telecommunications by satellites

07 p1099 A69-18463

Photoparametric up-converter with optimum SNR, noting suitability of direct detection of amplitude modulated optical signals

07 p1104 A69-18888

Lithium niobate based parametric image converter for IR to visible operation, discussing design factors performance calculations

07 p1150 A69-19048

Parametric light interactions application to optics stressing nonlinear spectrograph and cavity and traveling wave oscillator [IEEE PAPER B-3]

07 p1152 A69-19066

Incoherent scatter power measurements, comparing square law signal detection, phase coherent receiver and parametric amplifier methods

07 p1085 A69-19222

Degenerate parametric amplifier using self pumping action of oscillating domain capacitance in Gunn effect

07 p1107 A69-19450

Low noise wideband amplifier system for commercial satellite communication ground terminal receiver, noting cryogenically cooled parametric amplifier

09 p1458 A69-22470

Gain stabilization of parametric amplifier, using pumped conduction current of varactor diode

09 p1467 A69-22585

Parametric amplification in beam plasma system, analyzing amplification of electron current component dependent on second order terms of velocity and charge density

10 p1740 A69-23791

Coupling constants of fast space charge waves in three frequency parametric TWT amplifier and of stress waves in slow wave structure, using graphical methods

11 p1844 A69-24446

Parametric amplifying systems with lumped reactive nonlinear elements, emphasizing UHF systems

11 p1844 A69-24448

Single circuit parametric oscillator excitation by small external narrow band signal, using method of slowly varying amplitudes

11 p1845 A69-24453

Maximum voltage and power gain of modulator-demodulator type nonresonant parametric amplifiers

11 p1849 A69-24956

Parametric amplifier gain, deriving expressions for diode pumping power and nonlinear circuit element resistance

11 p1849 A69-24957

Singly resonant optical parametric oscillator, noting single mode and multimode oscillation for various pump powers, pump wave depletion and mode competition

11 p1897 A69-25038

Bandwidth potential increase of parametric amplifier obtained by adding active filter elements to signal circuit, noting satellite communication band

12 p2039 A69-26380

Negative resistance parametric amplifier used as tracking filter, noting resonant frequency dependence on pumping frequency and input and idler circuits

13 p2225 A69-27183

High efficiency LF oscillations in avalanche diodes, noting evidence for parametric generation and condition for high efficiency

13 p2227 A69-27239

Integrated S-band parametric amplifier design, combining low noise performance at room temperature with broadband flat gain and linear phase response

13 p2230 A69-27678

Two idler parametric amplifiers bandwidth properties investigated using equivalent circuit, noting role of idler circuit design

13 p2233 A69-28066

Differential equations of single loop parametric amplifier response, analyzing forced oscillations

13 p2234 A69-28329

Reactive parameter scatter effect on amplitude frequency characteristics of regenerative reflection amplifiers based on equivalent circuit

13 p2235 A69-28515

Double beam parametric electron amplifier with compensation of difference channel, noting beams noise removal

13 p2237 A69-28578

L-band parametric amplifier operated in liquid N for noise reduction, discussing measurement circuit for gain, bandwidth and noise figure

13 p2237 A69-28644

Noncollinear single cavity optical parametric oscillation with specified energy conversion using ruby laser-pumped lithium niobate, discussing tuning

14 p2460 A69-29605

Parametron preamplifier for X band super-heterodyne ESR spectrometer, noting sensitivity and SNR

14 p2423 A69-29757

Capacitive parametric modulator transient processes and second harmonic effect analysis, obtaining transient response and recovery time

15 p2574 A69-30125

Oscillation breakdown of varactor diodes in parametric amplifiers from studying I-V characteristics, noting resonant circuit retuning effect

15 p2574 A69-30127

Noise sources in S band parametric amplifier with GaAs varactor diode measured at liquid nitrogen temperature, considering noise reduction

15 p2578 A69-30636

Time dependent Green function method for premature saturation due to parametric amplification of nonuniform spin wave modes by one and two magnon processes

15 p2668 A69-30685

RF band multimode parametric pulsed oscillations in distributed system using one dimensional resonators

16 p2758 A69-31796

Parametric amplification of ion-acoustic oscillations in plasma with LF electric field, noting suppression and resonance

16 p2821 A69-31797

Wave propagation at different group velocities along parametric line in traveling wave parametric amplifier

16 p2805 A69-32254

Statistical properties of parametric amplifier and frequency converter by Schroedinger quantum mechanics and P-representation of density matrix

16 p2761 A69-32363

Noise reduction in parametric electron beam amplifier by cooling two frequency resonator noise to liquid nitrogen temperature

16 p2762 A69-32511

Optical parametric oscillator output/signal frequency locked to absorbing atomic transition, discussing effective linewidth

18 p3133 A69-34263

Parametric tunable amplifier as prestage for radar receiver, discussing pump frequency and midband gain stabilization

18 p3104 A69-35457

Parametric amplifier developed for unattended satellite communication ground stations, featuring low noise broadband characteristics

19 p3270 A69-36240

Resonant parametric oscillator stable and random phases, considering smooth frequency tuning and two quantum luminescence laser construction

20 p3554 A69-37723

Negative energy waves presence, showing qualitative difference on theoretically derived parametric amplification in plasmas

20 p3582 A69-38244

Radiometer for 4 cm wavelength range with receiver circuit incorporating tunnel and parametric HF amplifiers, describing design and operation including sub-units

21 p3724 A69-39076

Absolute and convective instability criteria of interacting electromagnetic waves in waveguide systems involving parametric oscillators and amplifiers

21 p3677 A69-39555

Combination resonance and instability regions of second type for parametrically excited oscillations with nonlinear/cubic/damping

23 p4230 A69-42107

Stimulated Brillouin scattering application to measurement of hypersonic velocities and absorption in

gigahertz frequency range, laser frequency shifting and Q switching, etc

23 p4167 A69-42183

PARAMETRIC DIODES

Microwave diodes on GaAs base, determining basic parameters and effects on crystal formation and device construction

05 p0730 A69-16222

Pneumatic diode function generator for simulating nonlinear control systems, discussing operating characteristics and programming methods

11 p1858 A69-24580

Parametric amplifier gain, deriving expressions for diode pumping power and nonlinear circuit element resistance

11 p1849 A69-24957

Barrier capacitance measurement in mm wavelength parametric and multiplication diodes eliminating socket capacitance influence, describing oscilloscope and indicator methods

12 p2043 A69-26885

PARAMETRIC FREQUENCY CONVERTERS

Wideband electronically scanned receiver, using varactor diode upper sideband parametric frequency upconverter for frequency mixing

01 p0048 A69-11036

Parametric frequency divider using reverse biased hyperabrupt junction diodes to provide nonlinear capacitance

02 p0217 A69-12152

Photoparametric up-converter with optimum SNR, noting suitability of direct detection of amplitude modulated optical signals

07 p1104 A69-18888

Multiple access techniques in civil satellite communications systems, noting proposed digital time and frequency division methods

08 p1272 A69-19959

Parametric frequency converter consisting of mixer head in bridge circuit with varactors for 12 GHz TV transmitters

11 p1854 A69-25614

Step-up mixer converting modulated IF signal to HF level by HF high power oscillator signal, discussing efficiency

11 p1854 A69-25615

Upconverter with gain and stabilized frequency, using sideband locking of IMPATT diode oscillator

12 p2036 A69-25909

Up-converter IR detector noise characteristics for pulse and CW signal detection compared with photoconductive detector

12 p2029 A69-26329

Different parametric converters amplitude characteristics analysis for determining necessary pumping power, allowing for saturation

15 p2574 A69-30119

Statistical properties of parametric amplifier and frequency converter by Schrodinger quantum mechanics and P-representation of density matrix

16 p2761 A69-32363

Microelectronic S band upconverter designed and fabricated in microstrip on alumina substrate

16 p2762 A69-32562

Parametric conversion kinetics of monochromatic light waves in nonlinear crystals, using quantized electromagnetic field to study amplification and generation

19 p3332 A69-35870

PARAMETRONS

State variables with delta functions for electrical network with discontinuously variable components, discussing application to parametron

19 p3287 A69-36763

PARASITES

Parasitic calcifications of soft parts in flight personnel studied radiologically, noting filariasis, bilharziasis and worms

09 p1446 A69-22729

Behavioral patterns and physiological parameters of medical leech Hirudo medicinalis determined in natural environment prior to biological experiment in space

24 p4268 A69-43402

Environmental stress effects on medical leech studied to determine tolerance to spacecraft launching, orbiting and reentry

24 p4268 A69-43403

PARASITIC DISEASES

Parasitic calcifications of soft parts in flight personnel studied radiologically, noting filariasis, bilharziasis and worms

09 p1446 A69-22729

PARAWINGS

One and two lobed conical, cylindrical and all-flexible parawing lift, drag and pitching moment and canopy shape

[AIAA PAPER 68-10] 01 p0007 A69-11027

Flexible parawing lifting decelerator research data from wind tunnel and flight tests, noting manned space vehicle recovery and aircraft escape systems

[AIAA PAPER 68-967] 24 p4254 A69-43715

Gliding cargo airdrop system including automatic homing and manual control

[AIAA PAPER 68-958] 24 p4254 A69-43723

PARKING ORBITS

Parking orbit optimal orientation for minimal impulsive maneuvers total velocity increment in three dimensional capture-escape mission

[AIAA PAPER 69-918] 21 p3808 A69-39347

Low thrust guidance for multirevolution trajectory required for earth parking orbit transfer to parabolic orbit insertion, noting advantages over high thrust scheme

[AAS PAPER 69-403] 24 p4379 A69-42832

PARTIAL DIFFERENTIAL EQUATIONS

NT BIHARMONIC EQUATIONS

NT BURGER EQUATION

NT ELLIPTIC DIFFERENTIAL EQUATIONS

NT FOKKER-PLANCK EQUATION

NT GAUSS EQUATION

NT HELMHOLTZ VORTICITY EQUATION

NT LIOUVILLE EQUATIONS

NT PARABOLIC DIFFERENTIAL EQUATIONS

NT VLASOV EQUATIONS

Simultaneous partial integro-differential equations governing natural vibrations of arbitrary cross section cylindrical tubes, suggesting Fourier series solution

01 p0164 A69-10065

Linear partial differential equations for nonlinear intensive heat and mass transfer, discussing analogy between transfer processes and electromagnetic waves distribution

01 p0174 A69-10104

Hollow finite cylinder stress-strain analysis under normal loads on end faces solved by four partial differential equations

01 p0168 A69-10359

Boundary value problems in thin shallow shells of arbitrary planform analyzed by partial differential equations

01 p0171 A69-11071

Partial differential equation for distribution function in transport of charged particles in earth magnetosphere

01 p0147 A69-11320

Group invariant solutions of differential equation systems applied to quasi-linear partial differential equations of motion of air masses

02 p0274 A69-11444

Asymptotic and approximate waves constructed for system of nonlinear partial differential equations for phases corresponding to multiple characteristics

02 p0271 A69-12034

Iterative transfer of boundary values to fictitious contour in numerical solution of partial differential equations

[ONERA-TP-646] 03 p0454 A69-12874

Iterative method to solve large sets of algebraic equations in approximate solution of multidimensional partial differential equations by implicit numerical techniques

03 p0456 A69-13554

Compatibility equations in plane micropolar thermoclasticity theory obtained by associated matrix method

03 p0525 A69-13607

Difference schemes to solve Navier-Stokes equations for viscous incompressible fluid by substituting fourth order partial differential equation

03 p0415 A69-13650

Independent variables reduction in nonlinear partial differential equations, detailing group theory method

03 p0456 A69-13740

Optimal control theory applied to systems described by partial differential/integral equations

04 p0581 A69-14571

Differential-difference equations and nonlinear initial boundary value problems for linear hyperbolic partial differential equations, noting procedure based on method of characteristics

04 p0623 A69-14949

Numerical integration of elliptic mixed boundary value problem in region with curved boundary programmed in FORTRAN for general linear second order partial differential equation

04 p0625 A69-15287

SALEM programming system developed for digital simulation of systems described by partial differential equations

04 p0565 A69-15340

Functional optimization techniques for serial hybrid computer solution of partial differential equations, emphasizing algorithms handled on digital computer

04 p0566 A69-15344

Hybrid assumed mode solution of nonlinear partial differential equations/initial value problems/ in time-like independent variable

04 p0566 A69-15345

Hybrid computer algorithm for numerical integration of partial differential equations, using assumed sum separation of variables

04 p0566 A69-15346

Hybrid computational method for partial differential equations to reduce time of solution and error propagation

04 p0566 A69-15347

Iterative solution of continuous-time-discrete- space /CTDS/ equations as approach to hybrid computation of certain partial differential equations

04 p0567 A69-15348

Partial differential equations solution using analog, digital and hybrid computers, discussing heat transfer in parallel flow exchanger

05 p0723 A69-15705

Finite differences for identifying partial differential equations and associated boundary conditions of distributed parameter system

[ASME PAPER 68-WA/AUT-1]

05 p0738 A69-16185

Analog simulation of water hammer type phenomena governed by linear constant coefficient partial differential equations

05 p0751 A69-16475

Maximum principle application to stochastic systems, developing set of stochastic partial differential equations

05 p0788 A69-16482

Methods to obtain uniqueness for partial differential /elliptic/ equations boundary problem extended to parabolic conditions, analyzing necessary conditions for existence

07 p1173 A69-18728

Complex variable theory usefulness in investigating existence and uniqueness of solutions for boundary values in partial differential equation

07 p1173 A69-18731

Uniqueness conditions of expansions in series of functions stressing Jacobi series applied to singular partial differential equations

07 p1174 A69-18805

Tensor partial differential equations having spherical symmetry, examining covariant differentiation and contraction of tensors

07 p1123 A69-18807

Incorrect problem solving method applied to Cauchy problem solution for nonlinear partial differential equations, considering Ritz method applicability

07 p1174 A69-19005

Laminar conducting wall jet injected in transverse magnetic field, analyzing partial differential equations obtained

07 p1192 A69-19020

Axisymmetric jet impingement against solid plane from tube at finite distance, using nonlinear partial differential equation in finite difference form

[AICHE PAPER 31F] 08 p1302 A69-19847

Stieltjes transform relating initial boundary value problems for partial differential equations of various classifications

08 p1342 A69-20352

Book on integral operators in theory of linear partial differential equations covering analytic functions, harmonic functions, differential equations, etc

08 p1343 A69-20725

Optimal control approximate synthesis partial differential equation solution in form of interpolation polynomial for functions of many variables

08 p1299 A69-21068

Book on optimal control of systems governed by partial differential equations, noting systems of automation, existence theorems and numerical analysis

09 p1471 A69-21580

Decrease existence at t approaching infinity solution of Sobolev linear partial differential equations describing rotating fluid small oscillations

09 p1481 A69-21899

Generalized orthogonality principles and expansion schemes for forced response of partial differential equations, noting applicability to rodlike structures

09 p1533 A69-21975

Kutta-Merson algorithm for converting partial differential equation for two dimensional unsteady state heat conduction to simultaneous ordinary differential equations

09 p1623 A69-22280

Liapunov direct method in stability problems for semilinear and quasi-linear systems of hyperbolic partial differential equations with independent variables

09 p1534 A69-22799

Natural frequencies and associated composite loss factor for laminated plate with alternate elastic and viscoelastic layers, deriving partial differential equations

[ASME PAPER 69-VIBR-68]

10 p1805 A69-24158

Wave propagation in connected space-time for linear second order hyperbolic partial differential equation, describing unitary invariant theory

11 p1908 A69-24356

Nonlinear partial differential equations for solution of steady stratified flows, noting hydrostatic pressure distribution and horizontal and vertical scales

11 p1869 A69-24889

Topologies introduced on state space for differential equations to obtain dynamical systems

11 p1909 A69-25409

Classification of second order quasi-linear partial differential equations with two independent variables in structural dynamics with emphasis on elastic structures

11 p1991 A69-25513

Boundedness criteria for second order hyperbolic equation boundary value problem solution in Banach space

12 p2122 A69-26573

Linear two dimensional partial differential equations solved by Laplace transforms on analog computer

12 p2123 A69-26717

Existence theorems for partial differential equations theory for traction boundary value problem of linearized elastostatics

12 p2188 A69-26928

Nonlinear hyperbolic partial differential equations with dissipation term for periodic solutions

12 p2124 A69-26929

Numerical solution to partial differential equations describing helical discharge in Ar with gas injection, discussing initial temperature distribution and radial distribution effects

12 p2141 A69-27131

Relaxing gas nonequilibrium flow in plane expansion, comparing partial differential equations with method of characteristics

13 p2244 A69-27322

Analytical expressions for nonlinear partial differential equation of heat conduction in solids, giving temperature as function of time and location

13 p2372 A69-27434

Partially characteristic boundary value problem for partial differential equations

13 p2288 A69-27527

Conditions governing application of reduced Nielsen equations to anholonomic systems dynamics, discussing kinetic energy function

13 p2288 A69-27924

Laminar temperature and velocity profiles near plane rectangular surface for free supersonic flow, solving partial differential equations for mass, momentum and energy conservation

13 p2309 A69-28025

Dynamic stability of elastic bodies with motion described by partial differential equation

15 p2652 A69-30860

Laminar boundary layer on rotating blades and yawed infinite wings, solving partial differential equations numerically by implicit finite difference scheme on computer

16 p2732 A69-31885

Interdependent behavior of Fourier solutions to sets of partial differential equations with variable coefficients

16 p2804 A69-32252

Optimal control approximate synthesis partial differential equation solution in form of interpolation polynomial for functions of many variables

16 p2765 A69-32483

Generalized finite difference approximations of linear partial differential operators in space based on functional approximations

16 p2756 A69-32552

Eigenvalue problems in partial differential equations solved by extended Kantorovich method, considering vibration of rectangular membrane and stability of elastic rectangular plate

16 p2876 A69-32783

Necessary and sufficient conditions for existence of smooth solution to quasi-linear partial differential equation

17 p2994 A69-32843

Stochastic differential game theory, discussing nonlinear partial differential equations for solution, dynamic programming validity conditions, finite difference scheme, etc

17 p2994 A69-32844

Book on quasi-reversibility application to partial differential equations covering parabolic, nonparabolic, elliptic equations and boundary conditions control

17 p2994 A69-33205

Ray methods application to partial differential equations for electromagnetic wave propagation in ionosphere, discussing strongly and weakly anisotropic inhomogeneous plasma

17 p2925 A69-33840

Nonlinear partial differential equations solutions in theory of thin elastic spherical shells subjected to temperature fields and external loading

17 p3067 A69-34147

Computer implementation of Bergman solution to initial value problem for partial differential equation of compressible fluid flow

18 p3164 A69-34614

Wave propagation in gas particle flow, obtaining fourth order particle differential equation from perturbation theory

18 p3121 A69-34772

Cauchy problem for homogeneous linear difference scheme with constant complex coefficients, giving stability lemmas

18 p3165 A69-35049

MHD flow, deriving equation system and boundary conditions for gas dynamic process

18 p3181 A69-35054

Peano-Baker method for integration of variational equations to produce partial derivatives used in satellite trajectory estimation

19 p3398 A69-35616

Partial differential equation representing influence of radiative and turbulent transfers of atmospheric heat, based on absorption coefficients for terrestrial radiation

19 p3363 A69-36498

Existence theorem for limits of minimizing sequences in optimal control problems, applying results to systems governed by partial differential equations

19 p3287 A69-36724

Transformation groups used to find similarity solutions for partial differential equations and heat equation

20 p3630 A69-36915

Finite elements general theory applied to wave propagation, gas kinetics, nonlinear partial differential equations, continuum mechanics and fluid dynamics

20 p3567 A69-36948

Computer solutions for nonlinear partial differential equations governing compressible flow patterns with shocks, using Lagrange coordinates

20 p3569 A69-38212

Partial differential equation initial value problems analyzed by ordinary differential equations via functional approximation method

21 p3756 A69-39132

Nonlinear problems involving large deflections of isotropic and orthotropic shallow shells of rectangular planform, deriving partial differential equations for solution

21 p3838 A69-39185

Axisymmetric solutions of magnetohydrostatic equations for large conductivity media satisfying second order partial differential equation containing two arbitrary functions

21 p3778 A69-39498

Operational calculus for n-variable functions analogous to Mikusinski method for single variable functions, giving applications to linear partial differential equations with constant coefficients

21 p3756 A69-39500

Upper and lower bounds for certain classes of partial differential equations associated with variational problems in theory of deterministic control processes

22 p3976 A69-41034

Positive solutions of parabolic and hyperbolic partial differential equations arising as viscoelastic media equations of motion, noting maximum principle utilization

22 p3976 A69-41035

Straight line method for boundary problems solutions with errors for partial differential equations

22 p3976 A69-41110

Boundary problem for differential equation of mixed type reduced to singular boundary problem for hyperbolic partial differential equations

23 p4181 A69-41409

Cauchy problem for partial differential equations linear parabolic system with coefficients depending on unknown functions

23 p4181 A69-41410

Linear partial differential equations derived from thermodynamic identities integrated by method of characteristics for relationships between temperature and pressure incomplete equations of state

23 p4239 A69-41569

Optimal generalized controls for systems under random forces described by hyperbolic partial differential equation system

23 p4144 A69-41957

Decrease existence at approaching infinity solution of Sobolev linear partial differential equations describing rotating fluid small oscillations

23 p4152 A69-41975

Boundary conditions for Tricomi equation in symmetric positive form, showing analytical and finite difference solutions

24 p4339 A69-42792

Wrong boundary conditions influence decay in overdetermined difference approximations to hyperbolic partial differential equation

24 p4340 A69-43227

Transverse shear influence on circular plates small displacement theory determined from coupled linear partial differential equations of plates

24 p4405 A69-43655

PARTIAL PRESSURE

NT HYPOXEMIA

NT OXYGEN TENSION

Oxygen partial pressure, temperature and olivine composition related, determining distribution coefficient of Fe and Mg between olivine and pyroxene

03 p0516 A69-14082

Temperature dependence of partial pressure of saturated As vapor over solid solutions of InAs-GaAs of different composition

04 p0642 A69-14938

Hydrothermal investigation of Ge trace quantity distribution between metal, silicate and sulfide phases at controlled oxygen partial pressure by oxygen buffer techniques

05 p0819 A69-15624

Blood oxygen metabolism, analyzing content and volume circulation in dogs under oxygen partial pressure decrease in inhaled air

12 p2019 A69-26346

High pressure Cs thermionic converter with cold region, measuring Cs partial pressure distribution in Ar filled tube

14 p2397 A69-29176

Lightweight sensor for telemetering oxygen partial pressure in respiration air

15 p2559 A69-31231

PARTICLE ACCELERATION

Solar cosmic radiation, particle acceleration, energetic particles as sample of sun and propagation of particles from sun to earth

03 p0498 A69-12934

Acceleration of charged particles in strong DC magnetic field by electrostatic waves with spatially varying phase velocities integrated numerically on IBM 360/65

03 p0479 A69-14028

Sudden acceleration of electrons in magnetosphere and magnetic tail related to magnetic bays, noting acceleration occurrence first in magnetosphere during polar substorm

04 p0594 A69-15122

Spectrum of accelerated particles on surface of stars revealed by observation of photospheric lithium and beryllium

05 p0817 A69-16711

Injection spectra of protons accelerated on sun to billion-trillion ev, discussing acceleration mechanisms

06 p0996 A69-17741

Electromagnetic ion acceleration in steady electric and magnetic fields chosen to match fields of Alkali Plasma Hall Accelerator /ALPHA/ [AIAA PAPER 69-111]

06 p0985 A69-18175

Ion cyclotron resonance acceleration and higher harmonic acceleration in axially nonuniformly magnetized plasma under influence of RF electric field

08 p1360 A69-20079

Bimodal diffusion mechanism for acceleration of trapped particles in earth magnetosphere, noting particle intensity profiles and energy spectra

08 p1307 A69-20183

Charged liquid droplets generator and acceleration through electric field for thrust vectoring, analyzing beam focusing and deflection [AIAA PAPER 69-283] 09 p1563 A69-21230

Charged particle acceleration in interplanetary medium, discussing protons and plasma oscillations interactions 09 p1575 A69-21541

Bimodal diffusion mechanism for acceleration of trapped electrons and protons in earth radiation belts, noting particle intensity profiles and energy spectra 09 p1576 A69-21708

Reflected particle acceleration at magnetospheric bow shock front attributed to interplanetary electric field 09 p1577 A69-21714

Cosmic charged particle acceleration in electromagnetic field described by vector and scalar potentials, constituting plane electromagnetic wave propagating along z axis 10 p1756 A69-22816

Line spectrum of flare gamma radiation due to atmosphere nuclei excitation by high energy proton acceleration 11 p1945 A69-24241

Low energy cosmic rays and plasma turbulence in heating and ionizing interstellar gas, discussing acceleration and galactic sources 11 p1945 A69-24380

Solar wind particles acceleration and transformation into radiation belt particles 11 p1948 A69-24855

High energy cosmic ray origin and acceleration by LF electromagnetic radiation produced by pulsars, noting maximum energy for protons 11 p1950 A69-24927

Cosmic radiation origin in terms of sudden injection of particles in time, momentum and space, considering statistical fluctuations role in observed spectrum 12 p2148 A69-26206

Potential mechanisms of electron acceleration inside magnetosphere, measuring power spectrum of X rays by electron braking in upper atmosphere 12 p2066 A69-26295

Cometary tail diffusion model based on luminous particle number decrease with time and particle accelerated motion and diffusion in space 14 p2523 A69-29705

Magnetic mirrors, Doppler and relativistic effects, wave attenuation and radiation pressure during gyroresonant particle acceleration in nonuniform magnetostatic and HF fields 14 p2499 A69-29845

Low energy electron and proton precipitation, discussing acceleration mechanisms and periodicity in relation to auroras and airglows 15 p2594 A69-30018

Fermi acceleration of energetic electrons trapped within dipole magnetic field analyzed to obtain quantitative results for wave-particle interaction within complex magnetospheric configuration 15 p2594 A69-30095

Charged particle acceleration in interplanetary medium, discussing protons and plasma oscillations interactions 16 p2851 A69-32536

Trapped protons acceleration through bimodal diffusion in magnetosphere, noting spatial patterns and temporal behavior of proton and electron belts 16 p2851 A69-32618

Development and applications of ion propulsion covering electrostatic acceleration of particles, Cs contact and electron bombardment ion thrusters, space missions, etc 17 p3020 A69-33354

Particle and light motions in Schwarzschild field, discussing acceleration beyond speed of light in reference /S/ frame of time independent coordinate systems 17 p3006 A69-33741

Trapped particle acceleration by random bimodal diffusion in inhomogeneous magnetic field accounting for high energy particles trapped in earth radiation belts 18 p3186 A69-34808

Mean lives of upper decay levels of lithium isotopes accelerated by electromagnetic isotope separator and directed through thin carbon foil 18 p3177 A69-35012

Ultrarelativistic electron acceleration in Crab Nebula maintaining synchrotron spectrum, obtaining power from compressional motion damping, gyrorelaxation effect and pitch angle anisotropy removal 19 p3424 A69-36336

Electrostatically accelerated iron spheres interaction with thin metal and nitrocellulose foils to develop detectors for cosmic dust collection and recording 21 p3719 A69-38344

Rocket measurements of primary auroral particles energy spectra indicating spectral structure acceleration peaks associated with electrostatic fields 21 p3707 A69-38490

Charged particle acceleration in interplanetary plasma from analysis of cosmic ray intensity increases accompanied by SC magnetic storms and Forbush effects 21 p3788 A69-38587

Cosmic rays composition, origin, acceleration and propagation, describing two component models 21 p3789 A69-38814

4 October 1965 type IV solar burst, studying acceleration mechanisms for fast electrons by comparing fine structure at various frequencies 22 p4001 A69-39983

Accelerating electric field model to interpret energy and angular distribution of auroral particles, noting electric potential limitations 22 p3938 A69-40445

Continuous electron acceleration in astrophysics, discussing Crab Nebula X ray flux and galactic and extragalactic radio source power law spectra 24 p4355 A69-42696

High energy nucleons and electrons accelerated in solar flares, considering interplanetary magnetic field effect on radiation properties near earth orbit 24 p4372 A69-43617

Low energy cosmic rays and plasma turbulence in heating and ionizing interstellar gas, discussing acceleration and galactic sources 24 p4375 A69-43770

PARTICLE ACCELERATORS

NT BETATRONS

NT CYCLOTRONS

NT ELECTRON ACCELERATORS

NT LINEAR ACCELERATORS

NT MICROTRONS

NT SYNCHROCYCLOTRONS

NT SYNCHROTRONS

Phase space concepts for beams, accelerators and confined particles, noting adiabatic invariants, phase space transformations, particle dynamics in accelerators and plasmas 06 p0966 A69-17673

Annular traveling wave resonator for feedback in resonance particle accelerator of smooth waveguide 07 p1107 A69-19160

Tritium contamination reduction in small ion accelerators for neutron production, discussing pumping problems and vacuum systems 12 p2059 A69-26499

Transverse momentum of fireball particles emitted in high energy inelastic collision related to emission angle and energy in accelerators 19 p3396 A69-36644

PARTICLE BEAMS

NT ATOMIC BEAMS

NT ELECTRON BEAMS

NT ION BEAMS

NT MOLECULAR BEAMS

NT NEUTRAL BEAMS

NT PION BEAMS

NT PROTON BEAMS

Beam-foil spectroscopy - NASA Conference, University of Arizona, November 1968, Volume I 03 p0470 A69-13160

Small silicon diodes to explore depth-dose distributions in water phantom of proton beams 03 p0430 A69-13481

Aperiodic hydrodynamic beam instability development and energy losses, discussing plasma oscillation enhancement and nonlinearities 03 p0480 A69-14137

Uniform external magnetic field effect on electric potential distribution within ion-electron beams near planar emitting surface 03 p0482 A69-14214

Beam foil spectroscopy for measuring wavelengths and spectral line intensities 04 p0595 A69-14276

Pumping requirements for nozzle skimmer region of neutral particle nozzle beam source, using two stage mechanical pump 04 p0600 A69-15026

H resonator for charged particle beams combination at output of double beam linear accelerator 05 p0727 A69-15639

Phase space concepts for beams, accelerators and confined particles, noting adiabatic invariants, phase

space transformations, particle dynamics in accelerators and plasmas 06 p0966 A69-17673

Electromagnetic waves excitation during interaction between density modulated beam and plasma in magnetic field, analyzing instabilities 07 p1189 A69-18508

Charged liquid droplets generator and acceleration through electric field for thrust vectoring, analyzing beam focusing and deflection [AIAA PAPER 69-283] 09 p1563 A69-21230

Density modulated charged particle beam interaction with plasma under paramagnetic resonance, analyzing longitudinal oscillations and parametric instability zone 10 p1741 A69-23947

Monograph on schlieren-optical technique for plasma beam temperature measurements using photoelectric scanning device 12 p2134 A69-26120

Oscillating electron ion discharge in magnetic field in system of alternating positive and negative electrodes to obtain fast neutral particle fluxes 13 p2311 A69-28109

Transverse particle and energy fluxes in toroidal magnetic traps magnetic fields with ionized plasmas, discussing particle diffusion coefficient and thermal conductivity 13 p2314 A69-28446

High energy neutron transport calculated using one dimensional discrete ordinates code with anisotropic scattering, comparing results with nucleon transport code calculations 14 p2481 A69-29592

H resonator for charged particle beams combination at output of double beam linear accelerator 16 p2762 A69-32497

Communication channel information capacity determination through particle ensembles entropy analysis 19 p3334 A69-35885

Magnetospheric stable charged particle beams for pearl pulsations and discrete VLF radiation in geomagnetic field, attributing synchronization to space charge 23 p4206 A69-41851

PARTICLE CHARGING

Rates of charging of thermionically emitting particles in space charge 06 p1035 A69-17928

PARTICLE CLOUDS

U CLOUDS

PARTICLE COLLISIONS

Heat and mass transfer coefficients derived for reacting gas mixtures by applying variational principle 01 p0006 A69-10400

Transition probabilities for collinear collision of particle with harmonic oscillator, noting reasons for discrepancy in Jackson and Mott form 01 p0124 A69-10688

Cosmic rays extensive air showers from interaction of particles with nuclei of elements in atmosphere 01 p0144 A69-10752

Landau damping in plasma, noting competing effects of nonlinearities and collisions on formation of plateau in spatially homogeneous distribution function 01 p0133 A69-11215

Numerical regularization of single binary collision in n body gravitational problem 02 p0322 A69-12268

Collision broadened homogeneous linewidth measurements for 6328 angstrom Ne line in Ne and He-Ne discharges, using nonlinear interaction between two traveling waves 02 p0257 A69-12613

Density gradient driven collisional drift waves, discussing identification, stabilization and enhanced plasma transport 03 p0474 A69-13145

Scattering of energetic charged particles in weakly unstable plasma for integrated spectrum of plasma electric field autocorrelation function 03 p0475 A69-13151

Rotation and orientation of cosmic dust particles due to collisions with interstellar gas particles 03 p0511 A69-13420

Empirical growth curve determined by using equivalent widths of absorption lines of quasar 3C 191, concluding ionization is mainly due to collisional processes 03 p0514 A69-13962

Parametric or impact parameter treatment for describing ion-atom collision at low or high impact velocities, reexamining approximate treatments 05 p0797 A69-16697

Monte Carlo method to calculate distributions describing particle behavior in Knudsen cell, clarifying relationship between gaseous collisions and Knudsen number
06 p0908 A69-17111

Ionizing electron collisions with He, determining energies and angular correlation distributions of scattered and ejected electrons
06 p0962 A69-17191

High energy pure photon showers in cosmic ray emulsions in relation to production of magnetic pole-dipole pairs
06 p0996 A69-17883

Spherical particle motion in vortex gas flow between planes of turbulence chamber perpendicular to axis of flow rotation, noting collisions effect
07 p1181 A69-19000

Loss rate of plasma from stellarator due to binary Coulomb collisions scattering particles in loss region, discussing diffusion coefficients
08 p1364 A69-20520

Vibrational excitation in He, H and N ion- molecule collisions on nitrogen first negative system, studying relative band intensities
08 p1356 A69-20739

Collisional theory of longitudinal wave propagation for two fluid viscous ionized plasmas formulated from coupled Maxwell and Boltzmann equations
08 p1367 A69-20796

Cosmic ray particle behavior in interplanetary medium, solving model equation for cosmic ray diffusion in cloud of outgoing scattering centers
09 p1575 A69-21598

Plasma transport properties derived from Boltzmann equation using Debye shielded Lande potential to represent collisions, noting viscosity and thermal conductivity
09 p1553 A69-22539

Secondary emission in low altitude satellite body dependent on inelastic collisions with primary cosmic ray protons
10 p1757 A69-22821

Local potential method extended to study plasma oscillations inhomogeneous kinetic equations in presence of linear or nonlinear collision operators
11 p1925 A69-24316

Extragalactic gamma ray fluxes predicted, discussing collisions, matter-antimatter annihilation and cosmological implications
11 p1946 A69-24466

Asymptotic solution for Fokker-Planck equation at low collision frequency, studying electron-ion collisions effect on universal instability in inhomogeneous plasma
11 p1930 A69-25358

Electron-ion recombination coefficient for triple collisions in dense low temperature plasma, deriving finite electron Fokker-Planck equation
11 p1933 A69-25541

Heat and mass transfer coefficients derived for reacting gas mixtures by applying variational principle
12 p2062 A69-26668

Energy loss during inelastic collisions between electrons and ionospheric particles, determining ionospheric heating by UV radiation
13 p2252 A69-27614

Finite Larmor radius and collision with neutral atoms simultaneous effects on plasma gravitational instability
13 p2346 A69-27708

Dissipative drift instability due to electron density gradient and dissipative mechanism /neutral-electron and ion-electron collisions/ in plasma in constant magnetic field
13 p2308 A69-27979

Elastic and inelastic elementary particle collisions described by Feinman diagrams, discussing computer results for high energy particle interactions
13 p2303 A69-28369

High energy particle collisions, calculating inelastic interactions between cosmic nuclei
13 p2330 A69-28370

Nuclear emulsion high energy nucleon-nuclei interaction model accounting for two maxima track formation
13 p2303 A69-28371

Multiple particle production and resonance events during high energy particle collisions
13 p2303 A69-28372

Four dimensional momenta transfer during high energy cosmic ray particle collisions, comparing various collision models
13 p2330 A69-28375

Vaporizer temperature and collision efficiency correlation data for magnesium oxide-argon dilute diffusion flames studied for determining inverse temperature dependence
13 p2380 A69-28461

Gas and polydispersed condensate parameters of nonequilibrium two phase flow in Laval nozzle, considering particle collisions and coagulation, energy exchange and momentum exchange
14 p2391 A69-29621

Collisional emission and absorption of longitudinal waves due to particle encounters in numerical experiments on one dimensional one species plasma
15 p2661 A69-30921

Ionosphere D region low field conductivity in presence of high field disturbing signal, assuming inelastic electron-neutral particle collisions
16 p2850 A69-32190

Diatom heavy particle collisions with emphasis on epithermal energy range, discussing elastic scattering and inelastic processes
16 p2815 A69-32259

Cosmic ray particle Pb nucleus interaction energy transfer to electron photon cascade in first inelastic collision, noting dependence on particle energy
17 p3008 A69-33387

Gas laser power dip in presence of elastic collisions, using equilibrium equations for particles velocity distribution function
17 p2983 A69-33972

Lorentz gas approximation to Boltzmann collision operator generalized for heavy molecule nonMaxwellian gas distribution function, obtaining equilibrium distribution applicable to ionized gas
18 p3179 A69-34438

Longitudinal plasma waves collision damping calculations using Rostoker test particle method
18 p3179 A69-34439

Collisional excitation of forbidden lines in planetary nebulae from 5337/5517 intensity ratio measurements, noting density and intensity relationship
19 p3422 A69-36221

Infinitesimal mass trajectories and possible double collision in gravitational field of two finite and unequal masses in plane elliptic restricted three body problem
21 p3795 A69-38443

Impact pressures during two body collisions, correlating pressure with particle speed
21 p3836 A69-38943

Cosmic X ray bremsstrahlung due to collisions of suprathermal protons with ambient electrons, giving clue about diffuse sky background of X rays
22 p4006 A69-40643

Shape resonances in low energy elastic scattering of electrons by C, N and O, discussing ground state configurations and close coupling equations corrections
23 p4193 A69-41452

Chemical reaction kinetics in high temperature gases in terms of collision theory, discussing gaseous statistics and Boltzmann equation
23 p4113 A69-41518

Ionization and light emission cross sections for collisions of protons and hydrogen atoms with atmospheric nitrogen used to analyze auroral events
24 p4368 A69-43177

Thermal nonequilibrium state and effective collision frequency between protons and electrons in solar wind plasma, explaining abnormal dissipation
24 p4368 A69-43187

PARTICLE COUNTERS

U RADIATION COUNTERS

PARTICLE DECAY

U RADIOACTIVE DECAY

PARTICLE DENSITY [CONCENTRATION]

NT ELECTRON DENSITY [CONCENTRATION]

NT ELECTRON DENSITY PROFILES

NT ELECTRON DISTRIBUTION

NT ION DENSITY [CONCENTRATION]

NT IONOSPHERIC ELECTRON DENSITY

NT IONOSPHERIC ION DENSITY

NT MAGNETOSPHERIC ELECTRON DENSITY

NT MAGNETOSPHERIC PROTON DENSITY

NT PLASMA DENSITY

NT PROTON DENSITY [CONCENTRATION]

Distance between measurement equipment and extensive air showers axis varied as function of particles number and number of hit
01 p0144 A69-10749

Frequency occurrence of small particles in meteor showers, discussing fragmentation and cosmic erosion as primary effects in small particle development
01 p0154 A69-10872

Electric discharge in gas flow with magnetic field, showing varying charged particle density as function of argon-cesium pressure
02 p0285 A69-11570

Diffusion effect on particle buildup in deionizing steady plasma flux linked to plasma concentration in presence of electron temperature gradients
02 p0291 A69-12483

Absorption oscillator strengths of S 1 and S 2 lines between 1100 and 2000 A, using arc burning light source
03 p0479 A69-13961

Charged particle density of unsteady plasma from Stark broadening of Balmer H beta line, using time-scanning image converter
03 p0481 A69-14145

Spectroscopic charged particle concentration determination, discussing error and limits of applicability low temperature plasma
05 p0762 A69-15899

Cosmic dust concentration in interplanetary space near earth, noting suitability of satellite observation
06 p0999 A69-16971

Transmittance and absorption cross sections of carbon particles suspended in flowing stream of nitrogen gas
06 p1034 A69-17804

Nonequilibrium low temperature plasma theory for ionization and particle distribution based on discrete and continuous spectra states, discussing electron distribution function
06 p0969 A69-17906

Night sky surface brightness and polarization measurements as basis for zodiacal dust cloud particle density distribution normal to ecliptic plane
07 p1222 A69-19588

Plasma flux measurements by charged particle traps in Venus vicinity by space vehicle Venus 4, discussing low concentration of charged particles
07 p1222 A69-19613

Nonlinear interactions between plasma waves of various intensities, noting changes in particle distribution
08 p1362 A69-20427

Zodiacal dust density in interplanetary space
08 p1407 A69-20938

Charged particles concentration change during vertical propagation of acoustic wave in F layer found transforming electric field into circularly polarized wave
09 p1484 A69-21528

Longitudinal electric field distribution and charged particle density in magnetic mirror under potential difference between magnetic equator and plane
10 p1689 A69-24204

Tunable Fabry-Perot interferometer for photoelectric measurements of absorption and emission line contours and line center particle concentrations
10 p1698 A69-24212

Radial distribution profiles of charge carriers in low temperature gas discharge plasma accounted for in terms of volume recombination
11 p1925 A69-24330

Charged particle concentration near electrodes in high current pulsed discharge with separated flames at atmospheric pressure determined by measuring quadratic Stark effect
11 p1927 A69-25219

Unicellular microorganisms size and concentration estimates based on light scattering measurements of suspensions in spectrophotometer cuvette compartment
11 p1829 A69-25643

Meteoritic dust particles collections prediction in atmosphere for low and high entry fluxes
12 p1558 A69-26342

Electromagnetic waves directional velocity, plasma temperature and particle density determined from analyzing electric field fluctuations amplification near body in plasma
12 p2137 A69-26531

Charged particle population dynamics in outer radiation zone of magnetosphere, discussing ring current particles, protons, electrons, alpha particles and electric field
12 p2150 A69-26743

Charged primary cosmic rays responsible for relative intensities of muon-poor extensive air showers at mountain and sea levels
12 p2152 A69-27099

Electric field determination from charged particle concentration in wake of body moving in rarefied plasma, noting hydrodynamics similarity
14 p2517 A69-29068

Stark effect applicability to charged particle concentration in nonstationary plasma
14 p2497 A69-29790

Relativistic corrections to particle distribution functions for high temperature plasma in thermodynamic equilibrium by integrating Gibbs distribution
14 p2499 A69-29847

Earth radiation belt data, discussing origin, density, distribution, etc, of protons, electrons and alpha particles
15 p2674 A69-30016

Drift wave instability due to particle number density gradient of plasmopause, considering velocity shear modification
15 p2595 A69-30096

Spectroscopic measurements of charged particle concentrations in jet produced by pulsed plasma generator
15 p2663 A69-30991

Time variation of altitude distribution of cosmic dust layer in upper atmosphere by Pandora II collector using inflight shadowing technique
15 p2698 A69-31353

Frequency of multiple muons from extensive air showers as function of zenith angle, noting mean transverse momentum and density spectrum
15 p2678 A69-31484

Possible existence in universe of large number of difficult-to-observe particles with zero rest mass left over from superdense phase
16 p2814 A69-31801

Azimuthal particle distribution expressions for analyzing cosmic ray jets
16 p2849 A69-32045

Solar wind velocity distribution anisotropy at earth explained by low density
16 p2849 A69-32097

Dimensions, concentration and spectrum of large precipitation particles in clouds and cloud water content by measuring reflectivity and absorptivity at different wavelength
16 p2807 A69-32268

Cosmic ray second harmonic daily variations explainable by symmetrical gradient rising away from solar equatorial plane
16 p2850 A69-32304

Charged particles concentration change during vertical propagation of acoustic wave in F layer found transforming electric field into circularly polarized wave
16 p2783 A69-32523

Moon density and nucleation of planets, explaining low density and absence of heavy core by late aggregation from nonmetallic particles
16 p2865 A69-32808

Self ignition of solid/fluid particles suspended in gas flow, discussing heat transfer coefficient, critical temperatures, etc
17 p3070 A69-33142

Luminous particles volumetric concentration calculation based on limiting surface density to determine bulk density in cometary head
17 p3032 A69-33189

Gas particle concentrations on moon due to solar wind, surface emissions and atmospheric contamination by lunar operations and rocket motor products
18 p3189 A69-34236

Self contained hand held battery operated aerosol particle analyzer, measuring aerosol concentration and size distribution for laboratory and space flight applications
18 p3136 A69-34691

Langmuir plate and spherical ion probe experiments aboard Explorer 31, measuring concentrations and temperatures of thermal electrons and ions
20 p3545 A69-37881

Mass spectrometric investigation of thermosphere at high latitudes, measuring number densities for nitrogen, Ar and molecular and atomic oxygen
20 p3533 A69-38086

Neutral particle density ratios in the thermosphere by rocket-borne monopole mass spectrometers
21 p3704 A69-38368

Cosmic ray muons for calibrating dE/dx counter used in particle identification by determining cosmic particles distribution as function of energy losses due to ionization
21 p3724 A69-39075

Normalized phase function and scattering coefficient of aerosols prediction from measurements of particle size distribution, density and refractivity based on Mie solution
21 p3719 A69-39774

PARTICLE DETECTORS

U RADIATION COUNTERS

PARTICLE DIFFUSION

NT ELECTRON DIFFUSION

Free access of low energy galactic particles to solar wind lines of force due to stochastic nature of lines
01 p0147 A69-11238

Solar cosmic rays diffusion relationship to interplanetary magnetic field power spectrum from high energy proton and electron observations
01 p0147 A69-11243

Diffusion of suspended particles in isotropic turbulence field of dispersed medium
02 p0234 A69-12579

Particle size distribution determination by measuring light beam extinction in turbid medium with photometer
03 p0428 A69-13110

Ideal gas spectra and density fluctuations correlations calculated during Markovian and nonMarkovian wandering of particles
03 p0477 A69-13414

Charged particle dynamics in spiral interplanetary magnetic field model, discussing electric drift velocity, point of origin and distribution
03 p0503 A69-14015

Equation describing statistically trapped particle motion under influence of fields varying in time and space
07 p1209 A69-19375

Dislocation climb theory of steady state creep, noting necessity of self diffusion mechanism in any high temperature creep theory
08 p1329 A69-20000

Bimodal diffusion mechanism for acceleration of trapped particles in earth magnetosphere, noting particle intensity profiles and energy spectra
08 p1307 A69-20183

Diffusion model for propagation of solar cosmic rays in interplanetary space, obtaining injection spectra for solar flare protons
08 p1379 A69-20613

Particle-wave interactions in weakly turbulent collisionless plasma, discussing ensemble average distribution function, diffusion, nonlinear Landau damping and nonlinear instabilities
08 p1368 A69-20803

Proton electrolyte application to fuel cells, discussing proton diffusion in solids and materials with vacancies /proton conductors/ in structures
08 p1269 A69-21053

Cosmic ray particle behavior in interplanetary medium, solving model equation for cosmic ray diffusion in cloud of outgoing scattering centers
09 p1575 A69-21598

Geomagnetically trapped particle loss processes and equilibrium distribution resulting from MHD wave field interaction described using sandbox model
11 p1948 A69-24856

Tellurium doping effect on phonon diffusion in GaSb, discussing thermal conductivity at low temperatures
12 p2142 A69-26294

Boundary layer parameters behind shock wave front in ionized gas calculated with allowance for charged particle diffusion
12 p2139 A69-26713

Earth radiation belts formation as function of particle injection into trapped radiation zones or proton and electron leakage
12 p2150 A69-26742

Diffusion of equatorial particles in outer radiation zone caused by expansions and contractions of permanently compressed magnetosphere, obtaining electric fields
14 p2510 A69-28937

Deposition and interdiffusion of W layers on Mo emitter of in-core thermionic reactor, investigating microstructure of transition zone
14 p2462 A69-29210

Particle diffusion and wave spectrum in unstable plasma calculated using Feynman diagrams, considering quasi-linear growth, resonant three wave coupling and nonlinear Landau damping
15 p2660 A69-30915

Low energy solar protons entry into magnetosphere on 26 May 1967 showing diffusion control
16 p2849 A69-31984

Cosmic ray second harmonic daily variations explainable by symmetrical gradient rising away from solar equatorial plane
16 p2850 A69-32304

Fuel cells with solid membranes with ion conductivity, discussing proton electrolyte
16 p2740 A69-32424

Trapped protons acceleration through bimodal diffusion in magnetosphere, noting spatial patterns and temporal behavior of proton and electron belts
16 p2851 A69-32618

Trapped particle acceleration by random bimodal diffusion in inhomogeneous magnetic field accounting for high energy particles trapped in earth radiation belts
18 p3186 A69-34808

Autoradiographic methods for diffusion and phase transformation in Fe-Cr alloys by application of photographic emulsion with tracer element on metal surface
20 p3561 A69-37416

Rocket measurement data of auroral particle precipitation classified in substorm phases of quiet and breakup period, breakup and postbreakup events and morning events
21 p3707 A69-38489

Charged particles beam penetration effects produced in atmosphere, determining particle diffusion and trajectory using Spencer moments and Monte Carlo methods
21 p3709 A69-38502

Field-aligned currents effect on ionosphere and precipitation of auroral primary particles, analyzing with mathematical model of ionospheric density height distribution
21 p3710 A69-38506

Small particle holography technique extended for dynamic properties of particle fields, determining velocity and density field, size distribution, flow structure and diffusion rate
21 p3726 A69-39776

Time dependent diffusion of light particles of Lorentz fluid approximated by Boltzmann equation leading to microscopic telegrapher equation
22 p3984 A69-40530

Outer anisotropic galactic cosmic particle flux distortion in interplanetary space, analyzing scattering in solar wind by isotropic diffusion equations
23 p4205 A69-41837

PARTICLE EMISSION

NT ELECTRON EMISSION

NT FIELD EMISSION

NT ION EMISSION

NT NEUTRON EMISSION

NT PHOTOELECTRIC EMISSION

NT SECONDARY EMISSION

NT THERMIONIC EMISSION

Neutrino radiation in universe with emphasis on stellar neutrino radiation, analyzing emission during nuclear fusion of C-N, He and Ne-Na cycles
01 p0145 A69-10754

Photon emission in germanium at high injection levels during uniaxial compression
04 p0643 A69-15255

Particle radiations and magnetic fields in metagalaxy, discussing galactic injection spectrum problems
06 p0991 A69-17310

Neutrino emission and carbon burning onset in 1.45 solar mass stellar models with pure He envelope, He burning shell and degenerate C-O core
08 p1384 A69-20059

Charged liquid droplets generator and acceleration through electric field for thrust vectoring, analyzing beam focusing and deflection
[AIAA PAPER 69-283]
09 p1563 A69-21230

Star collapse under energy losses due to neutrino emission, analyzing self similar asymptotic solutions
09 p1587 A69-21359

Neutron proton plasma properties in massive stars and supernovae, discussing neutrino emission
10 p1756 A69-22814

Radiation emission by scalar particle in field of two plane linearly polarized electromagnetic waves propagating toward each other
11 p1900 A69-25568

Poisson formula in double logarithmic approximation for photon emission cross section in analysis of bremsstrahlung involving high energy particles
11 p1922 A69-25758

Neutrino and antineutrino emission by URCA process calculated, assuming nuclear reactions in static and beta processes in kinetic equilibrium
15 p2674 A69-30542

Star collapse under energy losses due to neutrino emission, analyzing self similar asymptotic solutions
18 p3197 A69-34749

Transverse momentum of fireball particles emitted in high energy inelastic collision related to emission angle and energy in accelerators
19 p3396 A69-36644

Solid para hydrogen coated graphite particles expulsion into interstellar medium from star formation regions, considering mantles stability and particles extinction efficiency, albedo and phase function
20 p3601 A69-37492

- Atmospheric emissions - NATO Conference, Norway, July-August 1968
21 p3705 A69-38482
- Solid metal oxide particles temperature in premixed flames determined from intensity/ wavelength plots of continua
21 p3852 A69-39592
- PARTICLE ENERGY**
NT ELECTRON ENERGY
NT ELECTRON STATES
NT PROTON ENERGY
- Energetic cosmic radiation in deep mines, giving hypothesis of new particles more effective than muons
01 p0144 A69-10444
- Ring current particle energy density distribution for symmetric portion of magnetic storm derived from current magnetic field profile measurements
01 p0147 A69-11227
- Plasma waves and particle interaction in nonuniform magnetosphere, considering propagation across sheets of steep density gradient and auroral precipitation
02 p0235 A69-11429
- High energy interactions used to estimate energy of individual cosmic rays
03 p0498 A69-12941
- Balloon flown High Altitude Particle Physics Experiments /HAPPE/ for research on high energy cosmic rays and particle interactions
03 p0499 A69-12943
- Stormer problem of charged particle motion in magnetic dipole field, discussing analytical method for high and low energy particles
03 p0504 A69-14127
- Polar aurora incident energetic particles spectroscopic analysis, showing system of lines and bands intensity dependence on particle energy spectrum and magnetic activity
05 p0752 A69-15799
- High energy muons Cerenkov radiation, using water filled counter as function of muon momentum, noting no intensity decrease
06 p0991 A69-17306
- Low energy photon spectrum at balloon altitudes, noting small geomagnetic latitude dependence
06 p0992 A69-17313
- Distribution characteristics of radiation defects in materials irradiated by monoenergetic beams of protons and alpha particles
06 p0981 A69-17878
- Vela 4 satellite energetic particle experiment, describing instruments design and operation [IEEE PAPER 3C-2]
07 p1134 A69-19196
- Channel multiplier spectrometer for low energy electrons and protons at synchronous altitude on ATS-E satellite [IEEE PAPER 3C-5]
07 p1135 A69-19199
- Low energy charged particles in earth magnetosphere observed byOGO satellite
07 p1208 A69-19358
- Plasma instability with isotropic ion or electron velocity distribution function /nonMaxwellian/, discussing magnetic field and particle energy distribution functions
08 p1359 A69-19949
- Cosmic ray nuclei energy spectra and abundances above 20 Mev/nucleon determined by OGO-1 satellite experiment, considering He, B, C, N, O, Ne, Mg, Si, Mn, Fe, Co and Ni
08 p1378 A69-20067
- Photon momentum distribution role and relation to thermal radiation spectrum in fully ionized gases
08 p1357 A69-20747
- Magnetoactive plasma containing fast monoenergetic ions noting stability at drift frequencies and in terms of Alfvén wave buildup
09 p1546 A69-21566
- Low energy cosmic ray intensity increase on July 7, 1966 registered with high latitude neutron monitors
10 p1766 A69-23762
- Low energy particles during solar proton flare and effects on magnetosphere, cosmic ray intensity, ionosphere and geomagnetic activity
10 p1768 A69-23786
- Cosmic ray cut-off energy for synchronous satellites computed by trajectory tracing method using magnetospheric model
11 p1949 A69-24860
- Anisotropic fluxes of energetic particles in and near distant trapping region encountered by Explorer 33 satellite in outer magnetosphere
11 p1950 A69-25146
- Auroras and polar magnetic substorm observations limited comparison due to magnetospheric models inability to interpret daytime precipitation zones and particle energy spectra

12 p2072 A69-26740

Inner radiation zone including data on electrons, protons and heavier particles and results from high altitude nuclear tests

12 p2152 A69-27144

Negative charge production by H atoms collisions with rare gases and hydrogen, noting smooth rise of cross section with energy for rare gases

13 p2302 A69-27459

Laser Doppler method for measuring local particle velocities in two phase flows of liquid-metal MHD generators

13 p2260 A69-27476

Time of flight measurement for velocity of micron sized particles in two phase flow by light transmission method

13 p2263 A69-28243

Wilson chamber and ionization calorimeter determination of cosmic ray particle-carbon nuclei interaction energy characteristics

13 p2330 A69-28379

Nuclear component energy flux absorption in Fe measured with ionization calorimeter

13 p2330 A69-28386

Nuclear active particles energy in extensive air showers measured with ionization calorimeter, noting discrepancy attributed to ionization bursts

13 p2331 A69-28387

Ionization calorimeter energy measurement systematic errors

13 p2331 A69-28394

Primary particle energy and extensive air shower electron density relationship derived from vertical spectral profiles

13 p2331 A69-28396

High energy electron photon cascades event recorded with X ray photography, discussing origin in related atmospheric cosmic ray showers component subgroups

13 p2331 A69-28398

High energy muons energy spectrum in extensive cosmic ray showers from spectrum study of ionization bursts due to penetrating component

13 p2332 A69-28403

High energy ionization bursts in cosmic ray showers electron photon component, obtaining bursts power spectrum and component energy dependence

13 p2332 A69-28404

High energy mu-mesons component of atmospheric cosmic ray showers by particle impact penetration using multiple underground ionization chambers

13 p2332 A69-28409

Cosmic ray showers components relationships, analyzing superhigh energy nuclear cascade development, discussing components distribution function at constant proton energy

13 p2332 A69-28410

Primary particles energy determined by probability distribution functions of cosmic ray showers characteristics, using Monte Carlo computerized calculation

13 p2332 A69-28411

Cosmic ray chain reaction particles energy spectrum determination in heavy media, discussing cascade parameter application in showers development

13 p2303 A69-28412

Cosmic ray showers electron, positron and photon energy distribution functions calculated, considering positron annihilation, Compton effect and relativistic electrons formation

13 p2303 A69-28413

Electron photon cascades energy dependence on primary particle energy determined in lead by various instruments

13 p2304 A69-28418

Cosmic ray muons energy and angular distribution measurements, obtaining curve with respect to projection angles

13 p2332 A69-28420

Form factor of nucleus effect on high energy muons bremsstrahlung cross section

13 p2333 A69-28422

Distribution characteristics of radiation defects in materials irradiated by monoenergetic beams of protons and alpha particles

14 p2503 A69-28787

Spherical plate electrostatic analyzer transmission characteristics, emphasizing angular response to external particle sources as functions of angular coordinates and particle energy

14 p2449 A69-29560

High energy neutron transport calculated using one dimensional discrete ordinates code with anisotropic

scattering, comparing results with nucleon transport code calculations

14 p2481 A69-29592

Soviet book on solar cosmic rays covering origin, propagation, energy spectrum, diffusion dependence on particle energy and distance, solar flares, etc

14 p2514 A69-29816

Low energy positrons in cosmic radiation due to beta decay of carbon, nitrogen and oxygen isotopes, estimating positron fluxes and energy spectra

15 p2676 A69-30887

Ionospheric VLF emission and particle measurements, discussing energy, distribution and flux of protons and electrons

15 p2605 A69-31421

Diatomic heavy particle collisions with emphasis on epithermal energy range, discussing elastic scattering and inelastic processes

16 p2815 A69-32259

Cosmic ray particle Pb nucleus interaction energy transfer to electron photon cascade in first inelastic collision, noting dependence on particle energy

17 p3008 A69-33387

Resonances and doublets observation by neutron radiative capture and transmission of W and Zr isotopes in kev region, noting partial wave strength functions

18 p3175 A69-34314

Solar neutrons upper limits measured for 28 July 1967 importance 1 flares

18 p3187 A69-34959

Densities and angular distributions of fossil tracks in meteorites produced by slowing down heavy primary cosmic ray nuclei

19 p3410 A69-36096

Solar system low energy particle flux at 2-3 AU distance during last 10 million years, discussing cosmic radiation flux

19 p3411 A69-36097

High and medium energy molecular beams - Conference, Cannes, July 1969

19 p3375 A69-36171

Langmuir plate and spherical ion probe experiments aboard Explorer 31, measuring concentrations and temperatures of thermal electrons and ions

20 p3545 A69-37881

High energy cosmic rays primary spectrum determined from observations of secondary components including gamma rays, muons and air showers

21 p3790 A69-38822

Galactic cosmic rays, discussing chemical composition, isotopic separation, proton and alpha particles energy spectra, propagation, interactions, etc

21 p3791 A69-39502

Accelerating electric field model to interpret energy and angular distribution of auroral particles, noting electric potential limitations

22 p3938 A69-40445

Distribution function of output energies of polycrystalline metal surface used as plasma probe, considering homogeneous plasma flow and isotropic particle velocity distribution

23 p4196 A69-41696

Neutrons energy spectrum at sea level calculated and proved consistent with satellite cosmic ray data

23 p4205 A69-41701

Cosmic ray detectors design for medium, low and very low energy events on IMP-1 spacecraft, noting PCM format

23 p4118 A69-41738

Cs ionization by bromine, measuring relative cross section velocity dependence by crossed molecular beam technique

23 p4194 A69-42208

Air showers muon threshold energies deep underground as function of zenith angle, discussing nucleon-air-nucleus collision parameters variation effect

23 p4207 A69-42497

Cosmic ray pions and muons anomalous measurements above 1000 Gev explained by medium-strong contact interaction between protons

24 p4353 A69-43194

Solar high energy gamma ray flux abrupt increase detected by neutral particle plastic scintillators at balloon altitude

24 p4371 A69-43612

PARTICLE FLUX

U FLUX [RATE]

PARTICLE FLUX DENSITY

NT ELECTRON FLUX DENSITY
NT NEUTRON FLUX DENSITY
NT PROTON FLUX DENSITY

Spatial variations in particle intensity near and inside magnetosphere during September 1966 solar cosmic ray events, noting magnetosphere screening effectiveness

02 p0309 A69-12740

Large area proportional counter for cosmic ray design, construction and specifications

03 p0427 A69-12979

Cosmic ray intensity increase of January 28, 1967, noting pressure corrected hourly data and lack of association with visible solar flare

04 p0649 A69-15442

Elementary composition and origin of primary cosmic rays, discussing space techniques for observation of components

05 p0818 A69-16816

Mass influx and penetration rate of meteor streams

06 p1000 A69-17007

Helium component flux in primary cosmic rays determined, using corrected alpha particles number

06 p0988 A69-17275

Splash albedo flux measurement, using Cerenkov counter telescope surrounded by anticoincidence shield

06 p0989 A69-17278

Micron and submicron particle cumulative flux upper limits in satellite micrometeoroid environment of Gemini 12

07 p1215 A69-18845

Helium flux in lower thermosphere, using diffusion theory for multicomponent gas mixture to determine equation for equilibrium distribution

07 p1125 A69-18848

Cosmic ray negatron and positron spectra using balloon-borne magnetic spectrometer, obtaining absolute solar modulation of positron flux

08 p1380 A69-20728

Plasma flow from hot cathode discharge in magnetic field increases ion flux intensity and prevents flow divergence in vacuum

08 p1370 A69-21075

Brans-Dicke gravitation theory effects on solar evolution and neutrino flux, discussing solar luminosity

09 p1605 A69-22415

Low momentum muon directional coupling coefficients based on latitude survey of directional meson intensity

09 p1583 A69-22759

Speed distribution and density of molecular beam from time domain measurements of propagated beam perturbations, discussing gate functions

10 p1652 A69-23340

Time histories of Mev proton and alpha particle intensities during and after July 7, 1966 solar flare, noting abundance ratio and geophysical effects

10 p1768 A69-23768

Anisotropic fluxes of energetic particles in and near distant trapping region encountered by Explorer 33 satellite in outer magnetosphere

11 p1950 A69-25146

Particle fluxes in outer radiation belt and unstable radiation zone of outer geomagnetic field, discussing electron diffusion into magnetosphere and magnetic disturbances

12 p2150 A69-26744

Electron transport phenomenon in high pressure cesium diodes, noting quasi-static assumption of particle distribution functions

14 p2401 A69-29229

Solar corpuscular radiation component from satellite and interplanetary space probe geophysical data, discussing interplanetary magnetic field geometry and corpuscular fluxes

15 p2684 A69-30516

Cumulative flux of interplanetary and cislunar space dust particles by Mariner 4 andOGO 3 spacecraft, noting particle impact rate

15 p2699 A69-31394

Picogram dust particle flux in selenocentric space measurement by Lunar Explorer 35, showing enhancement during meteor showers

15 p2699 A69-31396

Ionospheric VLF emission and particle measurements, discussing energy, distribution and flux of protons and electrons

15 p2605 A69-31425

Cosmic ray shower axis mean distance from apparatus determined by measuring muon to charged particles densities ratio

17 p3024 A69-33580

Cosmic ray heavy nucleus enders flux by nuclear emulsions for balloon flights at various atmospheric depths

17 p3025 A69-34219

Solar system low energy particle flux at 2-3 AU distance during last 10 million years, discussing cosmic radiation flux

19 p3411 A69-36097

Thermal molecular beam sources fabricated from multichannel arrays, describing molecular flux leak rates and angular distributions

19 p3376 A69-36175

Corpuscular radiation distribution function with trapped particles maximum density fixed in equatorial plane and reflection points vicinity of magnetic force line

19 p3396 A69-36630

Rocket and satellite particle collection experiment to confirm reduced micrometeoroid flux near earth, noting inconclusive size frequency distributions of exposed flight samples

21 p3793 A69-38343

Auroral absorption relation to visual aurora and measured particle fluxes

21 p3707 A69-38488

Solar neutrinos emission mechanism for information on central region of sun, discussing detection and flux density

21 p3790 A69-38827

Particles integral and differential fluxes spectral distribution calculation for determining radiation load for synchronous satellite

22 p4035 A69-39909

Outer anisotropic galactic cosmic particle flux distortion in interplanetary space, analyzing scattering in solar wind by isotropic diffusion equations

23 p4205 A69-41837

Cosmic ray flux intensity increases, discussing effects of solar wind, corpuscular flux velocity and interplanetary magnetic field

23 p4205 A69-41838

PARTICLE IN CELL TECHNIQUE

Clouds-in-clouds and clouds-in-cells method /CIC/ for many body nonlinear plasma problems, calculating density and force of particles

12 p2138 A69-26625

PARTICLE INTENSITY

March 1966 Forbush decrease observed in underground meson component at 70 mwc compared with neutron and sea level meson intensity variations

01 p0146 A69-11129

Monte Carlo method used to calculate probability of muon penetration to deep underground levels with sea level energies

13 p2333 A69-28424

Supersonic molecular beam relative intensity represented as function of nozzle to collimator distance and gas admission pressure

20 p3579 A69-37432

PARTICLE INTERACTIONS

NT ELECTRON CAPTURE

NT ION ATOM INTERACTIONS

NT MOLECULAR COLLISIONS

NT MOLECULAR INTERACTIONS

NT NUCLEAR INTERACTIONS

NT SPIN-ORBIT INTERACTIONS

Weakly interacting neutrinos in anisotropic cosmological models with emphasis on equilibrium period, noting energy increment

01 p0123 A69-10348

Magnetic storm principal phase explained by interaction between quasi-trapped particles stream and magnetosphere

01 p0144 A69-10573

Electron impact spectrometer for obtaining molecular energy loss spectra used to investigate scattering cross sections for optically allowed and forbidden transitions

01 p0123 A69-10620

Nonexistence of Biota-Cloud recontamination hazard for planetary lander proved by analysis of interactions between small particles and physical fields around vehicle

02 p1201 A69-11771

Current carrier mobility in GaTe and tin selenide semiconducting stratified lattices, noting interaction of free carriers and polarized nonpolar phonons

02 p0295 A69-11777

Thermodynamic stability of plasma with strong interaction, discussing relationship to simultaneous oscillation forms

02 p0292 A69-12635

Induced combinational scattering /ICS/ on IR active transitions, deriving equations with allowance for population variation

02 p0282 A69-12636

Statistical description of nonelastic processes in nonequilibrium plasma in transverse magnetic field, using kinetic equations for distribution functions

03 p0476 A69-13412

Electromagnetic properties of bounded isotropic plasma in kinetic approximation

03 p0477 A69-13712

S matrix theory without restriction to asymptotic particle momentum measurements, introducing main nondynamical features

03 p0467 A69-13754

Atomic electron spontaneous transition in theory of direct particle interaction, considering electrodynamic field zero-point oscillations role

03 p0468 A69-13773

Grain boundary interaction energy with inclusion of second phase, describing equilibrium and boundary shape

03 p0449 A69-13880

Barometric coefficients of multiplicities calculated using cosmic ray interactions model and neutron monitors response to secondary nucleons

03 p0425 A69-14025

Hydrogen plasma transport properties for semiclassical quantum potential calculated by Chapman-Enskog-Hilbert theory

05 p0799 A69-15735

Dynamic response of solids induced by charged particle interaction noting laser interferometric measurement of surface stresses

05 p0771 A69-15817

Ion-molecule collisions of Ar-Co and N-No pairs, discussing charge exchange reaction rates and spiraling nature

05 p0797 A69-16428

Book on diffuse matter in space covering observations of interstellar gas, grains, particle interaction and star formation

06 p0997 A69-16833

Simultaneous parallel penetrating muons observed in multiple cloud chambers, obtaining information about sea level muons interactions and EAS

06 p0991 A69-17304

Packet of finite amplitude VLF whistler waves, examining cyclotron resonance interaction with high energy electrons and development in magnetosphere

06 p0917 A69-17378

Maximum number of binary collisions for three particles with zero range forces in relativistic rescattering singularities studies

08 p1353 A69-19788

Plasma diagnostics methods for evaluating collision and transport cross sections, discussing resonance fluorescence, steady state discharge and afterglow measurements

08 p1364 A69-20476

Slow distribution function of magnetoactive plasma, deriving kinetic equation in quasi-linear approximation for analyzing particle-HF electromagnetic wave interactions

08 p1365 A69-20550

Einstein space time concepts for unified formalism of matter interactions from elementary particles to astronomical bodies, discussing relativity theory

08 p1352 A69-20730

Partially ionized plasma oscillations in crossed magnetic and electric fields, noting role of LF particle collisions

08 p1370 A69-21079

Finite ion mass effect on stability of space charge neutralized electron beam

09 p1545 A69-21342

Effective cross sections of electron-neutron interaction in photosphere and sunspots, calculating electric conductivity and anisotropy coefficient

09 p1579 A69-22175

Galactic cosmic ray scattering and energy loss through solar wind interaction

09 p1580 A69-22202

Geomagnetically trapped particle loss processes and equilibrium distribution resulting from MHD wave field interaction described using sandbox model

11 p1948 A69-24856

Classical statistical mechanics of systems with identical or limited different particles, discussing particle collisions in dilute gases

11 p1870 A69-25009

Dense gas equilibrium plasma thermodynamic stability in case of high electrostatic interaction energy of charged particles, analyzing phase transition possibility

11 p1928 A69-25234

Inelastic interactions cross sections of slow electrons with adsorbed particles on W surface as function of temperature in surface bond vibrational region

12 p2132 A69-26114

Relativistic hydrodynamic equations for charged particles interacting in external scalar and gravitational fields, considering particle motion and scalar plasma dispersion
12 p2130 A69-26462

Charged state variations during protons and inert gas atoms interactions analyzed by coincidence method
12 p2133 A69-26543

Energy exchange between LF waves and magnetospheric energetic particle population by bounce resonant interaction
12 p2073 A69-26946

Effective tensors of elastic moduli and yielding of composite materials, considering multiparticle interactions and use of equilibrium and incompatibility equations
13 p2360 A69-27382

Oscillating electron ion discharge in magnetic field in system of alternating positive and negative electrodes to obtain fast neutral particle fluxes
13 p2311 A69-28109

Elastic and inelastic elementary particle collisions described by Feynman diagrams, discussing computer results for high energy particle interactions
13 p2303 A69-28369

High energy muons energy spectrum in extensive cosmic ray showers from spectrum study of ionization bursts due to penetrating component
13 p2332 A69-28403

Elastic materials with particle interactions of finite range, establishing continuum field and constitutive equations from particle mechanics
13 p2371 A69-28674

Fermi surface data of alkali metals interpreted in terms of interaction between conduction electrons and ionic lattice for deducing partial wave phase shifts
13 p2304 A69-28681

Electron magnon interaction in ferromagnetic and antiferromagnetic semiconductors, showing conduction band and electron effective mass and magnetic moment dependences on temperature and spin direction
14 p2504 A69-28991

Electrodynamics law between current elements consistent with Newtonian dynamics, noting consequences in discharge and plasma control
14 p2485 A69-29320

Small signal analysis of processes in klystron resonators involving beam-field interaction
15 p2573 A69-30117

Magnetic storm principal phase explained by interaction between quasi-trapped particles stream and magnetosphere
15 p2675 A69-30743

Ion-acoustic oscillations effect on weakly ionized plasma electrical conductivity, using BGK collision integral model
15 p2662 A69-30970

Particle-wave interaction in weak turbulent plasma in presence of uniform magnetic field, applying perturbation theory arbitrary order
16 p2819 A69-31683

Lasing influence on electron energy distribution in gas discharge measured with Langmuir probe, showing electron-electron interaction insufficient to maintain equilibrium
16 p2796 A69-31772

Single particle and collective excitations of plasmas in solids and interactions with acoustic and electromagnetic waves in magnetic field
16 p2821 A69-31820

Warm plasma probe, describing transit electrons interaction with electric field and generation of electroacoustic waves radiation
16 p2824 A69-32611

Ionization, recombination and charge transfer in upper atmosphere during aurora, considering quasi-equilibrium ion-electron concentrations
17 p2961 A69-33417

Coulomb interference corrections in pion-He scattering, discussing three specific formalisms
18 p3176 A69-35008

Comet-solar wind interaction model, determining contact discontinuity size and shape around comet nucleus and ion specular reflection
18 p3188 A69-35190

Cs jet device eliminating wall influence in nonlinear radiation-atom interaction phenomena
19 p3376 A69-36174

Ion production in K/diatom Br system by high energy K beam, obtaining total ionization cross section as function of energy
19 p3378 A69-36187

Hydromagnetic wave-charged particle resonant interaction described by diffusion equation in momen-

tum space, deriving diffusion coefficients and time evolution ultrarelativistic particle energy spectrum
19 p3424 A69-36335

Magnetospheric disturbances effect on radio wave propagation, discussing wave-particle interactions, VLF emissions and electrostatic waves
19 p3303 A69-36429

Electrostatically accelerated ion spheres interaction with thin metal and nitrocellulose foils to develop detectors for cosmic dust collection and recording
21 p3719 A69-38344

Venus magnetosphere induced by piling up magnetic field from solar wind due to ionospheric conductivity and collisions with planetary atmospheric particles
21 p3794 A69-38381

Unified theory of elementary particles assuming quantum mechanics as consequence of changes in time within microcosmos and particle-universe interaction
21 p3816 A69-39622

Scattering of high energy Ar beams by room-temperature Ar, He and H molecules, deriving interaction energies at internuclear distances
22 p3988 A69-41187

Black body radiation at very high temperatures, discussing pion-nucleon interaction in pion gas in thermal equilibrium
23 p4238 A69-41358

Inelastic collision cross sections for low energy interactions among electrons, ions, atoms and molecules determined as function of temperature, using approximate methods
23 p4194 A69-41520

Solar wind sample collection, describing experiment to determine ion flux capture efficiency for various metal foils
23 p4205 A69-41539

Integral transformation applicability to inverse problems concerning interaction potential energy between particle pairs in n-dimensional Euclidean space
23 p4182 A69-41960

Stellar neutrino energy loss due to electron-electron neutrino bremsstrahlung in nondegenerate gas determined from transition probability for charged baryons or leptons interaction
24 p4351 A69-42794

Cosmic ray pions and muons anomalous measurements above 1000 GeV explained by medium-strong contact interaction between protons
24 p4353 A69-43194

Diffuse cosmic X rays from Compton collisions between galactic leakage electrons and extragalactic background photons to verify microwave blackbody radiation properties
24 p4368 A69-43202

Crossed beam apparatus /evatron/ for studying energy spectra of crossed positive ethylene ion beams and neutral ethylene molecule beams
24 p4280 A69-43813

PARTICLE MASS

NT ELECTRON MASS

Finite ion mass effect on stability of space charge neutralized electron beam
09 p1545 A69-21342

Mass displacement in light path due to interaction with gravitational wave accompanying light pulse, discussing general relativity tests for time delay and starlight bending
09 p1540 A69-22081

Particle volume role in normal shockwave structure in gas-particle mixtures, discussing equations of motion formulation
13 p2244 A69-27327

Stable particles heavier than nucleons in extensive cosmic ray showers detected by delayed coincidences relative to shower electron photon component
13 p2331 A69-28402

Number and mass of sodium atoms in comet Ikeya-Seki 1965f head calculated from spectral observations, ascribing D lines to resonance scattering of photospheric radiation
15 p2685 A69-30526

Low velocity heavy mass particle detection in sea level cosmic radiation, assuming deuterons
16 p2846 A69-31600

Possible existence in universe of large number of difficult-to-observe particles with zero rest mass left over from superdense phase
16 p2814 A69-31801

Superluminal group velocities in relation to causality axion, considering sound propagation in ultradense matter and particles of imaginary mass /tachyons/
21 p3769 A69-38543

Meteoroid penetration damage to spacecraft system showing particle mass density distribution as protection criterion
21 p3805 A69-39222

Quark mass and charge interpretation during particle track photographic analysis of air shower cores by delayed expansion Wilson cloud chamber
24 p4383 A69-42944

PARTICLE MOTION

Particle moving in circular orbit perpendicular to axis of cylindrically symmetric magnetic field
01 p0120 A69-10811

Particles behavior after separation from meteor, considering deceleration for separation altitudes and initial velocities
02 p0314 A69-11644

Charged particle motion caused by ELF electromagnetic waves in presence of constant magnetic field, noting earth ionosphere application
02 p0240 A69-11712

Rotational motion of system of particles related to existence of reference frame to eliminate coupling terms between internal and rotational motion
02 p0280 A69-11867

Plasma jet motion in time constant and time variable magnetic field noting particle deflection, polarization loss, capture and cut-off
02 p0292 A69-12551

Solar cosmic radiation, particle acceleration, energetic particles as sample of sun and propagation of particles from sun to earth
03 p0498 A69-12934

S matrix theory without restriction to asymptotic particle momentum measurements, introducing mainly nondynamical features
03 p0467 A69-13754

Similarity motion of fluid particles in one dimensional gas flow, establishing limits of slip factor value change
03 p0419 A69-13920

Charged particle dynamics in spiral interplanetary magnetic field model, discussing electric drift velocity point of origin and distribution
03 p0503 A69-14011

Bound motion for particle in point electric dipole field, noting features of motion common to spherically pendulum motion
03 p0473 A69-14101

Stormer problem of charged particle motion in magnetic dipole field, discussing analytical method for high and low energy particles
03 p0504 A69-14121

Charged particle motion in time dependent external magnetic field
03 p0504 A69-14231

Charged particles motion in spatially modulated magnetic field solved using modification of Krylov-Bogoliubov asymptotic method
04 p0633 A69-14291

Asymptotic method for studying charged particle motion in spatially modulated magnetic field
04 p0634 A69-14292

Capture of electrically charged micrometeorites and corpuscles in magnetic field of gravitating dipole, noting necessary condition on particle motion
04 p0659 A69-14961

Random motion of particle with nonlinear damping obtaining velocity spectrum by solving associated nonstationary Fokker-Planck equation and using equivalent linearization technique
04 p0561 A69-15451

Charged particle motion in constant direction magnetic field varying exponentially with time, discussing electric field effect on particle motion
05 p0801 A69-15741

Solid phase particle motion in plasmatron with colliding jets, measuring W particle heating by optical method
05 p0802 A69-15971

Particles nonlinear motion in plasma in magnetic field with arbitrary electron velocity distribution discussing wave discontinuity patterns
05 p0804 A69-16371

Equation for charged particle motion in electromagnetic wave field propagated along magnetic field applied to nonlinear wave propagation in plasma near cyclotron resonance
06 p0963 A69-16901

Particle velocity measuring technique for two phase turbulent flows, using laser and Fabry-Perot interferometer
06 p0933 A69-17251

Spherical particle motion in vortex gas flow between planes of turbulence chamber perpendicular to axis of flow rotation, noting collisions effect
07 p1181 A69-19000

Instability in pyrolytic silicon dioxide films on Ge substrate under bias at room temperature consisting of positively charged ion motion
07 p1200 A69-19010

Auroral electron penetration into atmosphere analyzed on basis of independent electron particle motion, using auroral electron angular distributions and energy spectra above atmosphere
07 p1128 A69-19368

Particle dynamics measured by ATS satellite synchronous orbit, discussing flux time variations during geomagnetic disturbances
07 p1209 A69-19371

Particle motion, deriving Lagrangian formalism equivalent to Schroedinger equation for random motion theory
07 p1182 A69-19455

Rarefied plasma self similar motion qualitatively analyzed, particularly penetration and expansion, taking into account electric/magnetic field effects
08 p1359 A69-19951

Electromagnetic waves and photons coexistence, discussing wave mechanics and guidance of particles, photon guidance and corpuscular magnitudes, etc
08 p1351 A69-20117

Charged body moving at subsonic velocity normally through stratified elastic half space composed of film on homogeneous half space
08 p1417 A69-20753

Incoherent wave scattering of particle orbits as nonlinear effect of LF instabilities
08 p1367 A69-20801

Captured particles magnetic drift envelopes in magnetosphere calculated by model considering perpendicular geomagnetic dipole to solar wind
09 p1574 A69-21521

Charged particles equations of motion in earth magnetosphere in polar storms, considering auroral zone, diurnal variations and electron and proton velocities
09 p1485 A69-21535

Shock wave structure problems in plasma, including plasma particles random motion in term representing electric field
09 p1551 A69-22032

Differential equation for droplet motion along ballistic trajectory in gas flow, noting applicability to solid bodies via computer programming
09 p1483 A69-22222

Charged particles motion in geomagnetic field from analyzing spatial distribution within framework of two dipole magnetosphere model
10 p1756 A69-22818

Diffusion coefficient and cosmic ray motion in solar system, using satellite data of interplanetary magnetic field
10 p1757 A69-22822

Particulate radioactivity for study of stratospheric motions, demonstrating negligible long time particle settling with comparative measurements of particulate Sr 90 and gaseous C 14
10 p1682 A69-23410

Silicon carbide particle growth and motion in carbon star atmospheres
10 p1781 A69-23678

Electron confinement in magnetic mirror geometry supplemented with RF quasi-potential barriers, considering gas scattering
11 p1924 A69-24306

Dynamics of turbulent motion of incompressible viscous fluid particles, using Lagrangian functions
11 p1867 A69-24536

Adiabatic theory of charged particle motion in electromagnetic field, applying asymptotic methods of nonlinear oscillations theory
11 p1948 A69-24857

Stable particle trapping zone in magnetosphere, discussing results of adiabatic theory application to charged particle motion in earth magnetic field
11 p1948 A69-24858

Charged particle motion in periodic electromagnetic field, constructing dynamic variables describing motion
11 p1927 A69-25100

Transverse pulsating motion of spherical particle in turbulent flow, considering differential equation of motion transformation
11 p1876 A69-25489

Test particle classical dynamics in closed expanding universe, discussing Newtonian inertial mass decrease and canonical methods for determining momentum, velocity and energy
11 p1920 A69-25561

Cosmic radiation origin in terms of sudden injection of particles in time, momentum and space, considering statistical fluctuations role in observed spectrum
12 p2148 A69-26206

Quantitative magnetic field models of magnetosphere for analyzing field configuration variations and adiabatic particle motion
12 p2072 A69-26738

Model for self consistent time independent ring current of charged particle distribution under combined field of earth dipole and particle motion current
12 p2151 A69-26948

Electrohydrodynamic flows at large electric Reynolds numbers, obtaining Bernoulli and Cauchy-Lagrange integrals
13 p2305 A69-27379

Cosmic ray propagation theory for steady streaming along magnetic field and down cosmic ray density gradient, noting MHD wave generation by anisotropy
13 p2326 A69-27569

Vibrating camera for photographic measurement of flow velocities and trajectories of bodies marked by light spots
13 p2261 A69-27913

Angular distribution of nuclear particles dispersed during motion determined from photon energy and inelasticity coefficient
13 p2303 A69-28390

Low energy charged particle motion parallel with magnetic force lines analyzed in magnetosphere model with constant electric field
14 p2512 A69-29040

Geomagnetic cut-off influence on charged particle dynamics in geomagnetic field, applying charged particle motion theories to magnetosphere fields
14 p2513 A69-29099

Relativistic behavior of electromagnetic multipolar nongravitating particle, discussing integrability of field equations
14 p2486 A69-29594

Cometary tail diffusion model based on luminous particle number decrease with time and particle accelerated motion and diffusion in space
14 p2523 A69-29705

Coupled equations for heavy particle motion expressed by introducing generalized matrix operator for effective momentum in atomic collision processes
14 p2489 A69-29997

Plasma jet motion in time constant and time variable magnetic fields noting particle deflection, polarization loss, capture and cut-off
15 p2658 A69-30255

Gasdynamic model of comet nucleus region, discussing molecular collisions, surface brightness distribution and dust particle motion
15 p2684 A69-30520

Charged particle motion in magnetic mirror trap, observing time dependence with respect to orbital magnetic moment conservation
15 p2659 A69-30724

Final states of density, velocity and pressure in gas, comparing states reached after transition through single oblique hydromagnetic shock and two successive shocks
15 p2664 A69-31217

Relativistic generalization for polar Sommerfeld rosette of Fourier series expansions by Lagrange and Bessel for particle motion in Keplerian field
16 p2811 A69-31607

Nonlinear interaction between three monochromatic waves propagating parallel to magnetic field in plasma, considering relativistic drift motions of particles
16 p2816 A69-31640

Charged particle motion in superposed Heliotron and biconical cusp magnetic fields, considering particle confinement
16 p2817 A69-31643

Self consistent ring current of radiation belt under combined influence of earth dipole field and field due to currents of particle motions
16 p2776 A69-32096

Correlation between F region electrons vertical motion velocity variations and E region electrons horizontal motions in equatorial ionosphere
16 p2779 A69-32193

Captured particles magnetic drift envelopes in magnetosphere calculated by model, considering perpendicular geomagnetic dipole to solar wind
16 p2851 A69-32516

Charged particles equations of motion in earth magnetosphere in polar storms, considering auroral zone diurnal variations and electron and proton velocities
16 p2783 A69-32530

Linear irreversible thermodynamics theory as applied with conservation principles and Maxwell relations

to charged particle motion in electromagnetic field, noting Onsager coefficients role
17 p3075 A69-34142

Capture of electrically charged micrometeorites and corpuscles in magnetic field of gravitating dipole, noting necessary condition on particle motion
18 p3197 A69-34725

Solar cosmic ray anisotropies in terms of model with particles propagating along interplanetary magnetic field undergoing pitch-angle scattering
18 p3189 A69-35400

Plane electromagnetic wave scattering by motion of small ellipsoid in vacuum, noting total scattering and radar cross sections dependence on ellipsoid velocity
18 p3105 A69-35485

Active attitude control method with energy increases and decreases induced to modify attitude motions for particles and rigid bodies
19 p3429 A69-35958

Ion and electron fluxes and drag force dependence on electrostatic charge and velocity of interstellar dust particle
19 p3425 A69-36562

Gas dynamics in transition regime between continuum motion at high gas density and free particle motion at low density limit
19 p3300 A69-36658

Newtonian and general relativistic orbits of point mass in inverse square law force field, noting radar determination of spacecraft orbits
[AAS PAPER 68-098] 20 p3595 A69-37176

Negative time interval implications for meta particle at superluminal velocity with respect to two reference frames, noting causality paradoxes
20 p3598 A69-37412

Equilibrium velocity distributions of F region photoelectrons produced by solar ionizing radiation, discussing dayglow as impact result
20 p3591 A69-38061

Hydromagnetic waves equations of motion for non-relativistic case, discussing particle and fluid flow models
20 p3616 A69-38317

Magnetospheric electromagnetic phenomena explained by equations of motion for particle acceleration, forbidden regions and MHD processes
21 p3707 A69-38485

Low energy plasma escape flow from polar region /polar wind/, examining H, He and O ions participation in expansion
21 p3713 A69-38528

Drag effect on plasma motion in high current pulsed plasma accelerators of Marshall type, calculating current variations, voltage, particle velocity, efficiency and impulse
21 p3778 A69-39548

Spherical motion of solid body about fixed point with nonholonomic coupling, deriving equations for centrifugal moments of inertia effects on motion
21 p3773 A69-39840

Auroral UV and 3914 Å radiation during charged particle precipitation measured by satellite
22 p3939 A69-40507

Drift shell splitting in nondipolar distorted magnetosphere tested with data from electron spectrometer on ATS 1 and OGO 3 satellites
22 p4005 A69-40508

Self consistent flow calculation in dense space charge beams, including electrode design for portions isolation
22 p3985 A69-40668

PARTICLE PRODUCTION

Electron-hole collisions effect on drift and electron and hole diffusion in semiconductors at high injection levels
01 p0137 A69-10257

Initial production of metallic gases associated with sporadic E layers by processes other than vaporization or photodissociation, discussing Na atom production mechanisms
01 p0071 A69-11167

High energy strong interaction theory in cosmic ray physics, discussing Regge model, fireball production and quark problem
03 p0469 A69-12940

Solar X ray control of D layer based on Explorer 33 data, computing electron production rates due to typical X ray flux
03 p0500 A69-13224

Electron production and loss rates in F region from measurements of Faraday rotation imposed on VHF telemetry transmissions from geostationary satellite
03 p0503 A69-14016

Reducing decarburization of titanium carbide in argon plasma by carbon containing atmosphere, obtaining stable spheroidal particles
05 p0767 A69-15976

Gamma ray production and high energy electrons in cosmic radiation
05 p0817 A69-16712

Energy spectra of muons determined from knock-on electrons projected angles of emission in C, Al and Cu
06 p0991 A69-17305

Electron formation in lower ionosphere due to cosmic ray-atmosphere interaction, analyzing ionization of subrelativistic and relativistic solar and galactic cosmic rays
06 p0920 A69-17726

Direct muon production, discussing range vs energy relation for favorable experiment and difficulties with observed muon flux isotropy
07 p1209 A69-19406

High energy particles obtained by accelerating plasma with frozen-in magnetic field to relativistic velocities during scattering of fast electron beam
08 p1358 A69-19805

Very high energy gamma rays from pulsars, considering implications of various gamma ray production processes
08 p1377 A69-19897

Boron crystalline modification during transit through induction coupled Ar plasma producing better crystallized spheroids
08 p1372 A69-20687

Solar neutrinos and convective core mixing on short time scale resulting in flux reduction
09 p1574 A69-21453

Compton scattering of microwave radiation on cosmic ray electrons proposed as mechanism generating 100 Mev cosmic gamma rays
09 p1580 A69-22295

Renormalizable weak interaction mechanism for generation of high energy muons from Tev cosmic rays in upper atmosphere
09 p1581 A69-22530

Electron-hole collisions effect on drift and electron and hole diffusion in semiconductors at high injection levels
09 p1559 A69-22650

Electron production rates variations in lower ionosphere cosmic layer related to meteorological, geomagnetic and cosmic conditions
10 p1759 A69-22839

Spatial distribution of residual nuclei produced in thick Fe targets by one and three Gev protons, noting total production and longitudinal variation of production
10 p1760 A69-23411

Graphite particle formation in atmosphere of C type Mira variables, calculating particle size distribution by nucleation and coagulation theory
10 p1782 A69-23681

Neutron production cross sections prediction at proton bombarding energies below 50 Mev and above threshold for multiple nucleon emission
12 p2192 A69-26299

Tritium contamination reduction in small ion accelerators for neutron production, discussing pumping problems and vacuum systems
12 p2059 A69-26499

Multiple particle production and resonance events during high energy particle collisions
13 p2303 A69-28372

Gamma quantum spectrum shape from high altitude X ray film and nuclear emulsion blackening, discussing high energy pion production
13 p2330 A69-28378

Angular distribution of penetrating shower particles produced in nuclear interaction of cosmic rays with C, Sn, Cu and Pb
13 p2330 A69-28381

Pionization cross sections at 100 gev for interactions of cosmic ray neutrons and pions with C and Pb nuclei
13 p2330 A69-28382

Galactic and relativistic and subrelativistic solar cosmic rays effect on electron production rate in ionosphere, detailing low energy SCR-atmosphere interactions
13 p2333 A69-28544

Effective recombination coefficient in lower ionosphere determined from charged particle spectra obtained by rocket sounding in Canada
14 p2511 A69-28960

Formation cross sections of Li, Be and B isotopes produced from oxygen 16 spallation via high energy protons related to astrophysics and cosmic ray physics
14 p2512 A69-28968

Efficiency parameter beta for ion and electron production by meteoritic processes, noting importance to nighttime sporadic E ionization
14 p2520 A69-29372

Earth radiation belt data, discussing origin, density, distribution, etc, of protons, electrons and alpha particles
15 p2674 A69-30016

Low energy positrons in cosmic radiation due to beta decay of carbon, nitrogen and oxygen isotopes, estimating positron fluxes and energy spectra
15 p2676 A69-30887

Near horizontal air showers relationship to direct muon production and heavy triplet particles of unit charge, discussing nuclear interactions and muon bremsstrahlung
15 p2678 A69-31499

Particle production by gravitational fields in universe via quantum field theory, considering cosmological models
17 p3008 A69-33003

Electron production rate in low ionosphere, discussing parameters of ionizing solar cosmic rays and earth environment
17 p3022 A69-33035

Differential cross sections for secondary electron production in atomic ionization by charged particle impact, using classical binary encounter approximation
17 p3009 A69-34189

Hydrogen molecular ion dissociation due to ion-molecule inelastic collisions, comparing measured and calculated velocity distributions of protons produced
19 p3375 A69-35985

Noctilucent cloud particles nucleation and growth, noting time dependence and water vapor mixing ratio
21 p3702 A69-38346

Threshold photoneutron cross section for Mg 26, discussing resonances as primary production mechanism for stellar neutrons
21 p3788 A69-38599

Aluminum oxide droplets condensation from atmosphere of metal vapor and oxygen, studying temperature and time effects on particle nucleation, growth and distribution
21 p3783 A69-38799

Big bang and little bang nucleosynthesis, discussing electron-neutrino or electron-antineutrino excess role in He production
21 p3801 A69-38813

Pion production rate for proton-proton interactions in hydrogen, discussing relevance to hot massive stars, charged pion decay probability and mu-neutrino production
21 p3792 A69-39615

Chemical analysis of lunar surface by devices exploiting alpha particle backscattering and proton production by alphas placed by Surveyor 5, 6 and 7
22 p4012 A69-40088

Radiocarbon natural production by cosmic ray neutrons, utilizing proportional counters filled with N atmospheres
22 p4003 A69-40095

Cosmic gamma rays spectrum from neutral pions production and decay in metagalactic cosmic ray p-p collisions, deriving models based on Einstein general relativity theory
22 p4006 A69-40641

Solar L alpha and X ray emission contribution to lower ionosphere ion production, discussing altitudinal, latitudinal and temporal variations
22 p4008 A69-41096

Magnetospheric electron sudden intensity increases correlated with magnetic substorms occurrence at mid-night meridian from ATS 1 observation
24 p4367 A69-43173

Particle creation and quantized fields in expanding universe using covariant generalization of special relativistic free field equations, studying zero- and arbitrary-spin particles
24 p4352 A69-43193

PARTICLE SIZE DISTRIBUTION

Raindrop size distribution law effect on radio wave attenuation coefficient and differential effective backscattering cross section of rain
02 p0208 A69-12259

Particle size frequency distributions and lunar surface materials, showing impossibility of distinguishing between impact fragmentation of surface and pyroclastic rock deposition
02 p0325 A69-12567

Aerosol size distribution and variation with humidity effects on visual range, comparing computations with transmissometer and scattering recorder measurements
02 p0276 A69-12760

Particle size distribution determination by measuring light beam extinction in turbid medium with photometer
03 p0428 A69-13110

Asymptotic estimate derived for size distribution function of fragments resulting from brittle impact destruction of rigid object applied to meteorites and lunar craters
03 p0512 A69-13691

Mie total and differential backscattering cross sections at laser wavelengths for Junge size distribution aerosol models
04 p0609 A69-14290

Long term strength of Ni-Cr-Al-Ti alloys, studying gamma particles size and distribution effect
04 p0616 A69-14653

Helium-neon gas laser cavity beam for automatic high speed particle sizing
04 p0611 A69-15023

Diamond pyramid hardness dependence on grain size of recrystallized alpha titanium
06 p0943 A69-17235

Integrodifferential equation for plasma oscillations solved for effect of ion Larmor radius size and intrinsic electric field on flute instability of axially symmetric plasma
06 p0966 A69-17520

Tank collection and spectrophotometric tests in determining aluminum oxide particle size produced by small rocket engine
06 p0984 A69-18117

Grain size dependence of yield, flow and fracture stresses of Fe-Co-V alloy for 77-298 K
07 p1166 A69-19264

Polycrystalline beryllium specimens fabricated from powders, discussing initial powder particle size and distribution effects on microyield strength
07 p1168 A69-19598

Radiation scattering changes due to droplet size distribution change during stratus cloud formation calculated, using development model and Mie theory
08 p1346 A69-21093

Spatial size and velocity distributions for liquid or solid aerosols suspended in air flow using Q spoiled ruby laser and holography
09 p1492 A69-21418

Stratospheric dust, discussing terrestrial and meteoritic origins, volatility of particles smaller than few microns, and light scattering and direct sampling measurements
09 p1608 A69-22689

Interstellar grain model consisting of elongated dielectric particles represented by infinite circular cylinders reproducing observed interstellar extinction in IF far UV spectra
10 p1781 A69-23674

Graphite particle formation in atmosphere of C type Mira variables, calculating particle size distribution by nucleation and coagulation theory
10 p1782 A69-23681

Silicon particle sizes in Al-Si system investigated for interactions with dislocations as function of strain and for effect in dispersion hardening
10 p1714 A69-23980

Solar radiation pressure on interplanetary dust particles calculated as function of radius and density, noting asteroidal origin of dielectric and absorbing particles
11 p1956 A69-24397

Cloud and fog droplet spectra due to condensation of water vapor on nuclei solved by partial differential equation
12 p2126 A69-26017

Thermochemically synthesized high melting micropowders grinding by vibrational method and classification for polishing and finishing applications
12 p2113 A69-26256

Stony meteoric particles size and velocity during passage through atmosphere
12 p2157 A69-26341

Gaussian particle size distribution with porosity and surface irregularity corrections used to determine mean particle size of lunar surface material at Surveyor sites
12 p2158 A69-26371

Matrix grain size relation to dispersed particle size distribution and Zener-McLean equation description of microduplex structure in superplastic Ni-Fe-Cr alloy
13 p2278 A69-27411

Hypervelocity projectile size and density effect on ballistic limit of dual sheet spacecraft meteoroid protection structures, considering penetration of low and high density particles
13 p2367 A69-28306

Microstructure of light scattering media consisting of large size spherical particles

14 p2481 A69-28737

Multifoil thermal insulation using oxide particle layer separation, discussing insulation heat transfer characteristics as function of source temperature and oxide particle size

14 p2539 A69-29213

Thoria strengthened Ni-Cr alloys high temperature stability, noting thoria particle size influence

14 p2465 A69-29682

Meteor showers contribution to interplanetary dust flux based on relative number of particles of various size

15 p2697 A69-31308

Solid rocket motor propellant burning rate increased by adding special fine ammonium perchlorate /SFAP/ to optimize particle size distribution [AIAA PAPER 69-519]

16 p2793 A69-31850

Airborne particle size influence on gas turbine parts erosion, with attempts to relate to filtration and engine life

16 p2794 A69-32026

Dimensions, concentration and spectrum of large precipitation particles in clouds and cloud water content by measuring reflectivity and absorptivity at different wavelength

16 p2807 A69-32268

Metal oxide particle growth processes in rocket chambers and nozzles, using generalized kinetic-coagulation equation [AIAA PAPER 69-541]

16 p2844 A69-32724

Azimuth angle distribution of secondary particles forming cosmic ray diffused cone with high energy, showing asymmetry and deducing particle transverse momentum upper limit

17 p3024 A69-33763

Ice clouds near IR spectral reflectivity dependence on particle size, noting application to planetary atmospheres

18 p3126 A69-34283

Carbide phase growth rate in Mo-TZC alloy with particle size distribution maintained over time-temperature spectrum, noting diffusion and interface controlled processes

18 p3155 A69-34632

Self contained hand held battery operated aerosol particle analyzer, measuring aerosol concentration and size distribution for laboratory and space flight applications

18 p3136 A69-34691

Vertical air velocity in rain measured for size distribution of drops, using relation between drop fall rate and diameter

18 p3104 A69-35342

Particle size, velocity and position in moving streams measured by tilted film plane optical system with pulsed light source

19 p3306 A69-35733

Niobium carbide deposition from gaseous halogen compounds on graphite particles in pseudoliquefied state, noting stoichiometric coatings

20 p3566 A69-37369

Arbitrary circle distribution in plane transformed to corresponding distribution of spheres in space for size and shape distribution determination of disperse phase

20 p3627 A69-37764

Cepheus light attenuation curve explained by applying polymodal particle size distribution, obtaining interstellar dust density

20 p3608 A69-38048

Particle albedos and extinction cross sections computed by Mie theory showing dependence on refractivity, considering thermal radiation from cloudy planetary atmospheres

20 p3614 A69-38255

Rocket and satellite particle collection experiment to confirm reduced micrometeoroid flux near earth, noting inconclusive size frequency distributions of exposed flight samples

21 p3793 A69-38343

Noctilucent clouds total or partial extraterrestrial origin, deriving minimum particulate influx from satellite and rocket data

21 p3702 A69-38347

Aluminum oxide droplets condensation from atmosphere of metal vapor and oxygen, studying temperature and time effects on particle nucleation, growth and distribution

21 p3783 A69-38799

Sorting particles by shape using sieving equipment, noting results with crushed gravel

21 p3731 A69-38950

Normalized phase function and scattering coefficient of aerosols prediction from measurements of particle size distribution, density and refractivity based on Mie solution

21 p3719 A69-39774

Small particle holography technique extended for dynamic properties of particle fields, determining velocity and density field, size distribution, flow structure and diffusion rate

21 p3726 A69-39776

Free stream dispersion without permeation using nonporous glass beads and solutes, examining flow rate, particle size distribution, solute diffusivity, etc

22 p3894 A69-39873

Hydrogen permeability in Pd alpha phase measured, coupling with grain size measurements for grain boundary to bulk diffusivity ratio

23 p4175 A69-41502

Millimeter wave pseudorandom coded CW meteorological radar for precipitation drop size spectrum analysis and cloud studies, discussing overall system design

23 p4115 A69-41531

Instrumentation and data interpretation method for particle size determination by low-angle light scattering

24 p4313 A69-42764

Scattered light meter accuracy as function of aerosol particles atmospheric distribution according to size, analyzing measurement errors

24 p4343 A69-42966

Varying ratio between mean free path and spherical particle radius at 0-10 km, discussing free molecular flow effects in cloud physics

24 p4345 A69-43145

Solar radiation pressure on interplanetary dust particles calculated as function of radius and density, noting asteroidal origin of dielectric and absorbing particles

24 p4390 A69-43787

PARTICLE SPIN

NT ELECTRON SPIN

NT NUCLEAR SPIN

Chirp radar signal compression by proton spin echo phenomena, noting compression ratio and SNR

11 p1834 A69-24566

Atomic and molecular spins dynamic orientation in anisotropic radiation field, examining medium properties and astrophysical consequences

13 p2350 A69-27861

Validity of Lorentz invariance, discussing nuclear magnetic resonance test on torque for spin of electrons, muons and neutrons

18 p3176 A69-35007

PARTICLE TELESCOPES

March 1966 Forbush decrease observed in underground meson component at 70 mwe compared with neutron and sea level meson intensity variations

01 p0146 A69-11129

Geiger-Muller counter telescopes in conjunction with core selectors for studying geomagnetic effect of extensive air showers

03 p0430 A69-13303

Variational coefficients for vertical and inclined meson telescopes, deriving primary cosmic rays anisotropy parameters from daily variations

06 p0924 A69-17293

Large area scintillation telescopes with cubic geometry, measuring cosmic rays intensity from vertical and slant directions

06 p0925 A69-17296

Gamma ray telescope development for balloon-borne astronomy in search for discrete gamma sources and supernova explosions [IEEE PAPER 3A-5]

07 p1134 A69-19192

Fluorescer-photomultiplier mobile telescope for measurement of vertical cosmic ray intensity and equator points in atmosphere

09 p1493 A69-21420

High energy protons, helium and gamma rays observed by particle telescope on board OSO-C, obtaining integral rigidity spectra of proton and helium nuclei

09 p1579 A69-22172

Baryon passive nuclear state nonexistence indicated by above and below ground calorimetric telescope method of nuclear cascade observation

13 p2331 A69-28401

Proton and alpha particle fluxes above specified vertical geomagnetic cut-off rigidity measured by balloon-borne Cerenkov scintillation counter telescope

14 p2511 A69-28951

Fluorine nuclei in primary cosmic radiation identified by counter telescope measurements on Pioneer 8 spacecraft

15 p2676 A69-30886

Meteorological corrections of meson megatelescope data based on hourly ground-level pressures and temperatures, considering vector and regression analyses

19 p3308 A69-35991

Absorption mean free path for radiation absorbed by given medium, using zenith angle distribution from particle counter telescope

21 p3723 A69-38841

Diurnal variations in solar cosmic ray muon component near sea level, using scintillation counters assembled in muon telescope array

23 p4207 A69-42498

PARTICLE THEORY

Electromagnetic muon-nucleon interaction explanation for observed horizontal air showers, reexamining shower data in view of triplet particles

15 p2678 A69-31498

Cosmological constant and elementary particle theory

20 p3606 A69-38013

Computer experiment on 9000 particle plasma to test temporal echo theoretical prediction

21 p3777 A69-38713

PARTICLE TRAJECTORIES

NT ELECTRON TRAJECTORIES

Dust particle separation from inlet flow with S-bend duct to minimize engine dust ingestion, determining particle trajectories [AHS PAPER 211]

01 p0006 A69-10409

Uranium content in fragments from iron meteorites determined by fission fragment track recording

01 p0026 A69-11377

Etching techniques for revelation and viewing of fossil charged particle tracks in meteoritic and terrestrial minerals

02 p0245 A69-12569

Heavy ion track thermal spike model to account for LET and temperature effects in radiation biology and chemistry

03 p0371 A69-13479

Plasma diffusion in toroidal stellarator using integrals of drift equations for particle trajectories, determining distribution function

07 p1191 A69-18985

Density measurements of particle tracks in nuclear emulsions utilizing digitized video scan, discussing operation and instrumentation [IEEE PAPER 2A-7]

07 p1133 A69-19185

Trapped particles drift velocity in time dependent meridional magnetic and perpendicular electric field

08 p1368 A69-20809

Proportional counter pulse shapes calculation for point and extended ionization tracks, considering electron drift velocity and positive ion mobility

09 p1493 A69-21419

Quasi-trapped particle currents having discontinuities on daytime and nighttime sides of earth

09 p1577 A69-21767

Trajectories of particles entrained by gas flow in nozzles for study of erosion damage during passage of gas-particle mixture

11 p1818 A69-25355

Relation between planets axial moments and protoplanetary particles orbital eccentricity as explanation of outward winding of planets

12 p2154 A69-25818

Lagrangian solution for air mass element trajectory in free atmosphere using vortex invariant, noting application to atmospheric transport of contamination

16 p2805 A69-31611

Two dimensional analysis of isentropic perfect gas flow fields in axisymmetric nozzles for transonic two phase flow initial values, calculating particle trajectories [AIAA PAPER 69-572]

16 p2731 A69-31847

Numerical analysis of asymptotic solution for earth-moon particle trajectories in idealized restricted three body problem

16 p2857 A69-32155

Shock tube calibration for aerodynamic loading, determining flow parameters by observing particle trajectories with high speed photography of smoke tracers

18 p3085 A69-34469

Particle size, velocity and position in moving streams measured by tilted film plane optical system with pulsed light source

19 p3306 A69-35733

Infinitesimal mass trajectories and possible double collision in gravitational field of two finite and unequal masses in plane elliptic restricted three body problem

21 p3795 A69-38443

Charged particles beam penetration effects produced in atmosphere, determining particle diffusion and trajectory using Spencer moments and Monte Carlo methods

21 p3709 A69-38502

Auroral zone Birkeland currents in magnetosphere, analyzing particle trajectories for plasma sheet energy distribution and Alfvén layer position

21 p3792 A69-39567

Biological effects by cosmic ray heavy ions and solar flares, using direct correlation between damages caused and trajectories

23 p4089 A69-41831

Quark mass and charge interpretation during particle track photographic analysis of air shower cores by delayed expansion Wilson cloud chamber

24 p4383 A69-42945

Particle physics and discovery of K mesons and hyperons emphasizing track recording, cloud and bubble chamber techniques

24 p4352 A69-43039

PARTICLES

NT AEROSOLS
NT ALPHA PARTICLES
NT ANIONS
NT ANTINEUTRINOS
NT ANTINUCLEONS
NT ANTIPARTICLES
NT ANTIPROTONS
NT ARGON PLASMA
NT ARTIFICIAL RADIATION BELTS
NT ATOMIC BEAMS
NT BETA PARTICLES
NT BOSONS
NT CATIONS
NT CESIUM PLASMA
NT CHARGED PARTICLES
NT COLD NEUTRONS
NT COLD PLASMAS
NT COLLISIONLESS PLASMAS
NT CONDUCTION ELECTRONS
NT CORPUSCULAR RADIATION
NT COSMIC PLASMA
NT CYCLOTRON RADIATION
NT DEUTERIUM PLASMA
NT DEUTERONS
NT DROPS (LIQUIDS)
NT ELECTRON BEAMS
NT ELECTRON PLASMA
NT ELECTRON PRECIPITATION
NT ELECTRON RADIATION
NT ELECTRONS
NT ELEMENTARY PARTICLES
NT FAST NEUTRONS
NT FERMIONS
NT FINES
NT FOG
NT FREE ELECTRONS
NT HADRONS
NT HELIUM PLASMA
NT HIGH ENERGY ELECTRONS
NT HIGH TEMPERATURE PLASMAS
NT HOT ELECTRONS
NT HYDROGEN PLASMA
NT HYPERONS
NT INNER RADIATION BELT
NT ION BEAMS
NT ION CYCLOTRON RADIATION
NT KAONS
NT LEPTONS
NT LIGHT BEAMS
NT MAGNETICALLY TRAPPED PARTICLES
NT MESON RESONANCES
NT MESONS
NT METAL IONS
NT METAL PARTICLES
NT METAL POWDER
NT METALLIC PLASMAS
NT MICROPARTICLES
NT MIST
NT MOLECULAR BEAMS
NT NEGATONS
NT NEUTRAL BEAMS
NT NEUTRAL PARTICLES
NT NEUTRINOS
NT NEUTRONS
NT NONEQUILIBRIUM PLASMAS
NT NONUNIFORM PLASMAS
NT NUCLEONS
NT OUTER RADIATION BELT
NT PARTICLE BEAMS
NT PHOTOELECTRONS
NT PHOTON BEAMS
NT PHOTONEUTRONS
NT PHOTONS
NT PI-ELECTRONS
NT PION BEAMS
NT PLASMA CLOUDS
NT PLASMA JETS
NT PLASMA LAYERS
NT PLASMA SHEATHS

NT PLASMA SLABS
NT PLASMAS [PHYSICS]
NT POLARONS
NT POSITRONS
NT POWDER [PARTICLES]
NT POWDERED ALUMINUM
NT PRIMARY COSMIC RAYS
NT PROTON BEAMS
NT PROTON BELTS
NT PROTONS
NT QUARKS
NT RADIATION BELTS
NT RAINDROPS
NT RAREFIED PLASMAS
NT RELATIVISTIC PARTICLES
NT RELATIVISTIC PLASMAS
NT ROTATING PLASMAS
NT SOLAR CORPUSCULAR RADIATION
NT SOLAR COSMIC RAYS
NT SOLAR PROTONS
NT SOLAR WIND
NT SOOT
NT STELLAR WINDS
NT THERMAL NEUTRONS
NT THERMAL PLASMAS
NT TOROIDAL PLASMAS
NT TRAPPED PARTICLES

Oxidizer particle size and binder type effects on nonacoustic combustion instability of solid propellants [AIAA PAPER 69-175] 06 p0983 A69-18152

Luminous particles in space observed by Vostok, Mercury and Voskhod astronauts, discussing distribution, trajectories and terrestrial origin 07 p1222 A69-19617

Lifetime of highly soluble isolated dense spherical solute particle in solvent, taking into account molecular diffusion, kinetic limitations, etc 10 p1651 A69-22939

PARTICULATE FILTERS

U FLUID FILTERS

PARTITIONS [MATHEMATICS]

Partition coefficients between natural melts and plagioclase phenocrysts determined for rare earth elements and barium by mass spectrometry 08 p1310 A69-20944

Relative intensities of lines in vibration and rotation bands of isotopic carbon dioxide in planet Venus, tabulating partition functions 15 p2656 A69-31154

Reduction of partitioned submatrices functions for expediting calculations of hypercirculant and hyperhyper Jacobi analytic functions 18 p3163 A69-34330

Nonparametric partitioning algorithm for pattern classification, discussing pattern recognition, classifiers structure, real data applications, etc 24 p4285 A69-43062

PARTITIONS [STRUCTURES]

Large scale integration and batch-fabricated processing of logic and storage elements for fourth generation computer, discussing partitioning design 04 p0567 A69-15355

PARTS

U COMPONENTS

PASCHEN SERIES

Paschen series line contours for hydrogen in solar spectrum plotted from IR spectrophotometric data 01 p0148 A69-10126

IR and violet sulfur lines for Seyfert galaxies, noting substantial reddening in nuclei 02 p0325 A69-12593

Paschen line intensity measured as function of position across Orion Nebula 08 p1384 A69-20058

HD 217050 spectroscopic study, determining Balmer envelope temperature from comparison of homologous Balmer and Paschen lines intensities 18 p3201 A69-35144

PASSBANDS

U BANDPASS FILTERS

U BANDWIDTH

PASSENGER AIRCRAFT

NT A-300 AIRCRAFT
NT BAC 111 AIRCRAFT
NT BOEING 2707 AIRCRAFT
NT BOEING 707 AIRCRAFT
NT BOEING 747 AIRCRAFT
NT CH-46 HELICOPTER
NT CH-47 HELICOPTER
NT CH-54 HELICOPTER
NT CV-990 AIRCRAFT
NT DC 8 AIRCRAFT
NT DC 10 AIRCRAFT
NT DH 121 AIRCRAFT
NT L-1011 AIRCRAFT
NT SE-210 AIRCRAFT
NT TU-104 AIRCRAFT

NT TU-134 AIRCRAFT
NT TU-144 AIRCRAFT
NT VC-10 AIRCRAFT

BAC Three-Eleven 220 seat airliner for short and middle distance routes, discussing operating costs, thrust and range 02 p0193 A69-12067

Onboard electric power systems of transport aircraft, analyzing constant frequency systems for supersonic aircraft 02 p0196 A69-12166

Automatic all-weather landing system for scheduled civil passenger aircraft, discussing safety, display devices, Category 2 and 3 conditions 03 p0465 A69-13697

Light passenger aircraft of glass fiber reinforced plastic, using hose construction technique 03 p0454 A69-13822

Public health aspects of galactic radiation exposure at supersonic transport altitudes 03 p0375 A69-14072

Passenger aircraft design to cope with air traffic volume increase in 1970s, discussing economic aspects of high capacity aircraft 04 p0546 A69-14804

Coaxial multipurpose KA-26 helicopter design, discussing cruising speed, passenger capacity, range, flight ceiling, gross weight and piston engines 07 p1053 A69-18969

Acoustical measurements on MD-12 passenger aircraft before and after application of insulation for noise suppression 07 p1057 A69-19704

Lockheed 1011 Tristar with three turbofan engines for large capacity medium range service, noting configuration, aerodynamics, structure and cutaway drawings 08 p1255 A69-21143

Supersonic transport airline operations including safety, noise, traffic control, routing, etc 11 p2004 A69-24373

Multiengine helicopter scheduled passenger service operations in Europe 11 p2004 A69-24378

Onboard gas turbine auxiliary power units for executive jet transport aircraft [SAE PAPER 690332] 11 p1824 A69-24501

Passenger aircraft flight readiness verification, discussing flaw and corrosion detection and rivet joint inspection methods 11 p1822 A69-24526

Short range passenger aircraft, considering payloads, weights and economical classification 13 p2201 A69-27294

TU-134 jet passenger aircraft performance characteristics noting similarity to BAC 111 13 p2202 A69-27931

Aircraft noise control at source through high bypass ratio engine modification, FAA decibel standards and higher capacity aircraft for increased traffic density 14 p2509 A69-29156

Mass supersonic air transport physiological problems, reporting findings of FAUST committee concerning ozone toxicity, pressure drops, sonic booms, time zone physiology, etc 15 p2556 A69-31225

Aircraft role in future transport systems for passengers and goods, emphasizing shorter distances, intercity and interurban communication, etc 16 p2881 A69-31932

Medium range Tu-154 three jet transport aircraft, detailing fuselage, airfoil, tail unit, landing gear, propulsion unit and circuitry 16 p2735 A69-32073

Space requirements of departure lounges in airport buildings for large aircraft loading, discussing entry doors, boarding times, etc 16 p2766 A69-32330

Passenger cabin windows on Convair liner type aircraft, describing construction, installation, strength, etc 17 p3061 A69-33667

Skyvan 3 light passenger/freight carrier design, detailing power plant, installation and power management 17 p2902 A69-34192

Tail tip-evacuation limits, calculating aircraft balance effect of passenger relocations by graphical method [SAWE PAPER 765] 18 p3091 A69-34877

Aircraft interior conversion for passenger or cargo service, discussing convertible aircraft and quick change concepts [AIAA PAPER 69-784] 19 p3244 A69-35642

Passenger transport cruising at low supersonic speeds without sonic boom generation on ground, discussing overpressures, signature characteristics and corridor widths
[AIAA PAPER 69-776] 19 p3244 A69-35647

Jumbo jet audio entertainment and service systems, describing digital pulse multiplexing technique
19 p3285 A69-35806

DC 3 tail wheeled single skin piston aircraft conversion into first class luxury passenger aircraft for short haul service
20 p3460 A69-36918

Jumbo jet passenger loading devices including overwing bridges, transporters and terminal integration
20 p3511 A69-37916

All-plastic light passenger aircraft with inflated tube construction for shell, discussing design and performance
21 p3728 A69-38461

Economic effectiveness determination methods for commercial transport aircraft design analyzed quantitatively, using four engine 100-seat turbo-prop aircraft
21 p3855 A69-38873

Noise and vibration levels measured in An-24 Polish passenger aircraft indicating excess noise in crew compartment
22 p3862 A69-40005

Passenger safety during aircraft accidents in Arctic, discussing survival equipment and methods
23 p4107 A69-41811

Demand curves for VTOL intercity transportation, discussing conventional helicopters, compound helicopters, tilt rotor, tilt wing, stored rotor and fan or jet lift
24 p4254 A69-43721

PASSENGERS

Aviation industry passenger liability, discussing negligence litigation, compensation standards and roles of government, manufacturers and courts
06 p1042 A69-16851

Ground access routes between business districts and airports compared for passenger transport modes
[AIAA PAPER 69-1072] 12 p2059 A69-26773

Airport planning for large aircraft loading of passengers, baggage and cargo containers
17 p2948 A69-34208

Jumbo aircraft production technology causing economic setback, recommending added emphasis on passenger/cargo requirements and operating environments for greater profitability
18 p3232 A69-34542

Mass transit rail service between Manhattan and Kennedy Airport using Long Island Railroad mainline route, discussing baggage handling and time schedules
[AIAA PAPER 69-803] 19 p3453 A69-35596

Cosmic radiation exposure of passengers and crew in supersonic transport at high altitude
22 p4002 A69-40093

Air passenger traffic growth to 1980 in major sectors of air transport industry, emphasizing traffic volumes
22 p4052 A69-40425

Air traffic problems due to tourism, suggesting service modifications to meet future needs
22 p4053 A69-40434

Medical aid, equipment and organization for injured passengers in large aircraft accidents at airports and immediate neighborhood
24 p4270 A69-42602

Unscheduled aircraft landing to deplane passenger for medical reasons, discussing costs, time consumption and avoidance methods
24 p4278 A69-43393

PASSIVATION
U PASSIVITY

PASSIVE SATELLITES
NT BEACON SATELLITES
NT ECHO SATELLITES
NT ECHO 1 SATELLITE
NT EXPLORER 22 SATELLITE

Satellite communications history covering passive and active satellites and Communication Satellite Act impact
07 p1085 A69-19182

PASSIVITY

Austenitic stainless steels nonreproducible passivating tendencies, determining electrochemical and corrosion characteristics, discussing critical anodic current density role
20 p3562 A69-37750

PASTES

Plasticizer mechanical properties and content in paste, considering effects on texture of coagulation structure during die extrusion of compacts
12 p2118 A69-26257

PATCHING
U MAINTENANCE

PATHOGENESIS

Retinal lacerations and detachment in jet pilots, discussing pathogenesis, diagnosis and surgical reattachment methods
05 p0710 A69-16630

PATHOLOGICAL EFFECTS

Electron microscopic changes in lungs of rats after repeated exposure to pure oxygen
05 p0709 A69-16514

Pathological changes in respiratory and cardiovascular systems of white rats due to various levels of hyperoxia
10 p1646 A69-23577

Electron microscopic changes in lungs of rats after repeated exposure to pure oxygen
18 p3096 A69-34733

Flight and piloting influence on morbidity of civil aviation personnel, noting incidence of enteric, hemorrhoidal and respiratory diseases
18 p3098 A69-35303

Platelet role in decompression sickness pathology from experiments upon rats subjected to decompression after injection of antiplatelet serum
21 p3655 A69-38918

Pathological effects of single 120 Mev proton doses on rats blood in rotating cylinder, discussing leukopenia and benign and malignant tumors development
21 p3658 A69-39058

Pathological changes in solar ganglia cells of white rats following X ray exposure, using electron microscope
21 p3659 A69-39064

Normobaric oxygen toxicity pathology in baboons and Macaca, irus and squirrel monkeys during 14 day exposure
21 p3660 A69-39179

EKG, EEG, pneumograms and X ray pictures showed no pathological effect after prolonged confinement in sealed chamber having artificial atmosphere with variable gas composition
22 p3892 A69-40284

Hemodynamic characteristics of decortication in rabbits, noting upsets of compensatory and adaptive capabilities of cardiovascular system
22 p3888 A69-41271

Neodymium laser radiation effect on electrical and histomorphological properties of liver in rats and hamsters
23 p4111 A69-42344

Blood viscosity as possible key factor in physiology and pathology of circulation, suggesting causes of myocardial infarction and coronary occlusion
24 p4261 A69-42725

Biological and physiopathological effects of UHF electromagnetic radiation of radar antennas, reviewing localized effects
24 p4273 A69-42996

PATHOLOGY
NT HUMAN PATHOLOGY

Visceral lesions observed in mice and rats exposed to ultrashort waves indicating no pathological modification of physiology of reproduction
[AGARDOGRAPH-111] 08 p1266 A69-20679

Cold water immersion effects on man from physiological and physiopathological viewpoint, examining clothing effect
08 p1267 A69-20682

PATIENTS

Increased tolerance of orthostatic stress in heart failure patients
19 p3258 A69-36374

Patient transportation and evacuation system at disposal of Paris hospital, using short and long haul aircraft, turbosjets and helicopters
23 p4105 A69-41785

PATTERN DISTRIBUTION
U DISTRIBUTION [PROPERTY]

PATTERN RECOGNITION
NT CHARACTER RECOGNITION

Temporal pattern perception by human subjects required to integrate information presented in two modalities
02 p0200 A69-12724

Limited speech recognition system /LISPER/ simplifies recognition by computer designed as research vehicle and pattern recognition system
04 p0565 A69-15338

Pattern classification algorithms classified according to type of input information required
05 p0725 A69-16571

State variable techniques applied to optimal continuous linear feature extraction for binary Gaussian pattern recognition or detection problem
05 p0740 A69-16577

Stereoscopy effects on pattern recognition in visual noise
06 p0880 A69-17214

Recursive algorithms for pattern classification using misclassified samples
06 p0891 A69-17357

Deterministic pattern classification algorithms, discussing abstraction problem, stochastic algorithms, minimum error scheme and modified least squares scheme
06 p0892 A69-17395

Feature selection in pattern recognition, discussing techniques, crop classification problem and parametric multiclass pattern recognition
06 p0892 A69-17396

Adaptive pattern recognition, discussing classification techniques and merging into other aspects of artificial intelligence research
07 p1088 A69-18381

Pattern recognition method dependent on preselection of good variables, discussing SELFIC and relationship to Karhunen-Loeve expansion and factor analysis
07 p1088 A69-18386

Data handling by groups in perceptron type pattern recognition and decision making problems based on algorithm involving second degree polynomials
08 p1278 A69-20420

Pattern recognition as part of statistical communication theory, using Karhunen-Loeve expansion to minimize root-mean-square errors, showing application to handwritten numerals
09 p1461 A69-22292

Entropy minimization in feature extraction by dimensionality reduction with linear transformation of pattern vectors, noting recognition time and storage space savings
11 p1909 A69-25291

Pattern classification algorithms classified according to type of input information required
11 p1843 A69-25445

Adaptive pattern recognition system simulated and tested with agricultural radar images, describing predictive environmental model mathematically
12 p2097 A69-26990

Self adaptive system for recognition of dynamic shapes, discussing self structuring by learning, incomplete pattern recognition, logic element network, etc
12 p2054 A69-27080

Statistical analysis of radiation temperature structure for automatic recognition of meteorological situations from actinometric satellite observations
13 p2293 A69-27842

Largest scalar product of class and identification codes in diagnostic problems, discussing recognition
14 p2417 A69-29144

Image recognition algorithm for determination of hyperplane separating two finite sets of elements in Euclidean space
14 p2418 A69-29353

Pattern recognition and analysis, discussing definitions, rules of image transformation, pure and deformed patterns, etc
14 p2470 A69-29360

Remote sensor imaging techniques for simultaneous radar, IR and visible electromagnetic spectra of extensive land areas, presenting two clustering algorithms for multiple images
14 p2448 A69-29533

Data handling by groups in perceptron type pattern recognition and decision making problems based on algorithm involving second degree polynomials
14 p2418 A69-29658

Orthogonal signal recognition in set of false signals by resolving devices with limited sensitivity, giving design formulas for error probability
15 p2563 A69-30135

Recognition systems nonlinear discriminant function for separating linear inseparable patterns, describing orthogonal representation, correlation ratio and average variance criteria
15 p2645 A69-30806

Algorithm for calculating recognition error by applying pattern vectors having two multivariate Gaussian distribution to optimum Bayes classifier
15 p2572 A69-31113

Recognition system for discrete decision function generation to select one out of two classes of objects, deriving solutions for selection probability
17 p2932 A69-33119

- Adaptive filter with operational amplifier and digital to analog converters for bandpass characteristics, discussing pattern recognition application
17 p2942 A69-34093
- Digital simulation of biological model for visual images classification derived from human visual system aspects
17 p2911 A69-34094
- Frequency hopping technique applied to multiple access air-to-air/ground communication for tactical fighters, noting additive recognition
17 p2931 A69-34117
- Multilayer retina model with lateral couplings for visual pattern recognition, noting applications to data processing
19 p3260 A69-35898
- Gunn effect applied to digital electronics, discussing diode characteristics, microwave amplifier design, pattern recognition, analog-numerical conversion, etc
19 p3285 A69-36708
- Least square or least mean square approximation methods in abstract pattern recognition, noting unknown probability density function
20 p3504 A69-38285
- Storm location and severity prediction by pattern recognition theory, using quantized radar data, compared with statistical prediction
21 p3678 A69-39458
- Computer controlled TV cloud recognition equipment on meteorological satellites, discussing multistep process of automatic perspective distortion corrections by onboard computer
22 p3977 A69-40004
- Zoellner illusion in human visual system measured as function of background pattern density consisting of intersect angles and background line spacing
22 p3879 A69-40841
- Human visual response to moving spatially periodic patterns, analyzing critical frequencies, dependence on stimulus area and period, phase blindness and pattern reversal
22 p3880 A69-40850
- Spatiotemporal patterns learning among sensory and motor organs with linearly ordered components by nonlinear networks in terms of embedding fields theory
22 p3887 A69-41196
- Point images reference groups identification by human operator with limited visual perception in background noise, comparing results with automatic system using selection algorithms
23 p4109 A69-41955
- Pattern classification and iterative methods of linear/nonlinear dynamic plants identification, introducing phi machine as universal plants model
24 p4284 A69-42672
- Brain and machine model of pattern recognition, pattern synthesis, memory, learning and speech, using concept of similarity, context and signal analysis
24 p4273 A69-42909
- Nonparametric partitioning algorithm for pattern classification, discussing pattern recognition, classifiers structure, real data applications, etc
24 p4285 A69-43062
- Interpolated position and orientation perception by vision and active touch
24 p4275 A69-43116
- Adaptive multicategory pattern classification system, using independent samples to form mean-square approximations to Bayes discriminant functions
24 p4285 A69-43134
- Lambda waves EEG recording for evaluating eye movements during pattern vision
24 p4268 A69-43401
- PATTERSON MAP**
- Crystal and molecular structure of mu-oxo-bis(chlorobis(2,4-pentanedionato)titanium(IV)/chloroform solved by symbolic sign determination method and Patterson map interpretation
01 p0023 A69-10411
- PAVEMENTS**
- Construction practice for hot-mix bituminous pavements covering production, composition, application and quality control
01 p0057 A69-11276
- Airport runway surface construction materials requirements, taking into account factors different from highway pavement
17 p2948 A69-34215
- PAYLOAD MASS RATIO**
- Increased payload in orbit capability for future versions of Black Arrow vehicle, discussing propellant
02 p0335 A69-12681

- Synchronous orbit attainment with continuous electric propulsion, noting payload ratio dependence on various parameters and changing orbit inclination
[AIAA PAPER 69-275] 09 p1586 A69-21265
- Electrostatic thrusters using RF ion sources to optimize payload ratios, terminal velocities, propellants, life span and efficiencies
09 p1568 A69-21489
- Nuclear rockets as Saturn 5 third stages, emphasizing increased payload or velocity utility and resulting engine and stage requirements
[AIAA PAPER 69-555] 16 p2867 A69-31849
- PAYLOADS**
- Scientists involvement in planetary spacecraft missions, considering organization for particular instruments and more complex payloads
[AAS PAPER 68-192] 02 p0311 A69-11473
- Balloon, rocket probe and satellite payloads, noting French contributions and CNES role
02 p0333 A69-11914
- French space center in Guiana, discussing geographic location advantages for payload, rocket launching, space rendezvous, etc
02 p0228 A69-11920
- Mission mode and delivery method influence on payload maximization for Mars capsule system
02 p0335 A69-12822
- Onboard SDP-3 computer data system core for IMP spacecraft, considering payload
03 p0400 A69-13243
- Electric propulsion for payload transfer from low to synchronous orbit of ELDO launch vehicles
03 p0496 A69-13994
- Spacecraft launching facilities and payload capabilities in next decade, discussing orbits, spacecraft size and volume, attitude stabilization and positional accuracy
06 p1012 A69-16857
- Electrical propulsion for space maneuvers, discussing interrelationship of orbital changes, payloads and time
06 p0998 A69-16858
- Separable payload control for three axis orientation of sounding rocket instruments, discussing error sensors and pointing accuracies
06 p1014 A69-17583
- Maximum capacity estimation for one way transportation systems to moon and Mars, analyzing technical and economic aspects
09 p1586 A69-21297
- Manned spacecraft developments, considering Apollo Applications Program, space station establishment, space shuttle operations and payload cost
10 p1791 A69-22866
- Short range passenger aircraft, considering payloads, weights and economical classification
13 p2201 A69-27294
- Saturn 5 translunar payload capability enhancement by fuel biasing, propellant utilization systems, trajectory shaping and programmed mixture ratio scheme
[AIAA PAPER 69-451] 16 p2839 A69-32669
- Passive attitude stabilization of interplanetary probe, using conically shaped sails elastically connected to payload
17 p3047 A69-33225
- ASTRID high altitude sounding rockets orientation system aligning payload cones to target outside earth atmosphere, discussing software simulation with analog and digital computers, etc
17 p3001 A69-33424
- European launcher system based on modular principle for low orbit, geostationary and space probe missions payload requirements
17 p3050 A69-33428
- Heavy lift helicopter design with 30 ton payload, considering fanjet drive hot cycle and shaft drive propulsion systems
[AHS PAPER 330] 17 p2901 A69-33532
- Tail tip-evacuation limits, calculating aircraft balance effect of passenger relocations by graphical method
[SAWE PAPER 765] 18 p3091 A69-34877
- Rapid Targeting Procedures computer program for optimized orbital payload and associated launch vehicle targeting data with one submittal and minimum user intervention
[AAS PAPER 68-148] 19 p3402 A69-35951
- Spacecraft and boosters for earth resources surveys, discussing design, payloads, orbits, etc
21 p3799 A69-38629
- Recovery system for high altitude sounding rocket payloads, noting air inflated flotation device, payload separation and parachute deployment
[AIAA PAPER 68-959] 21 p3820 A69-39227

- Payload optimization factors for orbital storage of liquid hydrogen, considering payload cost of agitation, tank pressure, pressurant weight, etc
[AIAA PAPER 69-1007] 22 p4021 A69-40381
- Balloon flights with space available for secondary experiments, discussing launching agencies and experiment design restrictions
22 p3865 A69-40807
- Modular configuration of recoverable scientific MAP/Modular Auroral Probe/ payloads aboard Nike-Apache rockets, discussing payload design concepts
23 p4223 A69-41763
- PCM [MODULATION]**
- U PULSE CODE MODULATION**
- PCM TELEMETRY**
- Bandwidth limited PCM/PSK/PM telemetry system performance analysis for developing S band telemetry, including coherent and noncoherent detectors
07 p1081 A69-19098
- PCM telemetry system for sounding rocket payloads flown in polar light zone within German-American project AZUR
07 p1081 A69-19099
- PCM bit synchronizer/signal conditioners performance characteristics and specification
07 p1106 A69-19120
- Bit error probability estimation of NRZ PCM synchronizer and detector operating in presence of fluctuating data frequency source
07 p1083 A69-19121
- Spectral null from spectral characteristics and statistical properties of PCM signals used to estimate SNR
07 p1083 A69-19122
- Design of 126 channel PCM telemetry unit for C-5 aircraft flight test, discussing FET analog multiplexing
10 p1693 A69-23275
- ESRO Aurorae satellite telecommunication system, detailing information nature, PCM telemetry and remote control system standard
15 p2702 A69-31084
- Ground data operations system for large astronomical satellite comprising UHF telemetry, PCM telecommand and processing and display equipment
18 p3117 A69-34794
- PCM bit synchronizer signal to noise ratio measurement by input video signal zero crossings counting
19 p3271 A69-36248
- Ground data handling equipment characteristics for PCM telemetry link utilizing convolutional coding
19 p3273 A69-36267
- Addressable remote multiplexed PCM data system used on Titan III launch vehicles
19 p3274 A69-36279
- Stored program data processor used as PCM telemetry data acquisition system for postApollo applications, considering format and bit rate changes
19 p3274 A69-36280
- Computer based onboard satellite PCM telemetry, showing improved adaptability, size and cost reduction
20 p3500 A69-37382
- Machine independent telemetry oriented language /MITOL/ to develop computer programs for real time and postflight telemetry data processing
22 p3905 A69-40340
- PCM telemetry system for transferring information from many remote sources to single local processing point
24 p4281 A69-42620
- PDM [MODULATION]**
- U PULSE DURATION MODULATION**
- PEACETIME**
- Interpretation of term peaceful in Space Treaty and use of outer space including celestial bodies
07 p1244 A69-19234
- PEAKS**
- Rotating mirror Q switched carbon dioxide laser for high peak powers, analyzing pulse structure and duration dependence on collision induced relaxations
19 p3338 A69-36694
- PEARLITE**
- Eutectoid pearlite growth by pure iron-carbon specimen heat treatment
13 p2281 A69-28158
- Lunar volcanism origin of tektite and pearlite, noting no cosmic ray effects
20 p3597 A69-37338
- PEARSON DISTRIBUTIONS**
- Weapon systems integrated testing, determining test quantities as function of subsystems utilizing Neyman-Pearson confidence levels
15 p2619 A69-30400

- Differences in latitude readings obtained with two zenith telescopes, showing Pearson distribution of type VII and influence of observation conditions
17 p2959 A69-32879
- PEDOLOGY**
U SOIL SCIENCE
- PEENING**
U SHOT PEENING
- PELTIER EFFECTS**
Peltier measurements below 4 K capable of measuring low Seebeck coefficient on high resistivity alloys and in presence of magnetic field
14 p2449 A69-29563
Thermal EMF, electrical conductivity and Peltier effect in sintered refractory oxides at high temperature in air and in Ar
17 p3068 A69-32990
- PENALTIES**
Aircraft hijacking prevention through technical and legal means, discussing national and international air piracy laws
13 p2381 A69-27528
FAA jurisdictional procedures for law infringement, discussing civil codes, delegation of enforcement authorities and routine violations including low flying, weather, etc
16 p2882 A69-32335
- PENDULOUS GYROSCOPES**
U GYROSCOPIC PENDULUMS
- PENDULUMS**
NT GYROSCOPIC PENDULUMS
Torsional pendulum for stress and strain relaxation measurements of wire sample
01 p0079 A69-10221
Dynamic stability of double pendulum with vibrating point of suspension, obtaining differential equations of motion by Lagrange equations application in averaging method
11 p1884 A69-24768
Dual pendulum with tilt sensitivity at wide passband frequencies and damping due to horizontal oscillations
14 p2450 A69-29570
Asymptotic solutions to second order differential equations with slowly varying parameters and large resistance applied to mathematical pendulum damped swinging motion
16 p2804 A69-32253
Pendulum motion about stationary axis of solid body containing damper, ascribing instability to center of gravity shift with respect to cavity
18 p3135 A69-34557
Near resonant and nonresonant solutions of nonlinear equation describing rotating pendulum motion under periodic disturbance
21 p3771 A69-39004
Equation of motion for determining nonlinear vibration of rod pendulum in viscous flow of varying velocity
21 p3773 A69-39679
Bethenod pendulum behavior using coupled nonlinear differential equations, discussing synchronization methods
24 p4349 A69-42673
- PENETRANTS**
Two fold congruency method for statistical evaluation of fluorescent flaw detection penetrant sensitivity and reproducibility
10 p1700 A69-23374
Radioactive Kr as gaseous penetrant for nondestructive test inspections, noting high sensitivity
19 p3322 A69-35575
- PENETRATING PARTICLES**
U CORPUSCULAR RADIATION
- PENETRATION**
Force law determining impact processes of pyramidal and conical body penetration into smooth surface of rigid plastic metals
02 p0337 A69-11615
Screening of high density plasma from penetration by neutral gas, discussing prevention of high energy losses by charge exchange collisions
02 p0288 A69-12170
Meteoroid flux measured by Explorer 16 and Lunar Orbiter, analyzing penetration rate, average velocity and consistency with photographic meteors
13 p2349 A69-27820
Penetration mechanics of multisheet structures based on discrete particle modeling of impact debris [AIAA PAPER 69-371]
13 p2367 A69-28303
Thin foil penetration measurements for Fe microparticle impacts on metal and Mylar foils in space
15 p2641 A69-31339
- Interstellar particle penetration into solar system, discussing impact ionization of earth ionosphere by interstellar neutral hydrogen and helium
15 p2699 A69-31390
Liquid sodium penetration into stainless steel grain boundaries, using laser microprobe
18 p3154 A69-35473
Minority carriers penetration depth in solid aluminum gallium arsenide solutions with variable forbidden bandwidth determined from recombination radiation spectra
19 p3391 A69-36606
F layer penetration frequencies predictions compared with Alouette topside data
20 p3530 A69-37871
- PENETRATION BALLISTICS**
U TERMINAL BALLISTICS
- PENETROMETERS**
Lunar surface uppermost layer physical and mechanical properties investigated by soilmeter-penetrometer and radiation densimeter on Luna 13
18 p3113 A69-34239
- PENNING DISCHARGE**
Penning discharge in inhomogeneous magnetic mirror field, observing high burning voltage at low current in rarefied hydrogen plasma
01 p0133 A69-11218
Plasma heating dynamics by straight turbulent discharge current influenced by initial plasma parameters
07 p1195 A69-19592
Kaufman thruster with predominant radial field, noting electron mobility across ion extraction screen and advantages of uniform plasma distribution [AIAA PAPER 69-259]
09 p1569 A69-21877
Nonthermal microwave emission from cold cathode PIG discharge plasma, noting wide spectrum of electron cyclotron frequency harmonics
09 p1549 A69-22018
Plasma flow from Penning discharge with incandescent cathode in vacuum controllable by varying voltage, pressure and magnetic field strength
11 p1933 A69-25543
Current increase and voltage decrease in high voltage low pressure Penning discharge ascribed to hollow cathode effect
11 p1933 A69-25544
Screw instability in glowing discharge plasma column in longitudinal magnetic field generalized to instabilities in low pressure arc, Penning and high current discharges
13 p2315 A69-28526
Theory for current magnetic field characteristics of Penning discharge valid to extinction point
22 p3991 A69-40865
- PENNING EFFECT**
Auxiliary discharge thermionic converter with Penning mixture /Ne-Ar/, discussing pressure and Penning ionization effects, collector current discontinuities, etc
14 p2398 A69-29180
- PENTACHLORIDES**
U CHLORIDES
- PENTAERYTHRITOL TETRANITRATE**
U PETN
- PENTANES**
Isopentane and mesitylene index of refraction variations with pressure, determining average molecular radii and polarizabilities
01 p0123 A69-10685
Temperature and pressure measurements in low temperature combustion of n pentane covering slow reaction and cool flame regions
02 p0353 A69-12321
- PENTODES**
Wideband RF amplifier manufacturing problems, comparing operation of vacuum triodes and pentodes in passband circuits
11 p1849 A69-24958
Push-pull pentode frequency multipliers with sinusoidal undistorted outputs, studying grid bias effects on operating characteristics
22 p3912 A69-40260
- PENUMBRAS**
Wilson effect in sunspots, interpreting penumbra distortion near solar disk limb in terms of radiation transport
03 p0504 A69-12893
High resolution H alpha line photographs of solar chromosphere, showing superpenumbra-like dark fibrils around isolated sunspots
04 p0664 A69-15526
- Magnetically aligned flows between sunspots, considering Evershed effect on umbrae and penumbrae
10 p1772 A69-22907
Solar corona observed by X ray instrumentation of SOLRAD 8 satellite crossing moon penumbra during solar eclipse of 20 May 1966
15 p2698 A69-31363
Penumbra current distribution in plane electromagnetic waves diffraction by conducting cylinder, obtaining transient solution for impulsive excitation, discussing time harmonic problem
18 p3100 A69-34232
Relative penumbral intensity independent of spot position from data by pinhole photometer of large sunspots
20 p3603 A69-37542
Sunspot penumbra model in hydrostatic equilibrium accounting for continuum and Fraunhofer lines observations
22 p4019 A69-40290
Sunspots microstructure, discussing penumbra and umbral properties with respect to magnetic field configuration
24 p4378 A69-42690
- PEPTIDES**
Tryptic digestion of C terminal tritiated peptides analyzed with Scenedesmus ferrodoxin, noting use for protein structural study
10 p1648 A69-24190
Proline residue effects on hydrolysis of peptide bonds by thermolysin
15 p2561 A69-30083
Substrate specificity of cathepsin C derived from rat liver, describing polymeric structure and behavior as acidic protein
20 p3473 A69-37577
Cations of sulphates photosensitizing role in photolysis of amino acids and peptides in various atmospheres
20 p3477 A69-37626
DNA polymerase from Escherichia coli, discussing physical and chemical properties of enzyme and polypeptide chain consistency
22 p3898 A69-41070
Polypeptide synthesis as function of 5S ribosomal RNA dissociated from 50S ribosomal subunits by EDTA treatment
23 p4113 A69-41491
Tryptic pentapeptide Asp-Glu-Leu-Thr-Lys synthesis showing relation to Gm/a/ antigen of human gamma g-globulin
24 p4279 A69-42712
Sequence preparation of protected peptide polymer bond with anion exchange resin using solid phase transesterification
24 p4279 A69-42713
Amino acid sequence of dogfish lactic dehydrogenase, isolating acylated amino-terminal peptide and arginine residues, indicating four polypeptide chain composition
24 p4280 A69-43051
- PERCENTAGE**
U RATIOS
- PERCEPTION**
U AUDITORY PERCEPTION
U AUTOKINESIS
U CRITICAL FLICKER FUSION
U FLICKER
U OLFACTORY PERCEPTION
U PAIN SENSITIVITY
U SENSORY PERCEPTION
U SPACE PERCEPTION
U TACTILE DISCRIMINATION
U TASTE
U VERTICAL PERCEPTION
U VIBRATION PERCEPTION
U VISUAL DISCRIMINATION
U VISUAL PERCEPTION
- PERCEPTORS**
U SELF ORGANIZING SYSTEMS
- PERCHLORATES**
NT AMMONIUM PERCHLORATES
NT HYDROXYLAMMONIUM PERCHLORATES
NT MAGNESIUM PERCHLORATES
NT NITRONIUM PERCHLORATE
NT POTASSIUM PERCHLORATES
Diperchlorates different in organic part of structure and explosive transformation heats, showing strong dependence of combustion velocity on pressure
15 p2716 A69-30108
Thermal decomposition behavior of perchlorate oxidizers studied by flash mass thermal analysis for determining propellant combustion kinetics [WSCI PAPER 69-19]
16 p2832 A69-32357
- PERFECT GAS**
U IDEAL GAS

PERFLUORO COMPOUNDS

Perfluorocyclobutane-oxygen mixture combustion, measuring burning velocities and adiabatic equilibrium flame temperatures

21 p3852 A69-39594

PERFORATED PLATES

Stress analysis of multiply connected bodies under large elastic strains, deriving second order potentials for plate with elliptical holes

02 p0340 A69-12139

Stress concentrations around elliptical perforations in shrunk plates with bonded boundaries based on photoelastic models

02 p0345 A69-12391

Stresses in infinite elastic plate containing rigid rectangular inclusion subject to uniform stress field, using complex variable method and Schwartz-Christoffel conformal mapping

02 p0348 A69-12796

Stresses around two reinforced circular openings in thin elastic plate of isotropic material under biaxial loads

02 p0349 A69-12799

Successive approximations utilizing analytic stress functions used to obtain solution for infinite plate with arbitrary holes under biaxial stresses

[ASME PAPER 68-PVP-1] 03 p0523 A69-12998

Crack propagation near arbitrary curvilinear hole, discussing hole exterior mapping and critical loads for crack initiation

04 p0674 A69-14562

Stress field for skew hole determined from plane stress field for equivalent right hole, considering elastic plate penetrated by oblique circular cylinder

04 p0674 A69-14589

Creep stress concentration at circular hole in thin sheets under loads in own plane, discussing infinite thin plates

[AIAA PAPER 68-175] 04 p0676 A69-14708

Stress concentration around centrally placed circular bolt in axially loaded bar, using theory of infinite systems of linear equations

04 p0681 A69-15195

Stress-strain state for two dimensional physically nonlinear multiply connected elastic regions, noting plate with two identical circular holes

05 p0841 A69-16203

Stress distribution in infinite strip with equally spaced identical semicircular notches on one edge and subject to transverse bending

05 p0842 A69-16643

Stresses in finite width infinite elastic isotropic strip with equally spaced identical semicircular notches under uniform tension or pure bending

05 p0843 A69-16644

Stress-strain state of infinite plate with two holes of different diameter solved, using integral equation derived for two dimensional problem in elasticity theory for anisotropic medium

05 p0843 A69-16680

Deformation and stresses in biaxially loaded stretched thin plate with central small hole during stress redistribution caused by creep

06 p1022 A69-17368

Two dimensional stress distribution changes around rectangular hole with rounded corners for varying internal pressure and temperature

06 p1025 A69-17611

Transmission coefficient of plane electromagnetic wave obliquely incident on perforated metal screen in frequency range near primary resonance of structure

07 p1076 A69-18527

Couple stresses effect on thin plate stress distribution due to pressure of rivet on one side of circular hole

08 p1319 A69-20201

Two dimensional photoelasticity for minimizing stress concentration in perforated rectangular plate subjected to restrained shrinkage, discussing application to solid propellant rocket grains

08 p1412 A69-20255

Foil type strain gage for measurement of tangential strains along circumference of hole in plate under uniaxial and equibiaxial tension

08 p1314 A69-20258

Monograph on plane problem and bending problem for infinite elastic plate with doubly periodic set of circular holes

08 p1416 A69-20709

Stress concentration at circular hole in infinite plate for large strains and nonlinearity, analyzed by integral operator method

09 p1613 A69-21629

Stress-strain state of infinite plate with elliptical eccentric reinforced hole, using quadrature method

09 p1613 A69-21630

Surface heat transfer coefficients under perforated plate of multiple square array round impinging air jets

[ASME PAPER 69-GT-4] 09 p1624 A69-22508

Central circular hole effect on fundamental frequency of rectangular fixed edges plate, discussing hole size, square plates, etc

[ASME PAPER 69-VIBR-62] 10 p1805 A69-24156

Moment stresses effect on stress concentration in plates with common type hole, considering uniaxial and triaxial bending and torsion

11 p1971 A69-24646

Elastic unbounded isotropic plane weakened by doubly periodic system of identical holes, noting solution involving Cauchy type integral

11 p1972 A69-24652

Elastic isotropic half plane weakened by circular hole with concentrated force applied along hole contour, considering stress distribution

11 p1972 A69-24653

Stress concentration in isotropic plates weakened by curvilinear holes subjected to loading at infinity, noting curvature at corner points of holes

11 p1972 A69-24655

Three dimensional bending problem for thick isotropic plate with curvilinear hole and normal and tangential stress applied to edge of hole

11 p1973 A69-24657

Two dimensional contained plastic deformation in asymmetrical elasticity theory based on Cosserat medium, examining boundary value problems, stress concentration and elastic wave propagation at holes

11 p1973 A69-24659

Two dimensional problems solutions by contour smoothing methods, considering stress concentrations in reinforced or perforated thin elastic plates

11 p1973 A69-24661

Stress concentrations in bending of thin perforated plates, considering potential and vortex stresses due to edge effect

11 p1976 A69-24784

Residual thermal stresses and plastic strains at hole edges in perforated plates, considering heating and rapid cooling

11 p1982 A69-24947

Boundary determination for separating elastic and plastic regions of infinite perforated sheet with triangular network of circular holes

11 p1996 A69-25736

Stress concentration near circular hole in plate during bending, showing dependence on material constant

12 p2178 A69-25999

Stress concentration around square hole in celluloid plate subjected to creep under biaxial tension analyzed by photocreep method

12 p2178 A69-26000

Thermal stresses in infinite elastic plates containing insulated circular holes, using two dimensional bipolar coordinates

12 p2180 A69-26267

Stress concentration around rhombic hole in non-linear isotropic plate under pure shear

14 p2533 A69-28987

Stress concentration near circular nonreinforced hole at bending of transversely isotropic rectangular plate analyzed in terms of transverse shear theory

15 p2707 A69-30580

Couple-stresses effect on stress concentration of plate containing infinite row of holes, solving linear elastic problem in isotropic Cosserat continua for plate

15 p2708 A69-30640

Boundary layer solution in three dimensional bending for plate with curvilinear hole to study stress-strain state at hole and over entire plate

15 p2708 A69-30662

Stress concentration on circular holes and notches in anisotropic oriented glass fiber reinforced plastics determined by using photoelastic birefringent coatings

15 p2713 A69-31053

Hydrostatic stability and damping characteristics of perforated plates and screens for passive propellant control schemes from drop tower tests

[AIAA PAPER 69-531] 16 p2833 A69-32691

Stress-strain state analysis for brittle plate with circular holes of equal radius performed in cylindrical system of coordinates

17 p3055 A69-33127

Anisotropic elastic plate deflection weakened by circular hole with thin elastic ring reinforcement, assuming no load on ring and uniform stress-strain state of plate

17 p3055 A69-33128

Von Karman equations in dimensionless and finite difference forms for deflections of elastic circular plate with central hole under load solved by iteration

[ASME PAPER 69-APM-20]

18 p3214 A69-34395
Critical stresses and crack development near holes in compressed elastic plate

18 p3218 A69-34603

Plate bending theory modified for applying successive linear conjugates method to partially clamped isotropic plate and plate with circular hole

21 p3834 A69-38721

Stress-strain state in thin isotropic plate with circular hole under lateral bending and torsional moments

21 p3835 A69-38725

Enlargement of circular hole in disk with kinematic hardening and Tresca yield function compared with isotropic hardening

21 p3840 A69-39297

Deformation of uniformly thick elastic circular plates containing circular holes reinforced by thin rigid elastic rings

21 p3846 A69-39713

Dynamic stability of circular isotropic plate with central hole subjected to torsional moment uniformly distributed over both edges by equilibrium equation

22 p4043 A69-40455

Stress concentrations in circular plate with square hole subject to triaxial tension

23 p4227 A69-41712

Stressed state of thin plate with circular hole under normal and breaking force applied over hole perimeter

23 p4233 A69-42341

Perforated heat exchanger tube plates stiffness determination from hole diameter-to-spacing ratios

24 p4400 A69-43087

Tensile tests on fiber reinforced plates with circular holes, studying fiber orientation effects

24 p4404 A69-43602

PERFORATING

Perforation and penetration mechanisms of Styrofoam slabs, using impact tests with free falling and rifle powered projectiles

01 p0165 A69-10115

PERFORMANCE

Performance characteristics of hard limited and linear repeaters for satellite communications systems

01 p0032 A69-10966

Algorithm minimaxing performance index and sensitivity of controller design with and without saddle point

02 p0224 A69-11966

Thermal stability criteria for thermionic converter performance evaluation, noting electron cooling influence

09 p1441 A69-21838

Microwave avalanche diode oscillators performance estimates, discussing operation modes and transit time

10 p1665 A69-23873

High temperature electrochemical high performance batteries

17 p2904 A69-33663

Large scale axisymmetric inlet systems performance capabilities, reviewing theoretical and experimental programs

[AIAA PAPER 68-580] 17 p3022 A69-34018

Composite and structured material forms combination for obtaining high performance and low cost

18 p3161 A69-34608

Polymers in high performance applications - Conference, London, June 1969

18 p3150 A69-35420

Two level systems with overall performance as explicit function of first level performance, defining equivalence condition to prove coordinability for nonadditive case

24 p4294 A69-43308

PERFORMANCE PREDICTION

Digital loaded-line phase shift networks for microwave thin film applications, emphasizing design equations

01 p0040 A69-10198

Multiple configuration analysis of structures systematically predicting static and dynamic response of structures of single configuration class

01 p0169 A69-10639

Exploding wire detonators noting dependence of threshold burst current on bridgewise length and diameter, explosive surface, density, etc

01 p0119 A69-10672

Fracture toughness concept in predicting failure of materials due to sharp notches or cracks

02 p0336 A69-11431

Theoretical prediction for modified and hybrid plasma resonances discrimination, noting sensor axis angle to geomagnetic field

02 p0241 A69-11731

Propeller static performance calculations for infinite number of blades applied to four blade propeller at different blade angles

02 p0188 A69-11957

Performance cost functions for reaction jet controlled system during on-off limit cycle for stable and unstable plant

02 p0278 A69-11965

Notch stress procedure to predict low cycle fatigue life of specimens with fabrication flaws, discussing crack initiation and propagation lives effects [ASME PAPER 68-PVP-15]

03 p0523 A69-12997

Optimum receiver structure for estimating PSK information signal phase derived together with matched filter detector performance

03 p0403 A69-13203

Performance prediction by testing, considering stress analysis, temperature, multiaxial stresses, combined stress, corrosion, shock, etc

03 p0525 A69-13307

Diode mixer power series coefficients for spurious response prediction in superheterodyne receiver

03 p0399 A69-13905

Aircraft squadron performance effectiveness model

03 p0367 A69-13911

Cardiac function changes during orthostatic tests and problems in predicting reactions of cosmonauts in flight

03 p0381 A69-14229

Predictive model for risk in technological research and development

04 p0689 A69-14980

Jet pump head rise deterioration parameter for prediction of cavitation

05 p0745 A69-15791

Prediction technique for surface effect causing Si bipolar transistors gain degradation under ionizing radiation

06 p0976 A69-16879

Predictive scale of aircraft emergencies, analyzing human error rate under stress

06 p0880 A69-17208

Microwave semiconductor devices, discussing performance trends in detectors, tunnel diodes, mixers, varactors, transistors and Gunn effect devices

07 p1096 A69-18440

Predictor determining future position of TDMA /Time Division Multiple Access/ synchronous satellite communications system satellite from previously received bursts

07 p1076 A69-18553

Nondemographic model predicting market shares of V/STOL aircraft in competition with automobiles and conventional airliners for short haul intercity business travel markets

07 p1244 A69-18967

Seal swell prediction methods extended to include three dimensional solubility parameter concept [ASLE PAPER 68-LC-21]

07 p1171 A69-19306

Radome performance dependence on dielectric permittivity determined by digital program and simple design criterion

07 p1110 A69-19519

Small and full scale model tests for feasibility of retracted rotor aircraft for high speed flight [AIAA PAPER 69-219]

07 p1055 A69-19550

Control systems digital simulation based on coupling of prediction correction procedure with integration and differentiation procedure, discussing simulation errors

08 p1296 A69-20110

Performance boundaries of space propulsion systems containing nuclear electric stages [AIAA PAPER 69-249]

09 p1538 A69-21249

SERT 2 thruster system performance over expected mission parameters, noting operational lifetime excess over mission requirements [AIAA PAPER 69-235]

09 p1566 A69-21255

Power systems for future aircraft emphasizing growth in performance and reduction in weight

09 p1567 A69-21387

Performance prediction for planar and cylindrical electrode geometry fixed spacing thermionic converters

09 p1438 A69-21814

Cooled turbine performance evaluation methods, noting promise of analytical methods [ASME PAPER 69-GT-63]

09 p1572 A69-22517

Digital computer simulation as maintainability design and prediction tools, discussing fault localization in complex electronics systems

10 p1668 A69-22974

Existing predictive methods for determining high temperature low cycle fatigue life reexamination based on experiments on nickel

10 p1796 A69-23068

Celestial X ray source positions from rotating modulation collimator, predicting performance of collimator

10 p1722 A69-23328

Off design performance prediction method for radial inflow turbines compared with experimental results for small turbine and Brayton space power plant

10 p1754 A69-23891

Zinc electrode cycle life improvement by reducing change in electrode shape, noting effectiveness of teflonation

10 p1640 A69-23995

Highly resistant separator performance in Zn-Ag oxide battery, discussing zinc electrode limitations on battery performances

10 p1640 A69-23996

Airflow through open foam cellular structure, discussing mathematic model for predicting pressure buildup and foam response in shock and vibration isolation [ASME PAPER 69-VIBR-46]

10 p1803 A69-24144

Performance correction and nonstandard day performance prediction for analyzing turbocharged reciprocating aircraft engines in light aircraft applications [SAE PAPER 690309]

11 p1942 A69-24514

Aircraft structures fatigue strength determination, discussing test procedures, sample preparation, strength prediction, etc

11 p1970 A69-24525

Rapid low level commutator for temperature measuring circuit with thermocouples, discussing construction and performance

11 p1884 A69-24758

Weld defects effects on static and fatigue properties of weldments prediction, including tests of titanium-aluminum-vanadium joints

11 p1892 A69-24932

Propeller performance prediction for nonnegligible angle of attack, determining tip loss factor with model similar to Prandtl model for axial flight

11 p1819 A69-25375

Feedback control law preserving optimality for systems with unknown parameters, discussing optimally adaptive performance index

11 p1860 A69-25441

Wideband inverter operational amplifier frequency response, open and closed loop transfer functions, beta, settling time and slew rate limits, discussing HF performance prediction

11 p1857 A69-25666

Service life of system predicted by identifying and testing system variables of mission phases, using obtained data in statistical estimation

12 p2101 A69-25970

Nozzle erosion profile, char penetration and temperature response predicted for nozzle material for 260 SL-3 motor [AIAA PAPER 68-504]

12 p2118 A69-26784

Graphite improvement for high temperature applications by computerized properties analysis, failure criterion and improved testing for defective billets

12 p2115 A69-26845

Transistorized amplifiers reliability estimated from step by step failures during operation in intense external environment

12 p2043 A69-26886

Man machine model for prediction of human control behavior, generating model from analysis of helicopter pilot tasks

12 p2025 A69-27082

Computer simulation models for prediction of individual and crew performance in man machine environments

12 p2026 A69-27087

Computer simulation program for design and evaluation of digital Doppler processor, analyzing performance limitation due to quantization and white noise

12 p2035 A69-27096

Liquid metal two phase flow MHD generators efficiency prediction, discussing eddy losses and flow velocity

13 p2205 A69-27485

Liquid metal MHD induction generators design and performance, considering effect of geometry, operating conditions, fluid properties and power level on efficiency

13 p2207 A69-27503

Erosion type plasma accelerator using inductive energy storage compared with capacitive energy storage

13 p2311 A69-28110

Weighting factors relation in optimal systems integral squared error /ISE/ cost functional, characteristic coefficients and time response performance measures

14 p2534 A69-29317

Flight worthiness of mishandled electronic equipment, analyzing fragility and performance of shock exposed components and connections

15 p2576 A69-30362

Engineering models for wearout reliability prediction in dynamical systems subject to random loading, demonstrating practical and statistical methods

15 p2705 A69-30366

Leakage prediction through mechanical seal by theoretical equation developed from basic fluid mechanics [ASLE FICFS PREPRINT 17]

15 p2621 A69-30499

Computer aided design /CAD/ of component selection for circuit optimization applied to circuit performance and sensitivity calculations

15 p2628 A69-30849

Electrochemical test predicting stress corrosion performance of 2219 aluminum alloy in T851 and T87 tempers

16 p2798 A69-31716

ICRPG liquid propellant thrust chamber performance evaluation methodology, reviewing imperfections and limitations [AIAA PAPER 69-468]

16 p2838 A69-32657

Nonequilibrium initial condition combustion effects on propellant performance for hydrazine/ chlorine pentafluoride and hydrogen/fluorine with equilibrium, kinetic and frozen nozzle flow [AIAA PAPER 69-469]

16 p2832 A69-32659

Solid rocket motor performance prediction including motor pressure, thrust and propellant parameters, discussing mathematical modeling of flow fields [AIAA PAPER 69-732]

16 p2840 A69-32674

Agna propulsion system performance model for predicting propellant flow rate, mixture ratio, thrust time and specific impulse [AIAA PAPER 69-453]

16 p2841 A69-32683

Flight performance prediction for throttling bipropellant rocket engine utilizing ablative combustion chamber throat, discussing lunar module descent engine [AIAA PAPER 69-452]

16 p2841 A69-32690

Supersonic compressor blade sections performance prediction near maximum pressure ratio and efficiency by analyzing flow processes [AIAA PAPER 69-522]

16 p2843 A69-32711

Low cycle fatigue behavior prediction for 304 and 306 stainless steels based on temperature and strain rate ratio to tensile ductility

17 p2987 A69-33079

Apollo Lunar Module Environmental Control System /LM/ECS/ steady state performance simulation techniques, discussing vacuum chamber data of LTA-8/LM-3 [AIAA PAPER 69-616]

17 p2903 A69-33307

Mission task performance oriented approach to winged helicopters flying and handling qualities, considering wings and horizontal stabilizers influence [AHS PAPER 360]

17 p2900 A69-33522

Helicopter rotors and static propellers theory based on Prandtl-Betz theorem, calculating ideal performance [AHS PAPER 326]

17 p2894 A69-33533

Vertical takeoff aircraft propeller/rotor design and performance prediction, discussing vortex model, wake contraction, blade element aerodynamic properties, etc [AHS PAPER 325]

17 p2894 A69-33534

Helicopter hovering performance prediction from wake analysis by iteration, discussing wake interference significance and blade number influence [AHS PAPER 321]

17 p2895 A69-33538

Blade length effects on performance of flow straightener vanes influenced by secondary flow, noting high deflection and low aspect ratio

17 p2896 A69-33606

Superconducting antenna factors and matching circuit equivalents developed for predicting efficiency and Q increase on basis of Pb surface resistance

17 p2937 A69-33784

Fluidic attitude control systems performance prediction from conventional control analysis emphasizing steady state positioning accuracy

17 p2904 A69-34069

Soviet book on hydraulic servo drive covering design and performance, static and dynamic characteristics and stability problems

18 p3093 A69-34356

Reliability prediction in electronics, discussing basics, advances, limitations, etc

18 p3146 A69-34514

Reliability prediction limited to approximations related to past experience on similar equipment

18 p3147 A69-34517

Statistical testing techniques using small sample size at low component levels to predict product performance

18 p3117 A69-34528

Plastics behavior under loading and performance prediction, considering engineering design applications

18 p3161 A69-34609

Parameter sensitivity analysis of discrete suboptimal filters from optimal rmse estimate of actual system performance measure

18 p3110 A69-34675

Thermoelectric converter systems optimization by geometry independent functions

18 p3093 A69-34782

Solid propellant rocket motor predictive design by correlating performance and weight statistics via computer program [SAWE PAPER 775]

18 p3184 A69-34873

Nuclear powered surface effects machine performance estimates, calculating reactor power and payload fraction for various clearance heights, gross weights and velocities

18 p3171 A69-35180

Helicopter rotor rotational and vortex noises prediction methods and trends

18 p3088 A69-35224

Dynamic performance accuracy of astatic gyroscope with three degrees of freedom improved by inner gimbal mass increase

19 p3308 A69-35825

Mathematical basis for human operators purposeful behavior in complex systems control situation requiring decision reaching

19 p3260 A69-35895

Operational missile flight program validation plan noting mission analysis, computer programming, program preparation and performance prediction

19 p3279 A69-35955

Surveyor thermal vacuum test data comparison with flight results indicating performance prediction reliability of earth-based tests for vacuum and lunar environments

19 p3430 A69-36016

Man machine modeling technique for establishing personnel performance requirements, discussing field tests

19 p3261 A69-36025

Fracture mechanics applied to cylindrical pressure vessels containing longitudinal defects for fracture behavior prediction from fracture toughness or stress intensity factor

19 p3439 A69-36439

Volume prediction of human body exposed to vacuum based on animal skin elasticity and anatomical features

19 p3258 A69-36456

Acoustic filters performance determination, standing wave tube and anechoic termination methods

20 p3464 A69-37321

Propulsion system performance relationship to manned planetary mission capability, discussing anticipated performance of advanced propulsion concepts

20 p3586 A69-38118

Optimum and suboptimum synchronizers for extracting bit synchronization from binary data, showing performance dependence on pertinent system parameters

21 p3673 A69-38923

Multiple access techniques of SSB-PM and PCM-PM frequency translation for satellite communication system, comparing performance characteristics

21 p3678 A69-39807

Minimum bias criteria for selecting data fitting curves, allowing for unknown true equation in improving data predictability [AIAA PAPER 69-950]

22 p3975 A69-40332

Computerized simulation for performance evaluation of System/4 Pi-EP multiprocessor for use in aerospace vehicle

22 p3907 A69-40353

Hydrostatic bearings analysis for high pressure cryogenic rocket engine turbopumps to predict steady state and time dependent performance, noting turbulence, inertia and compressibility

22 p3955 A69-40408

Germanium microwave backward diodes optimum design and performance prediction through computer calculation for important parameters

22 p3916 A69-41224

Rotor operating limits, loads, performance prediction and airfoil development in rotary wing aerodynamics research

23 p4057 A69-41371

Delay line MTI receivers performance calculation accuracy, discussing error for general and restricted number of pulses from single and double cancellation at IF

23 p4117 A69-41605

Digital computer program for determining flight vehicle telemetry antenna performance from ground test readings

23 p4133 A69-41754

Radio telemetry system for evaluating protective masks dynamic performance by remote simultaneous monitoring of respiration, acceleration and temperature data generated by human subjects

23 p4121 A69-41765

Teleological systems behavior modeling based on input, output, goals, operation duration, etc

23 p4134 A69-42059

Thermoelectric generators using hot junction pressure contacted lead telluride technique, presenting model for long term performance characteristics

23 p4188 A69-42262

Space vehicle flight performance of Ni-Cd batteries noting reliability, consistency and predictability

23 p4072 A69-42285

Radar detection performance evaluation procedures based on integration, collapsing and fluctuation losses estimates for swirling target models and partially correlated targets

23 p4132 A69-42547

Space and missile guidance performance analysis through automatic generation of mission performance sensitivity with respect to error sources from Monte Carlo simulation [AAS PAPER 69-404]

24 p4347 A69-42836

PERFORMANCE TESTS

Performance characteristics of microstrip ferrite devices for hybrid microwave integrated circuit systems, including meander line phasers and YIG elements

01 p0040 A69-10191

T63 regenerative helicopter engine program, noting operational performance and engine-aircraft compatibility [AHS PAPER 212]

01 p0143 A69-10410

Stable fluxgate magnetometer sensor for exploration of space magnetic fields, discussing equipment specifications and performance tests [IEEE PAPER 10.2]

01 p0081 A69-10715

Low polarization error HF loop antenna array direction finder performance tests, comparing measured bearings with polarimeter and conventional crossed loops data

01 p0048 A69-11006

Test method to compare grazing incidence X ray telescope performance in visible light and in X rays

02 p0248 A69-11736

Propeller static performance calculations for infinite number of blades applied to four blade propeller at different blade angles

02 p0188 A69-11957

Operator handedness effect on control display movement stereotypes

02 p0203 A69-12212

Component total task relationships, analyzing simple and sequential practice effects with aid of Melton Complex Coordinator

02 p0203 A69-12214

Strain gage behavior on unstressed aluminum alloy under rapid heating using radiant heating, weld strength and high temperature test equipment

02 p0341 A69-12229

Rhenium-niobium cylindrical thermionic converters with mechanically polished or electroetched emitters, comparing performance

03 p0368 A69-13126

Performance prediction by testing, considering stress analysis, temperature, multiaxial stresses, combined stress, corrosion, shock, etc

03 p0525 A69-13307

Human inspection performance in quality control operations to assess visual inspection tasks accuracy

03 p0433 A69-13386

Weapons propulsion system off-design engine performance, noting installation loss effects [SAE PAPER 680712]

03 p0496 A69-13445

Low and high power pi-mode Laddertron oscillator design operation and performance characteristics

03 p0405 A69-13726

Performance index sensitivity of nominally optimal controls noting initial and final target manifolds relationship to trajectory sensitivity

05 p0737 A69-15866

Telemetered data obtained by lantar I automatic ionospheric laboratory, detailing argon-ion plasma engine performance

05 p0830 A69-16056

Inlet velocity profiles distortion effects on flow regimes and performance in two dimensional diffusers with turbulent boundary layers [ASME PAPER 68-WA/FE-25]

05 p0698 A69-16100

Inlet conditions influence on two annular diffusers performance, using low speed tests [ASME PAPER 68-WA/FE-38]

05 p0698 A69-16110

Gas turbine exhaust silencer performance correlated in laboratory and in service [ASME PAPER 68-WA/GT-9]

05 p0812 A69-16144

Mini trend hookup copper wire insulation performance evaluation

05 p0730 A69-16242

Solid insulator performance in vacuum, analyzing breakdown factors

05 p0731 A69-16243

Gain degradation under applied voltage and injection current during low dose gamma irradiation by Co-60 source for bipolar transistors

06 p0977 A69-16880

Optimized radiative heat transfer systems performance, comparing tubular radiators with various fin geometries and systems with belt radiator

06 p1033 A69-17600

Weightless simulators effectiveness for obtaining space systems maintainability criteria, using nonparametric experimental design for performance data

06 p0882 A69-17648

Army engineering flight testing of OH-6A helicopter, presenting test program and results

06 p0867 A69-17659

SGN-10 inertial navigation system evaluation by Pan American World Airways

06 p0955 A69-17663

General aviation flight testing philosophy and origin

06 p1043 A69-17667

BO-105 helicopter design, testing and characteristics noting four bladed rigid rotor [AHS PAPER 200]

07 p1052 A69-18869

Laboratory measurement data of low light level TV performance converted to anticipated real world performance data

07 p1132 A69-18948

Bandwidth limited PCM/PSK/PM telemetry system performance analysis for developing S band telemetry, including coherent and noncoherent detectors

07 p1081 A69-19098

Nickel-cadmium and Ag-Cd storage batteries performance, discussing methods to lengthen battery life and improvement of characteristics

08 p1261 A69-21051

Optical design of Wolter type I glancing incidence X ray telescope for 6-100 A wavelength region, describing results of laboratory and rocket flight tests of prototype

08 p1318 A69-21087

Electron bombardment effects on performance characteristics of UV gratings

08 p1318 A69-21097

Experimental program for tests to identify primary electric propulsion system integration problems and solutions, emphasizing design and initial testing [AIAA PAPER 69-236]

09 p1560 A69-21213

Life test of high temperature /2400 K/ 10 millipound resistor thrusters, comparing results to theoretical predictions [AIAA PAPER 69-294]

09 p1563 A69-21232

Segmented anode, carbon dioxide-hydrogen performance and hollow cathode erosion tests on low power MPD arc thruster, noting current measurements [AIAA PAPER 69-242]

09 p1563 A69-21236

Research and development program in annular slit colloid thruster technology, proving thruster feasibility by performance tests [AIAA PAPER 69-287]

09 p1566 A69-21257

Reproducibility of thermionic converters performance, comparing volt-ampere characteristics with reservoir and collector temperature

09 p1437 A69-21813

Thermionic converters with chloride and fluoride vapor deposited tungsten emitters, comparing performance characteristics and stability

09 p1438 A69-21819

Turbine stator blade performance determination from total pressure surveys downstream of blade row, noting problems in pressure measurement
[ASME PAPER 69-GT-103]

09 p1432 A69-22521

Radial inflow gas turbine engine performance testing, discussing instrumentation, recording systems and calibration techniques
[ASME PAPER 69-GT-104]

09 p1501 A69-22522

Shock ignition procedure to keep pyrotechnic composition in optimum condition in space environment, describing test layouts and theory

10 p1749 A69-23007

Primary explosives tested for effects of shock, friction, heat and electrical discharges

10 p1750 A69-23010

Learned behavior performance failure in hypothermia as temperature dependent phenomenon using rat, guinea pig, chinchilla, mouse, gerbil and hamster

10 p1643 A69-23124

Simplified model of ignition tests with liquid propellant rocket engines under high vacuum conditions, giving possible parameter for evaluation of simulation of real conditions

10 p1754 A69-24022

Thermionic converter SD-4 design and performance tests covering emitter, collector and Cs reservoir temperatures and power efficiency

11 p1827 A69-25398

Large astronomical mirrors support and testing - Conference, Tucson, December 1966

12 p2055 A69-26406

Optical tests of Hale telescope mirror and support system at Palomar, noting various maladjustments and malfunctions

12 p2057 A69-26411

Isaac Newton telescope, describing support of 98 inch mirror, structure between fabricated cell steel surface and mirror and tests with air bag support

12 p2058 A69-26416

Ablation performances of asbestos phenolic and silica phenolic compared at higher stagnation pressures in wave-superheater hypersonic tunnel

12 p2119 A69-26814

Electrodeless plasmatron coupled with oscillator operating at 5-30 kHz, discussing parameters effect on operation mode and performance

12 p2140 A69-27123

American, French and Soviet medium weight helicopters tested in terms of main rotor blades construction, rotor performances and comparative power plant data

13 p2201 A69-27329

Litton LTN-51E inertial navigation system accuracy and reliability evaluated on basis of transpacific flights [SAE PAPER 680299]

13 p2296 A69-28103

Flame extinguishing potential of various substances for low pressure premixed and diffusion flames

13 p2380 A69-28460

Scientific satellite checkout system tests by manual, automatic and self test control

13 p2243 A69-28480

S-band telemetry capability of Easter Test Range, discussing relationship to Telemetry Rehabilitation Project, major system decisions and performance characteristics

14 p2410 A69-28878

Carrier disappearance method for FM telemetry transmitter characteristics measurements including frequency deviation sensitivity, linearity and frequency response

14 p2411 A69-28881

Thermionic converter performance measured using test vehicles with guard ringed collectors and variable emitter-collector spacing

14 p2398 A69-29177

Cylindrical geometry in-pile and out-of-pile thermionic converters long term life tests, including unfueled and fueled versions

14 p2399 A69-29197

X-22A VSTOL aircraft testing, discussing control sensitivity, dutch roll mode period and performance test planning based on characteristics prediction

14 p2392 A69-29699

Design and test criteria for dynamically loaded structures from various viewpoints, discussing statistical variations, load strength and limitations

15 p2618 A69-30368

Combustion performance evaluation program demonstrating high performance with space storable propellant combination of FLOX, methane and ethane [AIAA PAPER 69-507]

16 p2829 A69-31848

L-500 inlet development program, discussing external forebody design, entry lip and diffuser geometries, configuration and technology developments, experimental techniques and test equipment
[AIAA PAPER 69-448]

16 p2733 A69-32684

Brake system components automatic testing for pneumatic or hydraulic integrity essential to safe system performance

17 p2978 A69-33377

CX-84 two propeller tilt wing deflected slipstream V/STOL Military Evaluation Program related to support of surface forces
[AHS PAPER 351]

17 p2900 A69-33526

Aircraft carrier landing system performance, variations in pilot experience, aircraft types and environment, emphasizing night carrier recovery

17 p2916 A69-34012

Twin spool hydrogen turbopump performance at zero net positive suction pressure /NPSP/ saturated fluid in propellant tank, including steady state and simulated transient engine tests
[AIAA PAPER 69-550]

18 p3140 A69-34414

Calorimetric methods for battery and cells testing, discussing heat generation data correlation

18 p3093 A69-34780

V/STOL model small scale tests compared with full scale tunnel or flight tests, considering normal differences in parameters and rotor instability

18 p3119 A69-35227

Semiconductor optical quantum amplifiers in pulse mode operation, describing arrangement for studying performance including pulse duration and current controls

18 p3153 A69-35258

Integral fuel tank sealant based on various hydrofluorocarbon polymers prepared, tested and compared for physical properties

19 p3356 A69-35533

Epoxy molding compounds performance on DIP integrated circuits, determining comparative moisture protection provided by encapsulants

19 p3280 A69-35546

Exposure tests of corrosion resistant claddings for high strength Al alloys protection, finding higher purity alloy cladding superiority

19 p3322 A69-35571

Signature analysis diagnostic methods for reliability tests involving final product checkout and early fault detection

19 p3322 A69-35574

Optimized flight crew training, evaluating safety, flight simulator efficiency, takeoff/landing practice and line experience based on test results
[AIAA PAPER 69-771]

19 p3245 A69-35653

Li variation effects on solar cell properties indicating cell performance control by amount introduced near p-n junction

19 p3252 A69-35695

Apollo optics system ground and flight performance tests results, suggesting possible design changes for sunlit space environments

19 p3307 A69-35796

Man machine modeling technique for establishing personnel performance requirements, discussing field tests

19 p3261 A69-36025

Optimal ratio predetection combiner used with diversity signals and various modulations, showing significant improvement in telemetry systems performance

19 p3270 A69-36241

Cascade wind tunnels performance experiments, investigating effect of exit side walls lengths

19 p3241 A69-36753

Low noise microwave devices performance and price, discussing transistor and tunnel diode amplifiers, traveling wave tubes and price reductions via manufacturing methods

20 p3504 A69-36913

Aerodynamic performance tests of autorotative unpowered rotor entry vehicle model at various Mach numbers and angles of attack
[AIAA PAPER 68-950]

20 p3458 A69-37155

Technical and metrological characteristics of short base strain gages and bonding to specimen, investigating sensitivity and creep

20 p3544 A69-37817

Telemetered data obtained by Iantar 1 automatic ionospheric laboratory, detailing argon-ion plasma engine performance

20 p3618 A69-37966

Large aperture Al alloy telescope mirrors consisting of Tenzalloy Al coated with Ni alloy, presenting performance data

20 p3546 A69-38193

Guidance and navigation flight tests, demonstrating system performance improvements by onboard inertial system communicating with external navigation aid
[AIAA PAPER 69-842]

21 p3765 A69-39429

High density environment-resistant circular connectors, discussing design, applications, test and performance data compliance with MIL-C-81511 specifications

22 p3910 A69-39947

Space simulation facility assembly and operational testing

22 p3919 A69-39959

Kyoto University hypersonic gun tunnel equipment and performance data, discussing central control system, automatic operating system and double diaphragm device

22 p3927 A69-40587

Ceramic-sealed Ni-Cd secondary batteries space environmental behavior testing to determine heat dissipation during spaceborne operation

22 p3869 A69-40591

Cs contact ion engine with tubular W ionizer tested for performance and reliability in vacuum chamber

22 p4000 A69-40592

Solid rocket motor static firing tests in low pressure environment, presenting data concerning vacuum chamber pressure, diffusers pressure distribution, chamber wall temperature distribution, etc

22 p4000 A69-40593

Balloon flights for testing remote sensor systems prior to space flight, considering return beam vidicon and tracking telescope suitability for experimentation

22 p3865 A69-40806

Piston driven shock tube at Kyoto University with performance tests results, investigating compression processes, shock speed and flow duration time

22 p3928 A69-41046

Flight performance analysis of airline pilot group related to flight recording monitoring system

22 p3868 A69-41145

Pigeon accelerated performance patterns as function of contiguity of brief visual stimuli and food reinforcement, noting pattern absence during stimuli omission

23 p4081 A69-41436

Fixed-tuned telemetry receiver as miss distance indicator /MDI/ to provide information in missile performance program

23 p4138 A69-41781

Performance test of German MPD plasma rocket engine with augmented magnetic field and 5-10 kw output, describing integral measurement procedure and observed phenomena
[DGLR-69-024D]

23 p4202 A69-41927

Heat pipe system performance of GEOS 2 satellite, noting transponders temperature differences

23 p4224 A69-42082

Large reflector paraboloid antenna performance under environmental loads

23 p4231 A69-42132

Pyrotechnical gas generator performance tests during Europa 1 rocket second and third stage separation, including generator design, ground and flight tests

23 p4224 A69-42153

Photomultiplier tubes performance enhancement by light incidence on photocathode at oblique angles explained by reflection

23 p4191 A69-42194

Electromagnetic compatibility /EMC/ filter design and test methods to achieve effectiveness and reliability, emphasizing transfer impedance characteristics

23 p4142 A69-42233

Apollo Telescope Mount /ATM/ solar cell module electrical performance testing using sunlight simulation

23 p4072 A69-42286

High efficiency boost regulator design and tests for planetary spacecraft, considering input and output voltages

23 p4075 A69-42302

Two fluid heat pipe performance, measuring temperatures and condenser end vapor pressures for two thermal power input conditions

23 p4240 A69-42306

High power density spacecraft hydrogen/oxygen fuel cells with open cycle heat and product-water removal subsystems and reactant tankage

23 p4076 A69-42309

Causes of ascent failures in high altitude balloons, discussing test methods and specifications revisions

24 p4251 A69-42714

Performance curves of cylindrical water heat pipe for performance map, observing free hydrogen accumulation
[ASME PAPER 69-HT-15]

24 p4413 A69-43554

PERFUSION

U DIFFUSION

PERIDOTITE

- U ENSTATITE
- U OLIVINE
- U PYROXENES

PERIHELIONS

Technological requirements for solar probe with close perihelion, discussing solar approach and space environment problems

03 p0519 A69-12855

Visual and photographic comet observations, including perihelion passage of P/Perrine-Mrkos in 1968

07 p1216 A69-19205

Recently discovered comets including Comet Thomas, discussing magnitudes and perihelions

12 p2172 A69-27161

Comet Ikeya-Seki phenomena near perihelion interpreted from mean surface and ice nucleus internal layers temperatures

14 p2523 A69-29706

Comet Ikeya-Seki 1965f photometric investigation during perihelion, determining tail type according to Bredikhin classification

14 p2524 A69-29709

Solar probes design for 0.3 to 0.1 AU perihelion distance, considering thermal control, power supply, communications, altitude control and alternative configurations

17 p3050 A69-33797

Jupiter swingby flight mode application to probe missions requiring solar polar regions overflight at close perihelion distances

19 p3401 A69-35915

Daylight observations of Comet Ikeya-Seki 1965-f at perihelion passage, discussing resulting emission line spectra within comet head

23 p4221 A69-42386

Space mission opportunities selection from analysis of short period comet perihelia, discussing flyby and rendezvous mission payloads [AAS PAPER 69-320]

24 p4381 A69-42866

PERIOD EQUATIONS

- U PERIODIC FUNCTIONS

PERIODIC FUNCTIONS

- NT SINE SERIES
- NT TANGENTS
- NT TRIGONOMETRIC FUNCTIONS

Iterative process for determining periodic solutions of nonlinear nonautonomous periodic differential equations without weak nonlinearity hypothesis applied to nonlinear synchronization

02 p0271 A69-11550

Periodic cubic differential equation of motion solved with special reference to location of fixed points and stability of solutions

02 p0280 A69-11816

Inverse Laplace transform determination method for periodic functions applied to rectangular pulse train and rectified sine wave

02 p0271 A69-11983

Necessary and sufficient conditions for solution boundedness for Liénard equation with forcing function

02 p0272 A69-12132

Frequency of periodic solutions of autonomous nonlinear systems determined by method using Duffing approximation

02 p0348 A69-12612

Existence and stability of periodic waves in cold collisionless plasma in magnetic field

03 p0474 A69-13143

Asymptotic behavior of periodic solution of neutral type equation with small delay

03 p0455 A69-13258

Wagon rolling toward piston executing HF oscillations, discussing periodic solutions of equations of motion corresponding to piston phase at collision

04 p0630 A69-14893

Existence theorem for periodic solutions of parabolic boundary value problem for infinite space time cylinder

04 p0624 A69-15004

Periodic solutions for linear and weakly nonlinear heat conduction equations, obtaining omega-periodic solutions for initial boundary value problems

04 p0625 A69-15109

One to one mappings of Fourier series of analytic almost periodic functions and Dirichlet series, discussing satisfaction of functional equation

05 p0786 A69-15882

Explicit solubility of asymptotically periodic linear systems of differential equations

05 p0788 A69-16483

Maximum index of exponential growth of solution of linear Hamiltonian equation with periodic operator

coefficient encountered in dynamic stability of elastic systems

07 p1231 A69-18501

Basic frequencies of uniformly almost periodic solutions of differential equations extended, noting application to orbit closures decomposition of almost periodic continuous flows

07 p1174 A69-18733

Periodic asymptotically stable MHD motions, proving uniqueness and existence theorems

07 p1194 A69-19437

Periodic solutions of autonomous system oscillations with many degrees of freedom based on Poincaré method applied to Liapunov systems

07 p1183 A69-19680

Numerical analysis of periodic solutions of restricted three body problem in sun-Jupiter system, noting genealogy of periodic orbits

08 p1382 A69-19874

Analog study of periodic permanent magnet focusing, considering ray equation, beam radius dependence on distance, amplitude variations, etc

08 p1285 A69-20555

Probable spectrum stability criterion and reducibility derived for linear differential equation having recursion or almost periodic coefficients

10 p1720 A69-23562

Nonsymmetric periodic solutions of second order nonlinear differential equations

10 p1721 A69-23641

Periodic functions approximated by linear methods of Fourier series

11 p1908 A69-24697

Periodic solutions of quasi-linear self contained system with several degrees of freedom in case of commensurate frequencies, showing coordinates functions breakdown

11 p1920 A69-25749

Steady state solution of periodically excited circuit, constructing Green function for use in convolution integral

12 p2036 A69-25918

Resonance circuit application to harmonic analysis of periodic functions on analog computer, considering transient period and sequential order

12 p2123 A69-26718

Nonlinear hyperbolic partial differential equations with dissipation term for periodic solutions

12 p2124 A69-26929

Periodic solutions for small nutation angle of quasi-linear autonomous system of equations of motion of heavy solid body moving around fixed point

14 p2445 A69-28896

Electromagnetic scatter from perturbed continuous medium, expressing problem in terms of periodic functions instead of conventional power series

14 p2414 A69-29513

Asymptotically almost periodic solutions of almost autonomous differential equation

15 p2645 A69-31096

Periodic solutions of variational equations near equilibrium, obtaining one parameter expansion of family of long period orbits

16 p2854 A69-31654

Quasi-periodic solutions for canonical systems of differential equations in plane n-body problem

17 p3035 A69-33620

Wave scattering from nonplanar periodic structures using periodicity method, including Green function and Mellin transform

17 p2929 A69-33880

Celestial mechanics, Part 1, covering almost periodic functions, relation to classical astronomy and modern mathematics, implicit function theorem, three body problem, etc

18 p3199 A69-34928

Periodic solution of boundary value problem involving motion equation of viscous fluid

18 p3123 A69-35053

Asymptotic behavior of solution to parabolic equation for t approaching infinity, proposing asymptotic formula to Cauchy problem for heat conduction

18 p3231 A69-35310

One degree of freedom systems nonlinear oscillations differential equations periodic solutions by successive approximations, obtaining proof for convergence

18 p3174 A69-35311

Monograph on periodic solutions and locking-in regions for differential equations with switching points describing motion of self excited oscillatory physical structures

20 p3577 A69-37923

Dynamic stability of linear systems with periodic coefficients based on iterative formulas, evaluating transition matrix

21 p3685 A69-38779

Periodic solutions of differential equation as example of locking in of frequencies, developing mapping procedure for perturbation methods application

22 p3979 A69-39894

Criterion for class of differential equations ensuring absence of nontrivial periodic solutions

22 p3974 A69-39897

Extension of Liapunov systems to time lag systems with small periodic parameter

22 p3980 A69-40107

Nonlinear system oscillations analysis based on small parameter method and difference equations, including resonant case and stability criterion for periodic solutions

22 p3980 A69-40108

Controllability and linear closed-loop controls in linear periodic systems

22 p3917 A69-40572

PERIODIC ORBITS

- U ORBITS

PERIODIC OSCILLATIONS

- U OSCILLATIONS

PERIODIC PROCESSES

- U CYCLES

PERIODIC VARIATIONS

- NT ANNUAL VARIATIONS
- NT DIURNAL VARIATIONS

Quasi-periodic VLF emissions associated with geomagnetic micropulsation activity in terms of comparable periodicity

01 p0063 A69-10274

26-month periodicity in quiet day range of geomagnetic field horizontal force, noting similar periodicity in sunspot number and 16-month oscillation in both phenomena

01 p0063 A69-10427

13-day cycle variation in cosmic radiation intensity confirmed by Vercelli method, giving values of amplitudes and correlation coefficients among variations

01 p0145 A69-11031

Spectral peaks for torsional oscillations of earth, estimating free periods from observations at six stations around earth

02 p0243 A69-12007

Measurements of pulsars CP 0834, CP 0950, CP 1133 and CP 1919, discussing pulse intensities and shape, submillisecond structure, intensity variations, periods and positions

02 p0328 A69-12726

Radio star scintillation data, establishing periodic variations in rates within 1 to 1.5 years

03 p0505 A69-13081

Time variations of chromospheric network of bright points covering solar disk in spectrograms, noting contrast and interspaces variation with 11-year solar cycle

04 p0651 A69-14372

Pulsating stars, cepheids, RR Lyrae and W Virginis, excitation mechanisms, period-luminosity relation, oscillation modes, location on Hertzsprung-Russell diagram, etc

04 p0653 A69-14625

0.1 Hz intensity variation in bright homogeneous auroras prior to and during breakup observed visually and with image orthicon TV systems

04 p0594 A69-15129

Liquid flow systems dynamic response to periodic disturbances of system structural supports

05 p0747 A69-16073

Increasing periodicities in radio pulses from pulsars

05 p0825 A69-16352

Pulsar pulse period stability, noting slowing down in several sources

05 p0825 A69-16353

Solar radio emissions analysis using radio telescope measurements, observing quasi-periodic LF fluctuations caused by chromospheric processes

06 p1004 A69-17535

Period fluctuations in ionospheric plasma resonance amplitude, proposing hypothesis in terms of quasi-electrostatic surface waves guided by antenna wire

07 p1125 A69-18847

Universal instability theory relevance to pulsating optical auroras and fast quasi-periodic variations of auroral X ray fluxes

07 p1125 A69-18852

Periodic pulling mechanism for explaining transition to turbulence in bounded plasma with weakly unstable drift modes

07 p1194 A69-19400

Frequency distribution curves of spot groups according to area, confirming existence of stable stages in evolution of sunspots

08 p1379 A69-20612

Quasar 3C454.3 optical variations, noting photographic and photometric evidence for period of 340 days

08 p1397 A69-20701

Correlated microwave and energetic X ray emission from solar flare with 16-sec periodic pulsations, discussing energy during modulation peaks

09 p1574 A69-21457

Mean temperature values accuracy determined from fixed period values by frequency graphs, discussing deviations from mean

09 p1534 A69-21511

Diurnal nutation and periodic terms of local coordinates using OPL model of Danjon astrolabe, presenting harmonic and Fourier analysis

09 p1596 A69-22059

Laser oscillations, discussing oscillation frequency, oscillation time, noise and spectrum width, pumping and lasing materials, line broadening and giant pulse generation

09 p1517 A69-22119

Three color observations of 16 magnetic stars and photometric properties of 23 stars, discussing periodicities in variations

09 p1599 A69-22196

Cepheids variations used to measure intergalactic distances, noting method of calibrating absolute Cepheid luminosity

10 p1780 A69-23646

Charged particle motion in periodic electromagnetic field, constructing dynamic variables describing motion

11 p1927 A69-25100

Unforced periodically varying systems, developing approximate solutions with Floquet theory

11 p1909 A69-25289

Period changes by variable stars in M13, showing

Variable 2 period lengthening

12 p2154 A69-25814

Pulsar PSR 0833-45 period decrease and rate of change in period increased between 24 February-3 March 1969, discussing contraction explanation

12 p2154 A69-25878

Solar radio emission bursts periodicity relation to burst intensity

12 p2157 A69-26234

Draconic period changes of satellite 1965-11-D /Cosmos 54 rocket/ during visual observations with Interob

12 p2174 A69-26444

Frequent periodic variations existence in daytime ozone content associated with solar activity

12 p2070 A69-26693

Linear closed loop control systems with periodically varying parameters analyzed by harmonics method using Fourier transforms

12 p2054 A69-26720

UBV observations of stars P and 36 Cygni including short period variations and secular changes in brightness

12 p2172 A69-27159

Periodicity decrease on 24 February to 3 March 1969 in decay of Molonglo pulsar PSR 0833-45

12 p2172 A69-27167

Photoelectric observations of blue light minima of U Geminorum variable Ex Hydrae indicating no change in orbital period

13 p2338 A69-27558

Jupiter decametric radio emission periodicity attributed to undiscovered satellite in unstable orbit, discussing application to satellite discovery

13 p2343 A69-27622

Linear polarization measurements at 6 cm, determining rotation period associated with Jupiter cm radiation

13 p2343 A69-27623

Sufficient conditions for periodic motion existence of autonomous nonlinear feedback systems derived in terms of linear system frequency response

13 p2238 A69-27923

Radio star scintillation data, establishing periodic variations in rates within 1 to 1.5 years

14 p2515 A69-28763

Relay sampled data phase plane trajectories periodic motions increased with increase of system duty factor

14 p2425 A69-28898

Interplanetary sector structure during rising portion of 1966-1967 sunspot cycle, giving recurrence period of interplanetary field

14 p2517 A69-28957

Periodicity of magnetothermal oscillations in pressure annealed pyrolytic graphite compared with hole carriers

14 p2504 A69-29005

Finite difference method for motion stability of periodic bipolar vibrational systems, considering perturbations

14 p2534 A69-29039

Oscillations intervals with diminishing period observed during magnetic storms, noting relationship to midlatitude disturbances in F region

14 p2436 A69-29060

Galactic OH emission sources time variations found in W49 and W75

14 p2517 A69-29085

White dwarfs periods of radial oscillations, considering ion gas contribution to adiabatic coefficient computation

14 p2517 A69-29090

Semimonthly lunar variation in D region absorption, discussing phase reversal of lunar tides between equatorial and high latitudes

14 p2439 A69-29113

Lacerta OB 1 B spectroscopic binaries periods and orbital elements, noting limits for secular variation

14 p2519 A69-29137

Pulsar model used to explain stellar shape oscillations as cause of radio emission intensity periodic variations

14 p2522 A69-29675

Cosmic ray intensity underground measurements, discussing solar modulation processes, sidereal day variations and interplanetary magnetic field influence

15 p2673 A69-30013

Cosmic ray variation theory, presenting data on coupling of solar activity with large scale characteristics of solar wind during 11-year cycle

15 p2673 A69-30015

Low energy electron and proton precipitation, discussing acceleration mechanisms and periodicity in relation to auroras and airglows

15 p2594 A69-30018

Variability of period of RR Lyrae type stars in globular cluster M3, deriving seasonal moments of stellar maxima and light curve elements

15 p2683 A69-30511

Periodic radial heat flux in infinite cylinder with varying heat sources, assuming time variable heat exchange on surface

15 p2717 A69-30575

Zeeman spectroscopy and UVB photometry of 17 Com and kappa Cnc, observing periodic magnetic and light variations

15 p2692 A69-30774

Almost periodical oscillations of nonlinear systems containing quasi-cyclic coordinates

16 p2813 A69-32286

Photoelectric observations of W Ursae systems, including observed and computed times of minimum light and period change

16 p2863 A69-32399

Meteor trails radar observations to measure zonal wind profiles between 80-110 km, noting short period oscillations

16 p2865 A69-32609

Radial oscillation periods of Hamada-Salpeter white dwarf models graphically compared with models by Harrison-Wheeler Wakano equation of state

17 p3037 A69-33642

Physical nature of HZ 22 short period hot subdwarf binary, noting arguments against normal B type binary hypothesis

17 p3044 A69-34181

Variable CoD minus 35 degrees 4257 noting primary period of 502 days superimposed on secondary beat period of 3000 days

18 p3195 A69-34431

Periodic motions in single mass impact vibration system by point transformations method, noting complexity characteristics

18 p3172 A69-34565

Models for pulsars periodicity and period range due to nonradial gravity wave in almost adiabatic matter of degenerate neutron stars

18 p3196 A69-34645

Pulsar PSR 0833-45 period decrease resulting from mass addition leading to radius and inertia moment decreases

18 p3196 A69-34646

Microfluctuations frequency and wavelength of electromagnetic, electric and magnetic field distributions in plasma shock wave front found consistent with ion-acoustic origin hypothesis

18 p3180 A69-35017

Relationship between micropulsation periods and size of magnetosphere expressed in power law form and interpreted with wave propagation

18 p3131 A69-35193

Pulsars theoretical period distributions derived, considering period change of period dependence

18 p3201 A69-35203

Jupiter decametric radio source analysis suggesting two component model of rotation at both constant and variable rotational periods

18 p3202 A69-35212

Meteor burst communication channel parameters for low data rate telemetry, considering signal amplitudes, decay, duty cycle, multipath, phase stability, trail location and variations

19 p3271 A69-36250

Autonomous functional differential equations with finite time interval dependent derivatives, resulting in periodicity theorem applicable to difference equations

19 p3361 A69-36600

Diurnal, seasonal and spatial variations in height and occurrence frequency of low electron density region below 3000 km

20 p3532 A69-37899

Periodicities in solar activity variation from correlation spectral analysis, establishing monotonically decreasing component and secular variations in activity

20 p3607 A69-38045

Twenty year wave in diurnal anisotropy component of galactic cosmic rays arriving at earth from asymptotic direction east of sun interpreted as magnetic reconnection

20 p3592 A69-38098

Near resonant and nonresonant solutions of nonlinear equation describing rotating pendulum motion under periodic disturbance

21 p3771 A69-39004

Periodic motions of mechanical oscillators with velocity discontinuities analyzed by differential equations

21 p3771 A69-39009

Convective cells and periodic variations in vertical gradient of electroatmospheric field

22 p3934 A69-39939

Dynamic systems stability with two degrees of freedom, determining second order time dependent integrals valid near periodic orbit

22 p4013 A69-40123

Periodic orbits obtained for special restricted three body problem in resonance using numerical integration

22 p4031 A69-40909

Lunar semimonthly variations in noon values of D region absorption at Singapore, noting opposite phases of lunar tides in D and F regions

22 p4035 A69-41211

Cosmic ray anisotropy direction during periodic intervals determination, noting application to event of December 1957

23 p4204 A69-41482

Relativistic Doppler shift effect observed from radio signal periodic variation of GEOS-1 satellite

23 p4126 A69-42389

Meter and decimeter wavelength range short period fading under conditions excluding optical sights, correlating specular and diffuse reflection

24 p4281 A69-42612

Jupiter Red Spot semiregular oscillations from photographic measurements, determining mean period and amplitude

24 p4383 A69-43002

PERIODICITY

U PERIODIC VARIATIONS

PERIODICITY [BIOLOGY]

U RHYTHM [BIOLOGY]

PERIPHERAL CIRCULATION

Circadian variations in human temperature regulation, measuring peripheral and rectal temperatures and peripheral heat and arterial blood flows in clothed resting males

22 p3872 A69-40201

Mathematical formulation for relative values of cardiac output and peripheral resistance as two contributing factors to arterial pressure change

23 p4085 A69-41473

Venous tone, peripheral venous pressure, skin and muscle blood flow, alterations of heart rate and respiration in men during leg exercise

23 p4096 A69-42090

Blood flow, volume and venous pressure measurements in right hand at low and high altitudes in residents and newcomers

23 p4098 A69-42106

Cardiopulmonary bypass developed for studies of long term weightlessness on cardiovascular system of mice, white rats and squirrel monkeys
24 p4278 A69-43394

PERIPHERAL JET FLOW

Fixed point support properties of quasi-vertical peripheral jet hovercraft with two pressure stages
06 p0857 A69-16820

Thin wall flow of circular jets in bounded transverse flow, showing hydrodynamical parameter of mixture effect on jets dimensionless path
10 p1679 A69-23567

Nuclear powered surface effects machine performance estimates, calculating reactor power and payload fraction for various clearance heights, gross weights and velocities
18 p3171 A69-35180

PERIPHERAL NERVOUS SYSTEM

Histological and histochemical studies of dephosphorylating enzyme distribution in muscle spindle capsule of guinea pig thigh muscles and cat calf muscles
15 p2554 A69-30406

Cerebral subcortical structures controlling effect on central and peripheral nervous systems, discussing motion coordination, space orientation, search reflexes and physiological sleep
22 p3889 A69-41275

PERIPHERIES

U BOUNDARIES

PERMALLOYS [TRADEMARK]

Isochronic annealing effect on coercive force of Mo Permalloy samples bombarded with neutrons in nuclear reactor
05 p0783 A69-16815

Electrodeposition of Te-containing Permalloy films with uniaxial magnetic anisotropy, noting electrolyte composition and film structure
11 p1935 A69-24332

Neutron irradiation and temperature effects on ferrite and Permalloy memory cores hysteresis loops
12 p2142 A69-26259

Dynamic Kerr observations of high speed flux reversal and relaxation process in permalloy thin films by magnetooptical camera with Q switched ruby laser
19 p3383 A69-36446

Bloch wall motion along hard direction of Permalloy films due to fast rising hard-axis pulses
20 p3584 A69-38191

Transformer for unilateral energy transfer using single domain uniaxial Permalloy film
21 p3684 A69-39454

PERMEABILITY

NT DIELECTRIC PERMEABILITY

Rarefied molecular gas flow past permeable surface, determining reflection law and flow parameters
20 p3459 A69-37438

Pumping pore size and permeability of wicks as part of heat pipes design
23 p4074 A69-42298

Wick capillary pressure, permeability and burnout heat flux measurements to provide data for heat pipe design
[ASME PAPER 69-HT-18] 24 p4412 A69-43548

PERMEATING

Gel permeation chromatography of nominally linear aliphatic polyesters, using tetrahydrofuran solvent at 37 degrees C
21 p3670 A69-39806

PERMUTATIONS

Fast Fourier Transform connection with circulant and permutation matrices for case with discrete time sample number equal to discrete frequency samples
23 p4182 A69-41761

PEROVSKITES

High pressure synthesis of dense ferrimagnetic perovskite allotropic form of yttrium-iron garnet
08 p1372 A69-20372

Spontaneous polarization onset in perovskite ferroelectrics, analyzing influence of Curie point, Jahn-Teller effect and atomic structure
22 p3995 A69-41159

PEROXIDES

NT HYDROGEN PEROXIDE

Perhydroxyl radical electron spin resonance spectrum in solution of hydrogen peroxide and water at 77 K, noting g factor, hyperfine splitting and molecular structure
01 p0024 A69-10683

Photolysis of t-butyl iodide at low temperatures as source of t-butyl peroxy radicals for synthesis of peroxides
07 p1073 A69-18375

Pseudosplitting/peroxide mechanism for O reduction at fuel cell cathodes, analyzing O molecule adsorption, H bonding and electron transfer at surface
16 p2748 A69-32809

PERSEID METEORIDS

Radar and photographic studies of meteors from Leonid and Perseid showers, presenting velocities, luminescence and ionization
10 p1783 A69-23895

Visual and photographic observations of Perseids meteor trails velocity noting discrepancy
13 p2353 A69-28035

Lyrid and Perseid meteor spectra for spectral line identifications in 3100-4000 A UV range, listing lines from six neutral atoms and five ions
15 p2700 A69-31500

PERSONALITY

Personality factors and job performance ratings relationship in radar controllers, computing Pearson correlation matrix based on age, education, motivational distortion, etc
21 p3665 A69-39169

PERSONALITY TESTS

External observer effect on human behavior during sensory deprivation tests conducted in isolation chambers as factor in estimating personality
02 p0200 A69-11516

Psychiatric study of master attack carrier aviators inability to fly, considering adult situational reaction diagnosis
03 p0369 A69-12883

Characteristics of accident experienced pilots based on personality and psychological tests
06 p0876 A69-18033

Military flying career choice as neurotic compensation for personality defects, stressing personality screening during interview
12 p2023 A69-26492

Personality characteristics of jet pilots measured by Edwards Personal Preference Schedule, including percentile norms table
14 p2408 A69-29294

Pilot selection procedure emphasizing integration of all-around personality picture from different approaches
24 p4278 A69-43395

PERSONNEL

NT AIRCRAFT PILOTS
NT ASTRONAUTS
NT COSMONAUTS
NT FLIGHT CREWS
NT FLIGHT SURGEONS
NT FLYING PERSONNEL
NT GROUND CREWS
NT INSTRUCTORS
NT MEDICAL PERSONNEL
NT OPERATORS [PERSONNEL]
NT PHYSICIANS
NT PILOTS [PERSONNEL]
NT PROGRAMMERS
NT QUALIFICATIONS
NT SCIENTISTS
NT SPACECREWS
NT TEST PILOTS

Industrial loyalty and trade secrets, discussing preservation of forms of intellectual property posed by mobile employee and management policies
01 p0180 A69-10991

Organizational identification of scientists as professional employees, exploring degree of loyalty and perceived self prestige
21 p3855 A69-38765

PERSONNEL DEVELOPMENT

Complex piloting simulation including fatigue for optimizing man machine synergy, emphasizing human adaptability and computer precision and speed
12 p2025 A69-27083

Reliability management simulation exercise training technique for government personnel, discussing decision making in development, production, testing and field usage of systems
18 p3117 A69-34487

Civil aviation center for R and D in aviation personnel education and training
[AIAA PAPER 69-785] 19 p3453 A69-35597

Air and space research at Goettingen Aerodynamic Testing Institute
19 p3295 A69-36684

Automated programmed instruction /API/ for training backup interceptor control personnel to conduct air defense operations
[AIAA PAPER 69-956] 22 p3905 A69-40338

PERSONNEL SELECTION

NT PILOT SELECTION

Human factors in aircraft systems, discussing personnel selection throughout design and manufacturing phases
01 p0019 A69-10449

Long range management forecasting by Delphi technique, describing expert panel selection, composite group replies and successive revisions
01 p0180 A69-11250

Essential hypertension in selection and evaluation of airline pilots, discussing use of thiazide therapy
06 p0875 A69-17850

Systolic murmurs and flight personnel evaluation, noting phonocardiographic definition and tracings of specific systolic murmurs
09 p1445 A69-2272

Value engineering application to engineer recruiting phase of industrial relations
13 p2382 A69-28090

Behavioral differences between engineers and scientists with reference to work environment
15 p2721 A69-31073

Vestibular function tested with angular acceleration, applying semicircular canal reflexes for flight crew selection and appraisal
20 p3481 A69-37271

Vestibulometric tests for flight surgeon appraisal of applicants in flying profession, comparing Coriolis forces cumulative load tests with conventional tests
20 p3481 A69-37278

Human factors methods importance in nonmilitary flight simulation training, discussing cost factors and skills evaluation
22 p3894 A69-41138

Retarded voice tests apparatus using graphical recording to determine intensity of deformations by autoaudition, considering application to recruitment investigation
24 p4270 A69-42604

Personnel training and selection systems, applying information processing models to diagnostic testing in job classification for performance improvement
24 p4274 A69-43020

PERSONNEL SUBSYSTEMS

Isolation of scientific and technical personnel and effect on lateral communication and intellectual cross fertilization in research and development program
11 p2004 A69-25303

Algorithm minimizing personnel number and training costs to meet uncertain skill requirements, applying to army aviation contingency force training composition
[AAS PAPER 69-116] 24 p4271 A69-42818

PERSPIRATION

Insensible water loss from human skin as function of ambient vapor concentration using IR gas analysis, applying results to water loss model revision
23 p4077 A69-41293

Human sweat glands reflex responses to diverse skin cooling rates in hot room, discussing bath temperature step decrease effect on lower limb
23 p4082 A69-41446

PERT

Survival of PERT/Cost technique without government impetus noting advantages for planning, monitoring and controlling technical performance objectives
01 p0180 A69-1125

ESRO 1 project management and organization, discussing cost control, time saving, program evaluation and review system /PERT/, etc
13 p2382 A69-27750

PERTURBATION

NT ORBIT PERTURBATION

NT SATELLITE PERTURBATION

Lifting rotor blades flapping response to atmospheric turbulence, discussing time averaging and perturbation schemes
[AIAA PAPER 69-206] 07 p1057 A69-19577

Motion stability over finite interval of time for perturbed mechanical systems
09 p1539 A69-21881

Singular perturbations for Cauchy and boundary value problems, considering differential operators and Hilbert space
10 p1720 A69-23635

Turbulence formation in conducting liquid at increasing Reynolds numbers, discussing cause of spontaneous magnetic field appearance
11 p1955 A69-24392

Sound generation by unsteady rotational flow as singular perturbation problem solved by matched asymptotic expansions, discussing flow and radiation fields
13 p2299 A69-28187

Wall flows and wake laws validity analyzed by wall balance technique, considering boundary layers under perturbation and core flow restrictions
13 p2251 A69-28633

Collisionless stability of relativistic, spherically symmetric star clusters against radial perturbations, considering one dimensional sufficient criteria
15 p2691 A69-30765

Monograph on dynamic behavior of jet engines especially during perturbations based on linear theory
15 p2671 A69-30931

Attenuation of small perturbations in shape of plane shock wave propagating into uniform medium in presence of rigid or interfacial boundaries
15 p2592 A69-31145

Microwave holograms generated by spinning dipole field perturbation technique, showing zone plates and moire fringe resolution
19 p3315 A69-36824

Thermal neutron flux perturbations in cylinders in test reactors, using regression analysis to obtain polynomials for flux perturbation, depression, self shielding factors, etc
20 p3575 A69-38274

Turbulence formation in conducting liquid at increasing Reynolds numbers, discussing cause of spontaneous magnetic field appearance
24 p4390 A69-43782

PERTURBATION THEORY

Optical pulse generator consisting of solid state laser with saturable absorber at cavity end using perturbation theory and Maxwell equations
01 p0089 A69-10179

Exact solution for coupling effects between two waves with complex coupling function, defining region of validity for earlier perturbation theory
01 p0027 A69-10252

Ground state energies of HeH divalent ion, comparing perturbation calculation values with variation-perturbation technique
01 p0123 A69-10547

Cost prediction equations used in perturbed environment of learning curves subjected to design change in industry
01 p0180 A69-10652

Figures of merit for polycrystalline uniaxial antiferromagnetic materials, for nonreciprocal devices at millimeter and submillimeter wavelengths, calculated from perturbation theory
[IEEE PAPER 17.11] 01 p0045 A69-10720

Matrix technique for transformation of equation of motion into first order equation in analyzing perturbation forces producing mechanical oscillations
01 p0170 A69-10827

Perturbations on major axes of slow moving comets in nearly parabolic original orbits by fast moving stars, discussing statistics of stellar encounters
01 p0153 A69-10871

Linearized perturbation treatment developed for photochemical and dynamical effects in gravity wave production of E-region ionospheric irregularities, including ion convergence
01 p0073 A69-11175

Secular perturbations produced by comet belt beyond Neptune on orbits of periodic comets of large aphelion
01 p0158 A69-11327

Singular perturbation method for reducing order of mathematical models in optimal sensitivity control problems
02 p0224 A69-11967

Alfven wave propagation in nonhomogeneous systems for relativistic MHD, discussing magnetic and velocity perturbations
02 p0290 A69-12254

Comparison of trajectories in optimum linear perturbation guidance
02 p0279 A69-12546

Equations of motion for arbitrary first order perturbations around any spherically symmetric metric
02 p0328 A69-12730

Nonlinear weak shock wave diffraction around convex angled corners in polytropic inviscid thermally nonconducting gas
03 p0412 A69-12848

Transport phenomena in crossed electric and strong magnetic fields, developing semiclassical and quantum treatments
03 p0473 A69-12926

Saturn ring gravitational field perturbations of space vehicle orbit on flyby mission solved by particle motion perturbation theory
03 p0508 A69-13260

Second order frequency dependent polarizabilities calculated by double perturbation theory
03 p0472 A69-13314

Double perturbation theory, deriving interchange theorem for polarizabilities at complex valued frequencies and formulation without assumption of existence of unperturbed Hamiltonian
03 p0472 A69-13315

Symmetric baroclinic instability role in Jupiter equatorial acceleration
03 p0508 A69-13347

Hansen planetary theory basic function, discussing perturbations expansion into trigonometric series
03 p0514 A69-13781

Unperturbed tube flow theory extended to flow through short axisymmetric tube
03 p0419 A69-13969

Upper bound for free energy of nonlocal superconductor in magnetic field, using variational method and perturbation theory
03 p0491 A69-13971

Satellite nonlinear spatial oscillations about center of mass during circular orbit, using perturbation theory and analog computer
04 p0665 A69-14270

Matrix perturbation method for hyperstatic structure modification by combining original solution elements with data on modification
04 p0668 A69-14380

Book on qualitative theory of sampled data systems
04 p0630 A69-14563

Two dimensional turbulent jet in uniform parallel stream, developing coordinate type perturbation expansion and applying series truncation method to predict downstream development
04 p0588 A69-14713

Perturbation method determination of gravitational induction for quasi-static axisymmetric systems
04 p0661 A69-15190

Laminar mixing of two semiinfinite parallel streams, deriving equations and boundary conditions by applying perturbation technique
05 p0744 A69-15714

Stationary solutions of Vlasov equation with external electric fields and BGK collision terms, using perturbation theory in moving frame
05 p0801 A69-15745

Asymptotic expansion of solution to linear singular perturbation problem of elliptic type in bounded strictly convex domain
05 p0786 A69-15928

Regularization of perturbed Keplerian motion in three dimensional space by means of Levi-Civita transformation generalized to three dimensions
05 p0827 A69-16602

Atomic Li photoionization cross sections calculated with Brueckner-Goldstone many body perturbation theory
06 p0961 A69-17134

Spectral line shapes broadened by electron impacts, taking into account contribution of radiation produced by perturbing electrons
06 p0961 A69-17136

Linear equations for three dimensional perturbations in boundary layer of viscous incompressible fluid flow on plane surface, discussing Tollmein-Schlichting waves
06 p0909 A69-17329

Spacecraft optimum low thrust trajectory analyzed by Hamilton-Jacobi perturbation theory, obtaining canonic constants of motion
06 p1007 A69-17574

Unperturbed Hamiltonian transformation applied to existing perturbation theories for exchange forces between atoms to obtain correct long range behavior
07 p1184 A69-18288

Linear differential system with boundary conditions, obtaining equivalent Fredholm integral equation and perturbation theorem
07 p1173 A69-18729

Perturbation methods for exchange and Coulomb energy of hydrogen molecule, calculating Hamiltonian by wave function
07 p1186 A69-19446

Numerical method for three dimensional boundary layer equations, applying perturbation technique and independence principle to rotating flat blade
[AIAA PAPER 69-227] 07 p1051 A69-19560

Positive column in longitudinal magnetic field in helium and neon, noting agreement with collision diffusion theory and Kadomtsev perturbation theory
08 p1361 A69-20212

Perturbation method in rectangular coordinates based on motions of Galilean satellites of Jupiter applied to nearly circular orbits of quasi-resonant systems
08 p1390 A69-20275

Stability and perturbation theory of abstract Cauchy problem with difference scheme, showing application to parabolic differential equations
08 p1343 A69-20537

Singular perturbation problem for elliptic linear partial differential equation, studying asymptotic expansion of solution in vicinity of singular points in nonconvex domain
08 p1352 A69-20751

Linear perturbation theory to predict instability threshold conditions caused by electric field in poorly conducting liquid subject to vertical temperature gradient
08 p1352 A69-20790

Perturbation theory for branching analysis of perfect and imperfect discrete conservative structural systems
08 p1417 A69-20822

Doppler effect in ionospheric acoustic perturbations caused by strong ground explosion, noting accord with nonlinear acoustic wave propagation theory
09 p1488 A69-21694

Perturbation theory for analyzing nonlinear boundary value problems
09 p1540 A69-21894

Uniformly rotating star models within first order perturbation theory in convective equilibrium and with radiation pressure, discussing radiative and gas pressure ratio
09 p1606 A69-22422

Analytical method for perturbations by spherical and cylindrical shock waves flowing toward common center
10 p1677 A69-22899

Subsonic channel flow of frictionless barotropic gas through oscillating grid, investigating perturbation velocity field and aerodynamic forces on airfoils
10 p1631 A69-22905

MHD first order partial differential equations used to investigate wave front between perturbed and unperturbed flow regions in magnetosonic propagation through homogeneous medium
10 p1727 A69-23090

Self consistent perturbation procedure for stationary homogeneous turbulence of incompressible fluid
10 p1680 A69-23648

Diakoptics applied in combination with perturbation method to determine natural frequencies of turbine buckets coupled by tie wires and/or cover
[ASME PAPER 69-VIBR-57] 10 p1804 A69-24151

Transport coefficients for almost Lorentzian mixture, computed as perturbation to coefficients for true Lorentzian mixture, compared to Chapman-Enskog method results
11 p1997 A69-24286

Perturbation theory applied to emitting density matrix in nonlinear polarization of resonance media, considering gas laser in coaxial magnetic field
11 p1895 A69-24630

B, L coordinates for mapping geomagnetically trapped particles distribution computed by perturbation method, using perfect dipole as zero order approximation
11 p1949 A69-24861

Perturbations of Volterra integral equation with vectors in n-dimensional real or complex Euclidean space, comparing solution with linear system solution
11 p1909 A69-24886

Boussinesq approximation for compressible fluids, discussing perturbation pressure and velocities and vertical scale motions
12 p2061 A69-26013

Perturbation theory of nonlinear control systems with periodic coefficients and small perturbation terms, exemplifying satellite attitude control
12 p2173 A69-26067

General perturbation theory for branching analysis of discrete structural systems, considering elastic post-buckling
12 p2179 A69-26213

Quasi-stochastic nonlinear one dimensional oscillations in periodically disturbed field applied to celestial mechanics of planetoids
12 p2130 A69-26373

Perturbation analysis in dielectric loaded rectangular waveguides, considering scattered modes and phase progression
12 p2039 A69-26381

London-van der Waals interaction energy of symmetric molecular pair calculated in perturbation theory

second order as infinite series in negative powers of separation
12 p2131 A69-26606

Gravity perturbations in Earth external field, treating anomalous potential using Green integral formula and spherical harmonics
12 p2077 A69-27139

Perturbation theory of antiplane elastoplastic deformations based on plasticity theory, considering circular hole in body under uniform shear
13 p2359 A69-27263

Rayleigh-Taylor instabilities in two fluid hydraulic model, noting perturbation direction and Lorentz forces effects on instabilities growth time
13 p2310 A69-28033

Perturbation method for nonlinear panel flutter at high Mach numbers, using von Karman large deflection plate theory and quasi-steady aerodynamic theory
13 p2364 A69-28204

Atmospheric ozone vertical distribution and total amount determined by radiative transfer and perturbation theory, presenting error analysis
13 p2255 A69-28493

Autonomous and nonautonomous transient processes in conservative and nonconservative nonlinear systems, deriving equations describing perturbations under loads, solving by asymptotic method
13 p2300 A69-28529

Secular instability of steadily rotating stars, analyzing meridional motions in radiation zones by linear perturbation theory
13 p2354 A69-28566

Weakly divergent intense light beam propagation in laminar optically inhomogeneous medium with self focusing possibility analyzed by perturbation theory
13 p2223 A69-28568

Galactic formation in Lemaitre universe from statistically probable density fluctuations, using perturbation theory and Newtonian cosmology
14 p2520 A69-29373

Eigenvalues of finite matrix Hamiltonian, considering convergence radius of perturbation series, limits and renormalization
14 p2470 A69-29451

Phase screen technique for deriving statistical characterizations of perturbations imposed on wave propagating through random medium applied to remote probing
14 p2414 A69-29511

Perturbed molecular distribution in translational and internal degrees of freedom in dilute chemically reacting gases with low ion concentrations
14 p2410 A69-29988

Density perturbation mode in Lifshitz relativistic theory for expanding universe gravitational instability, adopting Lagrangian coordinate condition to eliminate physically meaningless solution
15 p2652 A69-30203

Perturbation analysis for error estimates in algebraic eigenvalues and eigenvectors problems for solving skewed membrane vibrations
15 p2703 A69-30211

Plane planetary orbits construction extended to nearly circular and quasi-plane orbits by generalizing perturbations method to problems in space
15 p2690 A69-30622

Plane incompressible fluid interface stability in presence of transverse electric field, deriving equation of motion for perturbation amplitude
15 p2652 A69-30911

Perturbation formula for frequencies as function of Poisson coefficient, considering vibration modes of elastic body subject to boundary conditions
15 p2713 A69-31097

Asymptotic Liapunov stability of perturbed solutions to weakly coupled multifrequency systems
15 p2654 A69-31258

Vlasov-Poisson equations reformulation by arbitrary transformation to velocity variable, considering time or space secularity of perturbation theory
16 p2817 A69-31642

Particle-wave interaction in weak turbulent plasma in presence of uniform magnetic field, applying perturbation theory arbitrary order
16 p2819 A69-31683

Perturbation theory for nonlinear oscillations in ionized plasma, treating electron-neutral collisions effect by Boltzmann-Vlasov equation relaxation term, noting distribution function
16 p2820 A69-31702

Eigenvalues for class of nonself adjoint differential equations system treated as small perturbation of norm epsilon, assuming perturbation expansion
16 p2812 A69-31811

Perturbation solutions for planar cylindrical and spherical blast waves in air, considering third and fourth order approximations
16 p2770 A69-31900

Hansen method of partial anomalies for cometary orbits applied to comet Encke perturbed by earth and compared with perturbations by numerical integration
16 p2863 A69-32400

Weak nonlinear hydromagnetic waves in cold collisionless plasma, using nonlinear perturbation method
17 p3010 A69-32866

Monograph on interaction between flow and sound fields as singular perturbation problem, using matched asymptotic expansion
17 p2949 A69-32998

Star motion perturbations by invisible body, stressing bright bodies invisible by position near perturbed star
17 p3034 A69-33407

Wave propagation in two dimensional anisotropic media with several perturbation speeds, using Lundquist linear equations ensuring lacunas presence
17 p2925 A69-33841

Perturbation procedures applied to energy computation for ground and first excited state of hydrogen molecule at large separation
17 p3009 A69-34170

Wave propagation in gas particle flow, obtaining fourth order particle differential equation from perturbation theory
18 p3121 A69-34772

Electromagnetic wave scattering and depolarization by horizontally weakly inhomogeneous medium, using small perturbation method
18 p3101 A69-34788

Plane light wave propagation in homogeneous isotropic medium with fluctuating dielectric constant using perturbation theory and integrating energy conservation law
18 p3173 A69-35127

Fluctuations evolution in density perturbations analyzed to obtain free fall and free expansion universe models, showing no difference between expanding and static Newtonian universes
18 p3203 A69-35347

Bogoliubov averaging method of perturbation in wave mechanics for radiation and matter interaction, considering monochromatic and broad spectral incident wave for resonance study
18 p3175 A69-35483

Polynomial approximations in perturbational navigation and guidance schemes including Chebyshev and least square approximations
19 p3368 A69-35664

Perturbation technique application to stability criterion for rectilinear missile flight with arbitrary inclination, noting mass reduction and flow and gravity effect
19 p3429 A69-35779

Single junction vacuum thermocouple measuring thermal beam effect with reference to velocity distribution perturbation in molecular beam scattering
19 p3376 A69-36173

Coordinate perturbation and second order solution for early collapse phases of cylindrical or spherical detonation wave in equimolar acetylene-oxygen mixture
19 p3449 A69-36354

Clamped uniformly loaded rectangular plate large deflection elastic behavior approximate analysis, using perturbation method
20 p3620 A69-36998

Trajectory optimization of space vehicle with continuous thrust based on regularized equations, comparing perturbation method for earth-Jupiter rendezvous transfer
20 p3595 A69-37173

Perturbation matrix derivation in rectangular coordinates using Sitarsky two body variational equation for all motions
20 p3568 A69-37200

Trigonometric polynomials representing perturbation function and derivatives in three body problem
20 p3596 A69-37315

Hill method applied to motion theory for minor planet 11 Parthenope using computerized first order perturbations from principal planets
20 p3596 A69-37316

Singular perturbations and boundary layer theory for approximating solutions to simple ordinary differential equations
20 p3515 A69-37583

Perturbed motion of solid body containing axisymmetric cavities partially filled with ideal incompressible

fluid, solving boundary value problems of fluid oscillations
20 p3518 A69-38296

Gaseous rotating stars radial oscillations by perturbation method, considering angular velocity effects
21 p3795 A69-38470

Perturbation solution in power and asymptotic series for initial collapse phases of impulsively generated converging cylindrical and spherical shock waves in perfect gas
21 p3692 A69-38688

Nonlinear electromagnetic wave propagation by perturbation method previously employed to treat nonlinear boundary value problems involving partial differential equations
21 p3677 A69-39465

Impulsive velocity correction determination method for precise stationkeeping of stationary satellite, discussing perturbations
21 p3817 A69-39757

Periodic solutions of differential equation as example of locking in of frequencies, developing mapping procedure for perturbation methods application
22 p3979 A69-39894

Thermal perturbation propagation in nonlinear medium, considering thermal relaxation effects
22 p4051 A69-40712

Stueckelberg formulation for transition probabilities to interpret perturbation effects in elastic scattering differential cross section measurements
22 p3987 A69-41005

Magnetospheric natural toroidal oscillation periods solved by expression from perturbation method given by Landau and Lifshits where WKB method inapplicable
23 p4157 A69-41863

Linear diffraction equations in electronics in self consistent formulation reduced to complex transcendental equations, using perturbation method
23 p4124 A69-42033

Perturbation velocity potential of unsteady potential flow of barotropic gas past cascade of thin blades oscillating harmonically
24 p4244 A69-42716

Free convection from vertical surface using perturbation method
24 p4407 A69-42916

Mechanical model for dynamic buckling of elastic imperfection-sensitive structures under step loading, using perturbation method
24 p4405 A69-43656

Rotational microwave spectrum of 2-methylfuran, using fourth order perturbation method for internal rotation A-E doublet splittings
24 p4280 A69-43811

Many body perturbation theory with time dependent perturbations applied to frequency dependent polarizability of atomic oxygen
24 p4354 A69-43816

PERVEANCE

Convergent high-perveance electron gun design for use in microwave tubes, reducing anode aperture effect on current density
07 p1101 A69-18658

Space harmonics effect on helical TWT design, discussing operating voltage, beam radius, perveance and maximum allowable gain
07 p1105 A69-18950

PETN

Slowly exploding wires for igniting self sustaining deflagrations in PETN, RDX, HMX and tetryl, comparing circuit parameters for detonation initiation
01 p0141 A69-10678

Capacitance-voltage relationships for PETN initiation by various diameter gold exploding bridgewires, noting optimum capacitance dependence on energy transfer efficiency
01 p0141 A69-10679

PETROGRAPHY

Meteoritic extraterrestrial materials sampling for chemical, petrographic and metallurgical analyses, discussing microstructure and optimum specimen weight for representative analysis
01 p0150 A69-10480

Subsolidus equilibrium study in potassium tantalate K niobate system for dry and hydrothermal runs, using X ray powder diffraction and petrography
08 p1332 A69-20373

Chemical analysis and paragenesis of manganese ilmenite from Sierran adamellite using electron microprobe
19 p3302 A69-35977

Terrestrial planets high temperature evolution from solar system genesis theory, discussing meteorite chemical composition, petrography, mineralogy and age determination
19 p3407 A69-36079

Sharps chondrite chemical, petrographic and mineralogical studies suggesting formation from complex and repetitious high temperature events and agglomeration processes
19 p3408 A69-36086

Carbonaceous meteorites specimen petrographic observations, noting genetic interrelations with urelites regarding S-C and reduced Fe oxidized Fe ratios
19 p3413 A69-36112

Early Precambrian Onverwacht microstructures studied in petrographic thin sections and powdered preparations for possibility of oldest terrestrial fossils
24 p4263 A69-43221

PETROLEUM
U CRUDE OIL

PETROLOGY
NT PETROGRAPHY

Oxygen partial pressure, temperature and olivine composition related, determining distribution coefficient of Fe and Mg between olivine and pyroxene
03 p0516 A69-14082

Indium abundances in chondritic and achondritic meteorites and terrestrial rocks determined by radiochemical neutron activation analysis
08 p1404 A69-20917

C3 and C4 carbonaceous chondrites origin, evolution and classification based on mineralogic and petrologic data
19 p3413 A69-36109

Petrology, mineralogy and phase composition of Siena chondrite, interpreting meteorite as ignimbritic rock or welded tuff
20 p3602 A69-37534

Petrology of Czechoslovak moldavites, tabulating properties, mapping locations and distribution
23 p4210 A69-41350

Thermal conductivities /K/ of rock forming minerals reveals K as linear function of density for constant mean atomic weight
24 p4310 A69-43216

PFM [MODULATION]
U PULSE FREQUENCY MODULATION

PH

Nickel maraging steel polarization behavior in acidic solutions, noting corrosion potential dependence on pH
13 p2282 A69-28188

Fluorescence properties of nucleotides, polynucleotides and phosphorylated derivatives as function of temperature, pH and ionic strength
22 p3898 A69-41078

Hyperventilation induced hemolysis in dogs measured as function of exposure time, body temperature and blood pH
22 p3887 A69-41192

Severe heat stress effects on respiratory frequency, rectal temperature, blood gases and pH of conscious dog
23 p4081 A69-41432

EEG, ocular movements, gastric mobility and pH during human sleep from data transmitted by swallowed radio transmitter
23 p4093 A69-42063

DNA denaturation without variance from pH 7.0 by adding NaOH observed with viscosity measurements, obtaining similar results with hydrochloric acid
24 p4263 A69-43225

PHANTOM AIRCRAFT
U F-4 AIRCRAFT

PHARMACOLOGY

Pharmacological tools in autonomic nervous system research, discussing norepinephrine biosynthesis, storage, release and inactivation in mammals
02 p0200 A69-12722

Pharmacology for long term manned space flights
13 p2211 A69-28613

PHASE COHERENCE

Incoherent scatter power measurements, comparing square law signal detection, phase coherent receiver and parametric amplifier methods
07 p1085 A69-19222

TEM mode networks design for producing phase coherent pulse modulated microwave signals through spectrum S band
13 p2234 A69-28073

Laser pulse development dynamics taking into account phase relations between field and active medium polarization
17 p2983 A69-33695

Block coded telemetry systems design for phase coherent space communication employing double conversion superheterodyne phase locked receivers
19 p3277 A69-36487

Split phase PCM code modulated carrier transmission characteristics determined for amplitude, phase and frequency shift keying, assuming random bit pattern and noncoherent modulation
21 p3676 A69-39451

Holographic technique of coherent light field transformation with desirable phase distribution from laser light beams of arbitrary wavefront characteristics
22 p3950 A69-41115

PHASE CONTRAST

Holography applied to schlieren and phase contrast methods to enable visualization of minute phase change in light scattering object
08 p1313 A69-20176

Optical data processing techniques and phase contrast method variations for statistics of surface roughness
12 p2079 A69-25910

Vibrating surface relative phases visual observation by introducing small rotation between exposures of stroboscopic hologram
20 p3546 A69-38123

PHASE CONTROL
NT COUPLING CIRCUITS

Automatic phase control effective bandwidth determined by asymptotic method, presenting computer calculated dependence on circuit parameters
01 p0030 A69-10590

Phase modulator with phase locked loop oscillator as phase shifter, discussing unit cascading effect
05 p0729 A69-15965

Earth effect on signal correlation in space diversity microwave reception antennas, analyzing vertical separation and out of phase signals
05 p0720 A69-16530

Automatic phase control and transient processes in resonant amplifier in presence of phase discontinuities of input signal
05 p0721 A69-16533

Quasi-optical transmission lines having composite correction devices with/without phasing devices
05 p0723 A69-16784

Final stage of three phase DC/AC converter, noting three phase control circuit for power stages with germanium transistors
08 p1285 A69-20381

Automatic phase control effective bandwidth determined by asymptotic method, presenting computer calculated dependence on circuit parameters
10 p1653 A69-23105

Digital phase shift control of locked oscillator
12 p2052 A69-26382

Microwave bandpass linear phase filters design and synthesis for simultaneous flat amplitude and delay response
16 p2759 A69-31941

Earth effect on signal correlation in space diversity microwave reception antennas, analyzing vertical separation and out of phase signals
16 p2753 A69-32472

Automatic phase control and transient processes in resonant amplifier in presence of phase discontinuities of input signal
16 p2753 A69-32474

Phase and amplitude stability measurements in airborne pulse Doppler radar
20 p3492 A69-37711

Automatic phase control system stability range determination in piecewise linear approximation and in presence of proportional integrating filter
22 p3918 A69-40956

Symmetrically regulated AC/DC converters power characteristics improved by switching in phase rectifiers twice during control cycle
24 p4254 A69-42570

PHASE DEMODULATORS

Digital nth order phase locked loop for FM demodulation
04 p0561 A69-15452

PHASE DETECTORS

Digital phase locked loops synthesis for fading and sequential phase estimation in decoder using digital computation
03 p0388 A69-13178

Optimum receiver structure for estimating PSK information signal phase derived together with matched filter detector performance
03 p0403 A69-13203

PHASE DETECTORS

Simultaneous passage of useful and noise signals through differential frequency discriminator, determining spectrum by phase detection and detuned circuits
04 p0556 A69-14462

Optimum conditions for signal analysis determined for symmetrical binary communications channel with unknown signal phase
04 p0556 A69-14492

Phase method of photoelectric registration of stellar transition moments
04 p0601 A69-15252

Bit error probability estimation of NRZ PCM synchronizer and detector operating in presence of fluctuating data frequency source
07 p1083 A69-19121

Statistical analysis of cascade of bandpass limiter, ideal phase detector and video filter for mathematical modeling of coherent communication systems
07 p1084 A69-19147

Lock range and threshold defined, presenting experimental results for phase lock loop systems having modified nth order antilock phase detector [IEEE PAPER 67-TP-1178-COM]
10 p1663 A69-23531

Computer generated kinoform optical element operating on phase of incident waves and forming wave front reconstruction single image
10 p1697 A69-23867

Ionospheric plasma density vertical profile by measuring reflected radio waves phase frequency characteristics
12 p2070 A69-26685

Phase analysis in multiple-sensor receivers with high signal to noise ratio, considering phase difference between two stochastic input signals
13 p2220 A69-27938

Simultaneous passage of useful and noise signals through differential frequency discriminator, determining spectrum by phase detection and detuned circuits
14 p2410 A69-28833

Pull-in performance of phase locked loops with phase comparator having asymmetric triangular characteristic
14 p2413 A69-29482

Plasma diagnostics FM phase meter circuits tests, considering raster phase indicators, phase detectors and frequency integrators
14 p2497 A69-29797

Design and operation of two frequency phase meter for plasma diagnostics, using frequency modulation of microwave oscillator and waveguide bridge
14 p2451 A69-29798

Phase measurements at IF in microwave plasma diagnostics, examining phase stabilization processes
14 p2452 A69-29805

Signal phase measurement accuracy by discrete phase technique ensured by using wideband signals and automatic control of input SNR
15 p2574 A69-30130

Instrumental accuracy of discrete filter during measurement of initial phase of signal dependent on phase structure
15 p2574 A69-30139

False alarm stabilization circuits efficiencies compared in unsteady Gaussian noise, considering phase autocorrelator performance
15 p2567 A69-30342

Amplifier working in conjunction with solid state phase sensitive detector replacing existing commutator in Dobson ozone spectrophotometer
16 p2792 A69-32641

Vibrating objects phase determined by time average and real time holographic interferometry
17 p2974 A69-33324

Discrete information transmission synchronization in communication systems concerning optimal signal detection, HF, phase and coded synchronization, etc
18 p3104 A69-35264

Integrating filter analysis for effect of phase detector sawtooth characteristics on locking range of phase locked oscillator
20 p3486 A69-37011

Optimum phase reference detector obtained at low SNR with Costas loop for fully modulated PSK signals
20 p3492 A69-37710

Automatic phase control system stability range determination in piecewise linear approximation and in presence of proportional integrating filter
22 p3918 A69-40956

Digital transition tracking symbol synchronizer for low SNR coded telemetry systems, discussing phase locked loop analysis and phase detector simulation by Monte Carlo method
23 p4130 A69-42513

Cascaded limiter and phase detector, analyzing SNR transfer characteristics for specific PM signals
23 p4131 A69-42525

Laser cavity modes phase equality demonstrated by oscilloscope trace in two photon fluorescent method
24 p4327 A69-42981

PHASE DEVIATION

Coherence ratio of ionospherically propagated radio waves measured for phase difference between pairs of antennas
01 p0032 A69-10967

Directional antennas gain loss on ground sections calculated on basis of difference-phase measurements data
02 p0214 A69-11612

Anisotropically conducting spiral cone current phase distribution applied to frequency independent antennas analysis, discussing spiral motion and field azimuthal dependence effects
03 p0408 A69-14133

VLF radio wave phase time or motion variation emanating from ground based source at arbitrary point on earth
07 p1123 A69-18816

VLF diurnal phase change observations, showing deviations from theoretical first mode and second mode dominance
07 p1078 A69-18912

Common mode rejection technique to determine phasing differences in digital systems by measuring pulse delay
09 p1463 A69-21896

Directional antennas gain loss on ground sections calculated on basis of difference-phase measurements data
11 p1847 A69-24719

Phase analysis in multiple-sensor receivers with high signal to noise ratio, considering phase difference between two stochastic input signals
13 p2220 A69-27938

Phase distortion, conversion of delay coefficients into channel noise and determination of waveguide delay coefficients for FM satellite communication systems
[IEEE PAPER 68-TP-382-COM]
13 p2222 A69-28153

Absolute value type of early-late gate bit synchronizer phase noise performance determined by Fokker-Planck method, comparing results with different circuits performance
19 p3270 A69-36246

Diurnal and seasonal phase-difference fluctuation measurement of radio waves propagating along ground layer caused by atmospheric turbulence
20 p3485 A69-36971

Observation time influence on interferometers resolution limits due to radio wave phase fluctuations
21 p3682 A69-39122

Mode locked laser output intensity, studying effect of random phase variations on pulses
21 p3741 A69-39684

Frequency and phase instability characteristics of negative resistance amplifier due to changes in circuit parameters
22 p3916 A69-40962

PHASE DIAGRAMS

Soviet book on semiconductor compounds, production and properties covering crystal structures, phase diagrams, etc
01 p0137 A69-10353

Thermoelectric properties of GeTe-GaTe system, analyzing phase diagrams, solid solution formation, substitutions and zone structure influence
01 p0138 A69-10404

Solar and geophysical activity during February 1965 and March 1966 indicating geomagnetic activity on 27-day recurrence diagram
01 p0068 A69-11118

Phase diagram of BiTe degenerate semiconductor crystals synthesized by heat treatment, discussing crystallization methods and physical properties
02 p0294 A69-11540

Metallographic analysis of Zr corner structure in Zr-Al-Mo system phase diagram, plotting monovariant and nonvariant equilibria reactions
02 p0261 A69-11840

Zr corner of phase diagrams and microstructure, hardness and microhardness of Zr-Al-Nb system alloys
02 p0261 A69-11841

Zirconium corner of Zr-Al-Cr system phase diagram within concentration limits from 1350-700 C, considering corrosion resistance
02 p0262 A69-11842

Metallographic and radiographic analysis of zirconium corner in Zr-Be-Nb system, discussing phase transformation during quenching
02 p0262 A69-11843

Isothermal sections construction of zirconium corner of ternary phase diagram of Zr-Mo-V system from microstructure of cast and quenched alloy specimens
02 p0262 A69-11846

Structure of zirconium corner of Zr-V-Ni system phase diagram, using metallography, hardness and microhardness methods
02 p0262 A69-11847

Isothermal sections construction of Zr-V-Ni system phase diagram from study of alloys at 1000, 700 and 500 C
02 p0263 A69-11848

Omega phase and beta solid solution in Zr-V-Ta alloys quenched from 900 C
02 p0263 A69-11850

Zirconium corner of Zr-Fe-Nb phase diagram, studying alloy tempering at various temperatures
02 p0263 A69-11851

Zirconium corner of Zr-Cu-Mo phase diagram, using microstructure analysis of hardness and microhardness measurements, discussing plasticity variations and corrosion resistance
02 p0263 A69-11852

Zirconium corner in Zr-Nb-Cu phase diagram, plotting isothermal sections for high temperatures
02 p0263 A69-11854

Zirconium corner of Zr-Mo-Ni phase diagram using metallographic analysis, hardness and microhardness methods, constructing isothermal sections for high temperatures
02 p0264 A69-11855

Zirconium corner of Zr-Nb-Mo system phase diagram, using microstructure, microhardness, hardness and radiographic methods
02 p0264 A69-11856

Isothermal sections of Zr corner of Zr-Mo-Ta system phase diagram at high temperatures, noting composition vs hardness and omega phase
02 p0264 A69-11858

Isothermal sections of Zr corner of Zr-Mo-Ti phase diagram at various high temperatures, noting corrosion resistance in air and water
02 p0264 A69-11859

Isothermal sections of Zr-Ni-Nb system phase diagram at high temperatures, determining principal type of projection on concentration triangle
02 p0264 A69-11860

Isothermal sections of Zr corner of Zr-Nb-Cr system phase diagram at high temperatures, noting variation of stability with concentration
02 p0264 A69-11861

Nickel-rich region of Al-Ni-Y ternary system, emphasizing identification of solid phase equilibria through analysis of equilibrated alloy specimens
02 p0265 A69-12004

Phase diagram and heat resistance relation for ternary titanium alloys, considering component interactions and dissolution and dispersion effects
02 p0268 A69-12357

InAs-InP phase diagram taking into account equilibrium pressure of vapor over melts in preparing single crystals by controlled crystallization
03 p0483 A69-13024

Phenomena in III-V compounds and III-V compound-other compound solid solutions, examining equilibrium phase diagrams
04 p0641 A69-14505

Ferrite-austenitic stainless steels with Ti analyzed during aging at 450-600 C for excess phase nature
04 p0615 A69-14641

Röntgenographic and metallographic examinations for interaction between ZrC and Re in wide range of temperatures and concentrations, discussing phase diagram
04 p0617 A69-14900

Quasi-ternary titanium dichromide-V-Mo system composition at high temperatures, physical properties and phase diagrams
04 p0618 A69-15080

Solid phase equilibria in nickel-aluminum-scandium system at 1000 C
05 p0779 A69-15833

Vanadium-carbon and niobium-carbon binary systems revised phase diagrams, noting effect of sublattice order transformations
05 p0779 A69-15988

Equilibrium stability of horizontal layer of fluid in field of modulated temperature gradient having layer thickness greater than penetration depth of heat waves
07 p1241 A69-18696

Ti-Al-V alloys phase diagrams for isothermal cross sections and polythermal cross sections with constant Al/V ratios
07 p1161 A69-18768

Ti rich Ti-Al-Mo-Zr alloys phase diagrams at high temperatures, noting presence of solid solutions
07 p1161 A69-18769

Ti-Zr-Sn alloys phase equilibria and interaction between titanium stannide and solid solution of Ti and Zr
07 p1162 A69-18770

Heat resistance of Ti-Al-Mo-Zr alloys analyzed by bend tests, discussing phase diagrams
07 p1163 A69-18779

Components relationships in binary phase diagrams of III a and VI a transition metals on basis of electronic structure
08 p1331 A69-20191

Subsolidus equilibrium study in potassium tantalate K niobate system for dry and hydrothermal runs, using X ray powder diffraction and petrography
08 p1332 A69-20373

Phase equilibrium and dynamics of gas volume heated by cosmic rays and cooled by radiation
10 p1760 A69-23136

Phase equilibrium in cast Zr-Re-B and W-Re-B systems using microscopic and X ray analysis
10 p1711 A69-23332

Antenna point and astigmatic sources due to phase centers and phase diagrams relations and antenna caustic curves
10 p1664 A69-23798

Chromium-rhenium-boron ternary system using X ray diffraction and microstructure analysis, establishing phase equilibria at high temperatures
10 p1715 A69-24054

Zr-W high temperature phase relationships, noting Zr-zirconium tungstide eutectic temperature, zirconium tungstide peritectic temperature and Zr solubility in W
11 p1903 A69-24578

Vanadium side of V-Ni phase diagram, using X ray analysis, differential dilatometry, thermal analysis and metallographic methods
11 p1903 A69-24579

Nickel base superalloys long time carbide and intermetallic phases stability at high temperatures
13 p2277 A69-27405

W, Mo and heat treatment effects on phase composition and heat resistance of ferrite and austenitic steels
13 p2283 A69-28487

Phase diagram for physicochemical study of CdSb-Ge cross section of Cd-Sb-Ge ternary system, discussing exo-endothermal fusion effects, microstructure, etc
14 p2503 A69-28975

Chromium-cerium phase diagram determined by differential thermal, metallographic and X ray structural analysis
15 p2640 A69-30666

CR-B binary system phase diagram including lattice parameters, temperature of peritectic decomposition and characteristics of alloys
15 p2641 A69-31185

Multicomponent semiconductor compounds of non-stoichiometric composition, studying structure, behavior and correlation between electrical properties and phase diagrams
15 p2670 A69-31243

Phase equilibria in ternary systems Nb-Fe-B and Nb-Co-B, determining structural types and lattice constants by using X ray and microstructural analysis
15 p2641 A69-31246

TiC-Re phase diagram over wide range of temperatures and chemical compositions
15 p2641 A69-31247

Two component heat pipe operating characteristics on basis of thermodynamic phase equilibrium for binary mixtures
17 p3071 A69-33268

Highly concentrated hydrogen peroxide production, handling and storage, discussing crystallization process, equilibrium diagram, decomposition reduction and stabilizers
17 p3017 A69-33353

Binary Nb-Hf system phase diagram below solidus line noting lattice parameters and oxygen and nitrogen effects on phase equilibrium boundaries
18 p3157 A69-35247

Nb corner of Nb-Mo-Cr alloy phase diagram and oxidizability in air at high temperature
18 p3157 A69-35248

Chromium ternary systems phase diagrams and crystallographic structures, using heat treatment and X ray analysis

18 p3158 A69-35262

Fe-Ni-P phase diagram studies applied to schreibersite and rhabdite formation in iron meteorites

19 p3417 A69-36132

La-Rh system study by powder X ray diffraction, metallographic and differential thermal analysis, constructing equilibrium diagram and determining crystal structure data

21 p3744 A69-38739

V systems applications and phase diagrams, discussing binary metallic systems, Kurnakov law, alloy properties dependence on composition, superconductivity, melting point, etc

22 p3968 A69-39887

Fusibility diagrams for Ti-Ta-Cr by determining specimens melting points after homogenization at various temperatures in argon

22 p3969 A69-40075

Book on phase diagrams for ceramists, 1969 supplement

22 p3971 A69-40782

Phase diagram, dielectric and magnetic properties of Bi manganate/Pb titanate solid solutions of perovskite structure, showing dependence on composition and temperature

22 p3996 A69-41163

Cosmic ray diurnal phase and amplitude variations determined using superimposed records of cosmic ray stations inside limited rigidity region

23 p4204 A69-41481

Ternary diffusion at high temperature in Fe-Co-Ni alloy system covering entire ternary phase diagram, including computed interdiffusion coefficients

23 p4176 A69-41505

Radiation characteristics of dipole on wedge edge with sinusoidal current, discussing spatial phase and polarization calculations by computer

23 p4138 A69-41937

Al-Mn-V ternary system equilibrium diagram at various aluminum concentrations determined by magnetic and microhardness measurements, microstructural observations and X ray analysis

24 p4330 A69-42601

PHASE ERROR

Reliability of eliminating multivaluedness in two scale phase measurement method resolved by algorithm formulated on white Gaussian noise interference

02 p0206 A69-11603

Atmospheric noise amplitude distribution relation to rms phase errors in frequency components of VLF timing pulse

03 p0396 A69-13629

Random phase errors in end-fed linear antenna arrays

04 p0578 A69-15211

Difference schemes implementation through fractional time step and phase error methods reduce dispersion

04 p0591 A69-15282

Commutation antenna arrays with arbitrary amplitude distribution, considering phase error effect

05 p0729 A69-16082

Phase error mean square value in phase lock loop determined from linear differential equations to determine output SNR and noise threshold

05 p0720 A69-16342

Linear antenna synthesis for optimal separation of plane waves providing maximum SNR with allowance for statistical phase distribution of field

06 p0895 A69-17460

Statistical theory of traveling wave antennas for random phase-amplitude distribution of current, discussing phase errors

06 p0898 A69-17797

Statistical aspects of uncertainty function of linearly frequency modulated signals for nonstationary random process of phase errors

06 p0889 A69-17798

Swept-frequency complex return-gain response of injection locked oscillator over locking bandwidth, detecting and correcting phase errors between injection-locked diode oscillators

07 p1100 A69-18645

Single channel binary PSK communication systems performance influenced by degree of RF coherence between transmitter and receiver

07 p1082 A69-19109

Phase error and amplitude and phase modulation in aircraft VOR omni receiver in vicinity of reflecting objects, noting asymmetrical filter effect

08 p1271 A69-19863

Rapidly varying phase error effect on system performance in data detection process due to RF carrier tracking loop

09 p1456 A69-22459

Reliability of eliminating multivaluedness in two scale phase measurement method resolved by algorithm formulated on white Gaussian noise interference

11 p1835 A69-24710

Paraboloidal reflector antennas rms phase error minimization, describing axis location and determination of focus and focal length of best fit paraboloid

19 p3283 A69-35933

PCM bit synchronizer models, discussing phase errors gate and differentiating devices

19 p3271 A69-36249

Optimum power allocation for RF carrier phase error and synchronization error in two channel system

19 p3274 A69-36283

Phase error in synthetic aperture radar, discussing tolerance level, sources classification and effect on average response, resolution and ambiguity function

20 p3490 A69-37642

Phase error in monopulse antenna system attributed to far field background noise sources during passive or active objects tracking

20 p3492 A69-37707

Linear antenna synthesis for optimal separation of plane waves providing maximum SNR with allowance for statistical phase distribution of field

20 p3508 A69-37943

PHASE LOCK DEMODULATORS

Digital simulation of demodulator/tracking phase locked loop of navigation/traffic control satellite system in thermal noise diffuse multipath fading environment

03 p0390 A69-13204

Phase lock loops design with nonlinear filtering elements in low signal to noise region, considering signal demodulation, lock range and threshold

06 p0902 A69-17398

Approximate noise analysis of phase locked loop with signal clipping

08 p1270 A69-19857

Phase locked loop demodulator with quadrature channel modified for decision feedback to detect binary phase shift keyed signals

08 p1270 A69-19859

Phase-lock loop demodulator ability to acquire and remain locked on signal under noise and pulse interference

23 p4145 A69-42230

PHASE LOCKED SYSTEMS

Injection locked oscillator FM receiver consisting of linear mixer and negative resistance oscillator in phase locked configuration, solving receiver output differential equation

01 p0042 A69-10247

Voltage tunable magnetron used in conjunction with ferrite circulator as phase locked amplifier

01 p0045 A69-10632

Liquid lasers compound range of organic type, circulating system of inorganic type and power peaks

01 p0092 A69-11194

Injection phase locking for synchronizing oscillators and reducing FM noise

02 p0220 A69-12450

Low noise high power transistor oscillator using directional coupler, noting isolated port for injection phase locking

02 p0220 A69-12452

Nonlinear mode interactions in spatially inhomogeneous laser, analyzing suppression, phase locking and linear coupling among cavity modes

02 p0258 A69-12632

Synchronization in coded communication systems, considering phase lock loop and square wave correlation function

03 p0383 A69-12871

Digital phase locked loops synthesis for fading and sequential phase estimation in decoder using digital computation

03 p0388 A69-13178

Phase locked loop demodulators for binary PSK signals compared with and without decision directed feedback in presence of CW interference

03 p0409 A69-13201

Pseudorandom radar range /DIOMEDE/ using optical correlator and phase loop

03 p0393 A69-13254

Coherent PSK system in multipath environment /Rician fading and additive Gaussian white noise/ with phase locked loop for coherent reference extraction

03 p0393 A69-13255

Simultaneous phase locking of longitudinal and transverse laser modes in He-Ne laser

03 p0441 A69-14188

Nonlinear phase locked automatic frequency control system dynamics, noting asymptotic stability of equilibrium state in whole

04 p0559 A69-15137

Harmonic balance method to investigate phase locked oscillator stationary modes

04 p0559 A69-15138

Phase locked automatic frequency control system with additional frequency control loop and nonlinear filter in phase control loop, analyzing dynamics

04 p0559 A69-15140

Digital nth order phase locked loop for FM demodulation

04 p0561 A69-15452

Phase locked loop discriminator in threshold region, discussing effects of loop parameters, detuning error and modulation

04 p0580 A69-15471

Phase modulator with phase locked loop oscillator as phase shifter, discussing unit cascading effect

05 p0729 A69-15965

Phase error mean square value in phase lock loop determined from linear differential equations to determine output SNR and noise threshold

05 p0720 A69-16342

Phase measurement using phase lock loop, voltage controlled oscillator and synchronous counter

05 p0722 A69-16766

Signal/noise performance of frequency locked loop FM threshold extension demodulator compared to phase locked loop demodulator and conventional FM discriminator

06 p0886 A69-16934

Q switching and mode locking of neodymium selenium oxygen chlorine liquid laser, discussing power output and nature of pulses

06 p0935 A69-17776

Swept-frequency complex return-gain response of injection locked oscillator over locking bandwidth, detecting and correcting phase errors between injection-locked diode oscillators

07 p1100 A69-18645

Phase locking phenomenon of multitransverse longitudinal modes in He-Ne lasers, discussing mechanism of self locking phenomenon [IEEE PAPER Q-1]

07 p1153 A69-19076

Expected number of spikes of phase locked loop demodulators, extending determination method to FM discriminator threshold and maximum likelihood estimator

07 p1082 A69-19107

Approximate noise analysis of phase locked loop with signal clipping

08 p1270 A69-19857

Phase locked loop demodulator with quadrature channel modified for decision feedback to detect binary phase shift keyed signals

08 p1270 A69-19859

Normal multimode laser action with and without phase locking, using exact steady state solution of Fokker-Planck equation

08 p1325 A69-20291

Phase synchronized oscillators in microwave frequency multipliers with improved SNR

09 p1464 A69-22113

Mode locked laser operation, noting output and applications to optical communication, high speed photography, nonlinear optics and frequency standards

09 p1518 A69-22123

Van der Pol nonlinear oscillation theory adapted to microwave reflex klystrons, explaining locked and unlocked monotonic operational modes

09 p1466 A69-22444

Density functions analytic solution for Fokker-Planck equation representing cascaded phase locked loops

09 p1474 A69-22450

Lock range and threshold defined, presenting experimental results for phase lock loop systems having modified nth order tanlock phase detector [IEEE PAPER 67-TP-1178-COM]

10 p1663 A69-23531

Injection locked oscillator FM demodulator, analyzing signal distortion, intermodulation noise, differential gain and differential phase

11 p1845 A69-24565

He-Ne laser output phase fluctuations between adjacent modes during unlocked and self locked condition, noting cavity optical length short term fluctuations influence

11 p1898 A69-25048

Digital simulation of phase locked receiver in diffuse multipath fading environment with band limited thermal noise

11 p1839 A69-25298

Nonlinear crystal generated second harmonic power measured for multimode He-Ne 0.63 micron self locked laser

12 p2106 A69-26321

Microwave frequency synthesizer for digitally tuned UHF and microwave superhetrodyne receivers, considering phase locking voltage-tuned transistor oscillator

12 p2030 A69-26390

Output power and loss analysis of 2 n injection locked oscillators combined through magic tee hybrids

13 p2232 A69-28061

Noise reduction techniques using injection phase locking and high-Q cavities for HF oscillator high order multiplier and avalanche diode oscillator microwave sources

14 p2420 A69-29458

Pull-in performance of phase locked loops with phase comparator having asymmetric triangular characteristic

14 p2413 A69-29482

Semiconductor technology including radar, Gunn and limited space charge accumulation oscillators, phase locked antennas, data processing and solid state computerization

15 p2581 A69-31521

Multiple mode phase locking of He-Ne laser with fixed cavity length and laser tube fixed position in cavity, generating high speed optical pulses

17 p2980 A69-32957

Phase locked loop with flip-flop error detector compared to analog loop, discussing signal to noise ratio

17 p2931 A69-34115

Neodymium laser emission temporal structure in mode self locking regime with Q switching by saturable filter

18 p3152 A69-35016

Phase locked loop design of desensitized monolithic integrated circuits for FM multiplex signal filtering and demodulation, describing external tuning

19 p3273 A69-36274

Coherent phase locked loop receiver as carrier and modulation loops combination with parallel bandpass filter for ranging signal reception and FM demodulation

19 p3274 A69-36277

Block coded telemetry systems design for phase coherent space communication employing double conversion superhetrodyne phase locked receivers

19 p3277 A69-36487

Lock-on band of phase locked AFC system calculated by asymptotic method, considering frequency integrating filters with nonlinear capacitances

19 p3277 A69-36569

AM phase locked states switching behavior of PM He-Ne lasers, considering isotope mixtures effect

20 p3552 A69-36994

Nonlinear differential equations of injection phase locking solved by Riccati equation, discussing initial frequency offset to loop gain ratios

23 p4119 A69-41742

Phase locked UHF telemetry transponder for missile scoring applications, discussing design and performance

23 p4137 A69-41779

Acoustical holograms phase recording, combining external phase locked electronic reference beams

23 p4166 A69-42180

Digital transition tracking symbol synchronizer for low SNR coded telemetry systems, discussing phase locked loop analysis and phase detector simulation by Monte Carlo method

23 p4130 A69-42513

Laser cavity modes phase equality demonstrated by oscilloscope trace in two photon fluorescent method

24 p4327 A69-42981

PHASE MODULATION

Optimal coherent reception of frequency diversity signals in multipath channels investigated for noise immunity

01 p0028 A69-10375

Radio systems for discrete information transmission, emphasizing phase difference modulation, wideband, universal and adaptive systems

01 p0031 A69-10778

OMEGA radio navigation system optimization, emphasizing implementation of phase modulation to ensure lane identification

03 p0463 A69-13212

Sinusoidal phase modulation role in spectral broadening observed in trapped filaments of laser and Raman light

03 p0442 A69-14189

Phase input power characteristics of TWT, TDA and parametric amplifiers, noting crosstalk calculations and AM-PM conversion coefficients

04 p0573 A69-14336

Phase modulator with phase locked loop oscillator as phase shifter, discussing unit cascading effect

05 p0729 A69-15965

External and internal modulation methods in lasers noting phase, amplitude and frequency modulation, birefringence, electrooptics and Stark and Zeeman effects

06 p0937 A69-18010

High data rate coherent telemetry systems synthesis, discussing multiphase modulation and demodulation to achieve bandwidth requirements

07 p1083 A69-19123

Radio signal from magnetron transmitter, noting slow amplitude phase fluctuations distribution according to log-normal law

08 p1275 A69-20424

Ionospheric scattered radio wave field amplitude and phase variations assessed for diffraction at regular phase screen

09 p1453 A69-21526

Phase characteristics and magnetic mirrors effect on charge motion in spatially periodic magnetic field

09 p1551 A69-22036

Optimum selection of modulation indices for multitone phase modulation by graphical method, noting tolerance insensitivity

09 p1457 A69-22463

Gunn effect cavity controlled generator oscillations, noting phase trajectory closing conditions dependence on resonant mode parameters

09 p1468 A69-22596

Sporadic noise, false fronts and other noise effects on phase of output oscillations of resonance apparatus

09 p1460 A69-22641

Transmission system with baseband spectrum divided into subbands, cascade phase modulating carrier in multiplication chain

12 p2030 A69-26385

Mismatch between signal and filter effect on output response of matched filter for pseudorandom phase-manipulated signals in receiver

12 p2031 A69-26487

Oscillation spectrum with harmonic phase or frequency modulation, analyzing structural dependence on initial phase

14 p2412 A69-29427

Subcarrier phase modulated single sideband sinusoidal carrier synthesis, discussing signal power ratios, signal efficiency, design sensitivity, etc

14 p2413 A69-29489

Wideband PM communication system with synchronous reception and automatic control of reception bandwidth, providing improvement in noise stability

15 p2564 A69-30147

Waveform amplitude variation of phase modulation pulses affected by band limitation

15 p2569 A69-30803

360 degree varactor linear phase modulator, analyzing impedance matching, insertion loss, tuning design and serrodyne application

16 p2756 A69-31577

Ionospheric scattered radio wave field amplitude and phase variations assessed for diffraction at regular phase screen

16 p2754 A69-32521

Phase modulation in pseudo-noise ionospheric communication system for reducing F region CW signal fading

18 p3104 A69-35308

Phase and amplitude stabilization during phase modulated discrete data transmission

19 p3277 A69-36571

Optimal radar phase modulated waveform with optimal ambiguity function synthesized by solving variational equations for orthogonal series coefficients of expanded modulation

20 p3492 A69-37708

Linear filtering effects in channel with binary direct sequence antipodal biphase modulation in presence of white noise and sinusoidal interference, noting variance

23 p4122 A69-41774

Pseudorandom code development and possibilities for radar applications, considering signal processing,

antenna requirements, radar signal phase modulation, etc

24 p4281 A69-42741

Optical correlation for radar signals phase modulated by pseudorandom codes

24 p4282 A69-42742

PHASE SHIFT

Phase and amplitude variation at output of tuned amplifier, noting graphs and formulas

01 p0047 A69-10786

Self adaptive control circuit diagram examination, considering phase shift measurement reliability by eliminating distortion caused by system nonlinearities and noise

01 p0052 A69-10796

Laser beam phase fluctuations for propagation through turbulent atmosphere, noting interferometer for simultaneous measurements for pairs of rays

01 p0091 A69-10845

Holographic phase variation distribution recording by interference between reconstructed wave fronts from separate holograms

01 p0083 A69-10984

Methodological problems in studying ionosphere by phase measurements without taking into account geomagnetic field, noting value of main results

02 p0237 A69-11668

Polarization rotation and phase delay effects as function of frequency for ionospherically propagated HF signals

02 p0208 A69-12331

Equation for beam shift during beam steering of phased array by conjugate element phase shifting

02 p0219 A69-12340

Arbitrary phase shift vibrations of airfoil profiles in incompressible flow reduced to Fredholm equations, allowing for trailing vortices influence

02 p0190 A69-12574

Electrically controlled broadband microwave phase shifter consisting of coaxial line with varactors or ferroelectrics

03 p0408 A69-13987

Plasma density spatial distribution determined from HF electromagnetic wave phase shifts without assuming axisymmetry

03 p0480 A69-14138

Total ionospheric electron content determination from measurement of phase differences of satellite transmission, discussing data processing and differential Doppler effect measurements

04 p0592 A69-14766

Sudden VHF phase anomalies produced by solar flare induced ionospheric disturbances during July 1968

05 p0719 A69-15980

Suppressed rotation reciprocal ferrite phase shifter theory explained in terms of nonreciprocal coupling of cross polarized waveguide modes

06 p0896 A69-17484

Diurnal field strength and phase variations of VLF transmissions over transequatorial path from Australia to Japan

06 p0889 A69-17654

Coherent frequencies method for irregular component of satellite signal phase lead due to ionospheric inhomogeneities between satellite and ground station

06 p0890 A69-17799

Frequency-fluctuation correlation functions of radio wave field behind n random screens with random phase shifts calculated, obtaining statistical characteristics

07 p1076 A69-18525

Natural amplitude and phase fluctuations of originally monochromatic oscillations at output of regenerative frequency divider with thermal and shot noise

07 p1099 A69-18526

Phase shift and losses in wave propagation in dielectric environment, defining power transmission coefficient and insertion phase shift

07 p1087 A69-19518

Radome induced distortions of radioelectric axis analyzed by sectional phase analysis

07 p1110 A69-19521

Stable limiting cycles of laser resulting from mutual synchronization of phase shifted oscillation modes

07 p1158 A69-19752

Observations of Venus at 15.4 GHz establishing upper limit for brightness variation with phase angle

08 p1382 A69-19818

Propagation induced phase fluctuations reduction in widely separated oscillators, presenting microwave and optical methods

08 p1273 A69-20022

Temperature effect on phase stability and electrical length of braided coaxial cables, considering dielectric constant and mechanical length

08 p1283 A69-20225

Phase and amplitude variation at output of tuned amplifier, noting graphs and formulas

10 p1662 A69-23115

Telemetry data channel gain and phase correction with frequency response calibration technique using digital filtering

10 p1654 A69-23291

Qualitative analysis of recording phase only acoustic holograms of object wave instead of both phase and amplitude, considering fringe patterns and conjugate image

10 p1695 A69-23548

Quantum phase noise in He-Ne laser, considering amplitude fluctuation, spontaneous emission and oscillator linewidth

10 p1704 A69-23669

Polarized electromagnetic waves phase shift during total reflection from stratified dielectric region found dependent on transition zone width in addition to permittivity

10 p1657 A69-23862

Phase fluctuations measurements of obliquely incident signal reflected from ionosphere performed over distance of 1300 km, showing amplitude dependence

10 p1657 A69-23913

Mean losses in quasi-optical communication lines due to random irregularities in performance of waveguide phase correctors connected in series, noting random phase aberrations effect

10 p1658 A69-23954

Antenna array statistical synthesis, investigating signal detection capacity for large phase fluctuations

11 p1833 A69-24439

Tracking filter steady state oscillation amplitude and phase distributions determined from Fokker-Planck equation for high and low noise levels

11 p1844 A69-24441

Two oscillator signal combiner based on mutual synchronization, providing output signal free of phase jumps or amplitude fluctuations

11 p1849 A69-24928

He-Ne laser output phase fluctuations between adjacent modes during unlocked and self locked condition, noting cavity optical length short term fluctuations influence

11 p1898 A69-25048

Polarized Hartree-Fock model computing photoionization cross sections for Li isoelectronic sequence, listing phase shifts for partial waves of scattered electrons

11 p1922 A69-25260

Venus brightness temperatures vs phase angle to define spectra of day and night face at short wavelengths, using model atmosphere

12 p2153 A69-25806

Pulsed radio waves for measuring phase height in E region, showing short period fluctuations

12 p2066 A69-26111

Holography with pulsed lasers for high speed recording of amplitude and phase disturbances and rapid transient events, noting reconstruction evaluation problems

12 p2087 A69-26171

Hydromagnetic fluid flow between flat plates oscillating with phase difference, same frequency and different amplitudes

12 p2135 A69-26273

Digital phase-shift control of locked oscillator

12 p2052 A69-26382

Three dimensional log amplitude and phase fluctuation distributions of collimated and focused Gaussian beams propagated through random inhomogeneous medium, evaluating mean-square values

12 p2130 A69-26393

Differential absorption by measurement of phase difference of ionospherically propagated incoherent radio wave signals under quasi-longitudinal conditions

12 p2032 A69-26857

Antenna cross dipole array for vehicle tracking in VHF band, obtaining effect of local rotation by electrical phase shifting

13 p2226 A69-27185

Observability of phase state of nonlinear control system noting Liapunov function

13 p2238 A69-27742

Transmission line all pass equalizers theory and design for operation in TEM, TE or TM modes

13 p2233 A69-28065

Phase and amplitude changes of arbitrary-Q self excited oscillator under external disturbance, using differential equations

13 p2300 A69-28574

Fermi surface data of alkali metals interpreted in terms of interaction between conduction electrons and ionic lattice for deducing partial wave phase shifts

13 p2304 A69-28681

Methodological problems in studying ionosphere by phase measurements without taking into account geomagnetic field, noting value of main results

13 p2257 A69-28699

Electromagnetic wave phase characteristics after free space passage through statistical medium with wave disturbance producing density and ionization fluctuations

14 p2435 A69-29049

Fourier analysis of ionospheric wave reflection pulses for frequency contents and relative phase angles

14 p2440 A69-29351

Spatial distribution of plasma density from phase shift measurement in millimeter waves based on microwave multichannel probes

14 p2497 A69-29792

Plasma electron density measurement from phase shifts of electromagnetic wave groups propagation

14 p2497 A69-29796

Design and operation of two frequency phase meter for plasma diagnostics, using frequency modulation of microwave oscillator and waveguide bridge

14 p2451 A69-29798

Three channel microwave FM phase meter for studying plasma electron concentrations directional distribution without interferences between channels

14 p2497 A69-29799

FM homodyne phase meter with klystron oscillator for measuring plasma electron concentration, giving block diagrams of meter, detector and oscillator

14 p2451 A69-29800

Microwave interferometer with digital-logic elements for phase shift measurements in pulsed plasmas without frequency range limitations

14 p2452 A69-29802

Plasma density and conductivity radio interferometry during ultrarapid disturbances based on electromagnetic wave phase shift dependence on density

14 p2498 A69-29803

Direct phase measuring and measured phase compensating microwave devices designed for plasma diagnostics applications

14 p2452 A69-29804

Phase measurements at IF in microwave plasma diagnostics, examining phase stabilization processes

14 p2452 A69-29805

Reference oscillator frequency instability effect on radio signals phase shift in ionosphere measurements, evaluating errors

14 p2444 A69-29873

Short and ultrashort waves signals amplitude and phase displacement determination device, stressing sensitivity

15 p2570 A69-31088

Sudden phase anomalies on radio paths compared with calculated results for satellite observed solar X ray flux intensities to explain sudden ionospheric disturbances

17 p2959 A69-33006

Amplitude ratio measurement for two AC signals of given relative phase shift and same frequency

17 p2975 A69-33615

Phase fluctuation measurements of laser beam propagating through turbulent atmosphere

17 p2927 A69-33855

Laser beam propagation through turbulent medium, investigating statistical distribution of phase shift fluctuations

17 p2976 A69-33857

Absolute phase heights measurements in ionosphere for geometrical optics conditions, noting accuracy

17 p2927 A69-33859

Multiple interference effect introduced by nonlinear characteristics of photographic material, measuring phase variations by holographic multiple beam interferometry

17 p2977 A69-34159

Microwave propagation inside hollow cylinder using model plasma as dielectric, deriving relationship between phase shift and free electron density

17 p2932 A69-34218

Atom-atom scattering potential from phase shifts, using WKB formula and Jeffreys-Born approximation

19 p3378 A69-36189

Ionospheric data of local and integral electron concentration obtained by measuring phase shift of satellite emitted coherent radio waves

20 p3519 A69-37022

Vibrational displacement phase measurement by Michelson interferometer with laser source

20 p3538 A69-37320

Ground backscatter elevation angle recorded by phase comparison method, postulating ionospheric tilts to interpret data

20 p3535 A69-38188

National Physical Laboratory atomic clock improvements, describing use of cesium 133 as second of time standard and phase shift effects on precision

21 p3720 A69-38548

Ring laser bias in angular rotation measurement using optical phase shifters

21 p3735 A69-38651

Multistable logic circuitry with 10 stability levels based on phased pulse principle, noting efficiency and complexity in man machine interface

21 p3686 A69-39065

Distance measuring method limitations for modulated CW laser determined by laser transmitter receiver in conjunction with retroreflector target fixed position

21 p3739 A69-39457

Pulse width increase in mode locked laser caused by phase deviations, noting optical elements with quadratic dispersion of refractive index

21 p3741 A69-39683

Circadian rhythm phase shifts during ontogenesis produced by hormone concentration changes resulting from light variations

22 p3872 A69-40198

Free stream velocity in high enthalpy arc heated wind tunnel by measuring imposed temperature modulation apparent phase shift, describing circuit diagrams

22 p3926 A69-40444

Electronically controlled microwave phasers and time delay elements design and operation, discussing beam width, steering and effects, directivity and planar arrays

23 p4135 A69-41353

Positive phase shift relation to elastic modulus enhancement of smooth muscles of rabbit, cat and dog bladder, pulmonary artery and large veins

23 p4083 A69-41459

Array aperture amplitude and phase distortions effect on radiation field uniformity

23 p4138 A69-41940

Lunar photometric function near zero phase from Apollo 8 closeup photography, noting higher reflected brightness than at 1.5 degree phase angle

23 p4220 A69-42380

Measurement method for relative phase shift between density and potential oscillations in Cs plasma

24 p4354 A69-42676

Nonhuman primate circadian rhythms as functions of phase shift carried out in advance or delay

24 p4261 A69-42709

Ionized meteor trails reflection zone altitudes determination by interferometric measurements of phase differences

24 p4311 A69-43508

Inviscid hypersonic flow over oscillating slender wedge, defining equivalent phase shift

24 p4248 A69-43582

Thermal turbulence effects on phase fluctuations of laser beams, studying temporal decay of mean square refractive index fluctuation with fringe pattern displacements

24 p4329 A69-43754

PHASE SHIFT CIRCUITS

NT CIRCULATORS [PHASE SHIFT CIRCUITS]

Diode structure optimization for monolithic integrated circuit for Ku-band reflective phase shifter

01 p0040 A69-10195

Digital loaded-line phase shift networks for microwave thin film applications, emphasizing design equations

01 p0040 A69-10198

Semiconductor microwave phase shifters for electronic steering of phased array radar antennas noting cost, reliability and properties of steerable antennas

04 p0572 A69-14319

Reciprocal latching ferrite phase shifters application to lightweight scanned phased arrays, noting quasi-circularly polarized modes with lowest insertion loss

04 p0572 A69-14320

Electronic scanning antenna system consisting of ceramic rod linear array, power distributor, electronic ferrite phase shift feed and driver

04 p0572 A69-14327

- Circuit for accurate division of attenuation and phase shift changes, noting calculation errors
04 p0573 A69-14337
- Phase modulator with phase locked loop oscillator as phase shifter, discussing unit cascading effect
05 p0729 A69-15965
- X-band swept frequency oscillator using Gunn diode and ferrite phase shifter
05 p0734 A69-16573
- High accuracy microwave phase standard for calibration laboratories, discussing broadband differential phase shifter
06 p0896 A69-17487
- Equivalent network representation of feedthrough lens array taking into account mutual coupling between elements to predict performance characteristics
08 p1280 A69-20014
- Variable phase shifters and delay lines, discussing mechanical and electronic adjustments
08 p1290 A69-20978
- Reciprocal and nonreciprocal electronically adjustable ferrite phase shifters and application in scanning leaky wave antennas
08 p1290 A69-20979
- Applied magnetic field effects on longitudinally magnetized reciprocal ferrite phase shifters, showing shift type dependence on guide electrical thickness
13 p2229 A69-27673
- High power ferrite latching switch with forced air cooling, discussing nonreciprocal phase shifter materials and configurations
13 p2229 A69-27674
- Hybrid coupled low power digital microwave phase shifters design, discussing lumped element L-C and variable C shifter theories, power limitations and construction techniques
15 p2580 A69-31076
- Broadband continuously variable phase shifter with microstrip construction, describing phase rotation via stripline connected directional couplers
16 p2763 A69-32582
- Italian cross radio telescope noting added phase shifters to N-S arm, transistorized receiving system and modified data processing
19 p3295 A69-36643
- Semiconductor phase shifting for inertialess antenna scanning at microwave to millimeter wavelengths, describing diode construction with emphasis on solving insertion loss
[ONERA-TP-712] 23 p4143 A69-42519
- PHASE SHIFT KEYING**
- Phase locked loop demodulators for binary PSK signals compared with and without decision directed feedback in presence of CW interference
03 p0409 A69-13201
- Optimum receiver structure for estimating PSK information signal phase derived together with matched filter detector performance
03 p0403 A69-13203
- Coherent PSK system in multipath environment/Rician fading and additive Gaussian white noise/with phase locked loop for coherent reference extraction
03 p0393 A69-13255
- Time division multiple access satellite communication system employing pulse code modulation of voice channels and phase shift keying of RF carrier
07 p1077 A69-18759
- Bandwidth limited PCM/PSK/PM telemetry system performance analysis for developing S band telemetry, including coherent and noncoherent detectors
07 p1081 A69-19098
- Single channel binary PSK communication systems performance influenced by degree of RF coherence between transmitter and receiver
07 p1082 A69-19109
- Secondary maxima observed in pulses with binary phase shift keying for cases of large Doppler shifts
07 p1086 A69-19488
- Phase locked loop demodulator with quadrature channel modified for decision feedback to detect binary phase shift keyed signals
08 p1270 A69-19859
- Constant amplitude in-band additive interference for analysis of PSK signals in Gaussian noise, discussing coherent and differential detection
09 p1455 A69-21848
- Multichannel bit error probability for FSK and DPSK obtained for slow nonselective-fading multipath as function of multipath parameters and diversity order
10 p1656 A69-23533
- Received signal phase angle error probability in coherent PSK system in Gaussian noise and interference
13 p2219 A69-27665
- Compression capabilities of combined frequency and phase shift keying in radar and sonar pulse modulation using binary noise codes
15 p2568 A69-30628
- Double binary PSK system digital computer simulation for satellite communications, investigating filter and limiting effects on performance in error probability terms
20 p3492 A69-37705
- Optimum phase reference detector obtained at low SNR with Costas loop for fully modulated PSK signals
20 p3492 A69-37710
- Split phase PCM code modulated carrier transmission characteristics determined for amplitude, phase and frequency shift keying, assuming random bit pattern and noncoherent modulation
21 p3676 A69-39451
- Partially coherent PSK-modulated binary detection, deriving noisy phase reference by narrow band tracking filter, analyzing bit output error as function of SNR
23 p4122 A69-41772
- Error probability bounds for self synchronized binary PSK communication systems, simulating decision feedback, phase doubling and maximum likelihood systems
23 p4128 A69-42501
- Effective color TV transmission via satellite using PCM/PSK modulation, noting dependence on available equipment, bandwidth, desired error rate and SNR
23 p4130 A69-42520
- PCM satellite communication systems signal power and frequency bandwidth requirements, noting PCM-psk superiority over FDM-FM
24 p4283 A69-43200
- PHASE-SPACE INTEGRAL**
- Phase space concepts for beams, accelerators and confined particles, noting adiabatic invariants, phase space transformations, particle dynamics in accelerators and plasmas
06 p0966 A69-17673
- Master equation in quantum optics phase-space formulation based on Schroedinger equation of motion, noting application to Volterra integral equation and Born approximation
15 p2633 A69-30307
- System kinetics synthesis for nonlinear multiple lumped parameter system having responses in boundary region of phase-time space
16 p2812 A69-32247
- Optimal control parameters for gyroscopic devices with constrained phase coordinates obtained on analog computer by introducing equivalent phase coordinates system
24 p4317 A69-43708
- PHASE TRANSFORMATIONS**
- NT ARC MELTING
NT BOILING
NT EVAPORATION
NT FILM BOILING
NT FLASHING [VAPORIZING]
NT FREEZING
NT FUSION [MELTING]
NT LEIDENFROST PHENOMENON
NT MELTING
NT NUCLEATE BOILING
NT PROPELLANT EVAPORATION
NT SUBLIMATION
NT TRANSPIRATION
NT VACUUM MELTING
NT VAPORIZING
NT ZONE MELTING
- Space charge limited currents in SbSI single crystals with gallium electrodes during phase transition, discussing sticking probability and photoconductivity
01 p0137 A69-10258
- Structural transformations of quenched Fe-Ni-Nb austenitic alloy from X ray diffraction microstructure examination and hardness measurements
01 p0095 A69-10603
- Irradiation influence on chromium transition temperature explained by defect clusters and embrittling impurity redistribution
01 p0095 A69-10604
- Precipitation hardening of gamma phase in austenitic stainless steels studied for phase transformations by dilatometry after aging and quenching
01 p0096 A69-10613
- Ultrahigh pressure physics of materials, discussing apparatus, phase transitions and yield strength ductility relationships
02 p0260 A69-11803
- Martensite transformation by simple shear in equiatomic Ni-Ti alloy, using transmission electron microscopy
02 p0265 A69-12024
- Vanadium dioxide reflection spectra dependence on incident quantum energies during semiconductor/metal phase transition
02 p0298 A69-12100
- Sulfospinel polymorphism at high temperature and pressure and pressure-temperature phase relations
02 p0266 A69-12162
- Kinetic features of martensitic transformation of nickel steels dependent on plastic deformation degree at 525 C
02 p0267 A69-12190
- Heat conduction with change of phase in three dimensional melting and solidification problem under isotherm conditions and balanced energy at interface
02 p0354 A69-12548
- Ferrite and sigma phase formation in austenitic stainless steels with nickel and chromium content
02 p0269 A69-12764
- Metal/alumina interfaces strength, examining correlation with wetting and bonding and martensitic transformations
03 p0447 A69-13612
- Al/Zn/Mg alloys preprecipitation, discussing Guinier-Preston and critical zone sizes and reversible vacancy trap
03 p0447 A69-13613
- Second phase hardened materials recovery creep rate model, showing dependence on stress level
03 p0447 A69-13615
- Thermodynamic analysis of refractory compounds vapor transport conditions, illustrating integral free energy diagrams
03 p0453 A69-13619
- Moving and stationary interphase boundaries segregation during phase transformation, discussing embrittlement
03 p0450 A69-13883
- Aging of iron-nickel-titanium alloys during heating in reverse martensitic alpha to gamma transformation process, investigating phase parameter changes
04 p0613 A69-14558
- Bainite beta to alpha transformation in titanium-oxygen system, using high temperature metallography techniques
04 p0613 A69-14559
- High strength martensitic aging steels alloying effects, phase transformation and aging
04 p0615 A69-14644
- Alpha to gamma transformation kinetics in maraging steel during heating, studying alloying elements redistribution
04 p0616 A69-14648
- Long term strength of Ni-Cr-Al-Ti alloys, studying gamma particles size and distribution effect
04 p0616 A69-14651
- Martensitic transformation in Ti-Al-Mo alloys, noting specific features and effects of Mo content
04 p0617 A69-14940
- Electric field strength and helix pitch in induced cholesteric-nematic phase transitions, noting activation energy for charge carrier production
04 p0555 A69-14964
- Transitions in glasses at low temperatures, noting molecular relaxation dependence on copolymer composition
04 p0621 A69-15308
- Transient temperature distribution for finite slab in phase transformations via single face temperature changes
[ASME PAPER 68-WA/HT-37] 05 p0848 A69-16128
- Hot working temperature effects on Rene 63 mechanical properties and microstructures, using tensile and stress rupture tests, electron microscopy and X ray diffraction analysis
05 p0781 A69-16446
- Polymer glasses low temperature transitions, relating structure and transition temperature
05 p0717 A69-16493
- Metastable phases of binary zirconium-niobium system, defining decomposition of solid solution in cooling
05 p0781 A69-16614
- Lanthanum and hafnium effect on transition and recrystallization temperatures of tungsten and tungsten base alloys
05 p0782 A69-16797
- Sigma formation effects on cast nickel-based superalloys properties, discussing sigma occurrence prevention for longer service life of gas turbines
06 p0942 A69-17223
- Transmission electron microscopy used to study phase transformations in Ti-Mo and Ti-V alloys, determining crystal structures
06 p0943 A69-17230

Model for phase transition mechanism quantum-Coulomb plasmas, finding transition temperature for white dwarfs

06 p0968 A69-17785

Nimonic alloys recovery analyzed by X rays and electrolytic phase separation, showing precipitated gamma phase effect

07 p1159 A69-18533

Thermal and metallographic analyses of Ti-Zr-Al system vertical sections close to Ti-Al edge, considering phase equilibrium

07 p1162 A69-18771

Metastable phases in titanium alloys with beta alloying elements

07 p1162 A69-18773

Phase transformations in titanium alloys under nonequilibrium conditions

07 p1162 A69-18774

Tin and zirconium addition effect on transformations of titanium alloys during heat treatment

07 p1162 A69-18775

Phase and structural transformations in two phase quenched and aged titanium alloys, using electron microscopy and X ray analysis

07 p1162 A69-18776

Weld mechanical properties of Ti-6Al-2Sn-4Zr-2Mo titanium alloy as function of cooling rate changes or transformation rate shifts resulting in wide range of hardnesses

08 p1318 A69-19965

Metallographic and X ray study of cellular decomposition and precipitation in superconducting niobium zirconium alloy, noting heat treatment effect on current carrying properties

08 p1331 A69-20192

Phase identification and microstructural effects of gaseous nitrogen reaction with binary Nb-Ti alloys at 1000 C

08 p1331 A69-20195

Dislocations effect on intermediate body centered tetragonal phase precipitation in Fe-Ni-Cr-Be alloy using transmission electron microscopy

08 p1333 A69-20447

Spinodal decomposition effect on Al-Zn alloy mechanical properties noting strengthening, brittleness and work hardening capacity

09 p1522 A69-21501

Structure of spinodal decomposition in Al-Zn alloys by X ray diffraction noting anisotropy, periodicity and stability

09 p1522 A69-21502

Microstructure for spinodal decomposition in Al-Zn alloys noting Zn precipitation, fracture mechanics, dislocations and transmission electron microscopy results

09 p1522 A69-21503

Phase equilibria in V-Cr-C, Nb-Cr-C and Ta-Cr-C systems determined by microscope and X ray analyses

09 p1523 A69-21872

Space charge limited currents in SbSI single crystals with gallium electrodes during phase transition, discussing sticking probability and photoconductivity

09 p1559 A69-22651

Concentration changes in binary metal-gas solutions during simultaneous degassing kinetics and metal evaporation

09 p1528 A69-22732

Nickel alloy high temperature tests, noting coagulation of precipitated gamma prime phase, vacancies and creep rate increase

09 p1528 A69-22733

Radiometric observations of Venus brightness temperature variation used to determine phase effect at 8.6 mm wavelength

10 p1773 A69-22959

Omega phase transformation in binary and ternary Zr alloys after water quenching from within/alpha plus beta/ phase region

10 p1707 A69-22988

Spontaneous martensite phase transformation in Ti-Cr alloy thin foils formed electrolytically

10 p1708 A69-22994

Austenite to martensite strain induced transformation effect on energy absorption during crack propagation

10 p1709 A69-23074

Soviet book on fluid semiconductor properties at high temperatures during transition from solid to liquid state

10 p1744 A69-23316

Zirconium-rhenium-carbon ternary system, determining resistivity of melted alloys, discussing eutectic quasi-binary compounds

10 p1715 A69-24055

Thermal and microstructural analyses to determine phase interactions nature in Mg alloys of Mg- Nd-Al system

11 p1902 A69-24271

Monograph on effect of nitrogen on precipitation behavior of austenitic chromium-nickel steel covering carbides, intermetallics, phase transportations, corrosion resistance, etc

11 p1902 A69-24369

Monograph on effect of boron, zirconium and titanium on austenite transformation of CrMo steels bainite and martensite covering carbides, nitrides, mechanical properties, etc

11 p1903 A69-24634

Order-disorder in alloys with several phase transition temperatures, discussing crystal lattices, interstitial alloys, atomic and magnetic ordering

11 p1936 A69-24702

Superstructures in multicomponent alloys, transition mode and temperature, ordered state and atomic interactions

11 p1937 A69-24703

Pressure effects on hcp crystalline lattice alloys order-disorder transformations

11 p1937 A69-24704

Ignition of condensed homogeneous combustible materials in presence of phase transition in heated layer, discussing temperature distribution and ignition delay time in ammonium perchlorate

11 p2000 A69-25189

Dense gas equilibrium plasma thermodynamic stability in case of high electrostatic interaction energy of charged particles, analyzing phase transition possibility

11 p1928 A69-25234

Heat treatment effect on Ti-Mn alloy microstructure, discussing fcc martensite transformation into alpha, beta and intermediate phases as function of aging

11 p1906 A69-25578

Plasticity increase of molybdenum alloys during precipitation of second phase at high temperatures due to lattice defects redistribution and plastic deformation

11 p1906 A69-25685

Heat treatment effects on molybdenum-rhenium alloy field emission and surface structure in alpha and sigma phase regions

12 p2113 A69-26041

Lattice defects in annealed and plastically deformed cobalt, showing increase with increasing martensite transformations

12 p2113 A69-26042

Collection of papers on crystal structure imperfections covering dislocation mobility, kinetic recrystallization and volume changes during phase transformation

12 p2142 A69-26452

Volumetric and allotropic changes during heating in electrolytic cobalt multiple phase transformations

12 p2114 A69-26455

High strength steels, discussing ductility, austenite to martensite transformation for increased strain hardening rate and elongation and corrosion resistance

12 p2115 A69-26829

Shock waves in solids, discussing gas gun firing and explosive detonating at specimen, transformations measurement and materials processing applications

13 p2360 A69-27341

Martensite transformation in Ti-Cr binary alloys by thin foil electron microscopy, noting crystallographic theory

13 p2276 A69-27369

Homogenization of martensite formation in nickel 300 grade maraging steel, analyzing anisotropic transformation strains during thermal cycling

13 p2278 A69-27410

Stress and plastic deformation influence on allotropic transformation of cobalt-nickel single crystals studied by X ray diffraction

13 p2279 A69-27761

Precipitation influence on martensite formation kinetics and structure of Fe-Ni-Ti alloys

13 p2279 A69-27765

Ni alloys phase precipitation and Fe substitution effects on heat resistant alloys

13 p2283 A69-28488

Transition zone structure and phase composition in Ti/stainless steel bimetal as function of rolling conditions and heat treatment

13 p2283 A69-28490

Martensite transformation with fcc lattice in Ti alloys containing 5.9 percent Fe analyzed as function of cooling rate using X ray analysis

15 p2636 A69-30105

Vapor-liquid transition in inert gases based on Monte Carlo method, including comparison with van der Waal equation and plasma ionization equilibrium

15 p2655 A69-30981

Double shock method for detecting pressure limits in magnetic phase transition of solids

16 p2825 A69-31696

Slow forming forging and extrusion required for Ti alloys, discussing mechanical properties as function of beta transformation temperature

16 p2793 A69-31786

Time, temperature and transformation curves for Ti alloy by dilatometry, hardness measurements, X rays and micrography, discussing martensite and beta-alpha transformations

16 p2802 A69-32180

Interaction between two phase dynamical and combustion parameters in one dimensional gas-gas-metal combustion system [AIAA PAPER 69-540]

16 p2880 A69-32742

Book on gas dynamics of two phase media for thermal power engineering equipment, discussing phase transformations, condensation in high velocity flows, etc

17 p2948 A69-32951

Titanium alloy martensites crystallography by electron microscope, discussing lattice parameters and spontaneous transformation

18 p3154 A69-34245

Forming and heat treatment process for stainless steel pressure containers using liquid N₂, discussing austenite-martensite transformation role

18 p3161 A69-34605

Omega phase formation in Ti and Zr alloys with transition metals, discussing effects on mechanical and superconducting properties

18 p3155 A69-34634

Cumulative rapid thermal cycling influence on progressive disappearance martensitic transformation in 18 percent nickel maraging steel

18 p3155 A69-34650

Martensite transformation, C content and work hardening relations in stainless steels studied for magnetic detection of embrittlement during deformation

18 p3138 A69-35117

Beryllium diffusion coefficients in Zr and Ti bcc phases, using radioactive beryllium 7 at high temperatures

18 p3157 A69-35251

Phase shape deformation and austenite stabilization in Fe-Ni and Fe-Ni-Ti alloys following secondary alpha phase of reversed martensite-austenite transformation

18 p3159 A69-35448

Isothermal and thermal martensite transformations on polished surfaces of Fe-Ni-Mo alloys

19 p3344 A69-35983

Cr-S and Cr-Fe-S systems phase relations, using silica tube and collapsible tube experiments, correlating formation conditions of meteoritic sulfide assemblages

19 p3359 A69-36123

Vanadium thermistor fabrication influence on resistance jump at phase change temperature of vanadium dioxide, reproducing parameters by heat treating doped vanadium pentoxide

19 p3256 A69-36718

Heat conduction in medium with phase transitions, solving one dimensional nonlinear problem by calculation of isotherms and reduction to Cauchy problem

19 p3453 A69-36838

Phase transformations and strengthening mechanisms in Ti-Al-V alloy

20 p3556 A69-36954

F 2 layer midlatitude positive disturbances observed during IGY on quiet and disturbed days, noting positive to negative transition latitudes

20 p3527 A69-37674

Crystallographic relations between mother gamma phase and bulk martensitic structure of Fe-Ni alloys with less than 20 percent Ni, using radioisotopes

20 p3562 A69-37781

Phase analysis of systems Mn-S, Mn-Se and MnS-MnSe by X ray diffraction techniques, revealing homogeneity ranges

20 p3485 A69-38286

Titanium strengthened high strength hot-rolled steels, discussing cooling rates leading to complete ferrite phase transformation

21 p3743 A69-38652

Abnormal grain growth during secondary recrystallization of hydraulically extruded molybdenum as function of annealing

21 p3745 A69-38953

Phase softening transformations heat resisting alloys during cyclic heating, using X ray and electron microscope analyses

21 p3746 A69-38957

Phase plasticity in Ti-O alloy as function of temperature in alpha Ti and TiO, noting role of increased oxygen diffusion mobility

21 p3746 A69-38959

Soviet book on heat treatment of Ti alloys emphasizing structural and phase composition changes

21 p3749 A69-39526

Low melting point material selected model melt simulating shrinking process in castings of melt with broad liquidus-solidus interval

21 p3733 A69-39720

Enzyme transitions in RNA polymerase state during unprimed synthesis of r/I-C/ copolymer, noting dimer-monomer pattern during lag phase

22 p3895 A69-40050

Heat treated Ti-Al-Fe alloys thermal, microstructural and X ray analyses of phase transformations in Ti-rich corner

22 p3969 A69-40074

Jadeite/ high pressure sodium aluminum pyroxene/ shock-induced phase assemblage from oligoclase, noting relevance to lunar rock samples investigation

22 p3941 A69-40569

Phase equilibrium apparatus for measurement of thermodynamic properties of cryogenic fluid mixtures, including argon-methane data [NAS-NRC PAPER H-3]

22 p3947 A69-40630

Alloy Inconel 625 precipitation behavior and effect on short and long term properties, discussing tetragonal phase segregate and creep strength

22 p3971 A69-40802

Joints structure, phase and chemical composition in kinetics of titanium diffusion brazing with copper

22 p3958 A69-41203

Coherent matrix precipitates observation in Fe-Ni-Cr alloy by transmission electron microscopy, discussing yield strength and elongation dependence on aging conditions

23 p4176 A69-41508

Semiinverse method involving plane wave expansions to solve elliptical crack expansion and self similar phase transformation in anisotropic solid

24 p4397 A69-42749

InTe phase formation in thin film composed of two InTe phases, showing dependence on annealing in high vacuum and substrate temperature

24 p4361 A69-42994

PHASE VELOCITY

Acoustic plasma waves propagation in thin films in case of film quantization, showing phase velocities close to Fermi velocities of electrons

02 p0300 A69-12649

Bandwidth effect on wave recordings cross spectra interpretation from spatially separated sites, deriving relationship between propagation velocity and velocity bandwidth

05 p0756 A69-16272

Axial waves in blood vessels, determining phase velocities and damping, noting anisotropic behavior of artery wall

[SESA PAPER 1350] 07 p1069 A69-19726

Phase velocities and polarizations of linear waves in infinite uniform high beta plasma

08 p1359 A69-19986

OMEGA VLF navigational transmission phase delay variations and field strength measurements on transatlantic propagation path, noting effect of directional change

09 p1538 A69-22595

Transverse waves induced by disk oscillations about state of steady rotation in MHD, revealing circularly polarized waves with different phase velocities

10 p1728 A69-23239

Computer calculated phase velocities for surface wave and waveguide modes given for circular waveguide filled with inhomogeneous electron plasma

11 p1844 A69-24437

Backward plasma waves in region of anomalous dispersion indicated by opposite directions of RF wave phase and group velocities

11 p1927 A69-25116

Unstable weakly ionized HF magnetoplasma fluctuations with no axial drift, noting phase velocity parametric dependence

13 p2312 A69-28197

Wave parameters in coupled parallel surface wave transmission lines and dielectric waveguides, discussing phase velocities and spatial beat period

13 p2223 A69-28570

Surface wave study techniques, discussing digital moving window analysis of group and phase velocity and use of time variable filters

16 p2784 A69-32576

Slow electromagnetic wave propagation in superconducting thin film transmission lines, noting phase velocity dependence on film thickness and spacing

17 p2938 A69-33785

VLF wave propagation phase velocity prediction for airborne Omega computer, using scatter model based on abnormal ionosphere

17 p3002 A69-34077

Anisotropic ionospheric model for VLF TM and TE modes excitation, noting nighttime phase velocity variations

18 p3101 A69-34797

Linearized wave propagation digital simulation models to predict arterial blood flow characteristics and impedance, comparing phase velocity and transmission per wavelength

19 p3264 A69-36868

NonJeans gravitational instability of stars and interstellar gas in Galaxy due to wave interaction with stars having velocity near wave phase velocity

20 p3607 A69-38037

Pi 2 micropulsation waveform variation with time from simultaneous observations at low latitude stations, estimating phase velocity of higher frequency component

23 p4161 A69-42440

PHASED ARRAYS

Phased array radar cost improvement based on solid state devices and microwave integrated circuits application

01 p0048 A69-11039

Electron tubes in phased array radar systems, discussing replacement limits by solid state devices, reliability and cost reduction

01 p0048 A69-11040

Transistors vs electron tubes as microwave power sources in UHF phased array radars, noting transistor cost competitive limit

01 p0048 A69-11041

Phase, frequency and amplitude scanning, noting array design and applications

01 p0049 A69-11348

Phased array radar antennas emphasizing beam steering of transmitting linear array with number of phase shifters

01 p0049 A69-11390

Reflected and transmitted radiation fields for dielectric loaded infinite phased array of parallel plate waveguides as function of scan angle

02 p0218 A69-12326

Equation for beam shift during beam steering of phased array by conjugate element phase shifting

02 p0219 A69-12340

96 element wide band scanning array measurements, considering array simulators usability at frequencies above operating frequencies

02 p0219 A69-12343

Planar phased array of circular waveguides arranged in equilateral triangular grid, solving boundary value problem

03 p0406 A69-13829

Collimation of row and column steered phased arrays

04 p0570 A69-14304

Nonorthogonal beam steering commands for multielement two dimensional phased array antenna

04 p0570 A69-14305

Granularity of beam positions in digital phased arrays based on method of moments and phase distribution

04 p0570 A69-14306

Electronically steered and shaped beams for linear and ring phased array antennas by sampling element signals multiplexed into single channel

04 p0570 A69-14307

Element pattern nulls in phased arrays and relation to guided waves supported by array face

04 p0570 A69-14310

Impedance matching of volumetrically scanned waveguide arrays, stressing element spacing, surface wave impedance, etc

04 p0571 A69-14312

Linearly polarized waveguide phased array design, noting waveguide aperture size effect on admittance and minimization of zero radiation directions

04 p0571 A69-14313

Asymptotic decay of coupling for infinite phased arrays proved valid for infinite parallel linear plate array immersed in magnetized cold plasma

04 p0571 A69-14314

Driving point admittance of radiating aperture in infinite periodic planar phased array, determining coefficients of waveguide modal expansion and Floquet series

04 p0571 A69-14315

Infinite phased dipole array, discussing integral equation, current distributions and active admittances

04 p0571 A69-14316

Bandpass characteristic for wide instantaneous bandwidth microwave components for phased arrays, noting error effect on compressed signal and time delay design

04 p0571 A69-14318

Semiconductor microwave phase shifters for electronic steering of phased array radar antennas noting cost, reliability and properties of steerable antennas

04 p0572 A69-14319

Reciprocal latching ferrite phase shifters application to lightweight scanned phased arrays, noting quasi-circularly polarized modes with lowest insertion loss

04 p0572 A69-14320

Phased array antenna radiator element design, emphasizing configuration selection and reflection loss for beam steering

04 p0572 A69-14321

Impedance matching selection for phased array element, using element impedance data and equivalent circuit

04 p0572 A69-14323

HAPDAR-TACOL phased array radar design, discussing array patterns and multitarget tracking performance

04 p0556 A69-14324

Hybrid mode Ku-band mixer steering electronic scanning phased array design

04 p0572 A69-14325

Cassegrain two reflector antenna modification by discrete phased array, allowing for subunit redesign

04 p0572 A69-14326

Two dimensional electronically scanned k-band phased array antenna design and performance, discussing radiometric system

04 p0572 A69-14328

Radiation properties of spherical phased array of 16 flat spiral antennas and radiation field polarization characteristics

04 p0573 A69-14331

Radiation pattern of linear phased antenna array calculated during commutated scanning

04 p0577 A69-14785

Frequency controlled time delay network for broadband phased array antenna steering

04 p0580 A69-15469

Equivalent network representation of feedthrough lens array taking into account mutual coupling between elements to predict performance characteristics

08 p1280 A69-20014

Phasing of active region of log-periodic array antennas by modulated impedance feeders, discussing monopole and slot arrays

08 p1281 A69-20015

Resonance conditions in dielectric sheathed or plug loaded phase arrays of waveguides

08 p1281 A69-20034

Forced surface wave resonances in dielectric free 45 degree triangular grid circular waveguide phased arrays

08 p1282 A69-20038

Plane H polarized electromagnetic wave diffraction incident on array of rectangular rods described by linear algebraic equations

08 p1275 A69-20433

Electronically phased array antenna system design optimization and testing for application to spin stabilized satellites

08 p1289 A69-20969

Phased array radar system for UHF detection, identification and tracking of orbiting objects and ballistic missiles, noting system design and hardware

12 p2028 A69-25906

Electronically scanned and fixed multiple beam phased arrays for spaceborne microwave radiometric sensors

12 p2044 A69-26977

Helix antennas for phased arrays for spacecraft, discussing performance and development

13 p2228 A69-27632

Admittance of radiating elements in circular array with longitudinal slots on conducting cylinder, taking into account element interactions

13 p2234 A69-28505

Stepped scanned ring monopulse array, discussing pattern analysis, directivity, co-phased and quasi-phased model

14 p2419 A69-28894

Phased array blindness at inoperative scan angles explained in terms of elements excitation and termination caused by leaky wave
17 p2928 A69-33872

Driving point admittance of radiating aperture in infinite periodic phased array, determining Floquet series and coefficients of waveguide modal expansion
17 p2938 A69-33876

Bandwidth limitations for phase steered planar arrays in satellite applications, discussing weight reduction by modulo 2 pi beam steering
17 p2941 A69-34082

Phased arrays applied to inertialess electronic steering of satellite antennas, discussing digitally steered, retrodirective and hybrid matrix arrays
17 p2942 A69-34083

Beam control of optically fed two axis airborne electronically scanned phased arrays by on-array and off-array processing
17 p2942 A69-34085

Gain measurement of two element phased array aperture antenna during ATS-C tracking
19 p3272 A69-36254

Modified residue-calculus technique combined with scattering matrix multiple reflection techniques for boundary value problems in waveguide phased arrays, diffraction gratings, etc
20 p3505 A69-37298

Active admittance, realized gain and linear polarization degradation vs scan angle for infinite periodic phased arrays of circular apertures
20 p3507 A69-37844

Strapped down phased array radar tracker mechanization with digital loop closure electronics for homing missiles, noting cost advantages
[AIAA PAPER 69-873] 21 p3763 A69-39399

MERA /Molecular Electronics for Radar Applications/ modules testing in planar array simulator, measuring far field amplitude patterns in transmitting and receiving modes
22 p3912 A69-40067

Circular and spherical antenna arrays elements random distribution in three dimensional space using Monte Carlo method, considering arbitrary excitation and nonisotropic elements
22 p3914 A69-40704

Spacecraft phase array designed for use on synchronous communication satellite, discussing low structural weight packaging and unfurling problems and helix approach
22 p3915 A69-40705

Redirection of time varying signal between specified points by arbitrarily spaced antenna array elements with condition involving time delays for validity of retrodirection
23 p4136 A69-41580

Quantization sidelobe characteristics of phased array with triangular and rectangular element arrangement
23 p4137 A69-41591

S band phased array receiver developed to track automatically moving telemetry transmitter by electronic beam steering
23 p4120 A69-41751

Statistical analysis of random production errors on phasing section polarization field of antenna with elliptical polarization
23 p4125 A69-42041

Diffraction characteristics of electromagnetic wave by periodic two element arrays, noting amplitude measurement of harmonics in millimeter wavelength range
23 p4139 A69-42044

Microwave integrated circuit applications to reflective and transmissive phased arrays, discussing radar system elements
24 p4286 A69-43109

Microcircuit phased array electronic countermeasures system design and hardware techniques for aerospace applications, analyzing adaptive, retrodirective and combination array systems
24 p4287 A69-43110

PHASED LOCKED SYSTEMS

Injection phase-locking characteristics of LSA /limited space charge accumulation/ mode transferred-electron diode oscillators, employing negative conductance and equivalent circuit
14 p2421 A69-29544

PHENOL FORMALDEHYDE

Ionic and nonionic mineral oxide powder fillers influence on stereopolymers lattices formed from phenolformaldehyde oligomers, discussing mechanical properties
08 p1335 A69-20331

PHENOLIC RESINS

Quantitative determination of phenolic content in composite materials by pyrolysis gas chromatography method
01 p0025 A69-11267

Phenolic and epoxy adhesives for metal-metal and honeycomb bonding, discussing cold cure adhesives for aircraft structures and aircraft floor sandwich design optimization
04 p0606 A69-14845

Silica fabric reinforced phenolic composites mechanical properties at temperatures above cure level
09 p1530 A69-22321

Nozzle ablations based on chemical mechanism, discussing pure or reinforced phenolic resin
11 p1999 A69-24908

Time and temperature dependence of plastic properties of fiber reinforced phenolic heat shield materials
12 p2119 A69-26825

Phenolic resin and silica cloth laminates transparency to IR radiation, noting experimental results
18 p3136 A69-34640

Hexagonal and nonhexagonal cell phenolic honeycomb design as energy dissipating material noting processing, composite constituents, cell configuration and usage environment
19 p3353 A69-35503

Ablation effect on heat transfer coefficient of carbon, silica and ceramic cloths impregnated with phenolic resin subjected to torch testing and motor firing
21 p3753 A69-39800

PHENOLS

Thermodynamic dissociation constants of alkyl phenols in aqueous and methanol media based on UV spectroscopic analysis, noting anticarcinogenic properties
11 p1831 A69-24539

PHENOMENOLOGY

Lasers, reviewing phenomenology, physical and theoretical fundamentals, quantized energy levels, population of energy levels and laser components
06 p0936 A69-18003

Observations in quantum theory, considering object state, apparatus effects, eigenvalues probability distribution, etc
20 p3576 A69-37581

PHENYLS

Neat alpha styryl azide transformation into 2-phenylazirine, 3,6-diphenylpyridazine and 2,5-diphenylpyrrole after one month at room temperature in brown glass bottle
10 p1651 A69-23307

Free lysine and dinitrophenyl /DNP/ derivatives determined quantitatively by ion exchange chromatography
17 p2917 A69-33651

Compensatory hypertrophy effects on adrenal phenylethanolamine n-methyl transferase /PNMT/ activity in rats
23 p4080 A69-41404

PHILOSOPHY

NT PARADOXES

Philosophical problems of Einstein theory of gravitation and relativistic cosmology - Conference, Kiev, June 1966
14 p2482 A69-28856

Einstein general theory of relativity, discussing evolution and disunity among physicists and philosophers on universal relativity of mechanical motion
14 p2483 A69-28857

General relativity theory philosophical substance and meaning, discussing Einstein formulations and bases of classical, relativistic and quantum physics
14 p2483 A69-28859

Categorical structures in theoretical thinking for philosophical fundamental physical laws analysis, including space-time concept changes in classical physics and in theories of relativity
14 p2484 A69-28861

Soviet book on theories of origin, nature and evolution of life from viewpoint of dialectic materialism, covering evolution trends, cell differentiation, etc
19 p3259 A69-36746

PHOBOS

Deimos and Phobos mutual secular perturbations from calculated masses and orbital elements, using canonical systems of equations
10 p1780 A69-23615

PHOEBUS NUCLEAR REACTOR

Liquid hydrogen pumping for Phoebus reactor, discussing feed systems, nozzles, configurations, design, testing, etc
[AIAA PAPER 67-478] 21 p3769 A69-39751

PHONETICS

Speech intelligibility in air at ground level and in helium-oxygen mixture at 18,000 ft
12 p2019 A69-26548

PHONOCARDIOGRAMS

U PHONOCARDIOGRAPHY

PHONOCARDIOGRAPHY

Systolic murmurs and flight personnel evaluation, noting phonocardiographic definition and tracings of specific systolic murmurs
09 p1445 A69-22726

Intravascular pressure and sound measured in anesthetized dogs and humans using fiberoptic pressure catheter
17 p2917 A69-34172

Frequency analysis of second heart sound splitting in patients with coronary artery disease assessed clinically and by phonocardiography
24 p4261 A69-42726

Abnormally slow ultrasound diastolic slope detected by mitral valve motion study in patients with clinically pure mitral insufficiency
24 p4261 A69-42727

PHONON BEAMS

Phonon interactions with recoilless gamma rays, considering usability of Mossbauer effect as probe for VHF acoustic experiments
10 p1724 A69-23088

PHONONS

NT PHONON BEAMS

Multiphonon orbit-lattice relaxation of excited states of rare earth ions in crystals, measuring fluorescence lifetimes, quantum efficiencies and transition rates
01 p0134 A69-10011

Many valley n-type Ge and Si semiconductors dissipative current breakdown effects, noting dependence on symmetry of valleys and phonon scattering pattern
02 p0298 A69-12098

Electroacoustic amplifier based phonon devices, using surface waves on piezoelectric materials to speed radar data real time processing
03 p0394 A69-13353

Thermoelectric and thermomagnetic properties of bismuth at low temperatures, assuming thermal EMF due to phonon capture of carriers
03 p0488 A69-13885

Phonon capture by electrons in semiconductors with high permittivity in external electric field
03 p0489 A69-13891

Phonon states effective density in neodymium trichloride from vibronic spectra accompanying electronic transitions in trivalent Pr and Nd ions
03 p0473 A69-13907

Displacement correlations and frequency spectra for mass disordered lattices, deriving cluster expansion for phonon Green function
03 p0493 A69-14241

Raman spectra of optical phonons in semiconductors, using reflection techniques and Ar laser excitation
06 p0936 A69-17882

Electron and phonon tunneling spectroscopy in metal Ge contacts, noting improved agreement with one electron model
06 p0982 A69-18234

Electron plasma and magnetic field effects on polaritons in semiconducting GaAs studied by Raman scattering of light at small angles
07 p1200 A69-19401

Magnetophonon oscillations of transverse magnetoresistance of n-type epitaxial GaAs in pulsed magnetic field
08 p1373 A69-20760

Localized plasmons and optical phonons occurrence on local plasma levels, noting role of impurity atom in localized exciton-plasma resonance
09 p1548 A69-21674

Thermoelectric and thermomagnetic properties of bismuth at low temperatures, assuming thermal EMF due to phonon capture of carriers
11 p1938 A69-25686

Phonon capture by electrons in semiconductors with high permittivity in external electric field
11 p1939 A69-25692

Tellurium doping effect on phonon diffusion in GaSb, discussing thermal conductivity at low temperatures
12 p2142 A69-26294

Single crystals garnets Raman spectra using laser radiation, separating phonon spectra of host lattices from electronic Raman effect

14 p2507 A69-29334

Magnetoelastic resonant interaction of microwave longitudinal phonons propagating at right angles to magnetic bias applied to YIG rod axis

15 p2565 A69-30184

Hole mobilities in InSb due to phonon and ionized impurities scattering on basis of strain potential constants

16 p2824 A69-31575

Magnetoquantum-electric effect, analyzing center motion of cyclotron orbit during photon and phonon absorption and current quantity

16 p2826 A69-31823

Phonons, electrons and protons in ferro- paraelectric and hydrogen bonded ferroelectrics, examining higher frequency optical and lower frequency dielectric properties

16 p2827 A69-32262

Lattice vibration theory of solid state diffusion for Cu including anharmonic effects formulated using equilibrium statistical mechanics, considering interacting phonon events

17 p3015 A69-32822

Qualitative interpolation formula for phonon frequency spectrum of mass disordered alloys three dimensional systems at high concentrations

20 p3583 A69-37279

Optical frequencies and polarizations of IR active phonons of tysonite lanthanide fluorides based on Kramers-Kronig reflectance spectra analysis

22 p3993 A69-40729

Spin-phonon systems thermal noise, based on combined lattice and spin lattice Hamiltonian densities, applied to acoustic noise field measurements

24 p4350 A69-43061

PHOSPHATES

NT ADENOSINE TRIPHOSPHATE [ATP]
NT AMMONIUM PHOSPHATES
NT NUCLEOTIDES
NT POTASSIUM PHOSPHATES
NT PYRIDINE NUCLEOTIDES
NT URIDYLIC ACID

Phosphate cements for bonding mica ceramic to titanium in jet engine equipment

05 p0786 A69-16799

Uranyl ions interaction with phospholipid and cholesterol monolayers, using surface pressure and potential measurements

11 p1832 A69-25641

Corrosion resistance rate of duralumin sheet in aqueous superphosphate solutions dependence on concentration

12 p2113 A69-26124

Energy exchange of rare earth ions in uranyl phosphate liquids and glasses, studying sensitized luminescence origin

14 p2485 A69-29034

Chlorapatite and whitlockite compositions of phosphate minerals from chondrites determined by electron microprobe

15 p2690 A69-30706

Phosphate mineralogy of meteorites using X ray, electron-microprobe and chemical analyses, noting predominance of whitlockite

19 p3416 A69-36126

Active center chemical bond alteration influences on luminescence characteristics of phosphate glasses, noting quick energy transfer via ions

20 p3552 A69-37017

Magnetic ordering in dysprosium phosphate observed by high resolution spectral line intensity measurements, finding Neel temperature

21 p3773 A69-38331

Properties, relative magnitudes and relationship of pyrophosphate exchange reactions catalyzed by DNA polymerase from *Escherichia coli*

22 p3898 A69-41072

Deoxyribonucleoside triphosphate substrate binding to *Escherichia coli* DNA polymerase, conducting equilibrium dialysis

22 p3898 A69-41074

PHOSPHIDES

NT GALLIUM PHOSPHIDES
NT INDIUM PHOSPHIDES
NT SCHREIBERSITE

Optimal electroluminescent efficiencies for vapor grown gallium arsenide phosphide diodes, analyzing current spreading, absorption, impurity and composition effects

[ECS PAPER 103] 08 p1284 A69-20366

Optical and electrical properties of electroluminescent diffused gallium arsenide phosphide diodes with low donor concentrations, analyzing spectral emission and fabrication effects

16 p2758 A69-31699

Barringerite as Fe-Ni phosphide occurring in meteorite Ollague pallasite, indicating troilite and schreibersite crystallization at high temperatures

18 p3205 A69-35433

PHOSPHINES

Lewis acidity of alanes, discussing interactions of trimethylalane with amines, ethers and phosphines

07 p1074 A69-18630

Ligand field transitions in tertiary phosphine and arsine complexes of ruthenium and osmium

07 p1075 A69-19483

PHOSPHORESCENCE

Fluorescence and phosphorescence from tryptophan powders stimulated at low temperatures with UV, vacuum UV, fast electrons and X rays

03 p0372 A69-13487

Temperature effects on phosphorescence lifetimes and intensities of aromatic hydrocarbons in polymethyl methacrylate, estimating activation energy for thermally activated nonradiative decay mode

10 p1652 A69-23523

PHOSPHORS

Thermographic phosphor technique to provide transient temperature measurements in impulse wind tunnel

01 p0078 A69-10152

Thermographic phosphor coatings to obtain optical quantitative heat transfer distribution on wind tunnel models

12 p2099 A69-27150

Luminophors for carbon dioxide laser radiation visualization noting controlled sensitivity, quick response and resolution

18 p3153 A69-35259

Colors production on electroluminescent display using phosphors impressed-frequency/emission-color relationships together with chromatic biasing

24 p4286 A69-42900

PHOSPHORUS

Depth and planarity of zinc diffused junctions in GaP using temperature, phosphorus overpressure and time as independent variables

13 p2322 A69-28136

B-type stellar spectra, discussing atmospheres and local thermal equilibrium from considerations of He I and P II lines relative strength

15 p2679 A69-30046

Kamacite analysis for P and Ni in chondrites, pallasite and iron meteorites, considering cooling rate and rhadite

19 p3417 A69-36131

PHOSPHORUS COMPOUNDS

NT ADENOSINE TRIPHOSPHATE [ATP]
NT AMMONIUM PHOSPHATES
NT GALLIUM PHOSPHIDES
NT INDIUM PHOSPHIDES
NT NUCLEOTIDES
NT ORGANIC PHOSPHORUS COMPOUNDS
NT PHOSPHATES
NT PHOSPHIDES
NT PHOSPHINES
NT POTASSIUM PHOSPHATES
NT PYRIDINE NUCLEOTIDES
NT SCHREIBERSITE
NT URIDYLIC ACID

Gettering effect in silicon of phosphorsilicate glass surface layer and underlying phosphorus layer on gold and copper

03 p0487 A69-13640

PHOSPHORUS METABOLISM

High energy phosphate splitting for energy requirements not met by oxidation during supramaximal exercise, noting glycogen splitting into lactic acid after phosphate exhaustion

23 p4100 A69-41443

PHOSPHORUS POLYMERS

Thermal and mechanical properties UV of diazadiphosphetides, carbodiimides and phosphorus amide epoxies resins composites for use in environmental extremes

19 p3356 A69-35528

PHOSPHORUS 32

P32 distribution in protein of blood serum, liver and brains of rats bombarded with high energy protons

02 p0198 A69-11507

PHOSPHORYLATION

High oxygen concentration influence on animal organisms noting respiration, pulmonary gas exchange,

hypoxia, brain phosphorylation, immunological indices and morphological structure of rats and mice

05 p0709 A69-16512

High oxygen concentration influence on animal organisms noting respiration, pulmonary gas exchange, hypoxia, brain phosphorylation, immunological indices and morphological structure of rats and mice

18 p3095 A69-34731

Successive X ray doses effect on oxidative phosphorylation of vitamin B 1 in white rats liver tissue ultrastructure during and after irradiation, establishing thiamine biosynthesis suppression

21 p3658 A69-39056

Fluorescence properties of nucleotides, polynucleotides and phosphorylated derivatives as function of temperature, pH and ionic strength

22 p3898 A69-41078

PHOTOABSORPTION

Cultured Chinese hamster cells responses to UV light of different wavelengths indicating photon absorbing molecules inhibition of colony development

07 p1068 A69-19492

PHOTOCATHODES

Plasma flow from Penning discharge with incandescent cathode in vacuum controllable by varying voltage, pressure and magnetic field strength

11 p1933 A69-25543

Stellar photometric data for various photocathode materials used to calculate radiant energy falling on earth

17 p2973 A69-33092

PHOTOCELLS

U PHOTOELECTRIC CELLS

PHOTOCHEMICAL REACTIONS

NT PHOTOCROMISM
NT PHOTODECOMPOSITION
NT PHOTOLYSIS
NT PHOTOSYNTHESIS
NT RADIOLYSIS

Photochemistry and radiation chemistry - Conference, Natick, Massachusetts, April 1968

01 p0024 A69-10617

Long lived low level chemiluminescence due to gaseous reactions at low concentrations induced by mercury lamp irradiation or Tesla coil discharge

01 p0024 A69-10618

Linearized perturbation treatment developed for photochemical and dynamical effects in gravity wave production of E-region ionospheric irregularities, including ion convergence

01 p0073 A69-11175

Photochemistry in dry atmosphere, discussing ozone density vertical distribution in upper atmosphere and influence of O and ozone reactions with H compounds

02 p0245 A69-12694

Atmospheric ozone photochemistry, studying time dependence on hydrogen compounds, equilibrium concentration effects on reaction rates, latitude and season

06 p0916 A69-17004

Photochemical ignition of low pressure fuel-oxidizer mixtures applied to unsensitized stoichiometric mixtures of methane-oxygen and hydrogen-oxygen [WSCI PAPER 68-42]

06 p1034 A69-17791

Time dependent model of photochemical, advective and turbulent effects on meridional ozone distribution

07 p1122 A69-18253

Organic fluorine chemistry, discussing synthesis reactions and reaction of polyfluorocycloalkenes with various nucleophiles

08 p1269 A69-21129

Photochemical production of reduced organic compounds of C and N in primitive earth atmosphere

09 p1444 A69-21465

Photochemical attitude control rocket adaptable to self contained command signal or remote signal transmission, discussing light irradiation of propellant for thrust control

12 p2148 A69-26801

Ionic and biradical mechanisms in thermal and photo cis-trans isomerizations elucidated by planar and twisted configurations of polyenes

13 p2216 A69-27618

Venusian upper atmosphere dissociation and ionization, considering photochemical and dynamic processes and molecular, eddy and ambipolar diffusions

13 p2344 A69-27643

Diffusion of ozone distribution tracers in stratosphere, based on photochemistry in oxygen- only and oxygen-hydrogen atmospheres

13 p2294 A69-28492

Atmospheric ozone distribution in meridional plane including time effects of photochemistry, advection and turbulence assuming zonal symmetry

16 p2785 A69-32624

Ozone concentration photochemistry between 30-35 km, determining parameters in Hampson theory /hydrogen-oxygen atmosphere/ 16 p2787 A69-32636

Atmospheric ozone distribution as function of photochemical reactions, advection and vertical motions 16 p2787 A69-32643

Jupiter photochemistry above 1000 A, noting methane and ammonia photolysis zones, atmospheric pressures and hydrogen recombinations 17 p3032 A69-33165

Transient electrical responses from retinas, discussing visual pigment role in visual excitation, photochemistry, etc 19 p3258 A69-36377

Photographic film properties, discussing base material, emulsion, photochemical process, sensitometry, densitometry, granularity and color film 20 p3541 A69-37746

Airglow and vertical eddy transport photochemical models, analyzing O green line and OH emission distribution 21 p3713 A69-38523

Photodetachment of electrons from nitrogen dioxide ions by light in violet portion of visible spectrum, noting wavelength dependence 22 p3985 A69-40575

Model for ozone formation, distribution and decomposition at 15-45 km assuming zonal symmetry, including time effects of photochemistry, advection and turbulence 24 p4309 A69-43147

PHOTOCHEMISTRY
U PHOTOCHEMICAL REACTIONS

PHOTOCROMISM

Holography principles to design high capacity high speed storage devices, using photochrome recording medium 07 p1133 A69-19158

Photochromic panel for flash blindness protection using epoxy plastic plates containing aromatic hydrocarbon compounds excited to triplet states 21 p3668 A69-39783

Photochromic film behavior under high power argon ion laser excitation studied for display and computer memory applications, using excitation model 23 p4173 A69-41629

PHOTOCONDUCTIVITY

P-n-p junctions photoconductivity decay observation, determining signal bulk minority carrier lifetime in thin n regions 01 p0136 A69-10242

Space charge limited currents in SbSI single crystals with gallium electrodes during phase transition, discussing sticking probability and photoconductivity 01 p0137 A69-10258

Recombination effects in high resistivity Cu doped gallium arsenide single crystals determined by photoconductivity methods 02 p0294 A69-11627

Photocurrent carriers recombination in organic semiconductor rhodamine B films analyzed as function of illumination 03 p0489 A69-13890

Modulated photocurrent in CdS crystal obtained by irradiation with intensity modulated electron beam, noting relaxation time and trap concentration 03 p0490 A69-13946

Quality control of semiconductor materials, analyzing homogeneity by statistical distribution of nonequilibrium carriers based on photoconductivity measurement 04 p0642 A69-14856

Current carrier concentration temperature dependence in Te-doped silicon single crystals by analyzing photoconductivity spectra 04 p0644 A69-15267

Low temperature spectral distribution of impurity induced photoconductivity in p-type InSb crystals prepared by zone refining 04 p0644 A69-15270

Photoconductivity induced by laser pulses in semiconductor with parabolic dispersion law, linear transition and nonequilibrium carrier concentration higher than equilibrium carrier concentration 07 p1148 A69-18690

IR photoconductivity spectra at surface of gold doped silicon, establishing monopolarity 08 p1373 A69-21073

Current oscillations in semiinsulating O and Cr doped GaAs samples at room temperature, noting photoconductivity excitation spectra 09 p1557 A69-21753

Space charge limited currents in SbSI single crystals with gallium electrodes during phase transition, discussing sticking probability and photoconductivity 09 p1559 A69-22651

Photoelectric effects produced by polarized radiation in isotropic optical media, discussing photo EMF and photoconductivity in multivalley semiconductors and plasmas 10 p1701 A69-23138

IR radiation effects in cadmium sulfide crystals with green edge emission at low temperatures, discussing luminescence, photoconductivity and conductivity glow curves 10 p1746 A69-23565

Photoconductivity of semiconductors with multivalley electron energy and isotropic hole spectra, discussing nonlinearity of field dependence 11 p1937 A69-24913

Photocurrent carriers recombination in organic semiconductor rhodamine B films analyzed as function of illumination 11 p1939 A69-25691

CdS single crystals spectral dependence of photocurrent, photoconductivity quantum yield and photoelectromotive force in exciton absorption region 14 p2504 A69-28990

Automatic recording of spectral distribution of high resistance semiconductors photoconductivity using spectrograph monochromator 14 p2447 A69-29409

Majority carrier lifetime temperature dependence obtained from photoconductivity measurements of p-type GaAs crystals doped with Ge 15 p2666 A69-30056

Quality control of semiconductor materials, analyzing homogeneity by statistical distribution of nonequilibrium carriers based on photoconductivity measurement 15 p2667 A69-30248

Imperfection photoconductivity in electron irradiated Li-doped Si annealed at room temperature, noting level rearrangement in O rich material 19 p3382 A69-35696

Photocurrents and recombination luminescence in n-type diamonds subjected to UV, TI 204 and X ray irradiation indicating local electron centers formation 19 p3383 A69-36167

Transient recombination lifetimes in n-type float zone Si from 4.2 K to room temperature, obtaining electrical and photoconductivity values 19 p3383 A69-36447

Electrons and optical phonons interaction effects on optical and photoconducting properties of semiconductors, discussing phonon cyclotron resonance and oscillatory and magneto-oscillatory photoconductivity 19 p3385 A69-36517

Antimony trisulfide single crystals spectral dependence of impurity and stimulated impurity photoconductivities, comparing optical and thermal activation energies 22 p3994 A69-41042

Negative surface potential effect on noise and photoconductivity in Ge doped p-type InSb single crystals at low temperature in vacuum 24 p4362 A69-43738

PHOTOCONDUCTORS

Optimal modulation shape for light emission flux as function of photoresistance detector and resonance amplifier pulse characteristics 04 p0560 A69-15376

Pulse radiation effect on dielectric constant of sintered CdS photoresistors, discussing capacitance dependence on intensity, type and frequency of light 05 p0806 A69-15694

Phototubes, photodiodes, photoconductors, quantum detectors, nonlinear optical detectors and heterodyne receiving systems for photodetection of laser outputs 09 p1518 A69-22126

Photoconductor open circuit voltage determination, calculating responsivity and sensitivity of actual and ideal cases 12 p2093 A69-26481

One inch ceramic vidicon with slow scan photoconductor, electrostatic focusing and magnetic deflection to withstand sterilization and environmental testing for space applications 13 p2234 A69-28262

IR radiation detection by photoconductor in microwave resonator noting electric field influence 13 p2223 A69-28639

Optimal modulation shape for light emission flux as function of photoresistance detector and resonance amplifier pulse characteristics 16 p2752 A69-32123

Collector efficiency limitation of surface barrier-limited photoconductors attributed to photogenerated carrier diffusion into electrode 20 p3583 A69-37732

PHOTOCURRENTS
U ELECTRIC CURRENT
U PHOTOELECTRIC EMISSION

PHOTODECOMPOSITION

Photodegradation of organic polymers by UV radiation exposure, emphasizing polyvinyl chloride photochemistry and radiation stabilization 01 p0102 A69-10861

Photodestruction rate of H molecules by absorption of Lyman or Weber band radiation in interstellar space calculated at various distances from early stars 18 p3204 A69-35351

PHOTODETECTORS
U PHOTOMETERS

PHOTODIODES

Broadband signal and noise performance of direct detection optical receiver consisting of solid state photodiode and baseband amplifier 04 p0556 A69-14283

P-n planar avalanche photodiode without guard ring noting electrical properties, uniform multiplication and fabrication 05 p0733 A69-16559

Photoparametric up-converter with optimum SNR, noting suitability of direct detection of amplitude modulated optical signals 07 p1104 A69-18888

Ag-GaAs Schottky barrier photodiodes, describing fabrication and use as UV radiation detectors 09 p1462 A69-21334

Phototubes, photodiodes, photoconductors, quantum detectors, nonlinear optical detectors and heterodyne receiving systems for photodetection of laser outputs 09 p1518 A69-22126

Avalanche Schottky barrier photodiodes fabricated by plating GaAs with thin Pt layer and forming proton radiation guard ring, discussing gain bandwidth and SNR 13 p2226 A69-27195

GaAs photoelectric devices for radiation detection and light to electric energy conversion, considering photoresistors, photodiodes and solar cells 13 p2203 A69-27465

PHOTODISSOCIATION

Ionization, neutralization and charge exchange processes in ionosphere, detailing dependence of photodissociation and collision detachment of negative ions 01 p0066 A69-10598

Photodissociation and photoionization of diatomic molecules at high temperatures with calculation of absorption cross sections 03 p0473 A69-14147

Mass spectrometric measurements to determine energy distributions of ions produced in dissociative photoionization of O molecules 06 p0960 A69-17110

Carbon molecule photodissociation in cometary atmospheres, discussing intensity level distribution based on model 06 p1004 A69-17534

Recombination mechanism between CO and O produced by photodissociation of carbon dioxide in upper atmosphere of Venus and Mars 07 p1214 A69-18615

Wavelike photodissociation of gas molecules under quasi-monochromatic pulsed radiation, investigating associated supersonic disturbances 08 p1354 A69-19950

Primary processes leading to atomic and molecular hydrogen formation in hydrogen peroxide photolysis at 1236 A, noting OH formation 10 p1652 A69-23527

Interstellar molecular hydrogen and CH photodissociation, discussing molecular formation rates in interstellar medium 10 p1781 A69-23672

Diatomic hydrogen abundance evolution in uniform medium, discussing photodissociation effects and galactic evolution 15 p2680 A69-30205

Photodissociation of diatomic hydrogen by solar radiation for Venus atmosphere investigation, considering H atoms production rate by Stecher-Williams process 20 p3609 A69-38102

Negative ion concentrations in plasma by flash photodissociation, using Q switched laser for irradiation 21 p3778 A69-39574

Positively charged diatomic hydrogen molecules in interstellar extinction and photodissociation cross section in terms of formation mechanisms
24 p4375 A69-42610

PHOTOELASTIC ANALYSIS NT PHOTOGRAMMETRY

Stress concentrations around elliptical perforations in shrunk plates with bonded boundaries based on photoelastic models
02 p0345 A69-12391

Photoelastic analysis of HF stress waves propagating in bars and plates subjected to damped sinusoidal loading
[ASME PAPER 68-WA/APM-27]
04 p0669 A69-14397

Poincare sphere representation of polarized light used to predict rotation effect on optical observations in photoelastic shell analysis
04 p0683 A69-15495

Three dimensional photoelastic analysis based on optical theory of multilayer reflection technique
04 p0683 A69-15496

Piezooptical method applied to anisotropic bodies and reinforced plastics, deriving relation between dielectric tensors and stresses and strains
05 p0837 A69-16038

Photoelastic study of interaction between overlapping parallel cracks in tensile stress field
05 p0842 A69-16435

Strain distribution at crack base measured by Fabry-Perot interferometer and photoelastic coating
06 p1020 A69-17127

Anisotropic glass fiber reinforced epoxy resin composite under biaxial and uniaxial loads, noting isochromatics and isoclinics in photoelastic analysis
07 p1170 A69-18715

Two dimensional photoelasticity for minimizing stress concentration in perforated rectangular plate subjected to restrained shrinkage, discussing application to solid propellant rocket grains
08 p1412 A69-20255

Axisymmetric states of stress determined by photoelasticity, analyzing meridional slice under normal and oblique incidence
08 p1412 A69-20259

Structural reliability tests using photoelasticity and associated techniques, discussing computer methods, materials research, etc
09 p1479 A69-22734

Laser radiation induced stress waves in transparent media using dynamic photoelastic technique
10 p1707 A69-24213

Moire patterns for photoelastic strain analysis noting applications to elasticity, plasticity and creep problems
11 p1982 A69-24944

Stress concentration around square hole in celluloid plate subjected to creep under biaxial tension analyzed by photocreep method
12 p2178 A69-26000

Ultrahigh speed multiple framing photography system using sequentially modulated ruby laser and smear type camera applied to dynamic photoelasticity
12 p2086 A69-26166

Tempered glass plates strength nondestructive testing by scattered light photoelastic method, discussing application to aircraft windshield sandwich structures
[AIAA PAPER 68-323]
12 p2118 A69-26768

Stress distribution in matrix of unidirectionally fiber reinforced composite subject to shrinkage and normal transverse load, using three dimensional photoelastic analysis
12 p2189 A69-27162

Structural stress under acceleration loading simulated by two dimensional photoelastic model noting improvement of fringe patterns quality
14 p2532 A69-28885

Box girders stress distribution analyzed by stress-freezing method compared with photoelastic measurement
15 p2705 A69-30419

Automated shear difference analysis of three dimensional photoelastic model stress distribution by stress-freezing and slicing technique
15 p2609 A69-30680

Stress concentration on circular holes and notches in anisotropic oriented glass fiber reinforced plastics determined by using photoelastic birefringent coatings
15 p2713 A69-31053

Stresses in fixed two dimensional photoelastic models analyzed by hologram interferometry, displaying isochromatic and isopachic interference patterns
15 p2611 A69-31110

Photothermoelastic analysis of thermal stresses in turbine wheels with welded blades, noting stress concentration reduction
15 p2715 A69-31488

Schlieren and photoelastic methods for continuous and pulsed ultrasonic waves propagating in transparent media, discussing nondestructive testing applications
15 p2617 A69-31510

High speed photography using multiply pulsed ruby laser, Pockels cell modulation and smear camera for isochromatic and photoelastic pattern recording
19 p3306 A69-35731

Photoelastic model methods for two and three dimensional investigations of microstresses in composite materials
20 p3565 A69-36940

Cranz-Schardin camera for high speed recording in dynamic photoelastic fringe pattern studies, discussing framing rates, fringe gradients and design
20 p3541 A69-37778

Photoelastic data analysis for stress separations, discussing shear slope and Tesar methods
21 p3843 A69-39316

Poincare sphere properties representing birefringent behavior of materials and qualitative measurement technique for elliptically polarized light
21 p3844 A69-39318

Photoelastic and micromechanic studies of epoxy resins of varying Young moduli by simultaneous stress analysis of FRP and matrix materials
21 p3846 A69-39796

Isoclinic angle errors effects on photoelastic fringe order measurements accuracy
22 p3945 A69-40082

Moire effect applications to stress analysis, enumerating advantages over conventional grid techniques
22 p4042 A69-40315

Babinet compensator with birefringent wedges made of stress frozen photoelastic material rather than quartz
22 p4042 A69-40442

Scattered light methods inaccuracies for nondestructive analysis of generally stressed photoelastic models, noting modified Mini-max method
24 p4396 A69-42737

Isoclinics determination from fringe patterns, obtaining continuous principal stress direction data for photoelastic model in bonded polariscope
24 p4396 A69-42738

Photothermoelastic investigation of thermal stress concentrations around circular cavities and inclusions in two dimensional composite models
24 p4396 A69-42739

PHOTOELASTIC MATERIALS

Buckling deformation and stress fields around central slits in photoelastic models and metal sheets under tensile load
10 p1796 A69-23069

Electric vector transformation for three dimensional photoelastic medium irradiated by light in reverse direction, noting optical systems of birefringent plates and rotators
12 p2180 A69-26339

Photoelastic materials stressed state analysis by inserting analyzer and polarizer into sandwich medium, obtaining polarized light field
18 p3138 A69-35152

Surface stresses in rotating asymmetric profiled disks and axial deflection effects computed theoretically and compared to measurements on photoelastic models
19 p3447 A69-36862

Linear limit uniaxial stresses for stress-strain and stress-birefringence in photoelastic and mechanical model materials
20 p3628 A69-37777

Photoelastic behavior in amorphous solids, proposing microstructural mechanism for deformation birefringence
22 p3972 A69-40081

Epoxy resin materials assessed for model materials for three dimensional photoelasticity
22 p4042 A69-40311

Babinet compensator with birefringent wedges made of stress frozen photoelastic material rather than quartz
22 p4042 A69-40442

Principal stresses determination in optically active photoelastic models from fringe pattern while obtaining sum from Dirichlet problem solution by straight line method
23 p4228 A69-41987

Circular cylindrical photoelastic shells buckling modes under axial compression using high speed isoclinic photography, discussing shallow shell equations applicability to early stages
24 p4404 A69-43652

PHOTOELASTICITY

NT PHOTOVISCOELASTICITY

Three dimensional thermal stress distribution in case bonded solid propellant determined by scattered light

photoelastic technique coupled with transparent rocket motor model
02 p0345 A69-12371

Holographic interferometer for isopachic stress analysis, utilizing photochromic recording for real time interference
04 p0599 A69-15013

Collection of papers on photoelasticity by M. M. Frocht
08 p1410 A69-20116

Graphical methods for photoelastic effect behind system with stresses rotating about direction of light propagation, discussing circle technique
09 p1617 A69-22011

Structures analysis by photoelastic model techniques of stress visualization
10 p1794 A69-22941

Reversibility principle in transilluminated three dimensional photoelastic medium
14 p2535 A69-29359

Photoelasticity testing of stress gradient factor on notched tensile specimens
17 p3052 A69-32982

Rotation effect of secondary principal axes in scattered light photoelasticity by dual observation method, deriving light intensity
21 p3844 A69-39317

Pulse ruby laser-smear camera ultrahigh speed multiple frame recording system, describing applications to transmitted and scattered light photoelasticity
22 p3944 A69-40076

Photographic high speed recording system characteristics effects on dynamic photoelastic fringe patterns fidelity
22 p3945 A69-40077

Scattered light photoelasticity dual observation method, describing automatic data collecting and interpreting system
22 p3945 A69-40079

Epoxy resin materials assessed for model materials for three dimensional photoelasticity
22 p4042 A69-40311

PHOTOELECTRIC CELLS

NT PHOTOVOLTAIC CELLS

Laser longitudinal oscillation modes beat frequencies measurement by grouping photoelectron velocities by HF field containing photomultiplier cathode
03 p0440 A69-13265

Phase method of photoelectric registration of stellar transition moments
04 p0601 A69-15252

CdSe single crystal films vacuum deposition for use of photocells base with p-n heterojunctions
07 p1198 A69-18512

Photocells with p-n heterojunctions from sintered CdS, describing spectral sensitivity and temperature dependence of no-load photo EMF
08 p1374 A69-21084

Recombination parameters and depth of levels of p-n junctions in semiconductor photocells determined from position of maximum spectral sensitivity
09 p1560 A69-22718

Photocell base thickness for optimal power to weight ratio, noting photons spectral distribution and absorption coefficient dependence on frequency
09 p1443 A69-22719

Solar cells operation in space flight, considering Si photoelectric cells characteristics and complete systems construction for spacecraft power supplies
12 p2015 A69-25865

Electromagnetic accelerometer with symmetrically placed photocells detecting small steel ball position
17 p2971 A69-32897

PHOTOELECTRIC EFFECT

NT PHOTOIONIZATION

Photoelectric effect of thin gold films on silver and quartz substrates, analyzing work function dependence on thickness of deposited metal
02 p0300 A69-12630

Photoelectric effect of thin gold film under electric field, noting work function dependence on film thickness exhibits extremum
02 p0300 A69-12631

Photocurrent pinch-off effect in high resistivity thin CdS crystals for evaluating donors, acceptors and surface states
03 p0488 A69-13757

Quadratic and cubic response in photoelectric emission in potassium antimonide under laser irradiation observed with measurement of energy distribution of excited electrons
05 p0771 A69-15813

- Nonlinear coupling between background illumination and illumination signal producing lateral electrical fields in p-n junction, noting effect on sensitivity of position sensor
07 p1101 A69-18654
- Photoelectric effects produced by polarized radiation in isotropic optical media, discussing photo EMF and photoconductivity in multivalley semiconductors and plasmas
10 p1701 A69-23138
- Two photon photoelectron counting statistics and intensity fluctuations of incident radiation compared with single photon detectors and applied to laser outputs
10 p1704 A69-23658
- Variable stars in Large Magellanic Cloud from photoelectric measurements obtained in blue and violet, including periods of Cepheids and some period amplitude differences
14 p2526 A69-29853
- Indium antimonide crystals polarity effect on photoeffect, analyzing quantum yields and energy spectrum
15 p2667 A69-30076
- Alloying pairs of metal pellets to n and p type semiinsulating GaAs, discussing photo effects
17 p3015 A69-32824
- Photoelectric effect without photons, discussing classical field falling on quantized atomic electron
17 p3007 A69-32838
- Optical frequencies mixing based on photoelectric effect in metals and semiconductors, noting internal photoconductivity
19 p3332 A69-35871
- Low energy electron accelerator to produce measurably small fluxes through photoelectric effect from Au cathode UV irradiation to achieve high flux stability
19 p3313 A69-36492
- Friction bearing vibration recording device using light beam and photodiode
20 p3539 A69-37436
- Photoelectric methods for pulsed and CW lasers output power and energy measurements
22 p3961 A69-40239
- Photoelectric spectrometer observations of 1966 total solar eclipse, discussing limb darkening curves for regions of continuum 1.5 A wide around 5728 and 6404 A
22 p4027 A69-40659
- Chemical high pressure laser action produced by stimulated phototransition of electrons at contact moment between pair of reacting nonexcited gas molecules
22 p3965 A69-41117
- PHOTOELECTRIC EMISSION**
GaAs photoemissive yield spectrum analysis, discussing transition energies and energy band structure models
01 p0140 A69-11254
- Photoelectric properties of n-n junction interfaces in gallium phosphide and arsenide semiconductors
02 p0294 A69-11630
- Observation of photocurrents generated in Schottky barrier diodes on barium titanate, suggesting practical utility of photon-to-electron conversion efficiencies
07 p1104 A69-18905
- Photoelectric light diagrams for eclipsing binary star
08 p1392 A69-20565
- Time dependent recoverable isothermal decrease of photocurrent in CdS crystals in vacuum, noting trap mechanism involving electron redistribution
08 p1374 A69-21187
- Dark and photocurrent volt-ampere characteristics induced by capture of carriers injected into illuminated CdS single crystals
09 p1555 A69-21506
- Atmospheric extinction function in Chile by using photoelectric spectrum scans, observing neutral component, Rayleigh scattering and ozone absorption variations
10 p1777 A69-23386
- Early type stars spectrophotometric parameters, discussing hydrogen beta, gamma and delta line widths, magnitude, etc
10 p1777 A69-23387
- Statistical characteristics of photocurrent pulse amplitudes during cathode exposure to gas laser outputs
11 p1834 A69-24611
- CdS single crystals spectral dependence of photocurrent, photoconductivity quantum yield and photoelectromotive force in exciton absorption region
14 p2504 A69-28990
- GaAs photoelectric emission at different activation degrees by adsorbed Cs and BaO layers, noting spectral response characteristics differences and causes
14 p2504 A69-28993
- Indium antimonide crystals polarity effect on photoeffect, analyzing quantum yields and energy spectrum
15 p2667 A69-30076
- IR quenching of photocurrent under field effect in CdS crystal
16 p2827 A69-32044
- Time dependent recoverable isothermal decrease of photocurrent in CdS crystals in vacuum, noting trap mechanism involving electron redistribution
18 p3183 A69-35156
- Multiphoton luminescence and photocurrent excitation by ruby and neodymium laser beams of KCl-Eu single crystals, noting brightness dependence on laser beam power
19 p3335 A69-36165
- Ruby laser-ultrahigh vacuum device for studying electron and ion emissions and light absorption of materials, noting influence of adsorbed gas layers
20 p3553 A69-37406
- Multiquantum photoemissive effect in metals, semiconductors and dielectrics emphasizing laser application for studying electromagnetic field
22 p3964 A69-40690
- Ultrahigh vacuum cleaved GaAs-Cs and GaAs-cesium monoxide photoemission acceptor densities, noting crystal parameters role
23 p4198 A69-41548
- PHOTOELECTRIC GENERATORS**
GaAs photoelectric devices for radiation detection and light to electric energy conversion, considering photoresistors, photodiodes and solar cells
13 p2203 A69-27465
- Faceted reflector for solar power installations with photoelectric converters, discussing reflector construction, efficiency and energy balance
16 p2741 A69-32798
- Solar cell retractable array for spacecraft multikilowatt power generation
19 p3254 A69-35711
- PHOTOELECTRIC MATERIALS**
Light sensitivity dependence of semiconductor-metal systems on layer thickness
14 p2508 A69-29666
- PHOTOELECTRIC PHOTOMETRY**
U ELECTROPHOTOMETERS
PHOTOELECTRICITY
Temperature effects on primary photocurrent of base collector and collector substrate junctions of isolated transistors from microcircuits
06 p0977 A69-16881
- Photoelectronic imaging systems in space exploration emphasizing acquisition time, storage capacity and transmission time
07 p1136 A69-19591
- Photoelectric measurement of chromospheric heights by method requiring neither high telescopic resolution nor best seeing, discussing trials during September 1967
08 p1385 A69-20070
- Multichannel photoelectric spectrometer design for Hale telescope, noting effectiveness in red and IR observations
08 p1318 A69-21131
- Photoelectric, calorimetric and photon-momentum methods for measuring laser output energy and power emphasizing liquid, wire and pyroelectric calorimeters
11 p1899 A69-25196
- Photoelectric polarimeter to record sky light intensity in form of polarized components, detailing construction and operation
12 p2078 A69-25892
- Photoelectronic image devices, discussing detectors, electronography, Lallemand camera, spectracon and electron image multipliers
12 p2082 A69-26136
- Photoelectronic high speed image intensifier framing camera, showing single shot synchronized photography of electric spark in air
12 p2082 A69-26137
- Photoelectric characteristics of thin film CdS-CdTe heterojunction diodes, considering I-V illuminance, spectral characteristics and conduction band continuity
13 p2230 A69-27882
- CdS single crystals spectral dependence of photocurrent, photoconductivity quantum yield and photoelectromotive force in exciton absorption region
14 p2504 A69-28990
- Optophotoelectric pickup design for angular displacement measurements, considering application of moire pattern produced by radial diffraction gratings
14 p2447 A69-29327
- Electrical and photoelectrical properties of semiconductor heterojunctions prepared by Ge epitaxy on gallium arsenide bases, showing dependence on base surface treatment
15 p2667 A69-30078
- PHOTOELECTROMAGNETIC DETECTORS**
U RADIATION MEASURING INSTRUMENTS
U SENSORS
PHOTOELECTRONICS
U ELECTRONICS
U PHOTOELECTRICITY
PHOTOELECTRONS
F 2 layer cut-off frequency predawn increase caused by sunrise, resulting in photoelectrons transfer along force lines at magnetically conjugate point
02 p0238 A69-11681
- Photoelectron energy loss mechanisms in planetary atmospheres, considering possible constituents in Mars and Venus upper atmospheres
02 p0321 A69-12118
- Hall mobility of photoelectrons in cadmium sulfide layers
03 p0491 A69-14055
- Latitude dependence of 6300 A /O I/ twilight airglow enhancement attributable to conjugate photoelectrons
05 p0756 A69-16280
- Auger and photoelectron spectroscopy for chemical analysis, noting effects of sample thickness, sample potential, surface contamination and X ray incident angle
07 p1075 A69-19775
- Zone structure of silicon-silicon dioxide system for silica films obtained by pyrolytic dissociation, discussing kinetics of photoelectrons capture at traps
09 p1555 A69-21478
- Spectral distribution of X ray atmospheric absorption used to determine high energy photoelectrons spectrum
09 p1577 A69-21774
- Satellite measurements of suprathermal electrons at conjugate sunrise, indicating photoelectron escape from production level and movement along geomagnetic lines into conjugate ionosphere
11 p1950 A69-25144
- Optical satellite tracking system using multicoincidence method of photon signal counting by Q switched laser
11 p1841 A69-25579
- Temporal correlations in light field from laser at threshold of oscillation, measuring He-Ne CW gas laser by photoelectron count
13 p2271 A69-27399
- F 2 layer cut-off frequency predawn increase caused by sunrise, resulting in photoelectrons transfer along force lines magnetically conjugate point
13 p2257 A69-28712
- Zone structure of silicon-silicon dioxide system for silica films obtained by pyrolytic dissociation, discussing kinetics of photoelectrons capture at traps
15 p2669 A69-30723
- Quantum mechanics method for obtaining photocount distribution from optical maser photoelectron counting statistics
15 p2635 A69-31238
- Hall mobility of photoelectrons in cadmium sulfide layers
18 p3182 A69-35048
- Equilibrium velocity distributions of F region photoelectrons produced by solar ionizing radiation, discussing dayglow as impact result
20 p3591 A69-38061
- Dayglow O I lambda 1304 and 1356 A radiations photoelectron excitation rates theoretical calculation and experimental data on altitude dependence characteristics
22 p3939 A69-40517
- Conjugate regions 6300 A airglow enhancement during predawn, noting photoelectrons role in heating dark ionosphere region by producing fast electron flux
24 p4308 A69-43011
- PHOTOEMISSION**
U PHOTOELECTRIC EMISSION
PHOTOEMISSIVITY
U EMISSIVITY
U PHOTOELECTRIC EMISSION
PHOTOEMITTERS
U PHOTOELECTRIC MATERIALS

PHOTOENGRAVING

Electron beam exposure system to photoetch integrated circuit patterns without photomasks, using electronic computer for automatic pattern generation and registration 15 p2579 A69-31039

PHOTO GEOLOGY

Volcanic origin of lunar crater Dawes based on photogeological evidence obtained from Lunar Orbiter 5 photographs 11 p1952 A69-24264

Extraterrestrial imagery, discussing earth based telescopes, IR imagery, moon mapping, lunar and planetary probes, Lunar Orbiter photos interpretation and sensors for detecting life 15 p2690 A69-30711

Photogrammetric instruments applied to determination of spatial position of tectonic surfaces by aerial photography 20 p3539 A69-37511

PHOTOGRAMMETRY

Analytic photogrammetric determination of lunar control coordinates from Ranger photography 01 p0147 A69-10022

Mirror photogrammetry geometric principles, studying photo pairs, mirror reflection and reduction methods 01 p0077 A69-10025

Interpolation of deflections of vertical from horizontal gravity gradients, discussing potential applications to photogrammetry 02 p0243 A69-12012

Error analysis of orientation methods for extraterrestrial stereophotogrammetric mapping [JPL-TR-32-134] 03 p0429 A69-13299

Unified lunar control photogrammetric network produced by mapping satellite in 28 day polar orbit, using recurrent partitioning 05 p0819 A69-15628

Horizontal aerotriangulation by independent models using photogrammetric extension of horizontal control for small scale superwide angle photography, horizon photography and B 8 plotter 06 p0925 A69-17468

Calibration procedures for cameras and photographs in photogrammetry, noting least squares method and tolerance criteria 06 p0925 A69-17469

Wind vector in respect to orientation of large scale cirrus bands based on stereophotogrammetry and radar observations 08 p1346 A69-20442

Photogrammetric color negative prints, slides, etc, improved by scanning beam modulation 09 p1494 A69-21634

Photogrammetry for three dimensional geodesy, discussing satellite triangular methods, refraction anomalies, error corrections, etc 10 p1682 A69-23390

Multispectral photographic determination of reflectance of environmental features from aerial spectral photographs, noting EROS program application 11 p1880 A69-24266

Photogrammetric networks equalization by method of least squares, using external orientation elements of aerial photographs 12 p2079 A69-26032

Monograph on photogrammetry in satellite geodesy including photogrammetric measurement of satellite positions, German observation stations and work done in U.S., U.S.S.R. and France 16 p2790 A69-32202

Photogrammetry - Conference, Washington, D.C., March 1969 18 p3133 A69-34334

NASA photogrammetric lunar activities, discussing imagery and control data by Lunar Orbiter and photogrammetric data reduction for preparing manned lunar landing 18 p3133 A69-34336

Heights of cloud bases and convective cloud tops determined by stereoscopic photogrammetry of Apollo 6 mission 20 p3569 A69-36926

NASA lunar survey and mapping for generating Apollo satellite landing navigation control, using analytic photogrammetry, camera position and altitude data of lunar topography 20 p3536 A69-36931

Photogrammetric instruments applied to determination of spatial position of tectonic surfaces by aerial photography 20 p3539 A69-37511

Photographic interpretation, considering shape, size, tone, shadow, pattern, texture, site, association and resolution 20 p3540 A69-37739

Cameras photogrammetric parameters determined from stellar photographs, considering distortion components, reference points, etc 20 p3545 A69-38054

Aerial surveys flight functions cost plotted against degree of performance, allowing for obtainable accuracies 22 p3863 A69-40041

Holographic photogrammetry compared with conventional holography in monocular and binocular parallax reconstruction and stationary stability of objects 22 p3944 A69-40044

Photogrammetric contours plotting from aerial color films 22 p3944 A69-40045

Superwide angle camera with aerial photogrammetric lens system, discussing light distribution, rotary disk shutter, etc 22 p3944 A69-40047

Photogrammetric camera system developed from NASA requirements to document lunar surface environment during manned space flight exploration 22 p3948 A69-40989

Optical engineering and quality control of photogrammetric instruments for aerial color photography, discussing lenses, filters, projectors, plotters, electro-optical rectifier, etc 22 p3949 A69-40996

Terrain slope estimation of position errors of differential corrections in orthophoto production 22 p3951 A69-41245

Orthophoto maps production, discussing scales, aerial photography, control points, orthoreprojection, cartography and printing 22 p3951 A69-41246

Gridding technique for satellite APT pictures taken with camera axis perpendicular to earth surface 24 p4314 A69-42992

Electronic scanning and correlation techniques for terrain sensing required in automatic stereoperception 24 p4316 A69-43566

PHOTOGRAPHIC INTERPRETATION

U PHOTOINTERPRETATION

PHOTOGRAPHIC DEVELOPERS

Characteristics of astronomical photography, considering cameras, photographs, color films, photoemulsions and processing, etc 11 p1885 A69-24973

Multispectral processing of Apollo 6 earth photograph, evaluating geologic, vegetative and cultural features from red, green and blue portions of visible spectrum 22 p3941 A69-40987

Color chemistry concept producing high quality color negatives and prints in existing black and white processing systems 22 p3948 A69-40990

Photographic properties of Cibachrome silver dye bleach materials for yielding color reflection prints directly from color transparencies, discussing applications to aerial photography 22 p3949 A69-40991

Aerial color film processing systems 22 p3949 A69-40992

PHOTOGRAPHIC EMULSIONS

NT NUCLEAR EMULSIONS

Strain releasing method for reduction of small local movements of recording holographic emulsions resulting in degradation of holographically reconstructed wavefronts 06 p0923 A69-16930

Absolute sensitivity of Soviet UTs-3 photographic emulsion to vacuum UV radiation by method involving absolute calibration of photocathodes 07 p1136 A69-19620

Photographic emulsion layers depth dependence of darkening curve, modulation transfer function and granularity, determining properties by enzymatic and electrolytic treatments 12 p2089 A69-26196

Nonlinear holograms distortions analyzed by five point method utilizing relation between irradiance and amplitude transmittance of photographic emulsion 12 p2090 A69-26255

Nuclear interactions between high energy nuclear active particles and C nuclei, studying electron-photon component energy with nuclear photoemulsions 13 p2331 A69-28388

High resolution silver halide photoemulsions analyzed by holographic resolvometry using Ne-He laser to obtain interference patterns 15 p2606 A69-30052

Autoradiographic methods for diffusion and phase transformation in Fe-Cr alloys by application of photographic emulsion with tracer element on metal surface 20 p3561 A69-37416

Photographic film properties, discussing base material, emulsion, photochemical process, sensitometry, densitometry, granularity and color film 20 p3541 A69-37746

PHOTOGRAPHIC EQUIPMENT

NT BALLISTIC CAMERAS

NT CAMERA SHUTTERS

NT CORONAGRAPHS

NT FRAMING CAMERAS

NT HIGH SPEED CAMERAS

Aerial color photography for terrain analysis noting development of cameras, filters, high speed emulsions and processing equipment 01 p0077 A69-10023

Photographic control system requirements for Project Apollo manned launches, considering extreme heat, vibration and sound pressure environment [SMPTE PAPER 104-20] 04 p0596 A69-14360

Photographic system in Lunar Orbiter spacecraft 05 p0829 A69-15857

Automatic laser tracker system for close-up photographic coverage of rocket test [SMPTE PREPRINT 101-91] 07 p1116 A69-18949

Computer processed pictures including transformation of graphical material, picture generation from data or abstract rules, discussing procedures, instrumentation, color and applications 11 p1842 A69-24588

Characteristics of astronomical photography, considering cameras, photographs, color films, photoemulsions and processing, etc 11 p1885 A69-24973

Flare or stray light measured in long focus photographic objectives by photometric sphere and spherical segments without collimator 12 p2093 A69-26590

High speed curtain type photographic shutters testing by chronograph with phosphorescent and photographic recording, determining movement rate including acceleration and braking 12 p2093 A69-26598

Photographic system for astronaut training in Apollo Mission Simulator, using fixed camera and moving earth model coincident with strip color film past exposure slit 16 p2792 A69-32787

Portable electric lamp for work and photographic purposes in manned spacecraft, describing circuitry, construction and applications [IES PREPRINT 30] 18 p3138 A69-35173

PHOTOGRAPHIC FILM

NT MICROFILMS

Photographic film blackening under high intensity laser radiation indicating two photon mechanism as responsible 01 p0080 A69-10429

Scaled and translated composite curve technique for reducing calibration data for spectrograph film system response characteristics 01 p0082 A69-10839

Holographic film sensitometric properties, plotting density vs log exposure and time vs gamma curve 01 p0082 A69-10851

Hologram film nonlinearity effect in recording diffusely illuminated objects analyzed by means of amplitude transmittance 03 p0431 A69-13958

Holograms volume depth increased by reference beam splitting or by photographing holograms on same plate in sequence 05 p0761 A69-15651

Hologram storing on photochromic film, obtaining equations for optimal exposure time [IEEE PAPER F-1] 07 p1133 A69-19053

Color and black and white negatives effectiveness for photointerpretation, noting color imagery advantages 08 p1311 A69-19820

Holograms on photochromic films by split beam He-Ne laser using special mirror system 11 p1881 A69-24631

Holographic recording materials effect on optical reconstruction wave and hologram properties 11 p1882 A69-24681

Faint stars background exposure density and detection limit determined by astrosensitometer for Kodak Spectroscopic Plates
12 p2153 A69-25811

Hologram recording on photosensitive material based on photoinduced polymerization showing good resolution and diffraction efficiencies
13 p2258 A69-27199

Photographic layers darkening process, using widely spaced or single giant pulses of ruby laser
13 p2260 A69-27612

Image quality of color disks in aerial photographs using panchromatic, color positive, color negative and false color films, measuring reflected sunlight
14 p2450 A69-29600

Holograms volume depth increased by reference beam splitting or by photographing holograms on same plate in sequence
16 p2791 A69-32508

Modulation transfer function based on Fourier techniques, discussing nonlinear film development process
17 p3005 A69-33080

Previous radiation exposure effect on photographic film noting increased sensitivity at UV frequencies
19 p3314 A69-36626

Photographic interpretation, considering shape, size, tone, shadow, pattern, texture, site, association and resolution
20 p3540 A69-37739

Photographic film properties, discussing base material, emulsion, photochemical process, sensitometry, densitometry, granularity and color film
20 p3541 A69-37746

Photogrammetric contours plotting from aerial color films
22 p3944 A69-40045

Aerial color film processing systems
22 p3949 A69-40992

Hologram film nonlinearity effect on reconstructed image, discussing role of illumination type
23 p4165 A69-41636

Automatic analysis and classification of images stored on 35-mm film using CRT flying spot scanner with computer control and memory
24 p4286 A69-42744

PHOTOGRAPHIC MEASUREMENT
NT PHOTOGRAMMETRY

Confined vortex in air tangential and axial velocity distribution based on smoke profile pictures
01 p0060 A69-10413

Meteor photographic observation noting initial mass, motion, position and duration, disintegration in process of flaring, spectra and meteor flare classification scheme
01 p0159 A69-11372

Fluid flow velocity measurements by optical device having trigonal rectangular glass prisms and microscope objective
03 p0427 A69-12969

Photographic control system requirements for Project Apollo manned launches, considering extreme heat, vibration and sound pressure environment [SMPE PAPER 104-20]
04 p0596 A69-14360

Xenon flash lamps with electrolytic capacitors designed for photographic studies of laminar flows of viscous fluids
07 p1116 A69-18259

Absolute sensitivity of Soviet UTs-3 photographic emulsion to vacuum UV radiation by method involving absolute calibration of photocathodes
07 p1136 A69-19620

Picosecond light pulse measurement by two photon excitation of photographic film
08 p1313 A69-20165

Photographic magnitudes in UVB system based on photoelectric sequences for stars in NGC 2483 and NGC 2489 open clusters, obtaining spectral classes from objective prism plates
08 p1388 A69-20239

Photographic magnitudes in UVB system based on photoelectric sequence for stars in NGC 2546, Pi 1, NGC 2579 and Cr 185, obtaining spectral classes
08 p1388 A69-20240

Simultaneous photographic and radar observations of meteors, determining absolute stellar magnitude of meteor as function of parameters
08 p1390 A69-20337

Photographic measurement of parachute exit velocity during ejection from chute, describing electronic recording and unit operation with block diagram
08 p1317 A69-20875

Relative proper motions of stars measured by microscope projection technique
10 p1778 A69-23570

Expansion velocity of discharge plasma in exploding wires measured by X ray flash and streak photography, noting discrepancy
11 p1926 A69-24472

Rotating mirror streak cameras in quantitative measurements of extreme compressions by shock waves, analyzing spatial and temporal resolving power
12 p2084 A69-26151

Vilna meteorite bolide observation with all-sky camera noting seismic and analytic records
13 p2334 A69-27189

Flare star astrometric study to determine possible variable proper motion
13 p2348 A69-27810

Visual binary star parallax, motions and mass ratio determined using photographic data
13 p2349 A69-27815

Vibrating camera for photographic measurement of flow velocities and trajectories of bodies marked by light spots
13 p2261 A69-27913

Mirror correctors used with paraboloidal spaceborne telescopes in far UV, yielding enlarged photographic field
13 p2261 A69-27949

Vectormagnetograph to measure magnetic field vector components, obtaining field direction azimuth by servo circuit
14 p2453 A69-29972

Accurate optical position of quasars determined by plate overlap for radio interferometer calibration
16 p2859 A69-32229

UBV photometry of faint stars, discussing photographic plate effect on accuracy, emulsion standardization and use of electronography
17 p3031 A69-33099

Visual observation of pipe wall regions in turbulent flow by suspending colloidal size particles and photographing with high speed motion picture camera
17 p2956 A69-33598

Shock tube calibration for aerodynamic loading, determining flow parameters by observing particle trajectories with high speed photography of smoke tracers
18 p3085 A69-34469

High speed photography using multiply pulsed ruby laser, Pockels cell modulation and smear camera for isochromatic and photoelastic pattern recording
19 p3306 A69-35731

Ablating sphere viscous wake using image converter camera, computing luminance radial distribution by unit volume
19 p3306 A69-35739

Image converter camera and astronomical telescope arrangement for photographing metal diaphragm openings in shock tube
20 p3538 A69-37227

Auroral spectroscopy for high resolution coverage at maximum wavelength range, discussing plane diffraction grating
21 p3707 A69-38486

Gas dynamic processes during vaporization of solid material under Nd laser emission, using high speed photography
21 p3740 A69-39551

Photographic study of epoxy resin breakdown kinetics under pulsed laser beams, showing crack area as function of time
22 p3973 A69-40743

Orthophotography as technique for eliminating distortions in vertical aerial photographs during conversion into uniform scale reproductions
22 p3949 A69-40998

Spectral emissivity and radiation intensity spectral distribution measurements for heat-resistant materials at high temperature, using photographic method
23 p4238 A69-41330

PHOTOGRAPHIC RECORDING

Meteor photographic observation noting initial mass, motion, position and duration, disintegration in process of flaring, spectra and meteor flare classification scheme
01 p0159 A69-11372

Trailing camera technique to photograph impact and projectile penetration into earth materials from above and behind test vehicle
02 p0227 A69-11760

Hologram film nonlinearity effect in recording diffusely illuminated objects analyzed by means of amplitude transmittance
03 p0431 A69-13958

Fiber optic electrostatically focused image intensifier tube for recording star spectra with reduced exposure time [WERL-68-1C2-TAEC-P1]
04 p0603 A69-15444

Laser photolysis and spectroscopy for photographic recording of absorption spectra of transient intermediates in nanosecond reactions
05 p0772 A69-16025

Weld-nugget formation in resistance spot welding, using high-speed photography on model section of spot weld
05 p0769 A69-16539

Lippman-Bragg holograms production with high reconstruction efficiencies by suitable recording and processing techniques with commercially available photographic plates
06 p0926 A69-17481

Photorecording techniques for command and control systems requirements, discussing association with large screen computer generated CRT projection display equipment
06 p0928 A69-17923

Pulse intensity variations in pulsars observed at 113 MHz with parabolic antenna using photographic recording techniques, noting lack of periodicities
06 p1009 A69-17964

Photographic study of burning metalized composite propellant under acceleration, noting burning rate augmentation by heat transfer from alumina particles retained on propellant surface [AIAA PAPER 69-173]
06 p0983 A69-18151

Hologram storing on photochromic film, obtaining equations for optimal exposure time [IEEE PAPER F-1]
07 p1133 A69-19053

Book on photographic recording of high speed processes noting slit scanning, cinecameras, shutters, mirror rotation drive mechanisms, photographic materials, etc
08 p1317 A69-21033

Holographic displays using ultrasonic vibrations or laser outputs as optical sources, discussing recording materials, responses and computer applications
09 p1492 A69-21394

Photogrammetric color negative prints, slides, etc, improved by scanning beam modulation
09 p1494 A69-21634

Laser spark image in air photographed in scattered laser radiation light, showing singularities and absence of beadlike structure
09 p1519 A69-22531

Shearing interferometry by simultaneous reconstruction of two wavefronts on single photographic plate
10 p1690 A69-22952

Holographic motion picture recorded using CW Q switched laser and conventional camera
10 p1697 A69-24002

Photography role in experimental research with applications to flight analysis and comparison with human visual accuracy
11 p1881 A69-24573

Multicolor hologram recording and reconstruction gas lasers, discussing control of ghosts in three dimensional image
11 p1882 A69-24679

Holographic recording materials effect on optical reconstruction wave and hologram properties
11 p1882 A69-24681

Comet Berbon and minor planet positions photographically recorded /1964-1967/
11 p1962 A69-25121

Liquid crystals for photographically recording microwave holograms, noting impossibility of three dimensional image reconstruction with side-looking radar zone plates
12 p2079 A69-25917

Image intensifier for high speed spectrography of short duration faint radiation source, noting high speed shutter and resolution
12 p2085 A69-26160

Remote control spectrophotochronograph to study radiation of high speed high temperature processes, giving construction data and diagrams
12 p2085 A69-26161

Direct electron beam shadowgraph photographic /betagray/ technique for recording small high speed objects with 3 nanosecond exposure time
12 p2086 A69-26164

Holography with pulsed lasers for high speed recording of amplitude and phase disturbances and rapid transient events, noting reconstruction evaluation problems
12 p2087 A69-26171

Holographic position and velocity measurement techniques for high speed objects from explosions
12 p2087 A69-26174

Photographic emulsion layers depth dependence of darkening curve, modulation transfer function and granularity, determining properties by enzymatic and electrolytic treatments

12 p2089 A69-26196

Streak camera for continuous photographing of dark and bright satellites up to 9 stellar magnitude

12 p2092 A69-26451

High speed curtain type photographic shutters testing by chronograph with phosphorescent and photographic recording, determining movement rate including acceleration and braking

12 p2093 A69-26598

Photography for remote sensing, discussing aerial photography, side-looking radar and photography for recording, storing and retrieving data

12 p2096 A69-26975

Terrain photography applications and analysis including remote sensing of photographic systems and photointerpretation

12 p2098 A69-27006

Hologram recording by offsetting reference beam temporal frequency instead of using reference beam spatial offset

13 p2258 A69-27201

Soviet and foreign visual, photographic and photometric ground observations of satellites, emphasizing synchronous optical observations role in geodesy and geophysics

13 p2219 A69-27357

Photographic recording of parallax, proper motion, acceleration and orbital motion of Barnards star, noting mass ratios to jupiter

13 p2349 A69-27813

Relative parallax, fractional mass and luminosity of visual binary 1785 determined from photographs taken with Sproul refractor

13 p2349 A69-27814

Visual and photographic observations of Perseids meteor trails velocity noting discrepancy

13 p2353 A69-28035

Recording installation of ionospheric reflected radio signal fluctuations and amplitudes of resulting signals simultaneously at three points, discussing antenna commutator circuit

14 p2452 A69-29874

High speed picture thermography in nondestructive testing, describing IR scanning frame rate and thermal image recording

15 p2618 A69-30316

Aerial multiband remote sensors for wildland resources, considering multilens photographic systems, optical mechanical scanners and radar devices

15 p2609 A69-30458

Photodielectric tape camera with optical images stored on tape in form of charge pattern

16 p2792 A69-32558

Meteor station photorecorder of reflected radio signals, discussing design and performance during meteor shower

17 p2976 A69-33898

Photographic networks for meteors orbits and trajectories and meteorites impact points during nighttime, discussing fireball occurrence

19 p3415 A69-36120

Friction bearing vibration recording device using light beam and photodiode

20 p3539 A69-37436

Photographic studies of explosive reactions with description of ultrahigh speed cameras

21 p3719 A69-38446

Satellite phase and aberration corrections in processing photographic observations for geodetic purposes

21 p3720 A69-38606

Solar corona photographic study during 1961 total eclipse using quadruple camera, providing intensities, amount and direction of polarization

22 p4001 A69-40001

Diffuse coronal emission observation during total eclipse of February 1961 near solar prominences and polar ray form investigation in northern part of corona

22 p4002 A69-40002

Pulse ruby laser-smear camera ultrahigh speed multiple frame recording system, describing applications to transmitted and scattered light photoelasticity

22 p3944 A69-40076

Photographic high speed recording system characteristics effects on dynamic photoclastic fringe patterns fidelity

22 p3945 A69-40077

Holographic interferometry for surface strain and vibrations visualization, describing photographic recording techniques

22 p3945 A69-40244

Holography phototechnical and optical variants, discussing combination of conventional photography and wave front reconstruction

24 p4312 A69-42616

Linear motion blur compensation technique in photographic recordings by reconstruction of sharp image from hologram

24 p4314 A69-42972

PHOTOGRAPHIC RECORDING INSTRUMENTS

U OPTICAL MEASURING INSTRUMENTS

U RECORDING INSTRUMENTS

PHOTOGRAPHIC TRACKING

Optical spacecraft tracking organization in U.S.S.R., describing network of visual observation and photographic stations for satellite and space probe tracking

01 p0032 A69-10952

Geocentric orientation of quasi-geocentric coordinate network determined from simultaneous photographic satellite observations, using gravity force values

12 p2158 A69-26429

Earth stations coordinates determination from non-simultaneous photographic satellite observations by orbital method compared with simultaneous photographic observations of Echo 1

12 p2068 A69-26430

Observatory camera for satellite observation, discussing objective focusing and diameter and manual/automatic operation

12 p2092 A69-26450

Streak camera for continuous photographing of dark and bright satellites up to 9 stellar magnitude

12 p2092 A69-26451

Stellar image vibration amplitude dependence on trace direction by comparison with traces of moving satellites

15 p2647 A69-30166

PHOTOGRAPHS

NT CLOUD PHOTOGRAPHS

NT LUNAR PHOTOGRAPHS

NT MICROPHOTOGRAPHS

NT MOTION PICTURES

Calibration procedures for cameras and photographs in photogrammetry, noting least squares method and tolerance criteria

06 p0925 A69-17469

Computer processed pictures including transformation of graphical material, picture generation from data or abstract rules, discussing procedures, instrumentation, color and applications

11 p1842 A69-24588

Motion-distorted photograph deblurring method using extended range holographic Fourier transform division

22 p3944 A69-40020

PHOTOGRAPHY

NT AERIAL PHOTOGRAPHY

NT ALL SKY PHOTOGRAPHY

NT ASTRONOMICAL PHOTOGRAPHY

NT AUTORADIOGRAPHY

NT CHRONOPHOTOGRAPHY

NT CINEMATOPHOTOGRAPHY

NT CLOUD PHOTOGRAPHY

NT COLOR PHOTOGRAPHY

NT ELECTRO-OPTICAL PHOTOGRAPHY

NT ELECTRON PHOTOGRAPHY

NT FRAME PHOTOGRAPHY

NT INFRARED PHOTOGRAPHY

NT LUNAR PHOTOGRAPHY

NT PHOTOMICROGRAPHY

NT PHOTORECONNAISSANCE

NT RADAR PHOTOGRAPHY

NT ROCKET-BORNE PHOTOGRAPHY

NT SATELLITE-BORNE PHOTOGRAPHY

NT SCHLIEREN PHOTOGRAPHY

NT SHADOWGRAPH PHOTOGRAPHY

NT SPACEBORNE PHOTOGRAPHY

NT SPECTROHELIOGRAPHS

NT SPECTROPHOTOGRAPHY

NT STEREOPHOTOGRAPHY

NT ULTRAVIOLET PHOTOMETRY

Photographic image degradation resulting from wave front distortion due to atmospheric refractive density gradients over long oblique optical path

01 p1017 A69-10223

Exploding wire phenomenon during early expansion from time correlated X ray and optical streak photographs in vacuum chamber

01 p0119 A69-10670

High speed photography - Conference, Stockholm, June 1968

12 p2080 A69-26135

Regulated pulse lasers under free oscillation for photographing distant objects by illumination with shortened light pulses

12 p2089 A69-26190

Flash X ray unit with special film transport devices to obtain sequenced dynamic radiographs of ablating models during reentry simulation tests

19 p3291 A69-35720

Ruby laser goniometric and telemetric echoes by photographing Geos satellites

21 p3671 A69-38335

PHOTOINTERPRETATION

Aerial color photography for terrain analysis noting development of cameras, filters, high speed emulsions and processing equipment

01 p0077 A69-10023

Crater Copernicus photograph, discussing misinterpretation of Orbiter 2 lunar surface photograph on basis of effective temperature contours analysis

01 p0154 A69-10898

Lineament trend analysis of Gemini Red Sea synoptic terrain photography, noting computerized rotation from apparent to true angles

02 p0247 A69-12808

Annular and linear Martian surface formations nature and origin from analysis of Mariner 4 photographs

03 p0506 A69-13087

Photometric-polarimetric observations of planetary surfaces, discussing geological environment interpretation and spacecraft reconnaissance system mission planning

03 p0421 A69-13394

Tiros and ESSA weather satellites meteorological contributions, discussing photographic interpretation for weather predictions

04 p0626 A69-14690

Interpretation technique for weather satellite photographs of spatially coherent cloud distributions

04 p0628 A69-15090

Earth space image interpretation in various spectral regions, discussing effectiveness of photography, spectrophotometry, radar and microwave observations

05 p0763 A69-16054

Relative orientation elements of aerial photographs determined by iteration method

05 p0765 A69-16708

Meteorological satellites data for safe navigation of ships, discussing techniques to overcome difficulties in interpreting ice and cloud photographs

[UN PAPER 68-95776] 06 p0916 A69-17028

Atmospheric processes interpretation from cloud cover pictures televised by orbiting satellite, examining indirect weather forecasting

[UN PAPER 68-95713] 06 p0949 A69-17029

Meteorological satellite TV data of earth cloud cover for determining atmosphere pressure field

[UN PAPER 68-95654] 06 p0949 A69-17052

European cyclonic system developmental phases determined from characteristic structural features of satellite cloud pictures

[UN PAPER 68-95711] 06 p0950 A69-17070

Lunar geology information obtained by Ranger space missions

06 p1001 A69-17163

Ranger pictures improvement by computer, eliminating image distortion due to electronic imaging systems

06 p0924 A69-17164

Individual differences and relation to Witkin concept of perceptual style in target identification in aerial photographs

06 p0880 A69-17211

Map information display methods comparison for tactical image interpreters

06 p0924 A69-17212

Interpretation of IR cloud images transmitted by Nimbus 1 and Cosmos 122 satellites, using radiation temperature contrasts

06 p0952 A69-17984

Relative lunar altitudes determination from shadow measures on earth based lunar photographs by direction-cosine method

07 p1225 A69-19770

Comparator measures for relative lunar altitudes on Yerkes lunar photographs, estimating selenographic positions from grids of orthographic atlas of moon

07 p1225 A69-19771

Selenodetic measurements on Yerkes lunar star trailed photographs, considering limb and star trail

07 p1225 A69-19772

Yerkes star trailed lunar photographs with ephemeris values of moon libration for selenodetic coordinates of secondary points, discussing errors and altitudes

07 p1225 A69-19773

Photographic photometry of Saturn rings around times of disappearance /1966/

08 p1381 A69-19791

Color and black and white negatives effectiveness for photointerpretation, noting color imagery advantages 08 p1311 A69-19820

Aerial chronophotography of Southern Hemisphere conducted on around world polar flight analyzed for meteorological and geographical aspects and compared with satellite data 09 p1534 A69-21405

Space photography as sedimentological research tool demonstrated by space photographs application to projected Mars mission 09 p1490 A69-21797

Apollo 7 and weather satellite observation photographs of hurricane Gladys and typhoon Gloria 10 p1722 A69-22944

Large scale color and color IR aerial photography evaluation to determine interpretability for improving range resource inventories 11 p1880 A69-24265

Lunar far side craters vertical profiles plotted from photometric cross sections of Zond 3 photographs 11 p1959 A69-24726

TV IR cloud images interpretation transmitted by Cosmos 122, discussing specific features of cloud covers and underlying surfaces 11 p1912 A69-24826

Computer program for interpreting IR cloud pictures from Cosmos 122 satellite based on potential function method 11 p1884 A69-24833

Photogrammetric networks equalization by method of least squares, using external orientation elements of aerial photographs 12 p2079 A69-26032

Quantitative analysis of differential interferometer photographs using Wollaston prism with beam separation, applying method to sphere in low density hyper-sonic flow 12 p2089 A69-26187

Electro-optical scanning device and electro- optical matrix for mechanization of difference measurements in automatic photointerpretation of surveillance maps 12 p2090 A69-26302

Terrain photography applications and analysis including remote sensing of photographic systems and photointerpretation 12 p2098 A69-27006

Martian canals nature based on high contrast photographs obtained by Mariner 4 space probe 12 p2171 A69-27133

IR TV cloud pictures from meteorological satellites used for sky condition diagnostics and forecasting through automatic interpretation by image brightness quantization 13 p2291 A69-27728

Cartographic interpretation of TV cloud pictures transmitted by Molniya 1 satellite 13 p2292 A69-27730

Annular and linear Martian surface formations nature and origin from analysis of Mariner 4 photographs 14 p2515 A69-28769

Moon pictures from Apollo 8 spacecraft including full moon, crater Tsiolkovsky and unidentified area showing volcanism 14 p2527 A69-29889

Apollo 8 photooptics, considering TV camera and broadcasts, photographic equipment and visual observation 15 p2609 A69-30469

Photographic observations of comet Kiltson 1966b, estimating brightness, absolute magnitude and color index 15 p2685 A69-30529

Extraterrestrial imagery, discussing earth based telescopes, IR imagery, moon mapping, lunar and planetary probes, Lunar Orbiter photos interpretation and sensors for detecting life 15 p2690 A69-30711

Lasers and holography applications in astronomy including high resolution spectrographic diffraction gratings manufacture and astronomical objects photographic pictures evaluation 15 p2610 A69-30880

Nova Vulpeculae 1968 photographic observations analyzed for magnitudes, indicating 16 July 1968 explosion 16 p2855 A69-31659

Lunar rotation parameters determined from photographs and visual observations independent of moon profile 17 p3027 A69-32874

Electronic device utilizing scanning beam to evaluate limb photographs, reducing errors by introducing

second generator with frequency proportional to deflecting potential variation 17 p2970 A69-32884

Day sky brightness at altitude above 100 km obtained during rocket flight compared to night sky viewed from ground 17 p3037 A69-33664

Daily European weather surveys based on pictures transmitted by satellite during fourth quarter 1967 17 p3000 A69-33778

Aerospace images information suppressing and enhancing methods to aid interpreter in making more accurate recognition and measurement of earth resources subjects 18 p3133 A69-34338

Satellite photograph analysis to investigate interaction between subtropical and polar front jet streams 18 p3166 A69-34827

Satellite photography for snow cover mapping and depth estimation 18 p3167 A69-35084

Environmental studies using orbital photography, discussing color, color IR, black and white applications from Gemini and Apollo programs 18 p3132 A69-35275

Butterfly diagram of sunspot distribution, concluding physical processes not yet clarified 19 p3426 A69-36583

Horizontal wind components over U.S.S.R., Western Europe and Northeast Atlantic obtained from satellite photographs of vortex cloud systems 19 p3365 A69-36668

Photographic interpretation, considering shape, size, tone, shadow, pattern, texture, site, association and resolution 20 p3540 A69-37739

Earth space image interpretation in various spectral regions, discussing effectiveness of photography, spectrophotometry, radar and microwave observations 20 p3545 A69-37964

Cartographic tying-in of Zond 3 lunar surface photographs to verify maps of moon far side 20 p3608 A69-38051

Lunar surface erosion processes revealed by Lunar Orbiter photographs of boulder concentrations 21 p3794 A69-38378

Errors in sighting and identifying geodetic contour points on aerial photographs, considering stereocomparators parallaxes effect 21 p3719 A69-38404

Photographic studies of explosive reactions with description of ultrahigh speed cameras 21 p3719 A69-38446

Mars TV pictures from Mariner 7, describing prominent surface features 21 p3806 A69-39330

Comparative photointerpretation from panchromatic, color and Ektachrome IR aerial photography 22 p3944 A69-40039

Hyperlatitude photographs for geological mapping from Gemini spacecraft, noting remote sensing imagery 22 p3935 A69-40040

Surveying earth resources from space, covering orbital height photography in cartographic programs, hydrologic engineering, pollution control and geology 22 p3936 A69-40170

Harmonia and Parthenope /minor planets/ positions, establishing time dependence of relation between image diameter and planet magnitude 22 p4025 A69-40614

Long term computer produced multiple image satellite photomosaics for Southern Hemisphere, analyzing circulation, meridional bands, polar ice, cloud cover variations, etc 22 p3977 A69-40733

Photographic observations of supernovae including magnitudes, comparison star tables and instrument details 22 p4032 A69-40944

Orthophotography as technique for eliminating distortions in vertical aerial photographs during conversion into uniform scale reproductions 22 p3949 A69-40998

Automated air photo identification of crop types, utilizing stereo height as discriminating variable 23 p4155 A69-41721

Multispectral orbital photography used to obtain urban land-use data [AAS PAPER 69-483] 24 p4307 A69-42837

PHOTOIONIZATION

Photoionization curves and threshold energies for fluorocarbon and trifluoromethyl halide molecules and

ions, calculating ionic heats of formation and bond dissociation energies 02 p2025 A69-12464

Photodissociation and photoionization of diatomic molecules at high temperatures with calculation of absorption cross sections 03 p0473 A69-14147

Photoionization of donor impurities during absorption of IR radiation in n-type Te doped GaP at low temperatures 03 p0492 A69-14169

Ionization fronts stability, taking into account ionizing photons absorption effect in H II region and interstellar magnetic field 04 p0650 A69-14363

Mass spectrometric measurements to determine energy distributions of ions produced in dissociative photoionization of O molecules 06 p0960 A69-17110

Atomic Li photoionization cross sections calculated with Brueckner-Goldstone many body perturbation theory 06 p0961 A69-17134

Rational approximation for coefficients used in calculating hydrogenic photoionization Gaunt factors 08 p1354 A69-20153

Luminous discharge at nonabsorbing surface when exposed to single pulse ruby laser beam, suggesting photoionization in surface layer 08 p1327 A69-21021

Oscillator forces and photoionization and photorecombination cross sections of electron transitions in hydrogen atom, considering approximation for total radiation probability 09 p1588 A69-21365

Spectral distribution of X ray atmospheric absorption used to determine high energy photoelectrons spectrum 09 p1577 A69-21774

Simultaneous photoexcitation and photoionization of He near threshold at 186 A, measuring probability 11 p1921 A69-24926

Polarized Hartree-Fock model computing photoionization cross sections for Li isoelectronic sequence, listing phase shifts for partial waves of scattered electrons 11 p1922 A69-25260

Diffusion of ion-electron pairs produced by photoionization upstream of strong shock waves to shock tube walls based on particle flux and Poisson equations 11 p1866 A69-25275

Cross section for ionization of atoms by positive ion bombardment near threshold 11 p1922 A69-25322

Linearized perturbation for photochemical and dynamical effects in internal atmospheric gravity wave production of E region ionospheric irregularities 14 p2440 A69-29128

Photoionizing effect of hydrogen and helium UV glow in nighttime ionosphere compared with ground based IF ionosonde and sounding rocket observations 15 p2605 A69-31436

Unsteady model taking into account photoionization, neutralization and diffusion, describing electron concentration diurnal and seasonal variations in ionosphere F 2 region at midlatitudes 17 p2966 A69-33978

Oscillator forces and photoionization and photorecombination cross sections of electron transitions in hydrogen atom, considering approximation for total radiation probability 18 p3197 A69-34755

Ground and metastable state photoionization cross sections of BaI to explain artificial Ba clouds, using many channel quantum defect method 18 p3177 A69-35238

Precursor electrons due to photoionization ahead of pressure driven shock waves, presenting electron temperature and density theoretical analysis 20 p3511 A69-38238

Photon induced precursor ionization and electron produced wave separation from electrical shock tubes 20 p3511 A69-38240

Laser induced multiphoton ionization and cascade breakdown in high pressure gases, considering roles of refractive index, laser nonideal output and beam self focusing 21 p3738 A69-39445

Photoionization model of Seyfert galaxy extended to calculate temperatures, luminosities and sizes of zones emitting forbidden Fe X /6374 A/ and Fe XIV /5303 A/ 22 p4024 A69-40581

Atoms and ions collision strengths and photoionization cross sections for nitrogen, oxygen and neon fitted to interpolation formulas for temperature and frequency effects

22 p3988 A69-41244

Photoionization rates temperature dependence in upper atmosphere for O atoms and molecules and N molecules from computer calculations, allowing for earth sphericity

23 p4157 A69-41857

PHOTOLUMINESCENCE

NT X RAY FLUORESCENCE

Photoluminescence spectra of n-type GaAs films grown by gas transport reactions and from solution melt, noting recombination emission

03 p0488 A69-13887

Photoluminescence measurement of distribution of majority carrier concentration in GaAs

03 p0489 A69-13893

Epitaxial n-GaAs photoluminescence obtained from p-GaAs, considering emission intensity

03 p0492 A69-14167

Photoluminescence measurements of p-type thermal conversion in GaAs grown from silica boats, noting compensation by copper and shallow acceptors

04 p0639 A69-14434

IR radiation effects in cadmium sulfide crystals with green edge emission at low temperatures, discussing luminescence, photoconductivity and conductivity glow curves

10 p1746 A69-23565

Photoluminescence spectra of n-type GaAs films grown by gas transport reactions and from solution melt, noting recombination emission

11 p1939 A69-25688

Photoluminescence measurement of distribution of majority carrier concentration in GaAs

11 p1939 A69-25694

Heat treatment effects on Te-doped GaAs, using photoluminescence and carrier concentration measurements to study defects formed

16 p2825 A69-31708

UV excitation intensity increased for improving luminescent nondestructive testing, describing UV dosimeter and irradiation standards

18 p3138 A69-35115

F center formation and X ray and photostimulated F-band luminescence in europium ion-activated potassium halides as function of temperature and X ray dosage

19 p3383 A69-36164

Multiphoton luminescence and photocurrent excitation by ruby and neodymium laser beams of KCl-Eu single crystals, noting brightness dependence on laser beam power

19 p3335 A69-36165

Radiative recombination in GaAs, giving edge radiation spectra in p and n type crystals and photoluminescence method for measuring junction carrier concentration distribution

19 p3386 A69-36525

Injection lasers external quantum efficiency, stimulated and spontaneous emission and photoluminescence measurements

19 p3337 A69-36528

PHOTOLYSIS

NT RADIOLYSIS

Sulfur trioxide production in photolysis of sulfur dioxide at 1849 angstroms, noting oxygen addition effect on quantum yield

01 p0024 A69-10619

Photolysis of aliphatic amino acids by UV light in presence of salt ions forming ammonia, glyoxalic acid, acetaldehyde and formaldehyde

01 p0025 A69-11094

Metal oxides catalytic and inhibitory effects on photolysis of alanine by UV light

01 p0025 A69-11095

Photolytic conversion of allene to cyclopropylidene, discussing cyclononadiene in vapor phase and resulting product

02 p0205 A69-12721

Gas phase photolysis of carbon dioxide in far UV, searching for carbon trioxide

03 p0381 A69-13318

Nanosecond range flash photolysis technique and application to absorption spectra of excited singlet states

05 p0760 A69-15608

Laser photolysis and spectroscopy for photographic recording of absorption spectra of transient intermediates in nanosecond reactions

05 p0772 A69-16025

Photolysis of t-butyl iodide at low temperatures as source of t-butyl peroxy radicals for synthesis of peroxides

07 p1073 A69-18375

Collision broadening cross sections of OH UV transition at room temperature, using flash photolysis

09 p1543 A69-22252

Primary processes leading to atomic and molecular hydrogen formation in hydrogen peroxide photolysis at 1236 Å, noting OH formation

10 p1652 A69-23527

Photolytic cleavage of vic-triazole ring when unsubstituted at N, finding phenylacetone nitrile production mechanism

19 p3264 A69-35971

Laser action from atomic bromine produced by flash photolysis of gaseous iodine monobromide, discussing pulsed output, optical gain, chemical reversibility and atomic excitation

19 p3337 A69-36444

Cations of sulphates photosensitizing role in photolysis of amino acids and peptides in various atmospheres

20 p3477 A69-37626

Gases effects on UV irradiated thermal control materials spectral reflectance, discussing tests and photolysis mechanisms

[AIAA PAPER 69-1025] 22 p3923 A69-40395

Carbon trioxide formation during ozone photolysis in liquid carbon dioxide and sulfur hexafluoride, noting ozone disappearance quantum yield independence of oxygen/ozone ratio

23 p4112 A69-41338

PHOTOMAGNETIC EFFECTS

Surface recombination rate effect on lux-ampere characteristic of photomagnetic effect in CdS single crystals of low and high photosensitivity

05 p0809 A69-16377

Semiconductor current carriers surface recombination rates determined from photomagnetic effect

07 p1198 A69-18505

PHOTOMECHANICS

U PHOTOGRAPHY

U PRINTING

PHOTOMETERS

NT ELECTROPHOTOMETERS

NT ULTRAVIOLET SPECTROMETERS

NT ULTRAVIOLET SPECTROPHOTOMETERS

Twilight sky brightness measurements at 5200 angstroms for estimating upper atmospheric dust component, discussing error rates

01 p0075 A69-11191

Particle size distribution determination by measuring light beam extinction in turbid medium with photometer

03 p0428 A69-13110

Standard Leningrad-2 photoexposure meter applied to measurement of power of laser continuously operating in visual spectral range

04 p0602 A69-15405

Nonlinear coupling between background illumination and illumination signal producing lateral electrical fields in p-n junction, noting effect on sensitivity of position sensor

07 p1101 A69-18654

Optical heterodyning with single mode carbon dioxide laser and triglycine sulfate pyroelectric detector, noting detector sensitivity threshold

07 p1156 A69-19332

Celestial navigation system using photodetectors, comparing numbers and brightness of S4, S20 and silicon stars

10 p1775 A69-23190

High speed photodetector frequency characteristics using multimode gas laser and Kerr cell

10 p1707 A69-24211

Microphotometer for stellar magnitudes of galaxies determination from photographs

11 p1879 A69-24256

Tilting filter photometer for faint light source spectrophotometry, discussing digital approach used with photomultipliers

11 p1884 A69-24834

Stellar radial velocities derived from line positions measurements by precision screw microphotometer

12 p2153 A69-25810

Electronic nonimaging polarimeter/photometer for aircraft observations of pure red pine stand, suggesting application to terrestrial, airborne and satellite remote sensing

12 p2096 A69-26983

Sky mapping in IR, using IR photometer on TD1 ESRO satellite

13 p2260 A69-27606

Independently fluctuating Poisson light signals detected by receiver with inertialess photodetector, developing algorithm for estimating amplitude of useful signals

13 p2223 A69-28552

Photodetector requirements for autocollimators with beam splitters, considering spectral characteristics, photoresponse, time constant, positioning, etc

14 p2447 A69-29326

Portable photometer with red-sensitive photocathode and high SNR for O I 6300 airglow experiments

16 p2777 A69-32107

Photometer for simultaneous stellar photometry in UVB bands, purposes and performance characteristics and circuit diagrams

16 p2790 A69-32209

Iris microphotometer with measurement and reference beams traversing plate in neighboring regions designed for stellar images measurement

16 p2790 A69-32225

Optical information rates for photocount detection systems based on coherent field model, considering binary channels with or without Gaussian noise

20 p3485 A69-36923

Atmospheric ozone detection by three-color photometer measurements of solar UV radiation attenuation in Hartley continuum

20 p3543 A69-37802

N I nebular doublet and auroral and nebular lines of O I obtained with multifilter scanning photometer in France, Norway and at magnetic equator

21 p3712 A69-38519

Relative IR spectral reflectivity of selected lunar surface areas measured using double beam photoelectric filter photometer

21 p3815 A69-39588

PHOTOMETRY

NT ASTRONOMICAL PHOTOMETRY

NT ELECTROPHOTOMETRY

NT SPECTROPHOTOMETRY

NT STELLAR SPECTROPHOTOMETRY

NT TELEPHOTOMETRY

NT ULTRAVIOLET PHOTOMETRY

NT VISUAL PHOTOMETRY

Soviet and French coordinated geophysical studies at magnetically conjugate points in northern U.S.S.R. and Indian Ocean

06 p0918 A69-17391

Photometric effects of UVB color indices ineffective in detecting double stars in Galaxy

07 p1216 A69-18854

Quantitative spectroscopy and spectral photometry, discussing developed image properties and connection between exposure and image

08 p1315 A69-20467

Photometric methods for determination of H atom and hydroxyl radical concentrations in hot gases in convergent-divergent nozzles, noting Li/lithium hydroxide absorption

09 p1496 A69-21952

Lunar far side craters profile and structure determined from Zond 3 photographs using photometric method

11 p1959 A69-24725

Lunar far side craters vertical profiles plotted from photometric cross sections of Zond 3 photographs

11 p1959 A69-24726

Visual mapping and photometric scanning of Saturn with rings from earth, noting ring brightness edgewise linear dependence on rings opening

15 p2697 A69-31256

Baker-Nunn photometry from Apollo tracking utilizing photographs for brightness, dynamics and duration of rocket exhausts and venting clouds

15 p2571 A69-31338

Zenith and azimuthal photometric observations of red line atomic O airglow predawn enhancement over UK

16 p2775 A69-32086

Ti determination in presence of Nb or Ta by extraction-photometric method with diantipryl methane and thiocyanate

20 p3544 A69-37812

Martian surface and atmosphere interpretation through polarimetric and photometric simulation

20 p3614 A69-38253

PHOTOMICROGRAPHY

Pedoscope use in soil microbiological studies including ecology, infection susceptibility, etc

01 p0021 A69-11092

Diamond abrasive process for preparation of microminiature devices for metallographic analysis

03 p0402 A69-13007

Impact crater cross section in fused silica, describing photomicrographic technique for distinguishing hyper-velocity from low energy impacts [AIAA PAPER 69-367] 13 p2366 A69-28299

Photomicroscope film plane inclination adjusted to improve circle readings measurement, noting instrument errors role in star declinations errors 17 p2970 A69-32881

Micromatation and micrographics, discussing nonim- pact printing in computer activated output imbalance by high speed microfilm recorder 18 p3234 A69-35059

Fracture surfaces of stress corrosion cracks in Fe-Cr- Ni alloys studied by electron microfractography, noting cleavage fracture 19 p3350 A69-36891

PHOTOMULTIPLIER TUBES

Kerr effect apparatus for measurements of pure liquids and solutions involving comparison of two lu- minous fluxes with aid of photomultiplier 01 p0078 A69-10039

Photomultiplier geometry without use of light pipes for uniform response from large area single and double sheet plastic scintillation detectors 03 p0428 A69-13107

Time dependent photoelectron multiplier with low noise for recording long wave laser light pulses 03 p0440 A69-13264

Photoelectron counting in extreme UV using win- dowless photomultiplier detectors as photon counters 04 p0595 A69-14277

Stimulated emission properties of active fibers ob- tained from photomultipliers transmitting pulses to oscillosgraph 05 p0761 A69-15657

Photomultipliers response to energetic particles in terms of background current using data from OGO ex- periments 06 p0923 A69-16932

Coherent light fluxes detection, noting correlation characteristics of output signals of photomultiplier il- luminated by multimode He-Ne laser 09 p1515 A69-21438

Temperature effect on amplification factor of box type dynode system of photoelectron multipliers made of alloy AMGK, using single electron method 11 p1846 A69-24626

Low energy charged particle detectors reliability, analyzing windowless electron multipliers and effects of secondary emission layers on sensitivity 11 p1848 A69-24868

Continuous-channel electron multipliers degradation in spacecraft environment simulation laboratory equip- ment 14 p2449 A69-29565

Stimulated emission properties of active fibers ob- tained from photomultipliers transmitting pulses to oscillosgraph 16 p2792 A69-32514

Electrooptical /photomultiplier/ detection of satellite beacon flashes, establishing time of flash and measur- ing pulse shape and energy received 17 p2919 A69-33083

Color coded area sensitivity maps of photomultiplier tubes by multicolor display technique, noting focus electrode voltage 19 p3305 A69-35724

Astronomical observatory photomultiplier cell dark current fluctuations, showing statistical resemblance to binomial distribution 20 p3599 A69-37470

Radial velocities recording inaccuracies by solar magnetographs caused by dissimilarity between photomultipliers characteristics, describing photome- ter designs to eliminate errors 20 p3547 A69-38308

Flexible channel multiplier made of electron conduc- tive polymer, noting secondary yield and feedback ef- fect 22 p3917 A69-41234

Detection of metastable He, H, Ne, Ar, Kr, Xe and molecular nitrogen with continuous channel electron multipliers 22 p3917 A69-41235

HF data transmission system unaffected by high energy electromagnetic fields using GaAs IR emitting diode, glass fiber optic light guide and photomultiplier tube 23 p4121 A69-41768

Photomultiplier tubes performance enhancement by light incidence on photocathode at oblique angles ex- plained by reflection 23 p4191 A69-42194

PHOTON ABSORPTION
U ELECTROMAGNETIC ABSORPTION

PHOTON BEAMS
NT LIGHT BEAMS

Photographic film blackening under high intensity laser radiation indicating two photon mechanism as responsible 01 p0080 A69-10429

Inverse Compton effect and universal black body radiation from less energetic radio photons of galactic and metagalactic origin 08 p1381 A69-19786

Laser beams self focussing interpreted as photon contraction due to equivalent gravitational attraction with gravitational constant proportional to nonlinear refractive index 08 p1324 A69-20085

Photoelectric, calorimetric and photon-momentum methods for measuring laser output energy and power emphasizing liquid, wire and pyroelectric calorimeters 11 p1899 A69-25196

Stimulated reflection experiment for correlation between coherent photon beams from independent lasers 18 p3153 A69-35292

PHOTON DENSITY

Intensity interferometry by two photon excitation of fluorescence trace for three mode laser under phase locking, free running and FM-like conditions 10 p1705 A69-23811

Spectrum of clipped noise in optical spectroscopy, considering double clipping at zero photon number 15 p2571 A69-31486

Injection lasers external quantum efficiency, stimu- lated and spontaneous emission and photolu- minescence measurements 19 p3337 A69-36528

Indium arsenide injection laser observed for self modulation at LF modes, discussing nonMarkovian character of photon density relaxation 19 p3338 A69-36537

Quantum theory for single mode laser radiation, con- sidering photon distribution function and mean field damping decrement by phase quantum fluctuations 21 p3737 A69-38996

PHOTON-ELECTRON INTERACTION

Laser transition and photon energy of lightly doped GaAs, showing many body electron-hole- lattice in- teractions 02 p0257 A69-12615

Gallium phosphide luminescence near indirect transition during multiphoton excitation by Q switched ruby and Nd laser beams 03 p0489 A69-13892

Stimulated Compton effect for energy transfer between relativistic electrons and radio photons in quasi-stellar objects 05 p0828 A69-16652

Angular energy distribution in gamma quanta beam during collision between laser photons and relativistic electrons 10 p1701 A69-23132

Gallium phosphide luminescence near indirect transition during multiphoton excitation by Q switched ruby and Nd laser beams 11 p1939 A69-25693

Inverse problem method for reconstructing electrons differential spectral cross sections and photon pair for- mation in electron photon cascade 13 p2303 A69-28415

Energy transfer during fast electrons and photons in- teractions, indicating Compton energy losses related to space X ray and gamma radiation sources 15 p2676 A69-30953

Photon actuated switch consisting of 10 input binary logic gate and solid state relay to reduce aerospace vehicles self generated noise 20 p3505 A69-37289

Carbon dioxide laser amplifier operation, showing photon-induced current changes dependence on ampli- fier gain 23 p4172 A69-41398

PHOTONEUTRONS

Threshold photoneutron cross section for Mg 26, discussing resonances as primary production mechanism for stellar neutrons 21 p3788 A69-38599

PHOTONS
NT LIGHT BEAMS
NT PHOTON BEAMS

Multiphoton ionization cross section of atom via per- turbed Green function, considering light wave elec- tromagnetic field perturbing effects on atomic levels 02 p0283 A69-11539

Time correlation of photons emitted by krypton gas discharge tube and helium-neon multimode laser 02 p0255 A69-11611

Multiphoton ionization of molecular hydrogen and rare gases using Q switched Nd laser apparatus 02 p0283 A69-11701

Pulsar frequency Doppler shift due to general relativistic corrections to optical path of photons in field of sun 02 p0315 A69-11836

Photon emission in germanium at high injection levels during uniaxial compression 04 p0643 A69-15255

Photon number and amplitude fluctuations of laser radiation in case of inhomogeneously broadened atomic line and for steady state condition 05 p0770 A69-15631

Quadratic and cubic response in photoelectric emis- sion in potassium antimonide under laser irradiation observed with measurement of energy distribution of excited electrons 05 p0771 A69-15813

Low energy photon spectrum at balloon altitudes, noting small geomagnetic latitude dependence 06 p0992 A69-17313

High energy pure photon showers in cosmic ray emulsions in relation to production of magnetic pole- antipole pairs 06 p0996 A69-17883

Enhanced two photon emission between 6S and 4S levels of K, discussing stimulated three photon Raman scattering and four photon parametric coupling processes [IEEE PAPER S-8] 07 p1154 A69-19080

Electron plasma and magnetic field effects on polaritons in semiconducting GaAs studied by Raman scattering of light at small angles 07 p1200 A69-19401

Electromagnetic waves and photons coexistence, discussing wave mechanics and guidance of particles, photon guidance and corpuscular magnitudes, etc 08 p1351 A69-20117

Electron emission of probe caused by impinging ions and photons, discussing model for low plasma densities 08 p1361 A69-20232

Photon momentum distribution role and relation to thermal radiation spectrum in fully ionized gases 08 p1357 A69-20747

Angular distribution of photon radiance of spherical satellite irradiated by Lambertian earth, assuming nonemissive satellite 08 p1311 A69-21095

Photon whirls and formation of protogalaxies, discussing density inhomogeneities in hot model of universe in terms of pregalactic structure dynamics 09 p1361 A69-21355

Bose condensation and shock waves in photon spec- trum during scattering for equilibrium state of ionized plasma and radiation 09 p1546 A69-21574

Lunar photon leakage spectrum due to photons from capture and inelastic scattering of neutrons by galactic cosmic rays 09 p1597 A69-22088

Pulsar NP 0532 optical pulsations period, discussing time rates of change, pulse shape, amplitude, photons, etc 10 p1774 A69-23182

Two photon photoelectron counting statistics and in- tensity fluctuations of incident radiation compared with single photon detectors and applied to laser out- puts 10 p1704 A69-23658

Time correlation of photons emitted by krypton gas discharge tube and helium-neon multimode laser 11 p1895 A69-24718

Two photon and resonance parametric lasers non- linear polarization theory, deriving equations for elec- tromagnetic field oscillations 12 p2110 A69-26910

Proportional counter array for detection of soft X ray photons from OSO-4 observations, discussing solar event energy spectra 12 p2151 A69-26936

Photon loss coefficients in electron beam pumped GaAs laser showing dependence on doping type and impurity concentration, noting threshold current den- sity measurement 13 p2271 A69-27467

Carrier dragging in CdS single crystals under Q switched ruby laser light due to photon stream 13 p2271 A69-27661

Photon emission from highly relativistic stars, using computed differential light delays to calculate blurring of spherically symmetrical emission pulses 13 p2350 A69-27825

Tensor analysis of four photon interaction in rarefied plasma in magnetic field, determining cubic current of plasma wave self action

13 p2314 A69-28444

Rocket-borne scintillation spectrometer for cosmic photon radiation

14 p2449 A69-29566

Transition probabilities of spectral lines in helium-like ions estimated from hydrogen magnetic dipole transitions, discussing single photon decay

15 p2695 A69-30892

Two photon interaction between ultrashort light pulse and medium, showing pulse propagation through medium without absorption

15 p2634 A69-30966

Relative motion of 3 K cosmic background radiation with covariant photon equilibrium distribution

15 p2657 A69-31494

Photon bunching effect in spatially coherent noise field enhanced by superposing monochromatic coherent signal and/or shaping incident noise spectra

16 p2749 A69-31694

Photoelectric effect without photons, discussing classical field falling on quantized atomic electron

17 p3007 A69-32838

Photon whirls and formation of protogalaxies, discussing density inhomogeneities in hot model of universe in terms of pregalactic structure dynamics

18 p3197 A69-34745

Two photon excitation of luminescence in complex uranyl compound single crystals using Q switched ruby laser

19 p3334 A69-35982

IR detector limiting noise voltage /photon noise/ due to photon arrival fluctuations at responsive element determined using Planck radiation law

19 p3309 A69-36059

Two photon decay of metastable levels of hydrogenic and He-like ions in solar corona, depopulating via proton collisional excitation to 2p level

19 p3396 A69-36218

Paradox of incoming photons detection at two antennas without interference pattern disturbance explained by classical and quantum physics

20 p3538 A69-37415

Gas molecule collision influence on photon echo intensity produced by two linearly polarized laser pulses incident on sulfur hexafluoride

21 p3774 A69-38589

Renormalization of second order self energy part of photon and lowest order corrections to single photon vertex using Lagrange vector meson density

21 p3775 A69-39468

Spectral distribution of two photon emission from metastable state of singly ionized He by broadband spectroscopic coincidence counting technique

23 p4220 A69-42378

PHOTOOXIDATION

Photolysis of t-butyl iodide at low temperatures as source of t-butyl peroxy radicals for synthesis of peroxides

07 p1073 A69-18375

PHOTOPIEZOELECTRICITY

U PHOTOELECTRICITY

U PIEZOELECTRICITY

PHOTORECEPTORS

Live retinal photoreceptors studied by low angle X ray reflection, proposing electron density model

22 p3871 A69-40057

Cytoplasmic and ciliary connections between inner and outer segments of mammalian visual receptors

22 p3881 A69-40857

PHOTORECONNAISSANCE

Apollo 6 multisensor imagery of Wilcox Playa /prehistoric lake remnant/ in Arizona, using IR scanner, microwave radiometer, vidicon system and cameras

22 p3942 A69-40988

PHOTOREDUCTION

U PHOTOCHEMICAL REACTIONS

U REDUCTION [CHEMISTRY]

PHOTOSENSITIVITY

U PHOTOCONDUCTIVITY

PHOTORESISTORS

U PHOTOCONDUCTORS

PHOTOSENSITIVITY

NT LIGHT ADAPTATION

NT PHOTOTROPISM

Photographic film blackening under high intensity laser radiation indicating two photon mechanism as responsible

01 p0080 A69-10429

Laser holography using colored KBr crystals subjected to hard gamma radiation as photosensitive material

04 p0598 A69-14855

Photoconductor open circuit voltage determination, calculating responsivity and sensitivity of actual and ideal cases

12 p2093 A69-26481

Hologram recording on photosensitive material based on photoinduced polymerization showing good resolution and diffraction efficiencies

13 p2258 A69-27199

Photographic layers darkening process, using widely spaced or single giant pulses of ruby laser

13 p2260 A69-27612

Capture levels at photosensitive CdS crystals surface determined by studying field effect mobility dependence on electric field

13 p2318 A69-27884

Temperature effects on photosensitivity spectra of cadmium telluride thin films

13 p2318 A69-27889

Photodetector requirements for autocolimators with beam splitters, considering spectral characteristics, photoresponse, time constant, positioning, etc

14 p2447 A69-29326

Spectral distribution of photosensitivity for p-n junctions in silicon doped GaAs, showing agreement with state density model and absorption data

15 p2666 A69-30067

Laser holography using colored KBr crystals subjected to hard gamma radiation as photosensitive material

15 p2608 A69-30247

Photoresponse and minority carrier diffusion length long term stability of Li doped solar cells after proton, neutron and electron irradiation

19 p3252 A69-35697

Color coded area sensitivity maps of photomultiplier tubes by multicolor display technique, noting focus electrode voltage

19 p3305 A69-35724

Previous radiation exposure effect on photographic film noting increased sensitivity at UV frequencies

19 p3314 A69-36626

Cations of sulphates photosensitizing role in photolysis of amino acids and peptides in various atmospheres

20 p3477 A69-37626

Oxygen exchange in *Scenedesmus* and *Chlorella* as function of carbon dioxide, compensation point, Hill activity and photorespiration, using mass spectrometry

23 p4099 A69-42528

PHOTOSENSORS

U PHOTOELECTRICITY

U RADIATION MEASURING INSTRUMENTS

U SENSORS

PHOTOSPHERE

Chromospheric and photospheric solar observations made in Belgium in 1967, noting heliographic sunspot latitudes

02 p0313 A69-11533

Turbulent velocity in faculae and photosphere obtained from IR triplet of oxygen analysis

02 p0314 A69-11646

French solar research program, emphasizing photosphere-chromosphere transition zone

02 p0316 A69-11905

Goldberg-Unno method for determining Doppler width, microturbulence velocity and convection errors, considering photosphere as hot ascending and cold descending columns

02 p0328 A69-12752

Photosphere models comparison based on theoretical rotational temperatures of various diatomic molecular free radicals, using faint lines method

03 p0512 A69-13694

Analysis of equivalent widths as function of disk position for six photospheric neutral atomic oxygen Fraunhofer multiplets, noting O abundance

03 p0515 A69-14034

Spectra of hydrides of Mg 25 and Mg 26 in photosphere, searching for weak lines on basis of isotope shifts

03 p0515 A69-14035

Solar Fe abundance from photospheric permitted Fe and forbidden Fe II lines, noting equivalent widths of two Fe II lines

03 p0515 A69-14036

Photospheric brightness differences and structure of large scale intensity fluctuation, discussing association with solar supergranulation and chromospheric network

03 p0515 A69-14037

Time dependent variations in magnetic fields of active sunspot clusters in photosphere observed by magnetograph

04 p0651 A69-14369

Horizontal and vertical downward velocity components in developed solar active regions

04 p0651 A69-14370

Inner corona Fraunhofer lines invisibility at solar eclipses, emphasizing uncertainty of photospheric absorption lines appearance as electron scattering

04 p0654 A69-14628

Photospheric network obtained by spectroheliograms, discussing Fraunhofer lines weakening, nonsunspot magnetic fields and Zeeman sensitivity

04 p0664 A69-15523

Lithium abundance determination difficulties for undisturbed solar photosphere, noting Li I resonance line identification and model choice

05 p0821 A69-15849

Micro and macroturbulent motions velocity in solar photosphere based on Fraunhofer lines analysis

05 p0823 A69-16014

Spectrum of accelerated particles on surface of stars revealed by observation of photospheric lithium and beryllium

05 p0817 A69-16711

Solar supergranules and hydrogen convection zone analysis based on polytropic atmosphere convection physics

07 p1211 A69-18408

Solar photosphere model with two stream columnar representation of granulation for predicting continuous radiation field

07 p1217 A69-19238

Solar spectral line profiles for photosphere disturbed by short period acoustic waves

07 p1217 A69-19239

Radiative opacity in stellar atmospheres, discussing effect of UV continuum on photospheric radiation field

07 p1221 A69-19393

Solar photosphere abundances of various heavy elements from photoelectric spectrometer measurements of equivalent width of known Fraunhofer lines

08 p1390 A69-20393

Wing of solar line H-alpha for levels population of hydrogen atom in solar photosphere, discussing excitation temperature, absorption coefficient and thermodynamic equilibrium

08 p1390 A69-20394

Electron impacts role on dissociation rates of CO molecules in upper layers of solar photosphere

09 p1590 A69-21376

Effective cross sections of electron-neutron interaction in photosphere and sunspots, calculating electric conductivity and anisotropy coefficient

09 p1579 A69-22175

Solar magnetic fields compared in chromospheric and photospheric layers using magnetograph measurements, noting correlation with solar event

10 p1762 A69-23727

Alpha hydrogen plage 20934 /McMath no. 8362/ associated with July 1966 proton flare development and configuration along sunspot group axis

10 p1762 A69-23728

Center to limb variations of sunspot-photosphere brightness ratio, considering umbra darkening and radiative equilibrium

11 p1946 A69-24426

Magnetic fields, green corona emission and filaments relationship at high solar latitudes using synoptic charts

11 p1964 A69-25416

Photospheric magnetic fields, coronal emission and filaments distribution relationship with 1420 MHz radio emission, noting brightness and plasma density increase

11 p1964 A69-25417

Solar activity complex development based on magnetic, photospheric, chromospheric and coronal observations

11 p1964 A69-25418

Solar spectroscopic techniques, discussing instrumentation problems affecting photosphere line spectra, SNR in absorption spectra and near IR spectra

13 p2341 A69-27588

Tentative solar photospheric model meeting Noyes and Withbroe criticism

14 p2518 A69-29131

Ca II forbidden lines in photospheric spectrum identified with weak Fraunhofer line by photoelectric spectrometer scans

14 p2528 A69-29962

Dissociation equilibrium of diatomic molecules in solar atmosphere, comparing concentration above photosphere to MgH

14 p2528 A69-29963

Solar photosphere and sunspot magnetic fields structure and strength dependence on sunspot area
14 p2528 A69-29965

Fe II forbidden lines profiles and equivalent widths prediction for solar photospheric spectrum, deducing photospheric Fe abundance
16 p2854 A69-31652

Trieste astronomical observatory optical and radio solar photosphere observations in 1967, including solar cycle and north-south symmetry
16 p2858 A69-32206

Photospheric granulation near center of quiet sun, analyzing morphological properties from high definition Stratoscope photographs
17 p3029 A69-33045

Active solar centers interactions above photospheric level and through corona linkages, noting MHD shock waves and magnetic field lines
17 p3040 A69-33801

Temperature fluctuations in solar photosphere, noting transition from convective to radiative energy transport
17 p3040 A69-33810

Solar Fe II lines theoretical equivalent widths calculations, estimating influence of photosphere model on iron abundance data
18 p3191 A69-34305

Electron impacts role on dissociation rates of CO molecules in upper layers of solar photosphere
18 p3198 A69-34764

Molecular concentration-optical depth curves for combinations of two photospheric and two facular models, noting lines contrast dependence on dissociation energy
18 p3204 A69-35391

Interplanetary and photospheric magnetic fields polarities observed by Mariner 4 and with solar magnetograph, noting noncorrelated data along latitudinal strip
18 p3205 A69-35399

Criteria to prove incorrectness of two column model for photospheric granulation proposed by Margrave and Swihart /1969/
20 p3603 A69-37541

Photospheric radiation field role in temperature inversion of stellar chromospheres with dominant H ion opacity, postulating mechanical energy dissipation
20 p3613 A69-38173

Magnetic field fluctuations and radial velocity in undisturbed photosphere, discussing magnetic field relation to radial velocity, cross correlation asymmetry, etc
20 p3535 A69-38300

Revised solar iron abundance by photospheric Fe I lines analysis using Garz and Kock f values, noting influence on solar photospheric model
21 p3796 A69-38475

Mean intensity profiles of photospheric H alpha radiation illuminating solar prominences moving at different heights
22 p4011 A69-39995

Horizontally flowing eddies or Rossby waves in solar convection zone and photosphere, giving mathematical models showing hydromagnetic dynamo effects inducing reversing magnetic fields
22 p4019 A69-40294

Solar He abundance determined from solar model photospheres line and continuum radiation
22 p4031 A69-40911

Solar image selection device based on statistical analysis of photospheric contrast, noting use for electronic photography and location impaired observatory
23 p4213 A69-41697

Phenomenological sunspot model describing granules, supergranules, magnetic fields and photospheric convection
24 p4378 A69-42691

Interplanetary and geophysical conditions forecasting based on repetitions of low latitude photospheric background magnetic field patterns during solar activity cycles
24 p4387 A69-43626

PHOTOSTRESSES
Transparent dielectrics destruction by laser radiation noting stress development in medium
08 p1324 A69-19947

PHOTOSYNTHESIS
Interactions between intermediate fluorescence quenching trapping center and associated electron acceptor of oxygen evolving photosynthetic spinach chloroplast photosystem
01 p0024 A69-10928

Biological life support system for regenerating closed atmosphere by photosynthesis, using gas exchange between man and microalgae
01 p0021 A69-11078

Hydrogen adaptation effect on fluorescence of normal and Mn deficient algae, noting system II photosynthesis
04 p0554 A69-15325

Manganese catalyst photoreactivation in photosynthetic oxygen evolution in Mn deficient alga *Anacystis nidulans* cells
13 p2210 A69-28257

Photosynthesis and respiration rate in vegetables in controlled temperature, humidity, illumination levels, carbon dioxide and oxygen contents
17 p2912 A69-32933

Dual beam white or nearly monochromatic light source providing programmed repetitive sample illumination with variable intensity, pulse duration and sequence for photosynthesis research
19 p3312 A69-36378

Water purification through biological oxidation of organic wastes using controlled photosynthesis, discussing algae production and harvesting
21 p3668 A69-39711

Photosynthesis enhancement in seaweed after alternate exposure to gas laser and tungsten lamp white light passed through IR narrow band filter
24 p4270 A69-42580

PHOTOTHERMOTROPISM

U ANISOTROPY
U PHOTOTROPISM
U TEMPERATURE EFFECTS

PHOTOTROPISM
Q switches transparency as function of incident light intensity
04 p0610 A69-14385

Q switches transparency as function of incident light intensity
14 p2456 A69-28758

PHOTOTUBES

NT PHOTOMULTIPLIER TUBES
Phototubes, photodiodes, photoconductors, quantum detectors, nonlinear optical detectors and heterodyne receiving systems for photodetection of laser outputs
09 p1518 A69-22126

Random function output current obtained in phototube and scintillation detector including amplitude distribution, time measurements and pulse shape discrimination
22 p3947 A69-40670

PHOTOVISCOELASTICITY

Photoviscoelastic stress analysis to predict time dependent stress redistributions in polyphase system with viscoelastic binder under external loading conditions
03 p0524 A69-13061

Polymers stress-strain behavior and corresponding birefringence within limited temperature range and strain rates
15 p2642 A69-30678

PHOTOVOLTAGES

Cadmium sulfide films with larger than bandgap photovoltages, analyzing photovoltage decay and temperature and light intensity effects
06 p0980 A69-17772

PHOTOVOLTALIC CELLS

Linearized time dependent equation for photovoltage distribution in nonuniformly illuminated p-n junction
03 p0486 A69-13636

Photovoltaic solar cell power technology application to space use and exploration [ASME PAPER 68-WA/SOL-1]
05 p0705 A69-16158

Red, blue and no bias light effects on spectral response of copper sulfide-cadmium sulfide cell, using model incorporating photoconductive layer
05 p0808 A69-16358

Drift field photovoltaic cell performance with bulk and surface recombinations
06 p0870 A69-17473

Ceramic CdS photovoltaic solar cell properties and model, classifying junctions according to preparation method
14 p2508 A69-29886

Cu-Cd-S photovoltaic cell models correlated, reporting spectral response and electron microprobe test results
19 p3382 A69-35682

Radiation damage and recovery of lithium-diffused silicon p-n solar cells, measuring photovoltaic parameters as function of gamma radiation fluence
19 p3251 A69-35694

Photovoltaic solar cell power technology application to space use and exploration [ASME PAPER 68-WA/SOL-1]
19 p3255 A69-36418

Photovoltaic cells electrical characteristics, discussing Cd sulfide, single crystal Si and dendritic type Si cells for spacecraft power
22 p3868 A69-40130

PHOTOVOLTALIC CONVERSION

Photovoltaic properties of CdS thin film solar cells and silicon cells at Jupiter temperature and solar intensity
03 p0368 A69-13076

Advanced reconnaissance electric planetary spacecraft (AREPS) concept for repeated coverage of Mars or Venus surface, using solar-photovoltaic system [AIAA PAPER 69-253]
09 p1585 A69-21244

Liquid mercury cathode thrusters characteristics satisfying constraints imposed by solar flux variations with distance from sun [AIAA PAPER 69-237]
09 p1565 A69-21246

PHOTOVOLTALIC EFFECT

Surface photovoltaic effect in copper electroplated single crystal CdS solar cells, discussing Fermi level and Hall effect
05 p0704 A69-15958

Solar cells physical properties and functions, considering band structure of semiconductors, p-n junction diodes and photovoltaic effect, efficiency calculations and radiation damage
12 p2015 A69-25864

Photovoltaics - IEEE Conference, Pasadena, November 1968
19 p3249 A69-35678

Gold donor level impurity photovoltaic effect in silicon, noting solar cell efficiency reduction due to minority carrier recombination
19 p3381 A69-35679

Photovoltaic effects in cadmium mercury tellurides, considering band-gap variations, effective masses, mobilities, majority carrier concentration and pair lifetime
19 p3381 A69-35680

Cu-Cd-S photovoltaic cell models correlated, reporting spectral response and electron microprobe test results
19 p3382 A69-35682

Copper sulfide-cadmium sulfide heterojunction model for photovoltaic effect, considering surface layer intrinsic absorption and CdS photoconductivity
19 p3250 A69-35683

Photovoltaic effect at copper sulfide-cadmium sulfide heterojunction, studying depletion layer width, diffusion lengths and spectral response
19 p3382 A69-35684

PHUGOID OSCILLATIONS

U OSCILLATIONS
U PITCH (INCLINATION)

PHYSICAL CHEMISTRY

Soviet collection of articles on physicochemistry of zirconium alloys
02 p0261 A69-11839

Physicochemical synthesis of monosaccharides from human waste products at atmospheric and elevated pressures, considering methane oxidation by nitrogen oxides and ozone
07 p1071 A69-18971

Soviet collection of articles on physicochemical studies of heat resistant alloys
09 p1524 A69-22135

Heat resistant materials based on high melting point metals, summarizing achievements of chemical technology and vacuum metallurgy
09 p1524 A69-22137

Phase diagram for physicochemical study of CdSb-Ge cross section of Cd-Sb-Ge ternary system, discussing exo-endothermal fusion effects, microstructure, etc
14 p2503 A69-28975

Epoxy adhesives physical chemistry, curing processes, formulation, surface application methods, testing and health hazards
14 p2468 A69-29339

Physicochemical synthesis of monosaccharides from human waste products at atmospheric and elevated pressures, considering methane oxidation by nitrogen oxides and ozone
20 p3483 A69-38219

Soviet book on liquid binary systems covering physicochemical analysis and quantitative methods
21 p3670 A69-39529

Molecular radiobiology, discussing physicochemical processes caused by energy absorption in targets, leading to inactivation under various circumambient conditions
23 p4090 A69-41963

PHYSICAL CONSTANTS TESTING REACTOR
U NUCLEAR RESEARCH AND TEST REACTORS

PHYSICAL EXAMINATIONS

- Cardiovascular system medical examinations for selection of aircraft and spacecraft crew members from healthy men with no apparent disorders or complaints
07 p1066 A69-18983
- Cardiovascular system medical examinations for selection of aircraft and spacecraft crew members from healthy men with no apparent disorders or complaints
20 p3480 A69-38231
- NASA Lunar Receiving Laboratory functional areas and physical, chemical, biological and quarantine activities for crew and lunar samples
21 p3690 A69-38896

PHYSICAL EXERCISE

- Cosmonauts cardiac activity and respiration changes during physical exertion in orbital flight on Voskhod spacecraft
03 p0377 A69-14196
- Telemetry aortic blood pressure and heart rate from dogs under various physical activities and emotional stress
07 p1071 A69-19133
- Stability of male cardiovascular, respiratory and motor systems functional conditions after physical activity in pure O₂ medium at high altitude pressure
08 p1262 A69-19931
- Hypokinesia muscular activity deficit in males confined to bed rest compensated for by physical exercise, noting orthostatic resistance, acceleration endurance, immunity, etc
08 p1263 A69-19932
- Long term hypokinesia effect on cardiovascular system of athletes indicating human orthostatic resistance increase due to physical exercises
10 p1646 A69-23581
- Physical exercises to increase cosmonaut space environment tolerance, discussing effects of acceleration, altitude and hypoxia
15 p2560 A69-31460
- Motion coordination capacity of persons subjected to 40 days bed rest studied by dynamographic technique, discussing nature of slackening
17 p2906 A69-32937
- Prolonged hypokinesia effect on human resistance to physical stress, noting prophylactic influence of physical exercises
17 p2907 A69-32939
- Exercise effects on hepatic cholesterol of rats on diets high in saturated or unsaturated fats
21 p3653 A69-38903
- O uptake of middle aged men, comparing short and long term endurance running effects
21 p3654 A69-38904
- Human performance assessed by pulse rate increment at onset of exercise on bicycle ergometer and decrement during recovery after fasting
21 p3655 A69-38910
- Caucasian and Bantu males oxygen consumption at different work rates, gross body weight accounted for 70 percent of differences between individuals
21 p3655 A69-38911
- Physical activity programs in industry for selected employees as routine component of occupational health programs
21 p3663 A69-38919
- Seasonal effects on energy expenditure during rest and exercise at controlled ambient temperatures, noting effects on heart rate
22 p3890 A69-40211
- Oxygen uptake and circulatory response in human male subjects during maximal treadmill and bicycle exercise
22 p3874 A69-40226
- Arterial and deep venous blood from human forearm analyzed following rest and rhythmic exercise on ergometer in hyperbaric oxygen chamber
22 p3878 A69-40834
- Physical exercise effect on adolescent males, comparing oxygen uptake, heart volume and height in training and nontraining groups
23 p4077 A69-41312
- Stratified blood flow distribution in lung lobule from analyzing breath-holding changes on expired Ar and nitrous oxide tension plateaus during rest and exercise
23 p4078 A69-41315
- Rebreathing method for determining mixed venous oxygen pressure and cardiac output during rest and exercise in trained athletes
23 p4078 A69-41316
- Physical training effects under normal atmospheric pressure on high altitude hypoxia and acceleration resistance in rats, including survival times
23 p4079 A69-41383

- High energy phosphate splitting for energy requirements not met by oxidation during supramaximal exercise, noting glycogen splitting into lactic acid after phosphate exhaustion
23 p4100 A69-41443
- Hand and thumb exercise effects on acquisition tracking task performance
23 p4101 A69-41453
- Hypoxia acclimatization studied by subjecting groups to bicycle exercise at simulated high altitude and at ground level
23 p4086 A69-41678
- Exhaustion time extension in rats by altitude acclimation, noting adaptation loss resulting from physical exercise discontinuation
23 p4086 A69-41787
- Exercise prescription for hypokinetic airline pilots to prevent physiological deterioration and maintain performance, discussing predictive tests, tolerance evaluation, training regimens, etc
23 p4106 A69-41800
- Energy cost of muscular exercise in gastrocnemius muscle of dogs anesthetized with morphine, chloralose and urethane
23 p4093 A69-42065
- Rodent swimming and treadmill training effect on capacity of mitochondrial fraction from hind limb muscles to oxidize pyruvate triples
23 p4095 A69-42084
- Venous tone, peripheral venous pressure, skin and muscle blood flow, alterations of heart rate and respiration in men during leg exercise
23 p4096 A69-42090
- Training effect on fast muscle isometric contraction in rats, discussing mechanical characteristics
23 p4097 A69-42095
- Calorimetry-thermometry discrepancy during prolonged exercise in hot dry environment, measuring rectal temperature with increasing exposure time
23 p4098 A69-42104
- Oxygen consumption, ventilation and cardiac frequency relationship to body weight during submaximal exercise in normal human beings
23 p4099 A69-42169
- Central circulatory responses of humans to rapid skin temperature changes during continuous exercises
24 p4258 A69-42633

PHYSICAL FACTORS

- Human tolerance to SST sonic booms through scheduled community exposure, discussing physiological effects and acceptability level
14 p2541 A69-29153

PHYSICAL FITNESS

- Medical fitness regulations for pilots, including federal and internal airline regulations
06 p1041 A69-16844
- Tilt-table and acceleration tolerance of athletes and inactive students, comparing cardiovascular responses, heart rate and blackout level [DVL-834]
09 p1444 A69-21304
- Abnormalities of routine electrocardiograms in medical certification of pilots, indicating errors in screening
19 p3263 A69-36462
- Physical activity programs in industry for selected employees as routine component of occupational health programs
21 p3663 A69-38919
- Healthy, physically untrained students compared with trained athletes for differences in working capacity concerning orthostatic tolerance and blood pressure responses
22 p3889 A69-39940
- Heart rate responses and corresponding tolerance tests in trained athletes and nonathletes during simulated environmental extremes
23 p4102 A69-41683
- Healthy, physically untrained students compared with trained athletes for differences in working capacity concerning orthostatic tolerance and blood pressure responses
23 p4108 A69-41821
- Norms for quantitative vectorcardiography derived from statistical analysis of results from healthy young subjects, emphasizing medical evaluation of flying personnel
24 p4277 A69-43390
- Medical wastage of military and civil aviators in Great Britain /1963-1968/, discussing cardiovascular disease, fatal flying accidents and psychiatric disease
24 p4277 A69-43391

PHYSICAL OPTICS

- Radar cross sections for arbitrary bodies calculated with computerized ray optics method taking into account depolarization
02 p0209 A69-12332
- Conceptual problems of quantum optics, considering quantum mechanical and classical descriptions of effect of field on matter for damped and undamped modes
03 p0467 A69-13474
- Nonlinear optics noting harmonic generation of light, optical modulation, parametric oscillators, stimulated scattering, self focusing of light and resonance phenomena
05 p0770 A69-15704
- Nonlinear optics, noting polarization induced by electromagnetic waves, wave propagation, light wave coupling in dispersive medium and coupled laser modes
05 p0793 A69-15771
- Nonlinear optics, discussing frequency mixing, induced changes in dielectric constant and parametric amplification in microwave region of spectrum
05 p0772 A69-16229
- Ray optics method of far field scattering by discontinuity in parallel plane waveguide applied to strips, apertures, bifurcations, etc
14 p2423 A69-29753
- Fourier transform techniques applications in optics, converting optical signal amplitude and phase information into electrical signal information
19 p3374 A69-36737
- Coherent light focusing by helicoidal guide-extension to particle focusing, discussing analogy between index distribution for classical optics and potential distribution for electronic optics
22 p3981 A69-40475
- Lateral waves used to explain diffraction effects by light incident upon interface at critical angle of total reflection, discussing quasi-optical properties
23 p4191 A69-42148

PHYSICAL PROPERTIES

- Electrical resistivity, composition, and physical properties of titanium carbide, titanium oxide and titanium-oxygen-carbon alloys
03 p0446 A69-13575
- Book on properties of liquid and solid helium 3 and 4 physical characteristics, phase behavior and experimental techniques
04 p0630 A69-14688
- Whisker research history, discussing characteristic morphology, mechanical and physical properties and future applications as reinforcing components in reinforced metals
04 p0616 A69-14843
- Phase equilibria, phase transformation temperatures and relation between resistivity and chemical composition for alloys of Ti-Al-Mo-Zr system
04 p0618 A69-15079
- Low density polyurethane foam with and without honeycomb as ablative material for reentry vehicles, discussing oxidation resistance
04 p0688 A69-15513
- Randomly rough surface physical and geometrical remote determination by polychromatic bistatic radar
05 p0721 A69-16572
- Physical and physicochemical properties of anodic silica obtained by silicon oxidation in organic bath, discussing possible applications
05 p0810 A69-16589
- Physical electronics, discussing gas discharges, semiconductor devices, electron emission, noise in electronic devices and masers and lasers
05 p0735 A69-16666
- Preparation and properties of NbC-WC and TaC-WC carbides, analyzing hardness, resistivity, thermal expansion and dihedral angle
05 p0782 A69-16796
- Unified methods based on dislocation theory for direct solution of problems pertaining to physical properties of metals
06 p0944 A69-17502
- Australasian microtektite physical and chemical properties, comparing refractive indices, specific gravities, composition trends, etc
08 p1305 A69-19815
- Physical properties control in nickel powders obtained by hydrogen reduction of nickel diamine sulphate solutions
08 p1334 A69-21057
- Type two superconductors physical properties, discussing magnetic flux lines interaction with structural defects
09 p1555 A69-21490

Soviet book on fluid semiconductor properties at high temperatures during transition from solid to liquid state

10 p1744 A69-23316

Soviet book on methods of investigating semiconductors as applied to lead chalcogenides PbTe, PbSe and PbS covering physical and physicochemical properties

12 p2145 A69-26851

Physicochemical and operational properties of trimethylol propane esters as lubricating oils under static and dynamic conditions

12 p2103 A69-27090

Physical and physicochemical properties of ferrites - Conference, Minsk, Belorussian SSR, 1967

13 p2319 A69-27991

Homogeneous NbC and TiC specimens physical properties, discussing current carrier density and mobility dependence on composition

14 p2462 A69-28976

Pressure, temperature, vibrations and structural stresses data acquisition system for aeronautical applications

14 p2450 A69-29686

Semiconductor films synthesis and properties, discussing single crystal films, epitaxial nucleation, nuclei surface distribution, layer kinetics, doping and film-substrate interface

15 p2670 A69-31046

Lower oxides of Si, studying chemical composition, formation conditions, stability and chemical and physical properties

15 p2643 A69-31245

Reinforced textolite plastic dimensional and mass changes in water and oil immersion as function of surface, temperature and time

15 p2643 A69-31550

Precipitation processes and effect on properties of Cr-Ni-W-Ti heat resistant austenitic steel, using electron diffraction and transmission electron microscopy

17 p2984 A69-32833

Lunar based physics and chemistry, discussing exploration of and survival in lunar environment

18 p3112 A69-34235

Lunar surface uppermost layer physical and mechanical properties investigated by soilmeter-penetrometer and radiation densimeter on Luna 13

18 p3113 A69-34239

Polymer molecular structure influence on physical and mechanical properties, considering regularity, chain flexibility, crosslinking and intermolecular forces

18 p3099 A69-34606

B-epoxy and B-Al composites compared for strength/weight and modulus/weight ratios, moisture absorption, corrosion resistance, projected costs, etc

19 p3340 A69-35506

Integral fuel tank sealant based on various hydrofluorocarbon polymers prepared, tested and compared for physical properties

19 p3356 A69-35533

Interplanetary dust sources investigation based on physical and orbital parameters, noting derivation from asteroids and meteorites

19 p3415 A69-36119

Physical characteristics of young planetary nebulae and nuclei, discussing classification of objects II 4997, M 3-27 and M 1-2

19 p3423 A69-36226

Physicomechanical properties of tuff rock based on similarity to lunar surface rock, determining natural density, porosity and compression strength

22 p4034 A69-41105

Surface chemistry effect on physical properties of pressure sintered Be metal, suggesting surface alloying approach by powder metallurgical techniques

24 p4332 A69-42963

PHYSICAL SCIENCES

Physical sciences - USAF Conference, Albuquerque, June 1967

07 p1181 A69-18927

Book on special functions and approximations covering differential and integral equations and attendant theories arising in mathematical physics analysis

10 p1717 A69-22801

PHYSICAL WORK

Long term restriction of muscular activity noting effects on dynamics of cardiac contraction

02 p0198 A69-11515

Human endurance during isolation in closed space with prescribed велоergometric exercises, noting impairment of functional capacity

08 p1263 A69-19933

Human locomotion analysis, measuring metabolic expenditure and mechanical energy levels of principal body segments during walking

15 p2558 A69-30587

Bicycle ergometer combined with induction clutch, investigating effect of eccentric dynamic work with arms and legs

21 p3663 A69-38902

Strenuous physical training effects on human tolerance for work in heat, measuring rectal and mean skin temperatures and heart rates

22 p3890 A69-40199

Human metabolic response to hypothermia measured over wide range of work intensities and durations

22 p3891 A69-40215

Exercise-temperature regulation in men under constant submaximal workload at various simulated altitudes, discussing exercise core temperature equilibrium level setting mechanisms

22 p3891 A69-40219

Regression relations for energy expenditure in work predicted from heart rate and pulmonary ventilation in volunteers carrying loads upstairs

22 p3891 A69-40220

Respiratory gas exchange during workloads, comparing values for ventilation, oxygen uptake and carbon dioxide output measured in air and in helium-oxygen mixture

22 p3891 A69-40221

Heart rate measurements in ski jumpers with radio telemetric system revealing tachycardia during climbing and emotional stress

23 p4078 A69-41313

PHYSICIANS

Flight accident rate of U.S. physician pilots noting relation to number of takeoffs and landings

01 p0022 A69-11344

Aerospace medical educational programs for MD, post-MD and practicing physicians at medical faculties in U.S. and at Ohio State University

23 p4106 A69-41799

PHYSICS

Collection of papers on physics, Volume 31, Part 1, covering stellar evolution, electron transport in semiconductors, plasma microstability, etc

01 p0115 A69-10045

Bulgarian physics yearbook of higher technical institutes of learning, Volume 3

05 p0792 A69-15693

Nonlinear physics - Conference, Munich, June-July 1966

05 p0792 A69-15767

Physical electronics, discussing gas discharges, semiconductor devices, electron emission, noise in electronic devices and masers and lasers

05 p0735 A69-16666

Reports on progress in physics, Volume 31, Part 2

08 p1350 A69-19867

Physics, mathematics, mechanics - Conference Moscow, December 1964

13 p2300 A69-28430

Lunar physics and chemistry - IAA Conference, Belgrade, September 1967

18 p3112 A69-34234

Asymptotic solution, existence and uniqueness of integral equations occurring in elasticity theory and mathematical physics

21 p3772 A69-39618

General and applied physics - Conference, Alma-Ata, U.S.S.R., May 1967

21 p3853 A69-39841

Physics applications to earth and planetary interiors - NATO Conference, Newcastle-upon-Tyne, England, March-April 1967

22 p4015 A69-40172

Book on electronics and electron physics covering electron beams, far IR radiation, electron microscopy, scintillation detectors and breakdown in solids

22 p3981 A69-40667

Physics - Conference, Trieste, June 1968, Volume 1, Condensed matter, plasma physics, turbulence, quantum optics, statistical mechanics, astrophysics, quasars, pulsars, gravitation theory and cosmology

23 p4216 A69-42310

PHYSIOCHEMISTRY

Priming explosives analysis suggesting physicochemical methods for high purity products for space applications

10 p1750 A69-23012

Physicochemical methods of corrosion testing - Conference, Frankfurt am Main, April 1968

10 p1712 A69-23818

Lunar laboratory physical and chemical experiments including scattering phenomena, molecular and atomic beams and gas cloud photochemistry

18 p3113 A69-34237

Ammonia resistojet thruster, describing ammonia physicochemical properties and systems characteristics of pulsed mode operation and continuous thrust resistojets

23 p4203 A69-41931

PHYSIOGRAPHY

U GEOMORPHOLOGY

PHYSIOLOGICAL ACCELERATION

Hypokinesia and acceleration effects on human organism immunity and resistance to inflammatory diseases in 62 day test

02 p0198 A69-11513

Injury stress vs acceleration specification as valid criterion for pilots subjected to high acceleration, introducing models and illustrating with ejection example

17 p2913 A69-33008

Acceleration injury noting water immersion effect on cat lung due to intense body vibration, suggesting restraint as practical solution

17 p2913 A69-33009

PHYSIOLOGICAL EFFECTS

NT HEMODYNAMIC RESPONSES

Weak alternating electric field effects on human circadian rhythms

01 p0013 A69-10167

Soviet book on space physiology covering space flight and laboratory data on cerebral cortex function, digestive system, tissue changes, etc

01 p0014 A69-10743

Changes in organism during sudden decompression, analyzing pressure equalization, dissolved gases transformation and body fluids vaporization

01 p0020 A69-10753

Gemini and Mercury space flights medical results, summarizing physiological effects noted on body systems

01 p0017 A69-11074

Human endocrine-metabolic response to sequential decompression exposure during simulated orbital flight or extravehicular activity

01 p0022 A69-11337

Rodents exposure to neon enriched atmosphere for three weeks in sealed recycling system, discussing body weight pregnancies and litter

01 p0019 A69-11342

Physiological, cytochemical and histological effects on muscular activity, nervous system, adrenal and thyroid glands and liver of mice during 30 day hypokinesia

02 p0198 A69-11502

Physiological processes occurring in voluntary movements of animals under space flight weightlessness conditions

02 p0199 A69-11827

Space biomedical research trends, noting gastroenterology and lack of research on disease processes during space travel and overemphasis on space physiology

03 p0369 A69-12859

Physiological effects of space cabin environment variables during long and hazardous space missions with regard to engineering constraints and radiobiology

03 p0380 A69-13504

Manual performance relationship to men exposed to cold, thermal neutral and hot environments, discussing finger dexterity and motor coordination tests

03 p0381 A69-14074

Work and rest scheduling effect on working capacity and physiological state of male subjects in sealed chamber

03 p0381 A69-14201

Isolation effects on higher nervous activity, motor and vegetative reactions, muscular strength and emotional state

03 p0377 A69-14202

Daily sleep and wakefulness periodicity changes effect on heart rate, respiration and body temperature diurnal rhythms in human males under isolation conditions

03 p0377 A69-14203

Circadian rhythm effect between individuals of separate twin pairs, noting application to physiological research in medical genetics and human biometeorology

04 p0553 A69-15152

Histological investigation of internal organs of mice exposed to atmosphere with high oxygen content

05 p0709 A69-16513

Prolonged bed rest effect on brain bioelectrical activity from EEG reactions of subjects to acoustic signals followed by light signals

05 p0710 A69-16520

High temperature effects on physiological functions of man noting cardiovascular system and heart performance, body heat exchange and blood and urine composition

05 p0710 A69-16523

Clinical spectrum of postural hypotension, treating vasodepressor syncope, orthostatic anemia and idiopathic orthostatic hypotension

06 p0873 A69-17017

Physiological aspects of weightlessness

07 p1060 A69-18573

Oculomotor muscular tonus of rabbit during rocket flight acceleration and weightlessness

07 p1062 A69-18590

Drosophila melanogaster flies reproductive behavior and *Tridacna paludosa* chromosome patterns after weightlessness onboard Vostok 3 and 4

07 p1063 A69-18597

Immunological and histochemical methods for studying mice reactivity after long term exposure to hyperoxic atmosphere

07 p1065 A69-18975

Hypokinesia muscular activity deficit in males confined to bed rest compensated for by physical exercise, noting orthostatic resistance, acceleration endurance, immunity, etc

08 p1263 A69-19932

Aircrew members skin temperature changes in response to intense diffusive thermal radiation, noting psychological response to exposure [AGARDOGRAPH-111]

08 p1264 A69-20669

Thermoregulatory reactions of human body to sharp increase of ambient radiant temperature [AGARDOGRAPH-111]

08 p1264 A69-20670

Skin and subcutaneous temperature during exposure to intense thermal radiation, discussing estimation of subcutaneous temperature from skin temperature data [AGARDOGRAPH-111]

08 p1264 A69-20671

Thermal radiation effects on cutaneous vasomotor and sudomotor control of human organism [AGARDOGRAPH-111]

08 p1265 A69-20672

Long time physiological effects of rotating systems, surveying acceleration effects and rotation experiments on humans and rats

08 p1265 A69-21183

Landing and takeoff demonstration tests of OV-10A aircraft through rough terrain, noting pilots excessive physiological stresses [AIAA PAPER 69-316]

09 p1434 A69-22391

Physiological effects of breathing cool dehumidified air in hot humid environment, tabulating tolerance time, heart rate, temperature changes and sweat loss

09 p1446 A69-22543

Increased chronic acceleration physiological effects on chickens, comparing hematological observations with exercise capacity, survival and sexual development

10 p1641 A69-23041

Physiologic and metabolic effects in humans undergoing therapeutic hypothermia

10 p1643 A69-23125

Ocular injuries during bailout from Vampire aircraft, noting hemorrhages

10 p1649 A69-23380

Hypokinesia effects on human neurology on extended space flights simulated by 72-day bed rest

10 p1646 A69-23506

Automatic computer processing of physiological data during space flights, discussing choice of computers and computer programs

10 p1649 A69-23509

Prolonged bed rest effect on human myogenic tonus and proprioceptive reflexes, comparing test subjects with and without physical exercises

10 p1646 A69-23583

Combined effect of prolonged bed rest and acceleration exposure on human blood circulation, noting increased heart rate and arterial blood pressure

10 p1646 A69-23584

Altitude climates effects on human performance, discussing oxygen consumption at moderate altitudes during vigorous physical activity

11 p1827 A69-24924

Transensor implantation, sham implantation, no implantation and lighting effects on rat body composition, noting fat and water content

12 p2020 A69-26557

Book on earth atmosphere and outer space influence on human physiology for life support systems design

12 p2024 A69-27074

Gravity preference tests on rats subjected to simulated Aerobee 150 A rocket launching and flight in ground based spiral centrifuge

13 p2213 A69-28090

Physiopathological reactions of humans exposed to infrasonic vibrations applied via auricular canal, observing cardiac and circulatory hemodynamic troubles

13 p2215 A69-28590

Posture role in physiological effects of acceleration on motor activity, discussing gravitational importance to vital processes

13 p2211 A69-28593

Climatic environments development for physiological studies, considering ambient temperature, radiated heat and air velocity and movement

13 p2215 A69-28594

Physiological effects of intermittent light stimulation during helicopter flight, discussing visual and electric cortical functions at critical frequency threshold of subjective fusion

13 p2211 A69-28595

Lung ventilation mechanics affecting respiration in hyperbaric environment during deep diving, stressing biological necessity of equal pressure respiration

13 p2215 A69-28598

Circadian rhythms characteristics in humans, animals and plants, noting possible effects of rhythm disturbances on astronauts

13 p2211 A69-28614

Hypokinesia effects on transversostriated muscle fibers of mice, noting changes in myofibrillar apparatus, mitochondria and sarcoplasm

13 p2212 A69-28616

Autonomic nervous system role in controlling body functions after rapid decompression, increasing tolerance to pressure gradients by physical training

13 p2212 A69-28622

Noise measurement and scales in studying psychological and nonauditory physiological effects on human functioning

14 p2485 A69-29150

Human tolerance to SST sonic booms through scheduled community exposure, discussing physiological effects and acceptability level

14 p2541 A69-29153

Preferential shifts in consumption of metabolic fuels following exposure to hydrazine or monomethylhydrazine, considering biochemical and physiological responses

14 p2407 A69-29303

Oxygen physiological and biochemical effects on *Pseudomonas saccharophila*, discussing sucrose uptake, lipid synthesis and polysaccharide formation

15 p2556 A69-31045

Mass supersonic air transport physiological problems, reporting findings of FAUSST committee concerning ozone toxicity, pressure drops, sonic booms, time zone physiology, etc

15 p2556 A69-31225

Light effects on circadian rhythms in monkeys, describing changes in deep body temperature and locomotor activity phase relationships

15 p2556 A69-31336

High vacuum effects on oxidative processes in bacteria and physiological activities of enzymes

15 p2557 A69-31354

Alternating electric field effects on circadian rhythms in men, discussing period shortening and internal desynchronization

15 p2557 A69-31461

Long distance air flights through different time zones, discussing circadian physiological cycles, light-dark ratio shifts effects and methods of lessening desynchronization effects

16 p2745 A69-32444

Motion coordination capacity of persons subjected to 40 days bed rest studied by dynamographic technique, discussing nature of slackening

17 p2906 A69-32937

Human motion coordination under acceleration followed by weightlessness during jet flights along Keplerian orbits, discussing initial disturbance and subsequent subsiding

17 p2907 A69-32938

Physiological effects on men of 10 hour exposure to nitrogen-oxygen mixture followed by pure oxygen 4 hour exposure, simulating conditions during EVA

17 p2912 A69-32940

High positive g sub x acceleration effects on red cells destruction rate, measuring endogenous CO production of Gemini astronauts

17 p2908 A69-33176

Pulmonary mechanics during zero gravity maneuvers, noting decrease in flow rate and increase in expiration time without decrease in vital capacity

17 p2909 A69-33181

X irradiation and temperature effects on flour beetle *Tribolium confusum* pupae, noting wing abnormalities and pupal stage duration

17 p2910 A69-33748

Relationship between human response to noise and physical parameter, discussing controlled laboratory investigation to determine duration effect on annoyance

18 p3097 A69-34324

Histological investigation of internal organs of mice exposed to atmosphere with high oxygen content

18 p3096 A69-34732

Prolonged bed rest effect on brain bioelectrical activity from EEG reactions of subjects to acoustic signals followed by light signals

18 p3096 A69-34739

High temperature effects on physiological functions of man noting cardiovascular system and heart performance, body heat exchange and blood and urine composition

18 p3096 A69-34742

Toxic effects of Freon R FE 1301 on animals and human beings at different concentrations, assessing judgement, alertness and neuromuscular skill

18 p3098 A69-35061

Microbiological influence on astronauts efficiency during and after long space flights, stressing simulated microclimates and confinement effects on flora

18 p3097 A69-35304

Mechanical vibration effects on human body in industry and in terrestrial, aerial and nautical vehicles, discussing harmful frequencies and safety measures

19 p3259 A69-35605

Auditory analyzer functional changes due to prolonged slow rotation

20 p3470 A69-37251

Human sleep during prolonged rotation, discussing electroencephalograms, acoustic signal frequency producing waking reaction, cutaneous galvanic reflex and sleepiness of sleep

20 p3472 A69-37261

Vestibular analyzer dynamic characteristics under Coriolis acceleration, measuring heart beat rate, arterial pressure, head bending aftereffects, etc

20 p3472 A69-37262

Immunological and histochemical methods for studying mice reactivity after long term exposure to hyperoxic atmosphere

20 p3479 A69-38223

Psychology and physiology of vision in relation to large screen display design, discussing effects of symbol size and spacing, color usage, etc

21 p3662 A69-38330

Carbon dioxide levels monitoring in spacesuit research including limits of physiological acceptability

21 p3665 A69-39170

Heart electrical activity time sequence estimation based on multiple dipole binary model, deriving algorithm

21 p3668 A69-39865

Circadian rhythm phase shifts during ontogenesis produced by hormone concentration changes resulting from light variations

22 p3872 A69-40198

Maximum voluntary isometric muscle strength relation to endurance time in static work during partial curarization

22 p3890 A69-40213

Whole body LF mechanical vibration effects on anesthetized dogs peripheral circulation and vascular smooth muscle

22 p3875 A69-40228

Arterial and deep venous blood from human forearm analyzed following rest and rhythmic exercise on ergometer in hyperbaric oxygen chamber

22 p3878 A69-40834

Astronaut weight loss during space flight related to mission duration, noting dehydration and catabolism roles

23 p4100 A69-41303

Sotalol and propranolol cardiovascular effects, comparing toxicity and blocking action against circulatory and cardiac effects of catecholamines

23 p4080 A69-41403

Feline lung injury produced by vertical sinusoidal vibrations during upright water immersion attributed to chest wall impact

23 p4082 A69-41447

Flying effects on air hostesses, considering questionnaire data for various psychophysiological factors and flight modes

23 p4086 A69-41688

Pulmonary mechanics during zero gravity maneuvers, noting decrease in flow rate and increase in expiration time without decrease in vital capacity
23 p4089 A69-41825

Change in weight, plasma volume, urine flow and hematocrit in man before and after immersion up to chin in thermally neutral bath
23 p4096 A69-42087

Respiration effects on heart rhythm emphasizing direct mechanical influences
23 p4097 A69-42093

Central nervous, cardiovascular and metabolic data of Macaca nemestrina during simulated Biosatellite flight, testing data acquisitions systems
24 p4260 A69-42703

Physiological circadian rhythms in isolated and nonisolated Macaca Nemestrinas living under varied light intensities, noting telemetered deep body temperature, urine volume and sodium, etc
24 p4261 A69-42707

Noise level effects on pharmacological effectiveness of centrally acting drugs in rats
24 p4262 A69-42947

Continuous noise level effects on stabilized escape conditioning in male albino rats
24 p4262 A69-42948

Biological and physiopathological effects of UHF electromagnetic radiation of radar antennas, reviewing localized effects
24 p4273 A69-42996

Human circulatory reactions to cumulative flight vegetative stimuli evaluated by cumulative stress simulation method
24 p4266 A69-43375

Psychophysiological effects of fatigue and correlation with somatic parameters following circadian rhythm
24 p4268 A69-43407

Altitude decompression sickness in aviation, discussing physiological mechanisms underlying syndrome and treatment of conditions
24 p4269 A69-43412

PHYSIOLOGICAL FACTORS
NT PHYSICAL FACTORS

Neuromuscular actuation system model, noting compatibility with human physiological and anatomical data in tracking tasks
02 p0202 A69-11952

Physiological or survival training emphasizing psychological approach
06 p0879 A69-16965

Physiological functions of aged Japanese pilots, discussing height, weight, Rohrer index, obesity, vision deterioration and hearing disturbances
06 p0876 A69-18028

Optimum physiological parameters selection criteria for medical control of crew during space flights
07 p1071 A69-18978

Cold water immersion effects on man from physiological and physiopathological viewpoint, examining clothing effect
08 p1267 A69-20682

Heat susceptibility and tolerance in astronauts obtained by plot of skin and oral temperatures for subject under thermal stress
10 p1644 A69-23376

Physical factors affecting proximal and distal tubular sodium reabsorption in dogs undergoing water diuresis
13 p2210 A69-28482

Multichannel telemetry system for chronic implantation in animals to monitor physiological parameters
15 p2559 A69-31044

Space medicine to characterize nature and degree of changes in human functional capabilities due to space flight environment prolonged exposure
19 p3456 A69-36460

Soviet collection of papers on vestibular analyzer physiology
20 p3467 A69-37240

Optimum physiological parameters selection criteria for medical control of crew during space flights
20 p3483 A69-38226

EEG alpha activity relationship to laterality of reflective eye movements, indicating physiological correlates of hypotizability
22 p3887 A69-41213

Flight altitude effects on pilot performance with comparison of sensory and mental functions, considering oxygen use and flight safety
23 p4106 A69-41794

Space medicine to characterize nature and degree of changes in human functional capabilities due to space flight environment prolonged exposure
23 p4087 A69-41803

Risk factors in coronary diseases modified to provide base for estimating achievable mortality magnitude reduction
24 p4262 A69-43059

Mathematical input-output model for vestibular system, relating linear and angular motions to non-visual perception of orientation, motion and nystagmus for physiological characteristics
24 p4276 A69-43274

Behavioral patterns and physiological parameters of medical leech Hirudo medicinalis determined in natural environment prior to biological experiment in space
24 p4268 A69-43402

Physiological and psychological variables relationship in candidate pilots, noting age and educational level
24 p4268 A69-43406

PHYSIOLOGICAL RESPONSES

NT HEMODYNAMIC RESPONSES

Monkey psychomotor reactions during ballistic flight, noting alertness reduction during weightlessness
01 p0017 A69-11082

Physiologic and psychomotor changes during various acceleration stresses
01 p0019 A69-11340

Physiological studies of centripetal and Coriolis accelerations effects on vestibular function of humans in rotating chamber
02 p0197 A69-11498

Long term restriction of muscular activity noting effects on dynamics of cardiac contraction
02 p0198 A69-11515

Physiological causes and prevention of motion sickness during space flight, emphasizing conditioned reflex, different analysors interactions and vestibular-vegetative changes during weightlessness
02 p0200 A69-12122

Organic reaction and adaptation of rabbits and dogs to simulated weightlessness and acceleration compared with orbital flight data of human responses
03 p0376 A69-14192

Physiological mechanisms of weightlessness on human organism, discussing adaptation to weightlessness
03 p0377 A69-14197

X ray investigation of repeated simulated exposures to altitude and acceleration on healthy professional flyers
03 p0378 A69-14208

Sonic boom effect on corticosteroid level in human blood, noting no changes
03 p0378 A69-14209

White rat physiological processes while maintained on hypothermic cardiopulmonary bypass with small membrane type heart-lung machines
05 p0708 A69-15971

Biochemical indicators of pilot reactions to flights complicated by unexpected autopilot failures, using postflight chemical analysis of blood and urine
05 p0710 A69-16525

Renal excretion response to blood fluid volume shift resulting from altered orientation within gravity or from absence of gravity
06 p0873 A69-17015

Physiological response of human skeleton to hypogravity and hypodynamics studied by bed rest experiments, suggesting disuse atrophy of bone
06 p0873 A69-17019

Human physiology advances in connection with space exploration, discussing internal medium adaptation to space environment
06 p0873 A69-17061

Sympathoadrenal activity during and after impact stress measured from urinary excretion of catecholamines and 17-hydroxycorticosteroids
06 p0875 A69-17839

Soviet cosmonauts physiological reactions during weightlessness, analyzing EKG, arterial pressure, heart and respiratory rates and motion coordination
07 p1060 A69-18570

Physiological reactions of dogs during acceleration and weightlessness in suborbital flights of ballistic rockets
07 p1061 A69-18577

Phonocardiograms, EKGs, sphymograms, heart and respiration rates, body temperature and motor activity recorded/transmitted by TV during canine confinement in Soviet biological capsules
07 p1061 A69-18578

Statistical study of heart beat, respiration rate and arterial pressure of man during intermittent accelerations and short term weightlessness
07 p1061 A69-18579

Sensory and physiological reactions experienced by cosmonauts during parabolic training flights, tabulating arterial pressure, heart beat and respiration rate
07 p1061 A69-18580

Human and animal cardiovascular system reactions to weightlessness, noting vagus nerve role in adjusting organism
07 p1061 A69-18583

High oxygen concentration effect on conditioned reflex and associated EEG responses to light flash in rabbits occurs in well defined sequences
07 p1065 A69-18976

Human organism reaction to prolonged limitation of muscular activity during weightlessness simulated by bed rest, noting hypokinetic component of weightlessness
08 p1262 A69-19837

Mathematical, physical and physiological modeling for analysis of functional changes during varying gravity conditions
09 p1444 A69-22541

Rapid global transportation effect on circadian rhythmic patterns in human body functions, discussing kidney excretion and pituitary adrenal cortical system
09 p1444 A69-22545

X ray irradiated dogs subjected to heat stresses to determine thermoregulatory ability
09 p1445 A69-22548

Response rates of rats to periodic shocking for food reinforcement with added clock cue stimuli
10 p1644 A69-23304

Heat and humidity endurance limits in man
10 p1645 A69-23494

EEG, heart beat, respiration rates, body temperature, motor activity, physical and mental efficiency of man during anechoic chamber confinement
10 p1646 A69-23510

Hamsters responses to helium-oxygen and nitrogen-oxygen at ambient temperatures, comparing respiration rates, weights and body temperatures
10 p1646 A69-23564

Vegetable diet including 210 g of dry Chlorella biomass decreases effect on calcium and magnesium assimilation to produce insignificant negative balance of K and Mn
10 p1647 A69-23590

Human physiology for exposure to acute hypoxia studied with variation pulsograms and indices of external respiration and pulmonary gas exchange
10 p1647 A69-23592

EEG, EKG, respiratory motions and pulmonary ventilation recordings in study of carbon dioxide additions effect on human tolerance to hypoxic conditions
10 p1650 A69-23898

Blind goldfish behavioral responses to short lowered gravitational force cycles during vertical flight classified as vestibular reflexes resulting from otolith displacement
11 p1828 A69-25464

Biotelemetry of human physiological processes in space for assuring physiopsychological control and immediate intervention for emergencies, discussing application in Mercury and Gemini projects
12 p2023 A69-26491

European pilots accustomed to equatorial climate tested during regular flying missions, discussing heat effects on urinary steroids
12 p2024 A69-26560

Ventral posterolateral potentials in anesthetized immobilized cats in response to electric stimulation of mesenteric nerves and mechanoreceptors, studying thalamus nucleus role
12 p2020 A69-26562

Immobilization effects on alpha rhythm, locomotor coordination and visual alimentary motor reflexes of cats
13 p2212 A69-28617

High altitude acclimatization effects on cardiovascular system, external respiration, blood composition, optical and vestibular analyzers in human subjected to various stresses
13 p2212 A69-28623

Social and visual isolation effect on rat blood pressure, pulse pressure, heart rate, behavior and response to epinephrine
14 p2407 A69-29296

Visual, auditory and reaction-time responses in aging pilots, determining continuing capacity for choice and discrimination with advancing age
14 p2408 A69-29307

Food intake changes of female rats in response to changes in energy balance, discussing steroids as physiological tracer
15 p2555 A69-30693

Circadian rhythm in dermestid beetles *Trogoderma glabrum* Herbst as response to compulsory constant light and temperature conditions
15 p2557 A69-31469

Diurnal periodicity of physiological functions of flight crews flying through several time zones found to correspond to time zone of permanent residence
17 p2906 A69-32935

Acceleration injury noting water immersion effect on cat lung due to intense body vibration, suggesting restraint as practical solution
17 p2913 A69-33009

Leg volume changes in response to lower body negative pressure due to blood redistribution
17 p2908 A69-33171

Compensative adaptational reactions to weightlessness, discussing blood supply to thorax area, external respiration, gas exchange and energy loss during parabolic and orbital flights
17 p2909 A69-33384

Biochemical indicators of pilot reactions to flights complicated by unexpected autopilot failures, using postflight chemical analysis of blood and urine
18 p3096 A69-34744

Book on simulation in biology and medicine covering mathematical models, blood circulation, pulmonary ventilation, etc
19 p3260 A69-35894

Transient electrical responses from retinas, discussing visual pigment role in visual excitation, photochemistry, etc
19 p3258 A69-36377

Electrical response of frog and human visual cortex neurons to thermal vestibular and light flash stimulation
20 p3469 A69-37242

Cats vestibular neurons reactions to labyrinthine mon- and binaural polarization and caloric stimulation
20 p3471 A69-37255

Vestibular functions of humans subjected to Coriolis acceleration via prolonged rotation at different angular velocity rates
20 p3472 A69-37260

Test pilot vestibular training program to achieve higher tolerance of rotation, rocking and balancing and visual stimuli
20 p3472 A69-37266

Physiological and somatic effects on insects of radiation source onboard biosatellite 2, discussing wing abnormalities in flour beetle
20 p3476 A69-37619

High oxygen concentration effect conditioned reflex and associated EEG responses to light flash in rabbits occurring in well defined sequences
20 p3479 A69-38224

Eye elemental response to individual frequency jumps in oscillations of light, noting transient effect polarity
21 p3650 A69-38320

Male patients urine tests during sinusoidal vibration, noting catecholamine excretion as criterion of emotional stress under various environmental conditions
21 p3654 A69-38909

Human performance assessed by pulse rate increment at onset of exercise on bicycle ergometer and decrement during recovery after fasting
21 p3655 A69-38910

Physiological and psychological measurements of high pressure effects on man and animals, discussing decompression sickness, respiratory embarrassment, inert gas narcosis, helium tremble, etc
21 p3655 A69-38912

Nervous system reactions and resistance to ionizing radiation noting role of functional, morphological and physicochemical changes in nerve tissues
21 p3659 A69-39061

Histological changes in internal organs of rats after exposure to 400 r fast neutron dose, showing destructive processes followed by compensation reactions of cellular proliferation
21 p3659 A69-39062

Mandrax and barbiturates effects on aircrew reaction time, response time and tracking ability
21 p3661 A69-39274

Sympathetic nerve liberated noradrenaline increasing melatonin synthesis, using C 14 tracer for monitoring
22 p3871 A69-40051

Functional changes of somatosensory pathway from periphery to cortex during rapid eye movement (REM) and non-REM periods of deep sleep
22 p3872 A69-40161

Meaningful comparisons between single stimulus EEG records and average evoked potential
22 p3890 A69-40163

Strenuous physical training effects on human tolerance for work in heat, measuring rectal and mean skin temperatures and heart rates
22 p3890 A69-40199

Human metabolic response to hypothermia measured over wide range of work intensities and durations
22 p3891 A69-40215

Cerebellar cortex reactions to sciatic nerve stimulation in rats under transverse accelerations in centrifuge
22 p3877 A69-40279

Human heart chronotropic reactions during centrifuge acceleration tests up to tolerance limit, establishing sinus tachycardia in various degrees
22 p3877 A69-40283

Local electroretinogram responses produced in cats by light intensity incremental changes
22 p3878 A69-40835

Nocturnal and diurnal monkeys spectral sensitivity functions determined from simultaneous recordings of light-evoked cortical and retinal responses
22 p3882 A69-40867

Eye movement control mechanisms during binocular fixation used to determine corrective roles of flicks and drifts
22 p3883 A69-40876

Human electroretinogram (ERG) physiological variations as function of stimulation energy and wavelength
22 p3884 A69-40884

Antidiuretic hormone (ADH) and bradykinin effects on human thermal and cholinergic sweating after subdermal injection in forearm, abdomen and leg
23 p4077 A69-41311

Structural differences effect of gyral and sulcal areas of acoustic projection cortex on primary induced acoustic responses
23 p4079 A69-41380

Pigeon accelerated performance patterns as function of contiguity of brief visual stimuli and food reinforcement, noting pattern absence during stimuli omission
23 p4081 A69-41436

Human sweat glands reflex responses to diverse skin cooling rates in hot room, discussing bath temperature step decrease effect on lower limb
23 p4082 A69-41446

Circadian rhythms characteristics of healthy human beings as reference standards for comparing investigation data from different continents
23 p4083 A69-41457

Potent chemical factors released from anterior hypothalamus of rhesus monkeys in response to thermal stress during thermoregulation
23 p4084 A69-41472

Mathematical formulation for relative values of cardiac output and peripheral resistance as two contributing factors to arterial pressure change
23 p4085 A69-41473

Dependence of cochlear microphonics and summating potential on endocochlear potential
23 p4085 A69-41574

Physiological response to steady state hypoxia from exposure to 12 percent oxygen atmosphere, noting minimal heart rate and blood pressure changes
23 p4085 A69-41673

Human physiological responses to angular acceleration during breath holding, Mi, Valsalva and Mueller respiratory maneuvers in hollow spherical simulator
23 p4102 A69-41679

Physiological experiments to investigate aerospace flight stresses effects on oculomotor equilibrium, noting cardiovascular reaction and mechanism for interpretation
23 p4087 A69-41804

Jet pilot blood pressure response during positive acceleration in actual flight measured by telemetry compared with centrifuge test
23 p4089 A69-41822

Diurnal rhythms of heart rate and blood pressure reactions to posture changes on tilt table, finding orthostatic lability maxima
23 p4094 A69-42072

Efferent innervation influence of one ear to another in feline auditory system, based on afferent neurons responses to contralateral and binaural stimulation
23 p4094 A69-42073

Human thermal regulatory mechanism using analog simulation compared with experimental results of resting subjects responses to climatic chamber
23 p4111 A69-42079

Coronary circulation response to hyperoxia after vagotomy and combined alpha and beta adrenergic receptors blockade in anesthetized intact dog
23 p4096 A69-42088

Oxygen effect on X ray induced somatic crossing over frequency in *Drosophila melanogaster*, noting

bristle spots number modification on abdominal tergites
23 p4099 A69-42118

Adrenosympathetic reaction in flight, studying contributions of physical and nervous stresses in physically trained and untrained persons
23 p4099 A69-42363

Occipital eeg activity slowing and physiological changes during prolonged immobilization plus perceptual deprivation of human beings
24 p4256 A69-42554

X band pulsed microwaves effect on skin metabolism including respiratory activity, biochemistry and biosynthesis of intercellular materials, etc
24 p4270 A69-42575

M-1 Valsalva maneuver induced cardiovascular stresses effect on oculobulbar vergence of subjects observing Thorington scale, discussing probable physiological mechanisms
24 p4266 A69-43373

Aircraft passenger cabins pressure safety limits estimating factors, discussing human respiratory gas exchange mechanism, pressure drop and smoking effects, etc
24 p4269 A69-43411

PHYSIOLOGICAL TELEMETRY U BIOTELEMETRY

PHYSIOLOGICAL TESTS

NT BODY SWAY TEST

NT EAR PRESSURE TEST

NT VESTIBULAR TESTS

Physiological measurements onboard Soviet bioprobes and biosatellites including electrocardiography, phonocardiography, sphymography, seismocardiography and pneumography
01 p0015 A69-10947

Temporal pattern perception by human subjects required to integrate information presented in two modalities
02 p0200 A69-12724

Stability and habituation of nonspecific galvanic skin responses during light and sound stimulation periods in medical students
03 p0380 A69-13462

Permissible radiation doses for extended space missions, discussing clinical tests on dogs
05 p0708 A69-16508

Rules for selecting Soviet cosmonauts and physiological studies concerning heart and respiratory reactions to accelerations and weightlessness during preparation
07 p1060 A69-18569

Physiological and medical tests on Soviet cosmonauts onboard Voskhod spacecraft, assessing CNS, cardiovascular and respiratory systems and work-rest schedule
07 p1060 A69-18571

Auditory startle stimuli effect on human performance, noting decrease in mental and sensorimotor activity
07 p1066 A69-19421

Dogs cardiovascular activity mathematical analysis from physiological indices during long space flight
08 p1261 A69-19828

Tilt-table and acceleration tolerance of athletes and inactive students, comparing cardiovascular responses, heart rate and blackout level
09 p1444 A69-21304

Computer program for onboard medical checkups of spacecraft crews during extended space flights, discussing tests and intervals
10 p1649 A69-23505

Human intolerance to bacteria as food, considering response to *Hydrogenomonas eutropha* and *Aerobacter aerogenes*
13 p2213 A69-27265

Physiological and psychologic aging in professional pilots analyzed on basis of cardiovascular, pulmonary, exercise tolerance and sense testing
14 p2408 A69-29309

Permissible radiation doses for extended space missions, discussing clinical tests on dogs
18 p3095 A69-34727

Otolith apparatus functioning under weightlessness and accelerations in test stand experiments, discussing measuring techniques and nystagmic reaction durations
20 p3471 A69-37253

Surrounding noise effects on quick check audiometry test reliability, discussing pathological effects
21 p3725 A69-39286

Cortical responses by transient sensory stimulation of fingers EEG recorded, obtaining isomorphism between psychological and neurophysiological events
22 p3876 A69-40262

Whispered vowels pitch perception test using listen-and-compare method to determine formants for comparison with complex analysis procedure
23 p4190 A69-41575

Exercise prescription for hypokinetic airline pilots to prevent physiological deterioration and maintain performance, discussing predictive tests, tolerance evaluation, training regimens, etc
23 p4106 A69-41800

Physiological experiments to investigate aerospace flight stresses effects on oculomotor equilibrium, noting cardiovascular reaction and mechanism for interpretation
23 p4087 A69-41804

Subjects confined in caves for two to six months to note physiological rhythms time evolution and associated desynchronization and resynchronization
23 p4107 A69-41818

Test animals prolonged deep submersion in water, in mixed oxygen-H atmosphere at elevated pressure, noting EEG and EKG activities
24 p4262 A69-43025

PHYSIOLOGY

NT AUDIOLOGY

NT BODY COMPOSITION [BIOLOGY]

NT ELECTROPHYSIOLOGY

NT MENSTRUATION

NT NEUROPHYSIOLOGY

NT PSYCHOPHYSIOLOGY

NT RESPIRATORY PHYSIOLOGY

Magnetic fields role in neuropsychiatric and physiological experiments, noting effect on phagocyte activity
05 p0715 A69-16627

Physiological approach to tests and evaluation of aviation survival equipment, noting human reactions study under extreme conditions
06 p0877 A69-16953

Collection of papers on hypodynamics and hypogravics, physiology of inactivity and weightlessness
06 p0872 A69-17010

Digital computer program for physiological measurements, outlining interpolation of mathematical functions describing signals time variations
17 p2912 A69-32941

Physiological processes computer simulation with aorta modeling as example, noting difficulties and major problems
18 p3098 A69-34669

Organism growth physiology based on decisive enzyme reactions, considering synthesis of biological proteins from DNA and molecular life processes
21 p3652 A69-38787

Thermal physiology standardized symbols compilation for units of measurement
23 p4078 A69-41317

Space physiology, describing laboratory and onboard experiments
23 p4086 A69-41686

PI-ELECTRONS

Response of pi electrons in large organic molecule to scalar field for coronene, showing oscillator strength enhancement near single particle excitation band
20 p3580 A69-37497

PIASECKI MILITARY AIRCRAFT

U MILITARY AIRCRAFT

PICKLING

U CHEMICAL CLEANING

PICKOFFS

U SENSORS

PICKUPS

U SENSORS

PICTURE TUBES

Monochrome pictorial encoding, discussing pulse code modulation, delta modulation and buffer storage techniques
02 p0213 A69-12154

PICTURES

U PHOTOGRAPHS

PIERCING

Complete solution for punching smooth interface double layer Tresca material in plane deformation, including Coulomb material
09 p1617 A69-22048

PIEZOELECTRIC CRYSTALS

Acoustoelectric domains in CdS, making time evolution visible by means of modified optical strain birefringence and stroboscopic illumination
02 p0258 A69-12618

Parametric light generation employing KDP nonlinear crystals with mechanically tuned frequency
03 p0437 A69-13045

Electroacoustic amplifier based phonon devices, using surface waves on piezoelectric materials to speed radar data real time processing
03 p0394 A69-13353

Transverse electro-optical effect in piezoelectric crystals, using light modulation
04 p0639 A69-14427

Free carrier Faraday effect in piezoelectric semiconductors investigated for microwave frequencies, low temperatures, mixed deformation potential and piezoelectric scattering
04 p0643 A69-15201

Threshold velocities of acoustoelectric current oscillations in elemental piezo- and nonpiezoelectric semiconductors, taking into account amplification and losses of phonons
05 p0807 A69-15956

High power continuous and quasi-continuous wave UV generation by ADP and KDP crystals in argon-ion laser cavity [IEEE PAPER B-1]
05 p0773 A69-16308

Entrainment and acoustothermal effect in piezoelectric semiconductors having electrons with different energy
10 p1746 A69-23573

Acoustic wave amplification and generation in piezoelectric semiconductors and semimetals by supersonic carrier drift currents
11 p1926 A69-24641

Temperature behavior of resonant and antiresonant frequencies as function of electromechanical coupling and overtone order in piezoelectric resonators
14 p2421 A69-29542

Nonlinear analog of conical refraction in biaxial crystals, considering birefringence in piezoelectric uniaxial crystals and laser beam propagation
19 p3330 A69-35604

Piezoelectric characteristics of surface layers of Ba titanate single crystals, using static and dynamic electromechanical methods
22 p3995 A69-41156

Electrode interactions effects in interdigital surface wave transducers on piezoelectric materials, using Fourier analysis
24 p4312 A69-42615

Mechanization of analog electrical-to-fluidic transducer using carrier circuit techniques and piezoelectric bender drive assembly
24 p4315 A69-43026

PIEZOELECTRIC GAGES

FM/AM telemetry circuits with three axis piezoelectric accelerometer for measurements during impact tests of soft landing models
10 p1654 A69-23279

Piezoelectric variometer with reduced indicator time lag for measuring pressure gradients in fluid media
11 p1889 A69-25427

Reciprocity method for absolute calibration of piezoelectric accelerometer mounted on electrodynamic shaker table
15 p2615 A69-31283

PIEZOELECTRIC TRANSDUCERS

Meteorite particles recording by piezoelectric transducers, comparing data collected by Soviet and American scientists
01 p0152 A69-10587

Transverse sensitivity ratio of vibration transducer, discussing measurement by shaker method
04 p0603 A69-15432

Vacuum deposition of thin film microwave acoustic transducers of piezoelectric aluminum nitride
05 p0761 A69-15820

Ultrasonic search units in nondestructive tests, discussing piezoelectric materials and contact and immersion services
07 p1139 A69-18795

Signal conditioning for transducers covering piezoelectric devices, thermocouples, resistance transducers, reluctance and differential transformer sensors
10 p1691 A69-23228

Mechanical damping and electrical matching effects on bandwidth of piezotransducer in ultrasonic flaw detection equipment
10 p1697 A69-24073

Piezoelectric transducer theory, discussing acoustically matched sandwich type damper and calculating frequency characteristics
10 p1697 A69-24074

Meteorite particles recording by piezoelectric transducers, comparing data collected by Soviet and American scientists
15 p2691 A69-30757

Portable piezoelectric acceleration sensor, describing characteristics and principles of operation
17 p2975 A69-33594

Charge amplifier for piezoelectric transducer used in acceleration measurements
20 p3508 A69-37913

Piezoelectric microphone sensor flown on rocket for recording micrometeoritic impacts during noctilucent cloud display, determining cosmic dust particles flux
21 p3793 A69-38348

Piezoelectric transducer transient electrical response due to shock loaded stress using transform calculus
22 p3947 A69-40863

PIEZOELECTRICITY

Integrated circuit piezoelectric systems limitations and advantages
01 p0049 A69-11413

Transverse normal waves excitation in flat plate by applying piezoelectric plate or comb shaped emitter to surface or end face
04 p0678 A69-14901

Controlled transient signal distortion by shock monitoring instrumentation circuits using piezoelectric accelerometers
04 p0603 A69-15430

Resonance effects during piezoelectric interaction between charged drift wave and flexural wave in semiconductors with one sign current carriers
08 p1371 A69-19806

Electrical equivalent circuit for piezoelectric generation and detection of transient and sinusoidal ultrasonic waves by interdigital electrodes
12 p2039 A69-26376

Transverse normal waves excitation in flat plate by applying piezoelectric plate or comb shaped emitter to surface or end face
12 p2182 A69-26654

Acoustic effects in piezoelectric semiconductors due to sound-electrons interaction including sound absorption, sound velocity changes, electroacoustic effect, etc
14 p2503 A69-28786

Scanning Fabry-Perot interferometer with ultralow modulation frequencies, obtaining inverse piezoelectric effect curves of ceramic element
15 p2611 A69-31107

Linear piezoelectric plate vibrations, Elements of linear theory of piezoelectricity and vibrations of piezoelectric plates, covering differential equations, boundary conditions, etc
16 p2826 A69-31720

Piezoelectric shaker consisting of combination of damped resonant cylindrical elements for wide frequency calibration of vibration pickups
17 p2975 A69-33665

Transport mechanism in amorphous Ge films deposited on glass substrates studied by measuring piezoresistance as function of temperature during pure nitrogen immersion
19 p3391 A69-36559

PIEZORESISTIVE TRANSDUCERS

U PIEZOELECTRIC GAGES

PIGEONS

Threshold variations in caloric nystagmus in pigeons subjected to accelerations in head to tail direction in centrifuge at various temperatures
20 p3471 A69-37252

Pigeon accelerated performance patterns as function of contiguity of brief visual stimuli and food reinforcement, noting pattern absence during stimuli omission
23 p4081 A69-41436

Pigeon visual adaptation to flickering light, attributing ERG b-wave postadaptation rebound to retina bipolar cells inhibition
23 p4084 A69-41463

Attention shifts in maintained discrimination, discussing combined responses of varying and constant visual and auditory stimuli in pigeons
24 p4275 A69-43198

PIGGYBACK SYSTEMS

Truss framework for support of eight 100-lb satellites through Titan 3C launch and dispensing of satellites at predetermined times, discussing materials and fabrication
09 p1512 A69-22369

Secondary or abort mission maximized subject to primary mission constraints by variational treatment of optimal branched trajectories [AAS PAPER 68-138]
21 p3819 A69-39210

PIGMENTS

NT CHLOROPHYLLS

NT CYTOCHROMES

Color and appearance properties of paint films and relations to amounts and properties of colorants, noting translucent plastics and metallized paint films
04 p0620 A69-14886

Light transmission through body wall of living colorable desert iguanas measured by spectrophotometry, discussing skin pigment effects 07 p1059 A69-18373

Test program simulating solar wind outside magnetosphere to evaluate high melting point high density ceramic oxides as white thermal control coating pigments [AIAA PAPER 69-641] 17 p2993 A69-33762

Transient electrical responses from retinas, discussing visual pigment role in visual excitation, photochemistry, etc 19 p3258 A69-36377

Meteorites pigments identification as porphyrins for extraterrestrial life evidence, noting sample analyses of Orgueil, Murray, Cold Bokkeveld and Mokoia carbonaceous chondrites 22 p4008 A69-39889

PILOCARPINE

Ophthalmic 2 percent pilocarpine effect on normal ocular dynamics of various age groups, including visual acuity, accommodation and refraction 01 p0022 A69-11347

PILOT ERROR

Ocular motor failures in pilots due to convergent and divergent strabismus, discussing low pressure chamber tests and blood pressure effects on cranial nerve 03 p0370 A69-13470

Predictive scale of aircraft emergencies, analyzing human error rate under stress 06 p0880 A69-17208

Hearing errors in voice communication with radio telephone, noting effects of mean syllable number and consonants per syllable in pilots and controllers 06 p0891 A69-18034

Climatic factors affecting pilot vision and contributing to misjudgement during landing procedures, noting effect of downward slope in runway approach 06 p0884 A69-18036

Spatial disorientation as factor in accidents in operational command, noting relatively high experience level of involved pilots 07 p1072 A69-19431

Piloting errors due to false instrument readings during turbulent atmosphere flight 16 p2734 A69-32007

PILOT PERFORMANCE

Aircraft flight testing for determining airframe, engine and pilot degradation, examining flutter, handling characteristics, water ballast, propulsion, etc 01 p0054 A69-10292

All-weather landing factors for aircraft and pilots, describing instrument landing system, runway and visibility, pilot and crew procedures, etc 01 p0112 A69-10454

Medicinal therapy and flight safety of pilots and astronauts, discussing drug use, self treatment, tolerance and environmental factors 01 p0014 A69-10583

Head-Up Display (HUD) flight information applied to civil aviation, noting operational safety improvement and pilot work load reduction 01 p0020 A69-10635

Piloting aspects of jet V/STOL aircraft for poor weather operations without complicated ground aids, discussing deceleration transition, forward speed and final approach angle 01 p0010 A69-10868

Flight accident rate of U.S. physician pilots noting relation to number of takeoffs and landings 01 p0022 A69-11344

Error reduction in identifying pilot describing function from flight test data by shifting input signal by pilot delay time in simulated computer model 02 p0202 A69-11950

Validation study of pilots visual sampling behavior, using queuing model based on instrument and eye movement data from Link trainer mission flights 02 p0202 A69-11954

Aircraft cockpit displays design for flight control and navigation, discussing integration, pictorial realism, moving part, pursuit tracking, frequency separation and optimum scaling 02 p0203 A69-12213

Dynamic flight simulators fidelity assessment, discussing hybrid method based on pilot psychomotor responses 02 p0203 A69-12215

Psychiatric study of master attack carrier aviators inability to fly, considering adult situational reaction diagnosis 03 p0369 A69-12883

Vertical contact analog display /VCAD/ design, emphasizing need for integrated and supplementary information to pilots in systematic way 03 p0379 A69-13361

Glaucoma in commercial airline pilots noting value and safety of routine tonometry 03 p0376 A69-14078

Circadian rhythms disruption during long distance flights, discussing adverse effects on pilot and passenger performance 03 p0378 A69-14260

Aircraft in-flight collision, discussing difficulties and procedures of medical board of inquiry 05 p0715 A69-16628

Telemetric system for in-flight measurements of jet pilot heart and circulatory system to determine flight stresses leading to pilot failure 05 p0715 A69-16707

Aerodynamic instrumentation to improve helicopter takeoff and landing piloting performance under high gross weight conditions 05 p0767 A69-16776

Standards for EEG in pilot fitness examinations, analyzing effects of total flying hours 06 p0875 A69-18021

Approach light efficiency, discussing Calvert bar system and strobe flash on basis of pilot questionnaire polling 06 p0884 A69-18029

Manual performance of aircraft pilots under sustained acceleration using measurements of handwriting pressure 06 p0884 A69-18030

Characteristics of accident experienced pilots based on personality and psychological tests 06 p0876 A69-18033

Hearing errors in voice communication with radio telephone, noting effects of mean syllable number and consonants per syllable in pilots and controllers 06 p0891 A69-18034

Time perception capacity of astronauts and jet pilots during brief weightlessness, noting emotional state effects 07 p1065 A69-18981

System reliability influence on air accidents resulting from pilot errors, unforeseen obstacles, breakdowns and atmospheric effects 07 p1054 A69-19288

Aerial photography history, photographer qualities, airborne platforms, pilot briefing, air to air sortie, aerobatics, parachutes, etc 08 p1314 A69-20307

Flight deck equipment guidelines in aircraft, discussing pilots natural senses, visual information, displays, logic and memory capable computers and ground controller 08 p1266 A69-20450

Aircraft head-up display systems emphasizing all-weather operations and equipment characteristics 08 p1315 A69-20451

Subjective pilot ratings based on Cooper scale compared with aircraft handling criterion based on Shannon information theory, discussing pilot error and accident probability 08 p1254 A69-20458

Landing and takeoff demonstration tests of OV-10A aircraft through rough terrain, noting pilots excessive physiological stresses [AIAA PAPER 69-316] 09 p1434 A69-22391

Aviation combat performance criterion by analyzing questionnaires sent to combat deployed flight surgeons, noting possible value of peer rating 09 p1447 A69-22549

Jet fighter pilot spatial disorientation during flight and on ground, emphasizing vestibular neuronitis diagnosis 10 p1649 A69-23382

Human pilot adaptation in simulated multiloop VTOL hovering task with series loop closure model 10 p1650 A69-23378

Psychic stress effect on physiological parameters of helicopter pilots during critical flight situations, considering biotelemetric examination of heart and circulatory systems 11 p1829 A69-24347

VTOL aircraft flight control systems, considering computerization and automation approach with human pilot serving as monitor and emergency system 11 p1823 A69-25387

European pilots accustomed to equatorial climate tested during regular flying missions, discussing heat effects on urinary steroids 12 p2024 A69-26560

Complex piloting simulation including fatigue for optimizing man machine synergy, emphasizing human adaptability and computer precision and speed 12 p2025 A69-27083

Aircraft canopy scratches effects on pilot visual discrimination 13 p2214 A69-28533

Personality characteristics of jet pilots measured by Edwards Personal Preference Schedule, including percentile norms table 14 p2408 A69-29294

Medicinal therapy and flight safety of pilots and astronauts, discussing drug use, self treatment, tolerance and environmental factors 15 p2555 A69-30753

Blood pressure telemetry of pilot during flight including determination of psychophysical relations 15 p2559 A69-31229

EEG and pilots flight performance relations, discussing in-flight telemetric measurements from ground station 15 p2560 A69-31233

Painted helicopter rotor blades ruled out as cause of flicker induced vertigo, reporting pilots psychophysiological responses to formation flying 17 p2913 A69-33175

Color signal light gun for aircraft control at airport towers, noting pilot tests for familiarity with signal code 17 p2914 A69-33185

CH-46 helicopter flight simulation program for pilot response to large perturbation maneuvers, using six degrees of freedom mathematical models [AHS PAPER 361] 17 p2946 A69-33521

Analog correction method to suppress pilot maneuver effects during analysis of aircraft accelerations induced by atmospheric turbulence [ICAS PAPER 68-39] 17 p2901 A69-33590

Aircraft carrier landing system performance, variations in pilot experience, aircraft types and environment, emphasizing night carrier recovery 17 p2916 A69-34012

Flying offenses committed by private and professional pilots in Great Britain, discussing role of authorities involved 17 p3077 A69-34202

Accelerate-stop criteria examined from human engineering standpoint, discussing flight simulator study of pilot reaction times for transition to rejected takeoff configuration [AIAA PAPER 69-772] 19 p3244 A69-35650

Sensory physiology of pilot landing guided by runway lighting, stressing visibility influence 19 p3260 A69-35987

Manned aircraft air to air combat capabilities evaluated by simulator using two cockpits, digital computer and collimated displays [AIAA PAPER 68-253] 20 p3510 A69-37159

Time perception capacity of astronauts and jet pilots during brief weightlessness, noting emotional state effects 20 p3480 A69-38229

Pilots and automobile drivers functional impairment due to alcohol and drugs 21 p3663 A69-38792

Mandrax and barbiturates effects on aircrew reaction time, response time and tracking ability 21 p3661 A69-39274

Aircraft flying qualities research program, discussing Navy test pilot evaluations and longitudinal handling characteristics for simulated carrier landing task [AIAA PAPER 69-897] 21 p3648 A69-39421

Second order system handling qualities analysis for pilot rating through human transfer function and closed loop control 21 p3668 A69-39792

Energy cost of piloting helicopters and fixed wing aircraft calculated from expired minute volume and air oxygen content measured during basal state and flight 22 p3891 A69-40218

Flight performance analysis of airline pilot group related to flight recording monitoring system 22 p3868 A69-41145

Initial training and checking of airline pilots in new equipment to ensure competency, reduce nonrevenue flight time and use minimum airspace 22 p3894 A69-41150

Landing performance in T-33A aircraft with loss of binocular vision compared to performance with both eyes 23 p4102 A69-41675

Background flying experience of tactical fighter aircraft pilots accident potential, comparing accident and nonaccident groups 23 p4103 A69-41685

Flight altitude effects on pilot performance with comparison of sensory and mental functions, considering oxygen use and flight safety

23 p4106 A69-41794

Glider pilots fatigue attributed to nutritional habits

23 p4106 A69-41796

Exercise prescription for hypokinetic airline pilots to prevent physiological deterioration and maintain performance, discussing predictive tests, tolerance evaluation, training regimens, etc

23 p4106 A69-41800

Night vision requirements of Vietnam combat pilots investigated for relationship to Skyraider fatal crash during target strafing and H-34 helicopter crash landing

23 p4107 A69-41807

Klaxon hooter sudden sound used as auditory startle stimulus to determine hand sensorimotor activity and standing stability in pilot error causes

23 p4088 A69-41808

Jumbo jet role in air transportation, discussing future traffic growth, pilot problems and aircraft size limitations

23 p4063 A69-41819

Flight indicators monitoring by pilots, describing physiological and psychotechnical criteria for dials and clocks arrangement to improve efficiency

23 p4108 A69-41827

Senior commercial jet pilots ability to visualize flight instruments

23 p4089 A69-41829

Pilots body images determined by inkblot tests, considering effects of aircraft type, pilots experience, etc

23 p4112 A69-42364

Measurement methods for quantitative character of aircraft pilot rating scales for vehicle flying qualities, considering wording ambiguity, dual mission character, etc

24 p4276 A69-43326

Supersonic flying effect on urinary catecholamine excretion rates in pilots, noting emotional state

24 p4265 A69-43370

PILOT SELECTION

Medical fitness regulations for pilots, including federal and internal airline regulations

06 p1041 A69-16844

Rules for selecting Soviet cosmonauts and physiological studies concerning heart and respiratory reactions to accelerations and weightlessness during preparation

07 p1060 A69-18569

Cardiovascular system medical examinations for selection of aircraft and spacecraft crew members from healthy men with no apparent disorders or complaints

07 p1066 A69-18983

Military flying career choice as neurotic compensation for personality defects, stressing personality screening during interview

12 p2023 A69-26492

Witkin Rod and Frame Testing of pilots and engineers showing greater field independence in pilots, discussing applications to pilot instructor selection

12 p2023 A69-26556

Aviation health service for flight safety problems with emphasis on accident prevention, emphasizing physician role in man-machine relationship of personnel surveillance

18 p3098 A69-35305

Coronary angiography for evaluating cardiac problems of aircrew, giving case histories and clinical and laboratory findings

19 p3263 A69-36461

Abnormalities of routine electrocardiograms in medical certification of pilots, indicating errors in screening

19 p3263 A69-36462

Weightlessness tests during parabolic flight to supplement vestibular tests in astronaut selection

20 p3481 A69-37276

Vestibulometric test program for flight surgeon appraisal of flying personnel, emphasizing singling out persons prone to illusory sensations

20 p3473 A69-37277

Cardiovascular system medical examinations for selection of aircraft and spacecraft crew members from healthy men with no apparent disorders or complaints

20 p3480 A69-38231

Pilots and flight crews screening and training by supplemental air carriers

22 p4054 A69-41148

Initial training and checking of airline pilots in new equipment to ensure competency, reduce nonrevenue flight time and use minimum airspace

22 p3894 A69-41150

Thematic apperception test /TAT/ cards for assessing attitudes in naval recruiting, respiratory responses during ejections and aviation psychology

23 p4112 A69-42365

Pilot selection procedure emphasizing integration of all-around personality picture from different approaches

24 p4278 A69-43395

Physiological and psychological variables relationship in candidate pilots, noting age and educational level

24 p4268 A69-43406

PILOT TRAINING

Airline crew training, requalification, recurrent, upgrading and aircraft transition training for crew and pilot

01 p0019 A69-10450

Man machine relationship in V/STOL control display, discussing inflight simulators, emphasizing NASA X-14 and CH-3C programs

01 p0010 A69-10452

Business jet aircraft use for air transport pilot training instead of simulating devices, noting pilot cabins

03 p0366 A69-13643

Airline safety programs focused on developing reliable automatic landing system, realistic pilot training and airborne monitoring/recording system

06 p1041 A69-16840

Physiological or survival training emphasizing psychological approach

06 p0879 A69-16965

Electrohydraulic attitude servomechanism for controlling movements of pilot training cabin, describing hydraulic system and electric control circuit

06 p0906 A69-16966

Aerospace research pilot school /ARPS/ to train experimental test and aerospace research pilots and Manned Orbiting Laboratory /MOL/ astronauts

06 p0882 A69-17670

Optimized flight crew training, evaluating safety, flight simulator efficiency, takeoff/landing practice and line experience based on test results

[AIAA PAPER 69-771] 19 p3245 A69-35653

Annual general aviation aircraft accident rate variation related to annual variations in pilot flight training activity

19 p3262 A69-36448

Test pilot vestibular training program to achieve higher tolerance of rotation, rocking and balancing and visual stimuli

20 p3472 A69-37266

Rotary actuator to create realistic control effects in hydraulic loading system of jet flight-training simulators

20 p3511 A69-38182

Flight training using digital simulators, including maneuver analysis for TWA 707 program

22 p3928 A69-41137

Aircraft pilots medical disabilities as potential flight safety hazard, discussing aerospace medical specialist role and pilot education in symptoms evaluation

22 p3894 A69-41146

Pilots and flight crews screening and training by supplemental air carriers

22 p4054 A69-41148

Initial training and checking of airline pilots in new equipment to ensure competency, reduce nonrevenue flight time and use minimum airspace

22 p3894 A69-41150

Background flying experience of tactical fighter aircraft pilots accident potential, comparing accident and nonaccident groups

23 p4103 A69-41685

Annual general aviation accident rate prediction from annual flight training variations

23 p4062 A69-41793

Flight simulators role in airline pilot training, discussing skilled learning, performance measurements and future developments

23 p4112 A69-42366

PILOTED CENTRIFUGES

U HUMAN CENTRIFUGES

PILOTLESS AIRCRAFT

U DRONE AIRCRAFT

U FIREBEE 2 TARGET DRONE AIRCRAFT

U TARGET DRONE AIRCRAFT

PILOTS [PERSONNEL]

NT AIRCRAFT PILOTS

NT TEST PILOTS

Physiological functions of aged Japanese pilots, discussing height, weight, Rohrer index, obesity, vision deterioration and hearing disturbances

06 p0876 A69-18028

Visual, auditory and reaction-time responses in aging pilots, determining continuing capacity for choice and discrimination with advancing age

14 p2408 A69-29307

Physiologic and psychologic aging in professional pilots analyzed on basis of cardiovascular, pulmonary, exercise tolerance and sense testing

14 p2408 A69-29309

Injury stress vs acceleration specification as valid criterion for pilots subjected to high acceleration, introducing models and illustrating with ejection example

17 p2913 A69-33008

Flight and piloting influence on morbidity of civil aviation personnel, noting incidence of enteric, hemorrhoidal and respiratory diseases

18 p3098 A69-35303

Skiagrams results of retinoscopic measurements of eye peripheral refraction of pilots, attempting correlation between skiagram type and central refraction

24 p4267 A69-43399

PINCH EFFECT

NT PLASMA PINCH

NT THETA PINCH

Magnetic pinch effect in thermal RF induction plasma in argon, developing theory for calculating excess magnetic pressure

09 p1544 A69-21341

Junction lasers current-voltage characteristics, discussing coherence-pinch effect as explanation of threshold behavior

19 p3337 A69-36531

Collisional shocks in inverse pinch MHD shock producing device, discussing position in current sheet and effect on conductivity and diffusion

21 p3776 A69-38709

PINEAL GLAND

Mammalian pineal gland as neuroendocrine transducer, studying melatonin role in ovulation, gonadal growth, etc

20 p3480 A69-38284

C 14-tryptophan incorporation into C 14-protein in cultured rat pineals, noting norepinephrine stimulation

22 p3871 A69-40054

PINHOLES

Multiple pinhole camera for X ray astronomy, suggesting cross correlation image recovery technique based on Fourier convolution theorem

09 p1502 A69-22768

PINS

Rigidity of rotors with pin joints, calculating moments of inertia at connected sections of turbine shaft disks utilizing similarity concept

19 p3324 A69-35832

Critical signal assignments optimization in electrical/electronic connectors, considering bent pins, signal cross talk, adjacency requirements and corona

19 p3284 A69-36030

Titanium stress pin with headed straight-shank pin and collar for reducing fatigue stress around holes

22 p3957 A69-40832

PION BEAMS

Negative pion beams for therapy, radiobiology and dosimetry

03 p0371 A69-13478

Origin of galactic gamma rays, discussing evidence in support of interstellar gas in galactic disk and production of neutral pions and bremsstrahlung

16 p2852 A69-32806

Coulomb interference corrections in pion-He scattering, discussing three specific formalisms

18 p3176 A69-35008

High energy negative kappa meson-nucleon interactions with respect to multiplicity distribution of charged pions in nucleon-antinucleon annihilation, showing binomial distribution

24 p4351 A69-42791

PIONEER PROJECT

Interplanetary Pioneer spacecraft development and systems engineering aspects

06 p1017 A69-17605

Pioneer F/G mission to Jupiter by NASA for exploring interplanetary medium, asteroid belt, planet and environment

[AAS PAPER 69-290] 24 p4381 A69-42863

Monograph on Pioneer spacecraft program, discussing mission objectives, spacecraft design, etc

[AAS PAPER 69-066] 24 p4381 A69-42883

PIONEER SPACE PROBES

Magnetospheric plasma probe results with Pioneer 6 and 7, discussing plasma fluctuations and solar wind interaction with geomagnetic field

07 p1128 A69-19364

Monograph on Pioneer spacecraft program, discussing mission objectives, spacecraft design, etc [AAS PAPER 69-066] 24 p4381 A69-42883

PIONEER 6 SPACE PROBE

Solar wind electron component detection by plasma experiment on Pioneer 6, particularly class 2B flare and quiet period 05 p0816 A69-16275

Plasma and magnetic field measurements of tangential discontinuities in solar wind by Pioneer 6, considering velocity shears and rotation of sun 11 p1946 A69-24430

Pioneer 6 S band telemetry carrier Faraday rotation during corona occultation measured by deep space tracking antenna 15 p2700 A69-31419

Tabulated coherent S-band Doppler data from Pioneer 6 and 7 radio tracking, improving astronomical constants and ephemerides for earth-moon system [AAS PAPER 68-130] 20 p3595 A69-37179

PIONEER 7 SPACE PROBE

Relativistic electron confinement within geomagnetic tail neutral sheet measured by Pioneer 7 deep space probe, confirming kinetic energy observations of IMP 1 satellite 14 p2433 A69-28934

Tabulated coherent S-band Doppler data from Pioneer 6 and 7 radio tracking, improving astronomical constants and ephemerides for earth-moon system [AAS PAPER 68-130] 20 p3595 A69-37179

PIONEER 8 SPACE PROBE

Fluorine nuclei in primary cosmic radiation identified by counter telescope measurements on Pioneer 8 spacecraft 15 p2676 A69-30886

PIONEER 9 SPACE PROBE

Pioneer 9 deep space probe with telemetry link operated in coded mode with sequential decoding, discussing ground and flight test data 23 p4131 A69-42522

PIONS

Pionic 2p-1s X ray transition energy and natural linewidth and muonic 2p-1s X ray transition energy measurements for Na 23 01 p0122 A69-10035

Absorption cross section for 68 Mev positive pion absorption by 1p 3/2 neutron in C12 nucleus followed by single proton emission at 11 degrees 02 p0282 A69-11460

Radioactive decay of neutral pions generated in metagalactic cosmic ray interactions as source of high energy isotropic gamma rays observed by OSO-3 02 p0308 A69-12092

Extensive air showers characteristics based on models of high energy interactions of nucleons and pions with air nuclei 06 p0990 A69-17301

Lithium 6 and 7 fission following pion capture, searching for H 4 and 5 12 p2132 A69-26296

Negative pion from 600 MeV synchrocyclotron stopped in thin Li 6 target in search for excited states of triton 12 p2132 A69-26297

Pionization cross sections at 100 gev for interactions of cosmic ray neutrons and pions with C and Pb nuclei 13 p2330 A69-28382

Pion and nucleon interactions with nuclei, analyzing showers for symmetry and isotropy 13 p2331 A69-28389

Cosmic ray muons angular distribution measuring device for determining pion/kaon ratio 13 p2332 A69-28421

Elastic scattering cross sections of negative pions by deuterons compared with Glauber model calculations 17 p3007 A69-32885

Frequencies of charged secondaries numbers emitted from nucleon-nucleon and pion-nucleon inelastic collisions, observing multiplicity regularity 18 p3177 A69-35009

Pion production rate for proton-proton interactions in hydrogen, discussing relevance to hot massive stars, charged pion decay probability and mu-neutrino production 21 p3792 A69-39615

Cosmic gamma rays spectrum from neutral pions production and decay in metagalactic cosmic ray p-p collisions, deriving models based on Einstein general relativity theory 22 p4006 A69-40641

Black body radiation at very high temperatures, discussing pion-nucleon interaction in pion gas in thermal equilibrium 23 p4238 A69-41358

Negative pions elastic scattering from hydrogen, confirming differential cross section minimum for specific incident momentum-scattering angle region 24 p4352 A69-43049

Cosmic ray pions and muons anomalous measurements above 1000 Gev explained by medium-strong contact interaction between protons 24 p4353 A69-43194

PIPE FLOW

Incompressible fluid steady motion in curved tube investigated by Fourier series, solving coupled nonlinear equations numerically 01 p0058 A69-10142

Energy dissipation at rounded pipe entrance in viscous fluid, showing relation between entrance loss and radius of roundness 01 p0059 A69-10308

Semiempirical theory of turbulent MHD tube flow at small Reynolds numbers taking into account magnetic field presence 01 p0130 A69-10769

Stabilization of plane parallel MHD flow at inlet and outlet of flat rectangular tube with transverse magnetic field 01 p0130 A69-10770

Cryogenic expansion to pressures below triple point and resulting formation of solid-vapor mixtures, discussing flow and heat transfer characteristics in heated tubes 01 p0176 A69-11146

Frictional and heat transfer characteristics of laminar flow in porous tubes, using numerical solutions to flow and energy equations 01 p0177 A69-11408

Expression derived for flow characteristics in smooth pipe for entire Reynolds number range 02 p0230 A69-11870

Pressure pulses propagation in nonsteady fluid flow through expandable tubes, noting computer solution 02 p0232 A69-12477

Time dependent tube wall radial displacement during explosive welding as function of distance from initial explosion 02 p0254 A69-12675

Steady state temperature distribution in heat generating fluid in plug flow in circular tube with arbitrary inlet and wall temperature distribution 03 p0530 A69-12862

Boundary conditions for irrotational hydrodynamic field around sphere moving along axis of cylindrical tube containing incompressible fluid calculated by least squares method 03 p0415 A69-13362

Downstream secondary circulation resulting from sharp bend in fully developed turbulent pipe flow, noting departure from twin circulatory flow 03 p0419 A69-13952

Unperturbed tube flow theory extended to flow through short axisymmetric tube 03 p0419 A69-13969

Relaminarization of turbulent flow, studying velocity profiles at various axial cross sections in porous wall tube with fluid injection 04 p0586 A69-14409

Confined jet mixing region at entrance of tubular reactor, discussing mass and momentum transfer, chemical conversion and effect of Reynolds number [AICHE PAPER 25A] 04 p0586 A69-14508

Reynolds number similarity argument, establishing relation between mean velocity at pipe or channel center and shear stress at wall 04 p0589 A69-14895

Primary flow measuring element based on Chebyshev principle, noting differential pressure output loss and resistance to accumulation of contaminants 04 p0600 A69-15030

Frictional losses in straight tubing and effect of system on ball type valve, using polyurethane foam damped flexible silastic tube 04 p0608 A69-15331

Velocity profiles for laminar flow of homogeneous liquid in pipe inlet at small and moderate Reynolds numbers 05 p0743 A69-15578

Entry region flow and convective heat transfer prediction in cooled vertical pipe open at both ends, considering wall temperature 05 p0845 A69-15717

Simulation of two and three dimensional fluid transients by use of one dimensional equations in lattice-work of piping elements 05 p0747 A69-16071

Suction effect on incompressible flow through step expansion in circular pipe through sudden enlargement, considering inlet flow with thin boundary layer [ASME PAPER 68-FE-11] 05 p0748 A69-16074

Thermal entry problem solution for low Reynolds number turbulent gas flow based on Reynolds number dependent velocity profile [ASME PAPER 68-WA/FE-11] 05 p0748 A69-16090

Velocity profiles and eddy diffusivities for fully developed turbulent low Reynolds number pipe flow [ASME PAPER 68-WA/FE-34] 05 p0749 A69-16107

Heat transfer in turbulent pipe flow of radiating optically thin gas in circular tube [ASME PAPER 68-WA/HT-17] 05 p0847 A69-16121

Forced laminar flow convection in horizontal tube with variable viscosity and free convection effects [ASME PAPER 68-WA/HT-20] 05 p0847 A69-16123

Gas flow rate predictions for long and short tubes and annuli and at densities between laminar-continuum and free molecular regimes [ASME PAPER 68-WA/PID-5] 05 p0750 A69-16166

Quasi-method of characteristics with application to fluid lines with frequency dependent wall shear and heat transfer [ASME PAPER 68-WA/AUT-7] 05 p0750 A69-16181

Heat pipe for thermal control of terrestrial and aerospace energy conversion systems 06 p1030 A69-17189

Laminar constant pressure gradient flow of viscous incompressible conducting fluid through rotating straight circular pipe with perpendicular magnetic field 06 p0967 A69-17718

Thermal nonequilibrium of unsteady adiabatic gas flow in nonheat conducting tube with open ends 06 p0911 A69-17813

Analytical model of spoiler generated sound in jet pipe, presenting data on level, spectrum and directivity of sound 07 p1183 A69-19462

Corrected stability limit for Poiseuille flow in pipes, annuli and channels, discussing flow between cylinders 07 p1121 A69-19475

Heat transfer in horizontal and vertical tubes with viscous gravity flow with boundary conditions 07 p1243 A69-19733

Suction effect on temperature distribution and heat transfer in plane Couette flow and laminar flow in circular pipe 08 p1303 A69-20371

Turbulent heat transfer in conducting fluid flow through circular tube in longitudinal magnetic field and constant wall heat flux, using Lyon relation 09 p1621 A69-21590

Turbulent flow of viscous nonNewtonian fluids in smooth pipes, noting effects of viscous stresses 09 p1481 A69-21929

Expansion tube modification incorporating nozzle plate at secondary diaphragm for reducing flow nonuniformity and contamination [AIAA PAPER 68-371] 09 p1477 A69-21960

Impurity concentrations in expansion tube flow, measuring radiation intensities [AIAA PAPER 68-371] 09 p1477 A69-21961

Incident flow in variable cross section tubes using analytic asymptotic calculation 10 p1677 A69-22897

Response times for entire Knudsen number range in straight round pressure pipes, using digital computer in final integration 10 p1677 A69-22900

Solid cylindrical body entrainment by viscous incompressible fluid flow in tube under constant pressure gradients and absence of gravitational force 10 p1678 A69-23366

Equilibrium dissociating gas laminar flow in circular tube calculated for heat transfer and hydraulic resistance, using boundary layer equations 10 p1679 A69-23426

Velocity profiles of turbulent plasma flow in circular tube during application of longitudinal homogeneous magnetic field 11 p1922 A69-24234

Forced heat convection in steady turbulent air flow in circular cross sectioned tubes, noting laminar sublayer in wall regions 11 p2000 A69-25096

Viscous flow stability in rotating pipe, giving velocity components in cylindrical polar coordinates 11 p1871 A69-25125

Laminar Newtonian flow heat transfer to fluids with variable physical properties in vertical tubes with constant wall heat flux, considering viscosity and density
11 p2000 A69-25164

Friction coefficients for turbulent flow through smooth pipes, considering average and friction velocities relations, fluid velocity measurements and flow Reynolds number
11 p1874 A69-25429

Steady flow field for viscous incompressible fluid in rotating pipe with porous walls determined from Navier-Stokes equations
11 p1875 A69-25481

Forced discontinuous vibrations of liquid in conduit experimentally analyzed, discussing test devices and procedures
11 p1875 A69-25485

Temperature variation effects on heat transfer in laminar tube flow, taking into account constant wall temperature and heat flow density
12 p2189 A69-25762

Navier-Stokes equations of slow viscous fluid laminar flow near pipe inlet and exit with negligible mass forces, discussing velocity and pressure distribution
13 p2244 A69-27258

Resonance tube excitation from energy depletion in central part of subsonic jet supplying tube
13 p2247 A69-27738

Thermal entry problem solution for low Reynolds number turbulent gas flow based on Reynolds number dependent velocity profile
[ASME PAPER 68-WA/FE-11]
14 p2430 A69-29446

Axial and radial turbulence intensities for flow through smooth round tubes, measuring velocity profiles and drag coefficients
15 p2590 A69-30003

Transport properties interrelationship in turbulent pipe flow and free turbulence
15 p2591 A69-30792

Drag and friction coefficients for laminar pulsating incompressible fluid flow in circular tubes obtained from Navier-Stokes equation
15 p2592 A69-30988

Eigenvalue bounds for amplification rates, wave speeds and linear stability conditions for Orr-Sommerfeld equation governing parallel flow in boundary layer and round pipes
16 p2768 A69-31591

Asymptotic behavior of one dimensional laminar flow of incompressible viscous fluid in infinite cylindrical tube, giving equations for boundary conditions and flow rate
16 p2769 A69-31831

Inertia, compressibility and viscous friction effects on dynamic response of long fluid line, constructing models
16 p2771 A69-32066

Swirl decay of turbulent flow in tubes, showing decrease with increasing axial Reynolds number and independence of initial swirl angle
16 p2772 A69-32170

Forced laminar flow convection in horizontal tube with variable viscosity and free convection effects
[ASME PAPER 68-WA/HT-20]
17 p3068 A69-32902

Transverse turbulent pipe flow, obtaining limiting behavior of time averaged velocity gradient at wall
17 p2949 A69-33013

Turbulence measurements and roughness effects on viscous drag reduction with polymer solution in pipe flow, discussing friction factor, wall velocity profile, etc
17 p2951 A69-33252

Concentration, flow rate and tube diameter effects on viscous drag reduction in nonpolar soap solutions, using pressure drop measurements to observe turbulent flow behavior
17 p2951 A69-33253

Transverse magnetic field effect on shear turbulence structure of magneto-fluid-mechanic pipe flow with and without heat transfer
[AIAA PAPER 69-723]
17 p3012 A69-33497

Visual observation of pipe wall regions in turbulent flow by suspending colloidal size particles and photographing with high speed motion picture camera
17 p2956 A69-33598

Displacement of rectangularly mouthed pitot tubes in turbulent tube flow, determining roles of wall and shear effects
17 p2976 A69-34049

Static and impact pressure distributions for Mach number and velocity profiles of supersonic to subsonic flow transition in tube at low Reynolds numbers
[ASME PAPER 69-APM-23]
18 p3120 A69-34397

Rough wall turbulent boundary layer development in pipe flow determined for different roughness geometries in zero and adverse pressure gradients
18 p3125 A69-35387

Energy losses due to drag in unstable laminar fluid flow in tube
20 p3513 A69-36973

Prandtl mixing length theory for flow in pipes and channels described by spatial exponential form, developing velocity profile and friction factor
[ASME PAPER 69-FE-48]
20 p3516 A69-37978

Linear dynamic modeling of barotropic fluid in rigid circular tube, presenting axial velocity profile by confluent hypergeometric function with complex arguments
[ASME PAPER 69-FLCS-18]
20 p3516 A69-37982

Boundary layer velocity distribution in turbulent swirling pipe flow produced by twisted tape inserts
[ASME PAPER 69-FE-14]
20 p3516 A69-37990

Axial velocity and static pressure for incompressible fluid flow through straight smooth porous tube
[ASME PAPER 69-FE-44]
20 p3517 A69-38000

Hydraulic resistance of pipes with flow vorticity produced by helical swirlers
21 p3695 A69-38862

Skin friction and mean velocity profiles measured for fully developed 1000-10,000 Reynolds number flows in pipes and channels
22 p3932 A69-40897

Laminar flow in porous circular pipe with constant suction or injection applied at wall
24 p4298 A69-42618

Wave processes in pipelines during fluid filling, studying effects of flow resistance due to pumps and nozzles
24 p4300 A69-43075

Turbulent boundary layer at inlet section of gas blown tube based on solutions of energy and momentum equations, deriving relations for inlet section length
24 p4300 A69-43079

Dynamic pressure response of viscous compressible fluids in rigid tubes with dead ended volume termination, testing Ibrall theorem as function of Stokes number
24 p4301 A69-43287

Volatile wall vaporization gas flow expansion into vacuum from tube approximating unsteady mass and energy transfer and pressure at blocked end
24 p4408 A69-43489

Laminar flow in horizontal circular tubes with uniform heat flux, analyzing combined free and forced convection effects on secondary flow
24 p4409 A69-43519

Numerical program solving partial differential equations parabolic system for internal turbulent gas flow extended to flows undergoing circular tube laminarization by heating
[ASME PAPER 69-HT-52]
24 p4409 A69-43520

Eddy diffusivity hypothesis modified to fit observed heat transfer from smooth pipe wall to turbulent gas stream at low Reynolds numbers
[ASME PAPER 69-HT-H]
24 p4303 A69-43523

Radiative transport in nongray cylindrical medium using total band absorbance
[ASME PAPER 69-HT-38]
24 p4411 A69-43534

Choking and shock in flashing single component two phase flow in tube, including vibrational effects, predicting minimum stagnation pressure loss
[ASME PAPER 69-HT-61]
24 p4303 A69-43535

Turbulent flow in circular porous tube laminarized by uniform mass injection through tube wall, measuring velocity and turbulence intensity by impact probe
[ASME PAPER 69-HT-57]
24 p4303 A69-43537

Cylindrical bubbles stability in vertical pipes from photographs, describing wake, spacing, pressure pulsations and convection cells effects
[ASME PAPER 69-HT-28]
24 p4411 A69-43540

Film-nucleate boiling transition for liquid nitrogen in vertical forced flow in electrically heated tube, discussing conduction model and agreement with visual experiment
[ASME PAPER 69-HT-26]
24 p4412 A69-43542

Turbulent pipe flow with wall suction, calculating friction factor, pressure gradient, heat and mass transfer coefficients, velocity and temperature profiles
[ASME PAPER 69-HT-4]
24 p4414 A69-43562

PIPE NOZZLES

Fuel concentration effect on turbojet engine reheat jet pipe vibrations via tests
09 p1573 A69-22616

PIPELINES

Ultrasonic sounding for controlling dispersed gas phase in liquid pipelines under laboratory and practical conditions
04 p0596 A69-14489

Pressure losses in pipeline with venturi tube, calculating hydraulic resistance coefficient as function of structural parameters and pipeline length
15 p2612 A69-31180

Pressure drop in control element of gas generator during readjustment of throttle in hydraulic supply line, noting assumptions
19 p3393 A69-35819

Wave processes in pipelines during fluid filling, studying effects of flow resistance due to pumps and nozzles
24 p4300 A69-43075

PIPES [TUBES]

NT HEAT PIPES

Material memory effect in plastically prestrained thin welded brass tubes analyzed on basis of kinematic strain hardening theory
02 p0336 A69-11551

Gas dynamic choking limitation on heat transfer capacity of heat pipe operating at low vapor pressures from comparison of theory and experiment
03 p0531 A69-12989

Boundary conditions for irrotational hydrodynamic field around sphere moving along axis of cylindrical tube containing incompressible fluid calculated by least squares method
03 p0415 A69-13362

Tubular metal parts and assemblies, discussing flaring, forming, beading, tapering and step drawing
03 p0435 A69-13918

Laminar heat transfer in circular pipes in low Peclet number flow case with laminar velocity profile, discussing Hagen-Poiseuille flows
04 p0687 A69-15397

Transmission and reflection coefficients of cylindrical tubes moving in free molecular gas flow determined by Monte Carlo method
06 p0911 A69-17877

Soviet pipe production technology from Ti and Ti alloys, considering properties and methods improvement
07 p1164 A69-18787

Heat convection coefficient for wires enclosed in cylindrical tubes filled with water or ethanol, showing dependence on inclination angle
07 p1242 A69-18926

Hard-drawn steel wire wound pipes and tanks, properties and design calculation, discussing laminates and permissible stress
08 p1414 A69-20487

Histogram approximation of plastic deformation of metals, analyzing tube under internal load and sandwiche layer compression
10 p1793 A69-22850

Hydrostatic tube extrusion, discussing equipment, techniques and commercial applications
[SAE PAPER 690319]
15 p2617 A69-30093

Flexural vibrations of unstiffened doubly symmetric cylindrical tubes, obtaining natural frequencies of simply supported rectangular tube
15 p2703 A69-30210

Fracture safe design practices for pressure vessels and piping, stressing transition temperature and proof testing roles
17 p3060 A69-33562

Testing machine for in vacuo tensile testing of tubular metallic specimens at high temperatures and low pressures
18 p3117 A69-34604

Automatic ultrasonic instrument monitoring on-line welding conditions of RF longitudinally seamwelded tubes
18 p3136 A69-34778

Reinforced plastics static fatigue strength under various loads including thin walled tubes long term tests under constant internal pressure
18 p3162 A69-35353

Diffuser for high performance centrifugal compressors based on discrete pipe drillings
[ASME PAPER 68-GT-38]
19 p3240 A69-36420

Plastic bending of thin walled pipes taking into account cross section flattening
21 p3835 A69-38868

Cutting loads measured as function of cutting rate and cutting tool geometry during boring of Cr-Ni steel pipe blanks
21 p3731 A69-38878

PIRANI GAGES

Plasticity of tubular steel annealed in vacuum furnace and subjected to complex tension and torsion along deformation trajectories containing salient point
21 p3839 A69-39197

Optimal focusing of acoustic system for tube defectoscopy with circular normal waves
24 p4296 A69-42655

Composite and metal tubes compared to determine properties for various loadings
[AIAA PAPER 68-340] 24 p4405 A69-43653

PIRANI GAGES

Vertical atmospheric pressure distribution measured directly with Pirani-Israel gauge in Skylark rocket, transforming dynamic pressure data into static pressures on ground
17 p2971 A69-33037

PISTON ENGINES

NT WANKEL ENGINES

Quantitative amounts of contaminants oil from piston engine and life of oil lubricant in engine
04 p0604 A69-14500

Rotary engines, discussing scissor, eccentric rotor, multiple rotor and revolving block types
07 p1203 A69-18910

Coaxial multipurpose KA-26 helicopter design, discussing cruising speed, passenger capacity, range, flight ceiling, gross weight and piston engines
07 p1053 A69-18969

Performance correction and nonstandard day performance prediction for analyzing turbocharged reciprocating aircraft engines in light aircraft applications
[SAE PAPER 690309] 11 p1942 A69-24514

Soviet book on electric ignition systems for piston and jet engines and design aspects of different types of ignition systems
12 p2146 A69-26756

Glass fiber filled polytetrafluoroethylene materials for piston seals in high pressure oil-free reciprocating air compressors, discussing manufacturing and non-destructive tests
19 p3323 A69-35579

Wankel aircraft engines compared to piston and turbine aircraft engines for performance, maintenance and reliability
19 p3395 A69-36872

Optical devices for nondestructive testing of large piston engine equipment
20 p3547 A69-36921

Oil-free linear motor resonant piston gas compressor, hermetically sealable to handle radioactive and dangerous gases
[ASME PAPER 69-FE-36] 20 p3466 A69-37996

Rankine cycle power systems with reciprocating engines using organic working fluids, discussing engine development, system characteristics, etc
23 p4067 A69-42237

Positive displacement Rankine cycle rotary wet steam engine design compared with piston type, noting simplified evaporator and tests
23 p4069 A69-42252

Oil high temperature and oxidation conditions in aircraft piston engines, including physicochemical changes
24 p4321 A69-43141

PISTON THEORY

Gas velocity variations in ionizing shock wave propagating along magnetic field applied to conducting piston motion
05 p0801 A69-15787

Kinetic theory for weak shock generation by impulsive piston, using Fourier and Laplace transforms to solve BGK equation
08 p1304 A69-20783

Gun tunnel equilibrium piston technique by model analysis of piston weight, tunnel conditions and geometry
11 p1862 A69-25013

Two piston flow stability separated by thin wall in traveling magnetic field, finding piston inertia centers velocity equal to field velocity
14 p2500 A69-29903

Prestressed ceramic driver chamber energy efficiency for arc driven shock tube by pressure measurements with piezoelectric probe
18 p3116 A69-34456

Gas velocity variations in ionizing shock wave propagating along magnetic field applied to conducting piston motion
18 p3181 A69-35038

Fluid-shell interactions, using piston theory and cylindrical-wave approximations
18 p3223 A69-35174

Electrohydrodynamic supersonic flow over wavy wall by oscillating piston model, calculating streamlines and density distributions
19 p3297 A69-35838

Piston motion influence on gaseous motion set up by constant energy explosion, applying to steady high Mach number flow past blunt nosed object
22 p3931 A69-40892

Ionized plasma motion under plane piston action by self similar solution of Navier-Stokes equations
22 p3991 A69-41021

Polytropic gas unsteady motion in dihedral piston wake by solving mixed boundary value and Goursat problems
22 p3861 A69-41025

PISTONS

NT MAGNETIC PISTONS

Dense real gas thermodynamic relations in piston driven shock tube facilities operation
11 p1862 A69-25011

Piston driven facilities for hot high pressure gas production including gas tunnels, heavy piston facilities, piston driven shock tunnels and high speed guns
11 p1862 A69-25012

Isentropic compression tube with piston compressor for producing hypervelocity test flows, noting shock speeds
[AIAA PAPER 69-334] 13 p2249 A69-28270

Gas motion behind cylindrical shock wave created by piston motion in gravitating medium
19 p3298 A69-36386

Piston driven shock tube at Kyoto University with performance tests results, investigating compression processes, shock speed and flow duration time
22 p3928 A69-41046

Noise reduction research for hydraulic machines, examining piston pumps noise generating mechanism
22 p3870 A69-41238

PITCH

Human noise tolerance laboratory and community studies, discussing proposed tone corrections for aircraft noise
15 p2719 A69-30374

Hearing at LF, comparing noise and tone thresholds
21 p3664 A69-38986

Whispered vowels pitch perception test using listen-and-compare method to determine formants for comparison with complex analysis procedure
23 p4190 A69-41575

PITCH [INCLINATION]

Ballistic reentry vehicle roll-pitch coupling, showing influence of nose asymmetries
[AIAA PAPER 69-101] 06 p1018 A69-18156

Galaxies classification using rectified images, noting pitch and inclination angles
08 p1408 A69-21135

Pitch angle distribution function of thermal protons in magnetosphere taking into account earth gravitational field
12 p2067 A69-26354

Pitch angle diffusion of trapped electrons in terrestrial radiation zones, discussing diffusion theory based on Fokker-Planck equation, atmospheric Coulomb scattering mechanism, etc
12 p2150 A69-26746

Pitch determination of micrometer screw by scalar star pairs derived from FK3 and Washington zenith catalog noting temperature and dampness effects
16 p2859 A69-32218

Time optimal pitch motion of satellite in circular orbit based on maximum principle, considering variable and constant controls
18 p3207 A69-34677

Higher harmonic pitch angle inputs to eliminate oscillatory helicopter blade root shear determined through teetering rotor model
18 p3089 A69-35233

Torsionally flexible blade controllable twist rotor with pitch horn and servoflap control, discussing optimum inputs, airloads and angles of attack contours
18 p3089 A69-35234

Flux magnitude and pitch angle distribution relationship for postsubstorm auroral electrons, noting particle precipitation and acceleration models
20 p3592 A69-38083

Drift shell splitting in nondipolar distorted magnetosphere tested with data from electron spectrometer on ATS 1 and OGO 3 satellites
22 p4005 A69-40508

Spacecraft pitch and yaw angles measurement using environmental positive ion probes, discussing Gemini flight tests and attitude control systems
24 p4315 A69-43241

PITCH ATTITUDE CONTROL
U LONGITUDINAL CONTROL

PITCHING MOMENTS

Aerodynamics of bodies of revolution in nonplanar motion using nonlinear functional analysis of momenta for motion about center of gravity
[AIAA PAPER 68-20] 04 p0542 A69-14714

Small angle precessional motion of axisymmetric spin stabilized bodies subject to disturbing moments
10 p1724 A69-22932

Directional gyroscope with interframe correlation, discussing errors during object pitching and banking
14 p2446 A69-28922

Wind tunnel wall interference effects in wind tunnel testing of STOL aircraft by inducing interference velocities
[AIAA PAPER 68-399] 17 p2947 A69-34022

Stationary resonant nonlinear oscillatory and rotary states, stability and pitching motions of controlled satellite in slightly elliptical orbit
20 p3616 A69-37177

Schweikhard method for measuring changes in lift, drag and pitching moment of fixed wing aircraft as a function of distance from ground
20 p3462 A69-37423

Dynamic stall effect on helicopter rotor blades air-loading and blade pitching motion at high advance ratio
20 p3463 A69-37809

Aerodynamic pitch-roll coupling in spinning vehicles, showing unsteady components complicating data reduction
21 p3647 A69-39038

Flight control system providing variable stability in pitch axis of NF-8D Crusader, discussing flight evaluation of power approach short period configurations
[AIAA PAPER 69-896] 21 p3648 A69-39420

Pitching characteristics of three dimensional peripheral jet ground effect machines with compartment partition along pitch axis, considering longitudinal static stability and dynamic pitching motion
22 p3866 A69-40818

Single stage rocket body finite bending stiffness effect on pitching moment using approximate equation, noting applicability to multistage rockets
22 p4037 A69-41048

Dynamic model of ablation pitching moment derivative and time lag effect on spinning reentry vehicle applied to Black Knight flight results
24 p4245 A69-43249

PITOT STATIC TUBES
U SPEED INDICATORS

PITOT TUBES

Flow characteristics about curved lateral jet, discussing effect of pitot tube nozzle shape and turbulence
05 p0746 A69-16017

Boundary shear stress with unknown magnitude and direction measured by yaw probe used as Preston tube
05 p0751 A69-16396

Skin friction measurement with rectangular mouthed Preston tubes of constant thickness ratio, analyzing calibration curves and difference from circular tubes
11 p1880 A69-24376

Supersonic Preston tube correlations for Mach number and Reynolds number effects on hypersonic turbulent skin friction on adiabatic surfaces, simplifying correlation
[AIAA PAPER 69-345] 13 p2249 A69-28280

MHD properties of velocity measurement method using cylindrical glass filament probe and Pitot and Prandtl tubes
14 p2453 A69-29920

Pitot tubes diameter effect on pressure gradients during measurement through shock wave
16 p2771 A69-31927

Preston probe measurement of friction drag on subsonic and supersonic nozzle wall including effects of heat transfer, compressibility and pressure gradient
[AIAA PAPER 69-648] 17 p2893 A69-33496

Displacement of rectangularly mouthed pitot tubes in turbulent tube flow, determining roles of wall and shear effects
17 p2976 A69-34049

Pitot probe measurements of Hg drop growth rates and diameters, allowing for thermal and diffusion effects
24 p4316 A69-43583

PITTING

Orientation dependence of pitting and blistering in proton irradiated Al polycrystalline surfaces
04 p0640 A69-14451

Pitting corrosion resistance improvement in austenitic stainless steels with added molybdenum through electroslag remelting
05 p0781 A69-16499

Sulfite ion influence on pitting corrosion of stainless steels in sodium chloride solution
07 p1167 A69-19343

Thin foil preparation technique for transmission electron microscopy and selected etch pitting technique for CoO single crystals
12 p2112 A69-25944

PITUITARY GLAND

Hypoxia exposure effect on RNA synthesis in rat anterior pituitary cultured in vitro
01 p0015 A69-10923

Phosphodiesterase activity of anterior pituitary, median eminence, heart and cerebral cortex of rat, studying effects of caffeine, theophylline and hydrocortisone
02 p0199 A69-11885

Identity between growth hormone degrading activity of pituitary gland and plasmin
06 p0873 A69-17105

Resting EEG and parieto-occipital response changes evoked by slowly repeated flashes in case of severe hypothyroidism secondary to panhypopituitarism
07 p1064 A69-18634

Adrenal epinephrine and phenylethanolamine n-methyl transferase /PNMT/ activity in rat bearing transplantable pituitary tumor
08 p1263 A69-20374

Constant light/darkness effects on stress response rhythm of hypothalamic-pituitary-adrenocortical system in female rats
15 p2556 A69-31330

Rats adrenal corticosterone concentrations changes in response to ACTH, determining response sensitivity dependence on time after hypophysectomy
22 p3870 A69-39871

Pituitary-adrenocortical axis of rats in oxygen atmosphere at low pressure, finding depressed norepinephrine excretion
23 p4087 A69-41790

PITUITARY HORMONES

Rapid global transportation effect on circadian rhythmic patterns in human body functions, discussing kidney excretion and pituitary adrenal cortical system
09 p1444 A69-22545

PIVOTED WING AIRCRAFT

PIVOTS

Optimum automatic selection of redundancies, discussing weighting and pivot choice and rigid element incorporation
11 p1993 A69-25529

Load carrying capacity and friction calculated for pivoted pad journal bearings for machine design use [ASME PAPER 68-LUBS-27]
13 p2266 A69-27275

PLAGES [FACULAE]

U FACULAE

PLAN POSITION INDICATORS

Ground based control system via cockpit PPI display on transponder equipped aircraft broadcast with digital coding
03 p0464 A69-13244

Alphanumeric characters to identify radar targets on PPI display for air traffic control, considering technique for reducing smear
09 p1495 A69-21675

Meteorological Doppler radar information display for real time identification of hazardous winds and turbulence in storms
18 p3139 A69-35427

Sporadic E layer large scale irregularities direction and velocity determined by inclined backscatter method, using plan position indicator
20 p3528 A69-37682

PLANAR STRUCTURES

Planar arrays of linear antennas above stratified medium, showing antenna impedance and current distribution expressed in terms for free space environment
01 p0042 A69-10343

Planar transistor micromode operation during collector junction avalanche breakdown
01 p0047 A69-10884

Graphical method for determining rise time of planar transistors with constant collector space-charge capacitance
01 p0049 A69-11362

Planar technology application to germanium electronic components and integrated circuits
02 p0214 A69-11597

Planar transistor reliability test results noting failure rate, stability and effect of temperature
03 p0402 A69-13006

Planar phased array of circular waveguides arranged in equilateral triangular grid, solving boundary value problem
03 p0406 A69-13829

Complex power radiated by infinite planar array antenna, noting aperture field distribution influence on formula applicability
04 p0571 A69-14311

Planar linkages kinematic synthesis and design, using Newton-Raphson iteration technique to solve nonlinear equations
04 p0604 A69-14517

Double diffused planar Ge n-p-n and p-n-p transistors with high switching speed, noting fabrication and performance
05 p0809 A69-16557

P-n planar avalanche photodiode without guard ring noting electrical properties, uniform multiplication and fabrication
05 p0733 A69-16559

Steady flow circuit characteristics in square cross section channels of planar geometry fluid control elements in case of laminar flow
07 p1118 A69-18293

Surface recombination rate and retardation field effects on diffusion current in mesa diodes with low level injection
07 p1105 A69-19008

Fixed space planar thermionic diode with collector guard ring for studying various emitter materials, measuring emitter temperatures
09 p1438 A69-21815

Surface ion behavior on planar semiconductor devices determined by measuring effect of time, humidity, temperature, voltage and previous testing history
10 p1743 A69-23173

Breakdown voltage and avalanche drift instability factors in planar passivated p-n junctions as function of oxide thickness and mobile charge
10 p1743 A69-23174

Supersonic gas flow past plane and axisymmetric bodies with broken generatrix, determining tangential discontinuities and shock waves shape and position
11 p1820 A69-25470

Planar transistor micromode operation during collector junction avalanche breakdown
12 p2041 A69-26648

Difference schemes for elasticity theory plane dynamic problem with mixed boundary conditions, establishing scheme absolute stability
14 p2536 A69-29474

Bipolar HF p-type Si transistors preparation by B and P ion beams and planar technology masking technique, obtaining p-n-p structure
22 p3916 A69-40960

Plane-truss joints displacements determined by graph-analytic method, discussing representation of fictitious forces and moments
23 p4225 A69-41420

Diffuse configuration factors between small plane and large sphere by unit sphere method, presenting limiting cases
24 p4351 A69-43683

PLANCKS CONSTANT

Relative element abundances in Cyg, Her and Boo atmospheres, calculating curves of growth by Planck gradient method for stellar spectra
14 p2519 A69-29356

Planck law for black body radiation spectrum theoretically derived on basis of classical Lorentz-invariant electromagnetic radiation at absolute zero temperature without quantum assumption
22 p3982 A69-41001

PLANE WAVES

Plane wave propagation in infinite viscoelastic medium taking into account mutual effects of deformation and temperature fields
01 p0164 A69-10076

Plane wave scattering from modulated corrugated structures, obtaining reflection coefficients for multimode propagation
01 p0033 A69-10973

Diffraction of cylindrical and plane waves in system of two parallel circular cylinders, using equivalent circuit method
02 p0217 A69-12261

Reflection of plane electromagnetic wave from impedance cylinder in vacuum, using ray expansion method
02 p0217 A69-12262

Impedance sheet approximation to plasma slab, considering plane wave propagation, plasma covered slot antenna and transmission loss
02 p0209 A69-12348

Velocity measurement and flow pattern determination of plane shock waves during passage through channel diaphragm
02 p0234 A69-12589

HF approximations, discussing plane wave diffraction by conducting circular cylinder using Watson transform
03 p0384 A69-12903

Electromagnetic wave passage through plane gyrotropic layer of magnetized plasma, analyzing polarization and energy transfer
03 p0397 A69-13709

Legendre transformation application to plane elastoplastic loading waves, examining shock front formation in interaction region
04 p0673 A69-14495

HF plane sound waves in ideal gases with internal dissipation, considering particular applications to dissociating diatomic and vibrational relaxing gases
05 p0792 A69-15723

Submillimeter plane monochromatic wave amplitude and phase fluctuations during propagation in turbulent atmosphere surface layer, considering absorption by water vapor
05 p0722 A69-16778

Diffraction of plane electromagnetic waves obliquely incident on conducting rotated periodically tapered grating structure formed of infinite metal strips
05 p0723 A69-16788

Linear antenna synthesis for optimal separation of plane waves providing maximum SNR with allowance for statistical phase distribution of field
06 p0895 A69-17460

Plane wave scattering by conducting wire impedance loaded at center, discussing loading effect on backscattering cross sections
06 p0888 A69-17512

HF scattering of scalar plane wave by transparent sphere based on Watson transformation
07 p1181 A69-19033

Initial equations for plane wave diffraction at grids of squared beams, calculating transmission and reflection coefficients by reflection method and computer
07 p1084 A69-19149

Plane electromagnetic wave diffraction at oblique screen of circular cross section conducting wires solved, assuming smaller wire radius than grid spacing and wavelength
07 p1084 A69-19150

Real and imaginary parts of homogeneous isotropic electron plasma complex refractive index, noting application to plane electromagnetic wave propagation
07 p1193 A69-19183

Plane radiative shock wave propagation in homogeneous medium noting heating ahead and cooling behind shock front
08 p1302 A69-19798

Radar scattering cross section of finite perfectly conducting wedge for case of illumination by polarized plane wave
08 p1274 A69-20047

Constitutive equations for propagation of plane waves of finite amplitude in nonsimple elastic solids, discussing holohedral isotropic solids and transverse harmonic circularly polarized waves
08 p1411 A69-20141

Spherical wave generalization for plane light wave propagating in turbulent medium, describing circular objective averaging effect on intensity fluctuations
08 p1351 A69-20438

Quasi-linear differential constitutive equation of work hardenable elastoviscoplastic material in case of plane wave propagation in half space
08 p1415 A69-20662

Differential equations for normal propagation of plane electromagnetic waves in isotropic stratified inhomogeneous gyration medium, discussing boundary conditions and reflection properties
08 p1353 A69-21000

Dispersion equation to describe spectrum of LF density perturbations by pumping plane electromagnetic wave in transparent homogeneous plasma or fluid media
09 p1453 A69-21570

Electrothermal instabilities in small magnetic Reynolds number limit and ionization equilibrium at electron temperature using quasi-linear plane wave analysis
10 p1734 A69-23456

Quantitative analysis of plane waves for weak interaction of two dimensional sound and light fields in acoustical imaging by diffracted light
10 p1695 A69-23545

Plane wave solutions for acoustic propagation in polyatomic gas by using Sivovich-Thurber method for polyatomic kinetic models
11 p1920 A69-24287

Two dimensional wavefront shape induced in finitely strained elastic body by impulsive point body force
11 p1969 A69-24338

Electromagnetic plane wave scattering from slender semiinfinite cone, obtaining contribution to tip return arising from direct diffraction
11 p1836 A69-24988

Geometrical diffraction theory for bistatic scattering of plane wave by conducting frustum, calculating scattering matrix
11 p1837 A69-24999

Rapidly convergent series expansions for plane wave transmission coefficients for elliptical and rectangular apertures
11 p1837 A69-25001

Microwave antenna testing on small indoor ranges, discussing reflectors and feeds for generation of approximately uniform plane waves for antenna illumination
11 p1852 A69-25314

Radiation emission by scalar particle in field of two plane linearly polarized electromagnetic waves propagating toward each other
11 p1900 A69-25568

Plane transient electromagnetic wave from cold lossless plasma half space and slab
12 p2033 A69-26865

Nonuniform two dimensional hydromagnetic waves incident on idealized lower ionosphere, discussing validity of various models
12 p2074 A69-26960

Bhatnagar-Gross-Krook model for plane shock structure, considering moment and least squares methods and shock density gradient error analysis
12 p2063 A69-27112

Optimal thickness of inhomogeneous absorption layer subjected to normally incident plane monochromatic wave treated as Mayer-Boltz variational problem
13 p2297 A69-27381

Plane wave solution for wave propagation in inhomogeneous anisotropic time-varying media
13 p2219 A69-27397

Plane TM surface waves supported by plane ungrounded magnetoplasma slab with magnetostatic field parallel to two parallel interfaces and perpendicular to propagation direction
13 p2308 A69-27966

Plane elastoplastic shock waves propagation due to combined shear loadings assuming elastic isotropic work hardening materials
13 p2368 A69-28346

Electric field distribution in focal region of finite off-set paraboloid reflector illuminated by linearly polarized plane wave
13 p2234 A69-28427

Elastic medium properties recovered from reflected or transmitted plane waves at normal incidence, obtaining computational procedures and analytical solution from Schroedinger equation
13 p2300 A69-28664

Monochromatic plane waves propagation in anisotropic homogeneous cold plasmas, treating dispersion surface, reflection, refraction and waveguide applications
14 p2492 A69-29399

Plane wave reflection and transmission by unidirectionally conducting screen, considering oblique incidence and two polarizations
14 p2421 A69-29547

Plane electromagnetic wave refraction and scattering in solar corona during eclipsed observations of cosmic sources, calculating angular distribution of radiation intensity
15 p2688 A69-30555

Rayleigh assumption validity for wave scattering by analytic periodic surface predicated on solutions analytic continuation across boundary, discussing Green function role
15 p2652 A69-30673

Reflection of plane waves at boundary surface of two semiinfinite media in relative motion, calculating power reflection coefficients
15 p2568 A69-30796

Plane electromagnetic wave propagation normal and parallel to magnetic field in plasma analyzed by equivalent circuits and impedances
15 p2659 A69-30799

Attenuation of small perturbations in shape of plane shock wave propagating into uniform medium in presence of rigid or interfacial boundaries
15 p2592 A69-31145

Reflection of plane waves from stress free flat surface of micropolar elastic half space, presenting reflection laws and amplitude ratios
15 p2714 A69-31147

Scattering of time harmonic linearly polarized plane electromagnetic wave by uniformly axially moving cylinder, analyzing first order velocity effects
16 p2748 A69-31579

Inverse scattering technique for electromagnetic bistatic scattering by expressing field produced by incident plane wave as sum of incident field and Fourier transform
16 p2754 A69-32569

Shear layer effect on plane sound waves, discussing reflection and refraction at velocity discontinuity between two regions of fluid
17 p3005 A69-32954

Nonlinear interaction of plane electromagnetic wave with inhomogeneous plasma layer, noting concentration and electric field discontinuity
17 p2922 A69-33693

Plane shock wave interaction with plane rigid net-like wall, obtaining Mach numbers for reflected and penetrating shock waves
17 p2957 A69-33719

Plane wave scattering by multimode corrugated structure with H mode incidence, revealing theoretically scattering resonance as P type Wood anomalies
17 p2925 A69-33844

Physical mechanisms for nonlinearities in electromagnetic wave propagation, analyzing plane wave instability, self focused beams propagation and laser oscillations
17 p2928 A69-33867

Deformation of amplitude and frequency envelopes of plane modulated electromagnetic waves with dispersion in isotropic dielectric with cubic nonlinearity
17 p2928 A69-33869

Diffraction of skew incident plane electromagnetic wave by perfectly conducting right angled wedge embedded in uniaxially anisotropic medium
17 p2930 A69-33889

Angular spectrum representation of diffracted wave fields expressible by plane wave expansions containing only homogeneous waves
17 p3007 A69-34153

Penumbral current distribution in plane electromagnetic waves diffraction by conducting cylinder, obtaining transient solution for impulsive excitation, discussing time harmonic problem
18 p3100 A69-34232 [AFCL-69-0038]

Plane wave propagation due to combined compressive and shear stresses in half space, assuming elastoplastic material
18 p3213 A69-34388 [ASME PAPER 69-APM-12]

Polarization operator and Green function of photon for propagation of plane electromagnetic waves in constant crossed field, noting refractive indices
18 p3103 A69-35128

Plane wave scattering by semiinfinite turbulent dielectric slab, using Born approximation to develop asymptotic series for stochastic components of forward scattered field
18 p3174 A69-35245 [OSA PAPER WH-16]

Plane electromagnetic wave scattering by motion of small ellipsoid in vacuum, noting total scattering and radar cross sections dependence on ellipsoid velocity
18 p3105 A69-35485

Interference filter design for IR devices on Fresnel equation basis, analyzing plane electromagnetic wave propagation through stratified dielectric multilayer
19 p3373 A69-36053

Plane electromagnetic wave diffraction on conducting sphere situated in absorbing nonuniform plasma layer
19 p3275 A69-36340

Lateral and head-on interactions between plane shock wave and supersonic wedge, showing solution dependent on apex angle and incident flow Mach number
19 p3239 A69-36398

Scattered field of linear array of center loaded cylindrical elements illuminated by plane electromagnetic wave
20 p3494 A69-37838

Linear antenna synthesis for optimal separation of plane waves providing maximum SNR with allowance for statistical phase distribution of field
20 p3508 A69-37943

Biquadratic plane wave dispersion relation for gyrotropic waveguides with dielectric and magnetic properties, discussing associated quartic equation for refractivity
21 p3675 A69-39285

Wave trains of incident pulse diffraction in thin composite rod determined by transmission and reflection coefficients of plane waves at plane interfaces
21 p3845 A69-39677

Plane double front detonation wave attenuation by pursuing rarefaction waves, analyzing oscillations, onset mechanism and stability during transition to Chapman-Jouguet mode
22 p3929 A69-40112

Transient flow resulting from plane shock diffraction by analytic blunt body, basing analysis on Taylor series expansions in space and time variables
22 p3860 A69-40895

Plane EM wave transmission and reflection by semiinfinite isotropic plasma moving in arbitrary direction parallel to boundary, using Lorentz transformation
23 p4114 A69-41360

Plane electromagnetic wave scattering on turbulent fluctuations in electron density of finite volume ionized plasma, evaluating Booker-Gordon relation
23 p4116 A69-41587

Transverse spectra and structural functions of fluctuations for plane waves of different frequencies propagating in isotropic turbulent medium
23 p4117 A69-41728

Plane polarized electromagnetic wave diffraction incident on skewed metal ribbons array
23 p4125 A69-42043

Semiinverse method involving plane wave expansions to solve elliptical crack expansion and self similar phase transformation in anisotropic solid
24 p4397 A69-42749

Plane electromagnetic waves coherence properties, considering linear and arbitrary degree of polarization
24 p4350 A69-42982

Hot dense plasma used as driver gas producing plane stable current-free high Mach number shock fronts resembling plane blast waves
24 p4359 A69-43647

PLANET EPHEMERIDES

Icarus asteroid position measurements by astronomical photography, noting comparison for two South African observatories
01 p0150 A69-10373

Orbit corrections for lost minor planets 457, 1038, 1161, 1297, determining new ephemerides for oppositions
05 p0829 A69-16704

Relative positions of Neptune and BD minus 17 degrees 4388 star determined by Yale-Columbia refractor and double star camera, noting ephemerides correction from stellar occultation
17 p3041 A69-33814

Dichotomy of Venus in eastern and western elongations, determining time of occurrence by graphical method
18 p3203 A69-35336

Ephemeris calculations and lunar craters and reference stars coordinates measured from photographic plates, using digital computers
22 p4024 A69-40610

PLANET ORIGINS

U PLANETARY EVOLUTION

PLANETARIUMS

Network for fireball trajectories rapid analysis to recover meteorites and obtain orbital elements data, noting role of planetariums
19 p3295 A69-36121

PLANETARY ATMOSPHERES

NT JUPITER ATMOSPHERE

NT MARS ATMOSPHERE

NT VENUS ATMOSPHERE

Planetary atmosphere composition determination using mass spectrometry for neutral components, ion spectrometry for ionic components and data system optimization
02 p0247 A69-11468 [AAS PAPER 68-183]

Multiple light scattering in planetary atmospheres, discussing diffuse reflection and transmission by atmosphere of particles with anisotropic scattering pattern
02 p0319 A69-12105

Photoelectron energy loss mechanisms in planetary atmospheres, considering possible constituents in Mars and Venus upper atmospheres
02 p0321 A69-12118

Unmanned planetary exploration using Mariner class spacecraft for solar system and life origin
02 p0334 A69-12302

Planetary atmosphere determination error analysis using Kalman filter, noting results of simulated Martian atmosphere entry

02 p0331 A69-12806

Mars and Venus probes antenna problems in environments of near earth space, deep space and nonearth planetary atmospheres

02 p0223 A69-12811

Limiting conditions for gaseous atmospheres surrounding major and minor planets related to suitability for synoptic observation with optical telescopes and spectrometers

03 p0510 A69-13393

Structure and mean molecular weight measurement of unknown atmosphere assessed from high altitude tests in earth atmosphere [AIAA PAPER 68-1054]

03 p0512 A69-13699

Lateral transport of constituents in planetary exospheres, considering planetary rotation

03 p0515 A69-14010

Tetron flight observations of eddy velocities in planetary boundary layer, noting effects of height and seasonal variations

04 p0626 A69-14912

Neptune atmosphere height scale and density from photometric observation of star occultation

04 p0660 A69-15061

Multiple light scattering in spherical planetary atmosphere based on geometrical model, calculating twilight glow brightness

05 p0828 A69-16632

General atmospheric circulation characteristics estimation for earth, Mars, Venus and Mercury based on thermodynamic and hydrodynamic laws

05 p0828 A69-16635

Inverse problems in radiative transfer applied to remote measurements of IR radiation from planetary atmospheres, noting temperature and water vapor inversions

06 p0919 A69-17617

Radio occultation measurements of planetary atmospheres and ionospheres from orbiting pair [AIAA PAPER 69-53]

06 p1011 A69-18104

Radiative transfer problems in inhomogeneous anisotropically scattering plane parallel planetary atmospheres with internal source distributions solved by recursive method

07 p1213 A69-18610

Diurnal thermal wave form driven by harmonically oscillating ground temperature in nongray atmosphere, calculating results for terrestrial and Martian atmospheres

07 p1126 A69-19036

Vector equation of transfer for planetary atmosphere describing light scattering by anisotropic particles and analysis of resonance line scattering

08 p1385 A69-20063

Chemical abundances in planetary atmospheres based on spectroscopic determinations, considering terrestrial and Jovian planets

08 p1406 A69-20934

Unsteady atmospheric motions on planetary scale using Legendre polynomials

08 p1311 A69-21158

Optically thick planetary atmospheres in radiative-convective equilibrium investigated by models with adiabatic temperature gradient in troposphere, discussing gray stratospheric solution

09 p1600 A69-22200

Rotational Raman scattering in planetary atmospheres, analyzing spectra of deep solar Fraunhofer lines

09 p1601 A69-22207

Plane and spherical albedos of planet surrounded by infinite optical thickness atmosphere, with application to Venusian atmosphere

10 p1776 A69-23210

Unsteady baroclinic planetary atmosphere boundary layer turbulent states with various pressure and temperature gradient distributions, using boundary layer model

10 p1722 A69-23973

Methane absorption distribution in 6190 A band over Saturn disk at center and polar latitudes based on spectrograms

11 p1960 A69-24731

Model ion-exosphere for nonrotating planet with static dipole magnetic field generalized by permitting density and temperature variations over baropause

11 p1879 A69-25284

General atmospheric circulation characteristics estimation for earth, Mars, Venus and Mercury based on thermodynamic and hydrodynamic laws

14 p2516 A69-28791

Atmospheric dynamics parameters of Mercury, Venus, Mars and Jupiter, discussing generalized circulation theory

14 p2526 A69-29841

Reflected and absorbed solar radiation by planetary atmosphere and surface determined as function of atmosphere and surface optical properties

15 p2689 A69-30564

Multiple light scattering solutions accuracy by diffraction peak omission from cloud and haze analytic phase functions compared for optically thick and thin planetary atmospheres

17 p3032 A69-33159

Jupiter photochemistry above 1000 A, noting methane and ammonia photolysis zones, atmospheric pressures and hydrogen recombinations

17 p3032 A69-33165

Planetary atmospheres origin, discussing earth formation by planetesimals accumulation and similarity to Mars and Venus, volatiles in outer planets, etc

17 p3033 A69-33369

Suspected phase anomaly and Mercury atmosphere

17 p3034 A69-33414

Neptune radius, density and atmosphere deduced from observations during occultation of BD minus 17 degrees 4388 by Neptune

17 p3041 A69-33816

Ice clouds near IR spectral reflectivity dependence on particle size, noting application to planetary atmospheres

18 p3126 A69-34283

Half space applications regarding equation of transfer for planetary atmosphere

18 p3191 A69-34306

Planetary cosmogony problems involving protoplanetary cloud origin, matter condensation, planets formation and moon origin, noting iron content in chondrites

18 p3205 A69-35437

Diameter density and atmosphere of Neptune revised based on star eclipse, noting altitude and temperature

18 p3205 A69-35438

Approach navigation accuracy for planetary atmosphere braking to orbit about Mars and Venus [AAS PAPER 68-122]

19 p3402 A69-35937

Drop test method to obtain subsonic terminal velocity and base pressure data for planetary entry probe configurations

19 p3238 A69-35959

Radio measurements of nonionized media and planetary atmospheres, discussing uses of millimeter waves, line of sight propagation, scattering, etc

19 p3276 A69-36427

Optimal information selection for determining spacecraft trajectory, considering atmosphere, light speed and series expansion coefficients of planetary gravitational potentials

19 p3427 A69-36627

Radiating gas flows during hypersonic planetary reentry, discussing atmospheric composition, shock layer characteristics, nonequilibrium flows, etc

20 p3513 A69-36982

Particle albedos and extinction cross sections computed by Mie theory showing dependence on refractivity, considering thermal radiation from cloudy planetary atmospheres

20 p3614 A69-38255

Atmospheric structure, greenhouse effect and convective instability in window gray and nongray planetary atmospheres

20 p3615 A69-38257

Temperature structure of nongray planetary atmospheres, discussing scattering and absorption of solar energy by gas molecules, cloud aerosols and ground

20 p3615 A69-38258

Neptune equatorial radius, diameter, flattening and upper atmosphere optical properties determined from photometric curves of star BD-17 occultation

21 p3796 A69-38471

Planetary atmosphere structure and mean molecular weight determination from onboard measurements tested at high altitude in earth atmosphere, based on NASA Program [AIAA PAPER 68-1054]

21 p3715 A69-39023

Unsteady baroclinic planetary atmosphere boundary layer turbulent states with various pressure and temperature gradient distributions, using boundary layer model

21 p3760 A69-39659

RF voltage breakdown facility for studying spacecraft antenna characteristics in space and planetary atmosphere environments [AIAA PAPER 69-1028]

22 p3924 A69-40397

Molecular beams for simulating orbital flight through planetary atmospheres, considering various nozzle beam systems [AIAA PAPER 69-1031]

22 p3926 A69-40437

Neutral exosphere model for nonrotating planet permitting barosphere uniform rotation at certain angular velocity, determining velocity distribution and density

22 p4023 A69-40524

Steady state distribution of visible and IR radiation in planetary atmosphere illuminated from outside, calculating atmospheric temperature profile

22 p4031 A69-40910

Planetary atmosphere effect on Fresnel diffraction of ultrashort radio waves determined from short wave approximation of damping function

22 p3901 A69-40948

Spaceborne planetary UV spectroscopic search for atoms and molecules basic to life, specifically molecular N and water vapor photodissociation products

23 p4113 A69-41616

Solar wind collisionless hydromagnetic flow interaction with planetary atmosphere, using mathematical model to determine bow shock position limits in atmosphere

24 p4368 A69-43178

Magnetic dipole field variations effects on planetary atmosphere erosion by solar wind, discussing Mars and Venus atmospheres above ionosphere

24 p4385 A69-43224

PLANETARY BASES

Manned facilities design, construction and maintenance on extraterrestrial bodies, discussing astrophysical and lunar surface data requirements [AAS PAPER 69-208]

24 p4296 A69-42875

PLANETARY COMPOSITION

Mars surface photometric and spectrophotometric measurements, relating opposition effect details with corresponding laboratory sample measurements

07 p1212 A69-18601

Rare earths relative and absolute terrestrial abundances in shales, basalts, rhyolites and granites

08 p1310 A69-20942

Hypotheses concerning mechanism of lunar maria formation, discussing molten rock layer below lunar crust

10 p1782 A69-23710

Planetary interior convection analysis extended to include variable viscosity, heat source distribution, thermal expansion and diffusivity, etc

13 p2344 A69-27646

Chemical composition of earth, Venus, Mars, Mercury and moon calculated from mathematical models, constructing approximate equations of state at high pressure

14 p2526 A69-29878

Mars internal structure and composition modeling, considering core, mantle and temperature via earth analogy and Mariner 4 data

17 p3037 A69-33652

Mercury internal constitution and chemical composition, discussing models with iron cores and iron admixtures in mantle

20 p3597 A69-37331

Moon composition and similarities to Mars explained by silicates in solar system raw material

20 p3604 A69-37563

Planetary interiors from geophysical viewpoint emphasizing earth data

21 p3811 A69-39508

Fractionation mechanisms in early phases of planetary evolution sought to explain abundance problem in terrestrial planets

22 p4018 A69-40185

Extraterrestrial objects composition in defining cosmic abundance curve, including solar and meteoritic data

22 p4032 A69-40982

Martian surface mineralogical study of present state and past processes from rock analyses by unmanned spacecraft instruments to test planetary models

23 p4212 A69-41619

Model for accumulation of earth and planets from primitive solar nebula, implying inhomogeneous chemical composition of bodies in solar system

24 p4385 A69-43215

PLANETARY ENTRY

U ATMOSPHERIC ENTRY

PLANETARY ENVIRONMENTS

NT JUPITER ATMOSPHERE

NT MARS ATMOSPHERE

NT MARS ENVIRONMENT

NT VENUS ATMOSPHERE

Photometric-polarimetric observations of planetary surfaces, discussing geological environment interpretation

tion and spacecraft reconnaissance system mission planning
03 p0421 A69-13394

Product assurance role in spacecraft sterilization to maintain planetary biological environments integrity in space programs for extraterrestrial life determination
03 p0379 A69-13400

Particle and field environment of earth, discussing solar wind, bow shock, magnetosheath, magnetopause, magnetosphere and particle population
06 p1001 A69-17158

Solar system physical environments surveyed from exobiological viewpoint
17 p2907 A69-32968

Extraterrestrial optical microscopy, discussing experiment, telemetry, data interpretation and instrument characteristics concerning biological, cytochemical and petrographic microscopes
23 p4164 A69-41621

PLANETARY EVOLUTION

Monograph on nature of planets and solar system origin covering meteorite observations and age determination, chondrite composition, metallic elements, etc
01 p0152 A69-10702

Solar system origin and evolution by future space mission experiments, discussing theories and mission objectives
[AAS PAPER 68-191] 01 p0153 A69-10823

Introduction to planetary physics, Terrestrial planets, covering solid interior constituents, solar system dynamics and origin and evolution
01 p0154 A69-10920

Lunar surface early geologic evolution noting bearing on earth geologic history
[AAS PAPER 68-202] 02 p0312 A69-11478

Synodic month length variations since late Cambrian, noting paleontological evidence in mollusks and stromatolites and associated geological changes
02 p0241 A69-11807

NASA Planetary Exploration Program to gather data on origin of solar system and life, discussing planetary evolution and extraterrestrial life
02 p0200 A69-12804

Jupiter radio physics, discussing prebiological phase, low IR and microwave radio temperature and magnetic field
02 p0330 A69-12805

Annular and linear Martian surface formations nature and origin from analysis of Mariner 4 photographs
03 p0506 A69-13087

Secularly stable figures of equilibrium of rotating heterogeneous fluids of planetary size, noting dependence on laws of inertia and gravitation
03 p0513 A69-13780

Cometary origin of meteorites, discussing and rejecting origin from recent asteroidal collisions
05 p0818 A69-15588

Solar system evolution, noting angular momentum in planets and solar system and hypothesis of gravitationally contracting gaseous nebula
05 p0826 A69-16389

Possible evolution of earth continents and ocean basin, considering ultrabasic, basic, and intermediate to acidic lunar highlands chemical composition
06 p1000 A69-17006

Terrestrial and Cytherean atmospheres evolution based on gray atmosphere model, surface energy budget and partition of water and carbon dioxide
07 p1213 A69-18608

Commensurability among pairs of mean motions of natural satellites of major planets and hypothesis of tidal evolution of satellite systems
07 p1223 A69-19638

Martian structure theory, comparing mathematical model based on earth long term evolution and ad hoc models
08 p1387 A69-20092

Meteorites radiogenic and cosmic ray exposure ages, orbits and parent bodies, discussing H and L group chondrites
08 p1405 A69-20928

Boron in tektites determined by calorimetric technique for analysis of boron in silicates, comparing results with values from igneous and sedimentary parents
08 p1407 A69-20936

Radiogenic theory of origin of He in natural gas and absence of Ar from K 40 decay, discussing primordial earth atmosphere composition
08 p1311 A69-20947

Hypotheses concerning mechanism of lunar maria formation, discussing molten rock layer below lunar crust
10 p1782 A69-23710

Initial Sr isotopic composition at time of planetary objects formation in solar system and precision measurements for age determination of basaltic achondrites
11 p1953 A69-24357

Solar system age based on decay rate of natural radioactive elements
11 p1961 A69-24972

Mass distribution for bodies fallen on planets during formation estimated from present inclination of planetary axes of rotation, using limit theorems of probability theory
13 p2345 A69-27652

Lunar surface and earth early satellite system, discussing maria distribution, satellite impacts and close passage collisions
13 p2345 A69-27654

Moon-earth system origin emphasizing mass distribution
13 p2352 A69-27902

Annular and linear Martian surface formations nature and origin from analysis of Mariner 4 photographs
14 p2515 A69-28769

Comet scintillations and tail characteristics studied to obtain information on interplanetary flux field, magnetic fields and planetary structures
14 p2523 A69-29704

Venus atmosphere carbon dioxide content origin from interior degassing during molten phase, using atmospheric model
16 p2857 A69-32098

Moon density and nucleation of planets, explaining low density and absence of heavy core by late aggregation from nonmetallic particles
16 p2865 A69-32808

Planetary systems interrelationship with binaries and rotating stars, emphasizing occurrence frequency study based on stellar angular momentum orientation
17 p3032 A69-33105

Planetary atmospheres origin, discussing earth formation by planetesimals accumulation and similarity to Mars and Venus, volatiles in outer planets, etc
17 p3033 A69-33369

Planetary cosmogony problems involving protoplanetary cloud origin, matter condensation, planets formation and moon origin, noting iron content in chondrites
18 p3205 A69-35437

Meteorites data in planetary cosmogony, discussing iron meteorite ages, Xe retention in chondrites and synchronism of sun and protoplanetary cloud forming
19 p3406 A69-36075

Solar system matter evolutionary beginning traced to chemical elements synthesis by considering radioactive decay irreversible processes
19 p3406 A69-36076

Terrestrial planets high temperature evolution from solar system genesis theory, discussing meteorite chemical composition, petrography, mineralogy and age determination
19 p3407 A69-36079

Isotopic age determinations on iron and stone meteorites, discussing Rb-Sr and K-Ar results, internal isochrones, Kodaikanal data and planetary formation
19 p3413 A69-36108

Hypothetical planet captured by earth, becoming earth satellite/moon, discussing Mercury orbits peculiarities
20 p3603 A69-37562

Primitive earth upper atmosphere thermal models, considering roles of exospheric temperature and free hydrogen availability in methane dominated environment
20 p3608 A69-38056

Probability of biological development leading to human life on another planet
21 p3652 A69-38786

Chemical processes responsible for transformation of vast gas and dust cloud into planetary system
21 p3804 A69-39200

Atmospheric and hydrospheric evolution on primitive earth from geological point of view
21 p3806 A69-39290

Resonant spin and anomalous rotation of Mercury, analyzing influence of tidal degradation and permanent deformation of planet
21 p3814 A69-39568

Earth early thermal history with core formation before emplacement of earliest known rock possessing remanent magnetism
22 p3936 A69-40136

Paleontological evidence to verify varying G constant hypothesis for expanding earth theory, discussing uncertainties of geological dating
22 p4017 A69-40177

Dirac hypothesis on varying G constant considered in formulating earth expansion theory without resorting to Ramsey hypothesis
22 p4018 A69-40178

Paleogeographical evolution in support of earth expansion, discussing polar wandering, global continental drift and final complete disruption
22 p3936 A69-40181

Precambrian crustal geotectonic evidence of earth radius expansion based on dated orogenic fold belts distribution
22 p3936 A69-40182

Fractionation mechanisms in early phases of planetary evolution sought to explain abundance problem in terrestrial planets
22 p4018 A69-40185

Terrestrial type planetary evolution from early history and present internal configuration of earth, discussing gravitational energy associated with earth formation
23 p4212 A69-41613

Martian surface mineralogical study of present state and past processes from rock analyses by unmanned spacecraft instruments to test planetary models
23 p4212 A69-41619

Mariner 6 and 7 TV data, discussing implications for Mars present state, past history and biological status
24 p4384 A69-43195

Model for accumulation of earth and planets from primitive solar nebula, implying inhomogeneous chemical composition of bodies in solar system
24 p4385 A69-43215

PLANETARY EXPLORATION

U SPACE EXPLORATION

PLANETARY GRAVITATION

Limiting conditions for gaseous atmospheres surrounding major and minor planets related to suitability for synoptic observation with optical telescopes and spectrometers
03 p0510 A69-13393

Lagrange multipliers of variational problem of point motion and isochronal derivatives in field of attraction of axisymmetric planet
05 p0823 A69-16015

Biological systems response to inertial environment, escape from earth gravity, planetary gravity and artificial gravity
06 p0872 A69-17011

Jupiter unmanned flyby probes trajectory and mission analysis, considering planetary gravitational field role for trajectory shaping and flight times
06 p1007 A69-17598

Zonal harmonics of Legendre polynomial series of Jupiter attractive force function effects on motion of fifth satellite
14 p2521 A69-29463

Optimal information selection for determining spacecraft trajectory, considering atmosphere, light speed and series expansion coefficients of planetary gravitational potentials
19 p3427 A69-36627

Planetary gravitational fields and artificial satellite orbits determined by using earth based range rate measurements
24 p4388 A69-43650

PLANETARY LANDING

Planetary landing trajectory optimum single pulse correction determined by considering sum of correcting and retro pulses minimum
01 p0151 A69-10568

Multiengine Martian soft lander guidance and control system design with single engine failure accommodation based on six degrees of freedom computer simulation
02 p0277 A69-11740

Mars planetary entry and landing model tests, demonstrating technological feasibility of mission
02 p0333 A69-11746

Nonexistence of Biota-Cloud recontamination hazard for planetary lander proved by analysis of interactions between small particles and physical fields around vehicle
02 p1201 A69-11771

Biological monitoring during assembly of Technological Feasibility Spacecraft/Mars lander/ to evaluate thermal control techniques and microbiological burden prior to sterilization
02 p1201 A69-11774

Longitudinal range dispersion of unmanned Mars landers using VM-8 and VM-9 atmospheric models, discussing Syrtis Major as possible landing site
02 p0324 A69-12390

Mission mode and delivery method influence on payload maximization for Mars capsule system
02 p0335 A69-12822

Aeroshell structural development for Mars flyby and entry landing mission compatible with Atlas/Centaur launch vehicle
[AIAA PAPER 68-1159] 03 p0521 A69-13667

Entry and terminal deceleration systems for unmanned Martian landers, discussing parachute landing and lifting entry vehicles
[AIAA PAPER 68-1147] 03 p0521 A69-13670

Design of interface between Mariner Mars spacecraft and Mars planetary entry/landing capsule
[AIAA PAPER 68-1162] 03 p0521 A69-13671

Dynamic analysis and development of response histories and tradeoff study charts for spherical impact limiters for protecting hard landing planetary payloads
04 p0683 A69-15508

Planetary landing vehicle design optimization, considering effects of trajectory, guidance and environmental parameters under uncertainty
[AIAA PAPER 69-128] 06 p1018 A69-18107

Search theory application to planetary exploration overall strategy for improving landing site decisions
09 p1595 A69-21994

Mars planetary landing program schedule, COSPAR quarantine policy and biological losses from failures to collect data and from contamination
11 p1828 A69-25459

Spacecraft horizontal maneuvers in homogeneous gravitational field to achieve soft landing on planetary surface, including optimal liftoff and orbital transfer
13 p2356 A69-27685

Planetary landing trajectory optimum single pulse correction determined by considering sum of correcting and retro pulses minimum
15 p2691 A69-30738

Sterilized solid propellant motors applicability to planetary landing capsule spin stabilization
[AIAA PAPER 69-823] 16 p2840 A69-32675

Thermal stability elements in solid propellant liner insulation system for heat sterilized solid rocket motors used in unmanned planetary landers
[AIAA PAPER 69-437] 16 p2869 A69-32750

Mars lander thermal control system design parameters including environment, power duty cycle and lander size and weight
[AIAA PAPER 69-610] 17 p3072 A69-33274

Thermal design of landed vehicle on Mars surface, discussing instrument package covering inside surface coating and battery insulation
[AIAA PAPER 69-611] 17 p3049 A69-33295

Planetary lander model thermal design, analysis and testing, emphasizing lightweight multilayer insulation, discussing thermal/vacuum testing
[AIAA PAPER 69-612] 17 p3049 A69-33296

Mars landers impactable power subsystems, considering thermoelectric generators, batteries, conversion equipment, Mars environment, etc
23 p4069 A69-42253

PLANETARY LONGITUDE
U PLANET EPHEMERIDES

PLANETARY MAGNETIC FIELDS

Planetary magnetic field measurements near Venus, Mars, and moon, noting magnetic dipole comparison with earth and solar wind interactions
[AAS PAPER 68-186] 02 p0311 A69-11471

Jupiter radio physics, discussing prebiological phase, low IR and microwave radio temperature and magnetic field
02 p0330 A69-12805

Interplanetary magnetic field intensities, solar and stellar fields measured by Zeeman effect, discussing fields of Jupiter, Mars, Venus and moon
04 p0657 A69-14810

Particle flux and dose rates in Jupiter Van Allen belts based on assumed synchrotron radiation from trapped electrons in dipole magnetic field
[AIAA PAPER 69-18] 06 p0997 A69-18129

Magnetic field generation by dynamo action of liquid planetary cores, discussing evidence against magnetism around Mercury, Venus, Mars and Jupiter
07 p1210 A69-18371

Sun-like alternating field generators, discussing dynamo theory of stellar and planetary magnetic fields based on nonmirror symmetrical turbulent motion in conducting fluid
10 p1782 A69-23703

Model ion-exosphere for nonrotating planet with static dipole magnetic field generalized by permitting density and temperature variations over baropause
11 p1879 A69-25284

Soviet satellite and probe studies of earth, moon, Venus and Mars magnetic fields, noting automatic magnetometer
13 p2336 A69-27352

Time-invariant magnetic fields at planetary surfaces resulting from permanent magnetic bodies or distorting effect of inhomogeneous permeability on main field, computing components
20 p3609 A69-38105

Orbital Experimental Capsule /OEC/ as subsatellite concept for Martian fields and particles measurements, noting Voyager exploring vehicle applications
21 p3805 A69-39215

Dynamo action origin of stellar and planetary magnetic fields, considering turbulent helical motions of H convection zone of sun
22 p4011 A69-39998

PLANETARY MASS

Mass functions of real earth derived from satellite orbital perturbations
[UN PAPER 68-95385] 01 p0064 A69-10460

Pluto mass from observations of perturbation on motion of Neptune
02 p0315 A69-11808

Mass points substitution for mass of earth, giving gravitational effect equal to observed gravity values corrected for centrifugal acceleration
02 p0243 A69-12008

Anomalous gravitational geopotential as function of mass, discussing density anomalies in spherical shells for harmonics as obtained from satellite observations
02 p0244 A69-12178

Pluto mass from Neptune orbital longitude, comparing observations and theory
04 p0663 A69-15385

Venus research, discussing Mariner 5 and Venera 4 data, radar tracking, orbit, diameter, gravity, density distribution, etc
08 p1391 A69-20456

Earth center of mass determination from simultaneous satellite observations by photography or laser radar
12 p2068 A69-26425

Icarus radar and optical observations analyzed to verify general relativity predictions using Schwarzschild metrics and to estimate solar oblateness, Mercury mass, etc
13 p2350 A69-27823

Mercury, Venus, Mars, earth and lunar mass determinations by radio tracking and planetary radar systems
15 p2697 A69-31305

Mass of Jupiter system from motion of Doris, using variational equations for initial rectangular coordinates and velocities with respect to mass of Jupiter
16 p2863 A69-32403

Pluto mass and density accuracy, questioning values derived from Neptune observations
19 p3403 A69-35969

Jupiter mass determined by applying Cowell numerical integration to equations of motion for ninth satellite
21 p3795 A69-38468

Figure and inhomogeneities relationship for moon, Mercury, Venus, Mars and earth, discussing circular basins and mascons
21 p3803 A69-38980

Jupiter mass determined from observations of four minor planets perturbations
22 p4013 A69-40121

PLANETARY MOTION
U SOLAR ORBITS

PLANETARY NEBULAE

Planetary nebulae radio emission, observed with pencil beam of radio telescope, confirming thermal spectrum at radio frequencies
01 p0157 A69-11291

Spectral data for central stars of planetary nebulae from Lick 120-inch telescope, discussing stellar temperature and evolutionary track deduction
02 p0325 A69-12624

Spectrophotometric studies of planetary NGC 6543 gaseous nebula, measuring emission line intensities, electron density and temperature
[ARL-68-0200] 02 p0327 A69-12708

Planetary nebulae as possible low energy galactic X ray source
04 p0661 A69-15144

Electron temperatures and optical depths for planetary nebulae outer regions derived using radio spectra and Balmer line isophotes
06 p1009 A69-17962

Planetary nebulae NGC 7662 and IC 418 forbidden line spectra compared with computer model predictions, noting evidence for dynamical effects and filamentary structure
06 p1009 A69-17963

Planetary nebula IC 4642 spectral line intensities measured by photographic spectrophotometry compared to previous measurements, noting no evidence for changes
08 p1383 A69-19898

HF radio radiation from planetary nebulae
08 p1384 A69-20056

Absolute reddening curves derived for planetary nebulae by comparing radio continuum with hydrogen recombination lines
08 p1384 A69-20057

Southern planetary nebulae observed with Newtonian spectroscopic of Radcliffe Observatory in Pretoria, giving corrected data listing
08 p1392 A69-20561

Atmospheric structure and energy distribution of planetary nebulae central stars
08 p1393 A69-20570

Carbon 12 stars to simulate core evolution of planetary nebulae precursors, discussing nuclear shell burning
08 p1396 A69-20649

Photoelectric observations of nuclei of planetary nebulae He 1-5 and NGC 1514, noting changes in color and brightness characteristics
09 p1590 A69-21379

Absolute spectrophotometry of IR lines in planetary nebulae spectra determined by diffraction spectrograph
09 p1590 A69-21380

Detection of micron Ne emission line from planetary nebula IC 418 using IR spectrometer
09 p1591 A69-21452

Radiation fields of Lyman alpha to Lyman 10 calculated for model planetary nebulas with constant and exponential density distributions in spherical symmetry
09 p1604 A69-22407

Spectral lines relative intensities for bright medium excitation gaseous planetary nebula IC 3568, using photoelectric spectrum scanner and spectrophotometry technique
10 p1787 A69-24117

Optical depth at under 110 A due to continuous absorption by N, O and Ne ions estimated in high excitation planetary nebulae
10 p1790 A69-24140

Astronomical model indicating thin radial filaments in planetary nebula NGC 7293 formed by envelope density fluctuations attributed to ionizing and shock waves
11 p1955 A69-24384

Planetary nebulae radial velocities in large and small Magellanic Clouds compared with young objects rotational pattern and interstellar gas densities and velocities
12 p2155 A69-25891

Thermal and free-free emission from planetary nebulae based on graphite grain model, discussing IR fluxes
12 p2172 A69-27158

Polarization of continuum background of planetary nebulae in window in visible spectrum from scattering of nucleus star radiation by electron gas
13 p2339 A69-27567

Optical wavelength backscattering functions for nebulae in Pleiades cluster, noting color differences and surface brightness
13 p2340 A69-27577

Radio observations of planetary nebulae IC 418 and NGC 7027 at 9.5 mm indicating radio spectra thermal character, discussing electron temperature and density
13 p2343 A69-27625

Radiative and collisional ionization of H and He in planetary nebulae, discussing dielectronic recombination at high electron temperatures
14 p2518 A69-29133

Emission line fluxes of southern planetary nebulae in Magellanic Clouds and Galaxy measured photoelectrically, giving upper limit to H beta emission of Magellanic planetary
14 p2520 A69-29376

Radial velocities of planetary nebulae in Magellanic Clouds and Galaxy, discussing Population I and II kinematics
14 p2520 A69-29377

Planetary nebulae nuclei magnitudes in Magellanic Clouds and Galaxy measured photoelectrically, discussing early evolution
14 p2520 A69-29378

Ionization stratification and chemical abundances in planetary nebula NGC 7662, discussing density fluctuations effect on N II and O II lines
18 p3191 A69-34294

Pure carbon 12 stellar models evolution studied to determine production mechanism of planetary nebulae, discussing shell burning and surface layers unbinding role
18 p3191 A69-34298

Photoelectric observations of nuclei of planetary nebulae He 1-5 and NGC 1514, noting changes in color and brightness characteristics

18 p3198 A69-34767

Absolute spectrophotometry of IR lines in planetary nebulae spectra determined by diffraction spectrograph

18 p3198 A69-34768

Radio emission attributed to galactic nebula NGC 6857, suggesting origin in high density H II regions excited by OB star clusters

18 p3202 A69-35209

Collisional excitation of forbidden lines in planetary nebulae from 5537/5517 intensity ratio measurements, noting density and intensity relationship

19 p3422 A69-36221

Monochromatic energy flux measurement in H and forbidden lines of planetary nebulae indicating ionization level and optical depth

19 p3423 A69-36223

Electron density and electron temperatures determination in planetary nebulae, using maximum number of observed forbidden transitions

19 p3423 A69-36224

Physical characteristics of young planetary nebulae and nuclei, discussing classification of objects II 4997, M 3-27 and M 1-2

19 p3423 A69-36226

Statistical relation between expansion velocities and radii of planetary nebulae due to Lyman- α and diffuse Lyman- α radiation

19 p3426 A69-36575

Planetary nebulae observations, describing radio spectra characteristics, electron temperature measurement, hydrogen line emission, etc

20 p3598 A69-37425

Planetary nebulae imaging stratification effects on structural difference studies by slit and slitless spectrographs and narrow band photography

21 p3817 A69-39785

Photoelectric measurements of emission line intensities for low density planetary nebula with moderate excitation located near north galactic pole, deriving abundances

24 p4376 A69-42662

Tabulation of photographic and photoelectric spectrophotometrically obtained relative spectral line intensities for planetary nebula IC 5217, discussing interstellar absorption

24 p4376 A69-42663

Nebulosity around FG Sagittae for origin and evolution of planetary nebulae, suggesting ejection of nebular shell

24 p4381 A69-42887

Astronomical model indicating thin radial filaments in planetary nebula NGC 7293 formed by envelope density fluctuations attributed to ionizing and shock waves

24 p4390 A69-43774

PLANETARY ORBITS

NT SWINGBY TECHNIQUE

Existence of periodic solutions by Whittaker criterion to equations describing motion of satellite of spheroidal planet in planetocentric coordinate system

02 p0317 A69-11959

Equilibrium orientations of orbiting gyrostats, giving spectrum of solutions for bodies of varied shape and internal rotor angular momentum

03 p0522 A69-14246

Kepler third law application to radar determinations of astronomical unit of length in general relativity

04 p0657 A69-14698

Idealized point mass motion in axisymmetric gravitational field, discussing orbital stability about oblate planet

04 p0658 A69-14887

Soviet book on artificial satellite motion in noncentral gravitational field, discussing celestial axisymmetric planetary orbits, stationary centers, three body problem, etc

04 p0659 A69-15027

Pluto mass from Neptune orbital longitude, comparing observations and theory

04 p0663 A69-15385

Direct light pressure effect on evolution of limited planetocentric orbits of small bodies, noting longitudes of ascending node and pericenter

05 p0823 A69-16043

Approximate solution for determining satellite motion around axisymmetric planet

06 p1005 A69-17563

Radio occultation measurements of planetary atmospheres and ionospheres from orbiting pair

[AIAA PAPER 69-53] 06 p1011 A69-18104

Commensurability among pairs of mean motions of natural satellites of major planets and hypothesis of tidal evolution of satellite systems

07 p1223 A69-19638

Commensurability among pairs of mean motions of satellites of major planets and power law relation for orbital periods of satellites

07 p1224 A69-19639

Numerical analysis of periodic solutions of restricted three body problem in sun-Jupiter system, noting genealogy of periodic orbits

08 p1382 A69-19874

Canonical equations of planet satellite intermediate orbits using harmonics of gravitational potential

09 p1589 A69-21374

Motion of satellite of very oblate planet, investigating axisymmetric potential

10 p1774 A69-22969

Systematic errors caused by planet asphericity in measurements of orientation and motion parameters of orbiting object compensated by scanning navigation system

10 p1693 A69-23320

Orbits of asteroids surrounding commensurabilities with Jupiter, discussing theory for origin of Kirkwood gaps

10 p1778 A69-23604

Relation between planets axial moments and protoplanetary particles orbital eccentricity as explanation of outward winding of planets

12 p2154 A69-25818

Plane planetary orbits construction extended to nearly circular and quasi-plane orbits by generalizing perturbations method to problems in space

15 p2690 A69-30622

Outer planets exploration during 1976-80 period of unique solar system alignment

16 p2854 A69-31630

Simplified method for derivation of universal gravitation law from Kepler law of planetary orbits

16 p2813 A69-32481

Distributions of close planet-comet encounters for various orbital elements, calculating trajectory by conic matching

18 p3195 A69-34433

Canonical equations of planet satellite intermediate orbits using harmonics of gravitational potential

18 p3198 A69-34762

Optimal transfers between Keplerian orbits for time free case, considering hyperbolas, ellipses external to and intersecting attracting planet

19 p3399 A69-35669

Interplanetary swingby trajectory correcting maneuvers for space vehicles return to earth after planet orbiting with emphasis on singular points

19 p3427 A69-36613

Jupiter tenth satellite reobserved, discussing calculations and computer techniques for determining orbit

[AAS PAPER 68-140] 20 p3595 A69-37194

Direct light pressure effect on evolution of limited planetocentric orbits of small bodies, noting longitudes of ascending node and pericenter

20 p3606 A69-37952

Planet Mars opposition to earth, Jupiter and Saturn, including table showing Mars-Jupiter conjunctions

21 p3801 A69-38788

Reconnaissance missions for outer planets exploration, discussing spacecraft design constraints, multiple planet fly-by, planetary orbiter, etc

[AAS PAPER 69-291] 24 p4381 A69-42864

PLANETARY QUARANTINE

Mars planetary landing program schedule, COSPAR quarantine policy and biological losses from failures to collect data and from contamination

11 p1828 A69-25459

Sterilization assembly development laboratory /SADL/ quality assurance program for microbiological monitoring according to NASA planetary quarantine requirements

15 p2559 A69-31123

Microbiology quality assurance program for planetary mission, considering spacecraft sterilization during fabrication, test and launch site activities

15 p2559 A69-31124

Planetary quarantine constraints by NASA insuring low contamination probability from extraterrestrial biological exploration, giving contamination probability equations and sterilization procedures

16 p2746 A69-32435

PLANETARY RADIATION

Two element interferometer observing Saturn, Uranus and Neptune at 3.12 cm, determining equivalent black body disk temperature

01 p0148 A69-10052

Romanova method for solution of scalar equation of radiative transfer in plane parallel atmosphere

02 p0319 A69-12106

Brightness temperature maps for Jovian thermal radiation obtained through 8-14 micron window of atmosphere

02 p0309 A69-12715

Jupiter, Venus and Mars 8.6 mm radio emission, obtaining average disk brightness temperatures

02 p0327 A69-12716

Working breadboard model of planet tracker under various illuminating conditions, discussing hardware and closed loop tracking error analysis accounting for signal to noise effects

03 p0463 A69-13214

Polarized radio emission from Jupiter, giving hypothesis of radiation belts deformation by solar wind

03 p0512 A69-13703

Venus brightness temperature between 0.75 and 1.65 cm from radio emission measurements, taking into account water vapor in Venus atmosphere

04 p0658 A69-14960

Photoelectric photometry of Mercury, Venus, Mars, Jupiter and Saturn /1963-1965/, determining phase curves and monochromatic albedos

04 p0663 A69-15383

Non-Io controlled fifth source of Jupiter decametric radiation from/near visible planetary disk

05 p0813 A69-15604

IR astronomy with ground based instruments noting Mars and Venus spectra, Jovian disk scans, solar radiometry, IR stars, quasars and galaxies

05 p0821 A69-15842

Space radio astronomy techniques for problems in galactic radio emission, solar studies and planetary observations

05 p0821 A69-15844

Jupiter microwave radiation flux density at 81 MHz, noting spectrum of microwave emission

05 p0827 A69-16506

Groups of drifting lanes of emission in fine structure of dynamic spectra of Jupiter decasecond decametric radiation bursts

06 p1008 A69-17958

Microwaves from celestial objects noting radio emission from sun, moon and Jupiter, cosmic fireball and pulsars

08 p1407 A69-21125

Radiometric observations of Venus brightness temperature variation used to determine phase effect at 8.6 mm wavelength

10 p1773 A69-22959

Venus and Jupiter low resolution UV spectra obtained with servocontrolled star tracking telescope in Acrobee rocket, noting Lyman alpha radiation characteristics

[JHU-TR-15] 10 p1788 A69-24121

Brightness temperatures and spectra of Venus, Mars, Jupiter and moon measured from 8 to 14 microns by reflector and prismatic spectrometer

11 p1956 A69-24395

Venus and Jupiter brightness temperature and radio emission at 2.25 and 8 mm wavelengths observed with radio telescope

11 p1956 A69-24396

Atmospheric scintillation effect on planetary brightness distribution over disk from photometric measurements

11 p1960 A69-24729

Venus brightness temperatures vs phase angle to define spectra of day and night face at short wavelengths, using model atmosphere

12 p2153 A69-25806

Flux collectors and field imagers for IR astronomy, discussing design, construction and dimensions

13 p2239 A69-27605

Jupiter decametric radio emission periodicity attributed to undiscovered satellite in unstable orbit, discussing application to satellite discovery

13 p2343 A69-27622

Linear polarization measurements at 6 cm, determining rotation period associated with Jupiter cm radiation

13 p2343 A69-27623

Planet Mars stellar magnitude found dependent on processes occurring in atmosphere and at surface

15 p2689 A69-30565

Balloon-borne UV polarimetry of stars and planets, studying linear polarization between 2000 and 3000 Å

15 p2616 A69-31380

Venus microwave spectrum analyzed by comparing various thermal and nonthermal emission models, discussing surface temperature and atmospheric composition

16 p2853 A69-31597

Visual ashen light observation on Venus possibly attributable to solar particle bombardment from dark side emission detection by spectroscopic and photometric studies

16 p2861 A69-32300

Heliosphere boundary location significance for Jovian magnetosphere configuration, considering inverse correlation between sunspot number and Jovian decametric radio emission

17 p3033 A69-33379

Saturn emission peak and flux density at 408 MHz determined by cross telescope, discussing mechanism for enhanced radiation at long wavelengths

17 p3041 A69-33813

Venus brightness and polarization distributions measurement at centimeter wavelengths using two element interferometer, suggesting Venus atmosphere as main source of radiation

18 p3191 A69-34302

Jovian radio sources intermittency, recording difficulties, longitudinal drift and theories concerning origin

18 p3196 A69-34690

Venus brightness temperature between 0.75 and 1.65 cm from radio emission measurements, taking into account water vapor in Venus atmosphere

18 p3197 A69-34723

Crab Nebula radio brightness at 2.16 and 8.2 mm measured and compared to Jupiter flux density

19 p3428 A69-36875

Mayeda flare observed on Mars on 4 June 1937, suggesting oriented reflection of solar rays from ice crystals cloud or Martian surface feature

20 p5508 A69-38049

Polarization ellipse orientation at source from Faraday fringes on Jupiter decametric radio bursts swept frequency records

20 p3594 A69-38169

Orbital Experimental Capsule /OEC/ as subsatellite concept for Martian fields and particles measurements, noting Voyager exploring vehicle applications

21 p3805 A69-39215

Stellar scintillation spectra theory extended to rectangular apertures, generalizing to planetary scintillation and effects of diffraction, atmospheric dispersion and seeing

21 p3773 A69-39771

Planetary spectroscopy with McDonald 107 inch telescope, discussing role of molecular and atomic absorption lines, line broadening, Doppler shifts and Rayleigh criterion

21 p3727 A69-39786

Lightcurves for 624 Hektor with Radcliffe, Kitt Peak, Catalina and Cerro Tololo reflectors, noting asteroid shape and rotational axis

22 p4013 A69-40124

Jupiter spectrum observations in 2.8-14 micron range, describing absorption strength and brightness temperature, basing analysis on ammonia, methane and hydrogen absorption

22 p4028 A69-40662

Spectral reflectivity curves for Mars light and dark areas and seasonal changes of dark area simulated in laboratory

23 p4209 A69-41319

Brightness temperatures and spectra of Venus, Mars, Jupiter and moon measured from 8 to 14 microns by reflector and prismatic spectrometer

24 p4390 A69-43785

Venus and Jupiter brightness temperature and radio emission at 2.25 and 8 mm wavelengths observed with radio telescope

24 p4390 A69-43786

PLANETARY ROTATION

Atmospheric circulation on rotating and nonrotating planets with shallow atmospheres applied to Mars and Venus atmospheres

02 p0320 A69-12110

Mercury rotation period determination by surface photography, correcting earlier interpretation

03 p0517 A69-14233

Light curves for Vesta compared and rotation derived from aspect change effect on rotational period

04 p0657 A69-14677

Selenographic and celestial selenocentric coordinate systems, noting precession and nutation of lunar rotation axis

04 p0662 A69-15250

Resonance relations of rotational and orbital frequencies of solar system planets and satellites estimated for statistical significance

10 p1771 A69-22852

Model ion-exosphere for nonrotating planet with static dipole magnetic field generalized by permitting density and temperature variations over baropause

11 p1879 A69-25284

Relation between planets axial moments and protoplanetary particles orbital eccentricity as explanation of outward winding of planets

12 p2154 A69-25818

Theory for describing rotating fluid planets external geometry in state of hydrostatic equilibrium, noting role of equipotential surfaces

20 p3594 A69-37077

Earth polar wanderings attributed to rotation axis angular displacements generated by density redistribution on geologic time scale

20 p3535 A69-38192

Resonant spin and anomalous rotation of Mercury, analyzing influence of tidal degradation and permanent deformation of planet

21 p3814 A69-39568

PLANETARY SPACE FLIGHT

U INTERPLANETARY FLIGHT

PLANETARY SPACECRAFT

U INTERPLANETARY SPACECRAFT

PLANETARY SURFACES

NT MARS SURFACE

Orbital spectroscopic and radiometric IR experiments, considering moon and Mars surface [AAS PAPER 68-196]

02 p0312 A69-11474

Mercury radio emission phase dependence, discussing brightness temperature value approximation and surface layer properties

02 p0314 A69-11640

Unmanned planetary exploration using Mariner class spacecraft for solar system and life origin

02 p0334 A69-12302

Hard space suit for use on planetary surfaces and extravehicular activity, discussing design, fabrication and mobility

03 p0379 A69-12993

Photometric-polarimetric observations of planetary surfaces, discussing geological environment interpretation and spacecraft reconnaissance system mission planning

03 p0421 A69-13394

Satellite high resolution radar mapping of planets, discussing synthetic aperture and linear FM transmission radar techniques

03 p0430 A69-13399

Changes in bands of Jupiter /1962-1965/ from astronomical synoptic mapping program, tabulating overall and chromatic intensities and longitudinal velocities

03 p0512 A69-13696

Mercury rotation period determination by surface photography, correcting earlier interpretation

03 p0517 A69-14233

Ground coverage of oblate planets by spin stabilized satellites, determining ground areas visible to satellite by solution of quadratic equations

03 p0522 A69-14244

Optimal circular satellite orbits for planetary surface mapping mission minimizing overlap

03 p0518 A69-14247

Diffusive scattering effects on planetary surface reflection coefficient determined by radar observations

04 p0662 A69-15245

Predictive display technique for remote manual control of roving lunar and planetary surface vehicles

06 p0928 A69-17925

Radiating surface temperature and total atmospheric moisture content determinations based on meteorological earth satellite measurements of outgoing radiation in IR

06 p0952 A69-17988

Mars imaging mission and astrodynamic interaction, discussing arrival geometry and orbit size effects [AIAA PAPER 69-127]

06 p1011 A69-18169

Optical processing of planetary radar data for range Doppler image generation

08 p1270 A69-19816

Mars and Earth atmospheric carbon dioxide simulation and spectroscopic measurement for developing planetary surface pressure estimating procedures from IR transmission measurements

08 p1354 A69-20151

Bioorganic comparative analysis of desert soils, Precambrian shales and meteorites by automated pyrolysis-gas chromatography-mass spectrometry system for future Mars soil analysis [JPL-TR-32-1368]

11 p1832 A69-25640

Mars higher atmospheric transparency and changes in surface colors

12 p2154 A69-25823

Limits for Martian surface materials established by comparing visible and IR spectra with laboratory spectra

12 p2156 A69-26225

Photometric and polarimetric properties of Mars, discussing powder covering, chemical composition and particle size of bright and dark areas and blue haze

12 p2171 A69-27145

Reflected and absorbed solar radiation by planetary atmosphere and surface determined as function of atmosphere and surface optical properties

15 p2689 A69-30564

Flow over uniformly rough surface in planetary boundary layer from mixing length wind spiral model, using surface shear stress and wind direction data

17 p2997 A69-33153

Scale determination in spatial direction networks, using polygonal transverse measured along continental surfaces and Secor method over water surfaces

18 p3131 A69-35196

Depth distribution of primary cosmic radiation fluxes and secondary nuclear-active particles in stone meteorites and surface layer of planets, moon and asteroids

19 p3410 A69-36092

Radar astronomy, discussing planetary surfaces study techniques, target/signal interactions, planet cross sections, delay and Doppler spectra

20 p3491 A69-37650

Time-invariant magnetic fields at planetary surfaces resulting from permanent magnetic bodies or distorting effect of inhomogeneous permeability on main field, computing components

20 p3609 A69-38105

Saturn surface spectrum near ring shadow examined for water vapor content in ring and greenhouse effect on surface

20 p3616 A69-38305

Figure and inhomogeneities relationship for moon, Mercury, Venus, Mars and earth, discussing circular basins and mascons

21 p3803 A69-38980

Surface reflectivity mapping of Venus by radar interferometry at 3.8 cm, noting low reflectivity circular regions

21 p3806 A69-39331

Orbit selection rules for planetary cartographic spacecraft derived from relations connecting camera angle, view field and imaging resolution [AIAA PAPER 69-879]

21 p3763 A69-39405

Radar reflection techniques for planetary surface studies, considering surface properties effects on reflectivity and reflected wave characteristics, instrumentation and data for moon and planets

21 p3811 A69-39509

Martian atmosphere circulation compared to terrestrial, considering absence of oceans, radiative coupling and planetary scale motions

21 p3814 A69-39569

Rocket UV spectra indicating Venus atmosphere weak absorption and low ozone abundance and possible Jupiter surface depressions

22 p4028 A69-40661

Statistical model of cratered planetary surface slopes and elevation applied to radio wave scattering by moon and Venus

23 p4209 A69-41322

Mars landing site topography reconstructed via stereoscopic pictures returned by surface-based imaging systems

23 p4164 A69-41618

Bulk, selective particulate and hard rock samplers for landed extraterrestrial geological and biological instruments performing on-site analysis

23 p4146 A69-41620

Sequential analyses of planetary surface sample for extraterrestrial life detection, discussing chemistry, morphology, growth and metabolism for life attributes

23 p4213 A69-41623

PLANETARY TEMPERATURE

Photovoltaic properties of CdS thin film solar cells and silicon cells at Jupiter temperature and solar intensity

03 p0368 A69-13076

Planet Mercury rotation, showing reminiscence of apparent path of sun to Ptolemaic concept of planetary system

03 p0509 A69-13368

Scaled solar and gray-body temperature distribution models compared to determine stellar atmosphere

04 p0653 A69-14626

Venus brightness temperature between 0.75 and 1.65 cm from radio emission measurements, taking into account water vapor in Venus atmosphere

04 p0658 A69-14960

Atmospheric models for exospheric temperatures of Mars and Venus based on photoionization heating efficiency 12 p2155 A69-26020

Two channel IR radiometer for 1969 Mariner mission measuring equivalent black body surface temperature 17 p2972 A69-33085

Mars surface temperature calculated by applying Humphrey formula for planetary radiation energy, finding mean annual values of temperature for different albedo 17 p3034 A69-33412

Subsurface Martian temperature from sinusoidal temperature variation theory for semiinfinite homogeneous medium, plotting amplitude, mean surface and diurnal soil temperature curves 17 p3034 A69-33413

Mars internal structure and composition modeling, considering core, mantle and temperature via earth analogy and Mariner 4 data 17 p3037 A69-33652

Radio telescope observations at 11.13 cm for polarized E vector intensities of Saturn and disk temperature of Uranus and Neptune 17 p3039 A69-33731

Venus brightness temperature between 0.75 and 1.65 cm from radio emission measurements, taking into account water vapor in Venus atmosphere 18 p3197 A69-34723

Venusian atmospheric features obtained from Venus 5 and 6 and Mariner 5 observations, indicating extremely high temperatures and pressures 19 p3401 A69-35887

Book on thermal processes of earth and moon covering heat generation and transfer, internal temperatures, gravitational energy, etc 19 p3401 A69-35887

Mercury and Venus thermal histories based on analogy to earth models 20 p3597 A69-37333

Optical parameters of Martian surface and temperature, discussing brightness distribution along diameter in red spectral region, based on photoelectric cross sections 20 p3608 A69-38050

Earth early thermal history with core formation before emplacement of earliest known rock possessing remanent magnetism 22 p3936 A69-40136

Solid state chemical heat sources aboard unmanned planetary landing vehicles to maintain batteries and experiments operability during cold planetary nights 23 p4070 A69-42275

Mars thermal energy emission measurement by Mariner 1969 IR radiometer, indicating frozen carbon dioxide cap and minimum temperature 24 p4384 A69-43196

PLANETOCENTRIC COORDINATES

NT GEOCENTRIC COORDINATES

Existence of periodic solutions by Whittaker criterion to equations describing motion of satellite of spheroidal planet in planetocentric coordinate system 02 p0317 A69-11959

Selenographic and celestial selenocentric coordinate systems, noting precession and nutation of lunar rotation axis 04 p0662 A69-15250

Direct light pressure effect on evolution of limited planetocentric orbits of small bodies, noting longitudes of ascending node and pericenter 05 p0823 A69-16043

Direct light pressure effect on evolution of limited planetocentric orbits of small bodies, noting longitudes of ascending node and pericenter 20 p3606 A69-37952

PLANETOLOGY

Space systems use for planetary geology and geophysics - Conference, Boston, May 1967 03 p0509 A69-13390

French atlas of planets covering ancient and modern planetary system and discoveries, physical nature and movement, etc 03 p0513 A69-13778

Communications of lunar and planetary laboratory, Volume 7, covering lunar radiation, lunar craters, Vesta rotation, etc 04 p0655 A69-14668

Magnetic field generation by dynamo action of liquid planetary cores, discussing evidence against magnetism around Mercury, Venus, Mars and Jupiter 07 p1210 A69-18371

Permissible nonthermal convection modes in planetary interiors derived from conservation equations for

self gravitating homogeneous nonrotating compressible fluid spheres 07 p1213 A69-18611

Convection in planetary interiors produced by combined thermal and nonthermal mechanisms, noting self gravitating homogeneous nonrotating compressible fluid spheres 07 p1214 A69-18613

Communications of Lunar and Planetary Laboratory, Volume 7 07 p1225 A69-19769

Martian structure theory, comparing mathematical model based on earth long term evolution and ad hoc models 08 p1387 A69-20092

Earth and planets shallow seas tidal dissipation reflected in Q values, noting larger planet pressure effect 08 p1393 A69-20581

Radar probing of solar system noting contributions to knowledge on planets 09 p1595 A69-21765

Collection of Soviet papers on physics of moon and planets covering results of lunar, Mars and Jupiter photometric studies 11 p1959 A69-24723

Dependence of convection in planetary interiors upon magnitude of Rayleigh number for rigid and free surfaces 12 p2155 A69-26208

Planetary mantles thermal and nonthermal convection model, solving sphere density variations and radial velocity components due to internal time-independent motions 13 p2344 A69-27644

Planetary free vibrations, discussing models for earth, moon, Venus and Mars, rotation and ellipticity effects and measurement on seismometers, gravimeters and magnetometers 17 p3031 A69-33097

Mars 1969 opposition observations, discussing extremes in north and south hemispherical polar cap behavior, frosty deposit colorings and polar vapor/clouds 17 p3043 A69-34141

Book on thermal processes of earth and moon covering heat generation and transfer, internal temperatures, gravitational energy, etc 19 p3401 A69-35887

Boundary conditions for theory of solar system origin, discussing planetary atmospheres, surfaces, magnetic fields, composition and early solar wind 19 p3419 A69-36209

Planetary interiors from geophysical viewpoint emphasizing earth data 21 p3811 A69-39508

Earth temperature distribution using various models, noting excess of total heat production in interior vs heat flow during planet history 21 p3718 A69-39732

Physics applications to earth and planetary interiors - NATO Conference, Newcastle-upon-Tyne, England, March-April 1967 22 p4015 A69-40172

Physical and life supporting properties of hypothetical Martian biosphere, considering organism adaptation theories 22 p3876 A69-40271

Planetary exploration and NASA program objectives [AAS PAPER 69-286] 24 p4379 A69-42810

Solar activity empirical correlation with planetary positions used for long range forecast of solar flare proton events [AAS PAPER 69-069] 24 p4366 A69-42880

PLANETS

NT EARTH [PLANET]
NT JUPITER [PLANET]
NT MARS [PLANET]
NT MERCURY [PLANET]
NT NEPTUNE [PLANET]
NT PLUTO [PLANET]
NT SATURN [PLANET]
NT URANUS [PLANET]
NT VENUS [PLANET]

French atlas of planets covering ancient and modern planetary system and discoveries, physical nature and movement, etc 03 p0513 A69-13778

Capture of comets by large planets 03 p0517 A69-14128

Angular momenta of stars, planets and asteroids, plot log of angular momentum per unit mass against log of mass of astronomical object 09 p1608 A69-22716

Radioactivity levels estimation at surface and in bulk of solar system planets caused by galactic and solar cosmic rays 10 p1756 A69-22813

Total planet interaction energy of comets passing through solar system, showing non-Gaussian shape of distribution 10 p1774 A69-22970

Monograph on world of planets covering solar planetary system, atmospheres, water, seasons, organic life, etc 11 p1958 A69-24666

Quasi-stochastic nonlinear one dimensional oscillations in periodically disturbed field applied to celestial mechanics of planetoids 12 p2130 A69-26373

Mass distribution for bodies fallen on planets during formation estimated from present inclination of planetary axes of rotation, using limit theorems of probability theory 13 p2345 A69-27652

NASA planetary program, discussing Mars, Jupiter, Mercury, Venus and Saturn missions 15 p2723 A69-31318

Tabulated results of photographic plate measurements of minor planets positions at Leiden observatory 1938-1964/ 20 p3605 A69-37789

Probability of biological development leading to human life on another planet 21 p3652 A69-38786

Solar activity empirical correlation with planetary positions used for long range forecast of solar flare proton events [AAS PAPER 69-069] 24 p4366 A69-42880

PLANFORMS

NT CARET WINGS
NT DELTA WINGS
NT RECTANGULAR PANELS
NT RECTANGULAR PLANFORMS
NT RECTANGULAR PLATES
NT SWEPTBACK TAIL SURFACES
NT TRAPEZOIDAL WINGS
NT VARIABLE SWEEP WINGS
NT WING PLANFORMS

Bending of freely supported plates of polygonal planforms under transverse load with aid of R functions 02 p0341 A69-12140

Optimum planform stabilizer selection for damping of rotational motion and elastic torsional stresses of aircraft fuselage about longitudinal axis 11 p1966 A69-25327

PLANIMETRY

U AREA
U DIMENSIONAL MEASUREMENT

PLANNING

NT AIRPORT PLANNING

Future launch vehicle programs for automated space missions, discussing higher launch velocities and economics [AIAA PAPER 68-447] 09 p1610 A69-21983

Independent operations optimum performing sequence determined for parallel machines differing in technological characteristics and with assigned time using algorithm 16 p2763 A69-31626

PLANOTRONS

NT BACKWARD WAVE TUBES
NT CARCINOTRONS
NT CATHODE RAY TUBES
NT CESIUM DIODES
NT COLD CATHODE TUBES
NT GAS DISCHARGE TUBES
NT HELITRONS
NT IMAGE ORTHICONS
NT IMAGE TUBES
NT KLYSTRONS
NT PHOTOMULTIPLIER TUBES
NT PHOTOTUBES
NT PICTURE TUBES
NT THERMIONIC DIODES
NT THYRATRONS
NT TRAVELING WAVE TUBES
NT VIDICONS

Amplitrans use as broadband microwave amplifiers in high power radar systems with frequency agility, involving modified high vacuum tube modulator and modulator circuit 23 p4135 A69-41384

PLANTS [BOTANY]

NT ALGAE
NT ANABAENA
NT AUTOTROPHS
NT AZOTOBACTER
NT BACILLUS
NT BACTERIA
NT BLUE GREEN ALGAE

NT CHLORELLA
 NT ESCHERICHIA
 NT EUGLENA
 NT FOLIAGE
 NT FUNGI
 NT HYDROGENOMONAS
 NT LEAVES
 NT LICHENS
 NT MICROSPORES
 NT NEUROSPORA
 NT NITROBACTER
 NT PARASITES
 NT PSEUDOMONAS
 NT SCENEDESMUS
 NT SPORES
 NT STEAROTHERMOPHILUS
 NT TRADESCANTIA
 NT TREES [PLANTS]
 NT WOOD
 NT YEAST

Allelopathy, discussing application to gas liberating activity of edible plants as ingredients of space flight life support systems

02 p0198 A69-11509

Space flight factors, ionizing radiation and combined effects on vitamin C content in onion bulbs

05 p0708 A69-16510

Plants growth from seeds exposed to space environment onboard Cosmos 110 biological satellite compared with control plants

07 p1064 A69-18972

Change in content of dry matter, sugars and ascorbic acid in plants after action of space flight factors on seeds of these plants

10 p1645 A69-23495

Light interaction with stacked leaves and plant canopy, determining reflectance and transmittance

12 p2097 A69-26985

Plant and soil thermal behavior for various conditions of crop species, plant spacing, tillage, irrigation and aerial thermal scanner imagery

12 p2075 A69-26989

Gravity effects on plant growth, discussing horizontal clinostat experiments and auxin transport mechanism

15 p2555 A69-30470

Dynamic differential thermal analysis of dried plant and animal specimens and related substances yielding discrete decomposition peaks of exothermic type

15 p2555 A69-31000

Higher plants utilization as nutrition source in space missions, comparing weight requirements for cultivation equipment and food storage

15 p2560 A69-31408

Carrot plants growing during 374 days in conveyer type aeroponic assembly, noting yield and morphological features

17 p2912 A69-32943

Lignin presence in New Zealand moss gametophytes observed for characteristic color reaction and UV spectra, noting contrast with north temperate species

17 p2912 A69-34176

Space flight factors, ionizing radiation and combined effects on vitamin C content in onion bulbs

18 p3095 A69-34729

Radiation effects on microorganisms and plants during space flight on Biosatellite 2 and Gemini 11 missions

20 p3476 A69-37617

Geotropic response reciprocity in oat seedlings grown in two axis clinostat compared with acceleration constraints of biosatellites, considering imposition of centrifugal force

20 p3477 A69-37620

Plants growth from seeds exposed to space environment onboard Cosmos 110 biological satellite compared with control plants

20 p3479 A69-38220

Paleozoic plant fossils carbohydrate content

21 p3669 A69-39333

Carbohydrate analyses of upper carboniferous plant fossils in England, noting monosaccharides separation

21 p3661 A69-39534

Amino acid components in paleozoic plant fossils and rock samples noting glycine, serine and glutamic acid

21 p3662 A69-39535

Photosynthesis enhancement in seaweed after alternate exposure to gas laser and tungsten lamp white light passed through IR narrow band filter

24 p4270 A69-42580

PLANTS [INDUSTRIES]
 U INDUSTRIAL PLANTS

PLASMA ACCELERATION

Plasma slab acceleration along magnetic dipole guard field null, noting lack of equilibrium and no decrease of plasma losses

03 p0475 A69-13157

Space charge plasma acceleration in axially nonuniform magnetic field

03 p0477 A69-13760

Nonlinear mechanism for solar surge involving rapid acceleration of high electrical conductivity and macroscopic dimension plasma regions

03 p0516 A69-14044

Nonmagnetic plasma deceleration in quasi-stationary magnetic field with coaxial injector and barrier field

03 p0481 A69-14212

Cascade acceleration of plasma by two stage device noting plasma dispersion, plasma losses and highest final plasma velocity

03 p0482 A69-14215

Highly ionized plasma acceleration by intrinsic radiation achieved by deep cooling of free electrons

07 p1195 A69-19595

High energy particles obtained by accelerating plasma with frozen-in magnetic field to relativistic velocities during scattering of fast electron beam

08 p1358 A69-19805

Plasma acceleration by induced Hall currents, discussing Hall-to-current ratio maximum at critical magnetic field

[AIAA PAPER 69-280] 09 p1562 A69-21228

Quasi-steady state plasma acceleration in coaxial electrode geometry during synchronized application of tailored pulses of mass flow and current

[AIAA PAPER 69-267] 09 p1563 A69-21234

MPD plasma acceleration in West Germany, discussing Hall acceleration, electrodeless plasma acceleration by electromagnetic waves and space charge neutralized Hall ion thruster

[AIAA PAPER 69-279] 09 p1564 A69-21238

Plasma acceleration by pulsed electromagnetic traveling wave, discussing stable column formation and acceleration loss processes

09 p1544 A69-21301

Steady state spherically symmetric model for solar plasma acceleration with distance, showing essential role of viscosity

10 p1769 A69-23899

Mass transfer due to plasma recombination, ambipolar diffusion and electrode erosion and resistance forces effects on electrodynamic accelerated plasma

13 p2315 A69-28555

Energy relations and conversion for electrodynamic plasma acceleration with allowance for mass transfer processes resulting from recombination, diffusion and electrode erosion

15 p2664 A69-31176

Fringing effects on electric efficiency variation with slip for cylindrical induction MHD device operable as accelerator, generator or Joule heater

[AIAA PAPER 67-714] 16 p2736 A69-32152

Plasma acceleration away from rotating magnetized astrophysical objects analyzed and applied to pulsar NP 0532 for magnetic moment and mass loss rate calculations

20 p3598 A69-37419

Astrophysical ions acceleration model based on magnetic field annihilation theory

22 p3987 A69-41002

Conical induction plasma accelerator design for studying acceleration process characteristics

24 p4357 A69-43468

PLASMA ACCELERATORS

NT COAXIAL PLASMA ACCELERATORS

Steady one dimensional motion of current sheets in plasma accelerators, noting condition of zero initial conductivity

01 p0133 A69-11220

Cascade acceleration of plasma by two stage device noting plasma dispersion, plasma losses and highest final plasma velocity

03 p0482 A69-14215

Plasma rotation in current layer of pulsed inductive accelerator

[AIAA PAPER 68-86] 04 p0635 A69-14702

Energy transfer from pulse network to mass associated with propagating current sheet in linear pinch discharge, discussing pulsed plasma accelerator efficiency

[AIAA PAPER 69-113] 06 p0971 A69-18123

Current sheet pattern and gas flow stabilization in pulsed plasma accelerators

[AIAA PAPER 69-112] 06 p0971 A69-18140

Electromagnetic ion acceleration in steady electric and magnetic fields chosen to match fields of Alkali Plasma Hall Accelerator /ALPHA/

[AIAA PAPER 69-111] 06 p0985 A69-18175

Particle free path estimates for axisymmetric high specific impulse plasma accelerators, discussing collisionless plasma simulated by computer

[AIAA PAPER 69-278] 09 p1563 A69-21233

Experimental and theoretical investigation of mass injection effect on high current MPD arc

[AIAA PAPER 69-266] 09 p1564 A69-21242

Near cathode magnetic field effect on instability in linear Hall current accelerators, using geometry of field extending from anode to cathode region

[AIAA PAPER 69-381] 09 p1568 A69-21731

Hall type electromagnetic plasma accelerator, with thrust affected only by Lorentz forces in external magnetic field, compared to pure Hall accelerator

11 p1866 A69-25214

Erosion type plasma accelerator using inductive energy storage compared with capacitive energy storage

13 p2311 A69-28110

Tangential drag measurements at electrodes of arc in plasma accelerator, ion current partitioning at cathode and electrode damage

[AIAA PAPER 67-657] 13 p2312 A69-28219

Plasma jets from MPD accelerators, analyzing swirl, entrainment and pressure distribution using gasdynamic probes

13 p2313 A69-28242

Passive electric microwave probe with balancing capacitance for studying waveguide fields at high microwave power levels in radiative plasma accelerators

14 p2498 A69-29807

Hall ion thruster prime propulsion system, considering low and high voltage mode in plasma source I-V characteristics

17 p3019 A69-33338

Self induction of conical electrode type plasma accelerator with and without allowance for magnetic scattering field, investigating acceleration process

19 p3379 A69-35821

Drift effect on plasma motion in high current pulsed plasma accelerators of Marshall type, calculating current variations, voltage, particle velocity, efficiency and impulse

21 p3778 A69-39548

Conical induction plasma accelerator design for studying acceleration process characteristics

24 p4357 A69-43468

PLASMA ARC SPRAYING

U ARC SPRAYING

PLASMA ARC WELDING

High strength steel welding with physical properties equal to parent metal, discussing gas tungsten-arc, electron beam and plasma arc techniques

01 p0088 A69-11399

Plasma arc welding, discussing transferred and non-transferred arc systems application to spraying and welding techniques, including automated microplasma welding

04 p0608 A69-15482

Automatic plasma needle arc fusion welding for computer memory arrays and miniature electronic devices

09 p1511 A69-22355

Covered electrode, submerged arc, electroslag, gas metal arc, gas tungsten arc and plasma arc welding processes application to high strength steels

12 p2100 A69-25828

Plasma electron beam for welding, deriving beam current from secondary emission by ion bombardment, discussing gas pressure, equipment and applications

19 p3320 A69-35555

Microplasma, W inert gas and submerged arc welding processes for fabrication of rocket motor cases and pressure vessels, discussing material requirements and weldability

[SBAC PAPER 7] 20 p3550 A69-37449

Plasma arc systems and applications, noting transferred and nontransferred jets with emphasis on plasma spraying, surfacing, welding and cutting

[SBAC PAPER 18] 20 p3550 A69-37453

Repair welding methods for trailing edge cracks in nickel base superalloy used in turbine vanes, emphasizing plasma arc fusion welding

[ASM PAPER D8-16.3] 20 p3551 A69-38137

PLASMA CLOUDS

Target production device for deuterium plasma clouds in vacuum with Q switched neodymium laser

01 p0090 A69-10222

- Artificial visible plasma clouds in space interacting with electric and magnetic fields around earth
01 p0151 A69-10533
- Exploding wires as light source for quantitative spectroscopy, noting optically thin plasma clouds with radial symmetry
01 p0117 A69-10658
- Temperature and electron density distribution during late phase of wire explosion, analyzing optically thin plasma column by quantitative spectroscopy
02 p0286 A69-11711
- Simulation experiments using artificial plasma for astrophysical rocket exploration, discussing experiments leading to barium-copper oxide mixture choice for plasma cloud
06 p0999 A69-16973
- Arc cloud thermal conductivity effects on discharge temperature and radiation intensity, solving energy balance equation
06 p0964 A69-17254
- Plasma distribution and Alfvén wave velocity field in magnetosphere, discussing distortion of dipole magnetic field, ring current and wave propagation
10 p1742 A69-24205
- Auroral arcs drift as function of polar storm initial phase, noting agreement with satellite data on plasma motion in magnetosphere
12 p2071 A69-26694
- Ion cloud ambipolar diffusion and motion dependence on initial configuration and close magnetic field alignment above 95 km, discussing observations of meteor trains
12 p2074 A69-26961
- Radio wave diffraction by inhomogeneities arising from ionized gas clouds in interstellar medium
19 p3428 A69-36882
- Artificial ion plasma cloud experiment for studying auroral electric fields
21 p3710 A69-38507
- Magnetic field implications in stellar formation mechanism including gravitational collapse, magnetic gas cloud fragmentation and stellar winds magnetic braking
24 p4378 A69-42699
- PLASMA COMPOSITION**
- HF plasma ionic composition dependence on discharge conditions and ions translational energy
01 p0129 A69-10682
- Spherical and cylindrical probes emitting electrons and ions in unbounded plasma, deriving I-V characteristics equations
02 p0247 A69-11569
- Vacuum system for obtaining highly purified plasmas for thermionic investigations noting decontamination cycles and chamber characteristics
03 p0412 A69-13839
- Plasma jet mass structure investigated for decomposition during passage through vacuum by spectrometer and probe techniques
03 p0478 A69-13841
- Argon plasma composition in Saha equilibrium, using FORTRAN 4 program
07 p1193 A69-19168
- Fortran 4 program for computation of equilibrium compositions of gas mixtures at high temperatures
08 p1278 A69-20154
- Ionic species identification in argon-cesium discharges for thermionic converter design
09 p1440 A69-21830
- Electrohydrodynamic equations and transfer coefficients for multicomponent plasma with volumetric charge in electric field, discussing Ohm law and equations for plasma motion
12 p2135 A69-26399
- Soviet monograph on plasma diagnostics by lasers, describing interferometry, optical field visualization, schlieren and shadow photography
12 p2139 A69-27075
- Electron current, space potential and ionic composition obtained by Langmuir type probes on Explorer 31 for disturbance region dependence on ionic composition
14 p2518 A69-29122
- Hall generator electrical characteristics, discussing plasma homogeneity, stability and shock tube priming
15 p2658 A69-30298
- Density ratios of H ions to H atoms in ground state calculated as function of quasi-neutral plasma electron density
16 p2820 A69-31770
- Electromagnetic wave propagation in plasmas and plasma instabilities due to oscillations, deriving equations for frequency distributions in various plasma compositions
16 p2823 A69-32243

- Drift waves parametric excitation in resistive plasma derived from fluid equations, assuming plane geometry with periodic boundary conditions in magnetic field and azimuthal directions
18 p3179 A69-34440
- Steady state spherically symmetrical ejection of multicomponent plasma from sun determined with hydrogen approximation, considering ion composition
20 p3594 A69-37018
- Radioastronomical investigations of inhomogeneous near solar plasma structure
20 p3606 A69-38017
- Mach-Zehnder laser interferometer for measurements of electron density in transient Hg vapor plasma, noting agreement with microwave measurements
22 p3965 A69-40924

PLASMA CONDUCTIVITY

- Dense plasmas produced by explosions of wires and mercury filaments, discussing plasma conductivities
01 p0128 A69-10391
- Steady one dimensional motion of current sheets in plasma accelerators, noting condition of zero initial conductivity
01 p0133 A69-11220
- Born approximation for calculating low temperature plasma transport properties from quantum mechanical scattering cross sections on Debye potential
02 p0291 A69-12486
- Electron conductivity in low mass red giant core
02 p0327 A69-12709
- Electric field, current density and magnetic induction of plasma flow measured, obtaining plasma conductivity and flow velocity for electron temperature and density
03 p0473 A69-12877
- Magnetoconductance of nonequilibrium plasmas in indium antimonides, noting anisotropy effect of electric and magnetic field orientation
03 p0486 A69-13463
- Active and reactive impedance components of plane capacitor immersed in plasma and at LF noting dependence on plasma conductivity
03 p0477 A69-13713
- Xe gas discharge plasma resistivity dependence on current density measured in large turbulent flash lamps
03 p0478 A69-13846
- Electrodeless conductivity probe impedance in anisotropic plasma computed on basis of Maxwell equation
03 p0483 A69-14252
- Argon-K plasma electrical conductivity as function of electric current density at 1400-2400 K
05 p0798 A69-15614
- Electron distribution function effect on microwave emission and HF conductivity of weakly ionized discharge plasma
05 p0799 A69-15734
- Effective collision frequency deduced from ratio of microwave conductivity to electron density in PIG discharge plasma
05 p0804 A69-16442
- Ionized plasma electrical conductivity in magnetic field calculated by supplementing BGK collision terms with Vlasov equation
06 p0965 A69-17482
- Hydromagnetic plasma stability in infinite electrical conductivity approximation applied to smooth closed systems, discussing ballooning instability mode
06 p0965 A69-17519
- Finite conductivity or ohmic resistance effect on stationary axisymmetric self constricting MHD flow
06 p0966 A69-17548
- Potassium seeded argon plasma conductivity in induced electric field at static gas temperature for MHD generator model
06 p0871 A69-17909
- MHD generators with nonequilibrium conductivity, taking into account ionization instability of plasma
06 p0871 A69-17912
- Numerical analysis of stabilization of one component conducting plasma in two dimensional coaxial duct
07 p1190 A69-18757
- Longitudinal and transverse conductivities and anisotropy tangent for noncharged plasma in magnetic field
07 p1193 A69-19025
- Evaluation methods for DC electrical conductivity, heat conductivity and viscosity in plasmas
08 p1364 A69-20477
- Moderately ionized plasma electrical conductivity calculated by generalized Ohm law and measured along with other plasma properties
09 p1543 A69-21264

- Plasma conductivity tensor components in crossed fields calculated by Boltzmann kinetic equation, noting influence of magnetic field presence
09 p1546 A69-21565
- Electrical conductivity of partially ionized plasma, noting nonapplicability of Enskog-Chapman method and use of Lorentzian gas model
09 p1546 A69-21584
- High time resolution electrical conductivity measurement of ionized plasma gas flow, using changes in Q of circuit
09 p1546 A69-21585
- Conductivity probe design for tenuous plasmas and ionized gases, discussing experimental confirmation of theoretical behavior
09 p1496 A69-21936
- Photoelectric effects produced by polarized radiation in isotropic optical media, discussing photo EMF and photoconductivity in multivalley semiconductors and plasmas
10 p1701 A69-23138
- Finite Larmor radius, finite conductivity, rotation and Hall current effects on Jeans criterion for gravitational instability of plasma
10 p1729 A69-23408
- Electrical conductivity, electron energy balance, ionization equilibrium time and channel parameters in pulse discharge nonequilibrium Cs plasma containing inert gas addition
10 p1731 A69-23439
- Ar-K plasma studied as possible MHD generator working fluid by investigating influence of emission and external magnetic field on nonequilibrium electrical conductivity
10 p1732 A69-23441
- Rare gas-alkali plasma electrical conductivity dependence on gas temperature and preionization to determine optimum operating conditions for MHD generator
10 p1733 A69-23451
- MHD flows in MHD generator channel under magnetic field, analyzing steady laminar flow during entry and Hall effect on conductivity temperature dependence
10 p1734 A69-23455
- Turbulent plasma near stability limit in MHD generator with constant load coefficients, noting effect of conductivity and effects of gas temperature
10 p1735 A69-23460
- Conductivity and electron temperature in coaxial MHD generator plasma with magnetic field, studying Joule heating effect on performance
10 p1735 A69-23463
- Nonequilibrium electron heating effect on inert gas plasma conductivity during shock wave movement across magnetic field
10 p1737 A69-23470
- Pressure and temperature effects on electrical conductivity of dense plasma ejected from Laval nozzle
10 p1739 A69-23492
- Properties of superdense NaCl plasmas as model working substance for MHD generator, discussing ion concentration and collisions, charge reversal and conductivities
10 p1739 A69-23493
- Field effect on positive column plasma of glow discharge in air, analyzing near wall potential and conductivity
10 p1741 A69-23946
- Weakly ionized gas in crossed electromagnetic fields, formulating Ohm law from Ginzburg equations
11 p1925 A69-24319
- Electrical conductivity radial distribution in plasma flux from changes in Q factor and circuit inductance in presence and absence of skin effect
11 p1928 A69-25221
- Nonlinear HF conductivity of fully ionized plasma, considering applied electromagnetic field frequency close to electron plasma frequency
11 p1929 A69-25271
- Steady linearized aligned fields flow of collisionless plasma past slender body, noting effect of tensor conductivity
11 p1930 A69-25278
- Faraday type MHD energy converters in nonequilibrium conduction mode, analyzing two dimensional current and potential distributions in plane normal to magnetic field
11 p1826 A69-25397
- Electrostatic drift wave dissipative instability in framework of macroscopic theory, accounting for resistivity and viscosity using WKB method
11 p1934 A69-25655

- Electrical DC conductivity of turbulent plasma decreased in presence of ion waves
13 p2305 A69-27302
- Tensor conductivity measured and analyzed for MHD generator duct with electric and magnetic fields
13 p2309 A69-28026
- Current distribution in MHD duct with permeable electrodes with tensor conductivity, obtaining Riemann-Hilbert heterogeneous boundary value problem solution by finding electric field
13 p2310 A69-28030
- Current carrying cylindrical plasma column oscillations surrounded by electric excitation with multiple feedback radio, discussing stabilization possibility
13 p2311 A69-28106
- Coaxial three coil probe measuring local electrical conductivity and velocity in plasma streams, discussing operations in electrolytes and axisymmetric plasma stream
[AIAA PAPER 69-327] 13 p2313 A69-28264
- Load factor role in nonequilibrium ionization process in Faraday-type generator, determining relationship with conductivity
13 p2314 A69-28361
- Axisymmetric instabilities by Z-pinch and reverse axial current discharges in plasmas of arbitrary conductivity
13 p2315 A69-28449
- Plasma density and conductivity radio interferometry during ultrarapid disturbances based on electromagnetic wave phase shift dependence on density
14 p2498 A69-29803
- Density fluctuations effect on fully ionized plasma electrical conductivity in large or zero frequency external electric fields
14 p2502 A69-29990
- Conductivity tensor of collisional plasma in magnetic field, basing method on iterative procedure
14 p2503 A69-29999
- Electrical conductivity tensor of many component collisional relativistic plasma in magnetic field and near equilibrium, expressing collisional part as momentum integral
14 p2503 A69-30000
- Ion-acoustic oscillations effect on weakly ionized plasma electrical conductivity, using BGK collision integral model
15 p2662 A69-30970
- Air plasma electrical and thermal conductivity coefficients measured in wall stabilized DC arc at atmospheric pressure and high temperatures
15 p2663 A69-30979
- Current distribution and Hall voltage in crossed fields discharge with split electrodes in nonequilibrium Ar and Cs plasmas
15 p2663 A69-30980
- Geomagnetic ring current study, giving exact kinetic description based on Vlasov equation of plasma ring current in dipolar field
15 p2598 A69-31218
- Plasma conductivity measurements using RF induction probe
16 p2820 A69-31707
- Plasma cluster interaction with axially symmetric magnetic field, deriving plasma diamagnetic current, inductance and resistance from measured coil flux dependence on distance
16 p2823 A69-32365
- Raman scattering by coupled plasmon-cyclotron-harmonic modes in semiconducting plasmas in homogeneous static magnetic field
16 p2824 A69-32604
- Conducting fluid and plasma rotation between concentric cylinders due to crossed fields, determining velocity distribution, induced magnetic field and kinetic energy
[AIAA PAPER 69-726] 17 p3011 A69-33472
- Low density plasma electrical conductivity determined by temperature and electron density measurements, using Ohm law
18 p3181 A69-35072
- Scalar conductivity as governing parameter in determining current sheet diffusion and energy dissipation in MHD shock producing devices
21 p3776 A69-38708
- Nonlinear electron conductivity of Lorentz plasma subjected to frequency modulated electric field
21 p3778 A69-39573
- Inhomogeneous magnetically confined plasma stability, examining dissipative effects on spectra of drift oscillations with kinetic theory
01 p0126 A69-10187
- Transverse plasma velocity component effect on boundary layer structure between cold plasma and confined magnetic field
02 p0235 A69-11424
- Magnetic confinement of electric arc in alkali metal vapor containing gas flow, considering degree of ionization
02 p0286 A69-11585
- Statistical analysis of polarization of semiinfinite electron/ion plasma bounded by dielectric or conducting solid wall, deriving steady state and space potential
02 p0286 A69-11706
- General structure of magnetic surfaces of 3-turn helical magnetic field with axial current flow, noting closed magnetic trap production
02 p0288 A69-12168
- Ion cyclotron drift loss cone instability for cases of steep particle density gradients, magnetic field gradients and finite plasma dimensions
02 p0288 A69-12169
- Electromagnetic wave scattering by turbulent plasma pulsations in external magnetic field
02 p0289 A69-12174
- Anisotropic plasma cyclotron instability in magnetic trap with cold ion background and isotropic Maxwellian velocity distribution
02 p0292 A69-12554
- Plasma slab acceleration along magnetic dipole guard field null, noting lack of equilibrium and no decrease of plasma losses
03 p0475 A69-13157
- Critical pressure in mean magnetic well with closed lines, noting longitudinal resistivity annihilation of stabilizing effect of toroidal shear
03 p0476 A69-13382
- Plasma transverse injection into toroidal magnetic field created by linear current leads to plasma confinement along magnetic force lines
03 p0478 A69-13837
- Region of plasma electron capture during cyclotron electron resonance in magnetic trap with mirrors
03 p0478 A69-13849
- Monograph on electron waves and resonances in bounded plasmas covering theoretical and experimental methods, metallic and dielectric resonance probes, etc
04 p0633 A69-14296
- Min B magnetic trap, discussing induction coils, ponderomotive forces and mechanical stresses sustained by coils
04 p0634 A69-14299
- Magnetic field confinement of plasma produced by focusing Q switched laser output on solid deuterium pellet
05 p0798 A69-15585
- Fluctuations in multipole confined plasmas explained by solving general integral equation, yielding hydromagnetic and frequency modes
05 p0804 A69-16385
- Optimum magnetic field axial component and plasma gun discharge voltage for high velocity plasma injection into symmetrical cusp field
05 p0805 A69-16655
- Plasma confined in transverse magnetic field analyzed for drift rates, noting role of injection direction
06 p0963 A69-16907
- Hot plasma research at Polish Institute of Nuclear Research at Swierk
06 p0964 A69-17174
- Mathematical description of electromagnetic field containing plasma, discussing energy transfer modes between plasma and containing field
06 p0965 A69-17517
- Polynomial representations of mirror cusp fields produced by combination of mirror coils and Ioffe/multipole bars
06 p0966 A69-17522
- Plasma flute instability in magnetic trap with wall/plasma interface, using system of sensors and amplifiers
06 p0966 A69-17544
- Phase space concepts for beams, accelerators and confined particles, noting adiabatic invariants, phase space transformations, particle dynamics in accelerators and plasmas
06 p0966 A69-17673
- Theoretical population inversion in decaying nitrogen plasma column free from external fields and confined motionless in circular cylinder
[AIAA PAPER 69-48] 06 p0971 A69-18145
- Hot plasma containment by magnetic field, presenting results from stellarator for toroidal sheared magnetic field properties
07 p1190 A69-18929
- High density plasma dynamic stability in magnetic containment using variational calculations
08 p1359 A69-19984
- Nonlinear interaction of electromagnetic waves in bounded plasma, optimizing second order fields with reference to diagnostic applications
08 p1273 A69-20030
- Plasma lifetime in spherical multipole magnetic field trap compared to cusp trap
08 p1360 A69-20082
- Nuclear fusion reactor development, discussing magnetic field confinement of hot dense plasmas and electric power production economic possibilities
08 p1361 A69-20124
- Toroidal plasma nonequilibrium in multipole confinement devices with conventional magnetically shielded supports
08 p1369 A69-20819
- Magnetohydrostatic cavity formed round magnetic field of line dipole-line current combination by infinitely conducting plasma at uniform pressure
08 p1369 A69-20998
- Wave interaction in magnetically confined plasma taking into account body and surface waves
08 p1370 A69-21014
- Plasma flow motion and polarizing interaction in multipole magnetic field
08 p1370 A69-21015
- Arc jet generation and control noting application to hyperthermal aerospace environment studies, wind tunnels and materials heating and fabrication
08 p1371 A69-21128
- Electrostatic electron bombardment ion thruster with magnetoelectrostatically contained plasma
[AIAA PAPER 69-260] 09 p1567 A69-21262
- Lifetime and radial oscillations of magnetically confined laser produced plasma, solving hydrodynamical equations
09 p1545 A69-21493
- Discharge plasmas produced from solid materials at low pressures and temperatures and compressed against wall by magnetic field
09 p1547 A69-21594
- Warm plasma addition to mirror confined hot plasma stabilizing convective loss cone mode
09 p1551 A69-22040
- HF magnetic field effect on oscillations and instabilities of plasma confined by fixed magnetic field
10 p1739 A69-23623
- Nonlinear confining and deconfining forces of laser light interaction with inhomogeneous plasma, analyzing macroscopic motion based on ponderomotive force description
11 p1923 A69-24297
- Electric field fluctuations in inhomogeneous plasma calculated by test particle method, interpreting results in convective modes terms in plasma control and stability
11 p1924 A69-24301
- Electron confinement in magnetic mirror geometry supplemented with RF quasi-potential barriers, considering gas scattering
11 p1924 A69-24306
- Cesium plasma confinement time improvement in symmetrically heated tungsten end plates of Q machine
11 p1925 A69-24314
- Plasma confinement experiments with Tokamak type magnetic configuration device, giving schematics for thermonuclear reactor
11 p1927 A69-25099
- Spectrum space-time characteristics of electrically produced plasma discharge: magnetically compressed to discharge tube wall, using spectrochromograph and spectrographs
11 p1927 A69-25217
- Particle, momentum and heat balance of static and rotating magnetized plasmas in terms of macroscopic equations
11 p1928 A69-25248
- Neutron emission anisotropies in capacitor discharge produced plasma focus, detailing coaxial plasma gun energy spectrum and flux measurement
11 p1930 A69-25321
- LF electromagnetic waves stability and propagation conditions in plasma confined in central-conductor configuration measured, noting agreement with wave equation solution
11 p1931 A69-25362
- Current carrying inhomogeneous dense plasma instabilities confined in magnetic field, deriving dispersion relations in geometric optics approximation
11 p1932 A69-25537

PLASMA CONTROL

- Microinstabilities of plasma confined by magnetic trap, discussing stabilization, drift waves and anomalous diffusion of plasma by turbulence
01 p0125 A69-10048

Plasma flow from Penning discharge with incandescent cathode in vacuum controllable by varying voltage, pressure and magnetic field strength
11 p1933 A69-25543

Ionization instability in plasma enclosed by two infinitely segmented and ideally emitting electrode walls and two insulator walls
12 p2134 A69-26095

Charged particles influx from cusp shaped regions of stagnant plasma trapped in vicinity of two magnetic cusps on polar magnetopause
12 p2151 A69-26945

Plasma lens device for focusing ion or plasma beams with closed electron drift
13 p2307 A69-27658

Temperature effects on propagation of HF internal and surface waves in bounded plasma, deriving dispersion equations
14 p2410 A69-28733

Potassium plasma drift instability suppression by applied external HF electric field, noting plasma diffusion decrease toward container wall
14 p2489 A69-28740

Electrostatic screening in isothermal symmetrically charged and quasi-neutral plasmas, noting confinement in electrostatic trap
14 p2490 A69-29035

Electrodynamics law between current elements consistent with Newtonian dynamics, noting consequences in discharge and plasma control
14 p2485 A69-29320

Plasma scanner in obtaining current cross sections and current-voltage characteristics of hollow cathode magnetically confined arc plasma in argon
14 p2450 A69-29568

Anisotropic plasma cyclotron instability in magnetic trap with cold ion background and isotropic Maxwellian velocity distribution
15 p2658 A69-30251

Charged particle motion in magnetic mirror trap, observing time dependence with respect to orbital magnetic moment conservation
15 p2659 A69-30724

Wave regeneration by resonant particles interaction in inhomogeneous plasma of electrons confined in quadratic potential solved in WKB approximation
15 p2660 A69-30918

Hot electron plasma formation by injecting megaelectron volt ion beams followed by Lorentz trapping, noting advantages of DC operation
15 p2661 A69-30925

Interchange stability and drift motion of plasma with loss from ends of axisymmetric magnetic bottle, using hydromagnetic equations
15 p2664 A69-31100

Charged particle motion in superposed Heliotron and biconical cusp magnetic fields, considering particle confinement
16 p2817 A69-31643

One dimensional free expansion of collisionless plasma tested as function of thermal equilibrium and confinement, using Vlasov equations and computer
16 p2819 A69-31685

Multipole configuration toroidal plasma confinement device MHD equilibrium and stability from measured data
16 p2823 A69-32563

Electron beam injection into magnetic trap, obtaining plasma by ionization of supersonic argon flow passing through system
22 p3990 A69-40791

Bernstein modes initial value-boundary value problem for half space of plasma bounded by wall and parallel unperturbed magnetic field
23 p4196 A69-41875

Soviet high temperature plasma physics research, discussing magnetic plasma containment by Tokamak traps
23 p4196 A69-42167

Moving plasma partial capture in transverse magnetic field in experimental plasma source, noting influence of repulsion effect of plasma polarization volume charge
24 p4357 A69-43469

Drift characteristics of hydrogen plasma partially captured by transverse magnetic field, finding drift rate dependence on magnetic field level
24 p4357 A69-43470

PLASMA CYLINDERS

Electron plasma wave dispersion along cylindrical plasma column in magnetic field
01 p0126 A69-10277

Density gradient measurement method for plasma column with propagation and electric field perpendicular to external magnetic field
01 p0128 A69-10390

Electromagnetic waves propagation in cylindrical waveguide containing plasma column along axis in absence of constant magnetic field
02 p0285 A69-11463

Current carrying curved plasma column flute instability analysis, noting effect of increasing divergence from axial symmetry on Q values
02 p0289 A69-12175

Dispersion relations of axisymmetric and dipolar surface modes propagation along inhomogeneous plasma columns on dispersion relations
02 p0289 A69-12242

Plasma column density profile measurement by means of two resonant cavity modes for low pressure discharge in small diameter tubes
02 p0290 A69-12403

Electron radial distribution determination in positive Hg plasma column using simultaneous measurements with two different microwave cavities
02 p0290 A69-12404

Magnetic shear effect on stability of electron-neutral collision dominated plasma, noting helical perturbations onset
03 p0473 A69-12925

Helicon waves in nonresistive cylindrical and spherical plasmas
03 p0479 A69-13961

Pressure rise and thermal conductivity in cylindrical hydrogen plasma column in axial magnetic field, assuming local thermal equilibrium
03 p0479 A69-13967

Disintegration spectrum of Langmuir wave excited in plasma column by antenna, discussing conditions of resonance and parametric amplification
03 p0480 A69-14113

Ion and atom temperature distribution for two fluid model of Ar plasma in cylindrically symmetrical wall stabilized electric arc column
03 p0481 A69-14155

Absorption coefficients of plasmas in capillary discharge tubes, discussing measurement using gas laser light source
03 p0442 A69-14218

MHD instability in current discharges in magnetic field stabilized by current frequency modulation higher than perturbation increment of plasma column
04 p0635 A69-14549

Theoretical analysis of fixed stratification, taking into account nonlinear effects and variation in charged particle concentration along plasma column
04 p0636 A69-14783

Similarity law for ionization waves noting relations for frequency, wavelengths, amplification, propagation velocities and phase shifts
05 p0799 A69-15633

Similarity between characteristics of T layers in oxygen discharge positive column and Gunn instabilities in GaAs, noting role of negative O ions
05 p0800 A69-15739

Continuous radiation production in positive plasma column of inert gas considered as manifestation of plasma electrons bremsstrahlung from interaction with gas atoms
05 p0800 A69-15741

Equivalent circuit diagrams for impedance of plasma column in low current low pressure glow discharge
05 p0800 A69-15742

Mass spectrometric technique applied to positive column of hydrogen glow discharge for plasma properties, including relative densities of various hydrogen ions
05 p0802 A69-15913

Trapped mode wave propagation for cold uniform magnetoplasma cylinder in free space, studying dipole modes and one-wave approximation
06 p0967 A69-17756

Dispersion equation for dipolar surface waves in uniform cold lossless infinitely long magnetoplasma column in free space, obtaining numerical and asymptotic solutions
06 p0968 A69-17774

Surface wave propagation on circular plasma column moving in axial direction in free space region
06 p0968 A69-17775

Theoretical population inversion in decaying nitrogen plasma column free from external fields and confined motionless in circular cylinder
06 p0971 A69-18145

Microwave scattering by turbulent plasma column noting effects of plasma density
07 p1194 A69-19411

Cylindrical and spherical waves propagation in weakly inhomogeneous plasma treated by geometrical optics, noting caustic surfaces
07 p1195 A69-19747

Atomic flux from Cs and K ion recombination on hot end plates of Q machine measured, noting contribution to total plasma end loss rate
08 p1358 A69-19810

Positive column in longitudinal magnetic field in helium and neon, noting agreement with collision diffusion theory and Kadomtsev perturbation theory
08 p1361 A69-20212

Resonances in plasma column monitored by frequency and current modulation methods
08 p1365 A69-20552

Microwave scattering from longitudinal plasma waves propagating in collisionless plasma column
08 p1276 A69-20798

Plasma column of free burning electric arc, deriving temperature, electron concentration and electric field radial distributions
09 p1545 A69-21431

Electrons velocity-space instability in plasma column, analyzing unstable wave and dispersion characteristics
09 p1552 A69-22041

Slow electromagnetic wave propagation along cold collisionless cylindrical plasma in axial magnetic field, noting surface wave metamorphosis into bulk waves
10 p1739 A69-23659

Electromagnetic wave propagation along longitudinally magnetized plasma column surrounded by isotropic dielectric medium, without making quasi-static assumption
10 p1658 A69-24061

Coupling coefficient and impedance for excitation of isotropic plasma column by ring of magnetic current outside plasma, noting surface wave resonance effect
10 p1659 A69-24064

Electrostatic wave dispersion relation in uniformly rotating plasma cylinder used in interpreting Q machine experiments
11 p1924 A69-24300

Toroidal theta pinched plasma column collapse, using snowplow model for study of column position shift and cross section deformation
11 p1924 A69-24303

Tonks-Dattner resonances in plasma column, using linearized Vlasov equation for coupling to plasma waves of time varying electric fields
11 p1929 A69-25266

LF waves and instabilities on positive column in axial magnetic field, noting axisymmetric and asymmetric ion acoustic and electron wave modes and current convective instability
11 p1929 A69-25268

Centrifugal instability of plasma column generated by cyclotron absorption of microwave power in magnetic mirror field
11 p1931 A69-25366

Positive column contraction in Ar and Ar-Cs mixtures, developing theory for nonisothermal local collision arc
11 p1932 A69-25539

Microwave oscillations amplitude spatial distribution in gas discharge plasma excited by electron beam
11 p1933 A69-25542

Low power gradient uniform electric arc column in cross flow and transverse magnetic field, analyzing temperature, velocity, pressure and magnetic field distribution
11 p1933 A69-25556

Flute oscillation instability of dense plasma cylinder under nonuniform electric field, analyzing oscillation spectrum properties
11 p1934 A69-25707

Electromagnetic field penetration into plasma cylinder having electron mean free path comparable with plasma diameter, noting anomalous skin effect
12 p1233 A69-25833

Dynamic characteristics of plasma fluxes across magnetic field of diverter inside plasma cylinder formed during injection
12 p2134 A69-25977

Dynamic energy balance in positive column of electric arc, integrating expression to determine temperature time dependence
12 p2137 A69-26535

Surface dissipation effect induced by end electrodes on drift instabilities in cold ion plasma column described by differential equation with constant coefficient
12 p2138 A69-26710

Field patterns for wave radiation from electric dipole immersed in anisotropic plasma column excited by longitudinal DC magnetic field
12 p2034 A69-27103

Current carrying cylindrical plasma column oscillations surrounded by electric excitation with multiple feedback radio, discussing stabilization possibility
13 p2311 A69-28106

Convective-current instability in finite length plasma column, analyzing spectrum of unstable harmonics
13 p2314 A69-28441

Screw instability in glowing discharge plasma column in longitudinal magnetic field generalized to instabilities in low pressure arc, Penning and high current discharges
13 p2315 A69-28526

MHD waves and oscillations in cylindrical plasma column contained by longitudinal magnetic field, noting dispersion equations
14 p2489 A69-28732

Neutral gas pressure in positive column plasma between two coaxial insulated cylinders as function of cylinders radii
14 p2490 A69-29036

Balance equations for axial separation in anisothermal plasma columns with radial variation of neutral gas temperature applied to argon discharge with mercury vapor addition
14 p2493 A69-29690

Magnitude and type of wall losses from small opening in discharge tube for positive plasma column of low pressure glow discharge in hydrogen
14 p2493 A69-29691

Ionospheric inhomogeneity model for motion of infinite elliptical cylinder of cold plasma in neutral particle flow and ambient electrostatic and magnetostatic fields
14 p2500 A69-29864

Dynamic dispersion relation for bounded cylindrical beam plasma with temperature correction, including hot beam interaction
14 p2502 A69-29957

Calorimetric measurement of electron temperature in collisionless shock wave propagating in plasma column, discussing role of H beta line Stark broadening
15 p2657 A69-30104

Scattering by cylindrical post of complex permittivity /plasma/ in rectangular waveguide, calculating reflection, transmission and absorption coefficients by computer
16 p2756 A69-31578

Wide argon plasma column by axial current density measurements, confirming existence of instability and determining critical magnetic field
16 p2819 A69-31680

Electromagnetic wave diffraction in plasma cylinder of small nonuniform radius, analyzing interior field and radio wave reflection
16 p2751 A69-32031

Correlation coefficient of light fluctuations measured in Ar plasma in positive column of glow discharge, noting ionization wave appearance at critical gas pressure
16 p2822 A69-32039

Trapped modes in cold magnetoplasma slabs and rods in free space analyzed by Maxwell equation, assuming DC magnetic field and homogeneous electrons distribution
17 p2926 A69-33850

Microwave propagation inside hollow cylinder using model plasma as dielectric, deriving relationship between phase shift and free electron density
17 p2932 A69-34218

Microwave reflection and noise emission from cylindrical rare gas afterglow plasmas in axial magnetic field measured near electron cyclotron resonance
18 p3127 A69-34436

Anomalous absorption of electromagnetic wave in collisionless dense cylindrical plasma beam in circular waveguide, noting electric field strength for energy transfer
18 p3101 A69-34621

Scattering of electromagnetic waves obliquely incident on inhomogeneous plasma column of parabolic radial density distribution, noting applications to ionospheric irregularities
18 p3102 A69-34963

Plasma capture in stellarator diverter aperture with asynchronous plasma jets injection through diverter magnetic slots, discussing plasma cylinder density effect
21 p3776 A69-38585

Self induced magnetic field influence on plasma positive column stability in longitudinal magnetic field
24 p4356 A69-43366

PLASMA DECAY

Contact phenomena theory in decaying plasma applied to deionizing mercury vapor diode gas discharge plasma diagnostics
03 p0404 A69-13547

Plasma decay at high pressure in helium and argon with cesium vapor admixture and pure cesium vapor, using Saha equation
03 p0480 A69-14052

Time resolved electron number density and electron temperature in decaying plasma using laser interferometer
03 p0432 A69-14187

Double microwave interferometer for measuring hydrogen plasma decay
04 p0600 A69-15024

Theoretical population inversion in decaying nitrogen plasma column free from external fields and confined motionless in circular cylinder
[AIAA PAPER 69-48] 06 p0971 A69-18145

Nitrogen ion number density time dependence by mass spectrometric probing of decaying nitrogen plasmas, noting molecular ion production by colliding metastable nitrogen molecules
07 p1184 A69-19141

Free fall theory for afterglow decay of average electron density and temperature in pulsed cylindrical mercury vapor discharge plasma
08 p1358 A69-19811

Loss rate of plasma from stellarator due to binary Coulomb collisions scattering particles in loss region, discussing diffusion coefficients
08 p1364 A69-20520

Temperature dependence of dissociative recombination and molecular ion formation in decaying He, Ne and Ar plasmas in discharge tube energized with capacitor bank
08 p1356 A69-20741

Alfven oscillations in inhomogeneous decaying plasma from pulsed discharge with oscillating electrons
09 p1550 A69-22020

Plasma decay coefficient, charge recombination coefficient and electron scattering in cooling electron gas of quasi-steady cesium discharge plasma under high pressure
10 p1733 A69-23448

Flares development in form of loop tunnel, discussing role of filaments
11 p1945 A69-24238

Toroidal theta pinched plasma column collapse, using snowplow model for study of column position shift and cross section deformation
11 p1924 A69-24303

Collisional radiative electron-ion recombination rates measured in decaying rare gas plasmas produced by transient discharge
12 p2134 A69-25981

Alfven and slow and fast magnetoacoustic waves excited during decay instability of initial Alfven wave, noting dissipation effect on stability
14 p2489 A69-28735

Decaying arc discharge Cs plasma luminosity anomalous behavior due to combined effect of intrinsic monotonic and complex nonmonotonic emissions
14 p2490 A69-28996

Laser induced gas breakdown covering breakdown mechanism and plasma expansion and decay, with bibliography
17 p2980 A69-33026

Plasma decay at high pressure in helium and argon with cesium vapor admixture and pure cesium vapor, using Saha equation
18 p3181 A69-35045

Slot antenna radiation patterns in presence of aperture RF plasma breakdown sheath measured for various gas pressures and breakdown power levels
23 p4116 A69-41595

PLASMA DENSITY

Dense plasma with plasma frequency greater than cyclotron frequency, discussing flow past slender bodies
01 p0126 A69-10226

Plasma density dynamic measurements by Fabry-Perot microwave resonator, discussing resonator and coupling problems
01 p0080 A69-10318

Density gradient measurement method for plasma column with propagation and electric field perpendicular to external magnetic field
01 p0128 A69-10390

Dense plasmas produced by explosions of wires and mercury filaments, discussing plasma conductivities
01 p0128 A69-10391

Recombination reactions during postdischarge in helium plasma produced by laser beam, deriving equation for density evolution
01 p0128 A69-10394

Spectroscopic investigation of high density plasma from Li exploded wires
01 p0129 A69-10662

High temperature plasmas generation by exploding gold wires in vacuum, using time of flight technique for plasma densities and flow velocities
01 p0129 A69-10667

Relaxation processes and radiation stimulation in dense low temperature ionized plasma can lead to population inversion of several levels
01 p0131 A69-10789

End holes and glass tube effects in TM 010 mode measurements of average electron number density in cylindrical plasmas
01 p0131 A69-10812

Plasma wave properties relation to creation of electron plasma densities above critical density, discussing splitting of cold plasma resonance
01 p0131 A69-10818

Magnetospheric plasma distribution determination based on analysis of structured elements in micropulsations
01 p0076 A69-11229

Gaussian type microfield formation in plasma by placing constraints on plasma particles displacements
02 p0285 A69-11568

Screening of high density plasma from penetration by neutral gas, discussing prevention of high energy losses by charge exchange collisions
02 p0288 A69-12170

Barium plasma density measurements by Langmuir, microwave probes and resonance fluorescence scattering compared in Q device
02 p0288 A69-12172

Plasma column density profile measurement by means of two resonant cavity modes for low pressure discharge in small diameter tubes
02 p0290 A69-12403

Dense plasma temperature determination by gamma ray resonance scattering
02 p0291 A69-12481

Average plasma electron density measurement by feedback oscillator to determine dielectric constant
03 p0473 A69-13103

Electron fluid compression coefficient from simultaneous measurement and correlation of absolute magnitudes of ion acoustic wave potential and accompanying plasma density perturbation
03 p0475 A69-13148

Plasma density spatial distribution determined from HF electromagnetic wave phase shifts without assuming axisymmetry
03 p0480 A69-14138

Charged particle density of unsteady plasma from Stark broadening of Balmer H beta line, using time scanning image converter
03 p0481 A69-14145

HF gas discharges, discussing plasma temperature and density, plasmoid length and spectroscopic applications
03 p0482 A69-14217

Dense plasma radiation, analyzing spectrographically initial stages of wire explosion in vacuum
03 p0482 A69-14227

HF interaction of relativistic electron beam and plasma extended to include arbitrary variation of plasma density
04 p0637 A69-15046

Nondegenerate dense plasma thermodynamic stability by nonclassical methods, discussing atomic concentration dependence on ionic concentration
05 p0802 A69-15892

Langmuir probe to determine helium plasma density effect on electron temperature from relation between spectral line intensities
05 p0804 A69-16376

Theta pinch plasma electron density and temperature distributions measured using Thompson scattering of laser light and plasma bremsstrahlung
06 p0972 A69-18220

Plasma diagnostics using scattering of laser electromagnetic radiation by plasma density function, discussing plasma species collision effect on line profiles
07 p1131 A69-18485

Plasma column radial density profile measurement by electron plasma waves propagation in presence of strong magnetic field
07 p1194 A69-19323

Microwave scattering by turbulent plasma column noting effects of plasma density
07 p1194 A69-19411

Rarefied plasma self similar motion qualitatively analyzed, particularly penetration and expansion, taking into account electric/magnetic field effects
08 p1359 A69-19951

High density plasma dynamic stability in magnetic containment using variational calculations
08 p1359 A69-19984

Highly ionized low density plasmas production by strong UV radiation
08 p1360 A69-20080

Current fluctuations in Langmuir probe in turbulent plasma measured for various pressures, frequency bands, etc, noting plasma density fluctuations role
08 p1364 A69-20517

Warm plasma magnetic interactions, discussing density waves, pair correlation function and transport coefficients
08 p1366 A69-20749

Symmetric Alfvén waves propagation in hydrogen plasma with nonuniform density distribution, deriving dispersion relations for fully ionized plasma
08 p1367 A69-20794

Plasma oscillation modes perpendicular to magnetic field used to study energy conversion by wave coupling across density discontinuity
08 p1367 A69-20795

Flute instabilities in rarefied plasma with intrinsic electric field, discussing plasma density profile and uncompensation degree effects on plasma magnetic field stability
08 p1370 A69-21013

High temperature high density theta-pinch plasma refraction measurements by interference refractometer with beam perpendicular to plasma axis
09 p1544 A69-21302

Dispersion corrected three wavelength laser heterodyne system for plasma electron density and neutral density measurements
09 p1544 A69-21331

Mariner 2 data on large scale variations in magnetic field, solar wind density and temperature in interplanetary plasma
09 p1592 A69-21540

Equilibration potentials between dense thrust beam and dilute space plasma measured in wind tunnel [AIAA PAPER 69-263]
09 p1568 A69-21728

Time dependent plasma density variations studies by microwave interferometer having reflector for modulated or nonmodulated microwaves
09 p1496 A69-22030

Refraction errors in plasma density measurement by microwave interferometry
09 p1496 A69-22031

High density plasma in resonant cavity obtained by frequency shifting power source
10 p1727 A69-22955

Pressure and temperature effects on electrical conductivity of dense plasma ejected from Laval nozzle
10 p1739 A69-23492

Properties of superdense NaCl plasmas as model working substance for MHD generator, discussing ion concentration and collisions, charge reversal and conductivities
10 p1739 A69-23493

Thermodynamic stability of dense plasma consisting of electrons and charged ions, plotting ionization potential as function of electron density and temperature
11 p1922 A69-24232

Spectral broadening measurements of ruby laser light scattered by density fluctuations in theta pinch plasma
11 p1924 A69-24304

External modulated currents induced electromagnetic field effect on density distribution of bounded plasma, discussing fluctuations in various configurations
11 p1927 A69-24910

Dense gas equilibrium plasma thermodynamic stability in case of high electrostatic interaction energy of charged particles, analyzing phase transition possibility
11 p1928 A69-25234

Anisotropic plasma density measurement by launching circularly polarized plane electromagnetic wave at small angles to magnetic field direction
11 p1930 A69-25286

Ruby laser light scattered at 90 degrees by dense plasma focus, analyzing signal detection
11 p1899 A69-25324

Critical condition for electromagnetic radiation generation by energetic electrons gyrating in dense

magnetized plasma, proposing plasma instability mechanism
11 p1931 A69-25363

Temperatures and densities of atoms and electrons from spectroscopic methods in gas discharge plasma used for CW ion-argon lasers, evaluating inversion mechanism
12 p2106 A69-26319

Dense plasma flow across transverse inhomogeneous magnetic field, proving adiabatic nature of motion
12 p2137 A69-26528

Optical and spectral properties of dense plasma expanding after exploding electric wire in vacuum using high speed photography
12 p2137 A69-26533

Isoperimetric plasma thermodynamics problems, including plasma free energy and relativistic plasma density fluctuations energy
12 p2138 A69-26603

Population densities, pumping rates, lifetimes, etc, of singly ionized krypton ion laser
12 p2109 A69-26638

Ionospheric plasma density vertical profile by measuring reflected radio waves phase frequency characteristics
12 p2070 A69-26685

Soviet book on plasma thermionic energy conversion covering operation modes, transport processes, current-voltage characteristics, density, temperature, electric field distribution
12 p2017 A69-26850

Carbon dioxide laser as light source in Michelson interferometer for plasma electron density measurement
12 p2100 A69-27177

Alternating electric field parametric effects on inhomogeneous plasma in magnetic field, obtaining electrostatic wave coupling dispersion relation by density gradients considerations
13 p2304 A69-27298

Magnetic curvature effect on collisionless plasma density gradient drift instabilities, covering mean ion larmor radius and Alfvén modes
13 p2305 A69-27375

Stable geomagnetic pulsations related to plasma density shock position in magnetosphere and to magnitude of diurnal variations
13 p2253 A69-27692

Spatial density distribution and local values of attenuation of pulsed reflex discharge plasma determined from measured attenuation of microwave beam
13 p2312 A69-28112

Collective scattering of light from ruby laser by cold dense deuterium plasma produced by electrical discharge, deducing density and electron temperature
13 p2273 A69-28366

Laser radiation absorption in xenon plasma, noting dependence on intensity due to atoms ionization
13 p2314 A69-28442

Voltage drop of ignited mode related to current density in cesium diode, noting plasma zones
14 p2401 A69-29232

Probe and spectroscopic study of dense plasma thermionic converters noting parameters
14 p2404 A69-29256

Plasma potential and density distribution in near-electrode plasma sheath of thermionic converter
14 p2491 A69-29257

Nonlinear generation of sum and difference frequencies in ionized plasma current densities by nonuniform microwave fields noting electron scattering
14 p2507 A69-29350

Multiple scattering of electromagnetic waves in underdense plasma, deriving transport equation for radar backscatter
14 p2412 A69-29453

Polychromator measurement of hydrogen plasma electron density produced by normal ionizing shock wave, using Stark broadening study of H beta line
14 p2494 A69-29767

High speed streak cameras applicability to low density theta pinch studies, describing image converters design, operation and block diagrams
14 p2496 A69-29787

Stark effect applicability to charged particle concentration in nonstationary plasma
14 p2497 A69-29790

Spatial distribution of plasma density from phase shift measurement in millimeter waves based on microwave multichannel probes
14 p2497 A69-29792

Multifrequency interferometer for inhomogeneous plasma density soundings
14 p2497 A69-29795

Plasma density and conductivity radio interferometry during ultrarapid disturbances based on electromagnetic wave phase shift dependence on density
14 p2498 A69-29803

Plasma ion temperature measurement based on integral neutron yield, noting density determination
14 p2498 A69-29808

Relativistic corrections to particle distribution functions for high temperature plasma in thermodynamic equilibrium by integrating Gibbs distribution
14 p2499 A69-29847

Density fluctuations effect on fully ionized plasma electrical conductivity in large or zero frequency external electric fields
14 p2502 A69-29990

Sc X-1 fluctuating optical and X ray emission observed simultaneously, determining total energy flux and plasma radius and density
15 p2676 A69-30885

Te waves propagation along plasma sheet between conducting plates, determining vertical plasma density distribution
15 p2569 A69-30939

High beta theta pinch stability against tearing modes, determining necessary magnetic field conditions for slab and cylindrical cases
16 p2819 A69-31681

Temperature gradients effect on ion flute mode in low beta plasma having density gradients in x direction, obtaining instability condition
16 p2819 A69-31689

Holographical interferometry with laser spark radiation containing fundamental and second harmonic wavelengths, confirming heavy particle densities decrease in plasma with time
16 p2789 A69-31771

Mariner 2 data on large scale variations in magnetic field, solar wind density and temperature in interplanetary plasma
16 p2864 A69-32535

Magnetized solar wind model to evaluate temperature, density, velocity and magnetic field for various boundary conditions
17 p3041 A69-33812

Wave propagation in plasma filled cylindrical waveguide in axial magnetic field, approximating plasma density profile by WKB method
17 p2926 A69-33848

Artificial plasma properties at microwave frequencies, determining plasma electron density and effects on horn antenna radiation characteristics
18 p3100 A69-34271

High electron density in transient mercury vapor plasma determined using He-Ne laser interferometer measurements
18 p3153 A69-35307

Plasma density and potential distributions along circular cylinder surface in weakly ionized high speed low pressure gas flow, noting boundary layer separation point
19 p3380 A69-35839

Plasma density in magnetosphere by measuring geomagnetic pi 2 micropulsations in direction related to polar aurora oval southern boundary, determining period of pi 2 oscillations
19 p3303 A69-36205

Plasma concentration in nondipole magnetosphere model from pc 5 pulsations periods for high geomagnetic latitudes, noting solar winds effect
20 p3521 A69-37043

Mathematical model of nonlinear microwave breakdown for overdense and underdense plasma outside reentry vehicle, predicting nonlinear pulse transmission through high temperature plasma
20 p3495 A69-37853

Relaxation processes and radiation stimulation in dense low temperature ionized plasma leading to population inversion of several levels
20 p3582 A69-38006

Equatorial plasma sheet role in magnetotail assessed from Vela satellite data, noting diurnal density variations
21 p3711 A69-38512

Plasma capture in stellarator diverter aperture with asynchronous plasma jets injection through diverter magnetic slots, discussing plasma cylinder density effect
21 p3776 A69-38585

Parameters of DC discharge between concentric cylinders calculated for plasma probes by pressure theory, noting ion neutral collisions and magnetic field effects
21 p3776 A69-38712

- Microwave power coupling to high density plasmas for electrons heating, using dielectric plates
21 p3779 A69-39746
- Birefringent element within Fabry-Perot cavity for identification of direction of electron density change in z-pinch discharge
22 p3946 A69-40438
- Coherent MHD waves propagation in presence of plasma density fluctuations, applying perturbation technique to solve stochastic wave equation
22 p3990 A69-40529
- Rocket measurements of plasma densities and temperatures in visual aurora using electrostatic onboard and ejected Langmuir probes, observing hyperthermal electron
23 p4167 A69-42334
- Measurement method for relative phase shift between density and potential oscillations in Cs plasma
24 p4354 A69-42676
- Hydrogen plasmoids in axisymmetric magnetic field with acute angle geometry produced by opposing coils, measuring induction current field and plasmoid density distribution
24 p4358 A69-43473
- PLASMA DIAGNOSTICS**
- RF characteristics of electrodes immersed in magnetoplasma, discussing potential distribution around point charge and RF probe measurement of plasma parameters
01 p0029 A69-10550
- Time resolved spectroscopy of exploding wire plasmas in visible spectrum of various elements, determining plasma characteristics
01 p0119 A69-10671
- Power spectrum for energy transfer region in HF turbulent plasma by nonlinear equations, with results applied to subsonic ray acceleration
01 p0145 A69-10790
- End holes and glass tube effects in TM 010 mode measurements of average electron number density in cylindrical plasmas
01 p0131 A69-10812
- Rapid scan spectrometer design and calibration, noting application to diagnostics of high density transient Xe and H plasmas
01 p0082 A69-10838
- Soviet book on high temperature plasma diagnostics methods covering measurement errors, holographic interferometers and light scattering
01 p0132 A69-11199
- Electron distribution function of isotropic homogeneous Lorentzian plasma subjected to frequency modulated electric field calculated by successive approximation method
02 p0285 A69-11543
- Alkali metal quadrupole spectral doublets used as diagnostic for determining alkali-metal plasma electron temperature
02 p0286 A69-11584
- Lithium hydride microplasma expansion in vacuum using charge collectors, time of flight detectors and spectroscopy of light emission
02 p0286 A69-11704
- Statistical analysis of polarization of two component nonisothermal electron-ion Coulomb gas plasma containing microflukes
02 p0286 A69-11707
- Barium plasma density measurements by Langmuir, microwave probes and resonance fluorescence scattering compared in Q device
02 p0288 A69-12172
- Plasma physics experiments and theoretical studies, discussing plasma heating by magnetic compression and irreversible expansion, Cs plasmas, plasma diagnostics, etc
02 p0289 A69-12200
- Electron density measurement technique for dense thick steady state plasmas using swept microwave interferometer
02 p0290 A69-12349
- Plasma column density profile measurement by means of two resonant cavity modes for low pressure discharge in small diameter tubes
02 p0290 A69-12403
- Critical values of laser formed solid angle determined in plasma diagnostics of scattering spectrum density distribution
02 p0251 A69-12416
- Dense plasma temperature determination by gamma ray resonance scattering
02 p0291 A69-12481
- Plasma diagnostics in magnetic field with thin cylindrical probe based on Langmuir method
02 p0292 A69-12556
- Average plasma electron density measurement by feedback oscillator to determine dielectric constant
03 p0473 A69-13103
- Scattering of energetic charged particles in weakly unstable plasma for integrated spectrum of plasma electric field autocorrelation function
03 p0475 A69-13151
- Contact phenomena theory in decaying plasma applied to deionizing mercury vapor diode gas discharge plasma diagnostics
03 p0404 A69-13547
- Electromagnetic properties of bounded isotropic plasma in kinetic approximation
03 p0477 A69-13712
- Space charge plasma acceleration in axially nonuniform magnetic field
03 p0477 A69-13760
- Electric potential distribution in coaxial quasi-stationary plasma injector
03 p0478 A69-13838
- Electron emission from metal foils used to study lifetime, concentration and mean ion energy of hot plasma
03 p0481 A69-14211
- Absorption coefficients of plasmas in capillary discharge tubes, discussing measurement using gas laser light source
03 p0442 A69-14218
- Wave number frequency dependent spectral function and space-time correlation function in turbulent plasma, noting utility for probes and scattering analysis
03 p0483 A69-14255
- Radial profile measurement technique for individual emission line intensities in plasma applied to populations of excited atomic and ionic Ar in capillary discharges
04 p0634 A69-14441
- Microwave Fabry-Perot resonator for anisotropic plasma diagnostics in presence of static magnetic field
04 p0635 A69-14757
- Diagnostic techniques for high speed low density DVL plasma wind tunnel noting problems of pressure, temperature, hot-wire and calorimetric measurements [DVL-849]
04 p0584 A69-14823
- Ultrahigh speed holographic interferometry for studying plasmas produced by focused laser beam, noting electron density evolution in deuterium plasma
05 p0760 A69-15587
- Electron density measurement in rapidly varying plasma, using improved Mach-Zehnder interferometer
05 p0760 A69-15613
- Plasma refractive index determination by holographic interferometry with double pulse ruby laser
05 p0761 A69-15620
- Electrical properties of xenon pulse plasmas with high power dissipation, measuring discharge pressure and radiation distribution as function of voltage drop
05 p0801 A69-15746
- Microchemical analysis for diffusion measurement of laser produced lithium plasma in uniform magnetic field
05 p0762 A69-15960
- Low dispersion spectrograph for temperature and electron density determination in plasma beam
05 p0803 A69-15997
- Time resolved measurements, microwave interferometer and pulsed double probe for studying collision dominated plasma expansion in inductive HF He discharge
05 p0804 A69-16535
- Formulas describing reflection and transmission coefficients of plasma for plane electromagnetic wave, using Maxwell equations in variable medium
05 p0805 A69-16608
- Plasma characteristics in thermionic converter operating under low voltage arc conditions obtained by computer, probes and spectral techniques
06 p0963 A69-16910
- Electron concentration in pulsed plasma measured with Fabry-Perot interferometer and laser radiation source
06 p0963 A69-16911
- Coupled cavity carbon dioxide laser interferometer with feedback for measurement of transient plasma density in theta pinch, noting sensitivity
06 p0935 A69-17706
- Probe noise in quiescent plasmas investigated using back diffusion type discharge tubes producing low density plasmas and positive plasma columns
06 p0967 A69-17715
- Plasma diagnostics using scattering of laser electromagnetic radiation by plasma density function, discussing plasma species collision effect on line profiles
07 p1131 A69-18485
- Focused electromagnetic beam interferometers and antenna parameters for measuring electron density in plasma diagnostics
07 p1132 A69-18865
- Photoionization cross section measurements for sodium line by analyzing electron-ion recombination radiation from sodium seeded plasma, determining electron temperatures and concentrations
07 p1184 A69-19164
- Franck-Condon factors for high rotational levels of nitrogen calculated in Morse potential approximation for application to plasma diagnostics
07 p1185 A69-19169
- Argon plasma characteristics calculated from 8 mm interferometer data, interpreting transmission coefficients of dielectric film with permittivity gradient
07 p1194 A69-19324
- Complex transmission and reflection coefficients of dielectric film with permittivity gradient computed by modified Runga-Kutta method, noting plasma diagnostics application
07 p1194 A69-19334
- Plasma electron density and collision frequency determination, using CW maser interferometer
08 p1359 A69-19987
- Nonlinear interaction of electromagnetic waves in bounded plasma, optimizing second order fields with reference to diagnostic applications
08 p1273 A69-20030
- Axial striograms of noncylindrical focusing discharge for plasma structure in front of interior electrode of coaxial gun
08 p1362 A69-20279
- Collection of papers on plasma diagnostics
08 p1363 A69-20462
- Thermal and nonthermal radiation of hot gases using spectroscopic plasma diagnostics
08 p1363 A69-20463
- Quantitative spectroscopy methods for determining data on chemical constitution of plasmas, treating optically thin LTE plasmas
08 p1363 A69-20465
- Spectroscopic diagnostics for determining temperatures, electron densities and line shapes in optically thick plasmas
08 p1363 A69-20466
- Plasma diagnostics in X ray region, determining electron and ion temperatures and densities and energy losses by radiation
08 p1315 A69-20469
- Microwave plasma diagnostics, discussing electromagnetic radiation and wave propagation measurements
08 p1316 A69-20470
- Plasma diagnostics by use of lasers, discussing Thomson scattering and problems arising from light scattering applications
08 p1326 A69-20471
- Spatial distribution and temporal variation measurements of magnetic fields in plasma, emphasizing pulsed discharges
08 p1364 A69-20472
- Spacecraft applications of Langmuir probes, obtaining data from current-voltage characteristics for electron/ion concentrations, ion mass spectra and charged particle energy distribution
08 p1316 A69-20474
- Mass spectrometer application to plasma diagnostics, discussing mass spectra, particle extraction, low and high pressure discharges, supersonic flow, ion detection methods, etc
08 p1316 A69-20475
- Plasma diagnostics methods for evaluating collision and transport cross sections, discussing resonance fluorescence, steady state discharge and afterglow measurements
08 p1364 A69-20476
- Evaluation methods for DC electrical conductivity, heat conductivity and viscosity in plasmas
08 p1364 A69-20477
- Ar-H plasma arc radial temperature distribution determined by photoelectric spectroscopy in visible range
08 p1366 A69-20758
- Fluid equations for collisionless plasma including finite ion Larmor radius and finite beta effects
08 p1368 A69-20802
- SERT 2 mercury vapor fed hollow cathode operated in bell jar, determining volt-ampere characteristics and flow rates for plasma diagnostics [AIAA PAPER 69-258]
09 p1561 A69-21221
- Moderately ionized plasma electrical conductivity calculated by generalized Ohm law and measured along with other plasma properties [AIAA PAPER 69-277]
09 p1543 A69-21264

Electron multiplication during ionized H plasma exposure to annular electric field and magnetic field, including microwave diagnostics

09 p1543 A69-21299

High temperature high density theta-pinch plasma refraction measurements by interference refractometer with beam perpendicular to plasma axis

09 p1544 A69-21302

Dispersion corrected three wavelength laser heterodyne system for plasma electron density and neutral density measurements

09 p1544 A69-21331

Dominant ionic species in cesium plasma through mass spectrometer analysis, measuring total ion and electron currents

09 p1544 A69-21335

Low current arc discharge plasma diagnostics by light probe, analyzing deviation of resonance level population from equilibrium described by Saha equation

09 p1546 A69-21586

Diagnostic techniques to identify flow regimes of high enthalpy shock tunnel
[AIAA PAPER 68-729]

09 p1477 A69-21970

Electron concentration at front of anisotropic plasma expanding in axial direction in electrodeless induction discharge from measurements of reflected microwaves

09 p1550 A69-22027

Temperature pulsations radial distribution in plasma jet using plasmatron without mixing chamber

10 p1729 A69-23432

Electron density and collision frequency of MHD plasma determined directly by measuring phase shift and attenuation of propagating laser microwave signal

10 p1731 A69-23436

Interplanetary plasma subsequent to July 7, 1966 flare monitored by detectors on Pioneer 6 and Explorer 33

10 p1783 A69-23775

Laser applications to high temperature, gas dynamical and plasma phenomena

10 p1741 A69-23809

Heat propagation in discharge plasma heated by magnetosonic wave, constructing transverse temperature profile

10 p1741 A69-23896

Plasma concentration diagnostics in magnetosphere based on hydromagnetic whistlers/pearls dispersion

10 p1688 A69-23934

Ion and electron temperature and density measurement by Thomson scattering with low resolution monochromator for Salpeter parameter near unity

11 p1925 A69-24310

Plasma microwave diagnostics by multifrequency probes in geometric optics approximation, assuming inhomogeneous and semiinfinite plasmas with sharp boundaries and nonunity permittivities

11 p1926 A69-24602

Pulsed laser holography for recording interferograms of laser created plasma, discussing laser source properties, spatial and spectral coherence, double pulse mode, etc

11 p1895 A69-24683

Electrostatic probe measurements in gas warmer than probe, demonstrating applicability of continuum theory for highly negative probe

11 p1930 A69-25274

Positive column contraction in Ar and Ar-Cs mixtures, developing theory for nonisothermal local collision arc

11 p1932 A69-25539

Current increase and voltage decrease in high voltage low pressure Penning discharge ascribed to hollow cathode effect

11 p1933 A69-25544

Ar plasma diagnostics in pinch-discharge laser, determining electron temperature by spectroscopy and measuring plasma conductivity and ion concentration and temperature

11 p1933 A69-25548

High temperature plasma quasi-classical pseudopotential, binary function and free energy derived, using displacement and collective variable methods

11 p1934 A69-25701

Optical diagnostics methods for fast processes in rarefied plasma, using Michelson interferometers with ruby and Nd lasers as light sources

12 p2089 A69-26186

Plasma instability in magnetic and HF electric fields, observing aperiodic short wave and oscillatory instabilities

12 p2136 A69-26526

Low pressure arc discharge plasma, studying ion-acoustic oscillations development in magnetic field

12 p2136 A69-26527

Dense plasma flow across transverse inhomogeneous magnetic field, proving adiabatic nature of motion

12 p2137 A69-26528

Plasma-electron beam interaction induced HF oscillations, obtaining nearly noise free oscillations

12 p2137 A69-26529

Multi-electrode plasma probe with potential negative with respect to plasma, noting effect of microoptical features of probe on accuracy of I-V measurements

12 p2138 A69-26538

Multi-electrode probe performance in plasma diagnostics, considering effects of plasma pressure, probe geometry and space charge on current-voltage characteristics

12 p2138 A69-26539

Holographic plasma diagnostics covering phase, amplitude variations images, laser spark, theta pinch studies, etc

12 p2094 A69-26707

Plasma properties when carrying periodic magnetoacoustic wave expressed in terms of periodic functions, discussing small perturbation propagation

12 p2138 A69-26708

Solar wind plasma observations in geomagnetospheric wake compared at 1000 and 500 earth radii, considering ion energy spectra and geomagnetic tail

12 p2151 A69-26943

High pressure arc discharge diagnostics with spectroscopic method relating spectral profiles to central temperature, pressure and temperature distribution

12 p2094 A69-26968

Input impedance of quarter wavelength antenna in anisotropic plasma, discussing plasma parameters role and use of probe antenna in plasma diagnostics

12 p2044 A69-27071

Soviet book on microwave methods of plasma investigation based on electromagnetic wave interaction, covering microwave probes and plasma radiation

12 p2139 A69-27073

Soviet monograph on plasma diagnostics by lasers, describing interferometry, optical field visualization, schlieren and shadow photography

12 p2139 A69-27075

Parameter measurement technique for low pressure helical pulse plasma discharges, determining spatial distribution of HF electric and magnetic fields and current density

12 p2140 A69-27124

Field distribution in HF flame discharges by measuring electrical and geometrical parameters of discharge channel

12 p2140 A69-27128

Carbon dioxide laser as light source in Michelson interferometer for plasma electron density measurement

12 p2100 A69-27177

Inhomogeneous and anisotropic cold plasma filled plane capacitor resonance in steady magnetic field applied to plasma diagnostics, using calculus of variations

13 p2304 A69-27240

Optical maser induced electrical breakdown interaction with superhigh pressure ionized gases, using optical interferometry and holography

13 p2273 A69-28464

Electric field frequency effect on cyclotron resonance during gas discharge, establishing causes of discrepancy between theory and experiments

13 p2315 A69-28577

Solar wind quiet state thermal properties and chemical composition compared with coronal expansion hydrodynamic model predictions

14 p2513 A69-29098

RF impedance method for electron density and collision frequency in plasma

14 p2492 A69-29352

Plasma scanner in obtaining current cross sections and current-voltage characteristics of hollow cathode magnetically confined arc plasma in argon

14 p2450 A69-29568

Electron density, temperature and dimensions of helium breakdown induced by Q switched ruby laser beam as function of space and time

14 p2492 A69-29636

Balance equations for axial separation in anisothermic plasma columns with radial variation of neutral gas temperature applied to argon discharge with mercury vapor addition

14 p2493 A69-29690

Soviet papers on plasma diagnostics covering optical, microwave, corpuscular, correlation and bolometric methods

14 p2494 A69-29775

Michelson interferometers with large interference fields for plasma diagnostics emphasizing structural rigidity, monochromatic light pulse power, instruments vibrations resistance, etc

14 p2496 A69-29776

Fabry-Perot interferometer for studying spatial distribution of plasma electron concentration, discussing resolution using solid state gas laser light source

14 p2451 A69-29777

Laser spark plasma initial development phase showing high electron temperature and concentration, continuous spectrum emission, line broadening and shock wave formation

14 p2461 A69-29777

Helium plasma electron temperature and concentration measured in arc in magnetic field by laser light scattering at electrons

14 p2496 A69-29780

Plasma diagnostics facilities design, circuit diagrams and operation based on Q switched ruby laser and optical recording system

14 p2461 A69-29782

Plasma electron temperatures from electron bremsstrahlung spectra measurements in X ray region

14 p2496 A69-29783

High speed photographs of plasma emission spectra in UV and soft X radiation spectrum regions, discussing theory, design and operation of facilities

14 p2496 A69-29784

Electron temperature and concentration in plasma determined by measuring diamagnetic signal and IR radiation intensity, emphasizing usefulness in plasmoid head portion

14 p2496 A69-29785

Millimeter and submillimeter microwave spectrometric studies of high temperature plasmas and noise emission, discussing instrumentation and absolute measurements

14 p2451 A69-29786

Plasma surface HF harmonic oscillations amplitude determined by comparing side frequencies intensities of reflected microwave signal

14 p2497 A69-29794

Plasma electron density measurement from phase shifts of electromagnetic wave groups propagation

14 p2497 A69-29796

Plasma diagnostics FM phase meter circuits tests, considering raster phase indicators, phase detectors and frequency integrators

14 p2497 A69-29797

Design and operation of two frequency phase meter for plasma diagnostics, using frequency modulation of microwave oscillator and waveguide bridge

14 p2451 A69-29798

Microwave interferometer with digital-logic elements for phase shift measurements in pulsed plasmas without frequency range limitations

14 p2452 A69-29802

Direct phase measuring and measured phase compensating microwave devices designed for plasma diagnostics applications

14 p2452 A69-29804

Phase measurements at IF in microwave plasma diagnostics, examining phase stabilization processes

14 p2452 A69-29805

Three component fast neutral beam for hydrogen plasma ion density and electron temperature determination, improving accuracy and reliability

14 p2452 A69-29812

Time of flight mass spectrometers for plasmoids generated by theta pinch and discharge over organic glass, showing ion and electron currents oscillograms

14 p2498 A69-29813

Bibliography on laser applications in plasma physics covering plasma diagnostics and production

14 p2498 A69-29842

Electron densities measurement in plasmas in magnetic fields from profiles of spectral lines, noting Stark and Zeeman effect

15 p2657 A69-30027

Calorimetric measurement of electron temperature in collisionless shock wave propagating in plasma column, discussing role of H beta line Stark broadening

15 p2657 A69-30104

Plasma diagnostics in magnetic field with thin cylindrical probe based on Langmuir method

15 p2658 A69-30253

Electronic density of collisional cesium plasma, comparing measurements made by Langmuir and HF spherical probes

15 p2659 A69-30300

Steady state solutions for parametric excitations in various limits in plasmas, allowing for higher order mode coupling

15 p2661 A69-30919

Recording arrangement aperture effect on plasma scattering spectrum during plasma parameter determination by light scattering technique
15 p2664 A69-30996

Scattering of line focused electromagnetic waves by infinite cylinders obtained by modification of plane wave theory
15 p2664 A69-31478

Boltzmann equation for Lorentzian plasma in elliptic magnetic field solved by expanding distribution function in Legendre polynomials
17 p3009 A69-32827

Langmuir probe to determine space vehicle orientation in ionospheric or interplanetary plasma, discussing apparatus, accuracy and application
17 p3001 A69-33222

Test apparatus for determining radiative properties of Ar plasma as function of high temperature and pressure
[AIAA PAPER 69-601] 17 p3010 A69-33310

He-Ne laser plasma behavior, establishing parameters for electron gas, cross sections of formation and annihilation and excited states lifetimes
17 p2982 A69-33390

Collisionless cylindrical Langmuir probe response in turbulent plasma for mean and statistical properties
[AIAA PAPER 69-698] 17 p3010 A69-33438

RF high pressure plasma discharges contained within radial inflow vortex, measuring radiation efficiencies, power densities and radiation fluxes
[AIAA PAPER 69-695] 17 p3010 A69-33442

Collision free earth shock wave gross and fine structure deduced from OGO 5 plasma diagnostics
[AIAA PAPER 69-676] 17 p2961 A69-33452

VLF and ULF whistler propagation in magnetosphere for remote sensing magnetospheric plasma parameters, exhibiting characteristic patterns and interaction with plasma
17 p2962 A69-33712

Collisionless shock wave structure in plasmas, noting plasma and shock wave generation mechanisms
17 p3013 A69-33822

Trapped modes in cold magnetoplasma slabs and rods in free space analyzed by Maxwell equation, assuming DC magnetic field and homogeneous electrons distribution
17 p2926 A69-33850

Artificial plasma properties at microwave frequencies, determining plasma electron density and effects on horn antenna radiation characteristics
18 p3100 A69-34271

Plasma parameters relationship with double electrostatic probe volt-ampere characteristics, applying corrected formulas for temperature, ion density, etc., to flame diagnostics
18 p3137 A69-34932

Atmospheric whistlers and ion acoustic waves interaction in nonisothermal plasma, determining damping frequencies, decrements and wave polarization
18 p3180 A69-35024

Power spectrum for energy transfer region in HF turbulent plasma by nonlinear equations, with results applied to subcosmic ray acceleration
20 p3591 A69-38008

Parameters of DC discharge between concentric cylinders calculated for plasma probes by pressure theory, noting ion neutral collisions and magnetic field effects
21 p3776 A69-38712

Negative ion concentrations in plasma by flash photodissociation, using Q switched laser for irradiation
21 p3778 A69-39574

Magnetoplasma with Maxwellian velocity distribution, investigating quantitatively longitudinal dielectric function
22 p3988 A69-40066

Boltzmann equation analysis used to study near surface electron temperature for weakly ionized plasmas, showing nonequilibrium absorption layer governing electron temperature profile
22 p3989 A69-40528

Density, ion temperature, electron temperature and ion drifts in Ba or Ba doped plasmas determined by resonance fluorescence and optical pumping
22 p3962 A69-40532

Multifrequency dispersion interferometers applicability in plasma diagnostics, considering integral electron concentration measurements
22 p3947 A69-40959

Coupled set of differential equations describing generalized Volterra problem of conflicting populations and application to plasma oscillations
22 p3976 A69-41260

Electron energy measurement accuracy in carbon dioxide laser plasma by S band radiometer
24 p4327 A69-42613

Soviet collection of articles on plasmoids covering plasma accelerators and plasma interactions with magnetic fields
24 p4356 A69-43467

Conical induction plasma accelerator design for studying acceleration process characteristics
24 p4357 A69-43468

PLASMA DIFFUSION

Microinstabilities of plasma confined by magnetic trap, discussing stabilization, drift waves and anomalous diffusion of plasma by turbulence
01 p0125 A69-10048

Plasma stability criterion for universal mode, discussing cusp curvature stability
01 p0127 A69-10279

Diffusion effect on particle buildup in deionizing steady plasma flux linked to plasma concentration in presence of electron temperature gradients
02 p0291 A69-12483

Diffusion across magnetic field of unstable plasma with highly inhomogeneous density
03 p0478 A69-13840

Microchemical analysis for diffusion measurement of laser produced lithium plasma in uniform magnetic field
05 p0762 A69-15960

Magnetoplasma waves in semiconductor, discussing cold plasma dispersion, helicons, carrier densities, lattice dielectric constant and acoustic domain propagation
07 p1197 A69-18465

Plasma diffusion in toroidal stellarator using integrals of drift equations for particle trajectories, determining distribution function
07 p1191 A69-18985

Magnetosonic wave evolution in inhomogeneous dispersive plasma created by magnetic piston, discussing equation solution
07 p1181 A69-19001

Cross modulation of amplitude modulated wave propagating in nonlinear dispersive plasma, obtaining electric vector
07 p1086 A69-19228

Cold plasma stability during traversing by microwave beams in presence of external magnetic field, obtaining dispersion relations for longitudinal and transverse modes
07 p1195 A69-19465

HF wave propagation in unbounded electron-plasma systems using moment equations, discussing collisions effect and dispersion relation
07 p1086 A69-19468

Recombination coefficients for dense weakly ionized cesium plasma, treating recombination process as diffusion generated by electron collisions
08 p1359 A69-19844

Ambipolar diffusion in electron concentration inhomogeneities of weakly ionized plasma in magnetic field analyzed by linearized quasi-hydrodynamic equations
08 p1362 A69-20426

Cylindrical antenna input impedance in isotropic plasma, assuming weak three dimensional plasma diffusion
08 p1285 A69-20428

Quasi-linear theory of hydromagnetic waves in nonrelativistic collisionless plasma, noting resonant diffusion effect on plasma heating mode
08 p1367 A69-20797

Kaufman thruster with predominant radial field, noting electron mobility across ion extraction screen and advantages of uniform plasma distribution
[AIAA PAPER 69-259] 09 p1569 A69-21877

Plasma diffusion in toroidal stellarator, calculating collisional diffusion and diffusion constants
09 p1552 A69-22294

Nonequilibrium ionization in central regions of low temperature plasma, describing charged particle drift by using diffusion time concept
10 p1732 A69-23440

Electrostatic wave dispersion relation in uniformly rotating plasma cylinder used in interpreting Q machine experiments
11 p1924 A69-24300

Pfirsch-Schluter factor calculation for stationary toroidal plasma diffusion enhancement due to current along magnetic field over diffusion over that associated with diamagnetic current
11 p1925 A69-24312

Beam-plasma dispersion relations, obtaining dispersion equation for plasma waves and dispersion curves for longitudinal waves
11 p1925 A69-24366

HF instability of low pressure discharge in magnetic field, discussing plasma diffusion and oscillations
11 p1927 A69-24912

Backward plasma waves in region of anomalous dispersion indicated by opposite directions of RF wave phase and group velocities
11 p1927 A69-25116

Current carrying inhomogeneous dense plasma instabilities confined in magnetic field, deriving dispersion relations in geometric optics approximation
11 p1932 A69-25537

Ions and electrons in ionosphere diffusion tensor components and ambipolar diffusion coefficient expressions derived for nonisothermal plasma
12 p2071 A69-26700

Longitudinal electric field penetration into semibounded plasma using kinetic approximation, assuming diffusive plasma particles reflection from plasma boundary
12 p2138 A69-26711

Magnetospheric plasma instabilities, discussing pitch angle diffusion instabilities, auroral precipitation boundary location, radial diffusion and maximum dissipation limit
12 p2072 A69-26748

Diffusion and mass flow in steady state magnetically stabilized helium arc plasma effects on spectroscopic determinations of electron temperature, discussing degree of ionization
12 p2141 A69-27146

MHD generator analysis, formulating boundary value problem for ion diffusion and Fourier series solution for end effect of electrodes pair
13 p2208 A69-27613

Linearized dispersion equation for electron oscillations in isotropic plasma with known electron velocity distribution function
13 p2313 A69-28328

Magnetized plasma waveguide dispersion characteristics using Maxwell equations, stressing interaction of electron beam with wave modes
13 p2315 A69-28571

Potassium plasma drift instability suppression by applied external HF electric field, noting plasma diffusion decrease toward container wall
14 p2489 A69-28740

Electron and ion separation as function of plasma potential drop in Langmuir cathode layer in arc regime
14 p2490 A69-29237

Dynamic dispersion relation for bounded cylindrical beam plasma with temperature correction, including hot beam interaction
14 p2502 A69-29957

Ambipolar to free diffusion transition in magnetized slab plasmas, discussing basic equations, iterative numerical procedure, characteristic parameters and H plasma
15 p2657 A69-30023

Turbulent diffusion and ion heating in plasmas in presence of current instability
15 p2662 A69-30959

Covariant dispersion relations for relativistic plasma oscillations for many component plasma in external magnetic field
16 p2816 A69-31633

Electromagnetic wave propagation in unbounded compressible plasma under drift velocity and magnetic field, obtaining dispersion equation for current density
18 p3179 A69-34261

Applicability and limitations of diffusive equilibrium in topside ionosphere, noting plasma density distribution along magnetic field line
20 p3531 A69-37887

Linearized dispersion equation for isotropic electron plasma without external fields solved by harmonic function model
21 p3775 A69-38564

Electron plasma velocity distribution function determined from dispersion equation by harmonic function analog
21 p3776 A69-38565

Plasma dielectric constant and RF wave energy and power absorption in anomalous dispersion region, noting plasma permittivity inverse relation to absorption band frequency
23 p4195 A69-41385

PLASMA DIODES

Electron temperatures and densities in interelectrode plasma of close spaced high current cesium plasma diode
19 p3380 A69-36415

Plasma thermionic diode figure of merit based on Hatzopoulos model altered to include thermal conduction and electrical resistance

22 p3869 A69-40134

PLASMA DYNAMICS

Hydrodynamic model of laser produced solid particle plasma, giving distributions of pressure, density, temperature and velocity

01 p0132 A69-11210

One dimensional Vlasov plasma nonlinear response to external electric field varying in space and time

01 p0133 A69-11214

Anisotropic two component plasma relaxation taking into account dynamic shielding collective effects

01 p0134 A69-11419

Symmetric tensor of time averaged stresses for collisionless plasma in oscillating field derived by Maxwell equations

02 p0286 A69-11588

Lithium hydride microplasma expansion in vacuum using charge collectors, time of flight detectors and spectroscopy of light emission

02 p0286 A69-11704

Plasma production by laser irradiation of solid, calculating numerically time variations of temperature distribution, laser intensity and evaporated layer depth

02 p0256 A69-11935

Model for fast randomization of electron gas by trapped electroacoustical waves

02 p0289 A69-12236

Free fluid hydrodynamics equations applied to weakly ionized plasma stability, considering drift oscillations excitation

02 p0291 A69-12553

Density gradient driven collisional drift waves, discussing identification, stabilization and enhanced plasma transport

03 p0474 A69-13145

Plasma equation of motion in external electromagnetic field analyzed as generalization of Bernoulli equation in relativistic MHD

03 p0476 A69-13385

French research on electric propulsion dealing with plasma dynamics, discussing traveling wave accelerators, pulsed plasma guns, ion thrusters, etc [AIAA PAPER 67-740]

03 p0496 A69-13995

Distribution functions for fast electrons near anode calculated by kinetic theory, assuming weakly ionized plasma with smaller Debye length than collision mean free path

04 p0635 A69-14764

Kinetic model equation for electron plasma incorporating collision terms for model scattering

04 p0636 A69-15042

Curvilinear plasma motions in ionosphere same as cyclones and anticyclones in troposphere, solving ionospheric unstable wind as function of pressure gradients

06 p0919 A69-17722

Dynamics of Q spoiled neodymium laser created plasma expanding in vacuum magnetic field

06 p0970 A69-17952

Thickness of resistivity controlled hydromagnetic shock wave, using classical one fluid equations and generalized Ohm law

06 p0970 A69-17956

Design and performance of large vacuum system with central control desk to study plasma dynamics, discussing visual monitoring at desk

07 p1116 A69-18261

Quasi-static theory of antenna in magnetoactive plasma subjected to resonance, solving boundary value problem

07 p1099 A69-18522

Stabilization of plasma filament with alternating current by quadrupole magnetic field

07 p1191 A69-18987

Rarefied plasma self similar motion qualitatively analyzed, particularly penetration and expansion, taking into account electric/magnetic field effects

08 p1359 A69-19951

High density plasma dynamic stability in magnetic containment using variational calculations

08 p1359 A69-19984

Kinetic theory for plasma, considering electric field fluctuations time evolution simultaneously with one particle distribution time evolution and Landau damping in wave equation

08 p1360 A69-19991

Behavior of bounded and free arc discharges under action of transverse magnetic fields and gas flows

08 p1366 A69-20767

Plasma kinetic equation obtained by method similar to Chapman-Enskog method

08 p1369 A69-20816

Self focusing of plasma whistler wave along magnetic field at small threshold power

09 p1546 A69-21577

Electron drainage currents from dilute streaming plasmas to positively biased silicon and cadmium sulfide solar cell arrays [AIAA PAPER 69-262]

09 p1436 A69-21726

Integrodifferential equations describing longitudinal oscillation properties in nonlinear region of electron Maxwellian plasma waves and two cold electron beams

09 p1550 A69-22026

Two dimensional flat geometry for initial solar flare development stage, discussing tearing mode energy source for solar flares and plasma compressibility effects

09 p1583 A69-22757

Dynamics, stability and approach to equilibrium of bounded one dimensional collisionless plasma representing minimum energy states with nonlinear Vlasov equation solutions

11 p1924 A69-24305

Streamer based on model of perfectly conducting plasma produced on boundaries by entering and departing electrons, discussing streamer thickness and propagation velocity

11 p1935 A69-25759

Plasma velocity measurement by Doppler shifts of spectral lines with photoelectric recording, using Fabry-Perot interferometer

12 p2079 A69-26021

Dynamic growth of positive ion sheath on plane electrode in mercury plasma, measuring sheath thickness and current

12 p2134 A69-26099

Steady equilibrium collisionless plasma in oscillating electromagnetic field, describing formalism for linear relation between perturbation and charges and currents induced in plasma

12 p2135 A69-26284

Isoperimetric plasma thermodynamics problems, including plasma free energy and relativistic plasma density fluctuations energy

12 p2138 A69-26603

Boundary layer between cold plasma and vacuum magnetic field, considering transverse velocity component perpendicular to field

12 p2139 A69-26944

Theoretical model describing electrodynamic plasma properties of HF flame discharge in air, heating discharge envelopes by heat diffusion from discharge channel surface

12 p2140 A69-27125

Transport equation describing drift, diffusion and reaction of iron swarm influenced by electric field in gas

13 p2306 A69-27457

Vlasov equations solved for electrons and ions in electromagnetic field, coupling electric field to density oscillation modes of plasma

13 p2306 A69-27461

Ionization fraction as independent variable in plasma transport correlation, noting role in pressure effect increase

13 p2313 A69-28241

Magnetic field intensity, plasma pressure and energy density relations for macroscopic plasma motion inside neutral sheet from two dimensional model

14 p2440 A69-29119

Dynamic dispersion relation for bounded cylindrical beam plasma with temperature correction, including hot beam interaction

14 p2502 A69-29957

Free fluid hydrodynamics equations applied to weakly ionized plasma stability, considering drift oscillations excitation

15 p2658 A69-30250

Coupled kinetic equations for inhomogeneous systems treated as simultaneous equations in time, obtaining solutions by successive approximation

15 p2660 A69-30913

Interchange stability and drift motion of plasma with loss from ends of axisymmetric magnetic bottle, using hydromagnetic equations

15 p2664 A69-31100

Analytic expressions for motion of collisionless plasma created with isotropic velocities within uniform magnetic field, assuming equal electron and ion masses

16 p2818 A69-31673

Equivalent dielectric tensor for warm drifting electron plasma using model

16 p2820 A69-31701

Precurator plasma electron number densities calculations for blunt reentry vehicles, analyzing extreme UV radiation emanating from bow shock [AIAA PAPER 69-718]

17 p2893 A69-33487

Ionized plasma motion under plane piston action by self similar solution of Navier-Stokes equations

22 p3991 A69-41021

Interaction between two temperature plasma flux and electrodes in MHD channel with crossed electric and magnetic fields, studying boundary layer dynamics

22 p3991 A69-41022

Fokker-Planck plasma collision equation derived from Boltzmann equation, Markov process and Liouville equation

23 p4195 A69-41516

Stationary equilibrium of two dimensional plasmas with motion perpendicular to uniform magnetic field and gravitational field, considering resistive diffusion role

24 p4356 A69-43365

Hydrogen plasma-axisymmetric magnetic field interaction, studying plasmoid motions during exit from field

24 p4358 A69-43472

Crossed inhomogeneous electric and magnetic fields effect on H plasma fluxes dynamic behavior, deriving plasma motion formula

24 p4358 A69-43475

Actuator disk model for study of azimuthally nonuniform MPD arc plasma dynamics [AIAA PAPER 68-714]

24 p4359 A69-43570

PLASMA ELECTRODES

Bilateral plasma outflow plasmatron with variable electrode diameter, discussing efficiency, current-voltage characteristics and size

01 p0125 A69-10102

RF characteristics of electrodes immersed in magnetoplasma, discussing potential distribution around point charge and RF probe measurement of plasma parameters

01 p0029 A69-10550

Electron gun with plasma cathode consisting of gas discharge chamber, electron ejecting component and focusing system

04 p0598 A69-14857

Surface parameters influence on energy transfer to arc jet anode, discussing work function, accommodation coefficient and diffuse reflection coefficient of electrons [AIAA PAPER 69-107]

06 p1039 A69-18185

Current and voltage distribution in electromagnetic compressor channel with solid electrodes of finite resistance, noting error analysis

07 p1059 A69-19029

Power losses in MHD channel due to longitudinal end effects related to finite dimensions of electrodes and terminal insulators

07 p1193 A69-19030

Lithium vapor fueled applied field MPD arc jet performance using open end heat pipe vaporizer and hollow cathode [AIAA PAPER 69-241]

09 p1561 A69-21222

Plasma acceleration by induced Hall currents, discussing Hall-to-current ratio maximum at critical magnetic field [AIAA PAPER 69-280]

09 p1562 A69-21228

Quasi-steady state plasma acceleration in coaxial electrode geometry during synchronized application of tailored pulses of mass flow and current [AIAA PAPER 69-267]

09 p1563 A69-21234

Segmented anode, carbon dioxide-hydrogen performance and hollow cathode erosion tests on low power MPD arc thruster, noting current measurements [AIAA PAPER 69-242]

09 p1563 A69-21236

Predicting electrode geometry effect on saturation ion currents in diode exposed to ionizable vapor in equilibrium with liquid Ce

09 p1440 A69-21832

Plasma dissipative drift instability and nonlinear wave interaction from discharge with oscillating electrodes, investigating LF plasma oscillations

09 p1550 A69-22019

Current-voltage characteristics of combustion driven shock tube generated argon plasma

10 p1737 A69-23466

MHD generators with segmented electrodes at high Hall parameters, noting electron density, conductivity and Hall field reduction factor

10 p1637 A69-23476

Heat flux toward electrodes measured under high current discharge, showing conductive heat transfer and erosion effect

11 p1928 A69-25227

Porous cermet electrodes thermochemical protection by blowing neutral gas into electrode boundary layer, examining effect on volt-ampere characteristics

11 p1826 A69-25232

Current and voltage distribution around normal shock in MHD duct using conformal transformation,

considering continuous and segmented electrode boundary conditions

11 p1931 A69-25359

Angular distribution of electrons leaving plasma at electrode boundary, using kinetic Boltzmann equation with scattering function and specular reflection

11 p1933 A69-25546

Electrical breakdown between cold electrodes in contact with flowing plasma produced by electromagnetic shock tube

12 p2134 A69-26098

Multielectrode probe performance in plasma diagnostics, considering effects of plasma pressure, probe geometry and space charge on current-voltage characteristics

12 p2138 A69-26539

Surface dissipation effect induced by end electrodes on drift instabilities in cold ion plasma column described by differential equation with constant coefficient

12 p2138 A69-26710

Voltage characteristics in MHD generator with water cooled segmented electrodes using potential probes, considering forced convection heat transfer

12 p2017 A69-27178

MHD generator analysis, formulating boundary value problem for ion diffusion and Fourier series solution for end effect of electrodes pair

13 p2208 A69-27613

Conducting liquid boundary layer flow and heat flux on electrodes of MHD generator, including one dimensional flow outside boundary layer

13 p2309 A69-28028

Near electrode layer calculation in low temperature plasma, solving kinetic ion equation for quasi-neutral and Poisson equation for space charge regions

13 p2312 A69-28117

Mass transfer due to plasma recombination, ambipolar diffusion and electrode erosion and resistance forces effects on electrodynamic accelerated plasma

13 p2315 A69-28555

Low voltage arc in thermionic cesium vapor diode with lengthy electrodes and temperature variations along emitter, discussing plasma and current density distributions

14 p2402 A69-29244

Knudsen arcs kinetic theory with cesium/inert gas mixtures in narrow gap between parallel plate electrodes, discussing fast particle beams and electron scattering

14 p2491 A69-29245

Electron energy distribution function and nonequilibrium ionization rate in near cathode layer of thermionic converter

14 p2404 A69-29255

MHD channel flow calculations by quasi one dimensional approximation, considering potential drops at electrodes

14 p2500 A69-29904

Longitudinal pressure distribution in MHD channel with electrodes parallel to applied transverse magnetic field

14 p2501 A69-29918

Plasma three electrode source ion-optical characteristics, noting beam angular divergence dependence on spacing between discharge cavity and intermediate electrode

15 p2658 A69-30240

Current distribution and Hall voltage in crossed fields discharge with split electrodes in nonequilibrium Ar and Cs plasmas

15 p2663 A69-30980

Integral charge neutrality effect on local space charge density of MHD generator channel, examining electrode couple for Faraday generators

15 p2664 A69-31055

Regulating setup for controlling AC voltage surrounding polarization of magnetic electrode in plasma

15 p2664 A69-31094

I-V characteristics of caloelectric plasma converter with concentric electrodes measured for various hot electrode temperatures and mercury vapor flow rates

16 p2822 A69-32065

One dimensional viscous magnetofluidynamic flow in annulus formed by concentric cylindrical electrodes, reducing problem to linear partial differential equation set

[AIAA PAPER 69-725]

17 p3012 A69-33493

Self induction of conical electrode type plasma accelerator with and without allowance for magnetic scattering field, investigating acceleration process

19 p3379 A69-35821

Electron temperatures and densities in interelectrode plasma of close spaced high current cesium plasma diode

19 p3380 A69-36415

Gas velocity and pressure influence on electrical breakdown potential of Ar, N and He between parallel flat plate and concentric electrodes

24 p4359 A69-43693

PLASMA-ELECTROMAGNETIC INTERACTION

Absorption of linearly polarized light in reflecting surface layer of collisionless plasma, calculating layer lifetime for reflection of light

01 p0127 A69-10283

Artificial visible plasma clouds in space interacting with electric and magnetic fields around earth

01 p0151 A69-10533

Thermonuclear fusion program, discussing plasma instabilities suppression, toroidal installations, magnetic trap systems, plasma heating and dynamic stabilization

01 p0156 A69-11065

Resistive spherical plasma expansion into external magnetic field noting magnetic stream function

01 p0132 A69-11211

Moderately strong electromagnetic wave propagation in fully ionized plasma, noting nonlinear effects for frequency near plasma frequency

01 p0133 A69-11213

Normally incident linearly polarized electromagnetic wave reflection and transmission by semifinite longitudinally drifting magnetoplasma in static magnetic field

01 p0134 A69-11290

Electromagnetic waves propagation in cylindrical waveguide containing plasma column along axis in absence of constant magnetic field

02 p0285 A69-11463

Magnetic confinement of electric arc in alkali metal vapor containing gas flow, considering degree of ionization

02 p0286 A69-11585

Impedance sheet approximation to plasma slab, considering plane wave propagation, plasma covered slot antenna and transmission loss

02 p0209 A69-12348

Inert gas nonequilibrium MHD power generation in shock tube

02 p0196 A69-12425

Electromagnetic oscillations in ionized plasma, assuming higher oscillation frequency than collision frequency

02 p0292 A69-12643

Diffraction of cylindrical waves at half plane in cold anisotropic plasma, using Fresnel integrals

02 p0293 A69-12842

Helium plasma ion oscillations damping by external RF electric field at sheath-plasma resonance condition

03 p0476 A69-13323

Nonlinear interaction of steady state circularly polarized electromagnetic wave with cold plasma in constant longitudinal magnetic field

03 p0476 A69-13381

Energy partition between mechanical and magnetic modes in turbulent plasma in external field

03 p0476 A69-13384

Statistical description of nonelastic processes in nonequilibrium plasma in transverse magnetic field, using kinetic equations for distribution functions

03 p0476 A69-13412

Cold plasma motion caused by electromagnetic wave pressure propagating along uniform magnetic field

03 p0477 A69-13413

Electromagnetic wave passage through plane gyrotropic layer of magnetized plasma, analyzing polarization and energy transfer

03 p0397 A69-13709

Electromagnetic properties of bounded isotropic plasma in kinetic approximation

03 p0477 A69-13712

Helicon waves in nonresistive cylindrical and spherical plasmas

03 p0479 A69-13961

Nonmagnetic plasma deceleration in quasi-stationary magnetic field with coaxial injector and barrier field

03 p0481 A69-14212

Charged particles motion in spatially modulated magnetic field solved using modification of Krylov-Bogoliubov asymptotic method

04 p0633 A69-14297

Asymptotic method for studying charged particle motion in spatially modulated magnetic field

04 p0634 A69-14298

Nonlinear damping of circularly polarized electromagnetic wave propagating in plasma along magnetic field, noting particle motion in resonance region

04 p0558 A69-14982

Electromagnetic wave propagation in uniform anisotropic plasma, considering wave vectors perpendicular to magnetic field

04 p0637 A69-15048

Nonlinear demodulation of amplitude modulated wave propagating in plasma

04 p0559 A69-15210

Deuterium plasma heating by means of high power focused pulsed laser beam, noting initial energy of laser and pulse duration

05 p0769 A69-15583

Laser light scattering by plasma using theory of ionospheric scattering of radar signals, determining scattered spectrum

05 p0798 A69-15586

Interactions in classical relativistic plasmas, discussing Lorentz invariant statistical mechanical formalism and phenomenological electrodynamics

05 p0801 A69-15770

Electron plasma interaction with transverse EM wave propagating along magnetic field, calculating permittivity, density, field strength and applied frequency

05 p0805 A69-16699

Kinetic equation for plasma in external inhomogeneous nonstationary electromagnetic field, noting perturbation theory and Vlasov approximation

05 p0805 A69-16700

Spatial and temporal characteristics of two component electron-ion nonisothermal plasma and penetration of external LF electric field into plasma

05 p0806 A69-16745

Wave dispersion analysis for amplification in cold plasma filled cylindrical waveguide penetrated by electron beam of same radius

05 p0736 A69-16790

Electromagnetic waves transformation and scattering in plasma in electric field, showing abrupt increase at certain critical value

06 p0886 A69-16894

Spatial dispersion of electromagnetic waves reflection from moving plasma layer in magnetic field, determining transmission and energy absorption coefficients

06 p0886 A69-16895

Bounded and spatially separated plasmas wave oscillations stability in magnetic field, observing hydrodynamic slipping and drift instability

06 p0963 A69-16903

Equation for charged particle motion in electromagnetic wave field propagated along magnetic field applied to nonlinear wave propagation in plasma near cyclotron resonance

06 p0963 A69-16905

Propagation constant and radiation of center fed linear antenna with feed points displaced transverse to antenna axis and immersed in warm compressible plasma

06 p0896 A69-17476

Harmonic generation of S band signal inside plasma column at resonance

06 p0965 A69-17488

Arc phenomena and gas dynamic effects during shock heated plasma interaction with magnetic field

07 p1188 A69-18273

High power microwave interactions in pulsed electron beam plasma klystron

07 p1095 A69-18433

Energy losses of clusters of charged particles moving through unbounded isotropic plasma manifesting nonlinearity in interaction of particle generated fields

07 p1189 A69-18528

Shot noise in dipole antenna immersed in hot plasma related to antenna input resistance, using Maxwellian velocity distribution

07 p1079 A69-18920

Conducting gas acceleration in strong unsteady electromagnetic field, discussing channel flow in relation to time and pressure gradient

07 p1191 A69-18988

Cylindrical and spherical waves propagation in weakly inhomogeneous plasma treated by geometrical optics, noting caustic surfaces

07 p1195 A69-19747

Electromagnetic wave reflection from moving plasma characterized by conductivity for slow waves, calculating reflection and absorption factors

07 p1196 A69-19748

Self focusing of TM type electromagnetic waves in isotropic plasma and formation of waveguide channel

07 p1196 A69-19749

Nonlinear interaction of electromagnetic waves in bounded plasma, optimizing second order fields with reference to diagnostic applications
08 p1273 A69-20030

Coupled wave equation solution based on spectral resolution for longitudinal components of electric and magnetic fields when source currents are present in compressible anisotropic plasma
08 p1274 A69-20031

Plane electromagnetic wave reflection and transmission by semiinfinite moving compressible plasma fluid, noting interaction of transmitted H wave
08 p1360 A69-20097

Time-averaged value of forces of electromagnetic wave falling from vacuum and acting on magnetoactive plasma
08 p1361 A69-20200

Positive column in longitudinal magnetic field in helium and neon, noting agreement with collision diffusion theory and Kadomtsev perturbation theory
08 p1361 A69-20212

HF electromagnetic wave scattering at small scale plasma turbulence in magnetic fields, discussing interactions in frequent collisions region
08 p1275 A69-20435

Radiation field patterns of linear antennas immersed in weakly ionized plasma evaluated for propagation constants of current distribution
08 p1285 A69-20551

Complex microwave transmission coefficient of nominal cut-off plasma for several different types of electron distribution, noting discharge characteristics for cut-off
08 p1366 A69-20759

Wave interaction in magnetically confined plasma taking into account body and surface waves
08 p1370 A69-21014

Hall current influence on plasma jet interaction with space periodic magnetic field created by system of coaxial coils with alternating current directions
08 p1370 A69-21017

Longitudinal polarization behind front of plasma flow interacting with transverse magnetic field, showing electric potential and magnetic field exhibit structural fluctuations
08 p1370 A69-21018

Approximate solution of nonlinear differential equation describing interaction between galactic cosmic rays and solar wind, obtaining four domains
09 p1575 A69-21524

Amplitude modulated radio wave interaction with rarefied plasma in magnetic field, considering possible ionospheric heating by mechanism
09 p1453 A69-21543

Scientific data acquisition and interpretation effects on electric spacecraft plasmas and field directions, noting electron interchange reactions effect
[AIAA PAPER 69-276] 09 p1568 A69-21727

Radio frequency signal transmission between orbiting spacecraft and vehicle entering VM-10 model atmosphere, examining near wake approximations and plasma-electromagnetic interaction
09 p1455 A69-22002

Kinetic theory of electromagnetic wave passage through magnetoactive plasma, discussing dispersion and specular and diffuse reflection
09 p1550 A69-22022

Kinetic theory of electromagnetic wave propagation in infinite laminated plasma with different dielectrics, determining attenuation
09 p1550 A69-22023

Resonant interaction between traveling charge with superimposed magnetic field and Alfvén wave in plasma cylinder, showing cyclotron orbit variations
09 p1551 A69-22035

Charge and traveling wave interaction in circular waveguide in resonance regime solved by Krylov-Bogoliubov asymptotic method
09 p1551 A69-22037

Electromagnetic wave propagation direction in vacuum for reflection from semiinfinite plasma, noting effects of nonlinear transverse wave excitation
09 p1459 A69-22529

Plasma cavity shape formed by magnetic field effect due to several parallel line currents
[ISAS-433] 09 p1553 A69-22569

Second harmonic generation by electromagnetic wave incident on inhomogeneous plasma, determining power output
10 p1653 A69-23133

Plasma ions turbulent heating during electron-acoustic instability in field of circularly polarized electromagnetic wave at ion cyclotron frequency
10 p1728 A69-23137

Electromagnetic wave transmission through anisotropic plasma, discussing incident wave field strength effects near cyclotron frequency
10 p1728 A69-23167

Beam displacement at plasma under magnetic field connected with polarized electromagnetic wave reflections
10 p1740 A69-23724

Field effect on positive column plasma of glow discharge in air, analyzing near wall potential and conductivity
10 p1741 A69-23946

Landau type interaction between electron beam and whistler/helicon wave electric field within semiconductor/InSb/
10 p1742 A69-24107

Nonlinear confining and deconfining forces of laser light interaction with inhomogeneous plasma, analyzing macroscopic motion based on ponderomotive force description
11 p1923 A69-24297

Electric shock tube for measurement of plasma magnetic fields induced by shock plasma moving through DC magnetic field transverse to flow
11 p1925 A69-24311

Pfirsch-Schluter factor calculation for stationary toroidal plasma diffusion enhancement due to current along magnetic field over diffusion over that associated with diamagnetic current
11 p1925 A69-24312

Beam-plasma dispersion relations, obtaining dispersion equation for plasma waves and dispersion curves for longitudinal waves
11 p1925 A69-24366

Transient signal propagation through cold inhomogeneous plasma with electron density decreasing exponentially in direction of propagation
11 p1836 A69-24990

Tonks-Dattner resonances in plasma column, using linearized Vlasov equation for coupling to plasma waves of time varying electric fields
11 p1929 A69-25266

Normal mode representation of HF properties of inhomogeneous plasma, analyzing Vlasov equation for free oscillations under external driving field
11 p1929 A69-25269

Nonlinear HF conductivity of fully ionized plasma, considering applied electromagnetic field frequency close to electron plasma frequency
11 p1929 A69-25271

Electric field penetration into homogeneous plasma at frequencies near Langmuir frequency and current at surface of thin cylindrical antenna in plasma
11 p1853 A69-25551

Electromagnetic wave propagation cut-off in slightly noncompensated electron hole plasma, discussing wave evanescence above critical magnetic field value
12 p2133 A69-25926

Cyclotron harmonic waves/CHW/ nonlinear decay instability and parametric amplification, considering applicability to practical amplifiers
12 p2135 A69-26314

Plane transient electromagnetic wave from cold lossless plasma half space and slab
12 p2033 A69-26865

Interplanetary scintillation and angular spectrum of radio waves scattered by solar plasma, noting magnetospheric tail and solar wind
12 p2161 A69-26942

Soviet book on microwave methods of plasma investigation based on electromagnetic wave interaction, covering microwave probes and plasma radiation
12 p2139 A69-27073

Stationary magnetic field effect on sum and difference frequency generation due to nonuniform RF electric fields applied externally to plasma
13 p2305 A69-27376

Plasma lens device for focusing ion or plasma beams with closed electron drift
13 p2307 A69-27658

Waves propagating along rotating electron beam and interacting with magnetized plasma waveguide slow waves
13 p2312 A69-28118

Whistler type electromagnetic waves excitation by electron beam in plasma, noting intensity dependence on electron frequency
13 p2314 A69-28443

Magnetic and electric field effects on undamped electron-hole LF frequency plasma oscillations in spatially homogeneous nonpolar semiconductor
13 p2323 A69-28581

Reflection and absorption coefficients analyzed for obliquely incident electromagnetic wave from magnetoactive plasma in constant parallel magnetic field
14 p2411 A69-28997

Monochromatic plane waves propagation in anisotropic homogeneous cold plasmas, treating dispersion surface, reflection, refraction and waveguide applications
14 p2492 A69-29399

Longitudinal electric field penetration into plasma slab in constant magnetic field
14 p2493 A69-29665

Si III and O II spectral lines distortion in pulse HF plasma in rotating electromagnetic field, showing particle rotational speed dependence on discharge chamber radius
14 p2497 A69-29791

Passive electric microwave probe with balancing capacitance for studying waveguide fields at high microwave power levels in radiative plasma accelerators
14 p2498 A69-29807

Collisionless plasma slab drift mode stabilization at uniform temperature by oscillating electromagnetic field
14 p2499 A69-29851

MHD interaction between plasma and transverse magnetic field in shock tube, noting unsteady shock wave propagation in interaction zone
14 p2501 A69-29919

Plasma temperature measurement by resonant laser radiation absorption, assuming Saha-Boltzmann relation
14 p2501 A69-29954

Fermi acceleration of energetic electrons trapped within dipole magnetic field analyzed to obtain quantitative results for wave-particle interaction within complex magnetospheric configuration
15 p2594 A69-30095

Nonlinear effects and turbulent behavior in beam plasma instability, studying interactions in magnetic field
15 p2660 A69-30917

Thermodynamic Green function for Compton scatter cross section of photons by electrons in hot plasma
15 p2664 A69-31479

Weakly ionized plasma electron heating by interaction with HF electromagnetic field calculated using Boltzmann transport equation
15 p2665 A69-31480

Electromagnetic echo generation in collisionless spatially homogeneous plasma dependence on velocity distribution and magnetic interaction
16 p2818 A69-31677

Laser radiation absorption by inhomogeneous overdense plasma, discussing effects of plasma expansion on energy coupling efficiency
16 p2818 A69-31679

Particle-wave interaction in weak turbulent plasma in presence of uniform magnetic field, applying perturbation theory arbitrary order
16 p2819 A69-31683

Microwave field-plasma slab nonlinear interaction in rectangular waveguide, analyzing current and electron density and second harmonic TE and TM power
16 p2749 A69-31703

Nonlinear mixing of Ar plasma ion wave and externally applied electromagnetic wave
16 p2820 A69-31769

Single particle and collective excitations of plasmas in solids and interactions with acoustic and electromagnetic waves in magnetic field
16 p2821 A69-31820

Incident energy transfer to particles due to nonlinear interactions during passage of intense light beam through plasma, considering decay into plasma waves
16 p2822 A69-32046

Plasma cluster interaction with axially symmetric magnetic field, deriving plasma diamagnetic current, inductance and resistance from measured coil flux dependence on distance
16 p2823 A69-32365

Increase or decrease in light absorption by plasma particles found dependent on laser intensity level
16 p2797 A69-32382

Polarization characteristics of electromagnetic waves obliquely reflected from inhomogeneous isotropic plane stratified plasma
16 p2752 A69-32391

Approximate solution of nonlinear differential equation describing interaction between galactic cosmic rays and solar wind, obtaining four domains
16 p2851 A69-32519

Amplitude modulated radio wave interaction with rarefied plasma in magnetic field, considering possible ionospheric heating by mechanism

16 p2754 A69-32538

Wave front resistivity in laser produced plasma interacting with magnetic field enhanced by two stream instability

16 p2823 A69-32564

Polar substorms resulting from interaction between magnetized plasma stream and geomagnetic field in magnetosphere

16 p2852 A69-32620

Nonlinear interaction of plane electromagnetic wave with inhomogeneous plasma layer, noting concentration and electric field discontinuity

17 p2922 A69-33693

VLF and ULF whistler propagation in magnetosphere for remote sensing magnetospheric plasma parameters, exhibiting characteristic patterns and interaction with plasma

17 p2962 A69-33712

Electroacoustic-electromagnetic waves nonlinear coupling in compressible isotropic plasma, comparing slowly varying and resonant interaction approaches

17 p2928 A69-33870

Microwave propagation inside hollow cylinder using model plasma as dielectric, deriving relationship between phase shift and free electron density

17 p2932 A69-34218

HF electromagnetic waves penetration into slightly ionized plasma analyzed by Maxwell and kinetic equations, giving penetrating electric field by WKB formula

17 p2932 A69-34220

Electromagnetic wave propagation in unbounded compressible plasma under drift velocity and magnetic field, obtaining dispersion equation for current density

18 p3179 A69-34261

Artificial plasma properties at microwave frequencies, determining plasma electron density and effects on horn antenna radiation characteristics

18 p3100 A69-34271

Anomalous absorption of electromagnetic wave in collisionless dense cylindrical plasma beam in circular waveguide, noting electric field strength for energy transfer

18 p3101 A69-34621

Atmospheric whistlers and ion acoustic waves interaction in nonisothermal plasma, determining damping frequencies, decrements and wave polarization

18 p3180 A69-35024

Microwave background angular fluctuations investigated for relationship between whirl motion velocity and temperature dispersion, noting role of scattering by moving plasma

18 p3188 A69-35208

Radar design for target detection, tracking and identification, modeling plasma effects on radar cross section of reentry vehicles based on wave-plasma interactions

20 p3485 A69-36925

Negative energy waves presence, showing qualitative difference on the theoretically derived parametric amplification in plasmas

20 p3582 A69-38244

Matter and radiation interaction in hot model universe, investigating residual radiation spectrum deviation from Planck curve

21 p3797 A69-38536

Electromagnetic wave reflection and transmission from boundary between semiinfinite plasma and air by applying static magnetic field

21 p3672 A69-38743

Langmuir probe immersed in plasma RF response over range of signal amplitude and frequency and plasma electron density, showing sheath capacitance role

21 p3723 A69-38939

Jupiter magnetospheric radio emissions, discussing magnetic field and plasma-magnetic interactions

21 p3812 A69-39517

Microwave absorption by Ar plasma of positive column discharge in waveguide under inhomogeneous magnetic field

21 p3778 A69-39547

Homogeneous conducting moon-solar wind interactions, describing time dependent lunar magnetic and electric fields induced by interplanetary magnetic field variations

22 p4023 A69-40518

Prolate spheroidal antennas operation in isotropic plasmas, studying effects of collision frequency, electron temperature and antenna length on admittance, radiation and current distribution

22 p3914 A69-40702

Aperture distortions and spectral line shapes of electromagnetic radiation diffused by plasma

22 p3982 A69-40799

Radio wave scattering cross section in wake of body moving in ionosphere, using simplified procedure with asymptotic expressions

22 p3901 A69-41094

Electromagnetic wave propagation instabilities in semiconductor magnetoplasmas no diffusion limited to LF, using dispersion equation

22 p3902 A69-41223

Plane EM wave transmission and reflection by semiinfinite isotropic plasma moving in arbitrary direction parallel to boundary, using Lorentz transformation

23 p4114 A69-41360

Plasma dielectric constant and RF wave energy and power absorption in anomalous dispersion region, noting plasma permittivity inverse relation to absorption band frequency

23 p4195 A69-41385

Plane electromagnetic wave scattering on turbulent fluctuations in electron density of finite volume ionized plasma, evaluating Booker-Gordon relation

23 p4116 A69-41587

Slot antenna radiation patterns in presence of aperture RF plasma breakdown sheath measured for various gas pressures and breakdown power levels

23 p4116 A69-41595

Electromagnetic waves scatter propagation in isotropic plasma in plane waveguide, noting electron charge density fluctuations role

23 p4125 A69-42040

Electromagnetic scattering by small plasma ellipsoid moving in vacuum through external steady magnetic field, analyzing resonance phenomena

24 p4282 A69-42979

Rocket exhaust plume models for signal attenuation predictions, considering inhomogeneous plasma medium with varying electron density and collision frequency

24 p4408 A69-43253

Crossed inhomogeneous electric and magnetic fields effect on H plasma fluxes dynamic behavior, deriving plasma motion formula

24 p4358 A69-43475

Steady state interaction between collisionless plasma flow and immersed stationary magnetized or unmagnetized objects by inserting Cs ion accelerator into plasma wind tunnel

24 p4359 A69-43646

PLASMA ENGINES

Telemetered data obtained by Iantar 1 automatic ionospheric laboratory, detailing argon-ion plasma engine performance

05 p0830 A69-16056

Pulsed plasma microthruster propulsion system for synchronous orbit LES 6 satellite [AIAA PAPER 69-298]

09 p1562 A69-21227

Background pressure and magnetic field shape effect on MPD thruster performance, testing radiation cooled thrusters [AIAA PAPER 69-243]

09 p1564 A69-21239

Ion thrusters and various microthrusters/electron bombardment ion and pulsed plasma/ for proposed European missions [AIAA PAPER 69-274]

09 p1565 A69-21250

Segmented anode current and heat distribution in MPD engine measured with current shunts and calorimetric methods [AIAA PAPER 69-244]

09 p1566 A69-21260

MPD engine plasma flow investigated by Langmuir probe measurement of ion saturation current [AIAA PAPER 69-233]

09 p1567 A69-21266

Electric current spike in MPD operation, using segmented anode and image converter methods with argon and helium propellant gases

09 p1548 A69-21962

Ion spacecraft propulsion systems, discussing components and characteristics of reaction type rocket engines and electrical thrust devices

11 p1944 A69-25593

Axial velocities in ammonia MPD thruster exhaust by measuring Doppler shifts of spectral lines emitted by plasma constituents

16 p2835 A69-31890

Electric propulsion, discussing plasma research, MPD thruster and arcs, ion thruster research and spacecraft integration [AIAA PAPER 69-497]

16 p2838 A69-32655

Electric propulsion systems for manned planetary exploration flights, discussing arc jet, ion and plasma engines

18 p3185 A69-35108

Telemetered data obtained by Iantar 1 automatic ionospheric laboratory, detailing argon-ion plasma engine performance

20 p3618 A69-37966

Rotational arc motion in MPD accelerators with strong axial fields predicted by plasma physics equations

23 p4201 A69-41909

Radial pressure distribution in steady state rotationally symmetrical plasma jet subjected to axial magnetic field, emphasizing mass entrainment effect [DGLR-69-024A]

23 p4202 A69-41924

Spectroscopic azimuthal and axial measurement of jet velocity in MPD X9 rocket engine by spectrograph and Fabry-Perot interferometer [DGLR-69-024B]

23 p4202 A69-41925

Rocket engine plasma jet radial velocity measurement by induction-velometric method using moving probe [DGLR-69-024C]

23 p4202 A69-41926

Performance test of German MPD plasma rocket engine with augmented magnetic field and 5-10 kw output, describing integral measurement procedure and observed phenomena [DGLR-69-024D]

23 p4202 A69-41927

HF ion engine RIT 10, Kaufman ion engine ESKA, Hall effect ion engine HIT and MPD engine compared for state of development [DGLR-69-021]

23 p4202 A69-41928

PLASMA FLOW

U MAGNETOHYDRODYNAMIC FLOW

PLASMA FLUX MEASUREMENTS

Plasma flux measurements by charged particle traps in Venus vicinity by space vehicle Venus 4, discussing low concentration of charged particles

07 p1222 A69-19613

Electric shock tube for measurement of plasma magnetic fields induced by shock plasma moving through DC magnetic field transverse to flow

11 p1925 A69-24311

Electrical conductivity radial distribution in plasma flux from changes in Q factor and circuit inductance in presence and absence of skin effect

11 p1928 A69-25221

Dynamic characteristics of plasma fluxes across magnetic field of diverter inside plasma cylinder formed during injection

12 p2134 A69-25977

Slow theta pinch helium plasma measurements by Mach-Zender interferometer with Q switched laser

12 p2091 A69-26394

Low energy plasma fluxes in magnetosphere, discussing plasmopause position dependence on geomagnetic activity

12 p2150 A69-26747

Interplanetary plasma measurements by Luna, Mars 1, Zond 2 and Venera 3 probes, including solar plasma flux energy spectra diagram

13 p2336 A69-27354

Hydrogen plasmas motions in multipole magnetic fields, discussing plasma polarization, double vortex flow patterns and field line configurations

15 p2661 A69-30924

PLASMA FREQUENCIES

Dense plasma with plasma frequency greater than cyclotron frequency, discussing flow past slender bodies

01 p0126 A69-10226

Electromagnetic wave propagation across magnetic field under relative streaming motion, noting plasma frequency cut-off

01 p0134 A69-11247

Microwave oscillations during interaction between electron beam and plasma in electron tube

07 p1189 A69-18504

Plasma frequency resonances observed by topside sounders interpreted as slowly propagating waves suffering oblique reflection, noting effects of nonhorizontal magnetic field

07 p1124 A69-18837

Longitudinal electrostatic oscillations in plasma with Fermi distribution of energies, noting oscillation frequency dependence on electron density

08 p1359 A69-19985

Nondispersive LF mode in magnetized plasma with frequencies lower than ion cyclotron frequency, discussing plasma stability in presence of electron drift

08 p1366 A69-20750

Communication problems due to natural and artificial plasmas in spacecraft vicinity, discussing plasma effect theory

09 p1451 A69-21292

Transverse density nonuniformity effect on electromagnetic wave propagation in cylindrical plasma waveguide immersed in magnetic field, noting frequency increase
09 p1545 A69-21348

Soviet papers on high frequency properties of plasma, including microwave diagnostics, magnetohydrodynamic and shock waves
09 p1548 A69-22015

Theta pinch plasma microwave emission from electrodeless inductive discharge at low pressures recorded at near plasma frequencies
09 p1549 A69-22017

Plasma oscillation intensities at combination frequencies under assumption of plasma wave and ion acoustic wave propagating along z axis
09 p1550 A69-22024

High density plasma in resonant cavity obtained by frequency shifting power source
10 p1727 A69-22955

Normal mode dispersion at upper hybrid frequency propagating parallel to uniform magnetic field in spatially inhomogeneous plasma
11 p1924 A69-24302

Normal mode representation of HF properties of inhomogeneous plasma, analyzing Vlasov equation for free oscillations under external driving field
11 p1929 A69-25269

Nonlinear HF conductivity of fully ionized plasma, considering applied electromagnetic field frequency close to electron plasma frequency
11 p1929 A69-25271

Stationary magnetic field effect on sum and difference frequency generation due to nonuniform RF electric fields applied externally to plasma
13 p2305 A69-27376

Microwave and LF oscillations interactions in plasma beam system, showing oscillation amplitude dependence on frequency relationships
13 p2312 A69-28111

Nonlinear generation of sum and difference frequencies in ionized plasma current densities by nonuniform microwave fields noting electron scattering
14 p2507 A69-29350

Si III and O II spectral lines distortion in pulse HF plasma in rotating electromagnetic field, showing particle rotational speed dependence on discharge chamber radius
14 p2497 A69-29791

Energy absorption by cold nonuniform plasma from externally driven electric field, noting relation between plasma and driving frequencies
15 p2661 A69-30922

F region stratification during solar minimum and maximum, discussing regularities of plasma frequencies and diurnal variations
17 p2959 A69-33005

Oscillations excitation between ion cyclotron and electron plasma frequency in He ion beam generated plasma
17 p3014 A69-33830

PLASMA GENERATORS NT DUOPLASMATRONS NT PLASMATRONS

Heat transfer between arc column and discharge chamber wall of vortex linear plasmatron, using approximate similitude method
01 p0125 A69-10091

Recombination reactions during postdischarge in helium plasma produced by laser beam, deriving equation for density evolution
01 p0128 A69-10394

High temperature plasmas generation by exploding gold wires in vacuum, using time of flight technique for plasma densities and flow velocities
01 p0129 A69-10667

Thermonuclear fusion program, discussing plasma instabilities suppression, toroidal installations, magnetic trap systems, plasma heating and dynamic stabilization
01 p0156 A69-11065

Arc discharge in axially turbulent airflow producing equilibrium air plasma
02 p0285 A69-11571

Formation mechanism for heterogeneous structure of interplanetary plasma based on plasma instability from temperature anisotropy
02 p0314 A69-11638

Plasma production by laser irradiation of solid, calculating numerically time variations of temperature distribution, laser intensity and evaporated layer depth
02 p0256 A69-11935

Deuterium plasma evolution and creation modes obtained by short pulse laser discharge in gases,

discussing detonation and phase wave ionization mechanisms
02 p0288 A69-12040

Plasma generation in universe from temperature and pressure effects, ionizing radiation and stellar ejection of ionized particles
02 p0293 A69-12781

Electromechanical retracting pedestal for solid target injection into vacuum system and ionization by focused Q switched laser beam
03 p0439 A69-13105

Ionizing action of radiation due to heating substance in laser beam focus, discussing highly ionized plasma production
03 p0479 A69-13998

Breakdown plasmoids produced by lasers
03 p0480 A69-14058

Coaxial plasma accelerator for generation of pure injection plasmas, noting stability of propagating current sheath
03 p0481 A69-14213

Dense plasma radiation, analyzing spectrographically initial stages of wire explosion in vacuum
03 p0482 A69-14227

UHF discharge plasma, electron distribution over bound states and ionization stages
04 p0634 A69-14442

Toroidal gas discharge in waveguide by coupling of microwave power into gas to heat gas, noting plasma confinement [IMPI PAPER A4]
04 p0636 A69-14999

Plasma production by ultrashort pulse Q switched laser beam, discussing avoidance of initiation of breakdown wave
05 p0770 A69-15584

Mode locked laser as stroboscopic light source potential by investigating expansion of laser produced plasma by schlieren photography [IEEE PAPER H-1]
05 p0774 A69-16315

Plasma heating in two step theta pinch with coaxial coils yielding high temperature plasma at low capacitor storage charge
05 p0804 A69-16549

Mass spectrometric studies of plasmas produced by laser beam interaction with solid materials
06 p0932 A69-16921

Secondary emission and hollow cathode effects in low pressure hot cathode thyratron filled with hydrogen and with shield surrounded thermionic cathode
06 p0896 A69-17475

X rays detection from laser produced deuterium plasma through calibrated absorbers, presenting electron temperatures
06 p0964 A69-17479

Cesium plasma produced inside hot cylindrical tantalum cavity at 1400 K by contact ionization at wall while obtaining electrons from internal filament
06 p0927 A69-17707

Probe noise in quiescent plasmas investigated using back diffusion type discharge tubes producing low density plasmas and positive plasma columns
06 p0967 A69-17715

Plasma ionization enhancement by laser line radiation matched to specific atomic transitions [AIAA PAPER 69-47]
06 p0972 A69-18186

Radiation pressure effects on laser produced carbon plasma in vacuum, discussing target surface superheating, plume boundary, plume density precursor and electron and ion temperature merging
07 p1190 A69-18902

Stationary supersonic nonequilibrium plasma source in gas vacuum expansion and nozzle flows
07 p1191 A69-18986

Laser induced gas breakdown by focusing nanosecond pulses in air and deuterium [IEEE PAPER U-3]
07 p1155 A69-19085

Statistical theory of ionization for magnetoactive plasma with nonequilibrium concentration level and nonequilibrium energy distribution
07 p1193 A69-19142

Atomic flux from Cs and K ion recombination on hot end plates of Q machine measured, noting contribution to total plasma end loss rate
08 p1358 A69-19810

Highly ionized low density plasmas production by strong UV radiation
08 p1360 A69-20080

Arc jet generation and control noting application to hyperthermal aerospace environment studies, wind tunnels and materials heating and fabrication
08 p1371 A69-21128

Plasma generator for maintenance of space vehicle electrical neutrality during ejection of high velocity electron pulses [AIAA PAPER 69-273]
09 p1567 A69-21263

Discharge plasmas produced from solid materials at low pressures and temperatures and compressed against wall by magnetic field
09 p1547 A69-21594

Fission fragment generated plasma applicability to thermionic energy converters from electron density, temperature and transport studies
09 p1440 A69-21829

Enthalpy distribution in plasma tube arc heater inlet flow region with hot and cold gas core boundary in presence of electric field
09 p1553 A69-22538

Pulsed plasma production when focusing Q switched laser on solid target surface, noting high temperature effects and optical diagnostics methods
09 p1520 A69-22656

High temperature electron component of plasma produced by strong electron beam in adiabatic magnetic trap, deriving turbulent diffusion coefficient dependence
09 p1553 A69-22657

High density plasma in resonant cavity obtained by frequency shifting power source
10 p1727 A69-22955

Current-voltage characteristics of combustion driven shock tube generated argon plasma
10 p1737 A69-23466

Quasi-neutral plasma formation in hydrodynamic channel flow, discussing ignition and breakdown processes in preionized gaseous flow
10 p1737 A69-23467

Electrostatic wave dispersion relation in uniformly rotating plasma cylinder used in interpreting Q machine experiments
11 p1924 A69-24300

Cesium plasma confinement time improvement in symmetrically heated tungsten end plates of Q machine
11 p1925 A69-24314

Pulsed laser holography for recording interferograms of laser created plasma, discussing laser source properties, spatial and spectral coherence, double pulse mode, etc
11 p1895 A69-24683

Spectrum space-time characteristics of electrically produced plasma discharges magnetically compressed to discharge tube wall, using spectrochromograph and spectrographs
11 p1927 A69-25217

Temperature and electron concentration in plasma spark obtained in air by focusing Q switched laser radiation
11 p1928 A69-25235

Microwave analysis of plasmas produced by laser beam on aluminum spheres, noting expansion velocity and electron density
11 p1930 A69-25287

Neutron emission anisotropies in capacitor discharge produced plasma focus, detailing coaxial plasma gun energy spectrum and flux measurement
11 p1930 A69-25321

Current-voltage characteristics and ionization equilibrium of low voltage arc plasma in narrow gap of thermionic converter at high current density
11 p1933 A69-25554

Kinetics of air plasma formation in wake of shock wave propagating in air, taking into account nonequilibrium ionization
12 p2062 A69-26674

Load factor role in nonequilibrium ionization process in Faraday-type generator, determining relationship with conductivity
13 p2314 A69-28361

Time of flight mass spectrometers for plasmoids generated by theta pinch and discharge over organic glass, showing ion and electron currents oscillograms
14 p2498 A69-29813

Bibliography on laser applications in plasma physics covering plasma diagnostics and production
14 p2498 A69-29842

Synthesized plasma from neutralized mercury ion beam ejected from electron bombardment source, analyzing temperature, plasma sheath and stability
14 p2502 A69-29959

Longitudinal inhomogeneities in plasma of Q machines caused by ion emission from hot plate at different radial positions
15 p2661 A69-30925

Hot electron plasma formation by injecting megaelectron volt ion beams followed by Lorentz trapping, noting advantages of DC operation
15 p2661 A69-30925

Spectroscopic measurements of charged particle concentrations in jet produced by pulsed plasma generator
15 p2663 A69-30991

Electric arc plasma generator efficiency analysis including supply voltage, working current, current-source impedance, ballast resistor and optimum voltage-current selection
15 p2664 A69-31177

Laser radiation absorption by inhomogeneous overdense plasma, discussing effects of plasma expansion on energy coupling efficiency
16 p2818 A69-31679

I-V characteristics of caloroelectric plasma converter with concentric electrodes measured for various hot electrode temperatures and mercury vapor flow rates
16 p2822 A69-32065

Laboratory plasma produced by electromagnetically generated shock front propagation through ionized hydrogen
[AIAA PAPER 69-693] 17 p2945 A69-33447

Collisionless shock wave structure in plasmas, noting plasma and shock wave generation mechanisms
17 p3013 A69-33822

Turbulent heating of ions and electrons by interaction between magnetically collimated electron beam and electron beam self generated plasma
17 p3014 A69-33827

Plasma generation and heating by electron beam-plasma interactions, discussing HF fields excitation and absorption
17 p3014 A69-33828

Oscillations excitation between ion cyclotron and electron plasma frequency in He ion beam generated plasma
17 p3014 A69-33830

Heated Hg shock tube construction and operation, application to high electron density plasmas and problem of shock bifurcation in Hg monatomic gas
18 p3116 A69-34453

Fissioning plasma generated in shock tube with 235 uranium hexafluoride gas, selecting tube diameter, reflector depth and initial gas density for specific neutron multiplication
18 p3180 A69-34455

Semiconductor plasma production effects and pinching and microwave radiation in InSb plasma, discussing impact ionization, two photon absorption and plasma lifetime
19 p3389 A69-36545

Coherent radiation short pulses from mode locked laser permitting schlieren photography of plasma growth
21 p3736 A69-38795

Induction plasma device of continuous operation to simulate NASA designed gas core space propulsion reactor
[AIAA PAPER 68-712] 22 p3979 A69-40548

Electron beam injection into magnetic trap, obtaining plasma by ionization of supersonic argon flow passing through system
22 p3990 A69-40791

Spectrum characteristics of plasma generated by pulses of solid state laser radiation on metals and alloys in regular and quasi-stable regimes of emission
22 p3964 A69-40793

Nonlinear intensity transitions involving order of magnitude increases in visible luminosity of RF generated plasmas, noting inductive field and electron density influence
23 p4196 A69-41546

Eddy current plasmoids formation in potential magnetokinematic plasma flux found economical in terms of energy requirements
23 p4214 A69-41834

High temperature plasma generation by high power laser beam irradiation on small solidified gas particle, detailing experimental equipment and procedures
24 p4354 A69-42645

DC argon plasma generator operation, studying effects of gas flow direction and rate
24 p4255 A69-43077

PLASMA GUNS

Gas flow model of coaxial electromagnetic plasma gun front profiles and speeds for operation with positive central electrode
02 p0288 A69-12032

Optimum magnetic field axial component and plasma gun discharge voltage for high velocity plasma injection into symmetrical cusp field
05 p0805 A69-16655

Forward velocity of Bostick plasmoids demonstrated proportional to mean surge current through button source
06 p0964 A69-17480

Axial striograms of noncylindrical focusing discharge for plasma structure in front of interior electrode of coaxial gun
08 p1362 A69-20279

Pyrex spheres accelerated to 15 km/sec by plasma rail gun to study hypervelocity impact in thin stainless steel and Al targets
[AIAA PAPER 69-378] 13 p2368 A69-28308

Xenon atom and ion densities downstream from coaxial plasma gun measured using vacuum UV emission, absorption spectroscopy and Langmuir probe
16 p2819 A69-31690

Shock wave propagation through collisionless magnetized plasma, using gun driven, laser and cesium plasma flow methods
19 p3379 A69-35759

Time-variable pulsed transverse magnetic field used to cut off tails of plasmoids ejected from conical Plexiglas plasma gun into curvilinear magnetic field
24 p4358 A69-43476

PLASMA HEATING

Excitation heating energy pumping mechanism for explaining dynamic equilibrium in C rich arc plasmas with high ion temperature/electron temperature ratio
01 p0126 A69-10276

Thermonuclear fusion program, discussing plasma instabilities suppression, toroidal installations, magnetic trap systems, plasma heating and dynamic stabilization
01 p0156 A69-11065

Nonlinear interaction between longitudinal Langmuir waves and parallel wave vectors in heated plasma study, based on Cauchy problem of kinetic equation for electron distribution
02 p0285 A69-11461

Overheated semiconductor plasma instability in crossed electric and magnetic fields, deriving condition for occurrence
02 p0298 A69-12099

Heating of nonuniform plasma cylinder in constant magnetic field by magnetic pumping with oscillating magnetic field, determining energy absorption
02 p0288 A69-12167

Plasma physics experiments and theoretical studies, discussing plasma heating by magnetic compression and irreversible expansion, Cs plasmas, plasma diagnostics, etc
02 p0289 A69-12200

Collisionless plasma heating by hydromagnetic waves in solar wind
02 p0309 A69-12714

Electron emitter cooling and plasma heating of thermionic converters noting effects of plasma density, diode spacing, etc
03 p0368 A69-13127

Equilibrium and stability of strong current discharge in dense optically transparent plasma, determining cause of instability
04 p0636 A69-14983

Deuterium plasma heating by means of high power focused pulsed laser beam, noting initial energy of laser and pulse duration
05 p0769 A69-15583

Solid phase particle motion in plasmatron with colliding jets, measuring W particle heating by optical method
05 p0802 A69-15975

RF electron heating by beam-plasma interaction in uniform magnetic field
05 p0804 A69-16458

Plasma heating in two step theta pinch with coaxial coils yielding high temperature plasma at low capacitor storage charge
05 p0804 A69-16549

Transverse magnetic field effect on ohmic plasma heating in Tuman apparatus
06 p0963 A69-16906

Arc phenomena and gas dynamic effects during shock heated plasma interaction with magnetic field
07 p1188 A69-18273

Thermonuclear neutron emission from high temperature deuterium plasma produced by focusing high power laser radiation on lithium deuteride surface
[IEEE PAPER O-11] 07 p1153 A69-19072

Plasma heating dynamics by straight turbulent discharge current influenced by initial plasma parameters
07 p1195 A69-19592

Electron energy distribution function in plasma heated by electron-cyclotron resonance in adiabatic trap determined from bremsstrahlung spectrum
08 p1365 A69-20547

Quasi-linear theory of hydromagnetic waves in non-relativistic collisionless plasma, noting resonant diffusion effect on plasma heating mode
08 p1367 A69-20797

Heating of collisionless plasma in magnetic mirror by random electric field transverse to magnetic field
08 p1368 A69-20805

Numerical integration of motion equations of electrons subject to electrostatic waves, considering turbulent heating
08 p1368 A69-20806

Amplitude modulated radio wave interaction with rarefied plasma in magnetic field, considering possible ionospheric heating by mechanism
09 p1453 A69-21543

Plasma mixed ion heating by small scale HF turbulent electron sound pulsations
09 p1548 A69-21673

Semiempirical relation for electron cooling modified by plasma heating of thermionic converters, including effects of plasma density, diode spacing and surface potential difference
09 p1440 A69-21831

Electrons resonant heating in beam plasma discharge, discussing ion cyclotron wave excitation in hot electron plasma produced by electron beam
09 p1549 A69-22016

Stochastic model of electron cyclotron heating, calculating energy gain during transit of magnetic mirror field in presence of microwave electric field
09 p1551 A69-22038

Plasma wave excitation and dissipation in fast thetatron discharge, indicating electron nonadiabatic inductive acceleration without equilibrium orbit
09 p1552 A69-22046

Collisionless plasma heating by damping hydromagnetic waves applied to solar wind qualitative model, discussing magnetoacoustic wave energy
09 p1607 A69-22426

Plasma ion heating by external stochastic HF field, noting avoidance of special thermalization processes
09 p1553 A69-22527

Increased energy losses and microwave emission at cyclotron frequency harmonics during plasma electron heating at cut-off plasma concentrations in magnetic trap
10 p1728 A69-23130

Plasma ions turbulent heating during electron-acoustic instability in field of circularly polarized electromagnetic wave at ion cyclotron frequency
10 p1728 A69-23137

Nonequilibrium electron heating effect on inert gas plasma conductivity during shock wave movement across magnetic field
10 p1737 A69-23470

Heat propagation in discharge plasma heated by magnetosonic wave, constructing transverse temperature profile
10 p1741 A69-23896

Magnetospheric plasma heating by magnetosheath generated electromagnetic waves
11 p1950 A69-25149

Turbulent heating of toroidal plasma system with current contained in ceramic vacuum chamber with copper housing
11 p1935 A69-25752

Energy loss during turbulent plasma heating by current in open magnetic trap, attributing heating to ion-acoustic instability in plasma
11 p1935 A69-25753

Enhanced plasma heating in absorption zone of laser-induced gas breakdown at spherical blast wave shock front
14 p2460 A69-29604

Hydrogen plasma heating by fast large amplitude magnetoacoustic wave, measuring resonance excitation and absorption of wave
14 p2493 A69-29643

Turbulent diffusion and ion heating in plasmas in presence of current instability
15 p2662 A69-30959

Stochastic heating of protons by random magnetosonic wave propagating normal to magnetic field to explain proton energy excess in magnetotail plasma sheet
16 p2848 A69-31969

Electrostatic heating of solar wind ions from instability in two fluid solar wind model leading to preferential heating of protons over electrons
16 p2848 A69-31971

Amplitude modulated radio wave interaction with rarefied plasma in magnetic field, considering possible ionospheric heating by mechanism
16 p2754 A69-32538

Shock structure in RF heated partially ionized Ar plasma jet, using cylindrical free molecule Langmuir probe
[AIAA PAPER 69-697] 17 p3011 A69-33466

Collisionless plasma heating mechanisms from current layer turbulence in theta pinch experiment and shock wave front structure as function of initial magnetic field
17 p3013 A69-33824

Collisionless shock waves in plasma and ion and electron turbulent heating in high voltage theta pinches, noting magnetic disturbance
17 p3013 A69-33825

Turbulent heating of ions and electrons by interaction between magnetically collimated electron beam and electron beam self generated plasma
17 p3014 A69-33827

Plasma generation and heating by electron beam-plasma interactions, discussing HF fields excitation and absorption
17 p3014 A69-33828

Semiconductor plasma DC overheating instability in electric and magnetic fields, determining growth increments of oscillation amplitude
18 p3182 A69-35022

Propagation, damping, power coupling and plasma heating characteristics of harmonic ion cyclotron waves, noting temperature effects
21 p3777 A69-39455

Microwave power coupling to high density plasmas for electrons heating, using dielectric plates
21 p3779 A69-39746

PLASMA INSTABILITY

U MAGNETOHYDRODYNAMIC STABILITY

PLASMA INTERACTIONS

NT PLASMA-ELECTROMAGNETIC INTERACTION

Soviet book on atomic collisions and elementary processes in plasma covering atomic interactions, elastic and inelastic collisions, negative ions, autoionization, ion mobility and recombination
01 p0132 A69-11200

Rarefied plasma flow interactions with conductors having cross sections equal to Debye radius, noting production of self consistent electrostatic potential
01 p0134 A69-11307

Cosmic ray propagation in interplanetary space taking into account reverse effect on solar wind, deriving integrodifferential equation
02 p0306 A69-11657

Interactions of moving solar plasmas and solar magnetic fields, discussing solar velocity fields and fine structure observations
02 p0329 A69-12784

Solar wind interaction with moon, discussing core/surface layer conductivity and lunar limb shock wave formation
03 p0502 A69-14006

Transparency decrease in plexiglass during interaction with dense plasma, noting absorption independence of plasma pressure and dependence on wavelength
03 p0482 A69-14222

Quantum electrodynamics of radiation scattering from ionized interacting plasma, considering electron interactions
04 p0636 A69-15044

HF interaction of relativistic electron beam and plasma extended to include arbitrary variation of plasma density
04 p0637 A69-15046

RF electron heating by beam-plasma interaction in uniform magnetic field
05 p0804 A69-16458

Magnetosonic waves absorption in plasmas, studying collisions leading to HF energy resonant absorption at lower hybrid frequency
06 p0963 A69-16904

Shock formation in supersonic plasma flow guided by magnetic channel up to magnetic barrier
06 p0966 A69-17524

Supersonic plasma flow interaction with two dimensional magnetic dipole
06 p0967 A69-17738

Weakly ionized gas flow past discontinuous wall potential used to study edge effects and interaction problems for single and multiple flush electrostatic probes
[AIAA PAPER 69-80] 06 p0972 A69-18191

Electron bombardment ion source generated Ar plasma beam to study wakes of disks and spheres, considering plasma interaction with bodies
[AIAA PAPER 69-79] 06 p0865 A69-18200

Plasma diagnostics using scattering of laser electromagnetic radiation by plasma density function, discussing plasma species collision effect on line profiles
07 p1131 A69-18485

Model experiment on plasma flow about obstacle to simulate solar wind interaction with moon
07 p1205 A69-18851

Magnetospheric plasma probe results with Pioneer 6 and 7, discussing plasma fluctuations and solar wind interaction with geomagnetic field
07 p1128 A69-19364

Nonlinear interactions of positive and negative energy electrostatic modes of plasma immersed in magnetic field, discussing instability criterion and Landau damping
[IAEA PAPER CN-24/E-13] 07 p1196 A69-19768

Warm plasma magnetic interactions, discussing density waves, pair correlation function and transport coefficients
08 p1366 A69-20749

Nonlinear behavior of two stream instability between cold electron and ion streams
08 p1367 A69-20800

Plasma sheath-boundary interactions, analyzing emission, reflection and surface ionization effects on current densities and heat fluxes for cesium and argon
08 p1369 A69-20818

Plasma flow motion and polarizing interaction in multipole magnetic field
08 p1370 A69-21015

Frequency shift and Q change of microwave cavity caused by lossy dielectrics and plasmas, examining perturbing volume requirements for conductor behavior
09 p1544 A69-21323

Electric arc interaction with turbulent boundary layer in vortex stabilized plasmatron, noting variation in arc intensity
09 p1545 A69-21432

Mariner 2 measurements of geomagnetic field and interplanetary plasma parameters for analyzing interaction between interplanetary medium and magnetosphere during decreased solar activity
10 p1769 A69-23900

Magnetic lines of force penetration into magnetosphere accompanied by plasma insertion generating ring current responsible for main phase of magnetic storm
10 p1687 A69-23923

Voltage drop measurement across plasma anodized germanium film to determine anodization constant
10 p1742 A69-24004

Reflection of moving rarefied AR plasma from surface of nickel cylinder inserted into gas discharge tube
11 p1934 A69-25710

Trapping of plasmoids injected from two coaxial plasma sources through magnetic gaps of diverter, discussing alternate and simultaneous injection
12 p2133 A69-25976

Dynamic characteristics of plasma fluxes across magnetic field of diverter inside plasma cylinder formed during injection
12 p2134 A69-25977

Solar wind interaction with geomagnetic field simulation practically unrealizable, discussing partial simulation covering neutral magnetic layer formation on night side
12 p2149 A69-26681

Solar wind interaction with geomagnetic field, considering bow shock, field confinement in magnetosphere and stretching out of lines of force
12 p2072 A69-26735

Solar plasma flow around magnetosphere, discussing plasma velocity, density and temperature and magnetic field space and time variations
12 p2150 A69-26736

Laboratory models for solar wind and magnetosphere interactions with similarity laws of Vlasov theory as reference system
12 p2150 A69-26737

Magnetosphere model for plasma pressure by solar wind, discussing plasma drift from neutral sheet into geomagnetic tail
12 p2076 A69-27106

Incompressible conducting fluid turbulent flow velocity distribution in transverse magnetic field at small magnetic Reynolds numbers and constant MHD interaction frequency
13 p2246 A69-27498

Comet interaction with solar wind, assuming field tail coupling of ionized comet material to solar wind ions
13 p2349 A69-27817

Dissipative drift instability due to electron density gradient and dissipative mechanism /neutral-electron and ion-electron collisions/ in plasma in constant magnetic field
13 p2308 A69-27979

Collisions effect on wave propagation in homogeneous plasma, calculating permittivity tensor and electron equilibrium current using Boltzmann kinetic equation
13 p2311 A69-28104

Power output of ruby laser stimulated by strong pinch discharge plasma flux at 4000-7000 A in He
13 p2273 A69-28530

Cosmic ray propagation in interplanetary space taking into account reverse effect on solar wind, deriving integrodifferential equation
13 p2333 A69-28688

Interaction between shock tube gas discharge plasma and fast electrons ionized stationary gas, noting luminous discontinuities propagation
14 p2490 A69-28998

Magnetospheric plasma motion associated with Alfvén mode time fluctuations of magnetic field in solar wind
14 p2521 A69-29382

Ionospheric inhomogeneities models for plasma motions, considering electron-ion collisions
14 p2443 A69-29865

Conductivity tensor of collisional plasma in magnetic field, basing method on iterative procedure
14 p2503 A69-29999

Electrical conductivity tensor of many component collisional relativistic plasma in magnetic field and near equilibrium, expressing collisional part as momentum integral
14 p2503 A69-30000

Plasma-cyclotron interaction wave coupling mechanism in symmetrical double beam system in uniform magnetic field leading to unstable wave excitation along beam
17 p3015 A69-33831

Gas dynamics of interactions of tenuous ionosphere with moving satellites and diagnostic probes, using collision-free plasma kinetics methods
18 p3132 A69-35409

Microwave-plasma interaction instrumentation for supersonic channel constructed to investigate turbulent boundary layers formed over ablating heat shield materials
19 p3294 A69-35754

Electron-plasmon interaction in degenerate semiconductors, using mathematical model for rectifying metal contacts tunneling characteristics
19 p3382 A69-36049

Hydromagnetic wave-charged particle resonant interaction described by diffusion equation in momentum space, deriving diffusion coefficients and time evolution ultrarelativistic particle energy spectrum
19 p3424 A69-36335

Landau damping and echo in plasma, discussing theory, Van Kampen waves, finite amplitude wave attenuation, spin, cyclotron and plasma wave echoes
20 p3582 A69-38012

N and H plasmas and N-H plasma mixtures thermodynamic properties calculation, discussing numerical methods and corrections for electrostatic interactions
21 p3847 A69-38421

Solar atmosphere radio emission generation by hydrodynamic shock wave interaction with coronal plasma, treating corona as ideal gas consisting of protons and electrons
22 p4009 A69-39984

Josephson currents interaction with LF surface plasmons in superposed thin dielectric and superconducting metal films, noting I-V characteristics
22 p3992 A69-40420

Coupling coefficients and excitation increments determined for nonlinear interactions of surface waves in nonisothermal semibounded plasma
22 p3990 A69-40790

Interaction between two temperature plasma flux and electrodes in MHD channel with crossed electric and magnetic fields, studying boundary layer dynamics
22 p3991 A69-41022

Nonlinear plasma physics, discussing nonequilibrium effects, wave-wave coupling, wave-particle interactions, single nonlinear wave behavior, etc
23 p4197 A69-42312

Solar wind collisionless hydromagnetic flow interaction with planetary atmosphere, using mathematical model to determine bow shock position limits in atmosphere
24 p4368 A69-43178

Critique of magnetic response model for interaction of moon and interplanetary plasma magnetic field proposed by Blank and Sill
24 p4384 A69-43190

Magnetic and electron temperature interaction effects in fast MHD shock waves in slightly ionized plasma
24 p4356 A69-43361

Hydrogen plasma-axisymmetric magnetic field interaction, studying plasmoid motions during exit from field
24 p4358 A69-43472

Hydrogen plasmoids in axisymmetric magnetic field with acute angle geometry produced by opposing coils, measuring induction current field and plasmoid density distribution
24 p4358 A69-43473

PLASMA JET WIND TUNNELS

DC arc plasma torch as heat source in plasma tunnel, discussing nonuniformity of plasma flame
02 p0291 A69-12424

Diagnostic techniques for high speed low density DVL plasma wind tunnel noting problems of pressure, temperature, hot-wire and calorimetric measurements [DVL-849]
04 p0584 A69-14823

Continuous supersonic plasma wind tunnel obtained using magnetic Laval nozzle made by modification of Q device normal magnetic field configuration
15 p2589 A69-30909

Steady state plasma wind tunnel for flow around ionospheric satellites, studying wakes of cylinders and spheres [AIAA PAPER 69-673]
17 p2893 A69-33488

Free stream velocity in high enthalpy arc heated wind tunnel by measuring imposed temperature modulation apparent phase shift, describing circuit diagrams
22 p3926 A69-40444

Arc-heated hypersonic wind tunnel for simulated spacecraft reentry environment, aerodynamic heating characteristics and research applications
22 p3927 A69-40595

Arc-heated plasma jet wind tunnel flow properties in plenum chamber by spectroscopic techniques, measuring electron excitation, temperature and densities
22 p3990 A69-40596

PLASMA JETS

Faraday rotation of plane polarized microwave beam for measuring precursor ionization from exploding wire discharge in various gases
01 p0129 A69-10663

Plane MHD jets with variable conductivity, showing effective mixing length as function of distance
01 p0130 A69-10773

Structure of shock waves from MHD jet injected into zero viscosity, finite thermal and electrical conductivity medium analyzed by nonlinear differential equation system
01 p0130 A69-10774

Plasma discharge energy balance analysis to determine discharge power and temperature as function of electric field parameters
02 p0286 A69-11572

Thermal radiation effects on two dimensional steady MHD jet of conducting ionized gas confined by magnetic field
02 p0287 A69-11831

Quasi-one dimensional analysis of MPD arcs with nonequilibrium ionization taking into account finite rate processes and variable area [AIAA PAPER 68-87]
02 p0291 A69-12505

Radiation effect enhancement in supersonic plasma jet cooled by rapid expansion, giving energy equation for electron cooling rates to analyze electron temperature
02 p0292 A69-12557

Plasma jet motion in time constant and time variable magnetic fields noting particle deflection, polarization loss, capture and cut-off
02 p0292 A69-12558

Plasma jet mass structure investigated for decomposition during passage through vacuum by spectrometer and probe techniques
03 p0478 A69-13841

Pulsed arc source using plasma jet to obtain intense hydrogen ion beam
03 p0412 A69-13842

Frequency conversion in sheath capacitance of glow discharge plasma contained within metallic coaxial cylinders
04 p0634 A69-14456

LF electrical resonance oscillations in nonisothermal plasma jet flow, noting pressure and magnetic field effects on amplitude and frequency
04 p0638 A69-15174

Electron temperature time variation measurement in plasma-beam discharge by method based on single spectral line
04 p0638 A69-15368

Low temperature plasma electric arc source operation describing current voltage characteristics and potential distribution
05 p0802 A69-15902

Solid phase particle motion in plasmatron with colliding jets, measuring W particle heating by optical method
05 p0802 A69-15975

Energy balance of plasma radiation arcs based on mean pinch pressure and mean flow speed
05 p0802 A69-15996

Hall effect current influence on conductance of high current arcs
05 p0803 A69-15999

Doppler shift measurements of axial and rotational velocities in MPD arc, using reference lines from iron arc [AIAA PAPER 69-110]
06 p0972 A69-18171

Soviet collection of papers on turbulent jets of air, plasma and real gas
07 p1049 A69-18392

Electron acceleration in microtron through injection from low pressure gas discharge plasma
08 p1279 A69-19803

Spectroscopic analysis of hydrogen spark plasma discharge parameters at small PD values, discussing shock wave initiation accounting for transition to quasi-stable phases
08 p1360 A69-20100

Ar-H plasma arc radial temperature distribution determined by photoelectric spectroscopy in visible range
08 p1366 A69-20758

Electroslag welding using plasma jets with powdered material, discussing various parameters
08 p1321 A69-20766

Partially ionized argon plasma stagnation flow past blunt body using multifluid theory, obtaining flow profiles
08 p1369 A69-20817

Impurity elimination from hydrogen plasma jets injected from coaxial source normal to octupole magnetic field
08 p1370 A69-21016

Hall current influence on plasma jet interaction with space periodic magnetic field created by system of coaxial coils with alternating current directions
08 p1370 A69-21017

Plasma flow from hot cathode discharge in magnetic field increases ion flux intensity and prevents flow divergence in vacuum
08 p1370 A69-21075

Arc jet generation and control noting application to hyperthermal aerospace environment studies, wind tunnels and materials heating and fabrication
08 p1371 A69-21128

Rotating spoke in unstable pulsed MPD arc, noting rotation frequency and resemblance to plasma rotation [AIAA PAPER 69-234]
09 p1561 A69-21219

SERT 2 mercury vapor fed hollow cathode operated in bell jar, determining volt-ampere characteristics and flow rates for plasma diagnostics [AIAA PAPER 69-258]
09 p1561 A69-21221

Lithium vapor fueled applied field MPD arc jet performance using open end heat pipe vaporizer and hollow cathode [AIAA PAPER 69-241]
09 p1561 A69-21222

Hall effect and mass flow influence on MPD arc jet radial pressure profile calculated as function of pressure and magnetic field [AIAA PAPER 69-246]
09 p1562 A69-21226

Experimental and theoretical investigation of mass injection effect on high current MPD arc [AIAA PAPER 69-266]
09 p1564 A69-21242

Discharge plasmas produced from solid materials at low pressures and temperatures and compressed against wall by magnetic field
09 p1547 A69-21594

Carbon dioxide-nitrogen-helium laser with RF excitation of discharge plasma, noting high power per unit length
09 p1516 A69-21678

Fast Ba ion filament cloud injection into ionosphere using explosive shaped charge technique, noting application to ionospheric electric field measurement
09 p1539 A69-21752

Nonthermal microwave emission from cold cathode PIG discharge plasma, noting wide spectrum of electron cyclotron frequency harmonics
09 p1549 A69-22018

Plasma dissipative drift instability and nonlinear wave interaction from discharge with oscillating electrodes, investigating LF plasma oscillations
09 p1550 A69-22019

Alfven oscillations in inhomogeneous decaying plasma from pulsed discharge with oscillating electrons
09 p1550 A69-22020

Ionization and current growth in discharge in rotating plasma device with mirror shaped magnetic field
09 p1552 A69-22042

Rotating plasma gravitational instability during discharge as function of centrifugal acceleration, noting Coriolis and Larmor effects
09 p1552 A69-22043

Plasma wave excitation and dissipation in fast thetatron discharge, indicating electron nonadiabatic inductive acceleration without equilibrium orbit
09 p1552 A69-22046

Temperature pulsations radial distribution in plasma jet using plasmatron without mixing chamber
10 p1729 A69-23432

Ionization front propagation rate in crossed electric and magnetic fields in Ar-Cs, Hg-Cs and Ne-Xe discharge plasmas
10 p1733 A69-23447

Discharge plasma ionized waves, determining mechanism of wave propagation and instabilities
10 p1740 A69-23699

Neon discharges, discussing similarities in type p plasma ionization waves generated by pulsing
10 p1740 A69-23721

Explosive and reversible onset of helical instability in weakly ionized discharge plasmas, noting ambient noise level role
11 p1924 A69-24299

Radial distribution profiles of charge carriers in low temperature gas discharge plasma accounted for in terms of volume recombination
11 p1925 A69-24330

Expansion velocity of discharge plasma in exploding wires measured by X ray flash and streak photography, noting discrepancy
11 p1926 A69-24472

Dwell time of sample particles in plasma excitation zone, noting effect on spectral analysis of sample materials injected into spark discharge plasma
11 p1926 A69-24624

Spectrum space-time characteristics of electrically produced plasma discharges magnetically compressed to discharge tube wall, using spectrochromograph and spectrographs
11 p1927 A69-25217

Charged particle concentration near electrodes in high current pulsed discharge with separated flames at atmospheric pressure determined by measuring quadratic Stark effect
11 p1927 A69-25219

Temperature and electron concentration in plasma spark obtained in air by focusing Q switched laser radiation
11 p1928 A69-25235

Monograph on schlieren-optical technique for plasma beam temperature measurements using photoelectric scanning device
12 p2134 A69-26120

Electron concentrations in steady Ar and Ar-He plasma jets measured with microwave Fabry-Perot interferometer and Stark broadening of H beta line
12 p2317 A69-26537

Model, assuming electron thermal conductivity contribution, applied to studying solar plasma discharge characteristics in presence of three dimensional thermal sources in solar corona
12 p2149 A69-26680

Parameter measurement technique for low pressure helical pulse plasma discharges, determining spatial distribution of HF electric and magnetic fields and current density
12 p2140 A69-27124

Dense plasma jets in flowing HF flame discharges, discussing energy balance and longitudinal and radial temperature distribution
12 p2140 A69-27127

Oscillator parameter matching to flame discharge parameters to obtain optimal power for powering flame discharge for plasma jet source
12 p2140 A69-27129

Arc plasma jets radial velocity profiles measured by two probes in cyclic movement between jet edge and middle, including error estimation
13 p2307 A69-27611

Deuterium plasma jets passage through pulsed magnetic field by means of thermal and diamagnetic probes, noting magnetic field strength effect
13 p2311 A69-28107

Plasma jets tangential injection into toroidal magnetic field, discussing polarization interaction and depolarization effect
13 p2311 A69-28108

Alternating current plasma arc coaxial flow stabilization [AIAA PAPER 68-706] 13 p2313 A69-28232

Plasma jets from MPD accelerators, analyzing swirl, entrainment and pressure distribution using gasdynamic probes 13 p2313 A69-28242

LF wave propagation in DC discharge hydrogen plasma, noting self and artificial wave excitation 13 p2316 A69-28584

Interaction between shock tube gas discharge plasma and fast electrons ionized stationary gas, noting luminous discontinuities propagation 14 p2490 A69-28998

Electron and ion separation as function of plasma potential drop in Langmuir cathode layer in arc regime 14 p2490 A69-29237

Rasor phenomenological theory of space ionization in arc mode regime of Cs thermionic converter 14 p2402 A69-29242

Experimental and theoretical data correlation on low voltage arc in thermionic converters using cesium vapor, describing discharge plasma by solving differential equation system 14 p2404 A69-29254

Linear polarization achieved in He-Ne laser by applying external transverse magnetic field to plasma discharge 14 p2459 A69-29569

Pulsed HF discharge analysis in hydrogen based on laser light scattering at plasma electrons, noting presence of satellites 14 p2451 A69-29781

Light emission intensity correlation functions associated with LF oscillations in beam plasma discharge 14 p2498 A69-29814

Plasma energy and energy replacement time dependent on discharge pulse shape and magnitude 14 p2499 A69-29848

Flow phenomena associated with electrically conducting boundary layer jet injection through slot into uniform slipstream in presence of transverse magnetic field 14 p2501 A69-29917

Spectroscopic determination of temperature fields in water and transpiration cooled constricted Ar arc jets at atmospheric pressure 15 p2657 A69-30155

Semiautomatic recording device to determine gas discharge ion and electron sources operation modes optimum parameters 15 p2658 A69-30237

Radiation effect enhancement in supersonic plasma jet cooled by rapid expansion, giving energy equation for electron cooling rates to analyze electron temperature 15 p2658 A69-30254

Plasma jet motion in time constant and time variable magnetic fields noting particle deflection, polarization loss, capture and cut-off 15 p2658 A69-30255

Plasma arc characteristic and radiation at high pressure and temperature showing strong electrical field strength and radiation increases with pressure 15 p2659 A69-30377

Single and two phase subsonic plasma jets temperature and velocity distribution, noting reduction by condensed phase and use of Schlichting curves 15 p2663 A69-30989

Metal particles evaporation kinetics in plasma arc, determining total and unsteady evaporation time by spectroscopy and absorption radiography 15 p2663 A69-30990

Spectroscopic measurements of charged particle concentrations in jet produced by pulsed plasma generator 15 p2663 A69-30991

Iron and stone meteorites ablation using electrodeless plasmatron and filmed onto IR films 15 p2697 A69-31252

Electrical and thermal conductivities of high pressure arc plasmas from I-V characteristics and radial temperature profile 16 p2817 A69-31644

Temperature profiles in laminar boundary layer with endothermal reaction investigated using nitrogen plasma jet in rarefied gas wind tunnel 16 p2821 A69-31833

Micrometeorite simulation by wire explosion plasma, discussing energy requirements and simulator performance 16 p2821 A69-31839

High temperature ionized turbulent argon jet gasdynamics noting electron density 16 p2770 A69-31889

Electron temperature time variation measurement in plasma-beam discharge by method based on single spectral line 16 p2822 A69-32115

Discharge chamber plasma processes in electron bombardment ion thrusters, considering factors affecting thruster performance [AIAA PAPER 69-494] 16 p2845 A69-32735

Particles maximum diameter numerical values for melting during injection into plasma jet calculated for various metals and refractory dielectrics 17 p3009 A69-32825

RF high pressure plasma discharges contained within radial inflow vortex, measuring radiation efficiencies, power densities and radiation fluxes [AIAA PAPER 69-695] 17 p3010 A69-33442

Shock structure in RF heated partially ionized Ar plasma jet, using cylindrical free molecule Langmuir probe [AIAA PAPER 69-697] 17 p3011 A69-33466

LF electrical resonance oscillations in nonisothermal plasma jet flow, noting pressure and magnetic field effects on amplitude and frequency 18 p3180 A69-34716

Plasma arc systems and applications, noting transferred and nontransferred jets with emphasis on plasma spraying, surfacing, welding and cutting [SBAC PAPER 18] 20 p3550 A69-37453

Luminous tenuous collimated electron beam from plume of MPD arc in fiberglass vacuum tank, examining beam trajectory in geomagnetic fields 20 p3582 A69-38236

Plasma capture in stellarator diverter aperture with asynchronous plasma jets injection through diverter magnetic slots, discussing plasma cylinder density effect 21 p3776 A69-38585

Polymer films damage due to supersonic plasma jets, comparing fracture relief of oriented and unoriented polymers 21 p3752 A69-39081

Coronal jet resulting from chromospheric burst observed during 22 September 1968 total solar eclipse 22 p4028 A69-40716

Polymer film breakdown under impact of supersonic plasma beam pulses from capillary discharge chamber, including photomicrographs of cavities and structural defects 22 p3974 A69-41031

Argon plasma jet spectral radiation properties, considering electron density, recombination, excitation, argon density, etc 22 p3991 A69-41052

Radial pressure distribution in steady state rotationally symmetrical plasma jet subjected to axial magnetic field, emphasizing mass entrainment effect [DGLR-69-024A] 23 p4202 A69-41924

Spectroscopic azimuthal and axial measurement of jet velocity in MPD X9 rocket engine by spectrograph and Fabry-Perot interferometer [DGLR-69-024B] 23 p4202 A69-41925

Rocket engine plasma jet radial velocity measurement by induction-velometric method using moving probe [DGLR-69-024C] 23 p4202 A69-41926

Actuator disk model for study of azimuthally nonuniform MPD arc plasma dynamics [AIAA PAPER 68-714] 24 p4359 A69-43570

Error sources in magnetic field measurements using magnetic probes in high temperature plasmas, discussing detection, correction and elimination [AIAA PAPER 68-727] 24 p4316 A69-43571

Electrothermal waves in nonequilibrium electrical discharge in potassium seeded argon plasma 24 p4359 A69-43645

Electron density fluctuations in transition region of turbulent plasma jet, noting spiky waveform [AIAA PAPER 68-685] 24 p4360 A69-43697

PLASMA LAYERS

Stability of gravitating fluid layer of infinite extent but finite thickness including Hall effect 01 p0128 A69-10342

Coupled wave equations for propagation transverse to magnetostatic field in horizontally stratified and magnetized gyrotropic warm plasma 01 p0129 A69-10611

Horn antenna far field radiation pattern distortion by isotropic plasma slab, noting attenuation variation with electron density 02 p0218 A69-12335

Plasma pause and relation to ion composition in topside ionosphere, using Bohm coefficient for turbulent diffusion 02 p0246 A69-12741

Electromagnetic wave passage through plane gyrotropic layer of magnetized plasma, analyzing polarization and energy transfer 03 p0397 A69-13709

Fast time r moving striations in plasmas and dependence of ionization frequency on electron mean energy 03 p0477 A69-13801

Plasma rotation in current layer of pulsed inductive accelerator [AIAA PAPER 68-86] 04 p0635 A69-14702

Field strength, electron temperature and ion concentration fluctuations in axial direction determined from measurements between homogeneous and stratified plasma columns 05 p0800 A69-15736

High resolution electron and proton energy measurements by sounding rockets indicating plasma sheet as source of energetic auroral electrons 05 p0756 A69-16273

Spatial dispersion of electromagnetic waves reflection from moving plasma layer in magnetic field, determining transmission and energy absorption coefficients 06 p0886 A69-16895

Electromagnetic wave transmission and reflection at boundary of relativistic collisionless plasma, using Laplace transformation 06 p0968 A69-17783

Ion-acoustic wave excitation in plasma layer affected by incident p-polarized magnetic wave, deriving expressions for reflection, transmission and energy absorption coefficients 08 p1370 A69-21025

Kinetic theory of electromagnetic wave passage through magnetoactive plasma, discussing dispersion and specular and diffuse reflection 09 p1550 A69-22022

Kinetic theory of electromagnetic wave propagation in infinite laminated plasma with different dielectrics, determining attenuation 09 p1550 A69-22023

Excitation of plane plasma layer in magnetic field perpendicular to wave vector of excitation wave in gyrotropic waveguide 11 p1927 A69-24916

Te waves propagation along plasma sheet between conducting plates, determining vertical plasma density distribution 15 p2569 A69-30939

Low density cold plasma effect on stability of cylindrical layer of charged particles against electrostatic perturbations in uniform magnetic field 16 p2816 A69-31635

Electron temperature and number density measured at atmospheric pressure in plasma thermal laminar boundary layer adjacent to cooled wall [AIAA PAPER 69-692] 17 p3011 A69-33446

Nonlinear interaction of plane electromagnetic wave with inhomogeneous plasma layer, noting concentration and electric field discontinuity 17 p2922 A69-33693

Plane electromagnetic wave diffraction on conducting sphere situated in absorbing nonuniform plasma layer 19 p3275 A69-36340

Electromagnetic radiation from slot excited ground plane covered by inhomogeneous plasma layer, considering far field radiation pattern 20 p3495 A69-37852

Auroral zone Birkeland currents in magnetosphere, analyzing particle trajectories for plasma sheet energy distribution and Alfvén layer position 21 p3792 A69-39567

Reflection and transmission coefficients for harmonic electromagnetic wave incident at parabolic layer of stratified isotropic plasma 22 p3901 A69-41020

Thermal radiation diffraction of dielectric cylinder /cold plasma model/ containing N plus one layers with arbitrary temperatures and permittivities 23 p4123 A69-42028

PLASMA LIFETIME

Plasma lifetime in spherical multipole magnetic field trap compared to cusp trap 08 p1360 A69-20082

Time rates for growth and damping of resistive instability in gaseous plasma in crossed electric and magnetic fields 08 p1369 A69-20886

Lifetime and radial oscillations of magnetically confined laser produced plasma, solving hydrodynamical equations 09 p1545 A69-21493

Cesium plasma confinement time improvement in symmetrically heated tungsten end plates of Q machine 11 p1925 A69-24314

- Plasma experiments with TM-3 apparatus under stable discharge conditions in H, discussing energy loss mechanisms, transport coefficients, reciprocal lifetime, etc
16 p2820 A69-31795
- Semiconductor plasma production effects and pinching and microwave radiation in InSb plasma, discussing impact ionization, two photon absorption and plasma lifetime
19 p3389 A69-36545
- PLASMA LOSS**
- Atomic flux from Cs and K ion recombination on hot end plates of Q machine measured, noting contribution to total plasma end loss rate
08 p1358 A69-19810
- Warm plasma addition to mirror confined hot plasma stabilizing convective loss cone mode
09 p1551 A69-22040
- Equilibrium loss in closed cycle MHD generator using rare gases binary mixtures as working fluid
10 p1737 A69-23468
- Thermal balance of intergalactic gas, discussing plasma energy losses due to He emission and reverse Compton electron scattering and rapid cooling effect
11 p1954 A69-24381
- Back scattered electron inelastic LEED spectra of cesium plasma in W/100/-Cs system, noting strong loss peak
12 p2132 A69-26116
- Magnitude and type of wall losses from small opening in discharge tube for positive plasma column of low pressure glow discharge in hydrogen
14 p2493 A69-29691
- Interchange stability and drift motion of plasma with loss from ends of axisymmetric magnetic bottle, using hydromagnetic equations
15 p2664 A69-31100
- Thermal balance of intergalactic gas, discussing plasma energy losses due to He emission and reverse Compton electron scattering and rapid cooling effect
24 p4389 A69-43771
- PLASMA OSCILLATIONS**
- Inhomogeneous magnetically confined plasma stability, examining dissipative effects on spectra of drift oscillations with kinetic theory
01 p0126 A69-10187
- Asymptotic method for analyzing small long wave perturbations in plasma, showing instability with respect to perturbations propagating at angles to ion-acoustic wave
01 p0131 A69-10788
- Landau damping in plasma, noting competing effects of nonlinearities and collisions on formation of plateau in spatially homogeneous distribution function
01 p0133 A69-11215
- Ion acoustic wave dispersion in highly ionized Ar plasma in longitudinal magnetic field, noting effects of several phenomena
01 p0133 A69-11216
- Nonlinear interaction between longitudinal Langmuir waves and parallel wave vectors in heated plasma study, based on Cauchy problem of kinetic equation for electron distribution
02 p0285 A69-11461
- Plasma ion oscillation suppression by intensified electron plasma oscillations
02 p0287 A69-11934
- Nonlinear large amplitude electrostatic and electromagnetic oscillations in cold plasma having one dimensional spatial variations and fixed neutralized ion background
02 p0288 A69-12171
- Equations for studying plasma stability in sheared magnetic field examined for normal mode and wave packet perturbations
02 p0289 A69-12173
- Free fluid hydrodynamics equations applied to weakly ionized plasma stability, considering drift oscillations excitation
02 p0291 A69-12553
- Thermodynamic stability of plasma with strong interaction, discussing relationship to simultaneous oscillation forms
02 p0292 A69-12635
- Electromagnetic oscillations in ionized plasma, assuming higher oscillation frequency than collision frequency
02 p0292 A69-12643
- Radar observations of sun, determining reflected radio signal component formed by combination scattering in coronal plasma oscillation
03 p0505 A69-13082
- Relationship between instabilities and turbulence in plasma, using spectrum of plasma fluctuations
03 p0474 A69-13115
- Electrostatic acoustic wave mode with plasma motion in magnetic surfaces perpendicular to field in toroidal systems with geodesic curvature
03 p0475 A69-13147
- Dipole and quadrupole bremsstrahlung and damping of electron plasma oscillations, finding negative k-square collisional electron-ion contribution
03 p0475 A69-13149
- Helium plasma ion oscillations damping by external RF electric field at sheath-plasma resonance condition
03 p0476 A69-13323
- Frequency of damped oscillations in plasma in DC field, noting variation with electron density and DC field
03 p0479 A69-14050
- Dispersion equation for electron-ion and electron-hole plasma linear oscillations in crossed electric and magnetic fields
03 p0480 A69-14134
- Electron plasma oscillations diffusion due to scattering by large amplitude ion wave background, noting electron wave spectrum evolution
03 p0483 A69-14256
- Nonlinear electron oscillations in plasma, deriving asymptotic expression for plasma perturbation
04 p0635 A69-14552
- Electric field and energy dispersion law effects on plasma oscillations in semiconductors, calculating composite oscillation frequency
04 p0642 A69-14554
- Nonequilibrium ionization rate in arc discharge, studying perturbations effect in near cathode Langmuir layer
04 p0635 A69-14763
- Nonlinear damping of circularly polarized electromagnetic wave propagating in plasma along magnetic field, noting particle motion in resonance region
04 p0558 A69-14982
- LF electrical resonance oscillations in nonisothermal plasma jet flow, noting pressure and magnetic field effects on amplitude and frequency
04 p0638 A69-15174
- Perturbed wake behind spherical models in rarefied plasma flow, noting effects of electron temperature and electric potential of models
05 p0803 A69-16048
- Fluctuations in multipole confined plasmas explained by solving general integral equation, yielding hydromagnetic and frequency modes
05 p0804 A69-16385
- Ion plasma oscillations harmonics in helium plasma produced by back diffusion source, relating harmonics amplitude to electron density
05 p0804 A69-16459
- Electromagnetic waves transformation and scattering in plasma in electric field, showing abrupt increase at certain critical value
06 p0886 A69-16894
- Bounded and spatially separated plasmas wave oscillations stability in magnetic field, observing hydrodynamic slipping and drift instability
06 p0963 A69-16903
- Resonant four wave interaction for nonlinear energy transfer in electron plasma oscillations
06 p0963 A69-17143
- Resonance particle effects on flute oscillation kinetic stability when resonance particles drift under influence of magnetic field inhomogeneity
06 p0965 A69-17516
- Integrodifferential equation for plasma oscillations solved for effect of ion Larmor radius size and intrinsic electric field on flute instability of axially symmetric plasma
06 p0966 A69-17520
- Surface plasmons microscopic theory based on modified random phase approximation
06 p0967 A69-17711
- Dispersion relation for longitudinal oscillations of one component weakly ionized plasma without intercarrier collisions in uniform constant electric field
06 p0970 A69-17957
- Microwave oscillations during interaction between electron beam and plasma in electron tube
07 p1189 A69-18504
- Geometrical optics method for differential equations of fourth order in applications to LF plasma oscillations
07 p1190 A69-18697
- Periodic pulling mechanism for explaining transition to turbulence in bounded plasma with weakly unstable drift modes
07 p1194 A69-19400
- Longitudinal electrostatic oscillations in plasma with Fermi distribution of energies, noting oscillation frequency dependence on electron density
08 p1359 A69-19985
- Exact solution to kinetic equation for resonant three wave coupling in weakly turbulent plasmas, assuming only single triplet of modes interaction
08 p1360 A69-19989
- Collisionless shock waves in rarefied plasma, discussing dispersion effect and oscillatory shock wave structure
08 p1303 A69-19996
- Longitudinal excitations, discussing plasma equilibrium distributions
08 p1362 A69-20286
- Plasma oscillation modes perpendicular to magnetic field used to study energy conversion by wave coupling across density discontinuity
08 p1367 A69-20795
- LF electric potential oscillation of discharge plasma, describing oscillation behavior by theory of dissipative drift instability of weakly ionized plasma
08 p1370 A69-21020
- Partially ionized plasma oscillations in crossed magnetic and electric fields, noting role of LF particle collisions
08 p1370 A69-21079
- Scattering and transformation of electromagnetic waves in plasma in crossed electric and magnetic fields showing radiation spectrum maxima due to ion-acoustic oscillations propagation
08 p1277 A69-21080
- Rotating plasma disturbances onset in MPD arc, determining magnetic field dependence on mass flow, background pressure and propellant
[AIAA PAPER 69-232]
09 p1562 A69-21225
- Lifetime and radial oscillations of magnetically confined laser produced plasma, solving hydrodynamical equations
09 p1545 A69-21493
- Inhomogeneous collisionless plasma drift-oscillation stability in magnetic field augmented by E wave HF field
09 p1546 A69-21564
- Localized plasmons and optical phonons occurrence on local plasma levels, noting role of impurity atom in localized exciton-plasma resonance
09 p1548 A69-21674
- Plasma dissipative drift instability and nonlinear wave interaction from discharge with oscillating electrodes, investigating LF plasma oscillations
09 p1550 A69-22019
- Alfven oscillations in inhomogeneous decaying plasma from pulsed discharge with oscillating electrons
09 p1550 A69-22020
- Raman microwave scattering with low frequency oscillations caused by plasma drift instabilities
09 p1550 A69-22021
- Plasma oscillation intensities at combination frequencies under assumption of plasma wave and ion acoustic wave propagating along z axis
09 p1550 A69-22024
- Nonlinear longitudinal oscillations in nonisothermal electron plasma with Maxwellian distribution in velocity space and different temperatures of electrons and ions
09 p1550 A69-22025
- Unstable transverse potential oscillations in plasma with beam anisotropy and initial density modulation and analogy with known electrostatic oscillations
10 p1727 A69-23092
- Asymptotic method for analyzing small long wave perturbations in plasma, showing instability with respect to perturbations propagating at angles to ion-acoustic wave
10 p1653 A69-23107
- HF magnetic field effect on oscillations and instabilities of plasma confined by fixed magnetic field
10 p1739 A69-23623
- Transport of matter in nonisothermal weakly ionized plasma due to traveling ion-acoustic wave propagation, noting plasma oscillations and instability
10 p1741 A69-23945
- Density modulated charged particle beam interaction with plasma under paramagnetic resonance, analyzing longitudinal oscillations and parametric instability zone
10 p1741 A69-23947
- One dimensional electrostatic plasma oscillations in alternating external electric field, noting plasma stability and electron-electron two stream instability
11 p1924 A69-24298
- Electric field fluctuations in inhomogeneous plasma calculated by test particle method, interpreting results in convective modes terms in plasma control and stability
11 p1924 A69-24301

Electron number density LF oscillations for ionized gas identified with periodic solutions to neutral and charged particle plasma continuity equations
11 p1925 A69-24315

Local potential method extended to study plasma oscillations inhomogeneous kinetic equations in presence of linear or nonlinear collision operators
11 p1925 A69-24316

Hydromagnetic instability onset in dissipative flow of electrically conducting fluid between rotating permeable perfectly conducting cylinders, noting oscillatory axisymmetric critical modes
11 p1926 A69-24895

HF instability of low pressure discharge in magnetic field, discussing plasma diffusion and oscillations
11 p1927 A69-24912

Normal mode representation of HF properties of inhomogeneous plasma, analyzing Vlasov equation for free oscillations under external driving field
11 p1929 A69-25269

Natural oscillations excitation in magnetoactive plasma by modulated electron beam ascribed to Doppler or Cerenkov effects
11 p1932 A69-25535

Natural oscillations excitation instabilities by modulated ion beams in magnetoactive plasma ascribed to anomalous Doppler effect
11 p1932 A69-25536

Microwave oscillations amplitude spatial distribution in gas discharge plasma excited by electron beam
11 p1933 A69-25542

Flute oscillation instability of dense plasma cylinder under nonuniform electric field, analyzing oscillation spectrum properties
11 p1934 A69-25707

Correlation functions and spectral density of current fluctuations in weakly ionized plasma flows
11 p1934 A69-25715

Steady equilibrium collisionless plasma in oscillating electromagnetic field, describing formalism for linear relation between perturbation and charges and currents induced in plasma
12 p2135 A69-26284

Low pressure arc discharge plasma, studying ion-acoustic oscillations development in magnetic field
12 p2136 A69-26527

Plasma-electron beam interaction induced HF oscillations, obtaining nearly noise free oscillations
12 p2137 A69-26529

LF oscillations nonlinear excitation increment in plasma by electron beam found proportional to reciprocal of wave potential
12 p2138 A69-26709

Electron motion effects along magnetic field lines on axisymmetric torsional hydromagnetic oscillations in inhomogeneous low beta plasma, discussing resonance trapping
12 p2076 A69-27107

Plasma ion oscillations excited in plasma consisting of ion beam and thermal electrons produced by back diffusion sources
13 p2304 A69-27301

Vlasov equations solved for electrons and ions in electromagnetic field, coupling electric field to density oscillation modes of plasma
13 p2306 A69-27461

Laser light scattered from arc discharge, observing enhanced plasma oscillations
13 p2307 A69-27629

Semiconductor luminescent devices and laser pumping by solar radiation modulated to interact resonantly with solid state plasma oscillations and electric field in crystal
13 p2272 A69-27969

Collisions effect on wave propagation in homogeneous plasma, calculating permittivity tensor and electron equilibrium current using Boltzmann kinetic equation
13 p2311 A69-28104

Current carrying cylindrical plasma column oscillations surrounded by electric excitation with multiple feedback radio, discussing stabilization possibility
13 p2311 A69-28106

Microwave and LF oscillations interactions in plasma beam system, showing oscillation amplitude dependence on frequency relationships
13 p2312 A69-28111

Unstable weakly ionized HF magnetoplasma fluctuations with no axial drift, noting phase velocity parametric dependence
13 p2312 A69-28197

Linearized dispersion equation for electron oscillations in isotropic plasma with known electron velocity distribution function
13 p2313 A69-28328

Electromagnetic field induced plasma oscillation amplitude dependence on field frequency as function of field amplitude and discharge current at low N pressures
13 p2313 A69-28332

Variational method for time invariant states of collisionless plasma in oscillating electromagnetic field
13 p2314 A69-28365

Whistler type electromagnetic waves excitation by electron beam in plasma, noting intensity dependence on electron frequency
13 p2314 A69-28443

Magnetic and electric field effects on undamped electron-hole LF frequency plasma oscillations in spatially homogeneous nonpolar semiconductor
13 p2323 A69-28581

MHD waves and oscillations in cylindrical plasma column contained by longitudinal magnetic field, noting dispersion equations
14 p2489 A69-28732

Microwave oscillations in low pressure arc noting long gas discharge in small transverse dimensions
14 p2489 A69-28739

Radar observations of sun, determining reflected radio signal component formed by combination scattering in coronal plasma oscillation
14 p2515 A69-28764

Electron plasma oscillations and electron whistler of solar wind near Jupiter orbit
14 p2513 A69-29115

Secular terms for parallel component of electric current parallel to permanent magnetic field in toroidal MHD oscillations
14 p2492 A69-29369

Quasi-linear approximation for spectrum analysis of LF plasma wave oscillations in steady electric field
14 p2492 A69-29468

Plasma surface HF harmonic oscillations amplitude determined by comparing side frequencies intensities of reflected microwave signal
14 p2497 A69-29794

Plasma density and conductivity radio interferometry during ultrarapid disturbances based on electromagnetic wave phase shift dependence on density
14 p2498 A69-29803

Light emission intensity correlation functions associated with LF oscillations in beam plasma discharge
14 p2498 A69-29814

Collisionless Ce and K plasmas measurements to determine steady state parameters and LF oscillations, noting noise relationship to drift instability
14 p2499 A69-29849

Nonlinear longitudinal plasma oscillations, treating resonant particles, single mode and wave interactions
14 p2501 A69-29953

LF electrostatic oscillations of inhomogeneous solid state plasma with small number of current carriers in parallel external electric and magnetic fields
15 p2665 A69-30042

Free fluid hydrodynamics equations applied to weakly ionized plasma stability, considering drift oscillations excitation
15 p2658 A69-30250

Incident electromagnetic waves Raman scattering at turbulent plasma oscillations, obtaining plasma intrinsic radiation spectrum
15 p2659 A69-30728

Hydromagnetic stability calculations applied to umbral models, showing overstable oscillations relation to thermal hydromagnetic wave generation occurrence in sunspots
15 p2693 A69-30780

MHD stability and equilibrium of toroidal high beta configurations achieved by superimposing oscillating magnetic field on linear plasma column
15 p2660 A69-30877

Mode-mode coupling calculation for finite amplitude collisional drift waves demonstrating inherently nonlinear phenomena
15 p2660 A69-30916

Steady state solutions for parametric excitations in various limits in plasmas, allowing for higher order mode coupling
15 p2661 A69-30919

High order plasma wave echoes formulation and relation to initial perturbations based on Landau solution of initial value problem for Vlasov equation
15 p2661 A69-30926

Steady oscillations of active nonlinear system of nonisothermal plasma and charged particle flux, noting steady ion-acoustic waves
15 p2662 A69-30947

Ion-acoustic oscillations effect on weakly ionized plasma electrical conductivity, using BGK collision integral model
15 p2662 A69-30970

Small perturbations propagation in plasma at Newtonian acoustic velocity, determining temperature, pressure and current densities
15 p2663 A69-30993

Plasma modes, critical fluctuations and optical properties electric field dependence in two valley model of Gunn instability semiconductors
15 p2581 A69-31240

Covariant dispersion relations for relativistic plasma oscillations for many component plasma in external magnetic field
16 p2816 A69-31633

Stationary phase method of integration for growth and decay of resonant plasma oscillations excited by small pulsed dipole, noting Landau damping
16 p2817 A69-31641

Linearized kinetic equation for perturbed electron distribution function, detailing plasma oscillations along magnetic field by Landau collision term
16 p2818 A69-31674

Perturbation theory for nonlinear oscillations in ionized plasma, treating electron-neutral collisions effect by Boltzmann-Vlasov equation relaxation term, noting distribution function
16 p2820 A69-31702

Parametric amplification of ion-acoustic oscillations in plasma with LF electric field, noting suppression and resonance
16 p2821 A69-31797

Electromagnetic wave propagation in plasmas and plasma instabilities due to oscillations, deriving equations for frequency distributions in various plasma compositions
16 p2823 A69-32243

Discharge parameters modulation caused by acoustic wave propagating in partially ionized plasma, deriving perturbation current density and irradiated light intensity
16 p2752 A69-32364

Triple probes behavior in plasmas under AC electric field perturbations
17 p2920 A69-33592

Oscillations excitation between ion cyclotron and electron plasma frequency in He ion beam generated plasma
17 p3014 A69-33830

Damping of plane sinusoidal wave in cold collisionless plasma, studying supercritical amplitude oscillatory process
18 p3180 A69-34703

LF electrical resonance oscillations in nonisothermal plasma jet flow, noting pressure and magnetic field effects on amplitude and frequency
18 p3180 A69-34716

Plasma density in magnetosphere by measuring geomagnetic pi 2 micropulsations in direction related to polar aurora oval southern boundary, determining period of pi 2 oscillations
19 p3303 A69-36205

Plasma ion and electron concentration perturbations in wake of body moving at high velocity in collisionless plasma under steady magnetic field
20 p3459 A69-37659

Plasma oscillations of electrons of atomic system, using simple hydrodynamic model
20 p3580 A69-37818

Perturbed wake behind spherical models in rarefied plasma flow, noting effects of electron temperature and electric potential of models
20 p3581 A69-37957

Asymptotic method for analyzing small long wave perturbations in plasma, showing instability with respect to perturbations propagating at angles to ion-acoustic wave
20 p3582 A69-38005

Particle trapping and plasma oscillations in satellite disturbed ionosphere observed from Ariel and Aouette measurements, discussing frequency and wavelength relation
21 p3787 A69-38357

Nonlinear interaction of electron-acoustic oscillations in plasma, allowing for decay and inductive scattering in equation derivation for wave packet intensity
21 p3776 A69-38584

Nonlinear oscillations of inhomogeneous cold plasma in hybrid resonance region
21 p3672 A69-38588

Thermal effects of resonant coupling hydromagnetic oscillations in inhomogeneous finite-beta plasmas, ob-

taining equations for coupling modes between Alfvén and magnetosonic waves
21 p3776 A69-38710

Dispersion relations for surface plasma oscillations in normal metals for single and multiple films taking into account retardation effects, noting dielectric function
22 p3992 A69-40419

LF oscillations in electron number density of ionized deuterium, Ne and He identified from particle continuity equation
22 p3986 A69-40759

Diffuse reflection of electromagnetic longitudinal wave from magnetoactive plasma in oblique incidence
22 p3990 A69-40788

Homogeneous magnetoactive plasma longitudinal oscillations stability with fast monoenergetic ions addition, noting ion temperature increase stabilizing effect
22 p3990 A69-40789

Bernstein modes initial value-boundary value problem for half space of plasma bounded by wall and parallel unperturbed magnetic field
23 p4196 A69-41875

Rotational arc motion in MPD accelerators with strong axial fields predicted by plasma physics equations
23 p4201 A69-41909

Measurement method for relative phase shift between density and potential oscillations in Cs plasma
24 p4354 A69-42676

Moving striations as plasma oscillations arising from transit time delays of neutral and charged particles moving through ionized gas, using continuity equation
24 p4356 A69-43122

Polarization induced oscillations in forward portion of plasma flux crossing magnetic field, showing variations in maximum longitudinal potential of plasmoid
24 p4358 A69-43471

PLASMA-PARTICLE INTERACTIONS

Semiclassical wave emission and absorption theory applied to charged particles interaction with waves in magnetized plasmas
01 p0126 A69-10123

Plasma waves and particle interaction in nonuniform magnetosphere, considering propagation across sheets of steep density gradient and auroral precipitation
02 p0235 A69-11429

Screening of high density plasma from penetration by neutral gas, discussing prevention of high energy losses by charge exchange collisions
02 p0288 A69-12170

Synchrotron radiation excitation in system of relativistic monoenergetic electrons rotating in cold magnetoactive plasma
03 p0476 A69-13383

Nonlinear interaction between waves in relativistic plasma, determining probability between transverse and longitudinal waves with different phase velocities
03 p0397 A69-13710

Interaction between surface waves propagating along plane plasma boundary and parallel low density electron beam, noting wave amplification and excitation
03 p0480 A69-14135

Ion beam interaction with plasma in presence of charge exchange and zero external magnetic field, studying stability of system
03 p0481 A69-14200

Electron temperature time variation measurement in plasma-beam discharge by method based on single spectral line
04 p0638 A69-15368

Electrostatic waves interaction to electrons in plasma characterized by bump-in-tail distribution function, deducing mechanism of wave particle interaction
06 p0966 A69-17521

Backscattering due to collisions for electrons from emitter accelerated through positive ion sheath into plasma in thermionic diodes
06 p0898 A69-17773

Microwave oscillations during interaction between electron beam and plasma in electron tube
07 p1189 A69-18504

Electromagnetic waves excitation during interaction between density modulated beam and plasma in magnetic field, analyzing instabilities
07 p1189 A69-18508

Energy losses of clusters of charged particles moving through unbounded isotropic plasma manifesting nonlinearity in interaction of particle generated fields
07 p1189 A69-18528

Kinetic model describing collisions in nonequilibrium multicomponent plasma, studying pair collisions effect on stability of plasma-beam system
07 p1189 A69-18539

Wave propagation on cylindrical electron beam in vacuum and in plasma background, including relativistic effects
07 p1189 A69-18657

Comparative models of magnetoplasma, discussing wave propagation in cold plasma, warm plasma and microscopic model
07 p1190 A69-18919

Monoenergetic relativistic electrons stream gyrating along cold magnetoactive plasma with pitch angle radiatively unstable with respect to synchrotron radiation
07 p1191 A69-18958

HF wave propagation in unbounded electron-plasma systems using moment equations, discussing collisions effect and dispersion relation
07 p1086 A69-19468

High energy particles obtained by accelerating plasma with frozen-in magnetic field to relativistic velocities during scattering of fast electron beam
08 p1358 A69-19805

Plasma electron density and collision frequency determination, using CW maser interferometer
08 p1359 A69-19987

Electron cyclotron resonance absorption of injected radiation magnetic mirror, noting effect of RF heating on plasma electron distribution
08 p1364 A69-20519

Inhomogeneous collision plasma drift instabilities in strong magnetic field analyzed by solving nonlinear equations
08 p1365 A69-20549

Particle-wave interactions in weakly turbulent collisionless plasma, discussing ensemble average distribution function, diffusion, nonlinear Landau damping and nonlinear instabilities
08 p1368 A69-20803

Approximate solution of nonlinear differential equation describing interaction between galactic cosmic rays and solar wind, obtaining four domains
09 p1575 A69-21524

Charged particle acceleration in interplanetary medium, discussing protons and plasma oscillations interactions
09 p1575 A69-21541

High temperature electron component of plasma produced by strong electron beam in adiabatic magnetic trap, deriving turbulent diffusion coefficient dependence
09 p1553 A69-22657

Thermodynamic potential of rarefied plasma from Coulomb interactions of atoms with electrons and ions
10 p1728 A69-23134

Plasma electron beam nonlinear interaction, considering equations of motion of electron distribution function, plasma wave spectrum and mode coupling effects
10 p1729 A69-23407

Cosmic protons interaction with interplanetary plasma, analyzing beam energy loss due to excitation of longitudinal electrostatic oscillations
10 p1760 A69-23617

Parametric amplification in beam plasma system, analyzing amplification of electron current component dependent on second order terms of velocity and charge density
10 p1740 A69-23791

Density modulated charged particle beam interaction with plasma under parametric resonance, analyzing longitudinal oscillations and parametric instability zone
10 p1741 A69-23947

Rotational discontinuity in plasma, noting behavior for particle reflection off front side or back side of MHD wave
11 p1923 A69-24293

Dwell time of sample particles in plasma excitation zone, noting effect on spectral analysis of sample materials injected into spark discharge plasma
11 p1926 A69-24624

Linear interaction of electron beam and plasma in magnetic field noting convective wave instability, wave dispersion and properties behavior
11 p1929 A69-25267

Synchrotron radiation amplification by monoenergetic electron stream helically gyrating in static magnetic field of cold plasma, discussing amplification rate frequency dependence
11 p1931 A69-25361

Critical condition for electromagnetic radiation generation by energetic electrons gyrating in dense magnetized plasma, proposing plasma instability mechanism
11 p1931 A69-25363

Surface instabilities at tangential discontinuity between media caused by beam-plasma interaction, deriving dispersion relation
11 p1931 A69-25365

Natural oscillations excitation in magnetoactive plasma by modulated electron beam ascribed to Doppler or Cerenkov effects
11 p1932 A69-25535

Natural oscillations excitation instabilities by modulated ion beams in magnetoactive plasma ascribed to anomalous Doppler effect
11 p1932 A69-25536

Microwave oscillations amplitude spatial distribution in gas discharge plasma excited by electron beam
11 p1934 A69-25542

Convective wave instability resulting from modulated electron beam injection into plasma, noting amplitude restraint due to collisional damping effect
11 p1934 A69-25576

Plasma-electron beam interaction induced HF oscillations, obtaining nearly noise free oscillations
12 p2137 A69-26529

Average ionization cross sections of atomic and molecular H and He beams ionized by plasma electrons with Maxwellian velocity distribution
12 p2138 A69-26542

Clouds-in-clouds and clouds-in-cells method /CIC/ for many body nonlinear plasma problems, calculating density and force of particles
12 p2138 A69-26625

Longitudinal electric field penetration into semibounded plasma using kinetic approximation, assuming diffusive plasma particles reflection from plasma boundary
12 p2138 A69-26711

Plasma ion oscillations excited in plasma consisting of ion beam and thermal electrons produced by back diffusion sources
13 p2304 A69-27301

Electrical DC conductivity of turbulent plasma decreased in presence of ion waves
13 p2305 A69-27302

Microwave and LF oscillations interactions in plasma beam system, showing oscillation amplitude dependence on frequency relationships
13 p2312 A69-28111

Electron velocity distribution function in gaseous plasma with known collective oscillations and frequency/wave number relationship
13 p2313 A69-28327

Tensor analysis of four photon interaction in rarefied plasma in magnetic field, determining cubic current of plasma wave self action
13 p2314 A69-28444

Magnetized plasma waveguide dispersion characteristics using Maxwell equations, stressing interaction of electron beam with wave modes
13 p2315 A69-28571

Beam-plasma interactions by nonlinear Vlasov equation, describing amplification of longitudinal waves
14 p2493 A69-29692

Nonlinear longitudinal plasma oscillations, treating resonant particles, single mode and wave interactions
14 p2501 A69-29953

Wave regeneration by resonant particles interaction in inhomogeneous plasma of electrons confined in quadratic potential solved in WKB approximation
15 p2660 A69-30918

Collisional emission and absorption of longitudinal waves due to particle encounters in numerical experiments on one dimensional one species plasma
15 p2661 A69-30921

Steady oscillations of active nonlinear system of nonisothermal plasma and charged particle flux, noting steady ion-acoustic waves
15 p2662 A69-30947

Radial self focusing of low density electron beam by interaction with plasma in presence of beam plasma instability
15 p2662 A69-30964

Nonlinear wave scattering at plasma particles and weak plasma inhomogeneity effects on plasma current instability
15 p2662 A69-30965

Parametric amplification of ion-acoustic oscillations in plasma with LF electric field, noting suppression and resonance
16 p2821 A69-31797

Electron temperature time variation measurement in plasma-beam discharge by method based on single spectral line
16 p2822 A69-32115

Approximate solution of nonlinear differential equation describing interaction between galactic cosmic rays and solar wind, obtaining four domains
16 p2851 A69-32519

Charged particle acceleration in interplanetary medium, discussing protons and plasma oscillations interactions
16 p2851 A69-32536

Turbulent heating of ions and electrons by interaction between magnetically collimated electron beam and electron beam self generated plasma
17 p3014 A69-33827

Plasma generation and heating by electron beam-plasma interactions, discussing HF fields excitation and absorption
17 p3014 A69-33828

Time resolved beam distribution functions resulting from cyclotron instability and harmonics in electron injection machine during beam-plasma experiment
17 p3014 A69-33829

Book on nonlinear plasma theory covering nonlinear wave, wave-particle and wave-particle nonlinear interactions and weak plasma turbulence
18 p3180 A69-34930

Particle precipitation into auroral zone and plasma-energetic particle relationship in geomagnetic tail, discussing plasma sheet extent, energetic electron fluxes, etc
21 p3711 A69-38510

Kinetic model describing collisions in nonequilibrium multicomponent plasma, studying pair collisions effect on stability of plasma-beam system
21 p3776 A69-38691

Drag effect on plasma motion in high current pulsed plasma accelerators of Marshall type, calculating current variations, voltage, particle velocity, efficiency and impulse
21 p3778 A69-39548

Radiation fields from energetic electron moving in helical orbit in magnetoactive plasma, using Maxwell equations
22 p4008 A69-39965

Homogeneous magnetoactive plasma longitudinal oscillations stability with fast monoenergetic ions addition, noting ion temperature increase stabilizing effect
22 p3990 A69-40789

Infinites in statistical theory of radiative processes when applied to plasmas containing charged particles and radiation
22 p3991 A69-41055

Outer anisotropic galactic cosmic particle flux distortion in interplanetary space, analyzing scattering in solar wind by isotropic diffusion equations
23 p4205 A69-41837

Moving striations as plasma oscillations arising from transit time delays of neutral and charged particles moving through ionized gas, using continuity equation
24 p4356 A69-43122

PLASMA PHYSICS

Heat transfer situations in plasma flow indicates very high heat fluxes per unit area on surfaces with electric current
[ASME PAPER 68-HT-38] 01 p0175 A69-10314

Electron thermal relaxation length in positive column determined by plasma parameters variations in small amplitude moving striations
01 p0127 A69-10341

Numerical solution method for equation of electric field affected by permanent flux of identical ions
01 p0128 A69-10364

Soviet book on atomic collisions and elementary processes in plasma covering atomic interactions, elastic and inelastic collisions, negative ions, autoionization, ion mobility and recombination
01 p0132 A69-11200

Hydrodynamic model of laser produced solid particle plasma, giving distributions of pressure, density, temperature and velocity
01 p0132 A69-11210

Electric field in plasma half space determined by longitudinal wave normal mode analysis, using BKG particle conserving collision model
01 p0134 A69-11287

Anisotropic two component plasma relaxation taking into account dynamic shielding collective effects
01 p0134 A69-11419

Holtzmark plasma microfield, discussing neglect of term comparable to dipole moment during Fourier transform development for long range Coulomb field
02 p0287 A69-11871

Plasma physics experiments and theoretical studies, discussing plasma heating by magnetic compression and irreversible expansion, Cs plasmas, plasma diagnostics, etc
02 p0289 A69-12200

Transient signal propagation in lossless isotropic and homogeneous plasma for Gaussian pulse modulated carrier, discussing amplitude change and carrier phase distortion
02 p0290 A69-12351

Characteristic time on motion of magnetic lines of force in medium with Hall effect
02 p0290 A69-12399

Power radiated in magnetoionic mode by electron spiraling in magnetoplasma
02 p0309 A69-12720

Plasma astrophysics - Conference, Varenna, Italy, July 1966
02 p0328 A69-12780

Plasma generation in universe from temperature and pressure effects, ionizing radiation and stellar ejection of ionized particles
02 p0293 A69-12781

Plasma instabilities covering astrophysical phenomena, Rayleigh-Taylor instability, anisotropic and LF MHD, electrostatic and electromagnetics, warm plasmas, etc
02 p0293 A69-12783

Radiation due to collective effects in plasma physical aspects of astrophysics, discussing synchrotron radiation and bremsstrahlung
02 p0310 A69-12792

Plasma model of quasars and radio galaxies for observations of high energy radiation
02 p0329 A69-12794

Ion cyclotron wave generation in RF self sustained mode improved by installing grid structures in plasma near magnetic mirrors
03 p0474 A69-13113

Active and reactive impedance components of plane capacitor immersed in plasma and at LF noting dependence on plasma conductivity
03 p0477 A69-13713

Breakdown plasmoids produced by lasers
03 p0480 A69-14058

Natural and laboratory plasmas behavior and properties emphasizing particle interactions, MHD model and Boltzmann, Fokker-Planck and Vlasov equations
03 p0482 A69-14234

Discontinuities in plasma situated in magnetic field, noting drift of quasi-neutral inhomogeneities of electron and ion density
04 p0634 A69-14431

Model for predicting characteristics of short duration intense microwave pulse propagating in heated high temperature air
04 p0634 A69-14453

Quantum electrodynamics of radiation scattering from ionized interacting plasma, considering electron interactions
04 p0636 A69-15044

Electromagnetic wave propagation in uniform anisotropic plasma, considering wave vectors perpendicular to magnetic field
04 p0637 A69-15048

Hydromagnetic analogs calculated for Rayleigh-Taylor problem with Hall effect, confirming introduction of plasma instabilities
04 p0637 A69-15050

Hydrogen plasma transport properties for semiclassical quantum potential calculated by Chapman-Enskog-Hilbert theory
05 p0799 A69-15735

Electrical properties of xenon pulse plasmas with high power dissipation, measuring discharge pressure and radiation distribution as function of voltage drop
05 p0801 A69-15746

Interactions in classical relativistic plasmas, discussing Lorentz invariant statistical mechanical formalism and phenomenological electrodynamics
05 p0801 A69-15770

Evolutionarity of equations of MHD with Hall effect allowance for nondissipative plasma two dimensional flow
05 p0801 A69-15788

Hall effect current influence on conductance of high current arcs
05 p0803 A69-15999

Collision induced instability of partially ionized gases having large Ramsauer effect in external magnetic field, analyzing nonlinear characteristics
05 p0804 A69-16441

Plasma physics in space research, discussing solar wind, planetary atmosphere bow shock and convective motions of magnetosphere plasma
[ISAS-431] 06 p1000 A69-17026

Physics of plasmas, Volume 2, Weakly ionized gas, covering inelastic collision, free electron scattering, intermediary plasmas, etc
06 p0963 A69-17165

Surface plasmons microscopic theory based on modified random phase approximation
06 p0967 A69-17711

Variational solutions of one dimensional nonlinear Poisson-Boltzmann boundary value problems in theory of colloids and plasmas
06 p0968 A69-17784

Soviet collection of papers on MHD method of obtaining electrical energy, noting plasma properties in MHD generators
06 p0870 A69-17905

Ion-cyclotron instabilities in hot-ion cold-electron plasma resulting from left-hand circularly polarized wave propagating parallel to magnetic field
06 p0969 A69-17955

Harmonic ion cyclotron waves shown to possess stop and passband characteristics, supporting quasi-static ion cyclotron mode theory
06 p0970 A69-17953

Axisymmetric poloidal vacuum magnetic fields in low pressure plasmas in MHD equilibrium
06 p0972 A69-18230

Kinetic description of inhomogeneous plasma in ring approximation, discussing Vlasov equation and velocity distribution function
07 p1193 A69-19034

Cross sections for inelastic interactions of electrons with atoms and heavy impurity ions and processes of atomic excitation
07 p1195 A69-19652

Plasma spectral line shifting and broadening under ion and electron impact
07 p1187 A69-19720

Shock-like solutions of electrostatic Vlasov and Poisson equations, assuming zero temperature of positive ions and increasing electrostatic potential
08 p1359 A69-19982

Collective interactions of electromagnetic waves in plasma, discussing light scattering from electron fluctuations, stimulated emission and anomalous absorption
08 p1361 A69-20220

Radiative capture of electrons by chlorine, bromine and iodine atoms in shock heated plasma seeded with sodium halides from absolute intensities in continuous emission
08 p1355 A69-20735

Photon momentum distribution role and relation to thermal radiation spectrum in fully ionized gases
08 p1357 A69-20747

Discharge structure and stability of nonequilibrium plasma undergoing supersonic flow through linear MHD channel
08 p1366 A69-20788

Loss cones effect of anisotropic Maxwellian velocity distribution on EM waves propagating perpendicular to magnetic field in infinite plasma
08 p1369 A69-20820

Bose condensation and shock waves in photon spectrum during scattering for equilibrium state of ionized plasma and radiation
09 p1546 A69-21574

MHD stability of straight multipoles with shear, considering scalar-pressure perfectly conducting two dimensional MHD equilibria
09 p1546 A69-21576

Soviet papers on high frequency properties of plasma, including microwave diagnostics, magnetohydrodynamic and shock waves
09 p1548 A69-22015

Asymptotic toroidal equilibrium for guiding center plasma model based on stellarator expansion, considering toroidal curvature, helical currents and plasma pressures
09 p1552 A69-22044

Plasma transport properties derived from Boltzmann equation using Debye shielded Landé potential to represent collisions, noting viscosity and thermal conductivity
09 p1553 A69-22539

Finite Larmor radius, finite conductivity, rotation and Hall current effects on Jeans criterion for gravitational instability of plasma
10 p1729 A69-23408

Two temperature plasma model applicability in analyzing nonequilibrium MHD generator
10 p1731 A69-23438

Plasma ionization instability linear growth problem analyzed in bounded region
10 p1735 A69-23461

Boundary conditions for nonlinear equations of MHD for vicinity of zero magnetic field line, considering plasma pinch and current density
10 p1739 A69-23626

Charge transport in high pressure RF glow discharge in air at atmospheric pressure based on model plasma
10 p1740 A69-23662

One dimensional nonlinear model of anisotropic plasma instability with respect to Alfvén waves growth, noting applicability to solar wind processes
10 p1741 A69-23961

Charged particle motion in periodic electromagnetic field, constructing dynamic variables describing motion
11 p1927 A69-25100

Particle, momentum and heat balance of static and rotating magnetized plasmas in terms of macroscopic equations
11 p1928 A69-25248

Positive column contraction in Ar and Ar-Cs mixtures, developing theory for nonisothermal local collision arc
11 p1932 A69-25539

Plasma physics of electric arc transition from conducting plasma to insulating gas in electric circuit interruption, noting interrupter interaction with power system
12 p2133 A69-25905

Microwave harmonic generation in plasma capacitor, considering power resonances dependence on electron temperature and density
12 p2037 A69-25939

Relativistic hydrodynamic equations for charged particles interacting in external scalar and gravitational fields, considering particle motion and scalar plasma dispersion
12 p2130 A69-26462

Clouds-in-clouds and clouds-in-cells method /CIC/ for many body nonlinear plasma problems, calculating density and force of particles
12 p2138 A69-26625

Plasmapause, plasma sheet and energetic trapped electrons in earth magnetosphere, considering slot, peak intensity and trapping boundary
12 p2151 A69-26953

Soviet papers on physics of gas discharge plasma covering helical discharges, plasma jets, flame discharges, etc
12 p2139 A69-27121

Radiative energy losses in nonequilibrium plasmas, considering plasma geometries and distributions of Planck's function
13 p2305 A69-27374

Nose bluntness and model scale effect on radial and axial variation of wake fluid and plasma properties by hypervelocity shock tunnel
[AIAA PAPER 69-330] 13 p2242 A69-28266

Plasma screening effect on energy spectra of electrons localized at surface charges in weakly doped unipolar n-type semiconductor
14 p2505 A69-29170

Reflection of electromagnetic wave from magnetoactive plasma at inclined incidence, finding reflection and absorption coefficients
14 p2417 A69-29661

Bibliography on laser applications in plasma physics covering plasma diagnostics and production
14 p2498 A69-29842

Radio propagation in upper atmosphere and ionosphere noting rocket and satellite experiments including plasma physics research, tropospheric studies and space science services
14 p2526 A69-29854

Nonlinear longitudinal plasma oscillations, treating resonant particles, single mode and wave interactions
14 p2501 A69-29953

Longitudinal inhomogeneities in plasma of Q machines caused by ion emission from hot plate at different radial positions
14 p2502 A69-29959

Plasma instabilities due to anisotropic velocity distributions computer analyzed to study nonlinear phenomena and validity limits of linear theory
15 p2661 A69-30920

Stationary phase method of integration for growth and decay of resonant plasma oscillations excited by small pulsed dipole, noting Landau damping
16 p2817 A69-31641

Steady state density profile dependence on electron density dependence of net volume ionization rate by analyzing ambipolar diffusion in RF excited magnetized plasmas
16 p2818 A69-31672

Linearized Boltzmann equation in kinetic theory for weakly ionized plasma electrons under alternating electric and circularly polarized magnetic field, noting higher harmonics generation
16 p2820 A69-31752

Electron distribution function for weakly ionized plasma under alternating electric and circularly polarized rotating magnetic field, noting cyclotron resonance
16 p2820 A69-31753

Plasma physics and controlled nuclear fusion research - Conference, Novosibirsk, U.S.S.R., August 1968, Volume 1
17 p3012 A69-33817

Plasma physics and controlled nuclear fusion research - Conference, Novosibirsk, U.S.S.R., August 1968, Volume 2
17 p3014 A69-33826

Book on nonlinear plasma theory covering nonlinear wave, wave-particle and wave-particle nonlinear interactions and weak plasma turbulence
18 p3180 A69-34930

Evolutionarity of equations of MHD with Hall effect allowance for nondissipative plasma two dimensional flow
18 p3181 A69-35039

Time dependent equations for non-LTE occupation numbers of lower bound levels of hot gas or plasma outer layer atoms and ions
18 p3231 A69-35242

Equilibrium state of diamagnetic plasma configuration in inhomogeneous magnetic fields with complex potential near neutral point, noting solar flares and magnetic traps
19 p3380 A69-36467

Dielectric recombination in plasma, considering role in populating highly excited levels
20 p3580 A69-38016

Computer experiment on 9000 particle plasma to test temporal echo theoretical prediction
21 p3777 A69-38713

Laboratory experiments applicability to interplanetary plasma physics, describing simulations of solar wind interactions, magnetosphere, collisionless shock waves, etc
22 p4028 A69-40689

Classical path approximation in line broadening theory to derive impact and one-electron theories, with application to Stark broadening of Lyman series in hydrogen
23 p4193 A69-41379

Kinetic processes in gases and plasmas covering molecular transport equations, transport coefficients, chemical reactions as collision processes, etc
23 p4193 A69-41511

Kinetic equations for fully ionized plasmas and approximate derivation method for generalized Fokker-Planck equation including nonadiabatic effect
23 p4195 A69-41515

Soviet high temperature plasma physics research, discussing magnetic plasma containment by Tokamak traps
23 p4196 A69-42167

High temperature relatively dilute plasmas, discussing equations of motion, plasma oscillations, Landau damping, plasma confinement, etc
23 p4197 A69-42311

Nonlinear plasma physics, discussing nonequilibrium effects, wave-wave coupling, wave-particle interactions, single nonlinear wave behavior, etc
23 p4197 A69-42312

Boltzmann equation for electron distribution function of Lorentzian plasma traversed by transverse traveling wave, showing existence and uniqueness of solution
24 p4354 A69-42675

Nonthermal phenomena of astrophysics in relation to plasma physics, considering planetary and stellar regions, supernova envelopes, interstellar medium, cosmic rays, radio galaxies, etc
24 p4377 A69-42682

LF instability in plasmas and hydromagnetic fluids, discussing MHD equations, Rayleigh-Taylor instability, interchange mode, Kelvin-Helmholtz instability, etc
24 p4355 A69-42683

MHD tearing mode, considering most unstable wavelength, energetics and stability in two dimensional equilibria
24 p4355 A69-42684

PLASMA PINCH
NT THETA PINCH

Numerical estimates for degenerate pinch in InSb, determining pinch parameters
02 p0300 A69-12638

Tearing mode instability in Bessel function model preliminary to study of tearing mode in diffuse pinches
05 p0799 A69-15615

Energy balance of plasma radiation arcs based on mean pinch pressure and mean flow speed
05 p0802 A69-15996

Plasma impedance effect on time variation of inverse pinch
06 p0967 A69-17716

Energy transfer from pulse network to mass associated with propagating current sheet in linear pinch discharge, discussing pulsed plasma accelerator efficiency
[AIAA PAPER 69-113] 06 p0971 A69-18123

Continuum emission and forbidden lines in helium plasma in linear Z-pinch tube, noting plasma electron density
08 p1369 A69-20887

Pressure distribution in propagating current sheet structure in dynamic Z pinch discharge in argon, evaluating particle density, velocity and temperature profiles
[AIAA PAPER 69-264] 09 p1564 A69-21243

Formation and acceleration of luminescent current layer in Z pinch discharge, noting density and electron mean free path in cold gas
09 p1552 A69-22397

Boundary conditions for nonlinear equations of MHD for vicinity of zero magnetic field line, considering plasma pinch and current density
10 p1739 A69-23626

Ar plasma diagnostics in pinch-discharge laser, determining electron temperature by spectroscopy and measuring plasma conductivity and ion concentration and temperature
11 p1933 A69-25548

Axisymmetric instabilities by Z-pinch and reverse axial current discharges in plasmas of arbitrary conductivity
13 p2315 A69-28449

Power output of ruby laser stimulated by strong pinch discharge plasma flux at 4000-7000 Å in He
13 p2273 A69-28530

Electron and ion density distributions in propagating current sheet in Z pinch discharge in argon obtained by microwave reflection interferometer
16 p2816 A69-31639

Screw pinch stability explained by strong force free current carried by magnetic field around central plasma column
16 p2821 A69-32037

Collisionless shock wave generation and structure in zeta and theta pinches
17 p3013 A69-33819

Coherent emission from injection electron-hole plasma in indium antimonide without magnetic field, noting roles of crystal thickness and pinch effects
19 p3387 A69-36532

Semiconductor plasma production effects and pinching and microwave radiation in InSb plasma, discussing impact ionization, two photon absorption and plasma lifetime
19 p3389 A69-36545

Collisional shocks in inverse pinch MHD shock producing device, discussing position in current sheet and effect on conductivity and diffusion
21 p3776 A69-38709

PLASMA POTENTIALS

Electron density and temperature, ion density, composition and temperature and plasma space potential relative to space vehicle potential measured by spherical probe assembly
01 p0065 A69-10549

Statistical analysis of polarization of semiinfinite electron/ion plasma bounded by dielectric or conducting solid wall, deriving steady state and space potential
02 p0286 A69-11706

Space charge layer thickness determination in plasma filled capacitor by capacitance measurement, noting thickness dependence on plasma potential
03 p0477 A69-13714

Relation between energy spectrum and potential drop in plasma expelled from hot cathode tube into vacuum derived by electrostatic analyzer
06 p0963 A69-16899

Plasma flute instability in magnetic trap with wall/plasma interface, using system of sensors and amplifiers
06 p0966 A69-17544

Space plasma potential measurement based on RF impedance of plasma sheath/probe system
07 p1130 A69-18300

Shock-like solutions of electrostatic Vlasov and Poisson equations, assuming zero temperature of positive ions and increasing electrostatic potential
08 p1359 A69-19982

Metallic single and double plasma probes, discussing floating potential and ion saturation current
08 p1316 A69-20473

Integrated charged particle energy spectra from gridded electrostatic analyzers, relating retarding

potential curve to particle floating potential, kinetic temperature, etc
08 p1364 A69-20521

Debye potential for effective interaction between electron and proton of hydrogen atom in partially ionized plasma
08 p1365 A69-20746

Emissive probes for measuring plasma potentials over different ion density ranges on SERT spacecraft, detailing calibration and mechanical and electronic configurations
[AIAA PAPER 69-272] 09 p1492 A69-21217

Extraction and acceleration mechanism in RF ion motors, fixing plasma potential with extraction anode
[AIAA PAPER 69-284] 09 p1564 A69-21237

Nonlinearity of Hall voltage induced in plasma by external magnetic field under various assumptions
09 p1548 A69-21683

Thermodynamic potential of rarefied plasma from Coulomb interactions of atoms with electrons and ions
10 p1728 A69-23134

Moving striations in plasmas, presenting measurements of relative phases of electron temperature, plasma potential and luminous intensity near Pupp current limit
10 p1741 A69-23859

Field effect on positive column plasma of glow discharge in air, analyzing near wall potential and conductivity
10 p1741 A69-23946

Arc mode thermionic Cs converter nonlinear I-V characteristics explained by current-dependent temperature and potential fields in plasma
11 p1827 A69-25400

High temperature plasma quasi-classical pseudopotential, binary function and free energy derived, using displacement and collective variable methods
11 p1934 A69-25701

Rarefied plasma potential fluctuations when bounded by surface having complex conductivity and dispersing properties
12 p2139 A69-26712

Electron current, space potential and ionic composition obtained by Langmuir type probes on Explorer 31 for disturbance region dependence on ionic composition
14 p2518 A69-29122

Electron and ion separation as function of plasma potential drop in Langmuir cathode layer in arc regime
14 p2490 A69-29237

Plasma potential and density distribution in near-electrode plasma sheath of thermionic converter
14 p2491 A69-29257

Plasma energy and energy replacement time dependent on discharge pulse shape and magnitude
14 p2499 A69-29848

Hydrogen plasmas motions in multipole magnetic fields, discussing plasma polarization, double vortex flow patterns and field line configurations
15 p2661 A69-30924

Plasma density and potential distributions along circular cylinder surface in weakly ionized high speed low pressure gas flow, noting boundary layer separation point
19 p3380 A69-35839

Measurement method for relative phase shift between density and potential oscillations in Cs plasma
24 p4354 A69-42676

Polarization induced oscillations in forward portion of plasma flux crossing magnetic field, showing variations in maximum longitudinal potential of plasmoid
24 p4358 A69-43471

PLASMA POWER SOURCES

Gas discharge tubes and waveguide mounts as reference noise accuracy standards for S, C and X bands in WR284, WR137 and WR90 waveguides
02 p0210 A69-12439

Kaufman thruster with predominant radial field, noting electron mobility across ion extraction screen and advantages of uniform plasma distribution
[AIAA PAPER 69-259] 09 p1569 A69-21877

Soviet book on plasma thermionic energy conversion covering operation modes, transport processes, current-voltage characteristics, density, temperature, electric field distribution
12 p2017 A69-26850

Thermionic electrical power generation from reentry plasmas with nose cone as emitter and vehicle afterbody as collector
14 p2399 A69-29194

PLASMA PROBES

NT ELECTROSTATIC PROBES
NT MICROWAVE PLASMA PROBES

RF characteristics of electrodes immersed in magnetoplasma, discussing potential distribution around point charge and RF probe measurement of plasma parameters
01 p0029 A69-10550

Spherical and cylindrical probes emitting electrons and ions in unbounded plasma, deriving I-V characteristics equations
02 p0247 A69-11569

Plasma diagnostics in magnetic field with thin cylindrical probe based on Langmuir method
02 p0292 A69-12556

Probe and spectral techniques compared for investigation of low voltage arc of cesium plasma thermionic converter
03 p0478 A69-13836

Electrodeless conductivity probe impedance in anisotropic plasma computed on basis of Maxwell equation
03 p0483 A69-14252

Wave number frequency dependent spectral function and space-time correlation function in turbulent plasma, noting utility for probes and scattering analysis
03 p0483 A69-14255

Monograph on electron waves and resonances in bounded plasmas covering theoretical and experimental methods, metallic and dielectric resonance probes, etc
04 p0633 A69-14296

Charge carrier concentration determination by double probe in plasma with Druyvesteyn distribution of incident electron flow
05 p0800 A69-15737

Solar wind electron component detection by plasma experiment on Pioneer 6, particularly class 2B flare and quiet period
05 p0816 A69-16275

Explorer 35 measurements of low energy plasma in lunar orbit made by planar multigrid sensor programmed as retarding potential analyzer
05 p0825 A69-16278

Plasma characteristics in thermionic converter operating under low voltage arc conditions obtained by computer, probes and spectral techniques
06 p0963 A69-16910

Plasma flute instability in magnetic trap with wall/plasma interface, using system of sensors and amplifiers
06 p0966 A69-17544

Probe noise in quiescent plasmas investigated using back diffusion type discharge tubes producing low density plasmas and positive plasma columns
06 p0967 A69-17715

Space plasma potential measurement based on RF impedance of plasma sheath/probe system
07 p1130 A69-18300

Magnetospheric plasma probe results with Pioneer 6 and 7, discussing plasma fluctuations and solar wind interaction with geomagnetic field
07 p1128 A69-19364

Electron emission of probe caused by impinging ions and photons, discussing model for low plasma densities
08 p1361 A69-20232

Metallic single and double plasma probes, discussing floating potential and ion saturation current
08 p1316 A69-20473

Evaluation methods for DC electrical conductivity, heat conductivity and viscosity in plasmas
08 p1364 A69-20477

Emissive probes for measuring plasma potentials over different ion density ranges on SERT spacecraft, detailing calibration and mechanical and electronic configurations
[AIAA PAPER 69-272] 09 p1492 A69-21217

Low current arc discharge plasma diagnostics by light probe, analyzing deviation of resonance level population from equilibrium described by Saha equation
09 p1546 A69-21586

Saturation electron emission characteristics from incompletely outgassed Ta wire emitters immersed in Cs vapor using plasma anode technique, noting oxygen effects
09 p1437 A69-21812

Upper hybrid and modified plasma resonance on basis of rocket-borne gyroplasma probe data
10 p1726 A69-22807

Multielectrode plasma probe with potential negative with respect to plasma, noting effect of microoptical features of probe on accuracy of I-V measurements
12 p2138 A69-26538

Multielectrode probe performance in plasma diagnostics, considering effects of plasma pressure, probe

geometry and space charge on current-voltage characteristics
12 p2138 A69-26539

Parameter measurement technique for low pressure helical pulse plasma discharges, determining spatial distribution of HF electric and magnetic fields and current density
12 p2140 A69-27124

Arc plasma jets radial velocity profiles measured by two probes in cyclic movement between jet edge and middle, including error estimation
13 p2307 A69-27611

Deuterium plasma jets passage through pulsed magnetic field by means of thermal and diamagnetic probes, noting magnetic field strength effect
13 p2311 A69-28107

Plasma jets from MPD accelerators, analyzing swirl, entrainment and pressure distribution using gasdynamic probes
13 p2313 A69-28242

Coaxial three coil probe measuring local electrical conductivity and velocity in plasma streams, discussing operations in electrolytes and axisymmetric plasma stream
[AIAA PAPER 69-327] 13 p2313 A69-28264

Probe and spectroscopic study of dense plasma thermionic converters noting parameters
14 p2404 A69-29256

Plasma diagnostics in magnetic field with thin cylindrical probe based on Langmuir method
15 p2658 A69-30253

Gyroplasma probe data from rocket observations, determining winter ionospheric electron density profiles, electron temperature and electrostatic cyclotron waves effect
15 p2606 A69-31446

Maximum likelihood methods applied to device performing ion swarm experiments, measuring positive ion mobility in hydrogen
16 p2788 A69-31670

Electron trap behavior on charged spacecraft, obtaining expressions for current to aperture and internal retarding electrodes for all apertures and spacecraft potentials
16 p2849 A69-31976

Warm plasma probe, describing transit electrons interaction with electric field and generation of electroacoustic waves radiation
16 p2824 A69-32611

Electron heat transfer and spherical probe characteristics in moving nonequilibrium plasma analyzed at stagnation region as function of solid surface potential
[AIAA PAPER 69-699] 17 p3011 A69-33475

Triple probes behavior in plasmas under AC electric field perturbations
17 p2920 A69-33592

Gas dynamics of interactions of tenuous ionosphere with moving satellites and diagnostic probes, using collision-free plasma kinetics methods
18 p3132 A69-35409

Multiple electrode probe characteristics in rarefied plasma flow created by ion source, noting electrode potential role
19 p3314 A69-36622

Shock wave effect on ionization of detonation waves in propane-O mixtures producing stable high velocity plasma, measured by double probe method
21 p3853 A69-39745

Distribution function of output energies of polycrystalline metal surface used as plasma probe, considering homogeneous plasma flow and isotropic particle velocity distribution
23 p4196 A69-41696

Solar wind kinetic energy density using geomagnetic field horizontal component daily variation, treating earth as plasma probe
24 p4308 A69-42968

PLASMA PROPULSION

Mercury ion thrusters and facilities automatic controls durability testing, discussing vacuum chamber systems, unattended operation and control
[AIAA PAPER 68-576] 02 p0229 A69-12385

Electric propulsion research in Japan, considering cesium ion thruster, plasma acceleration and thrust by electric explosion of fine wires
06 p0984 A69-17629

Electron bombardment mercury ion thruster plasma properties and performance, computing ion beam current, discharge losses and propellant utilization efficiency
[AIAA PAPER 69-256] 09 p1560 A69-21214

Lithium vapor fueled applied field MPD arc jet performance using open end heat pipe vaporizer and hollow cathode
[AIAA PAPER 69-241] 09 p1561 A69-21222

- Rotating plasma disturbances onset in MPD arc, determining magnetic field dependence on mass flow, background pressure and propellant
[AIAA PAPER 69-232] 09 p1562 A69-21225
- Segmented anode, carbon dioxide-hydrogen performance and hollow cathode erosion tests on low power MPD arc thruster, noting current measurements
[AIAA PAPER 69-242] 09 p1563 A69-21236
- Electrothermal instabilities for explanation of MPD arc thruster rotating spoke phenomenon, noting agreement with experimental results
[AIAA PAPER 69-231] 09 p1566 A69-21254
- Kaufman thruster performance dependence on transmission of ion extraction optics and magnetic field shape
[AIAA PAPER 69-257] 09 p1569 A69-21878
- Electric and chemical rocket propulsion systems
13 p2325 A69-28255
- Induction plasma device of continuous operation to simulate NASA designed gas core space propulsion reactor
[AIAA PAPER 68-712] 22 p3979 A69-40548
- ### PLASMA RADIATION
- Light scattering from plasmas embedded in homogeneous magnetic field, discussing solid state and high temperature gas plasmas
01 p0125 A69-10015
- Light emission and transmission generated from laser interaction with lithium hydride in vacuum, noting laser energy variations effects
01 p0127 A69-10281
- LF radiation intensity oscillations of pulsed HF discharge in helium plasma, showing time dependence
01 p0128 A69-10347
- Relaxation processes and radiation stimulation in dense low temperature ionized plasma can lead to population inversion of several levels
01 p0131 A69-10789
- Pulsars features explained by model based on binary system of neutron stars, discussing associated stellar plasmas as directional HF radio wave source
01 p0156 A69-10981
- Ionized plasma radiation near plasma frequency, deriving formula for bremsstrahlung coefficient from Born approximation
02 p0286 A69-11589
- Lithium hydride microplasma expansion in vacuum using charge collectors, time of flight detectors and spectroscopy of light emission
02 p0286 A69-11704
- Integral spectral emissivity of gas arc plasmas at high temperatures and atmospheric pressure
02 p0291 A69-12484
- Laser produced sparks in 200 kG magnetic field in air, butane and helium at atmospheric pressure
02 p0260 A69-12659
- Procedure and apparatus for integral microwave and X ray and spectral measurements of quasi-steady plasma radiation
03 p0473 A69-12897
- Natural microwave radiation generation and propagation and wideband signal detection in problems connected with radio wave propagation, geophysics, radiometeorology and plasma physics
03 p0420 A69-12919
- Outer space electromagnetic radiation transfer in turbulent plasma with allowance for polarization effects, describing polarization induced changes in Stokes parameters
03 p0506 A69-13083
- Enhanced bremsstrahlung from supraluminous and subluminal waves in thermal isotropic homogeneous Maxwellian electron plasma, noting applicability to Crab Nebula
03 p0507 A69-13150
- Radiation intensity from system of monoenergetic relativistic electrons in plasma, discussing maser effect in coherent synchrotron radiation
03 p0500 A69-13407
- Dense plasma radiation, analyzing spectrographically initial stages of wire explosion in vacuum
03 p0482 A69-14227
- Plasma radiation, including atomic processes and radiation by variation of constituent kinetic energy
03 p0483 A69-14237
- Radial profile measurement technique for individual emission line intensities in plasma applied to populations of excited atomic and ionic Ar in capillary discharges
04 p0634 A69-14441
- High temperature air plasma total radiant intensity measurements in shock tube
04 p0685 A69-14719
- Gas laser pulse induced attenuated and nonattenuated plasma radiation recording, determining absorption coefficients
05 p0762 A69-15900
- Energy balance of plasma radiation arcs based on mean pinch pressure and mean flow speed
05 p0802 A69-15996
- Spectral line shapes broadened by electron impacts, taking into account contribution of radiation produced by perturbing electrons
06 p0961 A69-17136
- Continuous emission spectrum and continuous plasma absorption spectral coefficients for optically dense quasi-steady state electrical discharge plasma in sulfur capillary
06 p0964 A69-17251
- Radial electron concentration profile determination by spectroscopic examination of continuous plasma radiation of pulsed discharge in capillary
06 p0964 A69-17253
- X rays detection from laser produced deuterium plasma through calibrated absorbers, presenting electron temperatures
06 p0964 A69-17479
- Pulsar model based on rapidly rotating neutron star with radiating attached plasma, discussing test of radiation mechanism by means of coherence of emission
06 p1012 A69-18226
- Radiation transfer in resonance lines and in recombination continuum in plasma, discussing frequency redistribution during reradiation and optically dense systems
07 p1188 A69-18282
- Nitrogen plasma thermal radiation in spectral region from 0.5 to 1.1 micron, noting plasma state near local thermodynamic equilibrium
07 p1189 A69-18283
- Spectroscopic investigation of emission of air plasma in HF electrodeless plasmatron, analyzing near IR, UV and visible spectra
07 p1191 A69-18995
- Highly ionized plasma acceleration by intrinsic radiation achieved by deep cooling of free electrons
07 p1195 A69-19595
- Green function method for atomic line broadening in plasma radiation, including electron correlations and quantum effects
08 p1361 A69-20147
- Spectral distribution and energy of luminous radiation emitted during theta pinch in Ar plasma, noting energy maximum as function of pressure
08 p1362 A69-20280
- Transmission and reflection properties of materials for vacuum UV spectroscopy, using LTE plasmas for calibrating UV intensities
08 p1315 A69-20468
- Plasma diagnostics in X ray region, determining electron and ion temperatures and densities and energy losses by radiation
08 p1315 A69-20469
- Continuum emission and forbidden lines in helium plasma in linear Z-pinch tube, noting plasma electron density
08 p1369 A69-20887
- Epithermal microwave radiation from plasma produced by PIG Reflex in magnetic field with mirror geometry, discussing radiation at harmonics of electron cyclotron frequency
08 p1370 A69-21019
- Bose condensation and shock waves in photon spectrum during scattering for equilibrium state of ionized plasma and radiation
09 p1546 A69-21574
- Total radiation of dense low temperature argon arc discharge plasma measured by bolometer, showing increase with arc current and pressure
09 p1547 A69-21595
- Theta pinch plasma microwave emission from electrodeless inductive discharge at low pressures recorded at near plasma frequencies
09 p1549 A69-22017
- Nonthermal microwave emission from cold cathode PIG discharge plasma, noting wide spectrum of electron cyclotron frequency harmonics
09 p1549 A69-22018
- Helium-like ion resonance satellite lines in laboratory and solar plasmas, noting coincidence between solar satellite energy and energy level interval
09 p1598 A69-22158
- Stark broadening of Balmer H alpha, H beta, H gamma and H delta lines in plasma region in strong magnetic fields
09 p1542 A69-22248
- Neutron proton plasma properties in massive stars and supernovae, discussing neutrino emission
10 p1756 A69-22814
- Incoherent synchrotron radiation by relativistic electrons gyrating in cold magnetoactive plasma rederived, correcting errors
10 p1741 A69-23858
- Nitrogen plasma total radiation intensity under pressure and at high temperatures calculated from radiation spectrum
11 p1922 A69-24231
- Recombination emission spectrum relation to plasma recombination coefficient, determining plasma electron temperature from continuous spectrum intensity
11 p1934 A69-25566
- Plasma velocity measurement by Doppler shifts of spectral lines with photoelectric recording, using Fabry-Perot interferometer
12 p2079 A69-26021
- Plasmas role in emission mechanisms active in celestial sources of radiation, discussing sun and quasars
12 p2159 A69-26619
- Soviet book on microwave methods of plasma investigation based on electromagnetic wave interaction, covering microwave probes and plasma radiation
12 p2139 A69-27073
- Electromagnetic flux from nonlinear self interaction of electron plasma waves in far field of perturbation under anisotropic electron pressures
12 p2141 A69-27147
- Radiative energy losses in nonequilibrium plasmas, considering plasma geometries and distributions of Plancks function
13 p2305 A69-27374
- Cerenkov radiation from point charge uniformly moving along external magnetostatic field in warm anisotropic plasma, noting excitation modes and propagation frequencies
13 p2307 A69-27964
- Hypervelocity impact flash resolved into sub-microsecond continuum radiation pulse succeeded by slow rising long duration light pulse from neutral atomic line emission
[AIAA PAPER 69-364] 13 p2313 A69-28296
- Outer space electromagnetic radiation transfer in turbulent plasma with allowance for polarization effects, describing polarization induced changes in Stokes parameters
14 p2515 A69-28765
- Plasma arc characteristic and radiation at high pressure and temperature showing strong electrical field strength and radiation increases with pressure
15 p2659 A69-30377
- Radiative luminescence of gas discharge plasmas in channel with substantial radial heat transfer determined from energy balance measurement
15 p2662 A69-30978
- Electron temperature relaxation in shock heated Ar plasma, measuring plasma microwave radiation
15 p2663 A69-30995
- Macroscopic quasi-linear theory of HF radiation in cold electron-proton plasma allowing direct use of plasma and Maxwell equations
16 p2819 A69-31684
- Plasma magnetic field and electron density measured by Faraday rotation using resonant gas laser radiation
16 p2822 A69-32041
- Discharge parameters modulation caused by acoustic wave propagating in partially ionized plasma, deriving perturbation current density and irradiated light intensity
16 p2752 A69-32364
- Test apparatus for determining radiative properties of Ar plasma as function of high temperature and pressure
[AIAA PAPER 69-601] 17 p3010 A69-33310
- Radiation cooling behind strong shock in Kr as function of plasma luminosity near end of relaxation zone
18 p3171 A69-34450
- Coherent emission from injection electron-hole plasma in indium antimonide without magnetic field, noting roles of crystal thickness and pinch effects
19 p3387 A69-36532
- Semiconductor plasma production effects and pinching and microwave radiation in InSb plasma, discussing impact ionization, two photon absorption and plasma lifetime
19 p3389 A69-36545
- Radio wave propagation in anisotropic plasma consisting of oxygen ions and protons, deriving expressions for radio wave refractive index
20 p3486 A69-37052

- Relaxation processes and radiation stimulation in dense low temperature ionized plasma leading to population inversion of several levels
20 p3582 A69-38006
- Radiation sources fields and propagation in homogeneous lossy magnetoplasma, deducing wave equations for electric and magnetic current electron flux and mechanical body force sources
21 p3775 A69-38434
- Emissivity of nitrogen, oxygen and air plasmas in vacuum UV region of spectrum by photographic measurement, using He recombination radiation as brightness standard
21 p3774 A69-38944
- Differential approximation for radiant energy loss in nonequilibrium plasma generated from truncated Taylor series expansion of radiation source function
22 p3988 A69-40102
- Polymer film breakdown under impact of supersonic plasma beam pulses from capillary discharge chamber, including photomicrographs of cavities and structural defects
22 p3974 A69-41031
- Argon plasma jet spectral radiation properties, considering electron density, recombination, excitation, argon density, etc
22 p3991 A69-41052
- Infinites in statistical theory of radiative processes when applied to plasmas containing charged particles and radiation
22 p3991 A69-41055
- Classical path approximation in line broadening theory to derive impact and one-electron theories, with application to Stark broadening of Lyman series in hydrogen
23 p4193 A69-41379
- Nonlinear intensity transitions involving order of magnitude increases in visible luminosity of RF generated plasmas, noting inductive field and electron density influence
23 p4196 A69-41546
- IR radiation transmission in pulsed carbon dioxide discharge as function of time, proposing pumping and relaxation mechanism model
23 p4174 A69-42196
- Thermal continuum radiation from coronal plasmas at soft X ray wavelengths, investigating variations effect in element abundances
23 p4207 A69-42406
- Hydromagnetic radiation characteristics of electric and magnetic dipoles in homogeneous anisotropic cold plasma, obtaining field components and wave propagation modes
24 p4307 A69-42905
- PLASMA RESONANCE**
- Electron cyclotron harmonic waves in magnetoplasma irradiated by external microwaves
01 p0127 A69-10335
- Plasma wave properties relation to creation of electron plasma densities above critical density, discussing splitting of cold plasma resonance
01 p0131 A69-10818
- Ionospheric plasma electrostatic resonances from Alouette satellite signal observations
01 p0067 A69-10983
- Theoretical prediction for modified and hybrid plasma resonances discrimination, noting sensor axis angle to geomagnetic field
02 p0241 A69-11731
- Helium plasma ion oscillations damping by external RF electric field at sheath-plasma resonance condition
03 p0476 A69-13323
- Disintegration spectrum of Langmuir wave excited in plasma column by antenna, discussing conditions of resonance and parametric amplification
03 p0480 A69-14113
- Monograph on electron waves and resonances in bounded plasmas covering theoretical and experimental methods, metallic and dielectric resonance probes, etc
04 p0633 A69-14296
- Electron density variation in region of change of regime in gas discharge excited by HF capacitance and external electrode
04 p0637 A69-15060
- LF electrical resonance oscillations in nonisothermal plasma jet flow, noting pressure and magnetic field effects on amplitude and frequency
04 p0638 A69-15174
- Resonant four wave interaction for nonlinear energy transfer in electron plasma oscillations
06 p0963 A69-17143
- Harmonic generation of S band signal inside plasma column at resonance
06 p0965 A69-17488

- Quasi-static theory of antenna in magnetoactive plasma subjected to resonance, solving boundary value problem
07 p1099 A69-18522
- Period fluctuations in ionospheric plasma resonance amplitude, proposing hypothesis in terms of quasi-electrostatic surface waves guided by antenna wire
07 p1125 A69-18847
- Cylindrical antenna in uniaxial resonant plasmas, calculating current distribution and input admittance on basis of Wiener-Hopf technique
07 p1107 A69-19227
- Resonances in plasma column monitored by frequency and current modulation methods
08 p1365 A69-20552
- Electromagnetic wave attenuation propagating along external magnetic field ascribed to cyclotron wave energy absorption by resonant plasma particles
08 p1277 A69-21077
- Cold plasma magnetoacoustic resonance, showing nonlinear exciting magnetic field dependence on polarity and energy
09 p1548 A69-21668
- Localized plasmons and optical phonons occurrence on local plasma levels, noting role of impurity atom in localized exciton-plasma resonance
09 p1548 A69-21674
- Resonant interaction between traveling charge with superimposed magnetic field and Alfvén wave in plasma cylinder, showing cyclotron orbit variations
09 p1551 A69-22035
- Upper hybrid and modified plasma resonance on basis of rocket-borne gyroplasma probe data
10 p1726 A69-22807
- Ground wave propagation attainment of electron plasma resonance of F region, stressing need of wave vector orientation toward magnetic north
10 p1684 A69-23828
- Conductivity and permittivity for ion and electron resonance region of ionospheric plasma model calculated in quasi-hydrodynamic approximation
10 p1686 A69-23908
- Tonks-Dattner resonances in plasma column, using linearized Vlasov equation for coupling to plasma waves of time varying electric fields
11 p1929 A69-25266
- Resonance radiation output effect on electron distribution according to energies and concentration in low temperature plasma, solving relevant kinetic equations
11 p1935 A69-25757
- Energy exchange between LF waves and magneto-spheric energetic particle population by bounce resonant interaction
12 p2073 A69-26946
- Satellite observation of intensity and distribution of VLF emission at medium latitude during magnetic storm interpreted by transverse resonance plasma instability
12 p2073 A69-26947
- Nonlinear longitudinal plasma oscillations, treating resonant particles, single mode and wave interactions
14 p2501 A69-29953
- Resonance cones in angular distribution of short antenna RF electric field in anisotropic plasma noting variation with incident, cyclotron and plasma frequency
15 p2659 A69-30876
- Stationary phase method of integration for growth and decay of resonant plasma oscillations excited by small pulsed dipole, noting Landau damping
16 p2817 A69-31641
- Collisionless drift plasma wave instability growth rate calculation noting destabilization from resonant electrons
16 p2820 A69-31691
- Parametric amplification of ion-acoustic oscillations in plasma with LF electric field, noting suppression and resonance
16 p2821 A69-31797
- Noise emission and Landau damping of plasma resonances related by network theory including Nyquist formula, discussing noise temperature in free fall region
16 p2822 A69-32038
- Plasma electroacoustic resonance in reentry sheath of Trailblazer 2 vehicle excited by nonradiating coaxial antenna, deducing electron density gradient at vehicle surface
17 p3010 A69-32915
- Electroacoustic-electromagnetic waves nonlinear coupling in compressible isotropic plasma, comparing slowly varying and resonant interaction approaches
17 p2928 A69-33870

- LF electrical resonance oscillations in nonisothermal plasma jet flow, noting pressure and magnetic field effects on amplitude and frequency
18 p3180 A69-34716
- RF plasmoid properties, discussing bounded plasma resonance theory, basic experiments, resonance sustained discharges, role of negative ions, etc
18 p3181 A69-35487
- Cold plasma approximation of whistler excitation of lower hybrid resonance at wake of body moving through ionosphere, comparing results with Alouette satellite observations
20 p3519 A69-37025
- Ionospheric topside plasma resonances observed by fixed and swept frequency satellite-borne sounders
20 p3531 A69-37884
- Ionospheric resonances due to plasma nonlinearities near spacecraft, noting effects on radio signal propagation
20 p3495 A69-37886
- Frequency shifts observed in Alouette 2 cyclotron harmonic plasma resonances, noting antenna length and direction
20 p3496 A69-37892
- Landau damping and echo in plasma, discussing theory, Van Kampen waves, finite amplitude wave attenuation, spin, cyclotron and plasma wave echoes
20 p3582 A69-38012
- Nonlinear oscillations of inhomogeneous cold plasma in hybrid resonance region
21 p3672 A69-38588
- Resonant perturbation response of Vlasov magnetoplasma to source below electron gyrofrequency, explaining fractional resonances in Alouette 2 topside data
22 p4023 A69-40516
- Plasma resonances driven into nonlinear regime, using models of cold plasma driven by wave source and unmagnetized Vlasov plasma by two grid source
23 p4197 A69-42418
- Electromagnetic scattering by small plasma ellipsoid moving in vacuum through external steady magnetic field, analyzing resonance phenomena
24 p4282 A69-42979
- PLASMA RINGS**
- U TOROIDAL PLASMAS**
- PLASMA SHEATHS**
- Carbon monoxide ion dynamics in envelopes of comets exhibiting fountain behavior, discussing electron-collisional ionization within envelopes as main plasma production mechanism
02 p0310 A69-11423
- C and S band waveguide impedance measurements taken in flight in reentry plasma, noting results for plasma
02 p0218 A69-12333
- Reflection of plane electromagnetic wave from conducting plane covered with moving uniaxial sheath
02 p0209 A69-12334
- Kinetic theory model of plasma sheath transition, analyzing sheath structure in unignited mode of thermionic converter
03 p0368 A69-13125
- Helium plasma ion oscillations damping by external RF electric field at sheath-plasma resonance condition
03 p0476 A69-13323
- Reentry plasma sheath simulation in wind tunnel by injection of nitrogen plasma from model vehicle nose
03 p0412 A69-13679
- Coaxial plasma accelerator for generation of pure injection plasmas, noting stability of propagating current sheath
03 p0481 A69-14213
- Frequency conversion in sheath capacitance of glow discharge plasma contained within metallic coaxial cylinders
04 p0634 A69-14456
- Nonequilibrium ionization rate in arc discharge, studying perturbations effect in near cathode Langmuir layer
04 p0635 A69-14763
- Numerical values for cylindrical antenna admittance in uniaxial plasma, considering plasma compressibility and vacuum sheath
06 p0965 A69-17513
- Wall space charge layer effect on ion extraction from weakly ionized plasma, using quadrupole mass spectrometer
07 p1188 A69-18276
- Dynamics of pulsed microwave breakdown in nonuniform field at waveguide fed mica aperture, noting electric field distribution change due to initial plasma configuration
07 p1107 A69-19448

Plasma sheath-boundary interactions, analyzing emission, reflection and surface ionization effects on current densities and heat fluxes for cesium and argon
08 p1369 A69-20818

Electromagnetic field of infinite helical sheath, basing calculations on previous helical antenna studies
09 p1463 A69-21682

DC electrical resistance of magnetosphere between two satellites with sheaths and current-voltage relation of satellite sheath
09 p1489 A69-21710

Kinetic theory model of plasma sheath transition applied to sheath structure in unignited mode of thermionic converter
09 p1440 A69-21828

Ion-acoustic wave experiments for disturbance travel in plasma sheath, obtaining ion number density
11 p1929 A69-25272

Electric field penetration into homogeneous plasma at frequencies near Langmuir frequency and current at surface of thin cylindrical antenna in plasma
11 p1853 A69-25551

Dynamic growth of positive ion sheath on plane electrode in mercury plasma, measuring sheath thickness and current
12 p2134 A69-26099

Laminar MGD electrode boundary layer of thermal nonequilibrium plasma from collisionless Langmuir sheath and continuum theories
13 p2310 A69-28031

Inverse current in ignited mode diode linearly related to spacing, noting emitter sheath
14 p2401 A69-29230

Plasma potential and density distribution in near-electrode plasma sheath of thermionic converter
14 p2491 A69-29257

Ion and electron distributions in chemical nonequilibrium boundary layer flow over hypersonic reentry vehicle, discussing plasma sheath and boundary layer thickness relations
16 p2769 A69-31874

Plasma electroacoustic resonance in reentry sheath of Trailblazer 2 vehicle excited by nonradiating coaxial antenna, deducing electron density gradient at vehicle surface
17 p3010 A69-32915

Swept frequency microwave measurements in simulated reentry environments using dielectric layers, glow discharge plasma and aperture antenna-plasma layer model
[AIAA PAPER 69-701] 17 p2920 A69-33461

Electrical characteristics of equilibrium plasma sheaths at stagnation point of blunt body in high speed air, considering current collection regimes
[AIAA PAPER 69-702] 17 p3011 A69-33473

Severe magnetosphere distortions in north-south direction with parallel/antiparallel magnetosheath to magnetospheric field ascribed to solar wind property changes from Explorer 12 observations
18 p3128 A69-34947

Small continuum electrostatic probes calibration and operation in ionized plasma flow with sheath dimensions larger than boundary layer dimensions
19 p3304 A69-35719

HF backscattering characteristics of infinite conducting cylinder with radially inhomogeneous plasma sheath, using Bessel functions, geometrical optics and graphs
20 p3494 A69-37843

Langmuir probe immersed in plasma RF response over range of signal amplitude and frequency and plasma electron density, showing sheath capacitance role
21 p3723 A69-38939

Slot antenna radiation patterns in presence of aperture RF plasma breakdown sheath measured for various gas pressures and breakdown power levels
23 p4116 A69-41595

PLASMA SLABS

Horn antenna far field radiation pattern distortion by isotropic plasma slab, noting attenuation variation with electron density
02 p0218 A69-12335

Impedance sheet approximation to plasma slab, considering plane wave propagation, plasma covered slot antenna and transmission loss
02 p0209 A69-12348

Plasma slab acceleration along magnetic dipole guard field null, noting lack of equilibrium and no decrease of plasma losses
03 p0475 A69-13157

Particle measurements by Vela nuclear test detection satellites 7A and 2B/ noting plasma sheet in center of magnetotail
07 p1208 A69-19362

Ion Landau damping and finite Larmor radius effects on dispersion relation of Kelvin-Helmholtz instability due to shear in ion fluid velocity
08 p1367 A69-20799

Plane transient electromagnetic wave from cold lossless plasma half space and slab
12 p2033 A69-26865

Plane TM surface waves supported by plane ungrounded magnetoplasma slab with magnetostatic field parallel to two parallel interfaces and perpendicular to propagation direction
13 p2308 A69-27966

Longitudinal electric field penetration into plasma slab in constant magnetic field
14 p2493 A69-29665

Collisionless plasma slab drift mode stabilization at uniform temperature by oscillating electromagnetic field
14 p2499 A69-29851

Ambipolar to free diffusion transition in magnetized slab plasmas, discussing basic equations, iterative numerical procedure, characteristic parameters and H plasma
15 p2657 A69-30023

Microwave field-plasma slab nonlinear interaction in rectangular waveguide, analyzing current and electron density and second harmonic TE and TM power
16 p2749 A69-31703

Trapped modes in cold magnetoplasma slabs and rods in free space analyzed by Maxwell equation, assuming DC magnetic field and homogeneous electrons distribution
17 p2926 A69-33850

Parametric excitation theory involving Langmuir and ion-acoustic waves for homogeneous plasma slab with specular particle reflection at slab walls
20 p3582 A69-38245

PLASMA SOUND WAVES

U MAGNETOHYDRODYNAMIC WAVES

PLASMA SPECTRA

Rapid scan spectrometer design and calibration, noting application to diagnostics of high density transient Xe and H plasmas
01 p0082 A69-10838

Integral spectral emissivity of gas arc plasmas at high temperatures and atmospheric pressure
02 p0291 A69-12484

Probe and spectral techniques compared for investigation of low voltage arc of cesium plasma thermionic converter
03 p0478 A69-13836

Dense plasma radiation, analyzing spectrographically initial stages of wire explosion in vacuum
03 p0482 A69-14227

Relaxation method for separation of continuous electron/ion recombination spectrum from electron spectrum in nonequilibrium gas discharge plasma
04 p0639 A69-15369

Emission continuum intensity of negative nitrogen ion in nitrogen and air plasmas
04 p0639 A69-15370

Plasma characteristics in thermionic converter operating under low voltage arc conditions obtained by computer, probes and spectral techniques
06 p0963 A69-16910

Radial electron concentration profile determination by spectroscopic examination of continuous plasma radiation of pulsed discharge in capillary
06 p0964 A69-17253

Potassium seeded argon plasma conductivity in induced electric field at static gas temperature for MHD generator model
06 p0871 A69-17909

Spectroscopic investigation of emission of air plasma in HF electrodeless plasmatron, analyzing near IR, UV and visible spectra
07 p1191 A69-18995

Green function method for atomic line broadening in plasma radiation, including electron correlations and quantum effects
08 p1361 A69-20147

Thermal and nonthermal radiation of hot gases using spectroscopic plasma diagnostics
08 p1363 A69-20463

Quantitative spectroscopy methods for determining data on chemical constitution of plasmas, treating optically thin LTE plasmas
08 p1363 A69-20465

Spectroscopic diagnostics for determining temperatures, electron densities and line shapes in optically thick plasmas
08 p1363 A69-20466

Boltzmann plots derived from spatially integrated spectral line intensities emitted from nonuniform gaseous plasmas, discussing Boltzmann temperature
09 p1552 A69-22251

Spectrum analysis of aluminum plasma excited by giant pulse ruby laser radiation, discussing temperature and density
12 p2134 A69-26027

Back scattered electron inelastic LEED spectra of cesium plasma in W/100-Cs system, noting strong loss peak
12 p2132 A69-26116

Optical and spectral properties of dense plasma expanding after exploding electric wire in vacuum using high speed photography
12 p2137 A69-26533

High pressure arc discharge diagnostics with spectroscopic method relating spectral profiles to central temperature, pressure and temperature distribution
12 p2094 A69-26968

Convective-current instability in finite length plasma column, analyzing spectrum of unstable harmonics
13 p2314 A69-28441

Langmuir HF turbulence effect on anisotropic plasma oscillation spectra, determining instability conditions
13 p2315 A69-28448

Decaying arc discharge Cs plasma luminosity anomalous behavior due to combined effect of intrinsic monotonic and complex nonmonotonic emissions
14 p2490 A69-28996

Probe and spectroscopic study of dense plasma thermionic converters noting parameters
14 p2404 A69-29256

Quasi-linear approximation for spectrum analysis of LF plasma wave oscillations in steady electric field
14 p2492 A69-29468

Laser spark plasma initial development phase showing high electron temperature and concentration, continuous spectrum emission, line broadening and shock wave formation
14 p2461 A69-29779

Plasma electron temperatures from electron bremsstrahlung spectra measurements in X ray region
14 p2496 A69-29783

High speed photographs of plasma emission spectra in UV and soft X radiation spectrum regions, discussing theory, design and operation of facilities
14 p2496 A69-29784

Si III and O II spectral lines distortion in pulse HF plasma in rotating electromagnetic field, showing particle rotational speed dependence on discharge chamber radius
14 p2497 A69-29791

Electron densities measurement in plasmas in magnetic fields from profiles of spectral lines, noting Stark and Zeeman effect
15 p2657 A69-30027

Recording arrangement aperture effect on plasma scattering spectrum during plasma parameter determination by light scattering technique
15 p2664 A69-30996

Relaxation method for separation of continuous electron/ion recombination spectrum from electron spectrum in nonequilibrium gas discharge plasma
16 p2822 A69-32116

Emission continuum intensity of negative nitrogen ion in nitrogen and air plasmas
16 p2822 A69-32117

Electron impact broadening of isolated spectral lines emitted by neutral atoms in plasma
16 p2823 A69-32468

Spectrum characteristics of plasma generated by pulses of solid state laser radiation on metals and alloys in regular and quasi-stable regimes of emission
22 p3964 A69-40793

Thermal average derived with classical path treatment for line broadening theories of gases or plasmas
23 p4192 A69-41378

Spectroscopic azimuthal and axial measurement of jet velocity in MPD X9 rocket engine by spectrograph and Fabry-Perot interferometer [DGLR-69-024B]
23 p4202 A69-41925

PLASMA SPRAYING

Plasma arc welding, discussing transferred and non-transferred arc systems application to spraying and welding techniques, including automated microplasma welding
04 p0608 A69-15482

Tungsten coatings applied on stainless steel and titanium alloy surfaces by plasma jet
07 p1165 A69-18931

Zirconium and niobium carbide behavior during plasma spray coating, noting optimum oxygen content and mean carbide particle diameter in spray

07 p1165 A69-18933

Density distribution vs thickness in sprayed ZrC, NbC and aluminum oxide coatings obtained by plasma jet

12 p2118 A69-26258

Plasma spray quenched Al-V alloys resulting in dispersion strengthening of material

13 p2277 A69-27409

Electrical resistivity of aluminum oxide films deposited on tubular substrates by plasma and gas flame spraying, noting dependence on film thickness and substrate

15 p2630 A69-31179

Bonding strength of plasma coatings with substrate, testing aluminum oxide on steel

15 p2630 A69-31189

Particles maximum diameter numerical values for melting during injection into plasma jet calculated for various metals and refractory dielectrics

17 p3009 A69-32825

Residual tensile stress distribution during plasma spraying determined as function of temperature field in blank

20 p3548 A69-37328

Plasma coating formation mechanisms and parameters, studying metal surface and deposited particles temperatures, spraying time effects, etc

20 p3549 A69-37374

Plasma arc systems and applications, noting transferred and nontransferred jets with emphasis on plasma spraying, surfacing, welding and cutting [SBAC PAPER 18]

20 p3550 A69-37453

Plasma metal spray coating for Al and Mg alloy aircraft components adhesive bonding repair technique compared to welding and electroplating

21 p3728 A69-38462

Tungsten coatings applied on stainless steel and titanium alloy surfaces by plasma jet

21 p3746 A69-39152

PLASMA STABILITY

U MAGNETOHYDRODYNAMIC STABILITY

PLASMA TEMPERATURE

Plasma discharge energy balance analysis to determine discharge power and temperature as function of electric field parameters

02 p0286 A69-11572

Capillary arc source spectroscopy, determining plasma temperature and pressure dependence on capillary geometry and discharge current

02 p0286 A69-11573

Temperature and electron density distribution during late phase of wire explosion, analyzing optically thin plasma column by quantitative spectroscopy

02 p0286 A69-11711

Dense plasma temperature determination by gamma ray resonance scattering

02 p0291 A69-12481

Second virial coefficient of plasma at arbitrary temperature, noting small Coulomb interaction

02 p0292 A69-12639

Thermionic emission and dispersion of plasma created by monopulse of laser radiation focused on solid target, discussing plasma temperature determination methods

03 p0441 A69-14141

High temperature measurement based on spectral line displacement and broadening due to Stark effect, noting diagrams for O, Na, Mg, Al and Si at various temperatures

03 p0481 A69-14146

HF gas discharges, discussing plasma temperature and density, plasmoid length and spectroscopic applications

03 p0482 A69-14217

Electron temperature time variation measurement in plasma-beam discharge by method based on single spectral line

04 p0638 A69-15368

Flow characteristics and sound velocity in two temperature plasma

05 p0802 A69-15796

Free electron kinetic equation including inelastic electron-atom collisions derived for nonequilibrium low temperature plasma, showing interrelated electronic and atomic energy distribution

05 p0802 A69-15889

Spectroscopic charged particle concentration determination, discussing error and limits of applicability in low temperature plasma

05 p0762 A69-15899

Low dispersion spectrograph for temperature and electron density determination in plasma beam

05 p0803 A69-15997

Radial temperature profile in induction coupled argon plasmas at low and atmospheric pressures

06 p0964 A69-17193

Arc cloud thermal conductivity effects on discharge temperature and radiation intensity, solving energy balance equation

06 p0964 A69-17254

Transport properties of partially ionized low temperature plasmas, considering viscosity, electrical and heat conductivity of argon and nitrogen at high temperatures

06 p0969 A69-17907

Zeta discharge in low density regime characterized by strong turbulence, rapid loss of plasma, resistance higher than predicted and high ion temperature

06 p0970 A69-17955

Shock layer microwave radiation measurements during reentry flight of spherical nose cone, determining effective plasma temperature

[AIAA PAPER 69-183]

06 p0865 A69-18201

Nonequilibrium of electron and gas temperatures and reaction process for force-free plasma parallel beam produced in burner by expansion of argon plasma [DVL-875]

07 p1188 A69-18277

Hydrogen arc in axially parallel magnetic field produces higher plasma temperatures by reduced thermal conductivity coefficient

07 p1189 A69-18489

Simplification of equations for two temperature plasma composed of electrons, singly charged ions and neutral atoms, noting effect of viscosity and thermal force

07 p1190 A69-18693

Geomagnetic field line stretching outward due to energy entry in form of large number of charged particles or increase in particle temperature/inflation

07 p1127 A69-19357

Spectroscopic diagnostics for determining temperatures, electron densities and line shapes in optically thick plasmas

08 p1363 A69-20466

Recombination rate of electrons in high pressure helium-like plasma with gas temperature fixed at 300 K and electron temperature varied between 300-2000 K

08 p1356 A69-20742

Ar-H plasma arc radial temperature distribution determined by photoelectric spectroscopy in visible range

08 p1366 A69-20758

Plasma column of free burning electric arc, deriving temperature, electron concentration and electric field radial distributions

09 p1545 A69-21431

Mariner 2 data on large scale variations in magnetic field, solar wind density and temperature in interplanetary plasma

09 p1592 A69-21540

Local enthalpy measurements in atmospheric argon arc plasma jet at various arc currents, comparing calorimetric and spectrometric methods

09 p1547 A69-21602

Spectroscopic measurements of electron density and temperature for quasi-saturation region of ignited mode plasma in planar thermionic converter

09 p1439 A69-21826

Shock heated helium plasma temperature measurements by spectroscopy compared to Rankine-Hugoniot calculations including ionization effect

09 p1548 A69-21963

Boltzmann plots derived from spatially integrated spectral line intensities emitted from nonuniform gaseous plasmas, discussing Boltzmann temperature

09 p1552 A69-22251

Temperature pulsations radial distribution in plasma jet using plasmatron without mixing chamber

10 p1729 A69-23432

Low temperature optically thick boundary layers influence on spectroscopic temperature measurements in plasma MHD channels

10 p1731 A69-23434

Two temperature plasma model applicability in analyzing nonequilibrium MHD generator

10 p1731 A69-23438

Ionization instability in low temperature magnetized plasma, analyzing electron concentration perturbation caused by Joule heating during electron-ion collisions

10 p1741 A69-23962

Xenon pulse discharge plasma temperature distribution, spectral brightness density and light absorption across quartz tube section, noting temperature drop near wall

10 p1742 A69-24081

Electron-ion temperature relaxation near interface of two seminfinite nonmagnetized different temperature plasmas brought into thermal contact

11 p1923 A69-24296

Radiative cooling rates of bounded plasma of hydrogen isotopes, comparing dense deuterium plasma analytical results with brightness measurement

11 p1927 A69-25218

Temperature and electron concentration in plasma spark obtained in air by focusing Q switched laser radiation

11 p1928 A69-25235

Arc mode thermionic Cs converter nonlinear I-V characteristics explained by current-dependent temperature and potential fields in plasma

11 p1827 A69-25400

Temperatures and densities of atoms and electrons from spectroscopic methods in gas discharge plasma used for CW ion-argon lasers, evaluating inversion mechanism

12 p2106 A69-26319

Electromagnetic waves directional velocity, plasma temperature and particle density determined from analyzing electric field fluctuations amplification near body in plasma

12 p2137 A69-26531

Temperature measurement of plasma consisting of combustion products in MHD duct, measuring spectral line contours by Fabry-Perot interferometer for accuracies

13 p2309 A69-28023

Near electrode layer calculation in low temperature plasma, solving kinetic ion equation for quasi-neutral and Poisson equation for space charge regions

13 p2312 A69-28117

Cesium plasma electron temperature in narrow electrode space of thermionic converter determined using electrode and changeable space diode

14 p2491 A69-29243

Work function measurements of polycrystalline W, Re and Ni disks in high pressure cesium plasma for low probe temperature range

14 p2506 A69-29266

Plasma electron temperature determination by line intensity ratio of beryllium-like ions, noting excitation functions

14 p2496 A69-29789

Plasma ion temperature measurement based on integral neutron yield, noting density determination

14 p2498 A69-29808

Low beta fusion research in open end magnetic mirrors covering scope, end losses, fusion economics, flute instability, stabilization, etc

14 p2498 A69-29843

Convective and nonconvective two stream instability for hot plasmas, approximating equilibrium distribution function for given temperature by resonance functions

14 p2499 A69-29844

Plasma temperature measurement by resonant laser radiation absorption, assuming Saha-Boltzmann relation

14 p2501 A69-29954

Dynamic dispersion relation for bounded cylindrical beam plasma with temperature correction, including hot beam interaction

14 p2502 A69-29957

Electron concentration in low temperature nonequilibrium steady state plasma, including Saha equation applicability criterion

15 p2662 A69-30975

Single and two phase subsonic plasma jets temperature and velocity distribution, noting reduction by condensed phase and use of Schlichting curves

15 p2663 A69-30989

Iron and stone meteorites ablation using electrodeless plasmatron and filmed onto IR films

15 p2697 A69-31252

Propagation and linear transformation of HF electrostatic waves in hot magnetoactive radially inhomogeneous plasma, noting wavelength shortening

16 p2816 A69-31638

Electron temperature time variation measurement in plasma-beam discharge by method based on single spectral line

16 p2822 A69-32115

Mariner 2 data on large scale variations in magnetic field, solar wind density and temperature in interplanetary plasma

16 p2864 A69-32535

Magnetized solar wind model to evaluate temperature, density, velocity and magnetic field for various boundary conditions

17 p3041 A69-33812

Spectrum and cross section of radio wave scattering in two temperature plasma, relating differential

backscattering cross section to ionospheric electron density fluctuations 17 p2930 A69-33895

Radiation cooling behind strong shock in Kr as function of plasma luminosity near end of relaxation zone 18 p3171 A69-34450

Time variation of laser flare plasma temperature related to pulse parameters, using soft X radiation from plasma 18 p3154 A69-35496

Solar wind temperature, using distribution function for solar wind ions in anisotropic Maxwell distribution form 19 p3396 A69-36631

Plasma temperature and ion concentration profiles determined from simultaneous measurements by Alouette 2 and Explorer 31 satellites of electron density, temperature and ion abundance 20 p3532 A69-37896

Temperature gradient effect on plasma stability in maximum J configuration 21 p3776 A69-38711

Ionization formula linking nitrogen ion charge density ratio to plasma temperature 22 p3990 A69-40714

Interaction between two temperature plasma flux and electrodes in MHD channel with crossed electric and magnetic fields, studying boundary layer dynamics 22 p3991 A69-41022

Rocket measurements of plasma densities and temperatures in visual aurora using electrostatic onboard and ejected Langmuir probes, observing hyperthermal electron 23 p4167 A69-42334

Electron temperature distribution across shock wave in weakly ionized plasma, noting variable ionization across wave 24 p4356 A69-43362

PLASMA TURBULENCE

Microinstabilities of plasma confined by magnetic trap, discussing stabilization, drift waves and anomalous diffusion of plasma by turbulence 01 p0125 A69-10048

Generalized pair of space correlation and wave number spectrum functions applied to plasma electron density fluctuations and velocity fluctuations of background fluid 01 p0127 A69-10339

Power spectrum for energy transfer region in HF turbulent plasma by nonlinear equations, with results applied to subcosmic ray acceleration 01 p0145 A69-10790

Electromagnetic wave scattering by turbulent plasma pulsations in external magnetic field 02 p0289 A69-12174

Goldberg-Unno method for determining Doppler width, microturbulence velocity and convection errors, considering photosphere as hot ascending and cold descending columns 02 p0328 A69-12752

Outer space electromagnetic radiation transfer in turbulent plasma with allowance for polarization effects, describing polarization induced changes in Stokes parameters 03 p0506 A69-13083

Relationship between instabilities and turbulence in plasma, using spectrum of plasma fluctuations 03 p0474 A69-13115

Coulomb collision and microturbulence effect on plasma wave echo, noting echo dependence on perturbations in particle distribution 03 p0474 A69-13144

Energy partition between mechanical and magnetic modes in turbulent plasma in external field 03 p0476 A69-13384

Transport equation for electromagnetic waves multiple scattering by turbulent plasma 03 p0478 A69-13959

Electrodynamics of turbulent conducting media based on nonrelativistic MHD 03 p0479 A69-13972

Solar wind turbulence properties deduced from radio astronomical measurements 03 p0502 A69-14001

Electron viscosity coefficient in weakly turbulent plasma in strong magnetic field, noting electrical and thermal conductivity 03 p0480 A69-14136

Wave number frequency dependent spectral function and space-time correlation function in turbulent plasma, noting utility for probes and scattering analysis 03 p0483 A69-14255

Smeared out electron beam generation for experiments on weak plasma turbulence by passing beam through aluminum foils 04 p0636 A69-15020

Effective collision frequency deduced from ratio of microwave conductivity to electron density in PIG discharge plasma 05 p0804 A69-16442

Zeta discharge in low density regime characterized by strong turbulence, rapid loss of plasma, resistance higher than predicted and high ion temperature 06 p0970 A69-17955

Collisionless shock waves in high beta plasmas and in cold plasmas 07 p1194 A69-19366

Periodic pulling mechanism for explaining transition to turbulence in bounded plasma with weakly unstable drift modes 07 p1194 A69-19400

Microwave scattering by turbulent plasma column noting effects of plasma density 07 p1194 A69-19411

Exact solution to kinetic equation for resonant three wave coupling in weakly turbulent plasmas, assuming only single triplet of modes interaction 08 p1360 A69-19989

HF electromagnetic wave scattering at small scale plasma turbulence in magnetic fields, discussing interactions in frequent collisions region 08 p1275 A69-20435

Current fluctuations in Langmuir probe in turbulent plasma measured for various pressures, frequency bands, etc, noting plasma density fluctuations role 08 p1364 A69-20517

Particle-wave interactions in weakly turbulent collisionless plasma, discussing ensemble average distribution function, diffusion, nonlinear Landau damping and nonlinear instabilities 08 p1368 A69-20803

Longitudinal and transverse wave propagation in compressible isotropic turbulent plasma, noting mode coupling effect [AFCL-69-0289] 10 p1729 A69-23424

Turbulent plasma near stability limit in MHD generator with constant load coefficients, noting effective conductivity and effects of gas temperature 10 p1735 A69-23460

Spontaneous magnetic field excitation in turbulent plasma noting possible instability 10 p1740 A69-23715

Low energy cosmic rays and plasma turbulence in heating and ionizing interstellar gas, discussing acceleration and galactic sources 11 p1945 A69-24380

Electric field measurements for turbulence in collision-free shocks, noting power spectra of magnetic and electric fluctuations and electron density 11 p1930 A69-25276

Radio emission of fast cosmic ions by plasma wave conversion to electromagnetic waves, using nonlinear mechanism in turbulent plasma 12 p2149 A69-26209

Electrical DC conductivity of turbulent plasma decreased in presence of ion waves 13 p2305 A69-27302

Langmuir HF turbulence effect on anisotropic plasma oscillation spectra, determining instability conditions 13 p2315 A69-28448

Outer space electromagnetic radiation transfer in turbulent plasma with allowance for polarization effects, describing polarization induced changes in Stokes parameters 14 p2515 A69-28765

Kinetic theory of fluctuations in turbulent plasmas based on construction of many particle distribution functions 14 p2502 A69-29989

Incident electromagnetic waves Raman scattering at turbulent plasma oscillations, obtaining plasma intrinsic radiation spectrum 15 p2659 A69-30728

Ballistic wake structure and jump conditions for plane plasma shock waves with electrostatic turbulence 15 p2660 A69-30914

Particle diffusion and wave spectrum in unstable plasma calculated using Feynman diagrams, considering quasi-linear growth, resonant three wave coupling and nonlinear Landau damping 15 p2660 A69-30915

Nonlinear effects and turbulent behavior in beam plasma instability, studying interactions in magnetic field 15 p2660 A69-30917

Critical study of Tidman model for turbulent electrostatic shock wave structure in plasmas, noting velocity distribution function role 15 p2661 A69-30927

Turbulent diffusion and ion heating in plasmas in presence of current instability 15 p2662 A69-30959

Particle-wave interaction in weak turbulent plasma in presence of uniform magnetic field, applying perturbation theory arbitrary order 16 p2819 A69-31683

Plasma turbulence effect on magnetosonic wave attenuation, noting increased electron and ion collision frequency and appearance of anomalous resistance 16 p2820 A69-31794

Charge density irregularities of midlatitude ionospheric E region related to cross field plasma instability noting turbulence 16 p2773 A69-31972

Collisionless cylindrical Langmuir probe response in turbulent plasma for mean and statistical properties [AIAA PAPER 69-698] 17 p3010 A69-33438

Collisionless shock wave front turbulence in diluted plasma, including thickness, electron and ion component measurements 17 p3012 A69-33818

Collisionless plasma heating mechanisms from current layer turbulence in theta pinch experiment and shock wave front structure as function of initial magnetic field 17 p3013 A69-33824

Collisionless shock waves in plasma and ion and electron turbulent heating in high voltage theta pinches, noting magnetic disturbance 17 p3013 A69-33825

Signal wave scattering and transmission by ionized medium disturbed by high power pumping wave, studying wave interactions with Born approximation for bounded medium 17 p2928 A69-33871

Solar wind model for studying long wavelength turbulence as heat source for alpha particles and protons in solar plasma 18 p3186 A69-34299

Book on nonlinear plasma theory covering nonlinear wave, wave-particle and wave-particle nonlinear interactions and weak plasma turbulence 18 p3180 A69-34930

Spectral line scattering during propagation of radiation in turbulent plasma 19 p3396 A69-36573

Solar flares plasma turbulence mechanisms suggested from magnetic energy release studies of Petschek model of magnetic field annihilation 20 p3589 A69-37549

Power spectrum for energy transfer region in HF turbulent plasma by nonlinear equations, with results applied to subcosmic ray acceleration 20 p3591 A69-38008

Resonant perturbation response of Vlasov magnetoplasma to source below electron gyrofrequency, explaining fractional resonances in Alouette 2 topside data 22 p4023 A69-40516

Plane electromagnetic wave scattering on turbulent fluctuations in electron density of finite volume ionized plasma, evaluating Booker-Gordon relation 23 p4116 A69-41587

Optimization of Faraday MHD generators with nonequilibrium ionization and plasma turbulence, assuming electrons at Saha equilibrium at elevated temperatures 24 p4256 A69-43682

Electron density fluctuations in transition region of turbulent plasma jet, noting spiky waveform [AIAA PAPER 68-685] 24 p4360 A69-43697

Low energy cosmic rays and plasma turbulence in heating and ionizing interstellar gas, discussing acceleration and galactic sources 24 p4375 A69-43770

PLASMA WAVES

NT ELECTROSTATIC WAVES

Electron plasma wave dispersion along cylindrical plasma column in magnetic field 01 p0126 A69-10277

Quasi-monochromatic wave dispersion relation and energy transfer in inhomogeneous anisotropic medium 01 p0126 A69-10278

Transverse plasma mode excitation by nonlinear interaction analyzed by Hamiltonian function 01 p0127 A69-10280

Waves in inhomogeneous warm magnetoplasmas with static pressure gradients, applying dyadic to planar stratified plasma case 01 p0129 A69-10561

Plasma wave properties relation to creation of electron plasma densities above critical density, discussing splitting of cold plasma resonance

01 p0131 A69-10818

Electromagnetic waves trajectory distortion in moving plasma due to additional time delay noting propagation of pearl pulsations, whistling atmospherics and proton whistlers

01 p0068 A69-11114

Numerical method for determining group velocity of waves in homogeneous anisotropic medium, using implicit function from dispersion relation

01 p0131 A69-11117

Ionospheric irregularities and cross field plasma instability, analyzing nonlinear behavior of latter with two dimensional model

01 p0073 A69-11179

Stability of weakly inhomogeneous plasmas with free energy available for nonlinear resonant three wave interactions

01 p0133 A69-11212

VLF electric field measurements from 1 AU heliocentric orbit, noting field oscillations in solar wind and large amplitude HF noise bursts

01 p0035 A69-11224

Electric field in plasma half space determined by longitudinal wave normal mode analysis, using BKG particle conserving collision model

01 p0134 A69-11287

Plasma waves and particle interaction in nonuniform magnetosphere, considering propagation across sheets of steep density gradient and auroral precipitation

02 p0235 A69-11429

Book on propagation characteristics of various wave modes in ionized gas plasmas

02 p0285 A69-11518

Instability of longitudinal plasma waves propagating across magnetic field in plasma with electrons and ions drifting with different velocities across field

02 p0286 A69-11830

Total energy of plasma wave from second order energy, showing close approximation to wave packet energy

02 p0287 A69-11876

Plasma ion oscillation suppression by intensified electron plasma oscillations

02 p0287 A69-11934

Magnetoplasma wave propagation in periodic conducting solid, calculating electron drift effect on space harmonics

02 p0287 A69-11945

Standing ion-acoustic wave excitation in weakly ionized plasma, noting isothermal compression of electron gas

02 p0292 A69-12555

Acoustic plasma waves propagation in thin films in case of film quantization, showing phase velocities close to Fermi velocities of electrons

02 p0300 A69-12649

Wave analysis for energy propagation in plasma, discussing excitation spectrum and stability properties

02 p0293 A69-12782

Diffraction of cylindrical waves at half plane in cold anisotropic plasma, using Fresnel integrals

02 p0293 A69-12842

Wave fields and coupling of RF power to ion cyclotron waves in finite length thermal collisional plasma column

03 p0474 A69-13114

Existence and stability of periodic waves in cold collisionless plasma in magnetic field

03 p0474 A69-13143

Coulomb collision and microturbulence effect on plasma wave echo, noting echo dependence on perturbations in particle distribution

03 p0474 A69-13144

Density gradient driven collisional drift waves, discussing identification, stabilization and enhanced plasma transport

03 p0474 A69-13145

Enhanced bremsstrahlung from supraluminous and subluminal waves in thermal isotropic homogeneous Maxwellian electron plasma, noting applicability to Crab Nebula

03 p0507 A69-13150

Decay stability of large amplitude neutral wave into two ion acoustic waves in weakly ionized plasma

03 p0475 A69-13158

Magnetosonic wave propagation across magnetic field in warm collisionless Maxwellian multicomponent plasma studied for small electron cyclotron and ion cyclotron radii

03 p0479 A69-14020

Langmuir wave disintegration, analyzing instability criterion and growth rate

03 p0480 A69-14057

Disintegration spectrum of Langmuir wave excited in plasma column by antenna, discussing conditions of resonance and parametric amplification

03 p0480 A69-14113

Interaction between surface waves propagating along plane plasma boundary and parallel low density electron beam, noting wave amplification and excitation

03 p0480 A69-14135

Electron plasma oscillations diffusion due to scattering by large amplitude ion wave background, noting electron wave spectrum evolution

03 p0483 A69-14256

Monograph on electron waves and resonances in bounded plasmas covering theoretical and experimental methods, metallic and dielectric resonance probes, etc

04 p0633 A69-14296

Nonlinear electron oscillations in plasma, deriving asymptotic expression for plasma perturbation

04 p0635 A69-14552

Propagation velocity upper limits for plasma waves during state of equilibrium transition determined from nonlinear wave equation

04 p0630 A69-14553

Nonlinear demodulation of amplitude modulated wave propagating in plasma

04 p0559 A69-15210

Particles nonlinear motion in plasma in magnetic field with arbitrary electron velocity distribution, discussing wave discontinuity patterns

05 p0804 A69-16370

Coupled waves in ferromagnetic and antiferromagnetic semiconductors in constant electric and magnetic fields, discussing spin, electromagnetic and plasma waves dispersion

05 p0809 A69-16548

Hydrodynamic and lattice vibrations equations for coupled waves in ion semiconductors in external electric and magnetic fields, observing sound amplification

06 p0978 A69-16897

Equation for charged particle motion in electromagnetic wave field propagated along magnetic field applied to nonlinear wave propagation in plasma near cyclotron resonance

06 p0963 A69-16905

Power flow in cyclotron and plasma modes propagating in waveguide filled with cold collisionless axially magnetized plasma

06 p0897 A69-17760

Electrostatic waves in inhomogeneous plasma in finite magnetic field, noting dispersion relation for cold plasma and stabilization of instability

06 p0967 A69-17761

Nonlinear interaction between cyclotron harmonic waves propagating perpendicular to static magnetic field in warm magnetoplasma, noting parametric amplification and mode conversion

06 p0968 A69-17766

Surface plasma waves excitation by light and decay into photons applied to nonradiative modes

07 p1188 A69-18278

Nonlinear interaction between cyclotron harmonic waves, demonstrating synchronism conditions for traveling wave parametric amplification and passive mode conversion

07 p1189 A69-18439

Magnetoplasma waves in semiconductors, discussing cold plasma dispersion, helicons, carrier densities, lattice dielectric constant and acoustic domain propagation

07 p1197 A69-18465

Nonisothermal wave propagation in n-type indium antimonide in orthogonal static and magnetic fields, considering instabilities and acoustic and polar optical phonon scattering

07 p1197 A69-18467

Structure of plane shock wave of arbitrary force propagating across magnetic field in hot rarefied plasma

07 p1190 A69-18692

Comparative models of magnetoplasma, discussing wave propagation in cold plasma, warm plasma and microscopic model

07 p1190 A69-18919

Magnetosonic wave evolution in inhomogeneous dispersive plasma created by magnetic piston, discussing equation solution

07 p1181 A69-19001

Plasma column radial density profile measurement by electron plasma waves propagation in presence of strong magnetic field

07 p1194 A69-19323

Plasma waveguide parameter changes due to additional gas ionization from microwave field

07 p1196 A69-19750

Landau damping of long wavelength ion acoustic waves in collision-free one dimensional plasma with gravity field

08 p1359 A69-19983

Phase velocities and polarizations of linear waves in infinite uniform high beta plasma

08 p1359 A69-19986

Fresnel formulas for surface plasma waves excitation by light in thin metal foil embedded between dielectric layers, discussing transmissive and absorptive resonances

08 p1372 A69-20290

Nonlinear interactions between plasma waves of various intensities, noting changes in particle distribution

08 p1362 A69-20427

Cylindrical antenna input impedance in isotropic plasma, assuming weak three dimensional plasma diffusion

08 p1285 A69-20428

Energy density and transport velocity of RF wave in plasma in damped oscillations region, discussing resonance

08 p1365 A69-20553

Warm plasma magnetic interactions, discussing density waves, pair correlation function and transport coefficients

08 p1366 A69-20749

Collisional theory of longitudinal wave propagation for two fluid viscous ionized plasmas formulated from coupled Maxwell and Boltzmann equations

08 p1367 A69-20796

Microwave scattering from longitudinal plasma waves propagating in collisionless plasma column

08 p1276 A69-20798

Wave interaction in magnetically confined plasma taking into account body and surface waves

08 p1370 A69-21014

Electromagnetic wave attenuation propagating along external magnetic field ascribed to cyclotron wave energy absorption by resonant plasma particles

08 p1277 A69-21077

Cyclotron waves interaction when propagating in solid state plasma in magnetic field, determining amplification zones and factors

08 p1374 A69-21078

Plasma wave coupling in absence of magnetic field in revolving system containing dielectrics and circular waveguide

08 p1371 A69-21150

Inhomogeneous collisionless plasma drift-oscillation stability in magnetic field augmented by E wave HF field

09 p1546 A69-21564

Self focusing of plasma whistler wave along magnetic field at small threshold power

09 p1546 A69-21577

Quantum oscillations of magnetization, undamped magnetoplasma waves development and sound amplification by electron drift in crossed fields observed in semimetals

09 p1556 A69-21615

Plasma oscillation intensities at combination frequencies under assumption of plasma wave and ion acoustic wave propagating along z axis

09 p1550 A69-22024

Shock wave structure problems in plasma, including plasma particles random motion in term representing electric field

09 p1551 A69-22032

Electrons velocity-space instability in plasma column, analyzing unstable wave and dispersion characteristics

09 p1552 A69-22041

Plasma wave excitation and dissipation in fast thetatron discharge, indicating electron nonadiabatic inductive acceleration without equilibrium orbit

09 p1552 A69-22046

Second harmonic generation by electromagnetic wave incident on inhomogeneous plasma, determining power output

10 p1653 A69-23133

Correlation produced magnetoplasma mode in potassium confirmed by measurement of real part of surface impedance

10 p1728 A69-23168

Plasma electron beam nonlinear interaction, considering equations of motion of electron distribution function, plasma wave spectrum and mode coupling effects

10 p1729 A69-23407

Longitudinal and transverse wave propagation in compressible isotropic turbulent plasma, noting mode coupling effect

10 p1729 A69-23424

[AFCLR-69-0289]

- Discharge plasma ionized waves, determining mechanism of wave propagation and instabilities
10 p1740 A69-23699
- Transport of matter in nonisothermal weakly ionized plasma due to traveling ion-acoustic wave propagation, noting plasma oscillations and instability
10 p1741 A69-23945
- Plasma wave conversion into electromagnetic waves in strong magnetic field, studying nonlinear coalescence and scattering on thermal and epithermal ions
11 p1922 A69-24245
- Normal mode dispersion at upper hybrid frequency propagating parallel to uniform magnetic field in spatially inhomogeneous plasma
11 p1924 A69-24302
- Beam-plasma dispersion relations, obtaining dispersion equation for plasma waves and dispersion curves for longitudinal waves
11 p1925 A69-24366
- Backward plasma waves in region of anomalous dispersion indicated by opposite directions of RF wave phase and group velocities
11 p1927 A69-25116
- Landau dispersion relation solutions, noting higher order Landau poles and coupling of spatial Landau modes and least damped wave
11 p1929 A69-25265
- Tonks-Dattner resonances in plasma column, using linearized Vlasov equation for coupling to plasma waves of time varying electric fields
11 p1929 A69-25266
- Convective wave instability resulting from modulated electron beam injection into plasma, noting amplitude restraint due to collisional damping effect
11 p1934 A69-25576
- Transformation of longitudinal plasma wave into electromagnetic wave during collision with dielectric in plasma
11 p1934 A69-25708
- Acoustic wave generation in neutral particle component of weakly ionized gas by variation of electron temperature with low power RF signal
12 p2134 A69-26096
- Radio emission of fast cosmic ions by plasma wave conversion to electromagnetic waves, using nonlinear mechanism in turbulent plasma
12 p2149 A69-26209
- LF oscillations nonlinear excitation increment in plasma by electron beam found proportional to reciprocal of wave potential
12 p2138 A69-26709
- High speed photographic study of plasma luminescence front and charged particle concentration front counter to electrodynamic force in crossed electric and magnetic fields
12 p2141 A69-27130
- Electromagnetic flux from nonlinear self interaction of electron plasma waves in far field of perturbation under anisotropic electron pressures
12 p2141 A69-27147
- Nonlinear periodic wave propagation at angle to magnetic field in collisionless plasma studied by two fluid plasma equations
13 p2304 A69-27297
- Wave damping in plasma, developing Boltzmann analysis of electron mode dispersion relations involving momentum transfer and relaxations of electron-ion temperature and anisotropy
13 p2305 A69-27377
- MHD induction converters operational characteristics calculations with simultaneous considerations for finite length and channel width
13 p2207 A69-27496
- Finite Larmor radius effects on gravitational instability of rotating anisotropic plasma for transverse wave propagation mode
13 p2346 A69-27704
- Electromagnetic and plasma waves scattering by space vehicle excited by ground source in isotropic warm plasma, obtaining radar cross sections
13 p2221 A69-27965
- Collisions effect on wave propagation in homogeneous plasma, calculating permittivity tensor and electron equilibrium current using Boltzmann kinetic equation
13 p2311 A69-28104
- Waves propagating along rotating electron beam and interacting with magnetized plasma waveguide slow waves
13 p2312 A69-28118
- Unstable weakly ionized HF magnetoplasma fluctuations with no axial drift, noting phase velocity parametric dependence
13 p2312 A69-28197
- Whistler type electromagnetic waves excitation by electron beam in plasma, noting intensity dependence on electron frequency
13 p2314 A69-28443
- Tensor analysis of four photon interaction in rarefied plasma in magnetic field, determining cubic current of plasma wave self action
13 p2314 A69-28444
- LF wave propagation in DC discharge hydrogen plasma, noting self and artificial wave excitation
13 p2316 A69-28584
- Temperature effects on propagation of HF internal and surface waves in bounded plasma, deriving dispersion equations
14 p2410 A69-28733
- Quasi-linear approximation for spectrum analysis of LF plasma wave oscillations in steady electric field
14 p2492 A69-29468
- Radiative instability problem of stream plasma system in kinetic regime, discussing Fung letter
14 p2502 A69-29960
- Standing ion-acoustic wave excitation in weakly ionized plasma, noting isothermal compression of electron gas
15 p2658 A69-30252
- Particle diffusion and wave spectrum in unstable plasma calculated using Feynman diagrams, considering quasi-linear growth, resonant three wave coupling and nonlinear Landau damping
15 p2660 A69-30915
- Mode-mode coupling calculation for finite amplitude collisional drift waves demonstrating inherently nonlinear phenomena
15 p2660 A69-30916
- Wave regeneration by resonant particles interaction in inhomogeneous plasma of electrons confined in quadratic potential solved in WKB approximation
15 p2660 A69-30918
- Collisionless emission and absorption of longitudinal waves due to particle encounters in numerical experiments on one dimensional one species plasma
15 p2661 A69-30921
- High order plasma wave echoes formulation and relation to initial perturbations based on Landau solution of initial value problem for Vlasov equation
15 p2661 A69-30926
- Te waves propagation along plasma sheet between conducting plates, determining vertical plasma density distribution
15 p2569 A69-30939
- Nonlinear interaction between three monochromatic waves propagating parallel to magnetic field in plasma, considering relativistic drift motions of particles
16 p2816 A69-31640
- Quasi-linear theory of waves in collisionless plasma in absence of external fields, relating wave energy growth and decay to plasma stability
16 p2817 A69-31646
- Temporal damping rate for small amplitude linearly polarized TEM mode in plasma, using Landau equation
16 p2818 A69-31675
- Radar Thomson scatter from nonthermal steady state level of plasma waves in ionosphere measured, studying role of angle between wave vector and magnetic field
16 p2818 A69-31678
- Collisionless drift plasma wave instability growth rate calculation noting destabilization from resonant electrons
16 p2820 A69-31691
- Nonlinear mixing of Ar plasma ion wave and externally applied electromagnetic wave
16 p2820 A69-31769
- Plasma turbulence effect on magnetosonic wave attenuation, noting increased electron and ion collision frequency and appearance of anomalous resistance
16 p2820 A69-31794
- Incident energy transfer to particles due to nonlinear interactions during passage of intense light beam through plasma, considering decay into plasma waves
16 p2822 A69-32046
- Wave damping in current sheet in geomagnetic tail by radiating energy from sheet sides by electrostatic waves
16 p2781 A69-32318
- Plasma wave echoes concept extended to transverse electromagnetic wave excitation propagating parallel to external magnetic field
16 p2823 A69-32467
- Wave front resistivity in laser produced plasma interacting with magnetic field enhanced by two stream instability
16 p2823 A69-32564
- Waveforms analyzer for mixtures of exponentially damped sine waves, noting application to interferometer curves in plasma wave propagation
17 p2970 A69-32852
- Weak nonlinear hydromagnetic waves in cold collisionless plasma, using nonlinear perturbation method
17 p3010 A69-32866
- Collisionless shock wave front turbulence in diluted plasma, including thickness, electron and ion component measurements
17 p3012 A69-33818
- Collisionless shock wave structure in plasmas, noting plasma and shock wave generation mechanisms
17 p3013 A69-33822
- Plasma-cyclotron interaction wave coupling mechanism in symmetrical double beam system in uniform magnetic field leading to unstable wave excitation along beam
17 p3015 A69-33831
- Geomagnetic field latitudinal variation effect on cut-off frequencies of proton whistlers, discussing LF electromagnetic wave propagation in cold multicomponent plasma
18 p3100 A69-34253
- Longitudinal plasma waves collision damping calculations using Rostoker test particle method
18 p3179 A69-34439
- Microfluctuations frequency and wavelength of electromagnetic, electric and magnetic field distributions in plasma shock wave front found consistent with ion-acoustic origin hypothesis
18 p3180 A69-35017
- Electromagnetic and cyclotron waves interaction across opaque boundary in moving plasma in one dimensional approximation
18 p3181 A69-35027
- Transverse electromagnetic wave propagation in cylindrically stratified axially magnetized plasma, obtaining plasma properties profiles from method for isotropic media
19 p3266 A69-35619
- OGO 5 spacecraft detector instrumentation for measuring electrostatic and electromagnetic waves electric fields with coupled antennas, describing in-flight operation
19 p3315 A69-36683
- Sideband structure of transmitted frequency spectrum exhibited by plasma wave features on topside ionograms, noting harmonic resonances
20 p3496 A69-37891
- Induced Compton scattering of plasma and electromagnetic waves under astrophysical conditions, discussing HF radio emission spectra from cosmic objects and quasar
20 p3607 A69-38035
- Parametric excitation theory involving Langmuir and ion-acoustic waves for homogeneous plasma slab with specular particle reflection at slab walls
20 p3582 A69-38245
- Thermal effects of resonant coupling hydromagnetic oscillations in inhomogeneous finite-beta plasmas, obtaining equations for coupling modes between Alfvén and magnetosonic waves
21 p3776 A69-38710
- Coupled acoustic and spiral EM waves drift instabilities in bounded plasma of solid body found to be convective
21 p3782 A69-39556
- Relativistic solution by Landau procedure of initial value problem for one dimensional electron plasma wave coexisting with charged immobile background
21 p3778 A69-39579
- Monograph on whistler mode waves in plasma covering apparatus for studying gyroresonant interaction between whistler radiation and fast electrons
21 p3779 A69-39868
- Pitch angle distribution of cosmic ray electrons in decreasing magnetic field for waves in ionized plasma, noting anisotropy due to synchrotron radiation
22 p4006 A69-40642
- Coupling coefficients and excitation increments determined for nonlinear interactions of surface waves in nonisothermal semibounded plasma
22 p3990 A69-40790
- Collisionless damping of large amplitude ion acoustic waves excited externally in thermally ionized Cs plasma
22 p3991 A69-41008
- Electromagnetic wave propagation instabilities in semiconductor magnetoplasmas not diffusion limited to LF, using dispersion equation
22 p3902 A69-41223
- Electromagnetic radiation characteristics from vibrating electrons or electric dipole moving in com-

pressible isotropic plasma and from stationary dipole in moving medium, emphasizing Doppler effects
23 p4114 A69-41359

Plasma dielectric constant and RF wave energy and power absorption in anomalous dispersion region, noting plasma permittivity inverse relation to absorption band frequency
23 p4195 A69-41385

Nonlinear interaction between extraordinary waves propagating perpendicular to static magnetic field in cold homogeneous magnetoplasma
23 p4195 A69-41538

Acoustic wave propagation in plasma, analyzing ionic and electron sound caused by oscillation and relaxation processes using Landau and Vlasov kinetic equations
23 p4196 A69-41726

Transverse plasma waves propagating along parallel static electric and magnetic fields may lead to instabilities regardless of carriers sign
24 p4355 A69-42923

Electromagnetic waves incident upon anisotropic plasma, determining transmission and power reflection coefficients
24 p4282 A69-42978

Whistlers nonlinear interaction during cold magnetoplasma propagation, considering energy exchanges between waves
24 p4309 A69-43174

Surface wave terms found in long wavelength limit during solution of initial value problem for semiinfinite hot plasma
24 p4356 A69-43364

PLASMAGUIDES

Electromagnetic waves propagation in cylindrical waveguide containing plasma column along axis in absence of constant magnetic field
02 p0285 A69-11463

Plasma waveguide properties during high intensity electromagnetic wave propagation, discussing microwave waveguide coupling
03 p0482 A69-14228

Dispersive properties of axial and annular longitudinally magnetized plasma waveguides
05 p0802 A69-15925

Wave dispersion analysis for amplification in cold plasma filled cylindrical waveguide penetrated by electron beam of same radius
05 p0736 A69-16790

Self focusing of TM type electromagnetic waves in isotropic plasma and formation of waveguide channel
07 p1196 A69-19749

Plasma waveguide parameter changes due to additional gas ionization from microwave field
07 p1196 A69-19750

Broadband plasma waveguide switch application extended to 26-40 GHz range, discussing isolation, cold loss, switching time, trigger signal and ionized plasma
12 p2036 A69-25938

Waves propagating along rotating electron beam and interacting with magnetized plasma waveguide slow waves
13 p2312 A69-28118

Magnetized plasma waveguide dispersion characteristics using Maxwell equations, stressing interaction of electron beam with wave modes
13 p2315 A69-28571

Wave propagation in warm uniaxial plasma filled waveguide, analyzing TE modes, TM mode splitting and power transfer
16 p2756 A69-31576

Electromagnetic wave propagation in transversely magnetized warm plasma filled rectangular waveguide, analyzing TE and TM modes
16 p2756 A69-31581

Wave propagation in plasma filled cylindrical waveguide in axial magnetic field, approximating plasma density profile by WKB method
17 p2926 A69-33848

Helicon wave dimensional resonance in n-Nb plasma waveguides at different wavelengths relative to wall thickness
19 p3383 A69-36479

PLASMAS (PHYSICS)

NT ARGON PLASMA
NT BETA PARTICLES
NT CESIUM PLASMA
NT COLD PLASMAS
NT COLLISIONLESS PLASMAS
NT COSMIC PLASMA
NT DEUTERIUM PLASMA
NT ELECTRON PLASMA
NT HELIUM PLASMA
NT HIGH TEMPERATURE PLASMA
NT HYDROGEN PLASMA

NT METALLIC PLASMAS
NT NITROGEN PLASMA
NT NONEQUILIBRIUM PLASMAS
NT NONUNIFORM PLASMAS
NT RAREFIED PLASMAS
NT RELATIVISTIC PLASMAS
NT ROTATING PLASMAS
NT SOLAR WIND
NT STELLAR WINDS
NT THERMAL PLASMAS
NT TOROIDAL PLASMAS

Magnetoplasma wave propagation in periodic conducting solid, calculating electron drift effect on space harmonics
02 p0287 A69-11945

Plasmas in galaxies, spiral structures and radio galaxies, discussing quasar line and continuum spectra
02 p0329 A69-12790

Generation of UHF space charge waves by nonlinear interaction of two microwave signals in magnetoplasma, predicting optical mixing
03 p0475 A69-13146

Electron flow in stable negative electrostatic potential well produced by electronic injection at center of hollow open spherical anode
03 p0475 A69-13153

Charged particle density of unsteady plasma from Stark broadening of Balmer H beta line, using time scanning image converter
03 p0481 A69-14145

Current nature on infinite cylindrical antenna in compressible anisotropic lossy plasma medium, noting characteristic waves on infinite cylinder
04 p0578 A69-15215

Free energy of low density quantum plasmas derived statistically from exact two particle scattering phase shifts
05 p0799 A69-15629

Equations for frequency portions of electron-velocity distribution function in Lorentz plasma under influence of time periodic electromagnetic fields with two fundamental frequencies
05 p0800 A69-15743

Deceleration of conducting plasmoids moving in channels in nonuniform magnetic field
05 p0801 A69-15781

Forward velocity of Bostick plasmoids demonstrated proportional to mean surge current through button source
06 p0964 A69-17480

Modified truncation for BBGKY hierarchy for plasma, obtaining kinetic equation identical with Balescu-Lenard equation
08 p1360 A69-19990

Ion cyclotron resonance acceleration and higher harmonic acceleration in axially nonuniformly magnetized plasma under influence of RF electric field
08 p1360 A69-20079

Time dependent velocity distribution functions for carriers calculated in weakly ionized plasma in external electric field
08 p1362 A69-20265

Slow distribution function of magnetoactive plasma, deriving kinetic equation in quasi-linear approximation for analyzing particle-HF electromagnetic wave interactions
08 p1365 A69-20550

Time rates for growth and damping of resistive instability in gaseous plasma in crossed electric and magnetic fields
08 p1369 A69-20886

Communication problems due to natural and artificial plasmas in spacecraft vicinity, discussing plasma effect theory
09 p1451 A69-21292

Magnetoactive plasma containing fast monoenergetic ions noting stability at drift frequencies and in terms of Alfvén wave buildup
09 p1546 A69-21566

Free carrier magnetoplasma effect used for far IR phase matched difference frequency generation in semiconductors, discussing carbon dioxide laser transitions
09 p1556 A69-21578

Scientific data acquisition and interpretation effects on electric spacecraft plasmas and field directions, noting electron interchange reactions effect
[AIAA PAPER 69-276] 09 p1568 A69-21727

Plasma cavity shape formed by magnetic field effect due to several parallel line currents
[ISAS-433] 09 p1553 A69-22569

Solar system plasmas and X ray astronomy - Conference, Adelaide, Australia, August 1968
09 p1581 A69-22742

Radio wave generation in astrophysical plasmas, discussing various emission mechanisms
09 p1608 A69-22743

Correlation produced magnetoplasma mode in potassium confirmed by measurement of real part of surface impedance
10 p1728 A69-23168

High temperature gas mixture plasmas thermodynamical properties, emphasizing Debye electrostatic interactions and electron states
10 p1810 A69-23794

Trapping of plasmoids injected from two coaxial plasma sources through magnetic gaps of diverter, discussing alternate and simultaneous injection
12 p2133 A69-25976

Kinetics of air plasma formation in wake of shock wave propagating in air, taking into account nonequilibrium ionization
12 p2062 A69-26674

Magnetic field fluctuations of interplanetary plasma, considering anisotropic temperature instabilities
14 p2517 A69-29064

Rocket and satellites topside sounding of earth ionosphere, determining magnetoplasma structure and resonance
14 p2438 A69-29101

Time averaged stress tensor for ionized plasma in HF electromagnetic field, considering collisions
14 p2493 A69-29649

Fabry-Perot interferometer employing gas laser for plasmoid electron concentrations measurement at 3.39 micron wavelength
14 p2451 A69-29778

Particle drift velocity distribution of fully ionized plasma in magnetic field calculated by integration of Boltzmann equation
15 p2659 A69-30707

Time resolved Stark broadened spectral profiles for Na I 5682-88 Å and 4978-82 Å lines of plasma, comparing electron densities
15 p2656 A69-31155

Nonlinear generation of sum and difference frequency components in magnetoplasma current density due to alternating electric fields, electron density and temperature gradients
16 p2821 A69-32036

Continuity conditions for drifting magnetoplasmas without ionic effects, discussing eigenvalue equation of refractive index and electromagnetic modes propagation
17 p2926 A69-33851

Deceleration of conducting plasmoids moving in channels in nonuniform magnetic field
18 p3181 A69-35033

RF plasmoid properties, discussing bounded plasma resonance theory, basic experiments, resonance sustained discharges, role of negative ions, etc
18 p3181 A69-35487

Soviet collection of articles on plasmoids covering plasma accelerators and plasma interactions with magnetic fields
24 p4356 A69-43467

Time-variable pulsed transverse magnetic field used to cut off tails of plasmoids ejected from conical Plexiglas plasma gun into curvilinear magnetic field
24 p4358 A69-43476

PLASMATRONS

NT DUOPLASMATRONS

Heat transfer between arc column and discharge chamber wall of vortex linear plasmatron, using approximate similitude method
01 p0125 A69-10091

Solid phase particle motion in plasmatron with colliding jets, measuring W particle heating by optical method
05 p0802 A69-15975

Spectroscopic investigation of emission of air plasma in HF electrodeless plasmatron, analyzing near IR, UV and visible spectra
07 p1191 A69-18995

Electric arc interaction with turbulent boundary layer in vortex stabilized plasmatron, noting variation in arc intensity
09 p1545 A69-21432

DC plasmatron for heating argon with potassium additions at high temperatures and at near atmospheric pressure to obtain argon flow
09 p1547 A69-21596

Temperature pulsations radial distribution in plasma jet using plasmatron without mixing chamber
10 p1729 A69-23432

Electrodeless plasmatron coupled with oscillator operating at 5-30 kHz, discussing parameters effect on operation mode and performance
12 p2140 A69-27123

Current, magnetic field, flow velocity and plasmatron dimensions effects on arc voltage in coaxial plasmatron
13 p2306 A69-27388

Operating conditions influence on thermal stability of DC plasmatron arc to obtain high temperature source
15 p2663 A69-30994

PLASMOIDS
U PLASMAS [PHYSICS]

PLASMOLYSIS
Escherichia coli B/r cells plasmolyzed in sucrose observed under phase contrast, noting plasmolysis reduction in ions presence
19 p3257 A69-35973

PLASMONS
Surface plasmons microscopic theory based on modified random phase approximation
06 p0967 A69-17711

Surface plasma waves excitation by light and decay into photons applied to nonradiative modes
07 p1188 A69-18278

Surface plasmon excitation by tunneling electrons in GaAs-Pb junctions, discussing conductance at bias voltages, plasmon energy and concentration
07 p1200 A69-19402

Plasmon superconductivity mechanism in degenerate semiconductors and semimetals, noting interaction effect between electrons and plasma sound
09 p1556 A69-21573

Localized plasmons and optical phonons occurrence on local plasma levels, noting role of impurity atom in localized exciton-plasma resonance
09 p1548 A69-21674

Raman scattering by coupled plasmon-cyclotron-harmonic modes in semiconducting plasmas in homogeneous static magnetic field
16 p2824 A69-32604

Electron-plasmon interaction in degenerate semiconductors, using mathematical model for rectifying metal contacts tunneling characteristics
19 p3382 A69-36049

Dispersion relations for surface plasma oscillations in normal metals for single and multiple films taking into account retardation effects, noting dielectric function
22 p3992 A69-40419

Josephson currents interaction with LF surface plasmons in superposed thin dielectric and superconducting metal films, noting I-V characteristics
22 p3992 A69-40420

PLASTIC AIRCRAFT STRUCTURES
Glass fiber reinforced plastic in aircraft construction, considering cellular weight and economy
03 p0454 A69-13821

Light passenger aircraft of glass fiber reinforced plastic, using hose construction technique
03 p0454 A69-13822

Helicopter rigid rotor system with blades of glass fiber reinforced plastic
04 p0548 A69-14817

LFU 205 light aircraft design and construction with fiberglass reinforced plastic
08 p1321 A69-20867

Boron filaments reinforced epoxy aircraft landing gear structure prototype, discussing development, fabrication, and testing
09 p1508 A69-22340

Glass reinforced plastic molding compounds for OV-10A airplane structural components, noting cost savings [SAE PAPER 690342]
11 p1890 A69-24497

Composite airframe structural joint design and weight considerations for boron and glass fiber reinforced plastic materials [ASM PAPER W9-23.1]
14 p2535 A69-29448

Sailplanes design, discussing structural flexibility, deformations, acroclastic effects and plastics and man-made fibers
15 p2551 A69-30899

Fatigue properties and test procedures for glass reinforced plastic rotor blades used in twin engine helicopter [AHS PAPER 370]
17 p3060 A69-33518

Design and fabrication of plane and trapezoidal fiberglass wings with laminar plastic profiles for aerodynamic tests, including wing rigging and slotted wing
19 p3324 A69-35831

Helicopter rotor blade construction and developments, discussing mass balance, fatigue life, fail-safe characteristics, cost and weight ceiling and plastic materials
19 p3329 A69-36768

Boron fiber reinforced composite materials in aircraft structures, comparing rigidity with glass fiber plastics and weight gains
23 p4179 A69-42155

Redesigned Al wing structure using B-epoxy composite applied to pressurized fuel carrying section, including material, fabrication and test data
24 p4323 A69-43418

RTV silicone rubber for corrosion control coatings, high strength adhesives and low density sealants in aircraft structures
24 p4338 A69-43457

PLASTIC ANISOTROPY
Anisotropic plasticity in sheet metals under uniaxial and balanced biaxial tension
05 p0837 A69-16030

Plastic flow anisotropy and texture shifting by rolling in Ti-Mo-V alloy, analyzing slip rotation, grain boundary shear and deformation mode
17 p2987 A69-33078

PLASTIC COATINGS
Mechanical behavior of synthetic layer coatings for damping instrumental vibration and noise
01 p0168 A69-10399

Plastic backing films removal from carbon electron microscope replicas by maintaining specimens in horizontal position
09 p1495 A69-21651

Epoxy encapsulated transistors reliability, data from long term maximum rated life and accelerated tests
18 p3145 A69-34498

Wear resistance and antifriction measurement device for polymer coatings in high vacuum, various gases and during exposure to electron radiation
23 p4169 A69-41599

PLASTIC DEFORMATION
Shear accommodation kinking at second order twin bands in critically deformed magnesium investigated for dislocation mechanism
01 p0093 A69-10063

Repeated elastoplastic deformation of polycrystalline body analyzed by dynamic model
01 p0164 A69-10082

Yield condition of polycrystalline hcp metal, considering slip characteristics of hcp crystals
01 p0094 A69-10304

Fretting effect on fatigue of press fitted axle assemblies, analyzing relative slip amplitude dependence on size, shape, clamping pressure, nominal stress and cycles
01 p0167 A69-10305

Nb-W alloy solution hardening and deformation, noting flow stress dependence on strain rate and temperature plus activation energy of deformation
01 p0095 A69-10488

Deformation in aged Fe-Cr alloy studied for rate-controlling solid solution mechanism as function of stress
01 p0095 A69-10601

Interlayer slip in layered wood beams with nail joints analyzed in terms of small deflection theory
01 p0169 A69-10638

Plastic zone generation by slots cut in tensile test specimens before and during loading, discussing redistribution
01 p0098 A69-10762

Microfacets of metal surface cracks studied for plastic deformation and atomic separation mechanisms by electron diffraction
01 p0098 A69-10763

Strain distribution for fracture initiation and steady state crack propagation in plane strain tension of plastic materials
01 p0169 A69-10764

Mechanical finishing abrasion induced plastic deformation microtwinning observed in thin stainless steel films by transmission electron microscopy
02 p0251 A69-11542

Critical internal pressure induced plastic instability in membrane shells of revolution determined by graphical numerical method
02 p0338 A69-11719

Deformation thermodynamics, discussing mechanics and thermokinetics of continuous media and wave propagation problem
02 p0339 A69-11990

Kinetic features of martensitic transformation of nickel steels dependent on plastic deformation degree at 525 C
02 p0267 A69-12190

Finite deformation mode stability for finite amplitude first diameter nonlinear plastic wave initiation and growth at impact face in long rods
02 p0342 A69-12279

Plastic deformation wave propagation and heat generated near yield point of annealed aluminum
02 p0342 A69-12280

Aluminum deformation at various strain rates and temperatures under combined stress, comparing results with theoretical predictions
02 p0343 A69-12282

Constitutive equations for dynamic material behavior permit consideration of large deformations in direct manner
02 p0343 A69-12286

Plastic fatigue life of steel under rotary bending, proposing fracture criterion based on strain amplitude for low cycle stress levels
02 p0346 A69-12421

Finite difference numerical integration technique for large elastoplastic deformation transient and permanent deflection responses of thin shells
02 p0347 A69-12518

Elastic-plastic and creep deformation calculations of cylindrical shell, providing better estimate of critical time at higher stress levels by including plasticity
02 p0348 A69-12539

Friction induced plastic deformation of Be-Co-Zn single crystals with HCP structure
02 p0254 A69-12627

Aging and cold work hardening effect on deformability of aluminum-magnesium-silicon-copper alloy
02 p0254 A69-12677

Strain rate effect of large deflections of clamped circular viscoplastic plates subject to rigid mass impact
02 p0349 A69-12798

Asymptotic constitutive approximations for rapid finite deformation of general viscoelastic materials, noting isotropic solids and fluids
03 p0523 A69-13020

Plastically twisted prismatic bars with transverse discontinuous inhomogeneity, using sand hill analogy to determine stress field and limiting torque
03 p0524 A69-13021

Creep relaxation and kinking of aluminum-nickel whiskers at elevated temperature, noting permanent plastic deformation after heat treatment
03 p0443 A69-13119

Strain induced deformational instability of aluminum alloys
03 p0447 A69-13818

Model of creep in solids based on Markov process, discussing dislocation movement by means of thermal activation
03 p0529 A69-13942

Elastic-plastic boundaries velocities for combined longitudinal and torsional plastic wave propagation in thin walled tube during unloading [ASME PAPER 68-WA/APM-7]
04 p0670 A69-14403

Yield curve softening in hard Al subject to cyclic torsional loading, noting deformation resistance, surface hardness and yield strength
04 p0671 A69-14411

Resistance wire strain gages for measuring elastoplastic deformations in zones with high stress concentrations of strained machine elements
04 p0671 A69-14433

Impurity-dislocation interaction in Al alloy by vacancy mechanism and repeated yielding phenomenon, establishing activation energy
04 p0613 A69-14440

Alloying elements and cold rolling deformation effects on formation of texture in Ti alloys, noting inhomogeneity
04 p0617 A69-15077

Cold working considered for decreasing fatigue crack propagation rate in thin duraluminum sheets with various plastic deformations
04 p0681 A69-15170

Plastic deformation effect on structure, yield point and tensile strength of aged austenitic alloy containing Ni, Cr and Ti
04 p0618 A69-15177

Book on thermal time independent plastic and time dependent creep strains in structures through analogy permitting inelastic structures analysis
04 p0681 A69-15200

Truncated solid cones plastic yielding under quasi-static and dynamic axial loads at various strain rates
04 p0682 A69-15301

Exact geometrical equations and internal equilibrium for elastoplastic deflections of orthotropic shells of revolution using thin shell theory
05 p0831 A69-15680

Course slip during cyclic deformation of copper single crystals, discussing strain bursts dependence on stress amplitude rate, unidirectional prestrain and orientation
05 p0779 A69-15905

Elastic-plastic analysis of flat plates in membrane stretching and flexure, using method of initial strains [ASME PAPER 68-WA/PVP-10]

05 p0840 A69-16191

Book on plastic deformation of metals in terms of dislocation theory covering single crystals, alloying solid solutions, aggregates, annealing, etc

05 p0841 A69-16369

Crack nucleation in high strain fatigue based on plastic instability model

05 p0780 A69-16430

Plastic yield on inclined slip planes at tip of crack deformed in antipane strain

05 p0842 A69-16436

Crack tip displacements and strains in plastically yielded region measured with replica technique

05 p0780 A69-16437

Finite elastic-plastic deflections of orthotropic shells of revolution, deriving exact geometrical relations and equilibrium equations

05 p0842 A69-16642

Statically indeterminate elastoplastic problem under condition of complex shear

05 p0843 A69-16691

Magnetoplasticity induced in metal by high magnetic fields, examining stationary flow in two dimensional deformation

05 p0844 A69-16804

Plastic deformation, aging, heat treatment and machining effect on structure of thin films of AlMg11 alloy

05 p0783 A69-16814

Plastic yielding and strain distribution in Al reinforced with stainless steel wires determined by electron microscopy

06 p0940 A69-16947

Aluminum-stainless steel wire reinforced metal matrix composites, analyzing strain hardening and plastic deformation

06 p0940 A69-16950

Calculation of thin shell or beam structures with plasticity and isothermal creep based on linearization and local kinematic behavior [ONERA-TP-667]

06 p1020 A69-17099

Plastic deformation and bursting pressure of thin rupture disk as related to tensile strength

06 p1020 A69-17129

Plastic deformation in hypoeutectoid and hypereutectoid Ni-Ti alloys studied by compressive stress-strain analysis and transmission electron microscopy

06 p0941 A69-17222

Deformation and fracture of Be bicrystals grown by seeding and floating zone melting method from Be single crystal

06 p0942 A69-17225

Deformation and stresses in biaxially loaded stretched thin plate with central small hole during stress redistribution caused by creep

06 p1022 A69-17368

Numerical method for stress function of elastic-plastic torsion of hollow bars during quasi-static monotonic twist compared with relaxation method solution

06 p1023 A69-17370

Initially imperfect axially compressed cylindrical shells strength using variational principle, shell theory and deformation theory of plasticity [AIAA PAPER 69-91]

06 p1028 A69-18181

Plastic deformation of internally oxidized dispersion strengthened silver magnesium alloys, noting hardening effect dependence on oxidation temperature

07 p1159 A69-18627

Production technology of sheets, forgings and drop forgings from Ti and Ti alloys, discussing gas saturation prevention and plastic deformation

07 p1164 A69-18786

Section pressing from Ti alloy, noting procedure and temperature dependent deformation parameters effect on microstructure and properties

07 p1164 A69-18788

Transient heat evolution response to reappplied stress of alloys plastically predeformed at 4.2 K attributed to thermally softened defect structures

07 p1165 A69-18906

Plastic deformation in bcc, fcc and hcp metals as function of initial impact load energy, noting strain hardening effects

07 p1166 A69-19144

Fatigue gauge for plastic deformation based on plastic strain rates, cycles, temperature, etc

07 p1135 A69-19216

Minimum theorems in elastoplastic theory extended to continua for plastic strains governed by holonomic and nonholonomic stress-strain laws

07 p1235 A69-19442

Plasticity theories for nonisothermal loading, considering plastic strain

07 p1237 A69-19681

Accuracy of deformation theory in case of simple loading, analyzing external forces under conditions not satisfying loading theorem

07 p1237 A69-19684

Short cylinder of perfectly plastic Coulomb yield conditions compressed between rigid plates, discussing cylinder-plate interface frictions, angles of internal friction and cohesion

08 p1410 A69-19890

Free surface strain increment components on high carbon steel compression specimens to estimate tensile plastic instability onset, noting ductile fracture criterion

08 p1328 A69-19891

Heat generation effects by plastic deformations at tip of propagating crack in quasi-brittle materials, considering elastic stress field and crack velocity

08 p1412 A69-20144

Temperature dependence of polymethylmethacrylate deformation, yield and fracture in constant strain rate compressive and tensile tests

08 p1335 A69-20215

Continuum stress/plastic strain relations from Schmid Law of plastic slip in individual crystal grains

08 p1414 A69-20525

Incremental and corresponding total strain theories of plasticity used to analyze hydrostatic bulging of circular diaphragm

08 p1418 A69-20826

Cylindrically deformed fiber reinforced material, obtaining kinematics and constitutive equations

08 p1418 A69-21002

Elastoplastic response of intersecting hemispherical/cylindrical shell structures compared with plastic deformation predictions

09 p1615 A69-21922

Finite inelastic deformations under transverse impulsive loading of clamped thin rectangular platform shells idealized as membranes, using incremental plasticity theory

09 p1616 A69-21939

Complete solution for punching smooth interface double layer Tresca material in plane deformation, including Coulomb material

09 p1617 A69-22048

Heat resistant alloys plastic deformation, studying stress/strain systems, strain divisibility, strain rate and temperature effects, etc

09 p1504 A69-22145

Histogram approximation of plastic deformation of metals, analyzing tube under internal load and sandwiched layer compression

10 p1793 A69-22850

Deformation of thermoplastics under tensile loading, discussing types of loading

10 p1716 A69-22942

Negative creep in austenitic steel samples explained as possible redistribution of elements inside austenite grains at high temperatures

10 p1708 A69-22999

Strain fatigue mechanism of crack propagation in ductile metals, considering distribution of plastic cohesive stresses at crack tip

10 p1795 A69-23059

Plastic energy dissipation and crack surface displacement of penny shaped crack in elastoplastic material

10 p1803 A69-24030

Thermomechanical treatment effect on VT15 Ti alloy properties and welds after deformation, attaining high tensile strength and plastic properties

11 p1889 A69-24277

Strength analysis of revolving shallow shell with jumpwise thickness variations under axisymmetric distributed load, considering rigidity and plastic deformation

11 p1968 A69-24318

Alloying additions effect on plastic deformation anisotropy in GaAs single crystals, determining dislocation activation energies from creep tests

11 p1936 A69-24537

Two dimensional contained plastic deformation in asymmetrical elasticity theory based on Cosserat medium, examining boundary value problems, stress concentration and elastic wave propagation at holes

11 p1973 A69-24659

Stress-strain relation in crystalline media for pure tension and elongation epsilon several times conventional elastic limit, verifying by testing Al alloy [ONERA-TP-695]

11 p1975 A69-24754

Direct measurement device for metallic material response to mechanical stresses from stress force and global displacement/including material deformation/

11 p1884 A69-24757

Permanent displacement relationship to shell thickness following snap-through of loaded rigid boss in spherical metal shell

11 p1980 A69-24822

Residual thermal stresses and plastic strains at hole edges in perforated plates, considering heating and rapid cooling

11 p1982 A69-24947

Plastic strains in aluminum alloy under biaxial tensile and combined tensile and torsion tests, discussing small elastoplastic deformation theory

11 p1905 A69-24948

Analytical expressions for Gaussian constraint of continuum, using continuity conditions as equations of internal geometric couplings

11 p1984 A69-25170

Elastic and elastoplastic strains in materials under various loadings, determining temperature variations by thermoelectric method and verifying by tensile tests

11 p1985 A69-25178

Comparison of errors obtained by using linearly gliding and rotating strengthening moduli in stress-strain state on basis of linear stepwise approximation

11 p1986 A69-25342

Fcc metals cyclic deformation and fatigue dependence on cross slip of screw dislocations, considering strain hardening and crack propagation

11 p1906 A69-25389

Dynamic plastic response of finite bar subject to axial impact load noting reflected waves, stress-strain time histories and residual strain

11 p1991 A69-25512

Thermodynamics of strain rate sensitive elastoviscoplastic solids, considering kinematic description of plastic deformation and choice of state variables

11 p1994 A69-25601

Nimonic alloy single crystals strengthening during plastic deformation, analyzing jump phenomenon at high and low temperatures

12 p2112 A69-26038

Lattice defects in annealed and plastically deformed cobalt, showing increase with increasing martensite transformations

12 p2113 A69-26042

Large plastic deformation of two metallic cylindrical flat ended missiles in mutual longitudinal impact

12 p2179 A69-26217

Large deflection elastic-plastic analysis of axisymmetric shells of revolution indicating role of plastic yielding in buckling pressure reduction

12 p2186 A69-26839

Moire and gridwork methods of plastic strain analysis with application to plane strain and axisymmetric extrusion

13 p2359 A69-27256

Perturbation theory of antiplane elastoplastic deformations based on plasticity theory, considering circular hole in body under uniform shear

13 p2359 A69-27263

Molybdenum dislocation velocity and macrodeformation, noting thermal double kink mechanism inconsistencies and strain role in strain-rate relationship

13 p2276 A69-27392

Matrix grain size relation to dispersed particle size distribution and Zener-McLean equation description of microduplex structure in superplastic Ni-Fe-Cr alloy

13 p2278 A69-27411

Plastic deformation effects by hydrostatic fluid extrusion on mechanical properties of Ni maraging steels

13 p2278 A69-27414

Stress and plastic deformation influence on allotropic transformation of cobalt-nickel single crystals studied by X ray diffraction

13 p2279 A69-27761

Polycrystalline Re high temperature plastic deformation during creep, including activation energy and substructure dislocation study

13 p2280 A69-27767

Torsional testing facility for delayed elastic and non-recoverable strains in materials, noting application to diffraction limited reflecting optics

13 p2240 A69-27955

Classical plasticity theory modified to include finite elastic and plastic strain components by considering thermoelasticity and plastic work irreversible processes

13 p2362 A69-28119

Small strain plasticity theory for planar slip in specific nickel base alloy deformation

13 p2362 A69-28120

Discrete element plastic analysis of long prismatic bars under transverse loading in longitudinal direction, based on matrix displacement method

13 p2365 A69-28237

Grain size and deformation velocities effects on plasticity of dispersion hardened alloy

13 p2283 A69-28489

Minimum theorems for plastic strain rates and plastic strains governed by holonomic elastoplastic theory utilizing quadratic functions
13 p2370 A69-28629

Elastoplastic deformations of thin axisymmetric shells of revolution with variable thickness, exemplifying shell with piecewise constant thickness
14 p2533 A69-28982

Machine for measuring creep deformation of polytetrafluoroethylene under uniaxial compressive loads, discussing stress-strain relationship
14 p2469 A69-29412

Elastoplastic continua fire resistance at high temperatures, establishing plasticity condition and stress-strain relationships
14 p2536 A69-29598

Cold worked high purity Mo wire recovery after plastic deformation at room temperature, considering electrical resistivity decrease as function of annealing temperature
15 p2636 A69-30082

Experimental determination of strain /or strain rate/ tensor in plastic deformation analysis
15 p2707 A69-30639

Plastic strains at crack tips in thin plate under concentrated forces, analyzing slip bands during initial deformation
15 p2708 A69-30659

Interferometric technique for studying fracture specimens plastic zone using laser holography
15 p2609 A69-30681

Interface friction and adhesion of alloys workpieces and die materials under pressure and temperatures typical of plastic deformation
15 p2629 A69-30902

Similarity criteria for plastic deformation theory of body under pressure and nonuniform temperature field, considering strength calculations
15 p2714 A69-31200

Strain hardening experiments on single crystals of AlZn and AlAg alloys noting plastic behavior
16 p2800 A69-31776

Plastic expansion in metals due to alternating torsional and static tensile loading
16 p2875 A69-32291

Plastic failure under internal pressure of aluminum spherical shells with single radial or oblique nozzle based on limit analysis theory
17 p3052 A69-32983

Attitude and simple stability of deformable earth pointing satellite
17 p3047 A69-33229

Structure of meteorite Gibson section containing taenite grains and annealing twins indicating plastic deformation of taenite followed by recrystallization and grain growth
17 p3034 A69-33586

Loading path criterion for total strain /deformation/ plasticity theory based on Sanders loading function, discussing case of thermally loaded bar
17 p3062 A69-33711

Prestrained material plastic behavior experiments and deformation lines of influence analysis, noting importance in cold working
17 p3067 A69-34146

Craze formation and shear yielding considered for glassy polymers in terms of stress field requirements
17 p2993 A69-34169

Plastic energy dissipation rate during stable crack growth in sheet under uniaxial tension
18 p3212 A69-34345

Bending of rigid freely supported plastic plates under local axisymmetric dynamic load, discussing rectangular pulse effects and velocity fields
18 p3217 A69-34593

Sandwich beams optimal design determined for case of constraint on elastic deflection and for load factor at plastic collapse
18 p3218 A69-34623

Martensite transformation, C content and work hardening relations in stainless steels studied for magnetic detection of embrittlement during deformation
18 p3138 A69-35117

Nickel solid solutions strengthening under cold deformation studied by X ray, noting screw and edge dislocations role
18 p3157 A69-35246

Fiberglass-reinforced plastics longitudinal and transverse strain relations at various temperatures
18 p3163 A69-35366

Electron beam welds orientation effects on tensile and deformation properties of strengthened and welded austenitic stainless steels
18 p3151 A69-35432

Alpha Ti-Al and Ti alloys plastic deformation at low temperatures, noting slip and twin mechanisms role
18 p3158 A69-35444

Preliminary plastic deformations effect on dispersion hardened nimonic-80 alloy creep properties
18 p3159 A69-35446

Metal purity effect of nickel and Ni-Mo alloy on nucleation and recrystallization nuclei growth following 80 percent plastic deformation
18 p3159 A69-35449

Collection of articles on physical nature of plastic deformation and failure of metals
18 p3159 A69-35451

Nb single crystals plastic deformation influencing tensile strength, noting rolling directions
18 p3160 A69-35454

Preprogrammed deformation temperature influence on Ni creep strength, emphasizing smoothly changing loads effects
18 p3160 A69-35455

Yield condition of maximum constant distortion strain energy for anisotropic material without incompressibility assumption
18 p3227 A69-35494

Residual deformation of elastoplastically bent thin circular plate after perfect unloading from large deflection, considering equilibrium and compatibility conditions
19 p3438 A69-36306

Nondestructive test method using transducer action of flow in stress field causing plastic deformation with energy release as acoustic emission
19 p3314 A69-36634

Reducibility conditions of flow theory for smooth and piecewise smooth yield surfaces to relations of small elastoplastic deformations
19 p3443 A69-36794

Plastic deformation effect on dynamic buckling of elastic-plastic simple shallow truss subjected to step and impulsive loading
19 p3446 A69-36836

Stress and strain concentration factors under initial stages of elastoplastic deformation for circular hole in infinite medium, using method of successive approximation
19 p3447 A69-36860

Plane membranes finite deformation, deriving energy theorems for potential U bounds estimation
20 p3624 A69-37588

Thin cylindrical pressure vessels with circular cutouts and radial branches, observing limit pressures during plastic deformation
20 p3629 A69-38027

Stress strain state in thin circular elastoplastic disks under axially symmetric transient temperature distribution, noting moving annular plastic deformation region
20 p3629 A69-38028

B fiber reinforced Ni failure characteristics at high temperature, discussing plastic deformation and matrix role in crack inhibition
21 p3743 A69-38616

Plastic deformation and dislocation damping of cemented WC-Co alloys studied by compressive testing at room temperature
21 p3744 A69-38736

Depth dependent variations in texture in Nb due to inhomogeneous plastic deformation during cold rolling
21 p3744 A69-38737

Slip band etching procedure revealing Ni-base superalloy plastic deformation, accentuating slip bands and subgrain boundaries by electropolishing
21 p3744 A69-38741

Plastic bending of thin walled pipes taking into account cross section flattening
21 p3835 A69-38868

Creep measurements in Al alloy during uniaxial tensile stresses between 200-350 C, determining deformation dependence on time and stress
21 p3744 A69-38871

Plastic deformation combined effect with aging on mechanical properties of phase-hardened austenitic Fe-Ni-Ti alloys
21 p3746 A69-38956

Plastic deformation in hardened Ti alloys with thermally unstable beta phase under static compression and tensile loads by electron microscope
21 p3746 A69-39161

Levy-Mises equations for ideal plastic material derived from relationship between stress and rate of deformation tensors
21 p3840 A69-39287

Generalized strain-measure application to linearization of stress-strain curves of compressive, shear and tensile nature, discussing plastic deformations
21 p3844 A69-39321

Deformation localization and slip functions in statistical theory of plasticity, discussing approximations and untenability of Yosimura theory criticism
22 p4044 A69-40742

Creep at 400 degree C in Ti alloy sheets in short period plastic deformation due to work hardening by stepwise drawing in extensometric device
22 p3971 A69-41032

Energy equilibrium for crack growth in elastoplastic media, analyzing crack behavior during plastic deformation concentrated at edge of propagating crack
22 p4046 A69-41060

Plastic deformation by uniaxial tension during transition from dynamic to static loading from microscopic and macroscopic standpoint, noting slip lines
22 p4047 A69-41081

Rigid/plastic solids subjected partly to uniform fluid pressure and partly to general boundary conditions, analyzing uniqueness and stability criteria
23 p4235 A69-42460

PLASTIC FILMS

U POLYMERIC FILMS

PLASTIC FLOW

NT TRESCA FLOW

Plastic zone generation by slots cut in tensile test specimens before and during loading, discussing redistribution
01 p0098 A69-10762

Compaction kinetics in continuous quasi-viscous medium having plastic flow material under applied load, discussing hot pressing of nichrome powders
04 p0618 A69-15389

Crack tip plastic flow effect on strain energy release rate, considering Dugdale model for yielded crack [ASME PAPER 68-WA/MET-17]
05 p0838 A69-16155

Complementary variational principles for boundary value problems in continuum mechanics of solids, obtaining generalized Hamilton canonical formalism
07 p1232 A69-19173

Impurities effect on plastic flow stress and activation volume as functions of strain, strain rate and temperature in molybdenum crystals
10 p1710 A69-23089

Elongational viscosity coefficient determined from tensile measurements of materials under applied stress
10 p1681 A69-23976

Macroscopic states of stress criteria for plastic flow initial yielding, plastic flow and brittle fracture of ductile and brittle metals
11 p1975 A69-24671

Gas turbine disk calculation and plastic flow theory, considering loading conditions and elastoplastic strains due to centrifugal forces and nonuniform heating
11 p1982 A69-24945

Incompressible elastic-plastic solid flow through rough converging conical channel analyzed using Mises yield condition and Prandtl-Reuss equations
12 p2063 A69-27114

Physical limit model of fatigue in metals and alloys to determine stress producing plastic flow in surface layer
14 p2461 A69-28913

Necked tension specimens profiles for rigid-plastic nonhardening materials determined from compatibility equation for displacements and unloading rate
15 p2704 A69-30292

Monograph on stress fields in plane plastic flow as solutions to boundary value problems
15 p2711 A69-30932

Plastic tension of axisymmetric sample involving necking and small inhomogeneity, assuming Tresca yield condition and associated flow law
19 p3446 A69-36847

Fe crystals dislocations dynamic behavior during plastic flow development, describing stress and temperature effects on dislocations propagation and interactions
21 p3833 A69-38569

Axial through-cracks extension criteria in cylindrical pressure vessels, considering fracture toughness and plastic flow stress [ASM PAPER W9-13.3]
21 p3833 A69-38658

Creep theory with anisotropic hardening during early creep stages based on analogy with plastic flow theory
21 p3839 A69-39196

Axial through-cracks extension criteria in cylindrical pressure vessels, considering fracture toughness and plastic flow stress
22 p4046 A69-41040

PLASTIC MATERIALS

U PLASTICS

PLASTIC MEMORY

Material memory effect in plastically prestrained thin walled brass tubes analyzed on basis of kinematic strain hardening theory

02 p0336 A69-11551

Thermodynamics of viscoplastic materials under dynamic loads within framework of continuum mechanics of materials with memory

02 p0343 A69-12281

Controllable motions of compressible homogeneous isotropic solids, anisotropic solids and fluids with memory under constant body force

12 p2189 A69-27118

Mechanical properties associated with 55-Nitinol memory effect, presenting stress-strain and electrical resistivity as function of temperature

19 p3340 A69-35523

PLASTIC PROPELLANTS

Glass fiber reinforced plastic /GFRP/ roving end grains in rocket combustion chambers, discussing design and structural parameters

02 p0305 A69-12748

Elastomeric solid propellant grains viscoelastic flow, analyzing stresses and strains under various operating conditions and rocket engine geometry effect

10 p1801 A69-23702

Compositional and oxidizer particle size effects on combustion instability of plastic propellant based on ammonium perchlorate and polyisobutene [AIAA PAPER 69-478]

16 p2834 A69-32734

Flame propagation mechanism on plastic fuel in oxygen-nitrogen atmospheres with variable pressures and at different initial fuel temperatures, discussing safety and ignition problems

17 p3074 A69-33662

PLASTIC PROPERTIES

NT ELASTOPLASTICITY
NT THERMOPLASTICITY
NT VISCOPLASTICITY
NT YIELD POINT

Limit load analysis of three dimensional rigid perfectly plastic continua by approximate variational method

02 p0338 A69-11721

Dynamical strength of solid cylinder under axial loads increasing in time at given rate, using constitutive equations of thermodynamic theory

02 p0342 A69-12278

Surfaces role in superplasticity, demonstrating rate of neck growth dependence on surface irregularities

03 p0449 A69-13879

Laminar two dimensional free jet outflow of incompressible nonNewtonian pseudoplastic fluid from orifice into mass of same fluid

04 p0586 A69-14406

Plasticity of metals under isothermal conditions at elevated temperatures

04 p0671 A69-14454

Integration method for equations of plastic two dimensional stressed state with Mises yield condition, noting stress concentration at hole with pressure on contour

04 p0679 A69-14924

Soviet handbook on elasticity, plasticity and creep theories, emphasizing stresses and strains in solid thin walled shells and plates under bending, tension and torsion

04 p0683 A69-15499

Microplastic properties of arc-cast and Ti-Zr- Mo molybdenum sheet in tension at room temperature, measuring plastic strains with resistance strain gages

05 p0778 A69-15759

Thermodynamic theory of strain rate sensitive plastic material within framework of thermodynamics of materials with internal state variables

05 p0834 A69-15792

Anisotropic plasticity in sheet metals under uniaxial and balanced biaxial tension

05 p0837 A69-16030

Plastic moments calculation of continuous steel beams under various loading patterns

05 p0837 A69-16035

Elastic plastic stress distribution in compressed ring determined with postyield strain gages and stress-strain relationship from uniaxial tensile test

05 p0837 A69-16063

Book on continuum mechanics covering elasticity, fluid mechanics, plasticity and viscoelasticity, emphasizing basic concepts

05 p0843 A69-16713

Theoretical and experimental results on annealed tapered aluminum rods to assess one-dimensional rate independent theory of plastic wave propagation from longitudinal impact

06 p1022 A69-17365

Ti alloys thermomechanical treatment effect on strength and plasticity characteristics, noting single and double phase alloys and rupture

07 p1161 A69-18766

Complementary plastic work theorems in piecewise-linear elastoplasticity applied to plastic and nonlinear elastic problems

08 p1414 A69-20528

Minimum weight plastic design of circular and annular sandwich plates with piecewise constant cross section, discussing cost reduction

08 p1417 A69-20823

Compatibility theorem extension to three dimensional rigid plastic bodies with stress and velocity discontinuities, noting isotropic bodies with convex yield surface

08 p1418 A69-20845

Plastic yielding of tensile V-notched aluminum alloys elements with intermediate thickness and various shoulder ratios, studying thickness effect on yield load

09 p1612 A69-21499

Stresses and waves in highly conducting magnetoplastic metals as analogy of MHD processes in plasma

09 p1551 A69-22033

Plastic strain intensity distribution in aluminum alloy specimen with central hole measured with marked orthogonal lattice

09 p1617 A69-22221

Superplasticity in W-Re alloys, noting tensile properties, grain size and strain rate sensitivity for various Re contents at high temperatures

10 p1707 A69-22990

Plastic crack propagation in nonstrain hardening doubly grooved bending specimens with two surface slip, discussing crack angles, crack ductilities and fatigue striations

10 p1797 A69-23077

Dissolved gases and carbon effect on transition temperature from plastic to brittle state of high melting metals including niobium and vanadium

10 p1715 A69-24011

Polymer fatigue model from low cycle analysis of dynamic and thermal properties in structural plastics

10 p1717 A69-24217

Conformal mappings for solving boundary value problems in elasticity and plasticity theories for regions having singular points

11 p1973 A69-24662

Thin plastic shell theory based on static and geometrical relations for shallow and circular cylindrical shells

11 p1978 A69-24807

Plastic analysis of shallow spherical rigid plastic shell, using shell deflection equations to establish load-deflection relationship

11 p1980 A69-24823

Indentation of inhomogeneous rigid plastic solid by flat punch under plane strain conditions analyzed by perturbation method

11 p1986 A69-25244

Plasticity increase of molybdenum alloys during precipitation of second phase at high temperatures due to lattice defects redistribution and plastic deformation

11 p1906 A69-25685

Boundary determination for separating elastic and plastic regions of infinite perforated sheet with triangular network of circular holes

11 p1996 A69-25736

Stress discontinuity surface of three dimensional rigid plastic body arbitrary yield condition, considering equilibrium of regular four sided pyramid

11 p1996 A69-25738

Time and temperature dependence of plastic properties of fiber reinforced phenolic heat shield materials

12 p2119 A69-26825

Allowable thermodynamic processes and constitutive equation restrictions determined by Clausius-Duhem inequality, noting applications to plasticity theory and linear viscous fluids

13 p2371 A69-27319

Axisymmetric plastic buckling of complete spherical shells subjected to external hydrostatic pressure

13 p2361 A69-27439

Classical plasticity theory modified to include finite elastic and plastic strain components by considering thermoelasticity and plastic work irreversible processes

13 p2362 A69-28119

Small strain plasticity theory for planar slip in specific nickel base alloy deformation

13 p2362 A69-28120

Phenomenological macrorheology, discussing mechanical models designed for studying relation between stresses and strains in materials

13 p2369 A69-28562

Plasticity theory approximation variants for complex loading, analyzing strain trajectories using Prandtl-Reiss theory

14 p2532 A69-28978

Elastic-plastic bending of rectangular plates with asymmetrically inhomogeneous material in plastic range, using modified Ritz method

14 p2533 A69-28984

Maraging steel tensile strength increased, plasticity and toughness properties decreased with Ti content increase

15 p2639 A69-30630

Nonnewtonian solid propellant viscosity and pseudoplasticity utilizing rheological characterization for optimal casting and pot life determination [AIAA PAPER 69-518]

16 p2833 A69-32665

Aircraft and missile dynamic characteristics for heavy loads and large heat flux, noting small harmonic vibrations of heated structures in plastic domain [ICAS PAPER 68-38]

17 p3061 A69-33589

Loading path criterion for total strain /deformation/ plasticity theory based on Sanders loading function, discussing case of thermally loaded bar

17 p3062 A69-33711

Displacement bounding principle for work hardening plasticity theory based on Drucker inequality and stress space path existence [ASME PAPER 69-APM-7]

18 p3213 A69-34385

Soviet collection of papers on strength and plasticity of Ni and Ti and alloys covering high temperature internal friction, deformation and creep characteristics

18 p3158 A69-35442

Pure plastic bending of wide strip, determining stress strain state and plastic strain energy during constrained bending, noting application to corrugated panels

19 p3324 A69-35833

Boron thermal diffusion effects on plastic properties of pure Mo subjected to recrystallization

19 p3328 A69-36160

Collection of papers on mechanics including quantum theory, mechanics of micropolar continua, elasticity and plasticity, rheology, etc

20 p3623 A69-37580

Optimal plastic design of circular sandwich ring assuming symmetric loading, minimum plastic resistance and cost justification of stronger cross section

20 p3262 A69-37590

Analog method for determining structural creep displacement by setting up boundaries for linear elasticity and perfect plasticity

20 p3628 A69-37915

Soviet book on fundamentals of theory of plasticity and creep covering stress-strain state, bending, torsion, pressure, plane deformation, etc

20 p3630 A69-38206

Metals plastic behavior including strain hardening and Bauschinger effect

21 p3832 A69-38466

Phase plasticity in Ti-O alloy as function of temperature in alpha Ti and TiO, noting role of increased oxygen diffusion mobility

21 p3746 A69-38959

Variational problem for nonlinear functionals connected with finite plasticity, extending existence and uniqueness theorems to limit analysis

21 p3837 A69-39157

Plasticity of tubular steel annealed in vacuum furnace and subjected to complex tension and torsion under deformation trajectories containing salient point

21 p3839 A69-39197

Dynamic plasticity of nonsymmetrical free flight collision impact of crystalline solids, using linear temperature dependent stress-strain function and finite amplitude wave expansion

21 p3840 A69-39298

Bifurcation and hardening rate of rigid-plastic bodies presented on buckling of rectangular plate with lateral restraint

21 p3840 A69-39299

Single crystals dislocation dynamics and plasticity theory, discussing current tensor, conservation equation, slip systems, etc

21 p3845 A69-39676

Soviet collection of papers on static and dynamic problems in elasticity and plasticity theory covering plates, shells, beams, etc

22 p4038 A69-39911

Deformation localization and slip functions in statistical theory of plasticity, discussing approximations and untenability of Yosimura theory criticism

22 p4044 A69-40742

Time and plasticity effects on fracture determining solids strength as function of crack dimension

23 p4236 A69-42530

- Orthotropic aircraft materials plasticity theory, deriving stress-strain relationships in three mutually perpendicular symmetry planes for use in engineering calculations 24 p4400 A69-43083
- Plastic inhomogeneity effects on yield stress of isotropic spherical shell and long cylindrical tube under internal pressure 24 p4405 A69-43672
- PLASTIC TAPES**
- Pressure sensitive adhesives composition, tapes tacking and peeling theory and tests including electrolytic corrosion and insulation evaluation 14 p2468 A69-29342
- Photodiode tape camera with optical images stored on tape in form of charge pattern 16 p2792 A69-32558
- PLASTICITY**
- U PLASTIC PROPERTIES**
- PLASTICIZERS**
- Organic plasticizers molecular vaporization process kinetics, using isothermal and nonisothermal kinetic methods 04 p0620 A69-14956
- Temperature dependence of dynamic viscoelastic properties of plasticized epoxy resins 06 p0946 A69-17125
- Plasticizer mechanical properties and content in paste, considering effects on texture of coagulation structure during die extrusion of compacts 12 p2118 A69-26257
- Optimal conditions for extrusion compacting of hard alloy mixtures plasticized with paraffin, determining plasticizer content, upsetting, pressure and temperature 22 p3956 A69-40635
- PLASTICS**
- NT ACRYLIC RESINS
- NT EPOXY RESINS
- NT PHENOLIC RESINS
- NT POLYAMIDE RESINS
- NT POLYESTER RESINS
- NT POLYETHYLENE TEREPHTHALATE
- NT POLYETHYLENES
- NT POLYMETHYL METHACRYLATE
- NT POLYPROPYLENE
- NT POLYSTYRENE
- NT POLYTETRAFLUOROETHYLENE
- NT POLYVINYL CHLORIDE
- NT REINFORCED PLASTICS
- NT SYNTHETIC RESINS
- NT TEFLON [TRADEMARK]
- NT THERMOPLASTIC RESINS
- NT THERMOSETTING RESINS
- Simple wave solution existence for system of equations describing rapid plane flows of ideally plastic material 02 p0337 A69-11560
- Plastic material requirements for semiconductor device encapsulation noting electrical compatibility, mechanical and environmental protection and costs 02 p0270 A69-12161
- Aluminum plastic sandwich products production costs compatibility with conventional materials 02 p0348 A69-12749
- Flammability handbook for plastics noting characteristics, behavior under fire conditions and various fire hazard reduction mechanisms, tables, drawings, manufacturers, suppliers, etc 04 p0620 A69-14952
- Plastics in electronic packaging - Conference, Binghamton, New York, October 1968 04 p0620 A69-14953
- Oxygen index test for precise flammability ratings of plastics on numerical basis, eliminating drawbacks of ignition, end point and nonequilibrium conditions operation 04 p0621 A69-14957
- Fiberglass reinforced plastic bottoms design for integration with cylindrical shells, discussing design, shapes and boundary value problems 06 p1025 A69-17685
- Oxygen index test for precise flammability ratings of plastics on numerical basis, eliminating drawbacks of ignition, end point and nonequilibrium conditions operation 08 p1335 A69-20114
- Spacecraft component heat sterilization, discussing heat effects on electrical connections, polymers and adhesives 08 p1284 A69-20267
- Plastics - Conference, Washington, D.C., February 1969 08 p1336 A69-20478
- FAA regulations for improvements on crashworthiness and emergency evacuation from viewpoint of plastic applications and fire safety in aircraft 08 p1254 A69-20497
- Quasi-brittle fracture of plastic materials based on Griffith theory and crack propagation, analyzing real surface energy and work of plastic strain 09 p1614 A69-21883
- Part-through and through-thickness fatigue crack growth observations in glassy plastics, using linear elastic fracture mechanics [SESA PAPER 1348] 09 p1617 A69-22013
- Thermogravimetric plastics analysis data applied as constants to degradation kinetics equations used in charring-ablator digital computer programs 09 p1529 A69-22312
- Fatigue behavior of plastics classified noting temperature rises, crack initiation, etc 10 p1716 A69-23394
- Polymer fatigue model from low cycle analysis of dynamic and thermal properties in structural plastics 10 p1717 A69-24217
- Wear and friction properties of nylon and polyethylene sliding over unlubricated steel, considering adhesion theory 11 p1892 A69-25021
- Heat resistant composites, discussing composition, properties and high temperature behavior, plastic materials, reinforcement filaments, whiskers and test methods 12 p2117 A69-25855
- Plastics for electrical insulation - Conference, New York, January 1967 13 p2285 A69-27982
- Dielectric properties measurement of plastics for electrical insulation, stressing techniques for complex dielectric constants in various frequency ranges 13 p2285 A69-27984
- Fabrication techniques for plastic insulation in electronics, discussing packaging, low pressure molding, casting, etc 13 p2285 A69-27987
- Plastics engineering - Conference, Chicago, May 1969 14 p2469 A69-29411
- Pop-in mode of fracture obtained during investigation of fracture strength of glassy plastics, discussing mechanics 15 p2642 A69-30814
- Lifetime of structural plastics under vibration loading, considering polystyrene and polyformaldehyde samples under tension 15 p2643 A69-30972
- Molecular structure and uses of heat resistant plastics, discussing aromatic polyamides 18 p3161 A69-34279
- Plastics behavior under loading and performance prediction, considering engineering design applications 18 p3161 A69-34609
- Polymer selection and plastics contribution to technologies, noting trend toward improved performance at elevated temperatures 18 p3161 A69-34610
- Disk type or elastic melt extruders development based on Weissenberg effect permitting near uniform extrusion 18 p3148 A69-34612
- Plastics thermal properties and industrial structural applications dependency on temperature 18 p3161 A69-34839
- Moldable plastic shim material for structural airframe components, discussing application requirements 19 p3319 A69-35551
- All-plastic light passenger aircraft with inflated tube construction for shell, discussing design and performance 21 p3728 A69-38461
- Plastics applications in naval air systems command, discussing polymer families, nonstructural glass fiber-based products, radomes, electromagnetically transparent bodies, advanced composites, etc 21 p3751 A69-38532
- Plastics applications in Apollo-Saturn 5 program, considering foam, honeycomb, conformal coatings, embedment compounds, dielectrics, damping compounds, adhesives, sealants and gaskets 21 p3751 A69-38533
- Tensional and torsional forced vibration tester for viscoelastic plastic materials under tensile strain 21 p3720 A69-38591
- Levy-Mises equations for ideal plastic material derived from relationship between stress and rate of deformation tensors 21 p3840 A69-39287
- Grids applied to plastic samples for strain measurement using moiré fringe method, comparing tensile test results with Linley extensometer 22 p4042 A69-40312
- Scientific balloon vehicle design and development approaches for altitude, flight duration and payload capacity extension, discussing plastic balloons 22 p3865 A69-40812
- Static mechanical strength of syntactic foam tested by generating failure conditions based on combined biaxial and triaxial stress [ASME PAPER 69-APMW-24] 24 p4336 A69-43095
- PLATE [METAL]**
- U METAL PLATES**
- PLATE THEORY**
- Random temperature fields in plates and shells in thermal contact with two media with temperatures as separable random space-time functions 01 p0173 A69-10077
- Operational and integral heat balance method to obtain exact and approximate solution for monotonic heating of two layer unbounded plate 01 p0174 A69-10097
- Bending of micropolar plates using differential equations, considering transverse displacement and microrotation vector 01 p0167 A69-10324
- Differential equations for dynamical problems in plates obtained by symbolic approach involving power series substitution into linear elasticity dynamical equations 01 p0172 A69-11282
- Plate theories derived via strain energy potential integration through thickness, noting constitutive equations applicability to elastic buckling and postbuckling 02 p0340 A69-12055
- Heat transfer coefficient for physical protuberance on plate with turbulent boundary layer [ASME PAPER 68-HT-2] 02 p0351 A69-12204
- Direct matrix method for evaluation of critical loads and buckling modes for nonuniform flexural rigid plates having end and side constraints 03 p0522 A69-12866
- Mathematical models to investigate transient plane bending wave propagation in elastic plates, using elasticity and plate theories 03 p0525 A69-13606
- General solutions of three dimensional elasticity theory applied to isotropic disks and plates, emphasizing homogeneous solutions 03 p0526 A69-13738
- TUBA family of plate elements, discussing kinematically equivalent load matrices, initial loads due to initial strains, geometrical stiffness and square plates 03 p0530 A69-14090
- Thin cantilevered plate theory extended to large in-extensional deflections to account for geometry changes in bending moments [ASME PAPER 68-APM/BB] 04 p0670 A69-14401
- Conically bent plate cross section distortion analysis employing von Karman large deflection theory, noting effect of tapering [ASME PAPER 68-APM/Y] 04 p0670 A69-14402
- Plates yield point loads limit determination formulated as mathematical programming problem, using finite element representations for velocity and moment fields [ASME PAPER 68-WA/APM-21] 04 p0670 A69-14405
- Time harmonic vibrations and wave propagation in laminated plate, using elasticity theory equations and continuum theory for layered medium 04 p0675 A69-14685
- Annular plate clamped at inner and outer boundaries and subject to point load, computing deflection 04 p0676 A69-14725
- Compatible triangular plate elements for normal and in-plane displacements, discussing nine degree of freedom element, strain energy, simply supported and clamped plates 04 p0677 A69-14742
- Plate bending in presence of unsteady creep and with zero stress-strain state in middle surface solved by variational method 04 p0679 A69-14923
- Elastic strain and stress in ribbed circular plate bent skew-symmetrically, using orthotropic plates theory 04 p0681 A69-15172
- Bending of rectangular plate with partial clamping, obtaining solution by superposition method 04 p0681 A69-15289
- Symmetrical bending of laterally loaded circular micropolar plates 04 p0682 A69-15291

Vibration analysis of plates with discrete mass distribution based on Galerkin approach
04 p0682 A69-15293

Soviet handbook on elasticity, plasticity and creep theories, emphasizing stresses and strains in solid thin walled shells and plates under bending, tension and torsion
04 p0683 A69-15499

Pointwise limitation of field dislocation and bending moments in elastic plates
05 p0831 A69-15599

Book on plate formulas and tables for designing structure components of various geometrical shapes and thickness covering bending, compression, loading, etc
05 p0833 A69-15726

Clamped rectangular plate under lateral load stress analyzed by extended Kantorovich method to include bending moments and shearing forces
05 p0835 A69-15872

Vibration response of thin elastic plates to random loads
05 p0844 A69-16741

Dynamic behavior of three layer plates in supersonic gas flow
06 p1024 A69-17552

Initial defects influence on equilibrium states of compressed elastoplastic plates
06 p1025 A69-17684

Plate theories of linearly elastic materials under free undamped vibration, giving 500 references
[AIAA PAPER 69-24] 06 p1027 A69-18061

Initial stage of motion in Rayleigh problem, calculating time variable velocity of tangential stress on and velocity of gas near plate
07 p1118 A69-18701

Antisymmetric cross ply and angle ply laminated plates deflection under transverse loading with coupling between bending and middle-plane extension
07 p1231 A69-18711

Plane anisotropic rectangular plates with various boundary conditions, analyzing stability, natural frequencies, mode shapes and displacement under lateral loads
07 p1232 A69-18719

Fundamental problems of plate elastostatics with stress couples reduced to solution of integral equations, noting uniqueness theorem in plate bending theory
07 p1233 A69-19328

Explicit transverse bending stiffness and mass matrices for triangular finite plate element with linear thickness variation, using matrices for natural frequencies of vibration
08 p1414 A69-20526

Differential equation reduction for vibrational motion of rectangular plates subjected to variable tangential forces, discussing dynamic stability
08 p1415 A69-20666

Minimum weight plastic design of circular and annular sandwich plates with piecewise constant cross section, discussing cost reduction
08 p1417 A69-20823

Plane and three dimensional stress concentration studies involving asymmetrical stress tensors, noting contributions to moment theory of elasticity
08 p1419 A69-21177

Asymptotic two dimensional moment theory of elasticity, analyzing stress concentration at curvilinear holes and fluctuating boundary loads
09 p1614 A69-21884

Error estimates of stress concentration at free hole determined by two dimensional elasticity theory of thick plates
09 p1614 A69-21885

Plates stability and corner stress-strain state under variable loads calculated by method analogous to structural mechanics
10 p1792 A69-22849

Linear viscoelastic bending of anisotropic plates based on equation for Voigt plate, considering elliptic and rectangular plates
10 p1793 A69-22881

Eddy current nondestructive tests of nonmagnetic thin metallic sheets and plates from single surface
10 p1698 A69-23046

Crack propagation in plates and shells subjected to bending and direct loading, noting plate analysis modification for crack touching on compression side
10 p1795 A69-23061

Stress intensity magnification factors in surface flawed tension plates and notched round tension bars, evaluating fracture toughness
10 p1797 A69-23080

Elastic Cosserat plate and shell theory, considering constitutive equations imitating transversely isotropic material and elastic deformations
10 p1798 A69-23147

Large amplitude free vibration of isosceles right angled triangular plate with simply supported edges
10 p1800 A69-23236

Statistical theories of turbulence applied to thermal convection between infinite slippery plates at large Prandtl number
11 p1997 A69-24283

Elastic unbounded isotropic plane weakened by doubly periodic system of identical holes, noting solution involving Cauchy type integral
11 p1972 A69-24652

Three dimensional bending problem for thick isotropic plate with curvilinear hole and normal and tangential stress applied to edge of hole
11 p1973 A69-24657

Limiting equilibrium of plate weakened by curvilinear hole stress raiser with one or two cusps, obtaining stress-strain diagrams
11 p1973 A69-24658

Two dimensional elasticity and plate bending theories for calculating elastic isotropic panels and thin reinforced plates
11 p1974 A69-24664

Dynamic and fatigue crack propagation theories for brittle and quasi-brittle solids and plates
11 p1975 A69-24672

Free vibration modes of infinite uniform plate in linear coupled theory of thermoelasticity, considering heat transfer conditions
11 p1976 A69-24793

Limit loads for circular and annular plates of smoothly varying profile under uniformly distributed transverse loads
11 p1982 A69-24946

Linear differential equation solution for elastic systems stability problems, discussing applications to heated rectangular plates
11 p1982 A69-24950

Nodal lines shape in individual flats for long plates in combined shear and compression with sinusoidal edge rotations in longitudinal direction
11 p1983 A69-25137

Shear buckling of simply supported infinitely long plates orthogonally reinforced by stiffeners with flexural and torsional rigidity
11 p1984 A69-25142

Bent plates elastoplastic stress-strain state determination by elastic solution and finite differences, considering linear strengthening under uniform distribution of load
11 p1985 A69-25175

Free vibration frequencies of simply supported parallelogramic plates, noting skew angle splitting of degenerate frequencies and frequency crossing of modes
11 p1987 A69-25379

Modal coupling in thermally stressed plates, obtaining solution for frequencies and stiffness
11 p1990 A69-25509

Flutter analysis of plates with inplane boundary support flexibility exposed to transverse pressure loading or buckled by uniform thermal expansion
11 p1992 A69-25523

Plane stress state in plate with different glide moduli during tension and compression, considering axisymmetrical deformations
12 p2178 A69-26003

Aerodynamic field around symmetric profile two dimensional plates, visualizing velocity fields with Al particles
12 p2011 A69-26288

Mathematical bending theory for three layer elastic plates containing light or rigid fillers
12 p2182 A69-26678

Linear plate theory deficiency for large plate deflections, considering approximation of nonlinear behavior permitting changes in form without additional terms
12 p2185 A69-26822

Perturbation method for nonlinear panel flutter at high Mach numbers, using von Karman large deflection plate theory and quasi-steady aerodynamic theory
13 p2364 A69-28204

Rectangular plate buckling analyzed by finite element method with deflection function
13 p2364 A69-28225

Dynamic characteristics of Clough-Tocher triangle for natural frequency of simply supported plate, noting bending elements
13 p2365 A69-28246

Stress-strain state of circular annular plate with varying thickness subjected to concentrated axisymmetric load and shearing force applied to internal perimeter
13 p2369 A69-28563

Buckling of unsymmetric cross-ply rectangular plates under uniform shear, considering hinge-support boundary conditions
13 p2371 A69-28679

Finite thickness plate heat equation using Legendre polynomials
14 p2537 A69-28970

Stress concentration around rhombic hole in nonlinear isotropic plate under pure shear
14 p2533 A69-28981

Bending of elastic triangular plates with free and supported corners under uniformly distributed transverse load determined using Ritz method
14 p2535 A69-29410

Postbuckling of rectangular plates with exponential variation in thickness, analyzing large deflection equations using dynamic relaxation method
15 p2704 A69-30291

Finite element and iteration method for large deflection of rectangular plate, considering stiffness matrix for bending
15 p2706 A69-30435

Bending theory of orthotropic plates with variable elastic modulus under transverse loads, utilizing stress-strain relations and Kirchhoff-Love hypothesis
15 p2708 A69-30661

Minimum vibration frequency and compressive force for freely supported rectangular, triangular and circular plates simulated on analog computer
15 p2708 A69-30665

Equations for bending of elastic cantilever plate with parallelogram shape in oblique angle coordinate system, constructing functions satisfying Poisson conditions at contour
15 p2710 A69-30861

Elastic anisotropic panels mechanics analyzed using differential equations stressing transverse displacements, anisotropic thermal expansion, shape imperfections and slip deformations
15 p2711 A69-30904

Stress calculation for thermoelastic mixed boundary value problem in infinite isotropic plate with cylindrical stress free cavity
15 p2712 A69-31013

Bending theory for two layer plate made of isotropic material under sinusoidal load obtained by elasticity and classical theory based methods
15 p2714 A69-31198

Analogy between Timoshenko plate theory and moment theory of elasticity achieved by reducing Timoshenko equations to biharmonic and Helmholtz equation
15 p2715 A69-31205

Linear piezoelectric plate vibrations, Elements of linear theory of piezoelectricity and vibrations of piezoelectric plates, covering differential equations, boundary conditions, etc
16 p2826 A69-31720

Natural vibration of isotropic plates in temperature field with nonuniform distribution over plate
16 p2871 A69-31891

Parabolic and cardioid plates bending under uniform load by using point matching technique
16 p2874 A69-32166

Compressibility of material in stability problems of elastoplastic plates and shells
16 p2875 A69-32292

Bending problem of anisotropic/nonorthotropic plates solved by method of small parameter
16 p2875 A69-32294

Two dimensional plate theory with moment stress considerations derived from three dimensional elasticity theory, discussing reduction of equilibrium and compatibility equations
16 p2876 A69-32786

Stress-strain state analysis for brittle plate with circular holes of equal radius performed in cylindrical system of coordinates
17 p3055 A69-33127

Error estimation in thin elastic plate bending problem approximate solution by equal deflection lines method, constructing two sided bound for boundary value problems
17 p3062 A69-33713

Laminated anisotropic plate equations from thin plate theory including nonlinear terms, inertia and thermal stresses
[ASME PAPER 69-APM-15]

18 p3213 A69-34390

Uniform thickness rectangular plates bending with rigidly clamped or freely hinged edges solved by refined version on digital computer
18 p3215 A69-34535

Quadratic programming method for equations of elastic perfectly plastic solid applied to stress distribution in plate torsion and bending
18 p3218 A69-34661

Crack analysis in stiffened vibrating plate based on dynamic stress distribution, showing high bending stresses at intersection
18 p3223 A69-35168

Two dimensional theory for anisotropic plates motion derived, using asymptotic integration of three dimensional elasticity equations
18 p3224 A69-35297

Plate dynamics generalized equations independent of plate theory hypotheses, discussing algorithm and initial and boundary conditions
18 p3226 A69-35376

Secondary flow consisting of longitudinal vortices superposed on convection flow on inclined plate, obtaining flow pattern through flow visualization
18 p3124 A69-35383

Elliptic system of twelfth order equations describing elastic equilibrium of plate with kinematic functions analyzed by integration procedure
19 p3438 A69-36203

Plate material Poisson ratio determined by application of photoelastic interferometry to plate pure bending deformation contour lines
19 p3312 A69-36206

Von Karman equations for large deflection of simply supported square plates solved using dynamic relaxation method, recommending optimum mesh spacing
20 p3619 A69-36938

Clamped skew plates natural frequencies analysis using Galerkin method, expressing deflections as double series of beam characteristic functions, stating eigenvalues and eigenvectors
20 p3621 A69-37201

Composite laminates in cylindrical bending, discussing classical laminated plate theory limitations by comparing boundary value problems to corresponding theory of elasticity solutions
20 p3626 A69-37760

Unbalanced cross-ply elliptic laminated plates with bending membrane coupling, analyzing membrane boundary conditions with clamping assumed
20 p3626 A69-37762

Energy formulation extended for plane anisotropic rectangular plates, handling nonuniform properties and loadings
20 p3627 A69-37766

Stress and displacement in thin circular plates of ductile materials under axisymmetric loading predicted by nonlinear analysis
20 p3628 A69-37787

Asymptotic integration method of nonlinear elasticity equations for first approximation theory of anisotropic plates moderately large deflections
20 p3630 A69-38129

Rectangular plates bending boundary value problems, deriving formulas for plates with free edges
20 p3630 A69-38291

Plate bending theory modified for applying successive linear conjugates method to partially clamped isotropic plate and plate with circular hole
21 p3834 A69-38721

Composites elastic behavior, considering stress-strain in anisotropic lamina, composite plates and shells theory, thermal stresses and buckling for improving heterogeneous structures design
21 p3836 A69-38931

Approximate solution of unsteady thermal conductivity for plate with unlimited number of layers
21 p3851 A69-39083

Velocity and temperature distribution curves in turbulent boundary layer formed by natural convection on isothermal vertical plate, using Prandtl and Nusselt numbers
21 p3852 A69-39430

Concentration distribution of admixture in semibounded jet propagating along nonheat conducting plate, obtaining concentration profiles for various thermal and diffusion Prandtl numbers
21 p3854 A69-39844

Mathematical modeling techniques applied to thermoelastic cooling for plate without clamping and mechanical loads, examining integrator schematic diagram
21 p3680 A69-39851

Cosserat theory on couple stresses applied to stress distribution in semiinfinite plate, using Fourier transform method
22 p4038 A69-39902

Curvilinear planform plates natural oscillations, assuming small elastic bending strain obeying Hookes law
22 p4038 A69-39912

Stress analysis fundamental equation for variable thickness plate under concentrated load, using two dimensional Dirac delta function
22 p4041 A69-40144

Ambartsumian deflection theory applied to asymmetric bending problem for transversely isotropic circular plates
22 p4049 A69-41278

Mach 42 test measuring surface pressures, surface heat transfer rates and shock wave shapes in strong interaction regime for sharp and blunt plates
[AIAA PAPER 68-720] 23 p4059 A69-41886

Plates and shells under concentrated loads, analyzing stress-strain state
23 p4228 A69-41986

Green formula and fundamental solution for determining displacements and stresses in contour integral form for plate bending problems
23 p4230 A69-42002

Network method for stability of thin nonlinearly elastic compressible material plates, noting difference operators for rigidly clamped plates
23 p4230 A69-42003

Triangular plate bending element using Herrmann variational method, deriving matrices for finite elements
24 p4404 A69-43591

Single series solution for rectangular plate deflection under arbitrarily loaded concentrated load, considering monolithic slab beam connection case
24 p4404 A69-43593

Transverse shear influence on circular plates small displacement theory determined from coupled linear partial differential equations of plates
24 p4405 A69-43655

Buckling of thick homogeneous rectangular plates subjected to constant normal stress, noting error for thin plate approximation
24 p4406 A69-43696

PLATELETS

Platelet role in decompression sickness pathology from experiments upon rats subjected to decompression after injection of antiplatelet serum
21 p3655 A69-38918

PLATES

Heat flux applied to infinite plate contacting semiinfinite body determined from plate unsteady temperature, allowing for calorimeter heat losses
24 p4407 A69-42589

PLATES [STRUCTURAL MEMBERS]

NT ANISOTROPIC PLATES

NT ANNULAR PLATES

NT CANTILEVER PLATES

NT CIRCULAR PLATES

NT CORRUGATED PLATES

NT ELASTIC PLATES

NT END PLATES

NT ORTHOTROPIC PLATES

NT PERFORATED PLATES

NT POROUS PLATES

NT REINFORCED PLATES

Boundary layer of MHD flow past semifinite plate, using Navier-Stokes equations
01 p0130 A69-10771

Bending of freely supported plates of polygonal planforms under transverse load with aid of R functions
02 p0341 A69-12140

TUBA family of plate elements, discussing kinematically equivalent load matrices, initial loads due to initial strains, geometrical stiffness and square plates
03 p0530 A69-14090

Elastoplastic bending of plates with nonlinear stress-strain diagram
04 p0667 A69-14269

Flexural waves passage through obstacles in infinite plate, determining vibration arresting properties of rigid ribs, elastic inserts and hinged couplings
04 p0678 A69-14902

Flexural wave reflection from corner joint between plates, establishing reflection coefficient dependence on wave frequency
04 p0679 A69-14903

Absolute viscosity measurements from translational undamped oscillations of plate in liquid, considering viscosimeter walls effect
04 p0679 A69-14905

Monochromatic flexural waves passage through elastic insert between plates, determining wave absorptivity dependence on wave frequency
04 p0679 A69-14906

Laminated plates vibrational characteristics calculations by transition matrices, relating stresses and displacements under load
04 p0679 A69-14907

Numerical analysis for stresses in finite or infinite plate with arbitrary holes, considering boundary value problems
10 p1793 A69-22882

Reissner algorithms for displacements of bent plate represented in finite series form as solutions of Euler equations
10 p1793 A69-22883

Semibrittle material decompaction influence on stress distribution in infinite plate with edge loaded circular hole, noting stress-strain relation nonlinearities
11 p1972 A69-24656

Numerical analysis of natural oscillations of three layer sandwich plates of rectangular planform, considering end conditions
11 p1976 A69-24773

Finite difference method for transient and steady state response of vibrating plates, considering explicit and implicit formulas
11 p1983 A69-25020

Flexural waves passage through obstacles in infinite plate, determining vibration arresting properties of rigid ribs, elastic inserts and hinged couplings
12 p2182 A69-26655

Flexural wave reflection from corner joint between plates, establishing reflection coefficient dependence on wave frequency
12 p2182 A69-26656

Absolute viscosity measurements from translational undamped oscillations of plate in liquid, considering viscosimeter walls effect
12 p2182 A69-26658

Monochromatic flexural waves passage through elastic insert between plates, determining wave absorptivity dependence on wave frequency
12 p2182 A69-26659

Laminated plates vibrational characteristics calculations by transition matrices, relating stresses and displacements under load
12 p2182 A69-26660

Finite deflection discrete element analysis of sandwich plates and cylindrical shells with unbalanced laminated faces
12 p2185 A69-26821

Finite element displacement method extension to include geometric nonlinearity applied to arbitrary plate element, shallow cylindrical shell and shallow hyperbolic paraboloid
13 p2361 A69-27441

Spherical plate electrostatic analyzer transmission characteristics, emphasizing angular response to external particle sources as functions of angular coordinates and particle energy
14 p2449 A69-29560

Theory, function generator routine and testing for six node 18 degree of freedom triangular element for plate bending
15 p2706 A69-30430

Stiffness matrix for refined triangular plate bending finite element, considering Kirchhoff theory
15 p2706 A69-30434

Aluminum models of single cell simply supported folded plates to study instability phenomena possibly occurring in actual structure
15 p2709 A69-30679

Stiffness matrix of polygonal finite plate bending element derived using assumed stress distribution
15 p2710 A69-30867

Plane stress solution for stresses due to concentrated couple acting at any point on elliptic plate with fixed edge
15 p2712 A69-31014

Plate bending problems, comparing various approximate analytical methods including point matching, Galerkin, Ritz, Kantorovich and least squares techniques
16 p2874 A69-32160

Mixed plate element application to vibration and buckling eigenvalue problems based on Reissner variational principle, considering quadrilateral elements
16 p2874 A69-32176

Transient stress waves due to inputs of various types and time dependence in plates and revolving shells, discussing applications of elasticity theory analysis methods
16 p2876 A69-32785

Transverse bending of asymmetric sandwich plates with rigid filler taking into account stresses and strains in filler

17 p3055 A69-33129

Prestressed beams, columns and plates nonlinear response, statistical behavior and transverse cracking under axial compression, describing strength and stiffness

17 p3060 A69-33568

Transverse shear deformation and rotatory inertia effects on large amplitude lateral free vibrations of transversely isotropic plates
[ASME PAPER 69-APM-10]

18 p3213 A69-34386

Bending of rigid freely supported plastic plates under local axisymmetric dynamic load, discussing rectangular pulse effects and velocity fields

18 p3217 A69-34593

Heat transfer coefficient approximation under thermal instability conditions complicated by radiant heat exchange at plate surface, noting aircraft design applications

18 p3230 A69-34984

Isotropic plate critical strength measurements, evaluating role of material shear modulus

18 p3225 A69-35361

Viscous incompressible fluid flow around semi-infinite oscillating plate and skin friction on infinite cylinders oscillating parallel to length

19 p3237 A69-35620

Homogeneous heat flux effect on limit load of isotropic plate with rectilinear through crack, noting conditions for crack propagation

19 p3441 A69-36744

Number of forms of stability of plates and shells derived from eigenvalues of nonlinear boundary value problem containing generalized von Karman equations

19 p3445 A69-36816

Critical buckling loads for uniform compression of clamped or simply supported parabolic and semielliptic plates

20 p3622 A69-37223

Fourier heat equations functional corrections for determining temperatures of plate and cylinder heated simultaneously by radiation and convection

21 p3848 A69-38641

Curved shell elements in shell and plate analysis, discussing quadratic and cubic elements for space structures design

21 p3845 A69-39329

Thermal buckling of skew plates clamped along all edges under radiant heating, measuring various characteristics, solving differential equations by difference method

22 p4044 A69-40599

Dynamics of viscous electrically charged gas using Navier-Stokes equation

22 p3931 A69-40686

Photoelastic technique of stress-freezing and slicing to determine bending stresses in transversely loaded plate supported at corners

22 p4045 A69-40900

Unsteady thermal conductivity calculated by approximate analytical method in simple shape bodies/infinite plate, long cylinder, sphere/cooled or heated by thermal radiation

23 p4238 A69-41333

Plate and shell structures static and dynamic analysis by generalized variational principles in finite element method, discussing element displacement functions
[AIAA PAPER 68-290]

23 p4227 A69-41882

Computer program for natural oscillations of plates and shells, deriving differential equations of motion for thin elastic shell by variational method

23 p4230 A69-42004

Heated three layer plates stability under finite deflections in supersonic gas flow, deriving aerothermoelasticity equations

24 p4395 A69-42590

Three layer plate transverse bending in linear presentation, reducing problem to two displacement functions determination

24 p4395 A69-42594

Interlaminar shear stresses in cross-ply three ply symmetric laminated composite plate, analyzing interlaminar stress distribution under simple tension

24 p4399 A69-43052

Forced parametrically excited periodic vibration of finite length plate in plane supersonic flow, considering periodic forces applied at edges

24 p4407 A69-43733

Electroless deposition of various metals with emphasis on nickel, discussing mechanism, plating solutions, substrates, deposit properties and applications

01 p0099 A69-11060

Optimum conditions for producing Ti-V alloy sheet plated on one side with Nb by hot rolling

18 p3155 A69-34652

PLATINUM

Shock tube equilibrium method for determining vapor pressure of platinum submicron particles by suspension in xenon-argon carrier gas at high temperatures

03 p0532 A69-13319

Electrocatalysts for direct electrochemical oxidation on n-octane in fuel cells, discussing platinum consumption reduction
[ECS PAPER 8]

03 p0368 A69-13856

Treatment and testing of thin platinum and gold alloy wires used in thermoelements for studying liquid fuel vaporization in combustion chambers

07 p1130 A69-18258

Potential effect on wetting of platinum electrodes in acid electrolytes noting drainage role

08 p1268 A69-20362

Adsorption kinetics of hydrocarbon oxidation on platinum electrode

08 p1268 A69-21052

Spectral Pt II lines in Ap stars of Hg class observed during analysis of double lined spectroscopic binary HR 4072

15 p2695 A69-30891

Electrochemical oxidation of hydrocarbons on platinum electrode, discussing adsorption kinetics

16 p2740 A69-32423

Pt wire detector for flow regulation of atomic hydrogen beam, noting hydrogen maser application

22 p3950 A69-41232

PLATINUM ALLOYS

Room temperature lattice spacings of PdIn, PtIn and PtSn alloys including magnetic susceptibility

05 p0779 A69-15832

PLATINUM COMPOUNDS

Platinum based metal binary catalysts as anodes for hydrogen/carbon monoxide fuel mixtures oxidation, discussing alloy surface chemisorption of CO

12 p2026 A69-25937

PLAYBACKS

Buffer shift register with feedback control during tape recorder playback to obtain variable delay to compensate for recorder time base error

19 p3312 A69-36284

PLENUM CHAMBERS

Integrated lift, propulsion and control in Aeromobile air cushion vehicle, considering ram wing and gimbal fan plenum chamber vehicles

13 p2201 A69-27543

Plenum chamber obstructions influence on hovercraft lift fan performance, discussing tests and losses due to flat plate at impeller outlet

13 p2202 A69-27546

Multicell air cushion vehicle technology based on 1/4 scale and full scale tests, noting comparison with plenum systems and costs

13 p2202 A69-27547

Spectroscopic measurements of weakly ionized Ar plasma premixed with diatomic N in plenum chamber, demonstrating role of competitive reactions for metastable Ar atom

21 p3779 A69-39794

Arc-heated plasma jet wind tunnel flow properties in plenum chamber by spectroscopic techniques, measuring electron excitation, temperature and densities

22 p3990 A69-40596

PLETHYSMOGRAPHY

NT ELECTROPLETHYSMOGRAPHY
Nonsurgical methods of cardiac output measurement in aerospace medicine, considering simultaneous recording of carotid and femoral pulses and impedance plethysmography

23 p4088 A69-41813

Analog computer used to correct body plethysmographic chamber signal distortion due to inspired/expired air temperature and humidity differences

23 p4111 A69-42081

PLEURAE

Alveolar and pleural pressures affecting pulmonary interstitial pressure in anesthetized dogs, applying Starling law of transcapillary exchange

24 p4257 A69-42627

PLEXIGLASS [TRADEMARK]

U POLYMETHYL METHACRYLATE

PLOTTERS

NT X-Y PLOTTERS

Automatic plotting devices for graphic readouts in analog and digital computers

12 p2091 A69-26303

Data distortion elimination by improved superimposition of sinusoidal audio frequency signal on DC voltage of automatic Langmuir probe second derivative plotters

17 p2970 A69-32852

CRT graphic display/plotter for small digital computers, describing device operation, control and applications

21 p3679 A69-39608

Optical interpolation for GZ-I orthoprojector in storage mode, noting electronic contour plotter

22 p3951 A69-41247

PLOTTING

Radar range height angle charts for plotting earth based radio or radar system vertical plane coverage diagrams

01 p0031 A69-10632

Automatic heteroatomic plotting of high resolution mass spectral data, presenting relative intensity vs elemental composition in bar form

01 p0024 A69-10905

Hazard plot analysis of incomplete data involving times to failure for failed units and running times on unfailed units

18 p3147 A69-34515

Multiplexed censored data plotting on various type hazard papers for engineering information on time to failure distribution

20 p3567 A69-38288

Automatic contour plotting for orthoprojector based on adjacent profiles and linear interpolation

22 p3951 A69-41248

PLOTTING INSTRUMENTS

U PLOTTERS

PLUG NOZZLES

Interactions between outer and inner jets behind maximum cross section of jet engine nozzle
[ONERA-TP-600]

02 p0187 A69-11620

PLUM BROOK REACTOR

Beryllium reflector distortion in Plum Brook Reactor due to neutron embrittlement and gas formation, noting material surveillance, replacement, etc

03 p0465 A69-13131

PLUMBANE

U LEAD COMPOUNDS

U METAL HYDRIDES

PLUMES

NT ROCKET EXHAUST

Contaminants formation during pulse mode operation of liquid bipropellant attitude control rocket engine, discussing exhaust plume effects
[AIAA PAPER 69-574]

16 p2870 A69-32774

Current distribution and scattering cross section of missile with plume/ionized trail/ of tapered conductivity due to plane wave electromagnetic excitation

17 p2921 A69-33671

Buoyant plumes and thermals defined as vertical motions produced under gravity by density or temperature contrast between incompressible source fluid and environment

18 p3122 A69-34917

Carbon dioxide free jet expanding from conical nozzle into low density atmosphere, using freeze up method

22 p4000 A69-40594

Mixing spread of hydrogen plumes and air pollutants exhausted into open atmosphere, predicting subsonic free round jets air entrainment

24 p4300 A69-43257

PLUTO [PLANET]

Pluto mass from observations of perturbation of motion of Neptune

02 p0315 A69-11808

Pluto mass from Neptune orbital longitude, comparing observations and theory

04 p0663 A69-15385

Pluto mass and density accuracy, questioning values derived from Neptune observations

19 p3403 A69-35969

Pluto positions /1930-1965/ from photographic observations, ascribing declination errors to atmospheric dispersions

22 p4025 A69-40612

PLUTONIUM ISOTOPES

Pu 244 and 1 129 abundances in early solar system and continuous galactic synthesis model of element formation in stars

08 p1397 A69-20695

PLATING

NT ELECTROPLATING

NT NICKEL PLATE

Plutonium-244 existence in early solar system concluded from relative abundance ratios of excess meteoritic heavy Xe isotopes
08 p1401 A69-20900

Pu/U ratio from fossil track studies bearing on extinct Pu 244 in Campo del Cielo and Kodaikanal meteorites
19 p3407 A69-36077

PLUTONIUM 238

Pu-238 isotope organic Rankine cycle system analyzed for one year manned space station, using modified H-521 Space Power computer program
23 p4188 A69-42264

PLUVIOGRAPHS

U RECORDING INSTRUMENTS

PNEUMATIC CIRCUITS

Fluidic acceleration sensor based on vibrating string principle, discussing design, suspension system, driving-oscillator circuit, beat frequency circuit and detection circuits
02 p0249 A69-12091

Breadboard technique and interconnection for fluidic circuits in large systems
05 p0705 A69-16009

Hazards in pneumatic fluidic sequential circuits caused by delays in pneumatic tubing [ASME PAPER 68-WA/AUT-18]
05 p0706 A69-16174

Pneumatic instrumentation line transfer function approximated by system model for simplifying reactor control system analysis [IEEE PAPER 2D-6]
07 p1059 A69-19190

Second order system equations to approximate transfer function of homogeneous pneumatic instrumentation line terminated with pressure transducer
10 p1692 A69-23267

German monograph on theoretical and experimental investigations of tubes and lumped fluidic elements covering equivalent circuit
17 p2903 A69-33573

Pneumatic control circuits design based on logic functions and truth tables, noting fluid logic application
19 p3256 A69-36714

PNEUMATIC CONTROL

Pneumatics for aircraft systems integration, proposing engine bleed air use for high power short term duties, heat recovery from cabin air conditioning, etc
01 p0012 A69-10594

Pneumatic pressure ratio sensing element and associated high pressure switches and amplifiers for gas turbine engine control systems
02 p0249 A69-12088

Pneumatic elements, discussing development from process control via modules systems to logic elements and fluid sensors
02 p0197 A69-12795

Fluidic numerical controls of linear or rotating motors, discussing pneumatic, hydraulic, hybrid logic components and amplifiers
04 p0550 A69-15082

Hybrid electropneumatic and electrohydraulic servosystem for actuation of gas jet nozzles of sounding rocket automatic pointing system
04 p0550 A69-15182

Nonlinear lumped parameter model for long gas filled pressure sensing lines covering steady state, laminar or turbulent gas flow [AIAA PAPER 69-117]
06 p0913 A69-18106

AC fluidics for pressure pulse frequency control and monitoring in flow, discussing design and application to steam turbine speed control
07 p1058 A69-18938

Design criteria for pneumatic servo controls with fluidic elements stressing final transient, pilot circuits and amplifier elements
08 p1256 A69-20305

Book on industrial control engineering covering mathematics, semiconductor devices, feedback amplifier theory, closed loop systems, frequency response diagrams
12 p2051 A69-26244

Brake system components automatic testing for pneumatic or hydraulic integrity essential to safe system performance
17 p2978 A69-33377

Fluidic logic for high speed pneumatic stepping motor for high radiation environments, discussing belows pressure sequencing by open-loop counter, signal conversions and performance
18 p3092 A69-34310

Analytical, graphical and graph-analytical methods for synthesis of passive circuits ensuring air removal

from chambers of pneumatic logic control and servomechanisms
18 p3093 A69-34831

Pneumatic control circuits design based on logic functions and truth tables, noting fluid logic application
19 p3256 A69-36714

High temperature pneumatic systems for missile and space vehicle control, describing pressure regulators, flow controls, thrusters and analog valves
22 p3870 A69-41240

Pneumatic driving system for heart assist or total replacement pumps, discussing design features and performance characteristics
24 p4273 A69-42983

Nonlinear lumped parameter model for long gas filled pressure sensing lines covering steady state, laminar or turbulent gas flow [AIAA PAPER 69-117]
24 p4301 A69-43259

PNEUMATIC EQUIPMENT

NT GAS VALVES

Pneumatic stepping motor actuation system with pure fluid valves and signal processing and minimum number of moving mechanical parts for high g and temperature environments
02 p0196 A69-12086

Pneumatic analog to digital and digital to analog converters, noting diaphragm force balance capsules, converters using stepping motors and factors affecting accuracy [ASME PAPER 68-WA/AUT-16]
05 p0706 A69-16176

Self damped pneumatic vibration isolators by modifying characteristics throughout frequency range, noting inertia block for improving HF behavior
08 p1301 A69-20398

Pneumatic diode function generator for simulating nonlinear control systems, discussing operating characteristics and programming methods
11 p1858 A69-24580

Fluidic curved-wall electropneumatic converter optimization, presenting steady state, step and pulse mode responses for various positions and lengths of resistive heaters
15 p2553 A69-31298

Quasi-plastic impact resulting from incomplete elastic collision of two material points in presence of dry Coulomb friction, noting engineering role in pneumatic equipment
18 p3215 A69-34568

Discharge coefficient and opening time of pneumatic and hydraulic systems incorporating disks, nozzles and valves
18 p3094 A69-34981

Nomograph for rapid estimation of pressure drops across orifices in pneumatic systems using real gas data with illustration for nitrogen
20 p3467 A69-38186

Digital computers used in error calculation in calibration curves of turboengines and other pneumatic devices
21 p3724 A69-39100

Design features comparison and operation principles of gas strain gauges in application to structures, emphasizing independence of temperature variations in pneumatic circuits
21 p3725 A69-39324

Small signal amplitude/frequency response or transfer gain of volume-terminated pneumatic lines with circular and rectangular cross sections
24 p4301 A69-43288

PNEUMOGRAPHY

U PNEUMOGRAPHY

PNEUMOGRAPHY

Power spectral analysis feasibility for data reduction for medical interpretation of changes in pulmonary impedance pneumograph in remote monitoring
12 p2024 A69-26558

Venturi low resistance flowmeter for ventilatory measurements during rest and exercise on humans, noting suitability for analog integrator computation of tidal volumes
22 p3894 A69-40979

PNEUMONIA

Resistance to bacterial pneumonia and influenza infection in space cabin environment tested on mice in simulation chamber
07 p1067 A69-19432

PNEUMOTHORAX

Inflight spontaneous pneumothorax case of civilian pilot lung collapse experience during exposure to reduced ambient pressure, discussing etiology, incidence, treatment and disposition
17 p2909 A69-33183

POCKELS EFFECT

U BIREFRINGENCE

POCKET MICE

Diurnal pressure cycles found as zeitgeber to entrain body temperature endogenous circadian rhythm in pocket mice under constant environmental temperature and light
16 p2745 A69-32447

POIKILOTHERMIA

U FROGS

U LIZARDS

U TURTLES

POINCARÉ PROBLEM

Periodic solutions of autonomous system oscillations with many degrees of freedom based on Poincaré method applied to Liapunov systems
07 p1183 A69-19680

POINCARÉ SPHERES

Poincaré sphere representation of polarized light used to predict rotation effect on optical observations in photoelastic shell analysis
04 p0683 A69-15495

Poincaré sphere properties representing birefringent behavior of materials and qualitative measurement technique for elliptically polarized light
21 p3844 A69-39318

POINT DEFECTS

NT FRENKEL DEFECTS

NT VACANCIES [CRYSTAL DEFECTS]

Elastic constants of point defects for bcc and fcc crystals with vacancies and interstitials calculated by Born-Huang method for nonprimitive lattices
02 p0267 A69-12186

Ammonium perchlorate thermal decomposition, studying point defects role
03 p0494 A69-12896

Impurities effect on defects in oxygen deficient niobium, tantalum and zirconium oxide scales at high oxygen pressures, noting relationship to metal oxidation
03 p0444 A69-13312

Point defects in body centered cubic transition metals, discussing thermal equilibrium, irradiation cold work, high and low temperature recovery, etc
03 p0447 A69-13817

Interaction between point defects and magnesium atoms in aluminum irradiated by neutrons, analyzing magnesium concentration effect on recovery
05 p0781 A69-16613

Internal friction, Young modulus and resistivity measurements for stage I interstitials in electron irradiated tungsten
13 p2284 A69-28682

Book on defects and radiation damage in metals covering collision cascades, point defects clustering and impurities behavior
14 p2503 A69-28889

Point defect structure to control ammonium perchlorate burning rate, discussing thermal analysis data correlations, isothermal decomposition, etc [WSCI PAPER 69-17]
16 p2831 A69-32355

POINT IMPACT

Point load subjected deflections of cantilevers and circular rings found using electronic analog computers
03 p0522 A69-12865

Two dimensional wavefront shape induced in finitely strained elastic body by impulsive point body force
11 p1969 A69-24338

Quasi-plastic impact resulting from incomplete elastic collision of two material points in presence of dry Coulomb friction, noting engineering role in pneumatic equipment
18 p3215 A69-34568

POINT MATCHING METHOD [MATHEMATICS]

U BOUNDARY VALUE PROBLEMS

POINT SOURCES

Atmospheric diffusion measurement based on analysis of thoron emitted continuously from point source, permitting study of diffusion in atmospheric boundary layer
01 p0144 A69-10043

Green functions associated with electromagnetic radiation in moving medium, finding time dependent and harmonic Green functions
03 p0466 A69-13352

Flow pattern induced by oscillatory point source in rotating inviscid liquid
04 p0591 A69-15279

Reciprocal theorem for displacements of solid skeleton caused by fluid sources action in infinite consolidating space
05 p0835 A69-15869

Expression derived for correlation function and power spectrum of bearing of set of point radiators, taking into account receiver internal noise

05 p0719 A69-16219

Nonscattered, singly and multiply scattered light of beam from point source analyzed at boundary layer of turbid medium

05 p0789 A69-16640

IR radiation at 10.6 micron from two point sources mixed with collimated ruby laser radiation in proustite, obtaining visible image

06 p0928 A69-17904

Ray-optical description for point source excited surface waves in stratified anisotropic media

07 p1079 A69-18918

Minimal angle of resolution /MAR/ between point and extended circular source and between point source and simulated horizon, studying irradiation effects on manual navigation

07 p1177 A69-19208

Discrete extragalactic X ray sources model for explanation of diffuse X ray background, noting evolutionary aspects

07 p1206 A69-19255

Angular separation of two point sources measured through expressing antenna resolving power by a posteriori probability laws

08 p1288 A69-20961

Temperature and displacement fields in unbounded elastic space due to instantaneous point heat source action

09 p1621 A69-21495

Compressible gas flow problem in point body gravitational field solved with reference to sun and interstellar gas

09 p1577 A69-21769

Statistical estimation theory giving angular resolution of imaging systems in terms of noise characteristics and modulation transfer function

10 p1725 A69-24048

Holograms reconstructing images of points with diameters approximated by width of autocorrelation functions

11 p1886 A69-25058

Model for shock propagation from point energy source into cold atmosphere with exponential density variation

11 p1871 A69-25123

Nonscattered, singly and multiply scattered light of beam from point source analyzed at boundary layer of turbid medium

14 p2482 A69-28796

Point discharge measuring based on pulsed nature of discharge current, outlining field experiment results

15 p2610 A69-30698

Linear heat flux in thin composite plate with internal point source, assuming no heat transfer at surface and neglectable temperature changes

17 p3068 A69-33126

Shock waves propagation in inhomogeneous gases, considering time development and energy flux during point explosion in plane layers by quasi-stationary approximation

17 p2952 A69-33383

Spectral parameters effect on IR instrument SNR, discussing range equations of point and extended sources and radiation-noise-limited detectors

19 p3310 A69-36061

Plane, cylindrical and spherical point explosions in combustible gas mixtures for different gas motion models, formulating scaling law for detonation wave model

19 p3449 A69-36353

Holograms capable of multiple imaging or reconstructing point images, using extended and correlated signal and reference sources in recording process

21 p3727 A69-39777

Microwave background radiation in steady state cosmological model, attempting interpretation as discrete extragalactic radio sources population

22 p4029 A69-40765

High energy gamma rays point source in Sagittarius indicated from evidence obtained by high altitude balloon flights

24 p4365 A69-42606

Transmission functions probabilistic model for solving radiative transfer problems in spherical shell medium surrounding emitting black core or point source, using integrodifferential equations

24 p4415 A69-43637

POINT TO POINT COMMUNICATIONS

Point to point millimeter wave communication system design, discussing propagation and data transmission

03 p0405 A69-13723

Spectrum analysis of pulse signals by point to point measurements of magnitude and phase of pulse-like time functions, using narrow band filter output

03 p0399 A69-13939

Communication satellites applied to broadcasting, considering point to point satellite link and distribution systems

08 p1272 A69-19925

Satellite and terrestrial point-to-point communication circuit costs, considering multiple access and small antenna earth stations

19 p3456 A69-36822

POINTS [MATHEMATICS]

A priori and a posteriori estimates of direct methods accuracy in solving linear algebraic equations

01 p0105 A69-10727

Optimum addition of abscissas in quadrature formulas by expansion of abscissas equation in Legendre polynomials

03 p0455 A69-13372

Integration formulas based on set of Gauss or Lobatto points

03 p0455 A69-13374

Conformal mappings for solving boundary value problems in elasticity and plasticity theories for regions having singular points

11 p1973 A69-24662

Necessary and sufficient conditions for boundary point regularity in Dirichlet problem for heat conduction equation assuming Holder condition

15 p2716 A69-30047

POISEUILLE FLOW

U LAMINAR FLOW

POISONING [TOXICOLOGY]

U TOXIC DISEASES

POISONS

U CURARE

U DICHLORODIPHENYLTRICHLOROETHANE

U STRYCHNINE

U URETHANES

POISSON DENSITY FUNCTIONS

Fluctuation voltage mean square value at polar dielectric capacitor terminals determined by applying stochastic properties of Poisson point processes to statistical model

08 p1295 A69-21151

Poisson formula in double logarithmic approximation for photon emission cross section in analysis of bremsstrahlung involving high energy particles

11 p1922 A69-25758

Cumulative probability distribution of positive random variable from moment generating function, exemplifying exponential and Poisson functions

12 p2120 A69-25927

Huffman minimum redundancy coding extension to run-length information based on Poisson distribution, including optimization and data compression applications

19 p3272 A69-36262

M-ary detection for optical communication investigated for maximum likelihood detection of one of M Poisson processes in background noise

19 p3276 A69-36486

POISSON EQUATION

Liouville and Poisson equations solutions for locally ellipsoid stellar velocity distributions with constant coefficients

02 p0310 A69-11455

Cauchy-Poisson problem for viscous liquid, calculating free liquid surface response to point impulse or initial displacement

03 p0414 A69-13015

Field distribution in insulated gate FET determined by numerical solution of Poisson equation

10 p1662 A69-23170

Near electrode layer calculation in low temperature plasma, solving kinetic ion equation for quasi-neutral and Poisson equation for space charge regions

13 p2312 A69-28117

Green functions for Laplace, Poisson and transient heat diffusion equations solved by matrix multiplication

15 p2710 A69-30870

Iteration process by difference scheme for numerical solution to Dirichlet problem of two dimensional Poisson equation

18 p3164 A69-34701

Convergence properties of finite difference approximations to solutions of Dirichlet problem for Poisson equation

18 p3164 A69-34840

POISSON PROCESS

U STOCHASTIC PROCESSES

POISSON RATIO

Strain dependent modulus and Poisson ratio behavior of CTPB propellant, performing stress relaxation tests

04 p0646 A69-15510

Fiberglass reinforced plastics modulus of elasticity and Poisson ratio determined by strain gauges and frequency and resistivity measurements

08 p1335 A69-20330

Radial and tangential stresses in double glass fiber assuming different Poisson coefficients, determining conditions for axial stress redistribution prevention

09 p1614 A69-21741

Poisson ratio determination with bonded electrical resistance strain rosettes

11 p1995 A69-25652

Perturbation formula for frequencies as function of Poisson coefficient, considering vibration modes of elastic body subject to boundary conditions

15 p2713 A69-31097

Plate material Poisson ratio determined by application of holographic interferometry to plate pure bending deformation contour lines

19 p3312 A69-36206

Graphical representation of friction stresses produced on mechanical parts surface layers, using mathematical model based on Poisson ratio and friction coefficient

19 p3329 A69-36723

Structural flexure center position from shear stress analysis showing nondependence on Poisson ratio

20 p3622 A69-37213

Radial and tangential stresses in double glass fiber assuming different Poisson coefficients, determining conditions for axial stress redistribution prevention

20 p3630 A69-38217

Negative Poisson ratio of isotropic heat shield material pyrolytic graphite, noting thermodynamic validity

24 p4338 A69-43599

POLAND

Hot plasma research at Polish Institute of Nuclear Research at Swierk

06 p0964 A69-17174

Polish report on space sciences activities to COSPAR covering satellite position observations, geodesy, space physics, mechanics, computations, meteorology, etc

15 p2724 A69-31433

POLAR AURORAS

U AURORAS

POLAR CAP ABSORPTION

Polar cap event detected at low latitudes by effect on VLF propagation, noting VLF technique sensitivity to low proton fluxes

05 p0816 A69-16276

Energy dissipation of solar particles in atmosphere for 3914 and 5577 A bands, computing light emissions associated with PCA

08 p1378 A69-20186

Variable solar X ray emission from subflare activity in plage region producing polar cap absorption proton flare of July 7, 1966

10 p1764 A69-23745

Solar X ray emission and decay during proton flare of July 7, 1966 noting start of polar cap absorption

10 p1766 A69-23755

Time history of July 7-10 1966 PCA event analyzed using 16 riometers and concurrent satellite observations of solar cosmic radiation

10 p1683 A69-23770

VLF observations of July 7 1966 solar flare and PCA event

10 p1657 A69-23772

Sudden cosmic noise absorption /SCNA/ in polar cap during July 7, 1966 solar proton flare, estimating SCNA latitudinal distribution and protons magnetic cut-off boundary

10 p1770 A69-23907

Polar cap absorption riometer recorded during 2-6 September 1966 event compared to satellite measurements of solar protons, discussing diurnal variations and oxygen role in associative detachment reactions

14 p2440 A69-29126

Polar cap absorption effects on VLF transmission phase and amplitude in tabular form

18 p3103 A69-35185

Solar proton flare June 1968 analysis, discussing geophysical effects and possible polar cap absorption

20 p3587 A69-37332

Morphology of discrete polar cap and polar glow auroras, noting diurnal variations correlation with magnetic activity changes at low latitude

21 p3707 A69-38487

- Auroral absorption relation to visual aurora and measured particle fluxes 21 p3707 A69-38488
- Incident proton flux atmospheric altitude profile during PCA period, comparing balloon observations with preliminary satellite data 23 p4204 A69-41485
- Cosmic radio emission anomalous absorption measurements during PCA following July, August, September 1966 proton flares 23 p4156 A69-41845
- Solar energetic particle effects during polar cap absorption observed in earth upper atmosphere and at ground level 24 p4373 A69-43618
- Polar cap ionospheric response to solar cosmic ray events observed by Mariners 2 and 4 solar proton measurements used to test magnetosphere models 24 p4373 A69-43621
- POLAR CAPS**
- Magnetosphere studies in France noting magnetosphere characteristics, wave propagation, charged particles, particle precipitation mechanisms in auroral zones and polar caps 02 p0242 A69-11904
- Geoelectric field over polar cap based on proton flux detection 04 p0648 A69-14682
- Meteorological observations of Mars northern polar cap and Southern Hemisphere from northern summer solstice to early autumn 05 p0825 A69-16302
- Mars polar cap ice cap and dry ice theories, discussing dark wave and cloud distribution meteorological observations 07 p1212 A69-18603
- Ionization in lower ionosphere over polar cap under solar corpuscular fluxes measured by radio wave absorption 10 p1759 A69-22838
- Martian polar caps dimensions as function of planet heliocentric longitude examined from photographic observations, noting compatibility with spectroscopic data 11 p1959 A69-24728
- Polar cap sporadic E investigation with backscatter at 28 MHz, noting geographic distribution, annual and diurnal variations 12 p2069 A69-26464
- Kinetic energy balance equation of mean zonal flow in symmetrical polar cap derived from basic concepts of mechanics, discussing relative coordinate system rotation 15 p2595 A69-30219
- ESRO 2 satellite observations of solar proton event of 9 June 1968, comparing flux profile variations across polar cap with magnetic changes at earth surface 15 p2677 A69-31347
- Mars 1969 opposition observations, discussing extremes in north and south hemispherical polar cap behavior, frosty deposit colorings and polar vapor/clouds 17 p3043 A69-34141
- Jupiter observations /1966-1967/, discussing variations in size and position of polar caps and tropical belts 18 p3203 A69-35337
- Mariner 6 TV pictures with description of craters and south polar cap, noting moon-like crater abundance, form, arrangement and crater sizes 21 p3803 A69-38981
- Diurnal variations of electron flux based on balloon observations near polar cap consistent with geomagnetic cut-off variations of magnetospheric models 22 p4005 A69-40511
- Long term computer produced multiple image satellite photomosaics for Southern Hemisphere, analyzing circulation, meridional bands, polar ice, cloud cover variations, etc 22 p3977 A69-40733
- POLAR COORDINATES**
- Areas of expectation for single radar automatic tracking of flying objects derived on basis of equation of circle in polar coordinates 01 p0035 A69-11296
- Diurnal nutation and periodic terms of local coordinates using OPL model of Danjon astrolabe, presenting harmonic and Fourier analysis 09 p1596 A69-22059
- Saint Venant torsion and flexure of prismatic bars analysis in polar coordinates, discussing boundary errors 09 p1621 A69-22770
- Shock polar equation in polar coordinates, showing shock polar shape dependence on Mach number 16 p2772 A69-32178
- Earth polar coordinates determined from latitude observations, discussing weighting functions for determining polar motion 17 p2959 A69-32869
- Polar coordinates in Euclidean space applied to theory of satellite moving in gravitational field of spherically symmetrical body, introducing equipotential surfaces 19 p3397 A69-35610
- Numerical integration for continuously thrusting spacecraft optimal trajectory, considering rectangular Cartesian and polar cylindrical coordinates characteristics [AIAA PAPER 69-903] 21 p3798 A69-38546
- POLAR GASES**
- Polar molecule rotational excitation diffusion cross sections for electron scattering 06 p0961 A69-17139
- Viscosity, thermal conductivity and diffusion predicted for dilute nonpolar, polar and mixed gases, discussing methods for rotational relaxation collision numbers and resonant correction 21 p3850 A69-38951
- Computer made movies and time history plots for ion-dipole collisions involving polar molecules /CO, HCL and acetone/trile/ 24 p4352 A69-43124
- POLAR IONOSPHERE BEACON**
- U BEACON SATELLITES
- POLAR METEOROLOGY**
- Characteristics of electrovortices and auroral electrojets of polar disturbance field, discussing dynamics during geomagnetic storms 02 p0240 A69-11723
- Polar geomagnetic disturbance development and decay during solar quiet and moderately disturbed periods 02 p0240 A69-11724
- POLAR ORBITS**
- Circumpolar satellite orbits under lunar and solar perturbations based on two fixed centers problem, considering large amplitude disturbances 10 p1780 A69-23616
- Improved spheroidal method for calculation of almost polar orbit of artificial satellites, bypassing right ascension 12 p2152 A69-25799
- Solar and lunar effects on motions of polar orbiting satellites, discussing variable intermediate orbits 14 p2521 A69-29460
- POLAR RADIO BLACKOUT**
- Polar auroral region cosmic radio noise absorption bays diurnal variations attributed to drift of electrons captured in magnetosphere 03 p0423 A69-13520
- Auroral absorption distribution from arctic riometric observations mapped for evaluating radio communications reliability 17 p2967 A69-33990
- POLAR REGIONS**
- NT ANTARCTIC REGIONS
- NT ARCTIC REGIONS
- Micropulsations at magnetoconjugate points in Arctic and Antarctic, noting diurnal and seasonal variations and latitude dependence 01 p0068 A69-11112
- Solar protons observations by Satellite 1963 38C in polar regions at high altitude during spring 1966 01 p0146 A69-11123
- Polar wind, describing upward plasma expansion of topside polar ionosphere and acceleration of positive H and He ions 01 p0077 A69-11239
- Helium isotopes escape mechanism from earth atmosphere related to polar wind ionospheric plasma flow from earth 01 p0077 A69-11240
- Polar ionosphere heating by spill-over electron energy during strong geomagnetic disturbances, giving mathematical representation 02 p0237 A69-11664
- Relationship between polar geomagnetic disturbances and DR variations value of geomagnetic field 02 p0238 A69-11672
- Anomalous radio wave absorption in polar aurora region ionosphere, discussing disturbance characteristics 02 p0207 A69-11688
- Polar aurorae fine scale structure interpretation based on plasma instabilities characteristics 02 p0239 A69-11693
- Geophysical effects observed in Northern Hemisphere during low solar activity, discussing polar auroral intensities and positions 02 p0239 A69-11694
- Ionospheric current systems for various selected very quiet and slightly disturbed international quiet days based on Northern Hemisphere observatories data 03 p0423 A69-13518
- High latitude electrons boundary dependent on geomagnetic axis orientation, noting role of coupling between solar wind and magnetosphere 03 p0502 A69-14003
- High latitude outer zone electrons boundary region during geomagnetically quiet periods 03 p0502 A69-14004
- Energetic electron fluxes measured at 2000 km over auroral and polar regions and at 17 earth radii in magnetotail plasma sheet 03 p0503 A69-14013
- Equatorial semiaxis of magnetospheric tail at distances between 10 and 80 earth radii for various intensities of polar magnetic disturbances 05 p0753 A69-16050
- Field aligned Birkeland currents generation at auroral latitudes 05 p0755 A69-16266
- Magnetic disturbance vector distribution during polar magnetic substorm 05 p0755 A69-16271
- Satellite scintillation at high latitudes and possible relation to soft particle precipitation 05 p0757 A69-16406
- Book on polar and magnetospheric substorms including daily variation data, satellite observations, etc 06 p0915 A69-16832
- Radiation bursts in subpolar stratosphere recorded by gas discharge counters on board sounding balloons 06 p0921 A69-17744
- Electron density distribution stationary with respect to sun determined by Alouette 1 measurements over winter pole, noting relation to high density plasma 06 p0922 A69-18224
- Magnetospheric and high latitude ionospheric disturbances, bulk motion /convective/ flow pattern and electric field distribution 07 p1128 A69-19370
- Polar auroral far UV spectra using Ebert-Fastie monochromator flanked by photometers with same visual field 08 p1311 A69-21026
- Scientific report of Rockwell polar flight, November 14-17, 1965 09 p1484 A69-21401
- Aerial chronophotography of Southern Hemisphere conducted on around world polar flight analyzed for meteorological and geographical aspects and compared with satellite data 09 p1534 A69-21405
- Polar flight navigation charts showing feasibility of three dimensional celestial positioning 09 p1538 A69-21406
- Electron fluxes energy spectra determined from simultaneous photometric and riometric observations in polar regions 09 p1485 A69-21530
- Auroral oval boundary and median line variations with increasing magnetic storm time intensity, noting ring current effect on polar aurora location 09 p1485 A69-21532
- Charged particles equations of motion in earth magnetosphere in polar storms, considering auroral zone, diurnal variations and electron and proton velocities 09 p1485 A69-21535
- Solar flare energetic electron access to polar zones from measurements made by nine channel magnetic spectrometer on polar orbiting vehicle 09 p1577 A69-21709
- VLF polar chorus emission and geomagnetic variations caused by compressions or expansions of magnetosphere 10 p1681 A69-22803
- Polar geomagnetic disturbances global current systems representation by prototypes of equivalent current systems 10 p1688 A69-23937
- Various glacial periods mechanism ascribed to combination of long term solar activity cycle and polar migration 11 p1877 A69-24409
- Auroral infrasonic waves morphology related to temporal and spatial distributions of supersonic auroral motions during polar magnetic storms 11 p1878 A69-25152
- Theories for universal time controlled polar F region reevaluated in light of satellite low energy charged particle observations 12 p2065 A69-26103

Auroral arcs drift as function of polar storm initial phase, noting agreement with satellite data on plasma motion in magnetosphere

12 p2071 A69-26694

Electron concentration in polar ionosphere measured by coherent scattering method

12 p2071 A69-26703

Dynamics of magnetosphere, discussing auroral oval position, ring currents, plasma density and magnetic field variations in near polar region

12 p2072 A69-26741

Auroral and polar zone ionosphere effects on propagation in HF through low VHF spectrum, considering nongreat circle mode, sporadic E ionization, etc

12 p2032 A69-26859

Solar polar faculae observations, discussing relation to general solar magnetic field and coronal properties, solar high latitude rotation and susceptibility to atmospheric conditions

12 p2160 A69-26897

Unified model for spatial distribution of transpolar exospheric electron density for polar plasma study

12 p2151 A69-26952

Polar ionosphere heating by spill-over electron energy during strong geomagnetic disturbances, giving mathematical representation

13 p2257 A69-28695

Relationship between polar geomagnetic disturbances and DR variations value of geomagnetic field

13 p2257 A69-28703

Anomalous radio wave absorption in polar aurora region ionosphere, discussing disturbance characteristics

13 p2224 A69-28719

Polar aurorae fine scale structure interpretation based on plasma instabilities characteristics

13 p2258 A69-28724

Geophysical effects observed in Northern Hemisphere during low solar activity, discussing polar auroral intensities and positions

13 p2258 A69-28725

Electron concentration enhancement in upper atmosphere at polar latitudes, noting three independent zones and relation to magnetic local time

14 p2510 A69-28938

Magnetic storm time variations of electron concentrations in upper ionosphere near north geomagnetic pole, discussing magnetic time, altitude and latitude dependence

14 p2510 A69-28939

Suprathermal electrons energy distributions as function of magnetic latitude in polar ionosphere obtained by Explorer 31 satellite observation

14 p2512 A69-28963

Ionospheric effect sudden commencement parameters of magnetic storm related to distance from origin in polar regions

14 p2435 A69-29051

Ionized gas height scale changes in polar ionosphere obtained, assuming Chapman type ionization distribution

14 p2436 A69-29052

Correlation function of auroral reflection radio signals with allowance for polar ionospheric scattering and pulse signal transmission and reception

14 p2436 A69-29055

Polar auroral region displacement ascribed to distant magnetic field disturbances, proposing calculation method

14 p2436 A69-29059

Horizontal electric fields relations to charged particle fluxes in polar auroral ionosphere

14 p2437 A69-29070

Polar aurora rays mean length diurnal variations determined from photographic and visual observations in Tiksi bay

14 p2437 A69-29077

September 14, 1966 magnetic storm observation by Explorer 33 in geomagnetic tail and by polar stations, studying relation in magnetosphere and on earth

14 p2438 A69-29078

Sporadic electron flux contribution to high latitude geomagnetic disturbances at outer radiation belt boundary estimated from Elektron 1 and 2 observations

14 p2438 A69-29079

Polar aurora spectroscopic studies, discussing main spectral features, influence of observation time and location, analysis methods, etc

14 p2518 A69-29100

Magnetic field variations in magnetosphere and interplanetary space correlated with polar magnetic disturbances from dynamic morphology data

14 p2441 A69-29387

Solar corona magnetic field and polar rays, emphasizing field topology and local magnetic structure

14 p2525 A69-29718

Polar auroras temporal and spatial variations and relation to solar activity

14 p2442 A69-29719

Ozone concentration changes in polar regions and tropical zone due to meridional atmospheric circulation

14 p2442 A69-29830

Auroral displays observed in combined field of view of polar all sky camera networks, considering simultaneous geomagnetic disturbances over Alaska

15 p2595 A69-30215

Polar exosphere near solar maximum investigation by Explorer 19 and Explorer 24 drag satellites, considering density and atomic oxygen concentration measurements

15 p2600 A69-31351

Nighttime, twilight and daytime rocket experiments for ion composition of polar ionosphere at 100-180 km

15 p2604 A69-31414

Temperature measurements of neutral polar atmosphere at 120-170 km using artificial Na clouds

15 p2606 A69-31448

Solar protons nonuniformity over polar caps observed by OGO 2 ionization chamber during 24 March 1966 solar proton events

16 p2848 A69-31967

Electron fluxes energy spectra determined from simultaneous photometric and riometric observations in polar regions

16 p2783 A69-32525

Auroral oval boundary and median line variations with increasing magnetic storm time intensity, noting ring current effect on polar aurora location

16 p2783 A69-32527

Charged particles equations of motion in earth magnetosphere in polar storms, considering auroral zone diurnal variations and electron and proton velocities

16 p2783 A69-32530

Polar substorms resulting from interaction between magnetized plasma stream and geomagnetic field in magnetosphere

16 p2852 A69-32620

Polar ionosphere investigation based on vertical sounding and riometric observations, earth electromagnetic field and polar auroras spectrum intensity variations

17 p2963 A69-33950

Polar auroral zone boundaries from C-180 camera photographs related to magnetic disturbance level, noting evening-morning asymmetry

17 p2963 A69-33951

U shaped polar auroras development, examining relation with magnetic activity and current system configuration in lower ionosphere

17 p2963 A69-33952

Magnetic activity influence on polar auroras height

17 p2963 A69-33953

Polar auroras pulsation attributed to background brightness fluctuations, discussing intensity diurnal variation

17 p2963 A69-33954

Polar auroras appearance at solar activity maximum /IGY/ and minimum /ISQY/ at oval zone latitudes

17 p2963 A69-33955

Ionospheric processes associated with changes in polar aurora height, noting glow in E layer and soft electron emission into earth atmosphere

17 p2964 A69-33957

High latitude geomagnetic field quiet solar diurnal variations during magnetically quiet IGY winter days, relating type and amplitude at low and midlatitudes

17 p2964 A69-33960

Reexamination of polar F region electron density diurnal variation data contradicting King-Kohl theory of rotating neutral winds role

18 p3125 A69-34255

Anomaly of F region electron content vs polar geographic latitude and local mean time

18 p3126 A69-34257

Ion depletion in high latitude exosphere, considering OGO 2 simultaneous observations of positive ion concentration, VLF signal propagation and whistlers

18 p3187 A69-34939

Cosmic ray approach directions computation for high latitude stations, discussing results for low rigidity galactic cosmic rays and solar corpuscular events detection

18 p3187 A69-34940

Hydrogen bulge above springtime pole indicated by Lyman alpha radiation in earth geocorona, discussing

hydrogen horizontal transport and hydrogen compounds dissociation as causes

18 p3129 A69-34956

Ionospheric electric current systems dynamics in polar latitude in relation to 1966 geomagnetic storms

18 p3130 A69-35188

Earth ellipsoid determination by satellite observations, noting accuracy of polar flattening measurement on basis of perturbation or perigee argument

18 p3131 A69-35195

Jupiter swingby flight mode application to probe missions requiring solar polar regions overflight at close perihelion distances

19 p3401 A69-35915

Plasma density in magnetosphere by measuring geomagnetic pi 2 micropulsations in direction related to polar aurora oval southern boundary, determining period of pi 2 oscillations

19 p3303 A69-36205

Electron density distribution in northern and southern polar regions ionosphere based on 1958 and 1959 observations at high geomagnetic relatively low geographic latitudes

20 p3526 A69-37664

F 2 region critical frequencies obtained during winter at Northern and Southern Hemisphere stations located in auroral and polar zones, correlating changes with ionization

20 p3526 A69-37665

High latitude stations vertical ionograms in absence of ionospheric reflections due to low solar activity periods, discussing interpretation methods

20 p3529 A69-37690

High latitude ionosphere data from Alouette- ISIS program, describing various F, E and D regions parameters

20 p3530 A69-37868

High latitude limit of closed geomagnetic field lines indicated by high latitude electron boundary in outer radiation zone during Alouette satellite energy particle experiment

20 p3531 A69-37875

Equatorial semiaxis of magnetospheric tail at distances between 10 and 80 earth radii for various intensities of polar magnetic disturbances

20 p3532 A69-37959

Three dimensional current systems constructed semiquantitatively for polar magnetic substorms based on magnetic field distribution on earth surface

20 p3533 A69-38085

Mass spectrometric investigation of thermosphere at high latitudes, measuring number densities for nitrogen, Ar and molecular and atomic oxygen

20 p3533 A69-38086

Atmospheric gravity waves amplitude generated in equatorial electrojets and polar regions

20 p3593 A69-38107

Circulation near turbopause effect on lower thermosphere composition changes, noting heat source for warmth over winter polar region

21 p3704 A69-38366

Polar upper atmospheric phenomena interpreted as magnetospheric substorm manifestations, discussing role of asymmetric ring current formation

21 p3710 A69-38504

Low energy plasma escape flow from polar region /polar wind/, examining H, He and O ions participation in expansion

21 p3713 A69-38528

Cosmic ray proton cut-off increase at high latitudes during magnetospheric substorms, using balloon time observations of nuclear gamma ray flux

22 p4005 A69-40509

Daily variation of trajectory derived high latitude vertical cut-off rigidities in magnetospheric model consistent with proton and electron experiments

22 p4005 A69-40513

Spectral characteristics of structured areas of luminosity in polar cap region, reporting spatial and time variations plotted from NASA airborne survey

22 p3940 A69-40522

Ionospheric perturbations generation by time variable alternating electrical currents at polar latitudes, constructing radiation patterns for gravitational waves

23 p4155 A69-41842

Anomalies of isotropic cosmic ray secular variations at high latitudes based on superimposed neutron data

23 p4206 A69-41854

Geomagnetic ring current effect on position of auroral absorption zone in northern polar region, noting storm time part of disturbance

23 p4157 A69-41859

Concurrent geomagnetic micropulsations at equatorial and high latitude stations, discussing magnetospheric sources of Pi and Pc types
23 p4161 A69-42439

Equator-to-pole temperature gradient relation with planetary pressure belts, comparing observational data with theoretical circulation criterion
24 p4345 A69-43149

Solar protons delayed access into polar regions during 2 November 1967 solar particle event, discussing north-south asymmetry
24 p4368 A69-43183

POLARIMETERS

Partially polarized light and polarization degree measured by photoelectric polarimeter, obtaining scattering indicatrices and polarization degree dependences
01 p0075 A69-11190

Photometric-polarimetric observations of planetary surfaces, discussing geological environment interpretation and spacecraft reconnaissance system mission planning
03 p0421 A69-13394

Airborne polarimeter to measure Stokes parameters of linearly polarized visible atmospheric radiation in four narrow spectral regions
06 p0923 A69-16924

Photoelectric polarimeter to record sky light intensity in form of polarized components, detailing construction and operation
12 p2078 A69-25892

Electronic nonimaging polarimeter/photometer for aircraft observations of pure red pine stand, suggesting application to terrestrial, airborne and satellite remote sensing
12 p2096 A69-26983

Two channel polarimeter capable of eliminating atmospheric scintillation effects used for observation of magnetic stars and eclipsing binary U Herculis
13 p2347 A69-27713

Balloon for in situ measurements of atmospheric optical parameters using two axis sun pointer, spectropolarimeter and airborne telemetry
15 p2615 A69-31288

Solar radio bursts polarization measured with microwave correlation polarimeter, noting output recording rate
18 p3188 A69-35213

Polarimeter using 45 degree Bragg angle reflection applied to rocket payload design for determining polarization of celestial sources X rays
23 p4207 A69-42382

POLARIMETRY

Late type variable stars time dependent photometry and polarimetry in blue and violet, noting correlation for stellar brightness and degree of polarization
01 p0158 A69-11326

Instrumental Stokes vector calculating method involving light flow transformation matrix elements determination
04 p0601 A69-15248

Transistorized electrophotometer for polarimetric and photometric analysis of weak light fluxes, noting pulse amplifying and shaping circuits
11 p1884 A69-24735

Photometric and polarimetric properties of Mars, discussing powder covering, chemical composition and particle size of bright and dark areas and blue haze
12 p2171 A69-27145

Polarimetric observations of polarization percentage and position angle changes in T Tauri stars, confirming stellar polarization association with emission spectra
15 p2694 A69-30882

Balloon-borne UV polarimetry of stars and planets, studying linear polarization between 2000 and 3000 Å
15 p2616 A69-31380

Mars surface and atmospheric properties from polarization degree measurements, discussing optical properties of soil and detection of veils, mists and clouds
16 p2854 A69-31655

Martian surface and atmosphere interpretation through polarimetric and photometric simulation
20 p3614 A69-38253

POLARIS MISSILES

Polaris and Poseidon nuclear missile systems, considering efficiency and launching depth from nuclear submarine
19 p3432 A69-36687

POLARISCOPES

Isoclines determination from fringe patterns, obtaining continuous principal stress direction data for photoelastic model in bonded polariscope
24 p4396 A69-42738

POLARITY

Geomagnetic response asymmetry related to solar direction of polarity in interplanetary magnetic field
01 p0077 A69-11236

Myocardial repolarization changes in healthy persons with restricted motor activity
07 p1066 A69-18984

Indium antimonide crystals polarity effect on photoeffect, analyzing quantum yields and energy spectrum
15 p2667 A69-30076

Interplanetary and photospheric magnetic fields polarities observed by Mariner 4 and with solar magnetograph, noting noncorrelated data along latitudinal strip
18 p3205 A69-35399

Reversal rate of earth magnetic field deduced from observed and theoretical polarity interval length using hydraulic transmission line theory
19 p3304 A69-36869

Myocardial repolarization changes in healthy persons with restricted motor activity
20 p3480 A69-38232

POLARIZATION

Labyrinth polarization effect on stimulation and neuron activity in visual cortex of cats, using electroencephalograph
20 p3469 A69-37244

POLARIZATION [CHARGE SEPARATION]

NT DIELECTRIC POLARIZATION

NT ELECTROLYTIC POLARIZATION

Nonreciprocal tunable yttrium-iron garnet microstrip filter design through generation of circularly polarized field
01 p0041 A69-10202

Statistical analysis of polarization of semiinfinite electron/ion plasma bounded by dielectric or conducting solid wall, deriving steady state and space potential
02 p0286 A69-11706

Shock wave produced polarization effects in dielectrics, noting reflected shock waves and experimental results for polymethyl methacrylate and carbon tetrachloride
04 p0589 A69-14988

Tunnel diode univibrator, noting polarization influence on recovery time and pulse length stabilization dependence on resistive load
04 p0578 A69-15069

Electrical polarization effect on electroluminescence brightness waves in zinc sulfide films
05 p0807 A69-16213

Polarization effect on electroluminescent properties of zinc sulfide films
05 p0807 A69-16214

Repolarization processes in barium titanate single crystals by variable sinusoidal voltage pulses
05 p0808 A69-16215

Passive current maxima during anodic polarization of stainless steel in sulfuric acid, using electrochemical and electron microprobes
06 p0944 A69-17853

Thermodynamics and polarization of zinc electrode in alkaline media, discussing anodic dissolution and passivation
08 p1268 A69-21048

Microstructural analysis, determining junction orientation polarity effect on draw junction structure in GaSb crystals at room temperature
10 p1745 A69-23330

Plasma jets tangential injection into toroidal magnetic field, discussing polarization interaction and depolarization effect
13 p2311 A69-28108

Two center Coulomb integrals expressed in terms of center separation, noting applications to molecular calculations
14 p2471 A69-29926

Structure of solitary waves propagating in collisionless plasma perpendicular to magnetic field, considering soliton wavefronts charge separation and relativistic velocity
17 p2922 A69-33696

Polarizable ions effect on glass fibers strength retention, noting fatigue tests for hydrolytic stress corrosion
20 p3567 A69-37769

Repolarization processes in barium titanate single crystals by variable sinusoidal voltage pulses
20 p3584 A69-37785

Corrosion kinetics in metals using electrochemistry, stressing polarization techniques
21 p3749 A69-39494

Radio pulse emission from ionized disk of cosmic ray extensive air showers, noting importance of charge

separation in geomagnetic field and selective positron absorption
21 p3792 A69-39614

Spontaneous polarization onset in perovskite ferroelectrics, analyzing influence of Curie point, Jahn-Teller effect and atomic structure
22 p3995 A69-41159

Dielectric polarization of barium titanate and barium strontium titanate in pulsed fields in paraelectric phase, analyzing coefficient B in free energy function and equilibrium state
22 p3996 A69-41165

Moving plasma partial capture in transverse magnetic field in experimental plasma source, noting influence of repulsion effect of plasma polarization volume charge
24 p4357 A69-43469

POLARIZATION [SPIN ALIGNMENT]

Asymmetry of polarized protons scattered from He 4 at 540 Mev for laboratory angles between 4 and 42 degrees
04 p0632 A69-14966

Optical pumping at high temperatures using spin exchange signals for RF spectroscopy
07 p1148 A69-18893

Orientation of diamagnetic ground state Pb 207 atoms with nonzero orbital angular momentum by means of optical pumping and determination of nuclear moment
07 p1156 A69-19399

Relation between electron spin-spin interactions and polarization and relaxation of ruby nuclei at He temperatures
08 p1372 A69-20541

Planar ribbon winding for buildup control of material near polar openings of filament wound vessels, discussing ribbon width and density
09 p1507 A69-22328

Atomic and molecular spins dynamic orientation in anisotropic radiation field, examining medium properties and astrophysical consequences
13 p2350 A69-27861

Differential cross section and polarization measurements for elastic scattering of high energy protons from light nuclei
24 p4352 A69-43125

Many body perturbation theory with time dependent perturbations applied to frequency dependent polarizability of atomic oxygen
24 p4354 A69-43816

POLARIZATION [WAVES]

NT CIRCULAR POLARIZATION

NT ELLIPTICAL POLARIZATION

NT OPTICAL POLARIZATION

Faraday angle of rotation of radio signals polarization plane from satellites and celestial bodies
01 p0030 A69-10574

Analytical expressions for transfer function matrices of four terminal signal shaping networks, assuming rational matrix spectral density of randomly polarized signal
01 p0031 A69-10880

Normally incident linearly polarized electromagnetic wave reflection and transmission by semiinfinite longitudinally drifting magnetoplasma in static magnetic field
01 p0134 A69-11290

Quantum theory of electrical birefringence of noninteracting diamagnetic molecules /Kerr effect/ subjected to static electric field and polarized plane wave
02 p0279 A69-11538

Polarization rotation and phase delay effects as function of frequency for ionospherically propagated HF signals
02 p0208 A69-12331

Alfven wave propagation designations in terms of polarization and propagation velocity, resolving contradictory aspects
02 p0290 A69-12400

Linear polarization measurements of variable radio sources
02 p0325 A69-12592

Linear polarization measurements at 2.07 cm for 29 radio sources
02 p0326 A69-12705

Transverse magnetic field influence on power and polarization of helium-neon laser emission
02 p0260 A69-12844

Scattering matrices of complex configuration specified by cross polarized radar cross sections based on Green function, noting wire loop and wedge scatterers
03 p0384 A69-12904

Optical narrow bandpass filter designed for precision solar corona observations, utilizing interferential polarization and thermo-optical compensation
03 p0506 A69-13085

Polarization diversity analysis to avoid fading in microwave scatter links in D and E layers
03 p0394 A69-13378

Light polarization of night sky components scattered by troposphere
04 p0595 A69-15247

Extensive air shower radio pulse polarization, using log periodic EW- and NS-arm antennas
04 p0595 A69-15425

Resonance rotation of polarization plane in circular waveguide with ferrite resonator
05 p0718 A69-15640

Polarization-albedo relationship for selected lunar maria, highlands and mountains in five passbands suggest optical path length function of effective refractive index and particle size
05 p0829 A69-16663

Multimode direction tracking with polarization tracker used simultaneously, analyzing cross coupling and conical horn/reflector antenna
06 p0888 A69-17652

Output polarization rotation sensitivity to axial magnetic field varied by variable angle quartz flat inside He-Ne laser resonator
07 p1198 A69-18646

Polarization of ionospherically propagated HF radio waves for various times, frequencies and path azimuths applied to distortion in radio communication
07 p1078 A69-18916

Radiation resistance of short dipole immersed in cold magnetoionic medium, using polarized wave modes
07 p1107 A69-19226

Radioelectric axis deviation of radome in front of monopulse radar antenna
07 p1111 A69-19524

Phase velocities and polarizations of linear waves in infinite uniform high beta plasma
08 p1359 A69-19986

Log periodic antenna with vertically polarized omnidirectional radiation constant over bandwidth
08 p1281 A69-20033

Radar scattering cross section of finite perfectly conducting wedge for case of illumination by polarized plane wave
08 p1274 A69-20047

Radio observations of gamma Cygni source in Cygnus X complex showing nonthermal nature of source, noting weak but significant polarization
08 p1387 A69-20090

Plasma flow motion and polarizing interaction in multipole magnetic field
08 p1370 A69-21015

Longitudinal polarization behind front of plasma flow interacting with transverse magnetic field, showing electric potential and magnetic field exhibit structural fluctuations
08 p1370 A69-21018

Ion-acoustic wave excitation in plasma layer affected by incident p-polarized magnetic wave, deriving expressions for reflection, transmission and energy absorption coefficients
08 p1370 A69-21025

Polarization changes of R Coronae Borealis Star RY Sagittarii, tabulating percentage polarization and position angles
09 p1603 A69-22265

Level degeneracy effect on nonlinear interactions between traveling waves of different planes of polarization
10 p1705 A69-23815

Perturbation theory applied to emitting density matrix in nonlinear polarization of resonance media, considering gas laser in coaxial magnetic field
11 p1895 A69-24630

Polarized Hartree-Fock model computing photoionization cross sections for Li isoelectronic sequence, listing phase shifts for partial waves of scattered electrons
11 p1922 A69-25260

System switch, separating RF bands according to frequency and polarization for simultaneous transmission from parabolic horn antenna
11 p1854 A69-25618

Analytical expressions for transfer function matrices of four terminal signal shaping networks, assuming rational matrix spectral density of randomly polarized signal
12 p2031 A69-26644

Reflection coefficient of polarized radio waves at ionized meteoric trails obtained by numerical integration of differential equations
12 p2031 A69-26691

Chromospheric heating and polarization in late stars, considering association with Ca II K line emission cores
13 p2340 A69-27579

Optical narrow bandpass filter designed for precision solar corona observations utilizing interferential polarization and thermo-optical compensation
14 p2515 A69-28767

Polarization diversity analysis to avoid fading in microwave scatter links in D and E layers
14 p2410 A69-28829

Plane wave reflection and transmission by unidirectionally conducting screen, considering oblique incidence and two polarizations
14 p2421 A69-29547

Inhomogeneities effect on polarization of radio waves reflected from ionosphere, based on permittivity tensor
14 p2417 A69-29862

Faraday angle of rotation of radio signals polarization plane from satellites and celestial bodies
15 p2568 A69-30744

Regulating setup for controlling AC voltage surrounding polarization of magnetic electrode in plasma
15 p2664 A69-31094

Lunar radio emission linear polarization radial dependence at 0.8-cm wavelength using radio telescope, determining dielectric constant of emitting layer
15 p2697 A69-31251

VLF and particle rocket experiment for group delay time between rocket and ground, discussing wave polarization and energy flows meaning
15 p2571 A69-31424

Temporal damping rate for small amplitude linearly polarized TEM mode in plasma, using Landau equation
16 p2818 A69-31675

Resonance rotation of polarization plane in circular waveguide with ferrite resonator
16 p2762 A69-32498

Active admittance, realized gain and linear polarization degradation vs scan angle for infinite periodic phased arrays of circular apertures
20 p3507 A69-37844

Multimode He-Ne laser radiation polarization modulation as function of magnetic field, cavity anisotropy and frequency, using Macaluso-Corbino effect
21 p3739 A69-39447

Electron collisions effect on polarization of waves reflected from ionosphere
22 p3941 A69-40922

Fluctuations of polarization induced fading periods in short wave transmissions of Soviet earth satellites, showing relation to ionospheric inhomogeneities
22 p3942 A69-41095

Radiation characteristics of dipole on wedge edge with sinusoidal current, discussing spatial phase and polarization calculations by computer
23 p4138 A69-41937

POLARIZATION CHARACTERISTICS

Dynamic polarizability at imaginary frequencies, deriving upper and lower variational bounds with functionals containing trial functions
01 p0122 A69-10284

Low polarization error HF loop antenna array direction finder performance tests, comparing measured bearings with polarimeter and conventional crossed loops data
01 p0048 A69-11006

Solar corona electron density, polarization, temperature and monochromatic emission during November 1966 eclipse
02 p0310 A69-11457

Electromagnetic field interaction with polarizable elastic medium in gravitation theory resolves definition of electromagnetic energy in matter
02 p0279 A69-11537

Statistical analysis of polarization of two component nonisothermal electron-ion Coulomb gas plasma containing microfluctuations
02 p0286 A69-11707

Rocket released probe orientation determination from polarization measurements on telemetry signal
02 p0207 A69-11813

Polarization stability improvement of helical beam antenna by increased turns, smaller pitch angle and decreased transverse electromagnetic mode amplitude
02 p0219 A69-12345

Linear polarization measurements of variable radio sources
02 p0325 A69-12592

Unsteady phenomena during light pulses interaction in media with polarization, considering group delay, dispersion spreading and space-time analogy
02 p0259 A69-12646

Polarized orbital method for calculating electron-atom scattering amplitudes, noting discontinuous wave function, nonvariational technique and strong dependence on parameter
02 p0284 A69-12702

Linear polarization measurements at 2.07 cm for 29 radio sources
02 p0326 A69-12705

Light wave propagation in gyrotropic crystals, examining laser frequency shift circularly polarized by modulating field
03 p0436 A69-13037

Second order frequency dependent polarizabilities calculated by double perturbation theory
03 p0472 A69-13314

Double perturbation theory, deriving interchange theorem for polarizabilities at complex valued frequencies and formulation without assumption of existence of unperturbed Hamiltonian
03 p0472 A69-13315

Microwave solar burst data, analyzing flux intensity and polarization distributions
04 p0652 A69-14417

Lunar surface IR polarization measurements compared to visible and UV polarization
04 p0656 A69-14669

Polarization enhancements in solar microwave radiation, noting correlation with other solar events and geophysical effects
05 p0813 A69-15761

Mean number of polarization coefficient modulus zero crossings for field reduced at reception point to uncorrelated orthogonally polarized components
05 p0720 A69-16445

Domain structure of barium titanate single crystals during polarization reversal by sinusoidal AC field
06 p0981 A69-17893

Nonlinear interaction effects on frequency and polarization characteristics of dual polarization gas laser, discussing weak cavity anisotropies
07 p1145 A69-18473

Nonpolarized single frequency gas laser radiation produced by interferential effects in complex resonator
07 p1149 A69-18936

Linear polarized emission from pulsar CP 0328 dependent on frequency, discussing model for source with constant Faraday rotation
08 p1382 A69-19817

Validity of formula for oscillation frequency of nearly sinusoidal tunnel diode oscillator extended to operation in nonsinusoidal regime
08 p1279 A69-19924

Computer aided design program for testing equivalent circuits of bipolar transistors in static regime under various polarization conditions
08 p1280 A69-19972

Distributed type bipolar transistor model construction, considering methods of development and computer tests for transient conditions
08 p1280 A69-19976

Geometric optics and polarization properties of spherical reflector for integral representation of focal region fields, discussing stationary phase and field points
08 p1272 A69-20017

Lower ionosphere and earth-ionosphere waveguide effects on polarization characteristics of transmitted radio whistlers
08 p1306 A69-20181

Interferometric measurement of polarization distributions in Crab Nebula and 3C 315 radio sources by Fourier synthesis, discussing complex brightness
08 p1390 A69-20389

Spherical harmonic analysis of Stokes parameters for polarization of stars, discussing magnetic field of Galaxy
08 p1390 A69-20390

Lunar radio emission polarization characteristics, considering knife-edge type radiation pattern effect of antenna array
08 p1391 A69-20423

Focal antennas and receivers of Nancy radio telescope to measure flux density and incoming waves polarization, noting circular polarization in quasars
08 p1392 A69-20567

Polarization variations in radio pulses from pulsar CP 0328, noting possible origin in synchrotron radiation from collimated electron beam
08 p1397 A69-20694

Microwave absorption by free carriers in c domain barium titanate crystals inserted in waveguide during polarization reversal
08 p1374 A69-21189

Vela pulsar polarization and periodicity observations supporting rotational model vs radial pulsations as radio emission source
09 p1592 A69-21461

Lower ionosphere effect on LF electromagnetic disturbances, comparing propagation and damping of clockwise and counterclockwise polarized waves
09 p1487 A69-21637

Polarization changes of R Coronae Borealis Star RY Sagittarii, tabulating percentage polarization and position angles
09 p1603 A69-22265

Quadrupole splitting of Na 23 nuclear magnetic resonance /NMR/ to investigate spontaneous polarization, coercive field and domain characteristics in Rochelle salt ferroelectric phase
09 p1559 A69-22283

Book on thermodynamics of charged and polarized layers covering matter in electric fields, general framework theory, applications, etc
10 p1724 A69-23159

Polarization to extinction ratio criterion to choose interstellar cloud model, discussing magnetic field strength requirements
10 p1781 A69-23673

Spectroscopic, photometric and polarimetric observations of magnetic stars, discussing magnetic curves of periodic variables
11 p1954 A69-24362

Solar radio bursts observations with multielement compound interferometers, noting polarization distribution and magnetic field change
11 p1946 A69-24428

Radar transmitter and receiver antennas polarization parameters selection for obtaining maximum SNR at reception point
11 p1833 A69-24442

Hydrogen peroxide electrode cathodic polarization studied for liquid oxidant use in methanol fuel cells
11 p1825 A69-24523

Polarization effects of scattered coherent light on laser imagery, determining surface roughness and angle of incidence effects photographically on basis of Fung theory
11 p1896 A69-24849

Calcite crystals stability anisotropy to ruby laser radiation, studying threshold power as function of beam polarization
11 p1900 A69-25553

Microstructure of pc 3 and pc 4 geomagnetic pulsations, investigating polarization direction, period duration and latitude dependence
12 p2063 A69-25782

Atmospheric optics by spacecraft and high altitude probes concerning ozone and aerosol distributions, scattering indicatrix polarization and dust cloud inhomogeneities
12 p2055 A69-25815

Virtual power principles applied to solving force acting on fluid consisting of colloidal suspension of polarized particles in neutral vehicle
12 p2136 A69-26404

Surface waves effect on electromagnetic waves incoherent reflection from plasma-vacuum boundary, describing polarization and angular and spectral distributions
12 p2031 A69-26530

Laser active media polarization in strong electromagnetic fields, solving boundary value problems
12 p2110 A69-26907

Two photon and resonance parametric lasers nonlinear polarization theory, deriving equations for electromagnetic field oscillations
12 p2110 A69-26910

Polarization and structure of magnetic fields of quasars, E galaxies, normal galaxies and other extragalactic radio sources
12 p2165 A69-27034

Alloying effect on surface oxides determined from photoelectric polarization measurements for Ti-Nb and Ti-Ni
13 p2275 A69-27292

Jupiter polarization wavelength dependence noted in observations of 5 seconds diameter regions near poles and equator related to Rayleigh-Chandrasekhar molecular scattering theory
13 p2348 A69-27805

Polarization stabilization times dependence on risetime of external field pulse leading edge for semiconductor crystal, determining field concentration
13 p2317 A69-27880

Core polarization effects in inelastic scattering cross sections for several nuclei in 2s-1d shell, using Hartree-Fock wave functions and Born approximation
14 p2487 A69-29007

Coherence-polarization in remote sensing by microwave and laser means, analyzing scattering functions of rough surfaces
14 p2448 A69-29532

Linear polarization achieved in He-Ne laser by applying external transverse magnetic field to plasma discharge
14 p2459 A69-29569

Polarization characteristics of quasars, radio galaxies and galactic objects suggesting separate evolutionary processes
14 p2526 A69-29771

Polarimetric observations of polarization percentage and position angle changes in T Tauri stars, confirming stellar polarization association with emission spectra
15 p2694 A69-30882

Thermal radiation polarization in anisotropic and gyrotropic media described by Hermitian permittivity tensor, noting linearity
15 p2653 A69-30940

Wavelength dependence of linear polarization of sunlight scattered by Venus, noting temporal variations in UV
16 p2860 A69-32236

Amplitude distribution and correlation functions of signals reflected from precipitations at various polarizations of waves emitted and received
16 p2807 A69-32269

Depolarization degree of angel echo signals measured by radar station, indicating insects and other foreign particles in atmosphere as reflection sources
16 p2779 A69-32274

Polarization characteristics of electromagnetic waves obliquely reflected from inhomogeneous isotropic plane stratified plasma
16 p2752 A69-32391

Mean number of polarization coefficient modulus zero crossings for field reduced at reception point to uncorrelated orthogonally polarized components
16 p2753 A69-32478

Polarization, frequency and energy characteristics of lasers with resonators containing polarization transforming elements
17 p2983 A69-33967

Antarctic VLF emissions polarization and direction determination, using combination of antennas with planes lying in geomagnetic E-W and N-S directions
18 p3102 A69-34965

Microwave absorption by free carriers in c domain barium titanate crystals inserted in waveguide during polarization reversal
18 p3183 A69-35158

Solar disk edge polarization rate determined by applying Feautrier method to transfer equations for polarized radiation
19 p3427 A69-36728

Solar corona photographic study during 1961 total eclipse using quadruple camera, providing intensities, amount and direction of polarization
22 p4001 A69-40001

Linearly polarized electromagnetic wave diffraction during oblique incidence on crossed strip arrays, describing crossing angle effects on reflection, transmission and polarization conversion coefficients
23 p4124 A69-42030

Polarization characteristics of He-Ne ring laser emission with circularly anisotropic resonator, analyzing ellipticity as function of half wave cavity plate
24 p4328 A69-43160

POLARIZATION CHARTS
U GRAPHS [CHARTS]

POLARIZED ELASTIC WAVES

Forced recombination scattering of light on Rayleigh polarization waves in isotropic solid body with small elastooptical constants
21 p3770 A69-38963

POLARIZED ELECTROMAGNETIC RADIATION
NT SYNCHROTRON RADIATION

Linear polarization measurements at 2.07 cm for 29 radio sources
02 p0326 A69-12705

Electron concentration in lower ionosphere based on measurement of Faraday rotation of polarization plane of radio waves scattered by meteor trail
03 p0423 A69-13535

Strain effects on transverse electromagnetic modes of anisotropic dielectric waveguides at p-n junctions
03 p0406 A69-13830

Radiation properties of spherical phased array of 16 flat spiral antennas and radiation field polarization characteristics
04 p0573 A69-14331

Nonlinear damping of circularly polarized electromagnetic wave propagating in plasma along magnetic field, noting particle motion in resonance region
04 p0558 A69-14982

Polarization degree of type solar radio bursts dependent on heliographic longitude
04 p0649 A69-15242

Polarization enhancements in solar microwave radiation, noting correlation with other solar events and geophysical effects
05 p0813 A69-15761

Mean number of polarization coefficient modulus zero crossings for field reduced at reception point to uncorrelated orthogonally polarized components
05 p0720 A69-16445

Polarization tensor variation due to Faraday effect and differential absorption of ordinary and extraordinary waves for radiation propagating in magnetoactive cosmic plasma
05 p0805 A69-16650

Ion-cyclotron instabilities in hot-ion cold-electron plasma resulting from left-hand circularly polarized wave propagating parallel to magnetic field
06 p0969 A69-17951

Polarization of ionospherically propagated HF radio waves for various times, frequencies and path azimuths applied to distortion in radio communication
07 p1078 A69-18916

Electromagnetic multipole left- and right-hand circularly polarized modal fields for multiarm log spiral antennas, discussing current distributions, multipole coefficients and field patterns
08 p1281 A69-20018

Plane H polarized electromagnetic wave diffraction incident on array of rectangular rods described by linear algebraic equations
08 p1275 A69-20433

Orbiter and rotator models of pulsating radio sources, considering relationship between lack of Faraday rotation and similar polarization in decametric radiation from Jupiter
08 p1397 A69-20688

Electromagnetic microinstabilities of plasmas associated with transverse waves propagating perpendicular to external uniform magnetic induction, noting allowable frequencies
08 p1368 A69-20804

Passive electromagnetic circuit elements for laser light control such as circulators, isolators and phase shifters, discussing coherent light and polarization
09 p1518 A69-22127

Optimal receiving circuit determined for elliptically polarized signals in randomly polarized noise by deriving integral equation
09 p1456 A69-22285

Far IR radiation from water vapor laser, noting monochromaticity and strong linear polarization
10 p1702 A69-23160

Beam displacement at plasma under magnetic field connected with polarized electromagnetic wave reflections
10 p1740 A69-23724

Polarized electromagnetic waves phase shift during total reflection from stratified dielectric region found dependent on transition zone width in addition to permittivity
10 p1657 A69-23862

Polarized brightness distributions of supernova remnants IC 443 and W44 at 6-cm wavelength from observations with 6 minute resolution
10 p1787 A69-24113

Radiation emission by scalar particle in field of two plane linearly polarized electromagnetic waves propagating toward each other
11 p1900 A69-25568

Circular polarization of solar microwave radio emission in Southern and Northern Hemispheres due to solar magnetic field
13 p2326 A69-27550

Linear polarization measurements at 6 cm, determining rotation period associated with Jupiter cm radiation
13 p2343 A69-27623

Electric field distribution in focal region of finite offset paraboloid reflector illuminated by linearly polarized plane wave
13 p2234 A69-28427

Eclipsing close binary stars orbital planes spatial position determined from stellar emission polarization
15 p2688 A69-30560

- Balloon-borne UV polarimetry of stars and planets, studying linear polarization between 2000 and 3000 Å
15 p2616 A69-31380
- Scattering of time harmonic linearly polarized plane electromagnetic wave by uniformly axially moving cylinder, analyzing first order velocity effects
16 p2748 A69-31579
- Polarimetric observations of Be stars, noting dependence and self absorption by hydrogen of polarization produced by electron scattering
16 p2863 A69-32397
- Mean number of polarization coefficient modulus zero crossings for field reduced at reception point to uncorrelated orthogonally polarized components
16 p2753 A69-32478
- Monochromatic linearly polarized electromagnetic beam generator for submillimeter band, discussing applications
17 p2932 A69-34162
- Polarization operator and Green function of photon for propagation of plane electromagnetic waves in constant crossed field, noting refractive indices
18 p3103 A69-35128
- Mathematical relations for ring laser beams polarization conditions, using slanted isotropic plate and phase circulator to separate polarization plane
20 p3553 A69-37606
- Polarized radiation resonance scattering in weak uniform magnetic field, using Monte Carlo method to trace and count photons
20 p3577 A69-38157
- Diffraction of plane polarized electromagnetic wave incident on dielectric wedge formulated as singular integral equation, discussing electric field amplitude
22 p3903 A69-41258
- Linearly polarized electromagnetic wave diffraction during oblique incidence on crossed strip arrays, describing crossing angle effects on reflection, transmission and polarization conversion coefficients
23 p4124 A69-42030
- Plane electromagnetic waves coherence properties, considering linear and arbitrary degree of polarization
24 p4350 A69-42982
- POLARIZED LIGHT**
- Gas laser amplifier nonlinear behavior in axial magnetic fields and operating with two polarized light signals of strong or weak intensities
01 p0088 A69-10010
- Absorption of linearly polarized light in reflecting surface layer of collisionless plasma, calculating layer lifetime for reflection of light
01 p0127 A69-10283
- Light polarization properties in atmosphere noting aerosols effect
01 p0075 A69-11189
- Partially polarized light and polarization degree measured by photoelectric polarimeter, obtaining scattering indicatrices and polarization degree dependences
01 p0075 A69-11190
- Lunar surface composition, hardness, porosity, microstructure and transparency based on polarization of reflected light
04 p0658 A69-14958
- Angle of incidence influence on unpolarized and linear polarized light of solar cell short circuit current
04 p0551 A69-15312
- Poincare sphere representation of polarized light used to predict rotation effect on optical observations in photoelastic shell analysis
04 p0683 A69-15495
- Electric and magnetic fields of narrow coherent polarized light beam in free space, noting longitudinal field components due to beam narrowness
05 p0777 A69-16789
- Airborne polarimeter to measure Stokes parameters of linearly polarized visible atmospheric radiation in four narrow spectral regions
06 p0923 A69-16924
- Dayglow determination from aerosol spectrum obtained through data of brightness and polarization of day sky
07 p1211 A69-18545
- Fluorescent light polarization of neon atoms subjected to gas discharge, static magnetic field and laser beam
[IEEE PAPER T-9]
07 p1155 A69-19084
- Night sky surface brightness and polarization measurements as basis for zodiacal dust cloud particle density distribution normal to ecliptic plane
07 p1222 A69-19588
- Polarized light microscope for application to metallic crystallographic studies noting grain orientation, hcp grain basal pole orientation and etched fcc metals
09 p1499 A69-22302
- Light wave reconstruction including polarization, using single reference beam with depolarizing diffuser as source
10 p1690 A69-22951
- Stimulated emission of trivalent Nd ions in glass base, explaining connection between efficiency and emission polarization by interaction of laser modes with ions
10 p1703 A69-23618
- Interstellar dust distribution ideas to explain observed variability in starlight polarization and similar phenomena
10 p1785 A69-24050
- Airborne Q switched ruby laser for studying upper atmosphere meteoric formations optical characteristics and kinetics against background of underlying surface
12 p2125 A69-25955
- Sky polarization neutral points around sunset /spring-summer 1968/ at Bedford, Mass., inferring continuation and variations of enhanced stratospheric turbidity
12 p2067 A69-26343
- Polarimetric and photometric observations of comet Ikeya-Seki 1965f, plotting isophotes of head and polarized light distribution in tail
15 p2685 A69-30525
- Remote polarized light source photometric observation on background of polarized light scattered horizontally, considering atmosphere optical state effect on laser communications
15 p2649 A69-30655
- Mars surface and atmospheric properties from polarization degree measurements, discussing optical properties of soil and detection of veils, mists and clouds
16 p2854 A69-31655
- Lunar surface characteristics, discussing light polarization, lunar radiation, solar radiation and meteorite impact effects, etc
16 p2856 A69-32069
- Wavelength dependence of polarization of sunlight scattered by Venus atmosphere, including Rayleigh and Mie scattering mechanisms
16 p2860 A69-32237
- Light polarization diffusely reflected by earth atmosphere measured from balloon, using gain compensated photoelectric polarimeter
16 p2781 A69-32320
- Polarization of light from atmospheres of Mira variables, suggesting temperature variations over stellar surface
16 p2866 A69-32820
- Two polarization light interference scattered by moving and fixed atoms, obtaining forward scattered light intensity
17 p3005 A69-33109
- Lunar surface composition, hardness, porosity, microstructure and transparency based on polarization of reflected light
18 p3196 A69-34721
- Photoelastic materials stressed state analysis by inserting analyzer and polarizer into sandwich medium, obtaining polarized light field
18 p3138 A69-35152
- Gamma ray flux from processes associated with high energy electrons from pulsar NP 0532, noting light polarization
20 p3588 A69-37410
- Singular electromagnetic field rectilinear and elliptical polarization in general relativity, calculating light plane rotation in Schwarzschild space
20 p3576 A69-37431
- Polarization fluctuations of starlight indicating turbulent structure of interstellar medium, noting pulsar signal dispersion and Faraday rotation
22 p4030 A69-40771
- Human eye modulation transfer function in reflected light by analyzing depolarized and polarized components emerging from eye
22 p3884 A69-40888
- Mars light polarization observations noting unsatisfactory surface pressure determinations
23 p4212 A69-41615
- POLARIZED RADIATION**
- NT SYNCHROTRON RADIATION**
- Polarization of nightglow, line vs continuum
02 p0235 A69-11428
- Polarized low temperature laser excited Raman spectra of thulium gallium garnet
02 p0256 A69-11925
- OSO-B2 satellite zodiacal light observations at constant 90 degree elongation, measuring polarized component as function of time
02 p0245 A69-12718
- Outer space electromagnetic radiation transfer in turbulent plasma with allowance for polarization effects, describing polarization induced changes in Stokes parameters
03 p0506 A69-13083
- Polarized radio emission from Jupiter, giving hypothesis of radiation belts deformation by solar wind
03 p0512 A69-13703
- Linear polarization of cosmic radio emission measured near galactic anticenter at centimetric wavelengths
03 p0501 A69-13704
- Linear polarization of cosmic radio emission, discussing original measurement method and revised version based on discrimination of useful signal
03 p0501 A69-13705
- Polarization errors in phase type direction finder caused by antenna
04 p0561 A69-15404
- Polarization of diatomic molecular line radiation excited by electron impact
06 p0961 A69-17140
- Airborne S-band telemetry antennas for omnidirectional patterns of polarization component, discussing design, pattern measurements and application
07 p1106 A69-19112
- Electron density measurement in solar flare spray using discrepancy between measured and theoretical polarization
08 p1378 A69-20244
- Polarization and intensity distribution of extended supernova remnant in Centaurus, discussing remnant effect on galactic magnetic field
09 p1598 A69-22184
- Linearly polarized radiation from supernova remnants 3C 10, Taurus A, 3C 358 and Cassiopeia A, determining distributions by synthesizing fan beam
09 p1598 A69-22185
- Green and red coronal line nonpolarization observed during solar eclipses, discussing nonpolarization of red line and observation instrument error
09 p1600 A69-22204
- Photoelectric effects produced by polarized radiation in isotropic optical media, discussing photo EMF and photoconductivity in multivalley semiconductors and plasmas
10 p1701 A69-23138
- Position and polarization of 1720 MHz OH emission from W28, W44 and galactic center, considering unresolved concentrations of shell type nonthermal sources
10 p1776 A69-23220
- Polarization measurements of July 1966 proton flare, considering electron scattering and density
10 p1764 A69-23740
- Polarization observation of star BL Lac continuum by multichannel scanner, noting photoelectric UVB observations and identification with radio source
10 p1785 A69-24090
- Type 3 solar flare circular and linear polarization at 23.5 MHz frequency
11 p1945 A69-24244
- Condensation sources of maser radiation observed in W3 hydroxyl lines, discussing polarization and designation as protostars
11 p1954 A69-24379
- Wavelength dependence of polarization and UVRI photometry of highly polarized stars, correlating IR interstellar extinction with maximum polarization wavelength
12 p2153 A69-25809
- Frequency spectrum, time variations and polarization of source of synchrotron radio emission with expanding components flying apart at relativistic velocities
12 p2155 A69-26207
- Continuous polarized electron beam produced from spin conversion in ionizing reactions involving optically pumped metastable atoms in He discharge
12 p2130 A69-26312
- X ray polarization from Sco X-1, noting spurious instrumental polarization due to cosmic ray anisotropy using X ray polarimeter
12 p2149 A69-26315
- Blue, UV and yellow spectral observations of M 82 /NGC 3034/, obtaining polarization dependence on reciprocal of wavelength, polarization and color characteristics
12 p2169 A69-27057
- Galactic magnetic field along Orion arm from dispersion and rotation measures of linearly polarized radiation from pulsar psr 0833-45
13 p2335 A69-27311

Polarization of continuum background of planetary nebulae in window in visible spectrum from scattering of nucleus star radiation by electron gas
13 p2339 A69-27567

Two channel polarimeter capable of eliminating atmospheric scintillation effects used for observation of magnetic stars and eclipsing binary u Herculis
13 p2347 A69-27713

Gas ring lasers, discussing optimal parameters, colliding waves interference, nonmutual effect and radiation polarization
13 p2272 A69-28175

Vela pulsar PSR 0833-45 optical observations and Crab pulsar NP 0532 linear and circular polarization measurements by telescope- photomultiplier
13 p2354 A69-28470

Outer space electromagnetic radiation transfer in turbulent plasma with allowance for polarization effects, describing polarization induced changes in Stokes parameters
14 p2515 A69-28765

Laser beam discrete deflection method using Wollaston prism and electro-optical switch for changing polarization plane
14 p2459 A69-29391

Nonlinear interactions of linearly polarized carbon dioxide laser signals in sulfur hexafluoride measured as function of angle between polarization planes
14 p2460 A69-29602

Linear polarization of quasars, radio or normal spiral galaxies, galactic objects, etc, observed by Parkes telescope
14 p2526 A69-29770

Activity in Crab Nebula from 200-inch continuum and polarization plates, discussing nature and motion of wisps
15 p2691 A69-30758

Linear polarization in pulsating radio sources observed by galvanometric recordings, using Mark I radio telescope
17 p3036 A69-33635

Radio telescope observations at 11.13 cm for polarized E vector intensities of Saturn and disk temperature of Uranus and Neptune
17 p3039 A69-33731

Polarized emission from Nd activated glass, establishing S and P polarization component energy dependence on pumping energy
17 p2984 A69-33974

Irregularities distribution in antarctic ionosphere from polarization angle fluctuations of satellite S-66 radio signals, discussing diurnal magnetic and solar cycle effects
18 p3125 A69-34249

Extragalactic radiation depolarization through Milky Way transit determined from linear polarization and flux density measurements of discrete radio sources at 21.2 cm
18 p3190 A69-34287

Venus brightness and polarization distributions measurement at centimeter wavelengths using two element interferometer, suggesting Venus atmosphere as main source of radiation
18 p3191 A69-34302

Periodic fading in 42 MHz auroral backscatter by high speed polarization measurements, discussing scatter bursts and pulsating primary electron flux relationship
18 p3102 A69-34950

Solar radio bursts polarization measured with microwave correlation polarimeter, noting output recording rate
18 p3188 A69-35213

Pulsar PSR 0833-45 polarization structure frequency dependence measurement leading to model implying radiation emanated from magnetic poles neighborhood
18 p3202 A69-35215

Solar disk edge polarization rate determined by applying Feautrier method to transfer equations for polarized radiation
19 p3427 A69-36728

Modified geometrical diffraction theory applied to determination of vertically polarized radar backscattering from rear of cylinders and frustums
20 p3495 A69-37851

Linear and circular integrated polarization of extragalactic radio sources measured by two element interferometer at Owens Valley Radio Observatory
20 p3610 A69-38139

Polarization effect on diffusion equations of radiative transfer, noting anisotropy in Rayleigh scattering
21 p3847 A69-38473

Extragalactic radio sources linear polarized radiation distribution at 1418 MHz indicating ordered magnetic fields often oriented differently
22 p4015 A69-40155

Polarization measurement of slowly varying component of sun by pencil-beam antenna at 8.6 mm, analyzing data by magnetoionic theory
22 p4027 A69-40660

Pulsar magnetic models, coherent radio emission mechanisms, radiation polarization, data summary and astrophysical nature
22 p4030 A69-40905

Far IR gas laser with linearly polarized radiation output obtained by using echelette reflection grating in place of end mirror
23 p4172 A69-41400

Radiation scattering by thick planetary atmosphere according to Rayleigh law, considering luminance variation and absorption ray polarization
23 p4213 A69-41698

Plane polarized electromagnetic wave diffraction incident on skewed metal ribbons array
23 p4125 A69-42043

Ground antenna array for ionospheric physics experiments, consisting of wire dipoles connected to receive circular or linear polarization
24 p4286 A69-42607

Anisotropic carrier distribution effect on polarization of spontaneous recombination radiation during GaAs breakdown in electric field
24 p4362 A69-43736

Diagonal tunneling and radiation polarization in doped heterojunctions and p-n junctions of GaAs, using electroluminescence spectrum analysis
24 p4362 A69-43737

Condensation sources of maser radiation observed in W3 hydroxyl lines, discussing polarization and designation as protostars
24 p4389 A69-43769

POLARIZERS
Glan-Thompson and Rochon prisms modified by replacing one of two calcite halves of cemented oriented birefringent crystals with glass
02 p0280 A69-11924

Wideband device for rotating polarization plane of waves in waveguide between antennas, receivers and transmitters without affecting field linearity
09 p1469 A69-22643

Ellipsometric dimensions calculations with aid of laser radiation, stressing formulas for compensator and polarizer assemblies
15 p2636 A69-31474

Lummer-Gehrcke plate type polarizer made of birefringent material for Nd glass laser, discussing reflection coefficients in quartz crystals
21 p3739 A69-39541

POLAROGRAPHS
U POLAROGRAPHY

POLAROGRAPHY
Analytical determination of traces of metals caused by wear in aircraft liquid fuels, hydraulic fluids and lubricants, noting polarography and coulometry
03 p0435 A69-14101

POLARONS
Hall effect in semiconductors with polarons as majority carriers, noting variation with temperature of magnetic field dependence on Lorentz force
03 p0484 A69-13281

Hall effect in semiconductors with polarons as majority carriers, noting variation with temperature of magnetic field dependence on Lorentz force
14 p2508 A69-29654

Polarons large to nearly small transitions, studying ground state mass dependence on bare electron mass, electron-phonon interactions model, superconducting strontium titanate, etc
20 p3583 A69-37280

POLES
Earth polar wanderings attributed to rotation axis angular displacements generated by density redistribution on geologic time scale
20 p3535 A69-38192

North Pole trajectories and geomagnetic fields assuming motion of earth mantle and interior
22 p3942 A69-41120

POLICIES
Federal Government policies analysis, discussing disadvantages of planning-programming-budgeting system /PPBS/
10 p1811 A69-23353

POLISHED METALS
U METAL POLISHING

POLISHING
U ELECTROPOLISHING
U METAL POLISHING

POLITICS
Federal Government systems politics and budgeting, noting dichotomies, time dependence, taxonomy, etc
10 p1811 A69-23352

POLLUTANTS
U CONTAMINANTS

POLLUTION
NT AIR POLLUTION
Space controlled microbiology, discussing telemetry control of waste material conversion in air and water pollution
[UN PAPER 68-95861] 01 p0014 A69-10456

Fiddler crab absorption of DDT residues from organic detritus in estuaries, discussing DDT residue entrance into diverse food chains
14 p2406 A69-28872

POLONIUM ISOTOPES
Polonium 210 production for radiothermal propulsion via bismuth irradiation in graphite gas power reactor
05 p0791 A69-15594

POLYACRYLATES
U ACRYLIC RESINS

POLYAMIDE RESINS
Dynamic tests of mechanical properties of polyamide Tarlon X-A using free and resonant vibrations methods
09 p1528 A69-21496

Heat resistant polyamides and polyimides for electrical insulation, discussing properties and applications under extreme temperatures and basic reactions
13 p2286 A69-27988

Unlubricated wear characteristics of polyimide resin sliding against carbon steel in air, noting effects of surface temperature, bearing pressure and velocity
[ASLE PREPRINT 69AM 5C-2] 15 p2619 A69-30473

Low endurance fatigue in aluminum, Nylon 66 and epoxy resin compared, considering stress-strain relationships, fatigue damage, failure mechanisms and crack propagation
18 p3155 A69-34633

Nylon wear curves and friction coefficients for steel-on-nylon pairs determined as function of normal load
19 p3329 A69-36495

POLYATOMIC GASES
NT DIATOMIC GASES
Chapman-Enskog method applied to Boltzmann equations for transport coefficients for low density polyatomic gases
01 p0123 A69-10388

Thermodynamics of ideal multiatomic gases in local nonequilibrium, approximating real gas system by ergodic subsystems grouped by degrees of freedom
02 p0350 A69-11552

Dissociation and recombination of moderately complex molecules, using master equation with transition probabilities and decay rates obtained from reaction rates statistical theory
02 p0283 A69-12181

IR radiation heat transfer in polyatomic gases in limit of large path lengths
05 p0844 A69-15579

Kinetic equations for polyatomic gases obtained by extending 13 moment approximation to solve inelastic Boltzmann equation, resulting in 17 moment approximation
08 p1357 A69-20784

Plane wave solutions for acoustic propagation in polyatomic gas by using Sirovich-Thurber method for polyatomic kinetic models
11 p1920 A69-24287

Relaxation time influence on discharge coefficient of sonic nozzle of revolution, considering expanding polyatomic gas problem
19 p3241 A69-36721

Relaxing polyatomic gases transport properties from Boltzmann equations obtained without knowing excitation probabilities of internal molecular degrees of freedom
19 p3300 A69-36787

Relaxation time for rotational transitions of linear polyatomic carbon dioxide calculated by using Brout theory for diatomic H rotational relaxation calculations
20 p3581 A69-38121

Kinetic theory for macroscopic transport phenomena in N-component polyatomic gas mixtures with internal degrees of freedom under nonlocal thermodynamic equilibrium
23 p4238 A69-41435

POLYATOMIC MOLECULES
NT DIATOMIC MOLECULES

NT TRIATOMIC MOLECULES

Inverse population of vibrational levels generation in polyatomic molecules

02 p0259 A69-12647

Radiative decay of polyatomic molecules, applying Green function form for transition probability to decay of manifold of closely spaced coupled levels

14 p2488 A69-29924

POLYBENZIMIDAZOLE

High temperature structural adhesives at temperatures of 350 F and higher including epoxies, polyimides, amide-imides and polybenzimidazoles

15 p2642 A69-30329

Polyimides and polybenzimidazoles mechanical strength, heat resistance, electrical properties, radiation resistance and industrial applications

19 p3358 A69-35901

Low density polybenzimidazole composites as ablative heat shields, discussing arc-heated wind tunnel tests of linear and crosslinked structures

23 p3179 A69-41715

POLYCARBONATES

Welding of thermoplastic polycarbonate films, noting dryness requirement for satisfactory weld strength

06 p0930 A69-17094

Photographic observations of fatigue fracture of heat treated polycarbonate

06 p0946 A69-17205

Polycarbonate surface stiffness increase associated with fatigue induced by repetition of loads

06 p0946 A69-17206

Fatigue fracture due to heat generation in polycarbonate subjected to pulsating tensile load, presenting temperature change per unit stress increase

18 p3163 A69-35498

High speed brittle fracture of polycarbonate resin subjected to static bending in liquid nitrogen determined from crack propagation speed of surface coating

19 p3358 A69-35776

Tension tests of polycarbonate plates grooved at various angles, demonstrating necking dependence on mechanical instability

21 p3753 A69-39809

Polycarbonate and polysulfone thermoplastic bonding of Al and Ti in aircraft structures, discussing peel strength and stress crazing tests

24 p4326 A69-43459

POLYCRYSTALS

Hydrostatic pressure effects on mechanical properties of hot pressed, extruded and rolled polycrystalline beryllium sheet

01 p0092 A69-10059

Repeated elastoplastic deformation of polycrystalline body analyzed by dynamic model

01 p0164 A69-10082

Polycrystalline corundum thermal conductivity coefficients determination, describing measuring procedures at low temperatures

01 p0101 A69-10108

Yield condition of polycrystalline hcp metal, considering slip characteristics of hcp crystals

01 p0094 A69-10304

Strain hardening of alpha titanium studied for effects of grain size, strain rate, temperature and purity

01 p0095 A69-10610

Electrical conductivity of sintered polycrystalline cubic and monoclinic europium sesquioxide from DC current-voltage characteristics obtained in air at various pressures

02 p0296 A69-11874

Pressure and temperature dependence of isotropic elastic moduli of polycrystalline alumina, noting Gruisen parameter, equation of state and Debye temperature

02 p0268 A69-12407

Spontaneous emission of gadolinium ferrite polycrystals, discussing temperature dependence

03 p0487 A69-13731

High temperature physical, mechanical and thermal properties of polycrystalline graphites, relating properties to manufacturing techniques and processing [AIAA PAPER 68-297]

04 p0621 A69-15329

Dynamic measurements of modulus of elasticity for polycrystalline nickel-tungsten alloys at elevated temperatures

06 p0943 A69-17232

Polycrystalline Mg-Th-Zr alloy precipitation hardening investigated by tensile and hardness tests and transmission electron microscopy

07 p1167 A69-19265

Polycrystalline beryllium specimens fabricated from powders, discussing initial powder particle size and distribution effects on microyield strength

07 p1168 A69-19598

Ductile to brittle transition shown in tensile stress-strain curves of polycrystalline body centered cubic and hexagonal close packed materials

10 p1795 A69-23063

Thin polycrystalline film structure and formation, using electron beam instrument

11 p1936 A69-24601

Plasma anode technique for work functions measurements of polycrystalline W and Re wires in cesium vapor with cesium oxide additive

14 p2507 A69-29274

Polycrystalline BeO sound velocities determined as function of pressure and temperature using pulse superposition method

16 p2802 A69-32338

Creep tests on polycrystalline Be and Be alloy at various temperatures and stresses

17 p2986 A69-32912

Temperature and pressurization effects on tensile and compressive properties of polycrystalline arc-cast W

18 p3154 A69-34273

Dislocation structure of pure polycrystalline nickel subjected to high temperature creep, using electron microscopy following cold working and room temperature annealing

18 p3157 A69-35254

Polycrystalline diborides fabrication technology, discussing additives, thermal, physical and mechanical properties, specific applications, etc

19 p3355 A69-35526

Radiative heat transfer in polycrystalline corundum, studying photon thermal conductivity influence on lattice thermal resistivity

20 p3565 A69-36975

Model of isotropic polycrystal generalized to composite materials including mechanical mixtures, calculating macroscopic constants in heat conduction, diffusion and elasticity

21 p3752 A69-39193

Electron spin resonance /ESR/ of polycrystalline Mo(V) complexes with dipyrityl and phenanthroline, observing hyperfine interaction due to odd numbered isotopes

22 p3897 A69-40971

Polycrystalline ferroelectrics dielectric dispersion region in decimeter-centimeter wavelength range using waveguide resonance method employing wideband strip line

22 p3997 A69-41167

Distribution function of output energies of polycrystalline metal surface used as plasma probe, considering homogeneous plasma flow and isotropic particle velocity distribution

23 p4196 A69-41696

Polycrystalline ceramics chemical and microstructural control through thermomechanical and thermochemical hot forming techniques, discussing pressure sintering, hot extrusion, strain annealing, etc

24 p4321 A69-43338

Polycrystalline ammonium cyanide IR absorption spectrum as function of temperature, discussing ammonium ion hydrogen bonding to C or N atoms

24 p4280 A69-43809

POLYESTER RESINS

Fatigue properties and failure mechanisms of glass reinforced plastics based on chopped strand mat-polyester resin laminates

02 p0269 A69-11795

Long term weather and radar transmission effects on three ply fabric cloth fire-retardant polyester resin radome panel

08 p1414 A69-20485

Polymer structure effect on chemical resistance of reinforced plastics, sulfuric acid and sodium hydroxide corrosion of polyester resins and model copolymers

08 p1338 A69-20490

Flame resistant chlorine containing polyester resins, discussing preparation, curing characteristics, physical properties and reinforced plastics application

08 p1340 A69-20505

Creep strength of fiberglass reinforced polyester resins measured on structural components in long term tests under torsion

19 p3358 A69-35830

Glass fiber with epoxy resins compared to polyester resins, discussing chemical reactions, bonding and strength relations

19 p3358 A69-35902

POLYESTERS

Permittivity and loss tangent of unsaturated styrolene polyester copolymers at various temperatures and frequencies

[ONERA-TP-662]

04 p0621 A69-15114

Bromine containing unsaturated polyesters for fire retardancy and physical strengths, noting use in reinforced plastics for laminates, molding and corrosion

08 p1340 A69-20504

Polyesters reaction with dimethyl p-phenylene diamine compared under UV exposure from carbon arc and natural sunlight

10 p1716 A69-23978

Polyester/ammonium perchlorate combustion, determining degradation rate by loss in weight method at different intervals

13 p2324 A69-28234

Syntactic foam low density thermoplastic microspheres as hollow spherical filler in polyester matrix, noting applications

14 p2467 A69-29285

Reversion resistant polyether and polyester type urethanes, discussing applications, testing methods and material processing

19 p3357 A69-35566

Linear aliphatic polyesters preparation by acid chloride synthesis, acid exchange and ester exchange, stressing products purification

19 p3265 A69-36372

Gel permeation chromatography of nominally linear aliphatic polyesters, using tetrahydrofuran solvent at 37 degrees C

21 p3670 A69-39806

POLYETHYLENE TEREPHTHALATE

Mechanical anisotropy of polyethylene terephthalate and relation to molecular structure and cold drawing

05 p0785 A69-16489

Film processing effects on cryogenic mechanical properties of polyethylene terephthalate

05 p0785 A69-16490

Mechanical behavior of polyethylene terephthalate at cryogenic temperatures

05 p0785 A69-16494

Ultrahigh molecular weight polyethylene terephthalate synthesis from commercial solid state materials, noting effects of several parameters

05 p0797 A69-16496

POLYETHYLENES

NT POLYETHYLENE TEREPHTHALATE

High speed automatic osmometer applied to measurements of diffusible branched polyethylene samples, discussing apparent molecular weight observations

01 p0024 A69-10933

Inhomogeneous dielectric filling to simulate curvature in model earth-ionosphere waveguide

05 p0732 A69-16346

Polydiethylene glycol-bis-allyl carbonate /PBAC/ Hugoniot equation of state, reporting shock data, discussing applications to propellant testing

16 p2879 A69-32179

Polyethylene stainless steel lap joints and polyethylene samples yield strengths measurements at high temperature, suggesting yield mechanism based on dislocation loops

16 p2794 A69-32573

Fast neutron spectrum for subcritical section of homogeneous U 235-polyethylene thermionic critical assembly measured by pulsed source time-of-flight method

18 p3170 A69-34313

Spherulite boundaries and interspherulite breakdown in polyethylene, considering structure control by varying macromolecular microstructure

22 p3973 A69-40740

High energy oxygen-free hybrid propulsion system using polyethylene propellant and F oxygen mixture as oxidizer [DGLR-69-017]

23 p4202 A69-41930

POLYMERIZATION

Polymerization and strengthening effects simultaneous action at grain boundaries increased thermal stability of thermomechanically treated Ni-Cr alloy

17 p2991 A69-33940

POLYGONS

U PARALLELOGRAMS

U RECTANGLES

U SQUARES [MATHEMATICS]

U TRIANGLES

POLYHEDRONS

NT OCTAHEDRONS

NT PARALLELEPIPEDS

NT TETRAHEDRONS

Nonholonomic congruences of trihedrons in metric theory of straight line complex

03 p0457 A69-13865

POLYIMIDE RESINS

Polyimide glass fabric laminates with nonflammable characteristics for high O concentration spacecraft environments applications

09 p1531 A69-22366

Polyimide resin system for glass reinforced laminates, noting processing characteristics and curing

19 p3353 A69-35505

Mechanical properties and thermal aging of laminated specimens of collimated B monofilament reinforced composites preimpregnated with polyimide resin

19 p3354 A69-35514

High performance void free carbon fiber laminates preparation using polyimide resins, describing flexural strengths, moduli and interlaminar shear strengths

24 p4325 A69-43445

Postcured low void content graphite fiber reinforced polyimide resin composites fabrication including shear, flexural and tensile strength data

24 p4337 A69-43446

POLYIMIDES

Satellite, spacecraft and rocket components coatings and lubricants, noting high radiation resistance of polyimides

06 p0945 A69-17046

High temperature polyimide laminates for radomes and other supersonic aircraft components, discussing index flexural strength, dielectric constant and dissipation factor

07 p1171 A69-19545

Polyimide materials, discussing lamination and applications in electronic circuitry such as interconnection cables and multilayer interconnection boards

09 p1511 A69-22354

Glass reinforced polyimide laminate fabrication, discussing metal foil laminates

09 p1530 A69-22363

High temperature organic sealants for repairing small gas leakages in vacuum devices, tabulating test results for alkyd, epoxy, silicone and polyimide resins

11 p1907 A69-24742

Heat resistant polyamides and polyimides for electrical insulation, discussing properties and applications under extreme temperatures and basic reactions

13 p2286 A69-27988

High temperature structural adhesives at temperatures of 350 F and higher including epoxies, polyimides, amide-imides and polybenzimidazoles

15 p2642 A69-30329

Nuclear environment irradiation effects on materials, emphasizing radiation chemical processes affecting polyimide and copolymer of styrene and alpha-methylstyrene

19 p3356 A69-35530

Flexible-rigid hybrid polyimide-epoxy glass multilayer board to fill gap between all flexible and all rigid circuit boards

19 p3319 A69-35545

560 W deployable solar array consisting of very thin Si solar cells mounted on polyimide film, initiating deployment by duplicated pyrotechnic actuators

19 p3253 A69-35707

Polyimides and polybenzimidazoles mechanical strength, heat resistance, electrical properties, radiation resistance and industrial applications

19 p3358 A69-35901

Vacuum cured glass-reinforced polyimide laminate tests for use at elevated temperatures on F-111 aircraft

24 p4335 A69-42933

Damage repair techniques of polyimide honeycomb sandwich panels constructed with polyimide and Ti face sheets, using precured plugs, prepreg disks, sealants, etc

24 p4323 A69-43420

POLYISOPRENES

Geochemical synthesis of branched chain acyclic polymers from irradiated isoprene

24 p4269 A69-43750

POLYMER CHEMISTRY

Photodegradation of organic polymers by UV radiation exposure, emphasizing polyvinyl chloride photochemistry and radiation stabilization

01 p0102 A69-10861

Dispersion in gel permeation chromatograph, noting contributions of injection and detection systems to peak broadening and retention time

04 p0555 A69-14884

Ultrahigh molecular weight polyethylene terephthalate synthesis from commercial solid state materials, noting effects of several parameters

05 p0797 A69-16496

Polymeric Schiff bases synthesis, thermal stability and nature of pyrolytic decomposition of polyazines and derived polystilbenes

07 p1074 A69-18628

Binding of lysine-rich proteinoids to organismic or thermally synthesized polynucleotides, noting polyanhydramino acid interactions with polynucleotides

07 p1074 A69-18635

Polymer structure effect on chemical resistance of reinforced plastics, sulfuric acid and sodium hydroxide corrosion of polyester resins and model copolymers

08 p1338 A69-20490

Cross-linked polymers obtained by direct reaction of aryl polycarbonyls with aryl polyamines, studying char yields effect

08 p1269 A69-21059

Cross-links effect on char yields of azomethine polymers produced by aryl diamines with aryl diketones

08 p1269 A69-21060

Schiff base cross-links effect on synthesis of polymeric azomethines produced by bis exchange reactions, carbonyl and amine

08 p1269 A69-21061

Explosive acrylic polymers properties and preparation methods, noting chemical reactions and structure

08 p1376 A69-21152

Polyimide materials, discussing lamination and applications in electronic circuitry such as interconnection cables and multilayer interconnection boards

09 p1511 A69-22354

Experimental research concerned with origin of life, studying synthesis of precursor polymers and self assembly into protocells

10 p1641 A69-23035

Poly A-poly U synthesized by Azotobacter Vinelandi RNA polymerase in unprimed reaction containing ATP and UTP, following short lag period

10 p1647 A69-24185

Self assembly relation to origin of life and spontaneous generation applied to precellular polymers, biopolymers and cellular structures

12 p2018 A69-25776

Thermally stable polymers for high stress aerospace applications, noting chemical stability and structure of high polymers

12 p2117 A69-25853

Block tractable azomethine copolymers prepared by reaction of insoluble oligomers with monomers or of two different fusible oligomers, noting high thermal stability

13 p2217 A69-28317

Binder polymer network and microstructure effects on solid rocket propellant properties, emphasizing choice of polymer ingredients

17 p3017 A69-33668

Polyperfluoroalkylencimidoylperfluoroalkylene-amidine synthesized by reaction of perfluoroalkane dinitriles with ammonia or diamidine, giving elastomers of varying strength and elongation, noting thermal stability

19 p3264 A69-35535

High temperature structural adhesives developed from thermoplastic aromatic-heterocyclic polymers

19 p3357 A69-35560

Linear aliphatic polyesters preparation by acid chloride synthesis, acid exchange and ester exchange, stressing products purification

19 p3265 A69-36372

Molecular engineering of high organic polymers, discussing molecular weight, crystallization, elastomers, fiber formers and building construction materials

20 p3566 A69-37598

Model compounds and polymers solubility parameters correlated with refractive index data

21 p3751 A69-38552

Thermally stable polymers chemical and structural properties, discussing polymer use in aerospace technology

21 p3751 A69-38789

Cell origin in self organizing natural polymers in terms of molecular evolutionary priority of polynucleotides and poly alpha amino acids

22 p3896 A69-40781

Monograph on thermally stable polymeric azomethines synthesis by polycondensation reactions

23 p4113 A69-42019

Geochemical synthesis of branched chain acyclic polymers from irradiated isoprene

24 p4269 A69-43750

POLYMER PHYSICS

Stress-strain behavior of crazes in glassy polymers, discussing crack propagation, craze formation and failure and molecular weight effects

01 p1012 A69-10915

High speed automatic osmometer applied to measurements of diffusible branched polyethylene samples, discussing apparent molecular weight observations

01 p0024 A69-10933

Mechanical anisotropy of polyethylene terephthalate and relation to molecular structure and cold drawing

05 p0785 A69-16489

Polymer glasses low temperature transitions, relating structure and transition temperature

05 p0717 A69-16493

Temperature dependence of laser induced damage in plastic Q switch made of polyethylmethacrylate and vanadyl phthalocyanine for ruby laser

06 p0936 A69-17777

Ionic and nonionic mineral oxide powder fillers influence on stereopolymers lattices formed from phenolformaldehyde oligomers, discussing mechanical properties

08 p1335 A69-20331

Electromagnetic fields and magnetic and dielectric constants in fiberglass reinforced polymers determined by treating polymers as ideal dielectrics

08 p1336 A69-20336

Explosive acrylic polymers properties and preparation methods, noting chemical reactions and structure

08 p1376 A69-21152

Transversely isotropic elastic solid approximation for oriented fibers of polyethylene, nylon, polyethylene terephthalate and polypropylene, measuring elastic compliances

09 p1528 A69-21504

Network rupture hypothesis and molecular structure considerations used in obtaining constitutive equations for flow of polymer melts and solutions

10 p1800 A69-23369

Electrical properties of tetracyanoquinodimethane /TCNQ/ complexes representing unit segments of non-conjugated and conjugated polymers

11 p1832 A69-25675

Polymer structure relationship to thermal, mechanical and chemical properties of electrical insulating materials

13 p2285 A69-27986

Polyfluoroethylene resin breakdown under uniaxial tension, considering continuity disruption

13 p2286 A69-28321

Polymer molecular structure influence on physical and mechanical properties, considering regularity, chain flexibility, crosslinking and intermolecular forces

18 p3099 A69-34606

Polymer fibers tensile strength improved using sectional orientation strengthening at controlled temperature and tension conditions

19 p3358 A69-35984

Linear high polymer heat capacities by adding contributions from chain segments, deriving table of heat capacity contributions of polymer constituents

19 p3359 A69-36287

Thermally stable polymers chemical and structural properties, discussing polymer use in aerospace technology

21 p3751 A69-38789

Exposure rate influence on mechanical properties of polymer binder cross-linked by gamma radiation exposure from cobalt isotope source

23 p4179 A69-41711

POLYMERIC FILMS

Sulfide addition agents for diester lubricating grease and organic resin solid film lubricants, noting formulation and tests for steel and molybdenum

01 p0102 A69-10907

Polymeric film properties related to metal substrate interface corrosion, considering effects of stress concentration, surface cleanliness and adsorbed gases

02 p0265 A69-11896

Polymer films tensile properties after exposure to gamma radiation in vacuum, noting chain scission and cross linking

05 p0783 A69-16160

Cryogenic flexibility of thin polymeric film plies for use as spacecraft positive expulsion bladders

05 p0769 A69-16486

Film processing effects on cryogenic mechanical properties of polyethylene terephthalate

05 p0785 A69-16490

Welding of thermoplastic polycarbonate films, noting dryness requirement for satisfactory weld strength

06 p0930 A69-17094

Polyvinyl chloride coating for reducing aerodynamic skin friction drag, noting water saturation effect on polyurethane foam
[AIAA PAPER 69-165] 06 p0912 A69-18043

Polymers and organic optical cements transparent in 1 to 13 micron IR region, noting organosilicon resin
08 p1336 A69-20387

Plastic backing films removal from carbon electron microscope replicas by maintaining specimens in horizontal position
09 p1495 A69-21651

Methyl 2-cyanoacrylate adhesive bonding characteristics, noting importance of film thickness
09 p1529 A69-22316

Monograph on molecular structure and polymer properties, covering coherent adhesive layer of polymeric material for paint film in protective coatings
10 p1717 A69-24187

Polymeric insulation materials, discussing intrinsic properties dependence on temperature and atmosphere, stressing effect on aging
13 p2285 A69-27985

Corrosion at polymeric film-metal substrate interfaces, noting roles of film properties, bond strengths and primer coats
14 p2466 A69-29938

Dry lubricant films of soft metals, self lubricating plastics and crystalline powders, noting design and tests
15 p2642 A69-30328

Thin foil penetration measurements for Fe microparticle impacts on metal and Mylar foils in space
15 p2641 A69-31339

560 W deployable solar array consisting of very thin Si solar cells mounted on polyimide film, initiating deployment by duplicated pyrotechnic actuators
19 p3253 A69-35707

Polymer films damage due to supersonic plasma jets, comparing fracture relief of oriented and unoriented polymers
21 p3752 A69-39081

Stress analysis during solidification of binders in glass fiber reinforced plastic materials, using resin coated glass film simulation
22 p3973 A69-40746

Polymer film breakdown under impact of supersonic plasma beam pulses from capillary discharge chamber, including photomicrographs of cavities and structural defects
22 p3974 A69-41031

POLYMERIZATION

Radiation processed wood-plastic materials produced by impregnating natural wood with liquid monomer followed by ionizing radiation induced polymerization
04 p0605 A69-14582

Monograph on crystallization during polymerization, discussing categories, monomers capable of step reaction, chain reaction, nucleation crystal growth and perfection
05 p0783 A69-15967

Polymerization of monomers considered for direct synthesis of iminobenzylidene
10 p1651 A69-23308

Residual stresses and strains in wound reinforced plastic fiber cylinders subjected to polymerization by heat treating
11 p1907 A69-25679

Hologram recording on photosensitive material based on photoinduced polymerization showing good resolution and diffraction efficiencies
13 p2258 A69-27199

Silicone polymers and polymer formations for electrical applications including silicones for molded devices and components, potting resins, dielectric gel, RTV rubbers, etc
13 p2286 A69-27990

Time of heating effect on thermal polymerization of L-lysine free base
13 p2218 A69-28439

Molecular engineering of high organic polymers, discussing molecular weight, crystallization, elastomers, fiber formers and building construction materials
20 p3566 A69-37598

Sequence preparation of protected peptide polymer bond with amino exchange resin using solid phase transesterification
24 p4279 A69-42713

POLYMERS

Twisted yarns composed of continuous viscoelastic filaments dynamic response under periodic strain effect on dynamic modulus
04 p0619 A69-14686

Cryogenic properties of polymers - NASA/Case Conference, Cleveland, April 1967
05 p0784 A69-16485

Thermal expansion of polymers at cryogenic temperatures
07 p1172 A69-19730

Solid state laser radiation damage in polymers during tensile and compression loads using microstructural analysis
08 p1328 A69-21190

Shell theories for polymer and reinforced plastic shells, giving revised temperature and creep problem solutions due to mechanical behavior
09 p1611 A69-21481

Mass spectrometric determination of pyrolysis products generated from heated polymer samples
09 p1448 A69-22314

Book on strength and failure of viscoelastic materials covering linear and three dimensional polymers or polymer-based materials, flexibility and temperature effects
11 p1970 A69-24610

Origin of life in terms of polymers synthesis under thermodynamic and geological conditions
12 p2017 A69-25764

Origin of life data, discussing self ordered polymers, propagative cell-like systems, protozooids, cellular evolution, etc
12 p2018 A69-25781

Fiber polymer composite flexible insulating materials properties and applications stressing synthetic organic fibers
13 p2286 A69-27989

Outgassing behavior of polymers in spacecraft by thermal-vacuum weight-loss and contamination tests
13 p2286 A69-28089

Heterocyclic-aromatic organic polymer adhesives used for high temperature structural purposes, discussing processing, testing, formulating and impact on basic research
14 p2469 A69-29346

Polymers stress-strain behavior and corresponding birefringence within limited temperature range and strain rates
15 p2642 A69-30678

Nonlinear theoretical derivation of creep equations for three dimensional processes in polymers, based on Boltzmann-Volterra creep heredity concept using stress-strain summation
16 p2803 A69-32290

Luminescence spectra of aromatic polymers, monomers and dimers under high energy electron excitation using molecular resonance model
16 p2828 A69-32792

Machine for testing vibration stability of polymer samples subject to tension or compression, noting stability of plastic during vibration lower than during static loading
17 p2972 A69-33043

Turbulence measurements and roughness effects on viscous drag reduction with polymer solution in pipe flow, discussing friction factor, wall velocity profile, etc
17 p2951 A69-33252

Constitutive equation variation effect on near wall flow pattern of dilute polymer solutions
17 p2951 A69-33257

Polymer selection and plastics contribution to technologies, noting trend toward improved performance at elevated temperatures
18 p3161 A69-34610

Composite polymers thermophysical properties at thermal destruction temperatures, noting increased heating rate effect on kinetic curves
18 p3161 A69-34696

Solid state laser radiation damage in polymers during tensile and compression loads using microstructural analysis
18 p3152 A69-35159

Polymers in high performance applications - Conference, London, June 1969
18 p3150 A69-35420

Unfilled Pyrrone prepared from powder into molded parts for flexural tests at elevated temperatures observed for stability to electron irradiation in air
19 p3356 A69-35529

Integral fuel tank sealant based on various hydrofluorocarbon polymers prepared, tested and compared for physical properties
19 p3356 A69-35533

Nonlinear viscoelastic material properties evaluation from experimental data with illustration for polymers, deriving equations from thermodynamic principles
20 p3626 A69-37719

Automated rebound resilience apparatus for polymer dynamic mechanical properties studies over wide temperature range, using photoelectric device
21 p3689 A69-38593

Metal-polymer-metal and metal-polymer-silicon thin film structures analysis for polymers bulk properties and insulator-silicon interface, noting dipole-like relaxation
21 p3782 A69-39464

Flexible channel multiplier made of electron conductive polymer, noting secondary yield and feedback effect
22 p3917 A69-41234

Wear resistance and antifriction measurement device for polymer coatings in high vacuum, various gases and during exposure to electron radiation
23 p4169 A69-41599

Dynamic equilibrium of making and breaking adhesion bonds between polymer segments and dissimilar surfaces through water, allowing thermal stresses relaxation
24 p4326 A69-43458

POLYMETHYL METHACRYLATE

Polymethyl methacrylate irradiated by laser in vacuum to study mechanism responsible for gas formation
02 p0270 A69-11980

Transparency decrease in plexiglass during interaction with dense plasma, noting absorption independence of plasma pressure and dependence on wavelength
03 p0482 A69-14222

Fracture propagation in organic glasses, considering density of hyperbolic markings in polymethyl methacrylate and Dugdale model
05 p0784 A69-16429

Temperature dependence of polymethylmethacrylate deformation, yield and fracture in constant strain rate compressive and tensile tests
08 p1335 A69-20215

Liquid surface active media /kerosene, water, castor oil/ effect on strength of V notched polymethyl methacrylate specimens
09 p1528 A69-21852

Polymethyl methacrylate rupture time under stress determined from short and long time strength tests, noting relation to crack propagation time
09 p1528 A69-21853

Crack propagation properties of polymethyl methacrylate during bending and tension, noting temperature and loading time effect on crack size
09 p1529 A69-21854

Temperature effects on phosphorescence lifetimes and intensities of aromatic hydrocarbons in polymethyl methacrylate, estimating activation energy for thermally activated nonradiative decay mode
10 p1652 A69-23523

Biaxial stress effect on creep properties of thin walled tubes of polymethyl methacrylate at controlled temperature and humidity
10 p1717 A69-24216

Thermal expansion coefficients of Nb-Zr-Ti alloy and plexiglass at 10-300 K from dilatometric measurements
11 p1905 A69-24917

Polymethyl methacrylate burning rates in mixture with ammonium perchlorate or in hybrid systems when mixed with ammonium chloride
13 p3234 A69-28503

Simulated gravitational lens made of Plexiglass for demonstrating stellar gravitational lens phenomena, presenting partial cross section
15 p2653 A69-31163

Acoustic velocities in polymethylmethacrylate measured as functions of frequency, temperature and pressure, comparing data obtained with equation of state high pressure determinations
16 p2825 A69-31695

Linear pyrolysis of polymethyl methacrylate to verify Cantrell model and surface temperature determination method
17 p3017 A69-33132

Total gasification heat measurement during pyrolysis of polymethyl methacrylate and paraformaldehyde, discussing method and calorimetric equipment
17 p3069 A69-33133

Fracture kinetics of biaxial oriented polymethyl methacrylate, discussing crack development and propagation as compared to unoriented polymer
18 p3162 A69-35354

Mach reflection limiting parameters of conical shock wave in Plexiglas cylinders, showing head wave curvature radius linear relationship to cylinder diameter
19 p3302 A69-36845

Transparency and luminescence yield of plastic scintillators prepared from polymethyl methacrylate, comparing naphthalene and benzene compound additions with polystyrene 21 p3724 A69-39073

POLYMORPHISM

Polymorphic characteristics of titanium pentoxide prepared by reducing titania, examining oxidation products with X ray diffraction 07 p1168 A69-19601

Atomic size and outer electron effect on Fe, Co and Mn polymorphism, noting change in crystal lattices 15 p2638 A69-30321

Pressure and temperature effects on reversal transitions of stishovite, noting meteoritic impact formation at Meteor Crater, Arizona 22 p4021 A69-40412

POLYNOMIALS

NT DYADICS

NT HERMITIAN POLYNOMIAL

Ultraspherical potential approximation in nonlinear symmetric free oscillations applied to systems with hardening and softening cubic nonlinearities 01 p0107 A69-11418

Eigenvalue problem solutions for ordinary differential equations, discussing coefficient replacement, Ritz polynomial substitution and error limits 02 p0271 A69-12057

Mathematical analysis to determine complete characteristic of functions tolerating polynomial approximation in mean in crescent type noncaratheodory domains 02 p0272 A69-12164

Primitive trinomials of high degree for use in pseudorandom sequence generation of zeros and ones 03 p0455 A69-13373

Stability test functions for characteristic polynomials with real coefficients and even powers 05 p0833 A69-15710

Book on computer evaluation of mathematical functions, discussing errors, square and cube root, Chebyshev polynomials, approximation, rational function, asymptotic expansions, etc 05 p0723 A69-15955

Linear differential equations with sinusoidal coefficients analyzed with aid of trinomial recursions 05 p0787 A69-16464

Existence of minimal solutions of doubly infinite trinomial linear recursions of Poincare-Perron type 05 p0787 A69-16465

Polynomial representations of mirror cusp fields produced by combination of mirror coils and Ioffe /multipole/ bars 06 p0966 A69-17522

Current-voltage characteristic of tunnel diodes, with curve approximation by even degree polynomials of voltage, discussing quasi-linear analysis 06 p0898 A69-17802

Algorithms for polynomial resultants computation, considering extraneous factors, truncation errors, memory and computing speed 06 p0892 A69-17884

Quadratic form representation of multivariable polynomials expressing sufficient condition for positive definiteness of real multivariable polynomial 07 p1173 A69-18641

Iterative method for least square polynomial curve fitting with abscissas and ordinates subject to error 08 p1343 A69-20827

Least squares local smoothing by polynomials of noisy data in n dimensions 08 p1344 A69-20830

Optimal control approximate synthesis partial differential equation solution in form of interpolation polynomial for functions of many variables 08 p1299 A69-21068

Optimum number of terms in approximation of realizations of random process by polynomials 09 p1475 A69-22667

Filter network synthesis for realization of rational functions, discussing numerator polynomial inclusion by choice of divisor polynomial and branch introduction and parallel systems 10 p1667 A69-24038

Extremal controlled plants identification by Chebyshev orthogonal polynomials, comparing results with regression analysis 11 p1861 A69-25713

Modified scheme for simulation of delay with transient period independent of amount of delay, considering polynomial input 12 p2120 A69-25922

Polynomial coefficients multiplication by weighted damping factors for increased conformal mapping and boundary value problems solutions accuracy for doubly connected regions 12 p2178 A69-25998

Higher root loci of polynomials for multivariable systems with coefficients polynomials of real parameter 12 p2048 A69-26073

Polynomial and nonlinear equations of state for solids and liquids analyzed using uncommon statistical and least squares methods 14 p2486 A69-29470

Semidefinite Peano kernels of stable forms 15 p2644 A69-30450

Continued fraction inversion to rational fraction of two polynomials based on state space formulation and Routh algorithm 16 p2805 A69-32470

Optimal control approximate synthesis partial differential equation solution in form of interpolation polynomial for functions of many variables 16 p2765 A69-32483

Orthogonal polynomials for solving plane elasticity theory boundary value problems without constructing mapping functions, noting applications 17 p3067 A69-34144

Integration formulas involving integrand derivatives simplified by decreasing integrating power in terms of polynomials 18 p3164 A69-34615

Polynomial bases for orthogonal group irreducible representations, rederiving Wigner coefficients 18 p3164 A69-34807

Polynomial approximations in perturbational navigation and guidance schemes including Chebyshev and least square approximations 19 p3368 A69-35664

Dirichlet polynomials double sequences and double series with positive exponents, defining conditions for convergence in bicylinder 19 p3361 A69-36639

Trigonometric polynomials representing perturbation function and derivatives in three body problem 20 p3596 A69-37315

Algorithms testing characteristic polynomials and differential equation classical stability relations 21 p3755 A69-38925

Orthogonal polynomials in three dimensional contact problems without friction, discussing construction of kernels over finite and semiinfinite intervals 22 p4041 A69-40113

Geomagnetic zenith calculation at given point based on geomagnetic field model, using polynomial development 24 p4311 A69-43505

POLYPHENYL ETHER

Steel ball bearing high temperature fatigue life tested with synthetic paraffinic oil, fluorocarbon and polyphenyl ether [ASME PAPER 69-LUBS-18] 18 p3140 A69-34378

Polyphenyl ether lubricants and self lubricating materials compared for antifriction ball bearings in thrust reversing actuator gear box [SAWE PAPER 68-LC-1] 18 p3148 A69-35003

POLYPROPYLENE

Silane coupling effect on composite properties of glass fiber filled injection molded polypropylene, noting interface phenomenon 08 p1337 A69-20482

POLYSACCHARIDES

U CELLULOSE

U STARCHES

POLYSTYRENE

Monograph on heat transfer coefficients of polystyrene foams noting contribution of gas conduction, convection and radiation to total heat transfer 08 p1421 A69-20716

Polystyrene melt tensile viscosity prediction from shearing viscosities, using rheological network rupture theory 21 p3753 A69-39730

POLYTETRAFLUOROETHYLENE

Sliding surface tracks from hardened steel sliders on flat PTFE examined for molecular orientation with electron microscope 01 p0085 A69-10369

Molecular motion in polytetrafluoroethylene crystals at cryogenic temperatures, noting crystal defect permitting angular displacements of chain segments 05 p0797 A69-16495

Machine for measuring creep deformation of polytetrafluoroethylene under uniaxial compressive loads, discussing stress-strain relationship 14 p2469 A69-29412

Glass fiber filled polytetrafluoroethylene materials for piston seals in high pressure oil-free reciprocating air compressors, discussing manufacturing and non-destructive tests 19 p3323 A69-35579

Polytetrafluoroethylene ablation in high temperature argon, nitrogen, air and oxygen jets, discussing electric heater and heat flux measurement 20 p3632 A69-37522

Beryllium fluoride heat of formation from heat of combustion of Be-polytetrafluoroethylene mixture in fluorine 21 p3853 A69-39703

POLYTROPES

Spherical shock wave propagation in polytrope with poloidal magnetic field, noting application to shock waves in magnetic stars 04 p0664 A69-15438

Three dimensional gas flows near characteristic surface extended over homogeneous polytropic gas at rest 11 p1876 A69-25729

Water bag spherically symmetrical universe model, discussing system stability, distribution function representation and polytrope equivalency 16 p2866 A69-32813

Slow rotation of relativistic polytropes with linear corrections, showing inertia moment distribution and metric component 19 p3426 A69-36576

Equilibrium and stability of axisymmetric gaseous polytropes in toroidal magnetic fields, calculating harmonic oscillations by virial tensor method 21 p3797 A69-38534

POLYTROPIC PROCESSES

Generalization of characteristic relations for steady supersonic 3D motion of polytropic gas, obtaining complex screw motions 03 p0412 A69-12847

Two dimensional unsteady flow of inviscid polytropic gas using analysis of similarity solutions in homentropic flow 04 p0590 A69-15191

Solar supergranules and hydrogen convection zone analysis based on polytropic atmosphere convection physics 07 p1211 A69-18408

Solitary waves in stratified polytropic atmosphere allowing for convection and disregarding viscosity and turbulence 18 p3167 A69-35338

Polytropic gas unsteady motion in dihedral piston wake by solving mixed boundary value and Goursat problems 22 p3861 A69-41025

POLYURETHANE FOAM

Creep behavior of nonlinear rigid polyurethane foam under combined stress and applicability of multiple integral and modified superposition principle 04 p0680 A69-15155

Frictional losses in straight tubing and effect of system on ball type valve, using polyurethane foam damped flexible silastic tube 04 p0608 A69-15331

Low density polyurethane foam with and without honeycomb as ablative material for reentry vehicles, discussing oxidation resistance 04 p0688 A69-15513

Heat treatments in inert gas atmosphere improve elastic foam polyurethane by reducing capability of toxic outgassing 10 p1716 A69-23503

Airflow through open foam cellular structure, discussing mathematic model for predicting pressure buildup and foam response in shock and vibration isolation [ASME PAPER 69-VIBR-46] 10 p1803 A69-24144

Polyurethane foam high velocity deformation properties, discussing results of dynamic uniaxial stress tension and compression tests 11 p1907 A69-25648

Polyurethane with additives for fuel fire control in aircraft structures, achieving desired protection without impairing foams mechanical properties 15 p2561 A69-30311

Cellular carbon castings fabrication by carbonization of polyurethane polyfurfuryl alcohol foam for high temperature applications, noting properties 17 p2992 A69-33373

Bird impact resistance of polyurethane foam filled tailplane
17 p2901 A69-33648

Rigid PVC, urethanes and thermosets processing for high performance, noting injection molding and machine developments role
18 p3148 A69-34611

Friction coefficient and elastic deformation magnitudes relation in polyurethane during sliding friction in various liquids /lubricants/
18 p3149 A69-35362

Ablative materials thermal protection characteristics at low heating rates evaluated by convective heating tests, stressing polyurethane foam composite
19 p3357 A69-35536

Sprayable polyurethane foam lightweight insulation for Saturn s-2 booster tanks holding liquid H an liquid O at wide temperature ranges
21 p3732 A69-38967

Polyurethane foam composites for low heating rate thermal protection, noting astroquartz fiber additive effect on performance
21 p3753 A69-39236

Open cell ester-base polyurethane foam effect on fuel-utilizing microorganisms growth in jet fuel- water systems
24 p4271 A69-42700

Sprayable polyurethane foam external insulation for liquid hydrogen and oxygen storage aboard Saturn S-2 booster
24 p4337 A69-43453

POLYURETHANE RESINS

Ammonium perchlorate base propellant and polyurethane binder heat stability, dangers of aging under abnormal conditions and reaction products for components and tolylene diisocyanate
02 p0303 A69-11529

Fluorinated polyurethanes synthesis for liquid oxygen environments and cryogenic structural utility, noting structural effects on LOX compatibility
05 p0717 A69-16498

Shock attenuation and equation of state of polyurethane based on aquarium technique and free surface velocity measurement
16 p2828 A69-31810

Polyurethane corrosion resistance in various liquids determined from changes in sample hardness, weight, volume and deformation
18 p3162 A69-35360

Reversion resistant polyether and polyester type urethanes, discussing applications, testing methods and material processing
19 p3357 A69-35566

Device determining dynamic mechanical properties of tissues and various transducers, evaluating elastic properties of polyurethane, Hevea rubber and descending thoracic aorta
22 p3890 A69-40204

Polymeric polyurethane protective coatings for radar radome covers with improvement in service life, discussing performance, properties and production method
24 p4338 A69-43456

POLYVINYL CHLORIDE

Photodegradation of organic polymers by UV radiation exposure, emphasizing polyvinyl chloride photochemistry and radiation stabilization
01 p0102 A69-10861

Polyvinyl chloride coating for reducing aerodynamic skin friction drag, noting water saturation effect on polyurethane foam
[AIAA PAPER 69-165] 06 p0912 A69-18043

Rigid PVC, urethanes and thermosets processing for high performance, noting injection molding and machine developments role
18 p3148 A69-34611

PONDEROMOTIVE FORCES

Min B magnetic trap, discussing induction coils, ponderomotive forces and mechanical stresses sustained by coils
04 p0634 A69-14299

Ponderomotive forces and irregularities in earth rotation, considering core and lower mantle as closed system with respect to periodic electromagnetic and mechanical effects
09 p1487 A69-21636

Nonlinear confining and deconfining forces of laser light interaction with inhomogeneous plasma, analyzing macroscopic motion based on ponderomotive force description
11 p1923 A69-24297

Ponderomotive forces and sudden irregularities in earth rotation, discussing core-mantle electromagnetic coupling and toroidal field induction effects
19 p3302 A69-35769

Laser beam self focusing in plasma in terms of ponderomotive acceleration due to light intensity gradient
22 p3961 A69-40417

PONTRYAGIN PRINCIPLE

Dynamic programming to demonstrate sufficient conditions of optimality in maximum principle when regular control synthesis is realized
02 p0225 A69-11975

Minimum fuel attitude control of spacecraft by Pontryagin principle and extended steepest descent method
03 p0522 A69-14100

Pontryagin maximum principle used to solve optimal control problems on analog computer
05 p0739 A69-16473

Sensitivity coefficients to solve two point boundary value problem arising from Pontryagin principle, with application to time optimal control studies
08 p1296 A69-20297

Optimal rendezvous for two propelled spacecraft obtained by Pontryagin principle assuming small distance between vehicles compared to distances from center of gravity
10 p1791 A69-22923

Dynamic programming to demonstrate sufficient conditions of optimality in maximum principle when regular control synthesis is realized
10 p1666 A69-23884

Pontryagin principle application to incorporation of singular sections into optimal trajectories of controlled systems, considering conjugation of singular and nonsingular extremals
11 p1960 A69-24764

Nonlinear bang-bang optimal control problems solution based on differential dynamic programming, noting use of Pontryagin adjoint variables
11 p1860 A69-25444

Cantilever beam profile optimization methods using iterative analog computation to achieve minimum deflection, showing application of Pontryagin maximum principle
15 p2709 A69-30671

Pontryagin maximum principle applied to time optimal control of autonomous second order system with constant coefficients and differentiation in transfer function numerator
15 p2583 A69-31059

Adaptive random search algorithm utilizing boundary cost-function hypersurfaces measurement to implement Pontryagin maximum principle, discussing hybrid computer use, iterative solution and convergence properties
17 p2933 A69-33745

Optimal control theory applications for controllers not characterized by bang bang time responses using Pontryagin maximum principle
18 p3090 A69-34681

Optimal nutation damping of spin stabilized bodies, using Pontryagin maximum principle to optimize time, consumption and linear time-consumption combination
18 p3208 A69-34774

Law for time variations of modulus-restricted control action at trajectory end, two point boundary value problem solution and use of Pontryagin principle
18 p3175 A69-35324

Optimal fuel transfers between coplanar and non-coplanar coaxial elliptical orbits determined by Pontryagin maximum principle, using digital program for Hamiltonian equations solutions
19 p3399 A69-35670

Minimum impulse transfer between circular and nearby noncoplanar elliptic orbit, applying Pontryagin principle
19 p3400 A69-35675

Soviet monograph on mathematical methods of optimal control, discussing models and synthesis of optimal quick response systems by Pontryagin principle
21 p3757 A69-39524

Optimal pursuit control at constant moving velocity and limited angular velocities, using Pontryagin principle
21 p3825 A69-39629

POPULATION INVERSION

Relaxation processes and radiation stimulation in dense low temperature ionized plasma can lead to population inversion of several levels
01 p0131 A69-10789

Inverse population of vibrational levels generation in polyatomic molecules
02 p0259 A69-12647

Q switched Ruby laser metastable state population kinetics and resonator losses, discussing internal energy redistribution with subsequent absorption spectrum changes
04 p0610 A69-14381

Time dependence of laser output in C and N atoms following dissociative excitation transfer explained in terms of measured populations of excited states
05 p0795 A69-15663

Gas lasers involving gas-discharge collisions, selective pumping or chemical reactions to produce necessary inversion, giving theoretical analysis of excitation mechanisms
05 p0772 A69-16226

Critical population inversion for xanthene dye solution laser, analyzing optical loss due to triplet state concentration
[IEEE PAPER A-2] 05 p0773 A69-16307

Finite cross relaxation rate effect on spectral distribution in CW laser oscillator output with inhomogeneous broadening, noting population inversion distribution
[IEEE PAPER T-2] 05 p0776 A69-16327

Active element inverse population distribution effects on laser radiation angular divergence during lower and higher oscillation modes
06 p0932 A69-16913

Cross relaxation and spin-lattice relaxation probabilities determination in ruby crystal based on inversion coefficients
06 p0980 A69-17458

Radio recombination lines in populations of highly excited states of hydrogen, discussing collisional transition effects
06 p1010 A69-17970

Gas lasers principles of operation, discussing population mechanism, lifetime conditions, excitation processes, electron velocity distribution and types of discharges
06 p0937 A69-18008

Theoretical population inversion in decaying nitrogen plasma column free from external fields and confined motionless in circular cylinder
[AIAA PAPER 69-48] 06 p0971 A69-18145

Atomic, ionic and molecular gas lasers applications, population reversal conditions and processing technology
07 p1143 A69-18250

Tandem amplifier system of glass and selenium- oxychloride liquid lasers, discussing input power/output pulse relation and population inversion density measurement
07 p1147 A69-18487

Relaxation equations for oscillatory degrees of freedom of molecular supersonic binary gas flow in Laval nozzle, obtaining population inversion
07 p1118 A69-18540

Helium-neon laser output power dependence on spark-gap cross section geometry, analyzing diffusion equation and population inversion
07 p1147 A69-18541

Radiative lifetime for nitrous oxide 001-100 transition, laser level absolute population densities and saturation parameter measured in nitrous oxide-nitrogen-He laser
[IEEE PAPER G-10] 07 p1151 A69-19057

Population inversion of vibrational levels due to molecular collisions in carbon dioxide lasers, calculating transition probabilities, laser parameters and gain profile
[IEEE PAPER G-15] 07 p1151 A69-19061

Population inversion mechanism based on electron collisional excitation cross sections for molecular vibrational levels in carbon dioxide lasers
07 p1157 A69-19655

Degree of population inversion and inverse temperature measurement in medium
07 p1137 A69-19761

Molecular beam gas laser operating at transitions between ground state and resonance excited state of inert gas atom, obtaining population inversion
08 p1325 A69-20325

Population inversion in semiconductors obtained by applying electric field through dielectric sphere /field effect/
08 p1374 A69-21082

Heat transfer effect on population inversion time variation in pulsed carbon dioxide laser and molecules excitation rates dependence on gas mixture composition
09 p1519 A69-22289

Population inversion distribution and wave processes in optical amplifier, showing beam transformation of constant section and dependence on crystal characteristics
11 p1893 A69-24447

Population inversion in ground state sublevels of ruby laser, deriving required conditions
11 p1900 A69-25572

Temperatures and densities of atoms and electrons from spectroscopic methods in gas discharge plasma used for CW ion-argon lasers, evaluating inversion mechanism

12 p2106 A69-26319

Water vapor laser, discussing water vapor molecular structure, population inversion mechanism, perturbation model, etc

12 p2106 A69-26325

Standard phenomenological laser rate equations for population inversion and light intensity generalized by considering intensity dependent losses and Einstein coefficients

12 p2110 A69-27014

Q switched ruby laser metastable state population kinetics and resonator losses, discussing internal energy redistribution with subsequent absorption spectrum changes

14 p2456 A69-28754

Carbon dioxide laser inversion kinetics, combining pulse pumping with Q switching to observe rise, life and decay times

14 p2457 A69-28926

Lasing kinetics, emission spectrum and directivity of ruby laser with spatially homogeneous population inversion

15 p2634 A69-30729

Maser emission in interstellar OH ground state produced by IR pumping, noting population inversion mechanism

15 p2691 A69-30762

Power coupling among modes in semiconductor lasers in presence of spontaneous or forced microwave modulation of population inversion

15 p2634 A69-30875

Maser amplification of 9.5 GHz longitudinal elastic waves in divalent nickel impurity ions doped sapphire by stimulated emission from inverted spin population

16 p2795 A69-31554

Inversion coefficient for two orientations of ruby crystal with respect to external magnetic field perpendicular and push-pull orientations

16 p2795 A69-31570

Molecular beam gas laser operating at transitions between ground state and resonance excited state of inert gas atom, obtaining population inversion

17 p2981 A69-33315

Laser eigenmodes determined iteratively from eigenvalue equation including spatial inversion inhomogeneities, atomic density and local loss

17 p2984 A69-34046

Laser action in quantum system, analyzing absorption constant relation to spontaneous/ stimulated emission constants, energy level population inversion, pumping, etc

17 p2984 A69-34150

Population inversion in carbon dioxide laser related to pumping frequency, discussing molecular dissociation effect in gas mixture

18 p3151 A69-34620

Continuous explosion laser study of stationary detonation waves to determine conditions leading to partial population inversion and critical population density

19 p3336 A69-36360

Electroreflection study of inversion asymmetry and warping induced interband magneto-optical transitions in InSb, employing low temperature electric field modulation technique

19 p3386 A69-36521

Differential equations for field amplitude and level populations applicable to solid state lasers output power pulsations

20 p3554 A69-37726

Cross relaxation and spin-lattice relaxation probabilities determination in ruby crystal based on inversion coefficients

20 p3584 A69-37941

Relaxation processes and radiation stimulation in dense low temperature ionized plasma leading to population inversion of several levels

20 p3582 A69-38006

Optical pumping and selective population applications, considering double magneto-optic resonance and inelastic interatomic collisions

21 p3735 A69-38454

Ammonia inversion radiation in Sgr B2 region, observing distribution of density, velocity and rotational excitation

21 p3799 A69-38647

Relaxation equations for oscillatory degrees of freedom of molecular supersonic binary gas flow in Laval nozzle, obtaining population inversion

21 p3693 A69-38692

Helium-neon laser output power dependence on spark-gap cross section geometry, analyzing diffusion equation and population inversion

21 p3735 A69-38693

Protostar chemical processes responsibility for population inversion and properties in OH and water masers

22 p4018 A69-40267

POPULATIONS

Statistical equilibrium equations solution for thermodynamic equilibrium variations of populations of very high energy levels in hydrogen and complex atoms

01 p0150 A69-10395

Electron temperature relation to population ratio in Gunn effect

05 p0810 A69-16576

Temperature profile and power density distribution in metastable level of ruby laser rod during pumping in air

07 p1150 A69-18937

Wing of solar line H-alpha for levels population of hydrogen atom in solar photosphere, discussing excitation temperature, absorption coefficient and thermodynamic equilibrium

08 p1390 A69-20394

Time dependent statistical equilibrium equations solutions for describing time development of atomic populations by means of ergodic Markov chain

09 p1542 A69-22218

Energy level population of carbon dioxide molecules, noting intensity of spontaneous emission

13 p2274 A69-28580

Population feedback control in planarians by fission suppression by brain near other planarians

14 p2406 A69-28871

Population and excitation rates of working levels of carbon dioxide laser calculated on basis of emission power, amplification coefficient and spontaneous emission intensity

22 p3964 A69-40795

PORCELAIN

Corrosion prevention in beryllium, testing conversion coatings and low fired porcelain enamels under various humidity and temperature conditions

14 p2466 A69-29939

PORES

U POROSITY

POROSITY

Sheet steel composition effect on gas-tungsten arc welds porosity

04 p0607 A69-15219

Compressional and shear wave velocities vs porosity for sintered perlitic bricks

06 p1000 A69-17009

Titanium surface impurities effect on porosity in welds, proposing machining immediately before welding as solution

06 p0945 A69-17894

Titanium alloy interaction porosity with fillers during diffusion brazing, discussing joint strength as function of time, temperature and pressure

06 p0945 A69-17896

Surface treatment effect on weld porosity causes and removal in VT5-1 Ti alloy argon arc welding

06 p0945 A69-17897

Welding defects, processes, inspection and personnel training problems

10 p1700 A69-23372

Porosity sources in Ti alloy welds, discussing increased gas content and silica, edge surface finish and gas hose contaminants

11 p1892 A69-25668

Gas bubble formation in Ti welding associated with gas nuclei in metal, molten dwell time, gas diffusion coefficients, joint edge conditions, etc

11 p1892 A69-25669

Characteristic temperature, Young modulus and rms atomic displacement in metal borides of various porosities, using dynamic method based on ultrasonic oscillations measurement

12 p2115 A69-26615

Metallo-ceramic materials strength as function of porosity calculated for tension, shear, bending and torsion deformations

15 p2638 A69-30283

Magnetic anisotropy and porosity from approach to saturation of polycrystalline ferrites based on magnetization measurement

16 p2825 A69-31700

Weld porosity in Al alloys as function of composition variations, discussing water vapor contamination of welding arc

22 p3956 A69-40461

Porosity and composition effects on thermal conductivity of glass fiber reinforced plastics, noting tests of multilayer textolite sheets

22 p3973 A69-40747

Pumping pore size and permeability of wicks as part of heat pipes design

23 p4074 A69-42298

H concentration and pore formation in Ti fusion welds

24 p4319 A69-42885

Porosity and inclusions effects on Al arc weld fatigue properties at ambient and cryogenic temperatures

24 p4331 A69-42940

POROUS BOUNDARY LAYER CONTROL

Viscous liquid layer flow down inclined plane under boundary conditions, taking into account drag and penetration at porous bed surface

02 p0234 A69-12774

Van Driest-Bradshaw model for calculating sublayer function for self preserving laminarescent boundary layers, discussing porous surface suction or acceleration effects

[ASME PAPER 69-HT-12] 24 p4304 A69-43557

POROUS MATERIALS

NT POLYURETHANE FOAM

Gas flow analysis for externally pressurized porous journal gas bearing, considering circumferential flow in bearing clearance and porous bushing

01 p0085 A69-10312

Porous ceramic heat shields for lifting reentry vehicles, noting crack propagation resistance and load redistribution

[SAE PAPER 680643] 03 p0453 A69-13457

Coefficient of friction variations for MHD flow of electrically conducting liquid across porous medium under transverse magnetic field

03 p0480 A69-14112

Porous gas diffusion electrodes design for electrochemical energy converters, noting contribution of theory of electrode kinetics

04 p0551 A69-15309

Hardenability of ShKh-15 steel, establishing relationship of porosity to sintering method

04 p0619 A69-15390

Griffith biaxial fracture criterion for porous brittle materials based on continuum model with random infinitely sharp cracks

[ASME PAPER 68-WA/MET-12] 05 p0838 A69-16152

Thermal transpiration for performance prediction and development of gas pump

[ASME PAPER 68-WA/ENER-4] 05 p0706 A69-16162

Heat transfer performance of porous nozzle blade cascade represented by two dimensional mathematical model

05 p0812 A69-16400

Viscous electrically conducting liquid flow through insulating porous medium in presence of transverse magnetic field in region of validity of Darcy law

05 p0805 A69-16603

Properties of electrolytic and reduced titanium powders and sinterability of porous compacts

05 p0782 A69-16795

Compressional and shear wave velocities vs porosity for sintered perlitic bricks

06 p1000 A69-17009

Effects of multidimensional flow through porous matrices in mass transfer cooling, analyzing one dimensional model for blunt axisymmetric surfaces

[AIAA PAPER 69-149] 06 p1038 A69-18179

Ti metallurgy and production, discussing vacuum separation of sponge Ti, Ti melting in arc furnaces, Mg thermal reduction and chlorine processing method

07 p1161 A69-18761

Hydromagnetic steady forced flow against porous rotating disk, integrating equations of motion by Karmann-Pohlhausen and series methods

08 p1370 A69-21005

Fluid injection into flowfield from porous forward portion of blunt body in stagnation region flow, determining reservoir pressure and mass flow rate

09 p1430 A69-21973

Porous structures, using spherical tungsten powders, discussing metallurgy, sintering, temperature effects and performance characteristics in ion engines

10 p1710 A69-23166

Molybdenum fiber sintering activation by adding nickel, noting decrease in impact viscosity

10 p1711 A69-23336

Hartmann problem for motion of electroconductive fluid in homogeneous porous medium, modifying clas-

sical MHD equations by introduction of velocity of filtration

11 p1925 A69-24324

Diffusive flow with isopycnic lateral boundaries in porous medium and density distribution of diffusive motion, noting exact solution equivalence to previous solution

11 p1869 A69-24887

Porous cermet electrodes thermochromic protection by blowing neutral gas into electrode boundary layer, examining effect on volt-ampere characteristics

11 p1826 A69-25232

Cesium sorption in materials for thermionic converters reservoirs, discussing dimensional stability of porous alumina, W and C samples

14 p2463 A69-29220

Heat and mass transfer in porous medium with bulk flow in thin adjacent channel, applying Green function analysis to hydrogen-oxygen fuel cell

15 p2552 A69-31115

Boron effect on sintered porous Ni friction at high sliding velocities and temperatures, analyzing oxide film destruction restraint by decreased Ni plasticity

15 p2641 A69-31187

Tensile, bending and impact strengths of materials produced by metal porous blank impregnation with molten glass, noting metal density and sintering effects

15 p2643 A69-31188

Hydrogen oxygen fuel batteries with hydrophobic porous film electrodes and alkaline electrolyte

16 p2740 A69-32426

Similitude applied to dynamics of disperse media, discussing role of dimensionless numbers in mechanics of suspensions and two phase flows in porous media

19 p3300 A69-36775

Temperature and fluid distribution in porous solid subjected to large suction, convective heating and radiative cooling on one surface

20 p3514 A69-37225

Porous hydrophilic oxygen electrodes behavior, showing electrochemical reaction influence on shape of current density vs voltage curves

20 p3484 A69-38071

Heat resistance and strength properties of porous Ni-base cermet materials with mica additions under high temperature oxidation

21 p3751 A69-38615

Book on porous bodies hydrodynamics covering motion equations for free, filtration, perfect and Newtonian fluids

23 p4150 A69-41501

High pressure hydrogen-oxygen reversible fuel cells using calcia stabilized porous zirconia as membrane and aqueous KOH as electrolyte

23 p4076 A69-42308

Van Driest-Bradshaw model for calculating sublayer function for self preserving laminar boundary layers, discussing porous surface suction or acceleration effects

[ASME PAPER 69-HT-12] 24 p4304 A69-43557

POROUS PLATES

Two dimensional unsteady Rayleigh flow velocity of conducting and nonconducting viscous fluid past porous plate, analyzing suction and magnetic field effects

02 p0232 A69-12156

Heat transfer of steady laminar flow of incompressible, viscous and electrically conducting fluid between parallel porous plates

02 p0289 A69-12235

Transpiration cooling of porous flat plate by injection of carbon dioxide or air into carbon dioxide and air free streams

03 p0413 A69-12996

Heat transfer through turbulent boundary layer on porous plate with blowing and suction, determining Stanton numbers

04 p0586 A69-14356

Flow of two conducting immiscible liquids between parallel porous moving plates under transverse magnetic field

05 p0743 A69-15600

Decreasing secondary flows in spatial boundary layer on porous plate by boundary layer control /BLC/ through suction or blowing, using Prandtl partial differential equations

06 p0909 A69-17185

Laminar source flow of viscous incompressible liquid between two parallel coaxial rotating porous disks

06 p0909 A69-17243

Chemical reactions in boundary layer on porous plate in oxygen stream, discussing similar solution of laminar boundary layer equations with flame front

07 p1119 A69-18735

Radiative-convective heat transfer in gray gas plane layer blown into turbulent flow past permeable plate

07 p1242 A69-18991

Heat and mass transfer in laminar boundary layer on porous flat plate with variable suction or injection velocity and constant wall temperature

12 p061 A69-25947

Steady incompressible MHD laminar flow between parallel porous disks solved for large Reynolds and Hartmann numbers

15 p2662 A69-30968

Compressible flow over finite porous plate in supersonic stream with massive injection over surface analyzed using inviscid vortical flow model

16 p2770 A69-31884

Turbulent boundary layer gas mixture flow incident to porous plate surface

20 p3513 A69-37093

Unsteady boundary layer with distributed injection or suction on porous plate, determining acceleration and flow parameter functions from velocity profiles

21 p3692 A69-38609

Optimal boundary layer control ensuring minimum heat transfer to porous plate from incompressible flow of hot gas of cooling system

21 p3849 A69-38846

Thermal boundary layer formed during laminar jet flow over flat porous plate, discussing temperature distribution and mass transfer at plate surface

21 p3854 A69-39846

Corrosion of Ni through porous Au plate in humid sulfur dioxide atmospheric environments, analyzing product deposits and contact properties

23 p4176 A69-41534

Gas concentration measurement during injection into laminar boundary layer streaming along porous plate, using quadrupole resonance mass spectrometer

23 p4058 A69-41695

Anisotropic porous media model for fluid motion in rectangular fuel cell cavities, analyzing pressure, velocity, stream functions and purge time

23 p4075 A69-42300

POROUS WALLS

Frictional and heat transfer characteristics of laminar flow in porous tubes, using numerical solutions to flow and energy equations

01 p0177 A69-11408

Steady laminar flow in two dimensional channel with different permeability porous walls and large injection at both walls

03 p0417 A69-13795

Relaminarization of turbulent flow, studying velocity profiles at various axial cross sections in porous wall tube with fluid injection

04 p0586 A69-14409

Laminar flow of isotropic binary gas mixture in circular cylindrical tube with porous walls, determining concentration field variation with wall suction Reynolds number

05 p0744 A69-15618

Laminar and turbulent regimes of flame propagation studied by blowing explosive gas mixture through porous wall, determining Reynolds number by hot-wire anemometer

06 p1034 A69-17626

Unsteady MHD convective flow with suction of viscous incompressible electrically conducting fluid above vertical porous wall, noting horizontal magnetic field effect

07 p1195 A69-19477

MHD oscillatory flow along infinite plane porous wall with variable suction velocity, obtaining expressions for velocity and magnetic fields in boundary layer

09 p1547 A69-21607

Laminar elasticoviscous flow of liquid with short memory in two dimensional channel with porous walls

10 p1680 A69-23668

Differential equation for laminar flow of nonNewtonian fluid in annulus with porous walls of nonuniform permeability, considering inelastic and suction Reynolds numbers

10 p1680 A69-23690

Velocity distributions and skin friction coefficients in turbulent boundary layers over flat plate with injection or suction through porous wall

11 p1871 A69-25027

Temperature variations at porous wall surface as function of transpiration coolant flow rate

11 p2002 A69-25334

Steady flow field for viscous incompressible fluid in rotating pipe with porous walls determined from Navier-Stokes equations

11 p1875 A69-25481

Viscous incompressible conducting fluid flow through porous coaxial nonconducting cylinders under radial magnetic field with pressure gradients functions of time

12 p2062 A69-26275

Hydromagnetic flow of viscous conducting fluids through porous coaxial cylinders in radial magnetic field solved by Laplace transform

12 p2135 A69-26276

Model to study viscous flow characteristics in channel with porous walls and constant suction, noting non-monotonic velocity profile

14 p2429 A69-29015

Similar solution for free convective flow past vertical porous wall and unsteady flow past porous wall with dissipation term, using group transforms

15 p2592 A69-31010

Hele-Shaw and porous medium fuel tank systems behavior in simulated low gravity environment, studying sloshing, wetting, funnelling and fuel-driver gas interface stability

[AIAA PAPER 69-678] 17 p3021 A69-33444

Plane shock wave interaction with plane rigid net-like wall, obtaining Mach numbers for reflected and penetrating shock waves

17 p2957 A69-33719

Gas core reactor curved porous walls geometry tested with clear and smoky air injection, noting mass flow ratio in reactor cavity

18 p3171 A69-35181

Hydrodynamic stability of incompressible fluid boundary layer flow during blowing or suction through porous surface, determining Reynolds number lower bounds

18 p3124 A69-35381

Local heat transfer coefficients determined from temperature distribution on porous walls, deriving mathematical expressions for various surface geometries and transfer modes

20 p3630 A69-36977

Axial velocity and static pressure for incompressible fluid flow through straight smooth porous tube

[ASME PAPER 69-FE-44] 20 p3517 A69-38000

Law of wall parameters for compressible turbulent boundary layer with air injection through wall determined by analyzing data for hypersonic speeds

21 p3692 A69-38685

Temperature distribution determined for leading edge, convex and concave parts of turbine blade porous wall with effusion cooling

21 p3850 A69-38860

Heat transfer characteristics in evaporative, transpiration cooled porous systems

21 p3851 A69-39037

Viscoelastic fluid steady flow in porous walled channel, examining mass flow solution continuity

22 p3930 A69-40118

Laminar MHD flow in porous walled channel in transverse magnetic field, determining velocity distributions, induced fields and current over channel cross section

22 p3989 A69-40256

Laminar flow in porous circular pipe with constant suction or injection applied at wall

24 p4298 A69-42618

Turbulent flow in circular porous tube laminarized by uniform mass injection through tube wall, measuring velocity and turbulence intensity by impact probe

[ASME PAPER 69-HT-57] 24 p4303 A69-43537

Van Driest-Bradshaw model for calculating sublayer function for self preserving laminar boundary layers, discussing porous surface suction or acceleration effects

[ASME PAPER 69-HT-12] 24 p4304 A69-43557

PORPHYRINS

NT CHLOROPHYLLS

Biochemiluminescent luminol-peroxide reaction to detect iron porphyrin proteins in microorganisms for extraterrestrial life search, discussing reaction kinetics

15 p2556 A69-31325

Meteorites pigments identification as porphyrins for extraterrestrial life evidence, noting sample analyses of Orgueil, Murray, Cold Bokkeveld and Mokoia carbonaceous chondrites

22 p4008 A69-39889

Detection and spectral examination of trace porphyrin complexes by demetallation with methanesulfonic acid and spectrofluorometry, compared to absorption spectrophotometry

24 p4279 A69-42557

PORTABLE EQUIPMENT

Design aspects of 20 ft air transportable satellite earth station

08 p1272 A69-19926

Portable integrating sphere reflectometer, describing optical system, construction, etc
[AIAA PAPER 69-599] 17 p2973 A69-33264

Lithium peroxide utilization feasibility for oxygen supply and carbon dioxide control in extravehicular portable life support systems
[AIAA PAPER 69-620] 17 p2914 A69-33303

Portable piezoelectric acceleration sensor, describing characteristics and principles of operation
17 p2975 A69-33594

Self contained hand held battery operated aerosol particle analyzer, measuring aerosol concentration and size distribution for laboratory and space flight applications
18 p3136 A69-34691

Betatrions for nondestructive quality control for materials and products under special conditions
18 p3136 A69-34779

Portable electric lamp for work and photographic purposes in manned spacecraft, describing circuitry, construction and applications
[IES PREPRINT 30] 18 p3138 A69-35173

Electrostatic control for portable clean rooms, describing fabrication, assembly and checkout problems with Instrument Unit /IU/ control center for Saturn launch vehicles
19 p3428 A69-35550

Portable multiunit low pressure chamber with locks, permitting water replenishment, feeding of animals under continuous pressure and gas mixtures
22 p3891 A69-40217

Monopulse telemetry tracking system, describing equipment and mobile operation
22 p3900 A69-40681

Portable UHF telemetry receiving station for medium range surface-to-air missiles testing, analyzing antenna coverage over water and system prediction allowing variable parameters
23 p4122 A69-41780

Portable He-Ne laser design featuring positional adjustment for use in aligning optical systems
24 p4327 A69-42924

PORTS

Limitations of N-port concept in microwave technology, proposing definitions to avoid contradictions
11 p1841 A69-25624

POSITION [LOCATION]
NET SOLAR POSITION

Icarus asteroid position measurements by astronomical photography, noting comparison for two South African observatories
01 p0150 A69-10373

Optical identifications for 17 Ohio survey sources with peaked or flat spectra
01 p0153 A69-10854

Icarus positions from photographic observations with astrophot
01 p0159 A69-11331

Errors arising from inaccurate insertion of initial conditions in autonomous determination of coordinates of object moving along surface of spherical earth
02 p0281 A69-12137

Submicron particles spatial location in three dimensional volume detected by Fraunhofer holography
04 p0596 A69-14292

Galactic X ray sources noncoincident with conspicuous visible or radio objects, identifying visible and radio counterparts by determination of accurate celestial coordinates
05 p0813 A69-15845

Lunar occultations of radio source Sagittarius A observed at various frequencies between 230 and 2400 MHz, obtaining diameter, position and decimeter band flux densities
06 p1009 A69-17960

Predictor determining future position of TDMA /Time Division Multiple Access/ synchronous satellite communications system satellite from previously received bursts
07 p1076 A69-18553

Radio galaxies, quasars and radio stars between declinations plus 20 and plus 27 degrees, obtaining accurate positions and optical identifications
07 p1218 A69-19273

Crab Nebula pulsar NPO527 position measurement with split beam antenna, noting proximity and similar dispersion with NPO532
07 p1221 A69-19405

Vestibular analyzer role in spatial orientation under weightlessness conditions during aircraft flights, discussing underestimations of rotation angle of Barany chair
08 p1262 A69-19840

Time difference position determination system for space, surface and airborne vehicles, describing application to satellite navigation and air traffic control
08 p1348 A69-21066

Radio location system based on measuring distance between object and two stationary satellites, noting application to air traffic over North Atlantic
09 p1537 A69-21269

Polar flight navigation charts showing feasibility of three dimensional celestial positioning
09 p1538 A69-21406

Celestial X ray source positions from rotating modulation collimator, predicting performance of collimator
10 p1722 A69-23328

True position dimensioning and tolerancing /TPDT/ system usage in aerospace industry
10 p1700 A69-23355

Position of OH sources near seven galactic radio sources determined with two element variable-baseline interferometer, noting strong circular polarization
10 p1787 A69-24114

Radio sources optical positions for independent calibration sources
11 p1958 A69-24465

Plasmapause position measurements by ion mass spectrometers and broadband VLF receivers on OGO 1 and OGO 3 and by broadband recordings at Antarctica
11 p1878 A69-25153

Artificial noctilucent clouds or meteor trails positions determined by transforming photogrammetric coordinates
12 p2154 A69-25822

Inertial navigation platform principles including acceleration and position of vehicle, single axis platforms and stabilized element coordination
12 p2078 A69-25872

Large mirror support systems definition in terms of axial location and radial position
12 p2057 A69-26414

Spatial direction determination from simultaneous photographs of Echo 2 at Nikolaev and Helwan stations, using circle of simultaneity
12 p2068 A69-26427

Computer program solving for station coordinates and dynamical parameters at Smithsonian Astrophysical Observatory from optical data, laser range and range rate
12 p2068 A69-26428

Gustaffson pattern for variations in position of quiet homogeneous arcs, noting diurnal variations from visual observations at antarctic station
12 p2073 A69-26951

Satellite positions measurements by laser compared with radar and photographic methods, considering measurement errors
12 p2110 A69-27149

Optical identification of radio source 3C 230, suggesting removal from quasar list
12 p2173 A69-27171

Photographic observations of quasi-stellar objects for position determination
13 p2334 A69-27308

Spacecraft orientation from onboard stellar photographs, calculating absolute and relative elements, accuracy and camera parameters
13 p2296 A69-27696

Positions, spectral types and B magnitudes for possible field horizontal-branch stars at high galactic latitudes, selected from faint A star list
13 p2348 A69-27807

Photoelectric yellow and blue observations of variable V502 Ophiuchi, noting influence of partial eclipses on orbital determination reliability
13 p2348 A69-27809

Position determination from radio bearings using complex numbers, noting application to reconnaissance flight path
14 p2479 A69-29499

Cepheid variable 1 Carinae position in H-R diagram suggested from microturbulent velocity role in pulsational instability
14 p2522 A69-29590

Navy Navigation Satellite System /NAVSAT/ applications, considering nonmilitary marine and air all-weather navigation and positioning
14 p2479 A69-29856

Error assessment for 20 May 1966 annular eclipse observation point and observation time determination
15 p2686 A69-30533

Rescue locator beacons and airborne search equipment of VHF and UHF capabilities available to international civil aircraft operations
15 p2552 A69-30852

Orientation in proximity of moon and on moon surface utilizing maria, craters, etc
16 p2855 A69-31929

Exact positions of Ceres, Pallas, Juno and Vesta from 1941 to 1995 determined taking into account planets influence
16 p2859 A69-32224

Accurate optical position of quasars determined by plate overlap for radio interferometer calibration
16 p2859 A69-32229

Accurate positions at 2700 MHz and optical identification of radio sources with galaxies and quasi-stellar objects
17 p3035 A69-33611

CP 0950 and CP 1133 pulsating stars position, using radio telescope at two frequencies
17 p3036 A69-33639

Navigation and guidance systems for low altitude aircraft flight safety noting position determination, cockpit environment and fail-safe operation
17 p3002 A69-34080

Graphic representation of time dependence of sub-satellite points and orbital azimuths for relating satellite photographs to locality
18 p3128 A69-34818

Minor planets positions computer calculated and tabulated from Tashkent 1963 and 1964 astrophot observations, stating time and equatorial coordinates
20 p3596 A69-37312

Minor planets positions computer calculated and tabulated from 1966 and 1967 Crimean astrophot observations, using Yale catalog reference stars
20 p3570 A69-37313

Comet tails orientation determination for solar wind and interplanetary plasma investigation, considering geometrical difficulties and suggesting computation procedure
20 p3599 A69-37467

Space vehicle space-time position fiducial distribution and future location determinations based on inference theory
20 p3617 A69-37528

Tabulated results of photographic plate measurements of minor planets positions at Leiden observatory /1938-1964/
20 p3605 A69-37789

DIA satellite Doppler observations, noting effect of observation grouping on ground stations mutual position
21 p3701 A69-38336

Time difference position determination system for space, surface and airborne vehicles, describing application to satellite navigation and air traffic control
22 p3977 A69-39874

Compressor type cascade experiments to find closest possible traverse position to blade trailing edge
22 p3859 A69-40065

Airport location effect on facilities supply factors including atmospheric, environmental and economic conditions
22 p3926 A69-40431

Harmonia and Parthenope /minor planets/ positions, establishing time dependence of relation between image diameter and planet magnitude
22 p4025 A69-40614

Most probable position determination in astronomical navigation by tracing lines on nautical chart
23 p4186 A69-42025

Maritime navigation hyperbolic charts for aircraft position determination
23 p4186 A69-42026

Geographical position coordinates of radio operator determined by distance difference measurement using Loran and digital computer methods
23 p4186 A69-42027

Magnetic dip equator position at E layer and gradient with time and altitude, using geomagnetic field models
23 p4160 A69-42428

POSITION ERRORS

Ship navigation by altitude and azimuth measurements of artificial earth satellite, discussing position and reference errors and synchronous satellite advantages
[UN PAPER 68-95247] 01 p0112 A69-10461

Error reduction in initial azimuth alignment and azimuth and level axis gyro drifts in long range air transport gyro accelerator inertial systems
02 p0278 A69-12361

Probable errors in FK4 catalog of star positions and proper motions determined by Scott method
05 p0823 A69-16041

OMEGA position location equipment /OPLE/ test data to demonstrate feasibility of using OMEGA navigational system in conjunction with synchronous satellites

07 p1176 A69-19135

Hybrid OMEGA inertial system for following vehicle maneuver without lag developed by combining Schuler tuned inertial data and radio position data

07 p1177 A69-19209

Errors estimation in determination of radio signal source flux density, position and recorded half power widths

07 p1088 A69-19722

Pointing calibration of Haystack parabolic antenna by using radiometric measurements of cosmic ray sources

08 p1281 A69-20032

Range difference air navigation equations solution, discussing error updating of satellite position and constellation geometry

09 p1538 A69-21996

Stars astronomical positions elimination from photographic plates because of errors, discussing elimination criteria and picture taking method

10 p1784 A69-24034

Satellite position errors due to atmospheric instability, discussing altitude-temperature relation and stellar scintillation synchronism for stars at small angular distances

12 p2158 A69-26445

Navy Navigational Satellite System for position location accuracy in marine and oceanographic exploration applications [AIAA PAPER 68-471]

13 p2295 A69-27247

Fluidic attitude control systems performance prediction from conventional control analysis emphasizing steady state positioning accuracy

17 p2904 A69-34069

VOR/DME information augmentation by air data /airspeed/ for positional accuracy improvement, describing error sources, optimum data filter and system sensitivity and performance [AIAA PAPER 69-841]

21 p3762 A69-39372

Cumulative error in flight vehicle position determination by inertial navigation system, showing dependence on constant acceleration components

22 p3978 A69-40252

Pluto positions /1930-1965/ from photographic observations, ascribing declination errors to atmospheric dispersions

22 p4025 A69-40612

Mars positions determined from photographic observations by zone astrophotograph, establishing rms errors and objective centering error

22 p4025 A69-40613

Air traffic control transoceanic satellite system for minimizing navigation errors forcing wide separations, providing VHF voice communication and position surveillance

22 p3901 A69-41147

Terrain slope estimation of position errors of differential corrections in orthophoto production

22 p3951 A69-41245

Statistical analysis of position errors inherent in position-finding system utilizing position fixing planes in three dimensional space

22 p3979 A69-41253

Antenna pointing and tracking accuracy by identifying error sources in servo, structural, mechanical and alignment factors

23 p4125 A69-42126

Ionospheric irregularities effect on accurate satellite position determination in near real time

23 p4132 A69-42549

POSITION INDICATORS

NT PLAN POSITION INDICATORS

NT SPACECRAFT POSITION INDICATORS

Fluidic pulse time modulated angular position sensor for two axis hydrostatically supported gyroscope

02 p0249 A69-12087

High speed compression waves, rarefaction waves and gas interface regions position and velocity measurement in shock tube by sensing electrical impedance

03 p0428 A69-13104

Predictive logic control of on-off system with one position sensor [ASME PAPER 68-WA/AUT-14]

05 p0830 A69-16134

Phantom disk encoder for arc second digital position transducers

05 p0766 A69-16748

OMEGA position location equipment /OPLE/ test data to demonstrate feasibility of using OMEGA

navigational system in conjunction with synchronous satellites

07 p1176 A69-19135

Fluidic digital position sensor consisting of fluidic monostable amplifier, analyzing operation by characteristics method

15 p2554 A69-31301

Position sensitive sensors design of optical tracking systems with emphasis on amplitude, phase, frequency and pulse-time sensors

16 p2790 A69-32111

Electromagnetic accelerometer with symmetrically placed photocells detecting small steel ball position

17 p2971 A69-32897

Aircraft electromagnetic position finding system based on Doppler shift of CW carriers

17 p3002 A69-34078

Light aircraft emergency downed position indicators installation program, discussing transmitter minimum performance standards, listening watch insurance, etc

17 p2931 A69-34102

Artificial horizon indicator design modifications to facilitate maintaining horizontal aircraft position, discussing automatic pilot advantages in turbulence and flight simulators

17 p2903 A69-34214

Interpolated position and orientation perception by vision and active touch

24 p4275 A69-43116

POSITION SERVOS

U SERVOMOTORS

POSITIONING

Rib positioning effect on mechanical behavior of cantilevered rectangular plate in gas flow, considering critical flow velocities and rigidity relationships

01 p0165 A69-10085

Celestial navigation, discussing position fixing on rotating earth, time input, navigation aids and sextant angle

03 p0463 A69-13207

Optical sighting method for determining orientation of rocket on launch pad by laser collimator, noting lining up of Cassiopeia system

06 p0930 A69-17104

Optimum inertial/Doppler satellite navigation system, discussing position fixes application in resetting

08 p1349 A69-21199

Frequency domain stability criteria accuracy for application to fourth order nonlinear position control system

09 p1475 A69-22591

POSITIONING DEVICES [MACHINERY]

NT BOOMS [EQUIPMENT]

NT CAMS

Hydraulic-powered self propelled six degree of freedom loading vehicle moving tests assembly to test chamber with high accuracy positioning

20 p3511 A69-38181

Precision of gas turbine compressor blade positioning devices during machining, analyzing causes of inaccuracies

21 p3731 A69-38880

POSITIVE FEEDBACK

Positive feedback of spring mass system for mirror control on spectroheliometer of Apollo Telescope Mount flight

02 p0248 A69-11738

Dynamic mode locking of CW He-Ne laser by external regenerative feedback using RF beats between axial modes

02 p0260 A69-12657

Natural amplitude and phase fluctuations of originally monochromatic oscillations at output of regenerative frequency divider with thermal and shot noise

07 p1099 A69-18526

Signal processing regenerative technique used for multichannel predetection combining, including carrier suppressed signals

09 p1458 A69-22472

Regenerative amplifier to counteract cable damping due to narrow bandwidth in PCM systems

16 p2755 A69-31860

Regenerative Josephson effect detector with feedback-narrowed far IR response as tunable millimeter and submillimeter wave radiation detector

19 p3313 A69-36417

POSITRON ANNIHILATION

Positron annihilation in As, Sb, Bi, diamond, Ge, Si, S, Te and Se, noting contribution of valence electrons

03 p0485 A69-13295

Cosmic ray showers electron, positron and photon energy distribution functions calculated, considering

positron annihilation, Compton effect and relativistic electrons formation

13 p2303 A69-28413

POSITRONIUM

Positronium formation in positron-helium scattering, including polarizability in potentials appearing in final equations

24 p4353 A69-43815

POSITRONS

Gravitational force measurement on electrons and positrons in free fall through vertical metal tubes at low temperatures

01 p0125 A69-10979

Galactic halo chronology determination by positron component flux measurement in primary cosmic rays

08 p1386 A69-20084

Cosmic ray negatron and positron spectra using balloon-borne magnetic spectrometer, obtaining absolute solar modulation of positron flux

08 p1380 A69-20728

Annihilation gamma ray spectra from equilibrium spectra of secondary galactic positrons

14 p2514 A69-29948

Low energy positrons in cosmic radiation due to beta decay of carbon, nitrogen and oxygen isotopes, estimating positron fluxes and energy spectra

15 p2676 A69-30887

Electron-positron pair formation in electromagnetic field created by coherent laser light focused into vacuum with ideal lens

22 p3965 A69-41116

Positronium formation in positron-helium scattering, including polarizability in potentials appearing in final equations

24 p4353 A69-43815

POSTURE

Human postural muscle activity, motor reactions and dexterity during gravitational changes

07 p1063 A69-18593

Posture role in physiological effects of acceleration on motor activity, discussing gravitational importance to vital processes

13 p2211 A69-28593

Sensorimotor coordination of man performing graphic assignments in upright, reclining and prone position, discussing interaction of vestibular, visual and motor analysors

20 p3470 A69-37246

Diurnal rhythms of heart rate and blood pressure reactions to posture changes on tilt table, finding orthostatic lability maxima

23 p4094 A69-42072

POTABLE WATER

Analytical techniques for in-flight monitoring of aerospace water supplies for potability, emphasizing rapidity, sensitivity and reproducibility

01 p0019 A69-11339

POTASSIUM

NT LIQUID POTASSIUM

Alkali metal quadrupole spectral doublets used as diagnostic for determining alkali-metal plasma electron temperature

02 p0286 A69-11584

Potential energy functions based on electronegativities instead of spectroscopic parameters for Li and K molecules

03 p0472 A69-13805

Temperature dependence of isotope thermotransport in liquid K and Rb using steel capillary cells

03 p0533 A69-13970

Argon-K plasma electrical conductivity as function of electric current density at 1400-2400 K

05 p0798 A69-15614

Spectroscopy of potassium vapor using laser induced fluorescence, noting laser line coincides with several molecular transitions

05 p0771 A69-15907

Potassium ion resonant charge exchange, determining relation between effective cross section and ion velocity, using retarding field method

06 p0959 A69-16909

Enhanced two photon emission between 6S and 4S levels of K, discussing stimulated three photon Raman scattering and four photon parametric coupling processes

07 p1154 A69-19080

Barkhausen oscillator for LF domain by substituting Cs and K positive ions for electrons, giving oscillation curves and spectral analysis

08 p1280 A69-19981

Redistribution of potassium and argon in meteorites and rock samples, discussing thermal diffusion and grain size

08 p1405 A69-20926

DC plasmatron for heating argon with potassium additions at high temperatures and at near atmospheric pressure to obtain argon flow
09 p1547 A69-21596

Work function and desorption energy measurements of alkali metals from metallic substrates with modulated molecular beam, noting surface contamination
09 p1558 A69-21808

Correlation produced magnetoplasma mode in potassium confirmed by measurement of real part of surface impedance
10 p1728 A69-23168

Potassium vapor radiative perturbation by ruby laser radiation in glass cell with end windows, studying emission line structure
13 p2271 A69-27656

K and Ar 40 determination in iron meteorites by neutron activation for K/Ar dating
19 p3412 A69-36106

Ion production in K/diatom Br system by high energy K beam, obtaining total ionization cross section as function of energy
19 p3378 A69-36187

Drift velocity and lateral diffusion of positive hydronium, hydrogen and K ions in hydrogen with zero field mobilities
20 p3580 A69-38026

Pumping model for analyzing stimulated and enhanced potassium multiphoton emission primed by ruby laser-stimulated Raman electronic radiation
23 p4171 A69-41391

Electrothermal waves in nonequilibrium electrical discharge in potassium seeded argon plasma
24 p4359 A69-43645

POTASSIUM BROMIDES

Low temperature grinding technique for IR spectra of propellants and binders in potassium bromide disks
01 p0082 A69-10892

Laser holography using colored KBr crystals subjected to hard gamma radiation as photosensitive material
04 p0598 A69-14855

Laser holography using colored KBr crystals subjected to hard gamma radiation as photosensitive material
15 p2608 A69-30247

Velocity and angular distributions of KBr formed in reactive collisions between crossed molecular beams of K and thermal HBr/DBr/
18 p3178 A69-35476

POTASSIUM CHLORIDES

Paraelectric resonance spectroscopy on KCl, using bistable dipole model
06 p0982 A69-18235

PbTe single crystal films growth on KCl studied by electron microscope, observing vapor crystal mechanism without coalescence of contacting crystals
10 p1745 A69-23323

Multiphoton luminescence and photocurrent excitation by ruby and neodymium laser beams of KCl-Eu single crystals, noting brightness dependence on laser beam power
19 p3335 A69-36165

POTASSIUM CHROMATES

Catalytic effect of potassium bichromate and chromic oxide additives on burning of ammonium perchlorate and mixtures
08 p1375 A69-19997

Raman effect in potassium dichromate single crystal, discussing symmetrical and antisymmetrical internal vibrations of free ions
12 p2105 A69-26285

POTASSIUM COMPOUNDS

NT NEPHELINE
Subsolidus equilibrium study in potassium tantalate K niobate system for dry and hydrothermal runs, using X ray powder diffraction and petrography
08 p1332 A69-20373

POTASSIUM HYDROXIDES

Nonpolar gases solubilities in aqueous KOH solutions in temperature range 25 to 100 C, noting activity coefficients, salting out coefficients and heats of solution
10 p1651 A69-22937

POTASSIUM ISOTOPES

Early disturbances in active migration of potassium 42 ions in irradiated erythrocytes in rats, showing relation between influx and energy exchange in cells
10 p1647 A69-23966

POTASSIUM PERCHLORATES

Component ratio effect on pressure dependence of burning rate in ammonium and potassium perchlorate mixed with organic compounds, graphite and tungsten
12 p2027 A69-26474

POTASSIUM PHOSPHATES

Electro-optical device using KDP crystal for laser beam deflection at temperatures near Curie point
03 p0435 A69-12984

Parametric light generation employing KDP nonlinear crystals with mechanically tuned frequency
03 p0437 A69-13045

Second optical harmonic generation in uniaxial negative potassium dihydrogen phosphate, noting influence of generating process on angular structure and output power
03 p0439 A69-13057

Laser radiation influence on effectiveness of frequency doubling in KDP crystal
04 p0612 A69-15375

Second harmonic generation conversion efficiencies at 5300 A with KDP and lithium niobate crystals, using Nd-glass laser of high radiance and narrow bandwidth
09 p1514 A69-21333

Gas laser modulation steady state characteristics with KDP crystal in cavity, noting output power dependence on applied electric field
13 p2273 A69-28432

Laser radiation influence on effectiveness of frequency doubling in KDP crystal
16 p2797 A69-32122

Second harmonic emission in KDP crystal using ruby rod as active material, discussing difficulties encountered by diffused reflector
20 p3552 A69-36970

Electrocaloric effect from 78-130 K on crystalline potassium dihydrogen phosphate, showing quadratic dependence on applied field /and polarization/ in paraelectric phase
20 p3583 A69-37343

Nonmonochromatic laser emission frequency characteristics, studying second harmonic generation in nonlinear KDP crystal
20 p3554 A69-37727

Beam divergence and multimode laser visible emission influence on power and angular structure of second optical harmonic generated in KDP crystals
24 p4328 A69-43161

POTASSIUM 40

Body composition of USAF flying personnel, evaluating obesity by using radioactive potassium /K-40/ method
14 p2409 A69-29295

POTATOES

Radiosensitivity of potatoes to gamma ray and proton irradiation applied to whole tubers and to isolated eyes before planting
05 p0709 A69-16511

Sweet potatoes productivity and nutritive value as carbohydrates source in manned spaceflights
13 p2216 A69-28619

Radiosensitivity of potatoes to gamma ray and proton irradiation applied to whole tubers and to isolated eyes before planting
18 p3095 A69-34730

POTENTIAL

Completeness and relations between potentials and stress functions in micropolar elasticity and thermoelasticity
19 p3439 A69-36476

Retarding potential analyzers determining ionospheric structure, noting linearization of analysis
22 p3940 A69-40523

POTENTIAL ENERGY

NT BIOELECTRIC POTENTIAL

NT CONTACT POTENTIALS

NT COULOMB POTENTIAL

NT ELECTRIC POTENTIAL

NT GEOPOTENTIAL HEIGHT

NT IONIZATION POTENTIALS

NT LIENARD POTENTIAL

NT LOW VOLTAGE

NT PHOTOVOLTAGES

NT PLASMA POTENTIALS

NT SPIKE POTENTIALS

Potential energy functions based on electronegativities instead of spectroscopic parameters for Li and K molecules
03 p0472 A69-13805

Increasing vortex tubes energetic cooling efficiency for cooling aircraft components by using potential energy of gas emitted from tubes
04 p0684 A69-14488

Alkali metals thermoelectric power and energy dependence of Heine-Abarenkov pseudopotential, taking into account anisotropy effects
05 p0809 A69-16507

Vacancy relaxations in bcc crystals using energy dependence on radial displacements from defect of nearest neighbor sets, discussing crystal size and shape
05 p0809 A69-16529

Unsymmetrically laminated simply supported plates approximate solutions, considering potential energy and reduced stiffness matrix
07 p1232 A69-18725

Atmospheric circulation intensity measurement, using potential energy conversion to kinetic or kinetic energy dissipation by friction
07 p1175 A69-18947

Optical potentials for rotational and vibrational transitions in inelastic molecular collisions, considering adiabatic and sudden approximations
08 p1358 A69-21008

Plasma transport properties derived from Boltzmann equation using Debye shielded-Lande potential to represent collisions, noting viscosity and thermal conductivity
09 p1553 A69-22539

Total planet interaction energy of comets passing through solar system, showing non-Gaussian shape of distribution
10 p1774 A69-22970

Linearized atmosphere model above flat earth, applying variational principle to energy between geostrophic equilibrium and reestablished states
12 p2125 A69-25954

Exact solutions for two state potential curve crossing in subexcitation molecular collisions in terms of various decoupling schemes
12 p2131 A69-25983

Atmospheric energy budget of latent and sensible heat and potential energy between equator and 60 degree N
12 p2066 A69-26132

Energy budget equations applicable to limited atmospheric region using available potential energy concept, discussing relation to global energy
15 p2648 A69-30221

Temperature dependence of intermolecular interaction averaged potentials with respect to vibrational states
15 p2655 A69-30982

Potential and kinetic energy of cylindrical thin shell with cutout approximated by two dimensional finite difference methods, obtaining eigenvalue problem [AIAA PAPER 68-318]
16 p2874 A69-32158

Iterative potential between alkali ions and rare gas atoms, using model accounting for repulsive and attractive exchange forces
16 p2815 A69-32464

Elastic sandwich structures design for maximum strength, using potential energy functional to derive governing equations
17 p3062 A69-33708

Floating body attitude and stability analysis based on system potential energy balance, considering Archimedes principle, torques, equilibrium conditions, body shape, etc [SAWE PAPER 773]
18 p3172 A69-34874

Buckling stresses in thin walled box girder under bending determined using stationary potential energy criterion
18 p3224 A69-35344

Earth gravitational potential energy changes in examining expanding earth theory
22 p3936 A69-40180

Self consistent field molecular orbital method in LCAO/linear combination of atomic orbitals/ approximation applied to LiH ground state for potential energy curve
22 p3985 A69-40721

Energy equilibrium for crack growth in elastoplastic media, analyzing crack behavior during plastic deformation concentrated at edge of propagating crack
22 p4046 A69-41060

Stress-strain relations for materials with variable modulus of elasticity applied to internal work, obtaining potential strain energy
22 p4047 A69-41171

Potential energy modeling method for optimal design of structural systems with diverse performance criteria, giving truss design example
23 p4228 A69-41923

Integral transformation applicability to inverse problems concerning interaction potential energy between particle pairs in n-dimensional Euclidean space
23 p4182 A69-41960

Differential operators representing potential energy of thin shell, discussing self conjugacy of boundary value problems
23 p4229 A69-41999

POTENTIAL FIELDS

Positive ion beam probe for approximate static electric field distribution in low pressure RF discharges, analyzing deflection data for potential distributions

02 p0287 A69-11838

Stability margin difficulties in equilibrium application to continuum mechanics

03 p0418 A69-13816

Two dimensional magnetosphere with tail and neutral sheet, using Chapman-Ferraro approximation by mapping in potential plane

03 p0425 A69-14011

Closed analytic expressions for vector potential and magnetic field generated by axisymmetric multipole line currents

06 p0965 A69-17518

Quasi-random properties of dynamic system generated by solutions of second order differential equations

06 p0948 A69-17657

Quasi-integral operator applicability to analytical continuation of potential field into complex region arising during gravitational and magnetic anomalies interpretation

10 p1689 A69-24082

Stability of uniform rotations of gyrost at fixed point in potential force field, considering Routh rule

11 p1918 A69-24786

Knudsen arcs in argon showing potential well presence with anode barrier and cathode potential drop, establishing slow electrons thermal equilibrium

12 p2137 A69-26536

Waveguide higher order modes solved by finite-difference method, using successive overrelaxation to compute field potentials at discrete points in arbitrary guide shapes

13 p2228 A69-27670

Quasi-integral analytic continuation operator applicability to potential field approximated by certain truncated series expansion

14 p2470 A69-29032

Electron current, space potential and ionic composition obtained by Langmuir type probes on Explorer 31 for disturbance region dependence on ionic composition

14 p2518 A69-29122

Integrable cases of equations of motion of solid body around fixed point located in potential field of elastic supports

15 p2653 A69-31194

Steady state sunlit lunar surface electrostatic charge and potential distributions, noting electrons photoemission and solar wind particles collection

20 p3609 A69-38077

Motion of body with cavity completely filled with viscous fluid about center of mass in potential mass-force field, applying small parameter method

22 p3980 A69-40109

Geomagnetic multipole parameters changes using spherical harmonic coefficients of geomagnetic potential, relating to secular variation field

23 p4158 A69-42171

Continuous potential fields modeling based on electrohydrodynamic analogy extended to flows involving stream separation

24 p4300 A69-43089

POTENTIAL FLOW

NT EQUIPOTENTIALS

Potential flow of stream interaction with two dimensional thin jet, discussing jet penetration depth

01 p0007 A69-11019

Forced convection heat transfer coefficient invariance to flow reversal in Stokes and potential streaming flows past isothermal particles of arbitrary shape

04 p0590 A69-15274

Equations of motion derived for incompressible and irrotational viscous fluids in special relativity

05 p0792 A69-15682

Lift and drag coefficients for circular cylinder immersed in time dependent flow analyzed using potential flow model

[ASME PAPER 68-FE-15] 05 p0747 A69-16072

Unsteady potential flow and wake near oscillating circular cylinder noting velocity, pressure and correlation measurements

[ASME PAPER 68-WA/FE-23] 05 p0749 A69-16099

Integral method for backward boundary layers, developing third order polynomials for two dimensional potential flow toward opening

05 p0752 A69-16737

Numerical method for attacking-lifting problems of general three dimensional wing executing arbitrary motion in potential flow

[AIAA PAPER 69-23] 06 p0862 A69-18040

Circular turbulent air jet from flat plate into deflecting stream analyzed with potential flow model, noting applicability to V/STOL aircraft technology

[AIAA PAPER 69-223] 07 p1051 A69-19557

Flow rates characteristic of trapezoidal geometries encountered after schematization of noncylindrical ducts involving irrotational flow, leakage, heat exchanges and electrical conduction phenomena

08 p1303 A69-20270

Arbitrary stationary foil in perfect incompressible fluid moving at constant velocity at infinity assuming plane, steady and irrotational flow

08 p1303 A69-20272

Irrotational plane subsonic flow of compressible fluid about obstacle, reducing problem to integration of linear partial differential equation with boundary conditions

09 p1480 A69-21735

Finite difference numerical solutions to free stream-line axisymmetric potential fluid flow, noting independent and dependent variables consideration in boundary value problem

09 p1481 A69-21920

Incompressible two dimensional potential flow analysis with compressibility effects for thick highly cambered multibodies in cascade, noting slotted compressor blade performance

[ASME PAPER 69-GT-6] 09 p1432 A69-22507

Incompressible fluid flow engine spiral casing, considering flow as potential flow

10 p1632 A69-22914

Asymptotic boundary curves for two dimensional and axisymmetric incompressible irrotational flows into throat of convergent duct

10 p1680 A69-23893

Three dimensional compressible potential flow in curved circular duct analyzed by perturbation method

11 p1867 A69-24607

Large amplitude symmetric and asymmetric irrotational motion of inviscid incompressible fluid with liquid-vapor interface in accelerating cylindrical container of revolution

11 p1871 A69-25124

Thin deformable body motion in disturbed potential flow of ideal incompressible fluid

11 p1876 A69-25488

Potential triple traveling space waves in barotropic gas with arbitrary equation of state, analyzing adjacent and three dimensional self similar flows

12 p2061 A69-25889

Velocity fluctuation amplitude in potential cone of plane jet compared to properties of irrotational fluctuations induced by flow boundaries

13 p2247 A69-27736

Transonic ideal gas flow past semiinfinite bodies, determining flow potentials from body perturbations and surface boundary conditions

14 p2390 A69-29476

Book on mechanics of deformable media covering fluid and solid mechanics and applications to irrotational flows of compressible and incompressible fluids

16 p2813 A69-32789

Bag type deformation of incompressible viscous convective and nonevaporating droplets immersed in Stokes or potential flow pressure distributions, including Weber number

[AIAA PAPER 69-669] 17 p2954 A69-33456

Three dimensional potential surface flow past rotor blade in hover, accounting for compressibility and blade element theory limitations

[AHS PAPER 324] 17 p2895 A69-33537

Pressure distribution in two dimensional incompressible potential flow on Joukowski airfoils with normal upper surface spoilers, emphasizing potential flow theory

[AIAA PAPER 69-737] 18 p3083 A69-34402

Force on circular plate near screen due to incident potential incompressible jet flow

19 p3297 A69-35816

Generalized series solutions of boundary layer flows over pointed and blunt noses axisymmetric bodies, noting general potential flow extending Mangler transformation usefulness

20 p3514 A69-37211

Potential flow theory applied to determination of airfoil separated vortex flow and maximum lift and Reynolds number dependence

20 p3459 A69-37421

Second circle theorem for two dimensional irrotational flow of incompressible inviscid fluid in z plane

20 p3518 A69-38316

Potential flow interaction effects between blade rows in axial flow compressor stage, emphasizing inlet guide vane-rotor interaction

21 p3643 A69-38439

Potential flow past plane array of thin blades, analyzing perturbed dynamic behavior

21 p3696 A69-39243

Nonlinear incompressible potential flow with unbounded free surfaces, analyzing singularities in finite part of space

21 p3696 A69-39295

Plasma pause form in equatorial plane in presence of magnetospheric tail subsonic potential convective flow

22 p3942 A69-41103

Perturbation velocity potential of unsteady potential flow of barotropic gas past cascade of thin blades oscillating harmonically

24 p4244 A69-42716

Gas flow past bodies, deriving solution method without partial differential equations for flows with momentum potential

24 p4244 A69-43071

Unsteady axisymmetric potential flow of ideal incompressible fluid with free surfaces, deriving differential equations for gas bubble dynamics and surface geometry

24 p4302 A69-43500

POTENTIAL GRADIENTS

Critique of paper on theory of gradient instability in semiconductor currents, questioning boundary value problems solution validity

03 p0487 A69-13728

Potential distribution approximations for junction semiconductor devices, noting application to barrier layers and electron tunneling

03 p0408 A69-14107

Surface potential measurements for flat conductors or semiconductors using scanned electron beam probe

04 p0601 A69-15115

Potential gradient, small ion density and space charge density measurements for atmosphere on Atlantic Ocean during 1965

04 p0594 A69-15159

Low temperature plasma electric arc source operation describing current voltage characteristics and potential distribution

05 p0802 A69-15902

Solar flare influence on potential gradient and air-earth current properties at high mountain stations

05 p0759 A69-16634

Thermal EMF in epitaxial films, analyzing potential distribution in p-n junction with temperature gradients and film thickness effects

09 p1555 A69-21473

Increases of Newtonian potential, gradient and second derivative on gravitating body, considering positive and negative masses

13 p2300 A69-28545

Potential distribution between point in interelectrode gap and thermionic converter cathode in collisionless mode under transverse magnetic field

14 p2401 A69-29235

Thermal EMF in epitaxial films, analyzing potential distribution in p-n junction with temperature gradients and film thickness effects

15 p2669 A69-30718

Retarding potential analyzers to measure rocket vehicle potentials and ambient electric fields in active auroras

20 p3542 A69-37793

POTENTIAL THEORY

Vector potential used to express equations of incompressible fluid motion in form suitable for digital solution, discussing boundary conditions

01 p0058 A69-10228

Tensor character of fictitious potential function introduced to approximate locally tangent actual potential function, discussing planetary gravitational anomaly observation from orbiting vehicles

[AAS PAPER 68-198] 02 p0312 A69-11476

Cauchy problem and mixed boundary value problem for parabolic system solved with thermal potential theory

03 p0455 A69-13259

Vector potentials for Dirac equation derived assuming time independent external magnetic field without scalar potential

04 p0638 A69-15273

Thermal potential P and Q smoothness on surfaces, proving relevant theorems

05 p0849 A69-16452

Transverse motion of embedded or free semiinfinite beam with given initial displacement and velocity, using potentials leading to integral equations

[ONERA-TP-653] 07 p1230 A69-18264

Dirichlet and Neumann problems solvability using potential theory methods, limiting study to three dimensional domains

07 p1173 A69-18496

Gas breakdown in HF uniform electric field without steady transverse magnetic field

07 p1194 A69-19415

Metallic single and double plasma probes, discussing floating potential and ion saturation current

08 p1316 A69-20473

Intermolecular potential function relation to individual macroscopic properties extended to simultaneous fit of all possible pair combinations

10 p1652 A69-23391

Numerical orthonormalized system of functions for formulating functional equations in potential and elasticity theory, considering boundary value problems

10 p1801 A69-23687

Circle theorem for iterated equation of generalized axisymmetric potential theory, noting Stokes flow of viscous liquid

10 p1680 A69-23718

Equivalence of initial boundary value problem and integral equations obtained by regularization using potential theory

10 p1721 A69-23959

Boundary value problems of thermoelasticity, discussing existence and uniqueness theorems, ellipticity, thermoelastopotentials, Liapunov-Tauber theorem, Fredholm theorems, etc

12 p2182 A69-26726

Finite difference solution to TEM mode transmission line cross section for defining continuous potential function leading to capacitance upper bound

13 p2221 A69-28064

Potential functions applications to three dimensional static elasticity problems of parallelepipeds, using general stress solution

15 p2715 A69-31216

Monograph on ring airflow theory with nonuniform incidence covering steady flow and shear flow transition into boundary value problem of potential theory

17 p2889 A69-32995

Plane membranes finite deformation, deriving energy theorems for potential U bounds estimation

20 p3624 A69-37588

Equivalence of initial boundary value problem and integral equations obtained by regularization using potential theory

21 p3756 A69-39150

Protoelastic materials defined in terms of protopotential function, discussing stress tensor dependency on displacement gradients within body

22 p4042 A69-40452

POTENTIOMETERS [INSTRUMENTS]

Potentiometer transient contact resistance determined as function of contacts physical parameters

23 p4166 A69-41996

POTTING COMPOUNDS

Potting material reinforcing honeycomb structures for fastener installation prior to bonding face sheets to core, noting mechanical properties

24 p4326 A69-43466

POWDER [PARTICLES]

NT FINES
NT METAL POWDER
NT POWDERED ALUMINUM

Powders and explosives - Conference, Brussels, September 1966

02 p0301 A69-11519

Ionic and nonionic mineral oxide powder fillers influence on stereopolymers lattices formed from phenolformaldehyde oligomers, discussing mechanical properties

08 p1335 A69-20331

IR emissivities of powdered silicates and cloudy atmosphere model of spectral emission for radiative transfer in condensed powder

10 p1778 A69-23414

Pressure calcinering process in production of fine grained ceramics at low temperatures

12 p2119 A69-26832

Conformally plane solutions to Einstein equations derived with energy momentum tensor characteristic of pulverized material representing gravitational fields

13 p2298 A69-27796

Shear flow, cohesion and internal friction measurements of low bulk density particulate silicates of complex shape, noting significance for lunar comparison

24 p4383 A69-43040

POWDER METALLURGY

Substructural void formation in tungsten powder metallurgy as function of annealing temperature for doped, undoped and electron beam melted material

01 p0093 A69-10061

Nichrome bars production dispersion hardened by alumina and zirconia inclusions, noting extrusion temperature influence

01 p0085 A69-10397

Creep behavior of chemical vapor deposited tungsten at high temperatures by creep-rupture tests compared with powder metallurgy tungsten

01 p0097 A69-10647

Preparation of refractory alloys in powders, fibers and sintered billets by thermochemical method [ONERA-TP-636]

02 p0251 A69-11625

Lattice deformation relationship to dislocation density in vanadium carbide powders

02 p0265 A69-12001

Sintered molybdenum deoxidation effect with C, B and Si, analyzing hardness, tensile strength and ductility

02 p0265 A69-12002

Chromium bronze blanks compacted from granules for hardness and electrical conductivity, noting improved high strength characteristics over conventional production methods

02 p0266 A69-12127

Exothermal effects during sintering of nickel-aluminum powder mixture

02 p0269 A69-12838

Exothermal effects during sintering of nickel-aluminum powder mixture, showing role of liquid phase decomposition and intermetallics

02 p0269 A69-12843

Powder metallurgy, fusion and chemical vapor deposition techniques in manufacturing tungsten base alloys

07 p1165 A69-18792

Polycrystalline beryllium specimens fabricated from powders, discussing initial powder particle size and distribution effects on microyield strength

07 p1168 A69-19598

Physical properties control in nickel powders obtained by hydrogen reduction of nickel diamine sulphate solutions

08 p1334 A69-21057

Complicated power metallurgical shapes fabricated by hydrostatic pressing, noting spheres, cones, rods, tubes and combinations

09 p1511 A69-22353

Porous structures, using spherical tungsten powders, discussing metallurgy, sintering, temperature effects and performance characteristics in ion engines

10 p1710 A69-23166

Beryllium cermet compositions, discussing beryllium oxide content, mechanical strength and elastic and shear moduli

10 p1711 A69-23334

Fiber reinforced metals, discussing crystalline whiskers, metallic and ceramic fibers and mechanical characteristics

10 p1711 A69-23335

Slip casting powder mixture of zirconium carbide and tungsten, discussing optimum composition

10 p1716 A69-24056

Sintered metal powder process for metal-to-ceramic seals for thermionic converters, giving results for tensile strength, thermal cycling and cesium corrosion

14 p2454 A69-29211

Be billets fabrication from powders by cold hydrostatic pressing and pressureless sintering, noting hardness, density and grain size dependence on temperature

14 p2465 A69-29681

Yttrium effect on rate of thermal decomposition of silver carbonate powder and pressed pellets by isothermogravimetric analysis, examining water vapor, Co 60 gamma radiation and temperature effects

15 p2561 A69-30442

Powder properties effect on rolled strip thickness and compactness, angles, pressure at roll and torsion during rolling, analyzing Fe, Ni and Cu powders

15 p2630 A69-31183

Creep rate-stress-temperature relations for powder metallurgy rhenium, discussing activation energy

17 p2991 A69-34186

Re and Re alloy powder metallurgy, noting fabrication of Re coated W particles

20 p3562 A69-37749

H release, pressure and oxide layer formed by reaction during ball milling Cr in water

21 p3728 A69-38567

Powder metallurgy all inert processing method for producing nickel base superalloys forgings, discussing microstructure, reproducibility, mechanical properties, etc

[ASM PAPER GG-8-3-3] 21 p3745 A69-38929

Recrystallization during sintering of free flowing Nb and Ti carbide powders, determining grain growth dependence on temperature and activation energy

22 p3970 A69-40636

Surface chemistry effect on physical properties of pressure sintered Be metal, suggesting surface alloying approach by powder metallurgical techniques

24 p4332 A69-42963

POWDERED ALUMINUM

Aluminum corrosion and inhibition mechanisms in ethylene glycol/water solutions, using controlled powder immersion tests

02 p0265 A69-11895

High speed photographic study of finely dispersed Al particles combustion and ignition in high temperature gas flows, noting dependence on oxidizers concentration

08 p1375 A69-20341

Explosive compacting of aluminum powder, describing operational and experimental techniques, compacts hardness and density, mass production feasibility, etc

16 p2793 A69-31790

Combustion of isolated aluminum particles ignited by laser and burning in controlled gas mixture observed by cinephotomicrography [WSCIPAPER 69-3]

16 p2830 A69-32344

Nonsteady propellant burning theory for Al melting role in suppressing combustion instability in solid propellant rocket motors

19 p3393 A69-36814

POWDERED METALS

U METAL POWDER

POWER AMPLIFIERS

Solid state broadband RF power amplifier for airborne HF radio, eliminating total servosystem and all higher voltage components

17 p2942 A69-34114

One kw HF ground grid wideband untuned power amplifier in transformer coupled cascade stages

20 p3488 A69-37286

Carbon dioxide laser amplifiers gain saturation time dependence characteristics by theoretical model taking rotational relaxation into account

21 p3736 A69-38941

Thermal design of power amplifier for airborne HF transceiver, discussing component layout, air cooling and materials

22 p3909 A69-39942

POWER CONDITIONING

Power converter design for electrically propelled spacecraft, discussing weight, reliability, and thruster load requirements

[AIAA PAPER 69-240] 09 p1568 A69-21732

Aerospace NiCd batteries charge control, discussing depth of discharge, limiting voltage and environmental temperature interrelationship

23 p4071 A69-42282

Modularized static AC and DC inverters and converters for aerospace electrical power conditioning systems, discussing circuit functions and performance tests

23 p4073 A69-42292

Power conditioner for use with SERT II mercury ion thruster, describing electrical and mechanical design and operation

23 p4075 A69-42301

POWER CONVERSION

U ELECTRIC GENERATORS

POWER DENSITY

U FLUX DENSITY

POWER EFFICIENCY

Maximum power efficiency of pulsed injection laser with Fabry-Perot cavity expressed in terms of two dimensionless geometric variables

01 p0089 A69-10119

Gunn generator efficiency dependence on diode and regime parameters using computer model

01 p0042 A69-10319

Low and high power pi-mode Ladderton oscillator design operation and performance characteristics

03 p0405 A69-13726

Output power, efficiency and gain of two stage magnetron-type cascade amplifier

03 p0407 A69-13978

Bleaching of absorption hologram diffraction gratings for improved light efficiency, discussing bleaching materials results

04 p0596 A69-14284

High efficiency microwave oscillations in Si p-n and p-n-n positive avalanche diodes under pulsed conditions 04 p0580 A69-15491

High voltage mercury electron bombardment ion thruster power efficiency [ECS PAPER 170D] 05 p0812 A69-16233

High efficiency ion lasers without additional axial magnetic field 06 p0938 A69-18221

High power coupled cavity traveling wave tube for satellite communication, noting design techniques and performance characteristics 07 p1094 A69-18427

Streaming gas effect on carbon dioxide-nitrogen-helium laser power, discussing gas renewal phenomenon and evacuation rate 07 p1145 A69-18476

Epitaxial GaAs IMPATT diodes for generating CW X band power, noting high efficiencies and low noise characteristics 07 p1102 A69-18660

Space harmonics effect on helical TWT design, discussing operating voltage, beam radius, perveance and maximum allowable gain 07 p1105 A69-18950

Low density Hall ion thruster with application to Van Allen probe and orbit-to-orbit transfer [AIAA PAPER 69-281] 09 p1562 A69-21229

Radiation cooled MPD arc thruster design and performance, noting specific impulse relation to arc spoke rotation frequencies 09 p1566 A69-21259 [AIAA PAPER 69-245]

Cylindrical thermionic converter with vapor deposited rhenium emitter and niobium collector, measuring efficiency and power density 09 p1438 A69-21817

Out-of-core thermionic reactor power increase by using central heat pipe in coaxial cavity 09 p1441 A69-21836

Communication satellite power utilization optimized by matching final amplifiers to solar cell array [AIAA PAPER 68-437] 09 p1442 A69-21990

Turbine blade cooling research programs, discussing effects of increased trailing edge thickness and cooling air on turbine efficiency [ASME PAPER 69-GT-15] 09 p1432 A69-22501

Photocell base thickness for optimal power to weight ratio, noting photons spectral distribution and absorption coefficient dependence on frequency 09 p1443 A69-22719

Power conversion efficiency of diverging channel nonequilibrium MHD generator with small electrode losses, examining influence of channel design 10 p1637 A69-23472

Photoelectric, calorimetric and photon-momentum methods for measuring laser output energy and power emphasizing liquid, wire and pyroelectric calorimeters 11 p1899 A69-25196

Thermoelectric power generators energy output efficiency, discussing thermal and electric contact resistances influence for optimizing parameters 12 p2016 A69-26364

Power losses of varactor frequency multipliers with series connected circuits including open circuit tuned to second harmonic 12 p2043 A69-26888

Wet steam injector power losses in nozzle as function of humidity, noting compensation of nozzle throat diameter and fluid flow rates 13 p2246 A69-27490

Single wavelength design with compensation compared to multiwavelength design without compensation for liquid metal MHD induction converter, discussing optimization 13 p2207 A69-27504

Traveling wave tubes for high efficiency and extreme environments, discussing power output and RF drive 13 p2232 A69-28055

High power voltage tunable magnetron, discussing operating characteristics, life and applications 13 p2232 A69-28056

Traveling wave tubes with broadband CW power, discussing energy dissipation 13 p2232 A69-28057

Magnetically shielded O type backward wave oscillators for military and commercial applications 13 p2232 A69-28059

Nonlinear distortions in TWT for communication satellites applications, discussing relationship with efficiency 13 p2232 A69-28060

Error analysis in efficiency measurement of gas turbines, considering thermodynamics and power output 14 p2509 A69-29509

Power conversion efficiency of frequency doubler using ideal nonlinear capacitance with arbitrary output phase angle 14 p2421 A69-29537

Neutron irradiation effect on efficiency and other parameters of IMPATT diode 14 p2423 A69-29761

Resonance measurement of power percentage in single spurious mode of overmoded waveguide, using back to back transducers and reflection at input 15 p2577 A69-30611

Logic family with low power consumption subjected to 1 Mev electrons analyzed within telemetry circuit concept for space application 15 p2625 A69-30830

Equatorial mounted solar energy concentrator efficiency compared to unconcentrated sunlight and artificial UV-visible light source in reducing Pb tetraacetate solution in acetic acid 16 p2736 A69-31814

Zinc diffused GaAs avalanche diode high CW power and efficiency in normal mode 16 p2760 A69-32015

Solar cell characteristics at low temperatures, noting efficiency increase with decreasing temperature 19 p3251 A69-35691

Attitude control rocket exhaust plume impingement effect on electrical performance and mechanical damage of commercial silica covered silicon solar cells 19 p3252 A69-35700

Thermoelectric power generator with variable thermal conductivity and electrical resistivity, obtaining steady state temperature distribution, power output and thermal efficiency 22 p3868 A69-40131

Aperture efficiency, weight and control power requirements for hybrid matrix arrays in synchronous satellite applications, calculating residual array gains 22 p3915 A69-40707

Jet condenser at very low pressure in organic Rankine cycle power conversion system noting role in power efficiency 23 p4068 A69-42238

Mush cathode fabrication and characteristics for high power klystrons, comparing efficiency to oxide cathodes 23 p4144 A69-42532

POWER GAIN

On-axis gain of parabolic reflector antennas with rough reflecting surfaces as function of surface deviation, correlation distance, area and wavelength 01 p0041 A69-10246

Directional antennas gain loss on ground sections calculated on basis of difference-phase measurements data 02 p0214 A69-11612

Output power, efficiency and gain of two stage magnetron-type cascade amplifier 03 p0407 A69-13978

Reflections from input and output ducts influence on gain of TWT strophotron amplifier with/without allowance for back radiation 03 p0407 A69-13980

Rear gain control of dielectric rod antenna in airborne Doppler system with choke at feed point 04 p0576 A69-14770

Laser power increase noting influence of Mandelstam-Brillouin induced backscattering 04 p0612 A69-15414

Emitter base lateral diode carrier injection effect on current gain properties of small area double diffused planar transistors 05 p0728 A69-15808

Buildup modes of He-Ne laser in presence of other strongly oscillating modes, noting gain interaction effects 05 p0773 A69-16289

Gain degradation under applied voltage and injection current during low dose gamma irradiation by Co-60 source for bipolar transistors 06 p0977 A69-16880

Compact hydraulic power transfer units in aircraft with common connecting shaft for pump/motor elements, discussing integrated power package 06 p0930 A69-17168

X band CW traveling wave tube developed for communications, ECM and plasma research, discussing design, performance and gain ripple diminution 07 p1094 A69-18425

Power traveling wave tubes in ground stations for IN-TELSAT 3 direction finding system 07 p1094 A69-18426

Pumping power effect on He-Ne laser amplification factor dependence on temperature and discharge currents 07 p1149 A69-18935

Continuous wave and pulsed IR signals amplification on carbon dioxide laser amplifiers, discussing design, construction and performance of transmitter [IEEE PAPER J-1] 07 p1152 A69-19064

Beam distortion in low order Gaussian-Laguerre modes propagating through saturable laser amplifier, noting uniform and Bessel small signal gain distributions [IEEE PAPER J-3] 07 p1152 A69-19065

Miniature power amplifier stage for telemetry transmitters, discussing equipment size and weight reduction methods and hermetic envelope 07 p1106 A69-19115

Logic circuit for semiconductor current gain sensing switch 07 p1113 A69-19744

Cascaded avalanche diodes in negative resistance amplifying mode for increased output power and extended dynamic range 09 p1462 A69-21408

Gain, output power and radiation directivity of He-Ne traveling wave laser with nonresonant feedback 09 p1517 A69-21796

Gain stabilization of parametric amplifier, using pumped conduction current of varactor diode 09 p1467 A69-22585

High gain proportional and bistable fluidic amplifier design, noting high impedance role in pressure sensing and computer circuits in aircraft engine control 10 p1638 A69-23555

Antenna gain increase, using matched pair of Cassegrain reflectors with one primary source 10 p1664 A69-23799

Space charge waves amplification in semiconductors on coupling with forward circuit wave by transmission line analog, noting application to electromagnetic and acoustic waves 10 p1748 A69-24053

Directional antennas gain loss on ground sections calculated on basis of difference-phase measurements data 11 p1847 A69-24719

Maximum voltage and power gain of modulator-demodulator type nonresonant parametric amplifiers 11 p1849 A69-24956

Parametric amplifier gain, deriving expressions for diode pumping power and nonlinear circuit element resistance 11 p1849 A69-24957

Laser gain medium dispersion expressions applied to modulator ring laser operation with mode spacing less than pressure broadened atomic linewidth 12 p2106 A69-26324

Far field radiation pattern, radiation resistance, power gain, directivity and effective aperture for center fed dipole antenna with feed points displaced arbitrarily 12 p2039 A69-26352

Single frequency sealed off carbon dioxide amplifier, giving saturated gain 12 p2109 A69-26640

Power gain in TWT attenuators with linear tapered ends, considering conversion loss due to tapering 12 p2044 A69-27102

Gain optimization for dipole endfire array through orthogonalization of element directivity noting effects of element spacing, element gain and mutual coupling 13 p2226 A69-27186

Emitter self bias in power stages of transistor transmitters, considering transistor parameters dispersion 13 p2226 A69-27217

He-Ne laser transition line shape and gain curve through width, considering spectral frequency characteristics, output power and gas temperature and concentration 13 p2272 A69-28115

Crossed field backward wave tubes gain with stepwise varying interaction space found greater than with constant height interaction space 13 p2237 A69-28583

Avalanche diodes as high power pulsed microwave sources, noting power yields and efficiencies 14 p2418 A69-28890

High gain broadband amplifiers with triple tuned coaxial resonators and gridded power tubes, discussing phase stability 14 p2418 A69-28892

Polarization dependent gain saturation and nonlinearity induced anisotropy in He-Ne laser amplifier 14 p2457 A69-28931

Elastic collision effect on gas laser atoms velocity distribution and gain factor determined for strong collision model
14 p2459 A69-29388

VHF surface acoustoelectric amplifier investigated in DC drift field using composite spatially adjacent structure of lithium niobate and silicon film
14 p2422 A69-29559

Continuous IR parametric signal amplification in saturable absorber caused by carbon dioxide laser pumping
14 p2459 A69-29601

Varactors for frequency conversion circuits, discussing efficiency and output power
15 p2578 A69-30797

Traveling wave tube amplifier for wideband radio in SHF range containing periodically integrated magnetized system, discussing output power variation range
16 p2759 A69-31863

Frequency and time dependent gain characteristics of dye lasers, using computer program for rate equations for populations
17 p2980 A69-33025

Gain measurement of two element phased array aperture antenna during ATS-C tracking
19 p3272 A69-36254

Rotational-vibrational relaxation and molecular diffusion effect on saturation parameter of carbon dioxide laser, measuring gain as function of input power
19 p3338 A69-36692

Active admittance, realized gain and linear polarization degradation vs scan angle for infinite periodic phased arrays of circular apertures
20 p3507 A69-37844

Negative energy waves presence, showing qualitative difference on theoretically derived parametric amplification in plasmas
20 p3582 A69-38244

Carbon dioxide laser development, discussing gain, static amplifier and high pressure operations
22 p3962 A69-40474

GaAs laser diodes differential external quantum efficiency and gain per unit length dependence on laser reflectivity, taking into account optical losses
24 p4330 A69-43766

GaAs laser diodes differential external quantum efficiency and gain per unit length dependence on laser resonator length, taking into account optical losses
24 p4330 A69-43767

GaAs junction laser total stimulated light power dependence on resonator length taking into account optical losses
24 p4330 A69-43768

POWER GENERATORS

U ELECTRIC GENERATORS

POWER LIMITERS

Input signal random amplitude fluctuations suppression by parametric power limiter, discussing limiting frequency determination and dependence on signal amplitude
13 p2236 A69-28573

POWER LINES

Electromagnetic radiation below 1 GHz from gap type electrical discharges on electric power distribution lines
23 p4126 A69-42218

POWER PLANTS

Satellite solar power station proposed for power generation for future requirements, discussing world energy needs and finiteness of fossil fuel reserves
16 p2867 A69-31817

Aerodynamic characteristics of power plant installation, discussing nacelle design from viewpoint of aircraft performance and economic efficiency
17 p2898 A69-33215

POWER SERIES

NT TAYLOR SERIES

Diode mixer power series coefficients for spurious response prediction in superheterodyne receiver
03 p0399 A69-13905

Stability and weak oscillations of systems with distributed parameters, using method based on representation of characteristic equation in power series
06 p0956 A69-16822

Power series solutions of MHD boundary layer equations for flat plate with transverse magnetic field and arbitrary pressure gradient, discussing skin friction
09 p1545 A69-21396

Homogeneous parabolic differential equation for heat transfer of two finite bodies in thermal contact solved by power series
09 p1532 A69-21628

Consistent elastic shell theory based on expansion of sought solutions in power series over distance between point and middle surface
11 p1978 A69-24806

London-van der Waals interaction energy of symmetric molecular pair calculated in perturbation theory second order as infinite series in negative powers of separation
12 p2131 A69-26606

Two point boundary value problem converted into Cauchy problem, deriving power series solution method and algorithms for nonlinear problems
14 p2430 A69-29362

Asymptotic power series solutions of viscous solar wind equations
14 p2515 A69-29969

Power law fluids boundary layer near flat plate studied by series expansion and steepest descent methods, determining velocity gradient and skin friction coefficient
15 p2589 A69-30002

Double diffused transistor with Gaussian impurity distribution analyzed by power series for carrier density distribution and frequency response
16 p2758 A69-31616

Plasma flow structure near frontal point in earth magnetosphere, using quasi-hydrodynamic two dimensional model to obtain power series solution
20 p3594 A69-37019

First approximation stability of triangular Lagrange solutions of restricted elliptical three body problem, formulating power series for orbital eccentricity
20 p3575 A69-37318

POWER SPECTRA

Power spectral indices of March 6, 1968 solar radio burst, suggesting Razin effect
01 p0148 A69-10054

Power spectral density method of random loads analysis applied to V/STOL aircraft structural analysis, discussing statistical distribution
01 p0168 A69-10407

Power spectrum for energy transfer region in HF turbulent plasma by nonlinear equations, with results applied to subcosmic ray acceleration
01 p0145 A69-10790

Power saturation in isochronal traveling wave tube explained by motion of electron bunches relative to waves
01 p0047 A69-10882

Atmospheric turbulence power spectra for design criteria of future low altitude aircraft from LO-LOCAT program, analyzing turbulence scale lengths [AIAA PAPER 68-216]
01 p0011 A69-11023

Numerical filtering procedures for gust spectrum analyses compared for gain and phase lag frequency response characteristics, discussing gust acceleration spectra
01 p0084 A69-11052

Liquid lasers compound range of organic type, circulating system of inorganic type and power peaks
01 p0092 A69-11194

Solar cosmic rays diffusion relationship to interplanetary magnetic field power spectrum from high energy proton and electron observations
01 p0147 A69-11243

Radar cross section data interpretation, discussing calibration, unwanted signals, averaging, scattering matrix and power spectra
03 p0385 A69-12913

Pulsar CP 1919 pulse intensity fluctuations intensity with time scales could be strong scintillations
03 p0513 A69-13770

Time averaged products and squares of fluid turbulence signals at LF, using Hall effect multiplier device and integrating voltmeter
04 p0601 A69-15116

Standard Leningrad-2 photoexposure meter applied to measurement of power of laser continuously operating in visual spectral range
04 p0602 A69-15405

Static pressures, profiles of local longitudinal velocity, fluctuating wall pressures and power spectra of wall pressures measured for subsonic turbulent flow [ASME PAPER 68-WA/FE-36]
05 p0750 A69-16109

Expression derived for correlation function and power spectrum of bearing of set of point radiators, taking into account receiver internal noise
05 p0719 A69-16219

Statistical analysis of Radiorad/radar digitizing and recording/clutter and signal spectra and moving target detection by pulse radar
05 p0721 A69-16619

Atmospheric turbulence flight tests random data analysis to stimulate power spectra and transfer functions
05 p0767 A69-16756

Digital spectra analysis by Fourier transform and comb filter for determination of voltage and power spectra
05 p0722 A69-16762

Error probability vs SNR and power spectrum of PCM/PM signal with small phase deviation, noting applications in satellite tracking
06 p0889 A69-17656

Statistical frequency analysis of power spectrum of geomagnetic pulsations, discussing time and latitude dependence
07 p1122 A69-18297

Mode power spectra observations for ring and normal He-Ne lasers at 6328 A
07 p1155 A69-19087

Electronic optical system to process time-varying signals as optical spectrum analyzer for measuring power spectral density of input time function
08 p1317 A69-21086

Power spectral analysis of upper wind data of equatorial lower stratosphere noting quasi-biennial oscillation
09 p1537 A69-22297

Solar flare relation to interplanetary scintillation indices and power spectra
09 p1582 A69-22751

Earth currents and magnetic field variations recording in period range 10-200 sec, computing power density spectra on analog computer
10 p1682 A69-23593

Power spectrum analysis of photometric observations of white dwarf stars for measuring variability of stellar luminosity
10 p1788 A69-24124

Power spectrum of object flux transmittance using Fourier transform type holographic system compared to systems similar to correlator
12 p2090 A69-26254

Potential mechanisms of electron acceleration inside magnetosphere, measuring power spectrum of X rays by electron braking in upper atmosphere
12 p2066 A69-26295

Statistical characteristics of stationary stochastic pulse train specified by probability generating function, noting power density
12 p2030 A69-26383

Power spectral analysis feasibility for data reduction for medical interpretation of changes in pulmonary impedance pneumograph in remote monitoring
12 p2024 A69-26558

Power saturation in isochronal traveling wave tube explained by motion of electron bunches relative to waves
12 p2041 A69-26646

Statistical distribution of instantaneous frequency and power of signal associated with Doppler spectrum for exponentially distributed and determinate frequencies
12 p2032 A69-26863

Scattering characteristics of planet Venus at 3.8 cm wavelength, discussing frequency power spectra and radar cross section
13 p2349 A69-27818

Output power and loss analysis of 2 n injection locked oscillators combined through magic tee hybrids
13 p2232 A69-28061

High energy ionization bursts in cosmic ray showers electron photon component, obtaining bursts power spectrum and component energy dependence
13 p2332 A69-28404

Power spectrum of random process from discrete sequence of instantaneous values, assessing error
13 p2239 A69-28514

Power spectrum analysis and linear filtering for 27 day variation amplitude of geomagnetic disturbance subject to semiannual amplitude modulation
14 p2434 A69-28955

FORTAN program for calculation of magnitude and phase of digital filter transfer functions and power spectra of periodic waveforms
15 p2567 A69-30612

Power spectrum analyzer of weak periodic signal obscured by white noise by zero interactions count of signal and noise mixture
15 p2579 A69-30945

Power spectral density response of uniform beams to random pressures, evaluating joint acceptance of systems with pressure field [ASA PAPER SVT2]
15 p2713 A69-31143

POWER SUPPLIES

- Acoustic flow calorimeter for evaluating power transducers under loaded conditions
16 p2790 A69-32079
- Complex mechanical vibrations causes determined by sensor signals analysis
16 p2876 A69-32434
- Time variation of optical intensity of Sco X-1 X ray source, evaluating photometric data by power spectral analysis
16 p2852 A69-32805
- Power spectral analysis of chromospheric inhomogeneities in July 1967 and June 1968, tabulating mean heights of formation in solar atmosphere
17 p3040 A69-33811
- Solar cycle line in horizontal force of earth magnetic field resolved by power spectrum analysis suggesting 80 year cycle
18 p3205 A69-35414
- Vertical wind shears, structure functions, turbulence and power spectra for transverse velocity fluctuations in troposphere and stratosphere, noting clear air turbulence
20 p3570 A69-37506
- Power spectra of interplanetary magnetic field fluctuations determined from Pioneer 6 satellite data, relating results to galactic cosmic rays modulation
20 p3603 A69-37554
- Power spectrum for energy transfer region in HF turbulent plasma by nonlinear equations, with results applied to subcosmic ray acceleration
20 p3591 A69-38008
- Ionospheric scintillation power spectrum measurements from radio star and satellites related to F region radio refractive index fluctuations
20 p3534 A69-38093
- Output power spectra of Pb-Sn-Te diode laser above threshold of oscillation, demonstrating inverse dependence of line width on laser power
21 p3734 A69-38326
- Statistical analysis of wind velocity measurements at floating buoy stations, presenting velocity power spectra for different frequency bands
21 p3758 A69-39111
- Fourier spectrum analysis of solar line oscillation sequences, discussing power spectra and lifetime of oscillation phase
22 p4019 A69-40286
- Energy density distribution in power spectra of turbulence in long wave region in free atmosphere
24 p4346 A69-43155

POWER SUPPLIES

- Magnetic core logic circuit system for bidirectional stepping motor drive voltage power supply control in proper phase and time sequence
01 p0047 A69-11000
- Caterpillar diesel electric sets for powering NASA tracking station in Australia during Apollo 8 flight
07 p1117 A69-19632
- Power requirements for tracking, telecommand and telemetry of spacecraft over interplanetary distances, considering transmission problems, equipment weight and reliability
10 p1652 A69-22984
- Power sources - U.S. Army Conference, Atlantic City, May 1968
10 p1639 A69-23990
- Real time/process computer interface with electric power systems, discussing compatibility, reliability, etc, problems in connection with management and engineering personnel
11 p2004 A69-25302
- Operational amplifier integrated circuits applications, discussing simple and transducer amplifiers, operational circuits, wave shapers and generators and power supplies
11 p1857 A69-25665
- Oscillator parameter matching to flame discharge parameters to obtain optimal power for powering flame discharge for plasma jet source
12 p2140 A69-27129
- Square wave generator for junction laser power supply
13 p2274 A69-28643
- Ultrarelativistic electron acceleration in Crab Nebula maintaining synchrotron spectrum, obtaining power from compressional motion damping, gyrorelaxation effect and pitch angle anisotropy removal
19 p3424 A69-36336
- Rankine power cycle for fluid evaluation, discussing radiating area, thermodynamics, etc
23 p4239 A69-42276
- Seam welding processes and power supply effects on control efficacy based on electrode displacement for Al-Mg alloys
24 p4319 A69-42919

POWER SUPPLY CIRCUITS

- Pulsed ruby laser power supply incorporating facilities for variable output, automatic cutoff for fully charged capacitors and automatic manual triggering
02 p0256 A69-12095
- Circulator power splitting and isolating function in integrated microwave network
02 p0222 A69-12475
- Microwave energy generation with solid state equipment, noting Gunn effect diodes, avalanche diodes and limited space charge accumulation/LSA devices
03 p0402 A69-12971
- Solid state power supplies for turbine control and instrumentation, discussing control system manufacturer requirements and reliability specifications
03 p0368 A69-13432
- X ray proportional counter, analog to digital converter and power supply for gamma ray spectrometry used in satellite applications
07 p1134 A69-19194
- Thermal instability in power transistor structures, considering effects of design, emitter and base resistance at high currents
08 p1373 A69-20858
- Storage varactors and frequency dependent diode input power for multiplier cascades control, discussing series connections and limitations by thermal noise
11 p1841 A69-25607
- Electron-optical image converter camera for wide time intervals, considering nanosecond electronic control and high voltage stabilized power supply
12 p2083 A69-26140
- Single phase bidirectional AC/DC power convertor based on back-to-back SCR hybrid bridge
13 p2209 A69-28178
- Power supplies for ruby, YAG and glass lasers, emphasizing design equations and component selection
15 p2636 A69-31527
- Power supply circuits in spacecraft, DC voltage control systems, transistor and thyristor regulators and modulators, etc
17 p2937 A69-33582
- Overload protection guidelines for power subsystems, discussing source and protective device characteristics emphasizing spacecraft requirements
17 p2904 A69-34088

POWER TRANSMISSION

- Circulator power splitting and isolating function in integrated microwave network
02 p0222 A69-12475
- Production history of Model UH-1/Huey helicopter power transmission, discussing producibility
03 p0433 A69-13450
- Adaptive primary feed system for wide angle beam scanning from parabolic reflector antenna, using Fourier transformation to obtain uniform power distribution
08 p1279 A69-19908
- Radiant power flow, transmittance and absorbance of absorbing thin film multilayer in terms of characteristic matrix and admittance of surrounding media
11 p1896 A69-24850
- High speed shafting design for helicopter power transmission systems, discussing shaft in OH-6A Cayuse light observation helicopter
14 p2453 A69-28837
- Microwave power transmission to high or low altitude balloon systems for stationkeeping, describing flexible diode array rectifier antenna
22 p3870 A69-40809

POYNTING THEOREM

- Ray path geometry derived by Poynting vector to calculate surface fields due to creeping waves in sphere planes
08 p1274 A69-20046
- Polar elastic media pure torsion solved, noting couple-stresses influence on Poynting effect
08 p1414 A69-20527

PPI [POSITION INDICATORS]

U POSITION POSITION INDICATORS

PRANDTL-MEYER EXPANSION

- Stationary shock wave formation onset in Meyer-Prandtl flow, obtaining Marchal number for plane flow
09 p1429 A69-21688
- Leeward side of delta wing with sharp leading edges at hypersonic speeds, noting Prandtl-Meyer expansion
09 p1431 A69-21992
- Steady Prandtl-Meyer expansion of shock heated gases for recombination studies, measuring static pressure, stagnation point heat transfer, IR emission and optical absorption
18 p3228 A69-34466

PRANDTL NUMBER

- Transverse pressure gradient and streamwise derivatives effect on free convection laminar heat transfer on isothermal vertical plate at low Prandtl numbers
01 p0177 A69-11409
- Hydrodynamic analysis for determining steady flow region with closed separation area for Reynolds numbers to describe viscous mixing by Prandtl equations
02 p0190 A69-12570
- Heat transfer through vertical plane layer for various Prandtl numbers, discussing velocity and temperature profiles and effects of aspect ratio, Grashof and Rayleigh numbers
05 p0846 A69-16115
- Prandtl brittle fracture model modified for semi-finite crack in infinite body, discussing microscopic and macroscopic relation and crack propagation kinetics
07 p1237 A69-19682
- Wall temperature and Prandtl number effects on turbulent boundary layer thicknesses and shape factors for subsonic compressible gas flow over flat plate
09 p1432 A69-22513
- Statistical theories of turbulence applied to thermal convection between infinite slippery plates at large Prandtl number
11 p1997 A69-24283
- Steady incompressible fluids flow around stationary wings and through rotating blades cascades based on Prandtl airfoil theory of bound vortices
11 p1873 A69-25202
- Buoyancy-driven system instability mechanism, showing Prandtl number increment effect and relation to Coriolis-driven instability of rotating fluids
11 p1876 A69-25559
- Numerical solutions of equations for high Prandtl number boundary layers in two dimensional flat plate incompressible flow with mass injection
13 p2249 A69-28238
- Monograph on Prandtl number effect on heat transfer and pressure loss in artificially roughened channels
15 p2717 A69-30934
- Compressible laminar boundary layer equations solutions for nonunit Prandtl number by direct numerical integration
16 p2772 A69-32173
- Two term expansion for Nusselt number for laminar natural convection about isothermal horizontal cylinder in fluid with vanishingly small Prandtl number
17 p0368 A69-33014
- Coupling conditions by distinct equations for two laminar flow regions, studying near wake and considering Euler, Navier-Stokes and Prandtl correlations
19 p3299 A69-36649
- Free convection boundary layer singular character at low Prandtl numbers, deriving expression for Nusselt-Grashof relation
21 p3849 A69-38772
- Concentration distribution of admixture in semibounded jet propagating along nonheat conducting plate, obtaining concentration profiles for various thermal and diffusion Prandtl numbers
21 p3854 A69-39844
- Prandtl number influence on heat transfer and pressure drop characteristics of roughened channels, determining friction factor
24 p4407 A69-42915

PRASEODYMIUM

- Low temperature specific heat of praseodymium magnesium nitrate
12 p2026 A69-25784
- Praseodymium germanides resistivity and thermal EMF temperature dependence determined, discussing Hall effect, thermal expansion coefficient, melting point microhardness, etc
23 p4199 A69-42467
- Ultrasonic paramagnetic resonance investigations of Pr ions ground state energy levels in calcium fluoride
24 p4360 A69-42790

PREAMPLIFIERS

- Simultaneous measurement of gain and noise of linear two port device using noise generators as signal sources
02 p0210 A69-12430
- Low noise microwave amplifiers for radio astronomy and satellite communications receiving system preamplification
03 p0402 A69-13017
- Traveling wave maser and cooled parametric amplifier for ultralow noise preamplification in satellite communication earth terminal installations
05 p0728 A69-15670

Helium cooled low noise high gain parametric preamplifier for satellite communication by stagger tuning stages
07 p1098 A69-18460

Tunnel diode amplifiers for amplifying weak microwave signals, discussing low noise wideband preamplifier for communication satellites
07 p1099 A69-18464

PRECAMBRIAN PERIOD

Geomagnetic field strength in early Precambrian, discussing thermoremanent normal remnant and saturation inverse remnant magnetization studies of Botswana Modipe gabbro
08 p1309 A69-20580

Organic geochemical investigations of lunar rock samples based on analysis methods for carbonaceous meteorites and early Precambrian sedimentary rocks
20 p3476 A69-37616

Precambrian crustal geotectonic evidence of earth radius expansion based on dated orogenic fold belts distribution
22 p3936 A69-40182

Early Precambrian Onverwacht microstructures studied in petrographic thin sections and powdered preparations for possibility of oldest terrestrial fossils
24 p4263 A69-43221

PRECAUTIONS

U ACCIDENT PREVENTION

PRECESSION

NT LARMOR PRECESSION

Dynamically symmetric gyrostat steady motion stability in relation to satellite motion
01 p0163 A69-11301

Equivalence principle application to gyroscope motion in uniform gravitational field to obtain precessional angular velocity
05 p0764 A69-16367

Special and general relativity theories following Newtonian mechanics and gravitation theories, discussing metric tensor, sun oblateness and experiments with gyroscope spin axis precession
07 p1181 A69-18928

Biaxial gyro stabilizers mounting on rocking base, deriving expressions for constant components of stabilizer precession rate
09 p1498 A69-22112

Single axis gyro stabilizer stability analysis allowing for dry friction in precession axis, noting asymptotic tendency of motions toward steady rotation
09 p1502 A69-22701

Small angle precessional motion of axisymmetric spin stabilized bodies subject to disturbing moments
10 p1724 A69-22932

Hydropendulum bearing linear horizontal vibration effect on vortex vibration, analyzing zero initial phase using precession theory
10 p1697 A69-24086

Rotor shaft mounted on number of bearings and carrying masses and inertia angular precession and critical speeds, considering gyroscopic moments, rotary inertia and shear deformation
[ASME PAPER 69-VIBR-54]
10 p1805 A69-24154

Directional gyroscope accuracy increased by self adaptive systems, based on precession theory and drift amplitude dependence
11 p1881 A69-24559

Image motion trajectory in rotating angular mirror having converging reflections from two surfaces, using precession theory of gyroscopes
11 p1881 A69-24562

Helicoidal precession stability in sense of Liapunov, Poincare and Lagrange
12 p2130 A69-26286

Land gyrocompass on torsional suspensions in liquid filled chamber, considering design and operation in terms of precession theory
13 p2259 A69-27431

Instantaneous rotational impulse imparting steady motion of disk determined for coupled gyroscope
13 p2264 A69-28527

Circular membranes vibrational and stability characteristics under simultaneous constant spin and precessional motions, obtaining Hill equation for motion amplitude coefficients
13 p2370 A69-28665

Deep freezing of nuclear precession magnetometer elements for improving instrument characteristics
14 p2446 A69-29083

Earth quadrupole moment effects on precession of gyroscope in satellite in equatorial orbit
17 p2972 A69-33072

Boundary layer theory application to dynamics of gyroscope in gimbal suspension, defining nutational and precessional motion
18 p3135 A69-34559

Passive damper system for reducing precession in free symmetrical rotating space vehicle, noting linear torsional spring influence on precession decay
19 p3429 A69-35913

Coordinate transformation of Euler equations governing precession and nutation of self gravitating bodies of viscous fluid in inertial coordinates
21 p3797 A69-38539

Eulerian equations for precession and nutation of self gravitating fluid globes of arbitrary structures in inertial coordinates, discussing coplanar case, tidal breathing, etc
22 p4030 A69-40904

Autometric gyro for satellite general relativity experiments, particularly earth orbit measurement of Lense-Thirring precession
23 p4162 A69-41543

PRECIOUS METALS

U NOBLE METALS

PRECIPITATION [CHEMISTRY]

Grain boundary interaction energy with inclusion of second phase, describing equilibrium and boundary shape
03 p0449 A69-13880

Nodal precipitation and cellular solidification substructure in commercial purity nickel, discussing supercooling, NiO and eutectic composition
08 p1332 A69-20289

Carbide precipitation in stainless steels using metal foil and extraction replicas, discussing grain boundaries corrosion relation
10 p1713 A69-23820

Anodic stain etching technique for carbide precipitates of niobium-base alloy Cb 132, noting X ray diffraction
13 p2282 A69-28162

N precipitation kinetics in deformed Nb, finding constant in rate equation dependent on temperature and correlated to precipitates nature
15 p2639 A69-30585

Nb supersaturated solid solution in Co precipitation mechanism analyzed by X rays and electron microscope, noting diffusive scattering effects
21 p3750 A69-39788

PRECIPITATION [METEOROLOGY]

NT DEW

NT HAIL

NT RAIN

NT SNOW

Radar method of spiral scanning clouds and precipitation at constant altitude
03 p0459 A69-13286

Numerical radar information charts, plotting radio echo reflection boundaries from cloud and precipitation observations by weather radars
03 p0459 A69-13287

Quantitative estimations of cloud and precipitation by radar meteorology, assuming homogeneous reflectivity distribution of clouds
04 p0626 A69-14507

Microwave absorption and scattering by atmospheric precipitation as function of temperature and water droplet size
06 p0954 A69-17997

Radio wave brightness temperatures and contrast characteristics in presence of clouds and precipitation
06 p0954 A69-17999

Cometary, lunar and solar effects on precipitation, considering joint influence of meteoric streams and moon
11 p1965 A69-25420

Statistical rules for seasonal forecasts based on temperature and precipitation deviations analysis in long term climatological records, considering sunspot cycle role
12 p2125 A69-25895

Atmospheric models for electromagnetic scattering of monochromatic IR and microwave radiation by natural suspensions as hazes clouds and precipitation
12 p2030 A69-26467

Dimensions, concentration and spectrum of large precipitation particles in clouds and cloud water content by measuring reflectivity and absorptivity at different wavelength
16 p2807 A69-32268

Amplitude distribution and correlation functions of signals reflected from precipitations at various polarizations of waves emitted and received
16 p2807 A69-32269

Horizontal wind pulsations in precipitations obtained from pulsed Doppler radar data, including degree of turbulent flow anisotropy
16 p2807 A69-32271

Vertical wind velocity pulsations in precipitation and passage through subfrontal clouds measured by pulse radar
16 p2807 A69-32272

MRL-1 meteorological radar station detection of cloud types under steady rain, showers and storm conditions, describing radar data analysis procedure
16 p2808 A69-32278

Wind velocity and precipitation particle terminal fallspeeds component determination from continuity equation for data collected by Doppler radar
17 p2919 A69-33162

Air motion and precipitation patterns in travelling wave depression, considering Doppler radar data, rainfall rates, orographic influences, etc
18 p3166 A69-34419

Precipitation zone-cloud mass correlation based on Tiros cloud photographs, synoptic charts and weather maps for European U.S.S.R.
19 p3366 A69-36671

Cloud physics problems of precipitation release from interaction of air motions and microphysical events, discussing raindrop growth initiation, artificial cloud modification, etc
20 p3572 A69-37906

Doppler radar observations of precipitation induced mesoscale wind oscillations near melting layer produced by pressure perturbations due to horizontal variations in cooling
20 p3572 A69-37909

Meteor shower effects on rainfall, noting anomalous radar meteor influx increase and subsequent subnormal precipitation
20 p3609 A69-38062

Radar signal reflectivity and precipitation relationship revised on basis of radio signal damping for improved measurement accuracy
23 p4185 A69-42494

Precipitation physics, discussing cloud structure on mountains and in free atmosphere, precipitation measurement on ground, raindrop size distribution, etc
24 p4343 A69-43037

PRECIPITATION HARDENING

Nichrome bars production dispersion hardened by alumina and zirconia inclusions, noting extrusion temperature influence
01 p0085 A69-10397

Nb-W alloy solution hardening and deformation, noting flow stress dependence on strain rate and temperature plus activation energy of deformation
01 p0095 A69-10488

Precipitation hardening of gamma phase in austenitic stainless steels studied for phase transformations by dilatometry after aging and quenching
01 p0096 A69-10613

Aging and cold work hardening effect on deformability of aluminum-magnesium-silicon-copper alloy
02 p0254 A69-12677

Dispersed hard particles effect on high strain fatigue behavior of nickel at room temperature
03 p0443 A69-13121

Heavy titanium carbide precipitation on fatigue slip zones of stainless steel, noting rupture produced crystallographic facets
03 p0447 A69-13605

Al/Zn/Mg alloys preprecipitation, discussing Guinier-Preston and critical zone sizes and reversible vacancy trap
03 p0447 A69-13613

Second phase hardened materials recovery creep rate model, showing dependence on stress level
03 p0447 A69-13615

Impurity-dislocation interaction in Al alloy by vacancy mechanism and repeated yielding phenomenon, establishing activation energy
04 p0613 A69-14440

Properties of Ni-Mo-Al age hardening steels, discussing data confirming validity of low carbon low aluminum approach
04 p0613 A69-14527

Aging of iron-nickel-titanium alloys during heating in reverse martensitic alpha to gamma transformation process, investigating phase parameter changes
04 p0613 A69-14558

Al-Mg-Si alloy strain aging, noting effect of deformation stresses on kinetics and aging mechanism for prior and concurrent deformation
04 p0614 A69-14575

Precipitation hardening effects on Al-Zr recrystallization with Fe and Si additions, noting peak hardness increment with decrease in aging temperature

04 p0617 A69-14931

Work hardening in quenched fully hardened and overaged Mg-Mn alloy single crystals as function of temperature and strain rate

05 p0778 A69-15757

Low carbon maraging steel, studying age hardening behavior of iron-manganese-nickel alloys with titanium additions

05 p0781 A69-16541

Sintered W-Ni-Fe alloys strength and precipitation hardening characteristics for various compositions and cooling conditions

05 p0782 A69-16798

Precipitation hardening stainless steels, discussing corrosion resistance, high strength, weldability, fabricability, heat treatment, etc

06 p0932 A69-17874

Plastic deformation of internally oxidized dispersion strengthened silver magnesium alloys, noting hardening effect dependence on oxidation temperature

07 p1159 A69-18627

Plastic fractures of age hardened aluminum alloys analyzed by tensile tests and electron fractography, considering stresses, surface and intergranular effects

07 p1166 A69-18961

Polycrystalline Mg-Th-Zr alloy precipitation hardening investigated by tensile and hardness tests and transmission electron microscopy

07 p1167 A69-19265

Edge dislocations effect in perpendicular slip planes on work hardening and strain aging, calculating dilatation centers absorbed

07 p1238 A69-19695

Solution annealing and aging time and temperature effects on precipitation in quenched and aged beryllium

08 p1330 A69-20008

Weldability of precipitation-hardening stainless steels by gas tungsten arc process, discussing microstructure and shrinkage stress cracking

08 p1320 A69-20409

Dislocations effect on intermediate body centered tetragonal phase precipitation in Fe-Ni-Cr-Be alloy using transmission electron microscopy

08 p1333 A69-20447

Monograph on precipitation hardening and mechanical properties of various heat resistant alloys with Co contents to 35 percent

08 p1334 A69-20763

Crystal lattice and orientation of precipitate responsible for hardening water quenched Ni-Cr-Nb alloy

08 p1334 A69-20852

Wrought superalloys fusion welding behavior, discussing hot cracking, hot microfissuring and strain age cracking [SAE PAPER 690102]

09 p1503 A69-21558

Alloying elements effects on structure, mechanical properties, aging and composition of precipitation hardening intermetallic phases in Ni and Fe based alloys

09 p1525 A69-22143

High temperature metallic material strengthening methods, noting metallurgical factors and temperature effects on mechanical properties

10 p1712 A69-23630

Silicon particle sizes in Al-Si system investigated for interactions with dislocations as function of strain and for effect in dispersion hardening

10 p1714 A69-23980

Monograph on effect of nitrogen on precipitation behavior of austenitic chromium-nickel steel covering carbides, intermetallics, phase transportations, corrosion resistance, etc

11 p1902 A69-24369

Preliminary natural aging effects on maximum strength properties obtained at various artificial aging temperatures for aluminum ternary alloy

11 p1905 A69-24921

Highly alloyed steels weldability, considering nickel maraging and precipitation hardening stainless steels

12 p2111 A69-25829

Precipitated phase composition and structure of Co-Ti solid solution during aging

12 p2112 A69-26037

Intermetallic compound precipitation effects on mechanical properties of Fe-Mo alloy at high temperatures

12 p2116 A69-26925

Dynamic strain aging of Fe-Cr-C and Fe-Mo-C steels, analyzing strength, ductility and secondary

hardening by using microprobes, foils diffraction and extraction replicas

13 p2276 A69-27403

Quantitative separation of elements in gamma prime from precipitation hardened high temperature nickel-base alloys by anodic dissolution

13 p2277 A69-27408

Plasma spray quenched Al-V alloys resulting in dispersion strengthening of material

13 p2277 A69-27409

Precipitation influence on martensite formation kinetics and structure of Fe-Ni-Ti alloys

13 p2279 A69-27765

Dispersion-strengthened alloys from extraction replicas, determining volume fraction and spacing of dispersed phase particles

13 p2282 A69-28167

Ni alloys phase precipitation and Fe substitution effects on heat resistant alloys

13 p2283 A69-28488

Grain size and deformation velocities effects on plasticity of dispersion hardened alloy

13 p2283 A69-28489

Time and temperature effects on corrosion and structure of Hastelloy alloy C-276

14 p2466 A69-29930

Maraging steel weldability, discussing residual stresses, hydrogen cold cracking, age hardening and hot cracking

15 p2617 A69-30098

Strain aging of polycrystalline Nb containing interstitial impurities as function of temperature, discussing interstitials role in recovery substages

15 p2636 A69-30194

Al-Mg-Si alloy strain aging, noting effect of deformation stresses on kinetics and aging mechanism for prior and concurrent deformation

15 p2638 A69-30276

Discontinuous yielding characteristics of 2024 Al alloy determined for different conditions of solution, heat treatment and age hardening

15 p2639 A69-30598

Maximum strengthening due to second phase precipitation within operating temperatures maintainable to 20 hr during aging of Nb-Hf-O and Nb-Zr-O alloys

15 p2640 A69-30632

Trace elements influence on precipitation process and properties of Al-Cu, Al-Zn-Mg and Al-Mg alloys, using X ray diffraction

16 p2801 A69-31783

Precipitation processes and effect on properties of Cr-Ni-W-Ti heat resistant austenitic steel, using electron diffraction and transmission electron microscopy

17 p2984 A69-32833

Preliminary plastic deformations effect on dispersion hardened nimonic-80 alloy creep properties

18 p3159 A69-35446

Adhesive bonding of Al sheets for honeycomb sandwich material, using electrical conductivity to measure sheets age hardening progress during high temperature curing

19 p3321 A69-35565

Ti transition metals alloys omega phase precipitation, discussing composition, morphology, coherency, formation, etc

19 p3344 A69-35928

Precipitation hardening, microstructure and dislocation influence on intergranular stress corrosion cracking (SCC) of high strength Al alloys examined by transmission electron microscopy

19 p3351 A69-36898

Supersaturated solid solution decomposition in Ni-Cr-Ti system, discussing precipitation mechanism of eta phase

20 p3558 A69-36968

Precipitation hardening stainless steels applications in aerospace industry, discussing steel selection and heat treatment

20 p3563 A69-37931

Age hardening response of Mg-Th-Zr alloy at 60-450 C, discussing peak strengthening, superlattice formation, precipitation processes, etc

21 p3743 A69-38735

Composition and thermal treatment effects on weldability of precipitation hardened Ni base alloy, analyzing heat affected zone cracking sensitivity

22 p3968 A69-39885

Recovery process observation in pure binary Al-Cu alloy and commercial Al-Cu-Mg-Pb alloy, noting electron microscope applicability

22 p3968 A69-40062

Alloy Inconel 625 precipitation behavior and effect on short and long term properties, discussing tetragonal phase segregate and creep strength

22 p3971 A69-40802

Solid solutions precipitation effect during deformation process on static and dynamic tensile tests of Al alloy by electric resistance measurement

22 p3972 A69-41082

Al-Ni-Co alloys precipitation mechanism effect on magnetic properties, including heat treatment and Ti alloying effects

23 p4175 A69-41298

Ni based superalloy mechanical properties, determining chromium carbide discontinuous precipitation effects at various temperatures

23 p4176 A69-41507

Coherent matrix precipitates observation in Fe-Ni-Cr alloy by transmission electron microscopy, discussing yield strength and elongation dependence on aging conditions

23 p4176 A69-41508

PRECIPITATION PARTICLE MEASUREMENT

Radar calibration and precipitation measurements equation taking Gaussian approximation for antenna radiation pattern

16 p2806 A69-32264

Precipitation intensity measurements, obtaining distribution parameters from radar reflectivity at two wavelengths and microwave attenuation factor at third wavelength

16 p2806 A69-32265

Range effects on apparent height and frequency biases of radar precipitation echoes determined by regression technique for several stations

18 p3101 A69-34826

Waves in auroral ionosphere due to particle precipitation, indicating ionospheric plasma instabilities

18 p3130 A69-35187

Millimeter wave pseudorandom coded CW meteorological radar for precipitation drop size spectrum analysis and cloud studies, discussing overall system design

23 p4115 A69-41531

Precipitation physics, discussing cloud structure on mountains and in free atmosphere, precipitation measurement on ground, raindrop size distribution, etc

24 p4343 A69-43037

PRECIPITATORS

U ELECTROSTATIC PRECIPITATORS

PREDICTIONING

Semiconductor impressed voltage preconditioning, considering problems involving surface properties

16 p2758 A69-31713

PREDICTIONS

NT LINEAR PREDICTION

NT PERFORMANCE PREDICTION

Optimal predictor design by comparison of statistical input models, measuring signal filter performance by root-mean-squared errors

01 p0043 A69-10558

Adaptive compression system for predicting and encoding video data for transmission in noiseless channel

03 p0427 A69-12869

Distribution function of multiple correlation coefficient for various sampling volumes and various numbers of predictors calculated using Fisher formula

13 p2293 A69-27843

Predictability of deterministic fluid systems with many scales of motion using vorticity equation for two dimensional incompressible flow, noting application to earth atmosphere

19 p3303 A69-36404

Controlled-variable prediction display based on Taylor series computation, describing acceleration system simulator and human operator performance

19 p3313 A69-36414

Adaptive predicting filter mathematical model based on information probability, using adaptive systems latent memory

19 p3287 A69-36665

Biological responses to weightlessness prediction, considering gravity perception mechanisms, cellular metabolism, etc

21 p3656 A69-38921

Interference prediction models of equipment emissions and susceptibility thresholds based on limited spectrum signature data

23 p4126 A69-42223

PREDICTORS

U PREDICTIONS

PREFERRING TESTS

U COLD FLOW TESTS

PREFLIGHT OPERATIONS
NT COUNTDOWN

Mariner Mars 1969 spacecraft real time test support system and recorded data analysis including routing to printers, CRT displays and incremental plotters [AIAA PAPER 69-982] 22 p3907 A69-40362

PREFORMS

Etching, spray etching and photo-resist methods for producing CrNi steel heating elements for propeller deicing 12 p2102 A69-26370

PREHEATERS

U HEATING EQUIPMENT

PREHEATING

U HEATING

PRELAUNCH TESTS

NT STATIC FIRING

Europe 1 carrier rocket prelaunch wind load calculations as base for launch or delay decision 01 p0160 A69-10032

OGO program failure rate analysis with respect to cost, schedule and performance tradeoffs, considering component and systems design and reliability, prelaunch feedback, etc 18 p3207 A69-34519

Computer simulation model for Saturn 5 prelaunch system reliability analysis, using Bayesian techniques 18 p3207 A69-34529

Space vehicle data system synthesizer /SVDSS/ for dynamic calibration of automatic control and checkout systems during prelaunch and countdown operations 21 p3680 A69-39633

Spacecraft onboard computer for prelaunch targeting constants verification through checksum equation and error detection scheme, using generated number sequences [AIAA PAPER 69-946] 22 p3974 A69-40329

PRELOADING

U PRESTRESSING

PREMIXED FLAMES

Flame velocities of stable premixed tetrafluorethylene-oxygen mixture flames measured with bunsen-cone method 11 p1940 A69-24485

Turbulent burning velocity definition for one dimensional turbulent flow and average flame orientation perpendicular to flow direction, discussing transient flames in turbulent environment 13 p2379 A69-28452

Solid metal oxide particles temperature in premixed flames determined from intensity/ wavelength plots of continua 21 p3852 A69-39592

Laminar burning rate of premixed propane-air flames at one atmospheric pressure in DC electric fields, using cooled porous plug burned method 21 p3852 A69-39596

PREPARATION

U PRECONDITIONING

U PRESTRESSING

PREPOLYMERS

NT DIMERS

Curing agents for carboxy and hydroxy functional prepolymers synthesis and evaluation including sulfonyl, acyl and ureido aziridines [AIAA PAPER 69-436] 16 p2747 A69-32777

PRESINTERING

U SINTERING

PRESSES

Hydraulic press large closed die forging of various alloys and refractory materials, evaluating mechanical and metallurgical problems [ASM PAPER C7-5.4] 04 p0604 A69-14522

PRESSING [FORMING]

NT BLANKING [CUTTING]

NT COINING

Soviet book on press working of aviation materials, noting granulated and powdered materials and high strength and refractory materials 03 p0451 A69-14117

Large hydraulic press forgings for light metals, discussing 50,000 ton machine used for Al alloys, tooling and die considerations [ASM PAPER C7-5.1] 04 p0604 A69-14521

Section pressing from Ti alloy, noting procedure and temperature dependent deformation parameters effect on microstructure and properties 07 p1164 A69-18788

Complicated power metallurgical shapes fabricated by hydrostatic pressing, noting spheres, cones, rods, tubes and combinations 09 p1511 A69-22353

Slip casting powder mixture of zirconium carbide and tungsten, discussing optimum composition 10 p1716 A69-24056

PRESSURE

NT ATMOSPHERIC PRESSURE

NT BASE PRESSURE

NT BLOOD PRESSURE

NT CRITICAL PRESSURE

NT DENSIFICATION

NT DIFFERENTIAL PRESSURE

NT DYNAMIC PRESSURE

NT ELECTRON PRESSURE

NT GAS PRESSURE

NT HIGH ALTITUDE PRESSURE

NT HIGH PRESSURE

NT HYDROSTATIC PRESSURE

NT HYPERTENSION

NT HYPOTENSION

NT HYPOXEMIA

NT ILLUMINANCE

NT IMPACT LOADS

NT INLET PRESSURE

NT INTERNAL PRESSURE

NT INTRACRANIAL PRESSURE

NT INTRAOCULAR PRESSURE

NT LOW PRESSURE

NT LUMENS

NT LUMINANCE

NT LUMINOUS INTENSITY

NT OVERPRESSURE

NT OXYGEN TENSION

NT PARTIAL PRESSURE

NT RADIATION PRESSURE

NT SOUND PRESSURE

NT STAGNATION PRESSURE

NT STATIC PRESSURE

NT SUPERCRITICAL PRESSURES

NT SYSTOLIC PRESSURE

NT TRANSIENT PRESSURES

NT ULTRAHIGH VACUUM

NT VACUUM

NT VAPOR PRESSURE

NT WALL PRESSURE

NT WATER PRESSURE

NT WIND PRESSURE

Pressure on unsteadily oscillating cylindrical shell in external or internal supersonic flow derived from asymptotic theory 09 p1618 A69-22256

PRESSURE BREATHING

Forearm skin capacity vessels tonus as function of intrapulmonary pressure during positive and negative pressure breathing 23 p4093 A69-42068

Positive pressure breathing effects on cerebral arterial and venous blood pressure, hypothalamus and adrenal glands catecholamine content and cerebrum histological changes in dogs 24 p4265 A69-43371

PRESSURE BROADENING

Methane broadening and anomalously small pressure shift of 3.39 micron rotation-vibration line, using laser saturated molecular absorption 04 p0633 A69-15424

Collision broadened spectral line shape obtained in impact approximation using Anderson formulation compared to output of gas lasers [IEEE PAPER T-6] 07 p1154 A69-19083

PRESSURE CABINS

U PRESSURIZED CABINS

PRESSURE CHAMBERS

NT VACUUM CHAMBERS

Reinforced thin walled cylindrical pressure body nonlinear circumferential stress problem approximate solution, noting fatigue strength of aircraft pressurized cabins 04 p0548 A69-14838

Rectangular shock tube for use with pressure and vacuum, discussing sealing of circular end flanges to buildup tube 06 p0906 A69-16928

Device for producing high current high pressure arc discharge using water cooled chamber and Be bronze electrodes 09 p1547 A69-21593

Discharge rates of metabolic products in men confined in pressure chamber wearing airtight suits and gas masks 10 p1646 A69-23508

Prestressed ceramic driver chamber energy efficiency for arc driven shock tube by pressure measurements with piezoelectric probe 18 p3116 A69-34456

EEG monitoring during decompression illness /bends/ treatment by hyperbaric procedure using small multichannel telemetry pack 19 p3261 A69-36268

Bubble oscillations in water filled pressure chamber with alternating pressure generated by piston, measuring temporal development 19 p3302 A69-36871

Portable multiunit low pressure chamber with locks, permitting water replenishment, feeding of animals under continuous pressure and gas mixtures 22 p3891 A69-40217

EKG, EEG, pneumograms and X ray pictures showed no pathological effect after prolonged confinement in sealed chamber having artificial atmosphere with variable gas composition 22 p3892 A69-40284

PRESSURE COEFFICIENT

U AERODYNAMIC COEFFICIENTS

PRESSURE DISTRIBUTION

Static pressure field induced by steady subsonic flow of compressible inviscid fluid through two dimensional duct with statistically distributed wall roughness 01 p0062 A69-11279

Polygonal wing planform pressure distribution in incompressible flow calculated on basis of lifting surface theory 01 p0008 A69-11298

Pressure and shock shape determination for plane supersonic and low hypersonic flows past aerodynamic profiles 01 p0008 A69-11299

Turbulent boundary layer growth, pressure distributions and surface shear stresses on yawed semicircle cone [AIAA PAPER 68-98] 02 p0190 A69-12526

Unsteady pressure field in zone of aerodynamic proximity of free moving airscrew investigated with propeller blades replaced by surface singularities 02 p0192 A69-12827

Plane supersonic base flows studied using integral analysis of turbulent reattachment, noting prediction of wall pressure distribution 03 p0361 A69-12990

Pressure distribution at wedge wall during instantaneous small variation of supersonic motion 03 p0364 A69-13662

Rayleigh step journal bearings, considering pressure distribution, load capacity and attitude angle and optimal film thickness ratio for incompressible fluid lubrication 04 p0605 A69-14587

Shoulder pressure on slender cone/afterbody combinations in hypersonic inviscid flow of perfect gas 04 p0542 A69-14735

Axially symmetric bodies shape for static pressure at location independent of Mach number 04 p0542 A69-14738

Rotating spectral and spatial sound pressure distribution in propeller duct calculated on basis of propulsion quantities, noting effect of tip clearance 04 p0544 A69-14867

Mean meridional pressure profiles and atmospheric mass readjustment time dependence for initially at rest atmosphere with mean baroclinity, using frozen gradient model 04 p0627 A69-15086

Laminar compressible viscous boundary layer with arbitrary external pressure distribution, using implicit multiplace difference method 04 p0591 A69-15294

Local pressure and skin friction distribution around circular cylinder in cross flow in large range of Reynolds numbers 05 p0744 A69-15716

Weak shock wave diffraction at two dimensional obstacles, discussing time behavior of pressure distribution 05 p0746 A69-16018

Pressure distribution across short vortex chamber to exit radius with known inlet geometry based on incompressible flow model and visualization photographs [ASME PAPER 68-WA/FE-17] 05 p0748 A69-16093

Static pressures, profiles of local longitudinal velocity, fluctuating wall pressures and power spectra of wall pressures measured for subsonic turbulent flow [ASME PAPER 68-WA/FE-36] 05 p0750 A69-16109

Fixed point support properties of quasi-vertical peripheral jet hovercraft with two pressure stages 06 p0857 A69-16820

Visual investigation of flow field at swept wing, measuring pressure distribution at stall fence and vortices formation 06 p0858 A69-17341

Geometry changes influence on rigid plastic circular plate behavior under two independent distributed pressures 06 p1023 A69-17508

Pressure distribution, heat transfer rates and shear stresses in laminar boundary layer of supersonic viscous flow incident on corner point of body
06 p0861 A69-17641

Injector vaporizer performance in liquid metal MHD system, using model for total and static pressure distribution
06 p0871 A69-17918

Lower atmosphere pressure field determination based on meteorological satellite observations of amount and types of clouds and upper boundary altitude
06 p0952 A69-17987

Three dimensional compression problem for two elastic bodies in contact, determining contact pressure distribution by iteration procedure on computer
06 p1026 A69-18014

Pressure distribution determined from laminar viscous-inviscid interactions in supersonic flow, including flows with heat transfer
[AIAA PAPER 69-7] 06 p0913 A69-18095

Underexpanded nozzle ejected supersonic turbulent jet off-design behavior, discussing static pressure distribution, boundary layer and Mach number effect
07 p1049 A69-18397

Pressure distribution on star-shaped bodies in wind tunnel at Mach 4 and Reynolds number .000006
07 p1050 A69-18703

Gas pressure control in xenon lasers, using variable temperature surface partially insulated from liquid nitrogen coolant
07 p1155 A69-19090

Compressibility parameters role in pressure distribution derived for radial laminar compressible fluid flow between two disks
07 p1121 A69-19321

Shallow spherical shells equilibrium under uniformly distributed internal pressure, analyzing nonlinear boundary value problems by algorithm
07 p1237 A69-19685

Supersonic flows past slender bodies, calculating pressure by means of moving singularities
08 p1252 A69-20721

Boundary value problem for linearized system of Navier-Stokes equations in three dimensional space, determining velocity vector and pressure
08 p1344 A69-21156

Hall effect and mass flow influence on MPD arc jet radial pressure profile calculated as function of pressure and magnetic field
[AIAA PAPER 69-246] 09 p1562 A69-21226

Pressure distribution in propagating current sheet structure in dynamic Z pinch discharge in argon, evaluating particle density, velocity and temperature profiles
[AIAA PAPER 69-264] 09 p1564 A69-21243

Magnetic pinch effect in thermal RF induction plasma in argon, developing theory for calculating excess magnetic pressure
09 p1544 A69-21341

Cross-spectral density of pressure induced on lifting surface by isotropic atmospheric turbulence, solving integral equation
[ONERA-TP-681] 09 p1613 A69-21689

Lifting pressure distributions on oscillating surfaces in subsonic flows using doublet lattice method for various surface geometries
[AIAA PAPER 68-73] 09 p1430 A69-21946

Sonic boom reduction by azimuthal redistribution of supersonic aircraft pressure field variation
[AIAA PAPER 68-159] 09 p1434 A69-21948

Hypersonic slipper bearing problem in rocket boosted sleds, discussing flow model consisting of laminar stagnation region and boundary layers
[AIAA PAPER 68-736] 09 p1477 A69-22003

Base pressure fluctuations behind cone in supersonic gas flow, noting complicated superposition of harmonics associated with various factors
09 p1431 A69-22237

Fuel control systems using emulsified fuel, noting exposure effects and temperature and pressure characteristics
[ASME PAPER 69-GT-40] 09 p1571 A69-22486

Acoustic waves pressure field micropulsations in turbulent fluid, analyzing space-time spectrum
09 p1492 A69-22710

Pressure coefficients determination on slender body surface to estimate effects of quadratic terms, considering body of revolution with thin cruciform lifting surfaces
10 p1632 A69-22911

Interfacial pressure distribution during slip damping in clamped rectangular beams subjected to vibration
10 p1800 A69-23350

Invariant finite amplitude spherical shock wave propagation in medium with inversely radial density
10 p1778 A69-23405

Integral representation for velocity and pressure fields produced by horizontal motion of two dimensional bodies below or on free surface of viscous liquid
11 p1866 A69-24278

Characteristics method for solution of differential equations representing time changes of wind and pressure fields in divergent barotropic channel flow
11 p1911 A69-24585

Nonlinear partial differential equations for solution of steady stratified flows, noting hydrostatic pressure distribution and horizontal and vertical scales
11 p1869 A69-24889

Three dimensional theory of elasticity for finite hollow cylinder under axisymmetric deformation, considering stress and pressure distribution over surface
11 p1983 A69-25022

Pressure distribution measurement over sphere with cylindrical afterbody in magnetofluid dynamic flow, showing drag decrease at large magnetic field
11 p1873 A69-25136

Radial hydrostatic bearing parameters calculated by pressure distribution diagram in bipolar coordinates, obtaining equations of motion
11 p1892 A69-25341

Skin friction coefficient relation to pressure distribution in turbulent flow and development of momentum thickness along flow
11 p1819 A69-25385

Low power gradient uniform electric arc column in cross flow and transverse magnetic field, analyzing temperature, velocity, pressure and magnetic field distribution
11 p1933 A69-25556

Density stratified model of troposphere and constant gravity field for ground level pressure perturbations in mesoscale region
12 p2126 A69-26016

Inertia effect on incompressible fluid film pressure between two oscillating parallel plates, considering Reynolds number
12 p2102 A69-26241

Transverse symmetrical vibrations of thin elastic plates under Jacobi pressure distribution, giving displacement and velocity plots
12 p2180 A69-26271

Pressure distribution in finite width high speed self acting gas lubricated slider and partial arc bearings, noting trailing edge conditions and side leakage effects
[ASME PAPER 68-LUBS-15] 13 p2265 A69-27268

Pressure distribution in viscous flow between parallel disks with sinusoidal oscillation, noting effects of oscillation amplitude and vibrating disk velocity
[ASME PAPER 68-LUBS-1] 13 p2244 A69-27278

Flow models for externally pressurized gas bearings, discussing pressure distributions, load capacity and flow rate
[ASME PAPER 68-LUBS-2] 13 p2267 A69-27285

Nonuniform flowfield from supersonic penetration of plane shock by three dimensional pointed planar wing, using integral transform method to study field perturbation pressure
13 p2199 A69-27323

Suction effects on shockwave-turbulent boundary layer interactions at compression corner leading to reductions in upstream influence
13 p2244 A69-27326

Flux, density and pressure variations with position in vacuum system /nonuniform gas distribution/, discussing causes and consequences
13 p2299 A69-28019

Experimental and predicted shock axial pressure variations for semifinite metallic targets during high velocity impact, using Al alloys and Cu
[AIAA PAPER 69-361] 13 p2366 A69-28294

Boundary conditions for equilibrium diamagnetic plasma in magnetic dipole having constant and isotropic pressure in system
14 p2489 A69-28910

Neutral gas pressure in positive column plasma between two coaxial insulated cylinders as function of cylinders radii
14 p2490 A69-29036

High pressure Cs thermionic converter with cold region, measuring Cs partial pressure distribution in Ar filled tube
14 p2397 A69-29176

Time dependent evolution of probability pressure distribution maximum obtained from Liouville equation
14 p2472 A69-29406

Normalized correlation functions of dispersion values for pressure fields and geopotential obtained by low latitude stations, noting wind field features
14 p2478 A69-29833

Longitudinal pressure distribution in MHD channel with electrodes parallel to applied transverse magnetic field
14 p2501 A69-29918

Aircraft created pressure patterns responsible for sonic boom, discussing design techniques for noise reduction
15 p2550 A69-30369

Incompressible two dimensional turbulent boundary layer equations with arbitrary pressure distribution solved by weighted residual method
[AIAA PAPER 69-397] 15 p2591 A69-30478

Flow and pressure fields for spiral grooved pumping seal with specified groove dimensions and Reynolds number
[ASLE FICFS PREPRINT 30] 15 p2619 A69-30481

Mach numbers effect on pressure distribution and friction moment in nonisothermal layer of gas lubricant, using power series
15 p2629 A69-31021

Static pressure distribution induced by statistically roughened duct walls on supersonic stream
15 p2593 A69-31148

Boundary value problem for linearized system of Navier-Stokes equations in three dimensional space, determining velocity vector and pressure
15 p2645 A69-31249

Atmospheric models for pressure variation and neutral air winds in thermosphere, discussing wind velocity vector relation to satellites orbital inclination
15 p2603 A69-31403

Pressure distribution in wake produced by obstacle with secondary fluids injection into boundary layer, obtaining coefficient governing resistance of obstacle to forward motion
16 p2768 A69-31604

Double shock method for detecting pressure limits in magnetic phase transition of solids
16 p2825 A69-31696

Trailing shock wave position in air breathing jet engine channels, determining supersonic-subsonic boundary, noting Mach number effects on pressure ratio
16 p2768 A69-31743

Ablation injectants effect on supersonic stream pressure distribution inside cavity and upstream boundary layer velocity profiles
16 p2770 A69-31902

Acoustic waves pressure field micropulsations in turbulent fluid, analyzing space-time spectrum
16 p2782 A69-32489

Velocity and static pressure redistribution in distorted flow field upstream of axial flow compressors
[AIAA PAPER 69-485] 16 p2842 A69-32694

Turbulent base flowfields in multinozzle configurations, considering adiabatic flow and determining base pressure distribution from reverse jet impingement
[AIAA PAPER 69-570] 16 p2733 A69-32751

Impingement pressure analysis associated with two phase cryogenic propellant venting to space environment
[AIAA PAPER 69-571] 16 p2869 A69-32753

Monograph on determination of unsteady pressure field of freely rotating propeller covering blades, displacement and lift effects, distribution functions, etc
17 p2889 A69-32994

Linear aerospace structures vibrations in randomly distributed pressure field forecasted by applying Green function
[ONERA-TP-703] 17 p3054 A69-33064

Nonaxisymmetric stability loss /buckling/ of closed toroidal shell of circular cross section under uniformly distributed external pressure, considering Volmir linear theory
17 p3055 A69-33130

Bag type deformation of incompressible viscous convective and nonevaporating droplets immersed in Stokes or potential flow pressure distributions, including Weber number
[AIAA PAPER 69-669] 17 p2954 A69-33456

Flow field pressure distribution due to plane shock wave impinging by thin wing moving in opposite direction, discussing mathematical formulation, analytic solution and applications
[AIAA PAPER 69-647] 17 p2891 A69-33459

Surface pressure and heat transfer over blunt conical body in hypersonic flow with uniform mass addition of various gases
[AIAA PAPER 69-716] 17 p2891 A69-33463

Pressure distribution in self acting hydrodynamic journal bearings without end leakage, presenting closed form solution for nonhomogeneous Reynolds equation with turbulence considerations 18 p3139 A69-34270

Static and impact pressure distributions for Mach number and velocity profiles of supersonic to subsonic flow transition in tube at low Reynolds numbers
[ASME PAPER 69-APM-23] 18 p3120 A69-34397

Optimum pressure distribution and airfoil profiles for maximum lift without separation in incompressible flow determined by second order theory
[AIAA PAPER 69-739] 18 p3083 A69-34401

Pressure distribution in two dimensional incompressible potential flow on Joukowski airfoils with normal upper surface spoilers, emphasizing potential flow theory
[AIAA PAPER 69-737] 18 p3083 A69-34402

Method of characteristics for computing supersonic jets and wakes with given boundary pressure distribution
[ONERA-TP-721] 18 p3121 A69-34636

Objective analysis of pressure trend fields and surface pressure retaining field with scale of 100 km, using filtering procedure 18 p3166 A69-34816

Dynamic instability regions of parametric resonance of cylindrical shells with curved generating lines under axial and radial pressure 18 p3223 A69-34979

Stress-strain state calculations of ribs reinforcing cantilever shell under external pressure, using differential-difference equations 18 p3223 A69-34980

Subsonic and supersonic turbulent air jets expansion over perpendicularly positioned plane disk obstacle, deriving equations for pressure distribution and stagnation temperature 18 p3123 A69-34990

Forced pressure fluctuations in hydraulic systems of aircraft fuselages and engines, taking into account square law of losses at resistance points 18 p3094 A69-34991

Pressure distribution over lining of brake shoe for brake drums design, discussing pressure compensation after wear 18 p3149 A69-35287

Asymptotic theory of pressure on cylindrical shell subjected to unsteady oscillations in external and internal linearized supersonic flow using Laplace and Fourier transforms 18 p3089 A69-35461

Velocities and pressure in twisted jet in unbounded space containing same fluid as jet 19 p3298 A69-36388

Interaction effects between mixing and pressure distribution of heterogeneous flow in channel, deriving criteria for predicting pressure variation sign 19 p3300 A69-36785

Pressure increment due to inertia of rotating fluid film at journal bearing periphery theoretically estimated and measured 20 p3548 A69-37085

Supersonic inviscid flow past wing-body configuration, determining pressure distribution 20 p3458 A69-37099

Conical delta wings in supersonic-moderate hypersonic flow, studying yaw effects on pressure distribution behind shock wave 20 p3459 A69-37593

Sunspot spectra near solar limb for difference between Fraunhofer line continuum and line core formation levels, finding geometrical height scale and pressure equilibrium 22 p4019 A69-40292

STOL scaplane bottom pressure distribution from tests on scale model of PX-S scaplane, discussing boundary layer control effects 22 p3864 A69-40586

Space-time behavior of random pressure field of turbulent boundary layer on plane plate surface 22 p3933 A69-41027

Pressure distribution in gas lubrication layer of infinite radial sliding bearings, approximating differential equation by simple formulas 23 p4168 A69-41412

Mars light polarization observations noting unsatisfactory surface pressure determinations 23 p4212 A69-41615

Inviscid transonic flow past circular arc bodies of revolution, applying Hosokawa technique to pressure distribution solution 23 p4059 A69-41899

Radial pressure distribution in steady state rotationally symmetrical plasma jet subjected to axial magnetic field, emphasizing mass entrainment effect [DGLR-69-024A] 23 p4202 A69-41924

Digital simulation of oxygen pressure fields and supply conditions in biological tissues 23 p4097 A69-42098

Surface pressure field forecast by meteorological fields expansion into orthogonal components, estimating number of predictors in regression equation 23 p4184 A69-42491

Fluid flow around sphere at high Reynolds number by measuring pressure distribution, considering boundary layer separation, tunnel blockage, etc
[ASME PAPER 69-APMW-26] 24 p4245 A69-43093

Equator-to-pole temperature gradient relation with planetary pressure belts, comparing observational data with theoretical circulation criterion 24 p4345 A69-43149

Northern Hemisphere 500-mb height pattern series expansion, using optimal sets of orthonormal functions, obtaining rms error 24 p4346 A69-43157

Velocity and pressure fields produced by deformable load carrying filament studied for unsteady gas motion past slender body with nonpotential external forces 24 p4246 A69-43483

Gas phase self induced pressure field and laminar velocity distribution of working fluid within closed heat pipe channels analyzed by momentum integral method [ASME PAPER 69-HT-22] 24 p4412 A69-43546

Supersonic viscous flow around sharp corner at various expansion angles, giving pressure distributions and velocity profiles role [ASME PAPER 69-HT-14] 24 p4247 A69-43555

Irregular pressure profiles and pressure-time histories when using octofluorocyclobutane and sulfur hexafluoride in explosive driven shock tube [AIAA PAPER 68-730] 24 p4297 A69-43577

Mean velocity and pressure fields in turbulent boundary layer on flat plate at Mach 2 investigated for ratios of mass flow [AIAA PAPER 68-129] 24 p4304 A69-43581

Acrodynamic forces on hypersonic vehicle surfaces, deriving relations for weak interaction pressures induced in unsteady flow 24 p4306 A69-43676

Pressure distribution correlation over blunted slender cone at various angles of attack by tangent cone method, describing hypersonic wind tunnel tests 24 p4249 A69-43681

Computerized pressure distribution estimation for stalled airfoil with arbitrary wake geometry 24 p4250 A69-43726

PRESSURE DRAG

NT INTERFERENCE DRAG

NT SUPERSONIC DRAG

NT WAVE DRAG

Low Mach number airfoil profile drag calculation for various angles of attack and Reynolds numbers, noting effects of transition and airfoil thickness 01 p0006 A69-11017

Differential rotation of sphere in viscous incompressible liquid, discussing pressure and skin friction drag between two hemispheres with different angular velocities 04 p0590 A69-15278

Nonlifting blunt axisymmetric hypersonic shape determination to maximize pressure drag for given convective heat transfer, diameter and free-stream conditions 24 p4244 A69-42960

PRESSURE DROP

Dynamic gas flowmeter for ultrahigh vacuum based on transmission characteristics of diffuser screens and associated pressure drops 13 p2263 A69-28087

Pressure drop fluctuations amplitude and frequency effect on channel resistance and magnetic field effect on fluctuations intensity in laminar conducting fluid flow 14 p2501 A69-29909

Flame pressure drop and burning velocity related, discussing stream tube area expansion error 21 p3849 A69-38806

Liquid solid mixtures of parahydrogen flow characteristics in pipe, globe valve, orifices and venturi, determining pressure loss [NAS-NRC PAPER F-5] 22 p3998 A69-40626

PRESSURE EFFECTS

Hydrostatic pressure effects on mechanical properties of hot pressed, extruded and rolled polycrystalline beryllium sheet 01 p0092 A69-10059

Turbulent to laminar boundary layer reversal by applying negative pressure gradient 01 p0058 A69-10066

Diffusion welding of AMS 4921 titanium, discussing premature pressure removal before completion of first joining stage 01 p0086 A69-10535

Pressure and temperature dependence of slow crack growth in hardened steel in gaseous hydrogen environment 01 p0096 A69-10612

HF plasma ionic composition dependence on discharge conditions and ions translational energy 01 p0129 A69-10682

Isopentane and mesitylene index of refraction variations with pressure, determining average molecular radii and polarizabilities 01 p0123 A69-10685

Isothermal secant and tangent bulk moduli of silicon fluids and correlation with pressure, volume and temperature 01 p0102 A69-10913

Cryogenic expansion to pressures below triple point and resulting formation of solid-vapor mixtures, discussing flow and heat transfer characteristics in heated tubes 01 p0176 A69-11146

Cardiovascular changes in male students during tilt and negative pressure tests with bed rest studied from heart rate, blood pressure and leg volume measurements 01 p0021 A69-11334

Transverse pressure gradient and streamwise derivatives effect on free convection laminar heat transfer on isothermal vertical plate at low Prandtl numbers 01 p0177 A69-11409

Pressure and magnetostriction effects on magnetization curves of type 2 superconducting In-Tl alloy, noting Ginzburg-Landau parameter stress dependence 02 p0294 A69-11776

Ultrahigh pressure physics of materials, discussing apparatus, phase transitions and yield strength ductility relationships 02 p0260 A69-11803

Downstream pressure asymmetry effect on efflux angle and contraction coefficient of incompressible jet from two dimensional orifice 02 p0231 A69-12075

Vortex controlled fluid amplifiers, discussing static and dynamic performance characteristics 02 p0195 A69-12081

Fluid temperature sensor generating output differential pressure proportional to temperature of fluid entering device 02 p0249 A69-12089

Sulfospinel polymorphism at high temperature and pressure and pressure-temperature phase relations 02 p0266 A69-12162

Gaseous and liquid H refractive index variations with pressure and density below room temperature, noting Lorentz-Lorenz function variations 02 p0281 A69-12180

Relativistic heat transfer formula and pressure definition in relativistic thermodynamics 02 p0352 A69-12253

Pressure and temperature dependence of isotropic elastic moduli of polycrystalline alumina, noting Gruneisen parameter, equation of state and Debye temperature 02 p0268 A69-12407

Pressure and velocity couplings effects on oscillatory and transient motions in solid propellant rocket motors, emphasizing unsteady burning calculations 02 p0305 A69-12501

Anisotropic pressure influence on silicon diodes parameters 02 p0223 A69-12839

Finite amplitude surface wave excitation in infinitely deep ideal fluid by moving pressure, noting phase velocity increase with amplitude 03 p0466 A69-13277

Pressure induced microwave absorption in molecular N for various temperatures, determining dielectric loss, absorptivity and quadrupole moment 03 p0472 A69-13317

Equivalent pressure concept verification for arc discharge with incandescent cathode in mercury vapor 03 p0478 A69-13843

Uniaxial pressure applied to p-n junction of GaAs in injection laser, discussing effects on threshold current and wavelength

03 p0441 A69-13848

Pressure induced variations in stability constant characterizing bubble structure in two phase boundary layer of several liquids during boiling with natural convection

03 p0534 A69-14149

Constants in formulas describing temperature and pressure dependence of thermodynamic characteristics of high temperature monatomic ionized gases for positive ions

03 p0473 A69-14156

Human auditory function during exposure to prolonged low barometric pressure unaffected with normal oxygen partial pressure

03 p0378 A69-14206

X ray investigation of repeated simulated exposures to altitude and acceleration on healthy professional flyers

03 p0378 A69-14208

Hydrostatic pressure effect on recombination emission in indium phosphide p-n junctions

04 p0639 A69-14428

Thermodynamic computations for combustion product temperature and flow rate as function of pressure in burner and excess air ratio

04 p0684 A69-14487

Stressed state periodic problem in infinite strip under combined pressure and temperature field effect

04 p0673 A69-14497

Frequency dependent shear modulus for hexachlorobiphenyl measured under rare gas infusion at 5-25 C and from ambient atmospheric to 4000 psi

05 p0796 A69-15912

Liquid oxygen shear viscosity dependence on temperature and pressure obtained by measuring electrical characteristics of immersed torsional vibrating crystal

05 p0846 A69-15916

Relaxation time of carbon dioxide laser levels as function of water vapor, CO and Xe gas pressure measured by afterglow pulse gain technique [IEEE PAPER G-1]

05 p0774 A69-16314

Pressure stratification and transparency/geometrical depth expansion/ in Fricke-Elsasser and Zwaan sunspot models

06 p0999 A69-16976

Shock wave profiles in expansion flows determined with static and impact pressure probes, investigating pressure gradient effects

06 p0908 A69-17022

Plastic deformation and bursting pressure of thin rupture disk as related to tensile strength

06 p1020 A69-17129

Stability of rectangular transversely isotropic plate hinged at three sides under uniform pressure applied to two opposite hinged sides

06 p1021 A69-17178

Stability loss of shells of revolution under effect of axial compression and radial pressure with no restrictions on generatrix curvature, using strain energy method

06 p1021 A69-17179

Data on muons indicating temperature effect diurnal maximum and pressure corrected daily variation

06 p0924 A69-17294

Thin circular cylindrical shells steady creep behavior under combined lateral and axial pressures, using Tresca criterion and associated flow rule

06 p1023 A69-17506

Geometry changes influence on rigid plastic circular plate behavior under two independent distributed pressures

06 p1023 A69-17508

Moment equations of Vlasov plasma used for pressure effects on gravitational flute instability of nonuniform plasma

06 p0965 A69-17515

Two dimensional stress distribution changes around rectangular hole with rounded corners for varying internal pressure and temperature

06 p1025 A69-17611

Gas laser operation at high pressures, examining threshold pumping and power output dependence on pressure to optimize parameters

06 p0934 A69-17680

Collisionally induced microwave absorption by nonpolar gases, discussing dimer absorption

06 p0962 A69-17816

G suit inflation acute and prolonged effects on cardiovascular dynamics in recumbent and passively tilted individuals

06 p0883 A69-17843

Solid propellant burning rate behavior during abrupt environmental pressure excursions, using transient combustion model

[AIAA PAPER 69-172] 06 p1036 A69-18046

Extinction by depressurization of AP composite solid propellants theory to predict rate of pressure decrease required to achieve flameout

[AIAA PAPER 69-176] 06 p0983 A69-18102

Quasi-steady combustion model of fuel droplet with convection, including pressure effect

[AIAA PAPER 69-147] 06 p1037 A69-18114

Sustained combustion initiation in subatmospheric gaseous fuel-oxidant mixtures by UV radiation at room temperature, measuring parameters as function of mixture pressure

[AIAA PAPER 69-88] 06 p0983 A69-18118

Low pressure deflagration limit dependence on strand size in terms of cross section dimensions for composite ammonium chlorate propellant

[AIAA PAPER 69-144] 06 p0983 A69-18162

Cross hatching on various body surfaces due to periodic surface pressure fluctuations, discussing origin from counterrotating longitudinal vortices in boundary layer

[AIAA PAPER 69-11] 06 p0915 A69-18213

Calibration curve for constant temperature hot-wire anemometer, taking into account high wire temperature and gas pressure effects

06 p0930 A69-18218

Regression rate model for pressure sensitive hybrid combustion based on classical turbulent flame theory [WSCI PAPER 68-22]

07 p1240 A69-18362

Radiation pressure effects on laser produced carbon plasma in vacuum, discussing target surface superheating, plume boundary, plume density precursor and electron and ion temperature merging

07 p1190 A69-18902

Water vapor absorption line for nitrogen and oxygen mixtures with frequency measurements at various pressures and temperatures, discussing attenuation and line breadth

07 p1184 A69-18911

Pressure properties of fluorides and silicofluorides as cutting and grinding lubricants for titanium [ASLE PAPER 68-LC-20]

07 p1141 A69-19311

Pressure-temperature dependence of nitrogen solubility in tungsten at 2400-3000 C

07 p1168 A69-19602

Tensile strength of alloys under high pressure of hydrogen and helium, discussing embrittlement [ASM PAPER D8-14.2]

07 p1169 A69-19667

Local stability of thin walled elastic shells of revolution subjected to external pressure

07 p1237 A69-19686

Stability of cylindrical shell reinforced by circular ribs under combined action of external pressure and axial forces, using characteristic equation

07 p1238 A69-19687

Carbon dioxide laser radiation frequency controlled by varying boron trichloride pressure in cell inserted in resonator

08 p1323 A69-19804

Interaction between atom and plane monochromatic traveling wave taking into account pressure effect occurring in strong collision model

08 p1354 A69-19954

Wall temperature influence on intensity of transverse flow of three dimensional laminar boundary layer resulting from transverse pressure gradient

08 p1251 A69-20274

Recombination rate of electrons in high pressure helium-like plasma with gas temperature fixed at 300 K and electron temperature varied between 300-2000 K

08 p1356 A69-20742

Background pressure and magnetic field shape effect on MPD thruster performance, testing radiation cooled thrusters

[AIAA PAPER 69-243] 09 p1564 A69-21239

Flapper valves in high pressure hydraulic aircraft systems, with hydrodynamic equations and charts for design and performance characteristics

09 p1435 A69-21296

Bellows sealed valve for measurement of fluorine thermodynamic properties at moderately high pressures

09 p1493 A69-21428

Convective MHD channel flow in vertical channel subjected to temperature and pressure gradients, discussing wall conductance effects on flow rate and heat transfer

09 p1545 A69-21441

Gold diffusion and solubility in indium phosphide, analyzing temperature and vapor pressure effects

09 p1555 A69-21470

Stimulated Mandelstam-Brillouin scattering in compressed N and H as function of pressure, using ruby laser pulses

09 p1516 A69-21562

Thermionic converters stability and safety maintainable at high Ce pressures

09 p1441 A69-21837

Pure ammonium perchlorate single crystal self deflagration, determining energy transfer mechanisms from pressure effects, combustion characteristics and subsurface profile

[AIAA PAPER 69-142] 09 p1560 A69-21900

Laser radiation produced by continuous glow discharge within Al hollow cathode, determining laser power in terms of He-Ne mixture pressures

09 p1519 A69-22245

Thermosetting resin curing behavior characterized by differential thermal analysis performed above atmospheric pressure to prevent volatilization

09 p1500 A69-22311

Controlled expansion of captive silicone rubber used to achieve pressure control for adhesive bonding interface

09 p1512 A69-22367

Thermal and pressure environments analysis in Saturn S-1C stage base during flight tests, noting base gas flowfield and heating [AIAA PAPER 69-318]

09 p1611 A69-22383

Gas turbine combustion control at high pressure, considering mixing, fuel evaporation, spray penetration and cone angle

09 p1625 A69-22620

Linear theory of cylindrical panel buckling and circumferential restraint along straight edges under lateral pressure, using Donnell equations

09 p1621 A69-22782

Pressure and temperature effects on electrical conductivity of dense plasma ejected from Laval nozzle

10 p1739 A69-23492

Pressure effects on hep crystalline lattice alloys order-disorder transformations

11 p1937 A69-24704

Deformations of thick walled cylinder with internal surface subjected to uniform pressure and externally connected to rigid chamber, calculating solid rocket booster charge

11 p1942 A69-25347

Mass flow rates for nearly free molecular flow through two dimensional slit for several tank pressure ratios

11 p1874 A69-25357

Cylindrical shells spectral response to random acoustic pressure excitation, noting natural modes and inner air column effects

11 p1990 A69-25506

Flutter analysis of plates with inplane boundary support flexibility exposed to transverse pressure loading or buckled by uniform thermal expansion

11 p1992 A69-25523

Calcite IR absorption dependence on pressure, discussing calcite-aragonite transformation

12 p2141 A69-25783

Laser gain medium dispersion expressions applied to multimode ring laser operation with mode spacing less than pressure broadened atomic linewidth

12 p2106 A69-26324

Component ratio effect on pressure dependence of burning rate in ammonium and potassium perchlorate mixed with organic compounds, graphite and tungsten

12 p2027 A69-26474

Multi-electrode probe performance in plasma diagnostics, considering effects of plasma pressure, probe geometry and space charge on current-voltage characteristics

12 p2138 A69-26539

Carbon dioxide dissociation in carbon dioxide laser gas discharge plasma for various flow rates, pressures, discharge current densities and tube diameters

12 p2107 A69-26540

Finite plane deformations theory extended to incompressible materials with logarithmic change of volume proportional to pressure

12 p2181 A69-26613

Pressure and heating rate correlations for rocket exhausts impinging on flat plates and curved panels, generating axisymmetric real gas exhaust plumes

12 p2190 A69-26781

Pressure calcining process in production of fine grained ceramics at low temperatures

12 p2119 A69-26832

Temporal variation of metal content in galaxy, discussing stellar radiation pressure effects on heavy element abundance of interstellar gas

12 p2160 A69-26854

Steady helical discharges /skin effect/ in air and Ar under high pressure without gas injection, discussing discharge stability factors

12 p2140 A69-27122

Strain rate and pressurization effect on ductile-brittle transition temperature of polycrystalline sintered W, discussing yield stress

12 p2117 A69-27138

Resistance type bonded strain gages for seven adverse environments, discussing installations and transducers

12 p2099 A69-27165

Stress distributions in two normally intersecting cylindrical shells subjected to internal pressure, using Donnell and Flugge equations

13 p2359 A69-27255

Limiting pressure for deflagration related to initial solid temperature of single crystals and pressed pellets of ammonium perchlorate

13 p2324 A69-27364

Electric arc and hydrogen flow interaction at high pressure, showing radiation role in heat exchange

13 p2305 A69-27387

Ambient air pressure effects on fatigue crack growth rate in strain hardened aluminum

13 p2276 A69-27393

Hayashi effect modifications due to high opacity stellar atmosphere or presence of molecular hydrogen dissociation zone, discussing pressure dissociation role

13 p2342 A69-27594

Beryllium single crystals c axis compression behavior at three purity levels under hydrostatic pressures

13 p2279 A69-27760

Copper and aluminum fatigue in vacuum and ultrahigh vacuum, discussing effects of hydrogen, nitrogen and oxygen pressures

13 p2280 A69-28088

Depth and planarity of zinc diffused junctions in GaP using temperature, phosphorus overpressure and time as independent variables

13 p2322 A69-28136

Lung ventilation mechanics affecting respiration in hyperbaric environment during deep diving, stressing biological necessity of equal pressure respiration

13 p2215 A69-28598

Finite amplitude surface wave excitation in infinitely deep ideal fluid by moving pressure, noting phase velocity increase with amplitude

14 p2482 A69-28785

Graphites wear rates and structural changes in machine parts under dynamic stresses in air or vacuum, noting pressure role

14 p2467 A69-28912

Compressed ammonium perchlorate combustion rate and pressure requirements established from initial temperature effects

14 p2508 A69-28914

Frequency shifts of Lamb dip minimum in helium-neon laser, considering effects of discharge tube parameters and gas pressure

14 p2457 A69-28929

UV radiation decreased transmittance through quartz exposed to plasma at high temperature and pressure, showing dependence on heated surface layer absorption

14 p2490 A69-29159

Auxiliary discharge thermionic converter with Penning mixture /Ne-Ar/, discussing pressure and Penning ionization effects, collector current discontinuities, etc

14 p2398 A69-29180

Thermionic converter stability as function of cesium pressure, heat input, reservoir temperature, load voltage or resistance

14 p2402 A69-29236

Rare gases effect on thermionic converters volt-ampere characteristics, noting gas pressure, oxygen contamination and performance relations

14 p2403 A69-29251

Work function changes of tungsten single crystals as function of oxygen and CO gas pressure at high temperatures, using emission microscope

14 p2506 A69-29272

Auditory evoked response /AER/ as measure of narcosis induced at depth in diving personnel, discussing hyperbaric nitrogen and oxygen effects

14 p2407 A69-29302

Pressure sensitive adhesives composition, tapes tacking and peeling theory and tests including electrolytic corrosion and insulation evaluation

14 p2468 A69-29342

Compression molding of molecular salt-like intermediate Pyrrone powders by two pressure method, noting volatiles climination

14 p2469 A69-29415

Solar radiation pressure effects on satellite models in circular equinoctial orbits

14 p2522 A69-29595

Sonic boom produced earth particle velocities, noting seismic effect limitation to boom pressure envelope area and earth surface boundary

14 p2393 A69-29880

Diperchlorates different in organic part of structure and explosive transformation heats, showing strong dependence of combustion velocity on pressure

15 p2716 A69-30108

Shock hardening in Ni at high pressure observed by electron microscopy showing dominating thermal effects on microstructure

15 p2637 A69-30225

Collapse pressure of flush cylindrical nozzle axisymmetrically intersecting conical pressure vessel for rigid plastic shells

15 p2704 A69-30289

Plasma arc characteristic and radiation at high pressure and temperature showing strong electrical field strength and radiation increases with pressure

15 p2659 A69-30377

Gas barrier seal design producing varying unit loading on conventional contact seal faces, including geometric stability and test results [ASLE FICFS PREPRINT 26]

15 p2621 A69-30495

Gold diffusion and solubility in indium phosphide, analyzing temperature and vapor pressure effects

15 p2669 A69-30715

Power spectral density response of uniform beams to random pressures, evaluating joint acceptance of systems with pressure field [ASA PAPER SVT2]

15 p2713 A69-31143

Cylindrical shell bending subjected to internal pressure and force uniformly distributed on round section solved by numerical integration of differential equations

15 p2653 A69-31195

Similarity criteria for plastic deformation theory of body under pressure and nonuniform temperature field, considering strength calculations

15 p2714 A69-31200

Reinforced cylindrical shell stability under external compression load by pressurized air, determining critical pressure

15 p2715 A69-31204

Stagnation region dimensionless pressure effect on flow pattern, boundary conditions and oscillation mechanism in compressible flow through nozzle in circular duct

15 p2549 A69-31220

Rapid orbit prediction method for planning satellite observation programs, considering oblateness and radiation pressure effects

15 p2697 A69-31310

Fuel drop combustion under unsteady conditions at high pressure in unlimited and limited air volume

15 p2719 A69-31476

Uniaxial stress effect in Schottky barrier diodes measured by beam balance noting higher sensitivity

16 p2758 A69-31619

Acoustic velocities in polymethylmethacrylate measured as functions of frequency, temperature and pressure, comparing data obtained with equation of state high pressure determinations

16 p2825 A69-31695

Gas discharge tube graphite hollow cathode geometry leading to abnormal discharge operation under certain pressure conditions

16 p2814 A69-31838

Prebuckling deformations influence on circular cylindrical shell buckling under external pressure, applying Galerkin method to Donnell equations

16 p2872 A69-31905

Polycrystalline BeO sound velocities determined as function of pressure and temperature using pulse superposition method

16 p2802 A69-32338

Ammonium perchlorate sublimation models, discussing low temperature decomposition influence on pressure dependence of sublimation rate [WSCJ PAPER 69-22]

16 p2832 A69-32360

Hydrogen-oxygen ion exchange membrane fuel cells for sounding balloons, discussing flight duration and power requirements, gas supply pressure effects, etc

16 p2738 A69-32413

Diurnal pressure cycles found as zeitgeber to entrain body temperature endogenous circadian rhythm in pocket mice under constant environmental temperature and light

16 p2745 A69-32447

Jet engine compressor stalls in-flight investigation up to Mach 2 on F-111A by pressure sensors, noting steady state distortion role

[AIAA PAPER 69-488] 16 p2843 A69-32706

Supersonic compressor blade sections performance prediction near maximum pressure ratio and efficiency by analyzing flow processes

[AIAA PAPER 69-522] 16 p2843 A69-32711

Linear and nonlinear pressure coupled combustion instability of solid propellants

[AIAA PAPER 69-479] 16 p2834 A69-32725

Stresses in perforated ribbed cylindrical shell subjected to internal pressure using brittle coating, electrical strain gages, photoelasticity and micrometers

16 p2876 A69-32784

Plastic failure under internal pressure of aluminum spherical shells with single radial or oblique nozzle based on limit analysis theory

17 p3052 A69-32983

Preferential ion recombination in gases under high pressure, noting no dependence of recombination on average energy

17 p2949 A69-32999

Fatigue crack growth rates in stainless steel at elevated temperature measured as function of oxygen pressure in resonant fatigue machine

17 p2987 A69-33074

Nonaxisymmetric stability loss /buckling/ of closed toroidal shell of circular cross section under uniformly distributed external pressure, considering Volmir linear theory

17 p3055 A69-33130

Powdered oxidizer and infusible polymer binder combustion at various pressures, studying gaseous phase temperature field by optical color analysis

17 p3069 A69-33135

Temperature and pressure effects on flame propagation rates, burning time and combustion zone length in turbulent flows of homogeneous gas mixtures

17 p3069 A69-33140

Pulmonary ventilation and perfusion in normal supine subjects before and during exposure to lower body negative pressure measured using Xe-133

17 p2909 A69-33180

Inflight spontaneous pneumothorax case of civilian pilot lung collapse experience during exposure to reduced ambient pressure, discussing etiology, incidence, treatment and disposition

17 p2909 A69-33183

Thermal contact resistance measurement at various ambient pressures compared with theoretical predictions with each parameter analyzed over interface by computer program

[AIAA PAPER 69-629] 17 p3073 A69-33299

Turbulent boundary layer subject to sudden pressure variation due to rapid expansion or shock wave, noting application to hypersonic ramjet air intake

[ICAS PAPER 68-42] 17 p2895 A69-33587

Flame propagation mechanism on plastic fuel in oxygen-nitrogen atmospheres with variable pressures and at different initial fuel temperatures, discussing safety and ignition problems

17 p3074 A69-33662

Large deflections of thin nonlinearly elastic ring under external pressure, using two layer model

17 p3062 A69-33715

Interstellar H I regions and clouds heating and ionization by low energy cosmic rays from quantitative models, noting pressure equilibrium role

17 p3038 A69-33726

Stationary liquid under pressure effect on energy dissipation of rectilinear pipelines under pure bending

17 p2904 A69-33930

Temperature and pressurization effects on tensile and compressive properties of polycrystalline arc-cast W

18 p3154 A69-34273

Circular cylindrical shell nonlinear response to uniform radial impulsive pressure, noting intentionality constraint and equations of motion roles [ASME PAPER 69-APM-26]

18 p3214 A69-34399

Toroidal, spherical and conical shells limiting equilibrium under various loading and support conditions

18 p3216 A69-34572

Testing machine for in vacuo tensile testing of tubular metallic specimens at high temperatures and low pressures

18 p3117 A69-34604

Stability loss of shells of revolution under axial tension and radial pressure, considering shells of Gaussian curvature, calculating critical force

18 p3222 A69-34976

High temperature air spectral absorption indices determined at different pressures and temperatures
18 p3231 A69-35122

Electron current flow from metal target in gas due to laser radiation, showing increased dependence on gas pressure
18 p3152 A69-35124

Temperature and pressure effect on cobalt base alloy cavitation in liquid sodium, using vibratory apparatus and loss rate contour diagram
18 p3157 A69-35184

Plane LF oscillations of eccentric cylinder under harmonic pressure applied to lateral surfaces, noting natural oscillations
18 p3226 A69-35380

Pressure dependence of trapped spontaneous decay of resonant radiation carbon dioxide
18 p3179 A69-35478

Transfer molded epoxy dielectrics, comparing encapsulation rate, pressure and cure times to compression molding
19 p3281 A69-35548

Safety disk strength under static lateral pressure from rupture studies of thin circular plates under static and pulsating lateral pressure
19 p3434 A69-35773

Lunar interior chemical heterogeneity determined from model taking into account pressure, temperature and composition effects
19 p3425 A69-36421

Liquid driver shock tubes dynamic and thermodynamic properties as functions of diaphragm pressure ratio and initial conditions
19 p3295 A69-36471

Vertical profiles of pressure, temperature and density variations due to upper troposphere pressure changes with and without zero layer effect
19 p3365 A69-36580

HCN laser line gain measurements during continuous excitation as function of current and pressure for acetonitrile and water mixtures
19 p3339 A69-36695

Bubble oscillations in water filled pressure chamber with alternating pressure generated by piston, measuring temporal development
19 p3302 A69-36871

Hydrogen embrittlement mechanism in steel based on modified pressure theory, discussing crack propagation mechanisms and stress corrosion cracking
19 p3350 A69-36894

Maser submillimeter emission lines used to determine atmospheric and water vapor absorption, noting role of pressure
20 p3553 A69-37296

Supersonic molecular beam relative intensity represented as function of nozzle to collimator distance and gas admission pressure
20 p3579 A69-37432

Elastic properties of hot pressed polycrystalline quartz and rutile as function of pressure, obtaining pressure coefficients of compressional and shear wave velocities
20 p3583 A69-37502

Fluidic direct impact modulator design, studying effects of pressure levels and nozzle geometries [ASME PAPER 69-FLCS-38]
20 p3465 A69-37983

Superconductor research noting pressure effects, graphs and tables illustrate behavior of materials considered
20 p3584 A69-38015

Nitrogen gas breakdown threshold dependence on pressure during picosecond ruby laser pulse, discussing photoionization leading to breakdown in electromagnetic wave field
20 p3555 A69-38067

Inconel and aluminum tested in pressurized hydrogen at room temperature, using surface flawed fracture toughness specimens and preflawed pressure vessels
21 p3730 A69-38666

Diurnal variations of cosmic ray neutrons corrected for barometric and temperature effects by harmonic analysis
21 p3791 A69-38840

Physiological and psychological measurements of high pressure effects on man and animals, discussing decompression sickness, respiratory embarrassment, inert gas narcosis, helium tremble, etc
21 p3655 A69-38912

Oxygen pressure effect on oxide layer composition on W surface by secondary ion-ion emission
21 p3746 A69-39071

Stability of cylindrical shell of average length with elastic filler under uniform external radial pressure
21 p3837 A69-39088

Rat dental pulp hemorrhages following acute hypoxia from exposure to decompression chambers, atmospheric pressure variations or high acceleration
21 p3661 A69-39276

Temperature, applied stress and pressurization effects on materials corrosion by liquid F and F containing oxidizers
21 p3748 A69-39485

Power density and time history of pulsed molecular nitrogen laser, discussing dependence on fill pressure and electric circuit parameters
21 p3742 A69-39779

Static and fatigue strength of end-closed filament-wound vessels under internal pressure
21 p3846 A69-39797

Wear resistance of briquetted lubricants from fluoroplast and molybdenum disulfide under pressure
21 p3733 A69-39805

Ti and Zr diborides sintering with Cr, Mo, W and Re additions, discussing activation, pressure effects and density
22 p3968 A69-39888

Space cabin and suit pressures for decompression sickness avoidance and fire hazard alleviation
22 p3890 A69-40212

Lower body negative pressure (LBNP) effects on ventilation and lung volumes, presenting lung model for pulmonary gas exchange changes
22 p3891 A69-40222

Left ventricular function in intact anesthetized dogs analyzed during graded hypovolemia produced by lower body negative pressure
22 p3874 A69-40225

Gravitational fields and atmospheric pressure effects on soils subjected to static and dynamic loading, using aircraft parabolic gravity simulation [AIAA PAPER 69-1009]
22 p3921 A69-40382

Pressure and temperature effects on reversal transitions of stishovite, noting meteoritic impact formation at Meteor Crater, Arizona
22 p4021 A69-40412

Compactibility dependence of Fe, Co and Ni powders with Zr, Nb and Mo carbide additives on pressure, carbide content and lubricant
22 p3970 A69-40634

Detonation velocity variation in nitromethane with initial pressure, discussing relationships
22 p4051 A69-40713

Molecular N UV spectrum at various pressures, showing absorption band dependence on pressure induced dipole transitions
22 p3986 A69-40723

Pure quadrupole resonance spectrum of iodine-127 in solid stannic iodide measured in specific temperature range at atmospheric pressure
22 p3986 A69-40726

Arterial and deep venous blood from human forearm analyzed following rest and rhythmic exercise on ergometer in hyperbaric oxygen chamber
22 p3878 A69-40834

Pressure activated superfluid valve design and operation for liquid He transfer from reservoir to cold finger
22 p3870 A69-41237

Decreasing barometric pressure effects on abdominal gas volume in military men under simulated flight conditions, noting abdominal fullness and pain
23 p4076 A69-41291

Decompression sickness in simulated zoom flights, discussing bubble formation probability and instantaneous surface tension effect on bends resistance
23 p4077 A69-41292

Arterial pressure and heart rate responses to increased intrapulmonary pressure in anesthetized dogs via simulated Valsalva tests
23 p4078 A69-41365

Nitrogen-carbon dioxide-helium lasers CW operation at various pressures and N flow rates
23 p4173 A69-41496

Transport coefficients in neutral gases, discussing fundamental relations of parameters in viscosity, thermal conductivity and self, pressure and thermal diffusion
23 p4193 A69-41514

High speed radially resistant ball bearing, analyzing effect of lubrication film on axial rigidity
23 p4169 A69-41555

Initial pressure rise and consequent laminar boundary layer separation during interaction with shock wave
23 p4151 A69-41691

Pituitary-adrenocortical axis of rats in oxygen atmosphere at low pressure, finding depressed norepinephrine excretion
23 p4087 A69-41790

Burning solid propellant behavior under pressure fluctuations expressed in response function terms defining small mass flux change ratio to small pressure change
23 p4201 A69-41922

Hinged circular cylindrical shells reinforcing ribs effect on deflection and bending moments, assuming external pressure application
23 p4229 A69-42001

Sinusoidal pressure electric stimuli frequency effects in isolated carotid sinus on canine peripheral blood pressure, determining dynamic characteristics from observation data
23 p4092 A69-42062

Acoustic gravity waves propagation over spherical earth with isothermal windless atmosphere, determining pressure perturbations
23 p4158 A69-42175

Pressure ratio effect on supersonic turbine nozzle performance during off-design regime operation, noting effect of low specific heat gas ratio
23 p4203 A69-42250

Surface films effect on friction coefficient of sodium chloride and Zn single crystals under normal pressure loads, noting film thickness role
23 p4170 A69-42343

Nb single crystals oxidation in dry oxygen at high pressure and temperature indicating suboxide platelets existence as function of temperature
23 p4177 A69-42357

Steady constant density two dimensional flow in laminar boundary layer over permeable curved surfaces, showing effects of suction or blowing
23 p4153 A69-42399

Alveolar and pleural pressures affecting pulmonary interstitial pressure in anesthetized dogs, applying Starling law of transcapillary exchange
24 p4257 A69-42627

Test animals prolonged deep submersion in water, in mixed oxygen-H atmosphere at elevated pressure, noting EEG and EKG activities
24 p4262 A69-43025

Initial deflection and internal pressure effects on supersonic panel flutter boundary of simply supported rectangular plates under diverse middle-surface stress conditions
24 p4400 A69-43056

Initialization technique for primitive forecast equations balancing Coriolis and pressure forces effects on atmospheric observations
24 p4344 A69-43065

Ge films formation by evaporation technique, discussing background O pressure effect
24 p4361 A69-43345

Barometric pressure affecting convective heat transfer from human body in air, deriving empirical formula as function of air density, speed and temperature
24 p4267 A69-43384

White mice survival rates and blood morphology and sedimentation rates in low ambient pressure confinement following infectious bacteria injection
24 p4267 A69-43397

Aircraft passenger cabins pressure safety limits estimating factors, discussing human respiratory gas exchange mechanism, pressure drop and smoking effects, etc
24 p4269 A69-43411

Decompression disease symptoms from standpoint of gas bubbles formation in blood vessels, examining factors preventing air metabolism
24 p4269 A69-43414

Heat transfer during nitrogen tetroxide nucleate boiling at various pressures and heat fluxes [ASME PAPER 69-HT-58]
24 p4411 A69-43536

Damping influence on shallow arch static and dynamic snapping under step pressure load
24 p4405 A69-43654

Pressure effects in spontaneous ignition of interimpinging hydrazine and red fuming nitric acid (RFNA) liquid streams in evacuated test chamber
24 p4415 A69-43667

Gas velocity and pressure influence on electrical breakdown potential of Ar, N and He between parallel flat plate and concentric electrodes
24 p4359 A69-43693

Atmospheric gases emission spectra excited by electron beam as function of pressure
24 p4353 A69-43698

PRESSURE GAGES
NT BAYARD-ALPERT IONIZATION GAGES
NT IONIZATION GAGES

NT KNUDSEN GAGES
NT MANOMETERS
NT OSMOMETERS
NT PIEZOELECTRIC GAGES
NT PIRANI GAGES
NT VACUUM GAGES

Pressure measurements by gauges in rarefied gas flows past bodies of various shapes, discussing configurations effect on gauge readings 01 p0080 A69-10358

Shock reflection structure in ionizing xenon determined by fast rise pressure gauge mounted in shock tube end wall 01 p0132 A69-12105

Etched manganin gauge for shock pressure measurement in high noise environments containing radiation and electromagnetic effects 04 p0603 A69-15431

HF electromagnetic decoupling pressure gage, using transducer with solid state strain gages as sensing elements 15 p2611 A69-31029

PRESSURE GRADIENTS

Turbulent to laminar boundary layer reversal by applying negative pressure gradient 01 p0058 A69-10066

Waves in inhomogeneous warm magnetoplasmas with static pressure gradients, applying dyadic to planar stratified plasma case 01 p0129 A69-10561

Venus cloud layer thickness and lower boundary estimation from data on chemical composition, temperature and pressure profiles of atmosphere 01 p0152 A69-10580

Superlayer structure determination near turbulent boundary layer with zero pressure gradient, using constant temperature linearized hot-wire anemometers 01 p0061 A69-10759

Pressure and flow transients in liquid rocket engine feed systems predicted by method of characteristics 03 p0495 A69-12991

Turbulent boundary layer reversion to laminar state associated with departures from inner law velocity distribution in presence of favorable pressure gradients 03 p0414 A69-13016

Planetary boundary layer response to time varying pressure gradient force 03 p0460 A69-13337

Wind shear and reflectivity gradient effects on Doppler radar spectra 03 p0461 A69-13341

Pressure rise and thermal conductivity in cylindrical hydrogen plasma column in axial magnetic field, assuming local thermal equilibrium 03 p0479 A69-13967

Elastic-plastic thin walled cylindrical shell axisymmetric behavior under radial pressure difference, noting load for collapse [ASME PAPER 68-APM/AA] 04 p0670 A69-14404

Hypersonic turbulent boundary layer in adverse pressure gradients studied for transition, measuring static/pitot pressure, stagnation temperature and heat transfer rates [AIAA PAPER 68-44] 04 p0588 A69-14716

Incompressible turbulent boundary layer properties with arbitrary pressure gradient calculated by integral method resulting in single equation for skin friction coefficient [ASME PAPER 68-WA/FE-22] 05 p0749 A69-16098

Shock wave profiles in expansion flows determined with static and impact pressure probes, investigating pressure gradient effects 06 p0908 A69-17022

Curvilinear plasma motions in ionosphere same as cyclones and anticyclones in troposphere, solving ionospheric unstable wind as function of pressure gradients 06 p0919 A69-17722

Liquid metal MHD systems efficiency when operating with pressure jump in diffuser nozzle 06 p0872 A69-17921

Transformation theory for compressible turbulent boundary layer with arbitrary pressure gradient [AIAA PAPER 69-160] 06 p0912 A69-18073

Nonsimilar laminar boundary layer solutions with negative pressure gradient compared to experimental boundary layer velocity profiles, momentum and displacement thicknesses [AIAA PAPER 69-35] 06 p0913 A69-18094

Viscid-inviscid equations solution, describing flows with coupled mixing, combustion and lateral pressure gradients [AIAA PAPER 69-83] 06 p1037 A69-18109

Superlayer structure in turbulent boundary layer without pressure gradient, using constant temperature linearized hot wire anemometers 07 p1118 A69-18299

Conducting gas acceleration in strong unsteady electromagnetic field, discussing channel flow in relation to time and pressure gradient 07 p1191 A69-18988

Turbulent boundary layer in presence of longitudinal pressure gradient 07 p1122 A69-19735

Sonic boom minimum achievable shock front pressure rise and overpressure level prediction for given aircraft and flight conditions 08 p1253 A69-19903

Jet flow and wakes in external stream and tailored pressure gradients, deriving similarity solutions for boundary layer equations 08 p1252 A69-20782

Double adiabatic MHD fluid equations for electrons and ions with pressure gradients for collisionless plasma in magnetic field 08 p1369 A69-20815

Power series solutions of MHD boundary layer equations for flat plate with transverse magnetic field and arbitrary pressure gradient, discussing skin friction 09 p1545 A69-21396

Velocity profiles of turbulent boundary layers with constant and variable pressures using Cole formulation 09 p1484 A69-22780

Unsteady baroclinic planetary atmosphere boundary layer turbulent states with various pressure and temperature gradient distributions, using boundary layer model 10 p1722 A69-23973

Shock wave propagation in gravitational field with pressure and density gradients, considering nonlinear equations of fluid flow 11 p1961 A69-25106

Streamwise pressure gradient effect on velocity profile in viscous sublayer of two dimensional turbulent flow along smooth wall 11 p1872 A69-25131

Turbulent wall jet growth in streaming two dimensional incompressible flow over plane smooth wall with pressure gradient 11 p1873 A69-25139

Pressure and flow rate variations at any point of manifold with control units calculated using transfer functions 11 p1942 A69-25335

Piezoelectric variometer with reduced indicator time lag for measuring pressure gradients in fluid media 11 p1889 A69-25427

Floating element skin friction meter designed for adverse pressure gradients, discussing wall shear stress measurement 11 p1889 A69-25557

Jet stream winds direction correlated with direction of LF pressure disturbances crossing microbarograph array 12 p2125 A69-26015

Viscous incompressible conducting fluid flow through porous coaxial nonconducting cylinders under radial magnetic field with pressure gradients functions of time 12 p2062 A69-26275

Ablation wedge model design for testing in wave superheater under controlled pressure gradients and constant temperature 12 p2059 A69-26816

Atmospheric pressure and wind data at equatorial latitudes, determining relation between rms meridional and zonal wind and pressure gradient 13 p2293 A69-27845

Atmospheric pressure variation coefficients computation based on harmonic analysis of wave behavior 13 p2295 A69-28648

Laminar and turbulent hypersonic wakes trailing blunt bodies studied by finite difference method, taking into account pressure gradients and nonequilibrium chemical reactions effects 14 p2391 A69-29618

Sealing mechanism theory with face seal applications, taking into account load carrying capacity and no leakage pressure gradient [ASLE FICFS PREPRINT 18] 15 p2620 A69-30489

Venus cloud layer thickness and lower boundary estimation from data on chemical composition, temperature and pressure profiles of atmosphere 15 p2691 A69-30750

Wind tunnel investigation of turbulent gas flow heat transfer and hydrodynamic drag in variable pressure gradient field of divergent-convergent channel 15 p2548 A69-31173

Pitot tubes diameter effect on pressure gradients during measurement through shock wave 16 p2771 A69-31927

Pressure gradients and moving ions driven neutral-air winds in F region, using asymmetric pressure model 16 p2779 A69-32302

Lower solar corona composition changes due to pressure and thermal gradients calculated with multicomponent diffusion equations 17 p3030 A69-33059

Gas pressure differential across multilayer insulation blanket during rapid evacuation predicted, using one dimensional flow theory [AIAA PAPER 69-608] 17 p3072 A69-33275

Favorable pressure gradient effect on compressible two dimensional supersonic turbulent boundary using temperature and pressure probes and shear balance [AIAA PAPER 69-685] 17 p2956 A69-33489

Turbulent boundary layer subject to sudden pressure variation due to rapid expansion or shock wave, noting application to hypersonic ramjet air intake [ICAS PAPER 68-42] 17 p2895 A69-33587

Statistical analysis in inlet air flow dynamics, discussing inlet duct design and pressure variations [AIAA PAPER 68-649] 17 p2896 A69-34020

Hydrodynamic noise as pseudosound field resulting from pressure variations in turbulent fluid flow, using Lighthill acoustic analogy 18 p3123 A69-34921

Rough wall turbulent boundary layer development in pipe flow determined for different roughness geometries in zero and adverse pressure gradients 18 p3125 A69-35387

Axisymmetric laminar and turbulent wakes of body in flow with streamwise pressure gradient, discussing velocity defects and profiles 19 p3296 A69-35762

Surface tension gradients caused thermocapillary convection solved for spherical fluid film under weightlessness conditions 19 p3452 A69-36392

Pressure gradient produced steady plane flow of Maxwellian gas between infinite parallel planes, describing linearized Boltzmann equation solution 19 p3379 A69-36604

Wall temperature distributions predicted in turbulent boundary layer with arbitrary pressure gradients, basing calculations on Spalding function solutions 19 p3302 A69-36853

Turbulent boundary layer of injection gas flow calculated past surfaces with pressure gradient 20 p3513 A69-37091

Reynolds analogy factor approximate calculation for turbulent boundary layer with pressure gradient 20 p3514 A69-37183

Turbulent boundary layer growth predicted for adverse pressure gradients, using entrainment theory for two dimensional and axisymmetric flows [ASME PAPER 69-FE-16] 20 p3517 A69-37991

Nomograph for rapid estimation of pressure drops across orifices in pneumatic systems using real gas data with illustration for nitrogen 20 p3467 A69-38186

Upper atmosphere horizontal unsteady wind with pressure gradient time dependence, solving heat conduction type equation by integral representations 21 p3758 A69-38411

Temperature distributions and heat transfer in thermal entrance region for Hartmann liquid flows under constant pressure gradient between parallel electrically conducting walls at rest 21 p3847 A69-38442

Heat transfer and hydrodynamic resistance for turbulent gas flow in longitudinal positive and negative pressure gradients analyzed using Reynolds number data 21 p3848 A69-38635

Blowing effect on surface friction coefficient and heat transfer in turbulent boundary layer in compressible fluid with pressure gradient 21 p3643 A69-38636

Unsteady baroclinic planetary atmosphere boundary layer turbulent states with various pressure and temperature gradient distributions, using boundary layer model 21 p3760 A69-39659

Blood sheet flow velocity distribution and pressure gradients in pulmonary alveolar septa determined, allowing for system elasticity 22 p3874 A69-40216

Mass diffusion and heterogeneities in compression chamber gas mixture in shock tube ascribable to pressure and temperature gradients

23 p4146 A69-41547

Slender profile oscillations in subsonic flow near solid boundary, calculating pressure gradients by dipole method

23 p4058 A69-41713

Spanwise velocity profiles through cascades and axial flow turbomachines, analyzing loading, secondary losses and inlet conditions interacting on downstream profile

23 p4061 A69-42110

Shock wave/boundary layer interaction calculation methods circumventing simultaneous large longitudinal and transverse pressure gradients and viscous effects

24 p4243 A69-42582

Compressible gas flow into cavity of various volumes in presence of supercritical pressure gradients

24 p4298 A69-42587

Bubble flow evolution at various pressures up to critical value [ASME PAPER 69-HT-30]

24 p4411 A69-43529

Rough surface skin-friction relations expanded to provide turbulent boundary layer growth prediction in pressure gradient

24 p4304 A69-43580

Unsteady MHD conducting fluid flow in arbitrary ducts under transverse magnetic field, studying effects of pressure gradient impulsive change

24 p4359 A69-43678

Reverse flow profiles in turbulent free jet mixing with streamwise pressure gradient

24 p4306 A69-43684

PRESSURE HEADS

Spikes on sonic boom pressure waveforms due to simultaneous focusing and diffraction of planar N wave by inhomogeneous atmosphere layer

01 p0011 A69-11280

PRESSURE MEASUREMENTS

Cooled probes for gas measurements in high pressure arc jets, hyperthermal wind tunnels, rocket motors, scramjets and similar severe environments

01 p0078 A69-10150

Human systolic and diastolic blood pressure measuring apparatus and method

01 p0079 A69-10296

Pressure gain estimates in analog jet amplifier based on total pressure measurements in main jet interaction region

02 p0195 A69-12076

Viscous effects on impact pressure measurements in free jet low density gas flows at high Mach numbers

02 p0234 A69-12633

Wind tunnel pressure tests of Concorde air intake mockups in presence of aircraft wing and nose for Mach numbers 2, 2.2 and 2.35

03 p0361 A69-12879

Design and development of electrical transducer and associated instrumentation for fluid pressure measurement

03 p0427 A69-12914

Glaucoma in commercial airline pilots noting value and safety of routine tonometry

03 p0376 A69-14078

Unsteady potential flow and wake near oscillating circular cylinder noting velocity, pressure and correlation measurements [ASME PAPER 68-WA/FE-23]

05 p0749 A69-16099

Aircraft gas turbine component pressure data storage and scanning

05 p0726 A69-16768

Radiation effects on NERVA out-of-core instrumentation, discussing cryogenic temperature measurements and transducer measuring pressure at gamma heating rates

06 p0956 A69-16882

Manual performance of aircraft pilots under sustained acceleration using measurements of handwriting pressure

06 p0884 A69-18030

Condensation and probe interference in planar expansion deflection nozzle measurements [AIAA PAPER 69-170]

06 p0863 A69-18059

Flow measurements in near wake of 7 degree half angle cone at free stream Mach number 4.3, noting pressure measurements [AIAA PAPER 69-186]

06 p0863 A69-18068

Book on fundamentals of temperature, pressure and flow measurements covering standards, calibration, moving fluid effects, transient effects and installations in fluids and solids

07 p1131 A69-18410

Pneumatic instrumentation line transfer function approximated by system model for simplifying reactor control system analysis [IEEE PAPER 2D-6]

07 p1059 A69-19190

Low pressure measurement by electron scattering using Born approximation

07 p1181 A69-19218

Jet engine gas flow, temperature, velocity and pressure measurements by analog and digital systems

08 p1316 A69-20869

Coordination technique for pressure, density and temperature measurements by probes during parachute reentry into planetary atmospheres, taking into account reentry dynamics

09 p1609 A69-21775

Turbine stator blade performance determination from total pressure surveys downstream of blade row, noting problems in pressure measurement [ASME PAPER 69-GT-103]

09 p1432 A69-22521

Skin friction measurement with rectangular mouthed Preston tubes of constant thickness ratio, analyzing calibration curves and difference from circular tubes

11 p1880 A69-24376

Pressure distribution measurement over sphere with cylindrical afterbody in magnetofluid dynamic flow, showing drag decrease at large magnetic field

11 p1873 A69-25136

Static pressure measurements at surface of sharp plate in supersonic flow during gas/liquid jet injection

11 p1821 A69-25479

Different pressure and deflection measurements coherence in vortex flows verified assuming radial equilibrium conditions

12 p2012 A69-26362

Ionization sensors and detectors classification and dynamic calibration for pressure measurement

13 p2262 A69-28083

Diagnostic measurements in nonequilibrium nozzle flows compared to finite rate expansion calculations, measuring pressure, temperature and density [AIAA PAPER 69-328]

13 p2200 A69-28263

Atmospheric pressure variation coefficients computation based on harmonic analysis of wave behavior

13 p2295 A69-28648

Cavity mounted pressure transducers response in high speed pressure measurements

14 p2445 A69-28874

Contact between cylindrical surfaces in thermionic converters, determining thermal resistance and pressure in contact area

14 p2400 A69-29216

Worldwide observation of atmosphere with occultation satellites, correcting orbit perturbations to obtain air pressure

14 p2447 A69-29517

Saturated Li vapor pressure measured by static equilibrium technique based on use of null membrane, tabulating pressures for various temperatures

15 p2656 A69-30997

Pressure behind spherically divergent shock wave produced by explosion of metal wire measured and compared with calculated values

16 p2769 A69-31837

Buried collector ionization gage for measurements in 100 billionth torr pressure range using shielded collector to lower X ray current

16 p2791 A69-32324

Molecular flow network theory applicable to volumes interconnected by small orifices or porous membranes for transient pressure measurements

16 p2813 A69-32325

Vertical atmospheric pressure distribution measured directly with Pirani-Israel gauge in Skylark rocket, transforming dynamic pressure data into static pressures on ground

17 p2971 A69-33037

Pressure and temperature surveys of Mach 27-47 nozzle boundary layer at Ames M-50 He tunnel, determining velocity profiles, wall friction coefficient, etc [AIAA PAPER 69-686]

17 p2953 A69-33441

Wind tunnel model low pressure measuring system, discussing pressure transducers, automatic control and pressure distribution tests [AIAA PAPER 68-402]

17 p2947 A69-34023

High speed transient pressure measurement, emphasizing forcing function measurement

18 p3133 A69-34244

Fluidic pressure ratio computing device based on two free jets interaction principle, describing prototype system design and analysis, electronics and overall error

18 p3133 A69-34309

Ducted fan engine turbine air flow rate and frontal gas temperature determined from air tempera-

ture/pressure measurements behind compressor and engine fuel flow

18 p3086 A69-34986

Multichannel pressure telemetry system for base pressure measurements on small wind tunnel models, considering proximity effects on transducer-telemetry units

19 p3305 A69-35727

Error analysis for pressure measurements in blow-down supersonic tunnel

19 p3292 A69-35728

DYDRA data logger for dynamic measurements of pressure distributions on harmonically excited wind tunnel models, noting use as general transfer function analyzer

19 p3293 A69-35746

Pressure increment due to inertia of rotating fluid film at journal bearing periphery theoretically estimated and measured

20 p3548 A69-37085

Free flight telemetered base pressure test data correlation for high Mach numbers, noting facilities and instrumentation

20 p3458 A69-37196

Condensation and probe interference in planar expansion deflection nozzle measurements [AIAA PAPER 69-170]

21 p3645 A69-39769

Pressure measurements and gas flow analysis during thermal vacuum tests of manned spacecraft indicating adequate space vacuum simulation [AIAA PAPER 69-1033]

22 p3924 A69-40401

Single channel pressure telemetry unit with magnetic latching or RF switch for chronic implantation

23 p4100 A69-41295

Vacuum gage calibration standards and methods [AIAA PAPER 69-170]

23 p4162 A69-41530

Distortion processes in ear, discussing sound pressure level/SPL/measurements in rigid-walled couplers

23 p4085 A69-41573

Indentation tonometry for occult pathology and glaucoma in commercial pilots

23 p4088 A69-41805

Hypersonic turbulent flow heat transfer and pressure data for flat plate containing steps and cavities obtained in hypersonic wind tunnel [AIAA PAPER 68-673]

23 p4060 A69-41902

Pressure measurement modifications of quasi-steady flow model for interaction between reflected shock wave and laminar boundary layer in shock tube

23 p4152 A69-41903

Two fluid heat pipe performance, measuring temperatures and condenser end vapor pressures for two thermal power input conditions

23 p4240 A69-42306

PRESSURE OSCILLATIONS

Pressure oscillation production in wind tunnel by hinged plates in test section walls to test jet engine inlets under controlled conditions

02 p0229 A69-12537

Ideal liquid small oscillations in vessel under close to weightlessness conditions, discussing surface tension, equilibrium conditions and solution by decomposing vector function space

03 p0418 A69-13811

Primary frequency of oscillations of ideal liquid in cylindrical vessel with axially directed weak gravitational field

03 p0418 A69-13812

Pressure fluctuations in separated flow region behind thin fence, determining recombination point position, noise sources and frequency spectra variations

04 p0544 A69-14868

Initiation of HF combustion oscillation in premixed gas rocket [ISAS-430]

06 p1029 A69-17025

Nonmetalized composite propellant solid phase heterogeneities effect on oscillatory combustion, inducing coherent burning rate oscillations with external pressure oscillations

09 p1622 A69-22085

Fuel concentration effect on turbojet engine reheat jet pipe vibrations via tests

09 p1573 A69-22616

Forced discontinuous vibrations of liquid in conduit experimentally analyzed, discussing test devices and procedures

11 p1875 A69-25485

Combustion instability problems in rocket motors, emphasizing strongly coupled pressure oscillations in combustion chambers

11 p2003 A69-25597

Wall pressure fluctuations due to turbulent boundary layer flow, calculating statistical properties [AIAA PAPER 68-642]

13 p2244 A69-27246

- Pressure fluctuation relaxation model to close turbulent distribution function equations at one point level, solving equation for rectilinear flows and periodic wake decay
15 p2591 A69-30906
- Nonlinear response of single Helmholtz resonator subjected to finite amplitude pressure oscillations, detailing entrance, orifice and cavitation flow [AIAA PAPER 69-481]
16 p2844 A69-32719
- Semidiurnal oscillation in the thermogeostrophic atmosphere examined using atmospheric model for tidal oscillations response study
17 p2959 A69-33148
- Random oscillations of elastoacoustic systems, obtaining solution for spherical shell containing acoustic medium
17 p3057 A69-33199
- Pulsating flow analysis in finite and infinite conical nozzles under sinusoidal pressure disturbances [ASME PAPER 69-APM-16]
18 p3214 A69-34392
- Flame and pressure /or velocity/ oscillations interaction in unstable combustion regimes, considering tubes with propane-air mixtures
19 p3450 A69-36357
- Liquid propellant rocket injectors response to HF chamber pressure oscillations using one dimensional model
21 p3786 A69-39235
- Pressure wave transmission in liquid filled tubes, determining attenuation and phase shift for hemodynamics applications
24 p4279 A69-43798
- PRESSURE PULSES**
- Temperature and pressure measurements in low temperature combustion of n pentane covering slow reaction and cool flame regions
02 p0353 A69-12321
- Pressure pulses propagation in nonsteady fluid flow through expandable tubes, noting computer solution
02 p0232 A69-12477
- Dynamic pressure pulse over band on solid elastic cylinder surface, analyzing time stress distribution throughout elastic cylinder
04 p0670 A69-14408
- Longitudinal stress pulse propagation in finite length free-free bar with variable cross section, noting stresses in projectile impacting plane target
04 p0671 A69-14412
- Elastic behavior of large blood vessels in canine aorta by measuring dispersion and attenuation of artificially induced pressure waves
04 p0553 A69-14692
- Simulation of two and three dimensional fluid transients by use of one dimensional equations in lattice-work of piping elements
05 p0747 A69-16071
- White dwarfs atmospheric pulsation suggested as pulsar mechanism, considering thin adiabatic atmospheric model with constant lapse rate
05 p0828 A69-16659
- AC fluidics for pressure pulse frequency control and monitoring in flow, discussing design and application to steam turbine speed control
07 p1058 A69-18938
- Impulse noise damage risk criteria, discussing maximum tolerable exposure, hazardous exposure and methods of impulse noise measurement
07 p1066 A69-19171
- LF spectral analysis of flowing water pressure pulsations behind single bulge on hydrodynamic channel smooth wall at low disturbance level
13 p2246 A69-27535
- LF spectrum analysis of hydrodynamic flow near-wall pressure pulsations over rough surfaced wall
13 p2246 A69-27537
- Vortex ring production in liquid jet by vibration induced pressure pulses at orifice, discussing plates formed under high g vibration [AIAA PAPER 68-132]
16 p2770 A69-31880
- High speed transient pressure measurement, emphasizing forcing function measurement
18 p3133 A69-34244
- Dynamic pressure pulsations, temperature distribution and gas concentrations in discrete vortices zone in wake of plate in unbounded flow
18 p3124 A69-35120
- Spatiotemporal contours of pressure pulses emitted into surrounding fluid by collapsing cavitation bubble, using schlieren-optical observation method, electroacoustical detection device and microphone
19 p3302 A69-36870
- LF spectral analysis of flowing water pressure pulsations behind single bulge on hydrodynamic channel smooth wall at low disturbance level
20 p3518 A69-38202
- LF spectrum analysis of hydrodynamic flow near-wall pressure pulsations over rough surfaced wall
20 p3518 A69-38203
- Initially sharp plane pressure pulse propagation through linear elastic composite material, determining wave front shape change and stresses behind front [ASME PAPER 69-APMW-11]
24 p4401 A69-43103
- Interphase momentum transfer during propagation of infinitesimal pressure pulse through bubbly flow two phase mixture
24 p4409 A69-43511
- PRESSURE RECOVERY**
- Pressure recovery of straight channel divergence diffusers at high inlet Mach numbers [ASME PAPER 68-WA/FE-19]
05 p0698 A69-16095
- High energy recovery pressure and enthalpy sensor /HERPES/ for flow measurements in aerospace simulation facilities
19 p3307 A69-35750
- PRESSURE REDUCTION**
- NT EXPLOSIVE DECOMPRESSION**
- Changes in organism during sudden decompression, analyzing pressure equalization, dissolved gases transformation and body fluids vaporization
01 p0020 A69-10753
- Prolonged decompression stress effects on humans in simulated orbital flight or extravehicular activity, investigating endocrine-metabolic disturbance by urinalysis
01 p0022 A69-11336
- Human endocrine-metabolic response to sequential decompression exposure during simulated orbital flight or extravehicular activity
01 p0022 A69-11337
- Nitrogen and helium as factors affecting human decompression stress severity, using urinary measurements reflecting various endocrine and metabolic changes
01 p0018 A69-11338
- Smith correlation of turbine stage efficiency for relating achievable efficiency to stage loading and flow factors used for total pressure loss coefficient data [ASME PAPER 68-WA/GT-5]
05 p0812 A69-16140
- Human acceleration tolerance under reduced pressures corresponding to various high altitudes, noting visual disorders
07 p1065 A69-18982
- Air powered fluid jet engine compressor bleed control stressing closing, reset and override operations [ASME PAPER 69-GT-19]
09 p1571 A69-22498
- Elastic release wave and pressure drop measurement in 2024-T4 aluminum at 313 kb for dynamic yield strength, considering surface velocity and stress
10 p1712 A69-23665
- Bleed air environmental system utilizing air to air jet pumps as flow multipliers for cabin pressurization air supply in commercial turboprop aircraft [SAE PAPER 690331]
11 p1941 A69-24494
- Blood oxygen metabolism, analyzing content and volume circulation in dogs under oxygen partial pressure decrease in inhaled air
12 p2019 A69-26346
- Blood coagulation in animals under acute hypoxia at exposures to pressure corresponding to 5000 m altitude, noting blood morphology
12 p2019 A69-26348
- Radial electric field effect on pressure drop in isothermal laminar flow of dielectric liquid through stainless steel tube, considering ion drag
12 p2136 A69-26401
- Autonomic nervous system role in controlling body functions after rapid decompression, increasing tolerance to pressure gradients by physical training
13 p2212 A69-28622
- Bird respirator function at simulated high altitude, noting adequate support in case of rapid decompression
14 p2406 A69-29290
- Rapid decompression and recompression in stapectomized cat, noting fibrous tissue response in middle ear at reconstructions utilizing polyethylene struts on gelfoam
14 p2406 A69-29292
- Monograph on Prandtl number effect on heat transfer and pressure loss in artificially roughened channels
15 p2717 A69-30934
- Pressure losses in pipeline with venturi tube, calculating hydraulic resistance coefficient as function of structural parameters and pipeline length
15 p2612 A69-31180
- Hydrogen check valve with low cracking pressure and flow pressure drop for hydrogen vent system at Saturn launch pad [AIAA PAPER 69-578]
16 p2845 A69-32738
- Concentration, flow rate and tube diameter effects on viscous drag reduction in nonpolar soap solutions, using pressure drop measurements to observe turbulent flow behavior
17 p2951 A69-33253
- Solid propellant motor extinction by depressurization, determining extinction conditions by electrical analogy
17 p3021 A69-33355
- Solid propellant motor extinction by depressurization, determining extinction conditions by electrical analogy [ONERA-TP-722]
18 p3184 A69-34637
- Pressure drop in control element of gas generator during readjustment of throttle in hydraulic supply line, noting assumptions
19 p3393 A69-35819
- Human acceleration tolerance under reduced pressures corresponding to various high altitudes noting visual disorders
20 p3480 A69-38230
- Decompression study simulating supersonic aircraft cabin small structural failure at 60,000 ft, using monkeys as subjects
21 p3665 A69-39171
- Canine cerebellar Purkinje cells electron microscopy after rapid decompression to near vacuum
21 p3660 A69-39177
- Prandtl number influence on heat transfer and pressure drop characteristics of roughened channels, determining friction factor
24 p4407 A69-42915
- Choking and shock in flashing single component two phase flow in tube, including vibrational effects, predicting minimum stagnation pressure loss [ASME PAPER 69-HT-61]
24 p4303 A69-43535
- PRESSURE REGULATORS**
- Hybrid fluidic pressure regulator combining vortex amplifier and confined-jet amplifier with performance upgrading moving metering element, noting greater efficiency and reliability
10 p1639 A69-23560
- Back pressure control system for heat leak evaluation tests of cryogenic containers, discussing component selection and error analysis
15 p2702 A69-30397
- Self contained remote sense remote control pressure regulator using pure fluid amplifiers, controlling large or small flow over wide pressure range
15 p2554 A69-31303
- Temperature control below 5.2 K based on servoing He pressure above bath
18 p3136 A69-34641
- PRESSURE RELIEF VALVES**
- U RELIEF VALVES**
- PRESSURE SENSORS**
- Calibration of pressure transducers in liquid hydrogen to liquid helium temperature range using cryogenic test equipment
01 p0080 A69-10300
- Acoustic probe for measuring pressure fluctuations on hypersonic reentry vehicle, discussing flow characteristics and heat shield ablation effects on frequency response
01 p0008 A69-11278
- Pneumatic pressure ratio sensing element and associated high pressure switches and amplifiers for gas turbine engine control systems
02 p0249 A69-12088
- Design and development of electrical transducer and associated instrumentation for fluid pressure measurement
03 p0427 A69-12914
- Rotating hot wire and five hole pressure probes for determining complete velocity vector in subsonic flow
05 p0764 A69-16398
- Condensation and probe interference in planar expansion deflection nozzle measurements [AIAA PAPER 69-170]
06 p0863 A69-18059
- Nonlinear lumped parameter model for long gas filled pressure sensing lines covering steady state, laminar or turbulent gas flow [AIAA PAPER 69-117]
06 p0913 A69-18106
- Pressure-altitude transducers for atmospheric pressure measurements on balloon flights including diaphragm, thermoconductivity, radioactive density and hypsometer gauges
07 p1132 A69-18873

Fluoride light-off detector /FLOD/ for sensing and indicating minimum light-off or blow out conditions in turbojet engine afterburner
[ASME PAPER 69-GT-36] 09 p1501 A69-22488

Pressure transducers with variable reluctance and magnetic signal transmission techniques
10 p1690 A69-23226

Signal conditioning for transducers covering piezoelectric devices, thermocouples, resistance transducers, reluctance and differential transformer sensors
10 p1691 A69-23228

Capacitance pressure transducer capable of detecting pressure changes equivalent to 0.2 mm water
11 p1885 A69-24902

Single channel pressure telemetry unit for chronic implantation into cardiac chambers or major blood vessels in unrestrained animals for measuring ventricular pressure
11 p1831 A69-25642

Construction and calibration of combined temperature and pressure probe for compressible flow
13 p2242 A69-28226

Cavity mounted pressure transducers response in high speed pressure measurements
14 p2445 A69-28874

Monograph on investigation of rarefied gas flows by means of miniature pressure probes in transition region between molecular and continuum flows
14 p2430 A69-29289

Lightweight sensor for telemetering oxygen partial pressure in respiration air
15 p2559 A69-31231

Fluidic sensors for jet engine control, analyzing convergent divergent nozzles, vortex and acoustic oscillators for pressure and gas temperature measurements
[AIAA PAPER 69-542] 16 p2843 A69-32699

Fixed position pressure probe for measuring subsonic flow direction over range of Reynolds number, Mach number and flow angle
17 p2973 A69-33107

Wind tunnel model low pressure measuring system, discussing pressure transducers, automatic control and pressure distribution tests
[AIAA PAPER 68-402] 17 p2947 A69-34023

High speed transient pressure measurement, emphasizing forcing function measurement
18 p3133 A69-34244

Multichannel pressure telemetry system for base pressure measurements on small wind tunnel models, considering proximity effects on transducer-telemetry units
19 p3305 A69-35727

High energy recovery pressure and enthalpy sensor /HERPES/ for flow measurements in aerospace simulation facilities
19 p3307 A69-35750

Condensation and probe interference in planar expansion deflection nozzle measurements
[AIAA PAPER 69-170] 21 p3645 A69-39769

Pressure transducers using heterode strain sensors evaporated directly onto pressure diaphragm
22 p3950 A69-41222

Miniature transducer to measure low transient pressures on models in rarefied shock tunnel flows, emphasizing mechanical vibration, convective heating and miniaturization
22 p3950 A69-41222

Nonlinear lumped parameter model for long gas filled pressure sensing lines covering steady state, laminar or turbulent gas flow
[AIAA PAPER 69-117] 24 p4301 A69-43259

Dynamic pressure response of viscous compressible fluids in rigid tubes with dead ended volume termination, testing Ibrall theorem as function of Stokes number
24 p4301 A69-43287

Static and dynamic characteristics of fluid pressure signal transmitter between members with relative rotary motion
24 p4256 A69-43300

PRESSURE SUITS

NT SPACE SUITS

Flight test evaluation of small man lunar flying device /POGO/, discussing vehicle control, pressure suit factors and piloting differences
[AIAA PAPER 68-240] 02 p0229 A69-12379

G suit inflation acute and prolonged effects on cardiovascular dynamics in recumbent and passively tilted individuals
06 p0883 A69-17843

Finger dexterity in JMG-1 pressure gloves with regard to efficiency associated with fine adjustments
06 p0884 A69-18032

Pressure garments weight reduction methods, comparing partial pressure systems equipped with bladder, capstan, airpipe or foam rubber
06 p0884 A69-18037

Moisture losses of men wearing partial pressure suit with oxygen mask determined by changes in skin temperature and heat flow
10 p1647 A69-23591

PRESSURE VESSEL DESIGN

Cost effective pressure vessel design using fracture mechanics, discussing fabrication costs, service life requirements, etc
16 p2870 A69-31740

High modulus filament wound composites used for propellant and pressurization tanks, discussing overwrap and liner permeability, porosity, weight, etc
19 p3354 A69-35513

Fracture mechanics application to pressure vessel design and analysis, reviewing nondestructive inspection techniques
19 p3439 A69-36438

Linearization of relationship between stress concentration factor and reciprocal of strain hardening exponent enabling shakedown to pressure vessels formulated by mathematical model
20 p3620 A69-37002

Elastic interactions between cylindrical shell and added band reinforcement turns, analyzing stress relaxation magnitude and effect on pressure vessel design
20 p3621 A69-37064

Fracture mechanics concepts for cost effective booster pressure vessel design and fabrication from commercial steels using boiler plate techniques and minimal NDT quality control
21 p3837 A69-39028

PRESSURE VESSELS

Basic equations for optimum inhomogeneity in pressure vessels of maximum rigidity derived, using thick walled spherical shell
01 p0167 A69-10326

Spherical shell pressure vessels investigated for optimum inhomogeneity and rigidity using Lagrange polynomials
01 p0167 A69-10327

Fabrication of large arched bottoms for pressure vessels from aluminum alloys, discussing sheet cutting and welding, annealing, machining, etc
02 p0254 A69-12678

Computer method calculating stressed state of elliptical bottom of cylindrical pressure vessel based on differential bending equations for shell of revolution
04 p0668 A69-14275

Ultrahigh pressure test vessel for determining pressure vs burning rate characteristics of propellants and explosives
04 p0645 A69-14472

Glass, boron and graphite filament wound resin composites and liners for cryogenic pressure vessels
05 p0785 A69-16488

Leak testing of welded pressure and vacuum vessels, considering nature of flow of gases through small restrictions
07 p1140 A69-18799

Rupture times in analysis of creep tensile instability in uniformly pressurized thin walled membrane shells of revolution, comparing two criteria
07 p1234 A69-19378

High pressure storage vessels for gaseous hydrogen, discussing failure, manufacturing controls and access for internal nondestructive inspection
[ASM PAPER D8-14.1] 07 p1143 A69-19666

Pressure vessel design to alleviate hydrogen embrittlement of steels for shock tunnel drivers
[AIAA PAPER 68-367] 09 p1477 A69-21993

Multilayer pressure vessel load carrying capacity calculated, using Huber-Mises yield condition to estimate axial force influence
09 p1618 A69-22257

Planar ribbon winding for buildup control of material near polar openings of filament wound vessels, discussing ribbon width and density
09 p1507 A69-22328

Pressure vessels burst tests for investigating alloys, fabrication processes and biaxial loading effects, noting vessel configurations and test temperatures
10 p1714 A69-23974

Deformations and stresses in pressure vessel with elliptical cross section under uniform internal pressure, noting radial deflection and membrane, bending and skin stress
11 p1983 A69-25023

High pressure vessels welding reliability improvement, discussing edge profile, air expulsion from vessel and shielding atmosphere
11 p1892 A69-25670

Heat treatable low alloy steels weldability for lightweight ultrahigh strength pressure vessels, gear and shaft fabrication in aerospace applications
12 p2100 A69-25827

Axisymmetric elastic stresses in ring stiffened segmented shells of revolution, noting finite difference method for nonlinear analysis and computer program
12 p2185 A69-26818

Materials rating method in pressure vessel applications, considering impact on design of minimum cost space launch vehicle
12 p2175 A69-26844

Liquid sloshing in vessel of complex geometry reduced to boundary value problem
14 p2428 A69-28969

Collapse pressure of flush cylindrical nozzle axisymmetrically intersecting conical pressure vessel for rigid plastic shells
15 p2704 A69-30289

Thick walled pressurized cylinder fatigue test results compared with axial tension and rotating beam tests on same material
15 p2709 A69-30676

Repeated static stress limit of internal pressure vessels, emphasizing effect of redistribution of stresses and strains
15 p2712 A69-30973

Stress-strain rate of glass fiber reinforced plastic pressure vessels under internal pressure, determining optimal fiber pattern
17 p3057 A69-33195

Fracture safe design practices for pressure vessels and piping, stressing transition temperature and proof testing roles
17 p3060 A69-33562

Forming and heat treatment process for stainless steel pressure containers using liquid N, discussing austenite-martensite transformation role
18 p3161 A69-34605

Deformation detection by stress wave analysis technique /SWAT/, noting pressure vessel applications
18 p3223 A69-35080

Graphite fiber NOL rings and biaxial wound pressurized cylinders tested at ambient and cryogenic temperatures for tensile and cyclic fatigue properties
19 p3355 A69-35521

Fracture mechanics applied to cylindrical pressure vessels containing longitudinal defects for fracture behavior prediction from fracture toughness or stress intensity factor
19 p3439 A69-36439

Stress analysis of cylindrical shell-end closure junction for optimum pressure vessel configuration prediction for nuclear reactor applications
19 p3447 A69-36861

Microplasma, W inert gas and submerged arc welding processes for fabrication of rocket motor cases and pressure vessels, discussing material requirements and weldability
[SBAC PAPER 7] 20 p3550 A69-37449

Thin cylindrical pressure vessels with circular cutouts and radial branches, observing limit pressures during plastic deformation
20 p3629 A69-38027

Axial through-cracks extension criteria in cylindrical pressure vessels, considering fracture toughness and plastic flow stress
[ASM PAPER W9-13.3] 21 p3833 A69-38658

Texture hardening combined with age hardening for biaxial strength improvement of Ti-Al-V alloy, discussing applications to spherical pressure vessels
21 p3729 A69-38662

Computer program for stress analysis of cylindrical pressure vessel with flat-end closures by thin shell theory
21 p3842 A69-39306

Static and fatigue strength of end-closed filament-wound vessels under internal pressure
21 p3846 A69-39797

Axial through-cracks extension criteria in cylindrical pressure vessels, considering fracture toughness and plastic flow stress
22 p4046 A69-41040

High strength austenitic Cr-Mn-Ni steel applicability to welded pressure vessels for cryogenic fluid storage, discussing operating temperature stability, weldability, etc
23 p4175 A69-41475

Fracture and tensile properties of electron beam welded Al alloy for pressure vessels compared to gas tungsten arc welding results
24 p4319 A69-42941

Nondestructive detection of titanium hydride formation in threaded joints of Ti alloy pressurization tanks by neutron radiography
24 p4320 A69-42998

Aerospace pressure vessel materials selection and construction, applying Apollo program experience to future programs
24 p4324 A69-43430

PRESSURE WAVES
U ELASTIC WAVES

PRESSURE WELDING
NT DIFFUSION WELDING
NT EXPLOSIVE WELDING
NT ULTRASONIC WELDING

Fusion, resistance and pressure welding of titanium, discussing shielding, brazing, diffusion and adhesive bonding
02 p0253 A69-12064

Adhesive pressure welded joints tightness and fabrication stability analyzed on duraluminum sheet samples
17 p2978 A69-32949

PRESSURIZED CABINS

Reinforced thin walled cylindrical pressure body nonlinear circumferential stress problem approximate solution, noting fatigue strength of aircraft pressurized cabins
04 p0548 A69-14838

Bleed air environmental system utilizing air to air jet pumps as flow multipliers for cabin pressurization air supply in commercial turboprop aircraft
[SAE PAPER 690331] 11 p1941 A69-24494

Pressurized Navajo aircraft environmental system, discussing ventilation, pressurization, heating and air cooling systems
[SAE PAPER 690330] 11 p1829 A69-24504

Fuselage corrosion effect on structure and skin of older aircraft with emphasis on pressurized aircraft
21 p3646 A69-38392

Decompression study simulating supersonic aircraft cabin small structural failure at 60,000 ft, using monkeys as subjects
21 p3665 A69-39171

PRESSURIZATION
NT FUEL TANK PRESSURIZATION

Gas flow analysis for externally pressurized porous journal gas bearing, considering circumferential flow in bearing clearance and porous bushing
01 p0085 A69-10312

Whirl instability of externally pressurized gas journal bearing with peripheral feeding holes, discussing analytical natural frequency of shaft bearing systems
02 p0254 A69-12426

Pressurized fluid journal bearing with fluid fed into space between shaft and shell from plenum chamber in bearing housing through circumferential slots
06 p0931 A69-17529

Externally pressurized gas lubricated journal and thrust bearings designs, citing reference literature
[ASME PAPER 68-LUBS-8] 13 p2267 A69-27282

Externally pressurized gas lubricated bearings treated theoretically using unevenly distributed supercharging method, noting Reynolds equation numerical integration
[ASME PAPER 68-LUBS-44] 13 p2267 A69-27283

Pressurized cylindrical shell creep analysis by elastic procedure extension using computer program
17 p3067 A69-34211

Wrinkling of pressurized cylindrical and conical free membrane column under lateral load, considering membrane sheets elastic properties
22 p4045 A69-40814

PRESTON TUBES
U PITOT TUBES
U SPEED INDICATORS

PRETRAINING
U PRESTRESSING

PRESTRESSING

Yield surface after prestraining under radial loading, analyzing formation of yield corner
01 p0166 A69-10303

Prestraining of stainless steel EN58b sheet at room and cryogenic temperature, noting effect on tensile properties
01 p0099 A69-11151

Material memory effect in plastically prestrained thin walled brass tubes analyzed on basis of kinematic strain hardening theory
02 p0336 A69-11551

Predeformations of thin walled elastic isotropic spherical shells analyzed using Vlasov shell bending theory
02 p0336 A69-11555

Butt weld fatigue properties improvement in maraging steels, using shot peening and prestretching
03 p0434 A69-13762

Subsequent yield surfaces in cross shaped brass plates determined after prestraining or cold rolling
04 p0682 A69-15302

Prestressing of aircraft wing stringers in order to reduce weight, noting initial bending moment, initial axial stress and prestressing methods
05 p0832 A69-15690

Stress effect on laser damage crack orientation in transparent organic dielectrics, estimating gas pressure in cracks
10 p1703 A69-23621

Secondary fatigue curves slope variation to determine preloaded materials fatigue life under unstationary loading
17 p3052 A69-32976

Prestressed beams, columns and plates nonlinear response, statistical behavior and transverse cracking under axial compression, describing strength and stiffness
17 p3060 A69-33568

Prestrained material plastic behavior experiments and deformation lines of influence analysis, noting importance in cold working
17 p3067 A69-34146

Rectangular cross section pretwisted beams modal curves for turbine and compressor blading vibrational studies
20 p3621 A69-37080

Strain gage and mechanical types of load-determining bolts selected on basis of application requirements and installation costs
22 p3957 A69-40829

Interference fit fasteners role in improving aircraft structure fatigue life through preload barrier against fatigue stresses
22 p3957 A69-40830

Mechanical properties of glass and glass-ceramics products improvement through prestressing
24 p4335 A69-43034

Adhesive joints design with uniform shear stress for prestressing wood beams
24 p4323 A69-43425

PRETESTS
U TESTS

PRETREATMENT
U PRESTRESSING

PRETWISTING
U PRESTRESSING
U TWISTING

PREVENTION
U ACCIDENT PREVENTION
U CORROSION PREVENTION
U FIRE PREVENTION
U ICE PREVENTION

PRIMARY BATTERIES
U ALKALINE BATTERIES
U DRY CELLS
U THERMAL BATTERIES

PRIMARY COSMIC RAYS
NT SOLAR COSMIC RAYS

Primary cosmic radiation charge spectrum measurement during 1965 minimum solar activity, using balloon-borne Cerenkov scintillation counter
02 p3038 A69-12043

Underground search for massive strongly interacting cosmic ray particles, using shower selecting extension array and interaction detecting telescope
02 p0310 A69-12831

Deuteron microbeam for simulating biological effects of ionization by heavy cosmic ray particles
03 p0373 A69-13493

Numerical calculation of trajectories of high energy cosmic rays in galactic disk, using quasi-longitudinal model of magnetic field
03 p0501 A69-13960

Coupling coefficients between primary and secondary ionizing cosmic ray variations, using stratospheric observations in Siberia during IQSY
03 p0504 A69-14224

Heavy nuclei in cosmic rays analyzed in photographic emulsion tracks suggest supernova origin
04 p0649 A69-15422

Chemical composition of nuclear cosmic rays with Z greater than 22, noting etching techniques for utilizing meteoritic minerals as detectors
05 p0816 A69-16355

Energy spectrum and intensities of medium and very heavy nuclei in primary cosmic radiation
05 p0816 A69-16365

Heavy nuclei energy spectrum in primary cosmic rays explained by assuming two component charged nuclei
05 p0816 A69-16366

Elementary composition and origin of primary cosmic rays, discussing space techniques for observation of components
05 p0818 A69-16816

Heavy nuclei abundances and energy spectra in primary cosmic rays, using blob gap parameter as measure of primary ionization
06 p0988 A69-17274

Helium component flux in primary cosmic rays determined, using corrected alpha particles number
06 p0988 A69-17275

Oriented nuclear emulsion stack for determining differential rigidity spectrum of primary He nuclei between 12 and 35 bv
06 p0988 A69-17276

Rigidity spectra of total primary cosmic radiation by ascending or descending balloon-borne detectors in atmosphere, with changing mean response energy
06 p0989 A69-17279

Spark chambers for primary cosmic ray study in balloon flights, detailing construction and performance
06 p0924 A69-17285

Variational coefficients for vertical and inclined meson telescopes, deriving primary cosmic rays anisotropy parameters from daily variations
06 p0924 A69-17293

Primary cosmic ray intensity variation with cut-off energy of particular secondary component, using ground based monitors
06 p0925 A69-17295

Primary electrons implications on cosmic ray confinement in Galaxy, astrophysical aspects and problems of energy spectrum
06 p0991 A69-17308

Radio spectrum and cosmic ray electron data evaluated concerning conditions in Galaxy, deducing mean magnetic fields
06 p0991 A69-17309

Book on supernovae covering galactic supernovae, type II supernovae remnants, Crab Nebula, primary cosmic radiation, etc
07 p1210 A69-18379

Electron detector for OGO-E to measure flux and energy spectrum of electrons in primary cosmic rays
[IEEE PAPER 3C-4] 07 p1135 A69-19198

Cosmic ray nuclei energy spectra and abundances above 20 Mev/nucleon determined by OGO-1 satellite experiment, considering He, B, C, N, O, Ne, Mg, Si, Mn, Fe, Co and Ni
08 p1378 A69-20067

Low energy multiply charged cosmic ray nuclei propagation and source characteristics, considering two component model based on OGO satellite measurements
08 p1378 A69-20068

Galactic halo chronology determination by positron component flux measurement in primary cosmic rays
08 p1386 A69-20084

Energy spectrum of primary cosmic ray helium nuclei from nuclear emulsion stacks exposed in sounding rocket flights
08 p1378 A69-20264

Energy spectra of carbon and oxygen nuclei in primary cosmic radiation, comparing results to earlier measurements and satellite observation
08 p1380 A69-20632

Ablation rate of Saint-Severin amphoterite based on heavy primary cosmic ray track densities in surface samples
08 p1406 A69-20933

Geomagnetic activity correlation to cosmic ray solar daily variation underground, observing primary cosmic ray flux with meson telescopes
09 p1583 A69-22755

Weak interaction theory modifications needed for high energy cosmic ray muons to not violate conservation of probability
09 p1583 A69-22758

Satellite data on relative flux and group composition of heavy nuclei in primary cosmic rays
10 p1756 A69-22820

Secondary emission in low altitude satellite body dependent on inelastic collisions with primary cosmic ray protons
10 p1757 A69-22821

Mean distance between magnetic clouds in space determined from measuring anisotropy coefficient of high energy radiation
10 p1760 A69-23293

Primary cosmic rays, radiation belts and solar wind studies by semiconductor detectors installed on orbiting satellites
10 p1662 A69-23294

Secondary muon flux from primary cosmic ray particles monitored during minimum solar activity by telescopes at 60 mwe underground
10 p1769 A69-23827

Excess radiation in equatorial regions studied on-board Cosmos 137, noting contribution of primary particle multiplication to secondary radiation
10 p1783 A69-23922

High energy cosmic ray origin and acceleration by L.F. electromagnetic radiation produced by pulsars, noting maximum energy for protons
11 p1950 A69-24927

Cosmic ray composition and nuclear interactions at very high energies, comparing results of Monte Carlo simulations with various experimental data
12 p2149 A69-26475

Primary cosmic ray energy spectrum studies during 11-year cycle based on changes in intensity at various altitudes
12 p2149 A69-26682

Chemical composition of nuclear active particle component of primary cosmic rays in extensive air showers
13 p2326 A69-27464

Nuclear component energy flux absorption in Fe measured with ionization calorimeter
13 p2330 A69-28386

Primary particle energy and extensive air shower electron density relationship derived from vertical spectral profiles
13 p2331 A69-28396

Primary particles energy determined by probability distribution functions of cosmic ray showers characteristics, using Monte Carlo computerized calculation
13 p2332 A69-28411

Angular distribution function calculations for avalanche electrons at various stages of cascade development, discussing electron energies and primary electron roles
13 p2303 A69-28414

Primary electrons and gamma quanta generated electron photon cascades in Pb, obtaining error free cascade curves
13 p2304 A69-28416

Diurnal variation of cosmic ray muon intensity near geomagnetic equator and primary anisotropy monitored by cubical counter telescope
14 p2512 A69-28966

Fluorine nuclei in primary cosmic radiation identified by counter telescope measurements on Pioneer 8 spacecraft
15 p2676 A69-30886

Matter traversal of high energy primary galactic cosmic ray protons from antiproton flux and energy measurements
15 p2678 A69-31491

Charge sign ratio of primary cosmic ray electrons measured by balloon flown multilayer spark chamber, studying east-west asymmetry
15 p2678 A69-31497

Near horizontal air showers relationship to direct muon production and heavy triplet particles of unit charge, discussing nuclear interactions and muon bremsstrahlung
15 p2678 A69-31499

High energy cosmic ray proton, electron and photon propagation through cosmic microwave background, discussing mean free paths
16 p2852 A69-32819

Depth distribution of primary cosmic radiation fluxes and secondary nuclear-active particles in stone meteorites and surface layer of planets, moon and asteroids
19 p3410 A69-36092

Densities and angular distributions of fossil tracks in meteorites produced by slowing down heavy primary cosmic ray nuclei
19 p3410 A69-36096

Trans-iron nuclei flux in primary cosmic radiation determined through high altitude balloon exposure of interleaved layers of nuclear photographic emulsion and plastic detectors
21 p3787 A69-38327

Primary cosmic ray nuclei studies during Gemini 2 flight by nuclear emulsion detector with time resolution capability, describing experiment design and equipment operation
21 p3787 A69-38350

Primary cosmic rays solar diurnal modulation, measuring relative amplitudes and phases over full cycle
21 p3788 A69-38547

High energy cosmic rays primary spectrum determined from observations of secondary components including gamma rays, muons and air showers
21 p3790 A69-38822

Primary and secondary cosmic ray intensity variation with altitude from ascending balloon data, noting absorption length role
21 p3791 A69-39249

Extensive air showers temporal distribution of electrons by diffusion equations in A approximation compared with experiments and Monte Carlo calculations
22 p4007 A69-41054

Neutrons energy spectrum at sea level calculated and proved consistent with satellite cosmic ray data
23 p4205 A69-41701

PRIMATES

NT BABOONS
NT CHIMPANZEES
NT HUMAN BEINGS
NT MONKEYS

Biological effects of proton irradiation of monkeys investigated to provide improved protective shield design data with minimum weight penalty
03 p0373 A69-13496

Primates for space research, discussing selection, purchase, handling and use as controls in observations of disorders experienced by man
09 p1445 A69-22723

Statistical critique of Polyak values for tangential dendritic spread of primate retinal neurons
22 p3880 A69-40848

Circadian rhythms in nonhuman primates - Conference, Atlanta, July 1968
24 p4259 A69-42701

PRIMERS [COATINGS]

Low temperature bond failures of room temperature vulcanizing methyl-phenyl adhesive bonds attributed to thermal stress cracking of primer, presenting in-process tests
19 p3321 A69-35563

PRIMERS [EXPLOSIVES]

Primary explosives tested for effects of shock, friction, heat and electrical discharges
10 p1750 A69-23010

Silver and cadmium nitrides, copper chlorotetrazolate and barium and potassium dinitrobenzofuroxannates compared for priming explosive applications
10 p1750 A69-23011

Priming explosives analysis suggesting physicochemical methods for high purity products for space applications
10 p1750 A69-23012

Initiation of priming explosives by electrons, photons, electrical discharges and laser radiation
10 p1751 A69-23017

Secondary explosives ignition by primers and other explosive wire devices on missiles, discussing circuitry and resistance to severe climatic and electrical environments
10 p1751 A69-23021

PRINTED CIRCUITS

Printed circuits development based on use of grid without aid of draftsmen
02 p0216 A69-12051

Printed circuit board wiring technique for strain gage rosettes application in extensive airframe static tests
02 p0250 A69-12231

Flexible printed circuitry electrode arrays fabrication for surface cortical potentials recording in animals
02 p0204 A69-12601

Loss factors effects on substrate choice in production of microwave printed circuit components
04 p0578 A69-15199

Additive processing technique for fabrication of single sided, double sided and multilayer printed circuit boards
07 p1100 A69-18621

IR evaluation of multilayer etched circuit boards, discussing testing of circuit distributive properties and individual layers
07 p1117 A69-19698

Computer aided automatic drawing of printed circuits, including design and manufacture of films for engraving
08 p1296 A69-19979

Microsoldering techniques for thin and thick film hybrid circuits and microminiature printed circuit boards
09 p1510 A69-22349

Flat flexible printed circuitry in AWG-10 missile control system on F-4J, regarding wire harness packaging
09 p1511 A69-22356

Flexible printed circuits manufactured by offset rotogravure printing, noting production cost economies
09 p1511 A69-22357

Electronic module testing with integrated hardware/software system, noting module test console and manual capabilities
11 p1864 A69-25065

Doppler radar clearance hole packaging method for ruggedized dual in-line integrated circuits with conventional etching, tooling and double-sided printed wiring techniques
14 p2419 A69-29102

Automation of wiring diagrams and printed circuit conductor patterns by computerization
15 p2632 A69-31520

PRINTERS [DATA PROCESSING]

Alphanumeric listing and digital data x-y plotting by high speed printer, describing equipment modifications and control software
17 p2932 A69-33108

Micromation and micrographics, discussing nonimpact printing in computer avoiding output imbalance by high speed microfilm recorder
18 p3234 A69-35059

PRINTING

NT LITHOGRAPHY

Orthophoto maps production, discussing scales, aerial photography, control points, orthoreprojection, cartography and printing
22 p3951 A69-41246

PRISMATIC BARS

Plastically twisted prismatic bars with transverse discontinuous inhomogeneity, using sand hill analogy to determine stress field and limiting torque
03 p0524 A69-13021

Self excited aeroelastic galloping oscillations of long prismatic bodies subjected to wind velocity, noting effect of aerodynamically unstable cross sections
09 p1615 A69-21923

Saint Venant torsion and flexure of prismatic bars analysis in polar coordinates, discussing boundary errors
09 p1621 A69-22770

Transverse reinforcing straps effects on torsional stiffness and bending behavior of open cross section profile thin walled prismatic beams
10 p1802 A69-23890

Discrete element plastic analysis of long prismatic bars under transverse loading in longitudinal direction, based on matrix displacement method
13 p2365 A69-28237

Membrane analogy for flexure of prismatical beams with square cross section and longitudinal cavities, employing Saint-Venant solution
15 p2704 A69-30288

Torsion of composite prismatic rod consisting of three different isotropic materials with two interfaces converging on cross section contour corner point
15 p2707 A69-30579

Vibration modes and damping of rectangular cantilevered prismatic steel rods, showing effects of transverse vibration, material and stress on logarithmic decrement
17 p3065 A69-33936

Laser emission divergence reduced by compensating optical inhomogeneity of active elements with prismatic reflector in resonator
17 p2983 A69-33970

Torsion analysis of curvilinear rectangular prismatic beam reinforced by off-center circular rod, using conformal mapping
22 p4049 A69-41279

Prismatic beam stress-strain state under steady temperature field, deriving stresses, displacements and elastic curve equations
23 p4227 A69-41708

Nonlinear formulation for rigid jointed space frame comprised of prismatic linear elastic members, using Newton-Raphson and successive substitution methods
23 p4232 A69-42142

PRISMS

NT PRISMATIC BARS

One dimensional expansion of laser beam, using pairs of prisms with continuous wave output
01 p0091 A69-10852

Glan-Thompson and Rochon prisms modified by replacing one of two calcite halves of cemented oriented birefringent crystals with glass
02 p0280 A69-11924

Fluid flow velocity measurements by optical device having trigonal rectangular glass prisms and microscope objective
03 p0427 A69-12969

Pulsed ruby laser threshold and output energy for different relative orientations of rectangular prism and ruby crystal main crystallographic axis
05 p0777 A69-16526

Laser beam discrete deflection method using Wollaston prism and electro-optical switch for changing polarization plane
14 p2459 A69-29391

Initial flow turbulence effects on drag coefficient for prismatic bodies in low velocity gas flow determined by wind tunnels
14 p2391 A69-29625

Drag and lift coefficients of moderate aspect ratio prismatic bodies analyzed as function of angle of attack, Reynolds number and aspect ratio
17 p2896 A69-33717

Coupled dilatational and equivoluminal modes of free vibration for elastic prisms and polygonal plates, using Poisson ratio and wave path construction
19 p3444 A69-36801

PRIVATE AIRCRAFT
U GENERAL AVIATION AIRCRAFT

PRIVATE AVIATION
U CIVIL AVIATION
U GENERAL AVIATION AIRCRAFT

PROBABILITY DENSITY FUNCTIONS
NT NORMAL DENSITY FUNCTIONS
NT PEARSON DISTRIBUTIONS
NT RAYLEIGH DISTRIBUTION
NT WEIBULL DENSITY FUNCTIONS

Error probability distribution density at output of optimal Gaussian random signal detection, using approximate solution of integral equations
02 p0206 A69-11605

Computer program for calculating density distribution of deviation of F 2 layer critical frequency from median value
02 p0239 A69-11692

Probability density function measurement for microwave noise generator
02 p0221 A69-12459

Voltage probability density of wideband microwave noise, discussing measurement technique of dividing spectrum down by noise bandwidth
02 p0211 A69-12460

Probability density distribution of time shifts in binary signal fronts caused by fading, applying results to FM signal reception
05 p0719 A69-16087

Algorithm for discriminating random signals with unknown mean values, discussing decision functions possible existence to minimize error probability
05 p0719 A69-16218

Mean number of polarization coefficient modulus zero crossings for field reduced at reception point to uncorrelated orthogonally polarized components
05 p0720 A69-16445

Time averages for estimating probability distribution, density and moments of random functions applied to deterministic signals, considering sampling frequency dependence
05 p0722 A69-16729

Upper bound obtained for probability of zero Gaussian random process remaining above specified signal throughout prescribed interval of time
09 p1452 A69-21319

Density functions analytic solution for Fokker-Planck equation representing cascaded phase locked loops
09 p1474 A69-22450

Probability of completing countdown in single malfunction encounters, considering development of industry and government guidelines
10 p1792 A69-22979

Zero crossing statistics measurements for 1/f noise, noting statistically stationary character of probability density distributions of interval spacings between zero crossings
10 p1656 A69-23657

Optimal estimation of conditional mean of posterior probability density function in multistage nonlinear filters, using Monte Carlo techniques and Bayes theorem
10 p1667 A69-24039

Error probability distribution density at output of optimal Gaussian random signal detection, using approximate solution of integral equations
11 p1835 A69-24712

Rod load capacity changes due to random overloads constituting upper limit of stress probability distribution density function used in programmed fatigue tests
11 p1985 A69-25180

Nonlinear systems disturbed by random white noise analyzed by Fokker-Planck equation for probability density in state space
12 p2124 A69-27141

Computer program for calculating density distribution of deviation of F 2 layer critical frequency from median value
13 p2258 A69-28723

Probability density functions of waveforms from summation of digits in n-stage shift register generating m-sequence
15 p2568 A69-30617

Satellite signal probability density determined from scintillation plus Faraday effect in statistical terms
16 p2751 A69-32103

Mean number of polarization coefficient modulus zero crossings for field reduced at reception point to uncorrelated orthogonally polarized components
16 p2753 A69-32478

Robust detection of binary signal in additive noise, using extreme value theory /EVT/ to estimate probability density function and system error and threshold
17 p2944 A69-33624

Fokker-Planck equation applied to probability density for finding rays larger than correlation distance during propagation in random medium
17 p2926 A69-33854

Hazard and renewal rate and bathtub curves for electronic equipment reliability, noting single and multiple probability densities
20 p3504 A69-37070

Least square or least mean square approximation methods in abstract pattern recognition, noting unknown probability density function
20 p3504 A69-38285

Adaptive control system synthesis for reducing computation labor for controlled inertialess plant, reproducing probability density function to describe unknown parameters
22 p3918 A69-40739

Radar return from clutter target with circular polarization, finding probability density functions and cumulative distributions of power ratio
23 p4131 A69-42540

PROBABILITY DISTRIBUTION FUNCTIONS
Monte Carlo simulation procedure synthesizing probability distributions of reliability parameters with individually exponential components
01 p0036 A69-10707

Computer program for calculating density distribution of deviation of F 2 layer critical frequency from median value
02 p0239 A69-11692

Probability density distributions for monaural detection of tonal signal in continuous background of Gaussian noise as modified noncentral chi distribution
02 p1201 A69-11821

Optimal detection of random signals on background of noise of unknown intensity and persistent false alarm probability
02 p0208 A69-12264

Probability distribution of field strength fluctuations in p-n junctions taking into account impurities distribution
05 p0807 A69-16000

Time averages for estimating probability distribution, density and moments of random functions applied to deterministic signals, considering sampling frequency dependence
05 p0722 A69-16729

Double stochastic approximation algorithm for minimizing mean square error in finite expansion of unknown probability distribution functions
06 p0947 A69-17361

Synoptic meteorological predictions using statistical dynamic approach, considering probability distributions and nocturnal temperature decay
08 p1345 A69-20300

Continuous variate duration estimates by Markov process, giving example of surface air temperature conditional probability distribution
08 p1346 A69-20731

Computer programs for systems statistical reliability characteristics using reliability tests and time to failure data, giving optimal breakdown probability functions
08 p1322 A69-21101

Failure distribution functions based on Eyring component aging model, including failure probability density function for Weibull and gamma type distributions
08 p1322 A69-21104

Statistical regularization for obtaining a priori probability distribution information on mathematically incorrect inverse geophysical problems, deriving algorithm
10 p1689 A69-23968

Radio signals and concentrated noise amplitudes probability distributions reflected from ionosphere and scattered in troposphere calculated for Rayleigh and log-normal fading
11 p1833 A69-24440

GO/NO/GO logic synthesis for probability functions development for systems operational readiness tests
11 p1843 A69-25078

Rod load capacity changes due to random overloads constituting upper limit of stress probability distribution density function used in programmed fatigue tests
11 p1985 A69-25180

Probability distributions of characteristics of mass produced semiconductor rectifier diodes
12 p2035 A69-25832

Cumulative probability distribution of positive random variable from moment generating function, exemplifying exponential and Poisson functions
12 p2120 A69-25927

Random variables generation from distribution having given failure rate function
12 p2102 A69-26571

Joint probability distributions of electric microfield in hot ionized plasma consisting of noninteracting particles
12 p2139 A69-26871

Primary particles energy determined by probability distribution functions of cosmic ray showers characteristics, using Monte Carlo computerized calculation
13 p2332 A69-28411

Computer program for calculating density distribution of deviation of F 2 layer critical frequency from median value
13 p2258 A69-28723

Time dependent evolution of probability pressure distribution maximum obtained from Liouville equation
14 p2472 A69-29406

Optimum nonlinear digital filter synthesis for smoothing, predicting and differentiating measured quantity having uniform probability distribution over finite number of discrete values
14 p2426 A69-29421

FM discriminator click widths probability distribution function, defining click widths duration from input noise considerations
14 p2422 A69-29553

Moving targets trajectories determination from radar data, using posteriori probability distribution represented by Markov chain
15 p2566 A69-30334

Fluctuation spectra of monotonic gases, using two time probability distributions for distribution function autocorrelations
16 p2817 A69-31669

Modified pulse height analyzer /PHA/ for sample amplitude height occurrence frequency measurements obtaining amplitude probability distribution /APD/ and three moments of atmospheric noise
18 p3102 A69-34960

Thunderstorm probabilities at Cape Kennedy, giving data on frequency, duration, multiple occurrence, nonoccurrence, runs and conditional probabilities
18 p3167 A69-35100

Mechanical components life or cycles to failure probability distributions determined by Monte Carlo method, comparing theory with aircraft engine parts field data
19 p3327 A69-36031

Statistical description of turbulence of viscous incompressible fluid at large Reynolds numbers, using velocity distribution probability
20 p3517 A69-38007

Statistical regularization for obtaining a priori probability distribution information on mathematically incorrect inverse geophysical problems, deriving algorithm
21 p3680 A69-39654

Error probability of Gaussian signal detector in Gaussian noise background determined from quadratic form of probability distribution density
22 p3901 A69-40955

Radar return from clutter target with circular polarization, finding probability density functions and cumulative distributions of power ratio
23 p4131 A69-42540

Quantization optimization of continuous signals with known probability distribution, using quantizers with limited output values
24 p4288 A69-42671

PROBABILITY THEORY
Survival analysis based on probability theory for design of air cushion vehicle to determine height for operating over open sea
01 p0008 A69-10027

Asymptotic behavior of probabilities of large deviations of sums of independent random variables with moments of any order
01 p0104 A69-10264

Probabilities of error, correct reception and signal cancellation in radio communication systems channels with signal absorption fading
01 p0030 A69-10592

Meteorological probability assessors, describing framework for evaluation consistent with subjective probability theory

01 p0110 A69-10690

Monte Carlo method accuracy improvement for calculating probability characteristics of nonlinear ordinary differential equations, describing nonlinear automatic control

01 p0105 A69-10730

Probability characteristics of temperature and supply voltage dependent parameters of semiconductor equipment

01 p0047 A69-10783

Probabilistic Information Processing System using men and machines to perform diagnostic information processing and to guide decision making

01 p0037 A69-10954

Sequential probability ratio test for detecting changes in Gauss-Markov process characteristics, noting application to fault detection in gyro navigational system

01 p0083 A69-11002

Book on probabilistic information theory-discrete and memoryless models covering information transmission, digitalized sources, generating functions, decoding error, systematic codes and sequential decoding

01 p0037 A69-11030

Multistage detection systems probability characteristics with parallel stage realization, taking into account signal losses

02 p0206 A69-11604

Filter uncertainty for time or frequency resolution in analysis of waveform, decomposing characteristic functions and determining least uncertain realizable filter

02 p0226 A69-12306

Book on compound signals and uncertainty principle in radar observations, considering Woodward ambiguity function, determining accuracy and resolution of range and velocity measurements

03 p0385 A69-13000

Undetected defects and false alarm probabilities for automatic test equipment, emphasizing quality and confidence limits

03 p0428 A69-13187

Absorption as factor influencing correlation between solar activity, sporadic E layer probability of occurrence and reflection stability

03 p0423 A69-13537

Maximum probability technique for measuring angular coordinate with unknown signal and noise intensity

03 p0399 A69-14132

Optimal detection of deterministic signals with random initial phase on background of unknown intensity noise under condition of constant false alarm probability

04 p0557 A69-14788

Conditional probabilities, definition and algebra

04 p0623 A69-14948

Delay method of finite ergodic Markov chains, analyzing first moments of state probabilities with aid of asymptotic equation

04 p0624 A69-15002

Laws of wear and average life, noting application to electric connector reliability

04 p0579 A69-15320

Distribution free sequential probability ratio procedure for detecting signal in multiple resolution element radar

05 p0717 A69-15609

Standards of sterility for prevention of introduction of terrestrial microorganisms onto other planets during space missions, noting contamination probability

05 p0712 A69-15936

Probability theory and Laplace functions used to determine pulse coincidence probability of two random independent pulse streams in given time

05 p0719 A69-16224

Statistical aspects of uncertainty function of linearly frequency modulated signals for nonstationary random process of phase errors

06 p0889 A69-17798

Bit error probability for noncoherent binary FSK link involving Rician interfering signal

07 p1080 A69-19095

Bit error probability estimation of NRZ PCM synchronizer and detector operating in presence of fluctuating data frequency source

07 p1083 A69-19121

Antenna pattern loss factor for determination of average probability of detection vs SNR curves for three dimensional or pencil beam radars

08 p1270 A69-19858

Nonparametric ranking procedures based on order statistics/ guaranteeing preassigned probability for

selection from random samples populations as good as control

08 p1342 A69-20172

Book on stochastic convergence covering infinite sequences of random variables, stochastic integrals and derivatives, characterization of normal distribution and Wiener process

08 p1343 A69-20443

Angular separation of two point sources measured through expressing antenna resolving power by a posteriori probability laws

08 p1288 A69-20961

Error probability for transmission of one of M orthogonal, equally likely, equal energy signals over generalized incoherent channel

09 p1452 A69-21314

Round trip delay effect on probability of error in uncertainty feedback communication systems operating at channel capacity

09 p1453 A69-21322

One and two dimensional frequency distributions for probability estimates of climatological quantities, discussing temperature and interdiurnal changes

09 p1535 A69-21520

Coding schemes for memoryless Gaussian channels with feedback considering error probabilities

09 p1454 A69-21794

Probability approach to control system optimization problem for plant with incomplete information

09 p1473 A69-21856

Optimal detection of determinate signal and signal with random amplitude and phase, estimating probability of false and correct detection

09 p1456 A69-22286

Random data detection method applicable to low voltage SNR cases using real time correlation of probability functions

09 p1459 A69-22593

Probabilities of error, correct reception and signal cancellation in radio communication systems channels with signal absorption fading

10 p1653 A69-23106

Probability characteristics of temperature and supply voltage dependent parameters of semiconductor equipment

10 p1661 A69-23112

Variational approximation of probability measures and products of random matrices, discussing point distribution on Lobachevskii plane

10 p1719 A69-23399

Error correction of digital data with cyclic codes and probability function set extended to Bose-Chaudhuri-Hocquenghem codes and P super M codes

10 p1655 A69-23529

State probabilities of finite stochastic queueing system for calculating equipment reliability parameters

10 p1664 A69-23693

Optimizing two stage procedure for detecting fluctuating incoherent signal, estimating detection attempts reliability

11 p1833 A69-24444

Probability models used in statistical approach to fracture mechanics, noting role of weakest link model in representing brittle fracture

11 p1975 A69-24673

Multistage detection systems probability characteristics with parallel stage realization, taking into account signal losses

11 p1835 A69-24711

Probability of ocular damage for illumination by pulsed laser beam transmitted through atmosphere, developing safety nomograph for eye hazard analysis

11 p1830 A69-24843

Minimum test error probability test limits for known test equipment and signal tolerances, developing semi-graphically single equation for calculation

11 p1865 A69-25079

Microbial contamination release probability from solids fractured by impact, considering spacecraft sterilization requirements

11 p1828 A69-25461

Descriptive statistics in quality control dealing with variability and probability, discrete and continuous variables, frequency distributions and measures of central tendency and dispersion

12 p2100 A69-25846

Integral representation for continuous linear stochastic processes with independent pieces, assuming convergence in probability for sequence of random variables

12 p2121 A69-26365

Approximate solution of boundary value problems for Fokker-Planck equation to determine probability of exceeding limits in nonlinear automatic control systems

12 p2054 A69-26653

Probability analysis by methods simplifying calculations or providing bounds on reliability of complex system

12 p2103 A69-26751

Differential equations of probability theory for studying control systems and processes involving random variables

12 p2124 A69-27142

Inductive converters accuracy calculation by statistical method based on probability theory

13 p2259 A69-27424

Parallel processing in system of computers with identical output, including probability graph for algorithm

13 p2224 A69-27426

Bounding technique of first excursion probability for random vibration, considering relation to reliability of mechanical and structural systems under random disturbances

13 p2361 A69-27438

Probable sign-invariant periods of air temperature anomalies based on random Gaussian processes

13 p2294 A69-27855

Radar SEP /spherical error probable/ for defining error ellipsoid in three dimensional accuracy and CEP /circular error probable/ for defining two dimensional accuracy

13 p2221 A69-27963

Book on probability and stochastic processes, discussing applications

13 p2289 A69-28177

Probability matrix for n order transition independent of decision taking method, applying fundamental matrices to analysis of mean number of false targets

14 p2410 A69-28836

Thermionic converter components reliability under mechanical load and failure models, showing probabilistic nature of failures

14 p2400 A69-29227

Qualitative analysis of CAT parameters from radio sounding data, noting mean bumpiness probability dependence on Richardson number and wind vector shift

14 p2474 A69-29735

Complex pulsed radar signals synthesis with uncertainty function having principal maximum and small secondary maxima for radar stations and wideband communications systems

15 p2563 A69-30140

Probability diagnosis and prognosis for buffering zones based on Bayes formula, determining clear air turbulence zones

15 p2648 A69-30645

Initial uncertainties role in weather forecasting, discussing errors as represented by rms deviation of ensemble members from mean

15 p2649 A69-30894

Research and development planning and control models based on subjective probability estimates for failing projects identification

15 p2721 A69-31072

Probabilistic automata stochastic matrices algebraic properties of definite, quasi-definite, periodic and quasi-periodic sets

15 p2645 A69-31141

Hazards model for probabilistic prediction of casualties by exploding solid propellant rockets, deriving casualty expectation equation [AIAA PAPER 69-461]

16 p2869 A69-32749

Probabilistic analysis of code message distortion due to pulse noise in modulation systems and comparison between linear and quadratic detections

17 p2919 A69-33145

Spatial frequency distribution of linear array with randomly located elements from probabilistic analysis

17 p2929 A69-33873

Satellite attitude control mass properties, showing weight tradeoff analyses role in selecting control system [SAWE PAPER 743]

18 p3208 A69-34885

Evaluation method for strapdown spacecraft guidance systems on automated interplanetary missions, using cost and system performance efficiency probability model [AIAA PAPER 68-828]

19 p3370 A69-35953

System reliability with allowable downtime, calculating probability of on-line units staying operational during mission time using conditional availability

19 p3326 A69-36002

R and D program risk evaluation methodology in density functions form for program goals probabilities, noting random variables as parameters

19 p3455 A69-36008

Successful launch probability analyzed as function of launch strategy from past countdown hold data

19 p3430 A69-36034

Asymptotic behavior of probabilities of large deviations of sums of independent random variables with moments of any order
19 p3360 A69-36199

Perceptron probability algorithm for random events prediction based on previous histories, applying Bayes formulas, static solutions formulas and transition probability tables and graphs
19 p3287 A69-36664

Book on stochastic optimal linear estimation and control, discussing probability theory, models and continuous and discrete time linear systems
20 p3509 A69-37143

Time-space variations in occurrence probability of ionospheric E-2 layer during solar activity maximum and minimum
20 p3527 A69-37672

Probability theory applied to age and block replacement models in preventive maintenance of parts, noting inspection cost distribution
20 p3551 A69-38267

Antenna arrays subject to random excitation error analyzed by probability theory, noting relationship between antenna pattern and excitation distribution parameters
21 p3681 A69-38742

Spacecraft return probabilities with time constraints and redundant access, using Borel set concept for counting and summing coverage belts
21 p3819 A69-39017

Gaussian type densities estimated by representing unknown density in terms of convolution expansion of Gaussian probability density and arbitrary distribution, discussing convergence rates
21 p3756 A69-39499

Stacking fault formation probability in Ti and Zr by X ray diffraction techniques, using Fourier analysis and half-width measurements
21 p3749 A69-39600

Probability characteristics of total error in vertical gyroscope evaluated from component errors along suspension axes
22 p3946 A69-42051

Risk taking under uncertainty in individual and group decisions, analyzing gambling and group discussion situations
23 p4091 A69-42016

Most probable position determination in astronomical navigation by tracing lines on nautical chart
23 p4186 A69-42025

Error probability bounds for self synchronized binary PSK communication systems, simulating decision feedback, phase doubling and maximum likelihood systems
23 p4128 A69-42501

Algorithm for constructing random error correcting convolutional codes
24 p4284 A69-42723

Transmission functions probabilistic model for solving radiative transfer problems in spherical shell medium surrounding emitting black core or point source, using integrodifferential equations
24 p4415 A69-43637

Satellite system survival probability expressed as function of launch probability, time and number of satellites available
[AIAA PAPER 67-324] 24 p4249 A69-43665

PROBES

Cooled probes for gas measurements in high pressure arc jets, hyperthermal wind tunnels, rocket motors, scramjets and similar severe environments
01 p0078 A69-10150

Electron density and temperature, ion density, composition and temperature and plasma space potential relative to space vehicle potential measured by spherical probe assembly
01 p0065 A69-10549

PROBLEM SOLVING

NT ASYMPTOTIC METHODS
NT ITERATIVE SOLUTION
NT THEOREM PROVING

Exchange rule to solve system of linear matrix equations in sense of Chebyshev, giving various algorithms
01 p0105 A69-10705

FORTTRAN Deductive System to find solutions to theorem proving problems, discussing computer implementation
01 p0037 A69-10806

Finite element method for exact solution of more general problems with one independent variable and extension to many dependent variables
04 p0676 A69-14741

Stability of quasi-solutions for equations with closed and with continuous operators
13 p2289 A69-28483

Solution methods for differential heat conduction equations, discussing methods of variable separation, Green function, thermal potentials, etc
14 p2539 A69-29456

Convergence of methods of tangential parabolas and hyperbolas used in nonlinear equation solution with nondifferentiable operators
18 p3164 A69-34707

Technical problem solving model based on tape recorded protocols of engineers engaged in R and D project
20 p3640 A69-38020

Basic task archetypes in man-computer problem solving including detection, planning, optimization, designing, etc
24 p4274 A69-43019

PROCEDURES

U OPTICAL CORRECTION PROCEDURE

PROCESSORS [COMPUTERS]

U COMPUTERS

PROCUREMENT

Military aircraft procurement trends examined to forecast military aircraft market
01 p0009 A69-10147

Procurement procedures in management planning, discussing document flow charts, contract negotiation, etc
15 p2719 A69-30314

PRODUCT DEVELOPMENT

NT WEAPONS DEVELOPMENT

Handbook on fatigue properties for product design covering metals stress conditions, machine parts load and stress determination, cyclic stress, etc
01 p0170 A69-10918

Fabrication of large arched bottoms for pressure vessels from aluminum alloys, discussing sheet cutting and welding, annealing, machining, etc
02 p0254 A69-12678

Industrial and workman safety concept evolution, discussing role in product design engineering
[SAE PAPER 680676] 03 p0433 A69-13449

Optical and mechanical design of Anglo- Australian 150 inch telescope for observations of southern sky at Siding Spring Observatory, Australia
03 p0411 A69-13466

Cost effective aerodynamic deceleration and retardation systems for military and space programs, noting technical research and development areas in need of advancement
03 p0364 A69-13854

Single crystal cells for construction of large deployable solar cell arrays
03 p0368 A69-13993

Product development process diagram, systems engineering checklists and program plankit as devices to assist product manager
[ASME PAPER 68-WA/MGT-3] 05 p0850 A69-16146

Substrates containing silicon regions separated by silicon dioxide or ceramic dielectrics, prepared by lamination in hot press, noting applications to integrated circuits
07 p1100 A69-18617

Research and development programs for several advanced rotary wing VTOL concepts
[AIAA PAPER 69-199] 07 p1055 A69-19555

Avionic systems development, discussing criteria for realization of operational requirement and engineering product satisfying requirement
[AGARDOGRAPH-114] 08 p1317 A69-20982

Integrated circuit production, development and research in Germany
[AGARDOGRAPH-114] 08 p1292 A69-20994

Induction flowmeters design, discussing materials and structural details of sensor and transducer elements
11 p1887 A69-25208

Type 2 ceramic capacitor manufacture, selection and control in Concerto space program
11 p1853 A69-25393

Aircraft engine spark plugs development, reviewing ceramic and mica insulated plugs and four pole electrode spark plugs
13 p2324 A69-27333

Ultralightweight mirror blanks for astronomical telescopes, discussing weight saving low thermal expansion and fused monolithic core technology
13 p2261 A69-27953

Capital budgeting for R and D, discussing control of rising costs
14 p2541 A69-29281

Systems engineering approach to aerospace product defects minimization, discussing scope, contract

development, mainstream functions, component development, design data and subsystem integration
15 p2719 A69-30085

Barometric altimeters development, discussing servo and three pointer types, accuracy, Central Air Data Computer repeater function and future trends
15 p2610 A69-30859

Reliability testing of development models during production, considering short term and large batch tests
15 p2579 A69-31036

Mathematical model for money expenditure on product oriented research programs, based on accumulated profits
15 p2721 A69-31068

Propulsion system influence on aircraft reliability from viewpoint of engine manufacturer
15 p2629 A69-31122

Fatigue data adapted to conditions of specific design part including fatigue limits, S-N curves and various failure diagrams
16 p2794 A69-32433

JT8D turbofan engine composite fan blades design and fabrication methods using aluminum-Borsic fiber, noting direct and indirect weight reduction
[AIAA PAPER 69-465] 16 p2842 A69-32698

Engine and components reliability, discussing design stage and programming
[AIAA PAPER 69-476] 16 p2795 A69-32771

Small penetration axial rocket motors fabrication, discussing axial- and tangential-thrust integral assembly, impulse levels, delay line connection for igniters, production evolution, etc
[AIAA PAPER 69-520] 16 p2795 A69-32779

German VTOL aircraft development excluding helicopters, discussing technical problems, safety and economy in civil application
17 p2899 A69-33381

R and D for economic growth, discussing interaction between management, planning, engineering, marketing, production, customers and competitors
17 p3077 A69-34126

Development, manufacturing and logistic costs of reliability improvement in electronic equipment design
18 p2321 A69-34485

Electronic data processing facilitating engineering design development work, including computer programming
18 p3106 A69-34838

French helicopter industry projected development for existing types, production models or final development and long range design programs
19 p3248 A69-36848

Impact limiter system design for Mars landing vehicle noting balsa wood or phenolic honeycomb construction
[AIAA PAPER 68-161] 21 p3820 A69-39228

Linear elastic isotropic materials for model tests, describing properties of material composed of Araldite B and air
21 p3844 A69-39319

Thermal scale modeling for space hardware development from managerial and engineering viewpoints
[AIAA PAPER 69-1010] 22 p3922 A69-40383

NDT techniques relation to engineering design problems with failure potential, discussing management planning and cost analysis
24 p4318 A69-42769

Mechanical properties of glass and glass-ceramics products improvement through prestressing
24 p4335 A69-43034

PRODUCTION ENGINEERING

Silicon carbide filament fabrication by chemical vapor deposition, noting physical and mechanical properties and application to other refractories
01 p0097 A69-10645

Integrated circuit manufacturing status, discussing raw materials, crystal imperfections, surface damage, epitaxy and diffusion techniques
01 p0045 A69-10650

Fabrication of large parts in aircraft and space industry, discussing extrusion, forging, explosive forming and diffusion bonding
01 p0088 A69-11400

Reinforcing glass fiber fillers in thermoplastic commercial products, noting applicability to high speed fabrication by injection molding processes
02 p0269 A69-11794

Compressed air in aircraft manufacture, discussing versatility in production and testing of Concorde 002
02 p0253 A69-12069

Large scale integration /LSI/ arrays, discussing high yield manufacturing methods based on fixed nondiscretionary connections among components
02 p0254 A69-12467

Wafer chip assembling technique for high density interconnection of silicon devices in large monolithic electronic systems, noting application to MOS shift register
02 p0222 A69-12472

Microelectronic components joining technique by compliant bonding, utilizing deformable medium between tool and beam leads to eliminate intricate tool shapes and alignments
02 p0254 A69-12473

Industrial and workman safety concept evolution, discussing role in product design engineering
[SAE PAPER 680676] 03 p0433 A69-13449

Production history of Model UH-1/Huey helicopter power transmission, discussing producibility
[SAE PAPER 680675] 03 p0433 A69-13450

Electron beam welding procedure planning and production shop control parameters
04 p0605 A69-14529

Explosive welding application to dissimilar metals and tube to tube plate welding, noting influence of detonation and sound bulk velocity
04 p0608 A69-15481

Plasma arc welding, discussing transferred and non-transferred arc systems application to spraying and welding techniques, including automated microplasma welding
04 p0608 A69-15482

Electron beam process application to welding, machining and assembling in automobile mass production
04 p0608 A69-15484

Quality control in welding from design through experimental manufacture, product testing, large scale production and improvements
04 p0608 A69-15485

Self acting gas lubricated bearings production, discussing manufacture to ultraprecision tolerances by semiskilled labor
[ASME PAPER 68-WA/LUB-4] 05 p0768 A69-16130

Book on machinability and producibility of metals, plastics, nonmetallic materials and composites, emphasizing machine tools and tool holders
06 p0931 A69-17782

Additive processing technique for fabrication of single sided, double sided and multilayer printed circuit boards
07 p1100 A69-18621

Ti alloy blanks production technology and quality control, noting rolling of sectional profiles
07 p1161 A69-18765

Direct bead sampling by aspiration of molten metal in open hearth furnaces and converters
07 p1141 A69-19341

Alumina radomes manufacture by flame spraying process, discussing raw materials quality control, spraying operation, sintering and final inspection
07 p1142 A69-19528

Components production process effect on reliability based on values and functional relations of internal parameters, noting influence on accelerated testing
08 p1319 A69-20346

Cost control for project management based on detailed programming
08 p1423 A69-20629

Process control data in acceptance procedures for high reliability electronic components, discussing supplier and user cooperation
08 p1293 A69-21110

Bubble leak testing of components to understand effects of gas and liquid viscosity, surface tension, pressure differential and temperature
09 p1503 A69-21391

Metal castings around ceramic cores for economic manufacture of jet engines
09 p1503 A69-21907

Forming and processing facility for producing one million titanium alloy parts per month for Boeing 747 aircraft
09 p1504 A69-22063

Giant landing gear steel parts fabrication for Boeing 747 aircraft, discussing material and processing problems including Cr and Cd-Ti coatings application
09 p1434 A69-22064

Complicated power metallurgical shapes fabricated by hydrostatic pressing, noting spheres, cones, rods, tubes and combinations
09 p1511 A69-22353

Flexible printed circuits manufactured by offset rotogravure printing, noting production cost economies
09 p1511 A69-22357

Laser applications to production line metal working, discussing economics, welding, drilling, automation, thermal and atmospheric effects, etc
10 p1698 A69-22985

FM Lamb wave system for flaws and defects detection in thin metal sheets
10 p1699 A69-23048

Design management in next century covering computer methods, market needs, etc
11 p2004 A69-24371

Plain and rolling metal bearings manufacture and use, discussing materials structure and properties, operating conditions, lubrication, etc
11 p1903 A69-24517

Gas laser materials, fabrication and performance, analyzing gas cleanup, cathode degradation, bore erosion and optical surface contamination effects
11 p1896 A69-24743

Pressure calcining process in production of fine grained ceramics at low temperatures
12 p2119 A69-26832

Hard superconductors technology, stressing metallurgical processing factors effect on properties of niobium alloys and intermetallic compounds
12 p2103 A69-27120

Canadian air cushion vehicle industry, considering materials, design, production, tests, components and quality control
13 p2381 A69-27544

Fabrication techniques for plastic insulation in electronics, discussing packaging, low pressure molding, casting, etc
13 p2285 A69-27987

Relay reliability cost vs failure cost in spacecraft applications
13 p2231 A69-28044

Microminiature latching relay design and manufacturing cost
13 p2232 A69-28049

Value engineering and component/products improvement incentive contract clauses role in defense product quality improvement
13 p2383 A69-28100

Management and control techniques for aircraft product engineering changes
[ASME PAPER 69-DE-67] 14 p2540 A69-28850

Flat conductor cable technology, discussing design, manufacture, specifications, etc
[ASME PAPER 69-DE-8] 14 p2393 A69-28855

Book on integrated circuits covering fabrication techniques, basic semiconductor theory, thin film, monolithic, compatible circuits, packaging, etc
14 p2419 A69-29002

Production method for fabricating HF surface wave interdigital electrode transducers, discussing pattern replication, etching, etc
14 p2455 A69-29571

Hydrostatic tube extrusion, discussing equipment, techniques and commercial applications
[SAE PAPER 690319] 15 p2617 A69-30093

Hot extrusion process for steel and various metals in U.S. semifinished product industry, considering lubrication problems, research centers and development
15 p2618 A69-30228

VM-1 alloy investigated for creep mechanisms and ultimate strength for applications in reactors, rockets and aircraft construction
15 p2638 A69-30284

Foil bearings design, fabrication, applications to flexible material transport, rotor support, etc
15 p2618 A69-30327

Mass-produced silicon transistors reliability, presenting tables and curves of lifetime tests
15 p2626 A69-30833

Production line requirements for MOS and IC, considering high reliability at minimum cost for space applications
15 p2627 A69-30841

Ceramic condensers with very high reliability mass produced for Concerto program, describing component characteristics and production methods
15 p2627 A69-30844

Microelectronic technology for mass production of high reliability hybrid thin film circuits
15 p2628 A69-30845

Thin film tantalum nitride resistors technology and production, evaluating projected reliability of resistance circuits as function of operating and environmental conditions
15 p2628 A69-30846

Carbidothemic process for high melting metals and alloys production stressing Ti alloys
16 p2800 A69-31777

Integrated circuits effect on electronic equipment design and production technology
16 p2762 A69-32578

Wire-wrap solderless joints production technology in electronic equipment
16 p2763 A69-32579

Ammonium perchlorate grinding and blending facility, discussing process flow, machinery, etc
[AIAA PAPER 69-516] 16 p2767 A69-32664

Book on high purity beryllium metallurgy for nuclear reactor applications covering physical properties, crystallography, thermodynamics, production methods, etc
17 p2986 A69-32952

ELDO booster /EUROPA 1/ third stage management and construction problems
17 p3050 A69-33701

Disk type or elastic melt extruders development based on Weissenberg effect permitting near uniform extrusion
18 p3148 A69-34612

Machining processes effect on surface integrity of machine parts and effects on product quality
18 p3149 A69-35129

Polyimide resin system for glass reinforced laminates, noting processing characteristics and curing
19 p3353 A69-35505

Filament reinforced metal matrix composites made by continuous casting process, discussing tensile tests results and production costs
19 p3318 A69-35511

Tape placement machines to fabricate composite high modulus filamentary tape reinforced aerospace structures, anticipating future generations evolution into automatic control
19 p3323 A69-35584

Soviet book on interchangeability of structural elements in aircraft construction, discussing experiences in serial production of aircraft and helicopters
20 p3462 A69-37443

Microplasma, W inert gas and submerged arc welding processes for fabrication of rocket motor cases and pressure vessels, discussing material requirements and weldability
[SBAC PAPER 7] 20 p3550 A69-37449

Electronic packaging and production - Conference, Anaheim, February 1969 and Philadelphia, June 1969
22 p3909 A69-39941

Gas laser-Doppler radar system for moving materials velocity and length measurements in industrial processes
22 p3955 A69-40237

Metal matrix fiber-reinforced composite materials joining by welding and brazing techniques
22 p3956 A69-40480

Digital computer systems for automating machine parts design main metal cutting operations, emphasizing optimal instrument usage, reliability, digital algorithm language and economics
23 p4169 A69-41952

Waveguide below cut-off high pass filters fabrication technique using slot cut into waveguide section
23 p4170 A69-42231

Quality and reliability of electronic spacecraft devices and structural components produced in limited quantity, discussing documentation of production and testing
23 p4171 A69-42474

Numerical control as manufacturing tool, with application to aircraft engine precision components
24 p4318 A69-42710

Fatigue crack initiation mechanism as used in design to prevent fatigue failures in service
24 p4397 A69-42770

Self acting gas lubricated bearings production, discussing manufacture to ultraprecision tolerances by semiskilled labor
[ASME PAPER 68-WA/LUB-4] 24 p4320 A69-43035

PRODUCTIVITY

Research productivity in large organizations stressing interface problem minimization, recommending deferred bonus system
17 p3075 A69-32964

PROFICIENCY MEASUREMENT

U HUMAN PERFORMANCE

U PERFORMANCE TESTS

PROFLOMETERS

Radio profilograph designed for integrating aircraft excess altitudes and measured distances between aircraft and earth, discussing block diagram
07 p1132 A69-19006

Laser profilometer to measure sea wave profiles from airborne platform, describing transmitter, receiver and signal processor
21 p3739 A69-39461

PROGNOSIS
Geopotential and wind prediction by integration of prognostic equations of single level atmosphere
13 p2294 A69-27852

PROGRAM MANAGEMENT
U PROJECT MANAGEMENT
PROGRAMMERS
Temperature program generation for test chambers, describing temperature programmers and readout, verification and recording systems
22 p3954 A69-40038

PROGRAMMING [SCHEDULING]
NT THRUST PROGRAMMING
Cost control for project management based on detailed programming
08 p1423 A69-20629
Federal Government budgeting, discussing systems analysis, planning-programming, etc
10 p1811 A69-23351
Quantitative and qualitative reliability programs for commercial and aerospace products, considering Failure Effect Management System
18 p3143 A69-34486

PROGRAMS
NT APOLLO APPLICATIONS PROGRAM
NT APOLLO PROJECT
NT COMSAT PROGRAM
NT EARTH RESOURCES PROGRAM
NT ECHO PROJECT
NT EUROPEAN SPACE PROGRAMS
NT GEMINI PROJECT
NT LUNAR PROGRAMS
NT MARINER PROGRAM
NT MARS 69 PROJECT
NT MERCURY PROJECT
NT NASA PROGRAMS
NT NIMBUS PROJECT
NT PERT
NT PIONEER PROJECT
NT RESEARCH PROJECTS
NT ROVER PROJECT
NT SATURN PROJECT
NT SURVEYOR PROJECT
NT U.S.S.R. SPACE PROGRAM
NT UNIVERSITY PROGRAM
NT VOYAGER PROJECT
German analysis of preparatory technology of U.S. space programs, noting effects of hardware development for manned space travel on future planning
05 p0849 A69-15576

PROGRESS
National programs relationship to progress in technological societies
03 p0536 A69-14245

PROJECT MANAGEMENT
Avionics in forest resource inventories management, noting design of radar altimeter for low level aerial photography
01 p0080 A69-10352
Human engineering program plans for Phase 3 of SST Development Program in accordance with airframe and engine contracts
01 p0019 A69-10451
Project management in complex research, discussing incentive contracting decision model and resources allocation
02 p0356 A69-12476
Aerospace company engineering administration criteria and functions for chief project engineer [SAE PAPER 680682]
03 p0535 A69-13447
Aerospace manufacturing contribution to engineering function in design development [SAE PAPER 680668]
03 p0433 A69-13451
Book on economic management of research and engineering covering project plan impact, projects control and evaluation of research and engineering structure
04 p0688 A69-14530
Cost dependent utility characteristics in mathematical model for optimum research and development resource allocation, computing optimum fund distribution with Lagrange multipliers
04 p0689 A69-14807
Predictive model for risk in technological research and development
04 p0689 A69-14980
Graphical evaluation and review technique /GERT/ in R and D project planning processes
04 p0689 A69-15100

Estimate accuracy and project selection models in industrial research, examining company data for miscellaneous, technical and commercial failure
05 p0849 A69-15981
Project management decision making, noting decision nature, cost effectiveness concepts and incentives [ASME PAPER 68-WA/MGT-2]
05 p0850 A69-16145
Statistical analysis of aircraft programs engineering man hours, aircraft performance and weight, avionics systems, schedules, etc, as estimating standards
05 p0769 A69-16239
Cost and schedule planning and control /CSPC/ project progress reporting technique
05 p0850 A69-16300
German Air Force Center of Aeronautical Medicine, discussing organization, work projects and proposed mutual cooperation with French counterpart
05 p0850 A69-16629
Interplanetary Pioneer spacecraft development and systems engineering aspects
06 p1017 A69-17605
Organization behavior models compared in theory of scientific and professional personnel management, noting compromise between excess restrictions and freedom [AIAA PAPER 68-805]
08 p1422 A69-20196
Defense project management and discrepancies between estimates and final costs
08 p1423 A69-20628
Cost control for project management based on detailed programming
08 p1423 A69-20629
Project control cycle, cost monitoring and reporting to management
08 p1423 A69-20630
Organization and manpower utilization in R and D, determining criteria for organizational form selection
08 p1423 A69-21155
Incentive provisions used by mutual agreement between purchaser and contractor for project management covering planning, control, financial, technical and personnel functions
09 p1626 A69-22777
Potential hazards of government sponsored technology, examining SST and fluoridation projects and weather problems
10 p1811 A69-23392
Isolation of scientific and technical personnel and effect on lateral communication and intellectual cross fertilization in research and development program
11 p2004 A69-25303
Integrated management information system /IMIS/, discussing logistics, reliability and quality assurance disciplines
11 p2005 A69-25304
Program definition and government-industry relationships in entry research and development program management
11 p2005 A69-25726
FAA aircraft accident human factors investigation plan, discussing on-call pathologists, site organization and investigation, autopsy and result reporting
12 p2022 A69-25843
Civil aircraft accident investigation, discussing organization and procedures of Bureau of Aviation Safety of National Transportation Safety Board
12 p2191 A69-25844
Financial, political and engineering considerations influencing space flight programs implementation, including nuclear systems examination for propulsion and power capability
13 p2334 A69-27296
Esro 1 satellite program management, discussing scientific mission, structure, tracking system and history
13 p2355 A69-27360
ESRO 1 project management and organization, discussing cost control, time saving, program evaluation and review system /PERT/, etc
13 p2382 A69-27750
Galaxy C-5A aircraft Value Control Program stressing design organization, upper management authority, budgetary adjustments, etc
13 p2383 A69-28095
Cost estimates of R and D, considering planned profit and loss following products introduction to market
14 p2541 A69-29280
MACRO /methodology for allocating corporate resources to objectives/ for R and D, discussing program for optimal budget management
15 p2720 A69-30958

Program stretchout in aerospace procurement, discussing costs effect in relation to incentive contracts
15 p2721 A69-31071
Research and development planning and control models based on subjective probability estimates for failing projects identification
15 p2721 A69-31072
Integrated Logistics Support /ILS/ cost effectiveness, discussing management of systems elements in addition to prime equipment including computer programs, training, maintenance, etc
15 p2722 A69-31126
Book on space age management, considering large scale approach
16 p2881 A69-31766
Motivation and performance increase in R and D by incentive plans, discussing prestige, power, responsibility, recognition, work, salary, comfort, etc
17 p3075 A69-32963
International organization and project management procedures in design and construction of Heos 1 satellite for measuring charged particles energy distribution outside geomagnetic field
17 p3050 A69-33699
German research satellite Azur design and production management
17 p3050 A69-33700
ELDO booster /EUROPA 1/ third stage management and construction problems
17 p3050 A69-33701
Proposed projects selection for independent R and D development program in business entity, measuring merits in terms of future financial returns
17 p3077 A69-34129
Saturn software configuration accounting and reporting system for document change and information retrieval
18 p3105 A69-34269
Mathematical index model based on weighted factor analysis to facilitate management and technical decisions concerning achievement of numerous tasks with fixed funds
18 p3232 A69-34504
Operational system effectiveness information for reconnaissance drone system including test flights, discussing application to reliability and maintainability in project management
18 p3232 A69-34505
Failure mode and effect analysis integrating design and reliability engineering, discussing management controls and interdisciplinary coordination
18 p3147 A69-34526
Project management of Apollo short stack testing project, discussing organization, planning, operations and procurement to cut testing time
18 p3233 A69-34616
Apollo project by-products, emphasizing NASA project management methods application to large R and D projects
18 p3233 A69-34649
System approach to reliability demonstration, discussing design and impact on levels, risks, requirements, testing, cost and incentives
19 p3327 A69-36003
Systems effectiveness function from project and organization management viewpoint
19 p3454 A69-36006
Failure data role in management of launch operations reliability program
19 p3294 A69-36022
Ionospheric satellite series Alouette-ISIS, discussing successive engineering and management constraints leading to ISIS-C design
20 p3618 A69-37856
Technical problem solving model based on tape recorded protocols of engineers engaged in R and D project
20 p3640 A69-38020
International organizations and planning for earth observation satellite program involving exploitation in communications, meteorology and aircraft
21 p3855 A69-38622
Ariel 3 satellite management structure, responsibilities and orbit, stabilization, launch window, data acquisition and processing
21 p3856 A69-39255
Technical and economic factors of program to provide communications services via satellite facilities in continental U.S.
21 p3678 A69-39762
Thermal scale modeling for space hardware development from managerial and engineering viewpoints [AIAA PAPER 69-1010]
22 p3922 A69-40383

- Complex program management emphasizing systems engineering management, noting applications to aeronautical systems
[RAES PAPER 9] 22 p4053 A69-40489
- Management system for safety in NASA Manned Space Flight Program, discussing hazard analyses and reduction precedence sequence
[AAS PAPER 69-522] 24 p4418 A69-42851
- Space flight programs management cooperation and limited competition advantages, emphasizing single management team responsibility for effective multilateral activities
24 p4419 A69-43043
- PROJECTED AREAS**
U AREA
U PROJECTIVE GEOMETRY
- PROJECTILE CRATERING**
Numerical method for time dependent compressible Navier-Stokes equations applied to axisymmetric flow field produced by hypervelocity impact, examining viscous effects
[AIAA PAPER 69-354] 13 p2366 A69-28288
- Hypervelocity impact dynamics on copper cube targets imbedded with nickel wires, discussing terminal positions, Vickers hardness, flow fields, etc
[AIAA PAPER 69-368] 13 p2367 A69-28300
- Lunar relief mechanism based on experimental cratering by pasty projectiles, proposing terrestrial magma genesis
15 p2698 A69-31373
- Hypervelocity micrometeor impact sites identification on aluminumized glass, using conchoidal pattern as criterion in analysis
18 p3199 A69-34952
- PROJECTILE PENETRATION**
U TERMINAL BALLISTICS
- PROJECTILES**
NT HYPERVELOCITY PROJECTILES
- Perforation and penetration mechanisms of Styrofoam slabs, using impact tests with free falling and rifle powered projectiles
01 p0165 A69-10115
- Terradynamic research program for studying instrumented projectile penetration of terrestrial materials
02 p0228 A69-11767
- Attitude control system effect on roll resonance in rocket boosted projectile
09 p1610 A69-22001
- Parachute recovery system for spinning /250 rps/ 155 mm shell launched to 3000 ft/sec by 20,000 g acceleration
[AIAA PAPER 68-937] 12 p2014 A69-26805
- Gun projectiles assisted by solid propellant motor to increase range, discussing construction, performance and free-wheeling rotation band use
15 p2702 A69-30592
- Cylindrically shaped projectiles low velocity impact upon horizontal surface of dry commercial Ottawa sand mass, estimating penetration for soft landing
21 p3839 A69-39231
- Stability conditions determination for spinning projectile based on ballistic equations, discussing role of Magnus effect
21 p3772 A69-39294
- Ballistic equations for mass center movement in vertical plane defined by projectile initial velocity
23 p4183 A69-42482
- PROJECTIVE DIFFERENTIAL GEOMETRY**
U DIFFERENTIAL GEOMETRY
- PROJECTIVE GEOMETRY**
NT MERCATOR PROJECTION
- Orthogonal projection derived equation to optimally estimate state of nonstationary linear discrete systems with time delay, developing Kalman type filter
09 p1473 A69-22437
- PROJECTORS**
Laser color TV projection-display system using moving mirrors and dual polarization scanner
07 p1137 A69-19740
- Optical interpolation for GZ-1 orthoprojector in storage mode, noting electronic contour plotter
22 p3951 A69-41247
- Automatic contour plotting for orthoprojector based on adjacent profiles and linear interpolation
22 p3951 A69-41248
- PROJECTS**
U APOLLO PROJECT
U ECHO PROJECT
U GEMINI PROJECT
U MARS 69 PROJECT
U MERCURY PROJECT
U NIMBUS PROJECT
U ORBITER PROJECT
U PERT

- U PIONEER PROJECT
U RESEARCH PROJECTS
U ROVER PROJECT
U SATURN PROJECT
U SURVEYOR PROJECT
U VOYAGER PROJECT
- PROLATE SPHEROIDS**
Asymptotic solutions for prolate spheroidal wave functions satisfying given differential equation, producing asymptotic expansions in terms of confluent hypergeometric functions
04 p0623 A69-14892
- Prolate spheroidal antennas operation in isotropic plasmas, studying effects of collision frequency, electron temperature and antenna length on admittance, radiation and current distribution
22 p3914 A69-40702
- Electromagnetic backscattering by perfectly conducting prolate spheroid, predicting echo signal in resonance region
23 p4115 A69-41584
- PROLATENESS**
Prolateness of Venus radius on basis of satellite microwave temperature measurements, chemical compositions and ice cap model
10 p1784 A69-23958
- PROMINENCES**
NT SOLAR PROMINENCES
- Total solar eclipse of September 22, 1968 in Siberia, discussing instrumentation and solar light radiation, corona, prominences, spicules, etc
10 p1782 A69-23696
- Jupiter red spot prominence correlation with Zurich sunspot number
17 p3045 A69-34185
- PRONE POSITION**
Sensorimotor coordination of man performing graphic assignments in upright, reclining and prone position, discussing interaction of vestibular, visual and motor analyzers
20 p3470 A69-37246
- PROPAGATION**
Linear equations of motions of inviscid ideal gas atmospheres, describing climatology of propagation parameters for point impulse sources
22 p3938 A69-40446
- PROPAGATION [EXTENSION]**
U CRACK PROPAGATION
U FLAME PROPAGATION
- PROPAGATION MODES**
Forward and backward scattered modes over frequency range in multimode nonuniform waveguide, transforming coupled modes telegraphist equations into Volterra equations
01 p0043 A69-10621
- E field transmission and reflection coefficients in linearly tapered waveguide for fundamental and higher order modes, using point matching method
01 p0044 A69-10629
- Plane wave scattering from modulated corrugated structures, obtaining reflection coefficients for multimode propagation
01 p0033 A69-10973
- First normal modes characteristics and lateral wave in weak dielectric layer applicable to microwave propagation
01 p0033 A69-10975
- Electromagnetic wave propagation across magnetic field under relative streaming motion, noting plasma frequency cut-off
01 p0134 A69-11247
- Book on propagation characteristics of various wave modes in ionized gas plasmas
02 p0285 A69-11518
- Dispersion relation of internal acoustic gravity wave motion in compressible nonviscous and nonheatconducting atmosphere
02 p0242 A69-11868
- Dispersion relations of axisymmetric and dipolar surface modes propagation along inhomogeneous plasma columns on dispersion relations
02 p0289 A69-12242
- Polarization stability improvement of helical beam antenna by increased turns, smaller pitch angle and decreased transverse electromagnetic mode amplitude
02 p0219 A69-12345
- Mode theory of backscattered radar cross section of elongated dielectric bodies capable of sustaining traveling wave
03 p0384 A69-12907
- Parametric light generation in resonator with nonlinear medium, discussing continuous pumping with laser modes matched with pumping frequency
03 p0437 A69-13044

- Propagation tests of skywave field strength reduction by orthogonal transmission
03 p0395 A69-13597
- Finite element solution of Helmholtz equation and application to waveguides with complicated boundaries
03 p0404 A69-13598
- Sunrise modal interference patterns for VLF propagation, analyzing variations with latitude
03 p0396 A69-13628
- Strain effects on transverse electromagnetic modes of anisotropic dielectric waveguides at p-n junctions
03 p0406 A69-13830
- Optical waveguide with optimum refractive index distribution for equalizing group velocities of different modes and minimizing waveform distortion
04 p0575 A69-14749
- Dispersion relations for propagation of quasi-TEM mode and higher order symmetric modes in longitudinally magnetized ferrite filled coaxial waveguide
04 p0575 A69-14751
- Higher order modes suppression in square waveguides by bifurcating metal septa of finite length, analyzing periodic array of many finite-length septa
04 p0576 A69-14758
- Higher modes of longitudinal wave propagation in dispersive thin elastic rod, noting response to laser pulse
04 p0678 A69-14869
- Dielectric waveguide propagation, impedance and attenuation characteristics and insertion loss and launching efficiency of mode transducer
04 p0577 A69-14971
- VLF phase measurements for apparent and equivalent diurnal height variation for lower ionosphere waveguide
05 p0752 A69-15666
- Whistler mode propagation in homogeneous electron plasma situated in longitudinal electrostatic field, using Fokker-Planck model
05 p0758 A69-16417
- Solar cosmic rays anisotropies including solar flare particles propagation
06 p0990 A69-17288
- Deviation of dispersion equations for all modes existing in E-plane slabs of dielectrically loaded rectangular waveguides
06 p0888 A69-17486
- Multimode direction tracking with polarization tracker used simultaneously, analyzing cross coupling and conical horn/reflector antenna
06 p0888 A69-17652
- Trapped mode wave propagation for cold uniform magnetoplasma cylinder in free space, studying dipole modes and one-wave approximation
06 p0967 A69-17756
- VLF diurnal phase change observations, showing deviations from theoretical first mode and second mode dominance
07 p1078 A69-18912
- Formulas for ray paths in ionized layers with application to oblique ionograms and duct modes
07 p1078 A69-18913
- Circularly polarized waveguide mode simulation for multislot leaky waveguide harmonic content measurement
07 p1105 A69-19046
- Beam distortion in low order Gaussian-Laguerre modes propagating through saturable laser amplifier, noting uniform and Bessel small signal gain distributions
[IEEE PAPER J-3] 07 p1152 A69-19065
- Reflection and transmission scattering coefficients for step type transition between two uniform waveguides with surface impedance boundaries, discussing coupled differential equations
08 p1272 A69-20020
- Horizontal electric dipole excitation of spherical guide waves between earth and ionosphere, discussing TM and TE modes and ELF and VLF range
08 p1273 A69-20023
- Low energy multiply charged cosmic ray nuclei propagation and source characteristics, considering two component model based onOGO satellite measurements
08 p1378 A69-20068
- Disturbing TM mode generation effect on attenuation measurement accuracy in TE mode attenuators
08 p1283 A69-20126
- Wavefront Wilkins-Minnis, null selection and elevation scanning techniques for measuring radio signals elevation angles with vertical antenna arrays
08 p1275 A69-20293

- Propagation modes in corrugated cylindrical waveguides determined by imposing nonisotropic surface reactance boundary condition at corrugated walls
08 p1284 A69-20295
- Mode designation and propagation characteristics of dielectric tube waveguide, noting practicability at higher microwave frequencies
08 p1284 A69-20296
- Radiation field patterns of linear antennas immersed in weakly ionized plasma evaluated for propagation constants of current distribution
08 p1285 A69-20551
- Transverse density nonuniformity effect on electromagnetic wave propagation in cylindrical plasma waveguide immersed in magnetic field, noting frequency increase
09 p1545 A69-21348
- VLF electromagnetic wave propagation in earth-ionosphere waveguide with reflections from ionosphere, noting TE and TM mode coupling and mode conversion
09 p1460 A69-22699
- Micromechanism of crack propagation in brittle fracture, considering kinematics for steady state crack in plane strain and energy dissipation
10 p1796 A69-23070
- Transequatorial propagation mode for waves in VHF band twice scattered by field aligned irregularities in electron density
10 p1653 A69-23192
- Weakly attenuated components of VLF mode spectrum associated with propagation below anisotropic ionospheres as function of frequency and azimuth
10 p1655 A69-23417
- Shock front propagation in argon with electrode-drawn induced EMF, using shock tube with induced transverse magnetic field
10 p1737 A69-23469
- Slow electromagnetic wave propagation along cold collisionless cylindrical plasma in axial magnetic field, noting surface wave metamorphosis into bulk waves
10 p1739 A69-23659
- Electromagnetic wave propagation along longitudinally magnetized plasma column surrounded by isotropic dielectric medium, without making quasi-static assumption
10 p1658 A69-24061
- Normal mode dispersion at upper hybrid frequency propagating parallel to uniform magnetic field in spatially inhomogeneous plasma
11 p1924 A69-24302
- Computer calculated phase velocities for surface wave and waveguide modes given for circular waveguide filled with inhomogeneous electron plasma
11 p1844 A69-24437
- Air gap tolerances effect on admittance of TEM mode dielectric and plasma coated slot antennas determined by variational method
11 p1851 A69-24986
- Ideal mode conversion and transmission by circular aperture of cylindrically symmetric cavity
11 p1899 A69-25056
- Landau dispersion relation solutions, noting higher order Landau poles and coupling of spatial Landau modes and least damped wave
11 p1929 A69-25265
- LF waves and instabilities on positive column in axial magnetic field, noting axisymmetric and asymmetric ion acoustic and electron wave modes and current convective instability
11 p1929 A69-25268
- Wave-mode converter with feed for omnidirectional antenna excitation, discussing H to E wave conversion, waveguides, emitter, etc
11 p1854 A69-25616
- TEM-WAVE propagation between parallel conducting planes, stressing changes in curved waveguide sections
11 p1841 A69-25619
- Resonance method determining spurious modes excitation in natural mode converter, discussing construction, application and mathematical correlation
11 p1856 A69-25630
- Fresnel dragging effect on 3 cm microwaves by electron gas drift in low pressure glow discharge, noting electron density and excitation modes
12 p2133 A69-25766
- Characteristic equation for corrugated surface wave line loaded with uniformly spaced thin metallic disks excited in E mode, considering spacing and groove depth
12 p2028 A69-25899
- Radiation pattern of circular cylindrical dielectric rod antenna excited in mixed magnetic and electric modes, discussing mode transducer
12 p2035 A69-25900
- Distortionless propagation of light through optical two level atoms medium, considering relation to Poynting theorem, hyperbolic secant solution and pendulum analogy
12 p2130 A69-26313
- Short circuit and variable frequency technique for measurement of coupling efficiency between dielectric loaded rectangular and trough waveguides, noting propagation modes
12 p2039 A69-26374
- Internal guiding of microwaves by elevated tropospheric layer noting refractive index, radius of curvature and attenuation
12 p2032 A69-26856
- VLF wave propagation along mixed path in curved earth-ionosphere waveguide, considering reflection and transmission coefficients of modes
12 p2032 A69-26858
- Auroral and polar zone ionosphere effects on propagation in HF through low VHF spectrum, considering nongreat circle mode, sporadic E ionization, etc
12 p2032 A69-26859
- Elliptical waveguide design dimensions for minimum attenuation in fundamental mode, giving formulas for attenuation constant and minor-major axis ratio
12 p2044 A69-27070
- Horn exciter with fundamental and second mode in feeding waveguide of shallow paraboloid antennas
12 p2044 A69-27093
- Waveguide higher order modes solved by finite-difference method, employing successive overrelaxation to compute field potentials at discrete points in arbitrary guide shapes
13 p2228 A69-27670
- Microwave propagation in coupled pairs of microstrip transmission lines for integrated circuit design, discussing dielectric Green function
13 p2229 A69-27672
- Cerenkov radiation from point charge uniformly moving along external magnetostatic field in warm anisotropic plasma, noting excitation modes and propagation frequencies
13 p2307 A69-27964
- Plane TM surface waves supported by plane ungrounded magnetoplasma slab with magnetostatic field parallel to two parallel interfaces and perpendicular to propagation direction
13 p2308 A69-27966
- Numerical integration for coupling between two modes of propagation /electron and proton whistlers/
13 p2254 A69-27981
- Leaky helix and solid metal waveguides propagation losses measured by shuttle pulse method in SHF
13 p2233 A69-28063
- Diffraction and mirror analyses of right angle corner in overmoded waveguide for scattered modes, discussing transmission loss
13 p2234 A69-28426
- Two dimensional adiabatic transverse normal modes of inviscid compressible uniformly rotating fluid, discussing harmonic wave propagation in opposite directions and rotation effects
14 p2431 A69-29581
- Tunable band stop filter realization from characteristic equation solution for propagation modes by magnetized ferrite slab placed in rectangular waveguide
14 p2422 A69-29751
- Leaky waves propagation characteristics helix waveguide covered with slitted cylinder using transverse network representation, emphasizing small pitch angles, hybrid TE and TM modes, etc
14 p2422 A69-29752
- Impedance eigenvalues for eigenmodes of multiconductor transmission lines, discussing transverse field distributions along conical line
14 p2423 A69-29756
- Shields frequency ranges analysis to determine frequencies and parameters for electrostatic and magnetostatic modes transition to electromagnetic and microwave modes
15 p2562 A69-30120
- Corrugated cylindrical waveguides used as hybrid mode feeds for reflector antennas
15 p2575 A69-30175
- Corrugated conical horn used as antenna feed, studying modes in horn and associated radiation patterns by spherical hybrid functions analysis
15 p2575 A69-30176
- Cut-off wavelength of transverse magnetic mode related to cross section eccentricity of hollow conducting elliptical waveguide
15 p2575 A69-30178
- Waveguide mode propagation theory for determining earth-ionosphere spherical waveguide upper boundary height diurnal variation for VLF waves
15 p2595 A69-30224
- Resonance measurement of power percentage in single spurious mode of overmoded waveguide, using back to back transducers and reflection at input
15 p2577 A69-30611
- Time dependent Green function method for premature saturation due to parametric amplification of nonuniform spin wave modes by one and two magnon processes
15 p2668 A69-30685
- Coupled TEM lines arrays analysis in terms of odd and even modes, computing equivalent circuit elements, impedances and admittances
15 p2581 A69-31525
- Wave propagation in warm uniaxial plasma filled waveguide, analyzing TE modes, TM mode splitting and power transfer
16 p2756 A69-31576
- Electromagnetic wave propagation in transversely magnetized warm plasma filled rectangular waveguide, analyzing TE and TM modes
16 p2756 A69-31581
- Propagation modes attenuation and guidance on circular hollow dielectric waveguides dependent on dielectric loss tangent
16 p2757 A69-31587
- Hall current effect on thermal instability explaining nonself gravitating astronomical objects, discussing current effects on propagation modes
16 p2854 A69-31649
- Computerized finite element waveguide analysis for determining propagating modes and cut-off frequencies
16 p2760 A69-31942
- Waveguide bends fields expressed in coupled local annular modes derived by evaluating differential scattering coefficients
16 p2760 A69-31943
- Wave propagation in open periodic two dimensional iris waveguide and beam reconstruction by diffraction, considering existence and character of modal fields
16 p2753 A69-32394
- Ionosphere depression influence on VLF signals phase and amplitude calculated by mode theory and integral equations system representing aperture fields
17 p2920 A69-33418
- Asymptotic solutions for vector fields and propagation constants of axial modes in circular cylindrical waveguides, noting changes in dielectric constant
17 p2921 A69-33673
- Wave excitation in resonant dissipative and inhomogeneous structures, discussing resonator geometry, mode spectra, etc
17 p2926 A69-33849
- Trapped modes in cold magnetoplasma slabs and rods in free space analyzed by Maxwell equation, assuming DC magnetic field and homogeneous electrons distribution
17 p2926 A69-33850
- Continuity conditions for drifting magnetoplasmas without ionic effects, discussing eigenvalue equation of refractive index and electromagnetic modes propagation
17 p2926 A69-33851
- Mathematical model for aircraft antenna to antenna electromagnetic interference analysis, emphasizing techniques for propagation paths and shading factors
17 p2943 A69-34134
- Pulse propagation through antipode, calculating time domain response of fields near axial caustic
18 p3100 A69-34233
- Radio echo from south showing origin from irregularities in F but not E region, discussing propagation modes for particular record
18 p3125 A69-34252
- Whistlers propagation in cold plasma in uniform magnetic field, considering amplitude dispersion effect
18 p3179 A69-34437
- Anisotropic ionospheric model for VLF TM and TE modes excitation, noting nighttime phase velocity variations
18 p3101 A69-34797
- Transverse and longitudinal velocity components of detonation waves in stoichiometric hydrogen-oxygen propagating in fundamental mode in square section tube
19 p3451 A69-36367

Q factors of ideal antenna enclosed in imaginary sphere with excited TE and TM modes
20 p3506 A69-37836

Two-hop signals observed on high latitude Alouette 2 topside ionograms found propagating in field aligned cylindrical ionospheric ducts
20 p3531 A69-37890

Propagation characteristic model study of kinked Z trace observed on topside ionograms and explained by magnetoionic theory
20 p3531 A69-37893

Field patterns, propagation constants and losses determined for axially propagating modes guided by circular cylindrical inhomogeneous dielectric, using perturbation method
20 p3497 A69-38130

Monochromatic electromagnetic field in resonant medium, examining linear, incoherent and coherent nonlinear propagations and resonant scattering
21 p3769 A69-38382

Cosmic rays composition, origin, acceleration and propagation, describing two component models
21 p3789 A69-38814

Cosmic ray propagation from experimental data on cosmic ray nuclei
21 p3789 A69-38816

HF direction finder for display of time varying multimode propagation phenomena, using analog computer and phase sensitive interferometer
21 p3677 A69-39456

Equatorial radiation pattern of parallel plate TEM mode axial slot on elliptical conducting cylinders, using wedge diffraction and creeping wave theory
22 p3914 A69-40703

Mode conversion in nonuniform multimode waveguides and transitions using Maxwell equations, considering tapered and circular waveguides
23 p4135 A69-41354

HF backscatter, long delay signals and round-the-world echoes as radio wave propagation modes
23 p4116 A69-41602

VHF radio propagation over transequatorial circuit related to equatorial anomaly in F layer, suggesting F2/F2 propagation mode role
23 p4127 A69-42431

Rectangular dielectric waveguide propagation modes, describing computer analysis based on electromagnetic field expansion in circular harmonics series terms
24 p4288 A69-43330

PROPAGATION VELOCITY

Whistler rate and dispersion daily and annual variations derived relative to propagation conditions and magnetospheric behavior over North Italy
01 p0067 A69-11033

Granite compressional wave velocity and electrical resistivity variations with depth, explaining discrepancy between in situ and laboratory measurements on dry samples
02 p0241 A69-11806

Alfven wave propagation designations in terms of polarization and propagation velocity, resolving contradictory aspects
02 p0290 A69-12400

Pressure pulses propagation in nonsteady fluid flow through expansible tubes, noting computer solution
02 p0232 A69-12477

Velocity field generated by vibrations propagating at finite velocity over elastic wing surface
02 p0190 A69-12571

Light tachyons, tachyon velocity and relation to gravitational quanta
02 p0282 A69-12746

Theory of heat conduction with finite wave speeds for materials with memory
03 p0533 A69-13956

Elastic-plastic boundaries velocities for combined longitudinal and torsional plastic wave propagation in thin walled tube during unloading
[ASME PAPER 68-WA/APM-7]
04 p0670 A69-14403

Propagation velocity upper limits for plasma waves during state of equilibrium transition determined from nonlinear wave equation
04 p0630 A69-14553

Bandwidth effect on wave recordings cross spectra interpretation from spatially separated sites, deriving relationship between propagation velocity and velocity bandwidth
05 p0756 A69-16272

Compressional and shear wave velocities vs porosity for sintered perlitic bricks
06 p1000 A69-17009

Equations for electron scattering by sound in n-type semiconductors, giving corrections to sound propagation velocity during interactions
07 p1199 A69-18680

Quasi-linear differential constitutive equation of work hardenable elastoviscoplastic material in case of plane wave propagation in half space
08 p1415 A69-20662

Current sheet velocity in coaxial plasma accelerator, noting drag due to insulator ablation and degassing
[AIAA PAPER 69-265]
09 p1566 A69-21258

Mach number values and propagation rates of wear disturbances in interplanetary medium obtained from Mariner 2 data during low solar activity
09 p1575 A69-21523

Electron content of earth-Venus interplanetary medium measured by observing relative propagation time of radar pulses to Venus
09 p1594 A69-21697

Flame propagation normal velocity evaluated with heat transfer equation at flame front taking into account temperature, pressure and inert gas percentage
09 p1625 A69-22695

Crack propagation velocity in titanium alloys over varying stress intensities under adverse environment
10 p1709 A69-23058

Ionization front propagation rate in crossed electric and magnetic fields in Ar-Cs, Hg-Cs and Ne-Xe discharge plasmas
10 p1733 A69-23447

Turbulent flame propagation velocity in homogeneous premixed combustible gas, using one dimensional inviscid flame model
11 p1998 A69-24473

Flame velocities of stable premixed tetrafluoroethylene-oxygen mixture flames measured with bunsen-cone method
11 p1940 A69-24485

Electric fields effect on flame front propagation structure and velocity, obtaining color topletopograms by high speed photography
12 p2190 A69-26192

Velocity dependence of temperature waves /second sound/ in liquid He II measured as function of relative velocity for normal and superfluid
13 p2297 A69-27460

Shock wave velocity and gas flow parameters in shock tube with noninstantaneously opening diaphragm calculated by method of characteristics
14 p2432 A69-29623

Group delay time for dispersive wave propagation velocity determined using correlation method
15 p2562 A69-30094

Annealed aluminum rods dynamically compressive impact loading used to study longitudinal plastic waves propagation velocity
15 p2709 A69-30677

Small perturbations propagation in plasma at Newtonian acoustic velocity, determining temperature, pressure and current densities
15 p2663 A69-30993

Flame propagation velocity for different gas mixtures enclosed in glass tube determined by fiber optics devices
16 p2789 A69-31764

Relativistic exceptional wave propagating heat, computing speeds in direction orthogonal to heat vector
16 p2827 A69-32042

Initial temperature effects on flame propagation velocity in turbulent flow of homogeneous gasoline-air mixture under realistic conditions
16 p2837 A69-32138

Additives effect on flame propagation velocity and stability in N diluted hydrogen-chlorine propellants, noting entrained air role
[WSCIPAPER 69-13]
16 p2831 A69-32353

Mach number values and propagation rates of weak disturbances in interplanetary medium obtained from Mariner 2 data during low solar activity
16 p2851 A69-32518

VLF wave propagation phase velocity prediction for airborne Omega computer, using scatter model based on abnormal ionosphere
17 p3002 A69-34077

Hard cosmic radiation hypothesis for Newton gravitation law for neighboring bodies, obtaining gravitational energy quanta and propagation velocity relationship
18 p3172 A69-34627

High speed brittle fracture of polycarbonate resin subjected to static bending in liquid nitrogen determined from crack propagation speed of surface coating
19 p3358 A69-35776

Turbulent velocity of flame propagation in supersonic stream of hydrogen-air mixture determined by velocity distribution, exchange coefficient and burning time
19 p3448 A69-35854

Combustion turbulence effect on flame propagation velocity taking into account flame-generated pulsation velocity as function of temperature and flame velocity
21 p3850 A69-38861

Linear system propagation time measurement independent of input or output time functions
23 p4165 A69-41700

Heat finite propagation velocity effects on temperature distribution and heat flux for step temperature change at semiinfinite body surface
[ASME PAPER 69-HT-1]
24 p4414 A69-43564

PROPAGATORS

U PROPAGATION

PROPANE

Liquefied propane fog dispersal at Medford-Jackson airport, Oregon
04 p0585 A69-14918

Physicochemical and operational properties of trimethylol propane esters as lubricating oils under static and dynamic conditions
12 p2103 A69-27090

LF oscillations in simple combustion chamber using gaseous propane fuel, discussing association with progressive flame necking
18 p3230 A69-34837

Ammonia addition effect on laminar flame speeds of propane-air mixtures
21 p3849 A69-38809

Interferometric study of cool flame propagation in equimolar propane-oxygen mixtures, observing refractive index and temperature distribution changes
21 p3852 A69-39595

PROPELLANT ADDITIVES

NT SOLID ROCKET BINDERS

Plateau effect in burning of platonized propellants due to lead compound additives
03 p0494 A69-12881

Catalytic effect of potassium bichromate and chromic oxide additives on burning of ammonium perchlorate and mixtures
08 p1375 A69-19997

Aluminum effect on ammonium perchlorate/polyformaldehyde mixtures combustion properties noting heat transfer decrease into k phase
08 p1375 A69-20338

Vanadium pentoxide addition effect on combustion rates of mixtures of ammonium perchlorate and metallic fuels in nitrogen atmosphere
08 p1375 A69-20342

Jet fuel quality improvement by adding isopropylacetate and other substances because of surface-active and sorptive qualities
16 p2828 A69-31562

Burning velocity inhibitors effects on hydrocarbon-oxygen-nitrogen mixtures ignition temperature, reporting data on 20 additives at ambient temperature and pressure
[WSCIPAPER 69-14]
16 p2831 A69-32352

Point defect structure to control ammonium perchlorate burning rate, discussing thermal analysis data correlations, isothermal decomposition, etc
[WSCIPAPER 69-17]
16 p2831 A69-32355

Decomposition of ammonium perchlorate containing additives introduced by spray drying
[AIAA PAPER 69-502]
16 p2834 A69-32752

Book on chemical rockets and flame and explosives technology covering propulsion systems, combustion, propellant ingredients, etc
22 p3998 A69-40866

PROPELLANT BINDERS

NT SOLID ROCKET BINDERS

Low temperature grinding technique for IR spectra of propellants and binders in potassium bromide disks
01 p0082 A69-10892

Oxidizer particle size and binder type effects on nonacoustic combustion instability of solid propellants
[AIAA PAPER 69-175]
06 p0983 A69-18152

Combustion rates of condensed systems under positive and negative accelerations at atmospheric pressure
11 p2001 A69-25195

Combustion bomb testing of propellants containing fluorocarbon binder and ammonium perchlorate, noting unique ignition, combustion and extinction properties
[WSCIPAPER 69-9]
16 p2831 A69-32349

Composite propellants high pressure burning stability with various binders and oxidizers, showing ammoni-

- um perchlorate oxidized formulations susceptibility to instability
[AIAA PAPER 69-438] 16 p2834 A69-32704
- Powdered oxidizer and infusible polymer binder combustion at various pressures, studying gaseous phase temperature field by optical color analysis
17 p3069 A69-33135
- PROPELLANT CASTING**
- Nonnewtonian solid propellant viscosity and pseudoplasticity utilizing rheological characterization for optimal casting and pot life determination
[AIAA PAPER 69-518] 16 p2833 A69-32665
- PROPELLANT CHEMISTRY**
- High thrust fluorine engines and propellants
03 p0494 A69-12889
- Integrated Waste Management/Rocket Propulsion System, using human feces as propellant component
[SAE PAPER 680717] 03 p0495 A69-13442
- High performance chemical propulsion systems feasibility, discussing propellant combinations
06 p0983 A69-17627
- Propellant condensation on surfaces near electric rocket exhaust, calculating particle arrival rates, backflow and desorption energies
[AIAA PAPER 69-270] 09 p1565 A69-21252
- Chemical species and reactions determined for propellants in calculating nonequilibrium rocket engine performance
11 p1940 A69-24905
- Book on inorganic high energy oxidizers covering synthesis, structure and properties of fluoronitrogen, fluorine, fluorohalogen and oxygen compounds
12 p2146 A69-25824
- Description and automated research of correlation /DARC/ for establishing quantitative relationships between topology and properties of chemical substance
12 p2026 A69-26361
- Rocket propellants, propellant chemistry and rocket propulsion system performance
13 p3234 A69-27916
- Solid propellants formulation quantitative predictability for algorithmic modeling of functional selection, discussing specific impulse and burning rate
[AIAA PAPER 69-432] 16 p2828 A69-31845
- Chemical processing for manufacture of solid propellant motors, discussing mixing, casting and curing of composite propellants
16 p2829 A69-31992
- Additives effect on flame propagation velocity and stability in N diluted hydrogen-chlorine propellants, noting entrained air role
[WSCI PAPER 69-13] 16 p2831 A69-32353
- Free gas formation in propellant systems and effects on attitude control systems
[AIAA PAPER 69-434] 16 p2870 A69-32765
- Turbulent process employing product constituents dilute suspensions in inert carrier /Quickmix/ to obtain solid propellant mixtures, discussing plant design and analysis, economics, etc
[AIAA PAPER 69-517] 17 p2978 A69-33033
- Binder polymer network and microstructure effects on solid rocket propellant properties, emphasizing choice of polymer ingredients
[AICHE PAPER 37A] 17 p3017 A69-33668
- Thermodynamics of propellant combination of Li hydride containing solid fuel with ethylenimine base, coupled with Cl trifluoride oxidizer and ammonium nitrate added
22 p3997 A69-39919
- Book on chemical rockets and flame and explosives technology covering propulsion systems, combustion, propellant ingredients, etc
22 p3998 A69-40866
- Intermediate hydrazine-RFNA reaction product formed on injector nozzle and combustion chamber surfaces after fuel injection without ignition analyzed by various methods
24 p4365 A69-43669
- PROPELLANT COMBUSTION**
- NT SOLID PROPELLANT IGNITION**
- Book on combustion covering aerodynamic and chemical aspects, combustion instability, detonation and rocket propellant combustion
01 p0176 A69-10906
- Specific acoustic admittance of solid propellant burning surface for determining burning instability under rocket motor conditions
02 p0302 A69-11521
- Combustion instabilities in solid propellant rocket engines, emphasizing acoustic types for longitudinal and tangential modes
02 p0303 A69-11531
- Flame zone development of monopropellant droplets during heat-up period
02 p0352 A69-12310
- Solid propellant combustion instability models describing combustion zone dynamics applied to acoustic and nonacoustic instability in LF regime
[WSCI PAPER 67-13] 02 p0352 A69-12311
- Thermal decomposition of ammonium perchlorate and ammonium perchlorate-copper chromite mixtures
02 p0304 A69-12312
- Initiation of detonation by incident shock waves in hydrogen-oxygen-argon mixtures
02 p0304 A69-12313
- Hydrogen bromide, HI and HCl effects on hydrogen-air mixtures flammability, discussing flame propagation inhibition efficiency
02 p0304 A69-12315
- Fuel films ignition behind shock waves in air and oxygen
02 p0353 A69-12317
- Combustion oscillations in liquid and solid propellant engines, noting destructive effect of LF vibrations and acoustic instability
02 p0305 A69-12494
- Pressure and velocity couplings effects on oscillatory and transient motions in solid propellant rocket motors, emphasizing unsteady burning calculations
02 p0305 A69-12501
- Microcalorimetric measurement of radiation flux of flames of condensed burning material, noting surface temperature distribution
02 p0355 A69-12671
- Combustion model for rapidly burning involatile condensed materials, obtaining combustion rates
02 p0355 A69-12672
- Plateau effect in burning of platonized propellants due to lead compound additives
03 p0494 A69-12881
- Rocket engine combustion mechanism of ammonium perchlorate composite propellants
03 p0532 A69-13002
- Ultrahigh pressure test vessel for determining pressure vs burning rate characteristics of propellants and explosives
04 p0645 A69-14472
- Characteristics of liquid propellant explosions, analyzing detonation, shock wave formation and deflagration
04 p0645 A69-14474
- Saturn fireball thermal environment associated with liquid propellant explosions, using analytical model
04 p0645 A69-14475
- Yield and combustion physics of liquid propellant explosions determined from analytic charts
04 p0646 A69-14477
- Perturbation behavior of solid propellant combustion, discussing relevance of analytical models and use of qualitative models
04 p0685 A69-14726
- Initiation of HF combustion oscillation in premixed gas rocket
[ISAS-430] 06 p1029 A69-17025
- Deflagration of solid and hybrid propellants in steady state for missile and rocket propulsion applications
06 p0982 A69-17422
- Burning rates of solid propellants by variable pressure method, taking into account environmental heat loss and gaseous condensation
06 p0982 A69-17505
- Laminar and turbulent regimes of flame propagation studied by blowing explosive gas mixture through porous wall, determining Reynolds number by hot-wire anemometer
06 p1034 A69-17626
- Photochemical ignition of low pressure fuel-oxidizer mixtures applied to unsensitized stoichiometric mixtures of methane-oxygen and hydrogen-oxygen
[WSCI PAPER 68-42] 06 p1034 A69-17791
- Liquid hydrazine ignition by nitrogen tetroxide gas based on stagnation flow principle, presenting threshold measurements
06 p0983 A69-17792
- Unstable combustion of ammonium perchlorate /AP/, discussing correlation between propellant particle diameter and frequency in burning rate
[AIAA PAPER 69-177] 06 p1036 A69-18063
- Nonsteady combustion models for gases, liquid fuels and solid propellants, reviewing errors in physics and mathematics
[AIAA PAPER 69-178] 06 p1037 A69-18100
- Ammonium perchlorate high temperature decomposition by using carbon dioxide laser pyrolysis/mass spectrometry
[AIAA PAPER 69-143] 06 p0885 A69-18111
- Photographic study of burning metalized composite propellant under acceleration, noting burning rate augmentation by heat transfer from alumina particles retained on propellant surface
[AIAA PAPER 69-173] 06 p0983 A69-18151
- Low pressure deflagration limit dependence on strand size in terms of cross section dimensions for composite ammonium chlorate propellant
[AIAA PAPER 69-144] 06 p0983 A69-18162
- Solid propellant burning rates from condensed phase decomposition kinetics, discussing kinetic rates of thermal decomposition
[AIAA PAPER 69-145] 06 p1039 A69-18182
- Regression rate model for pressure sensitive hybrid combustion based on classical turbulent flame theory
[WSCI PAPER 68-22] 07 p1240 A69-18362
- Empirical and analytic modeling of propellant role in ignition, discussing ignition transient prediction to describe propellant ignitability characteristics
[WSCI PAPER 68-34] 07 p1202 A69-18364
- Strong electrostatic fields effects on burning rates of double base and composite propellants
[WSCI PAPER 68-24] 07 p1241 A69-18366
- Heat conduction equation for convective flow applied to gunpowder combustion under harmonic pressure variation
07 p1241 A69-18708
- Laboratory test stands for ignition, combustion and expansion processes experiments in hypergolic liquid fuels, noting minimal recombination gains
08 p1301 A69-20170
- Vanadium pentoxide addition effect on combustion rates of mixtures of ammonium perchlorate and metallic fuels in nitrogen atmosphere
08 p1375 A69-20342
- Monograph on ignition, combustion and expansion in hypergolic liquid propellant mixtures at gas temperatures up to 3000 K for small rocket engines
08 p1375 A69-20723
- Burning rate catalysts mechanism and location in composite propellant combustion at high pressure
09 p1622 A69-21954
- Solid propellant combustion, calculating burning, flame standoff distance, flame thickness, heat transfer, energy losses, and distributed and unsteady combustion
09 p1623 A69-22091
- Sublimation in ammonium perchlorate propellants combustion, discussing low temperature isothermal processes, linear regression rates measurements and low ambient pressure
11 p1940 A69-24481
- Critical diameter of ammonium perchlorate stable detonation as function of initial temperature, water content, density and particle size
11 p1940 A69-24553
- Ionizing radiation effects on combustion of ammonium perchlorate compacts with and without fuel addition, considering X ray, electron and plasma radiation
11 p1941 A69-25194
- Spherical monopropellant droplet radially symmetric burning during adiabatic vaporization and direct decomposition, examining near-equilibrium limit by asymptotic analysis
12 p2190 A69-25948
- Helmholtz resonance in rocket injectors as function of frequency response of interaction between chamber pressure and dissolved gas-fuel injection flow rate
12 p2148 A69-26806
- Polyester/ammonium perchlorate combustion, determining degradation rate by loss in weight method at different intervals
13 p2324 A69-28234
- Extinction kinetics of monopropellant droplet burning in inert gas reservoir with atmospheric temperature lower than adiabatic combustion temperature
13 p2378 A69-28250
- Polymethyl methacrylate burning rates in mixture with ammonium perchlorate or in hybrid systems when mixed with ammonium chloride
13 p2324 A69-28503
- Shorter combustors for high temperature jet engines of high speed aircraft, considering lifetime, shroud scoops, overheating, warpage, etc
14 p2509 A69-29433
- Nucleate boiling burnout heat flux data for ethane, ethylene and ethane-ethylene mixtures at various pressures, discussing applicability of Noyes equations
15 p2671 A69-31118
- Fuel injector-induced mass flux and mixture ratio distributions effects on combustion performance, chamber volume and stability, discussing combustion oscillation avoidance
16 p2877 A69-31731

Combustion in liquid propellant rockets, discussing aerothermochemical steady state and nonsteady behavior analysis and experiments
16 p2835 A69-31732

Solid propellants formulation quantitative predictability for algorithmic modeling of functional selection, discussing specific impulse and burning rate
[AIAA PAPER 69-432] 16 p2828 A69-31845

Solid propellants steady state combustion with emphasis on heterogeneous propellants
16 p2829 A69-31995

Combustion instability characteristics of solid propellants, discussing small scale testing methods
16 p2829 A69-31996

Solid fuel propulsion systems for tactical rockets design, discussing microwave attenuation, acceleration-combustion interactions and performance optimization
16 p2836 A69-31998

Compressible turbulent accelerating boundary layer flow model for convective heat transfer from rocket combustion gases, noting heat flux
16 p2878 A69-32000

Feed-system-coupled combustion instability linearized mathematical models for liquid fuel rocket engines, discussing nonrigid injector and method for instability elimination
16 p2836 A69-32001

Hybrid rockets combustion mechanism, discussing turbulent boundary layer with heat and mass transfer, chemical reactions, etc
16 p2879 A69-32002

Small disturbances and effect on processes of fast combustion of inflammable compressible mixture
16 p2837 A69-32137

Thermal layer theory of composite propellant combustion leading to minimum steady state burning rate under ideal thermal conditions
[WSCIPAPER 69-5] 16 p2830 A69-32346

Composite solid propellant burning rate by solving energy equation, yielding heat release, flame thickness and standoff distance
[WSCIPAPER 69-7] 16 p2830 A69-32348

Combustion bomb testing of propellants containing fluorocarbon binder and ammonium perchlorate, noting unique ignition, combustion and extinction properties
[WSCIPAPER 69-9] 16 p2831 A69-32349

IR spectrometric analysis of flames of composite rocket propellants, maintaining diffusion flames between surfaces of decomposing ammonium perchlorate and fuel source
[WSCIPAPER 69-10] 16 p2831 A69-32350

Linear pyrolysis of thermoplastics during combustion of composite solid propellants and ammonium perchlorate solid propellant deflagration mechanism studied by loose granule analog
[WSCIPAPER 69-16] 16 p2831 A69-32354

Doped recrystallized ammonium perchlorate effects on composite propellant burning rates
[WSCIPAPER 69-18] 16 p2831 A69-32356

Thermal decomposition behavior of perchlorate oxidizers studied by flash mass thermal analysis for determining propellant combustion kinetics
[WSCIPAPER 69-19] 16 p2832 A69-32357

Nonequilibrium initial condition combustion effects on propellant performance for hydrazine/chlorine pentafluoride and hydrogen/fluorine with equilibrium, kinetic and frozen nozzle flow
[AIAA PAPER 69-469] 16 p2832 A69-32659

Integrated double oblique shock scramjet for supersonic combustion tests and instrumentation development, discussing fuel injection through sonic orifices, combustion data, etc
[AIAA PAPER 69-827] 16 p2840 A69-32673

Composite solid propellant combustion using differential scanning calorimeter and mechanical model of steady state combustion
[AIAA PAPER 69-504] 16 p2833 A69-32679

Flame propagation in narrow slit and fine hole of solid propellant grain
[AIAA PAPER 69-561] 16 p2833 A69-32680

Premature exothermic decomposition suppression in propellant grade ammonium perchlorate, using differential thermal analysis
[AIAA PAPER 69-503] 16 p2833 A69-32688

Droplet vaporization model representing combustion processes of longitudinal oscillations in liquid rocket combustor
[AIAA PAPER 69-483] 16 p2841 A69-32689

Linear and nonlinear pressure coupled combustion instability of solid propellants
[AIAA PAPER 69-479] 16 p2834 A69-32725

Compositional and oxidizer particle size effects on combustion instability of plastic propellant based on ammonium perchlorate and polyisobutene
[AIAA PAPER 69-478] 16 p2834 A69-32734

Stability criteria for longitudinal combustion instability tested for generality using data from various solid propellant formulations
[AIAA PAPER 69-480] 16 p2834 A69-32736

Gas phase ignition theory with feedback of homogeneous propellant exposed to stagnant gas after shock reflection
[AIAA PAPER 69-559] 16 p2880 A69-32740

Combustion of pure crystalline boron single particles injected into hot oxidizing gases streams at atmospheric pressure
[AIAA PAPER 69-562] 16 p2880 A69-32741

Ammonium perchlorate linear pyrolysis by convective surface heating, discussing propellant deflagration models
[AIAA PAPER 69-501] 16 p2835 A69-32758

Hybrid propulsion chemical and technical problems, discussing solid fuel fragmentation and defining typical combustion modes
17 p3021 A69-33358

Liquid rocket combustion investigated by pulsed ruby laser holography at sea level rocket engine test stand, noting laminated glass acrylic window byproduct
[AIAA PAPER 69-471] 17 p3075 A69-34200

Nonsteady propellant burning theory for Al melting role in suppressing combustion instability in solid propellant rocket motors
19 p3393 A69-36814

Hydrogen and methane combustion to simulate expansion of storable propellants
[AIAA PAPER 68-635] 20 p3631 A69-37188

Laboratory unsteady burning data applied to analysis of small amplitude combustion instability in solid propellant rockets
20 p3586 A69-37224

Acceleration effects on solid propellant rocket motors combustion characteristics
[AIAA PAPER 68-530] 21 p3786 A69-39217

Shock front reaction and detonation initiation in low density ammonium perchlorate
21 p3784 A69-39590

Combustion considerations in fuel rich solid and hybrid propellant systems in air breathing propulsion for comparison with metal ignition requirements
23 p4199 A69-41894

Propellant ignition delay in contact of condensed fuel with hot reactive gas in shock tube, using graphical method and surface temperature fractional increase
23 p4199 A69-41897

Burning solid propellant behavior under pressure fluctuations expressed in response function terms defining small mass flux change ratio to small pressure change
23 p4201 A69-41922

Detonation wave instability and damping in gas containing liquid or solid inflammable aerosol, considering atomized propellants
23 p4240 A69-42339

Solid fuel ablation and supersonic combustion processes for various propulsion configurations, testing plastic models in wind tunnel
24 p4414 A69-43569

Solid propellant flame zone radiant energy flux emitted through side port of internal burning cylindrical rocket motor related to total heat flux at burning surface
24 p4415 A69-43595

Pressure effects in spontaneous ignition of interimpinging hydrazine and red fuming nitric acid (RFNA)/liquid streams in evacuated test chamber
24 p4415 A69-43667

Adiabatic model deflagration limits for steady linear monopropellant burning at Lewis number of unity and one step gas phase reaction
24 p4415 A69-43670

PROPELLANT DECOMPOSITION

Solid propellant burning rates from condensed phase decomposition kinetics, discussing kinetic rates of thermal decomposition
[AIAA PAPER 69-145] 06 p1039 A69-18182

Ammonium perchlorate exothermic decomposition control noting effects of preheating and ammonium fluoroborate additives
[WSCIPAPER 68-25] 07 p1202 A69-18363

Spherical monopropellant droplet radially symmetric burning during adiabatic vaporization and direct decomposition, examining near-equilibrium limit by asymptotic analysis
12 p2190 A69-25948

Steady deflagration of homogeneous monopropellant in condensed phase, considering nonequilibrium surface condition for mass decomposition rate
[WSCIPAPER 69-6] 16 p2830 A69-32347

Granular ammonium perchlorate thermal decomposition analyzed by cinemicrography, discussing sublimation role
[WSCIPAPER 69-20] 16 p2832 A69-32358

Ammonium perchlorate pyrolysis by convective surface heating, monitoring IR emission as measure of surface temperature
[WSCIPAPER 69-23] 16 p2832 A69-32361

Decomposition of ammonium perchlorate containing additives introduced by spray drying
[AIAA PAPER 69-502] 16 p2834 A69-32752

Turbulent heat and mass diffusion in catalytic reactors for hydrazine decomposition, developing computer program to calculate temperature and reactant concentration distributions
[AIAA PAPER 69-421] 16 p2846 A69-32768

Ammonium perchlorate decomposition, discussing high and low temperature reactions, combustion, catalysts and gaseous environment effects
21 p3784 A69-39593

PROPELLANT EVAPORATION

Propellants volatile fraction removal followed by gas chromatographical determination, noting use of heating method
02 p0302 A69-11522

Treatment and testing of thin platinum and gold alloy wires used in thermoelements for studying liquid fuel vaporization in combustion chambers
07 p1130 A69-18258

Fuel droplet evaporation and combustion in still air as unsteady diffusion controlling phenomenon, basing calculations on flame front model
20 p3632 A69-37520

PROPELLANT GRAINS

Glass fiber reinforced plastic (GFRP)/roving end grains in rocket combustion chambers, discussing design and structural parameters
02 p0305 A69-12748

Burning rate of solid grains of hybrid rocket engine, using calculated diagrams for quick computations of engine
08 p1376 A69-20590

Elastomeric solid propellant grains viscoelastic flow, analyzing stresses and strains under various operating conditions and rocket engine geometry effect
10 p1801 A69-23702

Flame propagation in narrow slit and fine hole of solid propellant grain
[AIAA PAPER 69-561] 16 p2833 A69-32680

Mathematical analysis of dendrite design of solid propellant grains for variant of modified wagon wheel design
22 p3997 A69-40553

PROPELLANT MASS RATIO

Relative weight of fuel required for flight along prescribed flight trajectory
03 p0519 A69-12964

Unannounced propellant weight and thrust of Soviet Luna spacecraft based on Luna 12 lunar orbit injection maneuver
08 p1409 A69-19969

Fuel injector-induced mass flux and mixture ratio distributions effects on combustion performance, chamber volume and stability, discussing combustion oscillation avoidance
16 p2877 A69-31731

Liquid propellant injector design for rocket thrust chambers, discussing mass and mixture ratio regulation
16 p2836 A69-31999

Cost optimization of mixture ratio control systems for liquid propellant launch vehicles, considering open and closed loop systems
[AIAA PAPER 69-441] 16 p2870 A69-32775

Chemical relaxation, optimum propellant mixture ratio, combustion chamber pressure, gas jet impulse, mass flow and drive capacity of space propulsion systems
18 p3229 A69-34773

PROPELLANT OXIDIZERS

U ROCKET OXIDIZERS

PROPELLANT PROPERTIES

Characteristics of liquid propellant explosions, analyzing detonation, shock wave formation and deflagration
04 p0645 A69-14474

Solid propellants formulation, processing physical properties, testing and rocket motor inspection
04 p0646 A69-14583

JP-4 fuel emulsions properties, handling characteristics and safety performance, noting satisfactory shelf life and thermal stability
[ASME PAPER 68-GT-24] 06 p0982 A69-17190

Fluid and thermodynamic modeling for ground test simulation of nuclear rocket vehicle liquid hydrogen propellant behavior
[SAE PAPER 690201] 07 p1178 A69-18306

Chemical reaction rate data for propellant systems containing boron or aluminum and hydrogen, chlorine and fluorine, based on finite kinetics expansions
[AIAA PAPER 69-182] 11 p1940 A69-24907

Fuel requirements for flights up to Mach 3.5, discussing heat stable mineral oil based SST fuels
11 p1941 A69-25422

Binder polymer network and microstructure effects on solid rocket propellant properties, emphasizing choice of polymer ingredients
[AICHE PAPER 37A] 17 p3017 A69-33668

PROPELLANT SENSITIVITY

Shock sensitivity of solid explosives and propellants, using calibrated gap testing techniques
02 p0302 A69-11520

Rocket propellant safety, discussing thermal, mechanical and impact sensitivity tests of solid and liquid propellants
02 p0302 A69-11525

Explosives and propellants sensitivity to fragment impact, establishing threshold detonation velocity
04 p0645 A69-14473

Shock initiation and sensitivity of granular explosives, noting heterogeneity effect in ammonium perchlorate
10 p1751 A69-23016

PROPELLANT SPRAYS

Charged particles generation by liquid subjected to high electric field for efficient bipolar microthruster
[AIAA PAPER 67-728] 13 p3235 A69-28220

PROPELLANT STORABILITY

Propellants volatile fraction removal followed by gas chromatographical determination, noting use of heating method
02 p0302 A69-11522

Film cooling design criteria for small rocket engines
[AIAA PAPER 68-617] 09 p1570 A69-21978

Combustion performance evaluation program demonstrating high performance with space storable propellant combination of FLOX, methane and ethane
[AIAA PAPER 69-507] 16 p2829 A69-31848

PROPELLANT STORAGE

Fluid support by capillary forces, fluid support by pressure with surface tension stabilization and capillary gas barriers for long life missions
[AIAA PAPER 68-465] 04 p0646 A69-15505

Thermal protection system optimization for storage of cryogenic propellants in space, noting vented systems
[AIAA PAPER 69-27] 06 p1039 A69-18211

Propellant orientation and expulsion methods in space vehicle tankage, discussing ullage rockets system, bladders and diaphragms, dielectrophoretic expulsion, etc
16 p2736 A69-31734

Highly concentrated hydrogen peroxide production, handling and storage, discussing crystallization process, equilibrium diagram, decomposition reduction and stabilizers
17 p3017 A69-33353

Payload optimization factors for orbital storage of liquid hydrogen, considering payload cost of agitation, tank pressure, pressurant weight, etc
[AIAA PAPER 69-1007] 22 p4021 A69-40381

PROPELLANT TANKS

Liquid propellant space launch vehicles longitudinal modes natural frequency, discussing coupled engine-propellant supply system stability
[AIAA PAPER 68-289] 02 p0335 A69-12393

Spherical false bottom influence on propellant sloshing in circular tank
[DVL-843] 03 p0416 A69-13665

Method for solving propellant sloshing in rotationally symmetric rocket tanks with arbitrary internal boundaries
04 p0665 A69-14840

Nondestructive weld tests of propellant tanks in Saturn V-S-1C stage
07 p1140 A69-18798

Maraging stainless steel for manufacturing liquid rocket propellant tanks, discussing composition determination and mechanical properties
07 p1166 A69-19236

Rigid top mass effect on longitudinal response of model vehicle propellant tank, determining natural frequencies and forced asymmetric response
09 p1616 A69-21979

Fluidic component application to propellant tank pressurization and controller design
[AIAA PAPER 68-629] 09 p1442 A69-21980

Cylindrical propellant tanks dynamic stability and parametric resonance, analyzing axial preload, liquid depth, top impedance and ullage pressure by Donnell theory
11 p1989 A69-25499

Liquid expulsion by direct pressurization of propellant tank in spinning missile system, demonstrating feasibility with subscale hardware
[AIAA PAPER 69-527] 16 p2838 A69-32651

Neutron and photon transport properties in liquid hydrogen obtained from measuring radiation environment in propellant tank mockup suspended above NERVA reactor
[AIAA PAPER 69-475] 16 p2810 A69-32716

Twin spool hydrogen turbopump performance at zero net positive suction pressure /NPSP/ saturated fluid in propellant tank, including steady state and simulated transient engine tests
[AIAA PAPER 69-550] 18 p3140 A69-34414

High modulus filament wound composites used for propellant and pressurization tanks, discussing overwrap and liner permeability, porosity, weight, etc
19 p3354 A69-35513

Boron epoxy strut prototype for support system of advanced nuclear flight stage with nonintegral cryogenic tankage configuration, achieving weight reduction
19 p3354 A69-35516

Main tank injection for packaged liquid missiles, discussing propulsion system design, pressurization, packaging and screen reservoir
[AIAA PAPER 68-627] 19 p3429 A69-35947

Sprayable polyurethane foam lightweight insulation for Saturn s-2 booster tanks holding liquid H an liquid O at wide temperature ranges
21 p3732 A69-38967

Simulated low gravity propellant sloshing in spherical, ellipsoidal and cylindrical tanks, discussing Bond number simulation and tank geometry effects
[AIAA PAPER 69-1004] 22 p3921 A69-40378

PROPELLANT TESTS

Low temperature grinding technique for IR spectra of propellants and binders in potassium bromide disks
01 p0082 A69-10892

Rocket propellant safety, discussing thermal, mechanical and impact sensitivity tests of solid and liquid propellants
02 p0302 A69-11525

Dry heat sterilization and ethylene oxide decontamination test equipment for bipropellant liquid propulsion system
02 p0228 A69-11764

Ultrahigh pressure test vessel for determining pressure vs burning rate characteristics of propellants and explosives
04 p0645 A69-14472

Liquid explosive testing from point of view of liquid mobility
04 p0646 A69-14481

Solid propellants formulation, processing physical properties, testing and rocket motor inspection
04 p0646 A69-14583

Test program for solid propellant rockets capability to withstand space environments
06 p0982 A69-17594

Short duration tube wind tunnel supersonic testing, noting Saturn S-1C base heating and solid propellant rocket base burning tests
[AIAA PAPER 69-335] 13 p2242 A69-28271

Solid rocket propellants tests, considering propulsion performance measurements, altitude simulation problems, internal flow patterns, nozzle geometry, etc
16 p2765 A69-31751

Polydiethylene glycol-bis-allyl carbonate /PBAC/ Hugoniot equation of state, reporting shock data, discussing applications to propellant testing
16 p2879 A69-32179

Integrated double oblique shock scramjet for supersonic combustion tests and instrumentation development, discussing fuel injection through sonic orifices, combustion data, etc
[AIAA PAPER 69-827] 16 p2840 A69-32673

Acceleration effects on solid propellant rocket motors combustion characteristics
[AIAA PAPER 68-530] 21 p3786 A69-39217

PROPELLANT TRANSFER

High pressure transfer system to deliver liquid hydrogen to testing equipment and liquid hydrogen/liquid oxygen engines
01 p0013 A69-11145

Cryogenic flexibility of thin polymeric film plies for use as spacecraft positive expulsion bladders
05 p0769 A69-16486

Propellant orientation and expulsion methods in space vehicle tankage, discussing ullage rockets system, bladders and diaphragms, dielectrophoretic expulsion, etc
16 p2736 A69-31734

Liquid expulsion by direct pressurization of propellant tank in spinning missile system, demonstrating feasibility with subscale hardware
[AIAA PAPER 69-527] 16 p2838 A69-32651

Capillary barriers to provide propellant positioning, expulsion capability and slosh damping for spacecraft propulsion systems during rotational maneuvers
[AIAA PAPER 69-529] 16 p2868 A69-32713

Analytical model for liquid fluorine no-vent loading operations noting application to flightweight upper stage systems
[AIAA PAPER 69-579] 16 p2767 A69-32715

Fluid flow problems during orbital refueling vehicle maneuvers and system operations in propellant transfer, including disturbances, liquid-vapor interface instability, vapor ingestion, etc
[AIAA PAPER 69-567] 16 p2868 A69-32721

Orbital refueling techniques, discussing vapor-liquid interface stability, pressurant requirements, transfer line chillover, propellant transfer dynamics, dielectrophoresis, suction speed estimating and system tradeoffs
[AIAA PAPER 69-564] 16 p2869 A69-32733

Pressurant gas requirements for pressurized discharge of liquid hydrogen from propellant tanks for optimum pressurization system designs
[AIAA PAPER 69-526] 16 p2845 A69-32737

Excessive extrapolation limitations in applying transient data to low gravity fluid behavior for orbital refueling systems, presenting orbital fluid transfer experiment
[AIAA PAPER 69-566] 16 p2870 A69-32755

Fluid transfer in orbit under low or zero g, stressing orientation
[AIAA PAPER 69-565] 16 p2865 A69-32770

Rocket engine with turbopump supplied liquid propellant, describing ejector, pump assembly, gas generator and control devices
17 p3019 A69-33341

Time-optimal nuclear rocket propellant start-up with thermal stress constraints based on distributed parameter model, deriving algorithm for flow rate increase
21 p3768 A69-39632

Cooldown of vacuum insulated transfer lines using liquid N and H, discussing flow characteristics reproduction by digital computer program
[NAS-NRC PAPER I-1] 22 p4050 A69-40625

Multiple outlets for reducing stratification-induced liquid propellant supply temperature rise, preventing cavitation problems in supply pumps
[AAS PAPER 69-395] 24 p4363 A69-42830

Dielectrophoretic zero gravity cryogenic liquid expulsion using lightweight high voltage ribbon electrode conduits and electrohydrodynamic bang-bang field effect
24 p4300 A69-43237

PROPELLANTS

- U AEROZINE
- U AIRCRAFT FUELS
- U CASE BONDED PROPELLANTS
- U COLLOIDAL PROPELLANTS
- U COMPOSITE PROPELLANTS
- U CRYOGENIC FLUIDS
- U CRYOGENIC ROCKET PROPELLANTS
- U DOUBLE BASE PROPELLANTS
- U DOUBLE BASE ROCKET PROPELLANTS
- U FLOX
- U GASEOUS ROCKET PROPELLANTS
- U GELLED ROCKET PROPELLANTS
- U GUN PROPELLANTS
- U HIGH ENERGY PROPELLANTS
- U HYBRID PROPELLANTS
- U HYPERGOLIC ROCKET PROPELLANTS
- U LIQUID HYDROGEN
- U LIQUID OXYGEN
- U LIQUID ROCKET PROPELLANTS
- U METAL PROPELLANTS
- U MONOPROPELLANTS
- U PLASTIC PROPELLANTS
- U RDX
- U ROCKET PROPELLANTS
- U SOLID PROPELLANTS
- U SOLID ROCKET PROPELLANTS

U STORABLE PROPELLANTS

U TETRYL

PROPELLER BLADES

Propeller static performance calculations for infinite number of blades applied to four blade propeller at different blade angles

02 p0188 A69-11957

Unsteady pressure field in zone of aerodynamic proximity of free moving airscrew investigated with propeller blades replaced by surface singularities

02 p0192 A69-12827

Helicopter rotor blades in metal sandwich bonding, discussing component parts assembly by adhesive films

07 p1143 A69-19731

Vibration eigenfrequencies of helicopter blades, discussing equation integration problems

11 p1995 A69-25673

Rotating static thrust propeller or hovering rotor flow field study by schlieren photography, considering vortex field, tip flow and shock wave formation

18 p3087 A69-35218

BORSIC Al composites for propeller blades, discussing designs, fabrication methods and tensile test results

[AIME PAPER S69-4] 21 p3733 A69-39473

PROPELLER DRIVE

NT HELICOPTER PROPELLER DRIVE

Propeller at static working state using vortex theory assuming infinite blade number, discussing thrust and torque coefficients

06 p0857 A69-17194

Wakkel engine development in Poland for powered military gliders at 18 hp and 5500 rpm

22 p3999 A69-40006

V/STOL propeller aerodynamics, considering thrust efficiency, roll and yaw control, flow visualization methods, etc

23 p4062 A69-41375

Wingtip mounted propellers effect on wing lift and induced drag, varying lift to drag ratio by changing inflight aspect ratio

24 p4250 A69-43713

PROPELLER EFFICIENCY

Propeller static performance calculations for infinite number of blades applied to four blade propeller at different blade angles

02 p0188 A69-11957

Lubrication and operation of Hamilton Standard propellers in high altitude and low temperature environments

[SAE PAPER 690323] 11 p1822 A69-24515

Helicopter rotors and static propellers theory based on Prandtl-Betz theorem, calculating ideal performance

[AHS PAPER 326] 17 p2894 A69-33533

PROPELLER SLIPSTREAMS

Streamlined rotors calculation, interpreting compatibility conditions between streamlining and airscrew stresses

08 p1252 A69-20655

Aerodynamic characteristics of propeller-wing-flap systems used on deflected slipstream STOL aircraft

09 p1431 A69-22278

CX-84 two propeller tilt wing deflected slipstream V/STOL Military Evaluation Program related to support of surface forces

[AHS PAPER 351] 17 p2900 A69-33526

Wind tunnel tests determining propeller slipstream effect on roll-damping derivative in transitional flight region, estimating STOL aircraft characteristics

22 p3863 A69-40145

PROPELLER SYNCHRONIZERS

U PROPELLERS

U SYNCHRONIZERS

PROPELLERS

NT SHROUDED PROPELLERS

NT TILTED PROPELLERS

Propeller performance prediction for nonnegligible angle of attack, determining tip loss factor with model similar to Prandtl model for axial flight

11 p1819 A69-25375

Monograph on determination of unsteady pressure field of freely rotating propeller covering blades, displacement and lift effects, distribution functions, etc

17 p2889 A69-32994

Book on experimental aerodynamics covering subsonic and supersonic wind tunnels, wall measurements, airfoils, aerodynamic characteristics of propellers, fixed and rotary wing aircraft

17 p2891 A69-33318

Helicopter rotors and static propellers theory based on Prandtl-Betz theorem, calculating ideal performance

[AHS PAPER 326] 17 p2894 A69-33533

PROPHYLAXIS

Motion sickness prophylaxis for rabbits subjected to rotation, investigating effects of adrenalin, ephedrine, sympatholytin, piperoxane and pyridoxyphene on nystagmus and respiration

20 p3472 A69-37265

Motion sickness prophylactic action of sodium hydrocarbonate in dogs subjected to vertical accelerations, using intravenous administration

20 p3473 A69-37269

PROPORTIONAL CONTROL

Random order linear homing systems analyzed by frequency methods employing method of proportional navigation, noting use of transfer functions

01 p0113 A69-10805

Fluidic proportional thruster system for sounding rocket control

[ASME PAPER 68-WA/FE-32] 05 p0763 A69-16105

Hysteresis of on-off element with proportional feedback around element, noting autooscillations and results for electromagnetic relay

12 p2053 A69-26506

Fluidic proportional level control and density control systems, discussing advantages of low initial and maintenance cost, long life and temperature, shock, radiation resistance, etc

22 p3870 A69-41241

Quasi-optimum proportional navigation for interceptor missiles, discussing feedback guidance law and attack geometry

24 p4348 A69-43292

PROPORTIONAL COUNTERS

Carbon dioxide ionization by Q switched laser beam, using proportional counter

02 p0255 A69-11702

Large area proportional counter for cosmic ray design, construction and specifications

03 p0427 A69-12979

Fast neutron fluxes at various atmospheric levels and geomagnetic northern midlatitudes measured by proportional counters using boron trifluoride

03 p0501 A69-13528

X ray proportional counter, analog to digital converter and power supply for gamma ray spectrometry used in satellite applications

[IEEE PAPER 3A-7] 07 p1134 A69-19194

Proportional counter pulse shape calculation for point and extended ionization tracks, considering electron drift velocity and positive ion mobility

09 p1493 A69-21419

X ray microanalyzer maximum sensitivity obtained using flow type proportional and scintillation counters with proper tuning and eliminating scattered electrons

12 p2093 A69-26596

Proportional counter array for detection of soft X ray photons from OSO-4 observations, discussing solar event energy spectra

12 p2151 A69-26936

Boron 10 absorption cross sections from counting ratios measurements of boron trifluoride proportional counter used to monitor neutron fluxes

17 p3008 A69-33753

Pulse height distribution changes of gas filled proportional counters ascribed to deposit accumulation on anode, using X ray fluorescence analysis

20 p3538 A69-37302

PROPRIOCEPTION

U AUTOKINESIS

PROPULSION

NT CHEMICAL PROPULSION

NT ELECTRIC PROPULSION

NT ELECTROMAGNETIC PROPULSION

NT ELECTROSTATIC PROPULSION

NT HYBRID PROPULSION

NT ION PROPULSION

NT JET PROPULSION

NT LOW THRUST PROPULSION

NT MARINE PROPULSION

NT NUCLEAR ELECTRIC PROPULSION

NT NUCLEAR PROPULSION

NT PLASMA PROPULSION

NT SOLAR PROPULSION

NT SPACECRAFT PROPULSION

NT UNDERWATER PROPULSION

Propulsion - Conference, Paris, October 1967

03 p0494 A69-12887

Aircraft propulsion by wake regeneration, noting supersonic transport oggee layout with maximum drag fraction

05 p0811 A69-15555

Propulsion and reentry - Conference, Belgrade, September 1967

06 p0859 A69-17625

Thermodynamics and aerothermodynamics for propulsion problems noting thermodynamic laws and quantities, steady flow, shock waves, nozzles, inlet and thermodynamic cycles

11 p1821 A69-25583

Propulsion systems for boosters and space vehicles including chemical, electric and nuclear

13 p2325 A69-27915

PROPULSION CALCULATIONS

U MATHEMATICAL MODELS

PROPULSION SYSTEM CONFIGURATIONS

Apogee stage and strap-on booster applications of solid propellant rocket motors, discussing configuration, functioning and performance

03 p0494 A69-12891

Airframe/propulsion blending in high performance fighter aircraft, discussing thrust augmentation, fuel consumption, induction system and exhaust nozzle balance with airframe

03 p0364 A69-13676

Power requirements of low thrust space engine for maneuvers and optimum overlappings theory for selection of power plant

04 p0666 A69-14920

Air deflection and modulation /ADAM/ turbofan propulsive wing V/STOL design

[AIAA PAPER 69-201] 07 p1056 A69-19573

Wind tunnel measurements on integrated shrouded propeller model proposed for power gliders

07 p1052 A69-19633

Pulsed MPD arc jet electric propulsion system requirements, examining physical constraints, pulse duration, duty cycle, power network structural details, etc

[AIAA PAPER 69-269] 09 p1560 A69-21215

Film cooling design criteria for small rocket engines

[AIAA PAPER 68-617] 09 p1570 A69-21978

Baseline requirements for commercial aircraft propulsion systems, stressing engine installation in aircraft

[ASME PAPER 69-GT-57] 09 p1572 A69-22514

Qualitative and quantitative hazards analysis of potential accidents/incidents in Post Boost Propulsion System with hypergolic propellants, considering recovery

10 p1753 A69-22972

Space station attitude control through resistojets and control moment gyros /CMG/, discussing propulsion, safety features, weight factors, etc

11 p1965 A69-24531

Space propulsion by radioisotope energy noting thermal heating, thruster configurations, propulsion system, mission capabilities and current thruster technology

11 p1914 A69-25591

Space propulsion system design with consideration for launch and mission requirements, noting upper stage structural design and computer techniques

12 p2148 A69-26834

Integrated lift, propulsion and control in Aeromobile air cushion vehicle, considering ram wing and gimbal fan plenum chamber vehicles

13 p2201 A69-27543

L-500 inlet development program, discussing external forebody design, entry lip and diffuser geometries, configuration and technology developments, experimental techniques and test equipment

[AHS PAPER 69-448] 16 p2733 A69-32684

Hall ion thruster prime propulsion system, considering low and high voltage mode in plasma source I-V characteristics

17 p3019 A69-33338

Propulsion power plant arrangements for rotary wing aircraft with thrust producer for forward flight, considering convertible fan/shaft engine configurations

[AHS PAPER 333] 17 p3021 A69-33529

Weights study of V/STOL aircraft types for similar mission and payload requirements with different propulsion systems and flight profiles

[SAWE PAPER 783] 18 p3091 A69-34869

NERVA technology development, discussing reactor technology program, downward firing and flight-like configuration engine

[AIAA PAPER 68-612] 19 p3371 A69-35942

VTOL aircraft lift systems, propulsion, airframes, dynamic and aerodynamic characteristics, control systems, missions, safety, configurations and environment

[AIAA PAPER 68-977] 20 p3461 A69-37149

Nonintegral burn of solid core nuclear rockets, discussing modular stage concepts approach to low cost space exploration

[AIAA PAPER 68-589] 21 p3768 A69-39026

- Lockheed 1011 propulsion system design relating to system and component maintainability, reliability, performance and noise
[SAE PAPER 690390] 23 p4201 A69-41665
- STOL transport aircraft propulsion requirements, discussing engine cycle selection, design variables effects, etc
[SAE PAPER 690380] 23 p4201 A69-41668
- PROPULSION SYSTEM PERFORMANCE**
- Vitiated inlet air effects on J60-P-6 turbojet engine performance at sea level for various simulated flight Mach numbers
01 p0143 A69-11063
- Disulfide effects on jet fuel operating characteristics and demercaptization influence on thermal stability, corrosive action and sedimentation
01 p0142 A69-11098
- Dry heat sterilization and ethylene oxide decontamination test equipment for bipropellant liquid propulsion system
02 p0228 A69-11764
- Book on electric propulsion systems for spacecraft covering thermoelectric, electromagnetic, electrostatic, plasmacore, thermonuclear and photon systems
02 p0305 A69-12233
- French solid propellant sounding rockets proposed launching from Guiana base using different fuel propulsion systems
03 p0518 A69-12851
- Apogee stage and strap-on booster applications of solid propellant rocket motors, discussing configuration, functioning and performance
03 p0494 A69-12891
- Weapons propulsion system off-design engine performance, noting installation loss effects
[SAE PAPER 680712] 03 p0496 A69-13445
- Monograph on exhaust gases mixing with cold airstream in ducted fanjet engine, noting thrust and efficiency increase
03 p0496 A69-14048
- High voltage mercury electron bombardment ion thruster power efficiency
[ECS PAPER 170D] 05 p0812 A69-16233
- High performance chemical propulsion systems feasibility, discussing propellant combinations
06 p0983 A69-17627
- Advanced electrical and nuclear propulsion systems for European launchers, comparing performances with chemical propulsion
06 p0984 A69-17628
- Advanced propulsion systems propulsive capabilities in connection with interstellar flights, considering rocket and ramjet propulsion, energy requirements and stellar plasma
06 p0984 A69-17631
- Method of characteristics for nonequilibrium internal flow fields in propulsion systems, discussing focusing, shock wave and accuracy
[AIAA PAPER 69-6] 06 p0915 A69-18170
- Aerobell extendible nozzle rocket engine design and performance, cold flow and simulated hot flow test results
[AIAA PAPER 69-4] 06 p0985 A69-18195
- Aircraft gas turbine engines control systems capabilities and future requirements, considering maximum propulsion system performance with minimum fuel consumption
[ASME PAPER 68-GT-62] 08 p1376 A69-19846
- HORA, flexible upper rocket stage, noting variable fuel tank capacity and high energy propulsion
08 p1409 A69-20094
- Water jet propulsion for air cushion vehicles, emphasizing inlet shape effect on performance and potential flow theory application to inlet design
08 p1254 A69-20115
- Turbojets, turbojets and Ramjet turbines compared as propulsion systems for aircraft with speeds to Mach 7
08 p1376 A69-20656
- Combustion in high power jet engine combustion chamber in case of continuous and intermittent liquid fuel injection
08 p1421 A69-20762
- Rocket propulsion with gaseous bipropellant systems and attitude control
08 p1376 A69-20870
- Particle free path estimates for axisymmetric high specific impulse plasma accelerators, discussing collisionless plasma simulated by computer
[AIAA PAPER 69-278] 09 p1563 A69-21233
- Space charge sheath electric thruster principles, construction and performance using laboratory test model
[AIAA PAPER 69-282] 09 p1563 A69-21235
- Background pressure and magnetic field shape effect on MPD thruster performance, testing radiation cooled thrusters
[AIAA PAPER 69-243] 09 p1564 A69-21239
- Performance boundaries of space propulsion systems containing nuclear electric stages
[AIAA PAPER 69-249] 09 p1538 A69-21249
- 30 cm diameter mercury bombardment low impulse thruster development for potential space applications, discussing performance and control
[AIAA PAPER 69-238] 09 p1566 A69-21256
- Kaufman thruster performance dependence on transmission of ion extraction optics and magnetic field shape
[AIAA PAPER 69-257] 09 p1569 A69-21878
- Space storable propulsion system comparison, discussing liquid propellants performance and thermodynamic analysis
[AIAA PAPER 68-614] 09 p1570 A69-21981
- Turbofan engines augmentation, evaluating duct heater, bluff body stabilizers, piloted can combustors, flameholding techniques and afterburner tests
09 p1573 A69-22617
- Book on rocket propellants covering propulsion fundamentals, liquid, solid and hybrid propellants properties, performance calculations, rocket technology, etc
10 p1752 A69-23806
- Propulsion optimization for various vehicles, considering power plant weight, specific fuel consumption, power and thrust ratios, etc
11 p1941 A69-24462
- Gas turbine propulsion engines for small single engine helicopters, discussing costs, performance and FAA tests
[SAE PAPER 690310] 11 p1942 A69-24513
- Chemical species and reactions determined for propellants in calculating nonequilibrium rocket engine performance
11 p1940 A69-24905
- Propeller performance prediction for nonegligible angle of attack, determining tip loss factor with model similar to Prandtl model for axial flight
11 p1819 A69-25375
- Rocket engine high energy hybrid propellant performance optimization, discussing engine enlargement, oxidizer injection geometry, fuel additives, combustion gas vorticity, etc
11 p1943 A69-25428
- Rocket propulsion devices classifications, discussing energy sources, propellants, performance, space vehicle applications, liquid propellant rockets, engines, selection criteria and cooling methods
11 p1943 A69-25587
- Nuclear rocket propulsion, discussing solid core and fluid core systems for reactors, nozzles, feed systems, control, component design and performance
11 p1914 A69-25590
- Ion spacecraft propulsion systems, discussing components and characteristics of reaction type rocket engines and electrical thrust devices
11 p1944 A69-25593
- Unsteady gas dynamics of explosions and detonation theory, noting applications to rocket propulsion systems performance
11 p1876 A69-25595
- Spacecraft propulsion systems comparison and evaluation, discussing quality, schedules and costs in relation to mission requirements
11 p1965 A69-25600
- Rocket propellants, propellant chemistry and rocket propulsion system performance
13 p2324 A69-27916
- Electric and chemical rocket propulsion systems
13 p2325 A69-28255
- Thermionic reactor systems, discussing hybrid nuclear rocket/nuclear electric Mars mission, design features, performance and electric power characteristics
14 p2480 A69-29183
- Performance potential of high speed ocean-going air cushion vehicles with aircraft nuclear power plants
[AIAA PAPER 69-416] 15 p2550 A69-30480
- Propulsion system influence on aircraft reliability from viewpoint of engine manufacturer
15 p2629 A69-31122
- Mixture ratio distribution, injector/chamber performance and nozzle effects on specific impulse of liquid propellant rocket engine using hydrazine and oxygen
16 p2828 A69-31724
- Bipropellant propulsion systems using Aerozine 50 and nitrogen tetroxide for Symphonie telecommunications satellite
16 p2828 A69-31733
- Solid rocket propellants tests, considering propulsion performance measurements, altitude simulation problems, internal flow patterns, nozzle geometry, etc
16 p2765 A69-31751
- Subsonic transport high bypass ratio engine evaluation in terms of fuel consumption, size, thrust-weight ratio, noise and price
16 p2835 A69-31803
- Nuclear rockets as Saturn 5 third stages, emphasizing increased payload or velocity utility and resulting engine and stage requirements
[AIAA PAPER 69-555] 16 p2867 A69-31849
- Solid fuel propulsion systems for tactical rockets design, discussing microwave attenuation, acceleration-combustion interactions and performance optimization
16 p2836 A69-31998
- Concorde propulsion and ejection systems reliability, testing reheating duct, primary nozzle, secondary assembly, etc
16 p2837 A69-32072
- ICRPG liquid propellant thrust chamber performance evaluation methodology, reviewing imperfections and limitations
[AIAA PAPER 69-468] 16 p2838 A69-32657
- Nuclear solid core rocket engine performance for interplanetary orbital launch of spacecraft by multiport injection
[AIAA PAPER 69-535] 16 p2810 A69-32660
- Vaporization interaction liquid rocket performance model, discussing performance loss evaluation and test data
[AIAA PAPER 69-470] 16 p2838 A69-32663
- Saturn 5 S-1C stage propulsion performance, using engine parameters from telemetry rather than accelerometer data, analyzed by iterative techniques and computer program
[AIAA PAPER 69-733] 16 p2839 A69-32672
- Agna propulsion system performance model for predicting propellant flow rate, mixture ratio, thrust time and specific impulse
[AIAA PAPER 69-453] 16 p2841 A69-32683
- Stator setting effect on single stage turbine performance, considering blade loss and surface velocity distribution
[AIAA PAPER 69-525] 16 p2841 A69-32686
- Solar electric propulsion system performance consisting of thrusters with thrust vector aligning actuators, switching network and flight type power conditioner
[AIAA PAPER 69-498] 16 p2843 A69-32708
- Analytical evaluation of secondary flow injection effects on rocket engine performance including cold flow and simulated hot flow data
[AIAA PAPER 69-473] 16 p2844 A69-32726
- Discharge chamber plasma processes in electron bombardment ion thrusters, considering factors affecting thruster performance
[AIAA PAPER 69-494] 16 p2845 A69-32735
- Nonequilibrium inlet conditions effect on combustor performance during H and vitiated air combustion, studying ignition delays
[AIAA PAPER 69-457] 16 p2881 A69-32767
- Space storable hydrocarbon fuel blended FLOX propellant performance with coaxial injector including characteristic velocity, chamber geometry, pressure and heat flux distribution
[AIAA PAPER 69-507] 16 p2835 A69-32772
- Constant chamber pressure thrust throttling of expansion-deflection rocket nozzle, calculating wall static pressure and thrust by characteristics method, discussing performance
[AIAA PAPER 69-435] 16 p2846 A69-32776
- Rocket performance optimization by extending injector design technology to high performance injectors for space storable FLOX/LPG propellants
[AIAA PAPER 69-506] 16 p2846 A69-32778
- Interagency Chemical Rocket Propulsion Group method of treating measurement error for liquid rocket engine performance parameters, using uncertainty model
[AIAA PAPER 69-734] 16 p2846 A69-32781
- RF ion thrusters using electrodeless self sustaining mercury discharge, describing basic theory, component design, performance optimization and test results
17 p3018 A69-33326
- Vernier motor for Europa 1 rocket third stage, discussing component design, system performance and fuel composition
17 p3018 A69-33328
- STOL and V/STOL short haul intercity airliners emphasizing propulsion systems, operational aspects and economics
17 p2898 A69-33356

PROPULSIVE EFFICIENCY

OH-6A drive system design for lightweight, low cost high performance helicopter, discussing reliability from RVN combat data
[AHS PAPER 374] 17 p2900 A69-33514

Helicopter power plant and drive and rotor systems influence on design, configuration, weight, payload and performance
[AHS PAPER 334] 17 p2901 A69-33528

Heavy lift helicopter design with 30 ton payload, considering fanjet drive hot cycle and shaft drive propulsion systems
[AHS PAPER 330] 17 p2901 A69-33532

Chemical relaxation, optimum propellant mixture ratio, combustion chamber pressure, gas jet impulse, mass flow and drive capacity of space propulsion systems
18 p3229 A69-34773

NERVA engine operational cycle and performance, discussing startup, thrust buildup and shutdown
[AIAA PAPER 69-515] 18 p3170 A69-34809

Advanced design weight analysis and fixed equipment and propulsion systems weight prediction, noting error probability
[SAWE PAPER 790] 18 p3220 A69-34867

Air breathing engines performance possibilities, describing design and testing difficulties, stability requirements, etc
18 p3185 A69-35139

Steady state and dynamic distortion influence on performance and stall of turbofan engine, discussing compressor instrumentation, tests and simulation data
18 p3185 A69-35175

Solar electric thrust system technology concerning performance, thruster control system stability and method for solution
19 p3394 A69-35941

BEEP /Best Estimate of Engine Performance/ program based on trajectory reconstruction and acceleration determination for evaluating Titan 3 propulsion system performance
[AIAA PAPER 68-585] 19 p3394 A69-35945

Main tank injection for packaged liquid missiles, discussing propulsion system design, pressurization, packaging and screen reservoir
[AIAA PAPER 68-627] 19 p3429 A69-35947

Titan 3 transtage attitude control system hydrazine rocket engine design and performance, emphasizing problems associated with monopropellant
[AIAA PAPER 69-422] 19 p3394 A69-36300

Propulsion performance of XB-70A aircraft calculated by gas generator method
[AIAA PAPER 68-594] 20 p3461 A69-37152

Propulsion system performance relationship to manned planetary mission capability, discussing anticipated performance of advanced propulsion concepts
20 p3586 A69-38118

Pulsed performance of saturated steam reaction jet, comparing steam performance to nine gases for equal temperatures and thrust levels
21 p3785 A69-39021

Mission and planetary vehicles characteristics affecting design of solid propellant motors and thrust vector control systems in planetary orbiters and landers
[AIAA PAPER 68-815] 21 p3819 A69-39031

Trajectory requirements and performance comparisons of single stage electrically propelled space vehicles
[AAS PAPER 68-106] 21 p3819 A69-39204

ATS 3 spacecraft ammonia-fueled resistojet engine test performance
[AIAA PAPER 68-553] 21 p3786 A69-39754

Equilibrium running points and performance data of turbojet engine with characteristic curves of dynamic intake, compressor, combustion chamber, turbine and ejection duct
21 p3786 A69-39858

MPD converters in pulsed and continuous modes, discussing inductive propulsion system
22 p3999 A69-39905

HF ion engine RIT 10, Kaufman ion engine ESKA, Hall effect ion engine HIT and MPD engine compared for state of development
[DGLR-69-021] 23 p4202 A69-41928

Low temperature mechanical properties of structural materials for high energy propulsion systems, using low boiling point propellants as liquid hydrogen, fluorine and oxygen
23 p4177 A69-42159

PROPULSIVE EFFICIENCY NT PROPELLER EFFICIENCY

Steady three dimensional flow through impeller of turbines with small number of blades and with edge cut hub, noting inefficiency of flow without impact
01 p0142 A69-10309

High pressure rocket engine design, considering complete combustion, propellant feed system overall efficiency and thermodynamic gain
03 p0495 A69-12888

Aerothermodynamics of subsonic-aircraft propulsion, analyzing performance of bypass engine, fuel consumption and specific weight
05 p0695 A69-15551

High turbine inlet temperature technology using thermosiphon cooling for gas turbine, possibly doubling specific horsepower of aircraft
[SAE PAPER 690034] 07 p1203 A69-18311

Unannounced propellant weight and thrust of Soviet Luna spacecraft based on Luna 12 lunar orbit injection maneuver
08 p1409 A69-19969

Electron bombardment mercury ion thruster plasma properties and performance, computing ion beam current, discharge losses and propellant utilization efficiency
[AIAA PAPER 69-256] 09 p1560 A69-21214

Book on rocket propellants covering propulsion fundamentals, liquid, solid and hybrid propellants properties, performance calculations, rocket technology, etc
10 p1752 A69-23806

Propulsion optimization for various vehicles, considering power plant weight, specific fuel consumption, power and thrust ratios, etc
11 p1941 A69-24462

Charged particles generation by liquid subjected to high electric field for efficient bipolar microthruster
[AIAA PAPER 67-728] 13 p2325 A69-28220

Fluidic systems for automatic control of fuel supply to ramjet engine combustor, coolant rationing and distribution to engine structure and performance efficiency maintenance
14 p2508 A69-28875

Monograph on jet turbine with small hub ratio for cases of complete and partial admission, considering masking effects, flow measurements, etc
20 p3586 A69-37924

Nonintegral burn of solid core nuclear rockets, discussing modular stage concepts approach to low cost space exploration
[AIAA PAPER 68-589] 21 p3768 A69-39026

Thrust increase methods for air breathing turbojet engines analyzed with respect to effectiveness, taking into account environmental supporting mass and fuel expenditures
23 p4199 A69-41578

Foamed liquid as potential coolants in rocket engine to overcome low efficiency and streaky coverage of conventional liquid film cooling
24 p4408 A69-43127

PROPYL COMPOUNDS
Propyl gallate radiation shielding effect variations with proton and gamma ray bombardment, noting growth and development of potato tuber eyes
08 p1262 A69-19927

PROPYLENE
Propylene imine IR and Raman spectra, calculating thermodynamic functions based on rigid rotator harmonic oscillator model
14 p2410 A69-29922

PROTECTION
U ACCELERATION PROTECTION
U CIRCUIT PROTECTION
U CORROSION PREVENTION
U EYE PROTECTION
U METEOROID PROTECTION
U RADIATION PROTECTION
U RADIATION SHIELDING
U SOLAR RADIATION SHIELDING
U THERMAL PROTECTION

PROTECTIVE CLOTHING
NT HELMETS
NT PRESSURE SUITS
NT SPACE SUITS

Occupant restraint systems for automobiles, aircraft and manned space vehicles, discussing cost, practicability, ease of use, acceptability and possible improvements
03 p0380 A69-13459

Water cooling jackets of plastic textile reinforced film for high inside temperature reduction in protective clothing
06 p0883 A69-18027

Protection against burn producing intense thermal exposures, noting double layer of fire resistant material
[AGARDOGRAPH-111] 08 p1266 A69-20674

Human body heat loss control during water immersion, discussing insulative garments and technologies of energy conversion systems
[AGARDOGRAPH-111] 08 p1267 A69-20681

Personal cooling in inadequately air conditioned cockpits, considering dry air, air ventilated suits and liquid circulated tubes near skin
[AGARDOGRAPH-111] 08 p1267 A69-20684

Ranque vortex tube as cooling device in MA-3 ventilating garment
09 p1447 A69-22550

Crash helmet impact protection capability, considering helmet construction
17 p2913 A69-33169

Composite ceramic armor systems for airborne vehicles and personnel, air cushion vehicles and ground troops, discussing weight and contour forming advantages
19 p3355 A69-35525

Radio telemetry system for evaluating protective masks dynamic performance by remote simultaneous monitoring of respiration, acceleration and temperature data generated by human subjects
23 p4121 A69-41765

Circulatory reactions of humans under g forces in centrifuge for various periods, with or without anti-g suit
24 p4267 A69-43385

PROTECTIVE COATINGS NT ANODIC COATINGS NT CERAMIC COATINGS NT PRIMERS [COATINGS]

Chemical vapor deposition of iridium coatings on graphites for high temperature oxidation protection, discussing parameters for iridium compounds and optimum depositing conditions
01 p0097 A69-10643

Passive ice protection of aerodynamic surfaces by icephobic coating, measuring removal of ice under simulated conditions in tunnel tests
01 p0056 A69-11047

Protective coatings for gas turbine engine components in marine environments, considering corrosion of diffuser, impeller, compressor case and turbine blades
01 p0099 A69-11057

Aircraft gas turbine compressor parts erosion tests
01 p0099 A69-11058

Silicic coatings effect on Mo mechanical properties subjected to tensile tests in vacuum and air at various temperatures
02 p0264 A69-11883

High temperature tensile strengths of uncoated boron filament and filament coated with silicon carbide
02 p0270 A69-12731

Aluminum corrosion by fungi isolated from jet fuel system with predominance of Cladosporium resinae, noting protective coatings
06 p0616 A69-14765

Satellite, spacecraft and rocket components coatings and lubricants, noting high radiation resistance of polyimides
06 p0945 A69-17046

Storable tubular extendible member /STEM/ booms for gravity gradient applications, emphasizing reflective coatings to minimize deflection by solar radiation
07 p1226 A69-18327

Chemical conversion coatings and low temperature enamels preventing corrosive attack on beryllium parts in environments containing moisture, chloride ions and/or high temperature oxidizers
07 p1169 A69-19762

Plastic backing films removal from carbon electron microscope replicas by maintaining specimens in horizontal position
09 p1495 A69-21651

Apparatus for depositing protective coatings on graphite by vacuum method in refractory metal carbonyl and halides mixtures and in molten metals
09 p1528 A69-21850

Earth reflected solar radiation and stability of satellite thermal control coatings, noting intensity distribution shifting toward UV region and coatings degradation rate
09 p1579 A69-22174

Refractory metal oxidation protection by inorganic compounds at high temperatures, discussing protective mechanisms
09 p1526 A69-22322

Refractory metal, precious metal and ceramic material compatibility tested by metallography and by microprobing for protective coatings possibilities
09 p1477 A69-22325

Refractory alloys electrodes used for surface coating Ti alloys by electric spark method, studying microhardness and wear resistance
10 p1711 A69-23339

Monograph on molecular structure and polymer properties, covering coherent adhesive layer of polymeric material for paint film in protective coatings
10 p1717 A69-24187

Gas film protection of quartz tube wall transparency loss due to hot plasma contact used to study UV emission during high power pulse discharges
11 p1926 A69-24616

Fiber optics application to fiberscopes and fused fiber optic plates, noting surface coating for light scattering prevention
12 p2084 A69-26150

Ductile metal clads and coatings of silicides, aluminides and noble metals to protect Cr alloys against nitrogen embrittlement and air oxidation
12 p2114 A69-26495

Book on oxidation and shielding of beryllium in gas media for nuclear and aircraft technology
13 p2280 A69-27927

Tungsten disilicide coated Ta-W alloy oxidation mechanisms, comparing coatings protective properties at high temperatures
13 p2280 A69-28137

Electrode surface bismuth coating selected for reducing electrostatic analyzers photocurrents
14 p2446 A69-29048

Self thermostatic phase-change coatings for active and passive spacecraft temperature control, discussing temperature dependent changeability in solar absorptance
14 p2530 A69-29434

Stress corrosion preventative metal-pigmented paints for titanium alloys, discussing chemicals added to increase cathodic potential
14 p2469 A69-29936

Corrosion at polymeric film-metal substrate interfaces, noting roles of film properties, bond strengths and primer coats
14 p2466 A69-29938

Corrosion prevention in beryllium, testing conversion coatings and low fired porcelain enamels under various humidity and temperature conditions
14 p2466 A69-29939

Calorimetric measurement of source and broadband spectral absorptances of spacecraft thermal control coatings during exposure to UV in vacuum environment
16 p2789 A69-31815

Simulated solar wind environment effects on zinc oxide/potassium silicate and lanthanum oxide/potassium silicate spacecraft thermal control coating pigments [AIAA PAPER 69-642]
17 p2991 A69-33273

UV irradiation effects on ZnO spacecraft thermal control coating pigments, discussing photo-Hall, luminescence and electron paramagnetic resonance measurements [AIAA PAPER 69-639]
17 p2992 A69-33288

Thermal design of landed vehicle on Mars surface, discussing instrument package covering inside surface coating and battery insulation [AIAA PAPER 69-611]
17 p3049 A69-33295

Electron energy effects on reflectance degradation and recovery of thermal control materials in vacuum, reporting test results for various protective coatings [AIAA PAPER 69-643]
17 p3005 A69-33306

Silicide coatings effect on Mo mechanical properties subjected to tensile tests in vacuum and air at various temperatures
18 p3156 A69-35043

Glass encased electronic components with conformal coatings, considering glass breakage at low temperature
19 p3281 A69-35547

Thin silicon solar cells environmental tests, evaluating temperature and humidity effects on various contacts and coatings
19 p3252 A69-35699

Cadmium sulfide solar cells and Kapton coverslides under proton irradiation, noting annealing of damage in samples exposed to air
19 p3253 A69-35705

Collection of papers on protective coatings of metals
19 p3328 A69-36155

Diffusion during high temperature exposure of protective coatings on Mo, noting compact layers and carbide forming elements effect on thermal stability
19 p3345 A69-36156

Al effect on B and Cr diffusion in protective coating on Cr-Ni heat resistant alloy, noting thermochemical kinetics for homogeneous layers
19 p3345 A69-36157

Heat resistance evaluation of ZrH6-K alloy subjected to multicomponent surface diffusion alloying combinations of Al, B, Cr, Si, Zr
19 p3345 A69-36159

Second surface mirror used as coating for spacecraft thermal control
20 p3632 A69-37290

Heat resistant coatings - Conference, Leningrad, may 1966
20 p3559 A69-37357

Coating deposition theory on high temperature materials, discussing interfacial energy and wetting properties of molten metal drop on solid base material surface
20 p3560 A69-37358

Protective coatings of oxygen-free high melting point Si compounds and silicate binder, noting chemical stability in corrosive media
20 p3566 A69-37371

Carbide coatings formation on graphite in molten media, determining diffusion coefficient of carbon in molten Zr
20 p3566 A69-37372

Tungsten carbide erosion resistant coatings, discussing optimum plasma deposition process and coating characteristics
20 p3561 A69-37373

Protective coatings for high melting point metals, discussing prevention of low temperature coating breakdown due to oxidation
20 p3561 A69-37375

Oxidation resistant coating methods and systems for Cb base materials protection for aerospace vehicles and aircraft propulsion systems structures
21 p3730 A69-38672

Oxidation resistant silicide coatings for tantalum and tungsten alloys at elevated temperatures
21 p3730 A69-38673

High strength steel landing gear components corrosion protective finishes, discussing paint over bare steel, porous Cd plating and vacuum deposited Cd
21 p3743 A69-38730

Sprayable polyurethane foam lightweight insulation for Saturn s-2 booster tanks holding liquid H an liquid O at wide temperature ranges
21 p3732 A69-38967

Stress corrosion cracking prevention by selection of material, stress relief, compressive stresses introduction, protective coatings and by simulated accelerated tests
21 p3748 A69-39490

Computer optimization of spacecraft optical coatings for temperature control, using finite element analysis and matrix inversion [AIAA PAPER 69-979]
22 p4050 A69-40359

Vacuum integrating sphere for measuring solar absorptance in space environment to determine thermal control coatings qualifications [AIAA PAPER 69-1021]
22 p3923 A69-40392

Galvanic corrosion prevention measures for airframe fasteners, discussing crevice sealants, primers, zinc chromate, cadmium and aluminum coatings
22 p3957 A69-40825

Silicide and B-modified coatings on Mo, noting improved high temperature oxidation resistance under thermocycling
22 p3957 A69-40972

Soviet collection of papers on bright electrolytic coatings including physicochemical principles of deposition
22 p3958 A69-41261

Physicochemical principles of electrolysis and electrodeposition of metals for obtaining bright galvanic coatings
22 p3958 A69-41262

Bright chromium electrodeposition principles and properties of coatings
22 p3958 A69-41263

IR directional and hemispherical emittance of spacecraft thermal control coatings, comparing values determined by various measurement techniques
23 p4164 A69-41633

Integral coverslip development for Si solar cells, considering borosilicate glass fusing on cell surface and RF and high vacuum ion beam sputtering
23 p4070 A69-42272

Wear protection of pressure loaded Ti-Mn alloy by heat diffused lubricated electrodeless Ni coatings
24 p4331 A69-42786

Soviet book on silicoorganic protective coatings preparation, physical, chemical and operational characteristics, with emphasis on silicates and metals
24 p4336 A69-43232

Chemical treatment of Ti during processing, discussing protective coating, scale conditioning, surface contaminant removal and acid pickling
24 p4324 A69-43432

Polymeric polyurethane protective coatings for radar radome covers with improvement in service life, discussing performance properties and production method
24 p4338 A69-43456

Protective coatings on Ni base superalloys for gas turbine engine blade and vane components for hot corrosion and oxidation resistance [SAE PAPER 690480]
24 p4335 A69-43515

PROTECTORS

AC ignitor priming of quartz-chlorine gas discharge X band waveguide limiter with fast recovery used as radar receiver protector
15 p2573 A69-30035

PROTEIN METABOLISM

NT LIPID METABOLISM

Chlorella and Scendesmus unicellular algae mixture tested for biological protein value in humans for possible food source
01 p0021 A69-11079

Protein contained purine free basal and yeast ribonucleic acid diets effect on plasma and urinary uric acid production in male subjects
05 p0708 A69-15968

Algae diet more effective than soya-protein diet in recovering metabolic processes in protein deficient white rats
07 p1065 A69-18977

Hypokinesia effects on rats noting body and organ weights, liver glycogen and N content and tissue proteolysis of skeletal muscles
08 p1262 A69-19928

Algae soil-protein diet more effective in recovering metabolic processes in protein deficient white rats
20 p3479 A69-38225

Muscular strength dynamometric measurements in subjects during prolonged inactivity with restricted caloric and protein intake, showing decrease in strength
21 p3653 A69-38901

Cholesterol-protein metabolism in muscles, liver and cerebrum of lethal X ray exposed guinea pigs compared with unexposed group
21 p3657 A69-39052

Protein rates and RNA synthesis in cerebra of rats analyzed as factor of high altitude hypoxia adaptation
22 p3886 A69-41122

Anoxia effects on leucine-super 3 H incorporation by submandibular gland cells of neonatal rats, discussing cytoplasmic proteins synthesis impairment
22 p3887 A69-41195

Cytoplasmic protein synthesis mechanism using rats heart-lung preparation with precise hemodynamic parameters control, noting variance with change in cardiac work level
23 p4083 A69-41456

Tension effects on amino acid incorporation rate into proteins of cross-striated muscles of rats
23 p4083 A69-41458

Whole body X irradiation effect on protein degradation in mice, using radioactive I labeled albumin
23 p4099 A69-42151

Cardiac myosin characteristics obtained from dogs with naturally occurring heart failure, showing reduced adenosinetriphosphatase activity as compared with normal dogs
24 p4258 A69-42630

Myocardium protein metabolism and heart physiology and pathophysiology, examining contractile function and energy transformation in hyperfunction, hypertrophy and heart failure
24 p4259 A69-42637

PROTEINOIDS

Acidic, neutral and basic proteinoids thermal synthesis, discussing characterization and tendency to form microparticles
07 p1074 A69-18633

Binding of lysine-rich proteinoids to organismic or thermally synthesized polynucleotides, noting polyanhydroamino acid interactions with polynucleotides
07 p1074 A69-18635

Self assembly relation to origin of life and spontaneous generation applied to precellular polymers, biopolymers and cellular structures
12 p2018 A69-25776

Origin of life data, discussing self ordered polymers, propagative cell-like systems, protenoids, cellular evolution, etc
12 p2018 A69-25781

PROTEINS

NT ADENOSINE TRIPHOSPHATE [ATP]
NT ALBUMINS
NT COENZYMES
NT FIBRINOGEN
NT GAMMA GLOBULIN
NT LIPOPROTEINS
NT NUCLEOTIDES

NT OXIDASE
NT OXYHEMOGLOBIN
NT PEPTIDES
NT PROTEINOIDS

Fluorescence spectroscopy of proteins, analyzing polarity, distances between groups, flexibility and conformational transitions

01 p0023 A69-10291

Low temperature effects on calf thymus deoxy-nucleoprotein, crystalline egg albumin and fibrillar actin, noting molecular weight and viscosity changes

01 p0018 A69-11089

Cell and tissue cultivation outside living organisms, discussing applications in space biology, space medicine and food protein sources

02 p0198 A69-11501

Nutritive value of protein from discolored algae biomasses on groups of rats kept on algae biomass, casein and soybean diets

02 p0198 A69-11510

High oxygen tension effect on transport and incorporation of exogenous leucine and protein synthesis in *Pseudomonas saccharophila* cells

03 p0369 A69-13433

Molecular mechanisms leading to mineralization of organic tissues, noting role of protein and glycoprotein matrices

04 p0555 A69-14888

Substrate and subunit interactions influence of beta 2 protein of *Escherichia coli* tryptophan synthetase on fluorescence properties of pyridoxal phosphate prosthetic groups

04 p0553 A69-15304

Protein free diets effects on rat intestinal microflora, noting decrease in lactic acid bacteria and increase in spore forming bacteria

05 p0709 A69-16516

Hydrogenomonas eutropha as means of protein food source independent of conventional agriculture for animal feed supplement

10 p1644 A69-23306

Tryptic digestion of C terminal tritiated peptides analyzed with *Scenedesmus ferrodoxin*, noting use for protein structural study

10 p1648 A69-24190

Protein and nucleic acid building blocks sequence differences influence on evolutionary relationship of living organisms, comparing fish and mammal globins

11 p1828 A69-25456

Gas-liquid chromatography of natural protein amino acids in biological substances, noting separation characteristics

13 p2217 A69-28258

Biochemiluminescent luminol-peroxide reaction to detect iron porphyrin proteins in microorganisms for extraterrestrial life search, discussing reaction kinetics

15 p2556 A69-31325

Dynamic differential thermal analysis with He flow performed on biological specimens, proteins and starches, showing discrete decomposition peaks monitoring pyrolysis process

16 p2747 A69-31807

Macromolecular ring shaped components corresponding to hemagglutinin studied in *Limulus polyphemus* hemolymph by electron microscopy

16 p2742 A69-31864

Protein free diets effects on rat intestinal microflora, noting decrease in lactic acid bacteria and increase in spore forming bacteria

18 p3096 A69-34735

Scenedesmus algae cell wall structure degrading to increase digestibility of cell bound protein, describing mechanical, enzymatic and chemical methods

21 p3667 A69-39701

Microbial protein extraction from *Chlorella* algae and *Torulla* yeasts using urea soaking method

21 p3662 A69-39712

Adenylates condensation in protein-associated amino acids as clue to peptide bond synthesis within protocellular structures

22 p3895 A69-40048

C 14-tryptophan incorporation into C 14-protein in cultured rat pineals, noting norepinephrine stimulation

22 p3871 A69-40054

NonDarwinian evolution of protein and DNA, comparing expectations of evolution models for protein and amino acid changes

22 p3871 A69-40060

Yield stress of normal human blood related to endogenous fibrinogen concentration as function of total protein concentration, proposing fibrinogen adsorption and coupling model

22 p3874 A69-40223

DNA interaction with ribosomes enhancing amino acid incorporation into cell-free protein synthesizing system extracted from *Chlorella pyrenoidosa*

23 p4080 A69-41430

Pyrimidine polyribonucleotides or purine polyribonucleotides binding to lysine- or arginine-rich proteinoids considered for abiogenesis

23 p4113 A69-41509

Biochemical evolution role in porphyrin synthesis forming hemoproteins base, discussing assimilation of carbon dioxide in early earth atmosphere

23 p4088 A69-41814

PROTOBIOLOGY

Cell-like structures containing biochemicals as inevitable event under various hypothetical primitive earth conditions

23 p4085 A69-41479

PROTON BEAMS

Proton energy distributions for passage through NaCl, KCl, KBr, Si and Ge single crystals at various angles relative to /100/ and /110/ crystallographic planes

01 p0140 A69-11109

Radiological properties of high energy proton beams from synchrocyclotron in tumor treatment and neurosurgery

03 p0373 A69-13495

Proton beams uniformity available at NASA synchrocyclotron designed for radiation biology research by simulating space radiation environment

05 p0742 A69-15992

Proton flare activity dependence on Bartel active longitudes and sector structure boundaries of interplanetary magnetic field

07 p1205 A69-19248

Carbon dioxide laser excitation by fast proton beams, noting generation power increase

08 p1323 A69-19802

Cosmic protons interaction with interplanetary plasma, analyzing beam energy loss due to excitation of longitudinal electrostatic oscillations

10 p1760 A69-23617

600 Mev proton synchrocyclotron at Space Radiation Effects Laboratory for space radiation environment simulation, discussing beam energy spread

16 p2814 A69-32201

Elastic scattering cross sections for 21-Mev incident protons measured for nuclei differing in mass, determining optical model potential

18 p3179 A69-35489

PPI bursts interpreted as proton beams cyclotron instability in geomagnetic field

20 p3521 A69-37039

PROTON BELTS

Inner Van Allen belt proton dose rate and spectral charged particle environment profiles correlated, noting agreement with theoretical values

01 p0145 A69-11081

Bimodal diffusion mechanism for acceleration of trapped electrons and protons in earth radiation belts, noting particle intensity profiles and energy spectra

09 p1576 A69-21708

Inner radiation zone including data on electrons, protons and heavier particles and results from high altitude nuclear tests

12 p2152 A69-27144

Proton dose in receiver behind combination electromagnetic and material shield, calculating dose for Van Allen and solar proton event spectra

15 p2652 A69-31522

Trapped protons acceleration through bimodal diffusion in magnetosphere, noting spatial patterns and temporal behavior of proton and electron belts

16 p2851 A69-32618

Ionospheric electron temperature profiles for mid-day equinoctial conditions noting protonospheric and conjugate heating effects

22 p3939 A69-40506

Cosmic ray albedo neutron decay (CRAND) source for trapped protons, showing disagreement with intensities in inner zone measured on OV1 2 spacecraft

22 p4005 A69-40512

Cosmic ray albedo-neutron decay source role in intensity measurements of high energy protons trapped on low L shells during satellite flights

24 p4367 A69-43176

Nighttime protonosphere thermal balance from Alouette 2 electrostatic probe measurements of electron temperature and concentration in magnetosphere

24 p4310 A69-43181

PROTON DAMAGE

Cadmium sulfide solar cells and Kapton coverslides under proton irradiation, noting annealing of damage in samples exposed to air

19 p3253 A69-35705

PROTON DENSITY [CONCENTRATION]

NT MAGNETOSPHERIC PROTON DENSITY

Ion cut-off whistlers observed during VLF experiment aboard OGO 2 and OGO 4, noting possible application to relative ionospheric proton concentration determination

03 p0426 A69-14029

Energy density of neutron star matter from Brueckner theory calculations of nuclear matter and pure neutron gas, determining proton relative density

08 p1381 A69-19785

Solar wind-magnetosphere pressure balance and proton density of solar wind

09 p1577 A69-21711

Cosmic rays sudden intensity increases during proton flares of 28 January 1967 and 7 July and 2 September 1966, plotting proton density vs pressure

20 p3587 A69-37045

PROTON ENERGY

Proton energy distributions for passage through NaCl, KCl, KBr, Si and Ge single crystals at various angles relative to /100/ and /110/ crystallographic planes

01 p0140 A69-11109

Thermal-neutron flux generated by high energy protons in water moderator surrounding thick targets calculated as function of position

02 p0279 A69-11837

High energy cosmic ray particles observed with SEZ-14 instrument aboard Proton 1 and 2 satellites

03 p0499 A69-12944

Acute somatic effects in monkeys irradiated with protons of various discrete energies representing significant portions of space proton spectrum

03 p0374 A69-13497

Charged particles injection into captured radiation zone of Van Allen belts during main phase of magnetic storm indicated by proton data analysis

05 p0815 A69-16057

Injection spectra of protons accelerated on sun to billion-trillion ev, discussing acceleration mechanisms

06 p0996 A69-17741

High electron-proton temperature ratios effect on solar wind double shock wave structure, using one dimensional and two fluid models

07 p1205 A69-18849

Solar protons balloon measurements following flare, noting integral proton flux and energy spectra

10 p1767 A69-23763

Microscale fluctuations in interplanetary magnetic field, considering proton thermal energy and magnetic field energy densities

10 p1785 A69-24100

High energy cosmic ray origin and acceleration by LF electromagnetic radiation produced by pulsars, noting maximum energy for protons

11 p1950 A69-24927

Pitch angle distribution function of thermal protons in magnetosphere taking into account earth gravitational field

12 p2067 A69-26354

Electron and proton spectra in 1-13 kev range relative to geomagnetic field lines measured by ESRO 1 satellite during Aurorae mission

13 p2328 A69-27755

Medium energy trapped and dumped protons at high latitudes and auroral zone, using semiconductor radiation detectors on ESRO 1 satellite

13 p2328 A69-27756

Low energy electron and proton precipitation, discussing acceleration mechanisms and periodicity in relation to auroras and airglows

15 p2594 A69-30018

Photometric rocket measurements in hydrogen auroras, finding vertical H beta emission profile estimate of proton energy spectrum for H beta production cross section

15 p2598 A69-31307

Magnetic storm effects on electrons and protons in outer belt, using satellite data for intensity and differential energy spectra

15 p2676 A69-31314

Matter traversal of high energy primary galactic cosmic ray protons from antiproton flux and energy measurements

15 p2678 A69-31491

Solar energetic proton penetration into magnetotail from proton data collected by Vela 4 energetic particle telescopes, comparing proton fluxes inside and outside magnetotail

16 p2847 A69-31966

Stochastic heating of protons by random magnetosonic wave propagating normal to magnetic field to explain proton energy excess in magnetotail plasma sheet

16 p2848 A69-31969

Electrostatic heating of solar wind ions from instability in two fluid solar wind model leading to preferential heating of protons over electrons
16 p2848 A69-31971

Low energy solar protons entry into magnetosphere on 26 May 1967 showing diffusion control
16 p2849 A69-31984

600 Mev proton synchrocyclotron at Space Radiation Effects Laboratory for space radiation environment simulation, discussing beam energy spread
16 p2814 A69-32201

Diurnal variations in gamma rays produced by proton bombardment ascribed to geomagnetic time dependence for low energy solar proton cut-off
16 p2850 A69-32308

Rocket instrumentation for electron and proton spectra measurement in aurora borealis
17 p2972 A69-33038

NaI/Tl/ and CsI/Tl/ scintillation counters effectiveness in recording low energy protons against counter noise background
18 p3138 A69-35255

Proton and deuteron energy used to study solid state chemical reactions effects on meteorites composition and properties, obtaining hydroxyl ions and hydrocarbons
19 p3414 A69-36114

Solar protons captured in earth dipole trap, discussing conditions for nonadiabatic escape
20 p3587 A69-37042

Charged particles injection into captured radiation zone of Van Allen belts during main phase of magnetic storm indicated by proton data analysis
20 p3591 A69-37967

Auroral electron and proton fluxes precipitation measurements by satellite, studying data in terms of spatial, energy and angular distributions
21 p3709 A69-38500

Daily variation of trajectory derived high latitude vertical cut-off rigidities in magnetospheric model consistent with proton and electron experiments
22 p4005 A69-40513

Cosmic X ray bremsstrahlung due to collisions of suprathermal protons with ambient electrons, giving clue about diffuse sky background of X rays
22 p4006 A69-40643

Cosmos 137 proton spectra data obtained in inner radiation belt agreeing with Relay I data
22 p4007 A69-41093

Thin films of infectious DNA of bacteriophage bombarded by slow protons, determining differential inactivation cross sections
23 p4081 A69-41431

Intermediate energy protons elastic and quasi-elastic scattering from light nuclei, correlating p-D, p-He-3, p-p and p-He-4 data with various scattering models
24 p4352 A69-43123

H beta production in hydrogen aurora measured during rocket flight, obtaining proton energy spectrum
24 p4309 A69-43170

PROTON FLUX DENSITY

Geoelectric field over polar cap based on proton flux detection
04 p0648 A69-14682

Satellite-borne auroral particle spectrometer calibration to minimize uncertainty in measuring absolute particle flux of electrons and protons
04 p0599 A69-15022

High energy proton and neutron fluxes and spectra from nuclear emulsion stacks on Cosmos satellites, calculating cosmic radiation doses
05 p0814 A69-16051

Cosmic ray electron flux and energy spectrum from balloon data obtained at Palestine, Texas, monitoring proton flux periodically
05 p0815 A69-16250

Polar cap event detected at low latitudes by effect on VLF propagation, noting VLF technique sensitivity to low proton fluxes
05 p0816 A69-16276

Hydrogen, helium and electron flux measurements by differential detectors at Fort Churchill in 1967
05 p0756 A69-16277

Nonadiabatic particle losses effect on integral proton flux in inner radiation belt, discussing proton energy spectrum
06 p0921 A69-17742

Low energy solar cosmic ray proton flux characteristics observed by Injun 1 satellite after July 1961 sudden commencement magnetic storm
09 p1576 A69-21707

Low energy proton flux in neighborhood of Moon measured by Luna 12 satellite indicating magnetized plasma region effect on burst
09 p1577 A69-21773

Recurrent Forbush decrease association with proton enhancement, discussing energetic storm particle events
09 p1582 A69-22752

Short term variability of solar proton flux in interplanetary space during solar flare activity, using data from cosmic ray detector on Pioneer 7
09 p1582 A69-22754

Solar cosmic rays proton intensity time variations and diffusion coefficient obtained by satellites, balloons and ground stations observations
10 p1755 A69-22812

Proton flux density at axial point of thin cylindrical and slab shell shields bombarded by isotropic inverse power law spectrum of protons in space
10 p1723 A69-23165

Solar protons balloon measurements following flare, noting integral proton flux and energy spectra
10 p1767 A69-23763

Energetic proton and electron fluxes spatial gradients after July 7, 1966 solar flare, noting satellite observations and injection mechanism geometry
10 p1767 A69-23767

ESRO 1 satellite measuring proton intensities and energy spectra of precipitated and magnetically trapped electrons
13 p2327 A69-27754

Integral particle flux of protons and electrons in upper atmosphere, discussing energy and angular distribution
13 p2328 A69-27757

Solar proton flux in two energy intervals measuring by ATS detectors during January 1967 event compared with data from satellites outside magnetosphere
14 p2509 A69-28935

Large amplitude pulsations in magnetic field magnitude and proton fluxes observed by satellite during magnetic storm compared with various models
14 p2434 A69-28947

Proton and alpha particle fluxes above specified vertical geomagnetic cut-off rigidity measured by balloon-borne Cerenkov scintillation counter telescope
14 p2511 A69-28951

ESRO 2 satellite observations of solar proton event of 9 June 1968, comparing flux profile variations across polar cap with magnetic changes at earth surface
15 p2677 A69-31347

Diurnal variations in gamma rays produced by proton bombardment ascribed to geomagnetic time dependence for low energy solar proton cut-off
16 p2850 A69-32308

Ground based solar proton monitoring, considering particle intensities and radiation dose rates from riometer absorption as function of time
16 p2850 A69-32321

D region electron densities from multifrequency absorption measurements by proton spectra analysis, noting cubic approximation
18 p3127 A69-34799

Low altitude trapped protons in inner radiation belt during solar minimum period, using emulsion detectors on polar-orbiting satellite
18 p3187 A69-34944

Precipitated low energy protons and electrons measurements during breakup aurora, discussing fluxes and poleward boundaries
18 p3187 A69-34946

Proton concentrations, magnetic field strength and temperatures distribution in interplanetary plasma flows as function of latitudinal distance from center of active region
20 p3594 A69-37020

Solar protons intensity increase observed by balloon-borne instruments over Antarctica, describing decay phases
20 p3589 A69-37556

High energy proton and neutron fluxes and spectra from nuclear emulsion stacks on Cosmos satellites, calculating cosmic radiation doses
20 p3591 A69-37961

Interplanetary proton and alpha particle radial gradients determined from Mariner data, considering Forbush decrease, particle solar origin, galactic cosmic radiation, etc
20 p3592 A69-38096

Charge exchange of solar wind protons passing shock front, noting turbulent subsonic motion of randomized hot solar wind protons in shadow cone
22 p4008 A69-41208

Incident proton flux atmospheric altitude profile during PCA period, comparing balloon observations with preliminary satellite data
23 p4204 A69-41485

PROTON IMPACT

First Born approximation cross sections for He excitation from ground state by proton impact calculated, using wave functions
06 p0960 A69-17027

Atomic H ionization by proton impact analyzed to calculate ejected electrons angular and energy distributions by extending Rudge and Seaton theory
19 p3375 A69-35911

Impact parameter versions of two state and Born approximations to calculate single excitation cross sections of H atoms ground state collisions
22 p3987 A69-41006

PROTON IRRADIATION

Explorer 26 observations of solar proton penetration inside trapped radiation near geomagnetic equator
01 p0146 A69-11122

P32 distribution in protein of blood serum, liver and brains of rats bombarded with high energy protons
02 p0198 A69-11507

Thermal-neutron flux generated by high energy protons in water moderator surrounding thick targets calculated as function of position
02 p0279 A69-11837

Slow proton irradiation of ribonuclease thin layers, determining differential inactivation cross section for various proton energies
03 p0371 A69-13482

Long lived radicals produced in crystalline ribonuclease and lysozyme by 120-Mev protons studied by ESR spectroscopy
03 p0372 A69-13485

Biological effects of proton irradiation of monkeys investigated to provide improved protective shield design data with minimum weight penalty
03 p0373 A69-13496

Acute somatic effects in monkeys irradiated with protons of various discrete energies representing significant portions of space proton spectrum
03 p0374 A69-13497

Biological effects on rhesus monkeys of high energy protons compared to effects of cobalt 60 gamma radiation
03 p0374 A69-13498

Surgical radiolesion in human brain by high energy protons
03 p0374 A69-13501

Orientation dependence of pitting and blistering in proton irradiated Al polycrystal surfaces
04 p0640 A69-14451

Pathomorphological aspects of radiation sickness in animals irradiated by high energy protons, showing changes in lymph node, stellate ganglion and spleen
05 p0708 A69-16509

Radiosensitivity of potatoes to gamma ray and proton irradiation applied to whole tubers and to isolated eyes before planting
05 p0709 A69-16511

Production rates of nuclides measured in stack of glass plates under proton irradiation for calculating cosmic ray production rates in stone meteorites
06 p0989 A69-17283

Distribution characteristics of radiation defects in materials irradiated by monoenergetic beams of protons and alpha particles
06 p0981 A69-17878

Bone marrow cell division disturbance in rats after proton irradiation
07 p1064 A69-18973

Propyl gallate radiation shielding effect variations with proton and gamma ray bombardment, noting growth and development of potato tuber eyes
08 p1262 A69-19927

Local shielding effectiveness of dogs against proton irradiation at minimum lethal dose, noting bone marrow role
08 p1263 A69-19939

Microvillar bleb formation in proton irradiated primate hepatocytes with electron microscope, noting sinusoidal lumen
10 p1641 A69-23045

Spatial distribution of residual nuclei produced in thick Fe targets by one and three Gev protons, noting total production and longitudinal variation of production
10 p1760 A69-23411

Electron and proton radiation doses impinging on orbiting satellites computed using orbit calculation and B, L coordinates
11 p1949 A69-24862

Computer program for electron and proton fluxes impinging on spacecraft, performing computation for Van Allen belts and solar flares
11 p1949 A69-24863

D-2 satellite radiation dose based on upper atmosphere electron and proton distribution model, simulating electron bombardment and aging of materials and subsystems
11 p1949 A69-24869

Electron, proton and gamma ray radiation effects on thin film CdS, GaAs and CdTe solar cells
11 p1825 A69-24872

Neutron production cross sections prediction at proton bombarding energies below 50 Mev and above threshold for multiple nucleon emission
12 p2192 A69-26299

Photoemulsion stacks irradiated by protons in magnetic field, determining nuclear isobar generation during quasi-nucleon interactions
13 p2303 A69-28373

Electron and proton components contribution to reverse current production after particle shower through upper Cu wall of ionization chamber with lower Pb wall
13 p2304 A69-28417

Distribution characteristics of radiation defects in materials irradiated by monoenergetic beams of protons and alpha particles
14 p2503 A69-28787

Histological changes in rat skin after 13 Mev proton irradiation, evaluating biopsies in tissue culture
14 p2407 A69-29299

Soviet book on nuclear interactions in spacecraft shielding covering proton-A1 nuclei inelastic interactions, secondary radiation, solar radiation effects, radiation belts, etc
14 p2481 A69-29817

Oxygen K-shell X ray production cross section and stopping power of aluminum oxide thin films for 20-100 kev protons
14 p2489 A69-29994

Diurnal variations in gamma rays produced by proton bombardment ascribed to geomagnetic time dependence for low energy solar proton cut-off
16 p2850 A69-32308

Pathomorphological aspects of radiation sickness in animals irradiated by high energy protons, showing channels in lymph node, stellate ganglion and spleen
18 p3095 A69-34728

Radiosensitivity of potatoes to gamma ray and proton irradiation applied to whole tubers and to isolated eyes before planting
18 p3095 A69-34730

Photoresponse and minority carrier diffusion length long term stability of Li doped solar cells after proton, neutron and electron irradiation
19 p3252 A69-35697

Proton irradiation effects on current degradation at fixed voltages of silicon solar cells with coverslips
19 p3252 A69-35701

Proton and electron auroral ovals, deriving H alpha intensity and frequency distributions as function of geomagnetic latitude and time from patrol spectrographs in Canada
19 p3302 A69-35993

Na 22 and H 3 production rates determined in stone meteorites exposed to 3 Gev isotropic protons, using radionuclide distribution data of exposed thick stone target
19 p3425 A69-36423

N-type GaAs optical properties after proton irradiation, noting transmission spectra dependence on initial electron concentration and irradiation dose
20 p3582 A69-36969

Bone marrow cell division disturbance in rats after proton irradiation
20 p3479 A69-38221

Pathological effects of single 120 Mev proton doses on rats blood in rotating cylinder, discussing leukopenia and benign and malignant tumors development
21 p3658 A69-39058

Solar proton bombardment of lunar surface, discussing luminescence and chemical effects
22 p4012 A69-40089

Thin films of infectious DNA of bacteriophage bombarded by slow protons, determining differential inactivation cross sections
23 p4081 A69-41431

PROTON MAGNETIC RESONANCE

Barrier to internal rotation from PMR spectrum for 1, 2-disubstituted ethanes, studying vicinal coupling parameters dependence
12 p2132 A69-25987

PROTON MASERS

Proton spin maser oscillator with emission coils coupled by prepolarized liquid, discussing tuning and detuning
08 p1324 A69-20231

Single hyperfine-state atomic beam selector effect on hydrogen maser stability, discussing DC magnetic field variation
18 p3153 A69-35306

PROTON-PROTON REACTIONS

Secondary particle spectra from proton-proton interactions analyzed in two temperature statistical model, considering momentum distributions
05 p0797 A69-16368

Pion production rate for proton-proton interactions in hydrogen, discussing relevance to hot massive stars, charged pion decay probability and mu-neutrino production
21 p3792 A69-39615

PROTON PROTUBERANCES

Cosmic radio emission anomalous absorption measurements during PCA following July, August, September 1966 proton flares
23 p4156 A69-41845

PROTON SATELLITES

Proton satellites measurements reconciliation with diurnal stellar variation data and cosmic rays origin models
19 p3396 A69-36621

PROTON SCATTERING

Differential cross sections for elastic scattering of 600 Mev protons from He 3 between 19 and 45 degrees
03 p0472 A69-13464

Asymmetry of polarized protons scattered from He 4 at 540 Mev for laboratory angles between 4 and 42 degrees
04 p0632 A69-14966

Multiple Coulomb scattering and range straggling effects in shielding against solar flare protons and trapped protons in Van Allen belt
10 p1723 A69-23164

Charged state variations during protons and inert gas atoms interactions analyzed by coincidence method
12 p2133 A69-26543

Elastic proton scattering measurements, noting consistency with statistical theory when diffraction is taken into account
13 p2302 A69-28368

High energy scattering approximation valid from small to large angles, discussing errors and proton scattering by He
14 p2487 A69-29008

Differential cross sections for elastic scattering of protons by Ar atoms in energy range 12.7-44.1 ev, estimating internuclear separation
20 p3580 A69-37499

Inelastic proton scattering cross sections for target nuclei in 2s-1d shell calculated in distorted wave Born approximation with projected Hartree-Fock wave functions
22 p3988 A69-41045

Intermediate energy protons elastic and quasi-elastic scattering from light nuclei, correlating p-D, p-He-3, p-p and p-He-4 data with various scattering models
24 p4352 A69-43123

Differential cross section and polarization measurements for elastic scattering of high energy protons from light nuclei
24 p4352 A69-43125

PROTON TELESCOPES

U PARTICLE TELESCOPES

PROTON 2 SATELLITE

Atmospheric density determination based on long period variations of drag coefficients from satellite Proton 2, considering satellite orientation
15 p2602 A69-31392

Satellite Proton 2 orientation from onboard measurement data, discussing general statistical method and data processing results
17 p3001 A69-33221

Proton 2 satellite orientation and motion about center of mass determined from telemetric data analysis under aerodynamic moment
22 p4037 A69-41090

PROTONS

NT SOLAR PROTONS

Spectra analysis of proton and He nuclei having different charge-to-mass ratios to obtain information on solar modulation and injection spectra
06 p0988 A69-17272

Differential energy spectrum of protons and helium nuclei using lithium drifted silicon detectors and scintillator-Cerenkov counter
07 p1204 A69-18833

Long lived streams of low energy solar electrons and protons and association with bright flares or solar active regions
07 p1206 A69-19249

Chemical effects of solar wind and cosmic protons on solid bodies in space, discussing possible relation to origin of life
08 p1407 A69-20935

Proton electrolyte application to fuel cells, discussing proton diffusion in solids and materials with vacancies /proton conductors/ in structures
08 p1269 A69-21053

Cosmic gamma ray spectra from metagalactic proton-antiproton annihilation
09 p1574 A69-21459

High energy protons, helium and gamma rays observed by particle telescope on board OSO-C, obtaining integral rigidity spectra of proton and helium nuclei
09 p1579 A69-22172

Chirp radar signal compression by proton spin echo phenomena, noting compression ratio and SNR
11 p1834 A69-24566

Ionization processes in Seyfert galaxies, considering thermal electrons, superthermal protons and electrons and nonthermal UV radiation
13 p2346 A69-27710

Proton initiated nuclear cascade in atmosphere calculated using Monte Carlo method, relating electron number to primary proton energy
13 p2331 A69-28397

Earth radiation belt data, discussing origin, density distribution, etc, of protons, electrons and alpha particles
15 p2674 A69-30016

Aurora electron and proton excitation patterns determined spectroscopically, discussing ground based observations of emission geomagnetic latitude-time distribution
15 p2593 A69-30017

Neutron star atmosphere and X ray emission spectrum, computing incident protons mean free path for two assumptions
15 p2686 A69-30535

Elementary processes cross sections in charged states changes during proton-hydrogen molecule interactions
15 p2655 A69-30963

Phonons, electrons and protons in ferro- paraelectric and hydrogen bonded ferroelectrics, examining higher frequency optical and lower frequency dielectric properties
16 p2827 A69-32262

Fuel cells with solid membranes with ion conductivity, discussing proton electrolyte
16 p2740 A69-32424

Hydrogen molecular ion dissociation due to ion-molecule inelastic collisions, comparing measured and calculated velocity distributions of protons produced
19 p3375 A69-35985

Synthesis of proton rich nuclei in highly evolved stars, considering p elements production in interior by isobaric transformation
19 p3428 A69-36837

Cosmic protons and high energy heavy nuclei interaction with radiation in expanding universe, including estimates of light radiation influence on cosmic ray spectra
20 p3591 A69-38034

ELF noise band observed by Alouette 2 receiver interpreted in terms of electrostatic power cyclotron harmonic waves, using digital power spectrum techniques
20 p3497 A69-38079

Ionospheric VLF electrostatic noise observed by sounding rocket, noting proton gyrofrequency harmonics effects within emission attenuation bands
21 p3714 A69-38550

Proton transfer mechanism of copper chromite catalyzed thermal decomposition of ammonium perchlorate, noting electron transfer
21 p3783 A69-38810

Thermodynamic properties of hydrogen atoms, protons and electrons, using canonical group analysis to determine bound and free states
21 p3850 A69-38964

Proton-antiproton high energy elastic scattering by bosons exchange, introducing vertex functions for non-local Lagrangian
21 p3775 A69-39467

Solar atmosphere radio emission generation by hydrodynamic shock wave interaction with coronal plasma, treating corona as ideal gas consisting of protons and electrons
22 p4009 A69-39984

Geomagnetically trapped protons and alpha particles, analyzing OGO 4 data
24 p4368 A69-43184

Proton cyclotron echoes on ionograms obtained from topside ionosphere by Alouette 2 satellite
24 p4310 A69-43189

Proton ejection as hydrogen ion clusters by low energy electron bombardment of solid hydrogen
24 p4389 A69-43747

PROTOPLASM

Mitochondrion-endoplasmic reticulum connection in hepatocytes, discussing possible protein molecule transfer
23 p4083 A69-41455

PROTOSTARS

NT T TAURI STARS

Plasmas in galaxies, spiral structures and radio galaxies, discussing quasar line and continuum spectra
02 p0329 A69-12790

Time scale of cooling/heating process compared with gaseous clouds contraction/expansion for one solar mass protostar evolution in transparent stage
04 p0651 A69-14366

Protostars as sources of anomalous OH emission, discussing densities, masses and temperatures of OH condensations
04 p0661 A69-15143

Submillimeter wavelength astronomy noting instruments, prestellar matter, interstellar and intergalactic matter state and composition, IR stars, planetary atmospheres, etc
05 p0821 A69-15843

Condensation sources of maser radiation observed in W3 hydroxyl lines, discussing polarization and designation as protostars
11 p1954 A69-24379

Residual interstellar gas from protostar formation detected as high luminosity IR object
13 p2327 A69-27593

Protostars collapse and flare up computations, including radiative and convective energy flow terms in hydrodynamic equations of motion
15 p2680 A69-30206

Preprotostar radio observations suggesting nonthermal radio sources formation with magnetic energy dissipated in particles acceleration
15 p2701 A69-31531

Protosun and solar system angular momentum losses analyzed from equations for convective star rotation change, noting almost total protosun initial momentum loss possibility
18 p3203 A69-35346

Primitive solar nebula physical model considered under angular momentum conservation in collapsing fragment
19 p3406 A69-36074

Protostar chemical processes responsibility for population inversion and properties in OH and water masers
22 p4018 A69-40267

Condensation sources of maser radiation observed in W3 hydroxyl lines, discussing polarization and designation as protostars
24 p4389 A69-43769

PROTOTYPES

Optical design of Wolter type 1 glancing incidence X ray telescope for 6-100 A wavelength region, describing results of laboratory and rocket flight tests of prototype
08 p1318 A69-21087

Electric outside-in attitude gyro display system prototype tested and compared with contemporary inside-out display
[SAE PAPER 690326] 11 p1890 A69-24507

VFW-H3 Sprinter prototype, discussing cost effectiveness, VFW-H2 test vehicle, hovering stability, dynamic takeoff characteristics, vibration level, noise level, reliability and maintenance
[AHS PAPER 303] 17 p2901 A69-33546

PROTOZOA

NT FLAGELLATA

NT MICROSPORES

NT PARAMACIA

NT SPORES

Continuous culture device for controlled growth of *Euglena gracilis*
15 p2555 A69-30445

Colpoda maupasis resistance to Martian atmospheric pressure and oxygen partial pressure noting adaptation, reproduction and existence
20 p3478 A69-37627

PROTUBERANCES

NT PROTON PROTUBERANCES

Orientation dependence of pitting and blistering in proton irradiated Al polycrystal surfaces
04 p0640 A69-14451

Three dimensional effects on Stanton tube data for skin friction determination for small protuberances drag immersed in turbulent boundary layer
16 p2771 A69-31920

PROVING

U THEOREM PROVING

PROXIMITY

Listen-in feature, allowing general aviation aircraft equipment to receive airborne SSR reply signals, provides air to air proximity warning
03 p0464 A69-13247

PSEUDOMONAS

High oxygen tension effect on transport and incorporation of exogenous leucine and protein synthesis in *Pseudomonas saccharophila* cells
03 p0369 A69-13433

Oxygen physiological and biochemical effects on *Pseudomonas saccharophila*, discussing sucrose uptake, lipid synthesis and polysaccharide formation
15 p2556 A69-31045

PSEUDONOISE

Pseudonoise generator producing controllable repetitive random signal patterns used to evaluate instrumentation system
03 p0403 A69-13188

Reference oscillator synchronization inaccuracy influence on SNR at output of correlation receiver during reception of signals with pseudonoise modulation
15 p2563 A69-30141

Hydrodynamic noise as pseudosound field resulting from pressure variations in turbulent fluid flow, using Lighthill acoustic analogy
18 p3123 A69-34921

Phase modulation in pseudo-noise ionospheric communication system for reducing F region CW signal fading
18 p3104 A69-35308

PSEUDORANDOM SEQUENCES

Pseudorandom radar ranger /DIOMEDE/ using optical correlator and phase loop
03 p0393 A69-13254

Primitive trinomials of high degree for use in pseudorandom sequence generation of zeros and ones
03 p0455 A69-13373

Properties and methods of generation of pseudorandom binary signals, developing linear modeling for multivariable systems
04 p0583 A69-15113

Incidental modulation effect on accuracy, signal loss and sensitivity of pseudorandom code systems
06 p0890 A69-17824

Drift elimination in linear system identification using binary m-sequences by crosscorrelating over two periods of output
11 p1834 A69-24547

Sampled data multichannel telemetry using pseudorandom sequences generated by linear shift registers
12 p2028 A69-25925

Pseudorandom uniformly distributed numbers generation from noise-like signals produced by shift register with feedback, noting statistical tests
13 p2218 A69-27248

Pseudorandom FM waveforms for simultaneous range and Doppler shift radar measurements
13 p2221 A69-27944

Quasi-uniform pseudorandom numbers program transmitter statistical characteristics suited for solving problems by Monte Carlo method
15 p2572 A69-30336

Millimeter wave pseudorandom coded CW meteorological radar for precipitation drop size spectrum analysis and cloud studies, discussing overall system design
23 p4115 A69-41531

Pseudorandom code development and possibilities for radar applications, considering signal processing, antenna requirements, radar signal phase modulation, etc
24 p4281 A69-42741

Optical correlation for radar signals phase modulated by pseudorandom codes
24 p4282 A69-42742

Coherent pulsed radars using pseudorandom modulation, explaining pulse position modulation and radar receiving equipment
24 p4282 A69-42743

PSYCHIATRY

U SOCIAL PSYCHIATRY

PSYCHOLOGICAL EFFECTS

NT ILLUSIONS

NT OCULOGRAPHIC ILLUSIONS

Human behavior during stressed underground confinement, discussing adaptation processes
01 p0020 A69-10757

Psychiatric study of master attack carrier aviators inability to fly, considering adult situational reaction diagnosis
03 p0369 A69-12883

Psychological aspects of crew members resistance to eject from aircraft in trouble
06 p0877 A69-16956

Macaque monkeys in weightless state on sounding rocket, noting vigilance level and characteristics
09 p1445 A69-22724

Psychic stress effect on physiological parameters of helicopter pilots during critical flight situations, considering biotelemetry examination of heart and circulatory systems
11 p1829 A69-24347

Noise measurement and scales in studying psychological and nonauditory physiological effects on human functioning
14 p2485 A69-29150

Engineer performance related to organizational factors, discussing colleague contact, work diversity, number of subordinates and involvement in work
15 p2721 A69-31069

Vertical vibrations effect on test subjects in supine position, noting human tolerances and mood changes
19 p3260 A69-35986

Psychology and physiology of vision in relation to large screen display design, discussing effects of symbol size and spacing, color usage, etc
21 p3662 A69-38330

Statistics on airline flight crew members grounding due to psychic disorders
21 p3665 A69-39181

Life in common by groups of four or five people isolated on high mountain under adverse conditions
21 p3661 A69-39267

In-flight illnesses in French Air Force, emphasizing psychological failures in etiology
21 p3666 A69-39270

Flying effects on air hostesses, considering questionnaire data for various psychophysiological factors and flight modes
23 p4086 A69-41688

Psychological, psychophysiological and biochemical effects of prolonged sleep deprivation in human males, noting transient ego disruption
23 p4099 A69-42195

Airline pilots simulated incapacitation involving myocardial infarction or cerebrovascular accident, discussing effect on crew behavior during flight task performance
24 p4277 A69-43386

Psychophysiological effects of fatigue and correlation with somatic parameters following circadian rhythm
24 p4268 A69-43407

PSYCHOLOGICAL FACTORS

Human psychological factors involved in genesis of contingent or conative negative variation using EEG activity measurements
01 p0015 A69-10904

Biological, psychological and technological requirements in astronaut nutrition programs, examining preservation and reconstitution techniques
04 p0554 A69-15388

Physiological or survival training emphasizing psychological approach
06 p0879 A69-16965

Medical factors as probable cause of aircraft accidents, discussing psychological factors, CO poisoning, hypoxia, alcohol, etc
07 p1067 A69-19433

Psychological study of stewardsesses for depressive, neurotic and psychosomatic episodes, discussing psychopathological structures corresponding to etiological sequences
07 p1067 A69-19434

Statistical, economic and psychological aspects of aeronautical and astronautical profitable reliability in relation to operation, using mathematical model
10 p1700 A69-23839

Military flying career choice as neurotic compensation for personality defects, stressing personality screening during interview
12 p2023 A69-26492

Lunar astronauts psychological problems, discussing isolation from outside world, gravitational and extreme light effects, protective space suits, etc
13 p2210 A69-27905

PSYCHOLOGICAL TESTS

NT RORSCHACH TESTS

Head injury clinical and laboratory long term follow-up data, discussing conscious state alterations, focal neurological deficit, EEG abnormalities, etc
01 p0022 A69-11346

Book on groups under stress covering psychological research in SEALAB 2, emphasizing planning of data collection and experimental results
04 p0552 A69-14533

Characteristics of accident experienced pilots based on personality and psychological tests
06 p0876 A69-18033

Flying safety and human factors relationships from job classification survey oriented toward social psychology
06 p0884 A69-18035

Man psychic activity interference resistance, discussing stress effects characterized by theta and delta rhythms
08 p1262 A69-19839

Visual, auditory and reaction-time responses in aging pilots, determining continuing capacity for choice and discrimination with advancing age
14 p2408 A69-29307

Physiologic and psychologic aging in professional pilots analyzed on basis of cardiovascular, pulmonary, exercise tolerance and sense testing
14 p2408 A69-29309

Physiological and psychological measurements of high pressure effects on man and animals, discussing decompression sickness, respiratory embarrassment, inert gas narcosis, helium tremble, etc
21 p3655 A69-38912

Multiple cues in paired comparisons, discussing mathematical model of psychological process in information extraction and combination
21 p3664 A69-38970

Thematic apperception test /TAT/ cards for assessing attitudes in naval recruiting, respiratory responses during ejections and aviation psychology
23 p4112 A69-42365

Pilot selection procedure emphasizing integration of all-around personality picture from different approaches
24 p4278 A69-43395

Physiological and psychological variables relationship in candidate pilots, noting age and educational level
24 p4268 A69-43406

PSYCHOLOGY

NT ACCIDENT PRONENESS
NT MILITARY PSYCHOLOGY
NT PSYCHOPHYSICS

Classical and differential conditioning of eyelid response with correctness of solutions of arithmetic problems as discriminandum
07 p1064 A69-18637

PSYCHOMOTOR PERFORMANCE

Monkey psychomotor reactions during ballistic flight, noting alertness reduction during weightlessness
01 p0017 A69-11082

Soviet book on human movements coordination during space flight covering space walks, lunar surface photographs, space docking, weightlessness, etc
01 p0018 A69-11180

Physiologic and psychomotor changes during various acceleration stresses
01 p0019 A69-11340

Physiological processes occurring in voluntary movements of animals under space flight weightlessness conditions
02 p0199 A69-11827

Dynamic flight simulators fidelity assessment, discussing hybrid method based on pilot psychomotor responses
02 p0203 A69-12215

Manual performance relationship to men exposed to cold, thermal neutral and hot environments, discussing finger dexterity and motor coordination tests
03 p0381 A69-14074

Psychomotor reactions to zero gravity during ballistic rocket flights, analyzing electrical activity of cortex in animals
06 p0874 A69-17649

Mild hypoxia effect on selective attention performance of human subjects at simulated 8000 ft altitude
09 p1445 A69-22553

Psychomotor reaction time and motions, myogenic tonus at rest and precision of monkeys during rocket flights along ballistic curve, noting weightlessness effect
10 p1646 A69-23575

Model for temporal structure of human behavior from analysis of temporal information treatment in subjective synchronization task
12 p2025 A69-27084

Models for cognitive behavior and psychomotor behavior for maintenance tasks
12 p2025 A69-27086

Mental patient performance in detecting and identifying visual signals under fixed interval schedule, noting nonuniform performance and comparing to normal subjects
23 p4091 A69-42014

Circadian rhythm phase relationships between photoperiodism and heart rate, locomotor activity and deep body temperature /DBT/ in unrestrained monkeys
24 p4260 A69-42706

PSYCHOPHYSICS

Psychophysical methods for determining perception threshold of angular acceleration in man during vertical rotation
05 p0708 A69-15969

Group observers magnitude estimation judgements of stationary spacecraft model apparent distance in simulated space, obtaining psychophysical functions for three stimulus ranges
07 p1069 A69-19501

Blood pressure telemetry of pilot during flight including determination of psychophysical relations
15 p2559 A69-31229

Psychophysical method of studying heart rate as indication of physiological fatigue
17 p2911 A69-34013

Brightness discrimination judgments for gray chips by humans, using psychophysical limits method and white, noncoherent red and He-Ne laser light sources
24 p4276 A69-43323

PSYCHOPHYSIOLOGY

External observer effect on human behavior during sensory deprivation tests conducted in isolation chambers as factor in estimating personality
02 p0200 A69-11516

Respiratory disturbances relationship to experience and attitudes toward gas anesthesia and response to different types of face mask
03 p0378 A69-12884

Psychochemical research theory and methodology, relating biochemical phenomena to human brain function
04 p0553 A69-14976

Psychophysiological factors in USAF aircraft mishaps involving ground egress
06 p0878 A69-16959

Biotelemetry of human physiological processes in space for assuring physiopsychological control and immediate intervention for emergencies, discussing application in Mercury and Gemini projects
12 p2023 A69-26491

F-102 pilot anticipatory and flight stress, noting endocrine-metabolic hyperactivity
12 p2023 A69-26552

Astronauts physical training for space flight requirements
13 p2215 A69-28611

Psychophysiological factors in USAF aircraft mishaps involving ground egress
15 p2558 A69-30462

Painted helicopter rotor blades ruled out as cause of flicker induced vertigo, reporting pilots psychophysiological responses to formation flying
17 p2913 A69-33175

Psychopharmacological drug effects on retinal neuron activity in cats measured by microelectrodes, noting spontaneous activity decrease
22 p3879 A69-40846

Psychopharmacological drug effect on visually evoked responses in cats from recordings from visual cortex, noting latencies increase with dose
22 p3879 A69-40847

Psychophysical threshold changes during subliminal monocular and interocular stimulation, studying conditioning flash size effects on temporal summation
22 p3881 A69-40860

Psychological, psychophysiological and biochemical effects of prolonged sleep deprivation in human males, noting transient ego disruption
23 p4099 A69-42195

Psychophysiological effects of fatigue and correlation with somatic parameters following circadian rhythm
24 p4268 A69-43407

PSYCHOSES

U PSYCHOTIC DEPRESSION

PSYCHOTHERAPY

Psychotherapeutic treatment of depressions and neuroses in flight crews, noting face to face method effectiveness
23 p4086 A69-41690

Psychiatric morbidity as absenteeism cause among ground and flight personnel in civil aviation, recommending psychotherapy and chemotherapy
24 p4266 A69-43378

PSYCHOTIC DEPRESSION

Man psychic activity interference resistance, discussing stress effects characterized by theta and delta rhythms
08 p1262 A69-19839

Psychotherapeutic treatment of depressions and neuroses in flight crews, noting face to face method effectiveness
23 p4086 A69-41690

PSYCHROMETERS

Aspiration psychrometric probe for measurements of relative humidity of gas-vapor phase of gas flow containing liquid droplets
06 p0927 A69-17689

PTM [MODULATION]

U PULSE TIME MODULATION

PUBLICATIONS

U DOCUMENTS

PULLEYS

Stress-strain state of shells of multicable elevator pulleys under asymmetric load for various friction coefficients and pulley shell lengths and widths
06 p1026 A69-18016

PULLING

Periodic pulling mechanism for explaining transition to turbulence in bounded plasma with weakly unstable drift modes
07 p1194 A69-19400

PULMONARY CIRCULATION

Control mechanisms of hemodynamic shifts from dogs subjected to acceleration under anesthesia
02 p0198 A69-11503

White rat physiological processes while maintained on hypothermic cardiopulmonary bypass with small membrane type heart-lung machines
05 p0708 A69-15971

High oxygen concentration influence on animal organisms noting respiration, pulmonary gas exchange, hypoxia, brain phosphorylation, immunological indices and morphological structure of rats and mice
05 p0709 A69-16512

Pulmonary capillary gas exchange and venous admixture model and inclusion into respiratory system model, discussing pressure and concentration gradients, pathological effects, etc
07 p1068 A69-19482

High oxygen concentration influence on animal organisms noting respiration, pulmonary gas exchange, hypoxia, brain phosphorylation, immunological indices and morphological structure of rats and mice
18 p3095 A69-34731

Transfer function in pulmonary ventilation and O tension in arterial blood analyzed by automatic control
19 p3260 A69-35897

Pulmonary arterial pressure for perfusion of excised dog lungs after inflation not due to shunt channels through atelectasis areas
21 p3651 A69-38386

Blood sheet flow velocity distribution and pressure gradients in pulmonary alveolar septa determined, allowing for system elasticity
22 p3874 A69-40216

Static pressure-diameter measurements on small pulmonary blood vessels of frogs, analyzing capillary septal area as function of intravascular pressures noting high compliance
22 p3885 A69-40974

Stratified blood flow distribution in lung lobule from analyzing breath-holding changes on expired Ar and nitrous oxide tension plateaus during rest and exercise
23 p4078 A69-41315

Pulmonary emphysema effect on expiratory flow limitation from static pressure-volume and flow volume curves during natural and forced deflation of hamster lungs
23 p4082 A69-41442

Pulmonary capillary blood flow pulse of healthy men in supine position recorded by nitrous oxide/plethysmograph and phonocardiogram
24 p4259 A69-42638

PULMONARY FUNCTIONS

Pulmonary mouth pressure and heart rate in Flack test for flight personnel by simultaneous double recordings
05 p0710 A69-16626

Lung ventilation mechanics affecting respiration in hyperbaric environment during deep diving, stressing biological necessity of equal pressure respiration
13 p2215 A69-28598

Pulmonary oxygen toxicity, analyzing reticulin and elastic tissue damage and hyaline membranes by histochemical techniques
14 p2407 A69-29298

Physiologic and psychologic aging in professional pilots analyzed on basis of cardiovascular, pulmonary, exercise tolerance and sense testing
14 p2408 A69-29309

Pulmonary ventilation and perfusion in normal supine subjects before and during exposure to lower body negative pressure measured using Xe-133
17 p2909 A69-33180

Pulmonary mechanics during zero gravity maneuvers, noting decrease in flow rate and increase in expiration time without decrease in vital capacity
17 p2909 A69-33181

Pulmonary surfactant identification on modified Wilhelmy balances, by measurement of areas corresponding to minimum surface tension, using tracheal lavage from dogs and rats
21 p3651 A69-38387

Hyperoxia and pulmonary surfactant washout in pulmonary compliance measurements of rats subjected to 100 percent diatomic oxygen before asphyxial death
21 p3659 A69-39066

Lower body negative pressure /LBNP/ effects on ventilation and lung volumes, presenting lung model for pulmonary gas exchange changes
22 p3891 A69-40222

Carbon monoxide effect on dog lung volume, mechanical properties and diffusing capacity
22 p3874 A69-40224

Oxygen uptake and circulatory response in human male subjects during maximal treadmill and bicycle exercise
22 p3874 A69-40226

Human lung ventilation-perfusion scatter decreasing gas exchange efficiency during high altitude adaptation
22 p3875 A69-40227

Unilateral hypoventilation effect during bronchospirrometry on human pulmonary blood flow
22 p3875 A69-40229

Alveolar and mixed venous carbon dioxide pressure during absence of gas exchange across mammalian lung
22 p3885 A69-40976

Arterial pressure and heart rate responses to increased intrapulmonary pressure in anesthetized dogs via simulated Valsalva tests
23 p4078 A69-41365

Air and saline P-V curves of rat lungs after hyperoxia, comparing hyperoxia effects to surfactant washout on pulmonary compliance
23 p4081 A69-41440

Carbon dioxide inhalation and intravenous isoproterenol effects on hemorrhagic consolidation occurring after left pulmonary artery ligation in dogs
23 p4082 A69-41441

Pulmonary capillary blood flow, stroke volume and heart rate measured in tilted and supine subjects during respiration, discussing tourniquets and intravenous atropine effects
23 p4082 A69-41445

Pulmonary mechanics during zero gravity maneuvers, noting decrease in flow rate and increase in expiration time without decrease in vital capacity
23 p4089 A69-41825

Forearm skin capacity vessels tonus as function of intrapulmonary pressure during positive and negative pressure breathing
23 p4093 A69-42068

Alveolar and pleural pressures affecting pulmonary interstitial pressure in anesthetized dogs, applying Starling law of transcapillary exchange
24 p4257 A69-42627

Steady state model for human respiratory system analysis, discussing controlled and controlling parts
24 p4276 A69-43272

PULMONARY LESIONS

Feline lung injury produced by vertical sinusoidal vibrations during upright water immersion attributed to chest wall impact
23 p4082 A69-41447

PULSARS

Pulsar discovery at position of suspected supernova remnant, suggesting pulsars as rotating neutron stars formed in stellar explosion
01 p0149 A69-10268

Pulsating magnetic white dwarfs as pulsar models, discussing radio emission mechanisms via shock wave interaction with stellar plasma atmosphere
01 p0149 A69-10269

Relative proper motion of blue star in field of pulsar CP 1919 determined from photographic data analysis
01 p0149 A69-10270

Neutral hydrogen content in directions of pulsars related to distance estimates
01 p0149 A69-10271

Pulsar radiation origin related to electromagnetic wave distortion during propagation through resonant media
01 p0149 A69-10272

Spectral fine structure in emission from pulsars, noting correlation between fading and spectral change
01 p0150 A69-10273

Pulsars features explained by model based on binary system of neutron stars, discussing associated stellar plasmas as directional HF radio wave source
01 p0156 A69-10981

Pulsar CP 1133 high energy gamma ray emission, using atmospheric Cerenkov detection technique for high energy neutral cosmic rays
02 p0307 A69-11823

Pulsar frequency Doppler shift due to general relativistic corrections to optical path of photons in field of sun
02 p0315 A69-11836

Pulsar CP 1133 pulse duration increase with decreasing RF from analysis of pulse shape data
02 p0318 A69-12093

Mass effect on frequency tested during approach of pulsar to sun
02 p0323 A69-12298

Radio telescopic detection of seven new pulsars lying close to galactic plane, noting one pulsar close to supernova remnant
02 p0327 A69-12725

Measurements of pulsars CP 0834, CP 0950, CP 1133 and CP 1919, discussing pulse intensities and shape, submillisecond structure, intensity variations, periods and positions
02 p0328 A69-12726

Solar corona delay effects on pulsar signals due to inhomogeneities in coronal electron density
02 p0328 A69-12727

Pulsar hypothesis based on oscillating white dwarf surrounded by hot rarefied corona to explain radio emission
03 p0505 A69-13077

Pulsar CP 1919 pulse intensity fluctuations intensity with time scales could be strong scintillations
03 p0513 A69-13770

Radio waves Faraday rotation measured from pulsars by recording difference in received power
03 p0513 A69-13771

Gamma ray fluxes from pulsating radio sources, using detection of Cerenkov light generated by energetic particles in atmosphere
03 p0513 A69-13772

Photographic recording to produce spatial analog of temporal Fourier spectrum of astronomical source used for distinguishing weak periodic signal from background signal
04 p0556 A69-14294

Pulsating radio sources near Crab Nebula noting possible coincidence with nebula, pulse dispersion and interstellar electron density
04 p0659 A69-14977

Spinning neutron star model for pulsars based on slowing down of pulse rate, proposing emission mechanism for radio energy and relativistic gas
05 p0825 A69-16351

Increasing periodicities in radio pulses from pulsars
05 p0825 A69-16352

Pulsar pulse period stability, noting slowing down in several sources
05 p0825 A69-16353

Pulsar amplitude variations due to scintillation effects arising from irregular plasma refraction by general interstellar medium between source and solar system
05 p0825 A69-16354

Pulsars, noting clusters associated with spiral arm tangential points, anomalous distribution and possible association with galactic disk or spiral arms
05 p0825 A69-16356

White dwarfs atmospheric pulsation suggested as pulsar mechanism, considering thin adiabatic atmospheric model with constant lapse rate
05 p0828 A69-16659

Frequency structure of pulse energy or pulsar intensity, emphasizing total energy density received per pulse
05 p0828 A69-16660

Pulse intensity variations in pulsars observed at 113 MHz with parabolic antenna using photographic recording techniques, noting lack of periodicities
06 p1009 A69-17964

Radio source CP 1133 at 408 Mc, noting upper and lower limit to continuous emission between pulses
06 p1009 A69-17969

Pulsar distance estimates based on evaluation of galactic H absorption of 21 cm radiation
06 p1012 A69-18225

Pulsar model based on rapidly rotating neutron star with radiating attached plasma, discussing test of radiation mechanism by means of coherence of emission
06 p1012 A69-18226

Pulsating radio source pulse arrival time measurements at 1919 plus 21, determining highest SNR
07 p1214 A69-18665

Pulsar characteristics absence in X ray sources, noting data for Scorpius XR-1
07 p1218 A69-19254

Crab Nebula pulsar NPO527 position measurement with split beam antenna, noting proximity and similar dispersion with NPO532
07 p1221 A69-19405

Linear polarized emission from pulsar CP 0328 dependent on frequency, discussing model for source with constant Faraday rotation
08 p1382 A69-19817

Pulsar emission possible connection with rotating neutron stars, discussing rotational energy transfer to circumstellar plasma and production of periodic shock waves
08 p1383 A69-19895

Very high energy gamma rays from pulsars, considering implications of various gamma ray production processes
08 p1377 A69-19897

Strong light flashes detected from fast pulsar NP 0532 in Crab Nebula, discussing time-averaged optical flux
08 p1394 A69-20622

Strong light flashes from pulsar NP 0532 in Crab Nebula, noting UVB photometric analysis of nebular brightness
08 p1394 A69-20623

Rotating and oscillating magnetic neutron stars causing pulsars radio and optical signals, stressing UV line emissions theory
08 p1394 A69-20624

Orbiter and rotator models of pulsating radio sources, considering relationship between lack of Faraday rotation and similar polarization in decametric radiation from Jupiter
08 p1397 A69-20688

Polarization variations in radio pulses from pulsar CP 0328, noting possible origin in synchrotron radiation from collimated electron beam
08 p1397 A69-20694

Galactic H II regions and projected electron density or dispersion measures of pulsars, noting early stars
08 p1397 A69-20696

Pulsar distance estimates, discussing effect of interstellar electron and H densities and temperature dependence of H density-electron density ratio within disk
08 p1397 A69-20698

Radio emission from magnetic neutron stars as possible model for pulsars, noting optical and IR emission bands
08 p1397 A69-20729

Instability of stellar structures intermediate between white dwarfs and neutron stars shown by stellar models, discussing pulsar signals periodicities
08 p1397 A69-20770

Microwaves from celestial objects noting radio emission from sun, moon and Jupiter, cosmic fireball and pulsars
08 p1407 A69-21125

Photoelectric monitoring broadband photometry and spectral scans of candidate star for pulsating radio source CP 1919
09 p1591 A69-21455

Pulsar NP 0532 identified with Baade south preceding star in Crab Nebula, noting pulsed optical radiation
09 p1592 A69-21458

Vela pulsar polarization and periodicity observations supporting rotational model vs radial pulsations as radio emission source
09 p1592 A69-21461

Crab Nebula pulsar properties including pulse shape, dispersion and strong pulse emission
09 p1592 A69-21462

Pulsars rotating neutron star model analyzed on basis of magnetic dipole rotating in vacuo
09 p1592 A69-21463

Two pulsars discovered during search with transit telescope at U.S. National Radio Astronomy Observatory, tabulating pulsar parameters
09 p1592 A69-21484

Jupiter model /cyclotron/ of pulsar radiation generation

09 p1608 A69-22761

Pulsar NP 0532 optical pulsations period, discussing time rates of change, pulse shape, amplitude, photons, etc

10 p1774 A69-23182

Electromagnetic wave buildup by induced Compton effect as possible radio emission source, considering data for quasars and pulsars

11 p1957 A69-24402

High energy cosmic ray origin and acceleration by LF electromagnetic radiation produced by pulsars, noting maximum energy for protons

11 p1950 A69-24927

Optical flashes recorded from Crab Nebula M1 close to central double star with periodicity equal to radio pulses discovered earlier

11 p1962 A69-25250

Crab Nebula pulsar detection by TV camera with image intensifier at focus of astronomical telescope, detailing instrumentation and observations

11 p1962 A69-25251

Pulsed radio source near Crab Nebula studied to estimate age of longer period pulsars and frequency of pulsar-producing events in galactic history

11 p1963 A69-25252

Pulsars and ancient chinese records of supernova explosions, relating luminous intensities, radio sources and evolution

11 p1963 A69-25253

Pulsar PSR 0833-45 period decrease and rate of change in period increased between 24 February-3 March 1969, discussing contraction explanation

12 p2154 A69-25878

Pulsar distances estimated from neutral hydrogen absorption, using observations from 140 ft telescope

12 p2156 A69-26224

Pulsar NP 0527 near Crab Nebula noting long period

12 p2156 A69-26227

Crab Nebula pulsar observations confirming wavelength independence of light velocity in space

12 p2157 A69-26233

Pulsars discovery, emission, regularity, narrow frequency band and pulse changes, physical nature and aspects of Crab Nebula source

12 p2160 A69-26895

Periodicity decrease on 24 February to 3 March 1969 in decay of Molonglo pulsar PSR 0833-45

12 p2172 A69-27167

Magnetic models of pulsars and rotating neutron stars to explain narrowness of radiation beam in polar diagram

12 p2172 A69-27168

Digital computer methods for weak pulsars search using radio noise picked by telescopes

12 p2172 A69-27169

Light curve shape as function of color, changing period and polarization angle of Crab Nebula optical pulsar

12 p2172 A69-27170

Vela pulsar investigated for optical pulsations, noting negative result for expected brightness

12 p2173 A69-27173

Galactic magnetic field along Orion arm from dispersion and rotation measures of linearly polarized radiation from pulsar psr 0833-45

13 p2335 A69-27311

Crab Nebula pulsar NP 0532 photoelectric spectrophotometry results, noting main pulse and interpulse spectral energy distributions similar to extended synchrotron radiation

13 p2335 A69-27317

Optical radiation detection from pulsar PSR 0833-45 associated with supernova remnant in Vela, noting UV excess from plates using U and B filters

13 p2337 A69-27516

Pulsars and neutron star formation based on stellar evolution theory, suggesting massive O stars as origin

13 p2337 A69-27517

Pulsars suggested as magnetic rotating neutron stars with unstable oscillations

13 p2352 A69-27912

X ray pulsations in Crab Nebula at frequency closely matching radio and optical pulsations, noting energy distribution

13 p2354 A69-28465

Vela pulsar PSR 0833-45 optical observations and Crab pulsar NP 0532 linear and circular polarization measurements by telescope- photomultiplier

13 p2354 A69-28470

Pulsar hypothesis based on oscillating white dwarf surrounded by hot rarefied corona to explain radio emission

14 p2515 A69-28759

Pulsars dynamic spectra, suggesting inadequacy of interstellar scintillation models to explain observed dependence of decorrelation band widths on frequency

14 p2517 A69-29087

Pulsar dispersion-removing technique, discussing pulsar mean flux density decrease with age

14 p2517 A69-29091

Pulsar model used to explain stellar shape oscillations as cause of radio emission periodic variations

14 p2522 A69-29675

Periodic stellar radiation at 3.5 mm from pulsar CP1919 measured by paraboloid antenna and radiometer

14 p2529 A69-29978

Pulsar NP 0532 period measurements at various frequencies, obtaining accuracy in timing data reduction by linking pulse arrivals over interval of months

15 p2680 A69-30232

Crab Nebula pulsar NP 0532 simultaneous optical and radio observations, noting influence of interstellar dispersion value uncertainty

15 p2680 A69-30233

Pulsar clock mechanisms on basis of relativistic gravitational effects, considering white dwarfs and neutron stars

15 p2694 A69-30855

Interstellar hydromagnetic waves due to streaming cosmic rays indicated by pulsar scintillations studies

15 p2676 A69-30889

Pulsar NP 0532 in Crab Nebula observed by rocket and telescope showing strong pulsed X ray signal

15 p2679 A69-31529

Pulsars properties, nature and utilization for interstellar medium study including radiation mechanisms, white dwarf stars and neutron star development

16 p2855 A69-31762

Nanosecond optical pulses from Crab pulsar NP 0532 detection indicating negative observations

16 p2865 A69-32801

Criticism of Chiu theory on radio emission from pulsars supposing electron radiation

16 p2865 A69-32802

Spin down effects on neutron stars, discussing decrease of period of PSR 0833-45 as result of differential rotation instability

16 p2865 A69-32803

Pulsars Mp 0450, Mp 1642 and Mp 1818 discovery, discussing role of Molonglo radio telescope and pulse amplitude variations in detection

17 p3026 A69-32857

Pulsars distance determined using H II region data covering line of sight stars and Galaxy hydrogen distribution

17 p3026 A69-32858

Pulsar emission and magnetic field in Crab Nebula, discussing magnetic flux amplification, gravitational to magnetic energy conversion and pulsars as pulsed signals

17 p3026 A69-32859

Collection of papers on pulsating stars covering discovery, signal characteristics, optical measurements, theories and applications

17 p3035 A69-33634

Linear polarization in pulsating radio sources observed by galvanometric recordings, using Mark I radio telescope

17 p3036 A69-33635

Emission from pulsating radio sources, discussing pulse amplitude variations and frequency structure for neutron stars and white dwarf

17 p3036 A69-33636

Pulsed radio source CP 1919 detection at 13 cm wavelength with maser receiver and 210 ft antenna

17 p3036 A69-33637

Impulsive radio emission from CP 0950 by Mark I telescope, plotting mean and interpulse profiles

17 p3036 A69-33638

CP 0950 and CP 1133 pulsating stars position, using radio telescope at two frequencies

17 p3036 A69-33639

Pulsed radio sources origin from models, emphasizing pulsating white dwarfs

17 p3037 A69-33640

Relativistic effect detection on pulsar frequencies by general relativity theory, assuming pulsars are orbiting objects

17 p3037 A69-33645

General relativity theory test using earth orbital motion and solar gravitational field effects on pulsars frequency stability

17 p3037 A69-33646

Pulsars properties and distribution in galactic coordinates, deriving interstellar medium properties and physical nature of objects based on neutron star rotation

17 p3040 A69-33800

Pulsed hard X radiation from NP 0532, discussing slow down rate and luminous intensity

18 p3186 A69-34316

NP 0532 slow down rate, using quadratic least squares method

18 p3191 A69-34317

IR and optical measurement of Crab pulsar NP 0532, analyzing energy density per pulse and smoothness of visual data

18 p3191 A69-34318

Faraday rotation in NP 0527 and CP 0328, measuring angular velocity and mean longitudinal magnetic fields

18 p3192 A69-34319

Pulsar search techniques, sources searched and discovery of NP 0527 and 0532

18 p3192 A69-34320

Light curve of pulsar NP 0532 represented with oblique rotator hypothesis, assuming concentrated emission at opposite spots on star

18 p3192 A69-34321

Pulsars observed for average energies at centimeter wavelengths, using azimuth elevation antenna

18 p3196 A69-34644

Models for pulsars periodicity and period range due to nonradial gravity wave in almost adiabatic matter of degenerate neutron stars

18 p3196 A69-34645

Pulsar PSR 0833-45 period decrease resulting from mass addition leading to radius and inertia moment decreases

18 p3196 A69-34646

Oblique rotator model for pulsars, discussing difficulties arising from two asymmetrically spaced pulses during each stellar rotation

18 p3196 A69-34647

Night sky Cerenkov light detectors observations of pulsars CP 1133, NP 0532 and NP 0527, noting instrumental limitation in detecting ultrashort light pulses

18 p3200 A69-34994

Low energy cosmic ray density in Galaxy due to pulsar PSR 0833-45 caused by mass ejection

18 p3187 A69-34995

Pulsars theoretical period distributions derived, considering period change of period dependence

18 p3201 A69-35203

Pulsars measured parameter data tabulation including right ascension, declination pulse repetition period, showing sources distribution and clusters

18 p3202 A69-35211

Pulsar PSR 0833-45 polarization structure frequency dependence measurement leading to model implying radiation emanated from magnetic poles neighborhood

18 p3202 A69-35215

Pulsars, pulse shape and duration, object size and spatial distribution, distinguishing between pulsars and supernovae

18 p3202 A69-35283

Pulsars pulse profiles data collected and interpreted with attempt to infer origin

20 p3597 A69-37335

Pulsar distance determined by electron content in line of sight to pulsar compared with neutral H amount integrated through galaxy in pulsar direction

20 p3597 A69-37409

Gamma ray flux from processes associated with high energy electrons from pulsar NP 0532, noting light polarization

20 p3588 A69-37410

Plasma acceleration away from rotating magnetized astrophysical objects analyzed and applied to pulsar NP 0532 for magnetic moment and mass loss rate calculations

20 p3598 A69-37419

Pulsars cosmic ray mass and charge spectra analyzed for evidence of neutron star origin

20 p3588 A69-37487

Radiation emission mechanism for NP 0532 associated with Crab Nebula, discussing shock- neutral sheet interaction

20 p3604 A69-37572

Radial pulsations of neutron star losing mass, interpreting Crab Nebula pulsar observed period and secular increase of period

20 p3604 A69-37573

Pulsed X ray emission associated with pulsar NP 0532 in Crab Nebula measured by six element detector on Aerobee 150 rocket

20 p3590 A69-37574

Optical flashes from PSR 0833-45 searched using 74 inch Radcliffe telescope with pulse counting photometers

20 p3604 A69-37575

Pulsar search signal processing and digital techniques, using fast folding /cross correlation/ or fast Fourier transform /FFT/ algorithms

20 p3605 A69-37824

Crab Nebula pulsar NP 0532 linear and circular optical polarization measurements

21 p3798 A69-38542

Rotating neutron star model to fit pulsar data, considering star crust formation and properties, angular velocity changes and starquake effects

21 p3798 A69-38544

Optical observations of pulsar NP 0532, comparing light curves in IR and UV, noting polarization

21 p3799 A69-38645

Spectroscopic observations of optical pulsar NP 0532, using technique permitting phase resolution of spectra of main pulse and interpulse

21 p3799 A69-38646

Spectra, fading and pulse structure of pulsars noting electron density, polarization, second periodic pulsation, etc

21 p3802 A69-38826

Rotating neutron stars with magnetic fields symmetric about rotation axis considered for pulsar model

22 p4027 A69-40657

Quasar features compared to pulsars, noting complete analogy except for energy output scale

22 p4029 A69-40762

Pulsar magnetic models, coherent radio emission mechanisms, radiation polarization, data summary and astrophysical nature

22 p4030 A69-40905

Pulsar CP 0328 radiation mechanism, considering relativistic effects of rapid rotation

22 p4035 A69-41206

Optical detection of pulsars with emphasis on CP 1919, discussing optical variation

23 p4218 A69-42325

Pulsars models and radiation mechanism, noting neutron stars with rotating magnetospheres

23 p4218 A69-42326

Pulsars dispersion measure and distance relationship, particularly for Crab Nebula pulsars

23 p4220 A69-42381

Neutron star formation, discussing influence of supernova explosions and need of pulsar study

23 p4222 A69-42393

Crab Nebula pulsars radio properties, possible neutron star origin, interstellar gas and magnetic fields, etc

24 p4375 A69-42556

Mean and variance of Faraday rotation and pulsar signal dispersion in galactic turbulent structure, applying to statistically homogeneous disk model of Galaxy

24 p4375 A69-42659

Pulsar model with seat as rotating neutron star having dipolar magnetic field not parallel to rotation axis

24 p4377 A69-42666

Pulsars relation with supernovae remains and radiation patterns and fluxes analysis, ascribing radio emission to relativistic plasma

24 p4383 A69-42985

Rotating neutron stars, pulsars and cosmic X ray sources, accounting for large and small diameter sources by rotating neutron star losing mass in magnetic field

24 p4369 A69-43222

Pulsars radio intensity fluctuations noting possible periodic pulse amplitude modulation

24 p4389 A69-43744

Pulsars turn off time compared to Galaxy age, discussing physical theory and pulsar models

24 p4389 A69-43745

Electromagnetic wave buildup by induced Compton effect as possible radio emission source, considering data for quasars and pulsars

24 p4391 A69-43792

PULSATING FLOW

U UNSTEADY FLOW

PULSE AMPLITUDE

Monolithic sense amplifier for laminated-ferrite memories including provision for strobing, detecting, pulse forming and internal inversion logic using thermal feedback control

01 p0039 A69-10174

Graphical method for determining rise time of planar transistors with constant collector space-charge capacitance

01 p0049 A69-11362

Pulsar CP 1919 pulse intensity fluctuations intensity with time scales could be strong scintillations

03 p0513 A69-13770

Pulse amplitude measurements comparison by sampling signal at given time and pulse peak detection, considering SNR

05 p0722 A69-16730

Transistorized multichannel pulse height analyzer and recording system for balloon-borne cosmic ray payloads, discussing performance capacity

06 p0924 A69-17284

High power microwave interactions in pulsed electron beam plasma klystron

07 p1095 A69-18433

Multichannel pulse height analyzer with memory, small size and low power consumption for application to satellites

07 p1135 A69-19200

Giant pulse production of Nd-glass laser with aid of coherent pumping by second harmonic of Q switched laser, noting pulse duration

07 p1156 A69-19333

Frequency conversion in microwave crystal mixer with EMF amplitude fluctuations in heterodyne

09 p1469 A69-22644

Noise rejection in linear amplitude detector during weak harmonic signal reception improved by limiting threshold voltage

09 p1460 A69-22645

Pulsar NP 0532 optical pulsations period, discussing time rates of change, pulse shape, amplitude, photons, etc

10 p1774 A69-23182

SNR variation with PCM using quantization distortion equations applied to coding-decoding facilities not exactly matched with respect to amplitude

10 p1656 A69-23692

Pulsed tunable lasers, emphasizing dye lasers for visible and near visible light in specialized spectroscopy

11 p1893 A69-24343

Amplitude spectra of periodic pulse sequences or pseudonoise sequences calculated using weighting and shape functions

12 p2030 A69-26389

Ferrites dynamic characteristics in alternating magnetization pulse with variable amplitude indicating linearity loss in strong fields

13 p2320 A69-27994

High latitude ionization spikes observed by POGO spacecraft, noting frequency correlation with magnetic disturbances and development by high energy electron injections

14 p2511 A69-28950

Plasma energy and energy replacement time dependent on discharge pulse shape and magnitude

14 p2499 A69-29848

Charge flow injection into MOS substrate attributed to gate pulses, correlating charge magnitude with pulse frequency

15 p2573 A69-30033

Q switched ruby laser giant pulses during pumping by another Q switched laser exhibit simple shape and low duration

15 p2634 A69-30727

Waveform amplitude variation of phase modulation pulses affected by band limitation

15 p2569 A69-30803

Peak amplitude selector for electrophysiological phenomena analysis, describing memory schemes, threshold crossing detectors and display, input and output circuits, timing, etc

15 p2612 A69-31266

Pulse height distributions, gain and counting rate characteristics of two magnetic strip multipliers and two channel multipliers in 1.5 to 44 A region of soft solar X-rays

17 p2972 A69-33082

Emission from pulsating radio sources, discussing pulse amplitude variations and frequency structure for neutron stars and white dwarf

17 p3036 A69-33636

Observed and computed radio pulse profiles of white dwarfs, noting resemblance of emissivity variation with latitude to magnetic field distribution on sun

17 p3037 A69-33644

Modified pulse height analyzer /PHA/ for sample amplitude height occurrence frequency measurements obtaining amplitude probability distribution /APD/ and three moments of atmospheric noise

18 p3102 A69-34960

Pulse height distribution changes of gas filled proportional counters ascribed to deposit accumulation on anode, using X ray fluorescence analysis

20 p3538 A69-37302

Phase and amplitude stability measurements in airborne pulse Doppler radar

20 p3492 A69-37711

PULSE AMPLITUDE MODULATION

Continuous random process spectral density at PAM system output

01 p0050 A69-10211

Transversal filters for equalization of data channels with pulse amplitude modulation, discussing pulse equalizability and convergence criteria for iterative search routine

01 p0027 A69-10251

Optimum demodulation of PAM-FM signal for case of minimum mean square error as performance criterion

03 p0392 A69-13250

Weighted pulse trains for clutter suppression during radar target detection

04 p0562 A69-15467

Continuous random process spectral density at PAM system output

14 p2424 A69-28748

Spectral characteristics of pulsed signal with determinate repetition period and amplitude and duration modulation by correlated random processes

15 p2567 A69-30347

Pulsars radio intensity fluctuations noting possible periodic pulse amplitude modulation

24 p4389 A69-43744

PULSE CODE MODULATION

NT DELTA MODULATION

Pulse code modulation /PCM/ time multiplex system companding by switching, discussing SNR measurement

01 p0031 A69-10739

Monochrome pictorial encoding, discussing pulse code modulation, delta modulation and buffer storage techniques

02 p0213 A69-12154

Mean error rates in microwave PCM systems with wave distortion due to multipath propagation

02 p0208 A69-12307

Optical correlator for fast acquisition of pseudorandom ranging codes, giving code delay estimation to synchronize local code generator of delay-lock loop

03 p0389 A69-13186

Optical receivers for deep space optical communications link assuming PCM scheme

03 p0389 A69-13194

Digital data processing equipment for space flight PCM telemetry

03 p0393 A69-13290

Radiation sensor PCM data processing by computer to detect radiation level using data decorrelation, data normalization and threshold test

03 p0400 A69-13313

Upper and lower bounds on mean reduced error of pulse code telemetry systems operating by binary code

03 p0396 A69-13687

Data handling equipment for Ariel 3 and future satellites emphasizing manufacturing of PFM and PCM systems

05 p0726 A69-16769

Error probability vs SNR and power spectrum of PCM/PM signal with small phase deviation, noting applications in satellite tracking

06 p0889 A69-17656

Time division multiple access satellite communication system employing pulse code modulation of voice channels and phase shift keying of RF carrier

07 p1077 A69-18759

Maximum likelihood bit synchronizer for baseband PCM signals in Gaussian noise, stressing system noise performance analysis and measurements

07 p1105 A69-19093

Block coding systems performance in digital PCM data transmission through N-ary discrete channels in white Gaussian noise presence, discussing SNR upper bounds

07 p1080 A69-19096

Bit probability of PCM/FM for receiver with IF bandwidth equal to or greater than data rate, limiter-discriminator detection and postdetection filter

07 p1082 A69-19106

Error probability for discriminator detection of wideband PCM/FM, considering IF bandwidth/bit duration product and low pass filtering effect

08 p1271 A69-19864

Delta modulation for analog to PCM encoding due to tapped binary shift register and up-down counter

09 p1455 A69-21844

Optimum timing extraction /bit synchronization/ in pulse code transmission, analyzing probabilistic structure by statistical parameter estimation and deriving system

09 p1455 A69-22115

SNR variation with PCM using quantization distortion equations applied to coding-decoding facilities not exactly matched with respect to amplitude

10 p1656 A69-23692

Atmospheric interference effects on optical PCM signal, analyzing absorption, beam bending, scintillation and correlation with visibility and weather

11 p1888 A69-25308

Ultrahigh speed microwave diode switch used as transmitter-modulator in PCM systems, utilizing varactor diode avalanche breakdown

13 p2229 A69-27671

PCM oscillator synchronization system stability, considering sampled model by digital nature of equipment

15 p2565 A69-30171

Demand assigned frequency division multiple access-PCM system designed by COMSAT for satellite communication

16 p2749 A69-31602

Regenerative amplifier to counteract cable damping due to narrow bandwidth in PCM systems

16 p2755 A69-31860

PCM data handling system for NASA Space Tracking and Data Acquisition Network with explanation for output capabilities, noting BIOSAT project

19 p3270 A69-36242

Nonlinear filter theory application to PCM bit synchronization, relating bit error rates to SNR and timing jitter

19 p3270 A69-36245

High bit rate signal conditioning, bit and group synchronization of NRZ PCM, considering gain and power bandwidth limitations and delays

19 p3271 A69-36247

PCM bit synchronizer models, discussing phase errors gate and differentiating devices

19 p3271 A69-36249

Digital data transmission by pulse code modulation considered for minimum mean square error

19 p3274 A69-36282

M-ary detection for optical communication investigated for maximum likelihood detection of one of M Poisson processes in background noise

19 p3276 A69-36486

Demultiplexing of high speed multichannel optical pulse code transmission systems, based on coincidence detection using locally generated reference pulses

19 p3279 A69-36764

Split phase PCM code modulated carrier transmission characteristics determined for amplitude, phase and frequency shift keying, assuming random bit pattern and noncoherent modulation

21 p3676 A69-39451

Multiple access techniques of SSB-PM and PCM-PM frequency translation for satellite communication system, comparing performance characteristics

21 p3678 A69-39807

PCM role in FDM-FM short haul low density cable communications systems used in exchange area and tactical military systems

22 p3900 A69-40678

TDMA/PCM system for communication tests via Applications Technology Satellites, discussing time synchronization and bit and frame coherency

23 p4129 A69-42510

Effective color TV transmission via satellite using PCM/PSK modulation, noting dependence on available equipment, bandwidth, desired error rate and SNR

23 p4130 A69-42520

PCM satellite communication systems signal power and frequency bandwidth requirements, noting PCM-psk superiority over FDM-FM

24 p4283 A69-43200

PULSE COMMUNICATION

Transversal filters for equalization of data channels with pulse amplitude modulation, discussing pulse equalizability and convergence criteria for iterative search routine

01 p0027 A69-10251

Power advantage of optimum system achieved with suboptimum feedback function for sequential binary detection system

02 p0225 A69-11996

VLF system simulation for evaluating digital communications systems operating in presence of additive atmospheric noise

03 p0390 A69-13205

Linear processing effect on digital communications systems performance by channel impulse response and

input-output relationship as distributional convolution equation

03 p0391 A69-13226

Digital detection of angle modulated signals including zero crossing detectors, digital phase locked loops, differentiation and arcsine demodulator

03 p0391 A69-13230

Atmospheric noise amplitude distribution relation to rms phase errors in frequency components of VLF timing pulse

03 p0396 A69-13629

Spectrum analysis of pulse signals by point to point measurements of magnitude and phase of pulse-like time functions, using narrow band filter output

03 p0399 A69-13939

Resonant amplifier response having stages identical to radio pulse with exponential envelope

05 p0720 A69-16444

Detection characteristics of coherent pulse packet with random initial phase on Gaussian noise background of unknown intensity

06 p0887 A69-17463

Gunn effect pulse devices with resistive loading, discussing logic, circuits and low power consumption

07 p1097 A69-18453

Secondary maxima observed in pulses with binary phase shift keying for cases of large Doppler shifts

07 p1086 A69-19488

Bandwidth restriction effect on performance of linear codes for digital communication with space vehicles, noting bit and word error probabilities

08 p1276 A69-20597

Sensitivity of microwave earth stations for analog and digital communications

09 p1453 A69-21409

Optimum timing extraction /bit synchronization/ in pulse code transmission, analyzing probabilistic structure by statistical parameter estimation and deriving system

09 p1455 A69-22115

Sunde model of troposcatter channel as transmission medium in computer simulation of adaptive digital communication scheme for selective fading channels

09 p1458 A69-22471

Probability analysis of distortions caused by pulse noise action on digital information

09 p1476 A69-22678

Pulsed RF spectra analyzer displays, noting responses to CW and pulsed signals and Fourier and pulsed repetition rate lines

09 p1460 A69-22791

Tandem interleaved cyclic codes for digital HF communication with improved error rate at reduced decay time

10 p1655 A69-23530

Statistical characteristics of photocurrent pulse amplitudes during cathode exposure to gas laser outputs

11 p1834 A69-24611

Digital logic techniques for high speed satellite communications, noting general purpose logic cards

12 p2040 A69-26465

Delay time of pulse signals in radio channel transmission described by standard deviation of channel properties

13 p2218 A69-27215

Signal to noise ratio requirements for sharp cut-off biphasic digital communication channel

13 p2221 A69-27959

Gallium arsenide injection laser for communication systems with pulse frequency modulation, noting power output dependence on crystal quality

14 p2459 A69-29349

Bayesian theory to determine maximum a posteriori estimation algorithms for optimum bit synchronization in digital communication systems

14 p2413 A69-29496

Algorithm for optimal digital processing of pulse signals during multilevel quantization in Markov noise, including error analysis

15 p2571 A69-30126

Noise sensitivity of FM discriminator/limiter in digital binary communication system with FM/PCM-FM/

15 p2564 A69-30145

Resonant amplifier response having stages identical to radio pulse with exponential envelope

16 p2753 A69-32476

Unidigit and multidigit communications systems performance and transmission characteristics, emphasizing SNR improvements

17 p2918 A69-33066

Electrooptical/photomultiplier/ detection of satellite beacon flashes, establishing time of flash and measuring pulse shape and energy received

17 p2919 A69-33083

Information storage of multichannel analyzer of continuous and pulsed processes

17 p2939 A69-33900

Optimum signal design to maximize SNR for pulse communications systems with signal energy detection, considering frequency, transmission and filtering characteristics and signal duration

18 p3104 A69-35484

Nonlinear filter theory applied to digital telemetry binary processes, using continuous time stochastic process

19 p3274 A69-36281

Tropospheric influence on pulse signal propagation, measuring pulse function of propagation path, hypothesizing signal reflection from tropospheric boundary layers

19 p3279 A69-36879

Detection characteristics of coherent pulse packet with random initial phase on Gaussian noise background of unknown intensity

20 p3496 A69-37946

Tradeoff between Doppler measurement capability and subcarrier demodulation in coherent digital communication system quantitatively presented for various SNR

23 p4122 A69-41771

PULSE COMPRESSION

Pulses generated by mode locked Nd glass laser, analyzing compression by gratings

01 p0091 A69-10817

Time compression system with ultrasonic diffraction cell allows coherent light optical spectrum analyzer to function at audiofrequencies

01 p0035 A69-11283

Dispersive two port components for application to microwave pulse compression, coupling YIG crystal magnetoelectric spin wave mode to acoustic transducer

02 p0217 A69-12149

Fourier synthesis procedure optimized to design of large time bandwidth product dispersive filters employing nondispersive tapped delay lines

03 p0403 A69-13217

Passive linear FM pulse compression radar systems detection capability compared with matched filter performance

03 p0390 A69-13218

Pulse compression by optical correlation techniques, discussing laser beam control by diffraction grating in ultrasonic delay line

03 p0397 A69-13732

Line filter compression and positioning of bipolar video pulse trains for conjunctive use with moving target indicator in echo elimination

04 p0558 A69-15071

Band inversion passive generation in pulse compression radar, noting influence on signal modulation laws

04 p0558 A69-15074

Single two dimensional coherent matched filter optical processor for simultaneous synthetic radar antenna beam sharpening and pulse compression

04 p0562 A69-15475

Sequences with small correlation functions as error correcting codes in word separation, synchronization and pulse compression systems

06 p0948 A69-17868

Pulse compression radar employing same dispersive line for signal generation and reception

08 p1271 A69-19918

Mode locked He-Ne laser pulses compression by multiple reflections from interferometer after application of linear electro-optic frequency sweep

09 p1516 A69-21745

Singular shock waves formation during pulsed forward motion of conducting piston in MHD medium

09 p1551 A69-22034

Optical pulse compression experiment illustrating performance of electro-optical Doppler shifter as linearly time varying frequency shift production device

09 p1519 A69-22445

Laser pulse picosecond substructure measurements, using pulse compression and second harmonic generation techniques

10 p1703 A69-23514

Output pulse duration calculation for compressing filter in presence of pulse or continuous FM noise, using parallelogram of arguments method

11 p1844 A69-24445

Chirp radar signal compression by proton spin echo phenomena, noting compression ratio and SNR

11 p1834 A69-24566

Elliptical polarization in ultrabandwidth YIG pulse compression networks, using reflections at rod faces
13 p2230 A69-27680

Adapter between dielectrically loaded waveguides with different cut-off frequencies and sizes for pulse compression systems
14 p2423 A69-29760

Compression capabilities of combined frequency and phase shift keying in radar and sonar pulse modulation using binary noise codes
15 p2568 A69-30628

Pulse compression using Hermitian functions, noting minimal rms error requirement in real system
16 p2755 A69-32585

Attainable signal compression coefficient in recirculator and relation to recirculator ring parameters, noting feedback coefficient stability
17 p2931 A69-33907

Acoustic surface waves on thin film for pulse compression radar dispersive delay line, describing delay characteristic synthesis and control
19 p3267 A69-35929

Sensitivity improvement for inertialess microwave signal scanning and readout by applying pulse compression concepts, discussing application to real time microwave imaging and holography
20 p3545 A69-37901

Optimum wideband signal for minimum Doppler distortion, describing pulse compression by linear-period modulation
21 p3671 A69-38406

Very short pulses effect on aircraft echoes, noting echoing area reduction as resolution cell diminishes
21 p3672 A69-38755

Radio FM pulse compression for vertical ionosphere sounding
21 p3674 A69-39082

Optical ultrashort pulse compression with paired diffraction gratings in terms of phase shift frequency dependence and Fresnel diffraction analogy
23 p4171 A69-41392

Active weighted pulse compression radar receiver output waveform analysis for amplitude, phase and frequency modulation, noting effects of spectrum weighting mismatch parameter
23 p4132 A69-42548

PULSE DIFFRACTION
Solid target output pulse magnitude and direction dependence on angle of incidence of intense laser beam
06 p0935 A69-17686

Wave trains of incident pulse diffraction in thin composite rod determined by transmission and reflection coefficients of plane waves at plane interfaces
21 p3845 A69-39677

PULSE DOPPLER RADAR
NT MONOPULSE RADAR
Pulse Doppler radar operation, discussing Doppler shift, range resolution and systems components
10 p1659 A69-24084

Horizontal wind pulsations in precipitations obtained from pulsed Doppler radar data, including degree of turbulent flow anisotropy
16 p2807 A69-32271

Nanosecond pulse coherent Doppler radar for monostatic measurements of turbulent wakes in shock tunnels and ballistic ranges
19 p3293 A69-35743

Holographic system to process signals received by pulse Doppler radar, noting real time operation with availability of instantaneous development image storage media
19 p3314 A69-36598

Phase and amplitude stability measurements in airborne pulse Doppler radar
20 p3492 A69-37711

Doppler radar based on triple pulse transmission at coherent frequencies, comparing echo pulses for targets cancellation and extraction
21 p3672 A69-38436

PULSE DURATION
Ultrashort light pulses in lasers with nonlinear absorber, evaluating random intensity peak probability created by intensity fluctuations and axial modes buildup
01 p0090 A69-10791

Pulses generated by mode locked Nd glass laser, analyzing compression by gratings
01 p0091 A69-10817

Step recovery switching silicon transistor combining planar and mesa technologies, discussing charge storage and fall times
02 p0215 A69-11937

Pulsar CP 1133 pulse duration increase with decreasing RF from analysis of pulse shape data
02 p0318 A69-12093

Laser pulse parameters generated in stationary locked mode regime with resonance modulation of losses
02 p0258 A69-12641

Oscilloscope display of sample of subnanosecond light pulse, using optical analog of electronic sampling oscilloscope
02 p0259 A69-12656

Pulsar CP 1919 pulse intensity fluctuations intensity with time scales could be strong scintillations
03 p0513 A69-13770

High voltage controlled amplitude rectangular pulse generators having nanosecond buildup time
04 p0597 A69-14849

Tunnel diode univibrator, noting polarization influence on recovery time and pulse length stabilization dependence on resistive load
04 p0578 A69-15069

Line filter compression and positioning of bipolar video pulse trains for conjunctive use with moving target indicator in echo elimination
04 p0558 A69-15071

Nonstationary nonlinear wave phenomena in ultrashort high intensity light pulse formation, discussing nonstationary stimulated Raman scattering and picosecond pump reduction of Raman amplification [IEEE PAPER H-5]
05 p0774 A69-16316

Generation and amplification of ultrashort optical pulses [IEEE PAPER H-12]
05 p0774 A69-16317

Upper limit of nonradiative relaxation time between specific states of absorption bands and fluorescence state emitting R lines in ruby laser
05 p0777 A69-16335

Light pulse duration and other parameters for ruby and Nd-glass lasers operating in synchronized mode regime determined by Armstrong method
06 p0934 A69-17549

Ultrashort light pulse generation and measurement of half width, using saturable dye to mode lock Nd-glass laser
06 p0935 A69-17769

Space and immersion suits physiological evaluation by pulse duration multiplexing telemetry, using commercial FM receiver
06 p0883 A69-17845

Picosecond laser pulses application to nonlinear optics, atomic and molecular systems transient response, optically generated plasmas, spectroscopy, high speed photography, etc
07 p1148 A69-18856

Pulse broadening in MHD copper vapor laser
07 p1149 A69-18904

Optical excitation process of energy states by light pulses of short duration compared to relaxation time, predicting Raman echoes [IEEE PAPER H-3]
07 p1152 A69-19062

Spontaneous and stimulated Raman emission in liquids, obtaining picosecond pulse duration and laser light linewidth [IEEE PAPER H-6]
07 p1152 A69-19063

Laser induced gas breakdown by focusing nanosecond pulses in air and deuterium [IEEE PAPER U-3]
07 p1155 A69-19085

Wide range current-to-frequency converter with pulse frequency linear to input current
07 p1107 A69-19170

Quantum paramagnetic amplifier saturating power dependence on input pulses length and frequency determined by kinetic equations solution
08 p1325 A69-20436

Picosecond light pulse generation by solid state laser interpreted by fluctuating intensity spikes arising from random emission interference in out-of-phase modes
08 p1326 A69-20548

Gas servo design utilizing floating flapper disk switching valves and pulse-length modulated pressure waves to actuate on-off switch [AGARDOGRAPH-118]
08 p1257 A69-20950

Proportional counter pulse shapes calculation for point and extended ionization tracks, considering electron drift velocity and positive ion mobility
09 p1493 A69-21419

Far IR laser pulse shape and duration
09 p1515 A69-21424

Laser triggered spark gap and Pockels cells producing consistently repeatable controlled duration pulses
09 p1515 A69-21427

Common mode rejection technique to determine phasing differences in digital systems by measuring pulse delay
09 p1463 A69-21896

Stability conditions for nonlinear pulse width and pulse time modulation systems, considering pulse element properties and system continuous part frequency characteristic
09 p1476 A69-22672

Ultrashort light pulses nonlinear amplification in medium with finite transverse relaxation time and linear radiation losses
10 p1702 A69-23139

Pulsar NP 0532 optical pulsations period, discussing time rates of change, pulse shape, amplitude, photons, etc
10 p1774 A69-23182

Geomagnetic crochet of July 7, 1966, discussing pulsations, recombination coefficient and electron density of ionospheric D region
10 p1683 A69-23757

Mode locked ruby laser for short duration pulse production, noting relation to reciprocal linewidth
10 p1705 A69-23813

Long and short duration pulses interactions with nonlinear dielectric, calculating frequency variations and spectral transformations
10 p1658 A69-23953

Output pulse duration calculation for compressing filter in presence of pulse or continuous FM noise, using parallelogram of arguments method
11 p1844 A69-24445

Output pulse parameters of short pulse thyristor generator as function of time constant, considering rise time of switch-on process
11 p1846 A69-24615

Electro-optically Q switched Nd doped calcium tungstate laser for producing two controlled pulses, noting application to other solid state lasers
11 p1899 A69-25052

Pulsed radio source near Crab Nebula studied to estimate age of longer period pulsars and frequency of pulsar-producing events in galactic history
11 p1963 A69-25252

Microstructure of pc 3 and pc 4 geomagnetic pulsations, investigating polarization direction, period duration and latitude dependence
12 p2063 A69-25782

Selective stroboscope with explosive bright light source and microsecond pulse duration for short flash period over large area, noting single frame separation method
12 p2086 A69-26162

Framing device capable of producing four pictures within 5 nsec, using Q switch laser for light source
12 p2086 A69-26168

Regulated pulse lasers under free oscillation for photographing distant objects by illumination with shortened light pulses
12 p2089 A69-26190

Pulsed HCN sealed laser long term operation, discussing behavior of 311 and 377 micron emissions
12 p2107 A69-26391

Giant pulses from laser with electro-optical quartz shutter, noting advantageous optical and mechanical properties of quartz
12 p2108 A69-26591

Analytic expressions for predicted widths of AM and FM mode locked pulses in homogeneous lasers
13 p2270 A69-27191

Intense ultrashort pulse widths determination by two photon fluorescence patterns, using model of partial laser mode locking
13 p2270 A69-27198

Ruby and neodymium glass lasers applicability to metal working, investigating factors affecting integral pulse power stability
13 p2273 A69-28431

Physiological effects of intermittent light stimulation during helicopter flight, discussing visual and electric cortical functions at critical frequency threshold of subjective fusion
13 p2211 A69-28595

Optically swept glass slab laser design, discussing pulse length and peak power
14 p2457 A69-28930

Passive Q switch laser single pulse formation time and spectral width using balance equations
14 p2458 A69-29166

Neodymium laser having adjustable pulse duration and homogeneous spatial radiation structure developed by two photon absorption
14 p2460 A69-29670

Electromagnetic noise radiation structure during lightning flash by measuring time duration distribution between pulses

14 p2445 A69-29885

Q switched ruby laser giant pulses during pumping by another Q switched laser exhibit simple shape and low duration

15 p2634 A69-30727

Radial pulsation mode of convective envelopes in adiabatic equilibrium for variable M red supergiant stars

15 p2692 A69-30766

Two photon interaction between ultrashort light pulse and medium, showing pulse propagation through medium without absorption

15 p2634 A69-30966

Atomic coherence and inhomogeneous broadening effects on laser amplifier ultrashort electromagnetic high peak power pulses

15 p2635 A69-31239

Laser flowmeter for pulse flow of highly corrosive rocket fuels and oxidizers with measured rise times less than 10 msec

15 p2616 A69-31292

Pulse duration control by two photon absorption, using GaAs as nonlinear element inserted in neodymium-glass laser cavity

16 p2796 A69-31798

Laser cavity optimization for producing minimum short light pulse width in fast Q switching of optical maser

16 p2796 A69-31802

Vertical incidence pulse dispersion with application to Alouette 1, discussing echo width, sounder system bandwidth and frequency gradient of ionospheric virtual height

16 p2750 A69-31977

Earth ionosphere cavity model for atmospheric waveform shape, considering ELF pulse distortion after propagation through antipode

16 p2750 A69-31978

Horizontal drifts and anisotropy of irregularities in ionospheric F 2 region by pulse fading drift records

17 p2960 A69-33164

Single radio pulse reception time relations by panoramic receiver, considering short wideband and long narrowband pulses

17 p2931 A69-33910

Night sky Cerenkov light detectors observations of pulsars CP 1133, NP 0532 and NP 0527, noting instrumental limitation in detecting ultrashort light pulses

18 p3200 A69-34994

Pulsed ultrasonic flaw detectors resolving power enhancement by shunting semiconductor diodes across piezoelectric elements of scanning heads to shorten scan pulse duration

18 p3137 A69-35112

Semiconductor optical quantum amplifiers in pulse mode operation, describing arrangement for studying performance including pulse duration and current controls

18 p3153 A69-35258

Second harmonic radiation generation in nonlinear dielectric by broadband short pulse optical signals

19 p3278 A69-36693

He-Ne laser subnanosecond intracavity coupler consisting of coaxial krypton pulse generator and electrooptic modulator

19 p3339 A69-36823

Ultrashort light pulses in lasers with nonlinear absorber, evaluating random intensity peak probability created by intensity fluctuations and axial modes buildup

20 p3555 A69-38009

Very short pulses effect on aircraft echoes, noting echoing area reduction as resolution cell diminishes

21 p3672 A69-38755

Coherent light emission by molecules excited by laser pulses having duration comparable to active medium polarization relaxation time

21 p3737 A69-38999

Pulse width increase in mode locked laser caused by phase deviations, noting optical elements with quadratic dispersion of refractive index

21 p3741 A69-39683

Circadian rhythm phase shifts during ontogenesis produced by hormone concentration changes resulting from light variations

22 p3872 A69-40198

Longitudinal modes locking and ultrashort light pulse generation in laser cavity resonator with nonlinear refractive index

23 p4171 A69-41389

Mode locked ruby laser with picosecond pulses using rooftop prism cavity with helical flashtube for pumping

23 p4172 A69-41395

Average total losses of H waves transmitted over waveguide communication lines by nanosecond pulse sequences

23 p4123 A69-41949

Diffusion times for saturated region in Hipernom tubes measured for various exciting magnetic fields and pulse duration

23 p4141 A69-42222

Ultrashort laser light pulses self focusing and determination of focal points coordinates

24 p4328 A69-43068

Auroral short period pulsations in 6300 A O I, discussing percentage modulation, quenching rate, etc

24 p4309 A69-43171

Oscillographic recording of GaAs laser ultrashort radiation pulses, using isolated injection regions and semiconductor photodiode as photoelectric converter

24 p4329 A69-43740

PULSE DURATION MODULATION

Circuit for linear voltage amplitude to pulse width conversion using controlled unijunction monostable multivibrator

02 p0217 A69-12151

Frequency domain stability criterion for pulse width modulated feedback

06 p0904 A69-17942

Operational principles and characteristics of pulse width modulator designed on basis of autooscillator amplifier, giving circuit diagrams

10 p1664 A69-23817

ELDO satellite command decoder performance in presence of noise, evaluating PDM bit decoder bit error probability and false command probability

11 p1834 A69-24563

Spectral characteristics of pulsed signal with determinate repetition period and amplitude and duration modulation by correlated random processes

15 p2567 A69-30347

PDM command coder meeting NASA Tone Digital Command Standard for German central ground station

16 p2755 A69-31859

Missile response-PDM guidance and control system parameters relationship, using phase plane representation

24 p4283 A69-43252

PULSE FREQUENCY MODULATION

Multivariable PFM control system stability analysis using Liapunov function as Hermitian quadratic form

01 p0050 A69-10207

Integral and sigma pulse frequency modulation effects on white noise, analyzing autocorrelation and spectral density functions of PFM system output

01 p0034 A69-11221

Periodic cycles in linear closed loop integral pulse FM systems, discussing existence conditions, periodic formulae and stability criterion

05 p0737 A69-15865

Pulsed control systems stability with frequency pulse modulation analyzed by Liapunov direct method

05 p0740 A69-16670

Data handling equipment for Ariel 3 and future satellites emphasizing manufacturing of PFM and PCM systems

05 p0726 A69-16769

Pulse frequency signal processing continuous and discrete differentiators, analyzing time delay, constant frequency, accuracy and codes

09 p1454 A69-21755

Stability conditions for control systems consisting of linear multivariable stationary neutral plant and multivariable pulse frequency modulator, using Liapunov direct method

12 p2049 A69-26080

Multivariable PFM control system stability analysis using Liapunov function as Hermitian quadratic form

14 p2424 A69-28743

Stable operation of pulsed system with signal modulated pulse frequency described by nonlinear integral equation

14 p2425 A69-28909

Numerical solution of differential equations for two channel PFM with pulse element, applying Dirac pulse sequence to input

14 p2426 A69-29148

Gallium arsenide injection laser for communication systems with pulse frequency modulation, noting power output dependence on crystal quality

14 p2459 A69-29349

PULSE FREQUENCY MODULATION TELEMETRY

Real time pulse frequency modulation telemetry receiving system for direct readout of ionograms from topside sounders, using off-shelf components

20 p3508 A69-37862

PULSE GENERATORS

Optical pulse generator consisting of solid state laser with saturable absorber at cavity end using perturbation theory and Maxwell equations

01 p0089 A69-10179

Carbon dioxide laser pulsed mode for generating giant pulses, noting applications and electron impact role

01 p0090 A69-10781

Active medium high gain during giant pulse generation shown to lead to radiation fluctuations

01 p0091 A69-10792

Probability density function measurement for microwave noise generator

02 p0221 A69-12459

Pulsed subharmonic oscillation in nonlinear regenerative selective circuits with reference to graphical analytical method for explaining behavior

03 p0385 A69-12918

High power pulse generators with four layer p-n-p-n structure, discussing design, principles and applications of semiconductor elements as modulators and switches

03 p0402 A69-12978

Giant pulse generation by Q switched water cooled CW ruby laser in narrow spectral range, discussing laser design and operation principles

03 p0435 A69-12982

High power sinusoidal pulsed current generator using Si controlled rectifiers/thyristors/as switches

03 p0404 A69-13262

Cavity arrangement to obtain pulse durations of 0.5-10 microseconds with ruby laser

03 p0441 A69-14142

Chirp pulse generation by carbon dioxide laser, discussing carrier frequency sweep

04 p0609 A69-14333

High voltage controlled amplitude rectangular pulse generators having nanosecond buildup time

04 p0597 A69-14849

Soviet book on impulse generators in transistors covering multivibrators and pulse generators with timer circuits, crystal controlled frequency and delayed feedback

04 p0578 A69-15053

Nonstationary nonlinear wave phenomena in ultrashort high intensity light pulse formation, discussing nonstationary stimulated Raman scattering and picosecond pump reduction of Raman amplification

05 p0774 A69-16316

Generation and amplification of ultrashort optical pulses

05 p0774 A69-16317

Gunn effect pulse generator for antenna arrays operating at decimeter wavelengths with external power source

06 p0895 A69-17459

Ultrashort light pulse generation and measurement of half width, using saturable dye to mode lock Nd-glass laser

06 p0935 A69-17769

Giant pulse generation by switched laser rapid pumping of neodymium doped glass laser

07 p1146 A69-18486

Picosecond laser pulses application to nonlinear optics, atomic and molecular systems transient response, optically generated plasmas, spectroscopy, high speed photography, etc

07 p1148 A69-18856

Tunnel diode pair unidirectional pulse regenerating circuits

07 p1104 A69-18892

Dynamics of injection lasers, discussing picosecond pulse generation

07 p1153 A69-19071

Pulse generation in Q switched traveling wave laser, noting effect of field amplification

07 p1154 A69-19077

Gunn diode operating to VHF range with coaxial line to generate rectangular waves and to function as memory element

09 p1467 A69-22587

Pulse generator switch consisting of avalanche transistors in series, describing voltage production and transmission, trigger pulse jitter and pulse amplitude

09 p1468 A69-22589

Pulsed J band Gunn effect oscillators performance, noting hybrid domain mode due to high bias fields

09 p1468 A69-22594

Lumped element line generators for high power pulsed sinusoidal oscillations utilizing recurrent triggering system, noting use in plasma physics experiments
10 p1662 A69-23344

Dynamics of external loss modulation and Q switching methods of generating ultrashort pulses in mode locking laser
10 p1703 A69-23624

Avalanche transistor pulse circuits temperature increase due to power dissipation, noting effects of external resistance grounding base and pinch in
11 p1845 A69-24570

Output pulse parameters of short pulse thyristor generator as function of time constant, considering rise time of switch-on process
11 p1846 A69-24615

High power short duration diffraction limited laser pulse generation with optically swept laser glass slab forming amplifier chain
11 p1897 A69-25036

Time-pulse function generator with piecewise parabolic approximation for converting value given by DC voltage or time interval into DC voltage for arbitrary functional relation
12 p2079 A69-25968

Multiframe image converter registration of space-time ruby laser spot structure changes in Q switched regime prior to giant pulse formation
12 p2083 A69-26142

Ultrahigh speed photographic cameras with exposure times between 5 and 500 nsec, using image tube and high voltage pulse generator
12 p2083 A69-26146

Synchronized microwave harmonic energy generation by filtering using DC step source feeding modified pulse forming network
12 p2041 A69-26630

Space-time characteristics of coherent light giant pulse development in laser with instantaneous Q switching, deriving equations to describe linear and nonlinear phases
12 p2110 A69-26909

Small signal quasi-stationary characteristics of pulse transistors including gain and input impedance calculations
13 p2227 A69-27423

Avalanche diodes as high power pulsed microwave sources, noting power yields and efficiencies
14 p2418 A69-28890

Nanosecond pulse generator for powering semiconductor lasers, examining circuit diagram and elements design
15 p2633 A69-30234

AM sinusoidal current pulse generator for semiconductor lasers, describing solid state circuit
15 p2633 A69-30235

Pulse generator to accommodate electronic system testing to shock response spectrum by simulating real world shock environment
15 p2585 A69-30360

RF band multimode parametric pulsed oscillations in distributed system using one dimensional resonators
16 p2758 A69-31796

Monomode giant pulse generation from neodymium glass laser by coherent pumping
16 p2797 A69-32018

Multiple mode phase locking of He-Ne laser with fixed cavity length and laser tube fixed position in cavity, generating high speed optical pulses
17 p2980 A69-32957

Shifted pulse multichannel generator producing pulses and pulse sequences time delayed with respect to reference channel
17 p2938 A69-33899

Diathermy instrument using solid state circuits to provide square wave pulses, discussing operating parameters for bipolar coagulation and advantages over spark gap instruments
18 p3134 A69-34537

Current generator circuit designed for semiconductor laser excitation with pulses modulated by sinusoidal signals at 4.75 MHz
18 p3153 A69-35256

Nanosecond pulse generator circuits based on four layer Si diodes designed for semiconductor laser excitation
18 p3153 A69-35257

Thermoanemometer filament frequency response measured by generator of velocity pulsations compared with conventional methods
19 p3308 A69-35856

He-Ne laser subnanosecond intracavity coupler consisting of coaxial krypton pulse generator and electrooptic modulator
19 p3339 A69-36823

Gunn effect pulse generator for antenna arrays operating at decimeter wavelengths with external power source
20 p3508 A69-37942

Carbon dioxide laser pulsed mode for generating giant pulses, noting applications and electron impact role
20 p3555 A69-38004

Active medium high gain during giant pulse generation shown to lead to radiation fluctuations
20 p3555 A69-38010

PULSE HEATING

Rapid annealing data for silicon transistors after reactor neutron pulse, deriving equation for defect recombination in cluster and subsequent diffusion outside cluster
06 p0975 A69-16870

Metal heating by laser, noting heating rates exponential increase with time due to optical characteristics changes
06 p0932 A69-16915

Combustion of pulse heated single Al and Be particles in various oxidizers
[WSCJ PAPER 69-2]
16 p2830 A69-32343

PULSE MODULATION

NT DELTA MODULATION

Pulse shape influence on electromagnetic compatibility and transmitter efficiency, discussing trapezoidal, raised-sine, sliced and complete error function shapes
01 p0030 A69-10631

Transient signal propagation in lossless isotropic and homogeneous plasma for Gaussian pulse modulated carrier, discussing amplitude change and carrier phase distortion
02 p0290 A69-12351

AM/PM noise conversion in solid state FM microwave signal sources, relating baseband noise power contribution to PM baseband noise power
02 p0212 A69-12462

Optimal control of open loop aperiodically modulated discrete time systems, discussing solution of associated two point boundary problem
02 p0226 A69-12732

Nonlinear operation of pulse control system by means of triple modulation
05 p0736 A69-15764

Error probability vs SNR and power spectrum of PCM/PM signal with small phase deviation, noting applications in satellite tracking
06 p0889 A69-17656

Nonlinear computer analysis of TWT small amplitude compression and small AM to PM conversion, noting coupling and circuit breaker effects
07 p1094 A69-18422

Optimum performance from planar metal ceramic triode oscillators by pulse modulation method selection, considering plate, cathode and grid modulation
09 p1470 A69-22793

Modulated wave holography for detecting and reconstructing ultrasonic beam path, noting applicability to vibrating objects analysis
10 p1694 A69-23368

Optimized receivers synthesized for narrow band radio signal filtration, comparing noise rejection properties of various pulse modulation types during speech transmission
14 p2413 A69-29464

Fast folding algorithm for detection and correlation of digital data with weak noisy pulse trains of differing periods
14 p2416 A69-29548

Compression capabilities of combined frequency and phase shift keying in radar and sonar pulse modulation using binary noise codes
15 p2568 A69-30628

Pulsed control systems sensitivity relationship to discreteness period described via differential equations
17 p2994 A69-33143

Current generator circuit designed for semiconductor laser excitation with pulses modulated by sinusoidal signals at 4.75 MHz
18 p3153 A69-35256

Laser and quasi-laser pulse modulation technique for global satellites telemetry system
19 p3272 A69-36257

Synthetic aperture radar principles, using periodic pulse modulation to construct terrain imaging radar
20 p3489 A69-37635

Analog telemetry signals generalizing frequency and pulse position modulations over coherent channels, noting added degrees of freedom function
20 p3492 A69-37713

Two-pulse limit cycle oscillation stability relation to physical parameters of pulse modulated feedback system used for satellite attitude control
21 p3688 A69-39756

Coherent pulsed radars using pseudorandom modulation, explaining pulse position modulation and radar receiving equipment
24 p4282 A69-42743

Pulse modulated feedback system for satellite attitude control, analyzing relationship between physical parameters to ensure two pulse limit cycle oscillation stability
24 p4295 A69-43318

PULSE RADAR

NT MONOPULSE RADAR

Radar cross section laboratory, discussing experimental techniques, electromagnetic range and pulse, FM/CW and CW radars
03 p0385 A69-12912

Level crossing rate meter correction for boxcar-ed and receiver noise readings in incoherent weather radars
04 p0557 A69-14915

Pulsed radar quantum paramagnetic amplifier protection from driving pulse leakage power by transient processes
05 p0728 A69-15644

Statistical analysis of Radicord/radar digitizing and recording/ clutter and signal spectra and moving target detection by pulse radar
05 p0721 A69-16619

Range-Doppler processing in pulsed radar applied to imaging of rigid rotating body with motion compensating resolution cells
08 p1270 A69-19861

Pulse compression radar employing same dispersive line for signal generation and reception
08 p1271 A69-19918

Digital simulation optimizing parameters of digital equipment to measure target azimuths in pulsed surveillance radar system, establishing optimum echo pulse quantization threshold
15 p2563 A69-30138

Complex pulsed radar signals synthesis with uncertainty function having principal maximum and small secondary maxima for radar stations and wideband communications systems
15 p2563 A69-30140

Residual phase term influence on compressed signal shape, analyzing linearly frequency modulated signal spectrum and sidelobe suppression in pulsed radar
15 p2564 A69-30143

Direction finding accuracy of pulsed radar with binary-quantized detector signals, discussing azimuth minimum variance and quantization threshold optimization
15 p2566 A69-30333

Pulse radar quantum paramagnetic amplifier protection from saturation by transmitter power, using linear electrical bias of EPR line
15 p2579 A69-30956

Pulsed radar quantum paramagnetic amplifier protection from driving pulse leakage power by transient processes
16 p2762 A69-32501

Frequency agility techniques applied to target detection in noncoherent pulsed radar systems
17 p2917 A69-32919

Radar target simulator approximating pulse radar receiver output for evaluating amplitude-sensing video target detection devices
17 p2921 A69-33629

Sampled data system with built-in data processing for observation of fine grain characteristics of pulsed signals used in radar systems
17 p2934 A69-34076

Acoustic surface waves on thin film for pulse compression radar dispersive delay line, describing delay characteristic synthesis and control
19 p3267 A69-35929

Radar astronomy, discussing planetary surfaces study techniques, target/signal interactions, planet cross sections, delay and Doppler spectra
20 p3491 A69-37650

Very short pulses effect on aircraft echoes, noting echoing area reduction as resolution cell diminishes
21 p3672 A69-38755

Active weighted pulse compression radar receiver output waveform analysis for amplitude, phase and frequency modulation, noting effects of spectrum weighting mismatch parameter
23 p4132 A69-42548

Coherent pulsed radars using pseudorandom modulation, explaining pulse position modulation and radar receiving equipment

24 p4282 A69-42743

Optimal allocation of pulses for array radar tracking large number of targets simultaneously, using discrete time maximum algorithm

24 p4283 A69-43311

PULSE RATE

Hot gas flows turbulence linear component intensity and frequency spectrum using optical measurement of pulse velocities

06 p0926 A69-17540

Pulsating radio source pulse arrival time measurements at 1919 plus 21, determining highest SNR

07 p1214 A69-18665

Sequence pulse stuffing technique for rate equalization of digital channels, discussing coding effect and capacity for word signaling

07 p1080 A69-19094

Pulse velocity in self locked He-Ne laser, noting air turbulence effects prevention

09 p1514 A69-21347

Human physiology for exposure to acute hypoxia studied with variation pulsograms and indices of external respiration and pulmonary gas exchange

10 p1647 A69-23592

Ultrawideband DC transistor amplifier for pulsed switching circuits with subnanosecond risetimes, discussing multistages with feedback dipoles, transient response and drift problems

11 p1854 A69-25612

Angle-to-code converter designed on basis of quantum magnetometers frequency sensors, transforming vector sum of bias magnetic fields into pulse repetition rates

12 p2016 A69-25963

Statistical characteristics of stationary stochastic pulse train specified by probability generating function, noting power density

12 p2030 A69-26383

Fourier analysis of ionospheric wave reflection pulses for frequency contents and relative phase angles

14 p2440 A69-29351

Ultrasonic pulse velocity and attenuation measurement in presence of noise, using coherent detection and signal averaging

14 p2449 A69-29564

Pulsar NP 0532 period measurements at various frequencies, obtaining accuracy in timing data reduction by linking pulse arrivals over interval of months

15 p2680 A69-30232

Emission from pulsating radio sources, discussing pulse amplitude variations and frequency structure for neutron stars and white dwarf

17 p3036 A69-33636

Pulsation periods for pure He white dwarfs calculated by Chandrasekhar equation including relativity and rotation effects

17 p3037 A69-33641

NP 0532 slow down rate, using quadratic least squares method

18 p3191 A69-34317

Recording instrument paper speed effect on pulse wave measurements precision, discussing multiple observer studies of left ventricular ejection time

19 p3258 A69-36449

Coriolis acceleration effect on vestibulo-vegetative and vestibulo-somatic reflexes of humans subjected to forward tilting, noting pulse and respiration rates

20 p3472 A69-37259

Coherent radiation short pulses from mode locked laser permitting schlieren photography of plasma growth

21 p3736 A69-38795

Human performance assessed by pulse rate increment at onset of exercise on bicycle ergometer and decrement during recovery after fasting

21 p3655 A69-38910

Output power dependence of repetitively Q switched carbon dioxide laser on repetition time measured with thermopile, noting decrease in mirror system

23 p4173 A69-41566

Pulsatile flow in coronary arteries simplified model compared with experiment in anesthetized dogs

23 p4098 A69-42103

Optical detection of pulsars with emphasis on CP 1919, discussing optical variation

23 p4218 A69-42325

Errors in estimating cardiac function from aortic and peripheral pulses, using cadaver experiments

24 p4262 A69-42728

PULSE RECORDERS

U COUNTERS

PULSE TIME MODULATION

Fluidic pulse time modulated angular position sensor for two axis hydrostatically supported gyroscope

02 p0249 A69-12087

Ultrashort light pulses problems in measurements of time characteristics and instantaneous power of laser radiation

09 p1516 A69-21575

Stability conditions for nonlinear pulse width and pulse time modulation systems, considering pulse element properties and system continuous part frequency characteristic

09 p1476 A69-22672

Time/frequency technology using time-ordered reporting digital data for air traffic control to avoid airborne collision

[AIAA PAPER 69-795]

19 p3367 A69-35635

False signals formation during random pulse noise in single command channels with PTM coding, noting code value and redundancy

19 p3278 A69-36595

PULSED JET ENGINES

Multipulse thruster module design and development tests for spacecraft attitude control, noting micropulse solid propellant rocket motor

02 p0194 A69-11762

Pulsed MPD arc jet electric propulsion system requirements, examining physical constraints, pulse duration, duty cycle, power network structural details, etc

[AIAA PAPER 69-269]

09 p1560 A69-21215

PULSED LASERS

NT Q SWITCHED LASERS

Maximum power efficiency of pulsed injection laser with Fabry-Perot cavity expressed in terms of two dimensionless geometric variables

01 p0089 A69-10119

Laser CRT with beam pumped aluminumized CdS crystals, discussing single spot low duty operation

01 p0039 A69-10175

Optical pulse generator consisting of solid state laser with saturable absorber at cavity end using perturbation theory and Maxwell equations

01 p0089 A69-10179

Exploding wire heating technique using combination of focused laser beam electric field intensity and pulsed power electric current

01 p0090 A69-10666

Carbon dioxide laser pulsed mode for generating giant pulses, noting applications and electron impact role

01 p0090 A69-10787

Active medium high gain during giant pulse generation shown to lead to radiation fluctuations

01 p0091 A69-10792

Pulses generated by mode locked Nd glass laser, analyzing compression by gratings

01 p0091 A69-10817

Pulsed nitrogen laser design involving gas discharge tube fed by low impedance parallel plate transmission line

01 p0091 A69-10842

Deuterium gas ionization over high pressure range under action of short pulse Q switched neodymium glass laser, noting breakdown wave existence

02 p0255 A69-11545

Deuterium plasma evolution and creation modes obtained by short pulse laser discharge in gases, discussing detonation and phase wave ionization mechanisms

02 p0288 A69-12040

Pulsed ruby laser power supply incorporating facilities for variable output, automatic cutoff for fully charged capacitors and automatic/manual triggering

02 p0256 A69-12095

Laser pulse parameters generated in stationary locked mode regime with resonance modulation of losses

02 p0258 A69-12641

Two photon fluorescence technique for display of picosecond laser pulses, discussing mode locking and ruby laser contrast ratios

02 p0259 A69-12654

Mode locking and ultrashort pulses in giant pulses in giant pulse ruby laser with heated nitrobenzene or alpha-chloronaphthalene in resonator

02 p0259 A69-12655

Giant pulse generation by Q switched water cooled CW ruby laser in narrow spectral range, discussing laser design and operation principles

03 p0435 A69-12982

Resonance light pulse propagation in one dimensional medium containing n and m quantum emitters located in Fabry-Perot resonator

03 p0437 A69-13039

Ruby laser light beam self focusing in sodium chloride and potassium bromide crystals

03 p0438 A69-13051

Time dependent photoelectron multiplier with low noise for recording long wave laser light pulses

03 p0440 A69-13264

Light pulse narrowing in laser in linear mode operation with inertialess bleachable filter

03 p0440 A69-13716

Single picosecond mode locked optical pulse selection from train of pulses of Q switched Nd-glass laser using optics external to oscillator cavity

03 p0441 A69-14185

Laser ranging and illumination systems, discussing direction of pulsed monochromatic radiation to illuminate scene and utilization of reflected radiation for imaging

03 p0442 A69-14191

Optical pumping distortion compensation in glass laser rod by changing coolant temperature, obtaining mode locked laser pulses

04 p0609 A69-14286

Power and time characteristics of He-Ne laser pumped by microwave pulses

04 p0610 A69-14423

Relaxation rates of water vapor laser lines obtained with split discharge laser

05 p0771 A69-15810

Generation and amplification of ultrashort optical pulses

[IEEE PAPER H-12]

05 p0774 A69-16317

Self Q switching of ruby lasers at 77 K, noting saturable absorber giant pulse process obtained by shielding part of laser rod from pump

05 p0776 A69-16332

Pulsed water vapor laser with single Brewster window for operation between 20 and 120 microns, comparing performance with ordinary laser

05 p0776 A69-16334

Lunar laser ranging for testing Einstein and Brans-Dicke gravitational theories, discussing pulse transit time and dominant nonNewtonian correction

05 p0825 A69-16362

Pulsed ruby laser threshold and output energy for different relative orientations of rectangular prism and ruby crystal main crystallographic axis

05 p0777 A69-16526

Computer tape controlled pulsed externally excited gas laser mask making machine with micropositioning coordinate table for integrated circuit fabrication

06 p0931 A69-17200

Pulsed laser emission of atomic N in mixture of molecular N and He, noting effects of pressure and frequency and duration of excitation pulses

06 p0933 A69-17258

Gas laser operating on pure O-He-Ne-Ar mixture at liquid N temperatures, noting atomic O transitions, pulsed operation and energy level populations

06 p0933 A69-17259

Mode locked Nd glass laser to pump organic dye laser, obtaining continuously tunable picosecond pulses

06 p0935 A69-17759

Ultrashort light pulse generation and measurement of half width, using saturable dye to mode lock Nd-glass laser

06 p0935 A69-17769

Plasma ionization enhancement by laser line radiation matched to specific atomic transitions

[AIAA PAPER 69-47]

06 p0972 A69-18186

Emission of Nd giant pulse laser with high repetition rate and peak power to generate second harmonic radiation in lithium niobate single crystals

07 p1144 A69-18469

Giant pulse generation by switched laser rapid pumping of neodymium doped glass laser

07 p1146 A69-18486

Tandem amplifier system of glass and selenium-oxichloride liquid lasers, discussing input power/output pulse relation and population inversion density measurement

07 p1147 A69-18487

Pulse synchronism of solid state lasers Q switched by same rotating prism, discussing pulse shifting to obtain radiation in filaments

07 p1147 A69-18488

Picosecond laser pulses application to nonlinear optics, atomic and molecular systems transient response, optically generated plasmas, spectroscopy, high speed photography, etc

07 p1148 A69-18856

Pulse broadening in MHD copper vapor laser

07 p1149 A69-18904

Pulses from Q switched carbon dioxide laser for studying Q switching techniques
[IEEE PAPER G-2] 07 p1150 A69-19054

Time resolved spectrum of high current pulsed argon laser discharge, noting primary laser output and afterglow
[IEEE PAPER L-12] 07 p1152 A69-19068

Circulating liquid laser system using neodymium in selenium oxychloride, discussing cooling advantages and components
[IEEE PAPER M-70] 07 p1153 A69-19069

Laser induced gas breakdown by focusing nanosecond pulses in air and deuterium
[IEEE PAPER U-3] 07 p1155 A69-19085

Giant pulse production of Nd-glass laser with aid of coherent pumping by second harmonic of Q switched laser, noting pulse duration 07 p1156 A69-19333

Nonlinear amplification of powerful light pulses in Nd glass 08 p1323 A69-19946

Ultrashort optical pulses of coherent light, discussing propagation in inhomogeneously broadened medium of two level systems 08 p1324 A69-20083

Small signal pulsed gas laser amplification limits, discussing time dependency, temperature effects, relaxation rates and energy transfer 08 p1324 A69-20098

Reflection holograms with single mode pulsed ruby laser 08 p1313 A69-20164

Carbon dioxide laser with two gas absorption cells in cavity for emission wavelength control and HF pulsed mode of operation 08 p1327 A69-21088

Mode locking via nonlinear polarizations in multimode solid state lasers 09 p1514 A69-21344

Pulse velocity in self locked He-Ne laser, noting air turbulence effects prevention 09 p1514 A69-21347

Electro-optical shutter for Nd-glass laser with high peak power pulses, discussing switching time, contrast ratio and synchronization 09 p1493 A69-21422

Far IR laser pulse shape and duration 09 p1515 A69-21424

Laser triggered spark gap and Pockels cells producing consistently repeatable controlled duration pulses 09 p1515 A69-21427

Ultrashort light pulses problems in measurements of time characteristics and instantaneous power of laser radiation 09 p1516 A69-21575

Mode locked He-Ne laser pulses compression by multiple reflections from interferometer after application of linear electro-optic frequency sweep 09 p1516 A69-21745

Laser oscillations, discussing oscillation frequency, oscillation time, noise and spectrum width, pumping and lasing materials, line broadening and giant pulse generation 09 p1517 A69-22119

Pulsed laser radar and applications to upper atmosphere observation equipment and distance measuring devices 09 p1456 A69-22132

Pulsed ruby laser of small output for hole drilling, studying correlation of vaporization, hole diameter and depth with laser output 09 p1504 A69-22247

Heat transfer effect on population inversion time variation in pulsed carbon dioxide laser and molecules excitation rates dependence on gas mixture composition 09 p1519 A69-22289

Temperature effect on pulsed laser action on electron transitions in diatomic molecules for rotational relaxation, discussing excitation mechanisms 09 p1520 A69-22654

Alkali halide single crystals disintegration by laser radiation differs as function of crystal physicochemical properties and band structure 10 p1745 A69-23322

Noble gas additives for triggering stability of pulsed argon ion lasers, discussing repetition rate and power loss 10 p1702 A69-23341

Pulsed and CW lasers glass crystals temperature fields determination, including tangential and axial thermal stresses 10 p1702 A69-23428

Laser pulse picosecond substructure measurements, using pulse compression and second harmonic generation techniques 10 p1703 A69-23514

Dynamics of external loss modulation and Q switching methods of generating ultrashort pulses in mode locking laser 10 p1703 A69-23624

Resonator interferometry of pulsed submillimeter wave lasers, analyzing mode structure, pulse shapes and molecular mechanism of laser emission 10 p1705 A69-23810

Sulfur dioxide-helium laser pulsed and CW submillimeter outputs 10 p1706 A69-24005

Pulsed tunable lasers, emphasizing dye lasers for visible and near visible light in specialized spectroscopy 11 p1893 A69-24343

Pulsed molecular nitrogen laser positive UV and IR systems interaction under varying gas pressure, applied voltage and tube diameters 11 p1893 A69-24346

Monograph on laser stroboscopy in megahertz range covering spark photography comparison, concept of modes, resonators, applications, etc 11 p1893 A69-24368

Pulsed solid state Nd doped calcium tungstate fundamental longitudinal modes selection by insertion of Fabry-Perot interferometers, lenses and diaphragms into resonator 11 p1894 A69-24471

Ruby laser unsteady modes with ruby filter, discussing conditions for pulsed, monopulse and steady mode transitions, with formulas for steady emission 11 p1894 A69-24619

Giant pulse buildup time in Nd-glass laser with passive shutter determined by comparing Q factor and peak power ratios of different modes 11 p1894 A69-24621

Pulsed laser holography advantages for recording small objects in motion and holographic interferometry advantages for complex surfaces and time-separated events 11 p1883 A69-24682

Pulsed laser holography for recording interferograms of laser created plasma, discussing laser source properties, spatial and spectral coherence, double pulse mode, etc 11 p1895 A69-24683

Coherent pulse laser holography for front and back lighted holograms of moving objects 11 p1895 A69-24686

Holographic reconstruction of spatial distribution of laser light field within and outside resonator, noting suitability for pulsed laser analysis 11 p1885 A69-24919

Airborne pulsed laser system for altimetry, determining height by measurement of transit time for pulse traveling to ground and back 11 p1885 A69-25035

High power short duration diffraction limited laser pulse generation with optically swept laser glass slab forming amplifier chain 11 p1897 A69-25036

Far IR CW gas laser design for maximum output, discussing pulsed operation, wavelength measurement and radiation detection 11 p1898 A69-25051

Pulsed laser emission from carbon dioxide collisionally pumped by vibrationally excited DF produced by reacting fluorine oxide with deuterium 12 p2104 A69-25986

Second harmonic conversion of giant pulse Nd laser emission related to beam divergence and space-time distribution of radiation, noting energy relationship 12 p2104 A69-26022

Temperature regime of pulsed laser with pump lamp located in cylindrical rod cavity, discussing adiabatic and nonadiabatic pumping 12 p2104 A69-26025

Photoelectric recorder with timebase image converter tube for investigating ultrashort light pulse transient response of laser 12 p2083 A69-26139

Holography with pulsed lasers for high speed recording of amplitude and phase disturbances and rapid transient events, noting reconstruction evaluation problems 12 p2087 A69-26171

Deformation measurement by laser pulse holographic method, discussing laser source choice criteria 12 p2087 A69-26175

Regulated pulse lasers under free oscillation for photographing distant objects by illumination with shortened light pulses 12 p2089 A69-26190

Simultaneous HCN and HOH laser emission in pulsed discharge through mixture containing H, C, N and O 12 p2107 A69-26330

Pulsed HCN sealed laser long term operation, discussing behavior of 311 and 377 micron emissions 12 p2107 A69-26391

Nd-doped glass pulsed laser with selected second harmonic radiation and KDP crystal frequency converter operating T 12Hz and 530 nm 12 p2108 A69-26594

Standing wave theory for steady state performance of Raman laser oscillator extended for time variation of exciting laser pulse 12 p2108 A69-26634

Analytic expressions for predicted widths of AM and FM mode locked pulses in homogeneous lasers 13 p2270 A69-27191

Breakdown in air produced by picosecond mode locked laser pulses showing evidence for self focusing 13 p2270 A69-27196

FM laser pulse formation time characteristics noting modulated resonator losses 13 p2272 A69-28114

Pulsed laser satellite tracking system, noting tracking mount adjustment 13 p2222 A69-28192

Pulsed laser holographic interferometry of density field created by high speed projectile motion in air [AIAA PAPER 69-347] 13 p2263 A69-28282

Trapped aerosols below temperature inversions causing lidar echoes in troposphere layers, discussing simultaneous balloon refractometer, thermometer and ground based lidar soundings 13 p2254 A69-28475

Carbon dioxide laser inversion kinetics, combining pulse pumping with Q switching to observe rise, life and decay times 14 p2457 A69-28926

Optically swept glass slab laser design, discussing pulse length and peak power 14 p2457 A69-28930

Pulsed lasers with pure carbon dioxide and mixture with N and He, discussing inversion mechanism, peak emission power and gas temperature effects in different modes 14 p2458 A69-29162

Passive Q switch laser single pulse formation time and spectral width using balance equations 14 p2458 A69-29166

Fluorite crystal laser activated by divalent samarium, discussing characteristics in pulsed operation mode 14 p2458 A69-29328

Undulation in output waveforms of pulsed water vapor laser observed with In-doped Ge detector 14 p2461 A69-29887

Airborne pulsed lasers for near shore bathymetric measurements, discussing feasibility results 15 p2609 A69-30459

Mechanical testing of high temperature materials subjected to thermal cycling by high power pulsed laser beam 15 p2636 A69-31512

Power supplies for ruby, YAG and glass lasers, emphasizing design equations and component selection 15 p2636 A69-31527

Pulse duration control by two photon absorption, using GaAs as nonlinear element inserted in neodymium-glass laser cavity 16 p2796 A69-31798

Monomode giant pulse generation from neodymium glass laser by coherent pumping 16 p2797 A69-32018

Passive mode locking of pulsed Nd-YAG laser using saturable absorber, noting two photon fluorescence contrast ratio 16 p2797 A69-32019

Repetitively Q switched ruby laser applied to frequency conversion, stimulated Raman scattering and vacuum UV generation 17 p2980 A69-33027

GaAs diode laser pulse train emission during pumping near threshold 17 p2982 A69-33421

Laser action and spontaneous emission at atomic oxygen transition, discussing pulsed emission mode in argon-oxygen laser 17 p2982 A69-33633

Laser pulse development dynamics taking into account phase relations between field and active medium polarization

17 p2983 A69-33695

Liquid rocket combustion investigated by pulsed ruby laser holography at sea level rocket engine test stand, noting laminated glass acrylic window byproduct [AIAA PAPER 69-471]

17 p3075 A69-34200

Electrooptical distance measurement based on laser pulse traveling time and phase measurements to determine satellite range

18 p3103 A69-35199

Semiconductor optical quantum amplifiers in pulse mode operation, describing arrangement for studying performance including pulse duration and current controls

18 p3153 A69-35258

Radiation dynamics of semiconductor GaAs injection laser with pulsed and continuous modes operation of diodes

18 p3154 A69-35495

Time variation of laser flare plasma temperature related to pulse parameters, using soft X radiation from plasma

18 p3154 A69-35496

High power pulsed laser welding system for structural alloys and parts, discussing pulse length, repetition rate, shielding and applicability

19 p3320 A69-35556

Focused Gaussian laser beam expansion due to thermal changes in refractive index of air, noting focused spot area increase with pulse energy

19 p3330 A69-35601

High speed photography using multiply pulsed ruby laser, Pockels cell modulation and smear camera for isochromatic and photoelastic pattern recording

19 p3306 A69-35731

Relation between angular divergence, spectral characteristics and kinetic behavior of laser operating in various pulsed modes

19 p3333 A69-35879

Frequency shift dependence in transition of Rb 87 atoms on pulsed pumping intensity, discussing continuous and pulsed indication and peak determination

19 p3336 A69-36345

Pulse ruby lasers with mercury lamps for pumping noting improved efficiency, power and temperature regime due to reduced IR radiation

19 p3336 A69-36347

Gas laser oscillation mode selection and self synchronization based on separation in two mirror cavity with nonlinear absorption

19 p3336 A69-36350

Pulsed water vapor laser high power operation and strongest component wavelength measurement

19 p3337 A69-36416

Second harmonic radiation generation in nonlinear dielectric by broadband short pulse optical signals

19 p3278 A69-36693

Rotating mirror Q switched carbon dioxide laser for high peak powers, analyzing pulse structure and duration dependence on collision induced relaxations

19 p3338 A69-36694

Flat wire grid calorimeter used as radiation sensor in measuring pulsed ruby laser

19 p3339 A69-36755

Surface cavity profiles created by pulsed laser on Ti, Al, Cu, Pb and Zn, compared with isotherms computed from heat conduction models

20 p3552 A69-36917

A scope laser radar system using Q switched solid state laser pulses, discussing configuration and performance

20 p3487 A69-37283

Holographic image range contouring produced by multifrequency emission from resonant output reflector in pulsed ruby laser cavity

20 p3540 A69-37733

Carbon dioxide laser pulsed mode for generating giant pulses, noting applications and electron impact role

20 p3555 A69-38004

Active medium high gain during giant pulse generation shown to lead to radiation fluctuations

20 p3555 A69-38010

Nitrogen gas breakdown threshold dependence on pressure during picosecond ruby laser pulse, discussing photoionization leading to breakdown in electromagnetic wave field

20 p3555 A69-38067

Primary excitation mechanism in pulsed carbon dioxide lasers found to be electron impact

20 p3556 A69-38122

Solid state traveling medium laser pulsed emission characteristics and nonlinear intensity distribution

21 p3735 A69-38438

Gas molecule collision influence on photon echo intensity produced by two linearly polarized laser pulses incident on sulfur hexafluoride

21 p3774 A69-38589

Giant Q switched laser pulse interaction with C target in background gas showing complex luminous shock structure near target as function of time

21 p3736 A69-38942

Coherent light emission by molecules excited by laser pulses having duration comparable to active medium polarization relaxation time

21 p3737 A69-38999

Mode locked laser output intensity, studying effect of random phase variations on pulses

21 p3741 A69-39684

Power density and time history of pulsed molecular nitrogen laser, discussing dependence on fill pressure and electric circuit parameters

21 p3742 A69-39779

Pulse ruby laser-smear camera ultrahigh speed multiple frame recording system, describing applications to transmitted and scattered light photoelasticity

22 p3944 A69-40076

Time dependent mathematical double acceptor model including heat effects for analyzing Q switching and stimulated emission time delays in pulsed junction lasers

22 p3962 A69-40560

Spiking behavior detection in Q switched light output from GaAs pulsed junction laser, noting width at high pumping levels

22 p3963 A69-40563

Carbon dioxide and carbon dioxide mixture mirror Q switched laser peak power generation, using pulsed excitation

22 p3963 A69-40564

Q switched pulsed discharge carbon dioxide laser, determining peak power dependence on delay between pulse excitation and Q switching

22 p3963 A69-40566

Emission dynamics and fine pulse structure in GaAs injection lasers, determining pulse duration and amplitude dependence on current and resonator length

22 p3963 A69-40603

Photographic study of epoxy resin breakdown kinetics under pulsed laser beams, showing crack area as function of time

22 p3973 A69-40743

Spectrum characteristics of plasma generated by pulses of solid state laser radiation on metals and alloys in regular and quasi-stable regimes of emission

22 p3964 A69-40793

Frequency discrimination in optical harmonic generators, discussing spectral width of wideband laser for supershort pulses and spectral device, using frequency dependence of mode locking direction

22 p3965 A69-40964

Longitudinal modes locking and ultrashort light pulse generation in laser cavity resonator with nonlinear refractive index

23 p4171 A69-41389

Pulsed Hg ion-He laser operation, revealing transition in near IR

23 p4171 A69-41393

Mode locked ruby laser with picosecond pulses using rooftop prism cavity with helical flashtube for pumping

23 p4172 A69-41395

Laser pulse effects on bones of rats, observing metabolic deviations in Ca 45 uptake

23 p4101 A69-41464

Intensity of optical pulses from CW GaAs injection lasers observed with fast sampling techniques

23 p4173 A69-41500

Ultrashort laser light pulses self focusing and determination of focal points coordinates

24 p4328 A69-43068

High power ruby laser pulse generation by diffraction modulator, employing modulated ultrasonic traveling waves at minimum resonator transmission losses

24 p4328 A69-43163

Transitions competition in He-Ne laser pulse operating in single mode with nonuniform gain saturation

24 p4328 A69-43165

PULSED RADIATION

NT ELECTROMAGNETIC PULSES

Spectral fine structure in emission from pulsars, noting correlation between fading and spectral change

01 p0150 A69-10273

Thermoelectric radiometer for transient radiant flux short duration pulse measurement, using thermally induced depolarization of polymer film dielectric [AIAA PAPER 68-403]

02 p0250 A69-12392

Ruby laser modifications for pulse transmission mode operation and cavity dumping, noting peak power output

02 p0257 A69-12410

Additive noise measurement in microwave power amplifiers under continuous wave and pulsed conditions

02 p0221 A69-12454

Short laser radiation pulses spectral characteristics determination with device converting laser emission frequency by nonlinear electro-optical crystals

02 p0257 A69-12560

Ferroelectric strontium barium niobate as sensitive detector of single pulse IR radiation, noting application to Q switched carbon dioxide laser output

02 p0300 A69-12623

Unsteady phenomena during light pulses interaction in media with polarization, considering group delay, dispersion spreading and space-time analogy

02 p0259 A69-12646

Two photon fluorescence technique for display of picosecond laser pulses, discussing mode locking and ruby laser contrast ratios

02 p0259 A69-12654

Mode locking and ultrashort pulses in giant pulses in giant pulse ruby laser with heated nitrobenzene or alpha-chloronaphthalene in resonator

02 p0259 A69-12655

Measurements of pulsars CP 0834, CP 0950, CP 1133 and CP 1919, discussing pulse intensities and shape, submillisecond structure, intensity variations, periods and positions

02 p0328 A69-12726

Pulsed electromagnetic signal reflection from plane boundary of absorbing medium

03 p0397 A69-13711

Single picosecond mode locked optical pulse selection from train of pulses of Q switched Nd-glass laser using optics external to oscillator cavity

03 p0441 A69-14185

Single punch through silicon avalanche diode structure and two distinct modes of oscillation making possible pulsed generation of microwaves

04 p0573 A69-14334

Moment method used to determine pulsed radiation instability propagating in luminescent scattering medium

04 p0610 A69-14425

Pulsating radio sources near Crab Nebula noting possible coincidence with nebula, pulse dispersion and interstellar electron density

04 p0659 A69-14977

High repetition rate pulsed illuminator using electrodeless halogen discharge for rapid light extinction

04 p0599 A69-15021

Extensive air shower radio pulse polarization, using log periodic EW- and NS-arm antennas

04 p0595 A69-15425

Pulse radiation effect on dielectric constant of sintered CdS photoresistors, discussing capacitance dependence on intensity, type and frequency of light

05 p0806 A69-15694

Electrical properties of xenon pulse plasmas with high power dissipation, measuring discharge pressure and radiation distribution as function of voltage drop

05 p0801 A69-15746

Dynamic response of solids induced by charged particle interaction noting laser interferometric measurement of surface stresses

05 p0771 A69-15817

Probability theory and Laplace functions used to determine pulse coincidence probability of two random independent pulse streams in time

05 p0719 A69-16224

Pulsar pulse period stability, noting slowing down in several sources

05 p0825 A69-16353

Nuclear pulsed radiation dosimeter based on strain gage measurement of induced thermal expansion, noting separation of neutron and gamma ray components

06 p0922 A69-16892

Solid target output pulse magnitude and direction dependence on angle of incidence of intense laser beam

06 p0935 A69-17686

Ultrashort light pulse generation and measurement of half width, using saturable dye to mode lock Nd-glass laser

06 p0935 A69-17769

Synchronizing ruby and Nd-glass laser pulses by means of passive bleachable dye solution liquid Q switch
07 p1147 A69-18530

Universal instability theory relevance to pulsating optical auroras and fast quasi-periodic variations of auroral X ray fluxes
07 p1125 A69-18852

Q switched laser quasi-periodic short pulse emission pattern evolution from broadband noise source, using fluctuating dipole model
07 p1149 A69-18897

Dynamics of pulsed microwave breakdown in nonuniform field at waveguide fed mica aperture, noting electric field distribution change due to initial plasma configuration
07 p1107 A69-19448

Hamilton-Jacobi equations of motion for classical electron in presence of traveling pulse of electromagnetic radiation, solving radiation pulse shape orbits
08 p1377 A69-19790

Picosecond light pulse measurement by two photon excitation of photographic film
08 p1313 A69-20165

Picosecond light pulse generation by solid state laser interpreted by fluctuating intensity spikes arising from random emission interference in out-of-phase modes
08 p1326 A69-20548

Polarization variations in radio pulses from pulsar CP 0328, noting possible origin in synchrotron radiation from collimated electron beam
08 p1397 A69-20694

Time dependent behavior of atomic light emitted from pulsed helium afterglow, noting absorption measurements and spectrometric system
08 p1356 A69-20743

Image orthicon tube to detect low intensity pulsed light signals, formulating SNR in terms of resolvable image points
08 p1317 A69-21085

Plasma acceleration by pulsed electromagnetic traveling wave, discussing stable column formation and acceleration loss processes
09 p1544 A69-21301

Pulsar NP 0532 identified with Baade south preceding star in Crab Nebula, noting pulsed optical radiation
09 p1592 A69-21458

Vela pulsar polarization and periodicity observations supporting rotational model vs radial pulsations as radio emission source
09 p1592 A69-21461

Crab Nebula pulsar properties including pulse shape, dispersion and strong pulse emission
09 p1592 A69-21462

Ultrashort light pulses problems in measurements of time characteristics and instantaneous power of laser radiation
09 p1516 A69-21575

Radio emission time variation from radio object associated with Sco X-1
09 p1603 A69-22268

Gravitational waves emitted by relativistic, nonrotating, nonradially pulsating stellar model, discussing polarization and energy and momentum transport
09 p1605 A69-22417

Anomalous mode avalanche diodes for pulse power generation noting output, efficiency, mode of operation, microwave oscillations and IMPATT diodes
09 p1466 A69-22455

Anharmonic pulsations of 15.6 solar mass star in helium burning phase, discussing radiation pressure, third order terms, higher modes and magnitude variation effects
10 p1771 A69-22853

Laser pulse picosecond substructure measurements, using pulse compression and second harmonic generation techniques
10 p1703 A69-23514

Capture of parametrically coupled waves by pulses and beams of pumping radiation in case of different group velocities directions
10 p1705 A69-23956

Probability of ocular damage for illumination by pulsed laser beam transmitted through atmosphere, developing safety nomograph for eye hazard analysis
11 p1830 A69-24843

High power short duration diffraction limited laser pulse generation with optically swept laser glass slab forming amplifier chain
11 p1897 A69-25036

Carbon dioxide laser for production of high peak power pulse, discussing mw peak power design and oscillation problem in high gain amplifiers
11 p1899 A69-25053

Nonadiabatic linear oscillations of stellar atmosphere, discussing wave coupling with stellar pulsation
11 p1961 A69-25104

Optical flashes recorded from Crab Nebula M1 close to central double star with periodicity equal to radio pulses discovered earlier
11 p1962 A69-25250

Auroral zone X ray pulsations during great geomagnetic disturbance and auroral electrojet development to maximum phase, noting atmospheric feedback modulation
12 p2065 A69-26109

Repetitive Q switched laser light source for interferometry, holography and high speed photography
12 p2087 A69-26170

Q switched ruby laser application to high speed shadow photography and holography in study of gas flow around ballistic body
12 p2088 A69-26177

Elastoplastic stress wave generation by penetration of impulsive electromagnetic radiation through thin surface layer of solid
12 p2179 A69-26215

Crab Nebula X ray pulse detection attempt during balloon flight of telescope
12 p2149 A69-26226

Pulsed or continuous radiation generated in laser having active element of neodymium glass fragments
12 p2109 A69-26715

Pulsars discovery, emission, regularity, narrow frequency band and pulse changes, physical nature and aspects of Crab Nebula source
12 p2160 A69-26895

Vela pulsar investigated for optical pulsations, noting negative result for expected brightness
12 p2173 A69-27173

Intense ultrashort pulse widths determined by two photon fluorescence patterns, using model of partial laser mode locking
13 p2270 A69-27198

Nuclear energized pulsational instability of stars based on linear quasi-adiabatic theory, including models with hydrogen burning shells
13 p2340 A69-27576

Hypervelocity impact flash resolved into sub-microsecond continuum radiation pulse succeeded by slow rising long duration light pulse from neutral atomic line emission
13 p2313 A69-28296

Optical signal conversion efficiency and threshold relationships in pulsed rangefinding systems, considering effects of noise obeying Poisson distribution
14 p2412 A69-29324

Short laser pulses reflection from artificial fog and smoke, showing dependence on reflecting medium attenuation coefficient
15 p2562 A69-30077

Short laser radiation pulses spectral characteristics determination with device converting laser emission frequency by nonlinear electro-optical crystals
15 p2633 A69-30257

Solar simulator with pulsed Xe arc tube, describing operating characteristics, spectral emission and simulator-sunlight correlation
15 p2586 A69-30385

Two photon interaction between ultrashort light pulse and medium, showing pulse propagation through medium without absorption
15 p2634 A69-30966

DQ Herculis photometric measurements synchronized with white dwarf component pulsation, discussing equipment, eclipse curve and binary period dependence on time
16 p2862 A69-32373

Nanosecond optical pulses from Crab pulsar NP 0532 detection indicating negative observations
16 p2865 A69-32801

Holographic recording of temporal coherence pattern of wave train from pulsed radiation source, investigating single mode ruby laser
17 p2973 A69-33114

Pulse propagation through antipode, calculating time domain response of fields near axial caustic
18 p3100 A69-34233

Pulsed hard X radiation from NP 0532, discussing slow down rate and luminous intensity
18 p3186 A69-34316

Radiation dynamics of semiconductor GaAs injection laser with pulsed and continuous modes operation of diodes
18 p3154 A69-35495

Second harmonic radiation generation in nonlinear dielectric by broadband short pulse optical signals
19 p3278 A69-36693

Ionosphere absolute phase height measurement methods independent of virtual height, using fixed frequency CW emission and pulsed sounding
20 p3520 A69-37032

Spectra, fading and pulse structure of pulsars noting electron density, polarization, second periodic pulsation, etc
21 p3802 A69-38826

Breakdown mechanism in GaAs, Si and CdSe semiconductors under intense light pulses ascribed to thermal impact
21 p3737 A69-39042

UHF radio pulses from zenith associated with extensive air showers, estimating threshold energy of scintillation trigger system
21 p3792 A69-39613

Radio pulse emission from ionized disk of cosmic ray extensive air showers, noting importance of charge separation in geomagnetic field and selective positron absorption
21 p3792 A69-39614

Device measuring light pressure and pulse energy of laser emission by converting kinetic energy into potential energy of twisted elastic suspension thread
22 p3961 A69-40246

Polymer film breakdown under impact of supersonic plasma beam pulses from capillary discharge chamber, including photomicrographs of cavities and structural defects
22 p3974 A69-41031

Optical ultrashort pulse compression with paired diffraction gratings in terms of phase shift frequency dependence and Fresnel diffraction analogy
23 p4171 A69-41392

Pulsating aurora diurnal variations and dependence on latitude and magnetic activity, photometric observations
24 p4308 A69-43004

PULSEJET ENGINES
Induced flow determination in pulsejet ejector, solving momentum and continuity equations by method of characteristics and mathematical model
[ASME PAPER 68-WA/FE-33]
05 p0812 A69-16106

Thermodynamic cycle analysis of various gas turbines and air breathing propulsion systems noting regenerators, heat exchangers and pulsejet engine
11 p1943 A69-25584

PULSES
NT ELECTRIC PULSES
NT ELECTROMAGNETIC PULSES
NT GEOMAGNETIC MICROPULSATIONS
NT GEOMAGNETIC PULSATIONS
NT MICROPULSATIONS
Cylindrical sound pulse propagation in homogeneous layer under inhomogeneous half space
04 p0630 A69-14531

Cross correlation function for two sequences of pulses arbitrarily distributed in time, noting noise stability of diversity reception systems
04 p0557 A69-14790

Pulsed solutions with fixed, floating and distributed pulses for optimal control of systems with differential equations unbounded and discontinuous on right side
09 p1471 A69-21435

PULVERIZING
U GRINDING [COMMINUTION]
PUMP IMPELLERS
Wear ring seals evaluation program for application to high pressure high speed liquid rocket turbopumps impeller wear rings
[ASME PAPER 68-WA/LUB-1]
05 p0768 A69-16129

Internal aerodynamics of centrifugal compressor impeller, discussing impeller channel airflow model, impeller exit flow, rotating channel flow, etc
[RAES PAPER 19]
22 p3859 A69-40498

PUMP SEALS
Wear ring seals evaluation program for application to high pressure high speed liquid rocket turbopumps impeller wear rings
[ASME PAPER 68-WA/LUB-1]
05 p0768 A69-16129

Spring supported hydrostatic shaft seal with floating members isolated from structure
[ASME PAPER 68-WA/LUB-9]
05 p0768 A69-16132

Flow and pressure fields for spiral grooved pumping seal with specified groove dimensions and Reynolds number
[ASLE FICFS PREPRINT 30]
15 p2619 A69-30481

Leakage in mechanical face seals with hydrodynamic films, noting misaligned seal theories for pumping with cavities and two fluids
[ASLE FICFS PREPRINT 19]

- 15 p2621 A69-30497
Helium gas shaft seal for spacecraft electrically driven LOX pump, noting advantages of floating carbon face seal type
[ASLE FICFS PREPRINT 24]

PUMPING

- 15 p2621 A69-30498
Pumping requirements for nozzle skimmer region of neutral particle nozzle beam source, using two stage mechanical pump
04 p0600 A69-15026
Parametric amplifier gain, deriving expressions for diode pumping power and nonlinear circuit element resistance
11 p1849 A69-24957
Pressure in sealing groove and increase time due to pumping action of moving wall applied to force cycloidal of translational motion, considering liquid in groove laminar
16 p2736 A69-32135
Peristaltic pumping in circular cylindrical tube, discussing viscous fluid flow induced by axisymmetric traveling sinusoidal wave imposed on flexible tube wall
[ASME PAPER 69-APMW-3]
24 p4275 A69-43108

PUMPS

- NT CENTRIFUGAL PUMPS
NT ELECTROMAGNETIC PUMPS
NT FUEL PUMPS
NT ION PUMPS
NT JET PUMPS
NT RAMS [PUMPS]
NT TURBINE PUMPS
NT VACUUM PUMPS
Thermal transpiration for performance prediction and development of gas pump
[ASME PAPER 68-WA/ENER-4]
05 p0706 A69-16162
Compact hydraulic power transfer units in aircraft with common connecting shaft for pump/motor elements, discussing integrated power package
06 p0930 A69-17168
Displacement pumps and fluids for extreme environments, discussing fluid types and operational parameters such as speed, pressure, temperature, power, displacement and size
06 p0931 A69-17188
Montardi circuit with sectioned electrodes to simulate isotropically conducting still liquid for application in MHD pump, discussing potentials distribution
07 p1059 A69-19031
Equilibrium theory of parametric pump using cyclic flow of binary mixture through column with heated and cooled bed of solid absorbent
09 p1481 A69-21910
Pump system to obtain indocyanine green dye-dilution curves without blood loss in small animals and infants
23 p4101 A69-41450
Pneumatic driving system for heart assist or total replacement pumps, discussing design features and performance characteristics
24 p4273 A69-42983

PUNCHES

- Indentation of inhomogeneous rigid plastic solid by flat punch under plane strain conditions analyzed by perturbation method
11 p1986 A69-25244

PUNCTURING
U PIERCING

- PUPA
X irradiation and temperature effects on flour beetle *Tribolium confusum* pupae, noting wing abnormalities and pupal stage duration
17 p2910 A69-33748

PURGING

- Anisotropic porous media model for fluid motion in rectangular fuel cell cavities, analyzing pressure, velocity, stream functions and purge time
23 p4075 A69-42300

PURIFICATION

- Gas chromatography technique for separation and purification of chemical compounds for ionizing radiation detectors
02 p0249 A69-12011
Carbon formation during production of high purity semiconductor Si, using C 14 tagged hydrogen impurities and methylated chlorosilanes contained in silicon tetrachloride
03 p0486 A69-13635
Linear aliphatic polyesters preparation by acid chloride synthesis, acid exchange and ester exchange, stressing products purification
19 p3265 A69-36372

- Protective layer material for high sludge capacity filters for fine purification of liquids used in aircraft hydraulic system
22 p3869 A69-40637

- H plasmoid tail cut-off eliminating plasma impurities during injection across octupole magnetic field from coaxial source
24 p4358 A69-43474

PURIFIERS

U PURIFICATION

PURINES

- NT ADENINES
NT URIC ACID
Protein contained purine free basal and yeast ribonucleic acid diets effect on plasma and urinary uric acid production in male subjects
05 p0708 A69-15968
Purines, pyrimidines and nucleosides absorption by Li-, Na-, Mg- and Ca-montmorillonite in aqueous solutions over range pH 2-12 by cation exchange
05 p0716 A69-15973
Absorption of nucleosides, purine and pyrimidine derivatives by Co-, Cu- and Ni-montmorillonite taking place by cation exchange process
05 p0716 A69-15974
Pyrimidine and purine bases analysis by time of flight mass spectrometry and paper chromatography
11 p1832 A69-24738

PURITY

- Charge materials purity found to increase beta-Ti alloys properties
01 p0094 A69-10216
Impurity transfer in doped and undoped epitaxially grown GaAs films, studying substrate dopants effect on carrier concentration profiles
05 p0807 A69-15957
Design theory of esaki diodes relation to internal parameters of degenerate semiconductors, discussing Fermi level position and maximum state density in purity band
05 p0732 A69-16298
Charge materials purity found to increase beta-Ti alloys properties
15 p2638 A69-30272
Metal purity effect of nickel and Ni-Mo alloy on nucleation and recrystallization nuclei growth following 80 percent plastic deformation
18 p3159 A69-35449

PURSUIT TRACKING

- Minimum fuel rendezvous maneuver for two space vehicles in circular orbit, considering propelled tracking equipment nonlinear equations of motion
05 p0823 A69-16036
Differential pursuit games solved by integrating Bellman equation for value function and determining set of possible positions in game with prescribed duration
05 p0788 A69-16536
Optimum evasion tactics for aircraft pursued by missile, using steepest ascent method for maximization of distance of closest approach
06 p0866 A69-17401
Differential games method solving pursuit problem for pursuer with greater maneuverability than pursued
09 p1476 A69-22671
Target displacement and track coherence in pursuit tracking tasks experiments for human performance studies
11 p1829 A69-24737
Differential approach game for unfavorable pursued motion, examining optimum control laws
13 p2288 A69-27525
Pursuit problem involving controllable pursuing plant, deriving condition for engagement with prescribed period of time
14 p2482 A69-28800
Flight times compared for intercept and pure pursuit missile trajectories
20 p3618 A69-37716
Strapped down phased array radar tracker mechanization with digital loop closure electronics for homing missiles, noting cost advantages
[AIAA PAPER 69-873]
21 p3763 A69-39399
Numerical algorithms for nonlinear optimal pursuit problems
21 p3757 A69-39536
Optimal pursuit control at constant moving velocity and limited angular velocities, using Pontryagin principle
21 p3825 A69-39629
Guidance control systems for moving plants pursuing targets, basing design on target characteristics and plant phase coordinates
21 p3687 A69-39643

- Policies and controller design for pursuing vehicle developed in terms of pursuit-evasion differential games
24 p4341 A69-43295

- Linear-quadratic pursuit-evasion game with dynamics perturbed by additive white Gaussian noise, obtaining linear minimax solutions
24 p4341 A69-43296

PUSH-PULL AMPLIFIERS

- Push-pull pentode frequency multipliers with sinusoidal undistorted outputs, studying grid bias effects on operating characteristics
22 p3912 A69-40260

PUSHING

- HRV-1 navy research pusher amphibian aircraft, discussing hydrofoils and operational problems
10 p1633 A69-23223

PWM [MODULATION]

U PULSE DURATION MODULATION

PYLON MOUNTING

U AIRCRAFT PRODUCTION

PYRAMIDAL BODIES

- Force law determining impact processes of pyramidal and conical body penetration into smooth surface of rigid plastic metals
02 p0337 A69-11615

PYRANOMETERS

- Solar radiation actinometric and pyranometric observations during 20 May 1966 eclipse, examining IR component and spectral radiation energies
15 p2697 A69-31257

PYRAZINES

NT AZINES

- Neat alpha styryl azide transformation into 2-phenylazirine, 3,6-diphenylpyridazine and 2,5-diphenylpyrrole after one month at room temperature in brown glass bottle
10 p1651 A69-23307

PYREX [TRADEMARK]

U BOROSILICATE GLASS

PYRIDINE NUCLEOTIDES

- Pyridine nucleotide-linked D-lactate dehydrogenase stereospecificity in various species of invertebrates
01 p0018 A69-11198
Flavoprotein/cytochrome b/559/ role as branch of Halobacterium electron transport in DPNH oxidase determined by salt dependence of reduced DPNH
20 p3484 A69-37101

PYRIDOXINE

- Macaque monkey behavior after injection of monomethylhydrazine with and without pyridoxine HCl, noting effects of aversively and appetitively rewarded training
03 p0375 A69-14068

PYRIMIDINES

NT MITOCHONDRIA

- Purines, pyrimidines and nucleosides absorption by Li-, Na-, Mg- and Ca-montmorillonite in aqueous solutions over range pH 2-12 by cation exchange
05 p0716 A69-15973
Absorption of nucleosides, purine and pyrimidine derivatives by Co-, Cu- and Ni-montmorillonite taking place by cation exchange process
05 p0716 A69-15974
Pyrimidine and purine bases analysis by time of flight mass spectrometry and paper chromatography
11 p1832 A69-24738

PYROCERAM [TRADEMARK]

- Glass/resin laminates behavior at high temperature
07 p1136 A69-19515

PYROELECTRICITY

- Pyroelectric crystals transparent at laser output wavelength used for recording transmitted radiation, noting response of triglycine sulfate crystal
03 p0438 A69-13050
Ferroelectric transition of barium titanates doped in OH or oxygen vacancies, using pyroelectric method
03 p0491 A69-14059
Pyroelectric thermometry for measurements at low temperatures with emphasis on calorimetry, discussing pyroelectric coefficients, dielectric constants and resistivities
09 p1493 A69-21423
Pyroelectric conductor sensors permitting continuous measuring and recording of air inhaled during chosen time intervals
15 p2559 A69-31230

PYROGRAPHALLOY

- U COMPOSITE MATERIALS
U PYROLYTIC GRAPHITE
U REFRACTORY MATERIALS

PYROLYSIS

Thermal model for interaction of exploding wires with methane atmosphere, discussing energy transfer efficiency in high temperature pyrolyses near explosion
 01 p0119 A69-10674
 Quantitative determination of phenolic content in composite materials by pyrolysis gas chromatography method
 01 p0025 A69-11267
 Nitronium perchlorate thermal decomposition under overpressure of He and O between 80 and 170 degrees noting weight loss processes and crystal phase change
 02 p0303 A69-11897
 Lithium aluminum hydride thermal decomposition using isothermal kinetics and differential thermal and thermogravimetric analyses, noting decomposition in four stages
 02 p0304 A69-11898
 Thermal decomposition of ammonium perchlorate and ammonium perchlorate-copper chromite mixtures
 02 p0304 A69-12312
 Nuclear radiation damage vs thermal decomposition of diaminitrobenzene and hexanitrostilbene, analyzing unchanged residual compound
 02 p0304 A69-12500
 Numerical solution for ambipolar diffusion and kinetic decomposition of rotating body of complex chemical composition in ionized airstream
 02 p0191 A69-12580
 Ammonium perchlorate thermal decomposition, studying point defects role
 03 p0494 A69-12896
 Thermal reaction kinetics of pyrolytic products of proline, leucine, arginine and lysine in aqueous solution
 05 p0716 A69-15627
 Charring phenolic nylon ablator material pyrolysis and surface recession for cyclic and constant combined convective and radiative heating
 [AIAA PAPER 69-151] 06 p1036 A69-18055
 Solid propellant burning rates from condensed phase decomposition kinetics, discussing kinetic rates of thermal decomposition
 [AIAA PAPER 69-145] 06 p1039 A69-18182
 Analog simulation of chemically reacting system applied to thermal decomposition of oxygen difluoride
 [WSCIPAPER 68-49] 07 p1073 A69-18318
 Reaction kinetics package for pyrolysis and combustion of aliphatic hydrocarbon molecule, considering reaction rates definition
 [WSCIPAPER 68-37] 07 p1073 A69-18353
 Ammonium perchlorate decomposition kinetics at high temperatures by measuring loss of weight in samples and gas evolution
 08 p1375 A69-20339
 Monograph on kinetic study of fast gas reactions with shock waves covering thermal decomposition of nitrous oxide, hydrazine tetrafluoride and nitrogen tetrafluoride
 08 p1304 A69-20707
 Mass spectrometric determination of pyrolysis products generated from heated polymer samples
 09 p1448 A69-22314
 SiC part fabrication by chemical vapor deposition through pyrolysis of chlorosilanes from vapor state onto machined substrates of graphite and metals
 09 p1509 A69-22344
 Mineralizing metabolic wastes by catalytic oxidation of pyrolysis products, noting nutritive value of ash solutions for *Chlorella* cultivation
 10 p1649 A69-23579
 Metal layers deposition, structure and properties obtained by H reduction of metal halides in vapor phase
 14 p2462 A69-29209
 Borane carbonyl pyrolysis in low pressure tubular flow reactor measured by mass spectrometry, noting wall collision role in diborane bond dissociation
 14 p2410 A69-29282
 Vacuum thermal decomposition of molybdenum sesquisulfide into metallic Mo, discussing reaction kinetics, mass transfer, diffusivity of sulfur gas, etc
 14 p2467 A69-29287
 Pyrolyzed refractory laminates for high temperature applications, analyzing mechanical and thermal properties
 15 p2618 A69-30313
 Yttrium effect on rate of thermal decomposition of silver carbonate powder and pressed pellets by isothermogravimetric analysis, examining water vapor, Co 60 gamma radiation and temperature effects
 15 p2561 A69-30442
 Dynamic differential thermal analysis of dried plant and animal specimens and related substances yielding discrete decomposition peaks of exothermic type
 15 p2555 A69-31000

Dynamic differential thermal analysis with He flow performed on biological specimens, proteins and starches, showing discrete decomposition peaks monitoring pyrolysis process
 16 p2747 A69-31807

Laminar-turbulent transition in boundary layer on thermally decomposing surface, discussing gasification rate, Reynolds number effects, heat transfer and turbulence onset mechanism
 16 p2878 A69-31951

Linear pyrolysis of thermoplastics during combustion of composite solid propellants and ammonium perchlorate solid propellant deflagration mechanism studied by loose granule analog
 [WSCIPAPER 69-16] 16 p2831 A69-32354

Thermal decomposition behavior of perchlorate oxidizers studied by flash mass thermal analysis for determining propellant combustion kinetics
 [WSCIPAPER 69-19] 16 p2832 A69-32357

Granular ammonium perchlorate thermal decomposition analyzed by cinemicrography, discussing sublimation role
 [WSCIPAPER 69-20] 16 p2832 A69-32358

Radiation effect on inorganic solids isothermal decomposition induction period, deriving equations for conditions representing various kinetics combinations during irradiation
 [WSCIPAPER 69-21] 16 p2832 A69-32359

Ammonium perchlorate pyrolysis by convective surface heating, monitoring IR emission as measure of surface temperature
 [WSCIPAPER 69-23] 16 p2832 A69-32361

Premature exothermic decomposition suppression in propellant grade ammonium perchlorate, using differential thermal analysis
 [AIAA PAPER 69-503] 16 p2833 A69-32688

Ammonium perchlorate linear pyrolysis by convective surface heating, discussing propellant deflagration models
 [AIAA PAPER 69-501] 16 p2835 A69-32758

Ammonium nitrate thermal decomposition activation by dyes and halides, noting endothermic and exothermic reactions, proposing models to study impurities role
 17 p3016 A69-32830

Linear pyrolysis of polymethyl methacrylate to verify Cantrell model and surface temperature determination method
 17 p3017 A69-33132

Total gasification heat measurement during pyrolysis of polymethyl methacrylate and paraformaldehyde discussing method and calorimetric equipment
 17 p3069 A69-33133

Linear pyrolysis of condensed materials in presence of heat loss into ambient medium expressed in terms of thermonutral and thermal reactions
 17 p3069 A69-33134

Low molecular weight fluorocarbons pyrolysis and oxidation in single pulse shock tubes, using vapor phase chromatography and mass spectral analyses
 18 p3099 A69-34467

Pyrolyzed tetraethoxysilane for carburizing steels and Ti alloys at 850-1050 C
 19 p3328 A69-36161

Low pressure ethylene decomposition on high temperature W ribbon surface
 19 p3265 A69-36729

Low pressure ethylene decomposition on high temperature Re ribbon surface
 19 p3266 A69-36730

Thermal decomposition of molybdenum carbonyl, deriving general equations, noting agreement with experimental data
 20 p3558 A69-37015

Negative electric potential effect on deposition rate of Mo from molybdenum carbonyl and on deposit chemical composition during pyrolysis
 20 p3559 A69-37016

Ammonium chlorate thermal decomposition by measuring formed noncondensable gas pressure and weight loss in solid state kinetic investigation
 21 p3669 A69-38800

Proton transfer mechanism of copper chromite catalyzed thermal decomposition of ammonium perchlorate, noting electron transfer
 21 p3783 A69-38810

High temperature pyrolysis of simple organic molecules in shock tube, considering diatomic C formation and decay rate
 23 p4113 A69-41693

PYROLYTIC GRAPHITE

Heat transfer in pyrolytic graphite analyzed by hybrid computer simulation
 02 p0353 A69-12387

Material requirements for uncooled nozzles of solid propellant rocket motors burning aluminized propellants, discussing successful testing of pyrolytic graphite
 06 p0946 A69-17530

Free vibrations of plates and beams of pyrolytic graphite type materials, analyzing transverse shear deformation and rotary inertia
 [AIAA PAPER 69-55] 06 p1027 A69-18070

Pyrolytic carbon felt composite development and properties, measuring and tabulating mechanical, thermal and ablation properties
 09 p1530 A69-22364

Periodicity of magnetothermal oscillations in pressure annealed pyrolytic graphite compared with hole carriers
 14 p2504 A69-29005

Pyrolytic graphite coated composite as nozzle throat material for high energy metallized solid propellant motors
 19 p3357 A69-35539

Nernst effect in pyrolytic graphite at low temperatures including thermal EMF, electrical conductivity, thermal conductivity and magnetoresistance coefficients
 21 p3753 A69-39562

Structural features and electrical resistivity of siliconated pyrolytic graphite, analyzing dependence on preparation conditions using X ray diffraction measurements
 24 p4335 A69-42926

Negative Poisson ratio of isotropic heat shield material pyrolytic graphite, noting thermodynamic validity
 24 p4338 A69-43599

PYROLYTIC MATERIALS

High temperature capacitor consisting of thin wafers of pyrolytic boron nitride noting fabrication, dissipation factor and capacitance
 04 p0551 A69-15299

Stress graphitizing and boron codeposition effect on dynamic mechanical properties of pyrolytic carbon, noting increase in internal friction and dynamic modulus
 10 p1716 A69-23036

Pyrolyzed refractory laminates for high temperature applications, analyzing mechanical and thermal properties
 15 p2618 A69-30313

Pyrolytic zirconium carbide emissivity during initial heating compared with results for specimens prepared by powder metallurgy
 15 p2640 A69-30985

PYROMETERS

NT OPTICAL PYROMETERS
 NT RADIATION PYROMETERS
 NT THERMOCOUPLE PYROMETERS

Pyrometer for turbine rotor blades surface temperature measurement, considering purged, line-of-sight viewing tube and signal processing to reject C particles interference
 [SAE PAPER 690431] 23 p4165 A69-41649

PYROMETRY

U TEMPERATURE MEASUREMENT

PYROTECHNICS

Hand operated visual signaling devices, discussing Mini Signals and cartridge load aerial signals
 06 p0878 A69-16962

Pyrotechnic and explosive elements in space systems - Conference, Tarbes, France, July 1968
 10 p1748 A69-23003

General and classical statistical techniques for cutting effectiveness and operational reliability of cutting fuses
 10 p1749 A69-23004

Space stage separation qualification of ONERA rocket vehicles based on angular perturbation measurements during variable roll speeds
 10 p1669 A69-23005

Electrical devices for detonation initiation in pyrotechnic equipment for space applications, tabulating characteristics
 10 p1749 A69-23006

Shock ignition procedure to keep pyrotechnic composition in optimum condition in space environment, describing test layouts and theory
 10 p1749 A69-23007

Silver and cadmium nitrides, copper chlorotetraazolate and barium and potassium dinitrobenzofuroxannates compared for priming explosive applications
 10 p1750 A69-23011

Igniferous materials for electrical initiation of explosive in extreme conditions, considering nitrophenol salts and pyrotechnics
 10 p1750 A69-23015

Q

Pyrotechnical devices for two stage solid propellant ballistic rocket, discussing self priming electric cells and auxiliary power and gas generators
10 p1752 A69-23024

Pyrotechnic activated calorimeter for reentry package design of vehicles entering earth atmosphere at lunar return velocities
10 p1669 A69-23026

Explosive and pyrotechnical elements for Grillo 1, Grillo 2 and Trigone 1 hot water rockets, detailing nozzle closure and chemical reaction activation
10 p1753 A69-23028

Pyrotechnics applications to Skylark upper atmosphere sounding rocket, discussing payload heads, nose cones, sensor covers, etc
10 p1792 A69-23029

Hollow charge pyrotechnic circuit closer, noting one piece construction, transportability, safety, quick action and reproducible delay
10 p1635 A69-23030

Pyrotechnic circuit closer using jet to achieve conduction between hollow charge lining and coaxial electrode
10 p1635 A69-23031

Rocket motors for ejection of instruments from sounding rocket payloads, considering powder cartridges and solid propellant motor characteristics
10 p1635 A69-23032

Two way pyrotechnic high pressure gas valve for D2 satellite, noting resistance to leakage due to nearly monolithic construction
10 p1635 A69-23033

Nose cone ejecting system with pyrotechnic devices for two stage Centaur rockets /Sud-Aviation/ with RF mass spectrometer
10 p1635 A69-23034

Quasi CW solid state doped lasers excited by pyrotechnic pump sources with potassium perchlorate oxidant and zirconium fuel, noting power to weight ratio
13 p2272 A69-28116

Brute battlefield illumination flare configuration, candle power, burn duration and hot air balloon-type suspension system
20 p3461 A69-37166

Pyrotechnical gas generator performance tests during Europa 1 rocket second and third stage separation, including generator design, ground and flight tests
23 p4224 A69-42153

PYROXENES

NT ENSTATITE

Disordered chondritic pyroxenes, analyzing X ray patterns of meteoritic and synthetic crystals
03 p0516 A69-14083

Mossbauer spectra of Fe minerals in unequilibrated ordinary chondrites, noting ratios of olivine to pyroxene iron
19 p3408 A69-36082

Orthopyroxenes cooling history, studying order-disorder transitions between ferrous iron and magnesium
20 p3523 A69-37518

Meteorite minerals as detectors for studying fossil record of cosmic ray nuclei, emphasizing feldspars and pyroxenes
20 p3590 A69-37568

Primitive low energy Fe-group nuclei irradiation of meteoritic crystals from studies of pyroxene and feldspar from meteorites, discussing astrophysical implications
20 p3590 A69-37569

Jadeite /high pressure sodium aluminum pyroxene/ shock-induced phase assemblage from oligoclase, noting relevance to lunar rock samples investigation
22 p3941 A69-40569

Pyroxene crystallization in meteoritic chondrules, noting normal spherulite crystallization
22 p4033 A69-41065

High temperature single crystal X ray studies of natural Fe-rich orthopyroxene, detecting high-low clinopyroxene inversions
24 p4311 A69-43218

PYROXYLIN

U CELLULOSE NITRATE

PYRRHOTITE

U TROILITE

PYRROLES

NT INDOLES

NT TRYPTOPHAN

Neat alpha styryl azide transformation into 2-phenylazirine, 3,6-diphenylpyridazine and 2,5-diphenylpyrrole after one month at room temperature in brown glass bottle
10 p1651 A69-23307

Q FACTORS

Varactor Q calculation from impedance vs bias measurements, circumventing circuit loss problem by procedure based on Weissfloch equivalent circuit of lossy two port network
04 p0575 A69-14753

Semiconductor laser generation efficiency increased by using external resonator and by signal amplification
05 p0777 A69-16378

High Q magnetically tunable microwave filters using magnetodynamic modes in ferrite spheres
06 p0892 A69-16831

Q factors dependence of IMPATT diode oscillator FM noise, noting excess noise temperature correlation with diode current
06 p0899 A69-17826

Microwave resonator characteristics, deriving expressions for Q for pure or coupled electric or magnetic modes
09 p1464 A69-22096

Varactor diodes for microwave frequency tuning of resonators used for oscillators of avalanche transit time and Gunn diodes, discussing Q factors
11 p1854 A69-25610

Operational Q factor of optimal differential relay system with inertial plant during tracking process, noting cadence pulses high repetition rate influence
12 p2052 A69-26279

Automatic search-free optimization by sensitivity functions, deriving algorithms by Q factor and discrepancy extrapolation
14 p2425 A69-28823

Optical IR yttrium-iron garnet rectifier increasing light intensity and system Q factor at low external magnetic field
17 p2981 A69-33117

Metrological measuring instrument scales selection principles for ensuring constant sensitivity and Q factor
17 p2975 A69-33614

Optimum automatic system for controlling helicopter formation flight, stressing transient response Q factor and transmission ratios
18 p3090 A69-34656

Q factors of ideal antenna enclosed in imaginary sphere with excited TE and TM modes
20 p3506 A69-37836

Design and performance of microwave open resonators with diffraction grating in mirror, describing Q factor calculation
23 p4139 A69-42045

Q SWITCHED LASERS

Target production device for deuterium plasma clouds in vacuum with Q switched neodymium laser
01 p0090 A69-10222

Optical radar for studying atmospheric water vapor, density, temperature and aerosols
01 p0090 A69-10540

Ultrashort light pulses in lasers with nonlinear absorber, evaluating random intensity peak probability created by intensity fluctuations and axial modes buildup
01 p0090 A69-10791

Amplification equations for calculating unsteady lasing in Q switched ruby laser, considering changes in populations and fields along cavity
01 p0092 A69-10888

Q switched laser excitation flash spectroscopic analysis of naphthalene, describing equipment arrangement and experimental results
02 p0254 A69-11544

Energy characteristics of laser with passive Q switch, taking into account internal reflections
02 p0256 A69-11999

Laser with passive Q switching with Faraday cell switch, studying induced recombination and Mandelsham-Brillouin scattering
03 p0435 A69-12983

Efficient conversion of Q switched neodymium-glass laser output into second harmonic obtained for low output levels at fundamental frequency
03 p0437 A69-13046

Q switched lasers powerful outputs obtainable at sum frequency, discussing frequency mixing in nonlinear dispersive media
03 p0438 A69-13047

Q switched neodymium-glass laser output conversion into second optical harmonic by passing beam through double Galilean telescope with adjustable focus
03 p0438 A69-13048

Q switched laser based on light waves parametric interaction in nonlinear medium operating at wavelengths from UV to IR
03 p0439 A69-13054

Q switched ruby laser nonlinear absorption in optically transparent organic liquids attributed to two quantum process with large cross section
03 p0439 A69-13055

Electromechanical retracting pedestal for solid target injection into vacuum system and ionization by focused Q switched laser beam
03 p0439 A69-13105

Solid state laser Q switched by rotating prism emitting giant pulse before two mirrors in parallel
03 p0440 A69-13365

Gallium phosphide luminescence near indirect transition during multiphoton excitation by Q switched ruby and Nd laser beams
03 p0489 A69-13892

High speed shadow photographs of Q switched laser triggered spark gap air discharge, showing sonic waves and development of discharge channel
04 p0610 A69-14349

Q switched Ruby laser metastable state population kinetics and resonator losses, discussing internal energy redistribution with subsequent absorption spectrum changes
04 p0610 A69-14381

Q switches transparency as function of incident light intensity
04 p0610 A69-14385

Pressurized spark gap triggered by focused Q switched laser beam introduced along axis
04 p0612 A69-15204

Output characteristics of slowly Q switched neodymium in calcium tungstate laser
04 p0612 A69-15206

Plasma production by ultrashort pulse Q switched laser beam, discussing avoidance of initiation of breakdown wave
05 p0770 A69-15584

Passive Q switching of solid state lasers based on stimulated Mandelstam-Brillouin light scattering
05 p0770 A69-15699

Phase grating formation in giant pulse laser Q switching liquid by reflecting light beam from Lippman plate at Bragg angle
05 p0771 A69-15811

Radiative flux density, spectrum and temporal behavior of Q switched laser induced underwater sparks
05 p0771 A69-15818

Line broadening possibility for Q switched iodine laser with aid of magnetic effect /Zeeman effect/, noting energy storage capability increase
05 p0773 A69-16288

Tunable Raman upconverter as coherent light generator, using Q switched Nd-YAG laser beam [IEEE PAPER B-2]
05 p0774 A69-16309

Mode locked laser as stroboscopic light source potential by investigating expansion of laser produced plasma by schlieren photography [IEEE PAPER H-1]
05 p0774 A69-16315

Self Q switching of ruby lasers at 77 K, noting saturable absorber giant pulse process obtained by shielding part of laser rod from pump
05 p0776 A69-16332

Radiation of laser active element with random inhomogeneities of refractive index, discussing beam divergence, operation modes and Q switched operation
05 p0777 A69-16550

Carbon dioxide Q switched laser nonlinear amplification characteristics in vibrational-rotational bands
06 p0933 A69-17118

Semiconductors reflectivity enhancement by irradiating with Q switched ruby laser output
06 p0935 A69-17768

Q switching and mode locking of neodymium selenium oxygen chlorine liquid laser, discussing power output and nature of pulses
06 p0935 A69-17776

Dynamics of Q spoiled neodymium laser created plasma expanding in vacuum magnetic field
06 p0970 A69-17952

Q switching of continuously pumped Nd/YAG laser using variable spacing Fabry-Perot interferometer as variable output coupler
06 p0938 A69-18229

Quantum electronics trends, discussing output power, mode control, stability and lifetime of CW and Q switched lasers and parametric interactions in nonlinear optics
07 p1144 A69-18468

Pulse synchronism of solid state lasers Q switched by same rotating prism, discussing pulse shifting to obtain radiation in filaments

07 p1147 A69-18488

Synchronizing ruby and Nd-glass laser pulses by means of passive bleachable dye solution liquid Q switch

07 p1147 A69-18530

Time stabilization method for lasing in electro-optically Q switched ruby laser with saturable absorber in cavity

07 p1147 A69-18531

Fresnel pulse holograms of three dimensional diffuse objects by single mode ruby laser with or without Q switching

07 p1132 A69-18801

Q switched laser quasi-periodic short pulse emission pattern evolution from broadband noise source, using fluctuating dipole model

07 p1149 A69-18897

Pulses from Q switched carbon dioxide laser for studying Q switching techniques [IEEE PAPER G-2]

07 p1150 A69-19054

Pulse generation in Q switched traveling wave laser, noting effect of field amplification [IEEE PAPER Q-5]

07 p1154 A69-19077

Spatially nonuniform laser model allowing for photon density and inversion variations, noting self Q switching mechanisms from stimulated scattering processes [IEEE PAPER Q-6]

07 p1154 A69-19078

Saturable dye filters used with ruby lasers, discussing relaxation time, residual absorption source and transient spectral hole burning

07 p1155 A69-19089

Stable limiting cycles of laser resulting from mutual synchronization of phase shifted oscillation modes

07 p1158 A69-19752

Frequency doubling of laser light with variable Q switched resonator

07 p1158 A69-19753

Q switched single mode ruby laser pulse passage through traveling wave amplifier decreases beam divergence

08 p1326 A69-20542

Formation and characteristics of flash produced in air by single pulse of Q switched ruby laser, using holographic interferograms

08 p1317 A69-21022

Pulsed plasma production when focusing Q switched laser on solid target surface, noting high temperature effects and optical diagnostics methods

09 p1520 A69-22656

Triplet-triplet transitions for Q switching, examining organics for passive Q switches

09 p1520 A69-22682

Q switching combined with pulsed pumping of carbon dioxide laser for observing optimal Q switching instant, noting pulse energy increase

10 p1703 A69-23619

Dynamics of external loss modulation and Q switching methods of generating ultrashort pulses in mode locking laser

10 p1703 A69-23624

Nd glass laser for emission of high radiance diffraction limited pulses, noting long path air breakdown and second harmonic generation

10 p1704 A69-23654

Traveling wave passive Q switched laser with bleachable absorber filter, analyzing unsteady processes without expanding field along natural resonator modes

10 p1705 A69-23949

Holographic motion picture recorded using CW Q switched laser and conventional camera

10 p1697 A69-24002

Q switching techniques for solid state lasers at room temperature for high peak power, discussing mechanical systems, electro-optic and magneto-optic shutters

10 p1706 A69-24018

Q switched carbon dioxide laser power increased by placing bleachable /boron tetrachloride/ filter in resonator

11 p1894 A69-24454

Electro-optically Q switched Nd doped calcium tungstate laser for producing two controlled pulses, noting application to other solid state lasers

11 p1899 A69-25052

Carbon dioxide laser for production of high peak power pulse, discussing mw peak power design and oscillation problem in high gain amplifiers

11 p1899 A69-25053

Gain decrease due to saturation during amplification of pulses from Q switched carbon dioxide laser oscillator, noting rotational sublevels relaxation rate

11 p1899 A69-25055

Q switching of ruby lasers by natural chlorophyll a and derivatives pheophytin a and Cu chlorophyllin Na

11 p1900 A69-25581

Gallium phosphide luminescence near indirect transition during multiphoton excitation by Q switched ruby and Nd laser beams

11 p1939 A69-25693

Transformation of Q switched neodymium laser radiation into Stokes component during stimulated combination scattering in liquid nitrogen

11 p1900 A69-25751

Emission from solutions of organic luminophores excited by harmonics of Q switched neodymium laser

12 p2104 A69-26030

Multiframe image converter registration of space-time ruby laser spot structure changes in Q switched regime prior to giant pulse formation

12 p2083 A69-26142

Ultrahigh speed multiple framing photography system using sequentially modulated ruby laser and smear type camera applied to dynamic photoelasticity

12 p2086 A69-26166

Q switched ruby laser stroboscope for high speed photography, using electro-optical crystals for Q switch

12 p2086 A69-26167

Framing device capable of producing four pictures within 5 nsec, using Q switch laser for light source

12 p2086 A69-26168

Repetitive Q switched laser light source for interferometry, holography and high speed photography

12 p2087 A69-26170

Q switched ruby laser application to high speed shadow photography and holography in study of gas flow around ballistic body

12 p2088 A69-26177

Slow theta pinch helium plasma measurements by Mach-Zender interferometer with Q switched laser

12 p2091 A69-26394

Q switched ruby laser with rotating prism, considering single pulse operation by increasing switching rate

12 p2107 A69-26588

Optical alignment for lasers with electro-optical Q switching and mutually misaligned ruby rod, KDP crystal and polarizing prism

12 p2107 A69-26589

Giant pulses from laser with electro-optical quartz shutter, noting advantageous optical and mechanical properties of quartz

12 p2108 A69-26591

Amplification equations for calculating unsteady lasing in Q switched ruby laser, considering changes in populations and fields along cavity

12 p2109 A69-26652

Space-time characteristics of coherent light giant pulse development in laser with instantaneous Q switching, deriving equations to describe linear and nonlinear phases

12 p2110 A69-26909

Single frequency ruby laser emission spectrum coincidence with interacting laser radiation at instant of Q switching

13 p2272 A69-27911

Passive Q switching of carbon dioxide laser with mixture of sulfur hexafluoride and chlorotrifluoro-ethylene gases within resonator

13 p2274 A69-28659

Q switched ruby laser metastable state population kinetics and resonator losses, discussing internal energy redistribution with subsequent absorption spectrum changes

14 p2456 A69-28754

Q switches transparency as function of incident light intensity

14 p2456 A69-28758

Carbon dioxide laser inversion kinetics, combining pulse pumping with Q switching to observe rise, life and decay times

14 p2457 A69-28926

Submillimeter wave generated in ZnTe by difference frequency mixing of Q switched ruby laser, discussing beat power [IEEE PAPER B-4]

14 p2457 A69-28927

Passive Q switch laser single pulse formation time and spectral width using balance equations

14 p2458 A69-29166

Electro-optical Q switched lasers with prismatic reflectors and phase shifter studied using Johns matrices for polarizer, Kerr cell and Porro prism elements

14 p2459 A69-29390

Q switched ruby laser designed for lidar probing of cosmic bodies and earth atmosphere

14 p2460 A69-29660

Plasma diagnostics facilities design, circuit diagrams and operation based on Q switched ruby laser and optical recording system

14 p2461 A69-29782

Pulsed IR laser optimal Q switching mode by using semiconductor mirror with nonparabolic dispersion law and changing mirror opening moment delay time

15 p2633 A69-30064

Q switched ruby laser giant pulses during pumping by another Q switched laser exhibit simple shape and low duration

15 p2634 A69-30727

Statistical characteristics of Q switched He-Ne laser emission gain fluctuations during transient process from subthreshold to superthreshold value

15 p2634 A69-30960

Q switched laser produced blast waves in low pressure Ar, discussing gas density and time dependence roles

16 p2796 A69-31705

Laser cavity optimization for producing minimum short light pulse width in fast Q switching of optical maser

16 p2796 A69-31802

Passive Q switching of chemical laser operating on vibrational-rotational line of vibrational transition of HCl

16 p2796 A69-31840

Spontaneous self pulsing and cavity dumping in carbon dioxide laser Q switched by internal GaAs electro-optic cell without saturable absorber

16 p2797 A69-32014

Tunable far IR radiation generated from difference frequency between two Q switched ruby lasers using lithium niobate and quartz as mixing crystals

16 p2798 A69-32603

Self Q switching of pumped neodymium-doped YAG and ruby lasers obtained by static misalignment of mirror and pumped laser filament

17 p2979 A69-32916

Repetitively Q switched ruby laser applied to frequency conversion, stimulated Raman scattering and vacuum UV generation

17 p2980 A69-33027

Q switching of CW 337 mu maser, gain factor measurements for pulse discharges and data on saturation and time dependence

17 p2981 A69-33088

Polymethine dyes in passive Q switches of neodymium lasers, noting effects of absorption band intensity, width and position on single pulse laser energy yield

17 p2983 A69-33968

Stable passive Q-switch of neodymium laser, presenting single pulses energy, time and spectral characteristics

17 p2983 A69-33969

Neodymium laser emission temporal structure in mode self locking regime with Q switching by saturable filter

18 p3152 A69-35016

Two photon excitation of luminescence in complex uranyl compound single crystals using Q switched ruby laser

19 p3334 A69-35982

Ruby laser Q switching with electro-optical shutter based on Li metaniobate crystals by applying static, single pulse or periodic potential to Pockels cell

19 p3336 A69-36346

Rotating mirror Q switched carbon dioxide laser for high peak powers, analyzing pulse structure and duration dependence on collision induced relaxations

19 p3338 A69-36694

Holographic camera using Q switched laser for recording high speed interferograms in plasma diagnostics

19 p3315 A69-36726

A scope laser radar system using Q switched solid state laser pulses, discussing configuration and performance

20 p3487 A69-37283

Ultrashort light pulses in lasers with nonlinear absorber, evaluating random intensity peak probability created by intensity fluctuations and axial modes buildup

20 p3555 A69-38009

Q switched laser pulse propagation in nonlinear laser amplifier using bitemporal relativity theory, deriving five dimensional wave equation revealing superlight signal existence

21 p3770 A69-38839

Giant Q switched laser pulse interaction with C target in background gas showing complex luminous shock structure near target as function of time
21 p3736 A69-38942

Fresnel pulse holograms of three dimensional diffuse objects by single mode ruby laser with or without Q switching
21 p3724 A69-38946

Spectral characteristics of Q switched single frequency ruby laser with tunable emission frequency in giant pulse mode
21 p3737 A69-38991

Deposited beta active thallium isotope materials angular distribution after vaporization by Q switched laser beam determined by target fragment recoil
21 p3737 A69-38992

Emission from polymethine dye solution during optical pumping with pulses from Q switched Nd glass laser, discussing emission spectral, temporal and energy characteristics
21 p3739 A69-39542

Emission kinetics of passive Q switched laser without constraints on relaxation time and switching characteristics of absorption centers and medium
21 p3740 A69-39550

Peak power ranges of Q switched CO-air-He molecular laser, noting recovery time and CO vibrational temperature
21 p3742 A69-39742

Transverse mode selection in rotating mirror neodymium doped calcium tungstate laser by inserting slit and edge into resonator
22 p3961 A69-40316

Time dependent mathematical double acceptor model including heat effects for analyzing Q switching and stimulated emission time delays in pulsed junction lasers
22 p3962 A69-40560

Digital computer determination of stimulated emission time delay, Q switching temperature and current region and impurity profile effect across junction in junction lasers
22 p3962 A69-40561

Spiking behavior detection in Q switched light output from GaAs pulsed junction laser, noting width at high pumping levels
22 p3963 A69-40563

Carbon dioxide and carbon dioxide mixture mirror Q switched laser peak power generation, using pulsed excitation
22 p3963 A69-40564

Q switched pulsed discharge carbon dioxide laser, determining peak power dependence on delay between pulse excitation and Q switching
22 p3963 A69-40566

Output power dependence of repetitively Q switched carbon dioxide laser on repetition time measured with thermopile, noting decrease in mirror system
23 p4173 A69-41566

Q VALUES

Earth and planets shallow seas tidal dissipation reflected in Q values, noting larger planet pressure effect
08 p1393 A69-20581

Metallicity index Q value difference between cluster and noncluster galaxies determined from UV, blue and violet observation data
10 p1774 A69-22964

Q multiplier UHF device as preselection filter for closely spaced channel signals, discussing channel interference reduction
23 p4141 A69-42220

QSO [RADIO SOURCES]

U QUASARS

QUADRATIC EQUATIONS

Quadratic form representation of multivariable polynomials expressing sufficient condition for positive definiteness of real multivariable polynomial
07 p1173 A69-18641

Quadratic programming and theory of elastic perfectly plastic structures under holonomic laws, proving theorems of limit analysis
07 p1235 A69-19443

Linear, quadratic, optimal control problems solved by sweep method, discussing time role, feedback control law and use of matrix equations
12 p2053 A69-26512

Minimum theorems for plastic strain rates and plastic strains governed by holonomic elastoplastic theory utilizing quadratic functions
13 p2370 A69-28629

Asymptotic solutions of optimum control for systems with constraints as linear differential equations and quadratic type functional
15 p2583 A69-31234

Quadratic programming method for equations of elastic perfectly plastic solid applied to stress distribution in plate torsion and bending
18 p3218 A69-34661

Computer quadratic method of evaluating ray propagation data for estimating inhomogeneous media properties
18 p3172 A69-34667

Quadratic Liapunov function existence for exponentially stable linear system with varying coefficients described by vector differential equations
19 p3359 A69-35617

Mathematical properties of involutorial matrix solutions to simple quadratic equation, obtaining symmetry properties, eigenvalues and recursion formulas
20 p3568 A69-37579

Biquadratic plane wave dispersion relation for gyrotropic waveguides with dielectric and magnetic properties, discussing associated quartic equation for refractivity
21 p3675 A69-39285

Memory gradient algorithm for reducing computing time by minimizing quadratic function of unconstrained variables compared with Fletcher-Reeves algorithm
24 p4340 A69-42957

QUADRATURE APPROXIMATION

U QUADRATURES

QUADRATURES

N-body problem in celestial mechanics, using differential equations, reduced to quadratures [UN PAPER 68-95268]
01 p0150 A69-10476

Optimum addition of abscissas in quadrature formulas by expansion of abscissas equation in Legendre polynomials
03 p0455 A69-13372

Approximate solution of celestial mechanics differential equations by reducing to quadratures for n body problems
06 p1006 A69-17566

All-pass transfer functions of new class type for design of quadrature filter networks, using Chebyshev approximation
08 p1277 A69-21167

Riemann sum definition and development of bounds for error in approximating integral, showing quadrature formulas as Riemann sums
10 p1719 A69-23521

Quadratic approximation at matrix level of dynamic equations for rotating bodies applied to gravity gradient satellite exhibiting nonlinear resonances
18 p3174 A69-35298

Iterative integration method of numerical quadrature over finite interval for analytic function, taking into account simple nonanalytic singularities in integrand
24 p4341 A69-43229

QUADRUPOLE NETWORKS

Direct couplings of autonomous noisy quadrupoles used for noise matching
01 p0043 A69-10591

Lumped element circuit producing directional coupling by electric and magnetic coupling of reactance quadrupoles, discussing insufficient coverage of calculated frequency range
16 p2763 A69-32581

Dispersive quadrupole network design using algorithm method
19 p3287 A69-36740

Quadrupole network transfer matrix calculation from known octupole matrix, describing frequency response determination of coupled transmission lines
22 p3912 A69-40257

Small losses measurement in circulators and reciprocal quadrupoles, using scattering matrix to eliminate mismatch errors
22 p3875 A69-40259

Transient processes in microwave quadrupoles with ferrite resonators
23 p4139 A69-41948

QUADRUPOLES

Cl 35 nuclear quadrupole resonance spectra of 3,6-dichloropyridazine, tetrachloropyridazine, 2,6-dichloropyrazine and chloropyrazine
01 p0123 A69-10290

Benzene quadrupole moment estimates from second virial coefficient data with polarizability in intermolecular potential function and from molecular susceptibility anisotropy
01 p0124 A69-10687

Alkali metal quadrupole spectral doublets used as diagnostic for determining alkali-metal plasma electron temperature
02 p0286 A69-11584

Hybrid loop properties determination using quadrupole algebra, noting frequency dependence of input impedance and voltage transmission
04 p0582 A69-15072

Electric quadrupole parameters, discussing relationship between voltages at terminals
04 p0579 A69-15228

Tsao-Curnutte line broadening calculations extended to include Raman scattering and quadrupole absorption
04 p0633 A69-15231

Stabilization of plasma filament with alternating current by quadrupole magnetic field
07 p1191 A69-18987

Electromagnetic diffraction for waves generated by electric quadrupole on perfectly conducting wedge, discussing finiteness and radiation emission
09 p1455 A69-22082

Nonmagnetic quadrupole ionization gauge, discussing systems design and electron oscillations
13 p2262 A69-28020

Nonmagnetic ionization gage consisting of quadrupole lens systems excited at HF, discussing electron focusing during operation
13 p2263 A69-28084

Earth quadrupole moment effects on precession of gyroscope in satellite in equatorial orbit
17 p2972 A69-33072

Electric quadrupole coupling for N 14 in aminedissulfonite studied by observation of second order transitions in electron spin resonance spectra
18 p3178 A69-35474

Boron 11 nuclear quadrupole coupling constants in solid boron halides, finding fine structure on nuclear magnetic resonance in boron fluoride
20 p3483 A69-36935

Pure quadrupole resonance spectrum of iodine-127 in solid stannic iodide measured in specific temperature range at atmospheric pressure
22 p3986 A69-40726

Quadrupole self and cross correlations of directional jet noise patterns, including frequency spectra and corrections
22 p3931 A69-40891

QUALIFICATIONS

Apollo spacecraft equipment qualification program for margin assurance, discussing ground and flight tests
19 p3430 A69-36015

QUALITATIVE ANALYSIS

Rarefied plasma self similar motion qualitatively analyzed, particularly penetration and expansion, taking into account electric/magnetic field effects
08 p1359 A69-19951

Friedrich qualitative analysis of ordinary differential operators modified to obtain quantitative information regarding eigenvalues distribution
17 p2995 A69-33404

QUALITY CONTROL

Ultrasonic quality control test methods for melt through welds in hydraulic line assemblies, noting equipment and surface roughness requirements
02 p0252 A69-11810

Undetected defects and false alarm probabilities for automatic test equipment, emphasizing quality and confidence limits
03 p0428 A69-13187

Human inspection performance in quality control operations to assess visual inspection tasks accuracy
03 p0433 A69-13386

Product assurance role in spacecraft sterilization to maintain planetary biological environments integrity in space programs for extraterrestrial life determination
03 p0379 A69-13400

Quality control of semiconductor materials, analyzing homogeneity by statistical distribution of nonequilibrium carriers based on photoconductivity measurement
04 p0642 A69-14856

Nondestructive testing of quality of electroexplosive devices based on determination of heat flow between bridge wire and surroundings
04 p0607 A69-14973

Quality control in welding from design through experimental manufacture, product testing, large scale production and improvements
04 p0608 A69-15485

Self acting gas lubricated bearings production, discussing manufacture to ultraprecision tolerances by semiskilled labor [ASME PAPER 68-WA/LUB-4]
05 p0768 A69-16130

Quality control for TV transmissions via communication satellites, considering transmission accuracy improvement and error measurement automation [UN PAPER 68-95773] 06 p0886 A69-17047

Holography for display devices, nondestructive testing, quality control, high speed, microscopy, acoustic testing, sonar, data storage, etc 06 p0928 A69-17873

Mechanical, electromagnetic and chemical signatures monitoring and analysis during system operation 06 p0932 A69-17875

Ti alloy blanks production technology and quality control, noting rolling of sectional profiles 07 p1161 A69-18765

Imaging systems for weld inspection, discussing physical factors and selection of radiation 07 p1139 A69-18796

Nondestructive tests for determining braze bond quality of open face honeycomb seal rings, using low viscosity liquids with fluorescent additives 07 p1140 A69-18797

Electromagnetic interference (EMI) created by noise coupling through conductive paths, discussing responsibility for control within systems management 07 p1079 A69-18944

Management control systems, discussing malfunction, inefficiency and needs of human elements 07 p1244 A69-18963

Direct bead sampling by aspiration of molten metal in open hearth furnaces and converters 07 p1141 A69-19341

Alumina radomes fabrication and control techniques to assure reproducibility of electrical and mechanical properties, detailing finished product inspection methods 07 p1142 A69-19529

High pressure storage vessels for gaseous hydrogen, discussing failure, manufacturing controls and access for internal nondestructive inspection [ASM PAPER D8-14.1] 07 p1143 A69-19666

Fabrication and processing techniques, tooling concepts and quality control for composite materials used in large aircraft, discussing honeycomb and sandwich structures [ASM PAPER D8-25.4] 07 p1172 A69-19670

Weld defects, discussing criteria for rejection, harmful and harmless defects, welding process and procedures and weld vs base metal defects 07 p1244 A69-19696

Integrated nondestructive testing systems to ensure welded assemblies reliability for Saturn 5 program, including surface defect detection 07 p1117 A69-19699

Components production process effect on reliability based on values and functional relations of internal parameters, noting influence on accelerated testing 08 p1319 A69-20346

Electronic components reliability tests, determining correlation between material quality and failure 08 p1293 A69-21109

Process control data in acceptance procedures for high reliability electronic components, discussing supplier and user cooperation 08 p1293 A69-21110

Bubble leak testing of components to understand effects of gas and liquid viscosity, surface tension, pressure differential and temperature 09 p1503 A69-21391

Efficiency of weather forecasts taking into account quality criteria and integrating index number, discussing optimization principle for new parameter 09 p1534 A69-21510

Quality control tests for adhesives used in structural parts including ultrasonic and nondestructive tests 09 p1513 A69-22564

Tests and quality control equipment used in German aeronautical and astronautical industries 09 p1513 A69-22565

Tumbling motion for testing gyroscopic devices quality 10 p1689 A69-22927

FM Lamb wave system for flaws and defects detection in thin metal sheets 10 p1699 A69-23048

Radiographic, ultrasonic, thermographic and leak test quality control for brazed liquid propellant rocket engine components 10 p1699 A69-23054

Welding defects, processes, inspection and personnel training problems 10 p1700 A69-23372

Metal surface distribution of electromagnetic field from striding transducer in eddy current flow detection, calculating magnetic field component 10 p1697 A69-24071

Mechanical damping and electrical matching effects on bandwidth of piezotransducer in ultrasonic flaw detection equipment 10 p1697 A69-24073

Flow detection inaccuracies in shadow method due to interference effects when using Babinet principle 10 p1675 A69-24075

Environmental requirements of military specifications tabulated according to tests for altitude, temperature, vibration, shock, humidity, temperature/altitude, etc 11 p1862 A69-24331

Passenger aircraft flight readiness verification, discussing flaw and corrosion detection and rivet joint inspection methods 11 p1822 A69-24526

Integrated management information system (IMIS), discussing logistics, reliability and quality assurance disciplines 11 p2005 A69-25304

TV test chart for evaluating Surveyor lunar spacecraft TV system covering resolution, photometric and colorimetric response and sun angular position [SMPT PAPER 105-71] 12 p2078 A69-25771

Reliability-quality control - Conference, Buffalo, May 1968 12 p2100 A69-25845

Descriptive statistics in quality control dealing with variability and probability, discrete and continuous variables, frequency distributions and measures of central tendency and dispersion 12 p2100 A69-25846

Configuration management, establishing uniform and mutually supporting methods of configuration identification, control and accounting for systems and equipment 12 p2192 A69-25849

Reliability-quality control - Conference, Ontario, April 1969 12 p2101 A69-25969

Reliability planning role in directing business functions to quality efforts integration in engineering, production and testing of electronic equipment 12 p2102 A69-25971

Graphite improvement for high temperature applications by computerized properties analysis, failure criterion and improved testing for defective billets 12 p2115 A69-26845

Soviet book on quality control of materials and machine parts by ionizing radiation covering radiation hazards and protection 13 p2268 A69-27935

Value engineering and component/products improvement incentive contract clauses role in defense product quality improvement 13 p2383 A69-28100

Titanium alloys for thermionic nuclear converters, discussing melting, forging, drawing and quality control of mechanical and physical properties 14 p2462 A69-29217

Electronic systems packaging substitution method for optimized malfunction isolation at succeeding levels to final discard-at-failure 14 p2420 A69-29494

Stainless steels stress corrosion susceptibility, detecting chromium carbide in martensitic matrix by galvanic nondestructive test method 14 p2466 A69-29935

Systems engineering approach to aerospace product defects minimization, discussing scope, contract development, mainstream functions, component development, design data and subsystem integration 15 p2719 A69-30085

Quality control of semiconductor materials, analyzing homogeneity by statistical distribution of nonequilibrium carriers based on photoconductivity measurement 15 p2667 A69-30248

Cost effectiveness of test selection when statistical distribution of load and strength are known, presenting curves for equally dispersed normal parameters distribution 15 p2720 A69-30401

Reliability control of 1/4-W resistors of tin oxide on glass substrate manufactured in quantity 15 p2627 A69-30837

Metal film resistor reliability for conventional and space use, outlining guidelines for fabrication and quality control 15 p2628 A69-30847

Quality assurance impact energy attenuation testing of U.S. Army flyer protective helmet, considering combined interaction of shell, foam liner and plastic pads 15 p2559 A69-30851

Quality control - ASQC Conference, Los Angeles, May 1969 15 p2721 A69-31119

Sterilization assembly development laboratory (SADL) quality assurance program for microbiological monitoring according to NASA planetary quarantine requirements 15 p2559 A69-31123

Electronic hardware optimum quality assurance selected by dynamic programming in terms of failure mechanism detection efficiency per source allocation 15 p2722 A69-31127

Quality control of high volume microelectronic circuit assembly of military computer emphasizing preventive action 15 p2580 A69-31129

Integrated circuits screens, developing sequence of life and environmental tests to remove units of potential reliability hazards 15 p2580 A69-31130

Large scale integrated MOS devices tests for space applications, establishing quality specifications 15 p2580 A69-31131

Integrated circuits failure analysis in space program applications, describing electrical analog for notification, fact gathering, part analysis and corrective action functions 15 p2580 A69-31132

High temperature ultrasonic testing to measure and control solid materials early in processing 15 p2632 A69-31514

Eddy current and ultrasonic applications to aircraft engine inspection, discussing electric and magnetic methods for quality control during fabrication 15 p2632 A69-31516

High reliability space system electronic parts control program to assure success of unmanned space missions 16 p2793 A69-31714

Book on ultrasonic testing of materials covering ultrasonics application to nondestructive testing, flaw detection and quality control 16 p2790 A69-32125

FORTAN computer program for quality control and calculation of total ozone measurements and lamp tests for Dobson ozone spectrophotometer 16 p2787 A69-32644

Solid propellant thrusters fabrication procedures, design considerations and quality control, stressing stress analysis and propellant choice with respect to geometry 17 p3018 A69-33331

Physics of Control program for electronic devices reliability, discussing qualified parts, chemical, physical and electrical properties, parameter ranges, specifications and corrective action 18 p3143 A69-34488

Semiconductor reliability evaluation program for economical experimental design, noting stress tests 18 p3232 A69-34496

Failure analyses of semiconductor devices for military use, suggesting modifications to MIL-STD reliability screen tests 18 p3108 A69-34499

Prefailure detection of unreliable electronics parts from random samples of received parts lots, noting cost reductions 18 p3146 A69-34508

Agna rocket vehicle production reliability evaluation program, testing specific representative equipment randomly selected from production stores 18 p3146 A69-34510

Automatic ultrasonic instrument monitoring on-line welding conditions of RF longitudinally seamwelded tubes 18 p3136 A69-34778

Betatrions for nondestructive quality control for materials and products under special conditions 18 p3136 A69-34779

Machining processes effect on surface integrity of machine parts and effects on product quality 18 p3149 A69-35129

X ray analyzer for residual stress measurement applied to quality control 18 p3150 A69-35423

Holographic interferometry for nondestructive testing of aircraft materials, discussing applications to quality control 19 p3322 A69-35576

System reliability evaluation based on failure analysis illustrated with examples covering initial requirement through parts production monitoring and control
19 p3454 A69-35782

Closed-loop system for test, failure analysis and corrective action in avionics reliability growth, showing cost effectiveness relationship to test program
19 p3282 A69-35784

Microwave equipment reliability considered in terms of various subsystems and components, showing carefully formulated and executed test program as essential
19 p3282 A69-35785

Microelectronics and IC process and quality control check list including conductor screening, resistor abrading and discrete part attachment
19 p3283 A69-36020

Cylindrical concave surface quality control by contactless comparison with reference surface, using interferometer with Twyman system and continuous laser
19 p3311 A69-36196

Quality control and dimensional accuracy in air-frame structures fusion welding
20 p3549 A69-37446

Fusion welding for thin gauge corrugated core sandwich airframe structures capable of operating at high temperature, discussing equipment, techniques and quality control
[SBAC PAPER 9] 20 p3549 A69-37448

Welding quality control in aircraft structures, considering weld design, process, weld and materials specifications, welding equipment and inspection
[SBAC PAPER 15] 20 p3550 A69-37452

Precision azimuth reference accuracy standards with confidence limits for gyrocompass evaluation, emphasizing astro and transfer angle repeatability
[AIAA PAPER 69-859] 21 p3725 A69-39387

Reliability testing and parts screening of electronic systems for best parts selection
22 p3953 A69-40029

Part selection, source control and application program for reliability of equipment design, noting derating
22 p3953 A69-40031

Engine oil analysis applied to commercial airline operations, ensuring lubricating qualities retention and detecting oil-wetted component failures
[SAE PAPER 69-0423] 23 p4169 A69-41647

Quality and reliability of electronic spacecraft devices and structural components produced in limited quantity, discussing documentation of production and testing
23 p4171 A69-42474

Management role in ensuring products and components quality and reliability, analyzing failure reasons
24 p4416 A69-42778

Self acting gas lubricated bearings production, discussing manufacture to ultraprecision tolerances by semiskilled labor
[ASME PAPER 68-WA/LUB-4] 24 p4320 A69-43035

Acrospace systems failures caused by stress corrosion, fatigue, overload, improper designing or inadequate processing control
24 p4323 A69-43428

Damage tolerance design concepts required to obtain reliability, maintainability and operational safety of complex aircraft
[ICAS PAPER 68-23] 24 p4254 A69-43717

QUALITY FACTORS U Q FACTORS

QUANTITATIVE ANALYSIS

Exploding wires as light source for quantitative spectroscopy, noting optically thin plasma clouds with radial symmetry
01 p0117 A69-10658

X Ray fluorescence of rock samples as applied to geological problems, noting standard deviations for element distribution
01 p0082 A69-10890

Quantitative determination of phenolic content in composite materials by pyrolysis gas chromatography method
01 p0025 A69-11267

Chemical composition of various types of chondrites, determining quantitative proportions soluble and insoluble in acids
01 p0026 A69-11381

Gas chromatographic determination of hydrocarbon quantity in methane in parts per billion range
03 p0382 A69-14115

Trace analysis /parts per billion/ of methane in helium, hydrogen and neon
03 p0382 A69-14116

Quantitative analysis of nonsteady temperature field in long cylinder for sudden heating of semiinfinite axisymmetric lateral surface
05 p0845 A69-15797

Quantitative spectroscopy and spectral photometry, discussing developed image properties and connection between exposure and image
08 p1315 A69-20467

Quality assessment of quantitative data on chemical composition of stony meteorites, considering precision and accuracy
11 p1953 A69-24359

Direct analysis of lunar surface chemical composition, considering soft landing probe and X ray isotope fluorescence method
11 p1832 A69-24629

Quantitative schlieren technique for one dimensional recording of light refraction in density gradients of high speed flow fields
12 p2088 A69-26181

Quantitative interferometric analysis of shock induced wavelength variations in glass and polished steel plates using Q switched ruby laser light source
12 p2089 A69-26185

Radioactivity induced in solid materials for components microautoradiography and radiograph information quantitative evaluation
13 p2297 A69-28157

Dispersion-strengthened alloys from extraction replicas, determining volume fraction and spacing of dispersed phase particles
13 p2282 A69-28167

Quantitative gas-liquid chromatography of sulfur amino acids trimethylsilyl derivatives
13 p2217 A69-28259

Quantitative gas-liquid chromatographic analysis of nucleic acid components including purine and pyrimidine bases, nucleosides or nucleotides
13 p2217 A69-28260

Quantitative analysis for N-acetylneuraminic acid by gas-liquid chromatography using trimethylsilyl derivative
13 p2217 A69-28315

Microstresses and distortions in quasi-isotropic solid bodies under strain evaluated by correlation functions
14 p2531 A69-28806

Quantitative analysis of interaction between spray and ambient atmosphere, discussing atomization of flat sheet and drop behavior relationship to operating conditions
15 p2717 A69-30465

Friedrich qualitative analysis of ordinary differential operators modified to obtain quantitative information regarding eigenvalues distribution
17 p2995 A69-33404

Quantitative analysis and classification of stony meteorites, including carbonaceous chondrites, by Mossbauer characteristics, discussing Prior plot and weather influence role in finds and falls
19 p3408 A69-36083

Quantitative mineralogical characterization of chondrites by modal analysis using electron microprobe
19 p3416 A69-36125

Spectroscopic quantitative analytical method for measuring atomic absorption in flame based on determining integral absorption magnitude during evaporation
20 p3539 A69-37605

QUANTIZATION

U MEASUREMENT

QUANTIZER

U COUNTERS

QUANTUM AMPLIFIERS

Quantum paramagnetic amplifier using andalusite single crystal and operating with three level pumping system
04 p0577 A69-14780

Quantum paramagnetic amplifier using natural andalusite single crystal and operating with four level pumping
04 p0577 A69-14781

Radio spectrometer with paramagnetic quantum amplifier for astronomical spectral measurements in 8 mm range
04 p0597 A69-14851

Pulsed radar quantum paramagnetic amplifier protection from driving pulse leakage power by transient processes
05 p0728 A69-15644

Quantum devices operation analyzed by introducing quasi-linear negative conductance into system by active substance, deriving equations to characterize saturation effects
05 p0719 A69-16223

Quantum paramagnetic amplifier saturating power dependence on input pulses length and frequency determined by kinetic equations solution
08 p1325 A69-20436

Radio spectrometer with paramagnetic quantum amplifier for astronomical spectral measurements in 8 mm range
15 p2607 A69-30243

Pulsed radar quantum paramagnetic amplifier protection from driving pulse leakage power by transient processes
16 p2762 A69-32501

Collection of papers on quantum electronics covering microwave, optical quantum generators and amplifiers, paramagnetic resonance, molecular excitation, etc
18 p3178 A69-35401

Gas and solid state microwave quantum generators and amplifiers, discussing radiation characteristics
18 p3153 A69-35407

Andalusite crystals as active media in paramagnetic quantum amplifiers, discussing design and performance
19 p3335 A69-35881

Possibility of combining individual yttrium ferrite single crystals to obtain noninteracting element for quantum paramagnetic traveling-wave amplifier operating at liquid nitrogen temperature
19 p3334 A69-35883

Amplitude and output spectra of optical quantum amplifier based on GaAs injection laser, noting values in traveling wave and regeneration mode
19 p3336 A69-36348

QUANTUM COUNTERS

Quantizing noise effect on reconstructed analog signal at reception terminal of digital data transmission system
01 p0027 A69-10250

Spectrum of clipped noise in optical spectroscopy, considering double clipping at zero photon number
15 p2571 A69-31486

QUANTUM ELECTRODYNAMICS

Cosmology and quantum electrodynamics, discussing zero point oscillations and predicted spontaneous emission rate
01 p0149 A69-10139

Microwave generation and amplification, noting microwave transit time tubes, semiconductor devices and methods utilizing quantum electronic effects to generate and amplify EHF oscillations
03 p0395 A69-13611

Quantum electrodynamics of radiation scattering from ionized interacting plasma, considering electron interactions
04 p0636 A69-15044

Multiphonon orbit lattice relaxation of excited states of rare earth ions in crystals, using results to design quantum electronic devices
[IEEE PAPER I-9] 05 p0774 A69-16318

Quantum electronics trends, discussing output power, mode control, stability and lifetime of CW and Q switched lasers and parametric interactions in nonlinear optics
07 p1144 A69-18468

Finite formulation of field theory applied to quantum electrodynamics, assuming Bogoliubov causality and TCP invariance of S operator
07 p1181 A69-18957

S matrix theory of electromagnetic interactions, obtaining equivalence of results with quantum electrodynamics by choice of subtraction constants
08 p1351 A69-20211

Interstellar extinction models of classical Mie particles and quantum mechanical polycyclic aromatic molecules
10 p1781 A69-23679

Relativistic coherence theory of black body radiation in transparent medium, deriving expressions for second order correlation tensors by phenomenological quantum electrodynamics
11 p1920 A69-25563

Transverse quantum thermodynamic phenomena in thin semiconducting films, noting effects of inelastic electron scattering at acoustic lattice vibrations
13 p2318 A69-27890

Magnetoquantum-electric effect, analyzing center motion of cyclotron orbit during photon and phonon absorption and current quantity
16 p2826 A69-31823

Quantum mechanical microwave frequency doubling in ruby, discussing output power variation with orientation
17 p3015 A69-33024

Quantum electronics theory, Volume 1, covering radiation-matter interactions, relaxation processes, spontaneous and stimulated emission, etc
17 p2982 A69-33686

Level shifts and spontaneous transitions in steady state of universe by path integral method of first quantization, considering time symmetric electromagnetic theory
22 p3980 A69-40169

Steady state cosmology for classical and quantum electrodynamics in local vicinity, deriving Lorentz-Dirac equation from variational principle
23 p4215 A69-42116

GaAs laser diodes differential external quantum efficiency and gain per unit length dependence on laser reflectivity, taking into account optical losses
24 p4330 A69-43766

GaAs laser diodes differential external quantum efficiency and gain per unit length dependence on laser resonator length, taking into account optical losses
24 p4330 A69-43767

QUANTUM GENERATORS
U STIMULATED EMISSION DEVICES

QUANTUM MECHANICS

Representation for real functions of quantum mechanical momentum operator obtained by functional integration in phase space
01 p0106 A69-10930

Conceptual problems of quantum optics, considering quantum mechanical and classical descriptions of effect of field on matter for damped and undamped modes
03 p0467 A69-13474

Maser model of single mode field coupled to N identical two level atoms, deriving threshold, stable and unstable steady states, relaxation oscillations, etc
03 p0441 A69-14108

Matrix elements calculation for one dimensional quantum-mechanical problems using transformation theory
04 p0632 A69-14866

Free energy of low density quantum plasmas derived statistically from exact two particle scattering phase shifts
05 p0799 A69-15629

Photon number and amplitude fluctuations of laser radiation in case of inhomogeneously broadened atomic line and for steady state condition
05 p0770 A69-15631

Quantum geometrodynamics in superspace, noting dynamical evolution of geometry with no real mass energy sources
05 p0793 A69-15773

Atomic hydrogen-bromine linear collision reaction intermediate formation and reactive scattering cross sections quantum mechanical calculation, using perturbed Morse oscillator approximation
05 p0796 A69-15911

Quantum oscillations of Maggi-Righi-Leduc (MRL) effect in n-InSb and n-InAs samples from single crystals at liquid helium temperature
06 p0979 A69-16992

Cyclotron resonance measurements of quantum effects in Ge valence bands by CW molecular gas laser, developing tunable submillimeter maser [IEEE PAPER C-6]
07 p1150 A69-19051

Experiments on Josephson tunneling junctions and superconducting contacts to demonstrate quantum electronic properties of superconductors [IEEE PAPER D-7]
07 p1200 A69-19052

Delta functions use in extending domain of Laplacian operator in quantum mechanics
07 p1174 A69-19495

Quantum theory of laser, discussing stationary photon distribution and correlation function for intensity fluctuations
08 p1324 A69-20221

Quantum mechanical description of ionizing reactions of highly charged positive ions in solar corona, obtaining approximate sum and selection rules
09 p1596 A69-22054

Fluid dynamical aspect of Schroedinger quantum mechanics and thermal equilibrium
09 p1541 A69-22394

Intrinsic quantum-mechanical behavior of fully ionized gas at high temperature and low density, defining classical limit
14 p2502 A69-29992

Master equation in quantum optics phase-space formulation based on Schroedinger equation of motion, noting application to Volterra integral equation and Born approximation
15 p2633 A69-30307

Quantum mechanics method for obtaining photocount distribution from optical maser photoelectron counting statistics
15 p2635 A69-31238

Klein theorem kinetic energy corrections taking into account breakdown of equipartition theorem
16 p2823 A69-32469

Collection of papers on quantum electronics covering microwave, optical quantum generators and amplifiers, paramagnetic resonance, molecular excitation, etc
18 p3178 A69-35401

Mathematical methods for quantum mechanical problems caused by electromagnetic field interaction with matter
18 p3175 A69-35402

Quantum transitions between molecular or atomic energy levels noting microwave spectroscopy utilization
18 p3099 A69-35405

Bogoliubov averaging method of perturbation in wave mechanics for radiation and matter interaction, considering monochromatic and broad spectral incident wave for resonance study
18 p3175 A69-35483

Paradox of incoming photons detection at two antennas without interference pattern disturbance explained by classical and quantum physics
20 p3538 A69-37415

Soviet book on quantum electronics covering electronic devices, nonrelativistic quantum mechanics, radiation field and matter interaction, black body radiation spectra, etc
20 p3556 A69-38210

Unified theory of elementary particles assuming quantum mechanics as consequence of changes in time within microcosmos and particle-universe interaction
21 p3816 A69-39622

Quantum-mechanical theory of unimolecular kinetics and predissociation developed from generalized Fano theory of resonant scattering
22 p3986 A69-40724

Quantum mechanical multimode correlation functions derivation and applications to laser theory
22 p3965 A69-41152

Quantum mechanical systems dynamics in diagonal coherent state representation, discussing applications
22 p3983 A69-41259

Variational formulation of nonlinear differential equations, treating vector fields in Hilbert spaces, finding relations useful in quantum mechanics
23 p4181 A69-41723

Collective rotational motion separation from internal motion in system of n point masses based on wave mechanics, emphasizing three body problem
24 p4349 A69-42650

QUANTUM NUMBERS

Absorption coefficient in three microwave lines of O with different rotational quantum numbers calculated, examining Zeeman effect in geomagnetic field
15 p2597 A69-30941

Transformed kinetic equation used to study relaxation of quantum oscillator to thermodynamic equilibrium state
18 p3152 A69-35126

QUANTUM STATISTICS

High temperature, fully ionized plasma equation of state, using quantum statistical theory of low density electron-ion plasma in thermal equilibrium
01 p0128 A69-10346

Self consistent field calculations of effective quantum numbers for nd, nf and ng electrons for atomic configurations from 2-126 Z
08 p1355 A69-20734

Chebyshev series approximations for Bose-Einstein functions of orders one to ten, noting computability of Fermi-Dirac functions and polylogarithms
24 p4341 A69-43231

QUANTUM THEORY

Quantum theory of electrical birefringence of noninteracting diamagnetic molecules /Kerr effect/ subjected to static electric field and polarized plane wave
02 p0279 A69-11538

Optimal reception of quantum signals at recording device aperture
02 p0206 A69-11607

Light tachyons, tachyon velocity and relation to gravitational quanta
02 p0282 A69-12746

First order equations for gravitational field quantized by methods developed for relativistic wave equations, describing elementary particles
03 p0466 A69-13422

Static formations in general theory of relativity and plankions
05 p0793 A69-15776

Symmetrical formulation of quantum theory of three wave optical parametric interactions in crystals
06 p0958 A69-17710

Model for phase transition mechanism quantum-Coulomb plasmas, finding transition temperature for white dwarfs
06 p0968 A69-17785

Difference frequency generation by multiple quantum transition from laser medium considered as resonant optical frequency mixing device
07 p1144 A69-18470

Quantum theory of electron gas with anomalous magnetic moments in intense magnetic fields, noting pair creation from thermodynamic energy in system
08 p1353 A69-19782

Quantum theory of laser, discussing stationary photon distribution and correlation function for intensity fluctuations
08 p1324 A69-20221

Quantum theory of line broadening and shift, relating adiabatic and diabatic collisions to elastic and inelastic scattering of perturbors
08 p1363 A69-20464

Laser operation through semiclassical dispersion theory, presenting dipole moment and population density equations derived from quantum theory
08 p1326 A69-20571

Quantum oscillations of magnetization, undamped magnetoplasma waves development and sound amplification by electron drift in crossed fields observed in semimetals
09 p1556 A69-21615

Functional equations of physical systems in strong coupling solved by quantum theory model of anharmonic oscillator, discussing relativistic invariant field theories
09 p1541 A69-22393

Universe origin, discussing big bang theory, effects of expansion time and temperature on elementary particles, RF quanta, etc
11 p1953 A69-24352

Coherence theory of electromagnetic field from classical /wave/ or quantum /particle/ standpoint, stressing information theory
11 p1915 A69-24455

Optimal reception of quantum signals at recording device aperture
11 p1835 A69-24714

Book on stellar atmospheres covering radiation theories, thermal equilibrium, measurement techniques, spectral analysis, etc, emphasizing sun
11 p1961 A69-25084

Quantum oscillators interaction with two level molecules system in circular laser
11 p1899 A69-25325

Maxwell theory-basis of special theory of relativity, discussing universal length constant
11 p1920 A69-25562

Stellar physics, Volume 1, covering stellar structure, evolution, physical processes, statistical physics, quantum theory, classical mechanics, etc
12 p2152 A69-25785

Shubnikov-de Haas effect and quantum limit phenomena concerning oscillatory magnetoresistance in semiconductors
16 p2827 A69-31826

Particle production by gravitational fields in universe via quantum field theory, considering cosmological models
17 p3008 A69-33003

Quantum electronics theory, Volume 1, covering radiation-matter interactions, relaxation processes, spontaneous and stimulated emission, etc
17 p2982 A69-33686

Quantum electronics, Volume 2, Maser amplifiers and oscillators
17 p2982 A69-33687

Laser action in quantum system, analyzing absorption constant relation to spontaneous/ stimulated emission constants, energy level population inversion, pumping, etc
17 p2984 A69-34150

Static formations in general theory of relativity and plankions
18 p3173 A69-35029

Soviet collection of papers on quantum electronics covering ruby laser actions, harmonic generation, laser outputs, etc
19 p3330 A69-35862

- Parametric conversion kinetics of monochromatic light waves in nonlinear crystals, using quantized electromagnetic field to study amplification and generation 19 p3332 A69-35870
- Lasers and maser devices in radio quantum electronics, discussing optical parametric and microwave devices including transistors, diodes, magnetrons, etc 19 p3284 A69-36433
- Electric field correlation to magnetic fields in quantum theory of coherence, deriving dynamical equations governing space-time development of correlation matrix 20 p3575 A69-37304
- Collection of papers on mechanics including quantum theory, mechanics of micropolar continua, elasticity and plasticity, rheology, etc 20 p3623 A69-37580
- Observations in quantum theory, considering object state, apparatus effects, eigenvalues probability distribution, etc 20 p3576 A69-37581
- Universe evolution from hot initial state, discussing element synthesis, quanta, radiation particles, etc 21 p3795 A69-38401
- Quantum theory for single mode laser radiation, considering photon distribution function and mean field damping decrement by phase quantum fluctuations 21 p3737 A69-38996
- Cavity Q dependence of intensity of single mode He-Ne laser above threshold for quantum and semiclassical theories 22 p3961 A69-40415
- Multiquantum photoemissive effect in metals, semiconductors and dielectrics emphasizing laser application for studying electromagnetic field 22 p3964 A69-40690
- Planck law for black body radiation spectrum theoretically derived on basis of classical Lorentz-invariant electromagnetic radiation at absolute zero temperature without quantum assumption 22 p3982 A69-41001
- Incoherent object threshold light detection by quantum limited optical system in presence of radiant thermal energy 23 p4191 A69-42147
- Quantum optics or electronics, discussing electromagnetic waves control and interactions with matter, maser oscillators theory and characteristics, nonlinear optics, induced transparency, etc 23 p4174 A69-42315
- Gravitational field quantization according to Einstein theory using classical Hamiltonian dynamics and quantum rules for constraints 23 p4192 A69-42332
- Laser quantum theory compared to stationary atoms semiclassical theory, emphasizing role of cavity mode spatial structure 24 p4327 A69-42789
- QUARKS**
- Leptonics quarks with various charges in cosmic rays, determining upper limit of flux in underground measurements 02 p0306 A69-11547
- Quark model to account for enormous energy from quasars 09 p1597 A69-22084
- Cosmic ray particles with fractional charge at sea level searched by scintillation counters with spark chambers, estimating quark flux intensity 13 p2333 A69-28425
- Quark detection in cosmic rays at sea level using scintillation counter and streamer chamber system 15 p2674 A69-30308
- Solar energy release by quark fusion catalysis of alpha reaction without production of neutrinos, noting temperature dependent reaction rate 18 p3186 A69-34643
- Quarkian core substance in superstars of great masses, discussing existence as primordial state forming baryon and nuclei and origin in stellar gravitational contraction 19 p3401 A69-35912
- Quark mass and charge interpretation during particle track photographic analysis of air shower cores by delayed expansion Wilson cloud chamber 24 p4383 A69-42945
- QUARTZ**
- Sustained high deceleration load effects on quartz crystals during atmospheric entry studied by centrifuge test program on oscillator circuits 01 p0042 A69-10417
- Tube and transistor type quartz crystal FM oscillators circuitry and operating characteristics, discussing generation of three frequencies 05 p0732 A69-16532

- Z magnetometer with quartz sensitive element suspended by thread in silicone oil design and operation 09 p1494 A69-21539
- Gas film protection of quartz tube wall transparency loss due to hot plasma contact used to study UV emission during high power pulse discharges 11 p1926 A69-24616
- UV radiation decreased transmittance through quartz exposed to plasma at high temperature and pressure, showing dependence on heated surface layer absorption 14 p2490 A69-29159
- Quartz oscillator with electronic temperature compensation, noting reduced size, weight and power consumption 14 p2420 A69-29398
- Quartz oscillator amplitude and frequency fluctuations due to elements tolerance fluctuations, examining oscillator parameters contributions to spectral line width 15 p2579 A69-30944
- Z magnetometer with quartz sensitive element suspended by thread in silicone oil design and operation 16 p2792 A69-32534
- Quartz fiber adhesion to Re measured in LEED/low energy electron diffraction/ apparatus for clean and O layer surfaces, noting brittle fracture 18 p3156 A69-35182
- Fiber reinforced carbon and graphite with application to reentry and propulsion systems and high temperature gas turbines, noting three dimensional woven quartz 19 p3354 A69-35519
- Elastic properties of hot pressed polycrystalline quartz and rutile as function of pressure, obtaining pressure coefficients of compressional and shear wave velocities 20 p3583 A69-37502
- Lummer-Gehrcke plate type polarizer made of birefringent material for Nd glass laser, discussing reflection coefficients in quartz crystals 21 p3739 A69-39541
- Quartz compasses designed for orientation of electronic devices with respect to magnetic meridians at low horizontal component values 23 p4166 A69-41869
- QUARTZ LAMPS**
- IR heating, discussing operation of IR emitters employing glass and quartz envelopes 03 p0411 A69-13548
- QUARTZ TRANSDUCERS**
- Rocket engines transient thrust measurement by quartz transducers 08 p1301 A69-20589
- Magnetosensitive quartz element with suspended magnet and two mirrors for recording magnetic variations 14 p2446 A69-29084
- QUASARS**
- Red shift pattern in quasar emission spectra consistent with fractional screening charges on emitting atom nuclei 01 p0153 A69-10855
- Cosmic rays properties and sources, considering origin in supernovae, galaxies, quasars and unknown sources 02 p0308 A69-12158
- Light fluctuations rise time, electron density, emission temperature and peak luminosity estimated for quasars powered by local gravitational collapse events 02 p0325 A69-12590
- Absorption and emission redshift distribution in quasars, N systems and similar compact and radio galaxies 02 p0325 A69-12591
- Linear polarization measurements at 2.07 cm for 29 radio sources 02 p0326 A69-12705
- Plasmas in galaxies, spiral structures and radio galaxies, discussing quasar line and continuum spectra 02 p0329 A69-12790
- Radio galaxies and quasars, discussing radio structure, observation methods, polarization, time variation, etc 02 p0329 A69-12791
- Energy sources and properties of quasars and radio galaxies by X ray astronomy 02 p0310 A69-12793
- Plasma model of quasars and radio galaxies for observations of high energy radiation 02 p0329 A69-12794

- Radio galaxies and quasars X ray emissions, calculating radiation fluxes produced by scattering of synchrotron radiation quanta at relativistic electrons 03 p0500 A69-13079
- Radio emission center of gravity from 3C 273 quasar determined by radio telescope together with A and B component fluxes 03 p0506 A69-13092
- Spectral line identification in quasars, noting emission lines characteristic of emission nebulas and absorption lines of stellar atmospheres 03 p0508 A69-13173
- Empirical growth curve determined by using equivalent widths of absorption lines of quasar 3C 191 concluding ionization is mainly due to collisional processes 03 p0514 A69-13962
- Radio spectra differences of quasars and radio galaxies, noting influence of frequency levels 04 p0652 A69-14418
- Continuum radiation of quasars, adopting cosmological interpretation of red shift 04 p0648 A69-14565
- Seyfert galaxies high excitation broad emission lines and quasars resemblance, discussing causes of spiral galaxies violent nuclear activity 04 p0657 A69-14689
- Optical variability of quasar 3C 273, suggesting radiation emission from single bodies rather than from large complex of independent sources 04 p0662 A69-15235
- Emission lines structure in quasar spectra, analyzing problem of weak absorption lines identification 04 p0662 A69-15236
- Evolutionary theory of origin and properties of Seyfert galaxies and quasars, postulating collisions within superdense clusters leading to supermassive stars and supernovae 05 p0819 A69-15703
- Radio observations of radio galaxies and quasars, noting double structure of many sources, some complex structures and association with optical objects 05 p0820 A69-15836
- Optical observations of radio galaxies and quasars, noting evidence for galactic explosions, surface distribution, physical properties, radio quiet quasars, etc 05 p0820 A69-15833
- Theoretical models explaining observed properties of radio galaxies and quasars, discussing quasar distance 05 p0821 A69-15851
- Quasar and radio galaxy evolution, discussing energy release rate and particle acceleration effects on radio and optical emissions 05 p0822 A69-15852
- MHD quasar model consisting of galaxy with supermassive plasma nucleus moving in magnetic field 05 p0822 A69-15853
- Variability in quasi-stellar objects, tabulating results of optical photographic survey 05 p0826 A69-16387
- Stimulated Compton effect for energy transfer between relativistic electrons and radio photons in quasi-stellar objects 05 p0828 A69-16652
- Quasars, stressing local Doppler and gravitational hypotheses for observed red shifts 06 p0998 A69-16968
- Optical mean energy distribution of quasars, discussing red shift effects, significance of physical origin of optical continuum radiation and K-term magnitude determination 06 p0999 A69-16975
- Relativity and stellar model stability, discussing energetics of quasars and gravitational collapse of supermassive stars 06 p1002 A69-17315
- Complex distribution of quasar red shift interpreted as due to two simple distributions of cosmological and gravitational red shift 06 p1009 A69-17968
- Cosmological model describing relation between red shift and magnitude of quasars 07 p1211 A69-18406
- Red shifts and intrinsic powers of radio galaxies and quasars, discussing local luminosity distribution, function of sources and cosmology 07 p1206 A69-19270
- Radio galaxies, quasars and radio stars between declinations plus 20 and plus 27 degrees, obtaining accurate positions and optical identifications 07 p1218 A69-19273

Cosmological models with antipole, determining models consistent with spatial distribution of quasars and radio galaxies

07 p1219 A69-19284

Radio spectrum of quasi-stellar object identified as Parkes 2134 plus 004

07 p1224 A69-19708

Relativistic astrophysics, discussing quasar phenomenology, red shift cosmology and relationship with galaxies

08 p1388 A69-20222

Quasars optical and electrical properties, distance, nature and role in cosmology

08 p1390 A69-20377

Focal antennas and receivers of Nancy radio telescope to measure flux density and incoming waves polarization, noting circular polarization in quasars

08 p1392 A69-20567

Quasar 3C454.3 optical variations, noting photographic and photometric evidence for period of 340 days

08 p1397 A69-20701

Quasi-stellar radio sources /QSS/ and radio galaxies structure and evolution, discussing nucleus nonuniform model

09 p1592 A69-21500

Theoretical models describing quasi-stellar objects and radio galaxies, noting objects locality, semilocality and cosmological distances

09 p1594 A69-21693

Quark model to account for enormous energy from quasars

09 p1597 A69-22084

Quasar red shifts due to cosmological and gravitational factors, assuming correlation of QSO intrinsic luminosity with gravitational red shift values

09 p1597 A69-22151

Red shifts of quasi-stellar objects obtained with image tube spectrograph, noting photoelectric magnitudes and colors

09 p1602 A69-22225

Spectroscopic observation of quasi-stellar objects noting red shifts

09 p1602 A69-22226

Absorption red shifts in quasi-stellar source due to dead galaxies in cosmologically flat model of universe

09 p1602 A69-22228

Absorption red shifts in quasar spectra from spectroscopic observations of PHL 5200 and B194

09 p1604 A69-22271

Quasi-stellar objects photometric selection in near IR

09 p1604 A69-22272

Quasars and explosive processes in galaxies as cosmic ray sources in expanding universe, studying relation between galactic and metagalactic cosmic rays

10 p1756 A69-22815

Homogeneous anisotropic cosmological models of pancake and cigar forms, discussing quasars and emission time effects on red shift and luminosity distance

10 p1771 A69-22856

Energy release in quasars through nonmassive gravitational collapse compared with local objects, noting cosmological luminosities

10 p1785 A69-24091

Spectroscopic observations of faint quasar near double galaxy NGC 3561, noting red shifts

10 p1785 A69-24092

Faint blue objects in intermediate to high galactic latitudes, summarizing results of UVB photoelectric photometry

10 p1788 A69-24123

Radiation probability of transmission through intervening galaxy and screening of quasar emission in universes with positive cosmological constant

10 p1790 A69-24135

Quasi-stellar radio sources interferometric observations at 2695 MHz, determining centroid of radio emission

10 p1790 A69-24138

Quasars optical polarization data, showing variable polarization for 3C 273

10 p1790 A69-24139

Quasar and radio galaxy spectra obtained on Cassegrainian focusing diffraction spectroscope

11 p1951 A69-24236

Quasars time dependent flux density variations at 6.6 cm, noting spectrum peaks tendency toward lower frequencies with time

11 p1954 A69-24382

Flux density of quasars 3C 270 and 3C 278 at 40 cm determined by digital computer with point source program

11 p1954 A69-24383

Electromagnetic wave buildup by induced Compton effect as possible radio emission source, considering data for quasars and pulsars

11 p1957 A69-24402

Plasmas role in emission mechanisms active in celestial sources of radiation, discussing sun and quasars

12 p2159 A69-26619

Quasars and radio-quiet objects numbers and properties, discussing red shifts interpretation by cosmological, gravitational and Doppler theories

12 p2161 A69-26937

Statistical data on space density of bright elliptical galaxies, radio galaxies, quasars, noting relation between space density and age

12 p2165 A69-27033

Polarization and structure of magnetic fields of quasars, E galaxies, normal galaxies and other extragalactic radio sources

12 p2165 A69-27034

Galactic and quasar radio sources distribution, discussing spectral indices

12 p2166 A69-27036

Radio sources angular dimensions determined by microwave interferometry, discussing distinctions between quasars, galaxies and unidentified sources

12 p2166 A69-27039

Frequency spectra of radio galaxies, supernova remnants and quasars observed by radio telescope operating in decimeter wave range

12 p2167 A69-27041

Quasars optical properties, hypotheses on nature, energy distribution, red shift, stellar magnitude and distance estimation on basis of absorption

12 p2167 A69-27042

Quasar spectra changes observed from 1962 to 1966 including flux density and antenna temperature for 3C 279 at cm wavelengths

12 p2167 A69-27043

Luminosity changes in quasar 3C 273, describing corrections introduced into luminosity curve obtained by iris photometer

12 p2167 A69-27044

Quasars intensity variations at various cm wavelengths confirming wavelength dependence

12 p2167 A69-27045

Quasar spectra, discussing 3C 345, 3C 191 absorption lines and model explaining quasar spectra

12 p2167 A69-27046

Red shift determinations and line identifications for quasars, using spectrograph with electro-optical converter

12 p2168 A69-27048

Quasar properties from cosmological nature, discussing red shift, luminosity, radiation intensity, absorption features, distribution, chemical composition, etc

12 p2168 A69-27049

Coherent radio emission mechanism in quasars and supernova remnants, discussing magnetic effects

12 p2168 A69-27050

Spectral energy distribution in quasars, using photoelectric spectral scanner in several wavelength ranges

12 p2168 A69-27051

Law of optical radiation and photometric characteristics of quasars, noting photometric effect of strong emission lines and color dependence on red shift

12 p2168 A69-27052

Optical identification of radio source 3C 230, suggesting removal from quasar list

12 p2173 A69-27171

Absorption line spectrum of quasar Ton 1530, discussing line widths and red shifts

13 p2334 A69-27306

Statistical tests for cosmological hypothesis for origin of absorption lines in spectra of quasars, considering red shifts

13 p2334 A69-27307

Photographic observations of quasi-stellar objects for position determination

13 p2334 A69-27308

Variable star BL Lacertae absolute spectral energy distribution in visible and IR regions, noting synchrotron features and possible quasar nature

13 p2335 A69-27315

Quasar applications as gravitational lenses within Hoyle-Fowler quasar model

13 p2340 A69-27575

IR extragalactic radio sources including normal radio galaxies, quasars and Seyfert galaxies

13 p2342 A69-27597

IR emission from quasars, noting quasar 3C 273 B and synchrotron mechanism probability

13 p2342 A69-27598

Quasar red shifts distance dependence indicated by visually bright quasar faintness in radio range

13 p2344 A69-27635

Extragalactic radio sources parameters analyzed for distinguishing quasars from dominant luminous radio galaxies by radio spectra

13 p2348 A69-27801

Extragalactic radio sources, observing nonlinear LF spectra for quasars and linear LF spectra for radio galaxies

13 p2351 A69-27867

Radio galaxies and quasars X ray emissions, calculating radiation fluxes produced by scattering of synchrotron radiation quanta at relativistic electrons

14 p2509 A69-28761

Radio emission center of gravity from 3C 273 quasar determined by radio telescope together with A and B component fluxes

14 p2516 A69-28774

Linear polarization of quasars, radio or normal spiral galaxies, galactic objects, etc, observed by Parkes telescope

14 p2526 A69-29770

Polarization characteristics of quasars, radio galaxies and galactic objects suggesting separate evolutionary processes

14 p2526 A69-29771

Symmetry between koinomatter and antimatter in universe, discussing koinonucleons production, big bang theory, protogalaxy model, quasi-stellar objects, galaxy evolution, etc

15 p2690 A69-30670

Quasar multiple absorption red shift lines caused by gas in extended galaxy halos, assuming broadened galactic cross section area

15 p2695 A69-30884

Quasi-stellar and related objects emission and absorption red shifts tabulation suggesting absorption lines origin

15 p2701 A69-31532

Quasi-stellar objects anomalous Hubble plot, suggesting explanation for steeper plot under assumption on red shift vs apparent magnitude relation

15 p2701 A69-31536

UBV photometry of southern quasars, radio galaxies and normal galaxies including two color diagrams, radio luminosity, brightness and color distribution

16 p2859 A69-32228

Accurate optical position of quasars determined by plate overlap for radio interferometer calibration

16 p2859 A69-32229

Accurate positions at 2700 MHz and optical identification of radio sources with galaxies and quasi-stellar objects

17 p3035 A69-33611

CP 0950 and CP 1133 pulsating stars position, using radio telescope at two frequencies

17 p3036 A69-33639

Quasars and intergalactic hydrogen density, using Schmidt law of increase in number density of quasars to construct plausible models

18 p3190 A69-34288

Radio sources identified as quasi-stellar objects through photographic detection of large brightness changes

18 p3201 A69-35206

Forbidden emission lines in spectra of normal, radio and Seyfert galaxies and quasars, giving information about quasi-stellar mean densities, temperatures, ionization, etc

19 p3424 A69-36236

Cosmological constant and elementary particle theory

20 p3606 A69-38013

Electron ejections from nuclei of radio galaxies and quasars explained on basis of plasma stability, discussing role of relativistic electrons and resulting unstable pinch

20 p3606 A69-38032

Induced Compton scattering of plasma and electromagnetic waves under astrophysical conditions, discussing HF radio emission spectra from cosmic objects and quasar

20 p3607 A69-38035

Cosmic ray electron role in energetics of solar flares, stellar flares and explosions, galactic eruptions and quasars

21 p3790 A69-38823

Quasars observations interpretation, discussing red shift origin, gravitational collapse, lifetime, distribution, cosmological aspects, etc

21 p3802 A69-38825

Quasi-stellar objects identification, distribution, emission lines interpretation, energy distribution, absorption spectra, radio properties, etc

21 p3811 A69-39515

Galactic nuclei as collapsed old quasars from dynamics of gas cloud collection in galactic nucleus, discussing cosmic radiation emission from synchrotron mechanism

21 p3815 A69-39610

Quasars red shifts distribution interpreted as due to cosmological and gravitational red shifts distribution, noting analysis error

22 p4024 A69-40580

Quasars observation failure for red shifts beyond z suggested due to absorption of intergalactic neutral H

22 p4024 A69-40582

Quasar features compared to pulsars, noting complete analogy except for energy output scale

22 p4029 A69-40762

Quasar association with galactic clusters, noting red shift and spectral correspondence

22 p4029 A69-40763

Radio galaxies and quasars number-flux density relations role in cosmology, discussing object identification, population, angular sizes, etc

23 p4218 A69-42324

Observational cosmology in terms of relation between red shift and apparent luminosity of galaxies /Hubble relation/

23 p4219 A69-42328

Red shift determinations and line identifications for quasars, using spectrograph with electro-optical converter

24 p4375 A69-42551

Law of optical radiation and photometric characteristics of quasars, noting photometric effect of strong emission lines and color dependence on red shift

24 p4375 A69-42552

Radio galaxies differences from quasi-stellar objects indicating relativistic particles generation from violent explosions releasing energy comparable with powerful supernova

24 p4378 A69-42697

Explosions mechanism in radio galaxies and quasars mechanism based on observed phenomena, emphasizing galactic flares

24 p4378 A69-42698

Book on physics and evolution of galaxies covering properties, stellar content, interstellar matter, high energy particles and radio galaxies

24 p4384 A69-43167

Quasars time dependent flux density variations at 6.6 cm, noting spectrum peaks tendency toward lower frequencies with time

24 p4389 A69-43772

Flux density of quasars 3C 270 and 3C 278 at 40 cm determined by digital computer with point source program

24 p4389 A69-43773

Electromagnetic wave buildup by induced Compton effect as possible radio emission source, considering data for quasars and pulsars

24 p4391 A69-43792

QUASI-PARTICLES

U ELEMENTARY EXCITATIONS

QUASI-STEADY STATES

Continuous emission spectrum and continuous plasma absorption spectral coefficients for optically dense quasi-steady state electrical discharge plasma in sulfur capillary

06 p0964 A69-17251

Quasi-steady state plasma acceleration in coaxial electrode geometry during synchronized application of tailored pulses of mass flow and current [AIAA PAPER 69-267]

09 p1563 A69-21234

Discrete automatic control systems determination by adjustable model, considering quasi-steady state conditions

13 p2238 A69-27253

Spectral distribution of fluctuations in stable plasma in absence of external fields, emphasizing electric field fluctuations, quasi-steady states, isotropic plasmas and thermodynamic equilibrium

14 p2490 A69-29103

Quasi-steady state supersonic gas flow past two closely spaced coaxial separating bodies at different velocities, showing dependence on separation rates

14 p2391 A69-29617

Validity range of nuclear quasi-equilibrium approximation for stellar silicon burning, discussing time rates of nuclear abundance changes and temperature effect

14 p2529 A69-29984

Kinetic theory of stationary laser emission under quasi-equilibrium conditions, analyzing emission modes

19 p3332 A69-35874

Laser multimode emission kinetic theory, discussing quasi-equilibrium disturbance effects and nature of inhomogeneity

19 p3333 A69-35875

Laser emission during disturbed quasi-equilibrium, considering emission spatial inhomogeneity due to arbitrary radiative transitions

19 p3333 A69-35876

Laser emission in system of four level centers, determining nonuniform emission line broadening due to disturbed quasi-equilibrium distribution of electron subsystem elementary excitations

19 p3333 A69-35877

QUASI-STELLAR RADIO SOURCES

U QUASARS

QUASILINEARITY

U NONLINEARITY

QUATERNARY ALLOYS

Ti rich Ti-Al-Mo-Zr alloys phase diagrams at high temperatures, noting presence of solid solutions

07 p1161 A69-18769

Heat resistance of Ti-Al-Mo-Zr alloys analyzed by bend tests, discussing phase diagrams

07 p1163 A69-18779

Dislocations effect on intermediate body centered tetragonal phase precipitation in Fe-Ni-Cr-Be alloy using transmission electron microscopy

08 p1333 A69-20447

Heat resistant fiber composites produced by oriented eutectic crystallization in Co and Ni quaternary alloys [ONERA-TP-710]

16 p2799 A69-31765

Fracture toughness of AlZnMgCu alloys, employing sharp notch tension, tear and precracked Charpy impact tests

16 p2800 A69-31780

Metallurgy, properties and applications of Co-Ni-Mo-Cr ultrahigh strength alloy, discussing corrosion

18 p3154 A69-34307

Tungsten influence on morphology and lattice parameter of fcc gamma prime phase in Ni-Cr-Ti-Al alloys

20 p3558 A69-36962

Corrosion and stress effects separation in stress corrosion of Al-Zn-Mg-Cu alloy, considering machined surface finishing role

21 p3747 A69-39435

QUATERNIONS

Programming technique using quaternion parameters for error reduction in simulation of spinning rigid body

05 p0724 A69-16469

Multispacecraft simultaneous simulation on hybrid computer using Encke perturbation method for translational motion and Hamilton quaternion method for inertial transformations [AIAA PAPER 69-937]

22 p4036 A69-40320

QUENCHING

Plasma spray quenched Al-V alloys resulting in dispersion strengthening of material

13 p2277 A69-27409

IR quenching of photocurrent under field effect in CdS crystal

16 p2827 A69-32044

QUENCHING [COOLING]

Precipitation hardening of gamma phase in austenitic stainless steels studied for phase transformations by dilatometry after aging and quenching

01 p0096 A69-10613

Heat transfer principles analyzed in development of new quenchants for aluminum, noting properties of inversely water soluble polyalkalene glycols

01 p0087 A69-10900

Migration and penetration of vacancies in quenched magnesium analyzed by electrical resistivity measurements and electron microscopy

02 p0267 A69-12187

Heat of solution and diffusivity of nitrogen in molybdenum analyzed by quenching technique and resistivity measurements at liquid helium temperature

02 p0267 A69-12188

Transitional hexagonal omega phase of Ti-Fe alloys quenched in water and tempered

03 p0451 A69-13999

Crystal lattice and orientation of precipitate responsible for hardening water quenched Ni-Cr-Nb alloy

08 p1334 A69-20852

Organic quenchant additive for distortion free heat treatment of dip-brazed aluminum parts

09 p1504 A69-22065

Supersaturation of dissolved B in splat quenched Fe-Ni-B alloys, noting interstitial and substitutional B in martensitic and austenitic phases

10 p1707 A69-22987

Quenched titanium-niobium alloy structure effect on superconductivity properties, using electron microscope and X rays

12 p2112 A69-26040

Nital etchant and sodium bisulfite stain for morphology of quenched dilute alloy Fe-Ni martensite

13 p2282 A69-28166

Electrical resistivity decrease in niobium-hydrogen alloys during isothermal aging at low temperature attributed to hydride precipitation, noting reaction rate and activation energy

14 p2463 A69-29288

Oil quench vacuum furnace with graphite cloth heating elements

14 p2456 A69-29894

Polyurethane with additives for fuel fire control in aircraft structures, achieving desired protection without impairing foams mechanical properties

15 p2561 A69-30311

Al cryogenic quenching using liquid N for slow and uniform heat removal to eliminate distortion

18 p3150 A69-35419

Quenching temperature and deformation conditions for Ti alloy bars optimal mechanical properties, emphasizing effect of primary structure

19 p3328 A69-36152

Ni-Ti maraging steel hardness impact strength and thermal EMF changes during quenching

19 p3345 A69-36154

Quench rate effect on martensite start temperature and fine structure of Fe-C and Fe-C-Ni steel, using transmission electron microscopy

20 p3557 A69-36956

Ti-Al-V sheets quenched from alpha plus beta field into salt bath at various high temperatures, studying effects of bath temperature and holding time on aging and mechanical properties

21 p3730 A69-38667

QUEUEING THEORY

Validation study of pilots visual sampling behavior, using queueing model based on instrument and eye movement data from Link trainer mission flights

02 p0202 A69-11954

Bulk queueing with service time distribution assuming customer arrival in batches and service discontinuance

02 p0271 A69-12060

Iterative method for numerical solution of linear algebraic equations for stationary probability distributions in queueing and reliability theory

10 p1721 A69-23691

State probabilities of finite stochastic queueing system for calculating equipment reliability parameters

10 p1664 A69-23693

Fluctuations effect in flow problems analyzed by waiting line theory to improve systems design based on operational needs

18 p3145 A69-34495

Parameters distinguishing analytic queueing models of time sharing algorithms, emphasizing techniques used for analyzing round-robin and multiple level queueing models

19 p3279 A69-35600

Equipment reliability determination from relations for efficiency characteristics of stochastic queueing system with finite number of sources having Markov character

24 p4287 A69-43129

R

RABBITS

Insignificant or recoverable changes observed in blood acetylcholine content and cholinesterase activity of rabbits subjected to 8 g acceleration

02 p0197 A69-11491

Increasing hypoxia effects on rabbit EEG and light flash conditioned alimentary reflex for simulated altitude ascent, noting subcortical stimulation

02 p0197 A69-11492

Retinal burns from intense light sources using rabbit eyes as function of irradiation rate, exposure time and image size

02 p0204 A69-12496

Transient changes in oxygen consumption, carbon dioxide elimination and respiratory quotients during and after induced hypoxia to rabbits

06 p0876 A69-18026

Oculomotor muscular tonus of rabbit during rocket flight acceleration and weightlessness

07 p1062 A69-18590

High oxygen concentration effect on conditioned reflex and associated EEG responses to light flash in rabbits occurs in well defined sequences

07 p1065 A69-18976

Clinicomorphological changes in rabbit eyes vascular system by exposing transverse accelerations
08 p1262 A69-19832

Transverse acceleration effect on male rabbit frontal hypothalamus nuclei neurosecretory function, noting blood plasma antidiuretic activity
08 p1262 A69-19930

Pulsed and CW microwave power effects on rabbit eyes, noting lens opacities produced
10 p1648 A69-23185

Corticosteroid and catecholamine metabolism change in rabbits during sharp limitation of motor activity
12 p2021 A69-26973

Central adrenergic mechanisms role in neurosecretory function of hypothalamo-hypophyseal system of rabbits under transverse accelerations in centrifuge
15 p2554 A69-30055

Myocardial changes in rabbits after general chronic ionizing irradiation attributed to lower cardiac activity, hypotrophy and dystrophy
17 p2906 A69-32929

Motion sickness prophylaxis for rabbits subjected to rotation, investigating effects of adrenalin, ephedrine, sympatholitin, piperoxane and pyridoxyphene on nystagmus and respiration
20 p3472 A69-37265

Nystagmus reactions in rabbits subjected to rotating vestibular tests, noting decrease following previous adaptation to stimulus
20 p3473 A69-37267

High oxygen concentration effect conditioned reflex and associated EEG responses to light flash in rabbits occurring in well defined sequences
20 p3479 A69-38224

Ventilatory responses to hypercapnia and hypoxia in anesthetized and unanesthetized rabbits before and after bilateral cervical vagotomy
21 p3651 A69-38390

Hyperbaric oxygen convulsions origin and site, studying pressure effect on brain electrical activity in rabbit by EEG
21 p3656 A69-38977

Single large X ray dose depressive effect on aminotransferase activity in rabbit blood serum, liver, kidney, heart, spleen, lungs, etc
21 p3657 A69-39051

Enzyme activity changes in liver, heart and cerebrum of X ray exposed rats and rabbits, noting individual enzyme differences in same X rayed organ
21 p3658 A69-39054

Single X ray dose effect on alpha-amylase and alpha-glucanophosphorylase in rabbit liver tissues and blood serum
21 p3658 A69-39055

Ionizing radiation histological and neurohistological effects in rabbits esophagus, stomach and ileocecal region intramural plexes
21 p3659 A69-39063

Electroretinogram a-wave relationship to early inhibition and excitation of retinal ganglion cells produced by flash superimposition in rabbits
22 p3878 A69-40836

Hemodynamic characteristics of decortication in rabbits, noting upsets of compensatory and adaptive capabilities of cardiovascular system
22 p3888 A69-41271

Positive phase shift relation to elastic modulus enhancement of smooth muscles of rabbit, cat and dog bladder, pulmonary artery and large veins
23 p4083 A69-41459

Rabbits long term reversible retinal function changes due to short high intensity light flashes, noting ERG suppression
23 p4084 A69-41468

Rhythmic wavelets electroretinogram recorded from rabbit retina in vitros preparation indicating dominant relatively low voltage waves compared to in vivos waves
23 p4101 A69-41471

Isolated pacemaker tissue from rabbit heart under dynamic and static stretching, discussing spontaneous frequency phenomena
23 p4096 A69-42092

Cardiovascular autonomic effects dynamic characteristics under severe arterial hypoxia in unanesthetized rabbit
24 p4258 A69-42632

Neural integration of cardiorespiratory responses and suprabulbar control during arterial hypoxemia in rhinencephalic thalamic pontine rabbits
24 p4258 A69-42635

Test animals prolonged deep submersion in water, in mixed oxygen-H atmosphere at elevated pressure, noting EEG and EKG activities
24 p4262 A69-43025

RACON BEACONS
U RADAR BEACONS

RADANT

Integrated radome antenna system design /radant/, comparing electrical performance with conventional systems
07 p1109 A69-19513

RADAR

NT COHERENT RADAR
NT CONTINUOUS WAVE RADAR
NT DOPPLER RADAR
NT METEOROLOGICAL RADAR
NT MONOPULSE RADAR
NT MOVING TARGET INDICATORS
NT OPTICAL RADAR
NT PULSE DOPPLER RADAR
NT PULSE RADAR
NT RANGE AND RANGE RATE TRACKING
NT SATELLITE-BORNE RADAR
NT SEARCH RADAR
NT SECONDARY RADAR
NT SIDE-LOOKING RADAR
NT SURVEILLANCE RADAR
NT TRACKING RADAR

Band inversion passive generation in pulse compression radar, noting influence on signal modulation laws
04 p0558 A69-15074

Digital signal processing in radar, sonar and communication
05 p0718 A69-15749

Book on new concepts in radars covering ideal reception, moving targets, autocorrelation, SNR, amplitude distribution, clutter, etc
24 p4283 A69-43168

RADAR ALTIMETERS
U RADIO ALTIMETERS

RADAR ANTENNAS

Nomograph for planning circular planar aperture antenna arrays, discussing element totalling and spacing, layout geometry, sidelobe suppression and scan loss from broadside
01 p0037 A69-10017

Phased array radar antennas emphasizing beam steering of transmitting linear array with number of phase shifters
01 p0049 A69-11390

Geodesic lens radar antennas, discussing air filled devices operated in TEM mode, inclusive Luneberg lenses, double layer pillboxes and parabolic lenses
03 p0402 A69-13184

Millimeter waves in communication navigation and research, discussing radar range resolution and remote sensing
03 p0397 A69-13722

Semiconductor microwave phase shifters for electronic steering of phased array radar antennas noting cost, reliability and properties of steerable antennas
04 p0572 A69-14319

HAPDAR-TACOL phased array radar design, discussing array patterns and multitarget tracking performance
04 p0556 A69-14324

Reflected radar signal random fluctuations suppressed by using antenna, receiving channels and logarithmic amplifiers
04 p0556 A69-14490

Contour pattern analysis of AN/FPQ-6 monopulse radar Cassegrainian antenna, giving three dimensional drawings
04 p0576 A69-14769

Electrohydraulic radar antenna telecontrol system, discussing pump assembly, hydraulic motor and pump control servojack
04 p0551 A69-15185

Military rotor blade radar antennas for all-weather low level flight and fire control
04 p0559 A69-15197

Single two dimensional coherent matched filter optical processor for simultaneous synthetic radar antenna beam sharpening and pulse compression
04 p0562 A69-15475

Electronically scanned X band array used as receiving antenna for target recognition radar
04 p0562 A69-15476

Secondary radar equipment functions and features forming IFF-SIF chain, discussing displacement controller and minor lobe suppression functions technical problems
05 p0721 A69-16591

Biological effects of VHF electromagnetic radiation from radar antennas
05 p0715 A69-16701

Integrated radome antenna system design /radant/, comparing electrical performance with conventional systems
07 p1109 A69-19513

Measurement bases in general, discussing theoretical data justifying ground level base and measurements results
07 p1136 A69-19516

Radioelectric axis deviation of radome in front of monopulse radar antenna
07 p1111 A69-19524

Paper-honeycomb sandwich radome structure for protecting monopulse UHF radar antennas used in BMEWS
07 p1111 A69-19537

Radiation pattern deformation due to sharp angle radome studied by analyzing diffraction in antenna dihedron system
07 p1112 A69-19539

Angular separation of two point sources measured through expressing antenna resolving power by a posteriori probability laws
08 p1288 A69-20961

Electronic multibeam switching X band antenna system design with separate transmitting and receiving antennas for use on continuous wave surveillance radar
08 p1289 A69-20967

Antenna noise temperature at earth station due to rain on radomes, solar and cosmic noise, noting SNR degradation
09 p1461 A69-21283

Radar transmitter and receiver antennas polarization parameters selection for obtaining maximum SNR at reception point
11 p1833 A69-24442

Microwave antenna testing on small indoor ranges, discussing reflectors and feeds for generation of approximately uniform plane waves for antenna illumination
11 p1852 A69-25314

Statistical gain characteristics of radar antennas at very short Fresnel zone ranges compared to Fraunhofer zone
12 p2040 A69-26470

Southern radio auroral zone observation with rhombic antennas, noting diffuse and discrete zones associated with proton and electron precipitation
12 p2033 A69-26950

Radar antenna radiation effects on man and biological material dependent on absorption degree and emission characteristics including wavelength, peak and mean power
13 p2215 A69-28597

Stepped scanned ring monopulse array, discussing pattern analysis, directivity, co-phased and quasi-phased model
14 p2419 A69-28894

Electronic boresight shift in space-borne monopulse radar system, expressing antenna and signal parameters in terms of equivalent branch and channel asymmetries
14 p2411 A69-28895

Radar calibration and precipitation measurements equation taking Gaussian approximation for antenna radiation pattern
16 p2806 A69-32264

Doubly curved reflectors for rotating search radar directional antenna, noting assembly of elliptical strips constituting segments of parabolic dishes and sidelobe suppression
16 p2763 A69-32790

Transmitting antenna design of multistation radar system for meteors and upper atmosphere investigation, discussing amplitude and phase of electromagnetic field
19 p3278 A69-36661

Phase error in synthetic aperture radar, discussing tolerance level, sources classification and effect on average response, resolution and ambiguity function
20 p3490 A69-37642

Biological and physiopathological effects of UHF electromagnetic radiation of radar antennas, reviewing localized effects
24 p4273 A69-42996

Microwave integrated circuit applications to reflective and transmissive phased arrays, discussing radar system elements
24 p4286 A69-43109

RADAR APPROACH CONTROL

FAA coded broadcasting to transponder equipped aircraft for air traffic control, navigation, collision avoidance and airfield approach
04 p0629 A69-15478

Lidar data obtained at Hamilton AFB, Calif., computer analyzed for lidar operational utility, determining cloud ceiling and visibility for aircraft landing operations
15 p2651 A69-30895

Air traffic control ground equipment developments including radio direction finders, surveillance radar, interconsole marking, etc
18 p3168 A69-34806

ATC medium range radar /SRE-LL1/, describing reflectors positions, information rate, installation, antenna parameters, etc
20 p3496 A69-37932

RADAR ASTRONOMY

Meteor grouping in meteor streams analyzed using radar records of meteor showers
01 p0154 A69-10873

Backscattering diagram of Venus at 40 cm determined from Doppler spectrum and reflected signals range energy distribution
02 p0314 A69-11639

Radar observations of sun, determining reflected radio signal component formed by combination scattering in coronal plasma oscillation
03 p0505 A69-13082

Diffusive scattering effects on planetary surface reflection coefficient determined by radar observations
04 p0662 A69-15245

Radar determination of exponent s for describing mass distribution of Geminid and Quadrantid meteoric bodies
05 p0823 A69-16033

Radar probing of solar system noting contributions to knowledge on planets
09 p1595 A69-21765

Mars photographic and radar data correlation indicating smoothness of dark areas and roughness of desert areas
11 p1964 A69-25406

Radar observations of sun, determining reflected radio signal component formed by combination scattering in coronal plasma oscillation
14 p2515 A69-28764

Received radar signal power maximizing problems in planetary exploration, analyzing abelian group real line and circle problems
17 p2993 A69-32831

Radio and radar astronomy with reference to extragalactic sources and solar system, noting astronomical instrumentation
19 p3425 A69-36430

Radar astronomy, discussing planetary surfaces study techniques, target/signal interactions, planet cross sections, delay and Doppler spectra
20 p3491 A69-37650

Astronomical unit determination, discussing dynamical and radar methods and Doppler shift of neutral hydrogen line spectra in radio astronomy method
22 p4022 A69-40464

Statistical model of cratered planetary surface slopes and elevation applied to radio wave scattering by moon and Venus
23 p4209 A69-41322

RADAR ATTENUATION

Altitude effects on radar attenuation in nonequilibrium solid propellant afterburning rocket exhaust plumes
04 p0685 A69-14730

Rocket exhaust plume models for signal attenuation predictions, considering inhomogeneous plasma medium with varying electron density and collision frequency
24 p4408 A69-43253

RADAR BACKSCATTER

U BACKSCATTERING

RADAR BEACONS

Interim radar improvement program for air route traffic control centers pending development of automated terminal radar programs
01 p0114 A69-11357

Radar detector for survivors, using inexpensive microwave mixer detector crystal
06 p0878 A69-16964

Airborne radar navigation with emphasis on semiautomatic fixing, describing beacon mode, map matching and airborne weather radar
18 p3169 A69-34851

RADAR BEAMS

Quantitative estimations of cloud and precipitation by radar meteorology, assuming homogeneous reflectivity distribution of clouds
04 p0626 A69-14507

Multiple target monopulse radar signal processing technique
04 p0562 A69-15470

Doppler navigation, explaining radar beam mechanization, Doppler spectrum, scanning noise, spectral compression and tracking
18 p3169 A69-34849

Optical correlation for radar signals phase modulated by pseudorandom codes
24 p4282 A69-42742

RADAR CHAFF

U CHAFF

RADAR CLUTTER MAPS

Clutter rejection using coded burst waveform for airborne early warning /AEW/ and airborne attack type radars
03 p0388 A69-13185

RADAR CORNER REFLECTORS

Radar cross section enhancement effect of corner reflectors, multiple reflectors and dielectric lenses
03 p0384 A69-12909

Geodesic lens radar antennas, discussing air filled devices operated in TEM mode, inclusive Luneberg lenses, double layer pillboxes and parabolic lenses
03 p0402 A69-13184

RADAR CROSS SECTIONS

Radar cross sections for arbitrary bodies calculated with computerized ray optics method taking into account depolarization
02 p0209 A69-12332

Book on calculating radar cross section characteristics of geometrically complex shapes using reflectivity characteristics, including electromagnetic theory and data interpretation
03 p0383 A69-12901

Electromagnetic diffraction theory for radar cross section of aircraft, missiles and satellites, discussing mathematical representation of electromagnetic field for extreme wavelengths
03 p0383 A69-12902

Scattering matrices of complex configuration specified by cross polarized radar cross sections based on Green function, noting wire loop and wedge scatterers
03 p0384 A69-12904

Monostatic radar cross section of simple shapes estimated using optics and Rayleigh region approximation with emphasis on multiple reflection
03 p0384 A69-12905

Bistatic radar cross sections of simple shapes calculated based on optics and resonance region, noting forward, nonforward and Rayleigh scattering
03 p0384 A69-12906

Mode theory of backscattered radar cross section of elongated dielectric bodies capable of sustaining traveling wave
03 p0384 A69-12907

Scattering from coated absorbing conducting bodies, considering flat plane and curved surfaces in Rayleigh region
03 p0384 A69-12908

Radar cross section enhancement effect of corner reflectors, multiple reflectors and dielectric lenses
03 p0384 A69-12909

Missile radar cross section based on modeling from simple forms, noting computer program
03 p0384 A69-12910

Radar cross section of missile and aircraft configurations, comparing theoretical and experimental results for Convair 990 static test model
03 p0384 A69-12911

Radar cross section laboratory, discussing experimental techniques, electromagnetic range and pulse, FM/CW and CW radars
03 p0385 A69-12912

Radar cross section data interpretation, discussing calibration, unwanted signals, averaging, scattering matrix and power spectra
03 p0385 A69-12913

Charts of horizontal cross sections of radio echo foci for radio echo reflections from cumulonimbus clouds
03 p0459 A69-13288

Scattering characteristics of planet Venus at 3.8 cm wavelength, discussing frequency power spectra and radar cross section
13 p2349 A69-27818

Electromagnetic and plasma waves scattering by space vehicle excited by ground source in isotropic warm plasma, obtaining radar cross sections
13 p2221 A69-27965

Statistical distribution functions for radar cross section of flying aircraft
14 p2414 A69-29500

Radar cross section of bird represented as unit density dielectric spheroid for bird hazard monitoring, discussing meteorological, insect and bird echoes
17 p2919 A69-33366

Plane electromagnetic wave scattering by motion of small ellipsoid in vacuum, noting total scattering and radar cross sections dependence on ellipsoid velocity
18 p3105 A69-35485

Radar design for target detection, tracking and identification, modeling plasma effects on radar cross section of reentry vehicles based on wave-plasma interactions
20 p3485 A69-36925

Numerical evaluation of geometrical optics radar cross sections of general doubly curved convex conducting body using surface fitting method
20 p3494 A69-37848

Moving model target for laboratory measurements of radar cross section to simulate satellite or reentry vehicle precession motion, noting signature data analysis
20 p3511 A69-37850

Satellite rotation from radar data analysis, requiring two full rotations and body characteristics to produce distinctive lobes in radar cross section
22 p3900 A69-40682

Randomly oriented disks and rods scatter pattern used to determine causes of log-normal distribution of radar cross section fluctuations
23 p4116 A69-41592

Bistatic radar scattering cross sections for reentry vehicle with ionized wake
23 p4116 A69-41593

Monostatic radar cross sections /RCS/ for 5 and 11 wavelength straight wires obtained from induced current integral equation solutions
23 p4116 A69-41594

RADAR DATA

Venus atmosphere and radius measurements by Mariner 5, Venera 4 and radar, comparing values
01 p0157 A69-11197

Ground based control system via cockpit PPI display on transponder equipped aircraft broadcast with digital coding
03 p0464 A69-13244

Multimode digital radar control paths and operating communication, discussing radar data, triggers, real time data and error localization
05 p0718 A69-15750

Optical processing of planetary radar data for range Doppler image generation
08 p1270 A69-19816

Radar and satellite TV clouds observation in meso and macroscale cloud systems
13 p2294 A69-27853

Graphical method for plotting contours of Rice distribution function as rocket-borne radar reflection data, determining leakage factor
14 p2416 A69-29536

Bird warning and forecast systems based on radar data covering 50 mile radius from airport
17 p2899 A69-33367

High speed analog to digital multiple channel wide-band data acquisition system designed for short pulse Doppler radar and probe measurements
19 p3307 A69-35745

Transport aircraft automatic altitude transmission requirements, discussing altimeter-transponder radar system to aid air traffic control
19 p3371 A69-36700

Storm location and severity prediction by pattern recognition theory, using quantized radar data, compared with statistical prediction
21 p3678 A69-39458

RADAR DETECTION

Adaptive detection mode for surveillance radar, using detection threshold proportional to spatially sampled clutter level estimates for regulation of false alarm probability
01 p0026 A69-10178

Radar attitude sensing system for determining vehicle roll, pitch, yaw, altitude and velocity of earth and lunar orbital vehicles
03 p0388 A69-13183

Digital modified discrete Fourier transform Doppler radar processor for tactical aircraft
03 p0389 A69-13196

Automatic sequential detector for noncoherent moving target indicator radar, describing noise and clutter residue control
03 p0389 A69-13197

Radar or ECM/ECCM system simulation by digital computer, using signal and jamming spectral inputs
03 p0400 A69-13200

Passive linear FM pulse compression radar systems detection capability compared with matched filter performance
03 p0390 A69-13218

Moving window radar detector design for moving targets, giving chart for SNR derivation to obtain given detection probability

04 p0558 A69-15073

Radar signal matched filters synthesis using linear digital filters and digital correlators noting role in radar detection

05 p0722 A69-16733

Radar detector for survivors, using inexpensive microwave mixer detector crystal

06 p0878 A69-16964

Antenna pattern loss factor for determination of average probability of detection vs SNR curves for three dimensional or pencil beam radars

08 p1270 A69-19858

Radar target detection and angular location estimation in amplitude comparison monopulse radar by simultaneous observation with group of antennas

09 p1452 A69-21312

Phased array radar system for UHF detection, identification and tracking of orbiting objects and ballistic missiles, noting system design and hardware

12 p2028 A69-25906

Radar SEP /spherical error probable/ for defining error ellipsoid in three dimensional accuracy and CEP /circular error probable/ for defining two dimensional accuracy

13 p2221 A69-27963

Panchromatic illumination in radar systems for image quality, tracking and detection problems, suggesting application to polypanchromatic radar

14 p2416 A69-29529

Frequency agility techniques applied to target detection in noncoherent pulsed radar systems

17 p2917 A69-32919

Radar geoscience application, discussing radar return relation to illuminated terrain in detecting buried river channels

20 p3491 A69-37651

Radar digital processing and display system for air traffic control with IC central processor and discrete data transmission over telephone lines from remote sites

21 p3760 A69-38328

Compound fading exponential /CFE/ clutter model for radar target detection, describing automatic detection applications

23 p4117 A69-41604

Radar detection performance evaluation procedures based on integration, collapsing and fluctuation losses estimates for swirling target models and partially correlated targets

23 p4132 A69-42547

Wavelike structure observed near tropopause with sensitive radar system, suggesting clear air turbulence as cause of breakdown of gravitational wave

24 p4342 A69-42893

RADAR DIRECTION FINDERS

U RADIO DIRECTION FINDERS

RADAR DISPLAYS

U RADARSCOPES

RADAR ECHOES

NT ANGELS

NT CLUTTER

NT LUNAR RADAR ECHOES

NT SOLAR RADAR ECHOES

NT VENUS RADAR ECHOES

Radar reflectivity and refractive index spectra in clear atmosphere simultaneously measured and compared with theoretical calculations

01 p0032 A69-10969

Sequential logic for improved signal detectability in frequency-agile search radars, discussing target echo fading models in radar range performance prediction

01 p0033 A69-11008

Fluctuating radar echoes from cloud targets with vibrating drops, noting amplitude modulation effect of changing cross section on backscattered signals

02 p0208 A69-12021

Radar target amplitude, angle and Doppler scintillation from analysis of echo signal propagation in space

02 p0211 A69-12447

Book on calculating radar cross section characteristics of geometrically complex shapes using reflectivity characteristics, including electromagnetic theory and data interpretation

03 p0383 A69-12901

Monostatic radar cross section of simple shapes estimated using optics and Rayleigh region approximation with emphasis on multiple reflection

03 p0384 A69-12905

Radar return signal generation for computer simulations of airborne radar systems, using digital computer program for time varying radar backscatter

03 p0429 A69-13199

Wind shear and reflectivity gradient effects on Doppler radar spectra

03 p0461 A69-13341

Reflected radar signal random fluctuations suppressed by using antenna, receiving channels and logarithmic amplifiers

04 p0556 A69-14490

Quasi-specular bistatic radar measurements of oblique scattering properties of lunar surface using telemetry carrier from Explorer 35 as lunar orbiting radar beacon

04 p0655 A69-14657

Sporadic background separation from radar observations of meteor showers, using echo range distribution, head echoes and antenna direction change

04 p0659 A69-15035

Sonar receiver reduced averaging processing in presence of extended and point targets compared with full averaging processor

04 p0562 A69-15477

Radar determination of exponent s for describing mass distribution of Geminid and Quadrantid meteoric bodies

05 p0823 A69-16033

Radio aurora radar measurement, determining echo and Doppler velocity distribution and dependence on aspect angle, magnetic latitude, height, azimuth and time

05 p0754 A69-16265

Radar echoes signal amplitude and phase digital recording with Radicord /radar digitizing and recording/ device

05 p0721 A69-16618

VHF radar observations of electron density irregularity in nighttime equatorial electrojet, comparing day and night time electron drift rates and directions

10 p1769 A69-23837

Chirp radar signal compression by proton spin echo phenomena, noting compression ratio and SNR

11 p1834 A69-24566

Trapped aerosols below temperature inversions causing lidar echoes in troposphere layers, discussing simultaneous balloon refractometer, thermometer and ground based lidar soundings

13 p2254 A69-28475

Equatorial electrojet VHF radar observations indicating nontwo stream electron concentration irregularities related to electron drift velocity

14 p2511 A69-28953

Doppler echo from random rough surface, discussing average power return, frequencies, amplitudes, antenna beamwidth and radar data correlation

14 p2413 A69-29488

Radar echoes observed from clear atmosphere, discussing scattering mechanisms of thin stable inversions, convective thermals, Benard convection cells, breaking gravity waves, etc

14 p2415 A69-29518

Earth radar studies, relating echo behavior to rocket altitude and surface electrical characteristics

14 p2416 A69-29531

Graphical method for plotting contours of Rice distribution function as rocket-borne radar reflection data, determining leakage factor

14 p2416 A69-29536

Ultrasonic pulse-echo-overlap method modified for simultaneous measurement of time delay and relative voltages in determining sound velocities and attenuation of solids

14 p2450 A69-29567

Relation between radar echoes spatial extent and synoptic conditions with reference to various fronts, noting significance for aviation

14 p2474 A69-29738

Algorithm for processing binary-quantized echo signal packets, obtaining useful and noise signals relation

15 p2571 A69-30331

Binary-quantized signal packet center for target azimuth determination, discussing antenna radiation pattern role

15 p2566 A69-30332

Digital method to produce radar reflectivity from analog audio frequency Doppler data extracted from terrain echo signal of CW scatterometer radar

15 p2572 A69-31111

Martian topography during rotation observed using radar round trip echo delay at 7840 MHz, discussing dark areas relation to elevation

16 p2860 A69-32238

Precipitation intensity measurements, obtaining distribution parameters from radar reflectivity at two wavelengths and microwave attenuation factor at third wavelength

16 p2806 A69-32265

Received radar signal power maximizing problems in planetary exploration, analyzing abelian group real line and circle problems

17 p2993 A69-32831

Radar cross section of bird represented as unit density dielectric spheroid for bird hazard monitoring, discussing meteorological, insect and bird echoes

17 p2919 A69-33366

Centrifugation effects on body composition and growth of mice

17 p2910 A69-33746

Range effects on apparent height and frequency biases of radar precipitation echoes determined by regression technique for several stations

18 p3101 A69-34826

Field aligned ionospheric F layer ion density irregularities, using simultaneous hourly radar echo and spread F data and detailed ray path calculations

18 p3129 A69-34958

Wind shear effects on radar echo decay constant for finite meteor trail, considering roles of trail length and electron density variations

19 p3276 A69-36482

Terrain radar returns emphasizing surface roughness influence in man-made target backscatter, determining radar cross section with radar range equation

20 p3490 A69-37646

Range-Doppler data processing of radar echoes from spread targets, considering quadratic filter theory, emphasizing received signal correlation functions

20 p3490 A69-37648

Radar geoscience application, discussing radar return relation to illuminated terrain in detecting buried river channels

20 p3491 A69-37651

Doppler radar based on triple pulse transmission at coherent frequencies, comparing echo pulses for targets cancellation and extraction

21 p3672 A69-38436

Very short pulses effect on aircraft echoes, noting echoing area reduction as resolution cell diminishes

21 p3672 A69-38755

Surface reflectivity mapping of Venus by radar interferometry at 3.8 cm, noting low reflectivity circular regions

21 p3806 A69-39331

Radar reflection techniques for planetary surface studies, considering surface properties effects on reflectivity and reflected wave characteristics, instrumentation and data for moon and planets

21 p3811 A69-39509

Monograph on selection of radar echoes from nearly colocated reflection centers, discussing guided missile multiple target resolution

22 p3899 A69-40533

Radar return from clutter target with circular polarization, finding probability density functions and cumulative distributions of power ratio

23 p4131 A69-42540

Thunderstorm turbulence relationship to weather radar echoes from storm penetrations in Oklahoma by instrumented aircraft

24 p4347 A69-43720

RADAR EQUIPMENT

NT PLAN POSITION INDICATORS

NT RADARSCOPES

Phased array radar cost improvement based on solid state devices and microwave integrated circuits application

01 p0048 A69-11039

Electron tubes in phased array radar systems, discussing replacement limits by solid state devices, reliability and cost reduction

01 p0048 A69-11040

Transistors vs electron tubes as microwave power sources in UHF phased array radars, noting transistor cost competitive limit

01 p0048 A69-11041

Radar cross section laboratory, discussing experimental techniques, electromagnetic range and pulse, FM/CW and CW radars

03 p0385 A69-12912

Array radar technology development offering multifrequency operations from common aperture

03 p0388 A69-13182

Millimeter wave lunar radar system component specifications and design with paraboloidal antenna, emphasizing reflectivity of moon

03 p0397 A69-13725

High power radar for investigating ionosphere by incoherent scatter technique

03 p0398 A69-13768

Digital radar systems, discussing control computers, beam steering computers, signal processors, mode control, displays and chirp networks 05 p0718 A69-15748

Stationary coherent /hologram/ radar and sonar using zone plate action to provide range information 05 p0721 A69-16578

Ferrite Y junction E plane circulator for airborne high power X band radar 07 p1100 A69-18639

Dielectric constant and loss angles measurement in Ku band used for onboard radars 07 p1112 A69-19544

Small amplitude surface irregularities effect on backscattering properties of radar calibration metal sphere, using full wave boundary perturbation method 08 p1273 A69-20027

Range measurement accuracy of radar automatic equipment, discussing nomograms for split-gate tracker, cyclic and pulse length errors and multipath reflections 08 p1275 A69-20228

Analog video processor in omnidirectional radar system for flight safety, discussing construction, transistorization and circuitry 08 p1276 A69-20605

Analysis and optimization of side-looking synthetic aperture radars carried out for resolution, SNR and least squares estimation of target field 08 p1277 A69-20960

Electronic beam-rotation systems operation using matrix network to feed circular arrays, noting applicability to direction finding or radar systems 08 p1288 A69-20964

Microelectronic multimode airborne radar system with modular construction, discussing system design, development, flight testing and operational results [AGARDOGRAPH-114] 08 p1277 A69-20989

Pulsed laser radar and applications to upper atmosphere observation equipment and distance measuring devices 09 p1456 A69-22132

Pulsed J band Gunn effect oscillators performance, noting hybrid domain mode due to high bias fields 09 p1468 A69-22594

Electrical, thermal and mechanical requirements in design of Landing Radar Electronic Assembly for Apollo Lunar Module 10 p1663 A69-23537

Secondary radar for air traffic control automation in France, discussing onboard equipment 10 p1723 A69-23705

Pulse Doppler radar operation, discussing Doppler shift, range resolution and systems components 10 p1659 A69-24084

Radar remote sensing for terrain data acquisition 12 p2098 A69-27005

Designs and capabilities of digital processing systems for automatic air traffic control radar information stressing future use of display for computerized control 13 p2295 A69-27332

Solid state radar feasibility, discussing circuit components, circuit design problems involving striplines and monoblocks, phase controlled antenna, solid state computers, etc 13 p2230 A69-27928

SHF solid state phased array radar with Gunn effect modular microwave IC design, discussing air and ground applications 14 p2420 A69-29435

Collection of papers on radar theory and technology, Volume 2, covering radar tracking, measurement, target acquisition, trajectory analysis, etc 15 p2565 A69-30330

Moving target selector radars subsystems amplitude and phase instability effects on interference signal suppression 15 p2576 A69-30339

Multifunctional radar errorless operation determined from relations between amount of received information, number of channels and SNR 15 p2576 A69-30354

Primary-secondary radar /SECAR/ integration for air traffic control, discussing problems of simultaneous display, transmission synchronization, signal multiplexing, etc 15 p2570 A69-31222

Semiconductor technology including radar, Gunn and limited space charge accumulation oscillators, phase locked antennas, data processing and solid state computerization 15 p2581 A69-31521

Radar control system based on load waveform monitoring by coupled control and modulating circuits 16 p2753 A69-32439

Microphonic noise measuring systems for airborne radar system design for noise reduction 17 p2937 A69-33628

Apollo lunar module landing radar, discussing descent phases, operating modes, assemblies and Surveyor radar 19 p3267 A69-35797

Onboard radar for light interceptor aircraft /Aida II/, discussing navigation, low altitude penetration and air to air missile interception 19 p3278 A69-36701

Secondary radar IFF/SIF /Identification Friend or Foe-Selective Identification Feature/ system, describing ground and onboard radar and data processing equipment 19 p3278 A69-36702

Imaging radars - Conference, University of Michigan, July-August 1969 20 p3488 A69-37631

Linear radar system theory including Fourier transforms, linear superposition and input/output ratio for deterministic and random signals, discussing filter and sampling theory 20 p3489 A69-37633

Synthetic aperture radar principles, using periodic pulse modulation to construct terrain imaging radar 20 p3489 A69-37635

Signal amplitude no memory nonlinearity effect on performance of synthetic aperture terrain imaging radar systems and simulation of CRT film systems 20 p3490 A69-37643

Airborne imaging radar drawbacks and advantages, describing techniques to overcome defects 20 p3493 A69-37735

MERA /Molecular Electronics for Radar Applications/ modules testing in planar array simulator, measuring far field amplitude patterns in transmitting and receiving modes 22 p3912 A69-40067

Amplitrans use as broadband microwave amplifiers in high power radar systems with frequency agility, involving modified high vacuum tube modulator and modulator circuit 23 p4135 A69-41384

Polymeric polyurethane protective coatings for radar radome covers with improvement in service life, discussing performance properties and production method 24 p4338 A69-43456

RADAR FILTERS

Clutter rejection using coded burst waveform for airborne early warning /AEW/ and airborne attack type radars 03 p0388 A69-13185

Digital processing of Doppler radar signals using matched filter concept 03 p0393 A69-13291

RADAR MAPS

Radar range height angle charts for plotting earth based radio or radar system vertical plane coverage diagrams 01 p0031 A69-10633

Satellite high resolution radar mapping of planets, discussing synthetic aperture and linear FM transmission radar techniques 03 p0430 A69-13399

Side looking radar for earth resources sensing, discussing geological and hydrographical mapping, oceanography, agricultural and biological phenomena 06 p0923 A69-17119

HF ionospheric radar ground scatter map showing separated land-sea backscattered radio waves by Doppler technique 09 p1454 A69-21681

Radar remote sensing for terrain data acquisition 12 p2098 A69-27005

Mathematical expressions for measuring heights of vertical and nonvertical features with both slant and ground range radar images 13 p2263 A69-28198

APQ-97 side-looking radar for topographic mapping of continually cloud covered areas, noting data reduction and compilation methods 20 p3519 A69-36928

Surface reflectivity mapping of Venus by radar interferometry at 3.8 cm, noting low reflectivity circular regions 21 p3806 A69-39331

RADAR MEASUREMENT

Specific effective scattering area on lunar surface using Luna 13 signals from Oceanus Procellarum measured with radar employing antenna with narrow radiation pattern 01 p0158 A69-11312

Book on compound signals and uncertainty principle in radar observations, considering Woodward ambiguity function, determining accuracy and resolution of range and velocity measurements 03 p0385 A69-13000

Radar method to estimate turbulent motions in clouds 03 p0459 A69-13289

Venus radius determined by planetary radar and Mariner 5 radio tracking data 03 p0508 A69-13348

Quasi-specular bistatic radar measurements of oblique scattering properties of lunar surface using telemetry carrier from Explorer 35 as lunar orbiting radar beacon 04 p0655 A69-14657

Level crossing rate meter correction for boxcar-ed and receiver noise readings in incoherent weather radars 04 p0557 A69-14915

Threshold signals and optimum signal parameters in radar range and velocity measurements 04 p0560 A69-15403

Radio aurora radar measurement, determining echo and Doppler velocity distribution and dependence on aspect angle, magnetic latitude, height, azimuth and time 05 p0754 A69-16265

Langmuir probe experiment measurement of upper region electron temperature on Explorer 32 conflict with Jicamarca Radar Observatory measurements 05 p0756 A69-16283

Randomly rough surface physical and geometrical remote determination by polychromatic bistatic radar 05 p0721 A69-16572

Meteoroid mass distribution determined by radar observations of underdense meteor trails at Springhill Meteor Observatory 06 p1003 A69-17493

Receiving system of CENFAM multistation radar project for meteoric and upper atmosphere studies composed of antennas connected to form product-interferometer pairs 07 p1077 A69-18674

Radar signal parameters measurements consisting of SNR estimation and optimum energy supply determination from SNR estimation 07 p1085 A69-19153

Quantitative radar determinations of radio wave scattering cross section of lunar surface layer 07 p1087 A69-19621

Wind vector in respect to orientation of large scale cirrus bands based on stereophotogrammetry and radar observations 08 p1346 A69-20442

Electron content of earth-Venus interplanetary medium measured by observing relative propagation time of radar pulses to Venus 09 p1594 A69-21697

Laser radar atmospheric applications, noting particulate matter mapping, backscatter density profiles and use of lidar 09 p1521 A69-22795

Remote geoscience sensing using properties of radar return noting scatterometry, imagery, altimetry and penetration measurements 11 p1835 A69-24692

Surface dielectric constant and microwave opacity of Venus atmosphere as function of wavelength determined by radar observations 12 p2153 A69-25805

Adaptive pattern recognition system simulated and tested with agricultural radar images, describing predictive environmental model mathematically 12 p2097 A69-26990

Cloud drift radar measurements for determining wind velocity profiles in mesosphere, using rocket released dipole reflectors 13 p2253 A69-27848

Refraction error in measurements with simple and radar interferometers, considering atmospheric effect 13 p2221 A69-27961

CENFAM radar receiving system for meteoric and upper atmospheric data on amplitude, range and direction of meteor echoes through interferometer pairs 13 p2354 A69-28649

Radar radiometer by adding radar to scanning microwave radiometer, discussing applications to spacecraft measurement of oceanic winds, waves and precipitation 14 p2421 A69-29528

Aerosol content of mesosphere with noctilucent clouds measured with optical radar in Norway 14 p2444 A69-29877

Binary-quantized signal packet center for target azimuth determination, discussing antenna radiation pattern role
15 p2566 A69-30332

Autonomous radiometers signals statistical properties used in space technology, discussing radar signals phenomenological models, measurement errors and energy characteristics
15 p2566 A69-30337

Regional slope measurement from two monoscopic radar images of same terrain area, discussing accuracy and applications to geomorphology and hydrology
15 p2610 A69-30710

Mercury, Venus, Mars, earth and lunar mass determinations by radio tracking and planetary radar systems
15 p2697 A69-31305

Planet Venus data from Venera 4, Mariner 5, radio astronomical and radar measurements
15 p2698 A69-31360

Martian topography during rotation observed using radar round trip echo delay at 7840 MHz, discussing dark areas relation to elevation
16 p2860 A69-32238

Cumulonimbus clouds phase structure and spatial distribution based on radar signal polarization analysis, showing high nonuniformity and variability
16 p2806 A69-32266

Vertical wind velocity pulsations in precipitation and passage through subfrontal clouds measured by pulse radar
16 p2807 A69-32272

Temperature profiles and associated wind profiles obtained with Jimsphere/FPS-16 radar system at Cape Kennedy, discussing remote CAT detector assessment
17 p2999 A69-33739

Meteoritic matter distribution by calculating orbital elements of 12,500 meteors from radar data, using diversity reception for radio waves scattered at meteor trails
17 p3041 A69-33894

Nanosecond pulse coherent Doppler radar for monostatic measurements of turbulent wakes in shock tunnels and ballistic ranges
19 p3293 A69-35743

Wind speed and direction determination accuracy of radar or theodolite methods
20 p3572 A69-37698

Mesospheric wind measurement by meteorological rockets based on radar determination of drift trajectories of chaff clouds
20 p3529 A69-37797

Radar observations of convective pattern types in clear atmosphere consisting of thermal- and Benard-like convection cells
20 p3573 A69-38059

Handbook of radar measurement covering noise measurement, error analysis, antenna performance, etc
21 p3678 A69-39668

RADAR NAVIGATION

Aircraft traffic control with cockpit self sufficiency for accurate and reliable navigation capability, discussing radar vector navigation and communication
07 p1177 A69-19210

Aircraft nose-mounted radome refraction errors influence on directional tracking and navigation, considering fire control and terrain following radars
07 p1086 A69-19512

Multifunction helicopter rotor blade radar for navigation, IFR approach and fire control, including flight test results
[AHS PAPER 315] 17 p2920 A69-33535

Airborne radar navigation with emphasis on semiautomatic fixing, describing beacon mode, map matching and airborne weather radar
18 p3169 A69-34851

Onboard radar for light interceptor aircraft/Aida II, discussing navigation, low altitude penetration and air to air missile interception
19 p3278 A69-36701

V/STOL aircraft radar inertial navigation system, describing approach and landing phase flight test results
[AAS PAPER 69-401] 24 p4252 A69-42831

RADAR PHOTOGRAPHY

Earth space image interpretation in various spectral regions, discussing effectiveness of photography, spectrophotometry, radar and microwave observations
05 p0763 A69-16054

Remote geoscience sensing using properties of radar return noting scatterometry, imagery, altimetry and penetration measurements
11 p1835 A69-24692

Imaging radar systems for employment on small spacecraft, fabricating small lightweight radar systems packages with integrated circuit techniques
11 p1835 A69-24695

Radar imagery for agricultural land mapping, noting field and crop discrimination and parameters influencing radar return
12 p2097 A69-26986

Integrated landscape analysis with radar imagery for earth resources
15 p2608 A69-30454

Aerial multiband remote sensors for wildland resources, considering multilens photographic systems, optical mechanical scanners and radar devices
15 p2609 A69-30458

Regional slope measurement from two monoscopic radar images of same terrain area, discussing accuracy and applications to geomorphology and hydrology
15 p2610 A69-30710

Side-looking radar and thermal IR photography as mapping system, discussing resolution and distortion
15 p2612 A69-31162

Atmospheric turbulence in cloudless region above thunderstorms and relation between turbulence and radar pictures of storms
15 p2649 A69-31211

Anamorphic holography, discussing optical and nonoptical wavelength processes and generation and reconstruction of holograms for radar applications
17 p2976 A69-34062

Imaging radar study based on optical imaging and electromagnetic wave processes, discussing Doppler signal processing, synthetic aperture radars and microwave holography
20 p3489 A69-37632

Airborne imaging radar motion compensation and sensing problems concerning perturbed signal correction, discussing spatial sensitivity measures and constraints
20 p3490 A69-37645

Atmospheric phenomena effects on terrain imaging radar systems performance, discussing tropospheric turbulence and ionospheric irregularities
20 p3490 A69-37647

Imaging radar applications noting military surveillance, navigation assistance, iceberg detection, sea rescue operations, all-weather traffic surveys, terrain mapping, etc
20 p3491 A69-37649

Radar astronomy, discussing planetary surfaces study techniques, target/signal interactions, planet cross sections, delay and Doppler spectra
20 p3491 A69-37650

Geological radar in regional and detail studies, discussing area side scanning imagery and lithology changes detection
20 p3491 A69-37652

Earth space image interpretation in various spectral regions, discussing effectiveness of photography, spectrophotometry, radar and microwave observations
20 p3545 A69-37964

RADAR RANGE

NT RANGE AND RANGE RATE TRACKING

Radar range height angle charts for plotting earth based radio or radar system vertical plane coverage diagrams
01 p0031 A69-10633

Pseudorandom radar ranger/DIOMEDE/ using optical correlator and phase loop
03 p0393 A69-13254

Millimeter waves in communication navigation and research, discussing radar range resolution and remote sensing
03 p0397 A69-13722

Radar range determination on any target based on parametric method and nomograms in decibels
04 p0560 A69-15227

Slide rule for radar range determination based on Neuvy formula
04 p0560 A69-15230

Threshold signals and optimum signal parameters in radar range and velocity measurements
04 p0560 A69-15403

Range measurement accuracy of radar automatic equipment, discussing nomograms for split-gate tracker, cyclic and pulse length errors and multipath reflections
08 p1275 A69-20228

Range effects on apparent height and frequency biases of radar precipitation echoes determined by regression technique for several stations
18 p3101 A69-34826

Optimal structural parameters of radar digital ranging servosystems derived from reproduction error, including computer simulation data
19 p3278 A69-36593

Radar data optical spatial-domain processor providing azimuth processing in range channels without range compression capability, reviewing coherent optical channels properties
20 p3489 A69-37636

Radar propagation in surface duct over water, describing range distribution estimation procedure
20 p3495 A69-37854

Ultrasonic diffraction delay lines technique to extend radar systems range without affecting target pinpointing capability
24 p4286 A69-42901

RADAR RECEIVERS

High range resolution by pulse to pulse frequency shifting, utilizing existing low resolution equipment by adding signal processing capability to receiver
03 p0388 A69-13181

Optimum gain control for diversity receivers used for radar and digital data transmission through fading media
03 p0410 A69-13833

Coherent moving target indicator radar receiver behavior as function of input situation, using improvement factor
04 p0556 A69-14338

Reflected radar signal random fluctuations suppressed by using antenna, receiving channels and logarithmic amplifiers
04 p0556 A69-14490

Level crossing rate meter correction for boxcar-ed and receiver noise readings in incoherent weather radars
04 p0557 A69-14915

Secondary radar equipment functions and features forming IFF-SIF chain, discussing displacement controller and minor lobe suppression functions technical problems
05 p0721 A69-16591

Receiving system of CENFAM multistation radar project for meteoric and upper atmosphere studies composed of antennas connected to form product-interferometer pairs
07 p1077 A69-18674

Transmit-receive device noise contribution effect on receiving system noise factor for device insertion immediately before low noise microwave amplifier
09 p1469 A69-22605

Radar transmitter and receiver antennas polarization parameters selection for obtaining maximum SNR at reception point
11 p1833 A69-24442

Ideal quantum receiver to detect coherent narrow band optical signal in presence of thermal background radiation, noting error probability
14 p2414 A69-29502

Microwave filter tailored for frequency response in L through S band regions for high range resolution radar receiver
14 p2423 A69-29759

AC ignitor priming of quartz-chlorine gas discharge X band waveguide limiter with fast recovery used as radar receiver protector
15 p2573 A69-30035

Digital receiver of radar signals for performing binary quantization of input data with subsequent processing by digital computer
15 p2563 A69-30136

Pulsed noise sensitivity in radar receivers having noise limiter for simple and complex signals
15 p2563 A69-30137

Pulse radar quantum paramagnetic amplifier protection from saturation by transmitter power, using linear electrical bias of EPR line
15 p2579 A69-30956

Automatic conversion receiver of meteorological radar data, examining reception amplitude sensitivity and frequency characteristics
16 p2791 A69-32280

Optimal radar receivers and waveforms with limited dynamic range for detecting point target masked by thermal noise and clutter returns
17 p2921 A69-33625

Radar target simulator approximating pulse radar receiver output for evaluating amplitude-sensing video target detection devices
17 p2921 A69-33629

Parametric tunable amplifier as prestige for radar receiver, discussing pump frequency and midband gain stabilization
18 p3104 A69-35457

RADAR RECEPTION

Fixed-tuned telemetry receiver as miss distance indicator /MDI/ to provide information in missile performance program 23 p4138 A69-41781

Active weighted pulse compression radar receiver output waveform analysis for amplitude, phase and frequency modulation, noting effects of spectrum weighting mismatch parameter 23 p4132 A69-42548

RADAR RECEPTION

Received radar signal power maximizing problems in planetary exploration, analyzing abelian group real line and circle problems 17 p2993 A69-32831

Pseudorandom code development and possibilities for radar applications, considering signal processing, antenna requirements, radar signal phase modulation, etc 24 p4281 A69-42741

RADAR REFLECTORS

Plane reflector with variable reflection coefficient for electromagnetic centimeter waves, consisting of plane grating of semiconductor diodes mounted in waveguide 03 p0406 A69-13938

RADAR RESOLUTION

Satellite high resolution radar mapping of planets, discussing synthetic aperture and linear FM transmission radar techniques 03 p0430 A69-13399

Distribution free sequential probability ratio procedure for detecting signal in multiple resolution element radar 05 p0717 A69-15609

Book on high resolution radar covering waveform analysis, resolution theory, radar mapping, target detection, etc 08 p1275 A69-20370

Analysis and optimization of side-looking synthetic aperture radars carried out for resolution, SNR and least squares estimation of target field 08 p1277 A69-20960

Angular separation of two point sources measured through expressing antenna resolving power by a posteriori probability laws 08 p1288 A69-20961

Airborne imaging radar motion compensation and sensing problems concerning perturbed signal correction, discussing spatial sensitivity measures and constraints 20 p3490 A69-37645

Monograph on selection of radar echoes from nearly colocated reflection centers, discussing guided missile multiple target resolution 22 p3899 A69-40533

Optimum signals for high resolution radar and communication systems, using transmitter waveform design of autocorrelation and cross correlation functions 23 p4132 A69-42545

RADAR SCANNING

Areas of expectation for single radar automatic tracking of flying objects derived on basis of equation of circle in polar coordinates 01 p0035 A69-11296

Radar method of spiral scanning clouds and precipitation at constant altitude 03 p0459 A69-13286

Electronic scanning radar systems design, discussing beam types, bandwidth, tracking, target acquisition, etc 04 p0556 A69-14301

Hybrid mode Ku-band mixer steering electronic scanning phased array design 04 p0572 A69-14325

Antenna pattern loss factor for determination of average probability of detection vs SNR curves for three dimensional or pencil beam radars 08 p1270 A69-19858

Signal processing method for achievement of very rapid space scanning with antenna array noting application to radar system 10 p1657 A69-23801

Real time electronically scanned radar control using digital computer with input and output conversion for information handling, noting interface equipment 11 p1834 A69-24544

Probability matrix for n order transition independent of decision taking method, applying fundamental matrices to analysis of mean number of false targets 14 p2410 A69-28836

Doppler navigation, explaining radar beam mechanization, Doppler spectrum, scanning noise, spectral compression and tracking 18 p3169 A69-34849

Side-looking radar and IR line scanning as method for simultaneous stereo height mapping, using images produced from same vantage point 20 p3536 A69-36929

Geometrical configuration for synthetic aperture terrain imaging radar scanning system, noting scanning methods in range and azimuth directions 20 p3489 A69-37634

Synthetic aperture radar principles, using periodic pulse modulation to construct terrain imaging radar 20 p3489 A69-37635

Signal spectrum and SNR of synthetic aperture terrain imaging radar using model, including two dimensional signal and Gaussian additive noise 20 p3489 A69-37638

Synthetic aperture terrain imaging radar system optimal design, considering noise-free and random noise conditions using least squares method and signal to noise ratios 20 p3489 A69-37639

RADAR SCATTERING

Tracking radar glint analysis model using diffraction theory to evaluate parameters of fields received from scattering centers on target aircraft 01 p0033 A69-11007

Specific effective scattering area on lunar surface using Luna 13 signals from Oceanus Procellarum measured with radar employing antenna with narrow radiation pattern 01 p0158 A69-11312

Backscattering diagram of Venus at 40 cm determined from Doppler spectrum and reflected signals range energy distribution 02 p0314 A69-11639

High power radar for investigating ionosphere by incoherent scatter technique 03 p0398 A69-13768

Correspondence between HF radar backscatter, optical aurora and electron precipitation, noting application to gross tracking of auroral oval 06 p0918 A69-17383

Radar scattering cross section of finite perfectly conducting wedge for case of illumination by polarized plane wave 08 p1274 A69-20047

Disturbed index of refraction scattering cross sections and aircraft acceleration increments for clear air turbulence, deriving correlation for measurements 10 p1656 A69-23651

Reversible ion heating by atmospheric tides, noting radar Thomson scatter observations of E region ion temperature height profiles 11 p1879 A69-25159

Radar backscatter and rocket profiles of ionospheric electron temperature, noting agreement in daytime flight measurements 11 p1951 A69-25162

Data analysis techniques for discrimination and identification of terrain surfaces from radar scatterometry information 12 p2099 A69-27010

Scattering characteristics of planet Venus at 3.8 cm wavelength, discussing frequency power spectra and radar cross section 13 p2349 A69-27818

Incoherent scatter observations of ionosphere, discussing radar equipment and measurement of electron density and temperature, ionic temperature and composition, etc 14 p2415 A69-29522

Radar backscatter analysis for Arctic ice identification, deriving ice surface roughness factors from Kirchhoff-Huygens principle 14 p2416 A69-29530

Radar Thomson scatter from nonthermal steady state level of plasma waves in ionosphere measured, studying role of angle between wave vector and magnetic field 16 p2818 A69-31678

NonMaxwellian electron velocity distribution influence on ionospheric measurements by Thompson scattering, explaining disagreement between scattering and probe measurements of electron temperature 16 p2788 A69-32647

HF radar scattering by finite circular cone as function of frequency and aspect angle using modified diffraction pattern theory 20 p3495 A69-37849

Modified geometrical diffraction theory applied to determination of vertically polarized radar backscattering from rear of cylinders and frustums 20 p3495 A69-37851

RADAR SIGNATURES

Simulation and display for radar ground-backscatter signatures by computer ray tracing, using model ionosphere containing realistic traveling disturbances 21 p3717 A69-39280

Satellite rotation from radar data analysis, requiring two full rotations and body characteristics to produce distinctive lobes in radar cross section 22 p3900 A69-40682

RADAR TARGETS

Tracking radar glint analysis model using diffraction theory to evaluate parameters of fields received from scattering centers on target aircraft 01 p0033 A69-11007

Radar target amplitude, angle and Doppler scintillation from analysis of echo signal propagation in space 02 p0211 A69-12447

Moving window radar detector design for moving targets, giving chart for SNR derivation to obtain given detection probability 04 p0558 A69-15073

Radar range determination on any target based on parametric method and nomograms in decibels 04 p0560 A69-15227

Weighted pulse trains for clutter suppression during radar target detection 04 p0562 A69-15467

Multiple target monopulse radar signal processing technique 04 p0562 A69-15470

Electronically scanned X band array used as receiving antenna for target recognition radar 04 p0562 A69-15476

Statistical analysis of Radiorcord /radar digitizing and recording/ clutter and signal spectra and moving target detection by pulse radar 05 p0721 A69-16619

Radar target detection and angular location estimation in amplitude comparison monopulse radar by simultaneous observation with group of antennas 09 p1452 A69-21312

Alphanumeric characters to identify radar targets on PPI display for air traffic control, considering technique for reducing smear 09 p1495 A69-21675

Digital signal tracking module operation and stability, considering use of interconnecting modules to achieve adaptive tracking 09 p1459 A69-22477

Digital simulation optimizing parameters of digital equipment to measure target azimuths in pulsed surveillance radar system, establishing optimum echo pulse quantization threshold 15 p2563 A69-30138

Airborne Doppler radar, estimating velocity distribution and density of pulse signals reflected from air and ground targets 15 p2567 A69-30349

Frequency agility techniques applied to target detection in noncoherent pulsed radar systems 17 p2917 A69-32919

Radar target simulator approximating pulse radar receiver output for evaluating amplitude-sensing video target detection devices 17 p2921 A69-33629

Pulse-to-pulse carrier frequency stability of microwave radar transmitter tube for fixed target suppression 20 p3485 A69-36943

Ambiguity function interaction with target scattering function in range-Doppler radar, discussing matched filtering application 20 p3490 A69-37641

Terrain radar returns emphasizing surface roughness influence in man-made target backscattering, determining radar cross section with radar range equation 20 p3490 A69-37646

Range-Doppler data processing of radar echoes from spread targets, considering quadratic filter theory, emphasizing received signal correlation functions 20 p3490 A69-37648

Doppler radar based on triple pulse transmission at coherent frequencies, comparing echo pulses for targets cancellation and extraction 21 p3672 A69-38436

Compound fading exponential /CFE/ clutter model for radar target detection, describing automatic detection applications 23 p4117 A69-41604

Radar return from clutter target with circular polarization, finding probability density functions and cumulative distributions of power ratio 23 p4131 A69-42540

Ultrasonic diffraction delay lines technique to extend radar systems range without affecting target pinpointing capability
24 p4286 A69-42901

RADAR TRACKING

Radar observation of Icarus at time of close approach, giving values of radius, rotation period and Doppler shift derived from spectrograms
02 p0323 A69-12300

Space surveillance radar system sensor misassociation of one space object for another, noting applicability to sonar and optical sensors
02 p0210 A69-12388

Errors in wind data due to wind response of parachute-borne sensor corrected with radar tracking, comparing corrected and uncorrected data
02 p0276 A69-12700

Automated real time monoradar surveillance system based on azimuthal monotonicity of radar plots and flexible tracking strategies
03 p0383 A69-12872

Delay line bandwidth reduction for video or digital information, noting radar tracking application
03 p0392 A69-13251

HAPDAR-TACOL phased array radar design, discussing array patterns and multitarget tracking performance
04 p0556 A69-14324

Sporadic background separation from radar observations of meteor showers, using echo range distribution, head echoes and antenna direction change
04 p0659 A69-15035

Wind turbulence measurement by shock wave tracking using Doppler radar, stressing relative location of antenna and sound source
04 p0628 A69-15149

Conversion of range telemetry systems /CORTS/ program noting installations and standardization
05 p0743 A69-16306

Correspondence between HF radar backscatter, optical aurora and electron precipitation, noting application to gross tracking of auroral oval
06 p0918 A69-17383

Aircraft nose-mounted radome refraction errors influence on directional tracking and navigation, considering fire control and terrain following radars
07 p1086 A69-19512

Signal processors for implementation of monopulse tracking radar with three instead of four beams, investigating accuracy
08 p1270 A69-19855

Anti-interference TV circuit using delay lines applied to radar systems, discussing false alarm probability and detection probabilities
08 p1271 A69-19919

Experimental circuit for simulating radar target tracking system based on split range gating, noting tracking role of error signal
08 p1300 A69-20109

Simultaneous photographic and radar observations of meteors, determining absolute stellar magnitude of meteor as function of parameters
08 p1390 A69-20337

Venus research, discussing Mariner 5 and Venera 4 data, radar tracking, orbit, diameter, gravity, density distribution, etc
08 p1391 A69-20456

Angel type radar echoes from coherent pulses in centimeter and decimeter wavelengths characterized by daytime convection and presence of inversion/ isothermal layers
09 p1491 A69-22706

Aircraft safety hazards due to birds, discussing radar role in plotting bird migrations
11 p1837 A69-25247

Kalman sequential estimation adaptation to target maneuvers without sacrificing tracking accuracy in nonmaneuvering portions of trajectory
11 p1861 A69-25455

Phased array radar system for UHF detection, identification and tracking of orbiting objects and ballistic missiles, noting system design and hardware
12 p2028 A69-25906

Radar application to meteorology, entomology and ornithology, discussing clear air turbulence detection and flight tracking of birds and insects
12 p2034 A69-27004

Secor 6 satellite /1966-51A/ orbital parameters determined from optical and radar observations noting use for upper atmosphere density and rotational speed studies
14 p2522 A69-29631

Moving targets trajectories determination from radar data, using posteriori probability distribution represented by Markov chain
15 p2566 A69-30334

Target trajectories determination based on radar data with allowance for association between neighboring readings, using statistical characteristics obtained with Markov chains
15 p2566 A69-30335

Airborne Doppler radar, estimating velocity distribution and density of pulse signals reflected from air and ground targets
15 p2567 A69-30349

Systematic error pattern in raw data obtained during tracking ROSE balloons by two radar systems, estimating range resolver error
15 p2649 A69-30897

Doppler tracking data from Lunar Orbiter missions for studying lunar gravity anomalies, plotting acceleration on lunar surface Mercator projection
15 p2697 A69-31313

Angle nature from backscattering patterns at radar station with one transmitting and two receiving antennas
16 p2779 A69-32275

Angel sources rate of motion observed at automatic tracking coherent pulse station, obtaining coincidence with wind and insect velocities
16 p2779 A69-32276

Angel type radar echoes from coherent pulses in centimeter and decimeter wavelengths characterized by daytime convection and presence of inversion/ isothermal layers
16 p2753 A69-32486

Meteor trails radar observations to measure zonal wind profiles between 80-110 km, noting short period oscillations
16 p2865 A69-32609

Centrifugation effects on body composition and growth of mice
17 p2910 A69-33746

Meteor trail drift radar observations in Kharkov, giving wind velocity diurnal and seasonal variations
17 p3041 A69-33897

Radar unit for network component /wind patrol/ in statistical observations of wind drift conditions in meteor trails
17 p2939 A69-33901

Automatic radar station for meteor observations, discussing separate transmitting and receiving antennas directive gain and radio echo power
17 p2939 A69-33902

Associative processor applied to interceptor radar system, noting processing time independence from target number and compatibility with real time systems
17 p2931 A69-34071

Doppler navigation, explaining radar beam mechanization, Doppler spectrum, scanning noise, spectral compression and tracking
18 p3169 A69-34849

Satellite observation data association, estimating consistency of radar object with orbiting prediction, using computer program including Monte Carlo run
18 p3103 A69-35098

Book on statistical communication and applications to radio and radar systems technology to provide guidelines for design decisions
19 p3267 A69-35900

Meteor radio electronics principles, methods and equipment, discussing ionized meteor trail formation, radar tracking and utilization of trails for communications
19 p3277 A69-36591

Radar design for target detection, tracking and identification, modeling plasma effects on radar cross section of reentry vehicles based on wave-plasma interactions
20 p3485 A69-36925

Satellite configurations and rotation parameters determined by radar analysis
20 p3488 A69-37295

Near-polar circular orbiting satellite for calibrating and evaluating ground-based radars observing space objects
20 p3617 A69-37714

ATC medium range radar /SRE-LL1/, describing reflectors positions, information rate, installation, antenna parameters, etc
20 p3496 A69-37932

Navigational accuracy of two way Doppler tracking of interplanetary spacecraft during heliocentric and planetary encounter trajectory phases
21 p3761 A69-39334

Strapped down phased array radar tracker mechanization with digital loop closure electronics for homing missiles, noting cost advantages
[AIAA PAPER 69-873] 21 p3763 A69-39399

Monopulse telemetry tracking system, describing equipment and mobile operation
22 p3900 A69-40681

Assignment algorithm for target recognition in multiradar tracking systems
22 p3902 A69-41250

Qualitative model of atmospheric mass circulation constructed from radar meteor trail drift observations, considering solar thermal radiation and zonal wind direction
23 p4214 A69-41862

Optimal allocation of pulses for array radar tracking large number of targets simultaneously, using discrete time maximum algorithm
24 p4283 A69-43311

RADAR TRANSMISSION

Reduction of ATR switch pulse peak in automatic frequency control system of radar station
01 p0047 A69-10784

Radar FM signal design with zigzag frequency variation, discussing relation between waveform characteristics and associated ambiguity function features
01 p0033 A69-11001

Digital processing of Doppler radar signals using matched filter concept
03 p0393 A69-13291

Continuous wave and pulsed IR signals amplification on carbon dioxide laser amplifiers, discussing design, construction and performance of transmitter
[IEEE PAPER J-1] 07 p1152 A69-19064

Long term weather and radar transmission effects on three ply fabric cloth fire-retardant polyester resin radome panel
08 p1414 A69-20485

Reduction of ATR switch pulse peak in automatic frequency control system of radar station
10 p1661 A69-23113

Radar signal cross correlation function calculation with reference function, applying acousto-optical modulator
10 p1694 A69-23539

Optical correlator for radar signal processing based on filtering first order diffracted light and integration on photomultiplier
12 p2028 A69-25911

Complex pulsed radar signals synthesis with uncertainty function having principal maximum and small secondary maxima for radar stations and wideband communications systems
15 p2563 A69-30140

Long distance FM radar signal relating to central station image processing, showing wideband sum signal especially suitable for transmission
16 p2750 A69-31862

Transmitting antenna design of multistation radar system for meteors and upper atmosphere investigation, discussing amplitude and phase of electromagnetic field
19 p3278 A69-36661

Optimal radar phase modulated waveform with optimal ambiguity function synthesized by solving variational equations for orthogonal series coefficients of expanded modulation
20 p3492 A69-37708

Radar signal design, considering ambiguity and modulation functions, envelope surfaces, coding conditions, etc
20 p3496 A69-37904

RADAR TRANSMITTERS

Pulse-to-pulse carrier frequency stability of microwave radar transmitter tube for fixed target suppression
20 p3485 A69-36943

RADARSCOPES

NT PLAN POSITION INDICATORS

Mathematical model of radar display, considering radar construction tube resolution, environment and eye perception parameters.
07 p1136 A69-19504

Cockpit TV-radar for providing pilots with navigation, weather and traffic data, discussing safety factors and radar picture transmission quality
[SAE PAPER 690327] 11 p1833 A69-24506

RADIAL DISTRIBUTION

Electron radial distribution determination in positive Hg plasma column using simultaneous measurements with two different microwave cavities
02 p0290 A69-12404

Radial diffusion coefficient for trapped electrons moving across field lines, obtaining time dependent solutions of Fokker-Planck equation
03 p0502 A69-14002

Horizontal and vertical downward velocity components in developed solar active regions
04 p0651 A69-14370

Radial profile measurement technique for individual emission line intensities in plasma applied to populations of excited atomic and ionic Ar in capillary discharges
04 p0634 A69-14441

Radial temperature profile in induction coupled argon plasmas at low and atmospheric pressures
06 p0964 A69-17193

Radial distribution of azimuthally averaged temperature and amplitude vacillation characteristics in rotating differentially heated fluid annulus determined by multiprobe technique
07 p1126 A69-19040

Radial distribution of H II regions in spiral galaxies, noting peak at 1/4 distance from center
08 p1384 A69-20052

Electron temperature and electron density variations with radial distance in 10 MHz electrodeless ring discharge in H, noting electric field
08 p1361 A69-20230

Ar-H plasma arc radial temperature distribution determined by photoelectric spectroscopy in visible range
08 p1366 A69-20758

Kaufman thruster with predominant radial field, noting electron mobility across ion extraction screen and advantages of uniform plasma distribution [AIAA PAPER 69-259]
09 p1569 A69-21877

Fundamental solutions of initial value problems related to Euler-Poisson-Darboux equation generalized for radially symmetric case, developing convolution integrals
09 p1533 A69-22796

Rotating plasma behavior in magnetic mirror trap, using radial electric field
10 p1740 A69-23716

Radial distribution profiles of charge carriers in low temperature gas discharge plasma accounted for in terms of volume recombination
11 p1925 A69-24330

Electrical conductivity radial distribution in plasma flux from changes in Q factor and circuit inductance in presence and absence of skin effect
11 p1928 A69-25221

Numerical solution to partial differential equations describing helical discharge in Ar with gas injection, discussing initial temperature distribution and radial distribution effects
12 p2141 A69-27131

Velocity, enthalpy and mass flux radial distributions in laminar boundary layer from calorimetry of argon subsonic flow [ASME PAPER 68-HT-6]
13 p2374 A69-27776

Nonreacting turbulent far wake problems, discussing centerline decay of viscosity models, similarity profiles and radial distributions at various Mach numbers
13 p2200 A69-28500

Radial velocities of planetary nebulae in Magellanic Clouds and Galaxy, discussing Population I and II kinematics
14 p2520 A69-29377

Radial distribution functions for dense hydrogenous plasma near ionization temperature by solving Percus-Yevick equations
14 p2502 A69-29998

Numerical analysis of charged particles radial distribution in radiation belts extended to geomagnetic tail for low energy auroral electrons
16 p2850 A69-32102

Cosmic ray shower axis mean logarithmic distance from apparatus calculated by transforming shower recording frequency radial distribution to lin-log coordinate system
17 p3024 A69-33581

Radial oscillation periods of Hamada-Salpeter white dwarf models graphically compared with models by Harrison-Wheeler Wakano equation of state
17 p3037 A69-33642

Electron intensities in Starfish belt /1963- 1965/, discussing radial diffusion loss mechanism and pitch-angle diffusion
18 p3187 A69-34945

Interplanetary proton and alpha particle radial gradients determined from Mariner data, considering Forbush decrease, particle solar origin, galactic cosmic radiation, etc
20 p3592 A69-38096

Radial pressure distribution in steady state rotationally symmetrical plasma jet subjected to axial magnetic field, emphasizing mass entrainment effect [DGLR-69-024A]
23 p4202 A69-41924

RADIAL FLOW

Magnetic knots /intergranular space strong small scale magnetic fields near sunspot/, longitudinal and transversal fields and radial velocities
07 p1217 A69-19244

Compressibility parameters role in pressure distribution derived for radial laminar compressible fluid flow between two disks
07 p1121 A69-19321

Off design performance prediction method for radial inflow turbines compared with experimental results for small turbine and Brayton space power plant
10 p1754 A69-23891

Radial liquid flow between flat annular rings /face seals/, discussing film cavitation
13 p2267 A69-27365

Arc plasma jets radial velocity profiles measured by two probes in cyclic movement between jet edge and middle, including error estimation
13 p2307 A69-27611

Azimuthal electric currents generation by Coriolis forces in hot stars with intensive radial flows in convective zones
13 p2350 A69-27862

Stationary radial source flow of liquid particles into vacuum, discussing boundary value problem equations, parameters effects on flow structure and flow field characteristics
13 p2248 A69-28210

Supersonic radial flow compressor producing flow with meridional component exceeding velocity of sound
17 p2889 A69-32992

Similarity solutions of viscous transonic equation describing spiral and radial flows, containing shock-like transitions of corresponding inviscid solutions
18 p3121 A69-34787

Turbocompressors, reviewing axial and radial compressors
19 p3395 A69-36749

Heat transfer in radial flow between two parallel plates, calculating Nusselt number for laminar and turbulent flows
20 p3633 A69-38176

Magnetic field and radial gas motion in sunspots from Crimean magnetograph observations at different depths of solar atmosphere
20 p3615 A69-38299

Flow field induced by spiral vortex sheet, noting existence of radial velocity component
21 p3692 A69-38610

Laminar boundary layer on funnel wall, considering internal vortical and radial flow
21 p3692 A69-38611

Gas flow characteristics in shrouded and unshrouded turbine wheel assemblies, emphasizing radial flow role in efficiency
21 p3785 A69-38865

Omicron Andromedae radial velocity measurements /1961-1966/ during normal B star periods
22 p4028 A69-40755

Pressure distribution in gas lubrication layer of infinite radial sliding bearings, approximating differential equation by simple formulas
23 p4168 A69-41412

RADIANCE

Outer solar coronal IR radiance measured by ground telescope and stratosphere balloon flight, noting interplanetary dust thermal emission
09 p1600 A69-22205

Statistical properties of spatial radiance distribution of sky and forest backgrounds in IR, noting one dimensional Wiener spectra
12 p2131 A69-27072

Mathematical model for determining time dependent terrain surface temperatures and radiances, considering radiative transfer convection, evaporation, ground vegetation temperature, etc [AIAA PAPER 69-592]
17 p3071 A69-33263

Superradiance and recombination radiation from CdTe with high compensation, using model assuming narrowing from superradiance onset for analysis
19 p3389 A69-36550

RADIANT COOLING

Long wave radiative water vapor cooling in troposphere determined by numerical prediction model, including vertical distribution of cloud and moisture effects
07 p1175 A69-18896

Radiative cooling layer behind shock front from neutral interstellar hydrogen cloud collision at Mach 20, discussing molecular hydrogen abundance during cooling
08 p1381 A69-19796

Semiempirical relation for electron cooling modified by plasma heating of thermionic converters, including effects of plasma density, diode spacing and surface potential difference
09 p1440 A69-21831

Phase equilibrium and dynamics of gas volume heated by cosmic rays and cooled by radiation
10 p1760 A69-23136

Radiative cooling rates of bounded plasma of hydrogen isotopes, comparing dense deuterium plasma analytical results with brightness measurement
11 p1927 A69-25218

Thermosphere radiative cooling by atomic O 62 micron line, noting cooling and heating rates
12 p3084 A69-26009

Nongray absorption and radiation cooling on smooth symmetric blunt bodies included in modified Maslen flow field method for radiation and large blowing [AIAA PAPER 69-637]
17 p2891 A69-33290

Heat pipe devices applied to radiative body heat transfer in space suit temperature control [AIAA PAPER 69-619]
17 p2914 A69-33293

Radiative and conductive heat transfer in heated finite gaseous body with emphasis on collisional and radiative relaxation, noting cooling as two stage process [AIAA PAPER 69-638]
17 p3073 A69-33311

Radiative energy emission by blunt vehicle shock layer under severe entry conditions, discussing flow properties and radiative transfer coupling [AIAA PAPER 69-719]
18 p3084 A69-34416

Radiation cooling behind strong shock in Kr as function of plasma luminosity near end of relaxation zone
18 p3171 A69-34450

Materials integral hemispheric radiative capacity determination based on cooling rate of thin walled specimen in vacuum, considering stainless steel, Ni and Cu
18 p3156 A69-34698

Long wave radiation influx toward atmospheric layers generated naturally by clouds, discussing radiation cooling of atmosphere in cloudy and clear weather
21 p3758 A69-39112

Ionization equilibrium and radiative cooling of high temperature low density plasma, noting cosmic gas cooling curve of line emission from oxygen ion transitions
24 p4376 A69-42661

Radiative cooling models for various midlatitude synoptic features, including stationary front and cyclones
24 p4343 A69-43064

RADIANT ENERGY

U RADIATION

RADIANT FLUX DENSITY

NT ELECTRON FLUX DENSITY

NT ILLUMINANCE

NT IRRADIANCE

NT LUMENS

NT LUMINANCE

NT LUMINOUS INTENSITY

NT NEUTRON FLUX DENSITY

NT PARTICLE FLUX DENSITY

NT PROTON FLUX DENSITY

NT RADIANCE

NT SOLAR CONSTANT

NT SOLAR FLUX DENSITY

Energetic X ray intensities from large and small Magellanic clouds investigated by balloon flight sky survey, noting energy flux upper limits
01 p0150 A69-10370

Ultrashort light pulses in lasers with nonlinear absorber, evaluating random intensity peak probability created by intensity fluctuations and axial modes buildup
01 p0090 A69-10791

13-day cycle variation in cosmic radiation intensity confirmed by Vercelli method, giving values of amplitudes and correlation coefficients among variations
01 p0145 A69-11031

Surface radiation balance measurements in India during IQSY, discussing diurnal, seasonal and spatial variations of net radiation
02 p0307 A69-11820

Ruby laser limiting gain, stimulated emission loss, noise loss and spectral distribution determined by radiation intensity, pumping power and mirror reflection
02 p0256 A69-12000

- Solar continuum intensity determination in middle IR, obtaining solar disk center brightness temperature measurement by comparison with black body model
02 p0318 A69-12041
- Thermoelectric radiometer for transient radiant flux short duration pulse measurement, using thermally induced depolarization of polymer film dielectric [AIAA PAPER 68-403]
02 p0250 A69-12392
- Retinal burns from intense light sources using rabbit eyes as function of irradiation rate, exposure time and image size
02 p0204 A69-12496
- Microcalorimetric measurement of radiation flux of flames of condensed burning material, noting surface temperature distribution
02 p0355 A69-12671
- Soft X ray spectrum of Sco XR-1, noting intensity change from previous measurement
02 p0309 A69-12711
- Free excited H atom Lyman alpha radiation intensity study using beam-foil excitation method
03 p0471 A69-13167
- Mean atmospheric downward radiation fluxes for large territories, using simple model atmospheres in derivation of computational formulas
03 p0422 A69-13410
- Bolide fireball radiation maximum efficiency from observed spectra, using monochromatic radiation efficiency data for rarefied atoms and ions in meteor comas
03 p0512 A69-13692
- Directional intensity of radiation emerging from top and bottom of Rayleigh scattering atmosphere
03 p0426 A69-14026
- High temperature air plasma total radiant intensity measurements in shock tube
04 p0685 A69-14719
- Photographs of intensity of radio emission in millimeter band, using luminophor based on ZnS and CdS
04 p0560 A69-15272
- Radiative flux density, spectrum and temporal behavior of Q switched laser induced underwater sparks
05 p0771 A69-15818
- Radiation intensity distribution from first negative and positive nitrogen system in equilibrium gas flow behind propagating shock front, discussing kinetics mechanism and electronic states
05 p0745 A69-15890
- Meteorological rocket measurement of corpuscular radiation intensity in upper atmosphere at various latitudes
05 p0814 A69-16052
- Jupiter microwave radiation flux density at 81 MHz, noting spectrum of microwave emission
05 p0827 A69-16506
- Arc cloud thermal conductivity effects on discharge temperature and radiation intensity, solving energy balance equation
06 p0964 A69-17254
- Primary cosmic ray intensity variation with cut-off energy of particular secondary component, using ground based monitors
06 p0925 A69-17295
- Large area scintillation telescopes with cubic geometry, measuring cosmic rays intensity from vertical and slant directions
06 p0925 A69-17296
- Isotropic background cosmic X ray flux measurements using low latitude balloon to minimize atmospheric background, obtaining hard solar X ray flux upper limits
06 p0992 A69-17311
- X ray sources intensity and spectrum variation with time, describing proposed balloon experiments with equatorial launching for performing measurements
06 p0992 A69-17312
- Flux density spectral dependence disagreement with power law for synchronous radiation mechanism for radio sources in 12.6 to 25 MHz interval
06 p1004 A69-17538
- Pulse intensity variations in pulsars observed at 113 MHz with parabolic antenna using photographic recording techniques, noting lack of periodicities
06 p1009 A69-17964
- Radiation measurements inside Apollo 4 and 6 command modules during passage through trapped radiation belts [AIAA PAPER 69-17]
06 p0884 A69-18202
- Shock tube measurements of radiation from simulated Jupiter atmosphere related to thermodynamic conditions encountered by entry probe [AIAA PAPER 69-184]
06 p0908 A69-18207
- Statistical study of solar radio flux fluctuations incidence, observing absorption and polarization effects
07 p1215 A69-18819
- Spectra and flux densities of cm wavelength radio sources
07 p1218 A69-19256
- Background radiation intensity upper limits for mm and submillimeter wavelengths in interstellar medium, noting intense flux in far IR
07 p1221 A69-19404
- Radio source counts log N-log S diagram slope uncertainty due to finite source number, discussing statistical analysis methods accuracy
08 p1383 A69-20048
- Temperature profile calculations for high pressure electric arcs using diffusion approximation for radiant flux density, taking energy transfer into account
08 p1420 A69-20148
- Power radiated by oscillating magnetic and electric dipoles in cold streaming plasma calculated by Poynting vector method
09 p1544 A69-21329
- Flux density variability and component age of radio sources at frequency of 5769 MHz measured by radio telescope
09 p1588 A69-21361
- Geomagnetic field irregular pulsations relationship with polar aurora and ULF radiation pulsations, stressing choruses appearance
09 p1485 A69-21536
- Cosmic ray intensity temperature dependence in stratosphere and anisotropy in interplanetary space determined from measurements over Arctic and Antarctic regions
09 p1575 A69-21542
- Cosmic ray intensity diurnal variations from super neutron monitor observations, discussing anisotropy resulting from reduced intensity in gardenhose direction in ecliptic plane
09 p1576 A69-21706
- Radiant flux reflected by mirror and incident on receiver for paraboloidal solar devices, obtaining heat loads and radiant energy formulas
09 p1436 A69-21803
- Circular central shading effect on energy distribution parameters of paraboloidal mirrors, noting reflected radiant flux power limitation
09 p1436 A69-21804
- Impurity concentrations in expansion tube flow, measuring radiation intensities [AIAA PAPER 68-371]
09 p1477 A69-21961
- Impulsive solar microwave bursts observed by parabolic reflector, obtaining bursts spectra and total flux density
09 p1579 A69-22178
- Weak X ray sources at 20-100 KeV photon energies observed during balloon flight, finding hard rays from Ara XR-1 and Nor XR-1
09 p1583 A69-22763
- Spectrum of high energy X ray flux from Sco XR-1 during balloon flight using active collimator detector and graded shield detector
09 p1584 A69-22766
- Solar activity influence on cosmic ray intensity 11 year variation, taking into account heliolatitudinal movement of sunspot regions in solar cycle as evidence of density gradient
10 p1754 A69-22802
- Neutrino groups generation in internal regions of sun, analyzing flux ambiguities due to error of cross section parameter of nuclear reactions
10 p1757 A69-22827
- Cosmic ray anisotropy and diurnal density variation, analyzing influence of interplanetary magnetic field and subsonic solar wind
10 p1757 A69-22828
- Galactic and solar cosmic ray modulation in interplanetary space during different phases of 11 year solar activity cycle
10 p1758 A69-22833
- Cosmic ray intensity variations by spectrographic method, noting geomagnetic effects
10 p1759 A69-22836
- Solar activity and 19 to 24 day variations in cosmic ray intensity
10 p1759 A69-22843
- Flux density and spectra measurements at 5 GHz for extraterrestrial and other discrete radio sources, noting spectral indices
10 p1773 A69-22958
- Relative band intensities of atmospheric and IR atmospheric systems of molecular oxygen compared with Franck-Condon factor calculations
10 p1681 A69-23163
- Two photon photoelectron counting statistics and intensity fluctuations of incident radiation compared with single photon detectors and applied to laser outputs
10 p1704 A69-23658
- Low energy cosmic ray intensity increase on July 7, 1966 registered with high latitude neutron monitors
10 p1766 A69-23762
- Secondary corpuscular stream effect on diurnal variations in cosmic ray intensity obtained from statistical analysis
10 p1769 A69-23904
- Interplanetary magnetic field sectoral structure effect on diurnal cosmic ray intensity and geomagnetic field, noting field direction influence
10 p1769 A69-23905
- High altitude balloon measurements of secondary gamma quanta intensity vertical distribution, using scintillation counter with CsI/Tl crystal
10 p1770 A69-23924
- Radio brightness map at 22.25 MHz of galactic plane including H II regions IC 1805 and IC 1848, discussing LF absorption
10 p1787 A69-24115
- Spectral lines relative intensities for bright medium excitation gaseous planetary nebula IC 3568, using photoelectric spectrum scanner and spectrophotometry technique
10 p1787 A69-24117
- Radio sources log N-log S diagram, red shifts and luminosity functions in zero cosmological constant and Lemaitre type Friedmann universes
10 p1789 A69-24134
- Nitrogen plasma total radiation intensity under pressure and at high temperatures calculated from radiation spectrum
11 p1922 A69-24231
- Mean absolute solar spectrum energy distribution from 1800 A to 4 mm, noting solar constant and radiation intensity determination
11 p1951 A69-24242
- Quasars time dependent flux density variations at 6.6 cm, noting spectrum peaks tendency toward lower frequencies with time
11 p1954 A69-24382
- Flux density of quasars 3C 270 and 3C 278 at 40 cm determined by digital computer with point source program
11 p1954 A69-24383
- Brightness temperatures and spectra of Venus, Mars, Jupiter and moon measured from 8 to 14 microns by reflector and prismatic spectrometer
11 p1956 A69-24395
- Specific level role in emission of optical radiation by ruby laser stimulated calcium fluoride crystals doped with divalent Dy ions
11 p1894 A69-24618
- Brightness temperature distributions from intensity interferometric measurements reconstructed by computation
11 p1888 A69-25256
- Calculated UV spectra of solar radiation reflected from atmosphere compared with satellites photometric measurements, attributing radiation intensity distribution asymmetries to seasonal dependence of ozone content
12 p2064 A69-25952
- Auroral zone X ray pulsations during great geomagnetic disturbance and auroral electrojet development to maximum phase, noting atmospheric feedback modulation
12 p2065 A69-26109
- Primary cosmic ray energy spectrum studies during 11-year cycle based on changes in intensity at various altitudes
12 p2149 A69-26682
- Cosmic radiation recorder designed for use onboard satellite to measure intensity space-time distribution under geomagnetic effect
12 p2094 A69-26697
- Radio galaxies luminosities distribution and spectral indices, galactic structures and diameters, considering relations between radio emission parameters
12 p2165 A69-27031
- Absolute radio luminosity relation to surface brightness of extragalactic radio sources, finding volume radiation coefficient of spiral and radio galaxies
12 p2166 A69-27035
- Quasars intensity variations at various cm wavelengths confirming wavelength dependence
12 p2167 A69-27045
- Extragalactic radio sources, discussing brightness distribution measurements and radio star scintillations
12 p2168 A69-27053

Variable radio sources observation at 9.55 mm wavelength, discussing flux density and electron cloud expansion

13 p2334 A69-27309

IR observations of ETA Carinae to 20 microns, noting continued increase in flux density into IR

13 p2335 A69-27316

Exterior field equations for radiating spheres with zero limb darkening in relativity and Bondi coordinates, determining radiative flux and pressures

13 p2339 A69-27566

Structure and thermometry of solar interior from measuring neutrino fluxes intensities emitted by unit mass

13 p2333 A69-28434

Diurnal variation of cosmic ray muon intensity near geomagnetic equator and primary anisotropy monitored by cubical counter telescope

14 p2512 A69-28966

Cosmic ray intensity preceding Forbush effects as function of chromospheric flares solar longitude and solar wind velocity

14 p2512 A69-29044

Frequency distribution of sudden cosmic ray intensity increases, considering Forbush phenomenon

14 p2514 A69-29773

Cosmic ray intensity during solar cycles, considering minima relationship to Bartel index maxima and solar wind modulation theory

14 p2515 A69-29967

Cosmic ray intensity underground measurements, discussing solar modulation processes, sidereal day variations and interplanetary magnetic field influence

15 p2673 A69-30013

Crab Nebula lunar occultation observed by Cassegrain array of deep space communication facility, finding radio brightness distribution similar to optical

15 p2687 A69-30539

Solar neutrino fluxes sensitivity to localized changes in opacity and equation of state, discussing solar models

15 p2675 A69-30768

Global multielement radio interferometer with autonomous reception synthesized for studying spatial radio brightness distribution over radiation sources

15 p2578 A69-30936

Radio interferometer with independent heterodynes to obtain radio brightness distribution over source by varying antenna spacing and reception frequency

15 p2578 A69-30937

Flux densities at 2695 MHz for radio sources, tabulating measured data, discussing spectral distribution indices

15 p2696 A69-31206

Corpuscular radiation intensity during geomagnetic disturbances measured during rocket flights at 50-100 km, discussing effects on lower ionospheric radio absorption

15 p2677 A69-31327

Discrete radio sources interferometer observations using trans-Pacific baseline, noting spectra and radiation intensity variations

15 p2701 A69-31530

Thick gas model for monochromatic one dimensional radiant flux near diffusely emitting and reflecting boundaries, discussing gray gas and exponential kernel approximations

16 p2769 A69-31871

Explorer 33 and Explorer 35 observations of solar flare of 8 July 1969 soft X rays, discussing absolute flux

16 p2849 A69-31988

Radio sources spectral flux densities at 22 MHz, considering ionospheric conditions, calibration and reduction

16 p2860 A69-32231

Geomagnetic field irregular pulsations relationship with polar aurora and ULF radiation pulsations, stressing choruses appearance

16 p2783 A69-32531

Cosmic ray intensity temperature dependence in stratosphere and anisotropy in interplanetary space determined from measurements over Arctic and Antarctic regions

16 p2851 A69-32537

Ozone and temperature profiles influence on atmospheric radiation intensities measurement by satellite in five spectral regions, noting pressure broadening effect

16 p2786 A69-32633

Reradiation and multiple reflection effects on radiant flux density distribution in cylindrical receivers of solar power installations

16 p2741 A69-32799

Line width and intensity correlation of laser radiation noting damping constant

17 p2980 A69-33012

Slowly varying component of solar radio emission /S component/, correlating 35 GHz S component flux and corresponding phase, discussing magnetic fields and electron density

17 p3030 A69-33056

Cosmic X rays diffused component absolute intensity measurement using rotating collimator borne on sounding rocket, noting flat spectrum and Sco X-1 intensity variation

17 p3023 A69-33068

Stellar photometric data for various photocathode materials used to calculate radiant energy falling on earth

17 p2973 A69-33092

RF high pressure plasma discharges contained within radial inflow vortex, measuring radiation efficiencies, power densities and radiation fluxes [AIAA PAPER 69-695]

17 p3010 A69-33442

Red dwarf star YZ CMi corona structure showing possible estimation of additional carried energy by shock waves after flare

17 p3043 A69-34166

Cosmic ray intensity short term stochastic variations in solar system related to turbulent solar wind day-to-day variations

18 p3186 A69-34300

Extrasolar X rays and sources from studying distribution, luminosity, diameters and variability of rays

18 p3193 A69-34364

Continuum survey at 1415-MHz between declinations of zero and 20 degrees N with radio telescope, noting flux densities and contour maps of sources

18 p3195 A69-34428

Flux density variability and component age of radio sources at frequency of 5769 MHz measured by radio telescope

18 p3197 A69-34751

Occurrence frequency distributions at microwave frequencies as function of peak intensity and directivities of solar bursts

18 p3187 A69-34969

Low energy cosmic ray density in Galaxy due to pulsar PSR 0833-45 caused by mass ejection

18 p3187 A69-34995

UV excitation intensity increased for improving luminescent nondestructive testing, describing UV dosimeter and irradiation standards

18 p3138 A69-35115

Radio sources spectrum measurement results at cm wavelengths in tabular form, noting flux density relationship to frequency

18 p3200 A69-35132

Ionization effects in hydrodynamic model of radiation driven breakdown wave propagation, obtaining wave velocity and absorbed laser flux density relationship

18 p3174 A69-35286

Radiometric measurement, discussing characteristics and calibration of instruments for measuring radiant intensity or radiance

19 p3311 A69-36071

Memory matrices sensitivity to laser beams with various emission power densities, considering matrices of thin metal layers on transparent base

19 p3335 A69-36198

Crab Nebula radio brightness at 2.16 and 8.2 mm measured and compared to Jupiter flux density

19 p3428 A69-36875

Radio emission intensity of Cas-A and Cyg-A at 30-60 cm, giving spectral indices

19 p3428 A69-36876

Intensities of translational lattice mode absorptions of alpha phase solid molecular nitrogen in far IR, noting temperature dependence

20 p3579 A69-37346

Solar radio emission parameters calculated, determining basic 327 MHz emission component and flux density-sunspot area correlation coefficient

20 p3588 A69-37478

Solar bremsstrahlung intensity dependence on heliographic longitude, noting maximum intensity shift toward electron beam direction

20 p3589 A69-37552

Radiative transport equation solution in two flow approximation for plane layer, considering absorption and dispersion characteristics dependence on radiation density

20 p3553 A69-37608

Threshold power, gain, output power and radiation energy during optical pumping of Q switched molecular laser by black body radiation

20 p3554 A69-37722

Meteorological rocket measurement of corpuscular radiation intensity in upper atmosphere at various latitudes

20 p3591 A69-37962

Ultrashort light pulses in lasers with nonlinear absorber, evaluating random intensity peak probability created by intensity fluctuations and axial modes buildup

20 p3555 A69-38009

Diurnal variations in cosmic ray intensity from observations by inclined meson telescopes scanning equatorial plane

20 p3593 A69-38109

Radio source flux density values in revised 3C catalog determining spectrum, discussing effects of relativistic electron energy distribution, self absorption and spatial distribution

20 p3609 A69-38138

Balloon-borne proportional counters to measure X rays intensity and spectral distribution from Taurus X-1 and Cygnus X-1

20 p3593 A69-38153

Variable BL Lac SHF flux density measurements, discussing periodicity and maxima spacing

21 p3798 A69-38545

Photodetector responses to radiant energy from many stars tabulated for various photocathode materials and silicon detector

21 p3800 A69-38680

Galactic radio sources high resolution observations at 178 MHz, determining flux densities and angular structures, noting supernovae remnants

21 p3801 A69-38701

X rays and gamma rays extragalactic components, calculating background component intensity for given model of universe

21 p3789 A69-38818

Primary and secondary cosmic ray intensity variation with altitude from ascending balloon data, noting absorption length role

21 p3791 A69-39249

Power density and time history of pulsed molecular nitrogen laser, discussing dependence on fill pressure and electric circuit parameters

21 p3742 A69-39779

Mean intensity profiles of photospheric H alpha radiation illuminating solar prominences moving at different heights

22 p4011 A69-39995

Diffuse galactic radiation intensity and distribution from photoelectric measurements compared with radiative transfer calculations using various interstellar dust models

22 p4013 A69-40096

Flux measurements of radio sources at 4.3 mm by 36 ft parabolic antenna, noting flux densities relative to Jupiter

22 p4014 A69-40126

Flux densities of radio sources in 3CR catalog measured at 2.8 cm wavelength

22 p4014 A69-40127

Declination measurements of sources in 4C Catalogue by Arecibo 1000 ft radio telescope

22 p4014 A69-40128

Radio observations of supernova remnant HB 21 at 2695 MHz, noting spectral brightness and curvature of northern shell segment

22 p4014 A69-40129

Photoelectric methods for pulsed and CW lasers output power and energy measurements

22 p3961 A69-40239

Radiant energy diffusion from spherical expanding matter for masses and velocities of model supernova outbursts, discussing thermonuclear and neutron star origins of supernovae

22 p4026 A69-40649

Quasar features compared to pulsars, noting complete analogy except for energy output scale

22 p4029 A69-40762

Flux density variations of radio sources at 2.8 and 4.6 cm wavelengths, suggesting relativistic particles prolonged injection into optically thin sources

22 p4029 A69-40764

Corpuscular radiation intensity measurements in upper atmosphere at midlatitudes by meteorological probe during geomagnetic storm, noting radio wave absorption

22 p4008 A69-41104

Stellar and diffuse galactic radiation intensity observations to obtain albedo values of interstellar dust particles

22 p4034 A69-41112

Electromagnetic waves emission intensity in one dimensional resonator, allowing for wave interference effects

22 p3966 A69-41172

Spectral emissivity and radiation intensity spectral distribution measurements for heat-resistant materials at high temperature, using photographic method

23 p4238 A69-41330

Radiative properties of Ta, Mo, Nb, graphite and niobium carbide at high temperatures

23 p4175 A69-41331

Day-to-day variability of daily variation of cosmic ray intensity during quiet solar activity period using high latitude neutron monitor data

23 p4204 A69-41484

Electric fields reducing recombination radiation intensity from bulk ionized GaAs and InP and shifting spectrum to lower energies, discussing self absorption

23 p4198 A69-41499

Instrumentation and data interpretation method for particle size determination by low-angle light scattering

24 p4313 A69-42764

Pulsars relation with supernovae remains and radiation patterns and fluxes analysis, ascribing radio emission to relativistic plasma

24 p4383 A69-42985

Cosmic ray albedo-neutron decay source role in intensity measurements of high energy protons trapped on low L shells during satellite flights

24 p4367 A69-43176

Solid propellant flame zone radiant energy flux emitted through side port of internal burning cylindrical rocket motor related to total heat flux at burning surface

24 p4415 A69-43595

Scanning Fabry-Perot interferometer interaction with laser source, calculating laser intensity and oscillation frequency changes for weak mode coupling

24 p4329 A69-43756

Quasars time dependent flux density variations at 6.6 cm, noting spectrum peaks tendency toward lower frequencies with time

24 p4389 A69-43772

Flux density of quasars 3C 270 and 3C 278 at 40 cm determined by digital computer with point source program

24 p4389 A69-43773

Brightness temperatures and spectra of Venus, Mars, Jupiter and moon measured from 8 to 14 microns by reflector and prismatic spectrometer

24 p4390 A69-43785

RADIANT HEATING

Instability of struts subjected to axial force and radiant heat, considering elastic and thermal deformation

02 p0337 A69-11716

Radiation heating characteristics of shock layer gases surrounding Venus entry vehicle, noting domination of carbon monoxide band and UV spectrum

02 p0351 A69-11751

Quantitative determination of reentry shock precursor absorption level and effect on surface radiation heating, calculating radiative flux from shock layer enthalpy distribution

02 p0354 A69-12528

Heavy ion track thermal spike model to account for LET and temperature effects in radiation biology and chemistry

03 p0371 A69-13479

IR heating, discussing operation of IR emitters employing glass and quartz envelopes

03 p0411 A69-13548

Book of engineering compendium on nuclear radiation shielding, discussing radiation sources, attenuation methods, induced heat generation, ducts and voids in shielding technology and design

05 p0791 A69-15830

Contact thermocouples to measure temperature of wall exposed to radiation, evaluating errors

17 p2975 A69-33596

Cryogenic liquid level temperature transducer with radiantly heated thermocouple sensitive element

17 p2975 A69-33670

Temperatures of radiantly heated sun and shade leaves of white oak measured in low speed wind tunnel, considering differences in convective heat dissipation

18 p3095 A69-34540

Equations governing stress waves generated by rapid nonuniform heating of solids, comparing elastoplastic with purely elastic solutions

21 p3837 A69-39158

Thermal buckling of skew plates clamped along all edges under radiant heating, measuring various characteristics, solving differential equations by difference method

22 p4044 A69-40599

Teflon dielectric properties evaluated during fast laser beam heating, noting presence of C by microwave measurement

24 p4336 A69-43266

RADIATION

Open cosmological model containing radiation and matter, noting matter density relationship to visible matter average

01 p0150 A69-10371

Arend-Roland comet head luminescence intensity, considering radiation scattering by dust component

21 p3804 A69-39080

RADIATION ABSORPTION

NT ATMOSPHERIC ATTENUATION

NT AURORAL ABSORPTION

NT ELECTROMAGNETIC ABSORPTION

NT MOLECULAR ABSORPTION

NT PHOTOABSORPTION

NT POLAR CAP ABSORPTION

NT SELF ABSORPTION

NT X RAY ABSORPTION

Organic dye lasers energy characteristics excited by monochromatic radiation, investigating radiation absorption during transitions from lower to higher electron-vibrational levels

01 p0090 A69-10381

Thermodynamics in homogeneous steady state fog over rough terrain representing absolutely absorbing surface

02 p0274 A69-11442

Kinetics of vaporization of metals with surface subjected to incident radiation flux noting pulse duration

02 p0350 A69-11577

Radiation attenuation cross sections of monatomic and diatomic xenon gas from UV absorption measurements near resonance line

02 p0284 A69-12551

Thermal tidal oscillations in earth atmosphere using circulation model attributed to solar radiation absorption by atmospheric vapor and ozone

03 p0457 A69-13030

Radiation absorption variations in KC-19 CdSe glass during ruby laser radiation, noting microcrystals and nonlinear effects role in determining optical properties

03 p0436 A69-13036

Ruby laser radiation nonlinear absorption coefficient measurement in CdS, ZnS and SiC semiconductor crystals, noting light limiting effects

03 p0436 A69-13038

Heavy ion track thermal spike model to account for LET and temperature effects in radiation biology and chemistry

03 p0371 A69-13479

Solar emission line absorption by oxygen and nitrogen atomic lines, discussing effect on upper atmosphere composition measurements

03 p0425 A69-14019

Observable horizons in expanding universe, considering absorption of extragalactic radiation

04 p0648 A69-14566

Viscoelasticity effect on tensile stress in absorption layer for free surface uniaxial motion

04 p0676 A69-14705

Nongray radiation absorption coefficients reformulation employing alternative angular moment averaged absorption coefficients with emission/Planck/

04 p0686 A69-14744

Book of engineering compendium on nuclear radiation shielding, discussing radiation sources, attenuation methods, induced heat generation, ducts and voids in shielding technology and design

05 p0791 A69-15830

Spectrophotometer and integral methods to determine solar radiation absorptivity for steady/ unsteady thermal regimes in solids

05 p0846 A69-15901

Cosmic radio noise absorption in ionosphere, discussing diurnal, seasonal and longer variations of integral absorption

06 p1008 A69-17727

Radio spectra analyzed for NGC 1052 and NGC 4278 elliptical galaxies, discussing 178 MHz flux density, anomalies and radiation absorption mechanisms

06 p1009 A69-17959

Terrestrial and Martian aerosols estimation based on carbon dioxide spectral and Mariner 4 RF occultation measurements

[AIAA PAPER 69-52] 06 p1011 A69-18199

Saturated absorption by Ne inside 6328 A He-Ne laser, discussing selection of Ne isotopes in gain and loss tubes

07 p1149 A69-18898

Single mode output power from 6328 A He-Ne laser through mode coupling induced by added absorption cell containing excited Ne

07 p1149 A69-18901

Relativistic cosmological models with radiation and matter, analyzing conversion from radiation-like models to dust-like models

07 p1222 A69-19587

Algorithm for high speed digital computers to evaluate stellar radiative opacities

07 p1222 A69-19589

Electron cyclotron resonance absorption of injected radiation magnetic mirror, noting effect of RF heating on plasma electron distribution

08 p1364 A69-20519

Laser stimulated gamma-optical transitions illustrated by gamma-optical absorption detection in dysprosium ethyl sulfate

08 p1328 A69-21185

Ruby laser emission absorption in transparent dielectrics, noting crack formation and propagation producing opacity

09 p1520 A69-22655

Cosmic ray absorption and modulation in lower ionosphere at midlatitudes, considering 11 year variations, Forbush effects and solar radiation on electron concentration

10 p1759 A69-22840

Starlight extinction by interplanetary medium evidenced from confirming correlation between star brightness on ecliptic and elongation

10 p1775 A69-23198

Radio brightness map at 22.25 MHz of galactic plane including H II regions IC 1805 and IC 1848, discussing LF absorption

10 p1787 A69-24115

Effective cross sections of UV radiation absorption by molecular oxygen in Schumann-Runge bands at high temperatures

11 p1921 A69-24617

Radiation attenuation in hazy lower atmosphere, calculating attenuation coefficients and using spherical model of haze particles and empirical formula for haze spectra

11 p1913 A69-25571

Gas motion and heating by radiation behind shock wave front, noting ionization and radiation absorption occurrence

12 p2061 A69-25880

Organic dye lasers energy characteristics excited by monochromatic radiation, investigating radiation absorption during transitions from lower to higher electron-vibrational levels

12 p2109 A69-26676

Monograph on atmospheric radiation transfer including absorption, scattering, direct, diffuse, global, thermal and net radiation

12 p2073 A69-26918

Hydrogen atoms in interstellar grains as source of stellar flux absorption, noting crystal environment effect on atomic hydrogen Lyman alpha transition

13 p2337 A69-27518

Synchrotron spectrum radiated by relativistic electrons below Razin cut-off, considering relation to radio spectra curvature of variable extragalactic sources

13 p2339 A69-27573

Germanium surface IR radiation absorption in vacuum at low temperatures, obtaining modulated interval reflection spectra

13 p2317 A69-27879

Gallium arsenide diode nonequilibrium carriers absorption of He-Ne laser radiation under emission conditions

13 p2272 A69-27893

Radiative transfer between two concentric gray opaque spheres separated by radiating gray gas, employing Fredholm equations

13 p2377 A69-28149

Laser radiation absorption in xenon plasma, noting dependence on intensity due to atoms ionization

13 p2314 A69-28442

Plasma temperature measurement by resonant laser radiation absorption, assuming Saha-Boltzmann relation

14 p2501 A69-29954

Synchrotron radiation and reabsorption theories

15 p2674 A69-30421

Molecular dissociation by line radiation absorption, applying results to hydrogen molecules in H I region dissociated by photons of mean interstellar UV radiation field

15 p2693 A69-30783

Distribution model for ionized interstellar gas over galactic disk for explaining radio emission absorption and depolarization from discrete sources

15 p2695 A69-30935

Partially coherent radiation scattering determined using Heisenberg operator, noting radiation absorption dependence on interfrequency band coherence

16 p2797 A69-32050

Asymptotic formulas for X and Y functions for resonance radiation scattering in layer, analyzing Doppler absorption and line profiles

16 p2813 A69-32588

Nongray absorption and radiation cooling on smooth symmetric blunt bodies included in modified Maslen flow field method for radiation and large blowing [AIAA PAPER 69-637] 17 p2891 A69-33290

Molecular gas absorption coefficient dependence on laser emission energy density, considering disturbed equilibrium distribution of molecules 17 p2983 A69-33973

UV absorption coefficients of high temperature air measured in shock tube reflected region 18 p3230 A69-35073

Laser stimulated gamma-optical transitions illustrated by gamma-optical absorption detection in dysprosium ethyl sulfate 18 p3152 A69-35154

Gas laser oscillation mode selection and self synchronization based on separation in two mirror cavity with nonlinear absorption 19 p3336 A69-36350

IR absorption in n-type gallium phosphide doped with telluride or Si in 1.5-2.0 micron range, analyzing wavelength dependence 19 p3385 A69-36518

Molecular oxygen rate of dissociation resulting from absorption in Schumann-Runge bands, calculating effects on chemistry of lower thermosphere and upper mesosphere 20 p3534 A69-38089

Absorption mean free path for radiation absorbed by given medium, using zenith angle distribution from particle counter telescope 21 p3723 A69-38841

Laser radiation increased absorption in opaque solid body attributed to vaporization, analyzing factors determining thermodynamic equilibrium between condensed and gaseous phases 21 p3736 A69-38962

Primary and secondary cosmic ray intensity variation with altitude from ascending balloon data, noting absorption length role 21 p3791 A69-39249

Synchrotron radiation and reabsorption for rapidly moving cloud of relativistic particles, considering errors 21 p3772 A69-39513

Radiation absorption and emission problem for material of unit density at rest solved by finite difference scheme 21 p3773 A69-39666

Vacuum integrating sphere for measuring solar absorptance in space environment to determine thermal control coatings qualifications [AIAA PAPER 69-1021] 22 p3923 A69-40392

Quasars observation failure for red shifts beyond z suggested due to absorption of intergalactic neutral H 22 p4024 A69-40582

Free-free intergalactic absorption at LF as function of red shift for uniform zero pressure cosmological models 22 p4025 A69-40640

Molecular collision pumping mechanism for anomalous microwave absorption by formaldehyde rotational transition in Galaxy dust cloud 22 p4029 A69-40768

Rocket measurement of far UV spectral intensity of theta Orionis for far UV interstellar extinction law in Orion nebula region 22 p4030 A69-40770

Interstellar extinction in UV from zeta and epsilon Persei spectra obtained with scanner attached to telescope mounted in pointed Aerobee rocket 22 p4030 A69-40772

Gaseous absorption cell variable attenuator for carbon dioxide laser radiation at specific wavelength, using forced convection to eliminate thermal defocusing effects 23 p4172 A69-41396

Fast neutron irradiation effect on IR absorption in single crystal GaAs for various fluences 23 p4198 A69-41540

Pure water vapor and water vapor-air mixture continuum absorption of carbon dioxide laser radiation measured to determine atmospheric attenuation 23 p4173 A69-41631

Radiation contribution to large scale atmospheric mass circulation simulation, considering short wave radiation, temperature variations, exponential and aerosol attenuation 23 p4184 A69-42487

Solar grazing ray absorption calculated by tracing through earth atmosphere, noting extinction for arbitrary ozone and aerosol profile 24 p4350 A69-43013

Ellipsometric liquid immersion method for optical parameters determination of system with nonabsorbing surface film on absorbing substrate 24 p4316 A69-43321

RADIATION BELTS

NT ARTIFICIAL RADIATION BELTS

NT INNER RADIATION BELT

NT OUTER RADIATION BELT

NT PROTON BELTS

Optimum control determination for low thrust spacecraft to minimize time for passing through radiation belt 01 p0113 A69-10571

Soviet book on dynamics of radiation belts of earth covering theories concerning magnetosphere, magnetic fields and plasma and electromagnetic pulsations 02 p0307 A69-11799

Radial diffusion coefficient for trapped electrons moving across field lines, obtaining time dependent solutions of Fokker-Planck equation 03 p0502 A69-14002

Bounce resonant scattering of particles trapped in geomagnetic field 03 p0503 A69-14014

Charged particles injection into captured radiation zone of Van Allen belts during main phase of magnetic storm indicated by proton data analysis 05 p0815 A69-16057

Particle and field environment of earth, discussing solar wind, bow shock, magnetosheath, magnetopause, magnetosphere and particle population 06 p1001 A69-17158

Synchrotron radiation from trapped high energy electrons in Van Allen belt 06 p0992 A69-17324

Particle flux and dose rates in Jupiter Van Allen belts based on assumed synchrotron radiation from trapped electrons in dipole magnetic field [AIAA PAPER 69-18] 06 p0997 A69-18129

Radiation measurements inside Apollo 4 and 6 command modules during passage through trapped radiation belts [AIAA PAPER 69-17] 06 p0884 A69-18202

Cyclotron- and bounce-resonance scattering of electrons trapped in geomagnetic field for pitch-angle scattering, noting whistler mode disturbances 07 p1208 A69-19367

Monte Carlo method applied to calculation of radiation transmission and dosage behind space vehicle shields during passage through earth radiation belt 08 p1377 A69-19843

Quasi-trapped particle currents having discontinuities on daytime and nighttime sides of earth 09 p1577 A69-21767

Multiple Coulomb scattering and range straggling effects in shielding against solar flare protons and trapped protons in Van Allen belt 10 p1723 A69-23164

Primary cosmic rays, radiation belts and solar wind studies by semiconductor detectors installed on orbiting satellites 10 p1662 A69-23294

Geomagnetic field Pc 3 and Pc 4 pulsation generation mechanism explained by resonance of MHD waves in force tubes adjoining radiation belt maximum 10 p1689 A69-24206

Solar wind particles acceleration and transformation into radiation belt particles 11 p1948 A69-24855

Geomagnetically trapped particle loss processes and equilibrium distribution resulting from MHD wave field interaction described using sandbox model 11 p1948 A69-24856

Stable particle trapping zone in magnetosphere, discussing results of adiabatic theory application to charged particle motion in earth magnetic field 11 p1948 A69-24858

B. L. coordinates for mapping geomagnetically trapped particles distribution computed by perturbation method, using perfect dipole as zero order approximation 11 p1949 A69-24861

Earth radiation belts formation as function of particle injection into trapped radiation zones or proton and electron leakage 12 p2150 A69-26742

Pitch angle diffusion of trapped electrons in terrestrial radiation zones, discussing diffusion theory based on Fokker-Planck equation, atmospheric Coulomb scattering mechanism, etc 12 p2150 A69-26746

Solar wind induced magnetospheric convection for interpretation of geomagnetic storms, aurora and trapped particle belts, noting electric fields 12 p2073 A69-26749

Model for self consistent time independent ring current of charged particle distribution under combined field of earth dipole and particle motion current 12 p2151 A69-26948

Plasmopause, plasma sheet and energetic trapped electrons in earth magnetosphere, considering slot, peak intensity and trapping boundary 12 p2151 A69-26953

Van Allen radiation belts proton and electron components recorded by Soviet lunar probes and Cosmos and Elektron satellites 13 p2326 A69-27350

Relativistic electron confinement within geomagnetic tail neutral sheet measured by Pioneer 7 deep space probe, confirming kinetic energy observations of IMP 1 satellite 14 p2433 A69-28934

Nonuniform ring current belt growth, discussing associated magnetospheric substorms 14 p2513 A69-29123

Saturated signals of GM counter from solar radiation monitoring satellite, showing Van Allen belt high energy particle origin 14 p2514 A69-29383

Earth radiation belt data, discussing origin, density, distribution, etc, of protons, electrons and alpha particles 15 p2674 A69-30016

Optimum control determination for low thrust spacecraft to minimize time for passing through radiation belt 15 p2651 A69-30741

Magnetic storm effects on electrons and protons in outer belt, using satellite data for intensity and differential energy spectra 15 p2676 A69-31314

Self consistent ring current of radiation belt under combined influence of earth dipole field and field due to currents of particle motions 16 p2776 A69-32096

Numerical analysis of charged particles radial distribution in radiation belts extended to geomagnetic tail for low energy auroral electrons 16 p2850 A69-32102

Spatial and temporal dependence of trapped particle energy spectra on basis of bimodal diffusion 16 p2852 A69-32619

Trapped particle acceleration by random bimodal diffusion in inhomogeneous magnetic field accounting for high energy particles trapped in earth radiation belts 18 p3186 A69-34808

Electron intensities in Starfish belt /1963- 1965/, discussing radial diffusion loss mechanism and pitch-angle diffusion 18 p3187 A69-34945

Pressure dependence of trapped spontaneous decay of resonant radiation carbon dioxide 18 p3179 A69-35478

Kinetic equation describing dynamics of inhomogeneous cloud of fast electrons and ions trapped in earth magnetic field 20 p3520 A69-37029

Solar protons captured in earth dipole trap, discussing conditions for nonadiabatic escape 20 p3587 A69-37042

Charged particles injection into captured radiation zone of Van Allen belts during main phase of magnetic storm indicated by proton data analysis 20 p3591 A69-37967

Dungey reconnection model of magnetosphere with dayside current sheet and pseudotrapping region compared with dayside observations of precipitation regions 21 p3711 A69-38511

Magnetospheric instabilities and whistler mode turbulence relationship to loss of high energy electrons from Van Allen belts 24 p4306 A69-42692

Geomagnetically trapped protons and alpha particles, analyzing OGO 4 data 24 p4368 A69-43184

RADIATION COUNTERS

NT CERENKOV COUNTERS

NT ELECTRON COUNTERS

NT GEIGER COUNTERS

NT NEUTRON COUNTERS

NT PARTICLE TELESCOPES

NT PROPORTIONAL COUNTERS

NT QUANTUM COUNTERS

NT SCINTILLATION COUNTERS

NT SPARK CHAMBERS

Distance between measurement equipment and extensive air showers axis varied as function of particles number and number of hit 01 p0144 A69-10749

- Cellulose nitrate sheets applicability in detecting cosmic ray relativistic heavy nuclei, considering etchable tracks
06 p0924 A69-17286
- Particle dynamics measured by ATS satellite synchronous orbit, discussing flux time variations during geomagnetic disturbances
07 p1209 A69-19371
- Nuclear particle plastic dielectric track detectors to record distribution of fissionable and heavy elements in nature and cosmic radiation
08 p1401 A69-20899
- Solar proton monitoring by particle detectors on-board rockets and IMP satellite
08 p1318 A69-21142
- Solid state AC voltage circuitry for measuring and controlling charged particle detector signals
10 p1662 A69-23256
- Differential energy losses of fission fragments in thin carbon films as function of mass and initial energy mapped by time of flight method
10 p1694 A69-23348
- Two photon photoelectron counting statistics and intensity fluctuations of incident radiation compared with single photon detectors and applied to laser outputs
10 p1704 A69-23658
- Extensive cosmic ray showers structure at sea level, using multiple hodoscopic counters and control system
13 p2332 A69-28405
- Spectrometric characteristics of He, H and molecular H ion recording counters as function of temperature
14 p2452 A69-29811
- Energetic gamma rays emission from radio source Cassiopeia A by high altitude balloon observations, using high resolution telescope
15 p2675 A69-30760
- Low velocity heavy mass particle detection in sea level cosmic radiation, assuming deuterons
16 p2846 A69-31600
- Low level beta, X and gamma radiation detector incorporating Geiger, proportional and scintillation counting features in various modes suiting radionuclide decay scheme
17 p2975 A69-33747
- NASA lunar receiving laboratory for lunar rock samples examination by gamma ray spectrometry for induced radioactive nuclides and naturally occurring isotopes
20 p3512 A69-38271
- Silicon junction radiation detectors applications in cryogenics, measuring junction response to beta particles at low temperatures
20 p3546 A69-38275
- Trans-iron nuclei flux in primary cosmic radiation determined through high altitude balloon exposure of interleaved layers of nuclear photographic emulsion and plastic detectors
21 p3787 A69-38327
- Cosmic ray muons for calibrating dE/dx counter used in particle identification by determining cosmic particles distribution as function of energy losses due to ionization
21 p3724 A69-39075
- Auroral zone X rays measurement counting rate vs time patterns from balloon flights at Kiruna
21 p3791 A69-39252
- Environmental neutron flux measured by various techniques, studying effects of soil and moisture on density
22 p4002 A69-40094
- Detection of metastable He, H, Ne, Ar, Kr, Xe and molecular nitrogen with continuous channel electron multipliers
22 p3917 A69-41235
- ### RADIATION DAMAGE
- Radiation damage and recovery of lithium-diffused silicon p-n solar cells, measuring photovoltaic parameters as function of gamma radiation fluence
19 p3251 A69-35694
- Solar cell integral covers optical losses in vacuum as function of degradation by UV exposure, noting accelerated testing for time-cost reduction
19 p3253 A69-35703
- Solar cell radiation damage during 416.8 days in synchronous orbit on satellite ATS 1, discussing radiation shields
19 p3253 A69-35704
- Physiological and somatic effects on insects of radiation source onboard biosatellite 2, discussing wing abnormalities in flour beetle
20 p3476 A69-37619
- Changes in CdS crystals spontaneous and coherent emissions caused by electron beam radiation damage, determining intensity and spectral composition dependence
21 p3780 A69-39047
- Nerve tissue oxidation processes relation to nervous system radiation sensitivity in dogs with cerebellum X rayed after enzyme poisons administration
21 p3658 A69-39053
- Enzyme activity changes in liver, heart and cerebrum of X ray exposed rats and rabbits, noting individual enzyme differences in same X rayed organ
21 p3658 A69-39054
- White rats hyperglycemia during blood sugar changes following single X ray dose, indicating increased sugar benefit in radiation damage treatment
21 p3658 A69-39057
- Pathological effects of single 120 Mev proton doses on rats blood in rotating cylinder, discussing leukopenia and benign and malignant tumors development
21 p3658 A69-39058
- Nervous system reactions and resistance to ionizing radiation noting role of functional, morphological and physicochemical changes in nerve tissues
21 p3659 A69-39061
- Histological changes in internal organs of rats after exposure to 400 r fast neutron dose, showing destructive processes followed by compensation reactions of cellular proliferation
21 p3659 A69-39062
- Ionizing radiation histological and neurohistological effects in rabbits esophagus, stomach and ileocecal region intramural plexes
21 p3659 A69-39063
- Pathological changes in solar ganglia cells of white rats following X ray exposure, using electron microscope
21 p3659 A69-39064
- Structural changes in Mo single crystal under action of laser radiation of various power densities
21 p3750 A69-39842
- Laser safety factors in open air applications, discussing pulse length, energy spatial distribution, atmospheric attenuation, human eye sensitivity, etc
22 p3892 A69-40241
- Polymer film breakdown under impact of supersonic plasma beam pulses from capillary discharge chamber, including photomicrographs of cavities and structural defects
22 p3974 A69-41031
- X ray radiation damage to white mice blood serum proteins disappearing following intraperitoneal administration of imidazole or benzimidazole
23 p4077 A69-41300
- Bacteriophage desoxyribonucleic acid (DNA)/degradation by gamma irradiation in vitro by Co 60, discussing breaks, cross links and molecular weight
23 p4079 A69-41402
- Lithium doped silicon acceptor concentration resulting from electron irradiation damage decreased by annealing at 300 degrees K
23 p4197 A69-41498
- Radiation hardened microcircuits and transistors for protection against transient radiation released by nuclear weapons
23 p4135 A69-41528
- Biological effects by cosmic ray heavy ions and solar flares, using direct correlation between damages caused and trajectories
23 p4089 A69-41831
- Radiation damage in chlamydomonas, discussing dark repair activities
23 p4090 A69-41964
- Microwave absorption by biological materials, noting energy distribution between reflected, transmitted and absorbed radiation as function of medium physical properties
24 p4270 A69-42574
- Solar protons and alpha particles measurements at synchronous orbit altitudes providing data for solar cell shield design to prevent radiation damage
24 p4369 A69-43265
- ### RADIATION DETECTORS
- #### NT DOSIMETERS
- #### NT SILICON RADIATION DETECTORS
- #### NT THRESHOLD DETECTORS [DOSIMETERS]
- DC biased microwave bolometer /barretter/ detector, describing small signal dynamic equivalent circuit for output voltage
01 p0044 A69-10626
- Distance between measurement equipment and extensive air showers axis varied as function of particles number and number of hit
01 p0144 A69-10749
- Gas chromatography technique for separation and purification of chemical compounds for ionizing radiation detectors
02 p0249 A69-12011
- Ferroelectric strontium barium niobate as sensitive detector of single pulse IR radiation, noting application to Q switched carbon dioxide laser output
02 p0300 A69-12623
- Low energy electrons on day side of magnetosphere observed with MIT electron detector onOGO 3 satellite
03 p0503 A69-14027
- Thermal conduction of chambers for selective and nonselective film detectors at low obturation frequencies
03 p0432 A69-14216
- Photoelectron counting in extreme UV using windowless photomultiplier detectors as photon counters
04 p0595 A69-14277
- Superconductors, discussing properties and materials for magnets, power systems, radiation detectors, HF devices and computer elements
04 p0642 A69-14584
- Magnetic electron multiplier used as particle detector in time-of-flight (TOF)/mass spectrometers can introduce mass discrimination effects
04 p0599 A69-15014
- Solar and terrestrial thermal radiometer absolute calibration noting standards and methods
04 p0602 A69-15429
- Balloon-borne SPARMO detector SC 67 used for measuring radiation at high altitudes
05 p0762 A69-15823
- Thin film thermocouple detector for molecular lasers operating in middle and far IR range
05 p0773 A69-16284
- Dynamics of laser response in IR detection by means of optical mixing in He-Ne laser, noting bandwidth
05 p0776 A69-16331
- Chemical composition of nuclear cosmic rays with Z greater than 22, noting etching techniques for utilizing meteoritic minerals as detectors
05 p0816 A69-16355
- Large area X ray collector, matrix detector for ionizing radiation and inflatable gas counter, considering application to X ray optics and astronomy
05 p0794 A69-16587
- Solar neutron production and propagation to earth, discussing particle detectors
06 p0989 A69-17281
- Multiplicity of secondary neutrons counted by IGY neutron monitor detecting cosmic radiation
06 p0925 A69-17297
- Low energy muons and nuclear active particles measured with extensive air showers array composed of scintillation detectors, spectrometer and Geiger counters
06 p0990 A69-17299
- Solar flare in-flight radiation detection and warning system for Concorde SST, noting radiation hazards due to solar cosmic rays
07 p1131 A69-18551
- Ag-GaAs Schottky barrier photodiodes, describing fabrication and use as UV radiation detectors
09 p1462 A69-21334
- Phototubes, photodiodes, photoconductors, quantum detectors, nonlinear optical detectors and heterodyne receiving systems for photodetection of laser outputs
09 p1518 A69-22126
- Slow atmospheric neutron energy spectrum determined by resonance detectors and l/v detectors, measuring cadmium ratio dependence on longitude and latitude
10 p1758 A69-22831
- Primary cosmic rays, radiation belts and solar wind studies by semiconductor detectors installed on orbiting satellites
10 p1662 A69-23294
- High energy cosmic radiation using Conversi detectors, noting design and internal efficiency
10 p1693 A69-23296
- Two photon photoelectron counting statistics and intensity fluctuations of incident radiation compared with single photon detectors and applied to laser outputs
10 p1704 A69-23658
- Solar UV radiation measurements by balloon-borne monochromatic illuminator, using Cd-cathode photomultiplier detector
11 p1945 A69-24410
- Low energy charged particle detectors reliability, analyzing windowless electron multipliers and effects of secondary emission layers on sensitivity
11 p1848 A69-24868

GaAs photoelectric devices for radiation detection and light to electric energy conversion, considering photoresistors, photodiodes and solar cells
13 p2203 A69-27465

Freons applications to radiation detector cooling, calculating specific volumes and compressibility factors for Freon 14
14 p2447 A69-29330

High energy gamma rays detection by balloon near geomagnetic equator, observing enhanced flux from galactic disk
15 p2675 A69-30695

Energetic gamma ray emission from Cygnus A and X-1, describing high altitude balloon telescope observation and gamma ray emulsion process
15 p2676 A69-30888

Gravitational radiation indicated by coincidences of detector observations over 1000 km, eliminating seismic and electromagnetic effects
16 p2784 A69-32565

Homodyne detection of IR radiation from carbon dioxide laser scattered from moving diffuse target, noting applicability to IR radar, heterodyne spectroscopy, etc
17 p2971 A69-32913

Pulse height distributions, gain and counting rate characteristics of two magnetic strip multipliers and two channel multipliers in 1.5 to 44 A region of soft solar X-rays
17 p2972 A69-33082

Low level beta, X and gamma radiation detector incorporating Geiger, proportional and scintillation counting features in various modes suiting radionuclide decay scheme
17 p2975 A69-33747

Lunar surface uppermost layer physical and mechanical properties investigated by soilmeter-penetrometer and radiation densimeter on Luna 13
18 p3113 A69-34239

Solar thermonuclear reactions studied by emitted neutrinos detection, plotting energy spectra for sensitivity of CI 37 detection system
18 p3185 A69-34278

Instruments for gamma ray astronomy including Ranger low energy detector, howitzer detector and cosmic spark chamber
18 p3138 A69-35135

Aircraft nucleonic fuel gauging system, using radioactive gas to emit gamma rays for fuel mass sensing
18 p3139 A69-35468

Coherent radiation detection using laser optical sine waves, considering detection by heterodyning, laser preamplifier and parametric amplification
19 p3335 A69-36070

Regenerative Josephson effect detector with feedback-narrowed far IR response as tunable millimeter and submillimeter wave radiation detector
19 p3313 A69-36417

Flat wire grid calorimeter used as radiation sensor in measuring pulsed ruby laser
19 p3339 A69-36755

Electromagnetic radiation detectors in nonphotographic sensing systems, describing performance as function of time constant, spectral response, cooling requirements and signal handling
20 p3540 A69-37736

Thermal scanner model block diagram presented including lens, filter, detector, CRT and camera, considering environmental factors affecting image character
20 p3541 A69-37740

Thermistor radiation detectors bias condition defined from equations and optimized in terms of responsivity, time constant and noise
21 p3727 A69-39782

Frequency response of thin film thermal detectors, discussing steady state harmonic response proportionality to film thickness and thermal conductivity
23 p4163 A69-41549

Cosmic ray detectors design for medium, low and very low energy events on IMP-1 spacecraft, noting PCM format
23 p4118 A69-41738

Einstein general theory of relativity and apparatus for gravitational radiation detection, discussing Dicke experiments and Riemann tensor measurement
23 p4192 A69-42331

RADIATION DISTRIBUTION

NT ANTENNA RADIATION PATTERNS

NT DIFFRACTION PATTERNS

NT SIDELOBES

Emission and frequency shift angles of antiStokes radiation from trapped filaments of laser light in liquids
01 p0114 A69-10012

Reflected and transmitted radiation fields for dielectric loaded infinite phased array of parallel plate waveguides as function of scan angle
02 p0218 A69-12326

Transverse radiation field distribution in CW laser found by geometrical optics approximation, assuming active two level medium and mode close to threshold
02 p0258 A69-12642

Ring lasers emission modes, studying nonlinearity effects on radiation field spatial-temporal distribution
03 p0437 A69-13040

Small silicon diodes to explore depth-dose distributions in water phantom of proton beams
03 p0430 A69-13481

Directional intensity of radiation emerging from top and bottom of Rayleigh scattering atmosphere
03 p0426 A69-14026

Outgoing radiation field based on interpretation of broad sector radiometer measurements made from meteorological earth satellites
04 p0627 A69-15032

Nonquadrupole nature of cosmological radio emission intensity distribution demonstrated for anisotropic homogeneous cosmological models without flat space
04 p0662 A69-15238

Large scale pattern in solar magnetic field correlated with interplanetary magnetic field
04 p0665 A69-15532

High power single mode ruby laser, using multielement rods with plane-parallel end surfaces for generating longitudinal and transverse mode
05 p0770 A69-15700

Latitudinal distribution of auroral and airglow emissions in Northern Hemisphere photometrically surveyed by jet aircraft
05 p0754 A69-16258

Active element inverse population distribution effects on laser radiation angular divergence during lower and higher oscillation modes
06 p0932 A69-16913

Slope optimization of antenna array difference radiation patterns coinciding with antenna directive gains
06 p0895 A69-17461

Flux density spectral dependence disagreement with power law for synchronous radiation mechanism for radio sources in 12.6 to 25 MHz interval
06 p1004 A69-17538

Actinometric and nephelometric data on outgoing short wave radiation obtained by Cosmos 122 satellite, tabulating cloud cover data, digital radiation data and brightness curves
06 p0952 A69-17983

Short wave radiation field reflected anisotropically from underlying surface into atmosphere calculated from brightness coefficient
06 p0952 A69-17985

Radiation profiles in ablating flat plate air-Teflon laminar boundary layer, discussing visible, UV and IR wavelengths
[AIAA PAPER 69-99] 06 p1037 A69-18086

Radiative transfer problems in inhomogeneous anisotropically scattering plane parallel planetary atmospheres with internal source distributions solved by recursive method
07 p1213 A69-18610

Green function applied to isotropic scattering of radiation in three dimensional homogeneous space
07 p1241 A69-18808

Irregularities producing partial radio wave reflection from midlatitude D region attributed to insufficient distribution
07 p1078 A69-18914

Solar photosphere model with two stream columnar representation of granulation for predicting continuous radiation field
07 p1217 A69-19238

Aircraft tire wear determination by measuring intensity of radiation originating from point source within thread, using thulium 170 isotope
07 p1143 A69-19703

Black body cavity radiation distribution as seen by observer in arbitrary uniform motion with respect to radiation mass center
08 p1380 A69-19784

Monte Carlo method applied to calculation of radiation transmission and dosage behind space vehicle shields during passage through earth radiation belt
08 p1377 A69-19843

Thermal and nonthermal radiation of hot gases using spectroscopic plasma diagnostics
08 p1363 A69-20463

Earth reflected solar radiation and stability of satellite thermal control coatings, noting intensity distribution shifting toward UV region and coatings degradation rate
09 p1579 A69-22174

Limits in applicability of earth equivalent radius to measuring microwave diffraction field in atmosphere
09 p1456 A69-22284

Radiation fields of Lyman alpha to Lyman 10 calculated for model planetary nebulas with constant and exponential density distributions in spherical symmetry
09 p1604 A69-22407

Radiation field at optical depths within plane parallel Rayleigh scattering atmosphere subjected to generalized free surface boundary conditions
09 p1606 A69-22441

Ultrashort light pulses nonlinear amplification in medium with finite transverse relaxation time and linear radiation losses
10 p1702 A69-23139

Amplification factor of He-Ne traveling wave light amplifier, discussing frequency stability and telescopic wave front broadening for uniform radiation distribution
11 p1894 A69-24623

Atmospheric scintillation effect on planetary brightness distribution over disk from photometric measurements
11 p1960 A69-24729

Two dimensional autocorrelation functions of outgoing radiation fields usable as quantitative characteristics of cloud distribution structures
11 p1913 A69-24832

Bias elimination in intensity pattern of incoherent holograms by introducing narrow band time modulation of light
11 p1885 A69-24846

Model for radiative transfer in atmosphere-ocean system by Monte Carlo method, considering Rayleigh and Mie scattering
11 p1877 A69-24851

Biological effects of cosmic ionizing radiation in supersonic commercial aircraft at high altitudes, showing spatial distribution based on balloon experiments
11 p1830 A69-24865

Radiating collinear open ended waveguides and near field coupling analyzed using simultaneous integral equations and Fourier series expansion of aperture field
11 p1850 A69-24984

Two dimensional radiation from apertures in conducting cylinders of arbitrary cross section, solving current distribution, admittances and radiation patterns
11 p1836 A69-24985

Long wave radiation fields calculations based on radiation transport equations, identifying differences between associated transmission functions
12 p1215 A69-25951

Second harmonic conversion of giant pulse Nd laser emission related to beam divergence and space-time distribution of radiation, noting energy relationship
12 p2104 A69-26022

Mode interaction in lasers with homogeneous line broadening, analyzing rate equations for radiation fields of operating modes for asymptotic values of mode intensities
12 p2106 A69-26323

Southern radio auroral zone observation with rhombic antennas, noting diffuse and discrete zones associated with proton and electron precipitation
12 p2033 A69-26950

Cosmic rays during 11-year solar cycle, short term variations and radial gradient based on Luna, Zond and Venera probes and Cosmos observations
13 p2326 A69-27351

Radiation fields and large scale atmospheric disturbances analyzed, using radiation maps from Cosmos satellites
13 p2291 A69-27727

Transport equation numerical solution for unsteady radiation field by straight lines method, allowing for scattering indicatrix forms with passage of time
13 p2350 A69-27858

Atomic and molecular spins dynamic orientation in anisotropic radiation field, examining medium properties and astrophysical consequences
13 p2350 A69-27861

Radiation field from sources on conical surface using Green functions
13 p2223 A69-28569

Solar cosmic rays diffusion enclosure in interplanetary space magnetic boundary suggested from balloon, satellite and ground observations of solar flare neutron component
14 p2513 A69-29067

Neodymium laser having adjustable pulse duration and homogeneous spatial radiation structure developed by two photon absorption

14 p2460 A69-29670

Plane electromagnetic wave refraction and scattering in solar corona during eclipsed observations of cosmic sources, calculating angular distribution of radiation intensity

15 p2688 A69-30555

Characteristics of neodymium-glass laser with unstable resonator noting transverse modes and radiation angular distribution

15 p2634 A69-30730

Relative motion of 3 K cosmic background radiation with covariant photon equilibrium distribution

15 p2657 A69-31494

Radiation diffusion in plane-parallel isothermal gas layer of two and three level atoms, considering stimulated emission and frequency redistribution

16 p2864 A69-32587

Reradiation and multiple reflection effects on radiant flux density distribution in cylindrical receivers of solar power installations

16 p2741 A69-32799

High energy cosmic ray proton, electron and photon propagation through cosmic microwave background, discussing mean free paths

16 p2852 A69-32819

Center to limb variation of solar hard X ray bursts, suggesting inverse Compton effect and bremsstrahlung from anisotropic electrons

17 p3023 A69-33055

Mode patterns and far field distribution for gas lasers operated in lowest order Gaussian transverse mode

17 p2981 A69-33090

Holographic recording of temporal coherence pattern of wave train from pulsed radiation source, investigating single mode ruby laser

17 p2973 A69-33114

Angular dependence of lunar nighttime IR radiation by invariant tensor techniques, noting surface roughness effect on radiation pattern [AIAA PAPER 69-597]

17 p3032 A69-33276

Line source excited ferrite layer radiation pattern reduced to one dimensional form by Fourier transform, obtaining angle of maximum leaky wave radiation

17 p2926 A69-33852

Extrasolar X rays and sources from studying distribution, luminosity, diameters and variability of rays

18 p3193 A69-34364

Macroscopic roughness effect on surface radiation characteristics for special cases

18 p3229 A69-34711

Local radiation characteristics calculation method, consisting of reducing integral equations to linear algebraic equations, applied to solve radiative heat exchange problems

18 p3229 A69-34713

Variable star in Large Magellanic Cloud having unusual light curve with complex maximum lasting 300 days

19 p3403 A69-35965

IR detector limiting noise voltage/phonon noise/ due to photon arrival fluctuations at responsive element determined using Planck radiation law

19 p3309 A69-36059

Numerical program for gas dynamics of hydrodynamic flow and radiation transport in diffusion and grey body approximations

19 p3450 A69-36356

Spectral line scattering during propagation of radiation in turbulent plasma

19 p3396 A69-36573

Photographic photometry investigation of Light distribution in spiral galaxies NGC 681, 972 and 1084, discussing mass distribution

20 p3599 A69-37476

M 31 nebula radio continuum survey, describing discrete sources catalog and Andromeda nebula radiation distribution

20 p3601 A69-37493

Lunar brightness variations during eclipse on 13 April 1968 measured photoelectrically, suggesting nonuniform diurnal distribution of atmospheric scatterers for observed asymmetry

20 p3601 A69-37510

Electromagnetic radiation from slot excited ground plane covered by inhomogeneous plasma layer, considering far field radiation pattern

20 p3495 A69-37852

Slope optimization of antenna array difference radiation patterns coinciding with antenna directive gains

20 p3508 A69-37944

Vertical turbulent diffusion and altitude distribution of radioactivity from short lived radon decay products in atmosphere

20 p3533 A69-38076

Atomic sources local multipolar field in anisotropic dielectrics determined from magnetic dipole radiation spatial distribution measurements

21 p3779 A69-38531

Monochromatic radiation diffusion in one dimensional bounded medium, deriving equations for probability density of quantum yield and intensity of light fluxes

21 p3769 A69-38586

Radiation field several wavelengths from dipole above plane earth, simplifying rigorous integral expression for Hertz vector by method of operators

21 p3770 A69-38748

Radiation fields from energetic electron moving in helical orbit in magnetoactive plasma, using Maxwell equations

22 p4008 A69-39965

Diffuse galactic radiation intensity and distribution from photoelectric measurements compared with radiative transfer calculations using various interstellar dust models

22 p4013 A69-40096

Surface integration technique used in conjunction with wedge diffraction theory to analyze TEM radiation patterns of parallel plate waveguides

23 p4136 A69-41581

Ionospheric perturbations generation by time variable alternating electrical currents at polar latitudes, constructing radiation patterns for gravitational waves

23 p4155 A69-41842

Anomalies of isotropic cosmic ray secular variations at high latitudes based on supermonitor neutron data

23 p4206 A69-41854

Numerical methods for radiation transport for inviscid stagnation flows, detailing spectral nature of radiation emission and absorption [AIAA PAPER 68-664]

23 p4059 A69-41890

Optimum design of spherical and ellipsoidal pumping chambers for solid state lasers determined from numerical calculation of radiation transfer efficiency

24 p4327 A69-42986

RADIATION DOSAGE

Surface dose rate and depth dose distribution for materials used for space vehicle and biological tissue protection from cosmic and internal radiation [UN PAPER 68-95260]

01 p0144 A69-10477

Nuclear radiation dose rate and atmospheric ionization from radioactive fallout and natural sources, discussing fallout effect on population

01 p0145 A69-10982

Inner Van Allen belt proton dose rate and spectral charged particle environment profiles correlated, noting agreement with theoretical values

01 p0145 A69-11081

Chronic gamma radiation biological damage in rats exposed to maximum nonlethal to minimum lethal doses for various periods

02 p0197 A69-11494

Solar flare radiation hazard in long duration space flight, discussing radiation distribution and dosage in human body

03 p0371 A69-13480

Small silicon diodes to explore depth-dose distributions in water phantom of proton beams

03 p0430 A69-13481

Radiation effects in man, searching for dose relationships in prodromal syndrome

03 p0374 A69-13503

Public health aspects of galactic radiation exposure at supersonic transport altitudes

03 p0375 A69-14072

Gamma radiation effects on transistors and diodes, discussing dosage and thermal changes within operational temperature range of germanium devices

05 p0728 A69-15695

High energy proton and neutron fluxes and spectra from nuclear emulsion stacks on Cosmos satellites, calculating cosmic radiation doses

05 p0814 A69-16051

Permissible radiation doses for extended space missions, discussing clinical tests on dogs

05 p0708 A69-16508

Kinetics of homogeneous and heterogeneous growth of centers of new phase of semiconductor during ion bombardment as function of radiation dose

06 p0978 A69-16985

Solar flare radiation protection requirements, considering bulk and plasma radiation shielding [AIAA PAPER 69-15]

06 p0884 A69-18079

Particle flux and dose rates in Jupiter Van Allen belts based on assumed synchrotron radiation from trapped electrons in dipole magnetic field [AIAA PAPER 69-18]

06 p0997 A69-18129

Solar cosmic ray dose rate and total dose magnitude predictions based on Epeak and isotropic diffusion models [AIAA PAPER 69-14]

06 p0997 A69-18160

Radiation measurements inside Apollo 4 and 6 command modules during passage through trapped radiation belts [AIAA PAPER 69-17]

06 p0884 A69-18202

Energy deposits from decay of tritium incorporated into bacteria, using computer simulation for radiation dose distribution

07 p1068 A69-19490

Permissible irradiation doses established for spacecraft crews making short and long flights, considering roles of life span, somatic effects, leukemia and genetics

07 p1069 A69-19618

Monte Carlo method applied to calculation of radiation transmission and dosage behind space vehicle shields during passage through earth radiation belt

08 p1377 A69-19843

Rabbit corneal damage thresholds for Gaussian beams of carbon dioxide laser IR radiation at various exposure times

11 p1830 A69-24844

Calculation of radiation doses in space - Conference, Toulouse, France, February 1968

11 p1947 A69-24854

Cosmic ray cut-off energy for synchronous satellites computed by trajectory tracing method using magnetospheric model

11 p1949 A69-24860

Electron and proton radiation doses impinging on orbiting satellites computed using orbit calculation and B, L coordinates

11 p1949 A69-24862

Computer program for electron and proton fluxes impinging on spacecraft, performing computation for Van Allen belts and solar flares

11 p1949 A69-24863

Supersonic aircraft radiation hazard due to solar flare proton exposure, using Monte Carlo method to estimate dosage as function of tissue slab

11 p1949 A69-24864

Biological radiation doses and protection from galactic, solar particle and trapped radiation in space, noting secondary radiation and bremsstrahlung in absorber

11 p1831 A69-24866

D-2 satellite radiation dose based on upper atmosphere electron and proton distribution model, simulating electron bombardment and aging of materials and subsystems

11 p1949 A69-24869

Radiation dose and radioactive isotopes induced in astronaut body by cosmic rays of various energies

11 p1831 A69-25463

Radiation dosimetry and shielding onboard Cosmos 110 artificial satellite, noting earth belt proton radiation

13 p2356 A69-27702

Admissible radiation doses for space crews and ionizing radiation protection, studying long term radiation effects on dogs

15 p2557 A69-31344

Proton dose in receiver behind combination electromagnetic and material shield, calculating dose for Van Allen and solar proton event spectra

15 p2652 A69-31522

Ground based solar proton monitoring, considering particle intensities and radiation dose rates from riometer absorption as function of time

16 p2850 A69-32321

Free radicals destruction rates by gamma irradiation at 77 K measured as first order function of dosage, using electron spin resonance spectroscopy

19 p3265 A69-36376

Supralethal doses of pulsed mixed gamma-neutron radiations from TRIGA reactor administered to unshielded, head shielded and trunk shielded beagles

19 p3259 A69-36459

High energy proton and neutron fluxes and spectra from nuclear emulsion stacks on Cosmos satellites, calculating cosmic radiation doses

20 p3591 A69-37961

Single large X ray dose depressive effect on aminotransferase activity in rabbit blood serum, liver, kidney, heart, spleen, lungs, etc

21 p3657 A69-39051

Single X ray dose effect on alpha-amylase and alpha-glucanophosphorylase in rabbit liver tissues and blood serum
21 p3658 A69-39055

White rats hyperglycemia during blood sugar changes following single X ray dose, indicating increased sugar benefit in radiation damage treatment
21 p3658 A69-39057

Histological changes in internal organs of rats after exposure to 400 r fast neutron dose, showing destructive processes followed by compensation reactions of cellular proliferation
21 p3659 A69-39062

Air ionization and beta and gamma dose rates measurements for natural radiation from cosmic rays compared to nuclear weapons tests fallout, considering biological effects
22 p4007 A69-40915

Absorbed dose and dose equivalent radiation rates at various depths in atmosphere due to proton spectrum of energetic solar flare
23 p4204 A69-41337

Exposure rate influence on mechanical properties of polymer binder cross-linked by gamma radiation exposure from cobalt isotope source
23 p4179 A69-41711

RADIATION EFFECTS

NT RADIOLYSIS

Cosmic radiation interactions with living viruses, considering X ray effects and optimal radiation dosage for cancer cell destruction
01 p0013 A69-10157

Electron cyclotron harmonic waves in magnetoplasma irradiated by external microwaves
01 p0127 A69-10335

Electron production rate and density created by galactic and solar cosmic rays in lower D region, considering ionization for PCA
01 p0063 A69-10426

Photographic film blackening under high intensity laser radiation indicating two photon mechanism as responsible
01 p0080 A69-10429

Irradiation influence on chromium transition temperature explained by defect clusters and embrittling impurity redistribution
01 p0095 A69-10604

Irradiation influence on yield stress of Ni-Al intermetallics noting temperature dependence and electron dosage
01 p0095 A69-10608

Photochemistry and radiation chemistry - Conference, Natick, Massachusetts, April 1968
01 p0024 A69-10617

Long lived low level chemiluminescence due to gaseous reactions at low concentrations induced by mercury lamp irradiation or Tesla coil discharge
01 p0024 A69-10618

Sulfur trioxide production in photolysis of sulfur dioxide at 1849 angstroms, noting oxygen addition effect on quantum yield
01 p0024 A69-10619

Photodegradation of organic polymers by UV radiation exposure, emphasizing polyvinyl chloride photochemistry and radiation stabilization
01 p0102 A69-10861

Photoinhibition of cell division and growth in Euglenoid flagellates by fluorescent and incandescent visible light
01 p0014 A69-10903

Cosmic radiation genetic, cytological and histological changes, particularly of pathological nature, on ecological systems employed in long duration Soviet manned flights
01 p0016 A69-10948

Nuclear radiation dose rate and atmospheric ionization from radioactive fallout and natural sources, discussing fallout effect on population
01 p0145 A69-10982

Shock layer gas radiation influence on deep space missile shape, noting evaluation by flow equations
01 p0007 A69-11070

UV and visible light interaction effect on biological activity of Paramecia unicellular infusoria, noting cell division rates and cell deaths
01 p0017 A69-11085

Lethal effect of solar UV radiations on dried Coliphage T-1 exposed to space at sounding rocket altitudes
01 p0017 A69-11086

Terrestrial microorganism survival in space aboard Gemini satellite, discussing lethal effects of solar radiation
01 p0018 A69-11087

Ionospheric and stratospheric UV radiation effects on survival of microorganisms
01 p0018 A69-11088

Electron irradiation induced damage in undoped GaSb single crystals at 77 K, noting dependence on energy and orientation
01 p0141 A69-11256

P32 distribution in protein of blood serum, liver and brains of rats bombarded with high energy protons
02 p0198 A69-11507

Mathematical models for Chlorella cell and biomass growth under illumination during space flight, noting ionizing radiation presence
02 p0198 A69-11508

Hypersonic gas flow past blunt body problem solved by integral correlation method, taking into account radiation effects and gas dynamic parameter distribution in shock wave layer
02 p0188 A69-11651

Thermal radiation effects on two dimensional steady MHD jet of conducting ionized gas confined by magnetic field
02 p0287 A69-11831

Radiation and electrical precursor effects in expansion tube of electromagnetic shock tube, discussing primary causes
02 p0229 A69-11936

Neutron and gamma irradiation effects on CdS crystals structure and properties, outlining electron energy level scheme
02 p0298 A69-12119

Nuclear radiation damage vs thermal decomposition of diaminitrobenzene and hexanitrostilbene, analyzing unchanged residual compound
02 p0304 A69-12500

Radiation effect enhancement in supersonic plasma jet cooled by rapid expansion, giving energy equation for electron cooling rates to analyze electron temperature
02 p0292 A69-12557

Radiation damage in CdS irradiated by normal mode or Q-switched ruby laser, discussing stimulated Brillouin scattering
02 p0257 A69-12614

Information theory application to study of biologically stimulating effects of low ionizing radiation doses, thermal energy and other environmental factors
03 p0369 A69-13434

Small silicon diodes to explore depth-dose distributions in water phantom of proton beams
03 p0430 A69-13481

Slow proton irradiation of ribonuclease thin layers, determining differential inactivation cross section for various proton energies
03 p0371 A69-13482

Inactivation by heavy ions of esterase activity of dried trypsin as function of temperature during irradiation
03 p0372 A69-13483

Long lived radicals produced in crystalline ribonuclease and lysozyme by 120-Mev protons studied by ESR spectroscopy
03 p0372 A69-13485

Trapped radical relationship to inactivation of trypsin exposed to UV by measuring radical concentration and inactivation degree
03 p0372 A69-13486

UV induced excited-state properties of DNA using optical emission and electron spin resonance methods
03 p0372 A69-13488

Genetic effects in yeast induced by heavy ion radiation, studying lethality, mitotic segregation, allelic recombination and reverse mutation
03 p0373 A69-13491

Biological effects of proton irradiation of monkeys investigated to provide improved protective shield design data with minimum weight penalty
03 p0373 A69-13496

Acute somatic effects in monkeys irradiated with protons of various discrete energies representing significant portions of space proton spectrum
03 p0374 A69-13497

Biological effects on rhesus monkeys of high energy protons compared to effects of cobalt 60 gamma radiation
03 p0374 A69-13498

Mammalian radiobiological studies of effects of heavy particles, discussing therapeutically advantageous characteristics
03 p0374 A69-13499

Biological effects in man due to heavy particles emission during major solar cosmic ray events, noting protective effect of human body
03 p0374 A69-13500

Radiation effects in man, searching for dose relationships in prodromal syndrome
03 p0374 A69-13503

Electrical resistance temperature dependence below room temperature for polycrystalline epitaxially grown Au and Ag films, noting effects of alpha irradiation
03 p0486 A69-13582

High energy X ray irradiation of head of Macaca mulatta, determining effect on cerebral blood flow and blood pressure
03 p0376 A69-14075

Aircraft cockpit and surface temperatures after solar radiation exposure in desert, showing inadequacies of meteorological data for thermal stress predictions
03 p0381 A69-14077

Reflection indicatrices of aluminum oxide, MgO, Au and Pt surfaces for normal irradiation noting temperature and surface treatment effects
03 p0534 A69-14161

Optical materials behavior after irradiation by high energy electrons, gamma rays or protons
03 p0493 A69-14190

Neodymium glass properties degradation during laser operation due to short wave pumping radiation and stimulated emission
03 p0442 A69-14219

Luminescence spectra due to radiative recombination of optically injected carriers in Co 60 gamma ray and neutron irradiated Si at low temperature
03 p0494 A69-14243

Explosive containment capsule for nuclear reactor irradiation
04 p0629 A69-14480

Radiation effects on III-V compounds, considering damage in solar cells and luminescence, light emitting and Esaki diodes
04 p0641 A69-14504

Radiation processed wood-plastic materials produced by impregnating natural wood with liquid monomer followed by ionizing radiation induced polymerization
04 p0605 A69-14582

Monograph on radiation gas dynamics, thermal radiation, applied spectroscopy and ablation and applications in high speed atmospheric entry
04 p0685 A69-14597

Burning rate of composite propellant with gamma irradiated ammonium perchlorate, noting enhancement at atmospheric pressure
04 p0647 A69-15519

Pulse radiation effect on dielectric constant of sintered CdS photoresistors, discussing capacitance dependence on intensity, type and frequency of light
05 p0806 A69-15694

Gamma radiation effects on transistors and diodes, discussing dosage and thermal changes within operational temperature range of germanium devices
05 p0728 A69-15695

Microorganisms and viruses susceptibility to sterilization by ionizing radiation, heat and combination of radiation and heat, considering space materials damage elimination
05 p0713 A69-15947

Earth radiation effect on space vehicle, using diffusely radiating sphere model
05 p0824 A69-16053

Polymer films tensile properties after exposure to gamma radiation in vacuum, noting chain scission and cross linking
[ASME PAPER 68-WA/RP-6]

Nuclear radiation influence on pool boiling heat transfer to liquid helium, using irradiated copper as boiling surface
[ASME PAPER 68-WA/PID-3]

Space flight factors, ionizing radiation and combined effects on vitamin C content in onion bulbs
05 p0791 A69-16164

Radiosensitivity of potatoes to gamma ray and proton irradiation applied to whole tubers and to isolated eyes before planting
05 p0708 A69-16510

Electric field effects on thermal annealing of electron irradiation damage in p-channel MOSFET device
05 p0733 A69-16562

Interaction between point defects and magnesium atoms in aluminum irradiated by neutrons, analyzing magnesium concentration effect on recovery
05 p0781 A69-16613

Nuclear and space radiation effects - IEEE Conference, University of Montana, July 1968
06 p0973 A69-16861

- Radiation defects stability in semiconductors, noting low temperature electron irradiation of Ge and effects of annealing 06 p0974 A69-16863
- Carrier scattering from defects in neutron irradiated semiconductors, noting mobility and relaxation time 06 p0974 A69-16864
- Recovery of carrier concentration and lifetime in n- and p-type Si during annealing after irradiation by 10 Mev electrons, noting impurities effects 06 p0974 A69-16865
- Recovery rate at room temperature in Li-doped p-n Si diodes and solar cells after 1 Mev electron irradiation, noting capacitance changes 06 p0974 A69-16867
- Neutron irradiation produced defects in p-type Si at 76 K, measuring Hall effect and electrical conductivity 06 p0975 A69-16868
- Majority and minority carrier trapping in neutron irradiated Si diodes, measuring transient junction capacitance recovery 06 p0975 A69-16869
- Neutron irradiated Si transistors radiation and annealing characteristics determined for inverse configuration 06 p0975 A69-16872
- Nearly abrupt X band Si avalanche IMPATT diodes irradiated by fast neutrons, noting effects on DC and microwave characteristics 06 p0976 A69-16874
- Neutron radiation effects on MOSFET, presenting model for neutron produced ionization in oxide layer 06 p0976 A69-16875
- Gamma radiation effects on gate threshold voltages in modified oxide insulators in MOS structures 06 p0976 A69-16876
- Electron radiation damage in MOSFET devices using bias temperature treatments 06 p0976 A69-16877
- Recovery and long term reliability of Si n-p-n transistors subject to gamma radiation, using military specifications for failure 06 p0976 A69-16878
- Prediction technique for surface effect causing Si bipolar transistors gain degradation under ionizing radiation 06 p0976 A69-16879
- Gain degradation under applied voltage and injection current during low dose gamma irradiation by Co-60 source for bipolar transistors 06 p0977 A69-16880
- Temperature effects on primary photocurrent of base collector and collector substrate junctions of isolated transistors from microcircuits 06 p0977 A69-16881
- Radiation effects on NERVA out-of-core instrumentation, discussing cryogenic temperature measurements and transducer measuring pressure at gamma heating rates 06 p0956 A69-16882
- Inverted transistor parameters required for accurate prediction of electrical and radiation storage time, discussing computer predictions of radiation responses 06 p0977 A69-16884
- Models to predict transient radiation responses in microcircuits, discussing model accuracy for junction and dielectrically isolated circuits 06 p0977 A69-16887
- Combined neutron degradation and gamma induced effects on closed loop system simulated by SECURE program 06 p0899 A69-16889
- Neutron and X ray radiation effects upon gallium arsenide devices including Gunn oscillators, transistors, Schottky barrier diodes and optoelectronic pulse amplifiers 06 p0978 A69-16890
- Radiation tests on Ovonic threshold switches performed with fast neutrons and broadband X rays 06 p0978 A69-16891
- Nuclear pulsed radiation dosimeter based on strain gage measurement of induced thermal expansion, noting separation of neutron and gamma ray components 06 p0922 A69-16892
- Spectral line shapes broadened by electron impacts, taking into account contribution of radiation produced by perturbing electrons 06 p0961 A69-17136
- Space radiation effect on spacecraft components and materials simulated by proton and fast electron bombardment of silicon, glass and skin materials 06 p0906 A69-17612
- Electron formation in lower ionosphere due to cosmic ray-atmosphere interaction, analyzing ionization of subrelativistic and relativistic solar and galactic cosmic rays 06 p0920 A69-17726
- Electron irradiation annealing and modification of 35 and 65 K defects in n-type Ge induced by 1 Mev electrons at low temperature 06 p0980 A69-17757
- Temperature dependence of laser induced damage in plastic Q switch made of polyethylmethacrylate and vanadyl phthalocyanine for ruby laser 06 p0936 A69-17777
- Distribution characteristics of radiation defects in materials irradiated by monoenergetic beams of protons and alpha particles 06 p0981 A69-17878
- Flour beetle under irradiation and weightlessness during space flight, analyzing effects on somatic wing development, germ cells and pupal period 06 p0876 A69-18177
- Storable tubular extendible member (STEM) booms for gravity gradient applications, emphasizing reflective coatings to minimize deflection by solar radiation 07 p1226 A69-18327
- Approximate solution to differential equations describing primary radiation defects transformation into secondary defects in semiconductors 07 p1199 A69-18679
- Hypersonic flow past blunt body near stagnation point, noting surface layer characterized by increased density and decreased entropy of gas 07 p1050 A69-18755
- Boundary value problem of temperature field and heat conduction in transparent media heated by laser radiation producing thermoelastic stresses leading to breakdown 07 p1149 A69-18925
- Vacuum, radiation and freeze drying effects on survival rate of microorganisms, noting influence of protective materials on extent of damage 07 p1064 A69-18943
- Permissible irradiation doses established for spacecraft crews making short and long flights, considering roles of life span, somatic effects, leukemia and genetics 07 p1069 A69-19618
- Inhibition of gamma ray induced DNA degradation by infection with bacteriophage 07 p1069 A69-19709
- Radiation effects on integrated circuits, stressing components design for maximum tolerance 07 p1113 A69-19779
- Bone marrow distribution in dogs as basis for study of compensatory reactions of hemopoietic organs in response to radiation damage 08 p1262 A69-19835
- Propyl gallate radiation shielding effect variations with proton and gamma ray bombardment, noting growth and development of potato tuber eyes 08 p1262 A69-19927
- Local shielding effectiveness of dogs against proton irradiation at minimum lethal dose, noting bone marrow role 08 p1263 A69-19939
- Transparent dielectrics destruction by laser radiation noting stress development in medium 08 p1324 A69-19947
- Linivll model for describing elementary phenomena of electronic equipment in terms of physical data applied to irradiated semiconductor diode and transistor 08 p1280 A69-19974
- Highly ionized low density plasmas production by strong UV radiation 08 p1360 A69-20080
- Synergistic effects of prolonged heat exposure and whole body irradiation with ionizing radiation on survival time in hamsters 08 p1263 A69-20174
- Collection of papers on thermal problems in aerospace medicine covering intense heat, cutaneous vasomotor and sudomotor control, water immersion, etc 08 p1263 A69-20667
- Aircrew members skin temperature changes in response to intense diffuse thermal radiation, noting psychological response to exposure [AGARDOGRAPH-111] 08 p1264 A69-20669
- Thermoregulatory reactions of human body to sharp increase of ambient radiant temperature [AGARDOGRAPH-111] 08 p1264 A69-20670
- Skin and subcutaneous temperature during exposure to intense thermal radiation, discussing estimation of subcutaneous temperature from skin temperature data [AGARDOGRAPH-111] 08 p1264 A69-20671
- Thermal radiation effects on cutaneous vasomotor and sudomotor control of human organism [AGARDOGRAPH-111] 08 p1265 A69-20672
- Protection against burn producing intense thermal exposures, noting double layer of fire resistant material [AGARDOGRAPH-111] 08 p1266 A69-20674
- Human reactions to increasing heat exposure, noting thermoregulation and metabolic and evaporative heat loss [AGARDOGRAPH-111] 08 p1265 A69-20675
- Biological effects of laser radiation on mammalian retina, noting thermal injury [AGARDOGRAPH-111] 08 p1266 A69-20676
- Microwave radiation effects on body weight and peripheral blood hemograms of mice, discussing maximum safe exposure related to generator output 08 p1266 A69-20678
- Visceral lesions observed in mice and rats exposed to ultrashort waves indicating no pathological modification of physiology of reproduction [AGARDOGRAPH-111] 08 p1266 A69-20679
- Nongray radiation effects on compressible turbulent free jet mixing of nonsimilar gases, using stepwise spectral absorption coefficient and Beer law 08 p1253 A69-20844
- Ionizing radiation effects on space charge of MOS devices, showing electron-hole pairs within oxide and electron injection from cathode 08 p1373 A69-20864
- Meteorites radiogenic and cosmic ray exposure ages, orbits and parent bodies, discussing H and L group chondrites 08 p1405 A69-20928
- Ablation rate of Saint-Severin amphoterite based on heavy primary cosmic ray track densities in surface samples 08 p1406 A69-20933
- Luminous discharge at nonabsorbing surface when exposed to single pulse ruby laser beam, suggesting photoionization in surface layer 08 p1327 A69-21021
- Angular distribution of photon radiance of spherical satellite irradiated by Lambertian earth, assuming nonemissive satellite 08 p1311 A69-21095
- Electron bombardment effects on performance characteristics of UV gratings 08 p1318 A69-21097
- Alkali halide crystals destruction by laser radiation for estimating optical strength, discussing impact ionization hypothesis 08 p1328 A69-21188
- Solid state laser radiation damage in polymers during tensile and compression loads using microstructural analysis 08 p1328 A69-21190
- Dislocation channeling process in polycrystalline Nb subject to tensile deformation after neutron irradiation 09 p1521 A69-21345
- Photoelectric ejection of grain electrons by solar quanta balance with solar wind electron capture by grain for interplanetary grain equilibrium potential 09 p1593 A69-21655
- Upper atmospheric density relation to AE indices sum and solar radio flux during geomagnetic disturbances 09 p1488 A69-21657
- Electron irradiation effect on surface potential of thermally grown silicon dioxide layers, noting conductivity and annealing effects 09 p1557 A69-21743
- Earth reflected solar radiation and stability of satellite thermal control coatings, noting intensity distribution shifting toward UV region and coatings degradation rate 09 p1579 A69-22174
- Electron beam radiation curing of mercaptan terminated butadiene-acrylonitrile liquid copolymers at ambient temperatures in air 09 p1512 A69-22368
- X ray irradiated dogs subjected to heat stresses to determine thermoregulatory ability 09 p1445 A69-22548
- Pulsed and CW microwave power effects on rabbit eyes, noting lens opacities produced 10 p1648 A69-23185
- Chemical and biological means of safeguarding body of astronaut against ionizing radiation and vibration 10 p1648 A69-23297
- Alkali halide single crystals disintegration by laser radiation differs as function of crystal physicochemical properties and band structure 10 p1745 A69-23322

IR radiation effects in cadmium sulfide crystals with green edge emission at low temperatures, discussing luminescence, photoconductivity and conductivity glow curves

10 p1746 A69-23565

Stress effect on laser damage crack orientation in transparent organic dielectrics, estimating gas pressure in cracks

10 p1703 A69-23621

Electron bombardment produced clustered displacements, paired vacancies and interstitial atoms in Si, discussing possible mechanism for developing defects

10 p1747 A69-23713

Early disturbances in active migration of potassium 42 ions in irradiated erythrocytes in rats, showing relation between influx and energy exchange in cells

10 p1647 A69-23966

Polyesters reaction with dimethyl p-phenylene diamine compared under UV exposure from carbon arc and natural sunlight

10 p1716 A69-23978

Annealing temperature of radiation defects in phosphorus doped silicon, discussing isochronal recovery characteristics of solar cells with different donor and oxygen concentrations

10 p1747 A69-24006

Soviet book on space radiobiology, discussing somatic effects, influence of flight factors, relative biological effectiveness of various radiations and radiation safety

11 p1827 A69-24263

Threshold criteria of gas phase thermal ignition for cellulose materials, considering heating by radiant energy

11 p1940 A69-24474

High energy radiation effects on electronic components in space missions, noting simulation tests and shielding

11 p1946 A69-24521

Nonthermal intergalactic bremsstrahlung model as isotropic X ray background due to subcosmic electron interactions with thermal ionized gas in expanding universe

11 p1947 A69-24595

Probability of ocular damage for illumination by pulsed laser beam transmitted through atmosphere, developing safety nomograph for eye hazard analysis

11 p1830 A69-24843

Rabbit corneal damage thresholds for Gaussian beams of carbon dioxide laser IR radiation at various exposure times

11 p1830 A69-24844

Biological effects of cosmic ionizing radiation in supersonic commercial aircraft at high altitudes, showing spatial distribution based on balloon experiments

11 p1830 A69-24865

Solar cells degradation by charged particles in space, considering protection by filter, silicon properties and use of cadmium cells

11 p1825 A69-24870

Electron, proton and gamma ray radiation effects on thin film CdS, GaAs and CdTe solar cells

11 p1825 A69-24872

Drift and tunnel effect of MOS transistors under ionizing electron and X ray irradiation, considering fabrication, electrical characteristics and D-2 satellite tests

11 p1848 A69-24873

Planar transistor gain degradation under weak ionizing radiation, considering operating voltage and temperature conditions

11 p1848 A69-24874

Laboratory simulation methods for cosmic nuclear radiation, discussing dosimetry methods

11 p1862 A69-24875

Single crystal solar cell degradations in space, duplicating radiation effect on minority carriers lifetime by laboratory tests

11 p1826 A69-24876

Lasers applied to simulation of effects of X ray or gamma ray bursts on semiconductor devices

11 p1896 A69-24877

Spherical and rod-plate spark gap response voltage as function of sawtooth wave, cosmic, gamma and UV radiation

11 p1851 A69-25086

Ionizing radiation effects on combustion of ammonium perchlorate compacts with and without fuel addition, considering X ray, electron and plasma radiation

11 p1941 A69-25194

Microorganism survival in space for exposure to solar UV radiation on balloons, rockets and satellites

11 p1828 A69-25457

Abiogenic synthesis of prebiological membranes under assumed primitive earth conditions by UV radiation of alkanes on phosphate and Mg ions aqueous solutions

11 p1828 A69-25462

Calcite crystals stability anisotropy to ruby laser radiation, studying threshold power as function of beam polarization

11 p1900 A69-25553

Laser radiation in vacuum effects on metals and alloys

11 p1906 A69-25684

Gas ionization by UV radiation emitted by pellet, target or portion of gas in laser beam focus, using polished metallic mirrors

11 p1901 A69-25754

Resonance radiation output effect on electron distribution according to energies and concentration in low temperature plasma, solving relevant kinetic equations

11 p1935 A69-25757

Laser beam damage in glass blocks, noting high speed photographic study and absorption of light by inclusions

12 p2117 A69-26193

Morphological microchanges in solar plexus ganglia of white rats after X irradiation

12 p2019 A69-26347

Soviet monograph on nuclear radiation effect on structure and properties of metals and alloys covering electron, gamma and neutron radiation

12 p2114 A69-26469

Solar flare proton radiation effects on earth satellites and solar probes, considering sunspot cycle 20, earth magnetic field shielding and Van Allen radiation belts

12 p2151 A69-26873

Neutron irradiated Nb single crystals tensile tested over temperature range, discussing athermal radiation hardening

13 p2275 A69-27368

MOS and junction transistors damage due to radiation, noting decrease in collector current under fast neutron dose

13 p2227 A69-27514

Frenkel defects in light irradiated p-type InSb single crystals at subthreshold radiation energies

13 p2318 A69-27885

Outgassed condensation effects in vacuum on magnesium difluoride overcoated UV irradiated Al mirrors, including temperature effects, Lyman alpha reflectance and IR analysis of deposits

13 p2299 A69-28015

Sublethal ionizing radiation doses effect on hemolytic immunocompetent spleen cells in mice upon using chemical radiation protectors

13 p2210 A69-28334

Forward current decrease in Si mesa diodes under fast neutron irradiation ascribed to increase in base resistance

13 p2236 A69-28549

Radar antenna radiation effects on man and biological material dependent on absorption degree and emission characteristics including wavelength, peak and mean power

13 p2215 A69-28597

Distribution characteristics of radiation defects in materials irradiated by monoenergetic beams of protons and alpha particles

14 p2503 A69-28787

Book on defects and radiation damage in metals covering collision cascades, point defects clustering and impurities behavior

14 p2503 A69-28889

Radiation damage in yeast cells irradiated by high energy C 12 ions evaluated from survival rate study

14 p2406 A69-28915

Ruby laser beam effects on CdS crystals optical properties, measuring absorption spectrum and light dispersion in crystal

14 p2457 A69-28999

Optical rectification effect in lithium metaniobate crystals under neodymium laser radiation, comparing results with data for potassium dihydrophosphate crystals

14 p2458 A69-29168

Sirene 302 thermionic converter lifetime during irradiation in Triton immersion pile, considering effects on conversion efficiency

14 p2481 A69-29198

Cylindrical in-core thermionic converters performance and life tests, discussing diode design, operation data and irradiation studies

14 p2399 A69-29199

Postirradiation investigation of uranium dioxide fuelled thermionic emitters by evaluating released fission gases, noting different neutron fluxes metallurgical effects

14 p2481 A69-29200

Radiation effects on Cs thermionic converter, discussing radiation interaction with alkaline atoms to complete space charge neutralization by supplementary ion creation

14 p2404 A69-29261

Histological changes in rat skin after 13 Mev proton irradiation, evaluating biopsies in tissue culture

14 p2407 A69-29299

Solar radiation pressure effects on satellite models in circular equinoctial orbits

14 p2522 A69-29595

Radiative effect on rotating gaseous magnetic mass stability in thermodynamic equilibrium, including small oscillations stability

14 p2522 A69-29596

Heat transfer at gas flow stagnation point past blunt body under radiation from air layer in shock wave wake, using gray gas model

14 p2390 A69-29614

Solar UV radiation effects on processes in comet head, interpreting surface brightness distribution of comet 1959k in terms of photodissociation

14 p2525 A69-29717

Neutron irradiation effect on efficiency and other parameters of IMPATT diode

14 p2423 A69-29761

Slow neutrons irradiation compensated high resistivity p-InSb current instability

15 p2666 A69-30058

Protostars collapse and flare up computations, including radiative and convective energy flow terms in hydrodynamic equations of motion

15 p2680 A69-30206

Radiation effect enhancement in supersonic plasma jet cooled by rapid expansion, giving energy equation for electron cooling rates to analyze electron temperature

15 p2658 A69-30254

Computer codes describing nuclear weapons effects associated with X ray transport, neutron transport and X ray interactions with material, fireball, blast environments, etc

15 p2652 A69-30381

Mortality kinetics of *Drosophila melanogaster*, comparing effects of gamma radiation-induced life shortening and natural aging

15 p2555 A69-30444

MOS devices for radiation environments utilizing aluminum oxide as gate insulator for developing resistance to radiation damage

15 p2577 A69-30595

Planar bipolar transistors degradation under thermal and ionizing radiation stresses, analyzing surface recombination currents of silica films and silica-silicon interfaces

15 p2625 A69-30826

Electrical parameters measurement for homogeneous batches of planar silicon transistors subjected to cobalt 60 gamma rays, considering isochronal and isothermal annealing

15 p2625 A69-30827

High temperature effects on electron and X ray irradiated MOS transistors for space charge analysis and defects in silica films

15 p2625 A69-30828

MIS devices with dielectric properties avoiding positive space charge formation, discussing radiation effect

15 p2625 A69-30829

Logic family with low power consumption subjected to 1 Mev electrons analyzed within telemetry circuit concept for space application

15 p2625 A69-30830

Unitary sorting influence on reliability of planar transistors subjected to irradiation recovery cycles and scaled stresses

15 p2626 A69-30834

Passive components reliability subjected to ionizing radiation for families, types, batches and individuals

15 p2627 A69-30838

Thermal radiation effects on subsonic flow of ideal gray gas, calculating streamwise variations of flow properties

15 p2717 A69-30908

Radiobiology of *Tradescantia* clone orbited in Biosatellite 2, analyzing space effects on spontaneous and radiation induced mutation and cytological changes

15 p2556 A69-31321

- Admissible radiation doses for space crews and ionizing radiation protection, studying long term radiation effects on dogs
15 p2557 A69-31344
- Escherichia coli B/r survival in high vacuum at different temperatures irradiated with UV or X rays tested as colony forming ability
15 p2557 A69-31388
- Mathematical solutions of Einstein cosmological equations for radiation universe, discussing model limitations for universes older than 5-6 billion years
15 p2700 A69-31496
- Microwave induced ionization wave propagation in rare gases, noting rapid electron density increase at wave front and subsequent slow plasma decay
16 p2818 A69-31671
- Lasing influence on electron energy distribution in gas discharge measured with Langmuir probe, showing electron-electron interaction insufficient to maintain equilibrium
16 p2796 A69-31772
- Gravitational effect of electromagnetic radiation evaluated on test particle using Einstein field equations
16 p2812 A69-32049
- Shock wave propagation in isothermal atmosphere, discussing radiation and ionization effects on thermal jump
16 p2858 A69-32207
- Solar corpuscular and UV radiation variation relationship to midlatitude airglow intensity in O I line
16 p2850 A69-32322
- Radiation effect on inorganic solids isothermal decomposition induction period, deriving equations for conditions representing various kinetics combinations during irradiation
[WSCI PAPER 69-21] 16 p2832 A69-32359
- Radiation and multiple reflection effects on radiant flux density distribution in cylindrical receivers of solar power installations
16 p2741 A69-32799
- Dielectric breakdown thresholds and cavitation in organic liquids observed during Q switched and pulsed ruby radiation
17 p2979 A69-32826
- Neutron bombardment and ionizing radiation resistance of aluminum oxide MOS devices using gate insulator fabricated by plasma anodization
17 p2935 A69-32888
- Myocardial changes in rabbits after general chronic ionizing irradiation attributed to lower cardiac activity, hypotrophy and dystrophy
17 p2906 A69-32929
- Corneal epithelium chromosome rearrangements in gamma irradiated white adult mice, noting radiation dosage and duration
17 p2907 A69-32944
- Aluminum capsule used in test reactor to irradiate explosive and propellant samples, determining radiation effects
17 p3004 A69-32945
- Simulated solar wind environment effects on zinc oxide/potassium silicate and lanthanum oxide/potassium silicate spacecraft thermal control coating pigments
[AIAA PAPER 69-642] 17 p2991 A69-33273
- UV irradiation effects on ZnO spacecraft thermal control coating pigments, discussing photo-Hall, luminescence and electron paramagnetic resonance measurements
[AIAA PAPER 69-639] 17 p2992 A69-33288
- Gas products evolved from selected thermal control coating materials during UV radiation in vacuum, noting permanent reflectance loss
[AIAA PAPER 69-640] 17 p2992 A69-33289
- Nonuniform wall radiation production of radiative equilibrium temperature and flux distributions in gray medium, discussing various approximation methods of solution
[AIAA PAPER 69-633] 17 p3072 A69-33294
- Electron energy effects on reflectance degradation and recovery of thermal control materials in vacuum, reporting test results for various protective coatings
[AIAA PAPER 69-643] 17 p3005 A69-33306
- Cosmic ionizing radiation effects on electronic elements operation based on radiation and matter interaction principles
17 p2937 A69-33583
- X irradiation and temperature effects on flour beetle/Tribolium confusum/ pupae, noting wing abnormalities and pupal stage duration
17 p2910 A69-33748
- Fast neutron irradiation effect on niobium nitride current carrying capacity, showing enhancement
17 p3008 A69-33765
- Damage thresholds to ocular tissues from laser radiation, presenting comparative theoretical curves and recommended safe working levels
18 p3097 A69-34312
- Space flight factors, ionizing radiation and combined effects on vitamin C content in onion bulbs
18 p3095 A69-34729
- Radiosensitivity of potatoes to gamma ray and proton irradiation applied to whole tubers and to isolated eyes before planting
18 p3095 A69-34730
- Radiation effects produced by high temperatures of shock waves and nuclear explosion fireballs, air cooling, laser emission-matter interaction and optical phenomena
18 p3230 A69-34926
- Photodisintegration of ultrahigh energy cosmic rays by universal radiation field, analyzing implications on origin and propagation time
18 p3188 A69-35006
- Alkali halide crystals destruction by laser radiation for estimating optical strength, discussing impact ionization hypothesis
18 p3152 A69-35157
- Solid state laser radiation damage in polymers during tensile and compression loads using microstructural analysis
18 p3152 A69-35159
- Nuclear environment irradiation effects on materials, emphasizing radiation chemical processes affecting polyimide and copolymer of styrene and alpha-methylstyrene
19 p3356 A69-35530
- Lithium doped solar cell irradiation by strontium 90 radioisotope, discussing electron flux rate, spectrum and recovery rates
19 p3251 A69-35693
- Imperfection photoconductivity in electron irradiated Li-doped Si annealed at room temperature, noting level rearrangement in O rich material
19 p3382 A69-35696
- Proton irradiation effects on current degradation at fixed voltages of silicon solar cells with coverslips
19 p3252 A69-35701
- Optimum solar cell cover glass systems selected by studying interplanetary space environment effects of proton impact, temperature and concurrent illumination on radiation damage
19 p3253 A69-35702
- Cadmium sulfide solar cells and Kapton coverslips under proton irradiation, noting annealing of damage in samples exposed to air
19 p3253 A69-35705
- Postirradiation growth of cultured Chinese hamster cells exposed to UV light, including comparison with X irradiation
19 p3257 A69-35975
- Biological effects of radioactivity and X rays irradiation of whole body and cells, considering DNA degradation
19 p3257 A69-35978
- Cosmic ray produced radionuclides and rare gas isotopes from Saint-Severin meteorite surface, showing relative Kr spallation mass yields dependence on cosmic ray energy spectra
19 p3410 A69-36093
- Meteoritic cosmic ray exposure time from method based on spallogenic Ar 36/Ar 38 ratio, noting impracticality for exposures longer than 5 million years
19 p3418 A69-36138
- Inelastic collisions and radiation effects on transport properties and shock structure in high temperature gases, obtaining density and temperature profiles
19 p3448 A69-36149
- Photocurrents and recombination luminescence in n-type diamonds subjected to UV, TI 204 and X ray irradiation indicating local electron centers formation
19 p3383 A69-36167
- Gas dynamics of material slah under radiation impact assuming thermal equilibrium reemission, discussing equations of motion and mean free path as function of frequency
19 p3449 A69-36355
- Free radicals destruction rates by gamma irradiation at 77 K measured as first order function of dosage, using electron spin resonance spectroscopy
19 p3265 A69-36376
- Photomechanical and electromechanical effects in semiconductors, considering indentation microhardness decrease caused by light irradiation or electric field
19 p3386 A69-36526
- Statistical relation between expansion velocities and radii of planetary nebulae due to Lyman-c and diffuse Lyman-alpha radiation
19 p3426 A69-36575
- Previous radiation exposure effect on photographic film noting increased sensitivity at UV frequencies
19 p3314 A69-36626
- Amorphous semiconductors based on noncrystalline materials compared to crystalline materials, noting radiation damage resistance
19 p3392 A69-36660
- N-type GaAs optical properties after proton irradiation, noting transmission spectra dependence on initial electron concentration and irradiation dose
20 p3582 A69-36969
- UV solar radiation variation effects on Mars and Venus upper atmosphere temperatures
20 p3595 A69-37136
- Astronomical observatory photomultiplier cell dark current fluctuations, showing statistical resemblance to binomial distribution
20 p3599 A69-37470
- Primitive low energy Fe-group nuclei irradiation of meteoritic crystals from studies of pyroxene and feldspar from meteorites, discussing astrophysical implications
20 p3590 A69-37569
- Life sciences and space research on biological effects of radiation in space - COSPAR Conference, Tokyo, May 1968
20 p3474 A69-37612
- Microorganisms death by exposure to high intensity visible and UV light, discussing effect of endogenous photosensitized oxidation on caratoid-containing Rhodotorula glutinis
20 p3475 A69-37613
- Radiation effects on microorganisms and plants during space flight on Biosatellite 2 and Gemini 11 missions
20 p3476 A69-37617
- Insects mutational responses to space flight and associated radiation on biosatellite 2 compared with ground based controls
20 p3476 A69-37618
- Biological effects of cosmic radiation on crewmen and protection measures, noting ground radiobiological and medical hygienic investigations
20 p3478 A69-37628
- Aluminum doped silicon solar cell energy loss coefficient under proton and high energy electron irradiation
20 p3465 A69-37911
- Radiation effects due to high altitude thermonuclear explosion measured by satellite, estimating fragments longitudinal drift velocity, plasma cloud expansion rate and fragment distribution
20 p3532 A69-37960
- Earth radiation effect on space vehicle, using diffusely radiating sphere model
20 p3606 A69-37963
- Transient effects of nuclear radiation bursts on dielectric properties of refractory low loss ceramics at L, S and X bands
20 p3584 A69-38065
- Nitrogen gas breakdown threshold dependence on pressure during picosecond ruby laser pulse, discussing photoionization leading to breakdown in electromagnetic wave field
20 p3555 A69-38067
- Gamma radiation effects on behavior of nickel and cadmium electrodes in alkaline solution
20 p3466 A69-38072
- Fast neutron irradiation effect in Ge crystals, using X ray diffraction and volumetric measurements
20 p3584 A69-38125
- Photospheric radiation field role in temperature inversion of stellar chromospheres with dominant H ion opacity, postulating mechanical energy dissipation
20 p3613 A69-38173
- OH emission rise after sunset and decay at sunrise attributed to strong solar dissociation of ozone
21 p3712 A69-38520
- Breakdown mechanism in GaAs, Si and CdSe semiconductors under intense light pulses ascribed to thermal impact
21 p3737 A69-39042
- Collection of papers on mechanisms of biological action of ionizing radiation covering radiation sickness dynamics, radiation damage, X ray effects, etc
21 p3656 A69-39049
- Intraperitoneal high polymer DNA administration normalizing effect on DNA and RNA contents in liver, spleen and intestinal mucosa of white rats exposed to X rays
21 p3657 A69-39050

Single large X ray dose depressive effect on aminotransferase activity in rabbit blood serum, liver, kidney, heart, spleen, lungs, etc

21 p3657 A69-39051

Cholesterol-protein metabolism in muscles, liver and cerebrum of lethal X ray exposed guinea pigs compared with unexposed group

21 p3657 A69-39052

Single X ray dose effect on alpha-amylase and alpha-glucanophosphorylase in rabbit liver tissues and blood serum

21 p3658 A69-39055

Successive X ray doses effect on oxidative phosphorylation of vitamin B 1 in white rats liver tissue ultrastructure during and after irradiation, establishing thiamine biosynthesis suppression

21 p3658 A69-39056

Photographic and photometric study of absorption and reflection of ruby laser light incident on biological objects

21 p3665 A69-39060

Ionizing radiation histological and neurohistological effects in rabbits esophagus, stomach and ileocecal region intramural plexes

21 p3659 A69-39063

Frenkel defects in light irradiated p-type InSb single crystals at subthreshold radiation energies

21 p3782 A69-39144

Somatic radiation effects on human organism related to manned space flights

21 p3660 A69-39172

Pumping and excitation spectra of solid solutions of cryptocyanine in glycerine irradiated by ruby laser, discussing population inversion and scattering and vibrational transitions

21 p3740 A69-39546

Particles integral and differential fluxes spectral distribution calculation for determining radiation load for synchronous satellite

22 p4035 A69-39909

Microwave radiation hazard data from experimental animals and surveys on humans, considering nonthermal effects, genetic and neurological effects, etc [MPI PAPER DA-6]

22 p3889 A69-40104

Curvature and temperature distribution in nonrotating long solid cylinders under solar radiation in interplanetary space

22 p4043 A69-40546

Restoration processes in *Chlorella pyrenoidosa* to distinguish intense and less intense gamma ray irradiations

22 p3878 A69-40792

Gain modification from spectral splitting of optical transition by incident light wave on higher frequency coupled transition

22 p3965 A69-41125

Hemoglobin inhomogeneity in rats irradiated with lethal doses of X rays and fast neutrons, using fractions prepared by column chromatography

22 p3888 A69-41274

Thin films of infectious DNA of bacteriophage bombarded by slow protons, determining differential inactivation cross sections

23 p4081 A69-41431

Laser pulse effects on bones of rats, observing metabolic deviations in Ca 45 uptake

23 p4101 A69-41464

Rabbits long term reversible retinal function changes due to short high intensity light flashes, noting ERG suppression

23 p4084 A69-41468

S-4 human blood experiment during Gemini 2 flight, studying spaceflight ionizing radiation interaction effects on single and multiple break chromosome aberrations

23 p4085 A69-41600

Exposure rate influence on mechanical properties of polymer binder cross-linked by gamma radiation exposure from cobalt isotope source

23 p4179 A69-41711

Radiation effects on population kinetics of granulocyte system forming bone marrow, discussing radiosensitivity and radiation-induced granulocytopenia

23 p4090 A69-41965

Insect gametes response to space flight and radiation in reduced gravity including plants and microorganisms

23 p4091 A69-42050

Oxygen effect on X ray induced somatic crossing over frequency in *Drosophila melanogaster*, noting bristle spots number modification on abdominal tergites

23 p4099 A69-42118

Whole body X irradiation effect on protein degradation in mice, using radioactive I labeled albumin

23 p4099 A69-42151

Apollo 11 observations of lunar surface glazing, considering radiation heating due to solar outbursts, rocket exhaust effects, shock heating or volcanism, erosion, etc

23 p4216 A69-42202

Human body responses to microwave irradiation, discussing thermal and nonthermal effects and damage to eyes and to information storage in living systems

23 p4111 A69-42216

Neodymium laser radiation effect on electrical and histomorphological properties of liver in rats and hamsters

23 p4111 A69-42344

Gamma radiation effect on AgCl-Cu redox state in AgCl activated, heat treated Na-Al-B-Si glass, using EPR method

23 p4180 A69-42471

X band pulsed microwaves effect on skin metabolism including respiratory activity, biochemistry and biosynthesis of intercellular materials, etc

24 p4270 A69-42575

Albino guinea pigs respiration rates and ear skin histology after exposures to coherent ruby laser light

24 p4270 A69-42578

Microwave radiation effects on biological systems, discussing categories according to radiation protection guide /RPG/ numbers, tissue properties and interactions

24 p4270 A69-42579

Cosmic rays properties and dynamical effects in Galaxy disk including origin, lifetime, magnetic field instability, etc

24 p4366 A69-42695

Biological and physiopathological effects of UHF electromagnetic radiation of radar antennas, reviewing localized effects

24 p4273 A69-42996

Thermal calculations of objects near lunar surface, considering IR emission directivity effects

24 p4385 A69-43254

Stagnation region heat transfer with nongray gas subjected to external radiation using two step continuum absorption coefficient model

24 p4415 A69-43590

Contraststreaming self gravitating gas streams stability taking into account thermal conduction and radiation effects

24 p4388 A69-43638

Measurement technique using dielectric waveguides for studying microwave fields influence on and energy imparted to body tissue

24 p4279 A69-43705

RADIATION HAZARDS

Laser radiation hazards due to direct or reflected viewing determined by evaluating output characteristics and environmental factors effects

02 p0204 A69-12497

Solar flare radiation hazard in long duration space flight, discussing radiation distribution and dosage in human body

03 p0371 A69-13480

Radiation accidents involving sudden brief exposure to penetrating radiation

03 p0374 A69-13502

Biological effects of VHF electromagnetic radiation from radar antennas

05 p0715 A69-16701

Pilot protection against laser hazards, discussing protective eyeglasses, fireproof clothing and materials

07 p1072 A69-19436

Radiation hazards during long duration space flights and suitable radiation shield design through radiobiological investigation

08 p1261 A69-19826

Air carrier liability for nuclear weapons damage, discussing international agreements

11 p2003 A69-24260

Probability of ocular damage for illumination by pulsed laser beam transmitted through atmosphere, developing safety nomograph for eye hazard analysis

11 p1830 A69-24843

Laser radar eye hazard for fixed and variable transmitter intensities, considering eye damage magnitude and successful detection magnitude of transmitter intensity

11 p1830 A69-24845

Soviet book on quality control of materials and machine parts by ionizing radiation covering radiation hazards and protection

13 p2268 A69-27935

Radar antenna radiation effects on man and biological material dependent on absorption degree and emission characteristics including wavelength, peak and mean power

13 p2215 A69-28597

Radiation exposure during orbital flight assessed for adverse effect on space stations and laboratories personnel, discussing shielding and dose rate tables

20 p3481 A69-37339

Cosmic radiation exposure of passengers and crew in supersonic transport at high altitude

22 p4002 A69-40093

Microwave radiation hazard data from experimental animals and surveys on humans, considering nonthermal effects, genetic and neurological effects, etc [MPI PAPER DA-6]

22 p3889 A69-40104

Solar flare radiation hazard to SST crew and passengers, discussing onboard and ground based warning systems and ICAO requirements

23 p4063 A69-41830

Human body responses to microwave irradiation, discussing thermal and nonthermal effects and damage to eyes and to information storage in living systems

23 p4111 A69-42216

Radio and microwaves biological effects, discussing differences between U.S. and Soviet assessments of radiation hazards

23 p4099 A69-42516

Laser hazard probability assessment in various applications, discussing power characteristics, attenuation by absorption and scattering and radiant energy spatial distribution

24 p4327 A69-42576

RADIATION HEATING

U RADIANT HEATING

RADIATION INDICATORS

U DOSIMETERS

U INDICATING INSTRUMENTS

RADIATION INJURIES

Prophylactic and therapeutic vitamin and organic compounds complexes in radiation damage reduction and death prevention for dogs exposed to X rays

02 p0197 A69-11493

Chronic gamma radiation biological damage in rats exposed to maximum nonlethal to minimum lethal doses for various periods

02 p0197 A69-11494

Radiation structural and transcription damage to deoxyribonucleic acid /DNA/, noting postirradiation repair on molecular level

03 p0372 A69-13489

Mammalian cell survival, chromosome abnormalities and recovery from heavy ion and X ray irradiation

03 p0373 A69-13492

Radiation accidents involving sudden brief exposure to penetrating radiation

03 p0374 A69-13502

Cosmic radiation and hibernation physiopathology of human organism, noting beryl as radiation resisting agent in spacecraft design

06 p0874 A69-17645

Dermal injury predictability for exposure to thermal radiation based on mathematical model using temperature-time histories

06 p0875 A69-17840

Microvillar bleb formation in proton irradiated primate hepatocytes with electron microscope, noting sinusoidal lumen

10 p1641 A69-23045

Laser radar eye hazard for fixed and variable transmitter intensities, considering eye damage magnitude and successful detection magnitude of transmitter intensity

11 p1830 A69-24845

RADIATION INTENSITY

U RADIANT FLUX DENSITY

RADIATION LAWS

NT KIRCHHOFF LAW OF RADIATION

Radiation problem in general theory of relativity investigated by momentum energy tensor, formulating criterion for gravitational radiation

01 p0116 A69-10435

Radiation models using discrete radiator ensembles having applications to analysis of forward and backscatter from rough surfaces, clutter and chaff models, etc

01 p0030 A69-10556

Planck law for black body radiation spectrum theoretically derived on basis of classical Lorentz-invariant electromagnetic radiation at absolute zero temperature without quantum assumption

22 p3982 A69-41001

RADIATION MEASUREMENT

Auroral zone X ray measurements emphasizing temporal intensity variations, energy spectra changes and source region movements during magnetospheric substorms

08 p1379 A69-20534

Energy spectra of carbon and oxygen nuclei in primary cosmic radiation, comparing results to earlier measurements and satellite observation

08 p1380 A69-20632

Aircraft measurements of earth atmosphere radiance in 8-14 micron window compared to calculated values as functions of altitude

08 p1311 A69-21094

Taurus A flux density measurement at 4.3 mm with 36-ft antenna at National Radio Astronomy Observatory to determine spectrum unambiguously

09 p1591 A69-21450

Cosmic ray intensity diurnal variations from super neutron monitor observations, discussing anisotropy resulting from reduced intensity in gardenhose direction in ecliptic plane

09 p1576 A69-21706

Solar flare energetic electron access to polar zones from measurements made by nine channel magnetic spectrometer on polar orbiting vehicle

09 p1577 A69-21709

Elektron 4 satellite radio emission data transmitted from July to December 1964, noting month-to-month variations in mean radiation level

09 p1578 A69-21776

Contour maps of supernova remnants HB 9, Simeis 147 and IC 443, noting spectra showing radiation nonthermal

09 p1604 A69-22408

Atmospheric thermal sounding by measuring outgoing thermal radiation with infinite resolution device, describing regularization method

09 p1491 A69-22707

Weak X ray sources at 20-100 Kev photon energies observed during balloon flight, finding hard rays from Ara XR-1 and Nor XR-1

09 p1583 A69-22763

High energy X ray observational data for Sagittarius sources scanned by active telescope during February 1968 balloon flight

09 p1583 A69-22764

Diffuse cosmic X ray background measured during balloon flight with actively shielded and collimated detector

09 p1584 A69-22767

Excess radiation in equatorial regions studied on-board Cosmos 137, noting contribution of primary particle multiplication to secondary radiation

10 p1783 A69-23922

Solar UV radiation measurements by balloon-borne monochromatic illuminator, using Cd-cathode photomultiplier detector

11 p1945 A69-24410

Small microwave antenna calibration by method of two black bodies exposed to different temperatures, reducing influence of cloudiness and humidity

11 p1844 A69-24450

Radiation measurements quality by wide angle receivers of Cosmos 122 satellite analyzed, showing agreement with data by other methods

11 p1912 A69-24830

Second tacite sounding rocket test for measuring UV radiation in transition zone between upper ionosphere and space

11 p1887 A69-25213

Radiation dose and radioactive isotopes induced in astronaut body by cosmic rays of various energies

11 p1831 A69-25463

H beta emission line in night sky spectrum measured with gas pressure scanned Fabry-Perot interferometer in Italian alps

12 p2074 A69-26963

Solar radiation in short wave, UV and X ray range recorded by rockets, probes and satellites, notably Elektron 2 probe

13 p2326 A69-27355

Cosmic X ray background measurements and Crab Nebula observation during sounding rocket flight

13 p2326 A69-27570

Dynamic Michelson interferometer equipped with Ge detector to obtain spectra of airglow from 1.2-1.6 microns

13 p2252 A69-27587

IR emission from quasars, noting quasar 3C 273 B and synchrotron mechanism probability

13 p2342 A69-27598

Radiation measurements by Cosmos 122 satellite over various regions, determining radiation temperature, long wave heat flux and albedo

13 p2291 A69-27726

Medium energy trapped and dumped protons at high latitudes and auroral zone, using semiconductor radiation detectors on ESRO 1 satellite

13 p2328 A69-27756

Cardiac output determined simultaneously in adult male humans by thoracic impedance changes and radioisotope dilution

14 p2408 A69-29304

Meteorological elements variation from measuring earth radiation in different spectral regions by satellites, determining temperature and humidity profiles

14 p2477 A69-29828

Periodic stellar radiation at 3.5 mm from pulsar CP1919 measured by paraboloid antenna and radiometer

14 p2529 A69-29978

Flux densities at 2695 MHz for radio sources, tabulating measured data, discussing spectral distribution indices

15 p2696 A69-31206

Disk and transmission line microstrip resonators radiation, measuring fractional amount of radiated power

16 p2760 A69-31946

Diurnal variations of IR atmospheric oxygen bands in airglow observed with filter photometer on balloon flights

16 p2776 A69-32091

Continuum radiation measurements for bremsstrahlung and recombination of neutral and ionized nitrogen

16 p2823 A69-32466

Atmospheric thermal sounding by measuring outgoing thermal radiation with infinite resolution device, describing regularization method

16 p2782 A69-32487

Neutron and photon transport properties in liquid hydrogen obtained from measuring radiation environment in propellant tank mockup suspended above NERVA reactor

[AIAA PAPER 69-475] 16 p2810 A69-32716

Antenna three dimensional radiation patterns, describing error analysis of various pattern measurement techniques

17 p2942 A69-34086

Metallic aerosol generator application in shock tube spectrometric measurements of radiation by molecules occurring as solids before decomposition to vapor phase

18 p3099 A69-34461

Differences concerning utilization of IR detectors, discussing nomenclature, fluctuations and definitions of detection, translation and readout

19 p3308 A69-35905

Spectral parameters effect on IR instrument SNR, discussing range equations of point and extended sources and radiation-noise-limited detectors

19 p3310 A69-36061

Radiometric measurement, discussing characteristics and calibration of instruments for measuring radiant intensity or radiance

19 p3311 A69-36071

Injection lasers external quantum efficiency, stimulated and spontaneous emission and photoluminescence measurements

19 p3337 A69-36528

Spherical, cylindrical and toroidal electrostatic analyzers with symmetrical angular characteristics for solar wind investigations

19 p3396 A69-36632

OGO-F neutron monitor for measuring cosmic ray neutron flux near earth, locating sensor on boom to minimize spacecraft produced neutrons

19 p3314 A69-36678

Solar protons in subpolar stratosphere during solar activity minimum indicated from proton measurements at Tiksi Bay

20 p3587 A69-37044

Electron and gamma quanta concentrations measurements by high altitude balloon, noting fluctuations at various altitudes

20 p3587 A69-37046

Spectral emissivity measurement of ablating phenolic graphite heated by subsonic air stream to high temperature to simulate reentry condition

20 p3565 A69-37187

Solar neutrinos capture rate estimation by using Li 7 as detector

20 p3588 A69-37420

Optical system for cosine-corrected radiation point to areal source measurement, discussing adaptation to spectral instruments, photocells and photoelements

20 p3538 A69-37429

Gamma ray emission of meteorite of 25 April 1969 measured by scintillation spectrometry, attributing peaks to annihilation radiation, Cs 137, Mn 54, etc

20 p3590 A69-37571

Pulsed X ray emission associated with pulsar NP 0532 in Crab Nebula measured by six element detector on Aerobee 150 rocket

20 p3590 A69-37574

Unresolved background radiation at 2695 MHz surveyed for galactic wing extent determination

20 p3606 A69-37830

Interplanetary proton and alpha particle radial gradients determined from Mariner data, considering Forbush decrease, particle solar origin, galactic cosmic radiation, etc

20 p3592 A69-38096

Solar cycle variation of extreme UV radiation from total solar disk under nonflare conditions by photoelectric measurements

20 p3592 A69-38103

X ray emission from high voltage microwave devices during high velocity electron braking measured using X ray sensitive film with superimposed aluminum scale

21 p3664 A69-39059

Quantitative criteria imposed on balloon measurements of auroral emissions from Kiruna, considering times of sunrise and sunset at different altitudes

21 p3716 A69-39250

Ariel 3 satellite attempted background radiation measurement between 2-4 MHz to show absorption onset in Galaxy

21 p3806 A69-39258

Electromagnetic radiation measurements in shielded enclosures, describing equipment and effects of frequency

21 p3683 A69-39439

Daily measurement of solar radio intensity at 810 MHz during 1964 minimum solar activity period

22 p4010 A69-39989

Photoelectric methods for pulsed and CW lasers output power and energy measurements

22 p3961 A69-40239

Calorimeters for laser energy measurement, discussing radiation damage avoidance and modifications for various modes

22 p3961 A69-40243

Neutron flux measurements on Cosmos 53, discussing equipment and calculation of secondary neutrons due to bombardment of satellite components

22 p4003 A69-40274

Auroral UV and 3914 A radiation during charged particle precipitation measured by satellite

22 p3939 A69-40507

Air ionization and beta and gamma dose rates measurements for natural radiation from cosmic rays compared to nuclear weapons tests fallout, considering biological effects

22 p4007 A69-40915

Quantization sidelobe characteristics of phased array with triangular and rectangular element arrangement

23 p4137 A69-41591

Day-to-day changes of cosmic ray diurnal variation measured on meson and neutron components, showing relationship with interplanetary magnetic field

23 p4206 A69-42012

Total solar radiation correlation with bright sunshine hours measured monthly on solarimeters and Campbell-Stokes recorders at various tropical stations

23 p4206 A69-42178

Forbidden O I 5577 A dayglow isotope equatorial measurements with rocket photometer, discussing altitude profiles and excitation mechanism

24 p4314 A69-43005

Cosmic ray albedo-neutron decay source role in intensity measurements of high energy protons trapped on low L shells during satellite flights

24 p4367 A69-43176

Solar protons and alpha particles measurements at synchronous orbit altitudes providing data for solar cell shield design to prevent radiation damage

24 p4369 A69-43265

IR measurements applications to meteorology, discussing IR radiation characteristics, atmospheric effects, thermal radiation detection and differences between real and black bodies

24 p4316 A69-43507

Solar cosmic ray anisotropy measurement by Explorer 34 satellite during solar flare events

24 p4373 A69-43619

RADIATION MEASURING INSTRUMENTS

NT ACTINOMETERS
NT BOLOMETERS
NT CERENKOV COUNTERS
NT DICKE RADIOMETERS
NT DOSIMETERS
NT ELECTRON COUNTERS
NT ELECTROPHOTOMETERS
NT ELECTROSTATIC PROBES
NT FABRY-PEROT SPECTROMETERS

NT GEIGER COUNTERS
 NT INFRARED DETECTORS
 NT INFRARED INSTRUMENTS
 NT INFRARED SCANNERS
 NT INFRARED SPECTROMETERS
 NT INFRARED SPECTROPHOTOMETERS
 NT MICROWAVE RADIOMETERS
 NT NEUTRON COUNTERS
 NT PARTICLE TELESCOPES
 NT PHOTOMETERS
 NT PROPORTIONAL COUNTERS
 NT PYRANOMETERS
 NT QUANTUM COUNTERS
 NT RADIOMETERS
 NT RIOMETERS
 NT SCINTILLATION COUNTERS
 NT SILICON RADIATION DETECTORS
 NT SOLAR SPECTROMETERS
 NT SPARK CHAMBERS
 NT SPECTROHELIOGRAPHS
 NT SPECTROPHOTOMETERS
 NT SPECTRODIAMETERS
 NT THRESHOLD DETECTORS [DOSIMETERS]
 NT ULTRAVIOLET SPECTROMETERS
 NT ULTRAVIOLET SPECTROPHOTOMETERS

Meteorological rocket measurement of ionizing radiation flux in upper atmosphere, noting flux decrease with increasing electron energy
 01 p0144 A69-10586

Space X ray background measurements, considering relativistic electrons Compton emission and metagalactic gas bremsstrahlung as possible sources
 01 p0147 A69-11310

Orbital spectroscopic and radiometric IR experiments, considering moon and Mars surface
 [AAS PAPER 68-196] 02 p0312 A69-11474

Lunar composition analysis by measuring atomic and nuclear radiation emission from orbiter
 [AAS PAPER 68-197] 02 p0312 A69-11475

Radiation sensor PCM data processing by computer to detect radiation level using data decorrelation, data normalization and threshold test
 03 p0400 A69-13313

Linear polarization of cosmic radio emission, discussing original measurement method and revised version based on discrimination of useful signal
 03 p0501 A69-13705

Stratospheric air sampling reliability instrumentation as part of radioactivity fallout detection program
 05 p0766 A69-16751

Solar constant measurement, reviewing instruments and results of Eppley-JPL program using high altitude jet aircraft and rocket research vehicle
 09 p1576 A69-21647

Gamma ray scattering gauge design optimum parameters to measure Mars atmospheric density
 09 p1495 A69-21842

Cosmos 149 meteorological satellite telephotometer, radiometer and other electronic equipment for measuring atmosphere and underlying surfaces physical parameters
 14 p2447 A69-29403

Cosmos 149 meteorological satellite telephotometers for measuring reflected solar radiation from earth
 14 p2447 A69-29404

Airglow research, discussing emission features, observation methods and instruments, ground station network, etc
 15 p2594 A69-30020

Meteorological rocket measurement of ionizing radiation flux in upper atmosphere, noting flux decrease with increasing electron energy
 15 p2675 A69-30756

Earth albedo instrument on OSO 3 spacecraft to measure solar reflectance of earth at various wavelengths
 15 p2614 A69-31279

UV excitation intensity increased for improving luminescent nondestructive testing, describing UV dosimeter and irradiation standards
 18 p3138 A69-35115

Probe for spectral radiation from luminous gas-cap stagnation region to determine driver gas in test section of hypersonic shock tunnel
 19 p3294 A69-35753

Measuring devices for near earth space radiation measurements
 20 p3591 A69-38018

Device measuring light pressure and pulse energy of laser emission by converting kinetic energy into potential energy of twisted elastic suspension thread
 22 p3961 A69-40246

RADIATION MEDICINE

U RADIOBIOLOGY

RADIATION NOISE

U ELECTROMAGNETIC NOISE

RADIATION PRESSURE

NT ELECTRON PRESSURE
 NT ILLUMINANCE
 NT LUMENS
 NT LUMINANCE
 NT LUMINOUS INTENSITY
 NT SOUND PRESSURE

Artificial lunar satellite orbital motion calculated by numerical integration, including solar and lunar electromagnetic radiation pressure effects
 04 p0662 A69-15251

Direct light pressure effect on evolution of limited planetocentric orbits of small bodies, noting longitudes of ascending node and pericenter
 05 p0823 A69-16043

Radiation pressure effects on laser produced carbon plasma in vacuum, discussing target surface superheating, plume boundary, plume density precursor and electron and ion temperature merging
 07 p1190 A69-18902

Time-averaged value of forces of electromagnetic wave falling from vacuum and acting on magnetoactive plasma
 08 p1361 A69-20200

Metagalaxy stationary model in terms of relativity theory, investigating radiation pressure balancing of gravitation as imaginary situation
 08 p1389 A69-20263

Solar wind-magnetosphere pressure balance and proton density of solar wind
 09 p1577 A69-21711

Uniformly rotating star models within first order perturbation theory in convective equilibrium and with radiation pressure, discussing radiative and gas pressure ratio
 09 p1606 A69-22422

Solar radiation pressure on interplanetary dust particles calculated as function of radius and density, noting asteroidal origin of dielectric and absorbing particles
 11 p1956 A69-24397

Temporal variation of metal content in galaxy, discussing stellar radiation pressure effects on heavy element abundance of interstellar gas
 12 p2160 A69-26854

Exterior field equations for radiating spheres with zero limb darkening in relativity and Bondi coordinates, determining radiative flux and pressures
 13 p2339 A69-27566

Potassium vapor radiative perturbation by ruby laser radiation in glass cell with end windows, studying emission line structure
 13 p2271 A69-27656

Solar radiation pressure effects on satellite models in circular equinoctial orbits
 14 p2522 A69-29595

Rapid orbit prediction method for planning satellite observation programs, considering oblateness and radiation pressure effects
 15 p2697 A69-31310

Earth reflected radiation pressure and perturbing effect on satellites
 15 p2599 A69-31324

Direct light pressure effect on evolution of limited planetocentric orbits of small bodies, noting longitudes of ascending node and pericenter
 20 p3606 A69-37952

Three dimensional coupled flexural and attitude dynamics of libration-damped cruciform gravity gradient satellite, discussing effects of orbital eccentricity, solar radiation pressure, etc
 [AAS PAPER 68-126] 21 p3819 A69-39211

Solar radiation pressure windmill effect in rotational bursting and elimination from solar system of small magnetic celestial bodies
 21 p3814 A69-39584

Device measuring light pressure and pulse energy of laser emission by converting kinetic energy into potential energy of twisted elastic suspension thread
 22 p3961 A69-40246

Light pressure induced secular effect contributing to planetary satellites and lunar orbits evolution calculated by numerical integration
 22 p4033 A69-41084

Class of one dimensional nonlinear waves and shock structure reduced to steady flows in radiation gas dynamics
 23 p4240 A69-42466

Solar radiation pressure on interplanetary dust particles calculated as function of radius and density, noting asteroidal origin of dielectric and absorbing particles
 24 p4390 A69-43787

RADIATION PROTECTION

NT SOLAR RADIATION SHIELDING

Surface dose rate and depth dose distribution for materials used for space vehicle and biological tissue protection from cosmic and internal radiation
 [UN PAPER 68-95260] 01 p0144 A69-10477

Prophylactic and therapeutic vitamin and organic compounds complexes in radiation damage reduction and death prevention for dogs exposed to X rays
 02 p0197 A69-11493

Solar radiation protection of radiometers and spectrometers on reentry vehicle by launching times and solar view field selection
 04 p0666 A69-15511

Radiation protection plan for Apollo lunar mission based on real time monitoring of solar activity and radiation in spacecraft
 [AIAA PAPER 69-19] 06 p0996 A69-18113

Pilot protection against laser hazards, discussing protective eyeglasses, fireproof clothing and materials
 07 p1072 A69-19436

Radiation resistance of animals in hibernation and hypothermia, noting temperature dependence of protective effect
 10 p1643 A69-23126

Chemical and biological means of safeguarding body of astronaut against ionizing radiation and vibration
 10 p1648 A69-23297

Biological radiation doses and protection from galactic, solar particle and trapped radiation in space, noting secondary radiation and bremsstrahlung in absorber
 11 p1831 A69-24866

Soviet book on quality control of materials and machine parts by ionizing radiation covering radiation hazards and protection
 13 p2268 A69-27935

Organosilicon-containing derivatives of 2-aminoethanethiols and 2-aminoethanethiosulphuric acids as radiation protective agents
 13 p2210 A69-28486

Admissible radiation doses for space crews and ionizing radiation protection, studying long term radiation effects on dogs
 15 p2557 A69-31344

Radiation resistant devices for minimizing neutron and gamma radiation effects on military electronic components, discussing selection features and sampling lot sizes
 18 p3144 A69-34491

Proton irradiation effects on current degradation at fixed voltages of silicon solar cells with coverslips
 19 p3252 A69-35701

Biological effects of cosmic radiation on crewmen and protection measures, noting ground radiobiological and medical hygienic investigations
 20 p3478 A69-37628

Radioprotective effects of 5-azacytidine on bone marrow and blood leukocytes of X ray irradiated AKR mice
 23 p4080 A69-41429

Co 60 kernel heat source for multimikrowatt space power supplies, stressing design for maximum safety
 23 p4187 A69-42257

Integral coverslip development for Si solar cells, considering borosilicate glass fusing on cell surface and RF and high vacuum ion beam sputtering
 23 p4070 A69-42272

Microwave radiation effects on biological systems, discussing categories according to radiation protection guide /RPG/ numbers, tissue properties and interactions
 24 p4270 A69-42579

RADIATION PYROMETERS

Thermistors for total optical radiation pyrometer and for temperature control system based on radiation pyrometer, noting thermistor response and control circuit
 04 p0601 A69-15119

RADIATION SHIELDING

NT SOLAR RADIATION SHIELDING

Biological effects of proton irradiation of monkeys investigated to provide improved protective shield design data with minimum weight penalty
 03 p0373 A69-13496

Radiation compensating thermocouple for gas temperature measurement, noting advantage over single thermocouples
 04 p0598 A69-14916

Book of engineering compendium on nuclear radiation shielding, discussing radiation sources, attenuation methods, induced heat generation, ducts and voids in shielding technology and design
 05 p0791 A69-15830

Radiation hazards during long duration space flights and suitable radiation shield design through radiobiological investigation
 08 p1261 A69-19826

Propyl gallate radiation shielding effect variations with proton and gamma ray bombardment, noting growth and development of potato tuber eyes
08 p1262 A69-19927

Local shielding effectiveness of dogs against proton irradiation at minimum lethal dose, noting bone marrow role
08 p1263 A69-19939

Proton flux density at axial point of thin cylindrical and slab shell shields bombarded by isotropic inverse power law spectrum of protons in space
10 p1723 A69-23165

Cryostat design, discussing vapor and radiation shielding, construction and insulation materials, safety features, cost considerations, etc
10 p1810 A69-24015

Solar cells degradation by charged particles in space, considering protection by filter, silicon properties and use of cadmium cells
11 p1825 A69-24870

Radiation dosimetry and shielding onboard Cosmos 110 artificial satellite, noting earth belt proton radiation
13 p2356 A69-27702

COHORT-II Monte Carlo computer program written in Fortran IV to model radiation shielding problems
14 p2417 A69-29004

Shock wave radiation screening by thermodynamically unstable gas, discussing brightness and gas temperature relative to shock wave front position
14 p2493 A69-29673

Proton dose in receiver behind combination electromagnetic and material shield, calculating dose for Van Allen and solar proton event spectra
15 p2652 A69-31522

Lunar module multilayer radiation insulation for thermal control, testing aluminum coated Mylar and Kapton sheets
[AIAA PAPER 69-609] 17 p3073 A69-33304

Monte Carlo method application to neutron streaming in hemispherical air-filled ducts in water tank to determine leakage through nuclear reactor shields
18 p3171 A69-35178

Multifoil thermal insulation for radiation shields from cryogenic temperatures to 3500 F, noting thermal conductivity
19 p3341 A69-35540

Solar cell radiation damage during 416.8 days in synchronous orbit on satellite ATS 1, discussing radiation shields
19 p3253 A69-35704

Supraethal doses of pulsed mixed gamma-neutron radiations from TRIGA reactor administered to unshielded, head shielded and trunk shielded beagles
19 p3259 A69-36459

Positive effect of shielding and cystamin administration on tonic and evacuator functions of rats gastrointestinal tract after gamma irradiation
22 p3877 A69-40285

Solar protons and alpha particles measurements at synchronous orbit altitudes providing data for solar cell shield design to prevent radiation damage
24 p4369 A69-43265

RADIATION SICKNESS

Radiation effects in man, searching for dose relationships in prodromal syndrome
03 p0374 A69-13503

Pathomorphological aspects of radiation sickness in animals irradiated by high energy protons, showing changes in lymph node, stellate ganglion and spleen
05 p0708 A69-16509

Pathomorphological aspects of radiation sickness in animals irradiated by high energy protons, showing changes in lymph node, stellate ganglion and spleen
18 p3095 A69-34728

Collection of papers on mechanisms of biological action of ionizing radiation covering radiation sickness dynamics, radiation damage, X ray effects, etc
21 p3656 A69-39049

RADIATION SOURCES

NT MONOCHROMATORS

NT NEUTRON SOURCES

NT POINT SOURCES

IR emission in NGC 7027 spectrum and role of discrete line emissions, discussing magnetic dipole transitions, temperature and density
01 p0148 A69-10051

Spectral lines source functions for formation in multiple atom and radiative transfer in atmosphere of three level Na atoms and four level O atoms
01 p0124 A69-10962

Cosmic rays properties and sources, considering origin in supernovae, galaxies, quasars and unknown sources
02 p0308 A69-12158

X ray source in constellation Vela lying close to galactic plane observed by attitude controlled Aerobee 150 rocket
02 p0308 A69-12594

Cosmic ray air shower distribution from Crab Nebula, M87, M82, quasars, X ray sources and recent supernovae
02 p0308 A69-12597

Soft X ray spectrum of Sco XR-1, noting intensity change from previous measurement
02 p0309 A69-12711

Structure of sources of noise storm enhancements and stationary type 4 bursts, discussing head and tail components
02 p0328 A69-12753

Metagalactic cosmic rays, galactic halo and sources of cosmic rays in Galaxy, noting models, electron component of cosmic rays and evolutionary cosmology
03 p0497 A69-12929

Galactic X ray sources, discussing location along spiral arms, age and properties of stars responsible for emission
03 p0497 A69-12930

Cosmic ray origins, considering hard protons, X rays, gamma rays, very soft protons, background radiation, charged particles and neutrinos
03 p0497 A69-12932

Cosmic X ray sources resolved against diffuse background radiation lying close to galactic plane
03 p0501 A69-13767

IR object discovered during T Tauri objects and diffuse nebulae study, discussing peculiarity
04 p0655 A69-14665

Planetary nebulae as possible low energy galactic X ray source
04 p0661 A69-15144

Optical variability of quasar 3C 273, suggesting radiation emission from single bodies rather than from large complex of independent sources
04 p0662 A69-15235

X ray astronomy, discussing sources associated with bremsstrahlung or synchrotron radiation, astrophysical models, black body radiation, relativistic electrons, etc
04 p0662 A69-15326

Earth X ray flux due to solar X rays reflected in atmosphere observed by Skylark rockets, noting observations of Sco XR-1 and Cen XR-2
04 p0649 A69-15440

Solar X ray source identification using D layer ionization behavior during eclipse
04 p0650 A69-15533

Cathode emission site analysis by measuring prebreakdown current under ultrahigh vacuum conditions
05 p0800 A69-15740

Book of engineering compendium on nuclear radiative shielding, discussing radiation sources, attenuation methods, induced heat generation, ducts and voids in shielding technology and design
05 p0791 A69-15830

X ray astronomy techniques, discussing X ray spectrographs, heliographs and nonsolar celestial X ray sources
05 p0762 A69-15840

Galactic X ray sources noncoincident with conspicuous visible or radio objects, identifying visible and radio counterparts by determination of accurate celestial coordinates
05 p0813 A69-15845

Tunable Raman upconverter as coherent light generator, using Q switched Nd-YAG laser beam [IEEE PAPER B-2]
05 p0774 A69-16309

Celestial X ray sources astronomy, discussing emission mechanism in 2 to 100 kev range and balloon observations in Cygnus and Taurus constellations
05 p0817 A69-16715

X ray sources intensity and spectrum variation with time, describing proposed balloon experiments with equatorial launching for performing measurements
06 p0992 A69-17312

Photoelectric observation of Sco X-1 variations with 91-cm reflector, tabulating results and estimating accuracy
06 p1008 A69-17695

Plasma instability role in radiant energy release from astronomical objects, noting plasma instabilities in solar system, cosmic rays, galactic and extragalactic objects
06 p1009 A69-17967

Galactic soft X rays observation with two rocket-borne gas filled counters, noting source near Wolf-Rayet star Gamma Velorum in Vela
07 p1204 A69-18599

Radiative transfer problems in inhomogeneous anisotropically scattering plane parallel planetary at-

mospheres with internal source distributions solved by recursive method
07 p1213 A69-18610

Organic lasers, discussing coherent laser light emission induced from organic dye molecules
07 p1149 A69-18908

Relaxation theory of highly ionized hydrogen plasma noting applications to stimulated emission, radiation source development and electromagnetic radiation amplification
07 p1191 A69-18996

Pulsar characteristics absence in X ray sources, noting data for Scorpius XR-1
07 p1218 A69-19254

Balloon observations of cosmic X ray sources in Cygnus and Crab Nebula, discussing data application to energy spectra analysis
07 p1210 A69-19716

Low energy multiply charged cosmic ray nuclei propagation and source characteristics, considering two component model based on OGO satellite measurements
08 p1378 A69-20068

Discrete source hypothesis for interpreting high energy cosmic gamma ray measurements obtained by OSO-3 spacecraft
08 p1380 A69-20699

OH emission source in constellation Canis Major discovered with interferometer in October 1968, noting nearby IR object
09 p1591 A69-21448

Low energy X ray spectra of Sco X-1 and Sagittarius sources measured by Be and Al window proportional counters during rocket flight
09 p1574 A69-21460

Temporal and spatial coherence effects of optical fields and relationship to multipole coherence effect
09 p1540 A69-22083

Sco X-1 optical spectrum magnitude and color changes, proposing variable black body model
09 p1601 A69-22213

Bright celestial IR sources in Ursa Major detected in spectral region by rocket-borne telescope, discussing luminosities of quasi-stellar sources
09 p1603 A69-22230

Iron line absence in emission spectrum of thermal X ray sources, constraining proposed thermal models
09 p1580 A69-22231

Far IR source in galactic center detected at 100 microns, noting thermal emission of interstellar dust grains as possible mechanism
09 p1603 A69-22264

X ray astronomy, tabulating properties of 22 discrete sources and discussing spectra, radio emission, optical identification, X ray production, etc
09 p1583 A69-22762

Weak X ray sources at 20-100 Kev photon energies observed during balloon flight, finding hard rays from Ara XR-1 and Nor XR-1
09 p1583 A69-22763

High energy X ray observational data for Sagittarius sources scanned by active telescope during February 1968 balloon flight
09 p1583 A69-22764

Quasars and explosive processes in galaxies as cosmic ray sources in expanding universe, studying relation between galactic and metagalactic cosmic rays
10 p1756 A69-22815

Modulation collimators determining angular sizes and celestial positions of X ray sources Sco X-1 and Taurus XR-1
10 p1678 A69-23326

Celestial X ray source positions from rotating modulation collimator, predicting performance of collimator
10 p1722 A69-23328

Antenna point and astigmatic sources due to phase centers and phase diagrams relations and antenna caustic curves
10 p1664 A69-23798

Spectra of low energy X ray source at position of Large Magellanic Cloud, noting flux
10 p1770 A69-24093

Spectroscopic observations of optical object identified with X ray source Cygnus X-2 noting radial velocity in absorption and emission lines
10 p1785 A69-24097

Double structure in IR near Trapezium region of M42 in Orion Nebula center
10 p1786 A69-24105

Condensation sources of maser radiation observed in W3 hydroxyl lines, discussing polarization and designation as protostars
11 p1954 A69-24379

Vacuum spark light source for extreme UV noting mechanical trigger, compatibility with clean vacuum system and magnetic confinement of ions
11 p1885 A69-24839

Radiation studies of pressure driven shock tubes with atomic ionization at high temperatures, discussing thermal light sources, autoionization, etc
11 p1863 A69-25014

Electroluminescence and electroluminescent devices, considering semiconductor lasers, radiation sources and image amplifiers
11 p1899 A69-25198

Crab Nebula X ray pulse detection attempt during balloon flight of telescope
12 p2149 A69-26226

Specularly vs diffusely reflecting cylinders for cavity type sources of approximately black body radiant energy, noting ray tracing of cones
12 p2130 A69-26245

Gravitational recoil due to gravitational emission of source analyzed in terms of Einstein equations
12 p2130 A69-26338

Plasmas role in emission mechanisms active in celestial sources of radiation, discussing sun and quasars
12 p2159 A69-26619

Correlation coefficients, comparing galactic X ray sources distribution with classical cepheids, old novae, planetary nebulae and Wolf-Rayet stars
12 p2171 A69-27155

Scorpius XR-1 X ray emission spectra, discussing Fe emission line near 7 kev plasma models, supernova mass and cosmic abundance
13 p3235 A69-27313

Microwave background radiation by intense sources studied by homogeneous and isotropic Friedmann and steady state models
13 p2339 A69-27574

Geomagnetic storm induced temporary radiation zones located by determining Explorer 30 attitude and spin axis orientation
14 p2514 A69-29384

Solar ionizing radiation sources, discussing activity at sunspot minimum, temperature, density and solar wind effects, X ray and UV spectra, etc
15 p2673 A69-30007

Decametric radio astronomy at frequencies from 10 to 40 MHz on wideband telescopes, discussing spectral types of discrete radiation sources
15 p2682 A69-30501

Global multielement radio interferometer with autonomous reception synthesized for studying spatial radio brightness distribution over radiation sources
15 p2578 A69-30936

Energy transfer during fast electrons and photons interactions, indicating Compton energy losses related to space X ray and gamma radiation sources
15 p2676 A69-30953

Extraterrestrial X ray galactic and extragalactic sources research fields, emphasizing identification with optical objects
15 p2696 A69-31213

Time variation of optical intensity of Sco X-1 X ray source, evaluating photometric data by power spectral analysis
16 p2852 A69-32805

Solar eclipse of 20 May 1966, comparing satellite-borne X ray and UV photometry with radio astronomical observations
17 p3023 A69-33058

Galactic X ray sources density nearly proportional to interstellar gas density squared, discussing X ray intensities estimation, galactic age, etc
17 p3030 A69-33069

Nocturnal D region conductivity enhancement relation to X radiation from Scorpius XR-1 and other sources, calculating ion production rate
17 p3024 A69-33378

Correlated bursts from separate distant sources on sun, noting occurrence in quiet periods and strength
17 p3024 A69-33804

Solar radio emission sources position changes observed in solar storm center
17 p3024 A69-33805

Line source excited ferrite layer radiation pattern reduced to one dimensional form by Fourier transform, obtaining angle of maximum leaky wave radiation
17 p2926 A69-33852

X ray absorption in surrounding gas sphere as function of continuous absorption, electron scattering and diffuse ionizing radiation, using radiative transfer theory
18 p3186 A69-34296

Extrasolar X rays and sources from studying distribution, luminosity, diameters and variability of rays
18 p3193 A69-34364

Source requirements for cosmic radiation origin model, noting fluctuations in momentum changing process
18 p3188 A69-35005

X ray sources model, describing possible ring of matter around white dwarf near end of active evolution
18 p3188 A69-35204

Source position of cosmic ray diurnal anisotropy relative to ecliptic plane from neutron monitor data at Mawson and Churchill stations
18 p3189 A69-35441

Thermal molecular beam sources fabricated from multichannel arrays, describing molecular flux leak rates and angular distributions
19 p3376 A69-36175

Continuous IR radiation source using electrically heated Mo ribbon, comparing emission from V shape and flat portions
19 p3313 A69-36491

Optical system for cosine-corrected radiation point to areal source measurement, discussing adaptation to spectral instruments, photocells and photoelements
20 p3538 A69-37429

Radiation emission mechanism for NP 0532 associated with Crab Nebula, discussing shock- neutral sheet interaction
20 p3604 A69-37572

Asymptotic evaluation of complex frequency integrals in theory of radiation from transient sources in dispersive media, interpreting results in terms of space-time rays
20 p3494 A69-37841

X ray spectra of Sco XR-1, Cyg XR-1 and Cyg XR-2 for proton energy range 1.5-13 kev from proportional counter measurements
20 p3593 A69-38152

Radiation sources fields and propagation in homogeneous lossy magnetoplasma, deducing wave equations for electric and magnetic current electron flux and mechanical body force sources
21 p3775 A69-38434

Interstellar absorption of 10 A X rays from sources in Scorpio-Sagittarius region, noting gas density between earth and Crab Nebula
21 p3788 A69-38648

Galactic nucleus observations in 1.65-19.5 micron range with evidence for strong radiation at 10 and 20 microns, noting mechanisms for IR radiation
21 p3799 A69-38650

Differential approximation for radiant energy loss in nonequilibrium plasma generated from truncated Taylor series expansion of radiation source function
22 p3988 A69-40102

Distinction between faint and bright sources of slowly varying solar microwave emission components applied to geomagnetic activity statistics
22 p4020 A69-40306

Identification, position and temperature of solar X ray sources derived from D layer ionization radio absorption behavior during eclipses and lunar reflection
22 p4004 A69-40308

Antenna array synthesis optimization for limited deviations of source distribution function from prescribed function
22 p3916 A69-40952

Galactic X ray sources observed in EM spectrum high energy region, discussing hot plasma cloud thermal radiation and electrons synchrotron radiation as emission sources
23 p4206 A69-42318

Distribution function for thermalization distances derived for infinite atmosphere with plane source in noncoherent light scattering
23 p4192 A69-42403

Transient sources of cosmic rays, discussing possible time variable intensity and momentum spectrum of Galaxy
24 p4367 A69-43006

Cosmic ray albedo-neutron decay source role in intensity measurements of high energy protons trapped on low L shells during satellite flights
24 p4367 A69-43176

Condensation sources of maser radiation observed in W3 hydroxyl lines, discussing polarization and designation as protostars
24 p4389 A69-43769

RADIATION SPECTRA

NT ABSORPTION SPECTRA

NT BALMER SERIES

NT D LINES

NT ELECTROMAGNETIC SPECTRA

NT ELECTRONIC SPECTRA

NT EMISSION SPECTRA

NT FRAUNHOFER LINES

NT H ALPHA LINE

NT H BETA LINE

NT H GAMMA LINE

NT H LINES

NT HERZBERG BANDS

NT INFRARED SPECTRA

NT K LINES

NT LINE SPECTRA

NT LYMAN SPECTRA

NT MICROWAVE SPECTRA

NT PASCHEN SERIES

NT RADIO SPECTRA

NT RAMAN SPECTRA

NT RYDBERG SERIES

NT SOLAR SPECTRA

NT STELLAR SPECTRA

NT TELLURIC LINES

NT UV SPECTRA

NT ULTRAVIOLET SPECTRA

NT VIBRATIONAL SPECTRA

Radiative heat transfer through transmission layers sandwiched between black bodies with variable blackness spectra
02 p0350 A69-11578

Solar flare X ray line and continuum spectra measured with crystal spectrometers aboard orbiting solar observatory
02 p0308 A69-12297

Extensive air showers at sea level, presenting experimental data for muon and electron numbers spectra
03 p0498 A69-12937

Solar X ray flares measurement by rocket and satellite, discussing X ray spectrum hardening, hard flares and SID
03 p0500 A69-13225

Continuum radiation of quasars, adopting cosmological interpretation of red shift
04 p0648 A69-14565

High power stable modes of operation of argon laser, observing stable output spectra
05 p0773 A69-16292

Radiative transfer equation solution for spectral line formed in two dimensionally varying atmosphere extended to continuum radiation in inhomogeneous atmospheres
08 p1386 A69-20077

Photon momentum distribution role and relation to thermal radiation spectrum in fully ionized gases
08 p1357 A69-20747

Radiation spectrum in nonrelativistic fully ionized gas in thermal equilibrium, obtaining dispersion relation for transverse electromagnetic waves and dielectric constant
08 p1357 A69-20748

Argon laser frequency spectrum instability caused by competing axial oscillations
08 p1327 A69-21023

Differential brightness of night airglow spectrum, obtaining rotational temperature by comparison with synthetic spectra
09 p1488 A69-21656

Continuous radiation spectrum of Taurus A in far IR using indium antimonide detector of Rollin type
09 p1597 A69-22156

Spectrum of high energy X ray flux from Sco XR-1 during balloon flight using active collimator detector and graded shield detector
09 p1584 A69-22766

Superhigh energy cosmic ray interaction with neutrinos in universe, shape of cosmic ray spectrum and universe development
10 p1757 A69-22826

Laser radiation spectrum scattered by low temperature plasma electrons at atmospheric pressure
11 p1922 A69-24233

Power output and radiation spectra of trivalent Nd doped liquid lasers based on phosphoryl chloride with tin and titanium chlorides
11 p1894 A69-24620

He-Ne laser radiation frequency spectrum as function of transverse magnetic field determined by photoheterodyne method
11 p1894 A69-24622

Nonuniform standing wave fields spatial distribution in active rod of ruby laser effects on laser radiation dynamic parameters, discussing radiation spectrum width
11 p1901 A69-25756

Remote control spectrophotochronograph to study radiation of high speed high temperature processes, giving construction data and diagrams
12 p2085 A69-26161

Frequency spectrum, time variations and polarization of source of synchrotron radio emission with ex-

panding components flying apart at relativistic velocities

12 p2155 A69-26207

To as unipolar inductor, analyzing interaction with Jupiter magnetosphere and decimetric synchrotron radiation

13 p2337 A69-27552

Stellar atmosphere models of pure hydrogen in hydrostatic, radiative and statistical equilibrium, including Lyman-alpha and continua, discussing nonLTE deviations

13 p2338 A69-27560

RR Lyrae gap stellar model atmospheres including radiation spectra, temperature radiation and convection, etc

13 p2338 A69-27561

Gamma quantum spectrum shape from high altitude X ray film and nuclear emulsion blackening, discussing high energy pion production

13 p2330 A69-28378

Secular instability of steadily rotating stars, analyzing meridional motions in radiation zones by linear perturbation theory

13 p2354 A69-28566

Intermediate band photometry of G, K and M stars in IR indicating continuous stellar radiation deviant from black bodies

14 p2520 A69-29375

Annihilation gamma ray spectra from equilibrium spectra of secondary galactic positrons

14 p2514 A69-29948

Earth atmosphere effect on cosmic ray variations, considering relation between extensive air showers and cosmic ray spectrum

16 p2851 A69-32381

Continuum radiation measurements for bremsstrahlung and recombination of neutral and ionized nitrogen

16 p2823 A69-32466

Radiation diffusion in plane-parallel isothermal gas layer of two and three level atoms, considering stimulated emission and frequency redistribution

16 p2864 A69-32587

Radiative recombination in GaAs, giving edge radiation spectra in p and n type crystals and photoluminescence method for measuring junction carrier concentration distribution

19 p3386 A69-36525

Minority carriers penetration depth in solid aluminum gallium arsenide solutions with variable forbidden bandwidth determined from recombination radiation spectra

19 p3391 A69-36606

Recombination radiation of tellurium and zinc doped GaAs alloy type diodes, discussing luminescence spectra, current-voltage characteristics and temperature effects

20 p3506 A69-37783

Critique of Shivanandan suggestion of background radiation spectrum distortions

21 p3815 A69-39612

Cosmic gamma rays spectrum from neutral pions production and decay in metagalactic cosmic ray p-p collisions, deriving models based on Einstein general relativity theory

22 p4006 A69-40641

Radiative properties of Ta, Mo, Nb, graphite and niobium carbide at high temperatures

23 p4175 A69-41331

RADIATION THERAPY

Negative pion beams for therapy, radiobiology and dosimetry

03 p0371 A69-13478

Mammalian radiobiological studies of effects of heavy particles, discussing therapeutically advantageous characteristics

03 p0374 A69-13499

Tissue pressurized oxygenation during radiation therapy emphasized for overcoming tumor radioreistance attributed to oxygen deficiency

23 p4091 A69-41967

RADIATION TOLERANCE

Radiation resistance of MOS transistors noting relationship with thermal stability, gate oxidation and metals used

02 p0221 A69-12468

NASA Plum Brook Reactor Facility (PBRF) for determining radiation tolerance to support nuclear power application in space for propulsion and power

03 p0465 A69-13128

Permissible radiation doses for extended space missions, discussing clinical tests on dogs

05 p0708 A69-16508

Radiosensitivity of potatoes to gamma ray and proton irradiation applied to whole tubers and to isolated eyes before planting

05 p0709 A69-16511

Thermal performance of pressure transducers, accelerometers, displacement transducers, resistance thermometers and control mechanisms for NERVA reactor

06 p0956 A69-16885

Satellite, spacecraft and rocket components coatings and lubricants, noting high radiation resistance of polyimides

06 p0945 A69-17046

Space radiation effect on spacecraft components and materials simulated by proton and fast electron bombardment of silicon, glass and skin materials

06 p0906 A69-17612

Radiation effects on integrated circuits, stressing components design for maximum tolerance

07 p1113 A69-19779

Synergistic effects of prolonged heat exposure and whole body irradiation with ionizing radiation on survival time in hamsters

08 p1263 A69-20174

Antenna tolerances theory, discussing illumination correlation function analytical evaluation for uniform and tapered illuminations

08 p1284 A69-20294

Radiation resistance of animals in hibernation and hypothermia, noting temperature dependence of protective effect

10 p1643 A69-23126

Limits of human tolerance to localized skin exposure to IR irradiation of various intensities from pain threshold observations, noting skin temperature role

10 p1647 A69-23589

Silicon n-p solar cell behavior during electron radiation, describing radiation resistant solar cell

11 p1825 A69-24871

Far field radiation pattern, radiation resistance, power gain, directivity and effective aperture for center fed dipole antenna with feed points displaced arbitrarily

12 p2039 A69-26352

MOS devices for radiation environments utilizing aluminum oxide as gate insulator for developing resistance to radiation damage

15 p2577 A69-30595

Admissible radiation doses for space crews and ionizing radiation protection, studying long term radiation effects on dogs

15 p2557 A69-31344

Diurnal variations in radiation sensitivity of mice and rats to irradiation with median lethal doses, noting sine curve survival function

15 p2557 A69-31458

Neutron bombardment and ionizing radiation resistance of aluminum oxide MOS devices using gate insulator fabricated by plasma anodization

17 p2935 A69-32888

Permissible radiation doses for extended space missions, discussing clinical tests on dogs

18 p3095 A69-34727

Radiosensitivity of potatoes to gamma ray and proton irradiation applied to whole tubers and to isolated eyes before planting

18 p3095 A69-34730

Unfilled Pyrrone prepared from powder into molded parts for flexural tests at elevated temperatures observed for stability to electron irradiation in air

19 p3356 A69-35529

Solar cells designed to survive exposure to fission/fusion neutrons and electromagnetic spectrum products of nuclear weapon detonation

19 p3251 A69-35689

Lithium-doped silicon solar cells development for radiation environments, discussing contractor functions, dopants, etc

19 p3251 A69-35692

Photoresponse and minority carrier diffusion length long term stability of Li doped solar cells after proton, neutron and electron irradiation

19 p3252 A69-35697

Multilayer lead oxide and cryolite dielectric coatings stability to ruby laser radiation, noting breakdown coherent radiation power densities

19 p3334 A69-35886

Supralethal doses of pulsed mixed gamma-neutron radiations from TRIGA reactor administered to unshielded, head shielded and trunk shielded beagles

19 p3259 A69-36459

Amorphous semiconductors based on noncrystalline materials compared to crystalline materials, noting radiation damage resistance

19 p3392 A69-36660

Radiation exposure during orbital flight assessed for adverse effect on space stations and laboratories personnel, discussing shielding and dose rate tables

20 p3481 A69-37339

Silicon dioxide film doped with Al to increase MOS structure radiation resistance

20 p3584 A69-38070

ESR comparative study of selenoamino acids and S analog radical formation and radiation resistance, noting selenium groups ability as acceptors for unpaired electrons

21 p3668 A69-38425

Nervous system reactions and resistance to ionizing radiation noting role of functional, morphological and physicochemical changes in nerve tissues

21 p3659 A69-39061

Survival rates of continuously cultivated Chlorella plants in air-carbon dioxide atmosphere after single exposure to gamma radiation, using microcolony counting technique

22 p3876 A69-40275

Radiation hardened microcircuits and transistors for protection against transient radiation released by nuclear weapons

23 p4135 A69-41528

Radiation damage in chlamydomonas, discussing dark repair activities

23 p4090 A69-41964

Radiation effects on population kinetics of granulocyte system forming bone marrow, discussing radiosensitivity and radiation-induced granulocytopenia

23 p4090 A69-41965

Tissue pressurized oxygenation during radiation therapy emphasized for overcoming tumor radioreistance attributed to oxygen deficiency

23 p4091 A69-41967

Cross sections of charge carrier capture by ions in gamma irradiated P-Al-Si glass with metal oxides additions measured for evaluating radiation stability improvement

23 p4180 A69-42470

Radiation hard device specifications, comparing data with environmental considerations

24 p4287 A69-43204

RADIATIVE HEAT TRANSFER

Radiant heat transfer in optically thick gray gas situated between parallel black diffusively emitting walls, using matched asymptotic expansion method

01 p0178 A69-11411

Radiative heat transfer through transmission layers sandwiched between black bodies with variable blackness spectra

02 p0350 A69-11578

Romanova method for solution of scalar equation of radiative transfer in plane parallel atmosphere

02 p0319 A69-12106

Radiant heat transfer prediction methods checked for validity and accuracy by irradiation measurements with materials of various surface properties [ASME PAPER 68-HT-42]

02 p0351 A69-12206

Heat transfer efficiency of triangular radiating fin in diathermal medium producing aerodynamic heating

02 p0354 A69-12490

Gray radiation and conductive heat transfer in Oseen-like free mixing flow, computing temperature distribution by inversion integral

02 p0354 A69-12504

Downstream radiation flux distribution calculated for blunt entry bodies, considering self absorption effects

02 p0354 A69-12547

Eddington approximation to solve radiative transfer equation

02 p0282 A69-12703

Probabilistic model for scattering function to solve radiative transfer problems in externally illuminated spherical shell atmosphere with perfectly absorbing core

02 p0328 A69-12751

Radiative heat loss effect on atmospheric cellular convection, analyzing critical Rayleigh number and width to height ratio of cells

02 p0276 A69-12776

Long wave radiative heat flux in boundary layers of cloud during solid overcast, discussing dependence on various cloud and atmospheric parameters

03 p0458 A69-13271

Radiative transfer equations solved for electron scattering stellar atmosphere, using transformation of integrodifferential transfer equations into singular integral equations

03 p0466 A69-13351

Reentry shock layer radiative heat transfer to surface of blunt superorbital vehicle [AIAA PAPER 68-1151]

03 p0532 A69-13560

RADIATION THERAPY

Atmospheric gas composition effects on shock layer radiative heat transfer and heat shield response in Venus entry simulated by earth reentry
[AIAA PAPER 68-1148] 03 p0412 A69-13672

Composite heat transfer by conduction and radiation in nongray medium, outlining electronic computer program for numerical solutions 03 p0533 A69-13884

Biot variational principle applied to combined conduction and radiation heat transfer 04 p0685 A69-14734

Correlations of stagnation point radiative heat transfer for earth reentry, noting use of nongray absorption coefficient models 04 p0685 A69-14736

Nongray radiation absorption coefficients reformulation employing alternative angular moment averaged absorption coefficients with emission/Planck/ 04 p0686 A69-14744

Flux equivalences of reflected and transmitted radiation among Rayleigh, isotropic and other scattering models 04 p0687 A69-15281

Reflection and transmission of radiation from very thick and semiinfinite homogeneous atmospheres with arbitrary phase function, using asymptotic fitting method 04 p0595 A69-15285

Thin foil heat flux sensor for radiative and convective heating rates over wide range and dynamic response, noting error mechanisms, calibration and accuracy 04 p0602 A69-15426

IR radiation heat transfer in polyatomic gases in limit of large path lengths 05 p0844 A69-15579

Energy transfer from radiating sphere to medium with molecular heat conduction 05 p0845 A69-15782

Regular thermal conditions in solid bodies with radiative heat transfer 05 p0845 A69-15896

Finned radiation emitter tube unsteady state temperature field as function of working body temperature and emitter geometry 05 p0846 A69-15898

Heat transfer in turbulent pipe flow of radiating optically thin gas in circular tube
[ASME PAPER 68-WA/HT-17] 05 p0847 A69-16121

Discrete radiative transfer in nonhomogeneous slabs, giving matrix solution 05 p0849 A69-16480

Radiative heat transfer between parallel plates separated by nongray gas with picket fence absorption coefficient using integral equations 06 p1033 A69-17554

IR radiative heat transfer in nongray gases for non-black bounding surfaces, considering diatomic gases with single vibration rotation band 06 p1033 A69-17559

Optimized radiative heat transfer systems performance, comparing tubular radiators with various fin geometries and systems with belt radiator 06 p1033 A69-17600

Optimizing radiating system consisting of radially diverging conical heat removing projections attached to cooled isothermal sphere 06 p1033 A69-17603

Inverse problems in radiative transfer applied to remote measurements of IR radiation from planetary atmospheres, noting temperature and water vapor inversions 06 p0919 A69-17617

Mathematical techniques for treating satellite based atmospheric data involving radiative transfer equation inversion, noting scattering and temperature measurement problems 06 p0957 A69-17618

Relaxation method for inversion of full radiative transfer equation, determining temperature profile in atmosphere from outgoing radiance
[JPL-TR-32-1351] 06 p0922 A69-17805

Combined radiation and conduction heat transfer equation applied to temperature profile around opaque hollow sphere and in solid condensed gas layer
[SAE PAPER 690197] 07 p1239 A69-18303

Thermal disturbance radiative decay time in carbon dioxide at low pressures and for nonzero vibrational relaxation times 07 p1215 A69-18843

Radiative-convective heat transfer in gray gas plane layer blown into turbulent flow past permeable plate 07 p1242 A69-18991

Radiative transfer equation for pure molecular scattering inverted for estimating vertical ozone distribution 07 p1126 A69-19042

Optical properties of hot air used to solve radiative transfer problems, including emissivities and absorption coefficients calculations 07 p1185 A69-19167

Radiative transfer iteration for gray medium between concentric spheres and for constant heat generating spherical region imbedded in gray medium 08 p1420 A69-20152

Thermal gradients in artificial satellites, considering heat exchange among various points of closed cavity surface by gray body diffuse radiation and reflection 08 p1421 A69-20157

Radiative-conductive heat transfer in plane layer of gray heat conducting medium, solving energy equation 09 p1621 A69-21433

Energy transfer in gases transmitting heat by interaction of thermal conduction and IR radiation 09 p1621 A69-21442

Temperature field in thin walled rods with spiral coil cross section in solar radiation, considering radiant heat exchange 11 p1999 A69-24779

Radiant heat transfer in hypersonic aerodynamic heating, discussing radiant flux and carbon dioxide concentration in reentry problems 11 p2002 A69-25233

Temperature variation and heat transfer in fins and relations between heat-flux-density and temperature difference 12 p2190 A69-25763

Long wave radiation fields calculations based on radiation transport equations, identifying differences between associated transmission functions 12 p2125 A69-25951

Thermosphere radiative cooling by atomic O 62 micron line, noting cooling and heating rates 12 p2064 A69-26009

Heat transfer in solid bodies, deriving thermal conductivity equation and surface boundary conditions in presence of radiative energy transfer 13 p2373 A69-27584

Radiative heat transfer of materials, discussing spectrum characteristics 13 p2373 A69-27768

Differential approximation for radiative transfer between concentric spheres enclosing gray gas
[ASME PAPER 68-HT-21] 13 p2373 A69-27774

Combined conduction and radiation transfer equations solutions for absorbing-emitting gas, obtaining slip coefficient for diffusion solution correct boundary condition 13 p2374 A69-27784

Radiative thermal losses of K in gases for MHD flow 13 p2308 A69-28022

Radiative heat transfer, discussing electromagnetic theory, transfer between surfaces and simultaneous conduction, convection and radiation 13 p2376 A69-28140

Radiative transfer between two concentric gray opaque spheres separated by radiating gray gas, employing Fredholm equations 13 p2377 A69-28149

Thermal behavior of space vehicle window systems predicted by mathematical analysis and computer methods for heat transfer through glass
[AIAA PAPER 68-65] 13 p2378 A69-28215

Energy transfer by simultaneous conduction and radiation between two media in intimate contact, detailing numerical solution method for resulting coupled nonlinear integrodifferential equations 13 p2378 A69-28340

Atmospheric ozone vertical distribution and total amount determined by radiative transfer and perturbation theory, presenting error analysis 13 p2255 A69-28493

Long wave radiative heat flux in boundary layers of cloud during solid overcast, discussing dependence on various cloud and atmospheric parameters 14 p2471 A69-28779

Radiative heat transfer calculations between parallel surfaces, applying approximations based on total emissivities to known spectral emissivities 14 p2539 A69-29223

Radiating gray gas laminar jet in thermodynamic equilibrium ejected from plane nozzle into wake analyzed using boundary layer, divergence and transfer equations 14 p2432 A69-29612

Radiation in atmospheric circulation, considering radiative equilibrium, cloudiness and surface interactions, surface temperature and heat input 14 p2477 A69-29826

Climate studies with allowance for radiative heat inputs, constructing nonadiabatic motions model for improving prognosis 14 p2477 A69-29827

Radiation method for temperature and heat flux measurement, discussing transducer with thermopile as sensor 15 p2607 A69-30154

Substitute kernel approximation for acoustic waves radiative transfer equations for nongray gas near equilibrium 15 p2717 A69-30799

Radiative luminescence of gas discharge plasmas in channel with substantial radial heat transfer determined from energy balance measurement 15 p2662 A69-30978

Radiative energy transfer through nongray absorbing and emitting medium generating heat with graphical presentation of temperature distribution and flux 15 p2718 A69-31153

Macroscopic quasi-linear theory of HF radiation in cold electron-proton plasma allowing direct use of plasma and Maxwell equations 16 p2819 A69-31684

Approximate expression for temperature dependent radiative heat flux in optically thin gas, considering reentry body hypersonic flight 16 p2877 A69-31892

Radiative heat transfer in nonisothermal scattering media of plane, spherical and cylindrical geometries separated by particle cloud 16 p2878 A69-31925

Heat pipes design for rocket engines cooling, discussing connections to space radiator and to heat rejection device and heat transfer capability
[AIAA PAPER 69-582] 16 p2839 A69-32668

Nongray equilibrium radiative heat transfer in viscous radiating shock layer around blunt body entering high temperature nonisothermal carbon dioxide-nitrogen atmosphere
[AIAA PAPER 69-636] 17 p3070 A69-33258

Radiant heat transfer predictions between isothermal plates based on diffuse plus specular directional property model
[AIAA PAPER 69-624] 17 p3070 A69-33259

Apparent thermal radiation properties for one dimensionally rough surface, discussing variance with property models employed in engineering analysis of radiant transfer
[AIAA PAPER 69-622] 17 p3071 A69-33271

Heat pipe devices applied to radiative body heat transfer in space suit temperature control
[AIAA PAPER 69-619] 17 p2914 A69-33293

Radiative heat transfer in nonisothermal media composed of spherical particles with complex refractive index emitting absorbing and scattering energy anisotropically, considering various geometries
[AIAA PAPER 69-626] 17 p3073 A69-33297

Heat transfer in evacuated multilayer insulation by radiation and conduction, considering optically thin media separating reflective layers
[AIAA PAPER 69-607] 17 p3073 A69-33300

Normal and directional emittance for two dimensional emitting, absorbing and scattering semiinfinite plane slab based on Monte Carlo method compared with Bobco approximation
[AIAA PAPER 69-625] 17 p3005 A69-33301

Radiative and conductive heat transfer in heated finite gaseous body with emphasis on collisional and radiative relaxation, noting cooling as two stage process
[AIAA PAPER 69-638] 17 p3073 A69-33311

Radiative and conductive heat transport mechanisms at cryogenic temperature applicable to thermal energy transport minimizing technique in containment system 17 p3074 A69-33680

Temperature fluctuations in solar photosphere, noting transition from convective to radiative energy transport 17 p3040 A69-33810

Radiation gas dynamics in shock tube, studying radiation coupled flows with flow field affected by radiant energy transport 18 p3116 A69-34447

Orthonormalization methods applied to heat conduction, convection and radiation problems, noting digital computer programs modifications 18 p3229 A69-34662

Materials integral hemispheric radiative capacity determination based on cooling rate of thin walled 18 p3229 A69-34662

specimen in vacuum, considering stainless steel, Ni and Cu

18 p3156 A69-34698

Local radiation characteristics calculation method, consisting of reducing integral equations to linear algebraic equations, applied to solve radiative heat exchange problems

18 p3229 A69-34713

Heat transfer coefficient approximation under thermal instability conditions complicated by radiant heat exchange at plate surface, noting aircraft design applications

18 p3230 A69-34984

Energy transfer from radiating sphere to medium with molecular heat conduction

18 p3230 A69-35034

Radiant heat transfer integral equations solutions accuracy determined from differences between geometric and resolving angular emission factors

18 p3230 A69-35119

Temperature distribution around radiating sphere in homogeneous gas medium with molecular heat transfer, solving energy transport equation

18 p3231 A69-35325

Partial differential equation representing influence of radiative and turbulent transfers of atmospheric heat, based on absorption coefficients for terrestrial radiation

19 p3363 A69-36498

Radiative heat transfer in polycrystalline corundum, studying photon thermal conductivity influence on lattice thermal resistivity

20 p3565 A69-36975

Stagnation point heating in hypersonic gas flow past blunt bodies, considering radiative transfer effects on shock wave temperature and density distribution, wave separation, etc

20 p3457 A69-36981

Combined heat transfer by radiation and conduction in disperse media /thermal insulation/ described by system of nonlinear integrodifferential equations

20 p3631 A69-37097

Temperature and fluid distribution in porous solid subjected to large suction, convective heating and radiative cooling on one surface

20 p3514 A69-37225

Boundary conditions for differential approximation to radiative transfer, noting optically thick slip conditions

20 p3633 A69-37524

Temperature and pressure relations in power plant with closed gas cycles with radiative heat transfer, noting radiation area reduction influence

20 p3464 A69-37603

Fourier heat equations functional corrections for determining temperatures of plate and cylinder heated simultaneously by radiation and convection

21 p3848 A69-38641

Radiative heat input to artificial satellite in orbit due to solar and earth radiations calculated and presented in graphs for satellite temperature calculation

22 p4006 A69-40589

Radiative transfer in interior of two concentric spheres in motion assuming low density of residual gas

22 p4031 A69-40907

Radiative energy transport in moving gaseous media in local thermodynamic equilibrium, assuming spectral line shifts by temperature and pressure variations

22 p3982 A69-41018

Combined heat transfer calculations, considering moving radiating media and simultaneous convection or conduction

23 p4237 A69-41328

Absorptivity of nonuniformly heated thin walled cylindrical radiator with central radiating hole, calculated by forward-reverse and integral methods

23 p4238 A69-41332

Mars atmosphere response to surface temperature changes by radiative and convective heating, noting strong solar control of mean wind distribution

23 p4212 A69-41614

Radiative heat transfer in nonisothermal absorbing and emitting media without scattering and with anisotropic and isotropic scattering

23 p4239 A69-41632

Radiative transfer effects in low Reynolds number or merged layer regime of hypersonic flow about axisymmetric blunt bodies, including thin shock layer theory

23 p4059 A69-41885

Arc heating of shock tube driver gas, describing radiative energy transfer mechanism

23 p4147 A69-41895

Space radiator system with hybrid, water heat pipes to transport waste heat from radioisotopic thermoelectric generator

23 p4190 A69-42304

Orographic inhomogeneities of underlying surfaces for radiating atmospheric waves formation, deriving formulas for plane stable atmosphere

23 p4185 A69-42492

Atmospheric gas composition effects on shock layer radiative heat transfer and heat shield response in Venus entry simulated by earth reentry

[AIAA PAPER 68-1148] 24 p4394 A69-43248

Radiant energy transfer in absorbing and emitting media, noting approximate equations reduced to correct optically thin and thick limits for multidimensional problems

[ASME PAPER 69-HT-E] 24 p4410 A69-43524

Radiative transport in nongray cylindrical medium using total band absorbance

[ASME PAPER 69-HT-38] 24 p4411 A69-43534

One dimensional numerical solution for steady state thermal behavior of trapezoidal profile annular fins transferring heat by conduction and radiation

[ASME PAPER 69-HT-6] 24 p4413 A69-43553

Reentry shock layer radiative heat transfer to surface of blunt superorbital vehicle

[AIAA PAPER 68-1151] 24 p4414 A69-43567

Lateral heat conduction and radiation along two parallel long plates separated by nonabsorbing dielectric with refractive index of unity

24 p4415 A69-43594

Quasi-isotropic semigray radiative transfer prediction using nongray model in bounded plane-parallel geometries for gas with spectrum from free-free processes

24 p4415 A69-43673

Heat conduction problems associated with radiant exchange in shells under discontinuous solar flux, considering spacecraft structures, illumination theory and astrophysics

24 p4416 A69-43689

RADIATIVE RECOMBINATION

Shock front structure in radiative relaxation region in atomic H, calculating Lyman continuum effects

01 p0122 A69-10125

Ionization, neutralization and charge exchange processes in ionosphere, detailing dependence of photodissociation and collision detachment of negative ions

01 p0066 A69-10598

Recombination radiation from excitons and free carriers in epitaxial GaAs with impurities at liquid He temperatures

01 p0140 A69-11253

Mechanical thermal stresses effects during laser flash illumination of GaAs, discussing temperature dependence of radiative recombination

02 p0256 A69-12245

Laser transition and photon energy of lightly doped GaAs, showing many body electron-hole- lattice interactions

02 p0257 A69-12615

Radiative recombination in p-n junctions in InP at various temperatures

03 p0492 A69-14166

Luminescence spectra due to radiative recombination of optically injected carriers in Co 60 gamma ray and neutron irradiated Si at low temperature

03 p0494 A69-14243

Recombination radiation of tellurium and zinc doped GaAs alloy type diodes, discussing luminescence spectra, current-voltage characteristics and temperature effects

05 p0729 A69-16210

Stimulated radiative recombination process for ramjet propulsion, investigating delay chamber required for vibration-to-translation conversion

06 p0984 A69-17630

Radiation transfer in resonance lines and in recombination continuum in plasma, discussing frequency redistribution during reradiation and optically dense systems

07 p1188 A69-18282

Oscillator forces and photoionization and photorecombination cross sections of electron transitions in hydrogen atom, considering approximation for total radiation probability

09 p1588 A69-21365

Radiative and collisional ionization of H and He in planetary nebulae, discussing dielectronic recombination at high electron temperatures

14 p2518 A69-29133

Hydrogen recombination in hot universe model, discussing emission of energetic quanta

15 p2690 A69-30734

Continuum radiation measurements for bremsstrahlung and recombination of neutral and ionized nitrogen

16 p2823 A69-32466

Oscillator forces and photoionization and photorecombination cross sections of electron transitions in hydrogen atom, considering approximation for total radiation probability

18 p3197 A69-34755

Radiative recombination of atomic oxygen ions in nighttime F region UV radiation detected by polar-orbiting OGO 4 satellite

18 p3129 A69-34957

Radiative recombination in GaAs, giving edge radiation spectra in p and n type crystals and photoluminescence method for measuring junction carrier concentration distribution

19 p3386 A69-36525

Injection lasers external quantum efficiency, stimulated and spontaneous emission and photoluminescence measurements

19 p3337 A69-36528

Coherent recombinational radiation of semiconductors excited by electron beam

19 p3387 A69-36539

Minority carriers penetration depth in solid aluminum gallium arsenide solutions with variable forbidden bandwidth determined from recombination radiation spectra

19 p3391 A69-36606

Fe-doped p-type gallium arsenide single crystal radiative recombination emission during current carriers transition from deep acceptor level into valence band

19 p3392 A69-36611

Recombination radiation of tellurium and zinc doped GaAs alloy type diodes, discussing luminescence spectra, current-voltage characteristics and temperature effects

20 p3506 A69-37783

Radiative recombination in GaAs p-n structures having region with concentrations of Ge atoms

21 p3780 A69-39044

Ionic excited states statistical equilibrium populations calculated for various electron densities and temperatures including effects of dielectronic, radiative and three body recombinations

22 p3985 A69-40666

RADIATORS

Radiation models using discrete radiator ensembles having applications to analysis of forward and backscatter from rough surfaces, clutter and chaff models, etc

01 p0030 A69-10556

Phased array antenna radiator element design, emphasizing configuration selection and reflection loss for beam steering

04 p0572 A69-14321

Monopulse parabolic antenna radiator design for decimeter and meter wavelengths, discussing characteristic properties at optimal dimensions

17 p2939 A69-33905

Antenna design, based on helical beam radiator data, providing checking facility giving automatic alarm

24 p4312 A69-42573

RADICALS

Ion pairing effects of cyclooctatetraene anion radical, studying electron spin resonance spectra temperature dependence

10 p1651 A69-22938

Ionic and biradical mechanisms in thermal and photois-trans isomerizations elucidated by planar and twisted configurations of polyenes

13 p2216 A69-27618

HO2 radical detection in rarefied H flame produced by HF discharges, recording high amplitude signals

15 p2716 A69-30054

RADII

Ionized meteor trails initial radii statistical characteristics determined for two models

10 p1783 A69-23917

Single and cladged glass fibers radii and refractive indices measurements on basis of laser light scattering

11 p1918 A69-25044

Neptune radius, density and atmosphere deduced from observations during occultation of BD minus 17 degrees 4388 by Neptune

17 p3041 A69-33816

Lunar gravitational potential and lunar surface radius vector binomial series coefficients determination from Luna 10 data used for lunar surface shape calculations

20 p3596 A69-37308

Ancient and present earth radii ratios determined by triangulation using paleomagnetic sites situated on different paleomeridians
22 p3937 A69-40183

RADIO ALTIMETERS

Avionics in forest resource inventories management, noting design of radar altimeter for low level aerial photography
01 p0080 A69-10352

Spacecraft radar altimetry with application to geodesy, discussing orbital and tracking errors
15 p2609 A69-30460

Spacecraft radar altimetry applied to study of sea surface slopes, tides, tsunamis, storm surges and submarine geology
15 p2609 A69-30461

FM radioaltimeter for Concorde aircraft, describing autocorrelation and automonitoring device, signal characteristics, reliability, etc
19 p3315 A69-36699

RADIO ANTENNAS

Mechanically despun VHF antenna for spin stabilized synchronous satellites, detailing electrical and mechanical design
01 p0161 A69-10350

Large paraboloid radio antennas structural setting for minimizing effects on performance due to deformation of surface by gravitational forces
06 p1023 A69-17372

Statistical theory of traveling wave antennas for random phase-amplitude distribution of current, discussing phase errors
06 p0898 A69-17797

TV transmission antenna radiation patterns measured with helicopter flown equipment and Decca navigation equipment
08 p1274 A69-20130

Failure causes for planetary reduction gear tooth for adjustment of radio telescopic antennas, studying fracture characteristics, working conditions and loading moments
08 p1321 A69-20853

Hertzian radiometric antennas and signal processing techniques for aerial mapping project for sun
08 p1290 A69-20976

Construction of large parabolic antennas for radio astronomy and satellite communication, noting dimensional accuracy, directional precision and dynamical behavior
09 p1476 A69-21650

Large aperture satellite communication antenna gain measurement technique, using extraterrestrial radio wave source or satellite
09 p1456 A69-22116

Multimode tracking/SYMMTRAC I and II/ feeds for low noise antennas, noting feed performance
11 p1852 A69-25317

Antenna switch for cascading and separating RF channels of high power wideband broadcasting systems
11 p1854 A69-25617

Noise sensitivity of space diversity reception system with narrow beam electrically switchable antennas for incomplete beam separation
12 p2030 A69-26485

Number 2 ground communications antenna system on Goonhilly Downs for British Post Office earth station
12 p2044 A69-26923

Microwave radiometric sensor operational principles and capabilities, discussing antennas and radiometric receivers
12 p2033 A69-26976

Soviet monograph on intrinsic noise emission in radio channels covering noise temperature at receiver input, thermal microwave radiation, etc
13 p2219 A69-27304

Two antenna radio direction finding system statistical synthesis, using quadratic linear process
15 p2562 A69-30110

Aoriste antenna to receive radioelectric signals from satellite emitter at distance of 10,000 km
15 p2580 A69-31095

Wideband frequency switch to connect narrow band auxiliary to wideband radio system antenna, describing components
16 p2759 A69-31861

Radio antenna consisting of truncated confocal paraboloids, discussing pencil beam pattern, antenna parameters and experimental results
17 p2939 A69-33904

Canadian radio observatory 150 ft telescope antenna, discussing dish structural feature for resisting gravity, wind and thermal stresses
23 p4149 A69-42134

RADIO ASTRONOMY

Planetary nebulae radio emission, observed with pencil beam of radio telescope, confirming thermal spectrum at radio frequencies
01 p0157 A69-11291

Space diversity reception as applied to radio astronomical investigation of large scale ionospheric inhomogeneities
02 p0237 A69-11665

French radio astronomy, presenting sky background radiation and solar emission results from Rubis 02 and 04 rockets
02 p0316 A69-11908

Radio telescope for Owens Valley Radio Observatory, noting interferometer array of steerable antennas and signal wavelength influence on telescope reflector accuracy
02 p0229 A69-11974

Radio signals from hydroxyl radicals by maser action in early stars, noting emission magnitude and intensity spectrum dissimilarity at different frequencies
02 p0324 A69-12493

Measurements of pulsars CP 0834, CP 0950, CP 1133 and CP 1919, discussing pulse intensities and shape, submillisecond structure, intensity variations, periods and positions
02 p0328 A69-12726

Radio galaxies and quasars, discussing radio structure, observation methods, polarization, time variation, etc
02 p0329 A69-12791

Energy sources and properties of quasars and radio galaxies by X ray astronomy
02 p0310 A69-12793

Radio star scintillation data, establishing periodic variations in rates within 1 to 1.5 years
03 p0505 A69-13081

Man-made and natural spatial communications
03 p0394 A69-13577

Ariel 3 receiver for measuring galactic noise spectrum, discussing loop antenna use with swept receiver, false terrestrial signals, etc
03 p0404 A69-13581

Submillimeter wave observation of sun to study anomalous absorption region
03 p0513 A69-13774

Solar wind turbulence properties deduced from radio astronomical measurements
03 p0502 A69-14001

Radio spectra differences of quasars and radio galaxies, noting influence of frequency levels
04 p0652 A69-14418

Radio spectrometer with paramagnetic quantum amplifier for astronomical spectral measurements in 8 mm range
04 p0597 A69-14851

Sporadic E irregularities in producing amplitude variations in radio star observations and satellite transmission
04 p0594 A69-15125

Protostars as sources of anomalous OH emission, discussing densities, masses and temperatures of OH condensations
04 p0661 A69-15143

Venus observation at 4.52 cm showing 654 K mean brightness temperature, negligible phase variation and polarization indicates thick atmosphere
05 p0818 A69-15601

Submillimeter wavelength astronomy noting instruments, prestellar matter, interstellar and intergalactic matter state and composition, IR stars, planetary atmospheres, etc
05 p0821 A69-15843

Space radio astronomy techniques for problems in galactic radio emission, solar studies and planetary observations
05 p0821 A69-15844

Radio astronomical methods for total atmospheric absorption of radio waves by atmospheric thermal radio emission measurements based on sky brightness temperature
05 p0723 A69-16779

Radio spectra of supernova remnants Cygnus Loop and IC443, noting possible radiation from shell source
06 p1003 A69-17322

Lunar occultations of galactic center region observed at 1667 MHz indicating OH absorption origin in uniform rotating cloud
06 p1009 A69-17961

Pulse intensity variations in pulsars observed at 113 MHz with parabolic antenna using photographic recording techniques, noting lack of periodicities
06 p1009 A69-17964

Radio sources detected in HF surveys not listed in 4C catalog
06 p1010 A69-17974

Joint radio-optical observations of flare star UV Ceti in Australasia during September-October 1967
07 p1214 A69-18666

Radio telescope survey of intense emission regions along galactic plane, considering antenna temperatures, spectrum and steps of observed emission
07 p1216 A69-19138

Radio sources flux densities from fan beam survey using Molongo radio telescope compared to flux densities of Parkes catalog, presenting revised spectra
07 p1218 A69-19278

HF radio radiation from planetary nebulae
08 p1384 A69-20056

Interplanetary scintillations of 3C 279 and CTA 21 combined to derive solar wind density fluctuation model, using random thin screen theory
08 p1385 A69-20069

Solar radio astronomy, discussing quiet sun radio emission, solar activity, slowly varying radio emission, radio bursts and possibility of observing lines
08 p1388 A69-20218

Galactic neutral hydrogen structure in region of Cygnus observed with parabolic antenna and frequency-switched radiometer
08 p1388 A69-20243

Photographic magnitudes of stars in various open clusters based on UVB system and photoelectric sequence
08 p1389 A69-20245

Quasars optical and electrical properties, distance, nature and role in cosmology
08 p1390 A69-20377

Galactic H 56 alpha recombination radio line observation in Omega Nebula in millimeter band with radio telescope, obtaining electron temperature
08 p1397 A69-20771

Microwaves from celestial objects noting radio emission from sun, moon and Jupiter, cosmic fireball and pulsars
08 p1407 A69-21125

Space systems and radio astronomy - Conference, Geneva, September-October 1968
09 p1448 A69-21268

Space systems and radioastronomy - Conference, Geneva, September-October 1968, Part 2
09 p1450 A69-21285

RF spectral lines due to OH molecule detected in interstellar space in absorption of RF radiation from Casiopeia A source
09 p1586 A69-21295

Astronomical data on background radiation examined for existence of galactic radio halo
09 p1590 A69-21395

Vela pulsar polarization and periodicity observations supporting rotational model vs radial pulsations as radio emission source
09 p1592 A69-21461

Crab Nebula pulsar properties including pulse shape, dispersion and strong pulse emission
09 p1592 A69-21462

Pulsars rotating neutron star model analyzed on basis of magnetic dipole rotating in vacuo
09 p1592 A69-21463

Neutral hydrogen content and distribution of late type spiral galaxy NGC 6946 from 21 cm line measurements
09 p1598 A69-22187

Venus and Jupiter observations by earth paraboloid antenna, discussing average brightness temperatures and upper limit for Venus water vapor abundance
09 p1600 A69-22206

Radio telescopic survey for OH emission at 1667 MHz in interstellar dust clouds for catalog compilation, tabulating results
09 p1603 A69-22267

Solar outburst and storm accompanying 9 June 1968 flare, noting radio evidence for coronal instability before flare
09 p1582 A69-22747

Solar radio astronomy in Australia including solar atmosphere, bursts, instruments, etc
10 p1777 A69-23383

Radio astronomical investigations of small scale inhomogeneity motion and dimensions in interplanetary plasma, using observations of 3C 48 scintillations in 1967
10 p1782 A69-23711

Crab Nebula radio emission spectrum in decimeter wavelength range indicating emission spectral index decrease from Taurus A
10 p1784 A69-23941

- Radiophysics Laboratory /Sidney/, discussing radio astronomy, radioheliographs, radio telescopes, cloud physics and research
10 p1784 A69-23988
- Quasars time dependent flux density variations at 6.6 cm, noting spectrum peaks tendency toward lower frequencies with time
11 p1954 A69-24382
- Solar flares theories, discussing data acquisition by space research and solar radio astronomy
11 p1946 A69-24516
- Pulsar PSR 0833-45 period decrease and rate of change in period increased between 24 February-3 March 1969, discussing contraction explanation
12 p2154 A69-25878
- Pulsar distances estimated from neutral hydrogen absorption, using observations from 140 ft telescope
12 p2156 A69-26224
- Pulsar NP 0527 near Crab Nebula noting long period
12 p2156 A69-26227
- Rotating central disk in galactic plane observed by radio telescope, assessing relation between expanding gas of disk and high velocity stream from center
12 p2163 A69-27018
- Velocity distribution and density of neutral hydrogen in southern portions of M 31 and Sc-type galaxy M 33 by 75 m radio telescope
12 p2166 A69-27038
- Radio sources angular dimensions determined by microwave interferometry, discussing distinctions between quasars, galaxies and unidentified sources
12 p2166 A69-27039
- Frequency spectra of radio galaxies, supernova remnants and quasars observed by radio telescope operating in decimeter wave range
12 p2167 A69-27041
- Quasar spectra changes observed from 1962 to 1966 including flux density and antenna temperature for 3C 279 at cm wavelengths
12 p2167 A69-27043
- Quasars intensity variations at various cm wavelengths confirming wavelength dependence
12 p2167 A69-27045
- Extragalactic radio sources, discussing brightness distribution measurements and radio star scintillations
12 p2168 A69-27053
- Periodicity decrease on 24 February to 3 March 1969 in decay of Molonglo pulsar PSR 0833-45
12 p2172 A69-27167
- Galactic magnetic field along Orion arm from dispersion and rotation measures of linearly polarized radiation from pulsar psr 0833-45
13 p2335 A69-27311
- Lambda-doublet radiation from excited state of interstellar OH detected at 5 cm wavelength
13 p2335 A69-27312
- Astronomical maps of integrated hydrogen density, dispersion and velocity of high galactic latitude neutral hydrogen concentration, discussing kinetic temperature
13 p2347 A69-27718
- Neutral hydrogen cloud observed at high galactic latitude, discussing top intensity velocity, peak intensity dispersion, age, hydrogen mass and density
13 p2347 A69-27719
- Extragalactic radio sources parameters analyzed for distinguishing quasars from dominant luminous radio galaxies by radio spectra
13 p2348 A69-27801
- HF emission spectra of radio pulses from cosmic ray showers confirming Dublin group observations
13 p2333 A69-28471
- Troposphere effects on millimeter wave radio astronomy measurements, discussing solar noise fluctuations due to clouds and precipitation
13 p2223 A69-28607
- Space diversity reception as applied to radio astronomical investigation of large scale ionospheric inhomogeneities
13 p2257 A69-28696
- Radio star scintillation data, establishing periodic variations in rates within 1 to 1.5 years
14 p2515 A69-28763
- Radio astronomical observations of shape and drift velocity of focusing ionospheric discontinuities
14 p2436 A69-29054
- Contour maps of Milky Way continuum radiation at 1410 and 2650 MHz from low latitude survey, listing sources with estimates of flux density
14 p2526 A69-29772
- Radio spectrometer with paramagnetic quantum amplifier for astronomical spectral measurements in 8 mm range
15 p2607 A69-30243
- Decametric radio astronomy at frequencies from 10 to 40 MHz on wideband telescopes, discussing spectral types of discrete radiation sources
15 p2682 A69-30501
- Extratmospheric long and short wave radio astronomy since first artificial satellite, including device carriers effectiveness of earth satellites, lunar orbiters, rockets and balloons
15 p2682 A69-30504
- Optical and radio estimations of galactic masses, analyzing radius of rotation curve inflection point
15 p2687 A69-30547
- Radio astronomical research developments including structural requirements for 100 m telescope
15 p2589 A69-30864
- RF spectral lines due to OH molecule detected in interstellar space in absorption of RF radiation from Cassiopeia A source
15 p2697 A69-31226
- Planet Venus data from Venera 4, Mariner 5, radio astronomical and radar measurements
15 p2698 A69-31360
- Doppler effect significance in radio astronomy including galaxies relative motion and information concerning isolated hydrogen clouds between galaxies
16 p2853 A69-31565
- Trieste astronomical observatory optical and radio solar photosphere observations in 1967, including solar cycle and north-south symmetry
16 p2858 A69-32206
- Pulsars Mp 0450, Mp 1642 and Mp 1818 discovery, discussing role of Molonglo radio telescope and pulse amplitude variations in detection
17 p3026 A69-32857
- Pulsed radio source CP 1919 detection at 13 cm wavelength with maser receiver and 210 ft antenna
17 p3036 A69-33637
- Cryogenic applications to low noise reception development in radio astronomy, planetary radar and communication with deep space probes
17 p2921 A69-33685
- Interstellar neutral hydrogen in mean galactic latitudes noting two different component types
17 p3039 A69-33766
- Frequency bands allocations for space research and radio astronomy development, noting Inter Union Commission of Frequency Allocations recommendations
18 p3100 A69-34376
- Pulsars observed for average energies at centimeter wavelengths, using azimuth elevation antenna
18 p3196 A69-34644
- Discrete radio sources spectra at decametric wavelengths, showing variation with frequency and radio wave generation mechanism leading to various spectral types
18 p3200 A69-35134
- Radio and radar astronomy with reference to extragalactic sources and solar system, noting astronomical instrumentation
19 p3425 A69-36430
- Crab Nebula radio brightness at 2.16 and 8.2 mm measured and compared to Jupiter flux density
19 p3428 A69-36875
- Detector radiometer design for radio astronomical measurements in 0.7-2 mm range, discussing sensitivity
19 p3285 A69-36877
- Radioastronomical investigations of inhomogeneous near solar plasma structure
20 p3606 A69-38017
- Radio observations of 30 May 1965 total solar eclipse at Manus Island, discussing radio brightness
20 p3616 A69-38304
- Radio sources observation by lunar occultation, interplanetary scintillations and interferometry techniques, outlining measurement theory
21 p3812 A69-39518
- Temperature fluctuations in microwave background radiation from primeval perturbations compared with perturbations from discrete radio sources
21 p3815 A69-39611
- Astronomical unit determination, discussing dynamical and radar methods and Doppler shift of neutral hydrogen line spectra in radio astronomy method
22 p4022 A69-40464
- Statistical model of cratered planetary surface slopes and elevation applied to radio wave scattering by moon and Venus
23 p4209 A69-41322
- Radio studies of galactic structure, discussing Milky Way origin and formation
23 p4217 A69-42320
- Observational cosmology developments with radio and X ray astronomy emphasizing existence, origin, effects and anisotropy of excess microwave background
23 p4219 A69-42327
- Antenna arrays for radio astronomy in meter-wavelength region including cross-polarized rhombics, steerable broadside collinear array and radio interferometer
23 p4143 A69-42353
- Carbon isotopes compared in interstellar formaldehyde transition for galactic nucleosynthesis, discussing spectrum analysis of radio astronomical telescope observations
23 p4220 A69-42376
- Spiral and irregular galaxies integral properties and relations, discussing optical and 21-cm observations, hydrogen masses, statistical corrections, hydrogen line optical depths, etc
23 p4220 A69-42383
- Equal velocity contour diagrams for interstellar matter emission and absorption study in Cassiopeia-Perseus region
24 p4384 A69-43050
- Quasars time dependent flux density variations at 6.6 cm, noting spectrum peaks tendency toward lower frequencies with time
24 p4389 A69-43772
- RADIO ASTRONOMY EXPLORER SATELLITE**
- RAE-A satellite design, simulation and flight performance, discussing gravity gradient stabilization
07 p1226 A69-18328
- RAE satellite boom deployment to achieve gravity gradient capture
07 p1228 A69-18346
- Magnetic attitude detection and control system for Radio Astronomy Explorer satellite
[AIAA PAPER 68-855] 12 p2174 A69-26779
- Radio Astronomy Explorer satellite boom deployment method resulting in gravity gradient capture, emphasizing role of predeployment attitude and antenna Vee angle
[AIAA PAPER 69-920] 21 p3821 A69-39350
- Radio astronomy Explorer A attitude determination via disk-oriented programming ground support system for reducing and calibrating telemetry data, attitude prediction and command, etc
[AIAA PAPER 69-983] 22 p3907 A69-40363
- Cosmic radio background noise spectrum near north galactic pole based on Radio Astronomy Explorer satellite experiments
23 p4219 A69-42375
- Tethered orbiting interferometer configurations for future Radio Astronomy Explorer satellites, discussing gravitational stabilization and delta launching into orbit as single payload
[AAS PAPER 69-255] 24 p4313 A69-42859
- Iterative weighted least squares method for reconstructing time history of coupled rotation and flexural oscillations of Radio Astronomy Explorer satellite
24 p4394 A69-43291
- RADIO ATTENUATION**
- NT MANDELSTAM REPRESENTATION**
- Total atmospheric moisture content by measuring radio wave absorption at water vapor molecule rotational spectrum absorption line
02 p0274 A69-11438
- Atmospheric water vapor content from summer-fall 1966 measurements of atmospheric radio wave absorption of thermal radio emission, describing experimental apparatus
02 p0274 A69-11439
- Ionosphere formed waveguide electromagnetic field determined by expression, accounting for radio wave absorption during communications via artificial satellites
02 p0206 A69-11661
- Sudden cosmic noise absorption in ionosphere confirms relationship with solar chromospheric flares
02 p0306 A69-11667
- Terrain roughness effect on ionospheric radio wave absorption measurement data compared with theoretical results
02 p0207 A69-11669
- Anomalous radio wave absorption in polar aurora region ionosphere, discussing disturbance characteristics
02 p0207 A69-11688
- Performance characteristics of 300 GHz Dicke type superheterodyne radiometer receiver for measuring atmospheric attenuation of electromagnetic waves
02 p0209 A69-12336
- Teichmann cost analysis extended to include frequency dependent and diversity dependent rain losses for satellite communication, using Bayes strategy
05 p0721 A69-16580

Electromagnetic waves attenuation and scattering by rainfalls calculated using droplet distribution function
08 p1275 A69-20430

Midlatitude ionospheric disturbances accompanied by auroral type radio absorption observed by radio astronomy and probes during May 26, 1967 storm
10 p1688 A69-23935

Millimeter and submillimeter radio waves attenuation in rain, showing effective loss cross section as function of raindrop diameter and wavelength
10 p1657 A69-23943

Vertical atmospheric absorption of radio waves by water vapor and oxygen molecules near rotational resonance based on radio emission measurements
10 p1658 A69-23944

Attenuation losses on curved dielectric waveguide in X band
11 p1856 A69-25633

Differential absorption by measurement of phase difference of ionospherically propagated incoherent radio wave signals under quasi-longitudinal conditions
12 p2032 A69-26857

F cosine θ theorem validity for VLF radio wave absorption in ionosphere tested using exponential electron density models, noting Brewster angle influence on reflection coefficient
13 p2222 A69-28473

Ionosphere formed waveguide electromagnetic field determined by expression, accounting for radio wave absorption during communications via artificial satellites
13 p2224 A69-28692

Sudden cosmic noise absorption in ionosphere confirming relationship with solar chromospheric flares
13 p2334 A69-28698

Terrain roughness effect on ionospheric radio wave absorption measurement data compared with theoretical results
13 p2224 A69-28700

Anomalous radio wave absorption in polar aurora region ionosphere, discussing disturbance characteristics
13 p2224 A69-28719

Riometric data processing method for radio wave absorption measurement, considering nighttime cosmic radio emission intensity
14 p2436 A69-29056

Radio wave absorption coefficient in lower ionosphere related to total radiation absorption and electron concentration profile
14 p2411 A69-29075

Ionospheric radio wave absorption at midlatitude, noting mesospheric zonal wind inversion
14 p2441 A69-29418

Interstellar radio absorption influence on spatial distribution of cosmic radio emission observations with fixed multiple dipole antenna arrays
15 p2687 A69-30545

Radio wave absorption by water vapor in Venusian and Martian atmospheres, constructing model from Venera 4 data
15 p2569 A69-30952

Regenerative amplifier to counteract cable damping due to narrow bandwidth in PCM systems
16 p2755 A69-31860

Radio wave emission bursts at 28 MHz at onset of nighttime absorption dip and close to auroral zone from riometer recordings, noting relation to geomagnetic storms
16 p2775 A69-32085

Radio emission and absorption of cumulus and stratus clouds at millimeter and centimeter wavelengths, giving maximum SNR defined by brightness temperature
16 p2807 A69-32270

Radio wave absorption in interstellar H I regions, considering mean absorption coefficient dependence on height above galactic plane, evaluating planar electron density
17 p3034 A69-33608

Cosmic radio emission absorption during IQSY at 24.6 MHz, relating diurnal variation of absorption and geomagnetic index F scatter occurrence
17 p2968 A69-33992

Ionospheric radio wave absorption measurements by A1 method at 2.2 MHz, showing height estimates of absorption region and winter anomaly
17 p2968 A69-33993

Ionosonde electric circuit modified to permit radio wave absorption measurements over wide frequency range, calculating electron collision frequencies in F region
17 p2968 A69-33994

D region electron densities from multifrequency absorption measurements by proton spectra analysis, noting cubic approximation
18 p3127 A69-34799

Preamplifier analysis for FM system optimization to maintain constant output signal to noise ratio throughout baseband
18 p3103 A69-35088

Residual nighttime radio wave absorption in ionosphere, noting absorption-magnetic activity relation existence
20 p3528 A69-37678

Frequency dependence of radio wave absorption in ionosphere at 2.2-4 MHz by impulse method, noting effect of sporadic layer
20 p3491 A69-37680

Ariel 3 satellite attempted background radiation measurement between 2-4 MHz to show absorption onset in Galaxy
21 p3806 A69-39258

Identification, position and temperature of solar X ray sources derived from D layer ionization radio absorption behavior during eclipses and lunar reflection
22 p4004 A69-40308

Free-free intergalactic absorption at LF as function of red shift for uniform zero pressure cosmological models
22 p4025 A69-40640

Ionospheric radio waves constant absorption term obtained from sunrise and sunset data
23 p4127 A69-42424

Ionospheric nondeviative radio wave absorption, noting roles of collisional and working frequencies and solar zenith angle
23 p4127 A69-42425

Space attenuation at VHF and UHF telemetry frequencies
24 p4281 A69-42622

RADIO AURORAS

Radio aurora radar measurement, determining echo and Doppler velocity distribution and dependence on aspect angle, magnetic latitude, height, azimuth and time
05 p0754 A69-16265

Radio aurora rate of occurrence from VHF bistatic radio system observations in eastern Canada
07 p1124 A69-18824

Southern radio auroral zone observation with rhombic antennas, noting diffuse and discrete zones associated with proton and electron precipitation
12 p2033 A69-26950

Radio waves propagation along polar auroras region, obtaining ionospheric parameters for magnetic disturbances based on penetration probability
14 p2436 A69-29058

Physical model for IGY radio aurora data correlated with Brice magnetospheric convection model
18 p3125 A69-34231

Waves in auroral ionosphere due to particle precipitation, indicating ionospheric plasma instabilities
18 p3130 A69-35187

Bistatic auroral backscatter communications conducted by recording CW transmissions from beacon transmitters to study radio aurora
21 p3709 A69-38498

RADIO BEACONS

Aircraft Searchmeter, discussing device fitted to locate emergency radio beacon signal
06 p0878 A69-16963

ORBIS-CAL designed to achieve three axis orientation to local vertical and velocity vector in eccentric orbit by gravity gradient stabilization
07 p1226 A69-18323

High latitude transition or scintillation boundary between high and low amplitude fluctuations of satellite radio beacon signals examined as function of time
07 p1125 A69-18846

Scintillation fading of VHF beacons on synchronous satellites, noting amplitude fluctuation depth and rate
09 p1457 A69-22461

Bearing errors from radio beacons with rotating or multilobe radiation patterns
15 p2567 A69-30343

Rescue locator beacons and airborne search equipment of VHF and UHF capabilities available to international civil aircraft operations
15 p2552 A69-30852

Direction defining radio beacons performance, discussing signal amplitude and phase comparison systems and Doppler techniques
17 p2918 A69-33028

RADIO BLACKOUT

U BLACKOUT [PROPAGATION]

RADIO BROADCASTING

U BROADCASTING

RADIO BURSTS

NT SOLAR RADIO BURSTS
NT TYPE 2 BURSTS
NT TYPE 3 BURSTS
NT TYPE 4 BURSTS
NT TYPE 5 BURSTS

VLF electric field measurements from 1 AU heliocentric orbit, noting field oscillations in solar wind and large amplitude HF noise bursts
01 p0035 A69-11224

Automatic recording device for cosmic ray burst: utilizing information time delay to allow detailed initial period study
03 p0430 A69-13545

VLF radiation bursts /July-October 1966/ in U.S.S.R., noting detection probability increase with increasing magnetic activity
06 p0920 A69-17731

Radiation bursts in subpolar stratosphere recorded by gas discharge counters on board sounding balloons
06 p0921 A69-17744

Solar X ray bursts decay curves and spectra in 10 to 150 kev range interpreted as hot coronal condensation during flare and electron bremsstrahlung
07 p1206 A69-19250

Radio wave emission bursts at 28 MHz at onset of nighttime absorption dip and close to auroral zone from riometer recordings, noting relation to geomagnetic storms
16 p2775 A69-32085

Red dwarf star /YZ Canis Minoris/ radio outbursts: observation noting stellar atmospheric spectrum, electron density and temperature and total flare energy
17 p3043 A69-34164

Solar proton flare June 1968 analysis, discussing geophysical effects and possible polar cap absorption
20 p3587 A69-37332

Polarization ellipse orientation at source from Faraday fringes on Jupiter decametric radio bursts swept frequency records
20 p3594 A69-38169

Auroral vLF emission bursts simultaneous with sharp ionospheric absorption dip and SC deflections in geomagnetic H, noting corpuscular ionization
24 p4308 A69-43001

Solar X ray bursts decay curves and spectra in 10 to 150 kev range interpreted as hot coronal condensation during flare and electron bremsstrahlung
24 p4372 A69-43613

RADIO COMMUNICATION

NT PULSE FREQUENCY MODULATION
TELEMETRY
NT TELEPHONY
NT TELEPHOTOMETRY

Critical parameters for optimum design of Cassegrain antenna used in space communications [UN PAPER 68-95280]
01 p0043 A69-10481

Probabilities of error, correct reception and signal cancellation in radio communication systems channels with signal absorption fading
01 p0030 A69-10592

Radio links between earth and deep space probes, summarizing bistatic radar astronomy results [AAS PAPER 68-182]
02 p0311 A69-11467

Maritime radio communications satellite service for ship safety, discussing stationary equatorial satellite systems [AIAA PAPER 68-232]
02 p0356 A69-12383

Soviet book on meteor trail scatter communications covering civil and military advantages over troposcatter systems, meteor trail scatter properties, etc
04 p0562 A69-15488

Meridional radio communication between radio station at South Geomagnetic Pole and amateur SSB radio stations in U.S.S.R.
06 p0889 A69-17753

Hearing errors in voice communication with radio telephone, noting effects of mean syllable number and consonants per syllable in pilots and controllers
06 p0891 A69-18034

Polarization of ionospherically propagated HF radio waves for various times, frequencies and path azimuths applied to distortion in radio communication
07 p1078 A69-18916

Duty cycle increase on meteor forward scatter radio communication paths by use of wide-beam transmitting antenna along great circle
08 p1394 A69-20609

Direct radio and TV broadcasting from satellite-borne radio transmitter to general public, giving visibility, gains, frequencies and bandwidths tables
09 p1586 A69-21286

Radiocommunications for Tiros and Nimbus meteorological satellites, noting weather data communications and hydrological experiments

09 p1451 A69-21289

Communication problems due to natural and artificial plasmas in spacecraft vicinity, discussing plasma effect theory

09 p1451 A69-21292

Radio waves behavior along paths between satellites and earth, studying preferred frequency bands for spacecraft transmitters used as beacons

09 p1451 A69-21293

Coherent FSK LF/VLF radio communication modem with large predetection bandwidth for improvement of reception in atmospheric noise

09 p1458 A69-22473

Probabilities of error, correct reception and signal cancellation in radio communication systems channels with signal absorption fading

10 p1653 A69-23106

Tandem interleaved cyclic codes for digital HF communication with improved error rate at reduced decay time

10 p1655 A69-23530

Carrier to interference ratio /CIR/ between desired path and every other path within predetermined range in microwave system calculated by computer

11 p1840 A69-25312

Computer techniques application to radio engineering functions related to system performance, layout engineering, frequency coordination and administration, discussing decision parameters interrelationship

11 p1840 A69-25313

Signal to noise ratio at output of three stage radio section with preselector, detector and ideal integrator, noting error

13 p2222 A69-28506

Ionospheric horizontal discontinuities of electron density distribution parameters effect on penetration frequency, skip distances and arrival angles

14 p2436 A69-29057

Potential noise stability of reception in binary communications system with active pause in channel for unknown signal arrival time

15 p2563 A69-30134

Radio waves behavior along paths between satellites and earth, studying preferred frequency bands for spacecraft transmitters used as beacons

15 p2570 A69-31227

Ionospheric data acquisition and utilization for improved radio communications, considering contact between engineers and physicists, ionosondes, data reliability for prediction, etc

17 p2961 A69-33402

Auroral absorption distribution from arctic riometric observations mapped for evaluating radio communications reliability

17 p2967 A69-33990

Book on statistical communication and applications to radio and radar systems technology to provide guidelines for design decisions

19 p3267 A69-35900

Soviet book on modern systems of wireless telecommunication covering radio communication and tropospheric, ionospheric and satellite wireless systems

20 p3487 A69-37235

German ground station radio communications via Intelsat satellites, discussing transmitting facilities, TV picture and sound signals, etc

22 p3902 A69-41249

RADIO CONTROL

Current carrying cylindrical plasma column oscillations surrounded by electric excitation with multiple feedback radio, discussing stabilization possibility

13 p2311 A69-28106

Ground station command transmission equipment for German AZUR satellite, describing components based on NASA Tone Digital Command System

16 p2759 A69-31856

Soviet book on radio control of rocket missiles and space vehicles covering control principles, systems analysis and synthesis, vehicle characteristics, etc

20 p3574 A69-37232

ELDO radio guidance station at Gove, discussing propulsion stage tracking and instruction transmitted to vehicle

22 p3919 A69-39920

Missile response-PDM guidance and control system parameters relationship, using phase plane representation

24 p4283 A69-43252

[AIAA PAPER 68-820]

RADIO DIRECTION FINDERS

TRANSIT satellite navigation system for all-weather diurnal position fixing, noting Doppler frequency measurement and ionospheric signal refraction

01 p0112 A69-10457

Low polarization error HF loop antenna array direction finder performance tests, comparing measured bearings with polarimeter and conventional crossed loops data

01 p0048 A69-11006

CRT direction finder with linear scanning to determine statistical data for azimuthal distribution of atmospherics

04 p0600 A69-15104

Polarization errors in phase type direction finder caused by antenna

04 p0561 A69-15404

Aircraft Searchmeter, discussing device fitted to locate emergency radio beacon signal

06 p0878 A69-16963

Shipboard direction finder calibration accuracy, emphasizing radio operator training

06 p0897 A69-17533

Power traveling wave tubes in ground stations for INTLSAT 3 direction finding system

07 p1094 A69-18426

Electronic beam-rotation systems operation using matrix network to feed circular arrays, noting applicability to direction finding or radar systems

08 p1288 A69-20964

Optimal direction finding systems based on bearing angle representation in multidimensional Markov process, considering white and interference noise

13 p2219 A69-27254

Bearing errors reduction in vertical loop HF direction finders for ionospherically propagated signals in dual channel system

14 p2413 A69-29493

Two antenna radio direction finding system statistical synthesis, using quadratic linear process

15 p2562 A69-30110

Direction finding accuracy of pulsed radar with binary-quantized detector signals, discussing azimuth minimum variance and quantization threshold optimization

15 p2566 A69-30333

Atmospheric sources automatic location by direction finding network based on triangulation network principle

18 p3102 A69-34961

HF direction finder for display of time varying multimode propagation phenomena, using analog computer and phase sensitive interferometer

21 p3677 A69-39456

Direction finding characteristics of nonlinear antenna, including current determination and optimal angle for sidelobe level

21 p3684 A69-39619

RADIO ECHOES

Ducted echoes on topside ionograms and whistler diffuseness at midlatitudes, noting common occurrence of phenomena

01 p0029 A69-10551

VHF transhorizon propagation by double reflection from elevated layer in troposphere

01 p0034 A69-11139

Envelope distribution of echo signal during reflection scattering by extended turbulent meteor trails

02 p0207 A69-11690

Centimeter radio wave reflections from explosion region produced by TNT and hexogen charge

02 p0282 A69-12415

Numerical radar information charts, plotting radio echo reflection boundaries from cloud and precipitation observations by weather radars

03 p0459 A69-13287

Charts of horizontal cross sections of radio echo foci for radio echo reflections from cumulonimbus clouds

03 p0459 A69-13288

Horizon focusing gain for radio waves reflected obliquely from ionosphere, noting effects of transmitter location and ionosphere geometry

03 p0395 A69-13627

Mass distributions of meteoroids obtained from underdense radio meteor echoes

03 p0518 A69-14254

Plasma frequency resonances observed by topside sounders interpreted as slowly propagating waves suffering oblique reflection, noting effects of nonhorizontal magnetic field

07 p1124 A69-18837

Conjugate echoes in Alouette 2 topside sounder ionograms explained by multiple reflections between

conjugate points of field line, noting magnetospheric waveguides role

08 p1274 A69-20045

D region electron density vertical profiles measured using partially reflected echoes from lower ionosphere

08 p1307 A69-20189

Combination backscattering on ionic sound waves assumed responsible for unexpected features of radio signals reflected from sun

10 p1776 A69-23219

Echo 1 aluminized plastic balloon satellite, discussing radio linkup by reflections, use in geodesy and atmospheric and radiation pressure effects on lifetime

10 p1792 A69-23804

Lunar surface pore water /or ice/ detection by active orbital or surface electromagnetic experiments, noting water effect on reflection coefficient

11 p1958 A69-24693

Wind structure in atmosphere meteor region from persistent meteor trail radio echoes amplitude fluctuations, noting horizontal wind velocity profiles

12 p2074 A69-26962

Envelope distribution of echo signal during reflection scattering by extended turbulent meteor trails

13 p2224 A69-28721

Object shapes automatically classified from reflected radio signals, considering correlation description of object effective dispersion surface diagram

14 p2411 A69-28917

Radio wave reflections from edge of large scale depressions of ionospheric electron density observed by topside sounding satellites, discussing ionogram recordings

14 p2415 A69-29521

Fresnel irregularities calculated from radio wave partial reflection from lower ionosphere measured by rocket probes

15 p2604 A69-31420

Meteorological effects on anomalous radio echo determined from simultaneous aerological and radar observations, noting maximum signal amplitude during high humidity and low wind speeds

16 p2808 A69-32277

Automatic radar station for meteor observations, discussing separate transmitting and receiving antennas directive gain and radio echo power

17 p2939 A69-33902

Radio echo from south showing origin from irregularities in F but not E region, discussing propagation modes for particular record

18 p3125 A69-34252

Leonid meteoroids mass distribution law exponent evaluation based on unstable meteoric radio echo durations integral distribution

18 p3203 A69-35334

Ionospheric electron density irregularities observed by topside sounders showing shape, dimensions across magnetic field and variation percent, discussing resulting radio echoes

20 p3530 A69-37870

Radio wave reflection from irregularly ionized meteor trains, discussing decay time scatter and electron line density

22 p3899 A69-39969

HF backscatter, long delay signals and round-the-world echoes as radio wave propagation modes

23 p4116 A69-41602

Radio echoes diffraction patterns determination from reflection coefficients of polarized radio waves reflected from ionized meteor trails

23 p4214 A69-41846

Ionosphere reflected radio waves field strength measurements, obtaining formula for ground wave discrimination

23 p4123 A69-41861

RADIO ELECTRONICS

Complex electronic systems optimum redundant element content determination for ensuring adequate supply

14 p2426 A69-29422

Lasers and maser devices in radio quantum electronics, discussing optical parametric and microwave devices including transistors, diodes, magnetrons, etc

19 p3284 A69-36433

Meteor radio electronics principles, methods and equipment, discussing ionized meteor trail formation, radar tracking and utilization of trails for communications

19 p3277 A69-36591

RADIO EMISSION

NT SOLAR RADIO BURSTS

NT SOLAR RADIO EMISSION

NT TYPE 2 BURSTS

NT TYPE 3 BURSTS

NT TYPE 4 BURSTS
NT TYPE 5 BURSTS

Pulsar radiation origin related to electromagnetic wave distortion during propagation through resonant media

01 p0149 A69-10272

Spectral fine structure in emission from pulsars, noting correlation between fading and spectral change

01 p0150 A69-10273

Quasi-periodic VLF emissions associated with geomagnetic micropulsation activity in terms of comparable periodicity

01 p0063 A69-10274

Planetary nebulae radio emission, observed with pencil beam of radio telescope, confirming thermal spectrum at radio frequencies

01 p0157 A69-11291

Cosmic radio emission at 1.68 MHz measured by Cosmos 142 satellite, discussing receiver, antenna and radiation temperature

01 p0158 A69-11322

Powerful flares close connection with filaments and loop prominences, discussing differences in physical characteristics

02 p0306 A69-11633

Mercury radio emission phase dependence, discussing brightness temperature value approximation and surface layer properties

02 p0314 A69-11640

Venus microwave phase effect analyzed assuming dry massive Venus atmospheric model, discussing heat transfer processes

02 p0319 A69-12108

Galactic Jupiter Probes investigating Jupiter atmosphere and emissions and deep space cosmic radiation

02 p0324 A69-12303

Normal galaxies radio emission and brightness of metagalactic radio background

02 p0325 A69-12564

Jupiter, Venus and Mars 8.6 mm radio emission, obtaining average disk brightness temperatures

02 p0327 A69-12716

Pulsar hypothesis based on oscillating white dwarf surrounded by hot rarefied corona to explain radio emission

03 p0505 A69-13077

Antennas with vertical radiation patterns to measure frequency spectrum of distributed cosmic radio emission between 6.3-40 MHz

03 p0500 A69-13080

Thermal conditions of upper blanket of lunar surface during eclipse, using data to calculate lunar radio emission

03 p0506 A69-13088

Radio emission center of gravity from 3C 273 quasar determined by radio telescope together with A and B component fluxes

03 p0506 A69-13092

Interstellar gas masers account for properties of 18 cm emission lines from OH molecules

03 p0511 A69-13465

Man-made and natural spatial communications

03 p0394 A69-13577

Mercury radio emission theory, calculating Mercurian brightness temperature as function of solar illumination and distance from sun

03 p0512 A69-13688

Polarized radio emission from Jupiter, giving hypothesis of radiation belts deformation by solar wind

03 p0512 A69-13703

Spontaneous emission of gadolinium ferrite polycrystals, discussing temperature dependence

03 p0487 A69-13731

Diurnal variations of low latitude VLF emissions observed at Hiraio, Japan

03 p0398 A69-13900

Ionospheric LF radio noise cut-off near proton gyrofrequency, discussing satellite ELF and VLF observations

03 p0399 A69-14021

Nonlinear effect of triggering pulse on electron distribution for triggering of VLF emissions

03 p0399 A69-14022

Ammonia gas molecules in interstellar medium, discussing detection in direction of galactic center by means of microwave emission

03 p0518 A69-14258

Venus brightness temperature between 0.75 and 1.65 cm from radio emission measurements, taking into account water vapor in Venus atmosphere

04 p0658 A69-14960

Protostars as sources of anomalous OH emission, discussing densities, masses and temperatures of OH condensations

04 p0661 A69-15143

Nonquadrupole nature of cosmological radio emission intensity distribution demonstrated for anisotropic homogeneous cosmological models without flat space

04 p0662 A69-15238

Photographs of intensity of radio emission in millimeter band, using luminophor based on ZnS and CdS

04 p0560 A69-15272

Extensive air shower radio pulse polarization, using log periodic EW- and NS-arm antennas

04 p0595 A69-15425

Gyro synchrotron emission spectrum and intensity from energetic solar electrons radiating in coronal magnetic fields applied to type IV solar radio bursts

04 p0650 A69-15529

Europa control of decametric emission from Jupiter

05 p0813 A69-15605

Quasar and radio galaxy evolution, discussing energy release rate and particle acceleration effects on radio and optical emissions

05 p0822 A69-15852

MHD quasar model consisting of galaxy with supermassive plasma nucleus moving in magnetic field

05 p0822 A69-15853

Elektron satellite recorded sporadic radio emission noting relationship to geomagnetic disturbances and dependence on satellite position

05 p0824 A69-16059

Increasing periodicities in radio pulses from pulsars

05 p0825 A69-16352

Radio sources quantity dependence on radio emission value, noting determination of spatial density variations of radio galaxies

05 p0826 A69-16426

Jupiter microwave radiation flux density at 81 MHz, noting spectrum of microwave emission

05 p0827 A69-16506

Radio astronomical methods for total atmospheric absorption of radio waves by atmospheric thermal radio emission measurements based on sky brightness temperature

05 p0723 A69-16779

Radio emission from supernova remnants, reviewing evolution, structure, spectra and polarization, plus identification, characteristics, surface brightness and radio emissive remnants distance

06 p1002 A69-17314

Magnetic activity dependence of VLF emission properties at magnetically conjugate points

06 p0920 A69-17735

Groups of drifting lanes of emission in fine structure of dynamic spectra of Jupiter decasecond decametric radiation bursts

06 p1008 A69-17958

Radio emission and microwave absorption spectrum dependence on physical properties of clouds in millimeter and centimeter wavelength range

06 p0954 A69-17998

Radio wave brightness temperatures and contrast characteristics in presence of clouds and precipitation

06 p0954 A69-17999

Antenna transmission and receiving system effects on radio brightness temperature measurements by airborne equipment

06 p0929 A69-18000

Ground based radio telescope sensitivity to radio emission from earth atmosphere and galactic sources

07 p1099 A69-18515

Dependence of microwave emission from n-InSb on crystalline orientations, noting anisotropy in case of rotation in perpendicular plane

07 p1198 A69-18647

Radio telescope survey of intense emission regions along galactic plane, considering antenna temperatures, spectrum and steps of observed emission

07 p1216 A69-19138

Radio noise generation in topside ionosphere, noting Cerenkov radiation from intense soft fluxes of auroral electrons

07 p1127 A69-19257

Whistlers and VLF emissions from ground based and satellite measurements, applying results to electron density mapping and ion detection

07 p1127 A69-19354

Bright galaxies observed at 408 MHz with fan beam of east-west arm of cross-type radio telescope for correlations between radio and optical properties

08 p1386 A69-20087

Lunar radio emission polarization characteristics, considering knife-edge type radiation pattern effect of antenna array

08 p1391 A69-20423

Polarization variations in radio pulses from pulsar CP 0328, noting possible origin in synchrotron radiation from collimated electron beam

08 p1397 A69-2069

Radio emission from magnetic neutron stars as possible model for pulsars, noting optical and IR emission bands

08 p1397 A69-2072

Wideband 1665 MHz OH emission source in Carina region of galaxy in weak continuous radiation region with low degree of polarization

08 p1397 A69-2077

Water molecules radio spectral lines from microwave emission sources in Galaxy studied for variability, size and polarization

09 p1587 A69-21307

OH emission source in W24 during July 19, 1967 lunar occultation, obtaining better position for brighter OH emission feature

09 p1591 A69-21449

Elektron 4 satellite radio emission data transmitted from July to December 1964, noting month-to-month variations in mean radiation level

09 p1578 A69-21776

Radio telescopic survey for OH emission at 1667 MHz in interstellar dust clouds for catalog compilation, tabulating results

09 p1603 A69-22267

Radio emission time variation from radio object associated with Sco X-1

09 p1603 A69-22268

Nonthermal cosmic radio emission spectral index angular variations during scanning of sky by receiver antenna, analyzing dependence on galactic latitude

10 p1784 A69-23940

Crab Nebula radio emission spectrum in decimeter wavelength range indicating emission spectral index decrease from Taurus A

10 p1784 A69-23941

Venus and Jupiter brightness temperature and radio emission at 2.25 and 8 mm wavelengths observed with radio telescope

11 p1956 A69-24396

Lunar radio emission constant component in presence of heat flow from interior, using stratified model of surface structure with two variants

11 p1956 A69-24398

Electromagnetic wave buildup by induced Compton effect as possible radio emission source, considering data for quasars and pulsars

11 p1957 A69-24402

Transmitter frequency increase effect on production of artificial stimulated VLF emissions in magnetosphere

11 p1878 A69-25156

Radio emission of fast cosmic ions by plasma wave conversion to electromagnetic waves, using nonlinear mechanism in turbulent plasma

12 p2149 A69-26209

Electron concentration fluctuation in ionospheric inhomogeneities estimated from Cassiopeia A radio emission

12 p2070 A69-26687

Pulsars discovery, emission, regularity, narrow frequency band and pulse changes, physical nature and aspects of Crab Nebula source

12 p2160 A69-26895

Satellite observation of intensity and distribution of VLF emission at medium latitude during magnetic storm interpreted by transverse resonance plasma instability

12 p2073 A69-26947

Radio emission from 18 galaxies noting accompaniment of optical spectrum emission and enhancement due to production of relativistic electrons in active nuclei

12 p2164 A69-27026

Radio galaxies luminosities distribution and spectral indices, galactic structures and diameters, considering relations between radio emission parameters

12 p2165 A69-27031

Radio emission correlation to nuclei shape in normal galaxies

12 p2166 A69-27040

Coherent radio emission mechanism in quasars and supernova remnants, discussing magnetic effects

12 p2168 A69-27050

Soviet monograph on intrinsic noise emission in radio channels covering noise temperature at receiver input, thermal microwave radiation, etc

13 p2219 A69-27304

Radio emission from high level transitions in hydrogen calculated by superposing emission lines on background continuum, using Gaunt factor for free-free emission

13 p2327 A69-27596

Jupiter decametric radio emission periodicity attributed to undiscovered satellite in unstable orbit, discussing application to satellite discovery

13 p2343 A69-27622

VLF morning and evening magnetosphere emission distinction by studying spectrum width as function of variations in K index

13 p2253 A69-27740

Radio emitting clouds properties as function of distance to parent galaxy nucleus

13 p2352 A69-27874

Radio emission of atmospheric cosmic ray showers observed with multiple wideband half wave dipole antenna system, obtaining radiation spatial distribution

13 p2332 A69-28407

Half wave dipole antenna operational factors analyzed for RF radiation spatial power distribution from atmospheric cosmic ray showers

13 p2332 A69-28408

Pulsar hypothesis based on oscillating white dwarf surrounded by hot rarefied corona to explain radio emission

14 p2515 A69-28759

Antennas with vertical radiation patterns to measure frequency spectrum of distributed cosmic radio emission between 6.3-40 MHz

14 p2509 A69-28762

Thermal conditions of upper blanket of lunar surface during eclipse, using data to calculate lunar radio emission

14 p2515 A69-28770

Radio emission center of gravity from 3C 273 quasar determined by radio telescope together with A and B component fluxes

14 p2516 A69-28774

Pulsar model used to explain stellar shape oscillations as cause of radio emission intensity periodic variations

14 p2522 A69-29675

Crab Nebula lunar occultation observed by Cassegrain array of deep space communication facility, finding radio brightness distribution similar to optical

15 p2687 A69-30539

Metagalactic electrons and relict radiation interaction calculations allowing for universe expansion, space curvature and X ray absorption

15 p2687 A69-30541

Sky cosmic radio emission absolute temperature measured at decimeter wavelengths and at two zenith angles to minimize atmospheric influence

15 p2687 A69-30544

Distribution model for ionized interstellar gas over galactic disk for explaining radio emission absorption and depolarization from discrete sources

15 p2695 A69-30935

Lunar radio emission linear polarization radial dependence at 0.8-cm wavelength using radio telescope, determining dielectric constant of emitting layer

15 p2697 A69-31251

Radio emission and absorption of cumulus and stratus clouds at millimeter and centimeter wavelengths, giving maximum SNR defined by brightness temperature

16 p2807 A69-32270

Criticism of Chiu theory on radio emission from pulsars supposing electron radiation

16 p2865 A69-32802

Radio emission from Cygnus X-2 reporting on observations at 4.5 cm wavelength

16 p2865 A69-32804

Heliosphere boundary location significance for Jovian magnetosphere configuration, considering inverse correlation between sunspot number and Jovian decametric radio emission

17 p3033 A69-33379

Impulsive radio emission from CP 0950 by Mark I telescope, plotting mean and interpulse profiles

17 p3036 A69-33638

Observed and computed radio pulse profiles of white dwarfs, noting resemblance of emissivity variation with latitude to magnetic field distribution on sun

17 p3037 A69-33644

Saturn emission peak and flux density at 408 MHz determined by cross telescope, discussing mechanism for enhanced radiation at long wavelengths

17 p3041 A69-33813

Radio wave trajectories for waves emitted at 15, 20 and 25 kHz within spherically stratified ionosphere below F 2 maximum

17 p2969 A69-34001

Sky brightness temperature spectra searched for neutral intergalactic atomic hydrogen radio emission, using horn-reflector antenna

18 p3190 A69-34285

Observations of W49 at 2800 MHz with East-West resolution, analyzing shape of thermal and nonthermal source

18 p3195 A69-34427

Jovian radio sources intermittency, recording difficulties, longitudinal drift and theories concerning origin

18 p3196 A69-34690

Venus brightness temperature between 0.75 and 1.65 cm from radio emission measurements, taking into account water vapor in Venus atmosphere

18 p3197 A69-34723

RF synchrotron emission from electrons trapped in earth magnetic field observed by satellite, using magnetospheric environment model

18 p3128 A69-34948

Radio emission attributed to galactic nebula NGC 6857, suggesting origin in high density H II regions excited by OB star clusters

18 p3202 A69-35209

Radio emission from Sco XR-1 shown as synchrotron radiation of relativistic electrons in low density region surrounding denser core producing X ray

20 p3597 A69-37334

Cosmic radio emission absorption in D, E region and in F 2 layer above and below electron concentration maximum from vertical ionospheric sounding 1959 over Moscow

20 p3590 A69-37676

Elektron satellite recorded sporadic radio emission noting relationship to geomagnetic disturbances and dependence on satellite position

20 p3606 A69-37969

Induced Compton scattering of plasma and electromagnetic waves under astrophysical conditions, discussing HF radio emission spectra from cosmic objects and quasar

20 p3607 A69-38035

Radio emission measurements of moon at 3.2 cm by artificial moon method, calculating radio temperature and phase amplitudes

20 p3608 A69-38052

Upper limits for OH microwave emissions from radio sources F transitions, discussing pumping mechanism role in emission detection

21 p3796 A69-38477

Jupiter magnetospheric radio emissions, discussing magnetic field and plasma-magnetic interactions

21 p3812 A69-39517

Radio pulse emission from ionized disk of cosmic ray extensive air showers, noting importance of charge separation in geomagnetic field and selective positron absorption

21 p3792 A69-39614

RF high resolution observations of edge on spiral galaxy NGC 4631, noting radio halo and spur absence, nonthermal radio emission region, etc

22 p4022 A69-40463

Radio observations of elliptical and spiral noncluster galaxies, noting correlation between magnitude and radio emission in elliptical galaxies

22 p4025 A69-40639

Radio recombination line data from H II regions interpreted in terms of single electron temperature, considering non-LTE/local thermodynamic equilibrium/and clumping

22 p4025 A69-40645

Pulsar magnetic models, coherent radio emission mechanisms, radiation polarization, data summary and astrophysical nature

22 p4030 A69-40905

Cosmic radio emission anomalous absorption measurements during PCA following July, August, September 1966 proton flares

23 p4156 A69-41845

Crab Nebula pulsar radio properties, possible neutron star origin, interstellar gas and magnetic fields, etc

24 p4375 A69-42556

Pulsars relation with supernovae remains and radiation patterns and fluxes analysis, ascribing radio emission to relativistic plasma

24 p4383 A69-42985

Radio emission from diffuse thermal radio sources in northern Milky Way, giving contour maps

24 p4388 A69-43641

Venus and Jupiter brightness temperature and radio emission at 2.25 and 8 mm wavelengths observed with radio telescope

24 p4390 A69-43786

Lunar radio emission constant component in presence of heat flow from interior, using stratified model of surface structure with two variants

24 p4390 A69-43788

Electromagnetic wave buildup by induced Compton effect as possible radio emission source, considering data for quasars and pulsars

24 p4391 A69-43792

RADIO ENERGY

U RADIANT FLUX DENSITY

RADIO EQUIPMENT

NT IONOSPHERES

NT RADIOMETROGRAPHS

NT RADIOSONDES

NT RAWINSONDES

NT SUPERHETERODYNE RECEIVERS

NT TRANSMITTER RECEIVERS

NT TRANSPONDERS

NT VERY HIGH FREQUENCY RADIO EQUIPMENT

NT WHISTLER RECORDERS

Soviet book on electronics and radio instruments of flight vehicles, covering radars and antennas, automatic pilots and design

09 p1463 A69-21930

Space and carrier frequency diversity determination for mutually interfering microwave radio equipments

11 p1835 A69-24952

Radio equipment for studying ionospheric inhomogeneities using space diversity reception, presenting vertical component of drift velocities of small scale inhomogeneities

14 p2453 A69-29876

Digital simulation for radio systems nonlinear elements, outlining procedures to obtain algorithms

15 p2582 A69-30111

Short and ultrashort waves signals amplitude and phase displacement determination device, stressing sensitivity

15 p2570 A69-31088

Solid state broadband RF power amplifier for airborne HF radio, eliminating total servosystem and all higher voltage components

17 p2942 A69-34114

Functional signal conversion operations in microelectronic radio equipment, examining components in analog and pulsed devices synthesis

18 p3109 A69-35162

Interference prediction models of equipment emissions and susceptibility thresholds based on limited spectrum signature data

23 p4126 A69-42223

Colocated radio equipment time-sharing scheme for interference avoidance, describing switching method and sampling signal shape

23 p4142 A69-42228

Heat pipe coupled to air cooled heat exchanger to cool high power airborne radio component by dissipating thermal load into ambient air [ASME PAPER 69-HT-16]

24 p4413 A69-43552

RADIO FILTERS

Optimal reception methods noise stability for AM radio signals based on nonlinear filtration of information parameters of signals received on noise background

01 p0030 A69-10589

Dynamic tracking filter analysis and capabilities as low threshold demodulator in frequency modulated frequency division multiplexing satellite system

01 p0034 A69-11140

Lossy transmission line filters and wideband impedance matching

03 p0406 A69-13906

Radar signal matched filters synthesis using linear digital filters and digital correlators noting role in radar detection

05 p0722 A69-16733

All-pass transfer functions of new class type for design of quadrature filter networks, using Chebyshev approximation

08 p1277 A69-21167

Optimal reception methods noise stability for AM radio signals based on nonlinear filtration of information parameters of signals received on noise background

10 p1653 A69-23104

Receiver filter nonoptimality effects on accuracy of nonenergetic signal parameter measurements

11 p1835 A69-24960

Filter circuits for stabilization of solid state microwave devices, noting input matching characteristics

11 p1849 A69-24961

RADIO FREQUENCIES

NT C BAND

NT EXTREMELY HIGH FREQUENCIES
 NT EXTREMELY LOW RADIO FREQUENCIES
 NT HIGH FREQUENCIES
 NT LOW FREQUENCIES
 NT LOW FREQUENCY BANDS
 NT MICROWAVE FREQUENCIES
 NT SUPERHIGH FREQUENCIES
 NT ULTRAHIGH FREQUENCIES
 NT VERY HIGH FREQUENCIES
 NT VERY LOW FREQUENCIES

Frequency diversity for communication in fading environment, relating performance variance to between channel correlation variance

01 p0026 A69-10177
 Pulsar CP 1133 pulse duration increase with decreasing RF from analysis of pulse shape data
 02 p0318 A69-12093

RF feedback amplifier analytical design, deriving open and closed loop feedback noise figure expressions by use of equivalent noise model

02 p0217 A69-12150
 Scaling laws for RF discharge experiments in ionized environments, considering proper limit variables for simulation of electron density

02 p0283 A69-12241
 Thermostructural analysis of large flexible paraboloid antenna indicates RF losses due to thermal distortions significant for X band and higher transmissions [AIAA PAPER 68-333]

02 p0345 A69-12372
 Josephson voltage-frequency relation independence of superconductor nature, noting c/h value and importance to voltage standards and quantum electrodynamics

02 p0299 A69-12599
 Sampled data delay-lock loop for synchronizing pulsed envelope RF signals, using digital circuitry

03 p0390 A69-13216
 Frequency-fluctuation correlation functions of radio wave field behind n random screens with random phase shifts calculated, obtaining statistical characteristics

07 p1076 A69-18525
 Integrated frequency selective amplifier design for radio frequencies based on feedback configuration with positive real zero in loop transmission function

07 p1104 A69-18886
 Single channel binary PSK communication systems performance influenced by degree of RF coherence between transmitter and receiver

07 p1082 A69-19109
 Energy density and transport velocity of RF wave in plasma in damped oscillations region, discussing resonance

08 p1365 A69-20553
 RF selection for interspacecraft or earth-spacecraft communication

09 p1449 A69-21270
 Propagation and noise effects on frequency choice for communication satellite service to aircraft and ships, noting tropospheric and ionospheric attenuation considerations

09 p1451 A69-21288
 Radio waves behavior along paths between satellites and earth, studying preferred frequency bands for spacecraft transmitters used as beacons

09 p1451 A69-21293
 Extraterrestrial cosmic emissions responsible for background noise of communications engineering, discussing factors affecting frequency sharing with other services

09 p1586 A69-21294
 RF spectral lines due to OH molecule detected in interstellar space in absorption of RF radiation from Casiopeia A source

09 p1586 A69-21295
 Electrostatic thrusters using RF ion sources to optimize payload ratios, terminal velocities, propellants, life span and efficiencies

09 p1568 A69-21489
 RF voltage breakdown in air for 50 ohm coaxial transmission line configuration [JPL-TR-32-1379]

09 p1470 A69-22790
 Electron confinement in magnetic mirror geometry supplemented with RF quasi-potential barriers, considering gas scattering

11 p1924 A69-24306
 Extragalactic gamma ray fluxes predicted, discussing collisions, matter-antimatter annihilation and cosmological implications

11 p1946 A69-24466
 System switch, separating RF bands according to frequency and polarization for simultaneous transmission from parabolic horn antenna

11 p1854 A69-25618

High sensitivity LF and HF frequency deviation meter with resonant RC amplifiers for frequency discrimination and filtering

12 p2038 A69-26337
 DC to RF energy conversion in ungridded klystron gaps, calculating efficiency and optimum load conductance as function of gap dimensions

12 p2041 A69-26629
 RF synchrotron radiation emitted by electrons trapped in geomagnetic fields above auroral zones, discussing electron flux and cosmic background

12 p2151 A69-26949
 Stationary magnetic field effect on sum and difference frequency generation due to nonuniform RF electric fields applied externally to plasma

13 p2305 A69-27376
 Quasar red shifts distance dependence indicated by visually bright quasar faintness in radio range

13 p2344 A69-27635
 Excited hydrogen RF spectral lines from nebula NGC 6618, calculating frequency for transitions by Balmer formula

13 p2353 A69-28433
 X ray pulsations in Crab Nebula at frequency closely matching radio and optical pulsations, noting energy distribution

13 p2354 A69-28465
 HF emission spectra of radio pulses from cosmic ray showers confirming Dublin group observations

13 p2333 A69-28471
 Resonance cones in angular distribution of short antenna RF electric field in anisotropic plasma noting variation with incident, cyclotron and plasma frequency

15 p2659 A69-30876
 RF spectral lines due to OH molecule detected in interstellar space in absorption of RF radiation from Casiopeia A source

15 p2697 A69-31226
 Radio waves behavior along paths between satellites and earth, studying preferred frequency bands for spacecraft transmitters used as beacons

15 p2570 A69-31227
 Steady state density profile dependence on electron density dependence of net volume ionization rate by analyzing ambipolar diffusion in RF excited magnetized plasmas

16 p2818 A69-31672
 RF band multimode parametric pulsed oscillations in distributed system using one dimensional resonators

16 p2758 A69-31796
 RF spectral line detection from ortho hydrogen ions in Omega Nebula and NML Cygnus

16 p2864 A69-32571
 Computerized prediction of RF instrumentation system signal margins for missile flight tests based on trajectory and range balance equation

18 p3103 A69-35097
 Ionospheric auroral anomalous radio wave absorption frequency dependence index determined from cosmic radio emission intensity data

20 p3587 A69-37033
 F layer penetration frequencies predictions compared with Alouette topside data

20 p3530 A69-37871
 Langmuir probe immersed in plasma RF response over range of signal amplitude and frequency and plasma electron density, showing sheath capacitance role

21 p3723 A69-38939
 FM tactical radios frequency assignments rule, considering transmitter-receiver and interfering transmitter-receiver distances, equipment power, information transfer probabilities, etc

23 p4126 A69-42229

RADIO FREQUENCY DISCHARGE

Positive ion beam probe for approximate static electric field distribution in low pressure RF discharges, analyzing deflection data for potential distributions

02 p0287 A69-11838
 Metal atom production by bombarding metal with positive ions from microwave discharge, obtaining isolation in inert gas matrix and UV spectra

06 p0957 A69-17113
 RF ion thrusters using self sustaining electrodeless discharge [AIAA PAPER 69-285]

09 p1565 A69-21247
 Charge transport in high pressure RF glow discharge in air at atmospheric pressure based on model plasma

10 p1740 A69-23662
 RF ion thrusters using electrodeless self sustaining mercury discharge, describing basic theory, component design, performance optimization and test results

17 p3018 A69-33326

RF high pressure plasma discharges contained within radial inflow vortex, measuring radiation efficiencies, power densities and radiation fluxes [AIAA PAPER 69-695]

17 p3010 A69-33442
 RF plasmoid properties, discussing bounded plasma resonance theory, basic experiments, resonance sustained discharges, role of negative ions, etc

18 p3181 A69-35487
 Inductively coupled RF excited toroidal Ar ion laser, confining current discharge by strong axial magnetic field to reduce wall losses

19 p3338 A69-36690
 Volatile oxygen organic compounds subjected to RF electrodeless discharge, explaining product distribution in terms of reaction sequences

21 p3670 A69-39737
 High temperature equilibria from hydrocarbon plasma sources subjected to 3000 W RF electrodeless discharge

21 p3670 A69-39738
 Mechanism for pink afterglow accompanying microwave discharge in pure nitrogen, emphasizing gas kinetic temperature role

24 p4353 A69-43749

RADIO FREQUENCY HEATING

RF electron heating by beam-plasma interaction in uniform magnetic field

05 p0804 A69-16458
 Nonadiabatic and stochastic mechanisms for cyclotron resonance trapping and heating in magnetic mirror geometries

08 p1364 A69-20518
 Electron cyclotron resonance absorption of injected radiation magnetic mirror, noting effect of RF heating on plasma electron distribution

08 p1364 A69-20519
 Cutaneous receptor response to microwave irradiation, measuring warmth sensory effects in human forehead with radiometer [AGARDOGRAPH-111]

RADIO FREQUENCY IMPEDANCE PROBES

RF characteristics of electrodes immersed in magnetoplasma, discussing potential distribution around point charge and RF probe measurement of plasma parameters

01 p0029 A69-10550
 Permittivity measurements by measuring impedance on thin cylinders in rectangular waveguide or in cavity formed by coaxial transmission line

02 p0222 A69-12756
 RF impedance method for electron density and collision frequency in plasma

14 p2492 A69-29352
 Plasma conductivity measurements using RF induction probe

16 p2820 A69-31707
 RF impedance probe digital system for ionospheric measurements based on antenna resonance phenomena

20 p3542 A69-37791
 RF impedance probe used for ionospheric composition measurements, describing antenna operation in ion-electron cyclotron frequency range

RADIO FREQUENCY INTERFERENCE

NT ATMOSPHERICS
 NT BLACKOUT [PROPAGATION]
 NT CHIRP SIGNALS
 NT COSMIC NOISE
 NT DAWN CHORUS
 NT ELECTROMAGNETIC NOISE
 NT HISS
 NT IONOSPHERIC CROSS MODULATION
 NT IONOSPHERIC NOISE
 NT IONOSPHERICS
 NT POLAR RADIO BLACKOUT
 NT SHOT NOISE
 NT SUDDEN ENHANCEMENT OF ATMOSPHERICS
 NT THERMAL NOISE
 NT WHISTLERS

Optimal AM radio reception in presence of fluctuating noise and one AM interference signal with random initial phase of carrier oscillation

01 p0031 A69-10782
 Mutual RF interference between satellite and terrestrial telecommunications microwave relay system at shared frequencies

03 p0392 A69-13242
 Intermodulation and cross modulation distortions in double balanced modulator

04 p0573 A69-14341
 Optimum antenna radiation patterns during suboptimum scattered Gaussian signal detection in

homogeneous interference level investigated with single channel antenna
05 p0736 A69-16782

Ground based radio telescope sensitivity to radio emission from earth atmosphere and galactic sources
07 p1099 A69-18515

Bit error probability for noncoherent binary FSK link involving Rician interfering signal
07 p1080 A69-19095

Anti-interference TV circuit using delay lines applied to radar systems, discussing false alarm probability and detection probabilities
08 p1271 A69-19919

Coordination distances and interference probabilities to control interference in frequency sharing between communication satellite systems and terrestrial radio services
09 p1450 A69-21280

Safety requirements of test ranges, considering RF hazards to electroexplosive devices
10 p1751 A69-23019

Optimal AM radio reception in presence of fluctuating noise and one AM interference signal with random initial phase of carrier oscillation
10 p1653 A69-23111

Space and carrier frequency diversity determination for mutually interfering microwave radio equipments
11 p1835 A69-24952

Carrier to interference ratio /CIR/ between desired path and every other path within predetermined range in microwave system calculated by computer
11 p1840 A69-25312

Optimal direction finding systems based on bearing angle representation in multidimensional Markov process, considering white and interference noise
13 p2219 A69-27254

Jamming susceptibility, noting corrections for multiple noise sources and sidelobe level for antenna pattern
14 p2414 A69-29501

Three channel microwave FM phase meter for studying plasma electron concentrations directional distribution without interferences between channels
14 p2497 A69-29799

TR tubes spurious harmonic power generation investigated for intersystem interference reduction and testing criteria, discussing effects of incident power, gas pressure and tube geometry
15 p2573 A69-30032

Moving target selector radars subsystems amplitude and phase instability effects on interference signal suppression
15 p2576 A69-30339

Signal reflection elimination from underlying surface during aircraft flights by using two antenna array with identical radiation patterns
15 p2567 A69-30345

Mathematical model for aircraft antenna to antenna electromagnetic interference analysis, emphasizing techniques for propagation paths and shading factors
17 p2943 A69-34134

Terrestrial radio noise source aspects including atmospheric, propagation influence, lightning-generated noise and whistlers, radio interference, etc
19 p3276 A69-36434

Receiving circuit for AM signal envelope separation in presence of AM interference and fluctuation noise, using converter cascades to effect input signal frequency spectrum symmetry
19 p3277 A69-36568

Propagation effects on lane ambiguity resolution ability of Omega VLF navigational system, noting waveguide mode interference
21 p3673 A69-38756

RFI effects of earth based emitters on operation of geosynchronous satellites for data relay from near earth orbiting satellites, noting frequency assignments
23 p4120 A69-41757

Natural and man-made radio noise measurements, including formula for calculating signal strength of coherent interference
23 p4126 A69-42217

Q multiplier UHF device as preselection filter for closely spaced channel signals, discussing channel interference reduction
23 p4141 A69-42220

Radiated interference and susceptibility prediction for unshielded wires in near field of vertical rod antenna
23 p4141 A69-42225

Colocated radio equipment time-sharing scheme for interference avoidance, describing switching method and sampling signal shape
23 p4142 A69-42228

Adaptive signal processing interference rejection technique for suppression of cochannel AM interference in congested VHF tracking receiver
23 p4128 A69-42503

RADIO FREQUENCY NOISE
U ELECTROMAGNETIC NOISE

RADIO FREQUENCY SHIELDING
Ferromagnetic composite materials for microwave absorption and shielding over frequency band 0.3 to 10.0 GHz
09 p1510 A69-22352

Near field effects on accuracy of LF shielded enclosure measurements compared to open field environment
23 p4141 A69-42226

RADIO GALAXIES
Radio galaxies radio luminosity function expressed by means of power dependence, assuming three absolute visual magnitudes for each galaxy
02 p0325 A69-12563

Absorption and emission redshift distribution in quasars, N systems and similar compact and radio galaxies
02 p0325 A69-12591

Plasmas in galaxies, spiral structures and radio galaxies, discussing quasar line and continuum spectra
02 p0329 A69-12790

Radio galaxies and quasars, discussing radio structure, observation methods, polarization, time variation, etc
02 p0329 A69-12791

Energy sources and properties of quasars and radio galaxies by X ray astronomy
02 p0310 A69-12793

Plasma model of quasars and radio galaxies for observations of high energy radiation
02 p0329 A69-12794

Radio galaxies and quasars X ray emissions, calculating radiation fluxes produced by scattering of synchrotron radiation quanta at relativistic electrons
03 p0500 A69-13079

Radio spectra differences of quasars and radio galaxies, noting influence of frequency levels
04 p0652 A69-14418

Radio emission spectra of radio galaxies from 3CR catalog
04 p0661 A69-15234

Radio observations of radio galaxies and quasars, noting double structure of many sources, some complex structures and association with optical objects
05 p0820 A69-15836

Optical observations of radio galaxies and quasars, noting evidence for galactic explosions, surface distribution, physical properties, radio quiet quasars, etc
05 p0820 A69-15837

Theoretical models explaining observed properties of radio galaxies and quasars, discussing quasar distance
05 p0821 A69-15851

Quasar and radio galaxy evolution, discussing energy release rate and particle acceleration effects on radio and optical emissions
05 p0822 A69-15852

Radio spectra analyzed for NGC 1052 and NGC 4278 elliptical galaxies, discussing 178 MHz flux density, anomalies and radiation absorption mechanisms
06 p1009 A69-17959

Red shifts and intrinsic powers of radio galaxies and quasars, discussing local luminosity distribution, function of sources and cosmology
07 p1206 A69-19270

Radio galaxies, quasars and radio stars between declinations plus 20 and plus 27 degrees, obtaining accurate positions and optical identifications
07 p1218 A69-19273

Cosmological models with antipole, determining models consistent with spatial distribution of quasars and radio galaxies
07 p1219 A69-19284

M82 galaxy as Seyfert-like galaxy seen edge-on, using radio and optical data showing H alpha emission collisionally excited, discussing circular polarization
08 p1383 A69-20051

H alpha emission line in nucleus of Virgo A radio galaxy observed on spectrograph, estimating gas electron density and mass
09 p1588 A69-21360

Quasi-stellar radio sources /QSS/ and radio galaxies structure and evolution, discussing nucleus nonuniform model
09 p1592 A69-21500

Theoretical models describing quasi-stellar objects and radio galaxies, noting objects locality, semilocality and cosmological distances
09 p1594 A69-21693

Neutral atomic H content of small angular diameter galaxies, noting systematic radial velocities and total mass of galaxies
10 p1773 A69-22956

Quasar and radio galaxy spectra obtained on Cassegrainian focusing diffraction spectroscopy
11 p1951 A69-24236

Radio emission from 18 galaxies noting accompaniment of optical spectrum emission and enhancement due to production of relativistic electrons in active nuclei
12 p2164 A69-27026

Radio galaxies luminosities distribution and spectral indices, galactic structures and diameters, considering relations between radio emission parameters
12 p2165 A69-27031

Radio galaxy identification and luminosity measurement, noting limitations of red shift observation methods
12 p2165 A69-27032

Statistical data on space density of bright elliptical galaxies, radio galaxies, quasars, noting relation between space density and age
12 p2165 A69-27033

Polarization and structure of magnetic fields of quasars, E galaxies, normal galaxies and other extragalactic radio sources
12 p2165 A69-27034

Absolute radio luminosity relation to surface brightness of extragalactic radio sources, finding volume radiation coefficient of spiral and radio galaxies
12 p2166 A69-27035

Galactic and quasar radio sources distribution, discussing spectral indices
12 p2166 A69-27036

X ray emission from radio galaxies as possible bremsstrahlung radiation of hot gas, noting Crab Nebula
12 p2166 A69-27037

Radio sources angular dimensions determined by microwave interferometry, discussing distinctions between quasars, galaxies and unidentified sources
12 p2166 A69-27039

Frequency spectra of radio galaxies, supernova remnants and quasars observed by radio telescope operating in decimeter wave range
12 p2167 A69-27041

Spectrum analysis of radio galaxy M82 nucleus, noting H alpha emission lines from analysis of IR photograph
13 p2335 A69-27310

Galactic H II regions of high surface brightness in radio continuum surveyed at 1.95 cm wavelength with high resolution and positional accuracy
13 p2339 A69-27568

IR extragalactic radio sources including normal radio galaxies, quasars and Seyfert galaxies
13 p2342 A69-27597

Extragalactic radio sources parameters analyzed for distinguishing quasars from dominant luminous radio galaxies by radio spectra
13 p2348 A69-27801

Extragalactic radio sources, observing nonlinear LF spectra for quasars and linear LF spectra for radio galaxies
13 p2351 A69-27867

Radio emitting clouds properties as function of distance to parent galaxy nucleus
13 p2352 A69-27874

Radio galaxies and quasars X ray emissions, calculating radiation fluxes produced by scattering of synchrotron radiation quanta at relativistic electrons
14 p2509 A69-28761

Galactic OH emission sources time variations found in W49 and W75
14 p2517 A69-29085

Photoelectric observations of NGC 1275, noting increase in nucleus brightness
14 p2517 A69-29086

Polarization characteristics of quasars, radio galaxies and galactic objects suggesting separate evolutionary processes
14 p2526 A69-29771

Seyfert galaxy NGC 4151 electrophotometric investigation in UVB, confirming nucleus optical variability observed in visible and IR
15 p2686 A69-30536

Radial brightness and color variation curves for Seyfert galaxies plotted from measurements with concentric diaphragm in UVB
15 p2686 A69-30537

Radio galaxy Messier 87 mass determined using virial theorem for nucleus velocity dispersion
15 p2695 A69-30883

UBV photometry of southern quasars, radio galaxies and normal galaxies including two color diagrams, radio luminosity, brightness and color distribution
16 p2859 A69-32228

H alpha emission line in nucleus of Virgo A radio galaxy observed on spectrograph, estimating gas electron density and mass
18 p3197 A69-34750

Electron ejections from nuclei of radio galaxies and quasars explained on basis of plasma stability, discussing role of relativistic electrons and resulting unstable pinch
20 p3606 A69-38032

Photoionization model of Seyfert galaxy extended to calculate temperatures, luminosities and sizes of zones emitting forbidden Fe X /6374 Å/ and Fe XIV /5303 Å/
22 p4024 A69-40581

Emission lines in optical spectra of radio galaxy nuclei, considering time dependent energy release nature
22 p4034 A69-41174

Radio galaxies and quasars number-flux density relations role in cosmology, discussing object identification, population, angular sizes, etc
23 p4218 A69-42324

Radio galaxies differences from quasi-stellar objects indicating relativistic particles generation from violent explosions releasing energy comparable with powerful supernova
24 p4378 A69-42697

Explosions mechanism in radio galaxies and quasars mechanism based on observed phenomena, emphasizing galactic flares
24 p4378 A69-42698

RADIO HORIZONS

Transhorizon UHF energy transmission via tropospheric scatter, using propagation path model
02 p0209 A69-13250

Wavelength dependence of microwave propagation beyond radio horizon
03 p0395 A69-13626

Horizon focusing gain for radio waves reflected obliquely from ionosphere, noting effects of transmitter location and ionosphere geometry
03 p0395 A69-13627

VHF radio transmission beyond horizon, discussing instrumentation, annual and diurnal signal fluctuations and diffraction role in signal propagation
08 p1274 A69-20112

Received electromagnetic fields fluctuations due to transhorizon propagation, emphasizing fading, tropospheric turbulence correlation and rapid fluctuations due to small scale index variations
20 p3494 A69-37810

RADIO INTERFEROMETERS

Digital matched filtering technique for RF interferometer filtering carrier modulated by pseudonoise sequence, discussing applications to antenna arrays
01 p0048 A69-11003

Doppler effect in centimeter wave range demonstrated by radio interferometer, noting amplitude difference between reference wave and wave reflected from moving reflector
03 p0393 A69-13333

Interferometer at lambda 21 cm using fully steerable paraboloids for processing output signal with on-line digital computer
03 p0411 A69-13468

Signal matching in radio interferometer with autonomous receiver, magnetic tape recorders and memory electron beam tube with target
03 p0431 A69-13706

Space-frequency equivalence between monochromatic correlator interferometer using directional antennas and wideband correlator interferometer using isotropic antennas
07 p1132 A69-18917

Radio interferometer antenna array spatial characteristics obtained as function of geographical coordinates of site for reducing observation errors
08 p1314 A69-20434

Dimensions, temperature and electron density of quiet solar corona from radio interferometer measurements, noting activity and temperature at solar maximum and minimum
08 p1393 A69-20573

Synoptic radio interferometer observations of July 1966 solar proton flare at microwave frequencies, correlating observed radio source with proton event
10 p1783 A69-23734

Quasi-stellar radio sources interferometric observations at 2695 MHz, determining centroid of radio emission
10 p1790 A69-24138

Solar radio bursts observations with multielement compound interferometers, noting polarization distribution and magnetic field change
11 p1946 A69-24428

Refraction error in measurements with simple and radar interferometers, considering atmospheric effect
13 p2221 A69-27961

Global multielement radio interferometer with autonomous reception synthesized for studying spatial radio brightness distribution over radiation sources
15 p2578 A69-30936

Radio interferometer with independent heterodynes to obtain radio brightness distribution over source by varying antenna spacing and reception frequency
15 p2578 A69-30937

Discrete radio sources interferometer observations using transPacific baseline, noting spectra and radiation intensity variations
15 p2701 A69-31530

Accurate optical position of quasars determined by plate overlap for radio interferometer calibration
16 p2859 A69-32229

Multielement compound high resolution quick scan interferometer for rapidly changing solar burst observations at 3.75 GHz
18 p3118 A69-34968

Active interferometer controlled telemetry tracking system for missile range, discussing automatic target acquisition, dish feed, costs and optimized data-channel antenna patterns
19 p3271 A69-36253

Quasi-optimal synthesis for reception indicator used in radio interferometers for measuring signal amplitudes in presence of normal noise
20 p3504 A69-37009

Radio interferometry for suppressing background variance between microwave radiometer antenna and random terrestrial background
20 p3506 A69-37712

HF direction finder for display of time varying multimode propagation phenomena, using analog computer and phase sensitive interferometer
21 p3677 A69-39456

Tethered orbiting interferometer configurations for future Radio Astronomy Explorer satellites, discussing gravitational stabilization and delta launching into orbit as single payload
24 p4313 A69-42859

Ionized meteor trails reflection zone altitudes determination by interferometric measurements of phase differences
24 p4311 A69-43508

RADIO METEOROLOGY

Radio telescope measurements of total vertical atmospheric absorption to determine effective mean free path of oxygen and water vapor for absorption
02 p0206 A69-11450

Quantitative estimations of cloud and precipitation by radar meteorology, assuming homogeneous reflectivity distribution of clouds
04 p0626 A69-14507

Microwave radiometer for measuring mesosphere and stratosphere temperature as function of altitude using atmospheric oxygen line
06 p0924 A69-17247

Remote sensing of lower atmosphere refractive structure, using Rake tropospheric scatter channel-sounding technique
14 p2448 A69-29525

Qualitative analysis of CAT parameters from radio sounding data, noting mean bumpiness probability dependence on Richardson number and wind vector shift
14 p2474 A69-29735

RADIO METEORS

Mass distributions of meteoroids obtained from underdense radio meteor echoes
03 p0518 A69-14254

Radio meteor ionization profiles, discussing electron line density measurements by backscatter system
19 p3283 A69-35992

Meteor radio electronics principles, methods and equipment, discussing ionized meteor trail formation, radar tracking and utilization of trails for communications
19 p3277 A69-36591

Lower ionosphere atmospheric density, temperature and pressure profiles diurnal variations from data of radio meteor echoes
24 p4311 A69-43504

RADIO NAVIGATION

NT DECCA NAVIGATION
NT HYPERBOLIC NAVIGATION

NT LORAN

NT LORAN C

NT TACAN

NT VHF OMNIRANGE NAVIGATION

OMEGA radio navigation system optimization, emphasizing implementation of phase modulation to ensure lane identification
03 p0463 A69-13212

Air traffic development related to control systems advances, discussing telecommunications effect and radio navigation systems enabling pilot to determine position
08 p1347 A69-20598

Radio location system based on measuring distance between object and two stationary satellites, noting application to air traffic over North Atlantic
09 p1537 A69-21269

Satellite-borne terrestrial radiodetermination systems, noting VLF transmissions usage to overcome coverage problem
09 p1537 A69-21287

Soviet book on radio navigation of flight vehicles covering systems classification, operational characteristics, satellite navigation, etc
12 p2129 A69-27076

Deep space network system for radio navigation of Mariner mission in 1969, discussing objectives, spacecraft, tracking and data system, mission accuracy, etc
16 p2749 A69-31725

Radio navigation principles, radio waves propagation characteristics and factors affecting navigation systems choice
18 p3169 A69-34848

Pictorial display area navigation system for air traffic control in terms of cockpit utilization, interface with ground navigation aids, parallel multiple routes, etc [AIAA PAPER 69-798]
19 p3367 A69-35632

Surface and aerospace navigation by VLF radio network, discussing Omega transmitting station location, operational modes and daytime-nighttime accuracies [AAS PAPER 69-405]
24 p4347 A69-42834

RADIO OBSERVATION

Observation of satellites, orbit calculation and use in upper atmosphere research [UN PAPER 68-95789]
01 p0064 A69-10459

Sporadic E microstructure and vertical motion, describing radio sounding system to observe ionospheric 3d structure and motions from ground
01 p0071 A69-11164

Radio telescope for Owens Valley Radio Observatory, noting interferometer array of steerable antennas and signal wavelength influence on telescope reflector accuracy
02 p0229 A69-11974

Wind measurements by radio observation of meteor trails compared with fading drift results
02 p0275 A69-12042

Radio occultation measurements of Venus and Mars atmospheres using Mariner spacecraft
02 p0320 A69-12115

Radio amplitude and phase measurements during Mariner-Mars encounter, providing evidence for Martian atmospheric models
02 p0320 A69-12116

Venus atmospheric structure from surface to 20,000 km radial distance from Mariner 5 radio experiments, noting large mass-2 hydrogen component in upper atmosphere
02 p0330 A69-12802

Intense discrete radio sources observation by antenna array with fan beam, determining right ascension and east-west structure
04 p0663 A69-15379

Radio observations of radio galaxies and quasars, noting double structure of many sources, some complex structures and association with optical objects
05 p0820 A69-15836

Polar cap event detected at low latitudes by effect on VLF propagation, noting VLF technique sensitivity to low proton fluxes
05 p0816 A69-16276

Auroral absorption position and height deduced from VLF phase measurements, discussing diurnal fluctuations in reflection layer
05 p0758 A69-16415

Galactic H 2 regions radio observation using Cassegrain antenna and Dicke radiometer
06 p1008 A69-17696

Radio occultation measurements of planetary atmospheres and ionospheres from orbiting pair [AIAA PAPER 69-53]
06 p1011 A69-18104

Radio aurora rate of occurrence from VHF bistatic radio system observations in eastern Canada
07 p1124 A69-18824

Radio interferometer antenna array spatial characteristics obtained as function of geographical coordinates of site for reducing observation errors
08 p1314 A69-20434

Radio wavelength range observations of NO molecule lines in interstellar space
09 p1590 A69-21377

Bright emission nebula components and electron temperature determined by radio telescope observation
10 p1778 A69-23603

VLF observations of July 7 1966 solar flare and PCA event
10 p1657 A69-23772

Radio astronomical observations of Venus at atmosphere interpreted noting agreement with model based on Venera 4 data
10 p1791 A69-24202

Flux densities and spectral indices of radio sources in 3C and 3 CR catalogs, noting measurements at 86 MHz frequency
11 p1951 A69-24237

LF observations of complex galactic radio source W51, discussing structure and radio spectra of resolved components
12 p2153 A69-25807

Radio observations of planetary nebulae IC 418 and NGC 7027 at 9.5 mm indicating radio spectra thermal character, discussing electron temperature and density
13 p2343 A69-27625

21 cm line emission surveyed for spatial distribution of random velocities of neutral hydrogen in solar neighborhood
14 p2520 A69-29371

Radio pulse sounding of ionospheric structure and motions, discussing digital ionosonde, data analysis methods, etc
14 p2415 A69-29519

Radio equipment for studying ionospheric inhomogeneities using space diversity reception, presenting vertical component of drift velocities of small scale inhomogeneities
14 p2453 A69-29876

Reflecting or reradiating obstacle proximity as cause of siting errors in azimuth radio measurements, discussing omnidirectional obstacles effect
15 p2651 A69-31090

Mercury, Venus, Mars, earth and lunar mass determinations by radio tracking and planetary radar systems
15 p2697 A69-31305

Preprotostar radio observations suggesting nonthermal radio sources formation with magnetic energy dissipated in particles acceleration
15 p2701 A69-31531

Radio observation of 20 May 1966 solar eclipse at 9470 and 3300 MHz, discussing brightness distribution of S component sources
17 p3030 A69-33057

Soviet collection of papers on radio engineering covering ionospheric signal scattering, E layer structure, meteor trail observation, antenna arrays, etc
17 p2938 A69-33893

Kinesonde radio sounding system for three dimensional ground observations of E region microstructure and vertical motion of neutral air and ions
18 p3125 A69-34250

Space station observations of stars, galaxies and quasars, stressing electromagnetic spectrum role in astronomy
18 p3194 A69-34370

Radio wavelength range observations of NO molecule lines in interstellar space
18 p3198 A69-34765

Radiometric measurement of lunar areas during eclipse of 18 October 1967 at mm wavelengths, considering temperature changes and cooling rates
20 p3613 A69-38247

Earth atmospheric density measurement by microwave radio occultation techniques, transmitting coherent radio signal to repeater spacecraft from master station
21 p3705 A69-38375

Venus atmosphere structure determined from Mariner 5 flyby S band radio occultation measurements of ionosphere and atmosphere at illuminated and dark sides
21 p3794 A69-38380

Solar observations at 21 and 43 cm during solar minimum by grating cross and total power radiometer, giving radio map of solar emission
22 p4001 A69-39988

Radio observations of supernova remnant HB 21 at 2695 MHz, noting spectral brightness and curvature of northern shell segment
22 p4014 A69-40129

RADIO PHYSICS

S-band radio occultation for probing atmospheres of Mars and Venus
[AAS PAPER 68-185] 02 p0311 A69-11470

Jupiter radio physics, discussing prebiological phase, low IR and microwave radio temperature and magnetic field
02 p0330 A69-12805

Collection of Soviet papers on radio engineering
06 p0889 A69-17796

Statistical characteristics of transverse shifts of ray directions in turbulent atmosphere for arbitrary wave parameter values
10 p1657 A69-23942

Accuracy and variance of nonergodicity estimates for random processes associated with radiophysical applications
15 p2582 A69-30946

Radio science - Conference, Ottawa, August 1969
19 p3276 A69-36425

RADIO PROBING

High gain-temperature ratios aerials design by radio modeling techniques for horn and planar antennas, prime feed parabolooids and Cassegrain systems
08 p1279 A69-19961

Radiophase mapping utilizing VLF radio signals to detect conductive sheets and surface impedance of earth
12 p2075 A69-26982

Radio measurements of nonionized media and planetary atmospheres, discussing uses of millimeter waves, line of sight propagation, scattering, etc
19 p3276 A69-36427

Radio FM pulse compression for vertical ionosphere sounding
21 p3674 A69-39082

RADIO RANGE

Compatibility requirements and considerations of range telemetry tape crossplay operations, discussing major classes
07 p1133 A69-19117

Secor data reduction to correct tropospheric refractive effects of radio ranging on earth satellites using tropospheric model
18 p3104 A69-35200

RADIO RECEIVERS

NT SUPERHETERODYNE RECEIVERS
NT TRANSMITTER RECEIVERS
NT WHISTLER RECORDERS

Injection locked oscillator FM receiver consisting of linear mixer and negative resistance oscillator in phase locked configuration, solving receiver output differential equation
01 p0042 A69-10247

Wideband electronically scanned receiver, using varactor diode upper sideband parametric frequency upconverter for frequency mixing
01 p0048 A69-11036

Low noise front end wideband amplifier for 100-150 MHz broadband receivers, using distributed amplifier techniques
02 p0216 A69-12028

Low noise microwave amplifiers for radio astronomy and satellite communications receiving system preamplification
03 p0402 A69-13017

Optimum receiver structure for estimating PSK information signal phase derived together with matched filter detector performance
03 p0403 A69-13203

Sensitivity of radio receiver detecting weak sinusoidal and noise signals by counting zero crossings by envelope or phase of signal sum
03 p0405 A69-13717

Electrically small beamed receiving arrays in HF band and random noise
03 p0398 A69-13904

AN/TSC-54 military satellite communications terminal for contingency deployment, discussing design, system tradeoffs and performance
[AIAA PAPER 68-439] 04 p0579 A69-15367

Low noise room temperature satellite broadcast receiver for UHF, using room temperature parametric amplifiers
05 p0728 A69-15672

Transistorized receiver for satellite telecommunications having adjustable receiver center frequency within 20 MHz
05 p0734 A69-16594

Optimal radio signal receiver analyzing output signal properties
06 p0888 A69-17464

Finite IF filter bandwidth degradation of SNR of receiver for biphase modulated signals using integrate and dump filter
08 p1270 A69-19851

Phase error and amplitude and phase modulation in aircraft VOR omni receiver in vicinity of reflecting objects, noting asymmetrical filter effect
08 p1271 A69-19863

Error in receiver sensitivity calculation using approximate equation for noise power at input
08 p1275 A69-20226

Airborne ILS marker beacon receivers and secondary surveillance radar transponder using microelectronic equipment, noting thermal dissipation problems [AGARDOGRAPH-114] 08 p1292 A69-20991

Interference noise in communication satellite receivers and terrestrial radio relay receivers, noting interference reduction transfer factor
09 p1450 A69-21279

Low noise wideband amplifier system for commercial satellite communication ground terminal receiver, noting cryogenically cooled parametric amplifier
09 p1458 A69-22470

Microwave amplifiers and receivers noise performance factors measurement noting thermal noise, definitions of noise temperatures and noise figure, noise generators, etc
11 p1840 A69-25301

Multimode tracking/SYMMTRAC I and II feeds for low noise antennas, noting feed performance
11 p1852 A69-25317

Microwave radiometric sensor operational principles and capabilities, discussing antennas and radiometric receivers
12 p2033 A69-26976

Noise stability of FM receiver with automatic control of IF amplifier resonance frequency in presence of weak noise
15 p2564 A69-30144

German ground station commercial receiving system for satellite broadcast reception
16 p2766 A69-31855

Selective amplifier for recording time signals on Time Recorder 2 and measuring time lag caused by Philips 8RO 501 radio receiver
16 p2790 A69-32217

Rocket-borne AM radio receiver for Faraday rotation experiments to measure lower ionosphere electron density, giving circuit diagrams
17 p2936 A69-33062

Single radio pulse reception time relations by panoramic receiver, considering short wideband and long narrowband pulses
17 p2931 A69-33910

Airborne communication receiver solid state interference blanker circuitry comprising black box insertable between antenna and RF input
17 p2943 A69-34132

Optimal radio signal receiver analyzing output signal properties
20 p3496 A69-37947

Spark gap protection of input transistors in radio receivers against antenna-collected static charge damage
21 p3681 A69-38395

S band phased array receiver developed to track automatically moving telemetry transmitter by electronic beam steering
23 p4120 A69-41751

HF receiver interference blanker, discussing limiter-blanker system, integration, effectiveness and squelch circuit
23 p4141 A69-42221

Receivers EMC, discussing single parameter to evaluate susceptibility to desensitization, cross modulation and intermodulation
23 p4142 A69-42232

RADIO RECEPTION

Optimal AM radio reception in presence of fluctuating noise and one AM interference signal with random initial phase of carrier oscillation
01 p0031 A69-10782

Constant beamwidth antenna consisting of parabolic reflector and ridge loaded horn, noting conical scan tracking antenna application
02 p0218 A69-12325

Ultra cone system for ultralow noise reception of RF space communication from Mariner 5 during occultation by Venus
[JPL-TR-32-1340] 02 p0220 A69-12429

Earth effect on signal correlation in space diversity microwave reception antennas, analyzing vertical separation and out of phase signals
05 p0720 A69-16530

Signal strength variations for balloon-borne VHF FM transmitter due to wave interference, noting application to balloon range estimation
06 p0886 A69-16925

Coherent FSK LF/VLF radio communication modem with large predetection bandwidth for improvement of reception in atmospheric noise
09 p1458 A69-22473

Optimal AM radio reception in presence of fluctuating noise and one AM interference signal with random initial phase of carrier oscillation
10 p1653 A69-23111

Multiple beam HF receiving antenna system for directivity, azimuthal coverage and noise limitation
13 p2228 A69-27631

Earth effect on signal correlation in space diversity microwave reception antennas, analyzing vertical separation and out of phase signals
16 p2753 A69-32472

Received electromagnetic fields fluctuations due to transhorizon propagation, emphasizing fading- tropospheric turbulence correlation and rapid fluctuations due to small scale index variations
20 p3494 A69-37810

RADIO RELAY SYSTEMS

Microwave frequency multipliers for radio relay systems based on VHF transistors and varactor diodes
02 p0216 A69-12097

Mutual RF interference between satellite and terrestrial telecommunications microwave relay system at shared frequencies
03 p0392 A69-13242

Soviet book on multichannel and TV signals transmission over radio relay links using microwave tropospheric scatter propagation
04 p0558 A69-14919

Broadband LC filters having prescribed amplitude response and constant group delay, emphasizing IF filters for radio relays
05 p0732 A69-16343

Measurement methods at IF and baseband sections of microwave links, calculating noise superimposed on each swept measurement curve
05 p0722 A69-16728

Carrier energy dispersal in communication satellite telephony and TV systems, noting attendant RF bandwidth increase as function of distortion
09 p1450 A69-21277

Interference noise in communication satellite receivers and terrestrial radio relay receivers, noting interference reduction transfer factor
09 p1450 A69-21279

Multipath fading reduction on line of sight microwave radio relay links by dual space diversity, noting effects of vertical antenna separation, frequency, etc
[IEEE PAPER 68-TP-350-COM]
10 p1656 A69-23535

Echo 1 aluminized plastic balloon satellite, discussing radio linkup by reflections, use in geodesy and atmospheric and radiation pressure effects on lifetime
10 p1792 A69-23804

Carrier to interference ratio /CIR/ between desired path and every other path within predetermined range in microwave system calculated by computer
11 p1840 A69-25312

Mean-minute thermal noise intensity distribution in telephony channels of tropospheric radio relay systems
14 p2412 A69-29425

Long distance FM radar signal relaying to central station image processing, showing wideband sum signal especially suitable for transmission
16 p2750 A69-31862

Radio relay FM channel data transmission, evaluating cumulative thermal noise due to IF amplification at each station
21 p3672 A69-38653

RADIO SCATTERING

Raindrop size distribution law effect on radio wave attenuation coefficient and differential effective backscattering cross section of rain
02 p0208 A69-12259

Very thin short metallic filament scattering and absorption cross sections for various values of filament conductivity
03 p0395 A69-13623

Induced and combination scattering of high HF radio waves in ionosphere and magnetosphere
07 p1076 A69-18521

Lunar scattering of meter radio waves emitted by Luna 11 and 12 satellites, relating glide angle scattering coefficients to satellite altitude
07 p1087 A69-19615

Quantitative radar determinations of radio wave scattering cross section of lunar surface layer
07 p1087 A69-19621

Inverse Compton effect and universal black body radiation from less energetic radio photons of galactic and metagalactic origin
08 p1381 A69-19786

Radio signal spectrum scattered at oscillating interface calculated in Kirchhoff approximation, determining scattering factors
08 p1275 A69-20432

Duty cycle increase on meteor forward scatter radio communication paths by use of wide-beam transmitting antenna along great circle
08 p1394 A69-20609

Radio ray scattering resulting from traversing anisotropically turbulent solar corona, noting refraction effect on signal pulse arrival time
10 p1773 A69-22960

Ionospheric measurements of electron density, electron and ion temperature profiles from strength of incoherent radio wave scattering
10 p1686 A69-23910

Surface radio wave scattering propagating along rough surfaces, measuring emission during transformation into space waves
10 p1658 A69-23952

Antenna suspension height variation effects on HF signals in ionospheric scattering lines
12 p2032 A69-26705

Radio wave scattering characteristics of lunar surface in 3 cm wavelength by Luna 8 and Luna 9 automatic stations and Surveyor spacecraft
15 p2571 A69-31359

Spectrum and cross section of radio wave scattering in two temperature plasma, relating differential backscattering cross section to ionospheric electron density fluctuations
17 p2930 A69-33895

Radio wave diffraction by inhomogeneities arising from ionized gas clouds in interstellar medium
19 p3428 A69-36882

RADIO SIGNAL ABSORPTION

U ELECTROMAGNETIC ABSORPTION

RADIO SIGNALS

Faraday angle of rotation of radio signals polarization plane from satellites and celestial bodies
01 p0030 A69-10574

Optimal reception methods noise stability for AM radio signals based on nonlinear filtration of information parameters of signals received on noise background
01 p0030 A69-10589

Amplitude scintillations of satellite radio signals during sunrise due to ionospheric turbulence induced electron content variations
01 p0067 A69-10980

Radar FM signal design with zigzag frequency variation, discussing relation between waveform characteristics and associated ambiguity function features
01 p0033 A69-11001

Amplification process for VLF whistler mode radio signals observed in study of magnetosphere frequency shifting mechanism
01 p0077 A69-11241

Ionospheric electron density determined from Faraday effect, using ATS-3 radio signals
02 p0237 A69-11660

Radio signals from hydroxyl radicals by maser action in early stars, noting emission magnitude and intensity spectrum dissimilarity at different frequencies
02 p0324 A69-12493

Correlation coefficient between frequency diversified signals amplitudes estimated by approximation for two beam short wave radio channels
04 p0560 A69-15401

Resonant amplifier response having stages identical to radio pulse with exponential envelope
05 p0720 A69-16444

Low power RF signal triggering of self sustaining Gunn oscillations in GaAs samples
05 p0734 A69-16575

Signal strength variations for balloon-borne VHF FM transmitter due to wave interference, noting application to balloon range estimation
06 p0886 A69-16925

VLF radio wave phase time or motion variation emanating from ground based source at arbitrary point on earth
07 p1123 A69-18816

Errors estimation in determination of radio signal source flux density, position and recorded half power widths
07 p1088 A69-19722

VHF radio transmission beyond horizon, discussing instrumentation, annual and diurnal signal fluctuations and diffraction role in signal propagation
08 p1274 A69-20112

Wavefront Wilkins-Minnis, null selection and elevation scanning techniques for measuring radio signals elevation angles with vertical antenna arrays
08 p1275 A69-20293

Radio signal from magnetron transmitter, noting slow amplitude phase fluctuations distribution according to log-normal law
08 p1275 A69-20424

Radio signal reflection from objects of complex configurations by statistical model
09 p1460 A69-22662

Optimal reception methods noise stability for AM radio signals based on nonlinear filtration of information parameters of signals received on noise background
10 p1653 A69-23104

Stellar occultations by moon observed with ear and eye method, not taking into account corrections to radio time signals
10 p1776 A69-23205

Combination backscattering on ionic sound waves assumed responsible for unexpected features of radio signals reflected from sun
10 p1776 A69-23219

Radio signals and concentrated noise amplitudes probability distributions reflected from ionosphere and scattered in troposphere calculated for Rayleigh and log-normal fading
11 p1833 A69-24440

Radio signal carrier frequency and arrival time measurements, deriving expressions for phase amplitude distortions effects
11 p1835 A69-24959

Ionospheric electron density determined from Faraday effect, using ATS-3 radio signals
13 p2256 A69-28691

Radio signal amplitude changes from Explorer 22 beacon satellite attributed to wave diffraction by tropospheric structures
14 p2411 A69-29107

Radio signals F region scattering related to electron density fluctuations in ionosphere
14 p2444 A69-29870

Reference oscillator frequency instability effect on radio signals phase shift in ionosphere measurements, evaluating errors
14 p2444 A69-29873

Recording installation of ionospheric reflected radio signal fluctuations and amplitudes of resulting signals simultaneously at three points, discussing antenna commutator circuit
14 p2452 A69-29874

Autonomous radiometers signals statistical properties used in space technology, discussing radar signals phenomenological models, measurement errors and energy characteristics
15 p2566 A69-30337

Faraday angle of rotation of radio signals polarization plane from satellites and celestial bodies
15 p2568 A69-30744

Aoristic antenna to receive radioelectric signals from satellite emitter at distance of 10,000 km
15 p2580 A69-31095

Satellite radio signal scintillation variations association with sporadic E and spread F and dependence on magnetic activity in Southern Hemisphere during sunspot minimum
16 p2780 A69-32307

Resonant amplifier response having stages identical to radio pulse with exponential envelope
16 p2753 A69-32476

Meteor station photorecorder of reflected radio signals, discussing design and performance during meteor shower
17 p2976 A69-33898

Single radio pulse reception time relations by panoramic receiver, considering short wideband and long narrowband pulses
17 p2931 A69-33910

Irregularities distribution in antarctic ionosphere from polarization angle fluctuations of satellite S-66 radio signals, discussing diurnal magnetic and solar cycle effects
18 p3125 A69-34249

UHF radio pulses from zenith associated with extensive air showers, estimating threshold energy of scintillation trigger system

21 p3792 A69-39613

Satellite scintillating signals amplitude distribution, correlating observations and theoretical results

23 p4115 A69-41486

RF and microwave signal variable delay and processing using laser-acoustic interactions, photodetector and electrical-to-acoustical transducer

24 p4283 A69-43027

RADIO SOURCES [ASTRONOMY]

NT CASSIOPEIA A

NT PULSARS

NT QUASARS

Optical identifications for 17 Ohio survey sources with peaked or flat spectra

01 p0153 A69-10854

Metagalaxy temperature brightness explained from radio sources combined radiation with inversion spectra

02 p0313 A69-11632

Radio emission fluxes in solar active regions, determining slope of spectral characteristics of radio sources from effective emission center

02 p0314 A69-11676

Radio signals from hydroxyl radicals by maser action in early stars, noting emission magnitude and intensity spectrum dissimilarity at different frequencies

02 p0324 A69-12493

Normal galaxies radio emission and brightness of metagalactic radio background

02 p0325 A69-12564

Linear polarization measurements of variable radio sources

02 p0325 A69-12592

Radio source near UV object identified with X ray source GX3 plus 1

02 p0308 A69-12595

Radio source positions and structures from occultation observations, suggesting optical identifications

02 p0326 A69-12704

Plasma model of quasars and radio galaxies for observations of high energy radiation

02 p0329 A69-12794

Radio emission sources nature in terms of special relativity theory

03 p0499 A69-13078

Linear polarization of cosmic radio emission measured near galactic anticenter at centimetric wavelengths

03 p0501 A69-13704

Spectrum and diameter of source of slowly varying component of solar radio emission between 3.3 mm and 21 cm

03 p0516 A69-14045

Pulsating radio sources near Crab Nebula noting possible coincidence with nebula, pulse dispersion and interstellar electron density

04 p0659 A69-14977

Solar radio emission sources associated with sunspot groups and flocculi at 1.6 cm

04 p0649 A69-15241

Diminished RF intensity of neutral hydrogen line near radio source W 49 due to diminished kinetic temperature of gas

04 p0662 A69-15253

Intense discrete radio sources observation by antenna array with fan beam, determining right ascension and east-west structure

04 p0663 A69-15379

Supernova remnant theories used to interpret results of 1-mile Molonglo cross type radio telescope survey of nonthermal galactic sources

04 p0664 A69-15441

Non-Io controlled fifth source of Jupiter decametric radiation from/near visible planetary disk

05 p0813 A69-15604

Radio sources quantity dependence on radio emission value, noting determination of spatial density variations of radio galaxies

05 p0826 A69-16426

Radio emission from supernova remnants, reviewing evolution, structure, spectra and polarization, plus identification, characteristics, surface brightness and radio emissive remnants distance

06 p1002 A69-17314

Flux density spectral dependence disagreement with power law for synchronous radiation mechanism for radio sources in 12.6 to 25 MHz interval

06 p1004 A69-17538

Lunar occultations of radio source Sagittarius A observed at various frequencies between 230 and 2400

MHz, obtaining diameter, position and decimeter band flux densities

06 p1009 A69-17960

Radio sources detected in HF surveys not listed in 4C catalog

06 p1010 A69-17974

Solar wind, discussing corona, radio sources, radio bursts, comet tails, cosmic rays, etc

06 p1012 A69-18239

Spectra and flux densities of cm wavelength radio sources

07 p1218 A69-19256

Southern Hemisphere galactic H II regions continuum thermal radiation at 6 cm, noting maps for 28 of 36 sources, peak temperatures and emission and half intensity widths

07 p1206 A69-19271

Cosmic radio noise brightness distribution in Southern Hemisphere at 10.02 MHz, noting spectra of sources observed

07 p1206 A69-19272

Radio sources flux densities from fan beam survey using Molonglo radio telescope compared to flux densities of Parkes catalog, presenting revised spectra

07 p1218 A69-19278

Rosette Nebula structure from high resolution observations at 178 MHz of galactic plane, deriving 8600 K electron temperature for Nebula, discussing Monoceros Nebulosity

07 p1223 A69-19625

Errors estimation in determination of radio signal source flux density, position and recorded half power widths

07 p1088 A69-19722

Radio source counts log N-log S diagram slope uncertainty due to finite source number, discussing statistical analysis methods accuracy

08 p1383 A69-20048

Radio observations of gamma Cygni source in Cygnus X complex showing nonthermal nature of source, noting weak but significant polarization

08 p1387 A69-20090

Number count formula in zero pressure model universe for extragalactic radio sources with arbitrary luminosity and evolution functions, discussing red shifts

08 p1390 A69-20388

Interferometric measurement of polarization distributions in Crab Nebula and 3C 315 radio sources by Fourier synthesis, discussing complex brightness

08 p1390 A69-20389

Wideband 1665 MHz OH emission source in Carina region of galaxy in weak continuous radiation region with low degree of polarization

08 p1397 A69-20772

Optical depth determination in absorption lines of interstellar neutral hydrogen clouds by spectral observation of variable intensity radio sources

08 p1398 A69-20774

Flux density variability and component age of radio sources at frequency of 5769 MHz measured by radio telescope

09 p1588 A69-21361

Spectra of opaque radio sources with synchrotron self absorption, discussing brightness temperature and magnetic field

09 p1591 A69-21447

OH emission source in W24 during July 19, 1967 lunar occultation, obtaining better position for brighter OH emission feature

09 p1591 A69-21449

Condensed supernova remnants in Crab Nebula, considering various hypotheses for radio source

09 p1592 A69-21485

Polarization and intensity distribution of extended supernova remnant in Centaurus, discussing remnant effect on galactic magnetic field

09 p1598 A69-22184

Linearly polarized radiation from supernova remnants 3C 10, Taurus A, 3C 358 and Cassiopeia A, determining distributions by synthesizing fan beam

09 p1598 A69-22185

Contour maps of H II regions W12, Orion A, W43 and W51, listing flux densities and angular sizes of components

09 p1598 A69-22186

Red shifts of radio sources obtained with Carnegie image tube spectrograph, noting quasi-stellar objects and galaxies

09 p1602 A69-22224

Contour maps of supernova remnants HB 9, Simeis 147 and IC 443, noting spectra showing radiation nonthermal

09 p1604 A69-22408

Radio wave generation in astrophysical plasmas, discussing various emission mechanisms

09 p1608 A69-22743

Absolute flux density of five radio sources and relative flux densities of 37 sources defining absolute flux density scale for Southern Hemisphere

10 p1772 A69-22857

Radio spectra and structure of H II regions in emission nebula NGC 281 and unnamed nebula near NGC 2264

10 p1773 A69-22957

Flux density and spectra measurements at 5 GHz for extraterrestrial and other discrete radio sources, noting spectral indices

10 p1773 A69-22958

Position and polarization of 1720 MHz OH emission from W28, W44 and galactic center, considering unresolved concentrations of shell type nonthermal sources

10 p1776 A69-23220

Preliminary observations of Tau-A, Cas-A and Cyg-A with multiple-element interferometer

10 p1777 A69-23397

Pseudodynamic programming for optimizing design of correlator supersynthesis antenna arrays used for radio source tracking

10 p1663 A69-23420

Bright emission nebula components and electron temperature determined by radio telescope observation

10 p1778 A69-23603

Antenna for lunar occultation observations at 81.5 MHz, detailing experimental procedure and data reduction

10 p1779 A69-23606

Polarization observation of star BL Lac continuum by multichannel scanner, noting photoelectric UVB observations and identification with radio source

10 p1785 A69-24090

Hyperfine transition line of He 3 II for abundance in Messier 17 source by radio telescope

10 p1785 A69-24098

Interstellar formaldehyde detection in absorption against galactic and extragalactic radio sources, discussing chemical evolution

10 p1786 A69-24108

Position of OH sources near seven galactic radio sources determined with two element variable-baseline interferometer, noting strong circular polarization

10 p1787 A69-24114

Radio sources log N-log S diagram, red shifts and luminosity functions in zero cosmological constant and Lemaitre type Friedmann universes

10 p1789 A69-24134

Radio nebula NRAO 591/593, discussing thermal and nonthermal source and models based on electron density distribution

10 p1790 A69-24136

Flux densities and spectral indices of radio sources in 3C and 3CR catalogs, noting measurements at 86 MHz frequency

11 p1951 A69-24237

Condensation sources of maser radiation observed in W3 hydroxyl lines, discussing polarization and designation as protostars

11 p1954 A69-24379

Radio sources optical positions for independent calibration sources

11 p1958 A69-24465

Northern sky scan for discrete sources of gamma rays in 240 to 1000 kev energy region by telescope on balloon flight

11 p1946 A69-24593

Galactic radio source W 49 /3C 398/ observed with Cambridge one-mile radio telescope

11 p1963 A69-25259

Hydroxyl microwave emission sources in Cygnus not connected with continuum emission

11 p1964 A69-25403

LF observations of complex galactic radio source W51, discussing structure and radio spectra of resolved components

12 p2153 A69-25807

Frequency spectrum, time variations and polarization of source of synchrotron radio emission with expanding components flying apart at relativistic velocities

12 p2155 A69-26207

Pulsars discovery, emission, regularity, narrow frequency band and pulse changes, physical nature and aspects of Crab Nebula source

12 p2160 A69-26895

Polarization and structure of magnetic fields of quasars, E galaxies, normal galaxies and other extragalactic radio sources

12 p2165 A69-27034

Absolute radio luminosity relation to surface brightness of extragalactic radio sources, finding volume radiation coefficient of spiral and radio galaxies

12 p2166 A69-27035

Extragalactic radio sources, discussing brightness distribution measurements and radio star scintillations

12 p2168 A69-27053

Interacting galaxies theories, characteristics and terminology, discussing galactic radio sources and properties of matter

12 p2169 A69-27055

Galactic formation by massive matter cloud passage through antimatter cloud, discussing radio sources genesis

12 p2170 A69-27064

Optical identification of radio source 3C 230, suggesting removal from quasar list

12 p2173 A69-27171

Variable radio sources observation at 9.55 mm wavelength, discussing flux density and electron cloud expansion

13 p2334 A69-27309

Exterior field equations for radiating spheres with zero limb darkening in relativity and Bondi coordinates, determining radiative flux and pressures

13 p2339 A69-27566

Radiative relaxation of relativistic particle distribution undergoing synchrotron radiation and reabsorption, discussing self absorbed radio source model

13 p2327 A69-27572

Synchrotron spectrum radiated by relativistic electrons below Razin cut-off, considering relation to radio spectra curvature of variable extragalactic sources

13 p2339 A69-27573

Balloon-borne instrumentation for detection of far IR extended emission regions and bright point sources, describing results of initial flights

13 p2342 A69-27599

Radio emission fluxes in solar active regions, determining slope of spectral characteristics of radio sources from effective emission center

13 p2355 A69-28707

Radio emission sources nature in terms of special relativity theory

14 p2509 A69-28760

Frequency selection, spectral index distributions and counts of extragalactic radio sources

14 p2518 A69-29134

Linear polarization of quasars, radio or normal spiral galaxies, galactic objects, etc, observed by Parkes telescope

14 p2526 A69-29770

Radio observations of emission nebulae for flux densities, deriving electron temperatures

[ASME PAPER 69-DE-46] 14 p2527 A69-29941

Negative curvature electron energy spectrum of discrete radio source model, assuming acceleration by Fermi mechanism and energy loss by synchrotron radiation

15 p2687 A69-30540

Radio source W 43 distance determined from analyzing neutral H line profile and radial velocity in excited H line 104 alpha

15 p2687 A69-30543

Interstellar radio absorption influence on spatial distribution of cosmic radio emission observations with fixed multiple dipole antenna arrays

15 p2687 A69-30545

Electron energy distribution determination from electron synchrotron radiation spectrum for various magnetic field configurations within radio source

15 p2655 A69-30546

Distribution model for ionized interstellar gas over galactic disk for explaining radio emission absorption and depolarization from discrete sources

15 p2695 A69-30935

Radio interferometer with independent heterodynes to obtain radio brightness distribution over source by varying antenna spacing and reception frequency

15 p2578 A69-30937

Observations of 123 southern radio sources made with two element variable spacing interferometer, tabulating and graphing results

15 p2696 A69-31166

Flux densities at 2695 MHz for radio sources, tabulating measured data, discussing spectral distribution indices

15 p2696 A69-31206

Discrete radio sources interferometer observations using transPacific baseline, noting spectra and radiation intensity variations

15 p2701 A69-31530

Preprotostar radio observations suggesting nonthermal radio sources formation with magnetic energy dissipated in particles acceleration

15 p2701 A69-31531

Spectrophotometry of elliptical galaxy NGC 1052 nucleus from 3400 to 6300 A for relating radio properties and optical characteristics

16 p2853 A69-31610

Radio sources spectral flux densities at 22 MHz, considering ionospheric conditions, calibration and reduction

16 p2860 A69-32231

X ray source Cyg XR-1 angular diameter upper limit determined from balloon experiment data obtained with collimated X ray telescopes

17 p3026 A69-32860

Interferometric observations of radio source VRO 42 22 01 listed with antenna separations in wavelengths and with resolution direction

17 p3026 A69-32861

Radio observation of 20 May 1966 solar eclipse at 9470 and 3300 MHz, discussing brightness distribution of S component sources

17 p3030 A69-33057

Radio map of Orion A region, resolving M 42 and M 43 nebulae at 1.94 cm wavelength, noting optical photographs comparison

17 p3035 A69-33609

Spectra for 16 radio sources, questioning classification as supernova remnants

17 p3035 A69-33610

Accurate positions at 2700 MHz and optical identification of radio sources with galaxies and quasi-stellar objects

17 p3035 A69-33611

Radio sources interplanetary scintillations and cross correlation coefficient real time determination

17 p3038 A69-33727

Solar radio sources heights at 1424 and 696 MHz during near minimum solar activity

17 p3040 A69-33808

Parkes catalog of 1780 radio sources, noting inclusion of data concerning polarization, source structure, optical identifications, etc

17 p3045 A69-34199

Extragalactic radiation depolarization through Milky Way transit determined from linear polarization and flux density measurements of discrete radio sources at 21.2 cm

18 p3190 A69-34287

Depolarization of extragalactic radio sources at low Galactic latitudes attributed to ionized hydrogen produced by B2 star tunneling through interstellar hydrogen cloud

18 p3194 A69-34425

Galactic plane at 9.26 cm between longitudes of 32 to 49 degrees, tabulating contour map of antenna temperature and sources

18 p3195 A69-34426

Observations of W49 at 2800 MHz with East-West resolution, analyzing shape of thermal and nonthermal source

18 p3195 A69-34427

Continuum survey at 1415-MHz between declinations of zero and 20 degrees N with radio telescope, noting flux densities and contour maps of sources

18 p3195 A69-34428

Jovian radio sources intermittency, recording difficulties, longitudinal drift and theories concerning origin

18 p3196 A69-34690

Flux density variability and component age of radio sources at frequency of 5769 MHz measured by radio telescope

18 p3197 A69-34751

Radio sources spectrum measurement results at cm wavelengths in tabular form, noting flux density relationship to frequency

18 p3200 A69-35132

Discrete radio sources spectra at decametric wavelengths, showing variation with frequency and radio wave generation mechanism leading to various spectral types

18 p3200 A69-35134

Radio sources identified as quasi-stellar objects through photographic detection of large brightness changes

18 p3201 A69-35206

Radio emission attributed to galactic nebula NGC 6857, suggesting origin in high density H II regions excited by OB star clusters

18 p3202 A69-35209

Jupiter decametric radio source analysis suggesting two component model of rotation at both constant and variable rotational periods

18 p3202 A69-35212

Interstellar hydroxyl molecular clouds as radio wave sources, using very long baseline interferometry, suggesting natural masers in space for OH emissions

19 p3427 A69-36659

Radio emission intensity of Cas-A and Cyg-A at 30-60 cm, giving spectral indices

19 p3428 A69-36876

Planetary nebulae observations, describing radio spectra characteristics, electron temperature measurement, hydrogen line emission, etc

20 p3598 A69-37425

M 31 nebula radio continuum survey, describing discrete sources catalog and Andromeda nebula radiation distribution

20 p3601 A69-37493

Circular polarization measurements of compact radio sources at 1420 MHz, finding no detectable polarization

20 p3606 A69-37831

Brightness distribution over source, discussing regularization algorithms for radio astronomical data reduction from crossed telescope

20 p3606 A69-38033

Right ascension and flux density of source in Crab Nebula measured at meter wavelengths, evaluating spectrum and relative position to binary star center

20 p3607 A69-38040

Radio source flux density values in revised 3C catalog determining spectrum, discussing effects of relativistic electron energy distribution, self absorption and spatial distribution

20 p3609 A69-38138

Linear and circular integrated polarization of extragalactic radio sources measured by two element interferometer at Owens Valley Radio Observatory

20 p3610 A69-38139

Satellite-anomalous OH radio emission sources, observing spatial distribution and Stokes parameters

20 p3610 A69-38146

Upper limits for OH microwave emissions from radio sources F transitions, discussing pumping mechanism role in emission detection

21 p3796 A69-38477

Radio spectra of 136 sources determined at various declination ranges noting flattening at frequencies below 408 MHz

21 p3797 A69-38480

Variable BL Lac SHF flux density measurements, discussing periodicity and maxima spacing

21 p3798 A69-38545

Galactic radio sources high resolution observations at 178 MHz, determining flux densities and angular structures, noting supernovae remnants

21 p3801 A69-38701

Radio source counts from cosmological standpoint, discussing terrestrial location relative to quasars

21 p3802 A69-38828

Radio sources observation by lunar occultation, interplanetary scintillations and interferometry techniques, outlining measurement theory

21 p3812 A69-39518

Flux measurements of radio sources at 4.3 mm by 36 ft parabolic antenna, noting flux densities relative to Jupiter

22 p4014 A69-40126

Flux densities of radio sources in 3CR catalog measured at 2.8 cm wavelength

22 p4014 A69-40127

Declination measurements of sources in 4C Catalogue by Arecibo 1000 ft radio telescope

22 p4014 A69-40128

Extragalactic radio sources linear polarized radiation distribution at 1418 MHz indicating ordered magnetic fields often oriented differently

22 p4015 A69-40155

Flux density variations of radio sources at 2.8 and 4.6 cm wavelengths, suggesting relativistic particles prolonged injection into optically thin sources

22 p4029 A69-40764

Microwave background radiation in steady state cosmological model, attempting interpretation as discrete extragalactic radio sources population

22 p4029 A69-40765

Absorption features of 21 cm neutral hydrogen line in part of Cygnus X and of W 49, showing equal velocity contour diagrams from right ascension scans

22 p4034 A69-41200

X ray spectra of four high energy sources near galactic center
23 p4206 A69-42114

Continuous electron acceleration in astrophysics, discussing Crab Nebula X ray flux and galactic and extragalactic radio source power law spectra
24 p4355 A69-42696

Extragalactic radio sources flux densities at 5009 MHz tabulated, ascribing accuracy variations to uncertainty in receiver gain and dish efficiency
24 p4382 A69-42922

Radio emission from diffuse thermal radio sources in northern Milky Way, giving contour maps
24 p4388 A69-43641

Condensation sources of maser radiation observed in W3 hydroxyl lines, discussing polarization and designation as protostars
24 p4389 A69-43769

RADIO SPECTRA NT MICROWAVE SPECTRA

Spectral fine structure in emission from pulsars, noting correlation between fading and spectral change
01 p0150 A69-10273

Optical identifications for 17 Ohio survey sources with peaked or flat spectra
01 p0153 A69-10854

Spectrum and diameter of source of slowly varying component of solar radio emission between 3.3 mm and 21 cm
03 p0516 A69-14045

Radio spectra differences of quasars and radio galaxies, noting influence of frequency levels
04 p0652 A69-14418

Radio emission spectra of radio galaxies from 3CR catalog
04 p0661 A69-15234

Intense continuum bursts energy, flux density and energetic proton production, noting V-spectrum in proton flares
06 p0985 A69-16980

Radio spectrum and cosmic ray electron data evaluated concerning conditions in Galaxy, deducing mean magnetic fields
06 p0991 A69-17309

Solar radio spectroscopy for 40 to 240 MHz frequency range, noting dynamic spectra of solar radio bursts
06 p0925 A69-17318

Radio spectra of supernova remnants Cygnus Loop and IC443, noting possible radiation from shell source
06 p1003 A69-17322

Flux density spectral dependence disagreement with power law for synchronous radiation mechanism for radio sources in 12.6 to 25 MHz interval
06 p1004 A69-17538

Radio spectra analyzed for NGC 1052 and NGC 4278 elliptical galaxies, discussing 178 MHz flux density, anomalies and radiation absorption mechanisms
06 p1009 A69-17959

Electron temperatures and optical depths for planetary nebulae outer regions derived using radio spectra and Balmer line isophotes
06 p1009 A69-17962

Radio recombination lines in populations of highly excited states of hydrogen, discussing collisional transition effects
06 p1010 A69-17970

Digital FM techniques, signal spectral properties, discrimination detection, phenomenological model, etc
07 p1081 A69-19105

Spectra and flux densities of cm wavelength radio sources
07 p1218 A69-19256

Radio spectrum of quasi-stellar object identified as Parkes 2134 plus 004
07 p1224 A69-19708

Radio signal spectrum scattered at oscillating interface calculated in Kirchhoff approximation, determining scattering factors
08 p1275 A69-20432

Radio spectra of normal galaxies noting transition in spectrum
08 p1398 A69-20777

Radio wavelength range observations of NO molecule lines in interstellar space
09 p1590 A69-21377

Spectra of opaque radio sources with synchrotron self absorption, discussing brightness temperature and magnetic field
09 p1591 A69-21447

Taurus A flux density measurement at 4.3 mm with 36-ft antenna at National Radio Astronomy Observatory to determine spectrum unambiguously
09 p1591 A69-21450

Meter wave radio spectrum observations during 9 June 1968 solar flare, suggesting sudden intensity and frequency change due to shock wave
09 p1582 A69-22748

Pulsed RF spectra analyzer displays, noting responses to CW and pulsed signals and Fourier and pulsed repetition rate lines
09 p1460 A69-22791

Radio spectra and structure of H II regions in emission nebula NGC 281 and unnamed nebula near NGC 2264
10 p1773 A69-22957

Flux density and spectra measurements at 5 GHz for extraterrestrial and other discrete radio sources, noting spectral indices
10 p1773 A69-22958

Dynamic spectrum of July 7, 1966 proton flare, considering short wave fadeout at 0027 UT and intense burst of spectral Type 2
10 p1765 A69-23750

Decametric radio spectra from 0053 to 0200 UT during July 7, 1966 solar proton flare, discussing Type 4 phase
10 p1765 A69-23751

Dynamic spectrum of Type 4 solar radio burst during July 7, 1966 proton flare, noting limb effect
10 p1765 A69-23752

Crab Nebula radio emission spectrum in decimeter wavelength range indicating emission spectral index decrease from Taurus A
10 p1784 A69-23941

Quasi-stellar radio sources interferometric observations at 2695 MHz, determining centroid of radio emission
10 p1790 A69-24138

Quasars time dependent flux density variations at 6.6 cm, noting spectrum peaks tendency toward lower frequencies with time
11 p1954 A69-24382

Interplanetary scintillation and angular spectrum of radio waves scattered by solar plasma, noting magnetospheric tail and solar wind
12 p2161 A69-26942

Synchrotron spectrum radiated by relativistic electrons below Razin cut-off, considering relation to radio spectra curvature of variable extragalactic sources
13 p2339 A69-27573

Dielectronic recombination influence on radio recombination lines of carbon under typical nebular conditions
13 p2346 A69-27703

Extragalactic radio sources, observing nonlinear LF spectra for quasars and linear LF spectra for radio galaxies
13 p2351 A69-27867

H II alpha and beta radio recombination lines strengths predicted, noting role of calculations of hydrogen energy levels non-LTE populations
14 p2517 A69-29088

Frequency selection, spectral index distributions and counts of extragalactic radio sources
14 p2518 A69-29134

Spin temperature of interstellar neutral hydrogen calculated from 21 cm absorption spectra line profiles
15 p2681 A69-30411

Decametric radio astronomy at frequencies from 10 to 40 MHz on wideband telescopes, discussing spectral types of discrete radiation sources
15 p2682 A69-30501

Excited hydrogen radio lines observations, analyzing neutral and excited hydrogen distribution in galaxies
15 p2682 A69-30502

RF spectra for hyperfine structure of ortho-hydrogen molecular ion, calculating doubling constant for vibrational effects
15 p2693 A69-30784

Discrete radio sources interferometer observations using transPacific baseline, noting spectra and radiation intensity variations
15 p2701 A69-31530

Solar radio bursts spectra fine structure, discussing observations of fast drift storm, drift pair and split pair bursts
17 p3024 A69-33607

Spectra for 16 radio sources, questioning classification as supernova remnants
17 p3035 A69-33610

Spectrum and cross section of radio wave scattering in two temperature plasma, relating differential backscattering cross section to ionospheric electron density fluctuations
17 p2930 A69-33895

RF recombination lines measurement of helium for abundance in nebulas, comparing optical and radio values for H II regions
18 p3190 A69-34293

Pulsars observed for average energies at centimeter wavelengths, using azimuth elevation antenna
18 p3196 A69-34644

Radio wavelength range observations of NO molecule lines in interstellar space
18 p3198 A69-34765

Radio sources spectrum measurement results at cm wavelengths in tabular form, noting flux density relationship to frequency
18 p3200 A69-35132

Planetary nebulae observations, describing radio spectra characteristics, electron temperature measurement, hydrogen line emission, etc
20 p3598 A69-37425

Right ascension and flux density of source in Crab Nebula measured at meter wavelengths, evaluating spectrum and relative position to binary star center
20 p3607 A69-38040

Radio spectra of 136 sources determined at various declination ranges noting flattening at frequencies below 408 MHz
21 p3797 A69-38480

Radio observations of supernova remnant HB 21 at 2695 MHz, noting spectral brightness and curvature of northern shell segment
22 p4014 A69-40129

Cosmic radio background noise spectrum near north galactic pole based on Radio Astronomy Explorer satellite experiments
23 p4219 A69-42375

NASA program for radio spectrum utilization in aerospace communication systems
23 p4128 A69-42502

Pulsars radio intensity fluctuations noting possible periodic pulse amplitude modulation
24 p4389 A69-43744

Quasars time dependent flux density variations at 6.6 cm, noting spectrum peaks tendency toward lower frequencies with time
24 p4389 A69-43772

RADIO SPECTROSCOPY

Radio spectrometer with paramagnetic quantum amplifier for astronomical spectral measurements in 8 mm range
04 p0597 A69-14851

Solar radio spectroscopy for 40 to 240 MHz frequency range, noting dynamic spectra of solar radio bursts
06 p0925 A69-17318

Astronomical unit determined by measuring Doppler shift of spectral features of galactic hydrogen
07 p1222 A69-19590

RF spectroscopy of OH molecule, RF absorption by galactic OH and radio emission from OH in dust clouds
10 p1781 A69-23671

Time splitting of solar radio bursts observed at Oslo Solar Observatory with high resolution radio spectrographs
11 p1946 A69-24590

Color excess and 21 cm line intensity of RR Lyrae stars at high latitudes, confirming correlation between dust and atomic hydrogen
12 p2063 A69-25808

Radio spectrometer with paramagnetic quantum amplifier for astronomical spectral measurements in 8 mm range
15 p2607 A69-30243

Design and electrical features of microwave measurement system for solid state spectroscopy, discussing waveguides, signal source, detector, etc
15 p2610 A69-30709

Jodrell Bank RF digital autocorrelation spectrometer based on time delay related to signal power spectrum through Fourier transform
17 p2970 A69-32856

Red dwarf star /YZ Canis Minoris/ radio outbursts observation noting stellar atmospheric spectrum, electron density and temperature and total flare energy
17 p3043 A69-34164

Discrete radio sources spectra at decametric wavelengths, showing variation with frequency and radio wave generation mechanism leading to various spectral types
18 p3200 A69-35134

RADIO STARS NT PULSARS

Radio star scintillation data, establishing periodic variations in rates within 1 to 1.5 years
03 p0505 A69-13081

RADIO TELEGRAPHY

- Statistical comparison of scintillation depths of Transit 4A satellite to radio star Cassiopeia A
07 p1215 A69-18821
- Radio galaxies, quasars and radio stars between declinations plus 20 and plus 27 degrees, obtaining accurate positions and optical identifications
07 p1218 A69-19273
- Spherical harmonic analysis of Stokes parameters for polarization of stars, discussing magnetic field of Galaxy
08 p1390 A69-20390
- Radio star scintillation data, establishing periodic variations in rates within 1 to 1.5 years
14 p2515 A69-28763
- Ionospheric scintillation power spectrum measurements from radio star and satellites related to F region radio refractive index fluctuations
20 p3534 A69-38093

RADIO TELEGRAPHY

- Artificial triggering of VLF magnetospheric noise by NAA Morse code transmission during whistler duct drift across magnetic shells on 17 June 1965
11 p1878 A69-25154
- Global communication techniques and trends, discussing radio telephone and telegraph, submarine systems, satellite communications, line of sight links, tropospheric scatter, waveguide transmission, etc
16 p2750 A69-31755

RADIO TELEMETRY NT PULSE FREQUENCY MODULATION TELEMETRY

- RF voltage breakdown in solid state telemetry transmitters on sounding rocket, noting glow discharge initiated by energetic dissociated electrons
02 p0222 A69-12691
- VHF to UHF conversion, noting modular UHF telemetry transmitter, miniature UHF special purpose transmitter, RF power amplifiers and telemetry receiver
05 p0732 A69-16305
- Conversion from VHF to UHF at White Sands Missile Range, discussing telemetry acquisition, tracking and receiving systems
07 p1077 A69-18828
- Radio profilograph designed for integrating aircraft excess altitudes and measured distances between aircraft and earth, discussing block diagram
07 p1132 A69-19006
- Time division telemetry technique resolving data and control flow to and from remote locations /tactical aircraft/, noting application to environmental pollution control
07 p1081 A69-19100
- Telemetry and tracking antenna feed system in EC-135N instrumented aircraft for Apollo moon project
07 p1105 A69-19110
- UHF telemetry flight tests at White Sands Missile Range, discussing multipath and target scintillation problems
07 p1082 A69-19116
- Data transmission techniques for aerospace and industrial applications, discussing radio link
08 p1271 A69-19906
- Multichannel miniature telemetry for vibration, strain and temperature measurements in high speed machinery by solid state encapsulated devices
10 p1654 A69-23251
- Miniature telemetry systems for gun launched projectile instrumentation and ejection payloads, noting voltage controlled oscillators, commutators and VHF FM transmitters
10 p1654 A69-23280
- Shipborne self pointing antenna for reception of telemetry signals from maneuverable missile, discussing tracking and compensation for ship platform motion
10 p1664 A69-23803
- Echo 1 aluminized plastic balloon satellite, discussing radio linkup by reflections, use in geodesy and atmospheric and radiation pressure effects on lifetime
10 p1792 A69-23804
- Deep space telemetry bit errors increased by reference signal phase noises and partial RF signal suppression, calculating equivalent signal to noise ratio degradation
13 p2223 A69-28609
- S-band telemetry capability of Easter Test Range, discussing relationship to Telemetry Rehabilitation Project, major system decisions and performance characteristics
14 p2410 A69-28878
- Space Ground Link Subsystem as S-band communication link within Air Force Satellite Control Facility

- including unified telemetry, tracking and command systems
14 p2427 A69-28879
- VHF to UHF telemetry bands transition implemented by Naval Weapons Center
14 p2411 A69-28880
- Carrier disappearance method for FM telemetry transmitter characteristics measurements including frequency deviation sensitivity, linearity and frequency response
14 p2411 A69-28881
- ESRO 1/Aurorae satellite telemetry system constraints, discussing encoder, pulsed operation and integrated circuit assembly
15 p2702 A69-31085
- Pioneer 6 S band telemetry carrier Faraday rotation during corona occultation measured by deep space tracking antenna
15 p2700 A69-31419
- FM/FM telemetry system for high altitude rocket research, using independent subcarrier oscillator for each measurement transmitted with individual frequency modulation
16 p2750 A69-31853
- AZUR research satellite HF communications system, describing telemetry transmitter, command receiver and data transmission
16 p2759 A69-31854
- Seven helix antenna array components and operation mode at Berlin weather station, including biaxial rotator, preamplifier servoamplifier and VHF telemetry receiver
17 p2946 A69-33768
- Advanced Meteorological Sounding System /AMSS/ for measurements up to 150,000 ft, discussing configuration, characteristics, radiosonde, ranging, telemetry data ground equipment and test
18 p3108 A69-35102
- Laboratory and flight tests of airborne solid state UHF telemetry transmitter, discussing miniaturized coaxial hardware from RF power conservation viewpoint
19 p3267 A69-35996
- Solid state S band to VHF converter design to obtain optimum system noise for radio telemetry, discussing cost effectiveness and system performance
19 p3270 A69-36238
- Telemetry transmitter-receiver RF links quality determination, emphasizing nonlinear effects measurement by notch noise tests
19 p3270 A69-36239
- Optimal ratio predetection combiner used with diversity signals and various modulations, showing significant improvement in telemetry systems performance
19 p3270 A69-36241
- Telemetric control of urban transportation systems and law enforcement, considering automobiles as prime vehicle
19 p3272 A69-36256
- Wireless telemetry system design for physiological signals in human diagnosis, discouraging casual use of wireless transmission
19 p3261 A69-36269
- Computer program designing multiplex taper to minimize FM/FM telemetry system carrier threshold SNR, examining noise behavior of multiplex system stages for system performance
19 p3273 A69-36275
- Monte Cardiga telemetry station associated with sounding rocket range at Salto di Quirra, Sardinia, describing equipment, telemetry system capabilities and flexibility
20 p3512 A69-38280
- Radiotelemetric EEG recording variation possibility, examining dynamic behavior of human cerebral rhythms
22 p3889 A69-40158
- Capacitive coupling vs DC coupling between data input and transmitter exciter in FM telemetry system, based on pulse series Fourier analysis
23 p4119 A69-41744
- Flexible format adaptive telemetry encoder design, discussing system design and implementation technique with modular units
23 p4119 A69-41748
- S band phased array receiver developed to track automatically moving telemetry transmitter by electronic beam steering
23 p4120 A69-41751
- S band antenna systems for missiles, designed in various types to obtain RF telemetry links reliability by sharing effort between airborne and ground station equipment
23 p4137 A69-41753

- Radio telemetry system for evaluating protective masks dynamic performance by remote simultaneous monitoring of respiration, acceleration and temperature data generated by human subjects
23 p4121 A69-41765
 - Apollo Extravehicular Communication Telemetry System for monitoring astronaut portable life support system, space suit performance and body functions on lunar surface
23 p4121 A69-41767
 - IRIG /Inter-Range Instrumentation Group/ telemetry standards for U.S. Department of Defense missile and weapons systems, reviewing evolution, content, scope, philosophy, revisions, etc
23 p4121 A69-41770
 - Frequency diversity technique simplifying airborne antennas for UHF telemetry, useful on spin stabilized vehicles requiring omnidirectional antenna coverage
23 p4122 A69-41777
 - UHF down-converter design used in various Navy missiles UHF telemetry/miss-distance information system
23 p4137 A69-41778
 - Phase locked UHF telemetry transponder for missile scoring applications, discussing design and performance
23 p4137 A69-41779
 - Portable UHF telemetry receiving station for medium range surface-to-air missiles testing, analyzing antenna coverage over water and system prediction allowing variable parameters
23 p4122 A69-41780
 - Fixed-tuned telemetry receiver as miss distance indicator /MDI/ to provide information in missile performance program
23 p4138 A69-41781
 - Pioneer 9 deep space probe with telemetry link operated in coded mode with sequential decoding, discussing ground and flight test data
23 p4131 A69-42522
 - Space attenuation at VHF and UHF telemetry frequencies
24 p4281 A69-42622
- ## RADIO TELESCOPES
- Radio telescope for Owens Valley Radio Observatory, noting interferometer array of steerable antennas and signal wavelength influence on telescope reflector accuracy
02 p0229 A69-11974
 - Compact high-gain chromium doped rutile traveling wave masers for Onsala radio telescope for galactic and extragalactic microwave emission studies
02 p0257 A69-12463
 - Radio telescopic detection of seven new pulsars lying close to galactic plane, noting one pulsar close to supernova remnant
02 p0327 A69-12725
 - Radio emission center of gravity from 3C 273 quasar determined by radio telescope together with A and B component fluxes
03 p0506 A69-13092
 - Dynamic behavior of large steerable radio telescope, showing structural resonance influence on error detection system
03 p0412 A69-14093
 - 22-m parabolic reflector radio telescope with 9525 mm focal length at Crimean Astrophysical Observatory, noting high performance in mm wavelength range
04 p0584 A69-14376
 - Supernova remnant theories used to interpret results of 1-mile Molonglo cross type radio telescope survey of nonthermal galactic sources
04 p0664 A69-15441
 - Hydrostatic bearings, hydraulic drive system and hydraulic braking system for radio telescope with 2550 tons moving weight
05 p0743 A69-16147
 - Large paraboloid radio antennas structural setting for minimizing effects on performance due to deformation of surface by gravitational forces
06 p1023 A69-17372
 - Solar radio emissions analysis using radio telescope measurements, observing quasi-periodic LF fluctuations caused by chromospheric processes
06 p1004 A69-17535
 - Ground based radio telescope sensitivity to radio emission from earth atmosphere and galactic sources
07 p1099 A69-18515
 - Bright galaxies observed at 408 MHz with fan beam of east-west arm of cross-type radio telescope for correlations between radio and optical properties
08 p1386 A69-20087

Antenna tolerances theory, discussing illumination correlation function analytical evaluation for uniform and tapered illuminations

08 p1284 A69-20294

Focal antennas and receivers of Nancy radio telescope to measure flux density and incoming waves polarization, noting circular polarization in quasars

08 p1392 A69-20567

Molecular line intensity requirement in line of sight for detecting interstellar water vapor cloud, assuming transparent atmosphere and ideal radio telescope

09 p1591 A69-21446

Construction of large parabolic antennas for radio astronomy and satellite communication, noting dimensional accuracy, directional precision and dynamical behavior

09 p1476 A69-21650

Large steerable mm wave radio telescope of Simeiz observatory in U.S.S.R. noting computer aided pointing system

10 p1674 A69-23805

Filled and unfilled aperture radio telescopes, noting uses in radar astronomy and for aperture synthesis antennas

10 p1674 A69-23866

Radiophysics Laboratory /Sidney/, discussing radio astronomy, radioheliographs, radio telescopes, cloud physics and research

10 p1784 A69-23988

Galactic radio source W 49 /3C 398/ observed with Cambridge one-mile radio telescope

11 p1963 A69-25259

Atmospheric thermal radio emission fluctuations effects on radio telescope sensitivity, evaluating dispersion at low angles to horizon

12 p2031 A69-26643

Digital computer methods for weak pulsars search using radio noise picked by telescopes

12 p2172 A69-27169

Radio emission center of gravity from 3C 273 quasar determined by radio telescope together with A and B component fluxes

14 p2516 A69-28774

Reflector radio telescope of Pulkovo astronomical observatory noting high resolution

15 p2679 A69-30102

Large telescope dome movements automatic control, considering central and eccentric telescope mounting

15 p2588 A69-30441

Slowly varying component of solar radio emission, evaluating resolution of radio telescopes in sunspot studies and localized areas luminescence

15 p2674 A69-30503

Radio astronomical research developments including structural requirements for 100 m telescope

15 p2589 A69-30864

Pulsars Mp 0450, Mp 1642 and Mp 1818 discovery, discussing role of Molonglo radio telescope and pulse amplitude variations in detection

17 p3026 A69-32857

CP 0950 and CP 1133 pulsating stars position, using radio telescope at two frequencies

17 p3036 A69-33639

Radio telescope for radio astronomy in Bonn, discussing structural and operational problems

17 p2975 A69-33702

Continuum survey at 1415-MHz between declinations of zero and 20 degrees N with radio telescope, noting flux densities and contour maps of sources

18 p3195 A69-34428

LASSO /modified S-4B/UV/ vehicle mission to place in orbit two unmanned Lunar Modules for landing of radio and optical telescopes on lunar surface

18 p3136 A69-34813

Italian cross radio telescope noting added phase shifters to N-S arm, transistorized receiving system and modified data processing

19 p3295 A69-36643

T shaped radio astronomical array, discussing time sharing technique providing simultaneous observation capability and merits of T and cross configuration telescopes

20 p3507 A69-37837

Radio telescope structure material selection criteria, developing deformability criteria for structures under various stresses

20 p3546 A69-38306

Rotation of antenna pattern of radio telescope parabolic mirror subjected to thermoelastic deformations due to asymmetric solar heating

20 p3497 A69-38307

Synthetic aperture radio telescopes analysis, noting resolution and sensitivity at radio wavelengths for correlator array in supersynthesis mode operation

21 p3677 A69-39512

Solar radio emission /S component/ observations with 22-m radio telescope at Crimean Astrophysical Observatory

22 p4020 A69-40295

Structural technology for large radio and radar telescope systems - Conference, Cambridge, Mass., October 1967

23 p4147 A69-42120

Computerized evaluation of elastic deformations of 100 m parabolic reflector designs for Max Planck Institute radio telescope, outlining supports and dish structure

23 p4148 A69-42122

Feasibility studies to optimized design for 440 ft steerable filled-aperture radio and radar telescope, discussing parabolic configuration, radome selection, etc

23 p4148 A69-42123

Structure, operation and performance of two reflector Nancy radio telescope consisting of plane and spherical portion reflectors

23 p4149 A69-42124

Time averaged and fluctuating wind load effects on large radio telescope structures, discussing wind shear and turbulence influence on steady and unsteady loading

23 p4230 A69-42125

Parkes paraboloid radio telescope structural performance, using rapid survey instrument to measure surface deformations for optimum focusing determination

23 p4231 A69-42130

Canadian radio observatory 150 ft telescope antenna, discussing dish structural feature for resisting gravity, wind and thermal stresses

23 p4149 A69-42134

Surface accuracy of large diameter radio telescopes maintained by uncoupling reflector surface from backup structure, using active compensation

23 p4149 A69-42136

Tilttable conventional radio telescopes possibilities of passing gravitational limit for diameter and shortest wavelength, discussing dead load

23 p4231 A69-42138

NASA structural analysis /NASTRAN/ program applied to large radio telescopes, discussing static and dynamic analysis, problem formulation, finite element method, etc

23 p4232 A69-42145

Multichannel spectral line receiver for 210 ft Australian radio telescope with front ends covering wide frequency range

24 p4283 A69-43115

RADIO TRACKING

Constant beamwidth antenna consisting of parabolic reflector and ridge loaded horn, noting conical scan tracking antenna application

02 p0218 A69-12325

Venus radius determined by planetary radar and Mariner 5 radio tracking data

03 p0508 A69-13348

Telemetry with unrestrained animals, discussing radio tracking of game animals and instrumentation requirements for studying green sea turtle goal finding ability

07 p1071 A69-19136

Rawin systems for upper air measurements of wind and thermodynamic parameters, using balloon-borne radiosonde

07 p1057 A69-19581

Pseudodynamic programming for optimizing design of correlator supersynthesis antenna arrays used for radio source tracking

10 p1663 A69-23420

Space Ground Link Subsystem as S-band communication link within Air Force Satellite Control Facility including unified telemetry, tracking and command systems

14 p2427 A69-28879

Planetary navigation using spacecraft measurements and Doppler data from earth-based radio tracking, determining accuracy for earth-Mars trajectory

19 p3368 A69-35791

Navigational accuracy dependence on spacecraft geometry, determining information content and critical error sources of earth based Doppler radio tracking data

[AAS PAPER 69-112] 19 p3402 A69-35935

Tabulated coherent S-band Doppler data from Pioneer 6 and 7 radio tracking, improving astronomical constants and ephemerides for earth-moon system

[AAS PAPER 68-130] 20 p3595 A69-37179

Adaptive signal processing interference rejection technique for suppression of cochannel AM interference in congested VHF tracking receiver

23 p4128 A69-42503

RADIO TRANSMISSION

NT AUTOMATIC PICTURE TRANSMISSION
NT IONOSPHERIC F-SCATTER PROPAGATION
NT IONOSPHERIC PROPAGATION
NT MANDELSTAM REPRESENTATION
NT MICROWAVE ATTENUATION
NT MICROWAVE TRANSMISSION
NT MULTIPATH TRANSMISSION
NT SHORT WAVE RADIO TRANSMISSION
NT SINGLE SIDEBAND TRANSMISSION
NT TRANSEQUATORIAL PROPAGATION

Multiple transmission principles, examining linear systems, synchronous and asynchronous codes and channel interference

01 p0026 A69-10068

Tropospheric structure studied with high resolution antennas having small common volume

01 p0043 A69-10560

Radio systems for discrete information transmission, emphasizing phase difference modulation, wideband, universal and adaptive systems

01 p0031 A69-10778

Finsler geometric apparatus applied to electromagnetic wave propagation in media having refractive index varying with position and time, calculating errors

01 p0031 A69-10879

VHF transhorizon propagation by double reflection from elevated layer in troposphere

01 p0034 A69-11139

Charts summarizing daily solar phenomena, cosmic rays, geomagnetic variation, ionosphere, radiowave propagation and airglow observations in Japan

02 p0315 A69-11732

Ionospheric radio signal reflection measurements based on ground to rocket pulse propagation

02 p0245 A69-12736

Natural microwave radiation generation and propagation and wideband signal detection in problems connected with radio wave propagation, geophysics, radiometeorology and plasma physics

03 p0420 A69-12919

ELF radio wave propagation characteristics using two layered ionospheric model, noting deeper penetration than VLF

03 p0421 A69-13326

Subsurface radio propagation experiments determining feasibility of communication between vertical linear antennas located in drill holes and similar antennas on surface

03 p0395 A69-13622

Sunrise modal interference patterns for VLF propagation, analyzing variations with latitude

03 p0396 A69-13628

Atmospheric noise amplitude distribution relation to rms phase errors in frequency components of VLF timing pulse

03 p0396 A69-13629

Complex Doppler effect for oscillating source moving in dispersive medium, analyzing time behavior of radiation field

03 p0396 A69-13630

Statistical characteristics of multibeam signals reflected obliquely from ionosphere

03 p0396 A69-13708

Radio wave diffraction by knife edge obstacle on conducting earth surface noting effect on radio propagation

[AFCRL-68-0375] 04 p0560 A69-15216

Pulsar amplitude variations due to scintillation effects arising from irregular plasma refraction by general interstellar medium between source and solar system

05 p0825 A69-16354

Diurnal field strength and phase variations of VLF transmissions over transequatorial path from Australia to Japan

06 p0889 A69-17654

Phase and amplitude record changes in sunrise and sunset transitions in VLF transmissions over long path

06 p0889 A69-17655

Long wave radio stations field intensity spectral analysis data evaluated to determine vertical ionospheric displacements at sunset and sunrise

06 p0922 A69-17752

Nonlinear modulation distortions of high power radio waves propagating in ionosphere, noting electron temperature increase from radio wave
07 p1088 A69-19746

Reflection and transmission scattering coefficients for step type transition between two uniform waveguides with surface impedance boundaries, discussing coupled differential equations
08 p1272 A69-20020

Radio wave propagation over smooth cylindrical surface with specified boundary impedance, discussing diffraction loss and effect of surmounted obstacle
08 p1273 A69-20024

VHF radio transmission beyond horizon, discussing instrumentation, annual and diurnal signal fluctuations and diffraction role in signal propagation
08 p1274 A69-20112

VLF wave electromagnetic properties in magnetosphere, noting whistler mode propagation and refractive index and electron density of medium
08 p1306 A69-20180

Galactic H II regions and projected electron density or dispersion measures of pulsars, noting early stars
08 p1397 A69-20696

Coordination distances and interference probabilities to control interference in frequency sharing between communication satellite systems and terrestrial radio services
09 p1450 A69-21280

Satellite-borne terrestrial radiodetermination systems, noting VLF transmissions usage to overcome coverage problem
09 p1537 A69-21287

Daily observational results of solar phenomena, cosmic rays, geomagnetic variations, ionosphere, radio wave propagation and airglow arranged according to solar rotation number
10 p1771 A69-22808

Weakly attenuated components of VLF mode spectrum associated with propagation below anisotropic ionospheres as function of frequency and azimuth
10 p1655 A69-23417

Radio wave propagation in unstable inhomogeneous medium with space-time dispersion, showing adiabatic compression or expansion of wave packet spectrum
10 p1658 A69-23955

Long wave propagation at 164 kHz in India during 1966 and 1967, determining D region recombination coefficient and long wave absorption diurnal variation
10 p1659 A69-24065

Propagated ray paths plotted as functions of frequency and launch angle to predict signal dispersions
11 p1837 A69-25003

Air movement component of winter anomaly effect on radio wave absorption in mesosphere directly detected by rocket sounding
11 p1913 A69-25436

Finsler geometric apparatus applied to electromagnetic wave propagation in media having refractive index varying with position and time, calculating errors
12 p2031 A69-26642

Radio wave propagation in anisotropic inhomogeneous medium, obtaining reflection and conversion coefficients and electromagnetic field distribution
13 p2218 A69-27182

Errors in Appleton-Bayton equation for skip distance of radio waves in ionosphere
13 p2218 A69-27214

Delay time of pulse signals in radio channel transmission described by standard deviation of channel properties
13 p2218 A69-27215

Soviet satellite-borne radio waves studies of ionosphere, considering wave amplitudes, Doppler frequency shifts and outer ionosphere properties
13 p2252 A69-27349

Statistical distributions of refractive index parameters in tropospheric radio propagation from psychrometer soundings, discussing lapse rate
13 p2254 A69-28428

Automatic device for impedances and complex transmission factors measurement at meter and decimeter wavelengths, noting reflection factor
13 p2235 A69-28520

Long range ionospheric propagation of ultrashort radio waves, obtaining diurnal and seasonal characteristics of reflected signals amplitude and duration
13 p2255 A69-28543

Radio waves propagation along polar auroras region, obtaining ionospheric parameters for magnetic disturbances based on penetration probability
14 p2436 A69-29058

Noon ionospheric absorption data for Freiburg on different frequencies for lunar variation of ionospheric absorption of radio waves
14 p2438 A69-29104

Radio propagation in upper atmosphere and ionosphere noting rocket and satellite experiments including plasma physics research, tropospheric studies and space science services
14 p2526 A69-29854

Satellite radio observation for ionospheric parameters, utilizing Doppler and Faraday phenomena, signals fluctuations and sporadic phenomena
15 p2594 A69-30028

VLF radio wave propagation in waveguide channel formed by earth and inhomogeneous anisotropic ionosphere
16 p2751 A69-32032

Second order correction to first order Faraday rotation equation for quasi-transverse propagation of ionospheric radio waves obtained from Appleton-Hartree equation
16 p2777 A69-32101

Ground conductivity effects on MF sky wave transmission strength, discussing transmission over open sea
17 p2918 A69-33029

Scattered ionospheric reflection distribution at evening/morning periods showing deviation, using coherent method
17 p2927 A69-33860

Radio navigation principles, radio waves propagation characteristics and factors affecting navigation systems choice
18 p3169 A69-34848

Polar cap absorption effects on VLF transmission phase and amplitude in tabular form
18 p3103 A69-35185

Near and antipodal fields in earth-ionosphere waveguide using mode theory, ray theory, zonal harmonics series and method of images to derive field representations
19 p3283 A69-35931

Scientific findings from interplanetary spacecraft radio propagation experiments, particularly Mariner 5 data
19 p3267 A69-35940

Radio measurement methods and standards including measurements of attenuation, phase shift, time delay, impedance, field strength, antenna characteristics, RF properties of materials, etc
19 p3276 A69-36426

Magnetospheric disturbances effect on radio wave propagation, discussing wave-particle interactions, VLF emissions and electrostatic waves
19 p3303 A69-36429

Radio wave information transmission, discussing propagation in various media, antenna arrays, diffraction, scattering, plasmas, guided waves and periodic structures
19 p3276 A69-36431

Information theory, circuit optimization and computer aided design in radio wave information transmission
19 p3286 A69-36432

Diurnal and seasonal phase-difference fluctuation measurement of radio waves propagating along ground layer caused by atmospheric turbulence
20 p3485 A69-36971

Ionospheric electron content and concentration variations analysis based on data of radio waves propagating from satellite, considering Doppler shift and Faraday effect
20 p3486 A69-37027

Radio wave propagation in anisotropic plasma consisting of oxygen ions and protons, deriving expressions for radio wave refractive index
20 p3486 A69-37052

Space vehicle electronic attitude measurement method for reference coordinate and fixed coordinate systems based on rectangular coordinates of RF wave propagation directions
20 p3574 A69-37703

Received electromagnetic fields fluctuations due to transhorizon propagation, emphasizing fading-tropospheric turbulence correlation and rapid fluctuations due to small scale index variations
20 p3494 A69-37810

Meteorological parameters-radio propagation characteristics correlation, studying feasibility of data acquisition by occultation satellite system
21 p3705 A69-38374

Sharply bounded homogeneous ionospheric model to solve modal equation, discussing lower ionospheric conductivity from VLF transmission sudden enhancements of strength /SES/
21 p3714 A69-38554

Propagation effects on lane ambiguity resolution ability of Omega VLF navigational system, noting waveguide mode interference
21 p3673 A69-38756

Vertical factor equation numerical solution for radio wave propagation in vertically inhomogeneous troposphere
21 p3674 A69-39121

Ray theory of radio propagation by two variation techniques of phase paths
21 p3675 A69-39279

Split phase PCM code modulated carrier transmission characteristics determined for amplitude, phase and frequency shift keying, assuming random bit pattern and noncoherent modulation
21 p3676 A69-39451

HF backscatter, long delay signals and round-the-world echoes as radio wave propagation modes
23 p4116 A69-41602

Optimum signals for high resolution radar and communication systems, using transmitter waveform design of autocorrelation and cross correlation functions
23 p4132 A69-42545

RADIO TRANSMITTERS

NT IONOSPHERES
NT RADIOMETEOROLOGRAPHS
NT RADIOSONDES
NT RAWINSONDES
NT TRANSMITTER RECEIVERS

RF voltage breakdown in solid state telemetry transmitters on sounding rocket, noting glow discharge initiated by energetic dissociated electrons
02 p0222 A69-12691

Lake Kickapoo Space Surveillance Transmitting Station in Texas, discussing surroundings, equipment, operating range, VHF transmission, etc
03 p0411 A69-13209

AN/TSC-54 military satellite communications terminal for contingency deployment, discussing design, system tradeoffs and performance [AIAA PAPER 68-439]
04 p0579 A69-15367

Earth station system for ground based communications with Intelsats 2 and 3 noting antennas, receivers, transmitters and power supplies
05 p0741 A69-15667

Adaptive airborne VHF/UHF transmitter system, discussing design, ground isolation, current limiting, internal telemetry, wideband frequency response, real time video signals, etc
07 p1106 A69-19114

Miniaturized transmitter for single channel biotelemetric system to transmit electromyograms incorporating thin film components
08 p1265 A69-19836

Miniature telemetry systems for gun launched projectile instrumentation and ejection payloads, noting voltage controlled oscillators, commutators and VHF FM transmitters
10 p1654 A69-23280

Temperature measurement miniature telemetry transmitter
15 p2607 A69-30156

Knife-edge obstacle diffraction of nonisotropic transmitter analyzed via isotropic source model propagation path noting accuracy
17 p2917 A69-32847

Light aircraft emergency downed position indicators installation program, discussing transmitter minimum performance standards, listening watch insurance, etc
17 p2931 A69-34102

Laboratory and flight tests of airborne solid state UHF telemetry transmitter, discussing miniaturized coaxial hardware from RF power conservation viewpoint
19 p3267 A69-35996

Lower ionosphere radiation absorption at 4.01 MHz determined using A-3 method in measuring radio wave field between radio transmitters
20 p3528 A69-37675

Doppler technique for ionospheric electron density measurement by VLF ground based radio transmitter, noting HF method
20 p3542 A69-37792

Balloon-borne transmitter consisting of oscillator, driver and final output and connectable automatic frequency control circuit
21 p3682 A69-39251

Thermal design of missile mounted S band telemetry transmitter package based on temperature control system, using heat-of-fusion characteristics of wax material
22 p3909 A69-39945

S band phased array receiver developed to track automatically moving telemetry transmitter by electronic beam steering
23 p4120 A69-41751

RADIO WAVE REFRACTION

Space diversity reception as applied to radio astronomical investigation of large scale ionospheric inhomogeneities

02 p0237 A69-11665

Pulsar amplitude variations due to scintillation effects arising from irregular plasma refraction by general interstellar medium between source and solar system

05 p0825 A69-16354

Irregularities producing partial radio wave reflection from midlatitude D region attributed to insufficient distribution

07 p1078 A69-18914

Aircraft nose-mounted radome refraction errors influencing on directional tracking and navigation, considering fire control and terrain following radars

07 p1086 A69-19512

Axis deviation and refraction errors to correct design in radome of monopulse antenna, comparing various RF radome performances

07 p1110 A69-19520

Refraction errors in plasma density measurement by microwave interferometry

09 p1496 A69-22031

Radio ray scattering resulting from traversing anisotropically turbulent solar corona, noting refraction effect on signal pulse arrival time

10 p1773 A69-22960

Plasma microwave interferometry error due to refraction and beam displacement at receiving antenna aperture

13 p2312 A69-28113

Microwave propagation in Venusian atmosphere, analyzing refraction angles, attenuation and field strength fluctuations

13 p2223 A69-28567

Space diversity reception as applied to radio astronomical investigation of large scale ionospheric inhomogeneities

13 p2257 A69-28696

Electromagnetic wave diffraction in plasma cylinder of small nonuniform radius, analyzing interior field and radio wave reflection

16 p2751 A69-32031

Horizontally stratified ionosphere radio wave reflection and transmission properties, calculating full wave by differential equations

17 p2927 A69-33862

Radio wave propagation in anisotropic plasma consisting of oxygen ions and protons, deriving expressions for radio wave refractive index

20 p3486 A69-37052

RADIO WAVES

NT COSMIC NOISE
NT DECAMETRIC WAVES
NT EXTRATERRESTRIAL RADIO WAVES
NT GALACTIC RADIO WAVES
NT IONOSPHERIC NOISE
NT LONG WAVE RADIATION
NT MICROWAVES
NT MILLIMETER WAVES
NT SHORT WAVE RADIATION
NT SKY WAVES
NT SOLAR RADIO BURSTS
NT SOLAR RADIO EMISSION
NT SUBMILLIMETER WAVES
NT TYPE 2 BURSTS
NT TYPE 3 BURSTS
NT TYPE 4 BURSTS
NT TYPE 5 BURSTS
NT WHISTLERS

Radio wave abnormal absorption in auroral zone of ionosphere, investigating index of frequency dependence in absorption vs frequency relation

01 p0063 A69-10425

Radio waves incoherent scattering to measure electron concentration profiles at mean latitudes, allowing for collisions

01 p0065 A69-10575

Coherence ratio of ionospherically propagated radio waves measured for phase difference between pairs of antennas

01 p0032 A69-10967

Specular component of ionospherically reflected radio waves between antenna array elements measured for statistical variations

01 p0032 A69-10968

Spectral parameters of VLF radio noise given as functions of azimuth from atmospherics analyzer observations

01 p0033 A69-10971

Lower ionosphere vertical motions found responsible for nighttime variation of radio waves total field strength

02 p0207 A69-11689

Statistical characteristics of magnetoionic components of obliquely incident waves, obtaining envelope distribution of signal reflected from F 2 layer

02 p0314 A69-11691

Fading characteristics of radio waves reflected from two different heights in F region over Ahmedabad, India

03 p0385 A69-12915

Ionospheric midday radio wave absorption as function of geomagnetic latitude, season and solar activity from pulsed vertical radar sounding data

03 p0394 A69-13521

Radio waves diffusive and oblique reflections from F region, noting diffusive properties decrease during magnetic storms, especially during maximum solar activity

03 p0423 A69-13529

Radio wave absorption in ionosphere at five fixed frequencies for determining correlation with changes in sporadic E layer parameters

03 p0423 A69-13539

Radio waves Faraday rotation measured from pulsars by recording difference in received power

03 p0513 A69-13771

Radio waves diffraction around earth with atmospheric dielectric constant having linearly quadratic height dependence

03 p0399 A69-14130

Radio wave diffraction by knife edge obstacle on conducting earth surface noting effect on radio propagation [AFCRL-68-0375]

04 p0560 A69-15216

Random walk theory for effective secondary radiation center produced by reflection from composite reflectors, investigating fluctuations of reflected radio waves

05 p0718 A69-15653

Ionospheric models for studying nature of difference in relationships between HF radio waves Doppler shifts and changing ionosphere

05 p0755 A69-16269

Radio astronomical methods for total atmospheric absorption of radio waves by atmospheric thermal radio emission measurements based on sky brightness temperature

05 p0723 A69-16779

Ionospheric D layer electron concentration profile from radio wave absorption frequency dependence

06 p0920 A69-17729

Radio wave absorption measurements in atmosphere at superhigh frequencies, considering earth radiation, antenna sidelobes anisotropy, instrument effects, etc

07 p1076 A69-18518

Frequency-fluctuation correlation functions of radio wave field behind n random screens with random phase shifts calculated, obtaining statistical characteristics

07 p1076 A69-18525

VLF diurnal phase change observations, showing deviations from theoretical first mode and second mode dominance

07 p1078 A69-18912

Formulas for ray paths in ionized layers with application to oblique ionograms and duct modes

07 p1078 A69-18913

Reflected radio wave amplitude distributions related to distributions of curvature at reflector

07 p1086 A69-19225

Numerical determination of Doppler effect and reduced Doppler frequency difference for two coherent radio waves emitted from earth satellite

07 p1087 A69-19610

Galactic H II regions and projected electron density or dispersion measures of pulsars, noting early stars

08 p1397 A69-20696

Forward and backscattering of radio waves at electron concentration discontinuity near reflecting ionospheric layer with vertical nonuniformity

09 p1453 A69-21525

Ionospheric scattered radio wave field amplitude and phase variations assessed for diffraction at regular phase screen

09 p1453 A69-21526

Radio waves polarization scattered at ionospheric discontinuities analyzed for vertical incidence, determining modulus distributions and polarization factor argument

09 p1453 A69-21527

Amplitude modulated radio wave interaction with rarefied plasma in magnetic field, considering possible ionospheric heating by mechanism

09 p1453 A69-21543

HF ionospheric radar ground scatter map showing separated land-sea backscattered radio waves by Doppler technique

09 p1454 A69-21681

VHF satellite signal scintillation by ionospheric irregularities with sharp boundary /such as sporadic E/, noting diffraction pattern dependence on phase shift

09 p1489 A69-21713

Holographic technique application to radio and sound wave ranges, discussing incoherent holography development to overcome difficulties in image reconstruction of stationary objects

09 p1498 A69-22133

Solar occulting disk diameter at radio wavelengths derived from consideration of slightly deviated rays

09 p1607 A69-22432

Magnetoionic formulas similarity in ionospheric radio propagation and atmospheric acoustic gravity wave propagation above electron gyrofrequency

10 p1655 A69-23419

Vertical probe observations of short radio waves propagation through sporadic E at various frequencies and path lengths

10 p1657 A69-23933

Surface radio wave scattering propagating along rough surfaces, measuring emission during transformation into space waves

10 p1658 A69-23952

Radio wave field distortions by dielectric prisms in lens waveguides, discussing beam transformation, noting both geometrical optics effects and diffraction role

11 p1833 A69-24436

Ionospheric electron content gradients from Faraday rotation observations of radio beacon satellites for direction finding of HF radio waves

11 p1837 A69-25004

Pulsed radio waves for measuring phase height in E region, showing short period fluctuations

12 p2066 A69-26111

E region radio waves triple splitting observed in probe ionograms, analyzing diurnal and seasonal variations in Z component reflections occurrence

12 p2031 A69-26686

Reflection coefficient of polarized radio waves at ionized meteoric trails obtained by numerical integration of differential equations

12 p2031 A69-26691

Horizontally moving body wake scattering cross section calculated with allowance for sphericity of incident and scattered radio waves, using Bessel functions

12 p2031 A69-26699

Differential absorption by measurement of phase difference of ionospherically propagated incoherent radio wave signals under quasi-longitudinal conditions

12 p2032 A69-26857

Horizontal gradients below satellite orbit effect on reduced and minimum difference in Doppler frequency shifts of coherent radio waves from satellite in inhomogeneous ionosphere

13 p2219 A69-27701

Lower ionosphere vertical motions found responsible for nighttime variation of radio waves total field strength

13 p2224 A69-28720

Statistical characteristics of magnetoionic components of obliquely incidence waves, obtaining envelope distribution of signal reflected from F 2 layer

13 p2355 A69-28722

Correlation function of auroral reflection radio signals with allowance for polar ionospheric scattering and pulse signal transmission and reception

14 p2436 A69-29055

Inhomogeneities effect on polarization of radio waves reflected from ionosphere, based on permittivity tensor

14 p2417 A69-29862

Radio waves incoherent scattering to measure electron concentration profiles at mean latitudes, allowing for collisions

15 p2597 A69-30745

Book on ionospheric radio waves covering geomagnetism and sun, whistler propagation, oblique propagation, satellite sounding, etc

16 p2749 A69-31715

Radio wave single scattering at particles randomly grouped in space, showing correlation function of water content fluctuations in scattered field in clouds

16 p2807 A69-32267

Random walk theory for effective secondary radiation center produced by reflection from composite reflectors, investigating fluctuations of reflected radio waves

16 p2754 A69-32510

Forward and backscattering of radio waves at electron concentration discontinuity near reflecting ionospheric layer with vertical nonuniformity

16 p2754 A69-32520

Ionospheric scattered radio wave field amplitude and phase variations assessed for diffraction at regular phase screen
16 p2754 A69-32521

Radio waves polarization scattered at ionospheric discontinuities analyzed for vertical incidence, determining modulus distributions and polarization factor argument
16 p2754 A69-32522

Amplitude modulated radio wave interaction with rarefied plasma in magnetic field, considering possible ionospheric heating by mechanism
16 p2754 A69-32538

Radio waves ionospheric absorption dependence on equivalent frequency, showing marked difference for summer and winter conditions
17 p2918 A69-32927

Radio wave propagation in homogeneous turbulent gyrotropic medium, presenting solution for fluctuations in direction of wave scattering by geometrical optics approximation
17 p2927 A69-33861

Horizontally stratified ionosphere radio wave reflection and transmission properties, calculating full wave by differential equations
17 p2927 A69-33862

LF radio waves propagation in ionosphere by combining ray tracing in complex space with geometrical theory of diffraction, including diffraction by earth
17 p2928 A69-33866

Radio navigation principles, radio waves propagation characteristics and factors affecting navigation systems choice
18 p3169 A69-34848

Ion and temperature effects on lower ionosphere refractive index for VLF radio wave propagation
18 p3102 A69-34971

Nonmetallic materials thickness measurements at SHF, describing factors affecting geometrical-optics method
18 p3138 A69-35116

Radio distance meter design for accurate distance measurement, discussing transit time and advantages over optical meters
18 p3139 A69-35493

Optimum power allocation for RF carrier phase error and synchronization error in two channel system
19 p3274 A69-36283

Ionospheric data of local and integral electron concentration obtained by measuring phase shift of satellite emitted coherent radio waves
20 p3519 A69-37022

Scattering cross sections of radio waves at wake of vertically moving body near reflecting ionospheric layer, noting wave sphericity influence
20 p3486 A69-37023

Radio wave sphericity influence on scattering at moving body wake in ionosphere, determining scattering cross section principal maximum
20 p3486 A69-37024

Perturbed ionospheric regions acting as radio wave focusing lens, discussing frequency, power and pattern selection
20 p3486 A69-37048

Lower ionosphere radiation absorption at 4.01 MHz determined using A-3 method in measuring radio wave field between radio transmitters
20 p3528 A69-37675

Lunar surface scattering properties at 2.5 cm wavelength determined using computerized backscattering diagram and equations for obtaining scattering data
20 p3606 A69-37971

Sudden frequency deviations of HF radio waves propagated through ionosphere correlated with solar microwave bursts and optical flare events
20 p3592 A69-38101

Phase amplitude recording of radio waves reflected from D and F regions of ionosphere, reversing smoothing process by Fourier methods
21 p3672 A69-38558

Observation time influence on interferometers resolution limits due to radio wave phase fluctuations
21 p3682 A69-39122

Planetary atmosphere effect on Fresnel diffraction of ultrashort radio waves determined from short wave approximation of damping function
22 p3901 A69-40948

HF radio waves auroral absorption in ionosphere reviewed for first decade of riometry
22 p3902 A69-41218

Radio and microwaves biological effects, discussing differences between U.S. and Soviet assessments of radiation hazards
23 p4099 A69-42516

Thin film bolometer for monitoring RF radiation of arbitrary polarization and direction of propagation
24 p4311 A69-42572

RADIOACTIVE AGE DETERMINATION

Rubidium, Sr and Sr isotopic composition of normal gray hypersthene chondrite falls, noting Rb/Sr and Sr87/Sr86 ratio determination of Bath Furnace L chondrite isochron
02 p0317 A69-12020

Excess radiogenic argon in deep sea basalts from crest of East Pacific Rise, noting relation to glass content
02 p0244 A69-12568

Stony meteorite Krahenberg, determining isotopic composition, rubidium and strontium age of dark and light portions by neutron activation analysis
05 p0826 A69-16439

Radioactive decay products concentration from extinct radioisotopes in meteorites with estimation of formation interval, discussing fissiogenic xenon and solar system nucleosynthesis
08 p1405 A69-20924

Radiation ages of silicate inclusions in iron meteorites based on Sr evolution diagrams
08 p1405 A69-20927

Meteorites radiogenic and cosmic ray exposure ages, orbits and parent bodies, discussing H and L group chondrites
08 p1405 A69-20928

Kodaikanal iron meteorite measurements for cosmogenic rare gases and K-Ar isotopes ages for glass inclusions
09 p1596 A69-22047

Age of Galaxy from decay of uranium, assuming prompt synthesis
09 p1605 A69-22414

Rb-Sr and other radioactive isotopes cosmochronology in solar system, analyzing age of elements and r process
11 p1955 A69-24393

Freshly fallen meteorites from Portugal and Mexico, determining exposure age and classifying into iron meteorite and carbonaceous chondrite types
12 p2160 A69-26935

Rb 87-Sr 87 age of bronzite chondrites, analyzing olivine bronzite chondrite falls for K, Rb and Sr elemental concentrations
14 p2526 A69-29881

Correction of thermally lowered fission track ages of australites
15 p2696 A69-31140

Ar 39 and Cl 36 production rates and ratios in stone and stony-iron meteorites metal phases, discussing terrestrial age calculation
19 p3411 A69-36100

Radiation ages of bronzite chondrites, amphoterite and hypersthene from cosmic ray activities
19 p3412 A69-36102

Cosmic ray produced Be 10 in iron meteorites for terrestrial age determination, considering Cl 36 and rare gas analysis
19 p3412 A69-36104

K and Ar 40 determination in iron meteorites by neutron activation for K/Ar dating
19 p3412 A69-36106

Calcium-rich achondrites age distribution determined from inert gas measurements and existing data of eucrites, shergottites and howardites
19 p3413 A69-36107

Isotopic age determinations on iron and stone meteorites, discussing Rb-Sr and K-Ar results, internal isochrones, Kodaikanal data and planetary formation
19 p3413 A69-36108

K 40-Ar 40 age measurements in separated mineral phases of chondrites, including production rates of spallation isotopes
19 p3418 A69-36137

Meteoritic cosmic ray exposure time from method based on spallogenic Ar 36/Ar 38 ratio, noting impracticality for exposures longer than 5 million years
19 p3418 A69-36138

Calcium rich achondrites radiation ages determined from measuring He, Ne and Ar in howardites, nakhlites and angrites
20 p3602 A69-37535

Amphoterite /LL/ chondrites Rb-Sr age determination, noting high brecciation
21 p3814 A69-39583

Dirac cosmological principle of nuclear decay compared to Rutherford theory with respect to radioactive ages of terrestrial rocks and meteorites
22 p4017 A69-40176

Hoba meteorite surface radioactive isotope composition measured, finding terrestrial age from Ni-59 activity
22 p4021 A69-40411

K-Ar dates on cores and excess radiogenic Ar in flanges of australites for age determination
23 p4209 A69-41343

Darwin and Macedon impact glasses related to Far Eastern tektites through age determination by fission track technique
23 p4210 A69-41344

Fission track ages of tektites, australites and related glasses, considering errors due to annealing and etch pits
23 p4210 A69-41345

Stellar evolutionary ages and gravitational theory relations based on initial abundance ratio U 235/U 238 and present interstellar medium heavy element content
23 p4219 A69-42329

Rb-Sr isotopic determinations for Olivenza olivine-hypersthene chondrite, noting isotopic ratio vs age
24 p4385 A69-43214

Allende carbonaceous meteorite age determination by thermoluminescence method, assuming internal radioactivity source
24 p4385 A69-43219

Rb-Sr and other radioactive isotopes cosmochronology in solar system, analyzing age of elements and r process
24 p4390 A69-43783

RADIOACTIVE CONTAMINANTS

Computerized autocorrelation function analysis of radioactivity distributions in atmosphere at different altitudes, showing no correlation between values
11 p1945 A69-24320

RADIOACTIVE DECAY

NT NEUTRON EMISSION

Lanthanum isotopes beta decay, analyzing excitation of near spherical daughter nuclei of barium isotopes
01 p0122 A69-10100

Radioactive decay of neutral pions generated in metagalactic cosmic ray interactions as source of high energy isotropic gamma rays observed by OSO-3
02 p0308 A69-12092

Iodine 123 decay via gamma ray emission, noting energies of several transitions
03 p0470 A69-13099

Energy deposits from decay of tritium incorporated into bacteria, using computer simulation for radiation dose distribution
07 p1068 A69-19490

Inactivation of T4 bacteriophage by tritium decay incorporated into DNA and phage protein
07 p1068 A69-19491

Radioactive decay products concentration from extinct radioisotopes in meteorites with estimation of formation interval, discussing fissiogenic xenon and solar system nucleosynthesis
08 p1405 A69-20924

Radiogenic theory of origin of He in natural gas and absence of Ar from K 40 decay, discussing primordial earth atmosphere composition
08 p1311 A69-20947

Gamma ray luminosity of typical type I supernovae remnant computed by assuming Ni 56 radioactive decay energy origin of optical luminosity
09 p1581 A69-22409

Age of Galaxy from decay of uranium, assuming prompt synthesis
09 p1605 A69-22414

Solar system age based on decay rate of natural radioactive elements
11 p1961 A69-24972

Nonmesonic to mesonic decay ratio estimated for delta hydrogen hyperfragments
12 p2133 A69-26298

Low energy positrons in cosmic radiation due to beta decay of carbon, nitrogen and oxygen isotopes, estimating positron fluxes and energy spectra
15 p2676 A69-30887

Low level beta, X and gamma radiation detector incorporating Geiger, proportional and scintillation counting features in various modes suiting radionuclide decay scheme
17 p2975 A69-33747

Beam foil technique to measure energy transition levels radiative lifetime for nitrogen ions
17 p3009 A69-34154

Uranium abundances in several eucrites measured by fission track method, discussing Pu-Xe decay interval question
17 p3044 A69-34167

Mean lives of upper decay levels of lithium isotopes accelerated by electromagnetic isotope separator and directed through thin carbon foil

18 p3177 A69-35012

GaAs laser used as optical sweep generator for display of Cs 133 spectral line shape, studying fluorescence and radiation lifetime

19 p3339 A69-36696

Vertical turbulent diffusion and altitude distribution of radioactivity from short lived radon decay products in atmosphere

20 p3533 A69-38076

Dirac cosmological principle of nuclear decay compared to Rutherford theory with respect to radioactive ages of terrestrial rocks and meteorites

22 p4017 A69-40176

Radioactive decay and conductivity changes with time in high and low resistivity CdS single crystals after irradiation with 14 Mev and reactor fast neutrons

22 p3993 A69-40728

RADIOACTIVE FALLOUT PARTICLES

U FALLOUT
U PARTICLES

RADIOACTIVE ISOTOPES

NT BERYLLIUM 7
NT BERYLLIUM 10
NT CARBON 14
NT COBALT 60
NT KRYPTON 85
NT NITROGEN 16
NT PHOSPHORUS 32
NT PLUTONIUM ISOTOPES
NT PLUTONIUM 238
NT POTASSIUM 40
NT RUBIDIUM 86
NT SODIUM 22
NT STRONTIUM 90
NT TRITIUM
NT XENON 133
NT ZIRCONIUM 95

Tyrosine transaminase activity estimation by radioactive isotopic assay method, discussing application to rat liver and other organs

01 p0014 A69-10902

Preatmospheric meteorite size determination from distribution of radioactive isotopes resulting from nuclear reactions produced by cosmic rays, discussing error sources

01 p0159 A69-11375

Heterodiffusion of metallic impurities in body centered phases of doped zirconium and titanium, determining diffusion coefficients via radioactive isotopes

04 p0613 A69-14557

Critical end-on impact velocities calculated for reentering solid and granular radioisotopic fuel rods with solid and granular earth materials

04 p0630 A69-14800

Lead isotope composition and concentrations of U, Th, Ra, total Pb and Pb 210 in recent volcanic rocks, noting disequilibrium due to chemical fractionations

04 p0593 A69-15011

Radioisotopic propulsion stage design with liquid hydrogen working fluid, stressing tank insulation and hydrostatic flight behavior

05 p0811 A69-15595

Isotopic propulsion engine development problems, emphasizing single channel thermal power engine with hydrogen working fluid

05 p0811 A69-15596

Thorium 228 production and shaping for radiothermal propulsion, discussing transformation from radium 226, irradiated target processing, etc

05 p0791 A69-15597

Aircraft tire wear determination by measuring intensity of radiation originating from point source within thread, using thulium 170 isotope

07 p1143 A69-19703

Chondrite meteorite fall /1969/ in Mexico, noting opaque and microcrystalline matrices and gamma rays from short lived isotopes

08 p1396 A69-20686

Radioactive decay products concentration from extinct radioisotopes in meteorites with estimation of formation interval, discussing fissiogenic xenon and solar system nucleosynthesis

08 p1405 A69-20924

Particulate radioactivity for study of stratospheric motions, demonstrating negligible long time particle settling with comparative measurements of particulate Sr 90 and gaseous C 14

10 p1682 A69-23410

Rb-Sr and other radioactive isotopes cosmochronology in solar system, analyzing age of elements and r process

11 p1955 A69-24393

Vacuum tube with cathode heated directly by external radioisotope source, noting heat pipe providing isothermal heat transfer

11 p1848 A69-24748

Radiation dose and radioactive isotopes induced in astronaut body by cosmic rays of various energies

11 p1831 A69-25463

Space propulsion by radioisotope energy noting thermal heating, thruster configurations, propulsion system, mission capabilities and current thruster technology

11 p1914 A69-25591

Electron microautoradiograph preparation determining trace element amount and distribution by utilizing radioactive isotopes and high resolution of electron micrographs

13 p2263 A69-28168

Primary isotope thermionic electric power module design, considering various assemblies

14 p2398 A69-29190

SNAP 13 generator designs to develop technology for isotope heated thermionic converters, describing tests, efficiencies, power outputs and life times

14 p2481 A69-29191

Radioisotope fueled miniature thermionic converter for fractional watt level operation, defining optimum interaction of variables

14 p2399 A69-29193

Cosmic ray produced radionuclides and rare gas isotopes from Saint-Severin meteorite surface, showing relative Kr spallation mass yields dependence on cosmic ray energy spectra

19 p3410 A69-36093

Cosmic ray produced radionuclides P 32, Cl 36, Ar 37 and Ar 39 determined in separate mineral phases of meteorites, emphasizing ratios in metals

19 p3410 A69-36094

Heat generation in meteorites by radioactive isotopes generated by early solar proton irradiation prior to solar system solidification

19 p3411 A69-36098

Meteoritic trace elements and radionuclides measured by gamma coincidence techniques, emphasizing Mn 53 and Al 26

19 p3412 A69-36103

Spallogenic rare gas concentrations and isotopic ratios in taenite of iron meteorites measured mass spectrometrically and compared with kamacite values

19 p3419 A69-36139

Gamma ray emission of meteorite of 25 April 1969 measured by scintillation spectrometry, attributing peaks to annihilation radiation, Cs 137, Mn 54, etc

20 p3590 A69-37571

Cascaded thermoelectric module for spacecraft power conversion via module integration with radio isotope heat source, bonding SiGe and PbTe stages

20 p3465 A69-37706

NASA lunar receiving laboratory for lunar rock samples examination by gamma ray spectrometry for induced radioactive nuclides and naturally occurring isotopes

20 p3512 A69-38271

Radiocarbon natural production by cosmic ray neutrons, utilizing proportional counters filled with N atmospheres

22 p4003 A69-40095

Hoba meteorite surface radioactive isotope composition measured, finding terrestrial age from Ni-59 activity

22 p4021 A69-40411

Impact origin of Ivory Coast tektites and Bosumtwi Crater indicated by gamma ray spectrometric study of U, Th and K abundance patterns

23 p4210 A69-41347

SNAP 21 radioisotope powered thermionic generator with multiple couple Pb-Sn-telluride/Bi-Sb-telluride flat plate configuration for deep sea applications

23 p4069 A69-42248

Radioisotope thermal energy /RITE/ source for integrated life support systems for two man 180 day space station mission, determining optimum material selection and design details

23 p4189 A69-42268

ISOTEC thermoelectric generators for space power, describing design features, operation, power output and radioisotope heat source

23 p4189 A69-42270

Radioisotope energized Stirling engine for spacecraft auxiliary electric power, discussing system configurations, weight and fuel requirements

23 p4190 A69-42281

Compartmental models for radioactive tracer experiments with known tracer material amount, using

generalized Spearman simultaneous estimation procedure

24 p4339 A69-42765

Rb-Sr and other radioactive isotopes cosmochronology in solar system, analyzing age of elements and r process

24 p4390 A69-43783

RADIOACTIVE MATERIALS

Stationary vertical distribution of weightless radioactive substance in surface air layer, accepting two layer exponent law for vertical turbulent diffusion coefficient

04 p0593 A69-15091

Fuel cells utilizing direct electrochemical conversion of energy of radioactive elements

08 p1269 A69-21054

Radioactive light sources in photoelectric photometry, analyzing characteristics, brightness and stability of light flux and energy spectrum

11 p1951 A69-25421

Depth distribution of primary cosmic radiation fluxes and secondary nuclear-active particles in stone meteorites and surface layer of planets, moon and asteroids

19 p3410 A69-36092

RADIOACTIVE WASTES

Particulate radioactivity for study of stratospheric motions, demonstrating negligible long time particle settling with comparative measurements of particulate Sr 90 and gaseous C 14

10 p1682 A69-23410

RADIOACTIVITY

Radioactivity levels estimation at surface and in bulk of solar system planets caused by galactic and solar cosmic rays

10 p1756 A69-22813

Cosmic ray induced radioactivity in lunar surface and meteorites calculated together with cosmic ray intensity variations

10 p1756 A69-22817

Radiation dose and radioactive isotopes induced in astronaut body by cosmic rays of various energies

11 p1831 A69-25463

Radioactivity induced in solid materials for components microautoradiography and radiograph information quantitative evaluation

13 p2297 A69-28157

Errors due to neutron counter radioactivity in cosmic rays nucleon measurements analyzed in reducing readings to barometric pressure

23 p4206 A69-41855

RADIOBIOLOGY

Cosmic radiation interactions with living viruses, considering X ray effects and optimal radiation dosage for cancer cell destruction

01 p0013 A69-10157

Space radiation biology - NASA Conference, Berkeley, September 1965

03 p0370 A69-13476

Negative pion beams for therapy, radiobiology and dosimetry

03 p0371 A69-13478

Radiation structural and transcription damage to deoxyribonucleic acid /DNA/, noting postirradiation repair on molecular level

03 p0372 A69-13489

Heavy cosmic ray particles effect in manned space flight, noting results of deuteron microbeam experiment

03 p0373 A69-13494

Mammalian radiobiological studies of effects of heavy particles, discussing therapeutically advantageous characteristics

03 p0374 A69-13499

Public health aspects of galactic radiation exposure at supersonic transport altitudes

03 p0375 A69-14072

Proton beams uniformity available at NASA synchrocyclotron designed for radiation biology research by simulating space radiation environment

05 p0742 A69-15992

Radiation hazards during long duration space flights and suitable radiation shield design through radiobiological investigation

08 p1261 A69-19826

Soviet book on space radiobiology, discussing somatic effects, influence of flight factors, relative biological effectiveness of various radiations and radiation safety

11 p1827 A69-24263

Radiobiology of Tradescantia clone orbited in Biosatellite 2, analyzing space effects on spontaneous and radiation induced mutation and cytological changes

15 p2556 A69-31321

Book on radiation research covering molecular radiobiology, radiation chemistry, damage in chlamydomonas, granulopoiesis, oxygen radiobiology, etc
23 p4090 A69-41962

Molecular radiobiology, discussing physicochemical processes caused by energy absorption in targets, leading to inactivation under various circumambient conditions
23 p4090 A69-41963

Radiation effects on population kinetics of granulocyte system forming bone marrow, discussing radiosensitivity and radiation-induced granulocytopenia
23 p4090 A69-41965

Steady state and time dependent concentration gradients in and around cells due to oxygen diffusion and depletion in radiobiology
23 p4090 A69-41966

RADIOCHEMISTRY

Rare earth elements and yttrium in meteoritic chondrites determined by radiochemical neutron activation analysis
08 p1403 A69-20916

Bogou iron meteorite Ni-Cu-Zn contents determined by radiochemical methods
23 p4209 A69-41321

Book on radiation research covering molecular radiobiology, radiation chemistry, damage in chlamydomonas, granulopoiesis, oxygen radiobiology, etc
23 p4090 A69-41962

RADIOGENIC MATERIALS

Excess radiogenic argon in deep sea basalts from crest of East Pacific Rise, noting relation to glass content
02 p0244 A69-12568

RADIOGRAPHY

NT AUTORADIOGRAPHY

Exploding wire phenomenon during early expansion from time correlated X ray and optical streak photographs in vacuum chamber
01 p0119 A69-10670

Beryllium nondestructive tests, discussing eddy current inspection, ultrasonics, film radiography and scintillation [SAE PAPER 680652]
03 p0444 A69-13546

X ray study of biomechanics of respiratory act under long term acceleration stresses
05 p0710 A69-16522

Stereoradiography using holographic techniques to examine internal structure of opaque objects
08 p1313 A69-20178

Neutron radiography facility for production non-destructive testing inspection of aerospace components, noting collimation, neutron/gamma ray ratio optimization and neutron source [AGN-TP-229]
10 p1699 A69-23051

Cineradiography based on repetitive flashes drawn from single field emission X ray tube energized by high voltage pulse generator
12 p2086 A69-26163

Flash radiography technique using tungsten wire explosion in vacuum to obtain ultrafast reproducible X ray pulse
12 p2092 A69-26480

X ray study of biomechanics of respiratory act under long term acceleration stresses
18 p3096 A69-34741

Standard reference radiographs for weld defects on steel sheets and plates
18 p3150 A69-35425

Flash X ray unit with special film transport devices to obtain sequenced dynamic radiographs of ablating models during reentry simulation tests
19 p3291 A69-35720

Nondestructive testing techniques for flaw and defect detection, discussing radiography, ultrasonics, penetrants, thermal and magnetic methods, etc
23 p4169 A69-41529

RADIOISOTOPE BATTERIES

NT SNAP 13
NT SNAP 21
NT SNAP 27

Radioisotope fueled miniature thermionic converter for fractional watt level operation, defining optimum interaction of variables
14 p2399 A69-29193

Lithium doped solar cell irradiation by strontium 90 radioisotope, discussing electron flux rate, spectrum and recovery rates
19 p3251 A69-35693

Nuclear thermal and electrovoltaic batteries design and operation, discussing applications
20 p3464 A69-37288

Gisette 5 thermoelectric radioisotopic generator for submarine use, discussing strontium 90 as isotopic source
21 p3768 A69-38458

Planar radioisotope thermoelectric generator system for NASA deep space missions and integrated spacecraft power supply
23 p4070 A69-42254

Radioisotope thermoelectric generators (RTG)/ design and performance analysis method applied to generators using Si-Ge Air-Vac type thermocouples
23 p4188 A69-42260

Multifuel-capsule radioisotope thermoelectric generator design procedure, applying statistical environment definition
24 p4349 A69-43191

RADIOLOGY

Radiological properties of high energy proton beams from synchrocyclotron in tumor treatment and neurosurgery
03 p0373 A69-13495

Radiology and thermography in nondestructive reliability testing of electronic equipment
15 p2610 A69-30850

Dynamic roentgenology of cervical spine noting ease of use in neutral profile, hyperflexion and hyperextension for aeronautical medicine
23 p4087 A69-41797

Book on radiation research covering molecular radiobiology, radiation chemistry, damage in chlamydomonas, granulopoiesis, oxygen radiobiology, etc
23 p4090 A69-41962

Radiology diagnosis of military jet pilots injuries during ejection and touchdown, discussing fractures, spine injuries and ejection seat spine position
24 p4266 A69-43379

RADIOLYSIS

Electron pulse radiolysis of NO₂, determining absolute yields and rates of formation of nitrogen dioxide and nitrogen trioxide
14 p2410 A69-29928

Low temperature fuel cell with mixed oxidizer and fuel and fuel cell based on water radiolysis under alpha and gamma radiation
16 p2740 A69-32425

Gamma radiolysis of silver nitrate ice forming neutral Ag in magnetically distinct sites, discussing water dipoles rotation and electron paramagnetic resonance
22 p3992 A69-40574

RADIOMETEOROGRAPHS

Meteor station photorecorder of reflected radio signals, discussing design and performance during meteor shower
17 p2976 A69-33898

RADIOMETERS

NT DICKE RADIOMETERS
NT INFRARED DETECTORS
NT INFRARED SCANNERS
NT INFRARED SPECTROMETERS
NT INFRARED SPECTROPHOTOMETERS
NT MICROWAVE RADIOMETERS
NT SPECTRORADIOMETERS

Selective chopper radiometer for remote atmospheric temperature sounding, discussing satellite versions for Nimbus D and Nimbus E [UN PAPER 68-95797]
01 p0080 A69-10531

Thermoelectric radiometer for transient radiant flux short duration pulse measurement, using thermally induced depolarization of polymer film dielectric [AIAA PAPER 68-403]
02 p0250 A69-12392

Radiometric measurement of attenuation, emission and noise fluctuations due to earth atmosphere in 4 cm to 8 mm range
02 p0210 A69-12432

Microcalorimetric measurement of radiation flux of flames of condensed burning material, noting surface temperature distribution
02 p0355 A69-12671

Airborne radiometric /8 to 14 micron/ temperature measurements, determining emissivities of ocean, stratus clouds, desert and snow
04 p0592 A69-14653

Outgoing radiation field based on interpretation of broad sector radiometer measurements made from meteorological earth satellites
04 p0627 A69-15032

Solar and terrestrial thermal radiometer absolute calibration noting standards and methods
04 p0602 A69-15429

Solar radiation protection of radiometers and spectrometers on reentry vehicle by launching times and solar view field selection
04 p0666 A69-15511

Multichannel radiometers calibration and testing for spacecraft and solar simulation applications, noting exposure to sun onboard X-15 aircraft at high altitudes
06 p0926 A69-17620

Wideband superheterodyne tunable radiometers of millimeter wave range using input mixer and high intermediate frequency
07 p1131 A69-18517

Cosmic radio noise intensity measurements by ATS 2 satellite-borne radiometer
07 p1224 A69-19715

High altitude radiant emittance of cirrus clouds and cloudless sky for IR transmissivity based on aircraft measurements
09 p1536 A69-21641

Satellite mounted radiometers for determining albedo variations, using Fredholm equation with allowance for instrument errors
10 p1689 A69-23969

Feed shift beam switch for radiometric measurements of astronomical objects emission at millimeter wavelengths
11 p1836 A69-24996

Thunderstorm thermal noise emission determined by radiometer and steerable parabolic antenna in preparing water content contours along radio rays
12 p2127 A69-27002

Autonomous radiometers signals statistical properties used in space technology, discussing radar signals phenomenological models, measurement errors and energy characteristics
15 p2566 A69-30337

Space radiometers energy characteristics calculation taking into account reflecting surface roughness and antennas directional patterns
15 p2575 A69-30338

Cloud distribution effect on global coverage of remote radiometric sounding of atmosphere, considering Nimbus 1 and 2 data
15 p2650 A69-31335

Solar spectral irradiance measured by airborne instruments, discussing construction, calibration, etc, of photoelectric filter radiometer and Leiss monochromator
16 p2861 A69-32261

Rocket stability monitoring by temporal radiometry, using exhaust radiance measurement to detect frequencies in thrust chamber combustion pressure [AIAA PAPER 69-580]
16 p2839 A69-32670

Broadband thermal radiometer containing InSb electronic bolometer under magnetic field, discussing astronomical applications
17 p2969 A69-32823

Two channel IR radiometer for 1969 Mariner mission measuring equivalent black body surface temperature
17 p2972 A69-33085

Optical instruments optimal design for given requirements, discussing tradeoff studies of airborne reconnaissance scanner, spacecraft rendezvous sensor and track-while-scan radiometers
19 p3310 A69-36065

Radiometric measurement, discussing characteristics and calibration of instruments for measuring radiant intensity or radiance
19 p3311 A69-36071

Detector radiometer design for radio astronomical measurements in 0.7-2 mm range, discussing sensitivity
19 p3285 A69-36877

Satellite mounted radiometers for determining albedo variations, using Fredholm equation with allowance for instrument errors
21 p3717 A69-39655

Solar observations at 21 and 43 cm during solar minimum by grating cross and total power radiometer, giving radio map of solar emission
22 p4001 A69-39988

Radiometer for measurement of cosmic rays at 200-400 km altitudes range by satellites, presenting block diagram of radiation detector units
23 p4165 A69-41732

Radiometer for measuring solar flux variations, discussing design, performance tests and use for spacecraft measurements [AAS PAPER 69-254]
24 p4313 A69-42858

Regression generated radiometric and contour height fields of North American Continent using Nimbus 2 IR equivalent black body temperature and geopotential data
24 p4343 A69-42896

RADIONUCLIDES

U RADIOACTIVE ISOTOPES

RADIOPATHOLOGY

- Pathomorphological aspects of radiation sickness in animals irradiated by high energy protons, showing changes in lymph node, stellate ganglion and spleen
05 p0708 A69-16509
- Pathomorphological aspects of radiation sickness in animals irradiated by high energy protons, showing channels in lymph node, stellate ganglion and spleen
18 p3095 A69-34728

RADIOPROTECTIVE AGENTS

U ANTIRADIATION DRUGS

RADIOSENSITIVITY

U RADIATION TOLERANCE

RADIOSONDES

NT IONOSONDES

NT RAWINSONDES

- Optical ozone radiosonde for vertical distribution analysis, using weak absorption of Chappuis bands
02 p0251 A69-12761
- Vertical distribution of ascending long wave radiation, employing actinometric radio sondes
06 p0953 A69-17990
- Pilot balloon and radiosonde measurements for p as function of wind direction, velocity and stability, discussing variation with air layers
09 p1535 A69-21516
- Transpondersondes for atmospheric measurements, considering ground tracking, radiosondes, rocket-sondes and flight results
10 p1692 A69-23257
- Automatic recording and data processing for ionospheric radiosonde observations from ground stations, giving block diagrams and subsystems
13 p2225 A69-27610
- Irregular data obtained by radiosondes in winter for charts of high isobaric levels, noting stratospheric temperature effects on radiosonde ascent height
14 p2473 A69-29731
- Digital IC radiosonde system, discussing sampling, pulse width modulation, time multiplexing, follow-on subsystems, etc
17 p2937 A69-33675
- Advanced Meteorological Sounding System /AMSS/ for measurements up to 150,000 ft, discussing configuration, characteristics, radiosonde, ranging, telemetry data ground equipment and test
18 p3108 A69-35102

RADIOTHERAPY

U RADIATION THERAPY

RADIUM 226

- Thorium 228 production and shaping for radiothermal propulsion, discussing transformation from radium 226, irradiated target processing, etc
05 p0791 A69-15597

RADIUS

U RADII

RADOME MATERIALS

- Radome material insertion loss measurement by radiometric method noting error analysis
02 p0251 A69-12434
- Radomes developments for supersonic/hypersonic aircraft and missiles, considering conditions imposed by speed and by electronic requirements
07 p1171 A69-19508
- Ceramic radomes for hypervelocity aerospace vehicles, considering wide temperature environment effects on stability and properties
07 p1171 A69-19511
- Radome materials with superior dielectric and temperature characteristics for constructing high tolerance microwave multiband radome
07 p1109 A69-19514
- Glass/resin laminates behavior at high temperature
07 p1136 A69-19515
- Cordierite application to radomes for high velocity engines, discussing dielectric properties at microwave frequencies, mechanical properties, temperature control and fabrication
07 p1168 A69-19525
- Radome design and manufacture, considering airborne requirements, antenna systems and electromagnetic energy, with emphasis on ceramic material melting, forming, grinding and finishing
07 p1142 A69-19526
- Processing techniques for fabrication of ceramic radomes from alumina and silica
07 p1142 A69-19527
- Alumina radomes manufacture by flame spraying process, discussing raw materials quality control, spraying operation, sintering and final inspection
07 p1142 A69-19528

Alumina radomes fabrication and control techniques to assure reproducibility of electrical and mechanical properties, detailing finished product inspection methods
07 p1142 A69-19529

Ceramic radome materials resistance to rain erosion at high Mach numbers
07 p1171 A69-19532

Radome materials design and performance for guided weapons systems, describing research conducted in UK
07 p1112 A69-19540

Dielectric constant and loss angles measurement in Ku band used for onboard radars
07 p1112 A69-19544

High temperature polyimide laminates for radomes and other supersonic aircraft components, discussing index flexural strength, dielectric constant and dissipation factor
07 p1171 A69-19545

Long term weather and radar transmission effects on three ply fabric cloth fire-retardant polyester resin radome panel
08 p1414 A69-20485

Polymeric polyurethane protective coatings for radar radome covers with improvement in service life, discussing performance properties and production method
24 p4338 A69-43456

RADOMES

Multifrequency three layer sandwich radomes design for reflectionless sandwich at second frequency
01 p0034 A69-11037

Dielectric sheath effect on far zone radiation characteristics of aperture bounded by perfectly conducting ground plane
04 p0579 A69-15450

Radomes developments for supersonic/hypersonic aircraft and missiles, considering conditions imposed by speed and by electronic requirements
07 p1171 A69-19508

Radomes design and manufacture for high speed flight vehicles, discussing interactions between aerodynamic and electrical requirements with reference to mechanism of aberration
07 p1141 A69-19510

Aircraft nose-mounted radome refraction errors influence on directional tracking and navigation, considering fire control and terrain following radars
07 p1086 A69-19512

Integrated radome antenna system design /radant/, comparing electrical performance with conventional systems
07 p1109 A69-19513

Measurement bases in general, discussing theoretical data justifying ground level base and measurements results
07 p1136 A69-19516

Closed loop and electronically calibrated radome measurement systems for beam deflection, boresight shift and transmission loss measurements
07 p1109 A69-19517

Radome performance dependence on dielectric permittivity determined by digital program and simple design criterion
07 p1110 A69-19519

Axis deviation and refraction errors to correct design in radome of monopulse antenna, comparing various RF radome performances
07 p1110 A69-19520

Radome induced distortions of radioelectric axis analyzed by sectional phase analysis
07 p1110 A69-19521

Symmetrical three layer A and B type sandwich reflectionless radomes design for multifrequency operation and insertion phase delay
07 p1110 A69-19522

Dielectric radome designs for operation at harmonically unrelated frequencies in C and K bands, discussing sandwich structure of A and B types
07 p1110 A69-19523

Radioelectric axis deviation of radome in front of monopulse radar antenna
07 p1111 A69-19524

Alumina radomes manufacture by flame spraying process, discussing raw materials quality control, spraying operation, sintering and final inspection
07 p1142 A69-19528

Alumina radomes fabrication and control techniques to assure reproducibility of electrical and mechanical properties, detailing finished product inspection methods
07 p1142 A69-19529

Aberration of dielectric patches and rings attached to radome surface described by insertion phase
07 p1111 A69-19530

Statistical radomes design, analyzing dielectric constant and wall thickness tolerances effects on amplitude and phase of transmitted wave
07 p1111 A69-19531

Water effect on air supported radome of ground station for satellite communication
07 p1111 A69-19533

Aircraft radomes lightning protection, discussing evaluation by experimental methods and simulation
07 p1142 A69-19535

Boresight error in missile radome-antenna combination due to reflection and surface wave effects
07 p1111 A69-19536

Paper-honeycomb sandwich radome structure for protecting monopulse UHF radar antennas used in BMEWS
07 p1111 A69-19537

Spherical sandwich radomes designs, discussing aerodynamic loads, wind pressure effect, electrical properties and mountings
07 p1112 A69-19538

Radiation pattern deformation due to sharp angle radome studied by analyzing diffraction in antenna dihedral system
07 p1112 A69-19539

Wind tunnel investigation of damage to aircraft radomes by water droplet encounter during cloud passage and gaseous molecule friction in air
07 p1054 A69-19541

Radome axis error due to phase /dielectrics/ and metallic obstacles
07 p1112 A69-19542

Radiation pattern solved for antenna enclosed in radome, deriving exact formulas for scalar field
07 p1112 A69-19543

Airborne radomes reliability and high temperature environments, discussing missile nose cones, light weight ceramic techniques, circular polarization, etc
17 p2942 A69-34084

Antenna losses produced by metal space frame radome determined by considering end effects, member junctions circulating currents, mutual scattering and near field effects
23 p4149 A69-42127

High sensitivity communication system design consisting of radome enclosed steerable antenna, 500 kw transmitter and microwave configuration compatible with low noise receivers
23 p4149 A69-42131

Metal space frame radome design, considering electromagnetic performance, structural integrity, cost, membrane structures stability, etc
23 p4231 A69-42139

Space frame radome shell structural stability with emphasis on analogous continua for reticulated framework, examining connection imperfections effect on stiffness
23 p4232 A69-42140

Large deflection of three dimensional bar structures stability analyzed by potential energy minimization method, considering radome design
23 p4232 A69-42141

Space frame radome model elastic buckling tests for load deflection and maximum load predictions, considering individual beam failure and complex instability
23 p4232 A69-42143

RADON

Atmospheric diffusion measurement based on analysis of thoron emitted continuously from point source, permitting study of diffusion in atmospheric boundary layer
01 p0144 A69-10043

Turbulent parameter and turbulent diffusion vertical profile diurnal variations determination based on measurements of Rn 220 and thorium-B concentrations near ground
03 p0459 A69-13273

Turbulent parameter and turbulent diffusion vertical profile diurnal variations determination based on measurements of Rn 220 and thorium-B concentrations near ground
14 p2472 A69-28781

Vertical turbulent diffusion and altitude distribution of radioactivity from short lived radon decay products in atmosphere
20 p3533 A69-38076

RAFTS

U LIFE RAFTS

RAIL TRANSPORTATION

Mass transit rail service between Manhattan and Kennedy Airport using Long Island Railroad mainline route, discussing baggage handling and time schedules [AIAA PAPER 69-803] 19 p3453 A69-35596

Intercity air transportation compared with automobile and train travel, attributing air travel dead time to ground route and airspace congestion 24 p4416 A69-42561

RAIN

Graphical data on atmospheric and rainfall attenuation of spacecraft earth signal, emphasizing transmission via satellites 03 p0397 A69-13727

Teichmann cost analysis extended to include frequency dependent and diversity dependent rain losses for satellite communication, using Bayes strategy 05 p0721 A69-16580

Rain repellent system providing transparent film on aircraft windshield surface 06 p0877 A69-16954

Antenna noise temperature at earth station due to rain on radomes, solar and cosmic noise, noting SNR degradation 09 p1461 A69-21283

Millimeter and submillimeter radio waves attenuation in rain, showing effective loss cross section as function of raindrop diameter and wavelength 10 p1657 A69-23943

Attenuation statistics due to rain measured on earth-space path at 16 and 30 GHz, using sun as signal source 17 p2920 A69-33398

RAIN EROSION

U WATER EROSION

RAIN IMPACT DAMAGE

Ceramic radome materials resistance to rain erosion at high Mach numbers 07 p1171 A69-19532

Water effect on air supported radome of ground station for satellite communication 07 p1111 A69-19533

Wind tunnel investigation of damage to aircraft radomes by water droplet encounter during cloud passage and gaseous molecule friction in air 07 p1054 A69-19541

Cumulative damage concept for rain erosion of solid materials, noting incubation period and similarity to microscopic damage in fatigue failure 12 p2187 A69-26848

Solid materials erosion rate as function of cumulative damage generated by liquid droplets impingement 16 p2794 A69-31904

Rain erosion problems in aircraft design, reviewing protective measures for all-weather aircraft 21 p3646 A69-38393

RAINDROPS

Raindrop size distribution law effect on radio wave attenuation coefficient and differential effective backscattering cross section of rain 02 p0208 A69-12259

Electromagnetic waves attenuation and scattering by rainfalls calculated using droplet distribution function 08 p1275 A69-20430

Cloud and fog droplet spectra due to condensation of water vapor on nuclei solved by partial differential equation 12 p2126 A69-26017

Cumulative damage concept for rain erosion of solid materials, noting incubation period and similarity to microscopic damage in fatigue failure 12 p2187 A69-26848

Vertical air velocity in rain measured for size distribution of drops, using relation between drop fall rate and diameter 18 p3104 A69-35342

Sulfur dioxide, nitrogen dioxide and Aitken nuclei washout by artificial rain of known intensity and droplet size distribution 24 p4345 A69-43146

RAINSTORMS

U THUNDERSTORMS

RAMAN SPECTRA

Emission and frequency shift angles of antiStokes radiation from trapped filaments of laser light in liquids 01 p0114 A69-10012

Raman spectra and temperature dependent nuclear quadrupole resonance frequencies of p-dichlorobenzene and p-dichlorobenzene-D, calculating librational amplitudes 01 p0122 A69-10286

IR and Raman spectra of solid and matrix isolated methylamine and deuterium derivatives, locating amine twisting vibration in solid phase IR spectra 01 p0023 A69-10287

Electric field induced IR absorption and Raman scattering by optical phonons in centrosymmetric crystals, discussing tensor coefficients 02 p0295 A69-11779

Polarized low temperature laser excited Raman spectra of thulium gallium garnet 02 p0256 A69-11925

Far IR and Raman spectra of ethylene carbonate, gamma butyrolactone and cyclopentanone, noting consistency with hindered pseudorotation 02 p0206 A69-12723

Raman effect in liquid glycerol obtained with 4880 A ionized argon laser, determining valence vibrational frequencies 03 p0440 A69-13366

Sinusoidal phase modulation role in spectral broadening observed in trapped filaments of laser and Raman light 03 p0442 A69-14189

Tsao-Curnutte line broadening calculations extended to include Raman scattering and quadrupole absorption 04 p0633 A69-15231

Tunable Raman upconverter as coherent light generator, using Q switched Nd-YAG laser beam [IEEE PAPER B-2] 05 p0774 A69-16309

Nonstationary nonlinear wave phenomena in ultrashort high intensity light pulse formation, discussing nonstationary stimulated Raman scattering and picosecond pump reduction of Raman amplification [IEEE PAPER H-5] 05 p0774 A69-16316

Spontaneous Raman band shapes and depolarization ratios in liquid nitrogen and oxygen measured and compared to gas, discussing time dependence of rotational motion 06 p0962 A69-17817

Raman spectra of optical phonons in semiconductors, using reflection techniques and Ar laser excitation 06 p0936 A69-17882

Optical excitation process of energy states by light pulses of short duration compared to relaxation time, predicting Raman echoes [IEEE PAPER H-3] 07 p1152 A69-19062

Spontaneous and stimulated Raman emission in liquids, obtaining picosecond pulse duration and laser light linewidth [IEEE PAPER H-6] 07 p1152 A69-19063

Quantum mechanical, dipole approximation, non-resonance light scattering cross sections expressed in terms of oscillator strengths and refractive indices 07 p1183 A69-19645

Raman microwave scattering with low frequency oscillations caused by plasma drift instabilities 09 p1550 A69-22021

Rotational Raman scattering in planetary atmospheres, analyzing spectra of deep solar Fraunhofer lines 09 p1601 A69-22207

Coherent radiation brightness increased from liquid N Raman laser, using off-axial pumping 09 p1520 A69-22533

IR and Raman spectra of gas and liquid phase methylhydrazine and deuterated methylhydrazines, discussing vibrational motions, H bonding and thermodynamic functions 10 p1752 A69-23528

Raman effect in potassium dichromate single crystal, discussing symmetrical and antisymmetrical internal vibrations of free ions 12 p2105 A69-26285

Standing wave theory for steady state performance of Raman laser oscillator extended for time variation of exciting laser pulse 12 p2108 A69-26634

Libroelastic wave propagation and dispersion characteristics /solid carbon dioxide/ evaluated by using Raman scattering measurements 13 p2286 A69-28668

Single crystals garnets Raman spectra using laser radiation, separating phonon spectra of host lattices from electronic Raman effect 14 p2507 A69-29334

Propylene imine IR and Raman spectra, calculating thermodynamic functions based on rigid rotator harmonic oscillator model 14 p2410 A69-29922

Incident electromagnetic waves Raman scattering at turbulent plasma oscillations, obtaining plasma intrinsic radiation spectrum 15 p2659 A69-30728

Raman scattering by coupled plasmon-cyclotron-harmonic modes in semiconducting plasmas in homogeneous static magnetic field 16 p2824 A69-32604

Pumping model for analyzing stimulated and enhanced potassium multiphoton emission primed by ruby laser-stimulated Raman electronic radiation 23 p4171 A69-41391

Raman spectrum of solid alpha-nitrogen at low temperatures, calculating scattering intensities and Raman active librational lattice vibrations 23 p4194 A69-42204

Raman spectra analysis of solid carbon dioxide, nitrous oxide, nitrogen and CO, determining lattice mode intensities from oriented gas model 23 p4194 A69-42205

Raman scattering during external and internal motion of oxygen molecules condensed phases, observing gamma and liquid phase bandwidths during stretching vibrations 24 p4353 A69-43808

RAMJET ENGINES

NT PULSEJET ENGINES

NT SUPERSONIC COMBUSTION RAMJET ENGINES

Air jet high temperature and low pressure influence on combustion stability in ramjet engine 03 p0531 A69-12968

Stimulated radiative recombination process for ramjet propulsion, investigating delay chamber required for vibration-to-translation conversion 06 p0984 A69-17630

Advanced propulsion systems propulsive capabilities in connection with interstellar flights, considering rocket and ramjet propulsion, energy requirements and stellar plasma 06 p0984 A69-17631

Optimum fixed geometry ramjet in Mach range of 3 to 7 with successively subsonic and supersonic combustion [ONERA-TP-656E] 07 p1203 A69-18415

Air intakes for fixed exhaust throat hypersonic ramjet engines, discussing configuration dependence on Mach number at beginning of combustion [ONERA-TP-658] 07 p1203 A69-18418

External burning ramjets in supersonic stream noting applications to drag reduction, lift-drag ratio and attitude control 11 p1941 A69-24261

Ramjets and air augmented rockets as propulsion systems for supersonic atmospheric flight, noting inlet design, combustors and nozzles 11 p1943 A69-25586

Fluidic systems for automatic control of fuel supply to ramjet engine combustor, coolant rationing and distribution to engine structure and performance efficiency maintenance 14 p2508 A69-28875

Trailing shock wave position in air breathing jet engine channels, determining supersonic-subsonic boundary, noting Mach number effects on pressure ratio 16 p2768 A69-31743

Nitrogen reaction with excess fuel in ramjet engines, noting kinetic limitations in applications [WSCJ PAPER 69-12] 16 p2831 A69-32351

Collection of articles on ramjets including reaction propulsion, hypersonic inlets, combustion problems, Griffon aircraft, storable liquid fuels, etc 16 p2837 A69-32608

Integrated propulsion control system for ramjet Hypersonic Research Engine to operate at 3-8 Mach numbers [AIAA PAPER 69-546] 16 p2845 A69-32744

Flight velocity changes from sonic to supersonic through turbojet/ramjet combination possibility 17 p3020 A69-33348

RAMPS [STRUCTURES]

M 3.5 two dimensional mixed compression inlet system with self restart using flexible variable ramp system [AIAA PAPER 69-447] 16 p2845 A69-32732

RAMS (PUMPS)

Ram recovery of flush intake for air cushion vehicles noting influence of intake geometry, placement and incidence angle 01 p0005 A69-10026

RAMSAUER EFFECT

Collision induced instability of partially ionized gases having large Ramsauer effect in external magnetic field, analyzing nonlinear characteristics 05 p0804 A69-16441

Ratios of gas kinetic electron-atom collision integrals of Ramsauer for Ar 06 p0963 A69-17822

RANDOM ACCESS MEMORY

U CORE STORAGE

RANDOM DISTRIBUTIONS

U STATISTICAL DISTRIBUTIONS

RANDOM ERRORS

Atmospheric temperature profiles by regularizing algorithm, discussing influence of random errors in measured radiation and kernel of integral equation on interpretation accuracy

02 p0274 A69-11448

Probable errors in FK4 catalog of star positions and proper motions determined by Scott method

05 p0823 A69-16041

Statistical aspects of uncertainty function of linearly frequency modulated signals for nonstationary random process of phase errors

06 p0889 A69-17798

Antenna arrays subject to random excitation error analyzed by probability theory, noting relationship between antenna pattern and excitation distribution parameters

21 p3681 A69-38742

Statistical analysis of random production errors on phasing section polarization field of antenna with elliptical polarization

23 p4125 A69-42041

Algorithm for constructing random error correcting convolutional codes

24 p4284 A69-42723

RANDOM LOADS

NT GUST LOADS

Gyroscope with rotational symmetry subjected to random input torques analyzed by Euler equation of motion

01 p0079 A69-10236

Power spectral density method of random loads analysis applied to V-STOL aircraft structural analysis, discussing statistical distribution

01 p0168 A69-10407

Dynamic stability of structural system excited by random load, discussing effect of nonlinearities and dynamic snapping problems

02 p0339 A69-11988

Nonlinear oscillatory systems with constant delay under random forces action, noting use of stochastic difference-differential equations

03 p0468 A69-13866

Skin panel stresses for random acoustic loading, determining aircraft structure responses

03 p0530 A69-14092

Vibration response of thin elastic plates to random loads

05 p0844 A69-16741

Structural fatigue life evaluation as cumulative damage analysis for irregularly varying loads [DVL-780]

10 p1802 A69-24020

Structure dynamic response for motion through homogeneous frozen random load field with spacewise variations, applying analysis method to beam [ASME PAPER 69-VIBR-38]

10 p1807 A69-24176

Random periodic forces effect on single frequency oscillations of nonlinear nonautonomous system with distributed parameters, discussing perturbed boundary value problem

11 p1916 A69-24761

Liapunov type analysis of linear structural dynamic system excited by stochastic parametric load, discussing radially loaded thin circular plates

11 p1990 A69-25507

Structural fatigue-inducing random load spectrum analyzed and computed for laboratory simulation

15 p2705 A69-30363

Time dependence of maximum structural response of single degree of freedom mechanical system under random loading

15 p2705 A69-30365

Engineering models for wearout reliability prediction in dynamical systems subject to random loading, demonstrating practical and statistical methods

15 p2705 A69-30366

Fatigue life estimation for irregularly varying loads with emphasis on ground-air-ground stress cycles in aircraft

17 p3052 A69-32977

Linear aerospace structures vibrations in randomly distributed pressure field forecasted by applying Green function [ONERA-TP-703]

17 p3054 A69-33064

Damped vibrations of elastic open cylindrical shell under arbitrary loading, obtaining mean square of bending from correlation theory

17 p3054 A69-33094

Strength margins for combined random stresses, discussing average crossing frequency of curve by Gaussian stationary random vector with correlation coefficients included

17 p3066 A69-34038

Statistical characteristics stabilization of random loads in fatigue tests, noting transfer function of testing machine and spring stiffness

18 p3215 A69-34544

Fatigue life testing apparatus with computerized simulation of random load maxima and minima, describing rotating bend test application

19 p3434 A69-35777

Structural design for minimum weight under random loads representing steady vector random function

21 p3731 A69-38870

Weighting function of statistically optimal automatic dynamic system generating stochastic loads, using Fredholm equations

21 p3688 A69-39861

Small curvature effect on prevention of vibration in shallow shells under random loading numerically analyzed for component modes using linear theory

22 p4044 A69-40600

Optimal generalized controls for systems under random forces described by hyperbolic partial differential equation system

23 p4144 A69-41957

RANDOM NOISE

Reliability of binary message in Gaussian noise impaired by amplitude limiting in case of evaluation by integration

01 p0031 A69-10736

Reliability of eliminating multivaluedness in two scale phase measurement method resolved by algorithm formulated on white Gaussian noise interference

02 p0206 A69-11603

Optimal calculator of detection of Gaussian random signal against Gaussian noise background by reducing input signal to white noise

02 p0206 A69-11606

Voltage probability density of wideband microwave noise, discussing measurement technique of dividing spectrum down by noise bandwidth

02 p0211 A69-12460

Electrically small beamed receiving arrays in HF band and random noise

03 p0398 A69-13904

Stability of stochastic systems, discussing continuous parameter models, Gaussian white noise, stabilization of unstable deterministic system and ITO equations

04 p0623 A69-14695

Correlation function and spectrum analysis of passage of random noise and signal through multistage frequency multiplier

04 p0557 A69-14777

Gaussian channels capacity, studying supremum of information transmission rates with small error probability

04 p0558 A69-15006

Steady state response of inertialess discrete multivariable extremal system with noise, noting stepwise search systems

04 p0583 A69-15139

First and second passage times of stationary random process consisting of sinusoidal signal with stationary Gaussian noise

04 p0561 A69-15453

Detection characteristics of coherent pulse packet with random initial phase on Gaussian noise background of unknown intensity

06 p0887 A69-17463

Energy fluxes statistical distribution produced by random and regular energy sources

07 p1076 A69-18510

Optimum and suboptimum detection of K binary symbols corrupted by white Gaussian noise, discussing searching procedure and average error probability

07 p1081 A69-19097

Thermal noise and other disturbances from mismatched two port isolator in low power microwave transmission antenna noise between generators and loads

07 p1108 A69-19486

Recursive method for estimating number, amplitudes and time delays of signals overlapping in time and in presence of additive white Gaussian noise

08 p1270 A69-19854

Approximate noise analysis of phase locked loop with signal clipping

08 p1270 A69-19857

Signal to noise ratio with stochastic and additive noise and signal, showing block diagram of modified estimator

09 p1452 A69-21320

Constant amplitude in-band additive interference for analysis of PSK signals in Gaussian noise, discussing coherent and differential detection

09 p1455 A69-21848

Single degree of freedom mechanical system under random excitation studied for creep effect on vibrations by harmonic analysis

09 p1617 A69-22095

Optimal receiving circuit determined for elliptically polarized signals in randomly polarized noise by deriving integral equation

09 p1456 A69-22285

Optimal detection of determinate signal and signal with random amplitude and phase, estimating probability of false and correct detection

09 p1456 A69-22286

Sporadic noise, false fronts and other noise effects on phase of output oscillations of resonance apparatus

09 p1460 A69-22641

Reliability of eliminating multivaluedness in two scale phase measurement method resolved by algorithm formulated on white Gaussian noise interference

11 p1835 A69-24710

Optimal calculator of detection of Gaussian random signal against Gaussian noise background by reducing input signal to white noise

11 p1835 A69-24713

Energy gain during diversity reception in presence of random noise calculated, considering signal and noise amplitudes Rayleigh fluctuations

11 p1835 A69-24968

Analytical method for optimum switching function of relay servosystem subjected to stationary Gaussian random noise, considering perturbation and dynamic programming

11 p1859 A69-25025

First excursion failure survival probability of randomly excited structures, considering single degree of freedom linear oscillator under Gaussian white noise

11 p1990 A69-25505

Optimal scale factor selection to ensure minimum error variance in signal detection against random noise background for input limited range of measuring instrument

12 p2079 A69-25966

Optimum nonstationary Gaussian signals estimation in presence of noise, generalizing Wiener stationary processes filtering theory

12 p2029 A69-26202

Detection of known signals in general noise, describing sufficient conditions for singular detection and estimation

12 p2029 A69-26203

Nondeterministic differential games with imperfect state information, emphasizing linear system with quadratic cost functional and additive white Gaussian noise

12 p2053 A69-26505

Pull-in oscillator for random noise coincident with synchronizing and frequency shift signals, discussing circuit parameters effect on signal discrimination and noise suppression

12 p2044 A69-27101

Nonlinear systems disturbed by random white noise analyzed by Fokker-Planck equation for probability density in state space

12 p2124 A69-27141

Received signal phase angle error probability in coherent PSK system in Gaussian noise and interference

13 p2219 A69-27665

Rms error for reproduction of satellite signal transmitted through continuous Gaussian channel assessed by numerical calculation

13 p2219 A69-27697

Energy detection of random processes in colored Gaussian noise, discussing filtering, threshold detection, false alarm, probability distribution and density

13 p2220 A69-27937

Signal to noise ratio at output of three stage radio section with preselector, detector and ideal integrator, noting error

13 p2222 A69-28506

Algorithm for optimal digital processing of pulse signals during multilevel quantization in Markov noise, including error analysis

15 p2571 A69-30126

- False alarm stabilization circuits efficiencies compared in unsteady Gaussian noise, considering phase autocorrelator performance
15 p2567 A69-30342
- Unknown channels classes epsilon capacity applied to estimating capacity of channels with additive noise, discussing models and upper and lower bounds
15 p2570 A69-31142
- Book on statistical theory of signal detection and resolution in random noise covering hypothesis testing, digital communications, stochastic signals, filters, etc
16 p2748 A69-31566
- Fokker-Planck equation applied to probability density for finding rays larger than correlation distance during propagation in random medium
17 p2926 A69-33854
- Relationship between human response to noise and physical parameter, discussing controlled laboratory investigation to determine duration effect on annoyance
18 p3097 A69-34324
- Mechanical single degree of freedom system mean square response to AM random noise, considering frequency response, input excitation spectrum, etc [ASME PAPER 69-APM-25]
18 p3214 A69-34398
- Random excitations effects on vibrating nonlinear single degree of freedom system, statistically estimating resonance mode probability
18 p3171 A69-34554
- False signals formation during random pulse noise in single command channels with PTM coding, noting code value and redundancy
19 p3278 A69-36595
- Optical information rates for photocount detection systems based on coherent field model, considering binary channels with or without Gaussian noise
20 p3485 A69-36923
- Synthetic aperture terrain imaging radar system optimal design, considering noise-free and random noise conditions using least squares method and signal to noise ratios
20 p3489 A69-37639
- Detection characteristics of coherent pulse packet with random initial phase on Gaussian noise background of unknown intensity
20 p3496 A69-37946
- Satellite orbit determination errors attributed to Gaussian noise effect on tracking measurements, assuming known Gaussian probability error distribution [AIAA PAPER 69-911]
21 p3807 A69-39343
- Error probability of Gaussian signal detector in Gaussian noise background determined from quadratic form of probability distribution density
22 p3901 A69-40955
- Empirical determination of equivalent frequency characteristics of nonlinear system in random noise, assessing measurement errors
24 p4289 A69-42950
- Suboptimal closed loop controller for linear time varying process subject to additive random disturbances and measurement noises
24 p4292 A69-43285
- Linear-quadratic pursuit-evasion game with dynamics perturbed by additive white Gaussian noise, obtaining linear minimax solutions
24 p4341 A69-43296
- ### RANDOM NUMBERS
- Pseudorandom uniformly distributed numbers generation from noise-like signals produced by shift register with feedback, noting statistical tests
13 p2218 A69-27248
- Homogeneous Markovian sum of sequence of random quantities series, deriving limiting theorem for sum density
21 p3757 A69-39538
- ### RANDOM PROCESSES
- Continuous random process spectral density at PAM system output
01 p0050 A69-10211
- Linear random processes including law of large numbers, covariance estimation and linear to normal process relationship
01 p0029 A69-10555
- Variational law of control elements for automatic control systems with parameters subject to random changes
01 p0052 A69-10800
- Analytical expressions for transfer function matrices of four terminal signal shaping networks, assuming rational matrix spectral density of randomly polarized signal
01 p0031 A69-10880
- Euler-Lagrange relationship from equations of motion of tagged particle in turbulent velocity field consisting of random dispersive waves
01 p0121 A69-11202
- Narrow band normal steady state random processes applied to signal dispersion by extended oscillating body, obtaining statistical characteristics
02 p0206 A69-11602
- Model for fast randomization of electron gas by trapped electroacoustical waves
02 p0289 A69-12236
- Statistical characteristics of random phase quasi-harmonic process investigated for application of mathematical representation
02 p0208 A69-12263
- Mean square amplitude and phase fluctuations for propagation of light beam with Gaussian amplitude distribution through medium with randomly varying refractivity
02 p0208 A69-12308
- Book on applications of information theory to dynamical systems with random initial conditions and cybernetic systems consisting of communication systems with feedback
04 p0580 A69-14520
- Cross correlation function for two sequences of pulses arbitrarily distributed in time, noting noise stability of diversity reception systems
04 p0557 A69-14790
- Random cumulative damage theory for fatigue failure of steel under sinusoidal loading taking into account randomness of time to failure and possession of memory
04 p0680 A69-15154
- First and second passage times of stationary random process consisting of sinusoidal signal with stationary Gaussian noise
04 p0561 A69-15453
- Random motion of particle with nonlinear damping, obtaining velocity spectrum by solving associated nonstationary Fokker-Planck equation and using equivalent linearization technique
04 p0561 A69-15454
- Random walk theory for effective secondary radiation center produced by reflection from composite reflectors, investigating fluctuations of reflected radio waves
05 p0718 A69-15653
- Random processes study by special integral calculus containing deltas and theorems, with application to stationary processes
05 p0718 A69-15881
- Stability of differential systems with random parameters, developing Liapunov function approach and application to Ito equation
05 p0788 A69-16484
- Response of single and multidegree of freedom systems to nonstationary random excitation, analyzing spectral density function of pressure field close to jet engine
05 p0844 A69-16763
- Quasi-random properties of dynamic system generated by solutions of second order differential equations
06 p0948 A69-17657
- Turbulent boundary layer loading function for use with finite element structural analysis system applied to elastic aircraft structures random vibration [AIAA PAPER 69-20]
06 p0914 A69-18132
- Random filters and stabilization of periodic signals mixed with noise, establishing second order statistics at output
07 p1089 A69-18281
- Frequency-fluctuation correlation functions of radio wave field behind n random screens with random phase shifts calculated, obtaining statistical characteristics
07 p1076 A69-18525
- Particle motion, deriving Lagrangian formalism equivalent to Schrodinger equation for random motion theory
07 p1182 A69-19455
- Multiloop control plant described by Jacobian transfer matrix to control spectral characteristics of random processes
08 p1296 A69-20233
- Heating of collisionless plasma in magnetic mirror by random electric field transverse to magnetic field
08 p1368 A69-20805
- Fast electron diffusion in stochastic magnetic field, obtaining diffusion coefficient as function of ratio of correlation time to Larmor period
08 p1368 A69-20807
- One dimensional distribution law of random process with arbitrary correlation function, verifying normality hypotheses by integral criterion
08 p1299 A69-21069
- Upper bound obtained for probability of zero Gaussian random process remaining above specified signal throughout prescribed interval of time
09 p1452 A69-21319
- Smoothing data stability by least squares method, noting applicability to computer processing at random sequences
09 p1532 A69-21754
- Optimum number of terms in approximation of realizations of random process by polynomials
09 p1475 A69-22667
- Reliability function for electronic device during initial period of operation, based on use of lower bound
10 p1662 A69-23318
- Boundary value problem for elliptic-parabolic partial differential equations in theory of random processes, obtaining analytical solution in terms of hypergeometric functions
10 p1719 A69-23516
- Homogeneous turbulence in incompressible fluid, expanding field variable on ideal random basis
11 p1867 A69-24282
- Analog signal transmission through randomly fading channels, proposing pseudorandom phase reversals method for slowly varying multipath communication channels
11 p1834 A69-24552
- Narrow band normal steady state random processes applied to signal dispersion by extended oscillating body, obtaining statistical characteristics
11 p1835 A69-24709
- Confidence limits determined for damping parameter of complex stationary Gaussian Markov process
11 p1910 A69-25700
- Polarity coincidence correlation method due to random processes state characterization applied to man machine systems
12 p2022 A69-25931
- Optimal control of discrete time linear system with random parameters, noting case of additive noise in measurements
12 p2052 A69-26501
- Digital computer simulation of multidimensional stationary or nonstationary Gauss-Markov random processes with specified autocorrelation function, discussing time step choice
12 p2122 A69-26523
- Analytical expressions for transfer function matrices of four terminal signal shaping networks, assuming rational matrix spectral density of randomly polarized signal
12 p2031 A69-26644
- Differential equations of probability theory for studying control systems and processes involving random variables
12 p2124 A69-27142
- Reliability functions and cycles number before breakdown of finite automaton with account of randomness of malfunctions, structure and input signal distribution
13 p2224 A69-27250
- Bounding technique of first excursion probability for random vibration, considering relation to reliability of mechanical and structural systems under random disturbances
13 p2361 A69-27438
- Energy detection of random processes in colored Gaussian noise, discussing filtering, threshold detection, false alarm, probability distribution and density
13 p2220 A69-27937
- Power spectrum of random process from discrete sequence of instantaneous values, assessing error
13 p2239 A69-28514
- Continuous random process spectral density at PAM system output
14 p2424 A69-28748
- Computerized calculation of likelihood coefficients for identifying steady random processes against background noise, minimizing mean risk of erroneous solution
14 p2410 A69-28818
- Optimization criterion for synthesizing discrete nonlinear control system subjected to random controlling and perturbing effects
14 p2425 A69-28825
- Statistical description of geomagnetic field as random vector field, presenting correlation functions from empirical estimates from geomagnetic charts
14 p2437 A69-29062

Modeling nonstationary random processes using linear time-invariant difference equation, with applications to Kalman filtering and gyro drift

14 p2479 A69-29486

Electronic systems packaging substitution method for optimized malfunction isolation at succeeding levels to final discard-at-failure

14 p2420 A69-29494

Monograph on wave propagation and multiple scattering in random continuum, emphasizing scalar wave equation solutions

15 p2564 A69-30150

Spectral characteristics of pulsed signal with determinate repetition period and amplitude and duration modulation by correlated random processes

15 p2567 A69-30347

Accuracy and variance of nonergodicity estimates for random processes associated with radiophysical applications

15 p2582 A69-30946

Boundedness in mean square of solutions derived for linear differential equations forced oscillations with nonwhite Gaussian random functions parameters

16 p2873 A69-32058

One dimensional distribution law of random process with arbitrary correlation function, verifying normality hypotheses by integral criterion

16 p2765 A69-32484

Random walk theory for effective secondary radiation center produced by reflection from composite reflectors, investigating fluctuations of reflected radio waves

16 p2754 A69-32510

Random stress statistical properties and relationship to fatigue life, discussing Fuller prediction, comparison with test data, and vehicle design evaluation

17 p3053 A69-32988

Random oscillations of elastostatic systems, obtaining solution for spherical shell containing acoustic medium

17 p3057 A69-33199

Stochastic failure models based on stress peak distributions, including randomly deteriorating strength model and including hazard reliability functions

18 p3148 A69-35079

Multidimensional discrete control systems for spectral characteristics of random processes in vibrational and fatigue strength testing of machines and equipment

19 p3286 A69-35890

Triaxial static gyro stabilizer drifts, assuming perturbing moment steady centered random force applied along stabilizing gimbal axis

19 p3311 A69-36195

Algorithm for determining multidimensional random process from canonical representation of current state, noting minimum rms prediction error

19 p3287 A69-36663

Perceptron probability algorithm for random events prediction based on previous histories, applying Bayes formulas, static solutions formulas and transition probability tables and graphs

19 p3287 A69-36664

Random arrays representing random filament packing of actual composite materials, discussing effects on transverse stiffness

20 p3626 A69-37758

Optimal generalized random controls using stochastic integral equation in deterministic problem

21 p3756 A69-39266

Gyro drift rate mathematical modeling based on stationary and nonstationary time series analysis techniques with random process reduction to white noise residuals

[AIAA PAPER 69-838] 21 p3761 A69-39369

Stable linear system/shaping filter/synthesis transforming stationary white noise into random process having given covariance function

21 p3688 A69-39661

Optimal explicit method for parameters estimation not restricted to linear Gaussian problem derived in canonical form

[AIAA PAPER 69-947] 22 p3975 A69-40330

Random processes integration and differentiation and spectral density determination, examining Markov, Gaussian and point processes

22 p3975 A69-40777

Diffusion in biological systems by random walks with emphasis on gaseous diffusion in lung, noting probabilistic tree model

22 p3885 A69-40978

Satellite trajectory parameters estimation by maximum likelihood method applied to continuous satellite observations assuming random Gaussian process as measurement error

22 p3979 A69-41087

Random processes correlation functions determined by stochastic differential equations applied to lunar surface statistical characteristics determination

22 p4033 A69-41092

Uniform random field model development by taking moments in linear transformation form of certain initial field

23 p4183 A69-41523

Randomly oriented disks and rods scatter pattern used to determine causes of log-normal distribution of radar cross section fluctuations

23 p4116 A69-41592

N-dimensional theorem for evaluating time continuous channel capacity or rate distortion function of random process

24 p4284 A69-42721

Correcting deficiencies in parametric expressions for rate distortion function of Gaussian process under weighted square error criterion

24 p4281 A69-42722

Geodetic and geophysical random uncertainties as fundamental limitations on terrestrial inertial navigation accuracy

[AIAA PAPER 68-847] 24 p4348 A69-43240

RANDOM SAMPLING

Nonparametric ranking procedures /based on order statistics/ guaranteeing preassigned probability for selection from random samples populations as good as control

08 p1342 A69-20172

Extremal system of adaptive circuits adjusted by random search with varying random step distribution function

14 p2425 A69-28824

Statistical testing techniques using small sample size at low component levels to predict product performance

18 p3117 A69-34528

Weighting function of linear dynamic plant with steady random sampling determined with iterative method similar to stochastic approximation

24 p4289 A69-42951

RANDOM SIGNALS

Continuous random process spectral density at PAM system output

01 p0050 A69-10211

Error probability distribution density at output of optimal Gaussian random signal detection, using approximate solution of integral equations

02 p0206 A69-11605

Optimal calculator of detection of Gaussian random signal against Gaussian noise background by reducing input signal to white noise

02 p0206 A69-11606

Optimal detection of random signals on background of noise of unknown intensity and persistent false alarm probability

02 p0208 A69-12264

Pseudonoise generator producing controllable repetitive random signal patterns used to evaluate instrumentation system

03 p0403 A69-13188

Optimum conditions for signal analysis determined for symmetrical binary communications channel with unknown signal phase

04 p0556 A69-14492

Spectral density of response of linear discrete filter with multiple input and output periods to random signal

04 p0584 A69-15419

Beam deflection fluid amplifiers dynamic properties determined by random signal testing

05 p0705 A69-16010

Fluid amplifier linear transfer functions at signal levels on order of internal noise identified by random signal testing method

[ASME PAPER 68-WA/AUT-2] 05 p0706 A69-16184

Algorithm for discriminating random signals with unknown mean values, discussing decision functions possible existence to minimize error probability

05 p0719 A69-16218

Probability theory and Laplace functions used to determine pulse coincidence probability of two random independent pulse streams in given time

05 p0719 A69-16224

Counter/discounter assembly with slow resolution time for random fine pulses, using grouped tunnel diodes

05 p0735 A69-16702

Optimum antenna radiation patterns during suboptimum scattered Gaussian signal detection in homogeneous interference level investigated with single channel antenna

05 p0736 A69-16782

Book on introduction to random signals and communication theory covering signal analysis, analog and digital data transmission, information theory, etc

06 p0887 A69-17144

Optical heterodyne detection of randomly distorted signal beam, noting time invariant scheme yielding largest average SNR in atmospheric turbulence

07 p1087 A69-19642

Hilbert transform properties and application to random signals, analyzing analytic signal associated with general Gaussian random signal

08 p1271 A69-19915

Random data detection method applicable to low voltage SNR cases using real time correlation of probability functions

09 p1459 A69-22593

Error probability distribution density at output of optimal Gaussian random signal detection, using approximate solution of integral equations

11 p1835 A69-24712

Optimal calculator of detection of Gaussian random signal against Gaussian noise background by reducing input signal to white noise

11 p1835 A69-24713

Quantization error reduction for stochastic signals processing problems

12 p2051 A69-26201

Mismatch between signal and filter effect on output response of matched filter for pseudorandom phase-manipulated signals in receiver

12 p2031 A69-26487

Book on random signal analysis covering Fourier analysis, circuit analysis, Fourier transform theory, operators, probability, random variables, stochastic processes

12 p2031 A69-26632

Fourier analysis of pseudorandom binary sequences, noting relation of sequence sampling properties to interchange of phase angles of sequence harmonic components

13 p2287 A69-27245

Singularities of optimal filtration for random signals given by differential equations with variable coefficients and white noise

13 p2218 A69-27251

Input signal random amplitude fluctuations suppression by parametric power limiter, discussing limiting frequency determination and dependence on signal amplitude

13 p2236 A69-28573

Random signals and real time analysis systems for environment testing and transient signals

13 p2264 A69-28603

Continuous random process spectral density at PAM system output

14 p2424 A69-28748

Correlated noise effect on accuracy of suboptimal servosystem velocity measurements from recording Doppler frequencies

15 p2567 A69-30341

Subtractor performance for processing correlated random signals with different spectral widths in signal delay time indicator, discussing errors

15 p2572 A69-30346

Vibration/acoustics digitally controlled environmental testing, describing random test signal generation and random vibration tests

15 p2587 A69-30389

S-N fatigue life small bondable resistance sensor, discussing random response data interpretation with emphasis on use of strain multipliers

15 p2613 A69-31270

Likelihood ratio for random signals detection in white Gaussian noise based on innovation process

17 p2920 A69-33622

Optimum detection of stochastic signals in Gaussian noise, obtaining eigenfunctions series expansion associated with probability density function

17 p2921 A69-33623

Random signal behavior in hybrid correlator with analog and sampling channels, noting SNR expression and weak signal detection

24 p4283 A69-43139

RANDOM VARIABLES

Asymptotic behavior of probabilities of large deviations of sums of independent random variables with moments of any order

01 p0104 A69-10264

Minimal conditions for association of binary variables, studying nondecreasing functions and equivalence in coherent binary systems theory

04 p0624 A69-15007

Random processes study by special integral calculus containing deltas and theorems, with application to stationary processes

05 p0718 A69-15881

Analysis and synthesis of optimal linear time invariant systems with uncertain or unknown parameters, considering mean square error 06 p0902 A69-17405

Book on stochastic convergence covering infinite sequences of random variables, stochastic integrals and derivatives, characterization of normal distribution and Wiener process 08 p1343 A69-20443

Postselection estimation of component reliability in multicomponent systems, considering cases of binomial and exponential distributions of random variables 08 p1322 A69-21099

Variational approximation of probability measures and products of random matrices, discussing point distribution on Lobachevskii plane 10 p1719 A69-23399

Rate estimates of convergence of multidimensional central limit theorem for sequence of identically distributed independent random variables with third order finite moments 10 p1719 A69-23400

Mean losses in quasi-optical communication lines due to random irregularities in performance of waveguide phase correctors connected in series, noting random phase aberrations effect 10 p1658 A69-23954

Upper bounds for Bernstein-Kolmogoroff multidimensional inequalities, analyzing independent random vectors 11 p1910 A69-25698

Iterated logarithm law proved for class of stationary series extended to systems of dependent random variables with complete couplings 11 p1910 A69-25699

Cumulative probability distribution of positive random variable from moment generating function, exemplifying exponential and Poisson functions 12 p2120 A69-25927

Integral representation for continuous linear stochastic processes with independent pieces, assuming convergence in probability for sequence of random variables 12 p2121 A69-26365

Random variables generation from distribution having given failure rate function 12 p2102 A69-26571

Differential equations of probability theory for studying control systems and processes involving random variables 12 p2124 A69-27142

Wiener-Hermite expansion extended to include time dependent ideal random functions, discussing application to shear flow turbulence 15 p2644 A69-30201

Force resonance oscillations of one degree of freedom system with randomly time varying natural frequency 16 p2813 A69-32285

Natural oscillations frequency spectrum of turbomachine impeller blades subjected to random variations determined with frequency distribution function obtained by moments method 19 p3436 A69-35844

Asymptotic behavior of probabilities of large deviations of sums of independent random variables with moments of any order 19 p3360 A69-36199

Random variable used as model for unknown parameter in linear system, describing orthonormal expansion for evaluating mean-integral-squared error 21 p3685 A69-38727

Book on systems stability with random parameters, considering linear and nonlinear control systems, with application to stochastic approximation 23 p4181 A69-41510

Tolerance limits for uncertain requirements vector in linear programming with random variation, introducing nonparametric statistics with sensitivity analysis [AAS PAPER 69-079] 24 p4340 A69-42821

Automatic system failure sequence statistical analysis, considering randomly time variable external effects 24 p4289 A69-42953

Optimal rule for decision to stop or continue observation of random variables after observing sequence of variables with continuous distribution function 24 p4341 A69-43235

RANDOM VIBRATION

Stress peak distribution effects on random load fatigue investigated for one and two degree of freedom systems 01 p0172 A69-11355

Linear mechanical systems idealized by single degree of freedom system with viscous damping subjected to combined deterministic and random excitation 04 p0680 A69-14968

Vibration response of thin elastic plates to random loads 05 p0844 A69-16741

On-line analysis with digital computer, noting system designed for vibration and random vibration analysis 05 p0726 A69-16761

Bilinear hysteretic system undergoing random vibration, substantiating linearization analysis with analog computer simulation and comparing lifetime to linear system [ASME PAPER 69-VIBR-25] 10 p1806 A69-24173

Magnitude limited random excitation effect on linear system response, using single degrees of freedom model representing idealized mechanical structure [ASME PAPER 69-VIBR-41] 10 p1807 A69-24179

Displacement and acceleration criterion for synthesizing optimum linear vibration isolator systems subject to random input [ASME PAPER 69-VIBR-44] 10 p1807 A69-24182

Random periodic forces effect on single frequency oscillations of nonlinear nonautonomous system with distributed parameters, discussing perturbed boundary value problem 11 p1916 A69-24761

Random oscillations of nonlinear elastic system described by nonlinear partial differential equations 11 p1918 A69-24781

Transition density function of randomly excited diffusion process and confinement probability at fixed spatial point satisfying integrodifferential equation involving functional derivatives 11 p1860 A69-25451

Bounding technique of first excursion probability for random vibration, considering relation to reliability of mechanical and structural systems under random disturbances 13 p2361 A69-27438

Vibrostand effects on statistical characteristics of random vibrations of elastic system, discussing simulation techniques 14 p2536 A69-29743

Vibration/acoustics digitally controlled environmental testing, describing random test signal generation and random vibration tests 15 p2587 A69-30389

Random functions applications to random vibrations, discussing spectral power density, ergodic steady functions, etc 17 p3054 A69-33063

Numerical Fourier transform and inversion in random vibration performed on computer, noting use for stochastic structural dynamic analysis of complex structures 17 p2996 A69-33710

Energy dissipation influence on elastic elements random vibrations, obtaining relations between displacements rms value and random disturbance intensity 17 p3064 A69-33921

Mechanical single degree of freedom system mean square response to AM random noise, considering frequency response, input excitation spectrum, etc [ASME PAPER 69-APM-25] 18 p3214 A69-34398

Random vibrations in linear systems during spectral and correlation analysis, noting nonlinear systems 18 p3227 A69-35491

Random vibratory environment simulation for spectra, noting electrodynamic generator employed to excite electric field force 19 p3294 A69-35904

Ordinary coherence functions for computing frequency response in mechanical systems under random excitation 20 p3537 A69-37162

Scalar waves propagation in bounded randomly fluctuating media, emphasizing interface effects on coherent wave motion 21 p3675 A69-39283

Nonlinear random vibrations excitation in rectangular flat plate with initial imperfection by white noise, assuming clamped boundary conditions 22 p4048 A69-41183

Power flow relations between randomly vibrating systems with weak linear elastic or dissipative coupling 23 p4227 A69-41877

RANEY NICKEL

U CATALYSTS

U NICKEL

RANGE [EXTREMES]

NT FREQUENCY RANGES

NT RADIO RANGE

NT ROCHE LIMIT

Bounds from asymptotic behavior of solutions of nonlinear integrodifferential equation arising from nonlinear oscillators in acoustics 01 p0103 A69-10001

Approximate boundary controllability for heat equation by considering temperature variation with time 01 p0173 A69-10008

Upper and lower bounds for eigenvalues of differential problem connected with transverse vibrations of wedge shaped simply supported beam 02 p0272 A69-12193

Lehmann-Machly procedure for lower and upper bounds to eigenvalues of Hermitian operators in Hilbert space 06 p1020 A69-17131

Optimal approximation of functional matrix, giving upper bounds for deviations of general matrices from closest spectral matrices 06 p0948 A69-17495

Upper and lower bounds for feedback decoding and definite decoding minimum distances of binary convolutional codes 06 p0904 A69-17865

Radio source CP 1133 at 408 Mc, noting upper and lower limit to continuous emission between pulses 06 p1009 A69-17969

Unperturbed Hamiltonian transformation applied to existing perturbation theories for exchange forces between atoms to obtain correct long range behavior 07 p1184 A69-18288

Bounds on electric field outside radiating system determined for application to UHF and VHF systems design, considering microwave breakdown 08 p1273 A69-20026

Bounds for real and imaginary parts of dynamic moduli of composite viscoelastic systems 08 p1417 A69-20824

Riemann sum definition and development of bounds for error in approximating integral, showing quadrature formulas as Riemann sums 10 p1719 A69-23521

Probability analysis by methods simplifying calculations or providing bounds on reliability of complex system 12 p2103 A69-26751

X ray source Cyg XR-1 angular diameter upper limit determined from balloon experiment data obtained with collimated X ray telescopes 17 p3026 A69-32860

Displacement bounding principle for work hardening plasticity theory based on Drucker inequality and stress path existence [ASME PAPER 69-APM-7] 18 p3213 A69-34385

Analog method for determining structural creep displacement by setting up boundaries for linear elasticity and perfect plasticity 20 p3628 A69-37915

Upper limits for OH microwave emissions from radio sources F transitions, discussing pumping mechanism role in emission detection 21 p3796 A69-38477

Mariner attitude control system limit cycle operation during cruise, noting variation from ideal case to single side operation [AIAA PAPER 69-844] 21 p3822 A69-39374

Sonic boom lower bounds determination in midfield based on modification of Jones results by minimizing overpressure or shock strength of boom wave positive component 24 p4254 A69-43662

RANGE AND RANGE RATE TRACKING

Computer program solving for station coordinates and dynamical parameters at Smithsonian Astrophysical Observatory from optical data, laser range and range rate 12 p2068 A69-26428

Alford and Gold light modulation effect expanded to include one frequency spectrum with Doppler shift, discussing applications to optical radar for range and velocity measurements 21 p3672 A69-38409

RANGE CONTROL

U TRAJECTORY CONTROL

RANGE ERRORS

Longitudinal range dispersion of unmanned Mars landers using VM-8 and VM-9 atmospheric models, discussing Syrtis Major as possible landing site 02 p0324 A69-12390

Long distance VLF multirange navigation fix errors as function of angles of cut of position lines and range errors, presenting error isograms 14 p2478 A69-29484

Omega/VLF transmission range rate measurements for satellite Doppler navigation to provide velocity and location data, noting propagation error
14 p2479 A69-29857

Systematic error pattern in raw data obtained during tracking ROSE balloons by two radar systems, estimating range resolver error
15 p2649 A69-30897

Navigational accuracy dependence on spacecraft geometry, determining information content and critical error sources of earth based Doppler radio tracking data
[AAS PAPER 69-112] 19 p3402 A69-35935

Ionospheric range difference errors after correction for position fixing from satellite, considering elevation angle, latitude, day time, spatial and time electron content correlation
23 p4128 A69-42505

RANGE FINDERS

NT OPTICAL RANGE FINDERS

Optimal structural parameters of radar digital ranging servo systems derived from reproduction error, including computer simulation data
19 p3278 A69-36593

RANGE INDICATORS

U INDICATING INSTRUMENTS

RANGE MEASUREMENT

U RANGEFINDING

RANGEFINDING

NT SOUND RANGING

Radar range determination on any target based on parametric method and nomograms in decibels
04 p0560 A69-15227

Signal strength variations for balloon-borne VHF FM transmitter due to wave interference, noting application to balloon range estimation
06 p0886 A69-16925

Navigation satellites system designed for ATC without requirement for onboard transmitter, discussing spectrum occupancy, satellite power, lane ambiguities and computational procedures
07 p1177 A69-19212

Experimental circuit for simulating radar target tracking system based on split range gating, noting tracking role of error signal
08 p1300 A69-20109

Range measurement accuracy of radar automatic equipment, discussing nomograms for split-gate tracker, cyclic and pulse length errors and multipath reflections
08 p1275 A69-20228

Range difference air navigation equations solution, discussing error updating of satellite position and constellation geometry
09 p1538 A69-21996

Pulse Doppler radar operation, discussing Doppler shift, range resolution and systems components
10 p1659 A69-24084

Pseudorandom FM waveforms for simultaneous range and Doppler shift radar measurements
13 p2221 A69-27944

Automatic navigation and sighting system for French specified Jaguar combat aircraft development
16 p2809 A69-31760

Software remechanization of conventional hyperbolic LORAN for totally passive closed loop one way direct range measurements to individual LORAN transmitters
17 p3002 A69-34079

Scale determination in spatial direction networks, using polygonal transverse measured along continental surfaces and Secor method over water surfaces
18 p3131 A69-35196

Radar propagation in surface duct over water, describing range distribution estimation procedure
20 p3495 A69-37854

RANGER LUNAR PROBES

Analytic photogrammetric determination of lunar control coordinates from Ranger photography
01 p0147 A69-10022

Lunar geology information obtained by Ranger space missions
06 p1001 A69-17163

Ranger pictures improvement by computer, eliminating image distortion due to electronic imaging systems
06 p0924 A69-17164

RANGES (FACILITIES)

U BALLISTIC RANGES

U MISSILE RANGES

U TEST RANGES

RANGING

U RANGEFINDING

RANK TESTS

Group relative values for system criteria, showing application to illustrative maintenance criteria
10 p1668 A69-22973

RANKINE CYCLE

Thermodynamic comparison of MHD generators using Brayton and Rankine cycles, showing Rankine cycle conversion at higher channel Mach numbers for nonequilibrium ionization
03 p0369 A69-14154

Thermodynamic and aerodynamic characteristics of organic Rankine cycle working fluids for ideal application to manufacturing
[SAE PAPER 690063] 07 p1057 A69-18308

Power generation in combat environment by tested self contained organic Rankine silent engine, discussing working fluid properties
[SAE PAPER 690062] 07 p1058 A69-18309

Linear induction MHD generator using Rankine cycle with K-Na working fluid noting longitudinal edge effect compensation
07 p1058 A69-19026

Mercury cesium plasma in crossed electric and magnetic fields as working fluid of MHD generators based on Rankine cycle
10 p1636 A69-23458

Throttling effect on thermodynamic efficiency of MHD generator Rankine cycle with various working fluids
11 p1824 A69-24222

Nuclear energy conversion for long space missions, comparing dynamic Brayton, liquid metal MHD gas, dynamic Rankine and LMMHD Rankine cycles
16 p2810 A69-31748

Power subsystem weight effects on temperature ratio of Rankine type cycle, discussing method for rapid estimation
19 p3254 A69-35957

Rankine cycle power systems with reciprocating engines using organic working fluids, discussing engine development, system characteristics, etc
23 p4067 A69-42237

Jet condenser at very low pressure in organic Rankine cycle power conversion system noting role in power efficiency
23 p4068 A69-42238

Freon boiler designed for Rankine cycle heater fired on hydrocarbons with over 2000 F flame front temperature, considering radiant/convective heat transfer
23 p4068 A69-42239

Positive displacement Rankine cycle rotary wet steam engine design compared with piston type, noting simplified evaporator and tests
23 p4069 A69-42252

Pu-238 isotope organic Rankine cycle system analyzed for one year manned space station, using modified H-521 Space Power computer program
23 p4188 A69-42264

Performance, size, weight, operational characteristics and cost estimates of ZrH reactor-organic Rankine power systems
23 p4189 A69-42265

Systems analysis of Rankine cycle nuclear-electric potassium space power system using Li cooled fast reactor and high temperature turbine inlet
23 p4189 A69-42266

Organic Rankine cycle system using heat absorption from turbine exhaust to provide increased electrical output and to power air conditioning
23 p4070 A69-42267

Dynamic power and life support systems electrical/thermal integration for manned spacecraft using low temperature Rankine cycle generator
23 p4189 A69-42269

Rankine power cycle for fluid evaluation, discuss radiating area, thermodynamics, etc
23 p4239 A69-42276

RANKINE-HUGONIOT RELATION

Shock heated helium plasma temperature measurements by spectroscopy compared to Rankine-Hugoniot calculations including ionization effect
09 p1548 A69-21963

MHD Rankine-Hugoniot equations for ion density, thermal pressure and convective velocity magnitude and orientation during Pioneer 6 traversal of earth bow shock
23 p4222 A69-42417

RANKINE TEMPERATURE SCALE

U TEMPERATURE SCALES

RANKING

Nonparametric ranking procedures /based on order statistics/ guaranteeing preassigned probability for

selection from random samples populations as good as control
08 p1342 A69-20172

RAPCON [CONTROL]

U RADAR APPROACH CONTROL

RAPID EYE MOVEMENT STATE

Stiles-Crawford effect measurements before and following eye movements to determine retina shearing during eye movements
15 p2555 A69-31035

Functional changes of somatosensory pathway from periphery to cortex during rapid eye movement /REM/ and non-REM periods of deep sleep
22 p3872 A69-40161

Saccadic eye movements comparison during fixation and reading by contact lens optical lever technique
22 p3880 A69-40855

Hypnotic compounds properties influencing REM /rapid eye movements/ stage, discussing insomnia problems with jet flight crew and passengers
24 p4277 A69-43389

RARE EARTH COMPOUNDS

NT CERIUM COMPOUNDS

NT EUROPIUM COMPOUNDS

NT NEODYMIUM COMPOUNDS

NT SAMARIUM COMPOUNDS

Magnetic and semiconducting properties of samarium boride, noting effect of decreasing temperature
07 p1200 A69-19403

Relative heats of formation and reduced melting temperatures of lanthanide compounds correlated to lanthanide contraction
07 p1168 A69-19597

Gadolinium-cobalt system investigation by X ray diffraction thermoanalysis and metallography for intermetallic compounds, noting structure transformation and homogeneity
11 p1903 A69-24574

Low temperature specific heat of praseodymium magnesium nitrate
12 p2026 A69-25784

Far IR electronic and vibronic transitions in single crystals of Nd ions in tysonite lanthanide fluorides
13 p2316 A69-27628

CW lasers based on composite yttriofluorite type crystals, noting large number of intense emission bands
13 p2273 A69-28316

Rare earth niobates magnetic properties measured in pulsed magnetic fields
15 p2667 A69-30195

Crystal structures of Ni-rich rare earth/Ni phases, including high temperature forms
15 p2637 A69-30213

IR lattice spectra of rare earth Al, Ga and Fe garnets, discussing oxygen anion, translational rare earth cation and crystal lattice external motions
24 p4360 A69-42974

RARE EARTH ELEMENTS

NT CERIUM

NT DYSPROSIUM

NT ERBIUM

NT EUROPIUM

NT GADOLINIUM

NT LANTHANUM

NT LANTHANUM ISOTOPES

NT NEODYMIUM

NT PRASEODYMIUM

NT SAMARIUM

NT SCANDIUM

NT SCANDIUM ISOTOPES

NT TERBIUM

NT THULIUM ISOTOPES

NT YTTRIUM

Multiphonon orbit-lattice relaxation of excited states of rare earth ions in crystals, measuring fluorescence lifetimes, quantum efficiencies and transition rates
01 p0134 A69-10011

Ground state population modulation in trivalent rare earth doped single crystals by means of optical double resonance, noting applications
01 p0134 A69-10013

Multiphonon orbit lattice relaxation of excited states of rare earth ions in crystals, using results to design quantum electronic devices
[IEEE PAPER I-9] 05 p0774 A69-16318

Rare earth elements and yttrium in meteoritic chondrites determined by radiochemical neutron activation analysis
08 p1403 A69-20916

Rare earths relative and absolute terrestrial abundances in shales, basalts, rhyolites and granites
08 p1310 A69-20942

Earth crust transition elements distribution and abundance compared to rare earths
08 p1310 A69-20943

Partition coefficients between natural melts and plagioclase phenocrysts determined for rare earth elements and barium by mass spectrometry
08 p1310 A69-20944

Continental diabases and oceanic tholeiites in light of rare earth and barium abundances and partition coefficients indicating fusion process
08 p1310 A69-20945

Coherent emission from rare earth ions in electro-optic crystals, noting oscillations and electric field modulation occurrence
09 p1514 A69-21339

Trivalent rare earth ions Stark structure based on spectroscopic observations of stimulated transitions in lasers
10 p1701 A69-23129

Liquid lasers properties and composition including organic complex compounds, organic dyes, rare earth elements in polyphosphoric acid, etc
11 p1893 A69-24353

Glass lasers with trivalent rare earth ions noting properties, characteristics and recent developments
11 p1898 A69-25043

Rare earths additives effects on arc instability and weld puddle fluidity of stainless steel bare wire electrodes
12 p2103 A69-26623

Polycrystalline Ca-V garnets and Mg-Cr ferrites magnetic properties after adding rare earth elements
13 p2320 A69-27999

Energy exchange of rare earth ions in uranyl phosphate liquids and glasses, studying sensitized luminescence origin
14 p2485 A69-29034

Crystal structures of intermediate phases in La-Co and Nd-Co systems by powder X ray diffraction technique
15 p2667 A69-30087

Ca-rich achondrites genesis implied from rare earth and Ba absolute and relative concentrations
19 p3409 A69-36091

Solar rare earth abundances determined from high resolution tracings of solar spectrum, comparing results with nucleosynthesis theories
20 p3602 A69-37539

Electrical conductivity of rare earth metals La, Ce, Pr and Nd in solid and liquid states by rotating magnetic field method
21 p3781 A69-39070

RARE GASES

NT ARGON
NT ARGON ISOTOPES
NT HELIUM
NT HELIUM ATOMS
NT HELIUM ISOTOPES
NT KRYPTON
NT LIQUID HELIUM
NT NEON
NT NEON ISOTOPES
NT RADON
NT XENON
NT XENON ISOTOPES
NT XENON 129
NT XENON 133

Refractory metals interactions with gases in vacuum and inert gas environment, noting temperature and pressure effects on reactions, extent and kinetics
01 p0099 A69-11042

Multiphoton ionization of molecular hydrogen and rare gases using Q switched Nd laser apparatus
02 p0283 A69-11701

Inert gas nonequilibrium MHD power generation in shock tube
02 p0196 A69-12425

Xenon, krypton, nitrogen and nitrous oxide effect on respiration rate of rat liver slices at various oxygen partial pressures
03 p0375 A69-14069

Transport diffusion cross sections of slow electrons during scattering at inert gas atoms by microwave method, calculating electron transfer coefficients
03 p0481 A69-14143

Prigogine-Nicolis-Misguich transport theory tested with inert gas liquids and compared with Rice-Allnatt theory, based on modified Lennard-Jones potential model
04 p0589 A69-14863

Second dielectric virial coefficient of rare gases derived by cluster method
04 p0632 A69-14865

Continuous radiation production in positive plasma column of inert gas considered as manifestation of plasma electrons bremsstrahlung from interaction with gas atoms
05 p0800 A69-15741

Low collision energy charge transfer and dissociative charge transfer between rare gas ions and molecular nitrogen, measuring nitrogen ion kinetic energy distributions
05 p0796 A69-15909

Frequency dependent shear modulus for hexachlorobiphenyl measured under rare gas infusion at 5-25 C and from ambient atmospheric to 4000 psi
05 p0796 A69-15912

Continuous UV noble gas ion lasers, noting small signal gain and power output limit at various current densities for strong lines
05 p0775 A69-16321

Rare gases in stony meteorites, noting premordial inheritance and complex Xe anomalies
05 p0826 A69-16440

Noble gas atom simultaneous ionization and excitation by removal of metastable electron in fast collision
06 p0961 A69-17137

Inert gas discontinuous injection into nonequilibrium laminar boundary layer
06 p0860 A69-17635

Ratios of gas kinetic electron-atom collision integrals of Ramsauer for Ar
06 p0963 A69-17822

Electrical characteristics of linear Faraday generator using binary mixture of noble gases with nonequilibrium ionization
08 p1359 A69-19880

Polarization of Lyman alpha radiation in hydrogen rare gas collisions calculated in Born and distortion approximations including rotational coupling
08 p1355 A69-20207

Electron transport parameters in noble gases at low electric field intensities, elastic and inelastic scattering and Boltzmann transport equation
08 p1362 A69-20285

Tables of effective electron cross sections and macroscopic coefficients, Volume 1, covering hydrogen and rare gas molecular and atomic interactions with electrons
09 p1541 A69-21579

Kodaikanal iron meteorite measurements for cosmogenic rare gases and K-Ar isotopes ages for glass inclusions
09 p1596 A69-22047

Primary specific ionization in noble gases by charged particles
10 p1726 A69-23128

Noble gas additives for triggering stability of pulsed argon ion lasers, discussing repetition rate and power loss
10 p1702 A69-23341

Nitrogen impurities effect on electron energy balance in DC arc burning in inert gas
10 p1732 A69-23442

Rare gas-alkali plasma electrical conductivity dependence on gas temperature and preionization to determine optimum operating conditions for MHD generator
10 p1733 A69-23451

Equilibrium loss in closed cycle MHD generator using rare gases binary mixtures as working fluid
10 p1737 A69-23470

Nonequilibrium electron heating effect on inert gas plasma conductivity during shock wave movement across magnetic field
10 p1737 A69-23470

MHD conversion experiments using rare gas, considering Typhoon loop, electron heating and correction effects
10 p1738 A69-23475

Heat treatments in inert gas atmosphere improve elastic foam polyurethane by reducing capability of toxic outgassing
10 p1716 A69-23503

Electrical conductivity of partially ionized noble gases Ar, He, Xe and Kr, considering electron temperature and electron-electron interactions
11 p1923 A69-24295

Hot inert gas bubble thermal stability in cool reactive liquid
11 p1998 A69-24475

Collisional radiative electron-ion recombination rates measured in decaying rare gas plasmas produced by transient discharge
12 p2134 A69-25981

Charged state variations during protons and inert gas atoms interactions analyzed by coincidence method
12 p2133 A69-26543

Negative charge production by H atoms collisions with rare gases and hydrogen, noting smooth rise of cross section with energy for rare gases
13 p2302 A69-27459

Extinction kinetics of monopropellant droplet burning in inert gas reservoir with atmospheric temperature lower than adiabatic combustion temperature
13 p2378 A69-28250

Ionization of rare gases /H and N/ by nitrogen ions, determining cross sections of formation of slow ions and electrons
13 p2304 A69-28440

Auxiliary discharge thermionic converter with Penning mixture /Ne-Ar/, discussing pressure and Penning ionization effects, collector current discontinuities, etc
14 p2398 A69-29180

Knudsen arcs kinetic theory with cesium/inert gas mixtures in narrow gap between parallel plate electrodes, discussing fast particle beams and electron scattering
14 p2491 A69-29245

Noble gas thermionic converters, discussing auxiliary discharge compensation of negative space charge, I-V characteristics, efficiency and comparison to ignited mode cesium vapor converter
14 p2403 A69-29249

Rare gases effect on thermionic converters volt-ampere characteristics, noting gas pressure, oxygen contamination and performance relations
14 p2403 A69-29251

Rare gases total excitation cross sections absolute values measured in collision chamber, noting energy distribution of exciting electron beam, fine structure, etc
14 p2493 A69-29693

Gas-gas interactions second virial coefficients measured at various temperatures, comparing experimental data with results calculated by Kihara potential
14 p2488 A69-29927

Electron ion recombination role in atomic collision process in rare gases ionization path, considering scintillation mechanism
15 p2655 A69-30961

Vapor-liquid transition in inert gases based on Monte Carlo method, including comparison with van der Waal equation and plasma ionization equilibrium
15 p2655 A69-30981

Low energy neutral bremsstrahlung cross sections for Ne, Ar and Xe, using rapid scanning spectrometer
15 p2657 A69-31159

Microwave induced ionization wave propagation in rare gases, noting rapid electron density increase at wave front and subsequent low plasma decay
16 p2818 A69-31671

Ultrasonic velocity dispersion in para hydrogen and mixtures with He, Ne and Ar at 300 K, obtaining rotational relaxation times
16 p2815 A69-32791

Kr and Ar flash lamps pumping efficiencies compared for Nd-doped YAG and glass lasers
17 p2980 A69-32958

Microwave reflection and noise emission from cylindrical rare gas afterglow plasmas in axial magnetic field measured near electron cyclotron resonance
18 p3127 A69-34436

Cosmic ray produced radionuclides and rare gas isotopes from Saint-Severin meteorite surface, showing relative Kr spallation mass yields dependence on cosmic ray energy spectra
19 p3410 A69-36093

Calcium-rich achondrites age distribution determined from inert gas measurements and existing data of eucrites, shergottites and howardites
19 p3413 A69-36107

K 40-Ar 40 age measurements in separated mineral phases of chondrites, including production rates of spallation isotopes
19 p3418 A69-36137

Spallogenic rare gas concentrations and isotopic ratios in taenite of iron meteorites measured mass spectrometrically and compared with kamacite values
19 p3419 A69-36139

Trapped rare gases in Fe phase and silicate inclusions of Campo del Cielo Meteorite, El Taco
19 p3419 A69-36140

Thermal rare gas release from mineral separates of Mocs meteorite, using method giving activation energies as function of temperature
19 p3419 A69-36141

Distribution and origin of primordial He, Ne and Ar in Fayetteville and Kapoeta meteorites extracted and analyzed by laser-microprobe mass spectrometer
19 p3419 A69-36142

Molecular N rotational temperature effect on rare gases scattering cross section
19 p3377 A69-36184

- Noble gases effect at low pressures on O consumption by mammalian tissue, noting Xe, Kr, N and nitrous oxides effect on rat liver
19 p3258 A69-36454
- Rare gas distribution in earth atmosphere explained as outgassing from primordial solid particles, discussing stony meteorites composition
20 p3600 A69-37489
- Calcium rich achondrites radiation ages determined from measuring He, Ne and Ar in howardites, nakhlites and angrite
20 p3602 A69-37535
- Decompression research on inert gas transport in body, discussing solubility factors in decompression damage
21 p3655 A69-38913
- Valving concepts and functional approaches for inert gas attitude control thruster systems providing redundancy safeguards at minimum weight, volume and power costs
[AIAA PAPER 69-843] 21 p3786 A69-39373
- Elastic electron scattering by metastable states of rare gases, using effective potential matching experimental binding energy of negative ions
24 p4354 A69-43818

RAREFACTION

- Rarefaction onset along streamline from rocket nozzle with small Knudsen number at exit plane
23 p4152 A69-41920

RAREFACTION WAVES

U ELASTIC WAVES

RAREFIED GAS DYNAMICS

- Impulse and kinetic energy transfer in rarefied gases analyzed on basis of kinetic theory, considering surface curvature effect
01 p0173 A69-10093
- Rarefied merged stagnation shock layer of hypersonic body, considering chemical reactions of nonequilibrium dissociative relaxation of air
02 p0189 A69-12521
- Monte Carlo direct simulation for treating rarefied supersonic flows about bodies in transitional regime between continuum and free molecular flow
02 p0189 A69-12523
- Viscous effects on impact pressure measurements in free jet low density gas flows at high Mach numbers
02 p0234 A69-12633
- High rank moment tensors in weakly rarefied gas for case of gas deviation from local equilibrium, analyzing density, velocity and temperature
04 p0587 A69-14542
- Time independent flow of highly rarefied neutral gas past finite cone at zero angle of attack with freestream, noting molecular distribution function
04 p0541 A69-14712
- Rarefied flow past sphere, analyzing collisionless flowfield structure and development as density increases
04 p0542 A69-14731
- Rarefied hypersonic flow model for sharp flat plate in strong interaction regimes, discussing inviscid and viscous shock and merged layers subregions
04 p0589 A69-14747
- Interaction of rarefied gas with solid surface, analyzing accommodation coefficients, energy and impulse exchange as function of atomic bulk size
04 p0632 A69-14991
- Class of uniform motions of continuous media and rarefied gases
05 p0751 A69-16677
- Monte Carlo solution of linearized Boltzmann equation in rarefied gas dynamics, noting Knudsen layer and Couette flow applications
06 p0910 A69-17345
- Time dependent technique for inviscid blunt body flows to analyze viscous rarefied shock layer regime, using Navier-Stokes equations
[AIAA PAPER 69-139] 06 p0865 A69-18173
- Collimated nozzle beam for probing low density gas flows, discussing transition from free molecular to isentropic flow and Knudsen numbers
07 p1136 A69-19467
- Multibeam Fabry-Perot interferometers for aerodynamics measurements of rarefied gas flows, determining density distribution, shape, structure and detachment of shock waves
08 p1314 A69-20385
- Steady motion through rarefied gas of circular cylinder due to surface temperature difference
08 p1305 A69-20888
- Hydrodynamic equations and Grad transport coefficients for nonequilibrium rarefied monatomic gases developed for molecular collisions
09 p1481 A69-21888

- Singular integral equation for velocity in linearized Rayleigh problem in rarefied gas flow field solved by applying Luke weight coefficients
10 p1679 A69-23596
- Monte Carlo method application to heat transfer analysis including radiation, rarefied gas energy transfer and conduction
11 p1997 A69-24457
- Kinetic theory for examining transition regime of rarefied gas dynamics, discussing Boltzmann equations and models with related boundary value problems
11 p1870 A69-25005
- Classical statistical mechanics of systems with identical or limited different particles, discussing particle collisions in dilute gases
11 p1870 A69-25009
- Gasdynamic and Boltzmann equations relations in rarefied gas kinetics, applying physical and mathematical boundedness concept to setting boundary conditions for moment equations
13 p2250 A69-28320
- Monograph on investigation of rarefied gas flows by means of miniature pressure probes in transition region between molecular and continuum flows
14 p2430 A69-29289
- Direct simulation Monte Carlo method for hypersonic rarefied gas flow past solids, modeling on digital computer
14 p2390 A69-29580
- Intrinsic quantum-mechanical behavior of fully ionized gas at high temperature and low density, defining classical limit
14 p2502 A69-29992
- Hydrogen gas role in galaxy formation, estimating quantity needed to dissipate gas cloud contraction energy, discussing formation mechanics of molecular hydrogen
15 p2680 A69-30204
- Unsteady nonadiabatic shock waves in stellar gas dynamics, analyzing energy losses due to ionization at shock fronts by extended Chiznell-Wisem method
15 p2682 A69-30508
- Heat transfer in rarefied gas plane Couette flow determined by BGK model and moments method of half range distribution functions
16 p2876 A69-31688
- Book on mathematical methods in kinetic theory covering boundary value problems associated with Boltzmann equation, model equations, rarefied gas dynamics, etc
16 p2811 A69-31721
- Boltzmann kinetic equation describing rarefied neutral or weakly ionized gas state evolution, showing solution existence, uniqueness and successive approximation convergence
16 p2814 A69-31958
- Nonlinear rarefied gas flow problems with thermal nonequilibrium solved by numerical methods, considering intermolecular collisions effect
17 p2952 A69-33325
- Exhaust plume rarefaction from sonic orifice, considering continuum to transitional behavior for perfect gas
[AIAA PAPER 69-657] 17 p2892 A69-33465
- Flow field study of merging between bow shock and viscous layer upstream of highly cooled axisymmetric blunt body in rarefied hypersonic stream
[AIAA PAPER 69-656] 17 p2893 A69-33498
- Strong shock wave structural model, considering near molecular beam, upstream hypersonic and downstream subsonic flows and beam-continuum conversion by collision
18 p3120 A69-34457
- Aerodynamic characteristics of sphere and blunt cone in highly rarefied gas flow, noting molecular collision effect
18 p3086 A69-34708
- Rarefied gases transfer coefficients stochastic process calculation models, comparing results with correlation functions derived from transport equation
18 p3121 A69-34710
- Rarefied gas dynamics for continuous medium and discrete molecules assemblage, discussing flow over blunt model and free jet flow from sonic orifice
18 p3122 A69-34812
- Rarefied gas dynamics of blunt and sharp-pointed slender bodies in supersonic stream and free jet sonic expansion into high vacuum
18 p3123 A69-34924
- Thermal accommodation coefficients determination, comparing techniques based on free molecule flow heat flux data
18 p3230 A69-35071

- Rarefied gas flow between parallel plates using linearized Boltzmann transport equation, deriving integral equation for mass flow velocity
19 p3296 A69-35621
- Hypersonic rarefied gas flow past flat plate with sharp leading edge and past circular cylinder, noting wake structure similarity to viscous theory prediction
19 p3294 A69-35755
- Monte Carlo simulation for studying rarefied hypersonic gas flow about slender cones and flat plates
20 p3459 A69-37902
- Molecular transport equations of dilute gases, considering relaxation time spectrum, obtaining kinetic equations and correlation function expressions for transport coefficients
23 p4193 A69-41512
- Aerodynamic characteristics of moving and rotating bodies of revolution in free molecular rarefied gas flow, assuming Maxwellian thermal velocity distribution and diffuse specular interaction
24 p4243 A69-42583
- Supersonic rarefied gas flow past circular cylinder, studying flow and shock parameters by multiple wave interferometry
24 p4244 A69-43070
- Rarefied gas one dimensional transverse motions consistent with Boltzmann kinetic equation, solving integrodifferential equations for shock wave structure
24 p4351 A69-43491
- Stagnation temperature determined in transition and free molecule region of rarefied gas flows from critical mass flow dependence on temperature and stagnation pressure
24 p4408 A69-43492
- Cylindrical models in hypersonic rarefied flow, determining drag data by free flight technique
24 p4249 A69-43677

RAREFIED GASES

NT COSMIC GASES

NT INTERPLANETARY GAS

NT INTERSTELLAR GAS

- Pressure measurements by gauges in rarefied gas flows past bodies of various shapes, discussing configurations effect on gauge readings
01 p0080 A69-10358
- Accommodation coefficient effect on linearized heat transfer in rarefied gas between parallel plates and concentric cylinders
01 p0177 A69-11405
- Hydrodynamic theory of light scattering by dilute monatomic gases generalized by using linearized Burnett equations instead of Navier-Stokes equations
03 p0466 A69-13135
- Kinetic theory of sound propagation in rarefied gas using generalized orthogonal polynomial expansion, evaluating adequacy of nonequilibrium distribution postulated by Mintzer
03 p0466 A69-13156
- Differential thermistor gauge using Wheatstone bridge for use in free molecule pressure probe measurement of macroscopic velocity in rarefied gases
04 p0601 A69-15117
- Free convective heat transfer of cylinder in rarefied gas yielding Nusselt number as function of Grashof, Prandtl and Knudsen numbers
05 p0846 A69-15904
- Model kinetic integral equation for describing flow in transition region at leading edge of tapered body in rarefied gas
05 p0697 A69-16040
- Law of corresponding states applied to temperature dependence of viscosity of rarefied gases
06 p0957 A69-16918
- Drag force measurement in low density flows using modulation techniques
06 p0861 A69-17638
- Weakly ionized wakes study in free quasi-molecular regime of supersonic flow, using Langmuir probe in wind tunnels, discussing ion density distribution
06 p0966 A69-17639
- Dynamic behavior of shock layer of supersonic rarefied gas flow past disk and sphere
06 p0861 A69-17812
- Heat transfer to wedge in nearly free-molecular hypersonic flow of strongly rarefied gas
07 p1050 A69-18707
- Time derivatives of Boltzmann H function with respect to dilute gas
07 p1121 A69-19407
- Rarefied gases back diffusion between parallel plates used for studying diffusion in capillaries, deriving volume flow equation valid for any density
10 p1677 A69-22903

Supersonic and hypersonic flow of rarefied gas around blunted cylinders at various angles of attack, noting pressure distribution on model surface
11 p1821 A69-25478

Hypervelocity shock wave propagation in rarefied gas, observing anomalous wave attenuation
14 p2433 A69-29846

HO₂ radical detection in rarefied H flame produced by HF discharges, recording high amplitude signals
15 p2716 A69-30054

Effective heat transfer coefficient lambda for micro-scopic Fe particles traversing rarefied air, oxygen and Ar target gases
16 p2769 A69-31870

Vibrational temperature of low density nitrogen measured by electron beam method, discussing relationship to ratio of integrated vibrational band intensities
20 p3579 A69-37222

Rarefied molecular gas flow past permeable surface, determining reflection law and flow parameters
20 p3459 A69-37438

Viscosity, thermal conductivity and diffusion predicted for dilute nonpolar, polar and mixed gases, discussing methods for rotational relaxation collision numbers and resonant correction
21 p3850 A69-38951

Aerodynamic forces under space-like conditions measured by swing balance, using large scale molecular beams for rarefied hypersonic gas flow simulation [AIAA PAPER 69-1032]
22 p3924 A69-40400

Numerical analysis of plane Couette flow of rarefied binary gas mixture using relaxation type kinetic model equations, discussing slip velocity, friction coefficient, etc
22 p3931 A69-40778

Monte Carlo method applied to heat transfer in rarefied gas flow between parallel plates involving temperature jump in Knudsen layer
24 p4246 A69-43490

RAREFIED PLASMAS

NT COSMIC PLASMA

Penning discharge in inhomogeneous magnetic mirror field, observing high burning voltage at low current in rarefied hydrogen plasma
01 p0133 A69-11218

Perturbed wake behind spherical models in rarefied plasma flow, noting effects of electron temperature and electric potential of models
05 p0803 A69-16048

Structure of plane shock wave of arbitrary force propagating across magnetic field in hot rarefied plasma
07 p1190 A69-18692

Rarefied plasma self similar motion qualitatively analyzed, particularly penetration and expansion, taking into account electric/magnetic field effects
08 p1359 A69-19951

Collisionless shock waves in rarefied plasma, discussing dispersion effect and oscillatory shock wave structure
08 p1303 A69-19996

Flute instabilities in rarefied plasma with intrinsic electric field, discussing plasma density profile and uncompensation degree effects on plasma magnetic field stability
08 p1370 A69-21013

Amplitude modulated radio wave interaction with rarefied plasma in magnetic field, considering possible ionospheric heating by mechanism
09 p1453 A69-21543

Equilibration potentials between dense thrust beam and dilute space plasma measured in wind tunnel [AIAA PAPER 69-263]
09 p1568 A69-21728

Conductivity probe design for tenuous plasmas and ionized gases, discussing experimental confirmation of theoretical behavior [AIAA PAPER 68-170]
09 p1496 A69-21936

O, Ne, Si and Fe ionization equilibria in low density plasma, including dielectronic recombination and autoionization processes in calculations
09 p1543 A69-22404

Thermodynamic potential of rarefied plasma from Coulomb interactions of atoms with electrons and ions
10 p1728 A69-23134

Optical diagnostics methods for fast processes in rarefied plasma, using Michelson interferometers with ruby and Nd lasers as light sources
12 p2089 A69-26186

Rarefied Ar plasma flow current-voltage characteristics in discharge tube, noting plasma boundary layer thickness influence on saturation current
12 p2137 A69-26532

Rarefied plasma potential fluctuations when bounded by surface having complex conductivity and dispersing properties
12 p2139 A69-26712

Electric field determination from charged particle concentration in wake of body moving in rarefied plasma, noting hydrodynamics similarity
14 p2517 A69-29068

Low density cold plasma effect on stability of cylindrical layer of charged particles against electrostatic perturbations in uniform magnetic field
16 p2816 A69-31635

Amplitude modulated radio wave interaction with rarefied plasma in magnetic field, considering possible ionospheric heating by mechanism
16 p2754 A69-32538

Collisionless shock wave front turbulence in diluted plasma, including thickness, electron and ion component measurements
17 p3012 A69-33818

Damping of plane sinusoidal wave in cold collisionless plasma, studying supercritical amplitude oscillatory process
18 p3180 A69-34703

Low density plasma electrical conductivity determined by temperature and electron density measurements, using Ohm law
18 p3181 A69-35072

Multiple electrode probe characteristics in rarefied plasma flow created by ion source, noting electrode potential role
19 p3314 A69-36622

Rarefied nonmagnetic plasma in wake of body moving at higher than electron and ion thermal velocities
20 p3525 A69-37660

Perturbed wake behind spherical models in rarefied plasma flow, noting effects of electron temperature and electric potential of models
20 p3581 A69-37957

Ion temperature measurement in rarefied multicomponent plasma by temperature relation to ion beam divergence rate, comparing results to pyrometric measurements
23 p4196 A69-41839

High temperature relatively dilute plasmas, discussing equations of motion, plasma oscillations, Landau damping, plasma confinement, etc
23 p4197 A69-42311

Ionization equilibrium and radiative cooling of high temperature low density plasma, noting cosmic gas cooling curve of line emission from oxygen ion transitions
24 p4376 A69-42661

RASERS

U MASERS

RATE METERS

U MEASURING INSTRUMENTS

RATES [PER TIME]

NT ACCELERATION [PHYSICS]

NT ACOUSTIC VELOCITY

NT AIRSPEED

NT ANGULAR ACCELERATION

NT ANGULAR VELOCITY

NT ARRHYTHMIA

NT ARTIFICIAL GRAVITY

NT BRADYCARDIA

NT BURNING RATE

NT COLLISION PARAMETERS

NT COLLISION RATES

NT CRITICAL VELOCITY

NT CURRENT DENSITY

NT DECAY RATES

NT DECELERATION

NT DRIFT RATE

NT ELECTRON DECAY RATE

NT ELECTRON FLUX DENSITY

NT ESCAPE VELOCITY

NT EVAPORATION RATE

NT EXHAUST VELOCITY

NT FLOW VELOCITY

NT FLUX [RATE]

NT FLUX DENSITY

NT GRAVITATION

NT GROUP VELOCITY

NT HEART RATE

NT HEAT FLUX

NT HIGH GRAVITY ENVIRONMENTS

NT HIGH SPEED

NT HYPERSONIC SPEED

NT HYPOVENTILATION

NT ILLUMINANCE

NT IMPACT ACCELERATION

NT ION PRODUCTION RATES

NT IRRADIANCE

NT LANDING SPEED

NT LIGHT SPEED

NT LOADING RATE

NT LOW SPEED

NT LUMENS

NT LUMINANCE

NT LUMINOUS INTENSITY

NT LUNAR GRAVITATION

NT LUNAR GRAVITATIONAL EFFECTS

NT MAGNETIC FLUX

NT MASS FLOW RATE

NT NEUTRON FLUX DENSITY

NT ORBITAL VELOCITY

NT PARTICLE ACCELERATION

NT PARTICLE FLUX DENSITY

NT PHASE VELOCITY

NT PHOTON DENSITY

NT PHYSIOLOGICAL ACCELERATION

NT PLANETARY GRAVITATION

NT PLASMA ACCELERATION

NT PROPAGATION VELOCITY

NT PROTON FLUX DENSITY

NT PULSE RATE

NT RADIANCE

NT RADIANT FLUX DENSITY

NT RECOMBINATION COEFFICIENT

NT REDUCED GRAVITY

NT RELATIVISTIC VELOCITY

NT RESPIRATORY RATE

NT ROTOR SPEED

NT SIGNAL FADING RATE

NT SOLAR CONSTANT

NT SOLAR FLUX

NT SOLAR FLUX DENSITY

NT SOLAR GRAVITATION

NT SOLAR VELOCITY

NT SOUND INTENSITY

NT SPIN REDUCTION

NT STRAIN RATE

NT SUBSONIC SPEED

NT SUPERSONIC SPEEDS

NT SYSTOLE

NT TACHYCARDIA

NT TERMINAL VELOCITY

NT TIP SPEED

NT TRANSONIC SPEED

NT WIND VELOCITY

Ratio of volume emission rate of 5577 A photons to volume emission rate of one band of positive nitrogen molecule first negative system in aurora
05 p0756 A69-16360

Time rates for growth and damping of resistive instability in gaseous plasma in crossed electric and magnetic fields
08 p1369 A69-20886

Solid state sampling circuit for low pulse repetition frequencies to improve signal to noise ratio, noting ratio of holding to learning time
11 p1849 A69-24900

Ion pair annihilation average rate by single aerosol particle action in lower ionosphere noctilucent clouds
14 p2434 A69-28941

Chemical reaction-rate theory for creep tests, analyzing extrapolation equations for time-to-rupture dependence on temperature and stress
14 p2464 A69-29442

Book on rate constants of chemical reactions from flames covering flame propagation, mass spectroscopy, electron spin resonance, particles diffusion, combustion physics, etc
22 p3895 A69-40318

Numerical computation of rate-distortion function R/D for certain memoryless message sources, discussing bounds, reduction to minimization problem and applications
24 p4284 A69-42719

RATINGS

Handling-qualities rating data evaluation for low computation cost information, noting reliability estimation
21 p3664 A69-38968

Personality factors and job performance ratings relationship in radar controllers, computing Pearson correlation matrix based on age, education, motivational distortion, etc
21 p3665 A69-39169

Second order system handling qualities analysis for pilot rating through human transfer function and closed loop control
21 p3668 A69-39792

Measurement methods for quantitative character of aircraft pilot rating scales for vehicle flying qualities, considering wording ambiguity, dual mission character, etc
24 p4276 A69-43326

RATIONAL FUNCTIONS

Book on computer evaluation of mathematical functions, discussing errors, square and cube root, Chebyshev polynomials, approximation, rational function, asymptotic expansions, etc
05 p0723 A69-15955

Filter network synthesis for realization of rational functions, discussing numerator polynomial inclusion by choice of divisor polynomial and branch introduction and parallel systems

10 p1667 A69-24038

RATIONS

U SPACE RATIOS

RATIOS

NT ASPECT RATIO
NT DIMENSIONLESS NUMBERS
NT FINENESS RATIO
NT FROUDE NUMBER
NT FUEL-AIR RATIO
NT GRASHOF NUMBER
NT HIGH ASPECT RATIO
NT INDEXES (RATIOS)
NT LEWIS NUMBERS
NT LIFT DRAG RATIO
NT LOW ASPECT RATIO
NT MACH NUMBER
NT MASS RATIOS
NT NUSSELT NUMBER
NT OPTICAL REFLECTION
NT PAYLOAD MASS RATIO
NT PERVEANCE
NT POISSON RATIO
NT PRANDTL NUMBER
NT PROPELLANT MASS RATIO
NT RAYLEIGH NUMBER
NT REYNOLDS NUMBER
NT RICHARDSON NUMBER
NT SCALE (RATIO)
NT SCHMIDT NUMBER
NT SIGNAL TO NOISE RATIOS
NT SIMILARITY NUMBERS
NT STANDING WAVE RATIOS
NT STANTON NUMBER
NT STRESS RATIO
NT STROUHAL NUMBER
NT THICKNESS RATIO
NT THRUST-WEIGHT RATIO
NT VOID RATIO

Gamma heating rate measured by aqueous dosimeter converted to rate in thin tungsten detector in water shield through transport theory calculations, obtaining correction factors

07 p1178 A69-18825

Star counts in star cluster neighborhoods, obtaining ratios of corona radius to nucleus radius as function of cluster mass

11 p1951 A69-24246

Amplitude ratio measurement for two AC signals of given relative phase shift and same frequency

17 p2975 A69-33615

RATS

Short latency antidiuresis following initiation of food ingestion by food deprived rats, noting possible signaling factor

01 p0014 A69-10860

Tyrosine transaminase activity estimation by radioactive isotopic assay method, discussing application to rat liver and other organs

01 p0014 A69-10902

Blood volume in rats exposed to high altitude and deacclimated at ambient pressure, noting changes and control level restoration

01 p0015 A69-10922

Hypoxia exposure effect on RNA synthesis in rat anterior pituitary cultured in vitro

01 p0015 A69-10923

Rats on casein, soybean and Chlorella diets for protein source noting soybean diet produced no appreciable changes in intestinal flora

02 p0197 A69-11490

Chronic gamma radiation biological damage in rats exposed to maximum nonlethal to minimum lethal doses for various periods

02 p0197 A69-11494

Cerebellar cortex function disorders of rats subjected to long acceleration under weak anesthesia

02 p0198 A69-11504

Hypoxia effects on vestibular analyzer function of rats in pressure chambers at simulated altitudes from 11,000 to 12,000 m

02 p0198 A69-11506

P32 distribution in protein of blood serum, liver and brains of rats bombarded with high energy protons

02 p0198 A69-11507

Nutritive value of protein from discolored algae biomasses on groups of rats kept on algae biomass, casein and soybean diets

02 p0198 A69-11510

Lactodehydrogenase activity and LDG isoenzymes ratio in various tissues of rats during exposure to prolonged hypoxia at simulated heights

02 p0199 A69-11982

Steroid hormones effect on nervous system and behavior from data on gonadectomized rats and monkeys treated with testosterone propionate

03 p0375 A69-13551

Critical body temperature for intracranial self stimulation in white rats

03 p0375 A69-13897

Xenon, krypton, nitrogen and nitrous oxide effect on respiration rate of rat liver slices at various oxygen partial pressures

03 p0375 A69-14069

White rat physiological processes while maintained on hypothermic cardiopulmonary bypass with small membrane type heart-lung machines

05 p0708 A69-15971

Electron microscopic changes in lungs of rats after repeated exposure to pure oxygen

05 p0709 A69-16514

Protein free diets effects on rat intestinal microflora, noting decrease in lactic acid bacteria and increase in spore forming bacteria

05 p0709 A69-16516

Thyroid gland role in resistance and myoglobin content of skeletal muscles of flat land and high altitude acclimatized white rats

05 p0709 A69-16517

Bone marrow cell division disturbance in rats after proton irradiation

07 p1064 A69-18973

Algae diet more effective than soya-protein diet in recovering metabolic processes in protein deficient white rats

07 p1065 A69-18977

Acetate carbon 14 utilization in centrifuged rats, analyzing metabolism by measuring plasma glucose, FFA and lipids synthesis

07 p1067 A69-19429

Prolonged exposure of rats to oxygen concentrations studied for effects on organisms

08 p1262 A69-19831

Hypokinesia effects on rats noting body and organ weights, liver glycogen and N content and tissue proteolysis of skeletal muscles

08 p1262 A69-19928

Prolonged hypokinesia effects on white rats resistance to convulsions induced by high altitude simulation

08 p1262 A69-19929

Adrenal epinephrine and phenylethanolamine n-methyl transferase /PNMT/ activity in rat bearing transplantable pituitary tumor

08 p1263 A69-20374

Regional uptake of melanotin from blood or cerebrospinal fluid by rat brain

09 p1444 A69-21466

Acclimation to altitude hypoxia and duration of resistance to muscular effort in white Wistar rats on treadmill

09 p1445 A69-22725

Metabolic relationship between hypoxia and hypoglycemia in Wistar rats, noting oxygen consumption, energy expenditure under insulin and hydrogen partial pressure decrease effect

09 p1445 A69-22727

Glucose, lactate, free fatty acids, hepatic glycogen and endocrine activity in fasting hibernating dormouse and rat in deep hypothermia

10 p1642 A69-23118

Hypothermia induced alterations in biochemical processes studied with isolated rat liver perfused at low temperature

10 p1642 A69-23119

Response rates of rats to periodic shocking for food reinforcement with added clock cue stimuli

10 p1644 A69-23304

Rats sensitivity to accelerations found dependent on excitation-inhibition ratio in central nervous system and hypophyseal-adrenal system reactions during acoustic excitation

10 p1645 A69-23497

Rats tolerance to impact accelerations from blood enzyme activity providing safety limits for living organisms

10 p1645 A69-23500

Glycolysis rate and lactic acid content in rats myocardium during adaptation to hypoxia, using pressure chamber

10 p1645 A69-23501

Amino alcohol regenerable absorbers of carbon dioxides toxicological characteristics, discussing absorbing ability in rats

10 p1646 A69-23502

Pathological changes in respiratory and cardiovascular systems of white rats due to various levels of hyperoxia

10 p1646 A69-23577

Oxidative and dephosphorylating enzymes and esterases in rat and squirrel monkey cerebral cortexes, noting neuron activity

12 p2018 A69-25773

Transensor implantation, sham implantation, no implantation and lighting effects on rat body composition, noting fat and water content

12 p2020 A69-26557

Protective effect of hydrocortisone in rats observed during hypoxia

13 p2210 A69-27800

Gravity preference tests on rats subjected to simulated Aerobee 150 A rocket launching and flight in ground based spiral centrifuge

13 p2213 A69-28090

Altitude effects on body chilling rate in rats noting hypoxia role in inducing hypothermia

13 p2210 A69-28532

High altitude environmental effects on adrenal glands and hypothalamic neurosecretion in rats

13 p2211 A69-28615

Calcium isotopes tracer migration in caged rats in metabolism study

13 p2212 A69-28618

Fluorides or AMOX increased concentrations effect on thyroid growth rate, uptake and adrenal weight in rats

14 p2406 A69-29291

Social and visual isolation effect on rat blood pressure, pulse pressure, heart rate, behavior and response to epinephrine

14 p2407 A69-29296

Histological changes in rat skin after 13 Mev proton irradiation, evaluating biopsies in tissue culture

14 p2407 A69-29299

Decreased antidiuretic activity measured in blood of chronically centrifuged rats, noting role of antidiuretic hormone /ADH/

14 p2407 A69-29301

Food intake changes of female rats in response to changes in energy balance, discussing steroids as physiological tracer

15 p2555 A69-30693

Constant light/darkness effects on stress response rhythm of hypothalamic-pituitary-adrenocortical system in female rats

15 p2556 A69-31330

Diurnal variations in radiation sensitivity of mice and rats to irradiation with median lethal doses, noting sine curve survival function

15 p2557 A69-31458

White rats diet containing alcohol-soluble fraction of Chlorella and Scenedesmus biomass, noting changes in adrenal cortex and renal glomerus

17 p2906 A69-32930

Antihypoxic preparations protective effect on white mice and rats subjected to gravitational accelerations

17 p2906 A69-32931

Vestibular reactions in rats under hypothermal conditions by measuring postrotatory nystagmus beats number and duration, respiration rates and rectal temperature

17 p2906 A69-32934

Drug action on decompression sickness in rats compared with action on nitrogen narcosis and oxygen toxicity

17 p2913 A69-33172

Electrode stimulated hypothalamic drinking in rats compared with drinking induced by water deprivation, noting difference in consumption

17 p2910 A69-33750

Hepatic tyrosine transaminase rhythm in rats under various conditions of lighting, food consumption and dietary protein content

17 p2910 A69-33755

Ventromedial hypothalamic /VMH/ lesions, body weight and food consumption changes in male and female rats, observing differential effects

17 p2910 A69-33756

Electron microscopic changes in lungs of rats after repeated exposure to pure oxygen

18 p3096 A69-34733

Protein free diets effects on rat intestinal microflora, noting decrease in lactic acid bacteria and increase in spore forming bacteria

18 p3096 A69-34735

Thyroid gland role in resistance and myoglobin content of skeletal muscles of flat land and high altitude acclimatized white rats

18 p3096 A69-34736

Acetate-2-C 14 conversion to C 14 carbon dioxide and C 14 fatty acids in rats with 2/3 of liver removed
19 p3257 A69-35976

Environmental crowding effect on individual and group behavior in rat colony, using implanted passive resonant circuits for identification and passage information
19 p3257 A69-36243

Norepinephrine, dinitrophenol and dicumaryl effect on brown adipose tissue of cold exposed rats
19 p3258 A69-36294

Rats locomotion in centrifugally generated gravity fields determined for in-space behavioral studies of earth organisms gravity requirements
19 p3263 A69-36457

Bone marrow cell division disturbance in rats after proton irradiation
20 p3479 A69-38221

Algae soil-protein diet more effective in recovering metabolic processes in protein deficient white rats
20 p3479 A69-38225

Lateral and ventromedial hypothalamic areas functional interaction in rats, noting bilateral cuts producing hyperphagia
21 p3650 A69-38322

Exercise effects on hepatic cholesterol of rats on diets high in saturated or unsaturated fats
21 p3653 A69-38903

Platelet role in decompression sickness pathology from experiments upon rats subjected to decompression after injection of antiplatelet serum
21 p3655 A69-38918

Intraperitoneal high polymer DNA administration normalizing effect on DNA and RNA contents in liver, spleen and intestinal mucosa of white rats exposed to X rays
21 p3657 A69-39050

Enzyme activity changes in liver, heart and cerebrum of X ray exposed rats and rabbits, noting individual enzyme differences in same X rayed organ
21 p3658 A69-39054

Successive X ray doses effect on oxidative phosphorylation of vitamin B 1 in white rats liver tissue ultrastructure during and after irradiation, establishing thiamine biosynthesis suppression
21 p3658 A69-39056

White rats hyperglycemia during blood sugar changes following single X ray dose, indicating increased sugar benefit in radiation damage treatment
21 p3658 A69-39057

Pathological effects of single 120 Mev proton doses on rats blood in rotating cylinder, discussing leukopenia and benign and malignant tumors development
21 p3658 A69-39058

Histological changes in internal organs of rats after exposure to 400 r fast neutron dose, showing destructive processes followed by compensation reactions of cellular proliferation
21 p3659 A69-39062

Pathological changes in solar ganglia cells of white rats following X ray exposure, using electron microscope
21 p3659 A69-39064

Hyperoxia and pulmonary surfactant washout in pulmonary compliance measurements of rats subjected to 100 percent diatomic oxygen before asphyxial death
21 p3659 A69-39066

Rat dental pulp hemorrhages following acute hypoxia from exposure to decompression chambers, atmospheric pressure variations or high acceleration
21 p3661 A69-39276

Rats adrenal corticosterone concentrations changes in response to ACTH, determining response sensitivity dependence on time after hypophysectomy
22 p3870 A69-39871

Electrical stimulation effect on drive specificity in lateral hypothalamus area of sated rat, suggesting fallacy in previous conclusion concerning appetite
22 p3876 A69-40269

Nutritive value of mycelium of *Cantharellus cibarius* mushroom on rats compared with eggs and fresh and sour milk
22 p3892 A69-40273

Rat survival rate after prolonged gradually decreased body temperature without motion restraint or kept in fixed position
22 p3877 A69-40278

Cerebellar cortex reactions to sciatic nerve stimulation in rats under transverse accelerations in centrifuge
22 p3877 A69-40279

Positive effect of shielding and cystamin administration on tonic and evacuator functions of rats gastrointestinal tract after gamma irradiation
22 p3877 A69-40285

Protein rates and RNA synthesis in cerebra of rats analyzed as factor of high altitude hypoxia adaptation
22 p3886 A69-41122

Anoxia effects on leucine-super 3 H incorporation by submandibular gland cells of neonatal rats, discussing cytoplasmic proteins synthesis impairment
22 p3887 A69-41195

Mechanical vibrations and noise effects on acetylcholine concentration, esterase activity and synthesis ability in rat brain
23 p4079 A69-41381

Regression process in acetylcholine level in rats after mechanical vibrations and noise exposure
23 p4079 A69-41382

Physical training effects under normal atmospheric pressure on high altitude hypoxia and acceleration resistance in rats, including survival times
23 p4079 A69-41383

Compensatory hypertrophy effects on adrenal phenylethanolamine n-methyl transferase /PNMT/ activity in rats
23 p4080 A69-41404

Enzymatic processes of glucose metabolism in immature rats lymphatic tissues during exercise-induced elevated corticosteroid secretion
23 p4080 A69-41405

Cerebral and retinal capillary permeability to ions in rats analyzed by electron microscope using Prussian blue reaction
23 p4081 A69-41433

Air and saline P-V curves of rat lungs after hyperoxia, comparing hyperoxia effects to surfactant washout on pulmonary compliance
23 p4081 A69-41440

Cytoplasmic protein synthesis mechanism using rats heart-lung preparation with precise hemodynamic parameters control, noting variance with change in cardiac work level
23 p4083 A69-41456

Tension effects on amino acid incorporation rate into proteins of cross-striated muscles of rats
23 p4083 A69-41458

Laser pulse effects on bones of rats, observing metabolic deviations in Ca 45 uptake
23 p4101 A69-41464

Exhaustion time extension in rats by altitude acclimation, noting adaptation loss resulting from physical exercise discontinuation
23 p4086 A69-41787

Pituitary-adrenocortical axis of rats in oxygen atmosphere at low pressure, finding depressed norepinephrine excretion
23 p4087 A69-41790

Increased oxygen tension adaptation and effects on adrenocortical and sympatho-adreno-medullary activity in rats, indicating toxic conversion of epinephrine to indoles
23 p4087 A69-41791

Space cabin environment simulation effects on resistance to infection caused by pneumonia and influenza virus in rats
23 p4108 A69-41832

Electrical self stimulation adaptability of hypothalamus or instrumental self reinforcing reaction in rats using skinner box technique
23 p4091 A69-42052

Unisensory and multisensory signal processing in cortical and brain stem regions of albino rat by electronic averaging and time histogram techniques
23 p4092 A69-42055

Spontaneous rhythmical activity and mean vascular tone dependence in isolated helical rat aorta strips on extracellular concentration of noradrenalin
23 p4093 A69-42069

Portal blood pressure decrease effects on diuresis in unanesthetized rats, discussing osmotic diuresis
23 p4094 A69-42074

Rodent swimming and treadmill training effect on capacity of mitochondrial fraction from hind limb muscles to oxidize pyruvate triples
23 p4095 A69-42084

Training effect on fast muscle isometric contraction in rats, discussing mechanical characteristics
23 p4097 A69-42095

Neodymium laser radiation effect on electrical and histomorphological properties of liver in rats and hamsters
23 p4111 A69-42344

Urine osmolality of centrifuged rats compared with ad libitum or pair-fed control animals, indicating enhanced free water excretion and antidiuretic hormone involvement
24 p4262 A69-42904

Noise level effects on pharmacological effectiveness of centrally acting drugs in rats
24 p4262 A69-42947

Continuous noise level effects on stabilized escape conditioning in male albino rats
24 p4262 A69-42948

Stillbirth and neonatal death in stressed rats exposed to mild and acute gravitational loads in automobile ride and aircraft flight
24 p4266 A69-43381

Radioisotopic determination of haemodynamic and bioelectric disturbances of rat striated muscles subjected to acceleration and hypokinesia
24 p4268 A69-43409

Hyperoxia and hypoxia effects on mitotic activity in regenerating and normal rat liver exposed to environmental conditions
24 p4269 A69-43565

RAWINSONDES

Middle stratospheric diurnal temperature variation based on model eliminating radiation error of rawinsonde
03 p0461 A69-13344

Rawin systems for upper air measurements of wind and thermodynamic parameters, using balloon-borne radiosonde
07 p1057 A69-19581

Clear air turbulence computerized analysis and forecast over U.S. using upper air rawinsondes measurements
22 p3976 A69-39927

Simultaneous lower atmosphere clear air turbulence analysis by multiwavelength radar, jet aircraft and special rawinsondes
24 p4342 A69-42894

RAY TRACING

Radar cross sections for arbitrary bodies calculated with computerized ray optics method taking into account depolarization
02 p0209 A69-12332

Antarctic spread F irregularities, examining models and performing ray tracing
04 p0595 A69-15439

Ray tracing of Z-mode in tilted layer ionosphere to explain Z-mode echoes in ionograms
05 p0758 A69-16412

Nonvertical propagation effects on high altitude topside ionosphere sounder data reduction, using ray tracing
07 p1124 A69-18838

Formulas for ray paths in ionized layers with application to oblique ionograms and duct modes
07 p1078 A69-18913

Ray-optical description for point source excited surface waves in stratified anisotropic media
07 p1079 A69-18918

Earth dipole magnetic field effect on bearing deviation in HF transionospheric propagation analyzed by computer ray tracing
07 p1086 A69-19224

Ray path geometry derived by Poynting vector to calculate surface fields due to creeping waves in sphere planes
08 p1274 A69-20046

Statistical characteristics of transverse shifts of ray directions in turbulent atmosphere for arbitrary wave parameter values
10 p1657 A69-23942

Ray tracing application to evaluating aberrations produced by Fresnel holograms for optimizing design of aplanatic lens holography system
11 p1885 A69-24848

Propagated ray paths plotted as functions of frequency and launch angle to predict signal dispersions
11 p1837 A69-25003

Ray tracing techniques applied to internal gravity waves in fluid with spatially varying mean flows
12 p2067 A69-26345

Ionograms in vertical depletion duct in horizontally stratified isotropically refractive plasma, considering vertical propagation and ray paths traces dependence on electron concentration
14 p2434 A69-28945

Polar aurora rays mean length diurnal variations determined from photographic and visual observations in Tiksi bay
14 p2437 A69-29077

Stellar image vibration amplitude dependence on trace direction by comparison with traces of moving satellites
15 p2647 A69-30166

Differential equations as Hamiltonian function for signal path, travel time and frequency variation in anisotropic nonpermanent absorbing medium
17 p2924 A69-33836

Fokker-Planck equation applied to probability density for finding rays larger than correlation distance during propagation in random medium
17 p2926 A69-33854

LF radio waves propagation in ionosphere by combining ray tracing in complex space with geometrical theory of diffraction, including diffraction by earth
17 p2928 A69-33866

Computer quadratic method of evaluating ray propagation data for estimating inhomogeneous media properties
18 p3172 A69-34667

Propagation characteristic model study of kinked Z trace observed on topside ionograms and explained by magnetoionic theory
20 p3531 A69-37893

Ray theory of radial propagation by two variation techniques of phase paths
21 p3675 A69-39279

Diffuse coronal emission observation during total eclipse of February 1961 near solar prominences and polar ray form investigation in northern part of corona
22 p4002 A69-40002

Acoustical ray tracing in horizontally layered and vertically sectioned atmosphere on digital computer using shifting Cartesian coordinate system
23 p4154 A69-41532

Solar grazing ray absorption calculated by tracing through earth atmosphere, noting extinction for arbitrary ozone and aerosol profile
24 p4350 A69-43013

RAYLEIGH DISTRIBUTION

Energy gain during diversity reception in presence of random noise calculated, considering signal and noise amplitudes Rayleigh fluctuations
11 p1835 A69-24968

RAYLEIGH EQUATIONS

Difference method for parabolic differential equations solution for Rayleigh boundary layer in dissociating gas, using integral estimates to determine stability
18 p3124 A69-35295

RAYLEIGH NUMBER

Relation between Rayleigh and dynamic Richardson numbers in atmospheric boundary layer in presence of cellular convection
09 p1491 A69-22709

Model evolution of flow in fluid layer suddenly heated from below at Rayleigh number convection sufficient for turbulence
11 p1874 A69-25351

Wavelength of convective motions, discussing effects of lid heat conductivity on Rayleigh number
11 p2003 A69-25354

Dependence of convection in planetary interiors upon magnitude of Rayleigh number for rigid and free surfaces
12 p2155 A69-26208

Cellular convection suppression by parallel vertical thermally conducting walls inserted into bottom-heated fluid, analyzing effect on critical Rayleigh number
13 p2374 A69-27782

Benard convective flow as function of Rayleigh and Taylor numbers in thin variable rotating silicone oil layer determined by flow photographs
13 p2377 A69-28172

Two dimensional laminar convection cells asymptotic behavior for high Rayleigh number, discussing Robinson and Pillow models for fluid between horizontal plates heated from below
16 p2767 A69-31588

Relation between Rayleigh and dynamic Richardson numbers in atmospheric boundary layer in presence of cellular convection
16 p2808 A69-32488

Thermal convection in horizontal fluid layer heated from below, with zero shear boundaries above and below, noting critical Rayleigh number measured value
20 p3518 A69-38234

Electrohydrodynamic Rayleigh-Taylor bulk instability in initially static stratified fluid under electric stress
20 p3578 A69-38235

RAYLEIGH-RITZ METHOD

Convergence of Rayleigh-Ritz approximations to solution of elliptic boundary value problem applied to subsonic airfoil problem for 2D steady isentropic irrotational flow
03 p0361 A69-12846

Rayleigh-Ritz finite element method for approximate solution of nonlinear energy functional describing large

deflection bending behavior of uniform beam under point loads
05 p0833 A69-15711

Large deflection behavior of shallow circular arch subjected to vertical point load by nonlinear Rayleigh-Ritz finite element method, discussing deformation path
08 p1411 A69-20140

Higher order Rayleigh-Ritz approximations to eigenvalues and eigenfunctions of elliptic boundary value problem
09 p1534 A69-22798

Modified Rayleigh-Ritz method for prediction of stress concentration in elastostatic problems for elastic continua, noting plate bending
11 p1969 A69-24413

Free vibrations of laminated anisotropic rectangular plates with clamped edges analyzed by Rayleigh-Ritz energy method
13 p2371 A69-28673

Finite element analysis of nonlinear elastoplastic material-geometric behavior problems, describing computer program and incremental stiffness matrices
18 p3219 A69-34664

Finite element techniques of structural analysis for missile and space structures, including Apollo computerized analysis and structural optimization
19 p3438 A69-36324

Convergence of Rayleigh-Ritz approximations for variational problem, considering functionals of scalar valued function
24 p4339 A69-42793

RAYLEIGH SCATTERING

Monostatic radar cross section of simple shapes estimated using optics and Rayleigh region approximation with emphasis on multiple reflection
03 p0384 A69-12905

Bistatic radar cross sections of simple shapes calculated based on optics and resonance region, noting forward, nonforward and Rayleigh scattering
03 p0384 A69-12906

Scattering from coated absorbing conducting bodies, considering flat plane and curved surfaces in Rayleigh region
03 p0384 A69-12908

Stokes and Rayleigh layer formation during solid body rotation of semiinfinite fluid and infinite disk
03 p0417 A69-13797

Directional intensity of radiation emerging from top and bottom of Rayleigh scattering atmosphere
03 p0426 A69-14026

Rayleigh scattering from circularly birefringent media generalized for medium with no preferred internal axes
04 p0609 A69-14291

Flux equivalences of reflected and transmitted radiation among Rayleigh, isotropic and other scattering models
04 p0687 A69-15281

Rayleigh scattering cross sections for He, C, N and O compared with corresponding absorption coefficients, noting opacity of H deficient stars
06 p1002 A69-17319

Rocket-borne Rayleigh scattering instrumentation to measure atmospheric density, discussing instrumentation and flight results
06 p0927 A69-17698

Depolarized Rayleigh line widths measured for carbon dioxide, nitrogen and hydrogen, using measurements to calculate reorientation cross sections [IEEE PAPER B-11]
07 p1157 A69-19485

Radiation field at optical depths within plane parallel Rayleigh scattering atmosphere subjected to generalized free surface boundary conditions
09 p1606 A69-22423

Atmospheric extinction function in Chile by using photoelectric spectrum scans, observing neutral component, Rayleigh scattering and ozone absorption variations
10 p1777 A69-23386

Jupiter polarization wavelength dependence noted in observations of 5 seconds diameter regions near poles and equator related to Rayleigh- Chandrasekhar molecular scattering theory
13 p2348 A69-27805

Light scattering in single component systems near critical point analyzed by critical phenomena classical theory and Rayleigh theory
14 p2485 A69-28995

Rayleigh assumption validity for wave scattering by analytic periodic surface predicated on solutions analytic continuation across boundary, discussing Green function role
15 p2652 A69-30673

Wavelength dependence of polarization of sunlight scattered by Venus atmosphere, including Rayleigh and Mie scattering mechanisms
16 p2860 A69-32237

Plane electromagnetic wave scattering by motion of small ellipsoid in vacuum, noting total scattering and radar cross sections dependence on ellipsoid velocity
18 p3105 A69-35485

Radiation scattering by thick planetary atmosphere according to Rayleigh law, considering luminance variation and absorption ray polarization
23 p4213 A69-41698

Book on new concepts in radars covering ideal reception, moving targets, autocorrelation, SNR, amplitude distribution, clutter, etc
24 p4283 A69-43168

RAYLEIGH WAVES

Incipient stress corrosion damage detection in aluminum alloys, using Rayleigh wave attenuation
12 p2114 A69-26306

Book on solid bodies collision theory covering elastic bodies with ruled surfaces, dynamic effects associated with Rayleigh surface waves, thermodynamic effects, etc
18 p3210 A69-34259

Forced recombination scattering of light on Rayleigh polarization waves in isotropic solid body with small elastooptical constants
21 p3770 A69-38963

RRE

U RELATIVE BIOLOGICAL EFFECTIVENESS [RBE]

RC CIRCUITS

Equivalent circuits for transient characteristics approximation of distributed RC circuits
01 p0046 A69-10779

Inverse Laplace transform determination method for periodic functions applied to rectangular pulse train and rectified sine wave
02 p0271 A69-11983

Analysis and design of synchronous filter compatible with microelectronics requirements, switching N monolithic RC thin film devices to signal source of resistance
03 p0403 A69-13206

Active RC low pass filters sensitivity to component changes, discussing effect of below minimum limit value
04 p0578 A69-15070

Autocorrelation function distortion determined for Barker signal passing through linear system and RC filter, noting passband influence on function shape
05 p0720 A69-16443

3-terminal gyrator circuits using operational amplifiers, noting exact cancellation of negative by positive resistance and unattainability of LF unstable modes
06 p0893 A69-16936

RC converter filters and delay lines by expanding transfer function into series of components
07 p1113 A69-19677

Delta functions spectrum in reciprocal time domain for LC and RC structures due to impulse response in distributed parameters
09 p1471 A69-21327

Transient analysis for uniform RC structures using impulse excitations in open and short circuit configurations
09 p1471 A69-21328

Precision trimmed RC active networks for high selectivity microelectronic filter fabrication for frequency division multiplex applications
09 p1466 A69-22452

Glass covered microwire technology to realize RC element, analyzing equivalent element errors by simulating irrational transfer functions
09 p1476 A69-22677

Multiple loop feedback systems synthesis utilizing extended node introduction synthesis theory, considering filter response functions characteristics
10 p1667 A69-24037

RC circuit with variable time constant using variable resistor
10 p1667 A69-24046

Rectangular RC distributed circuits with shaped electrodes, analyzing short circuit admittance parameters
11 p1858 A69-24938

Load admittance effect on low pass voltage transfer characteristics of RC lines, analyzing shaped lines at open circuit under terminated conditions
11 p1859 A69-24939

Multivibrator circuit for generation of oscillations with frequency stability against transistor ambient temperature changes

12 p2036 A69-25919

High sensitivity LF and HF frequency deviation meter with resonant RC amplifiers for frequency discrimination and filtering

12 p2038 A69-26337

Transistorized LF-HF RC filters and current amplifiers design, exhibiting polynomial type characteristics

12 p2040 A69-26488

Autocorrelation function distortion determined for Barker signal passing through linear system and RC filter, noting passband influence on function shape

16 p2753 A69-32475

Multiloop feedback in active distributed RC networks for low parameter sensitivity with low amplifier gain compared to single loop circuits

18 p3111 A69-34679

Statistical analysis of operation of precision electric spark machine servosystems with RC generator based on working pulse peak voltage distribution

23 p4168 A69-41307

Distributed RC networks combined with lumped passive and active elements to produce distributed-lumped-active (DLA) networks for filter requirements

23 p4144 A69-41401

RDX

Slowly exploding wires for igniting self sustaining deflagrations in PETN, RDX, HMX and tetryl, comparing circuit parameters for detonation initiation

01 p0141 A69-10678

REACTANCE

Parasitic reactance disturbing attenuation and return loss of reactance filters, discussing correction of numerator polynomial of characteristic function

08 p1283 A69-20128

Equivalent circuit synthesis with six reactances-two terminal network bridges

08 p1295 A69-21166

Antenna reactance from sounding rocket in ionosphere, showing variations relationship to rocket spin period

22 p3934 A69-39964

REACTION CONTROL

Sublimation solid reaction control, discussing propellants, nozzle performance, sublimation area, power, pressure drop, response and valueless design [AIAA PAPER 68-516]

04 p0552 A69-15322

REACTION JET ATTITUDE CONTROL

U ATTITUDE CONTROL

U JET THRUST

REACTION JETS

U JET FLOW

U JET THRUST

REACTION KINETICS

Resonance theory of thermomolecular recombination kinetics applied to hydrogen atoms

01 p0122 A69-10034

Diffusional, thermal-diffusional and thermal fluxes in multicomponent flames, discussing flame structure and reaction kinetics

01 p0175 A69-10144

Glycolysis rate role in regulation of substrate inhibition of dehydrogenases

01 p0015 A69-10931

Refractory metals interactions with gases in vacuum and inert gas environment, noting temperature and pressure effects on reactions, extent and kinetics

01 p0099 A69-11042

Reaction rate and mechanism for low temperature reaction between lithium hydride and liquid ammonia, noting chemisorbed ammonia dissociation at interface

01 p0025 A69-11285

Diacytlenic burning and spontaneous combustion regularities, determining reaction kinetics at moderate temperature

02 p0351 A69-11981

Adiabatic stirred reactor, discussing steady state nonlinear equations of reactant gases combustion

02 p0352 A69-12316

Explosion limits in hydrogen-oxygen reaction measured in diffusion regime, giving rate constant of branching step

02 p0353 A69-12319

Reactions kinetics contribution to nonequilibrium recombination occurring in supersonic nozzle flow of combustion products of hydrogen in air

02 p0353 A69-12488

Chain and branched halogen-hydrogen reactions kinetic analysis for developing chemical laser with radiation energy weakly dependent on pumping energy

02 p0259 A69-12645

Dissociative velocity rates of oxygen and ozone in ionosphere obtained by exponential approximation for molecular concentration distribution

02 p0246 A69-12769

Chemical reaction scheme effect on hot zone structure of hydrogen-oxygen diffusion flame, considering influence of hydroxyl radical

03 p0531 A69-12895

Subcritical crack growth kinetics in high strength materials, suggesting growth rate control by reaction rate or diffusion

03 p0449 A69-13874

Combination rate constants for H-F-O reactions, discussing expressions and relative efficiencies with Argon as third body

04 p0646 A69-14743

Hydrazine decomposition in glow discharge, analyzing emission spectra and threshold level of decomposition by gas chromatography

04 p0646 A69-14860

Thermal reaction kinetics of pyrolytic products of proline, leucine, arginine and lysine in aqueous solution

05 p0716 A69-15627

Equations describing chemical kinetics and conservation law derived for ionization relaxation processes behind shock wave front in air

05 p0746 A69-15891

Austenitic Fe-Ti alloys sulfur solubility and internal sulfidation rate computed, noting stronger Ti-S interaction with temperature decrease and sulfur diffusion role

06 p0942 A69-17226

Chain reaction theory defining kinetic mechanism giving rise to explosion, noting conservation of free valences and formation and disappearance of radicals

06 p1031 A69-17415

Slow oxidation and self ignition in gaseous phase, discussing cold flames and interpretation of experimental data

06 p1031 A69-17416

Flame establishment and propagation in gas phase taking into account aerodynamic and chemical kinetics

06 p1031 A69-17418

Liquid phase radical oxidation with intermediate and end products in same phase, discussing products, hydroperoxidation and liquid systems explosiveness

06 p1032 A69-17425

Reaction rates coefficients of oxygen ions with molecular oxygen and nitrogen in nighttime F region over Moscow based on loss coefficient estimate

06 p0919 A69-17724

Activation energies in baffle stabilized flame deduced from reaction zone using gas chromatography

06 p1035 A69-17930

Supersonic molecular beam sampling system for coupling mass spectrometer to alkali metal-air reacting flow system in kinetics study, noting gas dynamic effects

[AIAA PAPER 69-94]

06 p0930 A69-18099

Chemical kinetic model for hydrocarbon fuels combustion and application to multidimensional finite difference mixing analyses in hypersonic engines and nozzles

[AIAA PAPER 69-86]

06 p1037 A69-18119

Solid propellant burning rates from condensed phase decomposition kinetics, discussing kinetic rates of thermal decomposition

[AIAA PAPER 69-145]

06 p1039 A69-18182

Finite kinetics calculations by computer programs to generate reactions among prescribed reactants

[WSCIPAPER 68-54]

07 p1072 A69-18314

Chemical kinetic numerical integration techniques applied to equations for chemical relaxation

[WSCIPAPER 68-45]

07 p1073 A69-18315

Adiabatic kinetic calculations of chemical additive effects on ignition delay of hydrogen-oxygen-argon gas mixtures

[WSCIPAPER 68-52]

07 p1239 A69-18316

Kinetics calculations in shock tube data interpretation, determining elementary rate constants and complex reaction mechanism

[WSCIPAPER 68-50]

07 p1073 A69-18319

Chemical kinetic data evaluation, discussing compilation, production and publication programs, material content and arrangement and reliability estimates

[WSCIPAPER 68-47]

07 p1073 A69-18320

Gas dynamics effects of hot spot in explosive gas mixture using kinetic rate equations, discussing composition, enthalpy and time dependence

[WSCIPAPER 68-53]

07 p1240 A69-18322

Reaction kinetics package for pyrolysis and combustion of aliphatic hydrocarbon molecule, considering reaction rates definition

[WSCIPAPER 68-37]

07 p1073 A69-18353

Composite solid propellants ignition response measured by imbedded hot wires indicating distributed reaction

[WSCIPAPER 68-36]

07 p1201 A69-18354

Ignition time of methane and acetylene, considering concentration and thermodynamic properties during reaction

[WSCIPAPER 68-41]

07 p1240 A69-18356

Nitrogen ion number density time dependence by mass spectrometric probing of decaying nitrogen plasmas, noting molecular ion production by colliding metastable nitrogen molecules

07 p1184 A69-1914

Variational solution of linearized molecular chemical-kinetic Boltzmann equation, discussing perturbation of Maxwell distribution, nonequilibrium correction to reaction rate and activation energy

07 p1185 A69-19301

Two body rate coefficients for charge transfer reactions of nitrogen, oxygen and NO positive ions to Na atoms measured using flowing afterglow system

07 p1185 A69-19303

Oxidation kinetics of niobium titanium alloy in air and oxygen at 1000 C, analyzing nitrogen and pressure effects

08 p1331 A69-20193

Oxidation kinetics of niobium titanium alloy in air and oxygen between 650 and 1000 C, analyzing activation energies and nitrogen effects

08 p1331 A69-20194

Phase identification and microstructural effects of gaseous nitrogen reaction with binary Nb-Ti alloys at 1000 C

08 p1331 A69-20195

Ammonium perchlorate decomposition kinetics at high temperatures by measuring loss of weight in samples and gas evolution

08 p1375 A69-20339

Platinum electrode study of electrochemical oxygen reduction in nonaqueous media, including kinetic effects of different water concentration levels

08 p1268 A69-20361

Cobalt chromium alloys high temperature oxidation kinetics, discussing thermographic study of oxidation rate and oxygen pressure role

[ECS PAPER 413]

08 p1332 A69-20364

Monograph on kinetic study of fast gas reactions with shock waves covering thermal decomposition of nitrous oxide, hydrazine tetrafluoride and nitrogen tetrafluoride

08 p1304 A69-20707

Adsorption kinetics of hydrocarbon oxidation on platinum electrode

08 p1268 A69-21052

General expressions derived for numerical stellar-interior calculations for nuclear reaction rates, emphasizing density-temperature combinations

09 p1606 A69-22418

Nozzle flow temperature patterns of relaxing combustion gases compared at different temperatures and pressures, using kinetic-chemical calculations

[DVL-896]

10 p1809 A69-23644

Critical conditions in spherical reacting mass, noting oscillatory nature of critical parameters in truncated Arrhenius rate on basis of nontruncated form

11 p1998 A69-24480

Liquid rocket propellants chemical reactions identification during kinetic expansion

[WSCIPAPER 68-7]

11 p1942 A69-24906

Chemical reaction rate data for propellant systems containing boron or aluminum and hydrogen, chlorine and fluorine, based on finite kinetics expansions

[AIAA PAPER 69-182]

11 p1940 A69-24907

Planning, instrumentation and analysis of shock tube experiments in chemical kinetics, noting gas phase reaction rates at high temperatures

11 p1863 A69-25015

Combustion chemical reactions kinetics of gaseous phase systems, discussing temperature, reaction rates extrapolation, hydrogen and hydrocarbons

11 p2000 A69-25185

Combustion mechanism of condensed inflammable systems such as gunpowder and other explosives, discussing combustion stability

11 p2000 A69-25187

Ion-molecule reaction kinetics in nitrogen-hydrogen mixtures using ion cyclotron resonance

12 p2131 A69-25985

Annealing effects on titanium oxidation kinetics, indicating no relation between oxide formation and diffusion anisotropy of oxygen

12 p2112 A69-26039

Desorption kinetics of atomic and oxide phases, analyzing composition of surface film formed from W and Mo single crystals interaction with oxygen
12 p2026 A69-26115

Ruby and neodymium glass traveling wave laser free generation spectra kinetics, noting mode transitions as function of pumping levels
13 p2271 A69-27655

Extinction kinetics of monopropellant droplet burning in inert gas reservoir with atmospheric temperature lower than adiabatic combustion temperature
13 p2378 A69-28250

HNO role in hydrogen-NO reaction rate data reexamined by numerical integration of governing differential equations
13 p2218 A69-28457

Neutral gas ionization in lower ionosphere, discussing physicochemical reactions, recombination coefficients, equilibrium processes, etc
13 p2255 A69-28540

Reaction kinetics between hydrazine and esters in benzene solution at 55 C, using amides as catalytic agents
14 p2409 A69-29033

Carbon dioxide dissociation by electron impact, determining reaction rate in positive column of DC glow discharge
14 p2488 A69-29095

Vacuum thermal decomposition of molybdenum sesquisulfide into metallic Mo, discussing reaction kinetics, mass transfer, diffusivity of sulfur gas, etc
14 p2467 A69-29287

Nb-Ta alloys oxidation kinetics at high temperature and structure and composition of oxide films and scale layers, discussing anomaly in oxidation rate temperature dependence
14 p2464 A69-29650

Electron pulse radiolysis of NO, determining absolute yields and rates of formation of nitrogen dioxide and nitrogen trioxide
14 p2410 A69-29928

Advanced liquid fuels and oxidizers development from rocket propulsion reaction principle
16 p2828 A69-31747

Induction period of reactions behind incident shock waves traveling through undiluted high temperature CO and molecular oxygen mixtures, using CO flame spectra
16 p2877 A69-31768

Removal rate of reaction water from fuel cells by diffusion-condensation procedure as function of temperature and electrolyte concentration
16 p2736 A69-32200

Reaction rate constants of ion-molecule interchange reaction as function of temperature, flow velocity, activation energy and constant part of steric factor P
16 p2747 A69-32312

Nitrogen reaction with excess fuel in ramjet engines, noting kinetic limitations in applications
[WSCl PAPER 69-12] 16 p2831 A69-32351

Thermal decomposition behavior of perchlorate oxidizers studied by flash mass thermal analysis for determining propellant combustion kinetics
[WSCl PAPER 69-19] 16 p2832 A69-32357

Medium temperature fuel cells advantages including improved electrochemical reaction kinetics, water and heat removal
16 p2739 A69-32417

Electrochemical oxidation of hydrocarbons on platinum electrode, discussing adsorption kinetics
16 p2740 A69-32423

Collection of articles on ramjets including reaction propulsion, hypersonic inlets, combustion problems, Griffon aircraft, storable liquid fuels, etc
16 p2837 A69-32608

Chemical reactions in compressible turbulent mixing flows, analyzing flow characteristics, rate equation and Reichardt theory
[AIAA PAPER 69-537] 16 p2747 A69-32701

Kinetics of combustion promotion of hydrogen-hydrocarbon mixtures by active particles, free atoms and free radicals using differential equations
17 p3069 A69-33139

Chemical reactions activation energy at high temperature, noting cross section shape role for deducing activation energy from rate data
18 p3099 A69-34443

Criteria to predict flow instabilities triggered by exothermic reaction presence in high temperature reaction kinetic shock tube studies
18 p3116 A69-34462

Kinetics of titanium oxidation in transitional range at high temperatures, showing agreement with oxidation model
18 p3157 A69-35252

Sulfur hexafluoride dissociation in argon at various temperatures and pressures, using shock tube techniques to determine unimolecular parameters
18 p3100 A69-35475

Computer program for numerical integration of chemical reaction rate equations behind steady state hydrogen-oxygen shock wave
19 p3451 A69-36366

Free radicals destruction rates by gamma irradiation at 77 K measured as first order function of dosage, using electron spin resonance spectroscopy
19 p3265 A69-36376

Finite chemical reaction rate detonation wave interaction with rarefaction wave, noting mixture activation energy and heating power influence
19 p3298 A69-36384

Rate coefficient for primary process in removing molecular nitrogen in high vibrational levels from active nitrogen by N atoms
19 p3379 A69-36424

Electron reactivity of one equivalent oxidizing agents at ZnO surface by electrochemical reduction
19 p3392 A69-36731

Ordered sets of Massieu thermodynamic characteristic speeds for reacting gas mixtures relevant to nonequilibrium flow fields compared to Laplacian and Newtonian speeds
19 p3452 A69-36802

Thermal energy rate constants of ion-molecule reactions in gaseous hydrogen, deuterium and HD, using ion cyclotron resonance method
20 p3578 A69-36934

Rate coefficients for chemiluminescent reactions of excited He with N, O, carbon monoxide and dioxide determined from spatial dependence of visible emission
20 p3483 A69-36936

Deactivation rate constants of carbon dioxide vibrationally excited by high temperature collision with carbon dioxide or nitrogen molecules, describing laser apparatus and reaction cells
20 p3578 A69-36937

Resonance theory of thermolecular atomic recombination kinetics based on transition complexes identification as quasi-bound states or orbiting resonances
20 p3579 A69-37345

Niobium carbide formation on graphite from gaseous niobium pentachloride and Ar mixtures, discussing parameters affecting layer growth rate
20 p3566 A69-37367

Ion-molecule reaction rate constants measurement by ion cyclotron resonance, assuming no ion and neutral gas molecules collisions
20 p3579 A69-37495

Molybdenum disilicide oxidation kinetics at various temperatures by thermal conductivity method, determining oxidation rates and activation energy
20 p3567 A69-37780

Carbon monoxide displacement rate of oxygen from combination with oxyhemoglobin solutions from human adult and fetal, horse, goat, dog, cat and rabbit
21 p3650 A69-38384

Ammonium chlorate thermal decomposition by measuring formed noncondensable gas pressure and weight loss in solid state kinetic investigation
21 p3669 A69-38800

Corrosion kinetics in metals using electrochemistry, stressing polarization techniques
21 p3749 A69-39494

Ammonium perchlorate decomposition, discussing high and low temperature reactions, combustion, catalysts and gaseous environment effects
21 p3784 A69-39593

Elemental fluorine reactions with Ni, Cu, Fe, Ti, Be, Al, Zr and Ag, giving reaction rate constants, activation energies, etc
21 p3670 A69-39706

Spectroscopic measurements of weakly ionized Ar plasma premixed with diatomic N in plenum chamber, demonstrating role of competitive reactions for metastable Ar atom
21 p3779 A69-39794

Vibration relaxation time and dissociation rate constant of carbon dioxide in high temperature shock waves, using IR emission
21 p3775 A69-39801

Adsorption kinetics in ternary mixture of nitrogen, methane and hydrogen, using concentration-time/breakthrough/curves measurement on activated coconut shell charcoal
[NAS-NRC PAPER H-4] 22 p3981 A69-40629

Thermodynamic properties of exchange reaction of Ti, Nb, Mo and W disilicides with graphite and pyrographite systems
22 p3970 A69-40638

Doped silver carbonate defect structure and doping effect on reaction kinetics by X rays and electron paramagnetic resonance, finding new crystal structure
22 p3993 A69-40720

Major ions in chemi-ionization of hydrocarbon flames determined for heats of formation by photoionization mass spectrometer
22 p3896 A69-40727

Kinetic processes in gases and plasmas covering molecular transport equations, transport coefficients, chemical reactions as collision processes, etc
23 p4193 A69-41511

Chemical reaction kinetics in high temperature gases in terms of collision theory, discussing gaseous statistics and Boltzmann equation
23 p4113 A69-41518

Macroscopic rate coefficient relation to microscopic chemical reaction cross section, discussing microscopic reversibility and balance
23 p4113 A69-41519

Carbon monoxide dissociation at high temperatures observed spectroscopically, finding complex reaction chain with diatomic C as intermediate
23 p4113 A69-41692

Hydrogen-air reaction kinetics analyzed using standing wave normal shock noting wall effects, ignition delay and recombination
[AIAA PAPER 67-479] 23 p4239 A69-41893

Boron tribromide-oxygen reaction kinetics effects on IC base diffusion uniformity, correlating uniformity with electrical properties
24 p4360 A69-42760

Reaction broadening in hydrogen-oxygen diffusion flame for slow hydrogen dissociation, using matched asymptotic expansions
24 p4408 A69-42920

Molecular vibrational relaxation effect on dissociating airflow behind shock wavefront, giving relations to chemical reaction rates in diffusion approximation
24 p4302 A69-43486

Charring ablator char zone nonequilibrium flow and chemical reaction kinetics as function of temperature, using thermal environment simulator
24 p4409 A69-43512

Prebiological chemical evolution, studying synthesis and degradation rates relationship at primitive environment energy levels
24 p4269 A69-43514

Supersonic flow stability with energy input applied to reaction kinetics of processes in aircraft and rocket combustion chambers
24 p4248 A69-43642

REACTION TIME

Chemical kinetic data evaluation, discussing compilation, production and publication programs, material content and arrangement and reliability estimates
[WSCl PAPER 68-47] 07 p1073 A69-18320

Reaction kinetics package for pyrolysis and combustion of aliphatic hydrocarbon molecule, considering reaction rates definition
[WSCl PAPER 68-37] 07 p1073 A69-18353

Arbitrary human motions coordination in reorganization phases determined during weightlessness for cyclographic analysis of adjustment time
07 p1065 A69-18979

Chromium oxide additions effects on reaction rates decrease during ammonium perchlorate and nitrate combustion
08 p1375 A69-20340

Response time of semiconductor diode from dependence of equivalent capacitance on direct displacement current
08 p1287 A69-20889

Response rates of rats to periodic shocking for food reinforcement with added clock cue stimuli
10 p1644 A69-23304

Psychomotor reaction time and monkeys, myogenic tonus at rest and precision of monkeys during rocket flights along ballistic curve, noting weightlessness effect
10 p1646 A69-23575

Chlorine pentafluoride formation from chlorine in anhydrous hydrogen fluoride in electrochemical cell, noting formation rate
13 p2217 A69-28135

Yttrium effect on rate of thermal decomposition of silver carbonate powder and pressed pellets by isothermogravimetric analysis, examining water vapor, Co 60 gamma radiation and temperature effects
15 p2561 A69-30442

Reaction rate theory for dilatational failure of heterogeneous materials subjected to stress
15 p2710 A69-30813

Accelerate-stop criteria examined from human engineering standpoint, discussing flight simulator study of pilot reaction times for transition to rejected takeoff configuration [AIAA PAPER 69-772] 19 p3244 A69-35650

Ion-molecule reaction rate constants measurement by ion cyclotron resonance, assuming no ion and neutral gas molecules collisions 20 p3579 A69-37495

Arbitrary human motions coordination in reorganization phases determined during weightlessness for cyclographic analysis of adjustment time 20 p3479 A69-38227

Mandrax and barbiturates effects on aircrew reaction time, response time and tracking ability 21 p3661 A69-39274

Sensory auditory and visual signals characteristics effects on human reaction time, noting different results for unilateral and bilateral signal pairs 23 p4083 A69-41454

Propellant ignition delay in contact of condensed fuel with hot reactive gas in shock tube, using graphical method and surface temperature fractional increase 23 p4199 A69-41897

Circadian periodicity of human reaction times tested during normal diurnal cycles and 24 hour wakefulness, noting acoustic and visual stimuli effects on learning 24 p4267 A69-43387

Isotopic exchange reaction rate between O 18 and CO in shock tube coupled to time of flight spectrometer, noting rate increase with time 24 p4353 A69-43807

REACTION WHEELS

Semiautomatic gravity gradient stabilization system design for low altitude earth oriented spacecraft attitude control, using active reaction wheel scanner 07 p1227 A69-18334

Vibrating momentum exchange device (VMED) in single axis configuration as competitor for inertia wheel or twin gyro 09 p1538 A69-22435

Advanced reaction wheel controller for spacecraft attitude control, discussing brushless DC motor role in weight and power reduction and control precision [AIAA PAPER 69-855] 21 p3822 A69-39383

Suboptimal attitude control system for Nimbus satellite using motor-driven inertia wheels as control torque source for three dimensional control 21 p3826 A69-39642

REACTIVATION

U ACTIVATION

REACTOR CHEMISTRY

U RADIOCHEMISTRY

REACTOR CORES

In-core thermionic sodium cooled uranium oxide fueled reactor for space vehicle power plant 02 p0279 A69-12666

Beryllium reflector distortion in Plum Brook Reactor due to neutron embrittlement and gas formation, noting material surveillance, replacement, etc 03 p0465 A69-13131

Cavity reactor consisting of dilute fuel core surrounded by moderating reflector to attain very high temperatures in gaseous cores 07 p1179 A69-18954

Nuclear rocket propulsion, discussing solid core and fluid core systems for reactors, nozzles, feed systems, control, component design and performance 11 p1914 A69-25590

Uninsulated in-core thermionic reactor design permitting diode series connections to build output voltage 14 p2398 A69-29186

Out-of-core thermionic systems with heat pipes usable in space applications, meeting advanced auxiliary power and nuclear propulsion requirements 14 p2480 A69-29188

Thermal neutron flux perturbations in cylinders in test reactors, using regression analysis to obtain polynomials for flux perturbation, depression, self shielding factors, etc 20 p3575 A69-38274

Induction plasma device of continuous operation to simulate NASA designed gas core space propulsion reactor [AIAA PAPER 68-712] 22 p3979 A69-40548

West German research in thermionic diodes and reactors, describing terrestrial version of thermal in-core thermionic reactor project 23 p4188 A69-42258

REACTOR DESIGN

Thermionic reactor systems, discussing fissionable material content, power output, specific power, component mass, total mass and design 02 p0279 A69-12662

In-core thermionic sodium cooled uranium oxide fueled reactor for space vehicle power plant 02 p0279 A69-12666

Cavity reactor consisting of dilute fuel core surrounded by moderating reflector to attain very high temperatures in gaseous cores 07 p1179 A69-18954

Nuclear reactors for powering electrical engines and current supply for satellite devices, noting ROVER project and KIW1 reactors 07 p1179 A69-19739

Thermionic reactor systems, discussing hybrid nuclear rocket/nuclear electric Mars mission, design features, performance and electric power characteristics 14 p2480 A69-29183

Thermionic reactor design for electric propulsion with emphasis on reactor power and fuel energy and fast neutron flux 14 p2509 A69-29184

Uninsulated in-core thermionic reactor design permitting diode series connections to build output voltage 14 p2398 A69-29186

Water moderated beryllium reflected reactor design for testing NERVA or Rover type fuel elements in nuclear environment, noting core location [AIAA PAPER 69-513] 16 p2810 A69-32656

Reactor testing, fuel elements and support materials for nuclear rocket program, discussing Phoebe 2A, Pewee 1 and nuclear furnace [AIAA PAPER 69-556] 16 p2811 A69-32739

Heat exchanger type low power solid-core fast nuclear rocket design, discussing fuels, safety aspects and space propulsion applications 17 p3004 A69-33342

Gas core reactor curved porous walls geometry tested with clear and smoky air injection, noting mass flow ratio in reactor cavity 18 p3171 A69-35181

Performance, size, weight, operational characteristics and cost estimates of ZrH reactor-organic Rankine power systems 23 p4189 A69-42265

Brayton-B generator for 2-10 kwe production, describing design, heat source/rejection, efficiencies and preliminary test data analysis 23 p4071 A69-42278

REACTOR FUELS

U NUCLEAR FUELS

REACTOR MATERIALS

Beryllium cermet compositions, discussing beryllium oxide content, mechanical strength and elastic and shear moduli 10 p1711 A69-23334

Book on high purity beryllium metallurgy for nuclear reactor applications covering physical properties, crystallography, thermodynamics, production methods, etc 17 p2986 A69-32952

Mechanical and thermal properties of vanadium alloys and austenitic stainless steels compared to determine applicability in high temperature reactor fuel jackets 22 p3971 A69-40973

REACTOR PHYSICS

Packed bed catalytic reactors cooling capacity in promoting endothermic reactions of hydrocarbon fuels, using computerized temperature and composition profiles [AIAA PAPER 69-588] 17 p3071 A69-33265

REACTOR SAFETY

Safety problems associated with transient boiling of liquid metals in fast nuclear reactors, emphasizing behavioral differences between liquid metals and water 08 p1420 A69-20101

Thermal stability criteria for thermionic converter performance evaluation, noting electron cooling influence 09 p1441 A69-21838

Nuclear power plant licensing, discussing public safety considerations by AEC and applicant responsibility in assuring freedom from undue risk 10 p1723 A69-23398

Remote disassembly and inspection methods for evaluating NRX-AG reactor components performance [AIAA PAPER 69-511] 16 p2810 A69-32712

Heat exchanger type low power solid-core fast nuclear rocket design, discussing fuels, safety aspects and space propulsion applications 17 p3004 A69-33342

REACTOR TECHNOLOGY

Reactors technical characteristics for high temperature mineralization of closed life systems biological wastes, deriving equations to estimate energy balance 10 p1649 A69-23504

Induction plasma device of continuous operation to simulate NASA designed gas core space propulsion reactor [AIAA PAPER 68-712] 22 p3979 A69-40548

Power systems for unmanned spacecraft, noting improved performance for zirconium hydride reactors and thermoelectric converters 23 p4187 A69-42255

Performance, size, weight, operational characteristics and cost estimates of ZrH reactor-organic Rankine power systems 23 p4189 A69-42265

READERS

Charge image detector for reading information as extended spatial charge distribution on dielectric layer surface, using vibrating conducting probe scanner 02 p0248 A69-11822

Reading amplifier for thin magnetic film memory stores permitting tunnel diode register positioning 04 p0579 A69-15319

READING

Error correction of strain gage/cement combination reading relaxation under prolonged steady loading at elevated temperature 22 p4042 A69-40313

Illumination effect on air navigation chart reading during flight, using questionnaire data 24 p4271 A69-42605

READING MACHINES

U READERS

READOUT

Holographic laser type memory with bulk storage capacity and short readout time 03 p0428 A69-13116

Sensor suspension, damping and signal readout through use of fluids with applications to rate and acceleration sensors [AGARDOGRAPH-118] 08 p1257 A69-20949

Image intensifier and return beam sections of 4.5 inch high resolution vidicon and camera system for high definition signal readout 17 p2976 A69-34063

Real time pulse frequency modulation telemetry receiving system for direct readout of ionograms from topside sounders, using off-shelf components 20 p3508 A69-37862

REAL GASES

Soviet book on shock waves in real gases covering gas flow patterns in shock tube, perturbations, shock and detonation wave reflection, etc 04 p0589 A69-14937

Approximate hydrodynamic equations applied to analysis of heat transfer in real gas flow in tube, taking into account energy transfer by radiation 04 p0686 A69-14993

Semiperfect gases with enthalpy dependent only on temperature, discussing validity of concept and Joule experiment on equivalence of heat and work 05 p0848 A69-16336

Detonation characteristics of gaseous explosives using equations of state for real gases, noting compressibility effect in mixture of hydrocarbons, O and N 05 p0848 A69-16337

Supersonic free jet with real gas effects and chemical reactions calculated by approximation 10 p1631 A69-22898

Dense real gas thermodynamic relations in piston driven shock tube facilities operation 11 p1862 A69-25011

Gas-gas interactions second virial coefficients measured at various temperatures, comparing experimental data with results calculated by Kihara potential 14 p2488 A69-29927

Nonequilibrium, real gas and nose bluntness effects on hypersonic slender body flows, analyzing similitudes, free stream temperature, velocity and relaxation [AIAA PAPER 69-708] 17 p2894 A69-33501

Integral relation method analysis of supersonic gas flow past blunt body of revolution 18 p3086 A69-35051

Shock waves Mach reflection at various velocities in real gases, observing temperature and pressure distributions, double reflections, effects of internal degrees of freedom excitation, etc 19 p3450 A69-36363

Nomograph for rapid estimation of pressure drops across orifices in pneumatic systems using real gas data with illustration for nitrogen 20 p3467 A69-38186

REAL NUMBERS

U INTEGERS

REAL TIME OPERATION

Structure oriented parallel algorithms for matrix operations, noting applicability to real time calculations for discrete Kalman filter and control problems 02 p0224 A69-11743

Phase plane diagram utility in toppling stability analysis of spacecraft, emphasizing numerical integration time reduction 02 p0334 A69-12376

Two dimensional representation of Venus entry probe target data for determining probe capability to provide real time data transmission to earth 02 p0331 A69-12820

Automated real time monoradar surveillance system based on azimuthal monotonicity of radar plots and flexible tracking strategies 03 p0383 A69-12872

Simulation design of multiprocessing system to provide air traffic control capabilities through use of real time operations 04 p0629 A69-15365

Analog FM subcarrier modulation selected for real time TV picture transmission via electro-optic space communication system 04 p0562 A69-15474

Real time performance, ground control and data processing of Surveyor spacecraft during maneuvers [AIAA PAPER 67-644] 04 p0586 A69-15502

Holography, discussing one beam recording, real time interferometry, pulsed laser, etc 05 p0761 A69-15774

Air Force Eastern Test Range data processing systems perform real time operations during in-flight phases of ballistic missiles and orbiting vehicles 05 p0727 A69-16772

Laser displays for information transfer to provide improved computer driven read-out techniques, noting real image and holographic displays 06 p0928 A69-17924

Radiation protection plan for Apollo lunar mission based on real time monitoring of solar activity and radiation in spacecraft [AIAA PAPER 69-19] 06 p0996 A69-18113

Apollo lunar TV camera for real time pictures during all phases of Apollo lunar landing mission, describing camera tube, circuitry and optics 07 p1133 A69-19137

Computer graphics and manufacturing, discussing man computer system for transformation of blueprint to numerically controlled machine tape with no time delay 07 p1089 A69-19741

Stochastic model for real time on demand weather predictions using REEP /regression estimation of event probabilities/ equations in Markov chain 08 p1345 A69-20299

Apollo/Saturn V automatic checkout test verification and debug program using real time computer simulation with digital space vehicle system model [AIAA PAPER 69-321] 09 p1478 A69-22378

Asynchronous on-line digital data acquisition system with immediate access to on-site numerical real time printout for rocket engine performance tests [AIAA PAPER 69-323] 09 p1478 A69-22381

Random data detection method applicable to low voltage SNR cases using real time correlation of probability functions 09 p1459 A69-22593

Complex spatial filtering by holographic Fourier transform subtraction 10 p1690 A69-22953

Real time computer controlled telemetry system readiness testing and validation, describing automatic closed loop checkout methods and remote display controller 10 p1660 A69-23270

Electron beam addressed electrooptic light valve used as spatial filter, discussing electronic control and optical processing in real time 10 p1697 A69-23870

Real time electronically scanned radar control using digital computer with input and output conversion for information handling, noting interface equipment 11 p1834 A69-24544

Real time Fourier spectroscopic system for synthesis of spectrum of interferogram, noting polystyrene IR transmission spectra 11 p1884 A69-24837

Computer controlled flight line tester performing automatic real time testing of aircraft avionics systems on flight line or hanger 11 p1864 A69-25060

Flexible control module for real time automated checkout requiring programming by personnel with strong software background 11 p1843 A69-25072

Real time correlator in periodic signal extraction from noise background, discussing multichannel sampler as special case of cross correlation extraction 11 p1837 A69-25094

Real time/process computer interface with electric power systems, discussing compatibility, reliability, etc, problems in connection with management and engineering personnel 11 p2004 A69-25302

Real time 2000 line TV camera with 40 MHz bandwidth, 1600 line vertical resolution and 1000 line horizontal resolution [SMPTE PAPER 105-73] 12 p2077 A69-25769

Real time pressure simulation chambers for testing space vehicles, discussing slow and rapid evacuation and pumping systems 13 p2240 A69-28077

Random signals and real time analysis systems for environment testing and transient signals 13 p2264 A69-28603

Hybrid computer system for real time optimum feedback controller using iterative algorithms with rapid convergence, discussing simulation and performance 15 p2582 A69-30071

Real time shock response analysis advantages over sequential analysis, describing equipment 15 p2618 A69-30359

Electrophysiological /electroslanchnogram/ medical data transmission via satellite from France to U.S. for real time computer processing 16 p2746 A69-32070

Radio sources interplanetary scintillations and cross correlation coefficient real time determination 17 p3038 A69-33727

Associative processor applied to interceptor radar system, noting processing time independence from target number and compatibility with real time systems 17 p2931 A69-34071

Observer theory application to hybrid inertial navigation systems, discussing error estimation and correction, real time mechanization, eigenvalues, etc 17 p3003 A69-34099

Saturn 5 system simulation showing feasibility, efficiency and economy of real time simulation using large mathematical model and general purpose digital computer 18 p3113 A69-34268

Reliability engineering methods for software programs with emphasis on real time computation, describing SSD Exhibit 61-47 documentation 18 p3105 A69-34524

PDP8 digital computer and Trebel vertical balancing machine combined for real time presentation of trim weights and positions, noting noise in force components [SAWE PAPER 738] 18 p3220 A69-34888

Meteorological Doppler radar information display for real time identification of hazardous winds and turbulence in storms 18 p3139 A69-35427

Real time terrain following computer for C-5A transport, discussing automatic throttle system and speed bleedoff utilization [AIAA PAPER 69-797] 19 p3367 A69-35633

Holographic system to process signals received by pulse Doppler radar, noting real time operation with availability of instantaneous development image storage media 19 p3314 A69-36598

Aircraft simulation, discussing flight simulation, real time computer assembly operation, computer-auxiliary interfaces, etc 19 p3296 A69-36707

Roscau satellite onboard computer systems design, emphasizing simulator and assembly programs for real time operation verification 20 p3501 A69-37389

Onboard computer and environment simulation for real time programs development, discussing instructions analysis, variables extraction and values and peripheral components 20 p3502 A69-37395

Real time analyzers of acoustic signals for aircraft engine noise, noting automatic test 20 p3462 A69-37756

Real time pulse frequency modulation telemetry receiving system for direct readout of ionograms from topside sounders, using off-shelf components 20 p3508 A69-37862

Sensitivity improvement for inertialess microwave signal scanning and readout by applying pulse compression concepts, discussing application to real time microwave imaging and holography 20 p3545 A69-37901

Radar calibration techniques for accurate real time tracking data, describing GEOS-B C-band experiment [AIAA PAPER 69-872] 21 p3675 A69-39398

Gyro test package, dynamic test facility and real time attitude algorithm to investigate operational capabilities of strapdown inertial attitude package [AIAA PAPER 69-849] 21 p3765 A69-39424

Real time operating system /RTOS/ 360 for spaceflight control, describing hardware, applications, task management and capacity, etc 21 p3679 A69-39602

Real time targeting for Apollo lunar orbit insertion maneuver burn, discussing impulsive maneuvers for flight control [AIAA PAPER 68-848] 21 p3828 A69-39760

Real time FM-to-digital converter for measuring periods of demodulated FM/FM data, discussing systems design 22 p3903 A69-39923

Real time network support simulation allowing network configuration for nominal or perturbed trajectory for Saturn vehicles, applicable to any flight azimuth 22 p4020 A69-40319

Real time orbit determination system at NASA manned space center for Apollo missions [AIAA PAPER 69-938] 22 p4020 A69-40321

Real time digital computer hardware simulation of Apollo Telescope Mount /ATM/ mission [AIAA PAPER 69-940] 22 p3919 A69-40323

Machine independent telemetry oriented language /MITOL/ to develop computer programs for real time and postflight telemetry data processing 22 p3905 A69-40340

Data compression and transmission technique for real time system to monitor manned space missions, noting Apollo telemetry data [AIAA PAPER 69-970] 22 p3906 A69-40350

Real time multiprocessing telemetry ground support integrated system design with expanded definition of hardware/software decision tradeoffs [AIAA PAPER 69-971] 22 p3907 A69-40351

Operational reliability verification of Apollo real time mission program and testing structure, discussing environment, processing, controls, response criteria, etc [AIAA PAPER 69-981] 22 p3907 A69-40361

Mariner Mars 1969 spacecraft real time test support system and recorded data analysis including routing to printers, CRT displays and incremental plotters [AIAA PAPER 69-982] 22 p3907 A69-40362

Software/hardware interface testing of real time system, including possible improvements to computer program management flow 22 p3908 A69-40364

Meteorological data real time processing for automatic weather analysis and prognosis, program used and computer output charts 22 p3977 A69-40732

Real time telemetry, tracking and command links by synchronous satellite relay, describing ATS-Nimbus E S-band experiment 23 p4121 A69-41759

IBM 360-50 computer with I/O terminals to process PCM and analog data from Modular Auroral Probe series of sounding rockets on real time basis 23 p4133 A69-41764

Ionospheric irregularities effect on accurate satellite position determination in near real time 23 p4132 A69-42549

REAL VARIABLES

NT ASYMPTOTES

NT ASYMPTOTIC SERIES

NT BESSEL FUNCTIONS

NT BIHARMONIC EQUATIONS

NT BINARY INTEGRATION

NT BLASIUS EQUATION

NT BOREL SETS

NT BURGER EQUATION

NT CALCULUS OF VARIATIONS

NT COLLINEARITY

NT CONTINUITY [MATHEMATICS]

NT COPLANARITY

NT CUBIC EQUATIONS

NT CURL [VECTORS]

NT DELTA FUNCTION

NT DIFFERENTIAL EQUATIONS

NT DUFFING DIFFERENTIAL EQUATION

NT EINSTEIN EQUATIONS

NT ELLIPTIC DIFFERENTIAL EQUATIONS

NT EXISTENCE THEOREMS

NT EXTREMUM VALUES

NT FALKNER-SKAN EQUATION
 NT FOKKER-PLANCK EQUATION
 NT FOURIER SERIES
 NT FUNCTIONAL INTEGRATION
 NT GAUSS EQUATION
 NT GREEN FUNCTION
 NT HANKEL FUNCTIONS
 NT HELMHOLTZ VORTICITY EQUATION
 NT HYPERBOLIC FUNCTIONS
 NT HYPERPLANES
 NT INTEGRAL CALCULUS
 NT JACOBI INTEGRAL
 NT JACOBI MATRIX METHOD
 NT KERNEL FUNCTIONS
 NT LAME WAVE EQUATIONS
 NT LIAPUNOV FUNCTIONS
 NT LIMITS [MATHEMATICS]
 NT LINEAR EQUATIONS
 NT LIOUVILLE EQUATIONS
 NT LIPSCHITZ CONDITION
 NT MEASURE AND INTEGRATION
 NT MINIMA
 NT NEUMANN PROBLEM
 NT NONLINEAR EQUATIONS
 NT NUMERICAL INTEGRATION
 NT PADE APPROXIMATION
 NT PARABOLIC DIFFERENTIAL EQUATIONS
 NT PARTIAL DIFFERENTIAL EQUATIONS
 NT PERIODIC FUNCTIONS
 NT POISSON EQUATION
 NT POWER SERIES
 NT QUADRATIC EQUATIONS
 NT RUNGE-KUTTA METHOD
 NT SERIES [MATHEMATICS]
 NT SINE SERIES
 NT STIELTJES INTEGRAL
 NT STURM-LIOUVILLE THEORY
 NT TANGENTS
 NT TAYLOR SERIES
 NT TRIGONOMETRIC FUNCTIONS
 NT VECTOR ANALYSIS
 NT VLASOV EQUATIONS
 NT VORTICITY
 NT VORTICITY EQUATIONS
 NT WEIGHTING FUNCTIONS
 NT WHITTAKER FUNCTIONS

Tricomi theorem extension concerning intermediate value property of continuous real valued functions of real variable

09 p1533 A69-22797

Evolutionary hypoelliptic equations with real variable coefficients, analyzing positive solutions and application to parabolic equations

11 p1908 A69-24534

Higher root loci of polynomials for multivariable systems with coefficients polynomials of real parameter

12 p2048 A69-26073

Partial differential equation with stochastic characteristics reducible to parabolic equation by introducing additional variables

12 p2121 A69-26366

Numerical procedure for testing absolute stability and positive realness of free dynamic systems based on Routh algorithm

18 p3112 A69-34689

Autonomous second order recurrence with real variables, studying conditions for attractive limiting set stability region with several noninterconnected regions

19 p3287 A69-36651

Evolutionary hypoelliptic equations with real variable coefficients, analyzing positive solutions and application to parabolic equations

21 p3756 A69-39151

REATTACHED FLOW

Model for asymptotic separated flow in wake behind broadside of bluff body, discussing separation point, interaction, reattachment, base flow and near wake

02 p0188 A69-11986

Turbulent jet model of unsymmetrical velocity profile for design of wall attachment device

02 p0231 A69-12072

Switching action mechanism in wall attachment fluid amplifier, outlining theory based on turbulent jet entrainment

02 p0195 A69-12073

Fluid mechanics of supersonic flow separation and reattachment in fluidic devices

02 p0231 A69-12077

Meksyn method application to problems of jet mixing and jet reattachment

02 p0233 A69-12530

Plane supersonic base flows studied using integral analysis of turbulent reattachment, noting prediction of wall pressure distribution

03 p0361 A69-12990

Reattachment pressure correlated for any type of two dimensional turbulent supersonic separated flow

04 p0588 A69-14727

Wall attachment type fluidic logic devices with low power consumption requirements, noting monostable and bistable devices

05 p0704 A69-16002

Tangential stress distribution and heat transfer in circular cylinder with attached wall jet

05 p0746 A69-16022

Laminar boundary layer separation and reattachment near concave corner on cooled reentry body in supersonic flow

06 p0911 A69-17592

Two dimensional supersonic flow along adiabatic curved ramp noting separation, attached flow and laminar boundary layer interaction with external stream

[AIAA PAPER 68-109] 09 p1430 A69-21949

Two dimensional model for analyzing turbulent separation and reattachment at blade trailing edge at supersonic speed

[ONERA-TP-678] 16 p2733 A69-32258

Mean parameters calculation between widening of turbulent flow and point of reattachment, including similarity hypothesis concerning velocity profile

19 p3299 A69-36648

Flow separation and reattachment points and line of zero velocity jet mixing determined by injecting smoke

[ASME PAPER 69-FE-29] 20 p3517 A69-37994

Coanda effect of separated jets reattachment to wall at high Knudsen number in pneumatic fluidic devices, discussing Reynolds and Mach numbers effect

[ASME PAPER 69-FLCS-37] 21 p3692 A69-38602

Separation flows in flat channel with step recess, analyzing dynamic characteristics in mixing region, in wake of rarefaction waves and in attachment zone

24 p4247 A69-43498

REATTACHMENT U ATTACHMENT

REBREATHING

Cardiac output during space flight based on rebreathing method for estimation of gas tension in mixed venous blood and Fick equation

[UN PAPER 68-95746] 01 p0151 A69-10527

RECEIVERS

NT LOGARITHMIC RECEIVERS
 NT SUPERHETERODYNE RECEIVERS
 NT TELEVISION RECEIVERS

Broadband parametric amplifier used as front amplifier in satellite communication systems ground station receiver, noting cryogenic operation capability

01 p0041 A69-10243

Small earth stations in future communication satellite systems, discussing applications, characteristics and equipment

[UN PAPER 68-95751] 01 p0028 A69-10492

Sensitivity calculation for microwave receiver consisting of traveling wave tube preamplifier followed by square law detector and video amplifier

01 p0048 A69-11038

Frequency feedback receiver capabilities as low threshold demodulator in frequency modulated frequency division multiplexing satellite system

01 p0034 A69-11141

Adaptive processing limited memory receiver for synchronous detection of signals of unknown amplitude

03 p0400 A69-13228

Signal detection by four terminal receiver network optimal for background Gaussian noise

04 p0557 A69-14776

Sonar receiver reduced averaging processing in presence of extended and point targets compared with full averaging processor

04 p0562 A69-15477

Asymptotic performance of adaptive receivers and application to signals of unknown frequency, noting SNR role

05 p0722 A69-16727

SNR enhancement in optical receiver by amplification before detection of carrier of modulated optical signal, using quantum amplifier

[IEEE PAPER R-5] 07 p1154 A69-19079

Receiving systems for digital telemetry signals from spacecraft, analyzing receiver performance by statistical methods

08 p1276 A69-20591

Book on laser communication system design covering modulation and detection methods

08 p1277 A69-20884

Hard limiting effect on sum of three or four sinusoidal signals noting output amplitudes, signal suppression and negative suppression effect

09 p1451 A69-21311

Optimal receiving circuit determined for elliptically polarized signals in randomly polarized noise by deriving integral equation

09 p1456 A69-22285

Adaptive threshold detection, using stochastic approximation techniques to derive receiver structures capable of learning optimum threshold setting during actual operation

11 p1839 A69-25297

Digital simulation of phase locked receiver in diffuse multipath fading environment with band limited thermal noise

11 p1839 A69-25298

Noise sensitivity of space diversity reception system with narrow beam electrically switchable antennas for incomplete beam separation

12 p2030 A69-26485

Phase analysis in multiple-sensor receivers with high signal to noise ratio, considering phase difference between two stochastic input signals

13 p2220 A69-27938

Frequency diversity reception system for drift of small scale ionospheric inhomogeneities, noting circuit diagrams

14 p2452 A69-29875

Noise stability of receiver network during detection of finite duration noise signal on white noise background, considering various narrow band preselectors

15 p2563 A69-30142

Linear feedback additive noise communication systems formulated in terms of arbitrary operations at transmitting and receiving points

17 p2944 A69-33626

X ray stroboscope for moving objects in penetrating irradiation, considering synchronization of radiation receiver

18 p3138 A69-35114

Coherent phase locked loop receiver as carrier and modulation loops combination with parallel bandpass filter for ranging signal reception and FM demodulation

19 p3274 A69-36277

Optimum receiver design for binary coded data detection in two channel space communication system, discussing phase error distribution and optimum decision function

19 p3275 A69-36286

Italian cross radio telescope noting added phase shifters to N-S arm, transistorized receiving system and modified data processing

19 p3295 A69-36643

Receiving and display telemetry system for obtaining direct ionospheric topside ionograms from Alouette 1 satellite, discussing video data tape recording cost

20 p3507 A69-37861

Delay line MTI receivers performance calculation accuracy, discussing error for general and restricted number of pulses from single and double cancellation at IF

23 p4117 A69-41605

Multichannel spectral line receiver for 210 ft Australian radio telescope with front ends covering wide frequency range

24 p4283 A69-43115

RECEIVING SYSTEMS

U RECEIVERS

RECEPTACLES [CONTAINERS]

U CONTAINERS

RECEPTORS [PHYSIOLOGY]

Acoustical vestibular stimulation in guinea pig, showing activation of receptors

03 p0376 A69-14076

Cutaneous receptor response to microwave irradiation, measuring warmth sensory effects in human forehead with radiometer

[AGARDOGRAPH-111] 08 p1266 A69-20677

Retinal burn resulting from prolonged viewing of sun, laser or thermonuclear explosion, noting effects on choroid, receptors and pigment cells

08 p1267 A69-20680

Receptor and adrenergic blockade effects on blood loss, tolerated period and metabolic sequelae of hypotension in dogs

23 p4098 A69-42102

RECIPROCAL THEOREMS

Reciprocal variational formulation for optimal control, estimating difference between suboptimal system response and optimum

03 p0457 A69-13766

Corollary of reciprocity theorem in holography

04 p0602 A69-15377

- Reciprocal theorem for displacements of solid skeleton caused by fluid sources action in infinite consolidating space
05 p0835 A69-15869
- Reciprocity, variational and uniqueness theorems developed within linear theory of coupled thermoviscoelasticity
07 p1233 A69-19327
- Reciprocity theorems of coupled and uncoupled thermoelasticity for macroisotropic and microisotropic simple homogeneous solids with microstructure
09 p1618 A69-22259
- Reciprocity theorem applied to Somigliana relations for static loads and coupled thermoelasticity
09 p1618 A69-22260
- EEG lead sensitivity to location and orientation of sources in brain by applying reciprocity theorem
10 p1648 A69-23186
- Magnetothermoelasticity equations, uniqueness and reciprocity theorems and solutions emphasizing moving media
15 p2715 A69-31215
- Corollary of reciprocity theorem in holography
16 p2790 A69-32124
- Reciprocal theorem for obtaining relations between transmitting antenna effective area, radiation pattern and aperture distribution
19 p3281 A69-35765
- Dynamic reciprocity relationship for linear directed continuous viscoelastic media, using Stieltjes convolution
19 p3373 A69-36307
- RECIPROCATING ENGINES**
U PISTON ENGINES
- RECIRCULATIVE FLUID FLOW**
- Atmospheric exposure chamber design for small animals, discussing dynamic and recirculating operations and gas scrubbing system
04 p0584 A69-14678
- Exhaust gas recirculation for VTOL aircraft [AIAA PAPER 67-439]
12 p2013 A69-26760
- Supersonic wake recirculation flow over rearward facing two dimensional steps and blunt bases
14 p2389 A69-29031
- Book on heat and mass transfer in recirculating flows, presenting elliptic differential equations and numerical solutions by computer
21 p3691 A69-38333
- Recirculation concept for air cushion vehicle air curtain evaluated by two dimensional and circular models, discussing optimum cushion area/jet exit area ratio
22 p3866 A69-40816
- RECLAMATION**
NT MATERIALS RECOVERY
NT WATER RECLAMATION
- Oxygen reclamation from carbon dioxide using solid oxide electrolyte, noting water vapor catalytic effect
07 p1071 A69-19423
- RECOGNITION**
NT CHARACTER RECOGNITION
NT PATTERN RECOGNITION
NT SPEECH RECOGNITION
NT TARGET RECOGNITION
- Holography and similarity criterion for developing image recognition algorithm
08 p1314 A69-20417
- RECOMBINATION COEFFICIENT**
- Recombination rate dependence on nonequilibrium charge carriers concentration at semiconducting surface
01 p0136 A69-10253
- Semiconducting diode base Dember effect impedance studied for recombination rates approaching zero or infinity
01 p0137 A69-10260
- Alpha recombination coefficient of molecular helium ions measured in helium afterglow plasmas as function of electron density and gas temperature
02 p0283 A69-11834
- Dissociation and recombination of moderately complex molecules, using master equation with transition probabilities and decay rates obtained from reaction rates statistical theory
02 p0283 A69-12181
- Electron temperature and concentration and solar UV absorption data from sounding rockets, estimating ion exchange rate, recombination coefficient and heat flux
03 p0422 A69-13508
- Low density limit to three body ionic recombination coefficients in various gases
04 p0632 A69-14679
- Effective gradient method modification for analyzing three body ionic recombination compared with diffusion method
05 p0795 A69-15661
- Surface recombination rate effect on lux-ampere characteristic of photomagnetic effect in CdS single crystals of low and high photosensitivity
05 p0809 A69-16377
- High temperature effects on gallium arsenide crystals current carriers lifetime, discussing recombination characteristics and impurity photoconductivity
05 p0809 A69-16551
- Recombination constants of dissociated oxygen and nitrogen flow in supersonic nozzle at high temperatures using modified Bray method
06 p1030 A69-17349
- Reaction rates coefficients of oxygen ions with molecular oxygen and nitrogen in nighttime F region over Moscow based on loss coefficient estimate
06 p0919 A69-17724
- Ionization index, electron formation and effective recombination coefficient in E 2 layer, noting solar activity effect
06 p0920 A69-17725
- Semiconductor lasers, discussing electron transitions, radiative band-band transitions, emission and absorption spectra, recombination rates, carrier lifetime and lasing conditions
06 p0937 A69-18009
- Semiconductor current carriers surface recombination rates determined from photomagnetic effect
07 p1198 A69-18505
- Two fluid approximation of one dimensional steady state flow of inviscid plasma with thermal gradients, considering ionization and recombination processes
07 p1189 A69-18691
- Surface recombination rate and retardation field effects on diffusion current in mesa diodes with low level injection
07 p1105 A69-19008
- Recombination coefficients for dense weakly ionized cesium plasma, treating recombination process as diffusion generated by electron collisions
08 p1359 A69-19844
- Three body ionic recombination coefficient for moderate and high gas densities, taking into account variability in mean free path and trapping radii
09 p1542 A69-21624
- Recombination rate dependence on nonequilibrium charge carriers concentration at semiconducting surface
09 p1559 A69-22646
- Semiconducting diode base Dember effect impedance studied for recombination rates approaching zero or infinity
09 p1559 A69-22653
- Slow recombination centers parameters in CdSe single crystals during heat treatment in vacuum or hydrogen atmosphere
09 p1560 A69-22664
- Recombination parameters and depth of levels of p-n junctions in semiconductor photocells determined from position of maximum spectral sensitivity
09 p1560 A69-22718
- Ionization relaxation in atmospheric pressure Ar-Cs plasma, considering two and three body recombination and O impurity effects
10 p1733 A69-23445
- Plasma decay coefficient, charge recombination coefficient and electron scattering in cooling electron gas of quasi-steady cesium discharge plasma under high pressure
10 p1733 A69-23448
- Long wave propagation at 164 kHz in India during 1966 and 1967, determining D region recombination coefficient and long wave absorption diurnal variation
10 p1659 A69-24065
- Solar cell equation series resistance and junction recombination parameters determination, considering I-V characteristics
11 p1826 A69-25395
- Electron-ion recombination coefficient for triple collisions in dense low temperature plasma, deriving finite electron Fokker-Planck equation
11 p1933 A69-25541
- Recombination emission spectrum relation to plasma recombination coefficient, determining plasma electron temperature from continuous spectrum intensity
11 p1934 A69-25566
- Collisional radiative electron-ion recombination rates measured in decaying rare gas plasmas produced by transient discharge
12 p2134 A69-25981
- Vertical ionization drift in F region as function of electron density, ionization coefficient and recombination coefficient
12 p2070 A69-26584
- Nondrifting n-p-n semiconductor current gain dependence on surface recombination rate
13 p2236 A69-28547
- Effective recombination coefficient in lower ionosphere determined from charged particle spectra obtained by rocket sounding in Canada
14 p2511 A69-28960
- Rate constants for recombination of atomic hydrogen with hydrogen molecules, hydrogen atoms and argon atoms at high temperatures behind shock waves
14 p2488 A69-29637
- Frequency response of MIS capacitance beyond inversion voltage, discussing recombination rate and generation-recombination current in space charge region
15 p2565 A69-30179
- Solar flares with subcosmic radiation in proton active region of May 1967, discussing X ray emission effects, calculating D region recombination coefficient and electron concentration
17 p3025 A69-34226
- Recombination coefficients of oxygen and nitrogen ions with electrons related to electron temperature, using microwave afterglow/mass spectrometer
18 p3176 A69-34789
- Nighttime ionospheric F region velocity component and recombination coefficient computer calculation
20 p3521 A69-37049
- Upper atmosphere particles, luminosity and electron concentration measurements documented in input, storage and energy radiation classes, determining recombination coefficients
21 p3707 A69-38491
- Recombination and ionization coefficients for quasi-steady state homogenous H and hydrogenic ion plasmas based on collisional-radiative model
22 p3988 A69-41153
- Collisional radiative recombination and ionization coefficients for weakly ionized H plasmas using rate equations
22 p3988 A69-41154
- Tabulated numerical values of Burgess general formula for computing dielectronic recombination rates
23 p4207 A69-41281
- Atomic nitrogen collisional ionization and recombination rates under assumed quasi-steady nonequilibrium distribution of electron state populations
24 p4353 A69-43700
- RECOMBINATION REACTIONS**
NT ATOMIC RECOMBINATION
NT ELECTRON-ION RECOMBINATION
NT ELECTRON RECOMBINATION
NT HYDROGEN RECOMBINATIONS
NT ION RECOMBINATION
NT OXYGEN RECOMBINATION
NT RADIATIVE RECOMBINATION
- Recombination reactions during postdischarge in helium plasma produced by laser beam, deriving equation for density evolution
01 p0128 A69-10394
- Recombination effects in high resistivity Cu doped gallium arsenide single crystals determined by photoconductivity methods
02 p0294 A69-11627
- Dissociation and recombination of moderately complex molecules, using master equation with transition probabilities and decay rates obtained from reaction rates statistical theory
02 p0283 A69-12181
- Ionization and recombination in low temperature plasmas, noting fast electron distribution function deviation from Maxwellian form and calculation for Cs plasma
02 p0292 A69-12559
- Carrier generation-recombination in space charge region of asymmetrical p-n junction, noting experimental results for InSb diodes
03 p0487 A69-13641
- Photocurrent carriers recombination in organic semiconductor rhodamine B films analyzed as function of illumination
03 p0489 A69-13890
- Combination rate constants for H-F-O reactions, discussing expressions and relative efficiencies with Argon as third body
04 p0646 A69-14743
- Gallium arsenide injection lasers properties, analyzing band structure, optical transitions, recombination lifetimes, conduction band states, optical gain, etc
05 p0772 A69-16228

Recombination statistical model for neutron irradiated Si transistors, considering diffusion potential, junction voltage, temperature, activation energy and capture ratio for holes and electrons
06 p0975 A69-16871

Charge carrier lifetime measured in intrinsic conductivity range of Cd doped InAs to define recombination mechanism, relating temperature dependence to surface impurities recombination
06 p0979 A69-16997

Drift field photovoltaic cell performance with bulk and surface recombinations
06 p0870 A69-17473

Radio recombination lines in populations of highly excited states of hydrogen, discussing collisional transition effects
06 p1010 A69-17970

Gradual output degradation mechanism in GaAs injection lasers, attributing internal radiative quantum efficiency reduction to nonradiative recombination centers formation
07 p1148 A69-18857

Recombination rate of nitrogen atoms using NO titration method, tabulating reactions and emissions during various stages of titration
08 p1309 A69-20454

Temperature dependence of dissociative recombination and molecular ion formation in decaying He, Ne and Ar plasmas in discharge tube energized with capacitor bank
08 p1356 A69-20741

Nonequilibrium distribution functions for neutral atoms excited states in optically thin low temperature singly ionized plasma containing ions, electrons and neutrals
10 p1731 A69-23437

Ionization and recombination processes in He 3 plasmas produced by neutron irradiation of H 3
10 p1738 A69-23488

Surface recombination efficiencies on metals measured as function of exposure time in steady Oscen flows, providing step-function increase in oxygen atom concentration
10 p1726 A69-23526

Nonlinear charge exchange and dissociative recombination effects on night F region decay compared with linear theory
10 p1685 A69-23832

Nighttime ionospheric recombination studies by model reference heights varying diurnally, seasonally and with solar flux and geographic location
10 p1685 A69-23834

Ionization-recombination thermodynamic equilibrium upset causing spectral excitation in He arc plasma
10 p1742 A69-24077

Photocurrent carriers recombination in organic semiconductor rhodamine B films analyzed as function of illumination
11 p1939 A69-25691

Lattice defects in development of recombination centers on Ge semiconductor surfaces, discussing photoconductivity and field effect
12 p2142 A69-25978

Overlay technique for analysis of F region transition into F1 and F2, noting ionization and recombination
12 p2065 A69-26102

Dielectronic recombination influence on radio recombination lines of carbon under typical nebular conditions
13 p2346 A69-27703

Sodium atoms and NO molecules role in atomic O 6300 and 5577 Å emissions in comet Mrkos 1957d due to charge exchanges and dissociative recombination
14 p2523 A69-29707

Ionization and recombination in low temperature plasmas, noting fast electron distribution function deviation from Maxwellian form and calculation for Cs plasma
15 p2658 A69-30256

Unsuccessful attempt to observe high charge ion lines generated by dielectronic recombination in solar corona at 5-cm wavelength
15 p2689 A69-30568

Nitrous oxide-CO bimolecular reaction and O-CO recombination in single pulse shock tube
16 p2748 A69-32793

Ionization, recombination and charge transfer in upper atmosphere during aurora, considering quasi-equilibrium ion-electron concentrations
17 p2961 A69-33417

RF recombination lines measurement of helium for abundance in nebulas, comparing optical and radio values for H II regions
18 p3190 A69-34293

Steady Prandtl-Meyer expansion of shock heated gases for recombination studies, measuring static pressure, stagnation point heat transfer, IR emission and optical absorption
18 p3228 A69-34466

Transient recombination lifetimes in n-type float zone Si from 4.2 K to room temperature, obtaining electrical and photoconductivity values
19 p3383 A69-36447

Superradiance and recombination radiation from CdTe with high compensation, using model assuming narrowing from superradiance onset for analysis
19 p3389 A69-36550

Nitrogen and water vapor effects on hydrogen-oxygen system recombination, using shock tubes for design of exhaust nozzles for hypersonic flow vehicles
21 p3669 A69-38801

Forced recombination scattering of light on Rayleigh polarization waves in isotropic solid body with small elastooptical constants
21 p3770 A69-38963

Radio recombination line data from H II regions interpreted in terms of single electron temperature, considering non-LTE/local thermodynamic equilibrium/clumping
22 p4025 A69-40645

Electron density decrease in F 2 layer ascribed to 9 July 1962 thermonuclear explosion, noting dissociative recombination role
22 p3942 A69-41098

Electric fields reducing recombination radiation intensity from bulk ionized GaAs and InP and shifting spectrum to lower energies, discussing self absorption
23 p4198 A69-41499

Anisotropic carrier distribution effect on polarization of spontaneous recombination radiation during GaAs breakdown in electric field
24 p4362 A69-43736

RECOMPRESSION

U COMPRESSING

RECONNAISSANCE

U AERIAL RECONNAISSANCE

U PHOTO RECONNAISSANCE

RECONNAISSANCE AIRCRAFT

NT F-5 AIRCRAFT

NT G-91 AIRCRAFT

NT OV-10 AIRCRAFT

NT P-1127 AIRCRAFT

Helicopter self defense armament for fire support of British Army operations, discussing vulnerability, weapons selection and tactics, logistics, etc
01 p0010 A69-10869

Nimrod maritime reconnaissance aircraft, discussing high speed high altitude transit flights
05 p0702 A69-15885

Engine air intake for operational Harrier V/STOL strike/reconnaissance fighter, describing intake instrumentation ring, temperature and pressure probe development and pressure recording
05 p0767 A69-16773

First flight test phase of multipurpose Viggen aircraft designed as basic platform for attack, trainer, reconnaissance and fighter versions
06 p0867 A69-17662

Operational system effectiveness information for reconnaissance drone system including test flights, discussing application to reliability and maintainability in project management
18 p3232 A69-34505

RECONNAISSANCE DRONE AIRCRAFT

U DRONE AIRCRAFT

RECONSTRUCTION

NT WAVE FRONT RECONSTRUCTION

Saint-Severin amphotericite geometrically reconstructed from fragments in form prior to atmospheric breakup, noting agreement with track densities of iron ions
19 p3416 A69-36128

RECORDING

U DATA RECORDING

U DATA SMOOTHING

U MAGNETIC RECORDING

U PHOTOGRAPHIC RECORDING

RECORDING HEADS

Rotary head units used in telemetry magnetic recorders, explaining concepts and advantages of rotary scanning
07 p1077 A69-18826

RECORDING INSTRUMENTS

NT FLIGHT LOAD RECORDERS

NT FLIGHT RECORDERS

NT LUNAR SEISMOGRAPHS

NT OSCILLOGRAPHS

N1 PLOTTERS

NT RADIOMETEOROLOGRAPHS

NT SEISMOGRAPHS

NT WEATHER DATA RECORDERS

NT WHISTLER RECORDERS

NT X-Y PLOTTERS

Thermographic phosphor technique to provide transient temperature measurements in impulse wind tunnel
01 p0078 A69-10152

Micrometeorites acoustic recordings on Cosmos 135, investigating data reliability influenced by appearance of thermal noise
01 p0152 A69-10578

Shock and vibration data recording, discussing transducer selection, accelerometer mounting, conditioning electronics and recording devices
01 p0083 A69-11050

Electron concentration in ionospheric outer regions determined from coherent frequencies recorded on-board OGO-A
01 p0147 A69-11323

Optimal reception of quantum signals at recording device aperture
02 p0206 A69-11607

Rapid recording microspectrophotometer for IR to UV absorption spectra of living cells, cell organelles and half micron diameter particles
03 p0428 A69-13109

Time dependent photoelectron multiplier with low noise for recording long wave laser light pulses
03 p0440 A69-13264

Automatic recording device for cosmic ray bursts utilizing information time delay to allow detailed initial period study
03 p0430 A69-13545

Signal matching in radio interferometer with autonomous receiver, magnetic tape recorders and memory electron beam tube with target
03 p0431 A69-13706

Shipboard standard visibility measurements by means of AEG-FFM scattered light recorder aboard Meteor in Atlantic Ocean during 1965
04 p0628 A69-15158

Spatial distribution of background magnetic fields of quiet sun from photoelectric magnetograph observations, noting relation to supergranulation
04 p0663 A69-15396

Radar echoes signal amplitude and phase digital recording with Radicord/radar digitizing and recording device
05 p0721 A69-16618

Optical commutation to permit multifield monitoring and recording with one sensor by employing high resolution imaging fiber optics elements feeding common focusing lens
06 p0926 A69-17678

Electrostatic storage display tube characteristics, construction, applications and reliability
07 p1101 A69-18655

Control and recording device for parameters and information relating to takeoff and landing, using detection elements and cross wire on runway
08 p1347 A69-20780

Photographic measurement of parachute exit velocity during ejection from chute, describing electronic recording and unit operation with block diagram
08 p1317 A69-20875

UHF telemetry conversion program at Pacific Missile Range, describing antenna, receive-record and separation display systems
09 p1454 A69-21800

Maintenance recording systems for aircraft fleet, discussing operations objectives and research, data collection and implementation using systems engineering
10 p1671 A69-23261

Algorithm for determining readings dispersion during cosmic ray recording, considering cosmic rays variability, statistical nature and instrument errors
10 p1770 A69-23906

Holographic recording of three dimensional flow field velocities, applying theory of particle size assessment via Fraunhofer holography
11 p1884 A69-24691

Optimal reception of quantum signals at recording device aperture
11 p1835 A69-24714

Photoelectric polarimeter to record sky light intensity in form of polarized components, detailing construction and operation
12 p2078 A69-25892

Photoelectric recorder with timebase image converter tube for investigating ultrashort light pulse transient response of laser
12 p2083 A69-26139

Continuously operating mirror scanning system for high speed photographic cameras, emphasizing maximum scanning speeds and framing rates

12 p2085 A69-26154

Holography with pulsed lasers for high speed recording of amplitude and phase disturbances and rapid transient events, noting reconstruction evaluation problems

12 p2087 A69-26171

Optimum recording conditions for analog recorders with continuous recording in rectangular coordinate system

12 p2091 A69-26332

Cosmic radiation recorder designed for use onboard satellite to measure intensity space-time distribution under geomagnetic effect

12 p2094 A69-26697

Scientific equipment on Cosmos 237 satellite for recording extraterrestrial radiation data, discussing specifications, operation and mission purpose

14 p2446 A69-29047

Automatic recording of spectral distribution of high resistance semiconductors photoconductivity using spectrograph monochromator

14 p2447 A69-29409

Thermistor instrument for remote sensing, magnetic synchronous recording and linear display of temperature

14 p2449 A69-29562

Semiconductor materials and fabrication methods for surface barrier junction n-type and p-type silicon counters used in hydrogen ion flux recording

14 p2452 A69-29810

Vector magnetograph to measure magnetic field vector components, obtaining field direction azimuth by servo circuit

14 p2453 A69-29972

Measurement system for recording of small localized temperature changes in brain

15 p2606 A69-30152

Automatic recording inverted dilatometer employing fused quartz vertical pedestal and yoke type pushrod

15 p2607 A69-30153

Semiautomatic recording device to determine gas discharge ion and electron sources operation modes optimum parameters

15 p2658 A69-30237

Micrometeorites acoustic recordings on Cosmos 135, investigating data reliability influences by appearance of thermal noise

15 p2691 A69-30748

Crack growth monitoring and recording techniques during fracture testing, using foil gauge, potential flow and acoustic pickup methods

15 p2713 A69-31109

Test facility for qualification of satellite fairings jet-tisoning system, describing accelerating tower and recording and control instrumentation

16 p2765 A69-31739

Selective amplifier for recording time signals on Time Recorder 2 and measuring time lag caused by Philips BRO 501 radio receiver

16 p2790 A69-32217

NaI/Tl and CsI/Tl scintillation counters effectiveness in recording low energy protons against counter noise background

18 p3138 A69-35255

Recording instrument paper speed effect on pulse wave measurements precision, discussing multiple observer studies of left ventricular ejection time

19 p3258 A69-36449

Recording devices for storing bandwidth data in time sequence, studying design parameters using light beam recorder implemented with CRT for read-in process

20 p3540 A69-37640

Cranz-Schardin camera for high speed recording in dynamic photoelastic fringe pattern studies, discussing framing rates, fringe gradients and design

20 p3541 A69-37778

Radial velocities recording inaccuracies by solar magnetographs caused by dissimilarity between photomultiplier characteristics, describing photometer designs to eliminate errors

20 p3547 A69-38308

Rheography of blood circulation of forearm after tightening with pneumatic cuff, analyzing amplitude increase and information about vascular system

21 p3653 A69-38838

Cosmic ray electron recorder for measuring intensity, energy spectrum and angular distribution of electron fluxes within specific energy range

21 p3724 A69-39074

Wideband telemetry recording error compensator for reducing flutter and interchannel time-base error in magnetic tape instrumentation

23 p4137 A69-41775

High speed tape transport characteristics, discussing capstan design, negative progression, reel-capstan interface, etc

23 p4165 A69-41776

Isometric recording device for tensile stresses on muscle preparations in vitro, based on differential transformer

23 p4111 A69-42056

RECOVERABILITY

Recovery rate at room temperature in Li-doped p-n Si diodes and solar cells after 1 Mev electron irradiation, noting capacitance changes

06 p0974 A69-16867

Firebee 2 /BQM-34E/ turbojet-propelled recoverable supersonic aerial target construction, performance prediction and missions

09 p1434 A69-21901

Time optimal regulator problem with recoverability constraint as restriction on system state during control synthesis

12 p2052 A69-26504

RECOVERABLE LAUNCH VEHICLES

Reusable aircraft type satellite launchers, discussing first stage recovery by parachute, ballutes, flexible wings and gyroglider

24 p4250 A69-42562

RECOVERABLE SPACECRAFT

NT AEROSPACEPLANES
NT APOLLO SPACECRAFT
NT GEMINI SPACECRAFT
NT MERCURY SPACECRAFT
NT REUSABLE SPACECRAFT
NT VOSKHOD 1 SPACECRAFT
NT VOSKHOD 2 SPACECRAFT
NT VOSKHOD MANNED SPACECRAFT

Paraglider as recoverable sounding rocket dropped from helicopter, describing system design and flight tests

[UN PAPER 68-95445] 01 p0161 A69-10465

Modular configuration of recoverable scientific MAP /Modular Auroral Probe/ payloads aboard Nike-Apache rockets, discussing payload design concepts

23 p4223 A69-41763

Flexible parawing lifting decelerator research data from wind tunnel and flight tests, noting manned space vehicle recovery and aircraft escape systems

[AIAA PAPER 68-967] 24 p4254 A69-43715

RECOVERY PARACHUTES

Air to air recovery of reentry vehicles, discussing parachute/wing descent, aircraft/helicopter energy absorption, payload boarding and towing techniques

[AIAA PAPER 68-1163] 03 p0520 A69-13563

Parachute recovery system for spinning /250 rps/ 155 mm shell launched to 3000 ft/sec by 20,000 g acceleration

[AIAA PAPER 68-937] 12 p2014 A69-26805

Emergency escape and personnel recovery systems including F-111 explosive system, midair deployed buoyancy aerostat and fly-away flexible wing rotor

15 p2551 A69-30853

Recovery system for high altitude sounding rocket payloads, noting air inflated flotation device, payload separation and parachute deployment

[AIAA PAPER 68-959] 21 p3820 A69-39227

RECOVERY TEMPERATURE

U SKIN TEMPERATURE [NON-BIOLOGICAL]

RECOVERY ZONES

Spacecraft return probabilities with time constraints and redundant access, using Borel set concept for counting and summing coverage belts

21 p3819 A69-39017

RECREATION

Leisure time and recreation facilities during long duration space missions, discussing astronaut selection procedure, active recreation, passive enjoyment and exercise programs

06 p0880 A69-17209

RECRYSTALLIZATION

Titanium alloy VTZ-1 recrystallization and oxidation processes studied by heating within 700-1200°C temperature range

01 p0094 A69-10214

Chondrules in Sharps /H-3/ chondrite show evidence of recrystallization and homogeneous olivines and pyroxenes

01 p0156 A69-10977

Nickel-cobalt fcc alloys rolling and recrystallization textures established with filtered Aco K-alpha radiation, considering stacking fault energy effects

04 p0615 A69-14643

Diamond pyramid hardness dependence on grain size of recrystallized alpha titanium

06 p0943 A69-17235

Crystal growth and deformation induced recrystallization in pure aluminum [ONERA-TP-671]

07 p1167 A69-19340

Time and temperature dependence of Mo and W deformation structure variation and primary recrystallization from metallographic investigations using electron microscopy

08 p1334 A69-21058

Recrystallization diagrams of commercially pure Mo and Mo alloyed with Fe, Co or Fe plus Ni, noting additions effect on recrystallized grain size

10 p1715 A69-24012

Solid solution decomposition effect on binary Mg alloys recrystallization temperature containing Al and Nd, using X ray and microstructural analysis

11 p1902 A69-24272

Plasticity increase of molybdenum alloys during precipitation of second phase at high temperatures due to lattice defects redistribution and plastic deformation

11 p1906 A69-25685

Molybdenum additive role in deformed carbonylic nickel recrystallization process

12 p2114 A69-26454

Metallographic study of microstructure recrystallization of 50 Ni-50 Fe alloy during annealing using special etchants and methods

13 p2281 A69-28155

Titanium alloy VT3-1 recrystallization and oxidation processes studied by heating from 700-1200°C

15 p2637 A69-30270

Structure of meteorite Gibeon section containing taenite grains and annealing twins indicating plastic deformation of taenite followed by recrystallization and grain growth

17 p3034 A69-33586

Secondary recrystallization in cold rolled molybdenum foil as function of temperature using electron microscopy and diffraction

18 p3157 A69-35253

Metal purity effect of nickel and Ni-Mo alloy on nucleation and recrystallization nuclei growth following 80 percent plastic deformation

18 p3159 A69-35449

Recrystallization limit effects on coarse grain growth in aluminum alloys extruded sections, studying roles of additives, extruding temperature and heat treatment duration

18 p3160 A69-35472

Dynamic recrystallization in Ni and Ni-Fe alloys during torsional high temperature deformation

19 p3344 A69-36147

Boron thermal diffusion effects on plastic properties of pure Mo subjected to recrystallization

19 p3328 A69-36160

Recrystallization in thoria dispersed Ni sheet as function of strain-anneal cycles, using electron transmission technique quantitative determination

20 p3557 A69-36958

Extrusion variables influence on microstructure and hardness level of Ti-Al-Sn compared with recrystallization behavior after cold swaging [ASM PAPER W9-8.2]

21 p3729 A69-38660

Abnormal grain growth during secondary recrystallization of hydraulically extruded molybdenum as function of annealing

21 p3745 A69-38953

Recrystallization during sintering of free flowing Nb and Ti carbide powders, determining grain growth dependence on temperature and activation energy

22 p3970 A69-40636

InTe phase recrystallization in thin films composed of two InTe phase mixtures, showing random concentrations and distribution of centers growing as spherulites

24 p4361 A69-42993

InTe phase formation in thin film composed of two InTe phases, showing dependence on annealing in high vacuum and substrate temperature

24 p4361 A69-42994

RECTANGLES

Thermal contact rectangle with single side heat capacity, applying Fourier transform and Abel convergence tests

03 p0533 A69-13863

Unsteady three dimensional heating of finite solid rectangular parallelepiped, deducing expressions for rectangle and slab

15 p2717 A69-30790

RECTANGULAR BEAMS

Moment curvature models under reverse cyclic straining developed from stress-strain curves for rectangular beams

04 p0683 A69-15497

Rectangular thin beam Saint Venant deflection in case of moment stresses based on elasticity and shell theory

05 p0834 A69-15783

Large displacement bending of rods for constant deformation cross section, negligible shearing forces and exponential stress-strain relation

05 p0843 A69-16682

Torsional vibrations of unstiffened cylindrical tubes analysis by differential equations and applications to free-free rectangular cross section

09 p1620 A69-22769

Interfacial pressure distribution during slip damping in clamped rectangular beams subjected to vibration

10 p1800 A69-23350

Long rectangular rods stability and vibrations under elastic deformations using bending theory

10 p1802 A69-24024

Torsional shearing stress in thick walled hollow rectangular cross sections

13 p2358 A69-27212

Membrane analogy for flexure of prismatical beams with square cross section and longitudinal cavities, employing Saint-Venant solution

15 p2704 A69-30288

Calculation of natural twisting and bending vibrations of beam with characteristics varying along length

16 p2873 A69-32130

Vibration modes and damping of rectangular cantilevered prismatic steel rods, showing effects of transverse vibration, material and stress on logarithmic decrement

17 p3065 A69-33936

Rectangular thin beam Saint Venant deflection in case of moment stresses based on elasticity and shell theory

18 p3223 A69-35035

Acoustic and internal dampings in freely supported uniform beams of circular and rectangular section, showing frequency dependence and vacuum effect

20 p3620 A69-37062

Rectangular cross section pretwisted beams model curves for turbine and compressor blading vibrational studies

20 p3621 A69-37080

Transverse vibrations of isotropic solid rectangular beam with secondary effects of rotary inertia and shear deformation retained

21 p3832 A69-38447

Stability loss of beams analyzed under compression allowing for various creep conditions in loading and unloading regions, calculating time to failure

22 p4039 A69-39917

Compressed rectangular beam stability under different creep conditions, deriving relation between creep time and initial deflection

22 p4039 A69-39918

Torsion analysis of curvilinear rectangular prismatic beam reinforced by off-center circular rod, using conformal mapping

22 p4049 A69-41279

RECTANGULAR GUIDES

Phase constant of rectangular waveguide containing longitudinal dielectric slab of arbitrary cross section calculated using orthonormal waveguide functions with separated curl and potential fields

01 p0042 A69-10437

Symmetrically truncated right angle E-plane corner, placing electric and magnetic walls in symmetry plane, solving resulting boundary value problems

01 p0044 A69-10624

E field transmission and reflection coefficients in linearly tapered waveguide for fundamental and higher order modes, using point matching method

01 p0044 A69-10629

Calibration of coaxial line noise sources in terms of rectangular waveguide standard, discussing use of adapter for comparison

02 p0210 A69-12436

Higher order modes suppression in square waveguides by bifurcating metal septa of finite length, analyzing periodic array of many finite-length septa

04 p0576 A69-14758

Scattering matrix for internal diffraction in rectangular waveguide with transversely magnetized ferrite core

06 p0895 A69-17455

Characteristic impedance of rectangular waveguide computation curve explained on basis of computer program for cascade of transmission line sections

06 p0897 A69-17490

Propagation modes in corrugated cylindrical waveguides determined by imposing nonisotropic surface reactance boundary condition at corrugated walls

08 p1284 A69-20295

Nonohmic microwave conductivity in semiconductor posts in rectangular waveguide, measuring incident, transmitted and reflected microwave powers

08 p1373 A69-20859

Reflection coefficient of double discontinuity consisting of two closely spaced inductive irises in rectangular waveguide

09 p1453 A69-21444

Radiation field patterns from metal wall aperture in waveguide with rectangular cross section determined using elliptic cylinder

11 p1850 A69-24982

Limiting frequencies of inhomogeneously filled lossless rectangular waveguides and field states, using Maxwell equations

11 p1855 A69-25620

Perturbation analysis in dielectric loaded rectangular waveguides, considering scattered modes and phase progression

12 p2039 A69-26381

Transmission type E saki diode amplifier with stabilizing dielectric loaded rectangular waveguide

13 p2233 A69-28067

Variational method used to determine accuracy of approximation technique for dielectric slab on sidewall of rectangular waveguide

13 p2233 A69-28072

Wave propagation and bandwidth characteristics of rectangular waveguide loaded with H plane lossless dielectric slab

13 p2222 A69-28075

Tunable band stop filter realization from characteristic equation solution for propagation modes by magnetized ferrite slab placed in rectangular waveguide

14 p2422 A69-29751

Relative dielectric constant and permeability of inhomogeneously filled rectangular waveguide filling medium expanded into trigonometric series to calculate cut-off frequencies and field patterns

15 p2577 A69-30627

Equivalent circuits of dielectric loaded and unloaded rectangular waveguide Esaki diode reflection amplifier

15 p2578 A69-30801

Scattering by cylindrical post of complex permittivity /plasma/ in rectangular waveguide, calculating reflection, transmission and absorption coefficients by computer

16 p2756 A69-31578

Electromagnetic wave propagation in transversely magnetized warm plasma filled rectangular waveguide, analyzing TE and TM modes

16 p2756 A69-31581

Broadband low VSWR transitions between rectangular waveguides and coaxial transmission lines, discussing asymmetrical probe and ridge types

16 p2757 A69-31584

Microwave field-plasma slab nonlinear interaction in rectangular waveguide, analyzing current and electron density and second harmonic TE and TM power

16 p2749 A69-31703

Mode filters for oversized rectangular waveguides, considering resistive sheet with complex surface impedance

16 p2760 A69-31948

Wave propagation in rectangular guides, determining dispersion curves by continued fractions method allowing for infinite set of time-space harmonics

17 p2925 A69-33843

Electromagnetic wave scattering in two angled rectangular waveguides filled with isotropic homogeneous medium

17 p2930 A69-33887

Solid state SHF transmission amplifiers design using rectangular waveguides and biased bulk GaAs

21 p3683 A69-39452

Electromagnetic propagation in infinite rectangular waveguide surrounded by dielectric medium described by Green dyadic

23 p4115 A69-41570

Waveguide fed rectangular aperture antenna with dielectric plug load, describing admittance resonant perturbation due to excited TE mode

23 p4136 A69-41589

Rectangular waveguides coupled by oblique subsonant slots in common face, discussing slot orientation and geometry roles

23 p4123 A69-41941

Electromagnetic wave diffraction by multielement periodic metallic strips arrays positioned transversely in rectangular waveguide

23 p4124 A69-42035

Rectangular waveguide with periodic array of infinitely thin metallic strips, studying intrinsic oscillations critical frequencies and amplitude spectrum

23 p4124 A69-42036

Electromagnetic wave propagation in rectangular and plane parallel waveguides coupled by common wall with periodic transverse slots

23 p4124 A69-42037

Rectangular waveguide with inhomogeneity represented by half space dielectric filling with boundary causing polarization, obtaining reflection elimination or minimization reflection

23 p4125 A69-42047

Transmission properties and directional coupler determined for optical circuit dielectric rectangular waveguide with surrounding dielectrics of smaller refractivity

24 p4287 A69-43328

Rectangular dielectric waveguide propagation modes, describing computer analysis based on electromagnetic field expansion in circular harmonics series terms

24 p4288 A69-43330

RECTANGULAR PANELS

Optimization of plane smooth rectangular panels of constant cross section subjected to loading and heating conditions

08 p1417 A69-20821

Finite element analysis of flat rectangular panels, developing equilibrium equations based on specified displacement modes

15 p2708 A69-30667

Finite element analysis of flat rectangular orthotropic multilayer stiffened panels, proposing six degrees of freedom model

15 p2708 A69-30668

Supersonic flutter in square panels and cylindrical shells, measuring critical dynamic pressure

17 p3051 A69-32923

Lightweight structural design problem of stress concentration associated with load diffusion in rectangular panels with constant stress flanges

18 p3219 A69-34785

Stability of sandwich panel strip with lightweight core, formulating problem in terms of equilibrium conditions and potential energy of system

21 p3832 A69-38417

RECTANGULAR PLANFORMS

Rectangular planform shallow spherical shell stability with mixed boundary conditions, using Cauchy-Riemann equations and equation for plate on elastic base

10 p1792 A69-22848

Numerical analysis of natural oscillations of three layer sandwich plates of rectangular planform, considering end conditions

11 p1976 A69-24773

RECTANGULAR PLATES

Rib positioning effect on mechanical behavior of cantilevered rectangular plate in gas flow, considering critical flow velocities and rigidity relationships

01 p0165 A69-10085

Gyroscopically induced vibrational response of rectangular plates and membranes, determining spin and precession effects on natural frequencies

02 p0347 A69-12519

Integral equation solution for plate with internal support

03 p0528 A69-13799

Resonance analysis of forced vibration of rectangular plate in three dimensional supersonic flow

03 p0528 A69-13928

Bending of rectangular plate with partial clamping, obtaining solution by superposition method

04 p0681 A69-15289

NeoHookean /incompressible solid/ rectangular parallelepiped compressed between lubricated rigid plates, comparing stability bounds with predicted critical loads

04 p0682 A69-15303

Clamped rectangular plate under lateral load stress analyzed by extended Kantorovich method to include bending moments and shearing forces

05 p0835 A69-15872

Green function for computation of stress intensity factors for edge cracks in rectangular plates with arbitrary loadings
[ASME PAPER 68-WA/MET-18]

05 p0839 A69-16156

Green function for stress intensity factors of rectangular plate edge cracks, noting application to thermal stresses
[ASME PAPER 68-WA/MET-19]

05 p0839 A69-16157

Plate deflection in own plane under moments applied to ends using elasticity theory, deriving relation between stress tensor and stress function

06 p1021 A69-17177

Stability of rectangular transversely isotropic plate hinged at three sides under uniform pressure applied to two opposite hinged sides

06 p1021 A69-17178

Optimal computer calculation procedure for medium thickness anisotropic laminar plates with shear applied to rectangular and hinged plates

06 p1026 A69-18015

Free vibrations of plates and beams of pyrolytic graphite type materials, analyzing transverse shear deformation and rotary inertia
[AIAA PAPER 69-55]

06 p1027 A69-18070

Plane anisotropic rectangular plates with various boundary conditions, analyzing stability, natural frequencies, mode shapes and displacement under lateral loads

07 p1232 A69-18719

Analytical solution for plate velocity statistics of turbulent-flow-excited rectangular flat plate, discussing vibration excitation

07 p1236 A69-19461

Two dimensional photoelasticity for minimizing stress concentration in perforated rectangular plate subjected to restrained shrinkage, discussing application to solid propellant rocket grains

08 p1412 A69-20255

Vibration characteristics of rectangular plate with fatigue crack and subject to tensile load, applying results to crack propagation in fuselage panels

08 p1413 A69-20399

Differential equation reduction for vibrational motion of rectangular plates subjected to variable tangential forces, discussing dynamic stability

08 p1415 A69-20666

Castigliano variational principle applied to thermal stresses in rectangular plate by expanding stress function in double series of cosine binomials

08 p1419 A69-21178

Free transverse vibrations of rectangular flat plate simply supported along periphery and rigidly connected to interior columns
[ASCE PAPER 739]

09 p1616 A69-21928

Finite inelastic deformations under transverse impulsive loading of clamped thin rectangular planform shells idealized as membranes, using incremental plasticity theory

09 p1616 A69-21939

Central circular hole effect on fundamental frequency of rectangular fixed edges plate, discussing hole size, square plates, etc
[ASME PAPER 69-VIBR-62]

10 p1805 A69-24156

Linear differential equation solution for elastic systems stability problems, discussing applications to heated rectangular plates

11 p1982 A69-24950

Field approach for stress and deflection analysis in rectangular plates reinforced by straight ribs, noting kernel function

11 p1983 A69-25019

Supersonic flutter solutions using finite elements, analyzing rectangular plate bending elements, square simply supported and clamped panels, low aspect ratio configurations, etc

11 p1991 A69-25516

Simply supported laminated anisotropic rectangular plate with coupling occurring between bending and in-plane extension, discussing stiffness analysis by Fourier series method

12 p2184 A69-26808

Lateral bending and two dimensional thermal stress in rectangular orthotropic plates, considering alternating direction implicit method

12 p2188 A69-27100

Correlation between temperature and stress field in thermal buckling of square viscoelastic Maxwell plates under random temperature

12 p2188 A69-27113

Natural vibration modes of linearly tapered rectangular plates, approximating plate characteristic shapes with series of products of beam characteristic shapes

13 p2358 A69-27211

Vibration modes in four lowest natural frequencies of clamped rectangular plates with linear thickness variation, using Ritz method

13 p2361 A69-27442

Shear buckling of clamped rectangular linearly tapered plates, considering uniform shear stress and load

13 p2361 A69-27443

Sine series solution for flexural vibration of rectangular isotropic plates applied to free vibration of orthotropic plates

13 p2363 A69-28128

Rectangular plate buckling analyzed by finite element method with deflection function

13 p2364 A69-28225

Uniaxial compressive stability of rectangular boron-epoxy laminated plates clamped on loaded edges, determining buckling loads by Southwell plots

13 p2287 A69-28669

Free vibrations of laminated anisotropic rectangular plates with clamped edges analyzed by Rayleigh-Ritz energy method

13 p2371 A69-28673

Analogy between differential equations for skew isotropic plates and rectangular anisotropic plates

13 p2371 A69-28678

Buckling of unsymmetric cross-ply rectangular plates under uniform shear, considering hinge-support boundary conditions

13 p2371 A69-28679

Elastic-plastic bending of rectangular plates with asymmetrically inhomogeneous material in plastic range, using modified Ritz method

14 p2533 A69-28984

Postbuckling of rectangular plates with exponential variation in thickness, analyzing large deflection equations using dynamic relaxation method

15 p2704 A69-30291

Strains determination for laterally edge loaded rectangular plate and sagittas determination of perpendicularly loaded plate proved analogous

15 p2704 A69-30295

Finite element and iteration method for large deflection of rectangular plate, considering stiffness matrix for bending

15 p2706 A69-30435

Stress concentration near circular nonreinforced hole at bending of transversely isotropic rectangular plate analyzed in terms of transverse shear theory

15 p2707 A69-30580

Eigenvalue problems in partial differential equations solved by extended Kantorovich method, considering vibration of rectangular membrane and stability of elastic rectangular plate

16 p2876 A69-32783

Stability of nonuniformly heated rectangular plate reinforced by elastic longitudinal and rigid transverse ribs, accounting for influence of torsional and bending rigidities

17 p3057 A69-33198

Moire reflection technique applied to study of stress-strain state of partially clamped rectangular cantilever plates under various loads

17 p3058 A69-33203

Discrete element displacement method applied to buckling analysis of flat rectangular plates under arbitrary membrane loading, calculating critical load intensities

17 p3066 A69-34048

Uniform thickness rectangular plates bending with rigidly clamped or freely hinged edges solved by refined version on digital computer

18 p3215 A69-34535

Transverse vibrations of thin linear viscoelastic rectangular plate of constant thickness resting on elastic medium

18 p3223 A69-35171

Strength analysis of three layer rectangular plates under complex load and support distributions

19 p3434 A69-35827

Bending of normally loaded simply supported rectangular plates in large deflection range solved by nonlinear differential equations and minimum potential energy principle

19 p3445 A69-36828

Simply supported rectangular plates experiments showing prediction on buckling load

19 p3447 A69-36854

Rectangular plate bending element corresponding to finite difference method use, deriving stiffness matrix from strain energy approximation

20 p3619 A69-36949

Clamped uniformly loaded rectangular plate large deflection elastic behavior approximate analysis, using perturbation method

20 p3620 A69-36998

Flat rectangular plates large deflection due to uniform lateral pressure and compressive edge loading analyzed through partial differential equations, difference equations and computer program

20 p3620 A69-37000

Energy formulation extended for plane anisotropic rectangular plates, handling nonuniform properties and loadings

20 p3627 A69-37766

Transverse shear deformation effect on bending of laminated rectangular plates, obtaining solutions for bending deflections, flexural vibration frequencies and buckling loads

20 p3627 A69-37770

Nonlinear oscillations of rectangular plates of composite materials by Berger approach and Reissner variational principle, noting rotary inertial and transverse shear deformation

20 p3627 A69-37771

Rectangular plates bending boundary value problems, deriving formulas for plates with free edges

20 p3630 A69-38291

Bifurcation and hardening rate of rigid-plastic bodies presented on buckling of rectangular plate with lateral restraint

21 p3840 A69-39299

Rectangular plate under biaxial tension stress analyzed to determine onset of necking and stress-strain state

22 p4039 A69-39913

Supersonic panel flutter boundary of buckled and unbuckled clamped rectangular plates, discussing in-plane stress effects

22 p3930 A69-40584

Buckled rectangular plates with constrained edges, analyzing natural frequencies as basis for supersonic panel flutter analysis

22 p4046 A69-41049

Nonlinear random vibrations excitation in rectangular flat plate with initial imperfection by white noise, assuming clamped boundary conditions

22 p4048 A69-41183

Natural vibrational frequencies of uniform thin elastic isotropic flat plates, investigating rectangular and parallelogram plates with various edge conditions

23 p4233 A69-42348

Shearing force and shear buckling deformation influence on supersonic panel flutter boundary of simply supported rectangular plates, basing analysis on deflection approximation

24 p4400 A69-43055

Initial deflection and internal pressure effects on supersonic panel flutter boundary of simply supported rectangular plates under diverse middle-surface stress conditions

24 p4400 A69-43056

Single series solution for rectangular plate deflection under arbitrarily located concentrated load, considering monolithic slab beam connection case

24 p4404 A69-43593

Buckling of thick homogeneous rectangular plates subjected to constant normal stress, noting error for thin plate approximation

24 p4406 A69-43696

RECTIFICATION

Ranger pictures improvement by computer, eliminating image distortion due to electronic imaging systems

06 p0924 A69-17164

Optical rectification effect in lithium metaniobate crystals under neodymium laser radiation, comparing results with data for potassium dihydrophosphate crystals

14 p2458 A69-29168

RECTIFIERS

NT AVALANCHE DIODES
NT CRYSTAL RECTIFIERS
NT GERMANIUM DIODES
NT THYRATRONS
NT THYRISTORS

Self excitation conditions and output characteristics of tunnel diode DC to AC converters for spacecraft, discussing relaxation-oscillator and push-pull circuit converter types

01 p0046 A69-10755

Synthetic circuit equipment for semiconductor rectifier life testing with built-in fault analyzer for indicating shorted and broken diodes

08 p1293 A69-21113

Probability distributions of characteristics of mass produced semiconductor rectifier diodes

12 p2035 A69-25832

Semiconductor rectifiers economic life testing with synthetic circuits utilizing thyristor switch

15 p2579 A69-31041

Optical IR yttrium-iron garnet rectifier increasing light intensity and system Q factor at low external magnetic field

17 p2981 A69-33117

Symmetrically regulated AC/DC converters power characteristics improved by switching in phase rectifiers twice during control cycle

24 p4254 A69-42570

RECTUM

Calorimetry-thermometry discrepancy during prolonged exercise in hot dry environment, measuring rectal temperature with increasing exposure time

23 p4098 A69-42104

RECUPERATORS

U REGENERATORS

RECURSION FORMULAS

U RECURSIVE FUNCTIONS

RECURSIVE FUNCTIONS

Generalized digital low pass filter synthesis by recursion technique, noting coefficient sensitivity simplification

03 p0403 A69-13227

Linear differential equations with sinusoidal coefficients analyzed with aid of trinomial recursions

05 p0787 A69-16464

Existence of minimal solutions of doubly infinite trinomial linear recursions of Poincare-Perron type

05 p0787 A69-16465

Recursive formulas for numerical evaluation of real convolution integral for simulation of control systems and electrical networks on digital computer

06 p0947 A69-17250

Recursive algorithms for pattern classification using misclassified samples

06 p0891 A69-17357

Nonlinear programming computational algorithm for recursive optimal estimates of constrained states of linear system

06 p0902 A69-17403

Probable spectrum stability criterion and reducibility derived for linear differential equation having recursion or almost periodic coefficients

10 p1720 A69-23562

Dynamical systems technique for nonautonomous differential equations leading to recurrent motions

10 p1720 A69-23636

Kalman equations of optimal recursive filter for linear discrete system extended to continuous system through limiting procedure

11 p1859 A69-25408

Recursive estimation of noisy nonlinear multivariable systems in white noise by Kalman, second order nonlinear and iteration filters

12 p2046 A69-26062

Stationary inventory problems analysis, discussing inventory policy, recursive and or limiting procedures, stationary point processes, stock delivery time instants, etc

12 p2192 A69-26750

Book on estimation theory and applications covering stochastic processes, linear estimators and recursive formulations

16 p2764 A69-32386

Optimal linear recursive estimators for uncertain observation, considering false alarm probability

20 p3485 A69-36922

Recurrence formulas for calculating Fourier expansions in elliptic motion in terms of eccentric and mean anomaly

[AIAA PAPER 69-910]

21 p3807 A69-39342

Recursion formula for multilayer interferometer derived, with allowance for multiwave interference, to calculate resonant circuit maxima and minima

23 p4165 A69-41729

Recursive estimation of noisy nonlinear multivariable systems in white noise by Kalman, second order nonlinear and iteration filters

23 p4146 A69-42447

Unmodeled errors detection in recursive flight trajectory estimation, deriving equations for unmodeled parameters

24 p4387 A69-43585

RED ARCS

Low latitude m arcs in 6300 angstrom emission during intense geomagnetic storm related to auroral red oxygen emission peak

01 p0062 A69-10136

Auroral midlatitude red arcs ground and satellite data, noting field aligned electron density depression, plasma temperature increase and O plus-H plus transition altitude

20 p3532 A69-37897

RED BLOOD CELLS

U ERYTHROCYTES

RED SEA

Lineament trend analysis of Gemini Red Sea synoptic terrain photography, noting computerized rotation from apparent to true angles

02 p0247 A69-12808

RED SHIFT

General theory of relativity tests with aid of satellites, considering gravitational red shift measurements, light deflection in solar field, etc

01 p0152 A69-10751

Red shift pattern in quasar emission spectra consistent with fractional screening charges on emitting atom nuclei

01 p0153 A69-10855

Absorption and emission redshift distribution in quasars, N systems and similar compact and radio galaxies

02 p0325 A69-12591

Continuum radiation of quasars, adopting cosmological interpretation of red shift

04 p0648 A69-14565

Quasars, stressing local Doppler and gravitational hypotheses for observed red shifts

06 p0998 A69-16968

Optical mean energy distribution of quasars, discussing red shift effects, significance of physical origin of optical continuum radiation and K-term magnitude determination

06 p0999 A69-16975

Mass motions in flares and moustaches indicated by spectral features, discussing red asymmetry of line emission

06 p0994 A69-17432

Complex distribution of quasar red shift interpreted as due to two simple distributions of cosmological and gravitational red shift

06 p1009 A69-17968

Cosmological model describing relation between red shift and magnitude of quasars

07 p1211 A69-18406

Red shifts and intrinsic powers of radio galaxies and quasars, discussing local luminosity distribution, function of sources and cosmology

07 p1206 A69-19270

Redundant world models, discussing elimination through measurement of larger red shifts of galaxies and quasars

07 p1219 A69-19283

General relativistic gravitational red shift effect on frequency transmitted from satellite orbits, noting possibility of measurement

08 p1383 A69-19901

Relativistic astrophysics, discussing quasar phenomenology, red shift cosmology and relationship with galaxies

08 p1388 A69-20222

Time delay, red shift, equivalence principle, light deflection and perihelion motion tests of general relativity with Jupiter probe

09 p1597 A69-22089

Quasar red shifts due to cosmological and gravitational factors, assuming correlation of QSO intrinsic luminosity with gravitational red shift values

09 p1597 A69-22151

Red shifts of radio sources obtained with Carnegie image tube spectrograph, noting quasi-stellar objects and galaxies

09 p1602 A69-22224

Red shifts of quasi-stellar objects obtained with image tube spectrograph, noting photoelectric magnitudes and colors

09 p1602 A69-22225

Absorption red shifts in quasi-stellar source due to dead galaxies in cosmologically flat model of universe

09 p1602 A69-22228

Absorption red shifts in quasar spectra from spectroscopic observations of PHL 5200 and B194

09 p1604 A69-22271

Bolometric luminosity-red shift relations of Friedmann dust universes corrected for inhomogeneities, using locally inhomogeneous Swiss cheese models

09 p1605 A69-22411

Interstellar reddening material distribution within 2500 parsecs of sun, noting concentration in galactic plane, spiral arms and cloud complexes

10 p1773 A69-22961

Red shift hypothesis postulated on perfect cosmological principle and uniqueness of electromagnetic wavelength measurements, showing agreement with astronomical data

11 p1961 A69-25108

Quasars and radio-quiet objects numbers and properties, discussing red shifts interpretation by cosmological, gravitational and Doppler theories

12 p2161 A69-26937

Colorimetric studies of galaxies exhibiting red shift with increasing radial distance from center

12 p2164 A69-27025

Radio galaxy identification and luminosity measurement, noting limitations of red shift observation methods

12 p2165 A69-27032

Quasars optical properties, hypotheses on nature, energy distribution, red shift, stellar magnitude and distance estimation on basis of absorption

12 p2167 A69-27042

Red shift determinations and line identifications for quasars, using spectrograph with electro-optical converter

12 p2168 A69-27048

Law of optical radiation and photometric characteristics of quasars, noting photometric effect of strong emission lines and color dependence on red shift

12 p2168 A69-27052

Absorption line spectrum of quasar Ton 1530, discussing line widths and red shifts

13 p2334 A69-27306

Statistical tests for cosmological hypothesis for origin of absorption lines in spectra of quasars, considering red shifts

13 p2334 A69-27307

Quasar red shifts distance dependence indicated by visually bright quasar faintness in radio range

13 p2344 A69-27635

Relativistic version of generalized gravitation theory, establishing models to describe gravitars having large gravitational mass defect and red shift

13 p2351 A69-27864

Low density Friedmann universe models with non-zero cosmological constant and long ages, deducing galaxy evolution rates from magnitude-red shift relations

14 p2527 A69-29944

Quasar multiple absorption red shift lines caused by gas in extended galaxy halos, assuming broadened galactic cross section area

15 p2695 A69-30884

Quasi-stellar and related objects emission and absorption red shifts tabulation suggesting absorption lines origin

15 p2701 A69-31532

Quasi-stellar objects anomalous Hubble plot, suggesting explanation for steeper plot under assumption on red shift vs apparent magnitude relation

15 p2701 A69-31536

Red shift table for six galaxies near Coma Cluster from spectrograms of absorption lines

17 p3044 A69-34182

Red shift-distance relation for galaxies, discussing time dependence

20 p3597 A69-37411

Open cluster NGC 7128 distance and reddening determination by photometry

20 p3598 A69-37465

Quasars observations interpretation, discussing red shift origin, gravitational collapse, lifetime, distribution, cosmological aspects, etc

21 p3802 A69-38825

Discreteness of distances to extragalactic objects, tabulating red shift values from Wilson formula for galaxy clusters

21 p3802 A69-38843

Nonexistence of second order clustering of galaxies and relationship to gravitational cut-off, relativistic cosmologies and red shifted light by exponential decay of photon energy

22 p4024 A69-40579

Quasars red shifts distribution interpreted as due to cosmological and gravitational red shifts distribution, noting analysis error

22 p4024 A69-40580

Quasars observation failure for red shifts beyond z suggested due to absorption of intergalactic neutral H

22 p4024 A69-40582

Free-free intergalactic absorption at LF as function of red shift for uniform zero pressure cosmological models

22 p4025 A69-40640

Interstellar reddening in solar vicinity, analyzing roles of galactic latitude and longitude and heliocentric distance

22 p4026 A69-40648

Universe expansion model, integrating Einstein gravitation equations with cosmological constant lambda to interpret Hubble effect

22 p4029 A69-40756

Quasar association with galactic clusters, noting red shift and spectral correspondence

22 p4029 A69-40763

Observational cosmology in terms of relation between red shift and apparent luminosity of galaxies (Hubble relation/

23 p4219 A69-42328

Universe behavior in time, discussing expansion observed by red shift, closed universe with future contraction phase and unlimited expansion open model

23 p4221 A69-42391

Red shift determinations and line identifications for quasars, using spectrograph with electro-optical converter

24 p4375 A69-42551

Law of optical radiation and photometric characteristics of quasars, noting photometric effect of strong emission lines and color dependence on red shift

24 p4375 A69-42552

REDUCED GRAVITY

Lunar gravity simulation effect on human performance, discussing fidelity requirements, self locomotion, metabolic rate and psychomotor task decrement

02 p0203 A69-12217

Low g accelerometers including air-film, electrically suspended, vibrating string, semiconductor and ONERA

[ONERA-TP-449]

05 p0766 A69-16749

Sensory and motor activity of human subjects exposed to reduced gravitation during aircraft motions along parabolic trajectories

07 p1062 A69-18592

Space flight crew efficiency during prolonged weightlessness, stressing preflight adaptation and space vehicle technology improvement

07 p1063 A69-18596

Blind goldfish behavioral responses to short lowered gravitational force cycles during vertical flight classified as vestibular reflexes resulting from otolith displacement

11 p1828 A69-25464

Monograph on gravity covering gravimetric boundary value problem, iterative solutions, error analysis, gravity reduction, integral equations, etc

13 p2254 A69-27929

Excessive extrapolation limitations in applying transient data to low gravity fluid behavior for orbital refueling systems, presenting orbital fluid transfer experiment

[AIAA PAPER 69-566]

16 p2870 A69-32755

Nonlinear free surface effects in low gravity tank draining, finding domains of validity for linearized and nonlinear analyses

[AIAA PAPER 69-680]

17 p2953 A69-33450

Bjerhammer gravity reduction method applied to gravity in space, analyzing two test models with mass focused between topographical and reference surface

18 p3173 A69-35197

Circular baffle mounted above flat-bottomed cylindrical tank outlet, discussing effect on remaining tank fluid volume and flow behavior under low gravity conditions

21 p3696 A69-39232

Simulated low gravity propellant sloshing in spherical, ellipsoidal and cylindrical tanks, discussing Bond number simulation and tank geometry effects

[AIAA PAPER 69-1004]

22 p3921 A69-40378

Space manufacturing processes for orbital low and zero gravity environment, discussing buoyancy and thermal convection sensitive and molecular forces controlled methods

[AAS PAPER 69-486]

24 p4380 A69-42844

REDUCTION [CHEMISTRY]

NT DEOXIDIZING

NT HYDROGENATION

Electroless deposition of various metals with emphasis on nickel, discussing mechanism, plating solutions, substrates, deposit properties and applications

01 p0099 A69-11060

Thermodynamic and kinetic interactions of high melting point metal oxides reduction by carbon

03 p0445 A69-13568

Metal oxide and carbon interaction during spatial separation of reagents, noting influence of reducing agent activity on metal vapors

03 p0445 A69-13569

Titanium aluminum alloys two stage direct production by aluminothermal reduction of titanium tetrachloride

07 p1159 A69-18536

Titanium tetrachloride reduction to titanium by magnesium, showing autocatalytic process

07 p1163 A69-18784

Two stage sodium thermal reduction of Ti tetrachloride to metallic Ti, determining process parameters

07 p1164 A69-18785

Polymorphic characteristics of titanium pentoxide prepared by reducing titania, examining oxidation products with X ray diffraction

07 p1168 A69-19601

Platinum electrode study of electrochemical oxygen reduction in nonaqueous media, including kinetic effects of different water concentration levels

[ECS PAPER 7]

08 p1268 A69-20361

Physical properties control in nickel powders obtained by hydrogen reduction of nickel diamine sulphate solutions

08 p1334 A69-21057

Photochemical production of reduced organic compounds of C and N in primitive earth atmosphere

09 p1444 A69-21465

Equatorial mounted solar energy concentrator efficiency compared to unconcentrated sunlight and artificial UV-visible light source in reducing Pb tetraacetate solution in acetic acid

16 p2736 A69-31814

Pseudosplitting/peroxide mechanism for O reduction at fuel cell cathodes, analyzing O molecule adsorption, H bonding and electron transfer at surface

16 p2748 A69-32809

Nonmetallic inclusions formation mechanism after reducing iron by Al, Zr and Ti, noting oxygen/reducing agent ratio role

22 p3969 A69-40069

Gamma radiation effect on AgCl-Cu redox state in AgCl activated, heat treated Na-Al-B-Si glass, using EPR method

23 p4180 A69-42471

Chlorella enzymes activity in reducing nitrate to nitrite and nitrite to ammonia

24 p4263 A69-43136

REDUNDANCY

Multibeam recording technique producing speckle-free images in redundant holograms of transparencies

01 p0082 A69-10850

Book on laws of failures in technical equipment with emphasis on quantitative description and practicality of reliability theory, discussing redundancy problems

03 p0453 A69-13009

Curve fitting for optimum redundancy reduction on sampled data, describing polygonal and approximate polygonal techniques

09 p1533 A69-22458

Pure inertial navigation system support by supplying additional or redundant navigational information, considering space flight applications and earth related problems

12 p2128 A69-25873

Data compression, redundancy reduction and applications to space flight technology

12 p2027 A69-25876

Stability augmentation system for CX-84 tilt wing V/STOL aircraft, using redundancy techniques to achieve fail operational performance with two active channels

[AHS PAPER 310]

17 p2901 A69-33545

Slide methods for duplex parallel and switchover redundant mission availabilities based on cost, reliability and maintainability

18 p3147 A69-34531

Masking and standby redundancy approach to fault tolerance in space navigation computers with illustrations, discussing automatic maintenance

19 p3279 A69-35798

Maximum rms error comparison of redundancy reduction techniques, emphasizing limiting slope technique and worst case interpolation error

19 p3273 A69-36264

Spacecraft control systems with computer command redundant jets for linear and angular pulses, relating configuration design to level-of redundancy and task dimension

[AIAA PAPER 69-845]

21 p3822 A69-39375

Fail-soft operation in array processor with cellular redundancy, discussing cellular autonomy, long life and ultrareliability

[AIAA PAPER 69-965]

22 p3906 A69-40346

REDUNDANCY ENCODING

Binary block codes for correction of substitution and synchronization errors

09 p1452 A69-21316

Huffman minimum redundancy coding extension to run-length information based on Poisson distribution, including optimization and data compression applications

19 p3272 A69-36262

False signals formation during random pulse noise in single command channels with PTM coding, noting code value and redundancy

19 p3278 A69-36595

REDUNDANT COMPONENTS

Nonorthogonal multisensor strapdown inertial reference unit providing redundant capabilities and optimal performance

03 p0429 A69-13211

Digital computer simulation of nonlinear redundant structure variables including thermal influence, creep and arbitrary loads

[AIAA PAPER 69-120]

06 p1028 A69-18166

Triodes reliability for space application, emphasizing RH 7 Cc used during Mariner 4 expedition

08 p1295 A69-21122

Reliable operation duration distribution shown to be arbitrary for standby system consisting of basic device and n devices in nonloaded standby condition

09 p1513 A69-22676

Optimum automatic selection of redundancies, discussing weighting and pivot choice and rigid element incorporation

11 p1993 A69-25529

Digital computer redundancy, analyzing triple modular redundancy in Saturn vehicles and quad design in primary processor and data storage for OAO

12 p2034 A69-26567

Redundant systems reliability prediction for single mission in standby mode or without standby, using failure states concept and birth-death equations

12 p2102 A69-26569

Complex electronic systems optimum redundant element content determination for ensuring adequate supply

14 p2426 A69-29422

Satellite circuit assembly reliability achievement by high reliability components, redundancy and optimal utilization

15 p2624 A69-30819

Multistage systems high reliability design, describing branch and bound computer method for optimal resource allocation of redundant components

18 p3148 A69-35081

Sequential design for economic description of potentially redundant elastic structures, noting redesign sequence

21 p3842 A69-39302

Valving concepts and functional approaches for inert gas attitude control thruster systems providing redundancy safeguards at minimum weight, volume and power costs

[AIAA PAPER 69-843]

21 p3786 A69-39373

Triple redundant actuator for fly-by-wire control system, noting electrohydraulic servomechanisms in side-by-side arrangement

22 p3870 A69-41242

Two channel electronic system with one redundant channel for automatic replacement in case of failure evaluated for operational preparedness

23 p4136 A69-41559

Liapunov stochastic stability direct method analog used for estimating reliability of redundant systems with constant recovery time

23 p4144 A69-41953

F-111D computer complex to provide selective functional redundancy and flexibility to accommodate mechanization changes

[AIAA PAPER 68-837]

24 p4285 A69-43719

REENTRY

NT HYPERBOLIC REENTRY

NT HYPERSONIC REENTRY

NT MANNED REENTRY

NT SPACECRAFT REENTRY

Nonequilibrium electron temperature, concentration and reflection in reentry boundary layers, discussing heat transfer and ionization energy diffusion

[AIAA PAPER 69-82]

06 p0915 A69-18190

REENTRY ANGLE

U ANGLES [GEOMETRY]

REENTRY COMMUNICATION

C and S band waveguide impedance measurements taken in flight in reentry plasma, noting results for plasma

02 p0218 A69-12333

Radio frequency signal transmission between orbiting spacecraft and vehicle entering VM-10 model atmosphere, examining near wake approximations and plasma-electromagnetic interaction

09 p1455 A69-22002

Amplitude modulation of electromagnetic waves by modulated magnetic fields for communications through rocket exhausts and reentry plasma sheaths during blackout

14 p2417 A69-29591

Mathematical model of nonlinear microwave breakdown for overdense and underdense plasma outside

reentry vehicle, predicting nonlinear pulse transmission through high temperature plasma
20 p3495 A69-37853

REENTRY EFFECTS

Ground simulation of reentry observables with ablation, studying ablation products interaction with flow-field of wave superheater hypersonic tunnel
02 p0229 A69-12502

Quantitative determination of reentry shock precursor absorption level and effect on surface radiation heating, calculating radiative flux from shock layer enthalpy distribution
02 p0354 A69-12528

Infrasonic waves recordings from Saturn 5 vehicle, observing signal reversal occurrence
03 p0509 A69-13358

Reentry shock layer radiative heat transfer to surface of blunt superorbital vehicle
[AIAA PAPER 68-1151] 03 p0532 A69-13560

Critical end-on impact velocities calculated for reentering solid and granular radioisotopic fuel rods with solid and granular earth materials
04 p0630 A69-14800

Nose cone reentry simulation under low temperature subliming ablators, discussing dry ice, camphor and steel calibrations models fabrication, instrumentation and boundary layer measurements
[AIAA PAPER 69-152] 06 p0929 A69-18098

Shock layer microwave radiation measurements during reentry flight of spherical nose cone, determining effective plasma temperature
[AIAA PAPER 69-183] 06 p0865 A69-18201

Inverted spin testing techniques using jet trainer, emphasizing entry variations and effect on spin characteristics
14 p2392 A69-29696

Flash X ray unit with special film transport devices to obtain sequenced dynamic radiographs of ablating models during reentry simulation tests
19 p3291 A69-35720

Diamond shaped surface ablation patterns development mechanism for several ablation materials of ground test and recovered flight vehicles
[AIAA PAPER 68-671] 23 p4059 A69-41891

Swept frequency X band reflectometer for measuring antenna properties in simulated reentry environments
[AAS PAPER 69-282] 24 p4313 A69-42861

Reentry shock layer radiative heat transfer to surface of blunt superorbital vehicle
[AIAA PAPER 68-1151] 24 p4414 A69-43567

REENTRY GLIDERS

U LIFTING REENTRY VEHICLES

REENTRY GUIDANCE

Digital simulation of vehicle motion and control for six degree of freedom simulations of Gemini reentry and aircraft, missile control, etc
05 p0725 A69-16477

Reentry and planetary entry physics and technology, II, Advanced concepts, experiments, guidance-control and technology
11 p1967 A69-25718

Subsonic glide landing approach guidance for unpowered lifting vehicles, using perturbation feedback and approximation of heading and position coordinates
[AIAA PAPER 69-865] 21 p3763 A69-39391

REENTRY PHYSICS

Upgrading wave superheater for evaluation of reentry materials
01 p0054 A69-10917

Unsteady aerodynamics of ablating flared reentry body, noting complications due to blunted nose shear flow and entropy gradient effects
02 p0189 A69-12524

Reentry plasma sheath simulation in wind tunnel by injection of nitrogen plasma from model vehicle nose
03 p0412 A69-13679

Monograph on radiation gas dynamics, thermal radiation, applied spectroscopy and ablation and applications in high speed atmospheric entry
04 p0685 A69-14597

Correlations of stagnation point radiative heat transfer for earth reentry, noting use of nongray absorption coefficient models
04 p0685 A69-14736

Propulsion and reentry - Conference, Belgrade, September 1967
06 p0859 A69-17625

Lifting reentry dynamic stability of flare stabilizers and flap controls
[AIAA PAPER 69-182] 06 p1017 A69-18053

Autorotation characteristics of various shapes in subsonic and hypersonic flows for mechanics of free flight reentry to earth impact
[AIAA PAPER 69-132] 06 p0863 A69-18062

Coordination technique for pressure, density and temperature measurements by probes during parachute reentry into planetary atmospheres, taking into account reentry dynamics
09 p1609 A69-21775

Book on reentry and planetary entry physics and technology covering entry dynamics, thermodynamics, radiation, ablation and heat transfer
11 p1967 A69-25573

Reentry and planetary entry physics and technology, II, Advanced concepts, experiments, guidance-control and technology
11 p1967 A69-25718

Swept frequency microwave measurements in simulated reentry environments using dielectric layers, glow discharge plasma and aperture antenna-plasma layer model
[AIAA PAPER 69-701] 17 p2920 A69-33461

Systematic mathematical ordering of knowledge concerning three dimensional flow patterns around blunt bodies, emphasizing high speed computers role
18 p3089 A69-35269

Spectral emissivity measurement of ablating phenolic graphite heated by subsonic air stream to high temperature to simulate reentry condition
20 p3565 A69-37187

Parametric differentiation applied to radiation gas dynamics equations solution, considering energy transfer by thermal radiation in high speed reentry
[AIAA PAPER 68-668] 23 p4059 A69-41892

Apollo afterbody heat transfer, studying ablation effects for various reentry angles of attack
24 p4415 A69-43680

REENTRY RANGE

Spacecraft longitudinal control during reentry of lunar orbiter into atmosphere, analyzing final range prediction, trajectory tracking and accelerometers performance
13 p2355 A69-27681

Spacecraft range control algorithm during reentry at parabolic velocity into atmosphere with varying parameter distributions
13 p2355 A69-27682

REENTRY SHIELDING

Apollo thermal protection system, noting low density ablation, flight and ground tests
[AIAA PAPER 68-1142] 03 p0519 A69-13558

Microwave techniques for bondline defects and thickness of reentry elastomeric heat shield material bonded to titanium alloy
09 p1499 A69-22306

Sample data reduction methods combined in special purpose computer for measuring ablation in reentry vehicle heat shields
10 p1660 A69-23290

Thin multiple layer superinsulation protection against reentry heat, discussing composite design considerations and refractory materials selection
12 p2060 A69-26817

REENTRY TRAJECTORIES

Incidence for three dimensional reentry trajectories preprogrammed as function of velocity, finding bank angle as function of inclination
03 p0504 A69-12858

Synoptic density maps for postreentry altitudes derived from constant pressure charts and horizontal gradients
04 p0626 A69-14909

Orbital trajectories about Mars or Venus, considering reentry to earth, planet perturbation effect, total mission time and orbital distance from planet
05 p0823 A69-16042

Ballistic reentry trajectories, considering point mass motion in central force field under tangential thrust action and spherical atmospheric density distribution
06 p1006 A69-17564

Spacecraft trajectory during atmospheric reentry determined from projections of longitudinal acceleration onto coordinate axes connected with spacecraft
06 p1014 A69-17581

Ablative and insulative performance of reference heat shield materials under transient heating simulating ballistic vehicle reentry trajectory, using plasma jet facility
[AIAA PAPER 69-150] 06 p0907 A69-18110

Convergence extensions in quasi-linearization for optimal control, showing results for brachistochrone and reentry trajectory problems
09 p1590 A69-21414

Reentry trajectories from lunar surface and orbit obtained by computer with allowance for initial data spread
09 p1594 A69-21756

Integration time reduction for equations of motion of vehicle center of mass during parabolic reentry, using Runge principle
09 p1532 A69-21763

Lifting entry concepts for return from earth orbit, discussing deceleration, heating and heat protection
11 p1968 A69-25720

Aerodynamic measurements on Apollo CM model at hypersonic flow simulating earth orbital reentry trajectory
12 p2012 A69-26800

Optimal control for minimization of heating and acceleration forces to reduce kinetic energy of reentry vehicle in space missions
13 p2352 A69-27960

Optimum overestimate to obtain bound permitting use as convergence criterion for iterative process in orbital glider reentry trajectory optimization
[ONERA-TP-628] 16 p2805 A69-32332

Earth-moon and moon-earth trajectory parameters related to lunar orbit conditions for synthesizing lunar orbit trajectory
18 p3196 A69-34704

Steepest ascent convergence improved in orbital glider reentry trajectories optimization problems, discussing bang-bang and cosine control-variable changes
19 p3398 A69-35666

Orbital trajectories about Mars or Venus, considering reentry to earth, planet perturbation effect, total mission time and orbital distance from planet
20 p3606 A69-37951

Apollo type reentry trajectory optimization numerical methods
24 p4386 A69-43281

REENTRY VEHICLES

NT AEROSPACEPLANES
NT APOLLO SPACECRAFT
NT GEMINI SPACECRAFT
NT HL-10 REENTRY VEHICLE
NT LIFTING REENTRY VEHICLES
NT MERCURY SPACECRAFT
NT RECOVERABLE SPACECRAFT
NT REUSABLE SPACECRAFT
NT TRAILBLAZER 2 REENTRY VEHICLE
NT VOSKHOD 1 SPACECRAFT
NT VOSKHOD 2 SPACECRAFT
NT VOSKHOD MANNED SPACECRAFT
NT X-24 AIRCRAFT

Acoustic probe for measuring pressure fluctuations on hypersonic reentry vehicle, discussing flow characteristics and heat shield ablation effects on frequency response
01 p0008 A69-11278

Active control system augmentation of inherent aerodynamic damping assuring acceptable limits on oscillatory rotational motion during hypersonic Martian atmospheric entry
02 p0333 A69-11742

Nosetip cooling system based on discrete subsonic forward liquid injection through ablative nosetip opening of blunted reentry vehicle
[AIAA PAPER 68-1141] 03 p0532 A69-13559

Reentry shock layer radiative heat transfer to surface of blunt superorbital vehicle
[AIAA PAPER 68-1151] 03 p0532 A69-13560

Air to air recovery of reentry vehicles, discussing parachute/wing descent, aircraft/helicopter energy absorption, payload boarding and towing techniques
[AIAA PAPER 68-1163] 03 p0520 A69-13563

Boundary layer transition measurements on flight tests of experimental 22 degree conical reentry vehicle with Be heat shield and graphite nose
[AIAA PAPER 68-1152] 03 p0362 A69-13648

Active cooling systems for high performance reentry vehicles in thermal and shear stress environments
[AIAA PAPER 68-1154] 03 p0533 A69-13669

Reentry plasma sheath simulation in wind tunnel by injection of nitrogen plasma from model vehicle nose
03 p0412 A69-13679

Make wire, light pipe and spring wire ablation sensors development for measuring parameters of heat shield materials for reentry vehicles
04 p0602 A69-15428

Solar radiation protection of radiometers and spectrometers on reentry vehicle by launching times and solar view field selection
04 p0666 A69-15511

Angle of attack effect on motion throughout entry of spinning descending vehicle, noting effects of transverse angular velocity and spin rate
04 p0666 A69-15522

Laminar boundary layer separation and reattachment near concave corner on cooled reentry body in supersonic flow

06 p0911 A69-17592

Dynamic stability loss on ablating vehicles ascribed to boundary layer transition effect from turbulent aft body heating

[AIAA PAPER 69-106] 06 p1037 A69-18087

Roll acceleration influence on angle of attack convergence and windward meridian rotation rate of rolling reentry vehicles

[AIAA PAPER 69-100] 06 p1018 A69-18089

Ballistic reentry vehicle roll-pitch coupling, showing influence of nose asymmetries

[AIAA PAPER 69-101] 06 p1018 A69-18156

Anomalous roll behavior of spinning ballistic reentry vehicles with compound aerodynamic asymmetry consisting of lateral offset combined with trim angle of attack

[AIAA PAPER 69-103] 06 p1019 A69-18168

Transonic dynamic stability of free flight half angle cones in wind tunnel for high drag planetary entry vehicles, discussing Mars entry trajectories

[AIAA PAPER 69-105] 06 p1019 A69-18209

Transpiration cooling of reentry vehicle nose tips, noting two dimensional aspects of porous wall coolant flow and matrix-coolant energy exchange

[AIAA PAPER 69-96] 06 p1039 A69-18212

Homogeneous fused silica and quartz reinforced resins as dielectric materials for reentry vehicle antenna windows

07 p1090 A69-18400

Aerothermoelasticity problems for Mars entry vehicles, discussing deceleration loads, separated hot gas flow, shield thermal gradients and oscillatory body motion

[AIAA PAPER 68-283] 09 p1610 A69-21991

Coated refractory tantalum alloy as ductile, weldable material for application on hypersonic aircraft or reusable reentry vehicles at high temperatures

09 p1526 A69-22326

Pyrotechnic activated calorimeter for reentry package design of vehicles entering earth atmosphere at lunar return velocities

10 p1669 A69-23026

Radiant heat transfer in hypersonic aerodynamic heating, discussing radiant flux and carbon dioxide concentration in reentry problems

11 p2002 A69-25233

Environmental problems of entry vehicle returning from lunar or planetary mission, discussing heat protection system efficiency

11 p1968 A69-25721

Entry propulsion and lower systems technology for planetary entry and atmospheric reentry vehicles

11 p1945 A69-25723

Wing section of high lift/drag test vehicle for 2500 F reentry, describing design, manufacture and testing

12 p2103 A69-26837

Optimal control for minimization of heating and acceleration forces to reduce kinetic energy of reentry vehicle in space missions

13 p2352 A69-27960

Thermionic electrical power generation from reentry plasmas with nose cone as emitter and vehicle afterbody as collector

14 p2399 A69-29194

Hypervelocity reentry simulation problems for slender and blunt bodies, defining significant parameters

15 p2681 A69-30376

Reentry flight test vehicle development for West German space program, using hypersonic model to determine controllability and aerodynamic stability

16 p2867 A69-31934

Shape and surface roughness effects on turbulent ablation of reentry body nose tip, noting recession rate

[AIAA PAPER 69-717] 17 p2952 A69-33435

Precursor plasma electron number densities calculations for blunt reentry vehicles, analyzing extreme UV radiation emanating from bow shock

[AIAA PAPER 69-718] 17 p2893 A69-33487

Collection of papers on thermal design principles of spacecraft and entry bodies

18 p3227 A69-34372

Aerodynamic and flight characteristics of variable geometry entry spacecraft during subsonic wing deployment and landing

[AIAA PAPER 69-742] 18 p3084 A69-34407

Aerodynamic characteristics of ballistic reentry vehicles from flight test dynamic measurements, illustrating results

18 p3085 A69-34670

Earth orbital entry vehicles weight prediction, noting vehicle geometry as function of vehicle shape, hypersonic lift drag ratio and crew size

[SAWE PAPER 770] 18 p3208 A69-34876

Computer aided design analysis program to provide weight and sizing data for entry spacecraft

[SAWE PAPER 797] 18 p3208 A69-34903

Autopilot for flight simulation of stability and control of pilot-airframe combined performance on reentry missions, using airborne analog computer for vehicle response

18 p3208 A69-35000

Computer programs determining gaseous properties and aerodynamic characteristics for missiles, reentry vehicles and spacecraft at angles of attack

18 p3107 A69-35068

Ablation heat shields, emphasizing dielectric low cost fabrication and application to entry vehicles

19 p3318 A69-35538

Radar design for target detection, tracking and identification, modeling plasma effects on radar cross section of reentry vehicles based on wave-plasma interactions

20 p3485 A69-36925

Rice-Ramsperger-Kassel kinetic theory applied to sulfur hexafluoride injection into boundary layer of high speed reentry vehicle

20 p3514 A69-37226

Composites for weight sensitive aerospace vehicles including reentry vehicles and V/STOL aircraft, considering costs, fracture toughness, corrosion resistance, etc

20 p3565 A69-37291

Moving model target for laboratory measurements of radar cross section to simulate satellite or reentry vehicle precession motion, noting signature data analysis

20 p3511 A69-37850

Mathematical model of nonlinear microwave breakdown for overdrive and underdense plasma outside reentry vehicle, predicting nonlinear pulse transmission through high temperature plasma

20 p3495 A69-37853

Three dimensional laminar boundary layer hypersonic flow about slender conical vehicles, analyzing transverse surface curvature effect, studying Reynolds number, cone angle, etc

[ASME PAPER 69-FE-23] 20 p3460 A69-37992

Active cooling systems for high performance reentry vehicles in thermal and shear stress environments

[AIAA PAPER 68-39016] 21 p3851 A69-39016

Electrical conductivity in wake neck measured using RF bridge on boom extending from reentry vehicle

21 p3724 A69-39030

Spring restrained, momentum-wheel inertial orientation and stabilization system for exoatmospheric vehicles, noting mission constraints and hardware parameter variations allowances

21 p3819 A69-39214

Reentry Vehicle Altitude-Velocity Sensor for continuously measuring hypersonic vehicles free stream density and velocity in atmosphere at low angle of attack

[AIAA PAPER 69-866] 21 p3725 A69-39392

Reentry cones with mass and configuration asymmetries, studying nonlinear aerodynamic characteristics by wind tunnel and full scale flight tests

[AIAA PAPER 69-867] 21 p3823 A69-39393

Artificial damping of longitudinal winged reentry vehicle motions in earth atmosphere, discussing vibration damper dynamic characteristics

21 p3829 A69-39828

Speed conditions of environmental simulation of thermal scale models of reentry vehicles, considering ablatives with phase-change and involved chemical reaction

[AIAA PAPER 69-1011] 22 p3922 A69-40384

Mars entry capsule ionized wake producing circularly polarized antenna radiation null region, noting effect on communication blackout time

22 p3914 A69-40701

Bistatic radar scattering cross sections for reentry vehicle with ionized wake

23 p4116 A69-41593

Diamond shaped surface ablation patterns development mechanism for several ablation materials of ground test and recovered flight vehicles

[AIAA PAPER 68-671] 23 p4059 A69-41891

Hypersonic reentry spheres drag coefficients derived from radar measurements

23 p4059 A69-41898

Dynamic model of ablation pitching moment derivative and time lag effect on spinning reentry vehicle applied to Black Knight flight results

24 p4245 A69-43249

Reentry shock layer radiative heat transfer to surface of blunt superorbital vehicle

[AIAA PAPER 68-1151] 24 p4414 A69-43567

REFERENCE ATMOSPHERES

Gas dynamics, thermodynamics, chemical properties, energy and products of hydrocarbon-air detonations in tubes under standard atmospheric conditions

[WSCI PAPER 68-26] 07 p1241 A69-18369

Data tabulation and calculation for atmospheric refraction between 5-40 km based on GOST standard atmosphere

15 p2646 A69-30160

Soviet meteorological rocket sounding data for upper atmosphere compared to CIRA 1965 model

15 p2650 A69-31421

REFERENCE SYSTEMS

Rotational motion of system of particles related to existence of reference frame to eliminate coupling terms between internal and rotational motion

02 p0280 A69-11867

Coupling geodetic systems of coordinates linked to reference ellipsoids from determination of angle of inclination relative to earth rotation axis and equatorial plane

12 p2068 A69-26426

Impulsive trajectories optimal and nonoptimal solutions, classifying known results for reference purposes

16 p2857 A69-32146

Transit forecast of terrestrial satellite moving through fixed coordinate line in assigned reference

16 p2859 A69-32221

Multiple reference sources to improve field of view of lensless Fourier transform holography limitation due to modulation transfer function of film and turbulence

17 p2971 A69-32920

Neighboring optimum feedback guidance to motivate min-distance lookup parameter determined by minimizing metric function of perturbed state and reference trajectory

[AIAA PAPER 69-888] 21 p3765 A69-39414

Adaptive control system for aerospace vehicles, describing model reference network for control parameter determination

21 p3688 A69-39857

Schwarzschild metric properties in synchronous reference system, using succession of Schwarzschild interval holonomic transformations as function of gravitational radius

22 p3982 A69-41063

Performance characteristics of multivariable model reference adaptive systems synthesized by Liapunov method analyzed using computer simulation

22 p3919 A69-41201

Visual and tactual interaction in judgments of vertical in dark room experiments, discussing effects of various reference systems

24 p4271 A69-42752

REFERENCES (STANDARDS)

U STANDARDS

REFINING

U ELECTROSLAG REFINING

REFLECTANCE

NT SPECTRAL REFLECTANCE

E field transmission and reflection coefficients in linearly tapered waveguide for fundamental and higher order modes, using point matching method

01 p0044 A69-10629

Electroreflectance spectra of Ge-Si alloys, noting concentration dependence and band structure of Si and Ge

02 p0295 A69-11784

Reflection elimination for single dielectric film on solid laser material substrate, calculating reflectance as function of frequency

02 p0256 A69-11926

Energy characteristics of laser with passive Q switch, taking into account internal reflections

02 p0256 A69-11999

Vanadium dioxide reflection spectra dependence on incident quantum energies during semiconductor/metal phase transition

02 p0298 A69-12100

Reflection indicatrices of aluminum oxide, MgO, Au and Pt surfaces for normal irradiation noting temperature and surface treatment effects

03 p0534 A69-14161

Reflection coefficients of edge and center elements of large periodic two dimensional antenna array, noting TEM mode parallel plate horn arrays

04 p0572 A69-14322

Reflection coefficient determination of bent multiwave waveguide, considering reflected wave due to

REFLECTED WAVES

secondary conversion of parasitic waves interacting with primary wave

04 p0576 A69-14773

Flexural wave reflection from corner joint between plates, establishing reflection coefficient dependence on wave frequency

04 p0679 A69-14903

Diffusive scattering effects on planetary surface reflection coefficient determined by radar observations

04 p0662 A69-15245

Electron beam modulation of germanium reflectance

05 p0807 A69-15816

Formulas describing reflection and transmission coefficients of plasma for plane electromagnetic wave, using Maxwell equations in variable medium

05 p0805 A69-16608

Nonuniform distribution and concentration of doping materials in semiconductors determined by measuring optical reflection coefficient

05 p0764 A69-16664

Semiconductors reflectivity enhancement by irradiating with Q switched ruby laser output

06 p0935 A69-17768

Transmission and reflection coefficients of cylindrical tubes moving in free molecular gas flow determined by Monte Carlo method

06 p0911 A69-17877

Model for spectral bidirectional reflectance of rough surface producing good agreement with experimental data

[AIAA PAPER 69-64]

06 p0959 A69-18125

Thermal radiative reflectance characteristics of low density charring ablators subjected to planetary entry environment simulation

[AIAA PAPER 69-61]

06 p0947 A69-18148

InAs solid solutions reflection spectra with CdTe, CdS, CdSe and ZnTe compounds, determining conduction bands

07 p1198 A69-18511

ELF radio waves reflection coefficients calculated from two layer ionospheric model, noting ion collision frequency effect in Schumann resonance frequency band

07 p1124 A69-18820

Open resonator reflection coefficient resonance curve compared with transmission coefficient, noting low Q waves excitation role

07 p1106 A69-19152

Complex transmission and reflection coefficients of dielectric film with permittivity gradient computed by modified Runga-Kutta method, noting plasma diagnostics application

07 p1194 A69-19334

Symmetrical three layer A and B type sandwich reflectionless radomes design for multifrequency operation and insertion phase delay

07 p1110 A69-19522

Reflection and transmission scattering coefficients for step type transition between two uniform waveguides with surface impedance boundaries, discussing coupled differential equations

08 p1272 A69-20020

Reflection coefficient of double discontinuity consisting of two closely spaced inductive irises in rectangular waveguide

09 p1453 A69-21444

Oxidation influence on molybdenum disilicide coatings emissivity, determining degree of blackness over thermal stability range

09 p1522 A69-21588

Thermal conductivity, electrical resistivity and degree of blackness of refractory metals at high temperatures measured by Bode and Eger-Disselhorst methods

09 p1522 A69-21589

Tunnel diode amplifier operation in presence of noise

09 p1469 A69-22630

Diffusion pump oil reflectance and absorption coefficients measured in three thicknesses using light source, monochromator and detector

10 p1725 A69-23647

Reflection coefficient of electromagnetic wave reflected from thin ionization layer, using frequency dependence of amplitude to estimate ionospheric layer thickness

10 p1686 A69-23912

Silicon dioxide coated Al reflectance, solar absorptivity and total normal and hemispherical thermal emissivity, noting application to satellite temperature control

11 p1918 A69-24835

Transmission and reflection scattering coefficient measurements of microwave networks by Fourier analysis

of transient response to impulsive or steplike waveforms

12 p2038 A69-26056

Flexural wave reflection from corner joint between plates, establishing reflection coefficient dependence on wave frequency

12 p2182 A69-26656

Reflection coefficient of polarized radio waves at ionized meteoric trails obtained by numerical integration of differential equations

12 p2031 A69-26691

Characteristic impedance determination for transmission lines cascades terminated by resistor using recurrent relations, discussing reflection coefficient

13 p2221 A69-28074

F cosine i theorem validity for VLF radio wave absorption in ionosphere tested using exponential electron density models, noting Brewster angle influence on reflection coefficient

13 p2222 A69-28473

Microwave cavity bandwidth determined from reflection coefficient measurements, considering reflection magnitude and phase

13 p2223 A69-28606

Reflection and absorption coefficients analyzed for obliquely incident electromagnetic wave from magnetoactive plasma in constant parallel magnetic field

14 p2411 A69-28997

He-Ne laser traveling wave output power, obtaining end mirror reflection coefficient optimal value

14 p2458 A69-29165

Reflection of electromagnetic wave from magnetoactive plasma at inclined incidence, finding reflection and absorption coefficients

14 p2417 A69-29661

Secondary effects role in n-GaAs crystals electrical reflection spectra with low free carrier concentration at room temperature in external electric field

15 p2666 A69-30061

Bidirectional reflectance of solar radiation and IR temperature data from Nimbus 2 satellite to differentiate clouds above snow surfaces

15 p2596 A69-30455

Cotton leaves reflectivity and transmittance measurements, discussing substrate salinity effects on internal structure of hydroponically grown plants

15 p2558 A69-30456

Reflection of plane waves at boundary surface of two semiinfinite media in relative motion, calculating power reflection coefficients

15 p2568 A69-30796

Earth reflected radiation pressure and perturbing effect on satellites

15 p2599 A69-31324

Reradiation and multiple reflection effects on radiant flux density distribution in cylindrical receivers of solar power installations

16 p2741 A69-32799

Gas products evolved from selected thermal control coating materials during UV radiation in vacuum, noting permanent reflectance loss

[AIAA PAPER 69-640]

17 p2992 A69-33289

Electron energy effects on reflectance degradation and recovery of thermal control materials in vacuum, reporting test results for various protective coatings

[AIAA PAPER 69-643]

17 p3005 A69-33306

Reflection and transmission coefficient matrices for stratified magnetoionic medium determined by thin film optical technique and iteration procedure

17 p2927 A69-33863

Reflection coefficient of symmetric parallel plate waveguide operating in TEM mode illuminating lossless dielectric layer, using wedge diffraction and geometrical optics methods

18 p3108 A69-34802

Plane electromagnetic wave interaction with moving conductive dielectric medium to obtain reflection and transmission coefficients, noting energy transfer

18 p3105 A69-35486

Reflectivity and chemical composition of metallic phase minerals in stone meteorites, showing optical characteristics sensitivity to composition

19 p3415 A69-36124

Integrated reflection coefficient with unpolarized incident X radiation for mosaic and perfect LiF crystals, presenting coefficient as function of wavelength

20 p3582 A69-37137

Free electrons influence on reflection coefficient of semiconductor in IR spectra, showing selective modulation with change in carrier concentration

20 p3583 A69-37610

TEM mode reflection coefficient for symmetric parallel plate waveguide composed of adjacent conducting wedges composition and radiating into perfectly reflecting sheet

20 p3507 A69-37839

Angular dependence of ocean surface-cloudless atmosphere reflectance for solar radiation studied with digitized camera signals from ATS 1 satellite

21 p3704 A69-38372

Reflection indicatrices of rough surface subjected to heat radiation for stationary and variable incidence angle, noting spatial distribution

21 p3847 A69-38455

Absorption constant and reflectivity coefficient on semiconductor samples with nonideally prepared surfaces, calculating measurement errors

21 p3782 A69-39240

Surface reflectivity mapping of Venus by radar interferometry at 3.8 cm, noting low reflectivity circular regions

21 p3806 A69-39331

Lummer-Gehrcke plate type polarizer made of birefringent material for Nd glass laser, discussing reflection coefficients in quartz crystals

21 p3739 A69-39541

Wave trains of incident pulse diffraction in thin composite rod determined by transmission and reflection coefficients of plane waves at plane interfaces

21 p3845 A69-39677

Radio echoes diffraction patterns determination from reflection coefficients of polarized radio waves reflected from ionized meteor trails

23 p4214 A69-41846

Holographic interferometry for measuring small static displacements of diffusely reflecting surfaces

23 p4167 A69-42185

Solid cylindrical antenna current and admittance calculation, considering reflection coefficient and multiple reflection phenomena at antenna ends

23 p4142 A69-42336

Bidirectional reflectance of earth atmosphere and cloud formation above equatorial Pacific observed by synchronous satellite as function of angular dependence

24 p4346 A69-43154

GaAs laser diodes differential external quantum efficiency and gain per unit length dependence on laser reflectivity, taking into account optical losses

24 p4330 A69-43766

REFLECTED WAVES

Fading characteristics of radio waves reflected from two different heights in F region over Ahmedabad, India

03 p0385 A69-12915

Plane electromagnetic wave scattering from slightly rough surface tilted away from reference plane, noting polarization effects

03 p0395 A69-13625

Horizon focusing gain for radio waves reflected obliquely from ionosphere, noting effects of transmitter location and ionosphere geometry

03 p0395 A69-13627

Reflectivity of low Richardson number critical levels for internal gravity waves propagating in stably stratified fluids with shear, studying stability numerically

03 p0424 A69-13953

Reflection coefficient determination of bent multiwave waveguide, considering reflected wave due to secondary conversion of parasitic waves interacting with primary wave

04 p0576 A69-14773

Random walk theory for effective secondary radiation center produced by reflection from composite reflectors, investigating fluctuations of reflected radio waves

05 p0718 A69-15653

Zone behind reflected shock wave in shock tube using electron beam scattering, showing flow spectra and attenuation region of wave

05 p0752 A69-16688

Airborne polarimeter to measure Stokes parameters of linearly polarized visible atmospheric radiation in four narrow spectral regions

06 p0923 A69-16924

Plane electromagnetic wave reflection and transmission by semiinfinite moving compressible plasma fluid, noting interaction of transmitted H wave

08 p1360 A69-20097

Electromagnetic wave propagation direction in vacuum for reflection from semiinfinite plasma, noting effects of nonlinear transverse wave excitation

09 p1459 A69-22529

Photometric consequences of reflection effect in close binaries, tabulating light curves

10 p1776 A69-23218

Gaussian laser beam reflection and refraction at curved interface between media of different refractive indices, considering tilted ellipsoidal interfaces

10 p1725 A69-23309

Beam displacement at plasma under magnetic field connected with polarized electromagnetic wave reflections

10 p1740 A69-23724

Active scanning Fabry-Perot interferometer interaction with mode matched laser resonator, analyzing phase and intensity of reflected wave of active three mirror resonator

11 p1886 A69-25047

Electrical conductivity of air behind incident and reflected shock wave fronts as function of temperature and Mach numbers measured by electrode method

11 p1888 A69-25220

Spacecraft surfaces bidirectional reflectance flux distribution applications to space thermal control computations

[AIAA PAPER 68-26] 13 p2222 A69-28216

Spherical stress wave reflected from plane surface, discussing tensile stress in target

[AIAA PAPER 69-363] 13 p2366 A69-28295

Reservoir conditions of reflected shock wind tunnel by subjecting gas to direct shock and shock reflected at closed downstream end of shock tube

13 p2243 A69-28359

Elastic medium properties recovered from reflected or transmitted plane waves at normal incidence, obtaining computational procedures and analytical solution from Schroedinger equation

13 p2300 A69-28664

Ruby laser reflected and transmitted light intensity following radiation focusing on cuvette containing cyclohexane, noting dependence on incident pulse power

14 p2459 A69-29392

Cosmos 149 meteorological satellite telephotometers for measuring reflected solar radiation from earth

14 p2447 A69-29404

Solar UV radiation reflected from Echo satellites measured and compared with UV fluxes from Lyrae

14 p2447 A69-29408

Reflected and absorbed solar radiation by planetary atmosphere and surface determined as function of atmosphere and surface optical properties

15 p2689 A69-30564

Earth reflected solar radiation spatial, angular and spectral distributions measured by telephotometers on-board Cosmos 149

15 p2596 A69-30650

Ozonosphere inhomogeneities from UV spectra of reflected solar radiation, studying latitude dependence of seasonal behavior at different heights

15 p2597 A69-30654

Pressure, temperature, density and enthalpy of carbon dioxide behind primary and reflected shock waves determined by method suitable for computer

15 p2592 A69-31054

Temperature and electron number density behind reflected shock in helium gas in T tube, noting Z pinch discharges

15 p2593 A69-31161

Conditions behind incident and reflected shock waves in shock tube calculated from initial pressure, density, temperature and shock speed

15 p2593 A69-31487

Electron concentration and mass density behind reflected shock in ionizing argon, using time resolved two wavelength interferometry

16 p2771 A69-31918

Light polarization diffusely reflected by earth atmosphere measured from balloon, using gain compensated photoelectric polarimeter

16 p2781 A69-32320

Polarization characteristics of electromagnetic waves obliquely reflected from inhomogeneous isotropic plane stratified plasma

16 p2752 A69-32391

Random walk theory for effective secondary radiation center produced by reflection from composite reflectors, investigating fluctuations of reflected radio waves

16 p2754 A69-32510

Plane shock wave interaction with plane rigid net-like wall, obtaining Mach numbers for reflected and penetrating shock waves

17 p2957 A69-33719

Reflected shock and boundary layer interaction in shock tube, discussing bifurcation effect on flow and turbulence transition

18 p3116 A69-34448

Reflected shock front interaction with heated thin gaseous filament studied in shock tube by spark interferometric and schlieren technique

18 p3228 A69-34468

Shock tunnel steady flow starting process in two dimensional reflection nozzle, using multiple shadowgraphs and interferograms, noting nozzle geometry influences

18 p3085 A69-34471

Rereflected shock waves behind tapered shock tube section indicated by shock wave detectors, microwave absorption and optical emission measurements

18 p3085 A69-34474

Shock waves attenuation through multiple reflections at ends and interactions with expansion wave in shock tube by pressure transducer, noting exponential decay

18 p3121 A69-34475

Reflected signals detection with limited frequency spectrum and minimum velocity resolution considered, analyzing signal properties

18 p3104 A69-35265

Axial stagnation point flow in shock wave reflected from sphere or circular cylinder, determining velocity time variation, enthalpy pressure and reflection

19 p3298 A69-36385

Spectral density of outgoing radiation in 0.6-0.8 micron frequency range, noting reflected radiation and cloud fields correlation functions

19 p3366 A69-36672

Phase amplitude recording of radio waves reflected from D and F regions of ionosphere, reversing smoothing process by Fourier methods

21 p3672 A69-38558

Radar reflection techniques for planetary surface studies, considering surface properties effects on reflectivity and reflected wave characteristics, instrumentation and data for moon and planets

21 p3811 A69-39509

Test model thermal balance in space simulator, measuring effects of solar simulator irradiance reflected from carbon dioxide cryopanel deposits

[AIAA PAPER 69-1012] 22 p3922 A69-40385

Human eye modulation transfer function in reflected light by analyzing depolarized and polarized components emerging from eye

22 p3884 A69-40888

Electron collisions effect on polarization of waves reflected from ionosphere

22 p3941 A69-40922

Radio echoes diffraction patterns determination from reflection coefficients of polarized radio waves reflected from ionized meteor trails

23 p4214 A69-41846

Pressure measurement modifications of quasi-steady flow model for interaction between reflected shock wave and laminar boundary layer in shock tube

23 p4152 A69-41903

Dielectric materials permittivity determined by measuring amplitude ratios of reflected and transmitted plane electromagnetic waves

23 p4123 A69-41950

Lunar photometric function near zero phase from Apollo 8 closeup photography, noting higher reflected brightness than at 1.5 degree phase angle

23 p4220 A69-42380

Fully dispersed wave reflection from plane wall in stable relaxing gas, obtaining canonical equation of state

24 p4299 A69-42717

Flaw determinations accuracy from measuring ultrasonic shear wave reflection peak intensities

24 p4397 A69-42756

REFLECTING TELESCOPES

Reflecting telescope objective for far UV and X ray regions, discussing microfinishing and optical and mechanical tolerances

01 p0121 A69-10896

Single and double mirror systems geometrical optical image aberrations noting focal number, angle of field, secondary magnification and mutual position tolerances

11 p1918 A69-24836

Schmidt all-reflecting telescope for UV imaging in Apollo Earth Orbital Scientific Experiment

11 p1887 A69-25101

Segmented active mirror optics design concept for lightweight optically stable primary reflector used in large orbiting astronomical telescopes

13 p2261 A69-27950

Nova Delphini 1967 observational data and equipment including Cassegrain spectrograph, reflector telescope and photoelectric photometer

15 p2682 A69-30439

Vienna 60 inch telescope concept and design, discussing optical systems possible combinations under local conditions

24 p4314 A69-43000

REFLECTION

NT INFRARED REFLECTION

NT RETROREFLECTION

NT SIGNAL REFLECTION

NT SPECTRAL REFLECTION

NT ULTRAVIOLET REFLECTION

NT WAVE REFLECTION

Three dimensional photoelastic analysis based on optical theory of multilayer reflection technique

04 p0683 A69-15496

Raman spectra of optical phonons in semiconductors, using reflection techniques and Ar laser excitation

06 p0936 A69-17882

Boundary conditions for reflection and transmission properties of absorbing shell of arbitrary shape

08 p1273 A69-20025

Electro-optical Q switched lasers with prismatic reflectors and phase shifter studied using Johns matrices for polarizer, Kerr cell and Porro prism elements

14 p2459 A69-29390

Time dependent radiation diffusion in inhomogeneous stationary medium applied to diffuse reflection of light

16 p2813 A69-32591

Optical constants changes in germanium determined by modulation method of measuring light reflected at different angles

18 p3173 A69-35014

Electroreflection study of inversion asymmetry and warping induced interband magneto-optical transitions in InSb, employing low temperature electric field modulation technique

19 p3386 A69-36521

Maxwell coefficient change of Cd atoms /in molecular beam/ diffusely reflected from metal surfaces related to reflector temperature, material and fabrication method

20 p3580 A69-37814

REFLECTION COEFFICIENT

U REFLECTANCE

REFLECTIVITY

U REFLECTANCE

REFLECTOMETERS

NT MICROWAVE REFLECTOMETERS

High temperature directional reflectance measurements of ablative materials as function of sample temperature using paraboloid reflectometer

[AIAA PAPER 68-25] 04 p0604 A69-15512

High resolution swept frequency reflectometer suitable for impedance matching in waveguides or coaxial lines

16 p2759 A69-31940

Portable integrating sphere reflectometer, describing optical system, construction, etc

[AIAA PAPER 69-599] 17 p2973 A69-33264

ATS 3 satellite reflectometer experiment carrying test samples to measure specular reflectance, noting silica shield effects

[AIAA PAPER 69-644] 17 p3071 A69-33270

REFLECTOR SATELLITES

U PASSIVE SATELLITES

REFLECTORS

NT PARABOLIC REFLECTORS

NT PARABOLOID MIRRORS

NT RADAR CORNER REFLECTORS

NT RADAR REFLECTORS

NT SOLAR REFLECTORS

Radiation pattern shaping from circular aperture antenna with constant illumination amplitude

[UN PAPER 68-95756] 01 p0029 A69-10524

Beryllium reflector distortion in Plum Brook Reactor due to neutron embrittlement and gas formation, noting material surveillance, replacement, etc

03 p0465 A69-13131

Directional properties of electric vibrator positioned at reflecting circular cylinder, discussing radiation patterns and cylindrical wave diffraction

04 p0574 A69-14459

Input admittance of confocal Fabry-Perot resonator, with waveguide coupled infinitely long conic-section cylindrical reflectors, taking into account diffraction and resistive losses

05 p0731 A69-16295

Directional mirror antenna parameters measurement by finite focusing of radiating element

06 p0895 A69-17453

Sectoral hoghorn as line feed for correcting spherical aberration in offset spherical reflector antennas

06 p0898 A69-17823

Geometric optics and polarization properties of spherical reflector for integral representation of focal region fields, discussing stationary phase and field points
08 p1272 A69-20017

Coupling between array antennas shown to reduce reflecting properties of Van Atta reflector consisting of linear half wave dipoles
08 p1282 A69-20037

Directional properties of electric vibrator positioned at reflecting circular cylinder, discussing radiation patterns and cylindrical wave diffraction
14 p2418 A69-28830

Reflector radio telescope of Pulkovo astronomical observatory noting high resolution
15 p2679 A69-30102

Double aperture problem with partially coherent incident field, noting application to microwave antenna-reflector combination
17 p2929 A69-33877

Apollo 11 moon reflector-laser beam experiment, discussing range changes produced by axial rotation and orbital motion and use for earth-moon dynamics
19 p3339 A69-36766

Directional mirror antenna parameters measurement by finite focusing of radiating element
20 p3508 A69-37938

Surface accuracy of large diameter radio telescopes maintained by uncoupling reflector surface from backup structure, using active compensation
23 p4149 A69-42136

REFLEXES

NT CAROTID SINUS REFLEX
NT RESPIRATORY REFLEXES

Increasing hypoxia effects on rabbit EEG and light flash conditioned alimentary reflex for simulated altitude ascent, noting subcortical stimulation
02 p0197 A69-11492

Prolonged bed rest effect on human myogenic tone and proprioceptive reflexes, comparing test subjects with and without physical exercises
10 p1646 A69-23583

Phase and tonic activity of oculomotor apparatus of rabbits during vestibular reflexes and postrotational nystagmus
20 p3469 A69-37243

Orientation reflexes of animals in weightlessness, analyzing turnover, vestibular and cervix reactions using motion pictures
20 p3470 A69-37248

Reflex activity of single preganglionic sympathetic fibers during coronary occlusion in cats, discussing left third thoracic/T3/ ramus communicans
23 p4084 A69-41460

Human arterial pressure reflex regulation during sleep, assessing baroreflex sensitivity
24 p4257 A69-42626

REFRACTED WAVES

Electromagnetic wave refraction angles in earth atmosphere, noting effect of stratified discontinuities on angle magnitude
06 p0887 A69-17450

Conical refraction of magnetosonic waves occurring when Alfvén waves propagate at speed of sound in conducting fluid in presence of constant uniform magnetic field
10 p1727 A69-23091

Gaussian laser beam reflection and refraction at curved interface between media of different refractive indices, considering tilted ellipsoidal interfaces
10 p1725 A69-23309

Nonlinear analog of conical refraction in biaxial crystals, considering birefringence in piezoelectric uniaxial crystals and laser beam propagation
19 p3330 A69-35604

Electromagnetic wave refraction angles in earth atmosphere, noting effect of stratified discontinuities on angle magnitude
20 p3496 A69-37935

REFRACTING TELESCOPES

Solar telescope in Berlin observatory for prominences and other solar phenomena observations by public
15 p2611 A69-30881

Objective lens of AVR-2 reflector at Poltava Observatory measured for spherical aberration, astigmatism, field curvature, coma and distortion
17 p2970 A69-32883

REFRACTION

NT ATMOSPHERIC REFRACTION
NT BIREFRINGENCE
NT RADIO WAVE REFRACTION

High temperature high density theta-pinch plasma refraction measurements by interference refractometer with beam perpendicular to plasma axis
09 p1544 A69-21302

Refraction angles for objects between 5-300 km and zenith distances between 1-88 degrees, describing calculation method for corrections
09 p1490 A69-21918

Quasi-transverse /Q-T/ point time lag on Faraday rotation records at widely spaced frequencies during satellite pass explained by refraction theory
18 p3100 A69-34251

Figure of earth and refraction - Conference, Vienna, March 1967
18 p3131 A69-35194

Skiagrams results of retinoscopic measurements of eye peripheral refraction of pilots, attempting correlation between skiagram type and central refraction
24 p4267 A69-43399

REFRACTIVE INDEX

U REFRACTIVITY

REFRACTIVITY

Isopentane and mesitylene index of refraction variations with pressure, determining average molecular radii and polarizabilities
01 p0123 A69-10685

IR reflection and transmission properties of various semiconductor compounds, rubidium halides, strontium titanate, BN and Te
01 p0139 A69-10840

Finsler geometric apparatus applied to electromagnetic wave propagation in media having refractive index varying with position and time, calculating errors
01 p0031 A69-10879

Radar reflectivity and refractive index spectra in clear atmosphere simultaneously measured and compared with theoretical calculations
01 p0032 A69-10969

Solar limb image vibrations caused by turbulent pulsations in refractive index of lowest atmospheric layers
01 p0156 A69-11183

Gaseous and liquid H refractive index variations with pressure and density below room temperature, noting Lorentz-Lorenz function variations
02 p0281 A69-12180

Refractivity distribution at ground level and at one km over India, correlating surface refractivity with difference, noting seasonal and diurnal variations
03 p0393 A69-13304

Refractive index and expansion thermal coefficients along axis of oriented Nd-YAG laser rod
04 p0160 A69-14293

Atmospheric refractive index for IR radiation in one to six micron region
04 p0591 A69-14300

Optical waveguide with optimum refractive index distribution for equalizing group velocities of different modes and minimizing waveform distortion
04 p0575 A69-14749

Refractive index temperature dependence of cadmium sulfide single crystals grown from gas phase
04 p0644 A69-15268

Plasma refractive index determination by holographic interferometry with double pulse ruby laser
05 p0761 A69-15620

Thermal self focusing of argon laser beam passing through lead glass
05 p0771 A69-15819

Fresnel drag produced by relativistic addition of electron velocities in semiconductors measured by changes in refractive index
05 p0807 A69-16026

Thermal self defocusing effect of laser beam in self focusing liquids, measuring refractivity changes by high speed double exposure holography [IEEE PAPER J-7]
05 p0775 A69-16320

Radiation of laser active element with random inhomogeneities of refractive index, discussing beam divergence, operation modes and Q switched operation
05 p0777 A69-16550

Spectrum and amplitude fluctuations of laser light propagating through liquid helium, obtaining spatial correlation function of refractive index fluctuations
06 p0957 A69-17267

Laser beam absorption induced index changes associated with thermal blooming observed in iodine doped carbon tetrachloride, using Mach-Zehnder interferometer
07 p1149 A69-18899

Real and imaginary parts of homogeneous isotropic electron plasma complex refractive index, noting application to plane electromagnetic wave propagation
07 p1193 A69-19183

Quantum mechanical, dipole approximation, non-resonance light scattering cross sections expressed in terms of oscillator strengths and refractive indices
07 p1183 A69-196451

Optical parameters for system of isotropic nonabsorbing film on isotropic absorbing substrate determined by ellipsometric method, noting Si optical constants
07 p1201 A69-19647

Laser beams self focusing interpreted as photon contraction due to equivalent gravitational attraction with gravitational constant proportional to nonlinear refractive index
08 p1324 A69-2008

Electromagnetic wave reflection from subrefractive layers in inhomogeneous region
09 p1454 A69-21679

Light waves refractive index distribution from balloon sounding data found to decrease with height in winter regardless of time of day
09 p1536 A69-21917

Gaussian laser beam reflection and refraction at curved interface between media of different refractive indices, considering tilted ellipsoidal interfaces
10 p1725 A69-23309

Nonlinear susceptibility tensor components and refractive index variations of liquids and glasses in high intensity ruby laser field, using interference methods
10 p1703 A69-23622

Scalar wave diffraction at body in scattering medium analyzed on basis of determinate medium with complex inhomogeneous effective refractive index
10 p1658 A69-23957

Single and clad glass fibers radii and refractive indices measurements on basis of laser light scattering
11 p1918 A69-25044

Focusing factor in stratified medium with refractive index depending exponentially on height
12 p2029 A69-26100

Atmospheric turbulence degradation of holographs resolution improved by geometrical optics and series-expansion methods, noting role of Gaussian and exponential refractive index structure
12 p2090 A69-26250

Finsler geometric apparatus applied to electromagnetic wave propagation in media having refractive index varying with position and time, calculating errors
12 p2031 A69-26642

Refractive index and attenuation factor of ionosphere
12 p2070 A69-26689

Statistical distributions of refractive index parameters in tropospheric radio propagation from psychrometer soundings, discussing lapse rate
13 p2254 A69-28428

Optical refraction effects from refractive index gradients in stressed models as limitation on moiré interferometry usefulness in Boussinesq problem and expanding pulse studies
14 p2531 A69-28883

Focused beam wave applied to atmospheric turbulence probing for spectral density of index of refraction, structure constant and wind velocity
14 p2414 A69-29512

Light intensity during coherent scattering based on complex refraction index of medium, noting scattering by clouds and diffraction by semitransparent hole
15 p2635 A69-31108

Spontaneous and stimulated aspects of light scattering by absorbing media, relating refraction index to temperature variations and external stresses
16 p2798 A69-32449

Electron density measurement method in plasma or vacuum based on refraction index in optical frequency range using laser interferometer mismatch as criterion
16 p2798 A69-32583

Air refractivity variations across horizontal and vertical boundary planes between two air masses of slightly different temperatures
17 p3028 A69-32880

Complex index of refraction of naturally occurring rock and mineral as function of wavelength of incident radiation
17 p2973 A69-33093

Atmospheric stability influence on vertical spectra of refractive index and air velocity deduced from beam swinging experiments and compared with radiosonde data
17 p2960 A69-33157

Thin surface films effect on radiative properties of metal surfaces determined by thin film optics, noting dependence on refractive index [AIAA PAPER 69-623]
17 p3072 A69-33283

Schlieren method for visualization of refractive index changes in transparent materials, discussing application to study of elastic wave fields

17 p2973 A69-33322

Continuity conditions for drifting magnetoplasmas without ionic effects, discussing eigenvalue equation of refractive index and electromagnetic modes propagation

17 p2926 A69-33851

Complex refractive index profiles and wave polarizations calculated for electromagnetic waves transmission through ionosphere at micropulsation frequencies

17 p2927 A69-33864

Plane anisotropic dielectric p-n junction layer waveguide properties, deriving characteristic equations for refraction indices

17 p2983 A69-33971

Refractive indices for various glasses obtained as function of wavelengths and temperature, using spectrometer as collimator

17 p3007 A69-34158

Thermal coefficient of optical glasses refractive index determined by interferometry, noting relation to glass chemical composition

18 p3172 A69-35013

Optical distance measurement using laser and atmospheric dispersion method through average refractive index determination over path

18 p3152 A69-35198

Monochromatic undulating light vertical refraction path curvature radii calculation based on refractive index

18 p3174 A69-35201

Focused Gaussian laser beam expansion due to thermal changes in refractive index of air, noting focused spot area increase with pulse energy

19 p3330 A69-35601

Refractive index profiles yielding wave functions expressed in terms of standard transcendental functions for electric fields in spherically stratified isotropic media

19 p3372 A69-35618

Ionospheric scintillation power spectrum measurements from radio star and satellites related to F region radio refractive index fluctuations

20 p3534 A69-38093

Satellite onboard transmission measurements determining atmospheric water vapor influence on integrated refractivity at specific absorption line resonant frequency

20 p3545 A69-38097

Model compounds and polymers solubility parameters correlated with refractive index data

21 p3751 A69-38552

Interferometric study of cool flame propagation in equimolar propane-oxygen mixtures, observing refractive index and temperature distribution changes

21 p3852 A69-39595

Normalized phase function and scattering coefficient of aerosols prediction from measurements of particle size distribution, density and refractivity based on Mie solution

21 p3719 A69-39774

Electromagnetic wave propagation in semiconductor plate under constant electric field, studying nonstandard carrier energy dispersion law effects on refractive index

22 p3994 A69-40751

Corneal stroma collagen fibrils and ground substance refractive indices, discussing corneal transparency and clouding

22 p3884 A69-40886

Longitudinal modes locking and ultrashort light pulse generation in laser cavity resonator with nonlinear refractive index

23 p4171 A69-41389

Multiple index high contrast holographic contouring technique compared with analogous multiple frequency system

23 p4164 A69-41628

Transmission properties and directional coupler determined for optical circuit dielectric rectangular waveguide with surrounding dielectrics of smaller refractivity

24 p4287 A69-43328

Index of refraction turbulent fluctuations effect on beam traversing optically active medium, discussing far field diffraction pattern and incoherent scattering [AIAA PAPER 68-683]

24 p4304 A69-43578

Thermal turbulence effects on phase fluctuations of laser beams, studying temporal decay of mean square refractive index fluctuation with fringe pattern displacements

24 p4329 A69-43754

REFRACTOMETERS

Optimum emission wavelengths in atmospheric refractive index determination in optical range finder/refractometer system, noting laser applicability

13 p2260 A69-27826

REFRACTORY MATERIALS

NT CHROMIUM
NT IRIDIUM
NT MOLYBDENUM
NT MOLYBDENUM ALLOYS
NT NIOBIUM
NT NIOBIUM ALLOYS
NT OSMIUM
NT PORCELAIN
NT RHENIUM
NT RHENIUM ALLOYS
NT TANTALUM
NT TANTALUM ALLOYS
NT TUNGSTEN
NT TUNGSTEN ALLOYS

Preparation of refractory alloys in powders, fibers and sintered billets by thermochemical method [ONERA-TP-636]

02 p0251 A69-11625

Liquid oxides wetting and spreading capabilities on refractory metal surfaces, noting chemical reaction oxide reducing effect

02 p0265 A69-11884

Soviet book on high temperature materials covering metal and liquid oxides, electrical conductivity, chemical properties, etc

03 p0445 A69-13567

Thermodynamic and kinetic interactions of high melting point metal oxides reduction by carbon

03 p0445 A69-13568

Electrical resistivity of sintered high melting point metal oxides, noting width of semiconductor forbidden band

03 p0445 A69-13570

Thermodynamic evaluation of interaction between solid metals and dispersed high melting point oxides, stressing isobaric potentials

03 p0446 A69-13571

Thermodynamic analysis of refractory compounds vapor transport conditions, illustrating integral free energy diagrams

03 p0453 A69-13619

Shear strengths of polyimide and polybenzimidazole resin/fiberglass reinforced honeycomb materials compared to previous high temperature materials, noting lightweight sandwich aircraft structures

04 p0620 A69-14844

Braze bonds of refractory electrical contacts using induction heating

04 p0607 A69-15218

High temperature capacitor consisting of thin wafers of pyrolytic boron nitride noting fabrication, dissipation factor and capacitance

04 p0551 A69-15299

Material requirements for uncooled nozzles of solid propellant rocket motors burning aluminized propellants, discussing successful testing of pyrolytic graphite

06 p0946 A69-17530

High temperature polyimide laminates for radomes and other supersonic aircraft components, discussing inflexural strength, dielectric constant and dissipation factor

07 p1171 A69-19545

Elevated temperature mechanical properties data for commercially produced super-strength alloys supplemented by product description tables

08 p1328 A69-19913

Apparatus for depositing protective coatings on graphite by vacuum method in refractory metal carbonyl and halides mixtures and in molten metals

09 p1528 A69-21850

Dynamic modulus of elasticity measured for nonporous refractory compounds obtained by diffusion saturation

09 p1529 A69-21871

Refractory compounds static strength temperature dependence at high temperatures measured in reference to melting temperature

09 p1523 A69-21873

Soviet collection of articles on physicochemical studies of heat resistant alloys

09 p1524 A69-22135

Electron microscopy for continuous observation and recording of dynamic reactions in high temperature materials

09 p1499 A69-22304

Coated refractory tantalum alloy as ductile, weldable material for application on hypersonic aircraft or reusable reentry vehicles at high temperatures

09 p1526 A69-22326

Laser evaporation vapors from refractory materials to produce surface temperature for carrying out reactions in gaseous phase and thin film preparation

09 p1519 A69-22476

Refractory ceramic materials use for advanced combustion chamber design, stressing brittleness effect and current fabrication techniques

09 p1531 A69-22624

Integral normal emissivity of electrically conducting materials heated to high temperatures by HF field of inductor, discussing measurement procedure and equipment

11 p1888 A69-25230

Thermochemically synthesized high melting micropowders grinding by vibrational method and classification for polishing and finishing applications

12 p2113 A69-26256

Thermal stability of refractory and cermet materials, analyzing small samples subjected to cyclic high energy radiative heating and air-water cooling

12 p2118 A69-26262

Molten high melting compounds obtained by arc furnace with consumable electrode and adjustable protecting atmosphere

12 p2055 A69-26264

Refractory cone models made of copper and Co coated Be for force tests in high enthalpy hypersonic arc tunnels at high simulated altitudes

12 p2059 A69-26796

Graphite improvement for high temperature applications by computerized properties analysis, failure criterion and improved testing for defective billets

12 p2115 A69-26845

Chemical corrosion of zirconia-based refractories in MHD generators, considering thermal cycling and shock, seed migration and prevention

13 p2284 A69-27469

Electrical, thermal and thermoelectronic properties of refractory oxide materials including lanthanum chromite and strontium zirconate, discussing Hall effect, IR absorption, mixtures, etc

13 p2316 A69-27470

Oxide and carbide high-melting-point materials for MHD generator electrode walls

13 p2284 A69-27471

Refractory ceramic materials thermal stability in high temperature subsonic ionized gas flow products, emphasizing zirconia and magnesia

13 p2285 A69-27472

Ceramic and cermet materials insulating, physical and mechanical properties for use in thermionic converters

14 p2467 A69-29214

High temperature compatibility of Mo, W, Nb and Ta as canning materials with high melting point and formation energy filling materials

14 p2463 A69-29219

Heterocyclic-aromatic organic polymer adhesives used for high temperature structural purposes, discussing processing, testing, formulating and impact on basic research

14 p2469 A69-29346

Pyrolyzed refractory laminates for high temperature applications, analyzing mechanical and thermal properties

15 p2618 A69-30313

Vaporization rates of Ti, Zr, Hf, Nb and Ta carbides at high temperatures measured by Langmuir method

15 p2640 A69-30983

Refractory materials based on BN and silicon nitride, studying effect of sintering conditions and chemical composition on mechanical properties

15 p2643 A69-31244

Mechanical testing of high temperature materials subjected to thermal cycling by high power pulsed laser beam

15 p2636 A69-31512

Biaxial stress strain properties of graphite base refractory composites noting fracture strength predictions [AIAA PAPER 68-337]

16 p2803 A69-32150

Particles maximum diameter numerical values for melting during injection into plasma jet calculated for various metals and refractory dielectrics

17 p3009 A69-32825

Thermal EMF, electrical conductivity and Peltier effect in sintered refractory oxides at high temperature in air and in Ar

17 p3068 A69-32990

Cellular carbon castings fabrication by carbonization of polyurethane polyfurfuryl alcohol foam for high temperature applications, noting properties

17 p2992 A69-33373

Reliable structural joints and attachments design for components fabricated from nonmetallic refractory brittle materials, discussing departures from conventional practices

17 p3061 A69-33569

Liquid oxides wetting and spreading capabilities on refractory metal surfaces, noting chemical reaction oxide reducing effect

18 p3156 A69-35044

Emissivity of high melting point compounds measured, considering electronic structure and atomic weight

18 p3158 A69-35260

Polycrystalline diborides fabrication technology, discussing additives, thermal, physical and mechanical properties, specific applications, etc

19 p3355 A69-35526

Polyimides and polybenzimidazoles mechanical strength, heat resistance, electrical properties, radiation resistance and industrial applications

19 p3358 A69-35901

High temperature materials for aerospace and spacecraft applications, considering carbon/carbon composites, oxides, carbides, fibers and ablative systems

19 p3346 A69-36320

Facility for evaluating thermal stability of heat resistant materials and cermets in constant temperature gas flow

20 p3565 A69-36979

Book on high temperature materials covering creep phenomena, design considerations, load and temperature effects, various steels, superalloys, refractory metals, etc

20 p3559 A69-37148

Coating deposition theory on high temperature materials, discussing interfacial energy and wetting properties of molten metal drop on solid base material surface

20 p3560 A69-37358

Protective coatings of oxygen-free high melting point Si compounds and silicate binder, noting chemical stability in corrosive media

20 p3566 A69-37371

Dynamic electron beam devices for refractory materials evaporation, discussing electron guns and vaporization film data

[ASM PAPER D8-2.2]

20 p3551 A69-38131

Refractory materials thermal conductivity high temperature measurement technique, discussing sample geometry, furnace design, temperature modulation and computerized simulation

21 p3742 A69-38422

Aerodynamic skin heating at high Mach numbers affecting structural design, noting use of high temperature materials, insulation systems and shell construction method

21 p3646 A69-38460

Enthalpy and heat capacity of high melting point homogeneous Ti, Zr and Nb carbides, analyzing influence of Me-Me bonds and carbon sublattice defects

21 p3742 A69-38614

Destructive interaction of refractory carbides and graphite compositions with chemically active high temperature gas streams

21 p3751 A69-38640

External friction of refractory materials at high temperature in vacuum, discussing testing machine and methods including metallographic, X ray, spectral and electron diffraction analyses

21 p3690 A69-39154

Thermal conductivity precision tests for refractory materials using ASTM method C 201-47, emphasizing sample preparation and calorimeter calibration

22 p3956 A69-40671

Cathode materials role in high temperature zirconia electrolyte fuel cell performance, discussing metals, collector-embedded and electronically conducting oxides properties

22 p3869 A69-40734

Mechanical properties of aircraft fasteners high temperature materials

22 p3956 A69-40823

V contents influence on high temperature strength and fine structure interrelation in low alloy CrMoWV steels

22 p3972 A69-41083

Heat resistant materials integral and spectral radiative properties in IR and visible regions determined by calorimetry and IR spectrometer

23 p4237 A69-41329

Spectral emissivity and radiation intensity spectral distribution measurements for heat-resistant materials at high temperature, using photographic method

23 p4238 A69-41330

Radiative properties of Ta, Mo, Nb, graphite and niobium carbide at high temperatures

23 p4175 A69-41331

REFRACTORY METAL ALLOYS

NT MOLYBDENUM ALLOYS

NT NIOBIUM ALLOYS

NT RHENIUM ALLOYS

NT TANTALUM ALLOYS

NT TUNGSTEN ALLOYS

Cobalt base alloy for construction in high temperature corrosive environment, discussing mechanical properties, oxidation and corrosion resistance and phase stability

01 p0095 A69-10546

Chemical vapor deposition of refractory metals, alloys and compounds - Conference, Gatlinburg, Tennessee, September 1967

01 p0096 A69-10640

Structural stability of manganese austenitic steels at high temperatures, discussing phase transformations and carbide precipitation changes

01 p0100 A69-11294

Isothermal sections of Zr corner of Zr-Mo-Ta system phase diagram at high temperatures, noting composition vs hardness and omega phase

02 p0264 A69-11858

Isothermal sections of Zr corner of Zr-Mo-Ti phase diagram at high temperatures, noting corrosion resistance in air and water

02 p0264 A69-11859

Isothermal sections of Zr-Ni-Nb system phase diagram at high temperatures, determining principal type of projection on concentration triangle

02 p0264 A69-11860

Isothermal sections of Zr corner of Zr-Nb-Cr system phase diagram at high temperatures, noting variation of stability with concentration

02 p0264 A69-11861

Electrochemical grinding application to metal cutting of refractory alloys in aircraft jet engine overhaul

[SAE PAPER 680662]

03 p0433 A69-13453

Alloying elements effect on mechanical and refractory properties and structure of forging of age hardenable Ni base alloys

03 p0452 A69-14122

Bainite beta to alpha transformation in titanium-oxygen system, using high temperature metallography techniques

04 p0613 A69-14559

Preparation and properties of NbC-WC and TaC-WC carbides, analyzing hardness, resistivity, thermal expansion and dihedral angle

05 p0782 A69-16796

Lanthanum and hafnium effect on transition and recrystallization temperatures of tungsten and tungsten base alloys

05 p0782 A69-16797

Tantalum diffusion layer on refractory cobalt and nickel base alloys analyzed by electron microprobe

[ONERA-TP-665]

06 p0941 A69-17097

Refractory metal alloys metallurgy and technology - Conference, Washington, D.C., April 1968

07 p1164 A69-18790

Rhenium effect on lattice solid solubility of oxygen in tungsten, calculating rhenium-oxygen cluster minimum binding free energy

08 p1329 A69-20007

Refractory alloys electrodes used for surface coating Ti alloys by electric spark method, studying microhardness and wear resistance

10 p1711 A69-23339

High temperature metallic material strengthening methods, noting metallurgical factors and temperature effects on mechanical properties

10 p1712 A69-23630

Dispersion-strengthened alloys from extraction replicas, determining volume fraction and spacing of dispersed phase particles

13 p2282 A69-28167

Co base high temperature binary alloys microstructure, investigating diffusion coefficients, stacking faults, vacancies, etc

14 p2465 A69-29890

Thermionic emission parameters for faces of W- Re, Mo-Re and Ta-Mo single crystals determined by Richardson method of straight lines

17 p3015 A69-33630

Facility for studying energy dissipation in refractory materials during fatigue tests in vacuum at various temperatures, describing principal components

17 p2947 A69-33926

Deformation studies of high melting point metals and alloys at high temperatures in vacuum, noting crack formation resistance and annealing time variations

18 p3155 A69-34651

Stress rupture parameters for refractory metals and alloys from Larson-Miller, Dorn and Manson-Haferd constants, noting optimization procedure

[ASM PAPER D8-3.4]

20 p3564 A69-38135

Creep resistance increase of Ni refractory alloy by thermovibrational treatment under stress relaxation conditions

21 p3744 A69-38869

Stress concentration and surface strain hardening effects on fatigue strength of refractory alloy specimens with and without cut

21 p3745 A69-38875

Torsional moments and forces during Ti alloy and refractory alloy milling with cylindrical cutter

21 p3731 A69-38877

Weldability of alloy Ni-Cr-Fe base-filler alloy combinations, noting threaded mold test and surface fissures

22 p3968 A69-39886

Refractory metals in rocket propulsion devices, applying tungsten in uncooled rocket nozzles and tungsten and rhenium to electrothermal propulsion

23 p4177 A69-42161

NASA programs for development of high temperature alloys for advanced air breathing engines emphasizing cast Ni-base alloy

[ICAS PAPER 68-26]

24 p4335 A69-43718

REFRACTORY METALS

NT CHROMIUM

NT IRIDIUM

NT MOLYBDENUM

NT NIOBIUM

NT OSMIUM

NT RHENIUM

NT TANTALUM

NT TUNGSTEN

Chemical vapor deposition of refractory metals, alloys and compounds - Conference, Gatlinburg, Tennessee, September 1967

01 p0096 A69-10640

Refractory metals interactions with gases in vacuum and inert gas environment, noting temperature and pressure effects on reactions, extent and kinetics

01 p0099 A69-11042

Ti for high temperature use in supersonic aircraft, noting compressibility limit on maneuvering load factor and cooling by H

02 p0192 A69-11891

Cold drawing workability of Nb, Mo and Ta using dies with lubrication for metal sheets

03 p0452 A69-14124

Lithium metal spray structural cooling system for refractory materials

[AIAA PAPER 68-358]

04 p0688 A69-15509

Parameters and relative errors tabulated from IR spectral emittance of Mo, Nb, Zr and Ta near 1400 K

05 p0846 A69-15903

Refractory metal silicon device technology noting high temperature diffusion masking properties for possible use in MOSFET technology

06 p0930 A69-17152

Dislocation redistribution during annealing and shock deformation in liquid nitrogen of chromium, molybdenum and tungsten single crystals

07 p1159 A69-18534

Less common refractory metals /rhenium, technetium, hafnium, noble metals/ properties, phase equilibria, etc

07 p1165 A69-18793

Development of materials in aerospace structures and propulsion systems, discussing superelastic alloys, graphite fibers, composites, refractory metals and processing techniques

08 p1332 A69-20306

Thermal conductivity, electrical resistivity and degree of blackness of refractory metals at high temperatures measured by Bode and Eger- Disselhorst methods

09 p1522 A69-21589

Carbides and silicides temperature coefficient of electrical resistivity and Hall constant plotted as function of metal carbides solid solutions concentration

09 p1523 A69-21740

Heat resistant materials based on high melting point metals, summarizing achievements of chemical technology and vacuum metallurgy

09 p1524 A69-22137

Temperature dependence of high melting point metals mechanical properties

09 p1525 A69-22138

Structure and properties of high heat resistant alloys based on high melting point metals with bcc lattice explained by electron theory

09 p1525 A69-22139

Refractory metal oxidation protection by inorganic compounds at high temperatures, discussing protective mechanisms

09 p1526 A69-22322

Refractory metal, precious metal and ceramic material compatibility tested by metallography and by microprobing for protective coatings possibilities

09 p1477 A69-22325

Chemical composition of chromium steels for optimum heat resistance properties, noting effects of nickel, nitrogen and ferrite and austenite-forming elements

10 p1708 A69-23000

Nitrogen solubility in molten niobium and molybdenum at high temperatures in argon flow

10 p1710 A69-23213

High temperature metallic material strengthening methods, noting metallurgical factors and temperature effects on mechanical properties

10 p1712 A69-23630

Liquid sodium corrosive action on vanadium, niobium, titanium and zirconium involving oxygen exchange from liquid to solid metal phase and energy of formation

10 p1713 A69-23821

Refractory metals testing at high temperatures in vacuum, discussing equipment modifications, temperature measurement and residual gas problems

10 p1714 A69-23848

Dissolved gases and carbon effect on transition temperature from plastic to brittle state of high melting metals including niobium and vanadium

10 p1715 A69-24011

Fractures in refractory metals surface layers due to Q switched laser pulses

11 p1899 A69-25402

Crack initiation prediction in high temperature components subjected to arbitrary thermal-mechanical cycling

13 p2365 A69-28252

High temperature compatibility of Mo, W, Nb and Ta as canning materials with high melting point and formation energy filling materials

14 p2463 A69-29219

Micrographic reagent coloring grains of Mo in relation to crystalline orientation applied to refractory metal welding and diffusion studies

14 p2505 A69-29221

Work function measurements of polycrystalline W, Re and Ni disks in high pressure cesium plasma for low probe temperature range

14 p2506 A69-29266

Sessile drops contact angles of alkali liquid metals on Re, W, Mo, Ta and Nb substrates related to substrate surface bare work function

14 p2506 A69-29270

Carbidothemic process for high melting metals and alloys production stressing Ti alloys

16 p2800 A69-31777

Forge to determine refractory metals formability and ductility at high temperature in protective pressure

17 p2945 A69-33419

Refractory metals fracture, discussing interstitial impurity addition effects in Group 5a and 6a metals

17 p2989 A69-33556

Deformation studies of high melting point metals and alloys at high temperatures in vacuum, noting crack formation resistance and annealing time variations

18 p3155 A69-34651

Manufacturing in space based on nongravity and hard vacuum environment, considering crystal growth and refinement, perfectly shaped bodies, refractory metals ultrapurification, etc

18 p3234 A69-35066

Thermogravimetric study of oxidation protection of refractory metals by fused LiF coating, noting oxidation retardation of Ta, Nb and W

19 p3341 A69-35573

Surface alloying of high melting point metals in Al melts, noting prior oxidation enhancement and simplifying of calorizing techniques

19 p3328 A69-36158

Be diffusion during vapor phase saturation of W, Mo, Nb and Ta, noting time and temperature dependence of layer thickness

20 p3549 A69-37364

Protective coatings for high melting point metals, discussing prevention of low temperature coating breakdown due to oxidation

20 p3561 A69-37375

Stress rupture parameters for refractory metals and alloys from Larson-Miller, Dorn and Manson-Haferd constants, noting optimization procedure

20 p3564 A69-38135

Carbides and silicides temperature coefficient of electrical resistivity and Hall constant plotted as function of metal carbides solid solutions concentration

20 p3585 A69-38216

Superalloy technology applications to gas turbine engines

21 p3785 A69-38928

REFRACTORY PERIOD

Refractory period adaptation to sudden heart rate changes in dogs

24 p4257 A69-42628

REFRASIL [TRADEMARK]

U FIBERS
U SILICON DIOXIDE

REFRIGERATING

Refrigeration system for space flight use of cryogenic gas storage, suggesting mission time increase

15 p2587 A69-30395

REFRIGERATING MACHINERY

NT REFRIGERATORS

Maser for satellite communication consisting of traveling wave ruby maser and closed cycle liquid helium refrigerator, discussing design, operation and performance characteristics

02 p0256 A69-11992

Air conditioning system for transport airplane using combined simple/bootstrap cycle refrigeration unit, discussing thermodynamic performance and hardware implementation

19 p3243 A69-35641

REFRIGERATORS

He refrigerators, noting 4 K design for large scale fixed installations and 20 K small scale design for airborne applications

05 p0704 A69-15671

Thermal losses in thermal regenerators used in cryogenic refrigerators

05 p0706 A69-16163

Thermal losses in thermal regenerators used in cryogenic refrigerators

13 p2203 A69-27421

REFUELING

Fueling procedures for Boeing 747 aircraft, discussing design and operation of large capacity fuel trucks

10 p1674 A69-23631

Fueling procedures for Boeing 747 aircraft, discussing design of high rate mobile fuel dispensers

10 p1674 A69-23633

Optimal motion control of spacecraft refueling during flight by liquefying atmospheric gas along prescribed trajectory under constant thrust

13 p2356 A69-27686

Monograph on spreading of explosive vapor/air mixtures during aircraft fueling, covering underlying flow technology principles

15 p2551 A69-30930

Fluid flow problems during orbital refueling vehicle maneuvers and system operations in propellant transfer, including disturbances, liquid-vapor interface instability, vapor ingestion, etc

16 p2868 A69-32721

Orbital refueling techniques, discussing vapor-liquid interface stability, pressurant requirements, transfer line chilldown, propellant transfer dynamics, dielectrophoresis, suction speed estimating and system tradeoffs

16 p2869 A69-32733

Excessive extrapolation limitations in applying transient data to low gravity fluid behavior for orbital refueling systems, presenting orbital fluid transfer experiment

16 p2870 A69-32755

REGENERATION [ENGINEERING]

Regenerative digital transmission system error, representing memory of binary regenerative channel with Markov model

01 p0027 A69-10249

T63 regenerative helicopter engine program, noting operational performance and engine-aircraft compatibility

01 p0143 A69-10410

Regenerative amplification stability in nonretarded wave helitron and traveling wave mitron type devices

02 p0214 A69-11610

Efficient life support systems for prolonged space missions, discussing scientific and experimental research

06 p0879 A69-17040

Life support system energy efficiency, treating transfer equations of closed space regeneration systems

06 p0882 A69-17644

Lunar shelter regenerative life support system performance and manned test

07 p1071 A69-19427

Experimental program to evaluate regenerable sorbents for carbon dioxide removal in space cabin environments

09 p1447 A69-22552

Mathematical model of closed biological cycle regenerating part of life support products, incorporating astronaut, storage and regenerating waste disposal units

10 p1649 A69-23580

Regenerative amplification stability in nonretarded wave helitron and traveling wave mitron type devices

11 p1847 A69-24717

Reactive parameter scatter effect on amplitude frequency characteristics of regenerative reflection amplifiers based on equivalent circuit

13 p2235 A69-28515

Regenerative life support systems, discussing water reclamation, carbon dioxide removal, onboard oxygen generation and radio isotope thermal energy sources

19 p3262 A69-36318

REGENERATION [PHYSIOLOGY]

Regenerative life support system development, considering synthesized organic compounds and microorganisms as foods for long duration space missions

20 p3477 A69-37623

REGENERATIVE COOLING

Diathermal regenerative cooling of combustion chambers and engine nozzles with supercritical heat transfer mode

03 p0495 A69-12970

Space storable regenerative cooling with FLOX/methane under conditions for small pump fed engine, describing injector and chamber design

16 p2844 A69-32718

Scramjet engine active cooling with regenerative system using superalloy heat exchangers and hydrogen fuel as coolant

24 p4365 A69-43725

REGENERATIVE CYCLES

U REGENERATION [ENGINEERING]

REGENERATIVE FEEDBACK

U POSITIVE FEEDBACK

REGENERATIVE FUEL CELLS

Justi-Winsel extraction process by electro dialysis for removing product water from electrochemical reaction in H-O fuel cells

08 p1260 A69-21043

High pressure hydrogen-oxygen reversible fuel cells using calcia stabilized porous zirconia as membrane and aqueous KOH as electrolyte

23 p4076 A69-42308

REGENERATORS

NT THERMOSIPHONS

Idealized cycle of gas expansion machine with regenerator for cooling radio components

04 p0687 A69-15164

Small aircraft gas turbine regenerators employing heat pipes, noting excessive cost and weight

05 p0812 A69-16142

Thermal losses in thermal regenerators used in cryogenic refrigerators

05 p0706 A69-16163

Thermal losses in thermal regenerators used in cryogenic refrigerators

13 p2203 A69-27421

Cryogenic heat exchanger design and application including vaporizers, recuperators, regenerators, reversing exchangers, nonsteady state flow and thermoelectric techniques

17 p3074 A69-33681

REGIONS

U ANTARCTIC REGIONS

U ARCTIC REGIONS

U AUROREAL ZONES

U FRFNSL REGION

U NULL ZONES

U POLAR REGIONS

U TEMPERATE REGIONS

U TROPICAL REGIONS

REGISTERS [COMPUTERS]

U ACCUMULATORS [COMPUTERS]

U SHIFT REGISTERS

REGRESSION ANALYSIS

Simultaneous estimation of parameters in multiple equation regression model arising from radioactive tracer experiments using compartmental models

01 p0106 A69-10926

Factor analysis applied to identifying extremal planes, presenting regression analysis based on least squares techniques to calculate mathematical model coefficients

05 p0737 A69-15888

Stochastic model for real time on demand weather predictions using REEP /regression estimation of event probabilities/ equations in Markov chain

08 p1345 A69-20299

Zonal westerlies variations associated with tidal cycles, discussing principal component analysis, zonal index, bandpass filtering, aliasing, prediction and stepwise regression

09 p1537 A69-22242

Sublimation in ammonium perchlorate propellants combustion, discussing low temperature isothermal processes, linear regression rates measurements and low ambient pressure

11 p1940 A69-24481

Wind velocities statistical properties at various altitudes, noting linear regression of orthogonal components and prediction of wind velocities at all altitudes

11 p1911 A69-24694

Regression rate of solid fuel in hybrid combustion determined as eigenvalue by Rayleigh flow model with evaporating boundary

16 p2879 A69-32013

Nonlinear regression techniques for statistical simultaneous measurement of thermal properties including convergence criterion [AIAA PAPER 69-602]

17 p3070 A69-33260

Statistical weight estimation equations developed by constrained regression analysis, noting application to vertical tail of cargo/transport aircraft [SAWE PAPER 762]

18 p3220 A69-34879

Regression process in acetylcholine level in rats after mechanical vibrations and noise exposure

23 p4079 A69-41382

Noncyclic daily solar quiet variation in mean hourly geomagnetic field by including noncyclic variation term in regression model

23 p4158 A69-42170

Solid cloud cover moisture content relation to outgoing thermal radiation, obtaining correlation coefficient and regression equations

23 p4184 A69-42488

Formulas for discriminant and regressive weather analysis for computer calculations under operational weather forecasting conditions

23 p4184 A69-42490

Regression generated radiometric and contour height fields of North American Continent using Nimbus 2 IR equivalent black body temperature and geopotential data

24 p4343 A69-42896

REGRESSION COEFFICIENTS

Linear regression and related procedures in identifying dynamic processes

06 p0901 A69-17360

Regression coefficients obtained from satellite cloud observations applicability in constructing geopotential fields, tabulating coefficients obtained from ground stations

13 p2292 A69-27731

Nozzle throat ablative materials for controlled high regression rates in tactical rocket motors, primarily nylon reinforced thermosetting resins [AIAA PAPER 69-423]

16 p2804 A69-32710

Regression relations for energy expenditure in work predicted from heart rate and pulmonary ventilation in volunteers carrying loads upstairs

22 p3891 A69-40220

REGULARITY

Solution regularity for class of quasi-linear second order elliptic systems, applying results to regularity of extremals of particular integral

05 p0786 A69-15927

REGULATION

U CONTROL

REGULATIONS

Medical fitness regulations for pilots, including federal and internal airline regulations

06 p1041 A69-16844

U.S. policy for commercial surface effects ships regulation, discussing operational, construction and design requirements

08 p1254 A69-20199

FAA regulations for improvements on crashworthiness and emergency evacuation from viewpoint of plastic applications and fire safety in aircraft

08 p1254 A69-20497

Government flight recorder regulations, detailing approved systems

10 p1691 A69-23246

Flight data recorders history and regulations, discussing parameters and design of systems

10 p1691 A69-23247

Thrust reversers for business jet aircraft, discussing federal aircraft regulation requirements for ground and in-flight qualification [SAE PAPER 690311]

11 p1941 A69-24512

FAA jurisdictional procedures for law infringement, discussing civil codes, delegation of enforcement authority and routine violations including low flying, weather, etc

16 p2882 A69-32335

Technical and operational planning activities of airline resulting from airport restrictions in terms of congestion, performance and noise and runway strength

17 p2948 A69-34206

REGULATORS

NT AUTOMATIC FREQUENCY CONTROL

NT CURRENT REGULATORS

NT FLOW REGULATORS

NT FREQUENCY CONTROL

NT FUEL FLOW REGULATORS

NT PRESSURE REGULATORS

NT RELIEF VALVES

NT SPEED REGULATORS

NT THERMOSTATS

NT VOLTAGE REGULATORS

Optimal control problem for linear regulators with constant external disturbance

02 p0225 A69-11970

Sampled data regulator for maintenance of constant alveolar carbon dioxide during steady state and transient ventilatory responses to hypoxic stimulation

07 p1072 A69-19480

Optimal control trajectories computation for bilinear regulator problems including neutron kinetics of nuclear reactor

12 p2049 A69-26083

Near optimum regulator design technique for high order linear systems, using singular perturbation method to reduce system order

12 p2052 A69-26503

Time optimal regulator problem with recoverability constraint as restriction on system state during control synthesis

12 p2052 A69-26504

Suboptimal linear regulators design method yielding feedback controller for multivariable linear systems subject to parameter variations

22 p3918 A69-41012

Optimal gain theory for input vector and application to regulator problem describing aircraft dynamics

24 p4293 A69-43305

REHEATING

U HEATING

REIGNITION

U IGNITION

REINFORCED MATERIALS

U COMPOSITE MATERIALS

REINFORCED PLASTICS

Creep and stress rupture strength of unidirectional glass fiber reinforced plastics, using tensile tests

01 p1011 A69-10080

Fatigue properties and failure mechanisms of glass reinforced plastics based on chopped strand mat-polyester resin laminates

02 p0269 A69-11795

Thermal protection by ablation calculated, emphasizing blocking phenomenon and effectiveness of laminated and reinforced resins

02 p0351 A69-11890

Fiberglass reinforced plastic laminates failure under biaxial compression due to layer separation with strain energy as endurance criterion

02 p0270 A69-12142

Rapidly heated ablative reinforced plastics strength and stress-strain properties, considering heat shield designs

02 p0347 A69-12512

Internal elastoplastic stress distribution within reinforced plastics subjected to force normal to internal filaments direction

02 p0347 A69-12513

Glass fiber reinforced plastics - Conferences, Freudenstadt, West Germany, October 1968

03 p0453 A69-13819

Knee in stress-strain diagram and crack formation in glass fiber reinforced plastics, discussing effect on construction load capacity

03 p0453 A69-13820

Glass fiber reinforced plastic in aircraft construction, considering cellular weight and economy

03 p0454 A69-13821

Light passenger aircraft of glass fiber reinforced plastic, using hose construction technique

03 p0454 A69-13822

Glass fiber reinforced plastics aging behavior under heat and weathering influence

03 p0454 A69-13823

Damping properties of glass fiber reinforced plastics measured by flexural vibrations

03 p0454 A69-13824

Helicopter rigid rotor system with blades of glass fiber reinforced plastic

04 p0548 A69-14817

Shear strengths of polyimide and polybenzimidazole resin/fiberglass reinforced honeycomb materials compared to previous high temperature materials, noting lightweight sandwich aircraft structures

04 p0620 A69-14844

Piezooptical method applied to anisotropic bodies and reinforced plastics, deriving relation between dielectric tensors and stresses and strains

05 p0837 A69-16038

Composites reinforcement with single crystal flakes of aluminum diboride

05 p0785 A69-16581

Stress direction and mean stress effects on fatigue properties of fiberglass reinforced plastics

06 p0945 A69-17124

Stress-strain relations for laminar anisotropic medium from known mechanical properties of layers for application to fiber reinforced plastics

06 p1021 A69-17176

Water cooling jackets of plastic textile reinforced film for high inside temperature reduction in protective clothing

06 p0883 A69-18027

Anisotropic glass fiber reinforced epoxy resin composite under biaxial and uniaxial loads, noting isochromatics and isoclinics in photoelastic analysis

07 p1170 A69-18715

High temperature polyimide laminates for radomes and other supersonic aircraft components, discussing index flexural strength, dielectric constant and dissipation factor

07 p1171 A69-19545

Fiberglass reinforced plastics modulus of elasticity and Poisson ratio determined by strain gauges and frequency and resistivity measurements

08 p1335 A69-20330

Structural parameters influence on fiberglass reinforced plastics strength studied for optimal structure selection

08 p1335 A69-20332

Structural residual stresses determination in oriented fiberglass reinforced plastics by models taking into account mutual influence of fibers

08 p1335 A69-20333

Fiberglass reinforced plastic plates strength coupled to elastic base with allowance for tangential shearing stresses

08 p1412 A69-20334

Electromagnetic fields and magnetic and dielectric constants in fiberglass reinforced polymers determined by treating polymers as ideal dielectrics

08 p1336 A69-20336

Thermoplastics reinforcement with fiber and whisker fillers, evaluating graded asbestos, carbon, silicon nitride, silicon carbide and potassium titanate

08 p1337 A69-20479

Tensile stress and energy-to-break values compared for glass-fortified thermoplastic resins, discussing notched and unnotched Izod impact

08 p1337 A69-20480

Flexural fatigue of glass-reinforced thermoplastics as function of various parameters, discussing test for autogenous dissipative heating

08 p1337 A69-20481

Polymer structure effect on chemical resistance of reinforced plastics, sulfuric acid and sodium hydroxide corrosion of polyester resins and model copolymers

08 p1338 A69-20490

Tensile strength of glass-fiber reinforced epoxy resin laminates subjected to fluctuating tension, discussing crack density dependence on fatigue stress cycles

08 p1338 A69-20494

Matrix properties related to torsional fatigue life of fiberglass reinforced NOL rings, using polyester and epoxy resins as model systems

08 p1339 A69-20495

Laminates and filament wound structures using carbon fibers with silicon carbide whiskerized surfaces, noting compositing and laminating techniques

08 p1339 A69-20501

- Plastic composite reinforcements with boron, silicon carbide, graphite, single crystal alumina and laminating resins, discussing properties and fabrication
08 p1340 A69-20503
- Bromine containing unsaturated polyesters for fire retardancy and physical strengths, noting use in reinforced plastics for laminates, molding and corrosion
08 p1340 A69-20504
- Flame resistant chlorine containing polyester resins, discussing preparation, curing characteristics, physical properties and reinforced plastics application
08 p1340 A69-20505
- Three dimensional reinforcement composites for gear and bearing applications with improved interlaminar shear strength, thermal and wear properties
08 p1340 A69-20509
- Direct chemical bonding effect on flexural strength and flexural modulus of glass fiber reinforced plastics, noting degradation reactions
08 p1341 A69-20514
- Silicon carbide fiber surfaces nature and interaction with coupling agents, epoxy and resin components, noting chemical and electron microprobe analysis
08 p1341 A69-20515
- LFU 205 light aircraft design and construction with fiberglass reinforced plastic
08 p1321 A69-20867
- Shell theories for polymer and reinforced plastic shells, giving revised temperature and creep problem solutions due to mechanical behavior
09 p1611 A69-21481
- Failure modes in fiberglass reinforced epoxy laminates subjected to compression loadings, discussing cracks formation and delamination at glass-resin interface
09 p1529 A69-22305
- Fiber glass reinforced plastic backing phase of composite armor, noting test method for evaluation of performance
09 p1507 A69-22319
- Silica fabric reinforced phenolic composites mechanical properties at temperatures above cure level
09 p1530 A69-22321
- Fatigue behavior of composite disk modified from previously evaluated boron epoxy reinforced titanium compressor disk
09 p1619 A69-22323
- Prepreg based on S glass with HTS finish and B staged epoxy resin, discussing tensile strength and moisture exposure
09 p1530 A69-22327
- Compressive behavior of uniaxial filament reinforced epoxy tubes for aerospace structures, using hand layup method with Teflon mandrel and sleeve
09 p1508 A69-22339
- Boron filaments reinforced epoxy aircraft landing gear structure prototype, discussing development, fabrication, and testing
09 p1508 A69-22340
- Whiskerized graphite fiber in resin matrix composites, analyzing interstitial growth characteristics, resin infiltration, layup and compaction
09 p1511 A69-22360
- Glass reinforced polyimide laminate fabrication, discussing metal foil laminates
09 p1530 A69-22363
- Thermoplastic resins as matrices for glass reinforced plastics and aerospace structural and nonstructural adhesives
09 p1530 A69-22365
- Strength of laminated glass filament reinforced plastic material in biaxial loading, discussing strength theories
10 p1794 A69-22943
- Fiber content by weight of reinforced plastics measured by pyrolysis
10 p1716 A69-23695
- Glass reinforced plastic molding compounds for OV-10A airplane structural components, noting cost savings
[SAE PAPER 690342] 11 p1890 A69-24497
- Glass fiber reinforced plastics tensile strength at low and high temperatures
11 p1907 A69-25181
- Birefringent coatings application to plane stress in orthotropic glass-fiber reinforced plastic materials noting stress-strain relations
11 p1995 A69-25647
- Residual stresses and strains in wound reinforced plastic fiber cylinders subjected to polymerization by heat treating
11 p1907 A69-25679
- Glass fiber reinforced plastics shells stability under external hydrostatic pressure, discussing compression and axial tests for normal elastic modulus, shear modulus and Poisson coefficient
11 p1995 A69-25681
- Time and temperature dependence of plastic properties of fiber reinforced phenolic heat shield materials
12 p2119 A69-26825
- Fracture mechanics of polymers and fiberglass reinforced plastics, indicating microcracking under static and cyclic loading due to resin phase brittleness and low strength
12 p2120 A69-26849
- Glass reinforced plastics for Hovermarine HM.2 sidewall hovercraft designed for ferry routes
13 p2201 A69-27542
- Reinforced plastics corrosion resistance, showing dependences on coupling agent and chemical compatibility between resin and fibers
[ASME PAPER 69-DE-60] 14 p2467 A69-28853
- Syntactic foam low density thermoplastic microspheres as hollow spherical filler in polyester matrix, noting applications
14 p2467 A69-29285
- Composite airframe structural joint design and weight considerations for boron and glass fiber reinforced plastic materials
[ASM PAPER W9-23.1] 14 p2535 A69-29448
- Stress concentration on circular holes and notches in anisotropic oriented glass fiber reinforced plastics determined by using photoelastic birefringent coatings
15 p2713 A69-31053
- Fiberglass reinforced plastic tensile strength dependence on vibration time and temperature and vibrational effect on modulus of elasticity
15 p2643 A69-31203
- Reinforced textolite plastic dimensional and mass changes in water and oil immersion as function of surface, temperature and time
15 p2643 A69-31550
- Carbon fiber reinforced plastics properties improvement by applying organosilanes, discussing silanol bond formation
16 p2803 A69-31806
- Molded composites application to engine components, discussing turboprop reduction gear case design using polymer matrix boron composite
[AIAA PAPER 69-466] 16 p2795 A69-32763
- Shear modulus of fiberglass reinforced plastics determined from torsional tests on squared beam of orthotropic material, evaluating influence of end conditions
17 p3058 A69-33204
- Fiberglass reinforced plastics internal heat shielding for isopropyl nitrate rocket combustion chamber, considering lining resistance and safety during repeated firing /Ludion motor/
17 p3019 A69-33343
- Critical buckling stress for cylinders wound with fiber reinforced plastics /FRP/, establishing stability criteria for fiber reinforced shells
17 p3058 A69-33430
- Fatigue properties and test procedures for glass reinforced plastic rotor blades used in twin engine helicopter
[AHS PAPER 370] 17 p3060 A69-33518
- Carbon fiber reinforced plastics development for aerospace use, presenting criteria for resins selection
17 p2992 A69-33647
- Surface chemistry of plastics reinforced with strong fibers, stressing need for investigating coupling films, catalysts and metallic ions role in coupling compounds chemisorption
17 p2992 A69-33655
- Energy dissipation in fiberglass reinforced plastics subjected to axially induced sinusoidal stresses, noting absorption coefficient and hysteresis heating
17 p2993 A69-33937
- Axisymmetric deformation of cylindrical wound fiberglass reinforced plastic shell analyzed by methods of rigid normals and nonlinearly elastic fiber system
18 p3222 A69-34974
- Fiberglass reinforced plastics short and long term strength anisotropy, correlating stress and logarithm of time to rupture under tension along different directions
18 p3162 A69-35352
- Reinforced plastics static fatigue strength under various loads including thin walled tubes long term tests under constant internal pressure
18 p3162 A69-35353
- Fiber distribution in oriented fiberglass reinforced plastics, noting statistically isotropical distribution and use for regular structure model
18 p3162 A69-35355
- Optimal structure model of fiberglass reinforced materials with polymer matrix, obtaining strength utilization coefficient dependence on length/ diameter ratio
18 p3162 A69-35356
- Oriented glassfiber reinforced plastics elastic moduli and tensile strength along anisotropic axes determined nondestructively, considering component content and material porosity
18 p3162 A69-35359
- Statistical description of microstructural elements /fibers and fillers/ in unidirectional fiberglass reinforced plastics determined in lattice nodes
18 p3163 A69-35363
- Linearity range of viscoelastic properties of fiberglass reinforced plastics, calculating stress-strain state
18 p3163 A69-35364
- Longitudinal modulus of interlaminar slip during creep of fiberglass reinforced plastic determined by bending tests of beams under concentrated force
18 p3163 A69-35365
- Fiberglass-reinforced plastics longitudinal and transverse strain relations at various temperatures
18 p3163 A69-35366
- Phenomenological creep theory for woven fiberglass reinforced plastic under moderate loads
18 p3226 A69-35373
- Lightly loaded truss structures fabricated from Be, Be-Al alloy and uniaxial B filament reinforced epoxy tubing for unmanned spacecraft applications
19 p3340 A69-35504
- B-epoxy and B-Al composites compared for strength/weight and modulus/weight ratios, moisture absorption, corrosion resistance, projected costs, etc
19 p3340 A69-35506
- Military storage and environment effects on strength of filament wound glass reinforced epoxy structures, tested on plastic motor case and pressure vessels
19 p3321 A69-35567
- Glass fiber filled polytetrafluoroethylene materials for piston seals in high pressure oil-free reciprocating air compressors, discussing manufacturing and non-destructive tests
19 p3323 A69-35579
- Resin impregnated fiber reinforced expandable structures used for automatic cure or rigidizing in space and initially small compact packages on earth
19 p3433 A69-35585
- Creep strength of fiberglass reinforced polyester resins measured on structural components in long term tests under torsion
19 p3358 A69-35830
- Titanium monocoque fuselage reinforced by composite boron filaments in polyimide resin matrix tested for SST applications, noting weight savings over all titanium structure
[AIAA PAPER 69-763] 19 p3329 A69-36298
- Metal fiber reinforced thermoplastic composites, analyzing unidirectional, crossed and random orientation cases taking into account adhesion efficiency between fiber and matrix
20 p3559 A69-37083
- High performance graphite fiber reinforced plastic composites development and characterization, discussing fiber property data
[ASM PAPER W9-16.1] 21 p3728 A69-38655
- Stress-strain state of fiberglass reinforced plastics under load analyzed by anisotropic linear creep theory and Galerkin method
21 p3835 A69-38831
- Silico-organic liquid water repellent coatings for increasing binder adhesion to glass fiber in glass fiber reinforced plastic materials of aircraft components
21 p3752 A69-38876
- Fiber reinforced plastics mechanical behavior including thermosetting and thermoplastic polymers reinforcement mechanism
21 p3752 A69-38933
- Photoelastic and micromechanics studies of epoxy resins of varying Young moduli by simultaneous stress analysis of FRP and matrix materials
21 p3846 A69-39796
- Tensile strength of glass and graphite fibers for fiber reinforced plastics /FRP/ tested with modified balance type and strain gage type tensile testers
21 p3753 A69-39799
- Residual stress effect on strength of oriented glass fiber reinforced plastics under transverse and longitudinal tension
22 p3973 A69-40745
- Stress analysis during solidification of binders in glass fiber reinforced plastic materials, using resin coated glass film simulation
22 p3973 A69-40746

Porosity and composition effects on thermal conductivity of glass fiber reinforced plastics, noting tests of multilayer textolite sheets 22 p3973 A69-40747

Summation methods for multiple damages caused by static fatigue in glass fiber reinforced plastics under stepwise loads 22 p3974 A69-40748

Initial stress dependence on tensile load in glass fiber reinforced plastic rings during winding 22 p4045 A69-40749

Temperature influence on mechanical properties and creep curves of fiberglass reinforced textolites compared with data from elasticity theory 23 p4179 A69-41993

Mechanical properties of fiberglass reinforced textolite at normal temperature, noting applicability of elasticity formulas 23 p4179 A69-41994

Soft fiber reinforced plastics creep and recovery properties, discussing test equipment, rheological properties, polishing effects, etc 23 p4179 A69-42006

Carbon fiber reinforced plastic components aerospace applications, discussing honeycomb sandwich satellite structure for investigating lamination methods, shapes, bonding and machining 24 p4336 A69-43209

Composite-to-metal joints design and fabrication, using carbon yarn in epoxy matrix for missile interstage application 24 p4323 A69-43426

REINFORCED PLATES

Soviet handbook on stress analysis of anisotropic three layer reinforced plates and shells and of thick walled cylinders, Volume 2 04 p0683 A69-15500

Critical axial load for elastic instability of unidirectional equally spaced fibers in plane of composite plate and buckling modes 07 p1232 A69-18714

Fiberglass reinforced plastic plates strength coupled to elastic base with allowance for tangential shearing stresses 08 p1412 A69-20334

Stress-strain state of infinite plate with elliptical eccentric reinforced hole, using quadrature method 09 p1613 A69-21630

Two dimensional problems solutions by contour smoothing methods, considering stress concentrations in reinforced or perforated thin elastic plates 11 p1973 A69-24661

Two dimensional elasticity and plate bending theories for calculating elastic isotropic panels and thin reinforced plates 11 p1974 A69-24664

Field approach for stress and deflection analysis in rectangular plates reinforced by straight ribs, noting kernel function 11 p1983 A69-25019

Shear buckling of simply supported infinitely long plates orthogonally reinforced by stiffeners with flexural and torsional rigidity 11 p1984 A69-25142

Fatigue crack propagation and fail-safe design for stiffened large Al alloy panels with crack stoppers, using residual strength analysis method 12 p2186 A69-26835

Buckling loads for anisotropic fiber reinforced composite plates with strong bending membrane coupling terms 12 p2186 A69-26840

Rigid supporting ribs effect on annular plate critical loading, stability loss and buckling 14 p2533 A69-28983

Finite element analysis of flat rectangular orthotropic multilayer stiffened panels, proposing six degrees of freedom model 15 p2708 A69-30668

Stability of nonuniformly heated rectangular plate reinforced by elastic longitudinal and rigid transverse ribs, accounting for influence of torsional and bending rigidities 17 p3057 A69-33198

Crack analysis in stiffened vibrating plate based on dynamic stress distribution, showing high bending stresses at intersection 18 p3223 A69-35168

Stiffened integrally formed panel stability evaluation based on compression structural efficiency and manufacturing costs [AIAA PAPER 69-760] 19 p3434 A69-35660

Elastoplastic state of composite structures with applicability of elasticity law and yield conditions illustrated by reinforced plate under plane stress 19 p3444 A69-36808

Buckling of eccentrically stiffened thin circular elastic plate under circumferential uniform compression, obtaining equations and critical loads 20 p3622 A69-37221

Nonlinearly elastic plates with reinforced edges, deriving differential equations for boundary conditions 21 p3833 A69-38574

Stress concentration in elastic plate reinforced at edge by straight rib analyzed in finite form by Cauchy integrals and Fourier transforms 22 p4041 A69-40114

Limiting load of square plate subjected to shear and reinforced by vertical stiffener, computing membrane and bending stresses as function of flexural rigidity 24 p4399 A69-42967

Tensile tests on fiber reinforced plates with circular holes, studying fiber orientation effects 24 p4404 A69-43602

Crack propagation in plate with stiffening ribs /riveted stringers/ under concentrated and tensile loads, determining rivet points displacements 24 p4406 A69-43709

REINFORCED SHELLS

Strength analysis of cylindrical shells with rib and ring reinforcement under compression loads using network method 01 p0164 A69-10083

Imperfection sensitivity of axially compressed stringer stiffened cylinder analysis via shell equations formulation using finite differences 02 p0348 A69-12542

Stress diffusion from axially loaded stiffeners into cylindrical elastic shells 03 p0530 A69-14065

Impulse buckling threshold for elastic-plastic cylinder with elastic core after development of unstable motion 04 p0671 A69-14144

Reinforced thin walled cylindrical pressure body nonlinear circumferential stress problem approximate solution, noting fatigue strength of aircraft pressurized cabins 04 p0548 A69-14838

Soviet handbook on stress analysis of anisotropic three layer reinforced plates and shells and of thick walled cylinders, Volume 2 04 p0683 A69-15500

Elastic stability of thin circular cylindrical shell with elastic core, longitudinal and transverse reinforcement ribs, initial defects and under large strains 05 p0832 A69-15691

Elastic stability of thin circular cylindrical shell with elastic core, longitudinal and transverse ribs and initial defects under combined pressure and thermal stress 05 p0832 A69-15692

Approximate expressions for displacement state of orthotropically reinforced conical thin walled shell, finding stiffness matrix by numerical integration 05 p0835 A69-15829

Resonant frequencies for beam type bending oscillations of thin walled rib-reinforced circular cylindrical shell freely supported at outermost ribs 05 p0841 A69-16204

Annular stress in rib reinforced cylindrical shells under axial compression load and internal pressure, using successive approximation 05 p0841 A69-16208

Bending general instability of stiffened shallow orthotropic cylindrical shells, noting buckling stress and application to shell design for various loadings 06 p1022 A69-17369

Buckling of elastic cylinders with rectangular cut-outs and reinforcements under axial or lateral loading, using modified Newton method [AIAA PAPER 69-92] 06 p1027 A69-18060

Elastic stability of three dimensionally reinforced composite cylindrical shells [AIAA PAPER 69-122] 06 p1029 A69-18216

Stability of cylindrical shell reinforced by circular ribs under combined action of external pressure and axial forces, using characteristic equation 07 p1238 A69-19687

Optimal design of circular cylindrical sandwich shells under pressure and shear loads, showing acceptability of small shear coefficient values 08 p1416 A69-20722

Thermal stresses in longitudinally reinforced cylindrical shell, combining moment and semimomentless shell theories to obtain numerical results 11 p1981 A69-24942

Stress analysis of reinforced cylindrical shells under external loading, using Vlasov semimomentless theory 11 p1982 A69-24949

Optimal parameters selection for rib-reinforced cylindrical shells determined with respect to axial critical loading magnitude 11 p1985 A69-25173

Critical axial compressive load for cylindrical shells reinforced with longitudinal ribs, noting internal pressure and rib spacing effects 11 p1985 A69-25177

Maximum stress under bending for thin walled circular cylindrical shell stiffened with uniform stringers 11 p1987 A69-25380

Inplane and rotary inertia effects on free vibration frequencies of circular cylindrical shells eccentrically stiffened by orthogonal set of stringers and/or rings 11 p1992 A69-25520

Free vibration of discretely stiffened cylindrical shells with arbitrary end conditions programmed for digital computer, considering flexure, extension, torsion and nonsymmetric stiffener cross section 11 p1992 A69-25521

Dynamic analysis of axisymmetric ring stiffened shells with attached asymmetric elastic structures, noting vibration modes 11 p1993 A69-25525

Glass fiber reinforced plastics shells stability under external hydrostatic pressure, discussing compression and axial tests for normal elastic modulus, shear modulus and Poisson coefficient 11 p1995 A69-25681

Zero Gaussian curvature rib reinforced shells free oscillations reduced to nonreinforced shell forced oscillations under cyclic loads 12 p2177 A69-25996

Natural frequencies of ring-stiffened thin walled cylindrical shell determined by partial differential equations of motion, allowing for eccentricity 12 p2184 A69-26810

Axisymmetric elastic stresses in ring stiffened segmented shells of revolution, noting finite difference method for nonlinear analysis and computer program 12 p2185 A69-26818

Buckling of ring stiffened cylinders subject to axial compression, considering prebuckling lateral wall displacements 14 p2534 A69-29030

Stress distribution in variable rigidity reinforcing frame of circular cylindrical shell using strain energy method 17 p3055 A69-33131

Stress-strain rate of glass fiber reinforced plastic pressure vessels under internal pressure, determining optimal fiber pattern 17 p3057 A69-33195

Critical buckling stress for cylinders wound with fiber reinforced plastics /FRP/, establishing stability criteria for fiber reinforced shells 17 p3058 A69-33430

Stress level reduction in pressurized circular cylinder with circumferential ring stiffener and longitudinal crack, using shallow shell equations 18 p3212 A69-34347

Stability of thin walled eccentrically reinforced cylindrical shell, determining eccentricity influence and critical pressure formula from considerations of Poisson ratio, reinforcement parameters, etc 18 p3216 A69-34576

Stress-strain state calculations of ribs reinforcing cantilever shell under external pressure, using differential-difference equations 18 p3223 A69-34980

Microstresses in hollow-fiber reinforced cylindrical shell under longitudinal shear stress, determining modulus of elasticity and optimum component ratios 18 p3225 A69-35369

Cylindrical reinforced steel shells stability under external pressure 18 p3225 A69-35371

Natural frequencies and mode shapes of vibration of cylindrical shells orthogonally stiffened with rings and stringers [AIAA PAPER 68-349] 19 p3437 A69-35948

Boundary conditions for shells with reinforced nonasymptotic boundaries, assuming coincident beam axis deformation with shell boundary deformation 19 p3443 A69-36781

Elastic shell theory to regularize singular integrodifferential equation, investigating load transfer from reinforcing ribs to circular cylindrical shell and numerical solution correlation 19 p3443 A69-36792

Elastic interactions between cylindrical shell and added band reinforcement turns, analyzing stress relaxation magnitude and effect on pressure vessel design
20 p3621 A69-37064

Soviet book on shell and thin walled structure calculation methods covering stability and stress analysis, reinforced and sandwich shells, etc
20 p3630 A69-38199

Stability loss for hinged circular cylindrical elastic shells reinforced by thin walled closed profile ribs, proposing minimum weight design method
21 p3835 A69-38723

Dynamic behavior of infinitely long cylindrical shells of ideally rigid plastic materials strengthened with ring ribs, determining distribution of moments and displacements
21 p3837 A69-39156

Stiffness matrix for curved membrane shell, outlining discrete element representation of cylinders with widely spaced circumferential stiffeners
21 p3842 A69-39305

Deformation of thin walled spherical shell reinforced with equatorial hoop by concentric elastic forces
21 p3846 A69-39714

Buckling strength prediction for circular cylindrical shells reinforced by circumferential and longitudinal stiffeners, solving torsional buckling of orthotropic shells under internal pressure
22 p4042 A69-40171

Axisymmetric vibrations of semiinfinite cylindrical shell constructed of fiber reinforced composite layers, obtaining frequency equation from equations of motions
22 p4044 A69-40559

Discrete rib effect on buckling resistance of cylindrical shell under combined external and axial compression loads, using Laplace transforms
23 p4229 A69-41990

Stability of orthotropic cylindrical shells reinforced at edges by elastic ribs, analyzing axisymmetric buckling, natural oscillations and rigidity characteristics
23 p4229 A69-41992

Hinged circular cylindrical shells reinforcing ribs effect on deflection and bending moments, assuming external pressure application
23 p4229 A69-42001

Orthotropic stiffness layer models for buckling of eccentrically stiffened shells of revolution with two unbonded orthotropic layers uncracked and circumferentially cracked
24 p4405 A69-43657

Computer program determination of barreling effect on strength of ring and stringer stiffened shells designed to support axial compression loads
24 p4405 A69-43671

REINFORCEMENT [PSYCHOLOGY]
NT REWARD [PSYCHOLOGY]

Squirrel monkeys exposed to centrifugally generated artificial gravity trained to respond for food reinforcement at selected gravity levels
23 p4081 A69-41434

Fixed interval human performance control under various histories of conditioning and response cost conditions, considering effects of postreinforcement pauses
23 p4100 A69-41437

Human performance on button pressing task with fixed ratio fixed interval reinforcement schedules
23 p4081 A69-41439

Electrical self stimulation adaptability of hypothalamus or instrumental self reinforcing reaction in rats using skinner box technique
23 p4091 A69-42052

Constant illumination intensity effects fixed ratio lever pressing behavior for appetitive reinforcement with chimpanzee in temperature and humidity controlled environment
24 p4260 A69-42702

REINFORCEMENT [STRUCTURES]

Prestressing of aircraft wing stringers in order to reduce weight, noting initial bending moment, initial axial stress and prestressing methods
05 p0832 A69-15690

Fatigue behavior of composite disk modified from previously evaluated boron epoxy reinforced titanium compressor disk
09 p1619 A69-22323

Transverse reinforcing straps effects on torsional stiffness and bending behavior of open cross section profile thin walled prismatic beams
10 p1802 A69-23890

Damping of response of integrally stiffened skin structures to random acoustic pressures, reducing rms stress in case of broad band excitation
[ASME PAPER 69-VIBR-26]

10 p1806 A69-24172

Two dimensional elastic reinforcements effects on stress, strain and elasticity of quasi-homogeneous anisotropic elastic medium

11 p1981 A69-24941

Prototype system for continuous dielectrophoretic deposition and alignment of micron sized ultrahigh strength whisker reinforced composites

13 p2269 A69-28676

Wide panel Ti structural extrusions with integral stiffeners, discussing material, sizes, properties and tolerances

19 p3319 A69-35552

Reinforcement unbonding onset in composite materials determined by continuous dynamic moduli and damping measurements of tensile specimens

20 p3511 A69-37761

Reinforcement effect on stress relaxation and creep in hereditary elastic materials, assuming integral shear modulus operator with exponential kernel

22 p4045 A69-40744

Torsion analysis of curvilinear rectangular prismatic beam reinforced by off-center circular rod, using conformal mapping

22 p4049 A69-41279

Potting material reinforcing honeycomb structures for fastener installation prior to bonding face sheets to core, noting mechanical properties

24 p4326 A69-43466

REINFORCEMENT RINGS

Buckling of ring stiffened cylinders subject to axial compression, considering prebuckling lateral wall displacements

14 p2534 A69-29030

Anisotropic elastic plate deflection weakened by circular hole with thin elastic ring reinforcement, assuming no load on ring and uniform stress-strain state of plate

17 p3055 A69-33128

Aircraft landing gear cylinder reinforcement rings design for minimum weight, using optimization iteration method for planar frames with elastic supports
[AIAA PAPER 68-328]

17 p3066 A69-34030

Stress level reduction in pressurized circular cylinder with circumferential ring stiffener and longitudinal crack, using shallow shell equations

18 p3212 A69-34347

Steady state temperature fields and thermal stresses determined in finite cylindrical shell by optimal parameters of reinforcing circular rib

21 p3834 A69-38714

Dynamic behavior of infinitely long cylindrical shells of ideally rigid plastic materials strengthened with ring ribs, determining distribution of moments and displacements

21 p3837 A69-39156

Deformation of uniformly thick elastic circular plates containing circular holes reinforced by thin rigid elastic rings

21 p3846 A69-39713

REINFORCING FIBERS

Mass or energy transfer in reinforced media, discussing components characteristics and role of diffusion processes

01 p0173 A69-10079

Ribbon reinforcements in composite materials noting stiffness properties

01 p0172 A69-11265

Diffusion zones in filament reinforced metal matrix composites, using metallographic technique

01 p0103 A69-11269

Stress transfer from loaded matrix to single fiber in composite materials determined by series and step formulations

01 p0172 A69-11271

Reinforcing glass fiber fillers in thermoplastic commercial products, noting applicability to high speed fabrication by injection molding processes

07 p0269 A69-11794

Metal composite materials, discussing strengthening mechanism for inclusion of high elastic coefficient and creep limit fibers in weak ductile matrices

02 p0268 A69-12750

Fabrication of Cu-W composites with discontinuous fibers based on sintering and rolling

03 p0444 A69-13349

Glass fiber reinforced plastics - Conferences, Freudenstadt, West Germany, October 1968

03 p0453 A69-13819

Damping properties of glass fiber reinforced plastics measured by flexural vibrations

03 p0454 A69-13824

Thermal stress in fiber reinforced metals, assuming Young modulus variable when thermal stress is applied during heating and cooling

04 p0682 A69-15393

Piezoptical method applied to anisotropic bodies and reinforced plastics, deriving relation between dielectric tensors and stresses and strains

05 p0837 A69-16038

Flow stress of iron wire reinforced aluminum alloy composites
[ASME PAPER 68-WA/MET-10]

05 p0780 A69-16150

Statistical model for tensile fracture of parallel fiber composites based on stress criterion for crack propagation

[ASME PAPER 68-WA/RP-7]

05 p0783 A69-16159

Boron carbide continuous filaments preparation and properties, discussing use in resin and metal composites
[ECS PAPER 210]

05 p0783 A69-16236

Glass, boron and graphite filament wound resin composites and liners for cryogenic pressure vessels

05 p0785 A69-16488

Nickel reinforced with mullite whiskers produced by hot pressing

05 p0782 A69-16794

Metal matrix composites - ASTM Conference, Boston, June 1967

06 p0938 A69-16940

Sapphire whisker reinforced aluminum composites fabrication and evaluation

06 p0939 A69-16942

Fiber orientation and morphology effect on tensile behavior of aluminum-nickel whisker reinforced aluminum

06 p0939 A69-16943

Lattice strains in matrix phase of aluminum-boron and copper-tungsten composites measured by X ray diffraction

06 p0939 A69-16944

Metal matrix composites compression microstrain behavior, analyzing continuous fiber composites of magnesium-boron and copper-tungsten

06 p0939 A69-16945

Diffusion bonded aluminum-boron composite material, discussing mechanical, metallographic and radiographic properties

06 p0939 A69-16946

Micromechanics of boron filament reinforced aluminum composites

06 p0940 A69-16948

Aluminum-silica fiber reinforced metal composite, discussing mechanical behavior and effect upon engineering applications

06 p0940 A69-16949

Aluminum-stainless steel wire reinforced metal matrix composites, analyzing strain hardening and plastic deformation

06 p0940 A69-16950

Fatigue performance of composites consisting of W or Mo helical coils embedded in Cu matrix, discussing evaluation from microstructural behavior

06 p0940 A69-16951

Delamination effects on strength degradation of filament wound composites

06 p0946 A69-17126

Diffusion bonding of whisker reinforced aluminum in closed steel die in argon atmosphere

06 p0943 A69-17238

Metal fiber reinforced ceramic matrix composites, discussing model system, bond strength, loading and elastic properties

06 p0946 A69-17528

Fiberglass reinforced plastic bottoms design for integration with cylindrical shells, discussing design, shapes and boundary value problems

06 p1025 A69-17685

Statistical theory of material strength with application to composite materials reinforced with whiskers and continuous fibers

06 p1028 A69-18142

High strength carbon fibers development and applications in reinforced composite materials and aerospace industry

06 p0947 A69-18236

Compressive strength of boron fiber-epoxy matrix composite, noting matrix support of fibers against buckling

07 p1170 A69-18713

Critical axial load for elastic instability of unidirectional equally spaced fibers in plane of composite plate and buckling modes

07 p1232 A69-18714

Anisotropic glass fiber reinforced epoxy resin composite under biaxial and uniaxial loads, noting isochromatics and isoclinics in photoelastic analysis
07 p1170 A69-18715

Fiber geometry and partial debonding effects on bond stress distributions around single rigid fiber in infinite elastic plate subject to tensile stress
07 p1170 A69-18717

Fiber reinforced plastic and metallic composites for longevity and endurance of materials at high temperatures and extreme loads, discussing alumina whiskers
07 p1167 A69-19290

Fiber-metal matrix composites fabrication, applications, mechanical properties and powder metallurgy
08 p1332 A69-20204

Development of materials in aerospace structures and propulsion systems, discussing superelastic alloys, graphite fibers, composites, refractory metals and processing techniques
08 p1332 A69-20306

Structural parameters influence on fiberglass reinforced plastics strength studied for optimal structure selection
08 p1335 A69-20332

Thermoplastics reinforcement with fiber and whisker fillers, evaluating graded asbestos, carbon, silicon nitride, silicon carbide and potassium titanate
08 p1337 A69-20479

High modulus and high strength carbon fibers and composites, discussing mechanical properties and interlaminar shear strength
08 p1338 A69-20488

Filament winding process variables effect on carbon or fiberglass reinforced composites, determining mechanical properties
08 p1338 A69-20489

Fracture energy of unidirectional laminated composites related to diameter, debonding energy and strength of reinforcing filaments
08 p1414 A69-20493

Tensile characteristics of discontinuous unidirectional fiber reinforced glass-epoxy composites and filament wound material, discussing alignment and interfacial bonding
08 p1339 A69-20496

Nondestructive testing methods application to fiber-bonded composites, noting X ray diffraction, radiography and ultrasonics
08 p1339 A69-20498

Laser beam diffraction method for measurement of apparent filament diameters, emphasizing high modulus carbon filaments
08 p1316 A69-20499

Thermoelastic properties of particulate, filamentary and layered composites, summarizing Soviet theoretical and experimental work
08 p1339 A69-20500

Matched metal molding of short graphite fiber composites
08 p1339 A69-20502

Shop-ready high modulus carbon and fiberglass composite reinforcement system, stressing effect of modulus fibers amount in laminate
08 p1340 A69-20508

Whiskerizing technique for growing small beta SiC single crystals on graphite filament surfaces, noting changes in interface geometry and chemistry
08 p1341 A69-20511

Fiber composite design, discussing contribution of filament diameter, number, content and properties, ply parameters and void content to structural response
08 p1341 A69-20512

Direct chemical bonding effect on flexural strength and flexural modulus of glass fiber reinforced plastics, noting degradation reactions
08 p1341 A69-20514

Silicon carbide fiber surfaces nature and interaction with coupling agents, epoxy and resin components, noting chemical and electron microprobe analysis
08 p1341 A69-20515

Mechanical properties of ceramic material consisting of pure silica matrix reinforced by carbon fibers
08 p1341 A69-20700

Cylindrically deformed fiber reinforced material, obtaining kinematics and constitutive equations
08 p1418 A69-21002

Failure criteria for predicting filamentary composite strength under uniaxial and combined stresses from properties and fabrication process considerations
09 p1611 A69-21479

Boron and graphite fibers role in composites cost feasibility in 1970s
09 p1524 A69-22067

Boron-epoxy composites applications and properties, comparing strength to weight and stiffness to weight ratios with aluminum, titanium and beryllium
09 p1529 A69-22068

Development and fabrication of fiber-resin and fiber-metal composites, discussing application to aerospace technology
09 p1524 A69-22069

Boron carbide filaments as reinforcements for metal structures, noting vapor deposition use of silica
09 p1529 A69-22070

Tensile strengths and elasticity moduli of graphite fibers produced from textile organic thread, discussing application to composites, ablative and fiber reinforced materials
09 p1529 A69-22071

Metallic and nonmetallic matrices reinforcement by ceramic whiskers, describing mechanical properties
09 p1525 A69-22142

Automatic fabrication process for boron reinforced composite structures, concerning orienting and laminating jet flap skins
09 p1507 A69-22329

Magnesium boron composite fabrication by diffusion bonding and liquid metal infiltration, obtaining minimized property variations and high strength to density ratios
09 p1507 A69-22332

Subscale aircraft fuselage section fabricated with lightweight graphite fiber/epoxy resin composite material
09 p1509 A69-22341

Bonded Al-B metal matrix composite materials hot press fabrication and design, discussing temperature pressure time cycles and honeycomb sandwich structures
09 p1510 A69-22351

Ceramic whiskers and metallic matrix chemical reactions during composite formation, analyzing coated and uncoated SiC whiskers in titanium matrix
09 p1527 A69-22359

Whiskerized graphite fiber in resin matrix composites, analyzing interstitial growth characteristics, resin infiltration, layup and compaction
09 p1511 A69-22360

Graphite fiber electroplating with nickel on continuous basis for ribbon like continuous flexible twist free yarn
09 p1512 A69-22362

Static and dynamic strength tests and modulus data for graphite fiber/epoxy composite yarn, noting ply winding and dimensions
[ASME PAPER 69-GT-114]
09 p1531 A69-22520

Metal composites of Ni or Mo fibers in Be matrix, discussing chemical compatibility in terms of reactions, solid solubility and diffusion at various temperatures
10 p1707 A69-22991

Fiber reinforced metals, discussing crystalline whiskers, metallic and ceramic fibers and mechanical characteristics
10 p1711 A69-23335

Fiber content by weight of reinforced plastics measured by pyrolysis
10 p1716 A69-23695

Electroplating solutions test for filament winding and electroforming process used in fabricating fiber reinforced metal composites
11 p1890 A69-24337

Reinforced metals properties and applications including fibers and lamination, notch sensitivity, brittle fracture, failure and heat resistance characteristics
11 p1904 A69-24898

Nozzle ablations based on chemical mechanism, discussing pure or reinforced phenolic resin
11 p1999 A69-24908

Unidirectional fibrous materials stability, finding characteristic equation in form of infinite determinant by solving three dimensional stability of reinforcing fibers in binder
11 p1985 A69-25172

Graphite and B filament-epoxy resin composites application to aeroelastic scaled dynamic models, analyzing weight savings, fabrication and component stiffness
11 p1990 A69-25508

Birefringent coatings application to plane stress in orthotropic glass-fiber reinforced plastic materials noting stress-strain relations
11 p1995 A69-25647

Residual stresses and strains in wound reinforced plastic fiber cylinders subjected to polymerization by heat treating
11 p1907 A69-25679

Fiber reinforced materials shear and tensile strength effect on stress-strain state of composite materials machine parts, considering design requirements
11 p1907 A69-25680

Composite materials for aerospace applications, discussing high modulus filaments, structural and non-structural design considerations, nondestructive testing techniques, etc
12 p2111 A69-25852

Metallic and ceramic whiskers and fibers for material reinforcement, discussing properties and fabrication techniques
12 p2111 A69-25856

Fiber reinforced space vehicle combustion chambers and cryogenic fuel tanks, discussing design and elastomechanical problems
12 p2176 A69-25860

Stress distribution in elements of unidirectionally fiber reinforced composite materials analyzed as function of fiber content and fiber-matrix elastic properties
12 p2180 A69-26263

Book on ceramic fibers and fibrous composite materials as structural reinforcements covering dynamic testing of fine filaments and whiskers, material characterization, etc
12 p2118 A69-26340

Orthotropic properties and stress fields for configurations of fiber or whisker reinforced composite materials subjected to nonaxial loading, considering infinite elastic matrix
12 p2186 A69-26824

Stress distribution in matrix of unidirectionally fiber reinforced composite subject to shrinkage and normal transverse load, using three dimensional photoelastic analysis
12 p2189 A69-27162

Fiber polymer composite flexible insulating materials properties and applications stressing synthetic organic fibers
13 p2286 A69-27989

Finite control volume approach to shock Hugoniot in unidirectional fiber reinforced composite, computing shear force along matrix-fiber interface
[AIAA PAPER 69-359]
13 p2366 A69-28292

Boron nitride coated boron reinforced metal matrix composites, discussing continuous liquid infiltration, fiber-matrix reactions and heat treatment
13 p2283 A69-28671

Tungsten alloy fiber reinforced nickel base alloy composites stress-rupture strength, oxidation and impact resistance for high temperature turbojet engine buckets
14 p2462 A69-29010

Fiber reinforced adhesives, discussing adhesion definition and variables separation, applications and testing
14 p2455 A69-29343

Boron filament wound composite structures fabrication noting physical properties
14 p2455 A69-29413

Thermal stresses in fiber reinforced metals as function of volumetric content of fiber phase
15 p2638 A69-30285

Interlaminar shear strength development for utilization of unidirectional strength and stiffness of graphite fibers, discussing epoxy resin-fiber interface improvement
15 p2642 A69-30312

Organic and inorganic fabric reinforcements effects on thermal properties of composites noting thermal conductivity, diffusivity, specific heat constants and temperature ranges
15 p2642 A69-30466

Fiberglass reinforced plastic tensile strength dependence on vibration time and temperature and vibrational effect on modulus of elasticity
15 p2643 A69-31203

Heat resistant fiber composites produced by oriented eutectic crystallization in Co and Ni quaternary alloys
[ONERA-TP-710]
16 p2799 A69-31765

Optical measuring methods of cross sections and mechanical properties of heat resistant fiber reinforced materials
16 p2803 A69-31804

Carbon fiber reinforced plastics properties improvement by applying organosilanes, discussing silanol bond formation
16 p2803 A69-31806

Molded composites application to engine components, discussing turboprop reduction gear case design using polymer matrix boron composite
[AIAA PAPER 69-466]
16 p2795 A69-32763

Tensile and creep deformation of fiber reinforced composites consisting of Mg-Li alloy matrix with high strength precipitation hardening stainless steel wire 17 p2986 A69-33073

Critical buckling stress for cylinders wound with fiber reinforced plastics (FRP), establishing stability criteria for fiber reinforced shells 17 p3058 A69-33430

Carbon fiber reinforced plastics development for aerospace use, presenting criteria for resins selection 17 p2992 A69-33647

Surface chemistry of plastics reinforced with strong fibers, stressing need for investigating coupling films, catalysts and metallic ions role in coupling compounds chemisorption 17 p2992 A69-33655

Filamentary composites elastic constants calculation extended to hexagonal symmetry by long waves method 17 p3061 A69-33666

Thin walled cantilevered fiberglass reinforced shafts damping characteristics dependence on natural vibration modes and fibers orientation 17 p3065 A69-33938

Macrostructural differences between filaments of B and SiC vapor deposited onto small diameter W wire, discussing radial cracks due to dilatation 18 p3160 A69-34266

Axisymmetric deformation of cylindrical wound fiberglass reinforced plastic shell analyzed by methods of rigid normals and nonlinearly elastic fiber system 18 p3222 A69-34974

Thermal stress in fiber reinforced metals, assuming Young modulus variable when thermal stress is applied during heating and cooling 18 p3223 A69-35021

Composite material applications in space vehicle structures, noting strength and stiffness of boron fibers in plastic or metal matrices 19 p3340 A69-35502

B-epoxy and B-Al composites compared for strength/weight and modulus/weight ratios, moisture absorption, corrosion resistance, projected costs, etc 19 p3340 A69-35506

Beryllium wire reinforced Al composites, discussing layup techniques and coated filament advantages 19 p3340 A69-35508

Silicon carbide coated boron fibers in aluminum alloy matrix, discussing tensile and structural properties of braze bonded specimens 19 p3340 A69-35509

Electroforming of Al matrix composites by codeposition of short graphite fibers, obtaining increased strength and elastic modulus 19 p3318 A69-35510

Filament reinforced metal matrix composites made by continuous casting process, discussing tensile tests results and production costs 19 p3318 A69-35511

Mechanical properties and thermal aging of laminated specimens of collimated B monofilament reinforced composites preimpregnated with polyimide resin 19 p3354 A69-35514

Glass overlaid B filament laminates interleaved with C and silica fabrics, evaluating ablative properties in solid rocket motor tests 19 p3354 A69-35515

Silicon nitride staple fibers synthesis, development and characterization, noting tensile strength and sonic modulus 19 p3354 A69-35517

Fiber reinforced carbon and graphite with application to reentry and propulsion systems and high temperature gas turbines, noting three dimensional woven quartz 19 p3354 A69-35519

Tape placement machines to fabricate composite high modulus filamentary tape reinforced aerospace structures, anticipating future generations evolution into automatic control 19 p3323 A69-35584

Resin impregnated fiber reinforced expandable structures used for automatic cure or rigidizing in space and initially small compact packages on earth 19 p3433 A69-35585

Silicon carbide coated boron fiber reinforced /Bor-sic/ Al composites tensile strength and elastic properties 19 p3344 A69-35926

Titanium monocoque fuselage reinforced by composite boron filaments in polyimide resin matrix tested for SST applications, noting weight savings over all titanium structure [AIAA PAPER 69-763] 19 p3329 A69-36298

Metal fiber reinforced thermoplastic composites, analyzing unidirectional, crossed and random orientation cases taking into account adhesion efficiency between fiber and matrix 20 p3559 A69-37083

Boron fiber reinforced Al matrix composite material for high performance aircraft gas turbine engine compressor blading [AIAA PAPER 68-1037] 20 p3586 A69-37153

Transverse stiffness and strength of unidirectional fiber-reinforced composites determined as function of fiber volume content, using finite element method and stress functions 20 p3623 A69-37354

Strength characteristics of high performance fibers and application to reinforced composite materials noting whiskers, polycrystalline and vitreous fibers 20 p3567 A69-37748

Elastic constants of composite containing parallel cylindrical fibers, discussing disturbance in stress field 20 p3626 A69-37759

Composite materials application in aerospace industry, discussing boron and carbon filament properties, epoxy resins, etc 20 p3563 A69-37930

Diffusion bonding of Al and boron filament layers into continuous structural material, studying process variables including heat treatment and cross rolling effects [AIME PAPER S69-6] 20 p3564 A69-38197

Carbon fiber reinforced plastics application to aircraft metal components for weight reduction, low cost and high mechanical properties 21 p3750 A69-38428

B fiber reinforced Ni failure characteristics at high temperature, discussing plastic deformation and matrix role in crack inhibition 21 p3743 A69-38616

High performance graphite fiber reinforced plastic composites development and characterization, discussing fiber property data [ASM PAPER W9-16.1] 21 p3728 A69-38655

Metal matrix compatibility of metal coated graphitized, silicon carbide and boron fibers, discussing fiber weakening processes [ASM PAPER W9-20.1] 21 p3751 A69-38670

Graphite fiber reinforced graphite composites fabrication, discussing spray forming and physical and mechanical properties [ASM PAPER W9-20.4] 21 p3730 A69-38671

Fiber reinforced plastics mechanical behavior including thermosetting and thermoplastic polymers reinforcement mechanism 21 p3752 A69-38933

Carbon fiber reinforced materials applications in aerospace industry, discussing long term potential and applications in F-5 aircraft 21 p3732 A69-38989

Al-B composite aircraft structure fabrication, discussing wingspan segment, resistance spot welding, hot forming of joggles, etc [AIME PAPER S69-1] 21 p3732 A69-39471

Stress-strain curves of W wires and of aligned composites of same wires in Cu matrix 21 p3845 A69-39709

Fracture strength of glass fiber-reinforced cylinders made by unidirectional filament winding predicted by analyzing three dimensional stress distributions 21 p3846 A69-39795

Photoelastic and micromechanic studies of epoxy resins of varying Young moduli by simultaneous stress analysis of FRP and matrix materials 21 p3846 A69-39796

Tensile strength of glass and graphite fibers for fiber reinforced plastics (FRP) tested with modified balance type and strain gage type tensile testers 21 p3753 A69-39799

High E modulus, structure, strength and temperature characteristics of reinforcement fibers, considering B, silicon carbide, C and Be 22 p3951 A69-39907

Boron and carbon reinforced composite materials aerospace structural application, discussing weight savings, components structural design and connection and load input problems 22 p4038 A69-39908

Metal matrix fiber-reinforced composite materials joining by welding and brazing techniques 22 p3956 A69-40480

Loading rate effects on fracture characteristics of unidirectional fiber reinforced materials, discussing fiber-resin interface strength 22 p3974 A69-41212

Soft fiber reinforced plastics creep and recovery properties, discussing test equipment, rheological properties, polishing effects, etc 23 p4179 A69-42006

B, silicon carbide, C and Be reinforcing fibers technology, thermal and physicochemical properties, noting coating, surface defects and improvement over glass fibers 23 p4179 A69-42154

Boron fiber reinforced composite materials in aircraft structures, comparing rigidity with glass fiber plastics and weight gains 23 p4179 A69-42155

Carbon fiber composites in construction of rocket motor cases, pressure vessels and support structures, including carbonization for ablation and insulation applications 23 p4180 A69-42158

Law of mixture governing creep strength of composite materials reinforced unidirectionally by continuous filaments, taking into account fibers and matrix viscoelastic properties 24 p4400 A69-43054

Stress analysis of hollow viscoelastic cylinder reinforced with elastic helically wound wires [ASME PAPER 69-APMW-23] 24 p4401 A69-43096

Carbon fiber reinforced plastic components aerospace applications, discussing honeycomb sandwich satellite structure for investigating lamination methods, shapes, bonding and machining 24 p4336 A69-43209

Aircraft structure fabrication combining unidirectional strength and stiffness of B composite with metal, including test and weight/ cost data 24 p4323 A69-43419

High modulus carbon filament composite structural elements for missile interstage application, showing weight savings 24 p4325 A69-43444

High performance void free carbon fiber laminates preparation using polyimide resins, describing flexural strengths, moduli and interlaminar shear strengths 24 p4325 A69-43445

Postcured low void content graphite fiber reinforced polyimide resin composites fabrication including shear, flexural and tensile strength data 24 p4337 A69-43446

High modulus graphite/asbestos reinforced laminates, noting improved transverse strength and thermal properties 24 p4337 A69-43447

Molded fiber composites in aerospace components applications, considering weight, stiffness, production and cost 24 p4326 A69-43448

Tensile strength improvement in Al-B composites by heat treatment to T6 condition and subsequent cold rolling 24 p4334 A69-43449

Boron epoxy composites evaluation for use in aircraft dynamic components, considering fatigue failure mechanism identification 24 p4337 A69-43450

Al-B composites fracture toughness obtained by comparing notched tensile data with unnotched specimens 24 p4335 A69-43451

Tensile data and photomicrographs of explosively bonded metal matrix composites interfaces 24 p4326 A69-43452

Tensile tests on fiber reinforced plates with circular holes, studying fiber orientation effects 24 p4404 A69-43602

REISSNER THEORY

Galerkin method for solving dimensionless Reissner equation for symmetrically loaded thin nonshallow shells of revolution 01 p0168 A69-10380

Reissner nonlinear equations for nonshallow symmetrically loaded shells of revolution 04 p0684 A69-15538

Reissner algorithms for displacements of bent plate represented in finite series form as solutions of Euler equations 10 p1793 A69-22883

Galerkin method for solving dimensionless Reissner equation for symmetrically loaded thin nonshallow shells of revolution 12 p2182 A69-26679

Mixed plate element application to vibration and buckling eigenvalue problems based on Reissner variational principle, considering quadrilateral elements 16 p2874 A69-32176

Reissner variational principle applied to incompressible and nearly incompressible anisotropic thermoelasticity

22 p4040 A69-39980

RELATIVE BIOLOGICAL EFFECTIVENESS [RBE]

Accelerated helium and carbon ions effects on mutation-induction and nuclear inactivation in *Neurospora crassa* compared with X rays, discussing relative biological effectiveness [RBE/

03 p0373 A69-13490

RBE of fast neutrons on mice, rats and guinea pigs, discussing suppression of mitosis in isolated cells

20 p3478 A69-37629

RELATIVISTIC EFFECTS

Compressible relativistic flow in subsonic, transonic and supersonic regimes, noting pressure coefficient variations

01 p0007 A69-11203

Pulsar frequency Doppler shift due to general relativistic corrections to optical path of photons in field of sun

02 p0315 A69-11836

Mass effect on frequency tested during approach of pulsar to sun

02 p0323 A69-12298

Radio emission sources nature in terms of special relativity theory

03 p0499 A69-13078

Fresnel drag produced by relativistic addition of electron velocities in semiconductors measured by changes in refractive index

05 p0807 A69-16026

White dwarf general relativistic instability toward dynamic collapse and Type I supernovae

06 p1010 A69-17975

Small signal coupled mode analysis including relativistic effects for studying spiraling electron beam interaction with fast wave circuits

07 p1114 A69-18436

Wave propagation on cylindrical electron beam in vacuum and in plasma background, including relativistic effects

07 p1189 A69-18657

General relativistic gravitational red shift effect on frequency transmitted from satellite orbits, noting possibility of measurement

08 p1383 A69-19901

Corrections to relativistic plasma thermodynamic functions associated with electromagnetic field effect, demonstrating inapplicability of Darwin Hamiltonian to problem

08 p1359 A69-19953

Characteristic equation obtained by considering world line vector, basic thermodynamic variables and metric tensor as functions of Licherowicz class

09 p1480 A69-21614

Relativity theory examined critically, discussing spherical space, Lorentz transformation and Einstein conclusions

10 p1725 A69-23317

Dynamical model for spherical inhomogeneity in mean mass density of universe to predict velocity dispersion observed for Coma Cluster

10 p1789 A69-24133

Photon emission from highly relativistic stars, using computed differential light delays to calculate blurring of spherically symmetrical emission pulses

13 p2350 A69-27825

Radio emission sources nature in terms of special relativity theory

14 p2509 A69-28760

Angular momentum-gravitational field coupling in collapsing star, applying rotational perturbation to spherically symmetric time dependent interior solution of Einstein field equation

14 p2520 A69-29374

Collisionless stability of relativistic, spherically symmetric star clusters against radial perturbations, considering one dimensional sufficient criteria

15 p2691 A69-30765

Pulsar clock mechanisms on basis of relativistic gravitational effects, considering white dwarfs and neutron stars

15 p2694 A69-30855

Doppler geodetical measurements, emphasizing relative orientation between station and orbit influence on coordinates determination accuracy, presenting electromagnetic wave propagation theory

15 p2601 A69-31375

Pulsation periods for pure He white dwarfs calculated by Chandrasekhar equation including relativity and rotation effects

17 p3037 A69-33641

Relativistic effect detection on pulsar frequencies by general relativity theory, assuming pulsars are orbiting objects

17 p3037 A69-33645

Relativistic effect in pericenter motion of comets and natural satellites from major semiaxes and eccentricities of natural bodies

17 p3044 A69-34174

Slow rotation of relativistic polytropes with linear corrections, showing inertia moment distribution and metric component

19 p3426 A69-36576

Relativistic star clusters, discussing existence and quasi-static evolution before collapse through gravitational radius

21 p3814 A69-39570

Manned relativistic space flight limitations dependence on biomagnetic levitation of human body in inhomogeneous magnetic field to compensate inertial forces during acceleration

22 p3889 A69-39906

Antenna design considerations for spacecraft at relativistic velocities, discussing gain function, receiver power density and source apparent frequency and direction

22 p3914 A69-40700

One dimensional flow of perfect compressible relativistic fluids, obtaining expression showing wave velocity dependence on relativistic speed of sound

22 p3931 A69-40711

Pulsar CP 0328 radiation mechanism, considering relativistic effects of rapid rotation

22 p4035 A69-41206

Relativistic Doppler shift effect observed from radio signal periodic variation of GEOS-1 satellite

23 p4126 A69-42389

RELATIVISTIC PARTICLES

Thermodynamical and hydrodynamical relations for relativistic classical scalar fluid, obtaining energy momentum tensor

01 p0175 A69-10345

Radio galaxies and quasars X ray emissions, calculating radiation fluxes produced by scattering of synchrotron radiation quanta at relativistic electrons

03 p0500 A69-13079

Synchrotron radiation excitation in system of relativistic monoenergetic electrons rotating in cold magnetoactive plasma

03 p0476 A69-13383

Kinetic theory to determine wave increments propagating across magnetic field in system of relativistic electrons in cold plasma

04 p0635 A69-14555

Pulsations of relativistic and nonrelativistic narrow /paraxial/ electron beams with spatial axis curved according to various laws, deriving approximate descriptive equations

04 p0632 A69-14981

HF interaction of relativistic electron beam and plasma extended to include arbitrary variation of plasma density

04 p0637 A69-15046

Interplanetary relativistic electrons from solar flare events

04 p0650 A69-15528

Focusing of relativistic cylindrical electron beam in static axial electric and magnetic fields, using least action principle to derive trajectory differential equation

05 p0796 A69-15715

Cellulose nitrate sheets applicability in detecting cosmic ray relativistic heavy nuclei, considering etchable tracks

06 p0924 A69-17286

Monoenergetic relativistic electrons stream gyrating along cold magnetoactive plasma with pitch angle radiatively unstable with respect to synchrotron radiation

07 p1191 A69-18958

Maximum number of binary collisions for three particles with zero range forces in relativistic rescattering singularities studies

08 p1353 A69-19788

Synchrotron radiation from relativistic electrons in magnetosphere, calculating variation with frequency and height of lines of force

08 p1306 A69-20182

Rotational energy conversion of neutron star into relativistic electrons energy suggested by increasing period of pulsating radio source in Crab Nebula

09 p1591 A69-21454

Relativistic solar electron detection in interplanetary space during July 7, 1966 proton flare event, noting energy spectrum and time history

10 p1767 A69-23766

Energetic particles observed during proton flare noting relativistic electrons, protons to alpha particles ratio, low energy particles and bidirectional proton stream

10 p1768 A69-23785

Incoherent synchrotron radiation by relativistic electrons gyrating in cold magnetoactive plasma rederived, correcting errors

10 p1741 A69-23858

Frequency spectrum, time variations and polarization of source of synchrotron radio emission with expanding components flying apart at relativistic velocities

12 p2155 A69-26207

Radio emission from 18 galaxies noting accompaniment of optical spectrum emission and enhancement due to production of relativistic electrons in active nuclei

12 p2164 A69-27026

Radiative relaxation of relativistic particle distribution undergoing synchrotron radiation and reabsorption, discussing self absorbed radio source model

13 p2327 A69-27572

Synchrotron spectrum radiated by relativistic electrons below Razin cut-off, considering relation to radio spectra curvature of variable extragalactic sources

13 p2339 A69-27573

Galactic and relativistic and subrelativistic solar cosmic rays effect on electron production rate in ionosphere, detailing low energy SCR-atmosphere interactions

13 p2333 A69-28544

Radio galaxies and quasars X ray emissions, calculating radiation fluxes produced by scattering of synchrotron radiation quanta at relativistic electrons

14 p2509 A69-28761

Relativistic electron confinement within geomagnetic tail neutral sheet measured by Pioneer 7 deep space probe, confirming kinetic energy observations of IMP 1 satellite

14 p2433 A69-28934

Relativistic solar proton propagation fluctuation effects in interplanetary magnetic field during cosmic ray intensity increase

14 p2512 A69-29045

Relativistic behavior of electromagnetic multipolar nongravitating particle, discussing integrability of field equations

14 p2486 A69-29594

Quark detection in cosmic rays at sea level using scintillation counter and streamer chamber system

15 p2674 A69-30308

Shock wave structure dissipation in gaseous medium with microscopic particle velocities asymptotically approaching light velocity

17 p2958 A69-34145

Hydromagnetic wave-charged particle resonant interaction described by diffusion equation in momentum space, deriving diffusion coefficients and time evolution ultrarelativistic particle energy spectrum

19 p3424 A69-36335

Ultrarelativistic electron acceleration in Crab Nebula maintaining synchrotron spectrum, obtaining power from compressional motion damping, gyrorotation effect and pitch angle anisotropy removal

19 p3424 A69-36336

Anisotropy of relativistic cosmic ray electrons, considering electron exposure time to synchrotron effects, energy loss from inverse Compton effect, etc

20 p3593 A69-38145

Synchrotron radiation and reabsorption for rapidly moving cloud of relativistic particles, considering errors

21 p3772 A69-39513

Far IR radiation generation, considering incoherent sources, harmonic generators, electron tubes, relativistic electrons and quantum oscillators

22 p3982 A69-40669

Flux density variations of radio sources at 2.8 and 4.6 cm wavelengths, suggesting relativistic particles prolonged injection into optically thin sources

22 p4029 A69-40764

Radio galaxies differences from quasi-stellar objects indicating relativistic particles generation from violent explosions releasing energy comparable with powerful supernova

24 p4378 A69-42697

RELATIVISTIC PLASMAS

Alfven wave propagation in nonhomogeneous systems for relativistic MHD, discussing magnetic and velocity perturbations

02 p0290 A69-12254

Radiation intensity from system of monoenergetic relativistic electrons in plasma, discussing mass effect in coherent synchrotron radiation

03 p0500 A69-13407

Nonlinear interaction between waves in relativistic plasma, determining probability between transverse and longitudinal waves with different phase velocities

03 p0397 A69-13710

MHD waves, Landau damping and magnetosonic waves in homogeneous relativistic Vlasov plasma

04 p0636 A69-15043

Interactions in classical relativistic plasmas, discussing Lorentz invariant statistical mechanical formalism and phenomenological electrodynamics

05 p0801 A69-15770

Electromagnetic wave transmission and reflection at boundary of relativistic collisionless plasma, using Laplace transformation

06 p0968 A69-17783

Transverse waves instability in relativistic plasma, noting condition of isotropy and existence of electromagnetic waves

07 p1193 A69-19032

Corrections to relativistic plasma thermodynamic functions associated with electromagnetic field effect, demonstrating inapplicability of Darwin Hamiltonian to problem

08 p1359 A69-19953

Isoperimetric plasma thermodynamics problems, including plasma free energy and relativistic plasma density fluctuations energy

12 p2138 A69-26603

Relativistic electrons synchrotron radiation by calculating magnetoactive plasma permittivity tensor, determining normal waves polarization characteristics

13 p2315 A69-28451

Electrical conductivity tensor of many component collisional relativistic plasma in magnetic field and near equilibrium, expressing collisional part as momentum integral

14 p2503 A69-30000

Covariant dispersion relations for relativistic plasma oscillations for many component plasma in external magnetic field

16 p2816 A69-31633

Elastic collision operator for relativistic Lorentz gas converted to differential form using Fokker-Planck limit for anisotropy segments

16 p2817 A69-31668

Fire hose instability growth rate in relativistic plasma with anisotropic pressure, discussing importance to cosmic ray liberation and isotropization at galactic halo

24 p4376 A69-42660

Pulsars relation with supernovae remains and radiation patterns and fluxes analysis, ascribing radio emission to relativistic plasma

24 p4383 A69-42985

RELATIVISTIC THEORY

NT MANDELSTAM REPRESENTATION

Gravitation theory similar to special relativity and Newtonian theories, noting gravitational potential, metric and Newtonian charts

01 p0115 A69-10340

General theory of relativity tests with aid of satellites, considering gravitational red shift measurements, light deflection in solar field, etc

01 p0152 A69-10751

Gravitational fields in Hamiltonian formulation of relativistic theory of gravitation, noting geometrical aspects and equivalence to Einstein theory

02 p0280 A69-11715

Relativistic heat transfer formula and pressure definition in relativistic thermodynamics

02 p0352 A69-12253

Solar gravitational field influence on annual trigonometric parallaxes within relativistic theory framework

03 p0506 A69-13091

Covariant statistical mechanics for equilibrium thermodynamics

03 p0533 A69-13758

Electrodynamics of turbulent conducting media based on nonrelativistic MHD

03 p0479 A69-13972

Total conserved momentum-energy of electromagnetic interaction of system of point charges in Wheeler-Feynman theory, noting mass defect of connected system

04 p0631 A69-15058

Interaction between point charges in Wheeler-Feynman electrodynamics, noting impossibility of deducing momentum and energy conservation from variational principle

04 p0631 A69-15059

Variational formulation of Einstein general relativity related to geometric foundations, deriving Bianchi identities from general invariance property

05 p0791 A69-15632

Soviet book on relativistic astrophysics covering evolution and structure of universe with reference to galaxies, stars, quasars, relativity theory, gravitation theory, etc

07 p1216 A69-18960

Relativistic cosmological models with radiation and matter, analyzing conversion from radiation-like models to dust-like models

07 p1222 A69-19587

Solar atmosphere model calculations of solar oblateness, discussing flux difference and Dicke experiment on general relativity

08 p1383 A69-19899

Relativistic astrophysics, discussing quasar phenomenology, red shift cosmology and relationship with galaxies

08 p1388 A69-20222

Gravitational wave solution of Einstein field equations, deriving Ricci and Riemann tensors for Einstein space

08 p1352 A69-20755

Inertia of electrically charged spherical body calculated on basis of relativistic stress energy

08 p1352 A69-20756

General relativistic models of massive hot nonrotating stars with adiabatic temperature gradients consisting of ideal gas and radiation mixture

09 p1605 A69-22416

Hydrodynamic equations and conservation laws for nonviscous fluid in postNewtonian approximation of Brans-Dicke theory applied to gaseous mass dynamic instability

10 p1789 A69-24130

Total energy-momentum interaction of system with mass defect in Wheeler-Feynman theory of electromagnetic interaction, demonstrating existence of gauge invariance

11 p1915 A69-24326

Einstein interpretation of time in special relativity theory disputed by Fok dilatation theory

11 p1915 A69-24345

Space-time hypersurfaces representations of shock waves of relativistic MHD, discussing compressibility role in proving consistency with relativistic theory

11 p1928 A69-25246

Relativistic coherence theory of black body radiation in transparent medium, deriving expressions for second order correlation tensors by phenomenological quantum electrodynamics

11 p1920 A69-25563

Ferromagnetic transition in superdense nuclear matter and neutron stars, developing relativistic equation of state

11 p1965 A69-25564

Relativistic hydrodynamic equations for charged particles interacting in external scalar and gravitational fields, considering particle motion and scalar plasma dispersion

12 p2130 A69-26462

Relativistic kinematics of continuum motion by invariant derivatives of deformation measures, discussing rigid body motion in Born sense

12 p2189 A69-27116

Relativistic version of generalized gravitation theory, establishing models to describe gravitars having large gravitational mass defect and red shift

13 p2351 A69-27864

Solar gravitational field influence on annual trigonometric parallaxes within relativistic theory framework

14 p2516 A69-28773

Unlimited extrapolation into infinity to determine ranges of applicability of theories in relativistic cosmology noting paradoxes

14 p2516 A69-28867

Density perturbation mode in Lifshitz relativistic theory for expanding universe gravitational instability, adopting Lagrangian coordinate condition to eliminate physically meaningless solution

15 p2652 A69-30203

Extragalactic research to solve problems in cosmological and cosmogonic theory, including relativistic cosmology and observations

15 p2681 A69-30436

Classical and relativistic gravitation theories using harmonic coordinate system, interpreting Einstein equations for insular distribution of masses and applications in geodesy

15 p2596 A69-30573

Relativistic generalization for polar Sommerfeld rosette of Fourier series expansions by Lagrange and Bessel for particle motion in Keplerian field

16 p2811 A69-31607

Relativistic tensor theories of gravitation in flat space with Neumann and Newton forms of gravitational potential, deriving expressions to estimate differences perceived by observer

19 p3373 A69-36204

Newtonian and general relativistic orbits of point mass in inverse square law force field, noting radar determination of spacecraft orbits [AAS PAPER 68-098]

20 p3595 A69-37176

Galactic mass relativistic distribution calculated, considering spherically symmetric model differential rotation near sun

20 p3600 A69-37484

Relativistic solution by Landau procedure of initial value problem for one dimensional electron plasma wave coexisting with charged immobile background

21 p3778 A69-39579

Normal radial vibrations in Newtonian and general relativistic stellar objects and dynamic instability, determining modes and natural frequencies

22 p4014 A69-40142

Gravitational constant secular change from considering relativistic cosmology and galactic structure, deriving equations of Newtonian cosmology

22 p4017 A69-40173

Cosmological constant closed relativistic universe, showing constant-observational data inconsistency

22 p4029 A69-40757

Off-diagonal matrix elements of Breit interaction between singlet-triplet transitions for helium isoelectronic sequences

22 p3986 A69-40783

RELATIVISTIC VELOCITY

Cloud chamber for measuring specific ionization in relativistic region by muons in gases, using drop counting method

06 p0925 A69-17303

High energy particles obtained by accelerating plasma with frozen-in magnetic field to relativistic velocities during scattering of fast electron beam

08 p1358 A69-19805

Constant acceleration relativistic rocket flight from inertial rocket and terrestrial point of view compared, examining light flash transmission and arrival time

09 p1609 A69-21959

Relativistically corrected Vlasov equation solved as approximate solution of exact relativistic equations of motion for low density media

10 p1724 A69-22924

Magnetic mirrors, Doppler and relativistic effects, wave attenuation and radiation pressure during gyroresonant particle acceleration in nonuniform magnetostatic and HF fields

14 p2499 A69-29845

Relativistic corrections to particle distribution functions for high temperature plasma in thermodynamic equilibrium by integrating Gibbs distribution

14 p2499 A69-29847

Motion of medium at ultrarelativistic velocities in general theory of relativity, noting velocity minimum at radius limit

15 p2653 A69-31067

Relativistic exceptional wave propagating heat, computing speeds in direction orthogonal to heat vector

16 p2827 A69-32042

Structure of solitary waves propagating in collisionless plasma perpendicular to magnetic field, considering soliton wavefronts charge separation and relativistic velocity

17 p2922 A69-33696

Shock wave structure dissipation in gaseous medium with microscopic particle velocities asymptotically approaching light velocity

17 p2958 A69-34145

Interstellar minimum fuel and time optimal trajectories for acceleration limited rockets determined by applying Pontryagin maximum principle to relativistic rocket equations of motion

20 p3602 A69-37530

Nonlinear relativistic wave velocity distribution within spherical nucleus bounded by shock wave in superdense gas determined by Cauchy problem

22 p3827 A69-41114

Reduced flight time interstellar round trip propulsion system with relativistic velocity capabilities, discussing vehicle with solar sail and magnetic course reversal [AAS PAPER 69-388]

24 p4363 A69-42829

RELATIVITY

Approximate integrals of Einstein equations for dipole and quadrupole electromagnetic radiation

01 p0115 A69-10263

RELATIVITY

Asymptotic behavior of curvature and conformal curvature tensors on asymptotically flat space-time
01 p0116 A69-10393

Radiation problem in general theory of relativity investigated by momentum energy tensor, formulating criterion for gravitational radiation
01 p0116 A69-10435

Mach principle in scalar-tensor gravitation theory, discussing self energy calculations in canonical formalism for solitary neutral and charged point particles
01 p0120 A69-10858

Conservation laws of energy and linear momentum in general relativity formulated, noting application to radiating gravitational systems
01 p0121 A69-11286

Equatorial geodesic motion of rotating source in gravitational field, using exact empty space solutions of Einstein equations
01 p0157 A69-11289

Lorentz invariant theories of gravitation compared with Einstein general relativity tests with respect to one body motion observations
02 p0318 A69-12094

Invariant theory of gravitational radiation, using impulse energy tensor
02 p0332 A69-12835

Plane front gravitational waves analyzed on basis of gravitational radiation theory, discussing Einstein equations
02 p0332 A69-12836

Radio emission sources nature in terms of special relativity theory
03 p0499 A69-13078

Coordinates interpretation in Schwarzschild problem, projecting space of events by light beams onto Galilean system at infinity
03 p0506 A69-13090

Plasma equation of motion in external electromagnetic field analyzed as generalization of Bernoulli equation in relativistic MHD
03 p0476 A69-13385

General theory of relativity equations for homogeneous anisotropic three dimensional space with matter, deriving ultrarelativistic equation of state
03 p0466 A69-13423

Theory of relativity and role of time intervals in prediction experiments for rate of clocks
03 p0467 A69-13599

Electromagnetic and gravitational tensor fields in Riemannian space, generalizing Maxwell and Bel-Robinson tensors
03 p0467 A69-13755

Kepler third law application to radar determinations of astronomical unit of length in general relativity
04 p0657 A69-14698

General relativity confirmation, discussing mass equivalence and classical and new experiments such as gravitational shift, rotation effect on perihelion and precession test
04 p0661 A69-15165

Perturbation method determination of gravitation induction for quasi-static axisymmetric systems
04 p0661 A69-15190

Relativistic analysis of far zone electromagnetic scattering by conducting sphere moving through incident plane wave, calculating scattering cross section
04 p0559 A69-15212

Variational formulation of Einstein general relativity related to geometric foundations, deriving Bianchi identities from general invariance property
05 p0791 A69-15632

Equations of motion derived for incompressible and irrotational viscous fluids in special relativity
05 p0792 A69-15682

Energy definition in relativity for steady state universes, particularly Schwarzschild universes
05 p0792 A69-15683

Static formations in general theory of relativity and plankions
05 p0793 A69-15776

Relativity and stellar model stability, discussing energetics of quasars and gravitational collapse of supermassive stars
06 p1002 A69-17315

Monograph on classical electromagnetism via relativity, developing Maxwell equations from Coulomb law
07 p1180 A69-18404

Special and general relativity theories following Newtonian mechanics and gravitation theories, discussing metric tensor, sun oblateness and experiments with gyroscope spin axis precession
07 p1181 A69-18928

Relativistic systems and relativistic Hamiltonian systems defined by second order equation, discussing canonical transformations conserving vector field Hamiltonian character
07 p1182 A69-19331

Gravitational and inertial field equations of Maxwellian form leading to gravitation theory consistent with special relativity
07 p1182 A69-19408

Petrov classification of cylindrically symmetric space-time, giving Weyl conformal curvature tensor and surviving Ricci tensor components
07 p1182 A69-19409

Riemann metric leading to empty flat space from Rainich equations of already unified field theory
07 p1182 A69-19418

Axially symmetric static solutions of Einstein equations with singularities on z axis allowing for higher multipole moments in general relativity
08 p1350 A69-19783

Space-time evolution of one Petrov type into another, obtaining algorithm, flow diagram and discontinuous hypersurfaces results
08 p1350 A69-19789

Space time structure conditions derived for compatibility with simultaneous fulfillment of causality and equivalence principles
08 p1351 A69-19948

Dynamical friction on star in postNewtonian approximation of general relativity
08 p1386 A69-20072

Metagalaxy stationary model in terms of relativity theory, investigating radiation pressure balancing of gravitation as imaginary situation
08 p1389 A69-20263

Two gravitational fields theory of gravitation in general relativity for flat universe, discussing gravitational wave propagation
08 p1390 A69-20276

Relativistic kinematics analog model for deformable continua, introducing deformation gradient and tensors
08 p1416 A69-20693

Einstein space time concepts for unified formalism of matter interactions from elementary particles to astronomical bodies, discussing relativity theory
08 p1352 A69-20730

General theory of relativity and tensor field equations relating space time characteristics to local properties of matter and vacuum, using Palatini Lagrangian method
09 p1593 A69-21572

Kerr type metric empty space times starting from fixed reference system and associated Killing vectors
09 p1540 A69-22050

Mass displacement in light path due to interaction with gravitational wave accompanying light pulse, discussing general relativity tests for time delay and starlight bending
09 p1540 A69-22081

Time delay, red shift, equivalence principle, light deflection and perihelion motion tests of general relativity with Jupiter probe
09 p1597 A69-22089

Clock paradox of Einstein special theory of relativity, reviewing work of Prokhovnik, Schlegel and Arley
10 p1772 A69-22865

Relativity theory examined critically, discussing spherical space, Lorentz transformation and Einstein conclusions
10 p1725 A69-23317

Radial motion of uniform spheres in general relativity, finding conditions for initially inward motion to reverse/bounce/
10 p1779 A69-23607

Book on relativity and cosmos, space and time in physics, astronomy and cosmology covering theoretical and empirical research
10 p1784 A69-24019

Maxwell theory basis of special theory of relativity, discussing universal length constant
11 p1920 A69-25562

Covariant equations of motion of body of variable mass in general relativity, considering Schwarzschild field, rotating mass field and Einstein static universe
11 p1965 A69-25744

Singularity of Schwarzschild spherically symmetrical solution to Einstein equations of general relativity theory, exemplifying Lemaitre coordinate system
12 p2129 A69-25974

Elastic stress created by perpetual motion of isotropic elastic solid in static space-time
12 p2130 A69-26283

Equations of state for continuous media, using variational principles within framework of relativity theory
12 p2131 A69-26972

Exterior field equations for radiating spheres with zero limb darkening in relativity and Bondi coordinates, determining radiative flux and pressures
13 p2339 A69-27566

Einstein theory of space and time analyzed with emphasis on inertial systems
13 p2297 A69-27633

Icarus radar and optical observations analyzed to verify general relativity predictions using Schwarzschild metrics and to estimate solar oblateness, Mercury mass, etc
13 p2350 A69-27823

Critical parameters of isothermal quasi-degenerate white dwarfs calculated by energy method, allowing for relativity theory error and neutron irradiation effect
13 p2351 A69-27871

Einstein second postulate concerning invariability of light vector in vacuum experimented for validity, using earth and moon as light rays launching and reflecting media
13 p2354 A69-28650

Radio emission sources nature in terms of special relativity theory
14 p2509 A69-28760

Coordinates interpretation in Schwarzschild problem, projecting space of events by light beams onto Galilean system at infinity
14 p2516 A69-28772

Philosophical problems of Einstein theory of gravitation and relativistic cosmology - Conference, Kiev, June 1966
14 p2482 A69-28856

Einstein general theory of relativity, discussing evolution and disunity among physicists and philosophers on universal relativity of mechanical motion
14 p2483 A69-28857

Observed values concept applied to general relativity theory, considering gravitational energy problem
14 p2483 A69-28858

General relativity theory philosophical substance and meaning, discussing Einstein formulations and bases of classical, relativistic and quantum physics
14 p2483 A69-28859

Invariants method and applications in classical and relativistic physics emphasizing theory of relativity, physical and mathematical theories relations and group theory applications
14 p2484 A69-28860

Categorical structures in theoretical thinking for philosophical fundamental physical laws analysis, including space-time concept changes in classical physics and in theories of relativity
14 p2484 A69-28861

Macroscopic space-time meaning in theoretical physics in terms of mathematical definition and philosophical concept
14 p2484 A69-28864

Space-time interpretation of static Einstein universe model and Friedmann space with variable positive curvature
14 p2484 A69-28865

Asymmetry causes on cosmogenic scale in view of symmetry in small space-time regions/microworlds/determinable within framework of Einstein theory
14 p2516 A69-28866

Fundamental principles of thermodynamics incorporation into general relativity and geometrodynamics, interpreting entropy growth in terms of space dynamics
14 p2538 A69-29019

Newman-Penrose formalism for conserved quantities in general relativity, giving group theoretic interpretation
14 p2486 A69-29450

Asymptotic expansions for Einstein-Maxwell field representing gravitational and electromagnetic radiation from finite source of matter and charge
14 p2486 A69-29635

Relativity theorems applied to collapsing stars and expanding universe noting limitations of general relativity from prediction of singularities
15 p2694 A69-30854

Motion of medium at ultrarelativistic velocities in general theory of relativity, noting velocity minimum at radius limit
15 p2653 A69-31067

Newtonian invariant mechanics, giving inertial interpretation of gravitation and Hubble expansion of universe
15 p2654 A69-31214

Exact static exterior and interior solution of Einstein equations for thick plane plate, discussing surface energy-momentum tensor
15 p2654 A69-31477

Far field energy radiated by two body system using approximation method in general relativity and Minowski gravitation theory
16 p2812 A69-31836

Electromagnetic cavity resonances in rotationally induced gravitational field by relativistic approach
16 p2812 A69-32048

Einstein field equations solutions generated via static spherically symmetric mass and charge distributions
16 p2812 A69-32053

Monograph on creation and evolution of physico-theoretical concepts of space, time and matter
16 p2812 A69-32110

Conservation laws in general relativity, discussing Noether theorem, Bianchi identities, superpotential, Einstein-Klein theorem, momentum method and outgoing radiation
16 p2813 A69-32362

General relativity theory test using earth orbital motion and solar gravitational field effects on pulsars frequency stability
17 p3037 A69-33646

Particle and light motions in Schwarzschild field, discussing acceleration beyond speed of light in reference /S/ frame of time independent coordinate systems
17 p3006 A69-33741

General relativity theory applicability to cosmology, Einstein principle of equivalence and contradicting arguments of relativistic cosmology
18 p3200 A69-34997

Static formations in general theory of relativity and plankions
18 p3173 A69-35029

Einstein gravitational field equations series expansion in powers of gravity constant by Bondi method for gravitational waves
18 p3173 A69-35146

Cosmological model based on inertia and relativity principles, considering scalar gravitational and electrostatic potential, light velocity, gravitational interaction and observed galactic red shift
18 p3206 A69-35470

Group properties of adiabatic motion equations of medium in relativistic hydrodynamics, including solutions of subgroups applicable to multiple particle production
19 p3301 A69-36843

Translating Tolman problem of cosmic dust motion into centrally symmetrical reading system, showing relativistic and Newtonian motion laws coincidence
20 p3594 A69-37079

Negative time interval implications for meta particle at superluminal velocity with respect to two reference frames, noting causality paradoxes
20 p3598 A69-37412

Singular electromagnetic field rectilinear and elliptical polarization in general relativity, calculating light plane rotation in Schwarzschild space
20 p3576 A69-37431

Cosmic matter density and velocity in expanding universe with negative curvature within Einstein-Friedman theory
20 p3599 A69-37472

General relativity effects on isotropic stars evolution, discussing dynamic stability and white dwarfs
21 p3798 A69-38540

Q switched laser pulse propagation in nonlinear laser amplifier using bitemporal relativity theory, deriving five dimensional wave equation revealing superlight signal existence
21 p3770 A69-38839

Spherically symmetrical T models of dust matter yielding method for obtaining maximum total mass effect in general relativity theory different from Friedman closed model
21 p3803 A69-38994

Relativistic thermodynamics using entropy principle to find restrictions on constitutive functions
22 p4050 A69-40451

Matter surface distribution in general relativity, deriving matching conditions
22 p3982 A69-40753

MHD of ideal charged gravitating fluid by variational principle, considering Einstein general relativity theory
22 p3992 A69-41056

Autometric gyro for satellite general relativity experiments, particularly earth orbit measurement of Lense-Thirring precession
23 p4162 A69-41543

Conjugate points along lightlike geodesics in general theory of relativity, deriving existence from vector field matrix properties and Ricci curvature
23 p4213 A69-41724

Field theories of gravitation and experimental survey of general relativity theory, discussing red shift, Mercury orbit rotation, light deflection, solar oblateness, etc
23 p4192 A69-42330

Einstein general theory of relativity and apparatus for gravitational radiation detection, discussing Dicke experiments and Riemann tensor measurement
23 p4192 A69-42331

Planck-Einstein equation derivation in special theory of relativity, discussing relativistic measurement of thermodynamic values in terms of Lorentz transformations
24 p4349 A69-42748

Particle creation and quantized fields in expanding universe using covariant generalization of special relativistic free field equations, studying zero- and arbitrary-spin particles
24 p4352 A69-43193

General relativity uniqueness established by postulating derivability of equations of motion from gravitational field equations
24 p4365 A69-43668

RELAXATION [MECHANICS]

NT SPIN-LATTICE RELAXATION

NT STRESS RELAXATION

Shock front structure in radiative relaxation region in atomic H, calculating Lyman continuum effects
01 p0122 A69-10125

Anisotropic two component plasma relaxation taking into account dynamic shielding collective effects
01 p0134 A69-11419

Long term creep characteristics of metal structures from short duration relaxation tests, summarizing data on rheologically stable materials
02 p0337 A69-11626

Computer models of one dimensional stellar problems, discussing fast relaxation of unsteady state to Fermi-Dirac distribution and slow relaxation to thermal equilibrium
02 p0323 A69-12274

Automatic determination of relaxation and retardation spectra for linearly viscoelastic materials from experimental data using simple numerical techniques
02 p0348 A69-12605

Electrons relaxation caused by ionization and recombination in nonequilibrium plasma, using Kerrebrock model
03 p0477 A69-13609

Relaxation mechanism of low temperature internal friction peaks in niobium quenched to room temperature
03 p0447 A69-13617

Relaxation effect in epitaxial silicon MOS structures, formulating differential equation for doping distribution in epitaxial layer
03 p0490 A69-13947

Relaxation induced self oscillations during combustion of gunpowder in semiclosed volume, noting combustion instability
04 p0686 A69-14987

Multiphonon orbit lattice relaxation of excited states of rare earth ions in crystals, using results to design quantum electronic devices
05 p0774 A69-16318

Mechanical relaxation of poly 4 methyl pentene 1 at cryogenic temperatures, discussing temperature dispersion curve and secondary absorption associated with thermal motion of side chains
05 p0785 A69-16492

Vacancy relaxations in bcc crystals using energy dependence on radial displacements from defect of nearest neighbor sets, discussing crystal size and shape
05 p0809 A69-16529

Nonisotropic relaxation of Boltzmann gas in homogeneous space, expressing collision integral moments in terms of distribution function moments for any molecule
06 p0910 A69-17347

Subpicosecond structure in output spikes of Nd-glass laser observed by employing two photon fluorescence displays inside laser cavity
06 p0938 A69-18231

Relaxation theory of highly ionized hydrogen plasma noting applications to stimulated emission, radiation source development and electromagnetic radiation amplification
07 p1191 A69-18996

Vibrational relaxation effects on laminar boundary layer velocity profiles and temperature and on layer thicknesses and wall heat flow downstream of shock wave
08 p1303 A69-20269

Interfacial charge relaxation oversteability in tangential electrical field, discussing electromechanical

polarization surface waves propagation and dielectrophoretic orientation of liquids in zero gravity space
08 p1353 A69-20792

MGD stagnation point flow, discussing relaxation region influenced by magnetic field
09 p1543 A69-21300

Dielectric relaxation for analysis of defect structure, microstructure, surface behavior, structural changes kinetics and environmental effects in insulators and semiconductors
09 p1559 A69-22307

Quasi-linear relaxation of electron beam in magnetoactive plasma, noting instability of plateau in velocity distribution function
09 p1553 A69-22659

Relaxation method for configurations and energies of atoms and stress induced crack opening displacements in crystalline solids
10 p1796 A69-23067

Transient response of MOS capacitance caused by mechanisms dependent on electric field distribution between silicon and oxide
10 p1744 A69-23176

Argas test loop as model for MHD power plant study, discussing component testing including channel preionization and relaxation experiments
10 p1673 A69-23478

Relaxation phenomena in ionization process in argon shock front structure, using EM and pressure driven shock tube to drive high speed shock waves
10 p1726 A69-23685

Damping of solid state laser relaxation oscillations in power output due to diffusion of excitation
10 p1706 A69-24079

Electron-ion temperature relaxation near interface of two semiinfinite nonmagnetized different temperature plasmas brought into thermal contact
11 p1923 A69-24296

Relaxation oscillations in field ionized epitaxial n-GaAs Gunn oscillators on seminsulating substrates, discussing recombination of excess electrons and holes
13 p2227 A69-27236

Relaxing gas nonequilibrium flow in plane expansion, comparing partial differential equations with method of characteristics
13 p2244 A69-27322

Wave damping in plasma, developing Boltzmann analysis of electron mode dispersion relations involving momentum transfer and relaxations of electron-ion temperature and anisotropy
13 p2305 A69-27377

Love wave amplitude data satisfying earth model with intrinsic internal friction at depths assumed due to single thermally activated relaxation
15 p2596 A69-30624

Electron temperature relaxation in shock heated Ar plasma, measuring plasma microwave radiation
15 p2663 A69-30995

Lynden-Bell statistical mechanics of relaxation in collisionless one dimensional stellar system, discussing low energy particles distribution
16 p2862 A69-32376

Far and near field solutions for one dimensional unsteady flows in general inviscid relaxing gas, obtaining flow field structure by matching techniques
17 p2957 A69-33599

Transformed kinetic equation used to study relaxation of quantum oscillator to thermodynamic equilibrium state
18 p3152 A69-35126

Rotating mirror Q switched carbon dioxide laser for high peak powers, analyzing pulse structure and duration dependence on collision induced relaxations
19 p3338 A69-36694

Weak shock wave structure in temperature relaxation media determined using theory of sound absorption in fluids
19 p3301 A69-36842

Modified model for vibration-dissociation relaxation coupling phenomena in nonequilibrium high temperature gas flow, discussing parameter U variation with kinetic temperature
20 p3514 A69-37208

Thermal perturbation propagation in nonlinear medium, considering thermal relaxation effects
22 p4051 A69-40712

Numerical analysis of plane Couette flow of rarefied binary gas mixture using relaxation type kinetic model equations, discussing slip velocity, friction coefficient, etc
22 p3931 A69-40778

MHD waves attenuation in ionosphere due to gyrorelaxation, reducing analysis to determination of anomalous absorption of acoustic waves
23 p4155 A69-41841

RELAXATION [PHYSIOLOGY]

RELAXATION [PHYSIOLOGY]

Temperature dependence of action potential, isometric tension development and relaxation rate of mammalian myocardium at low temperature, considering Ca ions role

23 p0492 A69-42060

RELAXATION METHOD [MATHEMATICS]

Optimum overrelaxation factor in diagnostic and forecast calculations

03 p0458 A69-13033

Digital computer solution of Laplace equation using dynamic relaxation method to introduce dynamic terms into basic equation

05 p0697 A69-15713

Relaxation method for inversion of full radiative transfer equation, determining temperature profile in atmosphere from outgoing radiance

[JPL-TR-32-1351]

06 p0922 A69-17805

Dynamic relaxation method for elastic deformation in mirrors, using tensor equations of elasticity in nonorthogonal curvilinear coordinates

12 p2187 A69-26890

Monte Carlo relaxation method for physically self consistent model stellar atmospheres, discussing stability, accuracy and convergence of solution

19 p3425 A69-36337

Finite element relaxation method for computing stress distribution in thin walled structure, considering computer program, storage and solving time

21 p3843 A69-39313

RELAXATION OSCILLATORS

Negative differential resistance effect producing relaxation type oscillations in n-type gallium arsenide

01 p0138 A69-10557

Relaxation oscillations in Si p-n junction diode reverse-biased into avalanche calculated by computer program

07 p1101 A69-18651

Lasing characteristics of Nd-glass laser when cavity radiation varies with time, discussing rapid damping of relaxation oscillations of laser intensity

08 p1327 A69-21024

RELAXATION TIME

Limited space-charge accumulation mode efficiency for gallium-arsenide diodes, taking into account electron-lattice relaxation processes

01 p0137 A69-10321

Electron thermal relaxation length in positive column determined by plasma parameters variations in small amplitude moving striations

01 p0127 A69-10341

Vibrational relaxation of diatomic gases behind shock waves, with variable heat bath temperature extended to constant enthalpy and constant total enthalpy conditions

01 p0061 A69-11204

Relaxation rates of water vapor laser lines obtained with split discharge laser

05 p0771 A69-15810

Relaxation time of carbon dioxide laser levels as function of water vapor, CO and Xe gas pressure measured by afterglow pulse gain technique

[IEEE PAPER G-1]

05 p0774 A69-16314

Upper limit of nonradiative relaxation time between specific states of absorption bands and fluorescence state emitting R lines in ruby laser

05 p0777 A69-16335

Proton spin-lattice relaxation time in dilute liquid and gas solutions of orthohydrogen in parahydrogen, noting dependence on temperature, density and composition

06 p0961 A69-17141

Settling time estimation method for class of time varying feedback control systems of linear, nonlinear and multivariable natures

06 p0902 A69-17399

Absorption and amplification of sound in many valley semiconductors in strong electric field, noting dependence on electron heating and relaxation times

07 p1199 A69-18681

Trivalent iron doped andalusite crystals dielectric and mass properties, investigating spin-lattice relaxation, cross relaxation times and inversion ratio

[IEEE PAPER C-2]

07 p1150 A69-19049

Optical excitation process of energy states by light pulses of short duration compared to relaxation time, predicting Raman echoes

[IEEE PAPER H-3]

07 p1152 A69-19062

Saturable dye filters used with ruby lasers, discussing relaxation time, residual absorption source and transient spectral hole burning

07 p1155 A69-19089

Relaxation times of carbon dioxide laser levels induced by radiation

09 p1515 A69-21488

Vibrational relaxation times in pure O and in O with methane impurity determined with acoustic absorption measurements

09 p1542 A69-21721

Carbon dioxide laser upper level rotational relaxation rate constant measurement, observing CW gain

10 p1701 A69-22948

Ultrashort light pulses nonlinear amplification in medium with finite transverse relaxation time and linear radiation losses

10 p1702 A69-23139

Excitation and ionization relaxation of cesium seeded argon gas computed for stepwise increase of electron temperature

10 p1732 A69-23444

Magnetic field induced nonequilibrium argon plasma ionization relaxation processes obtained with allowance for flow parameters change in relaxation zone

11 p1922 A69-24225

Chapman-Enskog procedure extension for binary gas mixtures, obtaining diffusion equation from revised relaxation time of component velocities

11 p1921 A69-24308

Electrical conductivity of space charge surface layer in semiconductors with many-valley energy spectra of current carriers, discussing scalar relaxation time

11 p1937 A69-24915

Carbon dioxide-N-He laser amplifier, noting gain time dependence and thermal relaxation rate after gas heating

11 p1899 A69-25054

Mass point system moving in gravitational field, discussing statistical mechanics, relaxation time and evolution of stellar systems

14 p2530 A69-29987

Weak shock waves relaxation time and amplitude and acoustic velocity as functions of thermorelaxing media

15 p2590 A69-30103

Small amplitude motions of plane interface between fluids stressed by initially perpendicular electric field, modeling fluids as ohmic conductors

16 p2811 A69-31667

Carbon dioxide dissociation relaxation times measured in shock tube at 1900-2400 K and 1.5-2.5 km/sec

16 p2766 A69-31910

Ultrasonic velocity dispersion in para hydrogen and mixtures with He, Ne and Ar at 300 K, obtaining rotational relaxation times

16 p2815 A69-32791

Gas ionization relaxation times from ion density profiles in shock tubes at low Mach numbers, discussing influence of impurities on ionization process

18 p3116 A69-34451

Shock wave interaction and bow shock wave establishment near sphere in presence of ionization relaxation, using time resolved schlieren photography

19 p3450 A69-36361

Relaxation time influence on discharge coefficient of sonic nozzle of revolution, considering expanding polyatomic gas problem

19 p3241 A69-36721

Relaxation time for rotational transitions of linear polyatomic carbon dioxide calculated by using Brout theory for diatomic H rotational relaxation calculations

20 p3581 A69-38121

Coherent light emission by molecules excited by laser pulses having duration comparable to active medium polarization relaxation time

21 p3737 A69-38999

Absorption and fluorescent spectra, relaxation times and quantum efficiencies measured for glasses doped with trivalent erbium, reviewing spectroscopic parameters involved with laser effect

22 p3962 A69-40476

Molecular transport equations of dilute gases, considering relaxation time spectrum, obtaining kinetic equations and correlation function expressions for transport coefficients

23 p4193 A69-41512

RELAY

Self and forced oscillations in multivariable relay control system, considering relays with hysteresis and dead band and stability of periodic states

12 p2049 A69-26084

RELAY SATELLITES

Communications system considerations for lunar libration point relay satellite to support Apollo lunar far side mission

03 p0388 A69-13180

Aeronautical satellite system to relay communications at VHF or L band frequencies from aircraft flying over oceanic routes

03 p0464 A69-13235

Low altitude satellite relay system, discussing modulation, antennas, frequency plans, telemetry, tracking, command and earth terminals

03 p0391 A69-13241

Orbiting Data Relay Network communications system provides continuous wideband communication between ground and earth orbiting spacecraft via synchronous satellite repeaters

[AIAA PAPER 68-432]

09 p1455 A69-21989

Data relay satellite concept, discussing orbits, communications between widely separated earth stations, and satellite tracking, telemetry and commanding

11 p1839 A69-25295

Data relay satellite systems for support of NASA R and D missions, discussing communications between satellites and to mission control

11 p1839 A69-25296

Technological feasibility of satellite based global data relay service for small users

12 p2028 A69-25949

Libration point relay satellites for continuous communication link between earth and lunar far side, discussing trajectories and halo orbit stationkeeping

15 p2680 A69-30188

Tracking and Data Relay Satellite System with synchronous orbit satellites to relay data between low altitude earth orbital spacecraft and mission control centers

23 p4120 A69-41755

Tracking and data relay satellite system (TDRSS) compared to ground based mission support, considering altitude coverage capability, economy and communication requirements

23 p4120 A69-41756

RFI effects of earth based emitters on operation of geosynchronous satellites for data relay from near earth orbiting satellites, noting frequency assignments

23 p4120 A69-41757

Real time telemetry, tracking and command links by synchronous satellite relay, describing ATS-Nimbus E S-band experiment

23 p4121 A69-41759

Telecommunications performance of two lunar relay satellite system /LRSS/, determining operation capabilities with Apollo communications system

23 p4129 A69-42508

Distributed communications for earth orbiting global satellite network defined parametrically, describing relay/switching and terminal station satellites

23 p4130 A69-42515

RELIABILITY

NT AIRCRAFT RELIABILITY

NT CIRCUIT RELIABILITY

NT COMPONENT RELIABILITY

NT SPACECRAFT RELIABILITY

NT STRUCTURAL RELIABILITY

Stratospheric air sampling reliability instrumentation as part of radioactivity fallout detection program

05 p0766 A69-16751

Bayesian reliability growth model with random variable parameters, discussing multimode failures

09 p1504 A69-21912

Iterative method for numerical solution of linear algebraic equations for stationary probability distributions in queueing and reliability theory

10 p1721 A69-23691

Reliability functions and cycles number before breakdown of finite automaton with account of randomness of malfunctions, structure and input signal distribution

13 p2224 A69-27250

Human performance reliability, testing mathematical model application and implications of time to first error concept by vigilance task

18 p3097 A69-34478

Operational system effectiveness information for reconnaissance drone system including test flights, discussing application to reliability and maintainability in project management

18 p3232 A69-34505

System effectiveness for reliability and maintainability achievement, analyzing people, organizations, value systems and accomplishment criteria in development program

19 p3455 A69-36044

Generalized limit theorem for reliability replacing Drenick exponential theorem

20 p3547 A69-37068

Integer programming method for optimizing constrained reliability problems with several system failure modes

20 p3504 A69-37069

Surrounding noise effects on quick check audiometry test reliability, discussing pathological effects

21 p3725 A69-39286

- Reliability demonstration testing equipment, describing temperature chamber design and instrumentation, overall facility planning, etc
22 p3954 A69-40034
- RELIABILITY CONTROL**
QUALITY CONTROL
- RELIABILITY ENGINEERING**
- Electronic packaging techniques for long life spacecraft, discussing effects of mechanical and electrical stress, temperature cycling, vacuum, radiation and contamination
01 p0038 A69-10145
- Reliability analysis of technological systems, determining characteristics as distribution function of time to specified number of failures
01 p0085 A69-10210
- Power spectral density method of random loads analysis applied to V/STOL aircraft structural analysis, discussing statistical distribution
01 p0168 A69-10407
- Monte Carlo simulation procedure synthesizing probability distributions of reliability parameters with individually exponential components
01 p0036 A69-10707
- Analytical reliability ratio to operational reliability for airborne equipment taking into account electrical and thermal aspects
01 p0011 A69-11069
- Reliability of operational satellite systems consisting of two single purpose satellites in interchangeable orbits, discussing outage and replacement
02 p0333 A69-11805
- Book on laws of failures in technical equipment with emphasis on quantitative description and practicality of reliability theory, discussing redundancy problems
03 p0433 A69-13009
- Solid state power supplies for turbine control and instrumentation, discussing control system manufacturer requirements and reliability specifications
03 p0368 A69-13432
- Fluid stability, viscosity, compressibility, gas solubility and lubricating properties determination for high temperature hydraulic systems
04 p0550 A69-14662
- Reliability in air and space travel, quality/ quantity aspects, problems and cooperation
04 p0606 A69-14803
- Reliable computation in computing systems designed from unreliable components, considering two models for component malfunctions
04 p0569 A69-15456
- Soviet book of statistical and mathematical tables for calculation, analysis and control of reliability
04 p0608 A69-15540
- Defect localization in complex plants applied to damage cause determination and economic criteria
05 p0767 A69-15765
- Reliability in aeronautics and astronautics, discussing safety, economic cost of technical delays and effect on public, air transport, design, development, testing, utilization, etc
07 p1053 A69-19287
- System reliability influence on air accidents resulting from pilot errors, unforeseen obstacles, breakdowns and atmospheric effects
07 p1054 A69-19288
- Fail-safe goals, design criteria, analytical methods and test procedures to achieve reliable damage tolerant dynamic rotating parts for V/STOL and helicopter transports
[AIAA PAPER 69-215] 07 p1237 A69-19569
- Computer program reliability enhancement, discussing significance of underestimation
08 p1278 A69-19845
- Operating and storage conditions effects on reliability of Pd-Ag thick film resistors
08 p1283 A69-20131
- Reliability effect on operating costs of satellite communications system ground stations, calculating annual cost of channel with continuous time carry-over
08 p1276 A69-20586
- Microcircuits, integrated circuits and other monolithic solid state circuits failure mechanisms examined and applied to reliability methodology
[AGARDOGRAPH-114] 08 p1292 A69-20987
- Reliability in electronics - Conference, Budapest, October 1968, Volume A
08 p1321 A69-21098
- Computer programs for systems statistical reliability characteristics using reliability tests and time to failure data, giving optimal breakdown probability functions
08 p1322 A69-21101
- Assessing cost effectiveness of reliability and quality of semiconductor products, using mathematical models
08 p1292 A69-21102
- Reliability of individual components of multicomponent systems under variable loads, using asymptotic distribution of minimal values
08 p1322 A69-21103
- Reliability in electronics - Conference, Budapest, October 1968, Volume D
08 p1292 A69-21105
- Aircraft reliability under cyclic loads in flight taking into account stress fluctuations
08 p1322 A69-21106
- Reliability terms for electrical apparatus, equipment and systems, indicating need for international standardization
08 p1292 A69-21108
- Process control data in acceptance procedures for high reliability electronic components, discussing supplier and user cooperation
08 p1293 A69-21110
- Reliability in electronics - Conference, Budapest, October 1968, Volume B
08 p1293 A69-21111
- Second breakdown mechanisms in transistors, describing electrical and physical characteristics and effects of design and structural defects on resistance to initiation
08 p1294 A69-21120
- Thermionic converter metallography relationship between materials and fabrication methods and reliable performance life
09 p1439 A69-21824
- Electric propulsion design, considering effects of weight, impedance matching, beam voltage regulation and operating point variations in formulating system mass and reliability
[AIAA PAPER 69-254] 09 p1569 A69-21879
- Reliable fluid transmission systems by brazed joints, noting base and filler metals, fitting designs and various processes
09 p1507 A69-22333
- Metallic systems microbonding and joining reliability, noting electron and laser beam welding and deposited film connections
09 p1510 A69-22348
- Tests and quality control equipment used in German aeronautical and astronautical industries
09 p1513 A69-22565
- Reliable operation duration distribution shown to be arbitrary for standby system consisting of basic device and n devices in nonloaded standby condition
09 p1513 A69-22676
- Structural reliability tests using photoelasticity and associated techniques, discussing computer methods, materials research, etc
09 p1479 A69-22734
- Gunn diode reliability improvement by using device structures preventing high field domains from reaching anode
09 p1470 A69-22788
- Algorithm in fault detection and isolation, discussing test optimization for complex systems or structures subject to failure
10 p1698 A69-22978
- General and classical statistical techniques for cutting effectiveness and operational reliability of cutting fuses
10 p1749 A69-23004
- Saturn 5 holddown and service arm electrical system design program optimized by integrating reliability and maintainability at initial design phase
[AIAA PAPER 69-309] 10 p1670 A69-23043
- Optimum calibration interval program for determining test equipment calibration frequencies on basis of mean time between failures and acceptable reliability levels
10 p1699 A69-23288
- Reliability characteristics of service life determination, noting exponential distribution of failure time value
10 p1662 A69-23319
- Hybrid fluidic pressure regulator combining vortex amplifier and confined-jet amplifier with performance upgrading moving metering element, noting greater efficiency and reliability
10 p1639 A69-23560
- Statistical, economic and psychological aspects of aeronautical and astronautical profitable reliability in relation to operation, using mathematical model
10 p1700 A69-23839
- Reliability behavior of information transmission between transmitter-receiver pair in network of crasure channels without decoding and recoding at nodes
10 p1657 A69-23865
- Spacecraft electronic components design, environmental and reliability criteria including weight and power
11 p1843 A69-24340
- Solid logic technology /SLT/ computer circuits, discussing IBM 360 computer reliability, failure analysis information retrieval, SLT module and failure rate
11 p1843 A69-24341
- Large scale integration applications to avionics including self testing, self repair, cost factors, etc
11 p1845 A69-24530
- Electronic systems and component reliability in space, considering electric parameter variation effects
11 p1848 A69-24867
- Low energy charged particle detectors reliability, analyzing windowless electron multipliers and effects of secondary emission layers on sensitivity
11 p1848 A69-24868
- First excursion failure survival probability of randomly excited structures, considering single degree of freedom linear oscillator under Gaussian white noise
11 p1990 A69-25505
- High pressure vessels welding reliability improvement, discussing edge profile, air expulsion from vessel and shielding atmosphere
11 p1892 A69-25670
- Reliability-quality control - Conference, Buffalo, May 1968
12 p2100 A69-25845
- Statistical reliability tools and methods, graphs and charts, estimations, prediction techniques and demonstrations
12 p2101 A69-25847
- Reliability improvement influence on life cycle costs of high volume piece of military/commercial equipment
12 p2101 A69-25848
- Configuration management, establishing uniform and mutually supporting methods of configuration identification, control and accounting for systems and equipment
12 p2192 A69-25849
- Computer reliability by development and methodical employment of self repair techniques
12 p2034 A69-25941
- Reliability-quality control - Conference, Ontario, April 1969
12 p2101 A69-25969
- Reliability planning role in directing business functions to quality efforts integration in engineering, production and testing of electronic equipment
12 p2102 A69-25971
- Integrated computerized reliability monitoring program for detecting aircraft systems and components performance trends and optimizing cost, utility and response
12 p2055 A69-25972
- Digital computer-aided reliability engineering methods for electronic equipment design and analysis
12 p2037 A69-25973
- Dynamic properties and reliability of linear time invariant multivariable control systems
12 p2051 A69-26093
- Digital computer redundancy, analyzing triple modular redundancy in Saturn vehicles and quad design in primary processor and data storage for OAO
12 p2034 A69-26567
- Redundant systems reliability prediction for single mission in standby mode or without standby, using failure states concept and birth-death equations
12 p2102 A69-26569
- Lens shutters durability, analyzing break-in effect, cock-and-release cycles and cause of failures
12 p2094 A69-26600
- Shock pulse criterion limitations and HF transients technique for design and tests of structures and components
12 p2182 A69-26731
- Probability analysis by methods simplifying calculations or providing bounds on reliability of complex system
12 p2103 A69-26751
- Transistorized amplifiers reliability estimated from step by step failures during operation in intense external environment
12 p2043 A69-26886
- Vibration machine as vibration environment simulation for product reliability testing, analyzing spectrum of acceleration waveforms
12 p2060 A69-26940
- Mathematical relations presented for parameters of technological, transport and information systems reliability and life expectancy
13 p2268 A69-27436
- Failure engineering analysis of electromechanical switching devices, discussing preanalysis planning, open-ended data sheets, etc
13 p2231 A69-28043

Relay reliability cost vs failure cost in spacecraft applications
13 p2231 A69-28044

Electric relays reliability requirements, discussing specifications, minimum current, load and frequency effects, etc
13 p2231 A69-28045

Reliability analysis of technological systems, determining characteristics as distribution function of time to specified number of failures
14 p2453 A69-28747

Reliability and efficiency improvements for thermionic converters at JPL, giving failures analyses
14 p2397 A69-29175

Aircraft hydraulic equipment ultrafine filters effect on component life and system reliability
15 p2552 A69-30069

Unoccupied space utilization in aircraft compartments due to microminiaturization, considering reliability enhancement of electronic equipment
15 p2576 A69-30353

Engineering models for wearout reliability prediction in dynamical systems subject to random loading, demonstrating practical and statistical methods
15 p2705 A69-30366

Weapon systems integrated testing, determining test statistics as function of subsystems utilizing Neyman-Pearson confidence levels
15 p2619 A69-30400

Cost effectiveness of test selection when statistical distribution of load and strength are known, presenting curves for equally dispersed normal parameters distribution
15 p2720 A69-30401

Rate gyro life and reliability, discussing gas bearings separating rotor from stator by thin gas film with conventional oil film characteristics
15 p2608 A69-30410

Space equipment reliability, discussing manufacturing defects, design faults, component failures, maintenance, overloads, accidents and operating errors
15 p2624 A69-30817

Spacecraft electronic component reliability policy based on preferential lists, selection programs and component management
15 p2624 A69-30818

Satellite circuit assembly reliability achievement by high reliability components, redundancy and optimal utilization
15 p2624 A69-30819

Management and scientific computer reliability difference, considering circuits, component assembly, software, maintenance, etc
15 p2624 A69-30821

Space electronic component reliability, considering suppliers and laboratory-workshop partnership
15 p2624 A69-30822

Unitary sorting influence on reliability of planar transistors subjected to irradiation recovery cycles and scaled stresses
15 p2626 A69-30834

Reliability control of π -W resistors of tin oxide on glass substrate manufactured in quantity
15 p2627 A69-30837

Mesa-structure varactors p - n junction generating harmonics by nonlinear capacity variation/ reliability, determining selection criterion and optimal test duration period
15 p2627 A69-30839

Metal film resistor reliability for conventional and space use, outlining guidelines for fabrication and quality control
15 p2628 A69-30847

Reliability testing of development models during production, considering short term and large batch tests
15 p2579 A69-31036

Complex systems reliability, describing uses of computer programs in analysis of circuit design, component failure modes and faults due to drifts
15 p2572 A69-31042

Diode burn-in dissipation measurement for reliability testing
15 p2579 A69-31043

Military specifications validity with reference to reliability and metal finishing industry
15 p2722 A69-31120

Military systems trouble documentation and evaluation, emphasizing computerized monitoring of reliability and maintainability
15 p2722 A69-31121

Propulsion system influence on aircraft reliability from viewpoint of engine manufacturer
15 p2629 A69-31122

Failure analysis techniques in electronic component reliability laboratory, discussing electrical and physical tests to detect weaknesses in manufacturing and design
15 p2722 A69-31133

Markov chain applications to avionics weapons system reliability specifications starting with mission profile, failure rates, success probabilities, etc
15 p2581 A69-31136

Space vehicle subcontracted components reliability attainment, discussing reliability process specifications, motivation, product reliability and feedback programs
15 p2723 A69-31139

High reliability space system electronic parts control program to assure success of unmanned space missions
16 p2793 A69-31714

Concorde propulsion and ejection systems reliability, testing reheating duct, primary nozzle, secondary assembly, etc
16 p2837 A69-32072

Engine and components reliability, discussing design stage and programming [AIAA PAPER 69-476]
16 p2795 A69-32771

Reliability physics - IEEE Conference, Washington, D.C., December 1968
17 p2935 A69-32886

Automatically controlled dynamic systems reliability estimation in terms of failure probability illustrated with autopilot-aircraft case
17 p3001 A69-33144

Reliable structural joints and attachments design for components fabricated from nonmetallic refractory brittle materials, discussing departures from conventional practices
17 p3061 A69-33569

Airborne data processing systems reliability, discussing software and hardware reconfiguration techniques and man-machine interface problems
17 p2977 A69-34072

Airborne radomes reliability and high temperature environments, discussing missile nose cones, light weight ceramic techniques, circular polarization, etc
17 p2942 A69-34084

Airborne electric power systems maintenance aids, describing design and operation of annunciator for establishment and display of system failure causes
17 p2905 A69-34112

Aircraft secondary power sources reliability dependence on electric loads, charge control and maintenance, discussing hermetically sealed batteries features
17 p2905 A69-34113

Reliability - Conference, Chicago, January 1969
18 p3140 A69-34476

Fault tree for hardware multiple failure safety analysis and reliability analysis for single failure analysis, illustrating comparative advantages
18 p3142 A69-34479

System state phase modeling as method for evaluating safety and reliability by analysis of system states in mission phases through logic diagram
18 p3142 A69-34480

AGREE /Advisory Group on Reliability of Electronic Equipment/ testing philosophy, emphasizing environmental tests
18 p3143 A69-34481

Environmental testing role in qualification, acceptance, burn-in and reliability demonstration tests
18 p3143 A69-34482

Reliability tasks vs product reliability, discussing differences in effectiveness and management programming
18 p3143 A69-34484

Development, manufacturing and logistic costs of reliability improvement in electronic equipment design
18 p3231 A69-34485

Quantitative and qualitative reliability programs for commercial and aerospace products, considering Failure Effect Management System
18 p3143 A69-34486

Reliability management simulation exercise training technique for government personnel, discussing decision making in development, production, testing and field usage of systems
18 p3117 A69-34487

Physics of Control program for electronic devices reliability, discussing qualified parts, chemical, physical and electrical properties, parameter ranges, specifications and corrective action
18 p3143 A69-34488

Failure mechanisms time and stress dependence relations
18 p3144 A69-34490

Mean-time-to-repair of complex systems with consideration for repair policies and number of repairmen, noting application to systems reliability engineering
18 p3144 A69-34494

Semiconductor reliability evaluation program for economical experimental design, noting stress tests
18 p3232 A69-34496

Ballistic missile and aircraft operational effectiveness, discussing data collection, reliability, availability and capability surveillance by computer
18 p3145 A69-34500

Operations research methods applied to systems effectiveness study, using key decision models with optimized alternatives
18 p3145 A69-34503

Reliability demonstration by MIL-STD-781 for equipment failure and success, proposing useful alternatives
18 p3145 A69-34507

Accelerated temperature tests, calculating temperature behavior of hazard rates and activation energy from failure data using computer simulation
18 p3117 A69-34509

Agna rocket vehicle production reliability evaluation program, testing specific representative equipment randomly selected from production stores
18 p3146 A69-34510

Spacecraft structures reliability, discussing detection, identification, assessment and control of defects
18 p3146 A69-34513

Reliability prediction in electronics, discussing basics, advances, limitations, etc
18 p3146 A69-34514

Hazard plot analysis of incomplete data involving times to failure for failed units and running times on unfailed units
18 p3147 A69-34515

Failure rate data role in reliability analysis and design optimization
18 p3147 A69-34516

Reliability prediction limited to approximations related to past experience on similar equipment
18 p3147 A69-34517

C-141 aircraft reliability growth history, discussing fleet performance, aging trends and delivery vs production sequence
18 p3090 A69-34521

Mechanical drives effectiveness for large antenna tracking/communications systems evaluated in terms of reliability and availability
18 p3100 A69-34522

Reliability block diagrams for laser systems, discussing failure modes of solid state, semiconductor and gas lasers
18 p3151 A69-34523

Reliability engineering methods for software programs with emphasis on real time computation, describing SSD Exhibit 61-47 documentation
18 p3105 A69-34524

Failure mode and effect analysis integrating design and reliability engineering, discussing management controls and interdisciplinary coordination
18 p3147 A69-34526

Computerized Markov effectiveness models of repairable and nonrepairable complex aerospace systems
18 p3195 A69-34527

Statistical testing techniques using small sample size at low component levels to predict product performance
18 p3117 A69-34528

Computer simulation model for Saturn 5 prelaunch system reliability analysis, using Bayesian techniques
18 p3207 A69-34529

TD1/TD2 satellites power supply subsystem, stressing high power requirements and significant design features regarding battery and solar array controls
18 p3093 A69-34791

Stochastic failure models based on stress peak distributions, including randomly deteriorating strength model and increasing hazard reliability functions
18 p3148 A69-35079

Multistage systems high reliability design, describing branch and bound computer method for optimal resource allocation of redundant components
18 p3148 A69-35081

System reliability evaluation based on failure analysis illustrated with examples covering initial requirement through parts production monitoring and control
19 p3454 A69-35782

Communication equipment reliability improvement through testing and failure analysis
19 p3282 A69-35783

Closed-loop system for test, failure analysis and corrective action in avionics reliability growth, showing cost effectiveness relationship to test program
19 p3282 A69-35784

Microwave equipment reliability considered in terms of various subsystems and components, showing carefully formulated and executed test program as essential
19 p3282 A69-35785

Scanning electron microscopy for reliability studies in semiconductor devices
19 p3382 A69-35788

Reliability and maintainability - Conference, Denver, July 1969
19 p3324 A69-35999

FAA ARTS-III terminal air traffic control system reliability and maintainability, discussing module addition
19 p3370 A69-36000

System reliability with allowable downtime, calculating probability of on-line units staying operational during mission time using conditional availability
19 p3326 A69-36002

System approach to reliability demonstration, discussing design and impact on levels, risks, requirements, testing, cost and incentives
19 p3327 A69-36003

R and D program risk evaluation methodology in density functions form for program goals probabilities, noting random variables as parameters
19 p3455 A69-36008

Product reliability program for C-5A to provide high delay/abort reliability during operational usage
19 p3247 A69-36011

Reliability measurements based on maintenance records, considering human factor and life limiting and random chance design
19 p3327 A69-36013

Integrated test program based on mission requirements, failure mode and effects analysis with feedback from testing to design and development functions
19 p3327 A69-36014

Intermediate level mathematical reliability model relating failure mechanism, part strength and interaction of application stresses to parts failure rates, with emphasis on microcircuits
19 p3283 A69-36019

Failure data role in management of launch operations reliability program
19 p3294 A69-36022

Subsystem designs evaluated on basis of human reliability metric to select desirable design configurations
19 p3261 A69-36026

DC 10 aircraft reliability program, discussing passenger attractiveness, dispatch reliability, maintenance cost, flight safety and computer simulation for reliability engineering
19 p3248 A69-36027

Partial prior information utilization via confidence intervals for mean time to failure of exponential reliability model
19 p3360 A69-36038

Bayesian reliability demonstration tests for predetermining sample size producer and consumer risks for equipment with exponential and binomial failure distributions
19 p3327 A69-36039

Bayesian confidence limits for systems reliability, considering exponential and unspecified life distribution subsystems
19 p3328 A69-36041

Visual inspection, thermal and mechanical shock, burn-in and hermeticity tests of microelectronic equipment, reviewing test methods and procedures of MIL-STD-883 program
19 p3284 A69-36043

Hazard and renewal rate and bathtub curves for electronic equipment reliability, noting single and multiple probability densities
20 p3504 A69-37070

Component hazard rate distribution functions from unit time and failure analysis, noting confidence statements and simulation studies
20 p3548 A69-37158

Onboard computer reliability, discussing missile computers and maintenance procedures
20 p3503 A69-37400

Technological systems engineering effectiveness assurance elements, discussing roles of engineering, operations research, data utilization, production and installation, etc
20 p3550 A69-37709

Space vehicle launcher system reliability from trials and adopted corrections, basing formal computation on adoption of normalized form for reliability likelihood
20 p3618 A69-38278

MIL-STD-781B reliability tests with standard based on exponential distribution for equipment exhibiting constant failure rate, noting sampling
20 p3551 A69-38289

Mathematical model of probability of errorless human performance for time continuous tasks for use in systems reliability analysis
21 p3664 A69-38971

Error propagation and tolerance analysis in design and reliability engineering and stress analysis
21 p3842 A69-39303

Dual role core /Ducor/ memory system with unique core stack assembly feature to achieve cost reduction and structural integrity for severe environmental conditions
22 p3903 A69-39950

Wire, flip-chip and beam-lead bonding processes effects on hybrid microcircuits reliability
22 p3911 A69-39956

Reliability testing - Conference, Anaheim, April 1969
22 p3952 A69-40021

Reliability testing as complex element of reliability engineering noting nondestructive, destructive and selective demonstration testing, stress-time correlations, risk levels optimization, etc
22 p3952 A69-40022

Reliability prediction accuracy through reliability testing with reference to interplay between design, manufacture, test programs, environmental conditions, etc
22 p3952 A69-40023

Reliability incentive programs, considering linear and nonlinear curves for mean time before failure /MTBF/ vs incentive dollars and negative MTBF vs penalty dollars
22 p3952 A69-40024

Implementation of MIL-STD-781 reliability test specification from contractor viewpoint, detailing test procedures /procedural, decision, reporting and corrective action rules/
22 p3952 A69-40025

Techniques to control, measure and assure reliability of electronics systems and equipment, emphasizing Thorndike chart and Molina tables
22 p3953 A69-40026

Reliability test program based on MIL-STD-781 B specification, noting test environments with AGREE chamber
22 p3953 A69-40027

Reliability assessment of ballistic missile inertial guidance system, discussing objectives and requisites
22 p3953 A69-40028

Reliability testing and parts screening of electronic systems for best parts selection
22 p3953 A69-40029

Metallurgical, chemical and mechanical analyses and high stress tests application to verification of electronic device reliability, noting failure modes and rate
22 p3953 A69-40030

Part selection, source control and application program for reliability of equipment design, noting derating
22 p3953 A69-40031

Planning, design and implementation of reliability testing facility, investigating phases of project life cycle
22 p3954 A69-40033

MIL-STD-781A vibration requirements, using mechanical shakers for AGREE vibration testing
22 p3954 A69-40036

Design and economic concepts of Lockheed L-1011 wide body trijets, discussing airport and airways congestion alleviation, passenger appeal, etc
22 p3863 A69-40494

Cs contact ion engine with tubular W ionizer tested for performance and reliability in vacuum chamber
22 p4000 A69-40592

Reliability engineering application to aircraft safety, considering mathematical models involving safety, human errors and accident causes
22 p3867 A69-41129

Safety engineering programs for aircraft design, discussing organizational relations, failure and operational safety analyses
22 p3867 A69-41132

Two channel electronic system with one redundant channel for automatic replacement in case of failure evaluated for operational preparedness
23 p4136 A69-41559

Commercial jet aircraft thrust reversers and noise suppressors developed by Rolls-Royce, discussing compatibility, reliability and applications
23 p4200 A69-41638

S band antenna systems for missiles, designed in various types to obtain RF telemetry links reliability by sharing effort between airborne and ground station equipment
23 p4137 A69-41753

Battery subsystems optimization for earth satellite lifetimes greater than 5 years, analyzing flexibility, weight and reliability
23 p4068 A69-42243

Space vehicle flight performance of Ni-Cd batteries noting reliability, consistency and predictability
23 p4072 A69-42285

All-electric nonlinear actuator steering advanced tactical missiles, noting 99.29 percent delivered unit reliability during mass production
23 p4225 A69-42458

Quality and reliability of electronic spacecraft devices and structural components produced in limited quantity, discussing documentation of production and testing
23 p4171 A69-42474

Management role in ensuring products and components quality and reliability, analyzing failure reasons
24 p4416 A69-42778

All-equipments reliability test improved by removing usual truncation and extending accept-reject lines of test plan MIL-STD-781
24 p4321 A69-43203

Damage tolerance design concepts required to obtain reliability, maintainability and operational safety of complex aircraft
24 p4254 A69-43717

RELIEF MAPS
Representation for computer storage of contour map data for searching problem involving determination of aircraft ground track
01 p0036 A69-10704

Contour maps of H II regions W12, Orion A, W43 and W51, listing flux densities and angular sizes of components
09 p1598 A69-22186

Generalized techniques for contour maps problem solution applied to problem of locating ground track of aircraft from elevation readings obtained during flight
09 p1461 A69-22599

Surface structure asymmetry of near and far sides of moon, considering earth radiation and gravity pull
18 p3206 A69-35439

RELIEF VALVES
Three valve manifold for five self righting inflation bags in escape capsule on F-111, providing one directional flow and pressure relief and shutoff
20 p3467 A69-38185

RELIEVING
U STRESS RELIEVING

RELUCTANCE
Pressure transducers with variable reluctance and magnetic signal transmission techniques
10 p1690 A69-23226

RELUCTIVITY
U RELUCTANCE

REMAGNETIZATION
U MAGNETIZATION

REMANENCE
Magnetic properties of stone, stony-iron and iron meteorites, discussing natural remanent magnetization origin in parent bodies and magnetic susceptibility
19 p3415 A69-36122

REMELTING
U MELTING

REMOTE CONSOLES
Time sharing remote computer station allowing on-spot data processing and output answers, formulating best-fit equation representing statistical data
18 p3107 A69-34860

REMOTE CONTROL
NT RADIO CONTROL
Remotely controlled explosives processing facility for handling unfamiliar sensitive materials, noting safety aspects and inspection, testing, transporting and destroying techniques
02 p0226 A69-11523

Rocket guidance, discussing foreign systems with emphasis on German range miss/gradient orientation scheme used on World War II V-2 rockets
02 p0279 A69-12362

Remotely operated open-cup impact tester for studying impact initiation of reaction of various liquid fluorinating agents with metals and plastics
06 p0907 A69-17876

Predictive display technique for remote manual control of roving lunar and planetary surface vehicles
06 p0928 A69-17925

Automatic remotely operated sodium D line reversal temperature measuring apparatus, analyzing systematic errors
06 p1035 A69-17932

Dynamic IR inspection to detect fatigue cracks in aircraft and missile structure from distance
11 p1861 A69-24262

Dynamics of gyroscopic synchronous servo system intended for remote measurement of spatial orientation coordinates of sensor moving element
11 p1881 A69-24558

Flow control valve for hydraulic motor speed regulation operated by remote pressure signal
11 p1827 A69-25646

Communication systems in interplanetary space covering telemetry, remote control, Doppler and distance measurements, coherent PCM/PSK/PM, demodulation, deep space network, etc
12 p2027 A69-25875

Remote control spectrophotochronograph to study radiation of high speed high temperature processes, giving construction data and diagrams
12 p2085 A69-26161

Book on control theory covering automatic and remote position control, diagrams, transfer functions, operators, Laplace transform use with differential equations
13 p2238 A69-28345

Pursuit problem involving controllable pursuing plant, deriving condition for engagement with prescribed period of time
14 p2482 A69-28800

Remote manipulators applications in space, discussing joint configurations, master-slave systems design, control systems, etc
15 p2558 A69-30187

ESRO Aurorae satellite telecommunication system, detailing information nature, PCM telemetry and remote control system standard
15 p2702 A69-31084

ESRO 1 and 2 satellites onboard remote control system, discussing tone digital standard code and equipment design features
15 p2702 A69-31086

Self contained remote sense remote control pressure regulator using pure fluid amplifiers, controlling large or small flow over wide pressure range
15 p2554 A69-31303

Variable optical system with remote and continuous adjustment of beam for solar simulation, permitting maximum test facility utilization
[AIAA PAPER 69-997] 22 p3920 A69-40375

Remote manipulator spacecraft system for refurbishing synchronous communication satellite, emphasizing compatibility with standard shroud Titan 3C launch vehicle
24 p4297 A69-43041

REMOTE HANDLING

Remote manipulators applications in space, discussing joint configurations, master-slave systems design, control systems, etc
15 p2558 A69-30187

Remote disassembly and inspection methods for evaluating NRX-AG reactor components performance
[AIAA PAPER 69-511] 16 p2810 A69-32712

REMOTE SENSORS

Remote sensors utilization in earth orbital space for discovery, inventory, evaluation, development and conservation of earth natural resources, noting satellite design
[UN PAPER 68-10464] 01 p0065 A69-10532

Agricultural remote sensing information system composed of data acquisition, processing and information extraction and interpretation phases, providing knowledge of earth resources
03 p0400 A69-13195

Randomly rough surface physical and geometrical remote determination by polychromatic bistatic radar
05 p0721 A69-16572

Remote sensing platform requirements for oceanographic and meteorologic observations, discussing orbital and aircraft platforms
[AIAA PAPER 69-154] 06 p1044 A69-18122

Compressor inlet temperature /CIT/ sensors, describing bimetal strip and liquid expansion aspirated types
[ASME PAPER 69-GT-18] 09 p1571 A69-22499

Remote geosensing using properties of radar return noting scatterometry, imagery, altimetry and penetration measurements
11 p1835 A69-24692

Remote sensing of environment - Conference, University of Michigan, Ann Arbor, April 1968
12 p2094 A69-26974

Photography for remote sensing, discussing aerial photography, side-looking radar and photography for recording, storing and retrieving data
12 p2096 A69-26975

Microwave radiometric sensor operational principles and capabilities, discussing antennas and radiometric receivers
12 p2033 A69-26976

Electronically scanned and fixed multiple beam phased arrays for spaceborne microwave radiometric sensors
12 p2044 A69-26977

Earth resources remote sensing from spacecraft noting meteorology, oceanography, forestry, agriculture and IR detection of plant diseases and pollution
12 p2192 A69-26978

Optical/mechanical IR line scanner imagery role in remote sensing
12 p2096 A69-26979

Correlation spectrometer for air pollution surveillance from airborne and spaceborne platforms, noting scanning satellite system for continuous global coverage
12 p2096 A69-26981

Electronic nonimaging polarimeter/photometer for aircraft observations of pure red pine stand, suggesting application to terrestrial, airborne and satellite remote sensing
12 p2096 A69-26983

Geographic and cartographic mapping applications of remote sensor data from orbital heights, discussing hardware, instrumentation, NASA role in data selection, etc
12 p2192 A69-26984

Light interaction with stacked leaves and plant canopy, determining reflectance and transmittance
12 p2097 A69-26985

Information collection by remote sensing and related economic principles, presenting mathematical formulation of linear programming model
12 p2193 A69-26988

Plant and soil thermal behavior for various conditions of crop species, plant spacing, tillage, irrigation and aerial thermal scanner imagery
12 p2075 A69-26989

Remote sensing and forest survey sampling designs, discussing nonstereo stratification, conventional photography and IR or radar imagery
12 p2097 A69-26991

Remote sensing technology application to improving range resource inventories, discussing aerial photography, optical, IR and radar scanning, etc
12 p2098 A69-26992

Prevalent detection of vigor loss and mortality signs in ponderosa pine trees subject to bark beetle attack
12 p2098 A69-26993

Airborne IR line scanning systems for latent forest fire detection, discussing discrimination module for automatic identification of hot targets
12 p2193 A69-26994

Airborne IR remote sensing techniques for fire detection, considering marginal and submarginal targets
12 p2098 A69-26995

Remote oceanographic sensing from ships, aircraft and spaceborne platforms, using active /radar and laser/ and passive sensors in visible, IR and microwave regions
12 p2075 A69-26997

Airborne magnetometer application for remote measurement of ocean wave spectra, obtaining wave noise power spectra and wave height profile
12 p2075 A69-26998

Airborne scanning spectrometer for IR detection of clear air turbulence, presenting flight records
12 p2098 A69-26999

Airborne IR spectrometer for remote clear air turbulence detection, noting necessity for mirror stabilization in pitch axis
12 p2098 A69-27000

Optical radar studies of lower atmosphere, giving Mie theory calculations of clear atmosphere volume backscattering cross sections for four laser wavelengths
12 p2033 A69-27001

Radar remote sensing for terrain data acquisition
12 p2098 A69-27005

Airborne IR surveys in engineering studies of terrain, discussing instrumentation technology, data interpretability, economic feasibility, etc
12 p2098 A69-27007

Side-looking airborne radars /SLAR/ application to geological exploration of remote unmapped areas
12 p2099 A69-27009

Data analysis techniques for discrimination and identification of terrain surfaces from radar scatterometry information
12 p2099 A69-27010

Airborne and satellite IR survey over active effusive eruption at Surtsey, Iceland, comparing thermal energy yield and radiant emission to ground measurements
12 p2076 A69-27011

Remote sensing of urban environments for metropolitan information systems noting photographic, thermal IR, radar and microwave applications
12 p2193 A69-27012

Methodology for technical feasibility and economic analysis of remote sensing applications
12 p2193 A69-27013

Phase screen technique for deriving statistical characterizations of perturbations imposed on wave propagating through random medium applied to remote probing
14 p2414 A69-29511

Focused beam wave applied to atmospheric turbulence probing for spectral density of index of refraction, structure constant and wind velocity
14 p2414 A69-29512

Passive remote sensing at microwave frequencies for meteorology, oceanography and geology, reviewing physics of wave interactions, mathematics of data interpretation, etc
14 p2414 A69-29514

Line of sight atmospheric path measurements for atmospheric inhomogeneities, using phase quadrature, microwave and near IR techniques
14 p2415 A69-29516

High resolution azimuth and elevation arrays sensing remote ionosphere and sea surface characteristics, discussing backscatter data for ionosphere and sea scatter
14 p2448 A69-29520

Remote optical heterodyne measurement of Doppler shift as method for determining vector wind velocity, noting influence of air pollution
14 p2448 A69-29523

Remote sensing of lower atmosphere refractive structure, using Rake tropospheric scatter channel-sounding technique
14 p2448 A69-29525

Multiple ground based geophysical sensors for detecting ionospheric phenomena, discussing continuous magnetic tape data recording, common time base and station operation
14 p2448 A69-29526

Coherence-polarization in remote sensing by microwave and laser means, analyzing scattering functions of rough surfaces
14 p2448 A69-29532

Remote sensor imaging techniques for simultaneous radar, IR and visible electromagnetic spectra of extensive land areas, presenting two clustering algorithms for multiple images
14 p2448 A69-29533

Computer based data handling and display for relating remote sensor signals to ground truth information derived from aerial photographs
14 p2416 A69-29534

Thermistor instrument for remote sensing, magnetic synchronous recording and linear display of temperature
14 p2449 A69-29562

Satellite observation of ocean surface and subsurface features, discussing onboard equipment and proposed orbits
15 p2607 A69-30190

Electromagnetic waves as data carriers for earth resources and technology satellite sensors
15 p2607 A69-30231

Integrated landscape analysis with radar imagery for earth resources
15 p2608 A69-30454

Color IR film improvement for high altitude remote sensor, using auxiliary minus-visual filters
15 p2609 A69-30457

Aerial multiband remote sensors for wildland resources, considering multilens photographic systems, optical mechanical scanners and radar devices
15 p2609 A69-30458

Fluidic digital position sensor consisting of fluidic monostable amplifier, analyzing operation by characteristics method
15 p2554 A69-31301

Self contained remote sense remote control pressure regulator using pure fluid amplifiers, controlling large or small flow over wide pressure range
15 p2554 A69-31303

IR measuring techniques for water surface temperature remote sensing
15 p2617 A69-31543

Ocean and water surface temperature measurement by IR remote sensing from aircraft and satellites, discussing accuracy and data correction [AIAA PAPER 69-590] 17 p2973 A69-33286

VLF and ULF whistler propagation in magnetosphere for remote sensing magnetospheric plasma parameters, exhibiting characteristic patterns and interaction with plasma 17 p2962 A69-33712

Temperature profiles and associated wind profiles obtained with Jimsphere/FPS-16 radar system at Cape Kennedy, discussing remote CAT detector assessment 17 p2999 A69-33739

Multispectral imaging remote sensors, analyzing energy sources affecting systems synthesis 17 p2977 A69-34064

Sea surface temperature remote sensing by Nimbus 2 satellite using TV camera and medium and high resolution IR radiometer 18 p3130 A69-35057

Manned spacecraft earth resource sensing, discussing advantages and applications in agriculture, forestry, geography, hydrology, oceanography and geology 18 p3208 A69-35058

Oceanographic sensing satellite systems, discussing applications, data requirements, sensors, booster and earth coverage capabilities 18 p3210 A69-35091

Electromagnetic field signatures in optical IR spectrum of satellite-borne sensors, analyzing spectral, spatial and temporal distributions, polarization and phase 19 p3309 A69-36060

Optical instruments optimal design for given requirements, discussing tradeoff studies of airborne reconnaissance scanner, spaceborne rendezvous sensor and track-while-scan radiometers 19 p3310 A69-36065

Multispectral scanner with multichannel spectrometer for earth observations, describing video image generation from detector elements output signals 19 p3310 A69-36066

NASA Earth Resources Survey Aircraft Program, describing aircraft and remote sensors characteristics 19 p3312 A69-36259

Fundamentals of remote sensing - Conference, University of Michigan, July 1969 20 p3493 A69-37734

Airborne imaging radar drawbacks and advantages, describing techniques to overcome defects 20 p3493 A69-37735

Electromagnetic radiation detectors in nonphotographic sensing systems, describing performance as function of time constant, spectral response, cooling requirements and signal handling 20 p3540 A69-37736

Remote sensing by electromagnetic waves in microwave region, describing differences between microwave and optical sensing 20 p3493 A69-37741

Remote sensing systems costs, benefits and economic evaluation 20 p3493 A69-37742

Remote sensors discrimination and performance, discussing linear filter system, contrast ratio, tricolor systems and multispectral scanning system 20 p3493 A69-37743

Remote sensors geometrical optics, considering power flow direction, specular reflection, imaging and dihedral in case of specular reflectors, reflection and diffraction 20 p3577 A69-37744

Human optical system as remote sensor consisting of transducing, data transmission and processing subsystems, defining perception function and describing visual aids 20 p3483 A69-37745

Force fields to establish nature and position of remotely located conditions, discussing radiated power, electromagnetic waves, black body radiation, etc 20 p3494 A69-37747

Earth resources technology satellite global survey system carrying multispectral sensors in long life space platform 21 p3720 A69-38623

Earth resources observation technology from satellites, reviewing sensors and methods, electromagnetic spectrum, atmospheric attenuation and windows, passive-active devices 21 p3720 A69-38624

Airborne electromagnetic systems measuring complex dielectric constant in earth crust for mineral and water resources exploration [RAES PAPER 8] 22 p3946 A69-40481

Airborne correlation spectrometer for air pollution remote sensing, describing applications [RAES PAPER 7] 22 p3896 A69-40488

Balloon flights for testing remote sensor systems prior to space flight, considering return beam vidicon and tracking telescope suitability for experimentation 22 p3865 A69-40806

Aerial remote sensing data for earth resources program including agricultural, geothermal/ geological tests, hydrological, water pollution and soil and flood water control observations 22 p3949 A69-40994

Systems analysis method for determining spacecraft remote sensors earth resources survey effectiveness by integrating specifications, mapping requirements and orbital characteristics 23 p4163 A69-41567

Radio telemetry system for evaluating protective masks dynamic performance by remote simultaneous monitoring of respiration, acceleration and temperature data generated by human subjects 23 p4121 A69-41765

Synoptic remote sensing oceanography from ships, aircraft and spaceborne platform, discussing fisheries [AAS PAPER 69-062] 24 p4307 A69-42822

Earth orbital remote sensing applications to forest and range resources management, discussing conventional aerial photography [AAS PAPER 69-059] 24 p4307 A69-42823

Orbiting vehicles remote sensing of earth resources, discussing instrumentation and accuracy requirements, data management and analysis and effectiveness criteria 24 p4315 A69-43199

REMS

U RAPID EYE MOVEMENT STATE

RENAL CALCULI

U CALCULI

RENAL FUNCTION

Renal excretion response to blood fluid volume shift resulting from altered orientation within gravity or from absence of gravity 06 p0873 A69-17015

Renal pathology of acute methylhydrazine intoxication in dogs, noting hemolytic anemia and hemoglobinuric nephropathy 06 p0883 A69-17847

Intrarenal capillary hydrostatic pressure effect on hemodynamically induced changes in sodium excretion 07 p1063 A69-18629

Oxygen saturation in outflowing and inflowing renal blood in dogs under normal and hypoxic conditions, assessing cannula technique 14 p2406 A69-28916

Renal vascular circulation in carotid occlusion pressor reflex by vasoconstriction in absence of renal autoregulation 22 p3887 A69-41190

Renal calculus incidence among aircrews of long and short haul airlines, considering effects of dry cabin environment and dehydration 23 p4108 A69-41826

RENDEZVOUS

U ORBITAL RENDEZVOUS

U SPACE RENDEZVOUS

RENDEZVOUS GUIDANCE

Parallel rendezvous of space vehicles in central gravitational field, discussing relative motion of space vehicle and supplementary force required 05 p0789 A69-16047

Manual and automatic spacecraft rendezvous and docking, discussing docking of Cosmos 186 and 188 in 1967 [UN PAPER 68-95764] 06 p1013 A69-17057

Suboptimal guidance corrections for continuous thrust vehicle disturbances during minimum fuel rendezvous in Martian orbit, discussing physical and modified cost functional [AIAA PAPER 69-76] 06 p0956 A69-18081

Optimal rendezvous for two propelled spacecraft obtained by Pontryagin principle assuming small distance between vehicles compared to distances from center of gravity 10 p1791 A69-22923

Apollo 10 lunar landing module, detailing weight, shape, electronic system and rendezvous radar 18 p3207 A69-34629

Parallel rendezvous of space vehicles in central gravitational field, discussing relative motion of space vehicle and supplementary force required 20 p3574 A69-37956

Guidance control systems for moving plants pursuing targets, basing design on target characteristics and plant phase coordinates 21 p3687 A69-39643

Rendezvous control law for spacecraft moving in central gravitational field along trajectory representing target vehicle Keplerian orbit 22 p4036 A69-40115

Manual method for navigating and guiding spacecraft to rendezvous with orbiting target, using hand-held unpowered optical instruments and manual computations [AIAA PAPER 68-859] 24 p4348 A69-43243

RENDEZVOUS SPACECRAFT

Rendezvous maneuvers for vehicle and elliptically orbiting targets, formulating relative motion of two bodies 04 p0658 A69-14828

Optimal rendezvous between satellite and spacecraft, determining power and time optimal coplanar rendezvous in circular orbit 09 p1538 A69-21759

Optimal rendezvous for two propelled spacecraft obtained by Pontryagin principle assuming small distance between vehicles compared to distances from center of gravity 10 p1791 A69-22923

Optimal rendezvous maneuver of pursuing vehicle with minimum fuel expenditure in approach stage on elliptic and hyperbolic orbits 15 p2701 A69-31548

Rigid and flexible coupling devices for spacecraft rendezvous, describing general operating conditions 22 p4036 A69-40008

Rendezvous control law for spacecraft moving in central gravitational field along trajectory representing target vehicle Keplerian orbit 22 p4036 A69-40115

RENDEZVOUS TRAJECTORIES

Space rendezvous problem as applicable to interplanetary missions, discussing steps in rendezvous maneuvers to permit final docking 03 p0511 A69-13401

Capture and control in conservative dynamical systems, analyzing orbital mechanics of derelict and pursuit spaceships 05 p0826 A69-16462

Low thrust trajectories for minimum time rendezvous between continuous thrust interceptor and passive target vehicle, comparing calculus of variations and steepest ascent analyses 16 p2857 A69-32177

Halley Comet rendezvous mission, comparing low thrust mode with ballistic Jupiter or Saturn swingby mode [AIAA PAPER 69-933] 21 p3809 A69-39360

Optimal pursuit control at constant moving velocity and limited angular velocities, using Pontryagin principle 21 p3825 A69-39629

Space mission opportunities selection from analysis of short period comet perihelia, discussing flyby and rendezvous mission payloads [AAS PAPER 69-320] 24 p4381 A69-42866

REPAIRING

U MAINTENANCE

REPEATERS

Hybrid digital transmission systems, discussing joint optimization of analog and digital repeaters and information rate of coaxial cable systems 01 p0027 A69-10248

Performance characteristics of hard limited and linear repeaters for satellite communications systems 01 p0032 A69-10966

Local oscillator for space telecommunications F9 repeater, operating principles, design calculations and test results 08 p1286 A69-20596

Interference noise in communication satellite receivers and terrestrial radio relay receivers, noting interference reduction transfer factor 09 p1450 A69-21279

Joint filter optimization in combination analog-digital hybrid multilevel transmission system 09 p1457 A69-22465

High gain self steering microwave repeater for earth-satellite communications noting design, performance and results of color TV transmissions 11 p1839 A69-25294

Communication subsystem design of Defense Communication Satellite Program/DCSP for background information, noting repeater with toroidal pattern antenna 23 p4131 A69-42537

REPLACING

Probability theory applied to age and block replacement models in preventive maintenance of parts, noting inspection cost distribution 20 p3551 A69-38267

REPLICAS

Electron fractography techniques and fracture modes in metallic materials interpretation, giving special attenuation to classical fracture replication and shadowing techniques 04 p0619 A69-15395

Plastic backing films removal from carbon electron microscope replicas by maintaining specimens in horizontal position 09 p1495 A69-21651

REPORTS

Scientific report of Rockwell polar flight, November 14-17, 1965 09 p1484 A69-21401

Scientific research report on cosmic ray and X ray astronomy by constant altitude stratospheric plastic balloons, etc 15 p2723 A69-31431

REPRESENTATIONS

Extension of results of one dimensional representation theory treating nonGaussian processes as perturbations of log normal process to higher dimensions 03 p0392 A69-13248

REPRODUCTION [COPYING]

Self reproducing automata, noting description of cellular system and applications to systems science 05 p0723 A69-15826

REPRODUCTIVE SYSTEMS

Self reproducing automata, noting description of cellular system and applications to systems science 05 p0723 A69-15826

Drosophila melanogaster flies reproductive behavior and Tradescantia paludosa chromosome patterns after weightlessness onboard Vostok 3 and 4 07 p1063 A69-18597

Visceral lesions observed in mice and rats exposed to ultrashort waves indicating no pathological modification of physiology of reproduction [AGARDOGRAPH-111] 08 p1266 A69-20679

Axiomatic explanation of complete self reproduction, noting logical mathematical biological reasoning and evolution theories 10 p1645 A69-23385

Penile erection electrically evoked from Macaca mulatta forebrain, measuring density and distribution of responding points 12 p2018 A69-25775

Population feedback control in planarians by fission suppression by brain near other planarians 14 p2406 A69-28871

Mammalian pineal gland as neuroendocrine transducer, studying melatonin role in ovulation, gonadal growth, etc 20 p3480 A69-38284

REPTILES

U LIZARDS

REPUBLIC MILITARY AIRCRAFT

U MILITARY AIRCRAFT

REPULSION

U FORCE

RESCUE OPERATIONS

Navigation techniques for emergency helicopter services in medical evacuation and air/sea rescue missions, discussing displays and search patterns 02 p0279 A69-12363

Radar detector for survivors, using inexpensive microwave mixer detector crystal 06 p0878 A69-16964

Legal and technical aspects of international cooperation in spacecraft crew rescue operations signed by UN General Assembly 06 p1042 A69-17033

Passenger and crew members escape from aircraft following water accidents, discussing ditching, evacuation, survival and rescue facilities 08 p1254 A69-20453

FAA regulations for improvements on crashworthiness and emergency evacuation from viewpoint of plastic applications and fire safety in aircraft 08 p1254 A69-20497

Rescue locator beacons and airborne search equipment of VHF and UHF capabilities available to international civil aircraft operations 15 p2552 A69-30852

Problems connected with rescue of crew members ejected over water 15 p2551 A69-30866

Light aircraft emergency downed position indicators installation program, discussing transmitter minimum performance standards, listening watch insurance, etc 17 p2931 A69-34102

Space docking, personnel placement on space stations, rescue stations, etc 18 p3196 A69-34630

Agreement on Rescue and Return of Astronauts and Return of Objects Launched into Outer Space, discussing unintended landing 20 p3636 A69-37113

Agreement on Rescue and Return of Astronauts and Return of Objects Launched into Outer Space, noting humanitarian considerations and indemnity for services rendered 20 p3636 A69-37114

Amendments considered for international law regarding earth and space rescue services as result of contemporary U.S. manned space flight programs 20 p3637 A69-37115

UN agreement provisions on international cooperation for rescuing astronauts and objects in case of accident, distress, emergency or unintended landing 20 p3637 A69-37116

International lawyers proposal for compulsory registration of space activities in connection with astronauts rescue and damages liability 20 p3637 A69-37118

Passenger safety during aircraft accidents in Arctic, discussing survival equipment and methods 23 p4107 A69-41811

RESEARCH

NT CRITICAL PATH METHOD

NT DYNAMIC PROGRAMMING

NT GAME THEORY

NT HIGH TEMPERATURE RESEARCH

NT LINEAR PROGRAMMING

NT LOW DENSITY RESEARCH

NT MINIMAX TECHNIQUE

NT NONLINEAR PROGRAMMING

NT OPERATIONS RESEARCH

NT SADDLE POINTS [GAME THEORY]

Materials research - Conference, Tokyo, September 1967 06 p0941 A69-17120

Cost estimates of R and D, considering planned profit and loss following products introduction to market 14 p2541 A69-29280

Capital budgeting for R and D, discussing control of rising costs 14 p2541 A69-29281

RESEARCH AIRCRAFT

NT B-70 AIRCRAFT

NT FIREBEE 2 TARGET DRONE AIRCRAFT

NT VZ-2 AIRCRAFT

NT X-15 AIRCRAFT

NT X-22A AIRCRAFT

NT XH-51 HELICOPTER

NT XV-4 AIRCRAFT

Variable properties aircraft for flying simulator, discussing flight control system and stability behavior 07 p1052 A69-18254

Test techniques for X-22A VTOL research aircraft during ground simulator work and actual flight test, describing stability and control characteristics [AIAA PAPER 69-319] 10 p1633 A69-23044

HRV-1 navy research pusher amphibian aircraft, discussing hydrofoils and operational problems 10 p1633 A69-23223

RESEARCH AND DEVELOPMENT

National tasks in civil aeronautical research and development noting technological and social factors 08 p1422 A69-20171

Flight research testing facilities at Arnold Engineering Development Center for rockets, turbojets, ramjet engines, aircraft, missiles, satellites and spacecraft 08 p1302 A69-20883

Integrated circuit production, development and research in Germany [AGARDOGRAPH-114] 08 p1292 A69-20994

Organization and manpower utilization in R and D, determining criteria for organizational form selection 08 p1423 A69-21155

National plan for air navigation covering R and D and operational aspects 08 p1348 A69-21192

British electric propulsion research, discussing electron bombardment ion engines, conical theta pinch and rail devices and test facilities [AIAA PAPER 69-299] 09 p1564 A69-21241

30 cm diameter mercury bombardment low impulse thruster development for potential space applications, discussing performance and control [AIAA PAPER 69-238] 09 p1566 A69-21256

Research and development program in annular slit colloid thruster technology, proving thruster feasibility by performance tests 09 p1566 A69-21257

[AIAA PAPER 69-287] Lasers, reviewing output properties, control and modulation characteristics, and applications to communications, plasma generation, measurement, high temperature metallurgy, etc 09 p1517 A69-22118

Turbine blade cooling research programs, discussing effects of increased trailing edge thickness and cooling air on turbine efficiency 09 p1432 A69-22501

[ASME PAPER 69-GT-15] Solid electrolyte batteries development and current research, detailing Sprague cell and iodine complexes 10 p1640 A69-23999

MHD power plant research and development, discussing shock wave electric power generators and modulated systems 11 p1925 A69-24469

Isolation of scientific and technical personnel and effect on lateral communication and intellectual cross fertilization in research and development program 11 p2004 A69-25303

Program definition and government-industry relationships in entry research and development program management 11 p2005 A69-25726

Research and development organizations under pressure of corporate assessment and systems management approach, suggesting core-technology structure and training 12 p2192 A69-26732

Intracompany research and development, noting separate philosophies approach 12 p2192 A69-26733

Charged particles generation by liquid subjected to high electric field for efficient bipolar microthruster [AIAA PAPER 67-728] 13 p2325 A69-28220

European space program developmental and fabrication problems in satellite structure development covering booster constraints, mission constraints, tolerances, etc 13 p2357 A69-28479

European heat pipe research emphasizing transportable heat quantities, heating rate and life duration 14 p2538 A69-29201

National plan for air navigation covering R and D and operational aspects 14 p2480 A69-29858

Diffusion bonding for leaktight joints in connectors using intermediate metal system of Au-Cu-Au 15 p2617 A69-30100

Air cushion vehicle research and development laboratory testing, plans, support equipment, monitoring by TV, etc 15 p2589 A69-30865

MACRO /methodology for allocating corporate resources to objectives/ for R and D, discussing program for optimal budget management 15 p2720 A69-30958

Mathematical model for money expenditure on product oriented research programs, based on accumulated profits 15 p2721 A69-31068

Measurable and strategic characteristics of Army laboratories management, considering papers published, inventions and laboratory performance 15 p2721 A69-31070

Research and development planning and control models based on subjective probability estimates for failing projects identification 15 p2721 A69-31072

Australian space research including space flight programs in cooperation with NASA 15 p2724 A69-31450

Motivation and performance increase in R and D by incentive plans, discussing prestige, power, responsibility, recognition, work, salary, comfort, etc 17 p3075 A69-32963

Research productivity in large organizations stressing interface problem minimization, recommending deferred bonus system 17 p3075 A69-32964

Research management differences between European and American corporate structures, discussing cultural differences, cost comparisons, social mobility, etc 17 p3075 A69-32965

Concorde design, discussing planform, wing twist and camber, hypersustentation, kinetic heating, aeroelasticity, R and D, tests, etc 17 p2899 A69-33380

Plasma physics and controlled nuclear fusion research - Conference, Novosibirsk, U.S.S.R., August 1968, Volume 1

17 p3012 A69-33817

Expenditures for R and D effect upon U.S. economy

17 p3076 A69-34041

Space program design, discussing NASA centers and NASA R and D life sciences, technological developments and federal action

17 p3076 A69-34042

R and D for economic growth, discussing interaction between management, planning, engineering, marketing, production, customers and competitors

17 p3077 A69-34126

Aerospace R and D marketing decisions, considering capability identification, business opportunities, strategies and independent program funding

17 p3077 A69-34127

Proposed projects selection for independent R and D development program in business entity, measuring merits in terms of future financial returns

17 p3077 A69-34129

Technology or Research Quantitative Utility Evaluation (TORQUE) system genesis and operation, with implications affecting R and D

17 p3077 A69-34130

Laser technology applications stressing engineering, control, communications, medicine, space sciences, holography, computers, etc

17 p2984 A69-34163

Apollo project by-products, emphasizing NASA project management methods application to large R and D projects

18 p3233 A69-34649

Aerospace biomedical technology transfer analysis, discussing spinoff, popular interest, transfer barriers, etc

18 p3236 A69-35104

U.S. military aircraft technology, flight environments, trends toward larger aircraft and R and D

18 p3092 A69-35138

Civil aviation center for R and D in aviation personnel education and training [AIAA PAPER 69-785]

19 p3453 A69-35597

R and D program risk evaluation methodology in density functions form for program goals probabilities, noting random variables as parameters

19 p3455 A69-36008

Air and space research at Goettingen Aerodynamic Testing Institute

19 p3295 A69-36684

French helicopter industry projected development for existing types, production models or final development and long range design programs

19 p3248 A69-36848

Delphy technique of technological forecasting used for R and D planning

20 p3639 A69-37353

Technical communication patterns in R and D laboratories, discussing effects of work structure, social relations, etc

20 p3640 A69-38019

Technical problem solving model based on tape recorded protocols of engineers engaged in R and D project

20 p3640 A69-38020

In-house research on R and D management in government agencies, discussing manning, training, center programs, case studies, etc

20 p3640 A69-38022

Laser research from theoretical stage to present, discussing applications

21 p3736 A69-38781

Dornier R and D, discussing single and twin engined aircraft, utility aircraft, helicopter, VTOL transport, safety, etc

22 p3862 A69-39931

Research and development programs leading to heat sterilizable spacecraft battery separator material, describing bench tests

23 p4072 A69-42284

Turbofan jet engine research, discussing future compression and bypass ratios, weight and noise reduction, maintenance and reliability, temperature effects, etc

24 p4363 A69-42569

Technological forecasting as aid to aerospace planner in optimizing R and D resources allocation [AAS PAPER 69-105]

24 p4417 A69-42819

Cape Kennedy space research and national priorities, indicating performance and progress of future space operations [AAS PAPER 69-110]

24 p4419 A69-42879

Materials research structural design cycle, discussing simultaneous optimization, constituent materials, fabrication process, load environment and mission constraints

24 p4399 A69-42991

Beryllium R and D emphasizing brittleness and fracture toughness for safe working stress levels of structurally loaded components

24 p4332 A69-43208

RESEARCH FACILITIES

Scientific advances from space research in communications astronomy, electronics, transportation, etc

01 p0151 A69-10498

Electromagnetic forming principles and applications describing large capacitor bank facility design for multipurpose research [ASTME PAPER MR68-418]

02 p0252 A69-11798

High energy cosmic ray research facility at mountain altitudes, noting nucleon-proton interactions, particle identification and momentum analysis

03 p0499 A69-12942

Research center for investigating man/computer interaction, discussing display systems, computers, languages and data entities

04 p0566 A69-15342

Hot plasma research at Polish Institute of Nuclear Research at Swierk

06 p0964 A69-17174

French supersonic recycling wind tunnel for short duration experiments

07 p1116 A69-19289

Communications of Lunar and Planetary Laboratory, Volume 7

07 p1225 A69-19769

Flight research testing facilities at Arnold Engineering Development Center for rockets, turbojets, ramjet engines, aircraft, missiles, satellites and spacecraft

08 p1302 A69-20883

Organizational behavior of scientists noting working environments, effectiveness of work sections, research management and organizational development

08 p1423 A69-21124

U.S. Army Materiel Command R and D planning structure and technical planning processes influence on decisions improvement

08 p1423 A69-21153

MHD blowdown loop facility for alkali seeded noble gas MHD energy conversion, noting performance and plasma insulation from ground

10 p1674 A69-23482

Solar research objectives and instrumentation of Einstein turret in Potsdam

15 p2682 A69-30437

Variable stars research and facilities in Tautenburg, East Germany

15 p2682 A69-30438

French space research center in Toulouse, discussing organization and activities involving satellites, rocket probes, balloons and environmental tests

16 p2765 A69-31758

Experiments integrated into single automated laboratory to detect extraterrestrial life through measuring metabolism and growth in planetary surface material

17 p2912 A69-32969

Outer space rocket plumes simulation facility combining low density wind tunnel and molecular sink properties, discussing role of liquid nitrogen cooled diffuser-precooler

22 p3928 A69-40731

Flight simulator with large lateral motion for large and supersonic transport aircraft, emphasizing reproduction of cockpit accelerations due to supersonic engine thrust loss

24 p4297 A69-43044

RESEARCH PROJECTS

Atmospheric turbulence power spectra for design criteria of future low altitude aircraft from LO-LOCAT program, analyzing turbulence scale lengths [AIAA PAPER 68-216]

01 p0011 A69-11023

Terradynamic research program for studying instrumented projectile penetration of terrestrial materials

02 p0228 A69-11767

Project management in complex research, discussing incentive contracting decision model and resources allocation

02 p0356 A69-12476

Aerospace research and development projects selection and planning for success in manufacturing competition

03 p0393 A69-13252

NASA Space Application Program strategy, discussing research and development trend toward complexity, versatility and multidisciplinary use of larger spacecraft

03 p0511 A69-13427

Research and development project selection and planning, outlining system to identify capabilities contributing to increasing success probability

03 p0535 A69-13552

Book on economic management of research and engineering covering project plan impact, projects control and evaluation of research and engineering structure

04 p0688 A69-14530

Cost dependent utility characteristics in mathematical model for optimum research and development resource allocation, computing optimum fund distribution with Lagrange multipliers

04 p0689 A69-14807

Graphical evaluation and review technique (GERT) in R and D project planning processes

04 p0689 A69-15100

Estimate accuracy and project selection models in industrial research, examining company data for miscellaneous, technical and commercial failure

05 p0849 A69-15981

UK hovercraft research covering internal/external dynamics, propulsion systems and full scale tests

05 p0702 A69-16393

FAA research and development responsibility to National Airspace System, examining programs for ATC automation, solid state technology application, communications, etc

05 p0850 A69-16717

NASA civil aviation electronics research program, discussing feasibility of V/STOL aircraft all-weather operations

05 p0850 A69-16718

UK space research in 1970s emphasizing solar observations in UN, cosmic X ray astronomy, solar space astronomy and ionospheric investigation

06 p0997 A69-16853

Telescope dispersion role in research projects, discussing techniques for spectral classification and radial velocities

07 p1074 A69-19202

Heuristic methods to determine scientific activities planning emphasizing problem definition, purposes, possibilities of solution and difficulties

15 p2720 A69-30969

Scientific research report on cosmic ray and X ray astronomy by constant altitude stratospheric plastic balloons, etc

15 p2723 A69-31431

Japan space research covering sounding rockets, balloons, satellites and facilities

15 p2725 A69-31466

Welding research program at Polish Institute of Aviation concerning electron beam, AR shielded arc, resistance welding and soldering of heat resistant alloys

17 p2979 A69-33688

Gust probes in model of low altitude atmospheric turbulence during USAF research program LO-LOCAT, plotting relationship between peak count distribution curves

17 p2999 A69-33737

RESEARCH VEHICLES

Stratospheric balloons for space research, emphasizing stabilization equipment suitability

03 p0366 A69-13589

Attitude control system for 625 A-1 research earth satellite, detailing operation and test program

17 p3050 A69-33426

German research satellite Azur design and production management

17 p3050 A69-33700

RESIDUAL GAS

Mass spectrometer residual gas analyzer (RGA) for identifying and measuring subliminated substances from spacecraft construction materials, noting applications during vacuum testing

02 p0227 A69-11758

Residual gas effect on fatigue behavior of pure iron subjected to alternating bending load in ultrahigh vacuum

04 p0616 A69-14846

Residual interstellar gas from protostar formation detected as high luminosity IR object

13 p2327 A69-27593

Residual gas analyzer and leak detector by time of flight measurements on neutral metastable atoms and molecules between pulsed electron gun and auger surface detector

13 p2262 A69-28006

Vacuum restoration by laser evaporation of active media /getters/ and vapor condensation on cold substrate applicable to nonmetallic active media /titanium-magnesium oxide/

21 p3735 A69-38590

RESIDUAL STRESS

Yield surface after prestraining under radial loading, analyzing formation of yield corner

01 p0166 A69-10303

Ruby laser crystals optical inhomogeneity and residual mechanical stresses effects on laser beam angle of divergence

01 p0139 A69-10831

Nondestructive technique to measure residual and working stresses in machine parts, using specially designed circuit

06 p0926 A69-17497

TIG welding introduced residual stresses amplitude and distribution in Ti sheets, studying effects on mechanical properties [ASM PAPER GG-8-2]

07 p1169 A69-19674

Roll planishing and thermal treatments effects on gas tungsten arc welded Ti-6Al-4V alloy on residual stresses, tensile, formability and fracture toughness properties

08 p1319 A69-19966

Elastic springback and residual stress distribution in sheet metal formed by bending determined as function of radius sheet thickness and stress-strain characteristics

08 p1319 A69-20005

Structural residual stresses determination in oriented fiberglass reinforced plastics by models taking into account mutual influence of fibers

08 p1335 A69-20333

Ultrasonic technique for metal surface and near surface residual stress measurement, emphasizing aluminum alloys

10 p1794 A69-23052

Continuum theory of dislocations and internal stresses in generalized Cosserat continuum as theoretical model for crystals

10 p1799 A69-23153

Ruby laser crystals optical inhomogeneity and residual mechanical stresses effects on laser beam angle of divergence

11 p1936 A69-24698

Residual thermal stresses and plastic strains at hole edges in perforated plates, considering heating and rapid cooling

11 p1982 A69-24947

Residual stresses and strains in wound reinforced plastic fiber cylinders subjected to polymerization by heat treating

11 p1907 A69-25679

Vacuum evaporation effects on internal macrostresses in deposited metal films based on X ray analysis, showing substrate temperature contribution

12 p2143 A69-26457

Induced stressing method for complex castings by controlled cooling during heat treatment applied to front frame of J-79 turbojet engine

13 p2269 A69-28184

Stainless steel biaxial residual surface stresses from grinding and finish machining determined by dissection technique [ASME PAPER 68-WA/MET-9]

14 p2455 A69-29437

Maraging steel weldability, discussing residual stresses, hydrogen cold cracking, age hardening and hot cracking

15 p2617 A69-30098

X ray and ultrasonic methods for surface residual stresses induced in machined or ground specimen

15 p2631 A69-31511

X ray analyzer for residual stress measurement applied to quality control

18 p3150 A69-35423

Stress relaxation of heat-resistant steels as function of equal stress during different elevated temperatures, applying results to time residual stress prediction

19 p3342 A69-35778

Soviet monograph on metal fatigue in aircraft structures, discussing effects of temperature, loading, residual stresses, surface finish and contact corrosion

20 p3622 A69-37231

Residual tensile stress distribution during plasma spraying determined as function of temperature field in blank

20 p3548 A69-37328

Axially symmetric distribution of residual strain in multilayered filament wound ring analyzed and compared with experimental results

20 p3628 A69-37774

X ray diffraction as nondestructive technique for measuring residual surface stress

21 p3845 A69-39476

Residual stress effect on strength of oriented glass fiber reinforced plastics under transverse and longitudinal tension

22 p3973 A69-40745

Residual stress measurement in steels and composite materials by X ray diffraction, discussing specimen preparation, diffractometer alignment, elastic modulus determination, etc

24 p4331 A69-42736

RESIDUES

Residue contributions to integrals associated with admittance of plasma or dielectric covered circular aperture antenna used to calculate surface wave contribution to waveguides

06 p0896 A69-17477

RESILIENCE

Viscoelastic materials gradual resilience loss under tensile stress, discussing mathematical relations between stress, loading time, elastic deformation and experimental verification

20 p3625 A69-37600

Automated rebound resilience apparatus for polymer dynamic mechanical properties studies over wide temperature range, using photoelectric device

21 p3689 A69-38593

RESIN BONDING

Resin bonded glass cloth for large airframe structures rectification

06 p0931 A69-17713

Film thickness effect on wear life of resin bonded solid lubricant film compared for various load test conditions [ASLE PREPRINT 68AM 7C-4]

07 p1139 A69-18624

Load, speed and coating thickness effect on wear life of resin bonded solid lubricant, using oscillating motion and low pressure blocks [ASLE PREPRINT 69AM 5C-3]

15 p2619 A69-30474

Energy dissipation in bonded structures, analyzing vibration damping, hysteresis loop and absorption coefficient dependence on deformation energy

17 p3066 A69-33943

Beryllium bonding, evaluating various surface preparations and adhesives

19 p3320 A69-35561

Outdoor aging effects on unstressed Al-Al lap shear joints bonded by various polymeric adhesives

19 p3320 A69-35562

Low temperature bond failures of room temperature vulcanizing methyl-phenyl adhesive bonds attributed to thermal stress cracking of primer, presenting in-process tests

19 p3321 A69-35563

Reinforcement unbonding onset in composite materials determined by continuous dynamic moduli and damping measurements of tensile specimens

20 p3511 A69-37761

Adhesives and adhesive resin bonding, describing internal stresses in joints, joints design for bonding, strength, bonding processes and testing

21 p3752 A69-38932

Strain distribution on surface of adhesive bonded box beam in simple bending, using water based brittle coating and self adhesive strain gages

21 p3844 A69-39325

Lap-shear strengths of Mg-Al alloy bonded with nylon-epoxy adhesive, including anodized coating rolling schedule and honeycomb core fabrication

24 p4323 A69-43417

Adhesive bonding of optical components, discussing material types, test methods, problem of operation at cryogenic temperature, etc

24 p4326 A69-43465

RESINS

NT ACRYLIC RESINS

NT ALKYD RESINS

NT EPOXY RESINS

NT ION EXCHANGE RESINS

NT PHENOLIC RESINS

NT POLYAMIDE RESINS

NT POLYESTER RESINS

NT POLYIMIDE RESINS

NT POLYMETHYL METHACRYLATE

NT POLYURETHANE RESINS

NT SILICONE RESINS

NT SYNTHETIC RESINS

NT THERMOPLASTIC RESINS

NT THERMOSETTING RESINS

Carbon fiber reinforced plastics development for aerospace use, presenting criteria for resins selection

17 p2992 A69-33647

RESISTANCE COEFFICIENTS U COEFFICIENTS

RESISTANCE HEATING

Resistance welding monitoring systems including thermal expansion slow scan ultrasonic and electric energy monitor/limiter systems

02 p0253 A69-11864

Energy release by Joule magnetic field dissipation in solar atmosphere

03 p0516 A69-14041

Conductivity and electron temperature in coaxial MHD generator plasma with magnetic field, studying Joule heating effect on performance

10 p1735 A69-23463

Joule heating role in generating internal gravity wave energy in auroral electrojet region, using linear model

12 p2064 A69-26010

Vacuum effects on resistance spot welds in aluminum, stainless steel and titanium alloys, noting X ray and tensile shear test results

12 p2103 A69-26622

Fluidic curved-wall electropneumatic converter optimization, presenting steady state, step and pulse mode responses for various positions and lengths of resistive heaters

15 p2553 A69-31298

Fringing effects on electric efficiency variation with slip for cylindrical induction MHD device operable as accelerator, generator or Joule heater [AIAA PAPER 67-714]

16 p2736 A69-32152

RESISTANCE THERMOMETERS

Thin film heated Pt resistance thermometer for skin friction or velocity measurements in air, water or blood

04 p0601 A69-15118

Resistance temperature transducers and thermocouples covering characteristics, readout and design for aerospace requirements

10 p1690 A69-23225

Oxygen boiling point studied via calibration of capsule type platinum resistance thermometers

14 p2540 A69-29888

Thermistor thermometer with low energy dissipation for flow measurements, discussing design considerations

15 p2608 A69-30296

Resistance thermometers operation characteristics and applications, noting sensor metals, true temperature and instrumentation errors

18 p3139 A69-35480

Resistance thermometer for measuring rapidly varying gas temperatures, optimizing length to eliminate heat transfer to mounting

23 p4163 A69-41557

RESISTIVITY

U ELECTRICAL RESISTIVITY

RESISTOJET ENGINES

Biowaste propelled resistojet control systems selection criteria based on NASA Manned Orbital Research Laboratory with six man crew [AIAA PAPER 68-121]

04 p0554 A69-15506

Ammonia resistojet stationkeeping subsystem on-board ATS 4 satellite, noting flight test data agreement with ground tests

09 p1560 A69-21212

Resistojet control system combined with control moment gyro payload capability for long duration manned orbital spacecraft missions [AIAA PAPER 69-255]

09 p1561 A69-21220

Life test of high temperature /2400 K/ 10 millipound resistojet thrusters, comparing results to theoretical predictions [AIAA PAPER 69-294]

09 p1563 A69-21232

Space station attitude control through resistojets and control moment gyros /CMG/, discussing propulsion, safety features, weight factors, etc

11 p1965 A69-24531

Fast heat-up electrothermal ammonia thruster role in development of hybrid resistojet in millipound thrust range [AIAA PAPER 69-496]

16 p2838 A69-32649

ATS 3 spacecraft ammonia-fueled resistojet engine test performance [AIAA PAPER 68-553]

21 p3786 A69-39754

Ammonia resistojet thruster, describing ammonia physicochemical properties and systems characteristics of pulsed mode operation and continuous thrust resistojets

23 p4203 A69-41931

RESISTOJETS

U RESISTOJET ENGINES

RESISTORS

NT THERMISTORS

Universal NOR element design with resistors, determining permissible combinations for static mode of operation by computer method

01 p0037 A69-10746

Theory of capillary flow for fluidic resistor design

05 p0705 A69-16011

Voltage divider network board composed of composite carbon resistors for measurement of terminal voltage of 3 Mev Dynamitron electron accelerator recalibration

06 p0907 A69-17705

Operating and storage conditions effects on reliability of Pd-Ag thick film resistors

08 p1283 A69-20131

Optimum microcircuit analog to digital converter for aerospace environment by combining monolithic circuits and thin film resistors

10 p1636 A69-23282

Electromagnetic scattering from thin wire loops under various impedance loadings, considering positive and negative resistors effect combined with reactive networks

11 p1837 A69-25000

Thin film cermet resistors for integrated circuits produced by thermal vapor deposition in vacuum, cathodic sputtering and explosive vapor deposition

13 p2268 A69-27466

Reliability control of 1/4-W resistors of tin oxide on glass substrate manufactured in quantity

15 p2627 A69-30837

Thin film tantalum nitride resistors technology and production, evaluating projected reliability of resistance circuits as function of operating and environmental conditions

15 p2628 A69-30846

Metal film resistor reliability for conventional and space use, outlining guidelines for fabrication and quality control

15 p2628 A69-30847

Thin film carbon resistors cutting with carbon dioxide gas laser, considering cylindrical bodies and aging properties

15 p2635 A69-31038

Single balanced modulators using square law resistors /space charge limited diodes/, discussing noise properties, conversion losses and terminating conductance

16 p2758 A69-31756

RESOLUTION

NT ANGULAR RESOLUTION

NT HIGH RESOLUTION

NT RADAR RESOLUTION

NT SPECTRAL RESOLUTION

Signal resolution during space diversity reception with nondirective or weakly directive antennas and noncorrelated receiver background noise, discussing signal processing

06 p0890 A69-17800

Object restoration, discussing data processing method for single variable functions with small signal to noise ratios

07 p1137 A69-19721

Motion measurement using Doppler shift of scattered laser light, noting high resolution

09 p1492 A69-21398

Statistical estimation theory giving angular resolution of imaging systems in terms of noise characteristics and modulation transfer function

10 p1725 A69-24048

Real time 2000 line TV camera with 40 MHz bandwidth, 1600 line vertical resolution and 1000 line horizontal resolution [SMPTE PAPER 105-73]

12 p2077 A69-25769

Practical time resolution of streak camera, discussing streak camera transfer function and measurement of resolution with pulsed laser diode emission

12 p2084 A69-26152

Energy resolution improvement in cylindrical electrostatic energy selector by focusing and limiting electron beam before entrance into monochromator

14 p2450 A69-29572

Close visual binaries separations for checking large aperture telescope resolution, listing binaries, orbits and ephemeris

16 p2855 A69-31662

Tv transmission of two dimensional transparency hologram with reduced resolution requirements on camera tube, eliminating zero order terms

17 p2974 A69-33401

Compressed signal spectral analyzer resolving power, discussing dynamic amplitude range influence and weighting functions role

17 p2939 A69-33906

Resolving power and field of view relations of holographic device for images recording through inhomogeneous atmosphere

20 p3540 A69-37728

Propagation effects on lane ambiguity resolution ability of Omega VLF navigational system, noting waveguide mode interference

21 p3673 A69-38756

Observation time influence on interferometers resolution limits due to radio wave phase fluctuations

21 p3682 A69-39122

Resolution limitations in holographic images using single record, discussing lensless holography using plane reference waves

21 p3727 A69-39778

RESOLUTION CELL

Range-Doppler processing in pulsed radar applied to imaging of rigid rotating body with motion compensating resolution cells

08 p1270 A69-19861

RESOLVENTS

U PROBLEM SOLVING

RESOLVING POWER

U RESOLUTION

RESONANCE

NT CYCLOTRON RESONANCE

NT ELECTRON PARAMAGNETIC RESONANCE

NT FERROMAGNETIC RESONANCE

NT MAGNETIC RESONANCE

NT MAGNETOSONIC RESONANCE

NT MICROWAVE RESONANCE

NT NUCLEAR MAGNETIC RESONANCE

NT OPTICAL RESONANCE

NT PARAMAGNETIC RESONANCE

NT PLASMA RESONANCE

NT PROTON MAGNETIC RESONANCE

NT RESONANT VIBRATION

NT SPIN RESONANCE

Resonance theory of thermomolecular recombination kinetics applied to hydrogen atoms

01 p0122 A69-10034

Partial avoidance of jump resonance in nonlinear feedback system, applying procedure to feedback amplifier circuit

01 p0051 A69-10442

Resonance energy transfer mechanism in Forster-Dexter theory of electron energy transfer by resonance interaction in condensed media, using many particle treatment

01 p0121 A69-12527

Input impedance of slot antenna in primary resonance region

04 p0577 A69-14784

Lithium abundance determination difficulties for undisturbed solar photosphere, noting Li I resonance line identification and model choice

05 p0821 A69-15849

Paraelectric resonance spectroscopy on KCl, using bistable dipole model

06 p0982 A69-18235

Resonance conditions in dielectric sheathed or plug loaded phase arrays of waveguides

08 p1281 A69-20034

Nonlinear integrodifferential kinetic equation for weak turbulence of resonant four wave processes, considering spectral energy density

11 p1921 A69-24294

Resonances in cross sections for electron impact excitation of forbidden lines in oxygen molecular ion at near threshold energies for astrophysical applications

11 p1921 A69-24417

Periodic Trojan orbits for resonance 1/12 in restricted three body problem, noting bridge of stable and unstable orbit lanes

13 p2350 A69-27824

Resonances in elastic cross section for electron/hydrogen atom scattering noting wide structure

15 p2657 A69-31265

Ca 2 resonance line profiles in large disk flares and in surrounding plage, discussing H and K line behavior

17 p3023 A69-33054

Resonances and doublets observation by neutron radiative capture and transmission of W and Zr isotopes in kev region, noting partial wave strength functions

18 p3175 A69-34314

Bogoliubov averaging method of perturbation in wave mechanics for radiation and matter interaction, considering monochromatic and broad spectral incident wave for resonance study

18 p3175 A69-35483

Nonlinear roll-yaw attitude motion of spinning symmetric satellite in elliptical orbit near internal or external resonance [AAS PAPER 68-124]

20 p3616 A69-37178

Resonance theory of thermomolecular atomic recombination kinetics based on transition complexes identification as quasi-bound states or orbiting resonances

20 p3579 A69-37345

Alouette 2 ionograms secondary resonances data indicating day-night effect in relative frequency of occurrence

20 p3496 A69-37889

Periodic orbits obtained for special restricted three body problem in resonance using numerical integration

22 p4031 A69-40909

RESONANCE PROBES

Inhomogeneous and anisotropic cold plasma filled plane capacitor resonance in steady magnetic field applied to plasma diagnostics, using calculus of variations

13 p2304 A69-27240

Pure quadrupole resonance spectrum of iodine-127 in solid stannic iodide measured in specific temperature range at atmospheric pressure

22 p3986 A69-40726

RESONANCE SCATTERING

Barium plasma density measurements by Langmuir, microwave probes and resonance fluorescence scattering compared in Q device

02 p0288 A69-12172

Dense plasma temperature determination by gamma ray resonance scattering

02 p0291 A69-12481

Bounce resonant scattering of particles trapped in geomagnetic field

03 p0503 A69-14014

Lyman-alpha observations of Venus by Mariner 5 analyzed, assuming resonance scattering of flux by hydrogen or deuterium atoms in Venus atmosphere

05 p0815 A69-16255

Bounce resonant scattering of auroral zone electrons, noting contribution to microbursts and mirror point diffusion

05 p0754 A69-16260

Differential cross section frequency dependence for resonant scattering of monochromatic light by dilute gas atoms [IEEE PAPER T-8]

05 p0776 A69-16328

Twilight resonance emissions due to atmospheric sodium, lithium and potassium, noting similarity of annual sodium and lithium twilight abundance variations [AFRL-69-0097]

06 p0918 A69-17494

Cyclotron- and bounce-resonance scattering of electrons trapped in geomagnetic field for pitch-angle scattering, noting whistler mode disturbances

07 p1208 A69-19367

Electrons resonance scattering by diatomic molecules from elastic and inelastic channel measurements in transmission

11 p1921 A69-24418

Excitation sources distribution in chromosphere from observed H alpha line contour, considering resonant scattering and internal excitation

15 p2683 A69-30509

Number and mass of sodium atoms in comet Ikeya-Seki 1965f head calculated from spectral observations, ascribing D lines to resonance scattering of photospheric radiation

15 p2685 A69-30526

Asymptotic formulas for X and Y functions for resonance radiation scattering in layer, analyzing Doppler absorption and line profiles

16 p2813 A69-32588

Plane wave scattering by multimode corrugated structure with H mode incidence, revealing theoretically scattering resonance as P type Wood anomalies

17 p2925 A69-33844

Polarized radiation resonance scattering in weak uniform magnetic field, using Monte Carlo method to trace and count photons

20 p3577 A69-38157

Monochromatic electromagnetic field in resonant medium, examining linear, incoherent and coherent nonlinear propagations and resonant scattering

21 p3769 A69-38382

Flashlamp-pumped dye laser for resonance scattering studies of upper atmospheric composition, describing laser construction and tuning

22 p3962 A69-40440

Quantum-mechanical theory of unimolecular kinetics and predissociation developed from generalized Fano theory of resonant scattering

22 p3986 A69-40724

RESONANCE TESTING

Ground and air resonance measured with gimbaled whirl tower stand for soft inplane matched stiffness rotor, discussing body inertia and speed limits [AIAA PAPER 69-205]

07 p1055 A69-19559

RESONANT CAVITIES
U CAVITY RESONATORS
RESONANT FREQUENCIES

Structural vibration problems of SA 330 helicopter from test flight data, discussing natural frequency displacement of blades and dynamic response improvement of structure

01 p0009 A69-10158

Natural vibration properties of elastic free-free body obeying Hooke law analysis from equilibrium and motion equations, determining Green tensor

01 p0167 A69-10323

Semiautomatic computer for determining torsional oscillation natural frequency in multimass in-line systems

01 p0035 A69-10596

Runway roughness effects on aircraft, formulating relationship between weight and resonant frequency through simple harmonic motion analogy

01 p0057 A69-11274

Discrete model for investigating beam vibration under various end conditions, determining natural frequency dependence on degrees of freedom

02 p0336 A69-11462

Theoretical prediction for modified and hybrid plasma resonances discrimination, noting sensor axis angle to geomagnetic field

02 p0241 A69-11731

Superposition of discrete number of collinear amplitude modulated harmonic oscillations

02 p0281 A69-12252

Liquid propellant space launch vehicles longitudinal modes natural frequency, discussing coupled engine-propellant supply system stability [AIAA PAPER 68-289]

02 p0335 A69-12393

Whirl instability of externally pressurized gas journal bearing with peripheral feeding holes, discussing analytical natural frequency of shaft bearing systems

02 p0254 A69-12426

Earth ionosphere resonator natural frequencies, considering diurnal variation and geomagnetic field eccentricity

03 p0422 A69-13512

Natural frequencies and mode shapes of coupled bending vibrations of pretwisted rectangular cross section beams determined by Rayleigh-Ritz energy method

03 p0529 A69-13989

Current oscillations or instabilities in semiconductor wafer with one electromagnetic mode and one carrier mode, investigating resonant frequencies

03 p0408 A69-14049

Temperature distributions, thermal stresses and natural frequencies of radial vibrations in thin circular cylindrical shells

04 p0675 A69-14704

Normal modes and natural frequencies of combined linear elastic structures resting on immovable base

04 p0678 A69-14870

Testing techniques and graphical presentation of test results to determine resonant frequencies and oscillation modes in sporting gliders

04 p0549 A69-15420

Natural frequencies controllability by induced thermal membrane stresses examined for thin disk

04 p0682 A69-15494

Frequency vs power absorption characteristics of deactivated klystrons, noting resonance frequencies and perturbation effect of electron beam loading

05 p0729 A69-15978

Blade natural frequency distribution around rotor and mechanical coupling between blades effects on flexing amplitudes under forced vibration [ASME PAPER 68-WA/GT-3]

05 p0837 A69-16139

Bending-torsion mode of rotating tapered twisted turbomachine blade, analyzing coupled flexural and torsional vibrations effect on natural frequency [ASME PAPER 68-WA/GT-6]

05 p0838 A69-16141

Resonant frequencies for beam type bending oscillations of thin walled rib-reinforced circular cylindrical shell freely supported at outermost ribs

05 p0841 A69-16204

Continuous and triggered audio frequency noise bands associated with ionospheric lower hybrid resonance frequency observed on OGO 2

05 p0754 A69-16257

Natural frequencies and modes of skew membranes obtained by Rayleigh-Ritz method

06 p0121 A69-17146

Electrostatic ionospheric waves excited around lower hybrid resonance frequency by high energy electrons

06 p0918 A69-17381

Resonant frequencies and fields in circular cylindrical microwave cavity containing cold uniform magnetoplasma dielectric

06 p0968 A69-17763

Radiation transfer in resonance lines and in recombination continuum in plasma, discussing frequency redistribution during reradiation and optically dense systems

07 p1188 A69-18282

Nonlinear interaction effects on frequency and polarization characteristics of dual polarization gas laser, discussing weak cavity anisotropies

07 p1145 A69-18473

Traveling wave microwave and optical resonators synthesis, determining design conditions for resonant frequencies

07 p1145 A69-18477

Natural frequency of fluid oscillations in complex pipelines

07 p1119 A69-18745

Natural modes and eigenfunctions of low amplitude oscillation determined by Ritz averaging method for ideal fluid with equilibrium surface in weak force field

07 p1119 A69-18746

Plasma frequency resonances observed by topside sounders interpreted as slowly propagating waves suffering oblique reflection, noting effects of nonhorizontal magnetic field

07 p1124 A69-18837

Open resonator reflection coefficient resonance curve compared with transmission coefficient, noting low Q waves excitation role

07 p1106 A69-19152

Resonance effects during piezoelectric interaction between charged drift wave and flexural wave in semiconductors with one sign current carriers

08 p1371 A69-19806

Shunted resonators on transmission line with asymmetrical response offering selectivity from resonance frequency standpoint

08 p1271 A69-19917

Gas laser emission natural frequency fluctuations spectral density measured by auxiliary heterodyne laser

08 p1326 A69-20540

Forbidden resonance line of Ca II in Arcturus from spectrograms at widely different times of year

08 p1392 A69-20558

Resonant frequencies, vibration modes and stress distributions for naturally vibrating plane wide blades of turbomachines

08 p1376 A69-20764

Rigid top mass effect on longitudinal response of model vehicle propellant tank, determining natural frequencies and forced asymmetric response

09 p1616 A69-21979

Helium-like ion resonance satellite lines in laboratory and solar plasmas, noting coincidence between solar satellite energy and energy level interval

09 p1598 A69-22158

Natural vibration frequency of circular orthotropic plate with variable rigidity

09 p1618 A69-22238

Vibration natural frequencies and mode shapes in cylindrical shells clamped at both ends, using fundamental differential equation under dynamic surface loading

09 p1618 A69-22274

Turbomachinery multiple pure tone noise associated with acoustic resonance of inlet cavities examined by narrow band filter tracking integer multiples of rotative speed

[ASME PAPER 69-GT-2]

09 p1572 A69-22509

Two mirror resonators, discussing curvatures formation and stability conditions to derive natural frequencies

09 p1520 A69-22680

Gyromotor flanges axial rigidity measuring methods based on axial deflection of flange or natural frequency of oscillating system

09 p1513 A69-22704

Resonance relations of rotational and orbital frequencies of solar system planets and satellites estimated for statistical significance

10 p1771 A69-22852

Rotatory inertia and shear deformation effects on natural frequency and bending mode shape in equations of motion of rotating turbomachine blade [ASME PAPER 69-VIBR-50]

10 p1804 A69-24148

Diakoptics applied in combination with perturbation method to determine natural frequencies of turbine buckets coupled by tie wires and/or cover [ASME PAPER 69-VIBR-57]

10 p1804 A69-24151

Central circular hole effect on fundamental frequency of rectangular fixed edges plate, discussing hole size, square plates, etc [ASME PAPER 69-VIBR-62]

10 p1805 A69-24156

Weight minimizing of circular disk subjected to behavioral and side constraints, considering resonance frequency of vibration and tolerances [ASME PAPER 69-VIBR-1]

10 p1700 A69-24159

Natural frequencies and mode shapes for longitudinal oscillations of liquid filled elastic circular cylindrical tank with flexible inverted conical bulkhead [ASME PAPER 69-VIBR-11]

10 p1806 A69-24165

Transverse beam natural vibration frequency evaluation method from Timoshenko theory

11 p1970 A69-24581

Characteristic frequencies approximation formula for gas bubbles in liquids compared with exact solutions

11 p1915 A69-24582

Nonlinear resonance formation during spatial nonlinear vibrations of solid bodies, establishing relations between vibration and excitation frequencies

11 p1919 A69-25167

Frequency characteristics of flexible compensated manifolds for aircraft engines, considering axial force

11 p1826 A69-25332

Natural frequencies and forms of small vibrations of ideal liquid in spherical container with weak force field, considering surface tension forces

11 p1875 A69-25484

Optimal design of structures with constraints on strength and natural frequency, developing steepest descent boundary value method

11 p1989 A69-25496

Gaseous He bubbles injection into liquid propellant launch vehicle fuel lines to reduce vehicle pogo oscillations by lowering feed system natural frequencies

11 p1967 A69-25498

Inplane and rotary inertia effects on free vibration frequencies of circular cylindrical shells eccentrically stiffened by orthogonal set of stringers and/or rings

11 p1992 A69-25520

Free vibration of discretely stiffened cylindrical shells with arbitrary end conditions programmed for digital computer, considering flexure, extension, torsion and nonsymmetric stiffener cross section

11 p1992 A69-25521

Resonant load impedance effects on Gunn diode oscillators output fluctuations, noting maximum power conditions

11 p1853 A69-25609

Lumped element construction technique involving crossed coils to reduce ferrite produced heat in resonance isolators, using substituted YIG

11 p1856 A69-25632

Ideal resonance problem with single critical term for case of libration solved by modified Poincare method, considering 24-hr satellite

12 p2152 A69-25800

Surface wave patterns of truncated conical shells with free edges attributed to mechanical properties

12 p2178 A69-26002

Linear vibrational systems natural frequencies and damping characteristics determined from system reaction to pulse effect

12 p2178 A69-26004

Free vibration fundamental natural frequency of shallow shell or dished plate with simply supported square boundary

12 p2179 A69-26211

Resonance circuit application to harmonic analysis of periodic functions on analog computer, considering transient period and sequential order

12 p2123 A69-26718

Natural frequencies of ring-stiffened thin walled cylindrical shell determined by partial differential equations of motion, allowing for eccentricity

12 p2184 A69-26810

Negative resistance parametric amplifier used as tracking filter, noting resonant frequency dependence on pumping frequency and input and idler circuits

13 p2225 A69-27183

Natural vibration modes of linearly tapered rectangular plates, approximating plate characteristic shapes with series of products of beam characteristic shapes

13 p2358 A69-27211

Self controlled vibration of elastically supported cylinder in fluid stream due to von Karman shedding, considering fluidelastic interaction, structural deformation and natural frequency

13 p2360 A69-27437

Vibration modes in four lowest natural frequencies of clamped rectangular plates with linear thickness variation, using Ritz method

13 p2361 A69-27442

Variational method for weak second order resonant interactions among waves with position and time varying amplitudes and phase angles

13 p2297 A69-27634

Frequency memory in cavity controlled Gunn oscillators, discussing loop gain and bandwidth dependence on oscillation mode and bias voltage

13 p2229 A69-27677

Subelement geometrical stiffness determined, considering complete element natural modes

13 p2362 A69-27838

Frequency equation for thickness effects on axisymmetric radial and rotatory vibrations of empty or fluid filled isotropic spherical shell

13 p2363 A69-28185

Dynamic characteristics of Clough-Tocher triangle for natural frequency of simply supported plate, noting bending elements

13 p2365 A69-28246

Oscillation in resonance tubes excited by subsonic jet, analyzing pressure and frequency for small Mach numbers by using wave diagram

13 p2370 A69-28630

Axisymmetric thermoelastic vibrations of infinite and finite cylindrical shells, determining natural frequencies and stress wave propagation

14 p2532 A69-28979

Semifree elastic membranes standing waves fundamental frequency, developing variational principle for first eigenvalue

14 p2535 A69-29365

Temperature behavior of resonant and antiresonant frequencies as function of electromechanical coupling and overtone order in piezoelectric resonators

14 p2421 A69-29542

Coupled magnetoacoustic waves in conducting paramagnetic fluid in resonance region due to mechanical and magnetic motions, considering dissipation

14 p2492 A69-29609

Bladed disk assemblies vibrational properties, discussing dynamic characteristics of system with pairs of close natural frequency modes under forced vibration

15 p2704 A69-30304

Natural frequencies and modes of complex structures composed of beam elements, considering hysteretic damping for response and transmissibility

15 p2706 A69-30431

Resonance measurement of power percentage in single spurious mode of overmoded waveguide, using back to back transducers and reflection at input

15 p2577 A69-30611

Natural oscillation frequency of gyrocompass mounted in torsional suspension, taking into account moments of inertia of sensitive element

16 p2791 A69-32282

Force resonance oscillations of one degree of freedom system with randomly time varying natural frequency

16 p2813 A69-32285

Saturn 5 longitudinal instability /POGO/ precluded by lowering S-1C stage propulsion system resonance below structural frequency

[AIAA PAPER 69-548]

16 p2868 A69-32658

Test stand for free oscillations frequencies and mode shapes of truncated conical shells of revolution with clamped edges and one free edge

17 p3058 A69-33202

Aerodynamic aspects of tail rotor design and structural dynamics of stiff inplane configurations, discussing blade natural frequencies

[AHS PAPER 342]

17 p3059 A69-33504

Natural gyrofrequencies of rigid rotor during slowing/stopping at high forward speed, using simple approximation

17 p2899 A69-33507

Rb 87 vapor laser output power dependence on magnetic field strength and resonator detuning, discussing laser and atomic transition frequency tuning

17 p2983 A69-33694

Automatic tuning of superconducting cavity resonant frequency using optical feedback, discussing phase error processing and frequency deviation

17 p2937 A69-33781

Thin walled cantilevered fiberglass reinforced shafts damping characteristics dependence on natural vibration modes and fibers orientation

17 p3065 A69-33938

Rotating shafts impact damping efficiency increaseable by providing proper clearance to reduce shaft stress in critical resonance frequency region

17 p3066 A69-33946

Polarization, frequency and energy characteristics of lasers with resonators containing polarization transforming elements

17 p2983 A69-33967

Natural frequencies and vibration modal shapes of asymmetrical airfoil blades analyzed by differential equations of motion, noting flexure coordinates center variations effect

17 p3067 A69-34053

Elastic beam-plate vibration natural frequency and dynamic instability in transverse static or oscillating magnetic field

[ASME PAPER 69-APM-B]

18 p3215 A69-34400

Forced vibration testing of complex continuous systems, demonstrating suppression of certain resonant frequencies due to laboratory techniques

18 p3114 A69-34422

Critical speeds of high speed turbine rotors running in friction bearings determined by varying natural frequencies of rotor and supports

18 p3147 A69-34545

Supported shafts natural vibration frequencies determination by averaging shaft parameters, noting suitability in HF ranges

18 p3147 A69-34546

Resonance effects between H levels by induced electric dipole transitions, using spatially periodic potential barriers

18 p3179 A69-35488

Transverse oscillations of shallow multilayer shells, using tangential-stress distribution law in determining natural oscillation frequencies in single and sandwich layer panels

19 p3435 A69-35842

Natural oscillations frequency spectrum of turbomachine impeller blades subjected to random variations determined with frequency distribution function obtained by moments method

19 p3436 A69-35844

Natural frequencies and mode shapes of vibration of cylindrical shells orthogonally stiffened with rings and stringers

[AIAA PAPER 68-349]

19 p3437 A69-35948

Natural frequencies of thin oblique angled isotropic plates, discussing closed form solution to differential equations

19 p3438 A69-36312

Combined resonance transition in n-type InSb by IR radiation, plotting intensity against magnetic field for different carrier concentrations to infer band structure

19 p3385 A69-36520

Gallium arsenide junction lasers operating above threshold, showing resonant modes dependence of steady state gain function and frequency dependence of spatial gain distribution

19 p3338 A69-36691

Transient oscillations in ammonia maser oscillator observation based on switching achieved by signal injection into cavity at molecular resonance frequency

19 p3339 A69-36825

Clamped skew plates natural frequencies analysis using Galerkin method, expressing deflections as double series of beam characteristic functions, stating eigenvalues and eigenvectors

20 p3621 A69-37201

Mechanical loss factors calculated by approximation formula from resonance curves of Voigt-Kelvin and Maxwell models

20 p3623 A69-37435

Rocket observations of VLF ionospheric resonances, noting artificial stimulation of detectable amplitude noise with cut-off at low hybrid resonance frequency

21 p3671 A69-38356

Ionospheric lower hybrid resonance /LHR/ noise discovered by Alouette 1, describing possible mechanisms for origin

21 p3702 A69-38358

Natural oscillations of end-hinged solid beam with variable parameters and concentrated masses, determining natural frequencies

21 p3833 A69-38575

Asymmetrical oscillations of cylindrical shell with elastic bottom containing liquid, discussing liquid level influence on natural oscillation frequencies

21 p3834 A69-38718

Free vibration of thin cylindrical shells with thickness discontinuity, considering natural frequencies and mode shapes dependence on thick/thin ratio

21 p3836 A69-38984

Acoustoelastic interaction effects of sonic bangs on natural frequencies response of large windows backed by closed cavity

21 p3836 A69-38988

Response of three level particles system with equidistant spectrum under resonant action of acoustic and electromagnetic pulses sequence with different frequencies

21 p3737 A69-39068

Natural frequency equations for torsional vibration of fixed/fixed and fixed/ simply supported uniform thin walled beams of open section based on energy method

22 p4040 A69-39935

Lasing properties of Ni-doped GaAs diodes evaluated by plotting resonance, mode amplitudes and frequencies for various bias currents and external capacitance

22 p3912 A69-40606

Natural frequency of thin plate subject to cylindrical bending, analyzing panel flutter by three mode approximation for large buckling deflection

22 p4045 A69-40821

Resonance frequency behavior of waveguide cavity with evanescent air gap symmetrically loaded with dielectric

22 p3900 A69-40925

Natural frequencies of N open dielectric waveguides system, obtaining fields expressions and dispersion equation for propagation constants

22 p3901 A69-40954

Buckled rectangular plates with constrained edges, analyzing natural frequencies as basis for supersonic panel flutter analysis

22 p4046 A69-41049

Polycrystalline ferroelectrics dielectric dispersion region in decimeter-centimeter wavelength range using waveguide resonance method employing wideband strip line

22 p3997 A69-41167

Magnetospheric natural toroidal oscillation periods solved by expression from perturbation method given by Landau and Lifshits where WKB method inapplicable

23 p4157 A69-41863

Waveguide Y-circulator parameters thermal stability equation, considering temperature, magnetization level and magnetic field resonance effects on tuning frequency

23 p4123 A69-41951

Combination resonance and instability regions of second type for parametrically excited oscillations with nonlinear /cubic/ damping

23 p4230 A69-42107

Rosman I reflector antenna for collecting data from earth orbiting satellites, discussing dynamic analysis of structural response to natural frequencies

23 p4231 A69-42133

Book on interaction between oscillatory systems and energy source of limited capacity, examining stability and resonance phenomena

23 p4170 A69-42166

Natural vibrational frequencies of uniform thin elastic isotropic flat plates, investigating rectangular and parallelogram plates with various edge conditions

23 p4233 A69-42348

Electromagnetic scattering by small plasma ellipsoid moving in vacuum through external steady magnetic field, analyzing resonance phenomena

24 p4282 A69-42979

RESONANT VIBRATION

Acoustic resonance excitation in axial flow compressor annulus by wake shedding from blades

01 p0142 A69-10058

Damping capacity and resistance to resonance fatigue of titanium and aluminum based steels and alloys

03 p0443 A69-13025

Single and double resonance in system of coupled nonlinear differential equations describing vibration phenomena in mechanical and similar systems

03 p0527 A69-13748

Perturbed nonlinear systems with many degrees of freedom, analyzing resonant oscillatory and rotary motions

04 p0631 A69-15536

Natural longitudinal single frequency oscillations of system of n material points connected in series by nonlinear elastic threads and with energy dissipation

05 p0832 A69-15687

Resonant beam tuned vibration damping device, noting weight saving potential

[ASME PAPER 68-WA/GT-2]

05 p0837 A69-16138

Orthogonality of natural oscillation modes of shells of arbitrary geometry, using equations of motion from Vlasov engineering moment theory
05 p0840 A69-16200

Resonance particle effects on flute oscillation kinetic stability when resonance particles drift under influence of magnetic field inhomogeneity
06 p0965 A69-17516

Resonant frequencies, vibration modes and stress distributions for naturally vibrating plane wide blades of turbomachines
08 p1376 A69-20764

Dynamic tests of mechanical properties of polyamide Tarlon X-A using free and resonant vibrations methods
09 p1528 A69-21496

Vibratory acceleration limiting equipment attachment for resonance conditions, utilizing attachment stiffness reduction above predetermined value
[ASME PAPER 69-VIBR-23]
10 p1806 A69-24170

Multiparameter optimum damping for harmonically excited linear stable strictly dissipative n degrees of freedom system, locating multivariable saddle points
[ASME PAPER 69-VIBR-42]
10 p1807 A69-24180

Nonlinear large amplitude vibrations of flexible beam with pinned ends supported simply on rigid base noting frequencies, modes, waveforms and stress distribution
[ASME PAPER 69-VIBR-43]
10 p1807 A69-24181

Nonlinear resonance formation during spatial nonlinear vibrations of solid bodies, establishing relations between vibration and excitation frequencies
11 p1919 A69-25167

Cylindrical propellant tanks dynamic stability and parametric resonance, analyzing axial preload, liquid depth, top impedance and ullage pressure by Donnell theory
11 p1989 A69-25499

Natural oscillations excitation in magnetoactive plasma by modulated electron beam ascribed to Doppler or Cerenkov effects
11 p1932 A69-25535

Natural oscillations excitation instabilities by modulated ion beams in magnetoactive plasma ascribed to anomalous Doppler effect
11 p1932 A69-25536

Resonant vibrational energy transfer between specific mode of carbon dioxide and N molecules at high temperatures, monitoring IR emission
12 p2131 A69-25984

Helmholtz resonance in rocket injectors as function of frequency response of interaction between chamber pressure and dissolved gas-fuel injection flow rate
12 p2148 A69-26806

Resonance tube excitation from energy depletion in central part of subsonic jet supplying tube
13 p2247 A69-27738

Nonstatic gyroscope nonlinear oscillations caused by swaying of synchronous gyromotor rotor
13 p2264 A69-28438

Oscillation in resonance tubes excited by subsonic jet, analyzing pressure and frequency for small Mach numbers by using wave diagram
13 p2370 A69-28630

Parametric resonance motion in viscous fluid column in communicating vessels during vertical oscillations, calculating critical accelerations over viscosity range
14 p2432 A69-29628

Oscillations analysis in quasi-linear autonomous system with two degrees of freedom, using point mapping for case of resonance
15 p2653 A69-31193

Self excited vibrations of rotors supported in gas bearings from analyzing solutions to equations of rotor motion
16 p2875 A69-32250

Nonlinear vibrations of mechanical two degrees of freedom system during resonance described using Krylov-Bogoliubov method to obtain differential equations solutions
16 p2875 A69-32255

Plane oscillations of liquid in rectangular elastic vessel determined to obtain frequencies and mode shapes of natural oscillations from velocity potential boundary conditions
17 p2950 A69-33200

Near resonant oscillations of warped turbine or compressor blades, discussing stress-strain relations
17 p3064 A69-33918

Axisymmetric bending oscillations of thin circular plates of constant thickness with allowance for energy

dissipation in material, analyzing resonance and phase amplitude characteristics
17 p3064 A69-33919

Random excitations effects on vibrating nonlinear single degree of freedom system, statistically estimating resonance mode probability
18 p3171 A69-34554

Resonance effects in finite hollow cylinder immersed in ideal compressible fluid and exposed to compression wave
18 p3215 A69-34567

Machine parts vibration attenuation, discussing input vibration reduction, resonance avoidance, damping, vibrating parts strengthening and shakers
18 p3148 A69-34619

Dynamic instability regions of parametric resonance of cylindrical shells with curved generating lines under axial and radial pressure
18 p3223 A69-34979

Resonant oscillations amplitude of nonlinearly elastic hinged cylindrical shell determined with cubic equation taking into account Hooke law, linear stresses, shell theory displacements, etc
19 p3435 A69-35843

Steady resonance operation modes of nonlinear oscillatory and rotational systems described by differential equations with deviating argument, using averaging procedure
19 p3374 A69-36469

Rotational motion bounds of satellites exhibiting parametric resonance under small librations in orbital plane
20 p3617 A69-37191

Passive helicopter rotor isolation for alleviating rotor induced vibration, using dynamic antiresonant vibration isolator
20 p3463 A69-37807

Spacecraft natural vibrations analyzed using point transforms with allowance for control systems imperfections
21 p3826 A69-39637

Nonlinear system oscillations analysis based on small parameter method and difference equations, including resonant case and stability criterion for periodic solutions
22 p3980 A69-40108

Natural torsional-flexural vibrations of bars with single symmetry, using matrix equations of equilibrium, displacements and natural coupled vibrations
22 p4043 A69-40456

Turbomachinery periodic structures design to improve tolerance to inflow distortion and resonant oscillatory flows, considering large amplitude pressure waves propagation
[SAE PAPER 690388]
23 p4201 A69-41666

Magnetospheric natural toroidal oscillation periods solved by expression from perturbation method given by Landau and Lifshits where WKB method inapplicable
23 p4157 A69-41863

RESONATORS

NT CAVITY RESONATORS

NT MULTIMODE RESONATORS

Pulsar radiation origin related to electromagnetic wave distortion during propagation through resonant media
01 p0149 A69-10272

YIG single crystal resonator tuning of Gunn diode in coaxial line circuit
01 p0042 A69-10320

Perfect piezosemiconductor resonator /phaser/ with CdSe/CdS/ crystal, discussing vibration excitation in wurtzite type crystal in electric field of electron drift
03 p0431 A69-13930

Magnetic retuning of resonator with helical electron flux /gyromonoton/ in starting and prestarting modes
03 p0407 A69-13979

Errors of wavemeter employing open resonator with spherical mirrors
03 p0407 A69-13983

Circuit properties of microwave dielectric resonators, discussing mode identification, resonant frequencies, coupling control, loaded Q, frequency tuning and periodic arrays
04 p0575 A69-14750

Microwave Fabry-Perot resonator for anisotropic plasma diagnostics in presence of static magnetic field
04 p0635 A69-14757

Varian cesium resonator as prime frequency testing standard with accuracy dependent on electronic system for quartz slaving
04 p0600 A69-15068

H resonator for charged particle beams combination at output of double beam linear accelerator
05 p0727 A69-15639

Resonance rotation of polarization plane in circular waveguide with ferrite resonator
05 p0718 A69-15640

Mode suppression by mixed polarization in Michelson interferometer type of optical resonator
05 p0776 A69-16330

Selective resonators for laser emission spectral structure control, proposing dispersion power increase by inserting telescopic system
05 p0777 A69-16371

Mechanically and electronically tunable resonator for driving IMPATT and Gunn diodes
07 p1097 A69-18455

Open resonator reflection coefficient resonance curve compared with transmission coefficient, noting low Q waves excitation role
07 p1106 A69-19152

Annular traveling wave resonator for feedback in resonance particle accelerator of smooth waveguide
07 p1107 A69-19160

Shunted resonators on transmission line with asymmetrical response offering selectivity from resonance frequency standpoint
08 p1271 A69-19917

Atomic clocks frequency standards, discussing masers, atomic beam resonators and gas cells and various applications
09 p1501 A69-22598

Waveguides and resonators design by solving scalar problem for eigenvalues of elliptic operator
09 p1469 A69-22626

Input admittance response characteristics and input susceptance and input conductance of resonant reactive modulator with varactors and nonlinear losses
10 p1665 A69-24066

Resonators made of YIG single crystals exhibiting lowest linewidth in ferromagnetic resonance at microwave frequencies
11 p1855 A69-25627

Microwave directional filter using ring resonator and couplers to obtain low transmission loss and center frequency tuning
13 p2226 A69-27187

Book on open resonators and open waveguides
14 p2419 A69-29316

Temperature behavior of resonant and antiresonant frequencies as function of electromechanical coupling and overtone order in piezoelectric resonators
14 p2421 A69-29542

Disk and transmission line microstrip resonators radiation, measuring fractional amount of radiated power
16 p2760 A69-31946

H resonator for charged particle beams combination at output of double beam linear accelerator
16 p2762 A69-32497

Resonance rotation of polarization plane in circular waveguide with ferrite resonator
16 p2762 A69-32498

Radiation dynamics of GaAs injection semiconductor laser, plotting spike period dependence on resonator length
19 p3337 A69-36535

Electromagnetic waves emission intensity in one dimensional resonator, allowing for wave interference effects
22 p3966 A69-41172

Recursion formula for multiwave interferometer derived, with allowance for multiwave interference, to calculate resonant circuit maxima and minima
23 p4165 A69-41729

Double cellular surface geometry effect on dispersion and coupling impedance of two dimensional periodic resonator slow wave structure
23 p4140 A69-42048

RESOURCES

NT EARTH RESOURCES

NT EXTRATERRESTRIAL RESOURCES

Avionics in forest resource inventories management, noting design of radar altimeter for low level aerial photography
01 p0080 A69-10352

Earth resource satellites, discussing world ground station network for data reception and information dissemination and training and research center
[UN PAPER 68-95529]
06 p0917 A69-17067

RESPIRATION

NT HIGH ALTITUDE BREATHING

NT PRESSURE BREATHING

Changes in blood circulation, external respiration and gas exchange rates in humans during prolonged hypodynamia
03 p0377 A69-14204

High oxygen concentration influence on animal organisms noting respiration, pulmonary gas exchange, hypoxia, brain phosphorylation, immunological indices and morphological structure of rats and mice
05 p0709 A69-16512

Weightlessness effects on human external respiration, gas exchange and energy expenditure indices during flight of Voskhod 2
12 p2020 A69-26563

Glycolysis control by respiration in human leukocytes with and without Pasteur effect conditions
15 p2555 A69-30413

High oxygen concentration influence on animal organisms noting respiration, pulmonary gas exchange, hypoxia, brain phosphorylation, immunological indices and morphological structure of rats and mice
18 p3095 A69-34731

Chronic hypoxic hypoxia on oxygen-hemoglobin dissociation curve and respiratory gas transport in man, considering altitude residents and heart and lung diseased patients
21 p3650 A69-38383

Amlyl nitrite inhalation effects on cardiovascular system, discussing tachycardia and carotidograms
21 p3661 A69-39278

Respiratory gas exchange during workloads, comparing values for ventilation, oxygen uptake and carbon dioxide output measured in air and in helium-oxygen mixture
22 p3891 A69-40221

Respiration effects on heart rhythm emphasizing direct mechanical influences
23 p4097 A69-42093

Oxygen exchange in Scenedesmus and Chlorella as function of carbon dioxide, compensation point, Hill activity and photorespiration, using mass spectrometry
23 p4099 A69-42528

RESPIRATORS

Bird respirator function at simulated high altitude, noting adequate support in case of rapid decompression
14 p2406 A69-29290

Protective filter for inspiration valve of oxygen masks in high performance aircraft, reducing respiratory volume exchange with given pressure amplitude
17 p2916 A69-33773

RESPIRATORY DISEASES

NT ASTHMA
NT EMPHYSEMA
NT INFLUENZA
NT PNEUMONIA

Respiratory difficulties from breathing through mask compared with changes in respiration resulting from obstruction caused by physical respiratory disorder
17 p2916 A69-33774

Airway distensibility effect on elastic behavior of human lungs, noting compliance and resistance at different breathing frequencies for diseased lungs
22 p3873 A69-40205

RESPIRATORY IMPEDANCE

X ray study of biomechanics of respiratory act under long term acceleration stresses
05 p0710 A69-16522

Respiratory difficulties from breathing through mask compared with changes in respiration resulting from obstruction caused by physical respiratory disorder
17 p2916 A69-33774

X ray study of biomechanics of respiratory act under long term acceleration stresses
18 p3096 A69-34741

RESPIRATORY PHYSIOLOGY

Respiratory pressure recording with tracheal cannulae applied on cats to obtain pneumograms and oscillograms of respiratory neurons
07 p1131 A69-18538

Euglena gracilis grown heterotrophically, investigating respiratory physiology as function of glucose, acetate or ethanol growth supporting carbon source
10 p1647 A69-24186

Lung ventilation mechanics affecting respiration in hyperbaric environment during deep diving, stressing biological necessity of equal pressure respiration
13 p2215 A69-28598

Compensative adaptational reactions to weightlessness, discussing blood supply to thorax area, external respiration, gas exchange and energy loss during parabolic and orbital flights
17 p2909 A69-33384

Ventilatory response to hypoxia and hypercapnia in hypothermic anesthetized dogs, noting decreased sensitivity of central chemoreceptors to carbon dioxide
22 p3885 A69-40977

Pulmonary capillary blood flow, stroke volume and heart rate measured in tilted and supine subjects during respiration, discussing tourniquets and intravenous atropine effects
23 p4082 A69-41445

Human physiological responses to angular acceleration during breath holding, Mi, Valsalva and Mueller respiratory maneuvers in hollow spherical simulator
23 p4102 A69-41679

Analog computer used to correct body plethysmographic chamber signal distortion due to inspired/expired air temperature and humidity differences
23 p4111 A69-42081

Human heart rate changes resulting from diving and breath holding exercises
23 p4095 A69-42083

Respiratory effects of body temperature changes separation from blood osmolality changes in dehydrated man
23 p4097 A69-42094

Aircraft passenger cabins pressure safety limits estimating factors, discussing human respiratory gas exchange mechanism, pressure drop and smoking effects, etc
24 p4269 A69-43411

RESPIRATORY RATE

NT HYPOVENTILATION

Xenon, krypton, nitrogen and nitrous oxide effect on respiration rate of rat liver slices at various oxygen partial pressures
03 p0375 A69-14069

Cosmonauts cardiac activity and respiration changes during physical exertion in orbital flight on Voskhod spacecraft
03 p0377 A69-14196

Transient changes in oxygen consumption, carbon dioxide elimination and respiratory quotients during and after induced hypoxia to rabbits
06 p0876 A69-18026

Astronauts increased heart beat, respiration rates and higher blood pressure subsides during repeated weightlessness tests
07 p1061 A69-18582

Pneumograms and EKG used to determine heart beat, respiration rates and systolic index of cosmonauts during Voskhod 2 flight
07 p1062 A69-18585

Hamsters responses to helium-oxygen and nitrogen-oxygen at ambient temperatures, comparing respiration rates, weights and body temperatures
10 p1646 A69-23564

Heart rate and respiratory response correlations in men during surface and underwater work, showing reasonable approximations of workload in surface-equivalent terms
14 p2406 A69-29293

Photosynthesis and respiration rate in vegetables in controlled temperature, humidity, illumination levels, carbon dioxide and oxygen contents
17 p2912 A69-32933

Vestibular reactions in rats under hypothermal conditions by measuring postrotatory nystagmus beats number and duration, respiration rates and rectal temperature
17 p2906 A69-32934

Pulmonary mechanics during zero gravity maneuvers, noting decrease in flow rate and increase in expiration time without decrease in vital capacity
17 p2909 A69-33181

Respiratory gas exchange in exercise during He-O breathing, analyzing effects on O consumption, carbon dioxide production and minute ventilation of human subjects
17 p2910 A69-33751

Coriolis acceleration effect on vestibulo-vegetative and vestibulo-somatic reflexes of humans subjected to forward tilting, noting pulse and respiration rates
20 p3472 A69-37259

Motion sickness prophylaxis for rabbits subjected to rotation, investigating effects of adrenalin, ephedrine, sympatholytin, piperoxane and pyridoxyphene on nystagmus and respiration
20 p3472 A69-37265

Airway distensibility effect on elastic behavior of human lungs, noting compliance and resistance at different breathing frequencies for diseased lungs
22 p3873 A69-40205

Regression relations for energy expenditure in work predicted from heart rate and pulmonary ventilation in volunteers carrying loads upstairs
22 p3891 A69-40220

Venturi low resistance flowmeter for ventilatory measurements during rest and exercise on humans, not-

ing suitability for analog integrator computation of tidal volumes
22 p3894 A69-40979

Lobeline effect on oxygen pressure in giantocellular nucleus of medulla oblongata and respiration rates of dogs recorded automatically
22 p3888 A69-41273

Severe heat stress effects on respiratory frequency, rectal temperature, blood gases and pH of conscious dog
23 p4081 A69-41432

Pulmonary mechanics during zero gravity maneuvers, noting decrease in flow rate and increase in expiration time without decrease in vital capacity
23 p4089 A69-41825

Albino guinea pigs respiration rates and ear skin histology after exposures to coherent ruby laser light
24 p4270 A69-42578

RESPIRATORY REFLEXES

Respiratory disturbances relationship to experience and attitudes toward gas anesthesia and response to different types of face mask
03 p0378 A69-12884

Irreversible blunted respiratory response to ventilation in high altitude natives, considering hypoxic and hypercapnic stimuli
12 p2018 A69-26130

Transient ventilatory response to breaths of nitrogen at rest and during exercise in high altitude and sea level natives
12 p2019 A69-26131

Peripheral chemoreceptor carbon dioxide sensitivity, measuring human respiratory response to large carbon dioxide breath in oxygen at sea level and high altitude
22 p3890 A69-40207

Heart rate respiratory control model with inclusion of pressoreceptor feedback, considering posture effect in transient envelope alteration
22 p3894 A69-41202

Thematic apperception test /TAT/ cards for assessing attitudes in naval recruiting, respiratory responses during ejections and aviation psychology
23 p4112 A69-42365

RESPIRATORY SYSTEM

NT LUNGS NT TRACHEA

Respiratory system control processes hypotheses experimental verification
01 p0019 A69-10209

Reactions of respiratory and cardiovascular system of dogs in biocompartment of ballistic missiles, discussing biopotential of myocardium, arterial pressure, etc
07 p1060 A69-18576

Statistical correlation between cardiovascular activity and respiration dynamics of cosmonauts during orbital flight, discussing heart beat and respiration rates
07 p1061 A69-18584

Pulmonary capillary gas exchange and venous admixture model and inclusion into respiratory system model, discussing pressure and concentration gradients, pathological effects, etc
07 p1068 A69-19482

Pathological changes in respiratory and cardiovascular systems of white rats due to various levels of hyperoxia
10 p1646 A69-23577

Respiratory system control processes hypotheses experimental verification
14 p2408 A69-28745

Hypoxia reaction elimination in human beings by repeated exposure to hypoxia, discussing nitrogen inhalation experiments and adaptive behavior of respiratory system
23 p4214 A69-41789

Neural integration of cardiorespiratory responses and suprabulbar control during arterial hypoxemia in rhinencephalic thalamic pontine rabbits
24 p4258 A69-42635

Steady state model for human respiratory system analysis, discussing controlled and controlling parts
24 p4276 A69-43272

RESPIROMETERS

Respiratory pressure recording with tracheal cannulae applied on cats to obtain pneumograms and oscillograms of respiratory neurons
07 p1131 A69-18538

Pyroelectric conductor sensors permitting continuous measuring and recording of air inhaled during chosen time intervals
15 p2559 A69-31230

Lightweight sensor for telemetering oxygen partial pressure in respiration air
15 p2559 A69-31231

RESPONDERS

U TRANSPONDERS

RESPONSE BIAS

Diffusion current detection method applied to reverse biased volt-ampere characteristics of Ge diodes, noting surface leakage role
07 p1105 A69-19007

RESPONSE TIME [COMPUTERS]

Response time estimation for control system with constrained phase coordinates, determining conditions for optimal control problem solution
21 p3769 A69-38568

RESPONSES

NT DYNAMIC RESPONSE
NT GALVANIC SKIN RESPONSE
NT HEMODYNAMIC RESPONSES
NT MODAL RESPONSE
NT PHYSIOLOGICAL RESPONSES
NT TRANSIENT RESPONSE

Photomultiplier geometry without use of light pipes for uniform response from large area single and double sheet plastic scintillation detectors
03 p0428 A69-13107

REST

U BED REST

RESTARTABLE ROCKET ENGINES

Liquids in zero g environment for controlling position of propellant within tank for restart of rocket engine, noting minimum energy principle applications
11 p1944 A69-25599

Spontaneous reignition predictions for solid restartable rocket motors with solid propellant combustion terminated by liquid quenching
[AIAA PAPER 69-444] 16 p2842 A69-32695

RESTORATION

Restoration processes in *Chlorella pyrenoidosa* to distinguish intense and less intense gamma ray irradiations
22 p3878 A69-40792

RESTRAINTS

U CONSTRAINTS

RESTRICTIONS

U CONSTRUCTIONS

RESULTANTS

Algorithms for polynomial resultants computation, considering extraneous factors, truncation errors, memory and computing speed
06 p0892 A69-17884

RETARDERS [DEVICES]

Cost effective aerodynamic deceleration and retardation systems for military and space programs, noting technical research and development areas in need of advancement
03 p0364 A69-13854

Hydrostatic bearings, hydraulic drive system and hydraulic braking system for radio telescope with 2550 tons moving weight
[ASME PAPER 68-WA/PEM-2] 05 p0743 A69-16147

RETENTION [PSYCHOLOGY]

Holographic theory of visual memory behavior, discussing human tests in situation of prompted visual recall
01 p0083 A69-10985

Mathematical model for information processing of biological memory as cybernetic system
23 p4110 A69-41982

RETICLES

Encoding and decoding in IR tracking system, analyzing chopping rotating FM reticle pattern
19 p3268 A69-36058

RETICULOCYTES

Reticulocyte count comparison on trained and sedentary college male subjects before and after strenuous exercise, noting role in oxygen uptake
21 p3654 A69-38907

RETINA

NT FOVEA

Retinal burns from intense light sources using rabbit eyes as function of irradiation rate, exposure time and image size
02 p0204 A69-12496

Retinal lacerations and detachment in jet pilots, discussing pathogenesis, diagnosis and surgical reattachment methods
05 p0710 A69-16630

Biological effects of laser radiation on mammalian retina, noting thermal injury
[AGARDOGRAPH-111] 08 p1266 A69-20676

Retinal burn resulting from prolonged viewing of sun, laser or thermonuclear explosion, noting effects on choroid, receptors and pigment cells
08 p1267 A69-20680

Multilayer retina model with lateral couplings for visual pattern recognition, noting applications to data processing
19 p3260 A69-35898

Transient electrical responses from retinas, discussing visual pigment role in visual excitation, photochemistry, etc
19 p3258 A69-36377

Live retinal photoreceptors studied by low angle X ray reflection, proposing electron density model
22 p3871 A69-40057

Electroretinogram a-wave relationship to early inhibition and excitation of retinal ganglion cells produced by flash superimposition in rabbits
22 p3878 A69-40836

Squirrel monkey retinas spectral stimulation, determining differential color responses reaching striate and prestriate cortex
22 p3879 A69-40844

Psychopharmacological drug effects on retinal neuron activity in cats measured by microelectrodes, noting spontaneous activity decrease
22 p3879 A69-40846

Statistical critique of Polyak values for tangential dendritic spread of primate retinal neurons
22 p3880 A69-40848

Human peripheral retina contrast sensitivity determined by measuring psychophysically for sinusoidal grating target describing luminance effects
22 p3882 A69-40870

Retinal topography relation to blue arcs phenomenon, assessing disparity in photoreceptor location and associated neurones for analysis of critically sited plots
22 p3882 A69-40872

Retinal mechanisms determining visual band movement thresholds obtained by manipulation of retinal locus, luminance, arc length and spectral distribution of moving stimulus
22 p3883 A69-40879

Cat intraretinal DC component and b-wave separation based on sensitivity to visual stimuli, discussing electroretinogram recorded with microelectrodes
22 p3883 A69-40881

Arterial occlusion effects on retinal structure in cats, describing degrees of cell degeneration
22 p3884 A69-40883

Cerebral and retinal capillary permeability to ions in rats analyzed by electron microscope using Prussian blue reaction
23 p4081 A69-41433

Pigeon visual adaptation to flickering light, attributing ERG b-wave postadaptation rebound to retina bipolar cells inhibition
23 p4084 A69-41463

Optic nerve spikes elicited by acetylcholine application on isolated perfused retina of frog, varying response by prostigmine and atropine
23 p4084 A69-41465

Rhythmic wavelets electroretinogram recorded from rabbit retina in vitros preparation indicating dominant relatively low voltage waves compared to in vivos waves
23 p4101 A69-41471

Retinal eccentricity effects on horizontal-vertical illusion magnitude, considering eye flattening and astigmatic properties
24 p4263 A69-43117

Selective g-force application as centrifugation treatment for retinal detachment, applying minimal load on circulation and optimal load on retina
24 p4268 A69-43405

RETINAL ADAPTATION

NT DARK ADAPTATION
NT LIGHT ADAPTATION

Visual sonar target detectability probability function of retinal position and brightness contrast
02 p0203 A69-12218

Human visual systems ability to encode retinal images produced by different size objects
03 p0369 A69-13359

Stiles-Crawford effect measurements before and following eye movements to determine retina shearing during eye movements
15 p2555 A69-31035

Nocturnal and diurnal monkeys spectral sensitivity functions determined from simultaneous recordings of light-evoked cortical and retinal responses
22 p3882 A69-40867

Tritanope and trichromat experiments for parafoveal visual response of tritanope, measuring spectral sensitivity and absolute threshold values
22 p3882 A69-40869

Blue cone mechanism contribution to mesopic function in producing Purkinje shift with luminance decrease, measuring sensitivity by flicker technique
22 p3883 A69-40880

High intensity flash effects on local electroretinogram, late receptor and slow potentials and ganglion cell activity in area centralis of cat retina
22 p3883 A69-40882

Human electroretinogram [ERG] physiological variations as function of stimulation energy and wavelength
22 p3884 A69-40884

Response characteristics of human visual mechanisms sensitive to motion while varying adaptation stimulus contrast to control visual effectiveness
22 p3884 A69-40887

RETINAL IMAGES

Analytical model for frog retinal bug detector cell to make possible signal measurement in frog optic fibers
07 p1070 A69-18383

Small eye movements measurement and retinal image stabilization based on tracking edge of blood vessel in optic disk
09 p1446 A69-21908

Digital simulation of biological model for visual images classification derived from human visual system aspects
17 p2911 A69-34094

Model for lateral inhibitory interaction in human retina, providing systematic account of simultaneous brightness contrast
21 p3653 A69-38898

Target distance and direction monocular estimates with stabilized and nonstabilized retinal images, finding eye movements not improving spatial judgment accuracy
22 p3878 A69-40838

Eye optical system spherical aberration measured by knife-edge method derived from Foucault test, investigating retinal image quality
22 p3882 A69-40873

Visual ellipse phenomena excitation by sinusoidal stimulating currents, noting frequency effects on ellipse shape
23 p4095 A69-42077

RETRACTABLE EQUIPMENT

Electromechanical retracting pedestal for solid target injection into vacuum system and ionization by focused Q switched laser beam
03 p0439 A69-13105

Small and full scale model tests for feasibility of retracted rotor aircraft for high speed flight
[AIAA PAPER 69-219] 07 p1055 A69-19550

Solar cell retractable array for spacecraft multikilowatt power generation
19 p3254 A69-35711

Hydraulic power pack for automatically raising or lowering landing gear in small aircraft
20 p3467 A69-38183

RETRACTABLE LANDING GEAR

U LANDING GEAR

RETRIEVAL

U DATA RETRIEVAL
U INFORMATION RETRIEVAL

RETROACTION

U RETROTHRUST

RETROFIRING

Flow field for single or multiple jets firing forward into oncoming supersonic free stream, noting effect of forward extending cylindrical body
[AIAA PAPER 69-69] 06 p0864 A69-18164

RETROREFLECTION

Van Atta array reflector retrograde effect, studying influence of transmission line length, interelement spacing and line-dipole matching on incident reflected radiation phase correlation
17 p2929 A69-33878

Rereflected shock waves behind tapered shock tube section indicated by shock wave detectors, microwave absorption and optical emission measurements
18 p3085 A69-34474

Distance measuring method limitations for modulated CW laser determined by laser transmitter receiver in conjunction with retroreflector target fixed position
21 p3739 A69-39457

Laser range measurement from earth to lunar retroreflector to study earth tipping and gravitational constant secular decrease
22 p3960 A69-40190

Redirection of time varying signal between specified points by arbitrarily spaced antenna array elements with condition involving time delays for validity of retrodirection
23 p4136 A69-41580

Retroreflector and Scotchlite object images obtained in long range holography with Q switched ruby laser, noting atmospheric seeing conditions
23 p4167 A69-42184

Microcircuit phased array electronic countermeasures system design and hardware techniques for aerospace applications, analyzing adaptive, retrodirective and combination array systems
24 p4287 A69-43110

Lunar laser beam retroreflection observations, showing agreement with predicted ephemeris and signal strength
24 p4384 A69-43197

RETROSEQUENCING

U RETROFIRING
U SEQUENTIAL CONTROL

RETROTHRUST

Retrograde motion of electric arcs in transverse magnetic fields, using multifluid equation to predict inclination and properties
[AIAA PAPER 69-45] 06 p0971 A69-18091

Fuel-time optimal retrothrust control for vertical and gravity turn ballistic trajectories of soft landing nonlifting bodies based on Pontryagin principle
[AIAA PAPER 69-868] 21 p3809 A69-39394

RETURN TO EARTH SPACE FLIGHT

Pyrotechnic activated calorimeter for reentry package design of vehicles entering earth atmosphere at lunar return velocities
10 p1669 A69-23026

Spacecraft return probabilities with time constraints and redundant access, using Borel set concept for counting and summing coverage belts
21 p3819 A69-39017

REUSABLE SPACECRAFT

NT AEROSPACEPLANES

Manned reusable space transportation systems development, discussing requirements for future space mission planning
03 p0519 A69-13395

Space flight cost analysis, relative costs of various types of transportation and need for reusable single stage to orbit vehicles
15 p2719 A69-30186

Rocket launch system cost role in space operations, discussing low cost expendable drop tank and Triamese reusable launch vehicle/ spacecraft concepts
18 p3210 A69-35087

Large booster nozzle reuse, discussing design, refurbishment, performance, costs and test evaluation
[AIAA PAPER 68-657] 19 p3394 A69-35944

Low cost rate transportation as mandatory goal for future space program, discussing recovery and reuse, launch system costs, hardware development, etc
20 p3618 A69-38117

Cost reduction steps in reusable launch vehicle design, discussing aircraft design and development experience application
21 p3826 A69-39689

Reusable Crew Module, Reusable Orbital System and Reusable All Systems options for low cost space transportation system
21 p3827 A69-39693

Apollo 11 mission and future space exploration prospects including moon base, manned space station, reusable shuttle vehicles, etc
23 p4211 A69-41477

Reusable aircraft type satellite launchers, discussing first stage recovery by parachute, ballutes, flexible wings and gyroglider
24 p4250 A69-42562

REVERBERATION

SST fuselage response to reverberant and turbulent boundary layer noise calculated for computing equivalent reverberant acoustic fields
15 p2549 A69-30302

Frequency and space averaging effect on variability and standard deviation of multimode media transmission responses, with application to reverberant media
23 p4115 A69-41576

REVERSE TIME

U REACTION TIME

REVERSED FLOW

Turbulent to laminar boundary layer reversal by applying negative pressure gradient
01 p0058 A69-10066

Internal electric field effect of diode with inhomogeneously doped base on lifetime of strong reverse current generated during instantaneous switching
08 p1287 A69-20890

Ejector-diffuser performance improvement by reduction of backflow with orifice plate installed at inlet of straight diffuser duct
11 p1819 A69-25382

Motion of slender axisymmetric bodies in rotating fluid, relating Long hypotheses to flow reversal and dipole distribution effects on lee waves
13 p2248 A69-28170

Electron and proton components contribution to reverse current production after particle shower through upper Cu wall of ionization chamber with lower Pb wall
13 p2304 A69-28417

Similarity solutions for laminar compressible boundary layer with reverse flow, considering various wall/stagnation temperature ratios
15 p2591 A69-30907

Galerkin-Kantorovich-Dorodnitsyn /GKD/ multimoment integral method improved reversed flow formulation for lower branch similar flows
17 p2958 A69-34054

Aerodynamic behavior of airfoil oscillating in reverse flow defined for various angles of attack and oscillatory amplitudes at low Mach numbers
18 p3087 A69-35219

Flow field throughout wind tunnel containing rotor with sharply deflected blades, noting reversed flow effect in front of wake
18 p3119 A69-35228

Laminar flow swirling motion in circular duct, studying separation and reversal
24 p4301 A69-43355

Inverse transition from turbulent to laminar flow in radial diffusers, noting nonagreement of transition point prediction methods
[ASME PAPER 69-HT-33] 24 p4247 A69-43530

Reverse flow profiles in turbulent free jet mixing with streamwise pressure gradient
24 p4306 A69-43684

REVERSING

Fast reversible switching between highly resistive and conductive states in various disordered semiconductors, using electric field
01 p0140 A69-11248

Reversibility principle in transilluminated three dimensional photoelastic medium
14 p2535 A69-29359

Reversion resistant polyether and polyester type urethanes, discussing applications, testing methods and material processing
19 p3357 A69-35566

REWARD [PSYCHOLOGY]

Instrumental reward experiment using concept learning paradigm with word-color compounds as stimuli
07 p1064 A69-18636

REYNOLDS EQUATION

Digital computer program for gas bearing analysis, discussing Reynolds equation and numerical approximations
04 p0604 A69-14518

Flat disk squeeze film air bearing, determining motion of supported mass by computer program
[ASME PAPER 68-LUBS-38] 13 p2266 A69-27272

Flat disk squeeze film air bearing, determining motion of supported mass by computer program
[ASME PAPER 68-LUBS-35] 13 p2266 A69-27280

Pressure distribution in self acting hydrodynamic journal bearings without end leakage, presenting closed form solution for nonhomogeneous Reynolds equation with turbulence considerations
18 p3139 A69-34270

REYNOLDS NUMBER

Semiempirical theory of turbulent MHD tube flow at small Reynolds numbers taking into account magnetic field presence
01 p0130 A69-10769

Hydromagnetic stability of free boundary layer between two uniform streams in presence of aligned uniform magnetic field at large Reynolds number
02 p0287 A69-11832

Expression derived for flow characteristics in smooth pipe for entire Reynolds number range
02 p0230 A69-11870

Vortex valve characteristics, noting Reynolds number and geometry effects on flow and turndown ratio
02 p0195 A69-12079

Laminar flow of anisotropic Erickson fluid near wall at large Reynolds numbers, discussing Newtonian behavior, viscosity coefficient and particle orientation
02 p0231 A69-12141

Reynolds and Mach numbers influence on loss coefficient magnitude at straight airfoil lattice
03 p0364 A69-13788

Laminar two dimensional viscous wake behind finite flat plate, investigating upstream and downstream flow field of trailing edge region for high Reynolds numbers
[ASME PAPER 68-WA/APM-20] 04 p0541 A69-14387

Series solutions for compressible and incompressible flows at low Reynolds number, including axisymmetric and MHD Stokes flow
04 p0587 A69-14609

Reynolds number similarity argument, establishing relation between mean velocity at pipe or channel center and shear stress at wall
04 p0589 A69-14895

Quasi-neutral, steady, inviscid and nonheat conducting flow of conducting gas with high magnetic Reynolds number in plane channel with transverse magnetic field
04 p0636 A69-14984

Velocity profiles for laminar flow of homogeneous liquid in pipe inlet at small and moderate Reynolds numbers
05 p0743 A69-15578

Circular cylinder near wake in cross flow measured with hot-wire anemometry for various Reynolds numbers, noting data processing on digital computer
[ASME PAPER 68-FE-5] 05 p0747 A69-16068

Thermal entry problem solution for low Reynolds number turbulent gas flow based on Reynolds number dependent velocity profile
[ASME PAPER 68-WA/FE-11] 05 p0748 A69-16090

Conical diffuser/exit duct performance and model for estimating energy losses, discussing inlet flow and Reynolds number
[ASME PAPER 68-WA/FE-45] 05 p0698 A69-16112

Surface vibrations effect on forced convection heat transfer normal to cylinder, discussing convective coefficients dependence on Reynolds number
[ASME PAPER 68-WA/HT-5] 05 p0846 A69-16116

High enthalpy, Mach and Reynolds number flight studies on ballistic ranges, describing launchers, flight simulation, measuring and recording techniques
06 p0860 A69-17632

Lifting reentry spacecraft performance examined in context of realistic aerodynamic characteristics at low flight Reynolds numbers
06 p0860 A69-17634

Analytical model developed from turbulent shear flow study, discussing Reynolds number effect
[AIAA PAPER 69-163] 06 p0914 A69-18139

Strouhal and Reynolds numbers relation from data on vortex streets of circular cylinder in two dimensional flow
07 p1119 A69-18749

Matched asymptotic expansions method applied to magnetic field induction in thin toroidal wire and flow past circular cylinder at small Reynolds number
07 p1180 A69-18811

Turbulent incompressible MHD flow between two parallel smooth plates in transverse magnetic field, determining magnetic Reynolds number
07 p1195 A69-19736

Navier-Stokes equations solution applicable to source type low Reynolds number flow through conical nozzles
09 p1482 A69-21976

Unsteady relative flow in centrifugal impeller passage running at part capacity and zero flow observed by hydrogen bubble flow visualization method
[ASME PAPER 69-GT-35] 09 p1432 A69-22489

Requirements for numerical solution of Navier-Stokes equations by finite difference method found limited to Re values with no turbulence
10 p1678 A69-22917

Moving conducting media velocity measurement using Reynolds number and electrical conductivity values, based on magnetic field distortion
10 p1731 A69-23435

Boundary layers influence on external electrical characteristics of MHD generator
11 p1824 A69-24221

Linear MHD generator power characteristics at large magnetic Reynolds numbers, analyzing magnetic field distribution for sectioned and solid electrodes
11 p1824 A69-24224

Angle of attack and Reynolds number effect on hypersonic flow past circular cone, obtaining shock wave shape
[ONERA-TP-692] 11 p1818 A69-24751

Finite difference solutions for time dependent equations of motion for steady flow around cylinder at large Reynolds numbers
11 p1872 A69-25133

Criteria for reversion of turbulent to laminar flow /r-verse transition/ as special cases of Reynolds number criterion, noting boundary layer properties role
11 p1873 A69-25134

Low Reynolds number stability of incompressible fluid half jet flow, investigating free laminar boundary layer instability
11 p1874 A69-25280

Dynamic stall data for helicopter rotor blade analyses obtained by oscillatory tests in pitch and in vertical translation at full scale Reynolds number
11 p1819 A69-25374

Flow stability of axisymmetric jet with parabolic velocity profile in fluid at rest, calculating critical Reynolds numbers
13 p2244 A69-27300

Electrohydrodynamic flows at large electric Reynolds numbers, obtaining Bernoulli and Cauchy-Lagrange integrals
13 p2305 A69-27379

Surface vibrations effect on forced convection heat transfer normal to cylinder, discussing convective coefficients dependence on Reynolds number
[ASME PAPER 68-WA/HT-5]
13 p2374 A69-27781

Radiated aerodynamic noise effects on boundary layer transition on sharp leading edge hollow cylinders in wind tunnels, noting Reynolds numbers correlation
[AIAA PAPER 68-375]
13 p2241 A69-28211

Two dimensional Couette flow analysis showing stability at Reynolds number tending to infinity
14 p2428 A69-28802

Self diffusing substance /salt/ distribution in turbulent water flow at different Reynolds numbers by NMR, obtaining diffusion function consistent with experiments
14 p2430 A69-29424

Thermal entry problem solution for low Reynolds number turbulent gas flow based on Reynolds number dependent velocity profile
[ASME PAPER 68-WA/FE-11]
14 p2430 A69-29446

MHD generator design with electric conductivity waveform at small magnetic Reynolds numbers
14 p2405 A69-29911

Inlet shape and Reynolds number effects on entrance flow development, using laser flowmeter based on Doppler effect to obtain laminar velocity profiles
15 p2589 A69-30001

Reynolds number, incident flow turbulence and interblade channels roughness effects on friction losses in axial flow turbines
15 p2547 A69-30074

Vortex shedding and wake formation behind inclined flat plate at low Reynolds number, using dye injector method for streak line observation
16 p2768 A69-31767

Subliming ablation effects on boundary layer transition for cones in hypersonic flow, discussing Reynolds numbers measured in wind tunnel tests
[AIAA PAPER 68-40]
16 p2732 A69-31881

Analytical expressions validity for skin friction in compressible turbulent boundary layer over wide range of Reynolds numbers and heat transfer conditions
16 p2771 A69-31926

Hydrodynamic parameters of annular Couette flow in longitudinal magnetic field for variable Reynolds and Mach numbers
16 p2821 A69-31953

Swirl decay of turbulent flow in tubes, showing decrease with increasing axial Reynolds number and independence of initial swirl angle
16 p2772 A69-32170

Free stream disturbances influence on hypersonic boundary layer transition Reynolds number in heated and unheated flows
[AIAA PAPER 69-704]
17 p2953 A69-33453

Hypersonic boundary layer transition on blunt slender cones at M equal 10 obtained independent Reynolds number
[AIAA PAPER 69-705]
17 p2954 A69-33455

Cone boundary layer transition location and Reynolds number as function of nose bluntness combined effect with Ar, air and He mass injection
[AIAA PAPER 67-706]
17 p2955 A69-33476

Viscous convergent-divergent nozzle flow slender channel approximations, discussing roles of nozzle geometry, Reynolds number and wall temperature, calculating velocity, enthalpy, etc
[AIAA PAPER 69-654]
17 p2894 A69-33502

Minimum Reynolds number and Malkus theory of turbulent channel flow, discussing stability, equilibrium flow, and stationary turbulence via variational theorem
17 p2957 A69-33764

Skin friction drag formula for tapered and delta wings with allowance for coefficient variation and Reynolds number dependence on chord length
17 p2896 A69-34037

Transient uniform flow over sphere at intermediate Reynolds numbers with recirculatory wakes, utilizing difference approximation to time dependent Navier-Stokes equations
18 p3120 A69-34434

Low Reynolds number solutions for incompressible viscous flows resulting from finite disk steady rotation
18 p3121 A69-34784

Vortex wakes behind circular cylinder subject to transverse sinusoidal oscillations in uniform water flow at specific Reynolds numbers, photographing varied frequency flow patterns
18 p3086 A69-35169

Viscous electrically conducting fluid flow around thin profiles for equal Reynolds and magnetic Reynolds numbers, using Oseen method to linearize equations
18 p3124 A69-35285

Heat flux densities and Reynolds potentials in turbulent boundary layer on heated flat plate with wall suction
19 p3452 A69-36722

Reynolds number dependence of turbulent velocity profile in circular tube and parallel plate channel analyzed by von Karman similarity hypothesis
20 p3513 A69-37081

Rotta analysis for linear flow transformation into turbulent flow, discussing Reynolds numbers
20 p3513 A69-37086

Statistical description of turbulence of viscous incompressible fluid at large Reynolds numbers, using velocity distribution probability
20 p3517 A69-38007

Narrow band vortex shedding from circular cylinder in critical Reynolds number range, noting increase in Strouhal number
21 p3644 A69-38690

One dimensional spectra of turbulent wakes behind circular cylinders, discussing isotropy, anisotropy and Reynolds number
21 p3693 A69-38705

Heat loss from cylinders at low Reynolds numbers in N-He and N-Ne binary mixtures
21 p3848 A69-38706

Incompressible viscous fluid flow past sphere at low Reynolds number, evaluating stream function and drag on sphere
21 p3694 A69-38771

Spectral equation for decaying isotropic turbulence of incompressible inviscid flow at large Reynolds number, using spectral cascading
21 p3694 A69-38835

Heat transfer from spheres in free finite width flow, determining heat transfer coefficient distribution as function of flow width and Reynolds number
21 p3855 A69-39849

Hypersonic flow for low Reynolds number, including magnetic field and wall temperature effects on heat transfer and skin friction for blunt shapes
22 p3860 A69-40540

Aligned uniform magnetic field effect on hydromagnetic stability of two dimensional incompressible electrically conducting jet flow with large Reynolds number
22 p3931 A69-40687

Free viscous layers structure at large Reynolds numbers, using matched asymptotic expansions for two dimensional compressible flow
22 p3932 A69-40927

Radiative transfer effects in low Reynolds number or merged layer regime of hypersonic flow about axisymmetric blunt bodies, including thin shock layer theory
23 p4059 A69-41885

Turbulence theory in laminar-turbulent flow transition, nonlinear stability for flows with Reynolds number higher than critical and fully developed turbulence
23 p4152 A69-42313

Turbine blade edge cooling efficiency, investigating Reynolds number and gas temperature to cooling air ratio influence
24 p4364 A69-43082

Fluid flow around sphere at high Reynolds number by measuring pressure distribution, considering boundary layer separation, tunnel blockage, etc
[ASME PAPER 69-APMW-26]
24 p4245 A69-43093

Heat transfer to highly accelerated turbulent boundary layer with and without mass addition, presenting data in terms of Stanton number vs Reynolds number
[ASME PAPER 69-HT-53]
24 p4409 A69-43518

Local Nusselt number beyond abrupt circular channel expansion tested for Reynolds numbers with air as working fluid
[ASME PAPER 69-HT-35]
24 p4411 A69-43532

Mass injection effects on viscous hypersonic low Reynolds number shock layer downstream and at stagnation point in blunt forebody region analyzed for non-reacting gas
24 p2429 A69-43663

Low Reynolds number unsteady wake flows, using hydrogen bubble flow visualization in high concentration glycerine mixtures
24 p4298 A69-43691

RH- 2 HELICOPTER U UH- 1 HELICOPTER

RHENIUM

Rhenium-niobium cylindrical thermionic converters with mechanically polished or electroetched emitters, comparing performance
03 p0368 A69-13126

Roentgenographic and metallographic examinations for interaction between ZrC and Re in wide range of temperatures and concentrations, discussing phase diagram
04 p0617 A69-14900

Vacuum arc melted W and W-Re alloys mechanical properties, noting Re additions effects
08 p1331 A69-20190

Effective work function of Re and Mo electrode samples determined from Schottky plots and emission measurements from grains
09 p1557 A69-21807

Comparative performance of niobium cylindrical thermionic converters with vapor deposited rhenium, stressing emitters surface preparation
09 p1438 A69-21816

Cylindrical thermionic converter with vapor deposited rhenium emitter and niobium collector, measuring efficiency and power density
09 p1438 A69-21817

Cylindrical thermionic diode with rhenium emitter for diode kinetic experiments, presenting test data from prototype diode with thimble water cooled
09 p1438 A69-21818

Polycrystalline Re high temperature plastic deformation during tensile creep, including activation energy and substructure dislocation study
13 p2280 A69-27767

Plasma anode technique for work functions measurements of polycrystalline W and Re wires in cesium vapor with cesium oxide additive
14 p2507 A69-29274

TiC-Re phase diagram over wide range of temperatures and chemical compositions
15 p2641 A69-31247

Creep rate-stress-temperature relations for powder metallurgy rhenium, discussing activation energy
17 p2991 A69-34186

Quartz fiber adhesion to Re measured in LEED /low energy electron diffraction/ apparatus for clean and O layer surfaces, noting brittle fracture
18 p3156 A69-35182

Low pressure ethylene decomposition on high temperature Re ribbon surface
19 p3266 A69-36730

Re and Re alloy powder metallurgy, noting fabrication of Re coated W particles
20 p3562 A69-37749

RHENIUM ALLOYS

Chemical vapor deposited W and W-Re alloys for structural applications, discussing fabrication methods and effects on mechanical properties
01 p0096 A69-10641

Chemical vapor deposited W and W-Re alloys investigated for deposition variables and heat treatment effects on mechanical properties
01 p0097 A69-10648

A15 type phase in vapor deposited W-Re alloys identified by X ray diffraction, metallography and hardness measurements
01 p0098 A69-10649

Superplasticity in W-Re alloys, noting tensile properties, grain size and strain rate sensitivity for various Re contents at high temperatures
10 p1707 A69-22990

Heat treatment effects on molybdenum-rhenium alloy field emission and surface structure in alpha and sigma phase regions
12 p2113 A69-26041

Re and Re alloy powder metallurgy, noting fabrication of Re coated W particles
20 p3562 A69-37749

Refractory metals in rocket propulsion devices, applying tungsten in uncooled rocket nozzles and tungsten and rhenium to electrothermal propulsion
23 p4177 A69-42161

RHEOELECTRICAL SIMULATION

Resistor network electric analog consisting of arithmetic units block, proposing procedure for elliptic equation solution
21 p3680 A69-39854

Rheoelectrical analog technique for low speed aerodynamic characteristics of finite wings in incompressible flow, using deep electrolytic tank for lifting surface calculations
23 p4061 A69-42351

Two dimensional incompressible inviscid fluid flow problems solution by conducting-paper analog with electrical equipotentials tracing, based on Laplace equation applicability
24 p4299 A69-43024

RHEOGRAPHY

U RECORDING INSTRUMENTS
U RHEOMETERS

RHEOLOGY

Steady state circular motion of fluid with variable rheological characteristics between coaxial cylindrical surfaces, obtaining velocity distribution
01 p0061 A69-10733

Nonlinear viscoelastic bodies arising in 3d rheological models with hidden parameters behaving according to law compatible with objectivity and 2nd thermodynamics principles
01 p0171 A69-11131

High aspect ratio submicroscopic whiskers of beta-SiC, investigating rheological properties of suspensions in various fluids
01 p0102 A69-11260

Long term creep characteristics of metal structures from short duration relaxation tests, summarizing data on rheologically stable materials
[ONERA-TP-639] 02 p0337 A69-11626

Laminar flow of nonNewtonian fluids described via rheological three parameter model
05 p0744 A69-15678

NonNewtonian hydrodynamics equations for non-linearly viscous and viscoelastic media, analyzing dependence on rheological model
05 p0745 A69-15786

Convection in conducting fluid filled cavities with variable wall temperature due to magnetic field, with results applicable to rheological systems
07 p1241 A69-18921

Flow fracture and rheological properties of viscoelastic material under biaxial loading
07 p1202 A69-19386

Flow equations of rheological media derived using thermodynamics, assuming nonlinear stress-strain relation in incompressible medium
08 p1419 A69-21074

Deformation processes of geometrically nonlinear rotational membrane shells under internal pressure
11 p1980 A69-24821

Phenomenological macrorheology, discussing mechanical models designed for studying relation between stresses and strains in materials
13 p2369 A69-28562

Nonnewtonian solid propellant viscosity and pseudoplasticity utilizing rheological characterization for optimal casting and pot life determination
[AIAA PAPER 69-518] 16 p2833 A69-32665

Quasi-static crack growth in viscous bodies analyzed by continuum mechanics, rheological models and energy equation, discussing fine structure
18 p3215 A69-34570

Collection of papers on mechanics including quantum theory, mechanics of micropolar continua, elasticity and plasticity, rheology, etc
20 p3623 A69-37580

Rheology application to description, explanation and measurement of materials properties during deformation
20 p3561 A69-37599

Viscoelastic nonlinear and linear solids models and rheological equations, studying stress-strain states of various complex Hookean, Kelvin, Maxwellian and Zener elements
20 p3625 A69-37601

Biological material flow phenomena, discussing rheological approach, microcirculation, macrocirculation, instrumentation and mathematical model for quantitative observation
20 p3473 A69-37602

Brittle failure models, discussing rheological properties, Griffith energy criterion properties, crack behavior in elastic and linear viscoelastic media, etc
21 p3839 A69-39194

Polystyrene melt tensile viscosity prediction from shearing viscosities, using rheological network rupture theory
21 p3753 A69-39730

Yield stress of normal human blood related to endogenous fibrinogen concentration as function of total protein concentration, proposing fibrinogen adsorption and coupling model
22 p3874 A69-40223

Human blood viscosity measurement over wide range of shear rates, obtaining rheological data, suggesting osmotic red cell crenation role
23 p4095 A69-42078

Microrheological property of blood measured with microglass fiber viscosimeter, noting sensitivity to intercellular friction of erythrocytes
23 p4098 A69-42100

RHEOMETERS

Short fiber composites flow orientation in system of high volume glass fibers in epoxy resin measured by glass rheometer
13 p2287 A69-28670

Rheography of blood circulation of forearm after tightening with pneumatic cuff, analyzing amplitude increase and information about vascular system
21 p3653 A69-38838

RHODIUM

La-Rh system study by powder X ray diffraction, metallographic and differential thermal analysis, constructing equilibrium diagram and determining crystal structure data
21 p3744 A69-38739

RHODIUM ALLOYS

Ti sub 3, Rh sub 5 and Hf sub 3, Rh sub 5 existence and isomorphism confirmed by crystallographic and X ray methods
19 p3343 A69-35920

RHOMBIC ANTENNAS

Nested rhombic antenna spacing determined by measuring mutual coupling and interacting effect on radiation patterns
11 p1850 A69-24979

RHYTHM [BIOLOGY]

NT CIRCADIAN RHYTHMS

Resting EEG and parieto-occipital response changes evoked by slowly repeated flashes in case of severe hypothyroidism secondary to panhypopituitarism
07 p1064 A69-18634

Immobilization effects on alpha rhythm, locomotor coordination and visual alimentary motor reflexes of cats
13 p2212 A69-28617

Hepatic tyrosine transaminase rhythm in rats under various conditions of lighting, food consumption and dietary protein content
17 p2910 A69-33755

Spontaneous rhythmical activity and mean vascular tone dependence in isolated helical rat aorta strips on extracellular concentration of noradrenalin
23 p4093 A69-42069

Social entrainment of feeding rhythms in Rhesus monkeys with light, temperature and sound held constant
24 p4260 A69-42704

Abnormal biologic rhythm in rhesus monkeys associated with behavioral stress, noting brain temperature periodicities sensed with implanted extradural thermistor
24 p4261 A69-42708

RIBBON PARACHUTES

Flight tests of deployment of 20 ft diam ribbon parachute at high dynamic pressures and supersonic speeds
11 p1823 A69-25383

RIBBONS

Ribbon reinforcements in composite materials noting stiffness properties
01 p0172 A69-11265

Stressed state periodic problem in infinite strip under combined pressure and temperature field effect
04 p0673 A69-14497

Planar ribbon winding for buildup control of material near polar openings of filament wound vessels, discussing ribbon width and density
09 p1507 A69-22328

RIBONUCLEIC ACIDS

NT ADENINES

Hypoxia exposure effect on RNA synthesis in rat anterior pituitary cultured in vitro
01 p0015 A69-10923

Unique sequence of oligonucleotides located in tobacco mosaic virus ribonucleic acid
03 p0370 A69-13461

Protein contained purine free basal and yeast ribonucleic acid diets effect on plasma and urinary uric acid production in male subjects
05 p0708 A69-15968

Amber suppressors conversion to ochre suppressors in RNA of bacterium or bacteriophage using uracil mutagen
07 p1068 A69-19493

Poly A-poly U synthesized by Azotobacter Vinelandi RNA polymerase in unprimed reaction containing ATP and UTP, following short lag period
10 p1647 A69-24185

Intraperitoneal high polymer DNA administration normalizing effect on DNA and RNA contents in liver, spleen and intestinal mucosa of white rats exposed to X rays
21 p3657 A69-39050

Enzyme transitions in RNA polymerase state during unprimed synthesis of r11-C/ copolymer, noting dimer-monomer pattern during lag phase
22 p3895 A69-40050

Protein rates and RNA synthesis in cerebra of rats analyzed as factor of high altitude hypoxia adaptation
22 p3886 A69-41122

Polypeptide synthesis as function of 5S ribosomal RNA dissociated from 50S ribosomal subunits by EDTA treatment
23 p4113 A69-41491

Pyrimidine polyribonucleotides or purine polyribonucleotides binding to lysine- or arginine-rich proteinoids considered for abiogenesis
23 p4113 A69-41509

RIBS [SUPPORTS]

Rib positioning effect on mechanical behavior of cantilevered rectangular plate in gas flow, considering critical flow velocities and rigidity relationships
01 p0165 A69-10085

Elastic strain and stress in ribbed circular plate bent skew-symmetrically, using orthotropic plates theory
04 p0681 A69-15172

Field approach for stress and deflection analysis in rectangular plates reinforced by straight ribs, noting kernel function
11 p1983 A69-25019

Optimal parameters selection for rib-reinforced cylindrical shells determined with respect to axial critical loading magnitude
11 p1985 A69-25173

Zero Gaussian curvature rib reinforced shells free oscillations reduced to nonreinforced shell forced oscillations under cyclic loads
12 p2177 A69-25996

Rigid supporting ribs effect on annular plate critical loading, stability loss and buckling
14 p2533 A69-28983

Stress-strain state calculations of ribs reinforcing cantilever shell under external pressure, using differential-difference equations
18 p3223 A69-34980

Steady state temperature fields and thermal stresses determined in finite cylindrical shell by optimal parameters of reinforcing circular rib
21 p3834 A69-38714

Stability loss for hinged circular cylindrical elastic shells reinforced by thin walled closed profile ribs, proposing minimum weight design method
21 p3835 A69-38723

Stress concentration in elastic plate reinforced at edge by straight rib analyzed in finite form by Cauchy integrals and Fourier transforms
22 p4041 A69-40114

Rib cross sections distribution for cylindrical shell under concentrated longitudinal forces obtainable by designing for minimum strain energy
23 p4228 A69-41988

Discrete rib effect on buckling resistance of cylindrical shell under combined external and axial compression loads, using Laplace transforms
23 p4229 A69-41990

Stability of orthotropic cylindrical shells reinforced at edges by elastic ribs, analyzing axisymmetric buckling, natural oscillations and rigidity characteristics
23 p4229 A69-41992

Hinged circular cylindrical shells reinforcing ribs effect on deflection and bending moments, assuming external pressure application
23 p4229 A69-42001

RICCATI EQUATION

Linear optimal control problems with quadratic performance indices, developing system equivalence for matrix Riccati equation
[ASME PAPER 68-WA/AUT-17]

05 p0738 A69-16175

Matrix Riccati and matrix quadratic equations in problems of stochastic control and filtering
05 p0740 A69-16601

Command inputs handling by linear optimal control theory, investigating Riccati matrix differential equation convergence
08 p1298 A69-20856

Matrix Riccati equation duality and bounds, discussing duality in context of optimal control
11 p1909 A69-24885

Negative exponential solution of matrix Riccati equation associated with linear optimal regulator and filter problems for time invariant plants
12 p2122 A69-26513

Riccati equation solution for inhomogeneous and homogeneous lines obtained by Lagrangian method for differential equations
15 p2582 A69-30124

Nonlinear differential equations of injection phase locking solved by Riccati equation, discussing initial frequency offset to loop gain ratios
23 p4119 A69-41742

Optimal deterministic estimation and feedback control for linear nonstationary process and measurement systems defined by Riccati equations, including Kalman-Bucy filter
24 p4291 A69-43276

RICHARDSON-DUSHMAN EQUATION

U TEMPERATURE EFFECTS

U THERMIONIC EMISSION

RICHARDSON NUMBER

Correlations at regional scale between clear air turbulence aircraft observation, Richardson number and wind intensity and direction at flight level
03 p0462 A69-13966

Richardson constant for thermionic emission in Schottky barrier diodes, noting effect of surface shadows
08 p1286 A69-20865

Relation between Rayleigh and dynamic Richardson numbers in atmospheric boundary layer in presence of cellular convection
09 p1491 A69-22709

Buoyancy in turbulent shear flow, rotation or streamline curvature effects and meteorological parameters, drawing formal exact algebraic analogy
11 p1870 A69-24894

Richardson number in vertical tropospheric region of maximum wind computed from data on jet streams observed in winter over radiosonde stations in Italy
13 p2295 A69-28656

Qualitative analysis of CAT parameters from radio sounding data, noting mean bumpiness probability dependence on Richardson number and wind vector shift
14 p2474 A69-29735

Relation between Rayleigh and dynamic Richardson numbers in atmospheric boundary layer in presence of cellular convection
16 p2808 A69-32488

RIDGES

Sand ridge origin and dynamical setting, discussing morphology-tidal current system equilibrium indicated by theory and field measurements
15 p2596 A69-30443

RIEMANN INTEGRAL

U MEASURE AND INTEGRATION

RIEMANN MANIFOLD

Killing fields applied to nonsymmetric spaces specify coordinate lines with slowest possible metric tensor variation and gravitational radiation
01 p0115 A69-10018

Geometrical existence proof of elastically coupled nonlinear systems normal mode vibrations demonstrated by existence of extremal arcs in Riemann space
01 p0166 A69-10232

Electromagnetic and gravitational tensor fields in Riemannian space, generalizing Maxwell and Bel-Robinson tensors
03 p0467 A69-13755

Brans-Dicke scalar-tensor theory, showing radiative Riemann tensor existence in absence of usual spin-2 gravitational waves
07 p1216 A69-18894

Riemann metric leading to empty flat space from Rainich equations of already unified field theory
07 p1182 A69-19418

Geometrized theory of combined gravitational and electromagnetic fields, using metric tensor of four dimensional Riemannian continuum to describe both fields
09 p1540 A69-22134

Maxwellian field and second order invariant system in vacuum in three dimensional Riemannian space with

positive-definite metric, discussing Lorentz invariant equations
09 p1541 A69-22392

Generalized Riemann function obtained as solution of transformed Boltzmann-Vlasov equation, discussing one dimensional and multidimensional cases
10 p1724 A69-22908

Theory for approximation of analytic functions given on closed spaces with piecewise smooth boundaries
12 p2120 A69-26198

Physical space-time defined as four dimensional Riemann space based on available information for physical measurements
14 p2484 A69-28862

Time-similar and isotropic geodesic curves simulating paths of test bodies in Riemann space corresponding to gravitational field
21 p3772 A69-39621

RIEMANN PROBLEM

U CAUCHY PROBLEM

RIEMANN WAVES

Mach disk and Riemann wave location, size and strength in underexpanded jet flows, proposing model for conservation equation satisfaction
[AIAA PAPER 69-665] 17 p2954 A69-33460

RIESZ THEOREM

Operator methods in engineering sciences, discussing integral transformations, Riesz method application to Cauchy problem, etc
03 p0457 A69-13744

RIGID MOUNTING

Biaxial gyro stabilizers mounting on rocking base, deriving expressions for constant components of stabilizer precession rate
09 p1498 A69-22112

Elastohydrodynamic lubrication of square section high pressure face seals mounted on rigid housings, considering design charts for load and leakage
[ASLE FICFS PREPRINT 16] 15 p2621 A69-30493

RIGID ROTOR HELICOPTERS

U XH-51 HELICOPTER

RIGID ROTORS

Helicopter rigid rotor system with blades of glass fiber reinforced plastic
04 p0548 A69-14817

BO-105 helicopter design, testing and characteristics noting four bladed rigid rotor
[AHS PAPER 200] 07 p1052 A69-18869

Hingeless fiberglass rotary wings dynamics, discussing effects of in-plane bending to flapping frequency ratio
[AIAA PAPER 69-204] 07 p1054 A69-19548

Ground and air resonance measured with gimbaled whirl tower stand for soft inplane matched stiffness rotor, discussing body inertia and speed limits
[AIAA PAPER 69-205] 07 p1055 A69-19559

Matrix elements for asymmetric rotors using rigid rotor reduced energies, describing computations method
09 p1614 A69-21913

Undamped rigid rotor critical speed analysis for firm and flexible foundations, discussing effect of center of gravity and rotor shapes
[ASME PAPER 69-VIBR-49] 10 p1808 A69-24184

Helicopter rotors with rigid blades performance from viewpoint of controllability and load distribution
13 p2201 A69-27295

NASA flight test of hingeless rotor compound helicopter to determine lift sharing characteristics, showing rotor lift dependence on airspeed
14 p2393 A69-29702

Natural gyrofrequencies of rigid rotor during slowing/stopping at high forward speed, using simple approximation
17 p2899 A69-33507

Gyro controlled rigid rotor dynamic stability studied for stoppable rotor operation, developing analytical expressions for determining stability boundary of constant and rotor speed gyros
[AHS PAPER 343] 17 p2899 A69-33508

Slot height, position and trailing edge geometry effects on elliptically shaped rotors selected for hover efficiency, size, transitional gust insensitivity and rigidity
18 p3088 A69-35231

Rigidity of rotors with pin joints, calculating moments of inertia at connected sections of turbine shaft disks utilizing similarity concept
19 p3324 A69-35832

Herzenberg geomagnetic dynamo model extensions including rigid rotors calculus, laminated rotors, induction problem and fluid rotors in rigid conductor
22 p3989 A69-40193

RIGID STRUCTURES

Eccentric compression in elastic domain for rigid homogeneous structural elements, considering traction and stress
02 p0341 A69-12258

Structural designs for minimum flexibility or weight using energy intensity per unit mass parameter
02 p0345 A69-12380

Orthotropic stiffened multilayer circular cylindrical shells buckling under axial compression, lateral pressure, etc
02 p0346 A69-12510

Equilibrium stability of elastic circular arch constrained in rigid cavity and subjected to uniformly distributed parallel loading
03 p0524 A69-13066

Submerged rigid circular cylinder displacement under influence of plane acoustic pressure wave solved by operational method
04 p0667 A69-14261

Rotation deviation of rigid body around axis, discussing three point body measurement and applicability
04 p0599 A69-15017

Book on thermal time independent plastic and time dependent creep strains in structures through analogy permitting inelastic structures analysis
04 p0681 A69-15200

Stiffness matrices for buckling or vibration analysis of long thin flat plate structures connected at longitudinal edges
05 p0836 A69-16029

Programming technique using quaternion parameters for error reduction in simulation of spinning rigid body
05 p0724 A69-16469

Quasi-phonon model for acoustic scattering and diffraction from rigid real obstacle in fluid medium
05 p0797 A69-16649

Differential equations of rotational motion of systems of rigid bodies in gravitational field derived with Lagrange equation
06 p0957 A69-17130

Finite plane deformation of solid body, arbitrary deformation law and arbitrary hydrostatic stresses dependence on volume change solved by nonlinear equation
06 p1021 A69-17175

Longitudinal stability derivatives prediction for rigid and elastic airplanes, using influence coefficient method
[AIAA PAPER 69-131] 06 p0868 A69-18134

Mathematical formulas for rigidity distribution of inhomogeneous multilayer shells, discussing invariance property
07 p1232 A69-19011

Specialization of field equations and boundary conditions of elastic dielectric for special case of rigid dielectric, using Lagrange multipliers
07 p1200 A69-19174

Compatibility theorem extension to three dimensional rigid plastic bodies with stress and velocity discontinuities, noting isotropic bodies with convex yield surface
08 p1418 A69-20845

Two layer cylindrical shells stability under external pressure, assuming nonuniform shell rigidity
08 p1419 A69-21180

Reaction vs time relations in accidental impact of large commercial aircraft against rigid surface, detailing stress analysis of nuclear power plants structures
09 p1613 A69-21677

Buckling of eccentrically stiffened thin circular cylindrical shell under uniform combined axial compression and torsion loads with lateral pressure
09 p1616 A69-21955

Rigid top mass effect on longitudinal response of model vehicle propellant tank, determining natural frequencies and forced asymmetric response
09 p1616 A69-21979

Single rotation for reorienting rigid body from initial to arbitrary final attitude together with corresponding control torques
09 p1610 A69-21998

Rigid body rotational simultaneous equations of motion transformed into explicit form for digital simulation
10 p1661 A69-23855

Damping of response of integrally stiffened skin structures to random acoustic pressures, reducing rms stress in case of broad band excitation
[ASME PAPER 69-VIBR-26] 10 p1806 A69-24172

Natural mode structural analysis matrix methods for small displacements, discussing curved local subbeam in space and circular arch

11 p1969 A69-24374

Linear differential equation solution for elastic systems stability problems, discussing applications to heated rectangular plates

11 p1982 A69-24950

Indentation of inhomogeneous rigid plastic solid by flat punch under plane strain conditions analyzed by perturbation method

11 p1986 A69-25244

Elastic free-free body deformation during motion based on equations of motion valid for rigid body, noting dynamic Green tensor

11 p1994 A69-25604

Stress discontinuity surface of three dimensional rigid plastic body arbitrary yield condition, considering equilibrium of regular four sided pyramid

11 p1996 A69-25738

Elastoplastic cylindrical shell instability determination under axial compression applied to inelastic solids

13 p2363 A69-28124

Inelastic structural system stresses, strains and displacements analyzed by differential stress-strain relationships, using finite element method [AIAA PAPER 68-291]

13 p2364 A69-28208

Rigid structures high damping without loss of rigidity achieved by epoxy resin dampers, noting moderate cost

13 p2370 A69-28601

End constraints and length/width ratio influence on composites off axis tensile tests, considering rigid clamping with/without end rotation

13 p2286 A69-28667

Rigid obstacle unsteady motion in compressible fluid with load applied to surface layer, deriving numerical solution of pressure expansion

14 p2430 A69-29480

Necked tension specimens profiles for rigid-plastic nonhardening materials determined from compatibility equation for displacements and unloading rate

15 p2704 A69-30292

Free vibrations of thin truncated circular conical shell and reinforcing rings and stringers, determining resonant frequencies for stiffened and unstiffened configurations

17 p3051 A69-32955

Dynamic equations solution for interacting rigid or elastic body system models using Cosserat bodies elastic theory, considering engineering applications

17 p3067 A69-34143

Bending of rigid freely supported plastic plates under local axisymmetric dynamic load, discussing rectangular pulse effects and velocity fields

18 p3217 A69-34593

Resin impregnated fiber reinforced expandable structures used for automatic cure or rigidizing in space and initially small compact packages on earth

19 p3433 A69-35585

Conservation laws and Liapunov stability of free rotation of rigid body about principal axes derived from kinetic energy and angular momentum

19 p3397 A69-35612

Light rigid civil aircraft response to continuous atmospheric turbulence estimated using two rigid body degrees of freedom method for vertical and lateral gusts [AIAA PAPER 69-766]

19 p3433 A69-35657

Gravity torque influence on axisymmetric dual spin satellites in fixed attitudes, using attitude stability studies of spinning single rigid bodies

19 p3429 A69-35917

Closed form solutions for rigid viscoplastic cylindrical shell under dynamic loading based on constitutive equations for rate sensitive plastic material

19 p3439 A69-36478

Liquid filled rigid bodies motion stability defined and solved for system with infinite number of degrees of freedom

19 p3301 A69-36810

Bifurcation and hardening rate of rigid-plastic bodies presented on buckling of rectangular plate with lateral restraint

21 p3840 A69-39299

Dynamic stress concentrations and rigid body response of cylinder imbedded in elastic medium subjected to compressional wave

21 p3840 A69-39300

Nonlinear formulation for rigid jointed space frame comprised of prismatic linear elastic members, using Newton-Raphson and successive substitution methods

23 p4232 A69-42142

Rigid/plastic solids subjected partly to uniform fluid pressure and partly to general boundary conditions, analyzing uniqueness and stability criteria

23 p4235 A69-42460

Force maintaining rigid inclusion embedded in elastic plate with rigid boundaries

23 p4235 A69-42465

Large space erectable structures rigidity, stiffness, thermal stability, structural efficiency and integrity [AAS PAPER 69-152]

24 p4398 A69-42877

RIGID WINGS

Time optimal control for torsional vibrations of flight vehicle for limited energy case, illustrating uniform wing of constant rigidity

21 p3686 A69-38891

RIGIDITY

Gyromotor flanges axial rigidity measuring methods based on axial deflection of flange or natural frequency of oscillating system

09 p1513 A69-22704

Shear modulus of fiberglass reinforced plastics determined from torsional tests on squared beam of orthotropic material, evaluating influence of end conditions

17 p3058 A69-33204

Torkington progressive rigidity model with successive minimum requirements relation to diagonal matrix elements of molecular force constants

17 p3068 A69-34230

Flexible-rigid hybrid polyimide-epoxy glass multilayer board to fill gap between all flexible and all rigid circuit boards

19 p3319 A69-35545

RILLS

U VALLEYS

RING CURRENTS

Magnetic field behavior at synchronous orbit during magnetospheric substorms, interpreting satellite observed data in terms of partial ring currents

01 p0075 A69-11225

Ring current particle energy density distribution for symmetric portion of magnetic storm derived from current magnetic field profile measurements

01 p0147 A69-11227

Magnetospheric ring current effect on main phase of geomagnetic storms, calculating diurnal storm-time portion of perturbation field

07 p1122 A69-18296

Magnetospheric magnetic field ring current asymmetry during different phases of geomagnetic storm observed by Explorer 26 and Vela 2 satellites

07 p1129 A69-19611

Auroral oval boundary and median line variations with increasing magnetic storm time intensity, noting ring current effect on polar aurora location

09 p1485 A69-21532

Average geomagnetic storm ranges as function of latitude, noting disturbances caused by ring and ionospheric currents

09 p1489 A69-21715

Magnetic lines of force penetration into magnetosphere accompanied by plasma insertion generating ring current responsible for main phase of magnetic storm

10 p1687 A69-23923

Auroral oval and ring current in magnetosphere, analyzing boundaries of lines of force on night side of earth

10 p1689 A69-24203

Plasma distribution and Alfvén wave velocity field in magnetosphere, discussing distortion of dipole magnetic field, ring current and wave propagation

10 p1742 A69-24205

Dynamics of magnetosphere, discussing auroral oval position, ring currents, plasma density and magnetic field variations in near polar region

12 p2072 A69-26741

Model for self consistent time independent ring current of charged particle distribution under combined field of earth dipole and particle motion current

12 p2151 A69-26948

Magnetospheric ring current model from ground stations data to interpret observed magnetic field disturbances

13 p2253 A69-27699

Auroral electrojet index in relation to magnetic storm sudden commencements, ring current main phase and energetic solar protons

14 p2511 A69-28954

Nonuniform ring current belt growth, discussing associated magnetospheric substorms

14 p2513 A69-29123

Geomagnetic ring current study, giving exact kinetic description based on Vlasov equation of plasma ring current in dipolar field

15 p2598 A69-31218

Self consistent ring current of radiation belt under combined influence of earth dipole field and field due to currents of particle motions

16 p2776 A69-32096

Auroral oval boundary and median line variations with increasing magnetic storm time intensity, noting ring current effect on polar aurora location

16 p2783 A69-32527

Polar upper atmospheric phenomena interpreted as magnetospheric substorm manifestations, discussing role of asymmetric ring current formation

21 p3710 A69-38504

Geomagnetic ring current effect on position of auroral absorption zone in northern polar region, noting storm time part of disturbance

23 p4157 A69-41859

RING DISCHARGE

Electron temperature and electron density variations with radial distance in 10 MHz electrodeless ring discharge in H₂, noting electric field

08 p1361 A69-20230

Toroidal plasma nonequilibrium in multiple confinement devices with conventional magnetically shielded supports

08 p1369 A69-20819

RING LASERS

Frequency difference of traveling waves in accelerated rotating ring laser

02 p0257 A69-12417

Ring lasers emission modes, studying nonlinearity effects on radiation field spatial-temporal distribution

03 p0437 A69-13040

Ring laser field space-time pattern from light waves scattered at discontinuities, discussing equations of motion of solid state laser

03 p0441 A69-14140

Laminar and turbulent flow measurement in variety of tube diameters, using ring laser without insertion of mechanical probe

04 p0596 A69-14281

Mode power spectra observations for ring and normal He-Ne lasers at 6328 Å

07 p1155 A69-19087

Quantum oscillators interaction with two level molecules system in circular laser

11 p1899 A69-25325

Laser gain medium dispersion expressions applied to multimode ring laser operation with mode spacing less than pressure broadened atomic linewidth

12 p2106 A69-26324

Laser output power amplitude fluctuations effect on beat frequency stability for traveling waves in annular laser with broadened Doppler emission line

12 p2107 A69-26541

Gas ring lasers, discussing optimal parameters, colliding waves interference, nonmutual effect and radiation polarization

13 p2272 A69-28175

Wave interaction in gas ring laser, delineating single mode emission zones as function of pumping, emission frequency position and Q factor differences

17 p2982 A69-33632

Mode coupling effects in CW gas ring lasers, considering excitation density pulsations, traveling waves dispersion, polarization, etc

19 p3334 A69-36046

Mathematical model of CW ring laser mode coupling in limits of low excitation

19 p3334 A69-36047

Inductively coupled RF excited toroidal Ar ion laser, confining current discharge by strong axial magnetic field to reduce wall losses

19 p3338 A69-36690

Mathematical relations for ring laser beams polarization conditions, using slanted isotropic plate and phase circulator to separate polarization plane

20 p3553 A69-37606

Ring lasers basic operating principles and primary applications, discussing Fresnel drag, magneto-optical effect, etc

22 p3961 A69-40240

Emission spectrum of nonself locked He-Ne ring laser, deriving phase relations for LF intermode oscillations

24 p4328 A69-43159

Polarization characteristics of He-Ne ring laser emission with circularly anisotropic resonator, analyzing ellipticity as function of half wave cavity plate

24 p4328 A69-43160

RING STRUCTURES

NT REINFORCEMENT RINGS

Self gravitating pulsating cylindrical and ring shaped cosmic masses from group theory standpoint compared with oscillating stars

01 p0148 A69-10124

Point load subjected deflections of cantilevers and circular rings found using electronic analog computers

03 p0522 A69-12865

Solid viscosities effects on dynamic load factors of ring and hollow sphere subject to uniformly distributed impulsive loads along inner and outer edges

03 p0530 A69-14089

Elastic ring subject to uniform hydraulic pressure on inner boundary and with two opposite slipless quarter-arcs on outer boundary, noting stress and deformation [ASME PAPER 68-WA/APM-17]

04 p0669 A69-14395

Lunar and Martian annular formations and structures, discussing classification, morphological characteristics, incidence frequencies and area sizes

04 p0658 A69-14959

Saturn ring formation by satellite spiral into Roche limit and disintegration

04 p0660 A69-15128

Elastic plastic stress distribution in compressed ring determined with postyield strain gages and stress-strain relationship from uniaxial tensile test

05 p0837 A69-16063

Stress distribution and spring rates in cantilever cone ring combination [ASME PAPER 68-WA/DE-3]

05 p0839 A69-16168

Three dimensional deformation and buckling of circular ring, discussing in-plane and out of plane deformations and loads [ASME PAPER 68-WA/DE-4]

05 p0839 A69-16169

Korn constant for boundary value problem of linear elastostatics applied to circular ring domain

05 p0844 A69-16740

Aberration of dielectric patches and rings attached to radome surface described by insertion phase

07 p1111 A69-19530

Separation of principal stresses along sections of symmetry free from external loads with application to circular ring and grooved bar

08 p1412 A69-20256

Matrix properties related to torsional fatigue life of fiberglass reinforced NOL rings, using polyester and epoxy resins as model systems

08 p1339 A69-20495

Rotational spectrum of ethylene episulfoxide to determine molecular structure, particularly orientation of C sub 2 S ring

08 p1268 A69-20535

Large deflections and associated moments in circular ring of linearly viscoelastic material subjected to small strains

09 p1615 A69-21925

Gravitational potential of circular rings used to investigate motion stability of Saturn rings

10 p1771 A69-22855

Radiation fields induced by constant current in elliptic ring, discussing analysis results applicability to elliptic capacitive antennas and annular slot

11 p1850 A69-24981

Thin ring-strut structure resting on elastic foundation, analyzing deformation taking warping effects into account, noting applicability to engine design

12 p2184 A69-26812

Three dimensional deformation and buckling of circular ring, discussing in-plane and out of plane deformations and loads [ASME PAPER 68-WA/DE-4]

13 p2360 A69-27420

Stress and strain fields for circular rubber ring under diametrical compression between flat plates, using moire, large strain analysis and photoelastic verification

14 p2531 A69-28884

Macromolecular ring shaped components corresponding to hemagglutinin studied in Limulus polyphemus hemolymph by electron microscopy

16 p2742 A69-31864

Thin circular ring stability under uniform external transverse loading at various angles, discussing transverse shear deformation effects and buckling

17 p3061 A69-33707

Large deflections of thin nonlinearly elastic ring under external pressure, using two layer model

17 p3062 A69-33715

Buckling time of oval ring under unsteady creep based on strain hardening theory

17 p3062 A69-33716

Mean rotational velocity of finite width gaseous ring in close binary system from rotational velocity measured on spectrograms

17 p3044 A69-34180

Lunar and Martian annular formations and structures, discussing classification, morphological characteristics, incidence frequencies and area sizes

18 p3197 A69-34722

Graphite fiber NOL rings and biaxial wound pressurized cylinders tested at ambient and cryogenic temperatures for tensile and cyclic fatigue properties

19 p3355 A69-35521

Elastic oscillations of inhomogeneous orthotropic ring under time-variable axisymmetrical load analyzed by Fourier method

19 p3434 A69-35828

Saturn ring dynamical structure theory supported by observations of knots or condensations

20 p3600 A69-37482

Optimal plastic design of circular sandwich ring assuming symmetric loading, minimum plastic resistance and cost justification of stronger cross section

20 p3625 A69-37590

Axially symmetric distribution of residual strain in multilayered filament wound ring analyzed and compared with experimental results

20 p3628 A69-37774

Optical properties and thickness of Saturn rings from observations during ring plane crossing of earth or sun, determining Tethys diameter and albedo

20 p3605 A69-37821

Saturn surface spectrum near ring shadow examined for water vapor content in ring and greenhouse effect on surface

20 p3616 A69-38305

Equivalent circuit technique for dispersion equation and coupling impedance of slow wave structures of ring-rod systems, noting retardation

23 p4139 A69-41944

Dynamic uniaxial tensile stress-strain data obtained at high rates by measuring kinematics of symmetrically expanding thin ring specimens

24 p4330 A69-42735

Flexural vibrations of rectangular cross sectioned rings, solving characteristic value problem for finite circular cylindrical shell

24 p4404 A69-43629

Computer program determination of barreling effect on strength of ring and stringer stiffened shells designed to support axial compression loads

24 p4405 A69-43671

RING WINGS

Monograph on ring airfoil theory with nonuniform incidence covering steady flow and shear flow transition into boundary value problem of potential theory

17 p2889 A69-32995

RIOMETERS

Riometric data processing method for radio wave absorption measurement, considering nighttime cosmic radio emission intensity

14 p2436 A69-29056

Ground based solar proton monitoring, considering particle intensities and radiation dose rates from riometer absorption as function of time

16 p2850 A69-32321

Polar ionosphere investigation based on vertical sounding and riometric observations, earth electromagnetic field and polar auroras spectrum intensity variations

17 p2963 A69-33950

High latitude geomagnetic disturbances, incoming electron fluxes and riometric absorption relationship in lower ionosphere studied by X ray bremsstrahlung with sounding balloons

17 p2964 A69-33961

Spatial gradient and amount of auroral radio absorption measured by riometers at magnetically conjugate and closely spaced stations

22 p3934 A69-39966

HF radio waves auroral absorption in ionosphere reviewed for first decade of riometry

22 p3902 A69-41218

RIOMETRY

U MEASUREMENT

U RIOMETERS

RISK

Predictive model for risk in technological research and development

04 p0689 A69-14980

R and D program risk evaluation methodology in density functions form for program goals probabilities, noting random variables as parameters

19 p3455 A69-36008

Risk taking under uncertainty in individual and group decisions, analyzing gambling and group discussion situations

23 p4091 A69-42016

Risk factors in coronary diseases modified to provide base for estimating achievable mortality magnitude reduction

24 p4262 A69-43059

RITZ AVERAGING METHOD

Nonlinear boundary value problems direct generalized solutions based on linearization of Bubnov-Galerkin and Ritz method

02 p0272 A69-12136

Computerized solution of three dimensional problems of elasticity theory using Ritz method

03 p0527 A69-13743

Finite element method convergence introduced as general numerical technique related to Ritz method in structural analysis with digital computers

03 p0527 A69-13745

Incorrect problem solving method applied to Cauchy problem solution for nonlinear partial differential equations, considering Ritz method applicability

07 p1174 A69-19005

Nonradial oscillation modes of massive stars determined by Ritz method application to variational principle, allowing for gravitational perturbation

10 p1785 A69-24036

Modified Bubnov-Galerkin-Ritz method for determining approximation coefficients in stress and displacement analysis, using mixed variational principle of elasticity theory

18 p3215 A69-34566

RIVERS

Lunar rivers as coalesced chain craters resulting from gas emission along fracture beneath lunar regolith

18 p3205 A69-35436

Rivers on moon, discussing possibilities of water existence on lunar surface in view of temperature, gravity and atmospheric conditions

19 p3419 A69-36145

RIVETED JOINTS

Single row riveted joints, representing rivet forces by Chebyshev functions in homogeneous arrangements and obtaining equations for continuous joints from limit procedure

04 p0682 A69-15292

Sonic riveting of aircraft Al alloys, noting no evidence of forging bursts, cracking, splitting, tearing and springback

24 p4320 A69-43060

RIVETING

Sonic riveting of aircraft Al alloys, noting no evidence of forging bursts, cracking, splitting, tearing and springback

24 p4320 A69-43060

RIVETS

Couple stresses effect on thin plate stress distribution due to pressure of rivet on one side of circular hole

08 p1319 A69-20201

Crack propagation in plate with stiffening ribs /riveted stringers/ under concentrated and tensile loads, determining rivet points displacements

24 p4406 A69-43709

RL-10-A-1 ENGINE

Flox/methane pump fed engine, discussing RL-10-A engine tests and optimized 5000 lb thrust engine design [AIAA PAPER 69-510]

16 p2741 A69-32720

RL-10 ENGINES

U RL-10-A-1 ENGINE

RLC CIRCUITS

NT LC CIRCUITS

Unified theory of normal mode analysis of RLC networks based on Tellegen theorem of Kirchhoff law, discussing coupled networks

07 p1115 A69-18858

RLC filters transfer functions applied to development of high pass filter

08 p1300 A69-21176

Equations adaptable to computer for RLC circuits containing linear and nonlinear n-terminal networks derived by nodal method

09 p1472 A69-21779

RLC two terminal bridge network synthesis, considering two reactances, three resistances and constraints

09 p1464 A69-22291

Frequency selective mechanical filter and LCR circuits and applications, noting inductances in solid state and thin film technology

09 p1467 A69-22558

Multiple loop feedback systems synthesis utilizing extended node introduction synthesis theory, considering filter response functions characteristics
10 p1667 A69-24037

Log periodic dipole array antennas simulated with simple RLC circuit loading uniform transmission line
11 p1850 A69-24977

RLC integrated low inductance circuit for magneto-optical high speed camera shutters, Q switched ruby laser and short light pulses in spark gap
12 p2084 A69-26149

Differential equations application to electrical circuit problems, solving voltage for series LCR networks and transforming Mathieu into Hill equation
12 p2052 A69-26351

Time varying resistance wire to arrest oscillations in pulsed capacitor discharge circuit, deriving over, under and critical damping conditions
22 p3917 A69-41228

RNA
U RIBONUCLEIC ACIDS

ROADS
U HIGHWAYS

ROASTING
Pressure calcinering process in production of fine grained ceramics at low temperatures
12 p2119 A69-26832

ROBOTS
Robot command and control by computer assembly, describing engineering analog of vertebrate nervous system
21 p3679 A69-39603

ROCHE LIMIT
Low mass close binary systems evolution, describing components inside critical Roche lobe in initial detached phases
10 p1777 A69-23310

ROCK SALT
U HALITES

ROCKET BOOSTERS
U BOOSTER ROCKET ENGINES

ROCKET-BORNE INSTRUMENTS
Rocket released probe orientation determination from polarization measurements on telemetry signal
02 p0207 A69-11813

Canadian program of scientific rocket sounding of auroral phenomena, outlining systems approach, engineering and scientific cooperation requirements, etc
02 p0335 A69-12689

Alignment of rocket-borne instrument with sun, discussing mechanical system design, servocontrol and silicon photodiode sensors
03 p0427 A69-12980

Nocturnal electron concentrations and temperature at Manitoba measured by rocket-borne Langmuir probe, compared with F1 region
03 p0502 A69-14008

Solar hydrogen Lyman alpha line profile measurement by rocket-borne spectrophotograph, obtaining flux available for scattering by atomic hydrogen in geocorona
05 p0815 A69-16254

Upper atmosphere physics, atmospheric composition and separation of gases, nature of air flow, water vapor content and lower ionosphere structure determinations by rocket
[UN PAPER 68-95693] 06 p0949 A69-17058

Rocket-borne Rayleigh scattering instrumentation to measure atmospheric density, discussing instrumentation and flight results
06 p0927 A69-17698

Rocket transportation for upper atmospheric measurements, discussing sensors and cost effectiveness
[AIAA PAPER 69-159] 06 p1018 A69-18066

Multilens spectroheliograph for nonstabilized rockets, obtaining consecutive points recording along solar image chord
08 p1313 A69-20252

Solar proton monitoring by particle detectors on-board rockets and IMP satellite
08 p1318 A69-21142

Temperature profiles variability for data obtained by rocketsonde thermistors launched with small time and spatial separation
09 p1494 A69-21644

Solar research from rockets and satellites, considering solar instruments including EUV spectrographs
10 p1772 A69-22867

Rocket IR astronomy in support of big bang hypothesis, considering photoelectric detectors and instrument system
10 p1772 A69-22868

Miniature telemetry systems for gun launched projectile instrumentation and ejection payloads, noting voltage controlled oscillators, commutators and VHF FM transmitters
10 p1654 A69-23280

Rocket-borne spectroheliograph for monochromatic solar photography in Mg II 2802.7 A line noting filter bandwidth, film polarizers and temperature control
11 p1884 A69-24838

Aerobee rocket-borne liquid helium cooled telescope for IR night sky observations
11 p1885 A69-24852

Spinning rockets UV spectrophotometry of early type stars, discussing instrumentation, calibration, data recording and stellar spectra
12 p2153 A69-25812

Rocket-borne scintillation spectrometer for cosmic photon radiation
14 p2449 A69-29566

Rocket observations of protons and alpha particles energy spectra after solar flares, noting riometer and magnetometer recordings
15 p2677 A69-31329

Weak emissions in near IR daytime airglow using rocket-borne spectrometers
16 p2776 A69-32094

Rocket instrumentation for electron and proton spectra measurement in aurora borealis
17 p2972 A69-33038

Rocket-borne AM radio receiver for Faraday rotation experiments to measure lower ionosphere electron density, giving circuit diagrams
17 p2936 A69-33062

Attitude stabilized rocket-released magnetometer for detection of earth field magnitude and direction changes
19 p3309 A69-35994

Rocket-released magnetometer probe for upper atmospheric measurements, discussing construction, flight, sensitivity and ionosphere current detection
19 p3309 A69-35995

Sounding rocket S band telemetry antenna operation, proposing quasi-isotropic pattern criterion to reduce effects of shadowing and interference
19 p3271 A69-36252

Solar photography at extreme UV wavelengths using pinhole camera instrumentation on stabilized Skylark rocket
20 p3539 A69-37545

Small rocket instrumentation techniques - COSPAR Conference, May 1968
20 p3541 A69-37790

Retarding potential analyzers to measure rocket vehicle potentials and ambient electric fields in active auroras
20 p3542 A69-37793

Auroral sounding rocket research and instrumentation in Scandinavia, discussing auroral particles, optical measurements, probe experiments and scientific objectives
20 p3542 A69-37794

Rocket-borne IR astronomical telescope high altitude observations compared with balloon observations
20 p3605 A69-37800

X ray heliography by Fresnel-Soret type zoneplate camera to obtain solar photographs from rockets
20 p3544 A69-37803

Piezoelectric microphone sensor flown on rocket for recording micrometeoritic impacts during noctilucent cloud display, determining cosmic dust particles flux
21 p3793 A69-38348

Neutral components of arctic thermosphere measured with rocket-borne RF mass spectrometers, discussing origin of atomic hydrogen and water lines
21 p3704 A69-38367

Neutral particle density ratios in thermosphere by rocket-borne monopole mass spectrometers
21 p3704 A69-38368

Digital processing of rocket-borne mass spectrometers for measurements in upper atmosphere, discussing calibration
22 p3904 A69-40232

Rocket UV spectra indicating Venus atmosphere weak absorption and low ozone abundance and possible Jupiter surface depressions
22 p4028 A69-40661

Thin film temperature sensor material, response time, substrate material and flight instrumentation for rocket-borne application
22 p3950 A69-41229

ROCKET-BORNE PHOTOGRAPHY

Rocket-borne spectroheliograph for monochromatic solar photography in Mg II 2802.7 A line noting filter bandwidth, film polarizers and temperature control
11 p1884 A69-24838

Solar corona observations on eclipse day by Aerobee rocket launched in New Mexico correlated to Siberian total eclipse photograph
15 p2696 A69-31099

Magnetically focused electronographic image converters for far UV photography and spectroscopy from sounding rockets, discussing stellar observations
20 p3543 A69-37801

ROCKET CHAMBERS

U COMBUSTION CHAMBERS
U THRUST CHAMBERS

ROCKET COMBUSTORS

U COMBUSTION CHAMBERS
U THRUST CHAMBERS

ROCKET ENGINE CASES

Rocket motor integration into Scout vehicle to improve performance
02 p0335 A69-12384

Cost and weight optimization for solid rocket motors using various steel casings
[SAWE PAPER 777] 18 p3208 A69-34871

Microplasma, W inert gas and submerged arc welding processes for fabrication of rocket motor cases and pressure vessels, discussing material requirements and weldability
[SBAC PAPER 7] 20 p3550 A69-37449

Carbon fiber composites in construction of rocket motor cases, pressure vessels and support structures, including carbonization for ablation and insulation applications
23 p4180 A69-42158

Carbon fibers and resin composites used as rocket motor systems ablative liners and structures, noting role in motor weight reduction
24 p4336 A69-43210

ROCKET ENGINE CONTROL

Soviet book on rocket engines covering combustion, fuels, engine design, controls and employment of nuclear energy
01 p0143 A69-11196

Electrohydraulic guidance of second stage of Diamant rocket used for orbiting satellites employing thrust vector orientation
04 p0551 A69-15183

Fluidic proportional thruster system for sounding rocket control
[ASME PAPER 68-WA/FE-32] 05 p0763 A69-16105

Scout launch vehicle for launching small research satellites in near earth orbits, describing solid propellant stages, guidance, telemetry and beacon systems
06 p1016 A69-17597

Fluidic vortex valve warm gas flow control for rocket application
[AIAA PAPER 69-118] 06 p0872 A69-18147

Ammonium perchlorate exothermic decomposition control noting effects of preheating and ammonium fluoroborate additives
[WSCJ PAPER 68-25] 07 p1202 A69-18363

Rocket propulsion with gaseous bipropellant systems and attitude control
08 p1376 A69-20870

Rocket engine test facilities automation noting cost reduction and improved capabilities
10 p1671 A69-23258

Time optimal steering for rocket vehicle with trajectory defined between initial and final state, using minimum principle and boundary value problem solution
11 p1861 A69-25454

Control system design for Black Arrow satellite launch vehicle based on Black Knight test vehicle system
14 p2530 A69-29630

Contaminants formation during pulse mode operation of liquid bipropellant attitude control rocket engine, discussing exhaust plume effects
[AIAA PAPER 69-574] 16 p2870 A69-32774

Rocket nozzle control by side forces produced by secondary gas stream injection observed for relationship with inclination angle to nozzle axis
20 p3457 A69-37065

Automation application to rocketry, discussing process control in installations including control circuits and electronic direct digital control system
20 p3617 A69-37340

ROCKET ENGINE DESIGN

Book on material and design problems encountered in construction of high performance missiles, rockets and spacecraft, considering influence of space environment

01 p0084 A69-10021

Gamma type 2 rocket engine for second stage of Black Arrow satellite launcher

01 p0143 A69-10834

Black Arrow space vehicle uprating, considering engines burning kerosene with HTP and turbopumping systems

01 p0143 A69-10835

Soviet rocketry origin, technology, launch vehicles, boosters and orbital assembly concept

01 p0162 A69-11066

Soviet book on rocket engines covering combustion, fuels, engine design, controls and employment of nuclear energy

01 p0143 A69-11196

Glass fiber reinforced plastic /GFRP/ roving end grains in rocket combustion chambers, discussing design and structural parameters

02 p0305 A69-12748

High pressure rocket engine design, considering complete combustion, propellant feed system overall efficiency and thermodynamic gain

03 p0495 A69-12888

Solid propellant rocket engine designs for ELDO-PAS apogee motors, discussing use of advanced materials to improve mass ratio and strap-on boosters

03 p0495 A69-12890

Apogee stage and strap-on booster applications of solid propellant rocket motors, discussing configuration, functioning and performance

03 p0494 A69-12891

Sublimation solid reaction control, discussing propellants, nozzle performance, sublimation area, power, pressure drop, response and valueless design [AIAA PAPER 68-516]

04 p0552 A69-15322

Isotopic propulsion engine development problems, emphasizing single channel thermal power engine with hydrogen working fluid

05 p0811 A69-15596

Suborbital probes, discussing UK sounding rockets Skylark, Petrel and Skua configurations, capabilities and performances

06 p1012 A69-16859

Unsteady supersonic flow around thin circular cylinder representing rocket stage, calculating flutter and response to random environment [ONERA-TP-666]

06 p0857 A69-17098

Scout launch vehicle for launching small research satellites in near earth orbits, describing solid propellant stages, guidance, telemetry and beacon systems

06 p1016 A69-17597

Aerobell extendible nozzle rocket engine design and performance, cold flow and simulated hot flow test results [AIAA PAPER 69-4]

06 p0985 A69-18195

Liquid fuel rocket engine design for cooling by propellant counter flows

08 p1376 A69-20588

Optimal length conditions of liquid rocket combustion chambers, considering propellants, injection conditions, etc, noting graphs and differential equations solutions

08 p1376 A69-20606

NERVA rocket engine with 200,000-250,000 lb thrust to replace Saturn 5 upper stage for manned interplanetary flights, discussing Mars flight

08 p1410 A69-21029

Ion accelerators design for Kaufman thrusters in terms of beam optics and grid lifetime, using digital computer and electrolytic tank analog [AIAA PAPER 69-261]

09 p1567 A69-21261

Film cooling design criteria for small rocket engines [AIAA PAPER 68-617]

09 p1570 A69-21978

Rocket engine high energy hybrid propellant performance optimization, discussing engine enlargement, oxidizer injection geometry, fuel additives, combustion gas vorticity, etc

11 p1943 A69-25428

Book on theory and design of jet, rocket, nuclear, ion and electric propulsion systems noting combustion, detonation, fluid injection and space mission applications

11 p1943 A69-25582

Ion spacecraft propulsion systems, discussing components and characteristics of reaction type rocket engines and electrical thrust devices

11 p1944 A69-25593

Solid propellant rocket engine design for combustion stability, discussing length, pulse induced and acoustic instability types [AIAA PAPER 68-532]

12 p2191 A69-26788

Soviet book on liquid fuel rocket engines design covering gas expansion in nozzles, mixture formation, heat transfer, injectors and supply systems

12 p2148 A69-27078

Electric rocket propulsion, discussing roles of plasma and gas discharge physics in development of electromagnetic, electrostatic and thermoelectric nuclear systems

13 p2325 A69-28253

Nuclear rocket propulsion operation, design, properties and performance of electrostatic, electrothermal and electromagnetic systems

13 p2297 A69-28254

Rocket motors with combustion chambers of variable geometry for hybrid propellants, stressing toroidal chamber

15 p2671 A69-30600

Hybrid motor in sounding rocket using amino plastic as fuel and nitric acid as oxidizer, discussing advantages in cost, handling, thrust, performance, etc

16 p2835 A69-31744

Oxidizer injector face configuration for high power variable thrust rocket engine using hydrogen/oxygen propellant

16 p2835 A69-31749

Solid fuel rocket engine thrust and chamber pressure development curves from charge and engine geometry, heat of explosion and kinetic characteristics

16 p2836 A69-31994

Vaporization interaction liquid rocket performance model, discussing performance loss evaluation and test data [AIAA PAPER 69-470]

16 p2838 A69-32663

Heat pipes design for rocket engines cooling, discussing connections to space radiator and to heat rejection device and heat transfer capability [AIAA PAPER 69-582]

16 p2839 A69-32668

Oxygen difluoride-diborane propellant injector and chamber design criteria applied to unmanned spacecraft rocket engine development [AIAA PAPER 69-508]

16 p2839 A69-32671

Fluid controlled solid rocket motors design for Mars mission with acceleration level as parameter, discussing mission specifications, system design and component considerations [AIAA PAPER 69-446]

16 p2841 A69-32687

Nozzle throat ablative materials for controlled high regression rates in tactical rocket motors, primarily nylon reinforced thermosetting resins [AIAA PAPER 69-423]

16 p2804 A69-32710

Flox/methane pump fed engine, discussing RL-10-1-A engine tests and optimized 5000 lb thrust engine design [AIAA PAPER 69-510]

16 p2741 A69-32720

Engine and components reliability, discussing design stage and programming [AIAA PAPER 69-476]

16 p2795 A69-32771

Charged colloids generation by electrostatic spraying for thruster concept, subjecting metal capillary needles to AC voltage [AIAA PAPER 69-495]

16 p2846 A69-32773

Small penetration aid rocket motors fabrication, discussing axial- and tangential-thrust integral assembly, impulse levels, delay line connection for igniters, production evolution, etc [AIAA PAPER 69-520]

16 p2795 A69-32779

Europa 3 rocket design, comparing 2 ton geostationary satellites and 700 kg satellite conceptions

17 p3045 A69-33095

RF ion thrusters using electrodeless self sustaining mercury discharge, describing basic theory, component design, performance optimization and test results

17 p3018 A69-33326

Solid propellant thrusters fabrication procedures, design considerations and quality control, stressing stress analysis and propellant choice with respect to geometry

17 p3018 A69-33331

Hall ion thruster prime propulsion system, considering low and high voltage mode in plasma source I-V characteristics

17 p3019 A69-33338

Rocket motors using hydrazine as monopropellant, considering doping as means of using anhydrous hydrazine mixed with other products

17 p3019 A69-33340

German rocket engine industry reliability and performance, discussing solid fuel, two component fuel, single fuel hydrazine, mixed fuel and ramjet engines

17 p3021 A69-33361

Kaufman ion thruster ESKA 18 operation principles and design compared to RIT 10 and SERT 2, discussing discharge and focusing characteristics and propulsion parameters

17 p3022 A69-33605

Agna rocket vehicle production reliability evaluation program, testing specific representative equipment randomly selected from production stores

18 p3146 A69-34510

Solid propellant rocket motor predictive design by correlating performance and weight statistics via computer program [SAWE PAPER 775]

18 p3184 A69-34873

NERVA technology development, discussing reactor technology program, downward firing and flight-like configuration engine [AIAA PAPER 68-612]

19 p3371 A69-35942

Titan 3 transtage attitude control system hydrazine rocket engine design and performance, emphasizing problems associated with monopropellant [AIAA PAPER 69-422]

19 p3394 A69-36300

Soviet monograph on electrical rocket engines covering basics of nuclear, electrothermal, plasma and ion engines

20 p3586 A69-37236

Cryogenic core concept for flexible and economical delivery system [AIAA PAPER 68-812]

21 p3827 A69-39753

Laboratory prototype of RF ion engines for space test, discussing components optimization

22 p3998 A69-39904

Solid rocket motor static firing tests in low pressure environment, presenting data concerning vacuum chamber pressure, diffusers pressure distribution, chamber wall temperature distribution, etc

22 p4000 A69-40593

Thrust optimization for sounding rocket to reach maximum altitude with given initial and propellant weight, using polygonal time function and multiple-parameter numerical technique

22 p4037 A69-41050

Kaufman ionic thruster /ESKA 18/ principles, design, electrical circuit, working and experimental characteristics, compared with RIT 10 and SERT II

23 p4203 A69-41934

ROCKET ENGINES

NT ARC JET ENGINES
NT BOOSTER ROCKET ENGINES
NT CESIUM ENGINES
NT ELECTRIC ROCKET ENGINES
NT ELECTROSTATIC ENGINES
NT ELECTROTHERMAL ENGINES
NT F-1 ROCKET ENGINE
NT HOT WATER ROCKET ENGINES
NT HYBRID PROPELLANT ROCKET ENGINES
NT HYDRAZINE ENGINES
NT HYDROGEN OXYGEN ENGINES
NT ION ENGINES
NT LIQUID PROPELLANT ROCKET ENGINES
NT M-1 ENGINE
NT MICROROCKET ENGINES
NT NUCLEAR ENGINE FOR ROCKET VEHICLES
NT NUCLEAR ROCKET ENGINES
NT PLASMA ENGINES
NT RESISTOJET ENGINES
NT RESTARTABLE ROCKET ENGINES
NT RL-10-A-1 ENGINE
NT SOLID PROPELLANT ROCKET ENGINES
NT ULLAGE ROCKET ENGINES
NT VERNIER ENGINES

Soviet book on rocket engines covering combustion, fuels, engine design, controls and employment of nuclear energy

01 p0143 A69-11196

High thrust fluorine engines and propellants

03 p0494 A69-12889

Pressure and flow transients in liquid rocket engine feed systems predicted by method of characteristics

03 p0495 A69-12991

Chemical rockets theory for case of chemical equilibrium and frozen nozzle expansions

03 p0495 A69-13004

Performance, operational, economic and management selection criteria for choosing rocket engine for particular vehicle and mission, noting rocket engine propellants

04 p0647 A69-15296

Microorganism viability in rocket engine combustion environments used to determine probability of biological contamination of Mars by Voyager missions

05 p0714 A69-15949

Fluidic proportional thruster system for sounding rocket control [ASME PAPER 68-WA/FE-32]

05 p0763 A69-16105

- Initiation of HF combustion oscillation in premixed gas rocket
[ISAS-430] 06 p1029 A69-17025
- Advanced propulsion systems propulsive capabilities in connection with interstellar flights, considering rocket and ramjet propulsion, energy requirements and stellar plasma
06 p0984 A69-17631
- Flight research testing facilities at Arnold Engineering Development Center for rockets, turbojets, ramjet engines, aircraft, missiles, satellites and spacecraft
08 p1302 A69-20883
- Research and development program in annular slit colloid thruster technology, proving thruster feasibility by performance tests
[AIAA PAPER 69-287] 09 p1566 A69-21257
- MPD engine plasma flow investigated by Langmuir probe measurement of ion saturation current
[AIAA PAPER 69-233] 09 p1567 A69-21266
- Rocket motors for ejection of instruments from sounding rocket payloads, considering powder cartridges and solid propellant motor characteristics
10 p1635 A69-23032
- Ramjets and air augmented rockets as propulsion systems for supersonic atmospheric flight, noting inlet design, combustors and nozzles
11 p1943 A69-25586
- Rocket propulsion devices classifications, discussing energy sources, propellants, performance, space vehicle applications, liquid propellant rockets, engines, selection criteria and cooling methods
11 p1943 A69-25587
- Unsteady gas dynamics of explosions and detonation theory, noting applications to rocket propulsion systems performance
11 p1876 A69-25595
- Nozzle erosion profile, char penetration and temperature response predicted for nozzle material for 260 SL-3 motor
[AIAA PAPER 68-504] 12 p2118 A69-26784
- Charged particles generation by liquid subjected to high electric field for efficient bipolar microthruster
[AIAA PAPER 67-728] 13 p2325 A69-28220
- Tactical rocket propulsion - Conference, La Jolla, California, April 1965
16 p2836 A69-31991
- Compressible turbulent accelerating boundary layer flow model for convective heat transfer from rocket combustion gases, noting heat flux
16 p2878 A69-32000
- Small disturbances and effect on processes of fast combustion of inflammable compressible mixture
16 p2837 A69-32137
- Fast heat-up electrothermal ammonia thruster role in development of hybrid resistojet in millipound thrust range
[AIAA PAPER 69-496] 16 p2838 A69-32649
- Pilot chamber initiated thermal decomposition reactor concept for monopropellant thruster, discussing thrust levels and throttling ratios
[AIAA PAPER 69-420] 16 p2841 A69-32685
- Flight performance prediction for throttling bipropellant rocket engine utilizing ablative combustion chamber throat, discussing lunar module descent engine
[AIAA PAPER 69-452] 16 p2841 A69-32690
- Analytical evaluation of secondary flow injection effects on rocket engine performance including cold flow and simulated hot flow data
[AIAA PAPER 69-473] 16 p2844 A69-32726
- Cost reduction criteria for rocket propulsion systems and components, discussing literature searches, engineering criteria, total program cost vs mission accomplished, etc
[AIAA PAPER 69-440] 16 p2883 A69-32748
- Ammonia jet device to stabilize telecommunication satellites consisting of electric heating element, ejection nozzle and thermal screens
17 p3018 A69-33236
- Thrust vector control by secondary gas injection for predicting lateral thrust performance, applying method to rocket engines, secondary gas generator and injector configuration
17 p3019 A69-33333
- Continuous mode operation in hypergolic bipropellant low thrust rocket motors, discussing high temperatures reached by combustion chamber walls and cooling solutions
17 p3019 A69-33335
- Wire wound glass fibers for rocket motors, discussing rupture strength
17 p3021 A69-33357
- Aerodynamic characteristics of plane inviscid fluid jets expanding over curvilinear surface, deriving force equations for surfaces in jet and rocket engines
19 p3296 A69-35815
- LM descent engine behavior upon contact with lunar surface simulated, basing test condition on statistical trajectory analysis indicating fire until touchdown possibility
[AIAA PAPER 69-1020] 22 p3923 A69-40391
- Rocket motor combustion efficiency evaluated by chemical energy conversion to equilibrium, applicable to fuels, oxidizers and combustors at subsonic or supersonic velocity
23 p4239 A69-41919
- Performance test of German MPD plasma rocket engine with augmented magnetic field and 5-10 kw output, describing integral measurement procedure and observed phenomena
[DGLR-69-024D] 23 p4202 A69-41927
- ### ROCKET EXHAUST
- Optical measurements through retrorocket plumes of landing spacecraft, investigating reduced landing site visibility and modulation transfer function
02 p0248 A69-11765
- Diffraction by rocket exhausts, discussing electromagnetic signal attenuation based on two dimensional straight edge diffraction model
02 p0209 A69-12352
- Electrostatic potential generated by rockets on space vehicles, noting source of electric current in exhaust plumes and effect on instrumentation
03 p0522 A69-13903
- Altitude effects on radar attenuation in nonequilibrium solid propellant afterburning rocket exhaust plumes
04 p0685 A69-14730
- Nuclear rocket engine exhaust gas cooling by injecting water jet eliminates need for secondary cooling
[AIAA PAPER 68-604] 04 p0591 A69-15516
- Radar backscattering from turbulent rocket exhaust plumes
[AIAA PAPER 69-71] 06 p0891 A69-18071
- Optical absorption index for molten beryllium oxide based on measurements of small beryllium/solid propellant rocket motor exhaust plumes
08 p1351 A69-20149
- Propellant condensation on surfaces near electric rocket exhaust, calculating particle arrival rates, backflow and desorption energies
[AIAA PAPER 69-270] 09 p1565 A69-21252
- Electrostatic rocket exhaust condensation on spacecraft solar electric panels cover glasses, noting deleterious effects
[AIAA PAPER 69-271] 09 p1569 A69-21874
- Pressure and heating rate correlations for rocket exhausts impinging on flat plates and curved panels, generating axisymmetric real gas exhaust plumes
12 p2190 A69-26781
- Laser Doppler particle sensor to measure velocities in rocket exhausts, using He-Ne laser light source and Fabry-Perot interferometer frequency filter
[AIAA PAPER 68-723] 12 p2094 A69-26783
- Baker-Nunn photometry from Apollo tracking utilizing photographs for brightness, dynamics and duration of rocket exhausts and venting clouds
15 p2571 A69-31338
- Rocket stability monitoring by temporal radiometry, using exhaust radiance measurement to detect frequencies in thrust chamber combustion pressure
[AIAA PAPER 69-580] 16 p2839 A69-32670
- Stagnation point electrostatic probe for measuring local electrical properties of solid propellant rocket exhausts
[AIAA PAPER 69-573] 16 p2840 A69-32677
- Rocket exhaust plume flow fields studied for vehicle effects taking into account nozzle boundary layer, coalescence shock and nonisentropic flow
[AIAA PAPER 69-569] 16 p2842 A69-32696
- Test programs utilizing pitot probes to map exhaust plumes from liquid bipropellant engines in low ambient pressures conducted to verify calculations
[AIAA PAPER 69-575] 16 p2869 A69-32746
- Exhaust plume rarefaction from sonic orifice, considering continuum to transitional behavior for perfect gas
[AIAA PAPER 69-657] 17 p2892 A69-33465
- Attitude control rocket exhaust plume impingement effect on electrical performance and mechanical damage of commercial silica covered silicon solar cells
19 p3252 A69-35700
- Accelerometer force balance method for measuring aerodynamic rocket plume forces acting on flat plate model in short duration shock tunnel test environments
19 p3292 A69-35737
- Water injection cooling of exhaust gases during stage testing of NERVA engine, discussing exhaust duct configuration and flow characteristics, spray nozzle geometry, etc
[AIAA PAPER 69-514] 19 p3372 A69-36301
- Chemical and thermal behavior of materials corrosion in propellant exhaust gases with analysis of reactions involving hydrogen, nitrogen, water, carbon dioxide, etc
21 p3784 A69-39489
- Outer space rocket plumes simulation facility combining low density wind tunnel and molecular sink properties, discussing role of liquid nitrogen cooled diffuser-precooler
22 p3928 A69-40731
- Liquid alumina particles agglomeration in convergent and throat region of nozzle leading to performance decrease by increasing velocity and temperature difference between phases
22 p4001 A69-40929
- Apollo 11 observations of lunar surface glazing, considering radiation heating due to solar outbursts, rocket exhaust effects, shock heating or volcanism, erosion, etc
23 p4216 A69-42202
- Rocket exhaust plume models for signal attenuation predictions, considering inhomogeneous plasma medium with varying electron density and collision frequency
24 p4408 A69-43253
- ### ROCKET FIRING
- #### NT RETROFIRING
- Nozzle erosion profile, char penetration and temperature response predicted for nozzle material for 260 SL-3 motor
[AIAA PAPER 68-504] 12 p2118 A69-26784
- ### ROCKET FLIGHT
- Soviet look on inertial control of ballistic rockets covering rocket flight deviations measured by onboard sensors and computer
01 p0113 A69-10994
- Rocket guidance, discussing foreign systems with emphasis on German range miss/gradient orientation scheme used on World War II V-2 rockets
02 p0279 A69-12362
- Cosmos 253 rocket reentry and fragmentation over England
05 p0830 A69-16656
- Psychomotor reactions to zero gravity during ballistic rocket flights, analyzing electrical activity of cortex in animals
06 p0874 A69-17649
- Oculomotor muscular tonus of rabbit during rocket flight acceleration and weightlessness
07 p1062 A69-18590
- Variation in spinning velocity around axis of last stage of solid propellant rocket in flight
08 p1409 A69-20160
- Black arrow rocket vehicle flight path computer programming, discussing geographical restrictions on design
09 p1593 A69-21616
- Constant acceleration relativistic rocket flight from inertial rocket and terrestrial point of view compared, examining light flash transmission and arrival time
09 p1609 A69-21959
- Coasting arc determination in rocket trajectory problems by Lagrange multipliers
09 p1595 A69-21969
- Psychomotor reaction time and motions, myogenic tonus at rest and precision of monkeys during rocket flights along ballistic curve, noting weightlessness effect
10 p1646 A69-23575
- Rocket trajectory determination by tracking on-board light source against star background with image orthicon TV system
12 p2033 A69-26965
- Aerodynamic failure investigation of Black Brant 2 single stage sounding rockets
15 p2703 A69-31545
- Hazards model for probabilistic prediction of casualties by exploding solid propellant rockets, deriving casualty expectation equation
[AIAA PAPER 69-461] 16 p2869 A69-32749
- Regularization method for maximum height ascent of rocket uniformly approximating control function by gradient projection method
18 p3164 A69-34706
- Mechanics of missile dispersion due to dynamic imbalance and rocket spin stabilization problems
[SAWE PAPER 741] 18 p3208 A69-34886
- Operational missile flight program validation plan noting mission analysis, computer programming, program preparation and performance prediction
19 p3279 A69-35955
- Single stage rocket control and trajectories for maximum target strike probability within given range
21 p3818 A69-38857

ROCKET FUEL TANKS

Integrals of motion for minimum fuel rocket trajectories in inverse square field calculated for constant power and constant exhaust rockets
[AIAA PAPER 69-904] 21 p3806 A69-39336

Equations of motion of unguided rocket under wind effect, calculating launch angles for wind compensation 22 p4037 A69-40815

ROCKET FUEL TANKS

U PROPELLANT TANKS

ROCKET LAUNCHERS

Optical sighting method for determining orientation of rocket on launch pad by laser collimator, noting lining-up of Cassiopeia system 06 p0930 A69-17104

HORA, flexible upper rocket stage, noting variable fuel tank capacity and high energy propulsion 08 p1409 A69-20094

Belier rocket launching facilities in Guiana, describing pads, tracking system, telecommunications network, etc 09 p1477 A69-22161

Space vehicle launcher system reliability from trials and adopted corrections, basing formal computation on adoption of normalized form for reliability likelihood 20 p3618 A69-38278

ROCKET LAUNCHING

NT LUNAR LAUNCH

NT ORBITAL LAUNCHING

Europe 1 carrier rocket prelaunch wind load calculations as base for launch or delay decision 01 p0160 A69-10032

French space center in Guiana, discussing geographic location advantages for payload, rocket launching, space rendezvous, etc 02 p0228 A69-11920

Temporary launching sites for rocket probes, discussing CNES activity, Dragon and Titus programs and mobile launching units 02 p0228 A69-11921

Space vehicle checkout, launch control and data monitoring by general purpose ground system providing flexible stimuli generation, measurement acquisition, computation and information display 18 p3118 A69-35064

Rocket launch system cost role in space operations, discussing low cost expendable drop tank and Triamese reusable launch vehicle/spacecraft concepts 18 p3210 A69-35087

Successful launch probability analyzed as function of launch strategy from past countdown hold data 19 p3430 A69-36034

Trajectory optimization of second state of rocket launched into earth circular orbit in gravitational field by stepwise fuel control, using Pontryagin maximum principle 21 p3829 A69-39818

Equations of motion of unguided rocket under wind effect, calculating launch angles for wind compensation 22 p4037 A69-40815

Nonlinear model including rocket rotary and forward motion inside smoothbore launcher utilizing dynamic friction coefficient 22 p4037 A69-41038

ROCKET LININGS

Fiberglass reinforced plastics internal heat shielding for isopropyl nitrate rocket combustion chamber, considering lining resistance and safety during repeated firing/Ludion motor/ 17 p3019 A69-33343

ROCKET NOSE CONES

Nose cone ejecting system with pyrotechnic devices for two stage Centaur rockets/Sud-Aviation/ with RF mass spectrometer 10 p1635 A69-23034

Sounding rocket aerodynamic stability as function of nose length and mass, discussing wind tunnel test data 19 p3432 A69-36761

Dornier ASTRID attitude stabilization system design for spinning rocket nose cone with instrument payload, using first stage biaxial inertial platform and second stage star tracker 21 p3826 A69-39639

ROCKET NOZZLES

Precracked ceramic rocket nozzle throat inserts, discussing improved thermal displacement accommodation, load transmission, fracture tolerance, articulation capability, etc 02 p0334 A69-12369

Material requirements for uncooled nozzles of solid propellant rocket motors burning aluminumized propellants, discussing successful testing of pyrolytic graphite 06 p0946 A69-17530

Aerobell extendible nozzle rocket engine design and performance, cold flow and simulated hot flow test results [AIAA PAPER 69-4] 06 p0985 A69-18195

Hydraulic control valves for guidance of rockets by secondary liquid injection into nozzle skirt, discussing structure, single nozzle missile and mass gain 07 p1230 A69-19293

Passive temperature indicators for maximum temperatures attained within rocket nozzle ablative materials 15 p2613 A69-31273

Optimum nonequilibrium nozzle performance for hydrogen-fluorine propellant system, considering contour, engine/nozzle weights and recombination kinetics [AIAA PAPER 69-472] 16 p2733 A69-32652

Flow disturbances in supersonic rocket nozzles due to secondary injection analyzed by effective body approximation, including side forces [AIAA PAPER 69-443] 16 p2839 A69-32666

Free flow field from underexpanded rocket motor nozzle and impingement effects of pressure and heat transfer to flat plate [AIAA PAPER 69-568] 16 p2842 A69-32693

Metal oxide particle growth processes in rocket chambers and nozzles, using generalized kinetic-coagulation equation [AIAA PAPER 69-541] 16 p2844 A69-32724

Constant chamber pressure thrust throttling of expansion-deflection rocket nozzle, calculating wall static pressure and thrust by characteristics method, discussing performance [AIAA PAPER 69-435] 16 p2846 A69-32776

Ablative materials for solid rocket nozzles, discussing static firing tests, rating system, equipment design and cost reduction 19 p3357 A69-35537

Large booster nozzle reuse, discussing design, refurbishment, performance, costs and test evaluation [AIAA PAPER 68-657] 19 p3394 A69-35944

Rocket nozzle control by side forces produced by secondary gas stream injection observed for relationship with inclination angle to nozzle axis 20 p3457 A69-37065

Hydrogen and methane combustion to simulate expansion of storable propellants [AIAA PAPER 68-635] 20 p3631 A69-37188

Cement materials to attach thermocouple to stainless steel tubing in nuclear rocket engine nozzle, considering thermal conductivity, bond and tensile and compressive strengths 21 p3753 A69-39699

Computerized solid rocket motor nozzle design with computer program providing weight, envelope and performance values for vehicle optimization studies [AIAA PAPER 69-975] 22 p3999 A69-40355

Rarefaction onset along streamline from rocket nozzle with small Knudsen number at exit plane 23 p4152 A69-41920

Graphite rocket engine nozzles chemical erosion at various temperatures, comparing reaction and diffusion rates 23 p4180 A69-42156

Refractory metals in rocket propulsion devices, applying tungsten in uncooled rocket nozzles and tungsten and rhenium to electrothermal propulsion 23 p4177 A69-42161

ROCKET OXIDIZERS

NT FLOX

Treatment procedure and preventive programs outlined for acute exposure to toxic rocket fuels or oxidizers 02 p0204 A69-12498

Photochemical ignition of low pressure fuel-oxidizer mixtures applied to unsensitized stoichiometric mixtures of methane-oxygen and hydrogen-oxygen [WSCIPAPER 68-42] 06 p1034 A69-17791

Laser flowmeter for pulse flow of highly corrosive rocket fuels and oxidizers with measured rise times less than 10 msec 15 p2616 A69-31292

Advanced liquid fuels and oxidizers development from rocket propulsion reaction principle 16 p2828 A69-31747

Oxidizer injector face configuration for high power variable thrust rocket engine using hydrogen/oxygen propellant 16 p2835 A69-31749

Composite propellants high pressure burning stability with various binders and oxidizers, showing ammonium perchlorate oxidized formulations susceptibility to instability [AIAA PAPER 69-438] 16 p2834 A69-32704

Compositional and oxidizer particle size effects on combustion instability of plastic propellant based on ammonium perchlorate and polyisobutene [AIAA PAPER 69-478] 16 p2834 A69-32734

Powdered oxidizer and infusible polymer binder combustion at various pressures, studying gaseous phase temperature field by optical color analysis 17 p3069 A69-33135

Composite modified cast-double-base rocket propellants with large proportions of metallic fuel and oxidizer, discussing application rocket propulsion 17 p3017 A69-33349

Impurities effect on corrosion of fluorine containing propellant oxidizer systems, noting aqueous and anhydrous hydrogen fluoride corrosion 21 p3784 A69-39487

ROCKET PLANES

U X-15 AIRCRAFT

ROCKET PROPELLANT TANKS

U PROPELLANT TANKS

ROCKET PROPELLANTS

NT AEROZINE

NT CRYOGENIC ROCKET PROPELLANTS

NT DOUBLE BASE ROCKET PROPELLANTS

NT GASEOUS ROCKET PROPELLANTS

NT GELLED ROCKET PROPELLANTS

NT HYPERGOLIC ROCKET PROPELLANTS

NT LIQUID ROCKET PROPELLANTS

NT METAL PROPELLANTS

NT MONOPROPELLANTS

NT SOLID ROCKET PROPELLANTS

Treatment procedure and preventive programs outlined for acute exposure to toxic rocket fuels or oxidizers 02 p0204 A69-12498

Increased payload in orbit capability for future versions of Black Arrow vehicle, discussing propellant 02 p0335 A69-12681

Relative weight of fuel required for flight along prescribed flight trajectory 03 p0519 A69-12964

Integrated Waste Management/Rocket Propulsion System, using human feces as propellant component [SAE PAPER 680717] 03 p0495 A69-13442

Rocket propulsion with gaseous bipropellant systems and attitude control 08 p1376 A69-20870

Medical examinations of missile fuel handlers, noting some abnormal results in liver function tests and possible hydrazine toxicity 09 p1447 A69-22556

Book on rocket propellants covering propulsion fundamentals, liquid, solid and hybrid propellants properties, performance calculations, rocket technology, etc 10 p1752 A69-23806

Injected propellant behavior during one dimensional passage through rocket combustion gas chamber, considering Reynolds number and propellant characteristics 11 p1941 A69-24329

Combustion rates of condensed systems under positive and negative accelerations at atmospheric pressure 11 p2001 A69-25195

Mercury electron bombardment thrusters, discussing mission, design, ground tests, components and thrust vectoring 12 p2148 A69-26787

Photochemical attitude control rocket adaptable to self contained command signal or remote signal transmission, discussing light irradiation of propellant for thrust control 12 p2148 A69-26801

Lunar soil as building material and extraction of water, oxygen and rocket propellants from lunar materials for lunar colony needs 13 p2352 A69-27907

Rocket propellants, propellant chemistry and rocket propulsion system performance 13 p2324 A69-27916

Laser flowmeter for pulse flow of highly corrosive rocket fuels and oxidizers with measured rise times less than 10 msec 15 p2616 A69-31292

Propellant orientation and expulsion methods in space vehicle tankage, discussing ullage rockets system, bladders and diaphragms, dielectricphoretic expulsion, etc 16 p2736 A69-31734

Flight performance prediction for throttling bipropellant rocket engine utilizing ablative combustion chamber throat, discussing lunar module descent engine [AIAA PAPER 69-452] 16 p2841 A69-32690

- Aluminum capsule used in test reactor to irradiate explosive and propellant samples, determining radiation effects
17 p3004 A69-32945
- Vernier motor for Europa 1 rocket third stage, discussing component design, system performance and fuel composition
17 p3018 A69-33328
- Numerical integration of plane orbital transfers with multiple powered arcs, minimizing propellant expenditure of small thrust chemical rocket
19 p3400 A69-35673
- Rocket engines propellant feed systems dynamics analyzed by model using linear methods with distributed-parameter pipe representation
[ASME PAPER 69-FE-6] 20 p3586 A69-37987
- ### ROCKET PROPELLED SLEDS
- Hypersonic slipper bearing problem in rocket boosted sleds, discussing flow model consisting of laminar stagnation region and boundary layers
[AIAA PAPER 68-736] 09 p1477 A69-22003
- Multicomponent force transducer for measuring track generated forces acting on rocket sled, discussing combined load and vibration tests
[ASME PAPER 69-VIBR-21] 10 p1698 A69-24168
- Parachute deployment load control by use of line ties from rocket sled tests
11 p1823 A69-25386
- Rocket sled incorporating magnetic suspension system
15 p2585 A69-30361
- Lift and drag determination for moving rectangular coils over infinite plane sheet for magnetic suspension and guidance for rocket sleds
17 p2946 A69-33789
- ### ROCKET SONDES
- #### U SOUNDING ROCKETS
- ### ROCKET SOUNDING
- Sporadic E layer structure observed by rocket borne probes relation to ground based radio techniques, showing agreement between plasma and blanketing frequencies
01 p0070 A69-11161
- Nighttime sporadic E rocket measurements, discussing descending layer thickness and electron density and lower boundary
01 p0071 A69-11165
- Sporadic E structure and composition measured above White Sands by rocket-borne planar ion trap and two RF ion mass spectrometers
01 p0071 A69-11166
- LF continuous wave rocket propagation in D region presented in terms of electron density profiles
01 p0076 A69-11232
- Far IR rocket observations of night sky background radiation
01 p0121 A69-11249
- French radio astronomy, presenting sky background radiation and solar emission results from Rubis 02 and 04 rockets
02 p0316 A69-11908
- Middle ionosphere temperature diurnal variations analyzed on basis of rocket experiments and electron density asymmetry
02 p0246 A69-12768
- Ionospheric electron temperature probe analysis based on Japanese Kappa rocket data
05 p0761 A69-15701
- High resolution electron and proton energy measurements by sounding rockets indicating plasma sheet as source of energetic auroral electrons
05 p0756 A69-16273
- Simultaneous rocket measurements of D region temperatures and electron densities on anomalous winter day
05 p0758 A69-16411
- Lunar umbra interception by Titus rockets during solar eclipse, measuring UV and IR flux
06 p0986 A69-17101
- Rocket-borne Rayleigh scattering instrumentation to measure atmospheric density, discussing instrumentation and flight results
06 p0927 A69-17698
- Sporadic E layers compared with model of electron concentration profile, using rocket measured profile data for computing ionogram
06 p0922 A69-17750
- PCM telemetry system for sounding rocket payloads flown in polar light zone within German-American project AZUR
07 p1081 A69-19099
- Low latitude easterly wind measurements by optical tracking of chemicals from sounding rockets and gun probes during darkness
09 p1487 A69-21621
- Auroral electron flux from particle fluxes measured with shielded Geiger-Muller telescopes mounted in rocket launched into diffuse aurora
09 p1576 A69-21663
- Quadrupole mass filter for rocket-borne measurements of thermospheric helium content, discussing turbopause level and winter helium bulge
09 p1489 A69-21712
- Auroral French rocket probe in Norway, studying low energy particles, relations between electron showers and high altitude electric fields, etc
09 p1498 A69-22160
- Upper hybrid and modified plasma resonance on basis of rocket-borne gyroplasma probe data
10 p1726 A69-22807
- Venus and Jupiter low resolution UV spectra obtained with servocontrolled star tracking telescope in Aerobee rocket, noting Lyman alpha radiation characteristics
[JHU-TR-15] 10 p1788 A69-24121
- Radar backscatter and rocket profiles of ionospheric electron temperature, noting agreement in daytime flight measurements
11 p1951 A69-25162
- Air movement component of winter anomaly effect on radio wave absorption in mesosphere directly detected by rocket sounding
11 p1913 A69-25436
- Lower ionosphere electron densities measured during solar eclipse by Nike-Apache rockets
12 p2073 A69-26861
- Rocket observations of visible and UV dayglow, using electron density and temperature measurements for emission rates of various excitation mechanisms
12 p2076 A69-27108
- Collection of Soviet papers on U.S.S.R. outer space studies /1957-1967/ covering rocket and satellite sounding, meteorology, radiation belts, etc
13 p2335 A69-27346
- Soviet rocket and satellite studies of upper atmosphere and ionosphere
13 p2251 A69-27347
- Soviet meteorological and geophysical rockets, satellites and techniques in cloud studies and weather forecasting, noting Cosmos results
13 p2290 A69-27348
- Rocket spectrographic observations of Alpha Virginis noting hydrogen Lyman absorption lines
13 p2338 A69-27555
- Night sky background observation by near IR radiation flux, using rocket-borne telescope and ground based equipment
13 p2342 A69-27600
- Rocket grenade measurements of earth atmosphere, finding lowest temperature in Alaska
13 p2255 A69-28637
- Ionospheric electron and ion temperatures correlated with electron concentration profile as measured by rockets and satellites
14 p2510 A69-28942
- Rocket and satellites topside sounding of earth ionosphere, determining magnetoplasma structure and resonance
14 p2438 A69-29101
- Earth radar studies, relating echo behavior to rocket altitude and surface electrical characteristics
14 p2416 A69-29531
- Radio propagation in upper atmosphere and ionosphere noting rocket and satellite experiments including plasma physics research, tropospheric studies and space science services
14 p2526 A69-29854
- Solar corona observations on eclipse day by Aerobee rocket launched in New Mexico correlated to Siberian total eclipse photograph
15 p2696 A69-31099
- Photometric rocket measurements in hydrogen auroras, finding vertical H beta emission profile estimate of proton energy spectrum for H beta production cross section
15 p2598 A69-31307
- Diurnal variations of wind velocity, temperature and density at high altitude measured by Skylark rockets
15 p2598 A69-31319
- Diurnal change in equatorial electrojet parameters observed by magnetometers on Nike Apache rockets
15 p2598 A69-31320
- Wintertime short term density variability in upper atmosphere obtained from rocket measurements
15 p2601 A69-31374
- Rocket and satellite measurements of density, temperature and composition in lower thermosphere, considering altitude dependence
15 p2602 A69-31383
- Inflight shadowing device incorporated into dust particle collection devices borne in Aerobee rocket sampling noctilucent cloud display over Fort Churchill
15 p2602 A69-31386
- Rocket ejected vapor trails structure in lower thermosphere showing no evidence of atmospheric turbulence
15 p2602 A69-31393
- Rocket observations of ozone concentration above 50 km by absorption spectroscopy, noting altitude dependence
15 p2603 A69-31397
- Sporadic E layer nighttime electron density profiles obtained by Langmuir probe equipped sounding rockets
15 p2603 A69-31398
- Diurnal variations of atmospheric ion composition at 100-200 km from rocket experiments
15 p2603 A69-31401
- Ionospheric ion composition at 130-155 km during meteor shower Orionides activity from geophysical rocket-borne RF mass spectrometer data
15 p2603 A69-31406
- Ion-molecular reactions measurements in ionosphere by VV type device and RF mass spectrometer
15 p2603 A69-31407
- Nighttime, twilight and daytime rocket experiments for ion composition of polar ionosphere at 100-180 km
15 p2604 A69-31414
- Soviet meteorological rocket sounding data for upper atmosphere compared to CIRA 1965 model
15 p2650 A69-31421
- Simultaneous particle flux and VLF noise spectrum measurements by rocket sounding, discussing equipment, telemetry and calibration systems and experimental data
15 p2605 A69-31423
- VLF and particle rocket experiment for group delay time between rocket and ground, discussing wave polarization and energy flows meaning
15 p2571 A69-31424
- British rocket and satellite experiments in space research, considering neutral atmosphere, ionosphere and solar radiation, orbital analysis, etc
15 p2724 A69-31463
- Virgo XR-1 rocket observations, presenting count rate histograms, differential photon spectrum and X ray and M87 core radio spectra
15 p2701 A69-31535
- FM/FM telemetry system for high altitude rocket research, using independent subcarrier oscillator for each measurement transmitted with individual frequency modulation
16 p2750 A69-31853
- Data processing for scientific rocket research, considering pulse counters, multiplexers, converters and programmers
16 p2755 A69-31858
- Spectrometric rocket measurements of ion concentrations between 200 and 630 km
16 p2774 A69-31974
- LF ground based absorption results compared with rocket measured D region electron density profiles
16 p2778 A69-32188
- Night sky far IR observation by rocket-borne telescope, discussing minimum signal detection and origin
16 p2781 A69-32445
- Auroral electrons measurement by rocket, discussing difficulties due to secondary electrons and method permitting primary electrons detection threshold determination as function of rocket position
16 p2785 A69-32617
- Vertical atmospheric pressure distribution measured directly with Pirani-Israel gauge in Skylark rocket, transforming dynamic pressure data into static pressures on ground
17 p2971 A69-33037
- Rocket instrumentation for electron and proton spectra measurement in aurora borealis
17 p2972 A69-33038
- Tacite rocket probe to study space IR radiation, using passive stellar sensor for recording reference stars positions to recalibrate gyroscope kinetic motion for attitude restoration
[ONERA-TP-731] 17 p3001 A69-33220
- Vertical structure concepts for air density, wind and sound velocity profiles in rocket climatology, discussing vertical relationship of wind shear statistics
17 p3000 A69-33794

Noctilucent cloud layer spectral brightness and transparency in E region determined from transhorizon rocket observations

18 p3130 A69-35148

Quiet aurora atomic O red and green lines intensity ratio measured from rocket

18 p3201 A69-35192

Search for diffuse galactic light component between 2100-2800 Å by rocket measurements of night sky brightness, showing low albedo of interstellar dust

18 p3202 A69-35210

Franco-Soviet rocket probe launchings for measuring daytime/nighttime ions and neutrons

18 p3210 A69-35282

Rocket observations of ionospheric E layer winds using Na release method

20 p3529 A69-37796

Rocket probe devices based on thermometrical body principle for measuring upper atmosphere water vapor and atomic oxygen

20 p3543 A69-37798

Ambient atmospheric temperature and molecular nitrogen density measured simultaneously by rocket-borne electron beam luminescence method

20 p3543 A69-37799

Meteor winds analysis method used on tidal period wind measurement data obtained by chemical release from rocket in 95-135 km region

20 p3574 A69-38092

Rocket and satellite particle collection experiment to confirm reduced micrometeoroid flux near earth, noting inconclusive size frequency distributions of exposed flight samples

21 p3793 A69-38343

Noctilucent clouds formation relation to ice sublimation, discussing rocket soundings

21 p3701 A69-38345

Corpuscular radiation indicated as ionization source in lower ionosphere from rocket sounding data, noting role in D region formation

21 p3787 A69-38352

Rocket observation of ionospheric electron and positive ion densities and dayglow emission intensities in twilight conditions

21 p3702 A69-38355

Rocket observations of VLF ionospheric resonances, noting artificial stimulation of detectable amplitude noise with cut-off at low hybrid resonance frequency

21 p3671 A69-38356

Rocket photometer observations of midnight atomic oxygen glow at 6300 Å during ascending and descending flights

21 p3703 A69-38360

Auroral parameters coordinated measurements at varying rocket pitch angles during penetration of diffuse aurora breakup phase

21 p3703 A69-38361

Wind motion and turbulence in upper atmosphere from Rehbar 15 and 16 rocket observations

21 p3703 A69-38362

Rocket measurement • data of auroral particle precipitation classified in substorm phases of quiet and breakup period, breakup and postbreakup events and morning events

21 p3707 A69-38489

Rocket measurements indicating auroral electrons modulation near equatorial plane, noting intensity changes as function of rocket flight time and altitude

21 p3709 A69-38499

Ionospheric currents geophysical DC electric fields measurement from sounding rockets, indicating anticorrelation with auroral luminosity

21 p3710 A69-38508

Spectra and intensities of rocket releases for upper atmosphere composition, temperature and reaction kinetics, noting chemiluminescence and atomic and molecular emissions

21 p3712 A69-38522

Rocket optical experiment for determining water, methane, nitric oxide and ozone vertical profiles in stratosphere and mesosphere

22 p4035 A69-39910

Far IR nightglow emission from atomic oxygen observed by rocket-borne liquid He-cooled telescope

22 p3940 A69-40521

Low energy X ray flux existence in Cen X-2 observed by rocket flight

22 p4007 A69-40773

Sco X-1 X-ray source energy spectrum and time variation from rocket flights in India

22 p4030 A69-40774

Lower ionosphere vertical wind velocity profiles determined from rocket-released grenade glow cloud

photographs, developing cloud buoyancy effect empirical model

23 p4154 A69-41305

Midlatitude ionospheric electron density rocket data survey, including nighttime and daytime N/h profiles for specific solar activities

23 p4155 A69-41563

Rocket measurements of plasma densities and temperatures in visual aurora using electrostatic onboard and ejected Langmuir probes, observing hyperthermal electron

23 p4167 A69-42334

Polarimeter using 45 degree Bragg angle reflection applied to rocket payload design for determining polarization of celestial sources X rays

23 p4207 A69-42382

Equatorial stratosphere and mesosphere wind, temperature and density data from rocket and balloon sounding, noting seasonal variations and possible stratosphere-ionosphere coupling

23 p4159 A69-42423

H beta production in hydrogen aurora measured during rocket flight, obtaining proton energy spectrum

24 p4309 A69-43170

Soft cosmic X ray background flux from rocket observations on 21 September 1968 from White Sands, discussing flux origins

24 p4368 A69-43220

ROCKET TEST FACILITIES

White Sands Missile Range space and missile test facilities and support facilities for space exploration

02 p0227 A69-11761

Asynchronous on-line digital data acquisition system with immediate access to on-site numerical real time printout for rocket engine performance tests

[AIAA PAPER 69-323] 09 p1478 A69-22381

Rocket engine test facilities automation noting cost reduction and improved capabilities

10 p1671 A69-23258

Short duration tube wind tunnel supersonic testing, noting Saturn S-1C base heating and solid propellant rocket base burning tests

[AIAA PAPER 69-335] 13 p2242 A69-28271

Subcontractors documentation coordination system for Mississippi Test Facility, identifying end items for maintenance and spares provisioning

18 p3118 A69-35063

Test stand for measurement of forces and moments from thrust vector controlled rocket, analyzing dynamic characteristics of hydrostatic supports

21 p3691 A69-39631

ROCKET THRUST

NT RETROTHRUST

French solid propellant sounding rockets proposed launching from Guiana base using different fuel propulsion systems

03 p0518 A69-12851

Soviet book on gas dynamics of solid fuel rocket motors covering combustion chamber flow, nozzle and thrust characteristics, pressure relaxation and channel charge

04 p0647 A69-15493

NERO thrust power measurement, discussing electromagnetic and strain-gage test stands

08 p1301 A69-20156

Rocket engines transient thrust measurement by quartz transducers

08 p1301 A69-20589

Photochemical attitude control rocket adaptable to self contained command signal or remote signal transmission, discussing light irradiation of propellant for thrust control

12 p2148 A69-26801

Solid fuel rocket engine thrust and chamber pressure development curves from charge and engine geometry, heat of explosion and kinetic characteristics

16 p2836 A69-31994

Liquid propellant injector design for rocket thrust chambers, discussing mass and mixture ratio regulation

16 p2836 A69-31999

Agema propulsion system performance model for predicting propellant flow rate, mixture ratio, thrust time and specific impulse

[AIAA PAPER 69-453] 16 p2841 A69-32683

Constant chamber pressure thrust throttling of expansion-deflection rocket nozzle, calculating wall static pressure and thrust by characteristics method, discussing performance

[AIAA PAPER 69-435] 16 p2846 A69-32776

Small penetration aid rocket motors fabrication, discussing axial- and tangential-thrust integral assembly, impulse levels, delay line connection for igniters, production evolution, etc

[AIAA PAPER 69-520] 16 p2795 A69-32779

Aerothermodynamic problems during transition after activation of thrust inverter in solid propellant rocket engines

17 p3018 A69-33327

Thrust magnitude and direction modulation of hybrid propellant engine, noting applications

17 p3019 A69-33337

Kaufman ion thruster ESKA 18 operation principles and design compared to RIT 10 and SERT 2, discussing discharge and focusing characteristics and propulsion parameters

17 p3022 A69-33605

NERVA engine operational cycle and performance, discussing startup, thrust buildup and shutdown

[AIAA PAPER 69-515] 18 p3170 A69-34809

Numerical solution of equations of motion of rocket under thrust in inverse square force field, discussing effects of initial acceleration

20 p3595 A69-37203

Minimum fuel thrust limited transfer trajectories computation for coplanar elliptic orbits

[AIAA PAPER 69-914] 21 p3808 A69-39344

ROCKET VEHICLES

NT AEROBEE ROCKET VEHICLE
NT AGENA ROCKET VEHICLES
NT ATLAS CENTAUR LAUNCH VEHICLE
NT ATLAS SLV-3 LAUNCH VEHICLE
NT BERENICE ROCKET VEHICLE
NT BLACK BRANT 2 SOUNDING ROCKET
NT BLACK KNIGHT ROCKET VEHICLE
NT CENTAUR LAUNCH VEHICLE
NT DIAMANT LAUNCH VEHICLE
NT ELDO LAUNCH VEHICLE
NT KAPPA ROCKET VEHICLES
NT MULTISTAGE ROCKET VEHICLES
NT SATURN LAUNCH VEHICLES
NT SATURN S-1C STAGE
NT SATURN S-2 STAGE
NT SATURN S-4B STAGE
NT SATURN STAGES
NT SATURN 5 LAUNCH VEHICLES
NT SCOUT LAUNCH VEHICLE
NT SINGLE STAGE ROCKET VEHICLES
NT SKUA ROCKET VEHICLES
NT SKYLARK ROCKET VEHICLE
NT SOUNDING ROCKETS
NT TITAN LAUNCH VEHICLES
NT TITAN 3 LAUNCH VEHICLE
NT X-15 AIRCRAFT

Longitudinal stability of unsteady motion of flight vehicle along ballistic trajectory, using linear differential equations

07 p1230 A69-19701

Rocket vehicle inertial attitude reference system, discussing flight control

09 p1609 A69-21618

Time optimal steering for rocket vehicle with trajectory defined between initial and final state, using minimum principle and boundary value problem solution

11 p1861 A69-25454

Ballistically effective atmospheric parameters for rocket vehicle design manuals involving application of climatological concepts of meteorology

12 p2175 A69-26874

Soviet book on rocket aerodynamics covering configurations, lifting, stabilizing and control surfaces, friction and heat transfer characteristics

17 p2889 A69-32829

Vibration analysis, using rigid body and normal modes to solve interconnection problem, applied to free-free natural vibration modes of clustered rockets

20 p3621 A69-37195

ROCKETRY

U ROCKETS

ROCKETS

Professional programs for aeronautics, rocketry and astronautics development

18 p3233 A69-34552

Rocket body elastic vibrations, liquid fuel supply oscillations and engine thrust vibrations effects on station stability

20 p3617 A69-37604

ROCKS

NT ANDESITE
NT BASALT
NT BRECCIA
NT COAL
NT ECLIGITE
NT ENSTATITE
NT GRANITE
NT IGNEOUS ROCKS
NT LAVA
NT MAGMA
NT MOLDAVITE
NT OLIVINE
NT PYROXENES
NT QUARTZ

NT SANDSTONES

NT SHALES

X Ray fluorescence of rock samples as applied to geological problems, noting standard deviations for element distribution

01 p0082 A69-10890

Lunar rock composition monitored by Luna 9 and 13 soft landed lunar probes
[UN PAPER 68-95769]

06 p1000 A69-17041

Griffith crack in brittle material, discussing validity for rock-like material with nonlinear stress-strain relationship

06 p1020 A69-17128

Complex index of refraction of naturally occurring rock and mineral as function of wavelength of incident radiation

17 p2973 A69-33093

Data on mass distribution of terrestrial fragmented rocks to interpret lunar rock samples, noting origin of asteroids and meteorites

20 p3613 A69-38250

Lunar surface, asteroids and meteorites properties by mass distributions of fragmented rocks

21 p3800 A69-38677

Amino acid components in paleozoic plant fossils and rock samples noting glycine, serine and glutamic acid

21 p3662 A69-39535

Physicomechanical properties of tuff rock based on similarity to lunar surface rock, determining natural density, porosity and compression strength

22 p4034 A69-41105

Lunar rocks types determination by mass spectrometry, describing results of terrestrial rocks tests

22 p4034 A69-41106

RODENTS

NT GROUND SQUIRRELS

NT GUINEA PIGS

NT HAMSTERS

NT MICE

NT POCKET MICE

NT RABBITS

NT RATS

Rodents exposure to neon enriched atmosphere for three weeks in sealed recycling system, discussing body weight pregnancies and litter

01 p0019 A69-11342

Computer analysis of cortical and subcortical activity in yellow bellied marmot during sleep, hibernation and hypothermia

10 p1643 A69-23122

Learned behavior performance failure in hypothermia as temperature dependent phenomenon using rat, guinea pig, chinchilla, mouse, gerbil and hamster

10 p1643 A69-23124

RBE of fast neutrons on mice, rats and guinea pigs, discussing suppression of mitosis in isolated cells

20 p3478 A69-37629

RODS

Finite deformation mode stability for finite amplitude first diameter nonlinear plastic wave initiation and growth at impact face in long rods

02 p0342 A69-12279

Rear gain control of dielectric rod antenna in airborne Doppler system with choke at feed point

04 p0576 A69-14770

Higher modes of longitudinal wave propagation in dispersive thin elastic rod, noting response to laser pulse

04 p0678 A69-14869

Stability of elastoplastic clamped free rod, noting compressive force for production of new equilibrium state and occurrence of transition to state

04 p0679 A69-14925

Elastic rod buckling under dynamic longitudinal compression load, determining critical load

04 p0679 A69-14926

Elastic rods shape for maximum stability defined by solution of variational problem, assuming noninfinite compressive stresses

05 p0832 A69-15688

Iteration method for determination of critical buckling load for straight rods

05 p0832 A69-15689

Buckling of rod with initial deflection as sinusoidal half wave, using Bubnov-Galerkin method and Laplace transform, calculating stresses of rod when subjected to nonsteady creep

06 p1021 A69-17182

Longitudinal and transverse vibrations of viscoelastic rods excited by inertia with aid of linear oscillator subjected to harmonic stress, using Kelvin-Voigt model

07 p1233 A69-19326

Thin rods and shells elastic analysis, using Cosserat continua for representing bodies in kinematics and balance and constitutive equations

07 p1234 A69-19382

Plane H polarized electromagnetic wave diffraction incident on array of rectangular rods described by linear algebraic equations

08 p1275 A69-20433

Long rectangular rods stability and vibrations under elastic deformations using bending theory

10 p1802 A69-24024

Slender elastic rod stability under spatial finite deflection, analyzing critical load by using Kirchhoff analogy and gyroscope motion

11 p1970 A69-24609

Temperature field in thin walled rods with spiral coil cross section in solar radiation, considering radiant heat exchange

11 p1999 A69-24779

Rod load capacity changes due to random overloads constituting upper limit of stress probability distribution density function used in programmed fatigue tests

11 p1985 A69-25180

Unsteady heat conduction of semiinfinite thin rod with mobile end face, ideally insulated lateral surface and convective heat transfer on uninsulated portion

11 p2002 A69-25229

Rectangular aluminum alloy rods carrying capacity under compression loads applied eccentrically to rod ends

11 p1986 A69-25326

Longitudinal and transverse frequencies of cylindrical metallic rod with spherical tip for sliding motion with dry friction

12 p2102 A69-26290

Dynamic programming method applied to Cauchy problem of large deflections in compressed rods, using recurrent functional equations

14 p2533 A69-28988

External and internal energy dissipation coefficients in vibrating aerodynamic rod structures

14 p2537 A69-29748

Heat propagation in rod of two sections with different properties, formulating relevant boundary value problem, solving with Duhamel principle

15 p2718 A69-31066

Thermal conductivity of semiinfinite rod with insulated surface and constant internal heat source, considering finite heat propagation rate

15 p2719 A69-31181

Statistical calculation of three dimensional frames of thin walled rods, using method of initial parameters in matrix form

15 p2714 A69-31199

Elastic stability of warped rods, using small oscillations method for varying end conditions and torsional-moment vector behavior

17 p3057 A69-33196

Longitudinal oscillations of homogeneous elastic rod under nonconservative force at one end, deriving equations of motion and stability conditions

18 p3216 A69-34578

Rod buckling under impact load, discussing compression strain wave front propagation

18 p3217 A69-34580

Natural longitudinal oscillations of variable cross section straight rods, assessing errors due to use of finite difference schemes

18 p3217 A69-34581

Stressed state analysis in dynamic brittle breakdown wave front of compression waves propagating in brittle rod under longitudinal impact

18 p3217 A69-34592

Buckling behavior of idealized Shenley rod consisting of linearly reinforced elastoplastic materials under compression, formulating constraints for stability

19 p3446 A69-36846

Equivalent circuit technique for dispersion equation and coupling impedance of slow wave structures of ring-rod systems, noting retardation

23 p4139 A69-41944

Thin walled rods for girder and frame systems designed by matrix method, solving differential equations for tension, compression, bending and torsion

23 p4230 A69-42005

Permanent deformation of axial rod subjected to blast load predicted using partial differential equation in conjunction with stress-strain relationship

24 p4406 A69-43699

ROGALLO WINGS

U FLEXIBLE WINGS

U FOLDING STRUCTURES

ROLL

Blunt cone hypersonic roll damping derivative, using Mach number distribution and graphical integration

04 p0542 A69-14739

Ablation surface patterns and resulting roll torques and roll behavior of hypervelocity vehicles
[AIAA PAPER 69-180]

06 p1036 A69-18051

Ballistic reentry vehicle roll-pitch coupling, showing influence of nose asymmetries
[AIAA PAPER 69-101]

06 p1018 A69-18156

Laminar hypersonic roll damping derivatives for 10 degree half angle cone at zero angle of attack for environmental flow conditions of hypersonic wind tunnel

09 p1430 A69-21958

Angular velocity of aircraft rotation about longitudinal axis at arbitrary point of passive trajectory section, with assumptions on roll damping, momentum, etc

18 p3092 A69-34989

ROLL CONTROL

U LATERAL CONTROL

ROLL FORMING

Hysteresis properties of membrane structures with soldered or rolled edges noting superiority of added elastic element in clamped area

01 p0087 A69-10828

Ti alloy blanks production technology and quality control, noting rolling of sectional profiles

07 p1161 A69-18765

ROLLER BEARINGS

Soviet aircraft roller bearings design, operation, service life, defect testing, etc

04 p0606 A69-14936

Rolling elements for high temperatures, discussing solid film lubricants, unlubricated rolling contact and materials and surface treatment
[IME PAPER 2]

07 p1138 A69-18566

Life margin tests of oil lubricated oscillating caged needle roller bearings under service conditions duplicating helicopter rotor hinge pin locations
[ASME PAPER 68-LC-7]

15 p2622 A69-30609

Linear analysis of damped flexibly mounted rolling element bearings influence on dynamic rotor unbalance response, including optimum support characteristics
[ASME PAPER 69-LUBS-8]

18 p3212 A69-34382

Cage and roller slip in high speed roller bearings over steady radial loads by measurement and theory

20 p3547 A69-37066

ROLLING

Fabrication of Cu-W composites with discontinuous fibers based on sintering and rolling

03 p0444 A69-13349

Rolling direction tensile tests of alloy steel plate displaying various fracture configurations over distinct temperature ranges, noting stress state, void formation and anisotropy
[ASME PAPER 68-WA/MET-1]

14 p2464 A69-29440

ROLLING CONTACT BEARINGS

U ANTI-FRICTION BEARINGS

ROLLING CONTACT LOADS

Mechanical properties of free rolling contact surfaces subject to high loads, discussing effect of oil film separation and fatigue crack initiation

02 p0339 A69-11989

Microslip between concentrated contacts and design charts for maximum pressure, closing-in of contacting bodies and optimized shapes, giving computer programs

15 p2629 A69-30903

Elastohydrodynamic lubrication film thickness in finite elliptical contact determined by two dimensional Reynolds equation in inlet region, using finite difference approximation
[ASME PAPER 69-LUBS-17]

18 p3120 A69-34379

Ball bearing lubrication simulation by rolling disk apparatus, emphasizing surface slip and related thermal effects alterable by geometric expansion
[ASME PAPER 69-LUBS-16]

18 p3140 A69-34380

Stress field in elastic contact area vicinity of hollow sphere subjected to normal load through flat plate, noting contact life
[ASME PAPER 69-LUBS-5]

18 p3212 A69-34383

Elastohydrodynamic theory of spherical bodies in normal approach contact, discussing lubrication and elasticity equations
[ASME PAPER 69-LUBS-3]

18 p3213 A69-34384

ROLLING MOMENTS

Aerodynamics of bodies of revolution in nonplanar motion using nonlinear functional analysis of moments for motion about center of gravity
[AIAA PAPER 68-20] 04 p0542 A69-14714

Roll acceleration influence on angle of attack convergence and windward meridian rotation rate of rolling reentry vehicles
[AIAA PAPER 69-100] 06 p1018 A69-18089

Monograph on rapid rotations of aircraft with fixed controls, covering spin and roll movements differential equations 12 p2013 A69-26118

Aerodynamic pitch-roll coupling in spinning vehicles, showing unsteady components complicating data reduction 21 p3647 A69-39038

ROOM TEMPERATURE

Low noise room temperature satellite broadcast receiver for UHF, using room temperature parametric amplifiers 05 p0728 A69-15672

Room temperature lattice spacings of PdIn, PtIn and PtSn alloys including magnetic susceptibility 05 p0779 A69-15832

CdS single crystals excess conductivity observed at room temperature 08 p1374 A69-21083

Room temperature WC-Co compacts oxidation resistance in air noting increase with preliminary sintering temperature 13 p2275 A69-27345

Low viscosity/density RTV silicone rubber sealants obtained by using glass microballoon fillers 24 p4337 A69-43454

ROOMS

U CLEAN ROOMS

ROOT-MEAN-SQUARE ERRORS

Root-mean-square error determination in automatic control system by digital computer for realizing control function, investigating harmonic and random input effects 01 p0050 A69-10208

Optimal control of discrete and continuous stochastic linear dynamical systems, discussing algorithms for instantaneous weighted minimum mean square error performance 01 p0051 A69-10439

Rms approximation validity limits for satellite temperature variances by deriving equations for thin insulated plate in space 02 p0352 A69-12211

F 2 layer critical frequencies variation coefficients, analyzing variation and root-mean-square deviations in terms of geomagnetic latitude and Wolf number 03 p0422 A69-13514

Noise signal mean square value measurement in pulse noise conditions by using noise amplitude limiter with limitation threshold in receiver 05 p0719 A69-16086

Analog-hybrid computer configurations for average and rms values of signals with respect to time 06 p0891 A69-17220

Double stochastic approximation algorithm for minimizing mean square error in finite expansion of unknown probability distribution functions 06 p0947 A69-17361

Linear closed loop control system poorly damped response to deterministic inputs improved by stability constraint for minimization of mean squared error 06 p0905 A69-17950

Root mean square time delay error with respect to playback time and autocorrelation function of tape recorded sine wave for studying jitter spectra 07 p1132 A69-18827

Presampling filtering, discussing effects on rms interpolation error for sampled data systems 07 p1083 A69-19129

Synchronization errors effects on performance of compression-line demodulator, increasing mean-square error in measuring instantaneous frequency and locking probability 08 p1271 A69-19920

Discrete predicting filter optimal synthesis in terms of rms error by solving normal Gaussian equations 09 p1473 A69-21858

Pattern recognition as part of statistical communication theory, using Karhunen-Loeve expansion to minimize root-mean-square errors, showing application to handwritten numerals 09 p1461 A69-22292

Stochastic approximation procedure minimizing mean square error criterion for system identification, estimation and decomposition of mixtures 11 p1842 A69-24934

Rms error for reproduction of satellite signal transmitted through continuous Gaussian channel assessed by numerical calculation 13 p2219 A69-27697

Temperature vertical profiles rms deviations calculated from temperature measurements during unstable atmospheric stratification 13 p2293 A69-27847

Root-mean-square error determination in automatic control system by digital computer for realizing control function, investigating harmonic and random input effects 14 p2424 A69-28744

Dynamic process during rms deviation of nonlinear system from prescribed trajectory described by nonlinear differential equations 14 p2425 A69-28822

Chopper modulated IR detection system error analysis through minimizing mean square error of approximating output function 14 p2450 A69-29639

Restoration of photographic images by optical spatial filtering with least mean square error filter in presence of random additive noise 15 p2611 A69-31033

Pulse compression using Hermitian functions, noting minimal rms error requirement in real system 16 p2755 A69-32585

Energy dissipation influence on elastic elements random vibrations, obtaining relations between displacements rms value and random disturbance intensity 17 p3064 A69-33921

Parameter sensitivity analysis of discrete suboptimal filters from optimal rmse estimate of actual system performance measure 18 p3110 A69-34675

Paraboloidal reflector antennas rms phase error minimization, describing axis location and determination of focus and focal length of best fit paraboloid 19 p3283 A69-35933

Maximum rms error comparison of redundancy reduction techniques, emphasizing limiting slope technique and worst case interpolation error 19 p3273 A69-36264

Digital data transmission by pulse code modulation considered for minimum mean square error 19 p3274 A69-36282

Algorithm for determining multidimensional random process from canonical representation of current state, noting minimum rms prediction error 19 p3287 A69-36663

Least square or least mean square approximation methods in abstract pattern recognition, noting unknown probability density function 20 p3504 A69-38285

Random variable used as model for unknown parameter in linear system, describing orthonormal expansion for evaluating mean-integral-squared error 21 p3685 A69-38727

Parameter estimation using entropy of error as criterion function compared with mean square error analysis 21 p3757 A69-39664

Optimal explicit method for parameters estimation not restricted to linear Gaussian problem derived in canonical form [AIAA PAPER 69-947] 22 p3975 A69-40330

RMS surface error compensation in radome-housed Cassegrain parabolic antenna including weight analysis 23 p4150 A69-42137

Northern Hemisphere 500-mb height pattern series expansion, using optimal sets of orthonormal functions, obtaining rms error 24 p4346 A69-43157

ROOTS OF EQUATIONS

Constant thickness disk temperature field for inhomogeneous boundary conditions, considering roots of characteristic equations determination 04 p0685 A69-14498

Two dimensional elementary transformation for obtaining eigenvalues, considering programming aspects for computing characteristic roots of matrix 04 p0624 A69-14967

Asymptotic computation and graphical display of imaginary mu-zeros of combinations of cross product Bessel functions 05 p0836 A69-15874

Root sensitivity of linear feedback control systems calculated with signal flow graph and transforming circle 05 p0740 A69-16588

Control system analysis and synthesis by means of generalized root-locus method on digital computer 07 p1114 A69-18291

Root sensitivity of characteristic equation of linear automatic control system to system parameter changes applied to aircraft angular stabilization 10 p1666 A69-23610

Zero crossing statistics measurements for 1/f noise, noting statistically stationary character of probability density distributions of interval spacings between zero crossings 10 p1656 A69-23657

Higher root loci of polynomials for multivariable systems with coefficients polynomials of real parameter 12 p2048 A69-26073

Stabilization of nonlinear control systems steady motions for two pairs of imaginary roots 13 p2298 A69-27745

Root locus method for nonlinear systems analysis, determining existence, stability and parameters of periodic solutions 14 p2445 A69-28919

Motion stability in nonresonant case of four pairs of imaginary roots in characteristic equation 21 p3770 A69-38883

Trajectories of roots of two channel systems with antisymmetric cross couplings using geometrical and analytical methods, noting hodograph 21 p3686 A69-38886

Algebraic equations for determination of controller parameters, noting a priori fixed roots of characteristic equation 21 p3723 A69-38887

Critical case of stable motion for differential equations having two zero roots 21 p3771 A69-39108

RORSCHACH TESTS

Pilots body images determined by inkblot tests, considering effects of aircraft type, pilots experience, etc 23 p4112 A69-42364

ROSETTE SHAPES

Printed circuit board wiring technique for strain gage rosettes application in extensive airframe static tests 02 p0250 A69-12231

Poisson ratio determination with bonded electrical resistance strain rosettes 11 p1995 A69-25652

ROSHKO PREDICTION

Roshko correlation for estimating vortex shedding from circular cylinder in sheared flow with velocity in Strouhal and Reynolds numbers 20 p3515 A69-37228

ROSSBY REGIMES

Planetary Rossby waves vertical propagation through weak westerly wind wave guides, using adiabatic linear model 03 p0460 A69-13335

Asymptotic similarity in neutral barotropic planetary boundary layers, solving Ekman flow by singular perturbation methods 03 p0460 A69-13336

Planetary boundary layer response to time varying pressure gradient force 03 p0460 A69-13337

Planetary wave-zonal flow interaction interpretation in terms of potential vorticity eddy transport, deriving zonal wind change and temperature field 07 p1126 A69-19037

Linearized model for vertical propagation of Rossby waves through atmosphere with Newtonian cooling, discussing atmospheric wind effects 08 p1344 A69-19812

Horizontally flowing eddies or Rossby waves in solar convection zone and photosphere, giving mathematical models showing hydromagnetic dynamo effects inducing reversing magnetic fields 22 p4019 A69-40294

ROTARY DRIVES

U MECHANICAL DRIVES

ROTARY GYROSCOPES

NT FLUID ROTOR GYROSCOPES

Dynamic equations for offset unsymmetric gyroscope with obliquely placed rotor, using dual transformation matrices [ASME PAPER 68-WA/DE-5] 05 p0764 A69-16170

Critical speeds of multiple disk rotors with multiple supports, discussing continuous shaft sections including gyroscopic and transverse shear and rotary inertia effects [ASME PAPER 69-VIBR-51] 10 p1804 A69-24153

Steady state solutions of differential equations of motion for body with fixed point, considering Kharlamov cone for rotation of heavy gyrost

11 p1917 A69-24780

Dynamics of gyroscope having flexible axis under gravitational force and elastic coupling reactions, deriving motion equations, precessions angular velocities, etc

14 p2445 A69-28798

Magnetic suspension device replacing mechanical bearings of inertial guidance systems gyro rotors, evaluating device strength and stability

14 p2479 A69-29492

Rate gyro life and reliability, discussing gas bearings separating rotor from stator by thin gas film with conventional oil film characteristics

15 p2608 A69-30410

Vibrarotor gyroscope operated as rate gyro for simultaneously indicating two components of angular velocity by amplitude and phase of periodic output signal

18 p3139 A69-35299

Accuracy improvement of method of averages applied to equations of small motions and disturbances of two rotor gyrocompass on ship performing circular maneuvers

18 p3139 A69-35378

ROTARY STABILITY

NT GYROSCOPIC STABILITY

First approximation stability of single rotation of artificial earth satellite about center of mass in Newtonian gravitational force field

01 p0161 A69-10585

Whirl instability of externally pressurized gas journal bearing with peripheral feeding holes, discussing analytical natural frequency of shaft bearing systems

02 p0254 A69-12426

Motion and stability of solid body with cavity containing rotor and two incompressible nonmixing liquids with surface tension

03 p0418 A69-13814

Rotation deviation of rigid body around axis, discussing three point body measurement and applicability

04 p0599 A69-15017

Stability of high speed rotors with sliding bearings

04 p0607 A69-15163

Aeroelastic rotor and nonsteady rotor aerodynamics

05 p0695 A69-15549

Unstable regions prediction for reciprocal system governed by linear equations with periodic coefficients, noting application to rotating shaft and helicopter rotor

08 p1413 A69-20401

Rotation effect on homogeneous gravitating systems stability, noting lack of unity in approaches to cosmogony by various authors

09 p1589 A69-21372

Stability of high speed single mass rotor with internal friction on damped anisotropic supports, considering support stiffness

[ASME PAPER 69-VIBR-2]

10 p1805 A69-24160

Stability of uniform rotations of gyrost at fixed point in potential force field, considering Routh rule

11 p1918 A69-24786

Nonlinear theory for whirling of heavy string under constant axial tension, considering orbitally stable modes for eigenvalues of rotation

13 p2359 A69-27264

Herringbone grooved gas lubricated journal bearing stability, testing effects of geometries and clearances on onset speed for half frequency whirl

[ASME PAPER 68-LUBS-25]

13 p2266 A69-27271

Linearized theory for stability of self acting gas journal bearings with noncircular members and elements of flexibility and damping, noting three lobed rotor

[ASME PAPER 68-LUBS-45]

13 p2266 A69-27277

Asymptotic analysis for stability and vibration response of spherical squeeze-film hybrid bearing, obtaining perturbation solutions

[ASME PAPER 68-LUBS-37]

13 p2267 A69-27281

Secular instability of steadily rotating stars, analyzing meridional motions in radiation zones by linear perturbation theory

13 p2354 A69-28566

Autonomous canonical system with two degrees of freedom, determining equilibrium position stability in resonance case, calculating earth satellite rotational stability

14 p2482 A69-28813

First approximation stability of single rotation of artificial earth satellite about center of mass in Newtonian gravitational force field

15 p2702 A69-30755

Rotation effect on homogeneous gravitating systems stability, noting lack of unity in approaches to cosmogony by various authors

18 p3198 A69-34761

Conservation laws and Liapunov stability of free rotation of rigid body about principal axes derived from kinetic energy and angular momentum

19 p3397 A69-35612

Turbine rotors load dependent unstable motions, considering exciting forces origins, external and internal damping, etc

20 p3628 A69-37918

Stability conditions determination for spinning projectile based on ballistic equations, discussing role of Magnus effect

21 p3772 A69-39294

Solid body filled with ideal incompressible liquid, analyzing stability of permanent rotations

21 p3773 A69-39837

ROTARY WING AIRCRAFT

NT ALOUETTE HELICOPTERS

NT AUTOGYROS

NT BO-105 HELICOPTER

NT CH-34 HELICOPTER

NT CH-46 HELICOPTER

NT CH-47 HELICOPTER

NT CH-54 HELICOPTER

NT H-56 HELICOPTER

NT HELICOPTERS

NT MILITARY HELICOPTERS

NT OH-6 HELICOPTER

NT S-61 HELICOPTER

NT SA-330 HELICOPTER

NT SH-3 HELICOPTER

NT UH-1 HELICOPTER

NT XH-51 HELICOPTER

Vibrating rod automatic ice detection and control system for fixed and rotary wing aircraft

01 p0083 A69-11046

Heligyro type takeoff and landing maneuvers, discussing M 211 takeoff jet thrust, pressure ratio, tip speed, etc

04 p0547 A69-14816

Future development in rotorcraft, discussing autogyros, helicopters, tilt rotor and wing aircraft

05 p0702 A69-16392

Compound rotorcraft VTOL vehicle current programs

05 p0703 A69-16394

Remote terminal computer for rotary-wing vehicles design, discussing programming language, engineer-computer interface and applications

07 p1052 A69-18868

Small and full scale model tests for feasibility of retracted rotor aircraft for high speed flight

[AIAA PAPER 69-219]

07 p1055 A69-19550

TRAC variable diameter rotor design based on jackscrew mechanism applied to compound helicopter

[AIAA PAPER 69-221]

07 p1056 A69-19572

Rotor dynamics of stowed rotor aircraft, analyzing blade stiffness in wind tunnel

[AIAA PAPER 69-207]

07 p1057 A69-19578

High bypass ratio compound fan shaft engine design and performance for convertible rotor wing aircraft

[ASME PAPER 69-GT-51]

09 p1572 A69-22511

Rotary wing aircraft speed boundary widening without impairing low speed attributes, discussing structural design factors, airframe design and stability, etc

17 p2897 A69-33209

Rotary wing aircraft height-velocity testing, analyzing engine-out landing by combining flight tests with mathematical simulation model

[AHS PAPER 353]

17 p2900 A69-33524

Propulsion power plant arrangements for rotary wing aircraft with thrust producer for forward flight, considering convertible fan/shaft engine configurations

[AHS PAPER 333]

17 p3021 A69-33529

Instrumentation for rotorcraft aerodynamics, considering boundary layer measurements, hot-wire anemometer and schlieren system for rotors and propellers

[AHS PAPER 320]

17 p2895 A69-33539

Circulation control by blowing and application to stopped rotor aircraft, discussing data from model scale blade experiments

19 p3248 A69-36767

Aerodynamics of rotary wing and V/STOL aircraft - Conference, Buffalo, June 1969, Volume 3

23 p4057 A69-41369

ROTARY WINGS

NT LIFTING ROTORS

NT RIGID ROTORS

NT TILTING ROTORS

NT TIP DRIVEN ROTORS

Structural vibration problems of SA 330 helicopter from test flight data, discussing natural frequency displacement of blades and dynamic response improvement of structure

01 p0009 A69-10158

Elastomeric bearings for support of heavy loads and accommodation of oscillatory motions, considering molded type for helicopter tail rotor

01 p0085 A69-10406

Composite main rotor blade for Sud-Aviation SA-330 helicopter consisting of steel spar/epoxy-glass envelope

[SAE PAPER 680693]

03 p0366 A69-13444

Military rotor blade radar antennas for all-weather low level flight and fire control

04 p0559 A69-15197

Rotary wing handling qualities, discussing analytical tools, design and IFR capabilities for higher speed range

05 p0701 A69-15550

Solar sail structural design, discussing application as propulsion system for heliogyro interplanetary spacecraft

06 p1015 A69-17591

Self excited rotor blade oscillation at high subsonic Mach numbers during flight tests of Sikorsky NH-3A compound helicopter

07 p1053 A69-18870

Flexible rotor blade dynamic response to radially moving force, emphasizing helicopter rotor vibration characteristics associated with tip-vortex impingement

[AIAA PAPER 69-203]

07 p1054 A69-19546

Research and development programs for several advanced rotary wing VTOL concepts

[AIAA PAPER 69-199]

07 p1055 A69-19555

Sikorsky ABC/advancing blade concept/helicopter program, discussing advantages and small scale wind tunnel experiments

[AIAA PAPER 69-217]

07 p1055 A69-19558

Boundary layer discontinuity on helicopter rotor blade in hovering using flow visualization

[AIAA PAPER 69-197]

07 p1051 A69-19561

Computer programmed momentum theory for induced flow field of helicopter rotor in forward flight

[AIAA PAPER 69-224]

07 p1052 A69-19562

Helicopter rotor noise generation, propagation, reception and reduction, discussing design charts for rotational noise spectra as function of design and flight variables

[AIAA PAPER 69-195]

07 p1055 A69-19563

Compound rotary wing aircraft research, discussing XH-51A maneuverability program and UH-1 high Mach and high advance ratio program

[AIAA PAPER 69-218]

07 p1056 A69-19568

Helicopter rotor blades in metal sandwich bonding, discussing component parts assembly by adhesive films

[ASME PAPER 69-VIBR-2]

07 p1443 A69-19731

Engineering testing of aerodynamic efficiency of helicopter rotors during hovering with and without ground effect

08 p1254 A69-20169

Streamlined rotors calculation, interpreting compatibility conditions between streamlining and airscrew stresses

08 p1252 A69-20655

Gyrostatic moments effects on critical angular velocities of varying and constant cross section rigidly and elastically supported hinged rotors

09 p1567 A69-21384

Dynamic stall data for helicopter rotor blade analyses obtained by oscillatory tests in pitch and in vertical translation at full scale Reynolds number

11 p1819 A69-25374

Dynamic systems stability with periodically varying parameters analyzed by Hill type infinite determinant, exemplifying helicopter rotor aeroelastic stability in forward flight

11 p1990 A69-25510

Mathematical model with straight wake airfoil to determine aerodynamic forces on oscillating rotor blades in hovering flight

11 p1821 A69-25514

Vibration eigenfrequencies of helicopter blades, discussing equation integration problems

11 p1995 A69-25673

Helicopter rotors with rigid blades performance from viewpoint of controllability and load distribution

13 p2201 A69-27295

Analog computer simulation of helicopter dynamics after main and tail rotor blades partial loss, showing banking and controllability 14 p2393 A69-29744

Life margin tests of oil lubricated oscillating caged needle roller bearings under service conditions duplicating helicopter rotor hinge pin locations [ASME PAPER 68-LC-7] 15 p2622 A69-30609

Painted helicopter rotor blades ruled out as cause of flicker induced vertigo, reporting pilots psychophysiological responses to formation flying 17 p2913 A69-33175

Optimum adaptation of propulsion gas generators to power jet driven rotors with blown flap control, considering jet engine, fanjet and engine driven compressor 17 p3020 A69-33344

Critical review of paper on tail rotor structural design principles covering sizing, blade frequency and response and aeroelasticity [AHS PAPER 342A] 17 p3059 A69-33503

Aerodynamic aspects of tail rotor design and structural dynamics of stiff inplane configurations, discussing blade natural frequencies [AHS PAPER 342] 17 p3059 A69-33504

Fatigue test loading spectra calculation methods, discussing helicopter rotating and nonrotating components tests [AHS PAPER 373] 17 p2945 A69-33515

Maximum helicopter level flight speed loads spectrum shape and severity related to rotor component fatigue design strength [AHS PAPER 372] 17 p3059 A69-33516

Fatigue properties and test procedures for glass reinforced plastic rotor blades used in twin engine helicopter [AHS PAPER 370] 17 p3060 A69-33518

Main rotor bifilar absorber for vibration reduction during S-61 helicopter flight, describing shake and flight tests [AHS PAPER 354] 17 p2900 A69-33523

Helicopter power plant and drive and rotor systems influence on design, configuration, weight, payload and performance [AHS PAPER 334] 17 p2901 A69-33528

Helicopter rotors and static propellers theory based on Prandtl-Betz theorem, calculating ideal performance [AHS PAPER 326] 17 p2894 A69-33533

Three dimensional potential surface flow past rotor blade in hover, accounting for compressibility and blade element theory limitations [AHS PAPER 324] 17 p2895 A69-33537

Helicopter hovering performance prediction from wake analysis by iteration, discussing wake interference significance and blade number influence [AHS PAPER 321] 17 p2895 A69-33538

Far field helicopter rotor noise radiation, analyzing blade slap, rotation noise, vortex noise effects and loading harmonics utilizing computer program 18 p3090 A69-34322

Aerodynamic characteristics of elliptical airfoils with jet circulation control for VTOL rotors including dual jets and cyclic results [AIAA PAPER 69-741] 18 p3084 A69-34406

Aerodynamics of rotary wing and V/STOL aircraft - Conference, Buffalo, June 1969 18 p3087 A69-35216

Lifting line theory for hovering propellers deformed wakes based on continuous vortex sheet representation 18 p3087 A69-35217

Rotating static thrust propeller or hovering rotor flow field study by schlieren photography, considering vortex field, tip flow and shock wave formation 18 p3087 A69-35218

Rotor airfoils design for helicopter performance optimization, noting hovering figure of merit and blade profile characteristics relationship 18 p3087 A69-35220

Rotor static performance calculation with near wake interference effects on rotor inflow distribution, considering strip momentum theory 18 p3088 A69-35221

Distributive loading rotational theory for helicopter rotor noise generation, considering steady and fluctuating force radiation and impulsive blade slap 18 p3088 A69-35222

Vortex shedding effects on helicopter rotor noise with and without blade slap, noting far and near field noise 18 p3088 A69-35223

Helicopter rotors forward-flight noise characteristics determined by wind tunnel tests compared to rotor noise during flyover 18 p3119 A69-35225

Aerodynamics of rotary wing and V/STOL aircraft - Conference, Buffalo, June 1969, Volume 2, Wind tunnel testing, New concepts in rotor control 18 p3088 A69-35226

Flow field throughout wind tunnel containing rotor with sharply deflected blades, noting reversed flow effect in front of wake 18 p3119 A69-35228

Torsionally flexible blade controllable twist rotor with pitch horn and servoflap control, discussing optimum inputs, airloads and angles of attack contours 18 p3089 A69-35234

Helicopter rotor blade construction and developments, discussing mass balance, fatigue life, fail-safe characteristics, cost and weight ceiling and plastic materials 19 p3329 A69-36768

Aerodynamic performance tests of autorotative unpowered rotor entry vehicle model at various Mach numbers and angles of attack [AIAA PAPER 68-950] 20 p3458 A69-37155

Vortex lattice method correlation on rotor/wing configurations for aerodynamic characteristics, noting triangular and circular hub and blades 20 p3458 A69-37163

Helicopter rotor blades instabilities during starting and stopping cycles, predicting aerodynamic loads by wind tunnel tests, determining negative/positive angles of attack 20 p3463 A69-37804

Passive helicopter rotor isolation for alleviating rotor induced vibration, using dynamic antiresonant vibration isolator 20 p3463 A69-37807

Positive pitch-flap coupling for controlling helicopter rotor blade motion stability involving blade in-plane deflections 20 p3463 A69-37808

Dynamic stall effect on helicopter rotor blades airloading and blade pitching motion at high advance ratio 20 p3463 A69-37809

Helicopter main rotor noise from square tipped blades determined as function of tip speed, blade area and thrust 22 p3864 A69-40676

Rotor operating limits, loads, performance prediction and airfoil development in rotary wing aerodynamics research 23 p4057 A69-41371

Rotor aerodynamics research in terms of theoretical and experimental data comparison, rotor blade flow visualization and blade section camber 23 p4057 A69-41372

Aerodynamic research for rotary wing and V/STOL aircraft, suggesting analytical techniques with software packages designed around standard input/output formats 23 p4146 A69-41373

Helicopter rotors trailing vortices by flow visualization, comparing Euler and Runge-Kutta iterative solutions 23 p4150 A69-41376

High speed compound helicopter rotor loads flight test program, discussing measured parametric effects [AIAA PAPER 68-980] 24 p4250 A69-43712

ROTATING

U ROTATION

ROTATING BODIES

NT COMPRESSOR ROTORS

NT FLYWHEELS

NT IMPELLERS

NT LIFTING ROTORS

NT PUMP IMPELLERS

NT RIGID ROTORS

NT ROTARY WINGS

NT ROTORS

NT TILTING ROTORS

NT TIP DRIVEN ROTORS

NT TURBINE WHEELS

Solid body motion about fixed point representable by two dimensional motion of two points on complex plane 01 p0116 A69-10356

Differential rotation of celestial body maintained in resonance state by locking photosphere oscillation onto rotational period 01 p0156 A69-11136

Equatorial geodesic motion of rotating source in gravitational field, using exact empty space solutions of Einstein equations 01 p0157 A69-11289

Numerical solution for ambipolar diffusion and kinetic decomposition of rotating body of complex chemical composition in ionized airstream 02 p0191 A69-12580

Kerr family of solutions of Einstein and Einstein-Maxwell equations for gravitational field of rotating body, noting global structure and causality 03 p0466 A69-13473

Stokes and Rayleigh layer formation during solid body rotation of semifinite fluid and infinite disk 03 p0417 A69-13797

Mathematical analysis for mechanism of spherical comet nucleus division as effect of nonuniform surface heating during rotation 04 p0659 A69-14997

Rotation deviation of rigid body around axis, discussing three point body measurement and applicability 04 p0599 A69-15017

Poincare sphere representation of polarized light used to predict rotation effect on optical observations in photoelastic shell analysis 04 p0683 A69-15495

Angle of attack effect on motion throughout entry of spinning descending vehicle, noting effects of transverse angular velocity and spin rate 04 p0666 A69-15522

Secondary steady flow /Taylor vortices/ between rotating cylinders, discussing development due to stability loss of Couette flow 05 p0745 A69-15780

Whirl dynamics of partially liquid filled spinning rotor mounted on elastic shaft, noting synchronous critical speed and asynchronous whirl speed [ASME PAPER 68-WA/APM-25] 05 p0768 A69-16189

Integrability of equations for problem of motion of heavy solid body about fixed point 05 p0794 A69-16206

Newtonian theory of rotating configurations, noting use of algebraic equations 05 p0826 A69-16427

Programming technique using quaternion parameters for error reduction in simulation of spinning rigid body 05 p0724 A69-16469

Differential equations of rotational motion of systems of rigid bodies in gravitational field derived with Lagrange equation 06 p0957 A69-17130

Soviet achievements in space research, comparing satellites with U.S. counterparts 06 p1005 A69-17561

Galactic rotation constant calculated from radial velocities of O, B and A stars in Cassiopeia constellation, using Fehrenbach objective prism 07 p1214 A69-18664

Numerical method for three dimensional boundary layer equations, applying perturbation technique and independence principle to rotating flat blade [AIAA PAPER 69-227] 07 p1051 A69-19560

Range-Doppler processing in pulsed radar applied to imaging of rigid rotating body with motion compensating resolution cells 08 p1270 A69-19861

Rotation effect on homogeneous gravitating systems stability, noting lack of unity in approaches to cosmogony by various authors 09 p1589 A69-21372

Euler rotational equations for bodies with variable inertia tensor subjected to extreme variations of mass distribution and mass loss 09 p1616 A69-21956

Increasing rotation of axisymmetric body about velocity vector ascribed to asymmetry in mass distribution, defining conditions for occurrence 09 p1431 A69-22077

Rotation and mass of Sb galaxy NGC 1832, giving central and mean densities 09 p1599 A69-22188

Small angle precessional motion of axisymmetric spin stabilized bodies subject to disturbing moments 10 p1724 A69-22932

Rigid body rotational simultaneous equations of motion transformed into explicit form for digital simulation 10 p1661 A69-23855

Balancing criteria for rotors of rotating machines, discussing acceptable residual specific unbalance, center of gravity displacement and machine vibration tolerance [ASME PAPER 69-VIBR-60] 10 p1804 A69-24149

Convection heat transfer and flow in rotating bodies, discussing laminar, turbulent and mixed flow in cones and disks, spheres and cylinders 11 p1998 A69-24459

Rotational dynamics equations in linearized matrix form applied to satellite librations in circular orbit and gyroscope motion

11 p1970 A69-24608

Kowalewski solution for motion of heavy body with fixed point, noting hodographs

11 p1917 A69-24776

Variational equations for rotation of heavy solid body with fixed point about horizontal axis, noting mass distribution

11 p1917 A69-24778

Steady state solutions of differential equations of motion for body with fixed point, considering Kharlamov cone for rotation of heavy gyrostat

11 p1917 A69-24780

Stability of uniform rotations of gyrostat with fixed point in potential force field, considering Routh rule

11 p1918 A69-24786

Deformation processes of geometrically nonlinear rotational membrane shells under internal pressure

11 p1980 A69-24821

Covariant equations of motion of body of variable mass in general relativity, considering Schwarzschild field, rotating mass field and Einstein static universe

11 p1965 A69-25744

Nonrelativistic theory of rotating configurations in terms of gravitational potential, center mass density and variable angular velocity

12 p2159 A69-26662

Spiral galaxies rotation curve fluctuations attributed to kinematic properties of galactic matter and gas components

12 p2170 A69-27062

Optimal stochastic controller synthesis theory applied to stabilizing and controlling orientation of rotating bodies in central gravitational fields

13 p2300 A69-28326

Periodic solutions for small nutation angle of quasi-linear autonomous system of equations of motion of heavy solid body moving around fixed point

14 p2445 A69-28896

Contact problem between elastic cylinder and rigid punch analyzed using integral equation, singularity isolation and series expansion

14 p2532 A69-28972

Nongravitational force dynamic effect and model for rotating cometary nucleus, including changes in orbital elements

14 p2524 A69-29713

Differential equations for elastic stress distribution in thin rotating shell with arbitrary profile, obtaining analytical dimensionless solutions for potential profiles

15 p2703 A69-30158

KB-18A rotary prism moving film panoramic aerial strike camera

15 p2614 A69-31281

Exact solution for motion of conducting solid of revolution rotating in infinite conducting viscous fluid, describing magnetic field

16 p2817 A69-31666

Gravitational and magnetic torque effect on rotational motion of triaxial rigid body in regressing orbit about oblate primary mass

16 p2861 A69-32240

Magnetic field effects on rotating cone compressible boundary layer at zero angle of attack, describing changes in drag coefficient, torque and velocity profiles [AIAA PAPER 69-721]

17 p2892 A69-33484

Rotary motion stability of axisymmetric solid body or gyroscope suspended on string and containing ellipsoidal cavity filled with liquid

18 p3135 A69-34558

Drift of two connected gyroscopes, discussing equations of motion assuming unperturbed rotation and weightlessness

18 p3135 A69-34561

Equations of motion of rapidly rotating spacecraft, considering deformations of long clastic booms

18 p3207 A69-34582

Rotation effect on homogeneous gravitating systems stability, noting lack of unity in approaches to cosmogony by various authors

18 p3198 A69-34761

Tank configurations allowing for sloshing in liquid fuel reaction control system in spinning satellite

18 p3219 A69-34796

Dynamic balance for rotating aerospace vehicles, discussing error in principal axis location between rotor on machine and free body in space [SAWE PAPER 740]

18 p3137 A69-34887

Secondary steady flow /Taylor vortices/ between rotating cylinders, discussing development due to stability loss of Couette flow

18 p3123 A69-35032

Quadratic approximation at matrix level of dynamic equations for rotating bodies applied to gravity gradient satellite exhibiting nonlinear resonances

18 p3174 A69-35298

Passive damper system for reducing precession in free symmetrical rotating space vehicle, noting linear torsional spring influence on precession decay

19 p3429 A69-35913

Lumped parameter simulation model, based on vector mechanics for flexible spinning bodies, to study spin stabilized spacecraft or turbine rotors

19 p3280 A69-35990

Rayleigh criteria extension for boundary layers of rotationally symmetrical bodies with curved meridian, utilizing orthogonal coordinate system

19 p3298 A69-36309

Self rotary motions of nearly conservative systems with one degree of freedom, deriving periodic solution of equation for phase trajectories

19 p3374 A69-36466

Thermoelastic deformation and mean rotation divergence formulas for elastic simply connected micropolar body

19 p3440 A69-36586

Nonlinear rotational viscoelastic membranes creep rupture and failure found dependent on function of accumulated energy and power dissipation during deformation

19 p3444 A69-36806

Optimal control of rotational and transversal motions of elastic flight vehicles, considering torsional and flexural deformations

21 p3760 A69-38890

Near resonant and nonresonant solutions of nonlinear equation describing rotating pendulum motion under periodic disturbance

21 p3771 A69-39004

Rodrigues formula derivation procedure and summation formula derivation for finite rotations of solid body, noting simplifications from kinematic considerations

21 p3772 A69-39183

Solid body filled with ideal incompressible liquid, analyzing stability of permanent rotations

21 p3773 A69-39837

Antenna reactance from sounding rocket in ionosphere, showing variations relationship to rocket spin period

22 p3934 A69-39964

Pulsar CP 0328 radiation mechanism, considering relativistic effects of rapid rotation

22 p4035 A69-41206

Increasing rotation of axisymmetric body about velocity vector ascribed to asymmetry in mass distribution, defining conditions for occurrence

23 p4060 A69-41968

Aerodynamic characteristics of moving and rotating bodies of revolution in free molecular rarefied gas flow, assuming Maxwellian thermal velocity distribution and diffuse specular interaction

24 p4243 A69-42583

Collective rotational motion separation from internal motion in system of n point masses based on wave mechanics, emphasizing three body problem

24 p4349 A69-42650

Finite deformation of circular elastic membrane spinning with constant angular velocity, solving nonlinear differential equations by Runge-Kutta method for three boundary conditions

24 p4404 A69-43651

Wave generation in infinite micropolar elastic solid, determining displacement and rotation fields and strain state

24 p4406 A69-43731

ROTATING CONES

U CONICAL BODIES

ROTATING CYLINDERS

Tangential velocity profile growth in laminar axial flow through concentric annulus with rotating inner cylinder, using Navier-Stokes equations for prediction

01 p0058 A69-10143

Inertia effect of flow between eccentric cylinders with rotating outer cylinder, calculating pressure and shearing distribution and force on inner cylinder

01 p0059 A69-10307

Rotating bodies stability conditions relative to radial disturbances found to be field strength dependence on internal mass at any point

02 p0317 A69-11978

Unsteady transient flow of viscous fluid in suddenly rotating open pot, taking into account effect of bottom in determination of velocity profile

03 p0414 A69-13019

Numerical solution of axisymmetric incompressible viscous fluid flows about rotating cylinder, Taylor vortex between cylinders and through labyrinth seal

03 p0419 A69-13990

Equations formulated for space vehicle reaction to rotating machinery and internal mass motion, evaluating dynamics of cylindrical space station rotating about major axis

05 p0827 A69-16476

Laminar constant pressure gradient flow of viscous incompressible conducting fluid through rotating straight circular pipe with perpendicular magnetic field

06 p0967 A69-17718

Wave motion onset and waveforms in rotating annulus with sinusoidally varying temperature differences

07 p1126 A69-19039

Viscous fluids rotational flow in cylindrically symmetrical vessels, circumventing Navier-Stokes equations of motion by Wedemeyer approximation

10 p1677 A69-22896

Hydromagnetic instability onset in dissipative flow of electrically conducting fluid between rotating permeable perfectly conducting cylinders, noting oscillatory axisymmetric critical modes

11 p1926 A69-24895

Viscous flow stability in rotating pipe, giving velocity components in cylindrical polar coordinates

11 p1871 A69-25125

Steady flow field for viscous incompressible fluid in rotating pipe with porous walls determined from Navier-Stokes equations

11 p1875 A69-25481

Surface equilibrium configurations and bifurcation points for rotating homogeneous right fluid cylinder confined by surface tension forces

14 p2428 A69-28816

Rotating bodies stability conditions relative to radial disturbances found to be field strength dependence on internal mass at any point

15 p2680 A69-30260

Turbulent viscous gas ingestion and fluid inertia analysis using stability of dynamic gas-liquid interface between rotating cylinders [ASLE FICFS PREPRINT 31]

15 p2621 A69-30496

Bending surface of shells under crosswise load analyzed by moire method, considering rotating cylindrical surfaces

15 p2713 A69-31056

Numerical approximation of Taylor vortices in viscous incompressible fluid flow between concentric rotating cylinders, using truncated eigenexpansions

15 p2593 A69-31518

Rotatory cylindrical shells supported at corners under symmetric load, determining deformation in arbitrary locations by moire method

15 p2715 A69-31546

Thermal stresses in rotating cylindrical interplanetary body heated by solar radiation

16 p2871 A69-31901

Rotating cylinder or vortex motion in shear flow with friction, noting drag and rotor force combined influence

17 p2950 A69-33151

Normal and negative Magnus force experienced by rotating cylinder in air flow, discussing wind tunnel tests, laminar and turbulent boundary layers separation, pressure distribution, etc

17 p2958 A69-34213

Viscous fluid secondary flow stability between coaxial rotating cylinders, using nonlinear differential equations derived from equations of motion

19 p3299 A69-36391

Rotating stratified fluid in thermally insulated cylinder, studying angular velocity abrupt change effects under stable temperature distribution

21 p3694 A69-38768

Kinetic beam instability development in homogeneous dust /gas/ cylinder rotating in hot invariable medium under arbitrary perturbations

22 p4032 A69-41017

Thermoelastic stresses in rotating cylinders and disks with radial temperature distribution, deriving plane deformation approximate solutions

23 p4227 A69-41707

Transition from axisymmetric to nonaxisymmetric flow in rotating annulus, using two layer quasigeostrophic model

24 p4345 A69-43150

Centrifugal forces effect on stability of inviscid liquid film over rotating cylinder away from stagnation region, noting film thickness stabilization effect

24 p4305 A69-43597

Vortex shedding from circular cylinders rotating normal to free stream velocity, studying roles of rotation rate and Reynolds number 24 p4248 A69-43601

ROTATING DISKS

Unsteady laminar boundary layer near thermally insulated rotating disk, establishing solutions describing motion 01 p0059 A69-10361

Rotating bodies stability conditions relative to radial disturbances found to be field strength dependence on internal mass at any point 02 p0317 A69-11978

Resisting forces produced by transverse vibration of rotating disks in viscous fluid 02 p0232 A69-12257

Ekman boundary layer problem of steady axisymmetric viscous incompressible flow between infinite coaxial rotating disk, studying laminar range of Taylor number R 05 p0744 A69-15665

Flow and heat transfer on nonNewtonian fluid about disk rotating with time dependent velocity, using Runge-Kutta-Gill technique for numerical integration 05 p0745 A69-15793

Displacement, distortions and unit stresses in rotating circular disk under plane strain 05 p0835 A69-15807

Injection or suction at disk surface, noting effects on heat and mass transfer in laminar flow about rotating disk 06 p1029 A69-17002

Step function factor for laminar heat transfer from rotating disk with surface temperature changing stepwise in uniform forced stream 06 p1029 A69-17003

Laminar source flow of viscous incompressible liquid between two parallel coaxial rotating porous disks 06 p0909 A69-17243

Air film cooling of rotating turbine disk, suggesting applicability to gas flows 06 p1034 A69-17814

Mechanical stability of pressed and forged Ti alloy gas turbine disks at high temperatures and rates of rotation 06 p1026 A69-18018

Motion of viscous incompressible fluid in interspace between rotating and parallel fixed permeable plane having supplementary fluid injection solved by Navier-Stokes equations 07 p1119 A69-18743

Rotary head units used in telemetry magnetic recorders, explaining concepts and advantages of rotary scanning 07 p1077 A69-18826

Satellite components of lines formed in stellar type differentially rotating disk 07 p1219 A69-19336

Quasi-plane stress in rotating disks of unconventional profile emphasizing conic shaped disk analysis in terms of hypergeometric series 07 p1235 A69-19444

Unsteady suction motion of viscous incompressible fluid under action of slowly rotating suction disk, noting fluid velocity variation 08 p1302 A69-19875

Von Karman flow changes due to unsteady heat transfer from rotating disks impulsively changing temperatures, particularly steady state and response time 08 p1422 A69-20996

Hydromagnetic steady forced flow against porous rotating disk, integrating equations of motion by Karman-Pohlhausen and series methods 08 p1370 A69-21005

Broadband sound field generated aerodynamically by relatively smooth disk rotating in own plane, noting turbulent boundary layer flow and surface roughness effect 09 p1539 A69-21718

Hollow turbine disks for provision of coolant to high performance aircraft gas turbine engines, fabricating disk in two axial halves 09 p1509 A69-22345

Stability of thin rotating disks of stars with respect to axisymmetric disturbances, noting overstabilities dependence on epicycles sizes 09 p1605 A69-22413

Rotating disk induced viscous conducting fluid motion in axial magnetic field 10 p1727 A69-23099

MHD flow and heat transfer between coaxial rotating disks under axial magnetic field, using powers expansion of Reynolds number 10 p1728 A69-23234

Transverse waves induced by disk oscillations about state of steady rotation in MHD, revealing circularly polarized waves with different phase velocities 10 p1728 A69-23239

Moving conducting media velocity measurement using Reynolds number and electrical conductivity values, based on magnetic field distortion 10 p1731 A69-23435

Infinitesimal bending oscillations and/or responses of thin rotating disks applied to thin disk galaxies, discussing Magellanic Cloud passage near galactic center 10 p1786 A69-24110

Similarity solution for flow of fluid-particle suspension over disk rotating at constant velocity, solving differential equations for flow velocity distributions 11 p1867 A69-24280

Gas turbine disk calculation and plastic flow theory, considering loading conditions and elastoplastic strains due to centrifugal forces and nonuniform heating 11 p1982 A69-24945

Torsional flow of incompressible anisotropic fluid between parallel circular plates rotating with constant angular velocity, showing resemblance to shear flow 12 p0262 A69-26277

Rotating central disk in galactic plane observed by radio telescope, assessing relation between expanding gas of disk and high velocity stream from center 12 p2163 A69-27018

MHD Stokes flow for rotating disk in parallel magnetic field, showing Lorentz force inhibiting effect on fluid motion 13 p2305 A69-27325

Instantaneous rotational impulse imparting steady motion of disk determined for coupled gyroscope 13 p2264 A69-28527

High speed rotating disks design and stress analysis [ASME PAPER 69-DE-1] 14 p2453 A69-28838

Rotating disk of nonuniform thickness, establishing optimum geometry for minimum tangential stress [ASME PAPER 69-DE-36] 14 p2454 A69-28841

Rotating bodies stability conditions relative to radial disturbances found to be field strength dependence on internal mass at any point 15 p2680 A69-30260

Uncoupled field equations for free large amplitude axisymmetric transverse vibrations of spinning membrane disks 15 p2704 A69-30303

Stagnation flow of viscous fluid against rotating magnetized disk, determining effects on magnetic and velocity fields, currents and shear stresses 15 p2659 A69-30674

Thermal stresses and displacements in isotropic inhomogeneous rotating circular disk with axle hole under steady temperature field 15 p2712 A69-31016

Convective heat transfer in centrifugal force field of cavity between two rotating disks in turbulent gas flow 16 p2837 A69-32139

Stress-strain state determination for axisymmetric shells applied to design of circular/annular plates and rotating disks 17 p3057 A69-33194

Turbulent boundary layer on disk rotating in free air, using circumferential and radial momentum integral equations and entrainment equation 17 p2957 A69-33601

Elastic stresses in rotating anisotropic disks with constant thickness, discussing solid, circular rigid shaft mounted and center drilled disks 17 p3067 A69-34138

Low Reynolds number solutions for incompressible viscous flows resulting from finite disk steady rotation 18 p3121 A69-34784

Secondary flows in confined viscous vortex for nuclear rockets, employing rotating disk in chamber end wall for recirculation 19 p3296 A69-35756

Turbine disks stress-strain state, using wire strain gauge to determine residual stresses, radial and tangential stresses as function of disks rpm 19 p3436 A69-35850

Computer program using system simulation and Monte Carlo techniques to assess turbojet engine compressor disk reliability, discussing maintenance policy and engine design effects 19 p3394 A69-36042

Transverse vibration and wave solutions for nonlinear equations governing transverse motions of spinning circular membrane disks 19 p3440 A69-36637

Dimensionless radial and transverse velocity profiles for unstably incompressible boundary layer on rotating disk in rotating fluid 19 p3300 A69-36720

Surface stresses in rotating asymmetric profiled disks and axial deflection effects computed theoretically and compared to measurements on photoelastic models 19 p3447 A69-36862

Radial and tangential stress analysis of rotating disk during steady state creep, using equations solved by finite difference method 22 p4043 A69-40458

Thermoelastic stresses in rotating cylinders and disks with radial temperature distribution, deriving plane deformation approximate solutions 23 p4227 A69-41707

Time dependent unsteady flow of incompressible and electrically conducting fluid between two infinite disks rotating in uniform axial magnetic field 23 p4153 A69-42410

MHD flow of incompressible viscous fluid between rotating electrical insulator disks 24 p4354 A69-42599

Forced flow against infinite rotating disk, showing von Karman similarity equations solution for axial flow at large distances toward disk 24 p4244 A69-42718

ROTATING ENVIRONMENTS

Antimotion sickness drugs tested in slow rotation room with controlled Coriolis accelerations, noting summation effect of dextroamphetamine sulfate and scopolamine hydrobromide 03 p0381 A69-14079

Rotational velocity estimates by observers during angular acceleration, noting vestibular function interpretation 04 p0554 A69-15332

Coriolis acceleration dosages applied in vestibulometric tests of male subjects inclined in rotating chair 05 p0710 A69-16521

Human vestibular and sensory reactions to rotation and rocking, Coriolis acceleration and vestibular reaction inhibition on ground test stand for effects of temporary weightlessness 07 p1062 A69-18586

Overt motion sickness prevention by incremental exposure to Coriolis accelerations 07 p1067 A69-19425

Long time physiological effects of rotating systems, surveying acceleration effects and rotation experiments on humans and rats 08 p1265 A69-21183

Upper atmosphere rotation perturbation effect on satellite orbit when scale height varies with height, showing inclination reduction 09 p1594 A69-21660

Coriolis acceleration in rotating environment, discussing origins and role in human existence in rotating space station 09 p1540 A69-21891

Motion sickness studied with slow rotation room having controlled Coriolis accelerations, discussing oculogyral illusion, nystagmus, dizziness and neuromuscular incoordination 12 p2019 A69-26547

Human vestibular reactions at various bodily rotation rates and planes, including counterrotation illusion and nystagmic reaction 12 p2020 A69-26564

Human nystagmic reaction variations due to simultaneous rotation of head and body, studying coriolis couple in horizontal semicircular canals 12 p2020 A69-26565

Coriolis effect in rotating spacecraft simulation, discussing optokinetic reflex responses as function of head turning angle with spin axis 14 p2409 A69-29300

Atmospheric heat exchange and circulation simulated by rotating containers, reproducing temperature field and dynamic structure above large area 14 p2478 A69-29840

Head movements controlled for rapid vestibular adaptation in slow rotation room /SRR/, preventing motion sickness 17 p2908 A69-33178

Coriolis acceleration dosages applied in vestibulometric tests of male subjects inclined in rotating chair 18 p3096 A69-34740

Visual and vestibular analysors interrelation in subjects receiving light pulses before and after rotation, noting role of cortical elements 20 p3470 A69-37249

Auditory analyser functional changes due to prolonged slow rotation 20 p3470 A69-37251

Vestibular functions of humans subjected to Coriolis acceleration via prolonged rotation at different angular velocity rates 20 p3472 A69-37260

Motion sickness prophylaxis for rabbits subjected to rotation, investigating effects of adrenalin, ephedrine, sympatholytin, piperoxane and pyridoxophene on nystagmus and respiration
20 p3472 A69-37265

Nystagmus reactions in rabbits subjected to rotating vestibular tests, noting decrease following previous adaptation to stimulus
20 p3473 A69-37267

Bonded strain gages for experimental stress analysis of high speed rotating machinery under high centrifugal loads
24 p4397 A69-42740

ROTATING FLUIDS

Turbulent heat and mass transfer in rotating incompressible fluid flow analyzed by kinetic energy and shear stress equations
01 p0060 A69-10402

Steady state circular motion of fluid with variable rheological characteristics between coaxial cylindrical surfaces, obtaining velocity distribution
01 p0061 A69-10733

Thermal convection in rotating fluid annulus, discussing suppression of frictional constraint on lateral boundary
03 p0460 A69-13339

Three dimensional sonic flow downstream from shock wave in nondissipative perfect fluid, introducing pseudorotating flow to obtain velocity field
03 p0362 A69-13363

Secularly stable figures of equilibrium of rotating heterogeneous fluids of planetary size, noting dependence on laws of inertia and gravitation
03 p0513 A69-13780

Second order difference scheme for calculation of plane or rotational compressible flow, investigating stationary flow as asymptotic limit of unsteady flow [ONERA-TP-652]
03 p0419 A69-14111

Stability of nondissipative stratified rotating flows with constant density to axisymmetric disturbances
04 p0588 A69-14740

Heated liquid mercury rotation rate and direction counter to rotating bunsen flame related to Venus cloud formations high velocities
04 p0664 A69-15466

Ekman boundary layer problem of steady axisymmetric viscous incompressible flow between infinite coaxial rotating disk, studying laminar range of Taylor number R
05 p0744 A69-15665

Two dimensional supersonic rotational flow around convex corner solved using coordinate system consisting of left running characteristics and streamlines
05 p0697 A69-15722

Liquid rise in partially filled circular cylinder with free surface accelerated from rest to constant angular velocity [ASME PAPER 68-FE-13]
05 p0747 A69-16065

Navier-Stokes equations for steady rotational motions of incompressible viscous fluid at small Reynolds numbers between rotational surfaces
07 p1119 A69-18748

Wave motion onset and waveforms in rotating annulus with sinusoidally varying temperature differences
07 p1126 A69-19039

Radial distribution of azimuthally averaged temperature and amplitude vorticity characteristics in rotating differentially heated fluid annulus determined by multiprobe technique
07 p1126 A69-19040

Stability of inviscid swirling flow with finite axial velocity components and nonvanishing radial density gradients, noting criterion for infinitesimal disturbances
08 p1305 A69-20851

Fluid flow induced by horizontally moving bodies in stratified and rotating fluids determined by matched asymptotic expansion theory
08 p1253 A69-20997

Magnetic field decay modes due to nonuniform rotation having angular velocity as increasing function of distance from axis in infinite circular conducting fluid cylinder
08 p1369 A69-20999

Decrease existence at approaching infinity solution of Sobolev linear partial differential equations describing rotating fluid small oscillations
09 p1481 A69-21899

Topology of solar magnetic field differential rotation, using hydromagnetic equations
09 p1606 A69-22425

Permanent flow of solenoidal vector line rotation in steady nondegenerate rotational flow having complex lamellar unit normal to streamline
10 p1727 A69-22862

Free periods of oscillation of incompressible rotating fluid bounded by rigid concentric spheres, using Longuet-Higgins solution of Laplace tidal equation
11 p1876 A69-25558

Buoyancy-driven system instability mechanism, showing Prandtl number increment effect and relation to Coriolis-driven instability of rotating fluids
11 p1876 A69-25559

Virtual power principles applied to solving force acting on fluid consisting of colloidal suspension of polarized particles in neutral vehicle
12 p2136 A69-26404

MHD Stokes flow for rotating disk in parallel magnetic field, showing Lorentz force inhibiting effect on fluid motion
13 p2305 A69-27325

Viscous heat conducting compressible fluid response to abrupt change in circular cylinder angular velocity at stable temperature distribution, considering Boussinesq approximation
13 p2245 A69-27378

Motion of slender axisymmetric bodies in rotating fluid, relating Long hypotheses to flow reversal and dipole distribution effects on lee waves
13 p2248 A69-28170

Stratified rotating fluid time dependent motion characterized by stability frequency ratio and Coriolis parameter within quasi-geostrophic approximation
13 p2248 A69-28171

Benard convective flow as function of Rayleigh and Taylor numbers in thin variable rotating silicone oil layer determined by flow photographs
13 p2377 A69-28172

Unique solution proven for laminar boundary layer equations of flow of revolution in unsteady state
13 p2248 A69-28195

Surface equilibrium configurations and bifurcation points for rotating homogeneous right fluid cylinder confined by surface tension forces
14 p2428 A69-28816

Kelvin-Helmholtz instability noting effects of oblique magnetic field and rotation, deriving dispersion relation
14 p2491 A69-29335

Two dimensional adiabatic transverse normal modes of inviscid compressible uniformly rotating fluid, discussing harmonic wave propagation in opposite directions and rotation effects
14 p2431 A69-29581

Liquid filled toroidal shaped rotating damping tube containing bubble, discussing parameters variation effect on spacecraft nutation
16 p2868 A69-32561

Conducting fluid and plasma rotation between concentric cylinders due to crossed fields, determining velocity distribution, induced magnetic field and kinetic energy [AIAA PAPER 69-726]
17 p3011 A69-33472

Vortex breakdown in rotating fluids associated with wave motion along axis of rotation, considering effects of nonzero wave amplitude [AIAA PAPER 69-645]
17 p2892 A69-33478

Fluid dynamic simulation of gas core nuclear rocket chamber for separating light and heavy gas via centrifugal force produced by MHD-driven rotational flow [AIAA PAPER 69-727]
17 p3004 A69-33483

Cyclonic vortices production by horizontal convergence in rotating water bowl as function of bottom surface inclination, modeling cyclogenesis in jet stream entropy field
17 p3000 A69-33760

Model calculations for movement of barotropic and initially symmetric vortices in rotating fluids with Coriolis parameter or fluid depth varying horizontally
17 p3000 A69-33761

Mean rotational velocity of finite width gaseous ring in close binary system from rotational velocity measured on spectrograms
17 p3044 A69-34180

Wave equations governing evolution of long nonlinear axially symmetric wave motion in inviscid rotating fluids
18 p3120 A69-34441

Conservation theorems for energy and mean circulation in inviscid rotating fluid, noting inertial wave spectrum continuity
18 p3121 A69-34550

Dimensionless radial and transverse velocity profiles for incompressible boundary layer on rotating disk in rotating fluid
19 p3300 A69-36720

Theory for describing rotating fluid planets external geometry in state of hydrostatic equilibrium, noting role of equipotential surfaces
20 p3594 A69-37077

Jupiter Great Red Spot in terms of homogeneous fluid rapid rotation, Rossby number, stagnant region, Taylor column and stratification
20 p3609 A69-38060

Viscous incompressible nonNewtonian fluids flow with treatment for steady rotational problems and oscillatory motion, considering primary and secondary motions
20 p3519 A69-38319

Rotating stratified fluid in thermally insulated cylinder, studying angular velocity abrupt change effects under stable temperature distribution
21 p3694 A69-38768

Interaction between boundary layer and external vortex flows and stability transitions of heated rotating fluid annulus
21 p3698 A69-39869

Motion of body with cavity completely filled with viscous fluid about center of mass in potential mass-force field, applying small parameter method
22 p3980 A69-40109

Kinetic beam instability development in homogeneous dust /gas/ cylinder rotating in hot invariable medium under arbitrary perturbations
22 p4032 A69-41017

Conducting fluid flow in spherical container in rotating magnetic field, calculating induced field velocity and inside and outside components
23 p4196 A69-41609

Decrease existence at approaching infinity solution of Sobolev linear partial differential equations describing rotating fluid small oscillations
23 p4152 A69-41975

Free vertical shear layers structure solutions singularities in rotating fluids, considering motion by rising or spinning axisymmetric body
23 p4153 A69-42356

Axial and angular momentum flux, flow force and circulation to determine strength and structure of narrow rotating axisymmetric vortex and swirling core flows
24 p4298 A69-42598

Static and dynamic characteristics of fluid pressure signal transmitter between members with relative rotary motion
24 p4256 A69-43300

ROTATING GENERATORS
U AC GENERATORS
U DYNAMOMETERS
U TURBOGENERATORS

ROTATING LIQUIDS

Unsteady slow rotational motion of viscoelastic liquid contained between two concentric spheres rotating with constant angular velocities
02 p0230 A69-11563

Flow pattern induced by oscillatory point source in rotating inviscid liquid
04 p0591 A69-15279

Whirl dynamics of partially liquid filled spinning rotor mounted on elastic shaft, noting synchronous critical speed and asynchronous whirl speed [ASME PAPER 68-WA/APM-25]
05 p0768 A69-16189

Whirling liquid hydrogen layer thermal and hydrodynamical conditions, noting application to cold neutrons source in high flux beam reactor
05 p0849 A69-16818

Rotating incompressible liquid drop held together by surface tension noting spheroidal and toroidal shapes, energies and case of surrounding denser medium
07 p1120 A69-19267

Stability of rotating liquid mass held together by surface tension
07 p1121 A69-19268

Bubble spiral path motion toward axis of rotation of liquid rotating at constant angular velocity
09 p1483 A69-22006

Differential rotation of incompressible inviscid fluid of infinite electrical conductivity in spherical shell, noting toroidal magnetic field for sun
22 p4027 A69-40658

Transition temperature depression in rotating liquid He based on increased inertial density of excitations
23 p4192 A69-42335

ROTATING MATTER

Rotational motion of system of particles related to existence of reference frame to eliminate coupling terms between internal and rotational motion
02 p0280 A69-11867

Universe rotation from observations of microwave background and using closed universe model
10 p1771 A69-22851

Galactic mass relativistic distribution calculated, considering spherically symmetric model differential rotation near sun 20 p3600 A69-37484

ROTATING MIRRORS

Solid state laser Q switched by rotating prism emitting giant pulse before two mirrors in parallel 03 p0440 A69-13365

Laser color TV projection-display system using moving mirrors and dual polarization scanner 07 p1137 A69-19740

Image motion trajectory in rotating angular mirror having converging reflections from two surfaces, using precession theory of gyroscopes 11 p1881 A69-24562

Rotating mirror streak cameras in quantitative measurements of extreme compressions by shock waves, analyzing spatial and temporal resolving power 12 p084 A69-26151

Rotating mirror turbine with air cushion floating shaft for use in streak and framing cameras, noting framing rate 12 p2085 A69-26156

Rotating mirror framing camera with continuous access at f/18 aperture, discussing image transfer system, frame rate and capacity, etc 12 p2085 A69-26157

Ultrahigh speed cinematographic materials, discussing mirror turbines, streak and synchronized framing cameras 12 p2090 A69-26197

Q switched ruby laser with rotating prism, considering single pulse operation by increasing switching rate 12 p2107 A69-26588

Rotating mirrors used for light signal Doppler frequency shifting 24 p4351 A69-43806

ROTATING PLASMAS

Plasma gravitational stability problem with Hall effect, noting relevance to astrophysical systems 03 p0478 A69-13803

Gravitational instability of rotating anisotropic plasma for longitudinal wave propagation mode, obtaining dispersion by using modified Chew-Goldberger-Low equation 05 p0827 A69-16596

Magnetic field generation in nonuniformly rotating plasma by current density from electron drift relative to positive ion gases due to viscous forces 06 p1009 A69-17966

Wave propagation and instabilities in rotating anisotropic collisionless plasma, analyzing plane and cylindrical perturbations 07 p1195 A69-19438

Plasma wave coupling in absence of magnetic field in revolving system containing dielectrics and circular waveguide 08 p1371 A69-21150

Rotating spoke in unstable pulsed MPD arc, noting rotation frequency and resemblance to plasma rotation [AIAA PAPER 69-234] 09 p1561 A69-21219

Rotating plasma disturbances onset in MPD arc, determining magnetic field dependence on mass flow, background pressure and propellant [AIAA PAPER 69-232] 09 p1562 A69-21225

Electric current spoke in MPD operation, using segmented anode and image converter methods with argon and helium propellant gases 09 p1548 A69-21962

Ionization and current growth in discharge in rotating plasma device with mirror shaped magnetic field 09 p1552 A69-22042

Rotating plasma gravitational instability during discharge as function of centrifugal acceleration, noting Coriolis and Larmor effects 09 p1552 A69-22043

Rotating plasma behavior in magnetic mirror trap, using radial electric field 10 p1740 A69-23716

Electrostatic wave dispersion relation in uniformly rotating plasma cylinder used in interpreting Q machine experiments 11 p1924 A69-24300

Kink type instability of rotating linear theta pinch plasma, calculating perturbation behavior with bounce model 11 p1929 A69-25270

Magnetic field effects on rotational MHD flow in container, noting Taylor-Proudman theorem, Ekman layers and vertical Stewartson boundary layers 11 p1930 A69-25279

Finite ion Larmor radius effect on gravitational instability of two superposed fluids in uniform rotation, analyzing interchange perturbations and vortex sheet 12 p2062 A69-26461

Finite Larmor radius effects on gravitational instability of rotating anisotropic plasma for transverse wave propagation mode 13 p2346 A69-27704

Plasma rotation by Lorentz force in homopolar gas discharge device, considering centrifugal forces effect on flow pattern 13 p2315 A69-28556

Radiative effect on rotating gaseous magnetic mass stability in thermodynamic equilibrium, including small oscillations stability 14 p2522 A69-29596

Radial pressure distribution in steady state rotationally symmetrical plasma jet subjected to axial magnetic field, emphasizing mass entrainment effect [DGLR-69-024A] 23 p4202 A69-41924

ROTATING SHAFTS

NT SHAFTS [MACHINE ELEMENTS]

NT TURBOSHAFTS

Flexural vibration of unbalanced rotating shaft with nonlinear characteristic of elasticity and damping, using equations of motion 01 p0168 A69-10329

Whirl instability of externally pressurized gas journal bearing with peripheral feeding holes, discussing analytical natural frequency of shaft bearing systems 02 p0254 A69-12426

Critical speeds of multiple disk rotors with multiple supports, discussing continuous shaft sections including gyroscopic and transverse shear and rotary inertia effects [ASME PAPER 69-VIBR-51] 10 p1804 A69-24153

Rotor shaft mounted on number of bearings and carrying masses and inertia angular precession and critical speeds, considering gyroscopic moments, rotary inertia and shear deformation [ASME PAPER 69-VIBR-54] 10 p1805 A69-24154

Varying diameter anisotropic composite shafts torsion based on strain and stress functions 11 p1982 A69-24975

Critical rotation rates of homogeneous shaft with two bearings under tension, considering shaft mass, stretching force magnitude and console disk gyroscopic effect 13 p2269 A69-28323

High speed shafting design for helicopter power transmission systems, discussing shaft in OH-6A Cayuse light observation helicopter [ASME PAPER 69-DE-5] 14 p2453 A69-28837

Thomas fracture theory and compatibility conditions for fracture surface of elastic-plastic rotating hollow shaft, discussing plastic equilibrium 15 p2712 A69-31017

Bending vibratory motion instability of rotor on elastic shaft with uniform mass distribution along axis, using variational methods 16 p2875 A69-32249

Elastomer hardness criteria ensuring maximum life and performance of rotary shaft seals 16 p2794 A69-32432

Thin walled cantilevered fiberglass reinforced shafts damping characteristics dependence on natural vibration modes and fibers orientation 17 p3065 A69-33938

Rotating shafts impact damping efficiency increaseable by providing proper clearance to reduce shaft stress in critical resonance frequency region 17 p3066 A69-33946

Supported shafts natural vibration frequencies determination by averaging shaft parameters, noting suitability in HF ranges 18 p3147 A69-34546

Viscoelastic shaft stability rotating at harmonically variable angular velocity, considering internal and external damping 18 p3224 A69-35300

Keyway stresses in shafts under tension, bending and torsion, using frozen stress photoelastic technique 19 p3445 A69-36827

Rigid shaft dynamics in hinged and elastic bearings, eliminating inaccuracy by limiting analysis to forced vibration 23 p4171 A69-42483

Rotating wickless hollow shaft heat pipe utilizing centrifugal acceleration for return pumping of condensate and transferring high heat fluxes [ASME PAPER 69-HT-19] 24 p4413 A69-43550

ROTATING SPHERES

Schlieren method for studying rotating sphere heat transfer during natural convection 01 p0174 A69-10095

Unsteady slow rotational motion of viscoelastic liquid contained between two concentric spheres rotating with constant angular velocities 02 p0230 A69-11563

Rotating bodies stability conditions relative to radial disturbances found to be field strength dependence on internal mass at any point 02 p0317 A69-11978

Flow development around impulsively rotating dipole magnetized sphere in viscous incompressible conducting fluid, noting diffusing Alfvén waves and induced field 03 p0477 A69-13793

Differential rotation of sphere in viscous incompressible liquid, discussing pressure and skin friction drag between two hemispheres with different angular velocities 04 p0590 A69-15278

Steady rotation of insulating body of revolution in unbounded electrically conducting fluid permeated by applied axial magnetic field 07 p1190 A69-18814

Aerodynamic torque on spinning spherical satellite, noting applications to accommodation coefficient measurements and study of aerodynamic gas-surface interactions 09 p1611 A69-22087

Short memory elasticoviscous fluid motion in and around oscillating spherical shell 10 p1800 A69-23240

Thin liquid film equilibrium on rotating sphere, determining conditions for detachment as function of angular velocity 12 p2061 A69-25886

Time dependent magnetic field induced inside rotating spherical conductor by external sources applied to moon 14 p2518 A69-29121

Incompressible viscous fluid steady motion caused by rotating ellipsoid, determining drag moments for circular disk and sphere 14 p2432 A69-29627

Rotating bodies stability conditions relative to radial disturbances found to be field strength dependence on internal mass at any point 15 p2680 A69-30260

Stress distribution in isotropic spherical shell rotating uniformly about diametral axis, deriving equilibrium equations 15 p2712 A69-31005

Upper limit of solar oblateness determined from secular stability of differential rotation during evolution 18 p3202 A69-35214

Angular velocity torsional oscillations of solid sphere under elastic force couple rotating in viscous liquid bounded by immobile concentric sphere 18 p3175 A69-35320

Conservation laws and Liapunov stability of free rotation of rigid body about principal axes derived from kinetic energy and angular momentum 19 p3397 A69-35612

Spherically rotating symmetric body gravitational collapse within Schwarzschild radius, presenting trapped surface concept for asymmetrical cases and generalization of space-time singularities 23 p4219 A69-42333

ROTATING STALLS

Two dimensional airfoil data application to three dimensional rotor blade element environment, predicting stall induced structural loads [AHS PAPER 322] 17 p2895 A69-33536

Dynamic stall characteristics of high speed symmetrical and cambered helicopter rotor blade airfoils from two dimensional wind tunnel determinations [AHS PAPER 206] 20 p3463 A69-37806

ROTATING VEHICLES

U VEHICLES

ROTATION

NT AUTOROTATION
NT EARTH ROTATION
NT MOLECULAR ROTATION
NT PLANETARY ROTATION
NT SATELLITE ROTATION
NT SOLAR ROTATION
NT STELLAR ROTATION

Absolute rotation in space measured with microwave rotation sensor using polarization of electromagnetic wave 04 p0573 A69-14342

Analytic solution for whirl in finite journal bearing with continuous lubricating film using Fedor approach [ASME PAPER 69-VIBR-55]

10 p1700 A69-24147

Rotary oscillatory solution of parameterized system with stable unexcited motion using successive approximations

14 p2482 A69-28812

Rotation curve, mass and M/L ratio of Sc galaxy NGC 6574, discussing nucleus and systemic velocity

15 p2691 A69-30764

Angular velocity of aircraft rotation about longitudinal axis at arbitrary point of passive trajectory section, with assumptions on roll damping, momentum, etc

18 p3092 A69-34989

Autonomous system steady motion with rotating phase and deviating argument solved by successive approximation over infinite time interval

18 p3175 A69-35323

Green functions for displacement and rotation fields of infinite homogeneous isotropic centrosymmetric micropolar elastic body subjected to time dependent mass forces and momenta

18 p3226 A69-35459

Human sleep during prolonged rotation, discussing electroencephalograms, acoustic signal frequency producing waking reaction, cutaneous galvanic reflex and depth of sleep

20 p3472 A69-37261

Rotation effect of secondary principal axes in scattered light photoelasticity by dual observation method, deriving light intensity

21 p3844 A69-39317

Low pressure arc discharge motion between concentric electrodes in transverse magnetic field, noting Lorentz, stationary and retrograde modes due to temperature nonequilibrium [AIAA PAPER 68-708]

24 p4359 A69-43644

ROTATIONAL FLOW

U FLUID FLOW

U VORTICES

ROTOR AERODYNAMICS

Aeroelastic rotor and nonsteady rotor aerodynamics

05 p0695 A69-15549

Vortex motion of separated flow from slender wings and rotor loading, discussing computer role in low speed aerodynamic research

05 p0696 A69-15562

Hingeless fiberglass rotary wings dynamics, discussing effects of in-plane bending to flapping frequency ratio [AIAA PAPER 69-204]

07 p1054 A69-19548

Helicopter rotor wake distorted geometry prediction by analytical method, noting experimental results for rotor in forward flight [AIAA PAPER 69-196]

07 p1051 A69-19553

Computer programmed momentum theory for induced flow field of helicopter rotor in forward flight [AIAA PAPER 69-224]

07 p1052 A69-19562

TRAC variable diameter rotor design based on jackscrew mechanism applied to compound helicopter [AIAA PAPER 69-221]

07 p1056 A69-19572

Rotor dynamics of stowed rotor aircraft, analyzing blade stiffness in wind tunnel [AIAA PAPER 69-207]

07 p1057 A69-19578

Streamlined rotors calculation, interpreting compatibility conditions between streamlining and airscrew stresses

08 p1252 A69-20655

Rotor downwash in ground effect in presence of step, using two dimensional analysis for flow field calculation [AIAA PAPER 69-225]

08 p1253 A69-21032

Foil bearings design, fabrication, applications to flexible material transport, rotor support, etc

15 p2618 A69-30327

Aerodynamic aspects of tail rotor design and structural dynamics of stiff inplane configurations, discussing blade natural frequencies [AHS PAPER 342]

17 p3059 A69-33504

Critique of paper on comparison of dynamically scaled model rotor test data with discrete azimuth aeroelastic stability theory [AHS PAPER 341A]

17 p3059 A69-33505

Dynamically scaled model rotor tested in wind tunnel to evaluate blade aeroelastic limits constructed with realistic mass and stiffness distributions [AHS PAPER 341]

17 p3059 A69-33506

Natural gyrofrequencies of rigid rotor during slowing/stopping at high forward speed, using simple approximation

17 p2899 A69-33507

Gyro controlled rigid rotor dynamic stability studied for stoppable rotor operation, developing analytical expressions for determining stability boundary of constant and rotor speed gyros [AHS PAPER 343]

17 p2899 A69-33508

Lifting rotors with thrust or tilting moment feedback control, deriving blade equations of motion [AHS PAPER 340]

17 p2899 A69-33510

Helicopter engine dynamic analysis, discussing modeling techniques, rotor responses and turbine speed control simulations and transition from mathematical models to hardware components [AHS PAPER 332]

17 p2946 A69-33531

Helicopter rotors and static propellers theory based on Prandtl-Betz theorem, calculating ideal performance [AHS PAPER 326]

17 p2894 A69-33533

Instrumentation for rotorcraft aerodynamics, considering boundary layer measurements, hot-wire anemometer and schlieren system for rotors and propellers [AHS PAPER 320]

17 p2895 A69-33539

Tail rotor aerodynamics, discussing ambient conditions, maximum thrust, precession effects, fin interference, noise reduction, etc [AHS PAPER 300]

17 p2895 A69-33549

Aerodynamics of rotary wing and V/STOL aircraft - Conference, Buffalo, June 1969

18 p3087 A69-35216

Lifting line theory for hovering propellers deformed wakes based on continuous vortex sheet representation

18 p3087 A69-35217

Aerodynamic behavior of airfoil oscillating in reverse flow defined for various angles of attack and oscillatory amplitudes at low Mach numbers

18 p3087 A69-35219

V/STOL model small scale tests compared with full scale tunnel or flight tests, considering normal differences in parameters and rotor instability

18 p3119 A69-35227

Flow field throughout wind tunnel containing rotor with sharply deflected blades, noting reversed flow effect in front of wake

18 p3119 A69-35228

Slot height, position and trailing edge geometry effects on elliptically shaped rotors selected for hover efficiency, size, transitional gust insensitivity and rigidity

18 p3088 A69-35231

Circulation controlled rotor aerodynamics with tangentially ejected air from surface slots of lifting body, noting performance at advance ratios and thrust coefficients

18 p3089 A69-35232

Torsionally flexible blade controllable twist rotor with pitch horn and servoflap control, discussing optimum inputs, airloads and angles of attack contours

18 p3089 A69-35234

Rotor operating limits, loads, performance prediction and airfoil development in rotary wing aerodynamics research

23 p4057 A69-41371

Rotor aerodynamics research in terms of theoretical and experimental data comparison, rotor blade flow visualization and blade section camber

23 p4057 A69-41372

ROTOR BLADES

Boundary layer discontinuity on helicopter rotor blade in hovering using flow visualization [AIAA PAPER 69-197]

07 p1051 A69-19561

Laminar boundary layer on rotating blades and yawed infinite wings, solving partial differential equations numerically by implicit finite difference scheme on computer

16 p2732 A69-31885

Dynamic stall characteristics of high speed symmetrical and cambered helicopter rotor blade airfoils from two dimensional wind tunnel determinations [AHS PAPER 206]

20 p3463 A69-37806

Natural convective heat transfer to gas turbine rotor blade and thermal resistance of cooling system using centrifugal pump

21 p3785 A69-39103

ROTOR BLADES (TURBOMACHINERY)

Steady three dimensional flow through impeller of turbines with small number of blades and with edge cut hub, noting inefficiency of flow without impact

01 p0142 A69-10309

Circumferential inhomogeneity of flow through impeller blades of axial flow compressor

03 p0361 A69-12954

Stress-strain distribution in rotor wheel with radial side blades, giving differential equations system for circular disk strains

09 p1612 A69-21494

Rotating twisted blades vibrations, deriving equations and vibration tests with models

09 p1618 A69-22236

Supersonic axial compressor boost stages for small gas turbine engines, using passage flow approach and passage criteria to design airfoils [ASME PAPER 69-GT-44]

09 p1570 A69-22478

Dry friction whip role in radial rubs dynamic stability in labyrinth seals and blade tips of turbomachinery [ASME PAPER 69-VIBR-56]

10 p1804 A69-24146

Rotatory inertia and shear deformation effects on natural frequency and bending mode shape in equations of motion of rotating turbomachine blade [ASME PAPER 69-VIBR-50]

10 p1804 A69-24148

Aerodynamic design of subsonic and transonic axial flow compressors, discussing blade configurations and computerized design of turbomachinery

12 p2147 A69-25792

American, French and Soviet medium weight helicopters tested in terms of main rotor blades construction, rotor performances and comparative power plant data

13 p2201 A69-27329

Aerodynamic losses and stage efficiency in partial admission turbines, using flat bladed rotor experiments and rotors of different blade pitch

15 p2547 A69-30290

Bladed disk assemblies vibrational properties, discussing dynamic characteristics of system with pairs of close natural frequency modes under forced vibration

15 p2704 A69-30304

Photothermoelastic analysis of thermal stresses in turbine wheels with welded blades, noting stress concentration reduction

15 p2715 A69-31488

Two dimensional model for analyzing turbulent separation and reattachment at blade trailing edge at supersonic speed [ONERA-TP-678]

16 p2733 A69-32258

Blade vibration damper consisting of springs attached to blade, analyzing resonance stresses on basis of dynamic rigidities

17 p3066 A69-33944

Critical speeds of high speed turbine rotors running in friction bearings determined by varying natural frequencies of rotor and supports

18 p3147 A69-34545

Natural oscillations frequency spectrum of turbomachine impeller blades subjected to random variations determined with frequency distribution function obtained by moments method

19 p3436 A69-35844

Tilt propotor composite aircraft design, discussing performance and mission potential [AHS PAPER 202]

20 p3463 A69-37805

Pyrometer for turbine rotor blades surface temperature measurement, considering purged, line-of-sight viewing tube and signal processing to reject C particles interference [SAE PAPER 690431]

23 p4165 A69-41649

Discrepancy between theoretical and experimental coefficients of friction losses on blades of centrifugal compressor impeller wheels, using lattice theory

23 p4058 A69-41727

ROTOR DISKS

U TURBINE WHEELS

ROTOR HUBS

U HUBS

U ROTORS

ROTOR LIFT

Sikorsky ABC/advancing blade concept/ helicopter program, discussing advantages and small scale wind tunnel experiments [AIAA PAPER 69-217]

07 p1055 A69-19558

NASA flight test of hingeless rotor compound helicopter to determine lift sharing characteristics, showing rotor lift dependence on airspeed

14 p2393 A69-29702

Heavy lift helicopter design with 30 ton payload, considering fanjet drive hot cycle and shaft drive propulsion systems [AHS PAPER 330]

17 p2901 A69-33532

ROTOR SPEED

Whirl dynamics of partially liquid filled spinning rotor mounted on elastic shaft, noting synchronous critical speed and asynchronous whirl speed [ASME PAPER 68-WA/APM-25]

05 p0768 A69-16189

Axial torque effect on critical speeds of continuous rotor with motion described by partial differential equations [ASME PAPER 69-VIBR-52]

10 p1804 A69-24152

Critical speeds of multiple disk rotors with multiple supports, discussing continuous shaft sections including gyroscopic and transverse shear and rotary inertia effects [ASME PAPER 69-VIBR-51]

10 p1804 A69-24153

Rotor shaft mounted on number of bearings and carrying masses and inertia angular precession and critical speeds, considering gyroscopic moments, rotary inertia and shear deformation [ASME PAPER 69-VIBR-54]

10 p1805 A69-24154

Rotor angular velocity and flexural strain interdependence at critical velocity

11 p1987 A69-25390

Critical speeds of high speed turbine rotors running in friction bearings determined by varying natural frequencies of rotor and supports

18 p3147 A69-34545

High speed rotors with air lubricated foil bearings, studying motion in pressurized and self acting modes

22 p3955 A69-40405

ROTORCRAFT

U ROTARY WING AIRCRAFT

ROTORS

NT COMPRESSOR ROTORS

NT FLYWHEELS

NT IMPELLERS

NT LIFTING ROTORS

NT PUMP IMPELLERS

NT RIGID ROTORS

NT ROTARY WINGS

NT TILTING ROTORS

NT TIP DRIVEN ROTORS

NT TURBINE WHEELS

Bursts of high speed rotor occurring at diametric cross section and around hub as function of hub size

01 p0142 A69-10306

Forced oscillations of unbalanced rotor on elastic bearings with nonlinear characteristics investigated for resultant forces and amplitude using motion equations

01 p0170 A69-10824

Amplitude-frequency characteristics of rotor mounted on hydrostatic bearings calculated by equations of dynamic compliance method

03 p0432 A69-12961

Blade to rotor heat transfer in turbines determined from temperature distribution of rod in medium with nonuniform temperature

06 p1034 A69-17870

Fracture mechanics for predicting crack propagation rate in rotor spars

07 p1053 A69-18872

Rotors linear vibrations due to unbalanced shaft rotating on lubricated bearings taking into account lubricant damping

07 p1235 A69-19441

Torsiograph systems analysis for rotors angular acceleration recording, discussing dynamic characteristics, system, environmental problems, etc

10 p1692 A69-23252

Stability of high speed single mass rotor with internal friction on damped anisotropic supports, considering support stiffness [ASME PAPER 69-VIBR-2]

10 p1805 A69-24160

Vector equation for correction masses for dynamic balancing of rotor supported on n points derived from bearing structure vibrations amplitude and phase

12 p2180 A69-26243

Dynamics of triaxial gyrostabilizer with additional rotor mounted on base, showing systematic drift

13 p2259 A69-27428

Gyroscopic motion with unbalanced rotor in run-down mode, integrating equations for small oscillations

13 p2259 A69-27429

Nonstatic gyroscopic nonlinear oscillations caused by swaying of synchronous gyromotor rotor

13 p2264 A69-28438

Oscillation amplitude of rotor with hydraulic dampers on elastic supports by expanding forced vibration modes with friction in natural modes

16 p2837 A69-32136

Bending vibratory motion instability of rotor on elastic shaft with uniform mass distribution along axis, using variational methods

16 p2875 A69-32249

Self excited vibrations of rotors supported in gas bearings from analyzing solutions to equations of rotor motion

16 p2875 A69-32250

Rotor hazards in rotational behavior of gravity stabilized satellites, describing gyrostact applications

17 p3048 A69-33233

Linear analysis of damped flexibly mounted rolling element bearings influence on dynamic rotor unbalance response, including optimum support characteristics [ASME PAPER 69-LUBS-8]

18 p3212 A69-34382

Mean drift rates of single and two rotor gyroscopic linear acceleration integrators mounted on irregularly rocking base

18 p3135 A69-34586

Attitude stabilization of symmetrical nonrotating earth satellite using earth-pointing rotor as gravitational anchor

19 p3429 A69-35914

Finite element method in stress analysis for axisymmetric rotors design, describing computer program and applications

19 p3445 A69-36826

Mathematical formulation and error analysis of two rotor gyroorbit used in plotting orbital system of satellite coordinates

21 p3765 A69-39636

High speed rotors with air lubricated foil bearings, studying motion in pressurized and self acting modes

22 p3955 A69-40405

ROUGHNESS

U SURFACE ROUGHNESS

ROUND TRIP TRAJECTORIES

NT CIRCUMLUNAR TRAJECTORIES

Optimum low thrust interplanetary transfers involving swingby trajectory past intermediate planet analyzed, assuming impulsive velocity change at planet

06 p1006 A69-17572

CircumJovian powered and free return trajectories, analyzing round trip missions and departure opportunity [AAS PAPER 68-117]

21 p3805 A69-39207

Reduced flight time interstellar round trip propulsion system with relativistic velocity capabilities, discussing vehicle with solar sail and magnetic course reversal [AAS PAPER 69-388]

24 p4363 A69-42829

ROUNDED LEADING EDGES

U LEADING EDGES

ROUTES

BAC Three-Eleven 220 seat airliner for short and middle distance routes, discussing operating costs, thrust and range

02 p0193 A69-12067

ROVER PROJECT

Control system utilizing digital and linear integrated circuits for low power testing of Pewee 1 reactor of Rover program [IEEE PAPER 2B-6]

07 p1179 A69-19188

Wideband acceleration instrumentation for Rover ground test facility liquid hydrogen turbopumps to study structural and flow induced vibrations

10 p1692 A69-23250

ROVINGS

Woven roving construction and fill/warp ratio effects on flexural strengths of four ply laminates

14 p2469 A69-29414

RUBBER

Displacement function selection in calculating rubber-metal valve design, considering boundary conditions of material deformation

01 p0087 A69-10829

Rubber modified thermoplastics structure and mechanical properties, emphasizing stress concentration around composite particles and crazing role in creep and fracture

10 p1716 A69-23985

Elastohydrodynamic lubrication of cylindrical rubber surface sliding over glass plate, using optical interference technique

23 p4171 A69-42531

RUBBER COATINGS

Small hovercraft simple and bag skirts design characteristics, considering materials

13 p2202 A69-27545

RUBIDIUM

Rubidium self oscillating magnetometer long term stability, noting changes affecting accuracy and sensitivity

02 p0250 A69-12394

Temperature dependence of isotope thermotransport in liquid K and Rb using steel capillary cells

03 p0533 A69-13970

Optical absorption of vacuum deposited thin rubidium films, noting similarity to sodium and potassium

03 p0491 A69-14114

Pumping light filtration conditions effect on transition frequency of rubidium atoms

04 p0611 A69-14779

Indium, Rb and Cs abundances obtained from sunspot spectra by comparison with Zr and Ti lines

13 p2343 A69-27626

Arcturus and solar rubidium abundance compared using Mount Wilson photographic spectrograms of Arcturus

14 p2522 A69-29589

Moldavites and Ries crater material, studying Rb-Sr isochronal relationship

23 p4154 A69-41341

RUBIDIUM COMPOUNDS

Parametric excitation of spin waves during parallel pumping of rubidium nickel fluoride ferrite, relating relaxation time and temperature

21 p3781 A69-39069

RUBIDIUM ISOTOPES

Rubidium, Sr and Sr isotopic composition of normal gray hypersthene chondrite falls, noting Rb/Sr and Sr87/Sr86 ratio determination of Bath Furnace L chondrite isochron

02 p0317 A69-12020

Rb 87 vapor laser short term frequency stability independent of vapor concentration, noting use as frequency standard

05 p0770 A69-15656

Rb 87 vapor laser short term frequency stability independent of vapor concentration, noting use as frequency standard

16 p2798 A69-32513

Rb 87 vapor laser output power dependence on magnetic field strength and resonator detuning, discussing laser and atomic transition frequency tuning

17 p2983 A69-33694

Rb 87 vapor laser pumping, output, spectral line width and emission frequency approximated in three level system

19 p3335 A69-36342

Rb 87 vapor laser output power and spectral line width dependence on optical pumping intensity and atom density in resonator

19 p3336 A69-36343

Light induced shift of Rb 87 vapor laser emission frequency during modulated optical pumping, discussing elimination by filter temperature and tuning

19 p3336 A69-36344

Frequency shift dependence in transition of Rb 87 atoms on pulsed pumping intensity, discussing continuous and pulsed indication and peak determination

19 p3336 A69-36345

Rb-Sr isotope patterns in tektites from Southeast Australian strewn field, studying Rb volatilization role in Rb-Sr isochron production

23 p4154 A69-41342

Rb-Sr isotopic determinations for Olivenga olivine-hypersthene chondrite, noting isotopic ratio vs age

24 p4385 A69-43214

RUBIDIUM 86

Gastric perfusion rate in restrained animals determined by Rb 86 clearance technique

17 p2908 A69-33170

RUBY

Electric effect in ruby, discussing resonance magnetic field and transition

03 p0485 A69-13320

Cross relaxation and spin-lattice relaxation probabilities determination in ruby crystal based on inversion coefficients

06 p0980 A69-17458

Ruby absorption, fluorescence and lasing properties, calculating polarization effect on relative intensities and forms of R1 and R2 bands in macroscopic theory

07 p1201 A69-19646

Relation between electron spin-spin interactions and polarization and relaxation of ruby nuclei at He temperatures

08 p1372 A69-20541

Chromium concentrations induced line shift in ruby single crystals spectra, determining principal lines position

10 p1744 A69-23321

Two photon absorption excitation of luminescence in ruby crystals by neodymium laser radiation, determining luminous intensity dependence on pumping intensity

15 p2634 A69-30731

Quantum mechanical microwave frequency doubling in ruby, discussing output power variation with orientation

17 p3015 A69-33024

Tau-luminescence in thin gamma-colored and uncolored ruby crystals containing Cr ions measured, discussing ions absorption spectrum changes

19 p3335 A69-36166

- Cross relaxation and spin-lattice relaxation probabilities determination in ruby crystal based on inversion coefficients
20 p3584 A69-37941
- RUBY LASERS**
- Ruby laser crystals optical inhomogeneity and residual mechanical stresses effects on laser beam angle of divergence
01 p0139 A69-10831
- Transmission of coherent ruby laser radiation through traveling wave amplifier noting spatial field structure changes
02 p0255 A69-11608
- Ruby laser limiting gain, stimulated emission loss, noise loss and spectral distribution determined by radiation intensity, pumping power and mirror reflection
02 p0256 A69-12000
- Pulsed ruby laser power supply incorporating facilities for variable output, automatic cutout for fully charged capacitors and automatic/manual triggering
02 p0256 A69-12095
- Ruby laser output energy degradation due to pump light absorption by color centers of ruby rod
02 p0256 A69-12358
- Ruby laser modifications for pulse transmission mode operation and cavity dumping, noting peak power output
02 p0257 A69-12410
- Mode locking and ultrashort pulses in giant pulses in giant pulse ruby laser with heated nitrobenzene or alpha-chloronaphthalene in resonator
02 p0259 A69-12655
- Giant pulse generation by Q switched water cooled CW ruby laser in narrow spectral range, discussing laser design and operation principles
03 p0435 A69-12982
- Ruby laser radiation nonlinear absorption coefficient measurement in CdS, ZnS and SiC semiconductor crystals, noting light limiting effects
03 p0436 A69-13038
- Ruby laser light beam self focusing in sodium chloride and potassium bromide crystals
03 p0438 A69-13051
- Ruby laser to study stimulated Mandelstam- Brillouin scattering in liquids and in various crystals in UV
03 p0438 A69-13053
- Nonlinear influence of resonator losses on stimulated emission of ruby laser, noting cut-off action
03 p0439 A69-13058
- Ruby laser emission spectral line narrowing due to lasing modes reduction
03 p0439 A69-13059
- Ruby laser boring and welding apparatus cooled by evaporated nitrogen gas, suitable for diamond boring
03 p0434 A69-13720
- Cavity arrangement to obtain pulse durations of 0.5-10 microseconds with ruby laser
03 p0441 A69-14142
- Frequency mixing of organic dye solution laser radiation with ruby laser radiation, showing broader UV spectrum
04 p0610 A69-14424
- Resonant interaction of radiation from liquid nitrogen cooled ruby laser with ruby crystal in temperature range 4.2-100 K
04 p0611 A69-14439
- Plasma refractive index determination by holographic interferometry with double pulse ruby laser
05 p0761 A69-15620
- High power single mode ruby laser, using multielement rods with plane-parallel end surfaces for generating longitudinal and transverse mode
05 p0770 A69-15700
- Self Q switching of ruby lasers at 77 K, noting saturable absorber giant pulse process obtained by shielding part of laser rod from pump
05 p0776 A69-16332
- Upper limit of nonradiative relaxation time between specific states of absorption bands and fluorescence state emitting R lines in ruby laser
05 p0777 A69-16335
- Pulsed ruby laser threshold and output energy for different relative orientations of rectangular prism and ruby crystal main crystallographic axis
05 p0777 A69-16526
- Ruby laser characteristics at 78 K, discussing emission threshold, optimum feedback, modes, etc
05 p0777 A69-16546
- Light pulse duration and other parameters for ruby and Nd-glass lasers operating in synchronized mode regime determined by Armstrong method
06 p0934 A69-17549
- Semiconductors reflectivity enhancement by irradiating with Q switched ruby laser output
06 p0935 A69-17768
- Temperature dependence of laser induced damage in plastic Q switch made of polyethylmethacrylate and vanadyl phthalocyanine for ruby laser
06 p0936 A69-17777
- Frequency doubling due to nonlinear response from Zeeman levels of ruby, discussing output and paramagnetic resonance
07 p1144 A69-18471
- Emission frequency stabilizing effect in concentric sapphire-coated ruby laser, noting frequency independence from temperature fluctuations and thermal stresses
07 p1147 A69-18543
- Fresnel pulse holograms of three dimensional diffuse objects by single mode ruby laser with or without Q switching
07 p1132 A69-18801
- Temperature profile and power density distribution in metastable level of ruby laser rod during pumping in air
07 p1150 A69-18937
- Saturable dye filters used with ruby lasers, discussing relaxation time, residual absorption source and transient spectral hole burning
07 p1155 A69-19089
- Ruby laser beam incident on steel surface in air or water measured for energies, determining reflected energy dependence on incident energy for self insulation effect
07 p1157 A69-19594
- Ruby absorption, fluorescence and lasing properties, calculating polarization effect on relative intensities and forms of R1 and R2 bands in macroscopic theory
07 p1201 A69-19646
- Reflection holograms with single mode pulsed ruby laser
08 p1313 A69-20164
- Q switched single mode ruby laser pulse passage through traveling wave amplifier decreases beam divergence
08 p1326 A69-20542
- Nonlinear optical effects in He-Ne and ruby lasers noting laser gain, frequency splitting, frequency differences in coupled lasers and frequency band narrowing
08 p1327 A69-20768
- Design of ruby laser for stability, lifetime, maintenance and safety requirements of commercial users, discussing power, pulse duration and beam divergence
08 p1327 A69-20881
- Luminous discharge at nonabsorbing surface when exposed to single pulse ruby laser beam, suggesting photoionization in surface layer
08 p1327 A69-21021
- Formation and characteristics of flash produced in air by single pulse of Q switched ruby laser, using holographic interferograms
08 p1317 A69-21022
- Laser rubies emission characteristics operating at different temperatures in common resonator, studying kinetics for pumping powers
08 p1327 A69-21076
- Atmospheric effects on laser beam attenuation, noting application to optical visibility measurement by ruby laser
08 p1327 A69-21089
- Optical parametric noise in water by ruby laser beam for phase matched four photon process
09 p1539 A69-21751
- Pulsed ruby laser of small output for hole drilling, studying correlation of vaporization, hole diameter and depth with laser output
09 p1504 A69-22247
- Ruby laser emission absorption in transparent dielectrics, noting crack formation and propagation producing opacity
09 p1520 A69-22655
- Nonlinear susceptibility tensor components and refractive index variations of liquids and glasses in high intensity ruby laser field, using interference methods
10 p1703 A69-23622
- Mode locked ruby laser for short duration pulse production, noting relation to reciprocal linewidth
10 p1705 A69-23813
- Spectral broadening measurements of ruby laser light scattered by density fluctuations in theta pinch plasma
11 p1924 A69-24304
- Output power losses in lasers with inhomogeneous active rods, deriving formulas for losses in ruby and Nd-glass laser rods
11 p1926 A69-24603
- Ruby laser unsteady modes with ruby filter, discussing conditions for pulsed, monopulse and steady mode transitions, with formulas for steady emission
11 p1894 A69-24619
- Ruby laser crystals optical inhomogeneity and residual mechanical stresses effects on laser beam angle of divergence
11 p1936 A69-24698
- Transmission of coherent ruby laser radiation through traveling wave amplifier noting spatial field structure changes
11 p1895 A69-24715
- Free emission spectrum analysis of ruby laser with external mirrors and elimination of axial mode discrimination
11 p1900 A69-25547
- Ruby laser performance with perturbing effect of standing wave field on homogeneity of deexcitation of level populations eliminated by HF modulation
11 p1900 A69-25569
- Population inversion in ground state sublevels of ruby laser, deriving required conditions
11 p1900 A69-25572
- Q switching of ruby lasers by natural chlorophyll a and derivatives pheophytin a and Cu chlorophyllin Na
11 p1900 A69-25581
- Nonuniform standing wave fields spatial distribution in active rod of ruby laser effects on laser radiation dynamic parameters, discussing radiation spectrum width
11 p1901 A69-25756
- Transverse mode dependence of spiking behavior for ruby laser pumped by pulsed argon ion laser
12 p2104 A69-25928
- Spectrum analysis of aluminum plasma excited by giant pulse ruby laser radiation, discussing temperature and density
12 p2134 A69-26027
- Q switched ruby laser stroboscope for high speed photography, using electro-optical crystals for Q switch
12 p2086 A69-26167
- Cine-holographic apparatus consisting of ruby laser and semitransparent mirror, noting capability of photographing within 10-100 nsec intervals
12 p2087 A69-26172
- Ruby crystal optical homogeneity and relation to main laser emission characteristics, discussing optical and structural surface properties [IEEE PAPER U-7]
12 p2106 A69-26322
- Q switched ruby laser with rotating prism, considering single pulse operation by increasing switching rate
12 p2107 A69-26588
- Heat removal from laser ruby rod by Cu prism connected to cooling system, discussing limiting factors in heat transfer area size
12 p2108 A69-26592
- Ultrasonic vibrations effect on emission of ruby laser with externally mounted mirrors
13 p2271 A69-27534
- Single frequency ruby laser emission spectrum coincidence with interacting laser radiation at instant of Q switching
13 p2272 A69-27911
- Single mode ruby laser for application to holography of ultrahigh speed three dimensional objects
13 p2262 A69-27980
- Power output of ruby laser stimulated by strong pinch discharge plasma flux at 4000-7000 A in He
13 p2273 A69-28530
- Composite ruby laser optical inhomogeneity effect on spectral, temporal and angular emission characteristics
14 p2458 A69-29163
- Ruby laser filled with single emission mode of oscillation using uniform pumping
14 p2458 A69-29164
- Ruby laser reflected and transmitted light intensity following radiation focusing on cuvette containing cyclohexane, noting dependence on incident pulse power
14 p2459 A69-29392
- Ruby laser lasing modes spectral time dependence attributed to population inversion inertia responsible for mode competition
15 p2633 A69-30725
- Lasing kinetics, emission spectrum and directivity of ruby laser with spatially homogeneous population inversion
15 p2634 A69-30729
- Inversion coefficient for two orientations of ruby crystal with respect to external magnetic field perpendicular and push-pull orientations
16 p2795 A69-31570

Ruby laser output energy degradation due to pump light absorption by color centers, discussing roles of defects and impurities in center formation
16 p2795 A69-31697

Fluorescence noise in Q switched ruby laser atmospheric backscattering experiments, noting relation to optical radar spurious and enhanced returns
16 p2777 A69-32183

Ruby and gas lasers operation principles, discussing spatial coherence, frequency stability, energy conservation and concentration, Q spooling, resonators, etc
16 p2797 A69-32377

Tunable far IR radiation generated from difference frequency between two Q switched ruby lasers using lithium niobate and quartz as mixing crystals
16 p2798 A69-32603

Self Q switching of pumped neodymium-doped YAG and ruby lasers obtained by static misalignment of mirror and pumped laser filament
17 p2979 A69-32916

Repetitively Q switched ruby laser applied to frequency conversion, stimulated Raman scattering and vacuum UV generation
17 p2980 A69-33027

Holographic recording of temporal coherence pattern of wave train from pulsed radiation source, investigating single mode ruby laser
17 p2973 A69-33114

Ruby laser stimulated emission spatial, temporal, energetic and spectral characteristics during disruption in spherical cavity containing strongly scattering medium
18 p3152 A69-35026

Ruby laser resonator losses resulting from changes in mirror transmittance or inclination, or introduction of bleachable absorbers
19 p3331 A69-35863

Ruby laser Q switching with electro-optical shutter based on Li metaniobate crystals by applying static, single pulse or periodic potential to Pockels cell
19 p3336 A69-36346

Pulse ruby lasers with mercury lamps for pumping noting improved efficiency, power and temperature regime due to reduced IR radiation
19 p3336 A69-36347

Flat wire grid calorimeter used as radiation sensor in measuring pulsed ruby laser
19 p3339 A69-36755

Wavelength-surface temperature relationship of ruby laser, discussing thermal control of emission wavelength
20 p3552 A69-36967

Second harmonic emission in KDP crystal using ruby rod as active material, discussing difficulties encountered by diffused reflector
20 p3552 A69-36970

Ruby laser-ultrahigh vacuum device for studying electron and ion emissions and light absorption of materials, noting influence of adsorbed gas layers
20 p3553 A69-37406

Stable mode generation in ruby laser with ability for modulation, using convex resonator and uniform illumination
20 p3553 A69-37607

Nitrogen gas breakdown threshold dependence on pressure during picosecond ruby laser pulse, discussing photoionization leading to breakdown in electromagnetic wave field
20 p3555 A69-38067

Ultrasonic vibrations effect on emission of ruby laser with externally mounted mirrors
20 p3556 A69-38201

Daylight sky spectral radiance in ruby laser spectral range as functions of scattering angle, height over horizon of observed point and sun altitude
21 p3734 A69-38397

Emission frequency stabilizing effect in concentric sapphire-coated ruby laser, noting frequency independence from temperature fluctuations and thermal stresses
21 p3735 A69-38695

Fresnel pulse holograms of three dimensional diffuse objects by single mode ruby laser with or without Q switching
21 p3724 A69-38946

Spectral characteristics of Q switched single frequency ruby laser with tunable emission frequency in giant pulse mode
21 p3737 A69-38991

Spectral, angular and temporal characteristics of traveling wave mode ruby laser emission, noting high transverse divergence effect on mode operation
21 p3741 A69-39554

Flash holography using ruby laser, describing optical system arrangement
21 p3727 A69-39784

Pulse ruby laser-smear camera ultrahigh speed multiple frame recording system, describing applications to transmitted and scattered light photoelasticity
22 p3944 A69-40076

Ruby laser resonator mirror mechanical vibrations effects on emission temporal behavior, spectral output and far field pattern, describing conditions for spiking
22 p3962 A69-40562

Mode locked ruby laser with picosecond pulses using rooftop prism cavity with helical flashtube for pumping
23 p4172 A69-41395

Monte Carlo method for energy transfer efficiency of ruby laser pumping cavities by helical flash lamps, noting dependence on ruby parameters
23 p4173 A69-41630

Blast wave energy determination of laser-induced gas breakdown in hydrogen, nitrogen, helium, argon and xenon in pressure chamber
24 p4299 A69-42651

Ruby laser crystal energy emission related to crystal rate of motion
24 p4327 A69-42652

High power ruby laser pulse generation by diffraction modulator, employing modulated ultrasonic traveling waves at minimum resonator transmission losses
24 p4328 A69-43163

Ruby laser second harmonic generation statistical characteristics with dielectric surface scatterer, showing variety of modes and high cross sectional stability
24 p4328 A69-43164

Light scattering from ruby laser beam passing through collisionless shock produced by H plasma compression measured by photomultiplier
24 p4360 A69-43748

RUDDERS

U AERIAL RUDDERS

RULES

U INSTRUMENT FLIGHT RULES
U SUM RULES

RUMANIA

Photoelectric observations program at Astronomical Observatory of Bucharest to determine smallest moments of several eclipsing stars
15 p2696 A69-31224

RUMBLE INSTABILITY

U ACOUSTIC INSTABILITY

RUNGE-KUTTA METHOD

Nonlinear Volterra integral equation solved by Runge-Kutta method
05 p0787 A69-16456

Monograph on implicit Runge-Kutta formulas for numerical integration of first order differential equations
08 p1343 A69-20706

Order determination for single step Runge-Kutta methods for solving general system of differential equations
12 p2124 A69-26891

Numerical solution of nonlinear Volterra integral equation by Runge-Kutta-Felberg method
15 p2644 A69-30657

Runge-Kutta type method truncation error estimation, discussing validity conditions, evaluation processes and numerical tests
15 p2644 A69-30672

Pseudo Runge-Kutta methods stability in numerically integrating two point Cauchy problems
15 p2646 A69-31261

Cauchy problem solution for first order nonlinear Volterra integrodifferential equation, using Runge-Kutta method
20 p3569 A69-38294

Helicopter rotors trailing vortices by flow visualization, comparing Euler and Runge-Kutta iterative solutions
23 p4150 A69-41376

RUNNING

Telometered heart rate response to progressively increased distance swimming competition compared with equidistance running events for change patterns, magnitude and recovery
23 p4100 A69-41444

Alaska sled dogs cardiovascular performance and flow distribution during cross country runs
24 p4256 A69-42624

RUNUP

U ENGINE TESTS

RUNWAY CONDITIONS

All-weather landing factors for aircraft and pilots, describing instrument landing system, runway and visibility, pilot and crew procedures, etc
01 p0112 A69-10454

Drag and spray effects due to slush and water on runways during aircraft takeoffs
01 p0011 A69-11048

Runway roughness effects on aircraft, formulating relationship between weight and resonant frequency through simple harmonic motion analogy
01 p0057 A69-11274

Runway development for increased airport capability, discussing computer simulation model of airport operations
06 p0906 A69-17166

Instrument for measuring light transmission in atmosphere to determine runway visual range
07 p1132 A69-18673

Runways slipperiness and grooving, discussing influence of wetness, tire form and speed on friction coefficient
10 p1674 A69-23707

Variational statistics applied to hourly meteorological data for predicting airport runways icing conditions time and duration
12 p2127 A69-26900

Runway roughness induced vibrations in highly flexible aircraft, noting effect on pilot control of aircraft and airframe structure
14 p2392 A69-29504

Fog removal by high power carbon dioxide lasers, evaluating possibility of clearing airport runways [AIAA PAPER 69-670]
17 p2945 A69-33449

Jet aircraft runway friction due to mud and water noting relation to takeoff length
17 p2903 A69-34216

Runway grooving to improve aircraft tire traction in adverse weather tested by F-4D and Convair 990A under wet conditions [AIAA PAPER 69-773]
19 p3244 A69-35649

Problems caused by air traffic rate growth in London Terminal area, examining runway limits, safety and noise restrictions
19 p3371 A69-36736

Runway grade relation to jet aircraft takeoff length
19 p3296 A69-36874

Forces on aircraft during ground roll with slick runway surface and cross wind for deceleration and control on ground [SAE PAPER 690375]
23 p4062 A69-41652

Aircraft braking, discussing systems, brakes, tires, runway interface, heat sink materials, friction measurements, skid control, cooling and recovery equipment [SAE PAPER 690376]
23 p4063 A69-41671

RUNWAY LIGHTS

Approach light efficiency, discussing Calvert bar system and strobe flash on basis of pilot questionnaire polling
06 p0884 A69-18029

Sensory physiology of pilot landing guided by runway lighting, stressing visibility influence
19 p3260 A69-35987

RUNWAYS

Redevelopment program for Newark airport noting runway construction, underground fuel system and passenger terminal complex
01 p0057 A69-11275

Maintenance practices for rigid concrete pavement of runways including joint and crack sealing and patching, considering necessary surface preparation and equipment
01 p0057 A69-11277

Monograph on length requirements for takeoff and landing of jet transports covering airport classification, roll distance formulas and long range transport performance nomograms
08 p1301 A69-20717

Airport runway surface construction materials requirements, taking into account factors different from highway pavement
17 p2948 A69-34215

Air terminals plans for 1975 aircraft and air traffic based on runway configurations [AIAA PAPER 69-805]
19 p3288 A69-35591

Airport capacity increase in terms of operations delay, discussing computer aided approach systems and additional runways
22 p3925 A69-40429

Airport standards analysis for safe, efficient air carrier operations including airport funding, safety programs for runways and terminal facilities
22 p4054 A69-41144

Jet runway design, construction and operation, discussing surface texture, lightning, grooving, etc [SAE PAPER 690377] 23 p4147 A69-41670

RUPTURING

Bursts of high speed rotor occurring at diametric cross section and around hub as function of hub size 01 p0142 A69-10306

Plastic deformation and bursting pressure of thin rupture disk as related to tensile strength 06 p1020 A69-17129

Rupture times in analysis of creep tensile instability in uniformly pressurized thin walled membrane shells of revolution, comparing two criteria 07 p1234 A69-19378

Polymethyl methacrylate rupture time under stress determined from short and long time strength tests, noting relation to crack propagation time 09 p1528 A69-21853

Network rupture hypothesis and molecular structure considerations used in obtaining constitutive equations for flow of polymer melts and solutions [AIChE PAPER 42C] 10 p1800 A69-23369

Sinusoidal or random excitations equivalence from point of view of rupture risks, considering industrial applications 13 p2370 A69-28602

Unsteady oscillations after rupture in thin homogeneous isotropic elastic plate, assuming deflection amplitude smaller than thickness 16 p2873 A69-32033

Safety disk strength under static lateral pressure from rupture studies of thin circular plates under static and pulsating lateral pressure 19 p3434 A69-35773

Rigid thermoplastic cylindrical shell creep under axisymmetrical loads, giving computer algorithm and time dependent criterion for rupture strength 22 p4045 A69-40750

Deferred rupture as function of applied load noting test methods 24 p4407 A69-43801

RUTHENIUM

Absorption and emission spectra of ruthenium 2 complexes dissolved in rigid glasses, discussing crystal field theory and luminescence 07 p1200 A69-19219

Ligand field transitions in tertiary phosphine and arsine complexes of ruthenium and osmium 07 p1075 A69-19483

RUTILE

Compact high-gain chromium doped rutile traveling wave masers for Onsala radio telescope for galactic and extragalactic microwave emission studies 02 p0257 A69-12463

Friction and wear tests of synthetic rutile single crystals against diamond styli and spherical sliders of ruby, sapphire and hardened steel [ASLE PAPER 68-LC-3] 07 p1140 A69-19307

Elastic properties of hot pressed polycrystalline quartz and rutile as function of pressure, obtaining pressure coefficients of compressional and shear wave velocities 20 p3583 A69-37502

RYAN AIRCRAFT

U FIREBEE 2 TARGET DRONE AIRCRAFT

U XC-142 AIRCRAFT

RYAN MILITARY AIRCRAFT

U MILITARY AIRCRAFT

RYDBERG SERIES

Oscillator strengths of transitions in shock tube between nitric oxide Rydberg states in near IR 08 p1354 A69-20150

Lowest valence and Rydberg states assigned to ungerade singlet states in dipole allowed absorption spectrum of molecular nitrogen 09 p1542 A69-21916

Absorption spectrum of NO molecule, analyzing f complexes electron structure, ionization potential and quadrupole moment 22 p3984 A69-40477

S

S BAND

U SUPERHIGH FREQUENCIES

U ULTRAHIGH FREQUENCIES

S CURVES

Dust particle separation from inlet flow with S-bend duct to minimize engine dust ingestion, determining

particle trajectories [AHS PAPER 211] 01 p0006 A69-10409

Langmuir S curves for tungsten single crystals in presence of adsorbed cesium, discussing orientation, theoretical and experimental correlation and instrumentation 14 p2506 A69-29271

S GLASS

Prepreg based on S glass with HTS finish and B staged epoxy resin, discussing tensile strength and moisture exposure 09 p1530 A69-22327

S MATRIX THEORY

Test procedure for obtaining large signal S characterization of nonlinear power transistors 02 p0214 A69-11600

Scattering matrices of complex configuration specified by cross polarized radar cross sections based on Green function, noting wire loop and wedge scatterers 03 p0384 A69-12904

Radar cross section data interpretation, discussing calibration, unwanted signals, averaging, scattering matrix and power spectra 03 p0385 A69-12913

S matrix theory without restriction to asymptotic particle momentum measurements, introducing main nondynamical features 03 p0467 A69-13754

Equivalent generator approach to facilitate scattering matrix analysis of complicated microwave circuit 04 p0582 A69-14755

Transistor scattering matrix parameters determination, emphasizing directional coupler errors and impedance mismatches 04 p0582 A69-15067

General theorem of isotropic microwave waveguide junction ports imposed by reflection symmetry 06 p0893 A69-16935

Scattering matrix for internal diffraction in rectangular waveguide with transversely magnetized ferrite core 06 p0895 A69-17455

Transmission coefficient of double frequency regenerative parametric amplifier described by scattering matrices 06 p0895 A69-17456

Coupled and uncoupled terminals series connection for reactive multiport network determined by transforming scattering matrix columns into coordinate vectors 07 p1100 A69-18529

S matrix theory of electromagnetic interactions, obtaining equivalence of results with quantum electrodynamics by choice of subtraction constants 08 p1351 A69-20211

Degeneracy of hydrogenic states to sum S-matrix in Stark broadening calculations 09 p1543 A69-22405

Scattering matrix for pattern forming circuit for multiple beam antenna arrays with interacting elements, noting orthogonal pattern optimization 09 p1469 A69-22627

Computer program for analysis of linear microwave multiport circuit by means scattering matrix equivalent 11 p1858 A69-24572

Geometrical diffraction theory for bistatic scattering of plane wave by conducting frustum, calculating scattering matrix 11 p1837 A69-24999

Full wave calculation of gravity waves for thermospheric model, describing wave type reflection, transmission, conversion and coupling by scattering matrix elements 11 p1878 A69-25150

Error analysis in conversion of two port scattering parameters used in microwave transistor characterization 11 p1852 A69-25200

Output power and loss analysis of 2 n injection locked oscillators combined through magic tee hybrids 13 p2232 A69-28061

Transistors scatter matrix parameters determined, describing measuring bench calibration system 14 p2420 A69-29393

Orthonormalized partial radiation patterns for antenna array of N emitters developed by introducing scattering matrix 15 p2579 A69-30951

Numerical solution of boundary value problems, discussing spectral domain and scattering matrix formalisms 17 p2929 A69-33882

Small losses measurement in circulators and reciprocal quadrupoles, using scattering matrix to eliminate

mismatch errors 22 p3875 A69-40259

Numerical procedure obtaining scattering matrix of passive reciprocal two port from standing wave measurements, using image circle in Smith chart 24 p4281 A69-42617

S WAVES

Compressional and shear wave velocities vs porosity for sintered perlitic bricks 06 p1000 A69-17009

Fredholm equations from dual integral equations for studying penny shaped crack response to incident harmonic shear wave in elastic medium 07 p1233 A69-19175

Plane elastoplastic shock waves propagation due to combined shear loadings assuming elastic isotropic work hardening materials 13 p2368 A69-28346

Acoustic bulk-surface wave transducer for shear or longitudinal wave transformation in nonpiezoelectric material at HF 15 p2607 A69-30167

Stress corrosion cracks investigation by shear wave technique 16 p2876 A69-32334

Flaw determinations accuracy from measuring ultrasonic shear wave reflection peak intensities 24 p4397 A69-42756

S-N DIAGRAMS

Linear cumulative damage theory defining low cycle fatigue region of classic S-N curve, providing biaxial strain mode by centrifugally loading rotors [ASME PAPER 68-WA/MET-8] 05 p0838 A69-16151

Linear cumulative damage theory defining low cycle fatigue region of classic S-N curve, providing biaxial strain mode by centrifugally loading rotors [ASME PAPER 68-WA/MET-8] 14 p2535 A69-29438

S-N fatigue life small bondable resistance sensor, discussing random response data interpretation with emphasis on use of strain multipliers 15 p2613 A69-31270

Fatigue data adapted to conditions of specific design part including fatigue limits, S-N curves and various failure diagrams 16 p2794 A69-32433

Secondary fatigue curves slope variation to determine preloaded materials fatigue life under unstationary loading 17 p3052 A69-32976

S/N fatigue life gage response to constant frequency random amplitude input strain 20 p3537 A69-37007

Estimation of program fatigue life curves from equivalent load program using Miner law 21 p3846 A69-39810

Structural materials deformation response to loading conditions and stress or strain cycle analysis to predict failure, including creep and stress relaxation 24 p4398 A69-42771

S-18 SATELLITE

U OAO

S-27 SATELLITE

U ALOUETTE 1 SATELLITE

S-57 SATELLITE

U OSO-C

S-58 HELICOPTER

U CH-34 HELICOPTER

S-61 HELICOPTER

Main rotor bifilar absorber for vibration reduction during S-61 helicopter flight, describing shake and flight tests [AHS PAPER 354] 17 p2900 A69-33523

S-64 HELICOPTER

U CH-54 HELICOPTER

SA-330 HELICOPTER

Structural vibration problems of SA 330 helicopter from test flight data, discussing natural frequency displacement of blades and dynamic response improvement of structure 01 p0009 A69-10158

Composite main rotor blade for Sud-Aviation SA-330 helicopter consisting of steel spar/epoxy-glass envelope [SAE PAPER 680693] 03 p0366 A69-13444

SAAB 37 AIRCRAFT

Electronic system checkout in SAAB 37 Viggen, using computer controlled test equipment 05 p0726 A69-16767

First flight test phase of multipurpose Viggen aircraft designed as basic platform for attack, trainer, reconnaissance and fighter versions 06 p0867 A69-17662

Microwave scanning beam landing guidance system for Swedish tactical aircraft Saab 37 Viggen, reviewing ground station and onboard equipment
16 p2735 A69-32057

Digital computer system for navigation, landing, fire control, monitoring and checkout aboard Saab 37 Viggen aircraft handling attack, reconnaissance and fighter missions
[AIAA PAPER 69-985] 22 p3908 A69-40365

SACCHARIDES

U CARBOHYDRATES

SADDLE POINTS [GAME THEORY]

Optimum control with respect to minimum fuel and power consumption involving constraints based on Kuhn-Tucker conditions and saddle point theorem
02 p0223 A69-11564

Uniform asymptotic expansion series for saddle point integrals applied to probability distribution in noise interference problems
03 p0398 A69-13832

Saddle point analysis of electromagnetic ground wave propagation in source excited field in waveguide formed by two parallel plate dielectrics
12 p2028 A69-25898

Existence theorem for Markov chain finite state stochastic games applied to saddle point and optimal strategy or epsilon-optimal strategy pairs
22 p3975 A69-41010

SAFETY

NT AIRCRAFT SAFETY

NT FLIGHT SAFETY

NT INDUSTRIAL SAFETY

NT REACTOR SAFETY

Aerothermal-structural reentry safety evaluation for SNAP-27 radioisotope Graphite Lunar Module Fuel Cask at orbital and superorbital velocities
[AIAA PAPER 68-1166] 03 p0465 A69-13561

Fault tree for hardware multiple failure safety analysis and reliability analysis for single failure analysis, illustrating comparative advantages
18 p3142 A69-34479

Aerothermal-structural reentry safety evaluation for SNAP-27 radioisotope Graphite Lunar Module Fuel Cask at orbital and superorbital velocities
[AIAA PAPER 68-1166] 22 p3979 A69-40551

Passenger safety during aircraft accidents in Arctic, discussing survival equipment and methods
23 p4107 A69-41811

Safety and failure of components - Conference, Brighton, England, September 1969
24 p4397 A69-42767

SAFETY DEVICES

NT ABORT APPARATUS

NT ARRESTING GEAR

NT EJECTION SEATS

NT ESCAPE CAPSULES

NT HELMETS

NT SEAT BELTS

NT SPACE SUITS

Astronaut safety considerations impact on design of Apollo Lunar Surface Experiments Package (ALSEP)
[SAE PAPER 680721] 03 p0433 A69-13448

Occupant restraint systems for automobiles, aircraft and manned space vehicles, discussing cost, practicability, ease of use, acceptability and possible improvements
03 p0380 A69-13459

Pilot warning indicators to equip all aircraft at low cost, discussing Doppler system
05 p0790 A69-16726

Supersonic aircraft fire detection using coherent fiber bundles
06 p0926 A69-17679

Boron carbide body armor fabrication by hot pressing in graphite molds
08 p1320 A69-20411

Business aircraft injury protection and impact survival design considerations, stressing upper torso restraint installations
[SAE PAPER 690335] 11 p1829 A69-24493

Aviation pathology in aircraft accident investigation of accident survivability features and accident precipitation factors, noting cockpit structures and protective equipment
12 p2021 A69-25841

Detonation system for exploding missile warheads, discussing trigger detonation and safety release elements
17 p3050 A69-33698

Mechanical vibration effects on human body in industry and in terrestrial, aerial and nautical vehicles, discussing harmful frequencies and safety measures
19 p3259 A69-35605

Optimized flight crew training, evaluating safety, flight simulator efficiency, takeoff/landing practice and line experience based on test results
[AIAA PAPER 69-771] 19 p3245 A69-35653

Safety disk strength under static lateral pressure from rupture studies of thin circular plates under static and pulsating lateral pressure
19 p3434 A69-35773

Descent device for emergency egress from jumbo jets based on centrifugal brake, including test data on C-5 fuselage section
19 p3255 A69-36146

SAFETY FACTORS

Rocket propellant safety, discussing thermal, mechanical and impact sensitivity tests of solid and liquid propellants
02 p0302 A69-11525

Safety problems of jumbo jet airbus and SST, discussing operational safety procedures and techniques
03 p0365 A69-12882

Industrial and workman safety concept evolution, discussing role in product design engineering
[SAE PAPER 680676] 03 p0433 A69-13449

Safety planning for use of reactive cryogenics in large volume, noting FLOX and liquid fluorine
04 p0645 A69-14468

JP-4 fuel emulsions properties, handling characteristics and safety performance, noting satisfactory shelf life and thermal stability
[ASME PAPER 68-GT-24] 06 p0982 A69-17190

Fatigue strength and aircraft structural standards based on experimentally determined safety factors
09 p1619 A69-22571

Safety requirements of test ranges, considering RF hazards to electroexplosive devices
10 p1751 A69-23019

Damage thresholds to ocular tissues from laser radiation, presenting comparative theoretical curves and recommended safe working levels
18 p3097 A69-34312

Computerized system-safety fault trees, discussing drawing, configuration control and simulation program
19 p3280 A69-36029

Composite laminated glass structures employed to improve safety characteristics of glass or to achieve special optical properties
21 p3752 A69-38934

Engine powered lift civil aircraft certification factors taking into account traffic growth, accident rates, learning rate and acceptable safety level
22 p3862 A69-39962

Laser safety factors in open air applications, discussing pulse length, energy spatial distribution, atmospheric attenuation, human eye sensitivity, etc
22 p3892 A69-40241

Fatigue collapse probability of fail-safe structure compared to safety factor design
22 p4045 A69-40820

Statistics of jet aircraft accidents including worldwide data and safety trends
22 p4054 A69-41128

Safety standards for DC 10 aircraft, considering cockpit design, hydraulic, electric power, autoland and direct lift control systems, structural safety and crash worthiness
22 p3867 A69-41133

Safety implications of technological developments in aviation, discussing standards and statistical data for supersonic transports and jumbo jets
22 p3867 A69-41134

B-747 safety assurance program, discussing organization, management, hazard sources, accident statistics, night visual approach and maintainability
22 p3867 A69-41135

Boeing 747 safety engineering program, discussing organization, design review, system safety, systems design-analysis and tests
22 p4054 A69-41136

Systems safety for unmanned spacecraft, considering power supply, equipment operation, trajectory correction, etc
[AAS PAPER 69-520] 24 p4392 A69-42849

Management system for safety in NASA Manned Space Flight Program, discussing hazard analyses and reduction precedence sequence
[AAS PAPER 69-522] 24 p4418 A69-42851

Flammability control for aerospace avionics systems safety, considering risk, test method, acceptability criteria, confidence level and ignition source
24 p4336 A69-43422

SAFETY HAZARDS

U HAZARDS

SAGITTARIUS CONSTELLATION

Lunar occultations of radio source Sagittarius A observed at various frequencies between 230 and 2400 MHz, obtaining diameter, position and decimeter band flux densities
06 p1009 A69-17960

Electron temperatures and internal turbulence in H II regions of Sagittarius arm measured by high resolution interference method
08 p1392 A69-20566

Low energy X ray spectra of Sco X-1 and Sagittarius sources measured by Be and Al window proportional counters during rocket flight
09 p1574 A69-21460

Further microwave emission lines and ammonia clouds in Sagittarius region, tabulating relevant transitions in ammonia and water
09 p1597 A69-22150

Polarization changes of R Coronae Borealis Star RY Sagittarii, tabulating percentage polarization and position angles
09 p1603 A69-22265

High energy X ray observational data for Sagittarius sources scanned by active telescope during February 1968 balloon flight
09 p1583 A69-22764

Sagittarius A occultation by moon, determining peak brightness and flux density of radio source
11 p1958 A69-24592

Milky Way structure, discussing dust bridge and density of absorbing matter between spiral arms of Sagittarius and Carina Cygnus
15 p2683 A69-30514

Star counts in Ophiuchus nebula darkened region /Scorpius/Ophiuchus/ and in comparison fields Corona Australis and Sagittarius
20 p3604 A69-37788

High energy gamma rays point source in Sagittarius indicated from evidence obtained by high altitude balloon flights
24 p4365 A69-42606

Nebulosity around FG Sagittae for origin and evolution of planetary nebulae, suggesting ejection of nebular shell
24 p4381 A69-42887

SAHA EQUATIONS

Argon plasma composition in Saha equilibrium, using FORTRAN 4 program
07 p1193 A69-19168

Electron concentration in low temperature nonequilibrium steady state plasma, including Saha equation applicability criterion
15 p2662 A69-30975

SAILPLANES

U GLIDERS

SAILS

NT SOLAR SAILS

Flutter vibration of sails fixed along edge and single wing weather vanes in supersonic flows
02 p0192 A69-12824

Passive attitude stabilization of interplanetary probe, using conically shaped sails elastically connected to payload
17 p3047 A69-33225

Aerodynamic characteristics of two dimensional nonexpandable flexible sail in hypersonic inviscid flow, discussing roles of sail length and chord and angle of attack
19 p3237 A69-35814

SAINT VENANT PRINCIPLE

Rectangular thin beam Saint Venant deflection in case of moment stresses based on elasticity and shell theory
05 p0834 A69-15783

Axisymmetric elastoplastic bending theory for cylindrical shell by applying Saint Venant plasticity conditions, determining stress distribution
08 p1419 A69-21179

Bar flexure determination for Saint Venant torsional and transverse loading, solving differential equations by finite element methods
09 p1614 A69-21722

Saint Venant torsion and flexure of prismatic bars analysis in polar coordinates, discussing boundary errors
09 p1621 A69-22770

Analytical expressions for Gaussian constraint of continuum, using continuity conditions as equations of internal geometric couplings
11 p1984 A69-25170

Rectangular thin beam Saint Venant deflection in case of moment stresses based on elasticity and shell theory
18 p3223 A69-35035

Saint Venant torsion problem using rederivation of integral equation by transferring external geometrical problem into internal static problem

21 p3836 A69-39003

Saint Venant principle of elastic equivalence of kinematically equivalent displacement systems at small surface area of elastic body

22 p4048 A69-41276

SALT BATHS

Cotton leaves reflectivity and transmittance measurements, discussing substrate salinity effects on internal structure of hydroponically grown plants

15 p2558 A69-30456

Salt bath brazing for honeycomb structures, describing brazing techniques for thorium dispersed Ni and NiCr, Rene 41 and Ti honeycomb panels

19 p3320 A69-35557

Ti-Al-V sheets quenched from alpha plus beta field into salt bath at various high temperatures, studying effects of bath temperature and holding time on aging and mechanical properties

21 p3730 A69-38667

Hot salt stress corrosion of Ti alloy, discussing hydrogen generation during elevated temperature exposure and embrittlement as manifestation of strain rate

21 p3747 A69-39434

Forged corrosion in aqueous salt environment at various temperatures in unstressed and stressed conditions, considering Be usability in turbomachinery

21 p3749 A69-39493

SALT SPRAY TESTS

Titanium alloys hot salt stress corrosion cracking, studying effects of chlorides and surface oxides

19 p3352 A69-36905

Burner rig hot corrosion test facility for evaluating Ni-Co alloys used in gas turbine engines operating in marine environment

22 p3928 A69-40673

SALTS

Salts and organic solvents effect on halophile Halobacterium cutirubrum catalase, noting enzyme activity inhibition by cation and anion

18 p3096 A69-35291

Electron transport chain of monovalent and divalent cations and of polyamines, studying effects on menadione reductase activity to determine salt dependence

22 p3886 A69-41077

SAMARIUM

Magnetic and semiconducting properties of samarium boride, noting effect of decreasing temperature

07 p1200 A69-19403

Fluorite crystal laser activated by divalent samarium, discussing characteristics in pulsed operation mode

14 p2458 A69-29328

SAMARIUM COMPOUNDS

High temperature research on systems formed by zirconium dioxide with samarium and gadolinium sesquioxides near melting point

01 p0101 A69-10044

SAMPLED DATA

U DATA SAMPLING

SAMPLED DATA SYSTEMS

U DATA SAMPLING

SAMPLERS

Miniaturized adding sample and hold device with adjustable delay applied to digital filters

04 p0574 A69-14350

Modeling requirements and methods for monitoring microbial contamination, discussing vacuum probe sampler to recover microorganisms from large surface areas

05 p0713 A69-15948

Supersonic molecular beam sampling system for coupling mass spectrometer to alkali metal-air reacting flow system in kinetics study, noting gas dynamic effects

[AIAA PAPER 69-94] 06 p0930 A69-18099

Surveyor scientific instruments and operation on moon, reviewing TV camera, alpha scattering instrument and surface sampler

[JPL-TR-32-1358] 08 p1312 A69-19850

Sample changer for metal fatigue studies under ultrahigh vacuum conditions, noting successive testing in same vacuum

08 p1302 A69-20877

Bulk, selective particulate and hard rock samplers for landed extraterrestrial geological and biological instruments performing on-site analysis

23 p4146 A69-41620

Leak detection techniques efficiency determined for airtight atmospheric air sampling devices used at low pressure and concentration

24 p4296 A69-42656

SAMPLES

Recursive algorithms for pattern classification using misclassified samples

06 p0891 A69-17357

Apollo lunar sample collection and analysis, discussing astronauts activity and equipment, sample types, laboratories for radioactive counting and gas analysis, etc

22 p3919 A69-40191

SAMPLING

NT AIR SAMPLING
NT DATA SAMPLING
NT RANDOM SAMPLING

Meteoritic extraterrestrial materials sampling for chemical, petrographic and metallurgical analyses, discussing microstructure and optimum specimen weight for representative analysis

[UN PAPER 68-95381] 01 p0150 A69-10480

Oscilloscope display of sample of subnanosecond light pulse, using optical analog of electronic sampling oscilloscope

02 p0259 A69-12656

Microbiological surface sampling methods, noting role in detecting contamination on eating utensils, blankets, sheets, etc

05 p0715 A69-15982

Direct bead sampling by aspiration of molten metal in open hearth furnaces and converters

07 p1141 A69-19341

Single sideband modulation theory explained by sum representation of sampling theorem, comparing different signal generating methods

09 p1456 A69-22290

Upper bounds for increment of band limited signal in sampling interval by increasing integral expressions of increment

11 p1834 A69-24551

Distribution function of multiple correlation coefficient for various sampling volumes and various numbers of predictors calculated using Fisher formula

13 p2293 A69-27843

Electronic component life test sampling plans based on lognormal distribution and instantaneous failure rate or hazard rate criterion

15 p2630 A69-31137

SAMPLING DEVICES

U SAMPLERS

SAN MARCO SATELLITE

San Marco project, discussing Italian Space Commission and NASA cooperation, equatorial range concept and development

[UN PAPER 68-95862] 01 p0180 A69-10518

SAN MARCO 2 SATELLITE

Long range HF propagation in equatorial zone observed with San Marco 2 satellite, discussing overall conditions of ionosphere

08 p1276 A69-20593

F region atmospheric density measurements obtained from aerodynamic drag on San Marco 2 satellite in equatorial orbit, comparing data with San Marco 1

21 p3704 A69-38369

Direct detection of ionospheric irregularity by device onboard San Marco satellite, utilizing antenna impedance fluctuations

21 p3715 A69-38562

SANDS

Sand ridge origin and dynamical setting, discussing morphology-tidal current system equilibrium indicated by theory and field measurements

15 p2596 A69-30443

SANDSTONES

Geochemistry and element abundances for Henbury impact glass, Darwin glass and australites, noting evidence for meteorite impact on sandstone

08 p1407 A69-20937

SANDWICH PLATES

U PLATES [STRUCTURAL MEMBERS]

SANDWICH STRUCTURES

Multifrequency three layer sandwich radomes design for reflectionless sandwich at second frequency

01 p0034 A69-11037

Deflection of orthotropic sandwich plates with unequal facing thickness with edges subjected to uniform and concentrated loading

01 p0172 A69-11270

Silicon nitride gate insulator in metal-insulator-silicon (MIS) devices, noting sandwich structures with thermally grown oxides removes limitations

02 p0299 A69-12244

Aluminum plastic sandwich products production costs compatibility with conventional materials

02 p0348 A69-12749

Sandwich panel construction, examining design with respect to panel size, thickness and weight limit

03 p0524 A69-13124

Fokker bond tester and structural details of different types of sandwich structure, giving attention to adhesive bonding of panels, adhesive application, etc

03 p0434 A69-13791

Low temperature conductance peaks observed in tunneling measurements on aluminum-phosphosilicate glass-degenerate silicon sandwich structures

03 p0493 A69-14183

Bending theory for sandwich plates with layers having different elastic properties using asymptotic integration of three dimensional equations

04 p0684 A69-15534

Five layer thin film band elimination filters amplitude and phase frequency characteristics

05 p0729 A69-16088

Glow discharge technique for dielectric layer deposition between metal interconnection patterns in multilayer integrated circuits, noting adhesion and feedthrough problems

06 p0931 A69-17201

Three layer structure theory, discussing thin elastic sandwich shells with middle layer susceptible to transverse shear

06 p1025 A69-17615

Anodizing effect on flexural properties of Al-aluminum oxide sandwich composites, emphasizing properties of oxide coatings as function of thickness

07 p1159 A69-18723

Symmetrical three layer A and B type sandwich reflectionless radomes design for multifrequency operation and insertion phase delay

07 p1110 A69-19522

Dielectric radome designs for operation at harmonically unrelated frequencies in C and K bands, discussing sandwich structure of A and B types

07 p1110 A69-19523

Paper-honeycomb sandwich radome structure for protecting monopulse UHF radar antennas used in BMEWS

07 p1111 A69-19537

Spherical sandwich radomes designs, discussing aerodynamic loads, wind pressure effect, electrical properties and mountings

07 p1112 A69-19538

Fabrication and processing techniques, tooling concepts and quality control for composite materials used in large aircraft, discussing honeycomb and sandwich structures

[ASM PAPER D8-25.4] 07 p1172 A69-19670

Helicopter rotor blades in metal sandwich bonding, discussing component parts assembly by adhesive films

07 p1143 A69-19731

Finite aspect ratio sandwich plates flutter in supersonic gas flow analyzed by differential equation describing plates elastic equilibrium

08 p1412 A69-20324

Variational method for safety limits of perfectly plastic simply supported conical sandwich shells subjected to uniform internal pressure and obeying Mises yield criterion

08 p1416 A69-20702

Optimal design of circular cylindrical sandwich shells under pressure and shear loads, showing acceptability of small shear coefficient values

08 p1416 A69-20722

Minimum weight plastic design of circular and annular sandwich plates with piecewise constant cross section, discussing cost reduction

08 p1417 A69-20823

Governing equations for bending of fixed isotropic circular sandwich plate subjected to eccentric concentrated load

09 p1615 A69-21926

Buckling of cylindrical and conical sandwich shells with fiberglass/epoxy facings and aluminum honeycomb cores

[AIAA PAPER 68-294] 09 p1616 A69-21942

Quality control tests for adhesives used in structural parts including ultrasonic and nondestructive tests

09 p1513 A69-22564

Histogram approximation of plastic deformation of metals, analyzing tube under internal load and sandwiched layer compression

10 p1793 A69-22850

Schleicher glider AS-W15 prototype tests, discussing balsa sandwich structure and flight characteristics

10 p1633 A69-22872

Numerical analysis of natural oscillations of three layer sandwich plates of rectangular planform, considering end conditions

11 p1976 A69-24773

Stress concentration around curvilinear holes in three layer spherical and cylindrical isotropic shells with hard and soft fillers under external loads

11 p1984 A69-25171

Book on statics and dynamics of anisotropic and heterogeneous elastic structures covering thin heterogeneous anisotropic panels, elastic and sandwich plates, etc

11 p1986 A69-25236

Metal bonded and sandwich structures application to space vehicles, launch vehicles, rocket motors, ground equipment and balloon gondolas, noting inspection methods

12 p2101 A69-25859

Finite deflection discrete element analysis of sandwich plates and cylindrical shells with unbalanced laminated faces

12 p2185 A69-26821

Fabrication, machining and contouring of boron-epoxy composite for sandwich type aircraft structure, noting F-5 supersonic fighter main landing gear strut door

12 p2103 A69-26826

Diffusion bonded Ti honeycomb sandwich, demonstrating structural integrity, efficiency, low weight and cost effectiveness

12 p2115 A69-26828

Minimum volume face sheet design of circular cylindrical sandwich shell obeying Mises yield criterion for loads transverse to lateral surface and axisymmetric

12 p2189 A69-27117

Local failure of axially loaded plastic foam core sandwich panels, using face wrinkling analysis procedures

13 p2357 A69-27207

Resistivity, capacitance and dielectric loss measurements for diode reactive sputtering grown AlN films and film sandwich structures of Ta, Au and Al films

13 p2322 A69-28013

Elastic deformations of spherical sandwich shell of rigidly connected isotropic homogeneous layers, describing shell symmetrical expansion and inversion under stresses

15 p2707 A69-30582

Vibration control by alternate layers of high damping viscoelastic material, discussing damping and loss factors, beams design and attachment

15 p2622 A69-30704

Vibrations attenuation by viscoelastic sandwich shear damping, discussing examples of aircraft equipment racks, gyro and airborne circuit board mountings

15 p2622 A69-30705

Linear bending theory of elastic anisotropic sandwich plates with strong and weak cores

15 p2713 A69-31025

Bending theory for two layer plate made of isotropic material under sinusoidal load obtained by elasticity and classical theory based methods

15 p2714 A69-31198

Bending method for unfolded honeycomb cores shaping for curvilinear sandwich structures

16 p2794 A69-32006

Forced oscillations of three layer plate used as vibration dampers for engine components

16 p2873 A69-32143

Roll-up solar array based on erection of planar sandwich structure from two rolled constituent halves

16 p2762 A69-32559

Transverse bending of asymmetric sandwich plates with rigid filler taking into account stresses and strains in filler

17 p3055 A69-33129

Finite aspect ratio sandwich plates flutter in supersonic gas flow analyzed by differential equation describing plates elastic equilibrium

17 p3058 A69-33317

Elastic sandwich structures design for maximum strength, using potential energy functional to derive governing equations

17 p3062 A69-33708

Damping constant of sandwich samples with foam plastic filler subjected to torsional and flexural vibrations determined for aircraft design applications

17 p2993 A69-33942

Axisymmetrical vibration characteristics of circular sandwich shell with viscoelastic core layer analyzed via differential equation to obtain frequency equation and composite loss factors

18 p3211 A69-34327

Sandwich beams optimal design determined for case of constraint on elastic deflection and for load factor at plastic collapse

18 p3218 A69-34623

Photoelastic materials stressed state analysis by inserting analyzer and polarizer into sandwich medium, obtaining polarized light field

18 p3138 A69-35152

Elastic stability of sandwich materials in microvolume under compressive force analyzed using three dimensional linearized equations for small subcritical strains

18 p3226 A69-35374

Diffusion bonded Ti honeycomb sandwich, discussing production, structural efficiency, high strength/weight ratio, etc

19 p3320 A69-35558

Adhesive bonding of Al sheets for honeycomb sandwich material, using electrical conductivity to measure sheets age hardening progress during high temperature curing

19 p3321 A69-35565

Strength analysis of three layer rectangular plates under complex load and support distributions

19 p3434 A69-35827

Transverse oscillations of shallow multilayer shells, using tangential-stress distribution law in determining natural oscillation frequencies in single and sandwich layer panels

19 p3435 A69-35842

Book on structural sandwich panels analysis and design covering beams and struts, bending theory, buckling, strain energy use, differential equations, etc

19 p3438 A69-36380

Vibration response approximation of three layer sandwich beam with nonlinear viscoelastic material core during flexural vibrations

20 p3619 A69-36910

Fusion welding for thin gauge corrugated core sandwich airframe structures capable of operating at high temperature, discussing equipment, techniques and quality control [SBAC PAPER 9]

20 p3549 A69-37448

Optimal plastic design of circular sandwich ring assuming symmetric loading, minimum plastic resistance and cost justification of stronger cross section

20 p3625 A69-37590

Soviet book on shell and thin walled structure calculation methods covering stability and stress analysis, reinforced and sandwich shells, etc

20 p3630 A69-38199

Stability of sandwich panel strip with lightweight core, formulating problem in terms of equilibrium conditions and potential energy of system

21 p3832 A69-38417

Multilayer sandwich panels containing unequal facings with distinct orthotropic cores, calculating dynamic load and stability of triangular panels

21 p3832 A69-38418

Stress concentration near holes in three layer spherical shells, determining boundary conditions at hole perimeters for various loads

21 p3833 A69-38570

Ti honeycomb sandwich panels, comparing properties of Ti and Al based brazing alloys

21 p3730 A69-38665

Composite or sandwich construction design based on employing all available materials and setting up requirements for mechanical and physical properties

21 p3836 A69-38935

Sandwich beams interlaminar shear stress calculations, considering roles of moduli of elasticity and layers thickness relative to beam

22 p4041 A69-40080

Nonlinear differential equations for large deflections of multisandwich shells of arbitrary shape built of stiff and weak elastic layers, considering cylindrical shells

23 p4226 A69-41572

Truncated conical sandwich shell suspended in free condition measured and analyzed for vibrational characteristics

23 p4235 A69-42462

Three layered circular plate under harmonic excitation, analyzing forced vibrational characteristics by variational principle and Ritz method

23 p4236 A69-42495

Heated three layer plates stability under finite deflections in supersonic gas flow, deriving aerothermoelasticity equations

24 p4395 A69-42590

Three layer plate transverse bending in linear presentation, reducing problem to two displacement functions determination

24 p4395 A69-42594

Shallow spherical sandwich shells critical buckling loads using differential pressure method

24 p4396 A69-42734

Si integrated circuits single and composite layered metallization systems, comparing characteristics of various refractory and noble metals

24 p4286 A69-42761

Transverse acoustic wave excitation of elastic circular cylindrical sandwich shell submerged in infinite fluid medium, describing simultaneous equations development for modal response [ASME PAPER 69-APMW-17]

24 p4401 A69-43100

Damage repair techniques of polyimide honeycomb sandwich panels constructed with polyimide and Ti face sheets, using precured plugs, prepreg disks, sealants, etc

24 p4323 A69-43420

Concorde elevons sandwich construction to meet sonic environment, discussing core, adhesive, design and fabrication

24 p4403 A69-43429

Metallurgical and structural production of diffusion bonded titanium honeycomb sandwich panels for aerospace hardware weight saving

24 p4324 A69-43434

Al brazed Ti honeycomb sandwich structures brazed in vacuum and Ar, analyzing mechanical properties and corrosion resistance as functions of temperature and pressure

24 p4324 A69-43435

SST range-payload improvement by emphasizing Ti alloys honeycomb and trusscore sandwich panels fabrication for structural boxes in wing and empennage

24 p4324 A69-43436

Orthotropic fiberglass/epoxy faced honeycomb aircraft type sandwich structure elastic properties by edgewise compression test

24 p4403 A69-43443

F-111 sandwich structure adhesive joints gluelines, describing thickness measurement techniques and acceptance criteria

24 p4403 A69-43461

Adhesive bonded joints for glass resin composite sandwich helicopter structures, describing aircraft applications

24 p4403 A69-43462

Welded honeycomb sandwich structures of Ti, steel and similar materials for use in extreme thermal and acoustical environments [AIAA PAPER 68-973]

24 p4326 A69-43716

SAPPHIRE

Sapphire whisker reinforced aluminum composites fabrication and evaluation

06 p0939 A69-16942

Maser amplification of 9.5 GHz longitudinal elastic waves in divalent nickel impurity ions doped sapphire by stimulated emission from inverted spin population

16 p2795 A69-31554

SARCOMA

U CANCER

SATAN [SENSOR]

U SENSORS

U TERRAIN ANALYSIS

SATELLITE ANTENNAS

Ariel 3 receiver for measuring galactic noise spectrum, discussing loop antenna use with swept receiver, false terrestrial signals, etc

03 p0404 A69-13581

Electronic counterrotating antennas, developing turning model of antenna group of telecommunications satellite

04 p0578 A69-15065

Homogeneous fused silica and quartz reinforced resins as dielectric materials for reentry vehicle antenna windows

07 p1090 A69-18400

Miniature current discontinuity antennas for VHF and UHF, describing airborne electronically steerable array exhibiting efficiency and minimum structural disturbance

07 p1105 A69-19111

Monopole antenna behavior over grounded metal hemisphere, noting application to spacecraft and broadcasting antennas erected on hill

08 p1282 A69-20040

Counterrotating antenna for spin stabilized satellite, noting linear phase shift influence on radiation pattern

08 p1289 A69-20968

Electronically phased array antenna system design optimization and testing for application to spin stabilized satellites

08 p1289 A69-20969

Self focusing linear array for communication satellites, evaluating reradiated field taking into account mutual coupling between elements

08 p1289 A69-20970

Large aperture satellite communication antenna gain measurement technique, using extraterrestrial radio wave source or satellite

09 p1456 A69-22116

Directional solar thermal field /sunlight/ effect on coupled nonplanar transverse and torsional vibrations of satellite cylindrical antennas in orbit

11 p1994 A69-25534

Antenna systems design for ISIS-A scientific satellite, discussing antenna array of 13 radiators for telemetry, command, beacon and experimental purposes

17 p2918 A69-33030

Bearing system for mechanically despun antenna in spin stabilized communications satellite, offering greater directional stability, lower weight and power losses

17 p2978 A69-33431

Phased arrays applied to inertialess electronic steering of satellite antennas, discussing digitally steered, retrodirective and hybrid matrix arrays

17 p2942 A69-34083

OGO-F electric and electromagnetic fields measurement for ionosphere using dipole antenna, emphasizing broadband observation covering whistler mode waves

19 p3284 A69-36677

Explorer 20 satellite for obtaining fixed frequency pulse soundings of ionospheric topside, discussing transceiver-dipole antenna instrumentation and payload

20 p3618 A69-37857

Alouette spacecraft design and dynamics emphasizing antenna characteristics

20 p3618 A69-37858

Direct detection of ionospheric irregularity by device onboard San Marco satellite, utilizing antenna impedance fluctuations

21 p3715 A69-38562

Radio Astronomy Explorer satellite boom deployment method resulting in gravity gradient capture, emphasizing role of predeployment attitude and antenna Vee angle

[AIAA PAPER 69-920]

21 p3821 A69-39350

Intelsat 3 communications satellite mechanically despun high gain directive antenna, discussing system, control electronics, design and performance

22 p3913 A69-40691

ATS 3 mechanically despun communications antenna, using parabolic cylindrical reflectors, in-line feed and vernier type stepping motor drive positioning

22 p3913 A69-40692

Multifunction lightweight antenna system package for spin stabilized near synchronous satellite having axis normal to orbital plane

22 p3913 A69-40694

Circularly polarized VHF antenna systems for spin stabilized satellites, discussing design and performance test results

22 p3913 A69-40695

Aperture efficiency, weight and control power requirements for hybrid matrix arrays in synchronous satellite applications, calculating residual array gains

22 p3915 A69-40707

Frequency diversity technique simplifying airborne antennas for UHF telemetry, useful on spin stabilized vehicles requiring omnidirectional antenna coverage

23 p4122 A69-41777

Communication subsystem design of Defense Communication Satellite Program /DCSP/ for background information, noting repeater with toroidal pattern antenna

23 p4131 A69-42537

SATELLITE ATTITUDE CONTROL

Subsystems of ESRO research satellites Td 1 and Td 2, discussing telecommunication, attitude control, power supply and temperature control design and functions

01 p0160 A69-10031

Spacecraft attitude ion sensor using charged thermal ions of earth atmosphere as reference, stressing reliability, economy and response

01 p0079 A69-10293

Solid body automatic orientation, discussing data units for angular error and angular velocity

01 p0122 A69-11302

Multipulse thruster module design and development tests for spacecraft attitude control, noting micropulse solid propellant rocket motor

02 p0194 A69-11762

Stabilization and control techniques for future unmanned commercial space vehicles, emphasizing appli-

cation of projected technological advances in instrumentation

[AIAA PAPER 67-878]

02 p0334 A69-12367

Multijet electrothermal systems for attitude control and stationkeeping of synchronous communications satellite

[AIAA PAPER 67-723]

02 p0305 A69-12375

Attitude control system for gravity gradient stabilized satellite in synchronous and near synchronous equatorial orbits, discussing libration damping methods

03 p0504 A69-12857

Magnetic orientation and attitude control of spin stabilized satellites, synthesizing control circuits and calculating power requirements

03 p0521 A69-13644

Artificial intelligence application to design of off-line and on-line learning control systems for controlling spacecraft attitudes

04 p0581 A69-14568

Time optimal turn maneuver for rocket with tilting engine and control nozzles, noting rotation moments distribution

04 p0665 A69-14832

Apollo guidance, navigation, stabilization and control subsystems, detailing inertial, optical and computer units for data processing and collecting

04 p0665 A69-14881

Soviet book on attitude control of meteorological satellites noting reference systems, sensing units and control algorithms

04 p0666 A69-15012

Boom flutter effects on attitude dynamics of OV1-10 satellite, noting introduction of angular momentum by tip mass elliptical vibration

04 p0666 A69-15520

UV astronomy, discussing vehicle stabilization, un-stabilized sounding rockets, scanning satellites, balloons, stabilized rockets, pointing satellites, optics and detectors

05 p0821 A69-15839

Predictive logic control of on-off system with one position sensor

[ASME PAPER 68-WA/AUT-14]

05 p0830 A69-16134

Attitude perturbations of spin stabilized satellite describing highly eccentric orbit

06 p1014 A69-17568

Attitude control system design problems for earth oriented satellites

06 p1015 A69-17586

Active magnetic coils for attitude control of synchronous satellites by computer simulation and laboratory tests

06 p1017 A69-17944

ORBIS-CAL designed to achieve three axis orientation to local vertical and velocity vector in eccentric orbit by gravity gradient stabilization

07 p1226 A69-18323

Semipassive three axis stabilization for dumbbell type satellites, considering pitch, roll and yaw motions damping

07 p1226 A69-18324

Semipassive attitude control system providing one degree pointing accuracies in all axes

07 p1226 A69-18326

Three axis gravity gradient stabilization system to minimize stray magnetic fields

07 p1226 A69-18329

Three axis gravity gradient stabilization systems for OV-1 spacecraft design

07 p1227 A69-18330

Semiactive gravity gradient stabilization system design for low altitude earth oriented spacecraft attitude control, using active reaction wheel scanner

07 p1227 A69-18334

Hybrid simulation study of satellite attitude control system to replace momentum wheels and gas jets by commandable gravity gradient boom

07 p1227 A69-18335

Equilibria of orbiting gyrostabilized satellite with internal angular momenta along principal axes

07 p1227 A69-18336

Communication satellites attitude control and stabilization due to antenna beam pointing, with future systems forecast, discussing exchange, distribution and collection systems

07 p1228 A69-18339

Eddy current damping systems for gravity gradient stabilized satellites, discussing electromagnetic torque and various parametric relationships

07 p1228 A69-18341

Semiactive gravity gradient stabilization system /SAGS/ for active pitch control and semipassive roll/yaw control

07 p1228 A69-18342

Long life gravity gradient stabilization system using Vee configured control moment gyros to semipassively damp vehicle librations

07 p1228 A69-18345

Gravity gradient stabilization role in space missions in 1970s and 1980s

07 p1229 A69-18348

GEOS 2 attitude stabilization by means of gravity gradient principle and passive energy dissipator, noting effects of orbit eccentricity, thermal distortion, radiation, etc

07 p1229 A69-18349

Vertistat H gravity gradient configuration prevents elastic deformation, permitting high pointing accuracy at synchronous altitudes

07 p1229 A69-18351

Optimum attitude program for multistage satellite launch vehicle with impact restrictions

07 p1229 A69-18492

Fluidic devices application to attitude and guidance control of satellites, rockets and space probes

07 p1230 A69-19292

Satellite attitude control, discussing mission requirements, typical guidance sensors, actuating torque, systems reliability, etc

09 p1609 A69-21617

Damped mass expulsion for space vehicle attitude control reducing propellant consumption and pulsing frequency

[AIAA PAPER 67-535]

09 p1610 A69-21986

Computer program for continuous attitude determination for spin stabilized OGO-C satellite after malfunction of attitude control system, calculating angle between high rate data periods

09 p1610 A69-21987

Attitude determination and hydrogen peroxide control system for spacecraft orientation in Syncom, Early Bird and ATS

[AIAA PAPER 67-532]

09 p1610 A69-21988

Automatic flight control system /AOOSY/ for German Azur satellite

09 p1459 A69-22563

Ionic propulsion application to geostationary satellite attitude correction

10 p1753 A69-23841

Numerical solution for changing satellite orientation within circular orbit plane by applying force of onboard flywheel

10 p1792 A69-24194

Harmonic balance procedure to study periodic motions in nonlinear stabilization system of nonrigid satellite

10 p1792 A69-24195

Space station attitude control through resistojets and control moment gyros /CMG/, discussing propulsion, safety features, weight factors, etc

11 p1965 A69-24531

Spacecraft attitude control with minimum energy control logic for small constant disturbance torques, considering reaction jet torquers and fuel consumption

11 p1966 A69-25446

Dynamic modeling for spin stability of satellites with flexible parts, noting torques induced by attitude control

11 p1994 A69-25533

Perturbation theory of nonlinear control systems with periodic coefficients and small perturbation terms, exemplifying satellite attitude control

12 p2173 A69-26067

Control moment gyro /CMG/ and use in space vehicle attitude control system, emphasizing control laws

[AIAA PAPER 67-589]

12 p2129 A69-26777

Wobble-spin technique for spacecraft inversion for earth photography using flywheel

12 p2174 A69-26780

Photochemical attitude control rocket adaptable to self contained command signal or remote signal transmission, discussing light irradiation of propellant for thrust control

12 p2148 A69-26801

Solar array energy performance as function of orbital parameters and spacecraft attitude

13 p2203 A69-27419

Spacecraft attitude control and stabilization by three degree of freedom control moment gyro with controllable gyro spin angular velocity

13 p2355 A69-27445

Spacecraft and satellite attitude control, discussing payloads, optimization and simulation problems

13 p2356 A69-27919

Magnetometers role in Aurorae satellite attitude stabilization, discussing operation principle, characteristics and performances

15 p2611 A69-31087

Dynamics of spin stabilized satellite with long crossed dipoles or slender beams, including linearized equations of motion

15 p2703 A69-31332

Multipad externally pressurized spherical bearing fed with incompressible fluid for satellite attitude control systems tests

16 p2793 A69-31728

Permanent magnets optimal design and properties for attitude control of German research satellite Azur, considering environmental influences

16 p2868 A69-31936

Ion propulsion applied to geostationary satellites attitude control, discussing thrust levels, cesium ionization, colloidal propulsion, etc

16 p2837 A69-32068

Free gas formation in propellant systems and effects on attitude control systems [AIAA PAPER 69-434]

16 p2870 A69-32765

Satellite attitude control and stabilization - Conference, Paris, October 1968

17 p3045 A69-33219

Diademe satellites stabilization system to measure station-to-satellite distance by laser pulse, discussing reflector, magnet for attitude control, damping device, etc

17 p3046 A69-33224

Passive attitude stabilization of interplanetary probe, using conically shaped sails elastically connected to payload

17 p3047 A69-33225

Cosmos 149 satellite stabilization system, discussing three axis orientation and pitch, yaw and roll stabilizations by aerodynamic and/or gyroscopic moments

17 p3047 A69-33226

Attitude and simple stability of deformable earth pointing satellite

17 p3047 A69-33229

Gravity gradient stabilized satellite achieving best theoretical performance through Foucault current and magnetic hysteresis articulations

17 p3048 A69-33234

Magnetic materials simulation for satellite stabilization device based on magnetic hysteresis, using mathematical models and direct magnetic measurements

17 p2945 A69-33235

Orbital and attitude control tests for PAS (two stage perigee-apogee synchronous satellite) in conjunction with booster Europa 2, discussing functional configuration

17 p3048 A69-33238

Satellites and space vehicles attitude control mathematical model accounting for nonrigidity, sloshing and energy dissipation in vehicle interior

17 p3048 A69-33239

Satellite three axis attitude control analysis showing rolling and longitudinal stabilization possibility by flywheel, with validity tested by analog simulation

17 p3048 A69-33240

Fluidics for satellite and rocket attitude control and guidance, discussing computing block function and components, system reliability and resistance to aging, etc

17 p3049 A69-33243

Astronomical satellite direct digital attitude control using digital computer between sensor and actuator to achieve optimal filtering and stabilization

17 p3049 A69-33244

Microthrusters thrust requirements for attitude control and orbital transfer of gravity gradient geostationary satellite

17 p3019 A69-33336

Micropropulsion system with sublimable solid fuel for satellite attitude control, satisfying mechanical and thermal environmental conditions during launch and in space

17 p3021 A69-33359

Attitude control system for 625 A-1 research earth satellite, detailing operation and test program

17 p3050 A69-33426

Solar probes design for 0.3 to 0.1 AU perihelion distance, considering thermal control, power supply, communications, altitude control and alternative configurations

17 p3050 A69-33797

Satellite attitude control mass properties, showing weight tradeoff analyses role in selecting control system [SAWE PAPER 743]

18 p3208 A69-34885

Biosatellite attitude control systems design development and flight test results for payload perturbing effects, discussing simulation activity

18 p3210 A69-35094

Attitude stabilization of symmetrical nonrotating earth satellite using earth-pointing rotor as gravitational anchor

19 p3429 A69-35914

Jet engine risetime effect on spacecraft orientation control system performance, assuming monotonic or extremal thrust mode

19 p3370 A69-36619

Stationary resonant nonlinear oscillatory and rotary states, stability and pitching motions of controlled satellite in slightly elliptical orbit

20 p3616 A69-37177

Nonlinear roll-yaw attitude motion of spinning symmetric satellite in elliptical orbit near internal or external resonance [AAS PAPER 68-124]

20 p3616 A69-37178

Space vehicle electronic attitude measurement method for reference coordinate and fixed coordinate systems based on rectangular coordinates of RF wave propagation directions

20 p3574 A69-37703

Spinning satellite attitude perturbations due to oscillating mass in satellite rigid frame, discussing analytical approach and analog simulation results

20 p3618 A69-37912

Earth pointing spacecraft attitude control, discussing reference axis system

21 p3760 A69-38620

Time-independent feedback attitude control system for high accuracy earth pointing motion of stable and unstable satellites in elliptic orbits

21 p3804 A69-39020

Degrees of freedom requirements in hinge couplings of multibody satellites, examining main body attitude control

21 p3820 A69-39233

Capture and gravity gradient stabilization of LIDOS satellite in eccentric orbit [AIAA PAPER 69-921]

21 p3821 A69-39351

Constraint torque elimination from vector equations canonical system for attitude dynamics of satellite consisting of arbitrarily interconnected rigid bodies [AIAA PAPER 69-923]

21 p3821 A69-39354

Magnetic hysteresis dynamic model suitable for digital computer simulation of near-earth satellite attitude motions damping compared with experimentally generated loops [AIAA PAPER 69-833]

21 p3821 A69-39364

Reaction boom attitude control systems for improving stabilization and maneuvering capability of earth pointing satellites, describing configurations [AIAA PAPER 69-834]

21 p3822 A69-39365

Valving concepts and functional approaches for inert gas attitude control thruster systems providing redundancy safeguards at minimum weight, volume and power costs [AIAA PAPER 69-843]

21 p3786 A69-39373

Mariner attitude control system limit cycle operation during cruise, noting variation from ideal case to single side operation [AIAA PAPER 69-844]

21 p3822 A69-39374

Mass expulsion and momentum systems for orbiting space station attitude control optimized, considering reaction jet and control moment gyro systems [AIAA PAPER 69-846]

21 p3822 A69-39376

Advanced reaction wheel controller for spacecraft attitude control, discussing brushless DC motor role in weight and power reduction and control precision [AIAA PAPER 69-855]

21 p3822 A69-39383

Spacecraft wide angle attitude control system stability analysis, using air bearing table simulation [AIAA PAPER 69-856]

21 p3823 A69-39384

Motion and stability characteristics of dual spin satellite system with pendulous type nutation dampers, noting mass unbalance effect [AIAA PAPER 69-857]

21 p3823 A69-39385

Spacecraft attitude acquisition/reorientation and stabilization controller design implemented by control moment gyro, proposing control algorithm using control actuator nonlinearity

21 p3826 A69-39641

Suboptimal attitude control system for Nimbus satellite using motor-driven inertia wheels as control torque source for three dimensional control

21 p3826 A69-39642

Electromagnetic attitude control system for Lincoln Experimental Satellite 5 in near-synchronous equatorial orbit, noting onboard error detection in closed control loop

21 p3827 A69-39755

Two-pulse limit cycle oscillation stability relation to physical parameters of pulse modulated feedback system used for satellite attitude control

21 p3688 A69-39756

Fluid loop rotational kinetic energy dissipator reducing time required for reaching WRESAT 1 satellite spin stabilization axis

21 p3828 A69-39767

Satellite attitude stabilization synthesis by flywheels allowing independent control of angular motions, assessing perturbation type influence

21 p3768 A69-39831

Satellite attitude stabilization systems transient response optimization using combined feedback

21 p3830 A69-39833

Radio astronomy Explorer A attitude determination via disk-oriented programming ground support system for reducing and calibrating telemetry data, attitude prediction and command, etc [AIAA PAPER 69-983]

22 p3907 A69-40363

Attitude stability of orbiting vehicle containing gyrost, discussing asymptotic stability

22 p4037 A69-40555

Spinning satellite containing elastically restrained, viscously damped mass, analyzing attitude dynamics and stability, noting wide nutation possibility

23 p4224 A69-42396

Spacecraft pitch and yaw angles measurement using environmental positive ion probes, discussing Gemini flight tests and attitude control systems

24 p4315 A69-43241

Torqued two axis gimbaled boom actuator satellite attitude control [AIAA PAPER 68-857]

24 p4348 A69-43245

Optimal hinged two body satellite configurations in circular and elliptical orbits, discussing need for adaptive attitude control for transient and steady state operation

24 p4393 A69-43247

Multidimensional approximation algorithm for parameter optimization of nonlinear stochastic systems, detailing application to space vehicle attitude controller

24 p4291 A69-43275

Pulse modulated feedback system for satellite attitude control, analyzing relationship between physical parameters to ensure two pulse limit cycle oscillation stability

24 p4295 A69-43318

SATELLITE ATTITUDE DISTURBANCE

U ATTITUDE STABILITY

U SPACECRAFT STABILITY

SATELLITE-BORNE PHOTOGRAPHY

Analytic photogrammetric determination of lunar control coordinates from Ranger photography

01 p0147 A69-10022

Synchronous observations of satellites by photographic techniques from satellite stations, discussing reference stars plane coordinates and exposure time recording

01 p0027 A69-10224

Cloud pictures from weather satellites reception according to automatic picture transmission (APT) system, discussing design and field strength measurements

[UN PAPER 68-95451]

01 p0108 A69-10458

Utility of satellite cloud pictures to meteorological work, discussing weather observation in Israel Meteorological Service

[UN PAPER 68-95571]

01 p0109 A69-10482

Earth orbital satellites for geologic applications, discussing Gemini photograph qualities and influence on Earth Resources Observational Satellite program

[UN PAPER 68-95441]

01 p0065 A69-10509

Lineament trend analysis of Gemini Red Sea synoptic terrain photography, noting computerized rotation from apparent to true angles

02 p0247 A69-12808

Tiros and ESSA weather satellites meteorological contributions, discussing photographic interpretation for weather predictions

04 p0626 A69-14690

Mare Orientale basin satellite photographs suggest asteroid impact formation

04 p0664 A69-15421

Space photography to provide synoptic sedimentary environmental data analysis, discussing orbital sensing advantages

05 p0753 A69-15993

Meteorological satellites data for safe navigation of ships, discussing techniques to overcome difficulties in interpreting ice and cloud photographs

[UN PAPER 68-95776]

06 p0916 A69-17028

European cyclonic system developmental phases determined from characteristic structural features of satellite cloud pictures

[UN PAPER 68-95711]

06 p0950 A69-17070

Satellite picture signal reception from ESSA, Nimbus and ATS to ascertain instrument requirements
06 p0888 A69-17651

ATS satellite distorted photographs conversion into normal and Mercator projections, using computer programs
10 p1689 A69-22945

Time registration delays during photographic observations of satellites, describing NAFA type satellite camera and mechanical and electrical systems
11 p1880 A69-24365

Surveyor 7 TV system in photon integration mode, analyzing slow scan vidicon storage characteristics and dark current limitations
[SMPTE PAPER 105-72] 12 p2078 A69-25772

Earth TV pictures from Molniia 1 communication satellite, showing advantages of high orbit over low orbit photography for global weather analysis and forecasting
13 p2292 A69-27729

Earth resource satellites, discussing mapping, land evaluation, geological observation, agricultural and hydrological applications, electromagnetic spectrum information, sensors and photographs
16 p2881 A69-31763

Daily European weather surveys based on meteorological satellite pictures transmitted during third quarter 1967
17 p3000 A69-33769

Meteorological satellite research, ATS-3 program earth color picture from oceanographic and geomorphological viewpoints and U.S.S.R. research
17 p3000 A69-33777

Daily European weather surveys based on pictures transmitted by satellite during fourth quarter 1967
17 p3000 A69-33778

Graphic representation of time dependence of subsatellite points and orbital azimuths for relating satellite photographs to locality
18 p3128 A69-34818

Satellite photograph analysis to investigate interaction between subtropical and polar front jet streams
18 p3166 A69-34827

Satellite photography for snow cover mapping and depth estimation
18 p3167 A69-35084

Gemini program for geologic orbital photography, discussing equipment used
18 p3131 A69-35274

Horizontal wind components over U.S.S.R., Western Europe and Northeast Atlantic obtained from satellite photographs of vortex cloud systems
19 p3365 A69-36668

Cirrus clouds occurrence, position and wind velocities on jetstream axes based on statistical analysis of aerological data and satellite TV pictures
19 p3366 A69-36669

Satellite IR hyperaltitude imagery for earth resources application, obtaining geological, meteorological and hydrological information
20 p3536 A69-36930

Synoptic and mesoscale cloud patterns near low level jet from Tiros 7 and 8 photographs, noting stratus formation and dissipation
20 p3570 A69-37404

Orbital images for earth resources satellite mission planning using Mercury, Gemini and Apollo synoptic terrain photographs
21 p3721 A69-38632

Long term computer produced multiple image satellite photomosaics for Southern Hemisphere, analyzing circulation, meridional bands, polar ice, cloud cover variations, etc
22 p3977 A69-40733

Cloud cover forms in circulatory-climatic zones of earth based on Zond 5 picture analysis, discussing air-mass exchanges and motions direction
23 p4184 A69-42486

Earth orbital remote sensing applications to forest and range resources management, discussing conventional aerial photography
[AAS PAPER 69-059] 24 p4307 A69-42823

Multispectral orbital photography used to obtain urban land-use data
[AAS PAPER 69-483] 24 p4307 A69-42837

Equatorial anticyclones over eastern Pacific caused by large scale cross-equatorial flows determined by ATS-1 photographs, noting frictional convergence factor
24 p4342 A69-42895

Gridding technique for satellite APT pictures taken with camera axis perpendicular to earth surface
24 p4314 A69-42992

SATELLITE-BORNE RADAR

Radar attitude sensing system for determining vehicle roll, pitch, yaw, altitude and velocity of earth and lunar orbital vehicles
03 p0388 A69-13183

SATELLITE COMMUNICATIONS
U SPACECRAFT COMMUNICATION

SATELLITE CONFIGURATIONS

Attitude control system for maintaining orientation of experimental package relative to space stabilized platform, noting transient response and steady state accuracy
06 p0955 A69-17587

Small astronomy satellite /SAS/ design, power, command, telemetry and control systems
07 p1229 A69-19126

Optical sensing devices for angle measurement between celestial body and satellite axes
12 p2078 A69-25871

Dynamics of spin stabilized satellite with long crossed dipoles or slender beams, including linearized equations of motion
15 p2703 A69-31332

Temperature distribution of solid spherical satellite under solar radiant heating solved by variational calculus or point matching methods
16 p2877 A69-31922

Satellite configurations and rotation parameters determined by radar analysis
20 p3488 A69-37295

Equations of motion of elastic dumbbell satellite and two-mass spring-connected satellite in orbit, using energy and Floquet theory to investigate spinning motion stability
21 p3817 A69-39759

Satellite rotation from radar data analysis, requiring two full rotations and body characteristics to produce distinctive lobes in radar cross section
22 p3900 A69-40682

Book on commercial satellites covering characteristics, uses, design, rocket propulsion systems, flight trajectories, etc
23 p4224 A69-42367

Tethered orbiting interferometer configurations for future Radio Astronomy Explorer satellites, discussing gravitational stabilization and delta launching into orbit as single payload
[AAS PAPER 69-255] 24 p4313 A69-42859

Optimal hinged two body satellite configurations in circular and elliptical orbits, discussing need for adaptive attitude control for transient and steady state operation
24 p4393 A69-43247

SATELLITE CONTROL

Radar attitude sensing system for determining vehicle roll, pitch, yaw, altitude and velocity of earth and lunar orbital vehicles
03 p0388 A69-13183

Small astronomy satellite /SAS/ design, power, command, telemetry and control systems
07 p1229 A69-19126

Maintenance telemetering, tracking and telecommand for developmental and operational satellites, discussing possibilities of frequency sharing between satellites and terrestrial services
09 p1451 A69-21290

Cesium microthruster system using beam deflection for satellite control, describing ion engine subsystem and control logic/power conditioner subsystem
[AIAA PAPER 69-292] 09 p1569 A69-21875

Computer design for booster/satellite control, discussing systems reliability, low power and tradeoffs
11 p1843 A69-25320

Multidimensional mode shapes and frequencies of 100 ft space erectable parabolic antenna
11 p1994 A69-25532

Optimum thrust control of satellite along given trajectory to rendezvous at zero velocity with orbited satellite
13 p2356 A69-27684

Ground station network and facilities for control of and acquisition and processing data from ESRO 1 satellite
13 p2220 A69-27751

ESRO 1 and 2 satellites onboard remote control system, discussing tone digital standard code and equipment design features
15 p2702 A69-31086

Test facility for qualification of satellite fairings jet-tisoning system, describing accelerating tower and recording and control instrumentation
16 p2765 A69-31739

Electrically propelled TV satellite control maneuvers to reach target position in synchronous circular orbit from spiral ascent trajectory
16 p2868 A69-31935

Momentum control system for satellite maneuvering and pointing in pitch and roll developed by modifying existing libration damping gyro stabilizer
18 p3207 A69-34684

NASA lunar survey and mapping for generating Apollo satellite landing navigation control, using analytic photogrammetry, camera position and altitude data of lunar topography
20 p3536 A69-36931

Automatic stationkeeping /geosynchronization/ for maintaining satellite in circular synchronous orbit at all geocentric longitudes for prolonged time with low fuel consumption
21 p3805 A69-39213

Radio Astronomy Explorer satellite boom deployment method resulting in gravity gradient capture, emphasizing role of predeployment attitude and antenna Vee angle
[AIAA PAPER 69-920] 21 p3821 A69-39350

Orbital results for Automatic Orbit Control System of Lincoln Experimental Satellite LES 6, using pulsed plasma microthrusters and self contained orbit measurement and control methods
[AIAA PAPER 69-934] 21 p3824 A69-39428

Linear multichannel spatial motion control systems for vehicles orbiting in earth atmosphere at supersonic velocities
21 p3766 A69-39645

Optimal control system for earth satellite orbital transfer, using wandering ellipse technique to develop trajectory correction algorithm
21 p3767 A69-39652

Satellite motion orbital elements dependence on large short impulse arbitrarily directed in space, analyzing optimal orbits transfer and thrust control
21 p3818 A69-39821

Satellite stabilization by earth magnetic field through conservative magnetic moments application
21 p3830 A69-39834

SATELLITE DESIGN

Subsystems of ESRO research satellites Td 1 and Td 2, discussing telecommunication, attitude control, power supply and temperature control design and functions
01 p0160 A69-10031

TRANSIT satellite navigation system for all-weather diurnal position fixing, noting Doppler frequency measurement and ionospheric signal refraction
01 p0112 A69-10457

Direct TV broadcasting from satellites with incoherent thermionic reactor and electrical propulsion
[UN PAPER 68-95559] 01 p0114 A69-10466

Remote sensors utilization in earth orbital space for discovery, inventory, evaluation, development and conservation of earth natural resources, noting satellite design
[UN PAPER 68-10464] 01 p0065 A69-10532

International Radiation Investigation Satellite /IRIS/ mission, structural design, power supply and control systems
01 p0162 A69-11101

Book on Demeter-earth resources satellite system covering design, instrumentation, cost estimates, economic benefits and political considerations
01 p0163 A69-11333

French satellites structure, power and communications systems, stabilization and detector groups
02 p0333 A69-11917

French geodetic satellites tracking operations, on-board equipment and ground stations
[UN PAPER 68-95835] 06 p1013 A69-17065

Anna 1-B geodetic satellite design, instruments and data acquisition
[UN PAPER 68-96195] 06 p0917 A69-17082

Orbital station projects, concepts and future uses
06 p1013 A69-17266

Soviet achievements in space research, comparing satellites with U.S. counterparts
06 p1005 A69-17561

Attitude control system design problems for earth oriented satellites
06 p1015 A69-17586

ORBIS-CAL designed to achieve three axis orientation to local vertical and velocity vector in eccentric orbit by gravity gradient stabilization
07 p1226 A69-18323

RAE-A satellite design, simulation and flight performance, discussing gravity gradient stabilization
07 p1226 A69-18328

Three axis gravity gradient stabilization system to minimize stray magnetic fields
07 p1226 A69-18329

Three axis gravity gradient stabilization systems for OV-1 spacecraft design
07 p1227 A69-18330

Small astronomy satellite /SAS/ design, power, command, telemetry and control systems
07 p1229 A69-19126

Small Scientific Satellite program, discussing payload for investigating magnetosphere and near interplanetary space
[IEEE PAPER 3C-1] 07 p1230 A69-19195

Intelsat 2 satellite structural design for Apollo communications
08 p1408 A69-19907

Domestic satellite system for carrying maximum traffic by full use of rocket technology including Saturn 5 type propulsion systems, antennas, frequencies, etc
09 p1458 A69-22467

AZUR German research satellite main structure dynamic characteristics, solar panels, yo-yo despin system, electronic ignition devices and magnetometer boom
12 p2175 A69-26875

AZUR satellite structural development static and dynamic considerations, discussing center of gravity, notching technique and test results
12 p2187 A69-26876

ESRO 1/Aurora project for ionospheric phenomena connected with incoming protons and electrons, describing orbit and alignment with geomagnetic field
13 p2356 A69-27747

Nimbus D meteorological satellite construction, control system, orbit, etc
13 p2356 A69-27832

Satellite and spacecraft power supply and power converters
13 p2209 A69-27917

European space program developmental and fabrication problems in satellite structure development covering booster constraints, mission constraints, tolerances, etc
13 p2357 A69-28479

Earth Resources Technology Satellites design for complete spectrum of frequencies
14 p2453 A69-29952

COMSAT thermal vacuum chamber specification configurations, discussing chamber orientation, vacuum and roughing systems, pumping mechanism, wiring, installation, testing, etc
15 p2587 A69-30393

ESRO 1 satellite design coordination, assembly and tests
15 p2702 A69-31082

D-2 satellite stabilization system design and development, noting mission to determine hydrogen distribution around earth
17 p3046 A69-33223

International organization and project management procedures in design and construction of Heos 1 satellite for measuring charged particles energy distribution outside geomagnetic field
17 p3050 A69-33699

German research satellite Azur design and production management
17 p3050 A69-33700

Scientific satellites structural design problems, considering limitations imposed by weight, layout, environmental conditions, mission and manufacture
18 p3208 A69-34792

ESRO Large Astronomical Satellite /LAS/ observatory in orbit, discussing operation, design and instrument settings in scientific package
18 p3208 A69-34793

Tank configurations allowing for sloshing in liquid fuel reaction control system in spinning satellite
18 p3219 A69-34796

Ground controlled remote manipulator spacecraft system to perform unmanned satellite orbital maintenance, discussing refurbishment, laboratory simulation, system cost effectiveness and feasibility
19 p3430 A69-36001

Communication satellites equipment and techniques, considering global network, satellite design, millimeter wave systems, etc
19 p3275 A69-36314

OGO for conducting diversified experiments to study earth atmosphere, earth-sun relationship, etc
19 p3432 A69-36674

Ionospheric satellite series Alouette-ISIS, discussing successive engineering and management constraints leading to ISIS-C design
20 p3618 A69-37856

Alouette spacecraft design and dynamics emphasizing antenna characteristics
20 p3618 A69-37858

Tiros M requirements for earth resources sensor systems, discussing spacecraft structure, dynamics, power, command and communications subsystems
21 p3818 A69-38621

Orbital Experimental Capsule /OEC/ as subsatellite concept for Martian fields and particles measurements, noting Voyager exploring vehicle applications
21 p3805 A69-39215

Ariel 3 satellite shape and systems including heat balance, data storage and compatibility problems
21 p3820 A69-39256

Circularly polarized VHF antenna systems for spin stabilized satellites, discussing design and performance test results
22 p3913 A69-40695

Book on commercial satellites covering characteristics, uses, design, rocket propulsion systems, flight trajectories, etc
23 p4224 A69-42367

OGO-6 design, research program, orbits and instrumentation, emphasizing relationship between particle activity, aurora and airglow, geomagnetic field, atmospheric and solar energy interrelations
24 p3493 A69-43132

SATELLITE DRAG

Accelerometric measurement of atmospheric drag with satellite 1968-59B, obtaining upper atmosphere density profile at 130-160 km
02 p0245 A69-12728

Satellite drag data to determine upper atmospheric composition according to density distribution with height
03 p0423 A69-13532

Upper atmosphere semiannual density variations, using satellite drag analysis
06 p0918 A69-17380

Air density at 470 km from orbit of satellite 1966-118 A, confirming large semiannual variation
09 p1488 A69-21659

Cylindrical satellite drag rotating about transverse axis in earth magnetic field, including aerodynamic and magnetic moments
12 p2174 A69-26443

Small body drag in wake of large satellite using two dimensional model noting methods for calculating distribution function moments in wake regions
12 p2012 A69-26798

Polar exosphere near solar maximum investigation by Explorer 19 and Explorer 24 drag satellites, considering density and atomic oxygen concentration measurements
15 p2600 A69-31351

Low altitude atmospheric density satellite OV1-16 measurements, showing agreement between onboard accelerometer and orbital drag data
15 p2602 A69-31385

Atmospheric density determination based on long period variations of drag coefficients from satellite Proton 2, considering satellite orientation
15 p2602 A69-31392

Drag measuring requirements and comparison of accelerometer or drag-free satellite control systems usage for atmospheric density determination
16 p2788 A69-31722

Steady state plasma wind tunnel for flow around ionospheric satellites, studying wakes of cylinders and spheres
[AIAA PAPER 69-673] 17 p2893 A69-33488

Ground traces of artificial earth satellites with respect to perturbations due to atmospheric drag, earth oblateness and moon and sun as third body
19 p3398 A69-35614

Satellite orbits calculation in nonrotating atmospheres, considering atmospheric drag and zonal harmonics coupled effects
[AIAA PAPER 69-925] 21 p3808 A69-39352

SATELLITE GROUND SUPPORT

Monograph on photogrammetry in satellite geodesy including photogrammetric measurement of satellite positions, German observation stations and work done in U.S., U.S.S.R. and France
16 p2790 A69-32202

More earth station equipment and design for satellite communication in INTELSAT network including antenna, feed and tracking, interconnect system, etc
22 p3900 A69-40679

Traveling wave tubes in satellite earth stations, discussing single carrier tubes and multiple carrier technique
23 p4143 A69-42420

SATELLITE GUIDANCE

Range difference air navigation equations solution, discussing error updating of satellite position and constellation geometry
09 p1538 A69-21996

Peano-Baker method for integration of variational equations to produce partial derivatives used in satellite trajectory estimation
19 p3398 A69-35616

Minimum fuel guidance from hyperbolic into specified circular orbit
19 p3367 A69-35663

SATELLITE INSTRUMENTS

Selective chopper radiometer for remote atmospheric temperature sounding, discussing satellite versions for Nimbus D and Nimbus E
[UN PAPER 68-95797] 01 p0080 A69-10531

Remote sensors utilization in earth orbital space for discovery, inventory, evaluation, development and conservation of earth natural resources, noting satellite design
[UN PAPER 68-10464] 01 p0065 A69-10532

Scintillation gamma spectrometer on Luna 10, eliminating charged particle background by fabricating detector from NaI single crystal in scintillating plastic container
01 p0084 A69-11314

Balloon, rocket probe and satellite payloads, noting French contributions and CNES role
02 p0333 A69-11914

Satellite high resolution radar mapping of planets, discussing synthetic aperture and linear FM transmission radar techniques
03 p0430 A69-13399

Satellite-borne auroral particle spectrometer calibration to minimize uncertainty in measuring absolute particle flux of electrons and protons
04 p0599 A69-15022

Low DC current measurement on board satellite, noting absence of elaborate compensation
04 p0602 A69-15399

General purpose satellite computer, discussing on-board processor /OBP/ design, memory, central unit, input/output and software
05 p0725 A69-16710

Data handling equipment for Ariel 3 and future satellites emphasizing manufacturing of PFM and PCM systems
05 p0726 A69-16769

Anna 1-B geodetic satellite design, instruments and data acquisition
[UN PAPER 68-96195] 06 p0917 A69-17082

Mechanically and electronically despun spacecraft antennas, comparing designs and projected performances for spin stabilized Intelsat 3 satellite
06 p0897 A69-17590

Heat storage cells for satellite solar power plants based on latent heat of fusion and single phase heat carrying agent
06 p0870 A69-17604

Calibrating long wave actinometric instruments designed for Soviet meteorological satellites
06 p0929 A69-17978

Informative properties of IR scanning equipment of meteorological satellites, discussing radiative flux measurements and thermal mapping
06 p0929 A69-17979

IR scanning systems of meteorological satellites for detection of clouds and various underlying surfaces, determining detection probability and errors
06 p0952 A69-17986

Electronic tubes utilization in space flight, summarizing characteristics and satellite applications
07 p1093 A69-18421

Onboard calibration system for gamma ray spectrometers and X ray detector in earth satellites, describing fabrication and test results for radioactive sources
[IEEE PAPER 3A-6] 07 p1134 A69-19193

Small Scientific Satellite program, discussing payload for investigating magnetosphere and near interplanetary space
[IEEE PAPER 3C-1] 07 p1230 A69-19195

IMP F and G solar cosmic ray spectrometer utilizing FET analog multiplier for onboard particle identification data processing
[IEEE PAPER 3C-3] 07 p1135 A69-19197

Channel multiplier spectrometer for low energy electrons and protons at synchronous altitude on ATS-E satellite
[IEEE PAPER 3C-5] 07 p1135 A69-19199

Multichannel pulse height analyzer with memory, small size and low power consumption for application to satellites [IEEE PAPER 3C-6] 07 p1135 A69-19200

Structure of quasi-linear and wideband satellite transponders, discussing possible improvements 09 p1609 A69-21619

Primary cosmic rays, radiation belts and solar wind studies by semiconductor detectors installed on orbiting satellites 10 p1662 A69-23294

Radiation measurements quality by wide angle receivers of Cosmos 122 satellite analyzed, showing agreement with data by other methods 11 p1912 A69-24830

Astronomical wide field cameras of large aperture ratio to detect extended near UV light sources outside atmosphere 12 p2080 A69-26127

Logarithmic response electrometer for upper atmosphere satellite measurements using subminiature vacuum tube 12 p2092 A69-26476

Geographic and cartographic mapping applications of remote sensor data from orbital heights, discussing hardware, instrumentation, NASA role in data selection, etc 12 p2192 A69-26984

Latching high-voltage reed relays in satellite instrumentation systems 13 p2231 A69-28047

Cosmos 149 meteorological satellite telephotometer, radiometer and other electronic equipment for measuring atmosphere and underlying surfaces physical parameters 14 p2447 A69-29403

Cosmos 149 meteorological satellite telephotometers for measuring reflected solar radiation from earth 14 p2447 A69-29404

Atmospheric radiative balance measurement on board Cosmos 149, describing design and operation of device 15 p2597 A69-30652

Satellite Proton 2 orientation from onboard measurement data, discussing general statistical method and data processing results 17 p3001 A69-33221

Lunar surface uppermost layer physical and mechanical properties investigated by soilmeter-penetrometer and radiation densimeter on Luna 13 18 p3113 A69-34239

Steady motion stability of satellite gyroscope in Cardan suspension traveling along circular orbit in Newtonian central force field 18 p3135 A69-34585

ESRO Large Astronomical Satellite /LAS/ observatory in orbit, discussing operation, design and instrument settings in scientific package 18 p3208 A69-34793

Spacecraft data storage requirements, discussing use of servo-driven tape recorders in data processing systems 18 p3107 A69-35096

Instruments for gamma ray astronomy including Ranger low energy detector, howitzer detector and cosmic spark chamber 18 p3138 A69-35135

Electromagnetic field signatures in optical IR spectrum of satellite-borne sensors, analyzing spectral, spatial and temporal distributions, polarization and phase 19 p3309 A69-36060

Satellite-borne experiments of neutral molecular beam-solid surface interactions, describing Molsink chamber, densitometer, sphere and paddlewheel satellites 19 p3377 A69-36182

Onboard satellite computer design and programming language criteria, considering cost, reliability, weight, volume and energy requirements 20 p3499 A69-37379

Missile-borne and satellite-borne computers analogies, comparing design, operational conditions and functional requirements 20 p3500 A69-37380

Swedish satellite onboard computer for particle experiment, discussing functional design based on buffer unit for experimental data 20 p3501 A69-37386

Onboard data processor design for Swedish satellite to study spatial and temporal variations of auroral particles 20 p3501 A69-37387

Onboard satellite computer for project Roseau experiments for magnetosphere study, discussing program switches, monitors and data compilers 20 p3501 A69-37388

Roseau satellite onboard computer systems design, emphasizing simulator and assembly programs for real time operation verification 20 p3501 A69-37389

Data handling system design for large astronomical satellite /LAS/, discussing spacecraft configuration, basic aims, program functions, subsystems, signal flow, flight repair, etc 20 p3501 A69-37390

Wire type memory model for satellite onboard computers, discussing nondestructive readout, power requirements, marginal temperatures, material and volume 20 p3503 A69-37403

Explorer 20 satellite for obtaining fixed frequency pulse soundings of ionospheric topside, discussing transceiver-dipole antenna instrumentation and payload 20 p3618 A69-37857

Sweep frequency ionospheric topside sounder design for Alouette and ISIS satellites, discussing influence of experiment requirements and spacecraft limitation and environments 20 p3507 A69-37859

Measuring devices for near earth space radiation measurements 20 p3591 A69-38018

Explorer 22 observations of ionosphere electron content, describing measuring equipment and data evaluation 22 p3935 A69-39977

OGO-6 design, research program, orbits and instrumentation, emphasizing relationship between particle activity, aurora and airglow, geomagnetic field, atmospheric and solar energy interrelations 24 p4393 A69-43132

HgCdTe as IR satellite detector for terrestrial, atmospheric and ocean mapping, IR astronomy and optical communication 24 p4362 A69-43666

SATELLITE LAUNCHING

U SPACECRAFT LAUNCHING

SATELLITE LIFETIME

Environmental tests of space vehicles, determining parameter effects on ground storage and transportation, launching and orbital life 02 p0228 A69-11918

Elliptic integrals to determine orbital elements time dependence in three body problem, estimating satellite lifetime 10 p1791 A69-24196

Air density height distribution determined from satellite orbit decay analysis, noting semiannual density variations 22 p3935 A69-39971

Lifetime of artificial satellites by approximate integration method with application to Explorer 1, comparing analytical prediction 22 p4036 A69-39973

Battery subsystems optimization for earth satellite lifetimes greater than 5 years, analyzing flexibility, weight and reliability 23 p4068 A69-42243

SATELLITE MANEUVERS

U SPACECRAFT MANEUVERS

SATELLITE NAVIGATION SYSTEMS

Ship navigation by altitude and azimuth measurements of artificial earth satellite, discussing position and reference errors and synchronous satellite advantages [UN PAPER 68-95247] 01 p0112 A69-10461

Worldwide navigation system consisting of synchronous satellites equipped with pulse modulated microwave transmitters [UN PAPER 68-95205] 01 p0113 A69-10514

Ship and aircraft traffic conditions in Japan and neighboring areas and requirements for navigation satellite system [UN PAPER 68-95226] 01 p0113 A69-10520

Aircraft navigation using synchronous satellites based on position location by intersection of two circles with centers below satellites 01 p0114 A69-11011

Navy Navigation Satellite System TRANSIT providing all-weather continuous worldwide service for military and civil users 02 p0277 A69-11753

TRANSIT /Navy Navigation Satellite System/ military and commercial applications 02 p0278 A69-12359

Digital simulation of demodulator/tracking phase locked loop of navigation/traffic control satellite system in thermal noise diffuse multipath fading environment 03 p0390 A69-13204

SPOT /Speed, Position and Track/ transoceanic traffic surveillance and navigation system for aircraft and marine users 03 p0463 A69-13234

Transoceanic air traffic control system with independent surveillance of aircraft positions, decision making agency and undelayed communications, using satellites 03 p0464 A69-13236

Project Dioscures for permanent air traffic control centers, positive telecommunication links and satellite navigation 08 p1347 A69-20779

Satellite navigation system feasibility for accurate and continuous navigation capability for Army tactical aircraft 08 p1349 A69 21193

Optimum inertial/Doppler satellite navigation system, discussing position fixes application in resetting 08 p1349 A69-21199

Soviet book on radio navigation of flight vehicles covering systems classification, operational characteristics, satellite navigation, etc 12 p2129 A69-27076

Navy Navigational Satellite System for position location accuracy in marine and oceanographic exploration applications [AIAA PAPER 68-471] 13 p2295 A69-27247

Algorithm for solving autonomous artificial satellite orbital elements by using successive approximations 13 p2296 A69-27687

Space vehicles and marine navigation using navigation satellites, radar, Doppler navigation, etc 13 p2296 A69-27918

Navy Navigation Satellite System /NAVSAT/ applications, considering nonmilitary marine and air all-weather navigation and positioning 14 p2479 A69-29856

Satellite space navigation system providing three component position in geodetic coordinates instantly and accurately on or near earth 15 p2650 A69-30088

Artificial satellites as navigation aids, describing angle, range and range-angle systems, discussing orbital mechanics and communications difficulties 18 p3169 A69-34855

Correlation role in navigation satellite analysis noting reduction in ephemeris error effects [AAS PAPER 68-145] 21 p3761 A69-39222

SATELLITE NETWORKS

Navigation Service Satellite System for aiding aircraft and ships at sea in Pacific Ocean, noting equipment and functions [UN PAPER 68-95251] 01 p0112 A69-10470

World Weather Watch /WWW/ system and meteorological satellites, discussing observational networks, data centers, telecommunication facilities, research, education and training program [UN PAPER 68-95209] 01 p0178 A69-10478

Navigation services satellite systems including position determination, communication and telemetry for ships and aircraft [UN PAPER 68-95363] 01 p0113 A69-10479

Optical spacecraft tracking organization in U.S.S.R., describing network of visual observation and photographic stations for satellite and space probe tracking 01 p0032 A69-10952

Navigation by satellite systems, discussing vehicle position determination and communications link for traffic control with comment on French space program 02 p0278 A69-11912

Maritime radio communications satellite service for ship safety, discussing stationary equatorial satellite systems [AIAA PAPER 68-232] 02 p0356 A69-12383

Communication satellites systems, discussing Intelsat satellite specifications and modulation methods for multiple access 03 p0383 A69-12870

Error correcting coding on DCSP satellite channels, discussing single access communication through wide-band SHF repeaters in synchronous earth orbit 03 p0387 A69-13177

Economic importance of European communications satellite system development 03 p0535 A69-13583

European regional satellite communication systems, discussing EUROVISION TV program broadcasting and multiple access telephony 03 p0395 A69-13585

Domestic satellite communication system model for greatest possible amount of traffic using Saturn 5 propulsion systems, multibeam antennas, synchronous repeater platforms, etc
04 p0561 A69-15447

Soviet Orbita communication satellite system network operation, design and technical and economic aspects
06 p0886 A69-17043

U.S.S.R. system Meteor consisting of four Cosmos satellites in polar orbits to observe cloud distribution, snow and ice field boundaries, etc
06 p1013 A69-17053

Dioscours system for international air traffic control and navigation over North Atlantic by means of two geostationary satellites
[UN PAPER 68-95832] 06 p0954 A69-17063

Canadian domestic satellite system requirements to extend existing terrestrial communications systems to improve coverage, capacity, flexibility and cost factors
06 p1043 A69-17832

Space communication, discussing global network of Intelsat satellites ground facilities, regional switching, RF channels, etc
06 p0890 A69-17860

Predictor determining future position of TDMA/Time Division Multiple Access/synchronous satellite communications system satellite from previously received bursts
07 p1076 A69-18553

World satellite telecommunications network, discussing recommendations with reference to signal transmission, acoustic echoes, etc
07 p1079 A69-18942

Communication satellites applied to broadcasting, considering point to point satellite link and distribution systems
08 p1272 A69-19925

Communication satellite systems role in world telecommunication network, discussing traffic type, volume and routing, earth stations location and capacities and orbit selection
09 p1449 A69-21271

Earth station antennas for communication satellite service, discussing design, fabrication, main lobe gain, side and back lobe suppression and noise performance
09 p1461 A69-21281

Earth station antenna radiation patterns for studying mutual interference effects between radio relay stations and communication satellite earth stations
09 p1461 A69-21282

Communication satellite system design for operation with frequency bands above 10 GHz, noting wideband communication
09 p1450 A69-21284

INTELSAT for design, construction, launching and maintenance of global communication satellites, noting transponders
09 p1457 A69-22466

Domestic satellite system for carrying maximum traffic by full use of rocket technology including Saturn 5 type propulsion systems, antennas, frequencies, etc
09 p1458 A69-22467

Data relay satellite systems for support of NASA R and D missions, discussing communications between satellites and to mission control
11 p1839 A69-25296

Satellite technology for government and defense communications systems, noting effects of rainfall attenuation, weather and solar interference on performance and reliability
12 p2028 A69-25932

Tracking and data acquisition networks and communications systems for support of space missions, studying data processing, unified S Band System and Data Relay Satellite System
12 p2028 A69-25933

Technological feasibility of satellite based global data relay service for small users
12 p2028 A69-25949

Satellite networks for air traffic control and aircraft communications in North Atlantic
13 p2296 A69-27831

Dioscours project for worldwide telecommunications, air traffic control and navigation by satellites, discussing technical, operational and economic characteristics
16 p2749 A69-31601

Satellites and ground stations system providing transoceanic civil, air and marine traffic control in North Atlantic, discussing position determination, communication and navigation, etc
18 p3170 A69-35065

Satellite systems for air traffic control, navigation, communications and telemetry in view of regulations of frequency allocations
18 p3103 A69-35089

Communication satellites equipment and techniques, considering global network, satellite design, millimeter wave systems, etc
19 p3275 A69-36314

Satellite telecommunication systems coordination, discussing transformation feasibility of consortium or international organ into international organization
20 p3637 A69-37120

Juridical norms defined by Madrid, Belgrade and Washington conferences regulating exploration and utilization of extraterrestrial bodies and space, considering satellite communications networks
20 p3638 A69-37123

International cooperation regarding space telecommunication systems, discussing INTELSAT and INTERSPUTNIK roles in achieving international coordination and equality
20 p3638 A69-37125

Global communication satellite system with 12 to 16 hour period equatorial orbit, discussing satellite daily switchings, motions relative to earth, etc
20 p3497 A69-38189

Meteorological parameters-radio propagation characteristics correlation, studying feasibility of data acquisition by occultation satellite system
21 p3705 A69-38374

Orbital mechanics of near earth satellite arrangements /clusters/ for satellite service vehicle /SSV/ accessibility from orbital space stations
[AIAA PAPER 69-929] 21 p3809 A69-39358

Technical and economic factors of program to provide communications services via satellite facilities in continental U.S.
[AIAA PAPER 68-412] 21 p3678 A69-39762

Air traffic control transoceanic satellite system for minimizing navigation errors forcing wide separations, providing VHF voice communication and position surveillance
22 p3901 A69-41147

Communication satellite technology application to overlay network linking nationwide data machines for business mail service with virtually instantaneous delivery at low cost
23 p4117 A69-41669

Real time telemetry, tracking and command links by synchronous satellite relay, describing ATS-Nimbus E S-band experiment
23 p4121 A69-41759

Multichannel time division multiple access system for communication satellite networks, considering PSK modems, PCM codes and channel capacity
23 p4129 A69-42511

Multiple access discrete address system /MADA/ for digital modulation communication systems for satellite networks, using time division techniques
23 p4130 A69-42512

Distributed communications for earth orbiting global satellite network defined parametrically, describing relay/switching and terminal station satellites
23 p4130 A69-42515

Satellite communication system capacity for segment of geostationary orbit extended to models involving two angular dimensions
23 p4131 A69-42521

Satellite system survival probability expressed as function of launch probability, time and number of satellites available
[AIAA PAPER 67-324] 24 p4249 A69-43665

SATELLITE OBSERVATION

Synchronous observations of satellites by photographic techniques from satellite stations, discussing reference stars plane coordinates and exposure time recording
01 p0027 A69-10224

Cloud pictures from weather satellites reception according to automatic picture transmission /APT/ system, discussing design and field strength measurements
[UN PAPER 68-95451] 01 p0108 A69-10458

Observation of satellites, orbit calculation and use in upper atmosphere research
[UN PAPER 68-95789] 01 p0064 A69-10459

Ship navigation by altitude and azimuth measurements of artificial earth satellite, discussing position and reference errors and synchronous satellite advantages
[UN PAPER 68-95247] 01 p0112 A69-10461

Satellite automatic picture transmission application to meteorological and hydrological problems including

wind estimates, atmospheric stability and cloud distributions
[UN PAPER 68-95300] 01 p0108 A69-10462

Atmospheric model development relating temperature, density, moisture and energy measurements from satellite observations for long term weather forecasting
[UN PAPER 68-95397] 01 p0108 A69-10463

Tiros Operational Satellite system for global weather analysis data acquisition and cloud cover photography, noting sensor development for numerical weather prediction
[UN PAPER 68-95823] 01 p0108 A69-10473

Passive and active transmitters and receivers of electromagnetic radiation in earth orbital satellites to collect pictorial or numerical data to study hydrology
[UN PAPER 68-95333] 01 p0064 A69-10487

Satellite photography applications to geography and cartography based on Gemini 7 photographs
[UN PAPER 68-95401] 01 p0178 A69-10489

Orbiting satellite global all-weather oceanographic data acquisition to complement higher resolution data from ships, buoys and aircraft remote sensors
[UN PAPER 68-95878] 01 p0064 A69-10491

Meteorological satellite observations value to Southern Hemisphere
[UN PAPER 68-95213] 01 p0109 A69-10513

Earth surveying methods by artificial satellites, discussing applications to undeveloped regions
[UN PAPER 68-95793] 01 p0065 A69-10523

Earth surface shape determinations by geodetic networks connecting ground observation points and satellite positions
[UN PAPER 68-95377] 01 p0065 A69-10528

Remote sensors utilization in earth orbital space for discovery, inventory, evaluation, development and conservation of earth natural resources, noting satellite design
[UN PAPER 68-10464] 01 p0065 A69-10532

Diapason satellite geodetic results concerning measurement accuracy, terrestrial potential models and station synchronization
01 p0065 A69-10543

Tiros satellite meteorological observations, discussing perturbation morphology and cloud mass organization
01 p0109 A69-10545

Topside ionosphere average height distributions of electron density and geomagnetic field intensity from Alouette 2 data over Japan, noting ionic composition
01 p0065 A69-10548

Micrometeorites acoustic recordings on Cosmos 135, investigating data reliability influenced by appearance of thermal noise
01 p0152 A69-10578

General theory of relativity tests with aid of satellites, considering gravitational red shift measurements, light deflection in solar field, etc
01 p0152 A69-10751

Soviet studies of ionospheric electron densities by means of geophysical rockets and satellites
01 p0067 A69-10944

Ionospheric plasma electrostatic resonances from Alouette satellite signal observations
01 p0067 A69-10983

Solar, interplanetary and magnetospheric electromagnetic events before and during magnetic storm from ground observatory and earth satellite data
01 p0156 A69-11120

Explorer 26 observations of solar proton penetration inside trapped radiation near geomagnetic equator
01 p0146 A69-11122

Solar protons observations by Satellite 1963 38C in polar regions at high altitude during spring 1966
01 p0146 A69-11123

Solar proton event generating sudden commencement magnetic storm, discussing effects on outer belt electrons as observed by Explorer 26 and time delay
01 p0146 A69-11124

Magnetic field data fromOGO-2 spacecraft and surface magnetic observatories, noting magnetic storm occurrence and magnetosphere inflation and detection of polar ionospheric currents
01 p0069 A69-11125

Differential Faraday technique to determine electron content latitude dependence in Northern Hemisphere during magnetically disturbed periods in March 1966
01 p0146 A69-11128

Venus atmosphere and radius measurements by Mariner 5, Venera 4 and radar, comparing values
01 p0157 A69-11197

Sudden magnetic field increase associated with July 8, 1966 sudden commencement observed byOGO 3 satellite in magnetotail
01 p0075 A69-11226

- Solar plasma observations during magnetic storms, discussing shocks and tangential discontinuities, geomagnetic variations and He
01 p0076 A69-11234
- Cosmos satellites monitoring electrons distribution in inner radiation belt suggest intensity stability for solar activity cycle
01 p0147 A69-11309
- Electron intensity diagram of diurnal trapped electron variation from Cosmos 5 satellite data, including harmonic analysis of data
01 p0147 A69-11321
- Cosmic radio emission at 1.68 MHz measured by Cosmos 142 satellite, discussing receiver, antenna and radiation temperature
01 p0158 A69-11322
- Orbital spectroscopic and radiometric IR experiments, considering moon and Mars surface
[AAS PAPER 68-196] 02 p0312 A69-11474
- Tensor character of fictitious potential function introduced to approximate locally tangent actual potential function, discussing planetary gravitational anomaly observation from orbiting vehicles
[AAS PAPER 68-198] 02 p0312 A69-11476
- Satellite monitoring application to air traffic control in parallel track system, discussing lateral and longitudinal separation control
02 p0277 A69-11591
- Ion concentrations and temperature measurements by magnetic trap on Cosmos 5 between 1000-1200 km
02 p0306 A69-11656
- Electron measurements at 18 earth radii in Vela satellite program
02 p0307 A69-11735
- French geodetic work with aid of artificial satellites, describing equipment, mounting, observation technique and laser telemetry experiments
02 p0228 A69-11913
- Vela 3A and Explorer 33 elapsed time observations of earth bow shock
02 p0244 A69-12299
- European space programs requirements for satellite launch autonomy/independence from U.S. and U.S.S.R., discussing satellite applications for resource surveys, weather forecasting, etc
02 p0335 A69-12682
- OSO-B2 satellite zodiacal light observations at constant 90 degree elongation, measuring polarized component as function of time
02 p0245 A69-12718
- Solar atmosphere from two dimensional study of solar spectrum, discussing satellite observations of corona and upper chromosphere
02 p0329 A69-12785
- High energy cosmic ray particles observed with SEZ-14 instrument aboard Proton 1 and 2 satellites
03 p0499 A69-12944
- Infrasonic waves recordings from Saturn 5 vehicle, observing signal reversal occurrence
03 p0509 A69-13358
- Elektron 2 satellite magnetic measurement of high latitude nocturnal magnetosphere, discussing variations, antisolar effect and elongation of magnetic field
03 p0422 A69-13505
- Angular and spectral distribution of earth IR radiation near horizon from satellite observation and spectrograms
03 p0422 A69-13506
- Latitude dependence of earth spectral radiation intensities, discussing satellite observations in equatorial and subtropical regions
03 p0422 A69-13507
- Topside ionosphere composition data by energy spectrometer on satellite Ariel 1, discussing positive ions and diurnal, seasonal and secular variations
03 p0424 A69-13806
- Low energy electrons on day side of magnetosphere observed with MIT electron detector on OGO 3 satellite
03 p0503 A69-14027
- Midlatitude nighttime total ionospheric electron content during magnetically disturbed periods from geostationary satellites Canary Bird and ATS 3
03 p0426 A69-14030
- Ground coverage of oblate planets by spin stabilized satellites, determining ground areas visible to satellite by solution of quadratic equations
03 p0522 A69-14244
- Satellite data for reevaluating extraterrestrial particles origin found in polar ice, atmosphere and terrestrial surface collections
04 p0654 A69-14655
- Portable amplitude and frequency recording system for studying ionosphere by radio signals from artificial satellites
04 p0597 A69-14748
- Outgoing radiation field based on interpretation of broad sector radiometer measurements made from meteorological earth satellites
04 p0627 A69-15032
- Space radio astronomy techniques for problems in galactic radio emission, solar studies and planetary observations
05 p0821 A69-15844
- Space observations needed for solar flares study
05 p0814 A69-15859
- Space observation of flare sprays and solar limb surges, stressing X ray research
05 p0814 A69-15860
- UV solar spectra observation, discussing coordination of ground based and satellite programs
05 p0822 A69-15861
- Space photography to provide synoptic sedimentary environmental data analysis, discussing orbital sensing advantages
05 p0753 A69-15993
- Elektron satellite recorded sporadic radio emission noting relationship to geomagnetic disturbances and dependence on satellite position
05 p0824 A69-16059
- Moon effect on intensity and angular distribution of energetic electron and proton shadowing as observed by Explorer satellites
05 p0824 A69-16252
- Continuous and triggered audio frequency noise bands associated with ionospheric lower hybrid resonance frequency observed on OGO 2
05 p0754 A69-16257
- Magnetic disturbance vector distribution during polar magnetic substorm
05 p0755 A69-16271
- Solar wind electron component detection by plasma experiment on Pioneer 6, particularly class 2B flare and quiet period
05 p0816 A69-16275
- Explorer 35 measurements of low energy plasma in lunar orbit made by planar multigrad sensor programmed as retarding potential analyzer
05 p0825 A69-16278
- Langmuir probe experiment measurement of upper region electron temperature on Explorer 32 conflict with Jicamarca Radar Observatory measurements
05 p0756 A69-16283
- Lower ionospheric diurnal variations in electron density observed by beacon satellite, noting effect on high power VHF forward scatter circuits
05 p0757 A69-16405
- Atmospheric vertical density and pressure profiles determined from satellite measurements of light beam phase shift and refraction angle
05 p0760 A69-16694
- Satellites role in observing and forecasting global atmospheric behavior, discussing World Weather Watch and Global Atmospheric Research Program
06 p0916 A69-16854
- Earth resource information from spacecraft including landmapping, geological photographs, hydrological and oceanographic data, etc
06 p0916 A69-16855
- Photomultipliers response to energetic particles in terms of background current using data from OGO experiments
06 p0923 A69-16932
- Cosmic dust concentration in interplanetary space near earth, noting suitability of satellite observation
06 p0999 A69-16971
- Mass influx and penetration rate of meteor streams
06 p1000 A69-17007
- Soviet satellite exploration of space magnetic fields and charged particles, noting Proton satellites and protons and carbon nuclei inelastic interactions
[UN PAPER 68-95768] 06 p0986 A69-17031
- Satellite actinometric data computerized reduction in U.S.S.R., examining computer program features
[UN PAPER 68-95763] 06 p0916 A69-17038
- Onset and development of typhoons observed by Cosmos satellites using TV type IR apparatus
[UN PAPER 68-95774] 06 p0949 A69-17039
- Atmospheric heat sources and heat sinks distribution based on Cosmos satellite data
06 p0949 A69-17048
- Processing TV cloud data monitored by Molniya 1 and Meteor meteorological satellites, discussing computer interpretation of TV photographs
[UN PAPER 68-95759] 06 p0950 A69-17060
- Rectangular space coordinates for points on earth determined from observations of directions and distances to and from satellites
[UN PAPER 68-95265] 06 p0917 A69-17064
- Earth resource satellites, discussing world ground station network for data reception and information dissemination and training and research center
[UN PAPER 68-95529] 06 p0917 A69-17067
- Economic and scientific reasons for using artificial satellites to establish continental geodetic network, noting continental displacements and terrestrial pole motion observations
[UN PAPER 68-07445] 06 p0917 A69-17069
- French program of space geodesy, discussing spatial triangulation, telemetry, dynamic geodesy, Diapason and Diademe experiments
[UN PAPER 68-95834] 06 p0917 A69-17071
- Eole meteorological satellite secondary use, discussing cosmic rays monitoring, navigation purposes and oceanographic research
[UN PAPER 68-95833] 06 p1013 A69-17077
- Attitude stabilization for astronomical satellites
06 p1015 A69-17588
- Mathematical techniques for treating satellite based atmospheric data involving radiative transfer equation inversion, noting scattering and temperature measurement problems
06 p0957 A69-17618
- Vertical ozone distribution in upper atmosphere from satellite measurements of UV solar radiation scattering by solving integral Laplace equation
06 p0996 A69-17733
- Soviet papers on satellite meteorology covering equipment onboard meteorological satellites, data processing, photograph interpretation, etc
06 p0951 A69-17976
- Ground, aircraft and spacecraft actinometric data compared for clear sky
06 p0951 A69-17982
- Interpretation of IR cloud images transmitted by Nimbus 1 and Cosmos 122 satellites, using radiation temperature contrasts
06 p0952 A69-17984
- Lower atmosphere pressure field determination based on meteorological satellite observations of amount and types of clouds and upper boundary altitude
06 p0952 A69-17987
- Relation between satellite data concerning thermal microwave radiation and meteorological conditions in lower atmosphere for possible use in weather forecasting
06 p0953 A69-17995
- Atmospheric measurements from satellites, discussing ATS-1 cloud images for definition of wind and use of WEFAX through ATS 2 satellites for data transmission
[AIAA PAPER 69-158] 06 p0954 A69-18038
- Venusian atmosphere model developed from satellite and earth based radar data for environmental criteria in spacecraft design and mission planning
[AIAA PAPER 69-51] 06 p1011 A69-18096
- Radio occultation measurements of planetary atmospheres and ionospheres from orbiting parit
[AIAA PAPER 69-53] 06 p1011 A69-18104
- Remote sensing platform requirements for oceanographic and meteorologic observations, discussing orbital and aircraft platforms
[AIAA PAPER 69-154] 06 p1044 A69-18122
- Electron density distribution stationary with respect to sun determined by Alouette 1 measurements over winter pole, noting relation to high density plasma
06 p0922 A69-18224
- Satellite and aircraft radiation measurements in cm and mm wavelength range to provide information on underlying surfaces
07 p1130 A69-18257
- Visible radiation scattering around Venus spherical atmosphere computed on basis of Venus 4 and Mariner 5 data
07 p1213 A69-18609
- Optical device for measurement of temperature changes with height in upper atmosphere by rockets or satellites
07 p1132 A69-18676
- Micron and submicron particle cumulative flux upper limits in satellite micrometeoroid environment of Gemini 12
07 p1215 A69-18845
- Solar wind, bow shock and magnetosheath observations by charged particle analyzers on Vela satellites
07 p1208 A69-19361
- Particle measurements by Vela nuclear test detection satellites /2A and 2B/ noting plasma sheet in center of magnetotail
07 p1208 A69-19362
- Structure, temporal behavior, shape and length of earth magnetic tail via satellite mapping
07 p1208 A69-19363

Geomagnetic tail topology, reconnection and interaction with moon from Explorer 33 satellite data
07 p1128 A69-19365

Particle dynamics measured by ATS satellite synchronous orbit, discussing flux time variations during geomagnetic disturbances
07 p1209 A69-19371

Bow shock and magnetopause boundary observations with IMP 2 plasma detector
07 p1129 A69-19372

Low energy electrons in magnetosphere from OGO-1 and OGO-3 observations, discussing plasma sheet, magnetic bay activity, electron pressure, temperature and density gradient
07 p1209 A69-19373

Observability theory of dynamic objects application to composing measurements for space flights, solving parametric observability problem
07 p1087 A69-19605

Magnetospheric magnetic field ring current asymmetry during different phases of geomagnetic storm observed by Explorer 26 and Vela 2 satellites
07 p1129 A69-19611

Solar corona X ray emission during flares and under quiet sun conditions investigated by satellite with X ray heliograph
07 p1210 A69-19614

Cosmic radio noise intensity measurements by ATS 2 satellite-borne radiometer
07 p1224 A69-19715

Ballistics room of Royal Belgian Observatory for observation of geodetic satellites
08 p1272 A69-19993

Solar proton monitoring by particle detectors on-board rockets and IMP satellite
08 p1318 A69-21142

Cosmos 92 satellite observation of night airglow flare, discussing NO bands emission and origin
09 p1485 A69-21533

Geomagnetic secular variations calculated by comparison of satellite, oceanic and aeromagnetic surveys
09 p1485 A69-21534

VLF emissions intensity and spectra variations compared with energetic electron fluxes variations during magnetosphere storm periods
09 p1488 A69-21698

Irregular regions in Antarctic ionosphere from Polar Ionosphere Beacon Satellite S-66 recordings, obtaining irregularities density from nulls clarity
09 p1490 A69-21716

Elektron 4 satellite radio emission data transmitted from July to December 1964, noting month-to-month variations in mean radiation level
09 p1578 A69-21776

Atmospheric density profile from satellite measurements of light wave phase and refraction angles, discussing ionospheric, water vapor and diffraction effects on errors
09 p1490 A69-21862

Spin stabilized spherical satellite in high elliptical orbit for lower thermosphere measurements during entire solar cycle
09 p1610 A69-22009

Helium-like ion resonance satellite lines in laboratory and solar plasmas, noting coincidence between solar satellite energy and energy level interval
09 p1598 A69-22158

Solar extreme UV, soft and hard solar X rays, cosmic X rays and gamma rays, cosmic ray particles and near earth visible radiation observed by OSO-3
09 p1578 A69-22167

Solar far UV emissions observed from OSO-C by grazing incidence grating spectrometer, noting temporal variations and atmospheric absorption characteristics
09 p1578 A69-22168

Solar and cosmic X rays observed by OSO-C, stressing galaxy M 87 upper limits and Lupus XR-1 power law spectral form
09 p1578 A69-22171

High energy protons, helium and gamma rays observed by particle telescope on board OSO-C, obtaining integral rigidity spectra of proton and helium nuclei
09 p1579 A69-22172

Sudden commencement associated discontinuities in interplanetary magnetic field observed by 3 satellite, stressing shocks and tangential and rotational discontinuities
09 p1598 A69-22183

Meteorological observation problems from satellites, considering lower atmosphere measurements and accuracies
09 p1537 A69-22690

Auroral electrojet precursors and geomagnetic variations before onset of bays, noting satellite observations
10 p1681 A69-22804

Satellite data on relative flux and group composition of heavy nuclei in primary cosmic rays
10 p1756 A69-22820

Secondary emission in low altitude satellite body dependent on inelastic collisions with primary cosmic ray protons
10 p1757 A69-22821

Diffusion coefficient and cosmic ray motion in solar system, using satellite data of interplanetary magnetic field
10 p1757 A69-22822

Forbush decreases spectra in low energy region from satellite measurements of neutron and hard component of cosmic rays
10 p1758 A69-22829

Solar research from rockets and satellites, considering solar instruments including EUV spectrographs
10 p1772 A69-22867

Apollo 7 and weather satellite observation photographs of hurricane Gladys and typhoon Gloria
10 p1722 A69-22944

Spectral intensity of high energy solar X rays observed during July 7, 1966 polar event with satellite OGO 3, suggesting nonthermal bremsstrahlung origin
10 p1766 A69-23753

Solar X ray flare of July 7, 1966 with Explorer 33 satellite attributed to McMath plage region 8362, discussing solar and cosmic radio noise
10 p1766 A69-23754

Time dependence, anisotropy and spectral composition of cosmic radiation generated during series of flares during July 5-20, 1966 by Pioneer 6 observations
10 p1768 A69-23769

Simultaneous interplanetary magnetic field measurements by geocentric satellites Explorer 33 and IMP 3 of MHD shock wave associated with July 8, 1966 sudden storm commencement
10 p1783 A69-23773

Protons emitted by July 7, 1966 solar flare observed by low altitude high latitude Injun 4 satellite
10 p1768 A69-23778

Subauroral traveling ionospheric disturbances and fading due to diffraction observed by geostationary satellites
10 p1685 A69-23831

Visual observation of aerospacecraft, discussing object luminance, eye contrast sensitivity, atmospheric contrast transmission function and psychophysiological and atmospheric effects
10 p1649 A69-23872

Excess radiation in equatorial regions studied on-board Cosmos 137, noting contribution of primary particle multiplication to secondary radiation
10 p1783 A69-23922

Venus atmosphere observations compared with Venera 4 measurements of temperature, pressure and carbon dioxide content
10 p1791 A69-24200

Solar wind flux near earth observed by Venera 2 /1965/ and Venera 4 /1967/ probes, noting solar activity effects
10 p1771 A69-24201

Radio astronomical observations of Venus atmosphere interpreted noting agreement with model based on Venera 4 data
10 p1791 A69-24202

Denser material beneath lunar maria revealed by precise tracking of lunar orbiting spacecraft, discussing geology and evolution
11 p1953 A69-24339

Time registration delays during photographic observations of satellites, describing NAFA type satellite camera and mechanical and electrical systems
11 p1880 A69-24365

Satellite photographic astrometry and chronometry, determining spatial positions of satellites and observation stations by space triangulation
11 p1956 A69-24400

Remote geoscience sensing using properties of radar return noting scatterometry, imagery, altimetry and penetration measurements
11 p1835 A69-24692

Imaging radar systems for employment on small spacecraft, fabricating small lightweight radar systems packages with integrated circuit techniques
11 p1835 A69-24695

Soviet collection of articles on satellite data interpretation and use for meteorological services
11 p1911 A69-24824

Chemical composition of Venusian atmosphere by Mariner and Venera satellites, comparing upper atmospheres of Venus and earth
11 p1960 A69-24971

Ionospheric electron content gradients from Faraday rotation observations of radio beacon satellites for direction finding of HF radio waves
11 p1837 A69-25004

Satellite measurements of suprathermal electrons at conjugate sunrise, indicating photoelectron escape from production level and movement along geomagnetic lines into conjugate ionosphere
11 p1950 A69-25144

Anisotropic fluxes of energetic particles in and near distant trapping region encountered by Explorer 33 satellite in outer magnetosphere
11 p1950 A69-25146

Solar flare and magnetic storm signals from ATS geostationary satellite on May 28, 1967, deriving total electron content
11 p1951 A69-25161

Color TV system for Earth Resources Observation Satellite /EROS/, discussing resolution in relation to spectral separation through data simulation study [SMPT PAPER 105-79]
12 p2077 A69-25767

Planetary imaging systems design problems illustrated by Mars orbiter reconnaissance, discussing radiation effect on film, shielding, stereo method comparisons, color bands, etc [SMPT PAPER 105-78]
12 p2078 A69-25770

Low light level slow scan Owl TV camera system with secondary electron conduction camera tube for satellite-borne observation of auroral light emission
12 p2079 A69-25904

Theories for universal time controlled polar F region reevaluated in light of satellite low energy charged particle observations
12 p2065 A69-26103

Meteorology and space vehicle capabilities noting earth, outer space and earth atmosphere observations and measurements, relaying telecommunication signals, etc
12 p2126 A69-26126

Martian crater density determined by comparison of statistical counts from Mariner 4 photographs
12 p2157 A69-26309

Collection of Soviet papers on satellite observations covering geodetic applications, orbital mechanics, atmospheric measurements, etc
12 p2067 A69-26424

Earth center of mass determination from simultaneous satellite observations by photography or laser radar
12 p2068 A69-26425

Spatial direction determination from simultaneous photographs of Echo 2 at Nikolaev and Helwan stations, using circle of simultaneity
12 p2068 A69-26427

Geocentric orientation of quasi-geocentric coordinate network determined from simultaneous photographic satellite observations, using gravity force values
12 p2158 A69-26429

Earth stations coordinates determination from non-simultaneous photographic satellite observations by orbital method compared with simultaneous photographic observations of Echo 1
12 p2068 A69-26430

Cosmic triangulation by geometrical synchronization of astrometric satellite observation, with precise times unavailable
12 p2158 A69-26433

Coupled geodetic triangular grids obtained using satellite observations for azimuths
12 p2069 A69-26433

Subsatellite point velocity determination by interpolation method using observation data without knowledge of orbital elements
12 p2158 A69-26435

Satellite celestial equator intersection time calculation from visual satellite observation near equator including satellite draconic period determination, particularly for high altitude
12 p2069 A69-26438

Cosmos 17 and 44 draconic periods of rotation, discussing period variations determination from visual observations
12 p2173 A69-26439

Soviet satellites rotation periods from processing of photometric observations
12 p2069 A69-26440

Anomalous satellite periods of rotation from successive observations at same topocentric parallel
12 p2158 A69-26441

Draconic periods changes of satellites 1963 53A and 1964 76A, based on observations
12 p2174 A69-26446

Solar chromospheric flares effect on temperature of upper atmosphere observed by satellite at perigee altitude

12 p2149 A69-26447

Computer program in ALGOL for computing satellite ephemerides applicable to satellites with direct or retrograde motion observed in Northern or Southern Hemispheres

12 p2159 A69-26448

Budapest University satellite radio observation APT station design, equipment and methods

12 p2059 A69-26449

Observatory camera for satellite observation, discussing objective focusing and diameter and manual/automatic operation

12 p2092 A69-26450

Cosmic radiation recorder designed for use onboard satellite to measure intensity space-time distribution under geomagnetic effect

12 p2094 A69-26697

Satellite observations of geomagnetic tail in magnetosphere near midnight meridian plane, discussing formation, shape, plasma sheet and models

12 p2072 A69-26739

Orbit determination from satellite using linear combinations of time of flight measurements and based on expansion of satellite law of motion

12 p2159 A69-26778

Meteorological application of ATS observations in form of time lapse movies of weather in motion, describing camera and data flow [AIAA PAPER 68-1094]

12 p2174 A69-26804

Space research in U.S.S.R. including Venera 4 soft landing mission to measure temperature, pressure, density and atmospheric composition of Venus

12 p2160 A69-26921

Solar-terrestrial environment, discussing mathematical development of solar wind, satellite measurement, magnetic storms, aurora and cosmic rays

12 p2161 A69-26941

Satellite observation of intensity and distribution of VLF emission at medium latitude during magnetic storm interpreted by transverse resonance plasma instability

12 p2073 A69-26947

Earth resources remote sensing from spacecraft noting meteorology, oceanography, forestry, agriculture and IR detection of plant diseases and pollution

12 p2192 A69-26978

Correlation spectrometer for air pollution surveillance from airborne and spaceborne platforms, noting scanning satellite system for continuous global coverage

12 p2096 A69-26981

Geographic and cartographic mapping applications of remote sensor data from orbital heights, discussing hardware, instrumentation, NASA role in data selection, etc

12 p2192 A69-26984

Tenuous cirrus cloud influence on 6.4-6.9 micron Nimbus 2 water observations, discussing equivalent black body temperatures correspondence to cloud and clear areas

12 p2075 A69-27003

Airborne and satellite IR survey over active effusive eruption at Surtsey, Iceland, comparing thermal energy yield and radiant emission to ground measurements

12 p2076 A69-27011

Star twinkling absence for lunar observation laboratory, noting star distance measurement and laser action in stellar atmospheres

12 p2173 A69-27172

Collection of Soviet papers on U.S.S.R. outer space studies /1957-1967/ covering rocket and satellite sounding, meteorology, radiation belts, etc

13 p2335 A69-27346

Van Allen radiation belts proton and electron components recorded by Soviet lunar probes and Cosmos and Elektron satellites

13 p2326 A69-27350

Cosmic rays during 11-year solar cycle, short term variations and radial gradient based on Luna, Zond and Venera probes and Cosmos observations

13 p2326 A69-27351

Soviet satellite and probe studies of earth, moon, Venus and Mars magnetic fields, noting automatic magnetometer

13 p2336 A69-27352

Interplanetary plasma measurements by Luna, Mars 1, Zond 2 and Venera 3 probes, including solar plasma flux energy spectra diagram

13 p2336 A69-27354

Solar radiation in short wave, UV and X ray range recorded by rockets, probes and satellites, notably Elektron 2 probe

13 p2326 A69-27355

Soviet and foreign visual, photographic and photometric ground observations of satellites, emphasizing synchronous optical observations role in geodesy and geophysics

13 p2219 A69-27357

Sky mapping in IR, using IR photometer on TD1 ESRO satellite

13 p2260 A69-27606

Venusian atmospheric pressure and temperature measurements by Venera 4 probe, noting agreement with Mariner 5 observations

13 p2345 A69-27689

Greenhouse effect in Venusian atmosphere, discussing cause of vertical temperature distribution established by Venera 4 probe

13 p2345 A69-27690

Venus atmosphere optical properties on basis of Venera 4 data, proposing models for measured rotational temperature and subcloud atmosphere radiative equilibrium

13 p2345 A69-27691

Fast charged particles measurements by Cerenkov counter in Cosmos 137 satellite, noting hard electron flux and cosmic ray radiation spectrum

13 p2327 A69-27693

High latitude capture region boundary for electrons in upper radiation belt determined relative to current electrojets in ionosphere from satellite observations

13 p2327 A69-27700

Collection of articles on satellite meteorology including vertical air motions, clouds and radiation fields

13 p2291 A69-27723

Radiation measurements by Cosmos 122 satellite over various regions, determining radiation temperature, long wave heat flux and albedo

13 p2291 A69-27726

Radiation fields and large scale atmospheric disturbances analyzed, using radiation maps from Cosmos satellites

13 p2291 A69-27727

Auroral phenomena investigation by ESRO 1 satellite, measuring particle flux arriving at auroral height

13 p2381 A69-27748

Auroral luminosity determination by two photometers on ESRO 1 satellite

13 p2253 A69-27752

Global coverage of positive ion composition and temperature, and electron density and temperature measurements during AURORAE mission of ESRO 1 satellite

13 p2253 A69-27753

ESRO 1 satellite measuring proton intensities and energy spectra of precipitated and magnetically trapped electrons

13 p2327 A69-27754

Electron and proton spectra in 1-13 keV range relative to geomagnetic field lines measured by ESRO 1 satellite during Aurorae mission

13 p2328 A69-27755

Medium energy trapped and dumped protons at high latitudes and auroral zone, using semiconductor radiation detectors on ESRO 1 satellite

13 p2328 A69-27756

Nimbus D meteorological satellite construction, control system, orbit, etc

13 p2356 A69-27832

European earth resource satellite systems technology, applications and costs

13 p2356 A69-27833

Corrections for atmosphere thickness needed for satellite measurements of underlying surface temperature

13 p2293 A69-27850

Radar and satellite TV clouds observation in meso and macroscale cloud systems

13 p2294 A69-27853

Scientific aims, optical design, instrument data, control and orbit operation of European Large Astronomical Satellite used in UV observations

13 p2264 A69-28477

Lunar surface gamma radiation observed by Luna 10 spectrometer, suggesting basalt-like minerals composition of lunar maria

13 p2333 A69-28635

Ion concentrations and temperature measurements by magnetic trap on Cosmos 5 between 1000-1200 km

13 p2333 A69-28687

Solar proton flux in two energy intervals measuring by ATS detectors during January 1967 event compared with data from satellites outside magnetosphere

14 p2509 A69-28935

Ionospheric electron and ion temperatures correlated with electron concentration profile as measured by rockets and satellites

14 p2510 A69-28942

Sporadic E layer cloud configuration study based on explorer 20 satellite observations, discussing W echoes

14 p2434 A69-28943

Ionograms in vertical depletion duct in horizontally stratified isotropically refractive plasma, considering vertical propagation and ray paths traces dependence on electron concentration

14 p2434 A69-28945

Large amplitude pulsations in magnetic field magnitude and proton fluxes observed by satellite during magnetic storm compared with various models

14 p2434 A69-28947

Correlation coefficients between radial components of interplanetary magnetic field and solar wind velocity from Mariner 5 data due to Alfvén waves

14 p2510 A69-28949

High latitude ionization spikes observed by POGO spacecraft, noting frequency correlation with magnetic disturbances and development by high energy electron injections

14 p2511 A69-28950

Suprathermal electrons energy distributions as function of magnetic latitude in polar ionosphere obtained by Explorer 31 satellite observation

14 p2512 A69-28963

Tangential solar wind discontinuity observed by Vela 2A satellite, producing ground magnetic disturbances conjunctively with magnetospheric, ground and ionospheric currents

14 p2512 A69-29041

Night airglow variations observed during Cosmos 92 satellite orbits, determining atmospheric albedo wavelength dependence for solid and medium cloudiness and clear skies

14 p2435 A69-29042

Error correction for correlation coefficient between satellite data of earth radiation intensity and satellite vision field shift

14 p2435 A69-29043

September 14, 1966 magnetic storm observation by Explorer 33 in geomagnetic tail and by polar stations, studying relation in magnetosphere and on earth

14 p2438 A69-29078

Sporadic electron flux contribution to high latitude geomagnetic disturbances at outer radiation belt boundary estimated from Elektron 1 and 2 observations

14 p2438 A69-29079

Rocket and satellites topside sounding of earth ionosphere, determining magnetoplasma structure and resonance

14 p2438 A69-29101

Electron density profiles in outer ionosphere and integral of electron density measured with coherent radio waves emitted from Electron satellite

14 p2438 A69-29106

Polar cap absorption riometer recorded during 2-6 September 1966 event compared to satellite measurements of solar protons, discussing diurnal variations and oxygen role in associative detachment reactions

14 p2440 A69-29126

Monograph on reduction of satellite data using fixed stars covering ALGOL programming for computing satellite direction from photographic model

14 p2446 A69-29286

Saturated signals of GM counter from solar radiation monitoring satellite, showing Van Allen belt high energy particle origin

14 p2514 A69-29383

Geomagnetic storm induced temporary radiation zones located by determining Explorer 30 attitude and spin axis orientation

14 p2514 A69-29384

Worldwide observation of atmosphere with occultation satellites, correcting orbit perturbations to obtain air pressure

14 p2447 A69-29517

Radio wave reflections from edge of large scale depressions of ionospheric electron density observed by topside sounding satellites, discussing ionogram recordings

14 p2415 A69-29521

Radar radiometer by adding radar to scanning microwave radiometer, discussing applications to spacecraft measurement of oceanic winds, waves and precipitation

14 p2421 A69-29528

Micrometeoroid showers proximity to epsilon Leonid showers in earth orbit, analyzing Helfenzreider comet role from satellite data

14 p2522 A69-29588

High and low latitude cellular cloud patterns observed by meteorological satellites, noting frequent occurrence over oceans

14 p2473 A69-29727

Cloud pattern characteristics in intertropical convergence zone above Indian and Pacific oceans from meteorological satellite photographs and cloud formation maps

14 p2473 A69-29728

Satellite radiation maps for synoptic analysis regarding world weather maps, discussing front, intertropical convergence zones and typhoon location

14 p2473 A69-29729

Meteorological elements variation from measuring earth radiation in different spectral regions by satellites, determining temperature and humidity profiles

14 p2477 A69-29828

Radio propagation in upper atmosphere and ionosphere noting rocket and satellite experiments including plasma physics research, tropospheric studies and space science services

14 p2526 A69-29854

Discontinuities in interplanetary magnetic field direction presented on mesoscale from Pioneer 6 observation, emphasizing distribution in time

14 p2528 A69-29970

Solar wind Helmholtz-type velocity discontinuities, noting plasma density and temperature stabilities from Explorer 34 observations

14 p2515 A69-29971

Solar wind existence verified by direct measurements of interplanetary magnetic field and plasma, reviewing solar corona studies by satellites and space probes

15 p2679 A69-30010

IQSY low energy galactic and solar cosmic ray observations made by various satellites and space probes, including hydrogen and helium energy spectra

15 p2673 A69-30014

Satellite radio observation for ionospheric parameters, utilizing Doppler and Faraday phenomena, signals fluctuations and sporadic phenomena

15 p2594 A69-30028

Artificial earth satellites positional observations by graphical smoothing on azimuth and altitude, discussing advantages for space geodesy

15 p2594 A69-30029

Satellite triangulation by least squares method based on conditions relating to observing stations coordinates, concerning synchronous observations of directions and distances

15 p2594 A69-30030

Satellite observation of ocean surface and subsurface features, discussing onboard equipment and proposed orbits

15 p2607 A69-30190

Bidirectional reflectance of solar radiation and IR temperature data from Nimbus 2 satellite to differentiate clouds above snow surfaces

15 p2596 A69-30455

Spacecraft radar altimetry with application to geodesy, discussing orbit and tracking errors

15 p2609 A69-30460

Spacecraft radar altimetry applied to study of sea surface slopes, tides, tsunamis, storm surges and submarine geology

15 p2609 A69-30461

Extraatmospheric long and short wave radio astronomy since first artificial satellite, including device carriers effectiveness of earth satellites, lunar orbiters, rockets and balloons

15 p2682 A69-30504

Solar corpuscular radiation component from satellite and interplanetary space probe geophysical data, discussing interplanetary magnetic field geometry and corpuscular fluxes

15 p2684 A69-30516

Astronomical UV radiation observation by OAO 2 satellite, discussing solar images, corona, chromosphere and UV spectrum, stellar evolution, etc

15 p2689 A69-30597

Temperature of underlying surface and moisture content of atmosphere from satellite thermal radio emission measurements

15 p2648 A69-30641

Earth thermal emission intensity measured by two beam radiometer onboard Cosmos 149, noting discrepancy between empirical and theoretical transfer functions of atmosphere

15 p2596 A69-30651

Micrometeorites acoustic recordings on Cosmos 135, investigating data reliability influences by appearance of thermal noise

15 p2691 A69-30748

Antenna, frequency converter and automatic spectrum recorder system for closest approach times prediction and satellite identification, discussing errors

15 p2569 A69-30800

Radio wave absorption by water vapor in Venusian and Martian atmospheres, constructing model from Venera 4 data

15 p2569 A69-30952

ESRO 1/Aurora satellite for Arctic ionosphere and aurorae observation, discussing electrons and protons measurements and auroral photometry

15 p2702 A69-31081

Monograph on large scale cloud distribution in extratropical low pressure regions, using classical meteorological observations and Tiros weather satellites data

15 p2650 A69-31212

Scintillation of ground based spherical wave laser source viewed from space analyzed from Geos 2 satellite laser tracking, noting stellar scintillation correspondence

15 p2570 A69-31309

Rapid orbit prediction method for planning satellite observation programs, considering oblateness and radiation pressure effects

15 p2697 A69-31310

Magnetic storm effects on electrons and protons in outer belt, using satellite data for intensity and differential energy spectra

15 p2676 A69-31314

Cloud distribution effect on global coverage of remote radiometric sounding of atmosphere, considering Nimbus 1 and 2 data

15 p2650 A69-31335

Satellite orbits obtained by tracking by synchronous satellites, discussing accuracy for low altitude satellites

15 p2698 A69-31340

Lunar surface features as observed by orbiting and landing craft, discussing particle layer, rocks, craters, effects of erosion, meteorite impact, etc

15 p2698 A69-31356

Radio wave scattering characteristics of lunar surface in 3 cm wavelength by Luna 8 and Luna 9 automatic stations and Surveyor spacecraft

15 p2571 A69-31359

Comparisons and combinations of geodetic parameters from dynamic and geometric satellite solutions and Mariner flights

15 p2600 A69-31362

Solar corona observed by X ray instrumentation of SOLRAD 8 satellite crossing moon penumbra during solar eclipse of 20 May 1966

15 p2698 A69-31363

Space direction by compensation method of cosmic triangulation network, using laser and optical observations of artificial satellites

15 p2699 A69-31377

Atmospheric density measurements by triaxial accelerometer system, ionization gauges and orbital decay of OV1-15 satellite

15 p2602 A69-31384

Low altitude atmospheric density satellite OV1-16 measurements, showing agreement between onboard accelerometer and orbital drag data

15 p2602 A69-31385

European geostationary satellite orbit inclination and eccentricity modification for maximum observation time of Northern Hemisphere by high resolution IR radiometer

15 p2650 A69-31389

Photoelectric photometry of artificial satellites noting equipment, Pegasus satellite observations and light curves from Cosmos 151, 192 and 220

15 p2616 A69-31391

Picogram dust particle flux in selenocentric space measurement by Lunar Explorer 35, showing enhancement during meteor showers

15 p2699 A69-31396

UV OGO observations of atomic hydrogen and oxygen in airglow, comparing results to exospheric models of hydrogen geocorona

15 p2603 A69-31400

Geocoronal Lyman alpha short term and 27-day variations observed by OGO 4 spacecraft attributed to flux variability at solar emission line center

15 p2699 A69-31404

Ion whistlers recorded by Alouette 2 VLF receiver providing information on ion composition of terrestrial ionosphere, showing variation with latitude and relationship to solar cycle

15 p2604 A69-31410

OGO 5 satellite measurements of intensity and width of Lyman alpha line scattered by hydrogen geocorona

15 p2699 A69-31412

ISIS A satellite fixed and sweep frequency ionograms indicating electron density variations, ionospheric resonances and Cerenkov radiation

15 p2604 A69-31416

Israel research on space data for meteorological purposes, describing automatic picture transmission data and errors in surface temperature determination by satellite radiometry

15 p2650 A69-31422

Faraday rotation measurements of signals from Explorer 22 analyzed to determine scintillation boundary in auroral ionosphere

15 p2605 A69-31443

British rocket and satellite experiments in space research, considering neutral atmosphere, ionosphere and solar radiation, orbital analysis, etc

15 p2724 A69-31463

Plasma flow pattern in twilight regions of earth magnetosheath from positive ion observations of twin Vela 3 satellites

16 p2773 A69-31961

Solar wind direction by analysis of data from IMP 1 satellite, noting anticorotation tendency

16 p2847 A69-31962

Interplanetary magnetic field radial dependence from Mariner 4 measurements between earth and Mars, indicating fluctuations produced by dynamic processes in solar wind

16 p2856 A69-31964

Solar energetic proton penetration into magnetotail from proton data collected by Vela 4 energetic particle telescopes, comparing proton fluxes inside and outside magnetotail

16 p2847 A69-31966

Solar protons nonuniformity over polar caps observed by OGO 2 ionization chamber during 24 March 1966 solar proton events

16 p2848 A69-31967

Banded chorus, VLF discrete emissions in magnetosphere in single variable frequency band with frequency depending on equatorial electron gyrofrequency

16 p2774 A69-31981

Lunar magnetic field measurements by Mariner 4 near sun-moon line extension, discussing search for lunar wake

16 p2856 A69-31986

Explorer 33 and Explorer 35 observations of solar flare of 8 July 1969 soft X rays, discussing absolute flux

16 p2849 A69-31988

Atmospheric density at 130-160 km measured from satellite 1968-59B orbit, noting agreement with CIRA 1965

16 p2776 A69-32095

Monograph on photogrammetry in satellite geodesy including photogrammetric measurement of satellite positions, German observation stations and work done in U.S., U.S.S.R. and France

16 p2790 A69-32202

Satellites meridian and extrameridian observations by transit instrument, examining errors in ephemerides of bulletins

16 p2858 A69-32211

Dim astronomical sources observability from sunlit spacecraft, considering coma of micron sized ice crystals influence on scattering by condensation model

16 p2861 A69-32301

Interplanetary magnetic fields from Explorer 33 magnetometer relationship to surface geomagnetic variations emphasizing unified view

16 p2862 A69-32309

Cosmos 92 satellite observation of night airglow flare, discussing NO bands emission and origin

16 p2783 A69-32528

Geomagnetic secular variations calculated by comparison of satellite, oceanic and aeromagnetic surveys

16 p2783 A69-32529

Ozone and temperature profiles influence on atmospheric radiation intensities measurement by satellite in five spectral regions, noting pressure broadening effect

16 p2786 A69-32633

Atmospheric optical density vertical distribution curves in near UV from spectrophotometer data of Echo type satellites entry into earth shadow

16 p2787 A69-32638

Ozone vertical distribution in upper stratosphere determined from OGO 4 observations, describing calibration of satellite data and onboard instrumentation

16 p2788 A69-32645

Faraday rotation measurements in ionosphere by geostationary satellite ATS-3 as evidence of considerable nighttime electron transport

17 p2959 A69-32926

Survey of six year period of satellite observed tropical Pacific cloud mapping

17 p2996 A69-33001

Sudden phase anomalies on radio paths compared with calculated results for satellite observed solar X ray flux intensities to explain sudden ionospheric disturbances

17 p2959 A69-33006

D-2 satellite stabilization system design and development, noting mission to determine hydrogen distribution around earth

17 p3046 A69-33223

French space geodesy since Space Age, detailing Diapason and Diademe satellites program, techniques and results

17 p2961 A69-33382

Collision free earth shock wave gross and fine structure deduced from OGO 5 plasma diagnostics [AIAA PAPER 69-676]

17 p2961 A69-33452

Tropical storms wind speeds related statistically to characteristics as pictured from satellites

17 p2997 A69-33690

Daily European weather surveys based on pictures transmitted by satellite during fourth quarter 1967

17 p3000 A69-33778

Lower ionosphere electron concentration confirmed as function of electron and ion temperature by satellite and probe data

17 p2966 A69-33981

Solar soft X ray bursts observed by Solrad 8 satellite, considering relationship to microwave radio bursts

17 p3025 A69-34055

Vertical tropospheric humidity distribution estimation from IR spectra obtained by TIROS satellites

18 p3126 A69-34284

Lunar origin, geological composition and water existence controversies from data gathered by various lunar probes

18 p3196 A69-34631

Ground data operations system for large astronomical satellite comprising UHF telemetry, PCM telecommand and processing and display equipment

18 p3117 A69-34794

Ion depletion in high latitude exosphere, considering OGO 2 simultaneous observations of positive ion concentration, VLF signal propagation and whistlers

18 p3187 A69-34939

Earth bow shock waves in far upstream interplanetary medium observed from magnetic data of Explorer 34 satellite

18 p3199 A69-34941

Sea surface temperature remote sensing by Nimbus 2 satellite using TV camera and medium and high resolution IR radiometer

18 p3130 A69-35057

Manned spacecraft earth resource sensing, discussing advantages and applications in agriculture, forestry, geography, hydrology, oceanography and geology

18 p3208 A69-35058

Oceanographic sensing satellite systems, discussing applications, data requirements, sensors, booster and earth coverage capabilities

18 p3210 A69-35091

Satellite observation data association, estimating consistency of radar object with orbiting prediction, using computer program including Monte Carlo run

18 p3103 A69-35098

Earth ellipsoid determination by satellite observations, noting accuracy of polar flattening measurement on basis of perturbation or perigee argument

18 p3131 A69-35195

Geodetic satellite measurements employing curve fitting approach using least squares analysis to resolve atmospheric refraction and shimmer problem

18 p3104 A69-35202

Gas dynamics of interactions of tenuous ionosphere with moving satellites and diagnostic probes, using collision-free plasma kinetics methods

18 p3132 A69-35409

Spacecraft lunar observations, especially data from Surveyor landings

18 p3205 A69-35410

Orthogonal functions for determining atmospheric vertical temperature profile from satellite measurement of earth outgoing radiation in carbon dioxide absorption band

19 p3303 A69-36409

Proton satellites measurements reconciliation with diurnal stellar variation data and cosmic rays origin models

19 p3396 A69-36621

Nighttime F 2 region temperature distribution under geomagnetically calm and disturbed conditions calculated from Alouette 1 satellite data

19 p3304 A69-36623

Soviet collection of papers on satellite meteorology problems covering cloud physics, jet streams, cyclones, satellite photography, etc

19 p3365 A69-36667

OGO for conducting diversified measurements to study earth atmosphere, earth-sun relationship, etc

19 p3432 A69-36674

OGO triaxial search coil magnetometer for measuring earth magnetic fluctuations, discussing design rationale and observation results

19 p3284 A69-36675

Solid state detector for electron spatial distribution measurements on OGO-F satellite, discussing design emphasizing reliability

19 p3284 A69-36676

OGO 5 ion spectrometer for measuring oxygen, He and hydrogen ion concentration, noting functions as energetic particle analyzer and proton energy distribution measurement capability

19 p3314 A69-36679

Long range weather forecasts attempt from relation between northern Atlantic Ocean water temperature anomaly and monthly satellite cloud data changes

20 p3569 A69-36987

Ionospheric data of local and integral electron concentration obtained by measuring phase shift of satellite emitted coherent radio waves

20 p3519 A69-37022

Cold plasma approximation of whistler excitation of lower hybrid resonance at wake of body moving through ionosphere, comparing results with Alouette satellite observations

20 p3519 A69-37025

Jupiter tenth satellite reobserved, discussing calculations and computer techniques for determining orbit [AAS PAPER 68-140]

20 p3595 A69-37194

Satellite configurations and rotation parameters determined by radar analysis

20 p3488 A69-37295

Janus discovery, discussing solar distance, rotation period, diameter, opposition brightness and planetary parameters derived from pictures

20 p3597 A69-37337

X ray data in 44-60, 8-16 and 1-8 A bands telemeasured by Solrad 9 satellite

20 p3588 A69-37473

Power spectra of interplanetary magnetic field fluctuations determined from Pioneer 6 satellite data, relating results to galactic cosmic rays modulation

20 p3603 A69-37554

Satellite observations of solar proton events with halo structure or energetic storm proton event and SSC, noting similarity in origin

20 p3589 A69-37555

Satellite representations of earth gravity field portraying consistent pattern of mass anomalies due to density differences in layers

20 p3523 A69-37566

Near-polar circular orbiting satellite for calibrating and evaluating ground-based radars observing space objects

20 p3617 A69-37714

Alouette 1 and 2 topside sounder ionograms analyzed with emphasis on low electron density, spread F and field aligned propagation

20 p3529 A69-37863

Electron density profiles from topside ionograms compared to ground based sounding results, discussing error corrections

20 p3495 A69-37865

Global electron density distribution morphology in topside ionosphere during sunspot minimum from Alouette 1 and 2 ionograms

20 p3530 A69-37867

High latitude ionosphere data from Alouette- ISIS program, describing various F, E and D regions parameters

20 p3530 A69-37868

Alouette satellite VLF observations data of ionosphere ion composition determined from ion whistlers and noise bands with LF cut-off

20 p3530 A69-37873

Cylindrical electrostatic probe measurements on Alouette 2 and Explorer 31, considering implications for future missions

20 p3544 A69-37877

Planar thermal ion and electron trap experiments on Explorer 31 satellite, measuring ion and electron density and temperature and ionic composition

20 p3544 A69-37878

Explorer 31 ion mass spectrometer calibrated in flight and compared with Alouette 2 topside electron concentration data

20 p3545 A69-37879

Suprathermal electron flux in lower latitudes and polar region analyzed from measurements by retarding potential analyzers on Explorer 31 satellite

20 p3590 A69-37880

Ionospheric electron and ion concentration and temperature by Langmuir plate and spherical ion probe on Explorer 31 and ionosonde on Alouette 2

20 p3531 A69-37883

Ionospheric topside plasma resonances observed by fixed and swept frequency satellite-borne sounders

20 p3531 A69-37884

Topside ionospheric magnetic field aligned irregularities using satellite observations of nonvertical electromagnetic wave propagation and delayed echo generation

20 p3495 A69-37885

Ionospheric resonances due to plasma nonlinearities near spacecraft, noting effects on radio signal propagation

20 p3495 A69-37886

Frequency shifts observed in Alouette 2 cyclotron harmonic plasma resonances, noting antenna length and direction

20 p3496 A69-37892

Topside ionospheric structure from Alouette 2 data, discussing thermopause temperature, plasma temperature, electron density profiles, satellite plasma frequency, etc

20 p3532 A69-37895

Ionic composition determined by combining Alouette topside sounder electron density profiles with electron and ion temperatures measured by ground based Thomson scatter sounder

20 p3532 A69-37898

Diurnal, seasonal and spatial variations in height and occurrence frequency of low electron density region below 3000 km

20 p3532 A69-37899

Radiation effects due to high altitude thermonuclear explosion measured by satellite, estimating fragments longitudinal drift velocity, plasma cloud expansion rate and fragment distribution

20 p3532 A69-37960

Elektron satellite recorded sporadic radio emission noting relationship to geomagnetic disturbances and dependence on satellite position

20 p3606 A69-37969

Measuring devices for near earth space radiation measurements

20 p3591 A69-38018

Earth albedo in lower latitudes measured by satellites and surface stations, comparing solar energy absorption by oceans and atmosphere

20 p3591 A69-38058

Ionospheric scintillation power spectrum measurements from radio star and satellites related to F region radio refractive index fluctuations

20 p3534 A69-38093

Explorer 32 atmospheric density measurements revealing neutral thermosphere latitudinal variations during geomagnetically undisturbed times

20 p3535 A69-38100

Solar X-ray events observed by scintillation counter telescope on OSO 3 satellite, discussing X ray spectra during burst initial and decay phases

20 p3593 A69-38166

Diurnal entrainment deviations and atmospheric turbulence effects on flash photographs from Geos 1

21 p3793 A69-38339

Space contamination due to manned vehicles and debris atmosphere effects on dim light source observations

21 p3793 A69-38341

Satellite measurements of small particles near-earth space density compared with chemical estimates of terrestrial cosmic material, suggesting particles origin in meteoroid ablation

21 p3701 A69-38342

Rocket and satellite particle collection experiment to confirm reduced micrometeoroid flux near earth, noting inconclusive size frequency distributions of exposed flight samples

21 p3793 A69-38343

Particle trapping and plasma oscillations in satellite disturbed ionosphere observed from Ariel and Alouette measurements, discussing frequency and wavelength relation

21 p3787 A69-38357

Ionospheric lower hybrid resonance /LHR/ noise discovered by Alouette 1, describing possible mechanisms for origin

21 p3702 A69-38358

Wind and cloud velocities from ESSA 3 and 5 and ATS 1 pictures for typhoon and tropical vortices in intertropical convergence zone

21 p3758 A69-38371

Microwave refraction method for satellite horizontal probing of earth atmosphere, discussing phase delay data inversion, air density and intersatellite relative velocity

21 p3671 A69-38376

Lunar Explorer 35 measurements of lunar surface electromagnetic properties, magnetic fields and solar wind-moon interactions

21 p3794 A69-38379

VLF and LF emission characteristic features and origin mechanism in auroral regions of ionosphere, discussing satellite observation of noise spectrum in space

21 p3708 A69-38495

Simultaneous ground and Alouette 2 satellite measurements of enhanced electromagnetic band emission in 500-1000 Hz range

21 p3708 A69-38496

Optical data supporting satellite observations of soft electron precipitation on poleward side of normal auroral zone

21 p3709 A69-38501

Equatorial plasma sheet role in magnetotail assessed from Vela satellite data, noting diurnal density variations

21 p3711 A69-38512

Direct detection of ionospheric irregularity by device onboard San Marco satellite, utilizing antenna impedance fluctuations

21 p3715 A69-38562

Satellite phase and aberration corrections in processing photographic observations for geodetic purposes

21 p3720 A69-38606

International organizations and planning for earth observation satellite program involving exploitation in communications, meteorology and aircraft

21 p3855 A69-38622

Earth resources observation technology from satellites, reviewing sensors and methods, electromagnetic spectrum, atmospheric attenuation and windows, passive-active devices

21 p3720 A69-38624

Ozone measurement from satellite by direct beam and scattered light methods employing UV sunlight attenuation

21 p3721 A69-38625

Effusive volcanic eruptions recorded by high thermal sensitivity satellite-borne IR systems

21 p3721 A69-38631

Satellite synoptic meteorological data collection systems, discussing configurations, global location requirements and digital code platforms position determination

[AIAA PAPER 68-1095] 21 p3819 A69-39029

Satellite determination of underlying surface temperature by IR spectroscopy, measuring emitted radiation in atmospheric windows

21 p3759 A69-39114

Terrestrial radio noise from lightning discharges measured by Ariel 3 satellite to deduce sources distribution

21 p3759 A69-39259

Synoptic study of worldwide VLF electromagnetic wave fields distribution above ionosphere from Ariel 3 observations

21 p3717 A69-39262

Tropospheric refractivity height profile model, computing corrections to satellite Doppler or range data

21 p3678 A69-39748

Airborne microwave radiometric measurements of simulated ocean surface under various conditions, suggesting possible wind velocity measurement by satellite

21 p3726 A69-39750

Residuals from earth based coherent two way radio Doppler data from Lunar Orbiter three orders of magnitude larger than observations from spacecraft

[AAS PAPER 68-131] 21 p3828 A69-39766

Anomalous X ray signals from Explorer 30 satellite showing saturation in ionization chamber possibly due to enhanced solar and atmospheric X rays

21 p3792 A69-39808

Latitude variation of radio satellite scintillation related to small scale ionospheric irregularities

22 p3899 A69-39972

Explorer 22 observations of ionosphere electron content, describing measuring equipment and data evaluation

22 p3935 A69-39977

Computer controlled TV cloud recognition equipment on meteorological satellites, discussing multistep process of automatic perspective distortion corrections by onboard computer

22 p3977 A69-40004

Neutron flux measurements on Cosmos 53, discussing equipment and calculation of secondary neutrons due to bombardment of satellite components

22 p4003 A69-40274

Solar soft X rays observed from OSO-3, correlating to solar flares and radio bursts

22 p4003 A69-40297

Explorer 30 /Solrad 8/ satellite observation of 0.5-3 A solar X ray emission related to magnetic configuration in sunspot group

22 p4003 A69-40298

Solar wind north-south component sector dependent asymmetry implied from tangential discontinuities orientations as observed by Mariner 4

22 p4004 A69-40303

Shock discontinuities in solar wind measured by magnetic field and plasma instruments on Explorer 34, applying Rankine-Hugoniot relations

22 p4020 A69-40304

Explorer 34 observations of hydrogen and He ions in solar wind, noting number density variations and tentative association with geomagnetic storms

22 p4004 A69-40305

Satellite observations of auroral particle precipitations indicating latitude dependence of auroral electrons averaged pitch angle and energy spectral distributions

22 p3938 A69-40502

Injun 5 satellite VLF electric and magnetic fields observations, discussing antenna operation, Poynting flux and noise band measurements

22 p3938 A69-40503

Drift shell splitting in nondipolar distorted magnetosphere tested with data from electron spectrometer on ATS 1 and OGO 3 satellites

22 p4005 A69-40508

Faraday effect measurements by polar orbiting satellites for vertical distribution of ionospheric electron density

22 p3941 A69-40718

Solar X ray detector aboard OGO 5 satellite observing two components in energetic solar X ray bursts, attributing impulsive component to bremsstrahlung

22 p4007 A69-40775

Ionospheric electron content satellite measurements during 20 May 1966 annular solar eclipse

22 p4007 A69-40916

Satellite trajectory parameters estimation by maximum likelihood method applied to continuous satellite observations assuming random Gaussian process as measurement error

22 p3979 A69-41087

Cosmos 137 proton spectra data obtained in inner radiation belt agreeing with Relay 1 data

22 p4007 A69-41093

Radial velocity data monitored during Venera 4 descent used for determining vertical and horizontal atmospheric flows velocities

22 p4034 A69-41099

Autometric gyro for satellite general relativity experiments, particularly earth orbit measurement of Lense-Thirring precession

23 p4162 A69-41543

Radiometer for measurement of cosmic rays at 200-400 km altitudes range by satellites, presenting block diagram of radiation detector units

23 p4165 A69-41732

Radioactive debris distribution in space from 9 July 1962 thermonuclear explosion over Johnston island recorded by Cosmos 6 satellite

23 p4205 A69-41836

Disagreement between Mariner 2 and IMP 1 data concerning interrelation between solar wind velocity and geomagnetism ascribed to instrumental errors and changes in magnetospheric properties

23 p4205 A69-41848

Integral electron concentration in column of space between earth satellite and ground determined by integral equation, assessing errors minimization methods

23 p4157 A69-41858

Relativistic Doppler shift effect observed from radio signal periodic variation of GEOS-1 satellite

23 p4126 A69-42389

Ionospheric electron content measurement from Faraday fading on satellite BE-B, using computer program for data reduction as function of latitude

23 p4160 A69-42434

Topside ionosphere response to magnetic storms, using Explorer 22 satellite electron concentration and temperature measurements

23 p4161 A69-42438

IMP 4 satellite measurements of cosmic ray electrons in interplanetary space compared to predictions of electron intensity from interstellar proton-electron collisions

24 p4365 A69-42667

Fluctuating electric fields relations to MHD bow shock structure, using LF fluxgate magnetometer aboard OGO 5

24 p4306 A69-42693

Lunar gravitational field data from Lunar Orbiter spacecraft reprocessed, discussing mascon effects on moon structure and evolution theories

24 p4379 A69-42785

Satellite-based meteorological observation system for global atmospheric research program, discussing wind measurement, IR and microwave sounding possibilities, etc

[AAS PAPER 69-120] 24 p4307 A69-42817

Earth resources surveys by space flights and plans for future satellites, describing results of EROS and ERTS programs

[AAS PAPER 69-058] 24 p4307 A69-42824

Venus swingby and direct Mercury trajectories analysis for optical imaging from flyby missions

[AAS PAPER 69-258] 24 p4380 A69-42860

Mars atmosphere study by Mariner 6 and 7 spacecraft, discussing instrumentation on board

[AAS PAPER 69-091] 24 p4393 A69-42881

Multiple exposure averaging technique summarizing satellite cloud photographs for various periods, presenting entire earth cloud cover atlas

24 p4343 A69-42897

Ionospheric electron content and distribution at low altitudes from satellite S 66 data, describing seasonal variations of equatorial anomaly peak

24 p4367 A69-43010

OGO-6 design, research program, orbits and instrumentation, emphasizing relationship between particle activity, aurora and airglow, geomagnetic field, atmospheric and solar energy interrelations

24 p4393 A69-43132

Bidirectional reflectance of earth atmosphere and cloud formation above equatorial Pacific observed by synchronous satellite as function of angular dependence

24 p4346 A69-43154

Electron intensities and substorm drift effects in outer radiation belt using two satellite technique

24 p4309 A69-43172

Magnetospheric electron sudden intensity increases correlated with magnetic substorms occurrence at midnight meridian from ATS 1 observation

24 p4367 A69-43173

Atmospheric density above 158 km altitude measured near equator with cold cathode magnetron pressure gage on satellite OV1-15

24 p4310 A69-43179

Nighttime protonosphere thermal balance from Alouette 2 electrostatic probe measurements of electron temperature and concentration in magnetosphere

24 p4310 A69-43181

Geomagnetically trapped protons and alpha particles, analyzing OGO 4 data

24 p4368 A69-43184

Proton cyclotron echoes on ionograms obtained from topside ionosphere by Alouette 2 satellite

24 p4310 A69-43189

Orbiting vehicles remote sensing of earth resources, discussing instrumentation and accuracy requirements, data management and analysis and effectiveness criteria

24 p4315 A69-43199

Auroral activity and lunar phases correlation from IMP-1 measurements of lunar magnetic field

24 p4311 A69-43502

Solar flare soft X ray and EUV emission spectra data obtained on OSO-3 satellite compared with centimetric radio bursts

24 p4371 A69-43609

Time structure of solar X ray bursts from OSO 3 satellite observations showing impulsive and gradual components

24 p4371 A69-43610

Solar X ray flux measurements from OGO 4, comparing peak fluxes before, during and after flares with IQSY data

24 p4371 A69-43611

- Solar X-ray spectrum as function of sunspot group type based on Solrad satellites flux data, discussing relationship to lower ionosphere characteristics variations
24 p4372 A69-43615
 - Solar cosmic ray anisotropy measurement by Explorer 34 satellite during solar flare events
24 p4373 A69-43619
 - Satellite photographic astrometry and chronometry, determining spatial positions of satellites and observation stations by space triangulation
24 p4391 A69-43790
- SATELLITE ORBIT CALCULATION**
U ORBIT CALCULATION
- SATELLITE ORBITS**
NT PARKING ORBITS
NT POLAR ORBITS
NT STATIONARY ORBITS
NT TWENTY-FOUR HOUR ORBITS
- Equations of motion of satellite in rotating coordinate system, noting effects of precession and nutation on transformation of orbital elements
01 p0150 A69-10445
 - Observation of satellites, orbit calculation and use in upper atmosphere research
[UN PAPER 68-95789]
01 p0064 A69-10459
 - Satellite trajectories calculated in form of parameters derived from processing measured functions, considering optimum mathematical description selection
01 p0151 A69-10570
 - Near circular satellite orbits evolution taking into account gravitational fields zonal harmonics effect on motion
01 p0157 A69-11304
 - Satellite optimal transfers from elliptic to parabolic orbits within set time
01 p0157 A69-11306
 - Smoothing and prediction of satellite orbit elements by stochastic approximation method, solving nonlinear equations system
01 p0158 A69-11319
 - Existence of periodic solutions by Whittaker criterion to equations describing motion of satellite of spheroidal planet in planetocentric coordinate system
02 p0317 A69-11959
 - Motion stability of two tethered unsymmetrical earth pointing bodies in circular orbit, presenting nine degrees of freedom differential equations of motions
02 p0324 A69-12507
 - Satellite orbit selection for determining geopotential and spherical and tesseral harmonic coefficients, discussing propulsion systems and satellite observation cost feasibility
02 p0331 A69-12807
 - Release windows for auxiliary body ejection from satellite in eccentric orbit, discussing visibility, celestial body interference, etc
03 p0505 A69-13003
 - Mission analysis for applications satellites, discussing tradeoffs among mission objectives, launch vehicles, spacecraft and geopolitical considerations
03 p0511 A69-13428
 - Geopotential resonant orbital perturbations of existing satellites, noting high inclination role
03 p0521 A69-13777
 - Optimal circular satellite orbits for planetary surface mapping mission minimizing overlap
03 p0518 A69-14247
 - Soviet book on artificial satellite motion in noncentral gravitational field, discussing celestial axisymmetric planetary orbits, stationary centers, three body problem, etc
04 p0659 A69-15027
 - Artificial lunar satellite orbital motion calculated by numerical integration, including solar and lunar electromagnetic radiation pressure effects
04 p0662 A69-15251
 - Satellite orbit evolution under effect of small perturbing force with constant magnitude and direction
05 p0829 A69-16672
 - Approximate solution for determining satellite motion around axisymmetric planet
06 p1005 A69-17563
 - Attitude perturbations of spin stabilized satellite describing highly eccentric orbit
06 p1014 A69-17568
 - Sun-orbit plane relationship effects on mission planning
[AIAA PAPER 69-129]
06 p1011 A69-18093
 - Transfer orbits calculation between low and high satellite orbits, determining trajectories by method with minimum use of linearization
07 p1211 A69-18503
 - Coordinates and velocity components accuracy for artificial earth satellite moving in central Newtonian field, covering elliptic and circular orbits
07 p1178 A69-19606
 - Steady state motions stability of gyroscope mounted on satellite in gravitational orbit
07 p1137 A69-19679
 - General relativistic gravitational red shift effect on frequency transmitted from satellite orbits, noting possibility of measurement
08 p1383 A69-19901
 - Circular satellite orbit calculation from incomplete observations of one orbital pass
09 p1589 A69-21373
 - Canonical equations of planet satellite intermediate orbits using harmonics of gravitational potential
09 p1589 A69-21374
 - Earth equipotential surface shape determination from satellite orbit dynamics, obtaining triaxial ellipsoid
09 p1487 A69-21635
 - Upper atmosphere rotation perturbation effect on satellite orbit when scale height varies with height, showing inclination reduction
09 p1594 A69-21660
 - Periodic motion of satellite with magnetic damper along circular orbit, assuming small value of damping coefficient
09 p1609 A69-21761
 - Resonance relations of rotational and orbital frequencies of solar system planets and satellites estimated for statistical significance
10 p1771 A69-22852
 - Satellite altitude stabilization by gravity gradient capture in earth elliptical orbit, showing effect of increase in damping
10 p1791 A69-22926
 - Planar motion of satellite containing damping mechanism, considering small dampers case
10 p1791 A69-22935
 - Motion of satellite of very oblate planet, investigating axisymmetric potential
10 p1774 A69-22969
 - Earth gravitational field effect on satellite orbits, noting elliptical motion in central force field, energy criteria and rotational ratios
10 p1776 A69-23295
 - Circumpolar satellite orbits under lunar and solar perturbations based on two fixed centers problem, considering large amplitude disturbances
10 p1780 A69-23616
 - Numerical solution for changing satellite orientation within circular orbit plane by applying force of onboard flywheel
10 p1792 A69-24194
 - Ellipsoidal satellite translational rotational motion under spherical planet and point source sun gravitational fields influence, obtaining approximate solution for three body problem
11 p1956 A69-24399
 - Satellite 1968-5A orbit analyzed for atmospheric density at 140-180 km, noting semiannual variation
12 p2066 A69-26229
 - Earth stations coordinates determination from non-simultaneous photographic satellite observations by orbital method compared with simultaneous photographic observations of Echo I
12 p2068 A69-26430
 - Cosmos 17 and 44 draconic periods of rotation, discussing period variations determination from visual observations
12 p2173 A69-26439
 - Anomalistic satellite periods of rotation from successive observations at same topocentric parallel
12 p2158 A69-26441
 - Draconic period changes of satellite 1965-11-D /Cosmos 54 rocket/ during visual observations with Interochs
12 p2174 A69-26444
 - Draconic periods changes of satellites 1963 53A and 1964 76A, based on observations
12 p2174 A69-26446
 - Orbit determination from satellite using linear combinations of time of flight measurements and based on expansion of satellite law of motion
12 p2159 A69-26778
 - Horizontal gradients below satellite orbit effect on reduced and minimum difference in Doppler frequency shifts of coherent radio waves from satellite in inhomogeneous ionosphere
13 p2219 A69-27701
 - First order secular and aperiodic perturbations in Keplerian orbital elements of synchronous satellite due to earth gravitational field eccentricity
14 p2521 A69-29466
 - Secor 6 satellite /1966-51A/ orbital parameters determined from optical and radar observations noting use for upper atmosphere density and rotational speed studies
14 p2522 A69-29631
 - Satellite observation of ocean surface and subsurface features, discussing onboard equipment and proposed orbits
15 p2607 A69-30190
 - Satellite trajectories calculated in form of parameters derived from processing measured functions, considering optimum mathematical description selection
15 p2691 A69-30740
 - Antenna, frequency converter and automatic spectrum recorder system for closest approach times prediction and satellite identification, discussing errors
15 p2569 A69-30800
 - Satellite orbits obtained by tracking by synchronous satellites, discussing accuracy for low altitude satellites
15 p2698 A69-31340
 - Upper atmospheric density effects on satellite orbits, discussing variations due to solar activity, day-night and semiannual changes and atmospheric rotation
15 p2600 A69-31350
 - Average angular velocity of upper atmosphere from changes in orbital inclinations of satellites, discussing wind speeds
15 p2600 A69-31352
 - Satellites orbits analysis for semiannual variation of air density in upper atmosphere
15 p2601 A69-31378
 - Earth figure parameters from satellite orbit dynamics, including potential on geoidal surface and scale factor for lengths
15 p2602 A69-31387
 - Atmospheric models for pressure variation and neutral air winds in thermosphere, discussing wind velocity vector relation to satellites orbital inclination
15 p2603 A69-31403
 - Satellite orbit evolution data applied to refinement of geophysical parameters, including upper atmosphere parameters and zonal harmonic coefficients in gravitational potential expansion
15 p2604 A69-31417
 - Hill method for satellite motion with reference to rectangular rotating axes system with origin at moon center of gravity, obtaining intermediate orbits
16 p2855 A69-31656
 - Satellites trajectories under influence of earth oblateness and low radial thrust acceleration by nonlinear mechanics asymptotic method, discussing osculating orbits
16 p2856 A69-32009
 - Satellite orbital resonances due to geopotential analyzed by asymptotic expansion for nearly circular or equatorial orbits
16 p2863 A69-32401
 - Upper atmospheric gas density and temperature distribution diurnal and seasonal variations calculated from satellites orbiting time changes
17 p2959 A69-32924
 - Orbital and attitude control tests for PAS /two stage perigee-apogee synchronous satellite/ in conjunction with booster Europa 2, discussing functional configuration
17 p3048 A69-33238
 - Adaptive filter for estimating system noise inputs from actual residuals developed to control Kalman filter in satellite orbit estimation
18 p3110 A69-34676
 - Time optimal pitch motion of satellite in circular orbit based on maximum principle, considering variable and constant controls
18 p3207 A69-34677
 - Canonical equations of planet satellite intermediate orbits using harmonics of gravitational potential
18 p3198 A69-34762
 - Graphic representation of time dependence of sub-satellite points and orbital azimuths for relating satellite photographs to locality
18 p3128 A69-34818
 - Artificial satellites as navigation aids, describing angle, range and range-angle systems, discussing orbital mechanics and communications difficulties
18 p3169 A69-34855
 - Satellite observation data association, estimating consistency of radar object with orbiting prediction, using computer program including Monte Carlo run
18 p3103 A69-35098
 - Polar coordinates in Euclidean space applied to theory of satellite moving in gravitational field of spherically symmetrical body, introducing equipotential surfaces
19 p3397 A69-35610

Electrically charged earth satellite motion under action of Lorentz force produced by geomagnetic field interaction, relating field trajectories to acceleration
19 p3431 A69-36615

Relative motion of two bodies linked by flexible weightless tether in artificial earth satellite orbit, simulating extravehicular walk
19 p3427 A69-36618

Gyrostat satellite equilibrium positions in circular equatorial orbit under action of gravitational magnetic and aerodynamic moments based on gyrostatized satellite equations of motion
19 p3432 A69-36620

Balloon satellite orbital time and eccentricity correlated, investigating earth shadow and solar radiation effects
19 p3427 A69-36628

Rotational motion bounds of satellites exhibiting parametric resonance under small librations in orbital plane
20 p3617 A69-37191

Satellite orbit determination method allowing geogravitational field determination and correction of station coordinates
21 p3793 A69-38337

Periodic orbits of Poincare and Schwarzschild types in motion of artificial satellite in disturbed gravitational field of axisymmetric oblate spheroid
21 p3795 A69-38441

Orbital parameters of short-lived low altitude earth satellites assuming no atmospheric drag, no orbital precession and flat earth condition
21 p3798 A69-38626

Satellite tracking and orbit determination accuracy for system of two synchronous geostationary satellites [AIAA PAPER 68-449]
21 p3674 A69-39019

Ariel 3 satellite management structure, responsibilities and orbit, stabilization, launch window, data acquisition and processing
21 p3856 A69-39255

Satellite orbit determination errors attributed to Gaussian noise effect on tracking measurements, assuming known Gaussian probability error distribution [AIAA PAPER 69-911]
21 p3807 A69-39343

Satellite orbits calculation in nonrotating atmospheres, considering atmospheric drag and zonal harmonics coupled effects
21 p3808 A69-39352

Sun-moon short term disturbances effect on synchronous equatorial navigation satellite orbits, noting fuel expenditure [AIAA PAPER 69-927]
21 p3761 A69-39356

Computer program for eccentric geocentric satellite orbits evolution, discussing atmospheric drag, earth oblateness and soilunar effects [AIAA PAPER 69-928]
21 p3808 A69-39357

Orbital mechanics of near earth satellite arrangements /clusters/ for satellite service vehicle /SSV/ accessibility from orbital space stations [AIAA PAPER 69-929]
21 p3809 A69-39358

Mathematical formulation and error analysis of two rotor gyroorbit used in plotting orbital system of satellite coordinates
21 p3765 A69-39363

Satellite maneuver for changing plane of circular orbit to pass through given point, determining on-off engine switching and thrust vector control
21 p3765 A69-39364

Satellites resonant perturbations analysis, deriving mean mean motion formulas
22 p4035 A69-39968

Algorithms for close earth satellite orbit calculation developed by numerical integration methods, discussing solution efficiency [AIAA PAPER 69-948]
22 p4021 A69-40331

Molecular beams for simulating orbital flight through planetary atmospheres, considering various nozzle beam systems [AIAA PAPER 69-1031]
22 p3926 A69-40437

Neglected gravity coefficients influence on computed satellite orbits and geodetic parameters
22 p4023 A69-40556

Sun and moon effects on earth satellite orbit
22 p4030 A69-40901

Artificial satellite motion analysis and perturbation function, considering disturbances due to second satellite or sun
22 p4030 A69-40906

Satellite trajectory parameters estimation by maximum likelihood method applied to continuous satellite observations assuming random Gaussian process as measurement error
22 p3979 A69-41087

Satellite motion initial phase vector estimation for calculating satellite motion from selection of complete or increasing volume of measurements
22 p4033 A69-41088

Periodic solutions for gravity-gradient stabilized satellite librating in orbital plane, using elliptic sine function and harmonic balance method
23 p4224 A69-41876

Spherical trajectories control by star height maintenance, analyzing resulting cycloid and cartographic representations
23 p4186 A69-42023

Ionospheric irregularities effect on accurate satellite position determination in near real time
23 p4132 A69-42549

OGO-6 design, research program, orbits and instrumentation, emphasizing relationship between particle activity, aurora and airglow, geomagnetic field, atmospheric and solar energy interrelations
24 p4393 A69-43132

Sun-orbit plane relationship effects on mission planning [AIAA PAPER 69-164]
24 p4386 A69-43261

Planetary gravitational fields and artificial satellite orbits determined by using earth based range rate measurements
24 p4388 A69-43650

Ellipsoidal satellite translational rotational motion under spherical planet and point source sun gravitational fields influence, obtaining approximate solution for three body problem
24 p4390 A69-43789

SATELLITE ORIENTATION

Solid body automatic orientation, discussing data units for angular error and angular velocity
01 p0122 A69-11302

Three axis magnetometers to determine nonoriented satellite axial orientation in absolute coordinates
01 p0163 A69-11303

Multibody dual spin spacecraft spin axis motion with active internal devices, using digital simulation
02 p0332 A69-11739

Magnetic orientation and attitude control of spin stabilized satellites, synthesizing control circuits and calculating power requirements
03 p0521 A69-13644

Short period terms elimination for problem of motion of satellite with strong inclination and eccentricity, using von Zeipel method
03 p0514 A69-13783

Equilibrium orientations of orbiting gyrostats, giving spectrum of solutions for bodies of varied shape and internal rotor angular momentum
03 p0522 A69-14246

UV astronomy, discussing vehicle stabilization, unstabilized sounding rockets, scanning satellites, balloons, stabilized rockets, pointing satellites, optics and detectors
05 p0821 A69-15839

Soviet achievements in space research, comparing satellites with U.S. counterparts
06 p1005 A69-17561

Equilibria of orbiting gyrostat satellite with internal angular momenta along principal axes
07 p1227 A69-18336

Rotation and orientation parameters of earth satellites based on qualitative analysis of solar direction indicator readings
07 p1230 A69-19604

Attitude determination and hydrogen peroxide control system for spacecraft orientation in Syncom, Early Bird and ATS [AIAA PAPER 67-532]
09 p1610 A69-21988

Luna 9 automatic station flight control complex, detailing communication, orientation and stabilization systems operation after separation from acceleration module
10 p1792 A69-24197

Flight control system for automatic interplanetary stations /AIS/, comparing Venera series orientation and correction system to Mariner systems
10 p1792 A69-24198

Spacecraft orbit control laws determined by studying influence of controlling acceleration in plane perpendicular to absolute velocity vector
11 p1965 A69-25743

External perturbation effects of near earth environment on dynamics and attitude of slowly spinning multibody satellite [AIAA PAPER 68-856]
12 p2174 A69-26795

Space vehicle attitude stabilization based on rotating flywheel resistance to changes in rotation axis attitude, noting grease lubricated hydrodynamic bearing system
12 p2175 A69-26893

Atmospheric density determination based on long period variations of drag coefficients from satellite Proton 2, considering satellite orientation
15 p2602 A69-31392

Satellite Proton 2 orientation from onboard measurement data, discussing general statistical method and data processing results
17 p3001 A69-33221

Langmuir probe to determine space vehicle orientation in ionospheric or interplanetary plasma, discussing apparatus, accuracy and application
17 p3001 A69-33222

Cosmos 149 satellite stabilization system, discussing three axis orientation and pitch, yaw and roll stabilizations by aerodynamic and/or gyroscopic moments
17 p3047 A69-33226

Numerical integration of Eole satellite attitude equations compared with results obtained by analog simulation or hybrid computation
17 p3048 A69-33232

Attitude stabilization of symmetrical nonrotating earth satellite using earth-pointing rotor as gravitational anchor
19 p3429 A69-35914

Instantaneous and integral solar irradiance of earth oriented satellite surface, noting solar illumination nomogram representation
19 p3432 A69-36629

Nonlinear roll-yaw attitude motion of spinning symmetric satellite in elliptical orbit near internal or external resonance [AAS PAPER 68-124]
20 p3616 A69-37178

Time-independent feedback attitude control system for high accuracy earth pointing motion of stable and unstable satellites in elliptic orbits
21 p3804 A69-39020

Ariel 3 satellite attitude determination, using solar aspect sensors to define conical surface containing spin axis
21 p3820 A69-39260

Ariel 3 satellite spin axis direction determination by optical means from analyzing sunlight glints reflected from surfaces
21 p3820 A69-39261

Reaction boom attitude control systems for improving stabilization and maneuvering capability of earth pointing satellites, describing configurations [AIAA PAPER 69-834]
21 p3822 A69-39365

Spacecraft attitude acquisition/reorientation and stabilization controller design implemented by control moment gyro, proposing control algorithm using control actuator nonlinearity
21 p3826 A69-39641

Aperiodic feedback substitution for angular velocity component of control signal in stabilization systems of oriented satellites
21 p3829 A69-39832

Spacecraft spherical motion about mass center under inertial force using Euler differential equations
21 p3830 A69-39838

Satellite orientation by determining rotation parameters about centers of mass with respect to certain coordinates
22 p4037 A69-41089

Proton 2 satellite orientation and motion about center of mass determined from telemetric data analysis under aerodynamic moment
22 p4037 A69-41090

Satellite aerodynamic characteristics, considering orbital position and attitude of cylindrical body and separate plate
22 p4037 A69-41102

Satellite attitude estimation from onboard telescope celestial sightings using iterative least squares method, considering measurement error noise and axes wobble
24 p4348 A69-43244

Stability analysis of periodic solutions associated with planar librations of gravity oriented satellite using linear perturbation analysis
24 p4388 A69-43649

SATELLITE PERTURBATION

Mass functions of real earth derived from satellite orbital perturbations [UN PAPER 68-95385]
01 p0064 A69-10460

Dynamically symmetric gyrostat steady motion stability in relation to satellite motion
01 p0163 A69-11301

Satellite nonlinear spatial oscillations about center of mass during circular orbit, using perturbation theory and analog computer
04 p0665 A69-14270

Perturbations of stationary orbital vehicles of arbitrary latitude due to earth triaxiality, noting control by low thrust rocket engine
05 p0823 A69-16037

Direct light pressure effect on evolution of limited planetocentric orbits of small bodies, noting longitudes of ascending node and pericenter

05 p0823 A69-16043

Roll dynamics of spinning axisymmetric satellite in elliptical orbit, discussing eccentricity and gravity gradient torque effect

05 p0830 A69-16397

Anomalous spacecraft OGO-D motion explained by open section boom thermally induced oscillations, discussing corrective measures

07 p1231 A69-18331

Secular perturbations of remote satellites within lunar gravitational field, comparing observations and analytical data

10 p1779 A69-23614

Satellite motion short period perturbations by earth gravitational field tesseral and sectoral harmonics

12 p2069 A69-26431

Natural terrestrial satellites existence suggested by telescopic and photographic observations and artificial satellites orbital perturbations

13 p2344 A69-27642

Steady motion stability of satellite with gimbal suspended gyroscope in central gravitational field, showing no effect of satellite perturbations on gyrostatic stability

14 p2530 A69-29481

Generalized Fourier analysis for satellite motion deviations from arbitrarily chosen reference orbit generated analytically or numerically, determining equations for potential coefficients

15 p2697 A69-31323

Earth reflected radiation pressure and perturbing effect on satellites

15 p2599 A69-31324

Air density at various heights determined from analysis of satellite low perigee orbits, discussing periodic density variations and correlation with daily geomagnetic index

15 p2599 A69-31348

Air densities from satellite obtained orbital data, comparing accuracy of values and methods of analysis

15 p2600 A69-31349

Upper atmospheric density effects on satellite orbits, discussing variations due to solar activity, day-night and semiannual changes and atmospheric rotation

15 p2600 A69-31350

Literal algebra /SPASM/ computer program critical verification of Kozai short period lunar perturbations, discussing errors

15 p2699 A69-31381

Lunar mass and gravitational field determined from lunar satellite dynamics, using potential function in terms of spherical harmonics

15 p2699 A69-31405

Long range perturbations of satellites and asteroids with arbitrary inclination and eccentricity, illustrating motion around moon, oblate and spherical planets using energy integral

17 p3031 A69-33098

Equatorial moderately elliptical satellite orbit perturbations calculated in local invariants, assuming state vector dependence of acceleration

17 p3039 A69-33796

Polar flattening influence of Jupiter on artificial satellite motion around Callisto noting orbital perturbations

18 p3199 A69-34913

Satellite motion perturbations in vicinity of critical inclination, using Encke method of numerical integration

19 p3397 A69-35607

Ground traces of artificial earth satellites with respect to perturbations due to atmospheric drag, earth oblateness and moon and sun as third body

19 p3398 A69-35614

Short term motion of lunar satellite, discussing third body disturbing functions and perturbation solution of nonsingular orbit elements

19 p3402 A69-35934

Hansen method applied to Jupiter tenth satellite orbit correction and perturbations, describing computer program and formulas used

20 p3602 A69-37529

Direct light pressure effect on evolution of limited planetocentric orbits of small bodies, noting longitudes of ascending node and pericenter

20 p3606 A69-37952

Three dimensional coupled flexural and attitude dynamics of libration-damped cruciform gravity gradient satellite, discussing effects of orbital eccentricity, solar radiation pressure, etc

[AAS PAPER 68-126] 21 p3819 A69-39211

Satellite position perturbation due to earth oblateness using Hansen method

[AIAA PAPER 69-909] 21 p3807 A69-39341

Gravity gradient perturbing torque cast in terms of perturbing Hamiltonian, deriving long term changes in rotational motion of tumbling triaxial satellite in elliptical orbit

[AIAA PAPER 69-922] 21 p3821 A69-39353

Sun-moon short term disturbances effect on synchronous equatorial navigation satellite orbits, noting fuel expenditure

[AIAA PAPER 69-927] 21 p3761 A69-39356

Earth shape and areas of anomalous gravity from satellite orbital perturbations, tabulating results from various experimenters

21 p3718 A69-39734

Satellite attitude stabilization synthesis by flywheels allowing independent control of angular motions, assessing perturbation type influence

21 p3768 A69-39831

Geomagnetic field and aerodynamic perturbation effects on satellite motion about center of mass, using asymptotic methods of nonlinear oscillation theory

21 p3830 A69-39835

Closed form solution to stability of coupled libration motion of slender axisymmetric satellite in circular orbit limited to small amplitude vibrations

22 p4008 A69-39936

Satellites resonant perturbations analysis, deriving mean mean motion formulas

22 p4035 A69-39968

Sun and moon effects on earth satellite orbit

22 p4030 A69-40901

Artificial satellite motion analysis and perturbation function, considering disturbances due to second satellite or sun

22 p4030 A69-40906

SATELLITE RENDEZVOUS

U ORBITAL RENDEZVOUS

SATELLITE ROTATION

First approximation stability of single rotation of artificial earth satellite about center of mass in Newtonian gravitational force field

01 p0161 A69-10585

Numerical analysis of temperature variation of spherical spinning satellite with and without radiatively coupled inner shell containing heat source

01 p0162 A69-10761

Three axis magnetometers to determine nonoriented satellite axial orientation in absolute coordinates

01 p0163 A69-11303

Multibody dual spin spacecraft spin axis motion with active internal devices, using digital simulation

02 p0332 A69-11739

Energy dissipation effects on attitude stability of dual-spin satellites with damping mechanism on rotating sections

04 p0665 A69-14703

Optimum stabilization of uniformly rotating axisymmetric satellite, using Liapunov theorem on asymptotic stability

04 p0666 A69-14921

Roll dynamics of spinning axisymmetric satellite in elliptical orbit, discussing eccentricity and gravity gradient torque effect

05 p0830 A69-16397

Nutational stability of multibody spin stabilized satellites, discussing moment of inertia ratios role with energy dissipative damper on despin platform

06 p01015 A69-17585

West German test facility for simulating artificial satellite rotation about center of mass

07 p1116 A69-18260

Rotation and orientation parameters of earth satellites based on qualitative analysis of solar direction indicator readings

07 p1230 A69-19604

Coriolis acceleration in rotating environment, discussing origins and role in human existence in rotating space station

09 p1540 A69-21891

Aerodynamic torque on spinning spherical satellite, noting applications to accommodation coefficient measurement and study of aerodynamic gas-surface interactions

09 p1611 A69-22087

Small angle precessional motion of axisymmetric spin stabilized bodies subject to disturbing moments

10 p1724 A69-22932

Ellipsoidal satellite translational rotational motion under spherical planet and point source sun gravitational fields influence, obtaining approximate solution for three body problem

11 p1956 A69-24399

Rotational dynamics equations in linearized matrix form applied to satellite librations in circular orbit and gyroscope motion

11 p1970 A69-24608

Dynamic systems stability with periodically varying parameters analyzed by Hill type infinite determinant, exemplifying helicopter rotor aeroelastic stability in forward flight

11 p1990 A69-25510

Gyrostabilized satellite steady state motions in Newtonian force field having displaced satellite center of mass orbital plane relative to center of attraction

12 p2173 A69-25885

Cylindrical satellite drag rotating about transverse axis in earth magnetic field, including aerodynamic and magnetic moments

12 p2174 A69-26443

Wobble-spin technique for spacecraft inversion for earth photography using flywheel

12 p2174 A69-26780

External perturbation effects of near earth environment on dynamics and attitude of slowly spinning multibody satellite

[AIAA PAPER 68-856] 12 p2174 A69-26795

Photographic observations of fifth satellite and disk of Jupiter against stars background for mean motion and regression of nodes

13 p2345 A69-27653

Satellite motion relative to center of mass and resonances by approximate solutions to motion equations, applying asymptotic methods

13 p2357 A69-28502

Autonomous canonical system with two degrees of freedom, determining equilibrium position stability in resonance case, calculating earth satellite rotational stability

14 p2482 A69-28813

Magnetic damping of homogeneous cylindrical satellite rotation about transverse axis

14 p2530 A69-29065

Coriolis effect in rotating spacecraft simulation, discussing optokinetic reflex responses as function of head turning angle with spin axis

14 p2409 A69-29300

Linear dynamic stability of spinning satellite in elliptic orbit, applying perturbation method to determine Floquet solutions

14 p2534 A69-29318

First approximation stability of single rotation of artificial earth satellite about center of mass in Newtonian gravitational force field

15 p2702 A69-30755

Satellite motion about center of mass, discussing satellite stabilization and libratory motion in gravitational force field, planet resonances, etc

15 p2703 A69-31411

Capillary barriers to provide propellant positioning, expulsion capability and slosh dampening for spacecraft propulsion systems during rotational maneuvers

[AIAA PAPER 69-529] 16 p2868 A69-32713

Lunar rotation parameters determined from photographs and visual observations independent of moon profile

17 p3027 A69-32874

Lunar rotation elements determined from distances between Moesting A and limb craters, using Iakovkin position angle method

17 p3028 A69-32876

Rotational equations of motion for two body spacecraft on common spin axis required for simulated gravity environment or gyroscopic stability augmentation

17 p3047 A69-33227

Rotor hazards in rotational behavior of gravity stabilized satellites, describing gyrostabil applications

17 p3048 A69-33233

Minimum time single axis capture of satellite spinning about pitch axis by low thrust jets, considering gravity gradient phenomenon

17 p3048 A69-33237

Rotational locks for arbitrary eccentricity orbit satellites

19 p3397 A69-35609

Passive damper system for reducing precession in free symmetrical rotating space vehicle, noting linear torsional spring influence on precession decay

19 p3429 A69-35913

Gravity torque influence on axisymmetric dual spin satellites in fixed attitudes, using attitude stability studies of spinning single rigid bodies

19 p3429 A69-35917

Stationary resonant nonlinear oscillatory and rotary states, stability and pitching motions of controlled satellite in slightly elliptical orbit

20 p3616 A69-37177

Nonlinear roll-yaw attitude motion of spinning symmetric satellite in elliptical orbit near internal or external resonance
[AAS PAPER 68-124] 20 p3616 A69-37178

Rotational motion bounds of satellites exhibiting parametric resonance under small librations in orbital plane
20 p3617 A69-37191

Spacecraft rotation and astronaut head and body motion as stimuli for vestibular analysis function study during weightlessness
20 p3473 A69-37275

Satellite configurations and rotation parameters determined by radar analysis
20 p3488 A69-37295

Moving model target for laboratory measurements of radar cross section to simulate satellite or reentry vehicle precession motion, noting signature data analysis
20 p3511 A69-37850

Spinning satellite attitude perturbations due to oscillating mass in satellite rigid frame, discussing analytical approach and analog simulation results
20 p3618 A69-37912

Motion and stability of rotating connected two body space station satellite system, developing Lagrangian equations of motion and optimizing damping system parameters
[AIAA PAPER 69-919] 21 p3820 A69-39349

Gravity gradient perturbing torque cast in terms of perturbing Hamiltonian, deriving long term changes in rotational motion of tumbling triaxial satellite in elliptical orbit
[AIAA PAPER 69-922] 21 p3821 A69-39353

Equations of motion of elastic dumbbell satellite and two-mass spring-connected satellite in orbit, using energy and Floquet theory to investigate spinning motion stability
21 p3817 A69-39759

Fluid loop rotational kinetic energy dissipator reducing time required for reaching WRESAT 1 satellite spin stabilization axis
21 p3828 A69-39767

Geomagnetic field and aerodynamic perturbation effects on satellite motion about center of mass, using asymptotic methods of nonlinear oscillation theory
21 p3830 A69-39835

Satellite rotation from radar data analysis, requiring two full rotations and body characteristics to produce distinctive lobes in radar cross section
22 p3900 A69-40682

Errors in determining controlled satellite rotation periods, proposing scheme for corrected trajectory calculation of small eccentricity orbits
22 p4033 A69-41086

Satellite orientation by determining rotation parameters about centers of mass with respect to certain coordinates
22 p4037 A69-41089

Proton 2 satellite orientation and motion about center of mass determined from telemetric data analysis under aerodynamic moment
22 p4037 A69-41090

Motion stability of rapidly spinning satellite, discussing elastic booms effect
22 p4037 A69-41091

Concentric or eccentric rotation effect on burning rate and geometry of small hybrid rocket motors using hydrogen peroxide-organic fuel
23 p4203 A69-41932

Spinning satellite containing elastically restrained, viscously damped mass, analyzing attitude dynamics and stability, noting wide nutation possibility
23 p4224 A69-42396

Iterative weighted least squares method for reconstructing time history of coupled rotation and flexural oscillations of Radio Astronomy Explorer satellite
24 p4394 A69-43291

Ellipsoidal satellite translational rotational motion under spherical planet and point source sun gravitational fields influence, obtaining approximate solution for three body problem
24 p4390 A69-43789

SATELLITE TELEVISION

Direct TV broadcasting from satellites with incoherent thermionic reactor and electrical propulsion
[UN PAPER 68-95559] 01 p0114 A69-10466

Geostationary satellite transmissions for educational purposes
[UN PAPER 68-95533] 01 p0028 A69-10494

Satellite TV systems for India, alternatives and costs
[UN PAPER 68-95750] 01 p0028 A69-10495

Satellite educational TV, considering program distribution, satellite characteristics, ground terminals design, reliability, quality, programming and costs
[UN PAPER 68-95827] 01 p0029 A69-10499

Satellite digital video data analyzed by two dimensional filter computer technique, discussing biomedical applications
02 p0213 A69-12155

Educational TV satellites, considering stationary ASCEND system with high power transmitters
02 p0335 A69-12747

Satellite TV transmitter power requirements for adequate direct broadcasting field strength in existing UHF TV bands
03 p0394 A69-13578

European regional satellite communication systems, discussing EUROVISION TV program broadcasting and multiple access telephony
03 p0395 A69-13585

Sound and TV broadcasting from satellites, discussing systems for future individual user pickup
04 p0558 A69-15120

Atmospheric processes interpretation from cloud cover pictures televised by orbiting satellite, examining indirect weather forecasting
[UN PAPER 68-95713] 06 p0949 A69-17029

Quality control for TV transmissions via communication satellites, considering transmission accuracy improvement and error measurement automation
[UN PAPER 68-95773] 06 p0886 A69-17047

Meteorological satellite TV data of earth cloud cover for determining atmosphere pressure field
[UN PAPER 68-95654] 06 p0949 A69-17052

Processing TV cloud data monitored by Molniya 1 and Meteor meteorological satellites, discussing computer interpretation of TV photographs
[UN PAPER 68-95759] 06 p0950 A69-17060

Communication satellites application to domestic live TV, telephone and data communication and long distance telecommunication in Canada
[UN PAPER 68-95501] 06 p0887 A69-17075

Communication satellites in synchronous equatorial orbit for two types of educational TV, discussing picture quality, modulation, power, bandwidth and system costs
06 p1017 A69-17624

M-20 digital computer program designed for calculating statistical characteristics of signals from IR TV scanning system of Cosmos 122 meteorological satellite
06 p0929 A69-17980

TV system producing images with 5000 line resolution, proposing application in Earth Resources Observation Satellite
07 p1131 A69-18552

Satellite TV broadcast application for communication and education, discussing costs and benefits in single and multimission combinations
07 p1244 A69-18678

Preemphasis applications compared in active communication satellite systems for frequency division multiplex telephony and for TV
09 p1449 A69-21275

Carrier energy dispersal in communication satellite telephony and TV systems, noting attendant RF bandwidth increase as function of distortion
09 p1450 A69-21277

Ground station receiving antenna design and size for indirect distribution of TV programs by geostatic satellites
10 p1654 A69-23389

TV broadcasting from synchronous satellites direct to ordinary UHF receivers in 1980s
11 p1833 A69-24529

Air flow distribution and wind velocities in cyclones constructed from Cosmos 122 TV cloud images
11 p1912 A69-24825

TV IR cloud images interpretation transmitted by Cosmos 122, discussing specific features of cloud covers and underlying surfaces
11 p1912 A69-24826

Statistical analysis of convective layer thickness and moisture content effect on convective cloud configurations, using satellite TV pictures
11 p1912 A69-24827

Statistical analysis of lee wave clouds from satellite TV pictures, determining lengths and air flow direction
11 p1912 A69-24828

Computer program for interpreting IR cloud pictures from Cosmos 122 satellite based on potential function method
11 p1884 A69-24833

Color TV system for Earth Resources Observation Satellite /EROS/, discussing resolution in relation to spectral separation through data simulation study
[SMPTE PAPER 105-79] 12 p2077 A69-25767

Thermionic converter power from satellite nuclear reactor for TV satellites, discussing direct heat utilization and applications
12 p2016 A69-25869

Vertical air motions and cloud behavior relationship based on statistical analysis of TV cloud pictures from Cosmos 122 satellite
13 p2291 A69-27724

IR TV cloud pictures from meteorological satellites used for sky condition diagnostics and forecasting through automatic interpretation by image brightness quantization
13 p2291 A69-27728

Earth TV pictures from Molniya 1 communication satellite, showing advantages of high orbit over low orbit photography for global weather analysis and forecasting
13 p2292 A69-27729

Cartographic interpretation of TV cloud pictures transmitted by Molniya 1 satellite
13 p2292 A69-27730

Synchronous satellite TV broadcasting systems in UK, discussing equipment, transmission problems and economic factors
13 p2220 A69-27830

Radar and satellite TV clouds observation in meso and macroscale cloud systems
13 p2294 A69-27853

Educational TV satellite system design for U.S. in 1970s
18 p3235 A69-35076

TV picture and newspaper pages simultaneous transmission via earth satellite /Orbit/ system, measuring SNR and crosstalk
19 p3277 A69-36567

Cloud masses vertical thickness estimated from study of cloud shadows on satellite TV pictures
19 p3366 A69-36670

Earth resources satellite /ERS/ TV camera configurations, return beam vidicon camera characteristics and devices for TV picture reproduction on film
21 p3720 A69-38619

Multispectral radiometric analysis of ERTS images, discussing image registration, SNR and atmospheric and diffraction effects
21 p3721 A69-38627

Mariner 6 TV pictures with description of craters and south polar cap, noting moon-like crater abundance, form, arrangement and crater sizes
21 p3803 A69-38981

Computer program for satellite APT geographical grid production, discussing latitude-longitude intersections transformation to Cartesian coordinates
21 p3718 A69-39749

German ground station radio communications via Intelsat satellites, discussing transmitting facilities, TV picture and sound signals, etc
22 p3902 A69-41249

Geostationary satellite TV broadcasting to small contiguous areas with separate programs, discussing communication distribution problems
22 p3902 A69-41252

Communication satellites european development, discussing economic and technological problems, stressing color TV and SHF/FM transmission, compared to conventional ground station transmission
24 p4393 A69-43133

SATELLITE TRACKING

Satellite triangulation simultaneous and trailing methods, discussing timing devices design
[UN PAPER 68-95285] 01 p0064 A69-10475

Earth surface shape determinations by geodetic networks connecting ground observation points and satellite positions
[UN PAPER 68-95377] 01 p0065 A69-10528

CNES worldwide network of tracking stations, describing equipment, location, organization and center of operations
02 p0228 A69-11922

Computer programming of satellite orbit tracking angles for automatic picture transmission receiving stations
04 p0558 A69-14917

Predictor determining future position of TDMA /Time Division Multiple Access/ synchronous satellite communications system satellite from previously received bursts
07 p1076 A69-18553

Ballistics room of Royal Belgian Observatory for observation of geodetic satellites
08 p1272 A69-19993

Maintenance telemetering, tracking and telecommand for developmental and operational satellites, discussing possibilities of frequency sharing between satellites and terrestrial services
09 p1451 A69-21290

Technical characteristics of spacecraft telemetering, tracking and telecommand systems, stressing links between earth stations and spacecraft
09 p1451 A69-21291

- Automatic flight control system /AOOSY/ for German Azur satellite
09 p1459 A69-22563
- Satellite photographic astrometry and chronometry, determining spatial positions of satellites and observation stations by space triangulation
11 p1956 A69-24400
- Electrical servopositioning of telemetry reception antenna for tracking satellites, considering weight, stability, etc
11 p1852 A69-25118
- Optical satellite tracking system using multicoincidence method of photon signal counting by Q switched laser
11 p1841 A69-25579
- Satellite position errors due to atmospheric instability, discussing altitude-temperature relation and stellar scintillation synchronism for stars at small angular distances
12 p2158 A69-26445
- Streak camera for continuous photographing of dark and bright satellites up to 9 stellar magnitude
12 p2092 A69-26451
- Satellite positions measurements by laser compared with radar and photographic methods, considering measurement errors
12 p2110 A69-27149
- Antenna cross dipole array for vehicle tracking in VHF band, obtaining effect of local rotation by electrical phase shifting
13 p2226 A69-27185
- Esro 1 satellite program management, discussing scientific mission, structure, tracking system and history
13 p2355 A69-27360
- Satellite tracking cameras developed in East Germany, discussing optical systems
13 p2262 A69-27958
- Pulsed laser satellite tracking system, noting tracking mount adjustment
13 p2222 A69-28192
- Artificial earth satellites positional observations by graphical smoothing on azimuth and altitude, discussing advantages for space geodesy
15 p2594 A69-30029
- Satellite triangulation by least squares method based on conditions relating to observing stations coordinates, concerning synchronous observations of directions and distances
15 p2594 A69-30030
- Stellar image vibration amplitude dependence on trace direction by comparison with traces of moving satellites
15 p2647 A69-30166
- Scintillation of ground based spherical wave laser source viewed from space analyzed from Geos 2 satellite laser tracking, noting stellar scintillation correspondence
15 p2570 A69-31309
- NASA laser systems for satellite tracking, determining ranging accuracy by comparing laser and computed reference orbital data
15 p2571 A69-31312
- Satellite trajectory determination and expected errors for OGO 4 and Geos 1 orbits, noting geopotential, aerodynamic drag and integration contributions
15 p2698 A69-31331
- Lasers for satellite range measurements, discussing power output, mount, accuracy and data
15 p2571 A69-31337
- Satellite orbits obtained by tracking by synchronous satellites, discussing accuracy for low altitude satellites
15 p2698 A69-31340
- Laser measurements for DIADEME satellites tracking to reconstruct actual trajectory in semidynamic geodesy
15 p2600 A69-31365
- Tesseral harmonics of geopotential and station coordinates based on combined Baker-Nunn, laser and range and rate satellite data
15 p2601 A69-31372
- Monograph on photogrammetry in satellite geodesy including photogrammetric measurement of satellite positions, German observation stations and work done in U.S., U.S.S.R. and France
16 p2790 A69-32202
- Electrooptical distance measurement based on laser pulse traveling time and phase measurements to determine satellite range
18 p3103 A69-35199
- Secor data reduction to correct tropospheric refractive effects of radio ranging on earth satellites using tropospheric model
18 p3104 A69-35200
- Australia spatial triangulation and trilateration using geometric satellite geodesy, including station position accuracy tests
18 p3132 A69-35499
- Ground traces of artificial earth satellites with respect to perturbations due to atmospheric drag, earth oblateness and moon and sun as third body
19 p3398 A69-35614
- Orbit parameters identification method based on given tracking data span applied to lunar orbiter tracking using Fourier analysis
19 p3401 A69-35916
- Gain measurement of two element phased array aperture antenna during ATS-C tracking
19 p3272 A69-36254
- Balloon location by low orbit meteorological satellites, discussing balloon movement due to wind and geometric and nongeometric effects on errors
21 p3760 A69-38618
- Automatic speech recognition and tracking techniques of moving objects, considering applicability to processing data from earth resources satellites
21 p3721 A69-38630
- Satellite tracking and orbit determination accuracy for system of two synchronous geostationary satellites [AIAA PAPER 68-449]
21 p3674 A69-39019
- Doppler tracking of near synchronous DODGE satellite from single frequency data, noting error sources [AAS PAPER 68-128]
21 p3674 A69-39202
- Satellite position perturbation due to earth oblateness using Hansen method [AIAA PAPER 69-909]
21 p3807 A69-39341
- Satellite orbit determination errors attributed to Gaussian noise effect on tracking measurements, assuming known Gaussian probability error distribution [AIAA PAPER 69-911]
21 p3807 A69-39343
- Radar calibration techniques for accurate real time tracking data, describing GEOS-B C-band experiment [AIAA PAPER 69-872]
21 p3675 A69-39398
- Space simulation tests of satellite-borne quartz crystal oscillators for tracking based on Doppler effect
22 p3927 A69-40590
- Tracking and Data Relay Satellite System with synchronous orbit satellites to relay data between low altitude earth orbital spacecraft and mission control centers
23 p4120 A69-41755
- Tracking and data relay satellite system /TDRSS/ compared to ground based mission support, considering altitude coverage capability, economy and communication requirements
23 p4120 A69-41756
- Real time telemetry, tracking and command links by synchronous satellite relay, describing ATS-Nimbus E S-band experiment
23 p4121 A69-41759
- Rosman I reflector antenna for collecting data from earth orbiting satellites, discussing dynamic analysis of structural response to natural frequencies
23 p4231 A69-42133
- Ground to satellite laser ranging experiments for daylight satellite range measurements
23 p4174 A69-42193
- Ionospheric range difference errors after correction for position fixing from satellite, considering elevation angle, latitude, day time, spatial and time electron content correlation
23 p4128 A69-42505
- Satellite photographic astrometry and chronometry, determining spatial positions of satellites and observation stations by space triangulation
24 p4391 A69-43790

SATELLITE TRACKING AND DATA ACQ

NETWORK

U STADAN [SATELLITE TRACKING NETWORK]

SATELLITE TRANSMISSION

Mechanically despun VHF antenna for spin stabilized synchronous satellites, detailing electrical and mechanical design
01 p0161 A69-10350Cloud pictures from weather satellites reception according to automatic picture transmission /APT/ system, discussing design and field strength measurements [UN PAPER 68-95451]
01 p0108 A69-10458International experimentation with U.S. communications satellites, noting design variations with participants and restraintless information exchange [UN PAPER 68-95421]
01 p0108 A69-10474Fucino earth station operation with Early Bird and Intelsat 2-F3 satellites receiving equipment and transmission system [UN PAPER 68-95455]
01 p0028 A69-10493Faraday angle of rotation of radio signals polarization plane from satellites and celestial bodies
01 p0030 A69-10574Communication satellites development in U.S.S.R., discussing Molniya 1 satellite design and objectives and Echo 2 satellite transmission experiments
01 p0032 A69-10949Amplitude scintillations of satellite radio signals during sunrise due to ionospheric turbulence induced electron content variations
01 p0067 A69-10980Transmitting systems of ESRO 2/IRIS satellite for ground station contact, discussing telemetry system, mission requirements and telecontrol
01 p0034 A69-11103Monopulse ground station antenna configuration for improvement of sidelobe level in satellite transmission [DVL-856]
02 p0214 A69-11599Surveyor 5 alpha particle backscattering instrument measurement, TV pictures of lunar surface elemental composition and magnetic and mechanical measurements
02 p0317 A69-12023Satellite power generation and transmission system for solar energy conversion, noting estimates of surface area and weight of collectors
02 p0323 A69-12296Aeronautical satellite system to relay communications at VHF or L band frequencies from aircraft flying over oceanic routes
03 p0464 A69-13235WEFAX /Weather Facsimile/ experiment to explore operational feasibility of direct meteorological data transmission via satellite relay from central station to remote stations
03 p0411 A69-13240Graphical data on atmospheric and rainfall attenuation of spacecraft earth signal, emphasizing transmission via satellites
03 p0397 A69-13727Total ionospheric electron content determination from measurement of phase differences of satellite transmission, discussing data processing and differential Doppler effect measurements
04 p0592 A69-14766Sound and TV broadcasting from satellites, discussing systems for future individual user pickup
04 p0558 A69-15120Sporadic E irregularities in producing amplitude variations in radio star observations and satellite transmission
04 p0594 A69-15125Path length and path length rate variations in synchronous satellite communications link
04 p0561 A69-15448Satellite scintillation at high latitudes and possible relation to soft particle precipitation
05 p0757 A69-16406F region equatorial irregularity belt observed from satellite transmission scintillation, noting north-south elongated patches
05 p0758 A69-16418Satellite picture signal reception from ESSA, Nimbus and ATS to ascertain instrument requirements
06 p0888 A69-17651High power coupled cavity traveling wave tube for satellite communication, noting design techniques and performance characteristics
07 p1094 A69-18427Water effect on air supported radome of ground station for satellite communication
07 p1111 A69-19533Numerical determination of Doppler effect and reduced Doppler frequency difference for two coherent radio waves emitted from earth satellite
07 p1087 A69-19610Conjugate echoes in Alouette 2 topside sounder ionograms explained by multiple reflections between conjugate points of field line, noting magnetospheric waveguides role
08 p1274 A69-20045Direct radio and TV broadcasting from satellite-borne radio transmitter to general public, giving visibility, gains, frequencies and bandwidths tables
09 p1586 A69-21286Radio waves behavior along paths between satellites and earth, studying preferred frequency bands for spacecraft transmitters used as beacons
09 p1451 A69-21293Computer program for processing actinometric data transmitted from Cosmos 122 satellite
11 p1913 A69-24831

Worldwide clock synchronization by geostationary satellite transponder relaying VHF signals from

reference clock, noting accuracy of radio propagation delay prediction

12 p2080 A69-26053

Scintillation index variations based on 40 MHz Explorer 22 satellite signals recorded in Germany

12 p2034 A69-27094

Soviet satellite-borne radio waves studies of ionosphere, considering wave amplitudes, Doppler frequency shifts and outer ionosphere properties

13 p2252 A69-27349

Instructional broadcast satellites programming for time cost reduction, discussing frequency allocation, interference and ground station design

13 p2381 A69-27373

Satellite 40 mc signal scintillations near sunspot minimum, noting scintillation index dependence on angle between radio ray and magnetic field

14 p2439 A69-29114

Computer program for STV-F9 satellite communication parameters, using ELDO forecasting values as input data

14 p2530 A69-29689

Omega/VLF transmission range rate measurements for satellite Doppler navigation to provide velocity and location data, noting propagation error

14 p2479 A69-29857

Faraday angle of rotation of radio signals polarization plane from satellites and celestial bodies

15 p2568 A69-30744

Aoriste antenna to receive radioelectric signals from satellite emitter at distance of 10,000 km

15 p2580 A69-31095

Radio waves behavior along paths between satellites and earth, studying preferred frequency bands for spacecraft transmitters used as beacons

15 p2570 A69-31227

Satellite signal probability density determined from scintillation plus Faraday effect in statistical terms

16 p2751 A69-32103

Signal records from S 66 satellite with strong scintillations, noting fluctuation well described by Nakagami m-distribution and possibility of deriving relations between different indices

16 p2777 A69-32104

Satellite radio signal scintillation variations association with sporadic E and spread F and dependence on magnetic activity in Southern Hemisphere during sunspot minimum

16 p2780 A69-32307

First order Doppler shift in ionosphere and horizontal gradients influence, discussing total electron content determination method made from geodetic satellites using two coherent frequencies

16 p2755 A69-32614

Doppler shift measurements at two coherent frequencies from Diadem satellites to determine ionospheric electron content, discussing accuracy and parameters defining satellite passage

16 p2785 A69-32615

Waveguide feeder for Goonhilly Downs satellite communication antenna reducing feeder loss for use with low elevation Intelsat 3 satellite

17 p2935 A69-32849

Europa 3 rocket design, comparing 2 ton geostationary satellites and 700 kg satellite conceptions

17 p3045 A69-33095

Antenna array construction for reception of weather satellite transmissions, noting automatic picture transmission systems/APT

17 p2946 A69-33767

Irregularities distribution in antarctic ionosphere from polarization angle fluctuations of satellite S-66 radio signals, discussing diurnal magnetic and solar cycle effects

18 p3125 A69-34249

Quasi-transverse /Q-T/ point time lag on Faraday rotation records at widely spaced frequencies during satellite pass explained by refraction theory

18 p3100 A69-34251

Image dissector meteorological cameras, discussing ATS-III and Nimbus systems, high resolution camera and multispectral cameras

18 p3137 A69-35101

Digitized video cloud picture data from ESSA satellite, discussing mesoscale archive and computer products including time averages and composites

19 p3279 A69-35810

Ionosphere disturbances due to high altitude thermonuclear explosions, discussing experimental proof by Cosmos satellites short wave transmitter radio signal scintillation statistical evaluation

19 p3304 A69-36624

Satellite and terrestrial point-to-point communication circuit costs, considering multiple access and small antenna earth stations

19 p3456 A69-36822

Ionospheric electron content and concentration variations analysis based on data of radio waves propagating from satellite, considering Doppler shift and Faraday effect

20 p3486 A69-37027

Computer based onboard satellite PCM telemetry, showing improved adaptability, size and cost reduction

20 p3500 A69-37382

Satellite onboard transmission measurements determining atmospheric water vapor influence on integrated refractivity at specific absorption line resonant frequency

20 p3545 A69-38097

Diffraction pattern of satellite signal field-aligned amplitude scintillation during quiet geomagnetic conditions

20 p3497 A69-38108

Multispectral radiometric analysis of ERTS images, discussing image registration, SNR and atmospheric and diffraction effects

21 p3721 A69-38627

Discrete filters for optimal processing of down-linked satellite data, considering inverse filter development by Kalman filtering techniques

21 p3677 A69-39462

Fluctuations of polarization induced fading periods in short wave transmissions of Soviet earth satellites, showing relation to ionospheric inhomogeneities

22 p3942 A69-41095

Satellite scintillating signals amplitude distribution, correlating observations and theoretical results

23 p4115 A69-41486

Power combining network for high power UHF solid state satellite transmitters with low loss, compact size and input port selection capability

23 p4137 A69-41743

Relativistic Doppler shift effect observed from radio signal periodic variation of GEOS-1 satellite

23 p4126 A69-42389

Faraday rotation diurnal variation plotted by analyzing radio transmissions from Canary Bird geostationary satellite, considering ionospheric electron density peak

23 p4160 A69-42433

Ionospheric electron content measurements at low latitudes close spaced frequency and differential Doppler shift technique, using BE-B and BE-C satellite transmission

23 p4161 A69-42435

Multiple access discrete address system /MADA/ for digital modulation communication systems for satellite networks, using time division techniques

23 p4130 A69-42512

Distributed communications for earth orbiting global satellite network defined parametrically, describing relay/switching and terminal station satellites

23 p4130 A69-42515

Effective color TV transmission via satellite using PCM/PSK modulation, noting dependence on available equipment, bandwidth, desired error rate and SNR

23 p4130 A69-42520

PCM satellite communication systems signal power and frequency bandwidth requirements, noting PCM-psk superiority over FDM-FM

24 p4283 A69-43200

SATELLITES

NT ACTIVE SATELLITES
NT ALOUETTE SATELLITES
NT ALOUETTE 1 SATELLITE
NT ALOUETTE 2 SATELLITE
NT ANNA SATELLITES
NT APOLLO SPACECRAFT
NT APPLICATIONS TECHNOLOGY SATELLITES
NT ARIEL 3 SATELLITE
NT ARTIFICIAL SATELLITES
NT BEACON SATELLITES
NT BIOSATELLITE 2
NT BIOSATELLITES
NT COMMUNICATION SATELLITES
NT COSMOS SATELLITES
NT COSMOS 5 SATELLITE
NT COSMOS 6 SATELLITE
NT COSMOS 149 SATELLITE
NT D-1 SATELLITE
NT DEIMOS
NT DIADEME SATELLITE
NT DODGE SATELLITE
NT EARLY BIRD SATELLITES
NT EARTH RESOURCES SATELLITES
NT EARTH SATELLITES
NT ECHO SATELLITES
NT ECHO 1 SATELLITE

NT ELEKTRON SATELLITES
NT ELEKTRON 4 SATELLITE
NT ESRO 1 SATELLITE
NT ESRO 2 SATELLITE
NT ESRO SATELLITES
NT ESSA SATELLITES
NT EUROPEAN 1 SPACECRAFT
NT EXPLORER SATELLITES
NT EXPLORER 1 SATELLITE
NT EXPLORER 16 SATELLITE
NT EXPLORER 18 SATELLITE
NT EXPLORER 20 SATELLITE
NT EXPLORER 22 SATELLITE
NT EXPLORER 26 SATELLITE
NT EXPLORER 29 SATELLITE
NT EXPLORER 30 SATELLITE
NT EXPLORER 31 SATELLITE
NT EXPLORER 33 SATELLITE
NT EXPLORER 35 SATELLITE
NT EXPLORER 38 SATELLITE
NT EXPLORER 40 SATELLITE
NT FRENCH SATELLITE
NT GEODETIC SATELLITES
NT GEOPHYSICAL SATELLITES
NT GEOS 2 SATELLITE
NT GRAVITY GRADIENT SATELLITES
NT HEOS A SATELLITE
NT HEOS SATELLITES
NT IAPETUS
NT IMP
NT INJUN SATELLITES
NT INTESAT SATELLITES
NT ISIS-A
NT ISIS SATELLITES
NT LINCOLN EXPERIMENTAL SATELLITES
NT LUNAR ORBITER
NT LUNAR SATELLITES
NT METEOROLOGICAL SATELLITES
NT MICROMETEOROID EXPLORER SATELLITES
NT MOLNIYA SATELLITES
NT MOON
NT NATURAL SATELLITES
NT NAVIGATION SATELLITES
NT NIMBUS SATELLITES
NT NIMBUS 3 SATELLITE
NT OAO
NT OGO
NT OGO-D
NT OGO-E
NT OGO-F
NT ORBIS CAL SATELLITE
NT ORBITAL SPACE STATIONS
NT ORBITAL WORKSHOPS
NT OSO
NT OSO-3
NT OSO-C
NT PASSIVE SATELLITES
NT PHOBOS
NT PROTON SATELLITES
NT PROTON 2 SATELLITE
NT RADIO ASTRONOMY EXPLORER SATELLITE
NT RELAY SATELLITES
NT SAN MARCO SATELLITE
NT SAN MARCO 2 SATELLITE
NT SCIENTIFIC SATELLITES
NT SYNCHRONOUS METEOROLOGICAL SATELLITE
NT SYNCHRONOUS SATELLITES
NT SYNCOM SATELLITES
NT TIROS SATELLITES
NT TIROS 9 SATELLITE
NT TRANSIT 4A SATELLITE
NT TRANSIT SATELLITES
NT VELA SATELLITES
NT VENERA SATELLITES
NT VENERA 4 SATELLITE
NT ZODIACAL DUST

I-V characteristics of electron emitting satellite in ionosphere, analyzing spherical Langmuir probe in collisionless plasma in magnetic field

14 p2511 A69-28956

SATURATED HYDROCARBONS

U ALKANES

SATURATION

Saturation effect theory in gas system, taking into account Doppler expansion and collisions based on density matrix

03 p0437 A69-13042

Carbon dioxide band vibration-rotation transitions saturation characteristics, stressing role of collisions in molecular gas lasers

14 p2457 A69-28928

Laser-nonlinear crystal dynamical interactions, studying saturation and coherence properties of second harmonic wave generated inside laser cavity

15 p2632 A69-30026

- Different parametric converters amplitude characteristics analysis for determining necessary pumping power, allowing for saturation
15 p2574 A69-30119
- Pulse radar quantum paramagnetic amplifier protection from saturation by transmitter power, using linear electrical bias of EPR line
15 p2579 A69-30956
- Magnetic anisotropy and porosity from approach to saturation of polycrystalline ferrites based on magnetization measurement
16 p2825 A69-31700
- Q switching of CW 337 mu maser, gain factor measurements for pulse discharges and data on saturation and time dependence
17 p2981 A69-33088
- Diffusion times for saturated region in Hipernom tubes measured for various exciting magnetic fields and pulse duration
23 p4141 A69-42222

SATURN (PLANET)

- Two element interferometer observing Saturn, Uranus and Neptune at 3.12 cm, determining equivalent black body disk temperature
01 p0148 A69-10052
- Saturn ring gravitational field perturbations of space vehicle orbit on flyby mission solved by particle motion perturbation theory
03 p0508 A69-13260
- Saturn ring formation by satellite spiral into Roche limit and disintegration
04 p0660 A69-15128
- Saturn rings optical properties and thickness from edgewise photometric observations, noting luminance relationship to direct brightness
07 p1219 A69-19335
- Photographic photometry of Saturn rings around times of disappearance /1966/
08 p1381 A69-19791
- Latitude measurements for features on Saturn, discussing means and standard deviations
08 p1394 A69-20618
- Magnitude data for Saturn satellites compiled and analyzed, noting discrepancy for Iapetus
08 p1394 A69-20619
- Rocket-borne photoelectric photometers for UV observations of Saturn, using interference filters
09 p1602 A69-22216
- Thermal models for Jupiter and Saturn corresponding to completely convective structure, using De Marcus state equations
09 p1607 A69-22428
- Gravitational potential of circular rings used to investigate motion stability of Saturn rings
10 p1771 A69-22855
- Methane absorption distribution in 6190 A band over Saturn disk at center and polar latitudes based on spectrograms
11 p1960 A69-24731
- Visual mapping and photometric scanning of Saturn with rings from earth, noting ring brightness edgewise linear dependence on rings opening
15 p2697 A69-31256
- Mimas-Tethys commensurability of motions and inclinations, calculating libration amplitude variation by numerical integration
16 p2861 A69-32241
- Radio telescope observations at 11.13 cm for polarized E vector intensities of Saturn and disk temperature of Uranus and Neptune
17 p3039 A69-33731
- Saturn emission peak and flux density at 408 MHz determined by cross telescope, discussing mechanism for enhanced radiation at long wavelengths
17 p3041 A69-33813
- Janus discovery, discussing solar distance, rotation period, diameter, opposition brightness and planetary parameters derived from pictures
20 p3597 A69-37337
- Photographic and spectroscopic observation of Saturn at Cassegrain focus of 122 cm reflector during earth passage through ring plane, discussing Saturn satellites
20 p3600 A69-37481
- Saturn ring dynamical structure theory supported by observations of knots or condensations
20 p3600 A69-37482
- Optical properties and thickness of Saturn rings from observations during ring plane crossing of earth or sun, determining Tethys diameter and albedo
20 p3605 A69-37821

- Saturn surface spectrum near ring shadow examined for water vapor content in ring and greenhouse effect on surface
20 p3616 A69-38305

SATURN LAUNCH VEHICLES

- Saturn fireball thermal environment associated with liquid propellant explosions, using analytical model
04 p0645 A69-14475
- Electrostatic control for portable clean rooms, describing fabrication, assembly and checkout problems with Instrument Unit /IU/ control center for Saturn launch vehicles
19 p3428 A69-35550
- Manual guidance and control of Saturn launch vehicles, considering feasibility, reliability and hardware implementation [AIAA PAPER 69-876]
21 p3824 A69-39402
- Real time network support simulation allowing network configuration for nominal or perturbed trajectory for Saturn vehicles, applicable to any flight azimuth
22 p4020 A69-40319
- Cape Kennedy Space Center mobile launchers and auxiliary equipment for Saturn vehicles, discussing functions, design and systems
24 p4297 A69-43036

SATURN PROJECT

- Saturn software configuration accounting and reporting system for document change and information retrieval
18 p3105 A69-34269

SATURN S- 1C STAGE

- Digital computer systems design optimization based on operational experience in development of Saturn S-1C stage Automatic Test and Checkout System
03 p0400 A69-13233
- Nondestructive weld tests of propellant tanks in Saturn V-S-1C stage
07 p1140 A69-18798
- Thermal and pressure environments analysis in Saturn S-1C stage base during flight tests, noting base gas flowfield and heating [AIAA PAPER 69-318]
09 p1611 A69-22383
- Temperature profiles and frequency driftings of VHF telemetry transmitters for Saturn S-1C stage, using IR radiation data
10 p1653 A69-23049
- Short duration tube wind tunnel supersonic testing, noting Saturn S-1C base heating and solid propellant rocket base burning tests [AIAA PAPER 69-335]
13 p2242 A69-28271
- Saturn S longitudinal instability /POGO/ precluded by lowering S-1C stage propulsion system resonance below structural frequency [AIAA PAPER 69-548]
16 p2868 A69-32658
- Saturn S S-1C stage propulsion performance, using engine parameters from telemetry rather than accelerometer data, analyzed by iterative techniques and computer program [AIAA PAPER 69-733]
16 p2839 A69-32672

SATURN S- 2 STAGE

- Ultrasonic inspection systems to determine and record bond quality on all adhesive bonded assemblies of Saturn S-2 booster and Apollo Command and Service Modules
15 p2632 A69-31515
- Sprayable polyurethane foam external insulation for liquid hydrogen and oxygen storage aboard Saturn S-2 booster
24 p4337 A69-43453

SATURN S- 4B STAGE

- Liquid hydrogen and LOX boost pump design for Centaur missile and liquid hydrogen and LOX chill-down pump design for Saturn 4B missile
01 p0087 A69-11149
- Cryogenic behavior of adhesive materials used in fabrication of liquid hydrogen/liquid oxygen powered Saturn S-4B stage
05 p0784 A69-16487
- System designs for manned spacecraft gravity gradient stabilization of Saturn S-4B stage at 400 km and lunar module at synchronous altitude
07 p1228 A69-18338
- LASSO /modified S-4B/IU/ vehicle mission to place in orbit two unmanned Lunar Modules for landing of radio and optical telescopes on lunar surface
18 p3136 A69-34813

SATURN STAGES

- Feasibility of nuclear stage for space missions, discussing Saturn 5 third stage replacement, payload gain, reactor and engine size
08 p1409 A69-20158

- NERVA rocket engine with 200,000-250,000 lb thrust to replace Saturn 5 upper stage for manned interplanetary flights, discussing Mars flight
08 p1410 A69-21029
- Nuclear rockets as Saturn 5 third stages, emphasizing increased payload or velocity utility and resulting engine and stage requirements [AIAA PAPER 69-555]
16 p2867 A69-31849

SATURN 5 LAUNCH VEHICLES

- Pressurization system for liquid rockets, analyzing inert weight and complexity reduction using Saturn 5 S-4B stage
02 p0305 A69-12386
- Large convective clouds in superheated air generated by static tests of Saturn 5 first stage
03 p0462 A69-14125
- LOX preclude accumulator system with He pressurant for prevention of Pogo effect on Saturn 5
04 p0666 A69-15298
- Integrated nondestructive testing systems to ensure welded assemblies reliability for Saturn 5 program, including surface defect detection
07 p1117 A69-19699
- Saturn 5 holddown and service arm electrical system design program optimized by integrating reliability and maintainability at initial design phase [AIAA PAPER 69-309]
10 p1670 A69-23043
- Nondestructive testing methods for Saturn 5 space vehicle with emphasis on NDT equipment for Apollo program
10 p1699 A69-23050
- Computerized shake test facility for Saturn 5 moon rocket, describing data acquisition, magnetic tape units, X-Y plotters, display devices, etc
10 p1672 A69-23285
- Saturn 5 unstable longitudinal oscillation due to coupling of structure and LOX line frequencies solved by helium injection
11 p1967 A69-25497
- Saturn 5 boost phase environment simulation on Apollo stages, discussing fixtures, load devices, instrumentation and ground test
15 p2588 A69-30405
- Saturn 5 longitudinal instability /POGO/ precluded by lowering S-1C stage propulsion system resonance below structural frequency [AIAA PAPER 69-548]
16 p2868 A69-32658
- Saturn 5 transular payload capability encancement by fuel biasing, propellant utilization systems, trajectory shaping and programmed mixture ratio scheme [AIAA PAPER 69-451]
16 p2839 A69-32669
- Saturn 5 system simulation showing feasibility, efficiency and economy of real time simulation using large mathematical model and general purpose digital computer
18 p3113 A69-34268
- Computer simulation model for Saturn 5 prelaunch system reliability analysis, using Bayesian techniques
18 p3207 A69-34529
- Nondestructive testing methods for Saturn 5 space vehicle with emphasis on NDT equipment for Apollo program
19 p3431 A69-36329
- Plastics applications in Apollo-Saturn 5 program, considering foam, honeycomb, conformal coatings, embedment compounds, dielectrics, damping compounds, adhesives, sealants and gaskets
21 p3751 A69-38533
- Apollo-Saturn 5 propulsion and structure feedback loop, analyzing Pogo components and Nyquist plot application [AIAA PAPER 69-877]
21 p3824 A69-39403
- Navigation state vector update effect on lunar mission completion capability for Saturn 5, emphasizing hardware and scheme errors and accelerometer failure [AIAA PAPER 69-883]
21 p3764 A69-39409
- Manned flyby and stopover missions to Mars and Venus with chemical propulsion and Saturn 5 launch vehicles, noting short duration low energy missions [AAS PAPER 69-492]
24 p4380 A69-42839

SAWTOOTH WAVESFORMS

- Radar FM signal design with zigzag frequency variation, discussing relation between waveform characteristics and associated ambiguity function features
01 p0033 A69-11001
- Sawtooth generators production based on equivalent circuit theory, calculating linearity errors in voltages
08 p1296 A69-20105
- Spherical and rod-plate spark gap response voltage as function of sawtooth wave, cosmic, gamma and UV radiation
11 p1851 A69-25086

SC- 7 AIRCRAFT

Integrating filter analysis for effect of phase detector sawtooth characteristics on locking range of phase locked oscillator

20 p3486 A69-37011

SC- 7 AIRCRAFT

Skyvan 3 light passenger/freight carrier design, detailing power plant, installation and power management

17 p2902 A69-34192

Skyvan 2 aircraft aerodynamic design, describing modifications to increase fuel capacity, directional stability and range capability

17 p2896 A69-34193

Series 3 Skyvan design, describing controls, electric and electronics equipment, weather protection, environmental and fuel systems

17 p2906 A69-34194

Flight compartment and cabin layout of Skyvan 3 designed as freighter with passenger capability

17 p2903 A69-34195

SCALARS

Weighting functions effect in calculating average scalar electrical conductivity in Lorentzian gas

04 p0638 A69-15317

Black body radiation coherence properties characterization by stochastic Gaussian scalar potential correlation function

05 p0795 A69-16819

Brans-Dicke scalar-tensor theory, showing radiative Riemann tensor existence in absence of usual spin-2 gravitational waves

07 p1216 A69-18894

Plane symmetric perfect fluid cosmological model derived from class I considerations, evaluating scalar invariants for line element

07 p1222 A69-19586

Waveguides and resonators design by solving scalar problem for eigenvalues of elliptic operator

09 p1469 A69-22626

Largest scalar product of class and identification codes in diagnostic problems, discussing recognition

14 p2417 A69-29144

Integral scalar equation describing signal attenuation by acoustically soft disk for mirror-shadow method of ultrasonic flaw detection

18 p3137 A69-35109

SCALE [CORROSION]

Impurities effect on defects in oxygen deficient niobium, tantalum and zirconium oxide scales at high oxygen pressures, noting relationship to metal oxidation

03 p0444 A69-13312

Cobalt chromium high temperature oxidation and scale formation

08 p1332 A69-20363

Chemical treatment of Ti during processing, discussing protective coating, scale conditioning, surface contaminant removal and acid pickling

24 p4324 A69-43432

SCALE [RATIO]

Wind velocity evaluating device operating by scale enlargement

12 p2079 A69-25896

SCALE EFFECT

Smooth cylindrical shell stability under axial compression noting effects of scale factor, initial defects, initial stresses and deflections in welded seam, etc

04 p0680 A69-14929

Scale effect on gold films electrical conductivity, analyzing film thickness and electron parameters of mean free path, concentration and surface reflection

12 p2143 A69-26459

Scale factor determination for energy dissipation at clamped ends, analyzing geometric parameter and clamping force effect on oscillation damping constant

17 p3065 A69-33927

Scale factor in designing uniform strength structures for dynamic load effects determined by recording fatigue limit and failure location, using variable cross section samples

23 p4225 A69-41422

SCALE HEIGHT

Neptune atmosphere height scale and density from photometric observation of star occultation

04 p0660 A69-15061

Photoelectric observation of star occultation by Neptune for scale height determination

06 p1008 A69-17694

Mathematical expressions for measuring heights of vertical and nonvertical features with both slant and ground range radar images

13 p2263 A69-28198

Ionized gas height scale changes in polar ionosphere obtained, assuming Chapman type ionization distribution

14 p2436 A69-29052

Sunspot spectra near solar limb for difference between Fraunhofer line continuum and line core formation levels, finding geometrical height scale and pressure equilibrium

22 p4019 A69-40292

SCALE MODELS

Elastic wind tunnel models used for testing at full scale dynamic pressures, discussing scaling laws and manufacturing and testing problems

[AIAA PAPER 68-56] 01 p0011 A69-11018

Scaled solar and gray-body temperature distribution models compared to determine stellar atmosphere

04 p0653 A69-14626

Scaled models for spacecraft thermal control, considering radiation-conduction-convection heat transfer

[SAE PAPER 690196] 07 p1116 A69-18304

Small and full scale model tests for feasibility of retracted rotor aircraft for high speed flight

[AIAA PAPER 69-219] 07 p1055 A69-19550

Graphite and B filament-epoxy resin composites application to aeroelastic dynamic models, analyzing weight savings, fabrication and component stiffness

11 p1990 A69-25508

Thrust balance for scale model of powered nacelle fan jet engine from drag analysis in wind tunnel, deriving fan nozzle velocity coefficient

13 p2199 A69-27446

Multicell air cushion vehicle technology based on 1/4 scale and full scale tests, noting comparison with plenum systems and costs

13 p2202 A69-27547

Variable bypass ratio lift/thrust engine arrangement in relation to safety and economic requirements, using scale model of V/STOL

15 p2672 A69-31542

Scale models of M-1 rocket engine oxygen and hydrogen pump driven two stage turbines used to determine performance and compact inlet manifolds problems

[AIAA PAPER 69-553] 16 p2840 A69-32678

Scale modeling of multilayer insulated spacecraft for thermal design, considering solar probe and two meter telescope models

[AIAA PAPER 69-613] 17 p3049 A69-33267

Critique of paper on comparison of dynamically scaled model rotor test data with discrete azimuth aeroelastic stability theory

[AHS PAPER 341A] 17 p3059 A69-33505

Dynamically scaled model rotor tested in wind tunnel to evaluate blade aeroelastic limits constructed with realistic mass and stiffness distributions

[AHS PAPER 341] 17 p3059 A69-33506

Nonrecirculating wind tunnel configuration with minimum atmospheric wind disturbances for V/STOL vehicles aerodynamic testing

[AIAA PAPER 68-398] 17 p2947 A69-34024

Thermal scale modeling for space hardware development from managerial and engineering viewpoints

[AIAA PAPER 69-1010] 22 p3922 A69-40383

Speed conditions of environmental simulation of thermal scale models of reentry vehicles, considering ablatives with phase-change and involved chemical reaction

[AIAA PAPER 69-1011] 22 p3922 A69-40384

Buoyant Venus Station balloon for deployment and inflation during parachute descent into Venus atmosphere tested with scale model balloons in wind tunnels

[AIAA PAPER 69-1017] 22 p3922 A69-40389

STOL seaplane bottom pressure distribution from tests on scale model of PX-S seaplane, discussing boundary layer control effects

22 p3864 A69-40586

Solid fuel ablation and supersonic combustion processes for various propulsion configurations, testing plastic models in wind tunnel

24 p4414 A69-43569

Scale error correction technique for structural impact modeling using dissimilar materials, involving permanent deformation of spherical caps impacted into liquids

24 p4406 A69-43692

SCALING

Decibel scaling advantages in vibration measurements

04 p0602 A69-15324

Metrological measuring instrument scales selection principles for ensuring constant sensitivity and Q factor

17 p2975 A69-33614

Automated analog scaling for in hybrid computer systems imposing magnitude and frequency constraints, using equations for amplifier input factors

18 p3105 A69-34617

SCALING LAWS

Scaling laws for RF discharge experiments in ionized environments, considering proper limit variables for simulation of electron density

02 p0283 A69-12241

Geostrophic adjustment for neutral and lapse conditions, discussing similarity arguments based on appropriate length and velocity scales

02 p0276 A69-12699

Scaling laws for nose bluntness effects on hypersonic aerodynamics of bodies of revolution

[AIAA PAPER 68-1158] 03 p0362 A69-13566

Scenic holographic stereograms resolution and up/down scaling, discussing roles of projector lens and camera aperture

11 p1883 A69-24690

Proposed index for measuring ionospheric scintillations, describing simplified scaling method

16 p2752 A69-32106

Blast response of model structures fabricated from material differing from prototype structures, testing in dynamic, impulsive and quasi-static loading realms

16 p2874 A69-32164

Froude number for scaling wind stress at air-water interface, verifying logarithmic wind profile and relating shear velocity to surface roughness

17 p2996 A69-33152

Full scale and transonic wind tunnel store separation characteristics, outlining uses of heavy and light scaling methods

17 p2896 A69-34035

Plane, cylindrical and spherical point explosions in combustible gas mixtures for different gas motion models, formulating scaling law for detonation wave model

19 p3449 A69-36353

SCANDIUM

Meteoritic materials investigated for Sc, Ce and Eu content and distribution in various phases, using neutron activation analysis

01 p0026 A69-11376

X ray study of scandium containing ferrites, establishing lattice stresses due to ion replacement in octahedral interstices

03 p0491 A69-14053

X ray study of scandium containing ferrites, establishing lattice stresses due to ion replacement in octahedral interstices

18 p3182 A69-35046

SCANDIUM ISOTOPES

Angular distributions for Sc 45-Ti 46 nuclear reactions involving 41 Mev alpha particles bombardment described by Born approximation

22 p3988 A69-41044

SCANNERS

NT HORIZON SCANNERS
NT INFRARED SCANNERS
NT OPTICAL SCANNERS
NT SUBREFLECTORS

Current distribution in scanning rectangular array with all-directional constant sidelobe and narrowest beamwidth

04 p0570 A69-14302

Directivity and beamwidth determination of large scanning Dolph-Chebyshev arrays

04 p0570 A69-14303

Impedance matching of volumetrically scanned waveguide arrays, stressing element spacing, surface wave impedance, etc

04 p0571 A69-14312

Aircraft gas turbine component pressure data storage and scanning

05 p0726 A69-16768

Scanning beam landing systems for VTOL aircraft

07 p1178 A69-19631

High field domains in Gunn effect diode in transit time mode of operation probed with stroboscopic electron beam in scanning electron microscope

08 p1283 A69-20162

Focusing effect on far field directional pattern shifting of array normal, noting electronic scanning properties

08 p1285 A69-20400

Scanning antenna array design utilizing element coupling and telescope type cylindrical optical system

10 p1664 A69-23800

Signal processing and DC restoration in line scan devices used in land/water terrain analysis

12 p2096 A69-26980

Plasma scanner in obtaining current cross sections and current-voltage characteristics of hollow cathode magnetically confined arc plasma in argon
14 p2450 A69-29568

Microwave scanning beam landing guidance system for Swedish tactical aircraft Saab 37 Viggen, reviewing ground station and onboard equipment
16 p2735 A69-32057

Electronic device utilizing scanning beam to evaluate limb photographs, reducing errors by introducing second generator with frequency proportional to deflecting potential variation
17 p2970 A69-32884

Scanning electron microscopy to study device failure and performance, discussing limitations and progress
17 p2936 A69-32890

Scanning electron mirror microscope advantages over electron mirror and scanning electron microscopes for examining integrated circuits
17 p2971 A69-32891

Scanning electron microscopy of devitrifying solder glass seals for hermetic packages, biased integrated circuits and metallization corrosion
17 p2936 A69-32892

Scanning electron microscopy for reliability studies in semiconductor devices
19 p3382 A69-35788

Electronic scanning and correlation techniques for terrain sensing required in automatic stereoperception
24 p4316 A69-43566

SCANNING

NT FREQUENCY SCANNING
NT PANORAMIC SCANNING
NT RADAR SCANNING

Phase, frequency and amplitude scanning, noting array design and applications
01 p0049 A69-11348

Two dimensional electronically scanned k-band phased array antenna design and performance, discussing radiometric system
04 p0572 A69-14328

Butler matrix-fed circular array for continuous 360 degree beam scanning
04 p0573 A69-14329

Parabolic antenna beam scanning by defocusing, calculating relationship between reflector and beam tilt angles
07 p1089 A69-18248

Holography by scanning receiver, source, object or both source and receiver, discussing resolution, magnification, image position and aberrations
07 p1136 A69-19640

Hemispherical scanning with small aperture monopoles, spirals, scimitars and wire antennas, discussing various types for multiple beam operations
08 p1290 A69-20973

Northern sky scan for discrete sources of gamma rays in 240 to 1000 kev energy region by telescope on balloon flight
11 p1946 A69-24593

Holographic scanning technique for laser beam deflection, noting two and three dimensional raster scanning
11 p1885 A69-24847

Theory of field distribution in antenna aperture extended to scanning with desired shape beam
15 p2578 A69-30634

Phased array blindness at inoperative scan angles explained in terms of elements excitation and termination caused by leaky wave
17 p2928 A69-33872

Spectral analyzer for structural noise spectrum of scanning ray TV transmitter
17 p2939 A69-33909

Celestial sphere scanning by passive method applicable to space missions requiring long lifetime and moderate pointing accuracies
[AIAA PAPER 68-854] 21 p3767 A69-39764

SCANNING DEVICES

U SCANNERS

SCAT

U SUPERSONIC COMMERCIAL AIR TRANSPORT

SCATTER PROPAGATION

NT IONOSPHERIC F-SCATTER PROPAGATION
Three-dimensional holography using scatter plates applicable to transilluminated objects in particular distribution of particles or phase disturbances
01 p0079 A69-10217

Soviet book on multichannel and TV signals transmission over radio relay links using microwave tropospheric scatter propagation
04 p0558 A69-14919

Soviet book on meteor trail scatter communications covering civil and military advantages over troposcatter systems, meteor trail scatter properties, etc
04 p0562 A69-15488

High resolution azimuth and elevation arrays sensing remote ionosphere and sea surface characteristics, discussing backscatter data for ionosphere and sea scatter
14 p2448 A69-29520

Variable scatter mechanism in turbulent tropospheric propagation medium, employing dynamic meteorology concepts for frontal disturbances effect on scatter volume
17 p2927 A69-33856

Scattered ionospheric reflection distribution at evening/morning periods showing deviation, using coherent method
17 p2927 A69-33860

Electromagnetic waves scatter propagation in isotropic plasma in plane waveguide, noting electron charge density fluctuations role
23 p4125 A69-42040

SCATTERERS

U SCATTERING

SCATTERING

NT ACOUSTIC SCATTERING
NT ATMOSPHERIC SCATTERING
NT BACKSCATTERING
NT COHERENT SCATTERING
NT COMPTON EFFECT
NT ELASTIC SCATTERING
NT ELECTROMAGNETIC SCATTERING
NT ELECTRON SCATTERING
NT FORWARD SCATTERING
NT INCOHERENT SCATTERING
NT ION SCATTERING
NT IONOSPHERIC F-SCATTER PROPAGATION
NT LIGHT SCATTERING
NT MICROWAVE SCATTERING
NT MIE SCATTERING
NT NEUTRON SCATTERING
NT NUCLEAR SCATTERING
NT PROTON SCATTERING
NT RADAR SCATTERING
NT RAMAN SPECTRA
NT RAYLEIGH SCATTERING
NT RESONANCE SCATTERING
NT REVERBERATION
NT TROPOSPHERIC SCATTERING
NT WAVE SCATTERING
NT X RAY SCATTERING

Carrier scattering mechanisms in n-type GaP, measuring IR radiation absorptivity in Te doped GaP
03 p0492 A69-14168

N-type GaAs single crystal magnetoresistivity, noting charge carrier scattering mechanisms
03 p0492 A69-14177

Monograph on atmospheric radiation transfer including absorption, scattering, direct, diffuse, global, thermal and net radiation
12 p2073 A69-26918

Normal and directional emittance for two dimensional emitting, absorbing and scattering semiinfinite plane slab based on Monte Carlo method compared with Bobco approximation
[AIAA PAPER 69-625] 17 p3005 A69-33301

SCATTERING AMPLITUDE

Polarized orbital method for calculating electron-atom scattering amplitudes, noting discontinuous wave function, nonvariational technique and strong dependence on parameter
02 p0284 A69-12702

Long range ionospheric propagation of ultrashort radio waves, obtaining diurnal and seasonal characteristics of reflected signals amplitude and duration
13 p2255 A69-28543

Spotted scattered background contrast relation to scattering system geometry during laser scattering by suspended Lycopodium spores
13 p2273 A69-28550

Plane light wave propagation in homogeneous isotropic medium with fluctuating dielectric constant using perturbation theory and integrating energy conservation law
18 p3173 A69-35127

Raman spectrum of solid alpha-nitrogen at low temperatures, calculating scattering intensities and Raman active librational lattice vibrations
23 p4194 A69-42204

Negative pions elastic scattering from hydrogen, confirming differential cross section minimum for specific incident momentum-scattering angle region
24 p4352 A69-43049

SCATTERING COEFFICIENTS

Radiation from isothermal sphere in vacuum having spherical scattering indicatrix solved by Bubnov-Galerkin method with allowance for scattering
01 p0174 A69-10106

Atmospheric extinction coefficient and backscattering function determined by laser radar using differential equation
07 p1126 A69-18966

Lunar scattering of meter radio waves emitted by Luna 11 and 12 satellites, relating glide angle scattering coefficients to satellite altitude
07 p1087 A69-19615

Reflection and transmission scattering coefficients for step type transition between two uniform waveguides with surface impedance boundaries, discussing coupled differential equations
08 p1272 A69-20020

Plane and spherical albedos of planet surrounded by infinite optical thickness atmosphere, with application to Venusian atmosphere
10 p1776 A69-23210

Transmission and reflection scattering coefficient measurements of microwave networks by Fourier analysis of transient response to impulsive or steplike waveforms
12 p2038 A69-26056

Transport equation numerical solution for unsteady radiation field by straight lines method, allowing for scattering indicatrix forms with passage of time
13 p2350 A69-27858

Backscattering intensity measurements by optical elements at 180 degrees to beam propagation direction, using CW He-Ne laser as radiation source
20 p3554 A69-37609

Normalized phase function and scattering coefficient of aerosols prediction from measurements of particle size distribution, density and refractivity based on Mie solution
21 p3719 A69-39774

SCATTERING CROSS SECTIONS

Electron impact spectrometer for obtaining molecular energy loss spectra used to investigate scattering cross sections for optically allowed and forbidden transitions
01 p0123 A69-10620

Initial ionization rates and collision cross sections in shock heated argon in low pressure shock tube, using double electrostatic probes
01 p0132 A69-11206

Raindrop size distribution law effect on radio wave attenuation coefficient and differential effective backscattering cross section of rain
02 p0208 A69-12259

Born approximation for calculating low temperature plasma transport properties from quantum mechanical scattering cross sections on Debye potential
02 p2921 A69-12486

Angular distribution of radiation scattered by microscopic polyvinyl toluene sphere monolayer, noting intensity distribution approximation using Mie theory
[AIAA PAPER 68-30] 02 p0282 A69-12503

Elastic scattering cross section for low energy electrons on metastable He atoms, using polarized orbital method
03 p0469 A69-12922

Differential cross sections for elastic scattering of 600 Mev protons from He 3 between 19 and 45 degrees
03 p0472 A69-13464

Very thin short metallic filament scattering and absorption cross sections for various values of filament conductivity
03 p0395 A69-13623

Transport diffusion cross sections of slow electrons during scattering at inert gas atoms by microwave method, calculating electron transfer coefficients
03 p0481 A69-14143

Mie total and differential backscattering cross sections at laser wavelengths for Junge size distribution aerosol models
04 p0609 A69-14290

Angular distribution of reactive elastic scattering analyzed by opacity function/reaction probability/
04 p0554 A69-14859

Relativistic analysis of far zone electromagnetic scattering by conducting sphere moving through incident plane wave, calculating scattering cross section
04 p0559 A69-15212

Atomic hydrogen-bromine linear collision reaction intermediate formation and reactive scattering cross sections quantum mechanical calculation, using perturbed Morse oscillator approximation
05 p0796 A69-15911

Differential cross section frequency dependence for resonant scattering of monochromatic light by dilute gas atoms
[IEEE PAPER T-8] 05 p0776 A69-16328

Hydrogen ions collision-induced dissociation cross section angular dependence measured, showing qualitative agreement with theoretical predictions
05 p0798 A69-16698

First Born approximation cross sections for He excitation from ground state by proton impact calculated, using wave functions
06 p0960 A69-17027

Electron impact excitation cross sections for emission from first negative bands of positive N molecule ion
06 p0961 A69-17135

Polar molecule rotational excitation diffusion cross sections for electron scattering
06 p0961 A69-17139

Rayleigh scattering cross sections for He, C, N and O compared with corresponding absorption coefficients, noting opacity of H deficient stars
06 p1002 A69-17319

Atmospheric droplets diameter, number density and scattering cross sections determined from laser radar return equation and Mie theory
06 p0888 A69-17483

Plane wave scattering by conducting wire impedance loaded at center, discussing loading effect on backscattering cross sections
06 p0888 A69-17512

Angular dependence of low energy electron impact excitation cross section of lowest molecular hydrogen triplet states
06 p0962 A69-17820

Incoherent scatter power measurements, comparing square law signal detection, phase coherent receiver and parametric amplifier methods
07 p1085 A69-19222

Quantitative radar determinations of radio wave scattering cross section of lunar surface layer
07 p1087 A69-19621

Quantum mechanical, dipole approximation, non-resonance light scattering cross sections expressed in terms of oscillator strengths and refractive indices
07 p1183 A69-19645

Cross sections for inelastic interactions of electrons with atoms and heavy impurity ions and processes of atomic excitation
07 p1195 A69-19652

Electron collisional excitation cross sections for upper states in Ar ion lasers
07 p1157 A69-19656

Bounds on scattering lengths, phase shifts and other scattering parameters determining cross sections, noting variational bounds for zero incident energy
07 p1186 A69-19657

Electron collisional excitation cross section calculations for atoms and ions using modified Born approximation taking into account three physical effects
07 p1187 A69-19658

Cross section calculations for elastic and inelastic electron collisions with atoms, ions and molecules and ionization of atomic systems by electrons and photons
07 p1187 A69-19660

Atomic collision theory, discussing cross section calculations by Gryzinski classical method, variational methods and Fadeev equations for three particles
07 p1187 A69-19661

Electron collision excitation of positive ions, calculating collision cross sections for transitions between levels of P term
07 p1187 A69-19714

Coupling between array antennas shown to reduce reflecting properties of Van Atta reflector consisting of linear half wave dipoles
08 p1282 A69-20037

Radar scattering cross section of finite perfectly conducting wedge for case of illumination by polarized plane wave
08 p1274 A69-20047

Absolute excitation cross sections for emission of second positive bands of nitrogen under electron impact
08 p1355 A69-20208

Collision cross sections between monatomic gas impurities and metastable atoms in He-Ne laser from output curve and impurity partial pressure
08 p1325 A69-20278

Plasma diagnostics methods for evaluating collision and transport cross sections, discussing resonance fluorescence, steady state discharge and afterglow measurements
08 p1364 A69-20476

Excitation cross sections of Fe XIV lines in solar coronal spectra, comparing computations with Coulomb-Born approximation
08 p1392 A69-20563

Inelastic transport cross sections for Lyman alpha transitions in hydrogen
08 p1357 A69-20814

Tables of effective electron cross sections and macroscopic coefficients, Volume 1, covering hydrogen and rare gas molecular and atomic interactions with electrons
09 p1541 A69-21579

Temperature stability of slightly ionized gas for arbitrary collision cross sections, discussing electron temperature variation as function of electric field strength
09 p1551 A69-22039

Effective cross sections of electron-neutron interaction in photosphere and sunspots, calculating electric conductivity and anisotropy coefficient
09 p1579 A69-22175

Collision broadening cross sections of OH UV transition at room temperature, using flash photolysis
09 p1543 A69-22252

Line blanketing for two level atom with spectral line formed in pure absorption and noncoherent scattering, studying wavelength and depth dependence
09 p1606 A69-22424

Interplanetary magnetic fields characteristics and magnetic inhomogeneities spectra from cosmic ray variation studies used to obtain scattering mean free path
10 p1757 A69-22824

Rotational excitation and scattering cross sections for rigid diatomic molecules reduced to yield distorted wave approximation, resulting in inelastic transition probabilities
10 p1726 A69-23524

Disturbed index of refraction scattering cross sections and aircraft acceleration increments for clear air turbulence, deriving correlation for measurements
10 p1656 A69-23651

Surface currents, scattered field and scattering cross section for perfectly conducting cylinder found by reducing two dimensional problem to solving coupled differential equations
10 p1657 A69-23860

Cut-off Coulomb potential transport cross sections compared with exponentially screened potential for various cut-off radii
11 p1924 A69-24309

Resonances in cross sections for electron impact excitation of forbidden lines in oxygen molecular ion at near threshold energies for astrophysical applications
11 p1921 A69-24417

Neutron production cross sections prediction at proton bombarding energies below 50 Mev and above threshold for multiple nucleon emission
12 p2192 A69-26299

Horizontally moving body wake scattering cross section calculated with allowance for sphericity of incident and scattered radio waves, using Bessel functions
12 p2031 A69-26699

Molecular beam scattering analysis by four parameter B-C intermolecular potential, plotting expansion coefficients against reduced curvature
13 p2301 A69-27206

Negative charge production by H atoms collisions with rare gases and hydrogen, noting smooth rise of cross section with energy for rare gases
13 p2302 A69-27459

Inelastic interaction cross sections of nuclear active particles at C and Fe in 70 to 1000 GeV energy range
13 p2330 A69-28383

Inelastic interaction cross sections of nuclear active cosmic ray particles with atomic Fe and Pb in 100 to 1000 GeV range
13 p2330 A69-28384

Inelastic scattering cross sections calculated, comparing results for various nuclear states expressed as Wood-Saxon radial and harmonic oscillator functions
14 p2504 A69-29006

Core polarization effects in inelastic scattering cross sections for several nuclei in 2s-1d shell, using Hartree-Fock wave functions and Born approximation
14 p2487 A69-29007

Unignited mode converter and emitter work function patches, calculating electron-cesium momentum transfer cross sections from saturation current measurements
14 p2490 A69-29240

Rare gases total excitation cross sections absolute values measured in collision chamber, noting energy

distribution of exciting electron beam, fine structure, etc
14 p2493 A69-29693

Kinetic theory of gases collision cross section definition compared to usual definition, discussing time reversed collisions
14 p2488 A69-29993

Finite scattering cross section in current carriers scattering on impurities in compensated semiconductors, assuming unscreened Coulomb potentials
15 p2666 A69-30063

Partial wave description for calculating cross sections of fine structure transitions of Na in collision with He, discussing shape resonances
15 p2655 A69-30198

Low energy neutral bremsstrahlung cross sections for Ne, Ar and Xe, using rapid scanning spectrometer
15 p2657 A69-31159

Radiative scattering cross sections of electrons from neutral O and atomic and molecular N using rapid scanning spectrometer for bremsstrahlung intensity
15 p2657 A69-31160

Thermodynamic Green function for Compton scatter cross section of photons by electrons in hot plasma
15 p2664 A69-31479

Charge transfer cross section between mercury ion and Cs assessed, considering ion engine positive ion beam neutralization
16 p2835 A69-31895

Elastic scattering cross sections of negative pions by deuterons compared with Glauber model calculations
17 p3007 A69-32885

Current distribution and scattering cross section of missile with plume/ionized trail/of tapered conductivity due to plane wave electromagnetic excitation
17 p2921 A69-33671

Spectrum and cross section of radio wave scattering in two temperature plasma, relating differential backscattering cross section to ionospheric electron density fluctuations
17 p2930 A69-33895

Plane electromagnetic wave scattering by motion of small ellipsoid in vacuum, noting total scattering and radar cross sections dependence on ellipsoid velocity
18 p3105 A69-35485

Elastic scattering cross sections for 21-Mev incident protons measured for nuclei differing in mass, determining optical model potential
18 p3179 A69-35489

Wall boundary condition model modification applied to molecular beam-solid surface scattering, noting qualitative agreement with observed distributions
19 p3377 A69-36179

Heated supersonic beam study of He-Ar intermolecular potential, determining total elastic collision cross section as function of velocity in scattering chamber
19 p3377 A69-36183

Molecular N rotational temperature effect on rare gases scattering cross section
19 p3377 A69-36184

Ar-Kr integral collision cross sections based on density measurements of Ar beam passed through liquid nitrogen cooled Kr filled scattering chamber
19 p3378 A69-36185

Energy dependence of elastic total collision cross section of identical He molecules, using velocity selected primary beams at low target temperature
19 p3378 A69-36186

Atom-atom scattering potential from phase shifts, using WKB formula and Jeffreys-Born approximation
19 p3378 A69-36189

Scattering cross sections of radio waves at wake of vertically moving body near reflecting ionospheric layer, noting wave sphericity influence
20 p3486 A69-37023

Radio wave sphericity influence on scattering at moving body wake in ionosphere, determining scattering cross section principal maximum
20 p3486 A69-37024

Differential cross sections for elastic scattering of protons by Ar atoms in energy range 12.7-44.1 eV, estimating internuclear separation
20 p3580 A69-37499

Atom-atom collisional excitation cross sections obtained from ionization cross sections, noting Thomson classical theory
20 p3580 A69-37500

Coupled equations for determining cross sections for rotational transitions in CN induced by low energy electron impact
21 p3773 A69-38476

Semiempirical electron impact cross sections and energy loss functions applied to dayglow and auroral intensities calculation, discussing atomic and aeronomic implications

21 p3713 A69-38527

Electromagnetic wave scattering from rough layer with plane and rough interfaces, determining scattering cross sections from electrical field and power density

21 p3677 A69-39459

Diatomic-monomeric oxygen collision cross section determined from rotational line width in diatomic oxygen Schumann-Runge emission spectra

22 p3983 A69-40099

Metals conductivity under high pressure, giving theories for electrons scattering cross sections on ions and for Debye temperature

22 p3980 A69-40187

Stueckelberg formulation for transition probabilities to interpret perturbation effects in elastic scattering differential cross section measurements

22 p3987 A69-41005

Impact parameter versions of two state and Born approximations to calculate single excitation cross sections of H atoms ground state collisions

22 p3987 A69-41006

Hydrogen-hydrogen excitation collisions by impact parameter treatment, investigating rotation coupling influence in four state cross sections approximation

22 p3987 A69-41007

Nonresonant and resonant cross sections for gamma ray transitions involving isobaric-spin mixed states in Be 8

22 p3987 A69-41043

Inelastic proton scattering cross sections for target nuclei in 2s-1d shell calculated in distorted wave Born approximation with projected Hartree-Fock wave functions

22 p3988 A69-41045

Radio wave scattering cross section in wake of body moving in ionosphere, using simplified procedure with asymptotic expressions

22 p3901 A69-41094

Inelastic collision cross sections for low energy interactions among electrons, ions, atoms and molecules determined as function of temperature, using approximate methods

23 p4194 A69-41520

Randomly oriented disks and rods scatter pattern used to determine causes of log-normal distribution of radar cross section fluctuations

23 p4116 A69-41592

Bistatic radar scattering cross sections for reentry vehicle with ionized wake

23 p4116 A69-41593

Ionospheric heating and velocity dependence of collision cross sections on transversely propagated equatorial hydromagnetic waves, discussing ordinary and extraordinary modes

23 p4161 A69-42437

Lyman alpha radiation from electron collisions with simple H-containing molecules, finding dissociative excitation cross section role

24 p4351 A69-43033

Negative pions elastic scattering from hydrogen, confirming differential cross section minimum for specific incident momentum-scattering angle region

24 p4352 A69-43049

Differential cross section and polarization measurements for elastic scattering of high energy protons from light nuclei

24 p4352 A69-43125

Elastic differential Li ion scattering cross sections on helium, nitrogen and oxygen

24 p4354 A69-43817

SCATTERING FUNCTIONS

Specific effective scattering area on lunar surface using Luna 13 signals from Oceanus Procellarum measured with radar employing antenna with narrow radiation pattern

01 p0158 A69-11312

Probabilistic model for scattering function to solve radiative transfer problems in externally illuminated spherical shell atmosphere with perfectly absorbing core

02 p0328 A69-12751

Spatial autocorrelation functions of amplitude and phase fluctuations in plane parallel to wavefront of incident wave for conditions of multiple scatter

03 p0468 A69-13807

Flux equivalences of reflected and transmitted radiation among Rayleigh, isotropic and other scattering models

04 p0687 A69-15281

Maximum number of binary collisions for three particles with zero range forces in relativistic rescattering singularities studies

08 p1353 A69-19788

Diffuse reflection and transmission of parallel rays by homogeneous two layer slab, solving simultaneous integral equations governing auxiliary functions

08 p1350 A69-19799

Brightness coefficients for isotropic scattering of homogeneous plane layer in turbid medium, using Legendre polynomials

11 p1960 A69-24733

Angular distribution of electrons leaving plasma at electrode boundary, using kinetic Boltzmann equation with scattering function and specular reflection

11 p1933 A69-25546

Spatial distribution patterns of gaseous argon atoms scattered from solid argon surface

13 p2300 A69-28658

Coherence-polarization in remote sensing by microwave and laser means, analyzing scattering functions of rough surfaces

14 p2448 A69-29532

Anisotropic scattering of current carriers in semiconductors, obtaining general expression for mobility tensor with variational principle

14 p2508 A69-29667

Radiative heat transfer in nonisothermal scattering media of plane, spherical and cylindrical geometries separated by particle cloud

16 p2878 A69-31925

Asymptotic formulas for X and Y functions for resonance radiation scattering in layer, analyzing Doppler absorption and line profiles

16 p2813 A69-32588

Ambiguity function interaction with target scattering function in range-Doppler radar, discussing matched filtering application

20 p3490 A69-37641

Scattering equations for sonic boom waveform spike perturbations produced by atmospheric turbulence, discussing supersonic aircraft pressure signatures

21 p3646 A69-38689

Radiative heat transfer in nonisothermal absorbing and emitting media without scattering and with anisotropic and isotropic scattering

23 p4239 A69-41632

SCATTERING MATRIX

U S MATRIX THEORY

SCAVENGING

Jet engine intershaft bearing oil feed design, discussing use of nonrotating feed link and improvement of oil scavenging at high altitudes

15 p2671 A69-30702

SCENEDESMUS

Tryptic digestion of C terminal tritiated peptides analyzed with Scenedesmus ferredoxin, noting use for protein structural study

10 p1648 A69-24190

White rats diet containing alcohol-soluble fraction of Chlorella and Scenedesmus biomass, noting changes in adrenal cortex and renal glomerulus

17 p2906 A69-32930

Scenedesmus algae cell wall structure degrading to increase digestibility of cell bound protein, describing mechanical, enzymatic and chemical methods

21 p3667 A69-39701

Scenedesmus ferredoxin amino acid sequence

22 p3896 A69-40435

Oxygen exchange in Scenedesmus and Chlorella as function of carbon dioxide, compensation point, Hill activity and photorespiration, using mass spectrometry

23 p4099 A69-42528

SCF

U SELF CONSISTENT FIELDS

SCHEDULES

U COUNTDOWN

SCHEDULING

Cost and schedule planning and control /CSPC/ project progress reporting technique

05 p0850 A69-16300

Airport alternate facilities, restrictive flight schedules and fee schedules for relieving airport congestion during peak traffic hours [AIAA PAPER 69-820]

19 p3453 A69-35595

Human observers visual monitoring of multiple meter display differentially controlled by concurrent signal scheduling

23 p4081 A69-41438

SCHELKUNOFF PRINCIPLE

Magnetic field plane radiation patterns for tapered dielectric rod antennas computed by Schelkunoff principle, noting taper angle effect on lobes

09 p1464 A69-22097

SCHIFF BASES

U IMINES

SCHLEICHER AIRCRAFT

Schleicher glider AS-W15 prototype tests, discussing balsa sandwich structure and flight characteristics

10 p1633 A69-22872

SCHLIENEN PHOTOGRAPHY

Schlieren method for studying rotating sphere heat transfer during natural convection

01 p0174 A69-10095

Flow field in fluidic temperature sensor using schlieren and shadowgraph techniques [ASME PAPER 68-WA/FE-29]

05 p0763 A69-16102

Mode locked laser as stroboscopic light source potential by investigating expansion of laser produced plasma by schlieren photography [IEEE PAPER H-1]

05 p0774 A69-16315

Modified schlieren interferometer for quantitative investigation of free convection boundary layer temperature profiles

07 p1130 A69-18263

Velocity measurement by combination of Doppler principle and schlieren method involving reflection, refraction or diffraction of laser beam

07 p1135 A69-19259

Schlieren optics study of omega wave in water filled cuvette, noting propagation by wall reflected water wave

08 p1350 A69-19889

Holography applied to schlieren and phase contrast methods to enable visualization of minute phase change in light scattering object

08 p1313 A69-20176

Kine films of gas flows within highly luminous transient arc taken by laser schlieren technique

08 p1316 A69-20615

Monograph on schlieren-optical technique for plasma beam temperature measurements using photoelectric scanning device

12 p2134 A69-26120

Shadow and schlieren photography, interferometry and quantitative data treatment obtainable by high speed multiframe photographic arrangement, using laser beam

12 p2086 A69-26165

Pulsed laser holography used in conjunction with schlieren three dimensional system for observing gas density gradients at different test positions

12 p2088 A69-26179

Diffraction theory of schlieren photometric slot and wire methods for cylindrical light wave of even order, discussing Fresnel diffraction for spherical wave

12 p2088 A69-26180

Quantitative schlieren technique for one dimensional recording of light refraction in density gradients of high speed flow fields

12 p2088 A69-26181

Schlieren high speed photography systems for ballistic projectile studies, discussing use of gas lasers as nanosecond light sources

12 p2088 A69-26182

Flow field over plain or complex bodies with pressure density changes, using high speed schlieren apparatus with color strip filter

12 p2088 A69-26183

Schlieren and photoelastic methods for continuous and pulsed ultrasonic waves propagating in transparent media, discussing nondestructive testing applications

15 p2617 A69-31510

Schlieren method for visualization of refractive index changes in transparent materials, discussing application to study of elastic wave fields

17 p2973 A69-33322

Streak photographs by differential interferometer to study head wave standoff in shock tubes as function of time

18 p3085 A69-34473

Rotating static thrust propeller or hovering rotor flow field study by schlieren photography, considering vortex field, tip flow and shock wave formation

18 p3087 A69-35218

Double knife-edged double-crossing schlieren apparatus analyzed for operation principle and applied to measure hypersonic wake characteristics in hotshot tunnel

19 p3293 A69-35740

Quantitative density data from schlieren measurements by photomultiplier technique for axisymmetric flow outside diffraction bands

19 p3306 A69-35741

Shock wave interaction and bow shock wave establishment near sphere in presence of ionization relaxation, using time resolved schlieren photography

19 p3450 A69-36361

Coherent radiation short pulses from mode locked laser permitting schlieren photography of plasma growth

21 p3736 A69-38795

SCHMIDT CAMERAS

Novas in M 31 on Tautenburger Schmidt photographs

08 p1382 A69-19873

Schmidt all-reflecting telescope for UV imaging in Apollo Earth Orbital Scientific Experiment

11 p1887 A69-25101

Astronomical data collection and evaluation, discussing digital distance measurement, photoelectric photometry, servocontrols and electronic computers suited for Schmidt telescope output

20 p3539 A69-37525

Schmidt camera image quality examined with spot diagrams, emphasizing methods of color confusion reduction over wide wavelength range

20 p3546 A69-38272

SCHMIDT METHOD

Benard convection cells analyzed by Boussinesq approximation and Schmidt-Liapunov method, obtaining boundary value problem branching solution

19 p3301 A69-36791

SCHMIDT NUMBER

Turbulent Schmidt number as function of ratio between turbulent and molecular kinematic viscosities for He, carbon dioxide and normal octane eddy diffusivities

21 p3852 A69-39432

SCHOOLS

Aerospace research pilot school /ARPS/ to train experimental test and aerospace research pilots and Manned Orbiting Laboratory /MOL/ astronauts

06 p0882 A69-17670

SCHOTTKY EFFECT

U WORK FUNCTIONS

SCHREIBERSITE

Barringerite as Fe-Ni phosphide occurring in meteorite Ollague pallasite, indicating troilite and schreibersite crystallization at high temperatures

18 p3205 A69-35433

Fe-Ni-P phase diagram studies applied to schreibersite and rhodite formation in iron meteorites

19 p3417 A69-36132

Morphologies and mechanical properties for identification of phosphides /schreibersite/ and carbides /cohenite/ in iron meteorites, noting nucleation and growth

19 p3417 A69-36133

SCHROEDINGER EQUATION

Separation of center of mass and rotational coordinates from N electron diatomic Schrodinger equation

04 p0554 A69-14861

Particle motion, deriving Lagrangian formalism equivalent to Schrodinger equation for random motion theory

07 p1182 A69-19455

Elastic medium properties recovered from reflected or transmitted plane waves at normal incidence, obtaining computational procedures and analytical solution from Schrodinger equation

13 p2300 A69-28664

Master equation in quantum optics phase-space formulation based on Schrodinger equation of motion, noting application to Volterra integral equation and Born approximation

15 p2633 A69-30307

Stellar system stability for corresponding stable barotropic gaseous system, discussing Schrodinger operator role

16 p2862 A69-32374

Franck-Condon factors for band systems of molecular hydrogen, computing wave functions for each electronic state by numerical solutions of radial Schrodinger equation

21 p3774 A69-38758

SCHULER TUNING

Schuler gyroscopic pendulum, noting magnitude requirement for gravitational field used in inertial navigation

02 p0248 A69-11593

Hybrid OMEGA inertial system for following vehicle maneuver without lag developed by combining Schuler tuned inertial data and radio position data

07 p1177 A69-19209

Mathematical basis for inertial vertical gyro development, considering Schuler conditions fulfillment with integral position correction

19 p3311 A69-36193

SCHUMANN-RUNGE BANDS

Oscillator strength determination for Schumann-Runge band system in molecular oxygen

02 p0284 A69-12832

Oxygen absorption coefficients for atomic silicon in spectral range of Schumann-Runge bands

06 p0960 A69-17090

Oxygen line absorption at elevated temperatures in Schumann-Runge system, estimating line widths

06 p0962 A69-17803

Effective cross sections of UV radiation absorption by molecular oxygen in Schumann-Runge bands at high temperatures

11 p1921 A69-24617

Nighttime molecular O densities between 100-130 km determined from Schumann-Runge absorption data for successive far UV spectra of hot star

14 p2435 A69-28959

Molecular oxygen rate of dissociation resulting from absorption in Schumann-Runge bands, calculating effects on chemistry of lower thermosphere and upper mesosphere

20 p3534 A69-38089

Absorption spectrum of diatomic oxygen excited by AC silent discharge photographed with vacuum spectrograph, associating lines with Schumann-Runge band

20 p3581 A69-38276

Diatomic-monomeric oxygen collision cross section determined from rotational line width in diatomic oxygen Schumann-Runge emission spectra

22 p3983 A69-40099

SCHWARZSCHILD METRIC

Observable surface of part of Friedmann universe calculated using analytical continuation of Schwarzschild coordinate system, noting angular extent and angle of observation effect

02 p0314 A69-11644

Coordinates interpretation in Schwarzschild problem, projecting space of events by light beams onto Galilean system at infinity

03 p0506 A69-13090

Energy definition in relativity for steady state universes, particularly Schwarzschild universes

05 p0792 A69-15683

Schwarzschild perfect fluid spheres stability to radial perturbations, noting fluid adiabatic index relation to critical value

07 p1221 A69-19585

Coordinate transformations eliminating singularities in gravitational radius of Schwarzschild metric, noting local Lorentz transformations

08 p1351 A69-19952

Counterexample to Tangherlini argument, discussing inconsistency of postulates leading to Schwarzschild metric without field equations

09 p1540 A69-22100

Covariant equations of motion of body of variable mass in general relativity, considering Schwarzschild field, rotating mass field and Einstein static universe

11 p1965 A69-25744

Singularity of Schwarzschild spherically symmetrical solution to Einstein equations of general relativity theory, exemplifying Lemaitre coordinate system

12 p2129 A69-25974

Icarus radar and optical observations analyzed to verify general relativity predictions using Schwarzschild metrics and to estimate solar oblateness, Mercury mass, etc

13 p2350 A69-27823

Coordinates interpretation in Schwarzschild problem, projecting space of events by light beams onto Galilean system at infinity

14 p2516 A69-28772

Particle and light motions in Schwarzschild field, discussing acceleration beyond speed of light in reference /S/ frame of time independent coordinate systems

17 p3006 A69-33741

Schwarzschild metric properties in synchronous reference system, using succession of Schwarzschild interval holonomic transformations as function of gravitational radius

22 p3982 A69-41063

Spherically rotating symmetric body gravitational collapse within Schwarzschild radius, presenting

trapped surface concept for asymmetrical cases and generalization of space-time singularities

23 p4219 A69-42333

SCHWASSMANN-WACHMANN COMET

Comet Schwassmann-Wachmann I orbit computation, using perturbations of all planets from Venus to Neptune

01 p0158 A69-11328

SCIATIC REGION

Cerebellar cortex reactions to sciatic nerve stimulation in rats under transverse accelerations in centrifuge

22 p3877 A69-40279

Electric responses of anterior and posterior gyrus cinguli to stimuli of sciatic nerve in cats

22 p3886 A69-41175

SCIENTIFIC SATELLITES

NT APPLICATIONS TECHNOLOGY SATELLITES

NT ORBIS CAL SATELLITE

International Radiation Investigation Satellite /IRIS/ mission, structural design, power supply and control systems

01 p0162 A69-11101

Scientific mission of ESRO 2/IRIS satellite, study of X rays and particles from sun and galaxy and primary cosmic ray electron measurement

01 p0163 A69-11102

Transmitting systems of ESRO 2/IRIS satellite for ground station contact, discussing telemetry system, mission requirements and telecontrol

01 p0034 A69-11103

ESRO 2/IRIS satellite launching checkout, count-down and breakdown of operations

01 p0163 A69-11104

Orbiting ESRO 2/IRIS energy measuring experiments, satellite stabilization, power source, communications and data recovery

01 p0156 A69-11108

Adaptive multiplex telemetry use in scientific satellite data management

02 p0212 A69-12817

European space research program, discussing government, science and industry in developing satellites and sounding rockets

03 p0520 A69-13584

Stored program computer for small scientific spacecraft, noting program and data memory capacities

04 p0569 A69-15472

Small Scientific Satellite program, discussing payload for investigating magnetosphere and near interplanetary space

[IEEE PAPER 3C-1]

07 p1230 A69-19195

Vela 4 satellite energetic particle experiment, describing instruments design and operation

[IEEE PAPER 3C-2]

07 p1134 A69-19196

AZUR satellite movement simulator for thermal control tests, describing assembly

08 p1300 A69-20095

Spin stabilized spherical satellite in high elliptical orbit for lower thermosphere measurements during entire solar cycle

09 p1610 A69-22009

European space research program, discussing government, science and industry in developing satellites and sounding rockets

11 p1966 A69-25102

Scientific aims, optical design, instrument data, control and orbit operation of European Large Astronomical Satellite used in UV observations

13 p2264 A69-28477

European space program developmental and fabrication problems in satellite structure development covering booster constraints, mission constraints, tolerances, etc

13 p2357 A69-28479

Scientific satellite checkout system tests by manual, automatic and self test control

13 p2243 A69-28480

Scientific equipment on Cosmos 237 satellite for recording extraterrestrial radiation data, discussing specifications, operation and mission purpose

14 p2446 A69-29047

Scientific satellite 1 solar cell panels power output dependence on temperature and spin calculated and compared with results for outdoor sunlight

15 p2552 A69-30072

ESRO 1/Aurora scientific satellite for ionospheric phenomena observation, discussing management structure and development process

15 p2702 A69-31080

ESRO 1/Aurorae satellite for Arctic ionosphere and aurorae observation, discussing electrons and protons measurements and auroral photometry
15 p2702 A69-31081

Centro Ricerche Aerospaziali objectives, equipment and activities in aerospace research, including space flight simulation facilities and scientific satellite launching range
15 p2724 A69-31456

AZUR research satellite HF communications system, describing telemetry transmitter, command receiver and data transmission
16 p2759 A69-31854

Data processing for scientific rocket research, considering pulse counters, multiplexers, converters and programmers
16 p2755 A69-31858

Thermal control system for AZUR research satellite, tabulating extreme flight temperatures and permissible temperature range from simulation test data
17 p2903 A69-33427

European Space Research Program report on HEOS-A satellite, noting planetary physics research particularly in magnetic fields, cosmic radiation and solar wind
18 p3207 A69-34628

TD1/TD2 satellites power supply subsystem, stressing high power requirements and significant design features regarding battery and solar array controls
18 p3093 A69-34791

Scientific satellites structural design problems, considering limitations imposed by weight, layout, environmental conditions, mission and manufacture
18 p3208 A69-34792

ESRO Large Astronomical Satellite /LAS/ observatory in orbit, discussing operation, design and instrument settings in scientific package
18 p3208 A69-34793

OGO for conducting diversified measurements to study earth atmosphere, earth-sun relationship, etc
19 p3432 A69-36674

Research satellite, commercial satellite, lunar spacecraft and military satellite missions, discussing Intelsat, Comsat, Early Bird, MOL and ESRO space program
19 p3432 A69-36750

Programmable data handling and telemetry systems for scientific satellites, noting system checkout, spacecraft integration, software and ground data processing
23 p4132 A69-41735

Space research in past and expected scientific knowledge from manned and automated earth orbital science missions
[AAS PAPER 69-036] 24 p4379 A69-42825

SCIENTISTS

Scientists involvement in planetary spacecraft missions, considering organization for particular instruments and more complex payloads
[AAS PAPER 68-192] 02 p0311 A69-11473

Scientific and technical information flow sources, showing DOD user need within defense industry and importance of local work environment
02 p0204 A69-12219

Organization behavior models compared in theory of scientific and professional personnel management, noting compromise between excess restrictions and freedom
[AIAA PAPER 68-805] 08 p1422 A69-20196

Organizational behavior of scientists noting working environments, effectiveness of work sections, research management and organizational development
08 p1423 A69-21124

Unutilized ideas in university laboratories, showing generation and implementation enhancement by marketing experience and product development background
15 p2720 A69-30596

Behavioral differences between engineers and scientists with reference to work environment
15 p2721 A69-31073

Book on digital electronics for scientists covering digital circuits and instruments for measurement, control or computation
18 p3112 A69-34915

Organizational identification of scientists as professional employees, exploring degree of loyalty and perceived self prestige
21 p3855 A69-38765

SCINTILLATION

Ionospheric irregularities height measurement using spaced receivers for recording satellite signals
01 p0064 A69-10428

Amplitude scintillations of satellite radio signals during sunrise due to ionospheric turbulence induced electron content variations
01 p0067 A69-10980

Latitudinal variations in auroral and subauroral region F layer diurnal and magnetic storm pattern shown by scintillation measurements
01 p0069 A69-11127

Ionospheric electron content, slab thickness and scintillation occurrence measurements at low latitude stations
02 p0235 A69-11427

Radar target amplitude, angle and Doppler scintillation from analysis of echo signal propagation in space
02 p0211 A69-12447

Radio star scintillation data, establishing periodic variations in rates within 1 to 1.5 years
03 p0505 A69-13081

Beryllium nondestructive tests, discussing eddy current inspection, ultrasonics, film radiography and scintillation
[SAE PAPER 680652] 03 p0444 A69-13546

Pulsar amplitude variations due to scintillation effects arising from irregular plasma refraction by general interstellar medium between source and solar system
05 p0825 A69-16354

Satellite scintillation at high latitudes and possible relation to soft particle precipitation
05 p0757 A69-16406

F region equatorial irregularity belt observed from satellite transmission scintillation, noting north-south elongated patches
05 p0758 A69-16418

Statistical comparison of scintillation depths of Transit 4A satellite to radio star Cassiopeia A
07 p1215 A69-18821

High latitude transition or scintillation boundary between high and low amplitude fluctuations of satellite radio beacon signals examined as function of time
07 p1125 A69-18846

Proportionality between log-amplitude variance and 7/6 power of wavenumber for horizontal propagation from spherical wave transmitter to point detector
07 p1157 A69-19641

Interplanetary scintillations of 3C 279 and CTA 21 combined to derive solar wind density fluctuation model, using random thin screen theory
08 p1385 A69-20069

VHF satellite signal scintillation by ionospheric irregularities with sharp boundary [such as sporadic E], noting diffraction pattern dependence on phase shift
09 p1489 A69-21713

Laser beam optical scintillation under atmospheric turbulence conditions, showing log amplitude variance saturation and decrease
09 p1517 A69-22079

Laser beam scintillation at night over long atmospheric horizontal paths, showing log amplitude covariance observation in agreement with theoretical prediction
09 p1517 A69-22080

Scintillation fading of VHF beacons on synchronous satellites, noting amplitude fluctuation depth and rate
09 p1457 A69-22461

Solar flare relation to interplanetary scintillation indices and power spectra
09 p1582 A69-22751

Atmospheric scintillation effect on planetary brightness distribution over disk from photometric measurements
11 p1960 A69-24729

Photosimulation of electron hole and exciton mechanisms of NaI-Tl and KI-Tl single crystal scintillations
12 p2144 A69-26722

Interplanetary scintillation and angular spectrum of radio waves scattered by solar plasma, noting magnetospheric tail and solar wind
12 p2161 A69-26942

Scintillation index variations based on 40 MHz Explorer 22 satellite signals recorded in Germany
12 p2034 A69-27094

Radio star scintillation data, establishing periodic variations in rates within 1 to 1.5 years
14 p2515 A69-28763

Pulsars dynamic spectra, suggesting inadequacy of interstellar scintillation models to explain observed dependence of decorrelation band widths on frequency
14 p2517 A69-29087

Satellite 40 mc signal scintillations near sunspot minimum, noting scintillation index dependence on angle between radio ray and magnetic field
14 p2439 A69-29114

Log amplitude variance calculation methods compared in statistics of optical scintillation by application to measurements with laser
14 p2486 A69-29642

Stellar scintillation spectra for different zenith distances, correlating data with meteorological conditions at time of observation
15 p2647 A69-30165

Interstellar hydromagnetic waves due to streaming cosmic rays indicated by pulsar scintillations studies
15 p2676 A69-30889

Electron ion recombination role in atomic collision process in rare gases ionization path, considering scintillation mechanism
15 p2655 A69-30961

Scintillation magnitude related to range and turbulence strength in near earth optical propagation, using pulsed and helium-neon laser
15 p2570 A69-31030

Scintillation of ground based spherical wave laser source viewed from space analyzed from Geos 2 satellite laser tracking, noting stellar scintillation correspondence
15 p2570 A69-31309

Optical communications experiments for quantitative data at 6328 Å on system fading due to scintillation and atmospheric turbulence effects on coherent propagation at 10.6 micron
16 p2748 A69-31564

Satellite signal probability density determined from scintillation plus Faraday effect in statistical terms
16 p2751 A69-32103

Signal records from S 66 satellite with strong scintillations, noting fluctuation well described by Nakagami m-distribution and possibility of deriving relations between different indices
16 p2777 A69-32104

Scintillation index determination, discussing data reduction methods, standard test records, calibration at stations with modest equipment and simulation on digital computer
16 p2751 A69-32105

Satellite radio signal scintillation variations association with sporadic E and spread F and dependence on magnetic activity in Southern Hemisphere during sunspot minimum
16 p2780 A69-32307

Radio sources interplanetary scintillations and cross correlation coefficient real time determination
17 p3038 A69-33727

Wavelength dependence of stellar scintillation, discussing apparatus to detect color effect in twinkling
19 p3401 A69-35809

Ionosphere disturbances due to high altitude thermomolecular explosions, discussing experimental proof by Cosmos satellites short wave transmitter radio signal scintillation statistical evaluation
19 p3304 A69-36624

Aircraft measurements of scintillation of ground based light source, calculating autocorrelation functions and intensity fluctuations spectra
19 p3279 A69-36881

Ionospheric scintillation power spectrum measurements from radio star and satellites related to F region radio refractive index fluctuations
20 p3534 A69-38093

Diffraction pattern of satellite signal field- aligned amplitude scintillation during quiet geomagnetic conditions
20 p3497 A69-38108

Photosimulation of electron hole and exciton mechanisms of NaI-Tl and KI-Tl single crystal scintillations
21 p3781 A69-39135

Stellar scintillation spectra theory extended to rectangular apertures, generalizing to planetary scintillation and effects of diffraction, atmospheric dispersion and seeing
21 p3773 A69-39771

Latitude variation of radio satellite scintillation related to small scale ionospheric irregularities
22 p3899 A69-39972

Satellite scintillating signals amplitude distribution, correlating observations and theoretical results
23 p4115 A69-41486

Coherent light propagation through turbulent atmosphere observed by applying He-Ne lasers to simultaneous measurements of scintillation effects over homogeneous optical paths
24 p4344 A69-43114

SCINTILLATION COUNTERS

Scintillation gamma spectrometer on Luna 10, eliminating charged particle background by fabricating detector from NaI single crystal in scintillating plastic container
01 p0084 A69-11314

Photomultiplier geometry without use of light pipes for uniform response from large area single and double sheet plastic scintillation detectors

03 p0428 A69-13107

Balloon-borne SPARMO detector SC 67 used for measuring radiation at high altitudes

05 p0762 A69-15823

Large area scintillation telescopes with cubic geometry, measuring cosmic rays intensity from vertical and slant directions

06 p0925 A69-17296

X ray microanalyzer maximum sensitivity obtained using flow type proportional and scintillation counters with proper tuning and eliminating scattered electrons

12 p2093 A69-26596

Cosmic ray particles with fractional charge at sea level searched by scintillation counters with spark chambers, estimating quark flux intensity

13 p2333 A69-28425

Rocket-borne scintillation spectrometer for cosmic photon radiation

14 p2449 A69-29566

Scintillation counter to determine neutrons number and distribution in time in pulses generated in hot plasma

14 p2452 A69-29809

Quark detection in cosmic rays at sea level using scintillation counter and streamer chamber system

15 p2674 A69-30308

Faraday rotation measurements of signals from Explorer 22 analyzed to determine scintillation boundary in auroral ionosphere

15 p2605 A69-31443

Proposed index for measuring ionospheric scintillations, describing simplified scaling method

16 p2752 A69-32106

Variable time lapse videoscintiscopes in medical applications, discussing implementation of TV camera, signal tape recording and audio activation

18 p3134 A69-34541

NaI/Tl/ and CsI/Tl/ scintillation counters effectiveness in recording low energy protons against counter noise background

18 p3138 A69-35255

Transparency and luminescence yield of plastic scintillators prepared from polymethyl methacrylate, comparing naphthalene and benzene compound additions with polystyrene

21 p3724 A69-39073

Random function output current obtained in phototube and scintillation detector including amplitude distribution, time measurements and pulse shape discrimination

22 p3947 A69-40670

Diurnal variations in solar cosmic ray muon component near sea level, using scintillation counters assembled in muon telescope array

23 p4207 A69-42498

Solar high energy gamma ray flux abrupt increase detected by neutral particle plastic scintillators at balloon altitude

24 p4371 A69-43612

SCINTILLATION SPECTROMETERS

U SPECTROMETERS

SCINTILLATORS

U SCINTILLATION COUNTERS

SCINTILLOMETERS

U SCINTILLATION COUNTERS

SCISSION

U CLEAVAGE

SCORING

Scratch gages under water in open and at high temperature, including circular X-Y recording scratch strain gage

15 p2610 A69-30682

SCORPIO CONSTELLATION

U SCORPIUS CONSTELLATION

SCORPIUS CONSTELLATION

Soft X ray spectrum of Sco XR-1, noting intensity change from previous measurement

02 p0309 A69-12711

Photometric investigation in UVB and H alpha of early B stars in Scorpio-Centaurus association, computing intrinsic colors and magnitudes corrected for interstellar absorption

06 p1001 A69-17195

Photoelectric observation of Sco X-1 variations with 91-cm reflector, tabulating results and estimating accuracy

06 p1008 A69-17695

Pulsar characteristics absence in X ray sources, noting data for Scorpius XR-1

07 p1218 A69-19254

Sco XR 1 optical and X ray spectra simultaneous observations during rocket flights

07 p1220 A69-19391

Low energy X ray spectra of Sco X-1 and Sagittarius sources measured by Be and Al window proportional counters during rocket flight

09 p1574 A69-21460

Sco X-1 optical spectrum magnitude and color changes, proposing variable black body model

09 p1601 A69-22213

Radio emission time variation from radio object associated with Sco X-1

09 p1603 A69-22268

Photoelectric spectrum scanning and IR photometric observations of Scorpius XR-1 X ray source

09 p1604 A69-22401

Spectrum of high energy X ray flux from Sco XR-1 during balloon flight using active collimator detector and graded shield detector

09 p1584 A69-22766

Modulation collimators determining angular sizes and celestial positions of X ray sources Sco X-1 and Taurus XR-1

10 p1678 A69-23326

Proper motions and positions of X ray source Sco X-1 and surrounding stars derived from astrophysical plates using overlap technique

12 p2152 A69-25798

X ray polarization from Sco X-1, noting spurious instrumental polarization due to cosmic ray anisotropy using X ray polarimeter

12 p2149 A69-26315

Scorpius XR-1 X ray emission spectra, discussing Fe emission line near 7 kev plasma models, supernova mass and cosmic abundance

13 p2325 A69-27313

Sco-Cen B stars radial velocities, determining spectroscopic binaries

14 p2519 A69-29136

Spectral classifications and UVB photometry for southern association Sco OB 1 containing cluster NGC 6231

15 p2692 A69-30771

Sco X-1 fluctuating optical and X ray emission observed simultaneously, determining total energy flux and plasma radius and density

15 p2676 A69-30885

Five color photometry of X ray source SCO X-1 in 1966-1968, discussing luminosity pulsations and flare activity

16 p2847 A69-31648

Time variation of optical intensity of Sco X-1 X ray source, evaluating photometric data by power spectral analysis

16 p2852 A69-32805

Nocturnal D region conductivity enhancement relation to X radiation from Scorpius XR-1 and other sources, calculating ion production rate

17 p3024 A69-33378

Radio emission from Sco XR-1 shown as synchrotron radiation of relativistic electrons in low density region surrounding denser core producing X ray

20 p3597 A69-37334

Star counts in Ophiuchus nebula darkened region /Scorpius-Ophiuchus/ and in comparison fields Corona Australis and Sagittarius

20 p3604 A69-37788

Scorpius X-1 X ray star model based on relativistic electron distribution due to magnetic field fluctuations, considering role of Alfvén waves

20 p3593 A69-38154

Sco X-1 X-ray source energy spectrum and time variation from rocket flights in India

22 p4030 A69-40774

Radial velocities for O and B stars in Milky Way field in Scorpius determined from prism spectrograms with specific dispersion at H gamma line

23 p4211 A69-41489

SCOTCHLITE (TRADEMARK)

Retroreflector and Scotchlite object images obtained in long range holography with Q switched ruby laser, noting atmospheric seeing conditions

23 p4167 A69-42184

SCOUT LAUNCH VEHICLE

Rocket motor integration into Scout vehicle to improve performance

02 p0335 A69-12384

Scout launch vehicle for launching small research satellites in near earth orbits, describing solid propellant stages, guidance, telemetry and beacon systems

06 p1016 A69-17597

SCR (RECTIFIERS)

U SILICON CONTROLLED RECTIFIERS

SCRAMJET ENGINES

U SUPERSONIC COMBUSTION RAMJET ENGINES

SCRAMJETS

U SUPERSONIC COMBUSTION RAMJET ENGINES

SCREEN EFFECT

Screening of high density plasma from penetration by neutral gas, discussing prevention of high energy losses by charge exchange collisions

02 p0288 A69-12170

Charge accumulation elimination on dielectric electrodynamic channel walls, comparing resistive wall channel to high internal impedance generator

02 p0291 A69-12506

Metal surface degradation by constant density laser radiation, computing screening effect

03 p0442 A69-14221

Frequency-fluctuation correlation functions of radio wave field behind n random screens with random phase shifts calculated, obtaining statistical characteristics

07 p1076 A69-18525

Transmission coefficient of plane electromagnetic wave obliquely incident on perforated metal screen in frequency range near primary resonance of structure

07 p1076 A69-18527

Radiation probability of transmission through intervening galaxy and screening of quasar emission in universes with positive cosmological constant

10 p1790 A69-24135

Time harmonic electromagnetic waves diffraction by circular aperture in conducting plane screen between different media, using Hertz vector formulation

12 p2030 A69-26463

Electron shielding in heavily doped many valley semiconductors, discussing Thomas-Fermi screening and Mott transition

13 p3234 A69-28683

Electrostatic screening in isothermal symmetrically charged and quasi-neutral plasmas, noting confinement in electrostatic trap

14 p2490 A69-29035

Plane wave reflection and transmission by unidirectionally conducting screen, considering oblique incidence and two polarizations

14 p2421 A69-29547

Shock wave radiation screening by thermodynamically unstable gas, discussing brightness and gas temperature relative to shock wave front position

14 p2493 A69-29673

Plane electromagnetic wave diffraction by screened periodic metallic strips array with real ferrite transversely magnetized to saturation

23 p4124 A69-42032

SCREENING

Screening techniques for semiconductor devices, considering component classification with respect to population strength distribution

15 p2627 A69-30840

SCREENS

Plane screen electrical shielding effectiveness calculation, using incident wave impedances associated with current loop and magnetic dipoles in transmission line equations

19 p3267 A69-35932

SCREW DISLOCATIONS

Screw dislocation interaction with partially bonded bimetallic interface, using isotropic elastic continuum approximation

10 p1802 A69-24027

Antiplane strain model for describing cracks and dislocation arrays within circular cylindrical inhomogeneity surrounded by elastic material

10 p1803 A69-24031

Fcc metals cyclic deformation and fatigue dependence on cross slip of screw dislocations, considering strain hardening and crack propagation

11 p1906 A69-25389

Nickel solid solutions strengthening under cold deformation studied by X ray, noting screw and edge dislocations role

18 p3157 A69-35246

X ray analysis of rolled and compressed Ti powder produced by calcium hydride reduction, noting coexistence of screw dislocations

21 p3745 A69-38952

SCREWS

Waveguide capacitive screw tuners effects on dissipative loss, discussing microwave measurements with copper screw tuners

16 p2757 A69-31586

Screw-nut feeder and adjustor systems with compensation for clearance and wear of cutting tools, deter-

mining efficiency for conversion of rotary to translational motion
23 p4168 A69-41414

CRIBING
U SCORING

CUTUM CONSTELLATION
Photoelectric search for delta Scuti variables in Coma and NGC 752 clusters, discussing short period variability of B, A and F stars
13 p2343 A69-27620
Short period variability of B, A and F stars observed in photometry of New Delta Scuti stars
13 p2348 A69-27803
Spectrophotometric observations of delta Scuti short period variable stars compared with model atmospheres
22 p4015 A69-40150

SDP [COMPUTERS]
U SITE DATA PROCESSORS

SE- 210 AIRCRAFT
Caravelle aircraft halting tests with barrier net
10 p1674 A69-23706

SEA-A
U EXPLORER 30 SATELLITE
U EXPLORER 31 SATELLITE

SEA KING HELICOPTER
U SH- 3 HELICOPTER

SEA KNIGHT HELICOPTER
U CH- 46 HELICOPTER

SEA WATER
Survival analysis based on probability theory for design of air cushion vehicle to determine height for operating over open sea
01 p0008 A69-10027
Protective coatings for gas turbine engine components in marine environments, considering corrosion of diffuser, impeller, compressor case and turbine blades
01 p0099 A69-11057
Stress corrosion in smooth and prenotched maraging steels exposed to sodium chloride solution and natural sea water
14 p2467 A69-29940
Galvanostatic anodic and cathodic currents effect on stress corrosion of Be sheet in aerated synthetic sea water at 72 F
21 p3747 A69-39436
Aerospace and marine corrosion technology - Conference, Los Angeles, July 1968
21 p3747 A69-39484
Stress corrosion cracking of welded Al alloys in sea water solution, showing combined action of sustained stress, corrosive environment and heat treatment
21 p3748 A69-39492

SEALANTS
U SEALERS

SEALERS
Viscoseal sealing coefficient and friction factor under turbulent flow conditions
[ASLE PREPRINT 68AM 5B-1]
01 p0087 A69-10911
High temperature organic sealants for repairing small gas leakages in vacuum devices, tabulating test results for alkyd, epoxy, silicone and polyimide resins
11 p1907 A69-24742
Stress corrosion cracking of titanium alloys in contact with high temperature fuel tank sealants
12 p2112 A69-25945
Chemical composition of cermet material for radial sealing of high temperature gas turbines, ensuring structural stability and oxidation resistance
13 p2275 A69-27344
Room temperature vulcanizing silicone rubber adhesive sealants strength and self bonding, describing primerless adhesion to Ti and Al alloys, Al, Ni and stainless steels
19 p3356 A69-35532
Integral fuel tank sealant based on various hydrofluorocarbon polymers prepared, tested and compared for physical properties
19 p3356 A69-35533
Fuel resistant elastomers evaluated for seal compounds for low temperature capability, noting epichlorohydrin-ethylene oxide as promising sealant
19 p3356 A69-35534
Low viscosity/density RTV silicone rubber sealants obtained by using glass microballoon fillers
24 p4337 A69-43454
Elastomers for SST aircraft applications, discussing properties evaluation, material selection, sealant requirements, etc
24 p4338 A69-43455

RTV silicone rubber for corrosion control coatings, high strength adhesives and low density sealants in aircraft structures
24 p4338 A69-43457

SEALING
Mechanical and physical properties and cryogenic wear tests performed on composite materials, considering NERVA cryogenic turbopump bearing retainer development
[ASME PAPER 68-WA/LUB-10]
05 p0768 A69-16133
Rectangular shock tube for use with pressure and vacuum, discussing sealing of circular end flanges to buildup tube
06 p0906 A69-16928
Nondestructive tests for determining braze bond quality of open face honeycomb seal rings, using low viscosity liquids with fluorescent additives
07 p1140 A69-18797
Bellows sealed valve for measurement of fluorine thermodynamic properties at moderately high pressures
09 p1493 A69-21428
Book on Wankel RC engine design and performance covering sealing, timing, life, lubrication, etc
11 p1942 A69-25237
Gas turbine compressor end seals, discussing air leakage paths, primary and secondary seals, design and efficiency
[ASLE PREPRINT 68AM 4B-4]
13 p2267 A69-27366
Sealing mechanism theory with face seal applications, taking into account load carrying capacity and no leakage pressure gradient
[ASLE FICFS PREPRINT 18]
15 p2620 A69-30489
Load support and leakage from microasperity lubricated face seals, developing hydrodynamic lubricant films
[ASLE FICFS PREPRINT 21]
15 p2622 A69-30500
Leak tests for sealed electronic circuits using helium mass spectrometer
18 p3138 A69-35271
Oil-free linear motor resonant piston gas compressor, hermetically sealable to handle radioactive and dangerous gases
[ASME PAPER 69-FE-36]
20 p3466 A69-37996
Bonding mechanisms in Mo-Mn-Ti metallizing and Cu brazing in metal to ceramic seals by strength test, microscopy and electron probe microanalysis
21 p3733 A69-39599
Clamping and sealing fastener for single direction installation consisting of pin, collar and sealing collar with insert
22 p3957 A69-40831

SEALS [STOPPERS]
NT GASKETS
NT GLANDS [SEALS]
NT HERMETIC SEALS
NT O RING SEALS
NT PACKINGS [SEALS]
NT PUMP SEALS
Radial face seals lubricating mechanism noting surface waviness effect on film thickness fluctuations
01 p0087 A69-10910
Friction and wear behavior of mechanical face seals, considering techniques and lubricants for increasing product of pressure and sliding velocity
02 p0253 A69-12160
Dynamic and interfacial fluid effects in mechanical face seals, discussing hydrodynamic pressure generation
04 p0606 A69-14798
Orifice compensated hydrostatic face seal under pressure and thermal loading for aircraft gas turbine
[ASME PAPER 68-WA/LUB-6]
05 p0768 A69-16131
Seal swell prediction methods extended to include three dimensional solubility parameter concept
[ASLE PAPER 68-LC-21]
07 p1171 A69-19306
Radial liquid flow between flat annular rings /face seals/, discussing film cavitation
13 p2267 A69-27365
Turbomachinery buffer seals, buffer gas regulation and cleanup systems for operation of closed Brayton cycle power conversion system with gas cooled nuclear reactor
13 p2268 A69-27367
Sintered metal powder process for metal-to-ceramic seals for thermionic converters, giving results for tensile strength, thermal cycling and cesium corrosion
14 p2454 A69-29211

Metal insulating seals using preliminary metallization or direct brazing for applications in thermionic converter technology and irradiation capsules
14 p2455 A69-29212
Spiral grooved turbulent screw seal /viscoseal/ analysis, combining results of spiral grooved journal bearing study with turbulent fluid film theory
[ASLE FICFS PREPRINT 32]
15 p2619 A69-30482
Misalignment and eccentricity effect on face seal, discussing leakage dependence on phase angle
[ASLE FICFS PREPRINT 15A]
15 p2620 A69-30483
Eccentric face seal with tangentially varying film thickness, analyzing leakage flow proportional to eccentricity and surface waviness
[ASLE FICFS PREPRINT 15B]
15 p2620 A69-30484
Noncontacting minimum leakage dynamic seal requiring liquid-vapor interface with leakage tolerance
[ASLE FICFS PREPRINT 40]
15 p2620 A69-30485
Lubrication and leakage control mechanics of face seals, considering liquid to vapor boundary within interface
[ASLE FICFS PREPRINT 22]
15 p2620 A69-30486
Face seals for jet engine mainshaft bearing compartments, emphasizing oil film and gas film seals
[ASLE FICFS PREPRINT 28]
15 p2620 A69-30487
Seal selection criteria based on maintaining fluid film between faces, discussing facial heat generation and dissipation, speed and size effects, etc
[ASLE FICFS PREPRINT 25]
15 p2620 A69-30488
Sealing mechanism theory with face seal applications, taking into account load carrying capacity and no leakage pressure gradient
[ASLE FICFS PREPRINT 18]
15 p2620 A69-30489
Dynamic seals literature review covering contact, mechanical, fixed clearance, film riding and elastomeric seals, systems and materials
[ASLE FICFS PREPRINT 29]
15 p2620 A69-30490
Hot pressed molybdenum disulphide-nickel composite film friction and wear tests in air and face seal configuration
[ASLE FICFS PREPRINT 23]
15 p2620 A69-30491
Gas turbine engine shaft face seal with self acting lift augmentation preventing rubbing contact, noting disadvantages of labyrinth and conventional seals
[ASLE FICFS PREPRINT 27]
15 p2621 A69-30492
Elastohydrodynamic lubrication of square section high pressure face seals mounted on rigid housings, considering design charts for load and leakage
[ASLE FICFS PREPRINT 16]
15 p2621 A69-30493
Gas visco seals performance analyzed for continuum flow regime, noting coefficient agreement with laminar flow analysis
[ASLE FICFS PREPRINT 34]
15 p2621 A69-30494
Gas barrier seal design producing varying unit loading on conventional contact seal faces, including geometric stability and test results
[ASLE FICFS PREPRINT 26]
15 p2621 A69-30495
Turbulent viscoseals gas ingestion and fluid inertia analysis using stability of dynamic gas-liquid interface between rotating cylinders
[ASLE FICFS PREPRINT 31]
15 p2621 A69-30496
Leakage prediction through mechanical seal by theoretical equation developed from basic fluid mechanics
[ASLE FICFS PREPRINT 17]
15 p2621 A69-30499
Lubrication and lubrication systems literature including compressible and incompressible fluid films, automotive, bearing, gear, friction, wear and boundary lubrication, seals and sealing systems
15 p2628 A69-30900
Erosion wear of graphitic and mica-ceramic materials used for sealing turbine compressors at high temperatures, including test installation
15 p2643 A69-31186
Shaft speed limitations on close clearance seals, using test data on changes in fluid viscosity causing contact and damage
[ASLE PAPER 68-LC-13]
21 p3731 A69-38763

Seals leak testing for complex manned spacecraft structures
[AIAA PAPER 69-1030] 22 p3924 A69-40399

SEAMS [JOINTS]

Seam and stitch welding in miniaturized semiconductor package fabrication, including leak rate tables
18 p3149 A69-35272

SEAPLANES

Blowing boundary layer control /BLC/ system designed for STOL seaplanes
05 p0695 A69-15546

STOL seaplane bottom pressure distribution from tests on scale model of PX-S seaplane, discussing boundary layer control effects
22 p3864 A69-40586

Beriev Be-12 cranked wing seaplane design including technical and operational data
24 p4251 A69-42796

SEARCH RADAR

Sequential logic for improved signal detectability in frequency-agile search radars, discussing target echo fading models in radar range performance prediction
01 p0033 A69-11008

Radar detector for survivors, using inexpensive microwave mixer detector crystal
06 p0878 A69-16964

Pulse Doppler radar operation, discussing Doppler shift, range resolution and systems components
10 p1659 A69-24084

Probability matrix for n order transition independent of decision taking method, applying fundamental matrices to analysis of mean number of false targets
14 p2410 A69-28836

Doubly curved reflectors for rotating search radar directional antenna, noting assembly of elliptical strips constituting segments of parabolic dishes and sidelobe suppression
16 p2763 A69-32790

Avionics of Naval E-2C airborne sentry and command and control system, discussing digital computer, search radar, etc
18 p3108 A69-34811

SEARCHING

Optimal distribution of search effort for moving target location, suggesting Markovian decision models
01 p0104 A69-10653

Aircraft Searchmeter, discussing device fitted to locate emergency radio beacon signal
06 p0878 A69-16963

Trunk and tree searching properties of Fano sequential decoding algorithms
06 p0902 A69-17400

Adaptive random search algorithm utilizing boundary cost-function hypersurfaces measurement to implement Pontryagin maximum principle, discussing hybrid computer use, iterative solution and convergence properties
17 p2933 A69-33745

Pulsar search techniques, sources searched and discovery of NP 0527 and 0532
18 p3192 A69-34320

Search for maximum along admissible directions in optimal control systems
19 p3286 A69-35988

SEAS

NT RED SEA

Microwave thermal emission by water measured from aircraft, studying radiation dependence on surface roughness
18 p3127 A69-34421

SEASONAL VARIATIONS

U ANNUAL VARIATIONS

SEASONS

NT SUMMER

NT WINTER

Westerly air flow frequency decline resulting in lower seasonal temperatures, tabulating Lamb categories daily maximum and minimum temperatures
13 p2222 A69-28474

SEAT BELTS

Impact mechanism in hip safety belt protection in vehicles, deriving motion for natural oscillations of upper part of human body model
20 p3482 A69-37595

Linear viscoelastic model parameters optimization for designing automobile lap seat belts, assuming abrupt impact stop
[ASME PAPER 69-APMW-25] 24 p4275 A69-43094

SEATS

NT BARANY CHAIR

NT EJECTION SEATS

Universal vestibulometric chair for inducing irritation in tests involving vestibular analyzer interaction with other body functions
02 p0200 A69-11517

Concorde aircrew seats design for electric operated tracking and lift, vertical movement accommodation seat and back tilt
15 p2553 A69-31167

SECANTS

U TRIGONOMETRIC FUNCTIONS

SECONDARY AIR

U AIR

SECONDARY COSMIC RAYS

Barometric coefficients of multiplicities calculated using cosmic ray interactions model and neutron monitors response to secondary nucleons
03 p0425 A69-14025

Coupling coefficients between primary and secondary ionizing cosmic ray variations, using stratospheric observations in Siberia during IQSY
03 p0504 A69-14224

Muon component of extensive cosmic ray showers, discussing effect of multiplicity of secondary particles created by high energy nuclear interactions
07 p1207 A69-19325

Neutron counter for measurements of atmospheric and earth leakage flux of secondary cosmic ray neutrons, discussing design and calibration
07 p1209 A69-19454

Secondary muon flux from primary cosmic ray particles monitored during minimum solar activity by telescopes at 60 mwe underground
10 p1769 A69-23827

Secondary corpuscular stream effect on diurnal variations in cosmic ray intensity obtained from statistical analysis
10 p1769 A69-23904

Excess radiation in equatorial regions studied on-board Cosmos 137, noting contribution of primary particle multiplication to secondary radiation
10 p1783 A69-23922

High altitude balloon measurements of secondary gamma quanta intensity vertical distribution, using scintillation counter with CsI/Tl crystal
10 p1770 A69-23924

Azimuth angle distribution of secondary particles forming cosmic ray diffused cone with high energy, showing asymmetry and deducing particle transverse momentum upper limit
17 p3024 A69-33763

High energy cosmic rays primary spectrum determined from observations of secondary components including gamma rays, muons and air showers
21 p3790 A69-38822

Primary and secondary cosmic ray intensity variation with altitude from ascending balloon data, noting absorption length role
21 p3791 A69-39249

SECONDARY EMISSION

Frequency and polarization selection of neodymium glass laser oscillators by directing secondary radiation into laser cavity and duplicating spectral properties
[IEEE PAPER P-3] 05 p0775 A69-16324

Secondary emission and hollow cathode effects in low pressure hot cathode thyratron filled with hydrogen and with shield surrounded thermionic cathode
06 p0896 A69-17475

Ion formation and ion secondary emission during sputtering, discussing Saha-Langmuir equation, probability theory, simultaneous processes, mass spectroscopic analyses, etc
08 p1355 A69-20616

Secondary emission in low altitude satellite body dependent on inelastic collisions with primary cosmic ray protons
10 p1757 A69-22821

Low energy charged particle detectors reliability, analyzing windowless electron multipliers and effects of secondary emission layers on sensitivity
11 p1848 A69-24868

Radiation pattern as function of asymmetry in amplitude of secondary source excitation by primary aperture antenna
11 p1852 A69-25117

Gas laser secondary modes emission and beat frequency spectrum widths, using results of Lamb lasers theory
15 p2633 A69-30121

Electron beam rotational temperature, noting discrepancies between experimental values and iterative calculations due to secondary electron effects
16 p2814 A69-32175

Auroral electrons measurement by rocket, discussing difficulties due to secondary electrons and method permitting primary electrons detection threshold determination as function of rocket position
16 p2785 A69-32617

Secondary electron emission from gas covered metal surfaces, discussing results of neutral beam investigations
17 p3008 A69-33000

Differential cross sections for secondary electron production in atomic ionization by charged particle impact, using classical binary encounter approximation
17 p3009 A69-34189

Frequencies of charged secondaries numbers emitted from nucleon-nucleon and pion-nucleon inelastic collisions, observing multiplicity regularity
18 p3177 A69-35009

Plasma electron beam for welding, deriving beam current from secondary emission by ion bombardment, discussing gas pressure, equipment and applications
19 p3320 A69-35555

Neutron flux measurements on Cosmos 53, discussing equipment and calculation of secondary neutrons due to bombardment of satellite components
22 p4003 A69-40274

Flexible channel multiplier made of electron conductive polymer, noting secondary yield and feedback effect
22 p3917 A69-41234

SECONDARY FLOW

Downstream secondary circulation resulting from sharp bend in fully developed turbulent pipe flow, noting departure from twin circulatory flow
03 p0419 A69-13952

Numerical solution of axisymmetric incompressible viscous fluid flows about rotating cylinder, Taylor vortex between cylinders and through labyrinth seal
03 p0419 A69-13990

Secondary steady flow /Taylor vortices/ between rotating cylinders, discussing development due to stability loss of Couette flow
05 p0745 A69-15780

Decreasing secondary flows in spatial boundary layer on porous plate by boundary layer control /BLC/ through suction or blowing, using Prandtl partial differential equations
06 p0909 A69-17185

Transverse secondary gaseous injection penetration into confined supersonic flow
[AIAA PAPER 69-2] 06 p0913 A69-18080

Analytical evaluation of secondary flow injection effects on rocket engine performance including cold flow and simulated hot flow data
[AIAA PAPER 69-473] 16 p2844 A69-32726

Finite amplitude standing transverse resonant acoustic field effects upon flow behavior of viscous fluid in cylindrical enclosure to acoustically model combustion instability
[AIAA PAPER 69-667] 17 p2954 A69-33457

Blade length effects on performance of flow straightener vanes influenced by secondary flow, noting high deflection and low aspect ratio
17 p2896 A69-33606

Secondary vortex generation in near wake of circular cylinders under forced oscillation, analyzing motion dependent transition regimes using hydrogen bubbles flow visualization
[AIAA PAPER 69-755] 18 p3084 A69-34411

Turbomachinery aerodynamics, discussing secondary flow in blading and digital computer applications to annulus flow field
18 p3086 A69-34925

Secondary steady flow /Taylor vortices/ between rotating cylinders, discussing development due to stability loss of Couette flow
18 p3123 A69-35032

Secondary flow consisting of longitudinal vortices superposed on convection flow on inclined plate, obtaining flow pattern through flow visualization
18 p3124 A69-35383

Secondary flows in confined viscous vortex for nuclear rockets, employing rotating disk in chamber end wall for recirculation
19 p3296 A69-35756

Viscous fluid secondary flow stability between coaxial rotating cylinders, using nonlinear differential equations derived from equations of motion
19 p3299 A69-36391

Viscous incompressible nonNewtonian fluids flow with treatment for steady rotational problems and oscillatory motion, considering primary and secondary motions
20 p3519 A69-38319

Secondary flow occurrence and geometry in viscous turbulent flow in square channel, using iterative solution
24 p4303 A69-43501

Laminar flow in horizontal circular tubes with uniform heat flux, analyzing combined free and forced convection effects on secondary flow
24 p4409 A69-43519

SECONDARY HARMONIC GENERATION
U HARMONIC GENERATIONS

SECONDARY INJECTION

Secondary injection effect on supersonic parallel diffuser, analyzing flow patterns, pressure distribution and recovery and heat transfer
03 p0365 A69-13991

Injectant stagnation temperature and molecular weight variation effect on flow field generated from secondary injection into supersonic stream [AIAA PAPER 69-1]
06 p1039 A69-18196

Hydraulic control valves for guidance of rockets by secondary liquid injection into nozzle skirt, discussing structure, single nozzle missile and mass gain
07 p1230 A69-19293

Fluidic secondary injection thrust vector control systems for solid propellant and hydrogen-oxygen rocket engines
10 p1753 A69-23561

Flow field structure involving supersonic secondary jet interactions and separated regions in thrust vector control system
11 p1944 A69-25594

Pressure distribution in wake produced by obstacle with secondary fluids injection into boundary layer, obtaining coefficient governing resistance of obstacle to forward motion
16 p2768 A69-31604

Flow disturbances in supersonic rocket nozzles due to secondary injection analyzed by effective body approximation, including side forces [AIAA PAPER 69-443]
16 p2839 A69-32666

Directional thrust control for solid propellant rockets, describing swinging, bent rotating nozzles and secondary injection
17 p3019 A69-33332

Thrust vector control by secondary gas injection for predicting lateral thrust performance, applying method to rocket engines, secondary gas generator and injector configuration
17 p3019 A69-33333

Turbulent premixed ammonia-air flame stabilization on flameholders, discussing secondary oxygen injection into circulation zone at blowoff limits
21 p3849 A69-38808

SECONDARY RADAR

Listen-in feature, allowing general aviation aircraft equipment to receive airborne SSR reply signals, provides air to air proximity warning
03 p0464 A69-13247

Secondary radar equipment functions and features forming IFF-SIF chain, discussing displacement controller and minor lobe suppression functions technical problems
05 p0721 A69-16591

Synchronous extractor for simultaneous extraction and association of primary and secondary radar videos in civil system, discussing automatic identification process
05 p0721 A69-16592

Secondary radar for air traffic control automation in France, discussing onboard equipment
10 p1723 A69-23705

Primary-secondary radar /SECAR/ integration for air traffic control, discussing problems of simultaneous display, transmission synchronization, signal multiplexing, etc
15 p2570 A69-31222

Secondary radar system chosen by EUROCONTROL Agency for civil air traffic control at Shannon and Brussels airports
15 p2571 A69-31501

Secondary radar IFF/SIF /Identification Friend or Foe-Selective Identification Feature/ system, describing ground and onboard radar and data processing equipment
19 p3278 A69-36702

SECONDARY WAVES
U S WAVES

SECRECTIONS
NT ENDOCRINE SECRETIONS
NT HORMONES
NT SWEAT

Allelopathy, discussing application to gas liberating activity of edible plants as ingredients of space flight life support systems
02 p0198 A69-11509

SECTORS

Stiffness matrices for sector elements under membrane stress, considering alternative displacement distributions within element
04 p0676 A69-14728

Lift drag ratio for conical sector with V-shaped wing at zero incidence
06 p0858 A69-17340

SECULAR PERTURBATION

U LONG TERM EFFECTS

SEDIMENTARY ROCKS

U COAL
U SANDSTONES
U SHALES

SEDIMENTS

Space photography to provide synoptic sedimentary environmental data analysis, discussing orbital sensing advantages
05 p0753 A69-15993

Space photography as sedimentological research tool demonstrated by space photographs application to projected Mars mission
09 p1490 A69-21797

Demixed layer at wall in shear flow of nonsedimenting suspensions with different geometries due to viscous and inertia effect superposition
13 p2251 A69-28498

Sediments and crude oils analyzed for fatty acids, considering abiological or bacterial origin of acids
20 p3523 A69-37538

SEEBECK EFFECT

Peltier measurements below 4 K capable of measuring low Seebeck coefficient on high resistivity alloys and in presence of magnetic field
14 p2449 A69-29563

Semiconducting properties of lanthanum-cobalt oxide measured, using Seebeck coefficient for analysis as function of resistivity
21 p3780 A69-38612

SEEDS

Wheat seedling germination and growth processes in absence of gravitational force onboard Biosatellite 2
01 p0015 A69-10932

Change in content of dry matter, sugars and ascorbic acid in plants after action of space flight factors on seeds of these plants
10 p1645 A69-23495

Weightlessness and vibration effects on soft red winter wheat seedlings
15 p2557 A69-31368

SEEKERS

U HOMING DEVICES

SEGMENTS

Traveling wave tube segmentation, analyzing effects of drift, grouping and selecting sections on efficiency and amplification
03 p0407 A69-13985

SEGREGATION

U SEPARATION

SEISMIC ENERGY

Sonic boom produced earth particle velocities, noting seismic effect limitation to boom pressure envelope area and earth surface boundary
14 p2393 A69-29880

Lunar seismology, discussing Apollo 11 instrumentation and experiments, moonquakes and travel times measurements and lunar tides
19 p3315 A69-36765

SEISMIC WAVES

NT LOVE WAVES
NT RAYLEIGH WAVES

Air coupled seismic waves generated by jet fighters flying at high altitudes and supersonic speeds
01 p0077 A69-11281

Lunar seismic velocity distribution data indicates broad low velocity zone together with possible extensive melting at depth [AAS PAPER 68-205]
02 p0312 A69-11480

Granite compressional wave velocity and electrical resistivity variations with depth, explaining discrepancy between in situ and laboratory measurements on dry samples
02 p0241 A69-11806

Moving window analysis digital technique for complex seismic surface waves in presence of noise and multimode propagation
02 p0243 A69-12006

Spectral peaks for torsional oscillations of earth, estimating free periods from observations at six stations around earth
02 p0243 A69-12007

Seismic wave generation, propagation, dispersion and attenuation in gravitating sphere having

homogeneous elastic mantle and liquid core, giving theoretical seismograms

02 p0243 A69-12010

Velocity distribution in lower mantle, showing second major discontinuity in P wave travel time curve at 24 degrees
07 p1129 A69-19502

Surface wave study techniques, discussing digital moving window analysis of group and phase velocity and use of time variable filters
16 p2784 A69-32576

Seismic surface wave observations analyzed by applying moving window method to orthogonal detector recordings permitting lateral refraction measurement, wave separation, etc
16 p2784 A69-32577

Monte Carlo inversion of seismic body waves for transposing uncertainties of observations to velocity models
17 p2962 A69-33654

Semiinverse method for elastic nonhomogeneity problems, considering case of seismic wave propagation
20 p3624 A69-37589

Multiple filter technique for seismic multimode dispersed signals, checking time and frequency resolution by diagnostic diagram
22 p3934 A69-39872

Sensors array to determine propagation wave vector velocity via high resolution frequency wavenumber spectrum analysis, emphasizing seismic applications
22 p3902 A69-41220

SEISMOGRAMS

Seismic wave generation, propagation, dispersion and attenuation in gravitating sphere having homogeneous elastic mantle and liquid core, giving theoretical seismograms
02 p0243 A69-12010

Spheroidal disturbances theoretical seismograms on surface of gravitating elastic sphere with homogeneous mantle and liquid core, considering gravity and polar radial stress effects
23 p4158 A69-42020

SEISMOGRAPHS

NT LUNAR SEISMOGRAPHS

Telemetry by reflex klystron accelerometer and seismometer with on air or coaxial cable signal transmission
19 p3272 A69-36255

SEISMOLOGY

Seismic refraction study of internal structure of volcanic cinder cone
02 p0236 A69-11465

Seismic regions location prediction on visible lunar side based on transient events, hot spots and gravity anomalies
18 p3193 A69-34363

Spheroidal disturbances theoretical seismograms on surface of gravitating elastic sphere with homogeneous mantle and liquid core, considering gravity and polar radial stress effects
23 p4158 A69-42020

SEISMOMETERS

U SEISMOGRAPHS

SELECTION

NT PERSONNEL SELECTION
NT PILOT SELECTION

Feature selection in pattern recognition, discussing techniques, crop classification problem and parametric multiclass pattern recognition
06 p0892 A69-17396

Nonparametric ranking procedures /based on order statistics/ guaranteeing preassigned probability for selection from random samples populations as good as control
08 p1342 A69-20172

Selection effects on comets discovery, comparing effectiveness of photographic and visual observation techniques
17 p3045 A69-34221

Part selection, source control and application program for reliability of equipment design, noting derating
22 p3953 A69-40031

Computer selection for given automatic control system, considering efficiency criterion and operational constraints satisfaction
24 p4285 A69-42952

SELECTIVE FADING

Noncoherent binary communication detector for slow selective fading channel with additive quasi-stationary noise based on mathematical procedure of nonparametric classification
03 p0390 A69-13215

SELECTORS

Sunde model of troposcatter channel as transmission medium in computer simulation of adaptive digital communication scheme for selective fading channels
09 p1458 A69-22471

SELECTORS

Laser wavelength selection device for parallel wavelength separation or recombination of laser beams external to laser cavities
01 p0091 A69-10841

Fast digitalized scan laser using Nd-YAG as active medium and containing crossed array of lithium niobate electro-optic switches for mode selection [IEEE PAPER R-2]
05 p0775 A69-16326

Peak amplitude selector for electrophysiological phenomena analysis, describing memory schemes, threshold crossing detectors and display, input and output circuits, timing, etc
15 p2612 A69-31266

Single hyperfine-state atomic beam selector effect on hydrogen maser stability, discussing DC magnetic field variation
18 p3153 A69-35306

Q multiplier UHF device as preselection filter for closely spaced channel signals, discussing channel interference reduction
23 p4141 A69-42220

SELENIDES

NT CADMIUM SELENIDES

NT GALLIUM SELENIDES

NT LEAD SELENIDES

NT ZINC SELENIDES

SnTe, SnSe and SnS epitaxial layers obtained by deposition of sublimates on cellulose-nitrite-varnish and single crystal NaCl and KBr substrates
02 p0298 A69-12049

Bismuth selenide inhomogeneous distribution effect on thermoelectric properties of bismuth telluride alloy
04 p0644 A69-15265

Thermoelectric parameters of polycrystalline p-type bismuth antimony telluride and bismuth antimony tellurium selenide solid solutions
15 p2668 A69-30629

Electrical conductivity and thermoelectromotive force of bismuth telluride and bismuth telluride-bismuth selenide alloys obtained by sintering, hot pressing and annealing
15 p2670 A69-31248

Nonlinear voltage dependence on current in p-type indium selenide single crystals, detecting negative resistance under pulsed electric field
22 p3992 A69-40602

SELENIUM

Selenium diffusion in indium antimonide, determining concentration gradients in junction space charge region by capacitance method
09 p1554 A69-21469

Se activation energy dependence on crystals composition and Se concentration, based on Hall coefficient temperature dependence in gallium arsenic phosphides
13 p2317 A69-27875

Selenium diffusion in indium antimonide, determining concentration gradients in junction space charge region by capacitance method
15 p2669 A69-30714

Se activation energy dependence on crystals composition and Se concentration, based on Hall coefficient temperature dependence in gallium arsenic phosphides
21 p3782 A69-39141

Selenium distribution along GaSb single crystals during oriented crystallization determined by radiometry
23 p4198 A69-41725

SELENIUM COMPOUNDS

NT CADMIUM SELENIDES

NT GALLIUM SELENIDES

NT LEAD SELENIDES

NT SELENIDES

NT ZINC SELENIDES

ESR comparative study of selenoamino acids and S analog radical formation and radiation resistance, noting selenium groups ability as acceptors for unpaired electrons
21 p3668 A69-38425

SELENOGRAPHY

Selenographic and celestial selenocentric coordinate systems, noting precession and nutation of lunar rotation axis
04 p0662 A69-15250

Selenographic technique for tying in lunar far side space photographs based on earth disk position measurements with respect to moon limb
05 p0763 A69-16055

Comparator measures for relative lunar altitudes on Yerkes lunar photographs, estimating selenographic positions from grids of orthographic atlas of moon
07 p1225 A69-19771

Gaussian particle size distribution with porosity and surface irregularity corrections used to determine mean particle size of lunar surface material at Surveyor sites
12 p2158 A69-26371

Selenographic technique for tying in lunar far side space photographs based on earth disk position measurements with respect to moon limb
20 p3545 A69-37965

SELENOLOGY

Selenodetic data results and calculations of moon visible physical surface do not agree
02 p0314 A69-11643

Tectonic map compiled for visible and far sides of moon, noting correlations between earth and moon tectogenesis
03 p0505 A69-12899

Lunar geoscience role in lunar mission planning, discussing costs, reduced gravity effects, sample mass limits and seismology
03 p0510 A69-13391

Lunar crater count observations of mare surface and ejecta blanket in Orientale basin
04 p0656 A69-14672

Lunar premare and postmare craters distributions, discussing latitude independence and sources of impacting bodies
04 p0656 A69-14673

Lunar history reexamination including added mantle convection and recent rocket data
05 p0825 A69-16303

Lunar rock composition monitored by Luna 9 and 13 soft landed lunar probes [UN PAPER 68-95769]
06 p1000 A69-17041

Post-telescopic lunar exploration, discussing Apollo program and development of selenology [JPL-TR-32-1399]
06 p1001 A69-17159

Nature and origin of lunar far side Tsiolkovsky crater
06 p1003 A69-17386

Fine structure and geology of lunar surface from Luna, Ranger, Surveyor and Orbiter data
07 p1212 A69-18547

Regolith thickness distribution at Lunar Orbiter sites, correlating thickness directly with cratering density
07 p1213 A69-18604

Selenodetic measurements on Yerkes lunar star trailed photographs, considering limb and star trail
07 p1225 A69-19772

Yerkes star trailed lunar photographs with ephemeris values of moon libration for selenodetic coordinates of secondary points, discussing errors and altitudes
07 p1225 A69-19773

Tucson selenodetic triangulation for coordinated points, considering measures on Yerkes star trailed plates
07 p1225 A69-19774

Models for lunar density distribution consistent with available data on lunar physical properties
08 p1393 A69-20579

Lunar mass concentrations /mascons/ origin and nature, postulating primordial lunar atmosphere and hydrosphere and carbon derived from primordial organic compounds
08 p1397 A69-20697

Collection of Soviet papers on physics of moon and planets covering results of lunar, Mars and Jupiter photometric studies
11 p1959 A69-24723

Moon figure determined by DOD-66 Selenodetic Control System compared with second surface harmonic using computer analysis
14 p2527 A69-29942

Mascons implications in selenodetic data analysis conducted at U.S. space centers
17 p3028 A69-32922

Lunar photometric function determined using modified Hapke surface model and corrected Lommel-Seeliger law for surface roughness and crater distribution [AIAA PAPER 69-596]
17 p3033 A69-33308

Lunar surface bulk density determined from laboratory and spacecraft measurements of static bearing capacity as functions of depth and solids percentage
18 p3193 A69-34366

Standing waves on moon, discussing annular and radial structures of lunar craters and global tectonic patterns
20 p3604 A69-37565

Lunar regolith from Surveyor Program pictorial data of lunar maria
22 p4012 A69-40087

Miniaturized seismic refraction system for manned lunar landings consisting of geophones, three channel amplifier, calibrator and logarithmic compressor
23 p4162 A69-41533

Manned lunar exploration programs and site evaluation concerning volcanic processes, chemical and mineralogical differentiation, atmosphere and protobiological materials
23 p4216 A69-42200

Lunar gravitational field data from Lunar Orbiter spacecraft reprocessed, discussing mascon effects on moon structure and evolution theories
24 p4379 A69-42785

SELF ABSORPTION

Downstream radiation flux distribution calculated for blunt entry bodies, considering self absorption effects
02 p0354 A69-12547

Band profiles and emission spectra of shock heated AIO compared for self absorption of blue-green system, discussing electronic transition moment
07 p1184 A69-19163

Spectra of opaque radio sources with synchrotron self absorption, discussing brightness temperature and magnetic field
09 p1591 A69-21447

Radiative relaxation of relativistic particle distribution undergoing synchrotron radiation and reabsorption, discussing self absorbed radio source model
13 p3227 A69-27572

Polarimetric observations of Be stars, noting dependence and self absorption by hydrogen of polarization produced by electron scattering
16 p2863 A69-32397

Radiation self absorption effects on heating loads of blunt body during hyperbolic entry
21 p3644 A69-39040

SELF ADAPTIVE CONTROL SYSTEMS

Self adaptive control circuit diagram examination, considering phase shift measurement reliability by eliminating distortion caused by system nonlinearities and noise
01 p0052 A69-10796

Dynamic system for self adaptive control of inertial plant described by differential equations, noting synthesis method eliminates distortion
01 p0052 A69-10797

Synthesis of statistically optimal self adaptive system for dynamic characteristics stabilization of automatic control system main loop
03 p0410 A69-13256

Self adaptive circuit parameters synthesis of systems using amplitude-frequency characteristic by Chaplygin theorem
03 p0410 A69-13256

High gain self steering repeater for multibeam microwave array system for earth-satellite communications
04 p0573 A69-14330

Self adaptive systems stability analyzed using filter and correlation methods, considering higher harmonics at rectifier and synchronous detectors output
04 p0582 A69-14796

Sensitivity models for adaptive and self adaptive systems design
04 p0582 A69-14797

Self balancing single degree of freedom free fall space environment simulator, discussing coincidence of mass and rotation centers
04 p0586 A69-15468

Space vehicle flight automatic optimization for maximum L/D reentry, considering perturbations causing trajectory inclination changes during roller coaster reentry
05 p0830 A69-16045

Multivariable self adaptive control system design using sensitivity methods, obtaining adaptation stability by Liapunov synthesis
06 p0900 A69-17352

Pattern recognition method dependent on preselection of good variables, discussing SELFIC and relationship to Karhunen-Loeve expansion and factor analysis
07 p1088 A69-18386

Computer simulations, comparing self adaptive /neurotron/ control of spacecraft energy allocation subsystem to programmed control
07 p1058 A69-18389

Directional gyroscope accuracy increased by self adaptive systems, based on precession theory and drift amplitude dependence
11 p1881 A69-24559

Digital control algorithm based on self adaptive linear model of multivariable processes used for feed-forward control of output signals

12 p2046 A69-26063

Self adaptive system for recognition of dynamic shapes, discussing self structuring by learning, incomplete pattern recognition, logic element network, etc

12 p2054 A69-27080

Searchless gradient self adaptive system for adjusting servosystem parameters to reference model characteristics, using auxiliary operator method

14 p2426 A69-29146

Liapunov method applied to stability evaluation of multiparameter self adaptive nonsearch gradient servosystems

19 p3286 A69-35891

Missile and spacecraft guidance navigation and control, discussing fluidics, self adaptive and digital control and Kalman filtering

19 p3370 A69-36316

Failure test algorithm for sequential units with delay lines of control digital computers, detecting replacement of output terminals by sensitive paths

20 p3502 A69-37394

Space vehicle flight automatic optimization for maximum L/d reentry, considering perturbations causing trajectory inclination changes during roller coaster reentry

20 p3618 A69-37954

Soviet book on self adaptive systems design, operational principles and analysis and synthesis methods

21 p3687 A69-39532

SELF ALIGNMENT

Alignment of rocket-borne instrument with sun, discussing mechanical system design, servocontrol and silicon photodiode sensors

03 p0427 A69-12980

Shipborne self pointing antenna for reception of telemetry signals from maneuverable missile, discussing tracking and compensation for ship platform motion

10 p1664 A69-23803

Self steered retrodirective antenna arrays with phase synthesizer, combining signals from individual elements at LF levels

11 p1850 A69-24983

Multidimensional self adjusting systems design by achieving parametric invariance, using sensitivity theory

11 p1861 A69-25711

SELF BIAS

U BIAS

SELF CONSISTENT FIELDS

Linear combination of atomic orbitals-molecular orbitals self consistent fields calculation on beryllium dihydride, using Gaussian basis functions

05 p0811 A69-15910

Asymptotic formulas for field diffracted by conducting wedge illuminated by line source usable for self consistent field analyses

05 p0720 A69-16344

LCAO-MO-SCF wave functions determined for ground and excited states of nitrogen dioxide at five different ONO angles

06 p0960 A69-17109

Ground state energy of Anderson Hamiltonian calculated by cluster variation for cases of infinite d-d correlation energy

06 p0958 A69-17712

Rapid differential rotation effect on massive main sequence O and B stars, discussing bolometric magnitude deficiencies and shifted position in Hertzsprung-Russell diagram

07 p1220 A69-19390

Self consistent field calculations of effective quantum numbers for nd, nf and ng electrons for atomic configurations from 2-126 Z

08 p1355 A69-20734

Stability of spherically symmetrical nonrotating mass systems moving in self consistent gravitational Einstein field, considering quasar applicability

11 p1956 A69-24394

Self consistent solutions for collisionless plasma penetration across magnetic field, showing electrons ability to accompany ions across field

15 p2661 A69-30923

Self consistent flow calculation in dense space charge beams, including electrode design for portions isolation

22 p3985 A69-40668

Self consistent field molecular orbital method in LCAO linear combination of atomic orbitals/approximation applied to LiH ground state for potential energy curve

22 p3985 A69-40721

Self consistent fields in waveguides containing thin conductors, expanding induced field into Fourier series in normal waves for series coefficients

23 p4123 A69-41942

Linear diffraction equations in electronics in self consistent formulation reduced to complex transcendental equations, using perturbation method

23 p4124 A69-42033

Stability of spherically symmetrical nonrotating mass systems moving in self consistent gravitational Einstein field, considering quasar applicability

24 p4390 A69-43784

SELF DEPLOYING SPACE STATIONS

U SPACE STATIONS

SELF DIFFUSION

U DIFFUSION

SELF ERECTING ANTENNAS

U ANTENNAS

SELF ERECTING DEVICES

Triangulated pantograph structure for deploying antennas, special equipment and instruments from spacecraft, noting structural design and strength characteristics

02 p0252 A69-11752

SELF EXCITATION

Self excitation conditions and output characteristics of tunnel diode DC to AC converters for spacecraft, discussing relaxation-oscillator and push-pull circuit converter types

01 p0046 A69-10755

Parametric vibrations of self excited elastic and aeroelastic systems with traveling waves, determining stable vibration boundaries

02 p0337 A69-11561

Gases optical pumping by self radiation laser action, discussing high intensity oscillatory transitional wide bands of molecular gases

04 p0610 A69-14382

Electromotive force along magnetic field induced by liquid metal flow /alpha effect/, giving foundation for self excitation of electromagnetic field

04 p0635 A69-14547

Two cavity large storage box atomic hydrogen maser, obtaining self excited oscillations coupled with high gain amplifier [IEEE PAPER C-8]

05 p0774 A69-16310

Induction, helical and straight through liquid metal MHD generators tested under independent and self excitation conditions

13 p2208 A69-27512

Gases optical pumping by self radiation laser action, discussing high intensity oscillatory transitional wide bands of molecular gases

14 p2456 A69-28755

Self excited vibrating laminar diffusion flames, discussing coupling, jet spacing radial heat transfer and boundary layer interaction

16 p2876 A69-31711

Viscoelastic half space properties effect on self excited vibration boundaries determination

16 p2873 A69-32063

Self excited vibrations of rotors supported in gas bearings from analyzing solutions to equations of rotor motion

16 p2875 A69-32250

Self excited oscillations in systems with one linearity symmetrical with origin determined by harmonic balance method

21 p3685 A69-38463

Nonlinear theory of optically excited semiconductor laser for conditions of self excitation, steady state lasing amplitude and lasing frequency shift

23 p4174 A69-41733

Self rhythms of low audio frequencies in motor nerves under electric pulses influence at VLF related to viscosity changes of nerve substance

23 p4092 A69-42057

SELF FOCUSING

Sparks from laser induced air breakdown due to focusing of laser beam, noting evidence for initiation by self focusing

01 p0092 A69-11246

Kerr effect and electrostriction during self focusing of high power laser beam in gases and liquids

04 p0611 A69-14792

Thermal self focusing of argon laser beam passing through lead glass

05 p0771 A69-15819

Thermal self actions of CW laser beams in solids and liquids with wind or convection flow, discussing self focusing and defocusing [IEEE PAPER E-12]

05 p0774 A69-16311

Thermal self defocusing effect of laser beam in self focusing liquids, measuring refractivity changes by high speed double exposure holography [IEEE PAPER J-7]

05 p0775 A69-16320

Self focusing of TM type electromagnetic waves in isotropic plasma and formation of waveguide channel

07 p1196 A69-19749

Laser beams self focussing interpreted as photon contraction due to equivalent gravitational attraction with gravitational constant proportional to nonlinear refractive index

08 p1324 A69-20085

Inhomogeneous laser beams self focusing effects in organic liquids recorded on bases of induced stimulated scattering

08 p1326 A69-20538

Self focusing linear array for communication satellites, evaluating reradiated field taking into account mutual coupling between elements

08 p1289 A69-20970

Self focusing aerial antenna arrays with full angular coverage for two way airborne communications

08 p1289 A69-20971

Self focusing of plasma whistler wave along magnetic field at small threshold power

09 p1546 A69-21577

First Stokes component of stimulated Mandelstam-Brillouin scattering and line defects caused by self focusing of single pulse laser beam

09 p1521 A69-22686

Self focusing of CW argon laser beam due to absorptive heating in crown glass, emphasizing time dependence of beam diameter as function of distance

10 p1706 A69-24009

Breakdown in air produced by picosecond mode locked laser pulses showing evidence for self focusing

13 p2270 A69-27196

Weakly divergent intense light beam propagation in laminar optically inhomogeneous medium with self focusing possibility analyzed by perturbation theory

13 p2223 A69-28568

Laser beam light pressure bending of incompressible liquid surface leading to beam self focusing in linear medium

14 p2461 A69-29674

Physical mechanisms for nonlinearities in electromagnetic wave propagation, analyzing plane wave instability, self focused beams propagation and laser oscillations

17 p2928 A69-33867

Self channeling of light in nonlinear isotropic medium using exact solutions of nonlinear Maxwell equations for two dimensional case

17 p3007 A69-33975

Laser beam self focusing in plasma in terms of ponderomotive acceleration due to light intensity gradient

22 p3961 A69-40417

Ultrashort laser light pulses self focusing and determination of focal points coordinates

24 p4328 A69-43068

SELF INDUCED VIBRATION

NT PANEL FLUTTER

NT SUBSONIC FLUTTER

NT SUPERSONIC FLUTTER

Self excited vibration of flowing medium and infinite cylindrical duct wall in primary magnetic field, discussing vibration stability and critical speeds

18 p3226 A69-35462

SELF LUBRICATING MATERIALS

Two phase self lubricating composite materials for high temperature, detailing impact strength, friction and wear tests [IME PAPER 12]

07 p1137 A69-18560

Cooling requirements for high speed polytetrafluorethylene lubricated ball bearings operating in cold hydrogen gas, developing minimum gas flow rate equation [ASLE PAPER 68-LC-2]

07 p1141 A69-19310

Self lubricating bearings lifetime calculated as function of lubricant in pores and consumption rate, noting temperature effects

15 p2618 A69-30281

Dry lubricant films of soft metals, self lubricating plastics and crystalline powders, noting design and tests

15 p2642 A69-30328

Polyphenyl ether lubricants and self lubricating materials compared for antifriction ball bearings in thrust reversing actuator gear box [SAWE PAPER 68-LC-1]

18 p3148 A69-35003

SELF LUBRICATION

Self acting gas lubricated bearings design procedures and comparison with oil lubricated bearings [ASME PAPER 68-LUBS-10]

13 p2265 A69-27267

Pressure distribution in finite width high speed self acting gas lubricated slider and partial arc bearings, noting trailing edge conditions and side leakage effects [ASME PAPER 68-LUBS-15]

13 p2265 A69-27268

Linearized theory for stability of self acting gas journal bearings with noncircular members and elements of flexibility and damping, noting three lobe rotor [ASME PAPER 68-LUBS-45]

13 p2266 A69-27277

Radial clearance influence on self lubricating porous bearing friction coefficient and oil losses as function of operation duration

16 p2794 A69-32067

SELF ORGANIZING SYSTEMS

Self organizing and learning control systems, adaptive systems theory and defining self organizing control systems

07 p1114 A69-18382

Self organizing trainable logical networks /TLN/ as stable controllers in multiaxis vehicle control problem, reviewing TLN concepts and training theory

07 p1070 A69-18388

Data handling by groups in perceptron type pattern recognition and decision making problems based on algorithm involving second degree polynomials

08 p1278 A69-20420

Data handling by groups in perceptron type pattern recognition and decision making problems based on algorithm involving second degree polynomials

14 p2418 A69-29658

Perceptron probability algorithm for random events prediction based on previous histories, applying Bayes formulas, static solutions formulas and transition probability tables and graphs

19 p3287 A69-36664

Cell origin in self organizing natural polymers in terms of molecular evolutionary priority of polynucleotides and poly alpha amino acids

22 p3896 A69-40781

Stochastic fuel regulator problem investigated by optimal and self organizing techniques, emphasizing realizability of resulting controllers

24 p4292 A69-43284

SELF OSCILLATION

Relationship between cooled surface temperature and pressure self oscillation frequency during heat transfer to turbulent fluid flow, showing temperature variations

01 p0173 A69-10094

Self sustained oscillations of piston type valving system with conduit line at upstream and capacity at downstream

01 p0012 A69-10310

Rubidium self oscillating magnetometer long term stability, noting changes affecting accuracy and sensitivity

02 p0250 A69-12394

Self oscillations of dynamic systems representing space vehicles, considering periodic motions stability, bifurcation curves and energy consumption requirement limit

03 p0519 A69-13068

Self oscillating pulse relay control system investigated by approximate method for harmonic linearization of nonlinearities, noting external effects

03 p0410 A69-13684

Equations for self oscillating mode of operation for O-type backward wave generator with electrostatically focused electron beam and finite values of amplification parameter

03 p0407 A69-13986

Relaxation induced self oscillations during combustion of gunpowder in semiclosed volume, noting combustion instability

04 p0686 A69-14987

Low power RF signal triggering of self sustaining Gunn oscillations in GaAs samples

05 p0734 A69-16575

Self excited rotor blade oscillation at high subsonic Mach numbers during flight tests of Sikorsky NH-3A compound helicopter

07 p1053 A69-18870

Optimizer for shaping control signal of hunting type system with plant in form of nonlinear inertialess element, examining inadequacy for system operation

07 p1115 A69-19757

High speed stable system by combining hunting type control system without closed cycles designed for plant optimization with recycling type controller

07 p1116 A69-19759

Self oscillations in angular velocity sensor using electric spring and potentiometric pickup, examining friction moment and inductance coil effects

09 p1497 A69-22106

Response and stability of self sustained two degrees of freedom system with nonlinear damping, noting harmonic oscillations

[ASME PAPER 69-VIBR-24]

10 p1806 A69-24171

Second order dynamic systems stability, analyzing nonlinear and self excited oscillations by using two differential equations

11 p1915 A69-24535

Asymptotic method for single and multifrequency oscillations of quasi-linear control systems with distributed parameters and delayed time coordinate

11 p1916 A69-24766

Acoustic frequency of longitudinal self oscillations during vibrational fuel combustion in afterburner, taking into account nonlinear properties of heat supply zone

11 p2002 A69-25339

Self and forced oscillations in multivariable relay control system, considering relays with hysteresis and dead band and stability of periodic states

12 p2049 A69-26084

Monograph on nonlinear servosystems covering nonlinearity with/without inertia, self oscillations, linearization by forced oscillations, stability theorems and Liapunov function choice

12 p2054 A69-26966

Heat convection mechanism in two phase autooscillatory system generalized to convective heat transfer in cloudy atmosphere

13 p2292 A69-27798

Phase and amplitude changes of arbitrary-Q self excited oscillator under external disturbance, using differential equations

13 p2300 A69-28574

Self oscillations of dynamic systems representing space vehicles, considering periodic motions stability, bifurcation curves and energy consumption requirement limit

14 p2530 A69-28750

Equation system for asynchronous MHD generator operating in self oscillating mode derived and solved

14 p2405 A69-29457

Spontaneous self pulsing and cavity dumping in carbon dioxide laser Q switched by internal GaAs electro-optic cell without saturable absorber

16 p2797 A69-32014

Autooscillatory process in n-circuit tunnel diode LC oscillators acted upon by external sinusoidal voltages

16 p2764 A69-32256

Si planar IMPATT diodes anomalous mode continuous wave UHF oscillations, noting DC density and DC/RF power conversion efficiency

17 p2934 A69-32846

Tunnel diode oscillators theory applications, investigating self resonance phenomena relating to static characteristic variations under self oscillating conditions

19 p3285 A69-36738

Monograph on periodic solutions and locking-in regions for differential equations with switching points describing motion of self excited oscillatory physical structures

20 p3577 A69-37923

Pulse modulated feedback system for satellite attitude control, analyzing relationship between physical parameters to ensure two pulse limit cycle oscillation stability

24 p4295 A69-43318

SELF REGULATING

U AUTOMATIC CONTROL

SELF REPAIRING DEVICES

Nonreplicative self repairing control, describing prototype computer construction for testing feasibility

04 p0569 A69-15457

Self reproducing automata, noting description of cellular system and applications to systems science

05 p0723 A69-15826

Computer reliability by development and methodical employment of self repair techniques

12 p2034 A69-25941

Satellite onboard computers automatic reconfiguration and self repair

20 p3503 A69-37399

SELF STIMULATION

Critical body temperature for intracranial self stimulation in white rats

03 p0375 A69-13897

Electrical self stimulation adaptability of hypothalamus or instrumental self reinforcing reaction in rats using skinner box technique

23 p4091 A69-42052

SELSYNS [TRADEMARK]

U SERVOMOTORS

SEMANTICS

Space Treaty interpretation of ambiguity of term peaceful due to differing concepts of U.S. and U.S.S.R.

20 p3635 A69-37104

Juridical meaning of peaceful in 1967 Space Treaty interpreted in terms of real purpose of given space activity

20 p3635 A69-37105

Interpretation of peaceful uses of outer space in Space Treaty, emphasizing provision forbidding individual military space activities whether aggressive or nonaggressive

20 p3635 A69-37106

1967 Space Treaty peaceful activities definition, suggesting explicit provisions regarding treaty province, enforcement machinery and implementation

20 p3636 A69-37112

SEMICIRCULAR CANALS

Vestibular analyzer role in spatial orientation under weightlessness conditions during aircraft flights, discussing underestimations of rotation angle of Barany chair

08 p1262 A69-19840

Human nystagmic reaction variations due to simultaneous rotation of head and body, studying coriolis couple in horizontal semicircular canals

12 p2020 A69-26565

Prolonged iterative accelerations and decelerations on vestibular apparatus, discussing nystagmus measurement attempt and centrifugation tests on guinea pigs

13 p2211 A69-28592

Diphenidol and prochlorperazine effect on human semicircular canal function, noting failure of drug to alter vestibular responses

17 p2913 A69-33168

Vestibular function tested with angular acceleration, applying semicircular canal reflexes for flight crew selection and appraisal

20 p3481 A69-37271

Equipment with minimum semicircular canals stimulation for vestibular analyzer studies

20 p3481 A69-37274

SEMICONDUCTING FILMS

Dimensional effects on thermodynamic and kinetic properties of thin semiconductor and semimetal films, noting quantization influence

01 p0136 A69-10186

Vacuum deposited n-type InAs films magnetoresistance coefficient dependences on length-to-width ratio, homogeneity moving carriers size and magnetic inductance

01 p0136 A69-10254

Thin film transistors prepared from spray deposited cadmium sulfide, discussing carrier mobility and low stability

02 p0214 A69-11596

Gunn domains reduction in sheet type GaAs oscillators by spreading of field lines out of active region

02 p0215 A69-11933

Thin CuAs selenide films by vacuum deposition, electronographic study proves cubic spherulitic phase existence

02 p0298 A69-12045

Nondestructive measurement of thin transparent film thickness by interference method, noting diffusion profiles

03 p0430 A69-13634

Photoluminescence spectra of n-type GaAs films grown by gas transport reactions and from solution melt, noting recombination emission

03 p0488 A69-13887

Photocurrent carriers recombination in organic semiconductor rhodamine B films analyzed as function of illumination

03 p0489 A69-13890

Epitaxial GaAs films with high electron mobility, noting radiation recombination spectra dependence on substrate orientation

03 p0492 A69-14172

Electrical conductivity of high resistance epitaxial semiconducting films measured by three probe method

04 p0597 A69-14538

Impurity transfer in doped and undoped epitaxially grown GaAs films, studying substrate dopants effect on carrier concentration profiles

05 p0807 A69-15957

Electrical polarization effect on electroluminescence brightness waves in zinc sulfide films

05 p0807 A69-16213

Polarization effect on electroluminescent properties of zinc sulfide films

05 p0807 A69-16214

Cadmium sulfide films with larger than bandgap photovoltages, analyzing photovoltage decay and temperature and light intensity effects
06 p0980 A69-17772

Selective etching technique in study of dislocations in epitaxial layers of gallium arsenide
06 p0981 A69-17891

Structural and electrical properties of indium antimonide and arsenide films, noting dependence of electron concentration and mobility on thickness
06 p0981 A69-17892

Automatic test set for measuring dopant concentration profiles in epitaxial films
07 p1130 A69-18245

CdSe single crystal films vacuum deposition for use of photocells base with p-n heterojunctions
07 p1198 A69-18512

Structural and optical properties of vacuum deposited GaP films at below 240-850 C
09 p1554 A69-21332

Semiconducting films as collector work function in thermionic converters, with regard to I-V characteristics
09 p1558 A69-21825

Vacuum deposited n-type InAs films magnetoresistance coefficient dependences on length-to-width ratio, homogeneity, moving carriers size and magnetic inductance
09 p1559 A69-22647

PbTe single crystal films growth on KCl studied by electron microscope, observing vapor crystal mechanism without coalescence of contacting crystals
10 p1745 A69-23323

Photoluminescence spectra of n-type GaAs films grown by gas transport reactions and from solution melt, noting recombination emission
11 p1939 A69-25688

Photocurrent carriers recombination in organic semiconductor rhodamine B films analyzed as function of illumination
11 p1939 A69-25691

Substructural patterns of epitaxial PbTe films obtained by condensation of vaporized PbTe on NaCl crystal surfaces, discussing formation kinetics and morphology
12 p2144 A69-26675

Microminiature five point measuring head with linear point design for resistivity measurement of semiconductor films, noting four point head capabilities
12 p2099 A69-27104

Semiconductor thin films analysis using mass spectrometer with spark source
13 p2316 A69-27293

Transverse quantum thermogalvanomagnetic phenomena in thin semiconducting films, noting effects of inelastic electron scattering at acoustic lattice vibrations
13 p2318 A69-27890

Absorption band edge position in p type indium antimonide thin films after heating, showing forbidden bandwidth function relationship to film thickness
15 p2666 A69-30044

Semiconductor films synthesis and properties, discussing single crystal films, epitaxial nucleation, nuclei surface distribution, layer kinetics, doping and film-substrate interface
15 p2670 A69-31046

Electrical switching in thin film arsenic selenium telluride semiconducting glass diodes, observing formation of liquid phase and conducting filaments
16 p2760 A69-32017

Tunnel junctions with low background currents made by reacting active gas layer adsorbed on Nb film surface with Pb upper film to form barrier
17 p3016 A69-33788

InSb thin films prepared by flash evaporation, discussing Hall measurements at various temperatures and electron mobility dependence on film thickness
18 p3182 A69-34348

Copper sulfide-cadmium sulfide heterojunction model for photovoltaic effect, considering surface layer intrinsic absorption and CdS photoconductivity
19 p3250 A69-35683

Gold/polycrystalline cadmium selenide film contact found ohmic in darkness and barrier in light, noting potential distribution, electron concentration and energy gap
19 p3384 A69-36480

Transport mechanism in amorphous Ge films deposited on glass substrates studied by measuring piezoresistance as function of temperature during pure nitrogen immersion
19 p3391 A69-36559

Silicon dioxide film doped with Al to increase MOS structure radiation resistance
20 p3584 A69-38070

Chalcogenide semiconductor film switches time parameters, showing delay time decrement with thickness decrease and voltage increase
21 p3780 A69-39045

Thin PbTe semiconductor films electrical properties measured in air and vacuum, showing dependence on thickness and conditions of preparation
21 p3782 A69-39242

Spectral dependence of optical absorption in InSb thin films under conditions of quantum dimensional effect, considering allowance for nonparabolic conduction zone
21 p3783 A69-39560

Optimal CdS single crystals growth from gaseous phase achieved with 2 to 1 ratio between Cd and S concentration
23 p4199 A69-42468

Temperature gradients effects on GaAs crystals grown by Bridgman method
23 p4199 A69-42469

InTe phase recrystallization in thin films composed of two InTe phase mixtures, showing random concentrations and distribution of centers growing as spherulites
24 p4361 A69-42993

InTe phase formation in thin film composed of two InTe phases, showing dependence on annealing in high vacuum and substrate temperature
24 p4361 A69-42994

Component proportion and diffraction spectrum of macroblock thin films of indium telluride phase of In-Te system, using X ray and microanalysis
24 p4361 A69-42995

Dielectric and semiconductor films vacuum deposition by CW carbon dioxide laser, discussing optical properties
24 p4329 A69-43755

SEMICONDUCTOR DEVICES

NT AVALANCHE DIODES

NT FIELD EFFECT TRANSISTORS

NT GALLIUM ARSENIDE LASERS

NT GERMANIUM DIODES

NT JUNCTION DIODES

NT JUNCTION TRANSISTORS

NT METAL OXIDE SEMICONDUCTORS

NT PARAMETRIC DIODES

NT PHOTODIODES

NT PHOTOVOLTAIC CELLS

NT SILICON TRANSISTORS

NT THERMISTORS

NT THYRISTORS

NT TRANSISTOR AMPLIFIERS

NT TRANSISTORS

NT VARACTOR DIODES

Posistors heat capacity investigated as temperature function, showing maximum heat balance corresponds to Curie temperature
01 p0038 A69-10098

Output p-channel MOS transistor selection tree for display and information storage systems
01 p0039 A69-10173

Microwave applications of monolithic and hybrid semiconductor circuit technologies, considering cost and performance
01 p0039 A69-10188

Nonreciprocal tunable yttrium-iron garnet microstrip filter design through generation of circularly polarized field
01 p0041 A69-10202

Semiconducting diode base Dember effect impedance studied for recombination rates approaching zero or infinity
01 p0137 A69-10260

Semiconductor switching diode, evaluating operation with nonlinear time delay equivalent circuit
01 p0046 A69-10747

Probability characteristics of temperature and supply voltage dependent parameters of semiconductor equipment
01 p0047 A69-10783

Plastic material requirements for semiconductor device encapsulation noting electrical compatibility, mechanical and environmental protection and costs
02 p0270 A69-12161

Semiconductor center traps effect on characteristics of metal oxide semiconductor transistors
02 p0299 A69-12183

Epitaxial GaAs transferred electron oscillators pulsed operation at bias voltage ten times threshold voltage, noting power output and efficiency
03 p0402 A69-12854

High power pulse generators with four layer p-n-p-n structure, discussing design, principles and applications of semiconductor elements as modulators and switches
03 p0402 A69-12978

Electron scattering by neutral acceptors in semiconductors, noting relaxation time for Ge at very low temperatures
03 p0484 A69-13280

Broadbanding of S-band three port stripline circulator, discussing effect of tuning and mode suppressor screws
03 p0404 A69-13472

Gunn effect and resulting electron transfer mechanism in semiconductor devices
03 p0486 A69-13610

Microwave generation and amplification, noting microwave transit time tubes, semiconductor devices and methods utilizing quantum electronic effects to generate and amplify EHF oscillations
03 p0395 A69-13611

Two band model for determining linear and nonlinear electromagnetic responses of small band gap semiconductors in magnetic field
03 p0487 A69-13753

Transverse perturbation influence on helical instability in oscillistor
03 p0488 A69-13886

Book on Hall generators /magnetically controllable semiconductor elements/, discussing principles of operation, design, manufacture and applications
03 p0406 A69-13954

Current oscillations or instabilities in semiconductor wafer with one electromagnetic mode and one carrier mode, investigating resonant frequencies
03 p0408 A69-14049

Potential distribution approximations for junction semiconductor devices, noting application to barrier layers and electron tunneling
03 p0408 A69-14107

Electron emission into vacuum from forward biased Schottky barrier consisting of cesiated thin layer of Pt on n-type ZnS
03 p0493 A69-14186

Semiconductor microwave phase shifters for electronic steering of phased array radar antennas noting cost, reliability and properties of steerable antennas
04 p0572 A69-14319

Twin differential calorimeter for measuring heat dissipation by wire specimen under fatigue tests, using semiconductor thermopiles
04 p0618 A69-15205

Field distribution and potential drop in semiconductor field emitter, noting nonlinear effects in indium trisulfide, electron mobility and multiplication factor
05 p0806 A69-15630

Coupled waves in ferromagnetic and antiferromagnetic semiconductors in constant electric and magnetic fields, discussing spin, electromagnetic and plasma waves dispersion
05 p0809 A69-16548

Radiation tests on Ovonic threshold switches performed with fast neutrons and broadband X rays
06 p0978 A69-16891

Semiconductor standard memory circuits, discussing arrays and density
06 p0894 A69-17202

Semiconductor device failure modes temperature dependence, discussing bonds, metallization and packaging
06 p0894 A69-17218

Semiconductor glasses use for electronic devices
06 p0980 A69-17714

Microwave semiconductor devices, discussing performance trends in detectors, tunnel diodes, mixers, varactors, transistors and Gunn effect devices
07 p1096 A69-18440

Pulse power from X band LSA devices at centimeter through millimeter wavelengths
07 p1097 A69-18445

Solution regrowth method to prepare epitaxial GaAs for Gunn effect devices
07 p1197 A69-18451

Low temperature technique for preparing solid-solid diffusion sources for silicon device fabrication based on gaseous hydrides as reagents
07 p1198 A69-18619

Doped silicon dioxide films as controlled reproducible diffusion sources for silicon devices fabrication
07 p1198 A69-18620

Monolithic HF circuits stability in TV and HF devices noting need for appropriate amplifiers
07 p1103 A69-18883

Logic circuit for semiconductor current gain sensing switch

07 p1113 A69-19744

Differential capacity of Li doped zinc oxide crystals between vapor deposited asymmetrical In electrode contacts

08 p1371 A69-19883

Microwave amplification using silicon diodes in avalanche resonance pumped modes

08 p1279 A69-19909

Digital method for quantitative study of carrier circulation phenomena in semiconductors, noting Algol program and continuously polarized p-n junction

08 p1280 A69-19973

Linville model for describing elementary phenomena of electronic equipment in terms of physical data applied to irradiated semiconductor diode and transistor

08 p1280 A69-19974

Semiconductor current fluctuations associated with generation, recombination and annihilation of random electron-hole pairs at ohmic contacts

08 p1372 A69-20545

Composite transistor simulation of circuit inductor effect for synthesizing frequency selective circuits

08 p1286 A69-20834

Nonohmic microwave conductivity in semiconductor posts in rectangular waveguide, measuring incident, transmitted and reflected microwave powers

08 p1373 A69-20859

Normalized thermionic field emission in metal semiconductor barriers for forward and reverse current-voltage relation

08 p1373 A69-20861

Response time of semiconductor diode from dependence of equivalent capacitance on direct displacement current

08 p1287 A69-20889

Microelectronics technology and economics, discussing semiconductor integrated, discrete component and thin film hybrid circuits and MOSFET devices [AGARDOGRAPH-114]

08 p1291 A69-20983

Assessing cost effectiveness of reliability and quality of semiconductor products, using mathematical models

08 p1292 A69-21102

Synthetic circuit equipment for semiconductor rectifier life testing with built-in fault analyzer for indicating shorted and broken diodes

08 p1293 A69-21113

Failure mechanisms in semiconductors, discussing imperfections, fabrication errors and electrical, thermal and mechanical stresses

08 p1294 A69-21117

Integrated semiconductor circuits reliability in electronics and microelectronics, discussing hybrid and monolithic circuits in thin/thick film design and on Si monocrystals

08 p1294 A69-21118

Delta functions spectrum in reciprocal time domain for LC and RC structures due to impulse response in distributed parameters

09 p1471 A69-21327

Germanium solid state triode controlling electron currents of space charge limited regime by means of gate conductors in solid state diode

09 p1462 A69-21353

Book on special semiconductor devices covering photoelectric devices, Zener diodes, diffused junction silicon rectifiers, tunnel diodes, etc

09 p1462 A69-21638

Semiconducting diode base Dember effect impedance studied for recombination rates approaching zero or infinity

09 p1559 A69-22653

Hall effect theory and devices, noting application to measurement of several physical quantities and sources of errors in devices

09 p1541 A69-22698

Recombination parameters and depth of levels of p-n junctions in semiconductor photocells determined from position of maximum spectral sensitivity

09 p1560 A69-22718

Probability characteristics of temperature and supply voltage dependent parameters of semiconductor equipment

10 p1661 A69-23112

Surface ion behavior on planar semiconductor devices determined by measuring effect of time, humidity, temperature, voltage and previous testing history

10 p1743 A69-23173

Semiconductor strain gage balance with temperature compensation for conventional wind tunnels

10 p1672 A69-23265

Semiconductors with negative differential conductivity, investigating decreasing current-voltage characteristics, S or N shaped curves, perturbation parameters, instability, etc

10 p1744 A69-23300

Semiconductor properties, applications and problems including thin films, superconductivity, etc

11 p1937 A69-24736

Lasers applied to simulation of effects of X ray or gamma ray bursts on semiconductor devices

11 p1896 A69-24877

Transverse perturbation influence on helical instability in oscillator

11 p1939 A69-25687

High CW power K-band Gunn oscillators attained through control over doping level, profile and GaAs epitaxial layer thickness

12 p2036 A69-25907

Voltage and current waveforms of resonant domain and limited space charge accumulation modes in transferred electron oscillators, noting drift current

12 p2036 A69-25908

Meshless shutter tube with nine images double deflection capability, using deflection and semiconducting plates assembly

12 p2083 A69-26144

Book on industrial control engineering covering mathematics, semiconductor devices, feedback amplifier theory, closed loop systems, frequency response diagrams

12 p2051 A69-26244

Multiinput sine comparators graphical analysis and design considerations, emphasizing semiconductor circuit providing quadrilateral polar characteristic on impedance plane

12 p2039 A69-26350

Bias circuit LF oscillations in short Gunn devices, analyzing sinusoidal and relaxation oscillations and stable bias in terms of terminal I-V characteristics

12 p2041 A69-26628

Soviet collection of papers on semiconductor devices and application

12 p2042 A69-26877

Harmonic generation, using nonlinear current-voltage characteristics of Gunn diodes at 9500 MHz frequency

13 p2226 A69-27235

Semiconductor luminescent devices and laser pumping by solar radiation modulated to interact resonantly with solid state plasma oscillations and electric field in crystal

13 p2272 A69-27969

Dielectric thin film electrical and mechanical properties and preparation for semiconductor devices, emphasizing Si compounds

13 p2286 A69-28004

Electron scattering by neutral acceptors in semiconductors, noting relaxation time for Ge at very low temperatures

14 p2508 A69-29653

Push-pull circuit configurations for GaAs transferred electron oscillators, discussing CW X band and pulsed L band devices operation

15 p2574 A69-30168

Engineering problems in IC microminiaturization, dividing devices according to suitability for microminiaturization

15 p2576 A69-30352

MIS devices with dielectric properties avoiding positive space charge formation, discussing radiation effect

15 p2625 A69-30829

Screening techniques for semiconductor devices, considering component classification with respect to population strength distribution

15 p2627 A69-30840

Reliability of high resolution accelerometer composed of semiconductor integrated circuits

15 p2627 A69-30843

Semiconductor rectifiers economic life testing with synthetic circuits utilizing thyristor switch

15 p2579 A69-31041

Book on semiconductor devices physics covering principles and operational characteristics, carrier distribution and transport properties, materials, junctions, thin films, etc

15 p2670 A69-31062

Similarity between semiconductor discrete devices and integrated circuits, considering materials, processing and failure modes

15 p2580 A69-31128

Semiconductor technology including radar, Gunn and limited space charge accumulation oscillators, phase locked antennas, data processing and solid state computerization

15 p2581 A69-31521

Linear high resolution gate function in blocking out analog signals or reproducing signal amplitudes at output, noting semiconductor elements utilization

15 p2581 A69-31523

Semiconductor devices leak testing methods including liquids, helium mass spectrometer, Radiflo and hermetic seal tests

16 p2758 A69-31712

Semiconductor impressed voltage preconditioning, considering problems involving surface properties

16 p2758 A69-31713

Soviet book on reliability of semiconductor radio devices of flight vehicles covering failures through production errors, power source instability, environment induced changes, etc

18 p3108 A69-34350

Semiconductor life potential evaluation based on electrical parameters measurements at various voltages over wide temperature range

18 p3144 A69-34489

Semiconductor reliability evaluation program for economical experimental design, noting stress tests

18 p3232 A69-34496

Failure analyses of semiconductor devices for military use, suggesting modifications to MIL-STD reliability screen tests

18 p3108 A69-34499

Gunn effect theory and applications, discussing field domains in semiconductors, excited oscillations measurement, oscillators design, computer elements, etc

18 p3183 A69-35160

Gunn effect and devices effective use for specific purposes and as components of microwave systems

18 p3183 A69-35263

Four terminal silicon planar p-n-p-n model operating as semiconductor small signal linear tetrode amplifier, discussing properties and mathematical models

18 p3109 A69-35293

Scanning electron microscopy for reliability studies in semiconductor devices

19 p3382 A69-35788

Amorphous semiconductors based on noncrystalline materials compared to crystalline materials, noting radiation damage resistance

19 p3392 A69-36660

Light emitting diodes /LED/, discussing operating voltage vs color, diode materials and applications

20 p3505 A69-37702

Equivalent circuit for microwave cavity containing active GaAs device applied to waveguide and radial mode cavity design

20 p3508 A69-37900

Failure analysis on semiconductor devices and integrated circuits, discussing procedure for factual information representing present condition of device

22 p3953 A69-40032

Hungarian-made semiconductor silicon-base strain gages meeting specifications at half world market price

22 p3947 A69-40938

Semiconductor devices development based on amorphous materials, reviewing solid state physics implications

23 p4198 A69-41560

Semiconductor phase shifting for inertialless antenna scanning at microwave to millimeter wavelengths, describing diode construction with emphasis on solving insertion loss

23 p4143 A69-42519

SEMICONDUCTOR JUNCTIONS

NT JOSEPHSON JUNCTIONS

NT N-N JUNCTIONS

NT N-P-N JUNCTIONS

NT P-I-N JUNCTIONS

NT P-N JUNCTIONS

NT P-N-P JUNCTIONS

NT P-N-P-N JUNCTIONS

NT SILICON JUNCTIONS

Heterojunction band model and carrier transport mechanisms emphasizing applications to heterophotodiodes, solar cells and hetero field effect transistors

02 p0294 A69-11598

GaSb-ZnTe heterojunction fabrication method, noting photoresponse, fluorescence and light transmission

02 p0299 A69-12408

WKB approximation for metal-semiconductor junction tunneling and transmission coefficient of parabolic barrier, discussing density of states in degenerate semiconductors

02 p0301 A69-12652

Scanning electron beam display of space charge of defects and junction behavior of edge dislocation array in Ge and Si monocrystals

02 p0301 A69-12661

Impurity profiles and energy band diagram for cuprous sulfide-CdS heterojunction based on capacitance, Hall and electron microprobe measurements

03 p0368 A69-13075

Coherent emission in epitaxial structures with heterojunctions in AlAs-GaAs system

03 p0489 A69-13896

Potential distribution approximations for junction semiconductor devices, noting application to barrier layers and electron tunneling

03 p0408 A69-14107

Insulated junction integrated circuit transistor operation with various terminal connections corresponding to diode switching of transistor

05 p0730 A69-16217

Diffusion anomaly of native acceptor defect in zinc selenium telluride p-n junctions, discussing applications in triple diffusion technique of preparing p-n junction diodes

05 p0808 A69-16286

Deep trapping levels caused by ion implantation doping, discussing level effects on electrical characteristics of zinc implanted GaAs diodes

05 p0808 A69-16287

Injection characteristics of n-aluminum gallium arsenide-p-GaAs heterojunctions from recombination radiation spectra

06 p0979 A69-16993

Barrier capacitance of semiconductor diodes for exact temperature measurement, discussing application to temperature to frequency converters

07 p1100 A69-18556

Surface plasmon excitation by tunneling electrons in GaAs-Pb junctions, discussing conductance at bias voltages, plasmon energy and concentration

07 p1200 A69-19402

Passivated metal semiconductor IMPATT diode for microwave CW oscillation

08 p1286 A69-20862

Second breakdown in semiconductors, studying thermal feedback connected with temperature time dependence of junction electrical properties

08 p1294 A69-21115

Radiative tunneling shifting peak spectra in abrupt asymmetrically doped GaAs junctions

09 p1544 A69-21336

Selenium diffusion in indium antimonide, determining concentration gradients in junction space charge region by capacitance method

09 p1554 A69-21469

Trapping state effect on tunneling probability in Schottky barriers, discussing current-voltage characteristics

09 p1557 A69-21748

Emission characteristics of duplex vapor deposited tungsten emitter with molybdenum collector in variable spacing guard ring converter

09 p1438 A69-21820

Schottky barriers on n-type GaAs, measuring forward current characteristics for various electron concentrations and temperatures

10 p1745 A69-23358

Coherent emission in epitaxial structures with heterojunctions in AlAs-GaAs system

11 p1939 A69-25697

Probability distributions of characteristics of mass produced semiconductor rectifier diodes

12 p2035 A69-25832

High current density filaments formation in silicon p-n-n avalanche diodes caused by incremental negative resistance in static current-voltage characteristics

12 p2036 A69-25916

Gallium arsenide junction laser resonant modes from theoretical model, calculating frequency separation

12 p2108 A69-26637

Collector supply voltage and base width effects on transistor amplification and frequency characteristics at microampere currents

12 p2042 A69-26879

Ceramic CdS photovoltaic solar cell properties and model, classifying junctions according to preparation method

14 p2508 A69-29886

Electrical and photoelectrical properties of semiconductor heterojunctions prepared by Ge epitaxy on gallium arsenide bases, showing dependence on base surface treatment

15 p2667 A69-30078

Selenium diffusion in indium antimonide, determining concentration gradients in junction space charge region by capacitance method

15 p2669 A69-30714

Book on semiconductor devices physics covering principles and operational characteristics, carrier distribution and transport properties, materials, junctions, thin films, etc

15 p2670 A69-31062

Tunnel junctions with low background currents made by reacting active gas layer adsorbed on Nb film surface with Pb upper film to form barrier

17 p3016 A69-33788

Copper sulfide-cadmium sulfide heterojunction model for photovoltaic effect, considering surface layer intrinsic absorption and CdS photoconductivity

19 p3250 A69-35683

Photovoltaic effect at copper sulfide-cadmium sulfide heterojunction, studying depletion layer width, diffusion lengths and spectral response

19 p3382 A69-35684

Multilayer multijunction solar cells with carrier generation within diffusion length of junction, discussing epitaxial techniques

19 p3251 A69-35690

Electron-plasmon interaction in degenerate semiconductors, using mathematical model for rectifying metal contacts tunneling characteristics

19 p3382 A69-36049

GaAs-GaP heterojunctions, analyzing continuous conduction band, capacitance and current-voltage characteristics, photoresponse and modulation effect

21 p3779 A69-38424

Diagonal tunneling and radiation polarization in doped heterojunctions and p-n junctions of GaAs, using electroluminescence spectrum analysis

24 p4362 A69-43737

SEMICONDUCTOR LASERS

NT GALLIUM ARSENIDE LASERS

P-n junction cut-off current density and ohmic losses effect on injection laser efficiency determined by using quality parameter

01 p0091 A69-10883

Solid state liquid and semiconductor lasers, detailing conditions for producing stimulated emission and applications

01 p0092 A69-11068

Quadratic and cubic response in photoelectric emission in potassium antimonide under laser irradiation observed with measurement of energy distribution of excited electrons

05 p0771 A69-15813

Semiconductor laser generation efficiency increased by using external resonator and by signal amplification

05 p0777 A69-16378

Semiconductor lasers, discussing electron transitions, radiative band-band transitions, emission and absorption spectra, recombination rates, carrier lifetime and lasing conditions

06 p0937 A69-18009

Memory effect in injection lasers output characteristics, noting anomalous increases in pulsed emission intensity with increasing current-pulse repetition rate

07 p1147 A69-18542

Self modulated radiation modes of Te-doped n-type InAs injection lasers

07 p1148 A69-18685

Quantum mechanical perturbation treatment of optical parametric luminescence in nonlinear lithium niobate crystals, noting applications to noncolinear phase matching problems

07 p1152 A69-19067

Semiconductor laser with isolated diodes in cavity, noting watt-ampere characteristics during nonuniform excitation and threshold curves

08 p1326 A69-20539

Lasing characteristics of Nd-glass laser when cavity radiation varies with time, discussing rapid damping of relaxation oscillations of laser intensity

08 p1327 A69-21024

Semiconductor lasers, discussing materials, oscillation wavelengths, excitation methods, operating principles, fabrication, GaAs p-n junction laser and applications

09 p1518 A69-22122

Stimulated Mandelstam-Brillouin scattering at second harmonic of ruby laser and neodymium glass laser

09 p1520 A69-22684

Electroluminescence and electroluminescent devices, considering semiconductor lasers, radiation sources and image amplifiers

11 p1899 A69-25198

Laser diode output efficiency increased in presence of transverse magnetic field suppressing higher order TE and TM modes

12 p2039 A69-26353

Bismuth doped lead tin telluride diode lasers with low threshold currents at cryogenic temperatures, discussing doping effect

12 p2109 A69-26641

P-n junction cut-off current density and ohmic losses effect on injection laser efficiency determined by using quality parameter

12 p2109 A69-26647

Direct modulation characteristics of semiconductor junction laser, analyzing resonance phenomenon, bias current, admittance, modulation frequency limit and emission lifetime

12 p2110 A69-27069

Electroluminescence of p-GaAs diodes analyzed over temperature range of linear dependence of lasing on injection current

13 p2230 A69-27887

Active medium temperature effect on semiconductor laser emission spectra composition, discussing amplification coefficient frequency dependence at various temperatures

13 p2271 A69-27888

Cadmium telluride laser characteristics including emission wavelength and electron beam threshold current density

13 p2272 A69-27896

Semiconductor luminescent devices and laser pumping by solar radiation modulated to interact resonantly with solid state plasma oscillations and electric field in crystal

13 p2272 A69-27969

Square wave generator for junction laser power supply

13 p2274 A69-28643

Nanosecond pulse generator for powering semiconductor lasers, examining circuit diagram and elements design

15 p2633 A69-30234

AM sinusoidal current pulse generator for semiconductor lasers, describing solid state circuit

15 p2633 A69-30235

Power coupling among modes in semiconductor lasers in presence of spontaneous or forced microwave modulation of population inversion

15 p2634 A69-30875

Unsaturable frequency discriminator influence in semiconductor laser feedback loop on laser emission spectrum

15 p2635 A69-30967

Reliability block diagrams for laser systems, discussing failure modes of solid state, semiconductor and gas lasers

18 p3151 A69-34523

Spectral inhomogeneity effect on spectrum of modes emitted by semiconductor p-n junction/laser

18 p3152 A69-35023

Current generator circuit designed for semiconductor laser excitation with pulses modulated by sinusoidal signals at 4.75 MHz

18 p3153 A69-35256

Nanosecond pulse generator circuits based on four layer Si diodes designed for semiconductor laser excitation

18 p3153 A69-35257

Semiconductor optical quantum amplifiers in pulse mode operation, describing arrangement for studying performance including pulse duration and current controls

18 p3153 A69-35258

GaSb p-n injection laser output at 4.2 K in strong transverse magnetic field, deducing effective mass and g-factor from stimulated emission peak shift

19 p3387 A69-36530

Junction lasers current-voltage characteristics, discussing coherence-pinch effect as explanation of threshold behavior

19 p3337 A69-36531

Temperature effects on threshold current density, emission wavelength and polarization of PbSe diode lasers

19 p3337 A69-36533

Output power spectra of Pb-Sn-Te diode laser above threshold of oscillation, demonstrating inverse dependence of line width on laser power

21 p3734 A69-38326

Temperature dependence of stimulated light power from GaAs junction lasers operated at constant bias current above threshold

21 p3734 A69-38437

Memory effect in injection lasers output characteristics, noting anomalous increases in pulsed emission intensity with increasing current-pulse repetition rate

21 p3735 A69-38694

SEMICONDUCTORS [MATERIALS]

Electron beam pumped semiconductor laser light beam amplitude and phase distribution, studying effects of inhomogeneous excitation by model
21 p3737 A69-39041

Electroluminescence of p-GaAs diodes, analyzing temperature range of linear dependence of lasing on injection current
21 p3682 A69-39145

Active medium temperature effect on semiconductor laser emission spectra composition, discussing amplification coefficient frequency dependence at various temperatures
21 p3738 A69-39146

Digital computer determination of stimulated emission time delay, Q switching temperature and current region and impurity profile effect across junction in junction lasers
22 p3962 A69-40561

Lasing properties of spontaneous emission hemispherical semiconductor diode with AlAs-GaAs junctions measured by calibrated silicon photocell
22 p3964 A69-40608

Nonlinear theory of optically excited semiconductor laser for conditions of self excitation, steady state lasing amplitude and lasing frequency shift
23 p4174 A69-41733

SEMICONDUCTORS [MATERIALS]

NT ACCEPTOR MATERIALS

NT DONOR MATERIALS

NT METAL OXIDE SEMICONDUCTORS

NT N-TYPE SEMICONDUCTORS

NT P-TYPE SEMICONDUCTORS

NT PHOTOCONDUCTORS

Collection of papers on physics, Volume 31, Part 1, covering stellar evolution, electron transport in semiconductors, plasma microstability, etc
01 p0115 A69-10045

Electron transport theory for pure and doped low mobility semiconductors and for impurity conduction in disordered semiconductors, noting related optical phenomena
01 p0135 A69-10047

Direct reading device for minority carriers lifetimes measurement in semiconductor single crystals
01 p0078 A69-10073

Recombination rate dependence on nonequilibrium charge carriers concentration at semiconducting surface
01 p0136 A69-10253

Electron-hole collisions effect on drift and electron and hole diffusion in semiconductors at high injection levels
01 p0137 A69-10257

Microwave second harmonic, sum and difference frequencies generation for two different microwaves normally incident on low temperature semiconductor slab in DC field
01 p0137 A69-10334

Soviet book on semiconductor compounds, production and properties covering crystal structures, phase diagrams, etc
01 p0137 A69-10353

Thermoelectric properties of GeTe-GaTe system, analyzing phase diagrams, solid solution formation, substitutions and zone structure influence
01 p0138 A69-10404

Nonequilibrium carriers during semiconductor depolarization, noting microwave oscillation energy absorption in silicon and zinc sulfide crystals
01 p0138 A69-10434

IR reflection and transmission properties of various semiconductor compounds, rubidium halides, strontium titanate, BN and Te
01 p0139 A69-10840

Intense laser emission interaction with current carriers in semiconductors, analyzing dependence of thermoelectric field produced by light absorption on intensity, frequency and temperature
01 p0139 A69-10895

Proton energy distributions for passage through NaCl, KCl, KBr, Si and Ge single crystals at various angles relative to /100/ and /110/ crystallographic planes
01 p0140 A69-11109

Ionization losses of Ge 72 atoms stopping in Ge, noting no cut-off indicative of energy gap effects
01 p0140 A69-11245

Fast reversible switching between highly resistive and conductive states in various disordered semiconductors, using electric field
01 p0140 A69-11248

Minority carrier density and diode current obtained as Laplace transforms from analyzing differential equations, describing charge carriers in semiconductor
01 p0049 A69-11361

Phase diagram of BiTeI degenerate semiconductor crystals synthesized by heat treatment, discussing crystallization methods and physical properties
02 p0294 A69-11540

Current carrier mobility in GaTe and tin selenide semiconducting stratified lattices, noting interaction of free carriers and polarized nonpolar phonons
02 p0295 A69-11777

Vacancy diffusion in Ge, relation to precipitation of Cu impurities from supersaturated solid solution and determination of monovacancy migration energy
02 p0295 A69-11780

Tabular reduction of crystal structure chemical information for metals and semiconductors for material selection use
02 p0295 A69-11786

Diffusion data in binary compound semiconductors, tabulating impurities, electrical behavior, temperature variations and diffusion coefficients
02 p0296 A69-11809

Electrical conductivity of sintered polycrystalline cubic and monoclinic europium sesquioxide from DC current-voltage characteristics obtained in air at various pressures
02 p0296 A69-11874

Temperature dependence of semiconductivity of sintered polycrystalline EuO from current-voltage characteristics, measuring activation energy
02 p0296 A69-11875

Melting points of tetrahedral phases with stoichiometric vacancies found proportional to covalent bonds number in semiconductors
02 p0297 A69-11881

Solid solutions microstructure and electrical conductivity in InAs-CdS and InAs-CdSe and InAs-CdSe systems
02 p0297 A69-11882

Boron diffusion in silicon, using nitrogen carrier and boron trichloride diffusant at high temperature for determination of critical oxygen flow rate
02 p0297 A69-11994

Electronographic determination of ternary alloys of germanium antimony tellurides noting hexagonal laminarity with cell periods
02 p0298 A69-12046

Overheated semiconductor plasma instability in crossed electric and magnetic fields, deriving condition for occurrence
02 p0298 A69-12099

Traveling high electric field domains in bulk semiconductors use in high speed integrated electronics, noting domain properties of GaAs and CdS
02 p0216 A69-12144

Mechanical thermal stresses effects during laser flash illumination of GaAs, discussing temperature dependence of radiative recombination
02 p0256 A69-12245

Energy distribution and capture cross section ratio limiting factors in semiconductors with deep energy levels
02 p0299 A69-12562

Step voltage transient behavior of electron-hole plasma injected into Ge, noting current time dependence
02 p0301 A69-12651

WKB approximation for metal-semiconductor junction tunneling and transmission coefficient of parabolic barrier, discussing density of states in degenerate semiconductors
02 p0301 A69-12652

Dielectric dispersion in inhomogeneous dielectrics and semiconductors, discussing three layered equivalent circuit
02 p0301 A69-12837

Semiconductor nonlinear electron polarizability, using model to obtain correct order of magnitudes
03 p0483 A69-13035

Ruby laser radiation nonlinear absorption coefficient measurement in CdS, ZnS and SiC semiconductor crystals, noting light limiting effects
03 p0436 A69-13038

Carbon dioxide laser for observing nonlinear effects related to electron interaction with lattice vibration within semiconductors
03 p0437 A69-13041

EPR spectra and thermal conductivity measurement in excited organic semiconductor salt derivatives of tetracyanoquinodimethane
03 p0484 A69-13278

Hall effect in semiconductors with polarons as majority carriers, noting variation with temperature of magnetic field dependence on Lorentz force
03 p0484 A69-13281

Positron annihilation in As, Sb, Bi, diamond, Ge, Si, S, Te and Se, noting contribution of valence electrons
03 p0485 A69-13295

Exciton distribution in semiconductors below Bose condensation temperature differing from diffusion distribution
03 p0486 A69-13415

Exciton spectrum for limiting case of large radius leading to Wannier-Mott equation with static dielectric permeability
03 p0486 A69-13416

Electrical resistivity of sintered high melting point metal oxides, noting width of semiconductor forbidden band
03 p0445 A69-13570

Carbon formation during production of high purity semiconductor Si, using C 14 tagged hydrogen impurities and methylated chlorine silanes contained in silicichloroform
03 p0486 A69-13635

Critique of paper on theory of gradient instability in semiconductor currents, questioning boundary value problems solution validity
03 p0487 A69-13728

Photocurrent pinch-off effect in high resistivity thin CdS crystals for evaluating donors, acceptors and surface states
03 p0488 A69-13757

Phonon capture by electrons in semiconductors with high permittivity in external electric field
03 p0489 A69-13891

Second harmonic generation in ternary semiconductor compounds
03 p0489 A69-13894

Direct amplification of ultra and hypersonic surface waves in semiconducting crystals of wurtzite group, taking into account drift effects and boundary conditions
03 p0490 A69-13925

Heat capacity of diamond-like semiconducting Si, GaAs and GaP calculated on basis of quasi-chain dynamics of covalent crystals
03 p0490 A69-13943

Stray fields and domain dynamics in Gunn effect semiconductors covered with dielectric sheets
03 p0491 A69-13988

Acoustic wave fluctuations in semiconductors in external electromagnetic field, applying conduction electron and lattice elasticity kinetic equations
03 p0491 A69-14054

Transport phenomena in semiconductors in strong DC field, emphasizing electrical conductivity as function of crystallographic orientation
03 p0491 A69-14097

Energy structure parameters for ZnTe-CdTe and ZnSe-ZnTe crystals, obtaining forbidden bandwidth dependence on composition
03 p0492 A69-14173

Electron vs phonon superconductivity mechanism conditions for semiconductors, semimetals and molecular crystals
03 p0492 A69-14176

Collection of papers on III-V compound semiconductors and semimetals covering physical properties, solid solutions and electric field, pressure, radiation and impurity effects
04 p0641 A69-14501

Phenomena in III-V compounds and III-V compound-other compound solid solutions, examining equilibrium phase diagrams
04 p0641 A69-14505

Resistivity and Hall mobility periodic change effect on probe measurements in semiconductors
04 p0642 A69-14534

Electric field and energy dispersion law effects on plasma oscillations in semiconductors, calculating composite oscillation frequency
04 p0642 A69-14554

Semiconductor resistivity, discussing resonator field structure and specimen position effects on measurement errors by contactless method
04 p0642 A69-14853

Quality control of semiconductor materials, analyzing homogeneity by statistical distribution of nonequilibrium carriers based on photoconductivity measurement
04 p0642 A69-14856

Vacuum equipment for evaporation or sputtering in semiconductor industry
04 p0598 A69-14876

Free carrier Faraday effect in piezoelectric semiconductors investigated for microwave frequencies, low temperatures, mixed deformation potential and piezoelectric scattering
04 p0643 A69-15201

Drifting temperature fluctuations in semiconductors in presence of strong electric field

04 p0643 A69-15256

Temperature dependence of Hall coefficient, conductivity and carrier mobility in manganese doped indium antimonides

04 p0643 A69-15257

Semiinsulating GaAs mobile electric domains, determining electric field strength from electrooptical effect measurements

04 p0643 A69-15261

Approximate equations in matrix form for analyzing complex semiconductor structures with p-n junctions

05 p0806 A69-15658

Threshold velocities of acoustoelectric current oscillations in elemental piezo- and nonpiezoelectric semiconductors, taking into account amplification and losses of phonons

05 p0807 A69-15956

Fresnel drag produced by relativistic addition of electron velocities in semiconductors measured by changes in refractive index

05 p0807 A69-16026

Electrical conductivity anisotropy in isotropic germanium and silicon semiconductors, noting effect of metallic contact insertion

05 p0808 A69-16216

Design theory of esaki diodes relation to internal parameters of degenerate semiconductors, discussing Fermi level position and maximum state density in purity band

05 p0732 A69-16298

Nonlinear optical coefficients in group IV and III-V semiconductors, calculating contribution from longitudinal and core electrons

[IEEE PAPER V-7]

05 p0776 A69-16329

Ultrasound propagation amplification coefficient in high permittivity semiconductors with electric field based electron-phonon interaction

05 p0809 A69-16372

BiTeBr semiconductor band structure determined from electrical and optical properties

05 p0810 A69-16609

Critical electron drift velocity threshold in surface wave amplification in semiconductor in magnetic field, noting partial effect of diffusion

05 p0810 A69-16648

Nonuniform distribution and concentration of doping materials in semiconductors determined by measuring optical reflection coefficient

05 p0764 A69-16664

Selective etching process for microminiaturization of special circuits for aerospace

05 p0736 A69-16753

Radiation defects stability in semiconductors, noting low temperature electron irradiation of Ge and effects of annealing

06 p0974 A69-16863

Carrier scattering from defects in neutron irradiated semiconductors, noting mobility and relaxation time

06 p0974 A69-16864

Light absorption in semiconductors with electron hole pair formation noting conduction and valence band

06 p0978 A69-16901

Kinetics of homogeneous and heterogeneous growth of centers of new phase of semiconductor during ion bombardment as function of radiation dose

06 p0978 A69-16985

Transverse AC current influence on longitudinal current induced by constant electric field in anisotropic semiconductor

06 p0978 A69-16991

Ambipolar motion of light injected photocarriers in cadmium-mercury-telluride in terms of diffusion and drift in electric fields

06 p0979 A69-17154

Heat transfer and IC, discussing semiconductors thermal and electrical analogs and thermal properties

06 p0894 A69-17216

GaAs IR emitters efficiency due to semiconductor material band structure

06 p0894 A69-17248

Semiconductor glasses use for electronic devices

06 p0980 A69-17714

Semiconductors reflectivity enhancement by irradiating with Q switched ruby laser output

06 p0935 A69-17768

Stability of negative differential conductivity state with respect to small disturbances, based on hydrodynamic equations for two valley GaAs semiconductors

06 p0981 A69-17879

Electrothermal domains in semiconductors, examining domain velocity of motion under external potential

06 p0981 A69-17880

Raman spectra of optical phonons in semiconductors, using reflection techniques and Ar laser excitation

06 p0936 A69-17882

Electron and phonon tunneling spectroscopy in metal Ge contacts, noting improved agreement with one electron model

06 p0982 A69-18234

Halide salts, semiconductors and nonoxide glasses as materials for high power laser windows

07 p1144 A69-18401

Magnetoplasma waves in semiconductors, discussing cold plasma dispersion, helicons, carrier densities, lattice dielectric constant and acoustic domain propagation

07 p1197 A69-18465

Semiconductor current carriers surface recombination rates determined from photomagnetic effect

07 p1198 A69-18505

Minority carrier distribution in doped semiconductors space-charge layer assuming relation between diffusion and Debye length

07 p1198 A69-18506

Approximate solution to differential equations describing primary radiation defects transformation into secondary defects in semiconductors

07 p1199 A69-18679

Absorption and amplification of sound in many valley semiconductors in strong electric field, noting dependence on electron heating and relaxation times

07 p1199 A69-18681

Photoconductivity induced by laser pulses in semiconductor with parabolic dispersion law, linear transition and nonequilibrium carrier concentration higher than equilibrium carrier concentration

07 p1148 A69-18690

Electron-electron interaction effect on I-V characteristic and equivalent circuit of metal-semiconductor contact, noting conductivity and rectifying properties

07 p1107 A69-19162

Magnetic and semiconducting properties of samarium boride, noting effect of decreasing temperature

07 p1200 A69-19403

Silicon on sapphire semiconductor technology for diode arrays used as read-only memories, discussing capacitance, resistance and pattern encoding by laser

07 p1113 A69-19767

Resonance effects during piezoelectric interaction between charged drift wave and flexural wave in semiconductors with one sign current carriers

08 p1371 A69-19806

Interaction between semiconductor excitons, obtaining formulas for exciton concentrations ground state energy and dispersion, noting association with Pauli statistics

08 p1371 A69-19955

Eutectic anisotropic InSb-NiSb crystals applied to IR detection, noting sensitivity to carbon dioxide lasers

08 p1373 A69-20866

Thin semiconductor plates negative differential resistance associated with captures at surface, describing electron gas by electron temperature

08 p1374 A69-21081

Population inversion in semiconductors obtained by applying electric field through dielectric sphere /field effect/

08 p1374 A69-21082

Impurities effect on electron energy spectrum in semiconductors at zone boundary and arbitrary doping levels, using Green function

09 p1554 A69-21467

Kinetic coefficients of carrier motion in semiconductor obtained by Boltzmann equation, considering impacts between carriers

09 p1554 A69-21468

Differential capacitance of n-n heterojunction calculated by metal semiconductor contact method

09 p1555 A69-21476

Plasmon superconductivity mechanism in degenerate semiconductors and semimetals, noting interaction effect between electrons and plasma sound

09 p1556 A69-21573

Free carrier magnetoplasma effect used for far IR phase matched difference frequency generation in semiconductors, discussing carbon dioxide laser transitions

09 p1556 A69-21578

Antiferromagnetic semiconductor transformation into metal in magnetic field

09 p1556 A69-21672

Current oscillations in semiinsulating O and Cr doped GaAs samples at room temperature, noting photoconductivity excitation spectra

09 p1557 A69-21753

Dielectric relaxation for analysis of defect structure, microstructure, surface behavior, structural changes kinetics and environmental effects in insulators and semiconductors

09 p1559 A69-22307

Hybrid circuit technology application to packaging electronic systems

09 p1508 A69-22336

Recombination rate dependence on nonequilibrium charge carriers concentration at semiconducting surface

09 p1559 A69-22646

Electron-hole collisions effect on drift and electron and hole diffusion in semiconductors at high injection levels

09 p1559 A69-22650

Oxide coated thermionic cathodes, noting semiconducting properties of alkaline earth oxides, particularly barium oxide and adsorption and optical properties

09 p1470 A69-22700

Photoelectric effects produced by polarized radiation in isotropic optical media, discussing photo EMF and photoconductivity in multivalley semiconductors and plasmas

10 p1701 A69-23138

Soviet book on fluid semiconductor properties at high temperatures during transition from solid to liquid state

10 p1744 A69-23316

Electronic states and minority carrier transport in mixed semiconductors with graded composition, noting position dependent band gaps and effective masses

10 p1745 A69-23360

Shallow impurity states in semiconductors, calculating bulk and surface energy eigenvalues in Si and Ge

10 p1745 A69-23361

Soviet book on highly doped semiconductors covering energy spectrum analysis, kinetic effects, optical properties, fabrication and applications

10 p1746 A69-23522

Entrainment and acoustothermal effect in piezoelectric semiconductors having electrons with different energy

10 p1746 A69-23573

Amorphous semiconductors, emphasizing structure and theory of liquid and amorphous states, electron energy spectra and scattering, impurities, Hall effect, etc

10 p1747 A69-23807

Thin film thickness and composition determination through scattered electron and characteristic X ray radiation recording

10 p1747 A69-23847

Diamond-like glassy semiconductor compound of cadmium germanium arsenide, determining optical lattice vibrations from IR reflection spectra

10 p1747 A69-23963

Surface atomic structure effects on polar faces in InSb semiconductor crystal established from measurements of contact potential difference by dynamic capacitor

10 p1747 A69-23965

Electronic properties of beryllium doped silicon studied with IR absorption spectroscopy and electrical measurements, describing Be thermal diffusion

10 p1747 A69-23989

Transmission line analogs and kinetic power theorems for space charge waves amplification in semiconductors, considering internal effect and wave excitation

10 p1748 A69-24052

Space charge waves amplification in semiconductors on coupling with forward circuit wave by transmission line analog, noting application to electromagnetic and acoustic waves

10 p1748 A69-24053

Gaussian summation for ion implantation profile control in semiconductors, describing computer program selecting optimum energies to fit predetermined profiles

11 p1857 A69-24546

Coulomb interaction during optical transitions between Landau subbands of Ge semiconductor valence and conduction bands in magnetic field, observing diamagnetic excitons

11 p1936 A69-24640

Acoustic wave amplification and generation in piezoelectric semiconductors and semimetals by super-sonic carrier drift currents

11 p1926 A69-24641

Semiconductor properties, applications and problems including thin films, superconductivity, etc
11 p1937 A69-24736

Electrical conductivity of impurity semiconductors containing variable current carrier concentrations, discussing current-voltage characteristics
11 p1937 A69-24909

Photoconductivity of semiconductors with multivalley electron energy and isotropic hole spectra, discussing nonlinearity of field dependence
11 p1937 A69-24913

Electrical conductivity of space charge layer in semiconductors with many-valley energy spectra of current carriers, discussing scalar relaxation time
11 p1937 A69-24915

Effective masses of electrons and holes in HgSe and HgTe characterized by narrow forbidden bands and high charge carrier mobility
11 p1937 A69-24920

Electrons conduction and switching in noncrystalline semiconductors, discussing localized states and thermally activated hopping
11 p1938 A69-25239

Phonon capture by electrons in semiconductors with high permittivity in external electric field
11 p1939 A69-25692

Second harmonic generation in ternary semiconductor compounds
11 p1939 A69-25695

Solar cells physical properties and functions, considering band structure of semiconductors, p-n junction diodes and photovoltaic effect, efficiency calculations and radiation damage
12 p2015 A69-25864

Room temperature thermal conductivity of semiconducting alloys with stoichiometric distributions of vacancies in cation sublattice, discussing heat resistance
12 p2142 A69-25975

Lattice defects in development of recombination centers on Ge semiconductor surfaces, discussing photoconductivity and field effect
12 p2142 A69-25978

GeTe, SnTe and strontium titanate transition into superconducting state including induced superconductivity
12 p2144 A69-26620

Solution for kinetic energy equation for organic semiconductors with narrow conduction band situated in strong electric field
12 p2144 A69-26673

Spatial dispersion of HF dielectric constant in semiconductor based on electron-hole pair production
12 p2145 A69-26723

Band structure and reflection spectra of vanadium dioxide and pentoxide single crystals, noting changes in metal-semiconductor phase transition
12 p2145 A69-26724

Soviet book on methods of investigating semiconductors as applied to lead chalcogenides PbTe, PbSe and PbS covering physical and physicochemical properties
12 p2145 A69-26851

Organic semiconductors physical properties and intermolecular charge transfer between donor and acceptor
13 p2317 A69-27799

Dispersion relations in semiconductors in magnetic field indicating current anisotropic instability association with excessive noise
13 p2317 A69-27876

Interacting carriers acoustoelectric waves in semiconductors with high dielectric constant, analyzing dispersion equation
13 p2317 A69-27878

Polarization stabilization times dependence on risetime of external field pulse leading edge for semiconductor crystal, determining field concentration
13 p2317 A69-27880

GaS, GaSe and InSe crystals band structure from analyzing reflection spectra, noting sensitivity to visible, IR and hard radiation
13 p2317 A69-27883

Electric drift instability in semiconductors with hot electrons, discussing diffusion, electron heat conduction, energy transfer, space charge density, etc
13 p2318 A69-27891

Monograph on optical properties and band structure of semiconductors covering absorption and reflectivity measurement, electronic states transition, deformation, etc
13 p2323 A69-28200

Magnetic and electric field effects on undamped electron-hole LF frequency plasma oscillations in spatially homogeneous nonpolar semiconductor
13 p2323 A69-28581

Electron shielding in heavily doped many valley semiconductors, discussing Thomas-Fermi screening and Mott transition
13 p2324 A69-28683

Acoustic effects in piezoelectric semiconductors due to sound-electrons interaction including sound absorption, sound velocity changes, electroacoustic effect, etc
14 p2503 A69-28786

Stability of negative differential conductivity state with respect to small disturbances, based on hydrodynamic equations for two valley GaAs semiconductors
14 p2503 A69-28788

Electrothermal domains in semiconductors, examining domain velocity of motion under external potential
14 p2503 A69-28789

Electron magnon interaction in ferromagnetic and antiferromagnetic semiconductors, showing conduction band and electron effective mass and magnetic moment dependences on temperature and spin direction
14 p2504 A69-28991

Thermionic converters semiconducting collector surfaces, evaluating work functions of nickel-chromium steel and aluminum trioxide collectors
14 p2506 A69-29269

Automatic recording of spectral distribution of high resistance semiconductors photoconductivity using spectrograph monochromator
14 p2447 A69-29409

EPR spectra and thermal conductivity measurement in excited organic semiconductor salt derivatives of tetracyanoquinodimethane
14 p2508 A69-29652

Hall effect in semiconductors with polarons as majority carriers, noting variation with temperature of magnetic field dependence on Lorentz force
14 p2508 A69-29654

Linear approximation of electron temperature increment and electron mobility in nondegenerate polar semiconductor in crossed fields
14 p2508 A69-29662

Light sensitivity dependence of semiconductor-metal systems on layer thickness
14 p2508 A69-29666

Anisotropic scattering of current carriers in semiconductors, obtaining general expression for mobility tensor with variational principle
14 p2508 A69-29667

Inhomogeneous distribution of nonequilibrium current carrier concentrations in semiconductors with electrons and holes of different lifetimes, noting instability
15 p2665 A69-30041

Frequency dependence of light absorption by excitons obtained for allowed and forbidden zone transfers in semiconductors
15 p2632 A69-30057

Finite scattering cross section in current carriers scattering on impurities in compensated semiconductors, assuming unscreened Coulomb potentials
15 p2666 A69-30063

Pulsed IR laser optimal Q switching mode by using semiconductor mirror with nonparabolic dispersion law and changing mirror opening moment delay time
15 p2663 A69-30064

Indium antimonide crystals polarity effect on photoeffect, analyzing quantum yields and energy spectrum
15 p2667 A69-30076

Amorphous semiconducting alloys single band model characteristics
15 p2667 A69-30199

Semiconductor resistivity, discussing resonator field structure and specimen position effects on measurement errors by contactless method
15 p2667 A69-30245

Quality control of semiconductor materials, analyzing homogeneity by statistical distribution of nonequilibrium carriers based on photoconductivity measurement
15 p2667 A69-30248

Impurities effect on electron energy spectrum in semiconductors at zone boundary and arbitrary doping levels, using Green function
15 p2669 A69-30712

Kinetic coefficients of carrier motion in semiconductor obtained by Boltzmann equation, considering impacts between carriers
15 p2669 A69-30713

Differential capacitance of n-n heterojunction calculated by metal semiconductor contact method
15 p2669 A69-30721

Glass ceramic coated and bonded silicon semiconductor material in integrated circuits devices fabrication, noting matched thermal expansion
15 p2669 A69-31040

Book on semiconductor devices physics covering principles and operational characteristics, carrier distribution and transport properties, materials, junctions, thin films, etc
15 p2670 A69-31062

Plasma modes, critical fluctuations and optical properties electric field dependence in two valley model of Gunn instability semiconductors
15 p2581 A69-31240

Multicomponent semiconductor compounds of nonstoichiometric composition, studying structure, behavior and correlation between electrical properties and phase diagrams
15 p2670 A69-31243

Fluctuation kinetics of electron system in nonequilibrium state arising in semiconductor in strong electric field, considering lattice and interelectron scattering
16 p2824 A69-31569

Heat conductivity of liquid and solid gallium telluride in steady state regime, using graphite cylindrical device
16 p2824 A69-31572

Magneto-optical oscillation of absorption coefficient in semiconductors during direct electron transitions
16 p2824 A69-31574

Microwave power loss and semiconductor conductivity relationship measured for carrier lifetime and mobility, noting nonlinearity and accuracy
16 p2825 A69-31617

Normal modes of electrons-electromagnetic field coupled system for many valley semiconductors, calculating dielectric constant for electron gas for ellipsoidal energy surfaces
16 p2826 A69-31821

External magnetic force and internal Coulomb force influence on carriers in conduction or valence band of semiconductor, considering H atom spectra
16 p2826 A69-31824

Shubnikov-de Haas effect and quantum limit phenomena concerning oscillatory magnetoresistance in semiconductors
16 p2827 A69-31826

Approximate equations in matrix form for analyzing complex semiconductor structures with p-n junctions
16 p2827 A69-32515

Raman scattering by coupled plasmon-cyclotron-harmonic modes in semiconducting plasmas in homogeneous static magnetic field
16 p2824 A69-32604

Thermoelectric converter systems optimization by geometry independent functions
18 p3093 A69-34782

Semiconductor plasma DC overheating instability in electric and magnetic fields, determining growth increments of oscillation amplitude
18 p3182 A69-35022

Melting points of tetrahedral phases with stoichiometric vacancies found proportional to covalent bonds number in semiconductors
18 p3182 A69-35041

Solid solutions microstructure and electrical conductivity in InAs-CdS, InAs-CdS and InAs-CdSe systems
18 p3182 A69-35042

Acoustic wave fluctuations in semiconductors in external electromagnetic field, applying conduction electron and lattice elasticity kinetic equations
18 p3182 A69-35047

Photovoltaic effects in cadmium mercury tellurides, considering band-gap variations, effective masses, mobilities, majority carrier concentration and pair lifetime
19 p3381 A69-35680

Cu-Cd-S photovoltaic cell models correlated, reporting spectral response and electron microprobe test results
19 p3382 A69-35682

Transducer with single crystal Ge for high heat flux measurement, noting calibration by direct conduction
19 p3307 A69-35748

Optical frequencies mixing based on photoelectric effect in metals and semiconductors, noting internal photoconductivity
19 p3332 A69-35871

Laser emission theory for indirect band-band transitions, considering light absorption by free carriers in semiconductors with polar and unpolar scattering
19 p3332 A69-35873

Physics of semiconductors - Conference, Moscow, July 1968, Volume 1

19 p3384 A69-36513

Impurity levels in semiconductors with multiconduction bands, noting impurities influence on photoluminescence, laser action and Gunn effect

19 p3385 A69-36514

Electrons and optical phonons interaction effects on optical and photoconducting properties of semiconductors, discussing phonon cyclotron resonance and oscillatory and magneto-oscillatory photoconductivity

19 p3385 A69-36517

Optical mixing and harmonic generation in semiconductors, discussing magnetoconductivity tensors and magneto-optical phenomena due to free carriers

19 p3385 A69-36519

Exciton line broadening in II-VI compound semiconductors, discussing thermal broadening of n equals one exciton associated with LO phonon-induced scattering

19 p3386 A69-36524

Photomechanical and electromechanical effects in semiconductors, considering indentation microhardness decrease caused by light irradiation or electric field

19 p3386 A69-36526

Coherent recombinational radiation of semiconductors excited by electron beam

19 p3387 A69-36539

Semiconductor physics - Conference, Moscow, July 1968, Volume 2

19 p3387 A69-36540

Narrow band gap alloys and ferromagnetic semiconductors, using transport properties for characterization

19 p3388 A69-36541

Semiconductor plasma production effects and pinching and microwave radiation in InSb plasma, discussing impact ionization, two photon absorption and plasma lifetime

19 p3389 A69-36545

Low temperature energy band gap in n -type single semiconductor crystals of In-Sb-Bi alloys analyzed by measuring Hall constant and optical absorption coefficient

19 p3390 A69-36552

Energy band gap variation as function of composition in In-Ga-P semiconductor crystals

19 p3390 A69-36553

Energy spectrum and transport mechanism for current carriers in amorphous-crystalline semiconductors, measuring thermostimulated conductivity, induced photoconductivity, optical quenching, etc

19 p3391 A69-36558

Transport properties of liquid semiconductors, using model for liquid mercury with minimum state density

19 p3391 A69-36560

Glassy semiconductors from metallic alloy binary and ternary systems of sulfide, selenide and telluride noting properties

19 p3392 A69-36641

Free electrons influence on reflection coefficient of semiconductor in IR spectra, showing selective modulation with change in carrier concentration

20 p3583 A69-37610

Light emitting diodes (LED), discussing operating voltage vs color, diode materials and applications

20 p3505 A69-37702

Electrical conductivity anisotropy in isotropic germanium and silicon semiconductors, noting effect of metallic contact insertion

20 p3584 A69-37786

Hall coefficient and conductivity measured as function of temperature for liquid Au, Cu and Ag tellurides and liquid alloy systems Bi-Te and Tl-Te

20 p3584 A69-38024

In-Te-Se system alloys structure and semiconductor properties analyzed by X rays

21 p3779 A69-38579

Semiconductor properties of indium telluride alloys, conductivity and Hall effect

21 p3779 A69-38580

Semiconducting properties of lanthanum-cobalt oxide measured, using Seebeck coefficient for analysis as function of resistivity

21 p3780 A69-38612

Current carrier concentration and magnetic field as factors influencing laser frequency resonance mixing in semiconductors with narrow forbidden bands

21 p3737 A69-38998

Breakdown mechanism in GaAs, Si and CdSe semiconductors under intense light pulses ascribed to thermal impact

21 p3737 A69-39042

Metal semiconductor contact resistance determination from measuring voltage drop in current passing through contact and second metallic contact

21 p3780 A69-39046

S doped GaSb single crystals prepared by Crochral-ski method studied for temperature dependence of resistivity and Hall coefficient

21 p3781 A69-39048

Electromechanical effect dependence on CdS semiconductor surface state, noting relationship between microhardness and discharge current

21 p3781 A69-39072

Spatial dispersion of HF dielectric constant in semiconductor based on electron-hole pair production

21 p3781 A69-39136

Band structure and reflection spectra of vanadium dioxide and pentoxide single crystals, noting changes in metal-semiconductor phase transition

21 p3781 A69-39137

Dispersion relations in semiconductors in magnetic field indicating current anisotropic instability association with excessive noise

21 p3782 A69-39142

Absorption constant and reflectivity coefficient on semiconductor samples with nonideally prepared surfaces, calculating measurement errors

21 p3782 A69-39240

Transverse thermomagnetic EMF and Nernst-Ettingshausen coefficient in GaSb semiconductor with double conduction band and strong degeneracy of current carriers

21 p3783 A69-39558

Electrical properties of semiconductors in HF electromagnetic field, showing Dember type EMF dependence on carrier response to field inhomogeneity

22 p3993 A69-40605

Multiquantum photoemissive effect in metals, semiconductors and dielectrics emphasizing laser application for studying electromagnetic field

22 p3964 A69-40690

Electromagnetic wave propagation in semiconductor plate under constant electric field, studying nonstandard carrier energy dispersion law effects on refractive index

22 p3994 A69-40751

Inhomogeneities effect on thermoelectric power and thermal efficiency of semiconductor thermocouple with constant forbidden band width

22 p3994 A69-40933

Electric instabilities in semiconductors analyzed by subdividing instabilities into cathode and anode waves, considering recombination and electron and hole production processes

22 p3997 A69-41173

Electromagnetic wave propagation instabilities in semiconductor magnetoplasmas not diffusion limited to LF, using dispersion equation

22 p3902 A69-41223

Electric fields reducing recombination radiation intensity from bulk ionized GaAs and InP and shifting spectrum to lower energies, discussing self absorption

23 p4198 A69-41499

SEMIEMPIRICAL EQUATIONS

Unidirectional filamentary composites thermoelastic properties relation to constituent materials properties, using semiempirical micromechanics theory

09 p1530 A69-22320

Vapor pressure equation for oxygen and nitrogen derived by adding nonanalytic term, correlating equation with observed data

[NAS-NRC PAPER H-1] 22 p4051 A69-40628

SEMIMETALS

U METALLOIDS

SENDERS

U TRANSMITTERS

SENSE ORGANS

NT CHEMORECEPTORS
NT CHOROID MEMBRANES
NT COCHLEA
NT CORNEA
NT CORTI ORGAN
NT EAR
NT EYE [ANATOMY]
NT FOVEA
NT GRAVIRECEPTORS
NT LABYRINTH
NT MIDDLE EAR
NT OCULOMOTOR NERVES
NT OTOLITH ORGANS
NT PHOTORECEPTORS
NT RETINA
NT SEMICIRCULAR CANALS
NT THERMORECEPTORS
NT VESTIBULES

Human nervous system and vestibular and auditory analysors functional changes under combined hypokinesia and radial accelerations effects

02 p0197 A69-11496

SENSES

U SENSORY PERCEPTION

SENSIBILITY

U SENSITIVITY

SENSITIVITY

NT IMPACT RESISTANCE
NT LIGHT ADAPTATION
NT NOTCH SENSITIVITY
NT PAIN SENSITIVITY
NT PHOTOSENSITIVITY
NT PHOTOTROPISM
NT PROPELLANT SENSITIVITY
NT RADIATION TOLERANCE

Sensitivity of voltage transfer function relative to variation in value of components of resistance terminated reciprocal reactive network

01 p0049 A69-10069

Error and sensitivity analysis of on-line algorithms for fixed point linear smoothing

01 p0050 A69-10238

Sensitivity reduction in specific optimal control by use of dynamical controller

01 p0051 A69-10441

Optimal control system sensitivity definitions, analysis methods and design techniques, discussing equations of motion of dynamical system satisfying vector differential equation

01 p0051 A69-10553

Sensitivity calculation for microwave receiver consisting of traveling wave tube preamplifier followed by square law detector and video amplifier

01 p0048 A69-11038

Two parameter dynamic system of fourth order optimization based on gradient method modified for discrete optimization

02 p0224 A69-11594

Singular perturbation method for reducing order of mathematical models in optimal sensitivity control problems

02 p0224 A69-11967

Generalized digital low pass filter synthesis by recursion technique, noting coefficient sensitivity simplification

03 p0403 A69-13227

Sensitivity of radio receiver detecting weak sinusoidal and noise signals by counting zero crossings by envelope or phase of signal sum

03 p0405 A69-13717

Sensitivity models for adaptive and self adaptive systems design

04 p0582 A69-14797

Transverse sensitivity ratio of vibration transducer, discussing measurement by shaker method

04 p0603 A69-15432

Performance index sensitivity of nominally optimal controls noting initial and final target manifolds relationship to trajectory sensitivity

05 p0737 A69-15866

Minimum sensitivity deadbeat sampled data control system design by frequency domain technique, using two controllers

[ASME PAPER 68-WA/AUT-15]

05 p0738 A69-16177

Sensitivity matrix in multivariable feedback control systems, discussing loop gain matrix design to achieve desired insensitivity to system error sources

[ASME PAPER 68-WA/AUT-9]

05 p0738 A69-16179

Root sensitivity of linear feedback control systems calculated with signal flow graph and transforming circle

05 p0740 A69-16588

SNR enhancement in optical receiver by amplification before detection of carrier of modulated optical signal, using quantum amplifier

[IEEE PAPER R-5] 07 p1154 A69-19079

Absolute sensitivity of Soviet UTs-3 photographic emulsion to vacuum UV radiation by method involving absolute calibration of photocathodes

07 p1136 A69-19620

Error in receiver sensitivity calculation using approximate equation for noise power at input

08 p1275 A69-20226

Sensitivity coefficients to solve two point boundary value problem arising from Pontryagin principle, with application to time optimal control studies

08 p1296 A69-20297

Sensitivity of microwave earth stations for analog and digital communications

09 p1453 A69-21409

Low sensitivity electric circuits synthesis based on analytical and numerical analysis of sensitivity function characteristics of selective polynomial circuits
09 p1472 A69-21780

Two fold congruency method for statistical evaluation of fluorescent flaw detection penetrant sensitivity and reproducibility
10 p1700 A69-23374

Hot wire sensitivity to velocity, temperature and density fluctuations of temperature varying flow field, discussing calibration curves and special cases
11 p1886 A69-25088

Computational method for quasi-optimal control with parameter sensitivity function, noting application to dynamical system model
11 p1859 A69-25165

Multidimensional self adjusting systems design by achieving parametric invariance, using sensitivity theory
11 p1861 A69-25711

Atmospheric thermal radio emission fluctuations effects on radio telescope sensitivity, evaluating dispersion at low angles to horizon
12 p2031 A69-26643

Sensitivity decrease of reversible temper brittleness of low alloy steels due to Mo inhibiting effect on phosphorus diffusion
13 p2283 A69-28491

Automatic search-free optimization by sensitivity functions, deriving algorithms by Q factor and discrepancy extrapolation
14 p2425 A69-28823

Pulsed noise sensitivity in radar receivers having noise limiter for simple and complex signals
15 p2563 A69-30137

Short and ultrashort waves signals amplitude and phase displacement determination device, stressing sensitivity
15 p2570 A69-31088

IR radiation detection sensitivity emphasizing frequency up-conversion
17 p2969 A69-32839

Pulsed control systems sensitivity relationship to discreteness period described via differential equations
17 p2994 A69-33143

Metrological measuring instrument scales selection principles for ensuring constant sensitivity and Q factor
17 p2975 A69-33614

Linear computer-controlled closed loop systems sensitivity analysis, deriving estimation error incremental covariance to demonstrate quality deterioration under perturbed initial conditions, parameters, etc
17 p2944 A69-33742

Parameter sensitivity analysis of discrete suboptimal filters from optimal rmse estimate of actual system performance measure
18 p3110 A69-34675

Memory matrices sensitivity to laser beams with various emission power densities, considering matrices of thin metal layers on transparent base
19 p3335 A69-36198

Large parameter variations effect on linear feedback control systems performance, optimal or suboptimal
21 p3685 A69-38726

Dynamic system absolute stability and sensitivity to parameter variations in linear part of system calculated by graphical and analytical techniques
21 p3685 A69-38729

Space mission sensitivity to parameters of interest determined by Monte Carlo simulation samples
21 p3804 A69-39036

Nocturnal and diurnal monkeys spectral sensitivity functions determined from simultaneous recordings of light-evoked cortical and retinal responses
22 p3882 A69-40867

Cat intraretinal DC component and b-wave separation based on sensitivity to visual stimuli, discussing electroretinogram recorded with microelectrodes
22 p3883 A69-40881

SENSITIZING

Ammonium nitrate thermal decomposition activation by dyes and halides, noting endothermic and exothermic reactions, proposing models to study impurities role
17 p3016 A69-32830

SENSOR-AIRBORNE TERRAIN ANALYSIS

U SENSORS
U TERRAIN ANALYSIS

SENSORIMOTOR PERFORMANCE

NT PSYCHOMOTOR PERFORMANCE

Reduced sensory input states psychobiology, discussing brain-mind relationship and dynamic information transfer loop for normal brain-mental operations

mation transfer loop for normal brain-mental operations
06 p0873 A69-17020

Subjects sensory reactions to weightlessness during parabolic flight, studying coordination of writing, eating and drinking motions
07 p1060 A69-18575

Sensory and physiological reactions experienced by cosmonauts during parabolic training flights, tabulating arterial pressure, heart beat and respiration rate
07 p1061 A69-18580

Human motor reactions during weightlessness based on parabolic or orbital space flight observations, noting cosmonaut writing performance
07 p1063 A69-18595

Auditory startle stimuli effect on human performance, noting decrease in mental and sensorimotor activity
07 p1066 A69-19421

Vestibular analyzer role in spatial orientation under weightlessness conditions during aircraft flights, discussing underestimations of rotation angle of Barany chair
08 p1262 A69-19840

Thermal radiation effects on cutaneous vasomotor and sudomotor control of human organism [AGARDOGRAPH-111]
08 p1265 A69-20672

Man machine integration, detailing sensory input and motor /or output/ systems, control loop and social structure impact
11 p1831 A69-25656

Muscle motor performance under continuous practice conditions, analyzing individual differences, intraindividual variability and remoteness
17 p2911 A69-34003

Factor analysis of complex perceptual-motor performance of man, measuring speed, flexibility, balance and strength
18 p3098 A69-35085

Sensorimotor coordination of man performing graphic assignments in upright, reclining and prone position, discussing interaction of vestibular, visual and motor analyzers
20 p3470 A69-37246

Orientation reflexes of animals in weightlessness, analyzing turnover, vestibular and cervix reactions using motion pictures
20 p3470 A69-37248

Human sensorimotor reactions during rotation in small radius apparatus at different speeds and torso inclinations
20 p3471 A69-37258

Motion sickness forms in human subjects subjected to induced rocking, noting impaired performance and sensorimotor reactions to visual stimuli
20 p3472 A69-37263

Ear-hand coordination adaptability tested by exposure to auditory rearrangement entailing 30 degree rotation of interaural axis produced by electronic pseudophones
21 p3663 A69-38899

Spatial distribution of amplitude and onset of pre-motion positivity, readiness and motor potential changes in human cerebral cortex preceding voluntary finger movements
22 p3875 A69-40261

Biological model describing spacecraft operator sensorimotor activity in response to various spacecraft control stimuli, outlining computer algorithm
22 p3892 A69-40281

Human performance on button pressing task with fixed ratio fixed interval reinforcement schedules
23 p4081 A69-41439

Bisensory auditory and visual signals characteristics effects on human reaction time, noting different results for unilateral and bilateral signal pairs
23 p4083 A69-41454

Arterial oxygen partial pressures and heart beat rates measured in humans during acute hypoxia after altitude and ergometer training, noting sensorimotor performance
23 p4086 A69-41788

Klaxon hooter sudden sound used as auditory startle stimulus to determine hand sensorimotor activity and standing stability in pilot error causes
23 p4088 A69-41808

Occipital eeg activity slowing and physiological changes during prolonged immobilization plus perceptual deprivation of human beings
24 p4256 A69-42554

SENSORS

Make wire, light pipe and spring wire ablation sensors development for measuring parameters of heat shield materials for reentry vehicles
04 p0602 A69-15428

InAs thin film sensors using Hall effect to measure magnetic fields at cryogenic temperatures
10 p1696 A69-23717

Transensor implantation, sham implantation, no implantation and lighting effects on rat body composition, noting fat and water content
12 p2020 A69-26557

S-N fatigue life small bondable resistance sensor, discussing random response data interpretation with emphasis on use of strain multipliers
15 p2613 A69-31270

Acoustic fluidic sensor /sonicell/ combining sonic generator based on edgetone principles with sensor dependent on laminar stream acoustic disturbance
15 p2616 A69-31302

Level signaling device for high temperature conducting fluids, describing sensor construction and circuitry
20 p3536 A69-36980

Sensors array to determine propagation wave vector velocity via high resolution frequency waveform spectrum analysis, emphasizing seismic applications
22 p3902 A69-41220

SENSORY DEPRIVATION

External observer effect on human behavior during sensory deprivation tests conducted in isolation chambers as factor in estimating personality
02 p0200 A69-11516

Reduced sensory input states psychobiology, discussing brain-mind relationship and dynamic information transfer loop for normal brain-mental operations
06 p0873 A69-17020

Work capacity and adaptation characteristics of humans confined in small chamber and experiencing effects of isolation and sensory deprivation
08 p1262 A69-19838

Social isolation and other sensory deprivations effects on human organism
08 p1263 A69-19937

Prolonged visual deprivation effect on pressure sensitivity of finger, forearm, neck and leg, noting effects after restoration of normal visual stimulation
13 p2210 A69-28313

Social and visual isolation effect on rat blood pressure, pulse pressure, heart rate, behavior and response to epinephrine
14 p2407 A69-29296

Occipital eeg activity slowing and physiological changes during prolonged immobilization plus perceptual deprivation of human beings
24 p4256 A69-42554

SENSORY DISCRIMINATION

NT BRIGHTNESS DISCRIMINATION
NT TACTILE DISCRIMINATION
NT VISUAL DISCRIMINATION

Control circuits in nature and sensory information data processing in human work, including servomechanism of brain-muscle system
21 p3652 A69-38784

Dynamic reactions of mathematical model representing vision and hearing process adaptation
23 p4110 A69-41984

Combined eye and ear identification of bimodally presented signals in noise over oscilloscope and earphones, noting significance of independent observers model
23 p4111 A69-42168

Attention shifts in maintained discrimination discussing combined responses of varying and constant visual and auditory stimuli in pigeons
24 p4275 A69-43198

SENSORY FEEDBACK

Reduced sensory input states psychobiology, discussing brain-mind relationship and dynamic information transfer loop for normal brain-mental operations
06 p0873 A69-17020

Unit activities in cerebellar cortex by auditory stimulation in cats, discussing response patterns obtained by histograms
22 p3876 A69-40264

Biological model describing spacecraft operator sensorimotor activity in response to various spacecraft control stimuli, outlining computer algorithm
22 p3892 A69-40281

SENSORY PERCEPTION

NT AUTOKINESIS
NT CRITICAL FLICKER FUSION
NT PAIN SENSITIVITY
NT SPACE PERCEPTION
NT TACTILE DISCRIMINATION
NT TASTE
NT VERTICAL PERCEPTION
NT VIBRATION PERCEPTION
NT VISUAL DISCRIMINATION
NT VISUAL PERCEPTION

Human sensory reactions to short term weightlessness
07 p1060 A69-18574

Motion cues simulation system with seat of six differentially inflatable sections, discussing DYNASEAT
17 p2947 A69-34007

Sensory physiology of pilot landing guided by runway lighting, stressing visibility influence
19 p3260 A69-35987

Human taste perception mechanism and taste system anatomy
21 p3652 A69-38783

Control circuits in nature and sensory information data processing in human work, including servo-mechanism of brain-muscle system
21 p3652 A69-38784

Sensory and logic behavior model of sequence selection based on received information, considering perception, sense, desire, concept and criteria levels
23 p4109 A69-41976

Human hearing and vision mathematical simulation, relating signal perception parameters to corresponding adaptation processes
23 p4109 A69-41979

Sensory information processing model for tactile perception using array of airjet and piezoelectric stimulators applicable to display design and nervous system investigation
24 p4276 A69-43273

SENSORY STIMULATION

Stability and habituation of nonspecific galvanic skin responses during light and sound stimulation periods in medical students
03 p0380 A69-13462

Critical body temperature for intracranial self stimulation in white rats
03 p0375 A69-13897

Coriolis stimulus effect during centrifugal g load on spatial orientation and accompanying stick performance
06 p0876 A69-18023

Spacecraft rotation and astronaut head and body motion as stimuli for vestibular analysis function study during weightlessness
20 p3473 A69-37275

Motion sickness as sensory rearrangement phenomenon, proposing neural mismatch hypothesis to account for symptom pattern
20 p3483 A69-38266

Stimulation effects of reticular formation, hippocampus and septum on sensory responses of posterior hypothalamic neurones in cats
21 p3656 A69-38979

Cortical and thalamic evoked activities changes during sensory conditioning of freely moving cat
22 p3872 A69-40160

Cortical responses by transient sensory stimulation of fingers EEG recorded, obtaining isomorphism between psychological and neurophysiological events
22 p3876 A69-40262

Mapping of biological potentials evoked in primary somatosensory fields by electrical signals on dorso-lateral surface of brain cortex of cats
22 p3886 A69-41121

Unisensory and multisensory signal processing in cortical and brain stem regions of albino rat by electronic averaging and time histogram techniques
23 p4092 A69-42055

SEPARATED FLOW NT BOUNDARY LAYER SEPARATION

Nozzle separation for thrust vector control with applications to guidance problems
01 p0161 A69-10412

Supercritical flow effects on unsteady aerodynamic coefficients used for subsonic aircraft flutter analysis, emphasizing changes due to shock and flow separation
01 p0007 A69-11020

Model for asymptotic separated flow in wake behind broadside of bluff body, discussing separation point, interaction, reattachment, base flow and near wake
02 p0188 A69-11986

Fluid mechanics of supersonic flow separation and reattachment in fluidic devices
02 p0231 A69-12077

Hydrodynamic analysis for determining steady flow region with closed separation area for Reynolds numbers to describe viscous mixing by Prandtl equations
02 p0190 A69-12570

Photographic flow patterns of separated flows with vortex formation obtained in wind tunnel for different aerodynamic configurations of revolution
02 p0191 A69-12586

Heat transfer covering heat conduction, channel flow, boundary layer flow, separated flow, etc
04 p0684 A69-14354

Slow nonNewtonian flow in separation zone analyzed using finite difference scheme
04 p0587 A69-14594

Reattachment pressure correlated for any type of two dimensional turbulent supersonic separated flow
04 p0588 A69-14727

Pressure fluctuations in separated flow region behind thin fence, determining recombination point position, noise sources and frequency spectra variations
04 p0544 A69-14868

Modified Karman-Pohlhausen pulse integral equation for calculating boundary layers is more accurate when seeking flow separation point
04 p0591 A69-15408

Vortex motion of separated flow from slender wings and rotor loading, discussing computer role in low speed aerodynamic research
05 p0696 A69-15562

Local pressure and skin friction distribution around circular cylinder in cross flow in large range of Reynolds numbers
05 p0744 A69-15716

Plane supersonic flows separated by thin film shaped jet, deriving pressure as function of deviation
05 p0746 A69-16020

Lift and drag coefficients for circular cylinder immersed in time dependent flow analyzed using potential flow model
05 p0747 A69-16072

[ASME PAPER 68-FE-15] Asymmetric supersonic air flow at 60 degree angle of attack past ellipsoid with frontal spike creating separation area
06 p0858 A69-17337

Similarity functions defined for laminar or turbulent separation in nonuniform supersonic flow
07 p1050 A69-18417

[ONERA-TP-659F] Gas segregation in positive column of DC discharge due to axial ion motion analyzed using conservation equation
08 p1361 A69-20145

Equilibrium theory of parametric pump using cyclic flow of binary mixture through column with heated and cooled bed of solid absorbent
09 p1481 A69-21910

Two dimensional supersonic flow along adiabatic curved ramp noting separation, attached flow and laminar boundary layer interaction with external stream
09 p1430 A69-21949

[AIAA PAPER 68-109] Tangential air jet for separation control of two dimensional incompressible flow along circular cylindrical wall
09 p1431 A69-22277

Oblique shock wave separation conditions in supersonic gas flow past wedge
09 p1483 A69-22665

Axisymmetric detached flow past slender solid of revolution by ideal incompressible fluid at zero angle of attack and with small cavitation numbers
11 p1877 A69-25741

Heat flux in two dimensional laminar separation zone in supersonic flow, measuring convection coefficient and wall pressure
12 p2011 A69-26289

Heat and mass transfer in two dimensional turbulent free shear flows including separated and reattached flows
13 p2377 A69-28145

Semiempirical parameters in streamline division and momentum integral analyses for separated flows, using error function velocity profile and spreading parameter sigma
14 p2389 A69-29028

Supersonic gas flow past wedge at zero angle of attack with separated shock wave, calculating velocity gradient at stagnation point and pressure and drag distribution
14 p2390 A69-29615

Quasi-steady state supersonic gas flow past two closely spaced coaxial separating bodies at different velocities, showing dependence on separation rates
14 p2391 A69-29617

Supersonic jet flow with separated shock wave flowing past infinite wedge using Chaplygin method, assuming negligible entropy variations
14 p2391 A69-29619

Two piston flow stability separated by thin wall in traveling magnetic field, finding piston inertia centers velocity equal to field velocity
14 p2500 A69-29903

Aerodynamic forces acting on harmonically oscillating thin profile in stalled plane parallel flow of ideal incompressible fluid
16 p2732 A69-32142

Distributed boundary layer suction effectiveness for controlling supersonic transitional flow separation
16 p2772 A69-32149

Heat transfer in laminar separated flows with flat plate segment connections, indicating correlation between local heat transfer rates for successive regions
16 p2879 A69-32169

Separated flow patterns in base flow at body recesses, emphasizing shock wave boundary layer interaction, laminar flow and flow in front of recess
17 p2949 A69-33124

Leading edge vortices and shock detachment flow over delta wings, discussing drag reduction due to lift
17 p2896 A69-34025

Fluctuating heat transfer and flow measurements for circular cylinder in crossflow with simultaneously imposed transverse standing sound field
18 p3124 A69-35384

Pure gas suction through free jet shock structure, analyzing aerodynamic effect of molecular separation
19 p3240 A69-36650

Supersonic flow past antisymmetrical thin delta wing by flow separation from subsonic leading edges, noting wing surface pressures
19 p3241 A69-36779

Global properties of solution of inverse detached shock problem analyzed by characteristic coordinates at low Mach number
19 p3301 A69-36788

Flow characteristics and wall heat transfer in separated flow region of annular cavity at free stream hypersonic speed and high gas temperature
20 p3458 A69-37185

[AIAA PAPER 68-672] Potential flow theory applied to determination of airfoil separated vortex flow and maximum lift and Reynolds number dependence
20 p3459 A69-37421

Flow separation and reattachment points and line of zero velocity jet mixing determined by injecting smoke
20 p3517 A69-37994

Secondary losses in flat large scale turbine lattice attributed to LF pulsating flow separation on back of blade
21 p3645 A69-39717

Axisymmetric separated flow in Chapman model shown nonexistent by flow visualization technique
23 p4060 A69-41905

Detachment in incompressible turbulent flows around thick body analyzed to predict base pressure, vortex volume, etc
24 p4299 A69-42674

Continuous potential fields modeling based on electrohydrodynamic analogy extended to flows involving stream separation
24 p4300 A69-43089

Laminar flow swirling motion in circular duct, studying separation and reversal
24 p4301 A69-43355

Separation flows in flat channel with step recess, analyzing dynamic characteristics in mixing region, in wake of rarefaction waves and in attachment zone
24 p4247 A69-43498

SEPARATION

Moving and stationary interphase boundaries segregation during phase transformation, discussing embrittlement
03 p0450 A69-13883

Optimization problems solution applied to separable but bounded state variable problem, providing control over commercial errors
24 p4292 A69-43286

SEPARATORS

NT AIR FILTERS
NT DUST COLLECTORS
NT ELECTROSTATIC PRECIPITATORS
NT EVAPORATORS
NT FLUID FILTERS
NT SIEVES
NT STILLS

Highly resistant separator performance in Zn-Ag oxide battery, discussing zinc electrode limitations on battery performances
10 p1640 A69-23996

Research and development programs leading to heat sterilizable spacecraft battery separator material, describing bench tests
23 p4072 A69-42284

Separation system for collecting wash and waste water from gaseous environment and separating liquid and gaseous phases during space missions
24 p4272 A69-42845

SEPTUM

Higher order modes suppression in square waveguides by bifurcating metal septa of finite length, analyzing periodic array of many finite-length septa
04 p0576 A69-14758

Stimulation effects of reticular formation, hippocampus and septum on sensory responses of posterior hypothalamic neurones in cats
21 p3656 A69-38979

SEQUENCING

Book on nonlinear programming, discussing transformation of constrained minimization problem into sequence of unconstrained minimizations of appropriate auxiliary functions
04 p0563 A69-14421

Sequence pulse stuffing technique for rate equalization of digital channels, discussing coding effect and capacity for word signaling
07 p1080 A69-19094

Probability density functions of waveforms from summation of digits in n-stage shift register generating m-sequence
15 p2568 A69-30617

SEQUENTIAL ANALYSIS

Optimal distribution of search effort for moving target location, suggesting Markovian decision models
01 p0104 A69-10653

Sequential probability ratio test for detecting changes in Gauss-Markov process characteristics, noting application to fault detection in gyro navigational system
01 p0083 A69-11002

Sequential logic for improved signal detectability in frequency-agile search radars, discussing target echo fading models in radar range performance prediction
01 p0033 A69-11008

Power advantage of optimum system achieved with suboptimum feedback function for sequential binary detection system
02 p0225 A69-11996

Sequential signal design for feedback channels, emphasizing single set subject to peak and average power constraints in time continuous transmission
03 p0408 A69-12868

Cross correlation function for two sequences of pulses arbitrarily distributed in time, noting noise stability of diversity reception systems
04 p0557 A69-14790

Distribution free sequential probability ratio procedure for detecting signal in multiple resolution element radar
05 p0717 A69-15609

Invariant imbedding and sequential interpolating filters for nonlinear processes
[ASME PAPER 68-WA/AUT-3]
05 p0738 A69-16183

Identification of finite memory, time discrete linear systems by Kiefer-Wolfowitz stochastic approximation procedures, presenting two algorithms for sequential identification
06 p0900 A69-17359

Trunk and tree searching properties of Fano sequential decoding algorithms
06 p0902 A69-17400

Signal detection procedures preserving nonparametric detection properties and advantages of sequential procedures, assuming signal corruption by additive noise at input
06 p0888 A69-17531

Linear recurring sequences over finite fields, discussing application to error correcting codes
06 p0948 A69-17863

Sequences with small correlation functions as error correcting codes in word separation, synchronization and pulse compression systems
06 p0948 A69-17868

Optimum and suboptimum detection of K binary symbols corrupted by white Gaussian noise, discussing searching procedure and average error probability
07 p1081 A69-19097

Input signal history analysis in recognition of moving or changing objects based on classification definition and Wald sequential analysis
08 p1297 A69-20419

Infinite tree code ensemble upper bound on moments derived for sequential decoding governed by Fano algorithm
09 p1471 A69-21318

Computer simulation of unbiased digital recording composed of sequential computations intended for various bit densities
[IEEE PAPER 3.3]
09 p1461 A69-22562

Auditory temporal masking of tonal signal by narrow band noise and perception of temporal order noting effects of intensity, frequency and time
11 p1830 A69-24795

Kalman sequential estimation adaptation to target maneuvers without sacrificing tracking accuracy in nonmaneuvering portions of trajectory
11 p1861 A69-25455

Algebraic and sequential coding-decoding method for data communication rates up to capacity of discrete memoryless channel, discussing error probabilities
13 p2219 A69-27664

Finite automaton malfunctions, discussing input sequences construction and output sequences analysis for malfunction subsets recognition
13 p2239 A69-28536

Input signal history analysis in recognition of moving or changing objects based on classification definition and Wald sequential analysis
14 p2427 A69-29657

Dynamic meteorology quasi-stable problems solved using sequential approximations solution for barotropic model of Euler equations
14 p2476 A69-29821

Real time shock response analysis advantages over sequential analysis, describing equipment
15 p2618 A69-30359

Sequential Bayes procedure demonstrating mean time to failure exceeding acceptable value with given confidence coefficient
19 p3327 A69-36040

Cross correlation and probability metric in coded sequential detection telemetry system, giving optimum parameters, overflow and error probabilities using computer simulations
19 p3273 A69-36266

Dirichlet polynomials double sequences and double series with positive exponents, defining conditions for convergence in bicylinder
19 p3361 A69-36639

Existence theorem for limits of minimizing sequences in optimal control problems, applying results to systems governed by partial differential equations
19 p3287 A69-36724

Failure test algorithm for sequential units with delay lines of control digital computers, detecting replacement of output terminals by sensitive paths
20 p3502 A69-37394

Sequential design for economic description of potentially redundant elastic structures, noting redesign sequence
21 p3842 A69-39302

Nonlinear estimation with noisy data, considering least squares fit, sequential /Kalman/ estimate and iterated sequential scheme
21 p3686 A69-39370

Sequential analyses of planetary surface sample for extraterrestrial life detection, discussing chemistry, morphology, growth and metabolism for life attributes
23 p4213 A69-41623

Satellite communication system high speed sequential decoder design, discussing parameters, simulation and test results on satellite channels
23 p4131 A69-42523

Sequential vector estimation of matrix of second partial derivatives, suggesting alternative least squares method
24 p4340 A69-42958

SEQUENTIAL COMPUTERS

Infinite tree code ensemble upper bound on moments derived for sequential decoding governed by Fano algorithm
09 p1471 A69-21318

Asynchronous finite state sequential nonlinear controller synthesis with few flip-flops for dynamic space vehicle systems
[AIAA PAPER 67-988]
13 p2225 A69-28201

Algorithm for assigning binary codes to inputs, internal states and outputs for sequential machines by threshold logic
18 p3105 A69-34618

SDP-3 small serial computer for engineering experiment on IMP spacecraft, discussing design modifications to improve performance
23 p4133 A69-41737

SEQUENTIAL CONTROL

Atomic clock with sequential optical pumping using resonance frequency of hyperfine transition of ground state Rb 87
12 p2090 A69-26291

Synthesizable automata with sequential homogeneous structure formed by standard fixed units combination
13 p2224 A69-27249

Apparent movement in peripheral vision induced by sequential flashing of spatially unresolved two dots, studying dynamics of illusion
16 p2746 A69-31556

Fluidic logic for high speed pneumatic stepping motor for high radiation environments, discussing bellows pressure sequencing by open-loop counter, signal conversions and performance
18 p3092 A69-34310

Spacecraft onboard computer for prelaunch targeting constants verification through checksum equation and error detection scheme, using generated number sequences
[AIAA PAPER 69-946]
22 p3974 A69-40329

Optimal rule for decision to stop or continue observation of random variables after observing sequence of variables with continuous distribution function
24 p4341 A69-43235

SERIES [MATHEMATICS]

NT ASYMPTOTIC SERIES

NT FOURIER SERIES

NT PADE APPROXIMATION

NT POWER SERIES

NT SINE SERIES

NT TAYLOR SERIES

Summation of Legendre series by transformation into integrals and use of recurrence relations
01 p0171 A69-11072

Chebyshev polynomials maximum property, examining effect of roundoff errors in Horner scheme for floating point arithmetic
03 p0456 A69-13553

Matrizants construction for Keplerian motions, discussing Hamiltonian character of variational equations for planar two body problem
03 p0513 A69-13779

Phenomena satisfying inhomogeneous Helmholtz equation in cylindrical coordinates, inferring equivalent infinite series directly from integral-transform method
04 p0623 A69-14896

Boundary condition description effect on numerical accuracy of series solution to boundary value problem by direct method
04 p0681 A69-15283

Double stochastic approximation algorithm for minimizing mean square error in finite expansion of unknown probability distribution functions
06 p0947 A69-17361

Uniqueness conditions of expansions in series of functions stressing Jacobi series applied to singular partial differential equations
07 p1174 A69-18805

Time harmonic, spherical harmonic and power series expansion of Boltzmann equation
08 p1353 A69-20793

F 2 layer state prediction as function of solar activity by series expansion for describing space-time variations of monthly F 2 medians critical frequencies
10 p1687 A69-23927

Rapidly convergent series expansions for plane wave transmission coefficients for elliptical and rectangular apertures
11 p1837 A69-25001

Theorem for integral expansion applied to boundary value problems of mathematical physics and elasticity theory for single sheet hyperboloids of revolution
11 p1910 A69-25731

Analytic continuation of Appell hypergeometric series into linear combination of four infinite series
12 p2123 A69-26605

Matched asymptotic expansions to obtain slider bearing load carrying capacity
[ASME PAPER 68-LUBS-18]
13 p2266 A69-27270

Series and integral expansions of Jacobi polynomials with positive kernel, noting ultraspherical polynomials
14 p2470 A69-28905

Finite thickness plate heat equation using Legendre polynomials
14 p2537 A69-28970

Quasi-integral analytic continuation operator applicability to potential field approximated by certain truncated series expansion
14 p2470 A69-29032

Stress in elastic cylinder under thermal expansion with one end clamped expressed by series expansion of biharmonic function using least squares method
14 p2534 A69-29284

Eigenvalues of finite matrix Hamiltonian, considering convergence radius of perturbation series, limits and renormalization
14 p2470 A69-29451

Wiener-Hermite expansion extended to include time dependent ideal random functions, discussing application to shear flow turbulence
15 p2644 A69-30201

Lagrange expansion theorem for shielded surface waves, obtaining modal functions and power flows
16 p2750 A69-31947

Dirichlet polynomials double sequences and double series with positive exponents, defining conditions for convergence in bicylinder
19 p3361 A69-36639

Generalized series solutions of boundary layer flows over pointed and blunt nosed axisymmetric bodies, noting general potential flow extending Mangler transformation usefulness
20 p3514 A69-37211

Polya concept of maximum and minimum densities of series applied to entire functions of finite order with positive zeros
20 p3568 A69-37442

Residue series representation of radiation fields for azimuthal leaky wave antenna on conducting cylinder, showing zeroth term correspondence to omnidirectional antenna
20 p3506 A69-37834

Literat solution to equations of motion applied to lunar theory using electronic computer with series convergence
21 p3796 A69-38474

Solution procedure for torus with given surface loads or displacements, using series expansion of generalized analytical functions, discussing stress concentration near toroidal cavity
21 p3839 A69-39192

Bullard-Gellman dynamo, discussing magnetic field developed as series expansion, truncation levels and convergence
22 p4018 A69-40194

Northern Hemisphere 500-mb height pattern series expansion, using optimal sets of orthonormal functions, obtaining rms error
24 p4346 A69-43157

Chebyshev series approximations for Bose-Einstein functions of orders one to ten, noting computability of Fermi-Dirac functions and polylogarithms
24 p4341 A69-43231

Single series solution for rectangular plate deflection under arbitrarily located concentrated load, considering monolithic slab beam connection case
24 p4404 A69-43593

SERT [ROCKET TESTS]
U SPACE ELECTRIC ROCKET TESTS

SERUMS
U INOCULUM

SERVICE LIFE
Quantitative amounts of contaminants oil from piston engine and life of oil lubricant in engine
04 p0604 A69-14500

Statistical method to investigate time varying stresses in helicopter structures, considering service life evaluation
05 p0767 A69-16775

Helicopter flight safety as function of service duration, performance limitations and propulsion failure
07 p1054 A69-19313

Nickel-cadmium and Ag-Cd storage batteries performance, discussing methods to lengthen battery life and improvement of characteristics
08 p1261 A69-21051

Synthetic circuit equipment for semiconductor rectifier life testing with built-in fault analyzer for indicating shorted and broken diodes
08 p1293 A69-21113

Automatic transistor reliability testing system based on measured data and reliability research
08 p1294 A69-21119

Reliability in microelectronics estimated from failures expected during lifetime, describing various test methods
08 p1294 A69-21121

Life test of high temperature /2400 K/ 10 millipound resistojet thrusters, comparing results to theoretical predictions
[AIAA PAPER 69-294] 09 p1563 A69-21232

SERT 2 thruster system performance over expected mission parameters, noting operational lifetime excess over mission requirements
[AIAA PAPER 69-235] 09 p1566 A69-21255

Thermionic converter metallography relationship between materials and fabrication methods and reliable performance life
09 p1439 A69-21824

Heat pipes for thermionic converters, wicks development, high temperature life testing and performance
09 p1440 A69-21833

Stochastic model for calculating expected component failures in transient state from Weibull distribution failure data for first generation
09 p1504 A69-22149

Titanium-boron composites for gas turbines, mechanical properties and service life in high temperature environment
[ASME PAPER 69-GT-1] 09 p1527 A69-22510

Reliability characteristics of service life determination, noting exponential distribution of failure time value
10 p1662 A69-23319

Zinc electrode cycle life improvement by reducing change in electrode shape, noting effectiveness of teflonation
10 p1640 A69-23995

First excursion failure survival probability of randomly excited structures, considering single degree of freedom linear oscillator under Gaussian white noise
11 p1990 A69-25505

Reliability improvement influence on life cycle costs of high volume piece of military/commercial equipment
12 p2101 A69-25848

Service life of system predicted by identifying and testing system variables of mission phases, using obtained data in statistical estimation
12 p2101 A69-25970

Lens shutters durability, analyzing break-in effect, cock-and-release cycles and cause of failures
12 p2094 A69-26600

Mathematical relations presented for parameters of technological, transport and information systems reliability and life expectancy
13 p2268 A69-27436

Reliability and efficiency improvements for thermionic converters at JPL, giving failures analyses
14 p2397 A69-29175

Thermionic converters with different collectors, emitters and metal-ceramic seals reliability tested, determining life duration
14 p2398 A69-29179

SNAP 13 generator designs to develop technology for isotope heated thermionic converters, describing tests, efficiencies, power outputs and life times
14 p2481 A69-29191

Cylindrical geometry in-pile and out-of-pile thermionic converters long term life tests, including unfueled and fueled versions
14 p2399 A69-29197

Cylindrical in-core thermionic converters performance and life tests, discussing diode design, operation data and irradiation studies
14 p2399 A69-29199

European heat pipe research emphasizing transportable heat quantities, heating rate and life duration
14 p2538 A69-29201

Concorde aircraft and engine materials selection factors including mechanical properties of metals and nonmetals, corrosion resistance, service life, sealants, weight analysis, etc
15 p2639 A69-30464

Life margin tests of oil lubricated oscillating caged needle roller bearings under service conditions duplicating helicopter rotor hinge pin locations
[ASLE PAPER 68-LC-7] 15 p2622 A69-30609

Hydrogen laser operation time reduction attributed to hydrocarbon formation on inner surface of storage flask, promoting atomic hydrogen recombination
15 p2634 A69-30942

Long life repairable equipment reliability and mean time between failure with limited life components and material in normal life maintenance environment
15 p2581 A69-31134

Airborne particle size influence on gas turbine parts erosion, with attempts to relate to filtration and engine life
16 p2794 A69-32026

Small turbine development for long life applications in helicopters and unpresurized aircraft, describing Artouste, Turmo, Astazou and Bastan series
17 p3020 A69-33346

Turbine blade cooling emphasizing economics, service life and computerized calculations
17 p3020 A69-33352

Helicopter flight loads spectra data compared on statistical basis to establish component service lives
[AHS PAPER 301] 17 p2901 A69-33548

Gas turbine components life prediction, using Weibull distribution and Bayes theorem to estimate probability of crack initiation
19 p3394 A69-36004

Relationship between chronological and fatigue life in airframes, showing fatigue life dependence on operating conditions, pilot techniques and maintenance and inspection quality
20 p3461 A69-36920

Argon laser lower operating level decay probabilities, using spectrum analysis to study role of radiative decay
22 p3965 A69-40965

Bayesian estimate of individual truck maintenance costs based on optimum replacement maintenance age
23 p4241 A69-41577

Fatigue crack initiation mechanism as used in design to prevent fatigue failures in service
24 p4397 A69-42770

Diagnosis of service failures and reasons for primary failure isolation from secondary damage
24 p4398 A69-42772

Engineering components service failures involving fatigue crack propagation, analyzing causes
24 p4398 A69-42775

Military aircraft service life problems solved by alternative replacement policies comparative present value analysis
24 p4253 A69-43058

Aerospace fastener systems standardization proposal to reduce inventories, simplify design and provide extended structural life
24 p4325 A69-43439

Aerospace fastening system requirements to lower in-place costs, extend service life and reduce weight of aircraft
24 p4325 A69-43440

Polymeric polyurethane protective coatings for radar radome covers with improvement in service life, discussing performance properties and production method
24 p4338 A69-43456

SERVICE MODULES
Thermal insulation for cryogenic storage in space, discussing Apollo service module conversion to cryogenic service module
12 p2175 A69-26827

SERVICES
NT MEDICAL SERVICES
NT METEOROLOGICAL SERVICES
Bulk queuing with service time distribution assuming customer arrival in batches and service discontinuance
02 p0271 A69-12060

SERVO LOOPS
U FEEDBACK CONTROL
U SERVOCONTROL

SERVOACTUATORS
U ACTUATORS
U SERVOMOTORS

SERVOAMPLIFIERS
Hydraulic regenerative servoamplifier system for electrohydraulic actuator design, discussing specifications and test results
15 p2553 A69-31294

Servovalves with fluidic and electrical inputs compared for gas servoamplifiers performance, considering use as sensors in closed-loop hydraulic circuit
19 p3255 A69-36711

SERVOCONTROL
Positive feedback of spring mass system for mirror control on spectroheliometer of Apollo Telescope Mount flight
02 p0248 A69-11738

Servoelements and control methods for V/STOL aircraft, including lift and propulsion throttle configurations
04 p0547 A69-14815

Servosystems and control, discussing characteristics, types and stability of servomechanisms
04 p0550 A69-15179

Servosystems and control, discussing open and closed loops and parallel, decoupling, multivariable and adaptive control
04 p0550 A69-15180

Hybrid electropneumatic and electrohydraulic servosystem for actuation of gas jet nozzles of sounding rocket automatic pointing system
04 p0550 A69-15182

Electrohydraulic radar antenna telecontrol system, discussing pump assembly, hydraulic motor and pump control servojack
04 p0551 A69-15185

DC servo system with torque feedback to ensure insensitivity to load variation and provide optimal performance
05 p0736 A69-15659

- Self contained electrically servoed transducers for flight control, noting angle of attack transducer and force
05 p0766 A69-16750
- Modal response analysis of servocontrols as deduced from vibration test, for possible application to aircraft [ONERA-TP-668]
06 p0869 A69-17100
- Three axis attitude servomechanism design to adjust attitude and angular velocity of spacecraft
06 p0955 A69-17589
- Design criteria for pneumatic servo controls with fluidic elements stressing final transient, pilot circuits and amplifier elements
08 p1256 A69-20305
- Gas servo design utilizing floating flapper disk switching valves and pulse-length modulated pressure waves to actuate on-off switch [AGARDOGRAPH-118]
08 p1257 A69-20950
- Monitors to detect incipient failure during turbine engine development, describing servocontrol
10 p1692 A69-23253
- Electrohydraulic vibration isolation systems with feedback, considering band and notch isolation, system stability and adjustable frequency response [ASME PAPER 69-VIBR-40]
10 p1641 A69-24178
- Dynamics of gyroscopic synchronous servo system intended for remote measurement of spatial orientation coordinates of sensor moving element
11 p1881 A69-24558
- Electrical servopositioning of telemetry reception antenna for tracking satellites, considering weight, stability, etc
11 p1852 A69-25118
- Servocontrol to delay flutter onset of aeroelastic structures, discussing rapid amplitude and phase changes near instability point, wind tunnel models, instrumentation, analog simulation
11 p1992 A69-25518
- Hydraulic servo actuators load effect included in control loop actuator simulation
12 p2016 A69-26266
- Temperature control below 5.2 K based on servoing He pressure above bath
18 p3136 A69-34641
- Servovalve orifice characteristics described by discharge, flow or loss coefficients for laminar and turbulent flow, noting use of Mises model
19 p3256 A69-36712
- Astronomical data collection and evaluation, discussing digital distance measurement, photoelectric photometry, servocontrols and electronic computers suited for Schmidt telescope output
20 p3539 A69-37525
- SERVOMECHANISMS**
NT SERVOAMPLIFIERS
NT SERVOMOTORS
- Dynamic properties of electrohydraulic servomechanisms having variable structure analyzed by analog computer
03 p0368 A69-13686
- Servosystems and control, discussing characteristics, types and stability of servomechanisms
04 p0550 A69-15179
- Servosystems and control, discussing open and closed loops and parallel, decoupling, multivariable and adaptive control
04 p0550 A69-15180
- Servosystems components design, discussing detector, corrector, amplifier and motor
04 p0550 A69-15181
- Hybrid electropneumatic and electrohydraulic servosystem for actuation of gas jet nozzles of sounding rocket automatic pointing system
04 p0550 A69-15182
- Electric position servosystems for 50 ton telemetry reception antenna and 1200 ton loading turntable of nuclear power plant
04 p0585 A69-15184
- Spherical gyroscope servosystem probabilistic synthesis ensuring minimum dispersion of random drift
05 p0764 A69-16669
- Electrohydraulic attitude servomechanism for controlling movements of pilot training cabin, describing hydraulic system and electric control circuit
06 p0906 A69-16966
- Automatic control textbook covering theoretical and practical principles of control engineering, analysis, design, servomechanisms and instrumentation
06 p0904 A69-17856
- DC servo system with torque feedback, discussing bang-bang system comparison, analog simulation, damping and quasi-optimum behavior
07 p1059 A69-19229

- Book on feedback control theory for engineering and applied physics noting signal theory, servomechanisms, transfer functions, system stability and Nyquist diagrams
08 p1295 A69-19841
- Kinematics of vertical gyroscope mounted in additional servo frame, determining kinematic errors due to rotor axis deviation
09 p1498 A69-22108
- Correlation between responses of linear systems for transient input as performance criterion for servomechanisms
09 p1475 A69-22536
- Analytical method for optimum switching function of relay servosystem subjected to stationary Gaussian random noise, considering perturbation and dynamic programming
11 p1859 A69-25025
- Inertial servomechanisms actuators, discussing dynamic characteristics, power, vibration damping, matching, couplers, etc
11 p1826 A69-25119
- Monograph on nonlinear servosystems covering nonlinearity with/without inertia, self oscillations, linearization by forced oscillations, stability theorems and Liapunov function choice
12 p2054 A69-26966
- Human operator as servo system element of subassemblies in tracking and equilibrium tasks, stressing results of electromyographic analysis
12 p2025 A69-27081
- Searchless gradient self adaptive system for adjusting servosystem parameters to reference model characteristics, using auxiliary operator method
14 p2426 A69-29146
- Correlated noise effect on accuracy of suboptimal servosystem velocity measurements from recording Doppler frequencies
15 p2567 A69-30341
- Barometric altimeters development, discussing servo and three pointer types, accuracy, Central Air Data Computer repeater function and future trends
15 p2610 A69-30859
- Servosystems components design, discussing detector, corrector, amplifier and motor
16 p2741 A69-32431
- Soviet book on hydraulic servo drive covering design and performance, static and dynamic characteristics and stability problems
18 p3093 A69-34356
- Computerized analysis and design of nonlinear servomechanisms, using describing functions technique
18 p3110 A69-34672
- Feedback realization of continuous optimal filter applied to designing servomechanisms with stochastic inputs and disturbances
18 p3110 A69-34673
- Analytical, graphical and graph-analytical methods for synthesis of passive circuits ensuring air removal from chambers of pneumatic logic control and servoelements
18 p3093 A69-34831
- Automatic ultrasonic inspection device search head, servomechanism and electronic system used for detecting weld defects and cracks
18 p3137 A69-35111
- Liapunov method applied to stability evaluation of multiparameter self adaptive nonsearch gradient servosystems
19 p3286 A69-35891
- Optimal structural parameters of radar digital ranging servosystems derived from reproduction error, including computer simulation data
19 p3278 A69-36593
- First harmonic approximation method reformulated to interpret nonlinear characteristic directly, discussing oscillation stability of servosystems
19 p3287 A69-36709
- Electrohydraulic servomechanism harmonic response showing nonlinear behavior, including jump resonance, analyzed by mathematical model and analog simulation
20 p3464 A69-36999
- Electrohydraulic servosystem to counteract atmospheric turbulence effects on B-52 global bombers, noting reduction in aircraft fatigue and structural damage
20 p3467 A69-38184
- Design concepts and principles of systems for monitoring of Concorde flight control actuators, considering servo control, control interconnections and control input system
20 p3467 A69-38190
- Stability of nonlinear systems with state variable feedback applied to fuel valve servomechanism
21 p3687 A69-39460

Programmable digital compensator for single high performance control loop servomechanisms
21 p3688 A69-39704

Aircraft directional stability in terms of ideal non-holonomic coupling on mechanical system, noting servosystem role
21 p3830 A69-39836

Statistical analysis of operation of precision electric spark machine servosystems with RC generator based on working pulse peak voltage distribution
23 p4168 A69-41307

Fluidic servomotor controlled by hydraulic vortex valves using mechanical signals for helicopter stability augmentation system
24 p4255 A69-42800

SERVOMOTORS

- Servosystems components design, discussing detector, corrector, amplifier and motor
04 p0550 A69-15181
- Limiting amplitude of output shaft vibrations of servodrive operated in linear region as function of frequency
04 p0584 A69-15417
- Transfer function variation of invariant servodrive, comparing calculated and experimental transient response
04 p0584 A69-15418
- Synchronous servomotor for parabolic antenna of surveillance radar, discussing motor size and optimum gear ratio determination
08 p1274 A69-20108
- Dynamic behavior of electrohydraulic servomotors over wide range of loads using differential equations of motion
08 p1256 A69-20718
- Gas servo design utilizing floating flapper disk switching valves and pulse-length modulated pressure waves to actuate on-off switch [AGARDOGRAPH-118]
08 p1257 A69-20950
- Inertial servomechanisms actuators, discussing dynamic characteristics, power, vibration damping, matching, couplers, etc
11 p1826 A69-25119
- Servosystems components design, discussing detector, corrector, amplifier and motor
16 p2741 A69-32431
- Fluidic logic for high speed pneumatic stepping motor for high radiation environments, discussing bellows pressure sequencing by open-loop counter, signal conversions and performance
18 p3092 A69-34310
- Spacecraft data storage requirements, discussing use of servo-driven tape recorders in data processing systems
18 p3107 A69-35096
- Duplex servomotor package sized for stabilator channel of F-4 aircraft providing compact integrated control surface positioning [AIAA PAPER 69-788]
19 p3249 A69-35640
- Triple redundant actuator for fly-by-wire control system, noting electrohydraulic servomechanisms in side-by-side arrangement
22 p3870 A69-41242
- Stability criteria for electrical interconnection in parallel operating valve controlled hydraulic servomotors applied to gimbaled system
24 p4256 A69-43310
- SERVOS**
U SERVOMOTORS
- SERVOSTABILITY CONTROL**
U SERVOCONTROL
- SET THEORY**
NT BOREL SETS
NT EQUIVALENCE
- Minimal conditions for association of binary variables, studying nondecreasing functions and equivalence in coherent binary systems theory
04 p0624 A69-15007
- Spontaneous decomposition of image space into compact sets/images or classes/ using adaptive dispersion method to reduce system learning time
11 p1859 A69-24964
- Torsion theory for modules over integral domain, giving definition of injective sums
13 p2287 A69-27339
- Image recognition algorithm for determination of hyperplane separating two finite sets of elements in Euclidean space
14 p2418 A69-29353
- Probabilistic automata stochastic matrices algebraic properties of definite, quasi-definite, periodic and quasi-periodic sets
15 p2645 A69-31141

Autonomous second order recurrence with real variables, studying conditions for attractive limiting set stability region with several noninterconnected regions
19 p3287 A69-36651

N-dimensional vector functions branching process stability belonging to locally compact set in certain space
20 p3509 A69-37075

SFERICS
U ATMOSPHERICS
SH-3 HELICOPTER

Analytical design of SH-3 helicopter engine inlet ice deflector shield interior surfaces, defining potential flow pattern and moisture droplet trajectories
01 p0011 A69-11064

SHADOWGRAPH PHOTOGRAPHY
NT SCHLIENEN PHOTOGRAPHY

Boundary layer effects on shadow deformation, emphasizing two dimensional flow with image projected by parallel light beams perpendicular to flow plane
03 p0364 A69-13787

High speed shadow photographs of Q switched laser triggered spark gap air discharge, showing sonic waves and development of discharge channel
04 p0610 A69-14349

Feed support blockage loss in parabolic antennas evaluated by shadowgraph photography
04 p0576 A69-14771

Electron fractography techniques and fracture modes in metallic materials interpretation, giving special attenuation to classical fracture replication and shadowing techniques
04 p0619 A69-15395

Qualitative criterion for observing atmospheric turbulence structure by shadowgraph based on medium statistical properties, using ray optics
07 p1183 A69-19650

Mirror image and oblique shadow method forming moire patterns to measure surface topography
08 p1312 A69-20103

Direct electron beam shadowgraph photographic/betagraphy/ technique for recording small high speed objects with 3 nanosecond exposure time
12 p2086 A69-26164

Q switched ruby laser application to high speed shadow photography and holography in study of gas flow around ballistic body
12 p2088 A69-26177

Shadowgraph cinematography technique for testing attenuating influence of symmetrical diaphragm system on shock wave
12 p2088 A69-26184

Shadow, schlieren and interferometric methods for study of transonic, supersonic and hypersonic fields of aerodynamics, using refractivity variations in heterogeneous medium
12 p2060 A69-26934

Plane shock wave propagation around cylinders of various radii recorded with shadowgrams and Mach-Zehnder interferograms, discussing wave diffraction mechanics
18 p3120 A69-34472

Nonequilibrium processes behind shock wave in shock tube supersonic air and nitrogen flow, using photoelectrical shadow method
21 p3695 A69-38961

Shadow photography study of electrical discharge set off by laser spark
21 p3740 A69-39552

Laser shadowgraph technique for visual observation of projectiles surface flying at hypersonic velocity along ballistic trajectory
22 p3963 A69-40601

Stereoscopic shadow caster application to photographic stereoscopic projection for studying binocular stereopsis under kinetic viewing conditions in vision research
22 p3893 A69-40839

SHADOWGRAPHS
U SHADOWGRAPH PHOTOGRAPHY
SHADOWS
NT LUNAR SHADOW
NT PENUMBRAS

Magnetically aligned flows between sunspots, considering Evershed effect on umbrae and penumbrae
10 p1772 A69-22907

Light saturation development of line profile component of normal Zeeman triplet in sunspot umbrae
14 p2528 A69-29964

Combined distribution density of elevations and slopes for illuminated areas of stable statistically

homogeneous random surface exposed to parallel rays beam
15 p2569 A69-30948

Chromospheric inhomogeneities rapid changing properties observable in H and K lines above sunspot umbrae
18 p3204 A69-35389

Umbral chromosphere flashes visual and photometric observations at 5 sec intervals on K line filtergrams using Halle filter
18 p3204 A69-35390

Shadow effects on current-voltage characteristics of solar cell array circuits, developing mathematical models
19 p3254 A69-35709

Cloud masses vertical thickness estimated from study of cloud shadows on satellite TV pictures
19 p3366 A69-36670

Sunspot umbra observed on 21 September 1966, computing transparency in model equaling photosphere transparency at same optical depth
20 p3605 A69-37825

Sunspots microstructure, discussing penumbra and umbral properties with respect to magnetic field configuration
24 p4378 A69-42690

SHAFTS [MACHINE ELEMENTS]
NT TURBOSHAFTS

Numerical solutions of elastic problems by conformal mapping and finite difference method applied to circumferentially grooved shafts in torsion
02 p0346 A69-12419

Numerical solutions elastoplastic torsion of circumferentially grooved shafts based on flow and deformation type theories
02 p0346 A69-12420

Amplitude-frequency characteristics of rotor mounted on hydrostatic bearings calculated by equations of dynamic compliance method
03 p0432 A69-12961

Limiting amplitude of output shaft vibrations of servodrive operated in linear region as function of frequency
04 p0584 A69-15417

Spring supported hydrostatic shaft seal with floating members isolated from structure
[ASME PAPER 68-WA/LUB-9]
05 p0768 A69-16132

Noncontacting torqueometers using magnetoelastic properties of steel shafts, discussing gas turbine and industrial applications
[ASME PAPER 69-GT-64]
09 p1500 A69-22480

Heat treatable low alloy steels weldability for lightweight ultrahigh strength pressure vessels, gear and shaft fabrication in aerospace applications
12 p2100 A69-25827

High speed shafting design for helicopter power transmission systems, discussing shaft in OH-6A Cayuse light observation helicopter
[ASME PAPER 69-DE-5]
14 p2453 A69-28837

Transverse and torsional vibration characteristics of tapered cantilever beams and shafts analyzed by lumped inertia force method
17 p3066 A69-34052

Shaft speed limitations on close clearance seals, using test data on changes in fluid viscosity causing contact and damage
[ASLE PAPER 68-LC-13]
21 p3731 A69-38763

SHAKERS

Equalization of multiple electromagnetic shakers for environmental vibration testing, using analog computer
[JPL-TR-32-1364]
02 p0229 A69-12374

Vibration machine as vibration environment simulation for product reliability testing, analyzing spectrum of acceleration waveforms
12 p2060 A69-26940

Multiple shaker ground vibration test system for confidence in helicopter designs before flight testing and evaluation of force balancers
15 p2585 A69-30357

Reciprocity method for absolute calibration of piezoelectric accelerometer mounted on electrodynamic shaker table
15 p2615 A69-31283

Piezoelectric shaker consisting of combination of damped resonant cylindrical elements for wide frequency calibration of vibration pickups
17 p2975 A69-33665

Machine parts vibration attenuation, discussing input vibration reduction, resonance avoidance, damping, vibrating parts strengthening and shakers
18 p3148 A69-34619

MIL-STD-781A vibration requirements, using mechanical shakers for AGREE vibration testing
22 p3954 A69-40036

SHALES

Normal, isoprenoid, dicarboxylic, keto and various aromatic acids isolated from controlled stepwise degradation of Green River kerogen by successive chromic acid oxidations
15 p2606 A69-31533

Acid fraction extraction of Green River shale identified by gas chromatography-mass spectrometry-computer system, noting trimethyl pentadecanoic acid
21 p3669 A69-38983

SHALLOW SHELL EQUATIONS

Exact solution of shallow shells of revolution equations governing linear deformation compared with asymptotic integration procedure
01 p0166 A69-10234

Shear buckling test data for shallow corrugated webs compared with theoretical analysis with web buckling as orthotropic plate or local mode
01 p0170 A69-10866

Boundary value problems in thin shallow shells of arbitrary planform analyzed by partial differential equations
01 p0171 A69-11071

Existence of smooth solution for system of equations describing nonlinear oscillations of thin plate and shallow shell
02 p0337 A69-11654

Plane shock wave interaction with elastic shallow spherical shell in compressible fluid, formulating equations of motion
02 p0339 A69-11977

Elastic noncircular orthotropic conical shell stress-strain state, obtaining differential equations reducible to integrodifferential equations solvable by iteration
04 p0673 A69-14494

Shallow shell deformations based on nonlinear equations solved by Newton-Raphson iteration
04 p0674 A69-14591

Equations for nonshallow spherical shell deformations derived by Bubnov-Galerkin method
04 p0684 A69-15539

Creep buckling of shallow geometrically nonlinear spherical shell of linear viscoelastic material under constant external load
05 p0831 A69-15679

Bending equations for shallow elastic three layer asymmetric shell with different isotropic layers and transversely isotropic rigid filler at various temperatures
05 p0840 A69-16197

Bending general instability of stiffened shallow orthotropic cylindrical shells, noting buckling stress and application to shell design for various loadings
06 p1022 A69-17369

Stress distribution in shallow spherical shell with smooth cornered rectangular hole or biperiodically arranged set of holes, using computer program
06 p1027 A69-18020

Circular cylindrical spinning shells vibrations by gyroscopically induced inertia loads, formulating equations of motion based on shallow shell theory
07 p1236 A69-19459

Shallow spherical shells equilibrium under uniformly distributed internal pressure, analyzing nonlinear boundary value problems by algorithm
07 p1237 A69-19685

Large deflection behavior of shallow circular arch subjected to vertical point load by nonlinear Rayleigh-Ritz finite element method, discussing deformation path
08 p1411 A69-20140

Stability and bending of flexible plates and shallow shells obeying hereditary relations solved by singular kernel functions
08 p1413 A69-20335

Axisymmetric dynamic snap through critical load analysis for elastic clamped shallow spherical shells, considering impulsive and step loads
09 p1616 A69-21977

Rectangular planform shallow spherical shell stability with mixed boundary conditions, using Cauchy-Riemann equations and equation for plate on elastic base
10 p1792 A69-22848

Stiffness matrix for doubly curved shallow shell element with rectangular plane projection applied to circular cantilevered cylinder and barrel vault
10 p1802 A69-23892

Strength analysis of revolving shallow shell with jumpwise thickness variations under axisymmetric dis-

tributed load, considering rigidity and plastic deformation 11 p1968 A69-24318

Stress concentration during deformations in thin shallow shells, using conformal mapping and difference method 11 p1971 A69-24648

Static and dynamic stability of flexible shallow spherical shell under axisymmetric load and elastically hinged along contours 11 p1976 A69-24763

Thin plastic shell theory based on static and geometrical relations for shallow and circular cylindrical shells 11 p1978 A69-24807

Asymptotic methods for three dimensional equations in thin and thick elastic shell theory for determining two dimensional systems 11 p1978 A69-24810

Plastic analysis of shallow spherical rigid plastic shell, using shell deflection equations to establish load-deflection relationship 11 p1980 A69-24823

Bending and membrane stresses determination in shallow thin shells of revolution under large axisymmetric deflections, using normal and radial displacement relationship [SESA PAPER 1332] 11 p1995 A69-25651

Quasi-shallow shells theory applicability to thin elastic shallow shells, emphasizing use of function W/W_0 12 p2178 A69-26001

Variational method of displacements for calculating positive Gaussian curvature shells with allowance for shear strain, considering shallow shell equations and symmetrical load 12 p2178 A69-26006

Free vibration fundamental natural frequency of shallow shell or dished plate with simply supported square boundary 12 p2179 A69-26211

Symmetrical stressed state of shallow shell with crack edge loading solved in Cartesian coordinates 12 p2181 A69-26614

Shallow hyperbolic paraboloidal shell with large deflections, analyzing nonlinear behavior with numerical method based on integral equations 12 p2185 A69-26820

Elastic buckling and initial postbuckling behavior of clamped shallow spherical shells under axisymmetric load 12 p2187 A69-26842

Stiffness matrix derived for skewed curved shallow shell element with reference to oblique coordinate system 13 p2358 A69-27210

Finite element displacement method extension to include geometric nonlinearity applied to arbitrary plate element, shallow cylindrical shell and shallow hyperbolic paraboloid 13 p2361 A69-27441

Nonlinear Galerkin analysis of curved plate flutter, using shallow shell/von Karman equations and quasi-steady aerodynamic theory 13 p2364 A69-28207

Differential equations for shallow circular spherical shell transformation to equation describing stress-strain state of plate on elastic base 13 p2369 A69-28565

Vibrations of thick walled shallow circular cylinder with thickness change in time, applying dynamic elasticity and Volterra equations 14 p2533 A69-28985

Torsional stability of shallow shells of revolution, solving eigenvalue problem obtained from perturbation of nonlinear equations by finite differences 16 p2871 A69-31879

Linear static deformation and buckling of shallow spherical shells under asymmetric load by solving two dimensional finite difference equations 16 p2871 A69-31897

Stress level reduction in pressurized circular cylinder with circumferential ring stiffener and longitudinal crack, using shallow shell equations 18 p3212 A69-34347

Side force problem for shallow helicoidal shell, shown as static geometric analog of pure bending problem, solved by applying duality [ASME PAPER 69-APM-11] 18 p3213 A69-34387

Regular integral equations solvability for boundary value problems in shallow shell theory, using method of potential representations and Green matrices 18 p3224 A69-35309

Limiting equilibrium of variable thickness shallow spherical and conical shells of revolution under axisymmetric loads, assuming rigid plastic shell material 18 p3225 A69-35370

Transverse oscillations of shallow multilayer shells, using tangential-stress distribution law in determining natural oscillation frequencies in single and sandwich layer panels 19 p3435 A69-35842

Iterative algorithm applied to shell theory boundary value problem of stress concentrations at shallow shell holes 19 p3436 A69-35847

Matrix displacement method of structural analysis applied to dynamic buckling of clamped shallow spherical caps under step pressure loading 20 p3622 A69-37229

Linear hydrodynamic equations describing inviscid fluid flow past thin elastic cylindrical shells in circle with motions described by shallow shell equations 21 p3834 A69-38719

Nonlinear problems involving large deflections of isotropic and orthotropic shallow shells of rectangular planform, deriving partial differential equations for solution 21 p3838 A69-39185

Nonlinear stability of shallow elliptical paraboloidal dome under uniformly distributed compression, solving by Bubnov-Galerkin method on computer 21 p3838 A69-39186

Variational principle applicable to nonlinear theory of shallow shells, deriving potential for equations describing uniform boundary conditions, discussing shell stability 21 p3838 A69-39191

Small curvature effect on prevention of vibration in shallow shells under random loading numerically analyzed for component modes using linear theory 22 p4044 A69-40600

Pairs existence of symmetrical equilibrium forms in nonlinear shallow shell under load made applicable to nonshallow shells equilibrium 22 p4047 A69-41062

Shallow shells two dimensional theory including effects of transverse shear deformation and of moments turning about normal to middle surface 22 p4048 A69-41197

Nonlinear shallow shell theory of stress and strain formulated via shell of revolution problem 22 p4048 A69-41198

Homogeneous equilibrium equations of nonlinear shallow shell theory, obtaining six stress function solutions for strain measures 22 p4048 A69-41199

Stress concentration in shallow spherical perforated shell under loads, reducing boundary value problem to infinite algebraic equations solution 23 p4233 A69-42342

Collapse load of shallow conical shells clamped at base and loaded through finite rigid boss, using Tresca yield condition for sandwich shell 23 p4236 A69-42496

Local stress distribution in cylindrical shells at concentrated load area solved by shallow shell theory 24 p4395 A69-42593

Axisymmetric vibration of shallow spherical caps, using nonlinear dynamic equations and associated variational equation of motion for elastic spherical shells [ASME PAPER 69-APMW-6] 24 p4402 A69-43107

Circular cylindrical photoelastic shells buckling modes under axial compression using high speed isoclinic photography, discussing shallow shell equations applicability to early stages 24 p4404 A69-43652

SHANKS

U JOINTS [JUNCTIONS]

SHANNON INFORMATION THEORY

U INFORMATION THEORY

SHAPED CHARGES

Wedge shaped charge technique for evaluation of detonation hazards of liquid explosives 04 p0646 A69-14479

Hollow charge pyrotechnic circuit closer, noting one piece construction, transportability, safety, quick action and reproducible delay 10 p1635 A69-23030

SHAPES

NT ELLIPTICITY

NT LINE SHAPE

NT ROSETTE SHAPES

NT T SHAPE

Optimal body shape determination by mathematical-mechanical relations derivation, discussing variational problems and variational principles applicability 03 p0526 A69-13739

Elastic rods shape for maximum stability defined by solution of variational problem, assuming noninfinite compressive stresses 05 p0832 A69-15688

Computer analysis for optimizing size and shape of thin walled axisymmetric elastic rings, plates and shells with respect to tension, rigidity and weight 06 p1026 A69-18017

Reading and reliability efficiency comparison in round vs vertical aircraft displays 06 p0883 A69-18025

Hypersonic body shaping for minimum drag and improved performance from view of flight regimes, discussing implications of pressure laws [AIAA PAPER 69-181] 06 p0863 A69-18052

Rotating incompressible liquid drop held together by surface tension noting spheroidal and toroidal shapes, energies and case of surrounding denser medium 07 p1120 A69-19267

Quasi-plane stress in rotating disks of unconventional profile emphasizing conic shaped disk analysis in terms of hypergeometric series 07 p1235 A69-19444

Shape and surface roughness effects on turbulent ablation of reentry body nose tip, noting recession rate [AIAA PAPER 69-717] 17 p2952 A69-33435

Least squares method of smoothing curves or surfaces involving orthogonal base functions, discussing matrices conditioning and structure eigenmodes 18 p3218 A69-34642

Sorting particles by shape using sieving equipment, noting results with crushed gravel 21 p3731 A69-38950

SHARING

U COORDINATION

SHARP LEADING EDGES

Two dimensional flow of incompressible fluid near sharp leading edge of plate at zero incidence, discussing approximation error and friction stress 03 p0415 A69-13651

Kinetic theory of sharp leading edge parallel to supersonic flow using Boltzmann equation, determining flow field 06 p0861 A69-17637

Flow near leading edge of sharp insulated and cooled flat plates, using Monte Carlo direct molecular simulation [AIAA PAPER 69-141] 06 p0866 A69-18208

Leeward side of delta wing with sharp leading edges at hypersonic speeds, noting Prandtl-Meyer expansion [AIAA PAPER 68-675] 09 p1431 A69-21992

Boltzmann equation with BGK model as governing equation for sharp leading edge problem in supersonic flow 11 p1817 A69-24288

Radiated aerodynamic noise effects on boundary layer transition on sharp leading edge hollow cylinders in wind tunnels, noting Reynolds numbers correlation [AIAA PAPER 68-375] 13 p2241 A69-28211

Hypersonic rarefied gas flow past flat plate with sharp leading edge and past circular cylinder, noting wake structure similarity to viscous theory prediction 19 p3294 A69-35755

SHATTERING

U FRAGMENTATION

SHEAR DISTURBANCES

U S WAVES

SHEAR FLOW

Neutrally stable disturbances for nonplanar parallel shear flow with continuously varying mean velocity 03 p0415 A69-13155

Reflectivity of low Richardson number critical levels for internal gravity waves propagating in stably stratified fluids with shear, studying stability numerically 03 p0424 A69-13953

Internal gravity waves propagation in shear flow, detailing interaction stress in incompressible stratified Boussinesq liquid, conservation energy exchange and radiation stress 05 p0788 A69-15721

Quasi-method of characteristics with application to fluid lines with frequency dependent wall shear and heat transfer [ASME PAPER 68-WA/AUT-7] 05 p0750 A69-16181

Compressible combustor turbulent shear flow analysis, discussing eddy diffusivity, density fluctuations, vorticity intensification and turbulent transport [WSCI PAPER 68-27] 06 p1034 A69-17793

Analytical model developed from turbulent shear flow study, discussing Reynolds number effect [AIAA PAPER 69-163] 06 p0914 A69-18139

Mean shear in wall region and outer region of constant pressure turbulent boundary layer 09 p1482 A69-21967

Buoyancy in turbulent shear flow, rotation or streamline curvature effects and meteorological parameters, drawing formal exact algebraic analogy 11 p1870 A69-24894

Direction of maximum turbulent vorticity in turbulent shear flow, determining alignment 11 p1874 A69-25282

Power law profiles of mean wind velocity and temperature in thermally stratified shear flow, considering dependence on thermal stability and Richardson number 11 p1874 A69-25381

Torsional flow of incompressible anisotropic fluid between parallel circular plates rotating with constant angular velocity, showing resemblance to shear flow 12 p2062 A69-26277

Heat and mass transfer conditions in ablation of shear thinning and thickening fluids at stagnation point [ASME PAPER 67-HT-78] 13 p2374 A69-27778

Heat and mass transfer in two dimensional turbulent free shear flows including separated and reattached flows 13 p2377 A69-28145

Incompressible uniform shear flows merging behind trailing edge of semiinfinite flat plate, using inner-outer expansion method based on Navier-Stokes equation 13 p2248 A69-28223

Demixed layer at wall in shear flow of nonsedimenting suspensions with different geometries due to viscous and inertia effect superposition 13 p2251 A69-28498

Model equation for Reynolds stress in turbulent two dimensional shear flow 14 p2428 A69-29000

Drift wave instability due to particle number density gradient of plasmopause, considering velocity shear modification 15 p2595 A69-30096

Wiener-Hermite expansion extended to include time dependent ideal random functions, discussing application to shear flow turbulence 15 p2644 A69-30201

Horizontal shear flow effect on linear geostrophic adjustment in unbounded barotropic fluid, discussing gravity waves, vorticity equations, available energy, etc 15 p2648 A69-30217

Rate equation for effective turbulent viscosity variations, considering effects of generation, convection, diffusion and decay in quasi-parallel shear flows 15 p2591 A69-30905

Lifting surface theory for cascade of blades in subsonic shear flow, determining blade surface pressure distribution, distinguishing shear and uniform flow compressibility effects 16 p2731 A69-31592

Compressible shear flow linear theory applied to transonic flow past thin airfoil, determining pressure distribution, discussing compressibility effects of nonuniform Mach number 16 p2731 A69-31593

Monograph on ring airfoil theory with nonuniform incidence covering steady flow and shear flow transition into boundary value problem of potential theory 17 p2889 A69-32995

Rotating cylinder or vortex motion in shear flow with friction, noting drag and rotor force combined influence 17 p2950 A69-33151

Incompressible turbulent boundary layer analysis by two region characterization for eddy viscosity, using Spalding generalized function and Prandtl free shear flow model 17 p2951 A69-33255

Transverse magnetic field effect on shear turbulence structure of magneto-fluid-mechanic pipe flow with and without heat transfer [AIAA PAPER 69-723] 17 p3012 A69-33497

Displacement of rectangularly mouthed pitot tubes in turbulent tube flow, determining roles of wall and shear effects 17 p2976 A69-34049

Statistical dynamics and structure of turbulent shear flows in incompressible fluids of constant density, discussing Reynolds stress at critical layers 18 p3123 A69-34922

Roshko correlation for estimating vortex shedding from circular cylinder in sheared flow with velocity in Strouhal and Reynolds numbers 20 p3515 A69-37228

Small amplitude acoustic waves propagating in compressible fluid with parallel shear flow and within constant gravitational field 21 p3772 A69-39241

Polystyrene melt tensile viscosity prediction from shearing viscosities, using rheological network rupture theory 21 p3753 A69-39730

Parallel shear flow equilibrium in inviscid nonheat-conducting incompressible fluid with density varying as function of vertical coordinate 21 p3697 A69-39743

Mass injection by strong blowing across Couette-Poiseuille shear flow 24 p4301 A69-43354

SHEAR LAYERS

Turbulent free shear layers in isoeenergetic flow, correlating theory and experiment [ASME PAPER 68-FE-9] 05 p0748 A69-16077

Mixing zone between two dimensional free stream and fluid at rest, measuring turbulent shear layer velocity profile behind rearward facing steps and over cavities [ASME PAPER 68-WA/FE-21] 05 p0749 A69-16097

Boundary shear stress with unknown magnitude and direction measured by yaw probe used as Preston tube 05 p0751 A69-16396

Three dimensional laser Doppler velocity instrument for mean velocity and turbulence measurements in subsonic jet shear layer [SAE PAPER 690266] 09 p1494 A69-21555

Mixing zone between two dimensional free stream and fluid at rest, measuring turbulent shear layer velocity profile behind rearward facing steps and over cavities [ASME PAPER 68-WA/FE-21] 14 p2430 A69-29443

Ideal fluid unsteady rectilinear plane-parallel flow stability, calculating shear layers before breakdown by using modified Rayleigh method 14 p2431 A69-29606

Mean velocity distribution prediction in turbulent shear flows of variable density by coordinate stretching method [AIAA PAPER 68-41] 16 p2770 A69-31888

Shear layer effect on plane sound waves, discussing reflection and refraction at velocity discontinuity between two regions of fluid 17 p3005 A69-32954

Linear normal mode instability of three dimensional laminar and turbulent shear layers, analyzing relations between velocity profile, eddy viscosity and oscillations 22 p3932 A69-40893

Free vertical shear layers structure solutions singularities in rotating fluids, considering motion by rising or spinning axisymmetric body 23 p4153 A69-42356

SHEAR PROPERTIES

Shear accommodation kinking at second order twin bands in critically deformed magnesium investigated for dislocation mechanism 01 p0093 A69-10063

Magnetic shear effect on stability of electron-neutral collision dominated plasma, noting helical perturbations onset 03 p0473 A69-12925

Frequency dependent shear modulus for hexachlorobiphenyl measured under rare gas infusion at 5-25 C and from ambient atmospheric to 4000 psi 05 p0796 A69-15912

Liquid oxygen shear viscosity dependence on temperature and pressure obtained by measuring electrical characteristics of immersed torsional vibrating crystal 05 p0846 A69-15916

Free vibrations of plates and beams of pyrolytic graphite type materials, analyzing transverse shear deformation and rotary inertia [AIAA PAPER 69-55] 06 p1027 A69-18070

Experimental evidence of validity of shear coefficient in Timoshenko beam theory 10 p1801 A69-23538

Rotatory inertia and shear deformation effects on natural frequency and bending mode shape in equations of motion of rotating turbomachine blade [ASME PAPER 69-VIBR-50] 10 p1804 A69-24148

Shear buckling of clamped rectangular linearly tapered plates, considering uniform shear stress and load 13 p2361 A69-27443

Isotropic plate critical strength measurements, evaluating role of material shear modulus 18 p3225 A69-35361

Twisting of spherical shell of nonhomogeneous isotropic material with variable shear modulus and inner surface assumed to be stress free 20 p3619 A69-36911

Complex representation of strain and displacement state in spherical shell using membrane theory, deriving shear forces resulting from single moment loading 21 p3831 A69-38416

Elastic modulus of beta Ti alloy containing Mo, Cr, Fe and Al measured under vibrations and shear modulus determined under torsion 22 p3969 A69-40072

Shearing force and shear buckling deformation influence on supersonic panel flutter boundary of simply supported rectangular plates, basing analysis on deflection approximation 24 p4400 A69-43055

SHEAR STRAIN

Shear buckling test data for shallow corrugated webs compared with theoretical analysis with web buckling as orthotropic plate or local mode 01 p0170 A69-10866

Elastic stability equations solved in geometrical linearization for thin anisotropic plates under transverse shear, using variational method 03 p0525 A69-13130

Compatible triangular plate elements for normal and in-plane displacements, discussing nine degree of freedom element, strain energy, simply supported and clamped plates 04 p0677 A69-14742

Plane shear strain measurement by means of properly oriented strain gages on surface and proper disposition of gages in Wheatstone bridge circuit 04 p0603 A69-15498

Sign conventions definition and importance for shear stress and strain analysis in laminated anisotropic composite materials, noting role in studying response 07 p1170 A69-18720

Optimal design of circular cylindrical sandwich shells under pressure and shear loads, showing acceptability of small shear coefficient values 08 p1416 A69-20722

Elastic bending moments and shear forces uniformly loaded flat plate structures with rectangular symmetry, using collocation technique and complex variable methods 11 p1986 A69-25241

Variational method of displacements for calculating positive Gaussian curvature shells with allowance for shear strain, considering shallow shell equations and symmetrical load 12 p2178 A69-26006

Torsional oscillation of cylindrical shell of nonhomogeneous material under periodic shearing force 13 p2361 A69-27462

Plastic flow anisotropy and texture shifting by rolling in Ti-Mo-V alloy, analyzing slip rotation, grain boundary shear and deformation mode 17 p2987 A69-33078

Transverse shear deformation and rotatory inertia effects on large amplitude lateral free vibrations of transversely isotropic plates [ASME PAPER 69-APM-10] 18 p3213 A69-34386

Strain displacement and compatibility equations of finite symmetrical deflections of thin shells of revolution [ASME PAPER 69-APM-14] 18 p3214 A69-34391

Flanges flexural rigidity effect on load carrying capacity, failure mechanism and postbuckling behavior of webs in shear, noting permissible load 18 p3227 A69-35492

Shallow shells two dimensional theory including effects of transverse shear deformation and of moments turning about normal to middle surface 22 p4048 A69-41197

SHEAR STRENGTH

Shear strengths of polyimide and polybenzimidazole resin/fiberglass reinforced honeycomb materials compared to previous high temperature materials, noting lightweight sandwich aircraft structures 04 p0620 A69-14844

Shear strength of grossly deformed solids noting extrusion and opposed anvils techniques 04 p0631 A69-15465

Large displacement bending of rods for constant deformation cross section, negligible shearing forces and exponential stress-strain relation 05 p0843 A69-16682

Multidirectional boron-epoxy laminates shear strengths and elastic moduli, calculating in-plane tension and compression 08 p1337 A69-20484

High modulus and high strength carbon fibers and composites, discussing mechanical properties and interlaminar shear strength
08 p1338 A69-20488

Three dimensional reinforcement composites for gear and bearing applications with improved interlaminar shear strength, thermal and wear properties
08 p1340 A69-20509

Dislocation model of strength of elastically inhomogeneous crystalline materials based on elastic interactions between dislocations and periodic fluctuations of shear modulus
08 p1333 A69-20557

Finite control volume approach to shock Hugoniot in unidirectional fiber reinforced composite, computing shear force along matrix-fiber interface
[AIAA PAPER 69-359] 13 p2366 A69-28292

W shear moduli at high temperatures measured by forced torsional vibration in wide frequency ranges, discussing grain boundary effects
14 p2465 A69-29651

Interlaminar shear strength development for utilization of unidirectional strength and stiffness of graphite fibers, discussing epoxy resin-fiber interface improvement
15 p2642 A69-30312

Atmospheric wind shear velocity snapping effect on yarn suspending instrument package from balloon gondola during parachute recovery
17 p2975 A69-33613

Craze formation and shear yielding considered for glassy polymers in terms of stress field requirements
17 p2993 A69-34169

Low temperature adhesive shear tests to measure force to break ice away from stainless steel surfaces coated with various bonded solid lubricants
19 p3323 A69-35581

Lap-shear strengths of Mg-Al alloy bonded with nylon-epoxy adhesive, including anodized coating rolling schedule and honeycomb core fabrication
24 p4323 A69-43417

SHEAR STRESS

NT TORSIONAL STRESS

Off-axis test for hard orthotropic composite materials, discussing fixture design to reduce shear coupling effect
01 p0103 A69-11273

Turbulent boundary layer growth, pressure distributions and surface shear stresses on yawed semiangle cone
[AIAA PAPER 68-98] 02 p0190 A69-12526

Compressible and incompressible laminar boundary layer with constant wall shear stress, using initial profiles
02 p0233 A69-12535

Second normal stress difference measurement by annular flows, giving approximate method for experimental data inversion
02 p0234 A69-12604

Active cooling systems for high performance reentry vehicles in thermal and shear stress environments
[AIAA PAPER 68-1154] 03 p0533 A69-13669

Turbulent fluctuations of viscous sublayer of two dimensional flow, assessing wall shear stress spectrum
04 p0587 A69-14544

Reynolds number similarity argument, establishing relation between mean velocity at pipe or channel center and shear stress at wall
04 p0589 A69-14895

Dynamic shear stresses at interface of embedded thin elastic filament and elastic matrix after subjecting filament to concentrated longitudinal line load
05 p0831 A69-15577

Velocity fields and wall shear stress distributions in eccentric annuli
[ASME PAPER 68-WA/FE-35] 05 p0750 A69-16108

Tension stress and shearing strain vs time for simultaneous stress relaxation and creep in polyurethane
[ASME PAPER 68-WA/APM-8] 05 p0839 A69-16186

Boundary shear stress with unknown magnitude and direction measured by yaw probe used as Preston tube
05 p0751 A69-16396

Statically indeterminate elastoplastic problem under condition of complex shear
05 p0843 A69-16691

Boundary layer on flat plate with homogeneous suction, discussing dimensionless displacement/ momentum thickness and wall shearing stress
05 p0752 A69-16744

Three layer structure theory, discussing thin elastic sandwich shells with middle layer susceptible to transverse shear
06 p1025 A69-17615

Pressure distribution, heat transfer rates and shear stresses in laminar boundary layer of supersonic viscous flow incident on corner point of body
06 p0861 A69-17641

Sign conventions definition and importance for shear stress and strain analysis in laminated anisotropic composite materials, noting role in studying response
07 p1170 A69-18720

Laminar and turbulent stresses in plane asymmetric incompressible flows analyzed based on Boussinesq formula for turbulent shear stresses
07 p1121 A69-19330

Shear stress at wall, averaged velocity field and turbulent heat transfer coefficients in straight smooth non-circular channels used to compute temperature fields
07 p1243 A69-19734

Subgrain diameter relation to misorientation in melt-grown aluminum single crystals from etch pitting and X ray techniques, discussing critical shear stress
08 p1330 A69-20011

Finite elements for analysis of flexible shells, considering Kirchhoff theory for transverse shear deformation and problems involving rotations and buckling
08 p1411 A69-20142

Fiberglass reinforced plastic plates strength coupled to elastic base with allowance for tangential shearing stresses
08 p1412 A69-20334

Wall friction influence on three dimensional flow in axial flow turbomachines, introducing shear stresses between flow planes
08 p1252 A69-20724

Approximation method applied to closed viscous streamline flow in rectangular cavity, discussing constant shear stress boundary condition
08 p1304 A69-20811

Conformal mapping method for flexure function determination, discussing shear coefficients for arbitrary cross section beams in Timoshenko beam theory
09 p1612 A69-21611

Bond shear effects on dynamic behavior of two layered cylindrical shell, identifying bond stiffness parameters
[AIAA PAPER 68-354] 09 p1616 A69-21941

Shear field pattern theory modified to apply to determination of sweptback wings, calculating stress development
10 p1801 A69-23645

Nodal lines shape in individual flats for long plates in combined shear and compression with sinusoidal edge rotations in longitudinal direction
11 p1983 A69-25137

Buckling of long flat panel in combined compression and shear with sinusoidal edge moments and support on two edges and on point supports
11 p1984 A69-25138

Tresca shear stress fatigue failure criterion and experimental data for combined bending and torsion acting out of phase
11 p1984 A69-25140

Shear buckling of simply supported infinitely long plates orthogonally reinforced by stiffeners with flexural and torsional rigidity
11 p1984 A69-25142

Floating element skin friction meter designed for adverse pressure gradients, discussing wall shear stress measurement
11 p1889 A69-25557

Torsional shearing stress in thick walled hollow rectangular cross sections
13 p2358 A69-27212

Stress and plastic deformation influence on allotropic transformation of cobalt-nickel single crystals studied by X ray diffraction
13 p2279 A69-27761

Wall shear stress measurement by evaporating liquid film, determining optimum liquid viscosity
13 p2375 A69-27793

Shear stress and velocity profile in MHD duct, examining turbulence damping by electromagnetic coupling
13 p2309 A69-28024

Tension stress and shearing strain vs time for simultaneous stress relaxation and creep in polyurethane
[ASME PAPER 68-WA/APM-8] 13 p2362 A69-28121

Plane elastoplastic shock waves propagation due to combined shear loadings assuming elastic isotropic work hardening materials
13 p2368 A69-28346

Buckling of unsymmetric cross-ply rectangular plates under uniform shear, considering hinge support boundary conditions
13 p2371 A69-28679

Stress concentration around rhombic hole in nonlinear isotropic plate under pure shear
14 p2533 A69-28987

Turbulent boundary layer in corner, measuring velocities, wall shear and turbulent normal stresses by employing momentum integral and similarity analyses
14 p2431 A69-29576

Mixing length model to relate turbulent shear stress to mean velocity field within planetary boundary layer above surface roughness change
17 p2997 A69-33154

Shear modulus of fiberglass reinforced plastics determined from torsional tests on squared beam of orthotropic material, evaluating influence of end conditions
17 p3058 A69-33204

Normal stress effects in viscoelastic fluid theories applied to one dimensional Burgers model of weak turbulence predicting drag reduction
17 p2951 A69-33256

Chemical species flux decay in turbulent boundary layer with catalytic wall, obtaining solution of conservation equation by using shear stress distribution
[AIAA PAPER 69-709] 17 p2955 A69-33480

Thin circular ring stability under uniform external transverse loading at various angles, discussing transverse shear deformation effects and buckling
17 p3061 A69-33707

Shear stress theory of fatigue failure of ductile materials based on crystallographic orientation and probability of slip of neighboring crystals
18 p3211 A69-34344

Plane wave propagation due to combined compressive and shear stresses in half space, assuming elastoplastic material
[ASME PAPER 69-APM-12] 18 p3213 A69-34388

Electrohydrodynamics of fluids having uniform electrical properties, emphasizing shear effects for interfacially confined electromechanical coupling
18 p3123 A69-34919

Higher harmonic pitch angle inputs to eliminate oscillatory helicopter blade root shear determined through teetering rotor model
18 p3089 A69-35233

Long term stability of orthotropic cylindrical shells under transverse shear stresses, calculating critical stress using Kirchhoff-Love model
18 p3225 A69-35357

Microstresses in hollow-fiber reinforced cylindrical shell under longitudinal shear stress, determining modulus of elasticity and optimum component ratios
18 p3225 A69-35369

Skin friction balance in Mach 5 wind tunnel with high heat transfer, measuring shear forces
19 p3292 A69-35734

Skin friction balance for shear stress measurements in presence of ablation, describing balance construction, calibration, flexure range, etc
19 p3292 A69-35735

Molybdenum single crystals deformation in direct shear, determining stress temperature dependence and critical regions for various slip systems
19 p3342 A69-35811

Structural flexure center position from shear stress analysis showing nondependence on Poisson ratio
20 p3622 A69-37213

Transverse shear deformation effect on bending of laminated rectangular plates, obtaining solutions for bending deflections, flexural vibration frequencies and buckling loads
20 p3627 A69-37770

Active cooling systems for high performance reentry vehicles in thermal and shear stress environments
[AIAA PAPER 68-39016] 21 p3851 A69-39016

Buckling stability of thin cylindrical shell under torsion, allowing for finite displacements due to shear in initial stress-strain state
21 p3838 A69-39187

Photoelastic data analysis for stress separations, discussing shear slope and Tesar methods
21 p3843 A69-39316

Sandwich beams interlaminar shear stress calculations, considering roles of moduli of elasticity and layers thickness relative to beam
22 p4041 A69-40080

Dynamics of viscous electrically charged gas using Navier-Stokes equation
22 p3931 A69-40686

Limiting load of square plate subjected to shear and reinforced by vertical stiffener, computing membrane and bending stresses as function of flexural rigidity
24 p4399 A69-42967

- Interlaminar shear stresses in cross-ply three ply symmetric laminated composite plate, analyzing interlaminar stress distribution under simple tension
24 p4399 A69-43052
- Real shear modulus and mechanical damping characteristics of cured adhesives measured for temperature effect, using torsion pendulum apparatus
24 p4338 A69-43460
- Transverse shear influence on circular plates small displacement theory determined from coupled linear partial differential equations of plates
24 p4405 A69-43655
- Shear stress and free molecular drag for gas flow along concave cylindrical surface oriented at angle of attack, analyzing multiple surface collisions effect
24 p4249 A69-43660
- SHEAR WAVES**
U S WAVES
- SHEARING**
Skin friction measurement in aerodynamic tests using thin liquid crystal coatings with changes in maximum light scattering wavelength in response to shearing forces
14 p2427 A69-29029
- Stiles-Crawford effect measurements before and following eye movements to determine retina shearing during eye movements
15 p2555 A69-31035
- SHEARING STRESS**
U SHEAR STRESS
- SHEATHS**
U ION SHEATHS
U PLASMA SHEATHS
- SHEDDING**
Vortex shedding and wake formation behind inclined flat plate at low Reynolds number, using dye injector method for streak line observation
16 p2768 A69-31767
- Narrow band vortex shedding from circular cylinder in critical Reynolds number range, noting increase in Strouhal number
21 p3644 A69-38690
- Vortex shedding from circular cylinders rotating normal to free stream velocity, studying roles of rotation rate and Reynolds number
24 p4248 A69-43601
- SHEEP**
Myocardial muscle fibers transient inward current components during sheep ventricle voltage clamp analysis
23 p4095 A69-42080
- SHEET METAL**
U METAL SHEETS
- SHELL STABILITY**
Circular, cylindrical thin walled shell dynamic response to moving shock solved by Flugge equations in series form
01 p0164 A69-10057
- Exact solution of shallow shells of revolution equations governing linear deformation compared with asymptotic integration procedure
01 p0166 A69-10234
- Thin cylindrical shell deformation and stress under concentrated radial loading, analyzing singularity at load point
01 p0166 A69-10301
- Galerkin method for solving dimensionless Reissner equation for symmetrically loaded thin nonshallow shells of revolution
01 p0168 A69-10380
- Sheba family of shell elements for matrix displacement method applied to problems of thin shells under membrane and bending action
01 p0170 A69-10865
- Shear buckling test data for shallow corrugated webs compared with theoretical analysis with web buckling as orthotropic plate or local mode
01 p0170 A69-10866
- Critical internal pressure induced plastic instability in membrane shells of revolution determined by graphical numerical method
02 p0338 A69-11719
- Existence and uniqueness of weak solutions in linear theory of stable equilibrium position for inhomogeneous elastic thin walled shells
02 p0340 A69-12036
- Critical points separating stable and unstable branches of equilibrium curve of nonlinear elastic systems, discussing flexible shallow conical shell in temperature field
02 p0341 A69-12256
- Multilayered shells equivalence to single layer shells for stress analysis, vibrations and stability
02 p0346 A69-12509
- Orthotropic stiffened multilayer circular cylindrical shells buckling under axial compression, lateral pressure, etc
02 p0346 A69-12510
- Matrix displacement method for nonlinear elastic analysis of shells of revolution under symmetrical and asymmetrical loadings
02 p0346 A69-12511
- Buckling of electroformed thin conical shells under hydrostatic pressure, proving theory for cones of large taper ratio
02 p0347 A69-12515
- Recent advances in shell buckling, discussing imperfection sensitivity, boundary conditions and wall configuration [AIAA PAPER 68-103]
02 p0347 A69-12516
- Elastic-plastic and creep deformation calculations of cylindrical shell, providing better estimate of critical time at higher stress levels by including plasticity
02 p0348 A69-12539
- Imperfection sensitivity of axially compressed stringer stiffened cylinder analysis via shell equations formulation using finite differences
02 p0348 A69-12542
- Finite difference schemes for axisymmetric oscillations of shells of revolution filled with liquid
03 p0523 A69-12951
- Unreinforced circular cutouts effects on buckling behavior of circular cylindrical shells under axial compression, using photoelastic plastic shells
03 p0523 A69-12988
- Creep buckling of circular cylindrical shells under axial compression and bending, using Al alloy test specimens
03 p0523 A69-12995
- Helicoidally symmetrical stress in cylindrical thin shells
03 p0529 A69-14056
- Compressed cylindrical shell stability analyzed on basis of axisymmetric equilibrium form, noting dependence on mechanical characteristics and geometry
04 p0667 A69-14265
- Impulse buckling threshold for elastic-plastic cylinder with elastic core after development of unstable motion
04 p0671 A69-14414
- Circular cylindrical isotropic shell deformation rate under dynamic axial load described by second order linear differential equation
04 p0673 A69-14499
- Thin shells deformations described by finite element model accounting for transverse shear deformations
04 p0674 A69-14588
- Shallow shell deformations based on nonlinear equations solved by Newton-Raphson iteration
04 p0674 A69-14591
- Buckling equations for orthotropic cylindrical shells with eccentric spiral stiffeners derived through variation method of total potential
04 p0676 A69-14710
- Nonlinear boundary value problem of elastokinetics solved by step-by-step integration to study thin walled shells stability under axial impact [DVL-853]
04 p0677 A69-14836
- Postbuckling equilibrium calculation for pressure loaded thin walled cylinders of finite length, using Donnell nonlinear shell theory
04 p0677 A69-14837
- Stability of circular cylindrical viscoelastic and elastic shells with local effects due to radial load on circumference or thermally induced tangential stress
04 p0680 A69-14928
- Smooth cylindrical shell stability under axial compression noting effects of scale factor, initial defects, initial stresses and deflections in welded seam, etc
04 p0680 A69-14929
- Reissner nonlinear equations for nonshallow symmetrically loaded shells of revolution
04 p0684 A69-15538
- Equations for nonshallow spherical shell deformations derived by Bubnov-Galerkin method
04 p0684 A69-15539
- Creep buckling of shallow geometrically nonlinear spherical shell of linear viscoelastic material under constant external load
05 p0831 A69-15679
- Elastic stability of thin circular cylindrical shell with elastic core, longitudinal and transverse reinforcement ribs, initial defects and under large strains
05 p0832 A69-15691
- Elastic stability of thin circular cylindrical shell with elastic core, longitudinal and transverse ribs and initial defects under combined pressure and thermal stress
05 p0832 A69-15692
- Stresses in cylindrical shell with elastic core loaded on curved surface solved, using elasticity theory for core and membrane solutions for shell
05 p0835 A69-15871
- Critical axisymmetric loads for instability in orthotropic multilayer conical shells obeying Hooke law under axial compression or external pressure
05 p0840 A69-16198
- Stability of thin cylindrical shells of medium length with one or both ends rigidly clamped
05 p0840 A69-16199
- Annular stress in rib reinforced cylindrical shells under axial compression load and internal pressure, using successive approximation
05 p0841 A69-16208
- Stability of three layer cylindrical shell in gas stream, analyzing oscillation mode and critical flutter dependence on filler resistance to transverse shear
05 p0843 A69-16683
- Stability of Al-Mg alloy spherical shells under uniform external pressure beyond elastic limit
05 p0843 A69-16693
- Calculation of thin shell or beam structures with plasticity and isothermal creep based on linearization and local kinematic behavior [ONERA-TP-667]
06 p1020 A69-17099
- Stability loss of shells of revolution under effect of axial compression and radial pressure with no restrictions on generatrix curvature, using strain energy method
06 p1021 A69-17179
- Axisymmetric form of stability loss of cylindrical shell under effect of axial load suddenly applied along generatrix, considering inertia forces and obtaining differential equations
06 p1021 A69-17181
- Oscillations of cylindrical orthotropic three layer shell having ideal fluid flow at variable rate, establishing parametric resonance and determining limits of shell motion instability regions
06 p1022 A69-17186
- Bending general instability of stiffened shallow orthotropic cylindrical shells, noting buckling stress and application to shell design for various loadings
06 p1022 A69-17369
- Buckling of elastic cylinders with rectangular cutouts and reinforcements under axial or lateral loading, using modified Newton method [AIAA PAPER 69-92]
06 p1027 A69-18060
- Radial vibrations of thin cylindrical shells subjected to thermal loadings, discussing temperature distributions, thermal stresses and natural frequencies [AIAA PAPER 69-59]
06 p1028 A69-18143
- Initially imperfect axially compressed cylindrical shells strength using variational principle, shell theory and deformation theory of plasticity [AIAA PAPER 69-91]
06 p1028 A69-18181
- Initial geometric imperfections effect on buckling and postbuckling behavior of laminated composite cylindrical shells under axial compression, considering reinforcing fiber orientations
06 p1029 A69-18194
- Elastic stability of three dimensionally reinforced composite cylindrical shells [AIAA PAPER 69-122]
06 p1029 A69-18216
- Supercritical elastic states of closed spherical shell
07 p1232 A69-18934
- Mathematical formulas for rigidity distribution of inhomogeneous multilayer shells, discussing invariance property
07 p1232 A69-19011
- Rupture times in analysis of creep tensile instability in uniformly pressurized thin walled membrane shells of revolution, comparing two criteria
07 p1234 A69-19378
- Shallow spherical shells equilibrium under uniformly distributed internal pressure, analyzing nonlinear boundary value problems by algorithm
07 p1237 A69-19685
- Local stability of thin walled elastic shells of revolution subjected to external pressure
07 p1237 A69-19686
- Stability of cylindrical shell reinforced by circular ribs under combined action of external pressure and axial forces, using characteristic equation
07 p1238 A69-19687
- Stability of cylindrical shells under concentrated annular loads using finite difference method, discussing critical loads, moments and errors
07 p1238 A69-19688
- Large deflection behavior of shallow circular arch subjected to vertical point load by nonlinear Rayleigh-Ritz finite element method, discussing deformation path
08 p1411 A69-20140

Finite elements for analysis of flexible shells, considering Kirchhoff theory for transverse shear deformation and problems involving rotations and buckling
08 p1411 A69-20142

Creep buckling stability of shells, with emphasis on stress and strain states and critical time, considering circular cylindrical shell
08 p1411 A69-20143

Stability of finitely deformed thin cylindrical shell of rubberlike material, showing bending resistance and thickness effects
08 p1413 A69-20414

Variational method for safety limits of perfectly plastic simply supported conical sandwich shells subjected to uniform internal pressure and obeying Mises yield criterion
08 p1416 A69-20702

Optimal design of circular cylindrical sandwich shells under pressure and shear loads, showing acceptability of small shear coefficient values
08 p1416 A69-20722

Two layer cylindrical shells stability under external pressure, assuming nonuniform shell rigidity
08 p1419 A69-21180

Stress-strain problem of geometrically nonlinear conical shell subjected to creep, giving method for complex deformation solution
09 p1612 A69-21497

Multilayer orthotropic cylindrical shells stability under distributed external load and off-center compression, analyzing subcritical deformation on critical load
09 p1613 A69-21685

Surrounding fluid effects on free axisymmetric vibrations of thin elastic spherical shells, studying irrotational motions in compressible and incompressible ideal fluids
09 p1613 A69-21720

Accuracy of approximations using shell equations for predicting dynamic behavior of thin cylindrical shells, with exact solutions from Flugge shell equation [AIAA PAPER 69-447]
09 p1616 A69-21938

Buckling of cylindrical and conical sandwich shells with fiberglass/epoxy facings and aluminum honeycomb cores [AIAA PAPER 68-294]
09 p1616 A69-21942

Buckling of eccentrically stiffened thin circular cylindrical shell under uniform combined axial compression and torsion loads with lateral pressure
09 p1616 A69-21955

Buckling capabilities of inflation rigidized wire film and shell film cylinders in axial compression and bending
09 p1617 A69-21997

Supercritical elastic states in convex shells produced by load in presence of thermal flux, noting no flux effect on states
09 p1617 A69-22078

Pressure on unsteadily oscillating cylindrical shell in external or internal supersonic flow derived from asymptotic theory
09 p1618 A69-22256

Linear theory of cylindrical panel buckling and circumferential restraint along straight edges under lateral pressure, using Donnell equations
09 p1621 A69-22782

Rectangular planform shallow spherical shell stability with mixed boundary conditions, using Cauchy-Riemann equations and equation for plate on elastic base
10 p1792 A69-22848

Axisymmetric free edge buckling of semiinfinite heterogeneous orthotropic cylindrical shells in axial compression, noting stability condition
10 p1802 A69-23889

Vibration characteristics of circular cylindrical shells containing water under axial excitation, investigating bubble formation and shell-fluid interaction [ASME PAPER 69-VIBR-4]
10 p1805 A69-24162

Strength analysis of revolving shallow shell with jumpwise thickness variations under axisymmetric distributed load, considering rigidity and plastic deformation
11 p1968 A69-24318

Stress concentration during deformations in thin shallow shells, using conformal mapping and difference method
11 p1971 A69-24648

Static and dynamic stability of flexible shallow spherical shell under axisymmetric load and elastically hinged along contours
11 p1976 A69-24763

Postbuckling behavior and subsequent imperfection sensitivity of thin walled cylinders subjected to torsion, considering perturbation
11 p1979 A69-24814

Thin walled circular cylinders postbuckling behavior and stability under axial compression calculated for design loads
11 p1979 A69-24816

Nonlinear shell theory, determining elastic deformation as function of stress under external loads using Lagrange variational principle
11 p1979 A69-24817

Semiinfinite circular cylindrical shell buckling under axial load, computing forces, moments and displacements by thin shell equation
11 p1979 A69-24818

Incremental collapse of shells under cyclic loadings in terms of generalized variables, finding interaction surfaces of load multipliers
11 p1980 A69-24820

Deformation processes of geometrically nonlinear rotational membrane shells under internal pressure
11 p1980 A69-24821

Permanent displacement relationship to shell thickness following snap-through of loaded rigid boss in spherical metal shell
11 p1980 A69-24822

Plastic analysis of shallow spherical rigid plastic shell, using shell deflection equations to establish load-deflection relationship
11 p1980 A69-24823

Stress analysis of reinforced cylindrical shells under external loading, using Vlasov semimomentless theory
11 p1982 A69-24949

Deformations and stresses in pressure vessel with elliptical cross section under uniform internal pressure, noting radial deflection and membrane, bending and skin stress
11 p1983 A69-25023

Thin elastic conical shells asymmetric deformation under stresses and strains, deriving asymptotic solution
11 p1983 A69-25090

Analytical expressions for Gaussian constraint of continuum, using continuity conditions as equations of internal geometric couplings
11 p1984 A69-25170

Optimal parameters selection for rib-reinforced cylindrical shells determined with respect to axial critical loading magnitude
11 p1985 A69-25173

Stress-strain state of shells with opposite edges hinged and rigidly clamped solved by numerical method after reduction to boundary value problem
11 p1985 A69-25174

Bending and membrane stresses determination in shallow thin shells of revolution under large axisymmetric deflections, using normal and radial displacements relationship [SESA PAPER 1332]
11 p1995 A69-25651

Glass fiber reinforced plastics shells stability under external hydrostatic pressure, discussing compression and axial tests for normal elastic modulus, shear modulus and Poisson coefficient
11 p1995 A69-25681

Stochastic problems in thin elastic shell theory solved by equations obtained by linearizing shell equations near initial state of stress
11 p1996 A69-25732

Composite shell carrying capacity under general load, studying closing shape between laminate layers, transverse contraction, supporting layers thicknesses ratio, etc
12 p2176 A69-25851

Quasi-shallow shells theory applicability to thin elastic shallow shells, emphasizing use of function W/δ
12 p2178 A69-26001

Variational method of displacements for calculating positive Gaussian curvature shells with allowance for shear strain, considering shallow shell equations and symmetrical load
12 p2178 A69-26006

Dynamic programming method for upper bound on collapse load of rotationally symmetric thin cylindrical shell under ring loading
12 p2179 A69-26214

Postcritical deformations of thin conical elastic shells hinged along edges under external pressure using Pogorelov method for cylindrical shells
12 p2181 A69-26609

Optimal additional loading at zero moment stress-strain state in simply connected shell of complex design under external loads, using successive approximation
12 p2181 A69-26610

Symmetrical stressed state of shallow shell with crack edge loading solved in Cartesian coordinates
12 p2181 A69-26614

Galerkin method for solving dimensionless Reissner equation for symmetrically loaded thin nonshallow shells of revolution
12 p2182 A69-26679

Natural frequencies of ring-stiffened thin walled cylindrical shell determined by partial differential equations of motion, allowing for eccentricity
12 p2184 A69-26810

Complex two layered shell of revolution under static and dynamic asymmetric loads analyzed using SABOR/DRASTIC computer codes
12 p2184 A69-26811

Large deflection elastic-plastic analysis of axisymmetric shells of revolution indicating role of plastic yielding in buckling pressure reduction
12 p2186 A69-26839

Elastic buckling and initial postbuckling behavior of clamped shallow spherical shells under axisymmetric load
12 p2187 A69-26842

Buckling and postbuckling equilibrium behavior of fiber reinforced cylindrical shell under uniform axial compression
12 p2187 A69-26843

Stress distributions in two normally intersecting cylindrical shells subjected to internal pressure, using Donnell and Flugge equations
13 p2359 A69-27255

Dynamic response of imperfect circular cylinder to constant velocity load, noting applicability of Hoff nonlinear equation for dynamic buckling of columns
13 p2359 A69-27260

Axisymmetric plastic buckling of complete spherical shells subjected to external hydrostatic pressure
13 p2361 A69-27439

Torsional oscillation of cylindrical shell of non-homogeneous material under periodic shearing force
13 p2361 A69-27462

Astronomical model explaining shell instability of Pleione /28 Tauri/ extended atmosphere, discussing magnetic field amplification by differential rotation to explosive dissipation in 9.16 years
13 p2347 A69-27716

Bending state of shells of revolution due to edge effects using nonlinear stress strain relation
13 p2362 A69-27921

Imperfection surface effect on buckling load of circular cylindrical shell under axial compression, locating limit points of postbuckled states
13 p2362 A69-28122

Elastoplastic cylindrical shell instability determination under axial compression applied to inelastic solids
13 p2363 A69-28124

Stressed state of cylindrical circular shell clamped at edges and subjected to concentrated radial forces
13 p2368 A69-28322

Infinite cylindrical shell stability under circular load solved by linearization about bending moment stress state and Galerkin method
14 p2531 A69-28808

Orthotropic cylindrical shell stability under uniform axial compression and internal pressure, taking into account subcritical state duration
14 p2532 A69-28981

Geometric discrepancies influence on stability modes and loads for thin shells up to point of pcollapse
14 p2533 A69-29022

Heterogeneous orthotropic circular cylindrical shell stability during axial critical compression
14 p2533 A69-29024

Zero-moment cylindrical meshed shell equilibrium equations, discussing solution methods and difference analog
14 p2536 A69-29473

Elastic deformations of spherical sandwich shell of rigidly connected isotropic homogeneous layers, describing shell symmetrical expansion and inversion under stresses
15 p2707 A69-30582

Bending surface of shells under crosswise load analyzed by moire method, considering rotating cylindrical surfaces
15 p2713 A69-31056

Reinforced cylindrical shell stability under external compression load by pressurized air, determining critical pressure
15 p2715 A69-31204

Torsional stability of shallow shells of revolution, solving eigenvalue problem obtained from perturbation of nonlinear equations by finite differences
16 p2871 A69-31879

Prebuckling deformations influence on circular cylindrical shell buckling under external pressure, applying Galerkin method to Donnell equations 16 p2872 A69-31905

Buckling load of cylindrical shell with inclined stiffeners, using method for stability of thin walled cylinder under transverse end load at free end 16 p2872 A69-31912

Axially symmetric vibrations of thin elastic spherical shell partially filled with liquid, considering shell as joined hemispheres with or without same thickness 16 p2873 A69-32129

Heated cylindrical shell with braces subjected to given compression and internal pressure, having elastic beams along edges, analyzing local deformations effect on shell strength and stability 16 p2873 A69-32131

Eigenvalues of truncated orthotropic shells of revolution with degenerate poles and various rigidities and geometries 16 p2873 A69-32133

Cylindrical shell aeroelastic dynamic stability subjected to supersonic flow field, considering geometric imperfections, edge constraint and prestability deformation [AIAA PAPER 68-285] 16 p2874 A69-32159

Elastic spheroidal shell of revolution under external pressure described by buckling and postbuckling theory 16 p2874 A69-32162

Oscillations and stability of cylindrical shell in gas flow taking into account inertia forces 16 p2875 A69-32287

Transient wave processes of deformation in spherical shell under load abruptly applied to geometrical pole 16 p2875 A69-32288

Compressibility of material in stability problems of elastoplastic plates and shells 16 p2875 A69-32292

Stresses in perforated ribbed cylindrical shell subjected to internal pressure using brittle coating, electrical strain gages, photoelasticity and micrometers 16 p2876 A69-32784

Free vibrations of thin truncated circular conical shell and reinforcing rings and stringers, determining resonant frequencies for stiffened and unstiffened configurations 17 p3051 A69-32955

Damped vibrations of elastic open cylindrical shell under arbitrary loading, obtaining mean square of bending from correlation theory 17 p3054 A69-33094

Nonaxisymmetric stability loss /buckling/ of closed toroidal shell of circular cross section under uniformly distributed external pressure, considering Volmir linear theory 17 p3055 A69-33130

Critical buckling stress for cylinders wound with fiber reinforced plastics /FRP/, establishing stability criteria for fiber reinforced shells 17 p3058 A69-33430

Nonlinear flexural vibrations excitation in cylindrical shell by longitudinal harmonic load, discussing solution of partial differential equations of motion 17 p3064 A69-33920

Cylindrical aluminum shell dynamic stability, analyzing steady state parametric oscillations, mode shape, frequency, amplitude and damping 17 p3065 A69-33929

Longitudinal crack in cylindrical shell under internal pressure, calculating normal and bending stress singularity strengths against curvature/ cracklength parameter 18 p3212 A69-34346

Circular cylindrical shell nonlinear response to uniform radial impulsive pressure, noting inextensionality constraint and equations of motion roles [ASME PAPER 69-APM-26] 18 p3214 A69-34399

Toroidal, spherical and conical shells limiting equilibrium under various loading and support conditions 18 p3216 A69-34572

Local stability of viscoelastic shells of revolution under axisymmetric loads, discussing asymmetric snapthrough of dome 18 p3216 A69-34573

Cantilever truncated conical shell stability under tensile stresses solved by strain energy technique 18 p3216 A69-34574

Stability of thin walled eccentrically reinforced cylindrical shell, determining eccentricity influence and critical pressure formula from considerations of Poisson ratio, reinforcement parameters, etc 18 p3216 A69-34576

Cylindrical shell stability under axial compression, studying buckling process and wave formation 18 p3217 A69-34597

Growth rate of stability loss intrinsic modes in elastic shells under severe load, discussing stress distribution during buckling 18 p3217 A69-34598

Positive Gaussian curvature shell under concentrated forces, analyzing stresses and strains relation to load distance using Thompson and Legendre functions 18 p3218 A69-34601

Plastic cylindrical shell buckling under axial impact, predicting velocity required to cause flexural waves 18 p3218 A69-34624

Stress-strain state of shells under concentrated loading, emphasizing positive Gaussian curvature 18 p3219 A69-34832

Axisymmetric deformation of cylindrical wound fiberglass reinforced plastic shell analyzed by methods of rigid normals and nonlinearly elastic fiber system 18 p3222 A69-34974

Nonlinear axisymmetric oscillations and motion stability of cylindrical wound elastic glassfiber shell under time dependent uniform internal pressure 18 p3222 A69-34975

Stability loss of shells of revolution under axial tension and radial pressure, considering shells of Gaussian curvature, calculating critical force 18 p3222 A69-34976

Boundary conditions of orthotropic shell stability under external pressure and axial tension, analyzing critical pressure by strain energy method 18 p3222 A69-34977

Constrained elastoplastic torsion of closed thin walled cylindrical shells, analyzing tangential and normal stress by using equilibrium equations 18 p3222 A69-34978

Dynamic instability regions of parametric resonance of cylindrical shells with curved generating lines under axial and radial pressure 18 p3223 A69-34979

Spherical shells axisymmetric equilibrium properties under uniformly distributed external compression 18 p3224 A69-35318

Initial deflection effect on elastic cylindrical shell stability under compression, finding critical load by determining limiting point in successive loading 18 p3224 A69-35319

Thin brittle plastic shells mechanical properties differing under tension and compression described by solving differential equations in successive approximation 18 p3224 A69-35327

Long term stability of orthotropic cylindrical shells under transverse shear stresses, calculating critical stress using Kirchhoff-Love model 18 p3225 A69-35357

Limiting equilibrium of variable thickness shallow spherical and conical shells of revolution under axisymmetric loads, assuming rigid plastic shell material 18 p3225 A69-35370

Cylindrical reinforced steel shells stability under external pressure 18 p3225 A69-35371

Stress-strain state of open cylindrical shells with arbitrary cross section determined for clamped-clamped, clamped-free and free-free supported shells 18 p3225 A69-35372

Automatic control systems for plants with distributed parameters, discussing stabilizing resonance shell with space-time dispersion of controlled processes 19 p3372 A69-35893

Natural oscillations and flutter of three layer cylindrical shell in supersonic gas flow analyzed by semimomentless theory, discussing boundary value problems, damping effects, etc 19 p3437 A69-36201

Displacement patterns for buckled shapes of axially compressed thin walled circular, cylindrical and conical shells 19 p3443 A69-36793

Number of forms of stability of plates and shells derived from eigenvalues of nonlinear boundary value problem containing generalized von Karman equations 19 p3445 A69-36816

Buckling and postbuckling of complete spherical shells with symmetric initial shape deviations and plastic deformations 19 p3446 A69-36834

Thin circular cylindrical shells elastic equilibrium under loads producing deflection, elongation or contraction described by integrating equilibrium equations with constant coefficient 20 p3621 A69-37076

Shells of revolution bearing capacity under axisymmetric loads determined by linear programming and finite difference method 20 p3622 A69-37326

Nonlinear theory based on Euler-Bernoulli hypothesis for axisymmetric deformations of heterogeneous orthotropic shells of revolution under rotationally symmetric mechanical and thermal loads 20 p3625 A69-37592

Load carrying capacity of orthotropic circular cylindrical shell under uniformly distributed normal load, considering edge support conditions 20 p3629 A69-38075

Soviet book on shell and thin walled structure calculation methods covering stability and stress analysis, reinforced and sandwich shells, etc 20 p3630 A69-38199

Noncircular curved shell stability under axial compression, using strain energy method to determine upper and lower critical stresses 21 p3834 A69-38715

Elastic closed and truncated conical shell stability with initial deflections under dynamic critical loading 21 p3834 A69-38716

Stability loss for hinged circular cylindrical elastic shells reinforced by thin walled closed profile ribs, proposing minimum weight design method 21 p3835 A69-38723

Circular cylindrical freely supported shell moment state stability, solving critical parameters by infinite matrix eigenvalues determination 21 p3835 A69-38724

Stability of cylindrical shell of average length with elastic filler under uniform external radial pressure 21 p3837 A69-39088

Deformation of circular cylindrical shell of varying thickness, obtaining differential equation solutions through multiple scales method 21 p3837 A69-39159

Nonlinear problems involving large deflections of isotropic and orthotropic shallow shells of rectangular platform, deriving partial differential equations for solution 21 p3838 A69-39185

Nonlinear stability of shallow elliptical paraboloidal dome under uniformly distributed compression, solving by Bubnov-Galerkin method on computer 21 p3838 A69-39186

Buckling stability of thin cylindrical shell under torsion, allowing for finite displacements due to shear in initial stress-strain state 21 p3838 A69-39187

Stability of free and clamped spherical and circular cylindrical shells subjected to uniform or nonuniform heating, discussing effects of temperature stresses 21 p3838 A69-39190

Variational principle applicable to nonlinear theory of shallow shells, deriving potential for equations describing uniform boundary conditions, discussing shell stability 21 p3838 A69-39191

Cylindrical shell stability during loading by uniform external pressure represented by Fourier series, determining critical pressure by solving nonlinear equations 21 p3846 A69-39715

Postbuckling of filled circular cylindrical shell using Ritz energy method for load deformation relation, discussing stabilizing effect of core 22 p4038 A69-39895

Cylindrical shells vibrations using Lagrangian based on Flügge system of stress-strain relations 22 p4039 A69-39924

Buckling strength prediction for circular cylindrical shells reinforced by circumferential and longitudinal stiffeners, solving torsional buckling of orthotropic shells under internal pressure 22 p4042 A69-40171

Nonlinear stability for closed thin walled orthotropic cylindrical shell subjected to uniform external pressure, using Bubnov-Galerkin method for approximate solution 22 p4042 A69-40454

Axisymmetric vibrations of semifinite cylindrical shell constructed of fiber reinforced composite layers, obtaining frequency equation from equations of motions 22 p4044 A69-40559

Cylindrical shells bending by finite element /cylindrical strips/ method, considering shells of arbitrary shape and variable thickness 22 p4046 A69-40968

Curved rectangular elements stiffness matrices derived for finite element analysis of cylindrical shells bending 22 p4046 A69-40969

Meridional crack problem for cylindrical and spherical shells solved for uniform membrane load and bending moment, obtaining stress intensity components
22 p4046 A69-41041

Pairs existence of symmetrical equilibrium forms in nonlinear shallow shell under load made applicable to nonshallow shells equilibrium
22 p4047 A69-41062

Prebuckling deformation influence on compressive buckling load for orthotropic cylindrical shells with elasticity principal axes in axial and circumferential directions
22 p4047 A69-41182

Standing waves in running tire shell wall, considering internal pressure, cross sections, wall thickness, cord angle, critical speed, etc
22 p4048 A69-41185

Closed circular cylindrical shell stability and oscillations under ring-shaped axial load, defining stress-strain state by radial displacements and force function
22 p4049 A69-41280

Deformation of orthotropic layered elastic shells based on linear elasticity theory, assuming surface and stress constraints
23 p4226 A69-41535

Nonlinear differential equations for large deflections of multisandwich shells of arbitrary shape built of stiff and weak elastic layers, considering cylindrical shells
23 p4226 A69-41572

Statics of axisymmetric deformation of cylindrical and conical shells of revolution of moderate thickness under uniformly and nonuniformly distributed loads
23 p4226 A69-41705

Infinite systems of algebraic equations in periodic problems for spherical shells with circular holes approximated by reduction method
23 p4227 A69-41706

Supercritical elastic states in convex shells produced by load in presence of thermal flux, noting no flux effect on states
23 p4228 A69-41970

Supercritical elastic states of closed spherical shell
23 p4228 A69-41971

Cylindrical shell load carrying capacity under axial compression, considering middle surface initial distortions influence
23 p4228 A69-41989

Discrete rib effect on buckling resistance of cylindrical shell under combined external and axial compression loads, using Laplace transforms
23 p4229 A69-41990

Stability of orthotropic cylindrical shells reinforced at edges by elastic ribs, analyzing axisymmetric buckling, natural oscillations and rigidity characteristics
23 p4229 A69-41992

Hinged circular cylindrical shells reinforcing ribs effect on deflection and bending moments, assuming external pressure application
23 p4229 A69-42001

Space frame radome shell structural stability with emphasis on analogous continua for reticulated framework, examining connection imperfections effect on stiffness
23 p4232 A69-42140

Circular cylindrical thin walled shells creep buckling under uniform axial compression
23 p4234 A69-42413

Buckling of truncated conical shells under torsion with various boundary conditions, applying Galerkin method to estimate critical load and wave number
24 p4395 A69-42715

Time independent interaction surface bounds to shells shakedown domain obtained for multiparameter loadings
24 p4396 A69-42732

Shallow spherical sandwich shells critical buckling loads using differential pressure method
24 p4396 A69-42734

Spherical vessel partially liquid-filled and supported by equatorial ring, studying axisymmetric oscillations under external forces
24 p4300 A69-43069

Cylindrical shell with supersonic nozzle end, describing axisymmetric oscillations forced by burning filler in gas stream
24 p4300 A69-43073

Axisymmetric vibration of shallow spherical caps, using nonlinear dynamic equations and associated variational equation of motion for elastic spherical shells
[ASME PAPER 69-APMW-6]

Orthotropic stiffness layer models for buckling of eccentrically stiffened shells of revolution with two un-

bonded orthotropic layers uncracked and circumferentially cracked
24 p4405 A69-43657

Computer program determination of barrel effect on strength of ring and stringer stiffened shells designed to support axial compression loads
24 p4405 A69-43671

SHELL THEORY

Random temperature fields in plates and shells in thermal contact with two media with temperatures as separable random space-time functions
01 p0173 A69-10077

Elastic shell nonlinear theory, introducing nonsymmetric stress tensor and principles of virtual work and objectivity
01 p0166 A69-10166

Variational principles of dynamic shell theory using Legendre transform for relations and boundary conditions of Timoshenko theory
01 p0166 A69-10262

Asymptotic integration of three dimensional elasticity equations for thin anisotropic shells and plates, deriving variability exponent of stress under given load
01 p0170 A69-10878

Torsion of variable cross sectional thin walled bars using shell theory equations
02 p0337 A69-11559

Three dimensional elastic theory using parametric expansion method developed for cylindrical translation shell profiles
02 p0338 A69-11718

Boundary value problem solution for arbitrary nonshallow cylindrical shells by small parameter method, assuming arbitrary geometry and hinged rectilinear edges
02 p0339 A69-11960

Soviet book on vibrations of elastic shell partly filled with fluid covering different stages in procedure for shells of axisymmetric configuration
02 p0346 A69-12480

Imperfection sensitivity of axially compressed stringer stiffened cylinder analysis via shell equations formulation using finite differences
02 p0348 A69-12542

Stresses in circular cylindrical shell subjected to local heating
03 p0523 A69-12952

Thin shells deformations described by finite element model accounting for transverse shear deformations
04 p0674 A69-14588

Natural vibrations of cylindrical panels analyzed on basis of Lamé parameters, shell equations and energy method
04 p0674 A69-14592

Postbuckling equilibrium calculation for pressure loaded thin walled cylinders of finite length, using Donnell nonlinear shell theory
04 p0677 A69-14837

Axisymmetric oscillation modes and frequencies of hemispherical shell partially filled with liquid, using moment theory of shells
04 p0679 A69-14922

Kirchhoff-Love hypothesis error dependence on stressed state variability index in theory of elasticity for closed spherical shell under uniform surface load
04 p0680 A69-14927

Soviet handbook on elasticity, plasticity and creep theories, emphasizing stresses and strains in solid thin walled shells and plates under bending, tension and torsion
04 p0683 A69-15499

Exact geometrical equations and internal equilibrium for elastoplastic deflections of orthotropic shells of revolution using thin shell theory
05 p0831 A69-15680

Rectangular thin beam Saint Venant deflection in case of moment stresses based on elasticity and shell theory
05 p0834 A69-15783

Stresses in cylindrical shell with elastic core loaded on curved surface solved, using elasticity theory for core and membrane solutions for shell
05 p0835 A69-15871

Circumferential buckling of ellipsoid of revolution due to internal pressure, assuming linear deflection and uniform thin shell
[ASME PAPER 68-WA/PVP-12]

Orthogonality of natural oscillation modes of shells of arbitrary geometry, using equations of motion from Vlasov engineering moment theory
05 p0840 A69-16190

Orthogonality of natural oscillation modes of shells of arbitrary geometry, using equations of motion from Vlasov engineering moment theory
05 p0840 A69-16200

Asymptotic integration of equations in theory of elasticity to develop approximate theory of momentless shells
05 p0843 A69-16689

Stress calculation for internal pressure in momentless shell of revolution
05 p0843 A69-16690

Steady state frequency response of conical and cylindrical shells under lateral excitation
06 p1021 A69-17147

Automatic data processing method for analyzing multiply connected elastoplastic shells of revolution
06 p1025 A69-17614

Three layer structure theory, discussing thin elastic sandwich shells with middle layer susceptible to transverse shear
06 p1025 A69-17615

Spherical caps axisymmetric static and dynamic buckling under load, using axisymmetric nonlinear elastic shell theory approximation and finite difference equations
[AIAA PAPER 69-89]
06 p1028 A69-18133

Initially imperfect axially compressed cylindrical shells strength using variational principle, shell theory and deformation theory of plasticity
[AIAA PAPER 69-91]
06 p1028 A69-18181

Approximate solution for hollow circular cylinder with fixed ends under axial displacement and cylindrical surfaces free from traction, using boundary layer technique
07 p1230 A69-18265

Mathematical formulas for rigidity distribution of inhomogeneous multilayer shells, discussing invariance property
07 p1232 A69-19011

Traveling waves on elastic spherical shells derived from dynamic equations of motion, including transverse shear and rotatory inertia effects
07 p1236 A69-19460

Buckling of long cylinders with homogeneous random axisymmetric geometric imperfections under axial compression, using truncated hierarchy technique
07 p1236 A69-19473

Finite elements for analysis of flexible shells, considering Kirchhoff theory for transverse shear deformation and problems involving rotations and buckling
08 p1411 A69-20142

Shell theories for polymer and reinforced plastic shells, giving revised temperature and creep problem solutions due to mechanical behavior
09 p1611 A69-21481

Stress-strain problem of geometrically nonlinear conical shell subjected to creep, giving method for complex deformation solution
09 p1612 A69-21497

Green function type solutions of shell equations by small parameter technique for case of free terms consisting of Dirac delta function
09 p1614 A69-21886

Nonlinear boundary value problem algorithm in shell theory, showing aid of numerical technique
09 p1614 A69-21887

Static, kinematic and elastic basic equations of shell theory integrated into differential equation for minimal surface helical shells
10 p1793 A69-22886

Finite element concepts for continuum theory of shells, noting bilinear approximation for displacement and fundamental decomposition principle for large deflection
10 p1794 A69-22891

Eddy current nondestructive tests of nonmagnetic thin metallic sheets and plates from single surface
10 p1698 A69-23046

Elastic Cosserat plate and shell theory, considering constitutive equations imitating transversely isotropic material and elastic deformations
10 p1798 A69-23147

Theory of thin shells - Conference, Copenhagen, September 1967
11 p1977 A69-24801

Thin elastic shell interior equations based on stress and strain, discussing shell description, strain derivatives plate deformation into cylindrical shells, etc
11 p1977 A69-24802

Linear shell theory foundations, discussing two and three dimensional stress strain relations, couple stresses, circumferential length ratio to shell thickness, etc
11 p1977 A69-24803

Thin elastic shell theory, using iterative process to develop differential equation integrals for interior state of stress
11 p1977 A69-24804

Nonlinear theories of deformable surfaces as two dimensional generalized continua applied to elastic shells, emphasizing elastic Cosserat surface
11 p1978 A69-24805

Consistent elastic shell theory based on expansion of sought solutions in power series over distance between point and middle surface
11 p1978 A69-24806

Thin plastic shell theory based on statical and geometrical relations for shallow and circular cylindrical shells
11 p1978 A69-24807

Shell theory foundations and basic equations, discussing classical shell equations asymptotic nature and errors
11 p1978 A69-24808

Continuum theory for thin elastic shells with local structural effects, emphasizing shell constituted by Cosserat material
11 p1978 A69-24809

Asymptotic methods for three dimensional equations in thin and thick elastic shell theory for determining two dimensional systems
11 p1978 A69-24810

Linear thin shell theory in complex dependent variable form for determining fourth order partial differential equations, considering elastic shells with edge loads
11 p1978 A69-24811

Finite deformation equations for flat annular membranes deduced from equations for thin shells of revolution, discussing displacement equations and fixed edge forces
11 p1979 A69-24813

Nonlinear shell theory, determining elastic deformation as function of stress under external loads using Lagrange variational principle
11 p1979 A69-24817

Symmetrically loaded weak moment shells of revolution made of materials with different moduli of elasticity
11 p1980 A69-24819

Plastic analysis of shallow spherical rigid plastic shell, using shell deflection equations to establish load-deflection relationship
11 p1980 A69-24823

Thermal stresses in longitudinally reinforced cylindrical shell, combining moment and semimomentless shell theories to obtain numerical results
11 p1981 A69-24942

Bending theory for truncated multilayer anisotropic conical shells, defining relations between displacements and external forces
11 p1984 A69-25141

Stress-strain state of shells with opposite edges hinged and rigidly clamped solved by numerical method after reduction to boundary value problem
11 p1985 A69-25174

Stochastic problems in thin elastic shell theory solved by equations obtained by linearizing shell equations near initial state of stress
11 p1996 A69-25732

Composite shell carrying capacity under general load, studying closing shape between laminate layers, transverse contraction, supporting layers thicknesses ratio, etc
12 p2176 A69-25851

Quasi-shallow shells theory applicability to thin elastic shallow shells, emphasizing use of function W/ρ
12 p2178 A69-26001

Variational method of displacements for calculating positive Gaussian curvature shells with allowance for shear strain, considering shallow shell equations and symmetrical load
12 p2178 A69-26006

Shallow hyperbolic paraboloidal shell with large deflections, analyzing nonlinear behavior with numerical method based on integral equations
12 p2185 A69-26820

Monograph on shell calculations by linear three dimensional elasticity theory, relating displacements and stresses
12 p2188 A69-26902

Three dimensional equations of elasticity reduced to two dimensional equations of shell theory, discussing stressed states of thin elastic bodies
14 p2531 A69-28807

Zero-moment cylindrical meshed shell equilibrium equations, discussing solution methods and difference analog
14 p2536 A69-29473

Oscillations of freely supported cylindrical shell of arbitrary cross section with breaks along generatrix,

determining eigenvalue of infinite matrix with normal determinant
15 p2707 A69-30581

Coaxial deviator theory of nonlinear elasticity, applying deformation theory variant to shell theory
15 p2592 A69-31058

Cylindrical shell bending subjected to internal pressure and force uniformly distributed on round section solved by numerical integration of differential equations
15 p2653 A69-31195

Sloping helicoid median surface with given parameters, obtaining equilibrium equations, elasticity and formulas relating deformations to displacements
15 p2714 A69-31197

Transient stress waves due to inputs of various types and time dependence in plates and revolving shells, discussing applications of elasticity theory analysis methods
16 p2876 A69-32785

Stress-strain state determination for axisymmetric shells applied to design of circular/annular plates and rotating disks
17 p3057 A69-33194

Stress-strain rate of glass fiber reinforced plastic pressure vessels under internal pressure, determining optimal fiber pattern
17 p3057 A69-33195

Complete spherical shells transverse frequency analysis, comparing results of elastic theory and classical, improved and membrane shell theories
17 p3061 A69-33705

Complete spherical shells nonsymmetric vibrations frequencies and mode shapes calculated by matrix method
17 p3061 A69-33706

Nonlinear partial differential equations solutions in theory of thin elastic spherical shells subjected to temperature fields and external loading
17 p3067 A69-34147

Axisymmetrical vibration characteristics of circular sandwich shell with viscoelastic core layer analyzed via differential equation to obtain frequency equation and composite loss factors
18 p3211 A69-34327

Side force problem for shallow helicoid shell, shown as static geometric analog of pure bending problem, solved by applying analogy
[ASME PAPER 69-APM-11]
18 p3213 A69-34387

Strain displacement and compatibility equations of finite symmetrical deflections of thin shells of revolution
[ASME PAPER 69-APM-14]
18 p3214 A69-34391

Differential equations of shells of revolution theory assuming rotationally symmetric stress and strain in thin elastic shells
18 p3215 A69-34549

Toroidal, spherical and conical shells limiting equilibrium under various loading and support conditions
18 p3216 A69-34572

Positive Gaussian curvature shell under concentrated forces, analyzing stresses and strains relation to load distance using Thompson and Legendre functions
18 p3218 A69-34601

Plastic cylindrical shell buckling under axial impact, predicting velocity required to cause flexural waves
18 p3218 A69-34624

Rectangular thin beam Saint Venant deflection in case of moment stresses based on elasticity and shell theory
18 p3223 A69-35035

Fluid-shell interactions, using piston theory and cylindrical-wave approximations
18 p3223 A69-35174

Regular integral equations solvability for boundary value problems in shallow shell theory, using method of potential representations and Green matrices
18 p3224 A69-35309

Weak moment shells made from materials with different elastic moduli, developing theory based on nondeformable normals
18 p3225 A69-35367

Thin walled shell temperature and strain fields described by integrodifferential equations based on Kirchhoff hypothesis and coupled thermoelasticity reciprocity equations
18 p3225 A69-35368

Cylindrical reinforced steel shells stability under external pressure
18 p3225 A69-35371

Resonant oscillations amplitude of nonlinearly elastic hinged cylindrical shell determined with cubic equation taking into account Hooke law, linear stresses, shell theory displacements, etc
19 p3435 A69-35843

Iterative algorithm applied to shell theory boundary value problem of stress concentrations at shallow shell holes
19 p3436 A69-35847

Contact problem of two thin elastic shells within Kirchhoff-Love theory, discussing constitutive equations
19 p3438 A69-36305

Nonlinear shell theory for thin elastic circular cylinders, obtaining equations for investigating equilibrium configurations of postbuckled states
19 p3440 A69-36636

Boundary conditions for shells with reinforced nonasymptotic boundaries, assuming coincident beam axis deformation with shell boundary deformation
19 p3443 A69-36781

Thin elastic shells internal stress state by iteration of two dimensional equation of general linear theory
19 p3443 A69-36790

Elastic shell theory to regularize singular integrodifferential equation, investigating load transfer from reinforcing ribs to circular cylindrical shell and numerical solution correlation
19 p3443 A69-36792

Elastic interactions between cylindrical shell and added band reinforcement turns, analyzing stress relaxation magnitude and effect on pressure vessel design
20 p3621 A69-37064

Equilibrium equations reduced to single partial differential equation for membrane theory of shells having coefficients of first quadratic form and specified curvature radius
20 p3622 A69-37220

Nonlinear theory based on Euler-Bernoulli hypothesis for axisymmetric deformations of heterogeneous orthotropic shells of revolution under rotationally symmetric mechanical and thermal loads
20 p3625 A69-37592

Free vibrational characteristics of thin walled circular cylindrical shells with layers of anisotropic elastic material laminated about middle surface
20 p3627 A69-37767

Thin curved panels postbuckling behavior under axial compression, basing study on thin shell finite deformation theory and Galerkin method
20 p3629 A69-38112

Soviet book on thin plates and shells bending and stability during creep covering analytical and numerical solutions for various structural elements
20 p3630 A69-38207

Shell elasticity calculation method, discussing stress state model, equilibrium conditions, shell geometry, etc
21 p3832 A69-38419

Composites elastic behavior, considering stress-strain in anisotropic lamina, composite plates and shells theory, thermal stresses and buckling for improving heterogeneous structures design
21 p3836 A69-38931

Variational principle applicable to nonlinear theory of shallow shells, deriving potential for equations describing uniform boundary conditions, discussing shell stability
21 p3838 A69-39191

Small parameter method applied to axisymmetric problems of elastoplastic nearly spherical bodies undergoing exponential hardening process, deriving linearized expressions for boundary conditions
21 p3839 A69-39198

Computer program for stress analysis of cylindrical pressure vessel with flat-end closures by thin shell theory
21 p3842 A69-39306

Nonlinear stability for closed thin walled orthotropic cylindrical shell subjected to uniform external pressure, using Bubnov-Galerkin method for approximate solution
22 p4042 A69-40454

Shallow shells two dimensional theory including effects of transverse shear deformation and of moments turning about normal to middle surface
22 p4048 A69-41197

Nonlinear shallow shell theory of stress and strain formulated via shell of revolution problem
22 p4048 A69-41198

Homogeneous equilibrium equations of nonlinear shallow shell theory, obtaining six stress function solutions for strain measures
22 p4048 A69-41199

Vlasov thin shell theory extended for undamped bending, transforming partial differential equations and stress function into integral equation solvable by successive approximations

23 p4225 A69-41407

Deformation of orthotropic layered elastic shells based on linear elasticity theory, assuming surface and stress constraints

23 p4226 A69-41535

Plates and shells under concentrated loads, analyzing stress-strain state

23 p4228 A69-41986

Complex configuration shells described by single analytical expression using R-conjunctive and R-disjunctive functions yielding boundary equations

23 p4229 A69-41991

Rigid/plastic solids subjected partly to uniform fluid pressure and partly to general boundary conditions, analyzing uniqueness and stability criteria

23 p4235 A69-42460

Three dimensional and shell theory analysis of nonaxisymmetric harmonic elastic wave propagation in hollow elastic sphere

[ASME PAPER 69-APMW-7]

24 p4402 A69-43105

Computerized spectral analysis of vibrational frequency due to elastic waves in isotropic hollow spherical shells

[ASME PAPER 69-APMW-8]

24 p4402 A69-43106

SHELLS [STRUCTURAL FORMS]

NT ANISOTROPIC SHELLS
NT CIRCULAR SHELLS
NT CONICAL SHELLS
NT CORRUGATED SHELLS
NT CYLINDRICAL SHELLS
NT DOMES [STRUCTURAL FORMS]
NT ELASTIC SHELLS
NT HEMISPHERICAL SHELLS
NT LIQUID FILLED SHELLS
NT METAL SHELLS
NT ORTHOTROPIC SHELLS
NT RADOMES
NT REINFORCED SHELLS
NT SPHERICAL CAPS
NT SPHERICAL SHELLS
NT THIN WALLED SHELLS
NT TOROIDAL SHELLS

Numerical analysis of temperature variation of spherical spinning satellite with and without radiatively coupled inner shell containing heat source

01 p0162 A69-10761

Asymmetrically loaded systems composed of shells of revolution, developing digital computer algorithm for solution of statics problems

05 p0840 A69-16201

Automatic data processing method for analyzing multiply connected elastoplastic shells of revolution

06 p1025 A69-17614

Stress-strain state of shells of multicable elevator pulleys under asymmetric load for various friction coefficients and pulley shell lengths and widths

06 p1026 A69-18016

Computer program for axisymmetrically deformed shells of revolution and combinations of such shells

06 p1026 A69-18019

Optimum design of shells loaded by concentrated forces, discussing thickness relation to middle surface, loading point and manufacturing considerations

11 p1979 A69-24812

Symmetrically loaded weak moment shells of revolution made of materials with different moduli of elasticity

11 p1980 A69-24819

Triangular shell element SHEBA for arbitrary curvature variation as means of performing large displacement matrix analyses, discussing local subelement, natural modes, cross sectional resultants, etc

16 p2872 A69-32025

Bending of circular plate into shell, using stress-strain relation in finite strain, solving differential equations and boundary conditions

21 p3836 A69-39005

Curved shell elements in shell and plate analysis, discussing quadratic and cubic elements for space structures design

21 p3845 A69-39329

Plate and shell structures static and dynamic analysis by generalized variational principles in finite element method, discussing element displacement functions

[AIAA PAPER 68-290]

23 p4227 A69-41882

Complex configuration shells described by single analytical expression using R-conjunctive and R-disjunctive functions yielding boundary equations

23 p4229 A69-41991

SHELTERS

U LUNAR SHELTERS

SHIELDING

NT ELECTROMAGNETIC SHIELDING
NT ELECTROSTATIC SHIELDING
NT HEAT SHIELDING
NT MAGNETIC SHIELDING
NT RADIATION SHIELDING
NT RADIO FREQUENCY SHIELDING
NT REENTRY SHIELDING
NT SOLAR RADIATION SHIELDING
NT SPACECRAFT SHIELDING

Bumper materials effect on two component hypervelocity impact shields performance, noting material velocity influence

[AIAA PAPER 69-379]

13 p2283 A69-28309

SHIFT REGISTERS

Wafer chip assembling technique for high density interconnection of silicon devices in large monolithic electronic systems, noting application to MOS shift register

02 p0222 A69-12472

Nonlinear feedback shift register circuit design by logical sequences

08 p1298 A69-20835

Linear shift register synthesis algorithm found to coincide with Berlekamp iterative algorithm for decoding BCH codes

09 p1470 A69-21317

Error control coding noting cyclic codes, binary shift registers, shift register circuits, encoding and decoding

09 p1461 A69-21893

Decoding procedure for error locating binary code indicating location of single subblock containing errors in code word, employing feedback shift registers

11 p1857 A69-24549

Shift registers with binary switching elements for shaping signal spectrum in data transmission systems without phase distortions

12 p2040 A69-26486

Pseudorandom uniformly distributed numbers generation from noise-like signals produced by shift register with feedback, noting statistical tests

13 p2218 A69-27248

Probability density functions of waveforms from summation of digits in n-stage shift register generating m-sequence

15 p2568 A69-30617

Buffer shift register with feedback control during tape recorder playback to obtain variable delay to compensate for recorder time base error

19 p3312 A69-36284

Minimization algorithm for switching systems synthesis, describing design of mass spectrometer curve function generator and autonomous shift register

23 p4146 A69-42535

SHIMS

U COMPENSATORS

SHIP PROPULSION

U MARINE PROPULSION

SHIPS

NT AIRCRAFT CARRIERS
NT NUCLEAR POWERED SHIPS
NT SUBMARINES

Marine requirements possible satisfaction by using space techniques to improve long range communications to achieve safety at sea and shipping operations efficiency

01 p0161 A69-10503

Shipboard direction finder calibration accuracy, emphasizing radio operator training

06 p0897 A69-17533

Skin friction drag reducing high polymer solution injected into turbulent boundary layer to test effectiveness on marine vehicles

17 p2951 A69-33254

Kormoran airborne missile weapon system for attacking seagoing targets, discussing navigation guidance, radar tracking and homing system

17 p3050 A69-33697

SHIVERING

Primary muscle spindle afferents from gastrocnemius muscle of cat before, during and after cold shivering, utilizing ramp stretches of same muscle

23 p4096 A69-42091

SHOCK

Dogs cardiovascular responses to histamine liberator /compound 48/80/, describing shock and acidosis with elevated histamine levels

22 p3873 A69-40206

SHOCK ABSORBERS

Supercritical damping of nonlinear mass elastic system with damping force function dependent on fractional powers of velocity, noting impact deceleration

04 p0671 A69-14413

Dynamic analysis and development of response histories and tradeoff study charts for spherical impact limiters for protecting hard landing planetary payloads

04 p0683 A69-15508

Airflow through open foam cellular structure, discussing mathematic model for predicting pressure buildup and foam response in shock and vibration isolation

[ASME PAPER 69-VIBR-46]

10 p1803 A69-24144

Synchronous vibration absorbers using gyroscopic systems, noting antiresonance with Perissogyro

[ASME PAPER 69-VIBR-39]

10 p1807 A69-24177

Optimum and suboptimum shock and vibration isolators, discussing three criteria and tradeoff between relative motion and accelerative force

[ASME PAPER 69-VIBR-45]

10 p1808 A69-24183

Landing shock attenuation system for Surveyor spacecraft, describing hydraulic cylinder and piston arrangement for damping, computerized shock absorber design and landing process simulation

[ASME PAPER 69-DE-54]

14 p2530 A69-28848

Steady state motion of multiple unit impact damper attached to sinusoidally excited primary system, determining asymptotically stable regions

15 p2714 A69-31144

Parameter selection for optimum characteristics of machine part shock absorbers subject to orthogonal impact pulses

16 p2794 A69-32297

Landing shock struts of Surveyor 6, emphasizing silicone liquid springs role as absorbers and stabilizers

20 p3466 A69-38180

SHOCK DIFFUSERS

U DIFFUSERS

SHOCK DISCONTINUITY

Lighthill method based expressions derived for discontinuity shape formed during shock wave diffraction near small angle

02 p0234 A69-12588

Anisotropic nonlinear wave propagation in arbitrarily moving ideal gas, using singular surface/ray combined theories

04 p0630 A69-14532

MHD shock discontinuities above critical Alfvén-Mach numbers in two fluid plasma

06 p0970 A69-17954

Jump conditions across MHD shock waves, reducing relations to identities applicable to nonequilibrium situations

07 p1193 A69-19242

Steady shock discontinuity in perfectly conducting gas flow in arbitrarily oriented magnetic field for various Mach numbers

08 p1360 A69-19988

Mach wave and anisotropic supersonic flow interaction, considering constant entropy along streamline and layer of entropy discontinuities /interfaces/

10 p1631 A69-22906

Shock discontinuities in solar wind measured by magnetic field and plasma instruments on Explorer 34, applying Rankine-Hugoniot relations

22 p4020 A69-40304

Semianalytic solution for axisymmetrical supersonic inviscid flow near stagnation region of spherically blunted body with detached shock waves

22 p3861 A69-41178

Axisymmetric supersonic flow around spherically blunted body at small angles of attack, deriving equations for shock deformation perturbations and surface pressure

22 p3861 A69-41179

SHOCK FRONTS

Shock front structure in radiative relaxation region in atomic H, calculating Lyman continuum effects

01 p0122 A69-10125

Gas flow model of coaxial electromagnetic plasma gun front profiles and speeds for operation with positive central electrode

02 p0288 A69-12032

Luminous flow in front of sphere and behind cylinder under high temperature and low density conditions, discussing profiles of shock waves

02 p0189 A69-12182

Ionizing shock front structure in monatomic gas, considering atom-atom and electron-atom collisional ionization rates

03 p0414 A69-13138

Shock waves luminescence temperature dependence measured by UV and visible radiation, noting dependence on front glow duration

03 p0415 A69-13411

Legendre transformation application to plane elastoplastic loading waves, examining shock front formation in interaction region

04 p0673 A69-14495

Apparatus for generating HF shock fronted pressure waves in resonant tube

06 p0906 A69-17149

Width of strong shock wave front and transition layers estimated, using Boltzmann kinetic equation and H-theorem

07 p1118 A69-18702

Approximate solution to problem of estimating thickness of shock wave by statistical mechanics

07 p1119 A69-18704

Gas dynamic shock wave entry into magnetic field, discussing field distribution behind shock front and diffusion and medium motion effects on penetration depths

07 p1192 A69-19022

Radiative cooling layer behind shock front from neutral interstellar hydrogen cloud collision at Mach 20, discussing molecular hydrogen abundance during cooling

08 p1381 A69-19796

Sonic boom minimum achievable shock front pressure rise and overpressure level prediction for given aircraft and flight conditions

08 p1253 A69-19903

Flow behind shock front propagating along viscous fluid film surface, noting shock intensities as related to detonation velocities, using schlieren photographs

08 p1303 A69-20326

Displacement effect due to subsonic reaction heat front behind shock wave in two dimensional supersonic flows

08 p1252 A69-20691

Gas pressure variations behind autonomous stable detonation fronts in propane-O mixtures, noting effect of diameter tubes and initial pressures

08 p1421 A69-20757

Reflected particle acceleration at magnetospheric bow shock front attributed to interplanetary electric field

09 p1577 A69-21714

Bodies of revolution in sonic flow of ideal gas, showing same perturbational effect of source and dipole on flow before shock front

10 p1632 A69-23364

Shock front propagation in argon with electrode-drawn induced EMF, using shock tube with induced transverse magnetic field

10 p1737 A69-23469

Relaxation phenomena in ionization process in argon shock front structure, using EM and pressure driven shock tube to drive high speed shock waves

10 p1726 A69-23685

Electrical conductivity of air behind incident and reflected shock wave fronts as function of temperature and Mach numbers measured by electrode method

11 p1888 A69-25220

Gas motion and heating by radiation behind shock wave front, noting ionization and radiation absorption occurrence

12 p2061 A69-25880

Boundary layer parameters behind shock wave front in ionized gas calculated with allowance for charged particle diffusion

12 p2139 A69-26713

Enhanced plasma heating in absorption zone of laser-induced gas breakdown at spherical blast wave shock front

14 p2460 A69-29604

Shock wave radiation screening by thermodynamically unstable gas, discussing brightness and gas temperature relative to shock wave front position

14 p2493 A69-29673

Shock wave propagation in isothermal atmosphere, discussing radiation and ionization effects on thermal jump

16 p2858 A69-32207

Shock detachment distance for flow around cylinders and spheres determined by microphotometric tracing of negatives of photographs of forward stagnation streamlines

17 p2949 A69-32962

Wave motion nonsteadiness influence on detonation front thickness using quasi-steady kinetic model of induction process, discussing agreement with experimental observations

17 p2952 A69-33403

Collisionless shock wave front turbulence in diluted plasma, including thickness, electron and ion component measurements

17 p3012 A69-33818

Oblique hydromagnetic shock waves in magnetized hydrogen plasma enclosed in pyrex chamber by oscillatory zeta discharge, probing for front development and structure

17 p3013 A69-33823

Collisionless plasma heating mechanisms from current layer turbulence in theta pinch experiment and shock wave front structure as function of initial magnetic field

17 p3013 A69-33824

Shock wave propagation in two types of electromagnetically driven shock tubes, describing probe for shock front velocity measurement

18 p3119 A69-34260

Br molecular dissociation rate in argon excess determined, considering visible emission intensity behind shock front

18 p3176 A69-34465

Reflected shock front interaction with heated thin gaseous filament studied in shock tube by spark interferometric and schlieren technique

18 p3228 A69-34468

Microfluctuations frequency and wavelength of electromagnetic, electric and magnetic field distributions in plasma shock wave front found consistent with ion-acoustic origin hypothesis

18 p3180 A69-35017

Cylindrical concentric detonation front and stability mechanism space-time measurement

20 p3632 A69-37215

Precursor electrons due to photoionization ahead of pressure driven shock waves, presenting electron temperature and density theoretical analysis

20 p3511 A69-38238

Shock front reaction and detonation initiation in low density ammonium perchlorate

21 p3784 A69-39590

Charge exchange of solar wind protons passing shock front, noting turbulent subsonic motion of randomized hot solar wind protons in shadow cone

22 p4008 A69-41208

One dimensional shock waves and acceleration fronts in nonlinear isotropic viscoelastic materials using constitutive equations

23 p4235 A69-42463

Molecular vibrational relaxation effect on dissociating airflow behind shock wavefront, giving relations to chemical reaction rates in diffusion approximation

24 p4302 A69-43486

Irregular pressure profiles and pressure-time histories when using octofluorocyclobutane and sulfur hexafluoride in explosive driven shock tube

[AIAA PAPER 68-730] 24 p4297 A69-43577

Tube diameter effects on shock front propagation, observing front formation process with schlieren method

24 p4297 A69-43630

Hot dense plasma used as driver gas producing plane stable current-free high Mach number shock fronts resembling plane blast waves

24 p4359 A69-43647

SHOCK HEATING

Initial ionization rates and collision cross sections in shock heated argon in low pressure shock tube, using double electrostatic probes

01 p0132 A69-11206

Medium heating by explosion in presence of allotropic changes and thermochemical reactions concerning temperature field determination

03 p0534 A69-14159

Shock heated gas radiation frequency dependence and UB and B-V color indices determination, studying role in close binary systems luminescence

13 p2350 A69-27860

Shock hardening in Ni at high pressure observed by electron microscopy showing dominating thermal effects on microstructure

15 p2637 A69-30225

Electron temperature relaxation in shock heated Ar plasma, measuring plasma microwave radiation

15 p2663 A69-30995

Induction period of reactions behind incident shock waves traveling through undiluted high temperature CO and molecular oxygen mixtures, using CO flame spectra

16 p2877 A69-31768

Convective plus radiative shock tube model stagnation point heating rate measurements for planetary entry heating rate in air and Venus gas

[AIAA PAPER 69-635] 17 p2890 A69-33272

Absolute gf values for Fe I and Fe II lines between 3190 and 3315 A measured by spectral absorption through shock heated gas containing Fe

18 p3175 A69-34304

Radiation gas dynamics in shock tube, studying radiation coupled flows with flow field affected by radiant energy transport

18 p3116 A69-34447

Shock heated argon thermal conductivity studied by optical interferograms, deriving equation for measured mean value

18 p3228 A69-34459

Metallic aerosol generator application in shock tube spectrometric measurements of radiation by molecules occurring as solids before decomposition to vapor phase

18 p3099 A69-34461

Steady Prandtl-Meyer expansion of shock heated gases for recombination studies, measuring static pressure, stagnation point heat transfer, IR emission and optical absorption

18 p3228 A69-34466

Radiation effects produced by high temperatures of shock waves and nuclear explosion fireballs, air cooling, laser emission-matter interaction and optical phenomena

18 p3230 A69-34926

Sulfur hexafluoride dissociation in argon at various temperatures and pressures, using shock tube techniques to determine unimolecular parameters

18 p3100 A69-35475

Ramsdorf meteorite chondrules and metal particles formation attributed to shock-induced partial melting and rapid cooling

19 p3409 A69-36088

Shock histories of hexahedrites and Ga-Ge group III octahedrites based on metallographic and X ray diffraction analysis, noting meteorites shocked preterrestrially

19 p3418 A69-36136

Dispersion of paraffin cork after instantaneous shock heating, noting expansion at various isentropic indices

19 p3301 A69-36839

Stagnation point heating in hypersonic gas flow past blunt bodies, considering radiative transfer effects on shock wave temperature and density distribution, wave separation, etc

20 p3457 A69-36981

Photoelectric measurements of UV absorption coefficients of high temperature air at specific temperature and wavelength ranges in pressure-driven shock tube

22 p4049 A69-40098

Gaseous mixtures for hypervelocity applications, studying equilibrium conditions and thermodynamic properties for shock and constant volume heating processes

22 p4049 A69-40266

Unsteady aerodynamic heating at stagnation region including surface combustion in arc heated high enthalpy wind tunnel

22 p3860 A69-40597

Arc heating of shock tube driver gas, describing radiative energy transfer mechanism

23 p4147 A69-41895

SHOCK LAYERS

Shock layer gas radiation influence on deep space missile shape, noting evaluation by flow equations

01 p0007 A69-11070

Radiation heating characteristics of shock layer gases surrounding Venus entry vehicle, noting domination of carbon monoxide band and UV spectrum

02 p0351 A69-11751

Rarefied merged stagnation shock layer of hypersonic body, considering chemical reactions of nonequilibrium dissociative relaxation of air

02 p0189 A69-12521

Reentry shock layer radiative heat transfer to surface of blunt superorbital vehicle

[AIAA PAPER 68-1151] 03 p0532 A69-13560

Plasma flow in electromagnetic shock tube with various pressures and speeds, noting turbulence onset in shock layer

06 p0968 A69-17764

Dynamic behavior of shock layer of supersonic rarefied gas flow past disk and sphere

06 p0861 A69-17812

Electron density shock layer profiles measured by Langmuir probe in hypersonic tunnel on blunt body for air flows and gas densities

[AIAA PAPER 69-81] 06 p0863 A69-18101

- Experimental and numerical nonequilibrium shock layer around cones in hypersonic pure oxygen flows with simultaneous rotational, vibrational and dissociation relaxation
[AIAA PAPER 69-136] 06 p0864 A69-18141
- Time dependent technique for inviscid blunt body flows to analyze viscous rarefied shock layer regime, using Navier-Stokes equations
[AIAA PAPER 69-139] 06 p0865 A69-18173
- Shock layer microwave radiation measurements during reentry flight of spherical nose cone, determining effective plasma temperature
[AIAA PAPER 69-183] 06 p0865 A69-18201
- Shock waves internal structure in perfect monatomic gases, discussing density distribution in shock layer experimental measurement 07 p1120 A69-18930
- Bow shock and magnetopause boundary observations with IMP 2 plasma detector 07 p1129 A69-19372
- Supersonic gas flows in shock layer past blunt bodies taking into account selective radiation and radiative transfer in continuum, applying method of characteristics 14 p2390 A69-29477
- Plane shock layer structure in pseudoMaxwellian monatomic gas, integrating Krook equation for gas molecule velocity 14 p2432 A69-29613
- Heat transfer at gas flow stagnation point past blunt body under radiation from air layer in shock wave wake, using gray gas model 14 p2390 A69-29614
- Nongray equilibrium radiative heat transfer in viscous radiating shock layer around blunt body entering high temperature nonisothermal carbon dioxide-nitrogen atmosphere
[AIAA PAPER 69-636] 17 p3070 A69-33258
- Shock layer properties, radiative and convective heat transfer about two hypersonic blunt bodies at zero angle of attack in assumed Martian atmosphere
[AIAA PAPER 69-634] 17 p2891 A69-33281
- Nonequilibrium multicomponent ionization calculations for stagnation merged shock layer of hypersonic blunt body by successive accelerated replacement
[AIAA PAPER 69-655] 17 p2892 A69-33469
- MGD hypersonic shock layer at spherically blunted body analyzed by utilizing induction equation including Hall effect
[AIAA PAPER 69-722] 17 p3012 A69-33494
- Radiative energy emission by blunt vehicle shock layer under severe entry conditions, discussing flow properties and radiative transfer coupling
[AIAA PAPER 69-719] 18 p3084 A69-34416
- Blunt body stagnation point ionization by chemical nonequilibrium thin viscous shock layer analysis, predicting electron density 23 p4060 A69-41917
- Supersonic flows past blunt bodies, formulating approximate similarity law for shock layers in subsonic regions 24 p4246 A69-43495
- Reentry shock layer radiative heat transfer to surface of blunt superorbital vehicle
[AIAA PAPER 68-1151] 24 p4414 A69-43567
- Mass injection effects on viscous hypersonic low Reynolds number shock layer downstream and at stagnation point in blunt forebody region analyzed for non-reacting gas 24 p4249 A69-43663
- SHOCK LOADS**
NT BLAST LOADS
- Shock loading history effect on solid state response of iron meteorites to annealing at moderate temperatures permits deductions about thermal history 01 p0149 A69-10134
- Corrosion rates and stress corrosion cracking sensitivity of explosively shocked austenitic stainless steels 03 p0444 A69-13308
- Deformation microstructures in shock loaded olivine, discussing planar features 05 p0818 A69-15607
- Dislocation redistribution during annealing and shock deformation in liquid nitrogen of chromium, molybdenum and tungsten single crystals 07 p1159 A69-18534
- Mathematical formula for estimating cost and efficiency of parachuting supplies, noting shock load reduction 07 p1053 A69-19140
- Shockload on axial intake fan leading edge of radial flow compressor, calculating flow field 08 p1251 A69-20604

- High speed deformation of metals under pulse loading, noting role of maximum stress magnitude and deformation characteristics 12 p2113 A69-26043
- Quantitative interferometric analysis of shock induced wavelength variations in glass and polished steel plates using Q switched ruby laser light source 12 p2089 A69-26185
- Meteorite fragment from Arizona Meteor Crater, establishing probable history from shock loading experiments on iron alloys 12 p2158 A69-26344
- Dynamic response of distended carbon materials to shock loading defined by measuring equation of state, unloading behavior and spallation strength 12 p2119 A69-26847
- Experimental and predicted shock axial pressure variations for semiinfinite metallic targets during high velocity impact, using Al alloys and Cu
[AIAA PAPER 69-361] 13 p2366 A69-28294
- Shock load protection through energy absorption and dissipation in primary or composite structures, listing honeycomb, cellular plastics and rubber mechanical properties
[ASME PAPER 69-DE-37] 14 p2531 A69-28846
- Optimal active shock isolation by nonlinear elements for system subjected to shock type loadings, discussing impulse shapes 15 p2713 A69-31019
- Shock force calculation for parachute of arbitrary canopy design, illustrating simplification permitting differential equation solution in closed form 15 p2551 A69-31172
- X ray detectable preferred disorder in solids by shock loading studied in Ainsworth meteorite and in hexagonal alpha silicon dioxide 15 p2671 A69-31538
- Polycrystalline nickel foil microstructure after explosive shock loading and heat treatments, using transmission electron microscopy 20 p3563 A69-38126
- Hugoniot equation of state of shock loaded W determined at room temperature and 950 C 20 p3564 A69-38127
- Shocked Bamle enstatite transformed to disordered enstatite, noting Debye-Scherrer patterns similarity 21 p3792 A69-38321
- Shock hardening of Al alloys in annealed, solution heat treated and aged conditions compared with cold-rolled materials
[ASM PAPER W9-10.4] 21 p3729 A69-38664
- Piezoelectric transducer transient electrical response due to shock loaded stress using transfer calculus 22 p3947 A69-40863
- SHOCK MEASURING INSTRUMENTS**
- Shock and vibration data recording, discussing transducer selection, accelerometer mounting, conditioning electronics and recording devices 01 p0083 A69-11050
- In-flight measurement of shock and vibration effects on aircraft and propulsion systems 01 p0084 A69-11051
- Etched manganin gauge for shock pressure measurement in high noise environments containing radiation and electromagnetic effects 04 p0603 A69-15431
- Shock attenuation and equation of state of polyurethane based on aquarium technique and free surface velocity measurement 16 p2828 A69-31810
- Optimum ballast resistance of thin film heat transfer gage producing shock arrival time, thickness and structure data of low pressure shock tube 18 p3117 A69-34470
- SHOCK RESISTANCE**
NT IMPACT RESISTANCE
- Shock sensitivity of solid explosives and propellants, using calibrated gap testing techniques 02 p0302 A69-11520
- Shock initiation and sensitivity of granular explosives, noting heterogeneity effect in ammonium perchlorate 10 p1751 A69-23016
- Ruggedized ballistic range telemetry system survivability and in-flight stability after gun launching, presenting temperature, strain and stagnation point pressure measurements 10 p1654 A69-23281
- Shock load protection through energy absorption and dissipation in primary or composite structures, listing honeycomb, cellular plastics and rubber mechanical properties
[ASME PAPER 69-DE-37] 14 p2531 A69-28846

- Solar array configurations and performance on Martian surface, including hard lander design and surviving shock levels 23 p4073 A69-42289
- SHOCK SIMULATORS**
- Gun tunnel equilibrium piston technique by model analysis of piston weight, tunnel conditions and geometry 11 p1862 A69-25013
- Shock spectra practical applicabilities to simulated and real shock equivalence, including spectra definitions and determinations 13 p2369 A69-28600
- Sonic boom simulation methods using shock tube booth type simulators, ballistic ranges and explosives, discussing unmanned data recorder as monitoring device 15 p2585 A69-30371
- Mechanical linear accelerator simulating acceleration, shock and weightlessness, noting data acquisition and interpretation 17 p2945 A69-33423
- SHOCK SPECTRA**
- Shock testing methods using shock spectrum concept and description testing machines and instrumentation 11 p1862 A69-24408
- Shock spectra practical applicabilities to simulated and real shock equivalence, including spectra definitions and determinations 13 p2369 A69-28600
- Real time shock response analysis advantages over sequential analysis, describing equipment 15 p2618 A69-30359
- Collision free earth shock wave gross and fine structure deduced from OGO 5 plasma diagnostics
[AIAA PAPER 69-676] 17 p2961 A69-33452
- Relative displacement spectra analysis illustrating shock spectra errors, comparing real system response with simple single degree of freedom system response 20 p3548 A69-37301
- Sonic boom lower bounds determination in midfield based on modification of Jones results by minimizing overpressure or shock strength of boom wave positive component 24 p4254 A69-43662
- SHOCK TESTS**
- Controlled transient signal distortion by shock monitoring instrumentation circuits using piezoelectric accelerometers 04 p0603 A69-15430
- Deformation microstructures in shock loaded olivine, discussing planar features 05 p0818 A69-15607
- Primary explosives tested for effects of shock, friction, heat and electrical discharges 10 p1750 A69-23010
- Shock testing methods using shock spectrum concept and description testing machines and instrumentation 11 p1862 A69-24408
- Shock pulse criterion limitations and HF transients technique for design and tests of structures and components 12 p2182 A69-26731
- Shock spectra practical applicabilities to simulated and real shock equivalence, including spectra definitions and determinations 13 p2369 A69-28600
- Real time shock response analysis advantages over sequential analysis, describing equipment 15 p2618 A69-30359
- Pulse generator to accommodate electronic system testing to shock response spectrum by simulating real world shock environment 15 p2585 A69-30360
- Flight worthiness of mishandled electronic equipment, analyzing fragility and performance of shock exposed components and connections 15 p2576 A69-30362
- SHOCK TUBES**
NT MAGNETIC ANNULAR SHOCK TUBES
- Shock reflection structure in ionizing xenon determined by fast rise pressure gauge mounted in shock tube end wall 01 p0132 A69-11205
- Initial ionization rates and collision cross sections in shock heated argon in low pressure shock tube, using double electrostatic probes 01 p0132 A69-11206
- Flow nonuniformity measured in shock tubes by determining heat transfer rate to fine wire probes 01 p0062 A69-11219

Radiation and electrical precursor effects in expansion tube of electromagnetic shock tube, discussing primary causes

02 p0229 A69-11936

Inert gas nonequilibrium MHD power generation in shock tube

02 p0196 A69-12425

Electronic transition moment for C/Swan/ bands measured in shock tube in carbon dioxide and argon mixtures

02 p0285 A69-12833

Boundary layers and heat transfers at shock tube walls, establishing approximate solution of boundary layer equation for laminar and turbulent cases [ONERA-TP-647]

03 p0412 A69-12875

Surface temperature thermal fluxmeters used in measurements of shock tubes [ONERA-TP-648]

03 p0427 A69-12876

High speed compression waves, rarefaction waves and gas interface regions position and velocity measurement in shock tube by sensing electrical impedance

03 p0428 A69-13104

Shock tube equilibrium method for determining vapor pressure of platinum submicron particles by suspension in xenon-argon carrier gas at high temperatures

03 p0532 A69-13319

Nozzle geometry influence on argon plasma flow parameters in shock tube, discussing measurement data behind shock wave front

03 p0481 A69-14160

Shock tube and samples of fluoroethylene, difluorodichloroethylene and fluoromethane in argon diluent used to prepare carbon difluoride, discussing electronic oscillator strengths

04 p0632 A69-14944

Rectangular shock tube for use with pressure and vacuum, discussing sealing of circular end flanges to buildup tube

06 p0906 A69-16928

Emissivity of high temperature air and carbon dioxide-nitrogen mixtures in two diaphragm shock tube

06 p0911 A69-17348

High speed streak camera synchronization with shock tube process involving nonreacting gases or mixtures in pressure chamber

06 p0926 A69-17499

Plasma flow in electromagnetic shock tube with various pressures and speeds, noting turbulence onset in shock layer

06 p0968 A69-17764

Shock tube study of ammonia oxidation at high temperature, detecting molecular species in reaction zone by IR emission

06 p0885 A69-17936

Chemiluminescence in high temperature oxidation of methane studied in shock tube

06 p0885 A69-17937

Shock tube measurements of radiation from simulated Jupiter atmosphere related to thermodynamic conditions encountered by entry probe [AIAA PAPER 69-184]

06 p0908 A69-18207

Kinetics calculations in shock tube data interpretation, determining elementary rate constants and complex reaction mechanism [WSCI PAPER 68-50]

07 p1073 A69-18319

Flow diagnostics for high enthalpy nonequilibrium gas flows in shock tubes using long pulse ionized Ar gas laser

08 p1323 A69-19879

Oscillator strengths of transitions in shock tube between nitric oxide Rydberg states in near IR

08 p1354 A69-20150

Monograph on interferometric studies of unsteady shock waves in theta pinch driven shock tube, discussing flow characteristics in helium and hydrogen

08 p1304 A69-20710

Monograph on shock wave structure in binary gas mixtures covering gas kinetics and shock tube measurements of heavy component density distribution

08 p1304 A69-20711

Arc driven shock tube with alumina ceramic liner to reduce driver gas contamination, noting shock speed and test time increase [AIAA PAPER 68-366]

09 p1570 A69-21957

Gate for measurement of density variation between expansion chamber and driver gas of valve driven shock tube

10 p1673 A69-23342

Shock front propagation in argon with electrode-driven induced EMF, using shock tube with induced transverse magnetic field

10 p1737 A69-23469

Relaxation phenomena in ionization process in argon shock front structure, using EM and pressure driven shock tube to drive high speed shock waves

10 p1726 A69-23685

Electric shock tube for measurement of plasma magnetic fields induced by shock plasma moving through DC magnetic field transverse to flow

11 p1925 A69-24311

Viscous effects of wall boundary layer behind primary shock wave on flow in shock tube, noting pressure and temperature changes

11 p1870 A69-25010

Dense real gas thermodynamic relations in piston driven shock tube facilities operation

11 p1862 A69-25011

Piston driven facilities for hot high pressure gas production including gas tunnels, heavy piston facilities, piston driven shock tunnels and high speed guns

11 p1862 A69-25012

Radiation studies of pressure driven shock tubes with atomic ionization at high temperatures, discussing thermal light sources, autoionization, etc

11 p1863 A69-25014

Planning, instrumentation and analysis of shock tube experiments in chemical kinetics, noting gas phase reaction rates at high temperatures

11 p1863 A69-25015

Intermittent flow facilities for ballistic and lifting reentry flight simulation including shock tubes, ballistic ranges and shock and gun tunnels

11 p1863 A69-25016

Transistorized assembly for amplification of signals emitted by platinum film probes in shock tubes, discussing application to chronometric device triggering

11 p1887 A69-25095

Diffusion of ion-electron pairs produced by photoionization upstream of strong shock waves to shock tube walls based on particle flux and Poisson equations

11 p1866 A69-25275

Electrical breakdown between cold electrodes in contact with flowing plasma produced by electromagnetic shock tube

12 p2134 A69-26098

Shock wave gas flow density behind shock tube calculated by shadows measurements using interferometric techniques

13 p2245 A69-27384

Shock tubes and tunnels design and operation principles for investigating physical and chemical phenomena

13 p2240 A69-27930

Isentropic compression tube with piston compressor for producing hypervelocity test flows, noting shock speeds [AIAA PAPER 69-334]

13 p2249 A69-28270

Reservoir conditions of reflected shock wind tunnel by subjecting gas to direct shock and shock reflected at closed downstream end of shock tube

13 p2243 A69-28359

Interaction between shock tube gas discharge plasma and fast electrons ionized stationary gas, noting luminous discontinuities propagation

14 p2490 A69-28998

Blue continuum emission from hot carbon dioxide measured in shock tube, discussing applications to temperature measurement of gases containing carbon dioxide

14 p2427 A69-29014

Optical carrier single channel telemetry system providing complete electrical isolation between shock tube data acquisition and data recording instrumentation

14 p2449 A69-29561

Shock wave velocity and gas flow parameters in shock tube with noninstantaneously opening diaphragm calculated by method of characteristics

14 p2432 A69-29623

Shock development in electrothermal shock tube with performance simulation of mechanical shock tube with hot driver but turbulent or unstable driver-shock interface

14 p2427 A69-29768

MHD interaction between plasma and transverse magnetic field in shock tube, noting unsteady shock wave propagation in interaction zone

14 p2501 A69-29919

Cosmic shock waves simulation through correlations between shock equations in classical and relativistic fluid dynamics, using shock tube tests

14 p2433 A69-29981

Shock tube hot flow duration, contact surface configuration and boundary layer thickness

15 p2590 A69-30297

Hall generator electrical characteristics, discussing plasma homogeneity, stability and shock tube priming

15 p2658 A69-30298

Temperature and electron number density behind reflected shock in helium gas in T tube, noting Z pinch discharges

15 p2593 A69-31161

Microwave breakdown dependence on elevated gas temperature in electric arc shock tube, considering air, nitrogen and argon

16 p2749 A69-31693

Carbon dioxide dissociation relaxation times measured in shock tube at 1900-2400 K and 1.5-2.5 km/sec

16 p2766 A69-31910

Mach reflection shock-shock locus in shock tube implosions generation by area change

16 p2766 A69-31919

Two phase detonations of fuel in liquid layer on shock tube wall with gaseous oxidizer, presenting one dimensional approximation for film detonation propagation

16 p2879 A69-32151

Nitrous oxide-CO bimolecular reaction and O-CO recombination in single pulse shock tube

16 p2748 A69-32793

Temperature jumps at gas-solid interface in shock tube calculated by one dimensional approximation of thermal boundary layer behind reflected shock wave

17 p2949 A69-33023

Shock wave propagation in two types of electromagnetically driven shock tubes, describing probe for shock front velocity measurement

18 p3119 A69-34260

High temperature and short duration flows - Conference, Freiburg University, West Germany, April 1967

18 p3114 A69-34444

Schardin contributions to theory and applications of shock tube, including rapidly occurring events

18 p3115 A69-34445

Shock tube application to transition probability measurements with emphasis on thermodynamic state of radiating gas, noting temperature dependence of level population

18 p3176 A69-34446

Radiation gas dynamics in shock tube, studying radiation coupled flows with flow field affected by radiant energy transport

18 p3116 A69-34447

Reflected shock and boundary layer interaction in shock tube, discussing bifurcation effect on flow and turbulence transition

18 p3116 A69-34448

Widths measurements of van der Waals broadened Si I spectral lines by shock tube and scanning Fabry-Perot interferometer, using argon as perturbing gas

18 p3116 A69-34449

Gas ionization relaxation times from ion density profiles in shock tubes at low Mach numbers, discussing influence of impurities on ionization process

18 p3116 A69-34451

Heated Hg shock tube construction and operation, application to high electron density plasmas and problem of shock bifurcation in Hg monatomic gas

18 p3116 A69-34453

Fissioning plasma generated in shock tube with 235 uranium hexafluoride gas, selecting tube diameter, reflector depth and initial gas density for specific neutron multiplication

18 p3180 A69-34455

Prestressed ceramic driver chamber energy efficiency for arc driven shock tube by pressure measurements with piezoelectric probe

18 p3116 A69-34456

Shock wave profiles in molecular N-H gas mixtures in shock tube measured by optical electron beam method, noting disagreement with Navier-Stokes calculations

18 p3134 A69-34458

Shock tube with cylindrical explosive to implode glass wall and produce high velocity glass particle jet, studying jet velocity and behavior and test gas pressure effects

18 p3116 A69-34460

Metallic aerosol generator application in shock tube spectrometric measurements of radiation by molecules occurring as solids before decomposition to vapor phase

18 p3099 A69-34461

Criteria to predict flow instabilities triggered by exothermic reaction presence in high temperature reaction kinetic shock tube studies

18 p3116 A69-34462

Gas phase ignition shock tube analysis of solid propellant taking into account changing surface temperature and fuel vapor consumption
18 p3183 A69-34463

Low molecular weight fluorocarbons pyrolysis and oxidation in single pulse shock tubes, using vapor phase chromatography and mass spectral analyses
18 p3099 A69-34467

Reflected shock front interaction with heated thin gaseous filament studied in shock tube by spark interferometric and schlieren technique
18 p3228 A69-34468

Shock tube calibration for aerodynamic loading, determining flow parameters by observing particle trajectories with high speed photography of smoke tracers
18 p3085 A69-34469

Optimum ballast resistance of thin film heat transfer gage producing shock arrival time, thickness and structure data of low pressure shock tube
18 p3117 A69-34470

Rereflected shock waves behind tapered shock tube section indicated by shock wave detectors, microwave absorption and optical emission measurements
18 p3085 A69-34474

Shock waves attenuation through multiple reflections at ends and interactions with expansion wave in shock tube by pressure transducer, noting exponential decay
18 p3121 A69-34475

UV absorption coefficients of high temperature air measured in shock tube reflected region
18 p3230 A69-35073

Heat exchange in stagnation point region of blunt body, using shock test simulation of high speed flight
18 p3086 A69-35118

Biased electrostatic probes determining free stream charge density and ionization risetime in supersonic flows in arc heated pressure driven shock tube
19 p3291 A69-35715

Calibration of inertial and surface temperature heat transfer transducers for hotshot and shock tube measurements developed and tested at ONERA [ONERA-TP-683]
19 p3305 A69-35726

Liquid driver shock tubes dynamic and thermodynamic properties as functions of diaphragm pressure ratio and initial conditions
19 p3295 A69-36471

Image converter camera and astronomical telescope arrangement for photographing metal diaphragm openings in shock tube
20 p3538 A69-37227

Thermal dissociation rate of HBr in Ar in 2100-4200 K temperature range by shock tube analysis, using IR emission and UV absorption
20 p3484 A69-37347

Vacuum UV flux along T type shock tube axis and measurements of He I line precursor emission, indicating ionizing radiation contributions to precursor ionization and excitation
20 p3511 A69-38239

Photon induced precursor ionization and electron produced wave separation from electrical shock tubes
20 p3511 A69-38240

Shock tube boundary layers dependence on shock strength determined using vorticity transport to define boundary layer coordinate
22 p3930 A69-40531

Velocity and temperature boundary layers on plane wall developed by ideal shock tube flow for weak shock and expansion waves
22 p3932 A69-40894

Piston driven shock tube at Kyoto University with performance tests results, investigating compression processes, shock speed and flow duration time
22 p3928 A69-41046

Mirror mount for shock tube laser cavity with alignment capability, noting seal against internal pressures
22 p3951 A69-41233

Detonation driven shocks of high Mach number obtained in improved membrane shock tube by heating and compressing driver gas
23 p4198 A69-41545

Mass diffusion and heterogeneities in compression chamber gas mixture in shock tube ascribable to pressure and temperature gradients
23 p4146 A69-41547

Irregular pressure profiles and pressure-time histories when using octofluorocyclobutane and sulfur hexafluoride in explosive driven shock tube [AIAA PAPER 68-730]
24 p4297 A69-43577

Tube diameter effects on shock front propagation, observing front formation process with schlieren method
24 p4297 A69-43630

Shock formation mechanism in simple shock tube using multistage modification of White model, deriving variation of shock Mach number
24 p4305 A69-43631

Quasi-steady laminar flat plate boundary layer in shock tube determined by reducing boundary layer equations to linear differential equations
24 p4305 A69-43632

High enthalpy shock tube and nozzle gas flows for incident shock Mach numbers analyzed for laminar boundary layers and boundary layer transitions
24 p4305 A69-43664

SHOCK TUNNELS

High temperature air plasma total radiant intensity measurements in shock tube
04 p0685 A69-14719

Shock tunnel simulation of scramjet combustion chamber performance [AIAA PAPER 69-84]
06 p0985 A69-18165

Transition of hypersonic boundary layers on conical body using shock tunnel, obtaining surface heat transfer distributions [AIAA PAPER 68-39]
09 p1482 A69-21943

Diagnostic techniques to identify flow regimes of high enthalpy shock tunnel [AIAA PAPER 68-729]
09 p1477 A69-21970

Pressure vessel design to alleviate hydrogen embrittlement of steels for shock tunnel drivers [AIAA PAPER 68-367]
09 p1477 A69-21993

Gun tunnel equilibrium piston technique by model analysis of piston weight, tunnel conditions and geometry
11 p1862 A69-25013

Shock tubes and tunnels design and operation principles for investigating physical and chemical phenomena
13 p2240 A69-27930

Nose bluntness and model scale effect on radial and axial variation of wake fluid and plasma properties by hypervelocity shock tunnel [AIAA PAPER 69-330]
13 p2242 A69-28266

Diffuser performance in hypersonic shock wind tunnel for nitrogen flow, discussing steady shock wave and separation zone formation time
14 p2391 A69-29622

Density and density fluctuations in hypersonic turbulent boundary layer on shock tunnel nozzle wall measured using electron beam probe
16 p2770 A69-31907

Shock tunnel facility generating short duration high velocity high density air flow with equilibrium chemical simulation of free stream flight conditions [AIAA PAPER 68-17]
16 p2766 A69-32167

Shock tunnel steady flow starting process in two dimensional reflection nozzle, using multiple shadowgraphs and interferograms, noting nozzle geometry influences
18 p3085 A69-34471

Quantitative photographs of low density flowfields during shock tunnel tests using electron beam excitation with image intensifier tube detector
19 p3292 A69-35723

Nanosecond pulse coherent Doppler radar for monostatic measurements of turbulent wakes in shock tunnels and ballistic ranges
19 p3293 A69-35743

Digital data acquisition system with ultrahigh sampling rate for Ames electric arc shock tunnel, describing analog to digital conversion, data storage, system performance, etc
19 p3293 A69-35744

Probe for spectral radiation from luminous gas-cap stagnation region to determine driver gas in test section of hypersonic shock tunnel
19 p3294 A69-35753

Miniature transducer to measure low transient pressures on models in rarefied shock tunnel flows, emphasizing mechanical vibration, convective heating and miniaturization
22 p3950 A69-41227

Uniform flow and wall boundary layer growth measurement in conical nozzle of reflected shock tunnel operating at high enthalpy conditions
24 p4247 A69-43575

SHOCK WAVE ATTENUATION

MHD shock wave decay in one dimensional unsteady flow of ideal inviscid perfectly conducting compressible fluid subjected to transverse magnetic field
05 p0806 A69-16736

Shadowgraph cinematography technique for testing attenuating influence of symmetrical diaphragm system on shock wave
12 p2088 A69-26184

Hypervelocity shock wave propagation in rarefied gas, observing anomalous wave attenuation
14 p2433 A69-29846

Attenuation of small perturbations in shape of plane shock wave propagating into uniform medium in presence of rigid or interfacial boundaries
15 p2592 A69-31145

Shock attenuation and equation of state of polyurethane based on aquarium technique and free surface velocity measurement
16 p2828 A69-31810

Shock wave structure dissipation in gaseous medium with microscopic particle velocities asymptotically approaching light velocity
17 p2958 A69-34145

Shock waves attenuation through multiple reflections at ends and interactions with expansion wave in shock tube by pressure transducer, noting exponential decay
18 p3121 A69-34475

Coordinate perturbation and second order solution for early collapse phases of cylindrical or spherical detonation wave in equimolar acetylene-oxygen mixture
19 p3449 A69-36354

Perturbation solution in power and asymptotic series for initial collapse phases of impulsively generated converging cylindrical and spherical shock waves in perfect gas
21 p3692 A69-38688

Electromagnetic wave propagation in nonlinear media, considering evolution and decay of electromagnetic shocks
21 p3697 A69-39670

Plane double front detonation wave attenuation by pursuing rarefaction waves, analyzing oscillations, onset mechanism and stability during transition to Chapman-Jouguet mode
22 p3929 A69-40112

SHOCK WAVE CONTROL

Sonic boom reduction devices, discussing supersonic electroaerodynamic flow with shock waves, gas discharge one dimensional continuum analysis, power expenditure and aerodynamic interaction [AIAA PAPER 69-38]
06 p0869 A69-18150

Gage for measurement of density variation between expansion chamber and driver gas of valve driven shock tube
10 p1673 A69-23342

SHOCK WAVE GENERATORS

NT MAGNETIC ANNULAR SHOCK TUBES

Unsteady flow in blade passage of partial admission turbine for high energy fluids, predicting shock wave formation at entrance using one dimensional theory [ASME PAPER 68-FE-25]
05 p0698 A69-16075

Apparatus for generating HF shock fronted pressure waves in resonant tube
06 p0906 A69-17149

Shock formation in supersonic plasma flow guided by magnetic channel up to magnetic barrier
06 p0966 A69-17524

Kinetic theory for weak shock generation by impulsive piston, using Fourier and Laplace transforms to solve BGK equation
08 p1304 A69-20783

Energy characteristics of exploding wires considered as shock wave source
09 p1539 A69-21560

Shock ignition procedure to keep pyrotechnic composition in optimum condition in space environment, describing test layouts and theory
10 p1749 A69-23007

MHD power plant research and development, discussing shock wave electric power generators and modulated systems
11 p1925 A69-24469

MHD generator design using shock wave kinetic energy produced by explosion in shock tube with superconducting magnetic system
14 p2393 A69-28911

Detached MHD shock wave formation in front of magnetic field acting as piston moving collisionless plasma, discussing time dependence, Alfvén speed and plasma parameters
14 p2502 A69-29958

Detonation wave in gaseous media, current theories on wave initiation, structure and propagation
19 p3452 A69-36370

Electromagnetic piston produced shock wave interaction with detonation wave, producing overdriven detonations
20 p3631 A69-37209

Scalar conductivity as governing parameter in determining current sheet diffusion and energy dissipation in MHD shock producing devices

21 p3776 A69-38708

Collisional shocks in inverse pinch MHD shock producing device, discussing position in current sheet and effect on conductivity and diffusion

21 p3776 A69-38709

SHOCK WAVE INTERACTION

Pulsating magnetic white dwarfs as pulsar models, discussing radio emission mechanisms via shock wave interaction with stellar plasma atmosphere

01 p0149 A69-10269

Plane shock wave interaction with elastic shallow spherical shell in compressible fluid, formulating equations of motion

02 p0339 A69-11977

Hypersonic surface measurements and flowfield properties about slender cones in hypersonic viscous interaction regime

[AIAA PAPER 68-2]

02 p0189 A69-12520

Shock waves collision with supersonically moving axisymmetric slender bodies analyzed by integral transform method, noting application to shock-shock interaction

03 p0413 A69-13010

Linear wave interaction with oblique shock waves, noting dependence of transmission, reflection and generation coefficients on Mach number

03 p0414 A69-13137

Stokes-like region around yawed needle in hypersonic strong interaction regime, discussing asymptotic analysis under Stewartson conditions

04 p0542 A69-14732

Rarefied hypersonic flow model for sharp flat plate in strong interaction regimes, discussing inviscid and viscous shock and merged layers subregions

04 p0589 A69-14747

Shock wave produced polarization effects in dielectrics, noting reflected shock waves and experimental results for polymethyl methacrylate and carbon tetrachloride

04 p0589 A69-14988

Dynamic compatibility conditions for shock wave collision with material discontinuity surface and for superposing two shock waves propagating in opposite directions

05 p0745 A69-15867

Weak shock wave diffraction at two dimensional obstacles, discussing time behavior of pressure distribution

05 p0746 A69-16018

Shock wave-boundary layer interaction configurations for hypersonic propulsion device inlets under transitional and turbulent conditions, noting heat transfer rate

[AIAA PAPER 69-8]

06 p0915 A69-18172

Shock wave in two dimensional mixed transonic airfoil flows, discussing initial value problem for flow downstream of shock

[AIAA PAPER 69-43]

06 p0915 A69-18180

Arc phenomena and gas dynamic effects during shock heated plasma interaction with magnetic field

07 p1188 A69-18273

Interaction between shock wave and magnetic field of current carrying grid for ideal gas with constant coefficients, discussing dissipation, ionization and Joule heat

07 p1120 A69-18998

Shock-like solutions of electrostatic Vlasov and Poisson equations, assuming zero temperature of positive ions and increasing electrostatic potential

08 p1359 A69-19982

Flow behind shock front propagating along viscous fluid film surface, noting shock intensities as related to detonation velocities, using schlieren photographs

08 p1303 A69-20326

Stationary shock wave formation onset in Meyer-Prandtl flow, obtaining Marchal number for plane flow

09 p1429 A69-21688

Nonequilibrium electron heating effect on inert gas plasma conductivity during shock wave movement across magnetic field

10 p1737 A69-23470

Viscous effects of wall boundary layer behind primary shock wave on flow in shock tube, noting pressure and temperature changes

11 p1870 A69-25010

Fluid mechanics shock wave interaction with turbulent boundary layers at transonic to high supersonic speed ranges, noting examples in aviation

11 p1871 A69-25018

Sound field generation by isotropic turbulence through finite strength shock, estimating acoustic energy flux from supersonic jet containing shock waves

11 p1872 A69-25130

Diffraction accompanying reflection of plane shock wave obliquely impinging on walls of obtuse wedge at finite incidence, considering Lighthill method

11 p1873 A69-25135

Nonuniform flowfield from supersonic penetration of plane shock by three dimensional pointed planar wing, using integral transform method to study field perturbation pressure

13 p2199 A69-27323

Suction effects on shockwave-turbulent boundary layer interactions at compression corner leading to reductions in upstream influence

13 p2244 A69-27326

Compression forces during interaction of colliding shock waves in compressible fluid medium, discussing linear and nonlinear problems

13 p2246 A69-27523

Reservoir conditions of reflected shock wind tunnel by subjecting gas to direct shock and shock reflected at closed downstream end of shock tube

13 p2243 A69-28359

Flow structure in conical shock wave-sharp flat plate interaction zone in supersonic flow, noting turbulent boundary layer before separation

14 p2428 A69-28897

Shock wave and blunt faced cylinder interaction in supersonic gas flow in two chamber shock tube observed with high speed photography

14 p2390 A69-29467

Plane shock wave interaction with elastic shallow shell in compressible fluid, formulating equations of motion

15 p2704 A69-30262

Electron concentration and mass density behind reflected shock in ionizing argon, using time resolved two wavelength interferometry

16 p2771 A69-31918

Conical shock wave-turbulent boundary layer interaction data obtained for adiabatic wall conditions at supersonic free stream Mach numbers, including suction effects

[AIAA PAPER 69-450]

16 p2773 A69-32754

Separated flow patterns in base flow at body recesses, emphasizing shock wave boundary layer interaction, laminar flow and flow in front of recess

17 p2949 A69-33124

Plane shock wave interaction with plane rigid netlike wall, obtaining Mach numbers for reflected and penetrating shock waves

17 p2957 A69-33719

Active solar centers interactions above photospheric level and through corona linkages, noting MHD shock waves and magnetic field lines

17 p3040 A69-33801

Collisionless shock waves in plasma and ion and electron turbulent heating in high voltage theta pinches, noting magnetic disturbance

17 p3013 A69-33825

Reflected shock and boundary layer interaction in shock tube, discussing bifurcation effect on flow and turbulence transition

18 p3116 A69-34448

Reflected shock front interaction with heated thin gaseous filament studied in shock tube by spark interferometric and schlieren technique

18 p3228 A69-34468

Shock waves attenuation through multiple reflections at ends and interactions with expansion wave in shock tube by pressure transducer, noting exponential decay

18 p3121 A69-34475

Free jet shock wave structure penetrated by surrounding pure gas molecules

18 p3086 A69-34819

Laminar separation in incompressible fluid flowing past bluff body at high Reynolds number, investigating shock wave interaction with laminar boundary layers

18 p3122 A69-34918

Vibrational deexcitation shocks in expanding nonequilibrium nozzle flows extended to include embedded adiabatic shock

18 p3089 A69-35386

Shock wave interaction and bow shock wave establishment near sphere in presence of ionization relaxation, using time resolved schlieren photography

19 p3450 A69-36361

Shock waves Mach reflection at various velocities in real gases, observing temperature and pressure distributions, double reflections, effects of internal degrees of freedom excitation, etc

19 p3450 A69-36363

Transverse and longitudinal velocity components of detonation waves in stoichiometric hydrogen-oxygen propagating in fundamental mode in square section tube

19 p3451 A69-36367

Finite chemical reaction rate detonation wave interaction with rarefaction wave, noting mixture activation energy and heating power influence

19 p3298 A69-36384

Lateral and head-on interactions between plane shock wave and supersonic wedge, showing solution dependent on apex angle and incident flow Mach number

19 p3239 A69-36398

Gas ionizing shock waves structure in arbitrary magnetic field, considering greater magnetic viscosity than dissipative coefficients

19 p3381 A69-36773

Three dimensional velocity field disturbed by shock wave traveling across slender wing at supersonic speed

19 p3242 A69-36797

Electromagnetic piston produced shock wave interaction with detonation wave, producing overdriven detonations

20 p3631 A69-37209

Amplitude equations for magnetoacoustic and entropy waves diverging from normal MHD shock, obtaining energy flux ratios associated with incident and transmitted waves

20 p3582 A69-38242

Perturbation solution in power and asymptotic series for initial collapse phases of impulsively generated converging cylindrical and spherical shock waves in perfect gas

21 p3692 A69-38688

Thermal dissociation of chlorine trifluoride behind incident shock waves as function of temperature using UV absorption spectroscopy

21 p3670 A69-39739

Shock wave effect on ionization of detonation waves in propane-O mixtures producing stable high velocity plasma, measured by double probe method

21 p3853 A69-39745

Solar atmosphere radio emission generation by hydrodynamic shock wave interaction with coronal plasma, treating corona as ideal gas consisting of protons and electrons

22 p4009 A69-39984

Jadeite /high pressure sodium aluminum pyroxene/ shock-induced phase assemblage from oligoclase, noting relevance to lunar rock samples investigation

22 p3941 A69-40569

Transient flow resulting from plane shock diffraction by analytic blunt body, basing analysis on Taylor series expansions in space and time variables

22 p3860 A69-40895

Strong interaction between hypersonic boundary layer over flat plate and associated inviscid flow, discussing heating and vorticity effects, boundary layer edge, etc

22 p3860 A69-40896

Initial pressure rise and consequent laminar boundary layer separation during interaction with shock wave

23 p4151 A69-41691

Mach 42 test measuring surface pressures, surface heat transfer rates and shock wave shapes in strong interaction regime for sharp and blunt plates

[AIAA PAPER 68-720]

23 p4059 A69-41886

Pressure measurement modifications of quasi-steady flow model for interaction between reflected shock wave and laminar boundary layer in shock tube

23 p4148 A69-41903

Supersonic aircraft sonic bangs loudness level calculations by model waveforms with allowance for interaction between incident and ground reflected shock waves

23 p4063 A69-42454

Shock wave/boundary layer interaction calculation methods circumventing simultaneous large longitudinal and transverse pressure gradients and viscous effects

24 p4243 A69-42582

Magnetic and electron temperature interaction effects in fast MHD shock waves in slightly ionized plasma

24 p4356 A69-43361

Hypersonic viscous interaction, studying axisymmetric flow over slender sharp nose cones at zero angle of attack and three dimensional flow over sharp flat plate

24 p4248 A69-43579

Strong shock and Mach waves interaction generated downstream of thick wedge body shock in unsteady hypersonic and supersonic flows

24 p4306 A69-43674

SHOCK WAVE LUMINESCENCE

Luminous flow in front of sphere and behind cylinder under high temperature and low density conditions, discussing profiles of shock waves

02 p0189 A69-12182

Spectral brightness temperature of shock waves in air measured at 220-800 nm, obtaining 9-14 km/sec shock waves by detonating explosives

11 p1877 A69-25755

High speed photographic study of plasma luminescence front and charged particle concentration front counter to electrodynamic force in crossed electric and magnetic fields

12 p2141 A69-27130

Br molecular dissociation rate in argon excess determined, considering visible emission intensity behind shock front

18 p3176 A69-34465

Precursor electrons due to photoionization ahead of pressure driven shock waves, presenting electron temperature and density theoretical analysis

20 p3511 A69-38238

SHOCK WAVE PROFILES

Pressure and shock shape determination for plane supersonic and low hypersonic flows past aerodynamic profiles

01 p0008 A69-11299

Schematic chart prepared for shock wave geometry of Tungusk meteorite, discussing tree felling

01 p0159 A69-11379

Detonation wave structure in solid cylindrical shell explosive, noting attainment of steady state structure

02 p0349 A69-11526

Luminous flow in front of sphere and behind cylinder under high temperature and low density conditions, discussing profiles of shock waves

02 p0189 A69-12182

Two dimensional diffuse shock waves in carbon dioxide, noting effect of shock curvature equivalence to thickness

02 p0233 A69-12534

Trimodal solutions for strong shock structure in gas of spherocylindrical molecules

03 p0414 A69-13136

Parameter changes of diatomic gas behind direct shock wave with simultaneous oscillatory and dissociative relaxation

03 p0418 A69-13835

Spherical shock wave propagation in polytrope with poloidal magnetic field, noting application to shock waves in magnetic stars

04 p0664 A69-15438

Shock wave profiles in expansion flows determined with static and impact pressure probes, investigating pressure gradient effects

06 p0908 A69-17022

Collisionless shock waves in rarefied plasma, discussing dispersion effect and oscillatory shock wave structure

08 p1303 A69-19996

Multibeam Fabry-Perot interferometers for aerodynamics measurements of rarefied gas flows, determining density distribution, shape, structure and detachment of shock waves

08 p1314 A69-20385

Monograph on shock wave structure in binary gas mixtures covering gas kinetics and shock tube measurements of heavy component density distribution

08 p1304 A69-20711

Supersonic jet impingement on flat plate, showing shock wave profiles and slipstream surface at stations parallel to nozzle axis

08 p1252 A69-20841

Bow shock wave position and shape in rectilinear flight with constant acceleration

09 p1433 A69-21386

Shock wave structure problems in plasma, including plasma particles random motion in term representing electric field

09 p1551 A69-22032

Switch-on ionizing shock waves structure, analyzing condition of downstream state and effect on hydromagnetic wave speed

09 p1552 A69-22045

Hypersonic drag and shock wave characteristics of blunt bodies including cones, spherical nose and concave nose bodies

09 p1433 A69-22568

Shock wave structure determination in simple monatomic gas, using statistical counting and successive approximation algorithm

10 p1680 A69-23894

Type 2 radio burst dynamic spectra determination for finding shock wave and magnetic field parameters above active corona region

11 p1945 A69-24243

Kinetic theories applied to shock wave structure study of monatomic gas

11 p1870 A69-25007

Motion equations for ideal transonic gas flow, applying solutions to flow with incident shock waves of various profiles

11 p1820 A69-25468

Supersonic gas flow past plane and axisymmetric bodies with broken generatrix, determining tangential discontinuities and shock waves shape and position

11 p1820 A69-25470

Topological properties of plane flow in subsonic region behind smooth shock wave in uniform supersonic flow, discussing shock wave convexity

12 p2061 A69-25888

Bhatnagar-Gross-Krook model for plane shock structure, considering moment and least squares methods and shock density gradient error analysis

12 p2063 A69-27112

Particle volume role in normal shockwave structure in gas-particle mixtures, discussing equations of motion formulation

13 p2244 A69-27327

Shock wave gas flow density behind shock tube calculated by shadows measurements using interferometric techniques

13 p2245 A69-27384

High purity beryllium dynamic tests, determining Hugoniot equation of state, shock profile and spall threshold/onset of microcracking/for elastic pulses [AIAA PAPER 69-360]

13 p2283 A69-28293

Minimum error criteria for shock wave structure determined by applying Mott-Smith distribution to Boltzmann equations for rigid sphere gas

14 p2431 A69-29579

MHD quantities in linear wave and small intensity shock wave dissipation and structure determinable by right and left eigenvectors of matrix MHD flow equation

14 p2500 A69-29902

Supersonic flow past cone in presence of blowing normal to cone surface, calculating flow field parameters behind conical shock wave

15 p2548 A69-31175

Trailing shock wave position in air breathing jet engine channels, determining supersonic-subsonic boundary, noting Mach number effects on pressure ratio

16 p2768 A69-31743

Mach reflection shock-shock locus in shock tube implosions generation by area change

16 p2766 A69-31919

Shock polar equation in polar coordinates, showing shock polar shape dependence on Mach number

16 p2772 A69-32178

Strong shock wave structural model, considering near molecular beam, upstream hypersonic and downstream subsonic flows and beam-continuum conversion by collision

18 p3120 A69-34457

Shock wave profiles in molecular N-H gas mixtures in shock tube measured by optical electron beam method, noting disagreement with Navier-Stokes calculations

18 p3134 A69-34458

Streak photographs by differential interferometer to study head wave standoff in shock tubes as function of time

18 p3085 A69-34473

Shock wave structure in single component monatomic gas by expanding Boltzmann equation distribution function in terms of Hermite polynomial

18 p3124 A69-35170

Nonequilibrium behavior of shock standoff distance ahead of spheres at low supersonic Mach number

18 p3089 A69-35385

Computer program for numerical integration of chemical reaction rate equations behind steady state hydrogen-oxygen shock wave

19 p3451 A69-36366

Shock and detonation waves refraction due to small disturbances in medium, noting causes of wave cellular structure

19 p3451 A69-36369

Pure gas suction through free jet shock structure, analyzing aerodynamic effect of molecular separation

19 p3240 A69-36650

Pade method applied in aerodynamics for determining detached shock wave shapes and shock waves attached at vertex of cone

19 p3241 A69-36778

Global properties of solution of inverse detached shock problem analyzed by characteristic coordinates at low Mach number

19 p3301 A69-36788

Shock wave parameters from meteoric body moving at high supersonic speeds through atmosphere, calculating specific heat ratio

19 p3428 A69-36841

Weak shock wave structure in temperature relaxation media determined using theory of sound absorption in fluids

19 p3301 A69-36842

Shock structure in two dimensional or axisymmetric jet flows under transverse impingement by low energy jets [ASME PAPER 69-FLCS-41]

20 p3515 A69-37975

Windward shock angle parameters on yawed cones correlated in single variable for hypersonic flow

23 p4060 A69-41918

Interplanetary shock waves structure and evolution, discussing propagation in collision free media by wave-particle interactions

23 p4222 A69-42394

One dimensional shock waves and acceleration fronts in nonlinear isotropic viscoelastic materials using constitutive equations

23 p4235 A69-42463

Class of one dimensional nonlinear waves and shock structure reduced to steady flows in radiation gas dynamics

23 p4240 A69-42466

Rarefied gas one dimensional transverse motions consistent with Boltzmann kinetic equation, solving integrodifferential equations for shock wave structure

24 p4351 A69-43491

SHOCK WAVE PROPAGATION

Two dimensional diffuse shock waves in carbon dioxide, noting effect of shock curvature equivalence to thickness

02 p0233 A69-12534

Propagation of detonation wave in tube containing single stream of diethylcyclohexane droplets dispersed in gaseous oxygen

03 p0415 A69-13139

Shock wave produced polarization effects in dielectrics, noting reflected shock waves and experimental results for polymethyl methacrylate and carbon tetrachloride

04 p0589 A69-14988

Spherical shock wave propagation in polytrope with poloidal magnetic field, noting application to shock waves in magnetic stars

04 p0664 A69-15438

Gas velocity variations in ionizing shock wave propagating along magnetic field applied to conducting piston motion

05 p0801 A69-15787

Dynamic compatibility conditions for shock wave collision with material discontinuity surface and for superposing two shock waves propagating in opposite directions

05 p0745 A69-15867

Radiation intensity distribution from first negative and positive nitrogen system in equilibrium gas flow behind propagating shock front, discussing kinetics mechanism and electronic states

05 p0745 A69-15890

Equations describing chemical kinetics and conservation law derived for ionization relaxation processes behind shock wave front in air

05 p0746 A69-15891

Shock tube investigation of formation and flow characteristics of impulsively generated vortex street recorded interferometrically, using high speed framing camera [ASME PAPER 68-FE-32]

05 p0748 A69-16079

Oblique shock wave propagation through two dimensional steady nonuniform incoming flow, discussing higher order theory via irrotational or rotational disturbances of arbitrary amplitude [AIAA PAPER 69-39]

06 p0913 A69-18103

Collisionless shock waves in high beta plasmas and in cold plasmas

07 p1194 A69-19366

Detonation wave propagation in H-O mixtures in supersonic flow, noting detonation front structure and velocity

08 p1420 A69-19882

Spectroscopic analysis of hydrogen spark plasma discharge parameters at small PD values, discussing shock wave initiation accounting for transition to quasi-stable phases

08 p1360 A69-20100

Flow behind shock front propagating along viscous fluid film surface, noting shock intensities as related to detonation velocities, using schlieren photographs
08 p1303 A69-20326

Displacement effect due to subsonic reaction heat front behind shock wave in two dimensional supersonic flows
08 p1252 A69-20691

Laser produced blast wave expansion measured by microwave technique, obtaining surface temperature and electron density
09 p1514 A69-21324

Boundary layer at tube wall behind shock wave propagating in gas-vapor mixture, analyzing condensation rate
09 p1480 A69-21591

High velocity gas stream induced shattering of liquid drops, disintegration rate and breakup time
[AIAA PAPER 68-83] 09 p1482 A69-21947

Nonuniform propagation of imploding shock waves by extending self similar solution to earlier times in implosion process when shock strength is finite
10 p1678 A69-22931

Converging cylindrical shock waves produced by discharging condenser bank into single turn coil surrounding gas container /theta pinch discharge/
10 p1678 A69-22933

Invariant finite amplitude spherical shock wave propagation in medium with inversely radial density
10 p1778 A69-23405

Shock wave propagation in gravitational field with pressure and density gradients, considering nonlinear equations of fluid flow
11 p1961 A69-25106

Model for shock propagation from point energy source into cold atmosphere with exponential density variation
11 p1871 A69-25123

Electric field measurements for turbulence in collision-free shocks, noting power spectra of magnetic and electric fluctuations and electron density
11 p1930 A69-25276

Kinetics of air plasma formation in wake of shock wave propagating in air, taking into account nonequilibrium ionization
12 p2062 A69-26674

Nonequilibrium radiation from first negative band of molecular nitrogen ion excited by shock wave electron impact
13 p2245 A69-27380

Speed of sound and shock waves in two phase flows of liquid metal MHD generators, considering droplets uniformly dispersed in gaseous phase
13 p2245 A69-27475

Plane elastoplastic shock waves propagation due to combined shear loadings assuming elastic isotropic work hardening materials
13 p2368 A69-28346

Two temperature gasdynamics for binary gas mixtures of differing molecular weight components, analyzing ultrasound and shock wave propagation
13 p2250 A69-28447

Diffuser performance in hypersonic shock wind tunnel for nitrogen flow, discussing steady shock wave and separation zone formation time
14 p2391 A69-29622

Shock wave velocity and gas flow parameters in shock tube with noninstantaneously opening diaphragm calculated by method of characteristics
14 p2432 A69-29623

Shock development in electrothermal shock tube with performance simulation of mechanical shock tube with hot driver but turbulent or unstable driver-shock interface
14 p2427 A69-29768

Hypervelocity shock wave propagation in rarefied gas, observing anomalous wave attenuation
14 p2433 A69-29846

MHD interaction between plasma and transverse magnetic field in shock tube, noting unsteady shock wave propagation in interaction zone
14 p2501 A69-29919

Calorimetric measurement of electron temperature in collisionless shock wave propagating in plasma column, discussing role of H beta line Stark broadening
15 p2657 A69-30104

Hydromagnetic fast shock strength and direction in inhomogeneous gravitational atmosphere with uniform magnetic field, discussing heating in solar corona
15 p2680 A69-30202

Digital computers for aircraft engines control, discussing economic assessment, advantages and basic control system
15 p2671 A69-30323

Unsteady nonadiabatic shock waves in stellar gas dynamics, analyzing energy losses due to ionization at shock fronts by extended Chiznell-Wisem method
15 p2682 A69-30508

Pressure, temperature, density and enthalpy of carbon dioxide behind primary and reflected shock waves determined by method suitable for computer
15 p2592 A69-31054

Temperature and electron number density behind reflected shock in helium gas in T tube, noting Z pinch discharges
15 p2593 A69-31161

Shock waves from accelerated, decelerated and stationary axisymmetric bodies flying at supersonic velocities in stratified isothermal atmosphere
15 p2551 A69-31171

Conditions behind incident and reflected shock waves in shock tube calculated from initial pressure, density, temperature and shock speed
15 p2593 A69-31487

Shock wave growth or decay in atmospheres with density and temperature variation using singular surface theory
16 p2768 A69-31663

Compression waves observed ahead of luminous discharge plasma below Mach 12-15 in electric shock tube, describing shock structure by blast wave theory
16 p2768 A69-31664

N wave propagation across nonuniform medium described by cloud or front layer, using geometrical optics
16 p2812 A69-31924

Numerical simulation of flare generated shock wave propagation through solar wind, noting transit time and shock strength agreement with observations
16 p2848 A69-31970

Transmission of Alfvén waves through earth bow shock based on hydromagnetic shocks theory, discussing amplitude amplification
16 p2777 A69-32099

Shock wave propagation in isothermal atmosphere, discussing radiation and ionization effects on thermal jump
16 p2858 A69-32207

Gas phase ignition theory with feedback of homogeneous propellant exposed to stagnant gas after shock reflection
[AIAA PAPER 69-559] 16 p2880 A69-32740

Supersonic blowdown wind tunnel noting cylindrical diffusers efficiency in starting supersonic nozzles increased in proportion to Mach number
17 p2890 A69-33125

Shock waves propagation in inhomogeneous gases, considering time development and energy flux during point explosion in plane layers by quasi-stationary approximation
17 p2952 A69-33383

Gas and small particle diffusion in turbulent boundary layer of blast wave propagating over land or water, assuming logarithmic vertical velocity profile
[AIAA PAPER 69-672] 17 p2953 A69-33439

Laboratory plasma produced by electromagnetically generated shock front propagation through unionized hydrogen
[AIAA PAPER 69-693] 17 p2945 A69-33447

Flow field pressure distribution due to plane shock wave impinging by thin wing moving in opposite direction, discussing mathematical formulation, analytic solution and applications
[AIAA PAPER 69-647] 17 p2891 A69-33459

Collisionless shock wave generation and structure in zeta and theta pinches
17 p3013 A69-33819

Energy dissipation in collisionless shock waves generated in plasmas with 1-500 trillion/cm electron density by theta pinch, measuring axial ionic energy spectrum
17 p3013 A69-33820

Oblique hydromagnetic shock waves in magnetized hydrogen plasma enclosed in pyrex chamber by oscillatory zeta discharge, probing for front development and structure
17 p3013 A69-33823

Red dwarf star YZ CMi corona structure showing possible estimation of additional carried energy by shock waves after flare
17 p3043 A69-34166

Shock wave propagation in two types of electromagnetically driven shock tubes, describing probe for shock front velocity measurement
18 p3119 A69-34260

Shock wave propagation induced by nonuniform instantaneous internal heating of nonlinear elastic strain hardening solid material
[SAWE PAPER 69-APM-17]

18 p3214 A69-34393

Plane shock wave propagation around cylinders of various radii recorded with shadowgrams and Mach-Zehnder interferograms, discussing wave diffraction mechanics
18 p3120 A69-34472

Rereflected shock waves behind tapered shock tube section indicated by shock wave detectors, microwave absorption and optical emission measurements
18 p3085 A69-34474

Gas velocity variations in ionizing shock wave propagating along magnetic field applied to conducting piston motion
18 p3181 A69-35038

Flow viscosity and heat conduction effects on shock wave propagation in bent channel with weak Mach reflection
18 p3124 A69-35326

Shock wave propagation through collisionless magnetized plasma, using gun driven, laser and cesium plasma flow methods
19 p3379 A69-35759

Detonation wave in gaseous media, current theories on wave initiation, structure and propagation
19 p3452 A69-36370

Gas motion behind cylindrical shock wave created by piston motion in gravitating medium
19 p3298 A69-36386

Jet and Mach disk density measured by fluorescence electron beam technique, calculating Mach disk thickness from density profiles
19 p3239 A69-36396

Hugoniot prediction for shock moving along longitudinal direction of unidirectional fiber reinforced composite
20 p3627 A69-37768

Soviet book on shock waves propagated by meteorite intrusion into earth atmosphere, covering interaction with earth surface, Tunguska meteorite, etc
20 p3613 A69-38205

Precursors ahead of pressure driven shock waves in Ar, considering electron diffusion, temperature a density
20 p3518 A69-38237

Normal ionizing shock waves in H, analyzing shock velocities as function of drive magnetic field using Chapman-Jouguet hypothesis
21 p3691 A69-38332

Schlieren framing photography used for studying shock wave hydrodynamic structure and ignition dynamics during expansion into detonable gas region
21 p3849 A69-38803

Shock front reaction and detonation initiation in low density ammonium perchlorate
21 p3784 A69-39590

Equation of state measurements of earth materials by shock wave techniques, applying to olivine for earth mantle constitution problem
22 p3937 A69-40188

Shock wave detachment distance in front of spheres and cylinders in hypersonic flow, using magnetic shock tubes and Mach 5 and 18 wind tunnels
22 p3931 A69-40710

Adiabatic plane ideal gas flow past airfoil, studying shock waves propagation effect on dynamic behavior
22 p3861 A69-41024

Unsteady combustion wave passage through inert obstacle in gunpowder in N filled pressure vessel
22 p4051 A69-41119

Ionizing shock wave propagation and reflection in transverse magnetic field based on MHD theory, assuming gas thermal equilibrium
22 p3992 A69-41176

Reaction zone following overdriven detonation wave propagating into mixtures of fluorine oxide and hydrogen molecules showing HF laser emission
22 p4052 A69-41188

Detonation driven shocks of high Mach number obtained in improved membrane shock tube by heating and compressing driver gas
23 p4198 A69-41545

Interplanetary shock waves structure and evolution, discussing propagation in collision free media by wave-particle interactions
23 p4222 A69-42394

Shock wave transient motion during passage through ducts in inviscid gas containing convergences, using characteristics method
23 p4153 A69-42398

Ionization rate limiting processes behind strong shock waves in pure N, plotting electron density profile diagrams
24 p4302 A69-43367

Tube diameter effects on shock front propagation, observing front formation process with schlieren method

24 p4297 A69-43630

Light scattering from ruby laser beam passing through collisionless shock produced by H plasma compression measured by photomultiplier

24 p4360 A69-43748

SHOCK WAVES

NT DETONATION WAVES

NT MACH CONES

NT NORMAL SHOCK WAVES

NT OBLIQUE SHOCK WAVES

NT RIEMANN WAVES

NT SONIC BOOMS

Circular, cylindrical thin walled shell dynamic response to moving shock solved by Flugge equations in series form

01 p0164 A69-10057

Simple and shock waves in nonlinear unsteady heat and mass transfer, discussing conditions for transforming simple waves into shock waves

01 p0174 A69-10096

Three dimensional flow at large distance and in front of shock wave for three dimensional body traveling at sonic velocity

01 p0005 A69-10159

Sonic flow at large distance and behind shock wave for axisymmetric body of revolution of finite dimensions in inviscid fluid

01 p0058 A69-10160

Molecular velocity distribution function in nonequilibrium flows, detailing asymptotic expansions in different velocity domains for weak shock

01 p0059 A69-10330

Barrier penetration depth by meteorite particles at prethreshold impact velocities, taking into account energy dissipation on shock wave front

01 p0152 A69-10579

Structure of shock waves from MHD jet injected into zero viscosity, finite thermal and electrical conductivity medium analyzed by nonlinear differential equation system

01 p0130 A69-10774

Vibrational relaxation of diatomic gases behind shock waves, with variable heat bath temperature extended to constant enthalpy and constant total enthalpy conditions

01 p0061 A69-11204

Shock reflection structure in ionizing xenon determined by fast rise pressure gauge mounted in shock tube end wall

01 p0132 A69-11205

Detonation generation in granular explosive subject to different shock wave intensities due to variable impact velocity

02 p0349 A69-11527

Swirl flow through single and multistage Carnot shock diffuser, analyzing relation of pressure rise and diffuser aspect ratio

02 p0230 A69-11616

Hydraulic analogy for shock and expansion waves arising in supersonic compressors due to three dimensionality of flow [ONERA-TP-598]

02 p0187 A69-11621

Hypersonic gas flow past blunt body problem solved by integral correlation method, taking into account radiation effects and gas dynamic parameter distribution in shock wave layer

02 p0188 A69-11651

Numerical calculations for oscillatory solutions of system of nonlinear differential equations, noting circularly polarized magnetic oscillations observed near earth bow shock front

02 p0241 A69-11729

Equations, tables and charts for shock drag parameter in determination of shock wave drag of body in supersonic free stream of ideal gas

02 p0188 A69-11862

Electro-optical measurements to determine intermolecular interaction temperatures in organic liquids compressed by shock waves

02 p0230 A69-11979

Vela 3A and Explorer 33 elapsed time observations of earth bow shock

02 p0244 A69-12299

Initiation of detonation by incident shock waves in hydrogen-oxygen-argon mixtures

02 p0304 A69-12313

Fuel films ignition behind shock waves in air and oxygen

02 p0353 A69-12317

Quantitative determination of reentry shock precursor absorption level and effect on surface radiation

heating, calculating radiative flux from shock layer enthalpy distribution

02 p0354 A69-12528

Hypersonic flow past delta wings with attached shock wave, analysis leads to determination of closed flow pattern

02 p0191 A69-12577

Lighthill method based expressions derived for discontinuity shape formed during shock wave diffraction near small angle

02 p0234 A69-12588

Velocity measurement and flow pattern determination of plane shock waves during passage through channel diaphragm

02 p0234 A69-12589

Nonlinear weak shock wave diffraction around convex angled corners in polytropic inviscid thermally nonconducting gas

03 p0412 A69-12848

Velocity field generated by shock wave incident on slender symmetrical body resting in infinite compressible medium

03 p0362 A69-13418

Solar wind interaction with moon, discussing core/surface layer conductivity and lunar limb shock wave formation

03 p0502 A69-14006

Nozzle geometry influence on argon plasma flow parameters in shock tube, discussing measurement data behind shock wave front

03 p0481 A69-14160

Explosive detonated in external electric field to obtain data on gas state behind shock wave

04 p0634 A69-14430

Structures response to explosive blast, discussing damage criterion in terms of blast wave impulse and critical time

04 p0671 A69-14476

Book on transonic aerodynamics, emphasizing two dimensional and three dimensional problems involving transonic flow about airfoils with and without shocks

04 p0541 A69-14580

Numerical algorithm for supersonic gas flow past blunt bodies with shock wave separation, using Dorodnitsyn method of integral correlation

04 p0587 A69-14621

One-dimensional self similar motion of relaxing gas, noting ODEs of process and gas dynamic parameters of flow field

04 p0588 A69-14623

Detection of electric field turbulence in earth bow shock, noting wave amplitude correlation with magnetic field structure

04 p0592 A69-14681

Soviet book on shock waves in real gases covering gas flow patterns in shock tube, perturbations, shock and detonation wave reflection, etc

04 p0589 A69-14937

Collapsing cylindrical ionizing shock in axial magnetic field, solving governing equations numerically

04 p0637 A69-15049

Transverse ionizing MHD shock waves, discussing jump conditions with magnetic field in shock plane

04 p0637 A69-15052

Magnetic lines curvature behind pseudostationary hydromagnetic shock determined, assuming parallel magnetic field and velocity vectors

04 p0638 A69-15092

Adiabatic motion of hydromagnetic fluid behind spherical fast shock wave for Parker solar wind model

04 p0660 A69-15126

Mountain structures surrounding lunar craters, discussing possible origin by impacting planetesimals shock waves

04 p0661 A69-15142

Wind turbulence measurement by shock wave tracking using Doppler radar, stressing relative location of antenna and sound source

04 p0628 A69-15149

Variable energy blast waves analysis with reference to cylindrical spark channel formation, noting shock front velocity approximation

04 p0590 A69-15203

Steady plane supersonic gas flows with large number of shocks computed on basis of weak solutions of hyperbolic system

04 p0544 A69-15284

Shock wave damping at large distances from body situated in ideal gas three dimensional flow

04 p0591 A69-15535

Energetic electrons of terrestrial origin behind bow shock and upstream in solar wind

05 p0815 A69-16253

Zone behind reflected shock wave in shock tube using electron beam scattering, showing flow spectra and attenuation region of wave

05 p0752 A69-16688

Numerical calculation of density profiles of shock waves in expansion flows

06 p0908 A69-17021

Plasma physics in space research, discussing solar wind, planetary atmosphere bow shock and convective motions of magnetosphere plasma [ISAS-431]

06 p1000 A69-17026

Thickness of resistivity controlled hydromagnetic shock wave, using classical one fluid equations and generalized Ohm law

06 p0970 A69-17956

Gasdynamic flow shock wave phenomena during exploding wire dwell time inside metal vapor cylinder, noting effect on reignition

07 p1188 A69-18275

Thermal dissociation of chlorine trifluoride behind incident shock waves at high temperature, discussing bimolecular reaction rate constant [WSCI PAPER 68-40]

07 p1202 A69-18355

Electric signals by shock and detonation waves, describing detection technique [WSCI PAPER 68-44]

07 p1240 A69-18360

Structure of plane shock wave of arbitrary force propagating across magnetic field in hot rarefied plasma

07 p1190 A69-18692

Plasma diagnostics by spectroscopic techniques, measuring polarity dependences of temperature and charged particle concentration for flows with shock wave and periodic structure

07 p1190 A69-18695

Nonstationary flow past spheres and cylinders in electromagnetic shock tube, determining time required for flow to become stationary

07 p1119 A69-18744

Hypersonic flow past blunt body near stagnation point, noting surface layer characterized by increased density and decreased entropy of gas

07 p1050 A69-18755

High electron-proton temperature ratios effect on solar wind double shock wave structure, using one dimensional and two fluid models

07 p1205 A69-18849

Shock waves internal structure in perfect monatomic gases, discussing density distribution in shock layer experimental measurement

07 p1120 A69-18930

Jump conditions across MHD shock waves, reducing relations to identities applicable to nonequilibrium situations

07 p1193 A69-19242

Solar wind, bow shock and magnetosheath observations by charged particle analyzers on Vela satellites

07 p1208 A69-19361

Magnetopause, magnetosheath, bow shock and adjoining interplanetary domain study by IMP-1 satellite, discussing macroscopic plasma variables and fluid model for solar wind

07 p1129 A69-19374

Shock waveforms lengthening due to propagation to high altitudes derived from computed numerical values, studying N waves from SST

07 p1054 A69-19463

Plane radiative shock wave propagation in homogeneous medium noting heating ahead and cooling behind shock front

08 p1302 A69-19798

Steady shock discontinuity in perfectly conducting gas flow in arbitrarily oriented magnetic field for various Mach numbers

08 p1360 A69-19988

Vibrational relaxation effects on laminar boundary layer velocity profiles and temperature and on layer thicknesses and wall heat flow downstream of shock wave

08 p1303 A69-20269

Monograph on kinetic study of fast gas reactions with shock waves covering thermal decomposition of nitrous oxide, hydrazine tetrafluoride and nitrogen tetrafluoride

08 p1304 A69-20707

Monograph on interferometric studies of unsteady shock waves in theta pinch driven shock tube, discussing flow characteristics in helium and hydrogen

08 p1304 A69-20710

Frozen shock in steady one dimensional compression flow of relaxing gases weaker than equilibrium shock

08 p1304 A69-20785

- Vorticity behind shock waves in conducting gases when magnetic field is tangential or normal to shock surface using momentum equation
08 p1367 A69-20789
- Two fluid kinetic model for analyzing shock wave structure in binary mixtures of monatomic inert gases, noting no overshoot in velocity profiles
08 p1304 A69-20813
- Bose condensation and shock waves in photon spectrum during scattering for equilibrium state of ionized plasma and radiation
09 p1546 A69-21574
- Singular shock waves formation during pulsed forward motion of conducting piston in MHD medium
09 p1551 A69-22034
- Solar moving type 4 burst emitting synchrotron radiation, noting electron acceleration in collisionless shock wave in corona
09 p1578 A69-22058
- Envelope shock waves transitions between modulated wave amplitude and frequency in dispersive medium with relaxing nonlinearity
09 p1483 A69-22660
- D type dissociation ionization front structure and associated shock fronts using quasi-steady flow approximation for Stromgren sphere development in interstellar molecular hydrogen cloud
10 p1772 A69-22858
- Analytical method for perturbations by spherical and cylindrical shock waves flowing toward common center
10 p1677 A69-22899
- Transverse magnetic field and shock strength effects on curvature ratio of attached shock waves and wedge
10 p1728 A69-23238
- Invariant transformation of equations for ideal gas plane steady motions, noting application to gas flows with shock waves and eddies
10 p1680 A69-23709
- Simultaneous interplanetary magnetic field measurements by geocentric satellites Explorer 33 and IMP 3 of MHD shock wave associated with July 8, 1966 sudden storm commencement
10 p1783 A69-23773
- Existence of motions of second type in explicit self similar strong shock solutions of Euler equations when velocity is linear function of coordinate
10 p1680 A69-23789
- Rotational discontinuity in plasma, noting behavior for particle reflection off front side or back side of MHD wave
11 p1923 A69-24293
- Angle of attack and Reynolds number effect on hypersonic flow past circular cone, obtaining shock wave shape
[ONERA-TP-692] 11 p1818 A69-24751
- Shock induced boundary layer flow establishment on semiinfinite flat plate, measuring heat transfer rates and transition to turbulence
11 p1869 A69-24890
- Vibrational relaxation frequency of asymmetric stretching mode of carbon dioxide determined by measuring rate of thermal emission in shock waves near 4.3 microns
11 p1922 A69-25128
- Electrical conductivity of air behind incident and reflected shock wave fronts as function of temperature and Mach numbers measured by electrode method
11 p1888 A69-25220
- Carbon dioxide temperature distribution, absorption and concentration as functions of molecular dissociation behind shock wave determined by measuring IR bands intensity
11 p1873 A69-25226
- Space-time hypersurfaces representations of shock waves of relativistic MHD, discussing compressibility role in proving consistency with relativistic theory
11 p1928 A69-25246
- Unstable ion sound wave propagation across magnetic field in collisionless shock waves, noting drift instability
11 p1930 A69-25273
- Diffusion of ion-electron pairs produced by photoionization upstream of strong shock waves to shock tube walls based on particle flux and Poisson equations
11 p1866 A69-25275
- Solution of confluence in three dimensional shock and detonation polars for spinning detonation
11 p2002 A69-25353
- Shock wave structure in gas mixtures, discussing velocity and temperature undershoot and overshoot
11 p1874 A69-25356
- Current and voltage distribution around normal shock in MHD duct using conformal transformation, considering continuous and segmented electrode boundary conditions
11 p1931 A69-25359
- Gas velocity variation in ionizing shock waves arbitrarily oriented with respect to magnetic field, considering magnetic viscosity and conductive piston
11 p1935 A69-25740
- Spectral brightness temperature of shock waves in air measured at 220-800 nm, obtaining 9-14 km/sec shock waves by detonating explosives
11 p1877 A69-25755
- Rotating mirror streak cameras in quantitative measurements of extreme compressions by shock waves, analyzing spatial and temporal resolving power
12 p2084 A69-26151
- Gasdynamic stability of detonation shock wave in case of arbitrary heat evolution kinetics using detonation model
12 p2062 A69-26672
- Shock pulse criterion limitations and HF transients technique for design and tests of structures and components
12 p2182 A69-26731
- Spiral arms as wakes of gravitational shock waves arising at galactic nucleus boundary and propagating outward through interstellar gas
12 p2170 A69-27066
- Shock waves in solids, discussing gas gun firing and explosive detonating at specimen, transformations measurement and materials processing applications
13 p2360 A69-27341
- Vibrational energy exchange between diatomic molecules by IR emission of CO fundamental behind shock waves
13 p2301 A69-27361
- Monograph on gasdynamics and classical theory of shock waves covering viscosity, heat conduction, gas cloud expansion into vacuum, etc
13 p2246 A69-27639
- Stable geomagnetic pulsations related to plasma density shock position in magnetosphere and to magnitude of diurnal variations
13 p2253 A69-27692
- Constant density heating upstream and constant pressure cooling downstream formulas for radiating shock waves
13 p2249 A69-28240
- Finite control volume approach to shock Hugoniot in unidirectional fiber reinforced composite, computing shear force along matrix-fiber interface
[AIAA PAPER 69-359] 13 p2366 A69-28292
- Enhanced plasma heating in absorption zone of laser-induced gas breakdown at spherical blast wave shock front
14 p2460 A69-29604
- Supersonic gas flow past wedge at zero angle of attack with separated shock wave, calculating velocity gradient at stagnation point and pressure and drag distribution
14 p2390 A69-29615
- Supersonic jet flow with separated shock wave flowing past infinite wedge using Chaplygin method, assuming negligible entropy variations
14 p2391 A69-29619
- Rate constants for recombination of atomic hydrogen with hydrogen molecules, hydrogen atoms and argon atoms at high temperatures behind shock waves
14 p2488 A69-29637
- Shock wave radiation screening by thermodynamically unstable gas, discussing brightness and gas temperature relative to shock wave front position
14 p2493 A69-29673
- Cosmic shock waves simulation through correlations between shock equations in classical and relativistic fluid dynamics, using shock tube tests
14 p2433 A69-29981
- Weak shock waves relaxation time and amplitude and acoustic velocity as functions of thermorelaxing media
15 p2590 A69-30103
- Electro-optical measurements to determine intermolecular interaction temperatures in organic liquids compressed by shock waves
15 p2561 A69-30264
- Barrier penetration depth by meteorite particles at prethreshold impact velocities, taking into account energy dissipation on shock wave front
15 p2709 A69-30749
- Ballistic wake structure and jump conditions for plane plasma shock waves with electrostatic turbulence
15 p2660 A69-30914
- Critical study of Tidman model for turbulent electrostatic shock wave structure in plasmas, noting velocity distribution function role
15 p2661 A69-30927
- Two phase flow mixing shocks, obtaining expressions for pressure and entropy changes, discussing shock stability and gas entrapment mechanism
16 p2768 A69-31589
- Initial ionization processes in strong shock wave in hydrogen, determining ionization relaxation length and cross section of atom-atom excitation collisions
16 p2815 A69-31590
- Similarity concepts extended to shock initiated fluid compression devices for magnetic flux concentration
16 p2768 A69-31665
- Q switched laser produced blast waves in low pressure Ar, discussing gas density and time dependence roles
16 p2796 A69-31705
- Photoinduced shock processes involving metastable hydrogen atoms and molecules, discussing vibrational and rotational levels
16 p2813 A69-31754
- Pressure behind spherically divergent shock wave produced by explosion of metal wire measured and compared with calculated values
16 p2769 A69-31837
- Perturbation solutions for planar cylindrical and spherical blast waves in air, considering third and fourth order approximations
16 p2770 A69-31900
- Pitot tubes diameter effect on pressure gradients during measurement through shock wave
16 p2771 A69-31927
- Bow shock wave during rectilinear flight with varying acceleration, describing sonic boom loop mechanism
16 p2734 A69-32005
- MHD of interstellar gas-dust medium, analyzing gas-dust flow and gas-dust shock waves in magnetic fields
16 p2823 A69-32590
- Shocks in gases, giving differential equation set for ideal gas behavior
17 p2948 A69-32845
- Axisymmetric supersonic gas flow with attached shock wave past cone, calculating flow parameters between body and shock wave
17 p2890 A69-33123
- Shock structure in RF heated partially ionized Ar plasma jet, using cylindrical free molecule Langmuir probe
[AIAA PAPER 69-697] 17 p3011 A69-33466
- Flow field study of merging between bow shock and viscous layer upstream of highly cooled axisymmetric blunt body in rarefied hypersonic stream
[AIAA PAPER 69-656] 17 p2893 A69-33498
- Collisionless shock wave structure in plasmas, noting plasma and shock wave generation mechanisms
17 p3013 A69-33822
- Leading edge vortices and shock detachment flow over delta wings, discussing drag reduction due to lift
17 p2896 A69-34025
- High temperature and short duration flows - Conference, Freiburg University, West Germany, April 1967
18 p3114 A69-34444
- Radiation cooling behind strong shock in Kr as function of plasma luminosity near end of relaxation zone
18 p3171 A69-34450
- Gladstone-Dale constants for dissociating high temperature oxygen determined for molecule and atom from density changes across shock
18 p3176 A69-34452
- Shock wave studies of gaseous NO thermal ionization in Kr as function of temperature, using time-of-flight mass spectrometer
18 p3099 A69-34464
- Elastic circular cylindrical panel behavior in fluid with acoustic shock wave, allowing for propagation waviness of elastic stresses
18 p3216 A69-34579
- Transport processes effect in shock wave on hypersonic flow past blunt body in neighborhood of stagnant point, noting heat transfer
18 p3086 A69-34910
- Radiation effects produced by high temperatures of shock waves and nuclear explosion fireballs, air cooling, laser emission-matter interaction and optical phenomena
18 p3230 A69-34926
- Earth bow shock waves in far upstream interplanetary medium observed from magnetic data of Explorer 34 satellite
18 p3199 A69-34941

Rotating static thrust propeller or hovering rotor flow field study by schlieren photography, considering vortex field, tip flow and shock wake formation
18 p3087 A69-35218

Cumulative shock waves in vaporized products of electrical explosion of conical copper wire configuration, discussing atmospheric ionized vortical configuration formation
19 p3372 A69-35823

Skimmer interaction influences on nozzle beam production explaining intensity maxima, proposing model assuming normal shock across skimmer mouth
19 p3238 A69-36172

Solid surface roughness influence on reflection of thermal energy molecular jets, showing shock determined by incidence angle
19 p3377 A69-36180

Flow velocity, flow Mach number and weak disturbance velocity behind shock wave measured for nitrogen, oxygen and carbon dioxide
19 p3298 A69-36362

Construction of single headed spin detonation polar as confluence of shock and deflagration waves by two dimensional hodograph
19 p3451 A69-36368

Axial stagnation point flow in shock wave reflected from sphere or circular cylinder, determining velocity time variation, enthalpy pressure and reflection
19 p3298 A69-36385

Drag measurements for sharp and blunt-nosed bodies shot into wind tunnel supersonic gas counterflows, discussing shock waves for different configurations
19 p3239 A69-36401

Water jets with greater than half sound speed created by shock wave impinging on cavity within liquid, discussing mechanism, maximum speed, shape, etc
19 p3301 A69-36815

Mach reflection limiting parameters of conical shock wave in Plexiglas cylinders, showing head wave curvature radius linear relationship to cylinder diameter
19 p3302 A69-36845

Structure of isolated MHD shock wave in viscous heat-conducting radiating gas finite electrical conductivity and transverse magnetic field
20 p3581 A69-37189

Shock and current sheet separation in magnetic shock tubes, determining electron temperature behind shock and within current layer
20 p3511 A69-38241

Giant Q switched laser pulse interaction with C target in background gas showing complex luminous shock structure near target as function of time
21 p3736 A69-38942

Nonequilibrium processes behind shock wave in shock tube supersonic air and nitrogen flow, using photoelectrical shadow method
21 p3693 A69-38961

Shock waves in closed cycle MHD with gaseous working fluids, investigating MHD channel flow
21 p3778 A69-39482

Electron temperature profile across shock wave in weakly ionized nonequilibrium argon by numerical integration of energy conservation equation, noting three body recombination
21 p3698 A69-39791

Vibration relaxation time and dissociation rate constant of carbon dioxide in high temperature shock waves, using IR emission
21 p3775 A69-39801

Magnetic fluctuations in various frequency ranges, associated with earth bow shock, detected with search coil magnetometer on OGO 3
22 p3938 A69-40501

Radiation emission and ionization in precursor and nonequilibrium region behind shock wave during approach to equilibrium in argon-like gas
22 p4006 A69-40526

Shock tube boundary layers dependence on shock strength determined using vorticity transport to define boundary layer coordinate
22 p3930 A69-40531

Nonlinear relativistic wave velocity distribution within spherical nucleus bounded by shock wave in superdense gas determined by Cauchy problem
22 p3861 A69-41114

Transonic flows behind separated shock waves of ideal gases past bodies of various geometries
23 p4151 A69-41526

Atomic spectrophotometry to monitor O atom formation rate behind shock waves in oxygen-argon mixtures, noting dissociation over 2850-5550 K temperature range
23 p4194 A69-42209

MHD Rankine-Hugoniot equations for ion density, thermal pressure and convective velocity magnitude and orientation during Pioneer 6 traversal of earth bow shock
23 p4222 A69-42417

Blast wave energy determination of laser-induced gas breakdown in hydrogen, nitrogen, helium, argon and xenon in pressure chamber
24 p4299 A69-42651

Solar corona instabilities and shock waves indicated by type 3 and 2 bursts, considering electrons ejection
24 p4378 A69-42689

Fluctuating electric fields relations to MHD bow shock structure, using LF fluxgate magnetometer aboard OGO 5
24 p4306 A69-42693

Theoretical models for collisionless plasma shock waves in terms of nonlinear, magnetosonic, constant profile waves, turbulent- and electrostatic-shock structures, etc
24 p4355 A69-42694

Solar wind collisionless hydromagnetic flow interaction with planetary atmosphere, using mathematical model to determine bow shock position limits in atmosphere
24 p4368 A69-43178

Electron temperature distribution across shock wave in weakly ionized plasma, noting variable ionization across wave
24 p4356 A69-43362

Underexpanded plane hypersonic gas jet injection into resting medium from straight nozzle, discussing shock wave formation
24 p4246 A69-43484

Viscous shock wave chemical relaxation for diatomic nonequilibrium dissociating gas flow, using Navier-Stokes and chemical kinetics equations
24 p4302 A69-43487

Compressible laminar boundary layer behind shock or thin expansion wave past moving flat plate solved by transforming governing equations into Blasius equation
24 p4305 A69-43596

Shock formation mechanism in simple shock tube using multistage modification of White model, deriving variation of shock Mach number
24 p4305 A69-43631

SHOES

Two degrees of freedom control moment gyro for astronaut attitude control during EVA, discussing muscle-controlled shoe-mounted stilts and precessional feedback forces
24 p4272 A69-42846

SHORT AND HARLAND AIRCRAFT U SC- 7 AIRCRAFT

SHORT CIRCUITS

Rectangular RC distributed circuits with shaped electrodes, analyzing short circuit admittance parameters
11 p1858 A69-24938

Dynamic properties of supply sources in carbon dioxide shielded welding as function of short circuit current statistical parameters, noting metal spatter correlation
11 p1892 A69-25667

Plane linear induction pump design optimization without short circuiting bus bars, allowing for MHD effects induced by traveling magnetic field
14 p2405 A69-29913

SHORT SC-7 AIRCRAFT

U SC- 7 AIRCRAFT

SHORT TAKEOFF AIRCRAFT

STOL and VTOL aircraft characteristics in operation, considering impact on terminal navigation and air traffic control
03 p0465 A69-13452

Heligyro type takeoff and landing maneuvers, discussing M 211 takeoff jet thrust, pressure ratio, tip speed, etc
04 p0547 A69-14816

Blowing boundary layer control /BLC/ system designed for STOL seaplanes
05 p0695 A69-15546

STOL aircraft intercity test flights emphasizing curved ILS approach, using onboard computer for altitude and distance data
08 p1347 A69-20602

Aerodynamic characteristics of propeller-wing-flap systems used on deflected slipstream STOL aircraft
09 p1431 A69-22278

Short takeoff aircraft characteristics, discussing aircraft certification and airfield regulation in Great Britain
13 p2203 A69-28356

STOL and V/STOL short haul intercity airliners emphasizing propulsion systems, operational aspects and economics
17 p2898 A69-33356

Wind tunnel wall interference effects in wind tunnel testing of STOL aircraft by inducing interference velocities
17 p2947 A69-34022

Lockheed C-130 Hercules modified as STOL aircraft studied in laboratory by computerized simulation and graphics techniques for pilot view during landing
18 p3092 A69-35466

Airport facilities planning for conventional jet, STOL and SST aircraft ground handling, stressing facilities economy and transportation subsystems
19 p3289 A69-35623

Computerized clock sequenced ATC system, area navigation /R Nav/ systems and STOL flight control
19 p3370 A69-36317

Short haul air transportation traffic congestion problems in Northeast corridor, emphasizing STOL solution for economy
19 p3248 A69-36865

STOL aircraft to serve traffic needs of northeast corridor, discussing decision making regarding size, type, cost, speed and strip-length
20 p3462 A69-37352

Flight control and stability of STOL transport aircraft with powered-lift boundary layer control system augmented lift
20 p3462 A69-37513

STOL airline operation test programs involving aircraft, navigation equipment, systems and ATC
21 p3646 A69-38731

STOL takeoff optimal trajectory maximizing altitude at given runway distance, using aircraft models
21 p3649 A69-39427

Wind tunnel tests determining propeller slipstream effect on roll-damping derivative in transitional flight region, estimating STOL aircraft characteristics
22 p3863 A69-40145

Air traffic systems and diminishing airspace capacity problems requiring additional airport facilities and STOL aircraft
22 p3925 A69-40428

STOL aircraft characteristics emphasizing ground and air space operations requirements and noise levels
22 p3863 A69-40430

STOLport policy for New York City including travel time analysis, ground transport systems, political and community acceptance, aircraft noise, etc
22 p3927 A69-40484

STOL seaplane bottom pressure distribution from tests on scale model of PX-S seaplane, discussing boundary layer control effects
22 p3864 A69-40586

VTOL, STOL and CTOL transportation systems cost effectiveness comparison for Northeast Corridor operation, considering ground facilities, access time, etc
23 p4147 A69-41642

STOL program in Northeast Corridor demonstrating significant city-to-city block time reduction by STOL transportation system
23 p4185 A69-41644

Terminal facilities planning for STOL service to meet traffic demand, considering site selection, runway alignment, aircraft noise, ground accessibility, etc
23 p4147 A69-41645

Air traffic interfaces of VTOL, STOL and CTOL aircraft serving same metropolitan terminal, emphasizing navigation systems, geographical positions, ground communication, etc
23 p4185 A69-41646

Metropolitan downtown airports for STOL and VTOL aircraft stressing Los Angeles Metroport
23 p4147 A69-41660

STOL transport aircraft propulsion requirements, discussing engine cycle selection, design variables effects, etc
23 p4201 A69-41668

Czechoslovak L-400 high wing short range STOL transport aircraft powered turboprop engines, discussing passenger and cargo version
24 p4251 A69-42799

SHORT WAVE RADIATION

NT MICROWAVES

NT MILLIMETER WAVES

NT SUBMILLIMETER WAVES

GaAs diode laser short wave emission, discussing coherent radiation and photon energy
03 p0441 A69-14165

Actinometric and nephelometric data on outgoing short wave radiation obtained by Cosmos 122 satellite,
24 p4251 A69-42799

- tabulating cloud cover data, digital radiation data and brightness curves
06 p0952 A69-17983
- Short wave radiation field reflected anisotropically from underlying surface into atmosphere calculated from brightness coefficient
06 p0952 A69-17985
- Visceral lesions observed in mice and rats exposed to ultrashort waves indicating no pathological modification of physiology of reproduction
[AGARDOGRAPH-111] 08 p1266 A69-20679
- Solar radio emission S component at short waves, discussing role of higher frequency spectrum in proton flare occurrence
10 p1763 A69-23735
- Functional relations expressing short wave radiation absorption and scattering in atmosphere
15 p2648 A69-30222
- Extraatmospheric long and short wave radio astronomy since first artificial satellite, including device carriers effectiveness of earth satellites, lunar orbiters, rockets and balloons
15 p2682 A69-30504
- Field strength determination at reception point for long range short wave paths, taking into account multiple ray paths and antenna radiation patterns
20 p3520 A69-37035
- Soviet book on methods of calculating characteristics of solar radiation covering short wave radiation, relationship to meteorological factors, applications, etc
20 p3570 A69-37233
- SHORT WAVE RADIO TRANSMISSION**
- Diversity antenna continuous short wave radio signal envelope distribution, autocorrelation functions, damping rate and cross correlation coefficients
03 p0394 A69-13522
- Short wave bands for earth-space communications, considering propagation anomalies compensated systems and frequency bands availability
03 p0397 A69-13721
- Correlation coefficient between frequency diversified signals amplitudes estimated by approximation for two beam short wave radio channels
04 p0560 A69-15401
- Equivalent hop and equivalent ionospheric parameters for short wave long distance radio links in ionospheric radio propagation
04 p0560 A69-15402
- Vertical probe observations of short radio waves propagation through sporadic E at various frequencies and path lengths
10 p1657 A69-23933
- Noise sensitivity of space diversity reception system with narrow beam electrically switchable antennas for incomplete beam separation
12 p2030 A69-26485
- Two beam short wave channel capacity with beam separation at receiving end, noting dependence on channel properties and fading correlations
15 p2562 A69-30115
- Directional transmitting and receiving antenna arrays for short wave meteor studies in Kharkov
17 p2939 A69-33903
- Short radio wave damping of earth satellite transmitter due to ionospheric diffraction resulting from increasing satellite-ground station distance
20 p3491 A69-37689
- SHOT NOISE**
- Forward current shot noise in parametric amplifiers using GaAs varactors, noting additional noise due to stored minority carriers current
01 p0048 A69-11137
- Thermal and shot noise in pumped resistive diode for frequency conversion, analyzing equivalent circuits
03 p0406 A69-13828
- Shot noise in Si Schottky barrier diodes for frequencies between 100 Hz and 50 kHz
05 p0734 A69-16564
- Shot noise in dipole antenna immersed in hot plasma related to antenna input resistance, using Maxwellian velocity distribution
07 p1079 A69-18920
- Unsuccessful space charge noise suppression measurements on field emission tubes, obtaining diffusion and shot noise measurements at high currents
16 p2752 A69-32384
- SHOT PEENING**
- Shot peening effect on fatigue properties of maraging and Al-Zn-Mg alloy steel welds, using repeated tensile tests
02 p0253 A69-12061
- Butt weld fatigue properties improvement in maraging steels, using shot peening and prestretching
03 p0434 A69-13762
- Heat treatment and shot peening effects on Al alloy fatigue strength and fine crystallographic structure
04 p0614 A69-14576
- Stress corrosion cracking prevention by shot peening, considering aircraft industry applications
14 p2466 A69-29937
- Heat treatment and shot peening effects on Al alloy fatigue strength and fine crystallographic structure
15 p2638 A69-30278
- SHRINKAGE**
- Stress concentrations around elliptical perforations in shrunk plates with bonded boundaries based on photoelastic models
02 p0345 A69-12391
- Two dimensional photoelasticity for minimizing stress concentration in perforated rectangular plate subjected to restrained shrinkage, discussing application to solid propellant rocket grains
08 p1412 A69-20255
- Shrinkage and heat release of polyglycol maleinate binder during gamma radiation consolidation compared with thermochemical consolidation
12 p2117 A69-25991
- Shrinkage stresses in two phase materials, analyzing stress distribution in epoxy inclusions in plasticized matrix during curing by photoelastic method
13 p2371 A69-28675
- Shrinkage cavity volume formulas for alloy castings with wide liquidus to solidus range, considering effects of diffused porosity and clustering for Mg alloy
20 p3548 A69-37329
- Low melting point material selected model melt simulating shrinking process in castings of melt with broad liquidus-solidus interval
21 p3733 A69-39720
- Stress analysis of incompressible solid propellant rocket charges by point matching technique, considering differential thermal shrinkage and axial acceleration cases
24 p4402 A69-43263
- SHROUDED BODIES**
U SHROUDS
- SHROUDED PROPELLERS**
- Rotating spectral and spatial sound pressure distribution in propeller duct calculated on basis of propulsion quantities, noting effect of tip clearance
04 p0544 A69-14867
- Integrated shrouded propeller as glider thrust source permitting powered takeoffs and updraft independence
05 p0702 A69-16379
- Wind tunnel measurements on integrated shrouded propeller model proposed for power gliders
07 p1052 A69-19633
- SHROUDED TURBINES**
- Gas flow characteristics in shrouded and unshrouded turbine wheel assemblies, emphasizing radial flow role in efficiency
21 p3785 A69-38865
- SHROUDS**
- Cryogenic plants for space simulation chambers, examining processes for cooling shroud below 100 K at given temperature differences
01 p0057 A69-11154
- Field noise reduction frequency spectra afforded by spacecraft shroud, basing estimating criterion on flight test data
09 p1609 A69-21892
- SHUNTS**
U BYPASSES
U CIRCUITS
- SHUTDOWNS**
- NERVA engine operational cycle and performance, discussing startup, thrust buildup and shutdown
[AIAA PAPER 69-515] 18 p3170 A69-34809
- SHUTTERS**
- Electro-optical shutter for Nd-glass laser with high peak power pulses, discussing switching time, contrast ratio and synchronization
09 p1493 A69-21422
- High speed curtain type photographic shutters testing by chronograph with phosphorescent and photographic recording, determining movement rate including acceleration and braking
12 p2093 A69-26598
- Single crystal line block electro-optical shutter reflector operation based on double reflection and birefringence in anisotropic media, noting application to Nd glass laser
20 p3554 A69-37611
- Isolation technique using exploding mirror shutter in multistage high gain laser system to overcome amplified target feedback during pulse lasing of reflective targets
24 p4330 A69-43762
- SIBERIA**
- Total solar eclipse of September 22, 1968 in Siberia, discussing instrumentation and solar light radiation, corona, prominences, spicules, etc
10 p1782 A69-23696
- SIC [COEFFICIENT]**
U STRUCTURAL INFLUENCE COEFFICIENTS
- SICKNESSES**
NT ALTITUDE SICKNESS
NT DECOMPRESSION SICKNESS
- In-flight illnesses in French Air Force, emphasizing psychological failures in etiology
21 p3666 A69-39270
- Cardiovascular illnesses incidence among airline flight personnel, discussing coronary insufficiency detection
21 p3661 A69-39271
- Aircraft pilots medical disabilities as potential flight safety hazard, discussing aerospace medical specialist role and pilot education in symptoms evaluation
22 p3894 A69-41146
- SID [IONOSPHERIC DISTURBANCES]**
U SUDDEN IONOSPHERIC DISTURBANCES
- SIDE-LOOKING RADAR**
- Holographic and microwave technology relationship, noting side-looking radar photos and X band radiation
03 p0430 A69-13354
- Side looking radar for earth resources sensing, discussing geological and hydrographical mapping, oceanography, agricultural and biological phenomena
06 p0923 A69-17119
- Analysis and optimization of side-looking synthetic aperture radars carried out for resolution, SNR and least squares estimation of target field
08 p1277 A69-20960
- Photography for remote sensing, discussing aerial photography, side-looking radar and photography for recording, storing and retrieving data
12 p2096 A69-26975
- Side-looking airborne radars (SLAR) application to geological exploration of remote unmapped areas
12 p2099 A69-27009
- Equations derived for radar image coordinate transition to geodetic coordinates in aerial surveying by side-looking airborne radar
15 p2596 A69-30574
- Side-looking radar and thermal IR photography as mapping system, discussing resolution and distortion
15 p2612 A69-31162
- APQ-97 side-looking radar for topographic mapping of continually cloud covered areas, noting data reduction and compilation methods
20 p3519 A69-36928
- Side-looking radar and IR line scanning as method for simultaneous stereo height mapping, using images produced from same vantage point
20 p3536 A69-36929
- Geological radar in regional and detail studies, discussing area side scanning imagery and lithology changes detection
20 p3491 A69-37652
- SIDEBANDS**
- Amplitude modulation factors expressed as carrier and sideband power for sinusoid and square wave signals, considering negative clipping by modulator cut-off
01 p0028 A69-10419
- Sideband amplification via saturated gas resonance in 258 GHz reflection amplifier with hydrogen cyanide gas filled cylindrical cavity
07 p1145 A69-18479
- Sideband structure of transmitted frequency spectrum exhibited by plasma wave features on topside ionograms, noting harmonic resonances
20 p3496 A69-37891
- SIDELOBE REDUCTION**
- Monopulse ground station antenna configuration for improvement of sidelobe level in satellite transmission [DVL-856]
02 p0214 A69-11599
- Constant amplitude current excitations superposed on uniformly spaced array for sidelobe reduction, comparing results to Chebyshev arrays
12 p2040 A69-26473
- Residual phase term influence on compressed signal shape, analyzing linearly frequency modulated signal spectrum and sidelobe suppression in pulsed radar
15 p2564 A69-30143

Meteorological radar dead zone diminished by using hybrid electronic waveguide suppression system to eliminate antenna sidelobe reflections
16 p2791 A69-32281

Short backfire antenna based on yagi type equipped with end reflector, noting fewer elements and low sidelobe advantages
16 p2763 A69-32586

Doubly curved reflectors for rotating search radar directional antenna, noting assembly of elliptical strips constituting segments of parabolic dishes and sidelobe suppression
16 p2763 A69-32790

Quantization sidelobe characteristics of phased array with triangular and rectangular element arrangement
23 p4137 A69-41591

Cophase antenna aperture with shaded central region, considering sidelobe radiation reduction by varying field amplitude distribution
23 p4138 A69-41939

SIDELOBES

Statistical characteristics of radiation pattern of mirror antennas in region of irregular sidelobes
04 p0577 A69-14787

Jamming susceptibility, noting corrections for multiple noise sources and sidelobe level for antenna pattern
14 p2414 A69-29501

Multiplicative feed system for monopulse angle tracking antennas, discussing influence of sidelobe and backlobe responses on control function slope determining antenna bearing angle
20 p3510 A69-37704

Direction finding characteristics of nonlinear antenna, including current determination and optimal angle for sidelobe level
21 p3684 A69-39619

Envelope characteristics of earth station Cassegrain antenna sidelobes, deriving formulas for central and spar blocking and forward feed spillover
23 p4143 A69-42517

SIDERITE METEORITES

U IRON METEORITES

SIDESLIP

Aircraft stability during sideslip, discussing influence of fuselage/wing interference
04 p0548 A69-14824

SIEVES

Sorting particles by shape using sieving equipment, noting results with crushed gravel
21 p3731 A69-38950

SIGHT

U VISUAL PERCEPTION

SIGNAL ANALYSIS

Small signal characteristics and frequency response of diode-stabilized integrated linear circuits, discussing feedback, impedance, bias-diode, etc
01 p0041 A69-10204

P-n-p junctions photoconductivity decay observation, determining signal bulk minority carrier lifetime in thin n regions
01 p0136 A69-10242

Germanium tunnel diode capacitance as function of bias voltage and HF signal magnitude, considering circuit design
02 p0214 A69-11614

Envelope distribution of echo signal during reflection scattering by extended turbulent meteor trails
02 p0207 A69-11690

Radar target amplitude, angle and Doppler scintillation from analysis of echo signal propagation in space
02 p0211 A69-12447

Book on compound signals and uncertainty principle in radar observations, considering Woodward ambiguity function, determining accuracy and resolution of range and velocity measurements
03 p0385 A69-13000

Iterative method of determining orthogonalized bases for representation of sampled data signals
03 p0391 A69-13231

Infrasound waves recordings from Saturn 5 vehicle, observing signal reversal occurrence
03 p0509 A69-13358

Multichannel communication received signals irregular components, discussing signal phase and amplitude fluctuations correlation coefficients
03 p0394 A69-13519

Maximum probability technique for measuring angular coordinate with unknown signal and noise intensity
03 p0399 A69-14132

Electronically steered and shaped beams for linear and ring phased array antennas by sampling element signals multiplexed into single channel
04 p0570 A69-14307

Weak periodic signal separation from noise using single and multichannel analog adders
04 p0597 A69-14848

Optimal filter design for estimating state of linear dynamical system in presence of high measurement noise
04 p0582 A69-14877

Optical signal frequency method for measuring velocity of fluid flow
04 p0598 A69-14995

Near earth atmospheric spectrum characteristics determined by analytical expressions for elementary signals in 2-30 kHz range
04 p0593 A69-15105

Threshold signals and optimum signal parameters in radar range and velocity measurements
04 p0560 A69-15403

Spectral density of response of linear discrete filter with multiple input and output periods to random signal
04 p0584 A69-15419

First and second passage times of stationary random process consisting of sinusoidal signal with stationary Gaussian noise
04 p0561 A69-15453

Uniaxial loading effect determination by change of harmonics amplitude of inductive pickup signal
05 p0763 A69-15995

Noise signal mean square value measurement in pulse noise conditions by using noise amplitude limiter with limitation threshold in receiver
05 p0719 A69-16086

Earth effect on signal correlation in space diversity microwave reception antennas, analyzing vertical separation and out of phase signals
05 p0720 A69-16530

Nonlinear distortion of FM signal during passage through multipath medium, using analysis of linear passive four terminal network
05 p0721 A69-16531

Time averages for estimating probability distribution, density and moments of random functions applied to deterministic signals, considering sampling frequency dependence
05 p0722 A69-16729

Pulse amplitude measurements comparison by sampling signal at given time and pulse peak detection, considering SNR
05 p0722 A69-16730

Book on introduction to random signals and communication theory covering signal analysis, analog and digital data transmission, information theory, etc
06 p0887 A69-17144

Analog-hybrid computer configurations for average and rms values of signals with respect to time
06 p0891 A69-17220

Optimal radio signal receiver analyzing output signal properties
06 p0888 A69-17464

Spectral null from spectral characteristics and statistical properties of PCM signals used to estimate SNR
07 p1083 A69-19122

Frequency feed forward open loop technique for lowering threshold and linearity of FM demodulators
07 p1106 A69-19128

Recursive method for estimating number, amplitudes and time delays of signals overlapping in time and in presence of additive white Gaussian noise
08 p1270 A69-19854

Hilbert transform properties and application to random signals, analyzing analytic signal associated with general Gaussian random signal
08 p1271 A69-19915

Input signal history analysis in recognition of moving or changing objects based on classification definition and Wald sequential analysis
08 p1297 A69-20419

Radio signal from magnetron transmitter, noting slow amplitude phase fluctuations distribution according to log-normal law
08 p1275 A69-20424

Vortex valves and amplifiers small signal analysis using mathematical model to describe quantitative effects of vortex parameter changes [AGARDOGRAPH-118]
08 p1257 A69-20953

Error probability for transmission of one of M orthogonal, equally likely, equal energy signals over generalized incoherent channel
09 p1452 A69-21314

Upper bound obtained for probability of zero Gaussian random process remaining above specified signal throughout prescribed interval of time
09 p1452 A69-21319

Continuous signal over finite time intervals represented by impulse functions of linear channel
09 p1454 A69-21723

Wideband signal Doppler distortion influence on parameter estimate accuracy
09 p1454 A69-21725

Large signal analysis of IMPATT oscillators with carrier velocity saturation, discussing two frequency mode of operation
09 p1463 A69-21846

Power spectrum of nonstationary processes with periodicity in two dimensional autocorrelation function based on Fourier transform
09 p1455 A69-21847

Automatic level measuring system, consisting of decade control oscillator, digital level generator and selective level meter for 200Hz-2MHz range
09 p1501 A69-22577

Sporadic noise, false fronts and other noise effects on phase of output oscillations of resonance apparatus
09 p1460 A69-22641

Singular integral method in approximation for synthesizing sequence of functions with spectrum of limited length
09 p1460 A69-22642

Vortex amplifiers small signal analysis based on mathematical model and network theory
09 p1443 A69-22739

Large signal vortex amplifier analysis using load lines to evaluate series orifice and vortex flow control valve characteristics
10 p1639 A69-23558

Analytic investigation of spectrum of electrical signals induced by spherical defects in ferroprobe sensors
10 p1675 A69-24072

Algorithm for calculating Bayes estimates for unsteady Gaussian signals separation in presence of unsteady Gaussian noise by least squares method
11 p1833 A69-24443

HF measurements by phase and amplification control of signal in impulse oscillography, noting accuracy in nanosecond range and signal distortion
11 p1880 A69-24541

Upper bounds for increment of band limited signal in sampling interval by increasing integral expressions of increment
11 p1834 A69-24551

Cepstrum /Fourier transform of log-spectrum of signal/ as model for prediction of perception of pitches in harmonic residue /ambiguity of pitch/
11 p1834 A69-24571

Signal to noise ratio in spectral composition of FM signals in magnetic recorder channels, taking into account parasitic FM and AM
11 p1834 A69-24612

Germanium tunnel diode capacitance as function of bias voltage and HF signal magnitude, considering circuit design
11 p1847 A69-24722

Transient responses of mutually synchronized signal systems, obtaining design parameters
12 p2030 A69-26388

Book on random signal analysis covering Fourier analysis, circuit analysis, Fourier transform theory, operators, probability, random variables, stochastic processes
12 p2031 A69-26632

Statistical distribution of instantaneous frequency and power of signal associated with Doppler spectrum for exponentially distributed and determinate frequencies
12 p2032 A69-26863

Book on elements of detection and signal design covering transmitter optimization for coherent and noncoherent digital communication systems, statistical decision theory, radar detection, etc
12 p2033 A69-26867

Pull-in oscillator for random noise coincident with synchronizing and frequency shift signals, discussing circuit parameters effect on signal discrimination and noise suppression
12 p2044 A69-27101

Spectral criterion for distinguishing mode locked and nonmode locked laser signals
13 p2270 A69-27197

Small signal quasi-stationary characteristics of pulse transistors including gain and input impedance calculations
13 p2227 A69-27423

Signal strength of two beam interferometers with laser illumination, considering modulation depth of interference pattern
13 p2259 A69-27450

Signal to noise ratio at output of three stage radio section with preselector, detector and ideal integrator, noting error

13 p2222 A69-28506

Transistorized DC amplifier circuit with reversible and controllable transfer constant based on voltage conversion principle

13 p2235 A69-28511

E layer fine scale structure, F 1 reactions and F 2 reflected signals analysis during 20 May 1966 solar eclipse

13 p2255 A69-28541

Coherent signal addition in systems with multibeam channels and incomplete beam separation, deriving expressions for signal shape effect on noise rejection

13 p2223 A69-28551

Input signal random amplitude fluctuations suppression by parametric power limiter, discussing limiting frequency determination and dependence on signal amplitude

13 p2236 A69-28573

Random signals and real time analysis systems for environment testing and transient signals

13 p2264 A69-28603

Envelope distribution of echo signal during reflection scattering by extended turbulent meteor trails

13 p2224 A69-28721

Radio signal amplitude changes from Explorer 22 beacon satellite attributed to wave diffraction by tropospheric structures

14 p2411 A69-29107

Subcarrier phase modulated single sideband sinusoidal carrier synthesis, discussing signal power ratios, signal efficiency, design sensitivity, etc

14 p2413 A69-29489

Nonlinear interactions of linearly polarized carbon dioxide laser signals in sulfur hexafluoride measured as function of angle between polarization planes

14 p2460 A69-29602

Input signal history analysis in recognition of moving or changing objects based on classification definition and Wald sequential analysis

14 p2427 A69-29657

Recording installation of ionospheric reflected radio signal fluctuations and amplitudes of resulting signals simultaneously at three points, discussing antenna commutator circuit

14 p2452 A69-29874

Small signal analysis of processes in klystron resonators involving beam-field interaction

15 p2573 A69-30117

Distribution function of SNR from coherent optimal estimate of signal amplitude

15 p2564 A69-30149

Weak periodic signal separation from noise using single and multichannel analog adders

15 p2607 A69-30241

Autonomous radiometers signals statistical properties used in space technology, discussing radar signals phenomenological models, measurement errors and energy characteristics

15 p2566 A69-30337

Power spectrum analyzer of weak periodic signal obscured by white noise by zero interactions count of signal and noise mixture

15 p2579 A69-30945

Signal records from S 66 satellite with strong scintillations, noting fluctuation well described by Nakagami m-distribution and possibility of deriving relations between different indices

16 p2777 A69-32104

Cumulonimbus clouds phase structure and spatial distribution based on radar signal polarization analysis, showing high nonuniformity and variability

16 p2806 A69-32266

Meteorological effects on anomalous radio echo determined from simultaneous aerological and radar observations, noting maximum signal amplitude during high humidity and low wind speeds

16 p2808 A69-32277

Error analysis of one bit autocorrelation method of spectral estimation, noting decrease in spectral variance with increased sampling rate

16 p2752 A69-32390

Complex mechanical vibrations causes determined by sensor signals analysis

16 p2876 A69-32434

Signal propagation in channel subject to static investigated using Fokker-Planck type equation in statistical mechanics methods

16 p2753 A69-32437

Earth effect on signal correlation in space diversity microwave reception antennas, analyzing vertical separation and out of phase signals

16 p2753 A69-32472

Nonlinear distortion of FM signal during passage through multipath medium, using analysis of linear passive four terminal network

16 p2753 A69-32473

Seismic surface wave observations analyzed by applying moving window method to orthogonal detector recordings permitting lateral refraction measurement, wave separation, etc

16 p2784 A69-32577

Ionosphere depression influence on VLF signals phase and amplitude calculated by mode theory and integral equations system representing aperture fields

17 p2920 A69-33418

Preemphasis analysis for FM system optimization to maintain constant output signal to noise ratio throughout baseband

18 p3103 A69-35088

Computerized prediction of RF instrumentation system signal margins for missile flight tests based on trajectory and range balance equation

18 p3103 A69-35097

Reflected signals detection with limited frequency spectrum and minimum velocity resolution considered, analyzing signal properties

18 p3104 A69-35265

Signature analysis diagnostic methods for reliability tests involving final product checkout and early fault detection

19 p3322 A69-35574

Transient phenomenon analysis and filtering based on stage separation tests in vacuum chamber, with emphasis on selective integration method

19 p3293 A69-35747

Critical signal assignments optimization in electrical/electronic connectors, considering bent pins, signal cross talk, adjacency requirements and corona

19 p3284 A69-36030

Meteor burst communication channel parameters for low data rate telemetry, considering signal amplitudes, decay, duty cycle, multipath, phase stability, trail location and variations

19 p3271 A69-36250

Continuous signal over finite time intervals represented by impulse functions of linear channel

20 p3488 A69-37459

Wideband signal Doppler distortion influence on parameter estimate accuracy

20 p3488 A69-37461

Linear radar system theory including Fourier transforms, linear superposition and input/output ratio for deterministic and random signals, discussing filter and sampling theory

20 p3489 A69-37633

Signal spectrum and SNR of synthetic aperture terrain imaging radar using model, including two dimensional signal and Gaussian additive noise

20 p3489 A69-37638

Signal amplitude no memory nonlinearity effect on performance of synthetic aperture terrain imaging radar systems and simulation of CRT film systems

20 p3490 A69-37643

Sensitivity improvement for inertialess microwave signal scanning and readout by applying pulse compression concepts, discussing application to real time microwave imaging and holography

20 p3545 A69-37901

Radar signal design, considering ambiguity and modulation functions, envelope surfaces, coding conditions, etc

20 p3496 A69-37904

Optimal radio signal receiver analyzing output signal properties

20 p3496 A69-37947

Diffraction pattern of satellite signal field-aligned amplitude scintillation during quiet geomagnetic conditions

20 p3497 A69-38108

Microwave oscillations amplification in bulk GaAs, discussing experimental verification of small signal theory

21 p3781 A69-39127

Unknown parameter experimental estimation based on signal direct observations with solution by stochastic approximations method

21 p3756 A69-39265

Biomedical electrical signals analysis by optical data processing, discussing conversion, SNR and filtering techniques

21 p3666 A69-39440

Algorithmic approach to nonlinear signal estimation problem useful in fetal electrocardiography

21 p3668 A69-39866

Multiple filter technique for seismic multimode dispersed signals, checking time and frequency resolution by diagnostic diagram

22 p3934 A69-39872

Optimal control problems, discussing properties of signal producing response signals with transient functions at independent outlets of linear dynamic system

23 p4145 A69-41958

Digital analysis of surface wave observations, discussing moving window, multiple filter, multicomponent recording, time variable filtration and cross correlation techniques

23 p4157 A69-42018

Compatible single sideband /CSSB/ modulation suitability for broadcasting, analyzing signal spectrum, demodulation distortion and signal generation methods

23 p4125 A69-42111

Mechanical stress measurement in cylindrical steel subjected to loads inside coaxial transducer, using transducer signal in contactless eddy current method

24 p4296 A69-42654

Small signal amplitude/frequency response or transfer gain of volume-terminated pneumatic lines with circular and rectangular cross sections

24 p4301 A69-43288

SIGNAL ANALYZERS

Time compression system with ultrasonic diffraction cell allows coherent light optical spectrum analyzer to function at audiofrequencies

01 p0035 A69-11283

Multichannel amplitude analyzer for space applications, noting use as gamma-spectrometer component in Lunik 10 and 4096 bit/channel traffic capacity

01 p0084 A69-11315

Multichannel pulse height analyzer with memory, small size and low power consumption for application to satellites

07 p1135 A69-19200

Pulsed RF spectra analyzer displays, noting responses to CW and pulsed signals and Fourier and pulsed repetition rate lines

09 p1460 A69-22791

Receiver filter nonoptimality effects on accuracy of nonenergetic signal parameter measurements

11 p1835 A69-24960

Design and efficiency for signal-time compressors of spectral analyzers using electron beam tubes with charge storage

15 p2576 A69-30351

Peak amplitude selector for electrophysiological phenomena analysis, describing memory schemes, threshold crossing detectors and display, input and output circuits, timing, etc

15 p2612 A69-31266

Information storage of multichannel analyzer of continuous and pulsed processes

17 p2939 A69-33900

Compressed signal spectral analyzer resolving power, discussing dynamic amplitude range influence and weighting functions role

17 p2939 A69-33906

Sampled data system with built-in data processing for observation of fine grain characteristics of pulsed signals used in radar systems

17 p2934 A69-34076

Modified pulse height analyzer /PHA/ for sample amplitude height occurrence frequency measurements obtaining amplitude probability distribution /APD/ and three moments of atmospheric noise

18 p3102 A69-34960

SIGNAL DETECTION

NT CORRELATION DETECTION

Optimal rank algorithm construction for signal detection in noise investigated for use in information transmission systems

01 p0027 A69-10374

Sequential logic for improved signal detectability in frequency-agile search radars, discussing target echo fading models in radar range performance prediction

01 p0033 A69-11008

Tinted ophthalmic media effect on detection and recognition of red signal lights in daylight, noting allowable coloration for aviation use

01 p0022 A69-11341

Optimum linear filters for signal detection against background noise using Hodges-Lehmann method

02 p0223 A69-11565

Test procedure for obtaining large signal S characterization of nonlinear power transistors

02 p0214 A69-11600

Multistage detection systems probability characteristics with parallel stage realization, taking into account signal losses

02 p0206 A69-11604

Probability density distributions for monaural detection of tonal signal in continuous background of Gaussian noise as modified noncentral chi distribution

02 p1201 A69-11821

Optimal detection of random signals on background of noise of unknown intensity and persistent false alarm probability

02 p0208 A69-12264

Natural microwave radiation generation and propagation and wideband signal detection in problems connected with radio wave propagation, geophysics, radiometerology and plasma physics

03 p0420 A69-12919

Adaptive processing limited memory receiver for synchronous detection of signals of unknown amplitude

03 p0400 A69-13228

Digital detection of angle modulated signals including zero crossing detectors, digital phase locked loops, differentiation and arcsine demodulator

03 p0391 A69-13230

Sensitivity of radio receiver detecting weak sinusoidal and noise signals by counting zero crossings by envelope or phase of signal sum

03 p0405 A69-13717

Spatial autocorrelation functions of amplitude and phase fluctuations in plane parallel to wavefront of incident wave for conditions of multiple scatter

03 p0468 A69-13807

Broadband signal and noise performance of direct detection optical receiver consisting of solid state photodiode and baseband amplifier

04 p0556 A69-14283

Photographic recording to produce spatial analog of temporal Fourier spectrum of astronomical source used for distinguishing weak periodic signal from background signal

04 p0556 A69-14294

Optimum conditions for signal analysis determined for symmetrical binary communications channel with unknown signal phase

04 p0556 A69-14492

Signal detection by four terminal receiver network optimal for background Gaussian noise

04 p0557 A69-14776

Optimal detection of deterministic signals with random initial phase on background of unknown intensity noise under condition of constant false alarm probability

04 p0557 A69-14788

Optimal filter design for estimating state of linear dynamical system in presence of high measurement noise

04 p0582 A69-14877

Distribution free sequential probability ratio procedure for detecting signal in multiple resolution element radar

05 p0717 A69-15609

Algorithm for discriminating random signals with unknown mean values, discussing decision functions possible existence to minimize error probability

05 p0719 A69-16218

Bayes estimator in decision directed adaptive detection problem, noting allowance for decision errors

05 p0740 A69-16583

Expressions for calculating filtering errors resulting from insufficient information about useful signal and noise characteristics

05 p0740 A69-16668

Digital spectra analysis by Fourier transform and comb filter for determination of voltage and power spectra

05 p0722 A69-16762

Optimum antenna radiation patterns during suboptimum scattered Gaussian signal detection in homogeneous interference level investigated with single channel antenna

05 p0736 A69-16782

Sounding energy optimum spatial distribution during scanning and detection of several signals, noting reduction of mean energy losses

05 p0723 A69-16786

Aircraft Searchmeter, discussing device fitted to locate emergency radio beacon signal

06 p0878 A69-16963

Attenuation of visual vigilance decrement through visual stimulation combined with various sound conditions

06 p0880 A69-17213

Identification of finite memory, time discrete linear systems by Kiefer-Wolfowitz stochastic approximation procedures, presenting two algorithms for sequential identification

06 p0900 A69-17359

Detection characteristics of coherent pulse packet with random initial phase on Gaussian noise background of unknown intensity

06 p0887 A69-17463

Signal detection procedures preserving nonparametric detection properties and advantages of sequential procedures, assuming signal corruption by additive noise at input

06 p0888 A69-17531

Electric signals by shock and detonation waves, describing detection technique [WSCIPAPER 68-44]

07 p1240 A69-18360

Optical pumping at high temperatures using spin exchange signals for RF spectroscopy

07 p1148 A69-18893

Optimum and suboptimum detection of K binary symbols corrupted by white Gaussian noise, discussing searching procedure and average error probability

07 p1081 A69-19097

Communication satellite system design by use of baseband equation relating SNR after detection to CNR at detector input

07 p1085 A69-19180

Incoherent scatter power measurements, comparing square law signal detection, phase coherent receiver and parametric amplifier methods

07 p1085 A69-19222

Proportionality between log-amplitude variance and 7/6 power of wavenumber for horizontal propagation from spherical wave transmitter to point detector

07 p1157 A69-19641

Optical heterodyne detection of randomly distorted signal beam, noting time invariant scheme yielding largest average SNR in atmospheric turbulence

07 p1087 A69-19642

Discrete signal detection providing optimum SNR for frequency and time domain differences between signal and noise

07 p1088 A69-19676

Secondary acquisition systems analysis by semiMarkov process model, defining minimum average acquisition time

08 p1270 A69-19852

Approximate noise analysis of phase locked loop with signal clipping

08 p1270 A69-19857

Phase locked loop demodulator with quadrature channel modified for decision feedback to detect binary phase shift keyed signals

08 p1270 A69-19859

Book on laser communication system design covering modulation and detection methods

08 p1277 A69-20884

Image orthicon tube to detect low intensity pulsed light signals, formulating SNR in terms of resolvable image points

08 p1317 A69-21085

Constant amplitude in-band additive interference for analysis of PSK signals in Gaussian noise, discussing coherent and differential detection

09 p1455 A69-21848

Optimal detection of determinate signal and signal with random amplitude and phase, estimating probability of false and correct detection

09 p1456 A69-22286

Weak signal optimization of multilevel quantization and corresponding detection performance, discussing asymptotic limits

09 p1456 A69-22293

Rapidly varying phase error effect on system performance in data detection process due to RF carrier tracking loop

09 p1456 A69-22459

Detectability parameter for measuring performance of multiple and random access satellite communication system using PN codes

09 p1457 A69-22460

Signal processing regenerative technique used for multichannel predetection combining, including carrier suppressed signals

09 p1458 A69-22472

Constant envelope threshold detection for establishing signal energy in presence of input noise power density variations

09 p1459 A69-22474

Random data detection method applicable to low voltage SNR cases using real time correlation of probability functions

09 p1459 A69-22593

Monitors to detect incipient failure during turbine engine development, describing servocontrol

10 p1692 A69-23253

IR detection at sum or difference frequency by employing optically nonlinear crystal and laser in visible and photomultiplier

10 p1704 A69-23656

Coherent detection spectroscopy with laser oscillator, emphasizing high resolution and applications in astronomical spectroscopy and IR

10 p1696 A69-23684

Antenna array statistical synthesis, investigating signal detection capacity for large phase fluctuations

11 p1833 A69-24439

Optimizing two stage procedure for detecting fluctuating incoherent signal, estimating detection attempts reliability

11 p1833 A69-24444

Self tuning in active filter for detection of weak LF signals in noisy background

11 p1845 A69-24548

Multistage detection systems probability characteristics with parallel stage realization, taking into account signal losses

11 p1835 A69-24711

Polyharmonic predictive and self tunable filters synthesis based on signal periodic components detection, noting role in information transmission and processing systems

11 p1849 A69-24966

Real time correlator in periodic signal extraction from noise background, discussing multichannel sampler as special case of cross correlation extraction

11 p1837 A69-25094

Adaptive threshold detection, using stochastic approximation techniques to derive receiver structures capable of learning optimum threshold setting during actual operation

11 p1839 A69-25297

Optical satellite tracking system using multicoincidence method of photon signal counting by Q switched laser

11 p1841 A69-25579

Optimal scale factor selection to ensure minimum error variance in signal detection against random noise background for input limited range of measuring instrument

12 p2079 A69-25966

Computer controlled network analyzer performing automatic microwave measurements of passive and active networks, based on signal splitting and detecting

12 p2037 A69-26048

Optimum nonstationary Gaussian signals estimation in presence of noise, generalizing Wiener stationary processes filtering theory

12 p2029 A69-26202

Detection of known signals in general noise, describing sufficient conditions for singular detection and estimation

12 p2029 A69-26203

Error bounds for orthogonal signals in additive white Gaussian noise channels for class of generalized decision strategies permitting variable-size list decoding

12 p2029 A69-26204

Up-converter IR detector noise characteristics for pulse and CW signal detection compared with photoconductive detector

12 p2029 A69-26329

Book on elements of detection and signal design covering transmitter optimization for coherent and noncoherent digital communication systems, statistical decision theory, radar detection, etc

12 p2033 A69-26867

Optical detection signals optimization in optical pumping, discussing light beam propagation direction, spectral composition and polarization characteristics

12 p2111 A69-27180

Algorithm for hypothesis optimal tests by series during signal detection in presence of noise

13 p2222 A69-28509

Independently fluctuating Poisson light signals detected by receiver with inertialess photodetector, developing algorithm for estimating amplitude of useful signals

13 p2223 A69-28552

Optical signal conversion efficiency and threshold relationships in pulsed rangefinding systems, considering effects of noise obeying Poisson distribution

14 p2412 A69-29324

Ideal quantum receiver to detect coherent narrow band optical signal in presence of thermal background radiation, noting error probability

14 p2414 A69-29502

Fast folding algorithm for detection and correlation of digital data with weak noisy pulse trains of differing periods

14 p2416 A69-29548

Algorithms for optimal detection of signals on background of normal noise with time varying intensity

15 p2563 A69-30133

Noise stability of receiver network during detection of finite duration noise signal on white noise background, considering various narrow band preselectors

15 p2563 A69-30142

Linear distortions effect on signals detection in binary communication channel with fluctuating noise, determining error probability

15 p2564 A69-30146

False alarm stabilization circuits efficiencies compared in unsteady Gaussian noise, considering phase autocorrelator performance

15 p2567 A69-30342

Threshold signal gain estimated in Glaser frequency filter self adaptation process during transformation from square law summator into matched filter

15 p2576 A69-30344

General autocorrelation function for input signal composed of two amplitude modulated noise waves and background noise from detecting system composed of half wave element

15 p2569 A69-30805

Superheterodyne millimeter and submillimeter wave detection, allowing harmonics separation

15 p2570 A69-31093

Book on statistical theory of signal detection and resolution in random noise covering hypothesis testing, digital communications, stochastic signals, filters, etc

16 p2748 A69-31566

Logic circuits abstract synthesis for detecting signals against noise background using known conditional quantized signal distributions

16 p2749 A69-31627

Night sky far IR observation by rocket-borne telescope, discussing minimum signal detection and origin

16 p2781 A69-32445

Electrooptical/photomultiplier/ detection of satellite beacon flashes, establishing time of flash and measuring pulse shape and energy received

17 p2919 A69-33083

Likelihood ratio for random signals detection in white Gaussian noise based on innovation process

17 p2920 A69-33622

Optimum detection of stochastic signals in Gaussian noise, obtaining eigenfunctions series expansion associated with probability density function

17 p2921 A69-33623

Robust detection of binary signal in additive noise, using extreme value theory /EVT/ to estimate probability density function and system error and threshold

17 p2944 A69-33624

Discrete information transmission synchronization in communication systems concerning optimal signal detection, HF, phase and coded synchronization, etc

18 p3104 A69-35264

Reflected signals detection with limited frequency spectrum and minimum velocity resolution considered, analyzing signal properties

18 p3104 A69-35265

Optimum signal design to maximize SNR for pulse communications systems with signal energy detection, considering frequency, transmission and filtering characteristics and signal duration

18 p3104 A69-35484

Temporal discrimination based on signal fluctuations emphasizing signal detection in presence of noise

19 p3373 A69-36057

Optimal ratio predetection combiner used with diversity signals and various modulations, showing significant improvement in telemetry systems performance

19 p3270 A69-36241

M-ary detection for optical communication investigated for maximum likelihood detection of one of M Poisson processes in background noise

19 p3276 A69-36486

Representation theory of signal detection in non-Gaussian noise environments applied for improved near optimum system performance [IEEE PAPER 69-TP-10-COM]

19 p3277 A69-36488

Optical information rates for photocount detection systems based on coherent field model, considering binary channels with or without Gaussian noise

20 p3485 A69-36923

Paradox of incoming photons detection at two antennas without interference pattern disturbance explained by classical and quantum physics

20 p3538 A69-37415

Discrete signal detection providing optimum SNR for frequency and time domain differences between signal and noise

20 p3488 A69-37458

Range-Doppler data processing of radar echoes from spread targets, considering quadratic filter theory, emphasizing received signal correlation functions

20 p3490 A69-37648

Detection characteristics of coherent pulse packet with random initial phase on Gaussian noise background of unknown intensity

20 p3496 A69-37946

QRS complex detection time error in noisy electrocardiograms

21 p3667 A69-39442

Tradeoffs between measurement accuracy, false alarm and detection probability in practical setting of thresholds for Neyman-Pearson criterion, analyzing noise samples

22 p3902 A69-41221

Envelope detection threshold levels definition for low input SNR based on apparent modulation depth reduction

22 p3902 A69-41225

Partially coherent PSK-modulated binary detection, deriving noisy phase reference by narrow band tracking filter, analyzing bit output error as function of SNR

23 p4122 A69-41772

M-ary noncoherent signal structures requiring less transmission bandwidth than conventional FSK, deriving SNR

23 p4122 A69-41773

Combined eye and ear identification of bimodally presented signals in noise over oscilloscope and earphones, noting significance of independent observers model

23 p4111 A69-42168

Phase-lock loop demodulator ability to acquire and remain locked on signal under noise and pulse interference

23 p4145 A69-42230

Random signal behavior in hybrid correlator with analog and sampling channels, noting SNR expression and weak signal detection

24 p4283 A69-43139

Lunar laser beam retroreflection observations, showing agreement with predicted ephemeris and signal strength

24 p4384 A69-43197

SIGNAL DETECTORS

Error probability distribution density at output of optimal Gaussian random signal detection, using approximate solution of integral equations

02 p0206 A69-11605

Optimal calculator of detection of Gaussian random signal against Gaussian noise background by reducing input signal to white noise

02 p0206 A69-11606

Noncoherent binary communication detector for slow selective fading channel with additive quasi-stationary noise based on mathematical procedure of non-parametric classification

03 p0390 A69-13215

Closed form solution for two input correlator processing gain with error function transfer characteristics and operating in Gaussian environment

03 p0403 A69-13253

Linear polarization of cosmic radio emission, discussing original measurement method and revised version based on discrimination of useful signal

03 p0501 A69-13705

Phase locked loop discriminator in threshold region, discussing effects of loop parameters, detuning error and modulation

04 p0580 A69-15471

Transistorized single sideband detector-converter operation in presence of large signal and heterodyne voltage levels, deriving equation for transmission coefficient

05 p0730 A69-16220

Asymptotic performance of adaptive receivers and application to signals of unknown frequency, noting SNR role

05 p0722 A69-16727

Maximum transmission coefficient of distributed p-n junction signal detector compared with concentrated detector coefficient using ordinary and tunnel diodes

05 p0736 A69-16787

Temperature dependence of conversion coefficients and sensitivity of n-type InSb detectors in millimeter and submillimeter ranges

07 p1199 A69-18683

Frequency discrimination characteristics of elliptically polarized dual polarization gas laser, discussing intensity crossover phenomenon and frequency stabilization application

07 p1153 A69-19074

[IEEE PAPER P-5]

Optical heterodyning with single mode carbon dioxide laser and triglycine sulfate pyroelectric detector, noting detector sensitivity threshold

07 p1156 A69-19332

Noise rejection in linear amplitude detector during weak harmonic signal reception improved by limiting threshold voltage

09 p1460 A69-22645

Error probability distribution density at output of optimal Gaussian random signal detection, using approximate solution of integral equations

11 p1835 A69-24712

Optimal calculator of detection of Gaussian random signal against Gaussian noise background by reducing input signal to white noise

11 p1835 A69-24713

Collision avoidance system for air traffic, discussing false signal discrimination via electronic measurement of light pulse duration from aircraft Xenon discharge beacon lamp

12 p2129 A69-26772

Energy detection of random processes in colored Gaussian noise, discussing filtering, threshold detection, false alarm, probability distribution and density

13 p2220 A69-27937

Noise stability of nonoptimal radar detection system for noise and FM signals, deriving expressions for optimal spectral width

13 p2222 A69-28508

Noise sensitivity of FM discriminator/limiter in digital binary communication system with FM/PCM-FM/

15 p2564 A69-30145

Noise parameters at output of logarithmic detector separating two AM signals with overlapping spectra

15 p2564 A69-30148

Differential equations for optimum reception to synthesize detectors of deterministic signals against nonGaussian background noise using Markov process

15 p2567 A69-30340

Spectral characteristics of pulsed signal with determinate repetition period and amplitude and duration modulation by correlated random processes

15 p2567 A69-30347

Spectral correlation characteristics of amplitude modulated signal with background noise at envelope detector output

15 p2576 A69-30348

Phase locked loop with flip-flop error detector compared to analog loop, discussing signal to noise ratio

17 p2931 A69-34115

Receiving circuit for AM signal envelope separation in presence of AM interference and fluctuation noise, using converter cascades to effect input signal frequency spectrum symmetry

19 p3277 A69-36568

Quasi-optimal synthesis for reception indicator used in radio interferometers for measuring signal amplitudes in presence of normal noise

20 p3504 A69-37009

Multispectral imaging system to increase contrast using optical mechanical scanner, multielement dispersing spectrometer and electronic signal processing equipment

20 p3540 A69-37737

Error probability of Gaussian signal detector in Gaussian noise background determined from quadratic form of probability distribution density

22 p3901 A69-40955

Automatic discriminator design for identifying distorted image in noise based on ideal transmitter and use of split scanning beam

23 p4163 A69-41551

SIGNAL DISTORTION

Reliability of binary message in Gaussian noise impaired by amplitude limiting in case of evaluation by integration

01 p0031 A69-10736

Gas lens distortion of Gaussian light beam in sequence of lenses with same aberration, using shuttle pulse technique

01 p0120 A69-10849

Pseudorandom scanned TV signal distortion due to flutter and skew introduced by tape recorder, computing system SNR for distortion as additive random noise

01 p0033 A69-10999

Spectrum distortion of intermediate frequency signal in coherent Doppler navigation radar

01 p0034 A69-11013

Fluid amplifier signal noise sources, using large scale model for investigating jet-knife edge interaction

02 p0195 A69-12078

Horn antenna far field radiation pattern distortion by isotropic plasma slab, noting attenuation variation with electron density
02 p0218 A69-12335

Diffraction by rocket exhausts, discussing electromagnetic signal attenuation based on two dimensional straight edge diffraction model
02 p0209 A69-12352

Intermodulation and cross modulation distortions in double balanced modulator
04 p0573 A69-14341

Moving media influence on transient electromagnetic modal wave propagation in dispersive waveguides
04 p0557 A69-14752

Controlled transient signal distortion by shock monitoring instrumentation circuits using piezoelectric accelerometers
04 p0603 A69-15430

Wideband multichannel optical signals nonlinear distortions during transmission by electrooptical modulators using Pockels effect
05 p0718 A69-15655

Waveform distortions of trapezoidal wave passing through Gaussian filter in pulse transmission, discussing ideal filter effects on degradation
05 p0719 A69-16296

Autocorrelation function distortion determined for Barker signal passing through linear system and RC filter, noting passband influence on function shape
05 p0720 A69-16443

Resonant amplifier response having stages identical to radio pulse with exponential envelope
05 p0720 A69-16444

Nonlinear distortion of FM signal during passage through multipath medium, using analysis of linear passive four terminal network
05 p0721 A69-16531

Signal detection procedures preserving nonparametric detection properties and advantages of sequential procedures, assuming signal corruption by additive noise at input
06 p0888 A69-17531

Error and noise sources in analog differentiators, discussing signal distortion minimization techniques and augmentation with linear phase filter
06 p0897 A69-17702

Frequency modulated signal envelope passage through bandpass filter of inductively coupled circuits described by differential equation
07 p1100 A69-18555

Beam distortion in low order Gaussian-Laguerre modes propagating through saturable laser amplifier, noting uniform and Bessel small signal gain distributions [IEEE PAPER J-3]
07 p1152 A69-19065

Effects, measurement and analysis of flutter in instrumentation recorders
07 p1133 A69-19118

Radome induced distortions of radioelectric axis analyzed by sectional phase analysis
07 p1110 A69-19521

Nonlinear modulation distortions of high power radio waves propagating in ionosphere, noting electron temperature increase from radio wave
07 p1088 A69-19746

Wideband signal Doppler distortion influence on parameter estimate accuracy
09 p1454 A69-21725

Probability analysis of distortions caused by pulse noise action on digital information
09 p1476 A69-22678

Radio signal carrier frequency and arrival time measurements, deriving expressions for phase amplitude distortions effects
11 p1835 A69-24959

Intermodulation noise distorting arbitrary frequency-modulated multicarrier microwave signal in satellite transponder, emphasizing nonlinear energy dissipation and AM-FM conversion
11 p1841 A69-25634

Scintillation index variations based on 40 MHz Explorer 22 satellite signals recorded in Germany
12 p2034 A69-27094

Rms error for reproduction of satellite signal transmitted through continuous Gaussian channel assessed by numerical calculation
13 p2219 A69-27697

Nonlinear distortions in TWT for communication satellites applications, discussing relationship with efficiency
13 p2232 A69-28060

Nuclear explosions electromagnetic effects on electronic systems, considering signals emitted from

fireball and signal attenuation by changed atmospheric propagation
13 p2234 A69-28344

Deep space telemetry bit errors increased by reference signal phase noises and partial RF signal suppression, calculating equivalent signal to noise ratio degradation
13 p2223 A69-28609

Single-sideband signal nonlinear distortion and graphical methods for calculation of oscillator tube plate current pulse components
14 p2418 A69-28828

FM measurements of angle distortion introduced by single pole bandpass filters compared to theoretical distortion
14 p2416 A69-29552

Time domain method for hybrid simulation to compute interchannel distortions due to linear transducers in FM systems
14 p2417 A69-29556

Linear distortions effect on signals detection in binary communication channel with fluctuating noise, determining error probability
15 p2564 A69-30146

Junction diode field factor, comparing results of dynamic impedance and distortion measurement methods with deduced values of static characteristic
15 p2575 A69-30301

Earth ionosphere cavity model for atmospheric waveform shape, considering ELF pulse distortion after propagation through antipode
16 p2750 A69-31978

Nonlinear distortion of FM signal during passage through multipath medium, using analysis of linear passive four terminal network
16 p2753 A69-32473

Autocorrelation function distortion determined for Barker signal passing through linear system and RC filter, noting passband influence on function shape
16 p2753 A69-32475

Resonant amplifier response having stages identical to radio pulse with exponential envelope
16 p2753 A69-32476

Wideband multichannel optical signals nonlinear distortions during transmission by electro-optical modulators using Pockels effect
16 p2754 A69-32512

Probabilistic analysis of code message distortion due to pulse noise in modulation systems and comparison between linear and quadratic detections
17 p2919 A69-33145

Level crossing signal obtained by magnetic/electric field modulation, tabulating corrections to widths and centers for distortions
17 p3009 A69-34155

Light changes caused by distortion of binary components, computing theoretical brightness variations by numerical integration of emerging atmospheric intensities over visible surface
17 p3044 A69-34179

Neumann-Lommel formula generalization for obtaining Bessel functions product sums illustrated with FM wave distortion calculation in multichannel system
18 p3101 A69-34625

Wideband signal Doppler distortion influence on parameter estimate accuracy
20 p3488 A69-37461

FM data transmission distortion noise and error rate compared with AM and phase step modulation, noting role of bandwidth
20 p3496 A69-37905

Distortion of electromagnetic pulse propagating through inhomogeneous plasma medium with linear electron density variation
20 p3496 A69-38030

Optimum wideband signal for minimum Doppler distortion, describing pulse compression by linear-period modulation
21 p3671 A69-38406

Atmospheric natural turbulence effect of degradation of laser signal phase and amplitude characteristics, noting refractive index inhomogeneities effect on optical tracking system [AIAA PAPER 69-871]
21 p3675 A69-39397

Spatiotemporal signal distortions for multiple scattering from unsteady radiant energy transfer equations
22 p3899 A69-40247

Maximum errors of telemetering systems under interchannel transient distortions in multistage amplifier of video signals
22 p3899 A69-40250

Automatic discriminator design for identifying distorted image in noise based on ideal transmitter and use of split scanning beam
23 p4163 A69-41551

Distortion processes in ear, discussing sound pressure level/SPL/ measurements in rigid-walled couplers
23 p4085 A69-41573

Analog computer used to correct body plethysmographic chamber signal distortion due to inspired/expired air temperature and humidity differences
23 p4111 A69-42081

Numerical computation of rate-distortion function R/D/ for certain memoryless message sources, discussing bounds, reduction to minimization problem and applications
24 p4284 A69-42719

N-dimensional theorem for evaluating time continuous channel capacity or rate distortion function of random process
24 p4284 A69-42721

Correcting deficiencies in parametric expressions for rate distortion function of Gaussian process under weighted square error criterion
24 p4281 A69-42722

SIGNAL ENCODING

Multiple transmission principles, examining linear systems, synchronous and asynchronous codes and channel interference
01 p0026 A69-10068

Monochrome pictorial encoding, discussing pulse code modulation, delta modulation and buffer storage techniques
02 p0213 A69-12154

VLF system simulation for evaluating digital communications systems operating in presence of additive atmospheric noise
03 p0390 A69-13205

Fourier coding method for coding images for digital transmission, achieving bandwidth reduction for televised images
04 p0556 A69-14429

Book on information coding and transmission and error detection and correction
04 p0558 A69-15066

Digital computer optimization of representation of sampled data signals on orthogonal basis, using iterative method
06 p0901 A69-17363

Sequence pulse stuffing technique for rate equalization of digital channels, discussing coding effect and capacity for word signaling
07 p1080 A69-19094

Block coding systems performance in digital PCM data transmission through N-ary discrete channels in white Gaussian noise presence, discussing SNR upper bounds
07 p1080 A69-19096

Bandwidth restriction effect on performance of linear codes for digital communication with space vehicles, noting bit and word error probabilities
08 p1276 A69-20597

Detectability parameter for measuring performance of multiple and random access satellite communication system using PN codes
09 p1457 A69-22460

Color signal light gun for aircraft control at airport towers, noting pilot tests for familiarity with signal code
17 p2914 A69-33185

Ground data handling equipment characteristics for PCM telemetry link utilizing convolutional coding
19 p3273 A69-36267

Block coded telemetry systems design for phase coherent space communication employing double conversion superheterodyne phase locked receivers
19 p3277 A69-36487

Nonlinear encoding for picture transmission using nonlinear analog to digital converter
23 p4119 A69-41747

Flexible format adaptive telemetry encoder design, discussing system design and implementation technique with modular units
23 p4119 A69-41748

Rod signals elicited by flashes in human eye measured, deriving relation between nerve signal size in rods and flashes energy
23 p4099 A69-42119

Optical correlation for radar signals phase modulated by pseudorandom codes
24 p4282 A69-42742

SIGNAL FADING

NT SELECTIVE FADING

Frequency diversity for communication in fading environment, relating performance variance to between channel correlation variance
01 p0026 A69-10177

Probabilities of error, correct reception and signal cancellation in radio communication systems channels with signal absorption fading
01 p0030 A69-10592

Sequential logic for improved signal detectability in frequency-agile search radars, discussing target echo fading models in radar range performance prediction
01 p0033 A69-11008

Wind measurements by radio observation of meteor trails compared with fading drift results
02 p0275 A69-12042

Fading characteristics of radio waves reflected from two different heights in F region over Ahmedabad, India
03 p0385 A69-12915

Coherent PSK system in multipath environment /Rician fading and additive Gaussian white noise/ with phase locked loop for coherent reference extraction
03 p0393 A69-13255

Phase path variations at three closely spaced points, measuring horizontal drifts at E region level, investigating time shift variability in spaced fading records
03 p0421 A69-13329

Polarization diversity analysis to avoid fading in microwave scatter links in D and E layers
03 p0394 A69-13378

Nonattenuating signals spectra construction by means of generalized function method and Laplace transforms
04 p0583 A69-15134

Absorption effect on fluctuation of signal level propagating in turbulent atmosphere taking into account absorption in water vapor
05 p0717 A69-15634

Probability density distribution of time shifts in binary signal fronts caused by fading, applying results to FM signal reception
05 p0719 A69-16087

Automatic compensation of unwanted signal level fluctuation in measuring setups including microwave generators and detectors
06 p0903 A69-17489

Incidental modulation effect on accuracy, signal loss and sensitivity of pseudorandom code systems
06 p0890 A69-17824

Interrelation between parameters of statistical distribution of amplitude, angular and phase characteristics of signals scattered by extended body performing oscillations
07 p1085 A69-19154

Scintillation fading of VHF beacons on synchronous satellites, noting amplitude fluctuation depth and rate
09 p1457 A69-22461

Probabilities of error, correct reception and signal cancellation in radio communication systems channels with signal absorption fading
10 p1653 A69-23106

Multipath fading reduction on line of sight microwave radio relay links by dual space diversity, noting effects of vertical antenna separation, frequency, etc
[IEEE PAPER 68-TP-350-COM]
10 p1656 A69-23535

Subauroral traveling ionospheric disturbances and fading due to diffraction observed by geostationary satellites
10 p1685 A69-23831

Radio signals and concentrated noise amplitudes probability distributions reflected from ionosphere and scattered in troposphere calculated for Rayleigh and log-normal fading
11 p1833 A69-24440

Analog signal transmission through randomly fading channels, proposing pseudorandom phase reversals method for slowly varying multipath communication channels
11 p1834 A69-24552

Statistical characteristics of photocurrent pulse amplitudes during cathode exposure to gas laser outputs
11 p1834 A69-24611

Millimeter wave propagation over water, discussing fading characteristics and atmospheric absorption effects
11 p1836 A69-24989

Propagated ray paths plotted as functions of frequency and launch angle to predict signal dispersions
11 p1837 A69-25003

Digital simulation of phase locked receiver in diffuse multipath fading environment with band limited thermal noise
11 p1839 A69-25298

VLF signal strength minima during transition fading, considering asymptotic statistical distribution
12 p2032 A69-26862

Polarization diversity analysis to avoid fading in microwave scatter links in D and E layers
14 p2410 A69-28829

Latitudinal cut-off of manmade VLF signals in short path through ionosphere to OGO 2 satellite, noting strong noise following signal cut-off
14 p2434 A69-28958

Electro-optical automatic gain control system to reduce atmospheric turbulence produced fluctuations in received optical signal strength
14 p2459 A69-29491

Binary error investigation in noncoherent FSK communication link with nonselective fading, noting Doppler shift
14 p2414 A69-29498

Sporadic E layer frequency characteristics dependence on reflected signal fading, showing fine structure influence and maximum value of mean electron concentration
14 p2442 A69-29733

Two beam short wave channel capacity with beam separation at receiving end, noting dependence on channel properties and fading correlations
15 p2562 A69-30115

Optical communications experiments for quantitative data at 6328 Å on system fading due to scintillation and atmospheric turbulence effects on coherent propagation at 10.6 micron
16 p2748 A69-31564

SNR changes loss factor effect during passage through MTI coherent receiver followed by video integrator
16 p2753 A69-32438

Absorption effect on fluctuation of signal level propagating in turbulent atmosphere taking into account absorption in water vapor
16 p2754 A69-32492

Integral scalar equation describing signal attenuation by acoustically soft disk for mirror-shadow method of ultrasonic flaw detection
18 p3137 A69-35109

Phase modulation in pseudo-noise ionospheric communication system for reducing F region CW signal fading
18 p3104 A69-35308

Fluctuations of polarization induced fading periods in short wave transmissions of Soviet earth satellites, showing relation to ionospheric inhomogeneities
22 p3942 A69-41095

Daytime drift velocities and signal fading characteristics of equatorial and blanketing sporadic E layer irregularities, noting independence of electrojet intensity
23 p4160 A69-42429

Ionospheric electron content measurement from Faraday fading on satellite BE-B, using computer program for data reduction as function of latitude
23 p4160 A69-42434

Meter and decimeter wavelength range short period fading under conditions excluding optical sights, correlating specular and diffuse reflection
24 p4281 A69-42612

SIGNAL FADING RATE

Influence of winds aloft on fading rate of microwaves propagated beyond horizon
01 p0030 A69-10566

Fading velocity short period characteristics and duration and depth of field strength variations over transhorizon path compared with corresponding atmospheric parameters
12 p2028 A69-25897

Frequency measurement of moving spacecraft RF carrier waves at low SNR by analog recording of noisy signal and HF trigger tone, noting data processing and signal fading rate
12 p2038 A69-26051

Quasi-transverse /Q-T/ point time lag on Faraday rotation records at widely spaced frequencies during satellite pass explained by refraction theory
18 p3100 A69-34251

Periodic fading in 42 MHz auroral backscatter by high speed polarization measurements, discussing scatter bursts and pulsating primary electron flux relationship
18 p3102 A69-34950

SIGNAL FLOW GRAPHS

Transistor circuits analysis with aid of signal flow graphs
04 p0575 A69-14461

Signal flow graphs based on matrix methods, discussing loop currents, systems orientation and transfer functions
09 p1475 A69-22600

Transistor circuits analysis with aid of signal flow graphs
14 p2418 A69-28832

SIGNAL GENERATORS

NT FREQUENCY SYNTHESIZERS

NT FUNCTION GENERATORS

Radar return signal generation for computer simulations of airborne radar systems, using digital computer program for time varying radar backscatter
03 p0429 A69-13199

Properties and methods of generation of pseudorandom binary signals, developing linear modeling for multivariable systems
04 p0583 A69-15113

Electric signals by shock and detonation waves, describing detection technique
[WSCI PAPER 68-44]
07 p1240 A69-18360

Pulse compression radar employing same dispersive line for signal generation and reception
08 p1271 A69-19918

Circuit for generation of square wave with frequency as sum or difference of two periodic signal frequencies, discussing SSB modulation
10 p1665 A69-24047

Pseudorandom uniformly distributed numbers generation from noise-like signals produced by shift register with feedback, noting statistical tests
13 p2218 A69-27248

TEM mode networks design for producing phase coherent pulse modulated microwave signals through spectrum S band
13 p2234 A69-28073

Square wave generator for junction laser power supply
13 p2274 A69-28643

Vibration/acoustics digitally controlled environmental testing, describing random test signal generation and random vibration tests
15 p2587 A69-30389

IR detectors defined as transducers producing electrical signal proportional to IR power incident on detector, classifying types
19 p3310 A69-36068

Voltage variation frequency analysis for narrow-band sweep oscillators circuit design
20 p3486 A69-37010

Fluidic pressure signal generator for use in fluidic system frequency response studies, considering design and performance
[ASME PAPER 69-FLCS-40]
21 p3649 A69-38603

Compatible single sideband /CSSB/ modulation suitability for broadcasting, analyzing signal spectrum, demodulation distortion and signal generation methods
23 p4125 A69-42111

SIGNAL MEASUREMENT

Specific effective scattering area on lunar surface using Luna 13 signals from Oceanus Procellarum measured with radar employing antenna with narrow radiation pattern
01 p0158 A69-11312

Linear polarization of cosmic radio emission measured near galactic anticenter at centimetric wavelengths
03 p0501 A69-13704

Impulse bandwidth measurement error determination by trapezoidal numerical integration
03 p0398 A69-13902

Spectrum analysis of pulse signals by point to point measurements of magnitude and phase of pulse-like time functions, using narrow band filter output
03 p0399 A69-13939

Optimal filter design for estimating state of linear dynamical system in presence of high measurement noise
04 p0582 A69-14877

Radar echoes signal amplitude and phase digital recording with Radicord /radar digitizing and recording/ device
05 p0721 A69-16618

Radar signal parameters measurements consisting of SNR estimation and optimum energy supply determination from SNR estimation
07 p1085 A69-19153

Signal to noise ratio with stochastic and additive noise and signal, showing block diagram of modified estimator
09 p1452 A69-21320

Weak signal optimization of multilevel quantization and corresponding detection performance, discussing asymptotic limits
09 p1456 A69-22293

Electron density and collision frequency of MHD plasma determined directly by measuring phase shift and attenuation of propagating laser microwave signal
10 p1731 A69-23436

Phase fluctuations measurements of obliquely incident signal reflected from ionosphere performed over distance of 1300 km, showing amplitude dependence
10 p1657 A69-23913

Count rate meter for statistical frequency of signals applied to input of trigger with Poisson distribution of pulse intervals

11 p1884 A69-24734

Radio signal carrier frequency and arrival time measurements, deriving expressions for phase amplitude distortions effects

11 p1835 A69-24959

Receiver filter nonoptimality effects on accuracy of nonenergetic signal parameter measurements

11 p1835 A69-24960

Vertical parabolic antenna array and receiving system for S band transhorizon signal phase and amplitude measurement

11 p1851 A69-24987

Phase and field strength of transequatorial VLF signals, noting behavior during sunrise, day and nighttime

12 p2032 A69-26860

Large scale ionospheric inhomogeneities anisotropy, dimensions and drift velocities from simultaneously measured irregular refraction

14 p2436 A69-29053

TR tubes spurious harmonic power generation investigated for intersystem interference reduction and design criteria, discussing effects of incident power, gas pressure and tube geometry

15 p2573 A69-30032

Signal phase measurement accuracy by discrete phase technique ensured by using wideband signals and automatic control of input SNR

15 p2574 A69-30130

Instrumental accuracy of discrete filter during measurement of initial phase of signal dependent on phase structure

15 p2574 A69-30139

Space radiometers energy characteristics calculation taking into account reflecting surface roughness and antennas directional patterns

15 p2575 A69-30338

Resonance measurement of power percentage in single spurious mode of overmoded waveguide, using back to back transducers and reflection at input

15 p2577 A69-30611

Short and ultrashort waves signals amplitude and phase displacement determination device, stressing sensitivity

15 p2570 A69-31088

Faraday rotation measurements of signals from Explorer 22 analyzed to determine scintillation boundary in auroral ionosphere

15 p2605 A69-31443

Voltage standing wave ratio measurement technique at low power level, including tolerated errors, compared with Roberts-von Hippel method

17 p2918 A69-33031

Amplitude ratio measurement for two AC signals of given relative phase shift and same frequency

17 p2975 A69-33615

PCM bit synchronizer signal to noise ratio measurement by input video signal zero crossings counting

19 p3271 A69-36248

Temporal position of pulse signal on noise background determined by measuring signal passage time through linear filter zero point

19 p3278 A69-36596

Phase amplitude recording of radio waves reflected from D and F regions of ionosphere, reversing smoothing process by Fourier methods

21 p3672 A69-38558

Rod signals elicited by flashes in human eye measured, deriving relation between nerve signal size in rods and flashes energy

23 p4099 A69-42119

Quantization optimization of continuous signals with known probability distribution, using quantizers with limited output values

24 p4288 A69-42671

SIGNAL MIXING

Frequency mixing of IR signals with visible laser light in nonlinear crystals to detect IR signals

01 p0089 A69-10180

Microwave signal nonlinear interaction in isotropic positive column

01 p0127 A69-10282

Nonlinear optics, discussing frequency mixing, induced changes in dielectric constant and parametric amplification in microwave region of spectrum

05 p0772 A69-16229

Dynamics of laser response in IR detection by means of optical mixing in He-Ne laser, noting bandwidth

05 p0776 A69-16331

Difference frequency generation by multiple quantum transition from laser medium considered as resonant optical frequency mixing device

07 p1144 A69-18470

Siting two antennas for combining signals to obtain all-around coverage in aircraft communication

08 p1289 A69-20972

Self steered retrodirective antenna arrays with phase synthesizer, combining signals from individual elements at LF levels

11 p1850 A69-24983

Step-up mixer converting modulated IF signal to HF level by HF high power oscillator signal, discussing efficiency

11 p1854 A69-25615

Tunnel diode harmonic mode mixer having IF

14 p2424 A69-29763

Bisensory auditory and visual signals characteristics effects on human reaction time, noting different results for unilateral and bilateral signal pairs

23 p4083 A69-41454

SIGNAL PROCESSING

Microwave signal nonlinear interaction in isotropic positive column

01 p0127 A69-10282

Pulse code modulation /PCM/ time multiplex system companding by switching, discussing SNR measurement

01 p0031 A69-10739

Phase and amplitude variation at output of tuned amplifier, noting graphs and formulas

01 p0047 A69-10786

Narrow band normal steady state random processes applied to signal dispersion by extended oscillating body, obtaining statistical characteristics

02 p0206 A69-11602

Book on communication systems covering signal design, video signals, communication satellites and threshold decoding techniques

03 p0383 A69-12867

High range resolution by pulse to pulse frequency shifting, utilizing existing low resolution equipment by adding signal processing capability to receiver

03 p0388 A69-13181

Digital modified discrete Fourier transform Doppler radar processor for tactical aircraft

03 p0389 A69-13196

VLF system simulation for evaluating digital communications systems operating in presence of additive atmospheric noise

03 p0390 A69-13205

Sampled data delay-lock loop for synchronizing pulsed envelope RF signals, using digital circuitry

03 p0390 A69-13216

Linear processing effect on digital communications systems performance by channel impulse response and input-output relationship as distributional convolution equation

03 p0391 A69-13226

Adaptive processing limited memory receiver for synchronous detection of signals of unknown amplitude

03 p0400 A69-13228

Fast Fourier-Hadamard transform for digitized signal representation, classification, discrimination and efficiency

03 p0392 A69-13249

Optimum demodulation of PAM-FM signal for case of minimum mean square error as performance criterion

03 p0392 A69-13250

Digital processing of Doppler radar signals using matched filter concept

03 p0393 A69-13291

Signal matching in radio interferometer with autonomous receiver, magnetic tape recorders and memory electron beam tube with target

03 p0431 A69-13706

Linear and nonlinear filtering, discussing models for signal process, linear white noise problem, optimal estimates, colored noise and finite dimensional approximation

04 p0581 A69-14696

Band inversion passive generation in pulse compression radar, noting influence on signal modulation laws

04 p0558 A69-15074

Digital filter design with complex coefficients for analytic signals and complex envelopes

04 p0579 A69-15460

Multiple target monopulse radar signal processing technique

04 p0562 A69-15470

Single two dimensional coherent matched filter optical processor for simultaneous synthetic radar antenna beam sharpening and pulse compression

04 p0562 A69-15470

Digital signal processing in radar, sonar and communication

05 p0718 A69-15749

Static and dynamic performance of pancake vortex flow field and application to signal amplification

05 p0704 A69-16000

Signal detection procedures preserving nonparametric detection properties and advantages of sequential procedures, assuming signal corruption by additive noise at input

06 p0888 A69-17531

Differential equations for minimum variance linear filter separating signals from additive correlated noise, using discrete time optimum formulas

[AIAA PAPER 69-73] 06 p0905 A69-18121

Signal conversion by multiple modulation in optical communication system, discussing electrooptic modulators and modulation spectrum

07 p1075 A69-18472

Signal multiplexing within linear algebra framework permitting use of orthonormality in receiver construction without orthonormal functions generation in multiplexer

07 p1078 A69-18830

OMEGA 4 100-k Hz ground station telemetry system for acquiring and processing outputs up to 23 FM and two TDM signals applied simultaneously from instrumentation recorder

07 p1105 A69-19103

Signal processors for implementation of monopulse tracking radar with three instead of four beams, investigating accuracy

08 p1270 A69-19855

Approximate noise analysis of phase locked loop with signal clipping

08 p1270 A69-19857

Filters for sampled signals sequences using design simplicity and signal to noise ratio for evaluation and comparison factors

08 p1274 A69-20127

Design and construction of linear digital filters for signal processing, discussing digital filtering of various signals for space research

08 p1297 A69-20303

Signal processing arrays - Conference, Dusseldorf, July 1966

08 p1287 A69-20957

Literature survey and critique of signal processing arrays, discussing synthetic, self phasing, retrodirective correlation and decision theoretic arrays

08 p1287 A69-20958

Signal processing arrays characterized by Fourier series radiation sources, time gating and signal smoothing by narrow band filtering

08 p1287 A69-20959

Hemispherical scanning with small aperture monopoles, spirals, scimitars and wire antennas, discussing various types for multiple beam operations

08 p1290 A69-20973

Hertzian radiometric antennas and signal processing techniques for aerial mapping project for sun

08 p1290 A69-20976

Space frequency filter antennas, using multiple terminals for signal processing as function of frequency and angle

08 p1290 A69-20977

Electronic optical system to process time-varying signals as optical spectrum analyzer for measuring power spectral density of input time function

08 p1317 A69-21086

Pulse frequency signal processing continuous and discrete differentiators, analyzing time delay, constant frequency, accuracy and codes

09 p1454 A69-21755

Soviet book on statistical theory of discrete signal demodulation, covering demodulator analysis and synthesis methods

09 p1455 A69-21933

Two dimensional signal analog correlation in noise background using optical spatial filtering Fraunhofer hologram and input as functions

09 p1499 A69-22276

Signal processing regenerative technique used for multichannel predetection combining, including carrier suppressed signals

09 p1458 A69-22472

Phase and amplitude variation at output of tuned amplifier, noting graphs and formulas

10 p1662 A69-23115

- Signal conditioning for transducers covering piezoelectric devices, thermocouples, resistance transducers, reluctance and differential transformer sensors
10 p1691 A69-23228
- Signal conditioning amplifiers covering carrier and DC amplifiers, differential amplifiers, charge amplifiers and active filters
10 p1691 A69-23230
- Solid state AC voltage circuitry for measuring and controlling charged particle detector signals
10 p1662 A69-23256
- Specifying electrical isolation and error signals suppression due to presence of common mode voltage in passive signal handling and conditioning equipment
10 p1654 A69-23272
- Radar signal cross correlation function calculation with reference function, applying acousto-optical modulator
10 p1694 A69-23539
- Resolving power increase in multibeam antenna, discussing signal demodulation through incident field breakdown
10 p1664 A69-23797
- Signal processing method for achievement of very rapid space scanning with antenna array noting application to radar system
10 p1657 A69-23801
- Narrow band normal steady state random processes applied to signal dispersion by extended oscillating body, obtaining statistical characteristics
11 p1835 A69-24709
- Two oscillator signal combiner based on mutual synchronization, providing output signal free of phase jumps or amplitude fluctuations
11 p1849 A69-24928
- Optimal multidimensional sequential filtration of signal on background of time correlated noise
11 p1859 A69-24967
- Transistorized assembly for amplification of signals emitted by platinum film probes in shock tubes, discussing application to chronometric device triggering
11 p1887 A69-25095
- Data processing system for satellite telemetry signals, describing hardware construction and operation, data readout, etc
11 p1840 A69-25426
- Observation process optimization in system described by linear differential equations of motion reduceable to optimal control problem
12 p2027 A69-25882
- Optical correlator for radar signal processing based on filtering first order diffracted light and integration on photomultiplier
12 p2028 A69-25911
- Quantization error reduction for stochastic signals processing problems
12 p2051 A69-26201
- Bandwidth potential increase of parametric amplifier obtained by adding active filter elements to signal circuit, noting satellite communication band
12 p2039 A69-26380
- Shift registers with binary switching elements for shaping signal spectrum in data transmission systems without phase distortions
12 p2040 A69-26486
- Mismatch between signal and filter effect on output response of matched filter for pseudorandom phase-manipulated signals in receiver
12 p2031 A69-26487
- Signal processing and DC restoration in line scan devices used in land/water terrain analysis
12 p2096 A69-26980
- Computer simulation program for design and evaluation of digital Doppler processor, analyzing performance limitation due to quantization and white noise
12 p2035 A69-27096
- Control signal correction in microwave ferrite modulators, eliminating losses due to screening effect of feeder
13 p2226 A69-27216
- Singularities of optimal filtration for random signals given by differential equations with variable coefficients and white noise
13 p2218 A69-27251
- Bayes theory and nonclassical variation method to solve optimal energy distribution available for identifying weak signals in background noise
14 p2410 A69-28817
- Input signal piecewise linear approximation for investigating response of dynamic automatic control systems to nonstandard input signal
14 p2426 A69-29143
- Optical signal conversion efficiency and threshold relationships in pulsed rangefinding systems, considering effects of noise obeying Poisson distribution
14 p2412 A69-29324
- Limiting incoherent or coherent interference signals at frequency of biphasic or quadriphase digital signal
14 p2413 A69-29483
- Bearing errors reduction in vertical loop HF direction finders for ionospherically propagated signals in dual channel system
14 p2413 A69-29493
- Continuous IR parametric signal amplification in saturable absorber caused by carbon dioxide laser pumping
14 p2459 A69-29601
- Solid state programmable avionics converter for signal processing, information conversion and aircraft control
14 p2405 A69-29687
- Algorithm for optimal digital processing of pulse signals during multilevel quantization in Markov noise, including error analysis
15 p2571 A69-30126
- Orthogonal signal recognition in set of false signals by resolving devices with limited sensitivity, giving design formulas for error probability
15 p2563 A69-30135
- Digital receiver of radar signals for performing binary quantization of input data with subsequent processing by digital computer
15 p2563 A69-30136
- Pulsed noise sensitivity in radar receivers having noise limiter for simple and complex signals
15 p2563 A69-30137
- Complex pulsed radar signals synthesis with uncertainty function having principal maximum and small secondary maxima for radar stations and wideband communications systems
15 p2563 A69-30140
- Residual phase term influence on compressed signal shape, analyzing linearly frequency modulated signal spectrum and sidelobe suppression in pulsed radar
15 p2564 A69-30143
- CdS films vacuum deposited on optically polished single crystals used for converting microwave radio signals into hypersonic waves
15 p2575 A69-30236
- Algorithm for processing binary-quantized echo signal packets, obtaining useful and noise signals relation
15 p2571 A69-30331
- Subtractor performance for processing correlated random signals with different spectral widths in signal delay time indicator, discussing errors
15 p2572 A69-30346
- Linear high resolution gate function in blocking out analog signals or reproducing signal amplitudes at output, noting semiconductor elements utilization
15 p2581 A69-31523
- Photon bunching effect in spatially coherent noise field enhanced by superposing monochromatic coherent signal and/or shaping incident noise spectra
16 p2749 A69-31694
- Long distance FM radar signal relaying to central station image processing, showing wideband sum signal especially suitable for transmission
16 p2750 A69-31862
- Automatic conversion receiver of meteorological radar data, examining reception amplitude sensitivity and frequency characteristics
16 p2791 A69-32280
- Bandwidth requirement of single channel monopulse limiter, discussing signals conversion to IF
16 p2761 A69-32471
- Attainable signal compression coefficient in recirculator and relation to recirculator ring parameters, noting feedback coefficient stability
17 p2931 A69-33907
- Resolving power of spectral analyzer with in-phase storage increased by weighted signal treatment
17 p2931 A69-33908
- Analog signal processing concepts based on models simulating mechanical function of ear cochlea
17 p2911 A69-34092
- Phase locked loop with flip-flop error detector compared to analog loop, discussing signal to noise ratio
17 p2931 A69-34115
- Analog to digital conversion, describing successive approximation technique with built-in sample and hold and discrete analog amplitude modification
17 p2934 A69-34124
- Data compression using orthogonal functions, design curves for given functions, signal characteristics and error avoidance
18 p3103 A69-35060
- Functional signal conversion operations in microelectronic radio equipment, examining components in analog and pulsed devices synthesis
18 p3109 A69-35162
- Encoding and decoding in IR tracking system, analyzing chopping rotating FM reticle pattern
19 p3268 A69-36058
- High bit rate signal conditioning, bit and group synchronization of NRZ PCM, considering gain and power bandwidth limitations and delays
19 p3271 A69-36247
- Phase locked loop design of desensitized monolithic integrated circuits for FM multiplex signal filtering and demodulation, describing external tuning
19 p3273 A69-36274
- Binary storage system operation during binary quantization of signal, applying results to storage efficiency improvement
19 p3278 A69-36597
- Holographic system to process signals received by pulse Doppler radar, noting real time operation with availability of instantaneous development image storage media
19 p3314 A69-36598
- Energy criteria inconsistency in evaluating frequency band changes attributed to simultaneous narrowing and broadening of different signal power bands
19 p3278 A69-36716
- Fourier transform techniques applications in optics, converting optical signal amplitude and phase information into electrical signal information
19 p3374 A69-36737
- Book on linear digital filtering and discrete spectrum analysis, emphasizing frequency domain description of signals and systems
20 p3487 A69-37146
- Recording devices for storing bandwidth data in time sequence, studying design parameters using light beam recorder implemented with CRT for read-in process
20 p3540 A69-37640
- Double binary PSK system digital computer simulation for satellite communications, investigating filter and limiting effects on performance in error probability terms
20 p3492 A69-37705
- Analog telemetry signals generalizing frequency and pulse position modulations over coherent channels, noting added degrees of freedom function
20 p3492 A69-37713
- Time division multiplexing of asynchronous digital signals from independent sources in continuous or bit stuffing mode, evaluating reliability and efficiencies
20 p3493 A69-37715
- Multispectral imaging system to increase contrast using optical mechanical scanner, multielement dispersing spectrometer and electronic signal processing equipment
20 p3540 A69-37737
- Pulsar search signal processing and digital techniques, using fast folding /cross correlation/ or fast Fourier transform /FFT/ algorithms
20 p3605 A69-37824
- Near constant phase variable attenuator for RF signal containing Doppler information, centering design around p-i-n diode as control element
21 p3681 A69-38410
- Relation between smoothed and filtered linear least squares estimates of signal process in white noise from deriving resolvable identity of covariance function
21 p3754 A69-38432
- Cross correlation coefficient for submillimeter monochromatic wave amplitude and phase fluctuations in turbulent atmospheric boundary layer
21 p3674 A69-39129
- Strapdown redundant experimental sensor inertial navigation package containing gyros and accelerometers, discussing signal real time processing by digital computer
21 p3762 A69-39379
- [AIAA PAPER 69-851]
- Nonlinear compensator characteristics determination for modifying compensated system output signal under various disturbances with inputs subjected to white noise
21 p3688 A69-39862
- Agricultural and forestry applications of tethered balloons, discussing observation angle effect on spectral signature response and signal preprocessing
22 p4053 A69-40805
- Digital signal processing electronic device for linearizing signals from sensors with nonlinear frequency output by modifying time signal frequency
22 p3915 A69-40935
- Unisensory and multisensory signal processing in cortical and brain stem regions of albino rat by electronic averaging and time histogram techniques
23 p4092 A69-42055

SIGNAL RECEPTION

Q multiplier UHF device as preselection filter for closely spaced channel signals, discussing channel interference reduction

23 p4141 A69-42220

Adaptive signal processing interference rejection technique for suppression of cochannel AM interference in congested VHF tracking receiver

23 p4128 A69-42503

Optimum signals for high resolution radar and communication systems, using transmitter waveform design of autocorrelation and cross correlation functions

23 p4132 A69-42545

Pseudorandom code development and possibilities for radar applications, considering signal processing, antenna requirements, radar signal phase modulation, etc

24 p4281 A69-42741

RF and microwave signal variable delay and processing using laser-acoustic interactions, photodetector and electrical-to-acoustical transducer

24 p4283 A69-43027

SIGNAL RECEPTION

NT SYMBOLS

NT TELEVISION RECEPTION

Optimal coherent reception of frequency diversity signals in multipath channels investigated for noise immunity

01 p0028 A69-10375

Coherent diversity reception of discrete signals in presence of concentrated noise investigated for use of optimal solution circuits for noise elimination

01 p0028 A69-10376

Optimal reception methods noise stability for AM radio signals based on nonlinear filtration of information parameters of signals received on noise background

01 p0030 A69-10589

Probabilities of error, correct reception and signal cancellation in radio communication systems channels with signal absorption fading

01 p0030 A69-10592

Optimal reception of quantum signals at recording device aperture

02 p0206 A69-11607

Optical receivers for deep space optical communications link assuming PCM scheme

03 p0389 A69-13194

Wide signal and noise statistics range to determine noise rejection characteristics of communication system used for single path and diversity reception

03 p0394 A69-13376

Multichannel communication received signals irregular components, discussing signal phase and amplitude fluctuations correlation coefficients

03 p0394 A69-13519

Correlation of received signals with diversified angles of arrival due to scattering by turbulently excited ionosphere

03 p0399 A69-14129

Simultaneous recording of radio emission from five sections of solar active region, using parabolic antenna and single amplification/reception channel

04 p0651 A69-14377

Portable amplitude and frequency recording system for studying ionosphere by radio signals from artificial satellites

04 p0597 A69-14748

Noise correlation effect on noise stability of diversity reception receiver with weighted coherent summation of signals

04 p0557 A69-14789

Temperature distribution over receiving layer of absorption edge image transformer, discussing thermal conduction influence on performance of thin film IR image receiver

04 p0631 A69-15280

Sonar receiver reduced averaging processing in presence of extended and point targets compared with full averaging processor

04 p0562 A69-15477

Probability density distribution of time shifts in binary signal fronts caused by fading, applying results to FM signal reception

05 p0719 A69-16087

Asymptotic performance of adaptive receivers and application to signals of unknown frequency, noting SNR role

05 p0722 A69-16727

Satellite picture signal reception from ESSA, Nimbus and ATS to ascertain instrument requirements

06 p0888 A69-17651

VHF space communication signals with radio fluctuations along propagation path through turbulent atmosphere, giving diversity reception effect when transmitting linearly polarized waves

06 p0889 A69-17653

Signal resolution during space diversity reception with nondirective or weakly directive antennas and noncorrelated receiver background noise, discussing signal processing

06 p0890 A69-17800

Sensitivity problems in receiving microwave signals from communications satellite at deep space distances, considering noise factors

07 p1077 A69-18669

VLF radio wave phase time or motion variation emanating from ground based source at arbitrary point on earth

07 p1123 A69-18816

Multifunction Receiver System rationale, concepts, background requirements and technical justifications for tracking, telemetry and ranging data acquisition by Goddard Center

07 p1081 A69-19101

Bit probability of PCM/FM for receiver with IF bandwidth equal to or greater than data rate, limiter-discriminator detection and postdetection filter

07 p1082 A69-19106

Pulse compression radar employing same dispersive line for signal generation and reception

08 p1271 A69-19918

Receiving systems for digital telemetry signals from spacecraft, analyzing receiver performance by statistical methods

08 p1276 A69-20591

Microwave converters structural characteristics, calculating noise figure

08 p1285 A69-20594

Hard limiting effect on sum of three or four sinusoidal signals noting output amplitudes, signal suppression and negative suppression effect

09 p1451 A69-21311

Optimal receiving circuit determined for elliptically polarized signals in randomly polarized noise by deriving integral equation

09 p1456 A69-22285

Noise rejection in multichannel telephone signal reception with FM and multiplexing, determining SNR dependence on SNR at receiver input

09 p1459 A69-22640

Noise rejection in linear amplitude detector during weak harmonic signal reception improved by limiting threshold voltage

09 p1460 A69-22645

Optimal reception methods noise stability for AM radio signals based on nonlinear filtration of information parameters of signals received on noise background

10 p1653 A69-23104

Probabilities of error, correct reception and signal cancellation in radio communication systems channels with signal absorption fading

10 p1653 A69-23106

VHF space communication signals with radio fluctuations along propagation path through turbulent atmosphere, giving diversity reception effect when transmitting linearly polarized waves

10 p1775 A69-23191

Resolving power increase in multibeam antenna, discussing signal demodulation through incident field breakdown

10 p1664 A69-23797

Antenna point and astigmatic sources due to phase centers and phase diagrams relations and antenna caustic curves

10 p1664 A69-23798

Shipborne self pointing antenna for reception of telemetry signals from maneuverable missile, discussing tracking and compensation for ship platform motion

10 p1664 A69-23803

Ionospheric discontinuities drift velocities from diversity reception data indicating no dependence on solar activity

10 p1686 A69-23911

Optimal reception of quantum signals at recording device aperture

11 p1835 A69-24714

Energy gain during diversity reception in presence of random noise calculated, considering signal and noise amplitudes Rayleigh fluctuations

11 p1835 A69-24968

Visual receiving equipment for consistency determination of Loran-C sky wave signals apparent arrival times

12 p2029 A69-26052

Differential absorption by measurement of phase difference of ionospherically propagated incoherent radio wave signals under quasi-longitudinal conditions

12 p2032 A69-26857

Phase and field strength of transequatorial VLF signals, noting behavior during sunrise, day and nighttime

12 p2032 A69-26861

Received signal phase angle error probability in coherent PSK system in Gaussian noise and interference

13 p2219 A69-27666

Wide signal and noise statistics range to determine noise rejection characteristics of communication system used for single path and diversity reception

14 p2410 A69-28822

Single-sideband signal nonlinear distortion and graphical methods for calculation of oscillator tube plate current pulse components

14 p2418 A69-28822

Random motions velocity of ionospheric inhomogeneities by extreme lines delineation of diffraction pattern during amplitude recording of reflected signal

14 p2444 A69-29872

Two beam short wave channel capacity with beam separation at receiving end, noting dependence on channel properties and fading correlations

15 p2562 A69-30115

Potential noise stability of reception in binary communications system with active pause in channel for unknown signal arrival time

15 p2563 A69-30134

Reference oscillator synchronization inaccuracy influence on SNR at output of correlation receiver during reception of signals with pseudonoise modulation

15 p2563 A69-30141

Wideband PM communication system with synchronous reception and automatic control of reception bandwidth, providing improvement in noise stability

15 p2564 A69-30147

Differential equations for optimum reception to synthesize detectors of deterministic signals against nonGaussian background noise using Markov process

15 p2567 A69-30340

Multifunctional radar errorless operation determined from relations between amount of received information, number of channels and SNR

15 p2576 A69-30354

Aoriste antenna to receive radioelectric signals from satellite emitter at distance of 10,000 km

15 p2580 A69-31095

VLF and particle rocket experiment for group delay time between rocket and ground, discussing wave polarization and energy flows meaning

15 p2571 A69-31424

Received radar signal power maximizing problems in planetary exploration, analyzing abelian group real line and circle problems

17 p2993 A69-32831

Cryogenic applications to low noise reception development in radio astronomy, planetary radar and communication with deep space probes

17 p2921 A69-33685

Single radio pulse reception time relations by panoramic receiver, considering short wideband and long narrowband pulses

17 p2931 A69-33910

Coherent phase locked loop receiver as carrier and modulation loops combination with parallel bandpass filter for ranging signal reception and FM demodulation

19 p3274 A69-36277

Quasi-optimal synthesis for reception indicator used in radio interferometers for measuring signal amplitudes in presence of normal noise

20 p3504 A69-37009

Circular or linear polarization diversity reception for VHF earth-station-satellite communications through turbulent ionosphere, assuming Rayleigh distribution fading

23 p4115 A69-41585

Monopulse, high power, three channel antenna feed system design for communication satellites, noting orthogonal polarization of transmit and receive functions

23 p4120 A69-41750

Omega aircraft navigation, discussing digital computer applications, SNR environment, carrier interference and accuracy requirements for signal reception

23 p4186 A69-42539

Book on new concepts in radars covering ideal reception, moving targets, autocorrelation, SNR, amplitude distribution, clutter, etc

24 p4283 A69-43168

SIGNAL REFLECTION

- Multifrequency three layer sandwich radomes design for reflectionless sandwich at second frequency
01 p0034 A69-11037
- VHF transhorizon propagation by double reflection from elevated layer in troposphere
01 p0034 A69-11139
- Backscattering diagram of Venus at 40 cm determined from Doppler spectrum and reflected signals range energy distribution
02 p0314 A69-11639
- Ionospheric radio signal reflection measurements based on ground to rocket pulse propagation
02 p0245 A69-12736
- Radar observations of sun, determining reflected radio signal component formed by combination scattering in coronal plasma oscillation
03 p0505 A69-13082
- Statistical characteristics of multibeam signals reflected obliquely from ionosphere
03 p0396 A69-13708
- Pulsed electromagnetic signal reflection from plane boundary of absorbing medium
03 p0397 A69-13711
- Earth effect on signal correlation in space diversity microwave reception antennas, analyzing vertical separation and out of phase signals
05 p0720 A69-16530
- Multichannel HF resolution spectral analyzer of pulses reflected from ionosphere applied to dependence of cross correlation coefficient on frequency separation
06 p0897 A69-17740
- Interrelation between parameters of statistical distribution of amplitude, angular and phase characteristics of signals scattered by extended body performing oscillations
07 p1085 A69-19154
- Reflected radio wave amplitude distributions related to distributions of curvature at reflector
07 p1086 A69-19225
- Electron concentration at front of anisotropic plasma expanding in axial direction in electrodeless induction discharge from measurements of reflected microwaves
09 p1550 A69-22027
- Radio signal reflection from objects of complex configurations by statistical model
09 p1460 A69-22662
- Phase fluctuations measurements of obliquely incident signal reflected from ionosphere performed over distance of 1300 km, showing amplitude dependence
10 p1657 A69-23913
- Long range ionospheric propagation of ultrashort radio waves, obtaining diurnal and seasonal characteristics of reflected signals amplitude and duration
13 p2255 A69-28543
- Radar observations of sun, determining reflected radio signal component formed by combination scattering in coronal plasma oscillation
14 p2515 A69-28764
- Object shapes automatically classified from reflected radio signals, considering correlation description of object effective dispersion surface diagram
14 p2411 A69-28917
- Correlation function of auroral reflection radio signals with allowance for polar ionospheric scattering and pulse signal transmission and reception
14 p2436 A69-29055
- Sporadic E layer frequency characteristics dependence on reflected signal fading, showing fine structure influence and maximum value of mean electron concentration
14 p2442 A69-29733
- Algorithm for processing binary-quantized echo signal packets, obtaining useful and noise signals relation
15 p2571 A69-30331
- Signal reflection elimination from underlying surface during aircraft flights by using two antenna array with identical radiation patterns
15 p2567 A69-30345
- Airborne Doppler radar, estimating velocity distribution and density of pulse signals reflected from air and ground targets
15 p2567 A69-30349
- Photography of laser echoes on satellites, tabulating results
15 p2570 A69-31311
- Vertical incidence pulse dispersion with application to Alouette 1, discussing echo width, sounder system bandwidth and frequency gradient of ionospheric virtual height
16 p2750 A69-31977

- Amplitude distribution and correlation functions of signals reflected from precipitations at various polarizations of waves emitted and received
16 p2807 A69-32269
- Depolarization degree of angel echo signals measured by radar station, indicating insects and other foreign particles in atmosphere as reflection sources
16 p2779 A69-32274
- Earth effect on signal correlation in space diversity microwave reception antennas, analyzing vertical separation and out of phase signals
16 p2753 A69-32472
- Scattered ionospheric reflection distribution at evening/morning periods showing deviation, using coherent method
17 p2927 A69-33860
- Signal wave scattering and transmission by ionized medium disturbed by high power pumping wave, studying wave interactions with Born approximation for bounded medium
17 p2928 A69-33871
- Meteor station photorecorder of reflected radio signals, discussing design and performance during meteor shower
17 p2976 A69-33898
- Reflected signals detection with limited frequency spectrum and minimum velocity resolution considered, analyzing signal properties
18 p3104 A69-35265
- Recording technique for measuring short period variations of radio signal reflections altitudes from ionosphere applicable to fast ionospheric processes
20 p3521 A69-37054
- TEM mode reflection coefficient for symmetric parallel plate waveguide composed of adjacent conducting wedges composition and radiating into perfectly reflecting sheet
20 p3507 A69-37839
- Redirection of time varying signal between specified points by arbitrarily spaced antenna array elements with condition involving time delays for validity of retrodirection
23 p4136 A69-41580
- Radar signal reflectivity and precipitation relationship revised on basis of radio signal damping for improved measurement accuracy
23 p4185 A69-42494
- Ionized meteor trails reflection zone altitudes determination by interferometric measurements of phase differences
24 p4311 A69-43508
- SIGNAL STABILIZATION**
- Carbon dioxide laser stabilization using laser profile and three mirror system
01 p0089 A69-10183
- Random filters and stabilization of periodic signals mixed with noise, establishing second order statistics at output
07 p1089 A69-18281
- Filter circuits for stabilization of solid state microwave devices, noting input matching characteristics
11 p1849 A69-24961
- Phase and amplitude stabilization during phase modulated discrete data transmission
19 p3277 A69-36571
- SIGNAL TO NOISE RATIOS**
- Optimal rank algorithm construction for signal detection in noise investigated for use in information transmission systems
01 p0027 A69-10374
- Coherent diversity reception of discrete signals in presence of concentrated noise investigated for use of optimal solution circuits for noise elimination
01 p0028 A69-10376
- Antenna performance optimization, considering gain dependence on diameter, feed, tolerances, noise temperature, etc
[UN PAPER 68-95813] 01 p0043 A69-10517
- Optimum modulation technique determination for single channel voice communication under severe noise conditions
[UN PAPER 68-95851] 01 p0029 A69-10526
- Optimal reception methods noise stability for AM radio signals based on nonlinear filtration of information parameters of signals received on noise background
01 p0030 A69-10589
- Signal to cross modulation noise ratio in TWT tube during amplification of sinusoidal signals
01 p0031 A69-10780
- Optimal AM radio reception in presence of fluctuating noise and one AM interference signal with random initial phase of carrier oscillation
01 p0031 A69-10782

- Spatial filtering effectiveness determination by equivalent spatial operations, deriving expression for SNR
01 p0052 A69-10799
- Regular and noise signal scattering by uneven surface determined by correlation functions, assuming monochromatic components scattering obeys Kirchhoff approximation
01 p0032 A69-10886
- Pseudorandom scanned TV signal distortion due to flutter and skew introduced by tape recorder, computing system SNR for distortion as additive random noise
01 p0033 A69-10999
- Optimum linear filters for signal detection against background noise using Hodges-Lehmann method
02 p0223 A69-11565
- Probability density distributions for monaural detection of tonal signal in continuous background of Gaussian noise as modified noncentral chi distribution
02 p1201 A69-11821
- Fluid amplifier signal noise sources, using large scale model for investigating jet-knife edge interaction
02 p0195 A69-12078
- Noise emitted by gas filled cavity perturbed by strong coherent signal computed by Nyquist equation
02 p0211 A69-12448
- Waveguide band transition noise of gas discharge source, discussing measurement methods for establishing excess noise ratio
02 p0212 A69-12461
- VLF system simulation for evaluating digital communications systems operating in presence of additive atmospheric noise
03 p0390 A69-13205
- Working breadboard model of planet tracker under various illuminating conditions, discussing hardware and closed loop tracking error analysis accounting for signal to noise effects
03 p0463 A69-13214
- Noncoherent binary communication detector for slow selective fading channel with additive quasi-stationary noise based on mathematical procedure of non-parametric classification
03 p0390 A69-13215
- Wide signal and noise statistics range to determine noise rejection characteristics of communication system used for single path and diversity reception
03 p0394 A69-13376
- Noise reduction techniques in digital and analog data transmission over space program distances, emphasizing deep space missions
03 p0394 A69-13398
- Multichannel communication received signals irregular components, discussing signal phase and amplitude fluctuations correlation coefficients
03 p0394 A69-13519
- Noise susceptibility of integrated circuits in digital systems, discussing sources and specifications
03 p0410 A69-13579
- Electrically small beamed receiving arrays in HF band and random noise
03 p0398 A69-13904
- Maximum probability technique for measuring angular coordinate with unknown signal and noise intensity
03 p0399 A69-14132
- Broadband signal and noise performance of direct detection optical receiver consisting of solid state photodiode and baseband amplifier
04 p0556 A69-14283
- Simultaneous passage of useful and noise signals through differential frequency discriminator, determining spectrum by phase detection and detuned circuits
04 p0556 A69-14462
- Constrained layer damping and conventional techniques combination for vibration and noise control
04 p0606 A69-14691
- Weak periodic signal separation from noise using single and multichannel analog adders
04 p0597 A69-14848
- Moving window radar detector design for moving targets, giving chart for SNR derivation to obtain given detection probability
04 p0558 A69-15073
- Modems for high data transmission rates on available voice bandwidth channels, noting point to point and multipoint polled networks and signal to noise ratio
04 p0564 A69-15208
- Phase locked loop discriminator in threshold region, discussing effects of loop parameters, detuning error and modulation
04 p0580 A69-15471
- Low noise shaped beam Casssegrain antenna design for space communications earth station service, noting gain/noise temperature figure and antenna construction
05 p0728 A69-15669

SNR analysis at amplifier output with AGC, noting increase with signal strength

05 p0729 A69-16085

Frequency and noise characteristics of gyrator circuits, analyzing Q factor, stability and oscillation sensitivity

05 p0735 A69-16621

Expressions for calculating filtering errors resulting from insufficient information about useful signal and noise characteristics

05 p0740 A69-16668

Asymptotic performance of adaptive receivers and application to signals of unknown frequency, noting SNR role

05 p0722 A69-16727

Pulse amplitude measurements comparison by sampling signal at given time and pulse peak detection, considering SNR

05 p0722 A69-16730

Signal/noise performance of frequency locked loop FM threshold extension demodulator compared to phase locked loop demodulator and conventional FM discriminator

06 p0886 A69-16934

Phase lock loops design with nonlinear filtering elements in low signal to noise region, considering signal demodulation, lock range and threshold

06 p0902 A69-17398

Linear antenna synthesis for optimal separation of plane waves providing maximum SNR with allowance for statistical phase distribution of field

06 p0895 A69-17460

Detection characteristics of coherent pulse packet with random initial phase on Gaussian noise background of unknown intensity

06 p0887 A69-17463

Error probability vs SNR and power spectrum of PCM/PM signal with small phase deviation, noting applications in satellite tracking

06 p0889 A69-17656

Differential equations for minimum variance linear filter separating signals from additive correlated noise, using discrete time optimum formulas [AIAA PAPER 69-73]

06 p0905 A69-18121

Random filters and stabilization of periodic signals mixed with noise, establishing second order statistics at output

07 p1089 A69-18281

Pulsating radio source pulse arrival time measurements at 1919 plus 21, determining highest SNR

07 p1214 A69-18665

Sensitivity problems in receiving microwave signals from communications satellite at deep space distances, considering noise factors

07 p1077 A69-18669

Direct coupled monolithic IF amplifier with active gain control, analyzing large signal response, stability, available gain and noise behavior

07 p1104 A69-18885

Photoparametric up-converter with optimum SNR, noting suitability of direct detection of amplitude modulated optical signals

07 p1104 A69-18888

Optimized gain control configuration using field effect transistor with broadband control to maintain high signal to noise ratio with low distortion

07 p1115 A69-18889

SNR enhancement in optical receiver by amplification before detection of carrier of modulated optical signal, using quantum amplifier [IEEE PAPER R-5]

07 p1154 A69-19079

Maximum likelihood bit synchronizer for baseband PCM signals in Gaussian noise, stressing system noise performance analysis and measurements

07 p1105 A69-19093

Block coding systems performance in digital PCM data transmission through N-ary discrete channels in white Gaussian noise presence, discussing SNR upper bounds

07 p1080 A69-19096

Spectral null from spectral characteristics and statistical properties of PCM signals used to estimate SNR

07 p1083 A69-19122

Smooth limiter effect on output of SNR for unbalanced and balanced FM discriminators, noting role of error function

07 p1106 A69-19127

Double sideband suppressed carrier FM telemetry system as airborne data recorder, discussing noise, environmental conditions, laboratory and flight tests

07 p1084 A69-19132

Radar signal parameters measurements consisting of SNR estimation and optimum energy supply determination from SNR estimation

07 p1085 A69-19153

Communication satellite system design by use of baseband equation relating SNR after detection to CNR at detector input

07 p1085 A69-19180

Optimum linear feedback code for additive noise systems with average power constraint on transmitter to increase channel capacity

07 p1085 A69-19181

Optical heterodyne detection of randomly distorted signal beam, noting time invariant scheme yielding largest average SNR in atmospheric turbulence

07 p1087 A69-19642

Discrete signal detection providing optimum SNR for frequency and time domain differences between signal and noise

07 p1088 A69-19676

Object restoration, discussing data processing method for single variable functions with small signal to noise ratios

07 p1137 A69-19721

Noise-signal receiver amplitude-limitation effect on noise measurement in presence of pulsed interference

07 p1088 A69-19754

Finite IF filter bandwidth degradation of SNR of receiver for biphasic modulated signals using integrate and dump filter

08 p1270 A69-19851

Signal correlation functions measurement errors due to randomly fluctuating delay, investigating additive and multiplicative noise with periodic and random signals

08 p1296 A69-19923

Filters for sampled signals sequences using design simplicity and signal to noise ratio for evaluation and comparison factors

08 p1274 A69-20127

Analysis and optimization of side-looking synthetic aperture radars carried out for resolution, SNR and least squares estimation of target field

08 p1277 A69-20960

Optimal control synthesis for linear plant operating in noise environment, applying dual control theory

08 p1299 A69-21070

Image orthicon tube to detect low intensity pulsed light signals, formulating SNR in terms of resolvable image points

08 p1317 A69-21085

Signal to noise ratio with stochastic and additive noise and signal, showing block diagram of modified estimator

09 p1452 A69-21320

Channel output SNR optimization in AM/FM telemetry system by using automatic gain control, discussing AGC time response and general characteristics

09 p1454 A69-21799

Phase synchronized oscillators in microwave frequency multipliers with improved SNR

09 p1464 A69-22113

Optimal detection of determinate signal and signal with random amplitude and phase, estimating probability of false and correct detection

09 p1456 A69-22286

Constant envelope threshold detection for establishing signal energy in presence of input noise power density variations

09 p1459 A69-22474

Random data detection method applicable to low voltage SNR cases using real time correlation of probability functions

09 p1459 A69-22593

Transmit-receive device noise contribution effect on receiving system noise factor for device insertion immediately before low noise microwave amplifier

09 p1469 A69-22605

Minimum error probability and optimal system regime relationship to noise rejection in memoryless communication investigated for limited repeated transmissions

09 p1459 A69-22639

Noise rejection in multichannel telephone signal reception with FM and multiplexing, determining SNR dependence on SNR at receiver input

09 p1459 A69-22640

Noise rejection in linear amplitude detector during weak harmonic signal reception improved by limiting threshold voltage

09 p1460 A69-22645

Optimal reception methods noise stability for AM radio signals based on nonlinear filtration of information parameters of signals received on noise background

10 p1653 A69-23104

Signal to cross modulation noise ratio in TWT tube during amplification of sinusoidal signals

10 p1653 A69-23109

Optimal AM radio reception in presence of fluctuating noise and one AM interference signal with random initial phase of carrier oscillation

10 p1653 A69-23111

SNR variation with PCM using quantization distortion equations applied to coding-decoding facilities not exactly matched with respect to amplitude

10 p1656 A69-23679

Tracking filter steady state oscillation amplitude and phase distributions determined from Fokker-Planck equation for high and low noise levels

11 p1844 A69-24444

Radar transmitter and receiver antennas polarization parameters selection for obtaining maximum SNR at reception point

11 p1833 A69-24444

Algorithm for calculating Bayes estimates for unsteady Gaussian signals separation in presence of unsteady Gaussian noise by least squares method

11 p1833 A69-24444

Self tuning in active filter for detection of weak LF signals in noisy background

11 p1845 A69-24548

DC conversion amplifier commutation induced noises and signal ratio as function of shunt capacitance across vibrator load investigated for increased noise stability

11 p1845 A69-24555

Signal to noise ratio in spectral composition of FM signals in magnetic recorder channels, taking into account parasitic FM and AM

11 p1834 A69-24612

Solid state sampling circuit for low pulse repetition frequencies to improve signal to noise ratio, noting ratio of holding to learning time

11 p1849 A69-24900

Discrete continuous signals transmission with minimum noise along synchronous and asynchronous channels

11 p1835 A69-24953

Radio signal carrier frequency and arrival time measurements, deriving expressions for phase amplitude distortions effects

11 p1835 A69-24959

Optimal multidimensional sequential filtration of signal on background of time correlated noise

11 p1859 A69-24967

Energy gain during diversity reception in presence of random noise calculated, considering signal and noise amplitudes Rayleigh fluctuations

11 p1835 A69-24968

SNR measurement with time interval counter and computer, discussing accuracy

11 p1839 A69-25299

Telemetry system sensitivity as function of noise figure, noting SNR and noise and bandwidth effects on system information handling capability

11 p1840 A69-25300

Carrier to interference ratio /CIR/ between desired path and every other path within predetermined range in microwave system calculated by computer

11 p1840 A69-25312

Optimal scale factor selection to ensure minimum error variance in signal detection against random noise background for input limited range of measuring instrument

12 p2079 A69-25966

Frequency measurement of moving spacecraft RF carrier waves at low SNR by analog recording of noisy signal and HF trigger tone, noting data processing and signal fading rate

12 p2038 A69-26051

Recursive estimation of noisy nonlinear multivariable systems in white noise by Kalman, second order nonlinear and iteration filters

12 p2046 A69-26062

Optimum nonstationary Gaussian signals estimation in presence of noise, generalizing Wiener stationary processes filtering theory

12 p2029 A69-26202

Detection of known signals in general noise, describing sufficient conditions for singular detection and estimation

12 p2029 A69-26203

Error bounds for orthogonal signals in additive white Gaussian noise channels for class of generalized decision strategies permitting variable-size list decoding

12 p2029 A69-26204

Permutation modulation for waveform transmission of quantized bandlimited signal, deriving signal to noise ratio

12 p2030 A69-26386

Regular and noise signal scattering by uneven surface determined by correlation functions, assuming monochromatic components scattering obeying Kirchhoff approximation

12 p2031 A69-26650

- Pi 2 micropulsations at African low latitude stations, considering damping effect on ionospheric micropulsation transmission signal dispersion and SNR
12 p2074 A69-26959
- Noise rejection and carrying capacity of wideband and narrowband discrete systems transmitting complex signals in concentrated noise spectrum
13 p2218 A69-27213
- Pseudorandom uniformly distributed numbers generation from noise-like signals produced by shift register with feedback, noting statistical tests
13 p2218 A69-27248
- Phase analysis in multiple-sensor receivers with high signal to noise ratio, considering phase difference between two stochastic input signals
13 p2220 A69-27938
- Signal to noise ratio requirements for sharp cut-off biphasic digital communication channel
13 p2221 A69-27959
- Signal to noise ratio at output of three stage radio section with preselector, detector and ideal integrator, noting error
13 p2222 A69-28506
- Coherent signal addition in systems with multibeam channels and incomplete beam separation, deriving expressions for signal shape effect on noise rejection
13 p2223 A69-28551
- Deep space telemetry bit errors increased by reference signal phase noises and partial RF signal suppression, calculating equivalent signal to noise ratio degradation
13 p2223 A69-28609
- Wide signal and noise statistics range to determine noise rejection characteristics of communication system used for single path and diversity reception
14 p2410 A69-28826
- Simultaneous passage of useful and noise signals through differential frequency discriminator, determining spectrum by phase detection and detuned circuits
14 p2410 A69-28833
- SNR improvement during low level turbulence measurements, examining correlation between hot-wire anemometers, including error analysis
14 p2446 A69-29018
- Optical signal conversion efficiency and threshold relationships in pulsed rangefinding systems, considering effects of noise obeying Poisson distribution
14 p2412 A69-29324
- Analog correlator performance interpreted as output SNR dependence on input signals and integrating system characteristics, covering filters and finite time integrators
14 p2413 A69-29485
- Performance of oscillating limiter driven by noise corrupted FM signals covering frequency deviations, carrier to noise ratio, etc
14 p2413 A69-29497
- FM discriminator click widths probability distribution function, defining click widths duration from input noise considerations
14 p2422 A69-29553
- Ultrasonic pulse velocity and attenuation measurement in presence of noise, using coherent detection and signal averaging
14 p2449 A69-29564
- Signal phase measurement accuracy by discrete phase technique ensured by using wideband signals and automatic control of input SNR
15 p2574 A69-30130
- Reference oscillator synchronization inaccuracy influence on SNR at output of correlation receiver during reception of signals with pseudonoise modulation
15 p2563 A69-30141
- Noise stability of receiver network during detection of finite duration noise signal on white noise background, considering various narrow band preselectors
15 p2563 A69-30142
- Noise stability of FM receiver with automatic control of IF amplifier resonance frequency in presence of weak noise
15 p2564 A69-30144
- Noise sensitivity of FM discriminator/limiter in digital binary communication system with FM/PCM-FM/
15 p2564 A69-30145
- Linear distortions effect on signals detection in binary communication channel with fluctuating noise, determining error probability
15 p2564 A69-30146
- Noise parameters at output of logarithmic detector separating two AM signals with overlapping spectra
15 p2564 A69-30148
- Distribution function of SNR from coherent optimal estimate of signal amplitude
15 p2564 A69-30149
- Adaptive signal pattern dependent feedback delta modulation for improved signal/quantization-noise ratio
15 p2565 A69-30177
- Weak periodic signal separation from noise using single and multichannel analog adders
15 p2607 A69-30241
- Algorithm for processing binary-quantized echo signal packets, obtaining useful and noise signals relation
15 p2571 A69-30331
- Spectral correlation characteristics of amplitude modulated signal with background noise at envelope detector output
15 p2576 A69-30348
- Radial velocities measuring tracking rate meter performance for Doppler frequencies, allowing for multiplicative noise
15 p2576 A69-30350
- Multifunctional radar errorless operation determined from relations between amount of received information, number of channels and SNR
15 p2576 A69-30354
- Power spectrum analyzer of weak periodic signal obscured by white noise by zero interactions count of signal and noise mixture
15 p2579 A69-30945
- HF electromagnetic decoupling pressure gage, using transducer with solid state strain gages as sensing elements
15 p2611 A69-31029
- Unknown channels classes epsilon capacity applied to estimating capacity of channels with additive noise, discussing models and upper and lower bounds
15 p2570 A69-31142
- Logic circuits abstract synthesis for detecting signals against noise background using known conditional quantized signal distributions
16 p2749 A69-31627
- Single balanced modulators using square law resistors/space charge limited diodes/, discussing noise properties, conversion losses and terminating conductance
16 p2758 A69-31756
- Radio emission and absorption of cumulus and stratus clouds at millimeter and centimeter wavelengths, giving maximum SNR defined by brightness temperature
16 p2807 A69-32270
- Error analysis of one bit autocorrelation method of spectral estimation, noting decrease in spectral variance with increased sampling rate
16 p2752 A69-32390
- SNR changes loss factor effect during passage through MTI coherent receiver followed by video integrator
16 p2753 A69-32438
- Optimal control synthesis for linear plant operating in noise environment, applying dual control theory
16 p2765 A69-32485
- Maximum a posteriori estimate of modulation on carrier with noise, discussing iterative technique and FM test
17 p2994 A69-32917
- Voltage standing wave ratio measurement technique at low power level, including tolerated errors, compared with Roberts-von Hippel method
17 p2918 A69-33031
- Unidigit and multidigit communications systems performance and transmission characteristics, emphasizing SNR improvements
17 p2918 A69-33066
- Optical heterodyne communication system with single mode and frequency carbon dioxide laser, noting coherent photon noise limit
17 p2919 A69-33086
- Likelihood ratio for random signals detection in white Gaussian noise based on innovation process
17 p2920 A69-33622
- Optimum detection of stochastic signals in Gaussian noise, obtaining eigenfunctions series expansion associated with probability density function
17 p2921 A69-33623
- Robust detection of binary signal in additive noise, using extreme value theory/EVT/ to estimate probability density function and system error and threshold
17 p2944 A69-33624
- Beat frequency measurements in far IR due to harmonic mixing of klystrons, discussing noise role
17 p3006 A69-33674
- Phase locked loop with flip-flop error detector compared to analog loop, discussing signal to noise ratio
17 p2931 A69-34115
- Preemphasis analysis for FM system optimization to maintain constant output signal to noise ratio throughout baseband
18 p3103 A69-35088
- Optimum signal design to maximize SNR for pulse communications systems with signal energy detection, considering frequency, transmission and filtering characteristics and signal duration
18 p3104 A69-35484
- Temporal discrimination based on signal fluctuations emphasizing signal detection in presence of noise
19 p3373 A69-36057
- Spectral parameters effect on IR instrument SNR, discussing range equations of point and extended sources and radiation-noise-limited detectors
19 p3310 A69-36061
- Solid state S band to VHF converter design to obtain optimum system noise for radio telemetry, discussing cost effectiveness and system performance
19 p3270 A69-36238
- Telemetry transmitter-receiver RF links quality determination, emphasizing nonlinear effects measurement by notch noise tests
19 p3270 A69-36239
- Parametric amplifier developed for unattended satellite communication ground stations, featuring low noise broadband characteristics
19 p3270 A69-36240
- Optimal ratio predetection combiner used with diversity signals and various modulations, showing significant improvement in telemetry systems performance
19 p3270 A69-36241
- PCM bit synchronizer signal to noise ratio measurement by input video signal zero crossings counting
19 p3271 A69-36248
- Computer program designing multiplex taper to minimize FM/FM telemetry system carrier threshold SNR, examining noise behavior of multiplex system stages for system performance
19 p3273 A69-36275
- Antenna high noise temperature reduction in single channel combined transmission and reception of tracking and communication data
19 p3275 A69-36328
- AC technique using lock-in power amplifier SNR for measuring galvanomagnetic and Shubnikov-de Haas effects, noting error reduction
19 p3312 A69-36375
- Receiving circuit for AM signal envelope separation in presence of AM interference and fluctuation noise, using converter cascades to effect input signal frequency spectrum symmetry
19 p3277 A69-36568
- False signals formation during random pulse noise in single command channels with PTM coding, noting code value and redundancy
19 p3278 A69-36595
- Optimal linear recursive estimators for uncertain observation, considering false alarm probability
20 p3485 A69-36922
- Cramer-Rao and split-beam tracker techniques compared for optimum bearing error attainable with linear passive sonar array in spatially incoherent noise environment
20 p3576 A69-37322
- Discrete signal detection providing optimum SNR for frequency and time domain differences between signal and noise
20 p3488 A69-37458
- Signal spectrum and SNR of synthetic aperture terrain imaging radar using model, including two dimensional signal and Gaussian additive noise
20 p3489 A69-37638
- Synthetic aperture terrain imaging radar system optimal design, considering noise-free and random noise conditions using least squares method and signal to noise ratios
20 p3489 A69-37639
- Optimum phase reference detector obtained at low SNR with Costas loop for fully modulated PSK signals
20 p3492 A69-37710
- Normalized SNR of aperture antennas determined in terms of random signal and noise fields correlation functions
20 p3494 A69-37845
- Linear antenna synthesis for optimal separation of plane waves providing maximum SNR with allowance for statistical phase distribution of field
20 p3508 A69-37943
- Detection characteristics of coherent pulse packet with random initial phase on Gaussian noise background of unknown intensity
20 p3496 A69-37946

Radio relay FM channel data transmission, evaluating cumulative thermal noise due to IF amplification at each station

21 p3672 A69-38653

QRS complex detection time error in noisy electrocardiograms

21 p3667 A69-39442

Optimum filter design for noisy analog feedback system with forward and feedback disturbances, using mean square error criterion between signal and data

21 p3687 A69-39449

Filtering optimization prior to limiting digital signals in strong noise, detailing bandwidth choice of single pole low pass filter

21 p3676 A69-39450

Error probability of Gaussian signal detector in Gaussian noise background determined from quadratic form of probability distribution density

22 p3901 A69-40955

Envelope detection threshold levels definition for low input SNR based on apparent modulation depth reduction

22 p3902 A69-41225

Automatic discriminator design for identifying distorted image in noise based on ideal transmitter and use of split scanning beam

23 p4163 A69-41551

Partially coherent PSK-modulated binary detection, deriving noisy phase reference by narrow band tracking filter, analyzing bit output error as function of SNR

23 p4122 A69-41772

M-ary noncoherent signal structures requiring less transmission bandwidth than conventional FSK, deriving SNR

23 p4122 A69-41773

Analyzing conditions for variable magnetic and electric noise occurrence at input of nuclear precession magnetometer used in field strengths measurements

23 p4165 A69-41852

Waveguide band filter with reflecting ferrite resonators and frequency matched loads for improved microwave SNR

23 p4139 A69-41945

Combined eye and ear identification of bimodally presented signals in noise over oscilloscope and earphones, noting significance of independent observers model

23 p4111 A69-42168

Natural and man-made radio noise measurements, including formula for calculating signal strength of coherent interference

23 p4126 A69-42217

Interference prediction models of equipment emissions and susceptibility thresholds based on limited spectrum signature data

23 p4126 A69-42223

Phase-locked loop demodulator ability to acquire and remain locked on signal under noise and pulse interference

23 p4145 A69-42230

Recursive estimation of noisy nonlinear multivariable systems in white noise by Kalman, second order nonlinear and iteration filters

23 p4146 A69-42447

Digital data transition tracking loop mean square phase noise computed as function of input SNR by Fokker-Planck technique

23 p4130 A69-42514

Effective color TV transmission via satellite using PCM/PSK modulation, noting dependence on available equipment, bandwidth, desired error rate and SNR

23 p4130 A69-42520

Cascaded limiter and phase detector, analyzing SNR transfer characteristics for specific PM signals

23 p4131 A69-42525

Omega aircraft navigation, discussing digital computer applications, SNR environment, carrier interference and accuracy requirements for signal reception

23 p4186 A69-42539

Random signal behavior in hybrid correlator with analog and sampling channels, noting SNR expression and weak signal detection

24 p4283 A69-43139

SNR improvement by antenna array optimization

24 p4287 A69-43140

SIGNAL TRANSMISSION

NT AUTOMATIC PICTURE TRANSMISSION
NT BIOTELEMETRY
NT DATA TRANSMISSION
NT IONOSPHERIC F-SCATTER PROPAGATION
NT IONOSPHERIC PROPAGATION
NT MANDELSTAM REPRESENTATION
NT MESSAGES
NT MICROWAVE ATTENUATION
NT MICROWAVE TRANSMISSION

NT MULTIPATH TRANSMISSION
NT PCM TELEMETRY
NT PULSE FREQUENCY MODULATION
NT PULSE FREQUENCY MODULATION
TELEMETRY
NT RADAR ATTENUATION
NT RADAR TRANSMISSION
NT RADIO ATTENUATION
NT RADIO TELEMETRY
NT RADIO TRANSMISSION
NT SATELLITE TRANSMISSION
NT SHORT WAVE RADIO TRANSMISSION
NT SINGLE SIDEBAND TRANSMISSION
NT SYMBOLS
NT TELEMETRY
NT TELEVISION TRANSMISSION
NT TRANSEQUATORIAL PROPAGATION

Integrated circuit digital filters design characterized by weight coefficients containing Lanczos factor for application to processing of signal transmitted from space vehicles

01 p0038 A69-10071

Frequency diversity for communication in fading environment, relating performance variance to between channel correlation variance

01 p0026 A69-10177

Minimum measurement time of dynamic transmission coefficient of system by FM method, calculating error

01 p0031 A69-10785

Regular and noise signal scattering by uneven surface determined by correlation functions, assuming monochromatic components scattering obeys Kirchhoff approximation

01 p0032 A69-10886

Doppler signal envelope cross correlation coefficient in two channel system, determining mutual density distribution for envelopes

01 p0032 A69-10887

Multistage detection systems probability characteristics with parallel stage realization, taking into account signal losses

02 p0206 A69-11604

Directional antennas gain loss on ground sections calculated on basis of difference-phase measurements data

02 p0214 A69-11612

Transient signal propagation in lossless isotropic and homogeneous plasma for Gaussian pulse modulated carrier, discussing amplitude change and carrier phase distortion

02 p0290 A69-12351

Educational TV satellites, considering stationary ASCEND system with high power transmitters

02 p0335 A69-12747

Sequential signal design for feedback channels, emphasizing single set subject to peak and average power constraints in time continuous transmission

03 p0408 A69-12868

Adaptive compression system for predicting and encoding video data for transmission in noiseless channel

03 p0427 A69-12869

Communication satellites systems, discussing Intelsat satellite specifications and modulation methods for multiple access

03 p0383 A69-12870

Atmospheric limitations for laser communications, discussing scattering and absorption effects

03 p0389 A69-13193

Simultaneous passage of useful and noise signals through differential frequency discriminator, determining spectrum by phase detection and detuned circuits

04 p0556 A69-14462

Optical waveguide with optimum refractive index distribution for equalizing group velocities of different modes and minimizing waveform distortion

04 p0575 A69-14749

Correlation function and spectrum analysis of passage of random noise and signal through multistage frequency multiplier

04 p0557 A69-14777

Gaussian channels capacity, studying supremum of information transmission rates with small error probability

04 p0558 A69-15006

Waveform distortions of trapezoidal wave passing through Gaussian filter in pulse transmission, discussing ideal filter effects on degradation

05 p0719 A69-16296

Symmetric M-ary signaling scheme, considering given calls signal vector transmission through communication channel

05 p0720 A69-16297

Lower ionospheric diurnal variations in electron density observed by beacon satellite, noting effect on high power VHF forward scatter circuits

05 p0757 A69-16405

Automatic phase control and transient processes in resonant amplifier in presence of phase discontinuities of input signal

05 p0721 A69-16533

Interpolation filters with restricted transmission zeros in transmission function capable of reconstructing continuous function from equidistant sample values

05 p0735 A69-16617

Maximum transmission coefficient of distributed parameter signal detector compared with concentrated detector coefficient using ordinary and tunnel diodes

05 p0736 A69-16787

Radio channel circuit outlined for tracking interplanetary spacecraft and probes with signal delay time prediction

06 p0888 A69-17621

Statistical aspects of uncertainty function of linearly frequency modulated signals for nonstationary random process of phase errors

06 p0889 A69-17798

Coherent frequencies method for irregular component of satellite signal phase lead due to ionospheric inhomogeneities between satellite and ground station

06 p0890 A69-17799

Block coding for transmitting across noisy binary symmetric channel accompanied by noiseless delayless feedback channel

06 p0891 A69-17864

Two and three frequency techniques for measuring group delay time of communication channels

07 p1076 A69-18557

World satellite telecommunications network, discussing recommendations with reference to signal transmission, acoustic echoes, etc

07 p1079 A69-18942

Maximum likelihood bit synchronizer for baseband PCM signals in Gaussian noise, stressing system noise performance analysis and measurements

07 p1105 A69-19093

Statistical radomes design, analyzing dielectric constant and wall thickness tolerances effects on amplitude and phase of transmitted wave

07 p1111 A69-19531

Transponders for communication satellites, discussing design constraints, reliability and transmission capacity increase

08 p1279 A69-19905

Signal interference criteria in considering frequency sharing between communication satellite systems and terrestrial radio services

09 p1449 A69-21273

Minimum bandwidth of M real equal energy signals with specified code or correlation matrix, noting optimum waveforms

09 p1452 A69-21313

Error probability for transmission of one of M orthogonal, equally likely, equal energy signals over generalized incoherent channel

09 p1452 A69-21314

Intermittent feedback channel for transmitter using orthogonal signals, noting smaller error probability and improved communication reliability

09 p1452 A69-21315

Coding schemes for memoryless Gaussian channels with feedback considering error probabilities

09 p1454 A69-21794

Radio frequency signal transmission between orbiting spacecraft and vehicle entering VM-10 model atmosphere, examining near wake approximations and plasma-electromagnetic interaction

09 p1455 A69-22002

Optimum selection of modulation indices for multitone phase modulation by graphical method, noting tolerance insensitivity

09 p1457 A69-22463

Joint filter optimization in combination analog-digital hybrid multilevel transmission system

09 p1457 A69-22465

Sunde model of troposcatter channel as transmission medium in computer simulation of adaptive digital communication scheme for selective fading channels

09 p1458 A69-22471

OMEGA VLF navigational transmission phase delay variations and field strength measurements on transatlantic propagation path, noting effect of directional change

09 p1538 A69-22595

Energy spectra and angular dependence characteristics of electromagnetic wave scattered on statistically uneven surface studied by vector form of Kirchhoff integral

09 p1459 A69-22635

Minimum error probability and optimal system regime relationship to noise rejection in memoryless

communication investigated for limited repeated transmissions

09 p1459 A69-22639

Minimum measurement time of dynamic transmission coefficient of system by FM method, calculating error

10 p1653 A69-23114

Pressure transducers with variable reluctance and magnetic signal transmission techniques

10 p1690 A69-23226

VLF transequatorial propagation variance from magnetic equator to midlatitude confirmed through phase and amplitude records of multisite observations

10 p1655 A69-23416

Antenna gain increase, using matched pair of Cassegrain reflectors with one primary source

10 p1664 A69-23799

Mechanical damping and electrical matching effects on bandwidth of piezotransducer in ultrasonic flaw detection equipment

10 p1697 A69-24073

Single circuit parametric oscillator excitation by small external narrow band signal, using method of slowly varying amplitudes

11 p1845 A69-24453

Analog signal transmission through randomly fading channels, proposing pseudorandom phase reversals method for slowly varying multipath communication channels

11 p1834 A69-24552

Multistage detection systems probability characteristics with parallel stage realization, taking into account signal losses

11 p1835 A69-24711

Directional antennas gain loss on ground sections calculated on basis of difference-phase measurements data

11 p1847 A69-24719

Discrete continuous signals transmission with minimum noise along synchronous and asynchronous channels

11 p1835 A69-24953

Receiver filter nonoptimality effects on accuracy of nonenergetic signal parameter measurements

11 p1835 A69-24960

Transient signal propagation through cold inhomogeneous plasma with electron density decreasing exponentially in direction of propagation

11 p1836 A69-24990

System switch, separating RF bands according to frequency and polarization for simultaneous transmission from parabolic horn antenna

11 p1854 A69-25618

Wave reflections due to rotationally symmetrical jump in circular waveguide cross section, using orthogonal expansion to solve resulting boundary value problem

11 p1855 A69-25622

Transmission characteristics of narrow band microwave bandpass filters with power cascade and Chebyshev behavior

11 p1857 A69-25677

Optimal communication by signal feedback link between transmitter and receiver based on optimum control and dynamic programming

12 p2046 A69-26060

Control signal interconnection of subsystems at different levels of hierarchical structure systems

12 p2050 A69-26089

Focusing factor in stratified medium with refractive index depending exponentially on height

12 p2029 A69-26100

Transmission system with baseband spectrum divided into subbands, cascade phase modulating carrier in multiplication chain

12 p2030 A69-26385

Permutation modulation for waveform transmission of quantized bandlimited signal, deriving signal to noise ratio

12 p2030 A69-26386

Graphs determining interference levels for optimum shielding, suppression, signal parameters and waveforms for pulses, step functions, CW signals and for military technology

12 p2030 A69-26471

Regular and noise signal scattering by uneven surface determined by correlation functions, assuming monochromatic components scattering obeying Kirchhoff approximation

12 p2031 A69-26650

Doppler signal envelope cross correlation coefficient in two channel system, determining mutual density distribution for envelopes

12 p2031 A69-26651

Antenna suspension height variation effects on HF signals in ionospheric scattering lines

12 p2032 A69-26705

VLF wave propagation along mixed path in curved earth-ionosphere waveguide, considering reflection and transmission coefficients of modes

12 p2032 A69-26858

VLF signal strength minima during transition fading, considering asymptotic statistical distribution

12 p2032 A69-26862

Monograph on discrete signals transmission by FM, considering secondary signal compression device and wire communication channels

12 p2033 A69-26866

Noise rejection and carrying capacity of wideband and narrowband discrete systems transmitting complex signals in concentrated noise spectrum

13 p2218 A69-27213

Delay time of pulse signals in radio channel transmission described by standard deviation of channel properties

13 p2218 A69-27215

Rms error for reproduction of satellite signal transmitted through continuous Gaussian channel assessed by numerical calculation

13 p2219 A69-27697

Synchronized backward wave oscillator transmitting tube for space communication stations

13 p2232 A69-28058

Simultaneous passage of useful and noise signals through differential frequency discriminator, determining spectrum by phase detection and detuned circuits

14 p2410 A69-28833

Large signal transit time effects in MOS transistor, noting drain current response

14 p2418 A69-28891

Computer based data handling and display for relating remote sensor signals to ground truth information derived from aerial photographs

14 p2416 A69-29534

Monograph on wave propagation and multiple scattering in random continuum, emphasizing scalar wave equation solutions

15 p2564 A69-30150

Spectral correlation characteristics of amplitude modulated signal with background noise at envelope detector output

15 p2576 A69-30348

Satellite signal probability density determined from scintillation plus Faraday effect in statistical terms

16 p2751 A69-32103

Signal propagation in channel subject to static investigated using Fokker-Planck type equation in statistical mechanics methods

16 p2753 A69-32437

Automatic phase control and transient processes in resonant amplifier in presence of phase discontinuities of input signal

16 p2753 A69-32474

Interstellar communication in search for extraterrestrial intelligence, discussing radio objects, OH emission regions and pulsating stars

17 p3028 A69-32971

Unidigit and multidigit communications systems performance and transmission characteristics, emphasizing SNR improvements

17 p2918 A69-33066

Differential equations as Hamiltonian function for signal path, travel time and frequency variation in anisotropic nonpermanent absorbing medium

17 p2924 A69-33836

Phase and amplitude stabilization during phase modulated discrete data transmission

19 p3277 A69-36571

Temporal position of pulse signal on noise background determined by measuring signal passage time through linear filter zero point

19 p3278 A69-36596

Transient oscillations in ammonia maser oscillator observation based on switching achieved by signal injection into cavity at molecular resonance frequency

19 p3339 A69-36825

Tropospheric influence on pulse signal propagation, measuring pulse function of propagation path, hypothesizing signal reflection from tropospheric boundary layers

19 p3279 A69-36879

Asymptotic evaluation of complex frequency integrals in theory of radiation from transient sources in dispersive media, interpreting results in terms of space-time rays

20 p3494 A69-37841

Monopulse, high power, three channel antenna feed system design for communication satellites, noting

orthogonal polarization of transmit and receive functions

23 p4120 A69-41750

Numerical computation of rate-distortion function R/D/ for certain memoryless message sources, discussing bounds, reduction to minimization problem and applications

24 p4284 A69-42719

Static and dynamic characteristics of fluid pressure signal transmitter between members with relative rotary motion

24 p4256 A69-43300

Hologram transmission by heterodyne scanning reference beam technique

24 p4283 A69-43333

SIGNATURES

NT MAGNETIC SIGNATURES

NT RADAR SIGNATURES

Mechanical, electromagnetic and chemical signatures monitoring and analysis during system operation

06 p0932 A69-17875

Electromagnetic field signatures in optical IR spectrum of satellite-borne sensors, analyzing spectral, spatial and temporal distributions, polarization and phase

19 p3309 A69-36060

SIGNS (SYMBOLS)

U SYMBOLS

SIGNS AND SYMPTOMS

NT BRADYCARDIA

NT VERTIGO

Decompression disease symptoms from standpoint of gas bubbles formation in blood vessels, examining factors preventing air metabolism

24 p4269 A69-43414

SIKHOTE-ALIN METEORITE

Sikhote-Alin iron meteorite high temperature oxidation and ablation and simulation with Fe-Ni alloy, noting phase compositions and structure

01 p0025 A69-11373

Meteorite dust spherules at Tungusk and Sikhote-Alin falls investigated for mineral composition using X ray analysis

01 p0160 A69-11383

SIKORSKY AIRCRAFT

NT CH-34 HELICOPTER

NT CH-54 HELICOPTER

NT S-61 HELICOPTER

NT SH-3 HELICOPTER

Self excited rotor blade oscillation at high subsonic Mach numbers during flight tests of Sikorsky NH-3A compound helicopter

07 p1053 A69-18870

Sikorsky ABC/advancing blade concept/ helicopter program, discussing advantages and small scale wind tunnel experiments

07 p1055 A69-19558

Skorsky HH-3F helicopters electronic equipment, discussing communication and navigation aids, search and recovery missions, etc

10 p1662 A69-23222

SIKORSKY HSS-2 HELICOPTER

U SH-3 HELICOPTER

SIKORSKY MILITARY HELICOPTERS

U MILITARY HELICOPTERS

SIKORSKY S-61 HELICOPTER

U S-61 HELICOPTER

SIKORSKY S-64 HELICOPTER

U CH-54 HELICOPTER

SILANES

NT CHLOROSILANES

Silane coupling effect on composite properties of glass fiber filled injection molded polypropylene, noting interface phenomenon

08 p1337 A69-20482

Carbon fiber reinforced plastics properties improvement by applying organosilanes, discussing silanol bond formation

16 p2803 A69-31806

Pyrolyzed tetraethoxysilane for carburizing steels and Ti alloys at 850-1050 C

19 p3328 A69-36161

SILENCERS

Gas turbine exhaust silencer performance correlated in laboratory and in service

05 p0812 A69-16144

Power generation in combat environment by tested self contained organic Rankine silent engine, discussing working fluid properties

07 p1058 A69-18309

SILICA

U SILICON DIOXIDE

SILICA GLASS

Silica glass hardness relationship to pressure induced densification at low temperatures

03 p0453 A69-13616

Gettering effect in silicon of phosphosilicate glass surface layer and underlying phosphorus layer on gold and copper

03 p0487 A69-13640

Silicon dioxide glass thermal conductivity at very low temperature

09 p1493 A69-21426

Impact crater cross section in fused silica, describing photomicrographic technique for distinguishing hyper-velocity from low energy impacts [AIAA PAPER 69-367]

13 p2366 A69-28299

Composite laminated glass structures employed to improve safety characteristics of glass or to achieve special optical properties

21 p3752 A69-38934

Silicate glass impurity droplet formations on alumina single crystals polished surfaces analyzed by electron microprobe as function of high temperature

23 p4176 A69-41597

Cross sections of charge carrier capture by ions in gamma irradiated P-Al-Si glass with metal oxides additions measured for evaluating radiation stability improvement

23 p4180 A69-42470

Gamma radiation effect on AgCl-Cu redox state in AgCl activated, heat treated Na-Al-B-Si glass, using EPR method

23 p4180 A69-42471

SILICATES

NT ALUMINUM SILICATES

NT ANDESITE

NT BERYL

NT CORDIERITE

NT ENSTATITE

NT FAYALITE

NT FELDSPARS

NT GARNETS

NT MONTMORILLONITE

NT NEPHELINE

NT PYROXENES

NT YTTRIUM-ALUMINUM GARNET

NT YTTRIUM-IRON GARNET

Gettering effect in silicon of phosphosilicate glass surface layer and underlying phosphorus layer on gold and copper

03 p0487 A69-13640

Magnesium silicate crystal structure, discussing transformations under high pressure, crystallochemistry and implications for physics of earth mantle

08 p1267 A69-19904

Radiation ages of silicate inclusions in iron meteorites based on Sr evolution diagrams

08 p1405 A69-20927

IR emissivities of powdered silicates and cloudy atmosphere model of spectral emission for radiative transfer in condensed powder

10 p1778 A69-23414

Reddened M supergiant 119 Tauri IR spectra and IR absorption by CO and SiO molecules in stellar atmosphere and silicate mineral in interstellar grains

10 p1786 A69-24104

Chemical and mineralogical study of Kodaikanal meteorite silicate and metal phases, using optical, X ray and electron microprobe techniques

11 p1953 A69-24335

Electrostatic charge distribution on ultrahigh vacuum cleaved silicates including instrumentation, UV irradiation, half life, Paschen relation, etc

13 p2322 A69-28018

Percorite phase in nickel analog of clinchrosytile formed under hydrothermal conditions in Wolf Creek meteorite cracks

18 p3199 A69-34824

Moon composition and similarities to Mars explained by silicates in solar system raw material

20 p3604 A69-37563

Interstellar grains formation and composition, suggesting mixture of graphite particles in carbon stars and silicates in oxygen-rich giants

20 p3615 A69-38260

Data evaluation, measurement accuracy and statistical procedure, using silicates chemical analysis

22 p3897 A69-40984

Shear load, cohesion and internal friction measurements of low bulk density particulate silicates of complex shape, noting significance for lunar comparison

24 p4383 A69-43040

SILICIDES

NT DISILICIDES

Silicide coatings effect on Mo mechanical properties subjected to tensile tests in vacuum and air at various temperatures

02 p0264 A69-11883

Carbides and silicides temperature coefficient of electrical resistivity and Hall constant plotted as function of metal carbides solid solutions concentration

09 p1523 A69-21740

Silicide coatings effect on Mo mechanical properties subjected to tensile tests in vacuum and air at various temperatures

18 p3156 A69-35043

Temperature effect on grain size, crystal orientation, microhardness and heat resistance of diffusion Si coatings on Mo

20 p3560 A69-37361

Microstructure and X ray structure compared for two and three component chromide, titanide and silicide diffusion layers on Nb, discussing phase composition

20 p3563 A69-37820

Carbides and silicides temperature coefficient of electrical resistivity and Hall constant plotted as function of metal carbides solid solutions concentration

20 p3585 A69-38216

Oxidation resistant silicide coatings for tantalum and tungsten alloys at elevated temperatures

21 p3730 A69-38673

Silicide and B-modified coatings on Mo, noting improved high temperature oxidation resistance under thermocycling

22 p3957 A69-40972

SILICON

Temperature dependence of hot electron drift velocity in silicon at high electric fields, using space charge perturbation theory

01 p0135 A69-10120

Radiation, Stark and van der Waals level broadening constants for Mg I and Si I calculated to interpret solar and stellar spectral line widths

02 p0310 A69-11454

Boron diffusion in silicon, using nitrogen carrier and boron trichloride diffusant at high temperature for determination of critical oxygen flow rate

02 p0297 A69-11994

Localized vibration modes of defects and IR absorption bands in compensated Si doped GaAs

02 p0299 A69-12402

Structure of /111/ single crystal Si surface after chemical-mechanical polishing and ultrahigh vacuum annealing, noting presence of Fe impurity

02 p0301 A69-12660

Carbon formation during production of high purity semiconductor Si, using C 14 tagged hydrogen impurities and methylated chlorine silanes contained in silicochloroform

03 p0486 A69-13635

Heat capacity of diamond-like semiconducting Si, GaAs and GaP calculated on basis of quasi-chain dynamics of covalent crystals

03 p0490 A69-13943

Si and iron impurities effects on duraluminum alloy structure and mechanical and plastic properties for fabrication from granules and rolling from ingots

03 p0452 A69-14120

Luminescence spectra due to radiative recombination of optically injected carriers in Co 60 gamma ray and neutron irradiated Si at low temperature

03 p0494 A69-14243

Direct reading instrument using four point probe and two analog computing circuits for Si and Ge resistivity measurements

04 p0599 A69-15019

Distribution of current carrier concentration and mobility in p-type silicon doped with phosphorus ions

04 p0643 A69-15254

N-type Si surface photopotential, conductivity and capacitance during anodic oxidation in absolute ethylene glycol

04 p0643 A69-15260

Si diffusion rate in single crystal and polycrystalline Mo, using various donor materials

05 p0780 A69-15990

Electrical conductivity anisotropy in isotropic germanium and silicon semiconductors, noting effect of metallic contact insertion

05 p0808 A69-16216

Shot noise in Si Schottky barrier diodes for frequencies between 100 Hz and 50 kHz

05 p0734 A69-16564

Recovery of carrier concentration and lifetime in n- and p-type Si during annealing after irradiation by 10 Mev electrons, noting impurities effects

06 p0974 A69-16865

Disordered regions in electron irradiated silicon noting defect clusters concentration effect on electrical properties

06 p0974 A69-16866

Neutron irradiation produced defects in p-type Si at 76 K, measuring Hall effect and electrical conductivity

06 p0975 A69-16867

Majority and minority carrier trapping in neutron irradiated Si diodes, measuring transient junction capacitance recovery

06 p0975 A69-16868

Oxygen absorption coefficients for atomic silicon in spectral range of Schumann-Runge bands

06 p0960 A69-17009

Oxide impurity effects causing potential shifts in covered by thick oxide layer studied with metal-oxide Si electrical measurement and radiochemical analysis

07 p1072 A69-18272

Forward transient response characteristics of high resistivity, long base, low lifetime p-n-n silicon diodes doped with Au, noting voltage oscillations

07 p1101 A69-18652

Majority carrier concentration changes in P-doped n-type Si during fast electron bombardment, discussing relative effect of A and E centers

07 p1199 A69-18684

Optical parameters for system of isotropic nonabsorbing film on isotropic absorbing substrate determined by ellipsometric method, noting Si optical constants

07 p1201 A69-19648

Li atoms and O interactions with electron radiation produced defects in Si studied by IR spectroscopy

09 p1554 A69-21337

Diffusion method for fabricating negative resistance diodes consisting of Cd doped silicon, introducing Cd into n-type silicon plates in evacuated vials

09 p1462 A69-21477

Zone structure of silicon-silicon dioxide system for silica films obtained by pyrolytic dissociation, discussing kinetics of photoelectrons capture at traps

09 p1555 A69-21478

Strong p-type conductivity of silicon doped with beryllium by thermal diffusion, giving electrical and optical measurements

09 p1556 A69-21652

Forward volt-ampere characteristics and differential resistance peak of Schottky barrier diode on doped Si

09 p1557 A69-21744

Effects of opacity arising from silicon bound-free transition on emergent fluxes and hydrogen line profiles for A and late B stellar atmospheres

09 p1604 A69-22403

O, Ne, Si and Fe ionization equilibria in low density plasma, including dielectronic recombination and autoionization processes in calculations

09 p1543 A69-22404

Silicon vidicon for near IR and visible radiation viewing describing spectral response, energy transfer characteristics, resolution and dark leakage currents

09 p1466 A69-22456

Impurity heterogeneities in unoxidized and oxidized silicon slices from electron probe X ray microanalyzer, discussing thermal oxidation effects

10 p1743 A69-23171

Electron bombardment produced clustered displacements, paired vacancies and interstitial atoms in Si, discussing possible mechanism for developing defects

10 p1747 A69-23713

Electronic properties of beryllium doped silicon studied with IR absorption spectroscopy and electrical measurements, describing Be thermal diffusion

10 p1747 A69-23989

Annealing temperature of radiation defects in phosphorus doped silicon, discussing isochronal recovery characteristics of solar cells with different donor and oxygen concentrations

10 p1747 A69-24006

Si IMPATT diode current and voltage waveforms of oscillation, noting small signal theory inapplicability

12 p2036 A69-25914

Relative intensities of selected Si two multiplets calculated and compared with solar spectrum and plasma source ZETA values

13 p2326 A69-27551

Relative transition probabilities for visible Si atom lines, noting disagreement with LS coupling predictions and solar Si abundance determination

13 p2340 A69-27580

Stellar Si burning at constant temperature studied for various initial abundance compositions, noting convergence toward pure Si relaxation

14 p2529 A69-29983

Validity range of nuclear quasi-equilibrium approximation for stellar silicon burning, discussing time rates of nuclear abundance changes and temperature effect
14 p2529 A69-29984

Diffusion method for fabricating negative resistance diodes consisting of Cd doped silicon, introducing Cd into n-type silicon plates in evacuated vials
15 p2578 A69-30722

Zone structure of silicon-silicon dioxide system for silica films obtained by pyrolytic dissociation, discussing kinetics of photoelectrons capture at traps
15 p2669 A69-30723

Glass ceramic coated and bonded silicon semiconductor material in integrated circuits devices fabrication, noting matched thermal expansion
15 p2669 A69-31040

Oscillator strengths calculated for transitions in Si III using dipole length and velocity matrix elements, comparing many electron correlation problem approximations
15 p2656 A69-31158

Silicon in iron meteorites and earth core determined by activation analysis on octahedrites, hexahedrites and ataxites
16 p2865 A69-32807

Si planar IMPATT diodes anomalous mode continuous wave UHF oscillations, noting DC density and DC/RF power conversion efficiency
17 p2934 A69-32846

Widths measurements of van der Waals broadened Si I spectral lines by shock tube and scanning Fabry-Perot interferometer, using argon as perturbing gas
18 p3116 A69-34449

Oxygen 18 adsorption on silicon activation analysis measurements used to obtain kinetic curve for chemisorption from monolayers
18 p3183 A69-35107

Nanosecond pulse generator circuits based on four layer Si diodes designed for semiconductor laser excitation
18 p3153 A69-35257

Lithium-doped silicon solar cells development for radiation environments, discussing contractor functions, dopants, etc
19 p3251 A69-35692

Imperfection photoconductivity in electron irradiated Li-doped Si annealed at room temperature, noting level rearrangement in O rich material
19 p3382 A69-35696

Reactive scattering from solid surfaces, discussing atom beam reaction of O with heated Ge and Si single crystals
19 p3377 A69-36178

Transient recombination lifetimes in n-type float zone Si from 4.2 K to room temperature, obtaining electrical and photoconductivity values
19 p3383 A69-36447

Optical pumping in pure Si at 77 K, noting dichroism conditions for dipolar electric transitions in cubic crystal
19 p3389 A69-36548

GaAs IMPATT diodes breakdown voltage, impurity density and outer layer thickness compared with Si IMPATT diodes
20 p3504 A69-36914

Electrical conductivity anisotropy in isotropic germanium and silicon semiconductors, noting effect of metallic contact insertion
20 p3584 A69-37786

Metal-polymer-metal and metal-polymer-silicon thin film structures analysis for polymers bulk properties and insulator-silicon interface, noting dipole-like relaxation
21 p3782 A69-39464

Strong doping criterion for Si with deep level impurity centers based on electron spectra of fast surface traps
22 p3992 A69-40604

Microwave reflection technique for transient and quiescent electrical conductivity of Si, noting nonohmic contacts
22 p3997 A69-41226

Lithium doped silicon acceptor concentration resulting from electron irradiation damage decreased by annealing at 300 degrees K
23 p4197 A69-41498

Spacecraft Si cell solar array using self rigidizing folded panels with flexible substrates for increased power/weight and power/stowage volume ratios
23 p4073 A69-42290

Electron irradiation-temperature dependence of introduction rate and room temperature annealing of carrier-removal defects in Li-doped Si
24 p4360 A69-42647

SILICON ALLOYS

Electroreflectance spectra of Ge-Si alloys, noting concentration dependence and band structure of Si and Ge
02 p0295 A69-11784

Al-Mg-Si alloy strain aging, noting effect of deformation stresses on kinetics and aging mechanism for prior and concurrent deformation
04 p0614 A69-14575

Cr-Si diffusion layers on Ti, noting results of roentgenographic and metallographic studies
04 p0614 A69-14578

IR photoconductivity spectra at surface of gold doped silicon, establishing monopolarity
08 p1373 A69-21073

Primary silicon crystals content and grain size effect on wear of high silicon aluminum alloys
09 p1526 A69-22281

V phase structure and V and E phase lattice constants for ternary systems /Ti, Zr, Nb or Ta/-Ni, Co or Fe/-Si or Ge/
10 p1708 A69-22992

Silicon particle sizes in Al-Si system investigated for interactions with dislocations as function of strain and for effect in dispersion hardening
10 p1714 A69-23980

Al-Mg-Si alloy strain aging, noting effect of deformation stresses on kinetics and aging mechanism for prior and concurrent deformation
15 p2638 A69-30276

Cr-Si diffusion layers on Ti, noting results of roentgenographic and metallographic studies
15 p2638 A69-30279

Cu, Ni, Co, Cr and Ti effect on high temperature mechanical properties and stability after prolonged annealing of Al-Si alloy with added 1 percent Mg
22 p3968 A69-40063

SILICON CARBIDES

Silicon carbide filament fabrication by chemical vapor deposition, noting physical and mechanical properties and application to other refractories
01 p0097 A69-10645

High aspect ratio submicroscopic whiskers of beta-SiC, investigating rheological properties of suspensions in various fluids
01 p0102 A69-11260

X ray diffraction used to measure alpha-SiC whiskers orientation in polymeric matrices
01 p0102 A69-11262

Silicon carbide deposition from liquid organic compounds using film boiling applied on heated tungsten wire substrate
02 p0252 A69-11804

High temperature tensile strengths of uncoated boron filament and filament coated with silicon carbide
02 p0270 A69-12731

Laminates and filament wound structures using carbon fibers with silicon carbide whiskerized surfaces, noting compositing and laminating techniques
08 p1339 A69-20501

Whiskerizing technique for growing small beta SiC single crystals on graphite filament surfaces, noting changes in interface geometry and chemistry
08 p1341 A69-20511

Silicon carbide fiber surfaces nature and interaction with coupling agents, epoxy and resin components, noting chemical and electron microprobe analysis
08 p1341 A69-20515

Cubic /beta/ silicon carbide films deposition by volatilization in presence of acetylene
09 p1554 A69-21350

Chemical processes in silicon carbide due to reactive deposition and chemical conversion, noting silicon growth mechanism involving outward diffusion
09 p1554 A69-21351

Silicon carbide filaments strength at high temperatures noting vapor deposition, mechanical properties and applications
09 p1524 A69-22072

Mass spectrometric analysis of silicon carbide for inhomogeneity in sample, noting metallic impurities
09 p1448 A69-22313

SiC part fabrication by chemical vapor deposition through pyrolysis of chlorosilanes from vapor state onto machined substrates of graphite and metals
09 p1509 A69-22344

High performance silicon carbide backward diode, discussing device design and operational characteristics
09 p1470 A69-22787

Current voltage characteristics in silicon carbide diodes having negative differential resistance
10 p1663 A69-23571

Silicon carbide particle growth and motion in carbon star atmospheres
10 p1781 A69-23678

SiC and GaP diodes used as low power light sources, studying electroluminescence in p-n region under pulsed excitation
14 p2419 A69-29325

Current and electroluminescence brightness dependence on reverse voltage in n-SiC diodes including tunnel and avalanche processes
15 p2573 A69-30062

Macrostructural differences between filaments of B and SiC vapor deposited onto small diameter W wire, discussing radial cracks due to dilatation
18 p3160 A69-34266

Silicon and boron carbides wettability with liquid metals during contact reactions at various temperatures, discussing wetting mechanism
18 p3156 A69-35153

Multiaxial stress effect at room temperature on fracture strength of silicon carbide tubular specimens
20 p3565 A69-36939

Silicon carbide compact coatings deposition on graphite by silicon tetrachloride, H and benzene gaseous mixture, relating layer thickness to temperature and process duration
20 p3566 A69-37368

SILICON COMPOUNDS

NT ALUMINUM SILICATES
NT ANDESITE
NT BERYL
NT CHLOROSILANES
NT CORDIERITE
NT DISILICIDES
NT ENSTATITE
NT FAYALITE
NT FELDSPARS
NT GARNETS
NT MONTMORILLONITE
NT NEPHELINE
NT ORGANIC SILICON COMPOUNDS
NT PYROXENES
NT QUARTZ
NT SILANES
NT SILICATES
NT SILICIDES
NT YTTRIUM-ALUMINUM GARNET
NT YTTRIUM-IRON GARNET

Organosilicon-containing derivatives of 2-aminoethanethiols and 2-aminoethanethiosulphuric acids as radiation protective agents
13 p2210 A69-28486

Protective coatings of oxygen-free high melting point Si compounds and silicate binder, noting chemical stability in corrosive media
20 p3566 A69-37371

Landing shock struts of Surveyor 6, emphasizing silicone liquid springs role as absorbers and stabilizers
20 p3466 A69-38180

Fluosilicic acid in chemical milling of Ti and Ti alloys
21 p3669 A69-38966

SILICON CONTROLLED RECTIFIERS

High power sinusoidal pulsed current generator using Si controlled rectifiers /thyristors/ as switches
03 p0404 A69-13262

Electronic controller with integrated circuits and inexpensive SCR as coupler or interface between card reader and frequency synthesizer designed for untended operation
06 p0897 A69-17704

Single phase bidirectional AC/DC power converter based on back-to-back SCR hybrid bridge
13 p2209 A69-28178

High temperature electronic tensile testing device utilizing SCR to study strain rate effect on metals properties
21 p3727 A69-39811

SILICON DIOXIDE

NT QUARTZ

Aged boric acid coated silica reaction vessels, showing reduced surface effects and high reproducibility in oxidation reactions
02 p0205 A69-12322

Silicon dioxide dielectric isolation for high speed low power circuits, noting saturation resistance and transient characteristics
02 p0221 A69-12470

Aluminum-silica fiber reinforced metal composite, discussing mechanical behavior and effect upon engineering applications
06 p0940 A69-16949

Oxide impurity effects causing potential shifts in Si covered by thick oxide layer studied with metal-oxide-Si electrical measurement and radiochemical analysis
07 p1072 A69-18272

SILICON FILMS

Doped silicon dioxide films as controlled reproducible diffusion sources for silicon devices fabrication 07 p1198 A69-18620

Instability in pyrolytic silicon dioxide films on Ge substrate under bias at room temperature consisting of positively charged ion motion 07 p1200 A69-19010

Mechanical properties of ceramic material consisting of pure silica matrix reinforced by carbon fibers 08 p1341 A69-20700

Zone structure of silicon-silicon dioxide system for silica films obtained by pyrolytic dissociation, discussing kinetics of photoelectrons capture at traps 09 p1555 A69-21478

Electron irradiation effect on surface potential of thermally grown silicon dioxide layers, noting conductivity and annealing effects 09 p1557 A69-21743

Combined electron microprobe and ellipsometric study of thin silicon dioxide films on silicon, noting reliability and accuracy 10 p1742 A69-22946

Positive space charge buildup produced in silicon dioxide by low energy electrons as function of beam energy and oxide thickness 10 p1743 A69-23172

Interfacial stress between thermally grown silicon dioxide and single crystal silicon correlated with oxide compressive strength 10 p1744 A69-23177

Molar heat and entropy of adsorption and activity coefficient of adsorbed phase for methane-ethane-silica gel system 10 p1652 A69-23370

Single crystal growth by controlled diffusion in silica gel using metathetical and decomplexation reactions 10 p1652 A69-23371

Silicon single crystal substrate, preoxidation, oxidation and low temperature heat treatment effects on MOS transistor compared with Silicon-Silicon dioxide interface characteristics 10 p1665 A69-24051

Silicon dioxide coated Al reflectance, solar absorptivity and total normal and hemispherical thermal emissivity, noting application to satellite temperature control 11 p1918 A69-24835

Zone structure of silicon-silicon dioxide system for silica films obtained by pyrolytic dissociation, discussing kinetics of photoelectrons capture at traps 15 p2669 A69-30723

X ray detectable preferred disorder in solids by shock loading studied in Ainsworth meteorite and in hexagonal alpha silicon dioxide 15 p2671 A69-31538

Andalusite crystals as active media in paramagnetic quantum amplifiers, discussing design and performance 19 p3333 A69-35881

Silicon dioxide film doped with Al to increase MOS structure radiation resistance 20 p3584 A69-38070

Equilibrium absorption and desorption rates of carbon dioxide-argon mixtures from silica gel measured as function of temperature using gas dynamics method 21 p3848 A69-38707

Pressure and temperature effects on reversal transitions of stishovite, noting meteoritic impact formation at Meteor Crater, Arizona 22 p4021 A69-40412

Slush H and N gels preparation and characteristics, including measurements of weight bearing capacity of gel as function of percent mass silica gelant 22 p3998 A69-40632

SILICON FILMS

Silicon nitride gate insulator in metal-insulator-silicon (MIS) devices, noting sandwich structures with thermally grown oxides removes limitations 02 p0299 A69-12244

Relaxation effect in epitaxial silicon MOS structures, formulating differential equation for doping distribution in epitaxial layer 03 p0490 A69-13947

Technique for obtaining flawless silicon single crystal films on sapphire bases by vacuum deposition, noting base temperature effect on film quality 07 p1198 A69-18509

Instability in pyrolytic silicon dioxide films on Ge substrate under bias at room temperature consisting of positively charged ion motion 07 p1200 A69-19010

Combined electron microprobe and ellipsometric study of thin silicon dioxide films on silicon, noting reliability and accuracy 10 p1742 A69-22946

MOS transistor Hall voltage, mobility and constant verified by magnetoelectric measurements of Si p-inversion layer 13 p2323 A69-28331

Thin silicon solar cells environmental tests, evaluating temperature and humidity effects on various contacts and coatings 19 p3252 A69-35699

SILICON JUNCTIONS

Avalanche multiplication in abrupt silicon p-n junctions analyzed using ionization coefficient measurements for holes and electrons 01 p0135 A69-10038

Surface charge distribution in silicon p-n junctions noting luminescence of microplasmas and inhomogeneous properties 02 p0294 A69-11629

Anisotropic pressure influence on silicon diodes parameters 02 p0223 A69-12839

Transit time effects in Si n-nu-n space charge limited current solid state devices 03 p0483 A69-12852

Temperature and current distribution in avalanching silicon p-n junctions 03 p0487 A69-13637

Multiplication effects on noise in Si avalanche diodes, noting high resolution apparatus for measurement of spatial variations 04 p0573 A69-14332

High efficiency microwave oscillations in Si p-n and p-n-n positive avalanche diodes under pulsed conditions 04 p0580 A69-15491

Incremental conductance of heavily doped n-type Si semiconductor barrier tunneling as function of bias voltage, indicating Fermi level dependence on dopants 05 p0808 A69-16285

Microwave absorption and series resistance of silicon mesa parametric amplifier diodes, discussing p-n junction and dielectric loss mechanism 05 p0732 A69-16347

Si IMPATT diode oscillator and amplifier for CW operation at 50 GHz noting fabrication, performance and phase locking properties 05 p0733 A69-16560

Recovery rate at room temperature in Li-doped p-n Si diodes and solar cells after 1 Mev electron irradiation, noting capacitance changes 06 p0974 A69-16867

Nearly abrupt X band Si avalanche IMPATT diodes irradiated by fast neutrons, noting effects on DC and microwave characteristics 06 p0976 A69-16874

Solid state diodes made by pulsed laser irradiation of polished silicon surfaces, discussing application to integrated circuit design 06 p0893 A69-17157

Low temperature technique for preparing solid-solid diffusion sources for silicon device fabrication based on gaseous hydrides as reagents 07 p1198 A69-18619

Relaxation oscillations in Si p-n junction diode reverse-biased into avalanche calculated by computer program 07 p1101 A69-18651

Silicon on sapphire semiconductor technology for diode arrays used as read-only memories, discussing capacitance, resistance and pattern encoding by laser 07 p1113 A69-19767

Microwave amplification using silicon diodes in avalanche resonance pumped modes 08 p1279 A69-19909

Failure mechanism in high-voltage semiconductor diodes explained by effect of reverse voltage pulses, considering design reliability 08 p1294 A69-21116

Positive and negative sloped current-voltage characteristics of silicon tunnel diodes with p-n junctions 10 p1746 A69-23574

Silicon n-p solar cell behavior during electron radiation, describing radiation resistant solar cell 11 p1825 A69-24871

High current density filaments formation in silicon p-n avalanche diodes caused by incremental negative resistance in static current-voltage characteristics 12 p2036 A69-25916

Forward current decrease in Si mesa diodes under fast neutron irradiation ascribed to increase in base resistance 13 p2236 A69-28549

Spectral distribution of photosensitivity for p-n junctions in silicon doped GaAs, showing agreement with state density model and absorption data 15 p2666 A69-30067

Transit time effects in silicon space charge limited diodes, studying frequency characteristics of small signal equivalent circuit 15 p2575 A69-30181

Al interconnections discontinuities at integrated circuit contact windows observed by scanning electron microscope, noting catastrophic failure and Si presence 17 p2936 A69-32893

Gold donor level impurity photovoltaic effect in silicon, noting solar cell efficiency reduction due to minority carrier recombination 19 p3381 A69-35679

Radiation damage and recovery of lithium-diffused silicon p-n solar cells, measuring photovoltaic parameters as function of gamma radiation fluence 19 p3251 A69-35694

Silicon junction radiation detectors applications in cryogenics, measuring junction response to beta particles at low temperatures 20 p3546 A69-38275

Active Ni centers properties in Si with emphasis on increasing and reducing minority carrier lifetime in silicon integrated circuits, discussing energy levels 24 p4560 A69-42759

SILICON NITRIDES

Silicon nitride gate insulator in metal-insulator-silicon (MIS) devices, noting sandwich structures with thermally grown oxides removes limitations 02 p0299 A69-12244

Pressurized fluid journal bearing with fluid fed into space between shaft and shell from plenum chamber in bearing housing through circumferential slots 06 p0931 A69-17529

Silicon nitride as ambient alkali barrier liner analogous to silicon carbide in MIS devices for thermal growth of silicon oxide 12 p2142 A69-25935

Silicon nitride vaporization and thermodynamic properties analyzed using Langmuir and Knudsen methods 12 p2118 A69-26261

Refractory materials based on BN and silicon nitride, studying effect of sintering conditions and chemical composition on mechanical properties 15 p2643 A69-31244

Silicon nitride staple fibers synthesis, development and characterization, noting tensile strength and sonic modulus 19 p3354 A69-35517

Silicon nitride ceramics fabrication technology and dimensional stability during nitridation, discussing applicability to aerospace precision or joined ceramic shapes 24 p4336 A69-43211

SILICON OXIDES

NT QUARTZ

Physical and physicochemical properties of anodic silica obtained by silicon oxidation in organic bath, discussing possible applications 05 p0810 A69-16589

Refractory metal silicon device technology noting high temperature diffusion masking properties for possible use in MOSFET technology 06 p0930 A69-17152

Flame emission spectrophotometric method for ultramicro sodium contamination detection in thin silicon oxide films and cleaned silicon surfaces [ECS PAPER 306] 08 p1314 A69-20367

Impurity heterogeneities in unoxidized and oxidized silicon slices from electron probe X ray microanalyzer, discussing thermal oxidation effects 10 p1743 A69-23171

Three layer vacuum deposited silicon monoxide films current voltage and conduction current density temperature dependence 10 p1745 A69-23324

Silicon nitride as ambient alkali barrier liner analogous to silicon carbide in MIS devices for thermal growth of silicon oxide 12 p2142 A69-25935

Lower oxides of Si, studying chemical composition, formation conditions, stability and chemical and physical properties 15 p2643 A69-31245

Dissociation energy and ionization potential measured for gaseous SiO and GeO 22 p3896 A69-40725

SILICON POLYMERS

NT SILICONE RESINS

NT SILICONES

Isothermal secant and tangent bulk moduli of silicon fluids and correlation with pressure, volume and temperature 01 p0102 A69-10913

SILICON RADIATION DETECTORS

Celestial navigation system using photodetectors, comparing numbers and brightness of S4, S20 and silicon stars

10 p1775 A69-23190

SILICON RECTIFIERS

U CRYSTAL RECTIFIERS

SILICON SOLAR CELLS

U SOLAR CELLS

SILICON TRANSISTORS

Step recovery switching silicon transistor combining planar and mesa technologies, discussing charge storage and fall times

02 p0215 A69-11937

Base transit time of minority carriers in double diffused Si transistors with small emitter area, discussing cut-off frequency

02 p0297 A69-11995

Wafer chip assembling technique for high density interconnection of silicon devices in large monolithic electronic systems, noting application to MOS shift register

02 p0222 A69-12472

Substrate terminal current anomalous enhancement observed in n-channel Si MOS transistors beyond pinch-off

04 p0574 A69-14348

Current carrier concentration temperature dependence in Te-doped silicon single crystals by analyzing photoconductivity spectra

04 p0644 A69-15267

Emitter base lateral diode carrier injection effect on current gain properties of small area double diffused planar transistors

05 p0728 A69-15808

Statistical studies of current-voltage characteristics of zinc-doped silicon diodes

05 p0732 A69-16425

Double diffused Si transistors, discussing temperature dependence of gain, injection efficiency, emitter and base regions energy gaps and excess noise

05 p0733 A69-16558

Si transistor I sub CE sub 0 characteristics measurement on curve tracer, discussing generation of loop by junction capacitances and emitter base diode

05 p0734 A69-16569

Rapid annealing data for silicon transistors after reactor neutron pulse, deriving equation for defect recombination in cluster and subsequent diffusion outside cluster

06 p0975 A69-16870

Recombination statistical model for neutron irradiated Si transistors, considering diffusion potential, junction voltage, temperature, activation energy and capture ratio for holes and electrons

06 p0975 A69-16871

Neutron irradiated Si transistors radiation and annealing characteristics determined for inverse configuration

06 p0975 A69-16872

Thermal time constant in Si diffused transistors decreases with increased neutron dosage

06 p0975 A69-16873

Recovery and long term reliability of Si n-p-n transistors subject to gamma radiation, using military specifications for failure

06 p0976 A69-16878

Prediction technique for surface effect causing Si bipolar transistors gain degradation under ionizing radiation

06 p0976 A69-16879

Threshold failure levels of semiconductor diodes and transistors due to pulse voltages

06 p0977 A69-16883

Destructive breakdown in Schottky barrier diodes by evaporating contact metal through mask onto silicon, showing local heating by thin wax layer

08 p1286 A69-20860

Field effect transistors with Schottky-barrier gates using epitaxial layers of silicon on substrates and gallium arsenide on semiinsulating substrates

08 p1286 A69-20863

Microwave silicon technology applied to fabrication of high gain high efficiency transistor

09 p1462 A69-21410

N enhancement silicon MOST saturation current as function of temperature

10 p1743 A69-23175

Interfacial charges in MOS transistors determined as function of surface potential by measuring channel conductance as function of temperature

10 p1744 A69-23178

Electrical parameters measurement for homogeneous batches of planar silicon transistors subjected to cobalt 60 gamma rays, considering isochronal and isothermal annealing

15 p2625 A69-30827

Mass-produced silicon transistors reliability, presenting tables and curves of lifetime tests

15 p2626 A69-30833

Silicon MOS transistor characteristics, discussing stability, temperature effects and inherent noise, noting applications to amplifier circuits

18 p3109 A69-35161

Generation-recombination noise due to trapped charge fluctuation at impurity centers in Si junction gate field effect transistors transition regions, using lumped equivalent circuit

22 p3911 A69-40009

Bipolar HF p-type Si transistors preparation by B and P ion beams and planar technology masking technique, obtaining p-n-p structure

22 p3916 A69-40960

SILICONE RESINS

High temperature organic sealants for repairing small gas leakages in vacuum devices, tabulating test results for alkyd, epoxy, silicone and polyimide resins

11 p1907 A69-24742

Gravimetric and IR absorption spectra analysis for determining heat resistance and chemical changes in organosilicone resins during heating

17 p2992 A69-33744

Elastomeric thermosetting one part silicone encapsulant environmental tests, checking physical and electrical properties stability under temperature and relative humidity conditions

19 p3281 A69-35549

SILICONE RUBBER

High strength room temperature vulcanizing silicone rubber for tooling and fabrication of aircraft and missile components

09 p1507 A69-22331

Controlled expansion of captive silicone rubber used to achieve pressure control for adhesive bonding interface

09 p1512 A69-22367

Room temperature vulcanizing silicone rubber adhesive sealants strength and self bonding, describing primerless adhesion to Ti and Al alloys, Al, Ni and stainless steels

19 p3356 A69-35532

Low viscosity/density RTV silicone rubber sealants obtained by using glass microballoon fillers

24 p4337 A69-43454

RTV silicone rubber for corrosion control coatings, high strength adhesives and low density sealants in aircraft structures

24 p4338 A69-43457

SILICONES

Silicone polymers and polymer formations for electrical applications including silicones for molded devices and components, potting resins, dielectric gel, RTV rubbers, etc

13 p2286 A69-27990

Thermal silicone grease type filler materials for heat transfer across bolted or clamped sheet metal surfaces in electronic equipment for space applications

16 p2794 A69-32560

SILICONIZING

Structural features and electrical resistivity of siliconated pyrolytic graphite, analyzing dependence on preparation conditions using X ray diffraction measurements

24 p4335 A69-42926

SILOS [MISSILE STORAGE]

U MISSILE SILOS

SILVER

Electrical resistance temperature dependence below room temperature for polycrystalline epitaxially grown Au and Ag films, noting effects of alpha irradiation

03 p0486 A69-13582

Temperature rise of micron sized silver particles on carbon film due to electron beam heating, setting up heat balance equation

04 p0640 A69-14449

Ag-GaAs Schottky barrier photodiodes, describing fabrication and use as UV radiation detectors

09 p1462 A69-21334

Gamma radiolysis of silver nitrate ice forming neutral Ag in magnetically distinct sites, discussing water dipoles rotation and electron paramagnetic resonance

22 p3992 A69-40574

Mean adsorption lifetimes and activation energies of Ag and Au on polycrystalline tungsten substrate in ultrahigh vacuum system free of hydrocarbon contamination

23 p4198 A69-41542

SILVER ALLOYS

Plastic deformation of internally oxidized dispersion strengthened silver magnesium alloys, noting hardening effect dependence on oxidation temperature

07 p1159 A69-18627

Stored energy of cold work and electrical resistivity of Ag-Mg solid solution alloys measured as functions of strain, Mg concentration and initial state of order

24 p4332 A69-43029

SILVER CADMIUM BATTERIES

Nickel-cadmium and Ag-Cd storage batteries performance, discussing methods to lengthen battery life and improvement of characteristics

08 p1261 A69-21051

Ni-Cd and Ag-Cd storage batteries for space applications, discussing performance, life and reliability

16 p2740 A69-32422

SILVER COMPOUNDS

Gamma irradiated silver carbonate EPR at liquid nitrogen temperatures

05 p0716 A69-15915

Yttrium effect on rate of thermal decomposition of silver carbonate powder and pressed pellets by isothermogravimetric analysis, examining water vapor, Co 60 gamma radiation and temperature effects

15 p2561 A69-30442

Doped silver carbonate defect structure and doping effect on reaction kinetics by X rays and electron paramagnetic resonance, finding new crystal structure

22 p3993 A69-40720

SILVER HALIDES

High resolution silver halide photoemulsions analyzed by holographic resolvolmetry using Ne-He laser to obtain interference patterns

15 p2606 A69-30052

SILVER IODIDES

Cloud seeding effects due to inhomogeneous distribution of freezing nuclei, discussing silver iodide distributions by Gaussian plume diffusion model

09 p1535 A69-21639

Solid state battery utilizing high conductivity solid electrolytes /metal silver iodide/, demonstrating cell performance improvements

10 p1640 A69-23998

SILVER NITRATES

Gamma radiolysis of silver nitrate ice forming neutral Ag in magnetically distinct sites, discussing water dipoles rotation and electron paramagnetic resonance

22 p3992 A69-40574

SILVER ZINC BATTERIES

Highly resistant separator performance in Zn-Ag oxide battery, discussing zinc electrode limitations on battery performances

10 p1640 A69-23996

SIMICOR [IMAGE CORRELATOR]

U IMAGE CORRELATORS

SIMILARITIES

U ANALOGIES

SIMILARITY NUMBERS

Geostrophic adjustment for neutral and lapse conditions, discussing similarity arguments based on appropriate length and velocity scales

02 p0276 A69-12699

Maintaining of flow similarity in calibration of nozzle type water meters for study of working processes of pumps

16 p2772 A69-32145

SIMILARITY THEOREM

Similarity theory results for turbulent diffusion in atmospheric surface layer compared with concentration measurements from Project Prairie Grass

02 p0276 A69-12695

Asymptotic similarity in neutral barotropic planetary boundary layers, solving Ekman flow by singular perturbation methods

03 p0460 A69-13336

Rapid uniform expansion of spherical cavity in compressible elastic-plastic solid, obtaining similarity solution

03 p0528 A69-13798

Similarity law for ionization waves noting relations for frequency, wavelengths, amplification, propagation velocities and phase shifts

05 p0799 A69-15633

Similarity functions defined for laminar or turbulent separation in nonuniform supersonic flow [ONERA-TP-659F]

07 p1050 A69-18417

SIMILITUDE LAW

Holography and similarity criterion for developing image recognition algorithm
08 p1314 A69-20417

Self similar solutions for collapse of empty cylindrical cavity in gas with given equation of state, describing gas motion past cavity
10 p1679 A69-23367

Similar boundary layers in Prandtl approximation determining similarity conditions for second order effects due to curvatures and outer vorticity
10 p1632 A69-23700

Neon discharges, discussing similarities in type p plasma ionization waves generated by pulsing
10 p1740 A69-23721

Global characteristics and similarity of ventilated cavity flows by injecting air behind immersed profiles of symmetrical wedge at zero incidence
10 p1680 A69-23788

Convective heat transfer, discussing coordinate transformation, similarity analysis similitude and Meksyn integration of boundary layer equations
13 p2376 A69-28139

Nonreacting turbulent far wake problems, discussing centerline decay of viscosity models, similarity profiles and radial distributions at various Mach numbers
13 p2200 A69-28500

Similarity theory similar to Nusselt and Stanton numbers obtained by triple analogy for heat, mass and momentum transfer
13 p2380 A69-28560

Similar solution for free convective flow past vertical porous wall and unsteady flow past porous wall with dissipation term, using group transforms
15 p2592 A69-31010

Similarity criteria for plastic deformation theory of body under pressure and nonuniform temperature field, considering strength calculations
15 p2714 A69-31200

Similarity concepts extended to shock initiated flux compression devices for magnetic flux concentration
16 p2768 A69-31665

Transformation of two dimensional boundary value equations for laminar power law nonNewtonian fluid flow to yield similar solutions
17 p2957 A69-34016

Similarity solutions of viscous transonic equation describing spiral and radial flows, containing shock-like transitions of corresponding inviscid solutions
18 p3121 A69-34787

Similarity solutions describing buoyancy effect on laminar and turbulent wakes of heated body in incompressible fluid vertically ascending flow
19 p3296 A69-35761

Electric models optimization for heat exchange systems based on mathematical similarity between equations describing temperature and electrical potential fields
19 p3256 A69-36717

Similarity method applied to linear integrodifferential equations of neutron transport in homogeneous space
19 p3361 A69-36774

Transformation groups used to find similarity solutions for partial differential equations and heat equation
20 p3630 A69-36915

Similarity rule in hydrodynamically transcritical regime in ionized multifluid gas
20 p3515 A69-37594

Supersonic flows past blunt bodies, formulating approximate similarity law for shock layers in subsonic regions
24 p4246 A69-43495

Similarity solutions to massive blowing problem, discussing inviscid flow model compatible with no-slip condition
24 p4305 A69-43658

SIMILITUDE LAW

Electric arc properties, investigating volt-ampere characteristics by approximate similitude and dimensional analysis
01 p0125 A69-10099

Convective heat transfer, discussing coordinate transformation, similarity analysis similitude and Meksyn integration of boundary layer equations
13 p2376 A69-28139

Similitude applied to dynamics of disperse media, discussing role of dimensionless numbers in mechanics of suspensions and two phase flows in porous media
19 p3300 A69-36775

SIMPLE HARMONIC MOTION

Runway roughness effects on aircraft, formulating relationship between weight and resonant frequency through simple harmonic motion analogy
01 p0057 A69-11274

Finite length cylindrical shell dynamic response to uniform radial impulse, noting simple harmonic motion and flexural mode excitation instability
02 p0347 A69-12517

SIMULATED ALTITUDE

Mild hypoxia effect on selective attention performance of human subjects at simulated 8000 ft altitude
09 p1445 A69-22553

Human mental performance impairment at simulated 8000 ft altitude indicated in increasingly difficult tests
23 p4102 A69-41680

SIMULATION

NT ACOUSTIC SIMULATION
NT ALTITUDE SIMULATION
NT ANALOG SIMULATION
NT ATMOSPHERIC ENTRY SIMULATION
NT COMPUTERIZED SIMULATION
NT CONTROL SIMULATION
NT DIGITAL SIMULATION
NT ENVIRONMENT SIMULATION
NT EXHAUST FLOW SIMULATION
NT FLIGHT SIMULATION
NT LANDING SIMULATION
NT RHEOELECTRICAL SIMULATION
NT SOLAR SIMULATION
NT SPACE ENVIRONMENT SIMULATION
NT THERMAL SIMULATION
NT WEIGHTLESSNESS SIMULATION

Monte Carlo method used to construct optimal algorithms for simulating homogeneous Markov chains whose trajectories reach absorbing state with probability of one
01 p0105 A69-10726

Wind gust simulation procedures, discussing high altitude clear air turbulence and simulation of air perturbations
03 p0461 A69-13647

Water droplet simulation by glass spheres used in study of light scattering at cloud particles
06 p0953 A69-17992

Shock tunnel simulation of scramjet combustion chamber performance
06 p0985 A69-18165

Circularly polarized waveguide mode simulation for multislot leaky waveguide harmonic content measurement
07 p1105 A69-19046

Experimental circuit for simulating radar target tracking system based on split range gating, noting tracking role of error signal
08 p1300 A69-20109

Composite transistor simulation of circuit inductor effect for synthesizing frequency selective circuits
08 p1286 A69-20834

Electrical analogs with passive elements in combination with stepping switches for simulation of plants with distributed parameters
09 p1471 A69-21436

Microwave antennas optical simulation, discussing given phase amplitude distribution problems
09 p1469 A69-22625

Mississippi Test Facility /MTF/ hardware data acquisition system error analysis from extensive simulated static firing tests
10 p1673 A69-23287

Spectral measurement of luminous trails produced by injecting high velocity submicron diameter iron particles into gaseous targets compared with meteor spectra
10 p1790 A69-24142

Color TV system for Earth Resources Observation Satellite /EROS/, discussing resolution in relation to spectral separation through data simulation study
12 p2077 A69-25767

Modified scheme for simulation of delay with transient period independent of amount of delay, considering polynomial input
12 p2120 A69-25922

Fourth angle driving law for different four gimbal systems used for simulation display and inertial platform isolation
12 p2055 A69-26265

Photosimulation of electron hole and exciton mechanisms of NaI-Tl and KI-Tl single crystal scintillations
12 p2144 A69-26722

Human behavior simulation - NATO Conference, Paris, July 1967
12 p2024 A69-27079

Cosmic shock waves simulation through correlations between shock equations in classical and relativistic fluid dynamics, using shock tube tests
14 p2433 A69-29981

Magnetic materials simulation for satellite stabilization device based on magnetic hysteresis, using mathematical models and direct magnetic measurements
17 p2945 A69-33235

Flow simulation on wind tunnel test models for aerodynamic characteristics of aircraft design, discussing boundary layer and external flow coupling
17 p2945 A69-33471

Ball bearing lubrication simulation by rolling disk apparatus, emphasizing surface slip and related thermal effects alterable by geometric expansion
17 p2945 A69-33471

Earth atmospheric large scale motion simulated in laboratory and by numerical technique
18 p3127 A69-34668

Photosimulation of electron hole and exciton mechanisms of NaI-Tl and KI-Tl single crystal scintillations
21 p3781 A69-39135

Time-similar and isotropic geodesic curves simulating paths of test bodies in Riemann space corresponding to gravitational field
21 p3772 A69-39621

Low melting point material selected model melt simulating shrinking process in castings of melt with broad liquidus-solidus interval
21 p3733 A69-39720

Monte Carlo methods for electromagnetic showers simulation, noting electron track length distribution in Pb glass absorber
22 p4007 A69-41057

Dynamic simulation for gas turbine engine components design to assure stable operation and rapid response characteristics
23 p4200 A69-41655

SIMULATOR TRAINING

U TRAINING SIMULATORS

SIMULATORS

NT COCKPIT SIMULATORS
NT CONTROL SIMULATION
NT ENVIRONMENT SIMULATORS
NT FLIGHT SIMULATORS
NT HIGH VACUUM ORBITAL SIMULATOR
NT LUNAR GRAVITY SIMULATOR
NT SHOCK SIMULATORS
NT SOLAR SIMULATORS
NT SPACE SIMULATORS
NT SPACECRAFT CABIN SIMULATORS
NT TARGET SIMULATORS
NT TRAINING SIMULATORS
NT VIBRATION SIMULATORS

Man machine relationship in V/STOL control display, discussing inflight simulators, emphasizing NASA X-14 and CH-5C programs
01 p0010 A69-10452

Variable properties aircraft for flying simulator, discussing flight control system and stability behavior
07 p1052 A69-18254

Micrometeorite simulation by wire explosion plasma, discussing energy requirements and simulator performance
16 p2821 A69-31839

SIMULTANEOUS EQUATIONS

Simultaneous partial integro-differential equations governing natural vibrations of arbitrary cross section cylindrical tubes, suggesting Fourier series solution
01 p0164 A69-10065

Mixed boundary value problem for system of Navier-Stokes equations for viscous incompressible fluid in stationary motion in vessel, noting rotating fluid
02 p0272 A69-12223

Doubly infinite sets of simultaneous linear equations used in electromagnetic boundary value problems solved by Asymptotic Anticipation Method
04 p0560 A69-15214

Simultaneous nonlinear equation solving in absence of Jacobian elements
08 p1344 A69-20832

Kutta-Merson algorithm for converting partial differential equation for two dimensional unsteady state heat conduction to simultaneous ordinary differential equations
09 p1623 A69-22280

Matrix eigenvalues for nonlinear simultaneous algebraic equations, discussing computer program for numerical integration
13 p2289 A69-28227

Taylor expansion applied to solution of nonlinear simultaneous algebraic equations in analyses of nonlinear structural systems using finite differences or elements
15 p2711 A69-30871

Coupled kinetic equations for inhomogeneous systems treated as simultaneous equations in time, obtaining solutions by successive approximation
15 p2660 A69-30913

Book on solution of linear ordinary differential equations and simultaneous systems using bar statics-equivalent beam method
15 p2711 A69-30929

Mixed boundary value problem for system of Navier-Stokes equations for viscous incompressible fluid in stationary motion in vessel, noting rotating fluid
23 p4183 A69-41974

SIMULTANEOUS IMAGE CORRELATOR
U IMAGE CORRELATORS

SINE
U TRIGONOMETRIC FUNCTIONS

SINE SERIES

Hyperbolic sine creep law, discussing limiting stresses for approximation by linear or exponential relationship
07 p1235 A69-19384

Sine series solution for flexural vibration of rectangular isotropic plates applied to free vibration of orthotropic plates
13 p2363 A69-28128

SINE WAVES

Quasi-sinusoidal tunnel diode oscillator studied for frequency and amplitude of harmonic voltage components
01 p0038 A69-10070

Amplitude modulation factors expressed as carrier and sideband power for sinusoid and square wave signals, considering negative clipping by modulator cut-off
01 p0028 A69-10419

Signal to cross modulation noise ratio in TWT tube during amplification of sinusoidal signals
01 p0031 A69-10780

Sinusoidal phase modulation role in spectral broadening observed in trapped filaments of laser and Raman light
03 p0442 A69-14189

First and second passage times of stationary random process consisting of sinusoidal signal with stationary Gaussian noise
04 p0561 A69-15453

Sine wave oscillator circuits and performance prediction for NERO thrust measurement test stand
08 p1300 A69-20155

Hard limiting effect on sum of three or four sinusoidal signals noting output amplitudes, signal suppression and negative suppression effect
09 p1451 A69-21311

Signal to cross modulation noise ratio in TWT tube during amplification of sinusoidal signals
10 p1653 A69-23109

Waveforms analyzer for mixtures of exponentially damped sine waves, noting application to interferometer curves in plasma wave propagation
17 p2970 A69-32852

Pulsating flow analysis in finite and infinite conical nozzles under sinusoidal pressure disturbances [ASME PAPER 69-APM-16]
18 p3214 A69-34392

Pulses and sine waves coupling between parallel transmission lines obtained using Oliver elementary coupling theory
19 p3266 A69-35768

Coherent radiation detection using laser optical sine waves, considering detection by heterodyning, laser preamplifier and parametric amplification
19 p3335 A69-36070

SINGLE CRYSTALS
NT WHISKERS [SINGLE CRYSTALS]

Ground state population modulation in trivalent rare earth doped single crystals by means of optical double resonance, noting applications
01 p0134 A69-10013

Gallium arsenide single crystal epitaxy with doping/concentrations into semiinsulating microwave circuits
01 p0040 A69-10196

Mechanical properties of lithium fluoride single crystals, taking into account equilibrium lattice defect structures
01 p0138 A69-10602

Interstitial impurity effects on mechanical properties of molybdenum single crystals, considering temperature dependence of flow stress in bcc metals
01 p0095 A69-10609

Silicon doped p-n GaAs single crystals and epitaxial layers energy spectrum, studying shift in position of emission band maximum
01 p0139 A69-10833

Dielectric constants of barium titanate single crystals as function of electric field intensity at different frequencies
01 p0139 A69-10889

Proton energy distributions for passage through NaCl, KCl, KBr, Si and Ge single crystals at various angles relative to /100/ and /110/ crystallographic planes
01 p0140 A69-11109

Diffusion process in dislocation-free doped and undoped GaAs single crystals
02 p0296 A69-11792

Vanadium dioxide reflection spectra dependence on incident quantum energies during semiconductor/metal phase transition
02 p0298 A69-12100

Ni-Cr-Ti-Al /Nimonic/ alloy single crystal mechanical properties at room temperature, determining importance of structure
02 p0268 A69-12192

Strain rate effect on dislocation substructure in deformed niobium single crystals, investigating relationship between mechanical properties and dislocation substructure
02 p0268 A69-12287

Free flight impact tests showing deformation curve for aluminum and copper single crystals representable as 1/4 power law
02 p0344 A69-12288

Friction induced plastic deformation of Be-Co-Zn single crystals with HCP structure
02 p0254 A69-12627

Ammonium perchlorate thermal decomposition, studying point defects role
03 p0494 A69-12896

InAs-InP phase diagram taking into account equilibrium pressure of vapor over melts in preparing single crystals by controlled crystallization
03 p0483 A69-13024

Directional solidification and composite structures, discussing structure changes effect on mechanical properties
03 p0449 A69-13877

Single crystal cells for construction of large deployable solar cell arrays
03 p0368 A69-13993

Quantum paramagnetic amplifier using andalusite single crystal and operating with three level pumping system
04 p0577 A69-14780

Quantum paramagnetic amplifier using natural andalusite single crystal and operating with four level pumping
04 p0577 A69-14781

Temperature dependence of electrical properties of In and Cu doped CdSb single crystals prepared by zone refining
04 p0643 A69-15264

Te and Zn doped p-type GaAs single crystals optical homogeneity, using interferometry
04 p0644 A69-15266

Current carrier concentration temperature dependence in Te-doped silicon single crystals by analyzing photoconductivity spectra
04 p0644 A69-15267

Refractive index temperature dependence of cadmium sulfide single crystals grown from gas phase
04 p0644 A69-15268

Homogeneous electroluminescence at 77 K in n-type GaAs single crystals without artificial p-n junctions, noting effects of electric field strength and Zn doping
04 p0644 A69-15271

Work hardening of fcc single crystals, emphasizing transmission electron microscopy of thin foils, X ray topography and etch pitting techniques
05 p0778 A69-15753

Work hardening in quenched fully hardened and overaged Mg-Mn alloy single crystals as function of temperature and strain rate
05 p0778 A69-15757

Work hardening characteristics of Ta and Ta-base alloy single crystals as function of temperature and interstitial concentration
05 p0778 A69-15758

Surface photovoltaic effect in copper electroplated single crystal CdS solar cells, discussing Fermi level and Hall effect
05 p0704 A69-15958

Repolarization processes in barium titanate single crystals by variable sinusoidal voltage pulses
05 p0808 A69-16215

Semiconductor laser generation efficiency increased by using external resonator and by signal amplification
05 p0777 A69-16378

Composites reinforcement with single crystal flakes of aluminum diboride
05 p0785 A69-16581

Gunn effect verification using n-type semiconductor single crystals in DC field, noting microwave field polarization plane rotation
06 p0978 A69-16902

Magnetoresistance of tellurium single crystals with various current carrier concentration at liquid helium temperatures
06 p0978 A69-16986

Fatigue hardening in fcc metals, discussing dislocation distribution in unidirectionally deformed single crystals
06 p0944 A69-17503

Domain structure of barium titanate single crystals during polarization reversal by sinusoidal AC field
06 p0981 A69-17893

Emission of Nd giant pulse laser with high repetition rate and peak power to generate second harmonic radiation in lithium niobate single crystals
07 p1144 A69-18469

Technique for obtaining flawless silicon single crystal films on sapphire bases by vacuum deposition, noting base temperature effect on film quality
07 p1198 A69-18509

CdSe single crystal films vacuum deposition for use of photocells base with p-n heterojunctions
07 p1198 A69-18512

Dislocation redistribution during annealing and shock deformation in liquid nitrogen of chromium, molybdenum and tungsten single crystals
07 p1159 A69-18534

Approximate solution to differential equations describing primary radiation defects transformation into secondary defects in semiconductors
07 p1199 A69-18679

Friction and wear tests of synthetic rutile single crystals against diamond styli and spherical sliders of ruby, sapphire and hardened steel [ASLE PAPER 68-LC-3]
07 p1140 A69-19307

Differential capacity of Li doped zinc oxide single crystals between vapor deposited asymmetrical In electrode contacts
08 p1371 A69-19883

Subgrain diameter relation to misorientation in melt-grown aluminum single crystals from etch pitting and X ray techniques, discussing critical shear stress
08 p1330 A69-20011

Thermal faceting of tungsten single crystal surfaces in oxygen, using vibrating-capacitor work function probe with low energy electron diffraction
08 p1330 A69-20137

Temperature dependence of single crystal elastic constants of nickel aluminide determined by ultrasonic wave propagation measurement
08 p1332 A69-20288

Tensile deformation properties of copper single crystals strengthened by fine dispersions of BeO particles
08 p1334 A69-20575

CdS single crystals excess conductivity observed at room temperature
08 p1374 A69-21083

Dark and photocurrent volt-ampere characteristics induced by capture of carriers injected into illuminated CdS single crystals
09 p1555 A69-21506

Face effect in p- and n-type gallium antimonide single crystals doped with zinc and tellurium
09 p1558 A69-21870

Slow recombination centers parameters in CdSe single crystals during heat treatment in vacuum or hydrogen atmosphere
09 p1560 A69-22664

Dislocation substructure near fatigue fracture surface during tensile mode crack growth in copper single crystals by transmission electron microscopy
10 p1797 A69-23079

Interfacial stress between thermally grown silicon dioxide and single crystal silicon correlated with oxide compressive strength
10 p1744 A69-23177

Chromium concentrations induced line shift in ruby single crystals spectra, determining principal lines position
10 p1744 A69-23321

Drawn n-p and p-n junctions obtained in Te and Zn doped GaSb single crystals prepared in pure He atmosphere by Czochralski method
10 p1745 A69-23329

Single crystal growth by controlled diffusion in silica gel using metathetical and decomplexation reactions
10 p1652 A69-23371

High temperature metallic material strengthening methods, noting metallurgical factors and temperature effects on mechanical properties
10 p1712 A69-23630

Dislocations velocity in high purity aluminum single crystals determined as function of applied stress at 74 and 83 K
10 p1713 A69-23840

Alloying additions effect on plastic deformation anisotropy in GaAs single crystals, determining dislocation activation energies from creep tests
11 p1936 A69-24537

Silicon doped p-n GaAs single crystals and epitaxial layers energy spectrum, studying shift in position of emission band maximum
11 p1936 A69-24700

Single crystal solar cell degradations in space, duplicating radiation effect on minority carriers lifetime by laboratory tests
11 p1826 A69-24876

Silicon resistance strain gage sensitivity dependence on crystallographic orientation following cut-off from single crystal
11 p1887 A69-25209

Resonators made of YIG single crystals exhibiting lowest linewidth in ferromagnetic resonance at microwave frequencies
11 p1855 A69-25627

Structure of epitaxial single crystal layers of CdS vacuum deposited on mica surface at various temperatures
11 p1939 A69-25709

Etched surfaces inhomogeneity of n-type GaAs single crystals, noting oxide layers formation
12 p2142 A69-25980

Nimonic alloy single crystals strengthening during plastic deformation, analyzing jump phenomenon at high and low temperatures
12 p2112 A69-26038

Raman effect in potassium dichromate single crystal, discussing symmetrical and antisymmetrical internal vibrations of free ions
12 p2105 A69-26285

Thermodynamic method for determination of conditions for CdS single crystal synthesis from gas phase, analyzing equilibrium between solid and gas phases
12 p2144 A69-26585

Magnetic crystallographic anisotropy of Li-Ga ferrite single crystals at temperature range measured by ferromagnetic resonance techniques
12 p2144 A69-26721

Photosimulation of electron hole and exciton mechanisms of NaI-Tl and KI-Tl single crystal scintillations
12 p2144 A69-26722

Band structure and reflection spectra of vanadium dioxide and pentoxide single crystals, noting changes in metal-semiconductor phase transition
12 p2145 A69-26724

Saturation and distortion effects on magnetoelastic wave excitation in yttrium garnet single crystals by large amplitude microwave frequency field
12 p2145 A69-26725

Stress and plastic deformation influence on allotropic transformation of cobalt-nickel single crystals studied by X ray diffraction
13 p2279 A69-27761

Capture levels at photosensitive CdS crystals surface determined by studying field effect mobility dependence on electric field
13 p2318 A69-27884

Gallium distribution in YIG single crystals by X ray spectral analysis, observing concentration fluctuations
13 p2321 A69-28002

Optical measurement method for burning surface temperature of condensed systems, realizing radiation from surface of combustion by light guide of monocrystalline aluminum oxide
13 p2379 A69-28453

CdS single crystals spectral dependence of photocurrent, photoconductivity quantum yield and photoelectromotive force in excitation absorption region
14 p2504 A69-28990

Langmuir S curves for tungsten single crystals in presence of adsorbed cesium, discussing orientation, theoretical and experimental correlation and instrumentation
14 p2506 A69-29271

Work function changes of tungsten single crystals as function of oxygen and CO gas pressure at high temperatures, using emission microscope
14 p2506 A69-29272

Negative dispersion of light in neodymium activated calcium tungstate single crystal using neodymium glass laser source, analyzing interferential bands in spectral diagrams
15 p2632 A69-30051

Semiconductor films synthesis and properties, discussing single crystal films, epitaxial nucleation, nuclei surface distribution, layer kinetics, doping and film-substrate interface
15 p2670 A69-31046

Diffuse Zn layers structure in GaAs single crystals, showing dislocations formation by anomalous Zn diffusion
15 p2670 A69-31048

Nonuniform electrical resistivity distribution in InSb single crystals as function of growth direction
15 p2670 A69-31049

Electrical conductivity of cesium iodide single crystals with anion and cation impurities noting temperature dependence
16 p2824 A69-31573

Gas laser application to magnetospectroscopy of graphite, Bi, As and pyrolytic graphite single crystals
16 p2796 A69-31822

Ta single crystal growth condition by zone melting, discussing orientation and purity relationship
16 p2803 A69-32490

Thermionic emission parameters for faces of W-Re, Mo-Re and Ta-Mo single crystals determined by Richardson method of straight lines
17 p3015 A69-33630

Dielectric constants of barium titanate single crystals as function of electric field intensity at different frequencies
18 p3182 A69-34720

Nb single crystals plastic deformation influencing tensile strength, noting rolling directions
18 p3160 A69-35454

Molybdenum single crystals deformation in direct shear, determining stress temperature dependence and critical regions for various slip systems
19 p3342 A69-35811

Possibility of combining individual yttrium ferrite single crystals to obtain noninteracting element for quantum paramagnetic traveling-wave amplifier operating at liquid nitrogen temperature
19 p3334 A69-35883

Electron spin resonance spectra of gamma irradiated single crystals of 9-methyladenine, analyzing H abstraction radical and temperature effects
19 p3264 A69-35974

Two photon excitation of luminescence in complex uranyl compound single crystals using Q switched ruby laser
19 p3334 A69-35982

Reactive scattering from solid surfaces, discussing atom beam reaction of O with heated Ge and Si single crystals
19 p3377 A69-36178

Antimony trisulfide natural light reflection and transmission in and near IR region, noting spectral temperature and time dependence peculiarities
19 p3384 A69-36481

InSb single crystals impurities incorporation and distribution, concluding electrical properties vary with homogeneity or heterogeneity of dopant microdistribution
19 p3389 A69-36547

Crystallization front topography and stratified structure of melt extracted n-type GaAs single crystals from anodic etching method
20 p3582 A69-37013

Single crystal line block electro-optical shutter reflector operation based on double reflection and birefringence in anisotropic media, noting application to Nd glass laser
20 p3554 A69-37611

Repolarization processes in barium titanate single crystals by variable sinusoidal voltage pulses
20 p3584 A69-37785

Injection and excitation of charge carriers in CdS single crystals, analyzing current-voltage characteristics dependence on electrode separation, temperatures and electric field
21 p3779 A69-38423

Transient current change with minor change in voltage with double injection of electrons and holes in CdS single crystals, obtaining time dependence
21 p3780 A69-38833

Magnetic crystallographic anisotropy of Li-Ga ferrite single crystals measured by ferromagnetic resonance techniques
21 p3781 A69-39134

Photosimulation of electron hole and exciton mechanisms of NaI-Tl and KI-Tl single crystal scintillations
21 p3781 A69-39135

Band structure and reflection spectra of vanadium dioxide and pentoxide single crystals, noting changes in metal-semiconductor phase transition
21 p3781 A69-39137

Saturation and distortion effects on magnetoelastic wave excitation in yttrium garnet single crystals by large amplitude microwave frequency field
21 p3782 A69-39138

Dislocations multiplication and rearrangement structure in thermal fatigue of Mo single crystals produced by electron beam zone melting
21 p3746 A69-39162

Impurities effect on domain structure of barium titanate single crystals grown from solution in KF melt determined by inner stresses
21 p3783 A69-39559

YIG single crystal disk instability, noting dispersion of magnetoelastic and plane spin waves from supplementary absorption and LF oscillations recording
21 p3783 A69-39561

Single crystals dislocation dynamics and plasticity theory, discussing current tensor, conservation equation, slip systems, etc
21 p3845 A69-39676

Impurities effects on single crystal film formation of fcc metals on alkali-halide cleavage planes, stressing stacking fault energy importance
22 p3992 A69-39899

Radioactive decay and conductivity changes with time in high and low resistivity CdS single crystals after irradiation with 14 Mev and reactor fast neutrons
22 p3993 A69-40728

Compton profile from single crystal of LiH measured with X ray scattering, noting valence- electron momentum distribution role
22 p3993 A69-40730

Antimony trisulfide single crystals spectral dependence of impurity and stimulated impurity photoconductivities, comparing optical and thermal activation energies
22 p3994 A69-41042

Piezoelectric characteristics of surface layers of Ba titanate single crystals, using static and dynamic electromechanical methods
22 p3995 A69-41156

Dielectric constant and IR spectra of Ba titanate single crystals doped with hydroxyl, showing dependence on temperature and crystal thickness
22 p3995 A69-41157

Waveguide-resonance investigation of temperature dependence of dielectric constant and paraelectric dispersion of Ba and Sr titanate single crystals at millimeter wavelengths
22 p3995 A69-41158

Selenium distribution along GaSb single crystals during oriented crystallization determined by radiometry
23 p4198 A69-41725

Surface films effect on friction coefficient of sodium chloride and Zn single crystals under normal pressure loads, noting film thickness role
23 p4170 A69-42343

Nb single crystals oxidation in dry oxygen at high pressure and temperature indicating suboxide platelets existence as function of temperature
23 p4177 A69-42357

Single crystal Ta and Ta base bcc solid solution strengthening and weakening as function of temperature and strain rate
23 p4178 A69-42358

High temperature single crystal X ray studies of natural Fe-rich orthopyroxene, detecting high-low clinopyroxene inversions
24 p4311 A69-43218

Luminescence, I-V and pulse characteristics of high resistivity Ni doped GaAs single crystals, noting injection conductivity
24 p4362 A69-43734

SINGLE SIDEBAND TRANSMISSION

Transistorized single sideband detector-converter operation in presence of large signal and heterodyne voltage levels, deriving equation for transmission coefficient
05 p0730 A69-16220

Meridional radio communication between radio station at South Geomagnetic Pole and amateur SSB radio stations in U.S.S.R.
06 p0889 A69-17753

Single sideband modulation theory explained by sum representation of sampling theorem, comparing different signal generating methods
09 p1456 A69-22290

Circuit for generation of square wave with frequency as sum or difference of two periodic signal frequencies, discussing SSB modulation

10 p1665 A69-24047

Optical modulation through Doppler frequency shift obtained by rotating radial diffraction grating [AOLR-69-1]

11 p1889 A69-25394

Twin image elimination in holography using single sideband object waves without offset reference wave introduction

12 p2090 A69-26253

Single-sideband signal nonlinear distortion and graphical methods for calculation of oscillator tube plate current pulse components

14 p2418 A69-28828

Subcarrier phase modulated single sideband sinusoidal carrier synthesis, discussing signal power ratios, signal efficiency, design sensitivity, etc

14 p2413 A69-29489

Multiple access techniques of SSB-PM and PCM-PM frequency translation for satellite communication system, comparing performance characteristics

21 p3678 A69-39807

Compatible single sideband /CSSB/ modulation suitability for broadcasting, analyzing signal spectrum, demodulation distortion and signal generation methods

23 p4125 A69-42111

SINGLE STAGE ROCKET VEHICLES

NT AGENA ROCKET VEHICLES

NT BLACK BRANT 2 SOUNDING ROCKET

NT BLACK KNIGHT ROCKET VEHICLE

Single stage rocket vehicle design for rapid global air transportation noting size, range and economics

09 p1433 A69-21303

Space flight cost analysis, relative costs of various types of transportation and need for reusable single stage to orbit vehicles

15 p2719 A69-30186

Single stage rocket control and trajectories for maximum target strike probability within given range

21 p3818 A69-38857

Single stage rocket body finite bending stiffness effect on pitching moment using approximate equation, noting applicability to multistage rockets

22 p4037 A69-41048

SINGULAR INTEGRAL EQUATIONS

Contact problem of pair of nonhomogeneous semicircular regions solved by singular integral equations solution method

02 p0336 A69-11553

Approximate solution of linear functional, singular integral and integrodifferential equations by general theory of approximate methods

02 p0272 A69-12163

Radiative transfer equations solved for electron scattering stellar atmosphere, using transformation of integrodifferential transfer equations into singular integral equations

03 p0466 A69-13351

Soviet book on theory of approximate methods and applications to numerical solution of singular integral equations

07 p1174 A69-19580

Singular integral method in approximation for synthesizing sequence of functions with spectrum of limited length

09 p1460 A69-22642

Analytic functions representation and application to theory of singular integral equations in continuum mechanics, noting Cauchy kernels and boundary value problems

19 p3361 A69-36813

Diffraction of plane polarized electromagnetic wave incident on dielectric wedge formulated as singular integral equation, discussing electric field amplitude

22 p3903 A69-41258

SINGULARITY [MATHEMATICS]

Structure of shock waves from MHD jet injected into zero viscosity, finite thermal and electrical conductivity medium analyzed by nonlinear differential equation system

01 p0130 A69-10774

Paradoxes associated with elastic-plastic limit load analysis of material satisfying Drucker stability postulates

02 p0337 A69-11562

Unsteady pressure field in zone of aerodynamic proximity of free moving airscrew investigated with propeller blades replaced by surface singularities

02 p0192 A69-12827

Numerical solution of elliptic equations by iteration result in convergence prevention and solution of Laplace and Poisson equations with singular Laplace operator

04 p0625 A69-15133

Electrical impedance of semiconductor supporting two waves contains entire complex transcendental function with complex parameter and infinity of zeros in left half z plane

07 p1196 A69-18268

Differential equations with singular problem solutions analyzed by reducing problem to solution of integral equation

07 p1174 A69-19004

Axially symmetric static solutions of Einstein equations with singularities on z axis allowing for higher multipole moments in general relativity

08 p1350 A69-19783

Space time structure conditions derived for compatibility with simultaneous fulfillment of causality and equivalence principles

08 p1351 A69-19948

Supersonic flows past slender bodies, calculating pressure by means of moving singularities

08 p1252 A69-20721

Singular perturbation problem for elliptic linear partial differential equation, studying asymptotic expansion of solution in vicinity of singular points in nonconvex domain

08 p1352 A69-20751

Finite difference schemes of high order of accuracy for Strum-Liouville and boundary value problems with regular singularity

10 p1719 A69-23365

Singular perturbations for Cauchy and boundary value problems, considering differential operators and Hilbert space

10 p1720 A69-23635

Differential game for determining singular fuel optimal control of plant with uncertainty in dynamic equation

10 p1667 A69-24041

Singularity of Schwarzschild spherically symmetrical solution to Einstein equations of general relativity theory, exemplifying Lemaître coordinate system

12 p1219 A69-25974

Singularities of optimal filtration for random signals given by differential equations with variable coefficients and white noise

13 p2218 A69-27251

Weak superconducting contacts volt-ampere characteristics current steps and emission spectra, showing singularities due to superconducting current nonharmonicity

14 p2504 A69-28994

Singularity-free global solutions to nonlinear differential equations associated with variational principles, deriving necessary condition for existence from dilatation invariance considerations

14 p2470 A69-29367

Physical singularity reduced to imaginary by introducing arbitrary function in form of perturbation into gravitational equations general solution

18 p1373 A69-35018

Singular perturbations and boundary layer theory for approximating solutions to simple ordinary differential equations

20 p3515 A69-37583

Linear nonstationary system with singular point analyzed for stability necessary and sufficient conditions using Riemann-Mellin conversion integrals and Laplace transforms

21 p3685 A69-38451

First order linear differential equations subject to linear constraints, discussing solution uniqueness dependence on matrix nonsingularity

21 p3754 A69-38744

Nonlinear incompressible potential flow with unbounded free surfaces, analyzing singularities in finite part of space

21 p3696 A69-39295

Jacobi polynomial series analytical expansion, studying relationship to Taylor series singular points

21 p3757 A69-39537

Numerical integration of double integral with Cauchy type singularity for calculation of aerodynamic or hydrodynamic load on lifting body

23 p4182 A69-41913

Spherically rotating symmetric body gravitational collapse within Schwarzschild radius, presenting trapped surface concept for asymmetrical cases and generalization of space-time singularities

23 p4219 A69-42333

Free vertical shear layers structure solutions singularities in rotating fluids, considering motion by rising or spinning axisymmetric body

23 p4153 A69-42356

Supersonic flows around slender bodies calculated by method of moving singularities

23 p4061 A69-42407

Volterra problem with given singularities for exterior of circle applied to fluid mechanics

24 p4339 A69-42679

Singular optimal control problems theoretical and computational aspects

24 p4292 A69-43282

SINKS

NT HEAT SINKS

Source and sink method application to direct axisymmetric problems of hydrodynamics

05 p0747 A69-16039

SINTERED ALUMINUM POWDER

Vacuum heating and thermal cycling influence on mechanical and structural properties of aluminum sheets fabricated from sintered powder

02 p0266 A69-12126

Powdering temperature effect on mesh size, structure and mechanical properties of pressed semifinished sintered Al-Cr and Al-Fe alloys

03 p0452 A69-14119

Cold rolling and annealing effects on tensile strength, heat resistance and ductility of sintered Al powder sheets

03 p0452 A69-14121

Yielding of matrix material and cell size of substructure relationship to dry abrasion resistance of SAP type aluminum alloy at room temperature

08 p1319 A69-19995

Creep behavior of aluminum-alumina alloys analyzed using rupture time to determine deformation speed influence on elongation and crack formation

12 p2120 A69-26938

SINTERING

Preparation of refractory alloys in powders, fibers and sintered billets by thermochemical method [ONERA-TP-636]

02 p0251 A69-11625

Sintered molybdenum deoxidation effect with C, B and Si, analyzing hardness, tensile strength and ductility

02 p0265 A69-12002

Anomalous discontinuous stress relaxation in sintered tantalum

02 p0265 A69-12003

Exothermal effects during sintering of nickel-aluminum powder mixture

02 p0269 A69-12838

Exothermal effects during sintering of nickel-aluminum powder mixture, showing role of liquid phase decomposition and intermetallics

02 p0269 A69-12843

Fabrication of Cu-W composites with discontinuous fibers based on sintering and rolling

03 p0444 A69-13349

Hardenability of ShKh-15 steel, establishing relationship of porosity to sintering method

04 p0619 A69-15390

Two stage thermal treatment inhibiting influence on swelling and porosity linked to Kirkendall effect during sintering of Fe-Ni powder mixtures

05 p0782 A69-16616

Properties of electrolytic and reduced titanium powders and sinterability of porous compacts

05 p0782 A69-16795

Sintered W-Ni-Fe alloys strength and precipitation hardening characteristics for various compositions and cooling conditions

05 p0782 A69-16798

Microstructural changes during liquid phase sintering of alloys, considering temperature effect on carbide grain growth and activation energies

07 p1168 A69-19599

Polymorphic characteristics of titanium pentoxide prepared by reducing titania, examining oxidation products with X ray diffraction

07 p1168 A69-19601

Porous structures, using spherical tungsten powders, discussing metallurgy, sintering, temperature effects and performance characteristics in ion engines

10 p1710 A69-23166

Molybdenum fiber sintering activation by adding nickel, noting decrease in impact viscosity

10 p1711 A69-23336

Added metal oxides solid solutions effect on creep kinetics and strain rate of zirconia samples during sintering

12 p2118 A69-26260

Room temperature WC-Co compacts oxidation resistance in air noting increase with preliminary sintering temperature

13 p2275 A69-27345

Be billets fabrication from powders by cold hydrostatic pressing and pressureless sintering, noting hardness, density and grain size dependence on temperature

14 p2465 A69-29681

SINUSES

Sintered mixtures of Ni-Mo powder noting electrical resistance, alloy and shear strength and impact viscosity 15 p2638 A69-30280

Tensile, bending and impact strengths of materials produced by metal porous blank impregnation with molten glass, noting metal density and sintering effects 15 p2643 A69-31188

Ti and Zr diborides sintering with Cr, Mo, W and Re additions, discussing activation, pressure effects and density 22 p3968 A69-39888

Recrystallization during sintering of free flowing Nb and Ti carbide powders, determining grain growth dependence on temperature and activation energy 22 p3970 A69-40636

Surface chemistry effect on physical properties of pressure sintered Be metal, suggesting surface alloying approach by powder metallurgical techniques 24 p4332 A69-42963

SINUSES

Valsalva maneuver produced abrupt onset of ptosis and proptosis caused by ethmoidal air cell rupture, discussing etiologies 17 p2909 A69-33186

SINUSOIDS

U SINE WAVES

SITE DATA PROCESSORS

IMP-1 experiment, describing design and applications of SDP-3 computer 19 p3280 A69-36265

SDP-3-A general purpose stored program computer designed for small scientific spacecraft onboard data system, noting computerized simulation 20 p3500 A69-37385

SITES

NT LANDING SITES
NT LAUNCHING SITES
NT LUNAR LANDING SITES

Soil resistivity survey at earth telecommunication installation site to determine optimal grounding or electrode system 07 p1117 A69-19348

SIZE [DIMENSIONS]

Dimensional effects on thermodynamic and kinetic properties of thin semiconductor and semimetal films, noting quantization influence 01 p0136 A69-10186

Venus diameter determination from optical measurements, noting cloud layer height and height of suspended particles in upper atmosphere 05 p0818 A69-15621

Equatorial semiaxis of magnetospheric tail at distances between 10 and 80 earth radii for various intensities of polar magnetic disturbances 05 p0753 A69-16050

Computer analysis for optimizing size and shape of thin walled axisymmetric elastic rings, plates and shells with respect to tension, rigidity and weight 06 p1026 A69-18017

Oxidizer particle size and binder type effects on nonacoustic combustion instability of solid propellants [AIAA PAPER 69-175] 06 p0983 A69-18152

Low pressure deflagration limit dependence on strand size in terms of cross section dimensions for composite ammonium chlorate propellant [AIAA PAPER 69-144] 06 p0983 A69-18162

Dimensions of 19 variable eclipsing binaries from published photometric and spectral orbital elements 09 p1590 A69-21378

Ground station receiving antenna design and size for indirect distribution of TV programs by geostatic satellites 10 p1654 A69-23389

Helical and log conical helical antenna width reduction by loading of traveling wave antenna elements with isotropic material 11 p1852 A69-25315

Plane strain fracture toughness tests on maraging steel plates for various yield strengths and large dimensions 12 p2114 A69-26496

Dimensions of 19 variable eclipsing binaries from published photometric and spectral orbital elements 18 p3198 A69-34766

Weight estimation and forecast in manned spacecraft design, noting size and weight relationship [SAE PAPER 793] 18 p3208 A69-34864

Far and near side lunar crater chains regularities in distribution and size 18 p3202 A69-35329

Cargo aircraft future design regarding engine development, structural flexibility, airport compatibility, cargo handling, etc 18 p3092 A69-35467

Equatorial semiaxis of magnetospheric tail at distances between 10 and 80 earth radii for various intensities of polar magnetic disturbances 20 p3532 A69-37959

SIZE DETERMINATION

NT PRECIPITATION PARTICLE MEASUREMENT

Particle size frequency distributions and lunar surface materials, showing impossibility of distinguishing between impact fragmentation of surface and pyroclastic rock deposition 02 p0325 A69-12567

Human visual systems ability to encode retinal images produced by different size objects 03 p0369 A69-13359

Lunar libration clouds, discussing visual observation at small phase angles for estimation of dominant cloud particle size 05 p0827 A69-16527

Photoelectric observation of star occultation by Neptune for mean radius determination 06 p1007 A69-17693

Analytical technique for unmanned spacecraft sizing for planetary missions, considering scientific objectives, characteristics and requirements [AIAA PAPER 69-125] 06 p1018 A69-18076

Tank collection and spectrophotometric tests in determining aluminum oxide particle size produced by small rocket engine 06 p0984 A69-18117

Spatial size and velocity distributions for liquid or solid aerosols suspended in air flow using Q spoiled ruby laser and holography 09 p1492 A69-21418

Glass fibers size, finish and surface treatment identification by pyrolysis attenuated total reflectance IR spectroscopy 09 p1448 A69-22315

Unicellular microorganisms size and concentration estimates based on light scattering measurements of suspensions in spectrophotometer cuvette compartment 11 p1829 A69-25643

Radio sources angular dimensions determined by microwave interferometry, discussing distinctions between quasars, galaxies and unidentified sources 12 p2166 A69-27039

Vertically polarized log periodic antenna consisting of unipole vertical radiators with side radiators for achieving minimum size 16 p2763 A69-32580

X ray source Cyg XR-1 angular diameter upper limit determined from balloon experiment data obtained with collimated X ray telescopes 17 p3026 A69-32860

Venusian cloud layer radius, discussing error in determination of occultation level height of Regulus by Venus 18 p3203 A69-35331

Diameter density and atmosphere of Neptune revised based on star eclipse, noting altitude and temperature 18 p3205 A69-35438

Particle size, velocity and position in moving streams measured by tilted film plane optical system with pulsed light source 19 p3306 A69-35733

Dynamic cathode ray tube spot size measurement by two slit technique, noting relationship to beam current and luminance 21 p3719 A69-38329

Analytical technique for unmanned spacecraft sizing for planetary missions, considering scientific objectives, characteristics and requirements [AIAA PAPER 69-125] 21 p3828 A69-39770

SIZE PERCEPTION

U SPACE PERCEPTION

SIZE SEPARATION

Galaxies classified by matter content of nucleus, discussing evolution 11 p1953 A69-24351

Sorting particles by shape using sieving equipment, noting results with crushed gravel 21 p3731 A69-38950

SIZING [SEPARATION]

U SIZE SEPARATION

SIZING [SHAPING]

Titanium hot forming and sizing die fabrication concepts for aircraft structures [ASM PAPER D8-26.1] 07 p1143 A69-19671

Computer aided design analysis program to provide weight and sizing data for entry spacecraft [SAE PAPER 797] 18 p3208 A69-34903

SKELETON

U MUSCULOSKELETAL SYSTEM

SKEWNESS

Stress field for skew hole determined from plane stress field for equivalent right hole, considering elastic plate penetrated by oblique circular cylinder 04 p0674 A69-14581

Natural frequencies and modes of skew membranes obtained by Rayleigh-Ritz method 06 p1021 A69-17166

Clamped skew plates natural frequencies analyzed using Galerkin method, expressing deflections as double series of beam characteristic functions, stating eigenvalues and eigenvectors 20 p3621 A69-37210

Simultaneous lateral skewing regions existence in low speed three dimensional turbulent incompressible boundary layer flow [ASME PAPER 69-FE-24] 20 p3517 A69-37995

SKID LANDINGS

Steerable landing gear system consisting of freely casting corotating wheel nose gear, tiltable axle and main gear skids for lifting body spacecraft [AIAA PAPER 69-790] 19 p3243 A69-35633

Aircraft braking, discussing systems, brakes, tires, runway interface, heat sink materials, friction measurements, skid control, cooling and recovery equipment [SAE PAPER 690376] 23 p4063 A69-11670

SKIDDING

High speed ball bearing skidding, proposing analytical model as design tool, discussing effects of thrust load, speed, oil temperature and flow rate [ASME PAPER 69-LUBS-20] 18 p3140 A69-34377

Aircraft tire skidding on wet surfaces, measuring interstitial water pressure for various treads, velocities and surface textures 19 p3247 A69-35910

SKIN [ANATOMY]

NT EPIDERMIS
NT EPITHELIUM

Light transmission through body wall of living colorable desert iguanas measured by spectrophotometry, discussing skin pigment effects 07 p1059 A69-18373

Limits of human tolerance to localized skin exposure to IR irradiation of various intensities from pain threshold observations, noting skin temperature role 10 p1647 A69-23589

Histological changes in rat skin after 13 Mev proton irradiation, evaluating biopsies in tissue culture 14 p2407 A69-29299

Photographic and photometric study of absorption and reflection of ruby laser light incident on biological objects 21 p3665 A69-39060

Monomethylhydrazine absorption through canine skin noting metabolic aftereffects and methemoglobinemia 22 p3887 A69-41191

Insensible water loss from human skin as function of ambient vapor concentration using IR gas analysis, applying results to water loss model revision 23 p4077 A69-41293

Forearm skin capacity vessels tonus as function of intrapulmonary pressure during positive and negative pressure breathing 23 p4093 A69-42068

X band pulsed microwaves effect on skin metabolism including respiratory activity, biochemistry and biosynthesis of intercellular materials, etc 24 p4270 A69-42575

Albino guinea pigs respiration rates and ear skin histology after exposures to coherent ruby laser light 24 p4270 A69-42578

SKIN [STRUCTURAL MEMBER]

Skin panel stresses for random acoustic loading, determining aircraft structure responses 03 p0530 A69-14092

Titanium fuselage skin contouring to shallow compound curvature of supersonic aircraft by elastic draping, shot peen forming and cold stretching, discussing residual stresses 09 p1512 A69-22374

Damping of response of integrally stiffened skin structures to random acoustic pressures, reducing rms stress in case of broad band excitation [ASME PAPER 69-VIBR-26] 10 p1806 A69-24172

Aerodynamic skin heating at high Mach numbers affecting structural design, noting use of high temperature materials, insulation systems and shell construction method 21 p3646 A69-38460

SKIN FRICTION

NT AERODYNAMIC DRAG
NT FRICTION DRAG

NT SUPERSONIC DRAG
NT VISCIOUS DRAG

Transverse curvature effect on skin friction and heat transfer in laminar flows past slender circular cylinders 02 p0232 A69-12210

Thin film heated Pt resistance thermometer for skin friction or velocity measurements in air, water or blood 04 p0601 A69-15118

Differential rotation of sphere in viscous incompressible liquid, discussing pressure and skin friction drag between two hemispheres with different angular velocities 04 p0590 A69-15278

Local pressure and skin friction distribution around circular cylinder in cross flow in large range of Reynolds numbers 05 p0744 A69-15716

Incompressible turbulent boundary layer properties with arbitrary pressure gradient calculated by integral method resulting in single equation for skin friction coefficient [ASME PAPER 68-WA/FE-22] 05 p0749 A69-16098

Boundary layer transition detection at supersonic speeds, using thin film gages to infer local laminar and turbulent supersonic skin friction [AIAA PAPER 69-9] 06 p0912 A69-18075

Turbulent skin friction on compliant skins stretched over damping fluid in shallow bath in flat plate [AIAA PAPER 69-164] 06 p0914 A69-18163

Constant property turbulent boundary layer flow, developing finite difference solution for prediction of velocity profiles and skin friction coefficient 09 p1482 A69-21950

Axisymmetric bodies longitudinal contours for hypersonic flow minimum drag, considering Newtonian pressure distribution and skin friction 10 p1632 A69-23886

Skin friction measurement with rectangular mouthed Preston tubes of constant thickness ratio, analyzing calibration curves and difference from circular tubes 11 p1880 A69-24376

Heat transfer and skin friction in convective and stagnation flow laminar film boiling in boundary layer flows with appreciable radiation 11 p1873 A69-25242

Skin friction drag coefficient for right circular cylinder calculation coefficient on basis of Blasius solution for flow 11 p1819 A69-25384

Skin friction coefficient relation to pressure distribution in turbulent flow and development of momentum thickness along flow 11 p1819 A69-25385

Floating element skin friction meter designed for adverse pressure gradients, discussing wall shear stress measurement 11 p1889 A69-25557

Supersonic Preston tube correlations for Mach number and Reynolds number effects on hypersonic turbulent skin friction on adiabatic surfaces, simplifying correlation [AIAA PAPER 69-345] 13 p2249 A69-28280

Skin friction measurement in aerodynamic tests using thin liquid crystal coatings with changes in maximum light scattering wavelength in response to shearing forces 14 p2427 A69-29029

Three dimensional laminar boundary layer on semiinfinite permeable flat plate in viscous incompressible fluid flow, calculating velocity profiles and skin friction components 14 p2433 A69-29898

Power law fluids boundary layer near flat plate studied by series expansion and steepest descent methods, determining velocity gradient and skin friction coefficient 15 p2589 A69-30002

Laminar boundary layer control by combined blowing and suction, analyzing surface roughness influence concerned with underwater vehicle skin friction reduction [AIAA PAPER 69-387] 15 p2591 A69-30477

Three dimensional effects on Stanton tube data for skin friction determination for small protuberances drag immersed in turbulent boundary layer 16 p2771 A69-31920

Analytical expressions validity for skin friction in compressible turbulent boundary layer over wide range of Reynolds numbers and heat transfer conditions 16 p2771 A69-31926

Swept wing attachment line boundary layer, measuring skin friction in full turbulence and velocity profiles with and without trip wire 17 p2958 A69-34047

Viscous incompressible fluid flow around semiinfinite oscillating plate and skin friction on infinite cylinders oscillating parallel to length 19 p3237 A69-35620

Skin friction balance in Mach 5 wind tunnel with high heat transfer, measuring shear forces 19 p3292 A69-35734

Skin friction balance for shear stress measurements in presence of ablation, describing balance construction, calibration, flexure range, etc 19 p3292 A69-35735

Turbulent skin friction coefficients of compliant surfaces on flat plates determined as function of speed for different materials 21 p3695 A69-39039

Skin friction results from free stream velocity boundary layers with varying injection and suction wall conditions, describing flow characteristics 21 p3696 A69-39431

Velocity profile and skin friction in boundary layer on flat plate with periodic vorticity near leading edge 22 p3929 A69-40015

Hypersonic flow for low Reynolds number, including magnetic field and wall temperature effects on heat transfer and skin friction for blunt shapes 22 p3860 A69-40540

Laminar viscous flow and skin friction near trailing edge of flat plate analyzed by modified Oseen approximation, noting accuracy for high Reynolds numbers 22 p3930 A69-40683

Skin friction and mean velocity profiles measured for fully developed 1000-10,000 Reynolds number flows in pipes and channels 22 p3932 A69-40897

Velocity defect profile and skin friction law for incompressible equilibrium turbulent boundary layer, using mixing length relation 22 p3934 A69-41180

Laminar boundary layers on slender paraboloids, analyzing skin friction formula and extension for transverse curvature ranges 23 p4152 A69-41904

Rough surface skin-friction relations expanded to provide turbulent boundary layer growth prediction in pressure gradient 24 p4304 A69-43580

Turbulent skin friction on compliant skins stretched over damping fluid in shallow bath in flat plate [AIAA PAPER 69-164] 24 p4306 A69-43685

SKIN FRICTION DRAG
U FRICTION DRAG

SKIN TEMPERATURE [BIOLOGY]

Aircrew members skin temperature changes in response to intense diffuse thermal radiation, noting psychological response to exposure [AGARDOGRAPH-111] 08 p1264 A69-20669

Skin and subcutaneous temperature during exposure to intense thermal radiation, discussing estimation of subcutaneous temperature from skin temperature data [AGARDOGRAPH-111] 08 p1264 A69-20671

Cutaneous receptor response to microwave irradiation, measuring warmth sensory effects in human forehead with radiometer [AGARDOGRAPH-111] 08 p1266 A69-20677

Skin temperature and cutaneous pain during warm water immersion, refuting subcutaneous thermal gradient hypothesis for stimulation of heat pain 08 p1267 A69-20683

Passive thermal control system for space suit use in extravehicular environment, discussing skin temperature control at varying heat flow rates 12 p2023 A69-26549

Skin temperature change rate influence on sweating in male subjects, discussing role of central thermosensitive structures 22 p3874 A69-40210

Human sweat glands reflex responses to diverse skin cooling rates in hot room, discussing bath temperature step decrease effect on lower limb 23 p4082 A69-41446

Subjective feeling of dampness correlation with relative humidity of air at zero and below zero C temperatures 23 p4109 A69-41870

Central circulatory responses of humans to rapid skin temperature changes during continuous exercises 24 p4258 A69-42633

SKIN TEMPERATURE [NON-BIOLOGICAL]

Conductive heat transfer between aerodynamically heated skin and barrel of Aerobec 150 sounding rocket telescope, noting effect of residual gas pressure 09 p1610 A69-22005

Thermocouples dynamic response attached to thin skinned model under constant heating rate, considering error reduction in temperature measurement 13 p2375 A69-27785

Unsteady temperature field in plane skin of aerodynamic body in case of temperature dependent thermophysical characteristics of skin material 18 p3092 A69-34982

Corrections for eliminating anomalous skin effect on IR emissivity for Ag, Cu, Au and Al 23 p4177 A69-42212

SKIRTS

Skirts on hovercraft, noting rough water drag, plough in and overturning, and skirt oscillation and wear problems 10 p1634 A69-23629

Small hovercraft simple and bag skirts design characteristics, considering materials 13 p2202 A69-27545

Multicell air cushion vehicle technology based on 1/4 scale and full scale tests, noting comparison with plenum systems and costs 13 p2202 A69-27547

Flexible skirt design for air cushion vehicle consisting of semicylindrical elements and permitting horse power and cost reductions 13 p2203 A69-28179

Mountbatten /SR.N4/ hovercraft development, seakeeping, skirt design and service introduction 15 p2550 A69-30479

SKUA ROCKET VEHICLES

Meteorological and sounding British rockets Skylark, Petrel and Skua, showing capabilities, payloads and experiments [UN PAPER 68-95785] 01 p0161 A69-10530

Mesospheric fine winds structure, discussing data obtained by Skua II rocket with chaff payload 15 p2604 A69-31415

SKULL

NT CRANIUM

Ultrasound-echo-encephalography in diagnosis of posttraumatic intracranial hemorrhage of skull and brain trauma, noting neuroradiological techniques 21 p3652 A69-38790

Sound evoked DC changes on intact skull of adult humans using data from AgCl electrodes, investigating intensity function, analyzing data by computer 23 p4098 A69-42101

SKY

U NIGHT SKY

SKY BRIGHTNESS

Soviet rocket and satellite night, twilight, airglow and auroral studies, discussing day sky brightness, night airglow and atmospheric stratification 01 p0066 A69-10941

Earth atmosphere transmission coefficients determination by relation between transparency and daytime sky brightness, noting limits of applicability 01 p0074 A69-11185

Automatic spectroelectrophotometer for measuring sky spectral brightness at 6910-4040 angstroms, determining point of minimum brightness 01 p0074 A69-11187

Atmosphere spectral transparency and stability spectrophotometric studies based on measuring solar aureole brightness 01 p0074 A69-11188

Twilight sky brightness measurements at 5200 angstroms for estimating upper atmospheric dust component, discussing error rates 01 p0075 A69-11191

Linear integral equations for brightness coefficients and auxiliary functions in semiinfinite atmosphere, expressing atmospheric albedo using moments and Chandrasekhar function 04 p0662 A69-15237

Dayglow determination from aerosol spectrum obtained through data of brightness and polarization of day sky 07 p1211 A69-18545

Cosmic radio noise brightness distribution in Southern Hemisphere at 10.02 MHz, noting spectra of sources observed 07 p1206 A69-19272

Night sky surface brightness and polarization measurements as basis for zodiacal dust cloud particle density distribution normal to ecliptic plane 07 p1222 A69-19588

Clear atmosphere model based on path of sight equilibrium radiance and nonabsorption permitting integration of equation of transfer 07 p1130 A69-19643

SKY RADIATION

Low latitudes observations of 21 cm line of H I in galactic center direction, giving contours maps of brightness temperature
08 p1392 A69-20562

Upper atmosphere temperature distribution estimation on basis of twilight zenith sky intensity measurements, discussing influence of various parameters on accuracy
09 p1487 A69-21653

Irregular pulsations in morning sky brightness using all-sky photographic airborne auroral observations along auroral oval
09 p1594 A69-21666

Photoelectric polarimeter to record sky light intensity in form of polarized components, detailing construction and operation
12 p2078 A69-25892

Visual mapping and photometric scanning of Saturn with rings from earth, noting ring brightness edgewise linear dependence on rings opening
15 p2697 A69-31256

Day sky brightness at altitude above 100 km obtained during rocket flight compared to night sky viewed from ground
17 p3037 A69-33664

Sky brightness temperature spectra searched for neutral intergalactic atomic hydrogen radio emission, using horn-reflector antenna
18 p3190 A69-34285

Search for diffuse galactic light component between 2100-2800 A by rocket measurements of night sky brightness, showing low albedo of interstellar dust
18 p3202 A69-35210

Visibility degree of noctilucent cloud determined from ratio of brightness contrast against sky to eye contrast threshold
19 p3362 A69-36410

Daylight sky spectral radiance in ruby laser spectral range as functions of scattering angle, height over horizon of observed point and sun altitude
21 p3734 A69-38397

Altitude variation of mesospheric daytime sky brightness from earth based measurements of twilight sky brightness, noting inconsistency in calculations based on standard atmospheres
21 p3716 A69-39116

SKY RADIATION

NT AIRGLOW
NT DAYGLOW
NT GEOCORONAL EMISSIONS
NT NIGHTGLOW
NT TWILIGHT GLOW

French radio astronomy, presenting sky background radiation and solar emission results from Rubis 02 and 04 rockets
02 p0316 A69-11908

Stratospheric dust effect on twilight sky color, evaluating scattered radiation chromaticity for atmospheric models containing ozone
02 p0243 A69-12014

X ray airglow in daytime sky, suggesting origin in atmospheric N and O K alpha lines due to fluorescent excitation by solar X rays
02 p0307 A69-12022

Double scattering effects of sky radiation and outgoing radiation balance in disturbed atmosphere, using homogeneous plane parallel atmospheric model
07 p1175 A69-18270

Soviet monograph on UV radiation of sun and sky emphasizing biological effects
07 p1221 A69-19506

Sky background light automatic compensation in stellar photography, using single or double channel photometer
08 p1313 A69-20247

Sky background of soft X ray emission in spectral band explained by emission lines from galaxies
08 p1380 A69-20769

Daytime sky radiation measurements by high altitude vehicles with spectrophotometer noting spectral radiance, luminance, polarization, albedo and near IR
08 p1317 A69-21071

Daytime clear sky light polarization in UV and visual spectral regions calculated with considerations for aerosol components polarization effect
09 p1491 A69-22708

Multiple scattering of solar radiation in turbid atmosphere, considering equations of sky radiation and radiative transfer
11 p1911 A69-24587

Northern sky scan for discrete sources of gamma rays in 240 to 1000 kev energy region by telescope on balloon flight
11 p1946 A69-24593

Sky polarization neutral points around sunset /spring-summer 1968/ at Bedford, Mass., inferring continuation and variations of enhanced stratospheric turbidity
12 p2067 A69-26343

Statistical properties of spatial radiance distribution of sky and forest backgrounds in IR, noting one dimensional Wiener spectra
12 p2131 A69-27072

Sky mapping in IR, using IR photometer on TD1 ESRO satellite
13 p2260 A69-27606

Incoming IR flux measurements at high altitude, noting flux increase due to water vapor condensation in troposphere
13 p2256 A69-28647

Absorption band observation near 0.43 mu in solar spectra and scattered radiation of sky, determining nontelluric origin
14 p2441 A69-29407

Sky cosmic radio emission absolute temperature measured at decimeter wavelengths and at two zenith angles to minimize atmospheric influence
15 p2687 A69-30544

Cosmic X ray bremsstrahlung due to collisions of suprathermal protons with ambient electrons, giving clue about diffuse sky background of X rays
22 p4006 A69-40643

SKY WAVES

NT WHISTLERS

Propagation tests of skywave field strength reduction by orthogonal transmission
03 p0395 A69-13597

Visual receiving equipment for consistency determination of Loran-C sky wave signals apparent arrival times
12 p2029 A69-26052

Forward and backscatter soundings compared to verify focusing mechanism of HF sky waves
14 p2435 A69-28967

Ground conductivity effects on MF sky wave transmission strength, discussing transmission over open sea
17 p2918 A69-33029

SKYCRANE HELICOPTER

U CH-54 HELICOPTER

SKYLARK ROCKET VEHICLE

Meteorological and sounding British rockets Skylark, Petrel and Skua, showing capabilities, payloads and experiments
[UN PAPER 68-95785] 01 p0161 A69-10530

Pyrotechnics applications to Skylark upper atmosphere sounding rocket, discussing payload heads, nose cones, sensor covers, etc
10 p1792 A69-23029

SKYRAIDER AIRCRAFT

U A-1 AIRCRAFT

SKYVAN AIRCRAFT

U SC-7 AIRCRAFT

SLABS

Transient temperature distribution for finite slab in phase transformations via single face temperature changes
[ASME PAPER 68-WA/HT-37] 05 p0848 A69-16128

Discrete radiative transfer in nonhomogeneous slabs, giving matrix solution
05 p0849 A69-16480

Group cross section generating techniques to calculate neutron capture rates and spatial capture distribution in depleted thick U slab, using GAROL program
18 p3177 A69-35179

Gas dynamics of material slab under radiation impact assuming thermal equilibrium reemission, discussing equations of motion and mean free path as function of frequency
19 p3449 A69-36355

SLANT

U SLOPES

SLANT PERCEPTION

U SPACE PERCEPTION

SLATS

U LEADING EDGE SLATS

SLEDS

U ROCKET PROPELLED SLEDS

SLEEP

NT HYPNOSIS

Oxygen intake and body temperature of basal and sleeping Andean natives at high altitude
06 p0874 A69-17835

Computer analysis of cortical and subcortical activity in yellow bellied marmot during sleep, hibernation and hypothermia
10 p1643 A69-23122

Space crew performance subsequent to sudden sleep arousal, noting selection between simultaneous and staggered sleep schedules
19 p3263 A69-36453

Human sleep during prolonged rotation, discussing electroencephalograms, acoustic signal frequency producing waking reaction, cutaneous galvanic reflex and deepness of sleep
20 p3472 A69-37261

Sleep habits of radar operators working in alternate crews in radar station on continuous watch
21 p3666 A69-39269

Functional changes of somatosensory pathway from periphery to cortex during rapid eye movement /REM/ and non-REM periods of deep sleep
22 p3872 A69-40161

EEG, ocular movements, gastric mobility and pH during human sleep from data transmitted by swallowed radio transmitter
23 p4093 A69-42063

Human arterial pressure reflex regulation during sleep, assessing baroreflex sensitivity
24 p4257 A69-42626

SLEEP DEPRIVATION

Aircrew fatigue and sleep loss factors, discussing transition through various time zones and flying through normal sleeping times
21 p3666 A69-39275

Prolonged wakefulness effect on human work capacity in isolated chamber, determining physical, intellectual and sensory capacities
22 p3877 A69-40280

Psychological, psychophysiological and biochemical effects of prolonged sleep deprivation in human males, noting transient ego disruption
23 p4099 A69-42195

Hypnotic compounds properties influencing REM /rapid eye movements/ stage, discussing insomnia problems with jet flight crew and passengers
24 p4277 A69-43389

SLEEVES

Glass vacuum systems grease free assembly method using heat shrinkable polyolefin sleeve tubing connector for compression of O ring joints
08 p1320 A69-20529

SLENDER BODIES

Dense plasma with plasma frequency greater than cyclotron frequency, discussing flow past slender bodies
01 p0126 A69-10226

Vortex method within slender body theory for aerodynamic interference between missile in both captive and dropped positions and carrying aircraft
01 p0007 A69-11026

Hall effect in unperturbed flow of fluids near thin profiles at infinity
01 p0132 A69-11133

Transverse curvature effect on skin friction and heat transfer in laminar flows past slender circular cylinders
02 p0232 A69-12210

Lift from unsteady flow past cascade of slender profiles with stagger angle reduced to solution of Fredholm integral equation
02 p0190 A69-12575

Curved bodies substitution in unsteady hypersonic flow past slender sharp nosed bodies within framework of plane sections
02 p0191 A69-12576

Shock waves collision with supersonically moving axisymmetric slender bodies analyzed by integral transform method, noting application to shock-shock interaction
03 p0413 A69-13010

Velocity field generated by shock wave incident on slender symmetrical body resting in infinite compressible medium
03 p0362 A69-13418

Kinematic parameters for elastic slender body aid in description of motion of body
04 p0668 A69-14271

Stokes-like region around yawed needle in hypersonic strong interaction regime, discussing asymptotic analysis under Stewartson conditions
04 p0542 A69-14732

Sting diameter and cylindrical protuberance length effects on base pressure of axisymmetric body in turbulent supersonic flow
05 p0697 A69-15712

Axisymmetric hypersonic flow of model gas over slender bodies with strong viscous interaction and shock wave extended to power law viscosity variation
05 p0744 A69-15720

Model kinetic integral equation for describing flow in transition region at leading edge of tapered body in rarefied gas

05 p0697 A69-16040

MHD aligned flow of compressible fluid past slender body in wind tunnel

06 p0861 A69-17719

Turbulent density fluctuations in near wake of hypersonic axisymmetric slender body measured photometrically with near UV absorption of sulfur dioxide in flow [AIAA PAPER 69-70]

06 p0864 A69-18158

Thin rods and shells elastic analysis, using Cosserat continua for representing bodies in kinematics and balance and constitutive equations

07 p1234 A69-19382

Supersonic flows past slender bodies, calculating pressure by means of moving singularities

08 p1252 A69-20721

Pressure coefficients determination on slender body surface to estimate effects of quadratic terms, considering body of revolution with thin cruciform lifting surfaces

10 p1632 A69-22911

Mean flow measurements in supersonic wake of slender two dimensional body at zero incidence and heat transfer rate, noting predictability from similarity analysis

11 p1817 A69-24281

Slender elastic rod stability under spatial finite deflection, analyzing critical load by using Kirchhoff analogy and gyroscope motion

11 p1970 A69-24609

Unsteady heat conduction of semiinfinite thin rod with mobile end face, ideally insulated lateral surface and convective heat transfer on uninsulated portion

11 p2002 A69-25229

Steady linearized aligned fields flow of collisionless plasma past slender body, noting effect of tensor conductivity

11 p1930 A69-25278

Hypersonic viscous gas flow past thin bodies, deriving equations for interactions between boundary layer and external flow

11 p1820 A69-25472

Axisymmetric detached flow past slender solid of revolution by ideal incompressible fluid at zero angle of attack and with small cavitation numbers

11 p1877 A69-25741

Motion of slender axisymmetric bodies in rotating fluid, relating Long hypotheses to flow reversal and dipole distribution effects on lee waves

13 p2248 A69-28170

Near wake in axisymmetric supersonic flow past slender body with/without base injection, obtaining pressure, temperature, Mach number, velocity and concentration distributions

14 p2389 A69-29017

Hypervelocity reentry simulation problems for slender and blunt bodies, defining significant parameters

15 p2681 A69-30376

Turbulent and transitional near wake of adiabatic slender wedge with and without base injection at Mach 4 in supersonic wind tunnel

16 p2732 A69-31882

Mean near wake flow of adiabatic two dimensional wedge at Mach 4 with tripped turbulent boundary layers and base mass addition

16 p2733 A69-32147

Mixed supersonic/subsonic type steady wake flow fields in flat based slender bodies, using finite difference method

17 p2892 A69-33468

Nonequilibrium, real gas and nose bluntness effects on hypersonic slender body flows, analyzing similitudes, free stream temperature, velocity and relaxation

17 p2894 A69-33501

Rarified gas dynamics of blunt and sharp-jointed slender bodies in supersonic stream and free jet sonic expansion into high vacuum

18 p3123 A69-34924

Vortex breakdown on slender sharp edged and modified delta wings with varying sweep angles investigated in wind tunnel using schlieren system for flow visualization

19 p3237 A69-35644

Nose bluntness effect on hypersonic flow for slender blunt bodies with arbitrarily shaped lateral surfaces at small attack angle

19 p3239 A69-36402

Second order theory for steady or unsteady subsonic flow past slender lifting bodies of finite thickness

20 p3458 A69-37182

Slender profile oscillations in subsonic flow near solid boundary, calculating pressure gradients by dipole method

23 p4058 A69-41713

Laminar boundary layers on slender paraboloids, analyzing skin friction formula and extension for transverse curvature ranges

23 p4152 A69-41904

Supersonic flows around slender bodies calculated by method of moving singularities

23 p4061 A69-42407

Two dimensional diverging flow of ideal compressible fluid past slender profile, using Prandtl-Glauert rule and linearized equation

24 p4243 A69-42584

Velocity and pressure fields produced by deformable load carrying filament studied for unsteady gas motion past slender body with nonpotential external forces

24 p4246 A69-43483

SLENDER CONES

Hypersonic surface measurements and flowfield properties about slender cones in hypersonic viscous interaction regime

[AIAA PAPER 68-2]

02 p0189 A69-12520

Shoulder pressure on slender cone/afterbody combinations in hypersonic inviscid flow of perfect gas

04 p0542 A69-14735

Peculiarities of aerodynamic characteristics of flow past plate and pointed and blunt slender cones in viscous hypersonic thermodynamically ideal gas

05 p0699 A69-16673

Lift drag ratio attainable by optimal transversal contour slender conical lifting body at hypersonic speeds

06 p0861 A69-17640

Free flight static, dynamic stability and drag data for 10 degree semiangle cone obtained at 8-16 Mach numbers

[AIAA PAPER 69-133]

06 p0862 A69-18050

Ballistic range tests to study ablation effects on aerodynamic characteristics of ablating and nonablating slender cones

[AIAA PAPER 69-179]

06 p1036 A69-18083

Spatial distribution of three dimensional laminar boundary layer transition zone on sharp half angle cone from hypersonic wind tunnel tests

[AIAA PAPER 69-12]

06 p0863 A69-18112

Drag coefficients for spheres and sharp cones in rarefied hypersonic air flow obtained in shock tunnel using free flight technique

[AIAA PAPER 69-140]

06 p0865 A69-18184

Nonequilibrium three dimensional boundary layer over slightly yawed cone analyzed for air dissociation and ionization parameters, noting binary scaling application

09 p1430 A69-21965

Electromagnetic plane wave scattering from slender semiinfinite cone, obtaining contribution to tip return arising from direct diffraction

11 p1836 A69-24988

Mass transfer cooling data correlation for estimating mass injection effect on slender cone drag

13 p2199 A69-28224

Unsteady pressure on oscillating slender cone in hypersonic flow derived by expanding flow equations in powers of shock density parameter

14 p2389 A69-29020

Flow field around sharp slender cones with surface mass transfer at zero angle of attack in low density supersonic and hypersonic flow

[AIAA PAPER 68-66]

16 p2732 A69-31887

Mach number, cone angle, bluntness and wall to recovery temperature ratio effects on slender cones boundary layer transition measurements at hypersonic speeds

17 p2890 A69-33250

Hypersonic slender cone zero angle of attack drag in rarefied continuum and noncontinuum flow in shock tunnel, indicating body dimension influence in transition regime

[AIAA PAPER 69-711]

17 p2891 A69-33445

Hypersonic boundary layer transition on blunt slender cones at M equal 10 obtained independent Reynolds number

[AIAA PAPER 69-705]

17 p2954 A69-33455

Nonuniform heating rates during laminar boundary layer transition on slender cone at hypersonic speeds

18 p3085 A69-34435

Monte Carlo simulation for studying rarefied hypersonic gas flow about slender cones and flat plates

20 p3459 A69-37902

Three dimensional laminar boundary layer hypersonic flow about slender conical vehicles, analyzing transverse surface curvature effect, studying Reynolds number, cone angle, etc

[ASME PAPER 69-FE-23]

20 p3460 A69-37992

Fluid mechanical structure of laminar hypersonic wake behind sharp circular cone, investigating flow field at zero angle of attack and adiabatic wall temperature

24 p4247 A69-43576

Hypersonic viscous interaction, studying axisymmetric flow over slender sharp nose cones at zero angle of attack and three dimensional flow over sharp flat plate

24 p4248 A69-43579

Radiation equilibrium temperature measured downstream of transpiration cooled gas flow near slender cone vertex in continuous flow hypersonic tunnel

24 p4248 A69-43588

Free flight telemetry base pressure measurements on slender cones and domed afterbodies in hypersonic laminar flow, using shock tunnel test facility

[AIAA PAPER 68-698]

24 p4249 A69-43675

Pressure distribution correlation over blunt slender cone at various angles of attack by tangent cone method, describing hypersonic wind tunnel tests

24 p4249 A69-43681

SLENDER WINGS

Test of similarity theory of leading edge vortices above slender wings in subsonic conical flow

04 p0543 A69-14820

Slender wing theory extension to not-to-slender wings approached as singular perturbation problem, using matched asymptotic expansions method

04 p0544 A69-14891

Vortex motion of separated flow from slender wings and rotor loading, discussing computer role in low speed aerodynamic research

05 p0696 A69-15562

Zhukovskii lifting force theorem application to slender wing profile and airfoil lattice in linearized supersonic flow

05 p0697 A69-16023

Lifting force and moments acting on slender wing of finite span and arbitrary planform moving at constant mean velocity in unsteady flow

06 p0858 A69-17338

Aerodynamic properties calculations of arbitrary slender supersonic wings using sum of simple integrals

15 p2548 A69-31170

Three dimensional velocity field disturbed by shock wave traveling across slender wing at supersonic speed

19 p3242 A69-36797

SLIDING

Stress fields in Hertzian contact of parallel cylinders composed of anisotropic materials and transversely isotropic spherical bodies

08 p1414 A69-20524

Runways slipperiness and grooving, discussing influence of wetness, tire form and speed on friction coefficient

10 p1674 A69-23707

Sliding behavior of nonmetallic bearing materials /plastics, ceramics and cermets/, discussing non-lubricated bearing application

14 p2454 A69-28851

Slide methods for duplex parallel and switchover redundant mission availabilities based on cost, reliability and maintainability

18 p3147 A69-34531

Linear oscillations of sphere in compressible viscous fluid with slip at surface, noting drag variation

19 p3297 A69-35836

Optimal sliding regimes for controlling dynamic systems, proposing control parameters system extension

21 p3768 A69-39826

SLIDING CONTACT

Microslip between concentrated contacts and design charts for maximum pressure, closing-in of contacting bodies and optimized shapes, giving computer programs

15 p2629 A69-30903

Stochastic model extension of interface temperature of solids in sliding contact to include transients, noting interface activities dependence

22 p3955 A69-40404

SLIDING FRICTION

Surface fatigue significance in sliding wear studied from damage on copper single crystal using electron microscope techniques

01 p0085 A69-10368

Sliding surface tracks from hardened steel sliders on flat PTFE examined for molecular orientation with electron microscope

01 p0085 A69-10369

Friction and wear behavior of mechanical face seals, considering techniques and lubricants for increasing product of pressure and sliding velocity

02 p0253 A69-12160

Idealized slider bearings with Maxwell liquid as lubricant, analyzing elasticity effects on pressure, load capacity and friction

02 p0253 A69-12413

Metal strip angled profile shaping by sliding application of forces with draw plate, analyzing friction effect with thin plastic shell engineering theory

03 p0432 A69-12962

Grain boundary sliding influence on gross mechanical behavior and stress distributions, emphasizing creep behavior

03 p0450 A69-13882

Stability of high speed rotors with sliding bearings

04 p0607 A69-15163

Dry sliding friction and wear in ultrahigh vacuum, emphasizing slip rings and brushes for space applications [IME PAPER 7]

07 p1138 A69-18561

Surface preparation effects on Ni-Cr-Fe alloy boundary friction studied by repeated sliding of cylinders on hard Pd-Pt-Au alloy cylinder [ASLE PREPRINT 68AM 6D-4]

07 p1139 A69-18625

Friction and wear tests of synthetic rutile single crystals against diamond styli and spherical sliders of ruby, sapphire and hardened steel [ASLE PAPER 68-LC-3]

07 p1140 A69-19307

Sliding friction technique to determine contact area and surface microtopography between abraded metals and polymers

08 p1319 A69-19994

Hypersonic slipper bearing problem in rocket boosted sleds, discussing flow model consisting of laminar stagnation region and boundary layers [AIAA PAPER 68-736]

09 p1477 A69-22003

Wear and friction properties of nylon and polyethylene sliding over unlubricated steel, considering adhesion theory

11 p1892 A69-25021

Fatigue strength reduction in Ti alloy in sliding friction contact with metallic materials caused by fretting corrosion

12 p2113 A69-26125

Calculated and experimental surface wear damage data correlated for materials under friction conditions

15 p2618 A69-30106

Unlubricated wear characteristics of polyimide resin sliding against carbon steel in air, noting effects of surface temperature, bearing pressure and velocity [ASLE PREPRINT 69AM 5C-2]

15 p2619 A69-30473

Gas turbine engine shaft face seal with self acting lift augmentation preventing rubbing contact, noting disadvantages of labyrinth and conventional seals [ASLE FICFS PREPRINT 27]

15 p2621 A69-30492

Corrosive wear due to atmospheric O in sliding metal systems, noting oxidation rate relation to wear rate and activation energy [ASLE PAPER 68-LC-11]

15 p2622 A69-30605

Sliding friction tests of Cu and Cu-Be alloy plates in contact with various alloy sliders in air and vacuum [ASLE PAPER 68-LC-5]

15 p2622 A69-30610

Boron effect on sintered porous Ni friction at high sliding velocities and temperatures, analyzing oxide film destruction restraint by decreased Ni plasticity

15 p2641 A69-31187

Sliding friction and wear properties of metal ceramic composites applied to aircraft brakes

17 p2987 A69-33375

Jet aircraft runway friction due to mud and water noting relation to takeoff length

17 p2903 A69-34216

Solid solutions atomic ordering effect on friction and wear in vacuum, using CuAu and FeCo systems

18 p3149 A69-35183

Friction coefficient and elastic deformation magnitudes relation in polyurethane during sliding friction in various liquids/lubricants

18 p3149 A69-35362

Full circle Be brake disks in C-5 aircraft, discussing properties at elevated temperature and fastening of friction lining

18 p3095 A69-35424

MHD pivoted slider bearing with convex pad surface under azimuthal magnetic field

21 p3733 A69-39744

Electrical sliprings assembly development with low dynamic resistance and long lifetime for space simulation testing, noting wear rate of rings and brushes [AIAA PAPER 69-1035]

22 p3925 A69-40402

Seizing characteristics of metals using electrical resistance as measure of lattice imperfection density due to friction

22 p3957 A69-41111

Pressure distribution in gas lubrication layer of infinite radial sliding bearings, approximating differential equation by simple formulas

23 p4168 A69-41412

Elastohydrodynamic lubrication of cylindrical rubber surface sliding over glass plate, using optical interference technique

23 p4171 A69-42531

SLIP

Slip geometry in bcc metals, discussing slip-line observations by light and electron microscopy techniques

05 p0781 A69-16537

Fcc metals cyclic deformation and fatigue dependence on cross slip of screw dislocations, considering strain hardening and crack propagation

11 p1906 A69-25389

Longitudinal modulus of interlaminar slip during creep of fiberglass reinforced plastic determined by bending tests of beams under concentrated force

18 p3163 A69-35365

Cage and roller slip in high speed roller bearings over steady radial loads by measurement and theory

20 p3547 A69-37066

Deformation localization and slip functions in statistical theory of plasticity, discussing approximations and untenability of Yosimura theory criticism

22 p4044 A69-40742

Relative slip effect on fretting fatigue strength, deriving stress initiating fatigue cracks

24 p4404 A69-43628

SLIP BANDS

U EDGE DISLOCATIONS

SLIP CASTING

Slip casting powder mixture of zirconium carbide and tungsten, discussing optimum composition

10 p1716 A69-24056

SLIP FLOW

Argon flow characteristics in converging nozzle in continuum, slip and free molecular regimes [ASME PAPER 68-WA/FE-9]

05 p0698 A69-16089

Slip flow problem for general specular-diffuse boundary condition in kinetic theory of gases, noting molecular distribution function

11 p1869 A69-24893

Navier-Stokes equations for compressible gas, generalizing viscous channel flow of heat conducting gas to slip flow of rarefied gas

12 p2061 A69-25887

Gas molecular mean free path effect on performance of spiral grooved thrust bearing, discussing slip flow factor and He Knudsen number [ASME PAPER 68-LUBS-17]

13 p2266 A69-27273

Argon flow characteristics in converging nozzle in continuum, slip and free molecular regimes [ASME PAPER 68-WA/FE-9]

14 p2390 A69-29445

Fringing effects on electric efficiency variation with slip for cylindrical induction MHD device operable as accelerator, generator or Joule heater [AIAA PAPER 67-714]

16 p2736 A69-32152

SLIPPERS

U SHOES

SLIPSTREAMS

NT PROPELLER SLIPSTREAMS

Supersonic jet impingement on flat plate, showing shock wave profiles and slipstream surface at stations parallel to nozzle axis

08 p1252 A69-20841

Flow phenomena associated with electrically conducting boundary layer jet injection through slot into uniform slipstream in presence of transverse magnetic field

14 p2501 A69-29917

Aerodynamic characteristics of turbulent twisted jet in slipstream in open jet wind tunnel, determining static pressure, temperature and velocity component profiles

21 p3645 A69-39848

Jet dynamic characteristics injected into supersonic air slipstream incident on flat body, calculating configuration, shock wave geometry and parameters distribution in flow field

24 p4250 A69-43710

SLOPES

NT GLIDE PATHS

Slope optimization of antenna array difference radiation patterns coinciding with antenna directive gains

06 p0895 A69-17461

Radio source counts log N-log S diagram slope uncertainty due to finite source number, discussing statistical analysis methods accuracy

08 p1383 A69-20048

Parallel flow of viscous liquid film with free surface down inclined plane, noting growth of initially infinitesimal amplitude waves and finite amplitude wave stability

11 p1869 A69-24891

Regional slope measurement from two monoscopic radar images of same terrain area, discussing accuracy and applications to geomorphology and hydrology

15 p2610 A69-30710

Slope optimization of antenna array difference radiation patterns coinciding with antenna directive gains

20 p3508 A69-37944

SLOSHING

U LIQUID SLOSHING

SLOT ANTENNAS

Radiation pattern shaping from circular aperture antenna with constant illumination amplitude [UN PAPER 68-95756]

01 p0029 A69-10524

Dual band shunt slot linear array for S and X band radiation patterns generated from single aperture

02 p0219 A69-12344

Impedance sheet approximation to plasma slab, considering plane wave propagation, plasma covered slot antenna and transmission loss

02 p0209 A69-12348

Diffraction coefficient for higher order edge-edge interaction terms in two dimensional diffraction by narrow slit and small circular aperture

03 p0396 A69-13631

Input impedance of slot antenna in primary resonance region

04 p0577 A69-14784

Difference radiation patterns of circular aperture with axisymmetric amplitude distribution

05 p0717 A69-15636

Backfire log periodic cavity-backed slot array, giving H plane power patterns with near field plots along array

08 p1281 A69-20035

Center feed system for broadening frequency bandwidth in X-band edge slotted waveguide array antenna

08 p1286 A69-20836

Air gap tolerances effect on admittance of TEM mode dielectric and plasma coated slot antennas determined by variational method

11 p1851 A69-24986

Radiation pattern of axial slot on circular conducting cylinder based on wedge diffraction and creeping wave theory

11 p1836 A69-24993

Complete electric field of idealized infinite slot antenna with uniform excitation in infinite conducting plane

11 p1851 A69-24994

Radiation pattern as function of asymmetry in amplitude of secondary source excitation by primary aperture antenna

11 p1852 A69-25117

Far field radiation pattern, radiation resistance, power gain, directivity and effective aperture for center feed dipole antenna with feed points displaced arbitrarily

12 p2039 A69-26352

Difference radiation patterns of circular aperture with axisymmetric amplitude distribution

16 p2754 A69-32494

Swept frequency microwave measurements in simulated reentry environments using dielectric layers, glow discharge plasma and aperture antenna-plasma layer model [AIAA PAPER 69-701]

17 p2920 A69-33461

Reciprocal theorem for obtaining relations between transmitting antenna effective area, radiation pattern and aperture distribution

19 p3281 A69-35765

Geometrical configuration for synthetic aperture terrain imaging radar scanning system, noting scanning methods in range and azimuth directions

20 p3489 A69-37634

Synthetic aperture radar principles, using periodic pulse modulation to construct terrain imaging radar

20 p3489 A69-37635

Normalized SNR of aperture antennas determined in terms of random signal and noise fields correlation functions

20 p3494 A69-37845

Equatorial radiation pattern of parallel plate TEM mode axial slot on elliptical conducting cylinders, using wedge diffraction and creeping wave theory

22 p3914 A69-40703

Edge diffraction effects in TEM axially slotted finite ground plane on radiation pattern in waveguides of different geometries

23 p4116 A69-41588

Simple antenna with good circular polarization over wide space sector, showing geometry, normalized orthogonal field distributions and beamwidth range, considering slot combinations

23 p4137 A69-41590

Slot antenna radiation patterns in presence of aperture RF plasma breakdown sheath measured for various gas pressures and breakdown power levels

23 p4116 A69-41595

Synthesis of antenna arrays of longitudinal passive slot radiators on metallic cylinder excited by single active slot, including experimental patterns

23 p4138 A69-41936

Directional couplers applied to excitation of non-protruding surface wave antennas, examining ridge slot system

23 p4139 A69-41946

Antenna losses produced by metal space frame radome determined by considering end effects, member junctions circulating currents, mutual scattering and near field effects

23 p4149 A69-42127

Beam wave propagation in conducting hollow circular cylinder applied to shielding cylinders design for aperture antenna transmission

24 p4282 A69-42987

Asymmetric metal flanges effect on beam tilt of aperture antennas

24 p4288 A69-43765

SLOTS

Incompressible two dimensional potential flow analysis with compressibility effects for thick highly cambered multibodies in cascade, noting slotted compressor blade performance

[ASME PAPER 69-GT-6] 09 p1432 A69-22507

Asymmetrical waves diffraction field at wide slots in circular waveguides determined in Huygens- Kirchhoff approximation

15 p2570 A69-30955

Circulation controlled rotor aerodynamics with tangentially ejected air from surface slots of lifting body, noting performance at advance ratios and thrust coefficients

18 p3089 A69-35232

Rectangular waveguides coupled by oblique subresonant slots in common face, discussing slot orientation and geometry roles

23 p4123 A69-41941

Electromagnetic wave propagation in rectangular and plane parallel waveguides coupled by common wall with periodic transverse slots

23 p4124 A69-42037

Slot type jet interaction flow tests at free stream Mach 4 and 5, describing equipment, procedure and results

24 p4249 A69-43686

SLOTTED ANTENNAS

U SLOT ANTENNAS

SLOTTED WIND TUNNELS

Optimal V/STOL wind tunnel through interference study of slotted tunnel walls, including porosity and height to width ratio effects

[AIAA PAPER 69-171] 06 p0908 A69-18203

Subsonic wind tunnel solid and ventilated wall interference on air flow around aerodynamic models, discussing data corrections and slotted wall tests

[AIAA PAPER 68-360] 12 p2059 A69-26766

SLOW NEUTRONS

U THERMAL NEUTRONS

SLUDGE

Protective layer material for high sludge capacity filters for fine purification of liquids used in aircraft hydraulic system

22 p3869 A69-40637

SLUSH

Drag and spray effects due to slush and water on runways during aircraft takeoffs

01 p0011 A69-11048

Slush hydrogen for spacecraft propulsion, discussing fabrication, conservation and storage

17 p3017 A69-33339

Slush H and N gels preparation and characteristics, including measurements of weight bearing capacity of gel as function of percent mass silica gelant

22 p3998 A69-40632

SLV [SOFT LANDING VEHICLES]

U SOFT LANDING SPACECRAFT

SMALL PERTURBATION FLOW

Three dimensional flow at large distance and in front of shock wave for three dimensional body traveling at sonic velocity

01 p0005 A69-10159

Linear stability of parallel flow in concentric annulus for infinitesimal axisymmetric disturbances

01 p0061 A69-11201

Matched asymptotic expansions method applied to magnetic field induction in thin toroidal wire and flow past circular cylinder at small Reynolds number

07 p1180 A69-18811

Thin spherical layer flow stability with respect to small disturbances, showing unsteady motion above critical Reynolds numbers and secondary flow features

11 p1875 A69-25486

Small disturbances distribution in flow parameters along two dimensional combustion zone of finite width using thermal diffusion theory

14 p2537 A69-28986

Linear small perturbation approximation for supersonic nonequilibrium flows past oscillating airfoil in two dimensional wind tunnel, noting Laplace transform solution

23 p4061 A69-42349

SMEAR

Alphanumeric characters to identify radar targets on PPI display for air traffic control, considering technique for reducing smear

09 p1495 A69-21675

SMELL

U OLFACTORY PERCEPTION

SMITH CHART

Book on Smith chart electronic applications in waveguide, circuit and component analysis and synthesis

22 p3915 A69-40780

SMOKE

Polarization of laser radiation scattered forward and back in artificial fog and smoke

03 p0393 A69-13275

Gas turbine engines smoke emission, considering smoke measurement, flame structure, carbon production, pressure effects fuel-air ratio, etc

09 p1573 A69-22622

Polarization of laser radiation scattered forward and back in artificial fog and smoke

14 p2410 A69-28783

Short laser pulses reflection from artificial fog and smoke, showing dependence on reflecting medium attenuation coefficient

15 p2562 A69-30077

Noise abatement and smoke emission reduction from aircraft engines

[AIAA PAPER 69-489] 16 p2746 A69-32764

Gas turbine engines smoke reduction, aerated fuel sprays for smoke control on engine design and factors affecting visibility of exhaust plumes

17 p3020 A69-33350

Karman vortex street formation indicated by smoke visualization method study of laminar wake behind single cylinder

21 p3644 A69-38687

SMOKE ABATEMENT

Low smoke emission combustors for aircraft turbine engines, discussing effects on ignition and exit temperature distribution

[AIAA PAPER 69-493] 19 p3394 A69-36299

SMOKE TRAILS

Aerated fuel spray effect on smoke reduction from high pressure ratio aircraft gas turbine engines, including smoke measurement and visibility

19 p3395 A69-36770

SMOOTHING

NT DATA SMOOTHING

Differentiability of fundamental solution to elliptic equations based on exact theorems of smoothness

01 p0106 A69-10955

SMS

U SYNCHRONOUS

SATELLITE

METEOROLOGICAL

SLAKING

U LATERAL OSCILLATION

SNAP

U SPACE POWER UNIT REACTORS

SNAP 8

SNAP 8 developmental reactor vacuum system providing space environment simulation for nuclear reactor ground testing

13 p2241 A69-28086

SNAP 10A

Zirconium hydride thermoelectric power system for space missions, discussing compactness, shield weight, temperature capability, reliability and SNAP 10A program

16 p2809 A69-31723

SNAP 13

SNAP 13 generator designs to develop technology for isotope heated thermionic converters, describing tests, efficiencies, power outputs and life times

14 p2481 A69-29191

SNAP 21

SNAP 21 radioisotope powered thermionic generator with multiple couple Pb-Sn-telluride/Bi-Sb-telluride flat plate configuration for deep sea applications

23 p4069 A69-42248

SNAP 27

Aerothermal-structural reentry safety evaluation for SNAP-27 radioisotope Graphite Lunar Module Fuel Cask at orbital and superorbital velocities

[AIAA PAPER 68-1166] 03 p0465 A69-13561

Aerothermal-structural reentry safety evaluation for SNAP-27 radioisotope Graphite Lunar Module Fuel Cask at orbital and superorbital velocities

[AIAA PAPER 68-1166] 22 p3979 A69-40551

SNAP 27 radioisotope thermoelectric generator system designed as prime power supply for Apollo lunar surface experiment package [ALSEP]

23 p4187 A69-42249

SNATCHING

U SPACECRAFT RECOVERY

SNOW

Bidirectional reflectance of solar radiation and IR temperature data from Nimbus 2 satellite to differentiate clouds above snow surfaces

15 p2596 A69-30455

Satellite photography for snow cover mapping and depth estimation

18 p3167 A69-35084

SNOWFLOW EFFECT

U PLASMA DYNAMICS

SOAPS

Concentration, flow rate and tube diameter effects on viscous drag reduction in nonpolar soap solutions, using pressure drop measurements to observe turbulent flow behavior

17 p2951 A69-33253

SOCIAL FACTORS

Aerospace technology role in economic and social benefits

[UN PAPER 68-95321] 01 p0178 A69-10467

Aerospace management technology transferability to problems of society and government

02 p0355 A69-11754

National tasks in civil aeronautical research and development noting technological and social factors

08 p1422 A69-20171

Man machine integration, detailing sensory input and motor /or output/ systems, control loop and social structure impact

11 p1831 A69-25656

Engineer performance related to organizational factors, discussing colleague contact, work diversity, number of subordinates and involvement in work

15 p2721 A69-31069

Legal, social and physical effects of supersonic flight, discussing damage claims validity and recovery resulting from breaking of sound barrier

17 p3075 A69-32841

Space, technology and society - Conference, Cocoa Beach, Florida, March 1969, Volume 2

18 p3233 A69-35055

Space, technology and society - Conference, Cocoa Beach, Florida, March 1969, Volume 1

18 p3234 A69-35070

Social entrainment of feeding rhythms in Rhesus monkeys with light, temperature and sound held constant

24 p4260 A69-42704

Bigemini pattern in baboon social behavior, noting diurnal rhythm independence from social deprivation, light cycling and food supply

24 p4260 A69-42705

Feedback effects and social facilitation of human vigilance performance, evaluating mere coaction vs potential evaluation

24 p4271 A69-42751

SOCIAL ISOLATION

Daily sleep and wakefulness periodicity changes effect on heart rate, respiration and body temperature diurnal rhythms in human males under isolation conditions

03 p0377 A69-14203

Leisure time and recreation facilities during long duration space missions, discussing astronaut selection procedure, active recreation, passive enjoyment and exercise programs

06 p0880 A69-17209

Social isolation and other sensory deprivations effects on human organism 08 p1263 A69-19937

Underwater experiment to determine man capability to perform scientific mission during 60 days isolation, noting task performance, social interaction and personal adjustment 08 p1300 A69-20113

Barbamyl effect with and without somatotropic hormone injection in mice during prolonged isolation and hypokinesia, noting sleep duration 10 p1646 A69-23576

Isolation of scientific and technical personnel and effect on lateral communication and intellectual cross fertilization in research and development program 11 p2004 A69-25303

Closed life support systems tests, describing effects of long term /one year/ confinement of three human subjects 13 p2216 A69-28612

Social and visual isolation effect on rat blood pressure, pulse pressure, heart rate, behavior and response to epinephrine 14 p2407 A69-29296

Cardiovascular system, neuromuscular activity and mental fitness of subjects performing physical and mental assignments with prescribed work-rest schedule during confinement 17 p2906 A69-32936

Desynchronization and resynchronization of human circadian rhythms of activity, body temperature and urine excretion during isolation in underground bunker in various conditions 21 p3660 A69-39173

Subjects confined in caves for two to six months to note physiological rhythms time evolution and associated desynchronization and resynchronization 23 p4107 A69-41818

Physiological circadian rhythms in isolated and nonisolated Macaca Nemestrinas living under varied light intensities, noting telemetered deep body temperature, urine volume and sodium, etc 24 p4261 A69-42707

SOCIAL PSYCHIATRY

Flying safety and human factors relationships from job classification survey oriented toward social psychology 06 p0884 A69-18035

Military flying career choice as neurotic compensation for personality defects, stressing personality screening during interview 12 p2023 A69-26492

SOCIOLOGY

NT SOCIAL FACTORS

National programs relationship to progress in technological societies 03 p0536 A69-14245

UFOs from sociological viewpoint, stressing need for international cooperation in exobiological research 17 p3076 A69-32974

Technology and social progress - ASS Conference, Washington, D.C., March 1968 17 p3076 A69-34039

Technical communication patterns in R and D laboratories, discussing effects of work structure, social relations, etc 20 p3640 A69-38019

Universities and public service education noting NASA requirements and programs 20 p3641 A69-38282

Ecological foundations of Haley metalaw and implications of interstellar golden rule, discussing social interaction with alien life forms 23 p4240 A69-41304

SODIUM

NT LIQUID SODIUM

Seasonal variation of evening-morning difference in maximum density heights of twilight sodium layer 01 p0063 A69-10275

Automatic remotely operated sodium D line reversal temperature measuring apparatus, analyzing systematic errors 06 p1035 A69-17932

Intrarenal capillary hydrostatic pressure effect on hemodynamically induced changes in sodium excretion 07 p1063 A69-18629

Two stage sodium thermal reduction of Ti tetrachloride to metallic Ti, determining process parameters 07 p1164 A69-18785

Photoionization cross section measurements for sodium line by analyzing electron-ion recombination radiation from sodium seeded plasma, determining electron temperatures and concentrations 07 p1184 A69-19164

Flame emission spectrophotometric method for ultraminate sodium contamination detection in thin silicon oxide films and cleaned silicon surfaces [ECS PAPER 306] 08 p1314 A69-20367

Atmospheric sodium measured at night by tuned laser radar, giving average column number density 09 p1484 A69-21464

Physical factors affecting proximal and distal tubular sodium reabsorption in dogs undergoing water diuresis 13 p2210 A69-28482

Sodium atoms and NO molecules role in atomic O 6300 and 5577 A emissions in comet Mrkos 1957d due to charge exchanges and dissociative recombination 14 p2523 A69-29707

Partial wave description for calculating cross sections of fine structure transitions of Na in collision with He, discussing shape resonances 15 p2655 A69-30198

Number and mass of sodium atoms in comet Ikeya-Seki 1965f head calculated from spectral observations, ascribing D lines to resonance scattering of photospheric radiation 15 p2685 A69-30526

Time resolved Stark broadened spectral profiles for Na I 5882-88 A and 4978-82 A lines of plasma, comparing electron densities 15 p2656 A69-31155

Aldosterone and hydrocortisone introduced into bladders of adrenalectomized dogs to restore sodium metabolism contributing to normal water-salt homeostasis 21 p3656 A69-38965

Free Na atoms production for spectral line reversal procedure, facilitating procedure by replacing NaCl, NaI and chromium carbonyl by sodium azide 24 p4297 A69-43589

SODIUM AZIDES

Free Na atoms production for spectral line reversal procedure, facilitating procedure by replacing NaCl, NaI and chromium carbonyl by sodium azide 24 p4297 A69-43589

SODIUM CARBONATES

Motion sickness prophylactic action of sodium hydrocarbonate in dogs subjected to vertical accelerations, using intravenous administration 20 p3473 A69-37269

SODIUM CHLORIDES

Titanium alloy stress corrosion behavior in atmospheric salt environments at elevated temperatures related to aircraft engine part failures 01 p0099 A69-11056

Proton energy distributions for passage through NaCl, KCl, KBr, Si and Ge single crystals at various angles relative to /100/ and /110/ crystallographic planes 01 p0140 A69-11009

Properties of superdense NaCl plasmas as model working substance for MHD generator, discussing ion concentration and collisions, charge reversal and conductivities 10 p1739 A69-23493

Substructural patterns of epitaxial PbTe films obtained by condensation of vaporized PbTe on NaCl crystal surfaces, discussing formation kinetics and morphology 12 p2144 A69-26675

Stress corrosion in smooth and prenotched maraging steels exposed to sodium chloride solution and natural sea water 14 p2467 A69-29940

Hyperfine spectrum analysis of NaCl at low field using molecular beam electric resonance method, discussing Hamiltonian function representation 16 p2815 A69-32794

Electrode potentials of pure metals, Ni-Cr and Ni base alloys in molten salts applied to corrosion studies 17 p2990 A69-33650

SODIUM COMPOUNDS

NT CRYOLITE

NT NEPHELINE

Temperature dependent far IR absorption of ferroelectric sodium nitrite, discussing single and multiphonon processes 03 p0490 A69-13940

Nonlinear optical properties of barium sodium niobate in ferroelectric tetragonal phase above room temperature, noting spontaneous parametric emission 09 p1515 A69-21354

SODIUM D-LINE

U D LINES

SODIUM ISOTOPES

Pionic 2p-1s X ray transition energy and natural linewidth and muonic 2p-1s X ray transition energy measurements for Na 23 01 p0122 A69-10035

Quadrupole splitting of Na 23 nuclear magnetic resonance /NMR/ to investigate spontaneous polarization, coercive field and domain characteristics in Rochelle salt ferroelectric phase 09 p1559 A69-22283

SODIUM VAPOR

Electron density in arc discharge between carbon electrodes and in discharge with Na vapor, noting relation to temperature and current 01 p0128 A69-10433

Initial production of metallic gases associated with sporadic E layers by processes other than vaporization or photodissociation, discussing Na atom production mechanisms 01 p0071 A69-11167

Rocket observations of ionospheric E layer winds using Na release method 20 p3529 A69-37796

Turbulent field structure between 90-120 km estimated from sodium clouds diameters variation ejected from rockets 21 p3713 A69-38524

Heat transfer capability and startup behavior of sodium heat pipes, studying heat transfer limit due to vapor velocity at evaporator end [ASME PAPER 69-HT-21] 24 p4412 A69-43547

SODIUM 22

Na 22 and H 3 production rates determined in stone meteorites exposed to 3 Gev isotropic protons, using radionuclide distribution data of exposed thick stone target 19 p3425 A69-36423

SOFT LANDING

Constant thrust deceleration formula for gravity turn soft landing maneuvers expressed in elementary and trigonometric functions of initial conditions for descent 02 p0335 A69-12531

FM/AM telemetry circuits with three axis piezoelectric accelerometer for measurements during impact tests of soft landing models 10 p1654 A69-23279

Spacecraft horizontal maneuvers in homogeneous gravitational field to achieve soft landing on planetary surface, including optimal liftoff and orbital transfer 13 p2356 A69-27685

Cylindrically shaped projectiles low velocity impact upon horizontal surface of dry commercial Ottawa sand mass, estimating penetration for soft landing 21 p3839 A69-39231

Fuel-time optimal retrothrust control for vertical and gravity turn ballistic trajectories of soft landing nonlifting bodies based on Pontryagin principle [AIAA PAPER 69-868] 21 p3809 A69-39394

SOFT LANDING SPACECRAFT

NT AEROSPACEPLANES

NT APOLLO SPACECRAFT

NT GEMINI SPACECRAFT

NT LANDING MODULES

NT LUNAR LANDING MODULES

NT LUNAR MODULE

NT MARS EXCURSION MODULE

NT MERCURY SPACECRAFT

NT SURVEYOR LUNAR PROBES

NT SURVEYOR 1 LUNAR PROBE

NT SURVEYOR 5 LUNAR PROBE

NT SURVEYOR 6 LUNAR PROBE

NT SURVEYOR 7 LUNAR PROBE

NT VOSKHOD 1 SPACECRAFT

NT VOSKHOD 2 SPACECRAFT

NT VOSKHOD MANNED SPACECRAFT

Multiengine Martian soft lander guidance and control system design with single engine failure accommodation based on six degrees of freedom computer simulation 02 p0277 A69-11740

Direct analysis of lunar surface chemical composition, considering soft landing probe and X ray isotope fluorescence method 11 p1832 A69-24629

Vehicles for lunar surface exploration and transportation including flying machines and wheeled vehicles 13 p2352 A69-27908

SOFTENING

Cycle dependent fatigue hardening and softening of metals in terms of crystal structure and stress amplitude 01 p0165 A69-10133

Phase softening transformations heat resisting alloys during cyclic heating, using X ray and electron microscope analyses 21 p3746 A69-38957

Alloy softening in bcc Fe-N and Fe-Ni, discussing causes of thermal stress component reduction in interstitial and substitutional alloys 22 p3969 A69-40164

Solid solution softening in bcc alloys, discussing alloy atoms intervention in low temperature deformation process
22 p3969 A69-40165

Bcc metals strengthening and alloy softening mechanisms, studying temperature and additives effects
22 p3970 A69-40166

SOFTWARE [COMPUTERS]
U COMPUTER PROGRAMS

SOIL MECHANICS
Correlating IR lunar nighttime temperature and bearing strength of lunar materials, using expressions of thermal conductivity and bearing strength of porous media in vacuo
20 p3613 A69-38248

Lunar morphology evolution by dust transport on surface, discussing possibility of fluidization
23 p4221 A69-42392

SOIL SCIENCE
Soil resistivity survey at earth telecommunication installation site to determine optimal grounding or electrode system
07 p1117 A69-19348

Bioorganic comparative analysis of desert soils, Precambrian shales and meteorites by automated pyrolysis-gas chromatography-mass spectrometry system for future Mars soil analysis [JPL-TR-32-1368]
11 p1832 A69-25640

Sterile soil from Antarctica found to contain organic carbon, noting significance for biological exploration of Mars
16 p2746 A69-31552

Lunar surface bulk density determined from laboratory and spacecraft measurements of static bearing capacity as functions of depth and solids percentage
18 p3193 A69-34366

Urease activity determined by using C 14 urea in stored, preserved /Permafrost/ and irradiated soils
18 p3095 A69-34543

Consecutive reaction equations for idealized soil column solved for nitrifying metabolite concentrations as functions of time and depth
19 p3264 A69-35606

Adenosine triphosphate /ATP/ content of terrestrial soils, based on firefly bioluminescent reaction, for Mars soil problems
20 p3473 A69-37567

Environmental neutron flux measured by various techniques, studying effects of soil and moisture on density
22 p4002 A69-40094

SOILS
NT ANDESITE
NT BASALT
NT BRECCIA
NT COAL
NT ECLOGITE
NT ENSTATITE
NT GRANITE
NT IGNEOUS ROCKS
NT LAVA
NT LUNAR DUST
NT LUNAR SOIL
NT MAGMA
NT MOLDAVITE
NT OLIVINE
NT POLYURETHANE FOAM
NT POROUS MATERIALS
NT PYROXENES
NT QUARTZ
NT ROCKS
NT SANDS
NT SANDSTONES
NT SHALES

Pedoscope use in soil microbiological studies including ecology, infection susceptibility, etc
01 p0021 A69-11092

Plant and soil thermal behavior for various conditions of crop species, plant spacing, tillage, irrigation and aerial thermal scanner imagery
12 p2075 A69-26989

Microwave radiometric brightness temperature relationship to soil moisture content for estimating bearing strength
12 p2099 A69-27008

Gravitational fields and atmospheric pressure effects on soils subjected to static and dynamic loading, using aircraft parabolic gravity simulation [AIAA PAPER 69-1009]
22 p3921 A69-40382

SOLAR ACTIVITY
NT FACULAE
NT SPICULES
NT SUNSPOTS

Solar and geophysical activity during February 1965 and March 1966 indicating geomagnetic activity on 27-day recurrence diagram
01 p0068 A69-11118

Solar X-ray high activity level during spring 1966 connected with gamma type magnetic solar regions and correlated with ionospheric effects
01 p0146 A69-11119

Solar, interplanetary and magnetospheric electromagnetic events before and during magnetic storm from ground observatory and earth satellite data
01 p0156 A69-11120

Chromospheric and photospheric solar observations made in Belgium in 1967, noting heliographic sunspot latitudes
02 p0313 A69-11533

Longitudinal distribution of cycle sunspots in initial phase of solar activity from Greenwich Observatory data
02 p0314 A69-11647

Solar and galactic cosmic rays measurement data to investigate variation in time of relations between cosmic rays modulation amplitude and solar activity variations
02 p0306 A69-11658

Radio emission fluxes in solar active regions, determining slope of spectral characteristics of radio sources from effective emission center
02 p0314 A69-11676

Relation between solar activity and cyclic variation of pearl pulsations excitation frequency during sunspot cycle
02 p0239 A69-11696

Charts summarizing daily solar phenomena, cosmic rays, geomagnetic variation, ionosphere, radiowave propagation and airglow observations in Japan
02 p0315 A69-11732

Primary cosmic radiation charge spectrum measurement during 1965 minimum solar activity, using balloon-borne Cerenkov scintillation counter
02 p0308 A69-12043

Book containing 1960-1965 /including IQSY/ chronological tables of solar and geophysical events, discussing solar activity, geomagnetic, ionospheric, auroral and cosmic ray research
02 p0321 A69-12165

Cosmic MHD, discussing mechanisms responsible for solar phenomena and dynamics of interstellar medium
02 p0293 A69-12789

Ionospheric parameters variation during SC effect as function of solar and magnetic activities
03 p0423 A69-13534

Absorption as factor influencing correlation between solar activity, sporadic E layer probability of occurrence and reflection stability
03 p0423 A69-13537

Geomagnetic field quiet day solar variations current system calculated, using 2000 LT as zero level basis
03 p0424 A69-13541

Horizontal and vertical downward velocity components in developed solar active regions
04 p0651 A69-14370

Daily solar indices monthly averages errors due to evaluation for days presenting favorable weather conditions
04 p0657 A69-14700

Slowly varying solar radio emission caused by bremsstrahlung and cyclotron mechanisms within limits of active region model
04 p0662 A69-15240

Polarization degree of type solar radio bursts dependent on heliographic longitude
04 p0649 A69-15242

UK space research in 1970s emphasizing solar observations in UN, cosmic X ray astronomy, solar space astronomy and ionospheric investigation
06 p0997 A69-16853

Cosmic ray daily variations relationship to geomagnetic activity, sector structure of interplanetary magnetic field and sunspot activity
06 p0990 A69-17291

Flare-like phenomena in chromosphere, discussing moustaches, dashes and spicules and relation to changes in magnetic field
06 p0994 A69-17433

Solar disk surge distribution difference between eastern and western disk parts
06 p0995 A69-17440

Sunspot ejection of filaments, flare surges and flare sprays, discussing bright and dark matter divergence from western spot
06 p0995 A69-17441

Solar type stellar activity, considering solar activity origin and correlation with stellar distances
06 p0996 A69-17447

Long lived streams of low energy solar electrons and protons and association with bright flares or solar active regions
07 p1206 A69-19249

Bow shock and magnetopause boundary observations with IMP 2 plasma detector
07 p1129 A69-19372

Soviet monograph on diurnal solar cosmic ray variations from maximum to minimum solar activity, discussing model based on anisotropic particle scattering theory
07 p1209 A69-19500

Hydrogen concentration above earth surface during minimum solar activity from ionospheric rocket and satellite measurements
07 p1129 A69-19612

Solar radio astronomy, discussing quiet sun radio emission, solar activity, slowly varying radio emission, radio bursts and possibility of observing lines
08 p1388 A69-20218

Sunspot activity dependence on phase of eleven year cycle and heliographic latitude, discussing fine structure of butterfly diagrams
08 p1379 A69-20611

Proton flares statistical analysis regarding isolated and near activity complexes for long term forecasting
08 p1379 A69-20614

Dispersion and average monthly numbers of whistlers for propagation trajectories during solar activity minimum, discussing electron concentrations in magnetosphere
09 p1485 A69-21531

Solar quiet day variations studied by annual amplitude dependence on number of sunspots, considering E layer ionization
09 p1575 A69-21550

Zero reference field for quiet day solar variations, considering magnetic field levels and errors
09 p1575 A69-21551

Type 3 solar radio noise bursts at hectometer wavelengths, deducing coronal electron temperatures from decay rates
09 p1594 A69-21665

Galactic cosmic ray modulation and solar activity analyzed on basis of cosmic ray measurement in stratosphere
10 p1758 A69-22832

Solar diurnal variation amplitude and phase instability, considering anisotropic cosmic ray fluxes superposition
10 p1759 A69-22837

Solar activity and 19 to 24 day variations in cosmic ray intensity
10 p1759 A69-22843

Solar activity forecasting methods
10 p1777 A69-23312

Solar radio astronomy in Australia including solar atmosphere, bursts, instruments, etc
10 p1777 A69-23383

Solar activity complex development based on magnetic, photospheric, chromospheric and coronal observations
11 p1964 A69-25418

Iono-index about hard emission of solar active regions, analyzing field fluctuations and SID in D region under daytime conditions
12 p2148 A69-26107

Linear extrapolation of stationary stochastic process predicting fluctuations of minimum and maximum periods in solar cycle
12 p2149 A69-26221

Interplanetary plasma flow directional velocity distribution from solar atmosphere active regions found inhomogeneous
12 p2149 A69-26698

Solar quiet currents in three dimensional ionosphere, considering ionospheric conductivity and horizontal layer equations
12 p2074 A69-26955

Coronal features prediction compared to maximum solar activity observations, discussing variations in force free field
13 p2354 A69-28472

Solar activity forecasting methods based on sunspots and flares
13 p2333 A69-28657

Solar and galactic cosmic rays measurement data used to investigate variation in time of relations between cosmic rays modulation amplitude and solar activity variations
13 p2333 A69-28689

Radio emission fluxes in solar active regions, determining slope of spectral characteristics of radio sources from effective emission center

13 p2355 A69-28707

Relation between solar activity and cyclic variation of pearl pulsations excitation frequency during sunspot cycle

13 p2258 A69-28727

Solar proton flux in two energy intervals measuring by ATS detectors during January 1967 event compared with data from satellites outside magnetosphere

14 p2509 A69-28935

Solar activity indices based on Ca IIoculi, emphasizing index representing emission excess over chromospheric emission

14 p2525 A69-29722

Solar activity and large scale magnetic field distribution in discrete latitude zones, including interplanetary magnetic field above ecliptic

14 p2528 A69-29966

Solar activity history and morphology 1964-1965/

15 p2679 A69-30006

Solar ionizing radiation sources, discussing activity at sunspot minimum, temperature, density and solar wind effects, X ray and UV spectra, etc

15 p2673 A69-30007

Cosmic ray variation theory, presenting data on coupling of solar activity with large scale characteristics of solar wind during 11-year cycle

15 p2673 A69-30015

Solar exosphere near solar maximum investigation by Explorer 19 and Explorer 24 drag satellites, considering density and atomic oxygen concentration measurements

15 p2600 A69-31351

Exospheric temperature variations by Thomson scattering related to solar and geomagnetic activity, discussing seasonal effect on thermospheric variables

15 p2604 A69-31409

Book on cosmic ray variations and solar activity during IQSY covering energy spectrum, outer space radiation, magnetosphere, etc

16 p2849 A69-32052

Trieste astronomical observatory optical and radio solar photosphere observations in 1967, including solar cycle and north-south symmetry

16 p2858 A69-32206

Dispersion and average monthly numbers of whistlers for propagation trajectories during solar activity minimum, discussing electron concentrations in magnetosphere

16 p2783 A69-32526

Solar quiet day variations studied by annual amplitude dependence on number of sunspots, considering E layer ionization

16 p2851 A69-32545

Zero reference field for quiet day solar variations, considering magnetic field levels and errors

16 p2851 A69-32546

Turbulent diffusion inside sun as explanation of solar spindown, Li depletion at surface and neutrino discrepancy, discussing diffusion coefficient and stellar evolution

16 p2866 A69-32814

Photospheric granulation near center of quiet sun, analyzing morphological properties from high definition Stratoscope photographs

17 p3029 A69-33045

Finite resolution effect on solar granulation simulated by numerical experiments using two dimensional smeared pattern

17 p3029 A69-33046

Active solar centers interactions above photospheric level and through corona linkages, noting MHD shock waves and magnetic field lines

17 p3040 A69-33801

Solar radio sources heights at 1424 and 696 MHz during near minimum solar activity

17 p3040 A69-33808

Auroral absorption maximum frequency correlation with years of solar activity reduction and magnetic activity from riometric data long term variations

17 p2968 A69-33991

Time dependent diffuse reflections related to solar activity, showing diffusion intensity variations with sporadic E layer height and electron concentration

17 p2968 A69-33997

Low altitude trapped protons in inner radiation belt during solar minimum period, using emulsion detectors on polar-orbiting satellite

18 p3187 A69-34944

Solar activity /Madrid 1967/, detailing Wolf numbers, sunspots, chromospheric faculae, H filaments and prominences

18 p3202 A69-35290

Umbral chromosphere flashes visual and photometric observations at 5 sec intervals on K line filtergrams using Halle filter

18 p3204 A69-35390

Cosmic rays nucleonic component latitude at solar minimum activity, using IGY neutron monitor

19 p3396 A69-36411

Solar and geomagnetic activity persistence by variance spectrum analysis, noting sunspot numbers and radiation flux autocorrelation functions

20 p3601 A69-37508

Flares and fast processes interrelation with active region stationary filaments, filament field magnetic envelope explosion stimulation of surges, plasma stream ascents, etc

20 p3591 A69-38042

Periodicities in solar activity variation from correlation spectral analysis, establishing monotonically decreasing component and secular variations in activity

20 p3607 A69-38045

Solar activity center characteristics in floccula stage during eleven year sunspot cycle

20 p3616 A69-38302

Babcock solar activity periodicity theory, correlating spots displacement and coronal magnetic field intensity changes

23 p4208 A69-41283

Day-to-day variability of daily variation of cosmic ray intensity during quiet solar activity period using high latitude neutron monitor data

23 p4204 A69-41484

Solar physics outline, discussing composition, quiet and active sun characteristics, radiation, etc

24 p4379 A69-42781

Solar activity empirical correlation with planetary positions used for long range forecast of solar flare proton events

24 p4366 A69-42880

Solar activity long term forecasts determined from comparison between Mount Wilson magnetic field synoptic chart latitude zones and sunspot groups

24 p4374 A69-43625

Interplanetary and geophysical conditions forecasting based on repetitions of low latitude photospheric background magnetic field patterns during solar activity cycles

24 p4387 A69-43626

SOLAR ACTIVITY EFFECTS

Ionic composition and temperature of nighttime topside ionosphere from analysis of incoherent backscatter spectra, discussing solar activity effects

01 p0076 A69-11233

Relation between north-south asymmetry of F 2 region critical frequencies and geomagnetic axis inclination angle, establishing increase in asymmetry during increased solar activity

02 p0237 A69-11662

Unusual stratification of F region during solar activities, noting role of traveling inhomogeneities

02 p0237 A69-11663

11-year solar cycle influence on F 2 region critical frequency, investigating correlation coefficient between mean monthly values of F 2 variations and respective sunspot numbers

02 p0238 A69-11680

E region electron concentration measurements during large solar zenith angles, noting anomalous behavior during low solar activity periods

02 p0239 A69-11683

Geophysical effects observed in Northern Hemisphere during low solar activity, discussing polar auroral intensities and positions

02 p0239 A69-11694

Magnetic storm of January 1967 due to 3B solar flare noting spacecraft observations, intensity, magnetospheric distortions and solar wind dynamics

03 p0500 A69-13430

Cosmic rays intensity increase due to meteor showers noting maximum solar activity effects

03 p0500 A69-13509

Ionospheric midday radio wave absorption as function of geomagnetic latitude, season and solar activity from pulsed vertical radar sounding data

03 p0394 A69-13521

Solar flares effect on ozonosphere, calculating time necessary for solar radiation to increase ozone concentration by 50 percent

03 p0424 A69-13542

Cosmic ray intensity after solar flare shown greater than during quiet periods from balloon data at Murmansk and Mirny

04 p0648 A69-14375

Geoelectric field over polar cap based on proton flux detection

04 p0648 A69-14682

Delay between solar activity and density changes in upper atmosphere using Harris-Priester model

04 p0594 A69-15121

Electromagnetic radiation from solar flares based on rocket and satellite observations of 10-100 keV X ray emission and ground observation of cm-wavelength bursts

05 p0813 A69-15603

Type 3 bursts spectra graphical representation, giving probable solar origin and curves of corona temperature

05 p0824 A69-16060

Solar modulating function form changes resulting in hysteresis near solar minimum

05 p0815 A69-16249

Zodiacal light, cometary contribution and solar activity

05 p0826 A69-16391

Solar cycle influence on winds in lower ionosphere

05 p0759 A69-16421

Solar flare influence on potential gradient and air-earth current properties at high mountain stations

05 p0759 A69-16634

Thermoelastic effects on gravity gradient stabilization of artificial satellites, including role of solar activity

06 p1025 A69-17613

Ionization index, electron formation and effective recombination coefficient in E 2 layer, noting solar activity effect

06 p0920 A69-17725

Vertically moving ionized formations relation to solar and magnetic activity

06 p0920 A69-17730

Radiation protection plan for Apollo lunar mission based on real time monitoring of solar activity and radiation in spacecraft

06 p0996 A69-18113

Quasi-periodic variations of solar radio emission intensity related to solar activity variations

07 p1211 A69-18516

Solar end and lateral pumping apparatus for neodymium doped YAG crystal lasers, noting applicability to space communication

07 p1150 A69-18953

Local interstellar electron spectrum limits from measurements of cosmic ray electrons, nonthermal galactic radio emission and solar modulation effects

07 p1206 A69-19269

Solar activity modulation of galactic cosmic rays with more than 1 GeV energy

08 p1378 A69-20224

Long term modulation of cosmic rays by solar activity explained by Parker solar wind model, noting confirmation by direct satellite measurements

08 p1379 A69-20533

Solar phenomena correlation with brightness variations of comet Alcock 1963b, noting sunspot maximum followed by maximum in absolute magnitude of comet

08 p1394 A69-20620

Fast and slow neutron latitude variation at aircraft altitudes during solar minimum, noting environment effects on measurement

09 p1574 A69-21402

Interplanetary medium parameters strong variations during low solar activity derived from Mariner 2 data

09 p1575 A69-21522

Mach number values and propagation rates of wear disturbances in interplanetary medium obtained from Mariner 2 data during low solar activity

09 p1575 A69-21523

Geomagnetic field quiet solar variations variability explained by model, noting agreement with observations at various stations

09 p1486 A69-21549

Eleven year cyclicity of geomagnetic activity from Sverdrlovsk Observatory data, noting possible relation with structural features of solar activity cycles

09 p1486 A69-21552

Solar modulation of galactic cosmic rays, discussing disagreements between convection diffusion theory and observation

09 p1581 A69-22744

Solar flare relation to interplanetary scintillation indices and power spectra

09 p1582 A69-22751

Short term variability of solar proton flux in interplanetary space during solar flare activity, using data from cosmic ray detector on Pioneer 7

09 p1582 A69-22754

Toroidal magnetic fields in ionosphere associated with solar quiet daily variations producing electric current and equatorial auroral electrojets

10 p1681 A69-22805

Galactic and solar cosmic ray modulation in interplanetary space during different phases of 11 year solar activity cycle

10 p1758 A69-22833

Forbush effects energy spectra and cosmic ray anisotropy beyond magnetosphere analyzed during solar activity minimum, using data from neutron monitors global network

10 p1758 A69-22835

Solar activity effect on interplanetary electromagnetic field according to cosmic ray modulation data, noting ineffective correlation and solar wind effects

10 p1759 A69-22841

Sudden ionospheric disturbance effects of solar X ray emission from active region with proton flare

10 p1764 A69-23744

Time history of July 7-10 1966 PCA event analyzed using 16 riometers and concurrent satellite observations of solar cosmic radiation

10 p1683 A69-23770

Forbush decrease associated with July 7 1966 proton event from cosmic ray intensity variation measurements by neutron monitors

10 p1768 A69-23774

Interplanetary plasma subsequent to July 7, 1966 flare monitored by detectors on Pioneer 6 and Explorer 33

10 p1783 A69-23775

F region response to solar proton flare characterized by two phase ionospheric storm as measured at ground base stations

10 p1684 A69-23783

Incoherent scatter measurements of F region electron concentrations at solar activity minimum

10 p1684 A69-23825

Secondary muon flux from primary cosmic ray particles monitored during minimum solar activity by telescopes at 60 mwe underground

10 p1769 A69-23827

Mariner 2 measurements of geomagnetic field and interplanetary plasma parameters for analyzing interaction between interplanetary medium and magnetosphere during decreased solar activity

10 p1769 A69-23900

Ionospheric discontinuities drift velocities from diversity reception data indicating no dependence on solar activity

10 p1686 A69-23911

Geomagnetic micropulsations fluctuations during solar activity cycle showing changes in excitation frequency with change in corpuscular fluxes parameters

10 p1687 A69-23919

F 2 layer state prediction as function of solar activity by series expansion for describing space-time variations of monthly F 2 medians critical frequencies

10 p1687 A69-23927

Geomagnetic field pulsations frequency changes in relation to geomagnetic and solar activity level

10 p1689 A69-23939

Solar wind flux near earth observed by Venera 2 /1965/ and Venera 4 /1967/ probes, noting solar activity effects

10 p1771 A69-24201

Various glacial periods mechanism ascribed to combination of long term solar activity cycle and polar migration

11 p1877 A69-24409

Photoelectric measurements of nightglow intensities during sunspot minima by zenith photometer, considering background continuum

11 p1877 A69-24584

Solar spectra of Mg II doublet lines during September 22, 1968 eclipse, considering chromospheric activity effects on emission peaks

11 p1958 A69-24591

Jupiter red spot visibility, establishing partial dependence on solar activity

11 p1964 A69-25404

Recurrent geophysical disturbances associated with solar active regions and low latitude background field pattern on solar surface magnetic fields

11 p1964 A69-25415

Cometary, lunar and solar effects on precipitation, considering joint influence of meteoric streams and moon

11 p1965 A69-25420

Monochromatic midlatitude auroral arc /M arc/ observation on 28-29 September 1967 at Moscow, Idaho

12 p2065 A69-26105

Variable solar activity effect on earth upper atmosphere rotation at altitudes from 200 to 300 km

12 p2069 A69-26442

Solar chromospheric flares effect on temperature of upper atmosphere observed by satellite at perigee altitude

12 p2149 A69-26447

Oscillation cycle of atmospheric circulation, analyzing solar activity effects on lunar and solar semidiurnal tides and transition from zonal to meridional circulation

12 p2070 A69-26692

Frequent periodic variations existence in daytime ozone content associated with solar activity

12 p2070 A69-26693

Solar control of day-to-day variability in phase of solar diurnal variation of horizontal magnetic intensity on quiet days

12 p2073 A69-26954

Relation between north-south asymmetry of F 2 region critical frequencies and geomagnetic axis inclination angle, establishing increase in asymmetry during increased solar activity

13 p2256 A69-28693

Unusual stratification of F region during solar activities, noting role of traveling inhomogeneities

13 p2256 A69-28694

11-year solar cycle influence on F 2 region critical frequency, investigating correlation coefficient between mean monthly values of F 2 variations and respective sunspot numbers

13 p2257 A69-28711

E region electron concentration measurements during large solar zenith angles, noting anomalous behavior during low solar activity periods

13 p2258 A69-28714

Geophysical effects observed in Northern Hemisphere during low solar activity, discussing polar auroral intensities and positions

13 p2258 A69-28725

Solar radio emission data during IGY covering solar terrestrial disturbances, broadband bursts, solar indices, etc

14 p2513 A69-29321

Solar flare effect on polar chorus variation determined by comparing Antarctica VLF data with low latitude magnetograms

14 p2514 A69-29385

Polar auroras temporal and spatial variations and relation to solar activity

14 p2442 A69-29719

Epochs in atmospheric circulation development over Northern Hemisphere, emphasizing solar activity roles in epochs appearances

14 p2478 A69-29837

Cosmic ray intensity during solar cycles, considering minima relationship to Bartel index maxima and solar wind modulation theory

14 p2515 A69-29967

Solar corpuscular radiation characterization by stable four streamer structure at near minimum solar activity

15 p2674 A69-30517

Solar cycle effect on high latitude magnetic activity, discussing annual variations and Lassen auroral zone model confirmation

15 p2598 A69-31207

Atmospheric density and temperature variations between 200-600 km from Cosmos satellite data, noting solar activity effect

15 p2599 A69-31343

ESRO 2 satellite observations of solar proton event of 9 June 1968, comparing flux profile variations across polar cap with magnetic changes at earth surface

15 p2677 A69-31347

Upper atmosphere structure and variations including density and composition in lower thermosphere, diurnal variations, variations with solar activity, etc

15 p2600 A69-31355

Atmospheric density dependence on solar and geomagnetic activity at low latitudes, discussing atmospheric expansion

15 p2605 A69-31441

Book on ionospheric radio waves covering geomagnetism and sun, whistler propagation, oblique propagation, satellite sounding, etc

16 p2749 A69-31715

Polar Ionosphere Beacon Satellite S-66 signals measured for large scale horizontal gradients in total electron content of Antarctic ionosphere at sunspot minimum and maximum

16 p2774 A69-31989

Lunar surface characteristics, discussing light polarization, lunar radiation, solar radiation and meteorite impact effects, etc

16 p2856 A69-32069

Simultaneous solution of continuity and heat conduction equations for ionospheric plasma consisting of electrons, atomic O ions and neutral gas species, discussing varying solar flux effects

16 p2849 A69-32082

Geomagnetic storms generation interpreted using solar coronal arrangements above central meridian

16 p2777 A69-32100

Low latitude asymmetric disturbance field analyzed using equivalent current vectors during magnetic storms, allowing for solar quiet day variation and declination

16 p2778 A69-32184

Earth atmosphere effect on cosmic ray variations, considering relation between extensive air showers and cosmic ray spectrum

16 p2851 A69-32381

Lunar components in mean values of geomagnetic field daily variations, discussing lunar phase during selected quiet days

16 p2782 A69-32458

Semiannual variation in amplitude of solar daily quiet geomagnetic variation, discussing sunspot dependence of seasonal secondary minimum and maxima

16 p2782 A69-32459

Interplanetary medium parameters strong variations during low solar activity derived from Mariner 2 data

16 p2851 A69-32517

Mach number values and propagation rates of weak disturbances in interplanetary medium obtained from Mariner 2 data during low solar activity

16 p2851 A69-32518

Geomagnetic field quiet solar variations variability explained by model, noting agreement with observations at various stations

16 p2784 A69-32544

Eleven year cyclicity of geomagnetic activity from Sverdlvsk Observatory data, noting possible relation with structural features of solar activity cycles

16 p2784 A69-32547

Cosmic ray electron spectrum data obtained by balloon flights, showing electron flux reduction above 500 Mev with increasing solar activity

16 p2851 A69-32566

Lunar tidal oscillations in F 2 layer critical frequency and F region minimum virtual height at Huancayo during IGY/IGC to study solar cycle effects

16 p2784 A69-32613

Fast atmospheric neutrons flux and spectrum measurement during two balloon flights, tabulating results and evaluating albedo flux during quiet sun period

16 p2851 A69-32616

Solar and terrestrial phenomena correlated for March 1966 events

16 p2852 A69-32621

F region stratification during solar minimum and maximum, discussing regularities of plasma frequencies and diurnal variations

17 p2959 A69-33005

Sudden phase anomalies on radio paths compared with calculated results for satellite observed solar X ray flux intensities to explain sudden ionospheric disturbances

17 p2959 A69-33006

Ozone concentration worldwide anomaly above 40 km in annual variations, noting dissimilarity in seasonal maximum and minimum with lower level

17 p2960 A69-33166

Hydrodynamic approximation to interplanetary gas motion influenced by solar flare caused perturbations

17 p3035 A69-33627

E region horizontal drift measurements at Ahmedabad from 1956 to 1966, noting solar activity and seasonal influences

17 p2962 A69-33678

Circular polarization in moving type 4 burst compared to stationary type 4 burst and related to preceding type 2 sources

17 p3024 A69-33806

Polar auroras appearance at solar activity maximum /IGY/ and minimum /IQSY/ at oval zone latitudes

17 p2963 A69-33955

High latitude geomagnetic field quiet solar diurnal variations during magnetically quiet IGY winter days, relating type and amplitude at low and midlatitudes

17 p2964 A69-33960

Geomagnetic disturbances intensity spatiotemporal distribution at Northern Hemisphere high latitudes during IGY and IQSY

17 p2965 A69-33966

Annual variations of postsunset altitude peak of equatorial F region noting correlation with solar activity

17 p2966 A69-33983

Solar flares with subcosmic radiation in proton active region of May 1967, discussing X ray emission effects, calculating D region recombination coefficient and electron concentration
17 p3025 A69-34226

Cosmic ray diurnal anisotropy variations, correlating component annual means with magnetic activity
18 p3186 A69-34934

Surges statistical properties observed in Sweden /1957-1967/ noting latitude distribution pattern, radio emission association, rate dependence on solar cycle, etc
18 p3204 A69-35393

Geomagnetic storms data compilation /1957-1964/, showing solar activity effect on solar corpuscular stream velocity
20 p3587 A69-37036

Ion production rates vertical distribution and temporal changes at midlatitudes during solar activity minimum and maximum above F 2 layer
20 p3525 A69-37656

Altitude variations at and near maximum electron concentration in quiet F 2 layer during solar activity maximum from sounding at southern geomagnetic pole
20 p3526 A69-37662

Solar activity effect on F 2 layer geometrical parameters, plotting prognostic maps using nomographic methods
20 p3526 A69-37663

Seasonal anomaly of F 2 layer critical frequency in Northern and Southern Hemispheres during high and low solar activity, discussing geomagnetic effect
20 p3526 A69-37667

Latitudinal variations in conditions for F 1 layer occurrence probability and stability during solar activity minimum period
20 p3527 A69-37669

Diurnal F 1 layer development over Irkutsk, Siberia, during minimum and maximum solar activity, using semiquantitative method
20 p3527 A69-37670

F zero layer occurrence relation to solar, magnetic and ionospheric activity levels variations from Ashkhabad observations /1958- 1964/
20 p3527 A69-37671

Time-space variations in occurrence probability of ionospheric E-2 layer during solar activity maximum and minimum
20 p3527 A69-37672

Sporadic E layer structure and behavior during solar cycle from vertical sounding, discussing semioaque region, reflection multiplicity, active height, wind effects, etc
20 p3528 A69-37681

Solar activity effect on short term meteorological processes and dynamic state of mesosphere and ionosphere, emphasizing relationship to entire atmosphere dynamics
20 p3590 A69-37684

High latitude stations vertical ionograms in absence of ionospheric reflections due to low solar activity periods, discussing interpretation methods
20 p3529 A69-37690

Type 3 bursts spectra graphical representation, giving probable solar origin and curves of corona temperature
20 p3591 A69-37970

Sudden frequency deviations of HF radio waves propagated through ionosphere correlated with solar microwave bursts and optical flare events
20 p3592 A69-38101

Photodissociation of diatomic hydrogen by solar radiation for Venus atmosphere investigation, considering H atoms production rate by Stecher-Williams process
20 p3609 A69-38102

Lower ionosphere over geomagnetic equator during evening twilight characterized by solar disturbances, using rocket-borne Langmuir and plasma noise probes
21 p3702 A69-38353

Twilight airglow excitations governed by solar radiation, indicating presence of alkali metals, positive calcium ions and H lines, positive sodium ion bands, etc
21 p3711 A69-38515

Primary cosmic rays solar diurnal modulation, measuring relative amplitudes and phases over full cycle
21 p3788 A69-38547

Daytime electron and ion composition model for height range from 150 to 1500 km at moderate latitudes and minimum solar activity
21 p3714 A69-38555

Ariel 3 satellite observations, including topside ionospheric variations with time and solar activity, electron density, temperature measurements, etc
21 p3716 A69-39257

Soviet book on synoptic climatological and heliogeophysical long term weather forecasts, discussing monthly and seasonal anomalies, sun-earth interrelations, solar corpuscular elements, etc
21 p3759 A69-39523

Solar radiation pressure windmill effect in rotational bursting and elimination from solar system of small magnetic celestial bodies
21 p3814 A69-39584

Explorer 30 /Solrad 8/ satellite observation of 0.5-3 A solar X ray emission related to magnetic configuration in sunspot group
22 p4003 A69-40298

Geomagnetic disturbances and cosmic ray storm of 25-26 May 1967 caused by McMath plage region 8818, noting Forbush decreases and ring current effect
22 p4004 A69-40307

Sun and moon effects on earth satellite orbit
22 p4030 A69-40901

Midlatitude ionospheric electron density rocket data survey, including nighttime and daytime N/h/ profiles for specific solar activities
23 p4155 A69-41563

Sudden and gradually developing geomagnetic storms with 27 day recurrence period and relation to 11 year solar activity cycle
23 p4156 A69-41849

Apollo 11 observations of lunar surface glazing, considering radiation heating due to solar outbursts, rocket exhaust effects, shock heating or volcanism, erosion, etc
23 p4216 A69-42202

Solar quiet and lunar electric current systems deduced from geomagnetic data, discussing electrical conductivities and wind models in dynamo region
23 p4160 A69-42427

Equatorial anomaly during declining solar activity, treating seasonal and daily variations, longitude dependence and geomagnetic storm-time distortions
23 p4161 A69-42436

Cosmic ray electron energy spectrum and intensity measurements indicating time variations attributed to solar modulation effects
24 p4367 A69-43175

Solar flares associated optical phenomena including filaments enhancement, destabilization and distortion, high speed ejections, explosions and loop prominences
24 p4371 A69-43607

Solar X-ray spectrum as function of sunspot group type based on Solrad satellites flux data, discussing relationship to lower ionosphere characteristics variations
24 p4372 A69-43615

Solar energetic particle effects during polar cap absorption observed in earth upper atmosphere and at ground level
24 p4373 A69-43618

Solar wind disturbances associated with flares
24 p4373 A69-43620

SOLAR ATMOSPHERE

Solar flare mechanism from analysis of energy transfer in quiet solar atmosphere, discussing convection, radiation, mechanical and MHD waves and thermal conduction
01 p0145 A69-10990

Goldberg-Unno method for determining Doppler width, microturbulence velocity and convection errors, considering photosphere as hot ascending and cold descending columns
02 p0328 A69-12752

Solar atmosphere from two dimensional study of solar spectrum, discussing satellite observations of corona and upper chromosphere
02 p0329 A69-12785

Solar atmosphere physical properties tabulated to interpret radio bursts and noise storms
02 p0329 A69-12786

Solar chromosphere dark mottles size, shape and evolution, using high resolution photography near solar disk center
03 p0515 A69-14038

Chromosphere fine structure in Lyman alpha intensity, compiling isophote map
03 p0515 A69-14039

Energy release by Joule magnetic field dissipation in solar atmosphere
03 p0516 A69-14041

Be I and Be II lines in solar spectra show no evidence for Be 7 and Be 10 in solar atmosphere
04 p0655 A69-14666

Local hydromagnetic mechanism to increase magnetic fields and shape into bipolar sunspot group configuration, discussing applicability to solar atmosphere
04 p0662 A69-15243

Lithium abundance in sunspots and undisturbed solar atmosphere from measurements of solar atmosphere and spot spectra
05 p0821 A69-15850

Micro and macroturbulent motions velocity in solar photosphere based on Fraunhofer lines analysis
05 p0823 A69-16014

Model for Evershed effect postulating unipolar symmetrical sunspot surrounded by magnetic knots of opposite polarity
06 p0999 A69-16977

SH above photosphere in solar atmosphere, discussing dissociation equilibrium of diatomic molecules and possible abundances
06 p1002 A69-17317

Chromospheric /optical/ flares caused by dense material falling from corona into chromosphere
06 p0993 A69-17430

Small scale mass motions in chromospheric structures surrounding solar flare indicating changes in magnetic field
06 p0993 A69-17431

Flare-like phenomena in chromosphere, discussing moustaches, dashes and spicules and relation to changes in magnetic field
06 p0994 A69-17433

Solar flares acceleration processes related to solar atmospheric currents
06 p0995 A69-17442

Model to account for flare and sunspot phenomena, discussing uni- and bipolar spots
06 p0995 A69-17443

Beryllium abundance in solar atmosphere from spectra observed at Oslo Solar Observatory
06 p1010 A69-17971

Solar supergranules and hydrogen convection zone analysis based on polytropic atmosphere convection physics
07 p1211 A69-18408

Solar photosphere model with two stream columnar representation of granulation for predicting continuous radiation field
07 p1217 A69-19238

Solar spectral line profiles for photosphere disturbed by short period acoustic waves
07 p1217 A69-19239

Chromospheric velocity field temporal characteristics in quiet region of sun, determining power spectra of Doppler shifts of H alpha spectra
07 p1217 A69-19240

Quiescent solar prominences horizontal oscillations, explaining periods, damping times and prominence shape changes by model of freely oscillating prominence in corona
07 p1205 A69-19245

Solar flare initial development model assuming high temperature chromospheric point explosion, noting subsequent expansion and large density gradient effects
07 p1205 A69-19246

Solar atmosphere model calculations of solar oblateness, discussing flux difference and Dicke experiment on general relativity
08 p1383 A69-19899

Chemical composition and element abundance in solar atmosphere and photosphere, noting solar absorption and emission and energy spectrum data
08 p1402 A69-20905

Viscosity coefficients approximation for chemical compositions in chromosphere and coronal gas
09 p1602 A69-22217

Growth rates for convective disturbances propagation in atmosphere with linear entropy variation, noting WKB approximation
11 p1957 A69-24422

Book on stellar atmospheres covering radiation theories, thermal equilibrium, measurement techniques, spectral analysis, etc, emphasizing sun
11 p1961 A69-25084

Ionization equilibrium for ions of solar abundant elements between C and Ni calculated as function of electron temperature
11 p1928 A69-25262

Solar chromosphere and corona heat intensity above 1000 km attributed to tongues of turbulence, considering convective zone exciting MHD waves mechanism
13 p2337 A69-27549

Solar atmosphere five minute oscillations observed by Frazer divided into two harmonic atmospheric model for studying oscillation region height and mean temperature
13 p2343 A69-27627

Solar 3 cm flux density sensitivity to physical conditions in solar atmosphere related to maximum ex-

- p>
istence in flux density spectrum F gamma in active regions
-
- 13 p2327 A69-27721
-
- Solar atmosphere surface radiation intensity determined by initial value theory including source function and resolvent
-
- 13 p2350 A69-27859
-
- Tentative solar photospheric model meeting Noyes and Withbroe criticism
-
- 14 p2518 A69-29131
-
- Dissociation equilibrium of diatomic molecules in solar atmosphere, comparing concentration above photosphere to MgH
-
- 14 p2528 A69-29963
-
- CO absorption lines in solar spectrum analyzed theoretically and experimentally indicating random distribution of molecules
-
- 15 p2688 A69-30552
-
- Short period pulsations in solar magnetic fields and chromosphere, determining optimum conditions for formation of standing oscillations
-
- 15 p2688 A69-30556
-
- Solar Mg b and Na D line spectra, computing profiles for Doppler cores of lines for multilevel model atoms and selected chromospheric parameter ranges
-
- 15 p2693 A69-30779
-
- Solar chromosphere metal abundance determined taking into account local thermodynamic equilibrium departures
-
- 16 p2855 A69-31657
-
- Solar Ca chromospheric plage decay curves obtained from area measurements, showing similarity and exponential mean curve
-
- 16 p2859 A69-32222
-
- Nondivergent oscillations in solar atmosphere forming normal modes or free oscillations, assuming free surface of chromosphere coronal interface and large density in convective zone
-
- 17 p3029 A69-33048
-
- Heliosphere boundary location significance for Jovian magnetosphere configuration, considering inverse correlation between sunspot number and Jovian decametric radio emission
-
- 17 p3033 A69-33379
-
- Solar flare model based on force-free currents in solar atmosphere, noting rapid energy release due to exceeding current density critical limit
-
- 18 p3188 A69-35392
-
- Solar atmosphere line source function showing frequency dependence as consequence of spectral line disappearance at solar limb
-
- 20 p3588 A69-37540
-
- Radioastronomical investigations of inhomogeneous near solar plasma structure
-
- 20 p3606 A69-38017
-
- Solar He abundance limits and discrepancies of C137 solar neutrino count experiment
-
- 20 p3592 A69-38068
-
- Steady state atomic He distribution according to solar atmosphere levels, involving formulation and solution of equilibrium equations for single and triplet levels
-
- 20 p3615 A69-38298
-
- Magnetic field and radial gas motion in sunspots from Crimean magnetograph observations at different depths of solar atmosphere
-
- 20 p3615 A69-38299
-
- Magnetic measurements of active regions at various levels of solar atmosphere, discussing chromospheric cold and hot region, faculae magnetic fields, etc
-
- 22 p4010 A69-39991
-
- Chromospheric heating above sunspots by analyzing MHD wave generation and propagation in sunspots and solar atmosphere
-
- 22 p4010 A69-39992
-
- Type 3 solar radio bursts observed during April-October 1967 for two alternative models of active region streamers in outer corona
-
- 22 p4003 A69-40300
-
- Outer solar convection zone structure dependence on change of parameters in mixing length theory examined to construct model
-
- 24 p4387 A69-43634
-
- SOLAR AUXILIARY POWER UNITS**
-
- Mathematical model to design weight optimized silicon-germanium solar flat plate thermoelectric generator as spacecraft auxiliary power source in near sun missions
-
- 05 p0704 A69-15674
-
- Heat storage cells for satellite solar power plants based on latent heat of fusion and single phase heat carrying agent
-
- 06 p0870 A69-17604
-
- Computer simulation of satellite electric power systems concerning solar array, thermal, battery and charge models for end-of-mission-life orbits
-
- 23 p4068 A69-42241
-
- Solar cells arrays degradation in Intelsat spacecraft at synchronous altitude, noting shielding gaps and low energy proton influence
-
- 23 p4072 A69-42287
-
- SOLAR AZIMUTH**
-
- U AZIMUTH**
-
- SOLAR CELLS**
-
- Solar cell generator design problems for solar probes, discussing increased operational temperature
-
- 02 p0197 A69-12665
-
- Thermal cycling tests showing improvement in cadmium sulfide solar cell stability, noting effect of thermal cycling stresses
-
- 03 p0367 A69-13074
-
- Photovoltaic properties of CdS thin film solar cells and silicon cells at Jupiter temperature and solar intensity
-
- 03 p0368 A69-13076
-
- Single crystal cells for construction of large deployable solar cell arrays
-
- 03 p0368 A69-13993
-
- Radiation effects on III-V compounds, considering damage in solar cells and luminescence, light emitting and Esaki diodes
-
- 04 p0641 A69-14504
-
- Angle of incidence influence on unpolarized and linear polarized light of solar cell short circuit current
-
- 04 p0551 A69-15312
-
- Surface photovoltaic effect in copper electroplated single crystal CdS solar cells, discussing Fermi level and Hall effect
-
- 05 p0704 A69-15958
-
- Photovoltaic solar cell power technology application to space use and exploration
-
- [ASME PAPER 68-WA/SOL-1]
-
- 05 p0705 A69-16158
-
- Recovery rate at room temperature in Li-doped p-n Si diodes and solar cells after 1 Mev electron irradiation, noting capacitance changes
-
- 06 p0974 A69-16867
-
- Heat storage cells for satellite solar power plants based on latent heat of fusion and single phase heat carrying agent
-
- 06 p0870 A69-17604
-
- Electron drainage currents from dilute streaming plasmas to positively biased silicon and cadmium sulfide solar cell arrays
-
- [AIJA PAPER 69-262]
-
- 09 p1436 A69-21726
-
- Electrostatic rocket exhaust condensation on spacecraft solar electric panels cover glasses, noting deleterious effects
-
- [AIJA PAPER 69-271]
-
- 09 p1569 A69-21874
-
- Annealing temperature of radiation defects in phosphorus doped silicon, discussing isochronal recovery characteristics of solar cells with different donor and oxygen concentrations
-
- 10 p1747 A69-24006
-
- Solar cells degradation by charged particles in space, considering protection by filter, silicon properties and use of cadmium cells
-
- 11 p1825 A69-24870
-
- Silicon n-p solar cell behavior during electron radiation, describing radiation resistant solar cell
-
- 11 p1825 A69-24871
-
- Electron, proton and gamma ray radiation effects on thin film CdS, GaAs and CdTe solar cells
-
- 11 p1825 A69-24872
-
- Single crystal solar cell degradations in space, duplicating radiation effect on minority carriers lifetime by laboratory tests
-
- 11 p1826 A69-24876
-
- Solar cell equation series resistance and junction recombination parameters determination, considering I-V characteristics
-
- 11 p1826 A69-25395
-
- Solar cells physical properties and functions, considering band structure of semiconductors, p-n junction diodes and photovoltaic effect, efficiency calculations and radiation damage
-
- 12 p2015 A69-25864
-
- Solar cells operation in space flight, considering Si photoelectric cells characteristics and complete systems construction for spacecraft power supplies
-
- 12 p2015 A69-25865
-
- GaAs photoelectric devices for radiation detection and light to electric energy conversion, considering photoresistors, photodiodes and solar cells
-
- 13 p2203 A69-27465
-
- Thermionic converter matched with solar cells analyzed for parabolic mirrors, assuming heat conduction power supply to cathode and uniform temperature distribution
-
- 13 p2209 A69-27970
-
- Power supply subsystem for TD1/TD2 satellites with solar cells, discussing design including standby battery for solar eclipse periods
-
- 13 p2209 A69-28481
-
- Space environment simulation tests of cadmium sulfide thin film solar cells, noting output loss
-
- 14 p2405 A69-29538
-
- Ceramic CdS photovoltaic solar cell properties and model, classifying junctions according to preparation method
-
- 14 p2508 A69-29886
-
- Scientific satellite 1 solar cell panels power output dependence on temperature and spin calculated and compared with results for outdoor sunlight
-
- 15 p2552 A69-30072
-
- Cadmium sulfides thin film solar cells for supplying power to instrumentation and data telemetry on longer lived balloons
-
- 15 p2553 A69-31287
-
- Thermal control coatings for solar cells of solar probe Helios
-
- 16 p2867 A69-31741
-
- Power supplies for balloon-borne instruments, describing light flexible NiCd batteries and solar cells used in EOLE project
-
- 16 p2736 A69-31745
-
- Roll-up solar array based on erection of planar sandwich structure from two rolled constituent halves
-
- 16 p2762 A69-32559
-
- Heat pipe application to thermal equalization around ATS-E solar cell mounting panels, comparing predicted and actual performance
-
- [AIJA PAPER 69-630]
-
- 17 p3072 A69-33277
-
- Photovoltaics - IEEE Conference, Pasadena, November 1968
-
- 19 p3249 A69-35678
-
- Gold donor level impurity photovoltaic effect in silicon, noting solar cell efficiency reduction due to minority carrier recombination
-
- 19 p3381 A69-35679
-
- Cu-Cd-S photovoltaic cell models correlated, reporting spectral response and electron microprobe test results
-
- 19 p3382 A69-35682
-
- Copper sulfide-cadmium sulfide heterojunction model for photovoltaic effect, considering surface layer intrinsic absorption and CdS photoconductivity
-
- 19 p3250 A69-35683
-
- Resistivity, layer thickness, postbarrier heat treatment and impurity effects on cadmium sulfide-copper sulfide solar cell
-
- 19 p3250 A69-35685
-
- Ion beam sputtering, evaporation and electrical degradation of Al contacted Si solar cells observed in high temperature cyclic tests
-
- 19 p3250 A69-35686
-
- Electrochemically passivated Ti/Pd/Ag contacts for Si solar cells tested in humidity stress and temperature cycling
-
- 19 p3250 A69-35687
-
- Bonded solderless solar cell panel prototype withstanding high annealing temperature and thermal shock without electrical or mechanical degradation
-
- 19 p3251 A69-35688
-
- Solar cells designed to survive exposure to fission/fusion neutrons and electromagnetic spectrum products of nuclear weapon detonation
-
- 19 p3251 A69-35689
-
- Multilayer multijunction solar cells with carrier generation within diffusion length of junction, discussing epitaxial techniques
-
- 19 p3251 A69-35690
-
- Solar cell characteristics at low temperatures, noting efficiency increase with decreasing temperature
-
- 19 p3251 A69-35691
-
- Lithium-doped silicon solar cells development for radiation environments, discussing contractor functions, dopants, etc
-
- 19 p3251 A69-35692
-
- Lithium doped solar cell irradiation by strontium 90 radioisotope, discussing electron flux rate, spectrum and recovery rates
-
- 19 p3251 A69-35693
-
- Radiation damage and recovery of lithium-diffused silicon p-n solar cells, measuring photovoltaic parameters as function of gamma radiation fluence
-
- 19 p3251 A69-35694

Li variation effects on solar cell properties indicating cell performance control by amount introduced near p-n junction

19 p3252 A69-35695

Photoresponse and minority carrier diffusion length long term stability of Li doped solar cells after proton, neutron and electron irradiation

19 p3252 A69-35697

Injection level effects on minority carrier lifetimes in lithium-doped devices and solar cells irradiated by electrons and reactor neutrons

19 p3252 A69-35698

Thin silicon solar cells environmental tests, evaluating temperature and humidity effects on various contacts and coatings

19 p3252 A69-35699

Attitude control rocket exhaust plume impingement effect on electrical performance and mechanical damage of commercial silica covered silicon solar cells

19 p3252 A69-35700

Proton irradiation effects on current degradation at fixed voltages of silicon solar cells with coverslips

19 p3252 A69-35701

Optimum solar cell cover glass systems selected by studying interplanetary space environment effects of proton impact, temperature and concurrent illumination on radiation damage

19 p3253 A69-35702

Solar cell integral covers optical losses in vacuum as function of degradation by UV exposure, noting accelerated testing for time-cost reduction

19 p3253 A69-35703

Solar cell radiation damage during 416.8 days in synchronous orbit on satellite ATS 1, discussing radiation shields

19 p3253 A69-35704

Cadmium sulfide solar cells and Kapton coverslips under proton irradiation, noting annealing of damage in samples exposed to air

19 p3253 A69-35705

Energy dissipation of solder-covered and solderless solar cells with TiAg contacts as function of storage time, temperature and humidity

19 p3253 A69-35706

560 W deployable solar array consisting of very thin Si solar cells mounted on polyimide film, initiating deployment by duplicated pyrotechnic actuators

19 p3253 A69-35707

Large area Si solar cell arrays design, considering environment, cell layout, thermal expansion, coverslips fabrication, costs, etc

19 p3253 A69-35708

Shadow effects on current-voltage characteristics of solar cell array circuits, developing mathematical models

19 p3254 A69-35709

Integrated thin film solar cell array consisting of CdS cells deposited on Kapton single sheets connected in series and covered by Mylar single sheet

19 p3254 A69-35710

Solar cell retractable array for spacecraft multikilowatt power generation

19 p3254 A69-35711

Solar cells volt-ampere characteristics calibrated at various solar incidence angles on LES-6 satellite in synchronous orbit

19 p3254 A69-35712

Solar cell degradation experiments on LES 4 and 5 satellites, discussing decay values and times for Si and CdTe cells with different cover thicknesses

19 p3254 A69-35713

Secondary power sources for space applications in solar arrays, static and dynamic thermal systems, high power batteries and fuel cells, discussing NASA machinery procurement

19 p3255 A69-36323

Photovoltaic solar cell power technology application to space use and exploration [ASME PAPER 68-WA/SOL-1]

19 p3255 A69-36418

Aluminum doped silicon solar cell energy loss coefficient under proton and high energy electron irradiation

20 p3465 A69-37911

Optimization of RF ion thruster cluster engines for ascending trajectory, discussing unfolding mechanism of solar cell panels

23 p4203 A69-41933

Solar cell power systems for manned space stations, summarizing studies of battery power system designs

23 p4068 A69-42242

Fuel cell /battery and solar array/battery systems for manned Apollo Applications Program /AAP/ space vehicles, considering mission and power requirements

23 p4069 A69-42244

Performance degradation in cadmium sulfide solar cells, discussing cause identification technique, I-V curve parameter changes, etc

23 p4070 A69-42271

Integral coverslip development for Si solar cells, considering borosilicate glass fusing on cell surface and RF and high vacuum ion beam sputtering

23 p4070 A69-42272

Hot spot failure modes in solar cell arrays noting protection through I-V characteristic control

23 p4142 A69-42273

Silicon solar cell panels, studying roles of solder, interconnector metals and substrate materials in failures under thermal cycling

23 p4070 A69-42274

Apollo Telescope Mount /ATM/ solar cell module electrical performance testing using sunlight simulation

23 p4072 A69-42286

Solar cells arrays degradation in Intelsat spacecraft at synchronous altitude, noting shielding gaps and low energy proton influence

23 p4072 A69-42287

Solar array configurations and performance on Martian surface, including hard lander design and surviving shock levels

23 p4073 A69-42289

Spacecraft Si cell solar array using self rigidizing folded panels with flexible substrates for increased power/weight and power/stowage volume ratios

23 p4073 A69-42290

Lightweight large area solar cell arrays for space programs with multikilowatt predicted performance, noting rollout array orbital flight testing

23 p4073 A69-42291

Spacecraft solar cell near-maximum power operation by tracking optimum value with array temperature sensor

23 p4075 A69-42303

Asteroid exploration by solar photovoltaic powered ion propelled probe, discussing spacecraft design, mission and 1975 Mariner utilization [AAS PAPER 69-322]

24 p4381 A69-42868

Solar protons and alpha particles measurements at synchronous orbit altitudes providing data for solar cell shield design to prevent radiation damage

24 p4369 A69-43265

SOLAR CHROMOSPHERE U CHROMOSPHERE

SOLAR COLLECTORS

Computation and optimization of energy distribution over randomly oriented elements of radiation receiving surface of hollow collector of concentrator type solar device

09 p1442 A69-22534

Solar simulator with 20 kw xenon lamps, discussing performance, versatility and problems with collectors, folding mirrors and cooling system

15 p2586 A69-30384

Solar power concentrator-absorber system, discussing flux distribution in focal plane and cavity heater optimization

17 p3022 A69-33795

SOLAR COMPASSES

U BEACONS
U GYROCOMPASSES
U MAGNETIC COMPASSES
U RADAR BEACONS
U RADIO BEACONS

SOLAR CONSTANT

Clear atmosphere model based on path of sight equilibrium radiance and nonabsorption permitting integration of equation of transfer

07 p1130 A69-19643

Solar electromagnetic radiation spectral distribution from ground level, rocket and satellite observations to obtain value of energy received at top of atmosphere

09 p1575 A69-21645

Solar irradiance spectral distribution data normalized and combined with spectral absorptance of satellite surface coatings, obtaining absorbed energy for spectral range

09 p1576 A69-21646

Solar constant measurement, reviewing instruments and results of Eppley-JPL program using high altitude jet aircraft and rocket research vehicle

09 p1576 A69-21647

Solar constant and spectral irradiance curve for zero air mass obtained from aircraft measurements

23 p4216 A69-42191

SOLAR CORONA

Geomagnetic disturbance activity forecasting method using solar coronal streams, noting reliability of test forecasts

01 p0150 A69-10372

Solar corona electron density, polarization, temperature and monochromatic emission during November 1966 eclipse

02 p0310 A69-11457

Space observations of solar intermediate corona, discussing balloon and rocket experiments and limitation of ground based observations [AAS PAPER 68-217]

02 p0313 A69-11483

Solar coronal ion abundance analyses from extreme UV emission lines

02 p0327 A69-12719

Solar corona delay effects on pulsar signals due to inhomogeneities in coronal electron density

02 p0328 A69-12727

Radar observations of sun, determining reflected radio signal component formed by combination scattering in coronal plasma oscillation

03 p0505 A69-13082

Mean annual intensity distribution of 5303 angstrom coronal line on solar limb determined for 11-year solar activity cycle

03 p0506 A69-13084

Optical narrow bandpass filter designed for precision solar corona observations, utilizing interferential polarization and thermooptical compensation

03 p0506 A69-13085

Temperature dependence of O VIII Lyman alpha/Lyman beta radiation ratio in solar corona, noting coronal temperature

03 p0516 A69-14042

Solar wind abundance measurements at earth orbit related to solar corona

03 p0503 A69-14047

Collisional ionization cross section for Fe ions evaluated to estimate solar corona temperature

04 p0651 A69-14365

Inner corona Fraunhofer lines invisibility at solar eclipses, emphasizing uncertainty of photospheric absorption lines appearance as electron scattering

04 p0654 A69-14628

Gyro synchrotron emission spectrum and intensity from energetic solar electrons radiating in coronal magnetic fields applied to type IV solar radio bursts

04 p0650 A69-15529

Coronal X ray emission near limbs in 16-40 A during solar eclipse

04 p0650 A69-15531

Coronal structure predicted for September 22, 1968 solar eclipse by model constructed for large structure of coronal and interplanetary magnetic fields

05 p0818 A69-15602

Type 3 bursts spectra graphical representation, giving probable solar origin and curves of corona temperature

05 p0824 A69-16060

Type 2 radio bursts and corona magnetic field over active center

06 p0985 A69-16979

Solar corona effects on tail of comet Ikeya-Seki, describing model for interaction between tail and corona

06 p1000 A69-16982

Solar wind, discussing corona, radio sources, radio bursts, comet tails, cosmic rays, etc

06 p1012 A69-18239

Solar wind and magnetosphere, discussing hydrodynamic expansion of solar corona

07 p1207 A69-19353

Solar corona X ray emission during flares and under quiet sun conditions investigated by satellite with X ray heliograph

07 p1210 A69-19614

Hartree-Fock calculations of coronal forbidden transition lines in Ar I isoelectronic sequence, obtaining wavelengths, magnetic dipole and electric quadrupole transition probabilities

08 p1385 A69-20071

Excitation cross sections of Fe XIV lines in solar coronal spectra, comparing computations with Coulomb-Born approximation

08 p1392 A69-20563

Dimensions, temperature and electron density of quiet solar corona from radio interferometer measurements, noting activity and temperature at solar maximum and minimum

08 p1393 A69-20573

Spectrum variations of type 4 radio burst as source rises through solar corona, determining electron density and magnetic field distributions in corona

08 p1380 A69-20775

Formation ratios of light isotopes in spallation reactions compared to observed stellar and solar abundances of lithium, beryllium and boron, discussing astrophysical implications

08 p1401 A69-20902

Present state of abundance determination in solar corona, discussing forbidden and UV lines analysis
08 p1402 A69-20907

Type 3 solar radio noise bursts at hectometer wavelengths, deducing coronal electron temperatures from decay rates
09 p1594 A69-21665

Quantum mechanical description of ionizing reactions of highly charged positive ions in solar corona, obtaining approximate sum and selection rules
09 p1596 A69-22054

Solar moving type 4 burst emitting synchrotron radiation, noting electron acceleration in collisionless shock wave in corona
09 p1578 A69-22058

Coronal open helmet streamer configurations, noting minimum temperature requirement for constriction to true geometrical throat
09 p1598 A69-22177

Green and red coronal line polarization observed during solar eclipses, discussing nonpolarization of red line and observation instrument error
09 p1600 A69-22204

Outer solar coronal IR radiance measured by ground telescope and stratosphere balloon flight, noting interplanetary dust thermal emission
09 p1600 A69-22205

Viscosity coefficients approximation for chemical compositions in chromosphere and coronal gas
09 p1602 A69-22217

Solar outburst and storm accompanying 9 June 1968 flare, noting radio evidence for coronal instability before flare
09 p1582 A69-22747

Radio ray scattering resulting from traversing anisotropically turbulent solar corona, noting refraction effect on signal pulse arrival time
10 p1773 A69-22960

Total solar eclipse of September 22, 1968 in Siberia, discussing instrumentation and solar light radiation, corona, prominences, spicules, etc
10 p1782 A69-23696

Simultaneous photometric observations of coronal emission lines during July 1966 solar proton flare plotted on synoptic charts
10 p1763 A69-23731

Coronal line intensity distribution for period of proton flare
10 p1763 A69-23732

K coronameter observations used to construct electron density models of corona above proton flare region of July 1966
10 p1763 A69-23733

Coronal IR observations during solar eclipse revealing thermal emission zone at predicted interplanetary dust vaporization region
10 p1789 A69-24131

Type 2 radio burst dynamic spectra determination for finding shock wave and magnetic field parameters above active corona region
11 p1945 A69-24243

Green function solution to Maxwell equations for interplanetary and coronal magnetic fields above photosphere, considering field at source surface
11 p1958 A69-24429

Monograph on internal structure of sun corona covering variations in intensity and width of coronal lines, inhomogeneity, quasi-homogeneous and anisothermic coronas, etc
11 p1961 A69-25103

Magnetic fields, green corona emission and filaments relationship at high solar latitudes using synoptic charts
11 p1964 A69-25416

Photospheric magnetic fields, coronal emission and filaments distribution relationship with 1420 MHz radio emission, noting brightness and plasma density increase
11 p1964 A69-25417

Solar activity complex development based on magnetic, photospheric, chromospheric and coronal observations
11 p1964 A69-25418

Forbidden solar corona lines transition probability in vacuum UV region
12 p2157 A69-26334

Solar polar faculae observations, discussing relation to general solar magnetic field and coronal properties, solar high latitude rotation and susceptibility to atmospheric conditions
12 p2160 A69-26897

Solar corona 5303 and 6374 A emission enhancements correlated to 169 MHz S-component, discussing coronal temperature
13 p2347 A69-27717

Coronal features prediction compared to maximum solar activity observations, discussing variations in force free field
13 p2354 A69-28472

Radar observations of sun, determining reflected radio signal component formed by combination scattering in coronal plasma oscillation
14 p2515 A69-28764

Mean annual intensity distribution of 5303 A coronal line on solar limb determined for 11-year solar activity cycle
14 p2515 A69-28766

Optical narrow bandpass filter designed for precision solar corona observations utilizing interferential polarization and thermo-optical compensation
14 p2515 A69-28767

Forbidden transition probabilities of solar corona lines in vacuum UV range
14 p2519 A69-29355

Solar corona magnetic field and polar rays, emphasizing field topology and local magnetic structure
14 p2525 A69-29718

Solar wind origins, discussing corona composition, corpuscular streams, R and M disturbances, etc
15 p2673 A69-30009

Solar wind existence verified by direct measurements of interplanetary magnetic field and plasma, reviewing solar corona studies by satellites and space probes
15 p2679 A69-30010

Hydromagnetic fast shock strength and direction in inhomogeneous gravitational atmosphere with uniform magnetic field, discussing heating in solar corona
15 p2680 A69-30202

Surveyor lunar landing procedures and results including instrumentation, lunar topography, selenology, chemical and physical properties, solar corona and earth laser output observations
15 p2681 A69-30324

Solar corpuscular radiation characterization by stable four streamer structure at near minimum solar activity
15 p2674 A69-30517

Type 3 radio bursts time profile for estimating magnetic field strength in solar corona
15 p2675 A69-30554

Plane electromagnetic wave refraction and scattering in solar corona during eclipsed observations of cosmic sources, calculating angular distribution of radiation intensity
15 p2688 A69-30555

Unsuccessful attempt to observe high charge ion lines generated by dielectronic recombination in solar corona at 5-cm wavelength
15 p2689 A69-30568

Coronal structure during 22 September 1968 eclipse from photographs, showing agreement with prediction by model
15 p2690 A69-30696

Coronal limb enhancement photometric study by spectroheliograms, comparing maximum brightness profiles in lines of different temperature in extreme UV
15 p2693 A69-30781

Temperature and density models for coronal green line enhancements with and without magnetic field effects, using graded height spectrograms
15 p2693 A69-30782

Thermal conductivity coefficients in solar corona and chromosphere computed and tabulated for H plasma
15 p2694 A69-30788

Solar wind and solar breeze theories distinguished, discussing applications to geocoronal hydrogen emission and solar corona expansion
15 p2676 A69-30858

Solar corona observations on eclipse day by Aerobee rocket launched in New Mexico correlated to Siberian total eclipse photograph
15 p2696 A69-31099

Solar corona observed by X ray instrumentation of SOLRAD 8 satellite crossing moon penumbra during solar eclipse of 20 May 1966
15 p2698 A69-31363

Pioneer 6 S band telemetry carrier Faraday rotation during corona occultation measured by deep space tracking antenna
15 p2700 A69-31419

Coronal Fe ionization lines X, XIII and XIV photographed by UV coronagraph
16 p2847 A69-31661

Geomagnetic storms generation interpreted using solar coronal arrangements above central meridian
16 p2777 A69-32100

Nondivergent oscillations in solar atmosphere forming normal modes or free oscillations, assuming free surface of chromosphere coronal interface and large density in convective zone
17 p3029 A69-33048

Lower solar corona composition changes due to pressure and thermal gradients calculated with multicomponent diffusion equations
17 p3030 A69-33059

Solar corona heating ascribed to Landau damping of ionacoustic waves generated in motion of photospheric granules
17 p3030 A69-33060

Active solar centers interactions above photospheric level and through corona linkages, noting MHD shock waves and magnetic field lines
17 p3040 A69-33801

Spatial structure of solar proton flare of 5 April 1960, discussing top ascending emission filament velocity in H alpha and coronal lines
17 p3025 A69-34224

Quiet solar wind model with magnetic field numerically calculated, obtaining coronal electron densities and angular momentum near earth
18 p3186 A69-34301

Radio echoes relationship to active parts of solar corona, noting agreement with data on type 3 radio bursts source location
18 p3201 A69-35207

White light solar corona brightness distribution observations /1964-1967/, considering solar radio flux relationship and equatorial electron densities
18 p3205 A69-35394

Primitive solar nebula physical model considered under angular momentum conservation in collapsing fragment
19 p3406 A69-36074

Forbidden lines in solar corona, discussing ionization equilibrium and excitation of levels in highly ionized atoms
19 p3422 A69-36216

Emission line spectrum for ionization and excitation in solar coronal structures, tabulating intensities from ground based eclipses observations
19 p3422 A69-36217

Two photon decay of metastable levels of hydrogenic and He-like ions in solar corona, depopulating via proton collisional excitation to 2p level
19 p3396 A69-36218

Intensity ratios effect of forbidden Fe and Ca transitions in solar corona on Fe/Ca ratio, noting cascading configurations
19 p3422 A69-36219

H alpha filtergrams and spectra of solar corona arch filament systems indicating downward and upward motions produced by magnetic field
20 p3588 A69-37543

Stability analysis of Kippenhahn-Schluter model of solar corona filaments against arbitrary perturbations treated in MHD approximation using Bernstein energy principle
20 p3588 A69-37544

Monochromatic coronal emission line photographs improved by composite technique
20 p3539 A69-37547

Solar microwave emission relationship to geomagnetic activity, analyzing statistically source intensity and model of coronal condensation associated with sunspots based on electron densities
20 p3589 A69-37557

Type 3 bursts spectra graphical representation, giving probable solar origin and curves of corona temperature
20 p3591 A69-37970

Solar magnetic field measurements for fine structure of magnetic asymmetry at different heights and within sunspots, discussing asymmetry for corona and interplanetary space
22 p4010 A69-39990

Solar corona photographic study during 1961 total eclipse using quadruple camera, providing intensities, amount and direction of polarization
22 p4001 A69-40001

Diffuse coronal emission observation during total eclipse of February 1961 near solar prominences and polar ray form investigation in northern part of corona
22 p4002 A69-40002

Medium sized solar radio events from peak intensities, spectrum characteristics and coronal magnetic field role
22 p4020 A69-40299

Type 3 solar radio bursts observed during April-October 1967 for two alternative models of active region streamers in outer corona
22 p4003 A69-40300

SOLAR CORPUSCULAR RADIATION

Coronal jet resulting from chromospheric burst observed during 22 September 1968 total solar eclipse
22 p4028 A69-40716

Thermal continuum radiation from coronal plasmas at soft X ray wavelengths, investigating variations effect in element abundances
23 p4207 A69-42406

Solar corona instabilities and shock waves indicated by type 3 and 2 bursts, considering electrons ejection
24 p4378 A69-42689

SOLAR CORPUSCULAR RADIATION

Biological effects in man due to heavy particles emission during major solar cosmic ray events, noting protective effect of human body
03 p0374 A69-13500

Solar particle events of May 23 and 28 1967, noting related solar and terrestrial phenomena
03 p0516 A69-14046

Solar neutron production and propagation to earth, discussing particle detectors
06 p0989 A69-17281

Long lived streams of low energy solar electrons and protons and association with bright flares or solar active regions
07 p1206 A69-19249

Null solar neutrino flux possible relation to 2 year solar cycle, discussing energetic disturbances at solar core and sunspots
08 p1377 A69-19902

Coronal open helmet streamer configurations, noting minimum temperature requirement for constriction to true geometrical throat
09 p1598 A69-22177

Ionization in lower ionosphere over polar cap under solar corpuscular fluxes measured by radio wave absorption
10 p1759 A69-22838

Secondary corpuscular stream effect on diurnal variations in cosmic ray intensity obtained from statistical analysis
10 p1769 A69-23904

Geomagnetic micropulsations fluctuations during solar activity cycle showing changes in excitation frequency with change in corpuscular fluxes parameters
10 p1687 A69-23919

Solar neutron flux measurement at earth in energy region 20-120 Mev by detector in balloon flight
11 p1945 A69-24421

Solar wind particles acceleration and transformation into radiation belt particles
11 p1948 A69-24855

Solar wind origins, discussing corona composition, corpuscular streams, R and M disturbances, etc
15 p2673 A69-30009

Solar corpuscular radiation component from satellite and interplanetary space probe geophysical data, discussing interplanetary magnetic field geometry and corpuscular fluxes
15 p2684 A69-30516

Solar corpuscular radiation characterization by stable four streamer structure at near minimum solar activity
15 p2674 A69-30517

Solar corpuscular and UV radiation variation relationship to midlatitude airglow intensity in O I line
16 p2850 A69-32322

Magnetic storm energy balance, assessing solar corpuscular flux energy consumption in and beyond magnetosphere
17 p2964 A69-33959

F region during earth passage through solar corpuscular stream, analyzing critical frequencies, virtual height, magnetogram H component and ionospheric storm effects attributed to downward drift
17 p2967 A69-33989

Geomagnetic storms and Forbush decreases accounted for by interplanetary solar corpuscular streams effects described by interplanetary magnetic field structure, noting independence of flares
18 p3187 A69-34937

Stream structure in interplanetary magnetic field during 1966, analyzing geomagnetic activity and solar particles and Forbush decrease anisotropy
18 p3199 A69-34938

Cosmic ray approach directions computation for high latitude stations, discussing results for low rigidity galactic cosmic rays and solar corpuscular events detection
18 p3187 A69-34940

Solar neutrons upper limits measured for 28 July 1967 importance I flares
18 p3187 A69-34959

Geomagnetic storms data compilation /1957-1964/, showing solar activity effect on solar corpuscular stream velocity
20 p3587 A69-37036

Lepton nonconservation implications for experiments involving solar neutrinos, showing effect on capture rate at earth for pep neutrinos
23 p4194 A69-41596

Solar flare-associated radio bursts, reviewing solar radio measurements based on X ray and particle observations
24 p4372 A69-43614

Solar energetic particle effects during polar cap absorption observed in earth upper atmosphere and at ground level
24 p4373 A69-43618

SOLAR COSMIC RAYS

Solar cosmic rays diffusion relationship to interplanetary magnetic field power spectrum from high energy proton and electron observations
01 p0147 A69-11243

Sudden ionospheric disturbance development and characteristics of solar cosmic ray flares, associated X ray emissions and high energy particle generation
02 p0308 A69-12398

Spatial variations in particle intensity near and inside magnetosphere during September 1966 solar cosmic ray events, noting magnetosphere screening effectiveness
02 p0309 A69-12740

Solar cosmic radiation, particle acceleration, energetic particles as sample of sun and propagation of particles from sun to earth
03 p0498 A69-12934

Biological effects in man due to heavy particles emission during major solar cosmic ray events, noting protective effect of human body
03 p0374 A69-13500

Solar proton flares injecting cosmic ray bursts into solar system, discussing optical, radioastronomical and satellite observations
04 p0649 A69-15327

Isotopic composition in near-surface regions of meteorites due to nuclear processes with low energy solar particles
06 p0989 A69-17282

Solar cosmic rays anisotropies including solar flare particles propagation
06 p0990 A69-17288

Electron formation in lower ionosphere due to cosmic ray-atmosphere interaction, analyzing ionization of subrelativistic and relativistic solar and galactic cosmic rays
06 p0920 A69-17726

Solar cosmic ray dose rate and total dose magnitude predictions based on Epeak and isotropic diffusion models
06 p0997 A69-18160

IMP F and G solar cosmic ray spectrometer utilizing FET analog multiplier for onboard particle identification data processing
07 p1135 A69-19197

Sunspot groups area changes relationship to cosmic ray flare occurrences
07 p1206 A69-19252

Soviet monograph on diurnal solar cosmic ray variations from maximum to minimum solar activity, discussing model based on anisotropic particle scattering theory
07 p1209 A69-19500

Diffusion model for propagation of solar cosmic rays in interplanetary space, obtaining injection spectra for solar flare protons
08 p1379 A69-20613

Low energy solar cosmic ray proton flux characteristics observed by Injun 1 satellite after July 1961 sudden commencement magnetic storm
09 p1576 A69-21707

Peaks and time intensity profile of energetic X rays and cosmic rays observed by OGO-C ion chamber on May 23, 1967 flare event
09 p1579 A69-22182

Solar cosmic rays proton intensity time variations and diffusion coefficient obtained by satellites, balloons and ground stations observations
10 p1755 A69-22812

Radioactivity levels estimation at surface and in bulk of solar system planets caused by galactic and solar cosmic rays
10 p1756 A69-22813

Diffusion coefficient and cosmic ray motion in solar system, using satellite data of interplanetary magnetic field
10 p1757 A69-22822

Galactic and solar cosmic ray modulation in interplanetary space during different phases of 11 year solar activity cycle
10 p1758 A69-22833

Forbush effects energy spectra and cosmic ray anisotropy beyond magnetosphere analyzed during solar activity minimum, using data from neutron monitors global network
10 p1758 A69-22835

Solar diurnal variation amplitude and phase instability, considering anisotropic cosmic ray fluxes superposition
10 p1759 A69-22837

Proton flares of July 7, 1966, September 2, 1966 and January 28, 1967, noting energy spectra and time dependence of proton flux
10 p1767 A69-23764

Time history of July 7-10 1966 PCA event analyzed using 16 riometers and concurrent satellite observations of solar cosmic radiation
10 p1683 A69-23770

Solar cosmic ray event of July 7 1966, noting sudden cosmic noise absorption reduction and particle absorption domination start at 0120 UT
10 p1768 A69-23771

Secondary corpuscular stream effect on diurnal variations in cosmic ray intensity obtained from statistical analysis
10 p1769 A69-23904

Galactic and relativistic and subrelativistic solar cosmic rays effect on electron production rate in ionosphere, detailing low energy SCR-atmosphere interactions
13 p2333 A69-28544

Solar cosmic ray flare of 28 January 1967 observed by neutron monitors, determining emission and particle spectrum at atmosphere boundary
14 p2513 A69-29066

Solar cosmic rays diffusion enclosure in interplanetary space magnetic boundary suggested from balloon, satellite and ground observations of solar flare neutron component
14 p2513 A69-29067

Soviet book on solar cosmic rays covering origin, propagation, energy spectrum, diffusion dependence on particle energy and distance, solar flares, etc
14 p2514 A69-29816

Electron production rate in low ionosphere, discussing parameters of ionizing solar cosmic rays and earth environment
17 p3022 A69-33035

Solar flares with subcosmic radiation in proton active region of May 1967, discussing X ray emission effects, calculating D region recombination coefficient and electron concentration
17 p3025 A69-34226

Solar cosmic ray anisotropies in terms of model with particles propagating along interplanetary magnetic field undergoing pitch-angle scattering
18 p3189 A69-35400

Solar system low energy particle flux at 2-3 AU distance during last 10 million years, discussing cosmic radiation flux
19 p3411 A69-36097

Cosmic rays nucleonic component latitude at solar minimum activity, using IGY neutron monitor
19 p3396 A69-36411

Chemical composition of galactic and solar cosmic rays, discussing differences from universal cosmic abundances, using Cerenkov counters, emulsions, etc
22 p4002 A69-40090

Diurnal variations in solar cosmic ray muon component near sea level, using scintillation counters assembled in muon telescope array
23 p4207 A69-42498

Solar cosmic ray anisotropy measurement by Explorer 34 satellite during solar flare events
24 p4373 A69-43619

Polar cap ionospheric response to solar cosmic ray events observed by Mariners 2 and 4 solar proton measurements used to test magnetosphere models
24 p4373 A69-43621

SOLAR CYCLES

NT SUNSPOT CYCLE

Chromospheric flares photometric measurements during near minimum solar activity, discussing characteristics
01 p0149 A69-10127

Cosmos satellites monitoring electrons distribution in inner radiation belt suggest intensity stability for solar activity cycle
01 p0147 A69-11309

Ionospheric sporadic E layer reflection duration during solar activity cycle analyzed as function of critical frequency

02 p0207 A69-11684

Mean annual intensity distribution of 5303 angstrom coronal line on solar limb determined for 11-year solar activity cycle

03 p0506 A69-13084

Diurnal, magnetic and solar cycle dependences of auroral emission variations and auroral occurrence

03 p0420 A69-13325

F layer disturbance showing pronounced difference in corpuscular flux effect on day and nighttime ionosphere

03 p0512 A69-13517

Solar flux variations in 44-60 A band during ascent of current solar cycle /Number 20/ measured by Solrad 8 satellite

04 p0650 A69-15530

Solar modulating function form changes resulting in hysteresis near solar minimum

05 p0815 A69-16249

Sunspot group classifications made at Zurich and Catania during 19th solar cycle compared to determine seeing influence

05 p0826 A69-16388

Solar cycle influence on winds in lower ionosphere

05 p0759 A69-16421

Semiannual variations in exospheric density near 1100 km derived from Echo 2 orbit, noting phases during solar cycle

06 p0918 A69-17385

Central Fraunhofer line intensities near solar minimum compared to Soviet results for possible solar cycle variation

08 p1386 A69-20075

Sunspot activity dependence on phase of eleven year cycle and heliographic latitude, discussing fine structure of butterfly diagrams

08 p1379 A69-20611

Eleven year cyclicity of geomagnetic activity from Sverdlovsk Observatory data, noting possible relation with structural features of solar activity cycles

09 p1486 A69-21552

Solar activity influence on cosmic ray intensity 11 year variation, taking into account heliolatitudinal movement of sunspot regions in solar cycle as evidence of density gradient

10 p1754 A69-22802

Numerical decile value maps of sporadic E layer ionization critical frequency for each month of solar cycle minimum and maximum year

10 p1682 A69-23418

Geomagnetic micropulsations fluctuations during solar activity cycle showing changes in excitation frequency with change in corpuscular fluxes parameters

10 p1687 A69-23919

Solar and lunar/solar harmonics determination, noting effects of moon on values of horizontal magnetic component

11 p1965 A69-25555

Linear extrapolation of stationary stochastic process predicting fluctuations of minimum and maximum periods in solar cycle

12 p2149 A69-26221

Cosmic rays during 11-year solar cycle, short term variations and radial gradient based on Luna, Zond and Venera probes and Cosmos observations

13 p2326 A69-27351

Solar cycle kinematical model based on field amplification by solar differential rotation including fluctuations in eruption rate

13 p2337 A69-27548

Ionospheric sporadic E layer reflection duration during solar activity cycle analyzed as function of critical frequency

13 p2224 A69-28715

Mean annual intensity distribution of 5303 A coronal line on solar limb determined for 11-year solar activity cycle

14 p2515 A69-28766

Cosmic ray intensity during solar cycles, considering minima relationship to Bartel index maxima and solar wind modulation theory

14 p2515 A69-29967

Solar activity history and morphology /1964-1965/

15 p2679 A69-30006

Cosmic ray variation theory, presenting data on coupling of solar activity with large scale characteristics of solar wind during 11-year cycle

15 p2673 A69-30015

Solar cycle effect on high latitude magnetic activity, discussing annual variations and Lassen auroral zone model confirmation

15 p2598 A69-31207

Latitude variations of delays between spread F and magnetic activity shown to be different at various parts of solar cycle

16 p2779 A69-32194

Trieste astronomical observatory optical and radio solar photosphere observations in 1967, including solar cycle and north-south symmetry

16 p2858 A69-32206

Eleven year cyclicity of geomagnetic activity from Sverdlovsk Observatory data, noting possible relation with structural features of solar activity cycles

16 p2784 A69-32547

Lunar tidal oscillations in F 2 layer critical frequency and F region minimum virtual height at Huancayo during IGY/IGC to study solar cycle effects

16 p2784 A69-32613

Surges statistical properties observed in Sweden /1957-1967/ noting latitude distribution pattern, radio emission association, rate dependence on solar cycle, etc

18 p3204 A69-35393

Solar cycle line in horizontal force of earth magnetic field resolved by power spectrum analysis suggesting 80 year cycle

18 p3205 A69-35414

Solar cycle variation of extreme UV radiation from total solar disk under nonflare conditions by photoelectric measurements

20 p3592 A69-38103

Critical frequency variations of F 2 layer and M/3000/F 2 with sunspot number for 19th solar cycle, noting dependence on geomagnetic latitude

21 p3715 A69-38560

Solar cycle and slowly varying components correlation with soft X ray radiation based on spacecraft measurements

22 p4004 A69-40504

Ionospheric vertical columnar electron content at midlatitudes near solar cycle minimum based on Faraday rotation data from Explorer 22

22 p3939 A69-40505

Babcock solar activity periodicity theory, correlating spots displacement and coronal magnetic field intensity changes

23 p4208 A69-41283

Sudden and gradually developing geomagnetic storms with 27 day recurrence period and relation to 11 year solar activity cycle

23 p4156 A69-41849

Geomagnetic activity hourly and daily variations during solar cycle at Huancayo

23 p4162 A69-42442

Diurnal and solar cycle variations of thermosphere density and temperature generated by solar EUV input and tidal wave, using two dimensional model

24 p4367 A69-43003

SOLAR DISK

U SUN

SOLAR ECLIPSES

Solar corona electron density, polarization, temperature and monochromatic emission during November 1966 eclipse

02 p0310 A69-11457

Solar eclipse effect on geomagnetic field at and near dip equator observed at Huancayo Observatory, Peru

02 p0241 A69-11727

Solar eclipse effects on ionospheric conductivity and geomagnetic field at and near dip equator observed at Huancayo, Peru

02 p0241 A69-11728

Sunrise effects in lower D region by solar eclipse, discussing anomaly in ionospheric absorption due to negative ion factor or recombination coefficient

02 p0246 A69-12767

Narrowing of ionospheric absorption anomaly in D region during solar eclipses in long and medium wave ranges due to recombination equation variability

02 p0246 A69-12770

Inner corona Fraunhofer lines invisibility at solar eclipses, emphasizing uncertainty of photospheric absorption lines appearance as electron scattering

04 p0654 A69-14628

Coronal X ray emission near limbs in 16-40 A during solar eclipse

04 p0650 A69-15531

Solar X ray source identification using D layer ionization behavior during eclipse

04 p0650 A69-15533

Coronal structure predicted for September 22, 1968 solar eclipse by model constructed for large structure of coronal and interplanetary magnetic fields

05 p0818 A69-15602

Stratospheric temperature, wind and ozone concentration measurement during solar eclipse by sounding rocket system

06 p0916 A69-17008

Lunar umbra interception by Titus rockets during solar eclipse, measuring UV and IR flux

06 p0986 A69-17101

Solar eclipse variations of E layer critical frequency explained by quasi-equilibrium between electron density and ionizing soft X ray radiation

07 p1204 A69-18823

Heat sources in E region from electron temperature data analysis recorded by rockets during eclipses in July 1963

09 p1490 A69-21771

Solar occulting disk diameter at radio wavelengths derived from consideration of slightly deviated rays

09 p1607 A69-22432

Total solar eclipse of September 22, 1968 in Siberia, discussing instrumentation and solar light radiation, corona, prominences, spicules, etc

10 p1782 A69-23696

Lower ionosphere electron densities measured during solar eclipse by Nike-Apache rockets

12 p2073 A69-26861

Vertical drift velocity of ionospheric F region during eclipse and on control day based on chemical reaction coefficients models, discussing electron density distribution

12 p2077 A69-27109

Solar eclipses phases and elements calculation by Fortran language computer, using least squares method

13 p2336 A69-27447

E layer fine scale structure, F 1 reactions and F 2 reflected signals analysis during 20 May 1966 solar eclipse

13 p2255 A69-28541

Rocket sounding measurements of ionospheric D region electron density profile during 20 May 1966 solar eclipse, discussing D region ionization source

14 p2439 A69-29116

Collection of Soviet papers on annular solar eclipse of 20 May 1966

15 p2685 A69-30530

Geometric shape of lunar profile from annular phase of 20 May 1966 annular solar eclipse coronagraph plates, applying Fourier series and Pascal limaçon approximation

15 p2686 A69-30531

Lunar coordinate corrections from solar ring coronagraphic observations of 20 May 1966 annular solar eclipse

15 p2686 A69-30532

Error assessment for 20 May 1966 annular eclipse observation point and observation time determination

15 p2686 A69-30533

High speed plate holder and shutter mechanisms for observing 20 May 1966 annular solar eclipse

15 p2686 A69-30534

Coronal structure during 22 September 1968 eclipse from photographs, showing agreement with prediction by model

15 p2690 A69-30696

Solar corona observations on eclipse day by Aerobee rocket launched in New Mexico correlated to Siberian total eclipse photograph

15 p2696 A69-31099

Solar radiation actinometric and pyranometric observations during 20 May 1966 eclipse, examining IR component and spectral radiation energies

15 p2697 A69-31257

Solar corona observed by X ray instrumentation of SOLRAD 8 satellite crossing moon penumbra during solar eclipse of 20 May 1966

15 p2698 A69-31363

Equatorial electrojet north-south cross sections in Pacific observed by airborne equipment during magnetically quiet day, moderately disturbed day and solar eclipse

16 p2777 A69-32182

Chromospheric spectrum outside of eclipse, wave lengths 3040 to 9266 A, listing emission lines taken at McMath solar telescope

16 p2861 A69-32257

Radio observation of 20 May 1966 solar eclipse at 9470 and 3300 MHz, discussing brightness distribution of S component sources

17 p3030 A69-33057

Solar eclipse of 20 May 1966, comparing satellite-borne X ray and UV photometry with radio astronomical observations

17 p3023 A69-33058

Radio observations of 30 May 1965 total solar eclipse at Manue Island, discussing radio brightness

20 p3616 A69-38304

Radio emission data from 20 May 1966 partial solar eclipse, giving radio noise and brightness distribution data

22 p4010 A69-39986

Solar corona photographic study during 1961 total eclipse using quadrupole camera, providing intensities, amount and direction of polarization

22 p4001 A69-40001

Diffuse coronal emission observation during total eclipse of February 1961 near solar prominences and polar ray form investigation in northern part of corona

22 p4002 A69-40002

Identification, position and temperature of solar X ray sources derived from D layer ionization radio absorption behavior during eclipses and lunar reflection

22 p4004 A69-40308

Photoelectric spectrometer observations of 1966 total solar eclipse, discussing limb darkening curves for regions of continuum 1.5 Å wide around 5728 and 6404 Å

22 p4027 A69-40659

Coronal jet resulting from chromospheric burst observed during 22 September 1968 total solar eclipse

22 p4028 A69-40716

Ionospheric electron content satellite measurements during 20 May 1966 annular solar eclipse

22 p4007 A69-40916

Total solar eclipse of 5 February 1962 observed for spectrophotometry of flash spectrum, finding abnormal intensity gradients of H alpha and D3 lines

24 p4388 A69-43636

SOLAR ENERGY

Satellite power generation and transmission system for solar energy conversion, noting estimates of surface area and weight of collectors

02 p0323 A69-12296

Near mesopause atmospheric layer energy balance, noting atomic oxygen diffusion role in redistributing absorbed solar energy among atmospheric layers

03 p0422 A69-13408

Gyro synchrotron emission spectrum and intensity from energetic solar electrons radiating in coronal magnetic fields applied to type IV solar radio bursts

04 p0650 A69-15529

Sun as calibration signal source for L and S band telemetry, discussing receiving system noise temperature determination and antenna gains

07 p1082 A69-19113

Liquid mercury cathode thrusters characteristics satisfying constraints imposed by solar flux variations with distance from sun

[AIAA PAPER 69-237]

09 p1565 A69-21246

Radiant flux reflected by mirror and incident on receiver for paraboloidal solar devices, obtaining heat loads and radiant energy formulas

09 p1436 A69-21803

Solar radio emission bursts periodicity relation to burst intensity

12 p2157 A69-26234

Solar array energy performance as function of orbital parameters and spacecraft attitude

13 p2203 A69-27419

Equatorial mounted solar energy concentrator efficiency compared to unconcentrated sunlight and artificial UV-visible light source in reducing Pb tetraacetate solution in acetic acid

16 p2736 A69-31814

Digital simulation of transient solar still processes, using finite difference approach for heat flow to and from soil

16 p2765 A69-31816

Satellite solar power station proposed for power generation for future requirements, discussing world energy needs and finiteness of fossil fuel reserves

16 p2867 A69-31817

Earth-reflected solar energy /albedo energy/ distribution model, assuming isotropic scattering by homogeneous atmosphere

[AIAA PAPER 69-591]

17 p2961 A69-33292

Solar energy release by quark fusion catalysis of alpha reaction without production of neutrinos, noting temperature dependent reaction rate

18 p3186 A69-34643

SOLAR ENERGY ABSORBERS

Solar irradiance spectral distribution data normalized and combined with spectral absorptance of satellite surface coatings, obtaining absorbed energy for spectral range

09 p1576 A69-21646

Computation and optimization of energy distribution over randomly oriented elements of radiation receiving surface of hollow collector of concentrator type solar device

09 p1442 A69-22534

Solar power concentrator-absorber system, discussing flux distribution in focal plane and cavity heater optimization

17 p3022 A69-33795

Earth albedo in lower latitudes measured by satellites and surface stations, comparing solar energy absorption by oceans and atmosphere

20 p3591 A69-38058

SOLAR FACULAE

U FACULAE

SOLAR FLARES

Chromospheric flares photometric measurements during near minimum solar activity, discussing characteristics

01 p0149 A69-10127

Ionized calcium lines in spectra of light bridges of sunspots, observed by diffraction spectroscopy, indicating similarity to chromospheric flares

01 p0154 A69-10894

Solar flare mechanism from analysis of energy transfer in quiet solar atmosphere, discussing convection, radiation, mechanical and MHD waves and thermal conduction

01 p0145 A69-10990

Solar X ray flare absolute flux correction, taking into account geometric obliquity factor variation with angle between satellite spin axis and satellite-sun line

01 p0147 A69-11242

Powerful flares close connection with filaments and loop prominences, discussing differences in physical characteristics

02 p0306 A69-11633

Solar flare X ray line and continuum spectra measured with crystal spectrometers aboard orbiting solar observatory

02 p0308 A69-12297

Sudden ionospheric disturbance development and characteristics of solar cosmic ray flares, associated X ray emissions and high energy particle generation

02 p0308 A69-12398

Solar flare model assuming open magnetic field configuration, discussing flare properties by application of tearing mode instability and nonlinear development

02 p0309 A69-12788

Solar X ray flares measurement by rocket and satellite, discussing X ray spectrum hardening, hard flares and SID

03 p0500 A69-13225

Magnetic storm of January 1967 due to 3B solar flare noting spacecraft observations, intensity, magnetospheric distortions and solar wind dynamics

03 p0500 A69-13430

Solar flare radiation hazard in long duration space flight, discussing radiation distribution and dosage in human body

03 p0371 A69-13480

Solar flares effect on ozonosphere, calculating time necessary for solar radiation to increase ozone concentration by 50 percent

03 p0424 A69-13542

Dynamic H alpha phenomena in projection on solar disk for simultaneously appearing flare and eruptive prominence on January 29, 1968

03 p0516 A69-14043

Solar particle events of May 23 and 28 1967, noting related solar and terrestrial phenomena

03 p0516 A69-14046

Chromospheric flare development and motion with respect to magnetic field of sunspot clusters

04 p0648 A69-14371

Cosmic ray intensity after solar flare shown greater than during quiet periods from balloon data at Murmansk and Mirny

04 p0648 A69-14375

Solar flares and sunspots number decrease near central meridian

04 p0660 A69-15040

Solar proton flares injecting cosmic ray bursts into solar system, discussing optical, radioastronomical and satellite observations

04 p0649 A69-15327

Cosmic ray intensity increase of January 28, 1967, noting pressure corrected hourly data and lack of association with visible solar flare

04 p0649 A69-15442

Radio bursts at 3.3 mm and H alpha emission during flares, proposing thermal enhancement

04 p0650 A69-15527

Interplanetary relativistic electrons from solar flare events

04 p0650 A69-15528

Electromagnetic radiation from solar flares based on rocket and satellite observations of 10-100 keV X ray emission and ground observation of cm-wavelength bursts

05 p0813 A69-15603

Space observations needed for solar flares study

05 p0814 A69-15859

Space observation of flare sprays and solar limb surges, stressing X ray research

05 p0814 A69-15860

Solar gamma rays measurement role in knowledge of solar flares, discussing simultaneous satellite and ground based observations

05 p0814 A69-15863

Sudden VHF phase anomalies produced by solar flare induced ionospheric disturbances during July 1968

05 p0719 A69-15980

Solar flare influence on potential gradient and air-earth current properties at high mountain stations

05 p0759 A69-16634

Intense continuum bursts energy, flux density and energetic proton production, noting V-spectrum in proton flares

06 p0985 A69-16980

Charge and energy composition of particles in solar flare, discussing rigidity spectra of singly and multiply charged nuclei

06 p0989 A69-17280

Solar cosmic rays anisotropies including solar flare particles propagation

06 p0990 A69-17288

Mass motions in solar flares - Conference, Anacapri, Italy, June 1968

06 p0992 A69-17426

Mass motions in solar flares using line profiles and filtergrams

06 p0993 A69-17427

Optical evidence for mass motions in solar flares /1937-1967/

06 p0993 A69-17428

Mass motion in solar flares, discussing loop flares from emission line profile characteristics

06 p0993 A69-17429

Chromospheric /optical/ flares caused by dense material falling from corona into chromosphere

06 p0993 A69-17430

Small scale mass motions in chromospheric structures surrounding solar flare indicating changes in magnetic field

06 p0993 A69-17431

Mass motions in flares and moustaches indicated by spectral features, discussing red asymmetry of line emission

06 p0994 A69-17432

Spectrographic H alpha observations indicating effects of rotary mass motion in flares and prominences

06 p0994 A69-17434

Solar flares and surges origin, discussing role of supergranular convection, field gradients and spicules

06 p0994 A69-17437

Mass motions in flares, quiescent filaments or other eruption phenomena at solar surface, noting loops, sprays, surges, etc

06 p0994 A69-17438

Sprays in solar flares, discussing production in explosive and normal flares, occurrence, energy and relation to surges

06 p0995 A69-17439

Solar flares acceleration processes related to solar atmospheric currents

06 p0995 A69-17442

Model to account for flare and sunspot phenomena, discussing uni- and bipolar spots

06 p0995 A69-17443

Solar flare eruptions due to current disruption, leading to magnetic energy transfer from whole current circuit to very small volume

06 p0995 A69-17444

Solar flares, discussing transformation of magnetic energy into ion and electron kinetic energy by acceleration in high impedance region in current filaments

06 p0995 A69-17445

Solar flares and plages free energy origin in magnetic field dissipation

06 p0996 A69-17446

- Injection spectra of protons accelerated on sun to billion-trillion ev, discussing acceleration mechanisms 06 p0996 A69-17741
- Earth electromagnetic field micropulsations associated with proton flare, evaluating data from polar caps, auroral zones and midlatitudes 06 p0996 A69-17754
- Solar flare radiation protection requirements, considering bulk and plasma radiation shielding [AIAA PAPER 69-15] 06 p0884 A69-18079
- Solar flare in-flight radiation detection and warning system for Concorde SST, noting radiation hazards due to solar cosmic rays 07 p1131 A69-18551
- Solar flare initial development model assuming high temperature chromospheric point explosion, noting subsequent expansion and large density gradient effects 07 p1205 A69-19246
- Class 3 plus solar proton flare of August 28, 1966 and class 2 solar flare of August 30, 1966, summarizing stages of growth 07 p1205 A69-19247
- Proton flare activity dependence on Bartel active longitudes and sector structure boundaries of interplanetary magnetic field 07 p1205 A69-19248
- Atlas of energetic solar flare X rays and tentative atlas of proton events observed by OGO-1 and OGO-3 ionization chambers 07 p1206 A69-19251
- Sunspot groups area changes relationship to cosmic ray flare occurrences 07 p1206 A69-19252
- Electron density measurement in solar flare spray using discrepancy between measured and theoretical polarization 08 p1378 A69-20244
- Diffusion model for propagation of solar cosmic rays in interplanetary space, obtaining injection spectra for solar flare protons 08 p1379 A69-20613
- Proton flares statistical analysis regarding isolated and near activity complexes for long term forecasting 08 p1379 A69-20614
- High temperature regions cooling as applied to solar flares, considering energy losses due to heat conduction, bremsstrahlung, line emission and recombination radiation 09 p1588 A69-21362
- Correlated microwave and energetic X ray emission from solar flare with 16-sec periodic pulsations, discussing energy during modulation peaks 09 p1574 A69-21457
- Solar protons in magnetospheric tail after flare of July 7, 1966 with isotropic pitch angle distribution, expressing energy spectrum as exponential in rigidity 09 p1576 A69-21699
- Solar flare energetic electron access to polar zones from measurements made by nine channel magnetic spectrometer on polar orbiting vehicle 09 p1577 A69-21709
- Solar X ray and extreme UV spectra during flares, attributing intense emissions to optical transitions 09 p1578 A69-22169
- Flares and chromospheric absorption features locations: compared with H alpha magnetograms, noting double emission ribbons development 09 p1579 A69-22179
- Energetic solar proton and electron event observed in July 1966 by Explorer 33 and OGO-C, noting association with invisible solar hemisphere flare 09 p1579 A69-22181
- Peaks and time intensity profile of energetic X rays and cosmic rays observed by OGO-C ion chamber on May 23, 1967 flare event 09 p1579 A69-22182
- Synchrotron and X ray emission generation from upper chromosphere electrons during solar flares 09 p1580 A69-22203
- Solar X ray bursts observed by proportional counter on IMP-F satellite to correlate optical H alpha flares and radio bursts 09 p1582 A69-22746
- Solar outburst and storm accompanying 9 June 1968 flare, noting radio evidence for coronal instability before flare 09 p1582 A69-22747
- Meter wave radio spectrum observations during 9 June 1968 solar flare, suggesting sudden intensity and frequency change due to shock wave 09 p1582 A69-22748
- Two solar flare initiated type 4 radio bursts on 4 and 6 May 1968, noting prominence activity leading to meter wave generation 09 p1582 A69-22749
- Solar flare event on 17 June 1968 consisting of two type 2 bursts followed by enhanced emission /possibly type 4/ 09 p1582 A69-22750
- Solar flare relation to interplanetary scintillation indices and power spectra 09 p1582 A69-22751
- Short term variability of solar proton flux in interplanetary space during solar flare activity, using data from cosmic ray detector on Pioneer 7 09 p1582 A69-22754
- Two dimensional flat geometry for initial solar flare development stage, discussing tearing mode energy source for solar flares and plasma compressibility effects 09 p1583 A69-22757
- Multiple Coulomb scattering and range straggling effects in shielding against solar flare protons and trapped protons in Van Allen belt 10 p1723 A69-23164
- Collection of articles on proton flare project /July 1966 event/ during IQSY, covering solar magnetic field, chromosphere, photosphere, solar activity, etc 10 p1760 A69-23725
- Magnetic fields and proton flare, showing isogauss maps of longitudinal and transverse fields for active region 10 p1762 A69-23726
- Solar magnetic fields compared in chromospheric and photospheric layers using magnetograph measurements, noting correlation with solar event 10 p1762 A69-23727
- Alpha hydrogen plane 20934 /McMath no. 8362/ associated with July 1966 proton flare development and configuration along sunspot group axis 10 p1762 A69-23728
- Two component calcium plage associated with proton flare of July 1966, describing initial development in old region periphery and component merging 10 p1763 A69-23729
- Sunspot group associated with proton flare of July 1966, describing formation of spot cluster pairs on borders of adjoining network cells 10 p1763 A69-23730
- Simultaneous photometric observations of coronal emission lines during July 1966 solar proton flare plotted on synoptic charts 10 p1763 A69-23731
- Coronal line intensity distribution for period of proton flare 10 p1763 A69-23732
- K coronameter observations used to construct electron density models of corona above proton flare region of July 1966 10 p1763 A69-23733
- Synoptic radio interferometer observations of July 1966 solar proton flare at microwave frequencies, correlating observed radio source with proton event 10 p1783 A69-23734
- Solar radio emission S component at short waves, discussing role of higher frequency spectrum in proton flare occurrence 10 p1763 A69-23735
- Proton flares during July 1966, discussing flare magnitude classes on disk, behind west limb, in active region and proximity to sunspots 10 p1763 A69-23737
- H alpha, H beta and D sub 3 /helium/ emission photographs of active prominence of July 9, 1966 using monochromatic filters for characteristic emissions from hydrogen and helium 10 p1764 A69-23738
- Active prominence during solar flare with loop-like shape of spectral line profiles, discussing turbulent velocities and limb flares 10 p1764 A69-23739
- Polarization measurements of July 1966 proton flare, considering electron scattering and density 10 p1764 A69-23740
- Solar west limb activity observations in H alpha line, noting July 9, 1966 loop system and July 11, 1966 twisted eruptive prominence 10 p1764 A69-23741
- Radio bursts and proton flares associated with active region McMath 8362 of July 1966, discussing wavelengths 10 p1764 A69-23742
- Summation curves method for development of active region and time dependence of energy loss during proton flare 10 p1764 A69-23743
- Sudden ionospheric disturbance effects of solar X ray emission from active region with proton flare 10 p1764 A69-23744
- Variable solar X ray emission from subflare activity in plage region producing polar cap absorption proton flare of July 7, 1966 10 p1764 A69-23745
- Behavior of active region prior to proton flare based on lambda sweep records, considering emission and absorption 10 p1765 A69-23746
- Variations in active region around McMath plage 8362 prior to proton flare, noting disk structure and nearby prominence modification 10 p1765 A69-23747
- Sunspot group evolution after proton flare, discussing decay of central umbrae 10 p1765 A69-23748
- Optical observations of proton flare, discussing flash phase and sunspot umbrae 10 p1765 A69-23749
- Dynamic spectrum of July 7, 1966 proton flare, considering short wave fadeout at 0027 UT and intense burst of spectral Type 2 10 p1765 A69-23750
- Decametric radio spectra from 0053 to 0200 UT during July 7, 1966 solar proton flare, discussing Type 4 phase 10 p1765 A69-23751
- Dynamic spectrum of Type 4 solar radio burst during July 7, 1966 proton flare, noting limb effect 10 p1765 A69-23752
- Spectral intensity of high energy solar X rays observed during July 7, 1966 polar event with satellite OGO 3, suggesting nonthermal bremsstrahlung origin 10 p1766 A69-23753
- Solar X ray flare of July 7, 1966 with Explorer 33 satellite attributed to McMath plage region 8362, discussing solar and cosmic radio noise 10 p1766 A69-23754
- Solar X ray emission and decay during proton flare of July 7, 1966 noting start of polar cap absorption 10 p1766 A69-23755
- X ray and extreme UV radiation deduced from sudden ionospheric disturbances during proton flare, discussing time dependence of emission 10 p1766 A69-23756
- Geomagnetic crochet of July 7, 1966, discussing pulsations, recombination coefficient and electron density of ionospheric D region 10 p1683 A69-23757
- Optical observations of later development of center of activity of July 7, 1966 proton flare 10 p1766 A69-23758
- Magnetic field decay in sunspot group 21034 during July 7, 1966 proton flare 10 p1766 A69-23759
- Proton flare event of July 1966, summarizing active region birth, evolution of spots, configuration and activity of center and general development 10 p1766 A69-23760
- Low energy cosmic ray intensity increase on July 7, 1966 registered with high latitude neutron monitors 10 p1766 A69-23762
- Solar protons balloon measurements following flare, noting integral proton flux and energy spectra 10 p1767 A69-23763
- Proton flares of July 7, 1966, September 2, 1966 and January 28, 1967, noting energy spectra and time dependence of proton flux 10 p1767 A69-23764
- Solar proton event of July 7 1966, discussing sea level observations 10 p1767 A69-23765
- Relativistic solar electron detection in interplanetary space during July 7, 1966 proton flare event, noting energy spectrum and time history 10 p1767 A69-23766
- Energetic proton and electron fluxes spatial gradients after July 7, 1966 solar flare, noting satellite observations and injection mechanism geometry 10 p1767 A69-23767
- Time histories of Mev proton and alpha particle intensities during and after July 7, 1966 solar flare, noting abundance ratio and geophysical effects 10 p1768 A69-23768
- Time dependence, anisotropy and spectral composition of cosmic radiation generated during series of flares during July 5-20, 1966 by Pioneer 6 observations 10 p1768 A69-23769
- VLF observations of July 7 1966 solar flare and PCA event 10 p1657 A69-23772
- Magnetospheric perturbations as aftermath of proton flare discovered by whistlers, noting plasmopause movement toward earth 10 p1683 A69-23776

Earth thermal plasmasphere contraction subsequent to solar flare obtained from ion mass spectrometers on OGO satellites

10 p1683 A69-23777

Protons emitted by July 7, 1966 solar flare observed by low altitude high latitude injun 4 satellite

10 p1768 A69-23778

Earth electromagnetic micropulsations in connection with July 7 1966 proton flare, discussing peculiarities in occurrence of pearls before and after flare

10 p1683 A69-23779

Geomagnetic field variations in middle and high latitudes during proton flare event, discussing UV radiation and period and energy spectra

10 p1683 A69-23780

Ionospheric conditions following solar proton flare observed with topside sounders of Alouette satellites, showing electron density depletion and hydromagnetic wave relationship

10 p1684 A69-23781

Low energy particle effects on midlatitude lower ionosphere conditions after July 7, 1966 proton flare, using ground based measurement

10 p1684 A69-23782

F region response to solar proton flare characterized by two phase ionospheric storm as measured at ground base stations

10 p1684 A69-23783

Ionospheric disturbances after July 7, 1966 proton flare noting flare ionizing radiation, high energy solar proton effects and low energy solar plasma

10 p1684 A69-23784

Energetic particles observed during proton flare noting relativistic electrons, protons to alpha particles ratio, low energy particles and bidirectional proton stream

10 p1768 A69-23785

Low energy particles during solar proton flare and effects on magnetosphere, cosmic ray intensity, ionosphere and geomagnetic activity

10 p1768 A69-23786

Proton flare project covering magnetic structure of active center, photosphere and corona white light observations, interferometric and spectrometric records, etc

10 p1769 A69-23787

Sudden cosmic noise absorption /SCNA/ in polar cap during July 7, 1966 solar proton flare, estimating SCNA latitudinal distribution and protons magnetic cut-off boundary

10 p1770 A69-23907

Flares development in form of loop tunnel, discussing role of filaments

11 p1945 A69-24238

Line spectrum of flare gamma radiation due to atmosphere nuclei excitation by high energy proton acceleration

11 p1945 A69-24241

Type 3 solar flare circular and linear polarization at 23.5 MHz frequency

11 p1945 A69-24244

Sunspot groups large scale configuration in complex proton region, investigating probability of occurrence of accompanying groups/satellites/ in flare generation

11 p1946 A69-24427

Solar flares theories, discussing data acquisition by space research and solar radio astronomy

11 p1946 A69-24516

Space radiation phenomena, discussing auroral precipitations and characteristics and solar flare particle ejection

11 p1948 A69-24859

Supersonic aircraft radiation hazard due to solar flare proton exposure, using Monte Carlo method to estimate dosage as function of tissue slab

11 p1949 A69-24864

Solar flare X ray and extreme UV radiation contribution to E and F1 region ionospheric effects observed by sudden frequency deviations

11 p1950 A69-25160

Solar flare and magnetic storm signals from ATS 1 geostationary satellite on May 28, 1967, deriving total electron content

11 p1951 A69-25161

Solar chromospheric flares effect on temperature of upper atmosphere observed by satellite at perigee altitude

12 p2149 A69-26447

Solar flare proton radiation effects on earth satellites and solar probes, considering sunspot cycle 20, earth magnetic field shielding and Van Allen radiation belts

12 p2151 A69-26873

Cosmic ray intensity preceding Forbush effects as function of chromospheric flares solar longitude and solar wind velocity

14 p2512 A69-29044

Solar cosmic ray flare of 28 January 1967 observed by neutron monitors, determining emission and particle spectrum at atmosphere boundary

14 p2513 A69-29066

Solar cosmic rays diffusion enclosure in interplanetary space magnetic boundary suggested from balloon, satellite and ground observations of solar flare neutron component

14 p2513 A69-29067

Solar X ray flux deduced from flare effects on VLF propagation, showing total energy content as measure of ionizing radiation

14 p2411 A69-29105

Solar flare effect on polar chorus variation determined by comparing Antarctica VLF data with low latitude magnetograms

14 p2514 A69-29385

Geomagnetic storms caused by plasma streams impinging on earth related to preceding cosmic flares, discussing polar cap absorption and ground level effects

14 p2514 A69-29416

Fe and Ti line growth in 12 July 1961 solar flare spectrum, finding ionized titanium, neutral and ionized iron excitation temperatures

14 p2514 A69-29720

Soviet book on solar cosmic rays covering origin, propagation, energy spectrum, diffusion dependence on particle energy and distance, solar flares, etc

14 p2514 A69-29816

General algorithm for eruptive plasma instabilities in fusion plasmas, flares and novae, yielding time behavior and dissipative effects

14 p2499 A69-29850

Solar flares associated with intensive sodium D lines emission observed photoelectrically with telescope in unperturbed region, analyzing possibilities of comets solar origin

15 p2674 A69-30506

Rocket observations of protons and alpha particles energy spectra after solar flares, noting riometer and magnetometer recordings

15 p2677 A69-31329

Low energy solar protons and alpha particles from 28 May 1967 solar flare used as probes of interplanetary medium

16 p2847 A69-31965

Numerical simulation of flare generated shock wave propagation through solar wind, noting transit time and shock strength agreement with observations

16 p2848 A69-31970

Explorer 33 and Explorer 35 observations of solar flare of 8 July 1969 soft X rays, discussing absolute flux

16 p2849 A69-31988

Sudden enhancement of atmospherics recorded during IGY, noting time lag between flare and SEA maximum

16 p2778 A69-32192

Solar flares and bursts correlation, taking into account sunspot type associated with flare and frequency range of bursts

16 p2850 A69-32213

Active longitudes of indices for sunspot activity and solar flares detected and investigated by isoline method for period 1957 to 1962

17 p3022 A69-33049

Ca 2 resonance line profiles in large disk flares and in surrounding plage, discussing H and K line behavior

17 p3023 A69-33054

Hydrodynamic approximation to interplanetary gas motion influenced by solar flare caused perturbations

17 p3035 A69-33627

Fine structure of 9 June 1968 solar flare related to nonflare chromosphere in active regions

17 p3024 A69-33802

Homology within solar flare associated type 2 radio events from dynamic spectra

17 p3024 A69-33803

Solar flare flux density and dynamic spectrum on 30 October 1968 at 80 MHz, showing noise storm positions and type II-III burst sources

17 p3025 A69-33807

Spatial structure of solar proton flare of 5 April 1960, discussing top ascending emission filament velocity in H alpha and coronal lines

17 p3025 A69-34224

Solar magnetic field strength distribution in active region during proton flares, using statistical analysis

17 p3025 A69-34225

Solar flares with subsonic radiation in proton active region of May 1967, discussing X ray emission effects, calculating D region recombination coefficient and electron concentration

17 p3025 A69-34226

Geomagnetic crochets time relations to solar X rays, radio bursts and flares

17 p3025 A69-34227

High temperature regions cooling as applied to solar flares, considering energy losses due to heat conduction, bremsstrahlung, line emission and recombination radiation

18 p3197 A69-34752

Geomagnetic storms and Forbush decreases accounted for by interplanetary solar corpuscular streams effects described by interplanetary magnetic field structure, noting independence of flares

18 p3187 A69-34937

Solar neutrons upper limits measured for 28 July 1967 importance I flares

18 p3187 A69-34959

Solar flare model based on force-free currents in solar atmosphere, noting rapid energy release due to exceeding current density critical limit

18 p3188 A69-35392

Hydrodynamics of gas flow due to solar flares using point explosion model, determining shock wave travel time to earth orbit

18 p3189 A69-35397

Sunspots magnetic structure producing solar proton flares, considering role of sunspots rotational motion on photospheric surface

18 p3189 A69-35415

Solar flares less than 10 A X rays effect on ionospheric ionization between 60 and 100 km

19 p3397 A69-36754

Cosmic rays sudden intensity increases during proton flares of 28 January 1967 and 7 July and 2 September 1966, plotting proton density vs pressure

20 p3587 A69-37045

Solar proton flare June 1968 analysis, discussing geophysical effects and possible polar cap absorption

20 p3587 A69-37332

Solar flares plasma turbulence mechanisms suggested from magnetic energy release studies of Petschek model of magnetic field annihilation

20 p3589 A69-37549

Kinetic energy of sunspot rotational motion transferred to electromagnetic energy in filamentary currents, noting time variations in solar atmosphere preconditioning for flare

20 p3589 A69-37550

Solar flares microwave and hard X ray bursts, discussing gyrosynchrotron plasma, nonthermal electron bremsstrahlung and electron relaxation

20 p3589 A69-37551

Solar ionizing radiation increase during flares of 21 and 23 May 1967 determined from ionospheric electron density concentrations

20 p3590 A69-37558

Magnetic structure of active solar region as function of time for correlation between flares and magnetic field evolution

20 p3590 A69-37827

Flares and fast processes interrelation with active region stationary filaments, filament field magnetic envelope explosion stimulation of surges, plasma stream ascents, etc

20 p3591 A69-38042

Spectral characteristics of solar proton flare on 2 September 1966, noting light intensity variations

20 p3591 A69-38043

Auroral absorption relation to visual aurora and measured particle fluxes

21 p3707 A69-38488

Cosmic ray electron role in energetics of solar flares, stellar flares and explosions, galactic eruptions and quasars

21 p3790 A69-38823

Solar flare origin theories, considering energy storage, trigger mechanisms, shock profiles, particle emission, etc

21 p3791 A69-39507

Solar flares and prominences emission lines equivalent width correlated with relative differential velocity between filaments

22 p4001 A69-39994

Statistical analysis of chromospheric flares connections with sunspots, using frequency distributions of flares occurrences in sunspot groups

22 p4001 A69-39996

Solar flare optical, neutron and gamma emission, discussing ionization losses and nuclear interaction of accelerated particles in flares

22 p4003 A69-40296

Solar soft X rays observed from OSO-3, correlating to solar flares and radio bursts

22 p4003 A69-40297

Type V continuum emissions from solar flares suggested as due to synchrotron radiation from protons spiraling in magnetic field, noting Type III emission
22 p4003 A69-40301

Photoelectric photometer monitoring of flare star UV Cet, comparing time intervals between flares to those of YZ CMi
22 p4032 A69-40945

Continual photoelectric monitoring of flare star YZ CMi by photoelectric photometer attached to reflector, giving light curves for flares
22 p4032 A69-40947

Emerging magnetic tube type proton flare of 26 September 1963, investigating tube dynamic properties for lower flare and ascending turbulent emission ribbons
23 p4208 A69-41282

Absorbed dose and dose equivalent radiation rates at various depths in atmosphere due to proton spectrum of energetic solar flare
23 p4204 A69-41337

Solar flare radiation hazard to SST crew and passengers, discussing onboard and ground based warning systems and ICAO requirements
23 p4063 A69-41830

Biological effects by cosmic ray heavy ions and solar flares, using direct correlation between damages caused and trajectories
23 p4089 A69-41831

Solar flares energy supply origin from studying magnetic field behavior, flare position and initial evolution
24 p4366 A69-42687

Solar flares spectra X ray portion, considering spatial distribution, relation to magnetic fields and time sequence of emitting region
24 p4366 A69-42688

Solar flare and space research - COSPAR Conference, Tokyo, May 1968
24 p4369 A69-43603

Solar flares properties noting cool optical flare and high energy flare plasma, energy sources, generating regions, particle emission, etc
24 p4370 A69-43604

Optical solar flares, discussing flare classification, proton flares, development, limb observation, spectra, line broadening, electron density, etc
24 p4370 A69-43605

Magnetic field energy supply to solar flares from consideration of energies in solar active regions
24 p4370 A69-43606

Solar flares associated optical phenomena including filaments enhancement, destabilization and distortion, high speed ejections, explosions and loop prominences
24 p4371 A69-43607

Solar flares accompanied X ray emission temporal and spectral variations, showing departure from thermal equilibrium
24 p4371 A69-43608

Solar flare soft X ray and EUV emission spectra data obtained on OSO-3 satellite compared with centimetric radio bursts
24 p4371 A69-43609

Solar X ray flux measurements from OGO 4, comparing peak fluxes before, during and after flares with IQSY data
24 p4371 A69-43611

Solar flare-associated radio bursts, reviewing solar radio measurements based on X ray and particle observations
24 p4372 A69-43614

Single frequency microwave solar bursts correlation with flares and associated active regions based on spectral grouping
24 p4372 A69-43616

High energy nucleons and electrons accelerated in solar flares, considering interplanetary magnetic field effect on radiation properties near earth orbit
24 p4372 A69-43617

Solar cosmic ray anisotropy measurement by Explorer 34 satellite during solar flare events
24 p4373 A69-43619

Solar wind disturbances associated with flares
24 p4373 A69-43620

Solar flare models in terms of energy storage and release mechanisms
24 p4374 A69-43622

Solar flare energy source derived from energetic protons trapped in sunspot magnetic field prior to flare occurrence
24 p4374 A69-43623

Oscillatory convection, energy transport and structure of sunspots, suggesting fast changes in equilibrium conditions for magnetic reconstruction and solar flares origin
24 p4374 A69-43624

SOLAR FLUX

Photovoltaic properties of CdS thin film solar cells and silicon cells at Jupiter temperature and solar intensity
03 p0368 A69-13076

Solar flux variations in 44-60 Å band during ascent of current solar cycle /Number 20/ measured by Solrad 8 satellite
04 p0650 A69-15530

Statistical study of solar radio flux fluctuations incidence, observing absorption and polarization effects
07 p1215 A69-18819

Solar atmosphere model calculations of solar oblateness, discussing flux difference and Dicke experiment on general relativity
08 p1383 A69-19899

Null solar neutrino flux possible relation to 2 year solar cycle, discussing energetic disturbances at solar core and sunspots
08 p1377 A69-19902

Solar constant measurement, reviewing instruments and results of Eppley-JPL program using high altitude jet aircraft and rocket research vehicle
09 p1576 A69-21647

Geocoronal Lyman alpha short term and 27-day variations observed by OGO 4 spacecraft attributed to flux variability at solar emission line center
15 p2699 A69-31404

Surface roughness effects on equilibrium temperature of isolated adiabatic plane surface illuminated by collimated and uniform solar flux
22 p4050 A69-40558

Interplanetary magnetic field role in interaction between terrestrial magnetosphere, solar plasma and solar flux energy transfer
23 p4214 A69-41865

Solar high energy gamma ray flux abrupt increase detected by neutral particle plastic scintillators at balloon altitude
24 p4371 A69-43612

Heat conduction problems associated with radiant exchange in shells under discontinuous solar flux, considering spacecraft structures, illumination theory and astrophysics
24 p4416 A69-43689

SOLAR FLUX DENSITY

Microwave spectra of peak flux of solar radio bursts of March and July 1966, relating plage regions to spectral characteristics
01 p0069 A69-11121

Solar X ray flare absolute flux correction, taking into account geometric obliquity factor variation with angle between satellite spin axis and satellite-sun line
01 p0147 A69-11242

Solar neutrino flux dependence on rotation rate of solar core and fractional mass involved in interior mixing
02 p0325 A69-12600

Photospheric brightness differences and structure of large scale intensity fluctuation, discussing association with solar supergranulation and chromospheric network
03 p0515 A69-14037

Chromosphere fine structure in Lyman alpha intensity, compiling isophote map
03 p0515 A69-14039

Microwave solar burst data, analyzing flux intensity and polarization distributions
04 p0652 A69-14417

Isotropic background cosmic X ray flux measurements using low latitude balloon to minimize atmospheric background, obtaining hard solar X ray flux upper limits
06 p0992 A69-17311

Solar intensity measurements at 1.2 mm during partial solar eclipse, noting solar limb brightening and intense solar outburst near end of eclipse
07 p1217 A69-19243

Liquid mercury cathode thrusters characteristics satisfying constraints imposed by solar flux variations with distance from sun
09 p1565 A69-21246

Photospheric magnetic fields, coronal emission and filaments distribution relationship with 1420 MHz radio emission, noting brightness and plasma density increase
11 p1964 A69-25417

Solar 3 cm flux density sensitivity to physical conditions in solar atmosphere related to maximum existence in flux density spectrum F gamma in active regions
13 p2327 A69-27721

Solar atmosphere surface radiation intensity determined by initial value theory including source function and resolvable
13 p2350 A69-27859

Solar flare flux density and dynamic spectrum on 30 October 1968 at 80 MHz, showing noise storm positions and type II-III burst sources
17 p3025 A69-33807

Solar microwave flux density during solar activity cycle tabulated, noting discrepancies in absolute flux levels
22 p4001 A69-39987

Daily measurement of solar radio intensity at 810 MHz during 1964 minimum solar activity period
22 p4010 A69-39989

Radiometer for measuring solar flux variations, discussing design, performance tests and use for spacecraft measurements
24 p4313 A69-42858

SOLAR FURNACES

Solar furnace for metal soldering, brazing and welding, using Pb-Sn solder for various joint types, twisted wires and rod-flange joining
16 p2793 A69-31818

SOLAR GENERATORS

Direct energy conversion and materials limitations, discussing thermoelectricity, solar cells, thermionics and fuel cells
02 p0194 A69-11801

Satellite power generation and transmission system for solar energy conversion, noting estimates of surface area and weight of collectors
02 p0323 A69-12296

Solar cell generator design problems for solar probes, discussing increased operational temperature
02 p0197 A69-12665

Design and performance equations for panel type solar thermoelectric generator, based on single thermocouple as generator unit
05 p0704 A69-15675

ESRO satellites power supply design, operation and characteristics
05 p0829 A69-15919

Electrical testing of six converter solar energy thermionic generator, discussing overheating and dual current mode anomalies
09 p1439 A69-21823

Electric and ion propulsion with solar array or nuclear reactor energy sources, discussing thermal thrusters, electrostatic thrusters and plasma thrusters
11 p1944 A69-25592

Heat conversion coefficients and initial temperature of active elements of solar powered electric devices
13 p2209 A69-28314

Solar conversion efficiencies of p-n and n-p diodes calculated for specified semiconductor heterojunctions using Anderson diffusion model
15 p2552 A69-30034

Solar and nuclear electric power technology for electric propulsion
16 p2741 A69-32709

Thermal contacts effects on optimum operating conditions of solar thermoelectric power generator, discussing losses due to low thermal conductivity coefficient of insulating layers
16 p2741 A69-32797

Faceted reflector for solar power installations with photoelectric converters, discussing reflector construction, efficiency and energy balance
16 p2741 A69-32798

Reradiation and multiple reflection effects on radiant flux density distribution in cylindrical receivers of solar power installations
16 p2741 A69-32799

Solar power concentrator-absorber system, discussing flux distribution in focal plane and cavity heater optimization
17 p3022 A69-33795

Large solar array systems in space, discussing design and operation
18 p3094 A69-35056

Solar cell power systems for manned space stations, summarizing studies of battery power system designs
23 p4068 A69-42242

Hot spot failure modes in solar cell arrays noting protection through I-V characteristic control
23 p4142 A69-42273

Design, fabrication and evaluation of lunar base solar array power modules, emphasizing structural/dynamic, thermal vacuum and acoustic tests
23 p4072 A69-42288

SOLAR GRAVITATION

Pulsar frequency Doppler shift due to general relativistic corrections to optical path of photons in field of sun
02 p0315 A69-11836

Stability of elliptical Venus orbits with solar gravitational perturbations, using equation accuracy and influence on mission planning

02 p0331 A69-12819

Solar gravitational field influence on annual trigonometric parallaxes within relativistic theory framework

03 p0506 A69-13091

Taurus A 21 cm absorption line frequency decrease during optical path approach to sun, discussing gravitational and electromagnetic origin

04 p0661 A69-15148

Circumpolar satellite orbits under lunar and solar perturbations based on two fixed centers problem, considering large amplitude disturbances

10 p1780 A69-23616

Solar gravitational field influence on annual trigonometric parallaxes within relativistic theory framework

14 p2516 A69-28773

Solar and lunar effects on motions of polar orbiting satellites, discussing variable intermediate orbits

14 p2521 A69-29460

SOLAR HEAT FLOW U HEAT FLUX

SOLAR HEATING

Simulated solar radiation heating of cesium vapor thermionic converters with multicapillary transmitters

07 p1058 A69-18951

Empirical determination of heating efficiency of extreme solar UV radiation interacting with carbon dioxide atmosphere of Mars and Venus

12 p2155 A69-26019

Axial support system for controlling thermal distortion of 82 inch heliostat mirror for Kitt Peak solar telescope

12 p2058 A69-26422

Plane and cylindrical thermionic converters, considering electricity generation by heating through flame, solar radiation and nuclear flux

14 p2419 A69-29178

Self thermostatic phase-change coatings for active and passive spacecraft temperature control, discussing temperature dependent changeability in solar absorptance

14 p2530 A69-29434

Diurnal thermospheric density, temperature and wind variations due to direct solar EUV heat input and tidal wave from lower atmosphere

15 p2605 A69-31439

Thermal stresses in rotating cylindrical interplanetary body heated by solar radiation

16 p2871 A69-31901

Temperature distribution of solid spherical satellite under solar radiant heating solved by variational calculus or point matching methods

16 p2877 A69-31922

Solar corona heating ascribed to Landau damping of ionacoustic waves generated in motion of photospheric granules

17 p3030 A69-33060

Temperature determination of thick flat plate rotating in space in solar flux with one surface insulated compared with Apollo heat shield results [AIAA PAPER 69-614]

17 p3071 A69-33266

Temperatures of radiantly heated sun and shade leaves of white oak measured in low speed wind tunnel, considering differences in convective heat dissipation

18 p3095 A69-34540

Rotation of antenna pattern of radio telescope parabolic mirror subjected to thermoelastic deformations due to asymmetric solar heating

20 p3497 A69-38307

SOLAR INSTRUMENTS NT SPECTROHELIOGRAPHS

Instrument technology for solar optical astronomy from space, noting rocket and satellite vehicles, far UV detectors, filters, photographic film fogging, etc

05 p0762 A69-15838

Multilens spectroheliograph for nonstabilized rockets, obtaining consecutive points recording along solar image chord

08 p1313 A69-20252

Solar research from rockets and satellites, considering solar instruments including EUV spectrographs

10 p1772 A69-22867

Apollo telescope mount (ATM) for solar experiments conducted from manned earth orbiting laboratory

10 p1791 A69-22871

Magnetic field inhomogeneities effect on line contours and magnetographic measurements, constructing

two stream models using Unno solution of transfer equations

22 p4019 A69-40288

Solar image selection device based on statistical analysis of photospheric contrast, noting use for electronic photography and location impaired observatory

23 p4213 A69-41697

SOLAR LONGITUDE

Proton flare activity dependence on Bartel active longitudes and sector structure boundaries of interplanetary magnetic field

07 p1205 A69-19248

Local solar magnetic fields longitudinal component correlation with central intensities in various Fraunhofer lines, noting chromospheric levels effect

07 p1219 A69-19285

Active longitudes of indices for sunspot activity and solar flares detected and investigated by isoline method for period 1957 to 1962

17 p3022 A69-33049

SOLAR MAGNETIC FIELD

OSO-4 solar UV spectrum measurements, correlating chromospheric line intensity and photospheric magnetic field strengths [AAS PAPER 68-219]

02 p0313 A69-11485

Interactions of moving solar plasmas and solar magnetic fields, discussing solar velocity fields and fine structure observations

02 p0329 A69-12784

Solar flare model assuming open magnetic field configuration, discussing flare properties by application of tearing mode instability and nonlinear development

02 p0309 A69-12788

Velocity dispersion and temperature anisotropy with respect to magnetic field direction, discussing inertial solar wind cooling effects

03 p0500 A69-13525

Energy release by Joule magnetic field dissipation in solar atmosphere

03 p0516 A69-14041

High resolution magnetograph study of solar magnetic field, showing magnetic asymmetry and fluctuations

04 p0651 A69-14367

Longitudinal component of solar facular magnetic field measured by high resolution spectrograms

04 p0651 A69-14368

Time dependent variations in magnetic fields of active sunspot clusters in photosphere observed by magnetograph

04 p0651 A69-14369

Horizontal and vertical downward velocity components in developed solar active regions

04 p0651 A69-14370

Chromospheric flare development and motion with respect to magnetic field of sunspot clusters

04 p0648 A69-14371

Interplanetary magnetic field intensities, solar and stellar fields measured by Zeeman effect, discussing fields of Jupiter, Mars, Venus and moon

04 p0657 A69-14810

Dissipation time of sunspot magnetic field determined as function of minimum spot value

04 p0660 A69-15039

Spatial distribution of background magnetic fields of quiet sun from photoelectric magnetograph observations, noting relation to supergranulation

04 p0663 A69-15396

Photospheric network obtained by spectroheliograms, discussing Fraunhofer lines weakening, nonsunspot magnetic fields and Zeeman sensitivity

04 p0664 A69-15523

Large scale pattern in solar magnetic field correlated with interplanetary magnetic field

04 p0665 A69-15532

Coronal structure predicted for September 22, 1968 solar eclipse by model constructed for large structure of coronal and interplanetary magnetic fields

05 p0818 A69-15602

Solar and interplanetary magnetic fields and plasmas, noting in situ observations by satellites and space probes of sector patterns, solar cosmic rays and wind

05 p0821 A69-15841

Time independent solar wind equations applied to spherical symmetry and radial magnetic field at solar surface, noting thermal conductivity anisotropy

05 p0817 A69-16703

Model for Evershed effect postulating unipolar symmetrical sunspot surrounded by magnetic knots of opposite polarity

06 p0999 A69-16977

Magnetic field surface in isolated symmetrical sunspot during motion across solar disk, determining field vector angle of inclination variation as related to solar surface

06 p0999 A69-16978

Type 2 radio bursts and corona magnetic field over active center

06 p0985 A69-16979

Small scale mass motions in chromospheric structures surrounding solar flare indicating changes in magnetic field

06 p0993 A69-17431

Flare-like phenomena in chromosphere, discussing moustaches, dashes and spicules and relation to changes in magnetic field

06 p0994 A69-17433

Solar flares and surges origin, discussing role of supergranular convection, field gradients and spicules

06 p0994 A69-17437

Solar flares and plages free energy origin in magnetic field dissipation

06 p0996 A69-17446

Solar type stellar activity, considering solar activity origin and correlation with stellar distances

06 p0996 A69-17447

Magnetic knots /intergranular space strong small scale magnetic fields near sunspot/, longitudinal and transversal fields and radial velocities

07 p1217 A69-19244

Local solar magnetic fields longitudinal component correlation with central intensities in various Fraunhofer lines, noting chromospheric levels effect

07 p1219 A69-19285

Solar magnetic fields distribution regularity with autocorrelation analysis of magnetic synoptic charts

08 p1394 A69-20610

Solar wind model including effects of rotation, magnetic fields and anisotropic heat conduction

08 p1380 A69-20643

Spectrum variations of type 4 radio burst as source rises through solar corona, determining electron density and magnetic field distributions in corona

08 p1380 A69-20775

Magnetic fields of solar supergranulation convective cells based on electromagnetic induction equation, indicating bipolar sunspots occurrence

09 p1588 A69-21366

Solar magnetic field observations with high resolution equipment compared with results by Mount Wilson Observatory

09 p1593 A69-21582

Slowly varying component height for microwave radio emission during IQSY, noting magnetic field changing strength effect

09 p1598 A69-22176

Flares and chromospheric absorption features locations compared with H alpha magnetograms, noting double emission ribbons development

09 p1579 A69-22179

Topology of solar magnetic field differential rotation, using hydromagnetic equations

09 p1606 A69-22425

Magnetically aligned flows between sunspots, considering Evershed effect on umbrae and penumbrae

10 p1772 A69-22907

Magnetograph in Italian observatory for weak solar magnetic field longitudinal components avoiding differential amplifier by electronic compensation

10 p1693 A69-23311

Magnetic fields and proton flare, showing isogauss maps of longitudinal and transverse fields for active region

10 p1762 A69-23726

Solar magnetic fields compared in chromospheric and photospheric layers using magnetograph measurements, noting correlation with solar event

10 p1762 A69-23727

Magnetic field decay in sunspot group 21034 during July 7, 1966 proton flare

10 p1766 A69-23759

Flares development in form of loop tunnel, discussing role of filaments

11 p1945 A69-24238

Type 2 radio burst dynamic spectra determination for finding shock wave and magnetic field parameters above active corona region

11 p1945 A69-24243

Solar radio bursts observations with multielement compound interferometers, noting polarization distribution and magnetic field change

11 p1946 A69-24428

Green function solution to Maxwell equations for interplanetary and coronal magnetic fields above photosphere, considering field at source surface

11 p1958 A69-24429

Plasma and magnetic field measurements of tangential discontinuities in solar wind by Pioneer 6, considering velocity shears and rotation of sun

11 p1946 A69-24430

Spectroheliograph technique, obtaining high resolution magnetic maps of solar magnetic fields directly in single image without photographic subtraction

11 p1880 A69-24432

Stationary Babinet compensator for measuring longitudinal solar magnetic fields by means of fringes introduced in spectroheliograms

11 p1880 A69-24433

Recurrent geophysical disturbances associated with solar active regions and low latitude background field pattern on solar surface magnetic fields

11 p1964 A69-25415

Magnetic fields, green corona emission and filaments relationship at high solar latitudes using synoptic charts

11 p1964 A69-25416

Photospheric magnetic fields, coronal emission and filaments distribution relationship with 1420 MHz radio emission, noting brightness and plasma density increase

11 p1964 A69-25417

Solar activity complex development based on magnetic, photospheric, chromospheric and coronal observations

11 p1964 A69-25418

Circular polarization of solar microwave radio emission in Southern and Northern Hemispheres due to solar magnetic field

13 p2326 A69-27550

Solar corona magnetic field and polar rays, emphasizing field topology and local magnetic structure

14 p2525 A69-29718

Solar photosphere and sunspot magnetic fields structure and strength dependence on sunspot area

14 p2528 A69-29965

Solar activity and large scale magnetic field distribution in discrete latitude zones, including interplanetary magnetic field above ecliptic

14 p2528 A69-29966

Type 3 radio bursts time profile for estimating magnetic field strength in solar corona

15 p2675 A69-30554

Short period pulsations in solar magnetic fields and chromosphere, determining optimum conditions for formation of standing oscillations

15 p2688 A69-30556

Plasma viscosity relation to stellar magnetic fields generation, taking into consideration angular momentum transfer

15 p2700 A69-31492

Equations of transformation for hourly data harmonic terms used in computation and representation of solar and lunar daily magnetic variations

16 p2782 A69-32457

Splintering loop prominences, noting 7 October 1967 prominence interpretable as ejected prominence streamer capture by transverse magnetic fields of loop

17 p3029 A69-33052

Active solar centers interactions above photospheric level and through corona linkages, noting MHD shock waves and magnetic field lines

17 p3040 A69-33801

Solar magnetic field strength distribution in active region during proton flares, using statistical analysis

17 p3025 A69-34225

Interplanetary and photospheric magnetic fields polarities observed by Mariner 4 and with solar magnetograph, noting noncorrelated data along latitudinal strip

18 p3205 A69-35399

Sunspots magnetic structure producing solar proton flares, considering role of sunspots rotational motion on photospheric surface

18 p3189 A69-35415

Bright regions with loops (BRLS) in sunspot group development, discussing survey of time lapse movies from 1968

19 p3403 A69-35967

H alpha filtergrams and spectra of solar corona arch filament systems indicating downward and upward motions produced by magnetic field

20 p3588 A69-37543

Solar flares plasma turbulence mechanisms suggested from magnetic energy release studies of Petschek model of magnetic field annihilation

20 p3589 A69-37549

Magnetic structure of active solar region as function of time for correlation between flares and magnetic field evolution

20 p3590 A69-37827

Flares and fast processes interrelation with active region stationary filaments, filament field magnetic envelope explosion stimulation of surges, plasma stream ascents, etc

20 p3591 A69-38042

Magnetic field and radial gas motion in sunspots from Crimean magnetograph observations at different depths of solar atmosphere

20 p3615 A69-38299

Magnetic field fluctuations and radial velocity in undisturbed photosphere, discussing magnetic field relation to radial velocity, cross correlation asymmetry, etc

20 p3535 A69-38300

Solar magnetic field measurements for fine structure of magnetic asymmetry at different heights and within sunspots, discussing asymmetry for corona and interplanetary space

22 p4010 A69-39990

Magnetic measurements of active regions at various levels of solar atmosphere, discussing chromospheric cold and hot region, faculae magnetic fields, etc

22 p4010 A69-39991

Dynamo action origin of stellar and planetary magnetic fields, considering turbulent helical motions of H convection zone of sun

22 p4011 A69-39998

Variable magnetic field effect on rotation of solar outer layers, applying to spectroscopic observations of rotation velocity at solar limb

22 p4019 A69-40293

Horizontally flowing eddies or Rossby waves in solar convection zone and photosphere, giving mathematical models showing hydromagnetic dynamo effects inducing reversing magnetic fields

22 p4019 A69-40294

Explorer 30 /Solrad 8/ satellite observation of 0.5-3 A solar X ray emission related to magnetic configuration in sunspot group

22 p4003 A69-40298

Babcock solar activity periodicity theory, correlating spots displacement and coronal magnetic field intensity changes

23 p4208 A69-41283

Solar flares energy supply origin from studying magnetic field behavior, flare position and initial evolution

24 p4366 A69-42687

Solar flares spectra X ray portion, considering spatial distribution, relation to magnetic fields and time sequence of emitting region

24 p4366 A69-42688

Sunspots microstructure, discussing penumbra and umbral properties with respect to magnetic field configuration

24 p4378 A69-42690

Phenomenological sunspot model describing granules, supergranules, magnetic fields and photospheric convection

24 p4378 A69-42691

Magnetic field energy supply to solar flares from consideration of energies in solar active regions

24 p4370 A69-43606

Solar flare energy source derived from energetic protons trapped in sunspot magnetic field prior to flare occurrence

24 p4374 A69-43623

Oscillatory convection, energy transport and structure of sunspots, suggesting fast changes in equilibrium conditions for magnetic reconstruction and solar flares origin

24 p4374 A69-43624

Interplanetary and geophysical conditions forecasting based on repetitions of low latitude photospheric background magnetic field patterns during solar activity cycles

24 p4387 A69-43626

Solar chromospheric spicules acceleration mechanism based on magnetic field structure on supergranulation boundaries

24 p4374 A69-43635

SOLAR OBSERVATORIES

NT OSO

NT OSO- 3

NT OSO-C

Space observations of solar intermediate corona, discussing balloon and rocket experiments and limitation of ground based observations

[AAS PAPER 68-217] 02 p0313 A69-11483

Chromospheric and photospheric solar observations made in Belgium in 1967, noting heliographic sunspot latitudes

02 p0313 A69-11533

Solar granules structural and correlation functions indicate homogeneous random field within photograph and regular component in intensity fluctuations spatial distribution

02 p0317 A69-11958

Instrument technology for solar optical astronomy from space, noting rocket and satellite vehicles, far UV detectors, filters, photographic film fogging, etc

05 p0762 A69-15838

Space observations needed for solar flares study

05 p0814 A69-15859

Space observation of flare sprays and solar limb surges, stressing X ray research

05 p0814 A69-15860

UV solar spectra observation, discussing coordination of ground based and satellite programs

05 p0822 A69-15861

Hard solar X ray bursts characteristics and coordination of ground and space observations

05 p0814 A69-15862

Aerospace Corp. solar observatory /California/ compound telescope, vacuum spectroheliograph, instrumentation and applications

11 p1862 A69-24792

Atmospheric attenuation of solar radiation, discussing submillimeter astronomy at low altitude observatories

13 p2327 A69-27590

Soviet stratospheric solar observation projects compared with American

13 p2355 A69-27640

Solar research objectives and instrumentation of Einstein turret in Potsdam

15 p2682 A69-30437

Solar telescope in Berlin observatory for prominences and other solar phenomena observations by public

15 p2611 A69-30881

Sayan Sun Observatory experimental equipment, discussing instruments for solar observation, earth currents measurement and cosmic ray neutron components recording

22 p3943 A69-39997

SOLAR ORBITS

NT PERIHELIONS

Secular perturbations produced by comet belt beyond Neptune on orbits of periodic comets of large aphelion

01 p0158 A69-11327

Planet Mercury rotation, showing reminiscence of apparent path of sun to Ptolemaic concept of planetary system

03 p0509 A69-13368

Interplanetary orbits for probe launched from earth to reencounter earth, noting relationship to three body problem

03 p0514 A69-13782

Solar motion in distant objects kinematics, suggesting simultaneous solutions of local motion and galactic rotation parameters

04 p0654 A69-14627

Mathematical analysis for mechanism of spherical comet nucleus division as effect of nonuniform surface heating during rotation

04 p0659 A69-14997

Orbit corrections for lost minor planets 457, 1038, 1161, 1297, determining new ephemerides for oppositions

05 p0829 A69-16704

11 Canis Minor meteor stream orbit computed, noting retrograde orbit and 4.2 million km perihelion

08 p1394 A69-20621

Meteorites radiogenic and cosmic ray exposure ages, orbits and parent bodies, discussing H and L group chondrites

08 p1405 A69-20928

Asteroidal and cometary orbits and origin of meteorites, discussing eccentricities, exposure ages and mass yield

08 p1406 A69-20929

Photographic and reflector observations of comets including orbit determinations and recoveries

08 p1408 A69-21140

Spacecraft trajectory using microthrust and lunar gravitational attraction for acceleration into heliocentric orbit

09 p1593 A69-21620

Catalog of orbital elements for periodic comets during perihelion passage

10 p1777 A69-23396

- Intermediate orbits to construct motion theory of natural satellites of all planets 11 p1952 A69-24253
- Zodiacal light models /including spherical and nonspherical models/, discussing mechanisms for orientation of particles in solar orbits 15 p2698 A69-31366
- Outer planets exploration during 1976-80 period of unique solar system alignment 16 p2854 A69-31630
- Perturbations of planet motion in planetary coordinates, noting unperturbed motion 18 p3199 A69-34912
- Hill method applied to motion theory for minor planet 11 Parthenope using computerized first order perturbations from principal planets 20 p3596 A69-37316
- Numerical integration of lunar motion equations to investigate lunar theory for high precision applications and to examine motion departures from gravitational theory 20 p3603 A69-37560
- Hypothetical planet captured by earth, becoming earth satellite /moon/, discussing Mercury orbits peculiarities 20 p3603 A69-37562
- Periodic orbits for interplanetary flight, using patched conic analysis for determining inclined elliptic free fall trajectory shutting between earth and Venus [AAS PAPER 68-102] 21 p3804 A69-39203
- Perturbative effects of Jupiter moons on spacecraft flyby and postencounter heliocentric trajectories, noting precision targeting [AIAA PAPER 69-932] 21 p3809 A69-39361
- ### SOLAR PHYSICS
- Solar growth curves constructed for solar disk center using various metal lines 02 p0314 A69-11637
- French solar research program, emphasizing protosphere-chromosphere transition zone 02 p0316 A69-11905
- Goldberg-Unno method for determining Doppler width, microturbulence velocity and convection errors, considering photosphere as hot ascending and cold descending columns 02 p0328 A69-12752
- Type 4 bursts mobile spectrum of september 14, 1966 interpreted by considering plasma effects on synchrotron emission mechanism 02 p0309 A69-12754
- Plasma instabilities covering astrophysical phenomena, Rayleigh-Taylor instability, anisotropic and LF MHD, electrostatic and electromagnetics, warm plasmas, etc 02 p0293 A69-12783
- Interactions of moving solar plasmas and solar magnetic fields, discussing solar velocity fields and fine structure observations 02 p0329 A69-12784
- Solar atmosphere physical properties tabulated to interpret radio bursts and noise storms 02 p0329 A69-12786
- Force free magnetic fields and solar filaments, describing model for explaining filament characteristics 02 p0329 A69-12787
- Solar flare model assuming open magnetic field configuration, discussing flare properties by application of tearing mode instability and nonlinear development 02 p0309 A69-12788
- Cosmic MHD, discussing mechanisms responsible for solar phenomena and dynamics of interstellar medium 02 p0293 A69-12789
- Wilson effect in sunspots, interpreting penumbra distortion near solar disk limb in terms of radiation transport 03 p0504 A69-12893
- Sunspot structure from two dimensional radiative transfer analysis of center limb intensity profiles made at several heliocentric angles 03 p0516 A69-14040
- Nonlinear mechanism for solar surge involving rapid acceleration of high electrical conductivity and macroscopic dimension plasma regions 03 p0516 A69-14044
- Solar microwave type 4 bursts spectra and decay rate time variations 04 p0648 A69-14364
- Slowly varying solar radio emission caused by bremsstrahlung and cyclotron mechanisms within limits of active region model 04 p0662 A69-15240
- Mixing effect on solar neutrino fluxes, assuming solar convective core with rapid thorough mixing 06 p1001 A69-17192
- Solar flares and surges origin, discussing role of supergranular convection, field gradients and spicules 06 p0994 A69-17437
- Magnetic fields of solar supergranulation convective cells based on electromagnetic induction equation, indicating bipolar sunspots occurrence 09 p1588 A69-21366
- Solar magnetic field observations with high resolution equipment compared with results by Mount Wilson Observatory 09 p1593 A69-21582
- Effective cross sections of electron-neutron interaction in photosphere and sunspots, calculating electric conductivity and anisotropy coefficient 09 p1579 A69-22175
- Solar interior rotational angular velocity influence on solar oblateness, noting reduction by turbulent mixing 09 p1600 A69-22201
- Differential solar rotation noting strong quasi-kineticity effect on solar convective zone and rotation influence on viscosity tensor and rotation law 11 p1955 A69-24390
- Solar flares theories, discussing data acquisition by space research and solar radio astronomy 11 p1946 A69-24516
- Ionization equilibrium for ions of solar abundant elements between C and Ni calculated as function of electron temperature 11 p1928 A69-25262
- Light saturation development of line profile component of normal Zeeman triplet in sunspot umbrae 14 p2528 A69-29964
- Convergent solutions of inviscid solar wind equations in expansions form including dimensionless distance from sun 14 p2515 A69-29968
- Asymptotic power series solutions of viscous solar wind equations 14 p2515 A69-29969
- Solar-terrestrial physics, Solar aspects - IQSY/COSPAR Conference, London, July 1967, Part 1 15 p2672 A69-30005
- Solar research objectives and instrumentation of Einstein turret in Potsdam 15 p2682 A69-30437
- Excitation sources distribution in chromosphere from observed H alpha line contour, considering resonant scattering and internal excitation 15 p2683 A69-30509
- Chromospheric spicules formation, density, pressure gradient, vertical motion, velocity fluctuations and luminosity 15 p2675 A69-30551
- Solar neutrino fluxes sensitivity to localized changes in opacity and equation of state, discussing solar models 15 p2675 A69-30768
- Temperature fluctuations in solar photosphere, noting transition from convective to radiative energy transport 17 p3040 A69-33810
- Solar flare model based on force-free currents in solar atmosphere, noting rapid energy release due to exceeding current density critical limit 18 p3188 A69-35392
- Steady state spherically symmetrical ejection of multicomponent plasma from sun determined with hydrogen approximation, considering ion composition 20 p3594 A69-37018
- Criteria to prove incorrectness of two column model for photospheric granulation proposed by Margrave and Swihart /1969/ 20 p3603 A69-37541
- Limb effect of solar Fraunhofer lines determined by telescope equipped with autocollimated type diffraction spectrograph 20 p3607 A69-38044
- Solar neutrinos emission mechanism for information on central region of sun, discussing detection and flux density 21 p3790 A69-38827
- Solar flare origin theories, considering energy storage, trigger mechanisms, shock profiles, particle emission, etc 21 p3791 A69-39507
- Solar physics and hydromagnetics - Conference, Sopot, Poland, September 1966 22 p4009 A69-39982
- Sunspot penumbra model in hydrostatic equilibrium accounting for continuum and Fraunhofer lines observations 22 p4019 A69-40290
- Extraterrestrial objects composition in defining cosmic abundance curve, including solar and meteoritic data 22 p4032 A69-40982
- Solar flares energy supply origin from studying magnetic field behavior, flare position and initial evolution 24 p4366 A69-42687
- Solar physics outline, discussing composition, quiet and active sun characteristics, radiation, etc 24 p4379 A69-42781
- Differential solar rotation noting strong quasi-kineticity effect on solar convective zone and rotation influence on viscosity tensor and rotation law 24 p4390 A69-43780
- ### SOLAR POSITION
- Variation in critical E layer frequencies at large solar zenith angles 06 p0921 A69-17748
- Rotation and orientation parameters of earth satellites based on qualitative analysis of solar direction indicator readings 07 p1230 A69-19604
- Magnetic declination from moving objects measured by geomagnetic vector projection in solar direction 09 p1486 A69-21538
- Magnetic declination from moving objects measured by geomagnetic vector projection in solar direction 16 p2783 A69-32533
- Diurnal and seasonal variations of primary atmospheric ions in topside ionosphere correlated with solar zenith angle, using ion mass spectrometer on Explorer 32 20 p3534 A69-38087
- Ionospheric nondeviative radio wave absorption, noting roles of collisional and working frequencies and solar zenith angle 23 p4127 A69-42425
- ### SOLAR PROBES
- Solar cell generator design problems for solar probes, discussing increased operational temperature 02 p0197 A69-12665
- Technological requirements for solar probe with close perihelion, discussing solar approach and space environment problems 03 p0519 A69-12855
- Space flight launches, interplanetary transfer orbits, flyby orbits and capture orbits for solar probe with 0.3 AU perihelion and Jupiter satellite probe 04 p0657 A69-14826
- German-American interplanetary vehicle to investigate interplanetary space and solar characteristics 06 p1012 A69-16970
- Solar flare proton radiation effects on earth satellites and solar probes, considering sunspot cycle 20, earth magnetic field shielding and Van Allen radiation belts 12 p2151 A69-26873
- Interplanetary dust and distribution study by micrometeorite analyzer and by zodiacal light observations using solar probe 15 p2694 A69-30879
- Thermal control coatings for solar cells of solar probe Helios 16 p2867 A69-31741
- Solar probes design for 0.3 to 0.1 AU perihelion distance, considering thermal control, power supply, communications, altitude control and alternative configurations 17 p3050 A69-33797
- Jupiter swingby flight mode application to probe missions requiring solar polar regions overflight at close perihelion distances 19 p3401 A69-35915
- Two dimensional gravity assisted trajectories for solar probe missions in ecliptic plane, discussing Venus and Jupiter assist missions 21 p3804 A69-39022
- Spacecraft central data system for deep space solar probe data management 24 p4284 A69-42621
- ### SOLAR PROMINENCES
- Powerful flares close connection with filaments and loop prominences, discussing differences in physical characteristics 02 p0306 A69-11633
- Fabry-Perot etalon for obtaining monochromatic weak solar prominences 02 p0248 A69-11634

Dynamic H alpha phenomena in projection on solar disk for simultaneously appearing flare and eruptive prominence on January 29, 1968

03 p0516 A69-14043

Space observation of flare sprays and solar limb surges, stressing X ray research

05 p0814 A69-15860

Solar limb prominence areas variation with latitude and solar activity cycle, noting changes in yearly mean latitude of prominences during cycle

05 p0816 A69-16390

Spectrographic H alpha observations indicating effects of rotary mass motion in flares and prominences

06 p0994 A69-17434

Solar prominence structures observed in H alpha emission, determining radial velocities as function of distance from limb

06 p0994 A69-17436

Mass motions in flares, quiescent filaments or other eruption phenomena at solar surface, noting loops, sprays, surges, etc

06 p0994 A69-17438

Quiescent solar prominences horizontal oscillations, explaining periods, damping times and prominence shape changes by model of freely oscillating prominence in corona

07 p1205 A69-19245

Emission spectrum analysis of faint solar prominences noting kinetic temperature, turbulent velocity and electron density

07 p1210 A69-19718

Electron density measurement in solar flare spray using discrepancy between measured and theoretical polarization

08 p1378 A69-20244

Synoptic charts of chromosphere, giving position and magnitude of sunspots, facula plages and prominences during synodic revolution of sun

08 p1379 A69-20378

Flares and chromospheric absorption features locations compared with H alpha magnetograms, noting double emission ribbons development

09 p1579 A69-22179

H alpha, H beta and D sub 3 /helium/ emission photographs of active prominence of July 9, 1966 using monochromatic filters for characteristic emissions from hydrogen and helium

10 p1764 A69-23738

Active prominence during solar flare with loop-like shape of spectral line profiles, discussing turbulent velocities and limb flares

10 p1764 A69-23739

Solar west limb activity observations in H alpha line, noting July 9, 1966 loop system and July 11, 1966 twisted eruptive prominence

10 p1764 A69-23741

Flares development in form of loop tunnel, discussing role of filaments

11 p1945 A69-24238

Solar quiescent prominences spectra with bright metallic lines, discussing turbulent angular velocity and kinematic temperature of filaments

11 p1945 A69-24387

Mercury transits in 1970 and 1973 to resolve prominence threads and spicules, sunspot fine structures, etc

11 p1958 A69-24434

Spectral emission of active prominences, showing looplike lines during quiet phases and differences in turbulent velocities magnitude

15 p2674 A69-30510

Solar telescope in Berlin observatory for prominences and other solar phenomena observations by public

15 p2611 A69-30881

H alpha/D3 intensity ratio variations in peripheral regions of prominences may be due to dynamic conditions of material emitting radiations

17 p3029 A69-33051

Splintering loop prominences, noting 7 October 1967 prominence interpretable as ejected prominence streamer capture by transverse magnetic fields of loop

17 p3029 A69-33052

Two flare unconnected prominence eruptions on 15, 29 January 1968, discussing emission at arch top

17 p3023 A69-33053

Solar flares and prominences emission lines equivalent width correlated with relative differential velocity between filaments

22 p4001 A69-39994

Mean intensity profiles of photospheric H alpha radiation illuminating solar prominences moving at different heights

22 p4011 A69-39995

Optical and mechanical systems of Wroclaw Observatory Lyot type coronagraph for prominence observations in H alpha line

22 p3943 A69-39999

Diffuse coronal emission observation during total eclipse of February 1961 near solar prominences and polar ray form investigation in northern part of corona

22 p4002 A69-40002

Solar flares associated optical phenomena including filaments enhancement, destabilization and distortion, high speed ejections, explosions and loop prominences

24 p4371 A69-43607

Solar quiescent prominences spectra with bright metallic lines, discussing turbulent angular velocity and kinematic temperature of filaments

24 p4375 A69-43777

SOLAR PROPULSION

Multimission interplanetary probe using solar electric propulsion

06 p0984 A69-17593

Advanced reconnaissance electric planetary spacecraft /AREPS/ concept for repeated coverage of Mars or Venus surface, using solar-photovoltaic system [AIAA PAPER 69-253]

09 p1585 A69-21244

Solar electric propulsion mission simplification by staging concept, discussing thrust combination, weight tradeoffs, design and Jupiter flyby probe [AIAA PAPER 69-251]

09 p1586 A69-21245

Spacecraft design, trajectory and mission analyses for multipurpose solar electric propulsion missions, emphasizing modular ion engine and fixed attitude spacecraft designs [AIAA PAPER 69-252]

09 p1568 A69-21729

Solar electric propulsion system performance consisting of thrusters with thrust vector aligning actuators, switching network and flight type power conditioner [AIAA PAPER 69-498]

16 p2843 A69-32708

Solar and nuclear electric power technology for electric propulsion [AIAA PAPER 69-826]

16 p2741 A69-32709

SOLAR PROTONS

Explorer 26 observations of solar proton penetration inside trapped radiation near geomagnetic equator

01 p0146 A69-11122

Solar proton observations by Satellite 1963 38C in polar regions at high altitude during spring 1966

01 p0146 A69-11123

Solar proton event generating sudden commencement magnetic storm, discussing effects on outer belt electrons as observed by Explorer 26 and time delay

01 p0146 A69-11124

Solar proton flares injecting cosmic ray bursts into solar system, discussing optical, radioastronomical and satellite observations

04 p0649 A69-15327

Energy flux into earth thermosphere due to fast corpuscular neutrals arising from charge transfer collisions between solar protons and neutral interstellar H

05 p0817 A69-16654

Intense continuum bursts energy, flux density and energetic proton production, noting V-spectrum in proton flares

06 p0985 A69-16980

Injection spectra of protons accelerated on sun to billion-trillion ev, discussing acceleration mechanisms

06 p0996 A69-17741

Earth electromagnetic field micropulsations associated with proton flare, evaluating data from polar caps, auroral zones and midlatitudes

06 p0996 A69-17754

Partial reflections from ionosphere, analyzing electron number densities, noting relation between D region ionization increases and small solar proton events

07 p1205 A69-18956

Class 3 plus solar proton flare of August 28, 1966 and class 2 solar flare of August 30, 1966, summarizing stages of growth

07 p1205 A69-19247

Atlas of energetic solar flare X rays and tentative atlas of proton events observed by OGO-1 and OGO-3 ionization chambers

07 p1206 A69-19251

Proton flares statistical analysis regarding isolated and near activity complexes for long term forecasting

08 p1379 A69-20614

Solar proton monitoring by particle detectors on-board rockets and IMP satellite

08 p1318 A69-21142

Solar protons in magnetospheric tail after flare of July 7, 1966 with isotropic pitch angle distribution, expressing energy spectrum as exponential in rigidity

09 p1576 A69-21699

Low energy solar cosmic ray proton flux characteristics observed by Injun 1 satellite after July 1961 sudden commencement magnetic storm

09 p1576 A69-21707

Energetic solar proton and electron event observed in July 1966 by Explorer 33 and OGO-C, noting association with invisible solar hemisphere flare

09 p1579 A69-22181

Short term variability of solar proton flux in interplanetary space during solar flare activity, using data from cosmic ray detector on Pioneer 7

09 p1582 A69-22754

Collection of articles on proton flare project /July 1966 event/ during IQSY, covering solar magnetic field, chromosphere, photosphere, solar activity, etc

10 p1760 A69-23725

Magnetic fields and proton flare, showing isogauss maps of longitudinal and transverse fields for active region

10 p1762 A69-23726

Solar magnetic fields compared in chromospheric and photospheric layers using magnetograph measurements, noting correlation with solar event

10 p1762 A69-23727

Alpha hydrogen plage 20934 /McMath no. 8362/ associated with July 1966 proton flare development and configuration along sunspot group axis

10 p1762 A69-23728

Two component calcium plage associated with proton flare of July 1966, describing initial development in old region periphery and component merging

10 p1763 A69-23729

Sunspot group associated with proton flare of July 1966, describing formation of spot cluster pairs on borders of adjoining network cells

10 p1763 A69-23730

Simultaneous photometric observations of coronal emission lines during July 1966 solar proton flare plotted on synoptic charts

10 p1763 A69-23731

Coronal line intensity distribution for period of proton flare

10 p1763 A69-23732

K coronameter observations used to construct electron density models of corona above proton flare region of July 1966

10 p1763 A69-23733

Synoptic radio interferometer observations of July 1966 solar proton flare at microwave frequencies, correlating observed radio source with proton event

10 p1783 A69-23734

Solar radio emission S component at short waves, discussing role of higher frequency spectrum in proton flare occurrence

10 p1763 A69-23735

Proton flares during July 1966, discussing flare magnitude classes on disk, behind west limb, in active region and proximity to sunspots

10 p1763 A69-23737

Polarization measurements of July 1966 proton flare, considering electron scattering and density

10 p1764 A69-23740

Solar west limb activity observations in H alpha line, noting July 9, 1966 loop system and July 11, 1966 twisted eruptive prominence

10 p1764 A69-23741

Radio bursts and proton flares associated with active region McMath 8362 of July 1966, discussing wavelengths

10 p1764 A69-23742

Summation curves method for development of active region and time dependence of energy loss during proton flare

10 p1764 A69-23743

Sudden ionospheric disturbance effects of solar X ray emission from active region with proton flare

10 p1764 A69-23744

Behavior of active region prior to proton flare based on lambda sweep records, considering emission and absorption

10 p1765 A69-23746

Variations in active region around McMath plage 8362 prior to proton flare, noting disk structure and nearby prominence modification

10 p1765 A69-23747

Sunspot group evolution after proton flare, discussing decay of central umbrae

10 p1765 A69-23748

Optical observations of proton flare, discussing flash phase and sunspot umbrae

10 p1765 A69-23749

Dynamic spectrum of July 7, 1966 proton flare, considering short wave fadeout at 0027 UT and intense burst of spectral Type 2

10 p1765 A69-23750

Decametric radio spectra from 0053 to 0200 UT during July 7, 1966 solar proton flare, discussing Type 4 phase

10 p1765 A69-23751

Dynamic spectrum of Type 4 solar radio burst during July 7, 1966 proton flare, noting limb effect

10 p1765 A69-23752

Spectral intensity of high energy solar X rays observed during July 7, 1966 polar event with satellite OGO 3, suggesting nonthermal bremsstrahlung origin

10 p1766 A69-23753

Solar X ray emission and decay during proton flare of July 7, 1966 noting start of polar cap absorption

10 p1766 A69-23755

Optical observations of later development of center of activity of July 7, 1966 proton flare

10 p1766 A69-23758

Magnetic field decay in sunspot group 21034 during July 7, 1966 proton flare

10 p1766 A69-23759

Proton flare event of July 1966, summarizing active region birth, evolution of spots, configuration and activity of center and general development

10 p1766 A69-23760

Ground level solar proton event recorded by neutron monitors

10 p1766 A69-23761

Low energy cosmic ray intensity increase on July 7, 1966 registered with high latitude neutron monitors

10 p1766 A69-23762

Solar protons balloon measurements following flare, noting integral proton flux and energy spectra

10 p1767 A69-23763

Proton flares of July 7, 1966, September 2, 1966 and January 28, 1967, noting energy spectra and time dependence of proton flux

10 p1767 A69-23764

Solar proton event of July 7 1966, discussing sea level observations

10 p1767 A69-23765

Relativistic solar electron detection in interplanetary space during July 7, 1966 proton flare event, noting energy spectrum and time history

10 p1767 A69-23766

Energetic proton and electron fluxes spatial gradients after July 7, 1966 solar flare, noting satellite observations and injection mechanism geometry

10 p1767 A69-23767

Time histories of Mev proton and alpha particle intensities during and after July 7, 1966 solar flare, noting abundance ratio and geophysical effects

10 p1768 A69-23768

Forbush decrease associated with July 7 1966 proton event from cosmic ray intensity variation measurements by neutron monitors

10 p1768 A69-23774

Magnetospheric perturbations as aftermath of proton flare discovered by whistlers, noting plasmopause movement toward earth

10 p1683 A69-23776

Protons emitted by July 7, 1966 solar flare observed by low altitude high latitude Injun 4 satellite

10 p1768 A69-23778

Earth electromagnetic micropulsations in connection with July 7 1966 proton flare, discussing peculiarities in occurrence of pearls before and after flare

10 p1683 A69-23779

Geomagnetic field variations in middle and high latitudes during proton flare event, discussing UV radiation and period and energy spectra

10 p1683 A69-23780

Ionospheric conditions following solar proton flare observed with topside sounders of Alouette satellites, showing electron density depletion and hydromagnetic wave relationship

10 p1684 A69-23781

Low energy particle effects on midlatitude lower ionosphere conditions after July 7, 1966 proton flare, using ground based measurement

10 p1684 A69-23782

F region response to solar proton flare characterized by two phase ionospheric storm as measured at ground base stations

10 p1684 A69-23783

Ionospheric disturbances after July 7, 1966 proton flare noting flare ionizing radiation, high energy solar proton effects and low energy solar plasma

10 p1684 A69-23784

Energetic particles observed during proton flare noting relativistic electrons, protons to alpha particles ratio, low energy particles and bidirectional proton stream

10 p1768 A69-23785

Proton flare project covering magnetic structure of active center, photosphere and corona white light observations, interferometric and spectrometric records, etc

10 p1769 A69-23787

Sudden cosmic noise absorption (SCNA) in polar cap during July 7, 1966 solar proton flare, estimating SCNA latitudinal distribution and protons magnetic cut-off boundary

10 p1770 A69-23907

Sunspot groups large scale configuration in complex proton region, investigating probability of occurrence of accompanying groups/satellites/ in flare generation

11 p1946 A69-24427

Supersonic aircraft radiation hazard due to solar flare proton exposure, using Monte Carlo method to estimate dosage as function of tissue slab

11 p1949 A69-24864

Solar flare proton radiation effects on earth satellites and solar probes, considering sunspot cycle 20, earth magnetic field shielding and Van Allen radiation belts

12 p2151 A69-26873

Solar proton flux in two energy intervals measuring by ATS detectors during January 1967 event compared with data from satellites outside magnetosphere

14 p2509 A69-28935

Auroral electrojet index in relation to magnetic storm sudden commencements, ring current main phase and energetic solar protons

14 p2511 A69-28954

Relativistic solar proton propagation fluctuation effects in interplanetary magnetic field during cosmic ray intensity increase

14 p2512 A69-29045

Rocket observations of protons and alpha particles energy spectra after solar flares, noting riometer and magnetometer recordings

15 p2677 A69-31329

ESRO 2 satellite observations of solar proton event of 9 June 1968, comparing flux profile variations across polar cap with magnetic changes at earth surface

15 p2677 A69-31347

Proton dose in receiver behind combination electromagnetic and material shield, calculating dose for Van Allen and solar proton event spectra

15 p2652 A69-31522

Low energy solar protons and alpha particles from 28 May 1967 solar flare used as probes of interplanetary medium

16 p2847 A69-31965

Solar energetic proton penetration into magnetotail from proton data collected by Vela 4 energetic particle telescopes, comparing proton fluxes inside and outside magnetotail

16 p2847 A69-31966

Solar protons nonuniformity over polar caps observed by OGO 2 ionization chamber during 24 March 1966 solar proton events

16 p2848 A69-31967

Low energy solar protons entry into magnetosphere on 26 May 1967 showing diffusion control

16 p2849 A69-31984

Diurnal variations in gamma rays produced by proton bombardment ascribed to geomagnetic time dependence for low energy solar proton cut-off

16 p2850 A69-32308

Ground based solar proton monitoring, considering particle intensities and radiation dose rates from riometer absorption as function of time

16 p2850 A69-32321

Spatial structure of solar proton flare of 5 April 1960, discussing top ascending emission filament velocity in H alpha and coronal lines

17 p3025 A69-34224

Solar magnetic field strength distribution in active region during proton flares, using statistical analysis

17 p3025 A69-34225

Solar wind model for studying long wavelength turbulence as heat source for alpha particles and protons in solar plasma

18 p3186 A69-34299

Sunspots magnetic structure producing solar proton flares, considering role of sunspots rotational motion on photospheric surface

18 p3189 A69-35415

Solar protons captured in earth dipole trap, discussing conditions for nonadiabatic escape

20 p3587 A69-37042

Solar protons in subpolar stratosphere during solar activity minimum indicated from proton measurements at Tiksi Bay

20 p3587 A69-37044

Cosmic rays sudden intensity increases during proton flares of 28 January 1967 and 7 July and 2 September 1966, plotting proton density vs pressure

20 p3587 A69-37045

Solar proton flare June 1968 analysis, discussing geophysical effects and possible polar cap absorption

20 p3587 A69-37332

Satellite observations of solar proton events with halo structure or energetic storm proton event and SSC, noting similarity in origin

20 p3589 A69-37555

Solar protons intensity increase observed by balloon-borne instruments over Antarctica, describing decay phases

20 p3589 A69-37556

Spectral characteristics of solar proton flare on 2 September 1966, noting light intensity variations

20 p3591 A69-38043

Solar proton bombardment of lunar surface, discussing luminescence and chemical effects

22 p4012 A69-40089

Type V continuum emissions from solar flares suggested as due to synchrotron radiation from protons spiraling in magnetic field, noting Type III emission

22 p4003 A69-40301

Cosmic ray proton cut-off increase at high latitudes during magnetospheric substorms, using balloon time observations of nuclear gamma ray flux

22 p4005 A69-40509

Charge exchange of solar wind protons passing shock front, noting turbulent subsonic motion of randomized hot solar wind protons in shadow cone

22 p4008 A69-41208

Emerging magnetic tube type proton flare of 26 September 1963, investigating tube dynamic properties for lower flare and ascending turbulent emission ribbons

23 p4208 A69-41282

Absorbed dose and dose equivalent radiation rates at various depths in atmosphere due to proton spectrum of energetic solar flare

23 p4204 A69-41337

Incident proton flux atmospheric altitude profile during PCA period, comparing balloon observations with preliminary satellite data

23 p4204 A69-41485

Solar protons delayed access into polar regions during 2 November 1967 solar particle event, discussing north-south asymmetry

24 p4368 A69-43183

Solar protons and alpha particles measurements at synchronous orbit altitudes providing data for solar cell shield design to prevent radiation damage

24 p4369 A69-43265

Solar flare energy source derived from energetic protons trapped in sunspot magnetic field prior to flare occurrence

24 p4374 A69-43623

SOLAR RADAR ECHOES

Radio echoes relationship to active parts of solar corona, noting agreement with data on type 3 radio bursts source location

18 p3201 A69-35207

SOLAR RADIATION

NT SUNLIGHT
NT TYPE 2 BURSTS
NT TYPE 3 BURSTS
NT TYPE 4 BURSTS
NT TYPE 5 BURSTS

Atmospheric noise at millimeter wavelengths, discussing solar radiation and antenna near and far field patterns

01 p0028 A69-10420

Spacecraft illuminance by reflected solar radiation calculated by computer method

01 p0151 A69-10576

Scattered solar Lyman alpha radiation measurement by Vertical Space Probe station in upper atmosphere including UV radiation

01 p0152 A69-10577

Solar absorptance, total hemispherical emittance and absorptance/emittance ratio for metals at cryogenic temperatures measured simultaneously with sinusoidally perturbed incident radiation

01 p0176 A69-10847

Soviet investigations of solar and cosmic electromagnetic and charged particle radiations by balloon, rocket and satellite measurements

01 p0145 A69-10945

Terrestrial microorganism survival in space aboard Gemini satellite, discussing lethal effects of solar radiation

01 p0018 A69-11087

- Radiation, Stark and van der Waals level broadening constants for Mg 1 and Si 1 calculated to interpret solar and stellar spectral line widths
02 p0310 A69-11454
- Global solar radiation flux measurements over India during IQSY
02 p0307 A69-11819
- French radio astronomy, presenting sky background radiation and solar emission results from Rubis 02 and 04 rockets
02 p0316 A69-11908
- Solar continuum intensity determination in middle IR, obtaining solar disk center brightness temperature measurement by comparison with black body model
02 p0318 A69-12041
- Iris satellite experiments in astrophysics including nuclear and solar induced electromagnetic radiation
03 p0427 A69-12849
- Wilson effect in sunspots, interpreting penumbra distortion near solar disk limb in terms of radiation transport
03 p0504 A69-12893
- Thermal tidal oscillations in earth atmosphere using circulation model attributed to solar radiation absorption by atmospheric vapor and ozone
03 p0457 A69-13030
- Submillimeter wave observation of sun to study anomalous absorption region
03 p0513 A69-13774
- Aircraft cockpit and surface temperatures after solar radiation exposure in desert, showing inadequacies of meteorological data for thermal stress predictions
03 p0381 A69-14077
- Solar and terrestrial thermal radiometer absolute calibration noting standards and methods
04 p0602 A69-15429
- Solar radiation protection of radiometers and spectrometers on reentry vehicle by launching times and solar view field selection
04 p0666 A69-15511
- Solar gamma rays measurement role in knowledge of solar flares, discussing simultaneous satellite and ground based observations
05 p0814 A69-15863
- Spectrophotometer and integral methods to determine solar radiation absorptivity for steady/ unsteady thermal regimes in solids
05 p0846 A69-15901
- Moon effect on intensity and angular distribution of energetic electron and proton shadowing as observed by Explorer satellites
05 p0824 A69-16252
- Atmospheric turbidity coefficient distribution in Northern Hemisphere from direct solar radiation measurements, noting application to IGY data
05 p0789 A69-16585
- Australian sounding rocket programs carried out in conjunction with U.S. satellite experiments [UN PAPER 68-95214]
06 p1013 A69-17076
- Mixing effect on solar neutrino fluxes, assuming solar convective core with rapid thorough mixing
06 p1001 A69-17192
- Charge and energy composition of particles in solar flare, discussing rigidity spectra of singly and multiply charged nuclei
06 p0989 A69-17280
- Inflatable solar shields for thermal protection of space vehicles utilizing cryogen propellants
06 p1017 A69-17609
- Solar absorptance and hemispherical emittance of metals at space conditions determined with cyclic incident radiation technique [AIAA PAPER 69-60]
06 p0945 A69-18154
- Storable tubular extendible member /STEM/ booms for gravity gradient applications, emphasizing reflective coatings to minimize deflection by solar radiation
07 p1226 A69-18327
- Thermally excited oscillation experienced by OGO 4 boom antenna demonstrated by mathematical model, showing nonplanar coupled bending-torsion oscillation by solar radiation
07 p1227 A69-18333
- Spherical and single axis passive oscillation energy dampers for gravity gradient oriented satellites, utilizing earth gravity field or solar pressure
07 p1229 A69-18347
- Simulated solar radiation heating of cesium vapor thermionic converters with multicapillary transmitters
07 p1058 A69-18951
- Solar photosphere model with two stream columnar representation of granulation for predicting continuous radiation field
07 p1217 A69-19238
- Soviet monograph on UV radiation of sun and sky emphasizing biological effects
07 p1221 A69-19506
- Energy dissipation of solar particles in atmosphere for 3914 and 5577 A bands, computing light emissions associated with PCA
08 p1378 A69-20186
- Solar particles and radiation - Conference, Kiel, October 1968
08 p1379 A69-20531
- Albedo over Antarctic, measuring solar radiation reflected by surface and atmosphere by Eppley radiometer
09 p1484 A69-21404
- Solar neutrinos and convective core mixing on short time scale resulting in flux reduction
09 p1574 A69-21453
- Solar electromagnetic radiation spectral distribution from ground level, rocket and satellite observations to obtain value of energy received at top of atmosphere
09 p1575 A69-21645
- Solar constant measurement, reviewing instruments and results of Eppley-JPL program using high altitude jet aircraft and rocket research vehicle
09 p1576 A69-21647
- Solar radiation absorption measurements by balloon for atmospheric water vapor distribution
09 p1536 A69-21864
- Helium-like ion resonance satellite lines in laboratory and solar plasmas, noting coincidence between solar satellite energy and energy level interval
09 p1598 A69-22158
- Solar extreme UV, soft and hard solar X rays, cosmic X rays and gamma rays, cosmic ray particles and near earth visible radiation observed by OSO-3
09 p1578 A69-22167
- Solar far UV emissions observed from OSO-C by grazing incidence grating spectrometer, noting temporal variations and atmospheric absorption characteristics
09 p1578 A69-22168
- Earth reflected solar radiation and stability of satellite thermal control coatings, noting intensity distribution shifting toward UV region and coatings degradation rate
09 p1579 A69-22174
- Modified nonstationary method for determining materials absorptivity with respect to incident solar radiation through heating and cooling rate measurements
09 p1528 A69-22720
- Solar Lyman alpha radiation scattering into antisolar geocorona, noting inaccessibility of region to solar wind
09 p1583 A69-22760
- Daily observational results of solar phenomena, cosmic rays, geomagnetic variations, ionosphere, radio wave propagation and airglow arranged according to solar rotation number
10 p1771 A69-22808
- Neutrino groups generation in internal regions of sun, analyzing flux ambiguities due to error of cross section parameter of nuclear reactions
10 p1757 A69-22827
- Cosmic ray absorption and modulation in lower ionosphere at midlatitudes, considering 11 year variations, Forbush effects and solar radiation on electron concentration
10 p1759 A69-22840
- Solar Lyman alpha, Lyman beta and Balmer alpha lines of He 2 for electron temperature and density and optical thickness of emitting layer
10 p1772 A69-22859
- Explorer 30 satellite monitoring of solar X ray emission during July 1-15 1966, noting plage region activation with increasing emission
10 p1763 A69-23736
- Polyesters reaction with dimethyl p-phenylene diamine compared under UV exposure from carbon arc and natural sunlight
10 p1716 A69-23978
- Mean absolute solar spectrum energy distribution from 1800 A to 4 mm, noting solar constant and radiation intensity determination
11 p1951 A69-24242
- Solar radiation pressure on interplanetary dust particles calculated as function of radius and density, noting asteroidal origin of dielectric and absorbing particles
11 p1956 A69-24397
- Solar UV radiation measurements by balloon-borne monochromatic illuminator, using Cd-cathode photomultiplier detector
11 p1945 A69-24410
- Center to limb variations of sunspot-photosphere brightness ratio, considering umbra darkening and radiative equilibrium
11 p1946 A69-24426
- Multiple scattering of solar radiation in turbid atmosphere, considering equations of sky radiation and radiative transfer
11 p1911 A69-24587
- Temperature field in thin walled rods with spiral coil cross section in solar radiation, considering radiant heat exchange
11 p1999 A69-24779
- Silicon dioxide coated Al reflectance, solar absorptivity and total normal and hemispherical thermal emissivity, noting application to satellite temperature control
11 p1918 A69-24835
- Biological radiation doses and protection from galactic, solar particle and trapped radiation in space, noting secondary radiation and bremsstrahlung in absorber
11 p1831 A69-24866
- Microorganism survival in space for exposure to solar UV radiation on balloons, rockets and satellites
11 p1828 A69-25457
- Thermally induced oscillatory instabilities in spacecraft booms, rederiving thermal torque equation to predict finite twist response
11 p1994 A69-25531
- Empirical determination of heating efficiency of extreme solar UV radiation interacting with carbon dioxide atmosphere of Mars and Venus
12 p2155 A69-26019
- Ocean circulation as climate regulator, discussing role in redistributing climate-changing energy input from solar radiation or lunar tidal friction into atmosphere
12 p2067 A69-26333
- Solar radiation in short wave, UV and X ray range recorded by rockets, probes and satellites, notably Elektron 2 probe
13 p2326 A69-27355
- Atmospheric attenuation of solar radiation, discussing submillimeter astronomy at low altitude observatories
13 p2327 A69-27590
- Solar atmosphere surface radiation intensity determined by initial value theory including source function and resolvent
13 p2350 A69-27859
- Human expansion in space, discussing moon landing and exploitation
13 p2352 A69-27901
- Semiconductor luminescent devices and laser pumping by solar radiation modulated to interact resonantly with solid state plasma oscillations and electric field in crystal
13 p2272 A69-27969
- Structure and thermometry of solar interior from measuring neutrino fluxes intensities emitted by unit surface
13 p2333 A69-28434
- Saturated signals of GM counter from solar radiation monitoring satellite, showing Van Allen belt high energy particle origin
14 p2514 A69-29383
- Cosmos 149 meteorological satellite telephotometers for measuring reflected solar radiation from earth
14 p2447 A69-29404
- Absorption band observation near 0.43 mu in solar spectra and scattered radiation of sky, determining nontelluric origin
14 p2441 A69-29407
- Solar UV radiation reflected from Echo satellites measured and compared with UV fluxes from Lyrae
14 p2447 A69-29408
- Solar radiation pressure effects on satellite models in circular equinoctial orbits
14 p2522 A69-29595
- Solar UV radiation effects on processes in comet head, interpreting surface brightness distribution of comet 1959k in terms of photodissociation
14 p2525 A69-29717
- Solar ionizing radiation sources, discussing activity at sunspot minimum, temperature, density and solar wind effects, X ray and UV spectra, etc
15 p2673 A69-30007
- Bidirectional reflectance of solar radiation and IR temperature data from Nimbus 2 satellite to differentiate clouds above snow surfaces
15 p2596 A69-30455
- Reflected and absorbed solar radiation by planetary atmosphere and surface determined as function of atmosphere and surface optical properties
15 p2689 A69-30564

Earth reflected solar radiation spatial, angular and spectral distributions measured by telephotometers on-board Cosmos 149

15 p2596 A69-30650

Ozonosphere inhomogeneities from UV spectra of reflected solar radiation, studying latitude dependence of seasonal behavior at different heights

15 p2597 A69-30654

Spacecraft illuminance by reflected solar radiation calculated by computer method

15 p2691 A69-30746

Scattered solar Lyman alpha radiation measurement by Vertical Space Probe station in upper atmosphere including UV radiation

15 p2691 A69-30747

Solar neutrino fluxes sensitivity to localized changes in opacity and equation of state, discussing solar models

15 p2675 A69-30768

Solar radiation actinometric and pyranometric observations during 20 May 1966 eclipse, examining IR component and spectral radiation energies

15 p2697 A69-31257

Earth albedo instrument on OSO 3 spacecraft to measure solar reflectance of earth at various wavelengths

15 p2614 A69-31279

Visual ashen light observation on Venus possibly attributable to solar particle bombardment from dark side emission detection by spectroscopic and photometric studies

16 p2861 A69-32300

He I/1.083 mu/ and O I/5577 A/ absolute brightness measured in solar aurora for various shadow heights of solar radiation, considering primary electron precipitation

16 p2780 A69-32311

Aircraft measurements and computer calculations of downward and upward solar radiation fluxes related to albedo, altitude and sun angle

17 p3023 A69-33158

Attenuation statistics due to rain measured on earth-space path at 16 and 30 GHz, using sun as signal source

17 p2920 A69-33398

Solar thermonuclear reactions studied by emitted neutrinos detection, plotting energy spectra for sensitivity of CI 37 detection system

18 p3185 A69-34278

Instantaneous and integral solar irradiance of earth oriented satellite surface, noting solar illumination nomogram representation

19 p3432 A69-36629

Solar disk edge polarization rate determined by applying Feautrier method to transfer equations for polarized radiation

19 p3427 A69-36728

UV solar radiation variation effects on Mars and Venus upper atmosphere temperatures

20 p3595 A69-37136

Soviet book on methods of calculating characteristics of solar radiation covering short wave radiation, relationship to meteorological factors, applications, etc

20 p3570 A69-37233

Mesosphere and lower thermosphere molecular O density from solar radiation atmospheric absorption, using satellite measurements

20 p3523 A69-37413

Solar neutrinos capture rate estimation by using Li 7 as detector

20 p3588 A69-37420

Solar bremsstrahlung intensity dependence on heliographic longitude, noting maximum intensity shift toward electron beam direction

20 p3589 A69-37552

Solar ionizing radiation increase during flares of 21 and 23 May 1967 determined from ionospheric electron density concentrations

20 p3590 A69-37558

Hg injection lamp with high power and variable spectral energy distribution as light source for testing solar radiation effects

20 p3510 A69-37630

Atmospheric ozone detection by three-color photometer measurements of solar UV radiation attenuation in Hartley continuum

20 p3543 A69-37802

Solar cycle variation of extreme UV radiation from total solar disk under nonflare conditions by photoelectric measurements

20 p3592 A69-38103

Solar UV emission lines from high resolution rocket observations

20 p3612 A69-38167

Angular dependence of ocean surface-cloudless atmosphere reflectance for solar radiation studied with digitized camera signals from ATS 1 satellite

21 p3704 A69-38372

Twilight airglow excitations governed by solar radiation, indicating presence of alkali metals, positive calcium ions and H lines, positive sodium ion bands, etc

21 p3711 A69-38515

OH emission rise after sunset and decay at sunrise attributed to strong solar dissociation of ozone

21 p3712 A69-38520

Solar neutrinos emission mechanism for information on central region of sun, discussing detection and flux density

21 p3790 A69-38827

Molecular O distribution in thermosphere from Ariel 3 observations of solar radiation attenuation, showing large and systematic variation with longitude

21 p3717 A69-39263

Solar radiation pressure windmill effect in rotational bursting and elimination from solar system of small magnetic celestial bodies

21 p3814 A69-39584

Mean intensity profiles of photospheric H alpha radiation illuminating solar prominences moving at different heights

22 p4011 A69-39995

Solar flare optical, neutron and gamma emission, discussing ionization losses and nuclear interaction of accelerated particles in flares

22 p4003 A69-40296

Vacuum integrating sphere for measuring solar absorptance in space environment to determine thermal control coatings qualifications [AIAA PAPER 69-1021]

22 p3923 A69-40392

Curvature and temperature distribution in nonrotating long solid cylinders under solar radiation in interplanetary space

22 p4043 A69-40546

Radiative heat input to artificial satellite in orbit due to solar and earth radiations calculated and presented in graphs for satellite temperature calculation

22 p4006 A69-40589

Zenith atmospheric attenuation in 183-325 GHz region measured by wideband Ge bolometer detector and spectral convolution technique

23 p4115 A69-41586

Qualitative model of atmospheric mass circulation constructed from radar meteor trail drifts observations, considering solar thermal radiation and zonal wind direction

23 p4214 A69-41862

Total solar radiation correlation with bright sunshine hours measured monthly on solarimeters and Campbell-Stokes recorders at various tropical stations

23 p4206 A69-42178

Human habitation conditions on moon from viewpoint of solar and lunar radiation, vacuum and gravitation effects including solar energy utilization

23 p4111 A69-42213

Type 4 bursts maximum intensities at different frequencies compared for centimeter and decimeter waves

24 p4366 A69-42964

Absorption observation of solar radiation at sunset by nitric acid in three wavelength intervals on different balloon flights

24 p4308 A69-42969

Solar grazing ray absorption calculated by tracing through earth atmosphere, noting extinction for arbitrary ozone and aerosol profile

24 p4350 A69-43013

Solar radiation pressure on interplanetary dust particles calculated as function of radius and density, noting asteroidal origin of dielectric and absorbing particles

24 p4390 A69-43787

SOLAR RADIATION SHIELDING

Gaseous hydrates formation in comet nuclei, discussing stability at given temperatures and pressures and solar radiation shielding by dust sheath

03 p0515 A69-14032

Solar flare radiation protection requirements, considering bulk and plasma radiation shielding [AIAA PAPER 69-15]

06 p0884 A69-18079

Multiple Coulomb scattering and range straggling effects in shielding against solar flare protons and trapped protons in Van Allen belt

10 p1723 A69-23164

SOLAR RADIO BURSTS

NT TYPE 2 BURSTS

NT TYPE 3 BURSTS

NT TYPE 4 BURSTS

NT TYPE 5 BURSTS

Power spectral indices of March 6, 1968 solar radio burst, suggesting Razin effect

01 p0148 A69-10054

Microwave spectra of peak flux of solar radio bursts of March and July 1966, relating plage regions to spectral characteristics

01 p0069 A69-11121

Solar noise storms structure and movement, discussing localization of type 1 burst emission into zones in solar corona

02 p0315 A69-11824

Solar atmosphere physical properties tabulated to interpret radio bursts and noise storms

02 p0329 A69-12786

Meter and decimeter solar radio bursts and sudden cosmic noise observed at Ahmedabad, India

03 p0518 A69-14259

Microwave solar burst data, analyzing flux intensity and polarization distributions

04 p0652 A69-14417

Radio bursts at 3.3 mm and H alpha emission during flares, proposing thermal enhancement

04 p0650 A69-15527

Electromagnetic radiation from solar flares based on rocket and satellite observations of 10-100 keV X ray emission and ground observation of cm-wavelength bursts

05 p0813 A69-15603

Space radio astronomy techniques for problems in galactic radio emission, solar studies and planetary observations

05 p0821 A69-15844

Hard solar X ray bursts characteristics and coordination of ground and space observations

05 p0814 A69-15862

Intense continuum bursts energy, flux density and energetic proton production, noting V-spectrum in proton flares

06 p0985 A69-16980

Solar radio spectroscopy for 40 to 240 MHz frequency range, noting dynamic spectra of solar radio bursts

06 p0925 A69-17318

Solar wind, discussing corona, radio sources, radio bursts, comet tails, cosmic rays, etc

06 p1012 A69-18239

Outstanding solar type 4 radio burst from spectrographic records at metric and decametric wavelengths from Weissenu Observatory

09 p1578 A69-22157

Impulsive solar microwave bursts observed by parabolic reflector, obtaining bursts spectra and total flux density

09 p1579 A69-22178

Solar X ray bursts observed by proportional counter on IMP-F satellite to correlate optical H alpha flares and radio bursts

09 p1582 A69-22746

Radio bursts and proton flares associated with active region McMath 8362 of July 1966, discussing wavelengths

10 p1764 A69-23742

Solar radio bursts observations with multielement compound interferometers, noting polarization distribution and magnetic field change

11 p1946 A69-24428

Time splitting of solar radio bursts observed at Oslo Solar Observatory with high resolution radio spectrographs

11 p1946 A69-24590

Solar radio emission bursts periodicity relation to burst intensity

12 p2157 A69-26234

Solar flares and bursts correlation, taking into account sunspot type associated with flare and frequency range of bursts

16 p2850 A69-32213

Solar microwave radiation burst of 29 October 1968 from active region behind west limb

16 p2865 A69-32811

Solar radio bursts spectra fine structure, discussing observations of fast drift storm, drift pair and split pair bursts

17 p3024 A69-33607

Correlated bursts from separate distant sources on sun, noting occurrence in quiet periods and strength

17 p3024 A69-33804

Solar radio burst fringes at 21 cm observed with high angular resolution using two element E-W interferometers

17 p3040 A69-33809

Solar soft X ray bursts observed by Solrad 8 satellite, considering relationship to microwave radio bursts

17 p3025 A69-34055

Geomagnetic crochets time relations to solar X rays, radio bursts and flares

17 p3025 A69-34227

Multielement compound high resolution quick scan interferometer for rapidly changing solar burst observations at 3.75 GHz

18 p3118 A69-34968

Occurrence frequency distributions at microwave frequencies as function of peak intensity and directivities of solar bursts

18 p3187 A69-34969

Radio echoes relationship to active parts of solar corona, noting agreement with data on type 3 radio bursts source location

18 p3201 A69-35207

Solar radio bursts polarization measured with microwave correlation polarimeter, noting output recording rate

18 p3188 A69-35213

Daily solar radio noise intensity at 10.7 cm with slowly varying components and quiet sun emission, revealing rise only and absorption bursts

19 p3401 A69-35758

Soviet monograph on large solar radio bursts covering global observation networks, monochromatic recordings, spectral classifications and catalog of IGY and IQSY observations

20 p3588 A69-37444

Solar flares microwave and hard X ray bursts, discussing gyrosynchrotron plasma, nonthermal electron bremsstrahlung and electron relaxation

20 p3589 A69-37551

Solar hard and soft X rays time-intensity profiles showing homology with centimeter radio bursts, suggesting origin from same electrons

20 p3589 A69-37553

Type I solar radio bursts linked in chains, giving graphical data for chain distributions frequency, photospheric height and lifetime

22 p4010 A69-39985

Medium sized solar radio events from peak intensities, spectrum characteristics and coronal magnetic field role

22 p4020 A69-40299

Synchrotron radiation HF cut-off resulting from electrons with anisotropic pitch angle distribution for type IV solar radio bursts

22 p4006 A69-40577

Solar flare soft X ray and EUV emission spectra data obtained on OSO-3 satellite compared with centimetric radio bursts

24 p4371 A69-43609

Solar flare-associated radio bursts, reviewing solar radio measurements based on X ray and particle observations

24 p4372 A69-43614

Single frequency microwave solar bursts correlation with flares and associated active regions based on spectral grouping

24 p4372 A69-43616

SOLAR RADIO EMISSION

NT TYPE 2 BURSTS

NT TYPE 3 BURSTS

NT TYPE 4 BURSTS

NT TYPE 5 BURSTS

Solar radio emission slowly varying component theory, discussing main characteristics of cyclotron and bremsstrahlung radiations of thermal electrons

02 p0314 A69-11636

Radio emission fluxes in solar active regions, determining slope of spectral characteristics of radio sources from effective emission center

02 p0314 A69-11676

Spectrum and diameter of source of slowly varying component of solar radio emission between 3.3 mm and 21 cm

03 p0516 A69-14045

Simultaneous recording of radio emission from five sections of solar active region, using parabolic antenna and single amplification/reception channel

04 p0651 A69-14377

Slowly varying solar radio emission caused by bremsstrahlung and cyclotron mechanisms within limits of active region model

04 p0662 A69-15240

Solar radio emission sources associated with sunspot groups and flocculi at 1.6 cm

04 p0649 A69-15241

Polarization enhancements in solar microwave radiation, noting correlation with other solar events and geophysical effects

05 p0813 A69-15761

Solar radio emissions analysis using radio telescope measurements, observing quasi-periodic LF fluctuations caused by chromospheric processes

06 p1004 A69-17535

Quasi-periodic variations of solar radio emission intensity related to solar activity variations

07 p1211 A69-18516

Statistical study of solar radio flux fluctuations incidence, observing absorption and polarization effects

07 p1215 A69-18819

Solar intensity measurements at 1.2 mm during partial solar eclipse, noting solar limb brightening and intense solar outburst near end of eclipse

07 p1217 A69-19243

Solar radio astronomy, discussing quiet sun radio emission, solar activity, slowly varying radio emission, radio bursts and possibility of observing lines

08 p1388 A69-20218

Microwaves from celestial objects noting radio emission from sun, moon and Jupiter, cosmic fireball and pulsars

08 p1407 A69-21125

Antenna noise temperature at earth station due to rain on radomes, solar and cosmic noise, noting SNR degradation

09 p1461 A69-21283

Correlated spectra of related sunspot number and solar 10.7 cm radiation component, noting variance for solar rotation periods

09 p1574 A69-21397

Correlated microwave and energetic X ray emission from solar flare with 16-sec periodic pulsations, discussing energy during modulation peaks

09 p1574 A69-21457

Upper atmospheric density relation to AE indices sum and solar radio flux during geomagnetic disturbances

09 p1488 A69-21657

Slowly varying component height for microwave radio emission during IQSY, noting magnetic field changing strength effect

09 p1598 A69-22176

Peaks and time intensity profile of energetic X rays and cosmic rays observed by OGO-C ion chamber on May 23, 1967 flare event

09 p1579 A69-22182

Synchrotron and X ray emission generation from upper chromosphere electrons during solar flares

09 p1580 A69-22203

Solar occulting disk diameter at radio wavelengths derived from consideration of slightly deviated rays

09 p1607 A69-22432

Solar radio astronomy in Australia including solar atmosphere, bursts, instruments, etc

10 p1777 A69-23383

Synoptic radio interferometer observations of July 1966 solar proton flare at microwave frequencies, correlating observed radio source with proton event

10 p1783 A69-23734

Solar radio emission S component at short waves, discussing role of higher frequency spectrum in proton flare occurrence

10 p1763 A69-23735

Photospheric magnetic fields, coronal emission and filaments distribution relationship with 1420 MHz radio emission, noting brightness and plasma density increase

11 p1964 A69-25417

Upper atmosphere density variations investigation using Eurobs system, correlating density to geomagnetic activity and 10.7 cm solar radio emission

12 p2069 A69-26437

Circular polarization of solar microwave radio emission in Southern and Northern Hemispheres due to solar magnetic field

13 p2326 A69-27550

Solar corona 5303 and 6374 A emission enhancements correlated to 169 MHz S-component, discussing coronal temperature

13 p2347 A69-27717

Solar 3 cm flux density sensitivity to physical conditions in solar atmosphere related to maximum existence in flux density spectrum F gamma in active regions

13 p2327 A69-27721

Troposphere effects on millimeter wave radio astronomy measurements, discussing solar noise fluctuations due to clouds and precipitation

13 p2223 A69-28607

Radio emission fluxes in solar active regions, determining slope of spectral characteristics of radio sources from effective emission center

13 p2355 A69-28707

Solar radio emission data during IGY covering solar terrestrial disturbances, broadband bursts, solar indices, etc

14 p2513 A69-29321

Slowly varying component of solar radio emission, evaluating resolution of radio telescopes in sunspot studies and localized areas luminescence

15 p2674 A69-30503

Slowly varying component of solar radio emission /S component/, correlating 35 GHz S component flux and corresponding plage, discussing magnetic fields and electron density

17 p3030 A69-33056

Solar radio emission sources position changes observed in solar storm center

17 p3024 A69-33805

Solar radio sources heights at 1424 and 696 MHz during near minimum solar activity

17 p3040 A69-33808

Surges statistical properties observed in Sweden /1957-1967/ noting latitude distribution pattern, radio emission association, rate dependence on solar cycle, etc

18 p3204 A69-35393

White light solar corona brightness distribution observations /1964-1967/, considering solar radio flux relationship and equatorial electron densities

18 p3205 A69-35394

Solar radio emission during quiet sun years 1964-1965 mapped using Stanford spectroheliograph, attributing slowly varying component to electron density enhancement

18 p3188 A69-35395

Solar microwave emission heliographic distribution during pronounced geomagnetic recurrence, noting brightness temperature nonuniformity due to coronal depression through polytropic models for solar wind

18 p3188 A69-35396

Solar radio emission parameters calculated, determining basic 327 MHz emission component and flux density-sunspot area correlation coefficient

20 p3588 A69-37478

Solar microwave emission relationship to geomagnetic activity, analyzing statistically source intensity and model of coronal condensation associated with sunspots based on electron densities

20 p3589 A69-37557

Radio observations of 30 May 1965 total solar eclipse at Manue Island, discussing radio brightness

20 p3616 A69-38304

Solar atmosphere radio emission generation by hydrodynamic shock wave interaction with coronal plasma, treating corona as ideal gas consisting of protons and electrons

22 p4009 A69-39984

Radio emission data from 20 May 1966 partial solar eclipse, giving radio noise and brightness distribution data

22 p4010 A69-39986

Solar microwave flux density during solar activity cycle tabulated, noting discrepancies in absolute flux levels

22 p4001 A69-39987

Solar observations at 21 and 43 cm during solar minimum by grating cross and total power radiometer, giving radio map of solar emission

22 p4001 A69-39988

Daily measurement of solar radio intensity at 810 MHz during 1964 minimum solar activity period

22 p4010 A69-39989

Solar radio emission /S component/ observations with 22-m radio telescope at Crimean Astrophysical Observatory

22 p4020 A69-40295

Solar soft X rays observed from OSO-3, correlating to solar flares and radio bursts

22 p4003 A69-40297

Distinction between faint and bright sources of slowly varying solar microwave emission components applied to geomagnetic activity statistics

22 p4020 A69-40306

Solar cycle and slowly varying components correlation with soft X ray radiation based on spacecraft measurements

22 p4004 A69-40504

Polarization measurement of slowly varying component of sun by pencil-beam antenna at 8.6 mm, analyzing data by magnetoionic theory

22 p4027 A69-40660

SOLAR REFLECTORS

Radiant flux reflected by mirror and incident on receiver for paraboloidal solar devices, obtaining heat loads and radiant energy formulas

09 p1436 A69-21803

SOLAR ROTATION

- Impulsive solar microwave bursts observed by parabolic reflector, obtaining bursts spectra and total flux density
09 p1579 A69-22178
- Solar simulator with 20 kw xenon lamps, discussing performance, versatility and problems with collectors, folding mirrors and cooling system
15 p2586 A69-30384
- Faceted reflector for solar power installations with photoelectric converters, discussing reflector construction, efficiency and energy balance
16 p2741 A69-32798

SOLAR ROTATION

- Geomagnetic response asymmetry related to solar direction of polarity in interplanetary magnetic field
01 p0077 A69-11236
- Solar neutrino flux dependence on rotation rate of solar core and fractional mass involved in interior mixing
02 p0325 A69-12600
- Solar wind model including effects of rotation, magnetic fields and anisotropic heat conduction
08 p1380 A69-20643
- Correlated spectra of related sunspot number and solar 10.7 cm radiation component, noting variance for solar rotation periods
09 p1574 A69-21397
- Solar interior rotational angular velocity influence on solar oblateness, noting reduction by turbulent mixing
09 p1600 A69-22201
- Topology of solar magnetic field differential rotation, using hydromagnetic equations
09 p1606 A69-22425
- Differential solar rotation noting strong quasi-kineticity effect on solar convective zone and rotation influence on viscosity tensor and rotation law
11 p1955 A69-24390
- East-west asymmetry in solar wind velocity due to solar rotation effects on interaction between fast and slow streams
11 p1950 A69-25148
- Solar oblateness and differential rotation time development due to solar wind torque
12 p2157 A69-26308
- Solar polar faculae observations, discussing relation to general solar magnetic field and coronal properties, solar high latitude rotation and susceptibility to atmospheric conditions
12 p2160 A69-26897
- Solar cycle kinematical model based on field amplification by solar differential rotation including fluctuations in eruption rate
13 p2337 A69-27548
- Solar rotation measured as function of latitude using Doppler compensator with magnetograph, noting daily rotation rate difference in H alpha and metallic lines
14 p2528 A69-29974
- Finite electrical conductivity effect on sun angular momentum loss due to solar wind
18 p3189 A69-35398
- Solar oblateness observed by Dicke and Goldenberg as interaction between slow uniform rotation and turbulent convection
22 p4017 A69-40175
- Variable magnetic field effect on rotation of solar outer layers, applying to spectroscopic observations of rotation velocity at solar limb
22 p4019 A69-40293
- Hydrodynamic equations for radial solar wind expansion linearized and specialized to treat co-rotating perturbations
22 p4003 A69-40302
- Differential solar rotation noting strong quasi-kineticity effect on solar convective zone and rotation influence on viscosity tensor and rotation law
24 p4390 A69-43780

SOLAR SAILS

- Solar sail structural design, discussing application as propulsion system for heliogyro interplanetary spacecraft
06 p1015 A69-17591
- Feasibility of automatic stationkeeping for synchronous satellites by using solar sailing techniques and low thrust systems
[AAS PAPER 68-151] 19 p3429 A69-35950
- Reduced flight time interstellar round trip propulsion system with relativistic velocity capabilities, discussing vehicle with solar sail and magnetic course reversal
[AAS PAPER 69-388] 24 p4363 A69-42829

SOLAR SENSORS

- Alignment of rocket-borne instrument with sun, discussing mechanical system design, servocontrol and silicon photodiode sensors
03 p0427 A69-12980
- Balloon for in situ measurements of atmospheric optical parameters using two axis sun pointer, spectropolarimeter and airborne telemetry
15 p2615 A69-31288
- Precision autocollimating solar sensor design for attitude alignment changes, including detector calibration and sounding rocket flight test results
[AIAA PAPER 69-858] 21 p3762 A69-39386
- Total solar radiation correlation with bright sunshine hours measured monthly on solarimeters and Campbell-Stokes recorders at various tropical stations
23 p4206 A69-42178
- Parallel wire array fluidic sun sensor for solar pointing fluidic attitude control, discussing design and breadboard test
24 p4348 A69-43297

SOLAR SIMULATION

- Multichannel radiometers calibration and testing for spacecraft and solar simulation applications, noting exposure to sun onboard X-15 aircraft at high altitudes
06 p0926 A69-17620
- Model, assuming electron thermal conductivity contribution, applied to studying solar plasma discharge characteristics in presence of three dimensional thermal sources in solar corona
12 p2149 A69-26680
- Solar wind interaction with geomagnetic field simulation practically unrealizable, discussing partial simulation covering neutral magnetic layer formation on night side
12 p2149 A69-26681
- Space environment simulation for vacuum, solar radiation, heat sink and orbital motion, discussing oil contamination of optical surfaces
13 p2241 A69-28079
- Solar thermal vacuum test for space flight qualification of military spin stabilized synchronous orbit communications satellite
15 p2587 A69-30391
- Handbook of solar simulation for thermal vacuum testing, discussing space environment, thermal control coatings, radiation sources, optical components, etc
21 p3690 A69-38894
- Variable optical system with remote and continuous adjustment of beam for solar simulation, permitting maximum test facility utilization
[AIAA PAPER 69-997] 22 p3920 A69-40375

SOLAR SIMULATORS

- Simulated solar radiation heating of cesium vapor thermionic converters with multicapillary transmitters
07 p1058 A69-18951
- Simulated solar EUV laboratory spectrophotometry used in preparing optical space flight experiments, discussing instrumentation and calibration
08 p1267 A69-19888
- Filtering system for xenon arc solar simulator to provide operation at air-mass-two /average sea level/ sunlight
09 p1476 A69-21648
- Thermal vacuum simulator for testing manned Lunar Module Test Vehicle, using conformal skin heaters to control heating rates and skin temperature
[AIAA PAPER 69-312] 09 p1479 A69-22386
- Solar simulator with xenon and krypton lamps designed for thermal balance tests, power conversion and material degradation experiments
15 p2586 A69-30383
- Solar simulator with 20 kw xenon lamps, discussing performance, versatility and problems with collectors, folding mirrors and cooling system
15 p2586 A69-30384
- Solar simulator with pulsed Xe arc tube, describing operating characteristics, spectral emission and simulator-sunlight correlation
15 p2586 A69-30385
- Boeing A-7000 Solar Simulator for Space Environment Simulation Laboratory, noting output characteristics
15 p2588 A69-30403
- Xenon high wattage short arc lamps for space/solar simulators, describing seals, electrodes shapes and cooling, operating characteristics, etc
[AIAA PAPER 69-998] 22 p3920 A69-40376
- Solar simulator built into multiwall ultrahigh vacuum chamber, describing simulator and chamber modifications
[AIAA PAPER 69-1001] 22 p3921 A69-40377

SOLAR SPECTRA

- Paschen series line contours for hydrogen in solar spectrum plotted from IR spectrophotometric data
01 p0148 A69-10126
- Solar copper abundance determined from measuring Cu I and 2 and resonance lines transition probabilities in electric arc emission under LTE conditions
02 p0204 A69-11456
- Fraunhofer lines hyperfine structure effect on solar abundances of V, Mn, Co, Cu and Ba, calculating equivalent line widths by ALGOL program
02 p0311 A69-11458
- OSO-4 solar UV spectrum measurements, correlating chromospheric line intensity and photospheric magnetic field strengths
[AAS PAPER 68-219] 02 p0313 A69-11485
- Solar flare X ray line and continuum spectra measured with crystal spectrometers aboard orbiting solar observatory
02 p0308 A69-12297
- Solar coronal ion abundance analyses from extreme UV emission lines
02 p0327 A69-12719
- Type 4 bursts mobile spectrum of september 14, 1966 interpreted by considering plasma effects on synchrotron emission mechanism
02 p0309 A69-12754
- Solar atmosphere from two dimensional study of solar spectrum, discussing satellite observations of corona and upper chromosphere
02 p0329 A69-12785
- Mean annual intensity distribution of 5303 angstrom coronal line on solar limb determined for 11-year solar activity cycle
03 p0506 A69-13084
- Fraunhofer lines in solar spectrum in 2950-8770 A wavelength region, noting 8000 additional unidentified lines
03 p0507 A69-13170
- Line identification methods in solar extreme UV and X ray regions
03 p0507 A69-13171
- Electron temperature and concentration and solar UV absorption data from sounding rockets, estimating ion exchange rate, recombination coefficient and heat flux
03 p0422 A69-13508
- Solar emission line absorption by oxygen and nitrogen atomic lines, discussing effect on upper atmosphere composition measurements
03 p0425 A69-14019
- Analysis of equivalent widths as function of disk position for six photospheric neutral atomic oxygen Fraunhofer multiplets, noting O abundance
03 p0515 A69-14034
- Spectra of hydrides of Mg 25 and Mg 26 in photosphere, searching for weak lines on basis of isotope shifts
03 p0515 A69-14035
- Solar Fe abundance from photospheric permitted Fe and forbidden Fe II lines, noting equivalent widths of two Fe II lines
03 p0515 A69-14036
- Spectrum and diameter of source of slowly varying component of solar radio emission between 3.3 mm and 21 cm
03 p0516 A69-14045
- Solar microwave type 4 bursts spectra and decay rate time variations
04 p0648 A69-14364
- Time variations of chromospheric network of bright points covering solar disk in spectrograms, noting contrast and interspaces variation with 11-year solar cycle
04 p0651 A69-14372
- Balloon observations of solar far IR spectrum and brightness temperature
04 p0652 A69-14419
- Be I and Be II lines in solar spectra show no evidence for Be 7 and Be 10 in solar atmosphere
04 p0655 A69-14666
- Instrument profile of birefringent Lyot filter for H alpha line determined from photographic spectra with grating spectrograph
04 p0664 A69-15524
- Bright streaks in H alpha disk chromosphere, noting predominantly horizontal loop structures
04 p0664 A69-15525
- Lithium abundance determination difficulties for undisturbed solar photosphere, noting Li I resonance line identification and model choice
05 p0821 A69-15849

Lithium abundance in sunspots and undisturbed solar atmosphere from measurements of solar atmosphere and spot spectra

05 p0821 A69-15850

UV solar spectra observation, discussing coordination of ground based and satellite programs

05 p0822 A69-15861

Type 3 bursts spectra graphical representation, giving probable solar origin and curves of corona temperature

05 p0824 A69-16060

Limb darkening and central intensity of solar disk measured in UV

05 p0827 A69-16466

Continuum position location and total line absorption in solar spectrum, using Houtgast high dispersion intensity measurements of UV region

05 p0828 A69-16611

Mass motions in solar flares using line profiles and filtergrams

06 p0993 A69-17427

Solar moustaches H alpha profiles spectroscopic studies indicating near symmetry

06 p0994 A69-17435

Solar prominence structures observed in H alpha emission, determining radial velocities as function of distance from limb

06 p0994 A69-17436

Communications of Lunar and Planetary Laboratory, Volume 7, covering IR solar spectrum atlas reports and solar spectrometer for airborne IR observations

06 p1008 A69-17807

Arizona-NASA atlas of IR solar spectrum, reproducing photometric tracings obtained from CV-990 aircraft flights

06 p1008 A69-17808

IR solar spectrum tables and graphs covering 10,657-12,857 A

06 p1008 A69-17809

NASA atlas of IR solar spectrum, reporting B and 4 meter spectrometer recordings over band containing methane telluric absorptions

06 p1008 A69-17810

Beryllium abundance in solar atmosphere from spectra observed at Oslo Solar Observatory

06 p1010 A69-17971

Forbidden S I lines due to transitions within ground configuration identified in Fraunhofer spectrum of sun, noting photospheric abundance of S

07 p1217 A69-19237

Solar spectral line profiles for photosphere disturbed by short period acoustic waves

07 p1217 A69-19239

Central Fraunhofer line intensities near solar minimum compared to Soviet results for possible solar cycle variation

08 p1386 A69-20075

Scattered light reduction in sunspot photometry, noting eliminating effect when observing spectral lines or narrow spectral regions

08 p1389 A69-20251

Wing of solar line H-alpha for levels population of hydrogen atom in solar photosphere, discussing excitation temperature, absorption coefficient and thermodynamic equilibrium

08 p1390 A69-20394

Excitation cross sections of Fe XIV lines in solar coronal spectra, comparing computations with Coulomb-Born approximation

08 p1392 A69-20563

Spectrum variations of type 4 radio burst as source rises through solar corona, determining electron density and magnetic field distributions in corona

08 p1380 A69-20775

Chemical composition and element abundance in solar atmosphere and photosphere, noting solar absorption and emission and energy spectrum data

08 p1402 A69-20905

Solar element abundances from nucleosynthesis standpoint, discussing measurements with high resolution spectrometer used in double pass with intermediate slit

08 p1402 A69-20906

Present state of abundance determination in solar corona, discussing forbidden and UV lines analysis

08 p1402 A69-20907

Correlated spectra of related sunspot number and solar 10.7 cm radiation component, noting variance for solar rotation periods

09 p1574 A69-21397

Stigmatic profiles of solar C II doublet resonance lines obtained by rocket-borne echelle spectrograph

09 p1592 A69-21456

Solar electromagnetic radiation spectral distribution from ground level, rocket and satellite observations to obtain value of energy received at top of atmosphere

09 p1575 A69-21645

Solar irradiance spectral distribution data normalized and combined with spectral absorptance of satellite surface coatings, obtaining absorbed energy for spectral range

09 p1576 A69-21646

Outstanding solar type 4 radio burst from spectrographic records at metric and decametric wavelengths from Weissenau Observatory

09 p1578 A69-22157

Solar far UV emissions observed from OSO-C by grazing incidence grating spectrometer, noting temporal variations and atmospheric absorption characteristics

09 p1578 A69-22168

Solar X ray and extreme UV spectra during flares, attributing intense emissions to optical transitions

09 p1578 A69-22169

Solar soft X ray components observed with ion chamber photometer, studying components relation to transient and slowly varying phenomena at other wavelengths

09 p1578 A69-22170

Impulsive solar microwave bursts observed by parabolic reflector, obtaining bursts spectra and total flux density

09 p1579 A69-22178

Green and red coronal line polarization observed during solar eclipses, discussing nonpolarization of red line and observation instrument error

09 p1600 A69-22204

Rotational Raman scattering in planetary atmospheres, analyzing spectra of deep solar Fraunhofer lines

09 p1601 A69-22207

Stellar evolution, computing sequences to establish solar model of primordial composition, comparing models with spectroscopic observations

10 p1788 A69-24126

Mean absolute solar spectrum energy distribution from 1800 A to 4 mm, noting solar constant and radiation intensity determination

11 p1951 A69-24242

Solar quiescent prominences spectra with bright metallic lines, discussing turbulent angular velocity and kinematic temperature of filaments

11 p1945 A69-24387

Equivalent line widths for solar disk Fe and Ti spectra determined for umbra models, noting role of sunspot location

11 p1955 A69-24388

Hydrogen balmer lines broadening by Stark and Doppler effects, finding prominences and chromosphere electron concentrations

11 p1955 A69-24389

Solar spectra of Mg II doublet lines during September 22, 1968 eclipse, considering chromospheric activity effects on emission peaks

11 p1958 A69-24591

Rocket-borne spectroheliograph for monochromatic solar photography in Mg II 2802.7 A line noting filter bandwidth, film polarizers and temperature control

11 p1884 A69-24838

Monograph on internal structure of sun corona covering variations in intensity and width of coronal lines, inhomogeneity, quasi-homogeneous and anisothermic coronas, etc

11 p1961 A69-25103

Solar X ray bursts analyzed by dynamic spectra based on time history of intensity of bursts

11 p1951 A69-25419

Relative intensities of selected Si two multiplets calculated and compared with solar spectrum and plasma source ZETA values

13 p2326 A69-27551

Atmosphere effects on solar IR spectra, discussing role of absorbing molecule distribution in transmittance calculations

13 p2341 A69-27589

Far IR and millimeter solar continuum, analyzing flatness of limb darkening curves and brightness temperature near minimum

13 p2341 A69-27591

Indium, Rb and Cs abundances obtained from sunspot spectra by comparison with Zr and Ti lines

13 p2343 A69-27626

Solar corona 5303 and 6374 A emission enhancements correlated to 169 MHz S-component, discussing coronal temperature

13 p2347 A69-27717

Solar 3 cm flux density sensitivity to physical conditions in solar atmosphere related to maximum excitation in flux density spectrum F gamma in active regions

13 p2327 A69-27721

Spectrometric and photometric investigation of spectral characteristics of large sunspot 45 degrees from solar disk center, tabulating characteristics of 134 spectral lines

13 p2218 A69-28324

Mean annual intensity distribution of 5303 A coronal line on solar limb determined for 11-year solar activity cycle

14 p2515 A69-28766

Absorption band observation near 0.43 mu in solar spectra and scattered radiation of sky, determining nontelluric origin

14 p2441 A69-29407

Arcturus and solar rubidium abundance compared using Mount Wilson photographic spectrograms of Arcturus

14 p2522 A69-29589

Fe and Ti line growth in 12 July 1961 solar flare spectrum, finding ionized titanium, neutral and ionized iron excitation temperatures

14 p2514 A69-29720

Source functions of IR Fraunhofer lines obtained using solar disk equivalent width method, noting LTE role

14 p2528 A69-29961

Ca II forbidden lines in photospheric spectrum identified with weak Fraunhofer line by photoelectric spectrometer scans

14 p2528 A69-29962

Solar rotation measured as function of latitude using Doppler compensator with magnetograph, noting daily rotation rate difference in H alpha and metallic lines

14 p2528 A69-29974

Solar ionizing radiation sources, discussing activity at sunspot minimum, temperature, density and solar wind effects, X ray and UV spectra, etc

15 p2673 A69-30007

Spectral emission of active prominences, showing looplike lines during quiet phases and differences in turbulent velocities magnitude

15 p2674 A69-30510

CO absorption lines in solar spectrum analyzed theoretically and experimentally indicating random distribution of molecules

15 p2688 A69-30552

Unsuccessful attempt to observe high charge ion lines generated by dielectronic recombination in solar corona at 5-cm wavelength

15 p2689 A69-30568

Solar Mg b and Na D line spectra, computing profiles for Doppler cores of lines for multilevel model atoms and selected chromospheric parameter ranges

15 p2693 A69-30779

Coronal limb enhancement photometric study by spectroheliograms, comparing maximum brightness profiles in lines of different temperature in extreme UV

15 p2693 A69-30781

Temperature and density models for coronal green line enhancements with and without magnetic field effects, using graded height spectrograms

15 p2693 A69-30782

Fe II forbidden lines profiles and equivalent widths prediction for solar photospheric spectrum, deducing photospheric Fe abundance

16 p2854 A69-31652

Center limb observations of Ca II emission core interpretations, discussing chromospheric thickness effects on Doppler width

16 p2854 A69-31653

Coronal Fe ionization lines X, XIII and XIV photographed by UV coronagraph

16 p2847 A69-31661

Chromospheric spectrum outside of eclipse, wave lengths 3040 to 9266 A, listing emission lines taken at McMath solar telescope

16 p2861 A69-32257

Solar spectral irradiance measured by airborne instruments, discussing construction, calibration, etc, of photoelectric filter radiometer and Leiss monochromator

16 p2861 A69-32261

Solar image motion frequency spectra analysis via photoelectric equipment, showing influence on photographic pictures, spectra and modulation transfer functions for diffraction telescope

17 p3029 A69-33047

H alpha/D3 intensity ratio variations in peripheral regions of prominences may be due to dynamic conditions of material emitting radiations

17 p3029 A69-33051

Solar radio bursts spectra fine structure, discussing observations of fast drift storm, drift pair and split pair bursts

17 p3024 A69-33607

Power spectral analysis of chromospheric inhomogeneities in July 1967 and June 1968, tabulating mean heights of formation in solar atmosphere

17 p3040 A69-33811

Spatial structure of solar proton flare of 5 April 1960, discussing top ascending emission filament velocity in H alpha and coronal lines

17 p3025 A69-34224

Solar Fe II lines theoretical equivalent widths calculations, estimating influence of photosphere model on iron abundance data

18 p3191 A69-34305

Spectroheliograms interpretation obtained in line cores of neutral oxygen IR multiplets

18 p3204 A69-35388

Forbidden transitions in absorption spectra of sun and normal and peculiar stars

19 p3422 A69-36215

Forbidden lines in solar corona, discussing ionization equilibrium and excitation of levels in highly ionized atoms

19 p3422 A69-36216

Emission line spectrum for ionization and excitation in solar coronal structures, tabulating intensities from ground based eclipses observations

19 p3422 A69-36217

Solar rare earth abundances determined from high resolution tracings of solar spectrum, comparing results with nucleosynthesis theories

20 p3602 A69-37539

Solar atmosphere line source function showing frequency dependence as consequence of spectral line disappearance at solar limb

20 p3588 A69-37540

H alpha filtergrams and spectra of solar corona arch filament systems indicating downward and upward motions produced by magnetic field

20 p3588 A69-37543

Solar photography at extreme UV wavelengths using pinhole camera instrumentation on stabilized Skylark rocket

20 p3539 A69-37545

Solar far UV images systematic photometry for thin solar models in terms of quiet sun intensity

20 p3603 A69-37546

Solar corona Fe XII emission spectral lines relative intensity analyzed as function of temperature electron density

20 p3603 A69-37548

Type 3 bursts spectra graphical representation, giving probable solar origin and curves of corona temperature

20 p3591 A69-37970

Spectral characteristics of solar proton flare on 2 September 1966, noting light intensity variations

20 p3591 A69-38043

Periodicities in solar activity variation from correlation spectral analysis, establishing monotonically decreasing component and secular variations in activity

20 p3607 A69-38045

Ce II line reversal from absorption to emission in solar spectrum, noting reversal position dependence on wavelength and line source function scattering term

20 p3613 A69-38168

Solar Fraunhofer spectrum, observing Fe 5576 and 6678, K 7699 and Ni 5436, 6129, 5847 and 6130 A lines

20 p3615 A69-38297

Sunspot size and shape in continuous spectrum regions from photometric observations in UV and red ranges

20 p3616 A69-38301

Atmospheric transmission determined in submillimeter solar radiation spectra using Bouguer law, identifying absorption lines in nocturnal and diurnal spectra

21 p3796 A69-38472

Revised solar iron abundance by photospheric Fe I lines analysis using Garz and Kock f values, noting influence on solar photospheric model

21 p3796 A69-38475

Intensity integral inversion for Doppler core of strong solar absorption lines to obtain line source function for solar atmosphere

21 p3796 A69-38478

Solar Na D lines analysis by direct inversion of line source function, finding Doppler core dependence on frequency

21 p3796 A69-38479

Papers of Lunar and Planetary Laboratory, Volume 9, covering IR solar spectrum

21 p3800 A69-38681

Solar spectrum data covering wavelength intervals from 13138-14707 and 12187-17731 A and 1.4 micron water band

21 p3800 A69-38682

Solar IR spectrum recorded by LPL B spectrometer on NASA CV-990 aircraft using one micron grating, noting resolution

21 p3800 A69-38683

Trial and error procedure applied to instrumental profile of Liege Solar Atlas, convoluting instrumental profile with telluric A band profile

21 p3722 A69-38698

First order profile of Utrecht Solar Atlas from second order profile and oxygen band refining procedure, deducing instrumental profile for first order spectra

21 p3722 A69-38699

Solar X rays observations, describing instrumentation, radiation characteristics, association with flares, spectrum analysis, etc

21 p3791 A69-39506

Core profiles of H alpha, H beta, H and K from spectrograms of plagues

22 p4010 A69-39993

Tabulation of solar UV spectrum features between 3650 and 3000 A from intercomparison of photoelectric records and Second Revised Rowland, indicating wavelength relocations

22 p4014 A69-40146

Fourier spectrum analysis of solar line oscillation sequences, discussing power spectra and lifetime of oscillation phase

22 p4019 A69-40286

Solar Zeeman triplet for excited atomic state comparable to or shorter than Larmor precession period, discussing polarization

22 p4019 A69-40287

Solar Zeeman triplet pseudo-pi-component at 5250 A /Fe I/, using Unno theory to calculate visibility, contrast and displacement

22 p4019 A69-40289

Sunspot position in H alpha core relative to continuum, discussing height differences between H alpha core and continuum levels

22 p4019 A69-40291

Sunspot spectra near solar limb for difference between Fraunhofer line continuum and line core formation levels, finding geometrical height scale and pressure equilibrium

22 p4019 A69-40292

Medium sized solar radio events from peak intensities, spectrum characteristics and coronal magnetic field role

22 p4020 A69-40299

Solar He abundance determined from solar model photospheres line and continuum radiation

22 p4031 A69-40911

Solar constant and spectral irradiance curve for zero air mass obtained from aircraft measurements

23 p4216 A69-42191

Thermal continuum radiation from coronal plasmas at soft X ray wavelengths, investigating variations effect in element abundances

23 p4207 A69-42406

Solar flares accompanied X ray emission temporal and spectral variations, showing departure from thermal equilibrium

24 p4371 A69-43608

Solar X-ray spectrum as function of sunspot group type based on Solrad satellites flux data, discussing relationship to lower ionosphere characteristics variations

24 p4372 A69-43615

Total solar eclipse of 5 February 1962 observed for spectrophotometry of flash spectrum, finding abnormal intensity gradients of H alpha and D3 lines

24 p4388 A69-43636

Solar quiescent prominences spectra with bright metallic lines, discussing turbulent angular velocity and kinematic temperature of filaments

24 p4375 A69-43777

Equivalent line widths for solar disk Fe and Ti spectra determined for umbra models, noting role of sunspot location

24 p4390 A69-43778

Hydrogen balmer lines broadening by Stark and Doppler effects, finding prominences and chromosphere electron concentrations

24 p4390 A69-43779

SOLAR SPECTROMETERS

Positive feedback of spring mass system for mirror control on spectroheliometer of Apollo Telescope Mount flight

02 p0248 A69-11738

Solar flare X ray line and continuum spectra measured with crystal spectrometers aboard orbiting solar observatory

02 p0308 A69-12297

Solar image or spectrum focal plane scanning technique with output beam displaced but undeviated relative to input beam for solar spectrophotometry

04 p0602 A69-15378

Solar radio spectroscopy for 40 to 240 MHz frequency range, noting dynamic spectra of solar radio bursts

06 p0925 A69-17318

Life raft thermal protection against exposure of aircrews to cold, noting chemically fueled heaters and IR reflective liners

06 p0883 A69-17841

IMP F and G solar cosmic ray spectrometer utilizing FET analog multiplier for onboard particle identification data processing

07 p1135 A69-19197

Three dimensional information pictures of chromospheric alpha H line using special camera attached to solar telescope diffraction grating spectrograph

07 p1217 A69-19241

Solar research from rockets and satellites, considering solar instruments including EUV spectrographs

10 p1772 A69-22867

Apollo telescope mount (ATM) for solar experiments conducted from manned earth orbiting laboratory

10 p1791 A69-22871

Laser beam for determining instrumental profile of high resolution double pass solar spectrograph, noting influence of slits width

11 p1893 A69-24431

Solar spectroscopic techniques, discussing instrumentation problems affecting photosphere line spectra, SNR in absorption spectra and near IR spectra

13 p2341 A69-27588

Guiding system of Spectro-Stratoscope /balloonborne solar telescope/, describing hydrostatic bearing and torque motor

13 p2262 A69-27957

Solar IR spectrum recorded by LPL B spectrometer on NASA CV-990 aircraft using one micron grating, noting resolution

21 p3800 A69-38683

Short region scanning of Arcturus spectrum with McMath solar spectrometer double pass system at Kitt Peak National Observatory compared to single pass system

21 p3721 A69-38697

Photoelectric spectrometer observations of 1966 total solar eclipse, discussing limb darkening curves for regions of continuum 1.5 A wide around 5728 and 6404 A

22 p4027 A69-40659

SOLAR STORMS

Solar noise storms structure and movement, discussing localization of type 1 burst emission into zones in solar corona

02 p0315 A69-11824

Nonlinear mechanism for solar surge involving rapid acceleration of high electrical conductivity and macroscopic dimension plasma regions

03 p0516 A69-14044

Solar type 4 bursts characteristics accounted for by cyclotron mechanism, assuming models of spot magnetic field configuration and electron density distribution

07 p1205 A69-18959

Solar outburst and storm accompanying 9 June 1968 flare, noting radio evidence for coronal instability before flare

09 p1582 A69-22747

Recurrent Forbush decrease association with proton enhancement, discussing energetic storm particle events

09 p1582 A69-22752

Solar radio emission sources position changes observed in solar storm center

17 p3024 A69-33805

Satellite observations of solar proton events with halo structure or energetic storm proton event and SSC, noting similarity in origin

20 p3589 A69-37555

SOLAR SYSTEM

Monograph on nature of planets and solar system origin covering meteorite observations and age determination, chondrite composition, metallic elements, etc

01 p0152 A69-10702

Solar system origin and evolution by future space mission experiments, discussing theories and mission objectives

01 p0153 A69-10823

[AAS PAPER 68-191]

Introduction to planetary physics, Terrestrial planets, covering solid interior constituents, solar system dynamics and origin and evolution
01 p0154 A69-10920

Stability characteristics of small and moderately sized short period Trojan librations in sun-Jupiter restricted three body problem
01 p0158 A69-11329

NASA Planetary Exploration Program to gather data on origin of solar system and life, discussing planetary evolution and extraterrestrial life
02 p0200 A69-12804

French atlas of planets covering ancient and modern planetary system and discoveries, physical nature and movement, etc
03 p0513 A69-13778

Life probability and origin on Milky Way planets with emphasis on solar system, discussing molecular biology role
05 p0707 A69-15966

Solar system evolution, noting angular momentum in planets and solar system and hypothesis of gravitationally contracting gaseous nebula
05 p0826 A69-16389

Pu 244 and I 129 abundances in early solar system and continuous galactic synthesis model of element formation in stars
08 p1397 A69-20695

S-process nucleosynthesis and temperature averaged neutron capture cross sections studied in relation to solar system, considering elemental and specific isotopic abundances
08 p1357 A69-20896

Plutonium-244 existence in early solar system concluded from relative abundance ratios of excess meteoritic heavy Xe isotopes
08 p1401 A69-20900

Model for nucleosynthesis of Li, Be and B in solar system from mass spectrometric measurements of high energy proton production of light elements
08 p1401 A69-20901

Solar system elements abundance compilation based on carbonaceous chondrites and nucleosynthesis in stars
08 p1401 A69-20903

Chemical composition of diffuse Orion Nebula and stars compared for lighter elements, considering solar system formation from interstellar medium
08 p1402 A69-20908

Primitive elemental abundances in solar system, discussing composition of sun, meteorites and lunar maria
08 p1403 A69-20914

Radioactive decay products concentration from extinct radioisotopes in meteorites with estimation of formation interval, discussing fissiogenic xenon and solar system nucleosynthesis
08 p1405 A69-20924

Meteoritic materials structure, composition and magnetic properties, supporting theory for solar system formation from supernova outbursts
09 p1593 A69-21581

Radar probing of solar system noting contributions to knowledge on planets
09 p1595 A69-21765

Solar system plasmas and X ray astronomy - Conference, Adelaide, Australia, August 1968
09 p1581 A69-22742

Primordial solar system chemical composition for studies of origin and evolution, compiling solar composition data
09 p1608 A69-22745

Radioactivity levels estimation at surface and in bulk of solar system planets caused by galactic and solar cosmic rays
10 p1756 A69-22813

Resonance relations of rotational and orbital frequencies of solar system planets and satellites estimated for statistical significance
10 p1771 A69-22852

Total planet interaction energy of comets passing through solar system, showing non-Gaussian shape of distribution
10 p1774 A69-22970

Rb-Sr and other radioactive isotopes cosmochronology in solar system, analyzing age of elements and r process
11 p1955 A69-24393

Monograph on world of planets covering solar planetary system, atmospheres, water, seasons, organic life, etc
11 p1958 A69-24666

Solar system age based on decay rate of natural radioactive elements
11 p1961 A69-24972

Jupiter red spot visibility, establishing partial dependence on solar activity
11 p1964 A69-25404

Solar system light elements investigated assuming Li, Be and B abundance as nuclear reaction products of high energy particles accelerated in early sun formation
13 p2354 A69-28495

Atmospheric dynamics parameters of Mercury, Venus, Mars and Jupiter, discussing generalized circulation theory
14 p2526 A69-29841

Comets considered as natural interplanetary space probes, stressing need for international cooperation on solar system studies
15 p2679 A69-30011

Interstellar particle penetration into solar system, discussing impact ionization of earth ionosphere by interstellar neutral hydrogen and helium
15 p2699 A69-31390

Outer planets exploration during 1976-80 period of unique solar system alignment
16 p2854 A69-31630

Tabulation of basic solar system data and formulas concerning trajectory length, escape velocity, orbits, etc
16 p2856 A69-32074

Solar system physical environments surveyed from exobiological viewpoint
17 p2907 A69-32968

Monograph on solar system space flight trajectory calculations covering solutions to differential equations, error analysis and gravitational effects
17 p3039 A69-33798

Protosun and solar system angular momentum losses analyzed from equations for convective star rotation change, noting almost total protosun initial momentum loss possibility
18 p3203 A69-35346

Meteorites data in planetary cosmogony, discussing iron meteorite ages, Xe retention in chondrites and synchronism of sun and protoplanetary cloud forming
19 p3406 A69-36075

Solar system matter evolutionary beginning traced to chemical elements synthesis by considering radioactive decay irreversible processes
19 p3406 A69-36076

Terrestrial planets high temperature evolution from solar system genesis theory, discussing meteorite chemical composition, petrography, mineralogy and age determination
19 p3407 A69-36079

Meteorite Li isotopic composition variations to determine neutron role in nucleosynthesis of solar system light elements
19 p3408 A69-36084

Solar system low energy particle flux at 2-3 AU distance during last 10 million years, discussing cosmic radiation flux
19 p3411 A69-36097

Boundary conditions for theory of solar system origin, discussing planetary atmospheres, surfaces, magnetic fields, composition and early solar wind
19 p3419 A69-36209

Radio and radar astronomy with reference to extragalactic sources and solar system, noting astronomical instrumentation
19 p3425 A69-36430

Soviet book on cosmos and hypotheses covering origin and physical characteristics of earth, moon, Venus and Mars
20 p3596 A69-37234

Moon composition and similarities to Mars explained by silicates in solar system raw material
20 p3604 A69-37563

Planet Mars opposition to earth, Jupiter and Saturn, including table showing Mars-Jupiter conjunctions
21 p3801 A69-38788

Chemical processes responsible for transformation of vast gas and dust cloud into planetary system
21 p3804 A69-39200

Optimum midcourse impulses effects on heliocentric launch window, comparing two and three impulse delta 5 performance for two and three dimensional solar system models
21 p3804 A69-39201

Stony meteorite composition and structure studied for conditions of preplanetary stage of solar system
22 p4012 A69-40084

Cometary nuclei composition as last samples of early solar system composition, discussing dirty snowball model and radical lifetime problem
22 p4013 A69-40097

Fractionation mechanisms in early phases of planetary evolution sought to explain abundance problem in terrestrial planets
22 p4018 A69-40185

Strategy for exploration of inner solar system leading to origin and history, detailing lunar exploration program
22 p4022 A69-40449

Antimatter motion in solar system and earth atmosphere, discussing vaporization and annihilation energy in collisions with interplanetary gas atoms
22 p4034 A69-41100

Nuclear propulsion for solar system exploration, discussing NERVA solid core nuclear fission rocket, nuclear-electric rockets and hybrid nuclear rocket/nuclear electric rocket systems
24 p4349 A69-42871

[AAS PAPER 69-330]
24 p4349 A69-42871

Mars and Venus flyby missions and Mercury planetary exploration plans, discussing future conditions permitting Jupiter, Saturn, Uranus, Neptune, Pluto flybys
24 p4384 A69-43137

Model for accumulation of earth and planets from primitive solar nebula, implying inhomogeneous chemical composition of bodies in solar system
24 p4385 A69-43215

Rb-Sr and other radioactive isotopes cosmochronology in solar system, analyzing age of elements and r process
24 p4390 A69-43783

SOLAR VELOCITY

Tachoheliograph /modified spectroheliograph/ for obtaining two dimensional solar velocity maps, discussing construction and theory of operation
17 p3030 A69-33061

SOLAR WIND

VLF electric field measurements from 1 AU heliocentric orbit, noting field oscillations in solar wind and large amplitude HF noise bursts
01 p0035 A69-11224

Solar plasma observations during magnetic storms, discussing shocks and tangential discontinuities, geomagnetic variations and He
01 p0076 A69-11234

Free access of low energy galactic particles to solar wind lines of force due to stochastic nature of lines
01 p0147 A69-11238

Polar wind, describing upward plasma expansion of topside polar ionosphere and acceleration of positive H and He ions
01 p0077 A69-11239

Solar wind directional fluctuation derived from wavy structure of comet Morehouse ionic tail rays, noting solar wind bulk velocity
02 p0311 A69-11459

Planetary magnetic field measurements near Venus, Mars, and moon, noting magnetic dipole comparison with earth and solar wind interactions
02 p0311 A69-11471

[AAS PAPER 68-186]
02 p0311 A69-11471

Cosmic ray propagation in interplanetary space taking into account reverse effect on solar wind, deriving integrodifferential equation
02 p0306 A69-11657

Parameters of solar wind responsible for geomagnetic activity, relating magnetic storm features to physical structure of interplanetary space and solar wind bubbles
02 p0240 A69-11725

Subsolar magnetosphere dimensions from ground observations of geomagnetic micropulsation period changes during magnetosphere deformations caused by solar wind inhomogeneities
02 p0244 A69-12356

Collisionless plasma heating by hydromagnetic waves in solar wind
02 p0309 A69-12714

Aurora displays distribution over earth, analyzing magnetosphere dependence on astronomical orientation of geomagnetic field in relation to solar wind
02 p0247 A69-12772

Cosmic ray and solar wind properties, discussing solar wind measurements, interplanetary magnetic field and solar wind sounding by cosmic rays
03 p0500 A69-13355

Velocity dispersion and temperature anisotropy with respect to magnetic field direction, discussing inertial solar wind cooling effects
03 p0500 A69-13525

Solar wind turbulence properties deduced from radio astronomical measurements
03 p0502 A69-14001

High latitude electrons boundary dependent on geomagnetic axis orientation, noting role of coupling between solar wind and magnetosphere
03 p0502 A69-14003

Solar wind interaction with moon, discussing core/surface layer conductivity and lunar limb shock wave formation
03 p0502 A69-14006

Lunar wake in solar wind at large distances, noting no satellite evidence of lunar magnetic field and evidence for lunar generated turbulence
03 p0514 A69-14007

Solar wind abundance measurements at earth orbit related to solar corona
03 p0503 A69-14047

F 2 layer formation and fast neutral particles ionization source due to charge exchange between solar wind protons and moving interstellar hydrogen
04 p0592 A69-15009

Solar and interplanetary magnetic fields and plasmas, noting in situ observations by satellites and space probes of sector patterns, solar cosmic rays and wind
05 p0821 A69-15841

Detached lunar compression wave, noting positive evidence from solar wind flux and direction measurements near lunar wake
05 p0824 A69-16251

Solar wind electron component detection by plasma experiment on Pioneer 6, particularly class 2B flare and quiet period
05 p0816 A69-16275

Time independent solar wind equations applied to spherical symmetry and radial magnetic field at solar surface, noting thermal conductivity anisotropy
05 p0817 A69-16703

Solar wind directional fluctuations at middle heliographic latitude, comparing Vela satellite measurements with comet Morehouse tail beam undulations
06 p0985 A69-16981

Solar wind model for electrons and collisionless ions temperatures and anisotropies
06 p0986 A69-16983

Plasma physics in space research, discussing solar wind, planetary atmosphere bow shock and convective motions of magnetosphere plasma
[ISAS-431] 06 p1000 A69-17026

27-day cosmic ray intensity variations related to solar wind velocity nonuniformity due to longitudinal distribution of coronal active regions
06 p0990 A69-17292

Simulation of solar wind interaction with earth magnetic field, discussing selection of dimensionless parameters
06 p0919 A69-17550

Solar wind, discussing corona, radio sources, radio bursts, comet tails, cosmic rays, etc
06 p1012 A69-18239

Lunar core electrical conductivity determination based on induced magnetic field arising from time varying interplanetary magnetic field associated with solar wind plasma
07 p1215 A69-18832

High electron-proton temperature ratios effect on solar wind double shock wave structure, using one dimensional and two fluid models
07 p1205 A69-18849

Model experiment on plasma flow about obstacle to simulate solar wind interaction with moon
07 p1205 A69-18851

Magnetosphere dynamical properties, discussing atmosphere, ionosphere, magnetopause, magnetosheath, bow shock, solar wind, collisionless plasmas, etc
07 p1127 A69-19352

Solar wind and magnetosphere, discussing hydrodynamic expansion of solar corona
07 p1207 A69-19353

Solar wind flow past earth and magnetosphere correspondence to external aerodynamics of round nosed bodies in supersonic stream
07 p1128 A69-19360

Solar wind, bow shock and magnetosheath observations by charged particle analyzers on Vela satellites
07 p1208 A69-19361

Magnetospheric plasma probe results with Pioneer 6 and 7, discussing plasma fluctuations and solar wind interaction with geomagnetic field
07 p1128 A69-19364

Interplanetary scintillations of 3C 279 and CTA 21 combined to derive solar wind density fluctuation model, using random thin screen theory
08 p1385 A69-20069

Geomagnetic storms, substorms and auroral displays as functions of processes in solar wind and upper atmosphere
08 p1307 A69-20188

Long term modulation of cosmic rays by solar activity explained by Parker solar wind model, noting confirmation by direct satellite measurements
08 p1379 A69-20533

Solar wind model including effects of rotation, magnetic fields and anisotropic heat conduction
08 p1380 A69-20643

Chemical effects of solar wind and cosmic protons on solid bodies in space, discussing possible relation to origin of life
08 p1407 A69-20935

Captured particles magnetic drift envelopes in magnetosphere calculated by model considering perpendicular geomagnetic dipole to solar wind
09 p1574 A69-21521

Approximate solution of nonlinear differential equation describing interaction between galactic cosmic rays and solar wind, obtaining four domains
09 p1575 A69-21524

Mariner 2 data on large scale variations in magnetic field, solar wind density and temperature in interplanetary plasma
09 p1592 A69-21540

Photoelectric ejection of grain electrons by solar quanta balance with solar wind electron capture by grain for interplanetary grain equilibrium potential
09 p1593 A69-21655

Interplanetary scintillation of radio sources to determine size and motion of plasma irregularities in solar wind for fine structure
09 p1594 A69-21658

Solar wind-magnetosphere pressure balance and proton density of solar wind
09 p1577 A69-21711

Galactic cosmic ray scattering and energy loss through solar wind interaction
09 p1580 A69-22202

Collisionless plasma heating by damping hydromagnetic waves applied to solar wind qualitative model, discussing magnetoacoustic wave energy
09 p1607 A69-22426

Cosmic ray variations as means of studying solar wind characteristics and interplanetary medium
10 p1755 A69-22811

Solar wind and galactic magnetic field buffer layer, analyzing cosmic rays effect and space-time distribution
10 p1757 A69-22825

Cosmic ray anisotropy and diurnal density variation, analyzing influence of interplanetary magnetic field and subsonic solar wind
10 p1757 A69-22828

Solar activity effect on interplanetary electromagnetic field according to cosmic ray modulation data, noting ineffective correlation and solar wind effects
10 p1759 A69-22841

Cosmic ray modulation by solar wind, discussing anisotropic diffusion during propagation through interstellar magnetic field
10 p1759 A69-22842

Asymmetrical solar wind volume variations of magnetic inhomogeneities and cosmic ray absorption in earth atmosphere, including barometric coefficients of neutron component
10 p1760 A69-22844

Primary cosmic rays, radiation belts and solar wind studies by semiconductor detectors installed on orbiting satellites
10 p1662 A69-23294

Ionospheric disturbances after July 7, 1966 proton flare noting flare ionizing radiation, high energy solar proton effects and low energy solar plasma
10 p1684 A69-23784

Steady state spherically symmetric model for solar plasma acceleration with distance, showing essential role of viscosity
10 p1769 A69-23899

Electrical phenomena in upper atmosphere and solar wind may control geomagnetic disturbances and aurorae
10 p1686 A69-23903

One dimensional nonlinear model of anisotropic plasma instability with respect to Alfvén waves growth, noting applicability to solar wind processes
10 p1741 A69-23961

Solar wind flux near earth observed by Venera 2 /1965/ and Venera 4 /1967/ probes, noting solar activity effects
10 p1771 A69-24201

Plasma and magnetic field measurements of tangential discontinuities in solar wind by Pioneer 6, considering velocity shears and rotation of sun
11 p1946 A69-24430

Solar wind particles acceleration and transformation into radiation belt particles
11 p1948 A69-24855

East-west asymmetry in solar wind velocity due to solar rotation effects on interaction between fast and slow streams
11 p1950 A69-25148

Solar oblateness and differential rotation time development due to solar wind torque
12 p2157 A69-26308

Model, assuming electron thermal conductivity contribution, applied to studying solar plasma discharge characteristics in presence of three dimensional thermal sources in solar corona
12 p2149 A69-26680

Solar wind interaction with geomagnetic field simulation practically unrealizable, discussing partial simulation covering neutral magnetic layer formation on night side
12 p2149 A69-26681

Solar wind interaction with geomagnetic field, considering bow shock, field confinement in magnetosphere and stretching out of lines of force
12 p2072 A69-26735

Solar plasma flow around magnetosphere, discussing plasma velocity, density and temperature and magnetic field space and time variations
12 p2150 A69-26736

Laboratory models for solar wind and magnetosphere interactions with similarity laws of Vlasov theory as reference system
12 p2150 A69-26737

Solar wind induced magnetospheric convection for interpretation of geomagnetic storms, aurora and trapped particle belts, noting electric fields
12 p2073 A69-26749

Solar-terrestrial environment, discussing mathematical development of solar wind, satellite measurement, magnetic storms, aurora and cosmic rays
12 p2161 A69-26941

Interplanetary scintillation and angular spectrum of radio waves scattered by solar plasma, noting magnetospheric tail and solar wind
12 p2161 A69-26942

Solar wind plasma observations in geomagnetospheric wake compared at 1000 and 500 earth radii, considering ion energy spectra and geomagnetic tail
12 p2151 A69-26943

Magnetosphere model for plasma pressure by solar wind, discussing plasma drift from neutral sheet into geomagnetic tail
12 p2076 A69-27106

Comet interaction with solar wind, assuming field tail coupling of ionized comet material to solar wind ions
13 p2349 A69-27817

Cosmic ray propagation in interplanetary space taking into account reverse effect on solar wind, deriving integrodifferential equation
13 p2333 A69-28688

Correlation coefficients between radial components of interplanetary magnetic field and solar wind velocity from Mariner 5 data due to Alfvén waves
14 p2510 A69-28949

Tangential solar wind discontinuity observed by Vela 2A satellite, producing ground magnetic disturbances conjunctively with magnetospheric, ground and ionospheric currents
14 p2512 A69-29041

Cosmic ray intensity preceding Forbush effects as function of chromospheric flares solar longitude and solar wind velocity
14 p2512 A69-29044

Solar wind quiet state thermal properties and chemical composition compared with coronal expansion hydrodynamic model predictions
14 p2513 A69-29098

Electron plasma oscillations and electron whistler of solar wind near Jupiter orbit
14 p2513 A69-29115

Magnetospheric plasma motion associated with Alfvén mode time fluctuations of magnetic field in solar wind
14 p2521 A69-29382

Cosmic ray intensity during solar cycles, considering minima relationship to Bartel index maxima and solar wind modulation theory
14 p2515 A69-29967

Convergent solutions of inviscid solar wind equations in expansions form including dimensionless distance from sun
14 p2515 A69-29968

Asymptotic power series solutions of viscous solar wind equations
14 p2515 A69-29969

Solar wind Helmholtz-type velocity discontinuities, noting plasma density and temperature stabilities from Explorer 34 observations
14 p2515 A69-29971

Solar wind origins, discussing corona composition, corpuscular streams, R and M disturbances, etc
15 p2673 A69-30009

Solar wind existence verified by direct measurements of interplanetary magnetic field and plasma, reviewing solar corona studies by satellites and space probes
15 p2679 A69-30010

Cosmic ray variation theory, presenting data on coupling of solar activity with large scale characteristics of solar wind during 11-year cycle
15 p2673 A69-30015

Solar wind and solar breeze theories distinguished, discussing applications to geocoronal hydrogen emission and solar corona expansion
15 p2676 A69-30858

Neutral point theory applied to solar wind and magnetospheric physics, discussing magnetic field reconstructions
16 p2846 A69-31596

Solar wind direction by analysis of data from IMP 1 satellite, noting anticorotation tendency
16 p2847 A69-31962

Worldwide changes in geomagnetic field, determining causes by examining magnetic field and plasma data for solar wind and classifying as SSC or SI
16 p2847 A69-31963

Interplanetary magnetic field radial dependence from Mariner 4 measurements between earth and Mars, indicating fluctuations produced by dynamic processes in solar wind
16 p2856 A69-31964

Numerical simulation of flare generated shock wave propagation through solar wind, noting transit time and shock strength agreement with observations
16 p2848 A69-31970

Electrostatic heating of solar wind ions from instability in two fluid solar wind model leading to preferential heating of protons over electrons
16 p2848 A69-31971

Solar wind speed transverse variation effect on cosmic ray intensity at earth analyzed using mathematical model
16 p2849 A69-32088

Solar wind velocity distribution anisotropy at earth explained by low density
16 p2849 A69-32097

Captured particles magnetic drift envelopes in magnetosphere calculated by model, considering perpendicular geomagnetic dipole to solar wind
16 p2851 A69-32516

Approximate solution of nonlinear differential equation describing interaction between galactic cosmic rays and solar wind, obtaining four domains
16 p2851 A69-32519

Mariner 2 data on large scale variations in magnetic field, solar wind density and temperature in interplanetary plasma
16 p2864 A69-32535

Simulated solar wind environment effects on zinc oxide/potassium silicate and lanthanum oxide/potassium silicate spacecraft thermal control coating pigments [AIAA PAPER 69-642]
17 p2991 A69-33273

Solar wind phenomenon, discussing angular momentum loss to sun, fluctuations at earth orbit and wind conditions at terminus and regions unvisited by spacecraft
17 p3023 A69-33370

European highly eccentric orbit satellite /HEOS/ cisunar probe to explore interplanetary space for magnetic fields, cosmic radiation, solar wind and earth shock wave
17 p3050 A69-33397

Test program simulating solar wind outside magnetosphere to evaluate high melting point high density ceramic oxides as white thermal control coating pigments [AIAA PAPER 69-641]
17 p2993 A69-33762

Magnetized solar wind model to evaluate temperature, density, velocity and magnetic field for various boundary conditions
17 p3041 A69-33812

Gas particle concentrations on moon due to solar wind, surface emissions and atmospheric contamination by lunar operations and rocket motor products
18 p3189 A69-34236

Solar wind model for studying long wavelength turbulence as heat source for alpha particles and protons in solar plasma
18 p3186 A69-34299

Cosmic ray intensity short term stochastic variations in solar system related to turbulent solar wind day-to-day variations
18 p3186 A69-34300

Quiet solar wind model with magnetic field numerically calculated, obtaining coronal electron densities and angular momentum near earth
18 p3186 A69-34301

Severe magnetosphere distortions in north-south direction with parallel/antiparallel magnetosheath to magnetospheric field ascribed to solar wind property changes from Explorer 12 observations
18 p3128 A69-34947

Comet-solar wind interaction model, determining contact discontinuity size and shape around comet nucleus and ion specular reflection
18 p3188 A69-35190

Finite electrical conductivity effect on sun angular momentum loss due to solar wind
18 p3189 A69-35398

Boundary conditions for theory of solar system origin, discussing planetary atmospheres, surfaces, magnetic fields, composition and early solar wind
19 p3419 A69-36209

Solar wind temperature, using distribution function for solar wind ions in anisotropic Maxwell distribution form
19 p3396 A69-36631

Spherical, cylindrical and toroidal electrostatic analyzers with symmetrical angular characteristics for solar wind investigations
19 p3396 A69-36632

Steady state spherically symmetrical ejection of multicomponent plasma from sun determined with hydrogen approximation, considering ion composition
20 p3594 A69-37018

Solar wind velocity cycles from fluid MHD viewpoint, applying Kelvin theorem on circulation stability in closed fluid system
20 p3587 A69-37041

Comet tails orientation determination for solar wind and interplanetary plasma investigation, considering geometrical difficulties and suggesting computation procedure
20 p3599 A69-37467

Solar wind plasma effects on lunar wake umbral and penumbral interplanetary magnetic field anomalies, evaluating roles of electrons and ions
20 p3609 A69-38095

Lunar Explorer 35 measurements of lunar surface electromagnetic properties, magnetic fields and solar wind-moon interactions
21 p3794 A69-38379

Venus magnetosphere induced by piling up magnetic field from solar wind due to ionospheric conductivity and collisions with planetary atmospheric particles
21 p3794 A69-38381

Helium in atmosphere, aurora and solar wind, discussing geophysical problems, interplanetary neutral H, etc
21 p3710 A69-38509

Geomagnetic field horizontal component daily variations in relation to solar wind, noting effects of ambient field night side decrease
21 p3714 A69-38549

Interstellar matter, considering objects size, solar wind structure, galactic parameters, magnetic fields and cosmic ray heating
21 p3802 A69-38819

Hydrodynamic equations for radial solar wind expansion linearized and specialized to treat co-rotating perturbations
22 p4003 A69-40302

Solar wind north-south component sector dependent asymmetry implied from tangential discontinuities orientations as observed by Mariner 4
22 p4004 A69-40303

Shock discontinuities in solar wind measured by magnetic field and plasma instruments on Explorer 34, applying Rankine-Hugoniot relations
22 p4020 A69-40304

Explorer 34 observations of hydrogen and He ions in solar wind, noting number density variations and tentative association with geomagnetic storms
22 p4004 A69-40305

Homogeneous conducting moon-solar wind interactions, describing time dependent lunar magnetic and electric fields induced by interplanetary magnetic field variations
22 p4023 A69-40518

Charge exchange of solar wind protons passing shock front, noting turbulent subsonic motion of randomized hot solar wind protons in shadow cone
22 p4008 A69-41208

Solar wind sample collection, describing experiment to determine ion flux capture efficiency for various metal foils
23 p4205 A69-41539

Outer anisotropic galactic cosmic particle flux distortion in interplanetary space, analyzing scattering in solar wind by isotropic diffusion equations
23 p4205 A69-41837

Cosmic ray flux intensity increases, discussing effects of solar wind, corpuscular flux velocity and interplanetary magnetic field
23 p4205 A69-41838

Disagreement between Mariner 2 and IMP 1 data concerning interrelation between solar wind velocity and geomagnetism ascribed to instrumental errors and changes in magnetospheric properties
23 p4205 A69-41848

Interplanetary magnetic field role in interaction between terrestrial magnetosphere, solar plasma and solar flux energy transfer
23 p4214 A69-41865

Solar wind kinetic energy density using geomagnetic field horizontal component daily variation, treating earth as plasma probe
24 p4308 A69-42968

Solar wind collisionless hydromagnetic flow interaction with planetary atmosphere, using mathematical model to determine bow shock position limits in atmosphere
24 p4368 A69-43178

Thermal nonequilibrium state and effective collision frequency between protons and electrons in solar wind plasma, explaining abnormal dissipation
24 p4368 A69-43187

Primordial hydrogen and helium concentration in Pesyanoe meteorite measured by gas chromatography, indicating solar wind injection source
24 p4384 A69-43213

Magnetic dipole field variations effects on planetary atmosphere erosion by solar wind, discussing Mars and Venus atmospheres above ionosphere
24 p4385 A69-43224

Solar wind disturbances associated with flares
24 p4373 A69-43620

SOLAR X-RAYS

Solar X-ray high activity level during spring 1966 connected with gamma type magnetic solar regions and correlated with ionospheric effects
01 p0146 A69-11119

Solar X ray flare absolute flux correction, taking into account geometric obliquity factor variation with angle between satellite spin axis and satellite-sun line
01 p0147 A69-11242

Sudden ionospheric disturbance development and characteristics of solar cosmic ray flares, associated X ray emissions and high energy particle generation
02 p0308 A69-12398

Line identification methods in solar extreme UV and X ray regions
03 p0507 A69-13171

Solar X ray control of D layer based on Explorer 33 data, computing electron production rates due to typical X ray flux
03 p0500 A69-13224

Solar X ray flares measurement by rocket and satellite, discussing X ray spectrum hardening, hard flares and SID
03 p0500 A69-13225

Coronal X ray emission near limbs in 16-40 A during solar eclipse
04 p0650 A69-15531

Solar X ray source identification using D layer ionization behavior during eclipse
04 p0650 A69-15533

Electromagnetic radiation from solar flares based on rocket and satellite observations of 10-100 kev X ray emission and ground observation of cm-wavelength bursts
05 p0813 A69-15603

X ray astronomy techniques, discussing X ray spectrographs, heliographs and nonsolar celestial X ray sources
05 p0762 A69-15840

Isotropic background cosmic X ray flux measurements using low latitude balloon to minimize atmospheric background, obtaining hard solar X ray flux upper limits
06 p0992 A69-17311

Solar eclipse variations of E layer critical frequency explained by quasi-equilibrium between electron density and ionizing soft X ray radiation
07 p1204 A69-18823

Solar X ray bursts decay curves and spectra in 10 to 150 kev range interpreted as hot coronal condensation during flare and electron bremsstrahlung
07 p1206 A69-19250

Atlas of energetic solar flare X rays and tentative atlas of proton events observed by OGO-1 and OGO-3 ionization chambers
07 p1206 A69-19251

Solar corona X ray emission during flares and under quiet sun conditions investigated by satellite with X ray heliograph

07 p1210 A69-19614

Spectral intensities and time variations of solar X ray bursts, discussing model for high energy flare plasma and resulting X ray flare

08 p1379 A69-20532

Correlated microwave and energetic X ray emission from solar flare with 16-sec periodic pulsations, discussing energy during modulation peaks

09 p1574 A69-21457

Solar X ray and extreme UV spectra during flares, attributing intense emissions to optical transitions

09 p1578 A69-22169

Solar soft X ray components observed with ion chamber photometer, studying components relation to transient and slowly varying phenomena at other wavelengths

09 p1578 A69-22170

Solar and cosmic X rays observed by OSO-C, stressing galaxy M 87 upper limits and Lupus XR-1 power law spectral form

09 p1578 A69-22171

Hard solar and cosmic X rays measured with satellite-borne telescope, considering flux and time variations

09 p1579 A69-22173

Hard X ray event spectrum representation by thermal bremsstrahlung spectrum emitted by energetic electrons, determining various physical parameters of source

09 p1579 A69-22180

Peaks and time intensity profile of energetic X rays and cosmic rays observed by OGO-C ion chamber on May 23, 1967 flare event

09 p1579 A69-22182

Synchrotron and X ray emission generation from upper chromosphere electrons during solar flares

09 p1580 A69-22203

K alpha lines in solar soft X ray spectra noting instrumental effect

09 p1580 A69-22232

Solar X ray bursts observed by proportional counter on IMP-F satellite to correlate optical H alpha flares and radio bursts

09 p1582 A69-22746

Explorer 30 satellite monitoring of solar X ray emission during July 1-15 1966, noting plage region activation with increasing emission

10 p1763 A69-23736

Sudden ionospheric disturbance effects of solar X ray emission from active region with proton flare

10 p1764 A69-23744

Variable solar X ray emission from subflare activity in plage region producing polar cap absorption proton flare of July 7, 1966

10 p1764 A69-23745

Spectral intensity of high energy solar X rays observed during July 7, 1966 polar event with satellite OGO 3, suggesting nonthermal bremsstrahlung origin

10 p1766 A69-23753

Solar X ray flare of July 7, 1966 with Explorer 33 satellite attributed to McMath plage region 8362, discussing solar and cosmic radio noise

10 p1766 A69-23754

Solar X ray emission and decay during proton flare of July 7, 1966 noting start of polar cap absorption

10 p1766 A69-23755

X ray and extreme UV radiation deduced from sudden ionospheric disturbances during proton flare, discussing time dependence of emission

10 p1766 A69-23756

Solar flare X ray and extreme UV radiation contribution to E and F1 region ionospheric effects observed by sudden frequency deviations

11 p1950 A69-25160

Solar X ray bursts analyzed by dynamic spectra based on time history of intensity of bursts

11 p1951 A69-25419

Iono-index about hard emission of solar active regions, analyzing field fluctuations and SID in D region under daytime conditions

12 p2148 A69-26107

Proportional counter array for detection of soft X ray photons from OSO-4 observations, discussing solar event energy spectra

12 p2151 A69-26936

Solar X ray flux deduced from flare effects on VLF propagation, showing total energy content as measure of ionizing radiation

14 p2411 A69-29105

Solar X rays intensity and spectrum effects on c layer critical frequency and D region ionospheric absorption

15 p2677 A69-31346

Explorer 33 and Explorer 35 observations of solar flare of 8 July 1969 soft X rays, discussing absolute flux

16 p2849 A69-31988

Sudden phase anomalies on radio paths compared with calculated results for satellite observed solar X ray flux intensities to explain sudden ionospheric disturbances

17 p2959 A69-33006

Center to limb variation of solar hard X ray bursts, suggesting inverse Compton effect and bremsstrahlung from anisotropic electrons

17 p3023 A69-33055

Solar eclipse of 20 May 1966, comparing satellite-borne X ray and UV photometry with radio astronomical observations

17 p3023 A69-33058

Pulse height distributions, gain and counting rate characteristics of two magnetic strip multipliers and two channel multipliers in 1.5 to 44 A region of soft solar X-rays

17 p2972 A69-33082

Solar soft X ray bursts observed by Solrad 8 satellite, considering relationship to microwave radio bursts

17 p3025 A69-34055

Solar flares with subcosmic radiation in proton active region of May 1967, discussing X ray emission effects, calculating D region recombination coefficient and electron concentration

17 p3025 A69-34226

Geomagnetic crochets time relations to solar X rays, radio bursts and flares

17 p3025 A69-34227

Solar flares less than 10 A X rays effect on ionospheric ionization between 60 and 100 km

19 p3397 A69-36754

X ray data in 44-60, 8-16 and 1-8 A bands telemetered by Solrad 9 satellite

20 p3588 A69-37473

Solar flares microwave and hard X ray bursts, discussing gyrosynchrotron plasma, nonthermal electron bremsstrahlung and electron relaxation

20 p3589 A69-37551

Solar hard and soft X rays time-intensity profiles showing homology with centimeter radio bursts, suggesting origin from same electrons

20 p3589 A69-37553

X ray heliography by Fresnel-Soret type zoneplate camera to obtain solar photographs from rockets

20 p3544 A69-37803

Solar X-ray events observed by scintillation counter telescope on OSO 3 satellite, discussing X ray spectra during burst initial and decay phases

20 p3593 A69-38166

Solar X rays observations, describing instrumentation, radiation characteristics, association with flares, spectrum analysis, etc

21 p3791 A69-39506

Anomalous X ray signals from Explorer 30 satellite showing saturation in ionization chamber possibly due to enhanced solar and atmospheric X rays

21 p3792 A69-39808

Solar soft X rays observed from OSO-3, correlating to solar flares and radio bursts

22 p4003 A69-40297

Explorer 30 /Solrad 8/ satellite observation of 0.5-3 A solar X ray emission related to magnetic configuration in sunspot group

22 p4003 A69-40298

Identification, position and temperature of solar X ray sources derived from D layer ionization radio absorption behavior during eclipses and lunar reflection

22 p4004 A69-40308

Atmospheric ionization rates due to attenuation of 1-100 A nonflare solar X rays, giving solar fluxes and absorption cross sections

22 p4004 A69-40447

Solar cycle and slowly varying components correlation with soft X ray radiation based on spacecraft measurements

22 p4004 A69-40504

Solar X ray detector aboard OGO 5 satellite observing two components in energetic solar X ray bursts, attributing impulsive component to bremsstrahlung

22 p4007 A69-40775

Solar L alpha and X ray emission contribution to lower ionosphere ion production, discussing altitudinal, latitudinal and temporal variations

22 p4008 A69-41096

Solar flares spectra X ray portion, considering spatial distribution, relation to magnetic fields and time sequence of emitting region

24 p4366 A69-42688

Solar flares accompanied X ray emission temporal and spectral variations, showing departure from thermal equilibrium

24 p4371 A69-43608

Solar flare soft X ray and EUV emission spectra data obtained on OSO-3 satellite compared with centimetric radio bursts

24 p4371 A69-43609

Time structure of solar X ray bursts from OSO 3 satellite observations showing impulsive and gradual components

24 p4371 A69-43610

Solar X ray flux measurements from OGO 4, comparing peak fluxes before, during and after flares with IQSY data

24 p4371 A69-43611

Solar X ray bursts decay curves and spectra in 10 to 150 kev range interpreted as hot coronal condensation during flare and electron bremsstrahlung

24 p4372 A69-43613

Solar flare-associated radio bursts, reviewing solar radio measurements based on X ray and particle observations

24 p4372 A69-43614

Solar X-ray spectrum as function of sunspot group type based on Solrad satellites flux data, discussing relationship to lower ionosphere characteristics variations

24 p4372 A69-43615

SOLDERED JOINTS

Hysteresis properties of membrane structures with soldered or rolled edges noting superiority of added elastic element in clamped area

01 p0087 A69-10828

Solder joint cracking in discrete component assemblies, discussing cracking mechanism and crack elimination methods

07 p1140 A69-19102

Wave soldering reliability and cost saving potential in miniature circuits manufacture for aerospace applications, noting process control and machine design relationship

18 p3146 A69-34512

Silicon solar cell panels, studying roles of solder, interconnector metals and substrate materials in failures under thermal cycling

23 p4070 A69-42274

SOLDERING

Microsoldering techniques for thin and thick film hybrid circuits and microminiature printed circuit boards

09 p1510 A69-22349

Wire-wrap solderless joints production technology in electronic equipment

16 p2763 A69-32579

Wave soldering reliability and cost saving potential in miniature circuits manufacture for aerospace applications, noting process control and machine design relationship

18 p3146 A69-34512

Diffusion welding and soldering of metallic wire with graphite and graphitized viscose applied to chromel, copel, chromel-alumel, Mo, W and W-Re

21 p3728 A69-38617

SOLENOIDS

High homogeneity sixth order superconducting solenoids with coil inner surface notch correction, describing graphical design techniques

10 p1665 A69-23857

Cryogenic solenoids with pure Al conductor for production of strong magnetic fields, discussing softness and strain resistivity problems

12 p2016 A69-26497

Book on solenoid magnet design covering magnetic and mechanical aspects of resistive and superconducting systems

20 p3464 A69-37145

SOLID ARGON

U SOLIDIFIED GASES

SOLID LUBRICANTS

Synthetic solid lubricants impurity detection by X ray diffraction and oxidation thermogravimetry

01 p0102 A69-10909

Ball bearing test apparatus for evaluation of greases and solid lubricants at high temperatures [ASLE PREPRINT 68AM 7C-2]

01 p0087 A69-10912

Atmospheric influence on friction endurance of solid powdered lubricants at constant layer thickness [IME PAPER 3]

07 p1138 A69-18563

Surface finish and hardness effects on wear life of inorganic solid lubricant film [ASLE PREPRINT 68AM 7C-3]

07 p1139 A69-18623

Film thickness effect on wear life of resin bonded solid lubricant film compared for various load test conditions [ASLE PREPRINT 68AM 7C-4]

07 p1139 A69-18624

Solid lubricant compacts for ball bearing separator materials, describing fabrication, design and friction and wear properties in air and vacuum
[ASLE PAPER 68-LC-16] 07 p1139 A69-18626

Physical sputtering deposition of molybdenum disulfide films as solid lubricant on rotating and sliding components, discussing lubrication properties in vacuum
[ASLE PAPER 68-LC-15] 07 p1140 A69-19308

Antifriction characteristics of hard lubricating coatings based on molybdenum disulfide and graphite in inert gas atmosphere and vacuum, determining thermal stability temperature ranges
13 p2269 A69-28053

Energetics in solid film lubricants vacuum deposition methods, showing dependence on interfacial and film characteristics
14 p2454 A69-29001

Dry lubricant films of soft metals, self lubricating plastics and crystalline powders, noting design and tests
15 p2642 A69-30328

Solid lubricant films friction and wear life determined under various conditions of contact, temperature, load and atmosphere
[ASLE PREPRINT 69AM 6C-1] 15 p2619 A69-30471

Load, speed and coating thickness effect on wear life of resin bonded solid lubricant, using oscillating motion and low pressure blocks
[ASLE PREPRINT 69AM 5C-3] 15 p2619 A69-30474

Microfibrous boehmite as binder for molybdenum disulfide in formation of ductile water resistant dry lubricant films
[ASLE PAPER 68-LC-14] 15 p2642 A69-30606

Solid lubricants on molybdenum disulfide base at various temperatures and low pressures, noting film mass losses and possible use with organic materials under high vacuum
16 p2793 A69-31561

Load capacities of graphite lined journal bearings, discussing factors affecting wear rates
[SAWE PAPER 68-LC-9] 18 p3148 A69-35002

Molybdenum disulfide dry film lubricant wear theory and test correlation problems, considering sintering self propagation due to chemical effect of environment
19 p3323 A69-35580

Low temperature adhesive shear tests to measure force to break ice away from stainless steel surfaces coated with various bonded solid lubricants
19 p3323 A69-35581

Wear protection of pressure loaded Ti-Mn alloy by heat diffused lubricated electrodeless Ni coatings
24 p4331 A69-42786

Solid film lubricants deposited by DC triode sputtering on Ni, Ni-Cr and Nb surfaces friction tested under ultrahigh vacuum conditions
24 p4321 A69-43126

SOLID NITROGEN

U SOLIDIFIED GASES

SOLID PHASES

A15 type phase in vapor deposited W-Re alloys identified by X ray diffraction, metallography and hardness measurements
01 p0098 A69-10649

Sulfur organic compound formation effect on composition and structure of solid phase formed during hydrocarbon jet fuels oxidation
01 p0142 A69-11097

Nickel-rich region of Al-Ni-Y ternary system, emphasizing identification of solid phase equilibria through analysis of equilibrated alloy specimens
02 p0265 A69-12004

Book on properties of liquid and solid helium 3 and 4 physical characteristics, phase behavior and experimental techniques
04 p0630 A69-14688

Structural microheterogeneities in monophase Ti alpha alloys, using complex phase analysis method
04 p0617 A69-14939

Martensitic transformation in Ti-Al-Mo alloys, noting specific features and effects of Mo content
04 p0617 A69-14940

Solid phase equilibria in nickel-aluminum-scandium system at 1000 C
05 p0779 A69-15833

Chemical composition and phase identification in commercial grades of cemented carbides
05 p0780 A69-15989

Transient temperature distribution for finite slab in phase transformations via single face temperature changes
[ASME PAPER 68-WA/HT-37] 05 p0848 A69-16128

Ti alloy beta phase variations in quantity, composition and dispersion during quenching, thermomechanical treatment and aging
07 p1163 A69-18777

Thermodynamic consequences of Lindemann mechanism for fusion of pure body, discussing application to isolated equilibrium system of solid and liquid phases
07 p1242 A69-19322

Structure of spinodal decomposition in Al-Zn alloys by X ray diffraction noting anisotropy, periodicity and stability
09 p1522 A69-21502

Microstructure for spinodal decomposition in Al-Zn alloys noting Zn precipitation, fracture mechanics, dislocations and transmission electron microscopy results
09 p1522 A69-21503

Nonmetalized composite propellant solid phase heterogeneities effect on oscillatory combustion, inducing coherent burning rate oscillations with external pressure oscillations
09 p1622 A69-22085

V phase structure and V and E phase lattice constants for ternary systems /Ti, Zr, Nb or Ta/-Ni, Co or Fe/-Si or Ge/
10 p1708 A69-22992

Solid hydrogen mantle condensation accounting for lack of detectable alpha hydrogen in star clusters and OB associations
10 p1776 A69-23214

Solid hydrogen condensation on graphite grains for microwave background, discussing hydrogen grain promotion of galactic and stellar formation
10 p1776 A69-23216

Near boundary zones in VT15 Ti alloy not involved in beta phase decomposition during aging below 500 C attributed to vacancy concentration decrease
11 p1902 A69-24275

Hydrogen solubility in solid and liquid Ti close to melting point, showing no effect on welds and castings porosity
11 p1905 A69-24963

Solid titanium surface energy determination, taking into account grain boundaries effect on accuracy
12 p2113 A69-26045

Nickel base superalloys long time carbide and intermetallic phases stability at high temperatures
13 p2277 A69-27405

Quantitative separation of elements in gamma prime from precipitation hardened high temperature nickel-base alloys by anodic dissolution
13 p2277 A69-27408

Thermal conductivity prediction technique for two and three phase solid heterogeneous mixtures
13 p2378 A69-28337

Mu phase lattice constants and cell volume in Nb-Zn system
15 p2636 A69-30086

Crystal structures of intermediate phases in La-Co and Nd-Co systems by powder X ray diffraction technique
15 p2667 A69-30087

Creep experiments on Mg alloys, discussing dispersed phases influence on creep cavitation and grain boundaries mobility
17 p2985 A69-32907

Orientation relationships between phases in Co-TaC pseudobinary eutectic alloy, discussing Co fcc-hcp allotropic transformation
[ONERA-TP-714] 17 p2988 A69-33395

Gaseous and solid phase properties of atomic and molecular systems, treating statistical energy distribution, kinetics, excited states and relaxation
18 p3178 A69-35406

Sigma phase and temperature effects on toughness of austenitic stainless steel weldments
18 p3150 A69-35429

Ti sub 3, Rh sub 5 and Hf sub 3, Rh sub 5 existence and isomorphism confirmed by crystallographic and X ray methods
19 p3343 A69-35920

Ti transition metals alloys omega phase precipitation, discussing composition, morphology, coherency, formation, etc
19 p3344 A69-35928

Cosmic ray produced radionuclides P 32, Cl 36, Ar 37 and Ar 39 determined in separate mineral phases of meteorites, emphasizing ratios in metals
19 p3410 A69-36094

Mass dependence of self diffusion in Fe by serial sectioning in alpha, gamma and delta phases, determining isotope effect with Fe radioactive isotopes
19 p3346 A69-36440

Nuclear magnetic resonance of epsilon and delta phases in NbN system with nitrogen mole fractions
19 p3383 A69-36445

Electrical conductivity of rare earth metals La, Ce, Pr and Nd in solid and liquid states by rotating magnetic field method
21 p3781 A69-39070

Soviet book on heat treatment of Ti alloys emphasizing structural and phase composition changes
21 p3749 A69-39526

Hydrogen permeability in Pd alpha phase measured, coupling with grain size measurements for grain boundary to bulk diffusivity ratio
23 p4175 A69-41502

InTe phase recrystallization in thin films composed of two InTe phase mixtures, showing random concentrations and distribution of centers growing as spherulites
24 p4361 A69-42993

SOLID PROPELLANT IGNITION

Temperature distribution and vaporization rate boundary conditions on metal particle surface during preignition heating in oxygen containing medium
02 p0355 A69-12670

Ignition pressure transient for solid propellant rockets predicted by computer program
[WSCIP PAPER 68-35] 07 p1203 A69-18352

Composite solid propellants ignition response measured by imbedded hot wires indicating distributed reaction
[WSCIP PAPER 68-36] 07 p1201 A69-18354

One dimensional lattice model for heterogeneous explosive detonation, discussing hot spots, grain burning ignition time, ignition site types and RDX detonation
[WSCIP PAPER 68-30] 07 p1240 A69-18357

Igniter design guidelines, types and characteristics of igniter materials
[WSCIP PAPER 68-32] 07 p1202 A69-18361

Ammonium perchlorate exothermic decomposition control noting effects of preheating and ammonium fluoborate additives
[WSCIP PAPER 68-25] 07 p1202 A69-18363

Empirical and analytic modeling of propellant role in ignition, discussing ignition transient prediction to describe propellant ignitability characteristics
[WSCIP PAPER 68-34] 07 p1202 A69-18364

Analytical model for thrust-time curve during ignition transient of solid propellant rocket engines, discussing flame spreading
[WSCIP PAPER 68-33] 07 p1203 A69-18365

Aluminum effect on ammonium perchlorate/polyformaldehyde mixtures combustion properties noting heat transfer decrease into k phase
08 p1375 A69-20338

Hypergolic filling materials for solid fuels with hybrid propellant combinations, discussing ignition and combustion of ethylenimine derivatives
10 p1753 A69-24023

Flame front propagation over solid fuel surface with hot igniting material injected into end-to-end cavity, discussing heat transfer by convection and radiation
11 p2001 A69-25193

Theoretical model of homogeneous solid propellant ignition in neutral nonflow environment, discussing ignition time
13 p2324 A69-28218

Chemical reaction between combustible solid fuel surface and oxidizer-containing gas in space capsule
16 p2877 A69-31896

Solid fuel ignition with gaseous oxygen in presence of copper chromate and other catalysts
16 p2829 A69-31913

Accidental ignition during solid propellant processing in terms of hazard to facilities and personnel, emphasizing mixing operation
16 p2829 A69-31993

Solid propellant rocket motors ignition and igniter performance, discussing ignition interior ballistics
16 p2829 A69-31997

Combustion of isolated aluminum particles ignited by laser and burning in controlled gas mixture observed by cinephotomicrography
[WSCIP PAPER 69-3] 16 p2830 A69-32344

Spontaneous reignition predictions for solid restartable rocket motors with solid propellant combustion terminated by liquid quenching
[AIAA PAPER 69-444] 16 p2842 A69-32695

Gas phase ignition shock tube analysis of solid propellant taking into account changing surface temperature and fuel vapor consumption
18 p3183 A69-34463

SOLID PROPELLANT ROCKET ENGINES

Combustion instabilities in solid propellant rocket engines, emphasizing acoustic types for longitudinal and tangential modes

02 p0303 A69-11531

Multipulse thruster module design and development tests for spacecraft attitude control, noting micropulse solid propellant rocket motor

02 p0194 A69-11762

Combustion oscillations in liquid and solid propellant engines, noting destructive effect of LF vibrations and acoustic instability

02 p0305 A69-12494

Pressure and velocity couplings effects on oscillatory and transient motions in solid propellant rocket motors, emphasizing unsteady burning calculations

02 p0305 A69-12501

Solid propellant rocket engine designs for ELDO-PAS apogee motors, discussing use of advanced materials to improve mass ratio and strap-on boosters

03 p0495 A69-12890

Apogee stage and strap-on booster applications of solid propellant rocket motors, discussing configuration, functioning and performance

03 p0494 A69-12891

Solid propellant rocket motor thrust vector control by swiveling or gimbaled exhaust nozzles or by secondary injection

03 p0495 A69-12892

Solid propellants formulation, processing physical properties, testing and rocket motor inspection

04 p0646 A69-14583

Sublimation solid reaction control, discussing propellants, nozzle performance, sublimation area, power, pressure drop, response and valueless design [AIAA PAPER 68-516]

04 p0552 A69-15322

Soviet book on gas dynamics of solid fuel rocket motors covering combustion chamber flow, nozzle and thrust characteristics, pressure relaxation and channel charge

04 p0647 A69-15493

Material requirements for uncooled nozzles of solid propellant rocket motors burning aluminized propellants, discussing successful testing of pyrolytic graphite

06 p0946 A69-17530

Test program for solid propellant rockets capability to withstand space environments

06 p0982 A69-17594

Scout launch vehicle for launching small research satellites in near earth orbits, describing solid propellant stages, guidance, telemetry and beacon systems

06 p1016 A69-17597

Tank collection and spectrophotometric tests in determining aluminum oxide particle size produced by small rocket engine [AIAA PAPER 69-146]

06 p0984 A69-18117

Ignition pressure transient for solid propellant rockets predicted by computer program [WSCI PAPER 68-35]

07 p1203 A69-18352

Analytical model for thrust-time curve during ignition transient of solid propellant rocket engines, discussing flame spreading [WSCI PAPER 68-33]

07 p1203 A69-18365

Direction changing of large solid propellant motors by changing jets angle or gas injection

07 p1230 A69-19291

Optical absorption index for molten beryllium oxide based on measurements of small beryllium/ solid propellant rocket motor exhaust plumes

08 p1351 A69-20149

Variation in spinning velocity around axis of last stage of solid propellant rocket in flight

08 p1409 A69-20160

Pyrotechnical devices for two stage solid propellant ballistic rocket, discussing self priming electric cells and auxiliary power and gas generators

10 p1752 A69-23024

Hot gas ignition devices for solid propellant rocket motors, discussing ignition rod and microrockets

10 p1752 A69-23025

Rocket motors for ejection of instruments from sounding rocket payloads, considering powder cartridges and solid propellant motor characteristics

10 p1635 A69-23032

Solid propellant motors nozzle design, analyzing structural and material problems, high temperature exhaust gases effects, thermal insulation, etc

10 p1716 A69-23403

Fluidic secondary injection thrust vector control systems for solid propellant and hydrogen-oxygen rocket engines

10 p1753 A69-23561

Solid propellant rockets, discussing composite and double base propellants and use of polymers

11 p1941 A69-25588

Combustion instability problems in rocket motors, emphasizing strongly coupled pressure oscillations in combustion chambers

11 p2003 A69-25597

Solid propellant rocket engine design for combustion stability, discussing length, pulse induced and acoustic instability types [AIAA PAPER 68-532]

12 p2191 A69-26788

Soviet book on solid propellant guided/unguided rocket design with emphasis on thrust control, including trajectory calculations, optimal parameters and components estimation by weight analysis

12 p2175 A69-27077

Gun projectiles assisted by solid propellant motor to increase range, discussing construction, performance and free-wheeling rotation band use

15 p2702 A69-30592

Chemical processing for manufacture of solid propellant motors, discussing mixing, casting and curing of composite propellants

16 p2829 A69-31992

Solid fuel rocket engine thrust and chamber pressure development curves from charge and engine geometry, heat of explosion and kinetic characteristics

16 p2836 A69-31994

Solid propellant rocket motors ignition and igniter performance, discussing ignition interior ballistics

16 p2829 A69-31997

Solid fuel propulsion systems for tactical rockets design, discussing microwave attenuation, acceleration-combustion interactions and performance optimization

16 p2836 A69-31998

Solid rocket motor ignition system based on exothermic alloying of bimetallic wire constituents [AIAA PAPER 69-425]

16 p2832 A69-32653

Solid rocket motor performance prediction including motor pressure, thrust and propellant parameters, discussing mathematical modeling of flow fields [AIAA PAPER 69-732]

16 p2840 A69-32674

Sterilized solid propellant motors applicability to planetary landing capsule spin stabilization [AIAA PAPER 69-823]

16 p2840 A69-32675

Stagnation point electrostatic probe for measuring local electrical properties of solid propellant rocket exhausts [AIAA PAPER 69-573]

16 p2840 A69-32677

Fluid controlled solid rocket motors design for Mars mission with acceleration level as parameter, discussing mission specifications, system design and component considerations [AIAA PAPER 69-446]

16 p2841 A69-32687

Spontaneous reignition predictions for solid restartable rocket motors with solid propellant combustion terminated by liquid quenching [AIAA PAPER 69-444]

16 p2842 A69-32695

Hazards model for probabilistic prediction of casualties by exploding solid propellant rockets, deriving casualty expectation equation [AIAA PAPER 69-461]

16 p2869 A69-32749

Thermal stability elements in solid propellant liner insulation system for heat sterilized solid rocket motors used in unmanned planetary landers [AIAA PAPER 69-437]

16 p2869 A69-32750

Aerothermodynamic problems during transition after activation of thrust inverter in solid propellant rocket engines

17 p3018 A69-33327

Solid propellant thrusters fabrication procedures, design considerations and quality control, stressing stress analysis and propellant choice with respect to geometry

17 p3018 A69-33331

Directional thrust control for solid propellant rockets, describing swiveling, bent rotating nozzles and secondary injection

17 p3019 A69-33332

Solid propellant motor extinction by depressurization, determining extinction conditions by electrical analogy

17 p3021 A69-33355

ELDO/PAS rocket motor for satellite launching from elliptic orbit apogee to synchronous orbit powered by ammonium perchlorate with organic binder and Al

17 p3022 A69-33604

Solid propellant motor extinction by depressurization, determining extinction conditions by electrical analogy [ONERA-TP-722]

18 p3184 A69-34637

Cost and weight optimization for solid rocket motors using various steel casings [SAWE PAPER 777]

18 p3208 A69-34871

Solid propellant rocket motor predictive design by correlating performance and weight statistics via computer program [SAWE PAPER 775]

18 p3184 A69-34873

Glass overlaid B filament laminates interleaved with C and silica fabrics, evaluating ablative properties in solid rocket motor tests

19 p3354 A69-35515

Ablative materials for solid rocket nozzles, discussing static firing tests, rating system, equipment design and cost reduction

19 p3357 A69-35537

Pyrolytic graphite coated composite as nozzle throat material for high energy metallized solid propellant motors

19 p3357 A69-35539

Liquid, solid, hybrid propellant and nuclear, electric and air breathing rocket engines, discussing orbiting payload cost, controllability, operating environments, velocity, etc

19 p3395 A69-36321

Nonsteady propellant burning theory for Al melting role in suppressing combustion instability in solid propellant rocket motors

19 p3393 A69-36814

Laboratory unsteady burning data applied to analysis of small amplitude combustion instability in solid propellant rockets

20 p3586 A69-37224

Mission and planetary vehicles characteristics affecting design of solid propellant motors and thrust vector control systems in planetary orbiters and landers [AIAA PAPER 68-815]

21 p3819 A69-39031

Acceleration effects on solid propellant rocket motors combustion characteristics [AIAA PAPER 68-530]

21 p3786 A69-39217

Nonstationary solid rocket fuel combustion scheme, using unsteady combustion model for quantitative analysis of rocket engine irregularities attributed to excessive fuel

22 p4050 A69-40457

Solid rocket motor static firing tests in low pressure environment, presenting data concerning vacuum chamber pressure, diffusers pressure distribution, chamber wall temperature distribution, etc

22 p4000 A69-40593

Solid rocket motors failure during static firing, discussing sequence of events

24 p4365 A69-43260

SOLID PROPELLANTS

NT CASE BONDED PROPELLANTS

NT COMPOSITE PROPELLANTS

NT DOUBLE BASE ROCKET PROPELLANTS

NT METAL PROPELLANTS

NT PLASTIC PROPELLANTS

Specific acoustic admittance of solid propellant burning surface for determining burning instability under rocket motor conditions

02 p0302 A69-11521

Solid propellant cartridges, discussing uses for starting large engines and providing auxiliary power in missiles or actuating devices

02 p0302 A69-11524

Gas chromatography used to determine residual solid propellant stabilizers content and nitro derivatives, including thin film chromatography

02 p0303 A69-11528

Solid propellant combustion instability models describing combustion zone dynamics applied to acoustic and nonacoustic instability in LF regime [WSCI PAPER 67-13]

02 p0352 A69-12311

Perturbation behavior of solid propellant combustion, discussing relevance of analytical models and use of qualitative models

04 p0685 A69-14726

Altitude effects on radar attenuation in nonequilibrium solid propellant afterburning rocket exhaust plumes

04 p0685 A69-14730

Deflagration of solid and hybrid propellants in steady state for missile and rocket propulsion applications

06 p0982 A69-17422

Burning rates of solid propellants by variable pressure method, taking into account environmental heat loss and gaseous condensation

06 p0982 A69-17505

Solid propellant burning rate behavior during abrupt environmental pressure excursions, using transient combustion model [AIAA PAPER 69-172]

06 p1036 A69-18046

Extinction by depressurization of AP composite solid propellants theory to predict rate of pressure decrease required to achieve flameout
[AIAA PAPER 69-176] 06 p0983 A69-18102

Oxidizer particle size and binder type effects on nonacoustic combustion instability of solid propellants
[AIAA PAPER 69-175] 06 p0983 A69-18152

Solid propellant burning rates from condensed phase decomposition kinetics, discussing kinetic rates of thermal decomposition
[AIAA PAPER 69-145] 06 p1039 A69-18182

Solid propellant combustion, calculating burning, flame standoff distance, flame thickness, heat transfer, energy losses, and distributed and unsteady combustion
09 p1623 A69-22091

Pressure waves interaction with solid fuel hot surface at HF based on linear theory of acoustic instability in condensed systems
13 p2371 A69-27383

Solid propellants formulation quantitative predictability for algorithmic modeling of functional selection, discussing specific impulse and burning rate
[AIAA PAPER 69-432] 16 p2828 A69-31845

Regression rate of solid fuel in hybrid combustion determined as eigenvalue by Rayleigh flow model with evaporating boundary
16 p2879 A69-32013

Composite solid propellant combustion using differential scanning calorimeter and mechanical model of steady state combustion
[AIAA PAPER 69-504] 16 p2833 A69-32679

Fluidic vortex valve to modulate solid propellant generated hot gas flow
[AIAA PAPER 69-424] 16 p2844 A69-32723

Low thrust reaction control for space missions, summarizing range and specific impulse characteristics for solid and hybrid systems
[AIAA PAPER 69-433] 16 p2834 A69-32745

Turbulent process employing product constituents dilute suspensions in inert carrier /Quickmix/ to obtain solid propellant mixtures, discussing plant design and analysis, economics, etc
[AIAA PAPER 69-517] 17 p2978 A69-33033

Hybrid propulsion chemical and technical problems, discussing solid fuel fragmentation and defining typical combustion modes
17 p3021 A69-33358

Solid propellant rocket motor predictive design by correlating performance and weight statistics via computer program
[SAWE PAPER 775] 18 p3184 A69-34873

Hydrodynamic stability of solid fuel combustion in presence of acoustic disturbances in gas phase, considering material erosion and particle dispersion
18 p3231 A69-35150

Combustion considerations in fuel rich solid and hybrid propellant systems in air breathing propulsion for comparison with metal ignition requirements
23 p4199 A69-41894

Burning solid propellant behavior under pressure fluctuations expressed in response function terms defining small mass flux change ratio to small pressure change
23 p4201 A69-41922

Solid fuel ablation by nitric acid, controlling reaction interface displacement rate by mass and heat transfer phenomena
24 p4363 A69-43568

Solid fuel ablation and supersonic combustion processes for various propulsion configurations, testing plastic models in wind tunnel
24 p4414 A69-43569

SOLID ROCKET BINDERS

Ammonium perchlorate base propellant and polyurethane binder heat stability, dangers of aging under abnormal conditions and reaction products for components and tolylene diisocyanate
02 p0303 A69-11529

Binder polymer network and microstructure effects on solid rocket propellant properties, emphasizing choice of polymer ingredients
[AICHE PAPER 37A] 17 p3017 A69-33668

SOLID ROCKET PROPELLANTS

NT DOUBLE BASE ROCKET PROPELLANTS

NT METAL PROPELLANTS

Shock sensitivity of solid explosives and propellants, using calibrated gap testing techniques
02 p0302 A69-11520

Rocket propellant safety, discussing thermal, mechanical and impact sensitivity tests of solid and liquid propellants
02 p0302 A69-11525

Ammonium perchlorate base propellant and polyurethane binder heat stability, dangers of aging under

abnormal conditions and reaction products for components and tolylene diisocyanate
02 p0303 A69-11529

Three dimensional thermal stress distribution in case bonded solid propellant determined by scattered light photoelastic technique coupled with transparent rocket motor model
[AIAA PAPER 68-512] 02 p0345 A69-12371

French solid propellant sounding rockets proposed launching from Guiana base using different fuel propulsion systems
03 p0518 A69-12851

Solid propellants formulation, processing physical properties, testing and rocket motor inspection
04 p0646 A69-14583

Point matching method for analysis of stress in incompressible solids of revolution, noting application to solid propellant rocket charges
04 p0683 A69-15518

Laminar and turbulent regimes of flame propagation studied by blowing explosive gas mixture through porous wall, determining Reynolds number by hot-wire anemometer
06 p1034 A69-17626

Unstable combustion of ammonium perchlorate /AP/, discussing correlation between propellant particle diameter and frequency in burning rate
[AIAA PAPER 69-177] 06 p1036 A69-18063

Ionizing radiation effects on combustion of ammonium perchlorate compacts with and without fuel addition, considering X ray, electron and plasma radiation
11 p1941 A69-25194

Deformations of thick walled cylinder with internal surface subjected to uniform pressure and externally connected to rigid chamber, calculating solid rocket booster charge
11 p1942 A69-25347

Limiting pressure for deflagration related to initial solid temperature of single crystals and pressed pellets of ammonium perchlorate
13 p2324 A69-27364

Polyester/ammonium perchlorate combustion, determining degradation rate by loss in weight method at different intervals
13 p2324 A69-28234

Solid rocket propellants tests, considering propulsion performance measurements, altitude simulation problems, internal flow patterns, nozzle geometry, etc
16 p2765 A69-31751

Solid rocket motor propellant burning rate increased by adding special fine ammonium perchlorate /SFAP/ to optimize particle size distribution
[AIAA PAPER 69-519] 16 p2793 A69-31850

Solid propellants steady state combustion with emphasis on heterogeneous propellants
16 p2829 A69-31995

Combustion instability characteristics of solid propellants, discussing small scale testing methods
16 p2829 A69-31996

Nonnewtonian solid propellant viscosity and pseudoplasticity utilizing rheological characterization for optimal casting and pot life determination
[AIAA PAPER 69-518] 16 p2833 A69-32665

Solid rocket motor performance prediction including motor pressure, thrust and propellant parameters, discussing mathematical modeling of flow fields
[AIAA PAPER 69-732] 16 p2840 A69-32674

Flame propagation in narrow slit and fine hole of solid propellant grain
[AIAA PAPER 69-561] 16 p2833 A69-32680

Linear and nonlinear pressure coupled combustion instability of solid propellants
[AIAA PAPER 69-479] 16 p2834 A69-32725

Stability criteria for longitudinal combustion instability tested for generality using data from various solid propellant formulations
[AIAA PAPER 69-480] 16 p2834 A69-32736

Thermal stability elements in solid propellant liner insulation system for heat sterilized solid rocket motors used in unmanned planetary landers
[AIAA PAPER 69-437] 16 p2869 A69-32750

Micropropulsion system with sublimable solid fuel for satellite attitude control, satisfying mechanical and thermal environmental conditions during launch and in space
17 p3021 A69-33359

Monograph on solid rocket propellants covering composition, combustion characteristics and energetic, mechanical and operational properties
20 p3585 A69-37441

Nonstationary solid rocket fuel combustion scheme, using unsteady combustion model for quantitative analysis of rocket engine irregularities attributed to excessive fuel
22 p4050 A69-40457

Mathematical analysis of dendrite design of solid propellant grains for variant of modified wagon wheel design
22 p3997 A69-40553

Stress analysis of incompressible solid propellant rocket charges by point matching technique, considering differential thermal shrinkage and axial acceleration cases
24 p4402 A69-43263

Solid propellant flame zone radiant energy flux emitted through side port of internal burning cylindrical rocket motor related to total heat flux at burning surface
24 p4415 A69-43595

SOLID ROTATION

U ROTATING BODIES

SOLID-SOLID INTERFACES

Fiber-fiber interaction effect on stress distribution and tensile strength of discontinuous aligned fiber composites
01 p0171 A69-11261

Heat transfer dependence on direction of heat flow in stainless steel/aluminum interfaces, showing surface roughness and flatness influence
01 p0177 A69-11406

Polymeric film properties related to metal substrate interface corrosion, considering effects of stress concentration, surface cleanliness and adsorbed gases
02 p0265 A69-11896

Thermodynamic evaluation of interaction between solid metals and dispersed high melting point oxides, stressing isobaric potentials
03 p0446 A69-13571

Metal/alumina interfaces strength, examining correlation with wetting and bonding and martensitic transformations
03 p0447 A69-13612

Low temperature technique for preparing solid-solid diffusion sources for silicon device fabrication based on gaseous hydrides as reagents
07 p1198 A69-18619

X ray and photomicrographic study of metal layer-ceramic seal interface reaction products, discussing phase transformations, temperature effects and time dependence
08 p1320 A69-20375

Polymeric composites mechanical energy dissipation dependence on dimensions of interfacial region between matrix and filler phases, considering particle size and strain magnification
10 p1794 A69-23037

Interfacial stress between thermally grown silicon dioxide and single crystal silicon correlated with oxide compressive strength
10 p1744 A69-23177

Screw dislocation interaction with partially bonded bimetallic interface, using isotropic elastic continuum approximation
10 p1802 A69-24027

Silicon single crystal substrate, preoxidation, oxidation and low temperature heat treatment effects on MOS transistor compared with Silicon-Silicon dioxide interface characteristics
10 p1665 A69-24051

Friction coefficient dependence on interfacial potential between solids
12 p2129 A69-25982

Heat flow resistance between solid bodies in contact in vacuum
13 p2378 A69-28338

Adhesive metal bonding methods including continuous surface bonds, core to face bonds, lap joints and structural adhesive materials
14 p2454 A69-28847

Contact problem between elastic cylinder and rigid punch analyzed using integral equation, singularity isolation and series expansion
14 p2532 A69-28972

Semiconductor films synthesis and properties, discussing single crystal films, epitaxial nucleation, nuclei surface distribution, layer kinetics, doping and film-substrate interface
15 p2670 A69-31046

Stress waves propagation through elastic-plastic medium with uniaxial displacement, discussing wave interactions and interface conditions
16 p2870 A69-31809

Test structure model for studying semiconductor-insulator interface related failure mechanisms in large scale integrated circuitry
17 p2936 A69-32894

Book on solid bodies collision theory covering elastic bodies with ruled surfaces, dynamic effects associated with Rayleigh surface waves, thermodynamic effects, etc
18 p3210 A69-34259

Nylon wear curves and friction coefficients for steel-on-nylon pairs determined as function of normal load
19 p3329 A69-36495

Dislocation effects on stress corrosion of metals, discussing behavior of porous structure and metal/corrosion film interface under applied stress
19 p3349 A69-36886

Electrostatically accelerated iron spheres interaction with thin metal and nitrocellulose foils to develop detectors for cosmic dust collection and recording
21 p3719 A69-38344

Orthogonal polynomials in three dimensional contact problems without friction, discussing construction of kernels over finite and semiinfinite intervals
22 p4041 A69-40113

Stochastic model extension of interface temperature of solids in sliding contact to include transients, noting interface activities dependence
22 p3955 A69-40404

Reaction impulse during steel spheres impacts at lead surface in vacuum dependent on kinetic energy, velocity and spheres material
22 p4047 A69-41101

Heat transfer and surface thermal conduction characteristics of contact of two solid bodies, discussing pressure effect, measurement and analytical techniques
23 p4237 A69-41327

Contact stability of hollow cylinder compressed between parallel planes measured optically, compared to approximation of elasticity theory
23 p4162 A69-41416

SOLID SOLUTIONS

Chemical composition effect on duraluminum supersaturated solid solution stability, presenting time vs temperature C curves of isothermal decomposition
01 p0094 A69-10396

Thermoelectric properties of GeTe-GaTe system, analyzing phase diagrams, solid solution formation, substitutions and zone structure influence
01 p0138 A69-10404

Nb-W alloy solution hardening and deformation, noting flow stress dependence on strain rate and temperature plus activation energy of deformation
01 p0095 A69-10488

Deformation in aged Fe-Cr alloy studied for rate-controlling solid solution mechanism as function of stress
01 p0095 A69-10601

Omega phase and beta solid solution in Zr-V-Ta alloys quenched from 900 C
02 p0263 A69-11850

Solid solutions microstructure and electrical conductivity in InAs-CdS and InAs-CdS and InAs-CdSe systems
02 p0297 A69-11882

Dislocations effect on decomposition rates of solid solutions of InAs and Au, Ag or Cu
03 p0484 A69-13283

Surface precipitation of carbides in solution treated and cooled molybdenum and tungsten
03 p0451 A69-14000

Energy structure parameters for ZnTe-CdTe and ZnSe-ZnTe crystals, obtaining forbidden bandwidth dependence on composition
03 p0492 A69-14173

Phenomena in III-V compounds and III-V compound-other compound solid solutions, examining equilibrium phase diagrams
04 p0641 A69-14505

Solid solutions of O in Ti and Zr, noting superstructure formation and physical properties
04 p0618 A69-15078

Structural characteristics of Ni-Mo alloys analyzed using electron microscopy and X ray diffusion scattering
05 p0782 A69-16808

InAs solid solutions reflection spectra with CdTe, CdS, CdSe and ZnTe compounds, determining conduction bands
07 p1198 A69-18511

Ti rich Ti-Al-Mo-Zr alloys phase diagrams at high temperatures, noting presence of solid solutions
07 p1161 A69-18769

Ti-Zr-Sn alloys phase equilibria and interaction between titanium stannide and solid solution of Ti and Zr
07 p1162 A69-18770

Cobalt-tungsten solid solutions thermodynamic properties calculated by Borelius method using phase diagram
07 p1165 A69-18941

Magnetic susceptibility of InP-GaAs solid solutions at various temperatures and for varying GaP content
07 p1200 A69-19013

Rhenium effect on lattice solid solubility of oxygen in tungsten, calculating rhenium-oxygen cluster minimum binding free energy
08 p1329 A69-20007

Increased Ti heat resistance by forming solid solutions and compounds having various dispersions and bond strength
09 p1525 A69-22140

Supersaturation of dissolved B in splat quenched Fe-Ni-B alloys, noting interstitial and substitutional B in martensitic and austenitic phases
10 p1707 A69-22987

Nb H alloys embrittlement, discussing hydride formation and resistance variation with temperature
10 p1707 A69-22989

Intermediate Ni-Nb intermetallic formation as decomposition product from supersaturated Ni rich Ni-Nb solid solution aged above room temperature
10 p1708 A69-22993

Repeated stepwise annealing process to obtain homogenized InSb-GaSb alloys continuous solid solutions
10 p1745 A69-23331

Solid solution decomposition effect on binary Mg alloys recrystallization temperature containing Al and Nd, using X ray and microstructural analysis
11 p1902 A69-24272

Zr-W high temperature phase relationships, noting Zr-zirconium tungstide eutectic temperature, zirconium tungstide peritectic temperature and Zr solubility in W
11 p1903 A69-24578

Precipitated phase composition and structure of Co-Ti solid solution during aging
12 p2112 A69-26037

Added metal oxides solid solutions effect on creep kinetics and strain rate of zirconia samples during sintering
12 p2118 A69-26260

InAs-InP solid solutions diffusion rate and lattice constant for various compositions
12 p2144 A69-26587

Mixed state of type 2 superconductors, stressing alloying elements effects in solid solution and structural inhomogeneities
12 p2145 A69-27119

Gamma prime phase coherent equilibrium solubilities in Ni alloys of Al, Si and Ti from magnetic studies of particle coarsening and electron metallographic observations
13 p2276 A69-27370

Supplementary absorption and Hall effect temperature dependence in solid solutions of gallium arsenic phosphide
13 p2318 A69-27894

Oriented composites obtained from organic system under various directional solidification conditions
13 p2287 A69-28680

Monograph on mechanical behavior of crystalline solids at elevated temperatures, discussing creep properties of metals, solid solutions and two phase alloys
14 p2465 A69-29749

Discontinuous yielding characteristics of 2024 Al alloy determined for different conditions of solution, heat treatment and age hardening
15 p2639 A69-30598

Thermoelectric parameters of polycrystalline p-type bismuth antimony telluride and bismuth antimony tellurium selenide solid solutions
15 p2668 A69-30629

GaAs zinc gallium selenide solid solutions properties, analyzing lattice constant, microhardness, forbidden zone and concentration relationships
15 p2670 A69-31050

Lattice components of heat conductivity and chemical composition relations of magnesium alloy solid solutions
16 p2824 A69-31567

Vibrational excess entropy in dilute solid solutions alloys calculated by changes in potential fields surrounding impurity atoms
16 p2798 A69-31706

Alloying elements effects on low temperature metal fracture, considering changes in ductile-brittle transition flow due to solute
17 p2988 A69-33551

Solid solutions microstructure and electrical conductivity in InAs-CdS, InAs-CdS and InAs-CdSe systems
18 p3182 A69-35042

Solid solutions atomic ordering effect on friction and wear in vacuum, using CuAu and FeCo systems
18 p3149 A69-35183

Nickel solid solutions strengthening under cold deformation studied by X ray, noting screw and edge dislocations role
18 p3157 A69-35246

Ni-Cr alloy unidirectionally solidified, grain and eutectic structure and alloy strength
19 p3343 A69-35921

Ni base superalloy stacking fault energy, studying effects of various solute additions
19 p3343 A69-35925

InSb-InAs, InSb-GaSb, InP-GaAs and InP-GaP quasi-binary systems solid solutions optical and electrical properties, determining energy gap change as function of composition
19 p3390 A69-36554

Minority carriers penetration depth in solid aluminum gallium arsenide solutions with variable forbidden bandwidth determined from recombination radiation spectra
19 p3391 A69-36606

Supersaturated solid solution decomposition in Ni-Cr-Ti system, discussing precipitation mechanism of eta phase
20 p3558 A69-36968

Ti and V sesquioxides and TiO-VO solid solutions crystallography and defect chemistry over entire range of compositions
20 p3484 A69-37526

Thermal expansion properties of oxides and oxide solid solutions measured for improved expansion coefficient search
20 p3567 A69-38066

Flow stress temperature dependence of Ni-Cr-Al alloys consisting of gamma prime dispersion in Ni base solid solution
21 p3744 A69-38738

Melt cooling rates effect on supersaturated solid solutions in Al ternary systems
21 p3745 A69-38955

Pumping and excitation spectra of solid solutions of cryptocyanine in glycerine irradiated by ruby laser, discussing population inversion and scattering and vibrational transitions
21 p3740 A69-39546

Nb supersaturated solid solution in Co precipitation mechanism analyzed by X rays and electron microscope, noting diffusive scattering effects
21 p3750 A69-39788

Solid solution softening in bcc alloys, discussing alloy atoms intervention in low temperature deformation process
22 p3969 A69-40165

Temperature dependence of heat capacity of Ba and Sr titanate solid solutions in ferroelectric phase transition region
22 p3996 A69-41162

Phase diagram, dielectric and magnetic properties of Bi manganate/Pb titanate solid solutions of perovskite structure, showing dependence on composition and temperature
22 p3996 A69-41163

Single crystal Ta and Ta base bcc solid solution strengthening and weakening as function of temperature and strain rate
23 p4178 A69-42358

Niobium solution hardening by nitrogen and oxygen, noting grain size effects in electron beam refining
23 p4178 A69-42362

Serrated flow characteristics in gold-indium solid solutions at various strain rates and temperatures
24 p4361 A69-43028

Stored energy of cold work and electrical resistivity of Ag-Mg solid solution alloys measured as functions of strain, Mg concentration and initial state of order
24 p4332 A69-43029

Temperature dependence of equilibrium solid solubility of C in Au, Cu and Ag foils with respect to graphite
24 p4334 A69-43413

SOLID STATE

Very far IR techniques applications in molecular and solid state spectroscopy and relationship with impurity band conduction
02 p0296 A69-11791

Optimal body shape determination by mathematical-mechanical relations derivation, discussing variational problems and variational principles applicability
03 p0526 A69-13739

Nonlinear problems in mechanics of deformable media and qualitative analysis of properties of mathematical models of physical processes involved
03 p0467 A69-13749

Characteristics of dynamic mechanical systems including solid state and hydrodynamic analogs of ideal incompressible fluids, based on statistical theory of turbulence
10 p1678 A69-23209

Anharmonic lattice vibrations, specific heats and coefficient of linear expansion of solids at high temperatures, noting interatomic spacing
10 p1809 A69-23653

Solid W enthalpy from 2800 K to melting point measured with drop calorimeter, tabulating heat capacity, entropy and free energy function
17 p2987 A69-33075

Proton and deuteron energy used to study solid state chemical reactions effects on meteorites composition and properties, obtaining hydroxyl ions and hydrocarbons
19 p3414 A69-36114

SOLID STATE DEVICES

NT AVALANCHE DIODES
NT CRYOTRONS
NT CRYSTAL RECTIFIERS
NT FIELD EFFECT TRANSISTORS
NT GALLIUM ARSENIDE LASERS
NT GERMANIUM DIODES
NT JUNCTION DIODES
NT JUNCTION TRANSISTORS
NT METAL OXIDE SEMICONDUCTORS
NT PARAMETRIC DIODES
NT PHOTODIODES
NT PHOTOVOLTAIC CELLS
NT RUBY LASERS
NT SEMICONDUCTOR DEVICES
NT SEMICONDUCTOR LASERS
NT SILICON TRANSISTORS
NT THERMISTORS
NT THYRISTORS
NT TRANSISTOR AMPLIFIERS
NT TRANSISTORS
NT VARACTOR DIODES

Phased array radar cost improvement based on solid state devices and microwave integrated circuits application
01 p0048 A69-11039

Electron tubes in phased array radar systems, discussing replacement limits by solid state devices, reliability and cost reduction
01 p0048 A69-11040

Technique for combining large numbers of solid state energy sources by using dense array of radiating elements
02 p0217 A69-12148

Dispersive two port components for application to microwave pulse compression, coupling YIG crystal magnetoelastic spin wave mode to acoustic transducer
02 p0217 A69-12149

Air gap isolated microcircuit beam-lead devices fabrication, operation, electrical performance and radiation resistance
02 p0221 A69-12469

RF voltage breakdown in solid state telemetry transmitters on sounding rocket, noting glow discharge initiated by energetic dissociated electrons
02 p0222 A69-12691

Transit time effects in Si n-nu-n space charge limited current solid state devices
03 p0483 A69-12852

Microwave energy generation with solid state equipment, noting Gunn effect diodes, avalanche diodes and limited space charge accumulation /LSA/ devices
03 p0402 A69-12971

Diamond abrasive process for preparation of microminiature devices for metallographic analysis
03 p0402 A69-13007

Solid state power supplies for turbine control and instrumentation, discussing control system manufacturer requirements and reliability specifications
03 p0368 A69-13432

Solid state precision frequency standard for L multiplex carrier equipment, using four precision quartz crystal oscillators
04 p0561 A69-15451

Onboard solid state neon cryostat for IR detector, noting resistance to missile vibration, acceleration and shock tests
06 p0906 A69-17103

Avalanche detector radioisotope X ray fluorescence analyzer development for XRF analysis of potassium and calcium, noting precision
[IEEE PAPER 3B-9] 07 p1135 A69-19201

Solid state electrochemical cells, discussing electrodes composition, battery construction and low, medium and high drainage under temperature extremes
[AICHE PAPER 22D] 08 p1256 A69-19848

Microwave silicon technology applied to fabrication of high gain high efficiency transistor
09 p1462 A69-21410

Microwave solid state power sources including transistors, varactor harmonic generator chains, tunnel diodes, avalanche transit time devices, etc
10 p1662 A69-23144

Solid state AC voltage circuitry for measuring and controlling charged particle detector signals
10 p1662 A69-23256

Solid state ozone generator for preparing ozone in known concentrations to 1000 ppm in air for laboratory studies
10 p1693 A69-23346

Solid state battery utilizing high conductivity solid electrolytes /metal silver iodide/, demonstrating cell performance improvements
10 p1640 A69-23998

Solid electrolyte batteries development and current research, detailing Sprague cell and iodine complexes
10 p1640 A69-23999

Solid logic technology /SLT/ computer circuits, discussing IBM 360 computer reliability, failure analysis information retrieval, SLT module and failure rate
11 p1843 A69-24341

Solid state synchro data interfaces for angular information, noting synchro to digital and digital to synchro conversion techniques and synchro repeaters
11 p1842 A69-24543

Microwave tube development, discussing cold cathodes, ferrite and semiconductor integration into tubes, tube failure physics, etc
11 p1847 A69-24745

Solid state sampling circuit for low pulse repetition frequencies to improve signal to noise ratio, noting ratio of holding to learning time
11 p1849 A69-24900

Filter circuits for stabilization of solid state microwave devices, noting input matching characteristics
11 p1849 A69-24961

Solid state IR imaging using monolithic Ge mosaics of isolated sensor elements, discussing design, structure, fabrication, system readout and operation
11 p1938 A69-25307

Solid state radar feasibility, discussing circuit components, circuit design problems involving striplines and monoblocks, phase controlled antenna, solid state computers, etc
13 p2230 A69-27928

SHF solid state phased array radar with Gunn effect modular microwave IC design, discussing air and ground applications
14 p2420 A69-29435

Solid state programmable avionics converter for signal processing, information conversion and aircraft control
14 p2405 A69-29687

Amplifier working in conjunction with solid state phase sensitive detector replacing existing commutator in Dobson ozone spectrophotometer
16 p2792 A69-32641

Scanning electron microscopy to study device failure and performance, discussing limitations and progress
17 p2936 A69-32890

Device quantity failure kinetics or time dependence effect on time-to-failure distribution resulting from given device degradation coefficients distribution
17 p2936 A69-32895

Solid state single unit digital control computer performing stability augmentation, pilot relief functions and generating minimum fuel flight paths for VTOL landing
17 p2934 A69-34075

Airborne communication receiver solid state interference blanker circuitry comprising black box insertable between antenna and RF input
17 p2943 A69-34132

Diathermy instrument using solid state circuits to provide square wave pulses, discussing operating parameters for bipolar coagulation and advantages over spark gap instruments
18 p3134 A69-34537

Laboratory and flight tests of airborne solid state UHF telemetry transmitter, discussing miniaturized coaxial hardware from RF power conservation viewpoint
19 p3267 A69-35996

Microelectronics role in maintenance and maintainability of subminiature solid state components, emphasizing functional packaging at module level
19 p3283 A69-36021

Solid state S band to VHF converter design to obtain optimum system noise for radio telemetry, discussing cost effectiveness and system performance
19 p3270 A69-36238

Solid state detector for electron spatial distribution measurements on OGO-F satellite, discussing design emphasizing reliability
19 p3284 A69-36676

Photon actuated switch consisting of 10 input binary logic gate and solid state relay to reduce aerospace vehicles self generated noise
20 p3505 A69-37289

Solid state SHF transmission amplifiers design using rectangular waveguides and biased bulk GaAs
21 p3683 A69-39452

MERA /Molecular Electronics for Radar Applications/ modules testing in planar array simulator, measuring far field amplitude patterns in transmitting and receiving modes
22 p3912 A69-40067

Power combining network for high power UHF solid state satellite transmitters with low loss, compact size and input port selection capability
23 p4137 A69-41743

Solid state chemical heat sources aboard unmanned planetary landing vehicles to maintain batteries and experiments operability during cold planetary nights
23 p4070 A69-42275

Microcircuit phased array electronic countermeasures system design and hardware techniques for aerospace applications, analyzing adaptive, retrodirective and combination array systems
24 p4287 A69-43110

SOLID STATE LASERS

NT RUBY LASERS

Continuous wave solid state lasers active elements temperature fields calculated by differential equations
01 p0089 A69-10105

Optical pulse generator consisting of solid state laser with saturable absorber at cavity end using perturbation theory and Maxwell equations
01 p0089 A69-10179

Solid state liquid and semiconductor lasers, detailing conditions for producing stimulated emission and applications
01 p0092 A69-11068

Deuterium gas ionization over high pressure range under action of short pulse Q switched neodymium glass laser, noting breakdown wave existence
02 p0255 A69-11545

Oppositely moving waves interaction during nonlinear transient process of oscillations buildup in annular solid state laser found dependent on coupling via scattering
02 p0259 A69-12648

Solid state laser Q switched by rotating prism emitting giant pulse before two mirrors in parallel
03 p0440 A69-13365

Ring laser field space-time pattern from light waves scattered at discontinuities, discussing equations of motion of solid state laser
03 p0441 A69-14140

Optical pumping distortion compensation in glass laser rod by changing coolant temperature, obtaining mode locked laser pulses
04 p0609 A69-14286

Refractive index and expansion thermal coefficients along axis of oriented Nd-YAG laser rod
04 p0609 A69-14293

Laser with combined active medium resulting from investigation of autoresonant energy transfer in composite crystals with optical centers
04 p0611 A69-14546

Passive Q switching of solid state lasers based on stimulated Mandelstam-Brillouin light scattering
05 p0770 A69-15699

Glass lasers, discussing neodymium properties in glass, flexibility of glass in size, shape and optical excellence, temperature coefficient of index of refraction, etc
05 p0772 A69-16227

Frequency and polarization selection of neodymium glass laser oscillators by directing secondary radiation into laser cavity and duplicating spectral properties [IEEE PAPER P-3]
05 p0775 A69-16324

Fast digitalized scan laser using Nd-YAG as active medium and containing crossed array of lithium niobate electro-optic switches for mode selection [IEEE PAPER R-2]
05 p0775 A69-16326

Active region doping effect on laser diode threshold current, noting current dependence on loss coefficient in interband transition model without selection rule
06 p0933 A69-17257

CW room temperature laser using lanthanum sodium molybdate crystals with positive trivalent Nd ion impurity
06 p0934 A69-17262

Dynamics of Q spoiled neodymium laser created plasma expanding in vacuum magnetic field
06 p0970 A69-17952

Optical pumping of solid state lasers, reviewing processes involved and properties of lasers
06 p0937 A69-18007

Q switching of continuously pumped Nd/YAG laser using variable spacing Fabry-Perot interferometer as variable output coupler
06 p0938 A69-18229

Subpicosecond structure in output spikes of Nd-glass laser observed by employing two photon fluorescence displays inside laser cavity
06 p0938 A69-18231

Giant pulse generation by switched laser rapid pumping of neodymium doped glass laser
07 p1146 A69-18486

Tandem amplifier system of glass and selenium-ox-ychloride liquid lasers, discussing input power/output pulse relation and population inversion density measurement
07 p1147 A69-18487

Pulse synchronism of solid state lasers Q switched by same rotating prism, discussing pulse shifting to obtain radiation in filaments
07 p1147 A69-18488

Synchronizing ruby and Nd-glass laser pulses by means of passive bleachable dye solution liquid Q switch
07 p1147 A69-18530

Solar end and lateral pumping apparatus for neodymium doped YAG crystal lasers, noting applicability to space communication
07 p1150 A69-18953

Giant pulse production of Nd-glass laser with aid of coherent pumping by second harmonic of Q switched laser, noting pulse duration
07 p1156 A69-19333

Amplitude modulation of radiation pulses of two level paramagnetic maser as affected by inhomogeneous broadening and spinning of resonance line
07 p1158 A69-19751

Doped crystal and gas lasers, discussing resonant cavities, axial modes, relaxation oscillation, mode locking and Lamb theory
08 p1323 A69-19869

Stimulated emission of laser employing crystal and glass lasers doped with neodymium ions, using high temperature spectroscopy
08 p1323 A69-19944

Nonlinear amplification of powerful light pulses in Nd glass
08 p1323 A69-19946

Picosecond light pulse generation by solid state laser interpreted by fluctuating intensity spikes arising from random emission interference in out-of-phase modes
08 p1326 A69-20548

Solid state laser radiation damage in polymers during tensile and compression loads using microstructural analysis
08 p1328 A69-21190

Mode locking via nonlinear polarizations in multimode solid state lasers
09 p1514 A69-21344

Nonlinear optical properties of barium sodium niobate in ferroelectric tetragonal phase above room temperature, noting spontaneous parametric emission
09 p1515 A69-21354

Solid state lasers, noting normal, continuous and single mode oscillations, Q switching, power output limitations, mode locking and liquid lasers
09 p1517 A69-22120

Periodic mode variations in ruby and neodymium lasers with tilted mirrors, discussing factors in resonator misalignment
09 p1520 A69-22663

Luminescence quantum yield in neodymium glass, noting independence to stimulating light frequency
10 p1702 A69-23211

Pulsed and CW lasers glass crystals temperature fields determination, including tangential and axial thermal stresses
10 p1702 A69-23428

Stimulated emission of trivalent Nd ions in glass base, explaining connection between efficiency and emission polarization by interaction of laser modes with ions
10 p1703 A69-23618

Nd glass laser for emission of high radiance diffraction limited pulses, noting long path air breakdown and second harmonic generation
10 p1704 A69-23654

Isotope shifts in 4416 Å cadmium laser, showing change of double peaked to single peaked profile with doubled active tube length
10 p1705 A69-23812

Neodymium doped YAG laser efficiency dependence on pump power level and spectral filtering of pump light
10 p1705 A69-23814

Elliptical cylindrical chambers optimum design for optical pumping of solid state lasers, discussing transfer efficiency and approximation by circular cylindrical chambers
10 p1706 A69-24010

Q switching techniques for solid state lasers at room temperature for high peak power, discussing mechanical systems, electro-optic and magneto-optic shutters
10 p1706 A69-24018

Damping of solid state laser relaxation oscillations in power output due to diffusion of excitation
10 p1706 A69-24079

Population inversion distribution and wave processes in optical amplifier, showing beam transformation of constant section and dependence on crystal characteristics
11 p1893 A69-24447

Pulsed solid state Nd doped calcium tungstate fundamental longitudinal modes selection by insertion of Fabry-Perot interferometers, lenses and diaphragms into resonator
11 p1894 A69-24471

Output power losses in lasers with inhomogeneous active rods, deriving formulas for losses in ruby and Nd-glass laser rods
11 p1926 A69-24603

Giant pulse buildup time in Nd-glass laser with passive shutter determined by comparing Q factor and peak power ratios of different modes
11 p1894 A69-24621

High power short duration diffraction limited laser pulse generation with optically swept laser glass slab forming amplifier chain
11 p1897 A69-25036

Glass lasers with trivalent rare earth ions noting properties, characteristics and recent developments
11 p1898 A69-25043

Stimulated emission cross section measurement of Nd ions in calcium tungstate using Edwards method
11 p1938 A69-25049

Electro-optically Q switched Nd doped calcium tungstate laser for producing two controlled pulses, noting application to other solid state lasers
11 p1899 A69-25052

Transformation of Q switched neodymium laser radiation into Stokes component during stimulated combination scattering in liquid nitrogen
11 p1900 A69-25751

Second harmonic conversion of giant pulse Nd laser emission related to beam divergence and space-time distribution of radiation, noting energy relationship
12 p2104 A69-26022

Emission from solutions of organic luminophores excited by harmonics of Q switched neodymium laser
12 p2104 A69-26030

Off axial mode selection in circular cross section solid state lasers due to nonuniformity of excitation by focusing of pump power
12 p2106 A69-26320

Transverse passive mode locking by dye technique for neodymium glass laser with confocal cavity
12 p2107 A69-26327

Nd-doped glass pulsed laser with selected second harmonic radiation and KDP crystal frequency converter operating T 12Hz and 530 nm
12 p2108 A69-26594

YAG-Nd laser continuous operation using incoherent injection luminescent pumping by gallium arsenide phosphide light emitting diodes at liquid nitrogen temperature
13 p2270 A69-27192

Ruby and neodymium glass traveling wave laser free generation spectra kinetics, noting mode transitions as function of pumping levels
13 p2271 A69-27655

Quasi CW solid state doped lasers excited by pyrotechnic pump sources with potassium perchlorate oxidant and zirconium fuel, noting power to weight ratio
13 p2272 A69-28116

CW lasers based on composite yttrium fluoride type crystals, noting large number of intense emission bands
13 p2273 A69-28316

Ruby and neodymium glass lasers applicability to metal working, investigating factors affecting integral pulse power stability
13 p2273 A69-28431

Fluorite crystal laser activated by divalent samarium, discussing characteristics in pulsed operation mode
14 p2458 A69-29328

Emission spectrum width of solid state lasers as function of temperature, investigating effects of active medium parameters, pumping and cavity
14 p2459 A69-29389

Stimulated emission of cerium trifluoride-positive trivalent Nd ion laser noting absorption, luminescence, excitation, emission spectra and metastable state lifetime
14 p2460 A69-29645

Neodymium laser having adjustable pulse duration and homogeneous spatial radiation structure developed by two photon absorption
14 p2460 A69-29670

Solid state and gas lasers operational parameters tabulation including pulse durations, powers, energy flux densities, electric and magnetic field strengths, etc
15 p2633 A69-30708

Characteristics of neodymium-glass laser with unstable resonator noting transverse modes and radiation angular distribution
15 p2634 A69-30730

Pumping energy absorbed by active element of neodymium glass during laser emission related to activator concentration
15 p2635 A69-31104

Power supplies for ruby, YAG and glass lasers, emphasizing design equations and component selection
15 p2636 A69-31527

Monomode giant pulse generation from neodymium glass laser by coherent pumping
16 p2797 A69-32018

Semiclassical theory of quantum generators, examining laser system response to effect of monochromatic standing wave based on kinetic equation for density matrix
16 p2798 A69-32480

Laser effect in neodymium glass, estimating efficiency of light energy output vs electric energy input
17 p2979 A69-32828

Kr and Ar flash lamps pumping efficiencies compared for Nd-doped YAG and glass lasers
17 p2980 A69-32958

Angular structure of second optical harmonic for cylindrical lens focusing of Nd laser beam into negative KDP crystal
17 p2981 A69-33110

Single frequency lasers using thin metal film mode selection filters, discussing film properties and experiments with Ar ion and Nd-YAG lasers
17 p2982 A69-33399

Polymethine dyes in passive Q switches of neodymium lasers, noting effects of absorption band intensity, width and position on single pulse laser energy yield
17 p2983 A69-33968

Stable passive Q-switch of neodymium laser, presenting single pulses energy, time and spectral characteristics
17 p2983 A69-33969

Polarized emission from Nd activated glasses, establishing S and P polarization component energy dependence on pumping energy
17 p2984 A69-33974

Reliability block diagrams for laser systems, discussing failure modes of solid state, semiconductor and gas lasers
18 p3151 A69-34523

Neodymium laser emission temporal structure in mode self locking regime with Q switching by saturable filter
18 p3152 A69-35016

Solid state laser radiation damage in polymers during tensile and compression loads using microstructural analysis
18 p3152 A69-35159

Gas and solid state lasers optical resonance and radiation generation, frequency properties, frequency shift, spectra and Zeeman effect
18 p3154 A69-35408

Solid state CW laser frequency control during operation, discussing emission properties and laser applications
19 p3331 A69-35864

Solid state laser emission frequency control and retuning using dispersive resonators, analyzing interference methods for wavelength measurement
19 p3331 A69-35865

Weak displacements of opaque objects and optical distortion in solid state lasers analyzed by holographic interferometry
19 p3308 A69-35909

Lasers and maser devices in radio quantum electronics, discussing optical parametric and microwave devices including transistors, diodes, magnetrons, etc
19 p3284 A69-36433

Single crystal line block electro-optical shutter reflector operation based on double reflection and birefringence in anisotropic media, noting application to Nd glass laser
20 p3554 A69-37611

Neodymium glass laser emission spatial characteristics, investigating higher laser modes excitation
20 p3554 A69-37725

Differential equations for field amplitude and level populations applicable to solid state lasers output power pulsations
20 p3554 A69-37726

Simultaneous mode locking of Nd YAG laser and intracavity second harmonic generation in high temperature Li niobate or BaNa niobate
20 p3555 A69-37731

Glass lasers development, operation, composition, applications, etc
21 p3734 A69-38407

Solid state traveling medium laser pulsed emission characteristics and nonlinear intensity distribution
21 p3735 A69-38438

Solid state traveling wave optical quantum amplifier for conversion of modulated signal carrier frequency, applying to frequency conversion in laser communication links
21 p3739 A69-39540

Lummer-Gehrcke plate type polarizer made of birefringent material for Nd glass laser, discussing reflection coefficients in quartz crystals
21 p3739 A69-39541

Emission from polymethine dye solution during optical pumping with pulses from Q switched Nd glass laser, discussing emission spectral, temporal and energy characteristics
21 p3739 A69-39542

Time characteristics and second harmonic of radiation of Nd laser containing lens systems, producing second harmonic in KDP crystal
21 p3740 A69-39544

Transverse mode selection in rotating mirror neodymium doped calcium tungstate laser by inserting slit and edge into resonator
22 p3961 A69-40316

Spectrum characteristics of plasma generated by pulses of solid state laser radiation on metals and alloys in regular and quasi-stable regimes of emission
22 p3964 A69-40793

Neodymium activated glass laser efficiency as function of absorption of pumping and emission energy by glass
22 p3964 A69-40797

High output laser amplifier consisting of glass and selenium oxychloride/Nd liquid lasers
23 p4173 A69-41565

Optimum design of spherical and ellipsoidal pumping chambers for solid state lasers determined from numerical calculation of radiation transfer efficiency
24 p4327 A69-42986

Optical properties of neodymium-doped YAG and glass laser materials including fluorescence lifetime and conversion efficiency, absorption spectra, sensitization effects, etc
24 p4329 A69-43751

SOLID STATE PHYSICS

Solid state physics - Conference, Alta Lake, British Columbia, August-September 1967
05 p0809 A69-16552

Cyclotron waves interaction when propagating in solid state plasma in magnetic field, determining amplification zones and factors
08 p1374 A69-21078

Collection of papers on solid state physics
11 p1935 A69-24524

Book on ultrasonic methods in solid state physics covering stress wave propagation in solids, pulse methods of velocity change and attenuation measurements and causes of losses
12 p2145 A69-26870

Solid state physics applications to fracture problems and structure of solids, considering crystallography, lattice vibrations, defects, electron bands, alloys and surface physics
13 p2316 A69-27221

Book on elements of solid state energy conversion covering quantum mechanics, thermodynamics, thermoelectricity and photovoltaic energy conversion
13 p2322 A69-28038

LF electrostatic oscillations of inhomogenous solid state plasma with small number of current carriers in parallel external electric and magnetic fields
15 p2665 A69-30042

Book on semiconductor devices physics covering principles and operational characteristics, carrier distribution and transport properties, materials, junctions, thin films, etc
15 p2670 A69-31062

Physics of solids in intense magnetic fields - Conference, Chania, Crete, July 1967
16 p2826 A69-31819

Single particle and collective excitations of plasmas in solids and interactions with acoustic and electromagnetic waves in magnetic field
16 p2821 A69-31820

Lattice vibration theory of solid state diffusion for Cu including anharmonic effects formulated using equilibrium statistical mechanics, considering interacting phonon events
17 p3015 A69-32822

Book on solid state electronics, discussing quantum mechanical approach, Fermi-Dirac statistics, electron theory of metals, semiconductors and magnetism
18 p3182 A69-34653

Physics of semiconductors - Conference, Moscow, July 1968, Volume 1
19 p3384 A69-36513

Semiconductor physics - Conference, Moscow, July 1968, Volume 2
19 p3387 A69-36540

Semiconductor devices development based on amorphous materials, reviewing solid state physics implications
23 p4198 A69-41560

SOLID SURFACES

NT CRYSTAL SURFACES

Streak interferometry method for measuring transient deformation data on metallic solid surfaces
01 p0078 A69-10117

Seismic refraction study of internal structure of volcanic cinder cone
02 p0236 A69-11465

Nonstationary wing motion in gas stream near solid surface, analyzing differential equation for acceleration potential
02 p0188 A69-12134

Electric potential effects on heat transfer from plasma to solid wall, measuring heat input rates
02 p0290 A69-12423

Plane electromagnetic wave scattering from slightly rough surface tilted away from reference plane, noting polarization effects
03 p0395 A69-13625

Interaction of rarefied gas with solid surface, analyzing accommodation coefficients, energy and impulse exchange as function of atomic bulk size
04 p0632 A69-14991

Solid insulator performance in vacuum, analyzing breakdown factors
05 p0731 A69-16243

Gas adsorption on solids, discussing statistical mechanical theory assuming localized adsorption for first adlayer and nonlocalized mobile layer adsorption on top
06 p0980 A69-17387

Chemical effects of solar wind and cosmic protons on solid bodies in space, discussing possible relation to origin of life
08 p1407 A69-20935

Heat transfer in solid bodies, deriving thermal conductivity equation and surface boundary conditions in presence of radiative energy transfer
13 p2373 A69-27584

Spatial distribution patterns of gaseous argon atoms scattered from solid argon surface
13 p2300 A69-28658

Velocity field in turbulent flow based on momentum transfer, determining velocity distribution for flow near solid surface
16 p2772 A69-32128

Electron heat transfer and spherical probe characteristics in moving nonequilibrium plasma analyzed at stagnation region as function of solid surface potential [AIAA PAPER 69-699]
17 p3011 A69-33475

Wall boundary condition model modification applied to molecular beam-solid surface scattering, noting qualitative agreement with observed distributions
19 p3377 A69-36179

Solid surface roughness influence on reflection of thermal energy molecular jets, showing shock determined by incidence angle
19 p3377 A69-36180

Gas molecules scattering by solid surface for monoenergetic and Maxwellian beams, discussing model with different values for magnitude and velocity direction
19 p3377 A69-36181

Unsteady heat transfer between gas flow and solid surface during melting
20 p3631 A69-37088

Heat conduction in thin layer near boundary surface of solid by approximating one dimensional conduction in half space with allowance for curvature
20 p3633 A69-38213

SOLID SUSPENSIONS

Heat conduction in viscous fluid flows with large concentration of suspended solid particles
02 p0351 A69-12052

Heat transfer involving particulate suspension, discussing characteristics of flowing suspension, inertia effects, impingement, deposition, radiation and electric charges
13 p2377 A69-28151

SOLIDIFICATION

Dendrite formation and solidification relationship in highly alloyed materials from quantitative determination of controlling factors for segregation
01 p0098 A69-10899

Directional solidification and composite structures, discussing structure changes effect on mechanical properties
03 p0449 A69-13877

Directional solidification of multicomponent metal alloys for matrix in fiber reinforced composites, using monovariant eutectic reactions
07 p1166 A69-19145

Nodal precipitation and cellular solidification substructure in commercial purity nickel, discussing supercooling, NiO and eutectic composition
08 p1332 A69-20289

Crystal microstructure and mechanical properties of unidirectionally solidified Ni-Ni-Nb intermetallic eutectic alloy at high temperature, examining deformation and fracture modes
13 p2276 A69-27402

Oriented composites obtained from organic system under various directional solidification conditions
13 p2287 A69-28680

Stress analysis during solidification of binders in glass fiber reinforced plastic materials, using resin coated glass film simulation
22 p3973 A69-40746

SOLIDIFIED GASES

Temperature field in plate heated at one end and situated in solidifying gas, leading to gas layer formation by sublimation
16 p2878 A69-31957

Star formation in interstellar solid hydrogen clouds originating from cellular pressure created by hydrogen condensation onto interstellar grains
16 p2862 A69-32375

Intensities of translational lattice mode absorptions of alpha phase solid molecular nitrogen in far IR, noting temperature dependence
20 p3579 A69-37346

Solid para hydrogen coated graphite particles expulsion into interstellar medium from star formation regions, considering mantles stability and particles extinction efficiency, albedo and phase function
20 p3601 A69-37492

Raman spectrum of solid alpha-nitrogen at low temperatures, calculating scattering intensities and Raman active librational lattice vibrations
23 p4194 A69-42204

Raman spectra analysis of solid carbon dioxide, nitrous oxide, nitrogen and CO, determining lattice mode intensities from oriented gas model
23 p4194 A69-42205

High temperature plasma generation by high power laser beam irradiation on small solidified gas particle, detailing experimental equipment and procedures
24 p4354 A69-42645

Order-disorder transitions in solid hydrogen, discussing model to explain molecular rotation angular momentum operator fluctuations
24 p4350 A69-43119

Dry ice ablating models for unheated supersonic and hypersonic wind tunnel tests, noting mass addition rate extension
24 p4297 A69-43255

Proton ejection as hydrogen ion clusters by low energy electron bombardment of solid hydrogen
24 p4389 A69-43747

Raman scattering during external and internal motion of oxygen molecules condensed phases, observing

gamma and liquid phase bandwidths during stretching vibrations 24 p4353 A69-43808

SOLIDS NT SOLIDIFIED GASES

Temperature evolution velocity parameter effect on behavior of elastoviscoplastic solids, noting demonstration by work hardening tests at variable temperatures [ONERA-TP-644] 01 p0164 A69-10036

Small oscillations in solid body with arbitrary cavity partially filled with viscous incompressible fluid 01 p0165 A69-10084

Solid body motion about fixed point representable by two dimensional motion of two points on complex plane 01 p0116 A69-10356

Radiative heat transfer through transmission layers sandwiched between black bodies with variable blackness spectra 02 p0350 A69-11578

Integration for equations governing linearized thermoelastic transformations of incompressible solids 02 p0340 A69-12033

Rapid uniform expansion of spherical cavity in compressible elastic-plastic solid, obtaining similarity solution 03 p0528 A69-13798

Motion and stability of solid body with cavity containing rotor and two incompressible nonmixing liquids with surface tension 03 p0418 A69-13814

Model of creep in solids based on Markov process, discussing dislocation movement by means of thermal activation 03 p0529 A69-13942

Dilatometer for measuring thermal expansion of solid bodies over temperature range at various gas media pressures 03 p0432 A69-14151

Dynamics of structured solids - ASME Conference, New York, December 1968 04 p0675 A69-14684

Approximate method to determine nonstationary thermal fields in solid bodies with thermal capacity and thermoconductivity coefficient depending linearly on temperature 04 p0688 A69-15409

Dynamic response of solids induced by charged particle interaction noting laser interferometric measurement of surface stresses 05 p0771 A69-15817

Reciprocal theorem for displacements of solid skeleton caused by fluid sources action in infinite consolidating space 05 p0835 A69-15869

Coupled heat equation to calculate transient and steady state temperature distributions in viscoelastic solids under cyclic deformations 05 p0836 A69-15878

Regular thermal conditions in solid bodies with radiative heat transfer 05 p0845 A69-15896

Spectrophotometer and integral methods to determine solar radiation absorptivity for steady/ unsteady thermal regimes in solids 05 p0846 A69-15901

Integrability of equations for problem of motion of heavy solid body about fixed point 05 p0794 A69-16206

Mass spectrometric studies of plasmas produced by laser beam interaction with solid materials 06 p0932 A69-16921

Free energy in linear viscoelastic solids 06 p1022 A69-17241

Detonations in gases and solids, discussing limits, speed, initiation by deflagration, chemical factors, dimensional effects, etc 06 p1032 A69-17424

Approximate expression for temperature distribution during heat transient in infinite solids of plane, cylindrical and spherical geometry 06 p1025 A69-17779

Solid body surface temperature relation to heat flux during cooling by fluid flow solved on computer 07 p1241 A69-18923

Steady state thermal stress distributions near external crack in solid, treating temperature distributions with respect to plane of crack 07 p1232 A69-19172

Damping flywheel to stabilize permanent rotation of weightless solid body moving by inertia, obtaining differential equations of motion 07 p1183 A69-19678

Mathematical models of crack propagation in solids noting similarity for equilibrium crack length 07 p1238 A69-19692

Consistency of high temperature equation of state of solids, considering Gruneisen parameter and lattice dynamics 08 p1419 A69-19814

Constitutive equations for propagation of plane waves of finite amplitude in nonsimple elastic solids, discussing holohedral isotropic solids and transverse harmonic circularly polarized waves 08 p1411 A69-20141

Proton electrolyte application to fuel cells, discussing proton diffusion in solids and materials with vacancies /proton conductors/ in structures 08 p1269 A69-21053

Heat transfer mechanism in solid body, deriving integrodifferential equation with classical equation and hyperbolic equation of heat propagation as special case 09 p1621 A69-21587

Ordinary and inverse variational methods for stress-strain state of solid body, using Lagrange multipliers to reduce variational problem 10 p1793 A69-22885

Relaxation method for configurations and energies of atoms and stress induced crack opening displacements in crystalline solids 10 p1796 A69-23067

Damping properties of nonlinear viscoelastic solids with applications to vibrating continua, using Gauss principle of least constraints 11 p1970 A69-24605

Dynamic and fatigue crack propagation theories for brittle and quasi-brittle solids and plates 11 p1975 A69-24672

Nonlinear resonance formation during spatial nonlinear vibrations of solid bodies, establishing relations between vibration and excitation frequencies 11 p1919 A69-25167

Mechanical model for oscillatory motion of solid body in Newtonian central force field 11 p1919 A69-25179

Indentation of inhomogeneous rigid plastic solid by flat punch under plane strain conditions analyzed by perturbation method 11 p1986 A69-25244

Stress wave propagation in thermoviscoelastic solids using extended Ritz method 11 p1993 A69-25527

Solid body motions containing cavity filled with viscous fluid under influence of gravity, formulating motion equations for fluid and body 12 p2061 A69-25884

Three dimensional problems in crack theory for unbounded brittle body, deriving critical loads from limiting equilibrium equation 12 p2178 A69-25997

Elastic stress created by perpetual motion of isotropic elastic solid in static space-time 12 p2130 A69-26283

Incompressible elastic-plastic solid flow through rough converging conical channel analyzed using Mises yield condition and Prandtl-Reuss equations 12 p2063 A69-27114

Controllable motions of compressible homogeneous isotropic solids, anisotropic solids and fluids with memory under constant body force 12 p2189 A69-27118

Book on microscopic and macroscopic fundamentals of fracture of solids covering structural, metallographic and physical aspects, dislocations, brittle fracture, etc 13 p2274 A69-27220

Solid state physics applications to fracture problems and structure of solids, considering crystallography, lattice vibrations, defects, electron bands, alloys and surface physics 13 p2316 A69-27221

Fracture and equilibrium position of dislocations in discrete and continuously distributed dislocations arrays including stress due to crack, energy considerations and crack initiation 13 p2358 A69-27222

Metallographic aspects of fracture, analyzing very brittle solids, Griffith cracks, ductile solids and ductile to brittle transition 13 p2274 A69-27225

Variational principle for admissible functions particular solution in elasticity theory involving solid bodies with cracks 13 p2359 A69-27290

Shock waves in solids, discussing gas gun firing and explosive detonating at specimen, transformations measurement and materials processing applications 13 p2360 A69-27341

Analytical expressions for nonlinear partial differential equation of heat conduction in solids, giving temperature as function of time and location 13 p2372 A69-27434

Diffraction images of coherently illuminated objects in presence of aberrations stressing images of edges, disks and bars 13 p2297 A69-27451

Unsteady temperature distribution in solid sphere with variable internal heat source and surface subjected to variable heat flux 13 p2373 A69-27773

Transient one dimensional temperature distribution determined for bodies with internal heat generation and nonlinear boundary condition, using Biot variational method [ASME PAPER 68-HT-6] 13 p2374 A69-27775

Friction wear of solid bodies based on microscopic contact system model, deriving particle distribution law from physico-statistical analysis 13 p2268 A69-28051

Transport processes under adiabatic conditions between external magnetic field and thermal and electrical gradients in solid, defining galvanomagnetic and thermomagnetic effects 13 p2299 A69-28129

Variational principle based on assumed stress hybrid method suitable for finite element analysis of incompressible solids 13 p2368 A69-28348

Periodic solutions for small nutation angle of quasi-linear autonomous system of equations of motion of heavy solid body moving around fixed point 14 p2445 A69-28896

Gas-surface interaction for trapping and energy exchange, comparing continuum and discrete lattice models for solids 14 p2409 A69-29092

Ultrasonic pulse-echo-overlap method modified for simultaneous measurement of time delay and relative voltages in determining sound velocities and attenuation of solids 14 p2450 A69-29567

Nonlinear oscillations stability of solid body connected to base by elastic springs of different rigidities under external forces 14 p2536 A69-29745

Soviet book on partially liquid filled solid body dynamics from viewpoint of space and aircraft applications 14 p2530 A69-29815

Variational principles of solid mechanics for finite element analysis of solid continua 15 p2705 A69-30429

Cylindrical wave propagation in thermoelastic incompressible isotropic solids, considering cases of zero and nonzero coefficient of thermic dilation 15 p2707 A69-30626

Integrable cases of equations of motion of solid body around fixed point located in potential field of elastic supports 15 p2653 A69-31194

Similarity criteria for plastic deformation theory of body under pressure and nonuniform temperature field, considering strength calculations 15 p2714 A69-31200

High temperature ultrasonic testing to measure and control solid materials early in processing 15 p2632 A69-31514

Double shock method for detecting pressure limits in magnetic phase transition of solids 16 p2825 A69-31696

Solid materials erosion rate as function of cumulative damage generated by liquid droplets impingement 16 p2794 A69-31904

Stresses due to nucleus of thermoelastic strain in infinite elastic solid with two rigid circular inserts 16 p2872 A69-31906

Temperature distribution of solid spherical satellite under solar radiant heating solved by variational calculus or point matching methods 16 p2877 A69-31922

Inhomogeneity effects on elastic waves generated by impulsive loading of surface using asymptotic method, discussing high stress intensification regions 16 p2873 A69-32157

Radiation effect on inorganic solids isothermal decomposition induction period, deriving equations for conditions representing various kinetics combinations during irradiation [WSCI PAPER 69-21] 16 p2832 A69-32359

Book on mechanics of deformable media covering fluid and solid mechanics and applications to irrotational flows of compressible and incompressible fluids 16 p2813 A69-32789

Wave generation in infinite micropolar elastic solid body analyzed by linearized equations of motion
17 p3053 A69-33018

Linear pyrolysis of condensed materials in presence of heat loss into ambient medium expressed in terms of thermoneutral and thermal reactions
17 p3069 A69-33134

Stable motions determination of solid bodies with liquid filled cavities and satellites motions stability in central Newtonian force field
17 p3005 A69-33228

Dynamic model of bodies with microstructure and nondissipative energy motion, discussing action steadiness, invariance conditions and Galilean relativity
17 p3067 A69-34149

Shock wave propagation induced by nonuniform instantaneous internal heating of nonlinear elastic strain hardening solid material [SAWE PAPER 69-APM-17]
18 p3214 A69-34393

Rotary motion stability of axisymmetric solid body or gyroscope suspended on string and containing ellipsoidal cavity filled with liquid
18 p3135 A69-34558

Inertial characteristics determination error influence of solid body on damping system parameters
18 p3171 A69-34562

Transposition formula for finite displacements of solid body having fixed point relative to fixed axes
18 p3172 A69-34589

Fixed point reaction force in mobile system of solids coupled kinematically, examining zero dynamic components
18 p3172 A69-34590

Torque calculations about joints of rigidly chain-like arranged clusters of flying bodies
18 p3208 A69-34776

Strains in solids of any form, using moire method combined with holographic interferometry
18 p3139 A69-35280

Limiting equilibrium of infinite brittle body weakened by internal plane elliptical crack, determining critical loads and stresses at crack
18 p3226 A69-35379

Longitudinal and transverse wave propagation in homogeneously deformed isotropic elastic solids, considering Hadamard and Green materials
19 p3440 A69-36588

Solid and structural mechanics theories noting continuum mechanics role
19 p3443 A69-36776

Body relations in continuum mechanics of solids, examining temperature influence varying in time and space
19 p3444 A69-36805

Thermal stresses in solids, discussing spaces and half spaces, thick walled systems, shells, plates, disks and bars
19 p3447 A69-36856

Continuum mechanics of micropolar fluids and solids, discussing thermodynamical restrictions on elasticity and viscosity coefficients, deriving field equations and boundary conditions
20 p3624 A69-37582

Viscoelastic nonlinear and linear solids models and rheological equations, studying stress-strain states of various complex Hookean, Kelvin, Maxwellian and Zener elements
20 p3625 A69-37601

Monograph on motion of solid body with cavities containing viscous liquid, covering kinetics involving completely or partly filled fluids
20 p3578 A69-38200

Forced recombination scattering of light on Rayleigh polarization waves in isotropic solid body with small elastooptical constants
21 p3770 A69-38963

Reaction forces calculated for system of connected solid bodies of various composition during accomplishment of given motion
21 p3771 A69-39085

Differential equations for variable mass solid body motion about fixed point having cavities filled with ideal fluid
21 p3771 A69-39106

Equations governing stress waves generated by rapid nonuniform heating of solids, comparing elastoplastic with purely elastic solutions
21 p3837 A69-39158

Rodrigues formula derivation procedure and summation formula derivation for finite rotations of solid body, noting simplifications from kinematic considerations
21 p3772 A69-39183

Constitutive equations for homogeneous viscous fluid and Kelvin-Voigt viscoelastic solid in electromagnetic field, using linear irreversible thermodynamics and continuum mechanics
21 p3851 A69-39289

Dynamic plasticity of nonsymmetrical free flight collision impact of crystalline solids, using linear temperature dependent stress-strain function and finite amplitude wave expansion
21 p3840 A69-39298

Gas dynamic processes during vaporization of solid material under Nd laser emission, using high speed photography
21 p3740 A69-39551

Coupled acoustic and spiral EM waves drift instabilities in bounded plasma of solid body found to be convective
21 p3782 A69-39556

Solid body filled with ideal incompressible liquid, analyzing stability of permanent rotations
21 p3773 A69-39837

Crack development in solid body, considering condition at crack tip not derivable from equation of motion and strain equation
22 p4047 A69-41123

Deformation tractions in undeformed and curved cuboid flexure and inverse flexure determined by stress-strain relations for homogeneous isotropic compressible materials
23 p4226 A69-41521

Stress-strain state in infinite medium with cavity under triaxial tensile force obtained from integrodifferential equation deduced from equilibrium equation
23 p4226 A69-41703

System asymptotic motion stability for given parameter values using algorithms with aid of R functions
23 p4191 A69-41704

Time and plasticity effects on fracture determining solids strength as function of crack dimension
23 p4236 A69-42530

Semiinverse method involving plane wave expansions to solve elliptical crack expansion and self similar phase transformation in anisotropic solid
24 p4397 A69-42749

Convective thermal flux at stagnation point in multicomponent partially ionized gas injected flow past body, considering effective ambipolar diffusion coefficient
24 p4246 A69-43485

SOLIDS FLOW
Small strain plasticity theory for planar slip in specific nickel base alloy deformation
13 p2362 A69-28120

SOLIDUS
Subsolidus equilibrium study in potassium tantalate K niobate system for dry and hydrothermal runs, using X ray powder diffraction and petrography
08 p1332 A69-20373

Binary Nb-Hf system phase diagram below solidus line noting lattice parameters and oxygen and nitrogen effects on phase equilibrium boundaries
18 p3157 A69-35247

SOLUBILITY
Saturation solubility of carbon in cobalt and nickel with respect to graphite determined by vapor transport experiments over large temperature range
01 p0092 A69-10060

Solubility of helium in liquid fluorine increases with temperature exhibiting reverse order
01 p0142 A69-11258

Nitrogen solubility measured in liquid Fe-Cr-Ni-Al alloys, noting solubility increase with increasing Al content
06 p0942 A69-17228

Nitrogen solubility in liquid Fe-Cr-Ni alloys increases with increased Cr concentration between 1550-1700 C and at one atm N pressure
06 p0942 A69-17229

Alloying elements effect on nitrogen solubility in liquid Fe-Cr-Ni alloys, defining quantitatively changes in solubility
06 p0943 A69-17234

Pressure-temperature dependence of nitrogen solubility in tungsten at 2400-3000 C
07 p1168 A69-19602

Rhenium effect on lattice solid solubility of oxygen in tungsten, calculating rhenium-oxygen cluster minimum binding free energy
08 p1329 A69-20007

Hydrogen solubility in solid and liquid phases of nickel-molybdenum and nickel-tungsten alloys at high temperatures
08 p1333 A69-20448

Gold diffusion and solubility in indium phosphide, analyzing temperature and vapor pressure effects
09 p1555 A69-21470

Nonpolar gases solubilities in aqueous KOH solutions in temperature range 25 to 100 C, noting activity coefficients, salting out coefficients and heats of solution
10 p1651 A69-22937

Nitrogen solubility in molten niobium and molybdenum at high temperatures in argon flow
10 p1710 A69-23213

Hydrogen solubility in solid and liquid Ti close to melting point, showing no effect on welds and castings porosity
11 p1905 A69-24963

Group 4A carbides and nitrides formation in Mo by arc melting, determining threshold solute metal-interstitial atom ratios
12 p2117 A69-27136

Gold diffusion and solubility in indium phosphide, analyzing temperature and vapor pressure effects
15 p2669 A69-30715

Model compounds and polymers solubility parameters correlated with refractive index data
21 p3751 A69-38552

SOLUTES
Field ion microscope study of imaging solute atoms of dilute Pt-based W, Pd, Co, Ni and Au alloys
01 p0092 A69-10055

Solute vertical stabilizing gradient inhibition of thermal convection of fluid layer under temperature gradient, discussing effects on two dimensional flows motion
03 p0532 A69-13012

Lifetime of highly soluble isolated dense spherical solute particle in solvent, taking into account molecular diffusion, kinetic limitations, etc
10 p1651 A69-22939

SOLUTION
Proton spin-lattice relaxation time in dilute liquid and gas solutions of orthohydrogen in parahydrogen, noting dependence on temperature, density and composition
06 p0961 A69-17141

SOLUTIONS
NT DETONABLE GAS MIXTURES
NT GAS MIXTURES
NT NUCLEAR EMULSIONS
NT PHOTOGRAPHIC EMULSIONS
NT SOLID SOLUTIONS

Nonpolar gases solubilities in aqueous KOH solutions in temperature range 25 to 100 C, noting activity coefficients, salting out coefficients and heats of solution
10 p1651 A69-22937

Nondestructive thermal tests using liquid crystals thermal sensitivity for measurement of temperature changes and visualization of temperature gradients
11 p1892 A69-25293

Helix to coil transition for triple stranded macromolecule in solution, calculating ring weighting and partition functions and intact bonds
24 p4353 A69-43812

SOLVENTS
Solution velocity and turbulence effects on solvent cleaning of corrosion resistant steel tubing, discussing fluidity forces and cleaning formulation
08 p1318 A69-19807

Halocarbon solvent for application of chlorosilane finish to heat cleaned glass fabric for reinforcement of plastic, noting relative humidity effect
08 p1341 A69-20513

Solvent effect in catalytic hydrogenation reaction of Schiff bases of alpha-keto acids with optically active alpha-alkylbenzylamine
12 p2026 A69-25779

SOMMERFELD APPROXIMATION
Eigenvalues for Orr-Sommerfeld equation by difference technique for Reynolds number range 5780-729000, determining Poiseuille flow stability in plane channel
03 p0416 A69-13654

Sommerfeld type and Fermi type approximation analytical solutions of Thomas-Fermi differential equations for positive ions
10 p1726 A69-23525

Relativistic generalization for polar Sommerfeld rosette of Fourier series expansions by Lagrange and Bessel for particle motion in Keplerian field
16 p2811 A69-31607

Asymptotic theory of Orr-Sommerfeld problem for symmetric channel flow stability
17 p2958 A69-34151

SONAR

- Visual sonar target detectability probability function of retinal position and brightness contrast
02 p0203 A69-12218
- Sonar receiver reduced averaging processing in presence of extended and point targets compared with full averaging processor
04 p0562 A69-15477
- Digital signal processing in radar, sonar and communication
05 p0718 A69-15749
- Stationary coherent /hologram/ radar and sonar using zone plate action to provide range information
05 p0721 A69-16578
- Hologram form of forward scatter bistatic radar or sonar
07 p1078 A69-18866
- Remote oceanographic sensing from ships, aircraft and spaceborne platforms, using active /radar and laser/ and passive sensors in visible, IR and microwave regions
12 p2075 A69-26997
- Cramer-Rao and split-beam tracker techniques compared for optimum bearing error attainable with linear passive sonar array in spatially incoherent noise environment
20 p3576 A69-37322

SONDES

- NT DROPSONDES
- NT IONOSONDES
- NT RADIOSONDES
- NT RAWINSONDES
- Ozoneonde based on modified Brewer electrochemical sonde
01 p0079 A69-10218
- Meteorological PTU /pressure, temperature, humidity/ probe for lower atmospheric layers, discussing detectors and assembly qualities
04 p0601 A69-15229
- Acoustic sounding of atmospheric structure, utilizing energy backscattered from temperature fluctuations in turbulent regions
14 p2448 A69-29527
- Vertical ozone distribution determination discrepancies between Brewer-Mast electrochemical sonde and Umkehr methods, discussing influence of seasonal and diurnal variations
16 p2786 A69-32630
- Optical probe for determining ozone vertical distribution at high altitudes, discussing optical method requirements and ozoneonde construction
16 p2792 A69-32637

SONIC ANEMOMETERS

- Sonic anemometer for wind velocity through pulse communication transducers noting applications to aerospace vehicle design
10 p1692 A69-23255
- Sonic anemometers for atmospheric turbulence, discussing variance spectra of vertical wind component and temperature in atmospheric surface layer
16 p2808 A69-32600

SONIC BOOMS

- Sonic bang intensities in stratified atmosphere obtained by geometrical acoustics and linear theory modifications to take account of nonlinear effects
01 p0008 A69-10056
- Aerodynamic configurations to reduce sonic boom at supersonic speeds
01 p0007 A69-11028
- Spikes on sonic boom pressure waveforms due to simultaneous focusing and diffraction of planar N wave by inhomogeneous atmosphere layer
01 p0011 A69-11280
- Air coupled seismic waves generated by jet fighters flying at high altitudes and supersonic speeds
01 p0077 A69-11281
- Sonic boom effect on corticosteroid level in human blood, noting no changes
03 p0378 A69-14209
- Human orienting reaction to sonic boom, determining degree of discomfort
03 p0378 A69-14210
- Concorde and Boeing supersonic transport overland sonic booms, discussing social, political and legal reactions
06 p0868 A69-17899
- Sonic boom reduction devices, discussing supersonic electroaerodynamic flow with shock waves, gas discharge one dimensional continuum analysis, power expenditure and aerodynamic interaction
[AIAA PAPER 69-38] 06 p0869 A69-18150

Sonic boom minimum achievable shock front pressure rise and overpressure level prediction for given aircraft and flight conditions
08 p1253 A69-19903

Sonic boom reduction by azimuthal redistribution of supersonic aircraft pressure field variation
[AIAA PAPER 68-159] 09 p1434 A69-21948

Acoustical, psychological, sociological and political aspects of human reaction to SST sonic booms over populated areas, tabulating Boeing and Concorde boom intensities
14 p2408 A69-29151

Human tolerance to SST sonic booms through scheduled community exposure, discussing physiological effects and acceptability level
14 p2541 A69-29153

Sonic boom damage legal claims, discussing causal relationship validity and claims processing
14 p2541 A69-29155

Sonic boom produced earth particle velocities, noting seismic effect limitation to boom pressure envelope area and earth surface boundary
14 p2393 A69-29880

Fast visual task performance indoors found dependent on sound pressure level
15 p2550 A69-30305

Aircraft created pressure patterns responsible for sonic boom, discussing design techniques for noise reduction
15 p2550 A69-30369

Sonic boom damage to structures from supersonic aircraft overflights using inductive and deductive approaches
15 p2585 A69-30370

Sonic boom simulation methods using shock tube, booth type simulators, ballistic ranges and explosives, discussing unmanned data recorder as monitoring device
15 p2585 A69-30371

Slender body aerodynamics combined with wave propagation theory for sonic booms of aircraft configurations, propeller and helicopter noise, sonic boom alleviation, etc
16 p2732 A69-31867

Bow shock wave during rectilinear flight with varying acceleration, describing sonic boom loop mechanism
16 p2734 A69-32005

Legal, social and physical effects of supersonic flight, discussing damage claims validity and recovery resulting from breaking of sound barrier
17 p3075 A69-32841

Sonic boom theory for steady flight in atmosphere without winds, discussing sonic boom reduction by aerodynamic means
17 p2902 A69-34017

Passenger transport cruising at low supersonic speeds without sonic boom generation on ground, discussing overpressures, signature characteristics and corridor widths
[AIAA PAPER 69-776] 19 p3244 A69-35647

Scattering equations for sonic boom waveform spike perturbations produced by atmospheric turbulence, discussing supersonic aircraft pressure signatures
21 p3646 A69-38689

Damped mass spring system response to sonic booms, considering effects of structural damping, total/ positive phase duration ratio and N wave rise time
21 p3647 A69-38987

Acoustoelastic interaction effects of sonic bangs on natural frequencies response of large windows backed by closed cavity
21 p3836 A69-38988

Supersonic aircraft sonic bangs loudness level calculations by model waveforms with allowance for interaction between incident and ground reflected shock waves
23 p4063 A69-42454

Supersonic aircraft design data, costs and benefits, discussing origin and significance of sonic boom
24 p4252 A69-42997

Sonic boom signatures produced by diverse SST configurations during cruise, indicating aircraft length as overpressure limit factor
24 p4253 A69-43661

Sonic boom lower bounds determination in midfield based on modification of Jones results by minimizing overpressure or shock strength of boom wave positive component
24 p4254 A69-43662

Isobaric inhomogeneous atmosphere effect on sonic boom determined, using analytic equation relating transmitted wave intensity to local free stream Mach number
24 p4254 A69-43728

SONIC FLOW

U TRANSONIC FLOW

SONIC NOZZLES

Sonic nozzle optimal profile determination with and without cylindrical throats, noting sonic line curvature importance on discharge coefficient
02 p0188 A69-12037

Sonic nozzle mass flow measurement errors at high supply pressures and moderate temperatures due to real gas effects
[ASME PAPER 68-WA/FM-4] 05 p0699 A69-16114

Controllable sonic flow orifice, discussing mass flow rate, area and upstream stagnation pressure
10 p1693 A69-23343

Exhaust plume rarefaction from sonic orifice, considering continuum to transitional behavior for perfect gas
[AIAA PAPER 69-657] 17 p2892 A69-33465

Rarefied gas dynamics for continuous medium and discrete molecules assemblage, discussing flow over blunt model and free jet flow from sonic orifice
18 p3122 A69-34812

Relaxation time influence on discharge coefficient of sonic nozzle of revolution, considering expanding polyatomic gas problem
19 p3241 A69-36721

Flowfield properties of two dimensional supersonic jet near sonic nozzle exit by numerical method of characteristics
22 p3860 A69-40920

SONIC SPEED

U ACOUSTIC VELOCITY

SONIC WAVEGUIDES

U ACOUSTIC DELAY LINES

SOOT

Oxygen addition to fuel stream effect on formation of soot and polycyclic aromatic hydrocarbons in ethane-air and ethylene-air diffusion flames
02 p0205 A69-12318

Optical constants of soot applied to heat flux calculations, discussing soot particles concentration determination in hydrocarbon combustion products
[ASME PAPER 68-HT-13] 13 p2374 A69-27777

SORBENTS

Experimental program to evaluate regenerable sorbents for carbon dioxide removal in space cabin environments
09 p1447 A69-22552

SORPTION

NT ADSORPTION

NT CHEMISORPTION

Cesium sorption in materials for thermionic converters reservoirs, discussing dimensional stability of porous alumina, W and C samples
14 p2463 A69-29220

SORTING

U CLASSIFYING

SOUND

U ACOUSTICS

SOUND AMPLIFICATION

Ultrasound propagation amplification coefficient in high permittivity semiconductors with electric field based electron-phonon interaction
05 p0809 A69-16372

Absorption and amplification of sound in many valley semiconductors in strong electric field, noting dependence on electron heating and relaxation times
07 p1199 A69-18681

Sound amplification role in increasing spread of bounded two dimensional smoke jet studied for application to fluid amplifiers
[ASME PAPER 69-VIBR-3] 10 p1640 A69-24161

SOUND BARRIER

U ACOUSTIC VELOCITY

SOUND FIELDS

Stability of tangential velocity discontinuity between two media with different densities situated in acoustic field
06 p0910 A69-17344

Broadband sound field generated aerodynamically by relatively smooth disk rotating in own plane, noting turbulent boundary layer flow and surface roughness effect
09 p1539 A69-21718

Boundary layer suction sound emission, analyzing turbulent flow past elastic plate with reinforced slots performing flexural and torsional vibrations
09 p1483 A69-22638

Sound generation by unsteady rotational flow as singular perturbation problem solved by matched asymptotic expansions, discussing flow and radiation fields 13 p2299 A69-28187

Acoustic hologram recorded by laser flying spot scanner 13 p2265 A69-28662

Ultrasound holography for imaging opaque structures, noting distortion due to long wavelength of sound field and distortion reduction techniques 13 p2265 A69-28663

Automated IR fatigue crack detection in sonic test facility capable of subjecting large aircraft or missile structures to intense sound fields 15 p2631 A69-31505

Monograph on interaction between flow and sound fields as singular perturbation problem, using matched asymptotic expansion 17 p2949 A69-32998

Far field helicopter rotor noise radiation, analyzing blade slap, rotation noise, vortex noise effects and loading harmonics utilizing computer program 18 p3090 A69-34322

Hydrodynamic noise as pseudosound field resulting from pressure variations in turbulent fluid flow, using Lighthill acoustic analogy 18 p3123 A69-34921

Helicopter rotor rotational and vortex noises prediction methods and trends 18 p3088 A69-35224

Fluctuating heat transfer and flow measurements for circular cylinder in crossflow with simultaneously imposed transverse standing sound field 18 p3124 A69-35384

Acoustic field due to jet aircraft in motion, describing convection parameter modification in generalized sound pressure equation 20 p3462 A69-37757

SOUND GENERATORS

Sound radiation from vibrating bodies, noting errors in Lighthill conclusion 02 p0282 A69-12800

Anomalous infrasonic signals observed during launching of space vehicles with thrust greater than 200,000 lb, noting supersonic and subsonic group velocity spreads 07 p1078 A69-18853

Analytical model of spoiler generated sound in jet pipe, presenting data on level, spectrum and directivity of sound 07 p1183 A69-19462

Acoustic energy generation for helium rich stars, discussing X ray radiation from helium star corona 08 p1380 A69-20645

Broadband sound field generated aerodynamically by relatively smooth disk rotating in own plane, noting turbulent boundary layer flow and surface roughness effect 09 p1539 A69-21718

Turbulent boundary layer sound emission effect on elastic plate, discussing pressure pulsation spectrum reflection 13 p2246 A69-27538

Rolls Royce noise and compressor test facility for continual lowering of engine sound pressure levels, considering sound generating mechanisms 13 p2240 A69-27616

Monograph on sound generation by turbulence and surfaces in arbitrary motion, discussing sound and multipole fields and governing equations 13 p2247 A69-27974

Acoustic power transferred to plane homogeneous elastic structures and cylindrical shells by neighboring sound sources 13 p2363 A69-28186

Sound generation by unsteady rotational flow as singular perturbation problem solved by matched asymptotic expansions, discussing flow and radiation fields 13 p2299 A69-28187

Vibration/acoustics environmental testing, discussing advantages of digital computer control system and digital noise generation techniques 15 p2586 A69-30387

Vibration/acoustics digitally controlled environmental testing, describing configuration and operation of control system and statistical requirements for noise generation 15 p2587 A69-30388

Acoustic fluidic sensor /sonicell/ combining sonic generator based on edgetone principles with sensor dependent on laminar stream acoustic disturbance 15 p2616 A69-31302

Turbulent boundary layer sound emission effect on elastic plate, discussing pressure pulsation spectrum reflection 20 p3518 A69-38204

SOUND INTENSITY

Intense transverse resonant acoustic field interaction with viscous fluid flows [ASME PAPER 68-WA/FE-8] 05 p0748 A69-16091

Intense transverse resonant acoustic field interaction with viscous fluid flows [ASME PAPER 68-WA/FE-8] 14 p2430 A69-29444

Helicopter rotor vortex noise data analyzed for noise suppression, obtaining sound power equations 17 p2896 A69-34034

Sound evoked DC changes on intact skull of adult humans using data from AgCl electrodes, investigating intensity function, analyzing data by computer 23 p4098 A69-42101

SOUND MEASUREMENT

U ACOUSTIC MEASUREMENTS

SOUND PERCEPTION

U AUDITORY PERCEPTION

SOUND PRESSURE

Rotating spectral and spatial sound pressure distribution in propeller duct calculated on basis of propulsion quantities, noting effect of tip clearance 04 p0544 A69-14867

Fast visual task performance indoors found dependent on sound pressure level 15 p2550 A69-30305

Acoustic pumping system for propellant control at zero gravity, describing system operation by hydraulic analogy for liquid sloshing prevention 20 p3548 A69-37294

Acoustic field due to jet aircraft in motion, describing convection parameter modification in generalized sound pressure equation 20 p3462 A69-37757

SOUND PROPAGATION

NT VOICE

Kinetic theory of sound propagation in rarefied gas using generalized orthogonal polynomial expansion, evaluating adequacy of nonequilibrium distribution postulated by Mintzer 03 p0466 A69-13156

Cylindrical sound pulse propagation in homogeneous layer under inhomogeneous half space 04 p0630 A69-14531

Monochromatic flexural waves passage through elastic insert between plates, determining wave absorptivity dependence on wave frequency 04 p0679 A69-14906

Equations for electron scattering by sound in n-type semiconductors, giving corrections to sound propagation velocity during interactions 07 p1199 A69-18680

Anomalous infrasonic signals observed during launching of space vehicles with thrust greater than 200,000 lb, noting supersonic and subsonic group velocity spreads 07 p1078 A69-18853

Acoustic holographic measurement of surface deformation generated by sound waves impinging on gas-liquid interface, discussing acoustic amplitude components 10 p1695 A69-23542

Plane wave solutions for acoustic propagation in polyatomic gas by using Sirovich-Thurber method for polyatomic kinetic models 11 p1920 A69-24287

Monochromatic flexural waves passage through elastic insert between plates, determining wave absorptivity dependence on wave frequency 12 p2182 A69-26659

Dissipative fluid sphere motion due to impulsive point source calculated by finite difference scheme, assuming Voigt and Maxwell type internal friction mechanisms limitations 14 p2485 A69-29026

Discrete sound radiation theory considering rotational noise as dominant rotor noise and stressing fluctuating forces as typical of helicopter rotor 18 p3090 A69-34323

Ion density, electric field and electron temperature responses to gas density perturbation calculated for acoustic wave propagation in gas discharge using hydrodynamic equations 20 p3578 A69-38243

Superluminal group velocities in relation to causality axion, considering sound propagation in ultradense matter and particles of imaginary mass /tachyons/ 21 p3769 A69-38543

SOUND RANGING

Waveguide arc location by sound ranging to determine RF breakdown onset in high power microwave system, describing experiment determining feasibility 04 p0576 A69-14762

SOUND TRANSDUCERS

NT ELECTROACOUSTIC TRANSDUCERS

NT HYDROPHONES

Vibrational characteristics of sonar transducer analyzed by optical holographic interferometry 04 p0598 A69-14871

Acoustic bulk-surface wave transducer for shear or longitudinal wave transformation in nonpiezoelectric material at HF 15 p2607 A69-30167

Acoustic fluidic sensor /sonicell/ combining sonic generator based on edgetone principles with sensor dependent on laminar stream acoustic disturbance 15 p2616 A69-31302

SOUND TRANSMISSION

NT TELEPHONY

Acoustic and electromagnetic energy propagation in lower ionosphere and atmosphere for energy pulse generation by chemical explosion 07 p1078 A69-18844

Sonic transmission of diatomic nitrogen during nozzle flow, presenting density dependence of natural oscillation energies and temperature 10 p1632 A69-22912

Atmospheric LF and HF sound transmission anomalies, discussing Tyndall paradox for fog signals propagation over ocean 13 p2301 A69-28666

Weak shock wave structure in temperature relaxation media determined using theory of sound absorption in fluids 19 p3301 A69-36842

Frequency and space averaging effect on variability and standard deviation of multimode media transmission responses, with application to reverberant media 23 p4115 A69-41576

SOUND VELOCITY

U ACOUSTIC VELOCITY

SOUND WAVES

NT AERODYNAMIC NOISE

NT AIRCRAFT NOISE

NT ELECTROACOUSTIC WAVES

NT ENGINE NOISE

NT JET AIRCRAFT NOISE

NT LAMB WAVES

NT NOISE [SOUND]

NT SONIC BOOMS

NT THERMAL NOISE

Electrostatic polarization field formation by acoustic wave propagation through ionosphere, calculating effect on ionization drift velocity 01 p0068 A69-11110

Ion acoustic wave dispersion in highly ionized Ar plasma in longitudinal magnetic field, noting effects of several phenomena 01 p0133 A69-11216

Standing ion-acoustic wave excitation in weakly ionized plasma, noting isothermal compression of electron gas 02 p0292 A69-12555

Acoustoelectric domains in CdS, making time evolution visible by means of modified optical strain birefringence and stroboscopic illumination 02 p0258 A69-12618

Sound radiation from vibrating bodies, noting errors in Lighthill conclusion 02 p0282 A69-12800

Linear wave interaction with oblique shock waves, noting dependence of transmission, reflection and generation coefficients on Mach number 03 p0414 A69-13137

Electron fluid compression coefficient from simultaneous measurement and correlation of absolute magnitudes of ion acoustic wave potential and accompanying plasma density perturbation 03 p0475 A69-13148

Kinetic theory of sound propagation in rarefied gas using generalized orthogonal polynomial expansion, evaluating adequacy of nonequilibrium distribution postulated by Mintzer 03 p0466 A69-13156

Planetary long waves behavior in atmospheric models, explaining unsteady components by means of filtered equations 03 p0459 A69-13274

Infrasonic waves recordings from Saturn 5 vehicle, observing signal reversal occurrence 03 p0509 A69-13358

Acoustic wave fluctuations in semiconductors in external electromagnetic field, applying conduction electron and lattice elasticity kinetic equations
03 p0491 A69-14054

Submerged rigid circular cylinder displacement under influence of plane acoustic pressure wave solved by operational method
04 p0667 A69-14261

Long distance propagation of acoustic gravity waves ducted in thermosphere, noting effect of seasonal variations in polar region
04 p0595 A69-15437

HF plane sound waves in ideal gases with internal dissipation, considering particular applications to dissociating diatomic and vibrational relaxing gases
05 p0792 A69-15723

Acoustic holograms, describing electronic method of reconstructing holographic image in order to avoid multiple image problem
06 p0923 A69-16933

Longitudinal acoustic waves propagation in partially ionized gas in external electric field, taking into account ionic collisions with electrons and neutral particles
06 p0963 A69-17079

Time averaged optical holographic interferometry of standing longitudinal acoustic waves in square cross section duct
06 p0923 A69-17150

Spatial distribution of vertically moving ionized formations in ionosphere suggests acoustic gravity waves excited in polar regions as cause
06 p0922 A69-17749

Solar spectral line profiles for photosphere disturbed by short period acoustic waves
07 p1217 A69-19239

Elastic constants of composite materials by dispersion relation of sound waves for long wavelength, assuming periodicity in three dimensional rectangular lattice
07 p1236 A69-19457

Acoustic emission from welds in stainless steel plates used for detecting defects in single and multiple pass machine welds
08 p1318 A69-19963

Landau damping of long wavelength ion acoustic waves in collision-free one dimensional plasma with gravity field
08 p1359 A69-19983

Ion-acoustic wave excitation in plasma layer affected by relatively smooth disk rotating in own plane, noting turbulent propagation layer flow and surface roughness effect
08 p1370 A69-21025

Charged particles concentration change during vertical propagation of acoustic wave in F layer found transforming electric field into circularly polarized wave
09 p1484 A69-21528

Broadband sound field generated aerodynamically by relatively smooth disk rotating in own plane, noting turbulent propagation layer flow and surface roughness effect
09 p1539 A69-21718

Holographic technique application to radio and sound wave ranges, discussing incoherent holography development to overcome difficulties in image reconstruction of stationary objects
09 p1498 A69-22133

Acoustic waves pressure field micropulsations in turbulent fluid, analyzing space-time spectrum
09 p1492 A69-22710

Combination backscattering on ionic sound waves assumed responsible for unexpected features of radio signals reflected from sun
10 p1776 A69-23219

Magnetoionic formulas similarity in ionospheric radio propagation and atmospheric acoustic gravity wave propagation above electron gyrofrequency
10 p1655 A69-23419

Microwave frequency room temperature acoustic surface wave propagation losses in lithium niobate measured by laser light deflection, discussing propagation and insertion losses
10 p1703 A69-23511

Acoustical transparencies illuminated by sound waves for optical imaging and ultrasonic diffraction, noting application to visualization of inhomogeneities in samples
10 p1695 A69-23546

Acoustic wave amplification and generation in piezoelectric semiconductors and semimetals by super-sonic carrier drift currents
11 p1926 A69-24641

Sound field generation by isotropic turbulence through finite strength shock, estimating acoustic energy flux from supersonic jet containing shock waves
11 p1872 A69-25130

Unstable ion sound wave propagation across magnetic field in collisionless shock waves, noting drift instability
11 p1930 A69-25273

Acoustic frequency of longitudinal self oscillations during vibrational fuel combustion in afterburner, taking into account nonlinear properties of heat supply zone
11 p2002 A69-25339

Multiple information storage in sampled hologram in space division multiplexing holography, constructing hologram with sound waves and reconstructing images with laser light
12 p2079 A69-25921

Acoustic wave generation in neutral particle component of weakly ionized gas by variation of electron temperature with low power RF signal
12 p2134 A69-26096

Acoustic waves in ionosphere relation to electron content fluctuations detected from beacon satellite BE-B signals
12 p2065 A69-26104

Velocity dependence of temperature waves /second sound/ in liquid He II measured as function of relative velocity for normal and superfluid
13 p2297 A69-27460

Planetary long waves behavior in atmospheric models, explaining unsteady components by means of filtered equations
14 p2472 A69-28782

VHF surface acoustoelectric amplifier investigated in DC drift field using composite spatially adjacent structure of lithium niobate and silicon film
14 p2422 A69-29559

Moving striations relations to ion acoustic waves in DC discharge in neon at various pressures, discharge currents and measurement excitation modes
14 p2494 A69-29695

Standing ion-acoustic wave excitation in weakly ionized plasma, noting isothermal compression of electron gas
15 p2658 A69-30252

Substitute kernel approximation for acoustic waves radiative transfer equations for nongray gas near equilibrium
15 p2717 A69-30791

Steady oscillations of active nonlinear system of nonisothermal plasma and charged particle flux, noting steady ion-acoustic waves
15 p2662 A69-30947

Ion-acoustic oscillations effect on weakly ionized plasma electrical conductivity, using BGK collision integral model
15 p2662 A69-30970

Disturbance currents from penetration of acoustic waves in weakly ionized gas, analyzing wave interaction with DC glow discharge
15 p2665 A69-31547

Single particle and collective excitations of plasmas in solids and interactions with acoustic and electromagnetic waves in magnetic field
16 p2821 A69-31820

Discrete layers criterion for multilayer approximation to real atmosphere in acoustic gravity wave propagation
16 p2774 A69-31980

Discharge parameters modulation caused by acoustic wave propagating in partially ionized plasma, deriving perturbation current density and irradiated light intensity
16 p2752 A69-32364

Acoustic waves pressure field micropulsations in turbulent fluid, analyzing space-time spectrum
16 p2782 A69-32489

Charged particles concentration change during vertical propagation of acoustic wave in F layer found transforming electric field into circularly polarized wave
16 p2783 A69-32523

Decimeter waves Doppler shift shown inversely proportional to wave frequency from electron density variation caused by acoustic wave propagation in ionosphere
16 p2755 A69-32610

Shear layer effect on plane sound waves, discussing reflection and refraction at velocity discontinuity between two regions of fluid
17 p3005 A69-32954

Sound effects on turbulent flame in gasoline-air mixture jet in Toeppler device with pulsed light source, measuring ionization in combustion zone
17 p3069 A69-33141

Electronically tunable lithium niobate optical filter utilizing collinear acousto-optic diffraction in anisotropic medium
17 p2943 A69-34157

Elastic circular cylindrical panel behavior in fluid with acoustic shock wave, allowing for propagation waviness of elastic stresses
18 p3216 A69-34579

Acoustic gravity waves generated in isothermal atmosphere by ground energy source calculated using stationary phase method and kinematic theory
18 p3129 A69-34953

Atmospheric whistlers and ion acoustic waves interaction in nonisothermal plasma, determining damping frequencies, decrements and wave polarization
18 p3180 A69-35024

Acoustic wave fluctuations in semiconductors in external electromagnetic field, applying conduction electron and lattice elasticity kinetic equations
18 p3182 A69-35047

Fluid-shell interactions, using piston theory and cylindrical-wave approximations
18 p3223 A69-35174

Scanned receiver acoustical holography for mapping or imaging sources of radiated acoustic energy on complex vibrator in water, noting application in air
20 p3576 A69-37323

Parametric excitation theory involving Langmuir and ion-acoustic waves for homogeneous plasma slab with specular particle reflection at slab walls
20 p3582 A69-38245

Acoustoclastic interaction effects of sonic bangs on natural frequencies response of large windows backed by closed cavity
21 p3836 A69-38988

Small amplitude acoustic waves propagating in compressible fluid with parallel shear flow and within constant gravitational field
21 p3772 A69-39241

Stellar atmospheres acoustic energy generation rate calculations, studying corona mass ejection effects on stellar rotation
21 p3813 A69-39521

Coronae around helium stars and X ray sources, calculating acoustic energy generation rates in convection zones
21 p3813 A69-39522

Coupled acoustic and spiral EM waves drift instabilities in bounded plasma of solid body found to be convective
21 p3782 A69-39556

Collisionless damping of large amplitude ion acoustic waves excited externally in thermally ionized Cs plasma
22 p3991 A69-41008

Acoustical ray tracing in horizontally layered and vertically sectioned atmosphere on digital computer using shifting Cartesian coordinate system
23 p4154 A69-41532

Acoustic gravity waves propagation over spherical earth with isothermal windless atmosphere, determining pressure perturbations
23 p4158 A69-42175

Stimulated Brillouin scattering application to measurement of hypersonic velocities and absorption in gigahertz frequency range, laser frequency shifting and Q switching, etc
23 p4167 A69-42183

Acoustical holography principles and reconstruction techniques, noting advantages of liquid-surface and temporal reference holography over optical counterpart
23 p4167 A69-42199

Optimal focusing of acoustic system for tube defectoscopy with circular normal waves
24 p4296 A69-42655

SOUNDERS

U SOUNDING

SOUNDING

NT BALLOON SOUNDING

NT IONOSPHERIC SOUNDING

NT ROCKET SOUNDING

Monograph on method and results of measurements of mobilities spectrum ion density and conductivity in upper troposphere and stratosphere
11 p1877 A69-24636

SOUNDING ROCKETS

NT AEROBEE ROCKET VEHICLE

NT BLACK BRANT 2 SOUNDING ROCKET

NT KAPPA ROCKET VEHICLES

NT SKUA ROCKET VEHICLES

NT SKYLARK ROCKET VEHICLE

Paraglider as recoverable sounding rocket dropped from helicopter, describing system design and flight tests
[UN PAPER 68-95445]

01 p0161 A69-10465

Meteorological rocket soundings and global synoptic observations, noting influence of atmospheric middle region
[UN PAPER 68-95405] 01 p0109 A69-10484

Japanese space research organizations, sounding rockets, meteorology, satellite communications, geodesy, etc
[UN PAPER 68-95563] 01 p0151 A69-10501

Destructible low cost meteorological sounding rocket Dart for global observation of upper atmosphere
[UN PAPER 68-95467] 01 p0161 A69-10510

Meteorological rocket measurement of ionizing radiation flux in upper atmosphere, noting flux decrease with increasing electron energy
01 p0144 A69-10586

Soviet studies of ionospheric electron densities by means of geophysical rockets and satellites
01 p0067 A69-10944

Balloon, rocket probe and satellite payloads, noting French contributions and CNES role
02 p0333 A69-11914

French /LRBA, ONERA and Sud-Aviation/ sounding rocket design emphasizing meteorological rockets and standard equipment
02 p0333 A69-11916

Canadian program of scientific rocket sounding of auroral phenomena, outlining systems approach, engineering and scientific cooperation requirements, etc
02 p0335 A69-12689

Astronomical alignment accuracy by rocket Casiopeia system, discussing scientific payload rotation and orientation by celestial bodies
03 p0462 A69-12850

French solid propellant sounding rockets proposed launching from Guiana base using different fuel propulsion systems
03 p0518 A69-12851

Alignment of rocket-borne instrument with sun, discussing mechanical system design, servocontrol and silicon photodiode sensors
03 p0427 A69-12980

European space research program, discussing government, science and industry in developing satellites and sounding rockets
03 p0520 A69-13584

Lower thermosphere composition over New Mexico, discussing rocket flight mass spectrometer measurements during summer 1967
03 p0425 A69-14009

Hybrid electropneumatic and electrohydraulic servosystem for actuation of gas jet nozzles of sounding rocket automatic pointing system
04 p0550 A69-15182

Fluidic proportional thruster system for sounding rocket control
[ASME PAPER 68-WA/FE-32] 05 p0763 A69-16105

Suborbital probes, discussing UK sounding rockets Skylark, Petrel and Skua configurations, capabilities and performances
06 p1012 A69-16859

Meteorological rockets for space meteorology, aeronomy and weather forecasting, noting international programs involving U.S.S.R.
06 p1043 A69-17056

Interamerican Experimental Network of Meteorological Investigation with Rockets/EXAMET-NET/, discussing atmospheric parameters measurement at high altitude
[UN PAPER 68-95903] 06 p0950 A69-17062

Australian sounding rocket programs carried out in conjunction with U.S. satellite experiments
[UN PAPER 68-95214] 06 p1013 A69-17076

Separable payload control for three axis orientation of sounding rocket instruments, discussing error sensors and pointing accuracies
06 p1014 A69-17583

Rocket transportation for upper atmospheric measurements, discussing sensors and cost effectiveness
[AIAA PAPER 69-159] 06 p1018 A69-18066

Trajectory calculation of unguided meteorological rocket by digital computers and by equations of motion, discussing wind influence on ceiling and horizontal ranges
08 p1409 A69-20457

Macaque monkeys in weightless state on sounding rocket, noting vigilance level and characteristics
09 p1445 A69-22724

Rocket motors for ejection of instruments from sounding rocket payloads, considering powder cartridges and solid propellant motor characteristics
10 p1635 A69-23032

Meteorological rocket probes in Spain for wind and temperature measurements, including stratospheric circulation data
11 p1877 A69-24519

European space research program, discussing government, science and industry in developing satellites and sounding rockets
11 p1966 A69-25102

Second tacite sounding rocket test for measuring UV radiation in transition zone between upper ionosphere and space
11 p1887 A69-25213

European Space Research Organization projects including satellites and sounding rocket launchings for various missions
12 p2175 A69-26922

Meteorological rocket measurement of ionizing radiation flux in upper atmosphere, noting flux decrease with increasing electron energy
15 p2675 A69-30756

Hybrid motor in sounding rocket using amino plastic as fuel and nitric acid as oxidizer, discussing advantages in cost, handling, thrust, performance, etc
16 p2835 A69-31744

ASTRID high altitude sounding rockets orientation system aligning payload cones to target outside earth atmosphere, discussing software simulation with analog and digital computers, etc
17 p3001 A69-33424

Fluidic attitude control systems performance prediction from conventional control analysis emphasizing steady state positioning accuracy
17 p2904 A69-34069

Sounding rocket S band telemetry antenna operation, proposing quasi-isotropic pattern criterion to reduce effects of shadowing and interference
19 p3271 A69-36252

Cassiopee device for spacecraft or sounding rocket attitude control, describing gyroscopic control unit, sensor element and jet control devices
[ONERA-TP-707] 19 p3432 A69-36686

Sounding rocket aerodynamic stability as function of nose length and mass, discussing wind tunnel test data
19 p3432 A69-36761

Auroral sounding rocket research and instrumentation in Scandinavia, discussing auroral particles, optical measurements, probe experiments and scientific objectives
20 p3542 A69-37794

Japanese meteorological sounding rocket for atmospheric temperature and wind from 60 km down to balloon observation level, discussing principles and payload separation
20 p3543 A69-37795

Mesospheric wind measurement by meteorological rockets based on radar determination of drift trajectories of chaff clouds
20 p3529 A69-37797

Magnetically focused electronographic image converters for far UV photography and spectroscopy from sounding rockets, discussing stellar observations
20 p3543 A69-37801

VLF electric and magnetic fields observed in auroral zone with Javelin 8.46 sounding rocket, noting HF electrostatic noise bursts
20 p3533 A69-38080

Air launched sounding rockets design, development and testing noting aerodynamic loading and surface, propulsion unit, cost effectiveness, etc
21 p3820 A69-39218

Recovery system for high altitude sounding rocket payloads, noting air inflated flotation device, payload separation and parachute deployment
[AIAA PAPER 68-959] 21 p3820 A69-39227

Antenna reactance from sounding rocket in ionosphere, showing variations relationship to rocket spin period
22 p3934 A69-39964

Thrust optimization for sounding rocket to reach maximum altitude with given initial and propellant weight, using polygonal time function and multiple-parameter numerical technique
22 p4037 A69-41050

IBM 360-50 computer with I/O terminals to process PCM and analog data from Modular Auroral Probe series of sounding rockets on real time basis
23 p4133 A69-41764

Sounding rocket measurements of electric and magnetic fields near auroral electrojet
24 p4310 A69-43188

SOUTH AMERICA

Educational TV coverage extension via synchronous satellites to areas of limited coverage, emphasizing South American countries
19 p3268 A69-36163

SOUTHERN HEMISPHERE NT ANTARCTIC REGIONS

Meteorological satellite observations value to Southern Hemisphere
[UN PAPER 68-95213] 01 p0109 A69-10513

Meteorological observations of Mars northern polar cap and Southern Hemisphere from northern summer solstice to early autumn
05 p0825 A69-16302

Atmospheric wind velocity in Northern and Southern Hemisphere, noting increase with height
06 p0921 A69-17747

Southern Hemisphere galactic H II regions continuum thermal radiation at 6 cm, noting maps for 28 of 36 sources, peak temperatures and emission and half intensity widths
07 p1206 A69-19271

Cosmic radio noise brightness distribution in Southern Hemisphere at 10.02 MHz, noting spectra of sources observed
07 p1206 A69-19272

Cosmic gamma radiation with energies above 100 Mev in southern sky, discussing results of balloon-borne spark chamber flight
08 p1377 A69-19787

Aerial chronophotography of Southern Hemisphere conducted on around world polar flight analyzed for meteorological and geographical aspects and compared with satellite data
09 p1534 A69-21405

Absolute flux density of five radio sources and relative flux densities of 37 sources defining absolute flux density scale for Southern Hemisphere
10 p1772 A69-22857

Tropospheric zonal wind semiannual oscillations in Southern Hemisphere tropics with westerly maxima and easterly minima in May and November
12 p2064 A69-26011

Spiral galaxies with connectors observed in Southern Hemisphere, noting galactic nuclei differences and nucleus relation to galaxy morphological type
12 p2165 A69-27030

Blocking processes synchronous development involving atmospheric circulation disturbances in Northern and Southern Hemispheres, noting localization in Pacific and Atlantic oceans
13 p2292 A69-27840

Temperatures and geopotentials of isobaric surfaces in Northern and Southern Hemispheres compared for summer and winter seasons
14 p2473 A69-29724

Troposphere behavior and stratosphere structure over Southern Hemisphere based on rocket measurements, comparing hemispheric atmospheric circulation intensities
14 p2477 A69-29832

Secular fluctuations of atmospheric circulation over Northern Hemisphere analyzed using isobaric and composite-kinematic surface maps, discussing analogies with Southern Hemisphere
14 p2478 A69-29836

Southern Milky Way spectral survey for selection, classification and photometry of interesting objects
17 p3031 A69-33101

Zonal winds in temperate latitude analyzed as function of latitude and month from GHOST balloon flights in Southern Hemisphere at 200 mb
17 p2997 A69-33163

Zonal flow intensity, velocity and kinetic energy of standing and traveling waves compared for Northern and Southern Hemispheres
17 p2997 A69-33392

F 2 region critical frequencies obtained during winter at Northern and Southern Hemisphere stations located in auroral and polar zones, correlating changes with ionization
20 p3526 A69-37665

F 2 layer seasonal anomaly, discussing global distribution observed by network of ionospheric stations
20 p3526 A69-37666

Long term computer produced multiple image satellite photomosaics for Southern Hemisphere, analyzing circulation, meridional bands, polar ice, cloud cover variations, etc
22 p3977 A69-40733

SOVEREIGNTY

1967 space Treaty Article 11, discussing provisions concerning private exploitation and supernatural body authority
20 p3635 A69-37107

SOYBEANS

Rats on casein, soybean and Chlorella diets for protein source noting soybean diet produced no appreciable changes in intestinal flora
02 p0197 A69-11490

SOYUZ SPACECRAFT

Soviet space program /1969/ objectives, Soyuz vehicle and future missions

06 p1002 A69-17265

Upper atmosphere and outer space investigations by Zond and Soyuz spacecraft

15 p2724 A69-31451

SPACE BIOLOGY

U EXOBIOLOGY

SPACE BUSES

U FERRY SPACECRAFT

SPACE CAPSULES

NT ESCAPE CAPSULES

NT MERCURY SPACECRAFT

Mars capsule feasibility model terminal dry heat thermal sterilization cycle determined from microbial data

02 p1201 A69-11772

Design of interface between Mariner Mars spacecraft and Mars planetary entry/landing capsule [AIAA PAPER 68-1162]

03 p0521 A69-13671

Chemical reaction between combustible solid fuel surface and oxidizer-containing gas in space capsule

16 p2877 A69-31896

Sterilized solid propellant motors applicability to planetary landing capsule spin stabilization [AIAA PAPER 69-823]

16 p2840 A69-32675

Thermal control of Mars entry capsule with fiberglass honeycomb sandwich shell analyzed with and without aft thermal curtain, emphasizing cruise-flight phase

[AIAA PAPER 68-1082]

19 p3429 A69-35949

SPACE CHARGE

Silicon p-n junction avalanche current temperature dependence calculation by considering space charge current and multiplication factor as function of temperature

01 p0136 A69-10245

Space charge limited currents in SbSI single crystals with gallium electrodes during phase transition, discussing sticking probability and photoconductivity

01 p0137 A69-10258

Limited space-charge accumulation mode efficiency for gallium-arsenide diodes, taking into account electron-lattice relaxation processes

01 p0137 A69-10321

Space charge limited operation of insulated gate field effect transistors, discussing maximum transconductance and minimum parasitic capacitances

01 p0402 A69-10322

Klystron bunching analysis, adding electron overtaking formulation to existing nonlinear space-charge wave theory

02 p0215 A69-11939

Cavity excitation and support of limited space-charge accumulation mode oscillations in n-GaAs epitaxial diode

02 p0297 A69-11940

Fundamental microwave oscillations at high frequencies in GaAs epitaxial sandwich layers, using space charge growth control

02 p0297 A69-11941

Nonisothermal space charge wave analysis of transit time mode oscillations in bulk GaAs, studying device reactance at given negative resistance

02 p0299 A69-12240

Scanning electron beam display of space charge of defects and junction behavior of edge dislocation array in Ge and Si monocrystals

02 p0301 A69-12661

Transit time effects in Si n-nu-n space charge limited current solid state devices

03 p0483 A69-12852

Microwave energy generation with solid state equipment, noting Gunn effect diodes, avalanche diodes and limited space charge accumulation/LSA/ devices

03 p0402 A69-12971

Diffusion in conduction process in dielectric fluids, discussing space charge limited current-voltage characteristics

03 p0415 A69-13140

Generation of UHF space charge waves by nonlinear interaction of two microwave signals in magnetoplasma, predicting optical mixing

03 p0475 A69-13146

Space charge limited square law diodes as HF mixers, noting low conversion loss of asymmetrical type

03 p0404 A69-13580

Carrier generation-recombination in space charge region of asymmetrical p-n junction, noting experimental results for InSb diodes

03 p0487 A69-13641

Space charge layer thickness determination in plasma filled capacitor by capacitance measurement, noting thickness dependence on plasma potential

03 p0477 A69-13714

Space charge plasma acceleration in axially nonuniform magnetic field

03 p0477 A69-13760

Nonlinear cross sectional space charge density distribution in electron beam of traveling wave tube

03 p0407 A69-13984

Hybrid Gunn domain and LSA mode operation in oversized bulk and epitaxially grown GaAs, noting large signal impedance data

04 p0639 A69-14339

Aircraft charge measurements in stratus clouds, noting charge sign is independent of cloud space charge

04 p0549 A69-15108

Potential gradient, small ion density and space charge density measurements for atmosphere on Atlantic Ocean during 1965

04 p0594 A69-15159

Electron bunching improvement by combined effect of space charge and inhomogeneous electrostatic field on velocity modulated electron flux in microwave devices

05 p0799 A69-15646

Equivalent capacitance derivation of space charge limited current from filamentary cathode

05 p0734 A69-16567

Limited space charge accumulation/LSA/ oscillations in GaAs, noting frequency independent power interrelationships

05 p0810 A69-16568

Static problem of electric field intensity and space charge density distribution in semiconductor with hot electrons and holes

06 p0978 A69-16989

Immobile space charge in MOS semiconductors as function of external voltage

06 p0979 A69-17153

Rates of charging of thermionically emitting particles in space charge

06 p1035 A69-17928

Electrostatic field strength and conductivity dependence of expansion and contraction of space charge cloud in process of discharging during static electrification

06 p0959 A69-18219

Wall space charge layer effect on ion extraction from weakly ionized plasma, using quadrupole mass spectrometer

07 p1188 A69-18276

Traveling wave amplifiers beam defocusing by RF circuits and space charge fields under large signal operating conditions, discussing magnetic field strength

07 p1094 A69-18424

Current and voltage waveforms of transit time, resonant domain and LSA modes of operation of transferred-electron oscillators

07 p1097 A69-18443

Pulse power from X band LSA devices at centimeter through millimeter wavelengths

07 p1097 A69-18445

Domain oscillations removal in n-type gallium arsenides by externally applied microwave field, noting doping effect on LSA conversion efficiency

07 p1196 A69-18446

Minority carrier distribution in doped semiconductors space-charge layer assuming relation between diffusion and Debye length

07 p1198 A69-18506

Field effect in Ge and Si, noting relation between dependence of space charge on surface level charge and on surface potential

07 p1199 A69-18682

Analytic integration of Langmuir equation for spherical space charge flow obtained in terms of Airy equation or Bessel functions solution

07 p1115 A69-18864

Ionizing radiation effects on space charge of MOS devices, showing electron-hole pairs within oxide and electron injection from cathode

08 p1373 A69-20864

Space charge sheath electric thruster principles, construction and performance using laboratory test model [AIAA PAPER 69-282]

09 p1563 A69-21235

Finite ion mass effect on stability of space charge neutralized electron beam

09 p1545 A69-21342

Selenium diffusion in indium antimonide, determining concentration gradients in junction space charge region by capacitance method

09 p1554 A69-21469

Energy distribution in electron gun with single crystal spherical cathode, noting work function, space charge cloud and beam overlapping effects

09 p1464 A69-22396

Space charge limited currents in SbSI single crystals with gallium electrodes during phase transition, discussing sticking probability and photoconductivity

09 p1559 A69-22651

Positive space charge buildup produced in silicon dioxide by low energy electrons as function of beam energy and oxide thickness

10 p1743 A69-23172

Breakdown voltage and avalanche drift instability factors in planar passivated p-n junctions as function of oxide thickness and mobile charge

10 p1743 A69-23174

Transmission line analogs and kinetic power theorems for space charge waves amplification in semiconductors, considering internal effect and wave excitation

10 p1748 A69-24052

Space charge waves amplification in semiconductors on coupling with forward circuit wave by transmission line analog, noting application to electromagnetic and acoustic waves

10 p1748 A69-24053

Coupling constants of fast space charge waves in three frequency parametric TWT amplifier and of stress waves in slow wave structure, using graphical methods

11 p1844 A69-24446

Unrippled space-charge flow in dense axially symmetric electron beams as basis for electron gun design

11 p1846 A69-24598

Electrical conductivity of space charge surface layer in semiconductors with many-valley energy spectra of current carriers, discussing scalar relaxation time

11 p1937 A69-24915

Voltage and current waveforms of resonant domain and limited space charge accumulation modes in transferred electron oscillators, noting drift current

12 p2036 A69-25908

Paraxial electron beams from Pierce gun and spreading due to thermal velocities and space charge in nonuniform potential

12 p2036 A69-25920

Negative resistance effects computed for HF operation of SCL diodes, based on quantitative analysis of small signal response

12 p2038 A69-26349

Atmospheric electricity and space charges ionization and equilibrium in earth atmosphere, discussing electric fields in lower atmosphere, ionosphere and magnetosphere

12 p2076 A69-27105

Near electrode layer calculation in low temperature plasma, solving kinetic ion equation for quasi-neutral and Poisson equation for space charge regions

13 p2312 A69-28117

Rasor phenomenological theory of space ionization in arc mode regime of Cs thermionic converter

14 p2402 A69-29242

Cesium plasma electron temperature in narrow electrode space of thermionic converter determined using electrode and changeable space diode

14 p2491 A69-29243

Noble gas thermionic converters, discussing auxiliary discharge compensation of negative space charge, I-V characteristics, efficiency and comparison to ignited mode cesium vapor converter

14 p2403 A69-29249

Ionization mechanisms in ignited mode cesium thermionic converter, discussing positive ions production for electron space charge neutralization and ion density calculations

14 p2404 A69-29258

Radiation effects on Cs thermionic converter, discussing radiation interaction with alkaline atoms to complete space charge neutralization by supplementary ion creation

14 p2404 A69-29261

Injection phase-locking characteristics of LSA/limited space charge accumulation/ mode transferred-electron diode oscillators, employing negative conductance and equivalent circuit

14 p2421 A69-29544

Space charge effects on trigger current and reflector voltages of reflex klystron

15 p2574 A69-30131

Transit time effects in silicon space charge limited diodes, studying frequency characteristics of small signal equivalent circuit

15 p2575 A69-30181

Space charge formation in MHD generator channels ascribed to gas parameters nonuniformity and magnetic induction vector presence, assuming steady flow
15 p2659 A69-30635

Selenium diffusion in indium antimonide, determining concentration gradients in junction space charge region by capacitance method
15 p2669 A69-30714

High temperature effects on electron and X ray irradiated MOS transistors for space charge analysis and defects in silica films
15 p2625 A69-30828

Integral charge neutrality effect on local space charge density of MHD generator channel, examining electrode couple for Faraday generators
15 p2664 A69-31055

Semiconductor technology including radar, Gunn and limited space charge accumulation oscillators, phase locked antennas, data processing and solid state computerization
15 p2581 A69-31521

Single balanced modulators using square law resistors /space charge limited diodes/, discussing noise properties, conversion losses and terminating conductance
16 p2758 A69-31756

Unsuccessful space charge noise suppression measurements on field emission tubes, obtaining diffusion and shot noise measurements at high currents
16 p2752 A69-32384

Electron bunching improvement by combined effect of space charge and inhomogeneous electrostatic field on velocity modulated electron flux in microwave devices
16 p2823 A69-32503

Electrostatically focused klystron /EFSK/ small signal gain calculations based on lens cell space charge wave analysis
18 p3109 A69-35294

Conducting medium steady one dimensional motions determined by assuming space charge-electric field interaction, considering electrohydrodynamic behavior of medium
18 p3181 A69-35315

Self consistent flow calculation in dense space charge beams, including electrode design for portions isolation
22 p3985 A69-40668

Space charge wave propagation induced by electron beam moving in annular waveguide, considering radiated field and current redistribution
23 p4124 A69-42034

SPACE COMMUNICATION
NT INTERPLANETARY COMMUNICATION
NT LUNAR COMMUNICATION
NT REENTRY COMMUNICATION
NT SPACECRAFT COMMUNICATION

Critical parameters for optimum design of Cassegrain antenna used in space communications
[UN PAPER 68-95280] 01 p0043 A69-10481

Space broadcasting possibilities and problems, considering home reception and group participation at community centers
[UN PAPER 68-95287] 01 p0028 A69-10497

Signal absorption in negative ionospheric ions effect on maximal frequency for space radio communication
[UN PAPER 68-95272] 01 p0029 A69-10529

Space age communication, use of satellites by mass media - UNESCO Conference, Paris, December 1965
03 p0534 A69-13132

Optical receivers for deep space optical communications link assuming PCM scheme
03 p0389 A69-13194

Coherent PSK system in multipath environment /Rician fading and additive Gaussian white noise/ with phase locked loop for coherent reference extraction
03 p0393 A69-13255

Bibliography of interstellar travel and communication
03 p0510 A69-13397

Noise reduction techniques in digital and analog data transmission over space program distances, emphasizing deep space missions
03 p0394 A69-13398

Man-made and natural spatial communications
03 p0394 A69-13577

Short wave bands for earth-space communications, considering propagation anomalies compensated systems and frequency bands availability
03 p0397 A69-13721

Millimeter waves in communication navigation and research, discussing radar range resolution and remote sensing
03 p0397 A69-13722

Graphical data on atmospheric and rainfall attenuation of spacecraft earth signal, emphasizing transmission via satellites
03 p0397 A69-13727

Analog FM subcarrier modulation selected for real time TV picture transmission via electro-optic space communication system
04 p0562 A69-15474

Low noise shaped beam Cassegrain antenna design for space communications earth station service, noting gain/noise temperature figure and antenna construction
05 p0728 A69-15669

Traveling wave maser and cooled parametric amplifier for ultralow noise preamplification in satellite communication earth terminal installations
05 p0728 A69-15670

Low noise room temperature satellite broadcast receiver for UHF, using room temperature parametric amplifiers
05 p0728 A69-15672

Radio channel circuit outlined for tracking interplanetary spacecraft and probes with signal delay time prediction
06 p0888 A69-17623

VHF space communication signals with radio fluctuations along propagation path through turbulent atmosphere, giving diversity reception effect when transmitting linearly polarized waves
06 p0889 A69-17653

Signal resolution during space diversity reception with nondirective or weakly directive antennas and noncorrelated receiver background noise, discussing signal processing
06 p0890 A69-17800

Multiring antenna arrays for space telemetry and communication, analyzing distant field, radiation resistance, directive gain and mutual impedance
06 p0899 A69-17827

Space communication, discussing global network of Intelsat satellites ground facilities, regional switching, RF channels, etc
06 p0890 A69-17860

High power microwave oscillator /carpitron/ for pure or FM signal amplification, noting low output noise level
07 p1096 A69-18437

Desired laser characteristics for space communications compared to existing lasers
07 p1146 A69-18483

Solar end and lateral pumping apparatus for neodymium doped YAG crystal lasers, noting applicability to space communication
07 p1150 A69-18953

Lincoln experimental satellites, discussing transition to UHF bands and orbital launching
07 p1087 A69-19630

Data transmission techniques for aerospace and industrial applications, discussing radio link
08 p1271 A69-19906

Local oscillator for space telecommunications F9 repeater, operating principles, design calculations and test results
08 p1286 A69-20596

RF selection for interspacecraft or earth-spacecraft communication
09 p1449 A69-21270

Communication satellite systems role in world telecommunication network, discussing traffic type, volume and routing, earth stations location and capacities and orbit selection
09 p1449 A69-21271

Frequency modulation methods and multiple access for communication satellite systems, considering bandwidth for space station transponder
09 p1449 A69-21274

Multiple access in communication satellite systems for achieving maximum flexibility of interconnection between earth stations
09 p1450 A69-21276

VHF space communication signals with radio fluctuations along propagation path through turbulent atmosphere, giving diversity reception effect when transmitting linearly polarized waves
10 p1775 A69-23191

Hardware limitations on communications, instrumentation and data handling for manned deep space missions
13 p2219 A69-27666

Synchronized backward wave oscillator transmitting tube for space communication stations
13 p2232 A69-28058

SPACE ELECTRIC ROCKET TESTS

Short term frequency stability measured for Doppler radar and space tracking communication applications, reviewing FM theory for spectral purity relationship
18 p3100 A69-34277

Optimum receiver design for binary coded data detection in two channel space communication system, discussing phase error distribution and optimum decision function
19 p3275 A69-36286

Block coded telemetry systems design for phase coherent space communication employing double conversion superheterodyne phase locked receivers
19 p3277 A69-36487

ITU space communication projects, discussing frequency registration, progress reports from member countries and committees, UN resolutions, communication satellites, etc
19 p3456 A69-36821

INTELSAT 1964 agreements consistency with multilateral international agreements, including UN General Assembly and International Telecommunication Union
20 p3638 A69-37122

International cooperation regarding space telecommunication systems, discussing INTEL-SAT and INTERSPUTNIK roles in achieving international coordination and equality
20 p3638 A69-37125

NASA program for radio spectrum utilization in aerospace communication systems
23 p4128 A69-42502

Space attenuation at VHF and UHF telemetry frequencies
24 p4281 A69-42622

Nonblocking switching networks operating in ordinary and in simultaneous switching regime, including control algorithms for optimal space communication
24 p4289 A69-43138

SPACE DEBRIS
Gegenschein measurements for determining upper limit on asteroidal debris spatial density
02 p0324 A69-12545

Spacecraft debris atmosphere effects on observations, discussing contamination of exposed optical surfaces and light scattering by ice particles from cabin water vapor leakage
09 p1487 A69-21654

Linearly polarized radiation from supernova remnants 3C 10, Taurus A, 3C 358 and Cassiopeia A, determining distributions by synthesizing fan beam
09 p1598 A69-22185

Integrodifferential equation derived and solved for evolution of collisional model of asteroids and debris
14 p2526 A69-29879

Space contamination due to manned vehicles and debris atmosphere effects on dim light source observations
21 p3793 A69-38341

Undulating dunelike deposits of surface debris similar to base-surge deposits in maar volcanoes and tuff rings, discussing underground ice existence
23 p4216 A69-42203

SPACE DENSITY
Statistical data on space density of bright elliptical galaxies, radio galaxies, quasars, noting relation between space density and age
12 p2165 A69-27033

Stellar densities and luminosity function determined from stellar data concerning sphere with 20 pc radius around sun
13 p2351 A69-27869

Density perturbation mode in Lifshitz relativistic theory for expanding universe gravitational instability, adopting Lagrangian coordinate condition to eliminate physically meaningless solution
15 p2652 A69-30203

Satellite measurements of small particles near-earth space density compared with chemical estimates of terrestrial cosmic material, suggesting particles origin in meteoroid ablation
21 p3701 A69-38342

SPACE ELECTRIC ROCKET TESTS
Emissive probes for measuring plasma potentials over different ion density ranges on SERT spacecraft, detailing calibration and mechanical and electronic configurations
[AIAA PAPER 69-272] 09 p1492 A69-21217

SERT 2 mercury vapor fed hollow cathode operated in bell jar, determining volt-ampere characteristics and flow rates for plasma diagnostics
[AIAA PAPER 69-258] 09 p1561 A69-21221

SERT 2 thruster system performance over expected mission parameters, noting operational lifetime excess over mission requirements
09 p1566 A69-21255

- Mercury electron bombardment thrusters, discussing mission, design, ground tests, components and thrust vectoring 12 p2148 A69-26787
- Kaufman ion thruster ESKA 18 operation principles and design compared to RIT 10 and SERT 2, discussing discharge and focusing characteristics and propulsion parameters 17 p3022 A69-33605
- Power conditioner for use with SERT II mercury ion thruster, describing electrical and mechanical design and operation 23 p4075 A69-42301
- SPACE ENVIRONMENT**
- U AEROSPACE ENVIRONMENTS**
- SPACE ENVIRONMENT SIMULATION**
- NT WEIGHTLESSNESS SIMULATION**
- Human behavior during stressed underground confinement, discussing adaptation processes 01 p0020 A69-10757
- Molecular flow in space simulation chambers with cryowalls, noting nonuniform flux density distribution 01 p0057 A69-11153
- Cryogenic plants for space simulation chambers, examining processes for cooling shroud below 100 K at given temperature differences 01 p0057 A69-11154
- Prolonged decompression stress effects on humans in simulated orbital flight or extravehicular activity, investigating endocrine-metabolic disturbance by urinalysis 01 p0022 A69-11336
- Human endocrine-metabolic response to sequential decompression exposure during simulated orbital flight or extravehicular activity 01 p0022 A69-11337
- Space simulation tests in TFS/Technological Feasibility Spacecraft/ program, discussing two interplanetary cruise modes and deorbit mode selected for simulation 02 p0227 A69-11757
- Work and rest scheduling effect on working capacity and physiological state of male subjects in sealed chamber 03 p0381 A69-14201
- Daily sleep and wakefulness periodicity changes effect on heart rate, respiration and body temperature diurnal rhythms in human males under isolation conditions 03 p0377 A69-14203
- Residual gas effect on fatigue behavior of pure iron subjected to alternating bending load in ultrahigh vacuum 04 p0616 A69-14846
- Self balancing single degree of freedom free fall space environment simulator, discussing coincidence of mass and rotation centers 04 p0586 A69-15468
- Simulation of solar wind interaction with earth magnetic field, discussing selection of dimensionless parameters 06 p0919 A69-17550
- Test program for solid propellant rockets capability to withstand space environments 06 p0982 A69-17594
- Space radiation effect on spacecraft components and materials simulated by proton and fast electron bombardment of silicon, glass and skin materials 06 p0906 A69-17612
- Multichannel radiometers calibration and testing for spacecraft and solar simulation applications, noting exposure to sun onboard X-15 aircraft at high altitudes 06 p0926 A69-17620
- Ablative and insulative performance of reference heat shield materials under transient heating simulating ballistic vehicle reentry trajectory, using plasma jet facility [AIAA PAPER 69-150] 06 p0907 A69-18110
- Thermal radiative reflectance characteristics of low density charring ablators subjected to planetary entry environment simulation [AIAA PAPER 69-61] 06 p0947 A69-18148
- Miniature ball and jewel bearings and gear lubrication in ultrahigh vacuum tests for space environment operation [IME PAPER 6] 07 p1138 A69-18562
- Astronauts increased heart beat, respiration rates and higher blood pressure subsides during repeated weightlessness tests 07 p1061 A69-18582
- Enzymes in simulated Martian environment exhibit higher resistance than in earth atmosphere at 4 C 07 p1065 A69-18974
- Group observers magnitude estimation judgements of stationary spacecraft model apparent distance in

simulated space, obtaining psychophysical functions for three stimulus ranges 07 p1069 A69-19501

AZUR satellite movement simulator for thermal control tests, describing assembly 08 p1300 A69-20095

Man in loop computer facility for programmers to check out flight programs in simulated space flight environment [AIAA PAPER 69-324] 09 p1479 A69-22384

Thermal vacuum simulator for testing manned Lunar Module Test Vehicle, using conformal skin heaters to control heating rates and skin temperature [AIAA PAPER 69-312] 09 p1479 A69-22386

Space vehicle explosive components, discussing identification, screening and final qualification of explosives and severe environment simulation methods 10 p1749 A69-23008

Space flight hypokinesia simulation experiments to study oxygen balance in man 10 p1646 A69-23507

Low energy charged particle detectors reliability, analyzing windowless electron multipliers and effects of secondary emission layers on sensitivity 11 p1848 A69-24868

D-2 satellite radiation dose based on upper atmosphere electron and proton distribution model, simulating electron bombardment and aging of materials and subsystems 11 p1949 A69-24869

Laboratory simulation methods for cosmic nuclear radiation, discussing dosimetry methods 11 p1862 A69-24875

Single crystal solar cell degradations in space, duplicating radiation effect on minority carriers lifetime by laboratory tests 11 p1826 A69-24876

Distance discrimination in simulated space environment, studying just noticeable difference /JND/ to determine relations between distance threshold and observation distance 12 p0222 A69-26372

Thermostructural simulation of lifting vehicle panel design, considering safety and trajectory shaping of flying laboratory 12 p0260 A69-26836

Sealed and unsealed relay coils temperature rise at simulated outer space air pressure levels 13 p2231 A69-28048

Vacuum pumping methods for large space simulation chambers, discussing cryopumping, economic and operational considerations 13 p2241 A69-28078

Space environment simulation for vacuum, solar radiation, heat sink and orbital motion, discussing oil contamination of optical surfaces 13 p2241 A69-28079

Three meter spherical volume heat balance test facility for space vehicles at European Space Technology Center, describing vacuum system, solar simulation, etc 13 p2241 A69-28080

Molecular gas flows in containers for space environment simulation, discussing flux distribution 13 p2241 A69-28081

SNAP 8 developmental reactor vacuum system providing space environment simulation for nuclear reactor ground testing 13 p2241 A69-28086

Meteoroid perforation effects on space cabin design, discussing simulated destructive environmental tests [AIAA PAPER 69-365] 13 p2357 A69-28297

Space suit meteoroid protection for extravehicular activity, discussing Gemini and lunar surface EVA suits and bumper concept [AIAA-PAPER-69-366] 13 p2213 A69-28298

Coriolis effect in rotating spacecraft simulation, discussing optokinetic reflex responses as function of head turning angle with spin axis 14 p2409 A69-29300

Space environment simulation tests of cadmium sulfide thin film solar cells, noting output loss 14 p2405 A69-29538

Continuous-channel electron multipliers degradation in spacecraft environment simulation laboratory equipment 14 p2449 A69-29565

Space Environment Simulation (SES) facility at Goddard Space Flight Center, discussing operations and maintenance 15 p2586 A69-30386

Thermal vacuum /TV/ manned-test operations related to Apollo lunar module in simulated space environment 15 p2558 A69-30394

Simulation of two phase hydrogen venting to space environment, discussing thrust effect measurements, flow instabilities and instrumentation 15 p2701 A69-30396

Boeing A-7000 Solar Simulator for Space Environment Simulation Laboratory, noting output characteristics 15 p2588 A69-30403

Escherichia coli B/r survival in high vacuum at different temperatures irradiated with UV or X rays tested as colony forming ability 15 p2557 A69-31388

600 Mev proton synchrocyclotron at Space Radiation Effects Laboratory for space radiation environment simulation, discussing beam energy spread 16 p2814 A69-32201

Visual perception of three dimensional objects under simulated solar illumination in space considered in relation to manned spaceflight maneuvers 17 p2913 A69-33174

Simulated solar wind environment effects on zinc oxide/potassium silicate and lanthanum oxide/potassium silicate spacecraft thermal control coating pigments [AIAA PAPER 69-642] 17 p2991 A69-33273

Specification requirements for space vacuum simulation, considering vacuum requirements for simulating various effects 17 p2946 A69-33659

Low pressure and background radiation conditions via cryogenically cooled surfaces, citing data on cryopumping under vacuum conditions for space simulation chambers 17 p3006 A69-33683

EEG electrode stimulated simian mental activity in problem solving during simulated space flight, discussing skull implantation and EEG recordings of hippocampus activity 17 p2910 A69-33749

Test program simulating solar wind outside magnetosphere to evaluate high melting point high density ceramic oxides as white thermal control coating pigments [AIAA PAPER 69-641] 17 p2993 A69-33762

Bjerhammer gravity reduction method applied to gravity in space, analyzing two test models with mass focused between topographical and reference surface 18 p3173 A69-35197

Future combined environment space simulation tests duplicating environment interaction encountered during earth orbits, deep space probes and manned flights 19 p3288 A69-35531

Instrumentation in aerospace simulation facilities - Conference, Farmingdale, New York, May 1969 19 p3289 A69-35714

Flash X ray unit with special film transport devices to obtain sequenced dynamic radiographs of ablating models during reentry simulation tests 19 p3291 A69-35720

Environmental testing of space hardware, discussing failure detection by thermal vacuum tests and mechanical signature analysis 19 p3430 A69-36009

Space environmental simulation facilities, discussing digital computers and equipment for simulating oxygen atmosphere, vacuum, heating and cooling, etc 19 p3295 A69-36326

Rats locomotion in centrifugally generated gravity fields determined for in-space behavioral studies of earth organisms gravity requirements 19 p3263 A69-36457

Combined angular and centrifugal acceleration effects on human and animal eyes motion studied to explain weightlessness effects on humans 20 p3471 A69-37257

Device for equipment insertion into space vacuum simulation chamber to minimize interaction with walls [ONERA-TP-676] 20 p3510 A69-37405

Moving model target for laboratory measurements of radar cross section to simulate satellite or reentry vehicle precession motion, noting signature data analysis 20 p3511 A69-37850

Enzymes in simulated Martian environment exhibit higher resistance than in earth atmosphere at 4 C 20 p3479 A69-38222

Handbook of solar simulation for thermal vacuum testing, discussing space environment, thermal control coatings, radiation sources, optical components, etc 21 p3690 A69-38894

Space mission sensitivity to parameters of interest determined by Monte Carlo simulation samples 21 p3804 A69-39036

Mission simulation testing in thermal vacuum environment for Apollo Lunar Module, noting conformal skin heaters [AIAA PAPER 69-991] 22 p3920 A69-40369

Solar simulator built into multiwall ultrahigh vacuum chamber, describing simulator and chamber modifications [AIAA PAPER 69-1001] 22 p3921 A69-40377

Speed conditions of environmental simulation of thermal scale models of reentry vehicles, considering ablatives with phase-change and involved chemical reaction [AIAA PAPER 69-1011] 22 p3922 A69-40384

Test model thermal balance in space simulator, measuring effects of solar simulator irradiance reflected from carbon dioxide cryopanel deposits [AIAA PAPER 69-1012] 22 p3922 A69-40385

Simulated degrading environment effect on spacecraft thermal control surfaces subjected to plume heating during apogee firing and solar irradiation [AIAA PAPER 69-1024] 22 p3923 A69-40394

RF voltage breakdown facility for studying spacecraft antenna characteristics in space and planetary atmosphere environments [AIAA PAPER 69-1028] 22 p3924 A69-40397

Aerodynamic forces under space-like conditions measured by swing balance, using large scale molecular beams for rarefied hypersonic gas flow simulation [AIAA PAPER 69-1032] 22 p3924 A69-40400

Pressure measurements and gas flow analysis during thermal vacuum tests of manned spacecraft indicating adequate space vacuum simulation [AIAA PAPER 69-1033] 22 p3924 A69-40401

Electrical sliprings assembly development with low dynamic resistance and long lifetime for space simulation testing, noting wear rate of rings and brushes [AIAA PAPER 69-1035] 22 p3925 A69-40402

Space simulation tests of satellite-borne quartz crystal oscillators for tracking based on Doppler effect 22 p3927 A69-40590

Cs contact ion engine with tubular W ionizer tested for performance and reliability in vacuum chamber 22 p4000 A69-40592

Arc-heated hypersonic wind tunnel for simulated spacecraft reentry environment, aerodynamic heating characteristics and research applications 22 p3927 A69-40595

Space cabin environment simulation effects on resistance to infection caused by pneumonia and influenza virus in rats 23 p4108 A69-41832

SPACE ENVIRONMENTAL LUBRICATION
U SPACECRAFT LUBRICATION

SPACE ERECTABLE STRUCTURES
NT BEACON SATELLITES
NT EXPLORER 22 SATELLITE

Expandable D 21 airlock scheduled for testing on NASA Orbital Workshop Flight based on elastic materials technique, noting more complex chemically rigidized concept [IAF PAPER SD-49] 02 p0334 A69-11949

Testing program using electrical measurements for determining adequacy of erectable parabolic reflector for space missions 02 p0223 A69-12812

Wire screen deployable boom concept for avoiding thermal bending of slender tubes problem in application to gravity gradient stabilization and antennas of spacecraft 07 p1229 A69-18350

Dynamics of deployable space structures stiffened by centrifugal forces due to spin, discussing LF radio telescope 11 p1994 A69-25530

Multidimensional mode shapes and frequencies of 100 ft space erectable parabolic antenna 11 p1994 A69-25532

Erectable metal booms and meshes structural analysis, design and mounting and deployment techniques for space applications 19 p3433 A69-35544

Resin impregnated fiber reinforced expandable structures used for automatic cure or rigidizing in space and initially small compact packages on earth 19 p3433 A69-35585

Curved shell elements in shell and plate analysis, discussing quadratic and cubic elements for space structures design 21 p3845 A69-39329

Space erectable microwave truss antenna automatically deploying rigid parabolic reflector 22 p3913 A69-40696

Spacecraft phase array designed for use on synchronous communication satellite, discussing low structural weight packaging and unfurling problems and helix approach 22 p3915 A69-40705

Zero g deployment dynamics of erectable truss parabolic antennas, obtaining latchup loads as function of reflector mechanical energy [AAS PAPER 69-336] 24 p4398 A69-42827

Large space erectable structures rigidity, stiffness, thermal stability, structural efficiency and integrity [AAS PAPER 69-152] 24 p4398 A69-42877

SPACE EXPLORATION

National space program management, discussing NACA and NASA, lunar mission planning, procedures and program flexibility and responsibility 01 p0178 A69-10468

Soviet space astronomy including rocket, satellite and space probe measurements for solar, stellar, planetary and lunar studies 01 p0155 A69-10946

Life sciences and space research - COSPAR Conference, London, July 1967 01 p0016 A69-11073

Radio links between earth and deep space probes, summarizing bistatic radar astronomy results [AAS PAPER 68-182] 02 p0311 A69-11467

Scientists involvement in planetary spacecraft missions, considering organization for particular instruments and more complex payloads [AAS PAPER 68-192] 02 p0311 A69-11473

U.S. space program projections, discussing earth orbit operations, lunar and planetary explorations, costs and timetable 02 p0355 A69-11744

Unmanned planetary exploration using Mariner class spacecraft for solar system and life origin 02 p0334 A69-12302

Manned Mars and Venus missions role in overall planetary exploration program 02 p0324 A69-12304

Planetary exploration strategy for form and origin of universe, unified field theory and abiogenesis, discussing mission planning group 02 p0324 A69-12305

Structural design options for decelerative aeroshell configurations for atmospheric entry on unmanned planetary explorations [AIAA PAPER 68-344] 04 p0683 A69-15507

Permissible development direction for space research, discussing space station, required systems and cost estimates 05 p0829 A69-15920

Spacecraft sterilization techniques for space exploration, discussing mathematical models for planetary quarantine and contamination by nonlanding vehicles 05 p0712 A69-15935

Simulation experiments using artificial plasma for astrophysical rocket exploration, discussing experiments leading to barium-copper oxide mixture choice for plasma cloud 06 p0999 A69-16973

Soviet satellite exploration of space magnetic fields and charged particles, noting Proton satellites and protons and carbon nuclei inelastic interactions [UN PAPER 68-95768] 06 p0986 A69-17031

Biological aspects of space exploration, analyzing human response to artificial environment in prolonged space missions [UN PAPER 68-95715] 06 p0873 A69-17035

Satellite and space communications and data transmission systems, emphasizing improvements in amount and rate of information for future requirements 06 p0886 A69-17045

U.S.S.R. international cooperation in outer space exploration for peaceful purposes, stressing space meteorology, communications, biology and medicine [UN PAPER 68-95669] 06 p1043 A69-17054

Soviet explorations of moon, Venus, Mars and interplanetary space, noting objectives of future lunar explorations [UN PAPER 68-95719] 06 p1000 A69-17055

Manned space flight programs, discussing U.S. technological, scientific and practical contributions 06 p1001 A69-17074

Soviet achievements in space research, comparing satellites with U.S. counterparts 06 p1005 A69-17561

U.S. space research program and achievements, describing practical aspects 06 p1005 A69-17562

Interplanetary Pioneer spacecraft development and systems engineering aspects 06 p1017 A69-17605

Photoelectronic imaging systems in space exploration emphasizing acquisition time, storage capacity and transmission time 07 p1136 A69-19591

Cybernetic theory application to automatic spacecraft, discussing control problems in Mariner 4 and Surveyor 7 missions and attitude stabilization system 08 p1409 A69-20583

Common nuclear propulsion modules for wide spectrum of manned planetary missions, discussing payload, mission and program flexibility [AIAA PAPER 68-590] 09 p1539 A69-21984

Search theory application to planetary exploration overall strategy for improving landing site decisions 09 p1595 A69-21994

Space exploration plans adaptation, considering spacecraft design, programs, costs and schedules flexibility 10 p1811 A69-22863

Power requirements for tracking, telecommand and telemetry of spacecraft over interplanetary distances, considering transmission problems, equipment weight and reliability 10 p1652 A69-22984

Manned space stations for future space exploration, discussing earth-like environment, artificial gravity, human factors and time dependence 11 p1965 A69-25644

Space research in U.S.S.R. including Venera 4 soft landing mission for measuring temperature, pressure, density and atmospheric composition of Venus 12 p2160 A69-26921

Collection of Soviet papers on U.S.S.R. outer space studies /1957-1967/ covering rocket and satellite sounding, meteorology, radiation belts, etc 13 p2335 A69-27346

Soviet space efforts /1957-1967/, discussing rocket, probe, spacecraft and satellite launchings and scientific results 13 p2336 A69-27358

Integrated device to detect biological growth and catabolic and anabolic activity in extraterrestrial exploration 15 p2556 A69-31306

Upper atmosphere and outer space investigations by Zond and Soyuz spacecraft 15 p2724 A69-31451

Outer planets exploration during 1976-80 period of unique solar system alignment 16 p2854 A69-31630

Commercial utilization of space technology, discussing cost reduction and role of NASA Apollo Program 17 p3043 A69-34044

Advanced space experiments - AAS Conference, Ann Arbor, September 1968 18 p3192 A69-34359

Space exploitation for experimental research - AAS Conference, Dedham, Mass., May 1968, Volume 24 18 p3193 A69-34367

Mariner 6 and 7 Mars probes, describing mission profile, basic structure, trajectory design and scientific experiments 18 p3198 A69-34795

Space, technology and society - Conference, Cocoa Beach, Florida, March 1969, Volume 2 18 p3233 A69-35055

Space exploration influence on science education, showing NASA instructional materials for teachers in biology, chemistry, physics, mathematics, industrial arts, etc 18 p3235 A69-35077

Mars exploration by 1969 Mariner 6 and 7 flyby, discussing mission and instrumentation 18 p3201 A69-35141

Soviet space exploration including Cosmos and Proton satellites, Luna project and Zond and Venera probes 18 p3201 A69-35163

Scientific findings from interplanetary spacecraft radio propagation experiments, particularly Mariner 5 data 19 p3267 A69-35940

Philosophy of law in space following exploration by man 19 p3455 A69-36332

Juridical norms defined by Madrid, Belgrade and Washington conferences regulating exploration and utilization of extraterrestrial bodies and space, considering satellite communications networks 20 p3638 A69-37123

Space law and space research, detailing UN law proposals 20 p3638 A69-37129

Space law for outer space exploration applications, defining outer space and space activity for legal purposes 20 p3639 A69-37130

International space law basic ideas and future trends, considering freedom of exploration, UN proposals, space demilitarization, etc

20 p3639 A69-37131

Space law code based on space accomplishments by nations as acts involving welfare of humanity

20 p3639 A69-37135

Microbial contamination release from impact-fractured solids, examining bacterial spores growth in fractured methyl methacrylate plastic for application to space exploration

20 p3475 A69-37614

Propulsion system performance relationship to manned planetary mission capability, discussing anticipated performance of advanced propulsion concepts

20 p3586 A69-38118

Gravity gradient phenomena in orbiting vehicle used to explore planetary gravity

[AIAA PAPER 68-851]

21 p3804 A69-39024

Nonintegral burn of solid core nuclear rockets, discussing modular stage concepts approach to low cost space exploration

[AIAA PAPER 68-589]

21 p3768 A69-39026

PostApollo space goals based on manned and unmanned planetary exploration and space science programs, considering human factors and propulsion problems

21 p3856 A69-39167

Exploration capabilities provided by Jupiter gravity assisted trajectories compared to direct ballistic flight trajectories

[AAS PAPER 68-116]

21 p3805 A69-39224

Strategy for exploration of inner solar system leading to origin and history, detailing lunar exploration program

22 p4022 A69-40449

Trajectory analysis of multiplanet Grand Tour mission to four large outer planets on single flight, discussing mission planning

[AIAA PAPER 68-1055]

22 p4023 A69-40544

Apollo 11 mission and future space exploration prospects including moon base, manned space station, reusable shuttle vehicles, etc

23 p4211 A69-41477

Spatial region accessible to earth launched probes determined for mission planning for exploration of aperiodic comets, discussing orbit parameters

23 p4212 A69-41536

Mars exploration for life by Mariner flybys and orbiters and 1973 Viking landers

23 p4212 A69-41611

Optical activity measurement for exobiology applications, considering polarimetry, gas-liquid chromatography, mass spectrometry and radioactivity detection

23 p4213 A69-41622

Venus atmosphere and clouds exploration by entry probes, discussing ground temperature, greenhouse model, cloud layer, etc

23 p4216 A69-42201

Planetary exploration and NASA program objectives

[AAS PAPER 69-286]

24 p4379 A69-42810

Manned flyby/orbiter of Mars providing scientific information at low incremental cost

[AAS PAPER 69-180]

24 p4379 A69-42813

Space research in past and expected scientific knowledge from manned and automated earth orbital science missions

[AAS PAPER 69-036]

24 p4379 A69-42825

Launch vehicle upper stage requirements in space missions, discussing space engine for lunar, planetary and interplanetary exploration

[AAS PAPER 69-359]

24 p4418 A69-42828

Manned flyby and stopover missions to Mars and Venus with chemical propulsion and Saturn 5 launch vehicles, noting short duration low energy missions

[AAS PAPER 69-492]

24 p4380 A69-42839

Technology flow for future manned earth orbit and lunar operations and planetary exploration

[AAS PAPER 69-494]

24 p4380 A69-42840

Manned space flight history and spacecraft development

[AAS PAPER 69-501]

24 p4380 A69-42852

Pioneer F/G mission to Jupiter by NASA for exploring interplanetary medium, asteroid belt, planet and environment

[AAS PAPER 69-290]

24 p4381 A69-42863

Reconnaissance missions for outer planets exploration, discussing spacecraft design constraints, multiple planet fly-by, planetary orbiter, etc

[AAS PAPER 69-291]

24 p4381 A69-42864

Nuclear propulsion for solar system exploration, discussing NERVA solid core nuclear fission rocket, nuclear-electric rockets and hybrid nuclear rocket/nuclear electric rocket systems

[AAS PAPER 69-330]

24 p4349 A69-42871

Monograph on Pioneer spacecraft program, discussing mission objectives, spacecraft design, etc

[AAS PAPER 69-066]

24 p4381 A69-42883

Mars and Venus flyby missions and Mercury planetary exploration plans, discussing future conditions permitting Jupiter, Saturn, Uranus, Neptune, Pluto flybys

24 p4384 A69-43137

SPACE FLIGHT

NT APOLLO FLIGHTS

NT APOLLO 10 FLIGHT

NT APOLLO 11 FLIGHT

NT APOLLO 7 FLIGHT

NT APOLLO 8 FLIGHT

NT APOLLO 9 FLIGHT

NT GEMINI FLIGHTS

NT GEMINI 11 FLIGHT

NT HYPERBOLIC REENTRY

NT HYPERSONIC REENTRY

NT INTERPLANETARY FLIGHT

NT INTERSTELLAR TRAVEL

NT LUNAR FLIGHT

NT MANNED REENTRY

NT MANNED SPACE FLIGHT

NT RETURN TO EARTH SPACE FLIGHT

NT SPACECRAFT REENTRY

Physiological measurements onboard Soviet bioprobes and biosatellites including electrocardiography, phonocardiography, sphymography, seismocardiography and pneumography

01 p0015 A69-10947

Cytological analysis of *Tradescantia paludosa* microspores for space flight influence onboard Cosmos 110

01 p0018 A69-11317

Meteoroid hazard, discussing possible future collisional dangers for space traffic

01 p0160 A69-11412

Benefits accruing from swingby operation, considering space flights past Jupiter, Saturn and other planets

02 p0326 A69-12663

Digital computers in space flight simulation and vehicle performance optimization, examining mission analysis

04 p0652 A69-14519

Automatic processing of electrocardiograms recorded during space flight by computer

05 p0715 A69-16524

Leisure time and recreation facilities during long duration space missions, discussing astronaut selection procedure, active recreation, passive enjoyment and exercise programs

06 p0880 A69-17209

Flour beetle under irradiation and weightlessness during space flight, analyzing effects on somatic wing development, germ cells and pupal period

06 p0876 A69-18177

Electronic tubes utilization in space flight, summarizing characteristics and satellite applications

07 p1093 A69-18421

Oculomotor activity of cosmonauts during orbital flight, analyzing electrooculograms taken during vestibular tests

07 p1063 A69-18594

Human motor reactions during weightlessness based on parabolic or orbital space flight observations, noting cosmonaut writing performance

07 p1063 A69-18595

Optimum physiological parameters selection criteria for medical control of crew during space flights

07 p1071 A69-18978

Monte Carlo method applied to calculation of radiation transmission and dosage behind space vehicle shields during passage through earth radiation belt

08 p1377 A69-19843

IR camera determining surface temperatures, discussing construction and space applications

08 p1315 A69-20455

Mission model construction for power limited systems, discussing flight concepts, propulsion mixes and electric propulsion

09 p1584 A69-21205

Space flight trajectory analysis of aerospace systems, discussing Analytical Trajectory Optimization Model

09 p1585 A69-21207

Space flight fuel consumption optimization as function of acceleration of nozzle control

10 p1666 A69-22919

Automatic computer processing of physiological data during space flights, discussing choice of computers and computer programs

10 p1649 A69-23509

Flat plate in two dimensional low density hypersonic flow wind tunnel tested for aerodynamic effects on spacecraft reentry

11 p1819 A69-25424

Book on reentry and planetary entry physics and technology covering entry dynamics, thermodynamics, radiation, ablation and heat transfer

11 p1967 A69-25573

Spacecraft propulsion systems comparison and evaluation, discussing quality, schedules and costs in relation to mission requirements

11 p1965 A69-25600

Electrochemical energy storage and conversion for space flight, emphasizing hydrogen oxygen and silver zinc batteries, Gemini and Apollo programs, etc

12 p2015 A69-25866

Space flight research programs including stellar and biological evolutions and environmental control

12 p2155 A69-26003

Biotelemetry of human physiological processes in space for assuring psychophysiological control and immediate intervention for emergencies, discussing application in Mercury and Gemini projects

12 p2023 A69-26491

X-15 research aircraft program piloting problems, ground facilities, heat transfer, space flight and steep reentry

12 p2014 A69-26872

Financial, political and engineering considerations influencing space flight programs implementation, including nuclear systems examination for propulsion and power capability

13 p2334 A69-27296

Boosters and space vehicles including earth satellites, lunar probes and interplanetary spacecraft

13 p2356 A69-27914

Propulsion systems for boosters and space vehicles including chemical, electric and nuclear

13 p2325 A69-27915

Space flight cost analysis, relative costs of various types of transportation and need for reusable single stage to orbit vehicles

15 p2719 A69-30186

Refrigeration system for space flight use of cryogenic gas storage, suggesting mission time increase

15 p2587 A69-30395

Liquid free surface response to mass force variation during space flight near zero-g, discussing effects on ignition

16 p2866 A69-31735

Monograph on solar system space flight trajectory calculations covering solutions to differential equations, error analysis and gravitational effects

17 p3039 A69-33798

Flight failure analysis, discussing methods and restrictions due to hardware unavailability, minimum data, urgency and publicity

18 p3145 A69-34502

Automatic processing of electrocardiography recorded during space flight by computer

18 p3098 A69-34743

Space flight optimization - Conference, Liege, Belgium, June 1967

19 p3398 A69-35662

Operational missile flight program validation plan noting mission analysis, computer programming, program preparation and performance prediction

19 p3279 A69-35955

Radiation exposure during orbital flight assessed for adverse effect on space stations and laboratories personnel, discussing shielding and dose rate tables

20 p3481 A69-37339

Insects mutational responses to space flight and associated radiation on biosatellite 2 compared with ground based controls

20 p3476 A69-37618

Optimum physiological parameters selection criteria for medical control of crew during space flights

20 p3483 A69-38226

Real time operating system (RTOS/ 360 for spaceflight control, describing hardware, applications, task management and capacity, etc

21 p3679 A69-39602

Space transportation cost saving options including booster systems, spacecraft/payload systems and support systems, discussing recovery and launching operations

21 p3857 A69-39690

Launch systems evolution, cost reduction breakthrough approach and application to future space transportation

21 p3857 A69-39692

Collection of papers on space flight mechanics covering trajectories, motion about center of mass, optimization, control systems

21 p3828 A69-39816

Long range space flight trajectory correction problem, obtaining algorithm for determining minimum number of corrections
21 p3818 A69-39822

SPACE FLIGHT FEEDING

Biological problems in prolonged space voyages including oxygen replacement, water supply and food regeneration
01 p0020 A69-11075

Chlorella and Scenedesmus unicellular algae mixture tested for biological protein value in humans for possible food source
01 p0021 A69-11079

Cell and tissue cultivation outside living organisms, discussing applications in space biology, space medicine and food protein sources
02 p0198 A69-11501

Physicochemical method for converting human urine and feces into carbohydrates in closed ecological systems
03 p0381 A69-14199

Biological, psychological and technological requirements in astronaut nutrition programs, examining preservation and reconstitution techniques
04 p0554 A69-15388

Test dogs feeding through enteropancreatic fistula homogenized mixture containing juice excretion stimulating agents during long space flight
08 p1265 A69-19829

Sweet potatoes productivity and nutritive value as carbohydrates source in manned spaceflights
13 p2216 A69-28619

Higher plants utilization as nutrition source in space missions, comparing weight requirements for cultivation equipment and food storage
15 p2560 A69-31408

Astronaut feeding in space and NASA criteria for space foods, eliminating foods in metal tubes and directing development efforts to dehydrated foods
15 p2560 A69-31459

Human requirements for nutrients under stress responses to space flight, considering synthetic food and hothouse plants
15 p2560 A69-31462

Space flight food evaluation by metabolic balance techniques during space flight simulation, considering food consumption during weightlessness
15 p2560 A69-31470

Monosaccharide production from carbon dioxide from respiration or human waste incineration, evaluating toxicological effects of synthetic monosaccharides
15 p2557 A69-31471

Human performance and adaptation to space flight effects under low calorie diet including optimal proportion of basic nutrients and amino acids
20 p3482 A69-37621

Fire hazard in closed chamber associated with intestinal hydrogen and methane formed by space diets, comparing Gemini-type and bland diets
20 p3482 A69-37622

Regenerative life support system development, considering synthesized organic compounds and microorganisms as foods for long duration space missions
20 p3477 A69-37623

Nutritive value of mycelium of *Cantharellus cibarius* mushroom on rats compared with eggs and fresh and sour milk
22 p3892 A69-40273

SPACE FLIGHT STRESS

Extraterrestrial vestibular research, discussing human otolith apparatus regulation subjected to change from geocentric to heliocentric orientation [UN PAPER 68-95389]
01 p0014 A69-10508

Soviet book on space physiology covering space flight and laboratory data on cerebral cortex function, digestive system, tissue changes, etc
01 p0014 A69-10743

Gemini and Mercury space flights medical results, summarizing physiological effects noted on body systems
01 p0017 A69-11074

Differential and threshold sensitivity of acoustic analyzer of humans under space flight factors
02 p0197 A69-11500

Physiological processes occurring in voluntary movements of animals under space flight weightlessness conditions
02 p0199 A69-11827

Physiological causes and prevention of motion sickness during space flight, emphasizing conditioned reflex, different analyzer interactions and vestibular-vegetative changes during weightlessness
02 p0200 A69-12122

Solar flare radiation hazard in long duration space flight, discussing radiation distribution and dosage in human body
03 p0371 A69-13480

Antimotion sickness drugs tested in slow rotation room with controlled Coriolis accelerations, noting summation effect of dextroamphetamine sulfate and scopolamine hydrobromide
03 p0381 A69-14079

Simulation of regulatory function of cardiovascular system during weightlessness
03 p0376 A69-14193

Cardiovascular system, respiratory system and metabolism of cosmonauts on three man flight of Voskhod, noting physiological and biochemical studies
03 p0377 A69-14195

Changes in blood circulation, external respiration and gas exchange rates in humans during prolonged hypodynamia
03 p0377 A69-14204

Cardiac function changes during orthostatic tests and problems in predicting reactions of cosmonauts in flight
03 p0381 A69-14229

Space flight factors, ionizing radiation and combined effects on vitamin C content in onion bulbs
05 p0708 A69-16510

Book on space clinical medicine covering hypoxia, ebullism, decompression, aerotitis, dehydration, hypothermia, cabin atmosphere contamination, urinary calculus, etc
05 p0711 A69-16801

Reactions of respiratory and cardiovascular system of dogs in biocompartment of ballistic missiles, discussing biopotential of myocardium, arterial pressure, etc
07 p1060 A69-18576

Recessive lethal mutations frequency in gametes of male and female *Drosophila melanogaster* onboard Vostok spacecraft
07 p1063 A69-18598

Radiation hazards during long duration space flights and suitable radiation shield design through radiobiological investigation
08 p1261 A69-19826

Biomedical experiment onboard Cosmos 110 concerning nonpathological changes
08 p1261 A69-19827

Dogs cardiovascular activity mathematical analysis from physiological indices during long space flight
08 p1261 A69-19828

Dogs blood coagulation system functional state after 22 day space flight onboard Cosmos 110
08 p1262 A69-19830

Change in content of dry matter, sugars and ascorbic acid in plants after action of space flight factors on seeds of these plants
10 p1645 A69-23495

Hypokinesia effects on human neurology on extended space flights simulated by 72-day bed rest
10 p1646 A69-23506

Weightlessness effects on human external respiration, gas exchange and energy expenditure indices during flight of Voskhod 2
12 p2020 A69-26563

Pharmacology for long term manned space flights
13 p2211 A69-28613

Transient and long lasting space environment stresses, discussing accelerations, vibrations, shocks, rapid descent in vacuum, temperature variations, gravity, etc
15 p2625 A69-30824

Human requirements for nutrients under stress responses to space flight, considering synthetic food and hothouse plants
15 p2560 A69-31462

Space research centrifuge counteracting null gravity physiological deconditioning, discussing linear and angular accelerations sensitivity and deconditioning effect on reentry task performance
18 p3114 A69-34368

Space flight factors, ionizing radiation and combined effects on vitamin C content in onion bulbs
18 p3095 A69-34729

Astronaut vestibular and motor analyzer functions during flight and simulation tests, discussing illusory space orientation and role of cortical dynamics
20 p3469 A69-37241

Human performance and adaptation to space flight effects under low calorie diet including optimal proportion of basic nutrients and amino acids
20 p3482 A69-37621

Physiological experiments to investigate aerospace flight stresses effects on oculomotor equilibrium, not-

ing cardiovascular reaction and mechanism for interpretation
23 p4087 A69-41804

Insect gametes response to space flight and radiation in reduced gravity including plants and microorganisms
23 p4091 A69-42050

Environmental stress effects on medical leech studied to determine tolerance to spacecraft launching, orbiting and reentry
24 p4268 A69-43403

SPACE FLIGHT TRAINING

Space flight crew efficiency during prolonged weightlessness, stressing preflight adaptation and space vehicle technology improvement
07 p1063 A69-18596

Astronauts physical training for space flight requirements
13 p2215 A69-28611

Astronaut selection and training in U.S. and U.S.S.R.
13 p2216 A69-28636

SPACE GLIDERS

U LIFTING REENTRY VEHICLES

SPACE LABORATORIES

NT MANNED ORBITAL LABORATORIES

NT MANNED ORBITAL RESEARCH LABORATORIES

Space station design requirements, Apollo applications program and various experimental programs
01 p0163 A69-11395

Moon environment for scientific experiments, emphasizing lunar surface properties, lack of man-made electromagnetic waves, vacuum and weak gravity force
13 p2240 A69-27910

Extraterrestrial life detection experiments integrated into single multipurpose space laboratory, including chemical analyses, metabolism identification, observation for molecular and/or cellular growth and replication
17 p2912 A69-32970

Lunar physics and chemistry - IAA Conference, Belgrade, September 1967
18 p3112 A69-34234

Lunar laboratory physical and chemical experiments including scattering phenomena, molecular and atomic beams and gas cloud photochemistry
18 p3113 A69-34237

Space manufacturing processes for orbital low and zero gravity environment, discussing buoyancy and thermal convection sensitive and molecular forces controlled methods [AAS PAPER 69-486]
24 p4380 A69-42844

SPACE LAW

Legal problems in space navigation and solution through international law including air and outer space limits, regulating authority and damage liability [UN PAPER 68-95475]
01 p0179 A69-10511

International liability for damage caused by launching of objects into outer space [UN PAPER 68-95337]
01 p0180 A69-10525

Book on international law and uses of outer space covering effects of UN General Assembly Resolutions and Outer Space Treaty
02 p0356 A69-12676

Legal problems in space navigation and solution via international law including air and outer space limits, regulating authority and damage liability
07 p1244 A69-19233

Yearbook of air and space law /1966/ covering documents on legal doctrines, treaties, regional arrangements, national bibliographies, Warsaw Convention, Hague Protocol, etc
10 p1811 A69-23986

International space law definitions, technology, regulations, role of industry and government, etc
13 p2381 A69-27529

International law governing aerospace activities /1966 to 2066/
13 p2382 A69-27829

Outer space law principle sources including divine law, UN and NASA contractors regulations
15 p2720 A69-31052

Philosophy of law in space following exploration by man
19 p3455 A69-36332

Space law - Conference, New York, October 1968
20 p3634 A69-37102

Treaty on Outer Space interpretation regarding establishment of international space agency with sufficient authority
20 p3635 A69-37103

Space Treaty interpretation of ambiguity of term peaceful due to differing concepts of U.S. and U.S.S.R.
20 p3635 A69-37104

Juridical meaning of peaceful in 1967 Space Treaty interpreted in terms of real purpose of given space activity

20 p3635 A69-37105

Interpretation of peaceful uses of outer space in Space Treaty, emphasizing provision forbidding individual military space activities whether aggressive or nonaggressive

20 p3635 A69-37106

1967 space Treaty Article 11, discussing provisions concerning private exploitation and supernational body authority

20 p3635 A69-37107

ESRO and legal liability in damage suits concerning satellite protection and environmental control

20 p3635 A69-37108

Outer Space Treaty of 1967, discussing Article 4 and arms control

20 p3636 A69-37109

Space law legal liability definitions for damage caused by space objects, discussing juridical principle and procedure

20 p3636 A69-37110

1967 Space Treaty legal aspects of consultation, suggesting international permanent body setup for resolving technical and political matters

20 p3636 A69-37111

1967 Space Treaty peaceful activities definition, suggesting explicit provisions regarding treaty province, enforcement machinery and implementation

20 p3636 A69-37112

Agreement on Rescue and Return of Astronauts and Return of Objects Launched into Outer Space, discussing unintended landing

20 p3636 A69-37113

Agreement on Rescue and Return of Astronauts and Return of Objects Launched into Outer Space, noting humanitarian considerations and indemnity for services rendered

20 p3636 A69-37114

Amendments considered for international law regarding earth and space rescue services as result of contemporary U.S. manned space flight programs

20 p3637 A69-37115

UN agreement provisions on international cooperation for rescuing astronauts and objects in case of accident, distress, emergency or unintended landing

20 p3637 A69-37116

Space vehicles registration within Treaty on Outer Space to provide protection for vehicle and third parties in cases of damage

20 p3637 A69-37117

International lawyers proposal for compulsory registration of space activities in connection with astronauts rescue and damages liability

20 p3637 A69-37118

Manned lunar bases from legal viewpoint, discussing national jurisdiction, personnel policies, mineral rights, etc

20 p3637 A69-37119

INTELSAT 1964 agreements consistency with multilateral international agreements, including UN General Assembly and International Telecommunication Union

20 p3638 A69-37122

Juridical norms defined by Madrid, Belgrade and Washington conferences regulating exploration and utilization of extraterrestrial bodies and space, considering satellite communications networks

20 p3638 A69-37123

Space law as foreseen in light of expected scientific progress in astronautics

20 p3638 A69-37126

International legal liability for personal injury or property damage caused by space activities

20 p3638 A69-37127

Space law history, discussing Space Treaty and UN Declaration of Legal Principles

20 p3638 A69-37128

Space law and space research, detailing UN law proposals

20 p3638 A69-37129

Space law for outer space exploration applications, defining outer space and space activity for legal purposes

20 p3639 A69-37130

International space law basic ideas and future trends, considering freedom of exploration, UN proposals, space demilitarization, etc

20 p3639 A69-37131

Domestic and international law compared in connection with space program, considering legal aspects of using satellites in discovering and exploiting earth resources

20 p3639 A69-37132

Multiple use doctrines in space law for resource utilization, discussing formation of planning commissions and licensing agencies

20 p3639 A69-37133

Planetary resources control and use from legal and policy standpoints, discussing space treaty effects on international law

20 p3639 A69-37134

Space law code based on space accomplishments by nations as acts involving welfare of humanity

20 p3639 A69-37135

Ecological foundations of Haley metalaw and implications of interstellar golden rule, discussing social interaction with alien life forms

23 p4240 A69-41304

Liability for personal and property damage due to space activities

[AAS PAPER 69-042] 24 p4418 A69-42826

SPACE LOGISTICS

Integrated management information system (IMIS), discussing logistics, reliability and quality assurance disciplines

11 p2005 A69-25304

SPACE MAINTENANCE

Split-seam process for inserting sterile objects into isolated sterile environment without contamination as method for sterile spacecraft repair

05 p0714 A69-15950

Maintenance telemetering, tracking and telecommand for developmental and operational satellites, discussing possibilities of frequency sharing between satellites and terrestrial services

09 p1451 A69-21290

Reliability and maintainability analysis of two year spacecraft mission combining earth orbits and Mars program, using computerized mathematical model

[AIAA PAPER 68-1059] 12 p2174 A69-26797

Lunar based optical workshop and repair facility, using ion beam technique to polish and repair optical element surfaces

18 p3113 A69-34243

Space manufacturing operations program, discussing zero gravity effect during earth orbit flight, Apollo Applications Program Orbital Workshop Flight 2, etc

18 p3208 A69-35067

Ground controlled remote manipulator spacecraft system to perform unmanned satellite orbital maintenance, discussing refurbishment, laboratory simulation, system cost effectiveness and feasibility

19 p3430 A69-36001

Satellite onboard computers automatic reconfiguration and self repair

20 p3503 A69-37399

Orbital mechanics of near earth satellite arrangements/clusters for satellite service vehicle (SSV)/accessibility from orbital space stations

[AIAA PAPER 69-929] 21 p3809 A69-39358

Self testing and repairing (STAR)/aerospace computer for automatic maintenance of unmanned interplanetary spacecraft

[AIAA PAPER 69-966] 22 p3906 A69-40347

Neutral buoyancy simulation of astronaut performing module replacement and repair task in zero-g environment

[AIAA PAPER 69-1005] 22 p3921 A69-40379

Tools and equipment for extra- and intravehicular activities in space and on lunar surface

[AAS PAPER 69-438] 24 p4319 A69-42802

Space manufacturing processes for orbital low and zero gravity environment, discussing buoyancy and thermal convection sensitive and molecular forces controlled methods

[AAS PAPER 69-486] 24 p4380 A69-42844

Remote manipulator spacecraft system for refurbishing synchronous communication satellite, emphasizing compatibility with standard shroud Titan 3C launch vehicle

24 p4297 A69-43041

SPACE MECHANICS

NT ASTRODYNAMICS

NT CELESTIAL MECHANICS

NT KEPLER LAWS

NT ORBITAL MECHANICS

Autonomous canonical system with two degrees of freedom, determining equilibrium position stability in resonance case, calculating earth satellite rotational stability

14 p2482 A69-28813

Flight and space mechanics problems from engineer standpoint, discussing flight path calculation, stability and control characteristics and experimental techniques for high reliability

17 p3076 A69-33041

Homogeneous deformations of space and Cauchy problem for homogeneous free molecular motions, considering velocity fields and accelerations

19 p3444 A69-36803

SPACE MISSIONS

Solar system origin and evolution by future space mission experiments, discussing theories and mission objectives

[AAS PAPER 68-191] 01 p0153 A69-10823

Scientific mission of ESRO 2/IRIS satellite, study of X rays and particles from sun and galaxy and primary cosmic ray electron measurement

01 p0163 A69-11102

Book on electric propulsion systems for spacecraft covering thermoelectric, electromagnetic, electrostatic, plasmacore, thermonuclear and photon systems

02 p0305 A69-12233

Manned reusable space transportation systems development, discussing requirements for future space mission planning

03 p0519 A69-13395

Noise reduction techniques in digital and analog data transmission over space program distances, emphasizing deep space missions

03 p0394 A69-13398

Space rendezvous problem as applicable to interplanetary missions, discussing steps in rendezvous maneuvers to permit final docking

03 p0511 A69-13401

Lunar Orbiter mission objectives and orbit design

[AIAA PAPER 68-47] 04 p0664 A69-15503

Fluid support by capillary forces, fluid support by pressure with surface tension stabilization and capillary gas barriers for long life missions

[AIAA PAPER 68-465] 04 p0646 A69-15505

Technological base for planning space flight missions to obtain data on earth resources, detailing earth resources technology satellites/ERTS/

05 p0830 A69-15921

Permissible radiation doses for extended space missions, discussing clinical tests on dogs

05 p0708 A69-16508

Efficient life support systems for prolonged space missions, discussing scientific and experimental research

[UN PAPER 68-95778] 06 p0879 A69-17040

Multimission interplanetary probe using solar electric propulsion

06 p0984 A69-17593

Manned space flight safety, discussing astronaut exposure to danger on ground, in training and in space mission

06 p0882 A69-17650

Apollo 4, 5 and 6 space missions, with preview of Apollo 7, 8 and 9 missions

06 p1017 A69-17672

Gravity gradient stabilization role in space missions in 1970s and 1980s

07 p1229 A69-18348

Feasibility of nuclear stage for space missions, discussing Saturn 5 third stage replacement, payload gain, reactor and engine size

08 p1409 A69-20158

Spacecraft electric propulsion parameters and launching vehicle characteristics in low thrust mission simulation, discussing spacecraft path

09 p1584 A69-21202

Electric propulsion missions analysis for spacecraft design engineer, discussing out-of-ecliptic and Jupiter flyby probes

09 p1584 A69-21203

Automated parameter search techniques applied to low thrust mission design, stressing trajectories and mission optimization

09 p1585 A69-21211

Monograph on requirements for high speed interplanetary flights with nuclear engines and refueling at destination

09 p1586 A69-21298

Spacecraft design, trajectory and mission analyses for multipurpose solar electric propulsion missions, emphasizing modular ion engine and fixed attitude spacecraft designs

[AIAA PAPER 69-252] 09 p1568 A69-21729

Human adaptation to various environments, emphasizing experimental space psychoneurology role in human behavior examinations during space missions

10 p1647 A69-23587

High energy radiation effects on electronic components in space missions, noting simulation tests and shielding

11 p1946 A69-24521

Space experiments analysis involving standardization for economy and mission thesis compromise, detailing aeronomic satellite project with integrated utilization 12 p2173 A69-26128

Problem areas within cryogenic chemical and nuclear propulsion systems for space missions, noting available technology and limitations [AIAA PAPER 67-454] 12 p2174 A69-26782

Reliability and maintainability analysis of two year spacecraft mission combining earth orbits and Mars program, using computerized mathematical model [AIAA PAPER 68-1059] 12 p2174 A69-26797

Soviet space program, discussing launch sites, series of launch vehicles and mission identification 13 p2381 A69-27303

Esro 1 satellite program management, discussing scientific mission, structure, tracking system and history 13 p2355 A69-27360

Logic family with low power consumption subjected to 1 Mev electrons analyzed within telemetry circuit concept for space application 15 p2625 A69-30830

Microbiology quality assurance program for planetary mission, considering spacecraft sterilization during fabrication, test and launch site activities 15 p2559 A69-31124

Flight instrument package for change of energy absorption and energy radiation of vehicle surfaces during various phases of space vehicle mission 15 p2613 A69-31269

NASA planetary program, discussing Mars, Jupiter, Mercury, Venus and Saturn missions 15 p2723 A69-31318

Book on space age management, considering large scale approach 16 p2881 A69-31766

System state phase modeling as method for evaluating safety and reliability by analysis of system states in mission phases through logic diagram 18 p3142 A69-34480

Permissible radiation doses for extended space missions, discussing clinical tests on dogs 18 p3095 A69-34727

Mariner 6 and 7 Mars probes, describing mission profile, basic structure, trajectory design and scientific experiments 18 p3198 A69-34795

Integrated test program based on mission requirements, failure mode and effects analysis with feedback from testing to design and development functions 19 p3327 A69-36014

Missile and space support planning, objectives, technology development, functions, maintenance and in-flight maintainability 19 p3295 A69-36327

Research satellite, commercial satellite, lunar spacecraft and military satellite missions, discussing Intelsat, Comsat, Early Bird, MOL and ESRO space program 19 p3432 A69-36750

Worldwide cloud cover simulation procedure providing data for computer simulation of earth oriented space missions, describing computer program using Monte Carlo mission simulation 20 p3573 A69-38120

Space mission sensitivity to parameters of interest determined by Monte Carlo simulation samples 21 p3804 A69-39036

CircumJovian powered and free return trajectories, analyzing round trip missions and departure opportunity [AAS PAPER 68-117] 21 p3805 A69-39207

Celestial sphere scanning by passive method applicable to space missions requiring long lifetime and moderate pointing accuracies [AIAA PAPER 68-854] 21 p3767 A69-39764

Laboratory prototype of RF ion engines for space test, discussing components optimization 22 p3998 A69-39904

Aerodynamic deceleration systems for space missions, considering deployment of subsonic parachute and inflatable configuration following atmospheric entry [AIAA PAPER 68-1081] 22 p4036 A69-40542

Centrifuge on board orbiting spacecraft as research tool for biological and physical experiments relevant to prolonged missions and spacecraft design 23 p4108 A69-41833

Navigation systems analysis for space missions planning, discussing onboard equipment and lunar landing accuracies [AAS PAPER 69-406] 24 p4347 A69-42833

Separation system for collecting wash and waste water from gaseous environment and separating liquid and gaseous phases during space missions [AAS PAPER 69-473] 24 p4272 A69-42845

SPACE NAVIGATION
NT INTERPLANETARY NAVIGATION

Legal problems in space navigation and solution through international law including air and outer space limits, regulating authority and damage liability [UN PAPER 68-95475] 01 p0179 A69-10511

Apollo landmark sighting by astronaut using Apollo onboard navigation system, simulating cloud cover effects with Monte Carlo technique 01 p0110 A69-10692

Autonomous solution to orbital navigation problem yielding direct measure of orbital parameters 01 p0114 A69-11005

Two dimensional representation of Venus entry probe target data for determining probe capability to provide real time data transmission to earth 02 p0331 A69-12820

Ground based guidance systems for supplementing onboard guidance of manned space vehicles 06 p0955 A69-17580

Sight reduction tables for orbital plane determination checked out by sextant sightings onboard Gemini 7 07 p1177 A69-19206

Legal problems in space navigation and solution via international law including air and outer space limits, regulating authority and damage liability 07 p1244 A69-19233

Manual onboard computation procedures and devices for determination of maneuvers for orbital navigation and guidance 08 p1348 A69-21184

Pure inertial navigation system support by supplying additional or redundant navigational information, considering space flight applications and earth related problems 12 p2128 A69-25873

Space vehicles and marine navigation using navigation satellites, radar, Doppler navigation, etc 13 p2296 A69-27918

Optimal linear space navigation policies including integrated nongravitational acceleration output from inertial measuring unit 14 p2479 A69-29487

Satellite space navigation system providing three component position in geodetic coordinates instantly and accurately on or near earth 15 p2650 A69-30088

Initial-convergence examination of Kalman filter for various autonomous navigation modes [AIAA PAPER 67-623] 16 p2809 A69-31875

Peano-Baker method for integration of variational equations to produce partial derivatives used in satellite trajectory estimation 19 p3398 A69-35616

Space navigation - Conference, Houston, April 1969 19 p3368 A69-35789

Mars autonomous entry navigation, discussing flight path angle control with onboard sensors using realistic sun, Canopus and planet line of sight tracker accuracies 19 p3368 A69-35790

Earth orbit estimation by manual stadimeter, space sextant and small data processor, discussing orbital parameter errors due to instrument and environment uncertainties 19 p3369 A69-35793

Masking and standby redundancy approach to fault tolerance in space navigation computers with illustrations, discussing automatic maintenance 19 p3279 A69-35798

Star/horizon measurements for onboard spacecraft navigation without cloud cover obscuration, discussing sightings, data processing and evaluation 19 p3369 A69-35800

Navigation, guidance and control developments for manned space missions, discussing earth orbital exploration bases 19 p3369 A69-35801

Strapdown electrostatic aerospace navigator /SEAN/ using electrostatically suspended gyros /ESG/ for inertial reference, including drift and computer tests 19 p3369 A69-35802

Navigational accuracy dependence on spacecraft geometry, determining information content and critical error sources of earth based Doppler radio tracking data [AAS PAPER 69-112] 19 p3402 A69-35935

Approach navigation accuracy for planetary atmosphere braking to orbit about Mars and Venus [AAS PAPER 68-122] 19 p3402 A69-35937

Continuously powered deep space vehicle orbit determination, discussing state estimation accuracy and use of continuous data filtering [AAS PAPER 68-144] 19 p3402 A69-35939

Missile and spacecraft guidance navigation and control, discussing fluidics, self adaptive and digital control and Kalman filtering 19 p3370 A69-36316

Horizon definition for Apollo space navigation references from examining earth atmosphere visible and far IR spectrum [AIAA PAPER 69-869] 21 p3763 A69-39395

Statistical error analysis of autonomous manned spacecraft navigation in long duration eccentric Mars orbits [AIAA PAPER 69-880] 21 p3763 A69-39406

Navigation state vector update effect on lunar mission completion capability for Saturn 5, emphasizing hardware and scheme errors and accelerometer failure [AIAA PAPER 69-883] 21 p3764 A69-39409

Guidance and control in space - Conference, Warsaw, June 1969 21 p3825 A69-39628

Navigation systems analysis for space missions planning, discussing onboard equipment and lunar landing accuracies [AAS PAPER 69-406] 24 p4347 A69-42833

Manual method for navigating and guiding spacecraft to rendezvous with orbiting target, using hand-held unpowered optical instruments and manual computations [AIAA PAPER 68-859] 24 p4348 A69-43243

SPACE ORIENTATION

Soviet astronaut experiences and visual impressions during space walk outside Voskhod 2, noting dominance of optical analyzer in space perception and orientation [UN PAPER 68-95717] 06 p1000 A69-17049

Human perception in space as function of nervous relationships involving optic, kinesthetic, vestibular and other analysors 08 p1263 A69-19938

Visual systems of hamster brain, discussing relative visual localization and discrimination blindness produced by ablation of cortical or tectal areas 08 p1265 A69-20685

Visual orientation near moon and at surface, considering terrestrial and lunar objects reflectivity and light reflection at various angles of incidence 14 p2525 A69-29750

SPACE PERCEPTION
NT AUTOKINESIS

Hyperstereoscopic and hypostereoscopic hologram images with doubled or halved interocular distance, noting effect on image depth 02 p0249 A69-11931

Soviet astronaut experiences and visual impressions during space walk outside Voskhod 2, noting dominance of optical analyzer in space perception and orientation [UN PAPER 68-95717] 06 p1000 A69-17049

Visual distortion in discrimination of figure proportion 06 p0875 A69-18022

Coriolis stimulus effect during centrifugal g load on spatial orientation and accompanying stick performance 06 p0876 A69-18023

Spatial disorientation as factor in accidents in operational command, noting relatively high experience level of involved pilots 07 p1072 A69-19431

Group observers magnitude estimation judgements of stationary spacecraft model apparent distance in simulated space, obtaining psychophysical functions for three stimulus ranges 07 p1069 A69-19501

Human perception in space as function of nervous relationships involving optic, kinesthetic, vestibular and other analysors 08 p1263 A69-19938

Maximum indicative absolute magnitudes of 33 supernovae, discussing usefulness as distance indicators 10 p1774 A69-22967

Jet fighter pilot spatial disorientation during flight and on ground, emphasizing vestibular neuronitis diagnosis 10 p1649 A69-23382

Distance discrimination in simulated space environment, studying just noticeable difference /JND/ to determine relations between distance threshold and observation distance 12 p2022 A69-26372

SPACE PHOTOGRAPHY

Visual orientation near moon and at surface, considering terrestrial and lunar objects reflectivity and light reflection at various angles of incidence
14 p2525 A69-29750

Luminescence effects on apparent size and shape of foveally fixated targets of various forms
19 p3259 A69-36458

Orientation reflexes of animals in weightlessness, analyzing turnover, vestibular and cervix reactions using motion pictures
20 p3470 A69-37248

Red shift-distance relation for galaxies, discussing time dependence
20 p3597 A69-37411

Mathematical models of human vestibular system for dynamic space orientation, using control theory
21 p3662 A69-38728

Mathematical models for describing visual perception of distance to ground during VTOL landing and takeoff
22 p3892 A69-40282

Target distance and direction monocular estimates with stabilized and nonstabilized retinal images, finding eye movements not improving spatial judgment accuracy
22 p3878 A69-40838

Stereoscopic shadow caster application to photographic stereoscopic projection for studying binocular stereopsis under kinetic viewing conditions in vision research
22 p3893 A69-40839

Device for studying stereoscopic field of vision applied to determining field of vision standards for healthy individuals
22 p3886 A69-41113

Head movement affecting visual and kinesthetic localization accuracy, discussing free and fixed head conditions
24 p4275 A69-43118

Mathematical input-output model for vestibular system, relating linear and angular motions to non-visual perception of orientation, motion and nystagmus for physiological characteristics
24 p4276 A69-43274

SPACE PHOTOGRAPHY

U SPACEBORNE PHOTOGRAPHY

SPACE POWER UNIT REACTORS

NT SNAP 8
NT SNAP 10A

Lunar surface power plants, considering weight constraint for various systems using nuclear power, solar cell/fuel cells and H-O reactant regeneration
01 p0013 A69-11396

Out-of-core thermionic space power generators using heat pipes, discussing feasibility in geometry, heat pipes, reactor, shield, heat exchanger and radiator
08 p1256 A69-19856

Thermionic space power reactor design, detailing Critical Experiment problems
09 p1441 A69-21835

SPACE PROBES

NT EXPLORER 18 SATELLITE

NT LUNAR PROBES

NT LUNIK LUNAR PROBES

NT LUNIK 9 LUNAR PROBE

NT LUNIK 10 LUNAR PROBE

NT LUNIK 12 LUNAR PROBE

NT LUNIK 13 LUNAR PROBE

NT MARINER SPACE PROBES

NT MARINER SPACECRAFT

NT MARINER 1 SPACE PROBE

NT MARINER 2 SPACE PROBE

NT MARINER 4 SPACE PROBE

NT MARINER 5 SPACE PROBE

NT MARINER 6 SPACE PROBE

NT MARINER 7 SPACE PROBE

NT MARINER-MERCURY 1973

NT MARS PROBES

NT PIONEER SPACE PROBES

NT PIONEER 6 SPACE PROBE

NT PIONEER 7 SPACE PROBE

NT PIONEER 8 SPACE PROBE

NT PIONEER 9 SPACE PROBE

NT RANGER LUNAR PROBES

NT SOLAR PROBES

NT SURVEYOR LUNAR PROBES

NT SURVEYOR 1 LUNAR PROBE

NT SURVEYOR 5 LUNAR PROBE

NT SURVEYOR 6 LUNAR PROBE

NT SURVEYOR 7 LUNAR PROBE

NT VENERA SATELLITES

NT VENERA 4 SATELLITE

NT VENUS PROBES

NT ZOND SPACE PROBES

NT ZOND 5 SPACE PROBE

NT ZOND 6 SPACE PROBE

Soviet space astronomy including rocket, satellite and space probe measurements for solar, stellar, planetary and lunar studies
01 p0155 A69-10946

Radio links between earth and deep space probes, summarizing bistatic radar astronomy results
[AAS PAPER 68-182] 02 p0311 A69-11467

S-band radio occultation for probing atmospheres of Mars and Venus
[AAS PAPER 68-185] 02 p0311 A69-11470

Satellites use in French space meteorology, discussing evolution, achievements, Eole project, etc
02 p0275 A69-11911

Temporary launching sites for rocket probes, discussing CNES activity, Dragon and Titus programs and mobile launching units
02 p0228 A69-11921

HORA, flexible upper rocket stage, noting variable fuel tank capacity and high energy propulsion
08 p1409 A69-20094

Low thrust space probe mission to Halley comet, utilizing nuclear electric propulsion
10 p1772 A69-22864

Tabular listing of Soviet satellites, spacecraft, probes and rockets launched between October 1957 and October 1967
13 p2355 A69-27359

Venusian atmospheric model based on Venera 4 measurements, calculating probe distance travel, temperature, density and pressure profiles
13 p2345 A69-27688

German solar and space probe Hora, discussing payload and propellant
13 p2357 A69-28638

Comets considered as natural interplanetary space probes, stressing need for international cooperation on solar system studies
15 p2679 A69-30011

IQSY low energy galactic and solar cosmic ray observations made by various satellites and space probes, including hydrogen and helium energy spectra
15 p2673 A69-30014

Earth sensor for spin stabilized spacecraft to maintain specific orientation with earth, discussing use of blue and red filters
15 p2609 A69-30593

Zodiacal light brightness and polarization measurements from space probes approximated by Mie scattering of interplanetary dust particles
16 p2857 A69-32092

Tacite rocket probe to study space IR radiation, using passive stellar sensor for recording reference stars positions to recalibrate gyroscope kinetic motion for attitude restoration
[ONERA-TP-731] 17 p3001 A69-33220

Future combined environment space simulation tests duplicating environment interaction encountered during earth orbits, deep space probes and manned flights
19 p3288 A69-35531

Optimal control stationkeeping for maintaining space probe stability around collinear points in three body problem
[AIAA PAPER 69-906] 21 p3807 A69-39338

Spatial region accessible to earth launched probes determined for mission planning for exploration of aperiodic comets, discussing orbit parameters
23 p4212 A69-41536

Spacecraft probes design for mapping meteoroid environment and penetration hazard through asteroid belt
[AAS PAPER 69-321] 24 p4392 A69-42867

Asteroid exploration by solar photovoltaic powered ion propelled probe, discussing spacecraft design, mission and 1975 Mariner utilization
[AAS PAPER 69-322] 24 p4381 A69-42868

SPACE PROGRAMS

NT APOLLO PROJECT

NT LUNAR PROGRAMS

NT SURVEYOR PROJECT

Space applications program including communications and navigation meteorology, earth resources survey and geodesy
[UN PAPER 68-95437] 01 p0178 A69-10472

Meteorological satellite research program, including unmanned satellite observations and possibilities with meteorologist on board manned spacecraft
[UN PAPER 68-95350] 01 p0109 A69-10483

Space program effects in education, science and engineering, noting impact of first satellite on U.S. research and technology
01 p0179 A69-10500

Japanese space research organizations, sounding rockets, meteorology, satellite communications, geodesy, etc
[UN PAPER 68-95563] 01 p0151 A69-10501

NASA university program, discussing participation in space and aeronautics development based on project oriented research grants and Sustaining University grants
[UN PAPER 68-95413] 01 p0179 A69-10506

NASA programs and opportunities for international cooperation in space
[UN PAPER 68-95367] 01 p0179 A69-10516

U.S. space program projections, discussing earth orbit operations, lunar and planetary explorations, costs and timetable
02 p0355 A69-11744

Space simulation tests in TFS /Technological Feasibility Spacecraft/ program, discussing two interplanetary cruise modes and deorbit mode selected for simulation
02 p0227 A69-11757

Galactic Jupiter Probes investigating Jupiter atmosphere and emissions and deep space cosmic radiation
02 p0324 A69-12303

Future space programs as governed by cost limitations, suggesting development of economical launch vehicle for shuttling between earth and orbital space stations
02 p0326 A69-12680

French solid propellant sounding rockets proposed launching from Guiana base using different fuel propulsion systems
03 p0518 A69-12851

NASA Space Application Program strategy, discussing research and development trend toward complexity, versatility and multidisciplinary use of larger spacecraft
03 p0511 A69-13427

U.S.-European cooperation in space activities, discussing implementation by COSPAR and jointly owned industrial corporations
03 p0535 A69-13586

Cooperation in developing space programs between Western Europe and U.S.
03 p0535 A69-13588

Cooperation between U.S. and Europe in space programs, discussing contracts and conditions
03 p0535 A69-13590

U.S.-European cooperation, stressing unsatisfactory role of European industry and governments in space projects
03 p0536 A69-13595

National programs relationship to progress in technological societies
03 p0536 A69-14245

Canadian upper atmosphere and space research programs organization, management and results
[UN PAPER 68-95551] 06 p1042 A69-17034

Australian sounding rocket programs carried out in conjunction with U.S. satellite experiments
[UN PAPER 68-95214] 06 p1013 A69-17076

Stimulating effects of space hypersonic experiments on technical and scientific progress, discussing steel degassing, welding, electroforming and geological applications
[UN PAPER 68-95459] 06 p0857 A69-17083

U.S. aerospace programs, reviewing manned space missions, space applications, space science, transportation, strategic and tactical warfare and influence on aerospace industry
07 p1243 A69-18376

Future launch vehicle programs for automated space missions, discussing higher launch velocities and economics
[AIAA PAPER 68-447] 09 p1610 A69-21983

Space exploration plans adaptation, considering spacecraft design, programs, costs and schedules flexibility
10 p1811 A69-22863

Space flight research programs including stellar and biological evolutions and environmental control
12 p1555 A69-26005

Space experiments analysis involving standardization for economy and mission thesis compromise, detailing aeronomic satellite project with integrated utilization
12 p1273 A69-26128

Boosters and space vehicles including earth satellites, lunar probes and interplanetary spacecraft
13 p2356 A69-27914

Earth orbital manned space astronomy, discussing long range program, instruments, facilities and data processing
13 p2240 A69-27947

Integrated circuits failure analysis in space program applications, describing electrical analog for notification, fact gathering, part analysis and corrective action functions
15 p2580 A69-31132

Indonesian space activities covering sounding rocket program, communication satellite ground station erection, etc
15 p2723 A69-31428

Report on Canadian space activities to COSPAR covering scientific satellite program, high altitude sounding rocket program, space radio communications, international cooperative programs, etc
15 p2723 A69-31429

Report on U.S. space science program to COSPAR on stellar and solar astronomy, lunar and planetary research, upper atmospheric physics, etc
15 p2723 A69-31430

Scientific research report on cosmic ray and X ray astronomy by constant altitude stratospheric plastic balloons, etc
15 p2723 A69-31431

Brazilian space activities covering launching sites, rocket experiments in meteorology, ionosphere and X ray astronomy, balloon experiments and ground observations
15 p2724 A69-31434

Australian space research including space flight programs in cooperation with NASA
15 p2724 A69-31450

Argentina space research report to COSPAR covering Orion II sounding rocket, balloon experiments, cosmic rays, X ray astronomy, international cooperative programs, etc
15 p2724 A69-31452

Pakistan space research covering meteorological rocket program, Na/K vapor experiment, satellite tracking, etc
15 p2724 A69-31455

Japan space research covering sounding rockets, balloons, satellites and facilities
15 p2725 A69-31466

Manned space stations role in future space plans, discussing prototypes and conceptual design
16 p2866 A69-31736

Space program design, discussing NASA centers and NASA R and D life sciences, technological developments and federal action
17 p3076 A69-34042

Commercial utilization of space - Conference, Dallas, May 1967
17 p3041 A69-34043

General technology history, stressing space technology and programs influencing developments in other fields
17 p3076 A69-34045

Scientific space research program /1968-1978/ outlining advanced lunar orbiter and Mars, Venus and Mercury probes
18 p3193 A69-34360

Frequency bands allocations for space research and radio astronomy development, noting Inter Union Commission of Frequency Allocations recommendations
18 p3100 A69-34376

Manufacturing in space based on nongravity and hard vacuum environment, considering crystal growth and refinement, perfectly shaped bodies, refractory metals ultrapurification, etc
18 p3234 A69-35066

Space manufacturing operations program, discussing zero gravity effect during earth orbit flight, Apollo Applications Program Orbital Workshop Flight 2, etc
18 p3208 A69-35067

AIAA view on Post-Apollo space program, considering multiple goals, unmanned application satellites and manned space flight objectives
18 p3236 A69-35136

Earth orbital space program mission effectiveness increased through utilization of standby launch vehicles, spacecraft and space station systems
19 p3430 A69-36010

Research satellite, commercial satellite, lunar spacecraft and military satellite missions, discussing Intelsat, Comsat, Early Bird, MOL and ESRO space program
19 p3432 A69-36750

Juridical meaning of peaceful in 1967 Space Treaty interpreted in terms of real purpose of given space activity
20 p3635 A69-37105

International lawyers proposal for compulsory registration of space activities in connection with astronauts rescue and damages liability
20 p3637 A69-37118

INTELSAT program, discussing U.S. proposals regarding domestic services, separate satellite programs, etc
20 p3637 A69-37121

Domestic and international law compared in connection with space program, considering legal aspects of using satellites in discovering and exploiting earth resources
20 p3639 A69-37132

Low cost rate transportation as mandatory goal for future space program, discussing recovery and reuse, launch system costs, hardware development, etc
20 p3618 A69-38117

PostApollo space goals based on manned and unmanned planetary exploration and space science programs, considering human factors and propulsion problems
21 p3856 A69-39167

Nuclear rocket program status and plans, presenting NERVA reactor and engine system tests
[AIAA PAPER 68-610] 21 p3768 A69-39219

Space transportation cost factors, discussing payload characteristics, carrier utilization, program duration, government participation and control, carrier design, hardware costs, launch costs, etc
21 p3857 A69-39687

Strategy for exploration of inner solar system leading to origin and history, detailing lunar exploration program
22 p4022 A69-40449

Satellite data management systems design, considering user-designer cooperation aspects for space programs
[AAS PAPER 69-366] 24 p4417 A69-42806

Fiscal requirements forecasting for space systems involving data analysis
[AAS PAPER 69-166A] 24 p4417 A69-42814

Space program planning, noting market requirements, acceptability and future characteristics
[AAS PAPER 69-083] 24 p4418 A69-42820

Space research in past and expected scientific knowledge from manned and automated earth orbital science missions
[AAS PAPER 69-036] 24 p4379 A69-42825

Economic aspects of future space activities noting systems analysis, operations research, manned and unmanned space capabilities, etc
[AAS PAPER 69-113] 24 p4418 A69-42878

Cape Kennedy space research and national priorities, indicating performance and progress of future space operations
[AAS PAPER 69-110] 24 p4419 A69-42879

Space flight programs management cooperation and limited competition advantages, emphasizing single management team responsibility for effective multi-lateral activities
24 p4419 A69-43043

SPACE RADIATION
U EXTRATERRESTRIAL RADIATION

SPACE RADIATORS
U SPACECRAFT RADIATORS

SPACE RATIONS
Higher plants utilization as nutrition source in space missions, comparing weight requirements for cultivation equipment and food storage
15 p2560 A69-31408

SPACE RENDEZVOUS
NT ORBITAL RENDEZVOUS

Space rendezvous problem as applicable to interplanetary missions, discussing steps in rendezvous maneuvers to permit final docking
03 p0511 A69-13401

Minimum fuel consumption for low thrust jet engine propelled space vehicles maneuvering in circular trajectories
05 p0829 A69-15879

Parallel rendezvous of space vehicles in central gravitational field, discussing relative motion of space vehicle and supplementary force required
05 p0789 A69-16047

Rendezvous maneuver with minimum fuel in circular orbit solved without restrictive conditions for accelerations due to approach thrust
16 p2852 A69-31558

Low thrust trajectories for minimum time rendezvous between continuous thrust interceptor and passive target vehicle, comparing calculus of variations and steepest ascent analyses
16 p2857 A69-32177

Optimal low thrust coplanar rendezvous control for thrusting vehicle and passive vehicle in elliptical orbit using linearized equations of motion and polar coordinates
20 p3617 A69-37192

Parallel rendezvous of space vehicles in central gravitational field, discussing relative motion of space vehicle and supplementary force required
20 p3574 A69-37956

Halley Comet rendezvous mission, comparing low thrust mode with ballistic Jupiter or Saturn swingby mode
[AIAA PAPER 69-933] 21 p3809 A69-39360

Computer program /TACTICS/ for simulating three vehicles simultaneous motion in space, considering interceptor-target guidance and intercept trajectories
[AIAA PAPER 69-890] 21 p3678 A69-39415

Space rendezvous methods from developmental environment to operational method
21 p3824 A69-39474

Rendezvous, intercept and injection optimal control laws derived from inhomogeneous linear differential equations with quadratic performance index
23 p4224 A69-41921

Quasi-optimum control law for minimum-time bounded acceleration rendezvous in central force field using Friedland technique, with application to lunar flight
24 p4349 A69-43313

SPACE RENDEZVOUS MANEUVERS
U SPACECRAFT MANEUVERS

SPACE SCIENCES
U AEROSPACE SCIENCES

SPACE SIMULATORS
NT HIGH VACUUM ORBITAL SIMULATOR

Solar thermal vacuum test for space flight qualification of military spin stabilized synchronous orbit communications satellite
15 p2587 A69-30391

Selectively pumped thermal vacuum test chamber for orbital heat transfer and environment simulation for flight vehicle performance prediction
15 p2587 A69-30392

Test facility for space vehicles simulating outer space gas pressure, heat sink behavior and relative motion to sun, detailing design and operation
21 p3689 A69-38420

Space simulation facility assembly and operational testing
22 p3919 A69-39959

Xenon high wattage short arc lamps for space/solar simulators, describing seals, electrodes shapes and cooling, operating characteristics, etc
[AIAA PAPER 69-998] 22 p3920 A69-40376

Space simulator vacuum facility for optical satellite tests, construction, operation and maintenance, emphasizing noncontaminating environment and pumping systems
[AIAA PAPER 69-1026] 22 p3924 A69-40396

Molecular beams for simulating orbital flight through planetary atmospheres, considering various nozzle beam systems
[AIAA PAPER 69-1031] 22 p3926 A69-40437

Unstabilized astronaut, hand-held and integrated life support EVA maneuvering units tested in gimbaled six degree of freedom servo driven moving base simulator
[AAS PAPER 69-516] 24 p4272 A69-42850

SPACE STATIONS
NT ORBITAL SPACE STATIONS
NT ORBITAL WORKSHOPS

Synchronous observations of satellites by photographic techniques from satellite stations, discussing reference stars plane coordinates and exposure time recording
01 p0027 A69-10224

Space station design requirements, Apollo applications program and various experimental programs
01 p0163 A69-11395

Buoyant station with science package designed for long duration missions with horizontal mobility in Venus atmosphere
02 p0333 A69-11745

Space-station-centrifuge configuration dynamic stability exhibiting instabilities at lower and higher centrifuge rotational speeds
[AIAA PAPER 68-142] 02 p0334 A69-12373

Permissible development direction for space research, discussing space station, required systems and cost estimates
05 p0829 A69-15920

Equations formulated for space vehicle reaction to rotating machinery and internal mass motion, evaluating dynamics of cylindrical space station rotating about major axis
05 p0827 A69-16476

Efficient life support systems for prolonged space missions, discussing scientific and experimental research
[UN PAPER 68-95778] 06 p0879 A69-17040

Wideband uncooled two stage reflecting parametric amplifiers with low noise temperature, noting application to space stations for telecommunications by satellites
07 p1099 A69-18463

SPACE STORAGE

Coriolis acceleration in rotating environment, discussing origins and role in human existence in rotating space station 09 p1540 A69-21891

Model simulation in program planning for space station with emphasis on accommodation of logistics 10 p1669 A69-22976

Large power systems integration in manned space stations, discussing design, selection and application criteria 13 p2209 A69-27939

Manned space stations role in future space plans, discussing prototypes and conceptual design 16 p2866 A69-31736

Satellite solar power station proposed for power generation for future requirements, discussing world energy needs and finiteness of fossil fuel reserves 16 p2867 A69-31817

Space station observations of stars, galaxies and quasars, stressing electromagnetic spectrum role in astronomy 18 p3194 A69-34370

Space docking, personnel placement on space stations, rescue stations, etc 18 p3196 A69-34630

Technological possibilities of gravity free production in space environment, discussing containerless manufacture of glass, liquid metal manipulation and defect free fibers 18 p3206 A69-35490

Earth orbital space program mission effectiveness increased through utilization of standby launch vehicles, spacecraft and space station systems 19 p3430 A69-36010

Manned lunar bases from legal viewpoint, discussing national jurisdiction, personnel policies, mineral rights, etc 20 p3637 A69-37119

Crew and passenger transportation to and from space station orbits, discussing cost reduction possibilities with current or future technology 21 p3827 A69-39691

Electric power system selection for long duration manned space station [AIAA PAPER 68-1034] 22 p3869 A69-40549

Space station safety, discussing damage containment and control, escape and rescue, etc [AAS PAPER 69-518] 24 p4392 A69-42842

SPACE STATION

Thermal protection system optimization for storage of cryogenic propellants in space, noting vented systems [AIAA PAPER 69-27] 06 p1039 A69-18211

Space storable propulsion system comparison, discussing liquid propellants performance and thermodynamic analysis [AIAA PAPER 68-614] 09 p1570 A69-21981

Mathematical model of closed biological cycle regenerating part of life support products, incorporating astronaut, storage and regenerating waste disposal units 10 p1649 A69-23580

Heat pipe boil-off control system for reducing cryogenic boil-off during long term space storage 12 p2191 A69-26793

Thermal insulation for cryogenic storage in space, discussing Apollo service module conversion to cryogenic service module 12 p2175 A69-26827

Combustion performance evaluation program demonstrating high performance with space storable propellant combination of FLOX, methane and ethane [AIAA PAPER 69-507] 16 p2829 A69-31848

Space storable regenerative cooling with FLOX/methane under conditions for small pump fed engine, describing injector and chamber design [AIAA PAPER 69-509] 16 p2844 A69-32718

Specific impulse deliverable performance of space storable propellant combination fluorine-oxygen/methane and oxygen difluoride/diborane [AIAA PAPER 69-505] 16 p2845 A69-32762

Space storable hydrocarbon fuel blended FLOX propellant performance with coaxial injector including characteristic velocity, chamber geometry, pressure and heat flux distribution [AIAA PAPER 69-507] 16 p2835 A69-32772

Rocket performance optimization by extending injector design technology to high performance injectors for space storable FLOX/LPG propellants [AIAA PAPER 69-506] 16 p2846 A69-32778

Payload optimization factors for orbital storage of liquid hydrogen, considering payload cost of agitation, tank pressure, pressurant weight, etc [AIAA PAPER 69-1007] 22 p4021 A69-40381

SPACE SUITS

Hard space suit for use on planetary surfaces and extravehicular activity, discussing design, fabrication and mobility 03 p0379 A69-12993

Sensible heat exchange from Gemini and Apollo space suits determined in environmental test facilities, presenting data for heat flux distributions 06 p0880 A69-17089

Astronaut extravehicular protection systems, discussing space suit, life support and thermal control subsystems and micrometeoroid protection 06 p0882 A69-17643

Space and immersion suits physiological evaluation by pulse duration multiplexing telemetry, using commercial FM receiver 06 p0883 A69-17845

Improved suit for lunar wear, noting production and qualifying schedule and astronaut tests 08 p1267 A69-21146

Discharge rates of metabolic products in men confined in pressure chamber wearing airtight suits and gas masks 10 p1646 A69-23508

Passive thermal control system for space suit use in extravehicular environment, discussing skin temperature control at varying heat flow rates 12 p2023 A69-26549

Space suit meteoroid protection for extravehicular activity, discussing Gemini and lunar surface EVA suits and bumper concept [AIAA-PAPER-69-366] 13 p2213 A69-28298

Heat pipe devices applied to radiative body heat transfer in space suit temperature control [AIAA PAPER 69-619] 17 p2914 A69-33293

Carbon dioxide levels monitoring in spacesuit research including limits of physiological acceptability 21 p3665 A69-39170

Hard space suit temperature history during lunar operational task simulation 21 p3666 A69-39182

Space cabin and suit pressures for decompression sickness avoidance and fire hazard alleviation 22 p3890 A69-40212

Manned testing of EVA equipment in thermal-vacuum environment for qualification of Apollo extravehicular mobility unit, using lunar surface thermal simulator [AIAA PAPER 69-992] 22 p3893 A69-40370

Real time metabolic rate analysis of suited astronaut using heart rate and O methods during thermal vacuum and extravehicular mobility tests [AIAA PAPER 69-993] 22 p3893 A69-40371

Computerized mass spectrometer for monitoring atmosphere in astronaut suits and cabin [AIAA PAPER 69-1016] 22 p3922 A69-40388

EVA/IVA fluid umbilical improved stowability and flexibility, discussing cross section development and tests [AAS PAPER 69-470] 24 p4272 A69-42847

SPACE SURVEILLANCE

Space surveillance radar system sensor misassociation of one space object for another, noting applicability to sonar and optical sensors 02 p0210 A69-12388

SPACE SURVEILLANCE [GROUND BASED]

Lake Kickapoo Space Surveillance Transmitting Station in Texas, discussing surroundings, equipment, operating range, VHF transmission, etc 03 p0411 A69-13209

Multiradar system development for total view of air situation from single air views, using digital computers interconnected with central computer 05 p0719 A69-15932

SPACE SURVEILLANCE [SPACEBORNE]

Photometric-polarimetric observations of planetary surfaces, discussing geological environment interpretation and spacecraft reconnaissance system mission planning 03 p0421 A69-13394

Ground coverage of oblate planets by spin stabilized satellites, determining ground areas visible to satellite by solution of quadratic equations 03 p0522 A69-14244

Aeronautical service satellites, considering communications, surveillance for navigation, traffic control, collision avoidance and search and rescue, weather and border control functions 04 p0666 A69-15295

Earth resources remote sensing from spacecraft noting meteorology, oceanography, forestry, agriculture and IR detection of plant diseases and pollution 12 p2192 A69-26978

Correlation spectrometer for air pollution surveillance from airborne and spaceborne platforms, noting scanning satellite system for continuous global coverage 12 p2096 A69-26981

Remote oceanographic sensing from ships, aircraft and spaceborne platforms, using active /radar and laser/ and passive sensors in visible, IR and microwave regions 12 p2075 A69-26997

Experimental SST terminal for satellite L band communications/surveillance ATC system, establishing terminal requirements for NASA and FAA studies 17 p2932 A69-34118

Tracking and data relay satellite system /TDRSS/ compared to ground based mission support, considering altitude coverage capability, economy and communication requirements 23 p4120 A69-41756

SPACE SYSTEMS ENGINEERING

U AEROSPACE ENGINEERING

SPACE-TIME CONTINUUM

U RELATIVITY

SPACE-TIME FUNCTIONS

Killing fields applied to nonsymmetric spaces specify coordinate lines with slowest possible metric tensor variation and gravitational radiation 01 p0115 A69-10018

Random temperature fields in plates and shells in thermal contact with two media with temperatures as separable random space-time functions 01 p0173 A69-10077

Asymptotic behavior of curvature and conformal curvature tensors on asymptotically flat space-time 01 p0116 A69-10393

Field theory of gravitation, discussing consequence of universality of gravitation /space-time geometry determination/ 01 p0116 A69-10443

Electromagnetic fields in vacuum extended to fields in presence of matter, deriving field equations covariant under Lorentz proper and improper transformations 02 p0281 A69-12196

Equations of motion for arbitrary first order perturbations around any spherically symmetric metric 02 p0328 A69-12730

Static locally flat solutions of Einstein vacuum field equation with line singularities and global space curvature, noting analogy to electromagnetic fields 03 p0466 A69-13389

Conformal change and connection relations in Einstein unified field theory, noting tensor applications 03 p0467 A69-13756

Ring laser field space-time pattern from light waves scattered at discontinuities, discussing equations of motion of solid state laser 03 p0441 A69-14140

Canonical equations for Lagrangian form of gravitational field equations in empty space 04 p0658 A69-14899

Existence theorem for periodic solutions of parabolic boundary value problem for infinite space time cylinder 04 p0624 A69-15004

Cosmology, experiments on gravitation, space-time theory and model of universal history 04 p0661 A69-15157

Space-time function for joint probability distribution of velocity and magnetic fields from hydromagnetic turbulence equations 04 p0638 A69-15277

Space-time diffraction for asymptotic solution of Klein-Gordon equation, studying one dimensional dispersive medium 05 p0802 A69-15930

Existence of cosmic time functions based on stable causality condition /absence of closed timelike or null curves in Lorentz metric/ 06 p0957 A69-17471

Necessary and sufficient conditions for Einstein spaces of second embedding class 06 p0957 A69-17547

Optimum length of Fourier time series approximating diurnal F2 critical frequency variation on planetary scale 06 p0921 A69-17746

Equation describing statistically trapped particle motion under influence of fields varying in time and space 07 p1209 A69-19375

Petrov classification of cylindrically symmetric space-time, giving Weyl conformal curvature tensor and surviving Ricci tensor components 07 p1182 A69-19409

Riemann metric leading to empty flat space from Rainich equations of already unified field theory
07 p1182 A69-19418

Plane symmetric perfect fluid cosmological model derived from class 1 considerations, evaluating scalar invariants for line element
07 p1222 A69-19586

Space-time evolution of one Petrov type into another, obtaining algorithm, flow diagram and discontinuous hypersurfaces results
08 p1350 A69-19789

Space time structure conditions derived for compatibility with simultaneous fulfillment of causality and equivalence principles
08 p1351 A69-19948

Primordial magnetic field effects on spatially homogeneous cosmological models with anisotropic Euclidean metric
08 p1383 A69-20049

Einstein space time concepts for unified formalism of matter interactions from elementary particles to astronomical bodies, discussing relativity theory
08 p1352 A69-20730

Analytical description of planetary distribution of space-time variations of fOF2, deriving Fourier series as function of UT
09 p1486 A69-21545

Space-time variations for approximating sporadic E layer critical frequencies of geographic and time distribution curves
09 p1486 A69-21547

General theory of relativity and tensor field equations relating space time characteristics to local properties of matter and vacuum, using Palatini Lagrangian method
09 p1593 A69-21572

Kerr type metric empty space times starting from fixed reference system and associated Killing vectors
09 p1540 A69-22050

Acoustic waves pressure field micropulsations in turbulent fluid, analyzing space-time spectrum
09 p1492 A69-22710

Four dimensional space-time immersion in conformally flat six dimensional space or flat eight dimensional space, noting group of isometries of tangent spaces
10 p1774 A69-23162

Relativity theory examined critically, discussing spherical space, Lorentz transformation and Einstein conclusions
10 p1725 A69-23317

F 2 layer state prediction as function of solar activity by series expansion for describing space-time variations of monthly F 2 medians critical frequencies
10 p1687 A69-23927

Book on relativity and cosmos, space and time in physics, astronomy and cosmology covering theoretical and empirical research
10 p1784 A69-24019

Wave propagation in connected space-time for linear second order hyperbolic partial differential equation, describing unitary invariant theory
11 p1908 A69-24356

Space-time hypersurfaces representations of shock waves of relativistic MHD, discussing compressibility role in proving consistency with relativistic theory
11 p1928 A69-25246

Elastic stress created by perpetual motion of isotropic elastic solid in static space-time
12 p2130 A69-26283

Cosmic radiation recorder designed for use onboard satellite to measure intensity space-time distribution under geomagnetic effect
12 p2094 A69-26697

Space-time characteristics of coherent light giant pulse development in laser with instantaneous Q switching, deriving equations to describe linear and nonlinear phases
12 p2110 A69-26909

Einstein theory of space and time analyzed with emphasis on inertial systems
13 p2297 A69-27633

Computer program for compressible fluid flows with space and time dependent variables, discussing hypervelocity impact
[AIAA PAPER 69-353] 13 p2365 A69-28286

Categorical structures in theoretical thinking for philosophical fundamental physical laws analysis, including space-time concept changes in classical physics and in theories of relativity
14 p2484 A69-28861

Physical space-time defined as four dimensional Riemann space based on available information for physical measurements
14 p2484 A69-28862

Macroscopic space-time meaning in theoretical physics in terms of mathematical definition and philosophical concept
14 p2484 A69-28864

Space-time interpretation of static Einstein universe model and Friedmann space with variable positive curvature
14 p2484 A69-28865

Asymmetry causes on cosmogonic scale in view of symmetry in small space-time regions /microworlds/ determinable within framework of Einstein theory
14 p2516 A69-28866

Seasonal variation in ionospheric radiation absorption related to time variation between sunrise and constant angle attainment of sun
14 p2437 A69-29072

Electron density, temperature and dimensions of helium breakdown induced by Q switched ruby laser beam as function of space and time
14 p2492 A69-29636

Successive approximations method applied to system of independent equations describing electromagnetic wave propagation in space with gravitational wave metric
14 p2487 A69-29669

Inertial systems in homogeneous isotropic expanding universe model, giving expression for line element accounting for Hubble effect
15 p2654 A69-31495

Monograph on creation and evolution of physico-theoretical concepts of space, time and matter
16 p2812 A69-32110

Magnetized minerals studied to investigate space-time structure and reversal of main geomagnetic field
16 p2782 A69-32462

Acoustic waves pressure field micropulsations in turbulent fluid, analyzing space-time spectrum
16 p2782 A69-32489

Analytical description of planetary distribution of space-time variations of fOF2, deriving Fourier series as function of UT
16 p2783 A69-32540

Space-time variations for approximating sporadic E layer critical frequencies of geographic and time distribution curves
16 p2784 A69-32542

Cylindrical concentric detonation front and stability mechanism space-time measurement
20 p3632 A69-37215

Thomas wave equation in fluid mechanics, examining coordinates system with normal hyperbolic metric of universe tube having given signature
20 p3598 A69-37430

Metric state-time dynamical polysystem with sequentially compact topological space, noting sliding state trajectories
22 p3975 A69-40573

Space-time behavior of random pressure field of turbulent boundary layer on plane plate surface
22 p3933 A69-41027

Spherically rotating symmetric body gravitational collapse within Schwarzschild radius, presenting trapped surface concept for asymmetrical cases and generalization of space-time singularities
23 p4219 A69-42333

Real space-time Green functions applied to turbulence induced infinite thin elastic plate vibration, analyzing mechanical dissipation effects
24 p4395 A69-42597

Weak magnetic field amplification in turbulent flow with velocity field as random function of space and time
24 p4375 A69-42657

SPACE TOOLS

Electrical explosive devices for space applications including explosive bolts, primers and igniters
01 p0141 A69-10544

Tools and equipment for extra- and intravehicular activities in space and on lunar surface
[AAS PAPER 69-438] 24 p4319 A69-42802

SPACE VEHICLE CHECKOUT PROGRAM

ESRO 2/IRIS satellite launching checkout, countdown and breakdown of operations
01 p0163 A69-11104

Digital computer systems design optimization based on operational experience in development of Saturn S-1C stage Automatic Test and Checkout System
03 p0400 A69-13233

Automatic checkout of space systems, discussing cost effectiveness tradeoffs, ground and onboard equipment utilization, vehicle design and mission success risk
03 p0411 A69-13392

Interpretive Checkout Test Language /CTL/ designed in near English form for aerospace checkout tasks
04 p0569 A69-15364

Apollo/Saturn V automatic checkout test verification and debug program using real time computer simulation with digital space vehicle system model
[AIAA PAPER 69-321] 09 p1478 A69-22378

Spacecraft onboard checkout systems and design of ground support equipment and software, noting adaptive dynamic analysis and maintenance /ADAM/ concept
[AIAA PAPER 69-307] 09 p1478 A69-22382

General purpose space vehicle ground support equipment adapted from special purpose systems, discussing checkout, launch control and data monitoring requirements
[AIAA PAPER 69-308] 09 p1479 A69-22385

Onboard checkout system concept, discussing philosophy, requirements, underlying considerations, system description, development and techniques of system selection
11 p1866 A69-25081

Space vehicle checkout, launch control and data monitoring by general purpose ground system providing flexible stimuli generation, measurement acquisition, computation and information display
18 p3118 A69-35064

Apollo Guidance, Navigation and Control system prelaunch checkup, flight experience and error analysis
[AIAA PAPER 69-89] 21 p3824 A69-39416

Integrated systems testing for unmanned spacecraft electromagnetic compatibility, discussing identification and elimination of interference sources
21 p3683 A69-39438

Space vehicle data system synthesizer /SVDS/ for dynamic calibration of automatic control and checkout systems during prelaunch and countdown operations
21 p3680 A69-39633

Spacecraft onboard computer for prelaunch targeting constants verification through checksum equation and error detection scheme, using generated number sequences
[AIAA PAPER 69-946] 22 p3974 A69-40329

Programming and checkout of computer for Eldo inertial guidance system, including flight simulation and autopilot tests
[AIAA PAPER 69-961] 22 p3978 A69-40342

Mariner Mars 1969 spacecraft real time test support system and recorded data analysis including routing to printers, CRT displays and incremental plotters
[AIAA PAPER 69-982] 22 p3907 A69-40362

General purpose space vehicle ground support equipment adapted from special purpose systems, discussing checkout, launch control and data monitoring requirements
[AIAA PAPER 69-308] 22 p3927 A69-40552

SPACE VEHICLE CONTROL

U SPACECRAFT CONTROL

SPACE VEHICLES

U SPACECRAFT

SPACE WEAPONS

Outer Space Treaty of 1967, discussing Article 4 and arms control
20 p3636 A69-37109

SPACEBORNE PHOTOGRAPHY

NT SATELLITE-BORNE PHOTOGRAPHY

Satellite photography applications to geography and cartography based on Gemini 7 photographs
[UN PAPER 68-95401] 01 p0178 A69-10489

Soviet space astronomy including rocket, satellite and space probe measurements for solar, stellar, planetary and lunar studies
01 p0155 A69-10946

Spacecraft device for photographing and transmitting TV pictures noting limitations and spatial conditions adaptations
02 p0207 A69-11829

Global cloud models construction techniques, discussing vertically pointing radars, airborne panoramic cameras, radiometry, meteorological satellites and light detection and ranging
02 p0275 A69-12381

Annular and linear Martian surface formations nature and origin from analysis of Mariner 4 photographs
03 p0506 A69-13087

Mars unmanned spacecraft mission profiles for surface imaging, noting influence of lighting requirements
[SMPT PAPER 104-21] 04 p0650 A69-14361

Interpretation technique for weather satellite photographs of spatially coherent cloud distributions
04 p0628 A69-15090

Unified lunar control photogrammetric network produced by mapping satellite in 28 day polar orbit, using recurrent partitioning

05 p0819 A69-15628

Photographic system in Lunar Orbiter spacecraft

05 p0829 A69-15857

Photographic results of Lunar Orbiter program noting possible Apollo sites

05 p0822 A69-15858

Space observations needed for solar flares study

05 p0814 A69-15859

Earth space image interpretation in various spectral regions, discussing effectiveness of photography, spectrophotometry, radar and microwave observations

05 p0763 A69-16054

Geophysical investigations on manned orbital space laboratories, discussing space photography, spectrophotometry, terrain pictures and aerosol layers

05 p0759 A69-16633

Blurred spaceborne photographic image reconstruction by spatial frequency filtration [UN PAPER 68-95240]

06 p0923 A69-17080

Mars surface features identification from comparison of Mariner 4 and ground bases telescopic photographs

07 p1213 A69-18605

Space photography as sedimentological research tool demonstrated by space photographs application to projected Mars mission

09 p1490 A69-21797

Apollo 7 and weather satellite observation photographs of hurricane Gladys and typhoon Gloria

10 p1722 A69-22944

Planetary imaging systems design problems illustrated by Mars orbiter reconnaissance, discussing radiation effect on film, shielding, stereo method comparisons, color bands, etc [SMPTE PAPER 105-78]

12 p2078 A69-25770

Low light level slow scan Owl TV camera system with secondary electron conduction camera tube for satellite-borne observation of auroral light emission

12 p2079 A69-25904

Wobble-spin technique for spacecraft inversion for earth photography using flywheel

12 p2174 A69-26780

Space photography for natural resource inventory, describing Gemini photographs role in assessing vegetation, geological, metal and soil resources in Western Hemisphere

12 p2097 A69-26987

Martian canals nature based on high contrast photographs obtained by Mariner 4 space probe

12 p2171 A69-27133

Spacecraft orientation from onboard stellar photographs, calculating absolute and relative elements, accuracy and camera parameters

13 p2296 A69-27696

Cartographic interpretation of TV cloud pictures transmitted by Molniia 1 satellite

13 p2292 A69-27730

Annular and linear Martian surface formations nature and origin from analysis of Mariner 4 photographs

14 p2515 A69-28769

Apollo 9 multispectral photography compared with photographs taken simultaneously by aircraft using same film filter combinations

15 p2608 A69-30452

Apollo 8 photooptics, considering TV camera and broadcasts, photographic equipment and visual observation

15 p2609 A69-30469

Magnetically focused electronographic image converters in far UV photography and spectroscopy in space astronomy applications

17 p2972 A69-33084

Tropical storms wind speeds related statistically to characteristics as pictured from satellites

17 p2997 A69-33690

Relative control data incorporation into sequential or simultaneous analytical triangulation systems, considering extraterrestrial photographs reduction

18 p3133 A69-34335

NASA photogrammetric lunar activities, discussing imagery and control data by Lunar Orbiter and photogrammetric data reduction for preparing manned lunar landing

18 p3133 A69-34336

Automated crop surveys from integrating observations made at different times (time dimensioning) during growing season, noting earth resources satellites role

18 p3126 A69-34337

Aerospace images information suppressing and enhancing methods to aid interpreter in making more accurate recognition and measurement of earth resources subjects

18 p3133 A69-34338

Environmental studies using orbital photography, discussing color, color IR, black and white applications from Gemini and Apollo programs

18 p3132 A69-35275

Hyperaltitude photographs from Gemini spacecraft for geological mapping

18 p3132 A69-35276

Earth space image interpretation in various spectral regions, discussing effectiveness of photography, spectrophotometry, radar and microwave observations

20 p3545 A69-37964

Lunar surface photographic mapping by Ranger, Surveyor and Lunar Orbiter projects, emphasizing image resolution and coverage

21 p3719 A69-38325

Diurnal entrainment deviations and atmospheric turbulence effects on flash photographs from Geos 1

21 p3793 A69-38339

Cloud velocity computations from ATS 1 and 3 satellites spin-scan photographs for prediction of neph systems motion and thunderstorms

21 p3757 A69-38370

Satellite phase and aberration corrections in processing photographic observations for geodetic purposes

21 p3720 A69-38606

Hyperlatitude photographs for geological mapping from Gemini spacecraft, noting remote sensing imagery

22 p3935 A69-40040

Apollo 6 multisensor imagery of Wilcox Playa /prehistoric lake remnant/ in Arizona, using IR scanner, microwave radiometer, vidicon system and cameras

22 p3942 A69-40988

Multiple exposure averaging technique summarizing satellite cloud photographs for various periods, presenting entire earth cloud cover atlas

24 p4343 A69-42897

SPACECRAFT

Digital data processing equipment for space flight PCM telemetry

03 p0393 A69-13290

Aeronautics - Conference, Beverly Hills, September 1968

06 p0866 A69-17658

Real time pressure simulation chambers for testing space vehicles, discussing slow and rapid evacuation and pumping systems

13 p2240 A69-28077

SPACECRAFT ANTENNAS

Triangulated pantograph structure for deploying antennas, special equipment and instruments from spacecraft, noting structural design and strength characteristics

02 p0252 A69-11752

C and S band waveguide impedance measurements taken in flight in reentry plasma, noting results for plasma

02 p0218 A69-12333

Mars and Venus probes antenna problems in environments of near earth space, deep space and nonearth planetary atmospheres

02 p0223 A69-12811

Testing program using electrical measurements for determining adequacy of erectable parabolic reflector for space missions

02 p0223 A69-12812

Current antenna system technology, particularly airborne and spaceborne applications

04 p0576 A69-14767

Decoupling techniques for antennas on aerospace vehicles, noting effects on far field radiation pattern and antenna gain

05 p0729 A69-15977

Thermally excited oscillation experienced by OGO 4 boom antenna demonstrated by mathematical model, showing nonplanar coupled bending-torsion oscillation by solar radiation

07 p1227 A69-18333

Wire screen deployable boom concept for avoiding thermal bending of slender tubes problem in application to gravity gradient stabilization and antennas of spacecraft

07 p1229 A69-18350

Onboard digital computer evaluation of trigonometric functions for antenna pointing

07 p1089 A69-19745

Electronically scanned and fixed multiple beam phased arrays for spaceborne microwave radiometric sensors

12 p2044 A69-26977

Helix antennas for phased arrays for spacecraft, discussing performance and development

13 p2228 A69-27632

Retrodirective antennas for spacecraft, discussing design, operations and applications

16 p2762 A69-32557

Spacecraft antennas properties, structure and problems including frequency ranges, external influences, omnidirectional radiation, input impedance, etc

16 p2763 A69-32584

Bandwidth limitations for phase steered planar arrays in satellite applications, discussing weight reduction by modulo 2 pi beam steering

17 p2941 A69-34082

RF impedance probe digital system for ionospheric measurements based on antenna resonance phenomena

20 p3542 A69-37791

Antenna reactance from sounding rocket in ionosphere, showing variations relationship to rocket spin period

22 p3934 A69-39964

RF voltage breakdown facility for studying spacecraft antenna characteristics in space and planetary atmosphere environments [AIAA PAPER 69-1028]

22 p3924 A69-40397

Deployable cross log periodic dipole /LPD/ array on conducting cone as potential application to spacecraft or missile requiring frequency independence in VHF-UHF band

22 p3913 A69-40693

Omnidirectional microwave parallel plate waveguide fed antenna design for flush mounted broadband spacecraft, noting equatorial and polar patterns

22 p3913 A69-40697

Radiation and impedance characteristics of spherically capped conical and monopole antennas protruding from spherical vehicle related to cone height, angle and vehicle diameter

22 p3908 A69-40699

Antenna design considerations for spacecraft at relativistic velocities, discussing gain function, receiver power density and source apparent frequency and direction

22 p3914 A69-40700

Mars entry capsule ionized wake producing circularly polarized antenna radiation null region, noting effect on communication blackout time

22 p3914 A69-40701

Prolate spheroidal antennas operation in isotropic plasmas, studying effects of collision frequency, electron temperature and antenna length on admittance, radiation and current distribution

22 p3914 A69-40702

Spacecraft phase array designed for use on synchronous communication satellite, discussing low structural weight packaging and unfurling problems and helix approach

22 p3915 A69-40705

Frequency diversity technique simplifying airborne antennas for UHF telemetry, useful on spin stabilized vehicles requiring omnidirectional antenna coverage

23 p4122 A69-41777

Space vehicle multibeam Cassegrain antenna system design meeting radiometric mapping requirements in microwave frequency range, discussing mounting, degrees of freedom, etc [ONERA-TP-713]

23 p4143 A69-42527

Swept frequency X band reflectometer for measuring antenna properties in simulated reentry environments [AAS PAPER 69-282]

24 p4313 A69-42861

SPACECRAFT CABIN ATMOSPHERES

Flight vehicle cabins ventilation for undesirable gas contaminants removal, discussing contaminant concentration calculation and automatic control

02 p0200 A69-11512

Physiological effects of space cabin environment variables during long and hazardous space missions with regard to engineering constraints and radiobiology

03 p0380 A69-13504

Corona and breakdown voltage in helium-oxygen atmospheres, analyzing conditions for manned space flight vehicles

05 p0730 A69-16241

Oxygen-helium cabin atmosphere effect on speech communication analyzed during simulated space mission

07 p1066 A69-19420

- Resistance to bacterial pneumonia and influenza infection in space cabin environment tested on mice in simulation chamber
07 p1067 A69-19432
- Spacecraft debris atmosphere effects on observations, discussing contamination of exposed optical surfaces and light scattering by ice particles from cabin water vapor leakage
09 p1487 A69-21654
- Digital computer program for heat and mass transfer characteristics of spacecraft carbon dioxide adsorption beds, discussing surface pressure of absorbent material [AICHE PAPER 19C]
09 p1446 A69-21931
- Polyimide glass fabric laminates with nonflammable characteristics for high O concentration spacecraft environments applications
09 p1531 A69-22366
- Experimental program to evaluate regenerable sorbents for carbon dioxide removal in space cabin environments
09 p1447 A69-22552
- Physiological effects on men of 10 hour exposure to nitrogen-oxygen mixture followed by pure oxygen 4 hour exposure, simulating conditions during EVA
17 p2912 A69-32940
- Artificial life support systems for sealed environments with application to specific missions, noting cryogenics use
17 p2915 A69-33682
- Infectious diseases in space flight, considering environment role in infection transmission, occurrence and severity
20 p3479 A69-37973
- Space cabin and suit pressures for decompression sickness avoidance and fire hazard alleviation
22 p3890 A69-40212
- Computerized mass spectrometer for monitoring atmosphere in astronauts suits and cabin [AIAA PAPER 69-1016]
22 p3922 A69-40388
- Space cabin environment simulation effects on resistance to infection caused by pneumonia and influenza virus in rats
23 p4108 A69-41832
- Separation system for collecting wash and waste water from gaseous environment and separating liquid and gaseous phases during space missions [AAS PAPER 69-473]
24 p4272 A69-42845
- SPACECRAFT CABIN SIMULATORS**
- Apollo mission simulation, discussing Command Module Simulator /CMS/, onboard computer system and dynamic visual presentation via infinity-optics display [SMPT E PAPER 105-74]
12 p2055 A69-25768
- Photographic system for astronaut training in Apollo Mission Simulator, using fixed camera and moving earth model coincident with strip color film past exposure slit
16 p2792 A69-32787
- SPACECRAFT CABINS**
- Mathematical simulation of temperature and humidity changes in compartments of hermetically sealed space vehicle cabins
02 p0200 A69-11489
- Low profile bulkheads for launch vehicles and spacecraft compartments to obtain structural weight reduction [AIAA PAPER 68-355]
02 p0334 A69-12370
- Meteoroid perforation effects on space cabin design, discussing simulated destructive environmental tests [AIAA PAPER 69-365]
13 p2357 A69-28297
- Parametric thermal control weight and power requirements for spacecraft life support systems, considering number of cabins, crew activity, heating, cooling and regeneration [AIAA PAPER 69-621]
17 p2914 A69-33305
- Closed compartment fire mathematical model to analyze combustion parameter effects, atmosphere pressure and temperature during fire [AIAA PAPER 69-618]
17 p3074 A69-33704
- SPACECRAFT COMMUNICATION**
- NT REENTRY COMMUNICATION**
- Integrated circuit digital filters design characterized by weight coefficients containing Lanczos factor for application to processing of signal transmitted from space vehicles
01 p0038 A69-10071
- Satellites and ocean platforms for civil aviation operations over North Atlantic, noting cost justification dependence on supersonic traffic increase [UN PAPER 68-95887]
01 p0113 A69-10521
- Spacecraft pencil beam parabolic antenna design and installation, discussing directivity factor variation with diameter and orientation accuracy effects
01 p0030 A69-10581
- Performance characteristics of hard limited and linear repeaters for satellite communications systems
01 p0032 A69-10966
- Dynamic tracking filter analysis and capabilities as low threshold demodulator in frequency modulated frequency division multiplexing satellite system
01 p0034 A69-11140
- Frequency feedback receiver capabilities as low threshold demodulator in frequency modulated frequency division multiplexing satellite system
01 p0034 A69-11141
- Ionosphere formed waveguide electromagnetic field determined by expression, accounting for radio wave absorption during communications via artificial satellites
02 p0206 A69-11661
- Maser for satellite communication consisting of traveling wave ruby maser and closed cycle liquid helium refrigerator, discussing design, operation and performance characteristics
02 p0256 A69-11992
- Ultra cone system for ultralow noise reception of RF space communication from Mariner 5 during occultation by Venus [JPL-TR-32-1340]
02 p0220 A69-12429
- Low noise microwave amplifiers for radio astronomy and satellite communications receiving system preamplification
03 p0402 A69-13017
- Communications system considerations for lunar libration point relay satellite to support Apollo lunar far side mission
03 p0388 A69-13180
- Low altitude satellite relay system, discussing modulation, antennas, frequency plans, telemetry, tracking, command and earth terminals
03 p0391 A69-13241
- High gain self steering repeater for multibeam microwave array system for earth-satellite communications
04 p0573 A69-14330
- AN/TSC-54 military satellite communications terminal for contingency deployment, discussing design, system tradeoffs and performance [AIAA PAPER 68-439]
04 p0579 A69-15367
- Earth station system for ground based communications with Intelsats 2 and 3 noting antennas, receivers, transmitters and power supplies
05 p0741 A69-15667
- High power transmitting tubes for INTEL SAT satellite communication earth stations, including multicavity klystrons and wideband TWT
05 p0728 A69-15668
- Teichmann cost analysis extended to include frequency dependent and diversity dependent rain losses for satellite communication, using Bayes strategy
05 p0721 A69-16580
- Transistorized receiver for satellite communications having adjustable receiver center frequency within 20 MHz
05 p0734 A69-16594
- Measurement methods at IF and baseband sections of microwave links, calculating noise superimposed on each swept measurement curve
05 p0722 A69-16728
- Ground station electronic environment, telemetry encoding and radio links for spacecraft communications and tracking
06 p0886 A69-16860
- Satellite communication channel number and distribution optimization, obtaining malfunction probability for telephone service communication system [UN PAPER 68-95772]
06 p0886 A69-17030
- Satellite and space communications and data transmission systems, emphasizing improvements in amount and rate of information for future requirements
06 p0886 A69-17045
- Communication satellites application to domestic live TV, telephone and data communication and long distance telecommunication in Canada [UN PAPER 68-95501]
06 p0887 A69-17075
- Coherent frequencies method for irregular component of satellite signal phase lead due to ionospheric inhomogeneities between satellite and ground station
06 p0890 A69-17799
- Mariner 1969 high rate telemetry system portions pertinent to combinatorial mathematicians, discussing coding and encoding
06 p0890 A69-17862
- High power coupled cavity traveling wave tube for satellite communication, noting design techniques and performance characteristics
07 p1094 A69-18427
- Satellite communications antenna system at Fucino earth station, describing transmitting and receiving equipment, facilities, power supply, etc
07 p1075 A69-18493
- Time division multiple access satellite communication system employing pulse code modulation of voice channels and phase shift keying of RF carrier
07 p1077 A69-18759
- High latitude transition or scintillation boundary between high and low amplitude fluctuations of satellite radio beacon signals examined as function of time
07 p1125 A69-18846
- Communications for Apollo Applications Program, considering extended duration manned missions in low earth orbit and Gemini, Saturn and Apollo hardware
07 p1083 A69-19124
- Mariner 1969 multimission high rate deep space telemetry system design, hardware and application
07 p1083 A69-19125
- Design aspects of 20 ft air transportable satellite earth station
08 p1272 A69-19926
- Large aperture low noise aerial design for satellite communication earth stations, discussing expected performance of 85-ft antenna at 4 GHz
08 p1279 A69-19956
- Ionospheric and tropospheric effects on microwave propagation including Faraday rotation, atmospheric refraction, attenuation and noise
08 p1272 A69-19958
- Multiple access techniques in civil satellite communications systems, noting proposed digital time and frequency division methods
08 p1272 A69-19959
- Reliability effect on operating costs of satellite communications system ground stations, calculating annual cost of channel with continuous time carry-over
08 p1276 A69-20586
- Receiving systems for digital telemetry signals from spacecraft, analyzing receiver performance by statistical methods
08 p1276 A69-20591
- Digital telemetry from spacecraft, discussing on-board processing, data compression, coding, sequence detection and receivers
08 p1276 A69-20592
- Bandwidth restriction effect on performance of linear codes for digital communication with space vehicles, noting bit and word error probabilities
08 p1276 A69-20597
- RF selection for interspacecraft or earth-spacecraft communication
09 p1449 A69-21270
- Interference noise in communication satellite receivers and terrestrial radio relay receivers, noting interference reduction transfer factor
09 p1450 A69-21279
- Coordination distances and interference probabilities to control interference in frequency sharing between communication satellite systems and terrestrial radio services
09 p1450 A69-21280
- Earth station antennas for communication satellite service, discussing design, fabrication, main lobe gain, side and back lobe suppression and noise performance
09 p1461 A69-21281
- Direct radio and TV broadcasting from satellite-borne radio transmitter to general public, giving visibility, gains, frequencies and bandwidths tables
09 p1586 A69-21286
- Satellite-borne terrestrial radiodetermination systems, noting VLF transmissions usage to overcome coverage problem
09 p1537 A69-21287
- Propagation and noise effects on frequency choice for communication satellite service to aircraft and ships, noting tropospheric and ionospheric attenuation considerations
09 p1451 A69-21288
- Radiocommunications for Tiros and Nimbus meteorological satellites, noting weather data communications and hydrological experiments
09 p1451 A69-21289
- Maintenance telemetering, tracking and telecommand for developmental and operational satellites, discussing possibilities of frequency sharing between satellites and terrestrial services
09 p1451 A69-21290
- Communication problems due to natural and artificial plasmas in spacecraft vicinity, discussing plasma effect theory
09 p1451 A69-21292

Radio waves behavior along paths between satellites and earth, studying preferred frequency bands for spacecraft transmitters used as beacons
09 p1451 A69-21293

Sensitivity of microwave earth stations for analog and digital communications
09 p1453 A69-21409

Construction of large parabolic antennas for radio astronomy and satellite communication, noting dimensional accuracy, directional precision and dynamical behavior
09 p1476 A69-21650

Orbiting Data Relay Network communications system provides continuous wideband communication between ground and earth orbiting spacecraft via synchronous satellite repeaters
[AIAA PAPER 68-432] 09 p1455 A69-21989

Large aperture satellite communication antenna gain measurement technique, using extraterrestrial radio wave source or satellite
09 p1456 A69-22116

Detectability parameter for measuring performance of multiple and random access satellite communication system using PN codes
09 p1457 A69-22460

Optimum time interval for constant data transmission rate during single pass of satellite over ground station
09 p1457 A69-22462

Frequency modulation feedback demodulator design procedure for satellite communications, noting importance of nonideal implementation
09 p1457 A69-22464

Commercial communication satellite earth station at Australia, noting antenna, autotracking capability, preamplifiers, and computer for control and monitor functions
09 p1458 A69-22469

Low noise wideband amplifier system for commercial satellite communication ground terminal receiver, noting cryogenically cooled parametric amplifier
09 p1458 A69-22470

Power requirements for tracking, telecommand and telemetry of spacecraft over interplanetary distances, considering transmission problems, equipment weight and reliability
10 p1652 A69-22984

Luna 9 automatic station flight control complex, detailing communication, orientation and stabilization systems operation after separation from acceleration module
10 p1792 A69-24197

High gain self steering microwave repeater for earth-satellite communications noting design, performance and results of color TV transmissions
11 p1839 A69-25294

Data relay satellite concept, discussing orbits, communications between widely separated earth stations, and satellite tracking, telemetry and commanding
11 p1839 A69-25295

Data relay satellite systems for support of NASA R and D missions, discussing communications between satellites and to mission control
11 p1839 A69-25296

Multimode tracking /SYMMTRAC I and II/ feeds for low noise antennas, noting feed performance
11 p1852 A69-25317

Data processing system for satellite telemetry signals, describing hardware construction and operation, data readout, etc
11 p1840 A69-25426

Intermodulation noise distorting arbitrary frequency-modulated multicarrier microwave signal in satellite transponder, emphasizing nonlinear energy dissipation and AM-FM conversion
11 p1841 A69-25634

Electrical power requirements in spacecraft, discussing communication, engine and control systems, data processing, electrochemical and nuclear sources
12 p2015 A69-25863

Data compression, redundancy reduction and applications to space flight technology
12 p2027 A69-25876

Satellite technology for government and defense communications systems, noting effects of rainfall attenuation, weather and solar interference on performance and reliability
12 p2028 A69-25932

Tracking and data acquisition networks and communications systems for support of space missions, studying data processing, unified S Band System and Data Relay Satellite System
12 p2028 A69-25933

Frequency measurement of moving spacecraft RF carrier waves at low SNR by analog recording of noisy signal and HF trigger tone, noting data processing and signal fading rate
12 p2038 A69-26051

Meteorology and space vehicle capabilities noting earth, outer space and earth atmosphere observations and measurements, relaying telecommunication signals, etc
12 p2126 A69-26126

Digital logic techniques for high speed satellite communications, noting general purpose logic cards
12 p2040 A69-26465

Traveling wave tube for European communication satellite power amplifiers, showing nonlinear distortions dependence on RF input/output power and helix voltage
[AIAA PAPER 68-430] 12 p2041 A69-26786

Number 2 ground communications antenna system on Goonhilly Downs for British Post Office earth station
12 p2044 A69-26923

ESRO 1 communication system and telemetering system compared to ESRO 2
13 p2220 A69-27749

Phase distortion, conversion of delay coefficients into channel noise and determination of waveguide delay coefficients for FM satellite communication systems
[IEEE PAPER 68-TP-382-COM] 13 p2222 A69-28153

Ionosphere formed waveguide electromagnetic field determined by expression, accounting for radio wave absorption during communications via artificial satellites
13 p2224 A69-28692

Latitudinal cut-off of manmade VLF signals in short path through ionosphere to OGO 2 satellite, noting strong noise following signal cut-off
14 p2434 A69-28958

Deep space data return, discussing system function, design, operational interfaces and interplanetary spacecraft data compression methods
14 p2517 A69-29096

Optimum thermal and nonlinear noise intensities distributions in frequency division multiplex satellite communications systems, relating relay station power, frequency band and channels
14 p2412 A69-29426

Computer program for STV-F9 satellite communication parameters, using ELDO forecasting values as input data
14 p2530 A69-29689

Communications mission of Symphonie project and satellite communications subsystem design
15 p2562 A69-30084

Spacecraft pencil beam parabolic antenna design and installation, discussing directivity factor variation with diameter and orientation accuracy effects
15 p2568 A69-30751

ESRO Aurorae satellite telecommunication system, detailing information nature, PCM telemetry and remote control system standard
15 p2702 A69-31084

ESRO 1/Aurorae satellite telemetry system constraints, discussing encoder, pulsed operation and integrated circuit assembly
15 p2702 A69-31085

Radio waves behavior along paths between satellites and earth, studying preferred frequency bands for spacecraft transmitters used as beacons
15 p2570 A69-31227

Global communication techniques and trends, discussing radio telephone and telegraph, submarine systems, satellite communications, line of sight links, tropospheric scatter, waveguide transmission, etc
16 p2750 A69-31755

Global satellite communication networks design by computer simulation, discussing politicotechnical interface problems, ground stations, atmospheric factors, system optimization, etc
16 p2750 A69-31852

AZUR research satellite HF communications system, describing telemetry transmitter, command receiver and data transmission
16 p2759 A69-31854

German ground station commercial receiving system for satellite broadcast reception
16 p2766 A69-31855

Ground station command transmission equipment for German AZUR satellite, describing components based on NASA Tone Digital Command System
16 p2759 A69-31856

Attenuation statistics due to rain measured on earth-space path at 16 and 30 GHz, using sun as signal source
17 p2920 A69-33398

Satellite system TDM techniques and prototype equipment capable of combining 12 unrelated start-stop and synchronous telegraph channels
17 p2920 A69-33420

Experimental SST terminal for satellite L band communications/surveillance ATC system, establishing terminal requirements for NASA and FAA studies
17 p2932 A69-34118

Artificial satellites as navigation aids, describing angle, range and range-angle systems, discussing orbital mechanics and communications difficulties
18 p3169 A69-34855

Ground data handling equipment characteristics for PCM telemetry link utilizing convolutional coding
19 p3273 A69-36267

Legal principles observed for international telecommunication systems establishment by means of artificial satellites regarding states interests and rights
20 p3638 A69-37124

Soviet book on modern systems of wireless telecommunication covering radio communication and tropospheric, ionospheric and satellite wireless systems
20 p3487 A69-37235

Double binary PSK system digital computer simulation for satellite communications, investigating filter and limiting effects on performance in error probability terms
20 p3492 A69-37705

Data acquisition and processing ionograms from Alouette satellites telemetered sweep frequency top-side sounding data
20 p3503 A69-37860

Communications, instrumentation and data handling for manned planetary missions, discussing data rate limitations
21 p3674 A69-39018

Daily communication link geometry between spacecraft in elliptical orbit and landed capsule, establishing spacecraft visibility contours for landing site latitude
[AAS PAPER 68-110] 21 p3805 A69-39223

Discrete filters for optimal processing of down-linked satellite data, considering inverse filter development by Kalman filtering techniques
21 p3677 A69-39462

Residuals from earth based coherent two way radio Doppler data from Lunar Orbiter three orders of magnitude larger than observations from spacecraft
[AAS PAPER 68-131] 21 p3828 A69-39766

Data compression and transmission technique for real time system to monitor manned space missions, noting Apollo telemetry data
[AIAA PAPER 69-970] 22 p3906 A69-40350

Moree earth station equipment and design for satellite communication in INTELSTAT network including antenna, feed and tracking, interconnect system, etc
22 p3900 A69-40679

Antenna design considerations for spacecraft at relativistic velocities, discussing gain function, receiver power density and source apparent frequency and direction
22 p3914 A69-40700

Circular or linear polarization diversity reception for VHF earth-station-satellite communications through turbulent ionosphere, assuming Rayleigh distribution fading
23 p4115 A69-41585

Intersatellite microwave laser communication system for ATS-F and ATS-G, discussing experiment, functional design and parameters
23 p4120 A69-41758

Apollo Extravehicular Communication Telemetry System for monitoring astronaut portable life support system, space suit performance and body functions on lunar surface
23 p4121 A69-41767

EHF earth-satellite link communication channel emphasizing down link, discussing weather models, atmospheric absorption and temperature, channel coherence bandwidth, etc
23 p4129 A69-42506

Deep space communication capability projection, considering data volume and rate, channel frequency, large apertures, data enhancement and system losses
23 p4129 A69-42507

Telecommunications performance of two lunar relay satellite system /LRSS/, determining operation capabilities with Apollo communications system
23 p4129 A69-42508

Short term frequency stability and spectral purity measurements of ATS 1 multiple access communication system
23 p4129 A69-42509

S-band pin-diode switch for high CW power satellite and deep space probe communication, using multiple quarter-wave transformers to stepdown diode impedance
23 p4143 A69-42518

Satellite communication system capacity for segment of geostationary orbit extended to models involving two angular dimensions
23 p4131 A69-42521

Satellite communication system high speed sequential decoder design, discussing parameters, simulation and test results on satellite channels
23 p4131 A69-42523

UHF satellites for mobile, broadcast and low cost services, discussing bandwidth expansion, interference effects, ground linking, UHF partition, satellite antenna sizes, etc
[AAS PAPER 69-333] 24 p4282 A69-42872

PCM satellite communication systems signal power and frequency bandwidth requirements, noting PCM-psk superiority over FDM-FM
24 p4283 A69-43200

SPACECRAFT COMPONENTS
NT LANDING MODULES
NT LUNAR LANDING MODULES
NT LUNAR MODULE
NT MARS EXCURSION MODULE

Space vehicle explosive components, discussing identification, screening and final qualification of explosives and severe environment simulation methods
10 p1749 A69-23008

Two way pyrotechnic high pressure gas valve for D2 satellite, noting resistance to leakage due to nearly monolithic construction
10 p1635 A69-23033

Wing section of high lift/drag test vehicle for 2500 F reentry, describing design, manufacture and testing
12 p2103 A69-26837

Space vehicle subcontracted components reliability attainment, discussing reliability process specifications, motivation, product reliability and feedback programs
15 p2723 A69-31139

Constant temperature heat pipe for thermal control of spacecraft components by direct coupling to external radiator
[AIAA PAPER 69-632] 17 p3070 A69-33262

Agna rocket vehicle production reliability evaluation program, testing specific representative equipment randomly selected from production stores
18 p3146 A69-34510

Lunar Orbiter Parts Program for selection and control of electronic and electrical parts, discussing reliability and flight failures
18 p3207 A69-34520

Spacecraft and components testing methods critical reassessment, discussing cost reduction, vacuum and thermal cycle tests
18 p3118 A69-35082

Handbook of electronic packaging including rigid and flexible printed wiring, soldering and mechanical interconnections, bonding, computer and military applications, etc
22 p3911 A69-40046

Quality and reliability of electronic spacecraft devices and structural components produced in limited quantity, discussing documentation of production and testing
23 p4171 A69-42474

Spacecraft single wall cryogenic storage system, discussing cost, pressure vessel and components, thermal and performance characteristics
24 p4393 A69-43045

Carbon fiber reinforced plastic components aerospace applications, discussing honeycomb sandwich satellite structure for investigating lamination methods, shapes, bonding and machining
24 p4336 A69-43209

SPACECRAFT CONFIGURATIONS
NT SATELLITE CONFIGURATIONS

Shock layer gas radiation influence on deep space missile shape, noting evaluation by flow equations
01 p0007 A69-11070

Spacecraft maneuvering by changing spacecraft geometry and utilizing different gravitational forces acting on finitely extended bodies
01 p0158 A69-11318

Multibody dual spin spacecraft spin axis motion with active internal devices, using digital simulation
02 p0332 A69-11739

Entry phase flight data of Missions AS-202, Apollo 4 and 6 compared with wind tunnel aerodynamics data [AIAA PAPER 68-1143] 03 p0519 A69-13556

Structural design options for decelerative aeroshell configurations for atmospheric entry on unmanned planetary explorations [AIAA PAPER 68-344] 04 p0683 A69-15507

Configuration, trajectory planning, instrumentation, calorimetry and aerodynamic heating for planetary atmosphere entry
11 p1968 A69-25719

Computer programs determining gaseous properties and aerodynamic characteristics for missiles, reentry vehicles and spacecraft at angles of attack
18 p3107 A69-35068

Drop test method to obtain subsonic terminal velocity and base pressure data for planetary entry probe configurations
19 p3238 A69-35959

Cone-conical-frustum configurations meeting center of gravity requirements for higher hypersonic lift-drag ratios in axisymmetric manned spacecraft
21 p3644 A69-39237

Mariner-Mercury 1973 flyby mission using Atlas-Centaur rocket and gravity-assisted maneuvers, discussing encounter geometrics, spacecraft configuration and Venus probe considerations [AAS PAPER 69-288] 24 p4381 A69-42862

SPACECRAFT CONSTRUCTION MATERIALS

Book on material and design problems encountered in construction of high performance missiles, rockets and spacecraft, considering influence of space environment
01 p0084 A69-10021

Mass spectrometer residual gas analyzer (RGA) for identifying and measuring subliminated substances from spacecraft construction materials, noting applications during vacuum testing
02 p0227 A69-11758

Antimicrobial spacecraft materials, discussing feasibility of impregnation or chemical combination of materials with bactericides
05 p0713 A69-15944

Cryogenic behavior of adhesive materials used in fabrication of liquid hydrogen/liquid oxygen powered Saturn S-4B stage
05 p0784 A69-16487

Space radiation effect on spacecraft components and materials simulated by proton and fast electron bombardment of silicon, glass and skin materials
06 p0906 A69-17612

Materials compatibility for space requirements, discussing shape retention, ductility, tensile strength, dissimilar materials stability, etc
06 p0945 A69-17872

Homogeneous fused silica and quartz reinforced resins as dielectric materials for reentry vehicle antenna windows
07 p1090 A69-18400

Strength increase in steel components of aircraft, missiles and submersibles in relation to chronological application sequence, discussing ultimate strength [ASM PAPER G68-9.4] 07 p1169 A69-19675

Composite materials for aerospace applications, discussing high modulus filaments, structural and non-structural design considerations, nondestructive testing techniques, etc
12 p2111 A69-25852

Materials rating method in pressure vessel applications, considering impact on design of minimum cost space launch vehicle
12 p2175 A69-26844

Spacecraft construction materials and strength problems including stress-strain determination, thin shell structural stability, dynamic loads, heat resistance, fiber-reinforced composites, ablation materials, etc
13 p2362 A69-27920

Simulated solar wind environment effects on zinc oxide/potassium silicate and lanthanum oxide/potassium silicate spacecraft thermal control coating pigments [AIAA PAPER 69-642] 17 p2991 A69-33273

Minimum cost design /MCD/ of space launch vehicle, discussing material and process selection based on fracture-safe conditions
19 p3433 A69-35587

Structural aerospace materials development with emphasis on Be and Ti alloys, discussing material combinations and composites
19 p3345 A69-36319

High temperature materials for aerospace and spacecraft applications, considering carbon/carbon composites, oxides, carbides, fibers and ablative systems
19 p3346 A69-36320

Space age metals supply and demand relationships, discussing system engineering criteria for maximum efficiency
19 p3346 A69-36635

Oxidation resistant coating methods and systems for Cb base materials protection for aerospace vehicles and aircraft propulsion systems structures
21 p3730 A69-38672

Metallic and nonmetallic materials for space applications with launch and orbit condition requirements, examining finishes and lubricants
24 p4332 A69-43207

Hazard rating for flammability of aerospace materials in air and oxygen environments applied to J-2 rocket engine insulation
24 p4336 A69-43423

SPACECRAFT CONTAMINATION

Planetary quarantine and biological search strategy, discussing Voyager-Mars mission configuration, sterilization, back contamination and decisions
01 p0021 A69-11090

Flight vehicle cabins ventilation for undesirable gas contaminants removal, discussing contaminant concentration calculation and automatic control
02 p0200 A69-11512

Nonexistence of Biota-Cloud recontamination hazard for planetary lander proved by analysis of interactions between small particles and physical fields around vehicle
02 p1201 A69-11771

Biological monitoring during assembly of Technological Feasibility Spacecraft (Mars lander) to evaluate thermal control techniques and microbiological burden prior to sterilization
02 p1201 A69-11774

Standards of sterility for prevention of introduction of terrestrial microorganisms onto other planets during space missions, noting contamination probability
05 p0712 A69-15936

Modeling requirements and methods for monitoring microbial contamination, discussing vacuum probe sampler to recover microorganisms from large surface areas
05 p0713 A69-15948

Microbial contaminants on space hardware, discussing detection and enumeration techniques
05 p0714 A69-15954

Spacecraft debris atmosphere effects on observations, discussing contamination of exposed optical surfaces and light scattering by ice particles from cabin water vapor leakage
09 p1487 A69-21654

Mars planetary landing program schedule, COSPAR quarantine policy and biological losses from failures to collect data and from contamination
11 p1828 A69-25459

Spacecraft sterilization requirements, evaluating viable organisms release probability from spacecraft as function of equipment fracturing
11 p1828 A69-25460

Outgassing behavior of polymers in spacecraft by thermal-vacuum weight-loss and contamination tests
13 p2286 A69-28089

Planetary quarantine constraints by NASA insuring low contamination probability from extraterrestrial biological exploration, giving contamination probability equations and sterilization procedures
16 p2746 A69-32435

Space contamination by spacecraft-borne terrestrial microorganisms, testing vacuum effect on water desorption rate using mass spectrometry on various cells
20 p3475 A69-37615

Space contamination due to manned vehicles and debris atmosphere effects on dim light source observations
21 p3793 A69-38341

Vacuum exposure nephelometer system for materials contamination screening in space applications
24 p4297 A69-42931

SPACECRAFT CONTROL
NT SATELLITE ATTITUDE CONTROL
NT SATELLITE CONTROL

Spacecraft periodic motion near center of mass determined by point transformation combined with bifurcation theory, studying stability and parametric dependence
01 p0161 A69-10205

Deceleration control system for aerobraking and skipout to orbit at Mars [AIAA PAPER 68-1146] 03 p0520 A69-13564

Minimum fuel attitude control of spacecraft by Pontryagin principle and extended steepest descent method
03 p0522 A69-14100

Real time performance, ground control and data processing of Surveyor spacecraft during maneuvers [AIAA PAPER 67-644] 04 p0586 A69-15502

Manual and automatic spacecraft rendezvous and docking, discussing docking of Cosmos 186 and 188 in 1967 [UN PAPER 68-95764] 06 p1013 A69-17057

Astrodynamics, guidance and control - Conference, Belgrade, September 1967, Volume 1 06 p1004 A69-17560

Three axis attitude servomechanism design to adjust attitude and angular velocity of spacecraft 06 p0955 A69-17589

Microscopic time lapse movies in solid/liquid interface profile during melting and freezing of materials for spacecraft thermal control as reversible heat sink [AIAA PAPER 69-95] 06 p1038 A69-18126

Aircraft and spacecraft guidance and control technology including computers, optimum and Kalman filtering, strapdown inertial navigation, sensors and test pads [AIAA PAPER 69-72] 06 p0956 A69-18136

Spacecraft control system and flexible structures interactions, discussing transient phenomena, limit-cycle oscillations and instabilities [AIAA PAPER 69-116] 06 p1019 A69-18187

Scaled models for spacecraft thermal control, considering radiation-conduction-convection heat transfer [SAE PAPER 690196] 07 p1116 A69-18304

Computer simulations, comparing self adaptive/neuron/control of spacecraft energy allocation subsystem to programmed control 07 p1058 A69-18389

Aircraft and spacecraft guidance and control technology including computers, optimum and Kalman filtering, strapdown inertial navigation, sensors and test pads [AIAA PAPER 69-72] 07 p1177 A69-19179

Human operator manual control of spacecraft under accelerations up to 18 g, noting performance and efficiency of males 08 p1265 A69-19936

Cybernetic theory application to automatic spacecraft, discussing control problems in Mariner 4 and Surveyor 7 missions and attitude stabilization system 08 p1409 A69-20583

Space guidance and control system components, noting control moment gyro, actuator, brushless DC motor, electrically supported gyro and laser gyro 09 p1500 A69-22434

Luna 9 automatic station flight control complex, detailing communication, orientation and stabilization systems operation after separation from acceleration module 10 p1792 A69-24197

Flight control system for automatic interplanetary stations [AIS], comparing Venera series orientation and correction system to Mariner systems 10 p1792 A69-24198

Spacecraft design for minimization of structure interaction with control system, noting susceptibility of extendible booms to solar environment 11 p1967 A69-25500

Reentry and planetary entry physics and technology, II, Advanced concepts, experiments, guidance-control and technology 11 p1967 A69-25718

Guidance and control concepts and hardware for atmospheric entry of Mercury, Gemini and Apollo spacecraft 11 p1914 A69-25724

Space vehicle angular velocities reduced to zero through linear and nonlinear optimal feedback control systems 12 p2054 A69-26516

Spacecraft longitudinal control during reentry of lunar orbiter into atmosphere, analyzing final range prediction, trajectory tracking and accelerometers performance 13 p2355 A69-27681

Spacecraft range control algorithm during reentry at parabolic velocity into atmosphere with varying parameter distributions 13 p2355 A69-27682

Optimal control algorithm for spacecraft descent in atmosphere based on nominal trajectory and acceleration measurements 13 p2355 A69-27683

Optimal motion control of spacecraft refueling during flight by liquefying atmospheric gas along prescribed trajectory under constant thrust 13 p2356 A69-27686

Spacecraft periodic motion near center of mass determined by point transformation combined with bifurcation theory, studying stability and parametric dependence 14 p2530 A69-28741

Earth sensor for spin stabilized spacecraft to maintain specific orientation with earth, discussing use of blue and red filters 15 p2609 A69-30593

ESRO 1 satellite centralized control system, discussing housekeeping system responsible for task execution in connection with power supply 15 p2702 A69-31083

Control methods for spacecraft reentry and landing, discussing adaptive systems, descent trajectory parameter prediction and angle of attack 16 p2867 A69-31742

Reentry flight test vehicle development for West German space program, using hypersonic model to determine controllability and aerodynamic stability 16 p2867 A69-31934

Low thrust reaction control for space missions, summarizing range and specific impulse characteristics for solid and hybrid systems [AIAA PAPER 69-433] 16 p2834 A69-32745

Free gas formation in propellant systems and effects on attitude control systems [AIAA PAPER 69-434] 16 p2870 A69-32765

Satellites and space vehicles attitude control mathematical model accounting for nonrigidity, sloshing and energy dissipation in vehicle interior 17 p3048 A69-33239

Navigation, guidance and control developments for manned space missions, discussing earth orbital exploration bases 19 p3369 A69-35801

Missile and spacecraft guidance navigation and control, discussing fluidics, self adaptive and digital control and Kalman filtering 19 p3370 A69-36316

Cassiopee device for spacecraft or sounding rocket attitude control, describing gyroscopic control unit, sensor element and jet control devices [ONERA-TP-707] 19 p3432 A69-36686

Soviet book on radio control of rocket missiles and space vehicles covering control principles, systems analysis and synthesis, vehicle characteristics, etc 20 p3574 A69-37232

Spacecraft discrete automatic control system computerized simulation, discussing logic elements, applications to design, etc 20 p3502 A69-37393

Density field surrounding leaking circular hatch of spacecraft treated as free molecular flow from annulus, superposing far field of effusive orifice flow 21 p3695 A69-39035

Spacecraft control systems with computer command redundant jets for linear and angular pulses, relating configuration design to level-of-redundancy and task dimension [AIAA PAPER 69-845] 21 p3822 A69-39375

Controllers design for reaction jet controlled aerospace vehicles, studying second order pitch-plane representation with actuator modeled as pure delay [AIAA PAPER 69-854] 21 p3822 A69-39382

Manual guidance and control of Saturn launch vehicles, considering feasibility, reliability and hardware implementation [AIAA PAPER 69-876] 21 p3824 A69-39402

Orbit selection rules for planetary cartographic spacecraft derived from relations connecting camera angle, view field and imaging resolution [AIAA PAPER 69-879] 21 p3763 A69-39405

Apollo Guidance, Navigation and Control system prelaunch checkup, flight experience and error analysis [AIAA PAPER 69-891] 21 p3824 A69-39416

Mathematical model of astronaut motion and spacecraft angular control during tethered reentry, discussing conditions preventing spinning and collisions 21 p3667 A69-39630

Guidance and control in space - Conference, Warsaw, June 1969 21 p3825 A69-39635

Spacecraft natural vibrations analyzed using point transforms with allowance for control systems imperfections 21 p3826 A69-39637

Guidance control systems for moving plants pursuing targets, basing design on target characteristics and plant phase coordinates 21 p3687 A69-39643

Guidance and control in space - Conference, Warsaw, June 1969 21 p3766 A69-39644

Spacecraft trajectory control algorithm for hypersonic reentry, describing onboard equipment role and simulation results 21 p3767 A69-39649

Stochastic motion control problems formulations in rocket dynamics 21 p3767 A69-39650

Space vehicles optimal pulsed control systems statistical synthesis, considering structural constraints on operation, memory capacity and algorithm coefficients 21 p3767 A69-39651

Real time targeting for Apollo lunar orbit insertion maneuver burn, discussing impulsive maneuvers for flight control [AIAA PAPER 68-848] 21 p3828 A69-39760

Deceleration control system for aerobraking and skipout to orbit at Mars [AIAA PAPER 68-1146] 21 p3828 A69-39761

Optimal sliding regimes for controlling dynamic systems, proposing control parameters system extension 21 p3768 A69-39826

General control theory for spacecraft motions, deriving dynamic equations of motion about center of mass for holonomic and nonholonomic control programs 21 p3829 A69-39829

Adaptive control system for aerospace vehicles, describing model reference network for control parameter determination 21 p3688 A69-39857

Biological model describing spacecraft operator sensorimotor activity in response to various spacecraft control stimuli, outlining computer algorithm 22 p3892 A69-40281

Nonlinear adaptive reaction jet attitude control for long life space vehicles, providing optimal performance over bias acceleration disturbances [AIAA PAPER 69-945] 22 p4036 A69-40328

Computer system functional requirements for autonomous Martian surface roving vehicle, emphasizing vehicle motion control system [AIAA PAPER 69-980] 22 p3907 A69-40360

Booster digital guidance and control system, discussing communication device providing data transfer between airborne digital computer and control device [AIAA PAPER 69-988] 22 p3978 A69-40368

Three axis motion simulator for in-orbit spacecraft attitude control evaluation using earth, sun and star sensor references [AIAA PAPER 69-1029] 22 p3924 A69-40398

Newton-Raphson function space algorithm for optimizing control systems with discontinuities and terminal constraints, discussing spacecraft examples 22 p3918 A69-41009

High temperature pneumatic systems for missile and space vehicle control, describing pressure regulators, flow controls, thrusters and analog valves 22 p3870 A69-41240

Manual method for navigating and guiding spacecraft to rendezvous with orbiting target, using hand-held unpowered optical instruments and manual computations [AIAA PAPER 68-859] 24 p4348 A69-43243

Attitude control system with rate of change limiter to minimize launch vehicle drift during first stage ascent through atmosphere 24 p4394 A69-43277

Launch vehicle control system synthesis based on mode control theory state variable formulations 24 p4394 A69-43278

Parallel wire array fluidic sun sensor for solar pointing fluidic attitude control, discussing design and breadboard test 24 p4348 A69-43297

SPACECRAFT DESIGN

NT SATELLITE DESIGN

Book on material and design problems encountered in construction of high performance missiles, rockets and spacecraft, considering influence of space environment 01 p0084 A69-10021

Electronic packaging techniques for long life spacecraft, discussing effects of mechanical and electrical stress, temperature cycling, vacuum, radiation and contamination 01 p0038 A69-10145

Space radiators for heat rejection from nuclear powered spacecraft doubling as primary structures to save weight, discussing conical or cylindrical configurations 01 p0160 A69-10151

Paraglider as recoverable sounding rocket dropped from helicopter, describing system design and flight tests
[UN PAPER 68-95445] 01 p0161 A69-10465

Surface dose rate and depth dose distribution for materials used for space vehicle and biological tissue protection from cosmic and internal radiation
[UN PAPER 68-95260] 01 p0144 A69-10477

Systematic approach to standard launch vehicle based on governmental expenditure minimization while attaining mission goals
01 p0162 A69-11096

Space station design requirements, Apollo applications program and various experimental programs
01 p0163 A69-11395

Meteoroid penetration detector development program for spacecraft construction, discussing design, materials and environmental tests
02 p0338 A69-11749

French /LRBA, ONERA and Sud-Aviation/ sounding rocket design emphasizing meteorological rockets and standard equipment
02 p0333 A69-11916

Hypervelocity impact effect on structural honeycomb spacecraft wall configurations, stressing design and wall thickness parameters
[AIAA PAPER 68-314] 02 p0345 A69-12389

Solar cell generator design problems for solar probes, discussing increased operational temperature
02 p0197 A69-12665

Explorer 33 and 35 satellites reliability achievement by design via AIMP program
03 p0519 A69-13232

Aeroshell structural development for Mars flyby and entry landing mission compatible with Atlas/Centaur launch vehicle
[AIAA PAPER 68-1159] 03 p0521 A69-13667

Entry corridor thermal entry limits for Apollo spacecraft defined for design of thermal protection system
[AIAA PAPER 68-1144] 03 p0521 A69-13673

Structural design options for decelerative aeroshell configurations for atmospheric entry on unmanned planetary explorations
[AIAA PAPER 68-344] 04 p0683 A69-15507

Manned spacecraft systems design optimization for extended space missions replacement modules
05 p0830 A69-16380

Equations formulated for space vehicle reaction to rotating machinery and internal mass motion, evaluating dynamics of cylindrical space station rotating about major axis
05 p0827 A69-16476

Dynamics of carrier rockets and space vehicles having complex three dimensional thin walled constructions with cavities containing liquids
[UN PAPER 68-95622] 06 p1013 A69-17051

Spacecraft systems, education - Conference, Belgrade, September 1967
06 p1015 A69-17596

Engineering designs and hardware required for low risk flight of long duration manned space stations
06 p1007 A69-17601

Interplanetary Pioneer spacecraft development and systems engineering aspects
06 p1017 A69-17605

Deployable appendages of OGO attitude controlled spacecraft design
06 p1017 A69-17606

Mercury atmospheric models for preliminary environmental criteria to be used in spacecraft design and engineering trade-off studies
[AIAA PAPER 69-54] 06 p1010 A69-18042

Analytical technique for unmanned spacecraft sizing for planetary missions, considering scientific objectives, characteristics and requirements
[AIAA PAPER 69-125] 06 p1018 A69-18076

Thermal considerations of spacecraft external panel effects on specular louvers systems, discussing heat dissipation and computer program
[AIAA PAPER 69-26] 06 p1037 A69-18097

Planetary landing vehicle design optimization, considering effects of trajectory, guidance and environmental parameters under uncertainty
[AIAA PAPER 69-128] 06 p1018 A69-18107

Manned orbital space stations design, purposes and applications, balancing costs against benefits
06 p1019 A69-18237

Explorer 40 satellite mathematical model and verification testing for close spacecraft flight temperature predictions
[SAE PAPER 690202] 07 p1239 A69-18305

Semiactive gravity gradient stabilization system design for low altitude earth oriented spacecraft attitude control, using active reaction wheel scanner
07 p1227 A69-18334

Electric propulsion missions analysis for spacecraft design engineer, discussing out-of- ecliptic and Jupiter flyby probes
09 p1584 A69-21203

Pre-design and mission analysis software capability for sizing, design, fabrication and developmental testing of flight hardware for electrically propelled inter-planetary spacecraft
09 p1585 A69-21210

Propellant condensation on surfaces near electric rocket exhaust, calculating particle arrival rates, backflow and desorption energies
[AIAA PAPER 69-270] 09 p1565 A69-21252

Single stage rocket vehicle design for rapid global air transportation noting size, range and economics
09 p1433 A69-21303

Spacecraft design, trajectory and mission analyses for multipurpose solar electric propulsion missions, emphasizing modular ion engine and fixed attitude spacecraft designs
[AIAA PAPER 69-252] 09 p1568 A69-21729

Space exploration plans adaptation, considering spacecraft design, programs, costs and schedules flexibility
10 p1811 A69-22863

Space stage separation qualification of ONERA rocket vehicles based on angular perturbation measurements during variable roll speeds
10 p1669 A69-23005

Spacecraft electronic components design, environmental and reliability criteria including weight and power
11 p1843 A69-24340

Data relay satellite concept, discussing orbits, communications between widely separated earth stations, and satellite tracking, telemetry and commanding
11 p1839 A69-25295

Spacecraft design for minimization of structure interaction with control system, noting susceptibility of extendible booms to solar environment
11 p1967 A69-25500

Space propulsion system design with consideration for launch and mission requirements, noting upper stage structural design and computer techniques
12 p2148 A69-26834

Esro 1 satellite program management, discussing scientific mission, structure, tracking system and history
13 p2355 A69-27360

Spacecraft construction materials and strength problems including stress-strain determination, thin shell structural stability, dynamic loads, heat resistance, fiber-reinforced composites, ablation materials, etc
13 p2362 A69-27920

Sensitivity function in time domain defined for control system design
13 p2238 A69-27936

Electric relays requirements for spacecraft with magnetic field constraints
13 p2231 A69-28046

Spacecraft surfaces bidirectional reflectance flux distribution applications to space thermal control computations
[AIAA PAPER 68-26] 13 p2222 A69-28216

Landing shock attenuation system for Surveyor spacecraft, describing hydraulic cylinder and piston arrangement for damping, computerized shock absorber design and landing process simulation
[ASME PAPER 69-DE-54] 14 p2530 A69-28848

Soviet book on partially liquid filled solid body dynamics from viewpoint of space and aircraft applications
14 p2530 A69-29815

Communications mission of Symphonic project and satellite communications subsystem design
15 p2562 A69-30084

Europa 1 first stage attitude control system adaptation to Europa 2 requirements, discussing design modifications and improvements and inertial guidance system introduction
16 p2866 A69-31726

Fluid flow problems during orbital refueling vehicle maneuvers and system operations in propellant transfer, including disturbances, liquid-vapor interface instability, vapor ingestion, etc
[AIAA PAPER 69-567] 16 p2868 A69-32721

Passive attitude stabilization of interplanetary probe, using conically shaped sails elastically connected to payload
17 p3047 A69-33225

Scale modeling of multilayer insulated spacecraft for thermal design, considering solar probe and two meter telescope models
[AIAA PAPER 69-613] 17 p3049 A69-33267

Planetary lander model thermal design, analysis and testing, emphasizing lightweight multilayer insulation, discussing thermal/vacuum testing
[AIAA PAPER 69-612] 17 p3049 A69-33296

Solar probes design for 0.3 to 0.1 AU perihelion distance, considering thermal control, power supply, communications, altitude control and alternative configurations
17 p3050 A69-33797

Lunar orbital mission plans intended to optimize spacecraft procurement, flight schedules, science objectives and available funds
18 p3193 A69-34362

Collection of papers on thermal design principles of spacecraft and entry bodies
18 p3227 A69-34372

TD1/TD2 satellites power supply subsystem, stressing high power requirements and significant design features regarding battery and solar array controls
18 p3093 A69-34791

Weight estimation and forecast in manned spacecraft design, noting size and weight relationship
[SAWE PAPER 793] 18 p3208 A69-34864

Computer aided design analysis program to provide weight and sizing data for entry spacecraft
[SAWE PAPER 797] 18 p3208 A69-34903

Minimum cost design (MCD) of space launch vehicle, discussing material and process selection based on fracture-safe conditions
19 p3433 A69-35587

Soviet space stations design based on orbital docking techniques for unrestricted mass size and number of modules, describing wheel shaped station
19 p3431 A69-36465

Spacecraft and boosters for earth resources surveys, discussing design, payloads, orbits, etc
21 p3799 A69-38629

Spacecraft control systems with computer command redundant jets for linear and angular pulses, relating configuration design to level-of- redundancy and task dimension
[AIAA PAPER 69-845] 21 p3822 A69-39375

Evaluation technique for astronautics subsystems in automated spacecraft designed for interplanetary missions, considering operation times, navigation updating and midcourse correction
[AIAA PAPER 69-882] 21 p3764 A69-39408

Cost reduction steps in reusable launch vehicle design, discussing aircraft design and development experience application
21 p3826 A69-39689

Vehicle designs and cost analyses for launch vehicle selection to minimize costs of 40,000- 150,000 pound payload placement into orbit
21 p3827 A69-39694

Low cost efficient shuttle system for personnel and cargo transport to earth orbit for NASA and DOD needs
21 p3827 A69-39695

Technology, design, development, qualification and operational elements noting effects on performance, economics and scheduling of nuclear vehicle
[AIAA PAPER 68-591] 21 p3769 A69-39752

Analytical technique for unmanned spacecraft sizing for planetary missions, considering scientific objectives, characteristics and requirements
[AIAA PAPER 69-125] 21 p3828 A69-39770

Modular configuration of recoverable scientific MAP /Modular Auroral Probe/ payloads aboard Nike-Apache rockets, discussing payload design concepts
23 p4223 A69-41763

Centrifuge on board orbiting spacecraft as research tool for biological and physical experiments relevant to prolonged missions and spacecraft design
23 p4108 A69-41833

Nuclear reactor/thermoelectric power system design for manned orbiting space station, discussing station integration and operation
23 p4187 A69-42256

Manned space flight history and spacecraft development
[AAS PAPER 69-501] 24 p4380 A69-42852

Spacecraft probes design for mapping meteoroid environment and penetration hazard through asteroid belt
[AAS PAPER 69-321] 24 p4392 A69-42867

Asteroid exploration by solar photovoltaic powered ion propelled probe, discussing spacecraft design, mission and 1975 Mariner utilization
[AAS PAPER 69-322] 24 p4381 A69-42868

- OSO spacecraft thermal design modified to operate University of Minnesota zodiacal light monitor experiment
[AAS PAPER 69-173] 24 p4393 A69-42873
- Adaptive control function technique to design lateral stability augmentation system for hypothetical manned, lifting body entry vehicle
24 p4394 A69-43301

SPACECRAFT DOCKING

- Manual and automatic spacecraft rendezvous and docking, discussing docking of Cosmos 186 and 188 in 1967
[UN PAPER 68-95764] 06 p1013 A69-17057
- Space vehicle docking dynamics and matrix equations of motion amenable to numerical solution on digital computer, using Hamilton principle and Lagrange multipliers
11 p1967 A69-25501
- Space docking, personnel placement on space stations, rescue stations, etc
18 p3196 A69-34630
- Soviet space stations design based on orbital docking techniques for unrestricted mass size and number of modules, describing wheel shaped station
19 p3431 A69-36465
- Rigid and flexible coupling devices for spacecraft rendezvous, describing general operating conditions
22 p4036 A69-40008

SPACECRAFT ELECTRONIC EQUIPMENT

- Magnetometric equipment on board Luna 10 and Venera 4 space stations for studying magnetic field in interplanetary space, describing circuit and metrological characteristics
01 p0080 A69-10582
- Self excitation conditions and output characteristics of tunnel diode DC to AC converters for spacecraft, discussing relaxation-oscillator and push-pull circuit converter types
01 p0046 A69-10755
- Satellite traveling wave tube for X band duplicating C and S band performance
03 p0405 A69-13678
- High temperature capacitor consisting of thin wafers of pyrolytic boron nitride noting fabrication, dissipation factor and capacitance
04 p0551 A69-15299
- Electronic circuits power supply onboard space vehicle, discussing chemical, solar and nuclear energy sources
07 p1225 A69-18251
- Electronic tubes utilization in space flight, summarizing characteristics and satellite applications
07 p1093 A69-18421
- Roll diffusion bonding technique for permitting complex design of coldplates and radiators of spacecraft electronic equipment
09 p1504 A69-22066
- Spacecraft electronics - Conference, Chicago, December 1968
09 p1465 A69-22433
- Spacecraft electronic components design, environmental and reliability criteria including weight and power
11 p1843 A69-24340
- Surveyor electronic engineering design for lunar environment, discussing vacuum and temperature effects
11 p1958 A69-24633
- High power TWT tube cooling in space vehicle, discussing thermal control system based on heat pipe radiator
11 p1847 A69-24747
- Electrical power requirements in spacecraft, discussing communication, engine and control systems, data processing, electrochemical and nuclear sources
12 p2015 A69-25863
- Electric relays requirements for spacecraft with magnetic field constraints
13 p2231 A69-28046
- Cosmos 149 meteorological satellite telephotometer, radiometer and other electronic equipment for measuring atmosphere and underlying surfaces physical parameters
14 p2447 A69-29403
- Magnetometric equipment on board Luna 10 and Venera 4 space stations for studying magnetic field in interplanetary space, describing circuit and metrological characteristics
15 p2610 A69-30752
- Spacecraft electronic component reliability policy based on preferential lists, selection programs and component management
15 p2624 A69-30818
- Satellite circuit assembly reliability achievement by high reliability components, redundancy and optimal utilization
15 p2624 A69-30819
- Integrated circuit failure analysis in military and space applications utilizing type-test programs
15 p2624 A69-30820
- Space electronic component reliability, considering suppliers and laboratory-workshop partnership
15 p2624 A69-30822
- Short term plan of European electronic component selection for ESRO satellite without established guaranteed failure rate
15 p2624 A69-30823
- Large scale integration /LSI/ and medium scale integration /MSI/ circuits evolution and requirements, noting onboard computers and space applications
15 p2625 A69-30825
- Large scale integrated MOS devices tests for space applications, establishing quality specifications
15 p2580 A69-31131
- High reliability space system electronic parts control program to assure success of unmanned space missions
16 p2793 A69-31714
- Soviet book on reliability of semiconductor radio devices of flight vehicles covering failures through production errors, power source instability, environment induced changes, etc
18 p3108 A69-34350
- Portable electric lamp for work and photographic purposes in manned spacecraft, describing circuitry, construction and applications
[IES PREPRINT 30] 18 p3138 A69-35173
- Magnetic core material and process technologies for space power electronic applications noting pulse transformers, nonlinear reactors and tapes
19 p3319 A69-35543
- Communication satellites equipment and techniques, considering global network, satellite design, millimeter wave systems, etc
19 p3275 A69-36314
- Spacecraft onboard processor for digital filtration and data compression, discussing prototype design, construction, sample memory, delay memory, arithmetic unit and programmer
20 p3500 A69-37383
- Onboard spacecraft computer design, programming and operation based on dual bussing system
20 p3500 A69-37384
- SDP-3-A general purpose stored program computer designed for small scientific spacecraft onboard data system, noting computerized simulation
20 p3500 A69-37385
- Satellite onboard computers automatic reconfiguration and self repair
20 p3503 A69-37399
- Spacecraft integration electronics modular packaging, discussing slice housing concept and design criteria including environmental resistance, reliability, performance, etc
22 p3910 A69-39949
- Flexible circuitry for reliable spaceborne data processing equipment electronic packaging
22 p3903 A69-39951
- Encapsulation effects on piece parts in high density package, considering unexpected part failures elimination in Lunar Module Signal Conditioning Electronic Assembly
22 p3910 A69-39953
- Spacecraft electronic components operating junction temperature control, considering role of thermal resistance in controlling radiative and conductive transfer
[AIAA PAPER 69-1015] 22 p3922 A69-40387
- Spacecraft onboard data handling system with MSI complementary MOS arrays, describing various components
23 p4133 A69-41739
- L and S band transmitters for space applications, discussing power and frequency stability, low intermodulation, inputs isolation, efficiency, size and weight
23 p4137 A69-41740
- Quality and reliability of electronic spacecraft devices and structural components produced in limited quantity, discussing documentation of production and testing
23 p4171 A69-42474

SPACECRAFT ENVIRONMENTS

- Rms approximation validity limits for satellite temperature variances by deriving equations for thin insulated plate in space
02 p0352 A69-12211

- Dog adaptation to 60 or 90 mm Hg carbon dioxide in 260 mm Hg total pressure environment, noting arterial pH and bicarbonate level
03 p0375 A69-14071

- Displacement pumps and fluids for extreme environments, discussing fluid types and operational parameters such as speed, pressure, temperature, power, displacement and size
06 p0931 A69-17188

- Statistical correlation between cardiovascular activity and respiration dynamics of cosmonauts during orbital flight, discussing heart beat and respiration rates
07 p1061 A69-18584

- Luminous particles in space observed by Vostok Mercury and Voskhod astronauts, discussing distribution, trajectories and terrestrial origin
07 p1222 A69-19617

- Physiological effects of breathing cool dehumidified air in hot humid environment, tabulating tolerance time, heart rate, temperature changes and sweat loss
09 p1446 A69-22543

- Electroexplosive devices protection by nonconducting composition against premature ignition by RFI in spacecraft environment, noting Apollo Standard Initiators
10 p1751 A69-23018

- Spacecraft electronic components design, environmental and reliability criteria including weight and power
11 p1843 A69-24340

- Computer program for electron and proton fluxes impinging on spacecraft, performing computation for Van Allen belts and solar flares
11 p1949 A69-24863

- Space mission medical heat problems covering thermal characteristics and heat control, protection and resistance of space vehicle and astronaut adaptation
12 p2023 A69-26493

- Self thermostatic phase-change coatings for active and passive spacecraft temperature control, discussing temperature dependent changeability in solar absorptance
14 p2530 A69-29434

- Continuous-channel electron multipliers degradation in spacecraft environment simulation laboratory equipment
14 p2449 A69-29565

- Weightlessness problems, discussing artificial gravitation on spacecraft and astronaut experiences
16 p2746 A69-31930

- Permanent magnets optimal design and properties for attitude control of German research satellite Azur, considering environmental influences
16 p2868 A69-31936

- UV irradiation effects on ZnO spacecraft thermal control coating pigments, discussing photo-Hall, luminescence and electron paramagnetic resonance measurements
[AIAA PAPER 69-639] 17 p2992 A69-33288

- Thermal design of landed vehicle on Mars surface, discussing instrument package covering inside surface coating and battery insulation
[AIAA PAPER 69-611] 17 p3049 A69-33295

- Apollo Lunar Module Environmental Control System /LM/ECS/ steady state performance simulation techniques, discussing vacuum chamber data of LTA-8/LM-3
[AIAA PAPER 69-616] 17 p2903 A69-33307

- Medical and biological laboratory ground experiments role in development of life support systems and suitable environments for prolonged manned space flights
18 p3098 A69-35165

- Optimum solar cell cover glass systems selected by studying interplanetary space environment effects of proton impact, temperature and concurrent illumination on radiation damage
19 p3253 A69-35702

- Space medicine to characterize nature and degree of changes in human functional capabilities due to space flight environment prolonged exposure
19 p3456 A69-36460

- Infectious diseases in space flight, considering environment role in infection transmission, occurrence and severity
20 p3479 A69-37973

- Ceramic-sealed Ni-Cd secondary batteries space environmental behavior testing to determine heat dissipation during spaceborne operation
22 p3869 A69-40591

- Space medicine to characterize nature and degree of changes in human functional capabilities due to space flight environment prolonged exposure
23 p4087 A69-41803

Space cabin environment simulation effects on resistance to infection caused by pneumonia and influenza virus in rats
23 p4108 A69-41832

SPACECRAFT GUIDANCE
NT SATELLITE GUIDANCE

Multiengine Martian soft lander guidance and control system design with single engine failure accommodation based on six degrees of freedom computer simulation
02 p0277 A69-11740

Proportional navigation guidance systems for interceptor missiles optimized by adding biased term to guidance equation
02 p0278 A69-11973

Manual optimal guidance schemes for space vehicles to minimize computational and display requirements for pilot task loading
02 p0279 A69-12365

Comparison of trajectories in optimum linear perturbation guidance
02 p0279 A69-12546

Nonorthogonal multisensor strapdown inertial reference unit providing redundant capabilities and optimal performance
03 p0429 A69-13211

Apollo guidance, navigation, stabilization and control subsystems, detailing inertial, optical and computer units for data processing and collecting
04 p0665 A69-14881

Astrodynamics, guidance and control - Conference, Belgrade, September 1967, Volume 1
06 p1004 A69-17560

Optimization procedure developed and applied to minimum fuel midcourse guidance of spacecraft, discussing optimal closed loop control of linear stochastic systems
06 p0955 A69-17576

Ground based guidance systems for supplementing onboard guidance of manned space vehicles
06 p0955 A69-17580

Suboptimal guidance corrections for continuous thrust vehicle disturbances during minimum fuel rendezvous in Martian orbit, discussing physical and modified cost functional
[AIAA PAPER 69-76] 06 p0956 A69-18081

Planetary landing vehicle design optimization, considering effects of trajectory, guidance and environmental parameters under uncertainty
[AIAA PAPER 69-128] 06 p1018 A69-18107

Aircraft and spacecraft guidance and control technology including computers, optimum and Kalman filtering, strapdown inertial navigation, sensors and test pads
[AIAA PAPER 69-72] 06 p0956 A69-18136

Linearized theory for minimum fuel guidance in neighborhood of minimum fuel space trajectory, unrestricted thrust magnitude and allowances for midcourse impulses
[AIAA PAPER 69-74] 06 p0956 A69-18183

Aircraft and spacecraft guidance and control technology including computers, optimum and Kalman filtering, strapdown inertial navigation, sensors and test pads
[AIAA PAPER 69-72] 07 p1177 A69-19179

Sight reduction tables for orbital plane determination checked out by sextant sightings onboard Gemini 7
07 p1177 A69-19206

Fluidic devices application to attitude and guidance control of satellites, rockets and space probes
07 p1230 A69-19292

Manual onboard computation procedures and devices for determination of maneuvers for orbital navigation and guidance
08 p1348 A69-21184

Trajectory error propagation upper bounds in many body field for impulsive initial error, relating error to mission tolerances
09 p1595 A69-21937

Space guidance and control system components, noting control moment gyro, actuator, brushless DC motor, electrically supported gyro and laser gyro
09 p1500 A69-22434

Guidance and control concepts and hardware for atmospheric entry of Mercury, Gemini and Apollo spacecraft
11 p1914 A69-25724

Fluidics for satellite and rocket attitude control and guidance, discussing computing block function and components, system reliability and resistance to aging, etc
17 p3049 A69-33243

Tracking and data acquisition systems for spacecraft and ground link through command, telemetry and tracking, noting data relay satellites, etc
17 p2919 A69-33371

Manual procedures for midcourse and terminal guidance, discussing onboard optical measurements and calculations
19 p3368 A69-35792

Apollo navigation, guidance and control systems in command module and lunar module, discussing inertial, optical and computer hardware operation
19 p3369 A69-35799

Navigation, guidance and control developments for manned space missions, discussing earth orbital exploration bases
19 p3369 A69-35801

Evaluation method for strapdown spacecraft guidance systems on automated interplanetary missions, using cost and system performance efficiency probability model
[AIAA PAPER 68-828] 19 p3370 A69-35953

Missile and spacecraft guidance navigation and control, discussing fluidics, self adaptive and digital control and Kalman filtering
19 p3370 A69-36316

Adaptive control for Mars entry based on sensitivity analysis
[AIAA PAPER 68-8355] 20 p3573 A69-37193

Spacecraft guidance analysis of multiple outer planet mission utilizing gravity assist swingbys to achieve planetary flybys with single spacecraft
[AAS PAPER 68-109] 21 p3761 A69-39205

GaAs laser tracking system for space guidance, describing equipment and operations
[AIAA PAPER 69-870] 21 p3763 A69-39396

Manual guidance and control of Saturn launch vehicles, considering feasibility, reliability and hardware implementation
[AIAA PAPER 69-876] 21 p3824 A69-39402

Neighboring optimum feedback guidance to motivate min-distance lookup parameter determined by minimizing metric function of perturbed state and reference trajectory
[AIAA PAPER 69-888] 21 p3765 A69-39414

Apollo Guidance, Navigation and Control system prelaunch checkup, flight experience and error analysis
[AIAA PAPER 69-891] 21 p3824 A69-39416

Guidance and control in space - Conference, Warsaw, June 1969
21 p3825 A69-39635

Guidance control systems for moving plants pursuing targets, basing design on target characteristics and plant phase coordinates
21 p3687 A69-39643

Guidance and control in space - Conference, Warsaw, June 1969
21 p3766 A69-39644

Long range space flight trajectory correction problem, obtaining algorithm for determining minimum number of corrections
21 p3818 A69-39822

ELDO radio guidance station at Gove, discussing propulsion stage tracking and instruction transmitted to vehicle
22 p3919 A69-39920

Variable time of arrival (VTA) guidance generalized, developing computational algorithms to supplement linear guidance method
22 p3979 A69-41186

Low thrust guidance for multirevolution trajectory required for earth parking orbit transfer to parabolic orbit insertion, noting advantages over high thrust scheme
[AAS PAPER 69-403] 24 p4379 A69-42832

Space and missile guidance performance analysis through automatic generation of mission performance sensitivity with respect to error sources from Monte Carlo simulation
[AAS PAPER 69-404] 24 p4347 A69-42836

Optimal transfer between hyperbolic asymptotes about finite size planet, discussing twelve types of analytical solutions in terms of arrival, departure and escape velocities
[AAS PAPER 69-242] 24 p4380 A69-42856

Manual method for navigating and guiding spacecraft to rendezvous with orbiting target, using hand-held unpowered optical instruments and manual computations
[AIAA PAPER 68-859] 24 p4348 A69-43243

Vector matrix second order sensitivity equation application to Mars entry guidance, performing numerical simulation of second order sensitivity guidance and tabulating results
24 p4388 A69-43690

SPACECRAFT INSTRUMENTS

NT SATELLITE INSTRUMENTS

Spacecraft attitude ion sensor using charged thermal ions of earth atmosphere as reference, stressing reliability, economy and response
01 p0079 A69-10293

Vector helium magnetometer for Mariner 4 /Mars 1964/ and Mariner 5 /Venus 1967/, discussing efforts to reduce spacecraft stray fields
[IEEE PAPER 10.1] 01 p0081 A69-10714

Stable fluxgate magnetometer sensor for exploration of space magnetic fields, discussing equipment specifications and performance tests
[IEEE PAPER 10.2] 01 p0081 A69-10715

Scientists involvement in planetary spacecraft missions, considering organization for particular instruments and more complex payloads
[AAS PAPER 68-192] 02 p0311 A69-11473

Triangulated pantograph structure for deploying antennas, special equipment and instruments from spacecraft, noting structural design and strength characteristics
02 p0252 A69-11752

Aerospace sensor systems, discussing adaptive multimode sensors and multispectral sensing, electronic recognition of image components, laser radar and Raman scattering technique
03 p0431 A69-13851

Electrostatic potential generated by rockets on space vehicles, noting source of electric current in exhaust plumes and effect on instrumentation
03 p0522 A69-13903

Instrument technology for solar optical astronomy from space, noting rocket and satellite vehicles, far UV detectors, filters, photographic film fogging, etc
05 p0762 A69-15838

Sterilization techniques for instruments and materials as applied to space research - COSPAR Conference, London, July 1967
05 p0711 A69-15934

Multichannel radiometers calibration and testing for spacecraft and solar simulation applications, noting exposure to sun onboard X-15 aircraft at high altitudes
06 p0926 A69-17620

Thermally induced vibration and flutter of flexible spacecraft boom, discussing stability by considering boom as cantilever beam
[AIAA PAPER 69-21] 06 p0869 A69-18144

Diode pump type circuit without diodes in signal path providing accurate transfer function analysis considered for spacecraft use
[IEEE PAPER 3A-3] 07 p1134 A69-19191

Surveyor scientific instruments and operation on moon, reviewing TV camera, alpha scattering instrument and surface sampler
[JPL-TR-32-1358] 08 p1312 A69-19850

Plasma generator for maintenance of space vehicle electrical neutrality during ejection of high velocity electron pulses
[AIAA PAPER 69-273] 09 p1567 A69-21263

Space systems and radioastronomy - Conference, Geneva, September-October 1968, Part 2
09 p1450 A69-21285

Satellite-borne terrestrial radiodetermination systems, noting VLF transmissions usage to overcome coverage problem
09 p1537 A69-21287

Spacecraft onboard checkout systems and design of ground support equipment and software, noting adaptive dynamic analysis and maintenance /ADAM/ concept
[AIAA PAPER 69-307] 09 p1478 A69-22382

Fundamentals of aerospace instrumentation - ISA Conference, Boston, June 1968, Volume 1
10 p1690 A69-23224

Sonic anemometer for wind velocity through pulse communication transducers noting applications to aerospace vehicle design
10 p1692 A69-23255

Low thrust propulsion devices high response impulse testing, describing limitations imposed by solenoid valve time response
10 p1672 A69-23278

Imaging radar systems for employment on small spacecraft, fabricating small lightweight radar systems packages with integrated circuit techniques
11 p1835 A69-24695

Low light level slow scan Owl TV camera system with secondary electron conduction camera tube for satellite-borne observation of auroral light emission
12 p2079 A69-25904

Spaceborne optical telescopes requirements and development including mirror material and construction, optical design, servocontrol, etc
13 p2261 A69-27946

Photogrammetric calibration of Surveyor 7 stereo mirror based on vector analysis
[JPL-TR-32-1390] 13 p2263 A69-28199

One inch ceramic vidicon with slow scan photoconductor, electrostatic focusing and magnetic deflection to withstand sterilization and environmental testing for space applications 13 p2234 A69-28262

Structure, equipment and weight breakdown of Black Arrow X3 spacecraft 13 p2357 A69-28478

Scientific equipment on Cosmos 237 satellite for recording extraterrestrial radiation data, discussing specifications, operation and mission purpose 14 p2446 A69-29047

Spacecraft radar altimetry with application to geodesy, discussing orbital and tracking errors 15 p2609 A69-30460

Spacecraft radar altimetry applied to study of sea surface slopes, tides, tsunamis, storm surges and submarine geology 15 p2609 A69-30461

Fluorine nuclei in primary cosmic radiation identified by counter telescope measurements on Pioneer 8 spacecraft 15 p2676 A69-30886

Flight instrument package for change of energy absorption and energy radiation of vehicle surfaces during various phases of space vehicle mission 15 p2613 A69-31269

Earth albedo instrument on OSO 3 spacecraft to measure solar reflectance of earth at various wavelengths 15 p2614 A69-31279

Electron trap behavior on charged spacecraft, obtaining expressions for current to aperture and internal retarding electrodes for all apertures and spacecraft potentials 16 p2849 A69-31976

Surface type airborne electrostatic probes in ambipolar diffusion flux, measuring ion saturation current, discussing electrode contamination and temperature and ablation tests [AIAA PAPER 69-700] 17 p2974 A69-33443

Electrostatic control for portable clean rooms, describing fabrication, assembly and checkout problems with Instrument Unit /IU/ control center for Saturn launch vehicles 19 p3428 A69-35550

Mars autonomous entry navigation, discussing flight path angle control with onboard sensors using realistic sun, Canopus and planet line of sight tracker accuracies 19 p3368 A69-35790

Planetary navigation using spacecraft measurements and Doppler data from earth-based radio tracking, determining accuracy for earth-Mars trajectory 19 p3368 A69-35791

Apollo optics system ground and flight performance tests results, suggesting possible design changes for sunlit space environments 19 p3307 A69-35796

Apollo lunar module landing radar, discussing descent phases, operating modes, assemblies and Surveyor radar 19 p3267 A69-35797

Apollo spacecraft equipment qualification program for margin assurance, discussing ground and flight tests 19 p3430 A69-36015

Distance of spacecraft descending on parachute through planetary atmosphere measured from center of planetary mass using onboard instrument data 19 p3432 A69-36633

OGO 4 UV airglow spectrometer consisting of Ebert-Fastie monochromator and photomultipliers with cesium telluride and cesium iodide channels 19 p3315 A69-36682

OGO 5 spacecraft detector instrumentation for measuring electrostatic and electromagnetic waves electric fields with coupled antennas, describing in-flight operation 19 p3315 A69-36683

Binary increment and residual class notation techniques for onboard spacecraft computer arithmetic 20 p3499 A69-37378

Explorer 31 ion mass spectrometer calibrated in flight and compared with Alouette 2 topside electron concentration data 20 p3545 A69-37879

Communications, instrumentation and data handling for manned planetary missions, discussing data rate limitations 21 p3674 A69-39018

Spacecraft-based navigation instruments for outer planet missions using celestial directions to outer planet natural satellites [AIAA PAPER 69-902] 21 p3761 A69-39348

Onboard processor servicing spacecraft sensors, programmable from ground, discussing functions and applications 22 p3903 A69-39921

Surveyor spacecraft instrumentation, describing TV camera design and operation, photographic requirements and techniques, lunar surface characteristics, etc 22 p4011 A69-40043

Apollo 6 multisensor imagery of Wilcox Playa /prehistoric lake remnant/ in Arizona, using IR scanner, microwave radiometer, vidicon system and cameras 22 p3942 A69-40988

Lunar TV camera for Apollo missions, discussing operational requirements and design 23 p4162 A69-41478

Systems analysis method for determining spacecraft remote sensors earth resources survey effectiveness by integrating specifications, mapping requirements and orbital characteristics 23 p4163 A69-41567

Centrifuge on board orbiting spacecraft as research tool for biological and physical experiments relevant to prolonged missions and spacecraft design 23 p4108 A69-41833

Mars atmosphere study by Mariner 6 and 7 spacecraft, discussing instrumentation on board [AAS PAPER 69-091] 24 p4393 A69-42881

SPACECRAFT LANDING

NT LUNAR LANDING

Optical measurements through retrorocket plumes of landing spacecraft, investigating reduced landing site visibility and modulation transfer function 02 p0248 A69-11765

Variable geometry features applied to lifting spacecraft to overcome inherent incompatibility and provide low speed and tangential landing capabilities [AIAA PAPER 68-1164] 03 p0520 A69-13562

Search theory application to planetary exploration overall strategy for improving landing site decisions 09 p1595 A69-21994

Soviet lunar probe Zond 6 achievements in controlled Earth landing and lunar surface photography 13 p2355 A69-27342

Landing shock attenuation system for Surveyor spacecraft, describing hydraulic cylinder and piston arrangement for damping, computerized shock absorber design and landing process simulation [ASME PAPER 69-DE-54] 14 p2530 A69-28848

Control methods for spacecraft reentry and landing, discussing adaptive systems, descent trajectory parameter prediction and angle of attack 16 p2867 A69-31742

Aerodynamic and flight characteristics of variable geometry entry spacecraft during subsonic wing deployment and landing [AIAA PAPER 69-742] 18 p3084 A69-34407

Spacecraft return probabilities with time constraints and redundant access, using Borel set concept for counting and summing coverage belts 21 p3819 A69-39017

Ground based guidance for land-landing manned spacecraft with low velocity descent systems, discussing high and low altitude glide path intercept and spiral [AIAA PAPER 69-864] 21 p3762 A69-39390

SPACECRAFT LAUNCHING

ESRO 2/IRIS satellite launching checkout, count-down and breakdown of operations 01 p0163 A69-11104

Status of European Space Operations Center /ESOC/ with ESRO 2/IRIS launching 01 p0163 A69-11105

Environmental tests of space vehicles, determining parameter effects on ground storage and transportation, launching and orbital life 02 p0228 A69-11918

All weather wind profile monitoring system using FPS-16 radar/Jimsphe system and flight simulation for protection of space vehicle and missile launches 03 p0462 A69-13852

Photographic control system requirements for Project Apollo manned launches, considering extreme heat, vibration and sound pressure environment [SMPTE PAPER 104-20] 04 p0596 A69-14360

Microwave power applications to propulsion, noting spacecraft launching, aircraft takeoff thrust assistance and power transmission in space [IMPI PAPER D2] 04 p0647 A69-15000

Spacecraft launching facilities and payload capabilities in next decade, discussing orbits, spacecraft size and volume, attitude stabilization and positional accuracy 06 p1012 A69-16857

Scout launch vehicle for launching small research satellites in near earth orbits, describing solid propellant stages, guidance, telemetry and beacon systems 06 p1016 A69-17597

Longitudinal structural vibration and lateral bending response mass and spring coupling in Saturn AS-502 during boost with longitudinal excitation by pogo effect [AIAA PAPER 69-58] 06 p1019 A69-18204

Anomalous infrasonic signals observed during launching of space vehicles with thrust greater than 200,000 lb, noting supersonic and subsonic group velocity spreads 07 p1078 A69-18853

Truss framework for support of eight 100-lb satellites through Titan 3C launch and dispensing of satellites at predetermined times, discussing materials and fabrication 09 p1512 A69-22369

General purpose space vehicle ground support equipment adapted from special purpose systems, discussing checkout, launch control and data monitoring requirements [AIAA PAPER 69-308] 09 p1479 A69-22385

Space propulsion system design with consideration for launch and mission requirements, noting upper stage structural design and computer techniques 12 p2148 A69-26834

European Space Research Organization projects including satellites and sounding rocket launchings for various missions 12 p2175 A69-26922

Control system design for Black Arrow satellite launch vehicle based on Black Knight test vehicle system 14 p2530 A69-29630

Europa 1 booster supplementing with perigee-apogee system for development of Europa 2, noting payload launching capability into 24-hr circular orbit 15 p2671 A69-31051

European launcher system based on modular principle for low orbit, geostationary and space probe missions payload requirements 17 p3050 A69-33428

Launch opportunity and window constraints, considering injection energy and precision, reference body occultation, communications range, etc 20 p3617 A69-37287

Low cost rate transportation as mandatory goal for future space program, discussing recovery and reuse, launch system costs, hardware development, etc 20 p3618 A69-38117

Space vehicle launcher system reliability from trials and adopted corrections, basing formal computation on adoption of normalized form for reliability likelihood 20 p3618 A69-38278

Europa 1 launch clearance procedure based on wind load precalculations from weather balloon determined wind profiles 20 p3619 A69-38281

Space transportation cost saving options including booster systems, spacecraft/payload systems and support systems, discussing recovery and launching operations 21 p3857 A69-39690

Synchronous communications satellite launch constraints for fixed time or node, noting application to IDCSP/A mission and sun angle, occultation and transfer orbit [AIAA PAPER 68-445] 22 p4036 A69-40543

General purpose space vehicle ground support equipment adapted from special purpose systems, discussing checkout, launch control and data monitoring requirements [AIAA PAPER 69-308] 22 p3927 A69-40552

Satellite system survival probability expressed as function of launch probability, time and number of satellites available [AIAA PAPER 67-324] 24 p4249 A69-43665

SPACECRAFT LUBRICATION

Space lubrication system for Orbiting Solar Observatory program, discussing theoretical high vacuum principles and flight performance and environmental test data 02 p0252 A69-11766

Satellite, spacecraft and rocket components coatings and lubricants, noting high radiation resistance of polyimides 06 p0945 A69-17046

European research on ultrahigh vacuum lubrication in space environments, emphasizing friction of materials under various loadings and temperatures [IME PAPER 10] 07 p1138 A69-18564

SPACECRAFT MANEUVERS

NT ORBITAL RENDEZVOUS

Spacecraft maneuvering by changing spacecraft geometry and utilizing different gravitational forces acting on finitely extended bodies 01 p0158 A69-11318

Constant thrust deceleration formula for gravity turn soft landing maneuvers expressed in elementary and trigonometric functions of initial conditions for descent 02 p0335 A69-12531

Spacecraft orbital maneuvers by means of low thrust, discussing optimization and several orbital transfer examples 03 p0522 A69-14086

Time optimal turn maneuver for rocket with tilting engine and control nozzles, noting rotation moments distribution 04 p0665 A69-14832

Power requirements of low thrust space engine for maneuvers and optimum overlappings theory for selection of power plant 04 p0666 A69-14920

Minimum fuel consumption for low thrust jet engine propelled space vehicles maneuvering in circular trajectories 05 p0829 A69-15879

Electrical propulsion for space maneuvers, discussing interrelationship of orbital changes, payloads and time 06 p0998 A69-16858

Ground based guidance systems for supplementing onboard guidance of manned space vehicles 06 p0955 A69-17580

Velocity meter for precision adjustment of orbits of vehicles in space for long periods using digital integrating accelerometer 08 p1348 A69-21063

Resistojet control system combined with control moment gyro payload capability for long duration manned orbital spacecraft missions [AIAA PAPER 69-255] 09 p1561 A69-21220

Rendezvous maneuvers for fixed elliptical target orbit, discussing numerical solution of problem and suitability of various points of target ellipse for rendezvous 09 p1538 A69-21649

Spacecraft horizontal maneuvers in homogeneous gravitational field to achieve soft landing on planetary surface, including optimal liftoff and orbital transfer 13 p2356 A69-27685

Midcourse maneuvers in interplanetary guidance, considering spin stabilized spacecraft flyby for Jupiter mission 13 p2354 A69-28504

Dynamic characteristics of model of spacecraft-astronaut-tether system during approach, deriving kinetic potential 15 p2696 A69-31064

Reaction control rocket engines for manned spacecraft, discussing operating and cycle life, thrust response, specific impulse and reliability 16 p2867 A69-31746

Electrically propelled TV satellite control maneuvers to reach target position in synchronous circular orbit from spiral ascent trajectory 16 p2868 A69-31935

Capillary barriers to provide propellant positioning, expulsion capability and slosh damping for spacecraft propulsion systems during rotational maneuvers [AIAA PAPER 69-529] 16 p2868 A69-32713

Fluid flow problems during orbital refueling vehicle maneuvers and system operations in propellant transfer, including disturbances, liquid-vapor interface instability, vapor ingestion, etc [AIAA PAPER 69-367] 16 p2868 A69-32721

Momentum control system for satellite maneuvering and pointing in pitch and roll developed by modifying existing libration damping gyrostabilizer 18 p3207 A69-34684

Interplanetary swingby trajectory correcting maneuvers for space vehicles return to earth after planet orbiting with emphasis on singular points 19 p3427 A69-36613

Lunar module motion during optimal ascent from moon surface into circular orbit of command module, noting descent maneuver similarity 19 p3431 A69-36617

Optimal low thrust coplanar rendezvous control for thrusting vehicle and passive vehicle in elliptical orbit

using linearized equations of motion and polar coordinates 20 p3617 A69-37192

Secondary or abort mission maximized subject to primary mission constraints by variational treatment of optimal branched trajectories [AAS PAPER 68-138] 21 p3819 A69-39210

Parking orbit optimal orientation for minimal impulsive maneuvers total velocity increment in three dimensional capture-escape mission [AIAA PAPER 69-918] 21 p3808 A69-39347

Reaction boom attitude control systems for improving stabilization and maneuvering capability of earth pointing satellites, describing configurations [AIAA PAPER 69-834] 21 p3822 A69-39365

Space rendezvous methods from developmental environment to operational method 21 p3824 A69-39474

Satellite maneuver for changing plane of circular orbit to pass through given point, determining on-off engine switching and thrust vector control 21 p3765 A69-39640

Real time targeting for Apollo lunar orbit insertion maneuver burn, discussing impulsive maneuvers for flight control [AIAA PAPER 68-848] 21 p3828 A69-39760

Optimal minimum fuel rendezvous maneuver variational problem, generalizing circular orbit results to conical orbits 22 p4028 A69-40754

Optimum functions for mass and energy flow during spacecraft orbital transfer, emphasizing time behavior of propulsion variables 24 p4382 A69-42921

SPACECRAFT MODELS

Mars planetary entry and landing model tests, demonstrating technological feasibility of mission 02 p0333 A69-11746

AZUR satellite movement simulator for thermal control tests, describing assembly 08 p1300 A69-20095

Spacecraft electric propulsion parameters and launching vehicle characteristics in low thrust mission simulation, discussing spacecraft path 09 p1584 A69-21202

Mission model construction for power limited systems, discussing flight concepts, propulsion mixes and electric propulsion 09 p1584 A69-21205

Aerodynamic measurements on Apollo CM model at hypersonic flow simulating earth orbital reentry trajectory 12 p2012 A69-26800

Gravity preference tests on rats subjected to simulated Aerobee 150 A rocket launching and flight in ground based spiral centrifuge 13 p2213 A69-28090

Solar radiation pressure effects on satellite models in circular equinoctial orbits 14 p2522 A69-29595

Dynamic characteristics of model of spacecraft-astronaut-tether system during approach, deriving kinetic potential 15 p2696 A69-31064

Scale modeling of multilayer insulated spacecraft for thermal design, considering solar probe and two meter telescope models [AIAA PAPER 69-613] 17 p3049 A69-33267

Planetary lander model thermal design, analysis and testing, emphasizing lightweight multilayer insulation, discussing thermal/vacuum testing [AIAA PAPER 69-612] 17 p3049 A69-33296

Thermal scale modeling for space hardware development from managerial and engineering viewpoints [AIAA PAPER 69-1010] 22 p3922 A69-40383

SPACECRAFT MODULES

NT LANDING MODULES

NT LUNAR LANDING MODULES

NT LUNAR MODULE

NT MARS EXCURSION MODULE

Cascaded thermoelectric module for spacecraft power conversion via module integration with radio isotope heat source, bonding SiGe and PbTe stages 20 p3465 A69-37706

SPACECRAFT MOTION

Hill method for satellite motion with reference to rectangular rotating axes system with origin at moon center of gravity, obtaining intermediate orbits 16 p2855 A69-31656

Liquid filled toroidal shaped rotating damping tube containing bubble, discussing parameters variation effect on spacecraft nutation 16 p2868 A69-32561

SPACECRAFT PERFORMANCE

Equations of motion of rapidly rotating spacecraft, considering deformations of long elastic booms 18 p3207 A69-34582

Motion and stability of rotating connected two body space station satellite system, developing Lagrangian equations of motion and optimizing damping system parameters [AIAA PAPER 69-919] 21 p3820 A69-39349

General control theory for spacecraft motions, deriving dynamic equations of motion about center of mass for holonomic and nonholonomic control programs 21 p3829 A69-39829

Spacecraft spherical motion about mass center under inertial force using Euler differential equations 21 p3830 A69-39838

Multispacecraft simultaneous simulation on hybrid computer using Encke perturbation method for translational motion and Hamilton quaternion method for inertial transformations [AIAA PAPER 69-937] 22 p4036 A69-40320

Kalman-Bucy filtering technique for estimation of initial conditions and smoothing in linear dynamic systems, noting rectilinear motion of randomly accelerated spacecraft 23 p4132 A69-42546

SPACECRAFT ORBITAL ASSEMBLY

U ORBITAL ASSEMBLY

SPACECRAFT ORBITS

NT INTERPLANETARY TRANSFER ORBITS

NT PARKING ORBITS

NT POLAR ORBITS

NT SATELLITE ORBITS

NT STATIONARY ORBITS

NT TRANSFER ORBITS

NT TWENTY-FOUR HOUR ORBITS

Orbiting ESRO 2/IRIS energy measuring experiments, satellite stabilization, power source, communications and data recovery 01 p0156 A69-11108

Saturn ring gravitational field perturbations of space vehicle orbit on flyby mission solved by particle motion perturbation theory 03 p0508 A69-13260

Spacecraft launching facilities and payload capabilities in next decade, discussing orbits, spacecraft size and volume, attitude stabilization and positional accuracy 06 p1012 A69-16857

Velocity meter for precision adjustment of orbits of vehicles in space for long periods using digital integrating accelerometer 08 p1348 A69-21063

Resistojet control system combined with control moment gyro payload capability for long duration manned orbital spacecraft missions [AIAA PAPER 69-255] 09 p1561 A69-21220

Spacecraft orbit control laws determined by studying influence of controlling acceleration in plane perpendicular to absolute velocity vector 11 p1965 A69-25743

Solar array energy performance as function of orbital parameters and spacecraft attitude 13 p2203 A69-27419

Fluid transfer in orbit under low or zero g, stressing orientation [AIAA PAPER 69-565] 16 p2865 A69-32770

Mathematical model for determining thrusted interplanetary spacecraft orbit, considering time history of position, velocity and thrust acceleration [AIAA PAPER 69-901] 21 p3806 A69-39335

Orbit selection rules for planetary cartographic spacecraft derived from relations connecting camera angle, view field and imaging resolution [AIAA PAPER 69-879] 21 p3763 A69-39405

Statistical error analysis of autonomous manned spacecraft navigation in long duration eccentric Mars orbits [AIAA PAPER 69-880] 21 p3763 A69-39406

Celestial sphere scanning by passive method applicable to space missions requiring long lifetime and moderate pointing accuracies [AIAA PAPER 68-854] 21 p3767 A69-39764

Minimum impulse transfer of vehicle between non-coplanar Kepler orbits, applying optimal control principles to formulation 23 p4214 A69-41878

SPACECRAFT PERFORMANCE

Variable geometry features applied to lifting spacecraft to overcome inherent incompatibility and provide low speed and tangential landing capabilities [AIAA PAPER 68-1164] 03 p0520 A69-13562

Digital computers in space flight simulation and vehicle performance optimization, examining mission analysis 04 p0652 A69-14519

Real time performance, ground control and data processing of Surveyor spacecraft during maneuvers [AIAA PAPER 67-644] 04 p0586 A69-15502

Earth radiation effect on space vehicle, using diffusely radiating sphere model 05 p0824 A69-16053

Lifting reentry spacecraft performance examined in context of realistic aerodynamic characteristics at low flight Reynolds numbers 06 p0860 A69-17634

RAE-A satellite design, simulation and flight performance, discussing gravity gradient stabilization 07 p1226 A69-18328

ESRO 1 satellite design coordination, assembly and tests 15 p2702 A69-31082

Saturn 5 translunar payload capability encumbrance by fuel biasing, propellant utilization systems, trajectory shaping and programmed mixture ratio scheme [AIAA PAPER 69-451] 16 p2839 A69-32669

Gravity gradient stabilized satellite achieving best theoretical performance through Foucault current and magnetic hysteresis articulations 17 p3048 A69-33234

Flight performance analysis of space systems, discussing preparation, implementation and communication 18 p3206 A69-34501

Earth orbital space program mission effectiveness increased through utilization of standby launch vehicles, spacecraft and space station systems 19 p3430 A69-36010

Jet engine risetime effect on spacecraft orientation control system performance, assuming monotonic or extremal thrust mode 19 p3370 A69-36619

Tiros-ESSA satellite operations, describing first and second generation systems 19 p3433 A69-36909

Earth radiation effect on space vehicle, using diffusely radiating sphere model 20 p3606 A69-37963

Navigation state vector update effect on lunar mission completion capability for Saturn 5, emphasizing hardware and scheme errors and accelerometer failure [AIAA PAPER 69-883] 21 p3764 A69-39409

Space rendezvous methods from developmental environment to operational method 21 p3824 A69-39474

Interactive graphics system for rocket vehicle trajectory simulation and performance analysis [AIAA PAPER 69-954] 22 p3905 A69-40336

SPACECRAFT POSITION INDICATORS

Navigation satellites system designed for ATC without requirement for onboard transmitter, discussing spectrum occupancy, satellite power, lane ambiguities and computational procedures 07 p1177 A69-19212

Instrument error analysis for spacecraft orientation and positioning near planet from planet disk observations 13 p2260 A69-27695

Spacecraft orientation from onboard stellar photographs, calculating absolute and relative elements, accuracy and camera parameters 13 p2296 A69-27696

SPACECRAFT POWER SUPPLIES

Subsystems of ESRO research satellites Td 1 and Td 2, discussing telecommunication, attitude control, power supply and temperature control design and functions 01 p0160 A69-10031

Storm-Shattuck and push-pull tunnel diode DC-to-DC converters suitable for spacecraft power supplies 01 p0013 A69-10750

Spacecraft voltage-limited charging system for sealed secondary batteries, discussing operating characteristics and battery parameters 01 p0013 A69-11010

Finned tube radiators optimum design for waste heat removal from space power plants 02 p0354 A69-12664

In-core thermionic sodium cooled uranium oxide fueled reactor for space vehicle power plant 02 p0279 A69-12666

Dissociating gas as working fluid for space plant, noting role in radiator area reduction 04 p0551 A69-15313

Mathematical model to design weight optimized silicon-germanium solar flat plate thermoelectric generator as spacecraft auxiliary power source in near sun missions 05 p0704 A69-15674

ESRO satellites power supply design, operation and characteristics 05 p0829 A69-15919

Liquid metals as coolants in breeder and space vehicle reactors for stable two phase flows 05 p0803 A69-15998

Photovoltaic solar cell power technology application to space use and exploration [ASME PAPER 68-WA/SOL-1] 05 p0705 A69-16158

Electronic circuits power supply onboard space vehicle, discussing chemical, solar and nuclear energy sources 07 p1225 A69-18251

Nuclear reactors for powering electrical engines and current supply for satellite devices, noting ROVER project and KiWI reactors 07 p1179 A69-19739

Out-of-core thermionic space power generators using heat pipes, discussing feasibility in geometry, heat pipes, reactor, shield, heat exchanger and radiator 08 p1256 A69-19856

Nuclear power supply with in-core thermionic reactor for space power source and use in satellite TV, discussing theory, design and components 08 p1350 A69-20871

Manned spacecraft electrical power systems requirements, noting Gemini and Apollo fuel cell system design and configuration 08 p1259 A69-21035

Electrical energy production on board space vehicles including solar batteries, chemical reagents and possible nuclear energy utilization 08 p1259 A69-21036

Energy source for space environments based on compact cold hydrogen-oxygen fuel cell, discussing heat control and water elimination methods 08 p1260 A69-21041

Electrostatic rocket exhaust condensation on spacecraft solar electric panels cover glasses, noting deleterious effects [AIAA PAPER 69-271] 09 p1569 A69-21874

High temperature and power gas diodes and thyristors for nuclear electrical space power systems 11 p1847 A69-24744

Astronautics - Conference, Braunschweig, West Germany, October 1968, Volume 2, Energy sources 12 p2014 A69-25862

Electrical power requirements in spacecraft, discussing communication, engine and control systems, data processing, electrochemical and nuclear sources 12 p2015 A69-25863

Solar cells operation in space flight, considering Si photoelectric cells characteristics and complete systems construction for spacecraft power supplies 12 p2015 A69-25865

Regulated voltage converter systems for onboard spacecraft electric power supplies, noting chopper circuits with rectifiers 12 p2015 A69-25867

Thermoelectric and thermal phenomena in thermoelectric generator development for spacecraft applications, considering element design and materials selection 12 p2016 A69-25868

Liquid-metal MHD space power generation system using intermittent vaporization slugs shooting at 2700 R peak temperature 13 p2206 A69-27492

Satellite and spacecraft power supply and power converters 13 p2209 A69-27917

Large power systems integration in manned space stations, discussing design, selection and application criteria 13 p2209 A69-27939

Power supply subsystem for TD1/TD2 satellites with solar cells, discussing design including standby battery for solar eclipse periods 13 p2209 A69-28481

Out-of-core thermionic reactor concept for space power supply using lithium heat pipes in crossed layers 14 p2480 A69-29187

Thermionic reactors U.S.S.R. space and other programs, considering power output, heat exchange and losses, neutron physics and design parameters 14 p2404 A69-29277

ESRO 1 satellite centralized control system, discussing housekeeping system responsible for task execution in connection with power supply 15 p2702 A69-31083

Storage batteries for satellite electrical power sources emphasizing operation in overcharged state 16 p2735 A69-31729

Nuclear energy conversion for long space missions, comparing dynamic Brayton, liquid metal MHD gas, dynamic Rankine and LMMHD Rankine cycles 16 p2810 A69-31748

Electrochemical generators for space applications - Conference, Paris, December 1967 16 p2736 A69-32405

Manned spacecraft fuel cell selection and design, discussing Gemini ion exchange membrane and Apollo Bacon cell systems 16 p2737 A69-32406

Electrochemical generators space applications, discussing nuclear, solar and rechargeable cells 16 p2737 A69-32407

Hydrogen-oxygen low power space use fuel cell, noting geometrical and electrical characteristics of electrodes 16 p2738 A69-32412

Double skeleton catalyst type VARTA fuel cell system for space power, using potassium hydroxide as electrolyte 16 p2739 A69-32418

Electrochemical generators utilizing anodically polarized zinc associated with oxygen, mercuric oxide or silver oxide for space power sources 16 p2739 A69-32420

Ni-Cd and Ag-Cd storage batteries for space applications, discussing performance, life and reliability 16 p2740 A69-32422

Parametric thermal control weight and power requirements for spacecraft life support systems, considering number of cabins, crew activity, heating, cooling and regeneration [AIAA PAPER 69-621] 17 p2914 A69-33305

Power supply circuits in spacecraft, DC voltage control systems, transistor and thyristor regulators and modulators, etc 17 p2937 A69-33582

Solar probes design for 0.3 to 0.1 AU perihelion distance, considering thermal control, power supply, communications, altitude control and alternative configurations 17 p3050 A69-33797

Overload protection guidelines for power subsystems, discussing source and protective device characteristics emphasizing spacecraft requirements 17 p2904 A69-34088

Rotary power transformer design for spin stabilized spacecraft power system, discussing efficiency and advantages 17 p3050 A69-34111

TD1/TD2 satellites power supply subsystem, stressing high power requirements and significant design features regarding battery and solar array controls 18 p3093 A69-34791

Large solar array systems in space, discussing design and operation 18 p3094 A69-35056

Magnetic core material and process technologies for space power electronic applications noting pulse transformers, nonlinear reactors and tapes 19 p3319 A69-35543

Solar cell retractable array for spacecraft multikilowatt power generation 19 p3254 A69-35711

Solar cells volt-ampere characteristics calibrated at various solar incidence angles on LES-6 satellite in synchronous orbit 19 p3254 A69-35712

Photovoltaic solar cell power technology application to space use and exploration [ASME PAPER 68-WA/SOL-1] 19 p3255 A69-36418

Cascaded thermoelectric module for spacecraft power conversion via module integration with radio isotope heat source, bonding SiGe and PbTe stages 20 p3465 A69-37706

Advanced reaction wheel controller for spacecraft attitude control, discussing brushless DC motor role in weight and power reduction and control precision [AIAA PAPER 69-855] 21 p3822 A69-39383

High voltage power supply electronic subsystem for electric propulsion of ATS-D satellite, describing packaging, temperature control and performance in simulated space environment 22 p3999 A69-39948

Photovoltaic cells electrical characteristics, discussing Cd sulfide, single crystal Si and dendritic type Si cells for spacecraft power 22 p3868 A69-40130

Electric power system selection for long duration manned space station [AIAA PAPER 68-1034] 22 p3869 A69-40549

Space power systems analysis, using computer program to correlate systems characteristics with mission parameters for automated satellite repair vehicle and space stations

23 p4068 A69-42240

Computer simulation of satellite electric power systems concerning solar array, thermal, battery and charge models for end-of-mission-life orbits

23 p4068 A69-42241

Solar cell power systems for manned space stations, summarizing studies of battery power system designs

23 p4068 A69-42242

Battery subsystems optimization for earth satellite lifetimes greater than 5 years, analyzing flexibility, weight and reliability

23 p4068 A69-42243

Fuel cell/battery and solar array/battery systems for manned Apollo Applications Program /AAP/ space vehicles, considering mission and power requirements

23 p4069 A69-42244

Thermionic reactors for auxiliary space power and electric propulsion applications, discussing converter development regarding nuclear fuel elements

23 p4186 A69-42246

SNAP 27 radioisotope thermoelectric generator system designed as prime power supply for Apollo lunar surface experiment package /ALSEP/

23 p4187 A69-42249

Mars landers impactable power subsystems, considering thermoelectric generators, batteries, conversion equipment, Mars environment, etc

23 p4069 A69-42253

Planar radioisotope thermoelectric generator system for NASA deep space missions and integrated spacecraft power supply

23 p4070 A69-42254

Power systems for unmanned spacecraft, noting improved performance for zirconium hydride reactors and thermoelectric converters

23 p4187 A69-42255

Co 60 kernel heat source for multikilowatt space power supplies, stressing design for maximum safety

23 p4187 A69-42257

Thermoelectric generators performance and life tests, describing JPL facilities and programs

23 p4188 A69-42263

Pu-238 isotope organic Rankine cycle system analyzed for one year manned space station, using modified H-521 Space Power computer program

23 p4188 A69-42264

Systems analysis of Rankine cycle nuclear- electric potassium space power system using Li cooled fast reactor and high temperature turbine inlet

23 p4189 A69-42266

Dynamic power and life support systems electrical/ thermal integration for manned spacecraft using low temperature Rankine cycle generator

23 p4189 A69-42269

ISOTEC thermoelectric generators for space power, describing design features, operation, power output and radioisotope heat source

23 p4189 A69-42270

Argon turboalternator design and testing for Brayton cycle space power system, discussing inlet operating temperature and shaft bearings and rotation

23 p4071 A69-42279

Analog computer simulation of single shaft Brayton cycle system dynamics, including startup and shutdown transients

23 p4071 A69-42280

Radioisotope energized Stirling engine for spacecraft auxiliary electric power, discussing system configurations, weight and fuel requirements

23 p4190 A69-42281

Aerospace NiCd batteries charge control, discussing depth of discharge, limiting voltage and environmental temperature interrelationship

23 p4071 A69-42282

Space vehicle flight performance of Ni-Cd batteries noting reliability, consistency and predictability

23 p4072 A69-42285

Apollo Telescope Mount /ATM/ solar cell module electrical performance testing using sunlight simulation

23 p4072 A69-42286

Solar cells arrays degradation in Intelsat spacecraft at synchronous altitude, noting shielding gaps and low energy proton influence

23 p4072 A69-42287

Spacecraft Si cell solar array using self rigidizing folded panels with flexible substrates for increased power/weight and power/stowage volume ratios

23 p4073 A69-42290

Lightweight large area solar cell arrays for space programs with multikilowatt predicted performance, noting rollup array orbital flight testing

23 p4073 A69-42291

Modularized static AC and DC inverters and converters for aerospace electrical power conditioning systems, discussing circuit functions and performance tests

23 p4073 A69-42292

Power conditioner for use with SERT II mercury ion thruster, describing electrical and mechanical design and operation

23 p4075 A69-42301

High efficiency boost regulator design and tests for planetary spacecraft, considering input and output voltages

23 p4075 A69-42302

Spacecraft solar cell near-maximum power operation by tracking optimum value with array temperature sensor

23 p4075 A69-42303

High power density spacecraft hydrogen/oxygen fuel cells with open cycle heat and product-water removal subsystems and reactant tankage

23 p4076 A69-42309

Space nuclear electric power systems applications and development, summarizing current status and near future programs

[AAS PAPER 69-305] 24 p4364 A69-42865

Battery/fuel cell hybrid power source, discussing fast transient response

[SAE PAPER 690205] 24 p4255 A69-42889

SPACECRAFT PRELAUNCH TESTS

U SPACE VEHICLE CHECKOUT PROGRAM

SPACECRAFT PROPULSION

NT ELECTROMAGNETIC PROPULSION

NT ELECTROSTATIC PROPULSION

NT ION PROPULSION

NT PLASMA PROPULSION

NT SOLAR PROPULSION

Solid, liquid and advanced propulsion techniques in France, discussing Diamant program and Europa booster

02 p0334 A69-11919

Book on electric propulsion systems for spacecraft covering thermoelectric, electromagnetic, electrostatic, plasmacore, thermonuclear and photon systems

02 p0305 A69-12233

Rocket motor integration into Scout vehicle to improve performance

02 p0335 A69-12384

French solid propellant sounding rockets proposed launching from Guiana base using different fuel propulsion systems

03 p0518 A69-12851

Power requirements of low thrust space engine for maneuvers and optimum overlappings theory for selection of power plant

04 p0666 A69-14920

Microwave power applications to propulsion, noting spacecraft launching, aircraft takeoff thrust assistance and power transmission in space

[IMPI PAPER D2] 04 p0647 A69-15000

Spacecraft propulsion - ELDO Conference, Paris, October 1967

05 p0791 A69-15593

Polonium 210 production for radiothermal propulsion via bismuth irradiation in graphite gas power reactor

05 p0791 A69-15594

Radioisotopic propulsion stage design with liquid hydrogen working fluid, stressing tank insulation and hydrostatic flight behavior

05 p0811 A69-15595

Isotopic propulsion engine development problems, emphasizing single channel thermal power engine with hydrogen working fluid

05 p0811 A69-15596

Thorium 228 production and shaping for radiothermal propulsion, discussing transformation from radium 226, irradiated target processing, etc

05 p0791 A69-15597

Low thrust nuclear engine using hydrogen suitable for transfer missions

05 p0791 A69-15598

Spacecraft optimum low thrust trajectory analyzed by Hamilton-Jacobi perturbation theory, obtaining canonic constants of motion

06 p1007 A69-17574

Solar sail structural design, discussing application as propulsion system for heliogyro interplanetary spacecraft

06 p1015 A69-17591

Feasibility of nuclear stage for space missions, discussing Saturn 5 third stage replacement, payload gain, reactor and engine size

08 p1409 A69-20158

Cesium electron bombardment microthruster system, discussing ion engine, feed, discharge neutralizer, power conditioning and control electronics

[AIAA PAPER 69-293] 09 p1561 A69-21223

SERT 2 thruster hollow cathode durability tested in bell jar

[AIAA PAPER 69-304] 09 p1562 A69-21224

Pulsed plasma microthruster propulsion system for synchronous orbit LES 6 satellite

[AIAA PAPER 69-298] 09 p1562 A69-21227

Background pressure and magnetic field shape effect on MPD thruster performance, testing radiation cooled thrusters

[AIAA PAPER 69-243] 09 p1564 A69-21239

Solar electric propulsion mission simplification by staging concept, discussing thrust combination, weight tradeoffs, design and Jupiter flyby probe

[AIAA PAPER 69-251] 09 p1586 A69-21245

Performance boundaries of space propulsion systems containing nuclear electric stages

[AIAA PAPER 69-249] 09 p1538 A69-21249

NASA long range planning of primary electric propulsion for automated space program

[AIAA PAPER 69-247] 09 p1565 A69-21251

Electron bombardment thrusters for low specific impulse operation, discussing electrode structures fabrication by bonding alumina disk to metal electrode

[AIAA PAPER 69-301] 09 p1568 A69-21730

Power converter design for electrically propelled spacecraft, discussing weight, reliability, and thruster load requirements

[AIAA PAPER 69-240] 09 p1568 A69-21732

Liquid mercury cathode electron bombardment thrusters applicability to electric propulsion missions

[AIAA PAPER 69-302] 09 p1569 A69-21876

Hollow cathode mercury electron bombardment thruster design, emphasizing low specific impulse operation and discharge chamber improvements

[AIAA PAPER 69-300] 09 p1569 A69-21880

Simulator for testing colloid microthruster, discussing spacecraft interfaces and time of flight thrust data

[AIAA PAPER 69-314] 09 p1478 A69-22380

Ionic propulsion application to geostationary satellite attitude correction

10 p1753 A69-23841

Book on theory and design of jet, rocket, nuclear, ion and electric propulsion systems noting combustion, detonation, fluid injection and space mission applications

11 p1943 A69-25582

Rocket propulsion devices classifications, discussing energy sources, propellants, performance, space vehicle applications, liquid propellant rockets, engines, selection criteria and cooling methods

11 p1943 A69-25587

Space propulsion by radioisotope energy noting thermal heating, thruster configurations, propulsion system, mission capabilities and current thruster technology

11 p1914 A69-25591

Electric and ion propulsion with solar array or nuclear reactor energy sources, discussing thermal thrusters, electrostatic thrusters and plasma thrusters

11 p1944 A69-25592

Ion spacecraft propulsion systems, discussing components and characteristics of reaction type rocket engines and electrical thrust devices

11 p1944 A69-25593

Electric propulsion systems characteristics, examining sputtering of metallic targets as thrust augmentor

11 p1944 A69-25598

Spacecraft propulsion systems comparison and evaluation, discussing quality, schedules and costs in relation to mission requirements

11 p1965 A69-25600

Entry propulsion and lower systems technology for planetary entry and atmospheric reentry vehicles

11 p1945 A69-25723

Fiber reinforced space vehicle combustion chambers and cryogenic fuel tanks, discussing design and elastomechanical problems

12 p2176 A69-25860

Space propulsion system design with consideration for launch and mission requirements, noting upper stage structural design and computer techniques

12 p2148 A69-26834

Thermionic reactor systems, discussing hybrid nuclear rocket/nuclear electric Mars mission, design

features, performance and electric power characteristics

14 p2480 A69-29183

Rocket motors with combustion chambers of variable geometry for hybrid propellants, stressing toroidal chamber

15 p2671 A69-30600

Electric propulsion, discussing plasma research, MPD thruster and arcs, ion thruster research and spacecraft integration [AIAA PAPER 69-497]

16 p2838 A69-32655

Minimal electric propulsion systems for interplanetary spacecraft, discussing payload, reduced trip time and low thrust systems for Jupiter flyby [AIAA PAPER 69-499]

16 p2844 A69-32714

Slush hydrogen for spacecraft propulsion, discussing fabrication, conservation and storage

17 p3017 A69-33339

Heat exchanger type low power solid-core fast nuclear rocket design, discussing fuels, safety aspects and space propulsion applications

17 p3004 A69-33342

Optimal overlapping theory to select nonthrottled low thrust spacecraft engines power, noting spacecraft mass invariability

18 p3184 A69-34583

Chemical relaxation, optimum propellant mixture ratio, combustion chamber pressure, gas jet impulse, mass flow and drive capacity of space propulsion systems

18 p3229 A69-34773

Electric propulsion systems for manned planetary exploration flights, discussing arc jet, ion and plasma engines

18 p3185 A69-35108

BEEP /Best Estimate of Engine Performance/ program based on trajectory reconstruction and acceleration determination for evaluating Titan 3 propulsion system performance [AIAA PAPER 68-585]

19 p3394 A69-35945

Pneumatic Vernier engines in aircraft and spacecraft, discussing weight, gas expansion and gas temperature

21 p3785 A69-39093

Trajectory requirements and performance comparisons of single stage electrically propelled space vehicles [AAS PAPER 68-106]

21 p3819 A69-39204

Liquid hydrogen pumping for Phoebus reactor, discussing feed systems, nozzles, configurations, design, testing, etc [AIAA PAPER 67-478]

21 p3769 A69-39751

Catalyst poisoning and hydrazine material compatibility during hydrazine propulsion systems sterilization and decontamination

21 p3786 A69-39768

Book on commercial satellites covering characteristics, uses, design, rocket propulsion systems, flight trajectories, etc

23 p4224 A69-42367

Spacecraft electric propulsion research in France, Great Britain and Germany

24 p4363 A69-42668

Launch vehicle upper stage requirements in space missions, discussing space engine for lunar, planetary and interplanetary exploration [AAS PAPER 69-359]

24 p4418 A69-42828

Reduced flight time interstellar round trip propulsion system with relativistic velocity capabilities, discussing vehicle with solar sail and magnetic course reversal [AAS PAPER 69-388]

24 p4363 A69-42829

Nuclear propulsion for solar system exploration, discussing NERVA solid core nuclear fission rocket, nuclear-electric rockets and hybrid nuclear rocket/nuclear electric rocket systems [AAS PAPER 69-330]

24 p4349 A69-42871

Optimum functions for mass and energy flow during spacecraft orbital transfer, emphasizing time behavior of propulsion variables

24 p4382 A69-42921

Weight limitations effect on optimum motion parameters of variable mass body in gravitational field applied to spacecraft optimum propulsion system controls and trajectory determination

24 p4383 A69-42956

SPACECRAFT RADIATORS

Dissociating gas as working fluid for space plant, noting role in radiator area reduction

04 p0551 A69-15313

Space radiator dynamic model for predicting outlet temperature transient response to environmental variations [AIAA PAPER 69-29]

06 p1039 A69-18205

Transient thermal analysis of space radiators excluding finite difference equations, noting computer adaptability and time saving [AIAA PAPER 69-615]

17 p3070 A69-33261

Heat pipe application to thermal equalization around ATS-E solar cell mounting panels, comparing predicted and actual performance [AIAA PAPER 69-630]

17 p3072 A69-33277

Space radiator system with hybrid, water heat pipes to transport waste heat from radioisotopic thermoelectric generator

23 p4190 A69-42304

SPACECRAFT RECOVERY

Air to air recovery of reentry vehicles, discussing parachute/wing descent, aircraft/helicopter energy absorption, payload boarding and towing techniques [AIAA PAPER 68-1163]

03 p0520 A69-13563

Soviet probe Zond 5 circumlunar flight to recover space vehicles from interplanetary paths

06 p1003 A69-17389

Agreement on Rescue and Return of Astronauts and Return of Objects Launched into Outer Space, discussing unintended landing

20 p3636 A69-37113

Agreement on Rescue and Return of Astronauts and Return of Objects Launched into Outer Space, noting humanitarian considerations and indemnity for services rendered

20 p3636 A69-37114

UN agreement provisions on international cooperation for rescuing astronauts and objects in case of accident, distress, emergency or unintended landing

20 p3637 A69-37116

Space transportation cost saving options including booster systems, spacecraft/payload systems and support systems, discussing recovery and launching operations

21 p3857 A69-39690

SPACECRAFT REENTRY

Upgrading wave superheater for evaluation of reentry materials

01 p0054 A69-10917

Apollo thermal protection system, noting low density ablation, flight and ground tests [AIAA PAPER 68-1142]

03 p0519 A69-13558

Space vehicle flight automatic optimization for maximum L/D reentry, considering perturbations causing trajectory inclination changes during roller coaster reentry

05 p0830 A69-16045

Cosmos 253 rocket reentry and fragmentation over England

05 p0830 A69-16656

Flat plate in two dimensional low density hypersonic flow wind tunnel tested for aerodynamic effects on spacecraft reentry

11 p1819 A69-25424

Mass transfer cooling of high velocity surfaces in gaseous environment noting applications to atmospheric entry

13 p2377 A69-28146

Control methods for spacecraft reentry and landing, discussing adaptive systems, descent trajectory parameter prediction and angle of attack

16 p2867 A69-31742

NASA planetary entry parachute program for rocket launched and balloon deployment tests [AIAA PAPER 68-934]

19 p3247 A69-35952

Space vehicle flight automatic optimization for maximum L/d reentry, considering perturbations causing trajectory inclination changes during roller coaster reentry

20 p3618 A69-37954

Optimal sliding regimes for controlling dynamic systems, proposing control parameters system extension

21 p3768 A69-39826

Arc-heated hypersonic wind tunnel for simulated spacecraft reentry environment, aerodynamic heating characteristics and research applications

22 p3927 A69-40595

SPACECRAFT RELIABILITY

Meteoroid penetration detector development program for spacecraft construction, discussing design, materials and environmental tests

02 p0338 A69-11749

Reliability of operational satellite systems consisting of two single purpose satellites in interchangeable orbits, discussing outage and replacement

02 p0333 A69-11805

Explorer 33 and 35 satellites reliability achievement by design via AIMP program

03 p0519 A69-13232

Reliability in air and space travel, quality/ quantity aspects, problems and cooperation

04 p0606 A69-14803

Spacecraft terminal dry heat sterilization procedures for minimal time and temperature conditions, using simple geometric configuration of spacecraft for thermal analysis

05 p0712 A69-15942

Engineering designs and hardware required for low risk flight of long duration manned space stations

06 p1007 A69-17601

Satellite attitude control, discussing mission requirements, typical guidance sensors, actuating torque, systems reliability, etc

09 p1609 A69-21617

Integrated management information system /IMIS/, discussing logistics, reliability and quality assurance disciplines

11 p2005 A69-25304

Reliability and maintainability analysis of two year spacecraft mission combining earth orbits and Mars program, using computerized mathematical model [AIAA PAPER 68-1059]

12 p2174 A69-26797

Electric relays requirements for spacecraft with magnetic field constraints

13 p2231 A69-28046

Three meter spherical volume heat balance test facility for space vehicles at European Space Technology Center, describing vacuum system, solar simulation, etc

13 p2241 A69-28080

Scientific satellite checkout system tests by manual, automatic and self test control

13 p2243 A69-28480

Space equipment reliability, discussing manufacturing defects, design faults, component failures, maintenance, overloads, accidents and operating errors

15 p2624 A69-30817

Static structure ground test for Saturn-Apollo vehicle short stack, describing air pressure simulation, data acquisition and readout systems

15 p2589 A69-31079

Space vehicle subcontracted components reliability attainment, discussing reliability process specifications, motivation, product reliability and feedback programs

15 p2723 A69-31139

Engine and components reliability, discussing design stage and programming [AIAA PAPER 69-476]

16 p2795 A69-32771

Fluidics for satellite and rocket attitude control and guidance, discussing computing block function and components, system reliability and resistance to aging, etc

17 p3049 A69-33243

Spacecraft and aircraft components failure analysis for ensuring high reliability of final products

18 p3143 A69-34483

Flight failure analysis, discussing methods and restrictions due to hardware unavailability, minimum data, urgency and publicity

18 p3145 A69-34502

Spacecraft structures reliability, discussing detection, identification, assessment and control of defects

18 p3146 A69-34513

Spacecraft and components testing methods critical reassessment, discussing cost reduction, vacuum and thermal cycle tests

18 p3118 A69-35082

Strapdown inertial reference unit system for inflight reliability and maintainability, discussing design and components

19 p3370 A69-35803

Space simulation facility assembly and operational testing

22 p3919 A69-39959

Operational reliability verification of Apollo real time mission program and testing structure, discussing environment, processing, controls, response criteria, etc [AIAA PAPER 69-981]

22 p3907 A69-40361

Orbiting Astronomical Observatory thermal test and evaluation program, discussing equipment and role in experimental design [AIAA PAPER 69-995]

22 p3920 A69-40373

Spacecraft test equipment based on balancing and vibration testing machines, emphasizing mass distribution experimental determination

24 p4296 A69-42669

Space station safety, discussing damage containment and control, escape and rescue, etc [AAS PAPER 69-518]

24 p4392 A69-42842

Systems supply for unmanned spacecraft, considering power supply, equipment operation, trajectory correction, etc [AAS PAPER 69-520]

24 p4392 A69-42849

High reliability of solenoid and pressure regulating valves under long duration space missions, considering design, tests and controls
[AAS PAPER 69-238] 24 p4319 A69-42854

SPACECRAFT RENDEZVOUS
U SPACE RENDEZVOUS

SPACECRAFT SHIELDING

Equation for calculating meteor shielded tubular panel heat radiators emissivity and weight optimization, considering surface thermal balance and temperature distribution
05 p0846 A69-15897

Cosmic radiation and hybernation physiopathology of human organism, noting beryl as radiation resisting agent in spacecraft design
06 p0874 A69-17645

Solar flare radiation protection requirements, considering bulk and plasma radiation shielding
[AIAA PAPER 69-15] 06 p0884 A69-18079

Monte Carlo method applied to calculation of radiation transmission and dosage behind space vehicle shields during passage through earth radiation belt
08 p1377 A69-19843

Field noise reduction frequency spectra afforded by spacecraft shroud, basing estimating criterion on flight test data
09 p1609 A69-21892

Super insulation blankets comprised of dacron sailcloth, silk net or aluminized mylar, describing crinkling, cutting, sewing and hole drilling techniques
09 p1507 A69-22330

Multiple Coulomb scattering and range straggling effects in shielding against solar flare protons and trapped protons in Van Allen belt
10 p1723 A69-23164

Proton flux density at axial point of thin cylindrical and slab shell shields bombarded by isotropic inverse power law spectrum of protons in space
10 p1723 A69-23165

Radiation dosimetry and shielding onboard Cosmos 110 artificial satellite, noting earth belt proton radiation
13 p2356 A69-27702

Multiwall meteoroid protection design in Apollo program, discussing bumper, backup sheet and honeycomb cells insulation
[AIAA PAPER 69-372] 13 p2367 A69-28304

Lightweight double walled meteoroid shield for Mariner Mars 1971, considering Teflon impregnated glass fabric outer sheet and multilayer thermal insulation
[AIAA PAPER 69-377] 13 p2357 A69-28307

Two plate meteoroid shields effectiveness determined by analyzing debris cloud ejected behind front plate after hypervelocity impact
[AIAA PAPER 69-380] 13 p2368 A69-28310

Soviet book on nuclear interactions in spacecraft shielding covering proton-A1 nuclei inelastic interactions, secondary radiation, solar radiation effects, radiation belts, etc
14 p2481 A69-29817

Calorimetric measurement of source and broadband spectral absorptances of spacecraft thermal control coatings during exposure to UV in vacuum environment
16 p2789 A69-31815

Lunar module multilayer radiation insulation for thermal control, testing aluminum coated Mylar and Kapton sheets
[AIAA PAPER 69-609] 17 p3073 A69-33304

Second surface mirror used as coating for spacecraft thermal control
20 p3632 A69-37290

Computer optimization of spacecraft optical coatings for temperature control, using finite element analysis and matrix inversion
[AIAA PAPER 69-979] 22 p4050 A69-40359

IR directional and hemispherical emittance of spacecraft thermal control coatings, comparing values determined by various measurement techniques
23 p4164 A69-41633

SPACECRAFT STABILITY

First approximation stability of single rotation of artificial earth satellite about center of mass in Newtonian gravitational force field
01 p0161 A69-10585

Data acquisition program for Apollo crew motion disturbances experiment consisting of ground simulations and orbital experiment establishing mathematical model of human body
02 p0201 A69-11759

Stabilization and control techniques for future unmanned commercial space vehicles, emphasizing application of projected technological advances in instrumentation
[AIAA PAPER 67-878] 02 p0334 A69-12367

Phase plane diagram utility in toppling stability analysis of spacecraft, emphasizing numerical integration time reduction
02 p0334 A69-12376

Self oscillations of dynamic systems representing space vehicles, considering periodic motions stability, bifurcation curves and energy consumption requirement limit
03 p0519 A69-13068

Energy dissipation effects on attitude stability of dual-spin satellites with damping mechanism on rotating sections
04 p0665 A69-14703

Apollo guidance, navigation, stabilization and control subsystems, detailing inertial, optical and computer units for data processing and collecting
04 p0665 A69-14881

Optimum stabilization of uniformly rotating axisymmetric satellite, using Liapunov theorem on asymptotic stability
04 p0666 A69-14921

Satellite relative equilibrium stability under action of gravitational and aerodynamic moments
05 p0830 A69-16503

Nutational stability of multibody spin stabilized satellites, discussing moment of inertia ratios role with energy dissipative damper on despun platform
06 p1015 A69-17585

Dynamic stability derivatives of large angle blunted conical spacecraft near transonic speed in simulated Mars environment for various angles of attack
[AIAA PAPER 69-104] 06 p1019 A69-18210

Semipassive three axis stabilization for dumbbell type satellites, considering pitch, roll and yaw motions damping
07 p1226 A69-18324

Thermal flutter effect on gravity gradient stabilized spacecraft, noting dependence on sunlight and time
07 p1226 A69-18325

Semipassive attitude control system providing one degree pointing accuracies in all axes
07 p1226 A69-18326

Storable tubular extendible member (STEM) booms for gravity gradient applications, emphasizing reflective coatings to minimize deflection by solar radiation
07 p1226 A69-18327

RAE-A satellite design, simulation and flight performance, discussing gravity gradient stabilization
07 p1226 A69-18328

Thermally excited oscillation experienced by OGO 4 boom antenna demonstrated by mathematical model, showing nonplanar coupled bending-torsion oscillation by solar radiation
07 p1227 A69-18333

Hybrid simulation study of satellite attitude control system to replace momentum wheels and gas jets by commandable gravity gradient boom
07 p1227 A69-18335

Equilibria of orbiting gyrostat satellite with internal angular momenta along principal axes
07 p1227 A69-18336

System designs for manned spacecraft gravity gradient stabilization of Saturn S-4B stage at 400 km and lunar module at synchronous altitude
07 p1228 A69-18338

Communication satellites attitude control and stabilization due to antenna beam pointing, with future systems forecast, discussing exchange, distribution and collection systems
07 p1228 A69-18339

Naval Research Laboratory experience with two and three axis gravity gradient satellites stabilization systems
07 p1228 A69-18344

RAE satellite boom deployment to achieve gravity gradient capture
07 p1228 A69-18346

Gravity gradient stabilization role in space missions in 1970s and 1980s
07 p1229 A69-18348

Damping criteria for satellite vibration based on energy dissipation by material hysteresis, friction in viscous flow, magnetic hysteresis and eddy currents
10 p1791 A69-22921

Atmospheric influence on plane oscillations of space vehicle moving at 100-150 km heights
10 p1792 A69-24208

Rotational dynamics equations in linearized matrix form applied to satellite librations in circular orbit and gyroscope motion
11 p1970 A69-24608

Saturn 5 unstable longitudinal oscillation due to coupling of structure and LOX line frequencies solved by helium injection
11 p1967 A69-25497

Magnetic attitude detection and control system for Radio Astronomy Explorer satellite
[AIAA PAPER 68-855] 12 p2174 A69-26779

Space vehicle attitude stabilization based on rotating flywheel resistance to changes in rotation axis attitude, noting grease lubricated hydrodynamic bearing system
12 p2175 A69-26893

Magnetic desaturation of inertia flywheels of satellite in equatorial or slightly inclined orbit, discussing satellite stabilization
13 p2357 A69-28476

Self oscillations of dynamic systems representing space vehicles, considering periodic motions stability, bifurcation curves and energy consumption requirement limit
14 p2530 A69-28750

Steady motion stability of satellite with gimbal suspended gyroscope in central gravitational field, showing no effect of satellite perturbations on gyrostaticity
14 p2530 A69-29481

First approximation stability of single rotation of artificial earth satellite about center of mass in Newtonian gravitational force field
15 p2702 A69-30755

Satellite gravitational stabilization system with maximum damping rate, discussing orbital plane oscillations
16 p2867 A69-31738

Flight and space mechanics problems from engineer standpoint, discussing flight path calculation, stability and control characteristics and experimental techniques for high reliability
17 p3076 A69-33041

Satellite attitude control and stabilization - Conference, Paris, October 1968
17 p3045 A69-33219

D-2 satellite stabilization system design and development, noting mission to determine hydrogen distribution around earth
17 p3046 A69-33223

Diademe satellites stabilization system to measure station-to-satellite distance by laser pulse, discussing reflector, magnet for attitude control, damping device, etc
17 p3046 A69-33224

Stable motions determination of solid bodies with liquid filled cavities and satellites motions stability in central Newtonian force field
17 p3005 A69-33228

Attitude and simple stability of deformable earth pointing satellite
17 p3047 A69-33229

Damping of gravity gradient stabilized satellites by hysteresis of materials, friction of viscous fluids, magnetic hysteresis and Foucault currents
17 p3047 A69-33230

Magnetic materials simulation for satellite stabilization device based on magnetic hysteresis, using mathematical models and direct magnetic measurements
17 p2945 A69-33235

Ammonia jet device to stabilize telecommunication satellites consisting of electric heating element, ejection nozzle and thermal screens
17 p3018 A69-33236

Satellite three axis attitude control analysis showing rolling and longitudinal stabilization possibility by flywheel, with validity tested by analog simulation
17 p3048 A69-33240

Flywheels desaturated by magnetic action for optimizing stabilization system of satellite in circular orbit [ONERA-TP-732] 17 p3049 A69-33241

Astronomical satellite direct digital attitude control using digital computer between sensor and actuator to achieve optimal filtering and stabilization
17 p3049 A69-33244

Bearing system for mechanically despun antenna in spin stabilized communications satellite, offering greater directional stability, lower weight and power losses
17 p2978 A69-33431

Aerospace vehicle mass property limits and dynamic balancing related, noting errors
[SAWE PAPER 772] 18 p3208 A69-34875

Differential synthesis technique application to design of multiaxis stability augmentation systems for aerospace vehicles
[AIAA PAPER 68-834] 20 p3616 A69-37156

Stability of periodic orbits in elliptic restricted three body problem
[AAS PAPER 68-086] 20 p3595 A69-37172

Stationary resonant nonlinear oscillatory and rotary states, stability and pitching motions of controlled satellite in slightly elliptical orbit
20 p3616 A69-37177

SPACECRAFT STERILIZATION

Nonlinear roll-yaw attitude motion of spinning symmetric satellite in elliptical orbit near internal or external resonance
[AAS PAPER 68-124] 20 p3616 A69-37178

Atmospheric entry-capsule dynamics, considering angle of attack motion under gravity forces influence and aerodynamic normal force stability relations
20 p3617 A69-37197

Photometry methods for spacecraft brightness in dynamical states of rapid spin and tumble
21 p3671 A69-38340

Planar tumbling in atmospheric entry, describing arrest by approximating Painleve equation
21 p3819 A69-39033

Motion and stability of rotating connected two body space station satellite system, developing Lagrangian equations of motion and optimizing damping system parameters
[AIAA PAPER 69-919] 21 p3820 A69-39349

Capture and gravity gradient stabilization of LIDOS satellite in eccentric orbit
[AIAA PAPER 69-921] 21 p3821 A69-39351

Aerodynamic and gravitational torque effects on orbiting satellites attitude stability, applying Liapunov direct method in case of conservative aerodynamic torque
[AIAA PAPER 69-832] 21 p3821 A69-39363

Adaptive tracking filter for bending mode stabilization of large flexible boosters
[AIAA PAPER 69-874] 21 p3823 A69-39400

Apollo-Saturn 5 propulsion and structure feedback loop, analyzing Pogo components and Nyquist plot application
[AIAA PAPER 69-877] 21 p3824 A69-39403

Spacecraft natural vibrations analyzed using point transforms with allowance for control systems imperfections
21 p3826 A69-39637

Dynamics of relay gas jet preliminary vibration damping system of gravity gradient stabilized satellite, allowing for sensor limitations and stabilizer flexural vibrations
21 p3826 A69-39638

Simulation of passively stabilized satellites using in-line hybrid computer
[AIAA PAPER 68-853] 21 p3680 A69-39758

Satellite stabilization by earth magnetic field through conservative magnetic moments application
21 p3830 A69-39834

Closed form solution to stability of coupled libration motion of slender axisymmetric satellite in circular orbit limited to small amplitude vibrations
22 p4008 A69-39936

Representative data of actual forces and moments applicable to large spacecraft attitude control system for typical crew activities obtained through simulation programs
[AIAA PAPER 69-1006] 22 p3921 A69-40380

Dynamic stability derivatives of large angle blunted conical spacecraft near transonic speed in simulated Mars environment for various angles of attack
22 p4036 A69-40550

Attitude stability of orbiting vehicle containing gyrost, discussing asymptotic stability
22 p4037 A69-40555

Motion stability of rapidly spinning satellite, discussing elastic booms effect
22 p4037 A69-41091

Periodic solutions for gravity-gradient stabilized satellite librating in orbital plane, using elliptic sine function and harmonic balance method
23 p4224 A69-41876

Spinning satellite containing elastically restrained, viscously damped mass, analyzing attitude dynamics and stability, noting wide nutation possibility
23 p4224 A69-42396

Tethered orbiting interferometer configurations for future Radio Astronomy Explorer satellites, discussing gravitational stabilization and delta launching into orbit as single payload
[AAS PAPER 69-255] 24 p4313 A69-42859

Stability analysis of periodic solutions associated with planar librations of gravity oriented satellite using linear perturbation analysis
24 p4388 A69-43649

SPACECRAFT STERILIZATION

Dry heat sterilization and ethylene oxide decontamination test equipment for bipropellant liquid propulsion system
02 p0228 A69-11764

Mars capsule feasibility model terminal dry heat thermal sterilization cycle determined from microbial data
02 p1201 A69-11772

Product assurance role in spacecraft sterilization to maintain planetary biological environments integrity in space programs for extraterrestrial life determination
03 p0379 A69-13400

Sterilization techniques for instruments and materials as applied to space research - COSPAR Conference, London, July 1967
05 p0711 A69-15934

Spacecraft sterilization techniques for space exploration, discussing mathematical models for planetary quarantine and contamination by nonlanding vehicles
05 p0712 A69-15935

Standards of sterility for prevention of introduction of terrestrial microorganisms onto other planets during space missions, noting contamination probability
05 p0712 A69-15936

Spacecraft sterilization techniques efficiency in terrestrial and extraterrestrial environments noting dry heat, radiation, ethylene oxide, isopropanol and formaldehyde in methanol
05 p0712 A69-15937

Dry heat destruction of spores, discussing dependence on spore water content and effect of surrounding gas volume on escape of water from spore
05 p0712 A69-15938

Dry heat sterilization of spacecraft, microorganism water content and recommendations for fabrication conditions for spacecraft
05 p0712 A69-15939

Ethylene oxide sterilization rate dependence on temperature, gas concentration, relative humidity and medium surrounding microorganisms
05 p0707 A69-15940

Mathematical model for estimating microbial survival in heat sterilization of spacecraft, including environmental and time cumulative effects
05 p0707 A69-15941

Spacecraft terminal dry heat sterilization procedures for minimal time and temperature conditions, using simple geometric configuration of spacecraft for thermal analysis
05 p0712 A69-15942

Spacecraft sterilization by hydrogen peroxide solutions mixed with selected anion active detergents
05 p0713 A69-15943

Antimicrobial spacecraft materials, discussing feasibility of impregnation or chemical combination of materials with bactericides
05 p0713 A69-15944

Modeling requirements and methods for monitoring microbial contamination, discussing vacuum probe sampler to recover microorganisms from large surface areas
05 p0713 A69-15948

Split-seam process for inserting sterile objects into isolated sterile environment without contamination as method for sterile spacecraft repair
05 p0714 A69-15950

Microbial contaminants on space hardware, discussing detection and enumeration techniques
05 p0714 A69-15954

Thermal stabilization and ethylene oxide effect on spaceborne electronic component sterilization and decontamination
08 p1283 A69-20266

Spacecraft component heat sterilization, discussing heat effects on electrical connections, polymers and adhesives
08 p1284 A69-20267

Technology Feasibility Spacecraft/TFS/ sterilization and bioassay program during assembly, analyzing sampling and cleaning procedures
09 p1446 A69-22358

Spacecraft sterilization requirements, evaluating viable organisms release probability from spacecraft as function of equipment fracturing
11 p1828 A69-25460

Microbial contamination release probability from solids fractured by impact, considering spacecraft sterilization requirements
11 p1828 A69-25461

Sterilization assembly development laboratory /SADL/ quality assurance program for microbiological monitoring according to NASA planetary quarantine requirements
15 p2559 A69-31123

Microbiology quality assurance program for planetary mission, considering spacecraft sterilization during fabrication, test and launch site activities
15 p2559 A69-31124

Dry heat destruction rates for microorganisms encapsulated in and on spacecraft hardware, concluding temperature and water conditions in spore as major factors
15 p2560 A69-31444

Spacecraft sterilization by destructive heating with thermite or high velocity entry friction before entering planet atmosphere
15 p2560 A69-31472

Planetary quarantine constraints by NASA insuring low contamination probability from extraterrestrial biological exploration, giving contamination probability equations and sterilization procedures
16 p2746 A69-32435

Sterilized solid propellant motors applicability to planetary landing capsule spin stabilization
[AIAA PAPER 69-823] 16 p2840 A69-32675

Thermal stability elements in solid propellant liner insulation system for heat sterilized solid rocket motors used in unmanned planetary landers
[AIAA PAPER 69-437] 16 p2869 A69-32750

Life support system sterilization maintenance problem for biosatellite experiment over one year
20 p3477 A69-37624

Loaded bipropellant liquid propulsion system sterilization studies on structural and nonmetallic materials suitability for use in oxidizer
[AIAA PAPER 68-631] 21 p3785 A69-39025

Catalyst poisoning and hydrazine material compatibility during hydrazine propulsion systems sterilization and decontamination
21 p3786 A69-39768

SPACECRAFT STRUCTURES

Space radiators for heat rejection from nuclear powered spacecraft doubling as primary structures to save weight, discussing conical or cylindrical configurations
01 p0160 A69-10151

Hypervelocity impact effect on structural honeycomb spacecraft wall configurations, stressing design and wall thickness parameters
[AIAA PAPER 68-314] 02 p0345 A69-12389

Optimal design of vibration tests based on decision theory
[SAE PAPER 680753] 03 p0525 A69-13436

Ground vibration testing of flight and space vehicles, noting structural damping asymmetries and nonlinearities
04 p0585 A69-14833

Digital computer methods and numerical techniques to evaluate temperature distributions in spacecraft structures, discussing thermal modeling
[SAE PAPER 690199] 07 p1239 A69-18301

Integrated nondestructive testing systems to ensure welded assemblies reliability for Saturn 5 program, including surface defect detection
07 p1117 A69-19699

Truss framework for support of eight 100-lb satellites through Titan 3C launch and dispensing of satellites at predetermined times, discussing materials and fabrication
09 p1512 A69-22369

Silicated alumina attachment for high temperature radomes and leading surface heat shields, discussing stress concentration and load transfer
09 p1477 A69-22370

Ultrasonically assisted installation of fasteners for weight savings in aircraft/spacecraft structures
09 p1478 A69-22373

Spacecraft design for minimization of structure interaction with control system, noting susceptibility of extendable booms to solar environment
11 p1967 A69-25500

Dynamics of deployable space structures stiffened by centrifugal forces due to spin, discussing LF radio telescope
11 p1994 A69-25530

Space vehicle dynamic structure response, discussing vibration problems, test methods and responses to periodic, stochastic and forced excitations
12 p2176 A69-25857

Metal adhesive bonding strength behavior in satellite and space vehicle applications, noting effects of various space environment factors
12 p2101 A69-25858

Metal bonded and sandwich structures application to space vehicles, launch vehicles, rocket motors, ground equipment and balloon gondolas, noting inspection methods
12 p2101 A69-25859

Fiber reinforced space vehicle combustion chambers and cryogenic fuel tanks, discussing design and elastomechanical problems
12 p2176 A69-25860

Thermal behavior of space vehicle window systems predicted by mathematical analysis and computer methods for heat transfer through glass
[AIAA PAPER 68-65] 13 p2378 A69-28215

Mathematical models for ballistic limit of single and double wall structures, yielding equations for relation to projectile and target characteristics
[AIAA PAPER 69-370] 13 p2367 A69-28302

Penetration mechanics of multisheet structures based on discrete particle modeling of impact debris
[AIAA PAPER 69-371] 13 p2367 A69-28303

Hypervelocity projectile size and density effect on ballistic limit of dual sheet spacecraft meteoroid protection structures, considering penetration of low and high density particles
[AIAA PAPER 69-376] 13 p2367 A69-28306

Lightweight double walled meteoroid shield for Mariner Mars 1971, considering Teflon impregnated glass fabric outer sheet and multilayer thermal insulation
[AIAA PAPER 69-377] 13 p2357 A69-28307

Structure, equipment and weight breakdown of Black Arrow X3 spacecraft
13 p2357 A69-28478

Spray deposition of low emittance gold thermal control coatings on aerospace structures
15 p2618 A69-30310

Variational principles and differential equations of thin elastic panels mechanics for aerospace structures
15 p2712 A69-30974

Static, transient and in-space environmental tests at satellite structures and heat shield test facilities in Italy
16 p2765 A69-31750

Scientific satellites structural design problems, considering limitations imposed by weight, layout, environmental conditions, mission and manufacture
18 p3208 A69-34792

Mariner 6 and 7 Mars probes, describing mission profile, basic structure, trajectory design and scientific experiments
18 p3198 A69-34795

Kennedy Space Center Vehicle Assembly Building construction, capacity and operation for manned spacecraft
19 p3288 A69-35500

Composite material applications in space vehicle structures, noting strength and stiffness of boron fibers in plastic or metal matrices
19 p3340 A69-35502

Lightly loaded truss structures fabricated from Be, Be-Al alloy and uniaxial B filament reinforced epoxy tubing for unmanned spacecraft applications
19 p3340 A69-35504

Environmental testing of space hardware, discussing failure detection by thermal vacuum tests and mechanical signature analysis
19 p3430 A69-36009

Finite element techniques of structural analysis for missile and space structures, including Apollo computerized analysis and structural optimization
19 p3438 A69-36324

Tiros M requirements for earth resources sensor systems, discussing spacecraft structure, dynamics, power, command and communications subsystems
21 p3818 A69-38621

Scattered light mean intensity determination in twilight aerosol atmosphere from satellite observations, formulating boundary value problem
21 p3717 A69-39656

Boron and carbon reinforced composite materials aerospace structural application, discussing weight savings, components structural design and connection and load input problems
22 p4038 A69-39908

Seals leak testing for complex manned spacecraft structures
[AIAA PAPER 69-1030] 22 p3924 A69-40399

Spacecraft booms thermally induced vibration and flutter, considering damping and solar exposure effects
22 p4043 A69-40545

Metallurgical and structural production of diffusion bonded titanium honeycomb sandwich panels for aerospace hardware weight saving
24 p4324 A69-43434

Heat conduction problems associated with radiant exchange in shells under discontinuous solar flux, considering spacecraft structures, illumination theory and astrophysics
24 p4416 A69-43689

SPACECRAFT TELEVISION
NT SATELLITE TELEVISION

Spacecraft device for photographing and transmitting TV pictures noting limitations and spatial conditions adaptations
02 p0207 A69-11829

TV test chart for evaluating Surveyor lunar spacecraft TV system covering resolution, photometric and colorimetric response and sun angular position
[SMPTE PAPER 105-71] 12 p2078 A69-25771

Surveyor 7 TV system in photon integration mode, analyzing slow scan vidicon storage characteristics and dark current limitations
[SMPTE PAPER 105-72] 12 p2078 A69-25772

Apollo 8 photooptics, considering TV camera and broadcasts, photographic equipment and visual observation
15 p2609 A69-30469

Apollo 10 field sequential color TV system, describing camera modifications, systems design and equipment compatibility problems
18 p3101 A69-34810

Mars TV pictures from Mariner 7, describing prominent surface features
21 p3806 A69-39330

Surveyor spacecraft instrumentation, describing TV camera design and operation, photographic requirements and techniques, lunar surface characteristics, etc
22 p4011 A69-40043

Mariner Mars 1969 TV system environmental test and calibration program
22 p3920 A69-40372

Lunar TV camera for Apollo missions, discussing operational requirements and design
23 p4162 A69-41478

Mariner 6 and 7 TV data, discussing implications for Mars present state, past history and biological status
24 p4384 A69-43195

SPACECRAFT TRACKING
NT SATELLITE TRACKING

Optical spacecraft tracking organization in U.S.S.R., describing network of visual observation and photographic stations for satellite and space probe tracking
01 p0032 A69-10952

Optical correlator for fast acquisition of pseudorandom ranging codes, giving code delay estimation to synchronize local code generator of delay-lock loop
03 p0389 A69-13186

Deep space tracking network development, discussing capabilities and operational quality assurance
07 p1078 A69-18831

Multifunction Receiver System rationale, concepts, background requirements and technical justifications for tracking, telemetry and ranging data acquisition by Goddard Center
07 p1081 A69-19101

Spacecraft tracking network for determining spacecraft motion parameters, noting application to coordinates and velocities determination for terrestrial observers
07 p1087 A69-19609

Processing of data obtained in continuous tracking of space objects using computer algorithms
10 p1791 A69-24193

Apollo Range Instrumented Aircraft /ARIA/ telemetry antenna system for trajectory tracking, discussing computer program for simulation of behavior
11 p1840 A69-25309

Phased array radar system for UHF detection, identification and tracking of orbiting objects and ballistic missiles, noting system design and hardware
12 p2028 A69-25906

Electromagnetic and plasma waves scattering by space vehicle excited by ground source in isotropic warm plasma, obtaining radar cross sections
13 p2221 A69-27965

Baker-Nunn photometry from Apollo tracking utilizing photographs for brightness, dynamics and duration of rocket exhausts and venting clouds
15 p2571 A69-31338

Tracking and data acquisition systems for spacecraft and ground link through command, telemetry and tracking, noting data relay satellites, etc
17 p2919 A69-33371

Navigational accuracy dependence on spacecraft geometry, determining information content and critical error sources of earth based Doppler radio tracking data
[AAS PAPER 69-112] 19 p3402 A69-35935

Continuously powered deep space vehicle orbit determination, discussing state estimation accuracy and use of continuous data filtering
[AAS PAPER 68-144] 19 p3402 A69-35939

Digital computer controlled antenna positioning system computing spacecraft tracking trajectory from given parameter input set
19 p3267 A69-35997

Navigational accuracy of two way Doppler tracking of interplanetary spacecraft during heliocentric and planetary encounter trajectory phases
[AIAA PAPER 69-899] 21 p3761 A69-39334

SPACECRAFT TRAJECTORIES
NT CIRCUMLUNAR TRAJECTORIES
NT EARTH-MARS TRAJECTORIES

NT EARTH-MOON TRAJECTORIES
NT INTERPLANETARY TRAJECTORIES
NT LUNAR TRAJECTORIES
NT MOON-EARTH TRAJECTORIES

Spacecraft motion parameters determination under controlled acceleration using information from inertial sensors
01 p0161 A69-10569

Optimum control determination for low thrust spacecraft to minimize time for passing through radiation belt
01 p0113 A69-10571

Low thrust spacecraft motion continuous correction by dynamic programming, assuming continuous information on system state including fuel consumption
01 p0113 A69-10572

Spacecraft trajectories computation from initial conditions by techniques involving construction of N body reference orbit
03 p0518 A69-14248

Minimum fuel consumption for low thrust jet engine propelled space vehicles maneuvering in circular trajectories
05 p0829 A69-15879

Algorithms construction for aerospace vehicle trajectory optimization, considering quasi-linearization method for computation of variable time optimum trajectories
06 p1006 A69-17569

Space vehicle trajectory optimization using computerized step by step steepest descent to minimum cost, considering cost gradient vs control
06 p1006 A69-17570

Spacecraft trajectory during atmospheric reentry determined from projections of longitudinal acceleration onto coordinate axes connected with spacecraft
06 p1014 A69-17581

Free fall vehicle dynamics for wind tunnel measurements of research shapes used in computer simulation of vehicle trajectories
[AIAA PAPER 69-229] 06 p0864 A69-18130

Observability theory of dynamic objects application to composing measurements for space flights, solving parametric observability problem
07 p1087 A69-19605

Coordinates and velocity components accuracy for artificial earth satellite moving in central Newtonian field, covering elliptic and circular orbits
07 p1178 A69-19606

Composition effect of flight path measurements on correction of space vehicles flight path, discussing single parameter correction of motion in force free field
07 p1178 A69-19607

Three dimensional atmospheric entry trajectories equations for satellite with aerodynamic lift, examining aerodynamic factors and bank angle effects
07 p1230 A69-19608

Spacecraft tracking network for determining spacecraft motion parameters, noting application to coordinates and velocities determination for terrestrial observers
07 p1087 A69-19609

Spacecraft trajectory using microthrust and lunar gravitational attraction for acceleration into heliocentric orbit
09 p1593 A69-21620

Spacecraft trajectory optimal determination without knowing measurements error distribution function, examining computer solution properties of linear programming
09 p1595 A69-21757

Minimum time turns for spacecraft about fixed axis lying beyond plane of vehicle forces
09 p1609 A69-21760

Spacecraft motion parameters and physical characteristics of space determined from statistical analysis of measurement data
09 p1495 A69-21764

Planar motion of satellite containing damping mechanism, considering small dampers case
10 p1791 A69-22935

Earth gravitational field effect on satellite orbits, noting elliptical motion in central force field, energy criteria and rotational ratios
10 p1776 A69-23295

Optimal motion control of spacecraft refueling during flight by liquefying atmospheric gas along prescribed trajectory under constant thrust
13 p2356 A69-27686

Canonical transformation and Hamilton-Jacobi theories applied to space vehicle trajectory analysis, discussing elliptical coast arc and optimal low thrust problems
13 p2353 A69-28202

SPACECREWS

Spacecraft motion parameters determination under controlled acceleration using information from inertial sensors 15 p2702 A69-30739

Optimum control determination for low thrust spacecraft to minimize time for passing through radiation belt 15 p2651 A69-30741

Low thrust spacecraft action continuous correction by dynamic programming, assuming continuous information on system state including fuel consumption 15 p2651 A69-30742

Generalized Fourier analysis for satellite motion deviations from arbitrarily chosen reference orbit generated analytically or numerically, determining equations for potential coefficients 15 p2697 A69-31323

Multistage rocket trajectories optimized by second order numerical technique and digital computer program, considering coasting, vacuum flight and transition times 16 p2857 A69-32154

Mariner 6 and 7 Mars probes, describing mission profile, basic structure, trajectory design and scientific experiments 18 p3198 A69-34795

Optimal landing of spacecraft on moon surface from low circular orbit, analyzing rocket thrust, altitude and landing site distance effect on spacecraft mass 19 p3431 A69-36616

Optimal information selection for determining spacecraft trajectory, considering atmosphere, light speed and series expansion coefficients of planetary gravitational potentials 19 p3427 A69-36627

Computation method for optimum finite thrust space trajectories based on approximation of state time history by polynomial [AAS PAPER 68-080] 20 p3595 A69-37170

Liapunov stability theory for motion of spacecraft with flexible and moving parts in force free space [AAS PAPER 68-125] 20 p3617 A69-37180

Space vehicle space-time position fiducial distribution and future location determinations based on inference theory 20 p3617 A69-37528

Numerical integration for continuously thrusting spacecraft optimal trajectory, considering rectangular Cartesian and polar cylindrical coordinates characteristics [AIAA PAPER 69-903] 21 p3798 A69-38546

Optimal transfer between coplanar elliptical orbits of spacecraft with combined small and large thrust propulsion system 21 p3803 A69-38848

Closed form solution for minimum fuel constant thrust trajectories for vehicle transfer in vacuum between arbitrary boundary conditions [AIAA PAPER 69-905] 21 p3806 A69-39337

Analytic approximation for initial adjoint vector for optimal/minimum propellant/space trajectories [AIAA PAPER 69-916] 21 p3808 A69-39345

Branched trajectory optimization for split rocket vehicles using projected gradient or steepest descent method [AIAA PAPER 69-917] 21 p3808 A69-39346

Perturbative effects of Jupiter moons on spacecraft flyby and postencounter heliocentric trajectories, noting precision targeting [AIAA PAPER 69-932] 21 p3809 A69-39361

Spacecraft descent trajectory optimization during atmospheric reentry, proposing algorithm for continuous trajectory determination 21 p3766 A69-39647

Flight dynamics boundary value problem for spacecraft trajectories optimization, using variational method 21 p3817 A69-39817

Controlled motion of space vehicle about center of mass analyzed by equation expressing nutation angle invariance 21 p3830 A69-39839

Real time orbit determination system at NASA manned space center for Apollo missions [AIAA PAPER 69-938] 22 p4020 A69-40321

Interactive graphics system for rocket vehicle trajectory simulation and performance analysis [AIAA PAPER 69-954] 22 p3905 A69-40336

Grobner method of Lie series applied to numerical integration of spacecraft trajectories and n-body problems 23 p4223 A69-42476

Venus swingby and direct Mercury trajectories analysis for optical imaging from flyby missions [AAS PAPER 69-258] 24 p4380 A69-42860

Meteoroid shower model for interplanetary flight hazard evaluation, suggesting shower zone defining on ecliptic plane 24 p4385 A69-43258

Fractional correction procedure for indirect trajectory optimization through extremal trajectory meeting boundary conditions 24 p4386 A69-43264

SPACECREWS

Man as main component of future spacecraft or planetary station closed ecological system, discussing spacecrew physiological monitoring for biological cycles optimization 01 p0020 A69-11076

Legal and technical aspects of international cooperation in spacecraft crew rescue operations signed by UN General Assembly 06 p1042 A69-17033

Optimum physiological parameters selection criteria for medical control of crew during space flights 07 p1071 A69-18978

Permissible irradiation doses established for spacecraft crews making short and long flights, considering roles of life span, somatic effects, leukemia and genetics 07 p1069 A69-19618

Computer program for onboard medical checkups of spacecraft crews during extended space flights, discussing tests and intervals 10 p1649 A69-23505

Admissible radiation doses for space crews and ionizing radiation protection, studying long term radiation effects on dogs 15 p2557 A69-31344

Biological effects of cosmic radiation on crewmen and protection measures, noting ground radiobiological and medical hygienic investigations 20 p3478 A69-37628

Optimum physiological parameters selection criteria for medical control of crew during space flights 20 p3483 A69-38226

Representative data of actual forces and moments applicable to large spacecraft attitude control system for typical crew activities obtained through simulation programs [AIAA PAPER 69-1006] 22 p3921 A69-40380

Crew survival ensurance under emergency situations during manned space flight, discussing Apollo abort system refinements [AAS PAPER 69-469] 24 p4272 A69-42848

SPACING

AIRCRAFT APPROACH SPACING

Dynamic programming application to synthesis of unequally spaced symmetrical antenna arrays 02 p0219 A69-12338

Optimum spacing of communication satellites on inclined circular synchronous orbits, applying figure 8 packing schemes 04 p0562 A69-15458

Synthesis of symmetrical linear array space factors in main beam and grating lobes by spacing distributions and element excitation adjustment 07 p1108 A69-19466

Performance prediction for planar and cylindrical electrode geometry fixed spacing thermionic converters 09 p1438 A69-21814

Zero crossing statistics measurements for 1/f noise, noting statistically stationary character of probability density distributions of interval spacings between zero crossings 10 p1656 A69-23657

Thinned arrays design based on array excitation autocorrelation function, considering element spacing 11 p1856 A69-25661

Transverse wave spacings for self sustaining detonations in oxygen and diluents mixtures with hydrogen, methane, acetylene or ethylene fuel, noting dilution 13 p2378 A69-28217

Three antenna interferometer angle measurement accuracy dependent on antenna spacing, deriving optimal spacing value 16 p2758 A69-31730

SPAIN

Solar activity /Madrid 1967/, detailing Wolf numbers, sunspots, chromospheric faculae, H filaments and prominences 18 p3202 A69-35290

SPALLATION

Cosmic-ray-produced stable and long-lived nuclides in iron meteorites, considering shielding effect on spallation production 19 p3411 A69-36099

K 40-Ar 40 age measurements in separated mineral phases of chondrites, including production rates of spallation isotopes 19 p3418 A69-36137

Spallogenic rare gas concentrations and isotopic ratios in taenite of iron meteorites measured mass spectrometrically and compared with kamacite values 19 p3419 A69-36139

SPALLING

Time dependence criterion in dynamic fracture determined by spall stress relation to stress pulse duration during plate impact 10 p1803 A69-24032

High purity beryllium dynamic tests, determining Hugoniot equation of state, shock profile and spall threshold /onset of microcracking/ for elastic pulses [AIAA PAPER 69-360] 13 p2283 A69-28293

SPARE PARTS

Manned spacecraft systems design optimization for extended space missions replacement modules 05 p0830 A69-16380

Spare kit evaluation model for problems with constraints on spare parts quantities, considering optimization and simulation routines for weapon system maintenance 10 p1669 A69-22981

Steady state availability of system with limited repairable spares for online units, considering statistical dependence among similar units 18 p3144 A69-34493

SPARK CHAMBERS

Spark chambers for primary cosmic ray study in balloon flights, detailing construction and performance 06 p0924 A69-17285

Instruments for gamma ray astronomy including Ranger low energy detector, howitzer detector and cosmic spark chamber 18 p3138 A69-35135

SPARK DISCHARGES

ELECTRIC SPARKS

SPARK GAPS

High speed shadow photographs of Q switched laser triggered spark gap air discharge, showing sonic waves and development of discharge channel 04 p0610 A69-14349

Pressurized spark gap triggered by focused Q switched laser beam introduced along axis 04 p0612 A69-15204

Electronically controlled spark gap system for HF optical frame separation based on Cranz-Schardin principle 05 p0763 A69-15985

He-Ne laser with small spark gap optimum parameters dependent on active medium and resonator field structure 06 p0935 A69-17683

Spherical and rod-plate spark gap response voltage as function of sawtooth wave, cosmic, gamma and UV radiation 11 p1851 A69-25086

RLC integrated low inductance circuit for magnetooptical high speed camera shutters, Q switched ruby laser and short light pulses in spark gap 12 p2084 A69-26149

Spark gap protection of input transistors in radio receivers against antenna-collected static charge damage 21 p3681 A69-38395

SPARK IGNITION

Spherical flames of spark-ignited dust clouds, discussing streak film photographs, flame propagation, particle burnout time and burning velocities 02 p0353 A69-12323

Laser induced breakdown spark ignition of detonable and nondetonable chemically reactive gas mixtures, noting blast waves [AIAA PAPER 68-146] 09 p1622 A69-21951

Spark ignition of liquid fuel droplets atomized in air analyzed by spark discharge visualization for two phase mixture 09 p1623 A69-22220

Steady propagation of flame front initiated by local ignitor /spark/ in gas mixture, discussing critical requirements, boundary conditions, etc 11 p2001 A69-25190

Aircraft fuel vent line sensitivity to lightning hazards, using flame propagation and arrester experiments with high voltage and high current facilities [SAE PAPER 690434] 23 p4062 A69-41651

SPARK MACHINING

- Electroerosion effect on fabrication of small disks for direct examination by electron microscopy, using refined and heat treated aluminum
03 p0427 A69-12880
- Beryllium chemical and mechanical machining in quantity production, examining salvage and safety precautions
[SAE PAPER 680649] 03 p0434 A69-13455
- Statistical analysis of operation of precision electric spark machine servosystems with RC generator based on working pulse peak voltage distribution
23 p4168 A69-41307
- Automation of single pass electric spark machining of high alloy steels and hard alloys, including anodic-mechanical profiling, cutting and drilling
23 p4168 A69-41308

SPARK PLUGS

- Aircraft engine spark plugs development, reviewing ceramic and mica insulated plugs and four pole electrode spark plugs
13 p2324 A69-27333

SPARK SHADOWGRAPH PHOTOGRAPHY

U SHADOWGRAPH PHOTOGRAPHY

SPARKS

NT ELECTRIC SPARKS

- Laser produced sparks in 200 kG magnetic field in air, butane and helium at atmospheric pressure
02 p0260 A69-12659
- Radiative flux density, spectrum and temporal behavior of Q switched laser induced underwater sparks
05 p0771 A69-15818
- Laser spark plasma initial development phase showing high electron temperature and concentration, continuous spectrum emission, line broadening and shock wave formation
14 p2461 A69-29779
- Shadow photography study of electrical discharge set off by laser spark
21 p3740 A69-39552
- Slow combustion laser spark at intensity below optical breakdown obtained by focusing radiation pulse of Nd glass laser in discharge gap
23 p4172 A69-41492

SPATIAL DEPENDENCIES

- Spatial and temporal dependence of trapped particle energy spectra on basis of bimodal diffusion
16 p2852 A69-32619
- Scale determination in spatial direction networks, using polygonal transverse measured along continental surfaces and Secor method over water surfaces
18 p3131 A69-35196

SPATIAL DISTRIBUTION

NT STAR DISTRIBUTION

- Spatial and kinetic distributions of molecules reflected by surface in rarefied atmosphere, discussing mathematical model
01 p0122 A69-10041
- H alpha emission symmetrical spatial distribution of night airglow observed with high transmission diffraction spectrographs
01 p0062 A69-10128
- Three dimensional holography using scatter plates applicable to transilluminated objects in particular distribution of particles or phase disturbances
01 p0079 A69-10217
- Meteorite scattering in geogravitational field and influence on lunar meteorite precipitation distribution
01 p0153 A69-10756
- Meteor grouping in meteor streams analyzed using radar records of meteor showers
01 p0154 A69-10873
- Midlatitude sporadic E layer vertical and horizontal structure and statistical properties, discussing theory of ion concentration by wind shear
01 p0073 A69-11177
- Soviet book on spectral, spatial and time characteristics of lasers covering luminescence and resonator theories, electromagnetic field structure and radiation dispersion
02 p0255 A69-11800
- Charge image detector for reading information as extended spatial charge distribution on dielectric layer surface, using vibrating conducting probe scanner
02 p0248 A69-11822
- Dipole antenna current distribution, deriving simple, accurate formula for infinite, semiinfinite and finite cases
02 p0218 A69-12330
- Gegenschein measurements for determining upper limit on asteroidal debris spatial density
02 p0324 A69-12545

Spatial variations in particle intensity near and inside magnetosphere during September 1966 solar cosmic ray events, noting magnetosphere screening effectiveness
02 p0309 A69-12740

Refractivity distribution at ground level and at one km over India, correlating surface refractivity with difference, noting seasonal and diurnal variations
03 p0393 A69-13304

Dipole model of geomagnetic field in terms of spatial distribution of vertical component, discussing computer program for calculating rectangular components
03 p0424 A69-13544

Geometric optics for media with spatial dispersion, describing procedures for equation solution
03 p0467 A69-13718

Spatial autocorrelation functions of amplitude and phase fluctuations in plane parallel to wavefront of incident wave for conditions of multiple scatter
03 p0468 A69-13807

Plasma density spatial distribution determined from HF electromagnetic wave phase shifts without assuming axisymmetry
03 p0480 A69-14138

Ring laser field space-time pattern from light waves scattered at discontinuities, discussing equations of motion of solid state laser
03 p0441 A69-14140

Photographic recording to produce spatial analog of temporal Fourier spectrum of astronomical source used for distinguishing weak periodic signal from background signal
04 p0556 A69-14294

Spatial distribution of background magnetic fields of quiet sun from photoelectric magnetograph observations, noting relation to supergranulation
04 p0663 A69-15396

Origin of binaries from angular momentum vectors orientation and separation distribution
05 p0822 A69-15856

Spatial and temporal conjugacy of visual auroras during magnetically quiet periods
05 p0753 A69-16247

Pulsars, noting clusters associated with spiral arm tangential points, anomalous distribution and possible association with galactic disk or spiral arms
05 p0825 A69-16356

Radio sources quantity dependence on radio emission value, noting determination of spatial density variations of radio galaxies
05 p0826 A69-16426

Sounding energy optimum spatial distribution during scanning and detection of several signals, noting reduction of mean energy losses
05 p0723 A69-16786

Cyclotron instability of outer radiation belt protons, taking into account data on spatial distribution and ion composition of exospheric plasma
06 p0919 A69-17721

Pc5 geomagnetic pulsations spatial characteristics, showing localized excitation in space and dependence on geomagnetic latitude
06 p0921 A69-17736

Mathematical theory of electromagnetic induction for spherical model of earth with conductivity distribution given by sine function
06 p0921 A69-17739

Spatial structure of residual anomalous magnetic field, determining parameters of eccentric horizontal dipole as main source of geomagnetic field
06 p0922 A69-17755

Distribution characteristics of radiation defects in materials irradiated by monoenergetic beams of protons and alpha particles
06 p0981 A69-17878

Cosmic radio noise brightness distribution in Southern Hemisphere at 10.02 MHz, noting spectra of sources observed
07 p1206 A69-19272

Cosmological models with antipole, determining models consistent with spatial distribution of quasars and radio galaxies
07 p1219 A69-19284

Noncoherent scattering of atoms with Maxwellian distribution in moving atmosphere, discussing Doppler broadening expansion in Legendre polynomials
07 p1219 A69-19286

Primordial magnetic field effects on spatially homogeneous cosmological models with anisotropic Euclidean metric
08 p1383 A69-20049

Radio interferometer antenna array spatial characteristics obtained as function of geographical coordinates of site for reducing observation errors
08 p1314 A69-20434

Spatial distribution and temporal variation measurements of magnetic fields in plasma, emphasizing pulsed discharges
08 p1364 A69-20472

Spatial density distribution in star clusters, determining relation between mean stellar mass and density range in subsystems
09 p1589 A69-21368

Galactic dust layer spatial structure and relation to brightness of Milky Way based on analysis of photoelectric color excesses in Aql and Cyg stars
09 p1590 A69-21381

Spatial distribution of velocity, spatial correlation and ergodicity of turbulent flow, using spectrum of intensity fluctuations of scattered laser light
09 p1493 A69-21491

Analytical description of planetary distribution of space-time variations of f0F2, deriving Fourier series as function of UT
09 p1486 A69-21545

Cloud seeding effects due to inhomogeneous distribution of freezing nuclei, discussing silver iodide distributions by Gaussian plume diffusion model
09 p1535 A69-21639

Rotation and mass of Sb galaxy NGC 1832, giving central and mean densities
09 p1599 A69-22188

Enthalpy distribution in plasma tube arc heater inlet flow region with hot and cold gas core boundary in presence of electric field
09 p1553 A69-22538

Charged particles motion in geomagnetic field from analyzing spatial distribution within framework of two dipole magnetosphere model
10 p1756 A69-22818

Interstellar reddening material distribution within 2500 parsecs of sun, noting concentration in galactic plane, spiral arms and cloud complexes
10 p1773 A69-22961

Galactic structure and space distribution of known Classical Cepheids, noting interstellar absorption and variation of period with distance to galaxy center
10 p1773 A69-22962

Spatial distribution of residual nuclei produced in thick Fe targets by one and three Gev protons, noting total production and longitudinal variation of production
10 p1760 A69-23411

Energetic proton and electron fluxes spatial gradients after July 7, 1966 solar flare, noting satellite observations and injection mechanism geometry
10 p1767 A69-23767

Structure dynamic response for motion through homogeneous frozen random load field with spacewise variations, applying analysis method to beam
[ASME PAPER 69-VIBR-38] 10 p1807 A69-24176

Differential solar rotation noting strong quasi-kineticity effect on solar convective zone and rotation influence on viscosity tensor and rotation law
11 p1955 A69-24390

Geomagnetically trapped particle loss processes and equilibrium distribution resulting from MHD wave field interaction described using sandbox model
11 p1948 A69-24856

Holographic reconstruction of spatial distribution of laser light field within and outside resonator, noting suitability for pulsed laser analysis
11 p1885 A69-24919

Aircraft dynamic response to three dimensional turbulence, establishing unique correspondence between spatial symmetry properties of ambient fields of turbulence and aircraft
11 p1823 A69-25503

Microwave oscillations amplitude spatial distribution in gas discharge plasma excited by electron beam
11 p1933 A69-25542

Nonuniform standing wave fields spatial distribution in active rod of ruby laser effects on laser radiation dynamic parameters, discussing radiation spectrum width
11 p1901 A69-25756

Observed frequencies of number of members in multiple systems of galaxies
12 p2156 A69-26222

Laser interferometer determining spatial distribution of neon metastable state in He-Ne active discharge, discussing lens effects
12 p2108 A69-26636

Kinetic equation solved for radiation propagation in atmosphere, considering neutron density variations and spatial distribution
12 p2149 A69-26683

SPATIAL DISTRIBUTION

- Spatial dispersion of HF dielectric constant in semiconductor based on electron-hole pair production 12 p2145 A69-26723
- Unified model for spatial distribution of transpolar exospheric electron density for polar plasma study 12 p2151 A69-26952
- Galactic and quasar radio sources distribution, discussing spectral indices 12 p2166 A69-27036
- Quasar properties from cosmological nature, discussing red shift, luminosity, radiation intensity, absorption features, distribution, chemical composition, etc 12 p2168 A69-27049
- Statistical properties of spatial radiance distribution of sky and forest backgrounds in IR, noting one dimensional Wiener spectra 12 p2131 A69-27072
- Galactic force law from observed stellar velocity and space density distribution 13 p2348 A69-27802
- Stellar densities and luminosity function determined from stellar data concerning sphere with 20 pc radius around sun 13 p2351 A69-27869
- Spatial density distribution and local values of attenuation of pulsed reflex discharge plasma determined from measured attenuation of microwave beam 13 p2312 A69-28112
- Half wave dipole antenna operational factors analyzed for RF radiation spatial power distribution from atmospheric cosmic ray showers 13 p2332 A69-28408
- Spatial harmonic spectrum and tangential field distributions in microwave devices showing separation of higher harmonics through delay structure 13 p2236 A69-28576
- Spatial distribution patterns of gaseous argon atoms scattered from solid argon surface 13 p2300 A69-28658
- Distribution characteristics of radiation defects in materials irradiated by monoenergetic beams of protons and alpha particles 14 p2503 A69-28787
- Asymmetric spherical temperature field reconstruction based on measuring temperature and derivatives at two points of field 14 p2537 A69-28888
- Frequency selection, spectral index distributions and counts of extragalactic radio sources 14 p2518 A69-29134
- Orientation distribution of lineal and areal elements in space, expanding density function definition of two dimensional lineal array 14 p2470 A69-29363
- Galactic anticenter region surveyed at 13.1 MHz, observing ionized hydrogen concentrations in galactic plane 14 p2519 A69-29370
- 21 cm line emission surveyed for spatial distribution of random velocities of neutral hydrogen in solar neighborhood 14 p2520 A69-29371
- Polar auroras temporal and spatial variations and relation to solar activity 14 p2442 A69-29719
- Relation between radar echoes spatial extent and synoptic conditions with reference to various fronts, noting significance for aviation 14 p2474 A69-29738
- Fabry-Perot interferometer for studying spatial distribution of plasma electron concentration, discussing resolution using solid state gas laser light source 14 p2451 A69-29777
- Spatial distribution of plasma density from phase shift measurement in millimeter waves based on microwave multichannel probes 14 p2497 A69-29792
- Spatial correlation function of Northern Hemisphere geopotential, using model based on random distribution of potential vortex fluctuations for atmospheric circulation 14 p2476 A69-29822
- Interstellar radio absorption influence on spatial distribution of cosmic radio emission observations with fixed multiple dipole antenna arrays 15 p2687 A69-30545
- Earth reflected solar radiation spatial, angular and spectral distributions measured by telephotometers on-board Cosmos 149 15 p2596 A69-30650
- Global multielement radio interferometer with autonomous reception synthesized for studying spatial radio brightness distribution over radiation sources 15 p2578 A69-30936

- Radio interferometer with independent heterodynes to obtain radio brightness distribution over source by varying antenna spacing and reception frequency 15 p2578 A69-30937
- Charge sign ratio of primary cosmic ray electrons measured by balloon flown multiplate spark chamber, studying east-west asymmetry 15 p2678 A69-31497
- Spatial distribution of stellar densities and velocity distributions in phase space, using Greenwich catalog of positions and proper motions of omega Centauri cluster stars 16 p2859 A69-32220
- Cumulonimbus clouds phase structure and spatial distribution based on radar signal polarization analysis, showing high nonuniformity and variability 16 p2806 A69-32266
- Galaxies clusters spatial distribution based on crude distance estimates, discussing serial correlation of counts and interpreting results 16 p2862 A69-32371
- Collisional equilibrium and nonuniform formation models for spatial gradient development of early afterglow of He plasma molecular excited state densities 16 p2782 A69-32465
- Analytical description of planetary distribution of space-time variations of f0F2, deriving Fourier series as function of UT 16 p2783 A69-32540
- Laser emission spatial structure transformation determined from ratio between focused spot radius and distance between lens and output mirror 17 p2981 A69-33111
- Spatial frequency distribution of linear array with randomly located elements from probabilistic analysis 17 p2929 A69-33873
- Meteoritic matter distribution by calculating orbital elements of 12,500 meteors from radar data, using diversity reception for radio waves scattered at meteor trails 17 p3041 A69-33894
- Geomagnetic disturbances intensity spatiotemporal distribution at Northern Hemisphere high latitudes during IGY and IQSY 17 p2965 A69-33966
- Space diversity reception and diurnal variations of F region ionospheric motions, comparing IQSY program 17 p2969 A69-33999
- Laser eigenmodes determined iteratively from eigenvalue equation including spatial inversion inhomogeneities, atomic density and local loss 17 p2984 A69-34046
- Spatial structure of solar proton flare of 5 April 1960, discussing top ascending emission filament velocity in H alpha and coronal lines 17 p3025 A69-34224
- H II regions distribution in nearby irregular I galaxies, attributing asymmetry to localized bursts of star formation 18 p3190 A69-34289
- Linear isotropic elastic continuum dislocations distribution, deriving transport equations by statistical methods, noting analogy between energy/ momentum and MHD equations 18 p3212 A69-34352
- Spatial density distribution in star clusters, determining relation between mean stellar mass and density range in subsystems 18 p3198 A69-34757
- Galactic dust layer spatial structure and relation to brightness of Milky Way based on analysis of photoelectric color excess in Aql and Cyg stars 18 p3198 A69-34769
- Ruby laser stimulated emission spatial, temporal, energetic and spectral characteristics during disruption in spherical cavity containing strongly scattering medium 18 p3152 A69-35026
- Laser emission during disturbed quasi-equilibrium, considering emission spatial inhomogeneity due to arbitrary radiative transitions 19 p3333 A69-35876
- Butterfly diagram of sunspot distribution, concluding physical processes not yet clarified 19 p3426 A69-36583
- Spatiotemporal contours of pressure pulses emitted into surrounding fluid by collapsing cavitation bubble, using schlieren-optical observation method, electroacoustical detection device and microphone 19 p3302 A69-36870
- Lower ionosphere geomagnetic field local gradients determination by partial reflection method 20 p3522 A69-37055
- IC 4499 cluster variable stars coordinates in tabular form, showing high percentage of short period 20 p3598 A69-37462

- Open cluster NGC 7128 distance and reddening determination by photometry 20 p3598 A69-37465
- Photogrammetric instruments applied to determination of spatial position of tectonic surfaces by aerial photography 20 p3539 A69-37511
- Time-space variations in occurrence probability of ionospheric E-2 layer during solar activity maximum and minimum 20 p3527 A69-37672
- Neodymium glass laser emission spatial characteristics, investigating higher laser modes excitation 20 p3554 A69-37725
- Arbitrary circle distribution in plane transformed to corresponding distribution of spheres in space for size and shape distribution determination of disperse phase 20 p3627 A69-37764
- Universal hydrogen distribution, discussing atomic hydrogen needed to close universe 20 p3610 A69-38140
- Satellite-anomalous OH radio emission sources, observing spatial distribution and Stokes parameters 20 p3610 A69-38146
- Autoradiographic technique for spatial distribution in solid of B at ppm concentration, using electron microscope 20 p3567 A69-38263
- Steady state atomic He distribution according to solar atmosphere levels, involving formulation and solution of equilibrium equations for single and triplet levels 20 p3615 A69-38298
- Energy spectrum, spatial characteristics and displacements of auroral zone X rays from X ray spectrometry 21 p3787 A69-38359
- Vertical neutral wind measurements in lower E region with wavelike spatial structure, noting vertical shear role in ionosphere dynamics 21 p3703 A69-38363
- Auroral electron and proton fluxes precipitation measurements by satellite, studying data in terms of spatial, energy and angular distributions 21 p3709 A69-38500
- Radio source counts from cosmological standpoint, discussing terrestrial location relative to quasars 21 p3802 A69-38828
- Spatial dispersion of HF dielectric constant in semiconductor based on electron-hole pair production 21 p3781 A69-39136
- Harrison primordial inhomogeneity postulate concerning baryon numbers distribution in universe, precluding possibility of considering cosmic rays bulk as universal 21 p3810 A69-39469
- Amplification saturation in spatially inhomogeneous laser field, relating power to active medium and resonator parameters 21 p3740 A69-39549
- EEG patterns computerized spatio-temporal display technique using CRT and motion picture camera 21 p3668 A69-39864
- Spatial gradient and amount of auroral radio absorption measured by riometers at magnetically conjugate and closely spaced stations 22 p3934 A69-39966
- Spin compensated state of localized magnetic impurity moment in space, calculating size range of magnetic impurity spin/conduction electron spin correlation function 22 p3983 A69-40061
- Space density of giant M stars as function of distance at galactic anticenter 22 p4014 A69-40125
- Spatial distribution of amplitude and onset of premonition positivity, readiness and motor potential changes in human cerebral cortex preceding voluntary finger movements 22 p3875 A69-40261
- Spatial coherence of He-Ne laser radiation diffused by turbid medium calculated by using diffraction and interference measurements 22 p3964 A69-40798
- Spatial interactions and thresholds in identification and detection of compound visual stimuli 22 p3883 A69-40878
- Radioactive debris distribution in space from 9 July 1962 thermonuclear explosion over Johnston island recorded by Cosmos 6 satellite 23 p4205 A69-41836
- Pulsars dispersion measure and distance relationship, particularly for Crab Nebula pulsars 23 p4220 A69-42381

Solar flares spectra X ray portion, considering spatial distribution, relation to magnetic fields and time sequence of emitting region
24 p4366 A69-42688

Differential solar rotation noting strong quasi-kineticity effect on solar convective zone and rotation influence on viscosity tensor and rotation law
24 p4390 A69-43780

SPATIAL FILTERING

Spatial filtering effectiveness determination by equivalent spatial operations, deriving expression for SNR
01 p0052 A69-10799

Laser Doppler meter model interpreting output frequency in terms of particle crossing set of fringes
06 p0932 A69-16927

Blurred spaceborne photographic image reconstruction by spatial frequency filtration
[UN PAPER 68-95240] 06 p0923 A69-17080

Two dimensional signal analog correlation in noise background using optical spatial filtering Fraunhofer hologram and input as functions
09 p1499 A69-22276

Complex spatial filtering by holographic Fourier transform subtraction
10 p1690 A69-22953

Typographical spatial correlation filtering methods for reconstructing holographic images with ultrasonic waves, noting application to flaw recognition
10 p1696 A69-23551

Electron beam addressed electrooptic light valve used as spatial filter, discussing electronic control and optical processing in real time
10 p1697 A69-23870

Lenses spherical aberration role in studying laser induced breakdown of gases, considering intense ionization collinear regions multiplicity along optic axis
15 p2634 A69-30878

Restoration of photographic images by optical spatial filtering with least mean square error filter in presence of random additive noise
15 p2611 A69-31033

Holographic method of a posteriori restoration of images formed by coherent and incoherent light by spatial frequency retrieval
19 p3304 A69-35603

System components for spatial discrimination implementation scheme, discussing IR detector arrays and optical imagery processing
19 p3373 A69-36055

Mechanical collimator using random aperture arrays for celestial observation at extreme UV and X rays
19 p3313 A69-36489

Image deblurring and aperture synthesis using a posteriori processing by Fourier transform holographic spatial filtering
21 p3722 A69-38793

SPATIAL ISOTROPY
U ISOTROPY

SPATIAL ORIENTATION
U ATTITUDE [INCLINATION]

SPECIES DIFFUSION

Micrographic reagent coloring grains of Mo in relation to crystalline orientation applied to refractory metal welding and diffusion studies
14 p2505 A69-29221

Z-micron sections removed from metal specimens by microtome for radiotracer study of mass dependence of self diffusion
19 p3313 A69-36490

SPECIFIC HEAT
NT HEAT OF SOLUTION

Posistors heat capacity investigated as temperature function, showing maximum heat balance corresponds to Curie temperature
01 p0038 A69-10098

Specific heats of Cu, GaAs, GaSb, InAs and InSb measured over low temperature ranges
01 p0140 A69-11252

Temperature dependence of thermal conductivity coefficient and specific heat of sublimating heat proof materials
02 p0350 A69-11580

Graphite specific heat temperature dependence at low temperatures, noting Wigner effect for neutron irradiation
02 p0269 A69-11782

Thermal contact rectangle with single side heat capacity, applying Fourier transform and Abel convergence tests
03 p0533 A69-13863

Heat capacity of diamond-like semiconducting Si, GaAs and GaP calculated on basis of quasi-chain dynamics of covalent crystals
03 p0490 A69-13943

Adiabatic elastic constants of molybdenum-rich rhenium alloys, studying concentration effects on bulk modulus, Debye temperatures and interatomic forces
04 p0613 A69-14455

Heat capacity at constant volume determined for nitromethane, trinitrotoluene and difluoramine alitanes
[WSCIPAPER 68-39] 07 p1202 A69-18368

Vanadium monoxides and oxycarbides heat capacity using adiabatic calorimeter, calculating entropy, enthalpy and characteristic temperatures
09 p1523 A69-21739

Specific heat dependence of beryllium at low temperatures on sample impurities, considering Debye temperature
09 p1527 A69-22399

Effect of degree of expansion of ionized gas in nozzle on specific power of MHD generator
10 p1636 A69-23103

Specific heats of oxygen at coexistence from triple point to critical point and corresponding values for liquid phase
10 p1808 A69-23187

Tabulating experimental constant volume specific heats of fluid oxygen from triple point to 300 K at pressures to 350 atm
10 p1808 A69-23188

Anharmonic lattice vibrations, specific heats and coefficient of linear expansion of solids at high temperatures, noting interatomic spacing
10 p1809 A69-23653

Specific heat of electron gas at temperatures approaching absolute zero, using method of displacements and collective variables
11 p1927 A69-24918

Specific isochoric heat capacity of pure fluids, considering thermal equation of state, vapor pressure and boundary conditions at critical point
11 p2001 A69-25201

Low temperature specific heat of praseodymium magnesium nitrate
12 p2026 A69-25784

Rigid heat conductor in continuum thermodynamics, discussing conductivity tensor symmetry and heat capacity positivity as restrictors
13 p2377 A69-28193

Half maximum temperature of diatomic gases determined by extending relation between specific heat and molecular dissociation to diatomic molecules
[DVL-899] 15 p2656 A69-31102

Streamline flow of ideal stable gas with constant ratio of specific heats around conical body with arbitrary taper, determining flow velocity components
16 p2732 A69-32126

Linear high polymer heat capacities by adding contributions from chain segments, deriving table of heat capacity contributions of polymer constituents
19 p3359 A69-36287

Shock wave parameters from meteoric body moving at high supersonic speeds through atmosphere, calculating specific heat ratio
19 p3428 A69-36841

Ammonium perchlorate experimental heat capacity data significance for rotational freedom of ammonium ion
20 p3484 A69-37344

Enthalpy and heat capacity of high melting point homogeneous Ti, Zr and Nb carbides, analyzing influence of Me-Me bonds and carbon sublattice defects
21 p3742 A69-38614

Metals conductivity under high pressure, giving theories for electrons scattering cross sections on ions and for Debye temperature
22 p3980 A69-40187

Temperature dependence of heat capacity of Ba and Sr titanate solid solutions in ferroelectric phase transition region
22 p3996 A69-41162

Thermal conductivity and specific heat of groups of liquid substances as functions of temperature, giving curves, tables and conversion factors
23 p4238 A69-41336

Frictionless supersonic and hypersonic flow of ideal gas of constant specific heat past cone with deformed axis at zero angle of attack
23 p4058 A69-41579

Computer calculation of adiabatic expansion of air, allowing for specific heat ratio and compressibility factor changes
24 p4244 A69-43088

SPECIFIC IMPULSE

Mixture ratio distribution, injector/chamber performance and nozzle effects on specific impulse of liquid propellant rocket engine using hydrazine and oxygen
16 p2828 A69-31724

Agena propulsion system performance model for predicting propellant flow rate, mixture ratio, thrust time and specific impulse
[AIAA PAPER 69-453] 16 p2841 A69-32683

Specific impulse deliverable performance of space storable propellant combination fluorine-oxygen/methane and oxygen difluoride/diborane
[AIAA PAPER 69-505] 16 p2845 A69-32762

Two stage vehicle gross weight minimization determined by slide rule computation using formula based on specific impulse differences between stages
19 p3429 A69-35918

SPECIFICATIONS

NT AIRCRAFT SPECIFICATIONS
NT EQUIPMENT SPECIFICATIONS

Military specifications validity with reference to reliability and metal finishing industry
15 p2722 A69-31120

Maintainability as design requirement in system specifications and contracts, noting MIL-STD-471 program of maintainability demonstration tests
20 p3551 A69-38268

Implementation of MIL-STD-781 reliability test specification from contractor viewpoint, detailing test procedures /procedural, decision, reporting and corrective action rules/
22 p3952 A69-40025

Reliability test program based on MIL-STD-781 B specification, noting test environments with AGREE chamber
22 p3953 A69-40027

SPECIMENS

Finite element analysis and strain gage results to verify end constraint on off-axis tensile coupons and to design test specimen
20 p3628 A69-37775

SPECTRA

NT ABSORPTION SPECTRA
NT ATOMIC SPECTRA
NT BALMER SERIES
NT D LINES
NT ELECTROMAGNETIC SPECTRA
NT ELECTRONIC SPECTRA
NT EMISSION SPECTRA
NT ENERGY SPECTRA
NT FRAUNHOFER LINES
NT H ALPHA LINE
NT H BETA LINE
NT H GAMMA LINE
NT H LINES
NT HERZBERG BANDS
NT INFRARED SPECTRA
NT K LINES
NT LINE SPECTRA
NT LYMAN SPECTRA
NT MASS SPECTRA
NT MICROWAVE SPECTRA
NT MOLECULAR SPECTRA
NT NEUTRON SPECTRA
NT NOISE SPECTRA
NT OXYGEN SPECTRA
NT PASCHEN SERIES
NT PLASMA SPECTRA
NT POWER SPECTRA
NT RADIATION SPECTRA
NT RADIO SPECTRA
NT RAMAN SPECTRA
NT RYDBERG SERIES
NT SCHUMANN-RUNGE BANDS
NT SHOCK SPECTRA
NT SOLAR SPECTRA
NT SPECTRAL BANDS
NT STELLAR SPECTRA
NT SWAN BANDS
NT TELLURIC LINES
NT UV SPECTRA
NT ULTRAVIOLET SPECTRA
NT VIBRATIONAL SPECTRA

Exciton spectrum for limiting case of large radius leading to Wannier-Mott equation with static dielectric permeability
03 p0486 A69-13416

Electrical conductivity and optical spectra changes of strontium titanate single crystals under constant electric field action
15 p2666 A69-30043

SPECTRAL ABSORPTION

U ABSORPTION SPECTRA

SPECTRAL ANALYSIS

U SPECTRUM ANALYSIS

SPECTRAL BANDS

SPECTRAL BANDS

NT ABSORPTION SPECTRA
NT FRAUNHOFER LINES
NT HERZBERG BANDS
NT SCHUMANN-RUNGE BANDS
NT SWAN BANDS
NT TELLURIC LINES

Spectral transmission for water vapor and carbon dioxide bands

02 p0236 A69-11451

Band profiles and emission spectra of shock heated AIO compared for self absorption of blue-green system, discussing electronic transition moment

07 p1184 A69-19163

IR zero one band of molecular O observed in day air-glow with ground based scanning grating spectrometer

08 p1306 A69-20096

Vibrational excitation in He, H and N ion-molecule collisions on nitrogen first negative system, studying relative band intensities

08 p1356 A69-20739

IR spectrum of NML Cygnus star with Michelson interferometer, noting CO bands and IR excess

09 p1602 A69-22229

Relative band intensities of atmospheric and IR atmospheric systems of molecular oxygen compared with Franck-Condon factor calculations

10 p1681 A69-23163

Methane absorption distribution in 6190 A band over Jupiter disk based on spectrograms, noting center to limb variations

11 p1960 A69-24730

Image tube spectra observations of interstellar absorption band at 4430 A, noting emission band at 4400 A

11 p1965 A69-25658

Cyanogen band absorption in nuclei of elliptical and spiral galaxies derived from photoelectric measurements indicating rich metal content in central cores

12 p2153 A69-25803

Transmission system with baseband spectrum divided into subbands, cascade phase modulating carrier in multipication chain

12 p2030 A69-26385

Monograph on optical properties and band structure of semiconductors covering absorption and reflectivity measurement, electronic states transition, deformation, etc

13 p2323 A69-28200

Pulsars dynamic spectra, suggesting inadequacy of interstellar scintillation models to explain observed dependence of decorrelation band widths on frequency

14 p2517 A69-29087

Franck-Condon factors for band systems of molecular hydrogen, computing wave functions for vibrational levels using potential energy function, Part I

15 p2656 A69-31156

Franck-Condon factors for band systems of molecular hydrogen, computing wave functions for vibrational levels using potential energy function, Part II

15 p2656 A69-31157

Spectroscopic observations of Venus atmosphere rotational temperature based on carbon dioxide band at 7883 A

16 p2852 A69-31563

Banded chorus, VLF discrete emissions in magnetosphere in single variable frequency band with frequency depending on equatorial electron gyrofrequency

16 p2774 A69-31981

Hydroxyl band contamination of emission and background radiation from night sky

16 p2774 A69-31987

Energy spectrum of secondary electrons and fluorescent efficiency in 3914 A band, obtaining ionization cross section

16 p2850 A69-32315

Ozone absorption coefficients in vicinity of Hartley band maximum verified by photographic spectrophotometry

16 p2785 A69-32626

Ozone and temperature profiles influence on atmospheric radiation intensities measurement by satellite in five spectral regions, noting pressure broadening effect

16 p2786 A69-32633

Static temperature measurement in arc-tunnel tests producing high velocity air streams by duplex scanning IR spectrometer

19 p3294 A69-35752

Atmospheric slant path molecular absorption and emission from band model methods, discussing computer program prediction capabilities

19 p3375 A69-36052

Undoped n-type gallium arsenide single crystals edge emission spectral band shape dependence on crystal type and ambient temperature

19 p3392 A69-36610

Electron band forces probable values of Meinel system positive N molecules and first positive system of nitrogen molecules at high temperatures

20 p3579 A69-37307

Rotational analysis of O₂O₂ band of gamma-prime system of TiO molecule, considering transition to ground state

20 p3577 A69-38170

Carbon dioxide band in Venus spectrum by dispersion analysis, deriving rotational temperature

20 p3614 A69-38254

First order profile of Utrecht Solar Atlas from second order profile and oxygen band refining procedure, deducing instrumental profile for first order spectra

21 p3722 A69-38699

Franck-Condon factors for band systems of molecular hydrogen, computing wave functions for each electronic state by numerical solutions of radial Schroedinger equation

21 p3774 A69-38758

Spectral transmittance of mixture of carbon monoxide and nitrous oxide for overlapping absorption bands [AIAA PAPER 67-600]

21 p3819 A69-39013

Thermal average derived with classical path treatment for line broadening theories of gases or plasmas

23 p4192 A69-41378

SPECTRAL EMISSION

Continuous and time-resolved absorption and emission spectra studies produced by exploding wires in gases, discussing effects of environment, pressure and electrical energy

01 p0118 A69-10664

Mechanism responsible for luminosity of long duration meteor trains, discussing color changes, band emission and train spectra as function of height and duration

01 p0154 A69-10874

Intensity ratio of first negative nitrogen band and oxygen line varies in auroral displays

02 p0235 A69-11425

Radio emission fluxes in solar active regions, determining slope of spectral characteristics of radio sources from effective emission center

02 p0314 A69-11676

Integral spectral emissivity of gas arc plasmas at high temperatures and atmospheric pressure

02 p0291 A69-12484

Weighting functions for finite optically thick atmospheres, discussing emission line formation

02 p0328 A69-12755

Astronomical needs for atomic spectra, discussing emissions in Wolf-Rayet lines and Of stars and forbidden lines in absorption in sun and F-K stars

03 p0508 A69-13172

Airborne radiometric /8 to 14 micron/ temperature measurements, determining emissivities of ocean, stratus clouds, desert and snow

04 p0592 A69-14653

Nongray radiation absorption coefficients reformulation employing alternative angular moment averaged absorption coefficients with emission /Planck/

04 p0686 A69-14744

Spectral output time variation of GaAs diode laser operating in Fabry-Perot modes

05 p0772 A69-15961

Total and spectral emittance of cobalt surfaces conditioned by evaporating some cobalt from surface at high temperature in vacuo

05 p0716 A69-16447

Chemiluminescence and chemionization in flames, considering electrically conducting properties and spectral analysis

06 p1032 A69-17423

Emission line formation in homogeneous chromosphere for noncoherent scattering, considering various chromosphere models

08 p1381 A69-19800

Spectral intensities and time variations of solar X ray bursts, discussing model for high energy flare plasma and resulting X ray flare

08 p1379 A69-20532

OH emission source in W24 during July 19, 1967 lunar occultation, obtaining better position for brighter OH emission feature

09 p1591 A69-21449

Boltzmann plots derived from spatially integrated spectral line intensities emitted from nonuniform gaseous plasmas, discussing Boltzmann temperature

09 p1552 A69-22251

IR excess from carbon-rich peculiar variable I Coronae Borealis and M7 variable associated with emission nebula R Aquarii attributed to circumstellar matter

09 p1603 A69-22261

Molecular ion C13H line found in zeta Ophiuchi 4232.08 A, measuring equivalent width and finding C12/C13 ratio

09 p1603 A69-22261

Radio recombination lines of galactic hydrogen and sensitive test for low energy cosmic ray existence in interstellar medium

09 p1580 A69-22273

Nonthermal cosmic radio emission spectral index and angular variations during scanning of sky by receiver antenna, analyzing dependence on galactic latitude

10 p1784 A69-23940

H beta emission line in night sky spectrum measured with gas pressure scanned Fabry-Perot interferometer in Italian alps

12 p2074 A69-26963

NGC 4151 bright lines intensity, electron density, temperature and ions quantity evaluation from spectrograms with 140 A/mm dispersion

12 p2164 A69-27021

IR airglow spectra measured by two beam interferometer on balloon, noting carbon dioxide and OH emission bands

13 p2252 A69-27586

Solar corona 5303 and 6374 A emission enhancements correlated to 169 MHz S-component, discussing coronal temperature

13 p2347 A69-27717

Optimum emission wavelengths in atmospheric refractive index determination in optical range finder/refractometer system, noting laser applicability

13 p2260 A69-27826

Goddard Experiment Package /automated spaceborne telescope design/ for stars and nebulae UV spectral emittance measurements

13 p2261 A69-27948

Time varying flow properties effects on hypersonic wind tunnel spectroscopic measurements, considering direct emission and electron beam techniques [AIAA PAPER 69-331]

13 p2242 A69-28267

Radio emission fluxes in solar active regions, determining slope of spectral characteristics of radio sources from effective emission center

13 p2355 A69-28707

Radiative heat transfer calculations between parallel surfaces, applying approximations based on total emissivities to known spectral emissivities

14 p2539 A69-29223

Solar simulator with pulsed Xe arc tube, describing operating characteristics, spectral emission and simulator-sunlight correlation

15 p2586 A69-30385

Unidentified cometary spectra line emission possible interpretations, examining atomic hydrogen abundance in cometary atmosphere and ionic hydrogen recombination

15 p2685 A69-30523

Weak emissions in near IR daytime airglow using rocket-borne spectrometers

16 p2776 A69-32094

Radio sources spectral flux densities at 22 MHz, considering ionospheric conditions, calibration and reduction

16 p2860 A69-32231

Two flare unconnected prominence eruptions on 19 January 1968, discussing emission at arch top

17 p3023 A69-33053

Probe for spectral radiation from luminous gas-cap stagnation region to determine driver gas in test section of hypersonic shock tunnel

19 p3294 A69-35753

Spectral emissivity measurement of ablating phenolic graphite heated by subsonic air stream to high temperature to simulate reentry condition

20 p3565 A69-37187

Relative oscillator strengths of 3500-5600 A Fe I lines in emission of arc burning in Ar with iron chloride admixture

20 p3581 A69-37823

Satellite-anomalous OH radio emission sources, observing spatial distribution and Stokes parameters

20 p3610 A69-38146

Excitation temperatures and OH microwave line optical depths measured for dust clouds, discussing optical absorption lines and LF radio absorption

20 p3611 A69-38147

Effective thinness approximation for spectral line formation from photon degradation processes and random walk of scattered photons, discussing optical thickness

20 p3612 A69-38155

Vacuum UV flux along T type shock tube axis and measurements of He I line precursor emission, indicating ionizing radiation contributions to precursor ionization and excitation
20 p3511 A69-38239

Daylight sky spectral radiance in ruby laser spectral range as functions of scattering angle, height over horizon of observed point and sun altitude
21 p3734 A69-38397

Luminous efficiency for electron induced molecular nitrogen bands, discussing thick- and thin-target measurements of fluorescent efficiencies
21 p3774 A69-38521

Emission from polymethine dye solution during optical pumping with pulses from Q switched Nd glass laser, discussing emission spectral, temporal and energy characteristics
21 p3739 A69-39542

Spectral reflectivity and emissivity observations of proposed Apollo landing sites compared with other lunar localities and unmanned lunar probe data
21 p3815 A69-39585

Argon plasma jet spectral radiation properties, considering electron density, recombination, excitation, argon density, etc
22 p3991 A69-41052

Heat resistant materials integral and spectral radiative properties in IR and visible regions determined by calorimetry and IR spectrometer
23 p4237 A69-41329

Spectral emissivity and radiation intensity spectral distribution measurements for heat- resistant materials at high temperature, using photographic method
23 p4238 A69-41330

Thermal average derived with classical path treatment for line broadening theories of gases or plasmas
23 p4192 A69-41378

Autoionized resonance transitions of He at 206.2-192.2 Å using He continuum produced by capillary spark, also producing He II line spectra
23 p4191 A69-42149

Light sources in 0.15-20 micron spectral range from published literature, unpublished reports, light source manufacturers and individuals
23 p4191 A69-42190

Spectral distribution of two photon emission from metastable state of singly ionized He by broadband spectroscopic coincidence counting technique
23 p4220 A69-42378

Photoelectric measurements of emission line intensities for low density planetary nebula with moderate excitation located near north galactic pole, deriving abundances
24 p4376 A69-42662

Tabulation of photographic and photoelectric spectrophotometrically obtained relative spectral line intensities for planetary nebula IC 5217, discussing interstellar absorption
24 p4376 A69-42663

SPECTRAL ENERGY DISTRIBUTION

Auroral emission rates and heating effects as function of altitudes
02 p0235 A69-11426

Angular and spectral distribution of earth IR radiation near horizon from satellite observation and spectrograms
03 p0422 A69-13506

Latitude dependence of earth spectral radiation intensities, discussing satellite observations in equatorial and subtropical regions
03 p0422 A69-13507

Wave number frequency dependent spectral function and space-time correlation function in turbulent plasma, noting utility for probes and scattering analysis
03 p0483 A69-14255

Low temperature spectral distribution of impurity induced photoconductivity in p-type InSb crystals prepared by zone refining
04 p0644 A69-15270

High energy proton and neutron fluxes and spectra from nuclear emulsion stacks on Cosmos satellites, calculating cosmic radiation doses
05 p0814 A69-16051

Finite cross relaxation rate effect on spectral distribution in CW laser oscillator output with inhomogeneous broadening, noting population inversion distribution [IEEE PAPER T-2]
05 p0776 A69-16327

Multiplicity of secondary neutrons counted by IGY neutron monitor detecting cosmic radiation
06 p0925 A69-17297

Extensive air shower high energy muons measurements noting energy spectrum, lateral spread and dependence on shower size
06 p0990 A69-17300

Complex distribution of quasar red shift interpreted as due to two simple distributions of cosmological and gravitational red shift
06 p1009 A69-17968

Planetary nebula IC 4642 spectral line intensities measured by photographic spectrophotometry compared to previous measurements, noting no evidence for changes
08 p1383 A69-19898

Radiative tunneling shifting peak spectra in abrupt asymmetrically doped GaAs junctions
09 p1544 A69-21336

Solar irradiance spectral distribution data normalized and combined with spectral absorbance of satellite surface coatings, obtaining absorbed energy for spectral range
09 p1576 A69-21646

Spectral distribution of X ray atmospheric absorption used to determine high energy photoelectrons spectrum
09 p1577 A69-21774

Photocell base thickness for optimal power to weight ratio, noting photons spectral distribution and absorption coefficient dependence on frequency
09 p1443 A69-22719

Ionization-recombination thermodynamic equilibrium upset causing spectral excitation in He arc plasma
10 p1742 A69-24077

IR spectral distribution from region between stars of Trapezium in Orion Nebula
10 p1786 A69-24106

NGC 4151 absolute intensities of wide emission of weak isolated and IR lines determined from photoelectric spectrophotometric measurements
12 p2164 A69-27023

Quasars optical properties, hypotheses on nature, energy distribution, red shift, stellar magnitude and distance estimation on basis of absorption
12 p2167 A69-27042

Spectral energy distribution in quasars, using photoelectric spectral scanner in several wavelength ranges
12 p2168 A69-27051

Variable star BL Lacertae absolute spectral energy distribution in visible and IR regions, noting synchrotron features and possible quasar nature
13 p2335 A69-27315

Crab Nebula pulsar NP 0532 photoelectric spectrophotometry results, noting main pulse and interpulse spectral energy distributions similarity to extended synchrotron radiation
13 p2335 A69-27317

Spectrophotometry of variable star SS Cyg, analyzing energy distribution in continuum, UV gradient and Balmer jump
13 p2351 A69-27868

Solar X ray flux deduced from flare effects on VLF propagation, showing total energy content as measure of ionizing radiation
14 p2411 A69-29105

Automatic recording of spectral distribution of high resistance semiconductors photoconductivity using spectrograph monochromator
14 p2447 A69-29409

Spectral distribution of photosensitivity for p-n junctions in silicon doped GaAs, showing agreement with state density model and absorption data
15 p2666 A69-30067

Absolute spectrophotometric gradients determined from energy distribution in UV beta Lyr spectrum, confirming gradual variations in light curve shape and spectral characteristics
15 p2688 A69-30557

Flux densities at 2695 MHz for radio sources, tabulating measured data, discussing spectral distribution indices
15 p2696 A69-31206

Solar radiation actinometric and pyranometric observations during 20 May 1966 eclipse, examining IR component and spectral radiation energies
15 p2697 A69-31257

Spectral density function derivation for energy scattered from underdense turbulent wake
16 p2732 A69-31893

BetaCrB atmospheric microturbulence velocity, ionization and excitation temperatures, electron pressure and abundances determined by spectrophotometry
16 p2864 A69-32592

Random functions applications to random vibrations, discussing spectral power density, ergodic steady functions, etc
17 p3054 A69-33063

Stable passive Q-switch of neodymium laser, presenting single pulses energy, time and spectral characteristics
17 p2983 A69-33969

YZ Canis Minoris red dwarf star flare event observation record, noting optical spectrum energy output and slow decay
17 p3043 A69-34165

Ionization stratification and chemical abundances in planetary nebula NGC 7662, discussing density fluctuations effect on N II and O II lines
18 p3191 A69-34294

Pulsars observed for average energies at centimeter wavelengths, using azimuth elevation antenna
18 p3196 A69-34644

Relation between angular divergence, spectral characteristics and kinetic behavior of laser operating in various pulsed modes
19 p3333 A69-35879

Spectral parameters effect on IR instrument SNR, discussing range equations of point and extended sources and radiation-noise-limited detectors
19 p3310 A69-36061

Spectral energy distribution of gamma-Cas in 1967 based on observations in seven color photometric system
19 p3426 A69-36565

Spectral density of outgoing radiation in 0.6-0.8 micron frequency range, noting reflected radiation and cloud fields correlation functions
19 p3366 A69-36672

Homogeneous isotropic turbulence spectrum asymptotic behavior for various spectral energy transfer models
19 p3301 A69-36818

Spectral intensity distribution of night airglow, noting visual spectra distribution difference from G2 stars
20 p3522 A69-37057

Hg injection lamp with high power and variable spectral energy distribution as light source for testing solar radiation effects
20 p3510 A69-37630

High energy proton and neutron fluxes and spectra from nuclear emulsion stacks on Cosmos satellites, calculating cosmic radiation doses
20 p3591 A69-37961

Balloon-borne proportional counters to measure X rays intensity and spectral distribution from Taurus X-1 and Cygnus X-1
20 p3593 A69-38153

Galactic X ray source spectral data observed by rocket, presenting graph with corrections
20 p3594 A69-38172

Magnetic ordering in dysprosium phosphate observed by high resolution spectral line intensity measurements, finding Neel temperature
21 p3773 A69-38331

Rocket measurements of primary auroral particles energy spectra indicating spectral structure acceleration peaks associated with electrostatic fields
21 p3707 A69-38490

Approximate formula for energy spectrum of isotropic turbulence at large wave numbers, showing agreement with Gaussian exponential form
21 p3694 A69-38834

Spectral equation for decaying isotropic turbulence of incompressible inviscid flow at large Reynolds number, using spectral cascading
21 p3694 A69-38835

NGC 7023 nebula physical characteristics observation based on flux and brightness measurement, noting spectral energy distribution and causes
21 p3816 A69-39724

IC 349 nebula in Pleiades investigated with diffraction spectrograph, observing spectral energy distribution relationship to illuminating star
21 p3817 A69-39728

Particles integral and differential fluxes spectral distribution calculation for determining radiation load for synchronous satellite
22 p4035 A69-39909

Power per unit volume of UV and forbidden lines emitted by ionized C, N, O and Ne as function of electron temperature and density
22 p3984 A69-40157

Spectral emissivity and radiation intensity spectral distribution measurements for heat- resistant materials at high temperature, using photographic method
23 p4238 A69-41330

Zenith atmospheric attenuation in 183-325 GHz region measured by wideband Ge bolometer detector and spectral convolution technique
23 p4115 A69-41586

SPECTRAL LINE WIDTH

Energy density distribution in power spectra of turbulence in long wave region in free atmosphere
24 p4346 A69-43155

Isotropic cosmic X rays measured by balloon-borne scintillation telescope, discussing agreement with electron energy spectral distribution
24 p4368 A69-43185

Quasi-isotropic semigray radiative transfer prediction using nongray model in bounded plane-parallel geometries for gas with spectrum from free-free processes
24 p4415 A69-43673

SPECTRAL LINE WIDTH

Negative Faraday effect and Doppler line width measurements for He-Ne IR gas laser tube by producing beat frequencies in ring laser system
01 p0088 A69-10028

Pionic 2p-1s X ray transition energy and natural linewidth and muonic 2p-1s X ray transition energy measurements for Na 23
01 p0122 A69-10035

Carbon dioxide spectral line broadening and self broadening coefficients, using carbon dioxide laser radiant energy
01 p0091 A69-10844

Nonequilibrium nitrogen plasma spectral line intensities calculated assuming optically thin plasma
01 p0124 A69-10960

Radiation, Stark and van der Waals level broadening constants for Mg I and Si I calculated to interpret solar and stellar spectral line widths
02 p0310 A69-11454

Fraunhofer lines hyperfine structure effect on solar abundances of V, Mn, Co, Cu and Ba, calculating equivalent line widths by ALGOL program
02 p0311 A69-11458

Collision broadened homogeneous linewidth measurements for 6328 angstrom Ne line in Ne and He-Ne discharges, using nonlinear interaction between two traveling waves
02 p0257 A69-12613

Ruby laser emission spectral line narrowing due to lasing modes reduction
03 p0439 A69-13059

Wind shear and reflectivity gradient effects on Doppler radar spectra
03 p0461 A69-13341

Telluric lines halfwidth and depth dependence on observation point altitude and intervening air mass, determining absorption line contours for isothermal atmosphere
03 p0512 A69-13695

Empirical growth curve determined by using equivalent widths of absorption lines of quasar 3C 191, concluding ionization is mainly due to collisional processes
03 p0514 A69-13962

Analysis of equivalent widths as function of disk position for six photospheric neutral atomic oxygen Fraunhofer multiplets, noting O abundance
03 p0515 A69-14034

Sinusoidal phase modulation role in spectral broadening observed in trapped filaments of laser and Raman light
03 p0442 A69-14189

Hydrogen spectral line broadening under combined action of ions and electrons, tabulating values for calculation of absorption coefficient
04 p0651 A69-14373

Seyfert galaxies high excitation broad emission lines and quasars resemblance, discussing causes of spiral galaxies violent nuclear activity
04 p0657 A69-14689

Tsao-Curnutte line broadening calculations extended to include Raman scattering and quadrupole absorption
04 p0633 A69-15231

Hydrogen spectral line widening by plasma electrons emphasizing Lyman, Balmer and Paschen series
04 p0638 A69-15239

Methane broadening and anomalously small pressure shift of 3.39 micron rotation-vibration line, using laser saturated molecular absorption
04 p0633 A69-15424

Photon number and amplitude fluctuations of laser radiation in case of inhomogeneously broadened atomic line and for steady state condition
05 p0770 A69-15631

Table of equivalent widths of isolated lines with combined Doppler and collision broadened profiles
05 p0796 A69-15747

Line broadening possibility for Q switched iodine laser with aid of magnetic effect / Zeeman effect/, noting energy storage capability increase
05 p0773 A69-16288

Gallium arsenide electro-optic switch measuring signal time response to radiation step of homogeneously broadened carbon dioxide, He and nitrogen laser amplifier
05 p0773 A69-16293

Finite cross relaxation rate effect on spectral distribution in CW laser oscillator output with inhomogeneous broadening, noting population inversion distribution [IEEE PAPER T-2]
05 p0776 A69-16327

Spectral line shapes broadened by electron impacts, taking into account contribution of radiation produced by perturbing electrons
06 p0961 A69-17136

Absorption edge broadening by electric field in Gunn domain of N-GaAs crystals
07 p1197 A69-18454

Water vapor absorption line for nitrogen and oxygen mixtures with frequency measurements at various pressures and temperatures, discussing attenuation and line breadth
07 p1184 A69-18911

Depolarized Rayleigh line widths measured for carbon dioxide, nitrogen and hydrogen, using measurements to calculate reorientation cross sections [IEEE PAPER B-11]
07 p1157 A69-19485

Calculated profiles of He I 4471 and 4922 A and forbidden components star spectra, using quasi-static and impact approximations
07 p1224 A69-19713

Plasma spectral line shifting and broadening under ion and electron impact
07 p1187 A69-19720

Spectra of envelope star HD 217050, analyzing metallic lines as function of central depths
08 p1387 A69-20121

Green function method for atomic line broadening in plasma radiation, including electron correlations and quantum effects
08 p1361 A69-20147

Equivalent widths of K line of single ionized calcium and central depths of unidentified broad absorption in O and B stars spectra
08 p1389 A69-20250

Quantum theory of line broadening and shift, relating adiabatic and diabatic collisions to elastic and inelastic scattering of perturbers
08 p1363 A69-20464

Mean square radii for assigned terms of Fe I energy diagram for Van der Waals line broadening
08 p1392 A69-20559

Self modulation, self steepening and spectral development of light in small scale trapped filaments, noting influence of relaxation time
08 p1352 A69-20745

Emission line galaxy NGC 5253, discussing radial velocity, line width and excitation and similarity to Seyfert galaxies
08 p1407 A69-21132

Frequency fluctuations in mode coupled gas laser used to determine natural emission line width
09 p1516 A69-21670

Helium I line profiles including forbidden component, discussing electron and ion Stark broadening and thermal Doppler broadening
09 p1601 A69-22209

Stark broadening of Balmer H alpha, H beta, H gamma and H delta lines in plasma region in strong magnetic fields
09 p1542 A69-22248

Nonadiabatic collision broadening theory for IR spectral lines applied to carbon dioxide-carbon dioxide and carbon dioxide-nitrogen collisions, estimating rotational line widths
09 p1543 A69-22250

Collision broadening cross sections of OH UV transition at room temperature, using flash photolysis
09 p1543 A69-22252

Molecular ion C13H line found in zeta Oph at 4232.08 A, measuring equivalent width and finding C12/C13 ratio
09 p1603 A69-22266

Laser induced line narrowing in coupled Doppler broadened transitions, noting mode crossing and spontaneous emission
09 p1519 A69-22282

Degeneracy of hydrogenic states to sum S-matrix in Stark broadening calculations
09 p1543 A69-22405

Line blanketing for two level atom with spectral line formed in pure absorption and noncoherent scattering, studying wavelength and depth dependence
09 p1606 A69-22424

Angular dependence of EPR line widths of trivalent Cr ions in zinc tungstate in rotating magnetic field, noting spin-phonon mechanism
10 p1743 A69-23131

Amplitude fluctuations and line width of traveling wave and standing wave He-Ne laser, considering saturation effects
10 p1701 A69-23135

Early type stars spectrophotometric parameters, discussing hydrogen beta, gamma and delta line widths, magnitude, etc
10 p1777 A69-23387

Nuclear sizes, emission line widths and densities in Sc galaxy M 51 and Seyfert galaxy NGC 4151, noting similarities and difference between nuclei
10 p1785 A69-24089

Spectral broadening measurements of ruby laser light scattered by density fluctuations in theta pinch plasma
11 p1924 A69-24304

Equivalent line widths for solar disk Fe and Ti spectra determined for umbra models, noting role of sunspot location
11 p1955 A69-24388

Hydrogen balmer lines broadening by Stark and Doppler effects, finding prominences and chromosphere electron concentrations
11 p1955 A69-24389

Solar spectra of Mg II doublet lines during September 22, 1968 eclipse, considering chromospheric activity effects on emission peaks
11 p1958 A69-24591

Monograph on internal structure of sun corona covering variations in intensity and width of coronal lines, inhomogeneity, quasi-homogeneous and anisothermic coronas, etc
11 p1961 A69-25103

Frequency stability of He-Xe laser with nonresonant feedback, noting spectral line width dependence on number of interacting modes
12 p2105 A69-26049

Shapes of extreme wings of collision-broadened carbon dioxide lines, noting absorption deviation from Lorentz-shaped lines
12 p2132 A69-26248

Disaligning and velocity changing collisions influence on laser light induced saturation peaks or holes in velocity distribution of Ne atoms
12 p2105 A69-26317

Mode interaction in lasers with homogeneous line broadening, analyzing rate equations for radiation fields of operating modes for asymptotic values of mode intensities
12 p2106 A69-26323

Laser gain medium dispersion expressions applied to multimode ring laser operation with mode spacing less than pressure broadened atomic linewidth
12 p2106 A69-26324

Surface gravities and detection of metallic line early A stars from spectral classification using equivalent line widths
12 p2171 A69-27151

Absorption line spectrum of quasar Ton 1530, discussing line widths and red shifts
13 p2334 A69-27306

Fe III line profiles and equivalent widths from spectrograms of zeta Cas and gamma Peg for Fe abundance, using model atmospheres
13 p2347 A69-27715

VLF morning and evening magnetosphere emission distinction by studying spectrum width as function of variations in K index
13 p2253 A69-27740

He-Ne laser transition line shape and gain curve through width, considering spectral frequency characteristics, output power and gas temperature and concentration
13 p2272 A69-28115

Spectral width of emission of laser resonator in nonstationary mode in presence of active medium, noting time dependence
14 p2456 A69-28736

Passive Q switch laser single pulse formation time and spectral width using balance equations
14 p2458 A69-29166

Emission spectrum width of solid state lasers as function of temperature, investigating effects of active medium parameters, pumping and cavity
14 p2459 A69-29389

Sunspot equivalent line widths calculated using sunspot models, considering influence of light scatter correction
14 p2525 A69-29721

Laser spark plasma initial development phase showing high electron temperature and concentration, continuous spectrum emission, line broadening and shock wave formation

14 p2461 A69-29779

Si III and O II spectral lines distortion in pulse HF plasma in rotating electromagnetic field, showing particle rotational speed dependence on discharge chamber radius

14 p2497 A69-29791

Source functions of IR Fraunhofer lines obtained using solar disk equivalent width method, noting LTE role

14 p2528 A69-29961

FM oscillations spectral width during modulation by finite sequences of multiple and nonmultiple frequencies

15 p2562 A69-30116

Gas laser secondary modes emission and beat frequency spectrum widths, using results of Lamb lasers theory

15 p2633 A69-30121

Subtractor performance for processing correlated random signals with different spectral widths in signal delay time indicator, discussing errors

15 p2572 A69-30346

Filamentary nebula IC 443 observation by Fabry-Perot etalon with image converter, determining radial, expansion velocities and H alpha line half width

15 p2686 A69-30538

Quartz oscillator amplitude and frequency fluctuations due to elements tolerance fluctuations, examining oscillator parameters contributions to spectral line width

15 p2579 A69-30944

Time resolved Stark broadened spectral profiles for Na I 5882-88 A and 4978-82 A lines of plasma, comparing electron densities

15 p2656 A69-31155

OGO 5 satellite measurements of intensity and width of Lyman alpha line scattered by hydrogen geocorona

15 p2699 A69-31412

Turbulence dissipation rate in clouds and precipitations determined from rms width of vertical sounding radar signal fluctuation spectra, distinguishing gravity and turbulence effects

16 p2807 A69-32273

Electron impact broadening of isolated spectral lines emitted by neutral atoms in plasma

16 p2823 A69-32468

Hydrogen line profiles, equivalent widths and electron impact for peculiar alpha 2 CVn and gamma Lyr stars

16 p2864 A69-32594

Line widths of 48 galaxies at 21 cm and spectroscopic data, estimating masses and angular momenta, finding mass-angular momentum relation

16 p2866 A69-32818

HCN laser line width measurement with high resolution spectrum analyzer indicating spectral widths caused by mechanical instability

17 p2979 A69-32850

Line width and intensity correlation of laser radiation noting damping constant

17 p2980 A69-33012

Spontaneous gas laser emission from level coupled by spontaneous transition with emitting level, obtaining atoms interaction with laser field velocity distribution and spectral line width

17 p2981 A69-33116

Level crossing signal obtained by magnetic/electric field modulation, tabulating corrections to widths and centers for distortions

17 p3009 A69-34155

Solar Fe II lines theoretical equivalent widths calculations, estimating influence of photosphere model on iron abundance data

18 p3191 A69-34305

Width measurements of van der Waals broadened Si I spectral lines by shock tube and scanning Fabry-Perot interferometer, using argon as perturbing gas

18 p3116 A69-34449

Atomic and molecular absorption lines and width measurement in spectrum of WZ Cassiopeiae carbon star in visual and IR region

18 p3204 A69-35350

Laser emission in system of four level centers, determining nonuniform emission line broadening due to disturbed quasi-equilibrium distribution of electron subsystem elementary excitations

19 p3333 A69-35877

Lamb theory of Doppler broadened gas laser extended to arbitrary intensities for single mode opera-

tion, calculating detuning curves and inversion densities

19 p3335 A69-36048

Rb 87 vapor laser pumping, output, spectral line width and emission frequency approximated in three level system

19 p3335 A69-36342

Rb 87 vapor laser output power and spectral line width dependence on optical pumping intensity and atom density in resonator

19 p3336 A69-36343

Exciton line broadening in II-VI compound semiconductors, discussing thermal broadening of n equals one exciton associated with LO phonon-induced scattering

19 p3386 A69-36524

Spectral line scattering during propagation of radiation in turbulent plasma

19 p3396 A69-36573

GaAs laser used as optical sweep generator for display of Cs 133 spectral line shape, studying fluorescence and radiation lifetime

19 p3339 A69-36696

Stark broadened H gamma profile, considering effect of strong collisions in electron perturbation and electron impact broadening of lower levels

20 p3579 A69-37305

Spectral line broadening and shift due to electron and ion shocks in impact theory

20 p3580 A69-37828

Output power spectra of Pb-Sn-Te diode laser above threshold of oscillation, demonstrating inverse dependence of line width on laser power

21 p3734 A69-38326

Equivalent absorption line widths of supergiant B1 IA /kappa Cassiopeia/ tabulated with log NH content of atmosphere for various elements

21 p3803 A69-38844

Absorption spectroscopy using resonance broadened atomic lines for two phase mixtures study

21 p3774 A69-39239

Solar flares and prominences emission lines equivalent width correlated with relative differential velocity between filaments

22 p4001 A69-39994

Calcium K line strengths in A stars measured by narrow band spectrometer compensated for seeing and transparency variations

22 p4015 A69-40154

Methane rotational temperature in Jovian atmosphere deduced from equivalent widths of lines at 1.1 micron band

22 p4028 A69-40663

Stark broadening of H-gamma for electron density measurement in plasma, noting temperature range

22 p3985 A69-40664

Electron and ion Stark broadening of allowed and forbidden, triplet and singlet transitions in neutral He at low electron densities, noting Doppler broadening

22 p3985 A69-40665

Aperture distortions and spectral line shapes of electromagnetic radiation diffused by plasma

22 p3982 A69-40799

Nonlinearity effect on spectral shape and bandwidth in connection with frequency modulation by noise

22 p3900 A69-40923

Frequency discrimination in optical harmonic generators, discussing spectral width of wideband laser for supershort pulses and spectral device, using frequency dependence of mode locking direction

22 p3965 A69-40964

Thermal average derived with classical path treatment for line broadening theories of gases or plasmas

23 p4192 A69-41378

Classical path approximation in line broadening theory to derive impact and one-electron theories, with application to Stark broadening of Lyman series in hydrogen

23 p4193 A69-41379

Electron spin memory in optical pumping cycle of potassium halides F centers, measuring relaxed excited state g factors and spin resonance line widths

23 p4198 A69-42419

Equivalent width measurements of Arcturus IR line spectra using Fourier transform spectroscopy, tabulating results

23 p4222 A69-42453

Equivalent line widths for solar disk Fe and Ti spectra determined for umbra models, noting role of sunspot location

24 p4390 A69-43778

Hydrogen balmer lines broadening by Stark and Doppler effects, finding prominences and chromosphere electron concentrations

24 p4390 A69-43779

Beta Orionis spectral line profiles data used to study atmospheric structure

24 p4391 A69-43804

SPECTRAL LINES

U LINE SPECTRA

SPECTRAL NOISE

U WHITE NOISE

SPECTRAL REFLECTANCE

Radar reflectivity and refractive index spectra in clear atmosphere simultaneously measured and compared with theoretical calculations

01 p0032 A69-10969

Plane wave scattering from modulated corrugated structures, obtaining reflection coefficients for multimode propagation

01 p0033 A69-10973

High temperature directional reflectance measurements of ablative materials as function of sample temperature using paraboloid reflectometer

04 p0604 A69-15512

Spectral reflectivity curves for bright and dark areas of Mars noting seasonal crossings

09 p1587 A69-21308

Multispectral photographic determination of reflectance of environmental features from aerial spectral photographs, noting EROS program application

11 p1880 A69-24266

Band structure and reflection spectra of vanadium dioxide and pentoxide single crystals, noting changes in metal-semiconductor phase transition

12 p2145 A69-26724

Light interaction with stacked leaves and plant canopy, determining reflectance and transmittance

12 p2097 A69-26985

Spectral reflectivity differences of selected dark and bright regions of Mars observed with double beam photometer

13 p2338 A69-27553

Lunar surface spectral reflectivity variations with time, noting phase angle effects on color contrast

13 p2349 A69-27819

Earth albedo instrument on OSO 3 spacecraft to measure solar reflectance of earth at various wavelengths

15 p2614 A69-31279

Spectral reflectivity differences /color differences/ on lunar surface in visible region, indicating compositional difference origins

17 p3037 A69-33653

Spectral reflectances of objects and vegetative backgrounds to generate color photographic technique increasing detection sensitivity and rate

18 p3133 A69-34247

CaO and MgO reflectance spectra measurements at high resolution and at low temperature including exciton spectra at 25 K, obtaining fine structure

18 p3181 A69-34274

Reflection reduction properties of symmetrical, light transmitting three layer coating consisting of zinc sulfide-magnesium fluoride-zinc sulfide films

18 p3173 A69-35147

Antimony trisulfide natural light reflection and transmission in and near IR region, noting spectral temperature and time dependence peculiarities

19 p3384 A69-36481

Cadmium sulfide-selenide single crystals vegetation coefficient polarimetric measurement, observing reflection peaks relationship to absorption spectral temperature dependence

19 p3391 A69-36607

Spectral reflectivities of sintered Ti-TiN-TiC and Zr-ZrN-ZrC alloys and Zr-ZrN-ZrC alloys

20 p3559 A69-37330

Band structure and reflection spectra of vanadium dioxide and pentoxide single crystals, noting changes in metal-semiconductor phase transition

21 p3781 A69-39137

Spectral reflectivity and emissivity observations of proposed Apollo landing sites compared with other lunar localities and unmanned lunar probe data

21 p3815 A69-39585

Visible and IR spectral reflectivity of Apollo lunar landing sites, attributing reflectivity differences to compositional and/or mineralogical differences

21 p3815 A69-39586

Relative IR spectral reflectivity of selected lunar surface areas measured using double beam photoelectric filter photometer

21 p3815 A69-39588

Gases effects on UV irradiated thermal control materials spectral reflectance, discussing tests and photolysis mechanisms

22 p3923 A69-40395

Optical frequencies and polarizations of IR active phonons of tysonite lanthanide fluorides based on Kramers-Kronig reflectance spectra analysis
22 p3993 A69-40729

Spectral reflectivity curves for Mars light and dark areas and seasonal changes of dark area simulated in laboratory
23 p4209 A69-41319

Donor and acceptor impurity effect on absorption and reflection spectra of CdTe single crystals, analyzing In, Ga, S and Se
24 p4362 A69-43735

SPECTRAL RESOLUTION

Europium complexes high resolution emission spectra in relation to molecular configuration
01 p0024 A69-10893

Selective resonators for laser emission spectral structure control, proposing dispersion power increase by inserting telescopic system
05 p0777 A69-16371

Photometric effects of UVB color indices ineffective in detecting double stars in Galaxy
07 p1216 A69-18854

Coupled wave equation solution based on spectral resolution for longitudinal components of electric and magnetic fields when source currents are present in compressible anisotropic plasma
08 p1274 A69-20031

HF ionospheric radar ground scatter map showing separated land-sea backscattered radio waves by Doppler technique
09 p1454 A69-21681

Recombination parameters and depth of levels of p-n junctions in semiconductor photocells determined from position of maximum spectral sensitivity
09 p1560 A69-22718

Color TV system for Earth Resources Observation Satellite /EROS/, discussing resolution in relation to spectral separation through data simulation study [SMPT PAPER 105-79]
12 p2077 A69-25767

Slowly varying component of solar radio emission, evaluating resolution of radio telescopes in sunspot studies and localized areas luminescence
15 p2674 A69-30503

Aberrations of Fabry-Perot interferometers with small nonuniformities in plate spacing used as spectral and optical filters
17 p2972 A69-33081

Remote sensors discrimination and performance, discussing linear filter system, contrast ratio, tricolor systems and multispectral scanning system
20 p3493 A69-37743

Spectroscopic observations of optical pulsar NP 0532, using technique permitting phase resolution of spectra of main pulse and interpulse
21 p3799 A69-38646

Solar IR spectrum recorded by LPL B spectrometer on NASA CV-990 aircraft using one micron grating, noting resolution
21 p3800 A69-38683

Image intensifier coupling to electron scanning image converter to increase time-resolving spectrograph sensitivity in simulated reentry studies
24 p4317 A69-43759

SPECTRAL THEORY

Book on linear boundary value problems of mathematical physics based on Green function covering Hilbert spaces, integral equations and spectral theory of differential operators
04 p0625 A69-15232

Book on stellar atmospheres covering radiation theories, thermal equilibrium, measurement techniques, spectral analysis, etc, emphasizing sun
11 p1961 A69-25084

Spectrum of ordinary second order differential operators, correlating spectral properties with analytic function-theoretic properties of differential equation solutions
17 p2996 A69-33793

Primary H nuclei flux and spectrum near geomagnetic equator, discussing emulsion stack exposure
22 p4005 A69-40520

Gain modification from spectral splitting of optical transition by incident light wave on higher frequency coupled transition
22 p3965 A69-41125

SPECTROGRAMS

Photometric standardization and calibration of meteor spectrograms for real meteor masses determination using spectroscensitometer
12 p2154 A69-25820

Magnetic A star HD 152107 anomalous intensification of Balmer series H lines observed by spectrograms
13 p2352 A69-27873

P Cyg star HD 190603 atmospheric parameters from spectrograms analyzed by curve of growth method, including ionization and excitation temperatures and electron density
14 p2519 A69-29357

Masses of visual binaries above main sequence with published orbits determined as function of position in H-R diagram, using spectroscopic parallaxes
18 p3195 A69-34429

MK system spectral types determination for B, A and F type stars from slit spectrograms near NGC 2264
23 p4211 A69-41487

M giant star possible evolution into S star, using high dispersion spectrograms
24 p4387 A69-43349

SPECTROGRAPHS

U SPECTROMETERS

SPECTROHELIOGRAPHS

Optical evidence for mass motions in solar flares /1937-1967/
06 p0993 A69-17428

Solar corona X ray emission during flares and under quiet sun conditions investigated by satellite with X ray heliograph
07 p1210 A69-19614

Sunspot observations with astrogaph telescope by tracing on projected image of solar disk
08 p1387 A69-20118

Multilens spectroheliograph for nonstabilized rockets, obtaining consecutive points recording along solar image chord
08 p1313 A69-20252

Radiophysics Laboratory /Sidney/, discussing radio astronomy, radioheliographs, radio telescopes, cloud physics and research
10 p1784 A69-23988

Spectroheliograph technique, obtaining high resolution magnetic maps of solar magnetic fields directly in single image without photographic subtraction
11 p1880 A69-24432

Stationary Babinet compensator for measuring longitudinal solar magnetic fields by means of fringes introduced in spectroheliograms
11 p1880 A69-24433

Aerospace Corp. solar observatory /California/ compound telescope, vacuum spectroheliograph, instrumentation and applications
11 p1862 A69-24792

Rocket-borne spectroheliograph for monochromatic solar photography in Mg II 2802.7 A line noting filter bandwidth, film polarizers and temperature control
11 p1884 A69-24838

Solar activity indices based on Ca flocculi, emphasizing index representing emission excess over chromospheric emission
14 p2525 A69-29722

Photoheliographic data tabulation of sunspots positions and areas for 1961 obtained from various astronomical observatories
15 p2700 A69-31490

Tachoheliograph /modified spectroheliograph/ for obtaining two dimensional solar velocity maps, discussing construction and theory of operation
17 p3030 A69-33061

Spectroheliograms interpretation obtained in line cores of neutral oxygen IR multiplets
18 p3204 A69-35388

Solar radio emission during quiet sun years 1964-1965 mapped using Stanford spectroheliograph, attributing slowly varying component to electron density enhancement
18 p3188 A69-35395

Solar microwave emission heliographic distribution during pronounced geomagnetic recurrence, noting brightness temperature nonuniformity due to coronal depression through polytrope models for solar wind
18 p3188 A69-35396

X ray heliography by Fresnel-Soret type zoneplate camera to obtain solar photographs from rockets
20 p3544 A69-37803

Neutral He lines at 537 A and 584 A obtained by spectroheliometer on OSO 4, studying differences between quiet and active regions
23 p4222 A69-42405

SPECTROHELIOSCOPES

U SPECTROHELIOGRAPHS

SPECTROMETERS

NT FABRY-PEROT SPECTROMETERS

NT INFRARED SPECTROMETERS

NT MASS SPECTROMETERS

NT SOLAR SPECTROMETERS

NT SPECTROHELIOGRAPHS

NT TIME OF FLIGHT SPECTROMETERS

NT ULTRAVIOLET SPECTROMETERS

H alpha emission symmetrical spatial distribution of night airglow observed with high transmission diffraction spectrographs
01 p0062 A69-10128

Electron impact spectrometer for obtaining molecular energy loss spectra used to investigate scattering cross sections for optically allowed and forbidden transitions
01 p0123 A69-10620

Rapid scan spectrometer design and calibration, noting application to diagnostics of high density transient Xe and H plasmas
01 p0082 A69-10838

Scaled and translated composite curve technique for reducing calibration data for spectrograph film system response characteristics
01 p0082 A69-10839

Scintillation gamma spectrometer on Luna 10, eliminating charged particle background by fabricating detector from NaI single crystal in scintillating plastic container
01 p0084 A69-11314

Multichannel amplitude analyzer for space applications, noting use as gamma-spectrometer component in Lunik 10 and 4096 bit/channel traffic capacity
01 p0084 A69-11315

Solar radiation protection of radiometers and spectrometers on reentry vehicle by launching times and solar view field selection
04 p0666 A69-15511

Low dispersion spectrograph for temperature and electron density determination in plasma beam
05 p0803 A69-15997

Cosmic ray magnetic spectrograph for measurement of momentum spectrum, charge ratio and specific ionization of muons, discussing magnetic and scattering displacement
06 p0925 A69-17302

Communications of Lunar and Planetary Laboratory, Volume 7, covering IR solar spectrum atlas reports and solar spectrometer for airborne IR observations
06 p1008 A69-17807

Instrument profile of grating spectrograph determined by applying He-Ne laser mode separated in Fabry-Perot interferometer
07 p1131 A69-18405

Parametric light interactions application to optics stressing nonlinear spectrograph and cavity and traveling wave oscillator [IEEE PAPER K-5]
07 p1152 A69-19066

Onboard calibration system for gamma ray spectrometers and X ray detector in earth satellites, describing fabrication and test results for radioactive sources [IEEE PAPER 3A-6]
07 p1134 A69-19193

X ray proportional counter, analog to digital converter and power supply for gamma ray spectrometry used in satellite applications [IEEE PAPER 3A-7]
07 p1134 A69-19194

Channel multiplier spectrometer for low energy electrons and protons at synchronous altitude on ATS-E satellite [IEEE PAPER 3C-5]
07 p1135 A69-19199

Stimulated emission of laser employing crystal and glass lasers doped with neodymium ions, using high temperature spectroscopy
08 p1323 A69-19944

Multichannel photoelectric spectrometer design for Hale telescope, noting effectiveness in red and IR observations
08 p1318 A69-21131

Cosmic ray intensity variations by spectrographic method, noting geomagnetic effects
10 p1759 A69-22836

Image intensifier for high speed spectrography of short duration faint radiation source, noting high speed shutter and resolution
12 p2085 A69-26160

Crossed beam apparatus with mass selected variable energy primary beam for study of angular and velocity spectra of ion-molecule reactions
12 p2092 A69-26477

Correlation spectrometer for air pollution surveillance from airborne and spaceborne platforms, noting scanning satellite system for continuous global coverage
12 p2096 A69-26981

H alpha line emission preceding auroral breakup by data analysis of Antarctica Meinel-type patrol spectrograph, noting magnetic activity role
14 p2441 A69-29386

Automatic recording of spectral distribution of high resistance semiconductors photoconductivity using spectrograph monochromator
14 p2447 A69-29409

Rocket-borne scintillation spectrometer for cosmic photon radiation
14 p2449 A69-29566

Parametron preamplifier for X band superheterodyne ESR spectrometer, noting sensitivity and SNR
14 p2423 A69-29757

Nova Delphini 1967 observational data and equipment including Cassegrain spectrograph, reflector telescope and photoelectric photometer
15 p2682 A69-30439

OGO 5 spectrometric studies of topside ionospheric ion concentrations, noting difference between nighttime and sunlit pass
15 p2599 A69-31345

Jodrell Bank RF digital autocorrelation spectrometer based on time delay related to signal power spectrum through Fourier transform
17 p2970 A69-32856

High energy cosmic ray muon charge ratios at large zenith angles measured as function of momentum by using spectrometer
17 p3023 A69-33321

Nondestructive ultrasonic, spectroscopic and TV test methods reducing time for inspection and increasing reliability of turbines
17 p2978 A69-33330

Ultrasonic spectrometry application to thickness measurement of thin and thick walled articles
18 p3137 A69-35110

Amplitude and intensity distributions of plane periodic Fresnel diffraction grating calculated by Fraunhofer theory, noting applicability to spectrometric and meteorological instruments
19 p3372 A69-35906

Multispectral scanner with multichannel spectrometer for earth observations, describing video image generation from detector elements output signals
19 p3310 A69-36066

Prismatic Cassegrainian-focus spectrograph of telescope at Shemakha Observatory, discussing camera inclination, instrumental contour for yellow neon line, astigmatism, optical temperature effects, etc
19 p3313 A69-36582

OGO 5 ion spectrometer for measuring oxygen, He and hydrogen ion concentration, noting functions as energetic particle analyzer and proton energy distribution measurement capability
19 p3314 A69-36679

Instrumental profile determination for high resolution stellar spectrograph, using profiles of telluric oxygen bands obtained from emission line observations
21 p3721 A69-38696

X ray scintillation spectrometers temperature stabilizing circuit, describing amplitude- frequency conversion technique for position stability
21 p3727 A69-39856

Cosmic ray electrons component measurements at balloon altitudes with electron spectrometers
22 p4002 A69-40091

Airborne correlation spectrometer for air pollution remote sensing, describing applications
[RAES PAPER 7] 22 p3896 A69-40488

Image intensifier coupling to electron scanning image converter to increase time-resolving spectrograph sensitivity in simulated reentry studies
24 p4317 A69-43759

SPECTROMETRY

U SPECTROMETERS

SPECTROPHOTOGRAPHY

Instrument profile of birefringent Lyot filter for H alpha line determined from photographic spectra with grating spectrograph
04 p0664 A69-15524

Apollo 9 multispectral photography compared with photographs taken simultaneously by aircraft using same film filter combinations
15 p2608 A69-30452

Spectral reflectances of objects and vegetative backgrounds to generate color photographic technique increasing detection sensitivity and rate
18 p3333 A69-34247

Monochromatic coronal emission line photographs improved by composite technique
20 p3539 A69-37547

SPECTROPHOTOMETERS

NT INFRARED SPECTROPHOTOMETERS

NT ULTRAVIOLET SPECTROPHOTOMETERS

Atmosphere spectral transparency and stability spectrophotometric studies based on measuring solar aureole brightness
01 p0074 A69-11188

Rapid recording microspectrophotometer for IR to UV absorption spectra of living cells, cell organelles and half micron diameter particles
03 p0428 A69-13109

Spectrophotometer and integral methods to determine solar radiation absorptivity for steady/ unsteady thermal regimes in solids
05 p0846 A69-15901

Daytime sky radiation measurements by high altitude vehicles with spectrophotometer noting spectral radiance, luminance, polarization, albedo and near IR
08 p1317 A69-21071

Remote control spectrophotochronograph to study radiation of high speed high temperature processes, giving construction data and diagrams
12 p2085 A69-26161

Statistical characteristics of ozone measurements with Dobson spectrophotometers and filter ozonometers, determining requirements for maximum effectiveness of ozone network
16 p2787 A69-32639

Amplifier working in conjunction with solid state phase sensitive detector replacing existing commutator in Dobson ozone spectrophotometer
16 p2792 A69-32641

Variations in difference between integrated ozone amount by soundings and total ozone by Dobson spectrophotometers
16 p2792 A69-32642

FORTAN computer program for quality control and calculation of total ozone measurements and lamp tests for Dobson ozone spectrophotometer
16 p2787 A69-32644

SPECTROPHOTOMETRY

NT STELLAR SPECTROPHOTOMETRY

Geophysical investigations on manned orbital space laboratories, discussing space photography, spectrophotometry, terrain pictures and aerosol layers
05 p0759 A69-16633

Mars surface photometric and spectrophotometric measurements, relating opposition effect details with corresponding laboratory sample measurements
07 p1212 A69-18601

Electron transport of Halobacterium cutirubrum, discussing spectrophotometric identification of cytochromes
07 p1068 A69-19481

Simulated solar EUV laboratory spectrophotometry used in preparing optical space flight experiments, discussing instrumentation and calibration
08 p1267 A69-19888

Flame emission spectrophotometric method for ultraminate sodium contamination detection in thin silicon oxide films and cleaned silicon surfaces
[ECS PAPER 306] 08 p1314 A69-20367

Absolute spectrophotometry of IR lines in planetary nebulae spectra determined by diffraction spectrograph
09 p1590 A69-21380

Solar soft X ray components observed with ion chamber photometer, studying components relation to transient and slowly varying phenomena at other wavelengths
09 p1578 A69-22170

Spectral lines relative intensities for bright medium excitation gaseous planetary nebula IC 3568, using photoelectric spectrum scanner and spectrophotometry technique
10 p1787 A69-24117

Tilting filter photometer for faint light source spectrophotometry, discussing digital approach used with photomultipliers
11 p1884 A69-24834

Ozone absorption coefficients in vicinity of Hartley band maximum verified by photographic spectrophotometry
16 p2785 A69-32626

Absolute spectrophotometry of IR lines in planetary nebulae spectra determined by diffraction spectrograph
18 p3198 A69-34768

Detection and spectral examination of trace porphyrin complexes by demetallation with methanesulfonic acid and spectrofluorometry, compared to absorption spectrophotometry
24 p4279 A69-42557

SPECTRORADIOMETERS

NT INFRARED SPECTROPHOTOMETERS

Radio spectrometer with paramagnetic quantum amplifier for astronomical spectral measurements in 8 mm range
04 p0597 A69-14851

Radio spectrometer with paramagnetic quantum amplifier for astronomical spectral measurements in 8 mm range
15 p2607 A69-30243

Multispectral radiometric analysis of ERTS images, discussing image registration, SNR and atmospheric and diffraction effects
21 p3721 A69-38627

SPECTROSCOPES

U SPECTROMETERS

SPECTROSCOPIC ANALYSIS

Spectroscopic investigation of high density plasma from Li exploded wires
01 p0129 A69-10662

Orbital spectroscopic and radiometric IR experiments, considering moon and Mars surface
[AAS PAPER 68-196] 02 p0312 A69-11474

Q switched laser excitation flash spectroscopic analysis of naphthalene, describing equipment arrangement and experimental results
02 p0254 A69-11544

X ray spectrographic camera for nondestructive spectrum analysis of small samples
03 p0427 A69-13101

Rapid recording microspectrophotometer for IR to UV absorption spectra of living cells, cell organelles and half micron diameter particles
03 p0428 A69-13109

Polar aurora incident energetic particles spectroscopic analysis, showing system of lines and bands intensity dependence on particle energy spectrum and magnetic activity
05 p0752 A69-15799

Spectroscopic charged particle concentration determination, discussing error and limits of applicability in low temperature plasma
05 p0762 A69-15899

Spectroscopy of potassium vapor using laser induced fluorescence, noting laser line coincides with several molecular transitions
05 p0771 A69-15907

Laser photolysis and spectroscopy for photographic recording of absorption spectra of transient intermediates in nanosecond reactions
05 p0772 A69-16025

Quantitative spectroscopy and spectral photometry, discussing developed image properties and connection between exposure and image
08 p1315 A69-20467

Southern planetary nebulae observed with Newtonian spectroscope of Radcliffe Observatory in Pretoria, giving corrected data listing
08 p1392 A69-20561

Glass fibers size, finish and surface treatment identification by pyrolysis attenuated total reflectance IR spectroscopy
09 p1448 A69-22315

Trivalent rare earth ions Stark structure based on spectroscopic observations of stimulated transitions in lasers
10 p1701 A69-23129

Low temperature optically thick boundary layers influence on spectroscopic temperature measurements in plasma MHD channels
10 p1731 A69-23434

Microimpurities in aluminum-yttrium garnets determined spectrographically by using gallium oxide as carrier and Teflon powder for fluorinator
10 p1747 A69-23843

Pulsed tunable lasers, emphasizing dye lasers for visible and near visible light in specialized spectroscopy
11 p1893 A69-24343

Nonpolar LF latitude variations based on spectroscopic and harmonic analysis of zenith telescope and prismatic astrolabe observations
11 p1956 A69-24401

Spectrometric oil analysis procedure [SOAP] for predicting failure of oil wetted parts in small turboprop aircraft engines
[SAE PAPER 690325] 11 p1941 A69-24508

Covalence degree of activator-ligand chemical bonds effect on spectroscopic properties of transition metals
11 p1907 A69-25031

Time varying flow properties effects on hypersonic wind tunnel spectroscopic measurements, considering direct emission and electron beam techniques
[AIAA PAPER 69-331] 13 p2242 A69-28267

Spectroscopic determination of temperature fields in water and transpiration cooled constricted Ar arc jets at atmospheric pressure
15 p2657 A69-30155

Spectroscopic measurements of charged particle concentrations in jet produced by pulsed plasma generator

15 p2663 A69-30991

Spectroscopic study of P Cygni showing ionization temperature, Balmer decrement agreement with calculated value and chemical composition

16 p2864 A69-32595

Mossbauer spectroscopy, discussing nuclear resonance fluorescence and equipment

18 p3099 A69-34622

Ion structure of keto and enol and McLafferty rearrangements determined by ion cyclotron resonance spectroscopy

19 p3265 A69-36288

Spectroscopic quantitative analytical method for measuring atomic absorption in flame based on determining integral absorption magnitude during evaporation

20 p3539 A69-37605

Spectrographic analysis for ferrous and nonferrous alloys as nondestructive testing

20 p3551 A69-38313

Nonpolar LF latitude variations based on spectroscopic and harmonic analysis of zenith telescope and prismatic astrolabe observations

24 p4391 A69-43791

SPECTROSCOPIC TELESCOPES

NT STRATOSCOPE TELESCOPES

Lasers and holography applications in astronomy including high resolution spectrographic diffraction gratings manufacture and astronomical objects photographic pictures evaluation

15 p2610 A69-30880

Solar image motion frequency spectra analysis via photoelectric equipment, showing influence on photographic pictures, spectra and modulation transfer functions for diffraction telescope

17 p3029 A69-33047

SPECTROSCOPY

NT ASTRONOMICAL SPECTROSCOPY

NT AUORAL SPECTROSCOPY

NT GAS SPECTROSCOPY

NT INFRARED SPECTROSCOPY

NT MAGNETIC SPECTROSCOPY

NT MASS SPECTROSCOPY

NT MOLECULAR SPECTROSCOPY

NT NUCLEAR RADIATION SPECTROSCOPY

NT OPTICAL EMISSION SPECTROSCOPY

NT RADIO SPECTROSCOPY

NT SPECTROPHOTOGRAPHY

NT SPECTROPHOTOMETRY

NT SPECTROSCOPIC ANALYSIS

NT STELLAR SPECTROPHOTOMETRY

NT ULTRAVIOLET SPECTROSCOPY

NT VACUUM SPECTROSCOPY

NT X RAY SPECTROSCOPY

Exploding wires as light source for quantitative spectroscopy, noting optically thin plasma clouds with radial symmetry

01 p0117 A69-10658

Time resolved spectroscopy of exploding wire plasmas in visible spectrum of various elements, determining plasma characteristics

01 p0119 A69-10671

Beam-foil spectroscopy - NASA Conference, University of Arizona, November 1968, Volume I

03 p0470 A69-13160

Beam-foil spectroscopy problems noting light collection, spectrograph design, broadening of spectral lines by Doppler effect and other complications

03 p0470 A69-13161

Spectroscopy of fast atoms resulting from fast ion impact with gas targets and electron capture into excited state

03 p0471 A69-13162

Beam-foil spectroscopy above 5.5 Mev for multiply ionized atoms, noting use of Tandem accelerator, spectral resolution, beam intensity and Doppler effect

03 p0471 A69-13163

Beam foil spectroscopy - NASA Conference, University of Tucson, November 1967, Volume 2

03 p0507 A69-13168

Beam foil spectroscopy for measuring wavelengths and spectral line intensities

04 p0595 A69-14276

Static beam deflection in beam foil spectroscopy for determining parent ionization stage of emitting ions

04 p0595 A69-14279

Superradiant and laser spectroscopy in second positive system of molecular nitrogen

04 p0609 A69-14285

Spectroscopy history from Newton to present, stressing need for standardized system of spectral classification

06 p0999 A69-16974

Paraelectric resonance spectroscopy on KCl, using bistable dipole model

06 p0982 A69-18235

Plasma diagnostics by spectroscopic techniques, measuring polarity dependences of temperature and charged particle concentration for flows with shock wave and periodic structure

07 p1190 A69-18695

Auger and photoelectron spectroscopy for chemical analysis, noting effects of sample thickness, sample potential, surface contamination and X ray incident angle

07 p1075 A69-19775

Shock heated helium plasma temperature measurements by spectroscopy compared to Rankine-Hugoniot calculations including ionization effect

09 p1548 A69-21963

Coherent detection spectroscopy with laser oscillator, emphasizing high resolution and applications in astronomical spectroscopy and IR

10 p1696 A69-23684

Spectroscopy application to spontaneous combination scattering of light

12 p2108 A69-26618

Stimulated emission of cerium trifluoride-positive trivalent Nd ion laser noting absorption, luminescence, excitation, emission spectra and metastable state lifetime

14 p2460 A69-29645

Remote sensing cross-beam cross correlation methods of determining spatially resolved average thermodynamic properties [AIAA PAPER 67-149]

16 p2789 A69-31868

Level crossing signal obtained by magnetic/electric field modulation, tabulating corrections to widths and centers for distortions

17 p3009 A69-34155

Quantum transitions between molecular or atomic energy levels noting microwave spectroscopy utilization

18 p3099 A69-35405

SPECTRUM ANALYSIS

Power spectral indices of March 6, 1968 solar radio burst, suggesting Razin effect

01 p0148 A69-10054

Hydrogen content effect on relaxation spectrum of alpha titanium, using nondestructive tests

01 p0096 A69-10614

Copper exploding wire Kerr-cell time-resolved absorption spectra analysis, considering copper atom transition

01 p0118 A69-10665

Perhydroxyl radical electron spin resonance spectrum in solution of hydrogen peroxide and water at 77 K, noting g factor, hyperfine splitting and molecular structure

01 p0024 A69-10683

Rapid scanning Fabry-Perot spectrometers, considering time resolution, wavelength resolution, wavelength interval size, aperture diameter and limitations of mechanical components

01 p0082 A69-10837

Laser beam spectra for modulation by electrooptic Doppler shift, considering sawtooth and triangular functions for applied electric field

01 p0091 A69-10843

Ionized calcium lines in spectra of light bridges of sunspots, observed by diffraction spectroscopy, indicating similarity to chromospheric flares

01 p0154 A69-10894

Spectral parameters of VLF radio noise given as functions of azimuth from atmospheric analyzer observations

01 p0033 A69-10971

Numerical filtering procedures for gust spectrum analyses compared for gain and phase lag frequency response characteristics, discussing gust acceleration spectra

01 p0084 A69-11052

Inner Van Allen belt proton dose rate and spectral charged particle environment profiles correlated, noting agreement with theoretical values

01 p0145 A69-11081

Automatic spectroelectrophotometer for measuring sky spectral brightness at 6910-4040 angstroms, determining point of minimum brightness

01 p0074 A69-11187

Atmosphere spectral transparency and stability spectrophotometric studies based on measuring solar aureole brightness

01 p0074 A69-11188

Time compression system with ultrasonic diffraction cell allows coherent light optical spectrum analyzer to function at audio frequencies

01 p0035 A69-11283

Nitrous oxide absorptance, deriving analytical expressions for transmission spectra

02 p0236 A69-11452

Eight color narrow band photometry of bright stars, discussing band system, instrumentation, data and calibration

02 p0313 A69-11487

Soviet book on spectral, spatial and time characteristics of lasers covering luminescence and resonator theories, electromagnetic field structure and radiation dispersion

02 p0255 A69-11800

Absorption oscillator strengths of Ba 2 lines in UV and visible spectral regions, using cascade arc in argon with barium vapor

02 p0242 A69-11872

Spectral measurements for matrix isolated lithium fluoride extended into far IR to obtain evidence for linear lithium fluoride dimer

02 p0205 A69-12465

Short laser radiation pulses spectral characteristics determination with device converting laser emission frequency by nonlinear electro-optical crystals

02 p0257 A69-12560

Automatic determination of relaxation and retardation spectra for linearly viscoelastic materials from experimental data using simple numerical techniques

02 p0348 A69-12605

High resolution spectroscopic study of stimulated rotational transitions of nitrogen molecules using crossed grating Echelle spectrograph

02 p0284 A69-12621

Stress and heat flux cospectra estimation using Busch-Panofsky observations

02 p0276 A69-12698

Type 4 bursts mobile spectrum of september 14, 1966 interpreted by considering plasma effects on synchrotron emission mechanism

02 p0309 A69-12754

Solar atmosphere from two dimensional study of solar spectrum, discussing satellite observations of corona and upper chromosphere

02 p0329 A69-12785

Procedure and apparatus for integral microwave and X ray and spectral measurements of quasi-steady plasma radiation

03 p0473 A69-12897

Fraunhofer lines in solar spectrum in 2950-8770 Å wavelength region, noting 8000 additional unidentified lines

03 p0507 A69-13170

Line identification methods in solar extreme UV and X ray regions

03 p0507 A69-13171

Spectral line identification in quasars, noting emission lines characteristic of emission nebulae and absorption lines of stellar atmospheres

03 p0508 A69-13173

Growth curve for analysis of stellar spectra, determining relative f values and abundance

03 p0508 A69-13174

F values for Ti II, Cr II and Fe II by empirical astrophysical line strength analysis, discussing f value determination from stellar growth curve

03 p0508 A69-13175

Stellar image and spectrum distortions during occultation observed from satellite, discussing recovery of atmospheric composition data from stellar spectra

03 p0421 A69-13346

Shock waves luminescence temperature dependence measured by UV and visible radiation, noting dependence on front glow duration

03 p0415 A69-13411

Bolide fireball radiation maximum efficiency from observed spectra, using monochromatic radiation efficiency data for rarefied atoms and ions in meteor comas

03 p0512 A69-13692

Bound excitons spectra in CdS, semiconductor band structure and tabulating positions of lines identified with excitons

03 p0488 A69-13784

Spectrum analysis of pulse signals by point to point measurements of magnitude and phase of pulse-like time functions, using narrow band filter output

03 p0399 A69-13939

Revision of RGU photometry fundamental data, noting main sequence curve position of O-B5 and distinction between zero age main sequence and class V

03 p0514 A69-13963

HF gas discharges, discussing plasma temperature and density, plasmoid length and spectroscopic applications

03 p0482 A69-14217

Mossbauer spectra of shocked and unshocked iron meteorite and fayalite
03 p0517 A69-14231

Photographic recording to produce spatial analog of temporal Fourier spectrum of astronomical source used for distinguishing weak periodic signal from background signal
04 p0556 A69-14294

Meteor spectrum from 1966 Leonid shower considered to be closer to comet nucleus spectra than previous spectra
04 p0655 A69-14664

Correlation function and spectrum analysis of passage of random noise and signal through multistage frequency multiplier
04 p0557 A69-14777

Nonadjustable Fabry-Perot scanning interferometer for gas laser spectra analysis, using barium titanate piezoceramic elements
04 p0598 A69-14854

Near earth atmospheric spectrum characteristics determined by analytical expressions for elementary signals in 2-30 kHz range
04 p0593 A69-15105

Nonattenuating signals spectra construction by means of generalized function method and Laplace transforms
04 p0583 A69-15134

Current nature on infinite cylindrical antenna in compressible anisotropic lossy plasma medium, noting characteristic waves on infinite cylinder
04 p0578 A69-15215

Fast Fourier transform, discussing algorithms for sampled Fourier spectra and FORTRAN programs
04 p0625 A69-15223

Spectral study of crystal lattice of gallium phosphides for influence of vacancies and impurities on band formation
04 p0643 A69-15258

Current carrier concentration temperature dependence in Te-doped silicon single crystals by analyzing photoconductivity spectra
04 p0644 A69-15267

Laser light scattering by plasma using theory of ionospheric scattering of radar signals, determining scattered spectrum
05 p0798 A69-15586

Crab Nebula and Cygnus XR-1 X ray spectra shown to have differential number power law spectra and same intensity
05 p0813 A69-15846

Spectra of close binary systems, analyzing abundance anomalies, noting metallicity results
05 p0822 A69-15854

Type 3 bursts spectra graphical representation, giving probable solar origin and curves of corona temperature
05 p0824 A69-16060

Bandwidth effect on wave recordings cross spectra interpretation from spatially separated sites, deriving relationship between propagation velocity and velocity bandwidth
05 p0756 A69-16272

Secondary particle spectra from proton-proton interactions analyzed in two temperature statistical model, considering momentum distributions
05 p0797 A69-16368

Ion temperature diurnal variations at 250-475 km obtained from Thomson scatter spectra
05 p0757 A69-16407

Frequency structure of pulse energy or pulsar intensity, emphasizing total energy density received per pulse
05 p0828 A69-16660

Spectrum of accelerated particles on surface of stars revealed by observation of photospheric lithium and beryllium
05 p0817 A69-16711

Atmospheric turbulence flight tests random data analysis to stimulate power spectra and transfer functions
05 p0767 A69-16756

Digital spectra analysis by Fourier transform and comb filter for determination of voltage and power spectra
05 p0722 A69-16762

Spectroscopy history from Newton to present, stressing need for standardized system of spectral classification
06 p0999 A69-16974

Single crystal InAs wafers reflection spectra from specular surfaces, obtaining direct interzone transition values and fine structure
06 p0979 A69-16995

Identification of emission lines from 3200 to 7000 Å in Eta Carinae spectrum, noting P Cygni-like absorption lines
06 p1002 A69-17263

Spectrum and amplitude fluctuations of laser light propagating through liquid helium, obtaining spatial correlation function of refractive index fluctuations
06 p0957 A69-17267

Cosmic radiation propagation in interstellar space, discussing differential kinetic energy spectra of protons, He, C and O nuclei and Fe
06 p0988 A69-17269

Spectra analysis of proton and He nuclei having different charge-to-mass ratios to obtain information on solar modulation and injection spectra
06 p0988 A69-17272

Mass motion in solar flares, discussing loop flares from emission line profile characteristics
06 p0993 A69-17429

Multichannel HF resolution spectral analyzer of pulses reflected from ionosphere applied to dependence of cross correlation coefficient on frequency separation
06 p0897 A69-17740

Long wave radio stations field intensity spectral analysis data evaluated to determine vertical ionospheric displacements at sunset and sunrise
06 p0922 A69-17752

Radio spectra analyzed for NGC 1052 and NGC 4278 elliptical galaxies, discussing 178 MHz flux density, anomalies and radiation absorption mechanisms
06 p1009 A69-17959

Spectral brightness of clouds and various terrains in visible and near IR regions measured from aircraft
06 p0953 A69-17991

Terrestrial and Martian aerosols estimation based on carbon dioxide spectral and Mariner 4 RF occultation measurements [AIAA PAPER 69-52]
06 p1011 A69-18199

Instrument profile of grating spectrograph determined by applying He-Ne laser mode separated in Fabry-Perot interferometer
07 p1131 A69-18405

InAs solid solutions reflection spectra with CdTe, CdS, CdSe and ZnTe compounds, determining conduction bands
07 p1198 A69-18511

Quasi-periodic variations of solar radio emission intensity related to solar activity variations
07 p1211 A69-18516

Dayglow determination from aerosol spectrum obtained through data of brightness and polarization of day sky
07 p1211 A69-18545

Spectroscopic binary 16 Piscium, showing unusual period of 47.25 days
07 p1214 A69-18662

Photoionization cross section measurements for sodium line by analyzing electron-ion recombination radiation from sodium seeded plasma, determining electron temperatures and concentrations
07 p1184 A69-19164

Hot gases optical properties based on real spectra, discussing radiative processes and cross sections calculation methods
07 p1185 A69-19166

Fe II lines relative intensities in eta Carinae spectrum, discussing possible intrinsic reddening of object and representation of visible and near IR continuum
07 p1217 A69-19253

Spectrum data of Nova Vulpeculae /1968/ summarized concerning dispersion figures
07 p1220 A69-19337

Spectrum of light scattered by particles suspended in turbulent fluid
07 p1157 A69-19417

Lines displacement in binary star spectrum due to blending, presenting graphs displaying magnitude of effect under various conditions
07 p1223 A69-19624

Radio spectrum of quasi-stellar object identified as Parkes 2134 plus 004
07 p1224 A69-19708

Emission spectrum analysis of faint solar prominences noting kinetic temperature, turbulent velocity and electron density
07 p1210 A69-19718

Plasma spectral line shifting and broadening under ion and electron impact
07 p1187 A69-19720

UV emission spectrum of double star Boss 1985, excitation potential effect on Fe II lines and table identifying emission lines
08 p1385 A69-20060

Electro-optical and magneto-optical effects in solids, noting high sensitivity and resolution in application to spectroscopic investigation of absolute spectra
08 p1371 A69-20217

Spectral distribution and energy of luminous radiation emitted during theta pinch in Ar plasma, noting energy maximum as function of pressure
08 p1362 A69-20280

Nine spectra of recurrent Nova T Pyxidis during fifth /1966/ outburst compared to previous outbursts
08 p1391 A69-20396

Transient response spectrum of nonlinear cubic spring mass system subjected to step function input, discussing viscous damping effects on peak response
08 p1413 A69-20402

Radio signal spectrum scattered at oscillating interface calculated in Kirchhoff approximation, determining scattering factors
08 p1275 A69-20432

Gas laser emission natural frequency fluctuations spectral density measured by auxiliary heterodyne laser
08 p1326 A69-20540

Emission spectrum of laser employing electron-vibrational transitions in samarium doped calcium fluoride crystal, noting spectrum shift with increasing crystal temperature
08 p1326 A69-20544

Rotating and oscillating magnetic neutron stars causing pulsars radio and optical signals, stressing UV line emissions theory
08 p1394 A69-20624

Cosmic ray negatron and positron spectra using balloon-borne magnetic spectrometer, obtaining absolute solar modulation of positron flux
08 p1380 A69-20728

Doublet structure suppression in mixtures of cesium and foreign gases, discussing absorption observations
08 p1356 A69-20736

Spectrum variations of type 4 radio burst as source rises through solar corona, determining electron density and magnetic field distributions in corona
08 p1380 A69-20775

Abundance determinations and spectrum intercomparisons in late type peculiar stars, discussing carbon and heavy metal star classes
08 p1403 A69-20910

IR photoconductivity spectra at surface of gold doped silicon, establishing monopolarity
08 p1373 A69-21073

Electronic optical system to process time-varying signals as optical spectrum analyzer for measuring power spectral density of input time function
08 p1317 A69-21086

Spectral study of Stokes vector for light scattered by natural objects, recommending phase and optical axis inclination angles for aircraft measurements
09 p1588 A69-21367

Correlated spectra of related sunspot number and solar 10.7 cm radiation component, noting variance for solar rotation periods
09 p1574 A69-21397

Differential brightness of night airglow spectrum, obtaining rotational temperature by comparison with synthetic spectra
09 p1488 A69-21656

Cross-spectral density of pressure induced on lifting surface by isotropic atmospheric turbulence, solving integral equation [ONERA-TP-681]
09 p1613 A69-21689

Vertical ionospheric motions near magnetic equator measured by Doppler shifts of incoherent scatter frequency spectra
09 p1489 A69-21704

Real configuration effect of magnetic field in moderately perturbed magnetosphere on whistlers dynamic spectra, stressing geomagnetic perturbation detection
09 p1490 A69-21766

High energy protons, helium and gamma rays observed by particle telescope on board OSO-C, obtaining integral rigidity spectra of proton and helium nuclei
09 p1579 A69-22172

Red autoionizing lines relative gf values for calcium measured by shock tube experiment
09 p1601 A69-22208

Pulsed RF spectra analyzer displays, noting responses to CW and pulsed signals and Fourier and pulsed repetition rate lines
09 p1460 A69-22791

Interplanetary magnetic fields characteristics and magnetic inhomogeneities spectra from cosmic ray variation studies used to obtain scattering mean free path
10 p1757 A69-22824

Optoelectronic spectrum analyzer with raster illuminator for producing two dimensional Fourier transform to analyze two dimensional functions
10 p1725 A69-23301

Transitions between heavy hole and spin orbit split bands in uniaxially stressed Ge and GaAs, noting spectra for various temperatures and valence band parameters
10 p1745 A69-23359

Atmospheric extinction function in Chile by using photoelectric spectrum scans, observing neutral component, Rayleigh scattering and ozone absorption variations
10 p1777 A69-23386

Soviet book on highly doped semiconductors covering energy spectrum analysis, kinetic effects, optical properties, fabrication and applications
10 p1746 A69-23522

Dynamic spectrum of July 7, 1966 proton flare, considering short wave fadeout at 0027 UT and intense burst of spectral Type 2
10 p1765 A69-23750

Discrete Fourier transforms, discrete linear filters and spectrum weighting for purpose of sidelobe reductions
10 p1666 A69-23888

Analytic investigation of spectrum of electrical signals induced by spherical defects in ferroprobe sensors
10 p1675 A69-24072

Power spectrum analysis of photometric observations of white dwarf stars for measuring variability of stellar luminosity
10 p1788 A69-24124

Nitrogen plasma total radiation intensity under pressure and at high temperatures calculated from radiation spectrum
11 p1922 A69-24231

Quasar and radio galaxy spectra obtained on Cassegrainian focusing diffraction spectroscopy
11 p1951 A69-24236

Flux densities and spectral indices of radio sources in 3C and 3CR catalogs, noting measurements at 86 MHz frequency
11 p1951 A69-24237

He I 10830 A line in beta Lyr shell observed by contact image converter tube, analyzing line structure and phase brightness
11 p1955 A69-24391

Brightness temperatures and spectra of Venus, Mars, Jupiter and moon measured from 8 to 14 microns by reflector and prismatic spectrometer
11 p1956 A69-24395

Venus albedo dependence on wavelength in UV spectrum between 4500 and 3200 A from reflector observations
11 p1957 A69-24406

Cepstrum/Fourier transform of log-spectrum of signal as model for prediction of perception of pitches in harmonic residue/ambiguity of pitch/
11 p1834 A69-24571

Power output and radiation spectra of trivalent Nd doped liquid lasers based on phosphoryl chloride with tin and titanium chlorides
11 p1894 A69-24620

Dwell time of sample particles in plasma excitation zone, noting effect on spectral analysis of sample materials injected into spark discharge plasma
11 p1926 A69-24624

Monograph on method and results of measurements of mobilities spectrum ion density and conductivity in upper troposphere and stratosphere
11 p1877 A69-24636

Real time Fourier spectroscopic system for synthesis of spectrum of interferogram, noting polystyrene IR transmission spectra
11 p1884 A69-24837

Spectrum space-time characteristics of electrically produced plasma discharges magnetically compressed to discharge tube wall, using spectrochromograph and spectrographs
11 p1927 A69-25217

Balloon-borne IR spectrometry to study atmospheric nitric acid vapor compared with absorption by ozone and methane
11 p1879 A69-25407

Solar X ray bursts analyzed by dynamic spectra based on time history of intensity of bursts
11 p1951 A69-25419

Free emission spectrum analysis of ruby laser with external mirrors and elimination of axial mode discrimination
11 p1900 A69-25547

Recombination emission spectrum relation to plasma recombination coefficient, determining plasma electron temperature from continuous spectrum intensity
11 p1934 A69-25566

Lunar far side surface spectral inhomogeneities in UV from Zond 3 measurements
12 p2154 A69-25817

Calculated UV spectra of solar radiation reflected from atmosphere compared with satellites photometric measurements, attributing radiation intensity distribution asymmetries to seasonal dependence of ozone content
12 p2064 A69-25952

IR absorption spectrum of Br-doped n-CdTe specimen, considering donor level transfer mechanism
12 p2142 A69-25979

Emission spectrum of ruby laser as function of relative orientation of resonator and active crystal axes, noting spectrum width
12 p2104 A69-26029

High speed streak camera for recording fast processes, noting changeability from optical to UV spectral range
12 p2085 A69-26155

Spectrum analysis of Jupiter atmospheric composition, obtaining abundances of minor constituents
12 p2155 A69-26205

Physical parameters and chemical composition of DD Lac atmosphere from spectral analysis
12 p2156 A69-26219

Element contents of supergiant HD 190603 at atmosphere based on spectrophotometric analysis including temperatures, turbulent velocity, gravity acceleration and electron concentration
12 p2157 A69-26336

Amplitude spectra of periodic pulse sequences or pseudonoise sequences calculated using weighting and shape functions
12 p2030 A69-26389

Photometric and colorimetric characteristics of hot gas optically thin in continuous spectrum with optical thickness of several units in Balmer series lines
12 p2159 A69-26667

Primary cosmic ray energy spectrum studies during 11-year cycle based on changes in intensity at various altitudes
12 p2149 A69-26682

Spectral model used for analysis of atmospheric turbulence as related to loads on gliders
12 p2127 A69-26931

High pressure arc discharge diagnostics with spectroscopic method relating spectral profiles to central temperature, pressure and temperature distribution
12 p2094 A69-26968

Multispectral and calibrated Alaskan Arctic aerial survey of sea ice, thaw lakes and polygonal soils
12 p2075 A69-26996

Successive explosions produced two gas systems observed in six Seyfert galaxy nuclei by spectrophotometry, using diffraction spectrographs
12 p2164 A69-27022

Colorimetric studies of galaxies exhibiting red shift with increasing radial distance from center
12 p2164 A69-27025

Blue, UV and yellow spectral observations of M 82 (NGC 3034), obtaining polarization dependence on reciprocal of wavelength, polarization and color characteristics
12 p2169 A69-27057

Spectral criterion for distinguishing mode locked and nonmode locked laser signals
13 p2270 A69-27197

LF spectral analysis of flowing water pressure pulsations behind single bulge on hydrodynamic channel smooth wall at low disturbance level
13 p2246 A69-27535

LF spectrum analysis of hydrodynamic flow near-wall pressure pulsations over rough surfaced wall
13 p2246 A69-27537

Oscillator strengths and wavelengths of X ray and EUV transitions in highly ionized iron line spectra
13 p2326 A69-27554

NGC 4194 galaxy emission line spectrum analysis showing presence of highly excited gas in nucleus and in bright central region similar to NGC 7714
13 p2339 A69-27571

Dynamic Michelson interferometer equipped with Ge detector to obtain spectra of airglow from 1.2-1.6 microns
13 p2252 A69-27587

Venus carbon dioxide spectral band analysis methods, discussing spectral lines and rotational temperatures obtained
13 p2344 A69-27649

VLF morning and evening magnetosphere emission distinction by studying spectrum width as function of variations in K index
13 p2253 A69-27740

GaS, GaSe and InSe crystals band structure from analyzing reflection spectra, noting sensitivity to visible, IR and hard radiation
13 p2317 A69-27883

Active medium temperature effect on semiconductor laser emission spectra composition, discussing amplification coefficient frequency dependence at various temperatures
13 p2271 A69-27888

Fluctuations in electric field induced by plasma flow in constant magnetic field, performing spectral analysis of voltage and current fluctuations in plasma
13 p2310 A69-28029

GaAs photoelectric emission at different activation degrees by adsorbed Cs and BaO layers, noting spectral response characteristics differences and causes
14 p2504 A69-28993

Sco-Cen B stars radial velocities, determining spectroscopic binaries
14 p2519 A69-29136

Spectral analysis of O and Ti based on O extraction, using Ni tank in A atmosphere with DC arc
14 p2446 A69-29158

Passive Q switch laser single pulse formation time and spectral width using balance equations
14 p2458 A69-29166

Oscillation spectrum with harmonic phase or frequency modulation, analyzing structural dependence on initial phase
14 p2412 A69-29427

Quasi-linear approximation for spectrum analysis of LF plasma wave oscillations in steady electric field
14 p2492 A69-29468

Supergiant HD-33579 in Magellanic cloud by model atmospheres, discussing abundances
14 p2529 A69-29979

Residual phase term influence on compressed signal shape, analyzing linearly frequency modulated signal spectrum and sidelobe suppression in pulsed radar
15 p2564 A69-30143

Nonadjustable Fabry-Perot scanning interferometer for gas laser spectra analysis, using barium titanate piezoceramic elements
15 p2608 A69-30246

Short laser radiation pulses spectral characteristics determination with device converting laser emission frequency by nonlinear electro-optical crystals
15 p2633 A69-30257

Design and efficiency for signal-time compressors of spectral analyzers using electron beam tubes with charge storage
15 p2576 A69-30351

Comet Ikeya-Seki tail spectra from nebular spectrograph, tabulating energy distribution in comet tail, noting similarity to solar spectrum
15 p2685 A69-30524

Radio source W 43 distance determined from analyzing neutral H line profile and radial velocity in excited H line 104 alpha
15 p2687 A69-30543

Ca XV spectrum in vacuum UV under laboratory conditions, discussing fine structure of ground level of Ca XV and coronal lines
15 p2688 A69-30553

Atmospheric transmission functions dependences on absorbing material, pressure and temperature in 15 micron band of carbon dioxide, introducing corrections
15 p2597 A69-30653

Spin doublet formation analysis in X ray satellite spectra, revealing K, L and M spin doublets existence
15 p2675 A69-30700

Ruby laser lasing modes spectral time dependence attributed to population inversion inertia responsible for mode competition
15 p2633 A69-30725

Power spectrum analyzer of weak periodic signal obscured by white noise by zero interactions count of signal and noise mixture
15 p2579 A69-30945

Optimal parameters of cuvette for use with helium-neon laser as excitation source to record combination light scattering spectra of powdery materials
15 p2635 A69-31105

Universal transfer function computer based on synchronous spectrum analyzer having outputs combined in cross spectrum correlation computer to yield plot in Bode form
15 p2615 A69-31282

Carbon atoms presence in Venus upper atmosphere from Venus spectrum obtained by Aerobee rocket experiment

15 p2698 A69-31341

Lyrid and Perseid meteor spectra for spectral line identifications in 3100-4000 Å UV range, listing lines from six neutral atoms and five ions

15 p2700 A69-31500

Induction period of reactions behind incident shock waves traveling through undiluted high temperature CO and molecular oxygen mixtures, using CO flame spectra

16 p2877 A69-31768

Atmospheric IR spectra determination from transmission functions overlapping effects of atmospheric gases

16 p2814 A69-31792

Gas laser application to magnetospectroscopy of graphite, Bi, As and pyrolytic graphite single crystals

16 p2796 A69-31822

Vertical ozone distribution from emission and absorption in 9.6 µ band determined during IGY in Switzerland

16 p2785 A69-32625

Luminescence spectra of aromatic polymers, monomers and dimers under high energy electron excitation using molecular resonance model

16 p2828 A69-32792

Hyperfine spectrum analysis of NaCl at low field using molecular beam electric resonance method, discussing Hamiltonian function representation

16 p2815 A69-32794

Cloud scattering corrections added to synthetic spectrum analysis of carbon dioxide bands and water vapor line in Venus spectrum

17 p3032 A69-33161

Acoustic spectrum averager for Mariner spacecraft environmental tests, calculating rms average 1/3 octave spectrum bands in real time [JPL-TR-32-1442]

17 p2946 A69-33658

13 color narrow band photometry of 1000 bright stars in tubular form, discussing sample points, Balmer discontinuity, absolute energy calibration, etc

17 p3038 A69-33692

Homology within solar flare associated type 2 radio events from dynamic spectra

17 p3024 A69-33803

Power spectral analysis of chromospheric inhomogeneities in July 1967 and June 1968, tabulating mean heights of formation in solar atmosphere

17 p3040 A69-33811

Numerical solution of boundary value problems, discussing spectral domain and scattering matrix formalisms

17 p2929 A69-33882

Compressed signal spectral analyzer resolving power, discussing dynamic amplitude range influence and weighting functions role

17 p2939 A69-33906

Resolving power of spectral analyzer with in-phase storage increased by weighted signal treatment

17 p2931 A69-33908

Spectral analyzer for structural noise spectrum of scanning ray TV transmitter

17 p2939 A69-33909

Absolute gf values for Fe I and Fe II lines between 3190 and 3315 Å measured by spectral absorption through shock heated gas containing Fe

18 p3175 A69-34304

Spectral study of Stokes vector for light scattered by natural objects, recommending phase and optical axis inclination angles for aircraft measurements

18 p3198 A69-34756

Radio sources spectrum measurement results at cm wavelengths in tabular form, noting flux density relationship to frequency

18 p3200 A69-35132

Discrete radio sources spectra at decametric wavelengths, showing variation with frequency and radio wave generation mechanism leading to various spectral types

18 p3200 A69-35134

Jupiter decametric radio source analysis suggesting two component model of rotation at both constant and variable rotational periods

18 p3202 A69-35212

Solar cycle line in horizontal force of earth magnetic field resolved by power spectrum analysis suggesting 80 year cycle

18 p3205 A69-35414

Random vibrations in linear systems during spectral and correlation analysis, noting nonlinear systems

18 p3227 A69-35491

Multidimensional discrete control systems for spectral characteristics of random processes in vibrational and fatigue strength testing of machines and equipment

19 p3286 A69-35890

Object discrimination based on IR spectral differences, reviewing calibrated radiometers, relative spectrometers and imaging sensors

19 p3373 A69-36056

Celestial spectra forbidden lines tabulated by element and ionization stages, describing laboratory spectrum analysis programs

19 p3421 A69-36212

M8 electron temperature and internal kinematics from photoelectric Fabry-Perot spectrometric recording of H alpha line profiles and N II

19 p3424 A69-36334

High index frequency modulated waveform spectrum analysis including upper bound on approximation error to avoid fallacy of Woodward theorem [IEEE PAPER 68-TP-74-COM]

19 p3276 A69-36485

Spectrum of axial modes of laser with inhomogeneous longitudinal pumping, dividing parameter space into steady emission regions

19 p3339 A69-36880

Spectrum measurement of He-Ne laser by Fabry-Perot interferometer, determining mirrors flatness

20 p3536 A69-36945

Vibration phenomena analysis by transfer function computer, discussing precision spectrum analyzers

20 p3498 A69-37003

Book on linear digital filtering and discrete spectrum analysis, emphasizing frequency domain description of signals and systems

20 p3487 A69-37146

Relative displacement spectra analysis illustrating shock spectra errors, comparing real system response with simple single degree of freedom system response

20 p3548 A69-37301

Energy level NMR spectral analysis for spin systems with sets of magnetically nonequivalent chemical-shift equivalent nuclei

20 p3579 A69-37348

WY Gem star spectroscopic observation showing peculiarity about forbidden and absorption spectra superposition

20 p3598 A69-37464

HD 200775 spectrum analyzed for absorption lines wavelengths and equivalent widths, noting role for NGC 7023

20 p3599 A69-37469

Zeta Tauri shell spectrum radial velocity measurement results compared with extrapolated seven year curve by Delplace

20 p3599 A69-37471

Solar and geomagnetic activity persistence by variance spectrum analysis, noting sunspot numbers and radiation flux autocorrelation functions

20 p3601 A69-37508

Solar rare earth abundances determined from high resolution tracings of solar spectrum, comparing results with nucleosynthesis theories

20 p3602 A69-37539

Spectral calculation deformations and errors estimation using Blackman-Tukey spectral formulas

20 p3571 A69-37697

Type 3 bursts spectra graphical representation, giving probable solar origin and curves of corona temperature

20 p3591 A69-37970

Periodicities in solar activity variation from correlation spectral analysis, establishing monotonically decreasing component and secular variations in activity

20 p3607 A69-38045

Radio source flux density values in revised 3C catalog determining spectrum, discussing effects of relativistic electron energy distribution, self absorption and spatial distribution

20 p3609 A69-38138

LF spectral analysis of flowing water pressure pulsations behind single bulge on hydrodynamic channel smooth wall at low disturbance level

20 p3518 A69-38202

LF spectrum analysis of hydrodynamic flow near-wall pressure pulsations over rough surfaced wall

20 p3518 A69-38203

Revised solar iron abundance by photospheric Fe I lines analysis using Garz and Kock f values, noting influence on solar photospheric model

21 p3796 A69-38475

Solar Na D lines analysis by direct inversion of line source function, finding Doppler core dependence on frequency

21 p3796 A69-38479

Spectrum, latitude dependence and diurnal variation of night airglow emission, noting space and time correlation and magnetic activity relationship to luminous intensity

21 p3711 A69-38514

Spectra and intensities of rocket releases for upper atmosphere composition, temperature and reaction kinetics, noting chemiluminescence and atomic and molecular emissions

21 p3712 A69-38522

Multispectral radiometric analysis of ERTS images, discussing image registration, SNR and atmospheric and diffraction effects

21 p3721 A69-38627

M 82 direct photographs sequence observation in optical IR region, noting small nucleus and unbroadened inclined emission lines

21 p3799 A69-38649

Argon ion laser single frequency output spectrum characteristics

21 p3738 A69-39140

Active medium temperature effect on semiconductor laser emission spectra composition, discussing amplification coefficient frequency dependence at various temperatures

21 p3738 A69-39146

Earth-pole wobble /1951-1966/ by spectral analysis using least square fit method

21 p3716 A69-39244

Solid metal oxide particles temperature in premixed flames determined from intensity/ wavelength plots of continua

21 p3852 A69-39592

Critique of Shivanandan suggestion of background radiation spectrum distortions

21 p3815 A69-39612

Catalog of reflection nebulae with known dimensions and flux characteristics noting spectrum characteristics

21 p3816 A69-39722

Fourier spectrum analysis of solar line oscillation sequences, discussing power spectra and lifetime of oscillation phase

22 p4019 A69-40286

Splash and return albedo electrons in cosmic ray electron spectrum between 12 Mev-1 Gev measured by high altitude balloon flight

22 p4005 A69-40510

Spectral characteristics of structured areas of luminosity in polar cap region, reporting spatial and time variations plotted from NASA airborne survey

22 p3940 A69-40522

Jupiter spectrum observations in 2.8-14 micron range, describing absorption strength and brightness temperature, basing analysis on ammonia, methane and hydrogen absorption

22 p4028 A69-40662

Quasar association with galactic clusters, noting red shift and spectral correspondence

22 p4029 A69-40763

Random processes integration and differentiation and spectral density determination, examining Markov, Gaussian and point processes

22 p3975 A69-40777

Agricultural and forestry applications of tethered balloons, discussing observation angle effect on spectral signature response and signal preprocessing

22 p4053 A69-40805

Glass filter systems for aerial color photography developed from spectral studies of sunlight, skylight and airlight in Rayleigh atmosphere

22 p3948 A69-40986

Multispectral processing of Apollo 6 earth photograph, evaluating geologic, vegetative and cultural features from red, green and blue portions of visible spectrum

22 p3941 A69-40987

Cosmos 137 proton spectra data obtained in inner radiation belt agreeing with Relay 1 data

22 p4007 A69-41093

Sensors array to determine propagation wave vector velocity via high resolution frequency wavenumber spectrum analysis, emphasizing seismic applications

22 p3902 A69-41220

Heat resistant materials integral and spectral radiative properties in IR and visible regions determined by calorimetry and IR spectrometer

23 p4237 A69-41329

Autoionized resonance transitions of He at 206.2-192.2 Å using He continuum produced by capillary spark, also producing He II line spectra

23 p4191 A69-42149

Carbon monoxide presence in Martian atmosphere from Mars line spectra, giving content, surface pressure and concentration

23 p4220 A69-42379

Blue component of HD 237006 and VV Cephei spectra, suggesting greater luminosity of blue star in late type supergiant

24 p4387 A69-43353

Solar flares accompanied X ray emission temporal and spectral variations, showing departure from thermal equilibrium

24 p4371 A69-43608

Total solar eclipse of 5 February 1962 observed for spectrophotometry of flash spectrum, finding abnormal intensity gradients of H alpha and D3 lines

24 p4388 A69-43636

Thermally scanned Fabry-Perot interferometer in flat-flat resonator configuration, featuring high transmission and large usable apertures, used for spectral analysis

24 p4329 A69-43757

He I 10830 A line in beta Lyr shell observed by contact image converter tube, analyzing line structure and phase brightness

24 p4390 A69-43781

Brightness temperatures and spectra of Venus, Mars, Jupiter and moon measured from 8 to 14 microns by reflector and prismatic spectrometer

24 p4390 A69-43785

Venus albedo dependence on wavelength in UV spectrum between 4500 and 3200 A from reflector observations

24 p4391 A69-43796

Rotational microwave spectrum of 2-methylfuran, using fourth order perturbation method for internal rotation A-E doublet splittings

24 p4280 A69-43811

SPECULAR REFLECTION

Specular component of ionospherically reflected radio waves between antenna array elements measured for statistical variations

01 p0032 A69-10968

Electromagnetic theory of surface radiation properties, analyzing specular reflectance of optically smooth surfaces

04 p0684 A69-14357

Single crystal InAs wafers reflection spectra from specular surfaces, obtaining direct interzone transition values and fine structure

06 p0979 A69-16995

Specular reflection computer program utilizing virtual image technique to determine reflection characteristics of enclosed diffusely emitting surface [AIAA PAPER 69-65]

06 p1040 A69-18215

Diffuse reflection of monochromatic radiation by semiinfinite plane layer in case of isotropic scattering, reducing problem to power series

11 p1960 A69-24732

Angular distribution of electrons leaving plasma at electrode boundary, using kinetic Boltzmann equation with scattering function and specular reflection

11 p1933 A69-25546

Specularly vs diffusely reflecting cylinders for cavity type sources of approximately black body radiant energy, noting ray tracing of cones

12 p2130 A69-26245

Light diffusive reflection from rough surface measured as function of angle of incidence in presence of specular component by goniospectrophotometer

14 p2485 A69-29171

Earth radar studies, relating echo behavior to rocket altitude and surface electrical characteristics

14 p2416 A69-29531

Cauchy system for reflection and transmission functions of finite isotropically scattering atmospheres with specular reflectors, noting use for ozone and cloud heights measurements

15 p2597 A69-31152

Radiant heat transfer predictions between isothermal plates based on diffuse plus specular directional property model [AIAA PAPER 69-624]

17 p3070 A69-33259

ATS 3 satellite reflectometer experiment carrying test samples to measure specular reflectance, noting silica shield effects [AIAA PAPER 69-644]

17 p3071 A69-33270

Coherent light scattering from rough surface, studying effects of target tilt, translation and rotation on speckle patterns produced

18 p3174 A69-35281

Remote sensors geometrical optics, considering power flow direction, specular reflection, imaging and dihedral in case of specular reflectors, reflection and diffraction

20 p3577 A69-37744

Parametric excitation theory involving Langmuir and ion-acoustic waves for homogeneous plasma slab with specular particle reflection at slab walls

20 p3582 A69-38245

Meter and decimeter wavelength range short period fading under conditions excluding optical sights, correlating specular and diffuse reflection

24 p4281 A69-42612

SPEECH

NT ARTICULATION
NT PHONETICS

Recorded vocal reactions of humans analyzed as characteristic of positive and negative emotions

05 p0709 A69-16518

Digitally controlled formant /spectral maximum/ generator for terminal analog speech synthesizer

11 p1852 A69-25292

Recorded vocal reactions of humans analyzed as characteristic of positive and negative emotions

18 p3096 A69-34737

Group leadership attempting behavior dependence on situational and perceptual variables

23 p4110 A69-42015

SPEECH DEFECTS

Retarded voice tests apparatus using graphical recording to determine intensity of deformations by autoaudition, considering application to recruitment investigation

24 p4270 A69-42604

SPEECH RECOGNITION

Limited speech recognition system /LISPER/ simplifies recognition by computer designed as research vehicle and pattern recognition system

04 p0565 A69-15338

Oxygen-helium cabin atmosphere effect on speech communication analyzed during simulated space mission

07 p1066 A69-19420

Speech intelligibility in air at ground level and in helium-oxygen mixture at 18,000 ft

12 p2019 A69-26548

He speech processor for aerospace applications, discussing He speech distortion nature

17 p2911 A69-34095

Machine recognition of continuous speech at acoustic level, noting low bit rate speech communication system

17 p2932 A69-34119

Aircraft noise acceptability tests based on listening in absence and presence of speech

18 p3097 A69-34325

Transmission filter to improve voice communication intelligibility and SNR, describing applications to nonlinear circuits

20 p3505 A69-37293

Automatic speech recognition and tracking techniques of moving objects, considering applicability to processing data from earth resources satellites

21 p3721 A69-38630

Speech interference aspects of noise measured as function of level and spectrum of speech and noise at listener ear, using simplifying nomogram

23 p4101 A69-41495

Whispered vowels pitch perception test using listen-and-compare method to determine formants for comparison with complex analysis procedure

23 p4190 A69-41575

Commercial aircraft peak cockpit noise level during cruise and high speed descent, discussing damage risk criteria and interplot speech interference

23 p4102 A69-41682

Brain and machine model of pattern recognition, pattern synthesis, memory, learning and speech, using concept of similarity, context and signal analysis

24 p4273 A69-42909

SPEED BRAKES

U BRAKES [FOR ARRESTING MOTION]

SPEED CONTROL

MOS technology developments for higher speeds in logic circuits

07 p1113 A69-19765

Fluidic overspeed sensor for small turboshaft power turbine, discussing requirements, circuit and system design, packaging, reliability and maintainability [ASME PAPER 69-GT-17]

09 p1571 A69-22500

Transistorized tachometer for rotational speed measurement and overspeed protection of automotive internal combustion engines

12 p2090 A69-26240

Hall generator DC brushless motors for aerospace use, discussing speed control and motor design

18 p3094 A69-35074

V/STOL wind tunnel data at low forward speeds, discussing test limit dependence on model size, downwash angle and tunnel geometry

18 p3119 A69-35229

SPEED INDICATORS

NT ANEMOMETERS
NT HOT-WIRE ANEMOMETERS
NT SONIC ANEMOMETERS
NT TACHOMETERS

Slide wire aircraft vertical velocity meter for application during aerogravimetric mapping, discussing calibration and gravitational force measurement accuracy

03 p0429 A69-13261

Boundary shear stress with unknown magnitude and direction measured by yaw probe used as Preston tube

05 p0751 A69-16396

Skin friction measurement with rectangular mouthed Preston tubes of constant thickness ratio, analyzing calibration curves and difference from circular tubes

11 p1880 A69-24376

Connecting duct influence on slide wire vertical airspeed indicator operating on barometric principle during aerial gravimetric surveying

13 p2260 A69-27828

Supersonic Preston tube correlations for Mach number and Reynolds number effects on hypersonic turbulent skin friction on adiabatic surfaces, simplifying correlation [AIAA PAPER 69-345]

13 p2249 A69-28280

Preston probe measurement of friction drag on subsonic and supersonic nozzle wall including effects of heat transfer, compressibility and pressure gradient [AIAA PAPER 69-648]

17 p2893 A69-33496

Reentry Vehicle Altitude-Velocity Sensor for continuously measuring hypersonic vehicles free stream density and velocity in atmosphere at low angle of attack [AIAA PAPER 69-866]

21 p3725 A69-39392

SPEED REGULATORS

Flow control valve for hydraulic motor speed regulation operated by remote pressure signal

11 p1827 A69-25646

SPEEDOMETERS

U SPEED INDICATORS

SPERMATOCYTES

U GAMETOCYTES

SPERMATOZOA

Axial units with basal plates in spermatozoa of Chlamydomonas negatively stained with phosphotungstic acid, showing doublet microtubules

07 p1066 A69-19263

SPHERES

NT CELESTIAL SPHERE
NT POINCARÉ SPHERES
NT ROTATING SPHERES

Radiation from isothermal sphere in vacuum having spherical scattering indicatrix solved by Bubnov-Galerkin method with allowance for scattering

01 p0174 A69-10106

Effect of steady flow of incompressible conducting fluid on magnetic dipole at center of sphere

01 p0128 A69-10363

Wake structure behind spherical bodies in rarefied plasma flow by measuring plasma parameters and disturbances with probes

01 p0134 A69-11308

Luminous flow in front of sphere and behind cylinder under high temperature and low density conditions, discussing profiles of shock waves

02 p0189 A69-12182

Heat transfer rates from high temperature spheres into subcooled liquid sodium during forced convection, noting surface vapor formation [ASME PAPER 67-WA/HT-32]

02 p0351 A69-12202

Heat transfer coefficient for spherical protuberance on plate with turbulent boundary layer [ASME PAPER 68-HT-2]

02 p0351 A69-12204

Boundary conditions for irrotational hydrodynamic field around sphere moving along axis of cylindrical tube containing incompressible fluid calculated by least squares method

03 p0415 A69-13362

Electromagnetic wave diffraction at uniformly expanding sphere solved by Kirchhoff method

03 p0397 A69-13719

Scattering data for optical diagnostic measurements on two component suspensions or gases, using random distributions of spheres

04 p0555 A69-14282

Rarefied flow past sphere, analyzing collisionless flowfield structure and development as density increases

04 p0542 A69-14731

Acoustic streaming near small spherical obstacles, obtaining stream functions

04 p0631 A69-14904

Free convective heat transfer in liquid filled spherical volume with constant thermal flux density at boundary
04 p0686 A69-14992

Relativistic analysis of far zone electromagnetic scattering by conducting sphere moving through incident plane wave, calculating scattering cross section
04 p0559 A69-15212

Velocities, accelerations and drag forces on spheres falling along center line in viscous fluid, considering different Reynolds numbers and Stokes approximation range
05 p0788 A69-15725

Energy transfer from radiating sphere to medium with molecular heat conduction
05 p0845 A69-15782

Nonequilibrium supersonic flow calculation of detonating mixture past blunt bodies applied to flow of hydrogen-oxygen mixture past sphere
06 p0859 A69-17343

Drag coefficients for spheres and sharp cones in rarefied hypersonic air flow obtained in shock tunnel using free flight technique
[AIAA PAPER 69-140] 06 p0865 A69-18184

Electron bombardment ion source generated Ar plasma beam to study wakes of disks and spheres, considering plasma interaction with bodies
[AIAA PAPER 69-79] 06 p0865 A69-18200

Laminar boundary layer flow on sphere in hypersonic flow of equilibrium dissociating air
07 p1050 A69-18756

Viscous gravitating sphere oscillations and velocity field, noting oscillations of Maxwell sphere
07 p1123 A69-18806

HF scattering of scalar plane wave by transparent sphere based on Watson transformation
07 p1181 A69-19033

Small amplitude surface irregularities effect on backscattering properties of radar calibration metal sphere, using full wave boundary perturbation method
08 p1273 A69-20027

Beam wave scattering by small sphere, discussing dielectric constant and difference from plane wave
08 p1273 A69-20028

Ray path geometry derived by Poynting vector to calculate surface fields due to creeping waves in sphere planes
08 p1274 A69-20046

Stress fields in Hertzian contact of parallel cylinders composed of anisotropic materials and transversely isotropic spherical bodies
08 p1414 A69-20524

Inertia of electrically charged spherical body calculated on basis of relativistic stress energy
08 p1352 A69-20756

Viscoelastic properties of heterogeneous media of composite sphere model type obtained from shear modulus formula
08 p1417 A69-20825

Self gravitating incompressible fluid sphere free oscillations, deriving characteristic equations for arbitrary viscosities
09 p1481 A69-21790

Diffraction of plane electromagnetic wave incident on conducting sphere segment, deriving secondary electromagnetic field equations in geometrical optics approximation
11 p1846 A69-24613

Pressure distribution measurement over sphere with cylindrical afterbody in magnetofluid dynamic flow, showing drag decrease at large magnetic field
11 p1873 A69-25136

Thin spherical layer flow stability with respect to small disturbances, showing unsteady motion above critical Reynolds numbers and secondary flow features
11 p1875 A69-25486

Transverse pulsating motion of spherical particle in turbulent flow, considering differential equation of motion transformation
11 p1876 A69-25489

Acoustic streaming near small spherical obstacles, obtaining stream functions
12 p2131 A69-26657

Radial and polar load support of squeeze film gas bearing in form of sphere pulsating radially or moving along polar axis
[ASME PAPER 68-LUBS-3] 13 p2266 A69-27279

Unsteady temperature distribution in solid sphere with variable internal heat source and surface subjected to variable heat flux
13 p2373 A69-27773

Differential approximation for radiative transfer between concentric spheres enclosing gray gas
[ASME PAPER 68-HT-21] 13 p2373 A69-27774

Radiative transfer between two concentric gray opaque spheres separated by radiating gray gas, employing Fredholm equations
13 p2377 A69-28149

Hypervelocity impact of spheres on thin targets studied with numerical solutions utilizing STEEP code two dimensional technique based on hydrodynamic elastoplastic model
[AIAA PAPER 69-357] 13 p2366 A69-28290

Dissipative fluid sphere motion due to impulsive point source calculated by finite difference scheme, assuming Voigt and Maxwell type internal friction mechanisms limitations
14 p2485 A69-29026

Subroutines for computing characteristics of electromagnetic radiation scattered by absorbing and homogeneous sphere employing logarithmic derivative method
14 p2412 A69-29283

Aerodynamic lift and moment fluctuations of sphere at supercritical Reynolds numbers measured by hot-wire anemometers, noting dependence on time
14 p2390 A69-29573

Near free molecule heat transfer and density distribution between concentric spheres using BGK model equation and Knudsen iteration technique
16 p2877 A69-31921

Temperature distribution of solid spherical satellite under solar radiant heating solved by variational calculus or point matching methods
16 p2877 A69-31922

Diffraction of electromagnetic waves produced by vertical dipole on impedance sphere of large radius in isotropic medium, using moment method
16 p2751 A69-32028

Water bag spherically symmetrical universe model, discussing system stability, distribution function representation and polytrope equivalency
16 p2866 A69-32813

Shock detachment distance for flow around cylinders and spheres determined by microphotometric tracing of negatives of photographs of forward stagnation streamlines
17 p2949 A69-32962

Elastohydrodynamic theory of spherical bodies in normal approach contact, discussing lubrication and elasticity equations
[ASME PAPER 69-LUBS-3] 18 p3213 A69-34384

Transient uniform flow over sphere at intermediate Reynolds numbers with recirculatory wakes, utilizing difference approximation to time dependent Navier-Stokes equations
18 p3120 A69-34434

Aerodynamic characteristics of sphere and blunt cone in highly rarefied gas flow, noting molecular collision effect
18 p3086 A69-34708

Electromagnetic induction in concentric thin shell-enclosed solid conducting sphere immersed in varying electromagnetic field
[AFRL-69-0082] 18 p3101 A69-34803

Energy transfer from radiating sphere to medium with molecular heat conduction
18 p3230 A69-35034

Temperature distribution around radiating sphere in homogeneous gas medium with molecular heat transfer, solving energy transport equation
18 p3231 A69-35325

Nonequilibrium behavior of shock standoff distance ahead of spheres at low supersonic Mach number
18 p3089 A69-35385

Ablating sphere viscous wake using image converter camera, computing luminance radial distribution by unit volume
19 p3306 A69-35739

Linear oscillations of sphere in compressible viscous fluid with slip at surface, noting drag variation
19 p3297 A69-35836

Plane electromagnetic wave diffraction on conducting sphere situated in absorbing nonuniform plasma layer
19 p3275 A69-36340

Shock wave interaction and bow shock wave establishment near sphere in presence of ionization relaxation, using time resolved schlieren photography
19 p3450 A69-36361

Axial stagnation point flow in shock wave reflected from sphere or circular cylinder, determining velocity time variation, enthalpy pressure and reflection
19 p3298 A69-36385

Hydrodynamic vertical or horizontal impact of sphere immersed in ideal heavy liquid of finite depth, considering container floor effect, surface pressure distribution, etc
19 p3299 A69-36393

Numerical integration of atmospheric motion equations in global domain using hexagonal grid, including sphericity corrections and Coriolis term
19 p3364 A69-36509

Combustible mixtures flow past bodies, discussing equation for shock polar for exothermal discontinuities at subsonic and supersonic velocities
19 p3241 A69-36780

Incompressible viscous fluid flow past sphere at low Reynolds number, evaluating stream function and drag on sphere
21 p3694 A69-38771

Spheres impulsive starting in incompressible viscous fluid, including Reynolds number and investigation time parameters in Navier-Stokes equation
21 p3696 A69-39296

Heat transfer from spheres in free finite width flow, determining heat transfer coefficient distribution as function of flow width and Reynolds number
21 p3855 A69-39849

Radiative transfer in interior of two concentric spheres in motion assuming low density of residual gas
22 p4031 A69-40907

Hypersonic reentry spheres drag coefficients derived from radar measurements
23 p4059 A69-41898

Spheroidal disturbances theoretical seismograms on surface of gravitating elastic sphere with homogeneous mantle and liquid core, considering gravity and polar radial stress effects
23 p4158 A69-42020

Sphere set in motion at constant velocity by impulsive force submerged in incompressible fluid in half space
24 p4298 A69-42585

Stokes stream function and forces acting on two spheres moving in contact along line of centers through viscous fluid
24 p4299 A69-42747

Fluid flow around sphere at high Reynolds number by measuring pressure distribution, considering boundary layer separation, tunnel blockage, etc
[ASME PAPER 69-APMW-26] 24 p4245 A69-43093

Hydrogen-air combustion in supersonic flow past sphere determined with allowance for chemical reactions nonequilibrium rates at high pressure and temperature
24 p4408 A69-43488

Diffuse configuration factors between small plane and large sphere by unit sphere method, presenting limiting cases
24 p4351 A69-43683

SPHERICAL CAPS

Spherical caps axisymmetric static and dynamic buckling under load, using axisymmetric nonlinear elastic shell theory approximation and finite difference equations
[AIAA PAPER 69-89] 06 p1028 A69-18133

Axisymmetric vibration of shallow spherical caps, using nonlinear dynamic equations and associated variational equation of motion for elastic spherical shells
[ASME PAPER 69-APMW-6] 24 p4402 A69-43107

Scale error correction technique for structural impact modeling using dissimilar materials, involving permanent deformation of spherical caps impacted into liquids
24 p4406 A69-43692

SPHERICAL HARMONICS

Algorithm computing spherical harmonic coefficients for eccentric geomagnetic dipole potential
02 p0245 A69-12735

Satellite orbit selection for determining geopotential and spherical and tesseral harmonic coefficients, discussing propulsion systems and satellite observation cost feasibility
02 p0331 A69-12807

Planetary distribution of ionospheric parameters analyzed, using geographic longitude and magnetic inclination as longitudinal and latitudinal coordinates
06 p0921 A69-17745

Spherical harmonic analysis of Stokes parameters for polarization of stars, discussing magnetic field of Galaxy
08 p1390 A69-20390

Time harmonic, spherical harmonic and power series expansion of Boltzmann equation
08 p1353 A69-20793

Radar SEP /spherical error probable/ for defining error ellipsoid in three dimensional accuracy and CEP /circular error probable/ for defining two dimensional accuracy
13 p2221 A69-27963

SPHERICAL SHELLS

Geomagnetic normal fields determination using spherical harmonic analysis, including extension to local fields

14 p2437 A69-29063

Kinetic energy conversion into heat in moving viscous media, formulating equations as volume integrals of spherical harmonics products

14 p2487 A69-29980

Large scale atmospheric wave motions analyzed by spherical harmonic representation of height fields over earth, detailing wave components and quasi-stationary fluctuations

15 p2647 A69-30216

Geopotential determination from gravity force measurements at known surface and error assessment for earth model with aid of spherical harmonic expansion

15 p2689 A69-30567

Coefficients of zonal spherical harmonics to 21st order in expression for earth gravitational potential

15 p2600 A69-31358

Arbitrary electromagnetic field prediction based on spherical harmonics expansion method using field points measurement data, determining electromagnetic properties of environments

17 p2929 A69-33881

Geomagnetic field lines coordinates calculation based on coefficients obtained in spherical harmonic analysis

20 p3522 A69-37060

Geomagnetic field spherical analysis from angular data and extrapolated values of time variable field coefficient

23 p4157 A69-41866

Geomagnetic multipole parameters changes using spherical harmonic coefficients of geomagnetic potential, relating to secular variation field

23 p4158 A69-42171

SPHERICAL SHELLS

Stress concentration near eccentric elliptical hole in spherical shell, using computer methods

01 p0165 A69-10089

Basic equations for optimum inhomogeneity in pressure vessels of maximum rigidity derived, using thick walled spherical shell

01 p0167 A69-10326

Spherical shell pressure vessels investigated for optimum inhomogeneity and rigidity using Lagrange polynomials

01 p0167 A69-10327

Predeformations of thin walled elastic isotropic spherical shells analyzed using Vlasov shell bending theory

02 p0336 A69-11555

Complex revolution vessels and multilobed structures analyzed by electronic computers, considering doubly stressed state of shells and bending moments from external forces

02 p0339 A69-11894

Plane shock wave interaction with elastic shallow spherical shell in compressible fluid, formulating equations of motion

02 p0339 A69-11977

Anomalous gravitational geopotential as function of mass, discussing density anomalies in spherical shells for harmonics as obtained from satellite observations

02 p0244 A69-12178

Postbuckling behavior of elastic spherical shells from pressure and volume-displacement instrumentation and photography

03 p0524 A69-13062

Solid viscosities effects on dynamic load factors of ring and hollow sphere subject to uniformly distributed impulsive loads along inner and outer edges

03 p0530 A69-14089

Kirchhoff-Love hypothesis error dependence on stressed state variability index in theory of elasticity for closed spherical shell under uniform surface load

04 p0680 A69-14927

Creep buckling of shallow geometrically nonlinear spherical shell of linear viscoelastic material under constant external load

05 p0831 A69-15679

Axisymmetric thermal stresses in spheroidal shell of arbitrary thickness due to thermoelastic strain nucleus

05 p0836 A69-15923

Stability of Al-Mg alloy spherical shells under uniform external pressure beyond elastic limit

05 p0843 A69-16693

Stress distribution in shallow spherical shell with smooth cornered rectangular hole or biperiodically arranged set of holes, using computer program

06 p1027 A69-18020

Supercritical elastic states of closed spherical shell

07 p1232 A69-18934

Gravitational field in static spherical shell of matter in vacuum, deducing exact junction conditions for thin shell

07 p1182 A69-19453

Traveling waves on elastic spherical shells derived from dynamic equations of motion, including transverse shear and rotatory inertia effects

07 p1236 A69-19460

Dynamic internal thermal shock in spherical shells of arbitrary thickness, considering uncoupled dynamic thermoelasticity problems with spherically symmetrical temperature fields

07 p1236 A69-19471

Shallow spherical shells equilibrium under uniformly distributed internal pressure, analyzing nonlinear boundary value problems by algorithm

07 p1237 A69-19685

Radiative transfer iteration for gray medium between concentric spheres and for constant heat generating spherical region imbedded in gray medium

08 p1420 A69-20152

Free vibration frequencies and mode shapes for thin orthotropic oblate spheroidal shells, noting isotropic oblate spheroidal shell and isotropic spherical shell

09 p1613 A69-21719

Axisymmetric dynamic snap through critical load analysis for elastic clamped shallow spherical shells, considering impulsive and step loads

09 p1616 A69-21977

Rectangular planform shallow spherical shell stability with mixed boundary conditions, using Cauchy-Riemann equations and equation for plate on elastic base

10 p1792 A69-22848

Short memory elasticoviscous fluid motion in and around oscillating spherical shell

10 p1800 A69-23240

Formula in Prandtl-Batchelor theory describing motion of incompressible fluid in sphere interior verified experimentally

11 p1868 A69-24755

Static and dynamic stability of flexible shallow spherical shell under axisymmetric load and elastically hinged along contours

11 p1976 A69-24763

Permanent displacement relationship to shell thickness following snap-through of loaded rigid boss in spherical metal shell

11 p1980 A69-24822

Plastic analysis of shallow spherical rigid plastic shell, using shell deflection equations to establish load-deflection relationship

11 p1980 A69-24823

Stress concentration around curvilinear holes in three layer spherical and cylindrical isotropic shells with hard and soft fillers under external loads

11 p1984 A69-25171

Axisymmetric oscillations of two spherical shells with noncoinciding centers of curvature immersed in compressible or incompressible fluids

11 p1875 A69-25467

Free periods of oscillation of incompressible rotating fluid bounded by rigid concentric spheres, using Longuet-Higgins solution of Laplace tidal equation

11 p1876 A69-25558

Axisymmetric deformation of thin orthotropic laminar spherical shells under internal loads calculated on computer using Legendre polynomials

12 p2181 A69-26611

Elastic buckling and initial postbuckling behavior of clamped shallow spherical shells under axisymmetric load

12 p2187 A69-26842

Monograph on shell calculations by linear three dimensional elasticity theory, relating displacements and stresses

12 p2188 A69-26902

Axisymmetric plastic buckling of complete spherical shells subjected to external hydrostatic pressure

13 p2361 A69-27439

Frequency equation for thickness effects on axisymmetric radial and rotatory vibrations of empty or fluid filled isotropic spherical shell

13 p2363 A69-28185

Differential equations for shallow circular spherical shell transformation to equation describing stress-strain state of plate on elastic base

13 p2369 A69-28565

Stress concentration around holes in thin shells, including analysis of stress-strain state in cylindrical and spherical shells

14 p2532 A69-28977

Syntactic foam low density thermoplastic microspheres as hollow spherical filler in polyester matrix, noting applications

14 p2467 A69-29285

Spherical plate electrostatic analyzer transmission characteristics, emphasizing angular response to external particle sources as functions of angular coordinates and particle energy

14 p2449 A69-29560

Plane shock wave interaction with elastic shallow shell in compressible fluid, formulating equations of motion

15 p2704 A69-30262

Elastic deformations of spherical sandwich shell of rigidly connected isotropic homogeneous layers, describing shell symmetrical expansion and inversion under stresses

15 p2707 A69-30588

Stress distribution in isotropic spherical shell rotating uniformly about diametral axis, deriving equilibrium equations

15 p2712 A69-31005

Linear static deformation and buckling of shallow spherical shells under asymmetric load by solving two dimensional finite difference equations

16 p2871 A69-31897

Axially symmetric vibrations of thin elastic spherical shell partially filled with liquid, considering shell as joined hemispheres with or without same thickness

16 p2873 A69-32129

Elastic spheroidal shell of revolution under external pressure described by buckling and postbuckling theory

16 p2874 A69-32162

Transient wave processes of deformation in spherical shell under load abruptly applied to geometrical pole

16 p2875 A69-32288

Air density measurement at high altitudes by falling instrumented sphere ejected by missile in upper atmosphere

17 p2971 A69-32898

Fluid filled spherical shell axisymmetric nontorsional motion analysis via differential equations obtained by Hamilton principle

17 p3051 A69-32956

Plastic failure under internal pressure of aluminum spherical shells with single radial or oblique nozzle based on limit analysis theory

17 p3052 A69-32983

Random oscillations of elastoacoustic systems, obtaining solution for spherical shell containing acoustic medium

17 p3057 A69-33199

Complete spherical shells transverse frequency analysis, comparing results of elastic theory and classical, improved and membrane shell theories

17 p3061 A69-33705

Complete spherical shells nonsymmetric vibrations frequencies and mode shapes calculated by matrix method

17 p3061 A69-33706

Nonlinear partial differential equations solutions in theory of thin elastic spherical shells subjected to temperature fields and external loading

17 p3067 A69-34147

Stress field in elastic contact area vicinity of hollow sphere subjected to normal load through flat plate, noting contact life [ASME PAPER 69-LUBS-5]

18 p3212 A69-34383

Spherical shells axisymmetric equilibrium properties under uniformly distributed external compression

18 p3224 A69-35318

Limiting equilibrium of variable thickness shallow spherical and conical shells of revolution under axisymmetric loads, assuming rigid plastic shell material

18 p3225 A69-35370

Hollow thin walled carbon spheres developed as filler material for resins in low weight high temperature applications

19 p3355 A69-35522

Buckling and postbuckling of complete spherical shells with symmetric initial shape deviations and elastic deformations

19 p3446 A69-36834

Twisting of spherical shell of nonhomogeneous isotropic material with variable shear modulus and inner surface assumed to be stress free

20 p3619 A69-36911

Matrix displacement method of structural analysis applied to dynamic buckling of clamped shallow spherical caps under step pressure loading

20 p3622 A69-37229

Shells of revolution bearing capacity under axisymmetric loads determined by linear programming and finite difference method

20 p3622 A69-37326

Complex representation of strain and displacement state in spherical shell using membrane theory, deriving shear forces resulting from single moment loading
21 p3831 A69-38416

Stress concentration near holes in three layer spherical shells, determining boundary conditions at hole perimeters for various loads
21 p3833 A69-38570

Stress-strain state of thin spherical shell of variable thickness in elastoplastic equilibrium, using Meissner variables to reduce equilibrium equations
21 p3834 A69-38717

Thermal stability of reactive spherical shell, investigating spontaneous ignition of volatile fuel drop exposed to hot oxidizing environment
21 p3849 A69-38804

Stability of free and clamped spherical and circular cylindrical shells subjected to uniform or nonuniform heating, discussing effects of temperature stresses
21 p3838 A69-39190

General system of equations derived for nonaxisymmetric oscillations of elastic spherical shells, obtaining expressions for oscillations from torsion, tension and bending
21 p3839 A69-39199

Deformation of thin walled spherical shell reinforced with equatorial hoop by concentric equal forces
21 p3846 A69-39714

Momentless orthotropic spherical shell of variable thickness stress analyzed, assuming large deformations under uniform axisymmetric load distribution
22 p4039 A69-39916

Solid viscosities effects on dynamic load factors of hollow sphere subjected to uniformly distributed impulsive loads, using three element model
22 p4044 A69-40598

Differential rotation of incompressible inviscid fluid of infinite electrical conductivity in spherical shell, noting toroidal magnetic field for sun
22 p4027 A69-40658

Meridional crack problem for cylindrical and spherical shells solved for uniform membrane load and bending moment, obtaining stress intensity components
22 p4046 A69-41041

Conducting fluid flow in spherical container in rotating magnetic field, calculating induced field velocity and inside and outside components
23 p4196 A69-41609

Infinite systems of algebraic equations in periodic problems for spherical shells with circular holes approximated by reduction method
23 p4227 A69-41706

Supercritical elastic states of closed spherical shell
23 p4228 A69-41971

Stress concentration in shallow spherical perforated shell under loads, reducing boundary value problem to infinite algebraic equations solution
23 p4233 A69-42342

Dynamic response of anisotropic elastic cylindrical and spherical shells determined by application of Hankel transforms, considering time dependence of loads
23 p4235 A69-42481

Shallow spherical sandwich shells critical buckling loads using differential pressure method
24 p4396 A69-42734

Three dimensional and shell theory analysis of nonaxisymmetric harmonic elastic wave propagation in hollow elastic sphere
[ASME PAPER 69-APMW-7]
24 p4402 A69-43105

Computerized spectral analysis of vibrational frequency due to elastic waves in isotropic hollow spherical shells
[ASME PAPER 69-APMW-8]
24 p4402 A69-43106

Energy dissipation in oscillating sphere filled with viscous fluid, giving fluid response by solving Navier-Stokes equation
24 p4305 A69-43587

Transmission functions probabilistic model for solving radiative transfer problems in spherical shell medium surrounding emitting black core or point source, using integrodifferential equations
24 p4415 A69-43637

Plastic inhomogeneity effects on yield stress of isotropic spherical shell and long cylindrical tube under internal pressure
24 p4405 A69-43672

SPHERICAL TANKS

Spherical false bottom influence on propellant sloshing in circular tank
[DVL-843]
03 p0416 A69-13665

Ritz method for natural oscillations of ideal liquid in spherical vessel with various filling levels, considering vertical perturbing force
06 p0910 A69-17333

Natural frequencies and forms of small vibrations of ideal liquid in spherical container with weak force field, considering surface tension forces
11 p1875 A69-25484

Simulated low gravity propellant sloshing in spherical, ellipsoidal and cylindrical tanks, discussing Bond number simulation and tank geometry effects
[AIAA PAPER 69-1004]
22 p3921 A69-40378

Spherical vessel partially liquid-filled and supported by equatorial ring, studying axisymmetric oscillations under external forces
24 p4300 A69-43069

SPHERICAL WAVES

Spherical elastic-plastic stress wave propagation analysis via finite difference procedure
02 p0348 A69-12610

Rapid uniform expansion of spherical cavity in compressible elastic-plastic solid, obtaining similarity solution
03 p0528 A69-13798

Spherical wave reflection from nondeformable plane in elastic viscoplastic medium
03 p0528 A69-13926

Helicon waves in nonresistive cylindrical and spherical plasmas
03 p0479 A69-13961

Adiabatic motion of hydromagnetic fluid behind spherical fast shock wave for Parker solar wind model
04 p0660 A69-15126

Spherical deflagration and detonation waves in diluted stoichiometric hydrogen-oxygen mixtures in hemispherical combustion chamber
06 p1034 A69-17927

Proportionality between log-amplitude variance and 7/6 power of wavenumber for horizontal propagation from spherical wave transmitter to point detector
07 p1157 A69-19641

Cylindrical and spherical waves propagation in weakly inhomogeneous plasma treated by geometrical optics, noting caustic surfaces
07 p1195 A69-19747

Spherical wave generalization for plane light wave propagating in turbulent medium, describing circular objective averaging effect on intensity fluctuations
08 p1351 A69-20438

Unsteady flow parameters for reaction products behind spherical detonation wave in gas mixtures based on Taylor solution
08 p1421 A69-20765

Analytical method for perturbations by spherical and cylindrical shock waves flowing toward common center
10 p1677 A69-22899

Kinetic theory for spherical expansion of hypersonic jet flow indicating translational freezing in hypersonic source expansion
11 p1870 A69-25006

Spherical wave propagation in homogeneous turbulent medium, discussing nonstationary statistics as applied to vertical propagation in atmosphere
12 p2029 A69-26251

Spherical stress wave reflected from plane surface, discussing tensile stress in target
[AIAA PAPER 69-363]
13 p2366 A69-28295

Digital computers for aircraft engines control, discussing economic assessment, advantages and basic control system
15 p2671 A69-30323

Scintillation of ground based spherical wave laser source viewed from space analyzed from Geos 2 satellite laser tracking, noting stellar scintillation correspondence
15 p2570 A69-31309

Perturbation solutions for planar cylindrical and spherical blast waves in air, considering third and fourth order approximations
16 p2770 A69-31900

Reflection of spherical stress wave against smooth indeformable plane in elastoviscoplastic medium, discussing Taylor series expansions for displacement, velocity and stress fields
18 p3226 A69-35463

Radio wave sphericity influence on scattering at moving body wake in ionosphere, determining scattering cross section principal maximum
20 p3486 A69-37024

Perturbation solution in power and asymptotic series for initial collapse phases of impulsively generated converging cylindrical and spherical shock waves in perfect gas
21 p3692 A69-38688

Reflection of spherical stress wave against plane clamped partition in elastoviscoplastic medium, investigating three dimensional problem by infinitesimal deformations theory
24 p4406 A69-43732

SPHEROIDS

NT OBLATE SPHEROIDS
NT PROLATE SPHEROIDS

Mass functions of real earth derived from satellite orbital perturbations
[UN PAPER 68-95385]
01 p0064 A69-10460

Existence of periodic solutions by Whittaker criterion to equations describing motion of satellite of spheroidal planet in planetocentric coordinate system
02 p0317 A69-11959

Axisymmetric stress field around spheroidal inclusions and cavities in transversely isotropic material
[ASME PAPER 68-WA/APM-14]
04 p0669 A69-14400

Motion of two rigid spheroids with mutual gravitational attraction based on Hamilton-Jacobi theory applicable to binary stars
16 p2863 A69-32402

Small parameter method applied to axisymmetric problems of elastoplastic nearly spherical bodies undergoing exponential hardening process, deriving linearized expressions for boundary conditions
21 p3839 A69-39198

SPHERULES

NT SPHERULITES

Meteorite dust spherules at Tungusk and Sikhotealin falls investigated for mineral composition using X ray analysis
01 p0160 A69-11383

Lifetime of highly soluble isolated dense spherical solute particle in solvent, taking into account molecular diffusion, kinetic limitations, etc
10 p1651 A69-22939

Black magnetite spherules electromagnetically separated from residue of Permian rock salt, determining content and properties of extraterrestrial material
12 p2154 A69-25821

Barbados airborne dust collections showing metal fragments and black magnetic spherules contaminants from handling, discussing deep sea cosmic spherules and zodiacal cloud
12 p2075 A69-26964

Oxide composition of silicate spherules from forest area devastated by Tunguka meteorite explosion using electron microprobe analysis
14 p2516 A69-28869

Black magnetite bearing spherules extracted from tektites, and magnetic fractions of impact glasses, determined by reflecting microscope and electron microprobe
23 p4210 A69-41349

SPHERULITES

Spherulite boundaries and interspherulite breakdown in polyethylene, considering structure control by varying macromolecular microstructure
22 p3973 A69-40740

Pyroxene crystallization in meteoritic chondrules, noting normal spherulite crystallization
22 p4033 A69-41065

SPICULES

Solar flares and surges origin, discussing role of supergranular convection, field gradients and spicules
06 p0994 A69-17437

Three dimensional information pictures of chromospheric alpha H line using special camera attached to solar telescope diffraction grating spectrograph
07 p1217 A69-19241

Mercury transits in 1970 and 1973 to resolve prominence threads and spicules, sunspot fine structures, etc
11 p1958 A69-24434

Chromospheric spicules formation, density, pressure gradient, vertical motion, velocity fluctuations and luminosity
15 p2675 A69-30551

Solar chromospheric spicules acceleration mechanism based on magnetic field structure on supergranulation boundaries
24 p4374 A69-43635

SPIKE ANTENNAS

U MONOPOLE ANTENNAS

SPIKE POTENTIALS

Expected number of spikes of phase locked loop demodulators, extending determination method to FM discriminator threshold and maximum likelihood estimator
07 p1082 A69-19107

SPIKES

Optic nerve spikes elicited by acetylcholine application on isolated perfused retina of frog, varying response by prostigmine and atropine
23 p4084 A69-41465

SPIKES

High latitude ionization spikes observed by POGO spacecraft, noting frequency correlation with magnetic disturbances and development by high energy electron injections
14 p2511 A69-28950

Radiation dynamics of GaAs injection semiconductor laser, plotting spike period dependence on resonator length
19 p3337 A69-36535

Ruby laser resonator mirror mechanical vibrations effects on emission temporal behavior, spectral output and far field pattern, describing conditions for spiking
22 p3962 A69-40562

SPIKING

Spiking behavior detection in Q switched light output from GaAs pulsed junction laser, noting width at high pumping levels
22 p3963 A69-40563

SPIN

NT ELECTRON CAPTURE
NT ELECTRON SPIN
NT NUCLEAR SPIN
NT SPIN-ORBIT INTERACTIONS
NT SPIN-SPIN COUPLING

Spin doublet formation analysis in X ray satellite spectra, revealing K, L and M spin doublets existence
15 p2675 A69-30700

SPIN DYNAMICS

Multibody dual spin spacecraft spin axis motion with active internal devices, using digital simulation
02 p0332 A69-11739

Boom flutter effects on attitude dynamics of OV1-10 satellite, noting introduction of angular momentum by tip mass elliptical vibration
04 p0666 A69-15520

Whirl dynamics of partially liquid filled spinning rotor mounted on elastic shaft, noting synchronous critical speed and asynchronous whirl speed
[ASME PAPER 68-WA/APM-25]
05 p0768 A69-16189

Mass distribution and inertia characteristics influence on spin susceptibility and spin recovery characteristics for eight current fighter aircraft
[AIAA PAPER 69-188]
06 p0868 A69-18057

Anomalous roll behavior of spinning ballistic reentry vehicles with compound aerodynamic asymmetry consisting of lateral offset combined with trim angle of attack
[AIAA PAPER 69-103]
06 p1019 A69-18168

Variation in spinning velocity around axis of last stage of solid propellant rocket in flight
08 p1409 A69-20160

Dynamics of deployable space structures stiffened by centrifugal forces due to spin, discussing LF radio telescope
11 p1994 A69-25530

Monograph on rapid rotations of aircraft with fixed controls, covering spin and roll movements differential equations
12 p2013 A69-26118

Solar oblateness and differential rotation time development due to solar wind torque
12 p2157 A69-26308

Atomic and molecular spins dynamic orientation in anisotropic radiation field, examining medium properties and astrophysical consequences
13 p2350 A69-27861

Inverted spin testing techniques using jet trainer, emphasizing entry variations and effect on spin characteristics
14 p2392 A69-29696

Spin temperature of interstellar neutral hydrogen calculated from 21 cm absorption spectra line profiles
15 p2681 A69-30411

Theory of temperature dependent magnon energies in antiferromagnets based on spin wave operator expansion of Hamiltonian, taking into account dynamical interaction between waves
15 p2668 A69-30684

Moon possible origin, discussing spin off from earth, accretion from same dust cloud or formed elsewhere and captured
20 p3603 A69-37559

Celestial sphere scanning by passive method applicable to space missions requiring long lifetime and moderate pointing accuracies
[AIAA PAPER 68-854]
21 p3767 A69-39764

Linear field gravitation theories, discussing spin dynamics
22 p3979 A69-39976

Spin compensated state of localized magnetic impurity moment in space, calculating size range of magnetic impurity spin/conduction electron spin correlation function
22 p3983 A69-40061

Spinning satellite containing elastically restrained, viscously damped mass, analyzing attitude dynamics and stability, noting wide nutation possibility
23 p4224 A69-42396

Spin-phonon systems thermal noise, based on combined lattice and spin lattice Hamiltonian densities, applied to acoustic noise field measurements
24 p4350 A69-43061

SPIN-LATTICE RELAXATION

Multiphonon orbit-lattice relaxation of excited states of rare earth ions in crystals, measuring fluorescence lifetimes, quantum efficiencies and transition rates
01 p0134 A69-10011

Acoustic paramagnetic resonance in arsenic doped germanium, measuring spin-lattice relaxation
02 p0296 A69-11835

Phonon states effective density in neodymium trichloride from vibronic spectra accompanying electronic transitions in trivalent Pr and Nd ions
03 p0473 A69-13907

Proton spin-lattice relaxation time in dilute liquid and gas solutions of orthohydrogen in parahydrogen, noting dependence on temperature, density and composition
06 p0961 A69-17141

Cross relaxation and spin-lattice relaxation probabilities determination in ruby crystal based on inversion coefficients
06 p0980 A69-17458

Optical pumping at high temperatures using spin exchange signals for RF spectroscopy
07 p1148 A69-18893

Trivalent iron doped andalusite crystals dielectric and maser properties, investigating spin-lattice relaxation, cross relaxation times and inversion ratio
[IEEE PAPER C-2]
07 p1150 A69-19049

Relation between electron spin-spin interactions and polarization and relaxation of ruby nuclei at He temperatures
08 p1372 A69-20541

Cross relaxation and spin-lattice relaxation probabilities determination in ruby crystal based on inversion coefficients
20 p3584 A69-37941

SPIN-ORBIT INTERACTIONS

NT ELECTRON CAPTURE

Spin-other-orbit matrix elements for F super 3 electron configurations
06 p0962 A69-17819

Venus and Mercury diurnal period commensurability associated with Venus spin-orbit resonance with earth orbit
22 p4018 A69-40270

Natural orbitals calculated from spin free one density matrix of open shell limited configuration-interaction wave function constructed from nonorthogonal basis
23 p4194 A69-42206

SPIN REDUCTION

Design evolution of mechanically despun antenna systems from ATS to INTELSTAT, discussing RF and control systems
03 p0403 A69-13239

Mechanically and electronically despun spacecraft antennas, comparing designs and projected performances for spin stabilized Intelstat 3 satellite
06 p0897 A69-17590

Resonant spin and anomalous rotation of Mercury, analyzing influence of tidal degradation and permanent deformation of planet
21 p3814 A69-39568

Intelstat 3 communications satellite mechanically despun high gain directive antenna, discussing system, control electronics, design and performance
22 p3913 A69-40691

SPIN RESONANCE

Proton spin maser oscillator with emission coils coupled by prepolarized liquid, discussing tuning and detuning
08 p1324 A69-20231

Temperature dependence of g-value in spin resonance in partially degenerate region in pure n-type InSb and InAs
19 p3389 A69-36549

Venus and Mercury diurnal period commensurability associated with Venus spin-orbit resonance with earth orbit
22 p4018 A69-40270

Nonresonant and resonant cross sections for gamma ray transitions involving isobaric-spin mixed states in Be 8
22 p3987 A69-41043

Electron spin memory in optical pumping cycle of potassium halides F centers, measuring relaxed excited state g factors and spin resonance line widths
23 p4198 A69-42419

SPIN-SPIN COUPLING

Coupled waves in ferromagnetic and antiferromagnetic semiconductors in constant electric and magnetic fields, discussing spin, electromagnetic and plasma waves dispersion
05 p0809 A69-16548

Relation between electron spin-spin interactions and polarization and relaxation of ruby nuclei at He temperatures
08 p1372 A69-20541

Barrier to internal rotation from PMR spectrum for 1, 2-disubstituted ethanes, studying vicinal coupling parameters dependence
12 p2132 A69-25987

Electric quadrupole coupling for N 14 in aminedisulfonate studied by observation of second order transitions in electron spin resonance spectra
18 p3178 A69-35474

SPIN STABILIZATION

Mechanically despun VHF antenna for spin stabilized synchronous satellites, detailing electrical and mechanical design
01 p0161 A69-10350

Magnetic orientation and attitude control of spin stabilized satellites, synthesizing control circuits and calculating power requirements
03 p0521 A69-13644

Ground coverage of oblate planets by spin stabilized satellites, determining ground areas visible to satellite by solution of quadratic equations
03 p0522 A69-14244

Energy dissipation effects on attitude stability of dual-spin satellites with damping mechanism on rotating sections
04 p0665 A69-14703

Optimum stabilization of uniformly rotating axisymmetric satellite, using Liapunov theorem on asymptotic stability
04 p0666 A69-14921

Roll dynamics of spinning axisymmetric satellite in elliptical orbit, discussing eccentricity and gravity gradient torque effect
05 p0830 A69-16397

Attitude perturbations of spin stabilized satellite describing highly eccentric orbit
06 p1014 A69-17568

Nutational stability of multibody spin stabilized satellites, discussing moment of inertia ratios role with energy dissipative damper on despun platform
06 p1015 A69-17585

Damping flywheel to stabilize permanent rotation of weightless solid body moving by inertia, obtaining differential equations of motion
07 p1183 A69-19678

Counterrotating antenna for spin stabilized satellite, noting linear phase shift influence on radiation pattern
08 p1289 A69-20968

Electronically phased array antenna system design optimization and testing for application to spin stabilized satellites
08 p1289 A69-20969

Computer program for continuous attitude determination for spin stabilized OGO-C satellite after malfunction of attitude control system, calculating angle between high rate data periods
09 p1610 A69-21987

Harmonic balance procedure to study periodic motions in nonlinear stabilization system of nonrigid satellite
10 p1792 A69-24195

Dynamic modeling for spin stability of satellites with flexible parts, noting torques induced by attitude control
11 p1994 A69-25533

Parachute recovery system for spinning /250 rps/ 155 mm shell launched to 3000 ft/sec by 20,000 g acceleration
[AIAA PAPER 68-937]
12 p2014 A69-26805

Optimal stochastic controller synthesis theory applied to stabilizing and controlling orientation of rotating bodies in central gravitational fields
13 p2300 A69-28326

Linear dynamic stability of spinning satellite in elliptic orbit, applying perturbation method to determine Floquet solutions 14 p2534 A69-29318

Solar thermal vacuum test for space flight qualification of military spin stabilized synchronous orbit communications satellite 15 p2587 A69-30391

Dynamics of spin stabilized satellite with long crossed dipoles or slender beams, including linearized equations of motion 15 p2703 A69-31332

Sterilized solid propellant motors applicability to planetary landing capsule spin stabilization [AIAA PAPER 69-823] 16 p2840 A69-32675

Bearing system for mechanically despun antenna in spin stabilized communications satellite, offering greater directional stability, lower weight and power losses 17 p2978 A69-33431

Rotary power transformer design for spin stabilized spacecraft power system, discussing efficiency and advantages 17 p3050 A69-34111

Optimal nutation damping of spin stabilized bodies, using Pontryagin maximum principle to optimize time, consumption and linear time-consumption combination 18 p3208 A69-34774

Time and fuel optimization of angular momentum alignment and nutation elimination of spin stabilized bodies with inertial reference direction 18 p3208 A69-34775

Mechanics of missile dispersion due to dynamic unbalance and rocket spin stabilization problems [SAWE PAPER 741] 18 p3208 A69-34886

Moment of inertia measurements facility for spacecraft dynamic balancing operations at low angular rates [SAWE PAPER 739] 18 p3118 A69-34889

Lumped parameter simulation model, based on vector mechanics for flexible spinning bodies, to study spin stabilized spacecraft or turbine rotors 19 p3280 A69-35990

Spinning satellite attitude perturbations due to oscillating mass in satellite rigid frame, discussing analytical approach and analog simulation results 20 p3618 A69-37912

Acrodynamic pitch-roll coupling in spinning vehicles, showing unsteady components complicating data reduction 21 p3647 A69-39038

Ariol 3 satellite management structure, responsibilities and orbit, stabilization, launch window, data acquisition and processing 21 p3856 A69-39255

Stability conditions determination for spinning projectile based on ballistic equations, discussing role of Magnus effect 21 p3772 A69-39294

Reaction boom attitude control systems for improving stabilization and maneuvering capability of earth pointing satellites, describing configurations [AIAA PAPER 69-834] 21 p3822 A69-39365

Motion and stability characteristics of dual spin satellite system with pendulous type nutation dampers, noting mass unbalance effect [AIAA PAPER 69-857] 21 p3823 A69-39385

Dornier ASTRID attitude stabilization system design for spinning rocket nose cone with instrument payload, using first stage biaxial inertial platform and second stage star tracker 21 p3826 A69-39639

Equations of motion of elastic dumbbell satellite and two-mass spring-connected satellite in orbit, using energy and Floquet theory to investigate spinning motion stability 21 p3817 A69-39759

Fluid loop rotational kinetic energy dissipator reducing time required for reaching WRESAT 1 satellite spin stabilization axis 21 p3828 A69-39767

ATS 3 mechanically despun communications antenna, using parabolic cylindrical reflectors, in-line feed and vernier type stepping motor drive positioning 22 p3913 A69-40692

Multifunction lightweight antenna system package for spin stabilized near synchronous satellite having axis normal to orbital plane 22 p3913 A69-40694

Dynamic model of ablation pitching moment derivative and time lag effect on spinning reentry vehicle applied to Black Knight flight results 24 p4245 A69-43249

SPIN TESTS

Spin tests to determine brittle fracture under plane strain, using cyclic thermal stress or hydrostatic pressure to generate fatigue crack in rotor blank 03 p0524 A69-13060

Nonlinear theory for whirling of heavy string under constant axial tension; considering orbitally stable modes for eigenvalues of rotation 13 p2359 A69-27264

Circular membranes vibrational and stability characteristics under simultaneous constant spin and precessional motions, obtaining Hill equation for motion amplitude coefficients 13 p2370 A69-28665

Inverted spin testing techniques using jet trainer, emphasizing entry variations and effect on spin characteristics 14 p2392 A69-29696

SPIN WAVES
U MAGNONS

SPINACH

Deoxyribonucleic acid conformations in spinach leaf chloroplasts by electron microscopy 20 p3479 A69-38001

SPIINAL CORD
NT SPINE

Ejection seat cushion dynamic characteristics influence on incidence of spinal injury during ejection, considering MIL specification dynamic model of human body 17 p2917 A69-34033

Thermoregulatory responses to cooling in spinal man, discussing deep temperature sensitive structures and relationship between skin and central regulatory structures 22 p3873 A69-40209

Lobeline effect on oxygen pressure in gigantocellular nucleus of medulla oblongata and respiration rates of dogs recorded automatically 22 p3888 A69-41273

Temperature dependence of afferent and efferent spontaneous activity of spinal cord, using filament recordings from ventral and dorsal roots in anesthetized cats 23 p4093 A69-42066

Spinal cord temperature effect on stretch responses of muscle spindle endings of triceps surae, anterior tibialis and extensor digitorum longus in anesthetized cats 23 p4093 A69-42067

Spinal cord temperature influence on stretch response of tonic and phasic alpha-motoneurons by filament recordings from ventral roots in anesthetized cats 23 p4098 A69-42099

High intensity and short duration acceleration effects on human beings, discussing mechanical resistance of spinal column and circulatory aspects 24 p4266 A69-43380

SPINE

Viscoelastic rod model of human spine subjected to accelerations 07 p1072 A69-19725

Dynamic roentgenology of cervical spine noting ease of use in neutral profile, hyperflexion and hyperextension for aeronautical medicine 23 p4087 A69-41797

Military pilots cervical spine dynamic X ray studies, comparing spine curvature and rectitude of jet and nonjet pilots and nonflying personnel 23 p4087 A69-41798

SPINEL

Sulfospinels polymorphism at high temperature and pressure and pressure-temperature phase relations 02 p0266 A69-12162

Thin sections of ringwoodite natural spinel in Tenham meteorite shower, observing various rounded purple isotropic grains 09 p1597 A69-22155

Artificial aging effect on spinel structure and properties of ferrites using X ray analysis, neutron diffraction and electron microscopy 13 p2320 A69-27997

Chromium composites mechanical properties, studying effects of alloying with spinel and magnesium oxides 23 p4177 A69-41672

SPINNING UNGUIDED ROCKET TRAJECTORY

Angle of attack effect on motion throughout entry of spinning descending vehicle, noting effects of transverse angular velocity and spin rate 04 p0666 A69-15522

SPINOR GROUPS

Factorizability of Einstein field equations in two dimensional spinor formulation 03 p0468 A69-13759

Gravitational analog of Mariot-Robinson theorem, obtaining two related theorems with Newman-Penrose spinor formalism 11 p1919 A69-25097

Second rank Dirac spinors with invariant components relative to Lorentz group transformations 19 p3361 A69-36817

SPIRAL ANTENNAS

NT LOG SPIRAL ANTENNAS

Balanced symmetrical four arm conical equiangular spiral antenna providing omnidirectional circularly polarized radiation pattern in azimuthal plane 03 p0404 A69-13471

Anisotropically conducting spiral cone current phase distribution applied to frequency independent antennas analysis, discussing spiral motion and field azimuthal dependence effects 03 p0408 A69-14133

Radiation properties of spherical phased array of 16 flat spiral antennas and radiation field polarization characteristics 04 p0573 A69-14331

Space frequency filter antennas, using multiple terminals for signal processing as function of frequency and angle 08 p1290 A69-20977

SPIRAL GALAXIES

NT MILKY WAY GALAXY

Seyfert galaxies high excitation broad emission lines and quasars resemblance, discussing causes of spiral galaxies violent nuclear activity 04 p0657 A69-14689

Seyfert galaxies nuclear regions, noting multicolor photometric measurements between 0.3 and 1.6 micron and measurements of M87 jet at 1.55 micron 04 p0663 A69-15386

X ray emission from Seyfert galaxy nuclei, noting model with bremsstrahlung from hot source 04 p0649 A69-15387

Galactic model with differential rotation, discussing experiments on bar and cylindrical galaxy and spiral and loop structures formation 07 p1216 A69-19204

Novas in M 31 on Tautenburg Schmidt photographs 08 p1382 A69-19873

Radial distribution of H II regions in spiral galaxies, noting peak at 1/4 distance from center 08 p1384 A69-20052

Neutral hydrogen content and distribution of late type spiral galaxy NGC 6946 from 21 cm line measurements 09 p1598 A69-22187

Rotation and mass of Sb galaxy NGC 1832, giving central and mean densities 09 p1599 A69-22188

Density wave theory of galactic spirals, discussing hydrogen distribution, young star distribution, stellar migration, magnetic field structure, density waves in stellar formation, etc 10 p1786 A69-24109

Cyanogen band absorption in nuclei of elliptical and spiral galaxies derived from photoelectric measurements indicating rich metal content in central cores 12 p1553 A69-25803

Interstellar gas and dust clouds inclination to plane of M31 galaxy spiral arms 12 p2159 A69-26664

Galactic nuclei congeneric and coexisting peculiarities, including hot star planar formations in spiral galaxies 12 p2164 A69-27027

Spiral galaxy nuclei, relating nuclei luminosity to galactic luminosity 12 p2165 A69-27028

Spiral galaxies with connectors observed in Southern Hemisphere, noting galactic nuclei differences and nucleus relation to galaxy morphological type 12 p2165 A69-27030

Absolute radio luminosity relation to surface brightness of extragalactic radio sources, finding volume radiation coefficient of spiral and radio galaxies 12 p2166 A69-27035

Spiral galaxies rotation curve fluctuations attributed to kinematic properties of galactic matter and gas components 12 p2170 A69-27062

Gasdynamic phenomena during subsonic or supersonic motion of isothermal gas under action of gravita-

tional forces in flatten axisymmetric galaxy containing spiral density waves

12 p2170 A69-27065

Spiral arms as wakes of gravitational shock waves arising at galactic nucleus boundary and propagating outward through interstellar gas

12 p2170 A69-27066

Spectrum analysis of radio galaxy M82 nucleus, noting H alpha emission lines from analysis of IR photograph

13 p2335 A69-27310

Hydromagnetic stability of spiral arm embedded in gravitating medium from analysis of instability of self gravitating incompressible cylinder

13 p2346 A69-27705

Messier 51 ionized hydrogen observations, discussing H II regions, radial velocities and galactic mass, rotation and noncircular nuclear motions

13 p2347 A69-27720

Integral equation solved by successive approximation procedure for determining mass distribution in galaxies on radial velocity basis, applying to NGC 7331

13 p2353 A69-28325

Linear polarization of quasars, radio or normal spiral galaxies, galactic objects, etc, observed by Parkes telescope

14 p2526 A69-29770

Supernova in Sc type spiral M83, discussing supernovae occurrence frequency

15 p2682 A69-30451

Spiral density waves formation in galaxy model with differentially rotating and nonrotating subsystems based on collective interactions

15 p2688 A69-30550

Rotation curve, mass and M/L ratio of Sc galaxy NGC 6574, discussing nucleus and systemic velocity

15 p2691 A69-30764

Irregular dwarf galaxies as source of faint objects in close galactic groups

16 p2864 A69-32597

Variation influence of total absorption to color excess ratio on galactic spiral structures indicating ineffective application of variable-extinction method to Q spectra

18 p3199 A69-34914

Spiral disk galaxies stability analysis assuming centrifugal force balancing self gravitation, transforming linearized equations of motion into eigenvalue equations

18 p3200 A69-35131

Spiral galaxy linear diameter relation to luminosity applied to Virgo galactic clusters, noting effect on distance modulus and Hubble constant

19 p3427 A69-36652

Spiral arms interpreted and derived as consequences of galactic nuclei explosion

20 p3599 A69-37468

Photographic photometry investigation of Light distribution in spiral galaxies NGC 681, 972 and 1084, discussing mass distribution

20 p3599 A69-37476

Nonlinear effects in spiral galaxies with emphasis on solar neighborhood region, discussing radial motion, stationary state with excited waves and vertex deviation

20 p3607 A69-38036

Spectra of peculiar S zero galaxy NGC 7625 with irregular dust distribution, discussing central spheroid rotation and mass

20 p3610 A69-38142

Galaxy NGC 3593 with large amounts of interstellar dust, calculating galactic mass and central density

20 p3610 A69-38143

Interferogram observations of central velocity of M 31 under constant rotational velocity assumption, noting galaxy inclination

21 p3797 A69-38481

Galaxy model for spiral structure origin

21 p3797 A69-38537

H II regions radial velocities ellipsoidal distribution in M 33 explained as distribution with minor axis in direction of rotation

21 p3797 A69-38538

RF high resolution observations of edge on spiral galaxy NGC 4631, noting radio halo and spur absence, nonthermal radio emission region, etc

22 p4022 A69-40463

Radio observations of elliptical and spiral noncluster galaxies, noting correlation between magnitude and radio emission in elliptical galaxies

22 p4025 A69-40639

Radio studies of galactic structure, discussing Milky Way origin and formation

23 p4217 A69-42320

Spiral and irregular galaxies integral properties and relations, discussing optical and 21-cm observations, hydrogen masses, statistical corrections, hydrogen line optical depths, etc

23 p4220 A69-42383

OB stars near emission nebula RCW 103, describing galactic structure in Norma

23 p4220 A69-42384

High radial velocity gas cloud near Seyfert type galaxy NGC 4939 nucleus investigated spectroscopically

24 p4375 A69-42609

Circular arm with elliptical cross section used as magnetohydrodynamical model of helical magnetic field in spiral arms to demonstrate interstellar gas flow path

24 p4388 A69-43640

SPLASH POINTS

U RECOVERY ZONES

U WATER LANDING

SPLICING

Machine cutting tool for cutting and splicing endless magnetic tape 30 microns thick, noting film safety feature and nonmagnetic steel scissors

08 p1321 A69-20876

SPLITTING

Partial difference methods from parabolic, elliptic and hyperbolic equations solved by splittings of locally one dimensional nature

21 p3754 A69-38745

Gain modification from spectral splitting of polarization transition by incident light wave on higher frequency coupled transition

22 p3965 A69-41125

SPOILERS

Analytical model of spoiler generated sound in jet pipe, presenting data on level, spectrum and directivity of sound

07 p1183 A69-19462

Spoiler effect on aerodynamic characteristics of airfoil with hinged flap in inviscid fluid plane flow

15 p2549 A69-31223

Pressure distribution in two dimensional incompressible potential flow on Joukowski airfoils with normal upper surface spoilers, emphasizing potential flow theory

[AIAA PAPER 69-737] 18 p3083 A69-34402

DC-10 aircraft CF6 engine thrust reverser and spoiler design features impacting operational characteristics, maintainability, noise reduction, structural concept, control and actuation system

[SAE PAPER 690411] 23 p4200 A69-41639

SPONTANEOUS COMBUSTION

Diacetylene burning and spontaneous combustion regularities, determining reaction kinetics at moderate temperature

02 p0351 A69-11981

Slow oxidation and self ignition in gaseous phase, discussing cold flames and interpretation of experimental data

06 p1031 A69-17416

Chemical mechanism of two stage spontaneous ignition controlled by cool flames of alkane-air mixtures under engine conditions to avoid knocking

11 p1998 A69-24479

Spontaneous reignition predictions for solid restartable rocket motors with solid propellant combustion terminated by liquid quenching

[AIAA PAPER 69-444] 16 p2842 A69-32695

Self ignition of solid/fluid particles suspended in gas flow, discussing heat transfer coefficient, critical temperatures, etc

17 p3070 A69-33142

Thermal stability of reactive spherical shell, investigating spontaneous ignition of volatile fuel drop exposed to hot oxidizing environment

21 p3849 A69-38804

Pressure effects in spontaneous ignition of interimpinging hydrazine and red fuming nitric acid/RF-NA/ liquid streams in evacuated test chamber

24 p4415 A69-43667

SPONTANEOUS EMISSION

Nonlinear optical properties of barium sodium niobate in ferroelectric tetragonal phase above room temperature, noting spontaneous parametric emission

09 p1515 A69-21354

Quantum phase noise in He-Ne laser, considering amplitude fluctuation, spontaneous emission and oscillator linewidth

10 p1704 A69-23669

Spontaneous gas laser emission from level coupled by spontaneous transition with emitting level, obtaining

atoms interaction with laser field velocity distribution and spectral line width

17 p2981 A69-33116

Laser action and spontaneous emission at atomic oxygen transition, discussing pulsed emission mode in argon-oxygen laser

17 p2982 A69-33632

Laser action in quantum system, analyzing absorption constant relation to spontaneous/stimulated emission constants, energy level population inversion, pumping, etc

17 p2984 A69-34150

Pressure dependence of trapped spontaneous decay of resonant radiation carbon dioxide

18 p3179 A69-35471

Carbon dioxide lasers near IR spontaneous emission spectra

19 p3339 A69-36697

Afterglow decay rates of Zn II laser lines in spontaneous emission measured, indicating thermal energy charge exchange excitation and CW oscillation

21 p3735 A69-38598

Changes in CdS crystals spontaneous and coherent emissions caused by electron beam radiation damage, determining intensity and spectral composition dependence

21 p3780 A69-39047

Lasing properties of spontaneous emission hemispherical semiconductor diode with AlAs-GaAs junctions measured by calibrated silicon photocell

22 p3964 A69-40608

Anisotropic carrier distribution effect on polarization of spontaneous recombination radiation during GaAs breakdown in electric field

24 p4362 A69-43736

SPONTANEOUS IGNITION TEMPERATURE

U IGNITION TEMPERATURE

SPORADIC E LAYER

Sporadic E layer boundary frequencies disturbances at midlatitudes, noting solar activity effects, diurnal variations and effect of meteor fluxes

01 p0066 A69-10600

Temperate latitude sporadic E origin and structure - Conference, Vail, Colorado, June 1968

01 p0069 A69-11156

Gross behavior patterns of intense sporadic E including seasonal, diurnal and geographic variations and latitudinal and longitudinal effects

01 p0070 A69-11157

Morphological behavior of blanketing sporadic E at middle latitudes, discussing wind shear time variations, solar cycle variation and geomagnetic storm effects

01 p0070 A69-11158

Time and latitude variations of blanketing sporadic E of different intensities

01 p0070 A69-11159

Numerical maps of sporadic E critical frequency for solar cycle maximum and minimum to estimate propagation

01 p0070 A69-11160

Sporadic E layer structure observed by rocket borne probes relation to ground based radio techniques, showing agreement between plasma and blanketing frequencies

01 p0070 A69-11161

Blob existence in temperate latitude sporadic E from ionosonde and VHF oblique incidence measurements

01 p0070 A69-11162

Sporadic E microstructure and vertical motion, describing radio sounding system to observe ionospheric 3d structure and motions from ground

01 p0071 A69-11164

Nighttime sporadic E rocket measurements, discussing descending layer thickness and electron density and lower boundary

01 p0071 A69-11165

Sporadic E structure and composition measured above White Sands by rocket-borne planar ion trap and two RF ion mass spectrometers

01 p0071 A69-11166

Initial production of metallic gases associated with sporadic E layers by processes other than vaporization or photodissociation, discussing Na atom production mechanisms

01 p0071 A69-11167

Metal ionic reactions with weak chemical bond breaking and three body reactions forming molecular ions without bond breaking, discussing sporadic E deionization

01 p0071 A69-11168

Cause and structure of temperate latitude sporadic E - Conference, Vail, Colorado, June 1968, Volume 2

01 p0072 A69-11169

Midlatitude sporadic E layer, examining hypothesis of wind action on metallic ions and metallic ion accumulation caused by gravity waves

01 p0072 A69-11173

Sporadic E layer formation, considering ion convergence effects due to neutral wind shears and drift ionization due to electrostatic field

01 p0072 A69-11174

Neutral gas temperature variations effect on electron-ion temperature height profile in tidally generated sporadic E layer with wind shear of gravity wave origin

01 p0073 A69-11176

Midlatitude sporadic E layer vertical and horizontal structure and statistical properties, discussing theory of ion concentration by wind shear

01 p0073 A69-11177

Ionospheric sporadic E layer reflection duration during solar activity cycle analyzed as function of critical frequency

02 p0207 A69-11684

Sporadic E layer critical frequencies seasonal and diurnal periodic variations, noting independence of solar activity cycle

02 p0239 A69-11685

Nighttime sporadic E layer occurrence due to ionization redistribution established, noting concurrent F region electron concentration decrease

03 p0423 A69-13536

Absorption as factor influencing correlation between solar activity, sporadic E layer probability of occurrence and reflection stability

03 p0423 A69-13537

Radio wave absorption in ionosphere at five fixed frequencies for determining correlation with changes in sporadic E layer parameters

03 p0423 A69-13539

Sporadic E irregularities in producing amplitude variations in radio star observations and satellite transmission

04 p0594 A69-15125

Sporadic E layers compared with model of electron concentration profile, using rocket measured profile data for computing ionogram

06 p0922 A69-17750

Time and latitude variations of blanketing sporadic E using wind shear theory, predicting ionization layer formation in ionospheric E layer

07 p1125 A69-18840

Space-time variations for approximating sporadic E layer critical frequencies of geographic and time distribution curves

09 p1486 A69-21547

F2 layer diffusion and sporadic E layer characteristics from equatorial ionosphere soundings on Zaria schooner

09 p1486 A69-21548

Sporadic E region HF backscatter observed during IQSY, using PPI display

09 p1489 A69-21701

VHF satellite signal scintillation by ionospheric irregularities with sharp boundary /such as sporadic E/, noting diffraction pattern dependence on phase shift

09 p1489 A69-21713

Numerical decile value maps of sporadic E layer ionization critical frequency for each month of solar cycle minimum and maximum year

10 p1682 A69-23418

Diurnal variations in sporadic E layer and wind in ionosphere during equinox and solstice periods, noting wind shear mechanism and ambient electron density

10 p1688 A69-23932

Vertical probe observations of short radio waves propagation through sporadic E at various frequencies and path lengths

10 p1657 A69-23933

Polar cap sporadic E investigation with backscatter at 28 MHz, noting geographic distribution, annual and diurnal variations

12 p2069 A69-26464

Correlation coefficient between changes in F2 layer critical frequency and sporadic E layer maximum frequency

13 p2254 A69-28330

Ionospheric sporadic E layer reflection duration during solar activity cycle analyzed as function of critical frequency

13 p2224 A69-28715

Sporadic E layer critical frequencies seasonal and diurnal periodic variations, noting independence of solar activity cycle

13 p2258 A69-28716

Sporadic E layer cloud configuration study based on explorer 20 satellite observations, discussing W echoes

14 p2434 A69-28943

Position stability of ionospheric sporadic E layer

14 p2435 A69-29038

Vertical motion of ionized formations in ionospheric F region related to sporadic E layer

14 p2437 A69-29074

Electron and ion temperatures height variations in sporadic E layers, noting effects of neutral gas temperature changes

14 p2440 A69-29127

Efficiency parameter beta for ion and electron production by meteoritic processes, noting importance to nighttime sporadic E ionization

14 p2520 A69-29372

Sporadic E layer frequency characteristics dependence on reflected signal fading, showing fine structure influence and maximum value of mean electron concentration

14 p2442 A69-29733

Ionospheric sporadic E layer inhomogeneities drift, discussing altitude dependence of velocity and direction

14 p2444 A69-29869

Sporadic E layer nighttime electron density profiles obtained by Langmuir probe equipped sounding rockets

15 p2603 A69-31398

Charge density irregularities of midlatitude ionospheric E region related to cross field plasma instability noting turbulence

16 p2773 A69-31972

Low latitude sporadic E layer associated with geomagnetic activity studied in Hong Kong using proton precession magnetometer and standard ionosonde

16 p2779 A69-32195

Sporadic E ionization by rocket sounding, comparing positive ion density measurements with separate wind shear observations

16 p2780 A69-32310

Space-time variations for approximating sporadic E layer critical frequencies of geographic and time distribution curves

16 p2784 A69-32542

F2 layer diffusion and sporadic E layer characteristics from equatorial ionosphere soundings on Zaria schooner

16 p2784 A69-32543

Relationship between sporadic E and 5577 A nightglow emission attributable to ionization redistribution in E region due to dynamic processes

16 p2788 A69-32782

Latitude variations of day and night ionospheric critical frequencies, inhomogeneity and ionization, discussing generation of r type sporadic E layer in auroral zone

17 p2964 A69-33963

Reflection and ionization heights diurnal variations in F region, obtaining data for sporadic E formation

17 p2968 A69-33995

Diurnal sporadic E layer height variations analyzed for singularities in height peak behavior as function of geography, season and magnetic activity

17 p2968 A69-33996

Time dependent diffuse reflections related to solar activity, showing diffusion intensity variations with sporadic E layer height and electron concentration

17 p2968 A69-33997

Midday aurora oval and polar cap region airborne observation, noting relation to sporadic E layer

18 p3126 A69-34258

Frequency dependence of radio wave absorption in ionosphere at 2.2-4 MHz by impulse method, noting effect of sporadic layer

20 p3491 A69-37680

Sporadic E layer structure and behavior during solar cycle from vertical sounding, discussing semiopaque region, reflection multiplicity, active height, wind effects, etc

20 p3528 A69-37681

Sporadic E layer large scale irregularities direction and velocity determined by inclined backscatter method, using plan position indicator

20 p3528 A69-37682

Small scale inhomogeneities motions in E and sporadic E layers, processing data with method of full correlation analysis and statistical method

20 p3528 A69-37683

Ion layer separation in temperate-zone sporadic E, obtaining layer shape by superimposition of density distributions

20 p3535 A69-38106

Equatorial E sub sq and daytime blanketing sporadic E occurrence frequencies compared in magnetic equatorial zone, considering diurnal, seasonal, latitudinal and vertical variations

23 p4160 A69-42426

Daytime drift velocities and signal fading characteristics of equatorial and blanketing sporadic E layer irregularities, noting independence of electrojet intensity

23 p4160 A69-42429

Midlatitude sporadic E model, discussing overdense ionization layers spatial distribution, wind shear effects, periodic variations, etc

24 p4311 A69-43743

SPORADIC METEOROIDS

Diffuse meteor stream separation from sporadic background, using orbital elements of individual meteors

04 p0659 A69-15034

Sporadic background separation from radar observations of meteor showers, using echo range distribution, head echoes and antenna direction change

04 p0659 A69-15035

SPORES

NT MICROSPORES

Dry heat destruction of spores, discussing dependence on spore water content and effect of surrounding gas volume on escape of water from spore

05 p0712 A69-15938

SPOT WELDS

Electrode indentation in resistance spot welds related to weld strength for titanium, steel and aluminum alloy

01 p0086 A69-10538

Spot weld strength of tungsten inert gas spot welding on Al-Mg-Si sheets greater than resistance welding, noting crack formation during inert gas welding

05 p0769 A69-16538

Weld-nugget formation in resistance spot welding, using high-speed photography on model section of spot weld

05 p0769 A69-16539

Vacuum effects on resistance spot welds in aluminum, stainless steel and titanium alloys, noting X ray and tensile shear test results

12 p2103 A69-26622

Seam and stitch welding in miniaturized semiconductor package fabrication, including leak rate tables

18 p3149 A69-35272

Resistance spot welds in Al, Ti and stainless steel in air and hard vacuum, showing feasibility for space assembly

19 p3319 A69-35554

SPRAY CHARACTERISTICS

Sprays in solar flares, discussing production in explosive and normal flares, occurrence, energy and relation to surges

06 p0995 A69-17439

Lateral spreading of liquids injected into supersonic flow, discussing dependence on Mach number and scattered light and schlieren photographs of spray structure

09 p1482 A69-21966

Quantitative analysis of interaction between spray and ambient atmosphere, discussing atomization of flat sheet and drop behavior relationship to operating conditions

15 p2717 A69-30465

Decomposition of ammonium perchlorate containing additives introduced by spray drying [AIAA PAPER 69-502]

16 p2834 A69-32752

Evaporation rate of liquid sprays involving atomization, droplets ballistics, drop size distribution, turbulence effects, etc

18 p3119 A69-34246

Spray cleaning and deoxidizing of Al surfaces for structural bonding using sulfuric acid-sodium dichromate deoxidizer, noting tests with proprietary solutions

19 p3321 A69-35564

Tilt wing V-STOL aircraft spray circulation characteristics in overwater operation, examining forces, moments and generated environmental conditions [AIAA PAPER 69-791]

19 p3243 A69-35638

SPRAY NOZZLES

Liquid metal sprayer design including calculation of nozzles for subsonic and supersonic gas outflow

21 p3728 A69-38613

SPRAYED COATINGS

Density distribution vs thickness in sprayed ZrC, NbC and aluminum oxide coatings obtained by plasma jet

12 p2118 A69-26258

Spray deposition of low emittance gold thermal control coatings on aerospace structures

15 p2618 A69-30310

Plasma coating formation mechanisms and parameters, studying metal surface and deposited particles temperatures, spraying time effects, etc
20 p3549 A69-37374

Sprayable polyurethane foam lightweight insulation for Saturn s-2 booster tanks holding liquid H an liquid O at wide temperature ranges
21 p3732 A69-38967

**SPRAYED PROTECTIVE COATINGS
U PROTECTIVE COATINGS**

SPRAYERS

Liquid metal sprayer design including calculation of nozzles for subsonic and supersonic gas outflow
21 p3728 A69-38613

SPRAYING

NT ARC SPRAYING
NT FLAME SPRAYING
NT PLASMA SPRAYING

Lithium metal spray structural cooling system for refractory materials
[AIAA PAPER 68-358] 04 p0688 A69-15509

Spray cooling techniques for thermal protection of aerospace structures including lithium spray cooling, vapor collection and condensation, etc
11 p1966 A69-24532

Etching, spray etching and photo-resist methods for producing CrNi steel heating elements for propeller de-icing
12 p2102 A69-26370

**SPRAYING APPARATUS
U SPRAYERS**

SPRAYS

U SPRAYERS

SPREAD F

Latitude variation of time of occurrence of maximum F height and maximum spread F probability
03 p0420 A69-13305

Antarctic spread F irregularities, examining models and performing ray tracing
04 p0595 A69-15439

Latitude variations of delays between spread F and magnetic activity shown to be different at various parts of solar cycle
16 p2779 A69-32194

Field aligned ionospheric F layer ion density irregularities, using simultaneous hourly radar echo and spread F data and detailed ray path calculations
18 p3129 A69-34958

**SPREAD REFLECTION
U DIFFUSE RADIATION
U REFLECTION**

SPREADING

Alloy elements effect on spreading of liquid titanium and zirconium alloys on graphite
03 p0446 A69-13573

Paraxial electron beams from Pierce gun and spreading due to thermal velocities and space charge in nonuniform potential
12 p2036 A69-25920

SPRINGS (ELASTIC)

Positive feedback of spring mass system for mirror control on spectroheliometer of Apollo Telescope Mount flight
02 p0248 A69-11738

Spring supported hydrostatic shaft seal with floating members isolated from structure
[ASME PAPER 68-WA/LUB-9]
05 p0768 A69-16132

Nonlinear oscillations stability of solid body connected to base by elastic springs of different rigidities under external forces
14 p2536 A69-29745

Blade vibration damper consisting of springs attached to blade, analyzing resonance stresses on basis of dynamic rigidities
17 p3066 A69-33944

Landing shock struts of Surveyor 6, emphasizing silicone liquid springs role as absorbers and stabilizers
20 p3466 A69-38180

Spring mass nonlinear systems under constant force excitation, studying step function responses of systems with various restoring force characteristics
21 p3836 A69-38985

Damped mass spring system response to sonic booms, considering effects of structural damping, total/positive phase duration ratio and N wave rise time
21 p3647 A69-38987

Time optimal control of soft spring showing switching locus changes
24 p4289 A69-42955

**SPUR [REACTORS]
U SPACE POWER UNIT REACTORS**

**SPURT [TRAJECTORIES]
U SPINNING UNGUIDED ROCKET TRAJECTORY**

SPUTTERING

Cathode sputtering and thermal evaporation in vacuum used for preparing thin dielectric coatings on mirrors of optical resonators containing nonlinear crystals
03 p0438 A69-13049

Angular distribution of particles sputtered from GaAs and GaP single crystals, bombarding faces with Ar ions at low energy
04 p0640 A69-14452

RF sputter etching of microcircuits and components
04 p0606 A69-14874

Vacuum equipment for evaporation or sputtering in semiconductor industry
04 p0598 A69-14876

Physical sputtering deposition of molybdenum disulfide films as solid lubricant on rotating and sliding components, discussing lubrication properties in vacuum
[ASLE PAPER 68-LC-15] 07 p1140 A69-19308

Electric propulsion systems characteristics, examining sputtering of metallic targets as thrust augmentor
11 p1944 A69-25598

Ion sputtering method for making electrodes in thermionic energy converters, discussing alumina and W surface layers preparation
23 p4170 A69-42259

SQUALLS

Probabilistic forecasts in meteorological support of aviation, comparing economic implications of squall forecasting
14 p2474 A69-29739

SQUARE WAVES

Diathermy instrument using solid state circuits to provide square wave pulses, discussing operating parameters for bipolar coagulation and advantages over spark gap instruments
18 p3134 A69-34537

Time domain expression derived for frequency varying nonperiodic square wave in FDM and FM systems, using orthogonal functions to obtain frequency spectrum
24 p4281 A69-42623

SQUARES [MATHEMATICS]

Square matrices decomposition into orthogonal and triangular matrices products for computer storage applications
13 p2290 A69-28485

Visual succession threshold for sides of square contour affected by presenting single line on parallel contour sides
22 p3882 A69-40868

**SQUEEZING
U COMPRESSING**

SQUELCH CIRCUITS

Linear integrated circuit communication systems based on subsystem approach, showing example of IF strip and audio AGC/squelch amplifier
01 p0035 A69-11389

HF receiver interference blanker, discussing limiter-blanker system, integration, effectiveness and squelch circuit
23 p4141 A69-42221

**SQUIRRELS
U GROUND SQUIRRELS**

**ST VENANT FLEXURE PROBLEM
U SAINT VENANT PRINCIPLE**

STABILITY

NT ACOUSTIC INSTABILITY
NT AERODYNAMIC STABILITY
NT AIRCRAFT STABILITY
NT ATTITUDE STABILITY
NT BOUNDARY LAYER STABILITY
NT COMBUSTION STABILITY
NT CONTROL STABILITY
NT DIMENSIONAL STABILITY
NT DIRECTIONAL STABILITY
NT DYNAMIC STABILITY
NT FLAME STABILITY
NT FLOW STABILITY
NT FREQUENCY STABILITY
NT GYROSCOPIC STABILITY
NT HOVERING STABILITY
NT LATERAL STABILITY
NT LONGITUDINAL STABILITY
NT LOW SPEED STABILITY
NT MAGNETOHYDRODYNAMIC STABILITY
NT MAGNETOSPHERIC INSTABILITY
NT MOTION STABILITY
NT ROTARY STABILITY
NT SHELL STABILITY
NT SPACECRAFT STABILITY
NT STATIC STABILITY

NT STORAGE STABILITY
NT STRUCTURAL STABILITY
NT SURFACE STABILITY
NT SYSTEMS STABILITY
NT THERMAL STABILITY

Stability of compound superconducting cables under conditions of controlled heat transfer from cable surface to liquid He
[IEEE PAPER 13.5] 01 p0176 A69-10718

Difference schemes stability for solving linearized gasdynamic equations obtained by representing transition matrices in form of two matrix sum
01 p0060 A69-10722

Stability of two coordinate automatic angular tracking systems
01 p0053 A69-10800

Reduction principle for study of linear differential equations stability
01 p0106 A69-10956

Unstable minimization problem of functional, examining construction of sequences and stability
02 p0271 A69-11648

Numerical integration stability of differential equations, noting limiting integration step size for unsteady distillation
02 p0273 A69-12478

Necessary conditions for stability of trivial solutions of parabolic systems of partial differential equations
03 p0456 A69-13405

Stability criteria for closed rigid feedback systems with stable linear part connected in series with parametric quick response nonlinear element
03 p0410 A69-13683

Critique of paper on theory of gradient instability in semiconductor currents, questioning boundary value problems solution validity
03 p0487 A69-13728

Stability of stochastic systems, discussing continuous parameter models, Gaussian white noise, stabilization of unstable deterministic system and ITO equations
04 p0623 A69-14695

Stability limits of regenerative echo amplifier during simultaneous variation of network capacitance and negative resistance
04 p0577 A69-14778

Periodic cycles in linear closed loop integral pulse FM systems, discussing existence conditions, periodic formulac and stability criterion
05 p0737 A69-15865

Stability of linear passive time variable circuits, discussing validity of circuit elements replacement by gyrator equivalents
05 p0739 A69-16348

Stability of time varying systems by construction of multipliers with prescribed phase characteristics
05 p0740 A69-16598

Stability analysis of nonlinear and time varying discrete feedback systems
05 p0740 A69-16600

L super P stability conditions for nonlinear time varying feedback systems derived with transformation technique and small gain theorem
06 p0903 A69-17411

Existence and uniqueness theorem for functional equation of optimal control problems, noting stability of solution
06 p0949 A69-17889

Rearrangement inequalities for positivity of nonquadratic transformations, discussing stability of nonlinear feedback loop described by difference equations
06 p0904 A69-17943

Circle criterion for stability of nonlinear time varying systems, considering integrator and infinite sequence of impulses in impulse response
06 p0905 A69-17949

Linear closed loop control system poorly damped response to deterministic inputs improved by stability constraint for minimization of mean squared error
06 p0905 A69-17950

Rotating stellar models oscillation and stability approximated by virial equations
07 p1220 A69-19389

Stability analysis of model reference adaptive control system with sinusoidal inputs, using reformulation of fourth order Runge-Kutta method
08 p1297 A69-20357

Stability region of second order nonlinear autonomous system determined by numerical computational method
08 p1297 A69-20358

Relativistic energy momentum tensor of electromagnetic field in moving multicomponent dispersive media and instability of wave
10 p1653 A69-23193

Instabilities of numerical integration of ordinary differential equations on digital computer, considering difference approximation containing extraneous solutions

10 p1721 A69-24042

Linear differential equation solution for elastic systems stability problems, discussing applications to heated rectangular plates

11 p1982 A69-24950

Initial conditions estimation problem for nonlinear system asymptotic stability and satisfaction of output constraints on state variables

11 p1909 A69-25290

Energy metric algorithm for Liapunov functions generation, discussing stability conditions in Wall and Moe work

12 p2122 A69-26521

Dahlquist linear multistep methods of stability analysis for ordinary differential equations extended to Volterra integrodifferential equations

12 p2123 A69-26753

Electric drift instability in semiconductors with hot electrons, discussing diffusion, electron heat conduction, energy transfer, space charge density, etc

13 p2318 A69-27891

Stability of quasi-solutions for equations with closed and with continuous operators

13 p2289 A69-28483

Semidefinite Peano kernels of stable forms

15 p2644 A69-30450

Chetaev /A, lambda/ estimates of approximate integrations of system of ordinary differential equations, analyzing stability with aid of Liapunov functions

15 p2644 A69-30664

Asymptotic Liapunov stability of perturbed solutions to weakly coupled multifrequency systems

15 p2654 A69-31258

Stability and asymptotic stability theorems related to Liapunov second method, considering linear differential equations zero solution

15 p2654 A69-31259

Pseudo Runge-Kutta methods stability in numerically integrating two point Cauchy problems

15 p2646 A69-31261

Stability determination for nonlinear automatic control systems, describing mathematical methods based on Liapunov functions

16 p2804 A69-32242

Digital simulation computer stability analysis scheme premised on use of perturbed transient responses

17 p2944 A69-32899

Stability conditions for time lag differential equation systems over finite interval employing Liapunov functions, noting similarity with systems having continuously acting disturbances

17 p2995 A69-33616

Ordinary differential equations integration method, presenting algorithm based on double constraint of maximum accuracy and stability

19 p3279 A69-35805

Liapunov first stability theorem generalized for differential equations in Banach space

19 p3360 A69-35860

Autonomous second order recurrence with real variables, studying conditions for attractive limiting set stability region with several noninterconnected regions

19 p3287 A69-36651

Elastic stability theory from thermodynamic viewpoint, considering postulates and energy equations

19 p3444 A69-36796

Adjoint system for determining equilibrium stability of elastic continuum subjected to follower type surface tractions

19 p3446 A69-36835

N-dimensional vector functions branching process stability belonging to locally compact set in certain space

20 p3509 A69-37075

Stability analysis of Kippenhahn-Schluter model of solar corona filaments against arbitrary perturbations treated in MHD approximation using Bernstein energy principle

20 p3588 A69-37544

Hydrostatic instability in high temperature stars in postNewtonian approximation

20 p3580 A69-37926

Stability criteria for integral manifold formed by intersection of hypersurfaces in Euclidean n-dimensional space

21 p3770 A69-38850

Asymptotic stability of differential equations solutions in linear normalized spaces via Liapunov theorems extension

21 p3755 A69-39105

Stability of two differential equations in critical case, obtaining Liapunov stability and instability

21 p3755 A69-39107

Absolute and convective instability criteria of interacting electromagnetic waves in waveguide systems involving parametric oscillators and amplifiers

21 p3677 A69-39555

YIG single crystal disk instability, noting dispersion of magnetostatic and plane spin waves from supplementary absorption and LF oscillations recording

21 p3783 A69-39561

Boundary value problem of hydrodynamic equations discontinuous solution stability under random perturbations, analyzing combustion and detonation models

23 p4239 A69-41961

Sufficient conditions theorems for investigation of instability of numerical integration methods to solve differential equations

24 p4339 A69-42646

STABILITY AUGMENTATION

U FEEDBACK CONTROL

U STABILIZATION

STABILITY DERIVATIVES

NT PITCHING MOMENTS

NT ROLLING MOMENTS

Stability derivative estimation at subsonic speeds for preliminary design engineer

05 p0700 A69-15545

Dynamic stability tests of tilt winged V/STOL aircraft model in ultralow speed range, discussing apparatus for stability derivatives

06 p0866 A69-17091

Lifting force and moments acting on slender wing of finite span and arbitrary planform moving at constant mean velocity in unsteady flow

06 p0858 A69-17338

Roll acceleration influence on angle of attack convergence and windward meridian rotation rate of rolling reentry vehicles

[AIAA PAPER 69-100]

06 p1018 A69-18089

Longitudinal stability derivatives prediction for rigid and elastic airplanes, using influence coefficient method

[AIAA PAPER 69-131]

06 p0868 A69-18134

Stability theorem for nonlinear mixed integral equations in boundary value problems

08 p1343 A69-20355

Unstable regions prediction for reciprocal cases governed by linear equations with periodic coefficients, noting application to rotating shaft and helicopter rotor

08 p1413 A69-20401

Laminar hypersonic roll damping derivatives for 10 degree half angle cone at zero angle of attack for environmental flow conditions of hypersonic wind tunnel

09 p1430 A69-21958

Newton-Raphson technique development for determining stability derivatives from flight data, noting use of a priori wind tunnel information

[AIAA PAPER 69-315]

09 p1434 A69-22379

Geometrical stability criterion similar to Popov criterion for single loop time varying nonlinear control systems analysis

09 p1476 A69-22784

Liapunov direct method in stability problems for semilinear and quasi-linear systems of hyperbolic partial differential equations with independent variables

09 p1534 A69-22799

Aircraft stability derivatives determined by adaptive method, emphasizing physical and mathematical characteristics of learning model

11 p1824 A69-25671

Asymptotic stability inferred by examining higher order derivatives of Liapunov function, noting application to learning and adaptive control

12 p2122 A69-26522

Accelerometer force balance used in measuring forces and moments acting on models in short duration rocket plume tests at simulated high altitude

[AIAA PAPER 69-351]

13 p2264 A69-28285

Stability theorems for barotropic vorticity equation integrated within limited region for flow through boundary without existing physical boundary conditions

13 p2294 A69-28494

Aerodynamic lift and moment fluctuations of sphere at supercritical Reynolds numbers measured by hot-wire anemometers, noting dependence on time

14 p2390 A69-29573

Popov type graphic criterion for determining absolute stability of modulation systems

16 p2764 A69-32440

Popov and Sandberg graphic methods for determining absolute stability of nonautonomous systems, noting role of single nonzero eigenvalue in matrix

16 p2765 A69-32441

Cosmos 149 satellite stabilization system, discussing three axis orientation and pitch, yaw and roll stabilizations by aerodynamic and/or gyroscopic moments

17 p3047 A69-33226

Cauchy problem for homogeneous linear difference scheme with constant complex coefficients, giving stability lemmas

18 p3165 A69-35049

Aircraft wing aerodynamic forces and moments due to lifting engine air intake simulated by wind tunnel experiment

19 p3239 A69-36400

Gyrostatt satellite equilibrium positions in circular equatorial orbit under action of gravitational magnetic and aerodynamic moments based on gyrostabilized satellite equations of motion

19 p3432 A69-36620

First approximation stability of triangular Lagrange solutions of restricted elliptical three body problem, formulating power series for orbital eccentricity

20 p3575 A69-37318

Wind tunnel tests determining propeller slipstream effect on roll-damping derivative in transitional flight region, estimating STOL aircraft characteristics

22 p3863 A69-40145

STABILITY TESTS

NT FLIGHT STABILITY TESTS

NT WIND TUNNEL STABILITY TESTS

Matrix transformation applications in dynamic system theory and stability test

02 p0281 A69-11943

Thermal cycling tests showing improvement in cadmium sulfide solar cell stability, noting effect of thermal cycling stresses

03 p0367 A69-13074

Stability margin difficulties in equilibrium application to continuum mechanics

03 p0418 A69-13816

Stability test functions for characteristic polynomials with real coefficients and even powers

05 p0833 A69-15710

Stability test for linear unit feedback control system with second order lag and dead time compensated by PIO controller

13 p2238 A69-27395

High strength alloys stress corrosion cracks, analyzing tensile ligament instability from plastic flow tests of bulk /compression/ specimens

13 p2277 A69-27404

Nickel base superalloys long time carbide and intermetallic phases stability at high temperatures

13 p2277 A69-27405

Numerical absolute stability test for nonlinear discrete systems using bilinear transformation

17 p2994 A69-32848

Finite difference schemes for barotropic fluid free surface model primitive equations tested for numerical integration stability and accuracy

17 p2997 A69-33691

Numerical procedure for testing absolute stability and positive realness of free dynamic systems based on Routh algorithm

18 p3112 A69-34689

Elastomeric thermosetting one part silicone encapsulant environmental tests, checking physical and electrical properties stability under temperature and relative humidity conditions

19 p3281 A69-35549

STABILIZATION

NT SIGNAL STABILIZATION

NT SPIN STABILIZATION

Garden hose instability quasi-linear stabilization employing macroscopic viewpoint, discussing fluid model

01 p0133 A69-11217

Stabilization system for klystron automatic frequency control, noting use in voice communication microwave generators and resonance spectroscopy

02 p0216 A69-12096

Cavity stabilization of microwave oscillator for noise reduction

02 p0220 A69-12451

Linear differential equations zero solution stabilization by control formed as linear combination of measured coordinates of object

03 p0408 A69-12972

Linear pulse control systems monotone stabilization, estimating required number of controls

03 p0409 A69-12975

Stabilization of steady motions of nonlinear controlled systems with two purely imaginary roots, using Liapunov stability theory

05 p0794 A69-15790

UV astronomy, discussing vehicle stabilization, un-stabilized sounding rockets, scanning satellites, bal-

loons, stabilized rockets, pointing satellites, optics and detectors

05 p0821 A69-15839

Stabilization method for composite cavity single frequency laser, noting insensitivity to oscillation power level variations

05 p0776 A69-16333

Stabilization rate of boundary value problem for parabolic equation in n dimensional space

09 p1532 A69-21627

Gain stabilization of parametric amplifier, using pumped conduction current of varactor diode

09 p1467 A69-22585

Fluid rotor angular accelerometer design for stabilization and control, noting applications to centrifuge speed and thruster gas consumption

10 p1633 A69-23273

Superconducting magnets steady state stability improvement by using composite conductors

10 p1746 A69-23634

Computer aided design of linear multivariable control systems applied to VTOL aircraft stability augmentation

12 p2013 A69-26068

Asymptotic controllability of linear system, giving stabilization procedures based on solutions to limiting differential equations

12 p2053 A69-26515

Helicopter stabilization systems design using optimal control theory to obtain multivariable feedback controller

12 p2014 A69-26764

Nonholonomic coupling effect on mechanical system stabilization characteristics in terms of generalized coordinates

14 p2482 A69-28814

Stabilization system design for stratospheric balloon gondolas, discussing optimal system with flywheel and weight combination

17 p2898 A69-33242

Stability augmentation system for CX-84 tilt wing V/STOL aircraft, using redundancy techniques to achieve fail operational performance with two active channels [AHS PAPER 310]

17 p2901 A69-33545

Statistical characteristics stabilization of random loads in fatigue tests, noting transfer function of testing machine and spring stiffness

18 p3215 A69-34544

Generalized Cauchy problem solution stabilization for ultraparabolic equation by integral representation of solution in positive initial functionals

18 p3165 A69-35312

C-5 aircraft stability augmentation and autopilot development with consideration for unusual design required by takeoff weight, inertia and low approach speed

20 p3461 A69-36927

Balloon-borne gondola azimuth stabilization using lunar tracker

20 p3538 A69-37300

Lifting body stability augmentation systems design, development, ground tests and flight data including frequency response, limit cycle and structural resonance [AIAA PAPER 69-887]

21 p3647 A69-39413

STABILIZED PLATFORMS

Stabilized platform vibration in inertial navigation system with integral correction

01 p0112 A69-10086

Brushless DC torque motor using reluctance magnetic circuit and toroidally distributed coil winding

01 p0012 A69-10154

Satellites and ocean platforms for civil aviation operations over North Atlantic, noting cost justification dependence on supersonic traffic increase [UN PAPER 68-95887]

01 p0113 A69-10521

Invariance of stabilized coordinates in power gyro stabilizers, using matrix equivalent of gyroscopic moments acting on platform

04 p0597 A69-14602

Multiframe platform stabilization, analyzing dynamic coupling due to possible avoidance of adjusting moment and effect of coupling on attitude control

04 p0629 A69-14830

Equations for instability of stabilized platform of inertial navigation system with viscous friction in accelerometers

06 p0954 A69-16824

Attitude stabilized balloon telescope for measuring interplanetary scattered light and nightglow

06 p0999 A69-16972

Attitude control system for maintaining orientation of experimental package relative to space stabilized platform, noting transient response and steady state accuracy

06 p0955 A69-17587

Attitude stabilization for astronomical satellites

06 p1015 A69-17588

Stabilized gyroscope platform internal dynamics analysis, outlining optimal orientation for full compensation of cross couplings

09 p1499 A69-22240

Gyroscopes orientation influence on dynamic drift of triaxial power gyrostabilizer on rocking platform, noting optimum orientations

11 p1881 A69-24560

Inertial navigation platform principles including acceleration and position of vehicle, single axis platforms and stabilized element coordination

12 p2078 A69-25872

Dynamics of triaxial gyrostabilizer with additional rotor mounted on base, showing systematic drift

13 p2259 A69-27428

Triaxial gyrostabilizer systematic drifts during rocking at large platform displacement angles, analyzing drift direction and rate dependence

13 p2259 A69-27430

Magnetic desaturation of inertia flywheels of satellite in equatorial or slightly inclined orbit, discussing satellite stabilization

13 p2357 A69-28476

Gyroscopic platforms automatic stability relative to inertial reference system, considering functional equations and error computation

21 p3760 A69-38734

Gyroplatform to stabilize gravimetric equipment on aircraft, noting channel stabilization by electrohydraulic servomechanism

21 p3723 A69-38885

Photographic platform applications of tethered balloons, discussing powered systems for low and high altitudes and free balloons

22 p3865 A69-40811

STABILIZERS

Optimum platform stabilizer selection for damping of rotational motion and elastic torsional stresses of aircraft fuselage about longitudinal axis

11 p1966 A69-25327

Ammonia jet device to stabilize telecommunication satellites consisting of electric heating element, ejection nozzle and thermal screens

17 p3018 A69-33236

STABILIZERS [AGENTS]

Gas chromatography used to determine residual solid propellant stabilizers content and nitro derivatives, including thin film chromatography

02 p3030 A69-11528

STABILIZERS [FLUID DYNAMICS]

NT HORIZONTAL TAIL SURFACES

Lifting reentry dynamic stability of flare stabilizers and flap controls

[AIAA PAPER 69-182] 06 p1017 A69-18053

Lift augmentation by lateral blowing over lifting surface, discussing wind tunnel pressure tests on wings, flaps and stabilizers [AIAA PAPER 69-193]

07 p1051 A69-19554

STABLE OSCILLATIONS

Nonlinear adiabatic pulsations of sequence of massive stars of uniform composition, allowing for radiation pressure variations

01 p0149 A69-10266

Asymptotic stability conditions for delayed quasilinear nonautonomous systems periodic solutions derived by Shimanov method

02 p0280 A69-11705

Free fluid hydrodynamics equations applied to weakly ionized plasma stability, considering drift oscillations excitation

02 p0291 A69-12553

Bistable zones in series oscillator circuit consisting of inductor and nonlinear p-n junction capacitance subjected to DC and AC voltage sources

04 p0575 A69-14463

Two mirror resonators, discussing curvatures formation and stability conditions to derive natural frequencies

09 p1520 A69-22680

Axisymmetric models for stable and unstable oscillations of rapidly rotating zero temperature white dwarfs, discussing kinetic and potential energy

10 p1789 A69-24129

Hydromagnetic fluid flow between flat plates oscillating with phase difference, same frequency and different amplitudes

12 p2135 A69-26273

Stable geomagnetic pulsations related to plasma density shock position in magnetosphere and to magnitude of diurnal variations

13 p2253 A69-27629

Time dependences of retardation effect, reversible magnetic permeability and magnetic viscosity during pulse magnetization of ferrite cores

13 p2319 A69-27999

Rotary oscillatory solution of parameterized system with stable unexcited motion using successive approximations

14 p2482 A69-28812

Bistable zones in series oscillator circuit consisting of inductor and nonlinear p-n junction capacitance subjected to DC and AC voltage sources

14 p2418 A69-28834

Nonlinear oscillations stability of solid body connected to base by elastic springs of different rigidities under external forces

14 p2536 A69-29745

Steady natural oscillations of unbounded brittle plane with cut under edge load, showing decreased critical load in presence of inertial effect

15 p2703 A69-30050

Bulk negative resistance material stability, discussing amplifier skin effect limitation and instability beyond critical length

15 p2575 A69-30172

Free fluid hydrodynamics equations applied to weakly ionized plasma stability, considering drift oscillations excitation

15 p2658 A69-30250

Oscillations analysis in quasi-linear autonomous system with two degrees of freedom, using point mapping for case of resonance

15 p2653 A69-31193

Satellite gravitational stabilization system with maximum damping rate, discussing orbital plane oscillations

16 p2867 A69-31738

Almost periodical oscillations of nonlinear systems containing quasi-cyclic coordinates

16 p2813 A69-32286

First harmonic approximation method reformulated to interpret nonlinear characteristic directly, discussing oscillation stability of servosystems

19 p3287 A69-36709

Two-pulse limit cycle oscillation stability relation to physical parameters of pulse modulated feedback system used for satellite attitude control

21 p3688 A69-39756

Oscillators frequency instability theories emphasizing difference between concepts of frequency instability and spectral purity

22 p3900 A69-40930

Book on interaction between oscillatory systems and energy source of limited capacity, examining stability and resonance phenomena

23 p4170 A69-42166

STACKING FAULT ENERGY

Nickel-cobalt fcc alloys rolling and recrystallization textures established with filtered Aco K-alpha radiation, considering stacking fault energy effects

04 p0615 A69-14643

Substructural changes during fatigue due to stacking fault energy variations related to morphology of fracture surface in solid solution Ni-Co alloys

10 p1795 A69-23060

Ni base superalloy stacking fault energy, studying effects of various solute additions

19 p3343 A69-35925

Stress corrosion cracking in stainless steel foils correlated with stacking fault energy and ordering, emphasizing environmental forming tendencies

19 p3350 A69-36892

Stacking fault formation probability in Ti and Zr by X ray diffraction techniques, using Fourier analysis and half-width measurements

21 p3749 A69-39600

Impurities effects on single crystal film formation of fcc metals on alkali-halide cleavage planes, stressing stacking fault energy importance

22 p3992 A69-39899

Dislocation structure of Al, Ni, Cu and Ag during creep, noting dependence of creep rate on stacking-fault energy

22 p3972 A69-41080

STACKING FAULTS

U CRYSTAL DEFECTS

STADAN [SATELLITE TRACKING NETWORK]

International 28-station global instrumentation ground support network for space tracking and data acquisition [UN PAPER 68-95912]

06 p1043 A69-17059

Tracking and data acquisition networks and communications systems for support of space missions, studying data processing, unified S Band System and Data Relay Satellite System

12 p2028 A69-25933

PCM data handling system for NASA Space Tracking and Data Acquisition Network with explanation for output capabilities, noting BIOSAT project

19 p3270 A69-36242

Data systems coordinating standards developed from experience with STADAN, discussing operating environment and administrative decisions influence on implementation

23 p4133 A69-41769

STAGE SEPARATION

Angular motion during first stage cut-off of Europa 1 launch vehicle from flight tests compared with theoretical predictions

03 p0519 A69-12856

Separation systems in Europa 1 booster vehicle, discussing thrust decay, ignition and control system characteristics

08 p1410 A69-21145

Space stage separation qualification of ONERA rocket vehicles based on angular perturbation measurements during variable roll speeds

10 p1669 A69-23005

Detonating fuses for separation of missile and rocket stages, noting separation ease, aftereffects, priming capability and fabrication

10 p1752 A69-23023

Transient phenomenon analysis and filtering based on stage separation tests in vacuum chamber, with emphasis on selective integration method

[ONERA-TP-684] 19 p3293 A69-35747

Pyrotechnical gas generator performance tests during Europa 1 rocket second and third stage separation, including generator design, ground and flight tests

23 p4224 A69-42153

Launch vehicle upper stage requirements in space missions, discussing space engine for lunar, planetary and interplanetary exploration

[AAS PAPER 69-359] 24 p4418 A69-42828

STAGING [ROCKETS]

U STAGE SEPARATION

STAGNATION FLOW

Ideal gas flow near stagnation line for blunt bodies, applying van Dyke series truncation method to numerical solution

03 p0364 A69-13660

Liquid hydrazine ignition by nitrogen tetroxide gas based on stagnation flow principle, presenting threshold measurements

[WSCI PAPER 68-43] 06 p0983 A69-17792

Partially ionized argon plasma stagnation flow past blunt body using multifluid theory, obtaining flow profiles

08 p1369 A69-20817

MGD stagnation point flow, discussing relaxation region influenced by magnetic field

09 p1543 A69-21300

Fluid injection into flowfield from porous forward portion of blunt body in stagnation region flow, determining reservoir pressure and mass flow rate

09 p1430 A69-21973

Stagnation flow of viscous fluid around rotating magnetized disk, determining effects on magnetic and velocity fields, currents and shear stresses

15 p2659 A69-30674

Hamiltonian variational principle for stationary bounded MHD flows, choosing suitable functions and rigid conducting boundary location

15 p2660 A69-30910

Shock detachment distance for flow around cylinders and spheres determined by microphotometric tracing of negatives of photographs of forward stagnation streamlines

17 p2949 A69-32962

Quasi-linear ordinary differential equations solutions for steady two dimensional stagnation point flows of nonNewtonian power law fluids

21 p3697 A69-39674

Numerical methods for radiation transport for inviscid stagnation flows, detailing spectral nature of radiation emission and absorption

[AIAA PAPER 68-664] 23 p4059 A69-41890

STAGNATION POINT

Ablation rate optical measurement near stagnation point of Teflon cylinder models, noting effect of nose curvature and temperature at supersonic speed

01 p0006 A69-10758

Heat transfer near stagnation point in axisymmetric turbulent jet impinging on circular disk

02 p0354 A69-12491

Rarefied merged stagnation shock layer of hypersonic body, considering chemical reactions of nonequilibrium dissociative relaxation of air

02 p0189 A69-12521

Exact solutions for Navier-Stokes equations for nonsteady incompressible viscous flow near two dimensional or axisymmetrical stagnation point

02 p0233 A69-12527

Correlations of stagnation point radiative heat transfer for earth reentry, noting use of nongray absorption coefficient models

04 p0685 A69-14736

Heat transfer between body and gas flow near stagnation point

04 p0544 A69-15412

Trailing edge velocity and stagnation points for isolated and latticed airfoils using Zhukovskii and Weing transformations

05 p0697 A69-15880

Free stream turbulence influence on stagnation zone heating in arc heated hypersonic facilities, obtaining stagnation point heating rates

[AIAA PAPER 69-167] 06 p1039 A69-18198

Nonstationary flow past spheres and cylinders in electromagnetic shock tube, determining time required for flow to become stationary

07 p1119 A69-18744

Hypersonic flow past blunt body near stagnation point, noting surface layer characterized by increased density and decreased entropy of gas

07 p1050 A69-18755

MGD stagnation point flow, discussing relaxation region influenced by magnetic field

09 p1543 A69-21300

Stagnation point heat transfer sensitivity to free stream turbulence attributed to external vorticity, noting correlation with Prandtl number

09 p1622 A69-21905

Stagnation point heat transfer for thin ablative coatings on sounding rockets in continuum supersonic and hypersonic flight regimes

10 p1808 A69-22934

Three dimensional MHD flow near forward stagnation point magnetic fields with large induction values described by differential equations, showing tendency towards two dimensional flow

10 p1727 A69-23100

Inviscid reacting flow free of molecular transport analyzed locally near stagnation point, using Lighthill-Freeman gas model

11 p1876 A69-25560

Heat and mass transfer conditions in ablation of shear thinning and thickening fluids at stagnation point

[ASME PAPER 67-HT-78] 13 p2374 A69-27778

Heat transfer at gas flow stagnation point past blunt body under radiation from air layer in shock wave wake, using gray gas model

14 p2390 A69-29614

Supersonic gas flow past wedge at zero angle of attack with separated shock wave, calculating velocity gradient at stagnation point and pressure and drag distribution

14 p2390 A69-29615

Boundary value problem in three dimensional boundary layer theory for incompressible flow near stagnation point

14 p2432 A69-29677

Stagnation point electrostatic probe for measuring local electrical properties of solid propellant rocket exhausts

[AIAA PAPER 69-573] 16 p2840 A69-32677

Convective plus radiative shock tube model stagnation point heating rate measurements for planetary entry heating rate in air and Venus gas

[AIAA PAPER 69-635] 17 p2890 A69-33272

Nonequilibrium multicomponent ionization calculations for stagnation merged shock layer of hypersonic blunt body by successive accelerated replacement

[AIAA PAPER 69-655] 17 p2892 A69-33469

Heat exchange in stagnation point region of blunt body, using shock test simulation of high speed flight

18 p3086 A69-35118

Probe for spectral radiation from luminous gas-cap stagnation region to determine driver gas in test section of hypersonic shock tunnel

19 p3294 A69-35753

Axial stagnation point flow in shock wave reflected from sphere or circular cylinder, determining velocity time variation, enthalpy pressure and reflection

19 p3298 A69-36385

Stagnation point heating in hypersonic gas flow past blunt bodies, considering radiative transfer effects on shock wave temperature and density distribution, wave separation, etc

20 p3457 A69-36981

Jupiter Great Red Spot in terms of homogeneous fluid rapid rotation, Rossby number, stagnant region, Taylor column and stratification

20 p3609 A69-38060

Unsteady aerodynamic heating at stagnation region including surface combustion in arc heated high enthalpy wind tunnel

22 p3860 A69-40597

Semianalytic solution for axisymmetrical supersonic inviscid flow near stagnation region of spherically blunted body with detached shock waves

22 p3861 A69-41178

Radiative transfer effects in low Reynolds number or merged layer regime of hypersonic flow about axisymmetric blunt bodies, including thin shock layer theory

23 p4059 A69-41885

Stagnation point Mach number gradient, sonic point location and drag coefficient of hemisphere at zero angle of incidence

23 p4060 A69-41910

Blunt body stagnation point air ionization by chemical nonequilibrium thin viscous shock layer analysis, predicting electron density

23 p4060 A69-41917

Chaplygin equation applied to eddy flow past semicylindrical surface, discussing stagnation points and boundary value problems

24 p4245 A69-43477

Convective thermal flux at stagnation point in multicomponent partially ionized gas injected flow past body, considering effective ambipolar diffusion coefficient

24 p4246 A69-43485

Heat exchange at stagnation point during interaction between underexpanded axisymmetric supersonic jet and flat obstruction, using method of characteristics

24 p4246 A69-43493

Stagnation region heat transfer with nongray subjected to external radiation using two step continuum absorption coefficient model

24 p4415 A69-43590

STAGNATION PRESSURE

Stagnation pressure losses of adiabatic flow of compressible fluids through abrupt area expansion and contraction in subsonic range, discussing base pressure

[ASME PAPER 68-WA/FE-46] 05 p0750 A69-16113

Ablation performances of asbestos phenolic and silica phenolic compared at higher stagnation pressures in wave-superheater hypersonic tunnel

12 p2119 A69-26814

Stagnation region dimensionless pressure effect on flow pattern, boundary conditions and oscillation mechanism in compressible flow through nozzle in circular duct

15 p2549 A69-31220

Stagnation temperature determined in transition and free molecule region of rarefied gas flows from critical mass flow dependence on temperature and stagnation pressure

24 p4408 A69-43492

Choking and shock in flashing single component two phase flow in tube, including vibrational effects, predicting minimum stagnation pressure loss

[ASME PAPER 69-HT-61] 24 p4303 A69-43535

STAGNATION TEMPERATURE

Internal temperature distributions of present and proposed calorimeter geometries operating at high pressure and extreme heating rates compared, using one and two dimensional heat conduction programs

01 p0079 A69-10299

Injectant stagnation temperature and molecular weight variation effect on flow field generated from secondary injection into supersonic stream

[AIAA PAPER 69-1] 06 p1039 A69-18196

Free stream turbulence influence on stagnation zone heating in arc heated hypersonic facilities, obtaining stagnation point heating rates

[AIAA PAPER 69-167] 06 p1039 A69-18198

Mixing regimes for flows with different stagnation enthalpies subject to mass flow limitation due to thermal choking

13 p2251 A69-28499

Similarity solutions for laminar compressible boundary layer with reverse flow, considering various wall/stagnation temperature ratios

15 p2591 A69-30907

Subsonic and supersonic turbulent air jets expansion over perpendicularly positioned plane disk obstacle, deriving equations for pressure distribution and stagnation temperature

18 p3123 A69-34990

Stagnation temperature determined in transition and free molecule region of rarefied gas flows from critical

STAINING

mass flow dependence on temperature and stagnation pressure
24 p4408 A69-43492

STAINING

Spectral absorption curves of hematoxylin stains in stained tissue sections of rat thyroid
01 p0015 A69-10924

STAINLESS STEELS

NT AUSTENITIC STAINLESS STEELS
NT MARTENSITIC STAINLESS STEELS

Prestraining of stainless steel En58b sheet at room and cryogenic temperature, noting effect on tensile properties
01 p0099 A69-11151

Mechanical finishing abrasion induced plastic deformation microtwinning observed in thin stainless steel films by transmission electron microscopy
02 p0251 A69-11542

Surface preparation effect on stress corrosion cracking of type 310 stainless steel wires in boiling aqueous magnesium chloride solutions
03 p0444 A69-13311

Stability of ductility and fatigue strength of stainless steel under longtime static loads in vacuum and in liquid lithium
03 p0450 A69-13912

Emissivity and other radiative characteristics of stainless steel oxides heated to various temperatures in air
03 p0453 A69-14157

Pool boiling heat transfer from stainless steel coated with Teflon to produce nonwetted surfaces
[ASME PAPER 68-WA/HT-12]
05 p0847 A69-16119

Aluminum-stainless steel wire reinforced metal matrix composites, analyzing strain hardening and plastic deformation
06 p0940 A69-16950

Nitrogen solubility measured in liquid Fe-Cr-Ni-Al alloys, noting solubility increase with increasing Al content
06 p0942 A69-17228

Stainless steel sensitization analyzed using Mossbauer spectroscopy and X ray diffraction, noting ferromagnetic phase
06 p0944 A69-17852

Passive current maxima during anodic polarization of stainless steel in sulfuric acid, using electrochemical and electron microprobes
06 p0944 A69-17853

Precipitation hardening stainless steels, discussing corrosion resistance, high strength, weldability, fabricability, heat treatment, etc
06 p0932 A69-17874

Tungsten coatings applied on stainless steel and titanium alloy surfaces by plasma jet
07 p1165 A69-18931

Maraging stainless steel for manufacturing liquid rocket propellant tanks, discussing composition determination and mechanical properties
07 p1166 A69-19236

Sulfite ion influence on pitting corrosion of stainless steels in sodium chloride solution
07 p1167 A69-19343

Long life creep rupture of Type 304 stainless steel for linear, Larson-Miller and Dorn parameter curves, discussing isothermal curves and creep rate
[ASM PAPER D8-9.6]
07 p1169 A69-19664

Acoustic emission from welds in stainless steel plates used for detecting defects in single and multiple pass machine welds
08 p1318 A69-19963

Weldability of precipitation-hardening stainless steels by gas tungsten arc process, discussing microstructure and shrinkage stress cracking
08 p1320 A69-20409

Ductile fracture behavior of two phase stainless steel examined by straining smoothed and notched tensile and Charpy impact specimens
08 p1333 A69-20574

Carbide precipitation in stainless steels using metal foil and extraction replicas, discussing grain boundaries corrosion relation
10 p1713 A69-23820

Highly alloyed steels weldability, considering nickel maraging and precipitation hardening stainless steels
12 p2111 A69-25829

Oxygen effects in Type 316 stainless steel, Nb-Zr alloy liquid potassium system, discussing thermal convection and forced circulation loops and corrosion rates
12 p2112 A69-25943

Hydrogen embrittlement of stainless steel and effects on mechanical properties, discussing martensitic phase role
12 p2115 A69-26616

Transition zone structure and phase composition in Ti/stainless steel bimetal as function of rolling conditions and heat treatment
13 p2283 A69-28490

Stainless steel biaxial residual surface stresses from grinding and finish machining determined by dissection technique
[ASME PAPER 68-WA/MET-9]
14 p2455 A69-29437

Chemical composition effect on Cr-Ni-Mo-Ti stainless maraging steels mechanical properties
15 p2640 A69-30631

Polyethylene stainless steel lap joints and polyethylene samples yield strengths measurements at high temperature, suggesting yield mechanism based on dislocation loops
16 p2794 A69-32573

Fatigue crack growth rates in stainless steel at elevated temperature measured as function of oxygen pressure in resonant fatigue machine
17 p2987 A69-33074

Low cycle fatigue behavior prediction for 304 and 306 stainless steels based on temperature and strain rate ratio to tensile ductility
17 p2987 A69-33079

Materials integral hemispheric radiative capacity determination based on cooling rate of thin walled specimen in vacuum, considering stainless steel, Ni and Cu
18 p3156 A69-34698

Low cycle fatigue leading to failure on AISI 321 stainless steel as function of elevated temperature and straining frequency
18 p3219 A69-34834

Martensite transformation, C content and work hardening relations in stainless steels studied for magnetic detection of embrittlement during deformation
18 p3138 A69-35117

Liquid sodium penetration into stainless steel grain boundaries, using laser microprobe
18 p3154 A69-35473

Low temperature adhesive shear tests to measure force to break ice away from stainless steel surfaces coated with various bonded solid lubricants
19 p3323 A69-35581

Hydrogen effect on embrittlement of Cr-Ni stainless steel from viewpoint of corrosion cracking, using reverse bending apparatus
19 p3358 A69-35774

Stress corrosion cracking of stainless steels and Incoloy and Inconel alloys in chloride, caustic, oxygenated and miscellaneous environments
19 p3349 A69-36890

Fracture surfaces of stress corrosion cracks in Fe-Cr-Ni alloys studied by electron microfractography, noting cleavage fracture
19 p3350 A69-36891

Stress corrosion cracking in stainless steel foils correlated with stacking fault energy and ordering, emphasizing environmental forming tendencies
19 p3350 A69-36892

Apparent dynamic modulus and damping under multilevel loading during fatigue cycling to estimate stainless steel specimens cumulation fatigue lives
20 p3620 A69-36997

Stainless steel cladding of metals to combine desirable properties into composite, describing bonding, product types and treatment
21 p3745 A69-38937

Tungsten coatings applied on stainless steel and titanium alloy surfaces by plasma jet
21 p3746 A69-39152

Thermal fatigue combined with mean stress, reversed mechanical stress, low cycle fatigue and static creep in stainless steel
21 p3847 A69-39813

Outgassing rates of stainless steel and Al with different surface treatments, including glass bead shot blasting, electropolishing, baking and vacuum cleaning
22 p3958 A69-41215

High temperature vacuum treatment of thick stainless steel sheets reducing hydrogen content and outgassing
22 p3958 A69-41217

Cyclic stress tests of stainless steel fiber Al alloy matrix composite, including strain hardening and stiffness characteristics
24 p4331 A69-42925

STAINING

U BOUNDARY LAYER SEPARATION

STANDARD ATMOSPHERES U REFERENCE ATMOSPHERES

STANDARD DEVIATION

X Ray fluorescence of rock samples as applied to geological problems, noting standard deviations for elemental distribution
01 p0082 A69-10899

Standard deviation of wind direction fluctuations by simultaneous measurements of wind wave displacements and number of wind direction reversals
04 p0626 A69-14911

Frequency and space averaging effect on variability and standard deviation of multimode media transmission responses, with application to reverberant media
23 p4115 A69-41579

STANDARD LAUNCH VEHICLE 3

U ATLAS SLV-3 LAUNCH VEHICLE

STANDARD LAUNCH VEHICLES

U ATLAS SLV-3 LAUNCH VEHICLE

STANDARDIZATION

Emergency oxygen supply systems for aircraft, discussing simplicity, standardization, safety, reliability and maintenance
[AIAA PAPER 67-965]
01 p0013 A69-11025

Reliability terms for electrical apparatus, equipment and systems, indicating need for international standardization
08 p1292 A69-21108

Zero reference field for quiet day solar variations, considering magnetic field levels and errors
09 p1575 A69-21551

Photometric standardization and calibration of meteor spectrograms for real meteor masses determination using spectroscintometer
12 p2154 A69-25820

Standardization requirement for laboratory and field research into vibration effects on humans, stressing subjective rating and performance measurements
13 p2213 A69-28091

Zero reference field for quiet day solar variations, considering magnetic field levels and errors
16 p2851 A69-32546

Digital computers standard programs for astronomical problems
20 p3596 A69-37317

High quality castings unified standards for European aerospace industry
20 p3551 A69-38029

Thermal physiology standardized symbols compilation for units of measurement
23 p4078 A69-41317

Aerospace fastener systems standardization proposal to reduce inventories, simplify design and provide extended structural life
24 p4325 A69-43439

STANDARDS

NT FREQUENCY STANDARDS

NT REFERENCE ATMOSPHERES

Electrical conductivity standards and eddy current measurements noting calibration facility
01 p0081 A69-10830

Microwave thermal noise standards, discussing construction, calibration and errors for field operational liquid nitrogen cooled waveguide noise standard
02 p0210 A69-12438

Low temperature microwave thermal noise standard discussing waveguide termination, cryogenic cooling and temperature and pressure controls
02 p0211 A69-12446

Precision coaxial connectors, giving IEEE standard mechanical, electrical and environmental specifications for general precision connectors using coplanar butt joints
02 p0222 A69-12757

Standards of sterility for prevention of introduction of terrestrial microorganisms onto other planets during space missions, noting contamination probability
05 p0712 A69-15936

Dual gas reference electrode system for molten carbonate cells with immobilized electrolyte
05 p0706 A69-16237

Computer use evaluation, discussing standards for automatic data processing /ADP/ investment and operations
05 p0850 A69-16299

High accuracy microwave phase standard for calibration laboratories, discussing broadband differential phase shifter
06 p0896 A69-17487

Standards for EEG in pilot fitness examinations, analyzing effects of total flying hours
06 p0875 A69-18021

Aircraft separation standards, considering separate space for VTOL in automated high density airways system
[AIAA PAPER 69-210] 07 p1178 A69-19579

Photometric standard based on calibration of Vega by Hayes compared with six color magnitudes
09 p1603 A69-22233

Standard reference radiographs for weld defects on steel sheets and plates
18 p3150 A69-35425

Radio measurement methods and standards including measurements of attenuation, phase shift, time delay, impedance, field strength, antenna characteristics, RF properties of materials, etc
19 p3276 A69-36426

Nonferrous metals and alloys conductivity standards development program resulting in fabrication, calibration and certification of 16 primary reference standards
20 p3537 A69-37008

Minor planets positions computer calculated and tabulated from 1966 and 1967 Crimean astrophot observations, using Yale catalog reference stars
20 p3570 A69-37313

MIL-STD-781B reliability tests with standard based on exponential distribution for equipment exhibiting constant failure rate, noting sampling
20 p3551 A69-38289

Precision azimuth reference accuracy standards with confidence limits for gyrocompass evaluation, emphasizing astro and transfer angle repeatability
[AIAA PAPER 69-859] 21 p3725 A69-39387

Vacuum gage calibration standards and methods
23 p4162 A69-41530

Data systems coordinating standards developed from experience with STADAN, discussing operating environment and administrative decisions influence on implementation
23 p4133 A69-41769

IRIG /Inter-Range Instrumentation Group/ telemetry standards for U.S. Department of Defense missile and weapons systems, reviewing evolution, content, scope, philosophy, revisions, etc
23 p4121 A69-41770

Telemetry Standards Coordination Committee annual report
23 p4241 A69-41782

FAA power spectral gust methods for computing design limit loads on commercial aircraft, noting British investigation
24 p2553 A69-43111

STANDING WAVE RATIOS

Wideband tunnel diode amplifier design, discussing implementation to out-of-band circulator characteristics and VSWR suppression
15 p2578 A69-30804

Pseudoexact bandpass filter design, presenting graphs for passband loss, voltage standing wave ratio and time delay as function of frequency
15 p2581 A69-31526

Broadband low VSWR transitions between rectangular waveguides and coaxial transmission lines, discussing asymmetrical probe and ridge types
16 p2757 A69-31584

Voltage standing wave ratio measurement technique at low power level, including tolerated errors, compared with Roberts-von Hippel method
17 p2918 A69-33031

STANDING WAVES

Ministriations in frequency graphs as evidence of standing waves in electrically exploded iron wires
01 p0118 A69-10661

Standing Alfvén wave resonances in liquid sodium
01 p0131 A69-10820

Bragg reflection of electrons by standing light waves of giant pulse laser
02 p0255 A69-11833

Standing ion-acoustic wave excitation in weakly ionized plasma, noting isothermal compression of electron gas
02 p0292 A69-12555

Standing wave methods for measuring permittivities of liquids having attenuation coefficients over considerable range
04 p0599 A69-15015

Time averaged optical holographic interferometry of standing longitudinal acoustic waves in square cross section duct
06 p0923 A69-17150

Standing waves effect on spectral and power characteristics of laser with plane mirrors, determining dependence on pumping power
07 p1148 A69-18800

Transverse LF oscillations in geomagnetic field observed during January 1967, noting possibility of being second harmonic of magnetospheric standing Alfvén waves
07 p1124 A69-18835

Amplitude fluctuations and line width of traveling wave and standing wave He-Ne laser, considering saturation effects
10 p1701 A69-23135

Multiple scattering in Kapitza-Dirac effect describing electron scattering by standing electromagnetic wave, noting transition probability less than unity
11 p1919 A69-25323

Ruby laser performance with perturbing effect of standing wave field on homogeneity of deexcitation of level populations eliminated by HF modulation
11 p1900 A69-25569

Nonuniform standing wave fields spatial distribution in active rod of ruby laser effects on laser radiation dynamic parameters, discussing radiation spectrum width
11 p1901 A69-25756

Absorption characteristics of thin metallic films in standing light wave for mode selection and conversion in lasers
12 p2104 A69-26024

Standing wave theory for steady state performance of Raman laser oscillator extended for time variation of exciting laser pulse
12 p2108 A69-26634

Standing waves and single mode room temperature laser emission from electron beam pumped cadmium sulfide thin crystal, discussing emission at 77 K
12 p2109 A69-26639

Semifree elastic membranes standing waves fundamental frequency, developing variational principle for first eigenvalue
14 p2535 A69-29365

Standing ion-acoustic wave excitation in weakly ionized plasma, noting isothermal compression of electron gas
15 p2658 A69-30252

Short period pulsations in solar magnetic fields and chromosphere, determining optimum conditions for formation of standing oscillations
15 p2688 A69-30556

Electron scattering due to Kapitza-Dirac effect in laser standing wave field
15 p2634 A69-30736

Semiclassical theory of quantum generators, examining laser system response to effect of monochromatic standing wave based on kinetic equation for density matrix
16 p2798 A69-32480

Zonal flow intensity, velocity and kinetic energy of standing and traveling waves compared for Northern and Southern Hemispheres
17 p2997 A69-33392

ELF and VLF wave propagation examined for heavy ions and lower ionospheric disturbance effects using numerical integration, noting standing wave field role for interpretation
18 p3125 A69-34254

Vibrating circular plate standing wave lateral displacements visualization by photographically recorded moiré patterns
20 p3537 A69-37067

Acoustic filters performance determination, standing wave tube and anechoic termination methods
20 p3464 A69-37321

Standing waves on moon, discussing annular and radial structures of lunar craters and global tectonic patterns
20 p3604 A69-37565

Standing waves effect on spectral and power characteristics of laser with plane mirrors, determining dependence on pumping power
21 p3736 A69-38945

Standing waves in running tire shell wall, considering internal pressure, cross sections, wall thickness, cord angle, critical speed, etc
22 p4048 A69-41185

Hydrogen-air reaction kinetics analyzed using standing wave normal shock noting wall effects, ignition delay and recombination
23 p4239 A69-41893

Amplitude and phase maps for annual global variations in atmospheric pressure based on harmonic data analysis, suggesting standing wave type distributions
23 p4185 A69-42493

Numerical procedure obtaining scattering matrix of passive reciprocal two port from standing wave measurements, using image circle in Smith chart
24 p4281 A69-42617

STANDS

U SUPPORTS

STANNATES

Stannate immersion process for reduction of magnesium-steel couples galvanic corrosion, discussing bath operating limits
14 p2466 A69-29933

STANNIDES

U NIOBIUM STANNIDES

STANTON NUMBER

Heat transfer through turbulent boundary layer on porous plate with blowing and suction, determining Stanton numbers
04 p0586 A69-14356

Heat transfer in accelerated turbulent boundary layer between converging planes with varying wall temperature and decreasing Stanton number
[ASME PAPER 68-WA/HT-13] 05 p0847 A69-16120

Heat transfer to highly accelerated turbulent boundary layer with and without mass addition, presenting data in terms of Stanton number vs Reynolds number
[ASME PAPER 69-HT-53] 24 p4409 A69-43518

STAR CLUSTERS

NT VIRGO STAR CLUSTER

Age and initial helium abundance of stars in M15 globular clusters estimated from stellar evolution lifetime ratio
01 p0149 A69-10135

Late type stars, discussing main sequence for Population 1 and Population 2 stars and ages and chemical composition of old galactic clusters and globular clusters
01 p0158 A69-11325

N body systems with/without external field, noting galactic field effect on system flattening
02 p0322 A69-12270

Computer study of collisionless self gravitating system using two dimensional model, obtaining gravitational field by solving Poisson equation
02 p0322 A69-12272

Evolutionary theory of origin and properties of Seyfert galaxies and quasars, postulating collisions within superdense clusters leading to supermassive stars and supernovas
05 p0819 A69-15703

Stellar escapes from clusters and temporary captures in restricted three body problem with equal masses
05 p0827 A69-16595

Stars of higher multiplicity, discussing numerical membership and gravitational binding of star clusters and binary stars
07 p1219 A69-19295

Photoelectric observations for stars in and near galactic cluster NGC 3680, discussing age and metal abundance
08 p1384 A69-20054

Three color photoelectric observations of stars near Orion Nebula, discussing gravitational contraction stars and color magnitude diagram
08 p1384 A69-20055

Paschen line intensity measured as function of position across Orion Nebula
08 p1384 A69-20058

Cluster star color indices determination by measuring intensities at nodes of extrafocal star spectra
08 p1387 A69-20122

Interlocking systems within Galaxy, deducing gravitational theory accounting for galactic spiral patterns
08 p1387 A69-20136

Open clusters age determination method to study giant star distribution as function of age
08 p1388 A69-20237

Color magnitude distribution as function of age for giant stars of open clusters, discussing error sources
08 p1388 A69-20238

Photographic magnitudes in UB_V system based on photoelectric sequences for stars in NGC 2483 and NGC 2489 open clusters, obtaining spectral classes from objective prism plates
08 p1388 A69-20239

Photographic magnitudes in UB_V system based on photoelectric sequence for stars in NGC 2546, Pi 1, NGC 2579 and Cr 185, obtaining spectral classes
08 p1388 A69-20240

Photographic magnitudes of stars in various open clusters based on UB_V system and photoelectric sequence
08 p1389 A69-20245

Photographic magnitudes in UB_V system for southern open clusters, giving table of photographic plates
08 p1389 A69-20253

Photographic magnitudes in UVB system based on photoelectric sequence for various open clusters stars, determining spectral classes for brighter stars
08 p1389 A69-20254

Mass loss in Red Giant stage from statistical analysis of H-R diagrams of galactic clusters
08 p1396 A69-20642

Stellar absolute magnitudes recalibration for consistency with photometric distance moduli of clusters
08 p1408 A69-21139

Galactic clusters absorption, discussing optical thickness in blue and red light
09 p1587 A69-21356

Spatial density distribution in star clusters, determining relation between mean stellar mass and density range in subsystems
09 p1589 A69-21368

Pleiades cluster structure, deriving visible density distribution curves for brighter stars
09 p1589 A69-21369

Radial velocities of stars near cluster NGC 7380, discussing discovered stars, double lined spectroscopic binaries and photometric information
09 p1597 A69-22060

Globular cluster origin as gravitationally bound gas clouds before galaxy formation from primeval fireball model
09 p1599 A69-22192

Spectrum analysis for early B type star Barnard 29 in M13 globular cluster
09 p1599 A69-22193

Spectral type and rotational velocity estimation for 83 stars near double cluster in Perseus, emphasizing Be stars
09 p1599 A69-22195

Stability of thin rotating disks of stars with respect to axisymmetric disturbances, noting overstabilities dependence on epicycles sizes
09 p1605 A69-22413

Solid hydrogen mantle condensation accounting for lack of detectable alpha hydrogen in star clusters and OB associations
10 p1776 A69-23214

Stellar models for chemical compositions to explain gap above main sequence in color-magnitude diagram of NGC 188
10 p1789 A69-24127

Dynamical model for spherical inhomogeneity in mean mass density of universe to predict velocity dispersion observed for Coma Cluster
10 p1789 A69-24133

Flare stars observational and known aggregate characteristics in Coal Sack region
10 p1790 A69-24141

Star counts in star cluster neighborhoods, obtaining ratios of corona radius to nucleus radius as function of cluster mass
11 p1951 A69-24246

Photoelectric and photographic observations in UVB system of open star clusters, analyzing dispersion in two color diagrams, noting absorbing material structure
11 p1951 A69-24247

Proper motions of low luminosity stars in Hyades cluster, noting photoelectric observations
12 p2152 A69-25797

Lacerta OB1 stellar spectral classes and photographic magnitudes, analyzing clusters and distributions in concentrated and dispersed areas
12 p2153 A69-25813

Period changes by variable stars in M13, showing Variable 2 period lengthening
12 p2154 A69-25814

Stellar evolution model for primeval He abundance in population II stars in globular clusters for big bang confirmation
12 p2156 A69-26228

Photoelectric observation of RR Lyrae stars in globular clusters to estimate reddening near galactic poles, considering color indices
12 p2172 A69-27157

Distance and mass-luminosity relation for Hyades stars relative to sun-Sirius type stars
13 p2339 A69-27565

Optical wavelength backscattering functions for nebulae in Pleiades cluster, noting color differences and surface brightness
13 p2340 A69-27577

Residual interstellar gas from protostar formation detected as high luminosity IR object
13 p2327 A69-27593

Photoelectric search for delta Scuti variables in Coma and NGC 752 clusters, discussing short period variability of B, A and F stars
13 p2343 A69-27620

Parallax and orbital motion of spectroscopic binary Tau Persei determined from Sproul refractor photographs
13 p2349 A69-27812

H-R diagrams of globular clusters, discussing evolution models with and without mass loss
14 p2527 A69-29943

Surface convection zone in atmospheres of global cluster and halo B stars determined to study He depletion efficiency
14 p2529 A69-29976

Mass point system moving in gravitational field, discussing statistical mechanics, relaxation time and evolution of stellar systems
14 p2530 A69-29987

Variability of period of RR Lyrae type stars in globular cluster M3, deriving seasonal moments of stellar maxima and light curve elements
15 p2683 A69-30511

Member stars number in globular clusters M3 and M5 determined from photometric and kinematic characteristics
15 p2688 A69-30561

Collisionless stability of relativistic, spherically symmetric star clusters against radial perturbations, considering one dimensional sufficient criteria
15 p2691 A69-30765

Atmospheric parameters for blue horizontal branch stars in globular cluster NGC 6397 by spectroscopic and photoelectric observations, obtaining mean stellar mass
15 p2692 A69-30770

Spectral classifications and UVB photometry for southern association Sco OB 1 containing cluster NGC 6231
15 p2692 A69-30771

Stellar group Ba 6 distance measured using three color photometry in RGU system
16 p2854 A69-31650

Open galactic cluster NGC 2254 distance determined by three color photometry in RGU system
16 p2854 A69-31651

Stellar diameters in galactic cluster stars determined using original and modified spectrophotometric method compared with spectral types BOV-FOV
16 p2858 A69-32210

Spatial distribution of stellar densities and velocity distributions in phase space, using Greenwich catalog of positions and proper motions of omega Centauri cluster stars
16 p2859 A69-32220

Four color and H beta photometry of stars in Coma and Ursa Major clusters compared to standard relations for Hyades Cluster
16 p2860 A69-32234

Galaxies clusters spatial distribution based on crude distance estimates, discussing serial correlation of counts and interpreting results
16 p2862 A69-32371

Stellar system stability for corresponding stable barotropic gaseous system, discussing Schroedinger operator role
16 p2862 A69-32374

Stationary galaxy dynamical theory, assuming constant velocity body of physically homogeneous star subsystems in space
17 p3031 A69-33102

Proper motions, color magnitude and distance modulus of stars in galactic cluster in direction of Large Magellanic Cloud using Cape wide angle photometry
17 p3034 A69-33411

Theoretical Hertzsprung-Russell diagram for star cluster NGC 1866, allowing stellar evolution study
17 p3038 A69-33720

Stars kinetic energy and escape rates from isolated cluster with arbitrary stellar mass distributions, assuming spherical symmetry and velocity distribution isotropy
17 p3038 A69-33721

UVB photoelectric investigation on southern globular clusters NGC 2808 and 1851, presenting star magnitudes and colors in tabular form and estimating reddening
18 p3190 A69-34290

Galactic clusters absorption, discussing optical thickness in blue and red light
18 p3197 A69-34746

Spatial density distribution in star clusters, determining relation between mean stellar mass and density range in subsystems
18 p3198 A69-34757

Pleiades cluster structure, deriving visible density distribution curves for brighter stars
18 p3198 A69-34758

UVB photoelectric observation of OB and open cluster Tr 16 stars in Carina-Centaurus, suggesting no limit in depth distribution
18 p3200 A69-35133

Fornax clusters integrated V magnitudes and B-V and U-B colors measurement
18 p3201 A69-35205

Radio emission attributed to galactic nebula NGC 6857, suggesting origin in high density H II regions excited by OB star clusters
18 p3202 A69-35209

Pulsars measured parameter data tabulation including right ascension, declination pulse repetition period, showing sources distribution and clusters
18 p3202 A69-35211

Book on Messier nebulae and star clusters covering current astronomical ideas, star maps, identification diagrams, telescope illustrations and astronomical data
18 p3206 A69-35471

IC 4499 cluster variable stars coordinates in tabular form, showing high percentage of short period
20 p3598 A69-37462

Open cluster NGC 7128 distance and reddening determination by photometry
20 p3598 A69-37465

Periods and magnitudes of RR Lyrae variable stars in M 2 cluster, tabulating photometric characteristics
20 p3599 A69-37477

Cepheid observation, nature and evolution
21 p3795 A69-38403

Statistical analysis of galactic structures subject to Newton gravitation covering globular clusters and spiral disk and rotating bar galaxies
21 p3803 A69-38924

Relativistic star clusters, discussing existence and quasi-static evolution before collapse through gravitational radius
21 p3814 A69-39570

Spectrophotometric analysis of interstellar absorption in direction of IC 1805 cluster, noting anomalies
21 p3814 A69-39576

Pleiades cluster and ambient interstellar medium structure analyzed for spectral distribution based on plane-parallel scattering model
21 p3817 A69-39727

Nonexistence of second order clustering of galaxies and relationship to gravitational cut-off, relativistic cosmologies and red shifted light by exponential decay of photon energy
22 p4024 A69-40579

Globular cluster star age and initial He abundance from main sequence, horizontal branch and red giant tip models using radiative opacities
22 p4035 A69-41205

Solar motions respecting high velocity atomic hydrogen clouds and local stellar group
22 p4035 A69-41209

Wolf-Rayet stars formation, evolution, age, galactic distribution and relation with open star clusters
23 p4208 A69-41288

Faint OB stars data tabulation between Carina and Centaurus, noting open clusters and MK classification
23 p4211 A69-41488

UVB magnitudes for open cluster NGC 559 stars determined from combined photoelectric and photographic measurements
23 p4211 A69-41490

Photographic observations of open cluster IC 4665 made on blue and yellow sensitive plates with Vatican refractor compared with photometric measurements
23 p4215 A69-42008

Narrow and intermediate band photometry of globular star clusters in uvby and beta photometric systems, relating reddening to metal abundances of member stars
24 p4387 A69-43352

STAR DISTRIBUTION

Stars of higher multiplicity, discussing numerical membership and gravitational binding of star clusters and binary stars
07 p1219 A69-19295

Galactic Wolf-Rayet star distances and distribution on galactic plane, noting concentration difference toward galactic center
07 p1223 A69-19636

Three color RGU system photometry in Milky Way field in direction of anticentrum, determining absolute brightness, luminosity and density of stars
08 p1387 A69-20119

Open clusters age determination method to study giant star distribution as function of age
08 p1388 A69-20237

Color magnitude distribution as function of age for giant stars of open clusters, discussing error sources

08 p1388 A69-20238

Color excesses in Kapteyn Selected Area 4 using photovisual /yellow/ and photographic /blue/ magnitudes from catalog data

08 p1388 A69-20241

Spatial distribution of stars and obscuring matter in Milky Way field in Kapteyn Selected Area 195 in Circinus, cataloging UVB photometry of stars

08 p1389 A69-20246

Photoelectric measurements of magnitudes and colors in UB system for stars in Puppis at Boyden Observatory

08 p1389 A69-20249

Sky areas search for stars with UV excesses listed in Luyten Two-Tenths Catalog of Proper Motions

08 p1392 A69-20560

Formation ratios of light isotopes in spallation reactions compared to observed stellar and solar abundances of lithium, beryllium and boron, discussing astrophysical implications

08 p1401 A69-20902

Spatial density distribution in star clusters, determining relation between mean stellar mass and density range in subsystems

09 p1589 A69-21368

Pleiades cluster structure, deriving visible density distribution curves for brighter stars

09 p1589 A69-21369

Motion and dispersion of peculiar velocities of stars in gravitational condensing interstellar gas

09 p1589 A69-21371

Stars astronomical positions elimination from photographic plates because of errors, discussing elimination criteria and picture taking method

10 p1784 A69-24034

Density wave theory of galactic spirals, discussing hydrogen distribution, young star distribution, stellar migration, magnetic field structure, density waves in stellar formation, etc

10 p1786 A69-24109

Proper motions and positions of X ray source Sco X-1 and surrounding stars derived from astrophysical plates using overlap technique

12 p2152 A69-25798

Correlation of stellar surface density distribution of young stars and neutral hydrogen gas in Small Magellanic Cloud

12 p2152 A69-25802

Lacerta OB1 stellar spectral classes and photographic magnitudes, analyzing clusters and distributions in concentrated and dispersed areas

12 p2153 A69-25813

Spacecraft orientation from onboard stellar photographs, calculating absolute and relative elements, accuracy and camera parameters

13 p2296 A69-27696

Positions, spectral types and B magnitudes for possible field horizontal-branch stars at high galactic latitudes, selected from faint A star list

13 p2348 A69-27807

Cepheid variable 1 Carinae position in H-R diagram suggested from microturbulent velocity role in pulsational instability

14 p2522 A69-29590

Interstellar absorption and spatial distribution in northern Aquila with absence of early O-B2 stars, including luminosity function

15 p2683 A69-30513

Milky Way structure, discussing dust bridge and density of absorbing matter between spiral arms of Sagittarius and Carina Cygnus

15 p2683 A69-30514

Member stars number in globular clusters M3 and M5 determined from photometric and kinematic characteristics

15 p2688 A69-30561

Star chains around Eta Carinae, discussing nonrandom real groupings and probability criteria using ADH red sensitive plate without filter

16 p2856 A69-31931

Spatial distribution of stellar densities and velocity distributions in phase space, using Greenwich catalog of positions and proper motions of omega Centauri cluster stars

16 p2859 A69-32220

Giant galaxy classified in terms of stellar population, discussing Orion, intermediate amorphous and combination categories

16 p2862 A69-32395

Southern Milky Way spectral survey for selection, classification and photometry of interesting objects

17 p3031 A69-33101

BCD classification for cepheids, discussing /sigma/ surface definition, locus of normal stars of population I and interstellar reddening

17 p3038 A69-33725

Pulsars properties and distribution in galactic coordinates, deriving interstellar medium properties and physical nature of objects based on neutron star rotation

17 p3040 A69-33800

Dwarf elliptical galaxies of local group, discussing star distribution and orbits, formation process, origin and distribution about Milky Way

18 p3194 A69-34424

Spatial density distribution in star clusters, determining relation between mean stellar mass and density range in subsystems

18 p3198 A69-34757

Pleiades cluster structure, deriving visible density distribution curves for brighter stars

18 p3198 A69-34758

Motion and dispersion of peculiar velocities of stars in gravitational condensing interstellar gas

18 p3198 A69-34760

UBV photoelectric observation of OB and open cluster Tr 16 stars in Carina-Centaurus, suggesting no limit in depth distribution

18 p3200 A69-35133

Pulsars measured parameter data tabulation including right ascension, declination pulse repetition period, showing sources distribution and clusters

18 p3202 A69-35211

Stellar populations in Milky Way galaxy, considering stellar motions, spectroscopy, spatial distribution and galactic dynamics

18 p3202 A69-35284

Star counts in Ophiuchus nebula darkened region /Scorpius-Ophiuchus/ and in comparison fields Corona Australis and Sagittarius

20 p3604 A69-37788

Luminosity calibration for subluminescent stars and space density of blue subluminescent stars south of declination minus 45 degrees based on white dwarfs and binaries

20 p3612 A69-38160

Stars of spectral class F 2 and earlier, brighter than magnitude 11.5, found in four regions of intermediate galactic latitude

20 p3612 A69-38162

Automatic instrument for star detection and azimuth derivation, scanning nighttime zenith star field [AIAA PAPER 69-861]

21 p3762 A69-39389

Resonant asteroids in statistically underpopulated Kirkwood gaps, noting oscillating mean motion distribution

22 p4013 A69-40122

Book on radial velocities and distances in southern Milky Way stellar fields, covering statistical study of star motions in Galaxy, instrumentation, procedures, etc

22 p4020 A69-40317

Wolf-Rayet stars formation, evolution, age, galactic distribution and relation with open star clusters

23 p4208 A69-41288

Absolute magnitude dispersion of galactic cluster brightest members as normally distributed random variable independent of cluster richness or faint members luminosity

23 p4215 A69-42113

Galactic evolution using concept of stellar populations and correlation with metal and He abundances

23 p4218 A69-42323

Elements origin and development in universe, discussing energy generation, structure and population of stars in Galaxy

24 p4386 A69-43335

STAR TRACKERS

Working breadboard model of planet tracker under various illuminating conditions, discussing hardware and closed loop tracking error analysis accounting for signal to noise effects

03 p0463 A69-13214

Stellar identification system using onboard sighting equipment and computer mathematical methods

08 p1347 A69-20657

Tacite rocket probe to study space IR radiation, using passive stellar sensor for recording reference stars positions to recalibrate gyroscope kinetic motion for attitude restoration [ONERA-TP-731]

17 p3001 A69-33220

Star magnitude variation caused by earth atmosphere related by equation to star altitude, station height, sensor response, spectral radiance, etc

18 p3168 A69-34814

Automatic celestial navigation, discussing star trackers design, mathematics of celestial fix and relationship to errors and physical and environmental constraints

18 p3169 A69-34852

Star/horizon measurements for onboard spacecraft navigation without cloud cover obscuration, discussing sightings, data processing and evaluation

19 p3369 A69-35800

Automatic instrument for star detection and azimuth derivation, scanning nighttime zenith star field [AIAA PAPER 69-861]

21 p3762 A69-39389

Satellite attitude estimation from onboard telescope celestial sightings using iterative least squares method, considering measurement error noise and axes wobble

24 p4348 A69-43244

STARCHES

Dynamic differential thermal analysis with He flow performed on biological specimens, proteins and starches, showing discrete decomposition peaks monitoring pyrolysis process

16 p2747 A69-31807

STARFIGHTER AIRCRAFT

U F-104 AIRCRAFT

STARK EFFECT

Europium complexes high resolution emission spectra in relation to molecular configuration

01 p0024 A69-10893

Stark effect meter for electric field measurement in space, discussing absorption cell development

03 p0429 A69-13222

Charged particle density of unsteady plasma from Stark broadening of Balmer H beta line, using time scanning image converter

03 p0481 A69-14145

High temperature measurement based on spectral line displacement and broadening due to Stark effect, noting diagrams for O, Na, Mg, Al and Si at various temperatures

03 p0481 A69-14146

He-Ne and He-Xe laser lines in IR tuned by axial magnetic field, observing Stark patterns of organic molecules [IEEE PAPER C-5]

07 p1150 A69-19050

Helium I line profiles including forbidden component, discussing electron and ion Stark broadening and thermal Doppler broadening

09 p1601 A69-22209

Stark broadening of Balmer H alpha, H beta, H gamma and H delta lines in plasma region in strong magnetic fields

09 p1542 A69-22248

Degeneracy of hydrogenic states to sum S-matrix in Stark broadening calculations

09 p1543 A69-22405

Trivalent rare earth ions Stark structure based on spectroscopic observations of stimulated transitions in lasers

10 p1701 A69-23129

Hydrogen balmer lines broadening by Stark and Doppler effects, finding prominences and chromosphere electron concentrations

11 p1955 A69-24389

Charged particle concentration near electrodes in high current pulsed discharge with separated flames at atmospheric pressure determined by measuring quadratic Stark effect

11 p1927 A69-25219

Electron concentrations in steady Ar and Ar-He plasma jets measured with microwave Fabry-Perot interferometer and Stark broadening of H beta line

12 p2137 A69-26537

Ultimate resolvable line dependence of Balmer series on electron density, considering line broadened by Stark and Doppler effects

13 p2351 A69-27865

Polychromator measurement of hydrogen plasma electron density produced by normal ionizing shock wave, using Stark broadening study of H beta line

14 p2494 A69-29767

Stark effect applicability to charged particle concentration in nonstationary plasma

14 p2497 A69-29790

Time resolved Stark broadened spectral profiles for Na I 5682-88 A and 4978-82 A lines of plasma, comparing electron densities

15 p2656 A69-31155

Stark broadened H gamma profile, considering effect of strong collisions in electron perturbation and electron impact broadening of lower levels

20 p3579 A69-37305

Stark broadening of H-gamma for electron density measurement in plasma, noting temperature range

22 p3985 A69-40664

Electron and ion Stark broadening of allowed and forbidden, triplet and singlet transitions in neutral He at low electron densities, noting Doppler broadening
22 p3985 A69-40665

Classical path approximation in line broadening theory to derive impact and one-electron theories, with application to Stark broadening of Lyman series in hydrogen
23 p4193 A69-41379

Rotational spectra of methylchlorodiazirine at room and dry ice temperature, using K band and Stark effect spectrometers
23 p4194 A69-42207

Hydrogen balmer lines broadening by Stark and Doppler effects, finding prominences and chromosphere electron concentrations
24 p4390 A69-43779

STARLIFTER AIRCRAFT

U C-141 AIRCRAFT

STARS

NT A STARS
NT B STARS
NT BINARY STARS
NT CEPHEID VARIABLES
NT DWARF STARS
NT EARLY STARS
NT ECLIPSING BINARY STARS
NT GIANT STARS
NT HERCULES NOVA
NT HOT STARS
NT MAGNETIC STARS
NT MAIN SEQUENCE STARS
NT NEUTRON STARS
NT NOVAE
NT O STARS
NT PROTOSTARS
NT PULSARS
NT RADIO STARS
NT SUN
NT SUPERGIANT STARS
NT SUPERNOVAE
NT T TAURI STARS
NT VARIABLE STARS
NT WHITE DWARF STARS
NT ZETA AURIGAE STAR

Eight color narrow band photometry of bright stars, discussing band system, instrumentation, data and calibration
02 p0313 A69-11487

Catalog of meridian program star observations made in Brorfelde, determining position relative to FK 4 stars by using impersonal photographic micrometer
02 p0315 A69-11815

Chemical composition of diffuse Orion Nebula and stars compared for lighter elements, considering solar system formation from interstellar medium
08 p1402 A69-20908

Angular momenta of stars, planets and asteroids, plot log of angular momentum per unit mass against log of mass of astronomical object
09 p1608 A69-22716

Faint blue objects in intermediate to high galactic latitudes, summarizing results of UVB photoelectric photometry
10 p1788 A69-24123

Spectroscopy and star classification on basis of spectra
12 p2155 A69-26122

Azimuth error from observations of circumpolar stars at greatest elongation using transit instrument
17 p3028 A69-32878

13 color narrow band photometry of 1000 bright stars in tubular form, discussing sample points, Balmer discontinuity, absolute energy calibration, etc
17 p3038 A69-33692

STARTERS

U ENGINE STARTERS

STARTING

Starting process in nozzle with one dimensional flow treated numerically by finite difference method using pseudoviscosity term
22 p3860 A69-40926

STATE EQUATIONS

U EQUATIONS OF STATE

STATE VECTORS

Linear filter performance degradation due to modeling error in estimate of state vector of stochastic linear dynamic systems
02 p0225 A69-11971

Optimal control of linear systems with state variables generated by linear feedback from output variables, considering time variance
06 p0903 A69-17406

Absolute stability of dynamic control systems with single nonlinear element function of two feedback state variables, giving sufficient conditions
06 p0905 A69-17948

Inertial navigation systems error analysis based on method of state variables
11 p1914 A69-25434

Optimization problem with bounded state variable, noting conditions on trajectories and relations for co-state vector at connecting or branching point
12 p2050 A69-26087

Lumped linear system state estimation with optimal linear smoothing instead of filtering, noting smoothing lag and variance
12 p2122 A69-26524

Equatorial moderately elliptical satellite orbit perturbations calculated in local invariants, assuming state vector dependence of acceleration
17 p3039 A69-33796

STATIC AERODYNAMIC CHARACTERISTICS

AZUR satellite structural development static and dynamic considerations, discussing center of gravity, notching technique and test results
12 p2187 A69-26876

STATIC DEFORMATION

Thermodynamic foundations of permanent deformation theory, noting parallel to viscoelastic material theory
02 p0350 A69-11714

Bar flexure determination for Saint Venant torsional and transverse loading, solving differential equations by finite element methods
09 p1614 A69-21722

Nonlinear programming for calculating static and kinematic failure of one dimensional structures by extending results from linear programming
14 p2418 A69-29597

Potential functions applications to three dimensional static elasticity problems of parallelepipeds, using general stress solution
15 p2715 A69-31216

Krylov functions determined by distribution theory and operational calculus, discussing deformations and statics of straight beams
15 p2715 A69-31475

Vibration properties of cantilever parallelogram box beam, using existing static deformation equations under large aspect ratio condition
21 p3846 A69-39803

Strain diagram with piecewise nonlinear curve for statically indeterminate systems stressed beyond elastic limit
24 p4400 A69-43072

STATIC ELECTRICITY

Electrostatic field strength and conductivity dependence of expansion and contraction of space charge cloud in process of discharging during static electrification
06 p0959 A69-18219

Signal propagation in channel subject to static investigated using Fokker-Planck type equation in statistical mechanics methods
16 p2753 A69-32437

Atmospheric ozone production by silent discharges near ground level during first stage of storm cell development
16 p2785 A69-32623

Electrical failures in aircraft due to static electrification of electrically heated windscreens, noting materials for reducing surface resistivity
19 p3256 A69-36769

Spark gap protection of input transistors in radio receivers against antenna-collected static charge damage
21 p3681 A69-38395

STATIC FIRING

Mississippi Test Facility (MTF) hardware data acquisition system error analysis from extensive simulated static firing tests
10 p1673 A69-23287

Ablative materials for solid rocket nozzles, discussing static firing tests, rating system, equipment design and cost reduction
19 p3357 A69-35537

Solid rocket motor static firing tests in low pressure environment, presenting data concerning vacuum chamber pressure, diffusers pressure distribution, chamber wall temperature distribution, etc
22 p4000 A69-40593

Solid rocket motors failure during static firing, discussing sequence of events
24 p4365 A69-43260

STATIC FRICTION

Stiction friction on magnetic tape and contact surfaces noting effect of binders, plasticizers, humidity and temperature
19 p3312 A69-36285

Film thickness and normal load effect in thin film solid friction, noting dependence on deformation at contact
22 p3955 A69-40400

STATIC INVERTERS

Airborne static inverter, called Digital Inverter, for conversion of DC to AC, single phase and/or three phase, noting precise frequency control
11 p1824 A69-24499

Modularized static AC and DC inverters and converters for aerospace electrical power conditioning systems, discussing circuit functions and performance tests
23 p4073 A69-42291

STATIC LOADS

Stability of ductility and fatigue strength of stainless steel under longtime static loads in vacuum and in liquid lithium
03 p0450 A69-13912

Effective slip systems in hexagonal close packed magnesium alloy under static and hydroexplosive loading, examining flow mechanism for fine structure formation
04 p0615 A69-146390

Reciprocity theorem applied to Somigliana relations for static loads and coupled thermoelasticity
09 p1618 A69-222604

Aluminum alloy thin sheets with central transverse fatigue cracks subjected to increasing static loads to fracture, investigating crack tip deformation
10 p1709 A69-230566

Subregions method in coupled thermoelasticity, discussing numerical values for thin steel circular disk
11 p1970 A69-246066

Energy dissipation in freely oscillating bodies under static stresses described by differential equation, assuming elliptical hysteresis loop
11 p1919 A69-250922

Energy dissipation and fatigue in metals under cyclic static loads, determining logarithmic decrements of vibrations and Bauschinger effect
12 p2181 A69-266122

Complex two layered shell of revolution under static and dynamic asymmetric loads analyzed using SABOR/DRASTIC computer codes
12 p2184 A69-268111

Fatigue cracks growth rate under combined static and cyclic stresses
15 p2709 A69-30808

Repeated static stress limit of internal pressure vessels, emphasizing effect of redistribution of stresses and strains
15 p2712 A69-30973

Plastic expansion in metals due to alternating torsional and static tensile loading
16 p2875 A69-32291

Static tensile stresses effect on energy dissipation in alloys used in compressor blades found dependent on composition and heat treatment
17 p2991 A69-33934

Laminated critical rate dampers consisting of ring shaped thin corrugated steel plates inserted between bearing and rotor, showing dependence on static load
17 p3066 A69-33945

Lunar surface bulk density determined from laboratory and spacecraft measurements of static bearing capacity as functions of depth and solids percentage
18 p3193 A69-34366

Load capacities of graphite lined journal bearings, discussing factors affecting wear rates
18 p3148 A69-35002

Reinforced plastics static fatigue strength under various loads including thin walled tubes long term tests under constant internal pressure
18 p3162 A69-35353

Plastic deformation in hardened Ti alloys with thermally unstable beta phase under static compression and tensile loads by electron microscope
21 p3746 A69-39161

Stress distribution on surface of stator vane loaded statically as cantilever derived by brittle coatings, strain gages and three dimensional photoelasticity
22 p4042 A69-40310

Summation methods for multiple damages caused by static fatigue in glass fiber reinforced plastics under stepwise loads
22 p3974 A69-40748

Plastic deformation by uniaxial tension during transition from dynamic to static loading from microscopic and macroscopic standpoint, noting slip lines
22 p4047 A69-41081

Solid solutions precipitation effect during deformation process on static and dynamic tensile tests of Al alloy by electric resistance measurement
22 p3972 A69-41082

Stress analysis of cylindrical tubes under torsional and transverse static loads based on vibrational theory, applied to rectangular cantilever tube
23 p4228 A69-41916

Mathematical method of processing test data air-frame panels subjected to repeated static loads to obtain lifetime equations and statistical characteristics
24 p4400 A69-43086

Total load factor static vertical component and lubricant flow rate square related to pocketed hydrostatic journal bearing revolutions
24 p4321 A69-43091

Static and cyclic tensile fatigue of alumina by ring test method, measuring time to failure
24 p4334 A69-43343

Deferred rupture as function of applied load noting test methods
24 p4407 A69-43801

STATIC PRESSURE
NT HYDROSTATIC PRESSURE

Axially symmetric bodies shape for static pressure at location independent of Mach number
04 p0542 A69-14738

Static pressures, profiles of local longitudinal velocity, fluctuating wall pressures and power spectra of wall pressures measured for subsonic turbulent flow [ASME PAPER 68-WA/FE-36]
05 p0750 A69-16109

Vortex incompressible flow in thin cylindrical chamber, analyzing outer and inner region and interface tangential velocity, shear and static pressures
10 p1679 A69-23557

Static pressure measurements at surface of sharp plate in supersonic flow during gas/liquid jet injection
11 p1821 A69-25479

Static pressure distribution induced by statistically roughened duct walls on supersonic stream
15 p2593 A69-31148

Monograph on static pressure and turbulence in free jets and jet flames covering radial velocity oscillations with and without chemical reactions, confined jets turbulence, etc
15 p2719 A69-31190

Static and dynamic characteristics of pressure compensated oil-hydraulic flow control valves and relief valves with emphasis on linearized effects
19 p3256 A69-36713

Axial velocity and static pressure for incompressible fluid flow through straight smooth porous tube [ASME PAPER 69-FE-44]
20 p3517 A69-38000

STATIC STABILITY
NT DIMENSIONAL STABILITY
NT SHELL STABILITY
NT STRUCTURAL STABILITY

Variational principles of dynamic shell theory using Legendre transform for relations and boundary conditions of Timoshenko theory
01 p0166 A69-10262

Multiple configuration analysis of structures systematically predicting static and dynamic response of structures of single configuration class
01 p0169 A69-10639

Phase plane diagram utility in toppling stability analysis of spacecraft, emphasizing numerical integration time reduction
02 p0334 A69-12376

Universal solution for static and dynamic response of structural components by method of initial parameters
03 p0527 A69-13746

Static stability of three dimensional elastic bodies under subcritical strains, noting application to stability of cylindrical shells and rods
05 p0834 A69-15784

Free flight static, dynamic stability and drag data for 10 degree semiangle cone obtained at 8-16 Mach numbers [AIAA PAPER 69-133]
06 p0862 A69-18050

Spherical caps axisymmetric static and dynamic buckling under load, using axisymmetric nonlinear elastic shell theory approximation and finite difference equations [AIAA PAPER 69-89]
06 p1028 A69-18133

Refractory compounds static strength temperature dependence at high temperatures measured in reference to melting temperature
09 p1523 A69-21873

Static characteristics of transistors dependence on current carriers surface recombination in inactive base region, noting strong electric field influence
09 p1464 A69-22287

Blood vessel model in form of cylindrical shell filled with liquid for studying cardiovascular system dynamic and static problems
12 p2018 A69-25989

Wind tunnel tests for static stability of Black Brant 4 vehicle second stage with flare and two fin flare combinations at supersonic speed
17 p2948 A69-34212

Soviet book on hydraulic servo drive covering design and performance, static and dynamic characteristics and stability problems
18 p3093 A69-34356

Two dimensional elastoplastic problems in static condition, discussing analytical, variational and finite difference methods
18 p3217 A69-34594

Static stability of three dimensional elastic bodies under subcritical strains, noting application to stability of cylindrical shells and rods
18 p3223 A69-35036

Static dynamic and damage tolerant strengths of advanced materials for VTOL aircraft with emphasis on Ti, cryoformed 301 stainless steels and filamentary composites [AIAA PAPER 69-764]
19 p3433 A69-35658

Cirrus cloud height above sea level and shape correlation with lower section static stability determined by stereophotogrammetric measurements
20 p3570 A69-37349

Static and fatigue strength of end-closed filament-wound vessels under internal pressure
21 p3846 A69-39797

Three dimensional welded structure of thin walled girders with stability loss, discussing welding strain gage measurements and simplified computational procedure
23 p4169 A69-42007

Static mechanical strength of syntactic foam tested by generating failure conditions based on combined biaxial and triaxial stress [ASME PAPER 69-APMW-24]
24 p4336 A69-43095

STATIC TESTS

Uniaxial strain static and gas gun compression tests result compared for syntactic foam
02 p0345 A69-12295

Large convective clouds in superheated air generated by static tests of Saturn 5 first stage
03 p0462 A69-14125

Static structure ground test for Saturn-Apollo vehicle short stack, describing air pressure simulation, data acquisition and readout systems
15 p2589 A69-31079

Automatic multichannel system for turbine blades static tests, discussing operation principles, component sections, programmed tape and vibration modes
15 p2672 A69-31209

Static, transient and in-space environmental tests at satellite structures and heat shield test facilities in Italy
16 p2765 A69-31750

STATICS

NT ELECTROSTATICS
NT HYDROSTATICS
NT MAGNETOHYDROSTATICS

Asymmetically loaded systems composed of shells of revolution, developing digital computer algorithm for solution of statics problems
05 p0840 A69-16201

Book on statics of thin walled shells of revolution covering stress-strain analysis for geometrical shapes
10 p1800 A69-23197

Book on solution of linear ordinary differential equations and simultaneous systems using bar statics-equivalent beam method
15 p2711 A69-30929

Matrix formulation for discrete element method applied to linear static and eigenvalue problems of thin walled segments, using homogeneous differential equations
19 p3445 A69-36831

Soviet collection of papers on static and dynamic problems in elasticity and plasticity theory covering plates, shells, beams, etc
22 p4038 A69-39911

STATIONARY ORBITS

Maritime radio communications satellite service for ship safety, discussing stationary equatorial satellite systems [AIAA PAPER 68-232]
02 p0356 A69-12383

Perturbations of stationary orbital vehicles of arbitrary latitude due to earth triaxiality, noting control by low thrust rocket engine
05 p0823 A69-16037

Dioscures system for international air traffic control and navigation over North Atlantic by means of two geostationary satellites [UN PAPER 68-95832]
06 p0954 A69-17063

Project Symphonie, discussing stationary communication satellite, coverage, frequencies and characteristics
06 p0886 A69-17072

Stable stationary positions for spacecraft determined by formulating variational equations for perturbing effects of earth triaxiality
06 p1006 A69-17565

Synchronous orbit attainment with continuous electric propulsion, noting payload ratio dependence on various parameters and changing orbit inclination [AIAA PAPER 69-275]
09 p1586 A69-21265

Ionic propulsion application to geostationary satellite attitude correction
10 p1753 A69-23841

European geostationary satellite orbit inclination and eccentricity modification for maximum observation time of Northern Hemisphere by high resolution IR radiometer
15 p2650 A69-31389

Ion propulsion applied to geostationary satellites attitude control, discussing thrust levels, cesium ionization, colloidal propulsion, etc
16 p2837 A69-32068

Geostationary satellite orbit used for communication satellites, noting ultimate limit of channels as related to separation angles between satellites
21 p3673 A69-38757

Satellite communication system capacity for segment of geostationary orbit extended to models involving two angular dimensions
23 p4131 A69-42521

STATIONKEEPING

Multijet electrothermal systems for attitude control and stationkeeping of synchronous communications satellite [AIAA PAPER 67-723]
02 p0305 A69-12375

Ammonia resistojet stationkeeping subsystem on-board ATS 4 satellite, noting flight test data agreement with ground tests [AIAA PAPER 69-296]
09 p1560 A69-21212

Feasibility of automatic stationkeeping for synchronous satellites by using solar sailing techniques and low thrust systems [AAS PAPER 68-151]
19 p3429 A69-35950

Stationkeeping motion effect on synchronous satellite orbit determination accuracy analyzed by two dimensional model, finding position uncertainty
20 p3595 A69-37218

Automatic stationkeeping /geosynchronization/ for maintaining satellite in circular synchronous orbit at all geocentric longitudes for prolonged time with low fuel consumption
21 p3805 A69-39213

Optimal control stationkeeping for maintaining space probe stability around collinear points in three body problem [AIAA PAPER 69-906]
21 p3807 A69-39338

Orbital results for Automatic Orbit Control System of Lincoln Experimental Satellite LES 6, using pulsed plasma microthrusters and self contained orbit measurement and control methods [AIAA PAPER 69-934]
21 p3824 A69-39428

Impulsive velocity correction determination method for precise stationkeeping of stationary satellite, discussing perturbations [AIAA PAPER 68-456]
21 p3817 A69-39757

High altitude balloon stationkeeping system combining battery powered propeller and drag chute
22 p3866 A69-40941

STATIONS

U DEEP SPACE INSTRUMENTATION FACILITY
U GLOBAL TRACKING NETWORK
U GROUND STATIONS
U ORBITAL SPACE STATIONS
U ORBITAL WORKSHOPS
U SPACE STATIONS
U STADAN [SATELLITE TRACKING NETWORK]
U TRACKING STATIONS
U WEATHER STATIONS

STATISTICAL ANALYSIS

NT AMPLITUDE DISTRIBUTION ANALYSIS
NT CORRELATION COEFFICIENTS
NT FACTOR ANALYSIS
NT MAXWELL-BOLTZMANN DENSITY FUNCTION
NT NONPARAMETRIC STATISTICS
NT NORMAL DENSITY FUNCTIONS
NT PEARSON DISTRIBUTIONS
NT POISSON DENSITY FUNCTIONS
NT PROBABILITY DENSITY FUNCTIONS

NT PROBABILITY DISTRIBUTION FUNCTIONS
 NT RANK TESTS
 NT RAYLEIGH DISTRIBUTION
 NT REGRESSION ANALYSIS
 NT REGRESSION COEFFICIENTS
 NT SEQUENTIAL ANALYSIS
 NT STANDARD DEVIATION
 NT VARIANCE [STATISTICS]
 NT WEIBULL DENSITY FUNCTIONS

Statistical equilibrium equations solution for thermodynamic equilibrium variations of populations of very high energy levels in hydrogen and complex atoms
 01 p0150 A69-10395

Optimal predictor design by comparison of statistical input models, measuring signal filter performance by root-mean-squared errors
 01 p0043 A69-10558

Statistical band model and line by line calculations of transmittance for IR bands in absorption spectra of ozone and water vapor
 [AFCR-68-0505] 01 p0124 A69-10919

Gross behavior patterns of intense sporadic E including seasonal, diurnal and geographic variations and latitudinal and longitudinal effects
 01 p0070 A69-11157

Euler-Lagrange relationship from equations of motion of tagged particle in turbulent velocity field consisting of random dispersive waves
 01 p0121 A69-11202

Integral and sigma pulse frequency modulation effects on white noise, analyzing autocorrelation and spectral density functions of PFM system output
 01 p0034 A69-11221

Statistical analysis of polarization of semiinfinite electron/ion plasma bounded by dielectric or conducting solid wall, deriving steady state and space potential
 02 p0286 A69-11706

Statistical analysis of polarization of two component nonisothermal electron-ion Coulomb gas plasma containing microfluctuations
 02 p0286 A69-11707

Dissociation and recombination of moderately complex molecules, using master equation with transition probabilities and decay rates obtained from reaction rates statistical theory
 02 p0283 A69-12181

Statistical characteristics of random phase quasi-harmonic process investigated for application of mathematical representation
 02 p0208 A69-12263

Composite tensile-failure modes, discussing failure load prediction, experimental data and statistical analysis of stress concentration effects
 [AIAA PAPER 68-173] 02 p0347 A69-12514

Statistical analysis of unsteady dynamic systems describable by unstable differential equations containing random parameters
 03 p0408 A69-12948

Statistical model of turbulent flow confirms Kolmogoroff hypothesis of equilibrium zone at large Reynolds numbers
 03 p0413 A69-12949

Optimal adaptive systems synthesis by statistical theory
 03 p0409 A69-12977

Statistical linearization of nonlinear memory type elements with stationary Gaussian input, applying Wiener method to one class of problems
 03 p0409 A69-13005

Statistical analysis of data concerning difference between real wind velocity and velocity of gradient wind for winds of various velocities
 03 p0458 A69-13268

Wide signal and noise statistics range to determine noise rejection characteristics of communication system used for single path and diversity reception
 03 p0394 A69-13376

Statistical description of nonelastic processes in nonequilibrium plasma in transverse magnetic field, using kinetic equations for distribution functions
 03 p0476 A69-13412

Statistics of central peaks in lunar craters drawn from catalog
 04 p0656 A69-14675

Statistical characteristics of radiation pattern of mirror antennas in region of irregular sidelobes
 04 p0577 A69-14787

Soviet book of statistical and mathematical tables for calculation, analysis and control of reliability
 04 p0608 A69-15540

Real shape of time correlation function computed from partially averaged data
 05 p0786 A69-15924

Data sampling and statistical verification in large scale sterilization procedures, discussing biological in-

dicator /bacillus stearothermophilus/ and incubation time
 05 p0714 A69-15952

Statistical relations for best value, standard deviation and confidence limits for engineering data, noting weighted least squares polynomial for fitting
 [ASME PAPER 68-WA/PTC-1] 05 p0768 A69-16192

Statistical analysis of aircraft programs engineering man hours, aircraft performance and weight, avionics systems, schedules, etc, as estimating standards
 05 p0769 A69-16239

Secondary particle spectra from proton-proton interactions analyzed in two temperature statistical model, considering momentum distributions
 05 p0797 A69-16368

Statistical studies of current-voltage characteristics of zinc-doped silicon diodes
 05 p0732 A69-16425

Response of single and multidegree of freedom systems to nonstationary random excitation, analyzing spectral density function of pressure field close to jet engine
 05 p0844 A69-16763

Transfer function coefficients from frequency response data determined to obtain information about dynamic system characteristics
 05 p0844 A69-16764

Statistical method to investigate time varying stresses in helicopter structures, considering service life evaluation
 05 p0767 A69-16775

Recombination statistical model for neutron irradiated Si transistors, considering diffusion potential, junction voltage, temperature, activation energy and capture ratio for holes and electrons
 06 p0975 A69-16871

Solar disk surge distribution difference between eastern and western disk parts
 06 p0995 A69-17440

Statistical processing of oscillograms of instantaneous values of wire tension during winding, determining stress characteristics
 06 p0927 A69-17691

Statistical theory of traveling wave antennas for random phase-amplitude distribution of current, discussing phase errors
 06 p0898 A69-17797

M-20 digital computer program designed for calculating statistical characteristics of signals from IR TV scanning system of Cosmos 122 meteorological satellite
 06 p0929 A69-17980

Statistical theory of material strength with application to composite materials reinforced with whiskers and continuous fibers
 [AIAA PAPER 69-123] 06 p1028 A69-18142

Statistical frequency analysis of power spectrum of geomagnetic pulsations, discussing time and latitude dependence
 07 p1122 A69-18297

Statistical study of heart beat, respiration rate and arterial pressure of man during intermittent accelerations and short term weightlessness
 07 p1061 A69-18579

Laminated composite fracture statistical theory with stress enhancements in elements next to primary fracture, comparing elastic and plastic matrices
 07 p1170 A69-18712

Statistical computations of elastic moduli of macroscopically isotropic particulate composites, discussing porosity and elastic properties of materials made by sintering
 07 p1159 A69-18722

Statistical comparison of scintillation depths of Transit 4A satellite to radio star Cassiopeia A
 07 p1215 A69-18821

Spectral null from spectral characteristics and statistical properties of PCM signals used to estimate SNR
 07 p1083 A69-19122

Statistical analysis of cascade of bandpass limiter, ideal phase detector and video filter for mathematical modeling of coherent communication systems
 07 p1084 A69-19147

Statistical properties of intensity fluctuations of light fields consisting of incoherent Gaussian component heterodyned with single frequency coherent beam
 07 p1182 A69-19416

Statistical radomes design, analyzing dielectric constant and wall thickness tolerances effects on amplitude and phase of transmitted wave
 07 p1111 A69-19531

Antenna pattern loss factor for determination of average probability of detection vs SNR curves from three dimensional or pencil beam radars
 08 p1270 A69-19858

Statistical theory of fluids in equilibrium based on correlation functions for pair interactions between constituent molecules, invoking superposition closure approximation
 08 p1350 A69-19863

Statistical techniques to develop nickel base superalloy with high temperature capabilities for jet engine turbine bucket applications
 08 p1329 A69-20001

Radio source counts log N-log S diagram slope uncertainty due to finite source number, discussing statistical analysis methods accuracy
 08 p1383 A69-20048

Statistical dynamics of turbulent incompressible fluid, discussing harmonic function in Navier-Stokes equation
 08 p1303 A69-20323

Receiving systems for digital telemetry signals from spacecraft, analyzing receiver performance by statistical methods
 08 p1276 A69-20591

Statistical approach to design and management, discussing multiple regression analysis, attributes, intuition, probability, simulation and applications
 08 p1344 A69-21162

Separation of normal geomagnetic field component from limited length measurements by moving averages, considering error and inhomogeneity of anomalous field
 09 p1486 A69-21537

Spacecraft motion parameters and physical characteristics of space determined from statistical analysis of measurement data
 09 p1495 A69-21764

Mathematical model for improving statistical approximation convergence and accuracy in estimating structural components parameters
 09 p1461 A69-21857

Soviet book on methods of optimal statistical solutions and problems of optimal control covering basic equations of random processes, stochastic differential equations, etc
 09 p1473 A69-21932

Soviet book on statistical theory of discrete signal demodulation, covering demodulator analysis and synthesis methods
 09 p1455 A69-21933

Time dependent statistical equilibrium equations solutions for describing time development of atomic populations by means of ergodic Markov chain
 09 p1542 A69-22218

Radio signal reflection from objects of complex configurations by statistical model
 09 p1460 A69-22662

Statistical theory and dynamic programming to synthesize optimal pulsed control systems having restrictions on control device storage capacity
 09 p1476 A69-22673

Probability analysis of distortions caused by pulse noise action on digital information
 09 p1476 A69-22678

Inverse problem in stochastic processes, considering random moving force and strip load in structural stress analysis
 10 p1793 A69-22876

General and classical statistical techniques for cutting effectiveness and operational reliability of cutting fuses
 10 p1749 A69-23004

Data interpretation, discussing correlation describing effectiveness of independent variable and table giving values directly from sample size, t, z, F and chi square values
 10 p1669 A69-23040

Double galaxies consisting of components moving away from each other with hyperbolic velocities from statistical tests of hypotheses
 10 p1775 A69-23203

Characteristics of dynamic mechanical systems including solid state and hydrodynamic analogs of ideal incompressible fluids, based on statistical theory of turbulence
 10 p1678 A69-23209

Two fold congruency method for statistical evaluation of fluorescent flow detection penetrant sensitivity and reproducibility
 10 p1700 A69-23374

Head injuries evaluation in aircrew, noting motor cycle accidents
 10 p1649 A69-23378

- Statistical, economic and psychological aspects of aeronautical and astronautical profitable reliability in relation to operation, using mathematical model
10 p1700 A69-23839
- Shock wave structure determination in simple monatomic gas, using statistical counting and successive approximation algorithm
10 p1680 A69-23894
- Secondary corpuscular stream effect on diurnal variations in cosmic ray intensity obtained from statistical analysis
10 p1769 A69-23904
- Ionized meteor trails initial radii statistical characteristics determined for two models
10 p1783 A69-23917
- Statistical characteristics of transverse shifts of ray directions in turbulent atmosphere for arbitrary wave parameter values
10 p1657 A69-23942
- Statistical regularization for obtaining a priori probability distribution information on mathematically incorrect inverse geophysical problems, deriving algorithm
10 p1689 A69-23968
- Brittle fracture of steel analyzed using statistical model, attributing occurrence to coalescence of arrested cracks initiated at different points
10 p1803 A69-24033
- Statistical estimation theory giving angular resolution of imaging systems in terms of noise characteristics and modulation transfer function
10 p1725 A69-24048
- Statistical theories of turbulence applied to thermal convection between infinite slippery plates at large Prandtl number
11 p1997 A69-24283
- Statistical parameters of critical load distribution in buckling of imperfection sensitive elastic structures, noting probability of failure
11 p1969 A69-24415
- Probability models used in statistical approach to fracture mechanics, noting role of weakest link model in representing brittle fracture
11 p1975 A69-24673
- Count rate meter for statistical frequency of signals applied to input of trigger with Poisson distribution of pulse intervals
11 p1884 A69-24734
- Statistical analysis of convective layer thickness and moisture content effect on convective cloud configurations, using satellite TV pictures
11 p1912 A69-24827
- Statistical analysis of lee wave clouds from satellite TV pictures, determining lengths and air flow direction
11 p1912 A69-24828
- Statistical method for determining accuracy of air-field weather reports on takeoff and landing conditions, visibility and cloud ceiling, correlating forecasts and actual conditions
11 p1913 A69-25205
- Dynamic properties of supply sources in carbon dioxide shielded welding as function of short circuit current statistical parameters, noting metal spatter correlation
11 p1892 A69-25667
- Lunar surface layer structure by statistical analysis of data concerning craters and stones distribution as shown by lunar orbiter photographs
12 p2154 A69-25816
- Statistical analysis of photometric curves for meteors undergoing fragmentation at onset of vaporization
12 p2154 A69-25819
- Descriptive statistics in quality control dealing with variability and probability, discrete and continuous variables, frequency distributions and measures of central tendency and dispersion
12 p2100 A69-25846
- Statistical reliability tools and methods, graphs and charts, estimations, prediction techniques and demonstrations
12 p2101 A69-25847
- Statistical turbulence theory applied to turbulent flow transport properties in lower atmosphere
12 p2125 A69-25894
- Stratospheric aerosol attenuation factor vertical distribution statistical structure, tabulating normalized correlation matrices, eigenvectors and eigenvalues
12 p2125 A69-25956
- Service life of system predicted by identifying and testing system variables of mission phases, using obtained data in statistical estimation
12 p2101 A69-25970
- Observed frequencies of number of members in multiple systems of galaxies
12 p2156 A69-26222
- Spherical wave propagation in homogeneous turbulent medium, discussing nonstationary statistics as applied to vertical propagation in atmosphere
12 p2029 A69-26251
- Statistical characteristics of stationary stochastic pulse train specified by probability generating function, noting power density
12 p2030 A69-26383
- Statistical data for visual binary systems with known spectral classes or colors and one component near main sequence
12 p2159 A69-26666
- Statistical method for calculating upper bound heights of sources responsible for magnetic anomalies
12 p2071 A69-26696
- Stationary inventory problems analysis, discussing inventory policy, recursive and or limiting procedures, stationary point processes, stock delivery time instants, etc
12 p2192 A69-26750
- Variational statistics applied to hourly meteorological data for predicting airport runways icing conditions time and duration
12 p2127 A69-26900
- Statistical analysis of UBv characteristics of blue objects located near galactic north pole by scintillation techniques
12 p2168 A69-27054
- Statistical properties of spatial radiance distribution of sky and forest backgrounds in IR, noting one dimensional Wiener spectra
12 p2131 A69-27072
- Inductive converters accuracy calculation by statistical method based on probability theory
13 p2259 A69-27424
- Vertical air motions and cloud behavior relationship based on statistical analysis of TV cloud pictures from Cosmos 122 satellite
13 p2291 A69-27724
- Statistical analysis of radiation temperature structure for automatic recognition of meteorological situations from actinometric satellite observations
13 p2293 A69-27842
- Friction wear of solid bodies based on microscopic contact system model, deriving particle distribution law from physico-statistical analysis
13 p2268 A69-28051
- Statistical theory of cumulative wear of machine parts with application to engine parts of passenger aircraft, automobiles, tractors, etc
13 p2268 A69-28052
- Wide signal and noise statistics range to determine noise rejection characteristics of communication system used for single path and diversity reception
14 p2410 A69-28826
- Statistical linearization of strong nonlinearity in series with random-gain amplifier element, deriving formulas for statistical gain parameters
14 p2425 A69-28920
- Statistical description of geomagnetic field as random vector field, presenting correlation functions from empirical estimates from geomagnetic charts
14 p2437 A69-29062
- Statistical synthesis of optimal control for quasi-harmonic systems by extending asymptotic method to include unremovable measurement error in output value
14 p2426 A69-29420
- Polynomial and nonlinear equations of state for solids and liquids analyzed using uncommon statistical and least squares methods
14 p2486 A69-29470
- Phase screen technique for deriving statistical characterizations of perturbations imposed on wave propagating through random medium applied to remote probing
14 p2414 A69-29511
- Vibrostand effects on statistical characteristics of random vibrations of elastic system, discussing simulation techniques
14 p2536 A69-29743
- Statistical analysis of data for 18-19 June 1936, estimating expressions involving external and internal components of geomagnetic field at storm time disturbances
14 p2444 A69-29883
- Two antenna radio direction finding system statistical synthesis, using quadratic linear process
15 p2562 A69-30110
- Orthogonal signal recognition in set of false signals by resolving devices with limited sensitivity, giving design formulas for error probability
15 p2563 A69-30135
- Quasi-uniform pseudorandom numbers program transmitter statistical characteristics suited for solving problems by Monte Carlo method
15 p2572 A69-30336
- Design and test criteria for dynamically loaded structures from various viewpoints, discussing statistical variations, load strength and limitations
15 p2618 A69-30368
- Statistical calculation of three dimensional frames of thin walled rods, using method of initial parameters in matrix form
15 p2714 A69-31199
- Statistical data concerning noctilucent clouds formation during IQSY, noting tendency to form along geographic longitudes and day and night existence
15 p2598 A69-31255
- Book on statistical theory of signal detection and resolution in random noise covering hypothesis testing, digital communications, stochastic signals, filters, etc
16 p2748 A69-31566
- Book on correlation theory of statistically optimal systems covering linear continuous, discrete, nearly optimal, nonlinear, decision element and adaptive systems
16 p2764 A69-32114
- Automatic nonrepairable control elements reliability evaluated statistically with differentiable lifetime distribution function
16 p2764 A69-32199
- Separation of normal geomagnetic field component from limited length measurements by moving averages, considering error and inhomogeneity of anomalous field
16 p2783 A69-32532
- Statistical analysis of Brewer-Mast electrochemical soundings of vertical ozone distribution for developing computer programs of climatological behavior
16 p2786 A69-32632
- Statistical characteristics of ozone measurements with Dobson spectrophotometers and filter ozonometers, determining requirements for maximum effectiveness of ozone network
16 p2787 A69-32639
- Rotating bending fatigue tests on aluminum alloys based on statistical analysis for material strength
17 p3052 A69-32979
- Random stress statistical properties and relationship to fatigue life, discussing Fuller prediction, comparison with test data, and vehicle design evaluation
17 p3053 A69-32988
- Satellite Proton 2 orientation from onboard measurement data, discussing general statistical method and data processing results
17 p3001 A69-33221
- Statistical dynamics of turbulent incompressible fluid, discussing harmonic function in Navier-Stokes equation
17 p2952 A69-33313
- Helicopter flight loads spectra data compared on statistical basis to establish component service lives [AHS PAPER 301]
17 p2901 A69-33548
- Tropical storms wind speeds related statistically to characteristics as pictured from satellites
17 p2997 A69-33690
- Radar unit for network component /wind patrol/ in statistical observations of wind drift conditions in meteor trails
17 p2939 A69-33901
- Statistical analysis in inlet air flow dynamics, discussing inlet duct design and pressure variations [AIAA PAPER 68-649]
17 p2896 A69-34020
- Linear isotropic elastic continuum dislocations distribution, deriving transport equations by statistical methods, noting analogy between energy/ momentum and MHD equations
18 p3212 A69-34352
- Statistical characteristics stabilization of random loads in fatigue tests, noting transfer function of testing machine and spring stiffness
18 p3215 A69-34544
- Statistical model for coherent functions obtained from laser equation, showing amplitude and frequency coupling of radiation fluctuations
18 p3152 A69-34820
- Time sharing remote computer station allowing on-spot data processing and output answers, formulating best-fit equation representing statistical data [SAWE PAPER 799]
18 p3107 A69-34860
- Rational vehicle weight estimation based on statistical data /REBOS/ including gross weight, weight coding, subdivisions, balance and size, inertia moments and products, etc [SAWE PAPER 791]
18 p3220 A69-34866

Meteor flakes nature and statistics from studying 318
meteors characterized by irregular brightness curve
18 p3203 A69-35333

Statistical regularization for determining vertical at-
mospheric temperature profile from measurements of
earth radiation in 15 micron carbon dioxide band
18 p3167 A69-35339

Statistical description of microstructural elements
/fibers and fillers/ in unidirectional fiberglass rein-
forced plastics determined in lattice nodes
18 p3163 A69-35363

Statistical relations between minute blood circula-
tion volume, O capacity and consumption rate in tis-
sues of men and dogs
19 p3260 A69-35896

Book on statistical communication and applications
to radio and radar systems technology to provide
guidelines for design decisions
19 p3267 A69-35900

Digital data compression system transmission error
statistical analysis, emphasizing addressing schemes ef-
fect on compression ratio
19 p3272 A69-36261

Ionosphere disturbances due to high altitude ther-
monuclear explosions, discussing experimental proof
by Cosmos satellites short wave transmitter radio signal
scintillation statistical evaluation
19 p3304 A69-36624

Two procedures for processing statistical data con-
cerning Gaussian processes made exchangeable by
manageable formula
19 p3361 A69-36646

Random gust design requirement and gust load
covariances to define boundaries of gust-loading region
for airframes
20 p3621 A69-37167

Small scale inhomogeneities motions in E and
sporadic E layers, processing data with method of full
correlation analysis and statistical method
20 p3528 A69-37683

Space vehicle launcher system reliability from trials
and adopted corrections, basing formal computation
on adoption of normalized form for reliability
likelihood
20 p3618 A69-38278

Mean importance variations of sunspot groups in
various latitude intervals, reducing data statistically
with dispersion analysis and autocorrelation method
20 p3616 A69-38303

Statistical analysis of galactic structures subject to
Newton gravitation covering globular clusters and
spiral disk and rotating bar galaxies
21 p3803 A69-38924

Statistical analysis of wind velocity measurements at
floating buoy stations, presenting velocity power spec-
tra for different frequency bands
21 p3758 A69-39111

Dispersion and correlation function for atmospheric
transparency due to water vapor from statistical model
of absorption bands and effective mass
21 p3759 A69-39113

Statistical characteristics of linear transformations of
gravity field anomalies by linear operators, noting com-
putation of covariance function
21 p3716 A69-39247

Nonlinear filter for optimal estimation of mean,
covariance and third central moments of system, noting
simulation tests stability for orbital navigation
[AIAA PAPER 69-852] 21 p3686 A69-39380

Statistical error analysis of autonomous manned
spacecraft navigation in long duration eccentric Mars
orbits
[AIAA PAPER 69-880] 21 p3763 A69-39406

Space vehicles optimal pulsed control systems
statistical synthesis, considering structural constraints
on operation, memory capacity and algorithm coeffi-
cients
21 p3767 A69-39651

Statistical regularization for obtaining a priori prob-
ability distribution information on mathematically incor-
rect inverse geophysical problems, deriving algorithm
21 p3680 A69-39654

Hydrodynamic turbulence in statistical prediction
for Burger equation, considering statistical inference
problem for initial conditions and prediction criterion
with estimable error
21 p3697 A69-39673

Weighting function of statistically optimal automatic
dynamic system generating stochastic loads, using
Fredholm equations
21 p3688 A69-39861

Statistical analysis of chromospheric flares connec-
tions with sunspots, using frequency distributions of
flares occurrences in sunspot groups
22 p4001 A69-39996

Resonant asteroids in statistically underpopulated
Kirkwood gaps, noting oscillating mean motion dis-
tribution
22 p4013 A69-40122

Distinction between faint and bright sources of
slowly varying solar microwave emission components
applied to geomagnetic activity statistics
22 p4020 A69-40306

LM descent engine behavior upon contact with lunar
surface simulated, basing test condition on statistical
trajectory analysis indicating fire until touchdown pos-
sibility
[AIAA PAPER 69-1020] 22 p3923 A69-40391

Deformation localization and slip functions in
statistical theory of plasticity, discussing approxima-
tions and untenability of Yosimura theory criticism
22 p4044 A69-40742

Statistical critique of Polyak values for tangential
dendritic spread of primate retinal neurons
22 p3880 A69-40848

Data evaluation, measurement accuracy and statisti-
cal procedure, using silicates chemical analysis
22 p3897 A69-40984

Infinites in statistical theory of radiative processes
when applied to plasmas containing charged particles
and radiation
22 p3991 A69-41055

Statistics of jet aircraft accidents including world-
wide data and safety trends
22 p4054 A69-41128

Jet transport operation and accidents statistics,
analyzing world data, accident causes and safety gap
22 p4054 A69-41130

Statistical analysis of position errors inherent in
position-finding system utilizing position fixing planes in
three dimensional space
22 p3979 A69-41253

Statistical analysis of operation of precision electric
spark machine servosystems with RC generator based
on working pulse peak voltage distribution
23 p4168 A69-41307

Statistical model of cratered planetary surface slopes
and elevation applied to radio wave scattering by moon
and Venus
23 p4209 A69-41322

Tolerance limits for uncertain requirements vector in
linear programming with random variation, introducing
nonparametric statistics with sensitivity analysis
[AAS PAPER 69-079] 24 p4340 A69-42821

Ruby laser second harmonic generation statistical
characteristics with dielectric surface scatterer, show-
ing variety of modes and high cross sectional stability
24 p4328 A69-43164

Norms for quantitative vectorcardiography derived
from statistical analysis of results from healthy young
subjects, emphasizing medical evaluation of flying per-
sonnel
24 p4277 A69-43390

Pilots myopia incidence statistical study after initiate
medical examination, emphasizing skiagram value in
prognosis
24 p4267 A69-43400

STATISTICAL COMMUNICATION THEORY U COMMUNICATION THEORY

STATISTICAL CORRELATION

Odd and even translational two sample test statistics
uncorrelated when combined sample distribution func-
tion is equally symmetric
01 p0106 A69-10925

One dimensional distribution law of random process
with arbitrary correlation function, verifying normality
hypotheses by integral criterion
08 p1299 A69-21069

Object shapes automatically classified from reflected
radio signals, considering correlation description of ob-
ject effective dispersion surface diagram
14 p2411 A69-28917

Spatial correlation function of Northern Hemisphere
geopotential, using model based on random distribu-
tion of potential vortex fluctuations for atmospheric
circulation
14 p2476 A69-29822

Statistical correlation of temperature and tail- wind
data for London-New York route at 50 mb for SST
operation
15 p2651 A69-30690

Galaxies clusters spatial distribution based on crude
distance estimates, discussing serial correlation of
counts and interpreting results
16 p2862 A69-32371

One dimensional distribution law of random process
with arbitrary correlation function, verifying normality
hypotheses by integral criterion
16 p2765 A69-32484

Line width and intensity correlation of laser radia-
tion noting damping constant
17 p2980 A69-33012

Analytical-statistical weight prediction to derive and
apply correlation expression, illustrated with bending
stress equation applied to aircraft wing group
[SAWE PAPER 810] 18 p3221 A69-34900

Hypercorrelation concept for statistical charac-
terization and structuring of systems with application to
management models, discussing multipoint systems
18 p3236 A69-35236

Random vibrations in linear systems during spectral
and correlation analysis, noting nonlinear systems
18 p3227 A69-35491

Statistical relation between expansion velocities and
radii of planetary nebulae due to Lyman-c and diffuse
Lyman-alpha radiation
19 p3426 A69-36575

Random processes correlation functions determined
by stochastic differential equations applied to lunar
surface statistical characteristics determination
22 p4033 A69-41092

STATISTICAL DECISION THEORY

Book on elements of detection and signal design
covering transmitter optimization for coherent and
noncoherent digital communication systems, statistical
decision theory, radar detection, etc
12 p2033 A69-26867

Recognition system for discrete decision function
generation to select one out of two classes of objects,
deriving solutions for selection probability
17 p2932 A69-33119

STATISTICAL DISTRIBUTIONS

NT PEARSON DISTRIBUTIONS

NT PROBABILITY DISTRIBUTION FUNCTIONS

NT RAYLEIGH DISTRIBUTION

Statistical characteristics of magnetoionic com-
ponents of obliquely incident waves, obtaining en-
velope distribution of signal reflected from F2 layer
02 p0314 A69-11691

Scattering data for optical diagnostic measurements
on two component suspensions or gases, using random
distributions of spheres
04 p0555 A69-14282

Energy fluxes statistical distribution produced by
random and regular energy sources
07 p1076 A69-18510

Frequency-fluctuation correlation functions of radio
wave field behind n random screens with random phase
shifts calculated, obtaining statistical characteristics
07 p1076 A69-18525

Interrelation between parameters of statistical dis-
tribution of amplitude, angular and phase charac-
teristics of signals scattered by extended body perform-
ing oscillations
07 p1085 A69-19154

Statistical distribution of chemical elements average
abundances in earth crust and meteorites and
nucleosynthesis of elements under specific astral condi-
tions
08 p1310 A69-20941

Mean temperature values accuracy determined from
fixed period values by frequency graphs, discussing
deviations from mean
09 p1534 A69-21511

Asymptotic behavior of frequency function of fluc-
tuations for generalized ensemble parameters, noting
characteristic function convergence to Gaussian at
thermodynamic limit
09 p1623 A69-22395

Variational approximation of probability measures
and products of random matrices, discussing point dis-
tribution on Lobachevskii plane
10 p1719 A69-23399

Zero crossing statistics measurements for 1/f noise,
noting statistically stationary character of probability
density distributions of interval spacings between zero
crossings
10 p1656 A69-23657

Two photon photoelectron counting statistics and in-
tensity fluctuations of incident radiation compared
with single photon detectors and applied to laser out-
puts
10 p1704 A69-23658

Statistical gain characteristics of radar antennas at
very short Fresnel zone ranges compared to Fraunhofer
zone
12 p2040 A69-26470

VLF signal strength minima during transition fading,
considering asymptotic statistical distribution
12 p2032 A69-26862

Statistical distribution of instantaneous frequency
and power of signal associated with Doppler spectrum

for exponentially distributed and determinate frequencies

12 p2032 A69-26863

Fiber axis distribution resulting from mechanical working deformation of matrix containing initially randomly oriented fibers

12 p2188 A69-26933

Statistical distributions of refractive index parameters in tropospheric radio propagation from psychrometer soundings, discussing lapse rate

13 p2254 A69-28428

Statistical characteristics of magnetoionic components of obliquely incidence waves, obtaining envelope distribution of signal reflected from F 2 layer

13 p2355 A69-28722

Statistical distribution functions for radar cross section of flying aircraft

14 p2414 A69-29500

Target trajectories determination based on radar data with allowance for association between neighboring readings, using statistical characteristics obtained with Markov chains

15 p2566 A69-30335

Autonomous radiometers signals statistical properties used in space technology, discussing radar signals phenomenological models, measurement errors and energy characteristics

15 p2566 A69-30337

Cost effectiveness of test selection when statistical distribution of load and strength are known, presenting curves for equally dispersed normal parameters distribution

15 p2720 A69-30401

CO absorption lines in solar spectrum analyzed theoretically and experimentally indicating random distribution of molecules

15 p2688 A69-30552

Statistical characteristics of Q switched He-Ne laser emission gain fluctuations during transient process from subthreshold to superthreshold value

15 p2634 A69-30960

Quantum mechanics method for obtaining photocount distribution from optical maser photoelectron counting statistics

15 p2635 A69-31238

Matrix eigenvalue problems with statistical properties, applying to dynamic structural systems and verifying solutions by Monte Carlo simulation

16 p2871 A69-31878

Statistical properties of parametric amplifier and frequency converter by Schrodinger quantum mechanics and P-representation of density matrix

16 p2761 A69-32363

Device quantity failure kinetics or time dependence effect on time-to-failure distribution resulting from given device degradation coefficients distribution

17 p2936 A69-32895

Fiber distribution in oriented fiberglass reinforced plastics, noting statistically isotropical distribution and use for regular structure model

18 p3162 A69-35355

Surges statistical properties observed in Sweden /1957-1967/ noting latitude distribution pattern, radio emission association, rate dependence on solar cycle, etc

18 p3204 A69-35393

Ozone vertical distribution predicted statistically, using total ozone amounts and backscattered UV spectral measurements

18 p3132 A69-35426

Astronomical observatory photomultiplier cell dark current fluctuations, showing statistical resemblance to binomial distribution

20 p3599 A69-37470

Atmospheric turbulence statistical distribution mass measurements using velocity, gravity and weight recordings based on calibration of aircraft as turbulence measuring instrument [ONERA-TP-699]

20 p3541 A69-37754

Random function output current obtained in phototube and scintillation detector including amplitude distribution, time measurements and pulse shape discrimination

22 p3947 A69-40670

Circular and spherical antenna arrays elements random distribution in three dimensional space using Monte Carlo method, considering arbitrary excitation and nonisotropic elements

22 p3914 A69-40704

Uniform random field model development by taking moments in linear transformation form of certain initial field

23 p4183 A69-41523

Randomly oriented disks and rods scatter pattern used to determine causes of log-normal distribution of radar cross section fluctuations

23 p4116 A69-41592

Absolute magnitude dispersion of galactic cluster brightest members as normally distributed random variable independent of cluster richness or faint members luminosity

23 p4215 A69-42113

Optimal scheme of combining moment estimators set derived for computational simplicity and asymptotic efficiency

24 p4342 A69-43704

STATISTICAL MECHANICS

Transport properties of steam, analyzing selection, correlation and prediction using statistical mechanical theories

01 p0174 A69-10110

Book on mathematical and physical fundamentals of molecular gasdynamics based on statistical mechanics, discussing free molecular flow

01 p0060 A69-10711

Statistical mechanics and thermodynamics for molecular systems applied to gravitational systems, discussing collisionless Boltzmann equation and Chandrasekhar binary collision model

02 p0323 A69-12273

Covariant statistical mechanics for equilibrium thermodynamics

03 p0533 A69-13758

Nonequilibrium statistical physics for kinetic theory of gases and statistical mechanics, noting irreversibility and entropy

05 p0793 A69-15769

Viscosity coefficient tensor in terms of autocorrelation functions, using linear reaction theory of mechanical disturbances

05 p0794 A69-15785

Gas adsorption on solids, discussing statistical mechanical theory assuming localized adsorption for first adlayer and nonlocalized mobile layer adsorption on top

06 p0980 A69-17387

Mechanical equilibrium and stability conditions for system of interacting atoms in crystal structure

06 p0944 A69-17504

Book on theory of kinetic equations covering classical mechanics, Liouville equation and distribution functions, kinetic equations relation to fluid dynamics, KBG equations, etc

07 p1180 A69-18411

Approximate solution to problem of estimating thickness of shock wave by statistical mechanics

07 p1119 A69-18704

Statistical theory of ionization for magnetoactive plasma with nonequilibrium concentration level and nonequilibrium energy distribution

07 p1193 A69-19142

Statistical properties of electromagnetic field diffracted by illuminated plane aperture studied in Fresnel zone on basis of partial coherence theory

11 p1836 A69-24978

Classical statistical mechanics of systems with identical or limited different particles, discussing particle collisions in dilute gases

11 p1870 A69-25009

Elastic proton scattering measurements, noting consistency with statistical theory when diffraction is taken into account

13 p2302 A69-28368

Statistical mechanics - Conference, Kyoto, September 1968

14 p2487 A69-29986

Mass point system moving in gravitational field, discussing statistical mechanics, relaxation time and evolution of stellar systems

14 p2530 A69-29987

Satellite signal probability density determined from scintillation plus Faraday effect in statistical terms

16 p2751 A69-32103

Lynden-Bell statistical mechanics of relaxation in collisionless one dimensional stellar system, discussing low energy particles distribution

16 p2862 A69-32376

Signal propagation in channel subject to static investigated using Fokker-Planck type equation in statistical mechanics methods

16 p2753 A69-32437

Lattice vibration theory of solid state diffusion for Cu including anharmonic effects formulated using equilibrium statistical mechanics, considering interacting phonon events

17 p3015 A69-32822

Closure conditions for Vlasov turbulence, discussing infinite systems of equations for dynamics of statistical quantities

17 p2958 A69-34228

Statistical dynamics and structure of turbulent shear flows in incompressible fluids of constant density, discussing Reynolds stress at critical layers

18 p3123 A69-34922

Viscosity coefficient tensor in terms of autocorrelation functions, using linear reaction theory of mechanical disturbances

18 p3173 A69-35037

Negative absolute temperatures physical meaning confirmed mathematically using statistical physics

18 p3231 A69-35403

Observation space transformed from statistical synthesis of nonlinear closed systems to multiple control system subjected to statistically assigned perturbations

19 p3287 A69-36662

Statistical equations for compressible gas, discussing turbulent quantities separated into fluctuating and macroscopic parts

19 p3300 A69-36784

Statistical mechanics applied to mechanical properties and thermodynamics studies of rapidly expanding or collapsing self gravitating systems

21 p3801 A69-38702

STATISTICAL MOMENTS

U DISTRIBUTION MOMENTS

STATISTICAL PROBABILITY

U PROBABILITY THEORY

STATISTICAL TESTS

NT RANK TESTS

Odd and even translational two sample test statistics uncorrelated when combined sample distribution function is equally symmetric

01 p0106 A69-10925

Algorithm for hypothesis optimal tests by series during signal detection in presence of noise

13 p2222 A69-28509

Nonlinear regression techniques for statistical simultaneous measurement of thermal properties including convergence criterion [AIAA PAPER 69-602]

17 p3070 A69-33260

Statistical testing techniques using small sample size at low component levels to predict product performance

18 p3117 A69-34528

Residual analysis prior to statistical tests on experimental data

21 p3755 A69-39120

Structural analysis and statistical fracture approach to design and testing for polycrystalline ceramic materials, including combined stress testing and load redistribution models

24 p4333 A69-43339

STATISTICAL WEATHER FORECASTING

Weather forecasting using statistical technique and Subsynoptic Advection Model of Weather Bureau, discussing mathematical background for various early morning predictions

08 p1345 A69-20298

Stochastic model for real time on demand weather predictions using REEP /regression estimation of event probabilities/ equations in Markov chain

08 p1345 A69-20299

Synoptic meteorological predictions using statistical dynamic approach, considering probability distributions and nocturnal temperature decay

08 p1345 A69-20300

Continuous variate duration estimates by Markov process, giving example of surface air temperature conditional probability distribution

08 p1346 A69-20731

Zonal westerlies variations associated with tidal cycles, discussing principal component analysis, zonal index, bandpass filtering, aliasing, prediction and stepwise regression

09 p1537 A69-22242

Statistical rules for seasonal forecasts based on temperature and precipitation deviations analysis in long term climatological records, considering sunspot cycle role

12 p2125 A69-25895

Synoptic process predictability, discussing forecasting of large and small scale processes by mathematical formulas and statistical description

12 p2126 A69-26576

Probabilistic forecasts in meteorological support of aviation, comparing economic implications of squall forecasting

14 p2474 A69-29739

STATOR BLADES

General atmospheric circulation instability factors for statistical weather forecasting, considering atmosphere as nonlinear oscillating system, analyzing relaxation time

14 p2476 A69-29820

Probability diagnosis and prognosis for buffeting zones based on Bayes formula, determining clear air turbulence zones

15 p2648 A69-30645

Nocturnal development of air mass stratus clouds in Texas and mechanism of formation, discussing turbulent mixing theory

15 p2649 A69-30893

Stochastic meteorological models based upon presence of weather regimes, illustrating association with statistical inference problems

18 p3166 A69-34822

Thunderstorm probabilities at Cape Kennedy, giving data on frequency, duration, multiple occurrence, nonoccurrence, runs and conditional probabilities

18 p3167 A69-35100

Weather prediction, considering mathematical and empirical procedures, computer applications, atmospheric instability, etc

21 p3757 A69-38324

Storm location and severity prediction by pattern recognition theory, using quantized radar data, compared with statistical prediction

21 p3678 A69-39458

STATOR BLADES

Transpiration cooling effect on turbine stator blade performance determined by annular cascade tests, using data to establish empirical correlation for loss coefficient

[ASME PAPER 69-GT-39] 09 p1432 A69-22487

Turbine stator blade performance determination from total pressure surveys downstream of blade row, noting problems in pressure measurement

[ASME PAPER 69-GT-103] 09 p1432 A69-22521

Dry friction whip role in radial rubs dynamic stability in labyrinth seals and blade tips of turbomachinery

[ASME PAPER 69-VIBR-56] 10 p1804 A69-24146

Stress distribution on surface of stator vane loaded statically as cantilever derived by brittle coatings, strain gages and three dimensional photoelasticity

22 p4042 A69-40310

STATORS

Stator setting effect on single stage turbine performance, considering blade loss and surface velocity distribution

[AIAA PAPER 69-525] 16 p2841 A69-32686

Wobble tolerance influence on axis deflection affecting accuracy during assembling of turbine rotors and stators

21 p3733 A69-39719

STEADY FLOW

NT COUETTE FLOW

NT HARTMANN FLOW

Effect of steady flow of incompressible conducting fluid on magnetic dipole at center of sphere

01 p0128 A69-10363

Indeformable gravity waves in horizontal cylindrical channel, using first and second order approximations for nearly uniform flow equations solutions

01 p0060 A69-10392

Steady one dimensional motion of current sheets in plasma accelerators, noting condition of zero initial conductivity

01 p0133 A69-11220

Static pressure field induced by steady subsonic flow of compressible inviscid fluid through two dimensional duct with statistically distributed wall roughness

01 p0062 A69-11279

Hydrodynamic analysis for determining steady flow region with closed separation area for Reynolds numbers to describe viscous mixing by Prandtl equations

02 p0190 A69-12570

Generalization of characteristic relations for steady supersonic 3D motion of polytropic gas, obtaining complex screw motions

03 p0412 A69-12847

Conservation equations for steady incompressible flow in variable area duct with mass transfer at walls simplified by linearizing inertial and convective terms

03 p0413 A69-13011

Supersonic flow region about blunt body calculated on basis of gasdynamic equations for steady flow of inviscid nonheat conducting gas

03 p0363 A69-13658

Steady flows of incompressible viscous fluid exterior or interior to circular cylinder

04 p0589 A69-14898

Steady plane supersonic gas flows with large number of shocks computed on basis of weak solutions of hyperbolic system

04 p0544 A69-15284

Secondary steady flow /Taylor vortices/ between rotating cylinders, discussing development due to stability loss of Couette flow

05 p0745 A69-15780

Solution to system of equations in boundary layer theory of steady incompressible fluid flow

05 p0751 A69-16454

Nonisentropic simple waves in two dimensional steady flow of ideal gas

05 p0752 A69-16687

Self similar solution for Navier-Stokes equations describing steady motion of submerged eddy jet of incompressible viscous fluid injected into half space

06 p0908 A69-16825

Steady two dimensional MHD flow of perfectly conducting fluid past nonconducting wedge with magnetic field orthogonal to flow velocity

06 p0964 A69-17244

Three dimensional hypersonic steady flow around blunt and pointed cones at nonzero angles of attack calculated by method of characteristics

[AIAA PAPER 69-187] 06 p0865 A69-18176

Steady two dimensional MHD flow in finite region of aligned fields

07 p1188 A69-18274

Steady flow circuit characteristics in square cross section channels of planar geometry fluid control elements in case of laminar flow

07 p1118 A69-18293

Unstationary characteristics method applied to numerical computation of steady compressible flow around airfoil

[ONERA-TP-630] 07 p1049 A69-18413

Boundary layer approximation for steady laminar flow of viscous incompressible fluid past paraboloid of revolution, obtaining vorticity distribution

07 p1120 A69-18812

Steady conical compressed flows in nonaxisymmetric ring nozzles characterized by discontinuities

07 p1120 A69-18989

One dimensional flow of conducting inviscid compressible fluid in channel in presence of transverse fields, discussing steady velocity flows

07 p1191 A69-19014

Arbitrary stationary foil in perfect incompressible fluid moving at constant velocity at infinity assuming plane, steady and irrotational flow

08 p1303 A69-20272

Two dimensional steady flow of finitely conducting compressible fluid subjected to magnetic field with two zero components

08 p1369 A69-20843

Hydromagnetic steady forced flow against porous rotating disk, integrating equations of motion by Karman-Pohlhausen and series methods

08 p1370 A69-21005

Plane steady transonic flow of perfect fluid around airfoils with constant curvature using hodographic method, discussing various boundary conditions

09 p1429 A69-21605

Permanent flow of solenoidal vector line rotation in steady nondegenerate rotational flow having complex lamellar unit normal to streamline

10 p1727 A69-22862

Steady three dimensional flow of gases with thermodynamic relaxation, noting flow field weak discontinuities and effect of discontinuities in wall curvature

10 p1677 A69-22894

Surface recombination efficiencies on metals measured as function of exposure time in steady Oseen flows, providing step-function increase in oxygen atom concentration

10 p1726 A69-23526

Finite difference technique for numerical computation of steady supersonic two dimensional gas flows, with or without diffusion normal to mean flow streamlines

10 p1679 A69-23595

Nonlinear partial differential equations for solution of steady stratified flows, noting hydrostatic pressure distribution and horizontal and vertical scales

11 p1869 A69-24889

Finite difference solutions for time dependent equations of motion for steady flow around cylinder at large Reynolds numbers

11 p1872 A69-25133

Steady incompressible fluids flow around stationary wings and through rotating blades cascades based on Prandtl airfoil theory of bound vortices

11 p1873 A69-25202

Steady flow of viscous incompressible fluid studied with system of equations equivalent to Navier-Stokes equations and finite difference method

11 p1875 A69-25480

Invariant transformation of Euler equations of motion for plane steady flows of perfect compressible fluid

11 p1877 A69-25739

Expansion of stream function of steady meridional flow of viscous fluid at small Reynolds numbers, giving expansion in spherical coordinates

13 p2247 A69-27737

Compressible gas MHD steady one dimensional flow in electric and magnetic fields

14 p2500 A69-29901

Space charge formation in MHD generator channels ascribed to gas parameters nonuniformity and magnetic induction vector presence, assuming steady flow

15 p2659 A69-30635

Steady incompressible MHD laminar flow between parallel porous disks solved for large Reynolds and Hartmann numbers

15 p2662 A69-30968

Steady inviscid compressible flow past wavy wall with simulated ablation, studying reflections effect on relationship between surface pressure and wall geometry

16 p2770 A69-31909

Monograph on ring airfoil theory with nonuniform incidence covering steady flow and shear flow transition into boundary value problem of potential theory

17 p2889 A69-32995

Exact similarity solutions of hypersonic small disturbance equations for steady flow, discussing equations of state and motion and dissociating gas flow

[AIAA PAPER 69-707] 17 p2953 A69-33448

Secondary steady flow /Taylor vortices/ between rotating cylinders, discussing development due to stability loss of Couette flow

18 p3123 A69-35032

Boundary layer equation for steady incompressible flow past flat plate with parabolic leading edge, obtaining series solution in inverse powers of Reynolds number

18 p3124 A69-35270

Equations governing steady diabatic gas flows in Crocco velocity vector field, discussing changes in total pressure

21 p3695 A69-39007

Navier-Stokes equations exact solutions for two dimensional steady flow of compressible viscous heat conducting perfect gas

22 p3929 A69-40117

Viscoelastic fluid steady flow in porous walled channel, examining mass flow solution continuity

22 p3930 A69-40118

Piston motion influence on gaseous motion set up by constant energy explosion, applying to steady high Mach number flow past blunt nosed object

22 p3931 A69-40892

Integral equations of motion for plane steady flow of viscous incompressible electrically conducting fluid around flat plate

22 p3992 A69-41109

Class of one dimensional nonlinear waves and shock structure reduced to steady flows in radiation gas dynamics

23 p4240 A69-42466

STEADY STATE

U EQUILIBRIUM

STEADY STATE CREEP

Deformation dependence on strain hardening and recovery rate during transient and steady state creep

06 p0943 A69-17236

Thin circular cylindrical shells steady creep behavior under combined lateral and axial pressures, using Tresca criterion and associated flow rule

06 p1023 A69-17506

Polycrystalline W steady state creep rate at high temperatures noting effects of stress, grain size and subgrain size

07 p1158 A69-18241

Dislocation climb theory of steady state creep, noting necessity of self diffusion mechanism in any high temperature creep theory

08 p1329 A69-20000

Beta parameter in exponential stress dependences of high temperature steady state creep rate and time to rupture of creep resistant alloys

10 p1712 A69-23719

Creep behavior of dispersion strengthened Nb base bcc alloy, studying temperature and stress effects on steady state creep rate

19 p3343 A69-35924

Radial and tangential stress analysis of rotating disk during steady state creep, using equations solved by finite difference method
22 p4043 A69-40458

STEADY STATE FLOW
U EQUILIBRIUM FLOW

STEAM
Steam ingestion tests on carrier aircraft gas turbine engines, analyzing inlet pressure and temperature distortion in steam-air environment
01 p0143 A69-11062
Sterilization without damage by mixing steam and formaldehyde at 80 C under subatmospheric pressure, noting thorough penetration
05 p0713 A69-15946
Aircraft steam catapult test facilities, noting construction and operational requirements
10 p1674 A69-24068

STEAM FLOW
Transport properties of steam, analyzing selection, correlation and prediction using statistical mechanical theories
01 p0174 A69-10110
Wet steam injector power losses in nozzle as function of humidity, noting compensation of nozzle throat diameter and fluid flow rates
13 p2246 A69-27490
Pulsed performance of saturated steam reaction jet, comparing steam performance to nine gases for equal temperatures and thrust levels
21 p3785 A69-39021

STEAM GENERATORS
U BOILERS

STEAM TURBINES
Positive displacement Rankine cycle rotary wet steam engine design compared with piston type, noting simplified evaporator and tests
23 p4069 A69-42252

STEARTHERMOPHILUS
Data sampling and statistical verification in large scale sterilization procedures, discussing biological indicator /bacillus stearothermophilus/ and incubation time
05 p0714 A69-15952

STEEL STRUCTURES
NT WELDED STRUCTURES
Fatigue strength reduction of structural steels fatigued in rotating bending after tensile deformation
03 p0450 A69-13916
Plastic moments calculation of continuous steel beams under various loading patterns
05 p0837 A69-16035
Noncontacting torque meters using magnetoelastic properties of steel shafts, discussing gas turbine and industrial applications
[ASME PAPER 69-GT-64] 09 p1500 A69-22480
Load carrying capacity of thin steel plates fatigued by cyclic shear buckling
17 p3052 A69-32980
Plasticity of tubular steel annealed in vacuum furnace and subjected to complex tension and torsion along deformation trajectories containing salient point
21 p3839 A69-39197
Mechanical stress measurement in cylindrical steel subjected to loads inside coaxial transducer, using transducer signal in contactless eddy current method
24 p4296 A69-42654
Structural detection in steel welded joints using higher harmonics from eddy current sensing element
24 p4319 A69-42886

STEELS
NT AUSTENITIC STAINLESS STEELS
NT BAINITIC STEEL
NT CARBON STEELS
NT CHROMIUM STEELS
NT HIGH STRENGTH STEELS
NT MARAGING STEELS
NT MARTENSITIC STAINLESS STEELS
NT NICKEL STEELS
NT STAINLESS STEELS
Corrosion of steel surfaces in contact with molybdenum disulphide noting influence of high humidity, milling and inhibitors
01 p0094 A69-10367
Pressure and temperature dependence of slow crack growth in hardened steel in gaseous hydrogen environment
01 p0096 A69-10612
Microscopic cleavage strength of high nitrogen steel notched bars determined from critical tensile stress criteria using elastoplastic analysis method
01 p0169 A69-10765

Steel selection for heat treated parts, discussing strength and hardness, service conditions, carbon content, quenching, cost, etc
01 p0101 A69-11397

Steel corrosion by iodine noting effects of water and oxygen
03 p0444 A69-13310

Vacuum effect on steel friction, noting changes in residual gases and heat transfer conditions
03 p0434 A69-13915

Methods of protecting industrial steel against hydrogen corrosion at high temperatures and pressures including cladding, carbon additions, surface film coating, etc
04 p0613 A69-14432

Prolonged loading effect on mechanical properties of 18Kh2N4VA steel at low temperature, discussing notched and unnotched specimens
04 p0614 A69-14573

Cr gas deposition on steel by means of chromium chloride salt, noting chromizing conditions effect on carbide growth and friction resistance
04 p0605 A69-14577

Nb and Cr additions effects on Hadfield type steel mechanical properties, noting improvement especially at low temperatures
04 p0614 A69-14579

Strain hardening and softening characteristics of maraging steels, Ni-Co and other steels and Ti-Al-Mo alloy
04 p0618 A69-15156

Sheet steel composition effect on gas-tungsten arc welds porosity
04 p0607 A69-15219

Hardenability of ShKh-15 steel, establishing relationship of porosity to sintering method
04 p0619 A69-15390

Creep properties of EP-376 steel under slowly varying loads
05 p0782 A69-16692

Fatigue tests on steel of various diameters using standard and accelerated methods
07 p1233 A69-19315

Atmospheric and alloying elements effects on casehardening by gas carburization of structural steels, noting carbon potential
07 p1167 A69-19344

Microstructural changes in 52100 steel bearing inner rings during cyclic stressing, obtaining thickening rate data on white-etching regions and lenticular carbides
08 p1319 A69-20004

Cr-Ni-Mo steel toughness with strain induced austenite to martensite transformation by TRIP /transformation induced plasticity/
08 p1330 A69-20012

Filler metals for HY steels, discussing tensile and yield strength, elongation and area reduction of butt welds deposited
08 p1320 A69-20406

Hard-drawn steel wire wound pipes and tanks, properties and design calculation, discussing laminates and permissible stress
08 p1414 A69-20487

Cyclic stress-strain and fatigue behavior in aircraft structural metals, discussing hardening and softening in aluminum alloys, steels and titanium alloys
10 p1714 A69-23981

Cyclic deformation resistance and fatigue damage accumulation in aluminum alloys, aircraft steels and titanium alloys
10 p1715 A69-23983

Brittle fracture of steel analyzed using statistical model, attributing occurrence to coalescence of arrested cracks initiated at different points
10 p1803 A69-24033

Arc welding aluminum to steel using bimetal transition insert piece
11 p1891 A69-24929

Steels classification for welded construction according to heat treatment and metallurgical structures
12 p2111 A69-25826

Fusion and solid state welding of steels, considering electron beam, HF resistance, friction and explosive welding
12 p2100 A69-25830

Quantitative interferometric analysis of shock induced wavelength variations in glass and polished steel plates using Q switched ruby laser light source
12 p2089 A69-26185

Fatigue fracture surfaces in cast steel and Al alloys, studying fracture morphology, crack propagation rate and striation spacing with microfractographic methods
12 p2116 A69-26916

Friction resistance between steel and ground basal in ultrahigh vacuum, showing increase by adhesion
13 p2298 A69-28014

Sensitivity decrease of reversible temper brittleness of low alloy steels due to Mo inhibiting effect on phosphorus diffusion
13 p2283 A69-28491

Stannate immersion process for reduction of magnesium-steel couples galvanic corrosion, discussing bath operating limits
14 p2466 A69-29933

Prolonged loading effect on mechanical properties of 18Kh2N4VA steel at low temperature, discussing notched and unnotched specimens
15 p2638 A69-30274

Titanium effect on structural steels mechanical properties noting anisotropy ascribed to sulfides, nitrides and borides
15 p2640 A69-30633

Brittle toughness determination method compared with Robertson and notch impact tests, evaluating steel susceptibility to brittle failure propagation
16 p2795 A69-32796

Fracture toughness of structural steels, discussing evaluation methods for brittle fracture resistance, toughness values and ratings correlation, etc
17 p2989 A69-33554

Dry dynamic friction of brass disk against steel surface reduced using ultrasonic oscillations creating air gap
18 p3135 A69-34587

Standard reference radiographs for weld defects on steel sheets and plates
18 p3150 A69-35425

Annealing effect on transition zone cohesion strength in two layer steel-titanium sheet, investigating role of TiC formation
18 p3159 A69-35450

Cyclic stress frequency on mild steel corrosion fatigue tests, showing strength dependence on potential and stress current
19 p3342 A69-35775

Stress relaxation of heat-resistant steels as function of equal stress during different elevated temperatures, applying results to time residual stress prediction
19 p3342 A69-35778

Pyrolyzed tetraethoxysilane for carburizing steels and Ti alloys at 850-1050 C
19 p3328 A69-36161

Nylon wear curves and friction coefficients for steel-on-nylon pairs determined as function of normal load
19 p3329 A69-36495

Fatigue strength tests of steels simulating boiler installation operating conditions, reproducing corrosion characteristics of water
19 p3347 A69-36741

C content and microstructure effect on electrochemical parameters of Fe and steels in dilute sulfuric acid, discussing Tafel constants and current density
20 p3563 A69-38002

Fatigue resistance of bimetallic sheets of steel and Al alloys by fatigue resonant machine, analyzing lifetime distribution and failure probability
21 p3835 A69-38773

Trace elements role in precision metallurgy for obtaining certain steel properties
21 p3750 A69-39870

Nonmetallic inclusions effect on steels cyclic strength dependence on inclusion composition and metallic matrix properties, derived from fatigue tests
22 p4047 A69-41064

Friction characteristics during diamond honing of different steel grades, determining lubricating and cooling liquids effect on friction coefficient
22 p3958 A69-41170

Mechanical properties of welded joints in Kh 18N9T steel at very low temperatures using austenitic-ferritic and austenitic welds
22 p3958 A69-41204

Residual stress measurement in steels and composite materials by X ray diffraction, discussing specimen preparation, diffractometer alignment, elastic modulus determination, etc
24 p4331 A69-42736

Low cycle fatigue strength tested on notched and unnotched round steel bars, distinguishing between fatigue lives for crack initiation and propagation
24 p4404 A69-43627

STEEP GRADIENT AIRCRAFT
U V/STOL AIRCRAFT

STEEPEST DESCENT METHOD

Minimum fuel attitude control of spacecraft by Pontryagin principle and extended steepest descent method
03 p0522 A69-14100

Baird-Hitchcock iterative method analog computer simulation by steepest descent
05 p0723 A69-15933

Continuous parameter identification methods for parameter optimization in automatic control system analysis and synthesis, using modified steepest descent optimization
05 p0725 A69-16474

Optimum evasion tactics for aircraft pursued by missile, using steepest ascent method for maximization of distance of closest approach
06 p0866 A69-17401

Power law fluids boundary layer near flat plate studied by series expansion and steepest descent methods, determining velocity gradient and skin friction coefficient
15 p2589 A69-30002

Stress and deformation in cross section of beam during complex loading using steepest-descent method
16 p2873 A69-32132

Steepest ascent convergence improved in orbital glider reentry trajectories optimization problems, discussing bang-bang and cosine control-variable changes
19 p3398 A69-35666

Kinetic model and steepest descent method to optimize one dimensional combustor
[AIAA PAPER 68-644] 19 p3448 A69-35943

Boundary layer equations solved for MHD version of Falkner-Skan problem, using Laplace transform and steepest descent technique
21 p3693 A69-38750

Unitary matrix representing generalized inverses, proving weak method of steepest descent for least squares solution of equations
21 p3755 A69-38926

Branched trajectory optimization for split rocket vehicles using projected gradient or steepest descent method
[AIAA PAPER 69-917] 21 p3808 A69-39346

STEEPNESS

U SLOPES

STEERABLE AN' ENNAS

NT INERTIALESS STEERABLE ANTENNAS

Nomograph for planning circular planar aperture antenna arrays, discussing element totalling and spacing, layout geometry, sidelobe suppression and scan loss from broadside
01 p0037 A69-10017

Equation for beam shift during beam steering of phased array by conjugate element phase shifting
02 p0219 A69-12340

Interferometer at lambda 21 cm using fully steerable paraboloids for processing output signal with on-line digital computer
03 p0411 A69-13468

Dynamic behavior of large steerable radio telescope, showing structural resonance influence on error detection system
03 p0412 A69-14093

Collimation of row and column steered phased arrays
04 p0570 A69-14304

Nonorthogonal beam steering commands for multielement two dimensional phased array antenna
04 p0570 A69-14305

Electronically steered and shaped beams for linear and ring phased array antennas by sampling element signals multiplexed into single channel
04 p0570 A69-14307

Phased array antenna radiator element design, emphasizing configuration selection and reflection loss for beam steering
04 p0572 A69-14321

Hybrid mode Ku-band mixer steering electronic scanning phased array design
04 p0572 A69-14325

High gain self steering repeater for multibeam microwave array system for earth-satellite communications
04 p0573 A69-14330

Electric position servosystems for 50 ton telemetry reception antenna and 1200 ton loading turntable of nuclear power plant
04 p0585 A69-15184

Electrohydraulic radar antenna telecontrol system, discussing pump assembly, hydraulic motor and pump control servojack
04 p0551 A69-15185

Frequency controlled time delay network for broadband phased array antenna steering
04 p0580 A69-15469

Digital radar systems, discussing control computers, beam steering computers, signal processors, mode control, displays and chirp networks
05 p0718 A69-15748

Miniature current discontinuity antennas for VHF and UHF, describing airborne electronically steerable array exhibiting efficiency and minimum structural disturbance
07 p1105 A69-19111

Onboard digital computer evaluation of trigonometric functions for antenna pointing
07 p1089 A69-19745

Broadband steerable arrays design, describing Wulvenberger array with doublet aeriels yielding good radiation patterns and low cost construction
08 p1288 A69-20963

Wideband array antenna IF time delay steering realization, showing steering independence of bandwidth
08 p1290 A69-20974

Large steerable mm wave radio telescope of Simeiz observatory in U.S.S.R. noting computer aided pointing system
10 p1674 A69-23805

Self steered retrodirective antenna arrays with phase synthesizer, combining signals from individual elements at LF levels
11 p1850 A69-24983

High gain self steering microwave repeater for earth-satellite communications noting design, performance and results of color TV transmissions
11 p1839 A69-25294

Number 2 ground communications antenna system on Goonhilly Downs for British Post Office earth station
12 p2044 A69-26923

Bandwidth limitations for phase steered planar arrays in satellite applications, discussing weight reduction by modulo 2 pi beam steering
17 p2941 A69-34082

Beam shape loss /BSL/ for electronically steerable array in search mode, determining optimum search beam locations from BSL computations
20 p3506 A69-37717

S band phased array receiver developed to track automatically moving telemetry transmitter by electronic beam steering
23 p4120 A69-41751

Structural features and performance of 300 ft steerable receiving antenna, discussing aiming error, aperture efficiency, azimuth and altitude drive
23 p4148 A69-42121

Feasibility studies to optimized design for 440 ft steerable filled-aperture radio and radar telescope, discussing parabolic configuration, radome selection, etc
23 p4148 A69-42123

Multisupport suspension arrangements for reducing reflector surface weight-loading distortion in steerable parabolic radio telescope antennas
23 p4149 A69-42128

Structural analysis program for obtaining steerable antenna surface deflections at various altitude angles and wind conditions as design parameters
23 p4230 A69-42129

High sensitivity communication system design consisting of radome enclosed steerable antenna, 500 kw transmitter and microwave configuration compatible with low noise receivers
23 p4149 A69-42131

Large paraboloidal reflector antenna computerized structural design, detailing framing, steering control, support structure, etc
23 p4231 A69-42135

STEERING

Gyroscopic apparent rate meters generating steering moments in inertial navigation systems for determining moving object position and course
18 p3134 A69-34556

Steerable landing gear system consisting of freely casting corotating wheel nose gear, tilttable axle and main gear skids for lifting body spacecraft
[AIAA PAPER 69-790] 19 p3243 A69-35639

STELLAR ATMOSPHERES

NT CHROMOSPHERE

NT SOLAR ATMOSPHERE

NT SOLAR CORONA

Pulsating magnetic white dwarfs as pulsar models, discussing radio emission mechanisms via shock wave interaction with stellar plasma atmosphere
01 p0149 A69-10269

Hydrogen line profiles in various early stars compared with profiles predicted from model atmosphere calculations for rotating and nonrotating early stars
01 p0154 A69-10876

Microturbulent velocity parameter correlation to iron-to-hydrogen ratio for G dwarfs, using model atmosphere abundance analyses
01 p0154 A69-10877

Pulsar hypothesis based on oscillating white dwarf surrounded by hot rarefied corona to explain radio emission
03 p0505 A69-13077

Stellar image and spectrum distortions during occultation observed from satellite, discussing recovery of atmospheric composition data from stellar spectra
03 p0421 A69-13346

Radiative transfer equations solved for electron scattering stellar atmosphere, using transformation of integrodifferential transfer equations into singular integral equations
03 p0466 A69-13351

Scaled solar and gray-body temperature distribution models compared to determine stellar atmosphere
04 p0653 A69-14626

Stellar spectra taken with rapid scanning Michelson interferometer, noting IR excess due to radiation from clouds surrounding stars
04 p0655 A69-14667

White dwarfs atmospheric pulsation suggested as pulsar mechanism, considering thin adiabatic atmospheric model with constant lapse rate
05 p0828 A69-16659

Temperature distribution for static stellar corona in presence of magnetic field, noting energy flow process
06 p1002 A69-17316

Rayleigh scattering cross sections for He, C, N and O compared with corresponding absorption coefficients, noting opacity of H deficient stars
06 p1002 A69-17319

Emission line profiles in spherical atmosphere expanding with constant radial velocity computed by Monte Carlo methods
06 p1009 A69-17965

Stellar atmospheres radiative opacity, computing metal absorption coefficients
07 p1220 A69-19392

Radiative opacity in stellar atmospheres, discussing effect of UV continuum on photospheric radiation field
07 p1221 A69-19393

Hydrogenic approximation validity in evaluation of atomic energy levels and radiative absorption cross sections for computation of stellar opacity
07 p1223 A69-19626

Dissociation equilibrium of negative H ions in solar type stellar atmospheres, noting H molecule vibrational and rotational levels and continuous thermal radiation
07 p1223 A69-19635

Strong line profiles computed for models of hot expanding extended atmospheres of OB supergiants
07 p1223 A69-19637

Preliminary model atmospheres for cepheid variable eta Aquilae, discussing mass loss processes
08 p1386 A69-20089

Expanding atmospheres in OB supergiants from radial velocity measurements, proposing tentative temperature and velocity fields
08 p1387 A69-20091

Atmospheric structure and energy distribution of planetary nebulae central stars
08 p1393 A69-20570

Acoustic energy generation for helium rich stars, discussing X ray radiation from helium star corona
08 p1380 A69-20645

Chemical composition of stellar atmospheres by model atmospheres, considering atomic transition, line broadening and thermodynamic equilibrium
08 p1402 A69-20904

Chemical composition of atmospheres of oldest Galactic stars, considering element abundances, metal and helium content and nuclear activity of massive stars
08 p1402 A69-20909

Stellar abundances of lithium, deuterium, beryllium and boron indicating nonthermal atmospheric origin
08 p1403 A69-20912

Aurigae star HD 35620 with respect to epsilon Virgins using model atmosphere and high dispersion spectra
08 p1403 A69-20913

Abundance analysis of B3 V star in Orion association, noting titanium and strontium overabundance and oxygen underabundance
08 p1407 A69-21133

- Stellar abundance and origin of elements, discussing stellar atmospheres and gaseous nebulae spectral determination, chronology of galactic halo, etc
09 p1587 A69-21306
- Density inversion in convective zone of stellar photospheres occurring in Eridani atmospheric model under certain conditions
09 p1595 A69-21843
- Atmospheric models for metal deficient stars of K and G spectral type, studying reduced metal abundance effect on atmospheric structure
09 p1596 A69-22055
- Subdwarf HD 25329 studied with model atmosphere approach, using H alpha, Na I and Mg I profiles for effective temperature
09 p1600 A69-22199
- Effects of opacity arising from silicon bound-free transition on emergent fluxes and hydrogen line profiles for A and late B stellar atmospheres
09 p1604 A69-22403
- Lyman alpha wing opacity effect on temperature scale and helium content in F and G subdwarf atmospheres
09 p1607 A69-22431
- Stellar atmosphere parameters analyzed over pulsation cycle by high dispersion spectra of cepheid variable RT Aurigae
10 p1778 A69-23605
- Silicon carbide particle growth and motion in carbon star atmospheres
10 p1781 A69-23678
- Graphite particle formation in atmosphere of C type Mira variables, calculating particle size distribution by nucleation and coagulation theory
10 p1782 A69-23681
- Circumstellar grain compositions of stars with various O to C abundance ratios, calculating molecular equilibrium of condensates and gaseous compounds in stellar atmospheres
10 p1786 A69-24103
- Nongray models of atmospheres of early stars, giving Avrett-Krook method of correcting temperature distribution
11 p1954 A69-24361
- Book on stellar atmospheres covering radiation theories, thermal equilibrium, measurement techniques, spectral analysis, etc, emphasizing sun
11 p1961 A69-25084
- Nonadiabatic linear oscillations of stellar atmosphere, discussing wave coupling with stellar pulsation
11 p1961 A69-25104
- Shock wave propagation in gravitational field with pressure and density gradients, considering nonlinear equations of fluid flow
11 p1961 A69-25106
- Physical structure of convective envelopes of population II main sequence stellar models by mixing length theory, emphasizing hydrogen molecule formation and pressure ionization
11 p1961 A69-25109
- Free electron density upper limits in plasma attributed to negative ion formation, noting effect on ionization equilibrium calculations for stellar atmospheres
11 p1928 A69-25255
- Computer program for model stellar envelopes of red supergiants with extended atmospheres
12 p2156 A69-26218
- Physical parameters and chemical composition of DD Lac atmosphere from spectral analysis
12 p2156 A69-26219
- Atmospheric element contents of F stars of Cyg, Her and Boo, using Planckian gradients and computer calculations for growth curves of atmospheric models
12 p2157 A69-26335
- Element contents of supergiant HD 190603 atmosphere based on spectrophotometric analysis including temperatures, turbulent velocity, gravity acceleration and electron concentration
12 p2157 A69-26336
- Hydrogenic transition derived excitation temperatures for Wolf-Rayet stars of WC sequence
12 p2160 A69-26904
- Dwarf and subdwarf stars limb darkening tables for unblanketed nongray radiative model atmospheres
12 p2171 A69-27153
- Star twinkling absence for lunar observation laboratory, noting star distance measurement and laser action in stellar atmospheres
12 p2173 A69-27172
- Steady state model envelopes of Be stars, determining excitation and ionization states for hydrogen atoms
13 p2338 A69-27559
- Stellar atmosphere models of pure hydrogen in hydrostatic, radiative and statistical equilibrium, including Lyman-alpha and continua, discussing nonLTE deviations
13 p2338 A69-27560
- RR Lyrae gap stellar model atmospheres including radiation spectra, temperature radiation and convection, etc
13 p2338 A69-27561
- Hydrogen to He ratio effect on stellar atmospheric structure, considering flux relations, UVB color indices, H line profiles, electron and gas pressures
13 p2339 A69-27562
- White dwarf atmospheric structure, analyzing masses and radii for DA stars and surface parameters of Eri B, based on grid of line blanketed models
13 p2339 A69-27563
- Hayashi effect modifications due to high opacity stellar atmosphere or presence of molecular hydrogen dissociation zone, discussing pressure dissociation role
13 p2342 A69-27594
- Electron gas behavior in nondegenerate envelope of magnetic white dwarf, discussing increased opacity due to magnetic fields
13 p2343 A69-27624
- Fe III line profiles and equivalent widths from spectrograms of zeta Cas and gamma Peg for Fe abundance, using model atmospheres
13 p2347 A69-27715
- Astronomical model explaining shell instability of Pleione /28 Tauri/ extended atmosphere, discussing magnetic field amplification by differential rotation to explosive dissipation in 9.16 years
13 p2347 A69-27716
- Pulsar hypothesis based on oscillating white dwarf surrounded by hot rarefied corona to explain radio emission
14 p2515 A69-28759
- Relative element abundances in Cyg, Her and Boo atmospheres, calculating curves of growth by Planck gradient method for stellar spectra
14 p2519 A69-29356
- P Cyg star HD 190603 atmospheric parameters from spectrograms analyzed by curve of growth method, including ionization and excitation temperatures and electron density
14 p2519 A69-29357
- Surface convection zone in atmospheres of global cluster and halo B stars determined to study He depletion efficiency
14 p2529 A69-29976
- Supergiant HD-33579 in Magellanic cloud by model atmospheres, discussing abundances
14 p2529 A69-29979
- B-type stellar spectra, discussing atmospheres and local thermal equilibrium from considerations of He I and P II lines relative strength
15 p2679 A69-30046
- Neutron star atmosphere and X ray emission spectrum, computing incident protons mean free path for two assumptions
15 p2686 A69-30535
- Nonlinear limb darkening corresponding to nongray stellar atmosphere model applied to light curve for compact eclipsing binary systems
15 p2689 A69-30563
- Radial pulsation mode of convective envelopes in adiabatic equilibrium for variable M red supergiant stars
15 p2692 A69-30766
- Atmospheric parameters for blue horizontal branch stars in globular cluster NGC 6397 by spectroscopic and photoelectric observations, obtaining mean stellar masses
15 p2692 A69-30770
- Pure hydrogen stellar atmosphere nonLTE models, calculating surface temperature rise due to H alpha line effect on continuum energy balance
15 p2693 A69-30777
- Surface gravity and temperature model atmospheres for O-type stars with UV line blanketing
15 p2693 A69-30778
- Photoelectric index of main sequence stars in F5 to G2 spectral range as indicator of atmospheric microturbulent velocities
15 p2695 A69-30999
- Magnetic field effect on thermal convection onset in compressible polytropic atmosphere compared with results from thin layer approximation
16 p2855 A69-31658
- Shock wave propagation in isothermal atmosphere, discussing radiation and ionization effects on thermal jump
16 p2858 A69-32207
- BetaCrB atmospheric microturbulence velocity, ionization and excitation temperatures, electron pressure and abundances determined by spectrophotometer
16 p2864 A69-32592
- Spectrophotometry of F stars 42 Cyg and nu Her atmospheres, analyzing microturbulence, excitation and ionization temperatures, electron pressures and abundances
16 p2864 A69-32596
- Effective temperature and gravity values for Mn Ap stars by comparing spectrum scans and H line profiles with predictions from atmospheric models
17 p3038 A69-33724
- Microturbulent velocities of A and F stars observed for reciprocal effective temperature range
17 p3039 A69-33729
- Red dwarf star /YZ Canis Minoris/ radio outbursts observation noting stellar atmospheric spectrum, electron density and temperature and total flare energy
17 p3043 A69-34164
- Radial velocities differences as indicator of stellar atmospheric turbulence, applying method to sun
17 p3044 A69-34177
- Alpha Serpentis spectrum study from model atmosphere and growth curves, finding metal abundance ratios five times as great as in Arcturus
18 p3200 A69-35130
- Balmer line spectrum formation in extended atmospheres of Be and shell stars, noting influence of angle of inclination to observer
18 p3204 A69-35349
- Monte Carlo relaxation method for physically self consistent model stellar atmospheres, discussing stability, accuracy and convergence of solution
19 p3425 A69-36337
- Atmospheric models for specified effective temperatures, hydrogen-to-metal ratios and surface gravities in studying metal deficiency effect on stellar atmosphere
19 p3425 A69-36338
- Effective thinness approximation for spectral line formation from photon degradation processes and random walk of scattered photons, discussing optical thickness
20 p3612 A69-38159
- Equivalent absorption line widths of supergiant B1 IA /kappa Cassiopeia/ tabulated with log NH content of atmosphere for various elements
21 p3803 A69-38844
- Stellar lithium and beryllium, discussing production and destruction processes in stellar atmospheres and abundance in various stars
21 p3810 A69-39505
- Stellar atmospheres acoustic energy generation rate calculations, studying corona mass ejection effects on stellar rotation
21 p3813 A69-39521
- Coronae around helium stars and X ray sources, calculating acoustic energy generation rates in convection zones
21 p3813 A69-39522
- Nongray models representing atmospheres of F and G supergiants computed and tabulated for 5400- 6600 K and various surface gravities
22 p4015 A69-40152
- P Cygni spectroscopy indicating existence and atmospheric structure of accelerating envelope about star, computing line profiles
22 p4023 A69-40471
- Helium-carbon star BD plus 10 degrees 2179 re-analyzed by grid of constant flux models containing right amount of C
22 p4026 A69-40652
- Model atmospheres of late type stars with solar abundances, effective temperatures between 2000-4000 K and gravities corresponding to dwarf, giant and supergiant stars
22 p4027 A69-40654
- Radiation transfer in circumstellar dust envelopes, considering thin and opaque clouds
22 p4027 A69-40655
- Exact solution of macroscopic line transfer equation including electron scattering terms for Milne-Eddington model atmosphere, discussing electron scattering effect on growth curves
22 p4007 A69-40903
- Atomic hydrogen departures from LTE computed for models of B star atmospheres, assuming detailed balance in hydrogen lines
24 p4376 A69-42665
- P Cygni characteristics and spectrum analysis, describing absorption lines, line widths, atmospheric composition, light variations, etc
24 p4391 A69-43803

Beta Orionis spectral line profiles data used to study atmospheric structure
24 p4391 A69-43804

STELLAR DOPPLER SHIFT

U DOPPLER EFFECT
U EXTRATERRESTRIAL RADIATION

STELLAR EVOLUTION

Collection of papers on physics, Volume 31, Part 1, covering stellar evolution, electron transport in semiconductors, plasma microstability, etc
01 p0115 A69-10045

Stellar evolution, discussing stellar structure, pre- and post-main sequence evolution, solar system origin, supernovae, white dwarfs, variable stars and close binaries
01 p0148 A69-10046

Age and initial helium abundance of stars in M15 globular clusters estimated from stellar evolution lifetime ratio
01 p0149 A69-10135

Pulsar discovery at position of suspected supernova remnant, suggesting pulsars as rotating neutron stars formed in stellar explosion
01 p0149 A69-10268

Late type stars, discussing main sequence for Population I and Population 2 stars and ages and chemical composition of old galactic clusters and globular clusters
01 p0158 A69-11325

Rotating star adiabatic axisymmetric motion solved numerically for small initial deviation from hydrostatic equilibrium
02 p0317 A69-11955

Computer study of collisionless self gravitating system using two dimensional model, obtaining gravitational field by solving Poisson equation
02 p0322 A69-12272

Red giants limiting helium core mass dependence on total stellar mass and initial composition from stellar evolutionary models
02 p0327 A69-12710

Supernova explosion theories, discussing neutrino and degenerate matter concepts, thermonuclear reactions in stellar explosions, oxygen conversion into sulfur, Crab Nebula, etc
03 p0509 A69-13356

Kinematic parameters of giant stars and stellar evolution, discussing variations as function of zone position in HR diagram
03 p0517 A69-14095

Time scale of cooling/heating process compared with gaseous clouds contraction/expansion for one solar mass protostar evolution in transparent stage
04 p0651 A69-14366

Mass exchange and evolution of close binaries /Main Sequence stars/
04 p0653 A69-14614

Evolution of close spectroscopic binaries and Am stars
05 p0822 A69-15855

Origin of binaries from angular momentum vectors orientation and separation distribution
05 p0822 A69-15856

Book on diffuse matter in space covering observations of interstellar gas, grains, particle interaction and star formation
06 p0997 A69-16833

Amount of flux carried by convection in late type stars, reevaluating drag role in mixing length theory
06 p1003 A69-17321

White dwarf general relativistic instability toward dynamic collapse and Type I supernovae
06 p1010 A69-17975

Pulsational properties of massive star in He burning evolutionary phase, determining inner structure from stellar model
07 p1218 A69-19279

Dynamical stability in premain sequence stars, discussing adiabatic models for pure hydrogen composition and collapse initiation by low opacity
07 p1220 A69-19388

Stellar samples with various luminosity and A star kinematic properties, discussing influence on application of hydrodynamics equations to evolution problems
07 p1224 A69-19712

Photoelectric observations for stars in and near galactic cluster NGC 3680, discussing age and metal abundance
08 p1384 A69-20054

Convection inhibition effects on premain sequence evolution of solar mass star, discussing largely radiative models
08 p1386 A69-20088

Photoelectric UVB photometry of stars in Puppis-Vela border region for associations of intermediate type stars
08 p1389 A69-20248

Period-age relations for delta Cephei stars based on stellar evolution theory and initial abundance of hydrogen
08 p1392 A69-20564

Binary stars systems with same total mass calculated for evolution from main sequence stage through mass exchange to white dwarfs
08 p1393 A69-20569

Close binaries evolution and Algol type systems origin, discussing hydrogen exhaustion in center
08 p1395 A69-20633

Wolf-Rayet star properties, model and mass loss
08 p1395 A69-20640

Mass loss in Red Giant stage from statistical analysis of H-R diagrams of galactic clusters
08 p1396 A69-20642

Carbon 12 stars to simulate core evolution of planetary nebulae precursors, discussing nuclear shell burning
08 p1396 A69-20649

Pu 244 and I 129 abundances in early solar system and continuous galactic synthesis model of element formation in stars
08 p1397 A69-20695

Helium production in Galaxy, assuming homogeneous evolution of some massive stars due to external factors
08 p1401 A69-20895

Abundance determinations and spectrum intercomparisons in late type peculiar stars, discussing carbon and heavy metal star classes
08 p1403 A69-20910

Cometary origin of meteors and element abundance in primitive solar nebula, discussing neutron capture products in chondrites
08 p1406 A69-20930

Star collapse under energy losses due to neutrino emission, analyzing self similar asymptotic solutions
09 p1587 A69-21359

Attractive and disruptive forces in conversion of interstellar gas into stars, discussing self gravitation, galactic magnetic field and cosmic ray pressure
09 p1599 A69-22190

Primordial helium and horizontal branch star luminosity, obtaining luminosities in He burning phase for different He and metal abundances from models
09 p1601 A69-22211

Stellar models for Population II lower main sequence stars, discussing uncertainties in radii and bolometric magnitude
09 p1601 A69-22214

Brans-Dicke gravitation theory effects on solar evolution and neutrino flux, discussing solar luminosity
09 p1605 A69-22415

General expressions derived for numerical stellar-interior calculations for nuclear reaction rates, emphasizing density-temperature combinations
09 p1606 A69-22418

Neutrino loss effects on evolution of pure iron stars, considering white dwarf, presupernova models and iron-helium transition
09 p1606 A69-22420

Anharmonic pulsations of 15.6 solar mass star in helium burning phase, discussing radiation pressure, third order terms, higher modes and magnitude variation effects
10 p1771 A69-22853

Solid hydrogen condensation on graphite grains for microwave background, discussing hydrogen grain promotion of galactic and stellar formation
10 p1776 A69-23216

Low mass close binary systems evolution, describing components inside critical Roche lobe in initial detached phases
10 p1777 A69-23310

Binary eclipsing visual star systems angular momentum, discussing evolution
10 p1777 A69-23313

Radial motion of uniform spheres in general relativity, finding conditions for initially inward motion to reverse /bounce/
10 p1779 A69-23607

Density wave theory of galactic spirals, discussing hydrogen distribution, young star distribution, stellar migration, magnetic field structure, density waves in stellar formation, etc
10 p1786 A69-24109

Virial theorem extended to investigate star condensations in large interstellar gas clouds
10 p1787 A69-24119

Red supergiants as old derivatives of main sequence O and B stars, discussing neutrino emissions and carbon core contraction
10 p1788 A69-24125

Stellar evolution, computing sequences to establish solar model of primordial composition, comparing models with spectroscopic observations
10 p1788 A69-24126

Stellar models for chemical compositions to explain gap above main sequence in color-magnitude diagram of NGC 188
10 p1789 A69-24127

Rb-Sr and other radioactive isotope cosmochronology in solar system, analyzing age of elements and r process
11 p1955 A69-24393

Stability of spherically symmetrical nonrotating mass systems moving in self consistent gravitational Einstein field, considering quasar applicability
11 p1956 A69-24394

Solar system age based on decay rate of natural radioactive elements
11 p1961 A69-24972

Evolutionary stages of visual binary components based on magnitudes and color indices
11 p1962 A69-25111

Gravitational stability of spheroidal expansions of rotating gas masses in astronomy, noting mechanism for fragmentation in cosmology
11 p1962 A69-25112

Pulsars and ancient chinese records of supernova explosions, relating luminous intensities, radio sources and evolution
11 p1963 A69-25253

Theoretical models corresponding to initial phases in thermal-gravitational collapse of spherical clouds from interstellar gas for stellar formation
11 p1963 A69-25261

Book on stellar, galactic and nucleosynthetic evolution covering nuclear, Fermi, electromagnetic and gravitational interactions roles
11 p1964 A69-25413

Close binaries evolution and mass exchange for stars of 5 solar masses with very short periods, using modified Henyey method
11 p1964 A69-25414

Stellar physics, Volume 1, covering stellar structure, evolution, physical processes, statistical physics, quantum theory, classical mechanics, etc
12 p2152 A69-25785

Hydrodynamic calculation of 1.42 solar mass white dwarf supernova, considering instability and collapse initiation by electron capture
12 p2156 A69-26210

Stellar evolution model for primeval He abundance in population II stars in globular clusters for big bang confirmation
12 p2156 A69-26228

Toroidal configuration in stellar evolution, noting polar magnetic fields in stars and inclined rotators
12 p2173 A69-27174

Gravitational parameters of highly condensed objects, considering white dwarf evolutionary stages, density and upper mass limit
13 p2334 A69-27190

Pulsars and neutron star formation based on stellar evolution theory, suggesting massive O stars as origin
13 p2337 A69-27517

Residual interstellar gas from protostar formation detected as high luminosity IR object
13 p2327 A69-27593

Activity center in Crab Nebula, noting symmetrical configuration
13 p2343 A69-27621

Solar system light elements investigated assuming Li, Be and B abundance as nuclear reaction products of high energy particles accelerated in early sun formation
13 p2354 A69-28495

IR astrophysics, discussing detection, instrumentation, IR stars and stellar evolution
14 p2516 A69-28868

Lithium depletion in main sequence stars of one solar mass, suggesting e-folding time scale indicated by Coma Cluster data
14 p2517 A69-29089

Intermediate band photometry of G, K and M stars in IR indicating continuous stellar radiation deviant from black bodies
14 p2520 A69-29375

Planetary nebulae nuclei magnitudes in Magellanic Clouds and Galaxy measured photoelectrically, discussing early evolution
14 p2520 A69-29378

H-R diagrams of globular clusters, discussing evolution models with and without mass loss
 14 p2527 A69-29943
 Heavy element abundances in peculiar A stars, investigating nucleosynthesis during massive stars evolution
 14 p2527 A69-29945
 Horizontal branch stars of metal-poor globular clusters in Galaxy evolved from very blue stars, noting substantial mass loss at He-flash
 14 p2529 A69-29977
 Stellar Si burning at constant temperature studied for various initial abundance compositions, noting convergence toward pure Si relaxation
 14 p2529 A69-29983
 Mass point system moving in gravitational field, discussing statistical mechanics, relaxation time and evolution of stellar systems
 14 p2530 A69-29987
 Convective neutral stability in Schwarzschild- Harm model for evolution of stars with large masses
 15 p2681 A69-30422
 Late type cool degenerate stars nonobservability or rarity in terms of internal energy available for radiation from surface
 15 p2681 A69-30423
 Internal structure of rotating stars, analyzing physical changes, circulation influence on mixing during evolution and angular velocity
 15 p2683 A69-30512
 Elastic and inelastic evolution of concentrated gravitational systems, discussing stellar diffusion, evaporation, halos and rotating systems
 15 p2687 A69-30548
 Relativity theorems applied to collapsing stars and expanding universe noting limitations of general relativity from prediction of singularities
 15 p2694 A69-30854
 Preprotostar radio observations suggesting nonthermal radio sources formation with magnetic energy dissipated in particles acceleration
 15 p2701 A69-31531
 Energy release efficiency in gravitational collapse, estimating rest energy fraction from energy conservation, neutron star stability and spherically symmetrical systems collapse considerations
 16 p2853 A69-31594
 Equilibrium models reliability for main sequence stars estimated from systematic applications of physical assumption sets and numerical methods
 16 p2859 A69-32219
 Star formation in interstellar solid hydrogen clouds originating from cellular pressure created by hydrogen condensation onto interstellar grains
 16 p2862 A69-32375
 Lynden-Bell statistical mechanics of relaxation in collisionless one dimensional stellar system, discussing low energy particles distribution
 16 p2862 A69-32376
 Turbulent diffusion inside sun as explanation of solar spindown, Li depletion at surface and neutrino discrepancy, discussing diffusion coefficient and stellar evolution
 16 p2866 A69-32814
 Stellar light element abundances, discussing evolution models for various star types
 16 p2866 A69-32816
 Evolutionary tracks along horizontal branch of models for Population II stars in postred giant phase
 17 p3030 A69-33071
 Theoretical Hertzsprung-Russell diagram for star cluster NGC 1866, allowing stellar evolution study
 17 p3038 A69-33720
 H II regions distribution in nearby irregular I galaxies, attributing asymmetry to localized bursts of star formation
 18 p3190 A69-34289
 Pure carbon 12 stellar models evolution studied to determine production mechanism of planetary nebulae, discussing shell burning and surface layers unbinding role
 18 p3191 A69-34298
 Star collapse under energy losses due to neutrino emission, analyzing self similar asymptotic solutions
 18 p3197 A69-34749
 X ray sources model, describing possible ring of matter around white dwarf near end of active evolution
 18 p3188 A69-35204
 Quarkian core substance in superstars of great masses, discussing existence as primordial state forming baryon and nuclei and origin in stellar gravitational contraction
 19 p3401 A69-35912

Primitive solar nebula physical model considered under angular momentum conservation in collapsing fragment
 19 p3406 A69-36074
 Solar system matter evolutionary beginning traced to chemical elements synthesis by considering radioactive decay irreversible processes
 19 p3406 A69-36076
 Photometric evolution of Nova Delphini 1967 /HR Del/ in UPXYZVS seven color intermediate waveband system, showing position on QQ diagram
 19 p3425 A69-36563
 Statistical relation between expansion velocities and radii of planetary nebulae due to Lyman-c and diffuse Lyman-alpha radiation
 19 p3426 A69-36575
 Synthesis of proton rich nuclei in highly evolved stars, considering p elements production in interior by isobaric transformation
 19 p3428 A69-36837
 Pulsars pulse profiles data collected and interpreted with attempt to infer origin
 20 p3597 A69-37335
 Pulsars cosmic ray mass and charge spectra analyzed for evidence of neutron star origin
 20 p3588 A69-37487
 Cepheid observation, nature and evolution
 21 p3795 A69-38403
 Galaxy model for spiral structure origin
 21 p3797 A69-38537
 General relativity effects on isotropic stars evolution, discussing dynamic stability and white dwarfs
 21 p3798 A69-38540
 Big bang and little bang nucleosynthesis, discussing electron-neutrino or electron- antineutrino excess role in He production
 21 p3801 A69-38813
 Physics of massive starlike objects, discussing high entropy requirement, eventual nonrelativistic collapse and gravitational fields produced by low entropy equilibrium
 21 p3811 A69-39516
 Relativistic star clusters, discussing existence and quasi-static evolution before collapse through gravitational radius
 21 p3814 A69-39570
 Nuclear gamma ray astronomy utilization for stellar interior detection, showing identification of key radioactive nuclei of supernova at explosion time
 21 p3792 A69-39572
 Book on white dwarf formation through mass exchange covering binary star system, primary star mass losses and evolution into white dwarf
 22 p4021 A69-40421
 Pulsational stability of pulsation modes of star in He burning evolution phase
 22 p4022 A69-40467
 Relative abundances U-235/U-238, Th-232/U-238, Pu-244/U-238 and I-129/I-127 at solar system formation time to obtain time evolution of gamma process nuclei
 22 p3986 A69-40766
 Globular cluster star age and initial He abundance from main sequence, horizontal branch and red giant tip models using radiative opacities
 22 p4035 A69-41205
 Main sequence star models for diverse solar masses, covering hydrogen burning phase in core and conditions for dynamic instability and mass exchange
 23 p4208 A69-41286
 Wolf-Rayet stars formation, evolution, age, galactic distribution and relation with open star clusters
 23 p4208 A69-41288
 Gaseous self gravitating mass equations applied to galactic evolution and star formation
 23 p4213 A69-41716
 Stellar evolutionary ages and gravitational theory relations based on initial abundance ratio U 235/U 238 and present interstellar medium heavy element content
 23 p4219 A69-42329
 Proper motions and spectroscopic data of bright members of II Per and I Lac associations analyzed to determine expansion age
 23 p4221 A69-42385
 Neutron star formation, discussing influence of supernova explosions and need of pulsar study
 23 p4222 A69-42393
 Magnetic field implications in stellar formation mechanism including gravitational collapse, magnetic gas cloud fragmentation and stellar winds magnetic braking
 24 p4378 A69-42699

Stellar structures and evolution stressing composition and processes of stellar interiors
 24 p4379 A69-42782
 Nebulosity around FG Sagittae for origin and evolution of planetary nebulae, suggesting ejection of nebular shell
 24 p4381 A69-42887
 Elements origin and development in universe, discussing energy generation, structure and population of stars in Galaxy
 24 p4386 A69-43335
 M giant star possible evolution into S star, using high dispersion spectrograms
 24 p4387 A69-43349
 Rb-Sr and other radioactive isotopes cosmochronology in solar system, analyzing age of elements and r process
 24 p4390 A69-43783
 Stability of spherically symmetrical nonrotating mass systems moving in self consistent gravitational Einstein field, considering quasar applicability
 24 p4390 A69-43784
STELLAR FIELDS
 U STAR DISTRIBUTION
STELLAR INERTIAL NAVIGATION
 U CELESTIAL NAVIGATION
 U INERTIAL NAVIGATION
STELLAR LUMINOSITY
 Stellar brightness attenuation in atmosphere, determining extinction factor using computer calculations
 01 p0157 A69-11192
 Radio galaxies radio luminosity function expressed by means of power dependence, assuming three absolute visual magnitudes for each galaxy
 02 p0325 A69-12563
 Hydrogen alpha line strength in 951 O, B and early A stars from narrow band photoelectric measurements for stellar luminosity
 03 p0511 A69-13435
 Relation between amplitude of light and radial velocity variations of beta Canis Majoris stars
 03 p0517 A69-14126
 Balloon observations of solar far IR spectrum and brightness temperature
 04 p0652 A69-14419
 Pulsating stars, cepheids, RR Lyrae and W Virginis, excitation mechanisms, period- luminosity relation, oscillation modes, location on Hertzsprung-Russell diagram, etc
 04 p0653 A69-14625
 Photometric investigation in UVB and H alpha of early B stars in Scorpio-Centaurus association, computing intrinsic colors and magnitudes corrected for interstellar absorption
 06 p1001 A69-17195
 Light variations of irregular eruptive variables known as RW Aurigae or T Tauri stars, discussing suitability of stochastic model
 06 p0996 A69-17448
 Photoelectric observation of star occultation by Neptune for mean radius determination
 06 p1007 A69-17693
 Photoelectric observation of star occultation by Neptune for scale height determination
 06 p1008 A69-17694
 Flare star AD Leo observations by continuous photoelectric monitoring, noting light curves properties
 06 p1008 A69-17697
 Joint radio-optical observations of flare star UV Ceti in Australasia during September-October 1967
 07 p1214 A69-18666
 Photometric effects of UVB color indices ineffective in detecting double stars in Galaxy
 07 p1216 A69-18854
 Evolution of galaxies, considering masses, gas masses, luminosities, spectra and motions
 07 p1219 A69-19297
 Algorithm for high speed digital computers to evaluate stellar radiative opacities
 07 p1222 A69-19589
 Galactic Wolf-Rayet star distances and distribution on galactic plane, noting concentration difference toward galactic center
 07 p1223 A69-19636
 Stellar samples with various luminosity and A star kinematic properties, discussing influence on application of hydrodynamics equations to evolution problems
 07 p1224 A69-19712
 Variable eruptive star in Hercules, discussing magnitude
 08 p1382 A69-19871

Three color RGU system photometry in Milky Way field in direction of anticentrum, determining absolute brightness, luminosity and density of stars
08 p1387 A69-20119

Photographic magnitudes in UVB system based on photoelectric sequences for stars in NGC 2483 and NGC 2489 open clusters, obtaining spectral classes from objective prism plates
08 p1388 A69-20239

Spatial distribution of stars and obscuring matter in Milky Way field in Kapteyn Selected Area 195 in Circinus, cataloging UVB photometry of stars
08 p1389 A69-20246

Photoelectric measurements of magnitudes and colors in UVB system for stars in Puppis at Boyden Observatory
08 p1389 A69-20249

Photographic magnitudes in UVB system for southern open clusters, giving table of photographic plates
08 p1389 A69-20253

Photographic magnitudes in UVB system based on photoelectric sequences for various open clusters stars, determining spectral classes for brighter stars
08 p1389 A69-20254

Coincidence error between star image and planet edge for entrance pupil and telescope magnification
08 p1314 A69-20383

Color index and mean light curves constructed for Cepheid Variables
08 p1395 A69-20635

Brightness in blue light and radial velocity variability of metallic line star 28 Andromedae
08 p1395 A69-20637

Photoelectric observations of SRA variable CH Cygni reveal strong variability, discussing existence of hot companion
08 p1396 A69-20650

Quasar 3C454.3 optical variations, noting photographic and photometric evidence for period of 340 days
08 p1397 A69-20701

Stars closer than five parsecs including binary systems, luminosity, spectral type and mass
08 p1407 A69-21130

Isophotal wavelengths of U, B, V and R bright star systems for replacing spectrophotometry with broadband multicolor data
08 p1408 A69-21134

Russell method application to combined data of both minima of eclipsing binary using electronic computers
08 p1408 A69-21136

Polaris cepheid variable star system color index and absolute magnitude from photometric observations
08 p1408 A69-21138

Stellar absolute magnitudes recalibration for consistency with photometric distance moduli of clusters
08 p1408 A69-21139

Cepheid stars as distance indicators in extragalactic space, using periodicity-luminosity relation
08 p1408 A69-21147

Limb darkening nonlinear effects on solutions for brightness curves of eclipsing binaries
09 p1588 A69-21364

Pleiades cluster structure, deriving visible density distribution curves for brighter stars
09 p1589 A69-21369

Galactic dust layer spatial structure and relation to brightness of Milky Way based on analysis of photoelectric color excesses in Aql and Cyg stars
09 p1590 A69-21381

Quasar red shifts due to cosmological and gravitational factors, assuming correlation of QSO intrinsic luminosity with gravitational red shift values
09 p1597 A69-22151

Distance of bright stars in Cepheus OB2 region by MK spectral classification and UVB photometry, noting early main sequence and supergiant stars
09 p1599 A69-22194

Radial velocity, light and magnetic variations of HD 10783 from concurrent UVB photometric and Zeeman spectroscopic observations
09 p1600 A69-22197

Primordial helium and horizontal branch star luminosity, obtaining luminosities in He burning phase for different He and metal abundances from models
09 p1601 A69-22211

Stellar models for Population II lower main sequence stars, discussing uncertainties in radii and bolometric magnitude
09 p1601 A69-22214

Half intensity angular diameter upper limit of Seyfert galaxy NGC 4151 nucleus, considering nonthermal continuum
09 p1602 A69-22227

Photometric standard based on calibration of Vega by Hayes compared with six color magnitudes
09 p1603 A69-22233

Maximum indicative absolute magnitudes of 33 supernovae, discussing usefulness as distance indicators
10 p1774 A69-22967

Celestial navigation system using photodetectors, comparing numbers and brightness of S4, S20 and silicon stars
10 p1775 A69-23190

Starlight extinction by interplanetary medium evidenced from confirming correlation between star brightness on ecliptic and elongation
10 p1775 A69-23198

Static envelope with no mass outflow for star static core constructed from opacity coefficient dependence on temperature and density
10 p1775 A69-23199

Cepheid variable stars light curves analyzed to determine radii and absolute magnitudes
10 p1775 A69-23200

Cepheids variations used to measure intergalactic distances, noting method of calibrating absolute Cepheid luminosity
10 p1780 A69-23646

Broadband photometry for circumstellar IR emission from cool stars, considering giant and carbon stars
10 p1786 A69-24102

Power spectrum analysis of photometric observations of white dwarf stars for measuring variability of stellar luminosity
10 p1788 A69-24124

Red supergiants as old derivatives of main sequence O and B stars, discussing neutrino emissions and carbon core contraction
10 p1788 A69-24125

Stellar evolution, computing sequences to establish solar model of primordial composition, comparing models with spectroscopic observations
10 p1788 A69-24126

Absolute dimensions of 34 eclipsing variables having both components near main sequence, comparing mass luminosity and mass spectrum to homogeneous model stars
11 p1952 A69-24248

Interstellar medium density distribution as function of stellar angular spherical coordinates applied to determining stellar motion forces and B stars brightness difference
11 p1955 A69-24386

He I 10830 A line in beta Lyr shell observed by contact image converter tube, analyzing line structure and phase brightness
11 p1955 A69-24391

Improved extraatmospheric wideband sensor nominal S-4 magnitudes of bright stars observed with narrowband UVBRI filter-sensor combinations
11 p1960 A69-24853

Proper motions of low luminosity stars in Hyades cluster, noting photoelectric observations
12 p2152 A69-25797

Faint stars background exposure density and detection limit determined by astrosensitometer for Kodak Spectroscopic Plates
12 p2153 A69-25811

Lacerta OB1 stellar spectral classes and photographic magnitudes, analyzing clusters and distributions in concentrated and dispersed areas
12 p2153 A69-25813

Photographic observations of Nova Her 1963 in 1967, showing nonreturn to prenova stage
12 p2156 A69-26223

White dwarfs structure model for deriving formula for phase density in color-luminosity diagram
12 p2159 A69-26665

Photoelectric and visual minima tabulated for eclipsing binaries, calculating light elements
12 p2160 A69-26853

UVB observations of stars P and 36 Cygni including short period variations and secular changes in brightness
12 p2172 A69-27159

IR objective-prism survey along southern Milky Way for identifying high luminosity stars
13 p2335 A69-27314

Superdense stars energy yield from neutrino emission, assuming incomplete degeneration of elementary particle Fermi gas
13 p2336 A69-27435

Distance and mass-luminosity relation for Hyades stars relative to sun-Sirius type stars
13 p2339 A69-27565

Quasar red shifts distance dependence indicated by visually bright quasar faintness in radio range
13 p2344 A69-27635

Short period variability of B, A and F stars observed in photometry of New Delta Scuti stars
13 p2348 A69-27803

Twelve color stellar photometry for studying galaxy synthesis, relating observations to temperature, luminosity and metal abundance
13 p2348 A69-27804

OB stars absolute magnitude and intrinsic colors
Cleveland system related to MK system
13 p2348 A69-27805

Photoelectric yellow and blue observations of variable TZ bootis light variation and orbital elements, noting maxima and secondary minimum causes
13 p2348 A69-27808

Parallax and mass ratio of visual type K6 dwarf binary system, ADS 1865, BD plus 30339
13 p2349 A69-27811

Relative parallax, fractional mass and luminosity of visual binary 1785 determined from photographs taken with Sproul refractor
13 p2349 A69-27814

Photon emission from highly relativistic stars, using computed differential light delays to calculate blurring of spherically symmetrical emission pulses
13 p2350 A69-27825

Stellar densities and luminosity function determined from stellar data concerning sphere with 20 pc radius around sun
13 p2351 A69-27869

Vela pulsar PSR 0833-45 optical observations and Crab pulsar NP 0532 linear and circular polarization measurements by telescope-photomultiplier
13 p2354 A69-28470

Balmer jumps for B star temperature scale, discussing relation between observed Balmer jumps and observed U-B color indices
14 p2518 A69-29132

Planetary nebulae nuclei magnitudes in Magellanic Clouds and Galaxy measured photoelectrically, discussing early evolution
14 p2520 A69-29377

Errors in magnitude equation and atmospheric dispersion calculated for 400 mm astrograph, emphasizing constant errors due to objective
15 p2646 A69-30162

Protostars collapse and flare up computations, including radiative and convective energy flow terms in hydrodynamic equations of motion
15 p2680 A69-30206

Late type cool degenerate stars nonobservability or rarity in terms of internal energy available for radiation from surface
15 p2681 A69-30423

Interstellar absorption and spatial distribution in northern Aquila with absence of early O-B2 stars, including luminosity function
15 p2683 A69-30513

Comet atmosphere dust component, relating physical properties to brightness characteristics in stellar magnitudes
15 p2685 A69-30528

Response color curves of U, B, V photometric system compatible for stellar observation, including U revision
15 p2689 A69-30562

ET Pegasi photoelectric observations in UVB colors, giving period different from Kaho and new time of maximum light
15 p2694 A69-30787

Five color photometry of X ray source SCO X-1 in 1966-1968, discussing luminosity pulsations and flare activity
16 p2847 A69-31648

Nova Vulpeculae 1968 photographic observations analyzed for magnitudes, indicating 16 July 1968 explosion
16 p2855 A69-31659

Star chains around Eta Carinae, discussing nonrandom real groupings and probability criteria using ADH red sensitive plate without filter
16 p2856 A69-31931

Magnetic star HD 173650 light curves showing maximum luminosity variation occurring in U light, noting minima flattening from U toward V
16 p2858 A69-32208

Two dimensional spectral classifications for bright A stars including magnitudes and colors
16 p2860 A69-32233

Photoelectric observations of W Ursae systems, including observed and computed times of minimum light and period change

16 p2863 A69-32399

Eclipsing binary CQ Cephei envelope variability determined from photoelectric light curve, using astronomical telescope

16 p2864 A69-32593

Bright and faint stars absolute declinations compared in vertical circle systems used in Golosev and Pulko catalogs

17 p3027 A69-32872

UBV photometry of faint stars, discussing photographic plate effect on accuracy, emulsion standardization and use of electronography

17 p3031 A69-33099

Light changes caused by distortion of binary components, computing theoretical brightness variations by numerical integration of emerging atmospheric intensities over visible surface

17 p3044 A69-34179

Limb darkening nonlinearity effects on solutions for brightness curves of eclipsing binaries

18 p3197 A69-34754

Pleiades cluster structure, deriving visible density distribution curves for brighter stars

18 p3198 A69-34758

Galactic dust layer spatial structure and relation to brightness of Milky Way based on analysis of photoelectric color excess in Aql and Cyg stars

18 p3198 A69-34769

Star magnitude variation caused by earth atmosphere related by equation to star altitude, station height, sensor response, spectral radiance, etc

18 p3168 A69-34814

Radio sources identified as quasi-stellar objects through photographic detection of large brightness changes

18 p3201 A69-35206

Wavelength dependence of stellar scintillation, discussing apparatus to detect color effect in twinkling

19 p3401 A69-35809

Bright regions with loops /BRLS/ in sunspot group development, discussing survey of time lapse movies from 1968

19 p3403 A69-35967

Nova luminosity sources during premaximum, considering stellar shell separation and intense ejection of matter

19 p3426 A69-36574

O stars spectrograms study for luminosity and temperature criteria

20 p3598 A69-37463

Fluxes and luminous efficiencies tabulated for main sequence and subgiant stars within reflection effect problem in eclipsing binaries and Chandrasekhar non-gray atmospheric models

20 p3600 A69-37479

M-87 X ray luminosity from balloon-borne detectors, considering background counting rate relation to azimuth

20 p3588 A69-37488

Hot star photogravitational acceleration determined from difference between apex and antiapex brightness, noting constant magnitude and direction of principal component of apex force

20 p3608 A69-38046

Luminosity calibration for subluminous stars and space density of blue subluminous stars south of declination minus 45 degrees based on white dwarfs and binaries

20 p3612 A69-38160

Stars of spectral class F 2 and earlier, brighter than magnitude 11.5, found in four regions of intermediate galactic latitude

20 p3612 A69-38162

IC 2118 nebula luminosity study by polarimetry and photometry, showing role of light scattering and color properties

21 p3817 A69-39726

Projected surface density upper limit of neutral atomic H between M31 and M33 galaxies, noting brightness temperature between NGC 4631 and 4656

22 p4024 A69-40578

Interstellar reddening in solar vicinity, analyzing roles of galactic latitude and longitude and heliocentric distance

22 p4026 A69-40648

Variable HDE 310376 spectroscopic and photometric data, discussing brightness fluctuations, color changes, emission and absorption spectra, etc

22 p4026 A69-40651

O stars absolute magnitudes scales, discussing use of Balmer discontinuity in magnitude calculations

23 p4213 A69-41699

Absolute magnitude dispersion of galactic cluster brightest members as normally distributed random variable independent of cluster richness or faint members luminosity

23 p4215 A69-42113

Observational cosmology in terms of relation between red shift and apparent luminosity of galaxies /Hubble relation/

23 p4219 A69-42328

VV Cephei type binaries cool and hot primary stars light variations, discussing duration, orbital cycle correlation, mass loss, etc

24 p4386 A69-43346

Radio emission from diffuse thermal radio sources in northern Milky Way, giving contour maps

24 p4388 A69-43641

Cassiopeia A luminous filaments motion study noting stellar remnant magnitude

24 p4389 A69-43746

Interstellar medium density distribution as function of stellar action spherical coordinates applied to determining stellar motion forces and B stars brightness difference

24 p4390 A69-43776

He I 10830 A line in beta Lyr shell observed by contact image converter tube, analyzing line structure and phase brightness

24 p4390 A69-43781

STELLAR MAGNETIC FIELDS

NT SOLAR MAGNETIC FIELD

Pulsating magnetic white dwarfs as pulsar models, discussing radio emission mechanisms via shock wave interaction with stellar plasma atmosphere

01 p0149 A69-10269

Interplanetary magnetic field intensities, solar and stellar fields measured by Zeeman effect, discussing fields of Jupiter, Mars, Venus and moon

04 p0657 A69-14810

Temperature distribution for static stellar corona in presence of magnetic field, noting energy flow process

06 p1002 A69-17316

Element abundances in magnetic stars, discussing Zeeman effect and anomalies in spectra

08 p1403 A69-20911

Sun-like alternating field generators, discussing dynamo theory of stellar and planetary magnetic fields based on nonmirror symmetrical turbulent motion in conducting fluid

10 p1782 A69-23703

Stellar model with magnetic field accelerating central core rotation to instability for determining rotating star energy and angular velocity distribution dependence

11 p1952 A69-24249

Spectroscopic, photometric and polarimetric observations of magnetic stars, discussing magnetic curves of periodic variables

11 p1954 A69-24362

Micrometric and photometric measurements of coude spectra of magnetic variable HD 125248, showing spectroscopic binary nature and computing orbital elements

11 p1963 A69-25264

Toroidal configuration in stellar evolution, noting polar magnetic fields in stars and inclined rotators

12 p2173 A69-27174

Electron gas behavior in nondegenerate envelope of magnetic white dwarf, discussing increased opacity due to magnetic fields

13 p2343 A69-27624

Local stability of rotating stars in toroidal and poloidal magnetic fields, using linear stability analysis

13 p2346 A69-27707

Two channel polarimeter capable of eliminating atmospheric scintillation effects used for observation of magnetic stars and eclipsing binary u Herculis

13 p2347 A69-27713

Astronomical model explaining shell instability of Pleione /28 Tauri/ extended atmosphere, discussing magnetic field amplification by differential rotation to explosive dissipation in 9.16 years

13 p2347 A69-27716

Pulsars suggested as magnetic rotating neutron stars with unstable oscillations

13 p2352 A69-27912

Stellar magnetic field generation by convective motions of surface layers of slowly rotating stars

15 p2688 A69-30559

Magnetic field effect on neutron beta decay rate, considering calculations applicability to elementary particle production

15 p2690 A69-30694

Metallic line /Am/ stars Zeeman observations, showing 16 Ori as spectroscopic binary, dubious binary nature of 15 Vul and doubtful presence of magnetic fields

15 p2692 A69-30775

Plasma viscosity relation to stellar magnetic fields generation, taking into consideration angular momentum transfer

15 p2700 A69-31492

Partial resolution of Zeeman patterns in spectrum for magnetic field existence in atmosphere of 53 Camelopardalis

20 p3611 A69-38155

HD 188041 magnetic field variations from Zeeman measurements correlated to spectral variations

20 p3611 A69-38156

Uniformly and differentially rotating stars taking into account magnetic fields effects, discussing radiative and hydrostatic equilibrium in nonspherical configurations, stellar atmospheres, etc

21 p3812 A69-39519

Rotating neutron stars with magnetic fields symmetric about rotation axis considered for pulsar model

22 p4027 A69-40657

A-type stars investigation for anomalous spectral line intensities, discussing Hertzprung-Russell diagrams, rotational velocities, magnetic fields and abundances

23 p4218 A69-43232

Magnetic field implications in stellar formation mechanism including gravitational collapse, magnetic gas cloud fragmentation and stellar winds magnetic braking

24 p4378 A69-42699

STELLAR MASS

Red giants limiting helium core mass dependence on total stellar mass and initial composition from stellar evolutionary models

02 p0327 A69-12710

Time scale of cooling/heating process compared with gaseous clouds contraction/expansion for one solar mass protostar evolution in transparent stage

04 p0651 A69-14366

Photographic plates based parallax determinations of nearby stars weights, relative and absolute values, probable error and observation interval

04 p0663 A69-15381

Galactic model with differential rotation, discussing experiments on bar and cylindrical galaxy and spiral and loop structures formation

07 p1216 A69-19204

Pulsational properties of massive star in He burning evolutionary phase, determining inner structure from stellar model

07 p1218 A69-19279

Element synthesis in stars of galactic halo as possible explanation for heavy elements presence in supermassive objects

07 p1219 A69-19296

Evolution of galaxies, considering masses, gas masses, luminosities, spectra and motions

07 p1219 A69-19297

Absolute magnitudes and intrinsic color photoelectric observations of Wolf-Rayet stars in Magellanic Clouds and Galaxy

07 p1221 A69-19583

Curve-of-growth abundance analysis for main sequence lambda Bootis stars, suggesting type Ap star characteristics

08 p1385 A69-20062

Convection inhibition effects on premain sequence evolution of solar mass star, discussing largely radiative models

08 p1386 A69-20088

Photographic magnitudes in UBV system based on photoelectric sequences for stars in NGC 2483 and NGC 2489 open clusters, obtaining spectral classes from objective prism plates

08 p1388 A69-20239

Photographic magnitudes in UBV system based on photoelectric sequence for stars in NGC 2546, Pi 1, NGC 2579 and Cr 185, obtaining spectral classes

08 p1388 A69-20240

Binary stars systems with same total mass calculated for evolution from main sequence stage through mass exchange to white dwarfs

08 p1393 A69-20569

Helium production in Galaxy, assuming homogeneous evolution of some massive stars due to external factors

08 p1401 A69-20895

Stars closer than five parsecs including binary systems, luminosity, spectral type and mass

08 p1407 A69-21130

Spatial density distribution in star clusters, determining relation between mean stellar mass and density range in subsystems

09 p1589 A69-21368

Structure and pulsational properties of massive stars with helium cores and thin hydrogen poor envelopes

09 p1606 A69-22421

Neutron proton plasma properties in massive stars and supernovae, discussing neutrino emission

10 p1756 A69-22814

Low mass close binary systems evolution, describing components inside critical Roche lobe in initial detached phases

10 p1777 A69-23310

Nonradial oscillation modes of massive stars determined by Ritz method application to variational principle, allowing for gravitational perturbation

10 p1785 A69-24036

Star counts in star cluster neighborhoods, obtaining ratios of corona radius to nucleus radius as function of cluster mass

11 p1951 A69-24246

Close binaries evolution and mass exchange for stars of 5 solar masses with very short periods, using modified Henyey method

11 p1964 A69-25414

Gravitational parameters of highly condensed objects, considering white dwarf evolutionary stages, density and upper mass limit

13 p2334 A69-27190

White dwarf atmospheric structure, analyzing masses and radii for DA stars and surface parameters of Eri B, based on grid of line blanketed models

13 p2339 A69-27563

Distance and mass-luminosity relation for Hyades stars relative to sun-Sirius type stars

13 p2339 A69-27565

Parallax and mass ratio of visual type K6 dwarf binary system, ADS 1865, BD plus 30339

13 p2349 A69-27811

Photographic recording of parallax, proper motion, acceleration and orbital motion of Barnards star, noting mass ratios to jupiter

13 p2349 A69-27813

Relative parallax, fractional mass and luminosity of visual binary 1785 determined from photographs taken with Sproul refractor

13 p2349 A69-27814

Visual binary star parallax, motions and mass ratio determined using photographic data

13 p2349 A69-27815

Radiative effect on rotating gaseous magnetic mass stability in thermodynamic equilibrium, including small oscillations stability

14 p2522 A69-29596

H-R diagrams of globular clusters, discussing evolution models with and without mass loss

14 p2527 A69-29943

Horizontal branch stars of metal-poor globular clusters in Galaxy evolved from very blue stars, noting substantial mass loss at He-flash

14 p2529 A69-29977

Validity range of nuclear quasi-equilibrium approximation for stellar silicon burning, discussing time rates of nuclear abundance changes and temperature effect

14 p2529 A69-29984

Convective neutral stability in Schwarzschild-Harm model for evolution of stars with large masses

15 p2681 A69-30422

Radial pulsation mode of convective envelopes in adiabatic equilibrium for variable M red supergiant stars

15 p2692 A69-30766

Atmospheric parameters for blue horizontal branch stars in globular cluster NGC 6397 by spectroscopic and photoelectric observations, obtaining mean stellar mass

15 p2692 A69-30770

Simulated gravitational lens made of Plexiglass for demonstrating stellar gravitational lens phenomena, presenting partial cross section

15 p2653 A69-31163

Frequency distribution of star masses formed from solid H grains clouds, noting agreement with Salpeter initial mass function

16 p2862 A69-32372

Stars kinetic energy and escape rates from isolated cluster with arbitrary stellar mass distributions, assuming spherical symmetry and velocity distribution isotropy

17 p3038 A69-33721

Masses of visual binaries above main sequence with published orbits determined as function of position in H-R diagram, using spectroscopic parallaxes

18 p3195 A69-34429

Spatial density distribution in star clusters, determining relation between mean stellar mass and density range in subsystems

18 p3198 A69-34757

Quarkian core substance in superstars of great masses, discussing existence as primordial state forming baryon and nuclei and origin in stellar gravitational contraction

19 p3401 A69-35912

Eta Cassiopeiae orbit analysis with emphasis on multiple exposure photographic observations, noting companion mass

22 p4013 A69-40120

Book on white dwarf formation through mass exchange covering binary star system, primary star mass losses and evolution into white dwarf

22 p4021 A69-40421

Semiconvection zone occurrence in massive stars determined by stability considerations

22 p4022 A69-40470

Evolutionary dynamic model for H II region produced by massive stars within dense dust-laden clouds, discussing grain sputtering and time scales

22 p4025 A69-40646

Main sequence star models for diverse solar masses, covering hydrogen burning phase in core and conditions for dynamic instability and mass exchange

23 p4208 A69-41286

Eclipsing binaries spectroscopic and photometric data compared to Iben and Horn models of main sequence stars, noting stellar mass effects

23 p4208 A69-41287

STELLAR MASS EJECTION

Radio emission sources nature in terms of special relativity theory

03 p0499 A69-13078

Mass motions in flares, quiescent filaments or other eruption phenomena at solar surface, noting loops, sprays, surges, etc

06 p0994 A69-17438

Sunspot ejection of filaments, flare surges and flare sprays, discussing bright and dark matter divergence from western spot

06 p0995 A69-17441

Stellar chromosphere and flare spectra observations with image tube spectrograph using He 10803 line, noting possible contribution to X ray background

06 p1003 A69-17449

Nonisotropic mass ejection from components of close binary system effects on orbital elements for small initial eccentricity case

08 p1395 A69-20634

Wolf-Rayet star properties, model and mass loss

08 p1395 A69-20640

Mass loss observed in Of, Wolf-Rayet and OB supergiant stars from P-Cygni profiles in far UV resonance lines

08 p1395 A69-20641

Mass loss in Red Giant stage from statistical analysis of H-R diagrams of galactic clusters

08 p1396 A69-20642

Stellar rotation braking due to mass loss from coronae through stellar wind based on calculation of acoustic energy generation from convective zone

08 p1396 A69-20644

Spectroscopic evidence for mass loss from CH Cygni based on observations of chromospheric lines of high dispersion spectrograms

08 p1396 A69-20651

Helium production in Galaxy, assuming homogeneous evolution of some massive stars due to external factors

08 p1401 A69-20895

Amplitudes and rates of brightness increase during supernova outbursts, calculating released energies

09 p1587 A69-21358

Static envelope with no mass outflow for star static core constructed from opacity coefficient dependence on temperature and density

10 p1775 A69-23199

Galaxies classified by matter content of nucleus, discussing evolution

11 p1953 A69-24351

Dynamical effects of mass exchange in close binary systems ejection modes from point of view of orbital elements evolution

11 p1962 A69-25113

Orbital parameters changes computation in table form for binary systems with more massive component mass decrease

11 p1962 A69-25120

Nonmesonic to mesonic decay ratio estimated for delta hydrogen hyperfragments

12 p2133 A69-26298

Intergalactic matter capture by NGC 1614 nucleus, stellar ejection from galaxies, explosive separation of close binary and other unsteady phenomena in galaxies

12 p2169 A69-27061

Fine structure of absorption lines of circumstellar Ca ejected from Nova Delphini 1967, determining ejection dates and photospheric radius

13 p2346 A69-27709

Radio emission sources nature in terms of special relativity theory

14 p2509 A69-28760

Nova thermal explosion, analyzing hydrogen combustion after penetration from white dwarf shell into degenerate core

15 p2682 A69-30507

Wolf 359 flare spectra obtained with Palomar telescope, noting hydrogen and He line enhancement, broadening and violet shifting

16 p2852 A69-32817

Amplitudes and rates of brightness increase during supernova outbursts, calculating released energies

18 p3197 A69-34748

Low energy cosmic ray density in Galaxy due to pulsar PSR 0833-45 caused by mass ejection

18 p3187 A69-34995

Nova luminosity sources during premaximum, considering stellar shell separation and intense ejection of matter

19 p3426 A69-36574

Steady state spherically symmetrical ejection of multicomponent plasma from sun determined with hydrogen approximation, considering ion composition

20 p3594 A69-37018

Plasma acceleration away from rotating magnetized astrophysical objects analyzed and applied to pulsar NP 0532 for magnetic moment and mass loss rate calculations

20 p3598 A69-37419

Spiral arms interpreted and derived as consequences of galactic nuclei explosion

20 p3599 A69-37468

Radial pulsations of neutron star losing mass, interpreting Crab Nebula pulsar observed period and secular increase of period

20 p3604 A69-37573

Stellar mass loss in gravitational contraction and variation of rotation law during transition to main sequence

20 p3607 A69-38041

Stellar mass loss - Conference, Trieste, September 1968

21 p3812 A69-39520

Stellar atmospheres acoustic energy generation rate calculations, studying corona mass ejection effects on stellar rotation

21 p3813 A69-39521

Coronal jet resulting from chromospheric burst observed during 22 September 1968 total solar eclipse

22 p4028 A69-40716

Photoelectric photometer monitoring of flare star UV Cet, comparing time intervals between flares to those of YZ CMi

22 p4032 A69-40945

Continual photoelectric monitoring of flare star YZ CMi by photoelectric photometer attached to reflector, giving light curves for flares

22 p4032 A69-40947

STELLAR MOTIONS

Nonlinear adiabatic pulsations of sequence of massive stars of uniform composition, allowing for radiation pressure variations

01 p0149 A69-10266

Relative proper motion of blue star in field of pulsar CP 1919 determined from photographic data analysis

01 p0149 A69-10270

Perturbations on major axes of slow moving comets in nearly parabolic original orbits by fast moving stars, discussing statistics of stellar encounters

01 p0153 A69-10871

Rotating star adiabatic axisymmetric motion solved numerically for small initial deviation from hydrostatic equilibrium

02 p0317 A69-11955

Computer models of one dimensional stellar problems, discussing fast relaxation of unsteady state to Fermi-Dirac distribution and slow relaxation to thermal equilibrium

02 p0323 A69-12274

Sun motion with respect to extragalactic universe, discussing local supercluster kinematics

03 p0513 A69-13769

Relation between amplitude of light and radial velocity variations of beta Canis Majoris stars

03 p0517 A69-14126

- Light and radial velocity changes in close binary systems, including limb and gravity darkening of distorted stars in analysis of spectroscopic effects
04 p0653 A69-14612
- Probable errors in FK4 catalog of star positions and proper motions determined by Scott method
05 p0823 A69-16041
- Stellar escapes from clusters and temporary captures in restricted three body problem with equal masses
05 p0827 A69-16595
- Rotational velocity correlation to space velocity for early stars, suggesting attainment of spin momentum and space velocity during close encounter in small cluster
06 p1010 A69-17972
- Time variation of velocity spheroid dispersion, axis ratio and vertex deviation in Galaxy due to star-cloud encounters
07 p1215 A69-18668
- Evolution of galaxies, considering masses, gas masses, luminosities, spectra and motions
07 p1219 A69-19297
- Stellar galactic orbit perturbation by irregularities in distribution of gas cloud for motion inclined to galactic plane
07 p1223 A69-19634
- Stellar samples with various luminosity and A star kinematic properties, discussing influence on application of hydrodynamics equations to evolution problems
07 p1224 A69-19712
- Stellar orbits in galactic plane represented as generalized Keplerian motion
08 p1381 A69-19792
- Dynamical friction on star in postNewtonian approximation of general relativity
08 p1386 A69-20072
- Space motions of bright F type stars from parallaxes obtained by photometry
08 p1386 A69-20074
- Radial velocity curve, orbital elements and masses and radii of components of eclipsing binary system 9 Chamaleontis /BV 430/
08 p1391 A69-20395
- Nonisotropic mass ejection from components of close binary system effects on orbital elements for small initial eccentricity case
08 p1395 A69-20634
- Planckian stellar velocity distribution function, moduli and projections on coordinate planes determined by ellipsoidal approximation
09 p1589 A69-21370
- Motion and dispersion of peculiar velocities of stars in gravitational condensing interstellar gas
09 p1589 A69-21371
- Stability of thin rotating disks of stars with respect to axisymmetric disturbances, noting overstabilities dependence on epicycles sizes
09 p1605 A69-22413
- Eclipsing binary AU Puppis studied photoelectrically in yellow and blue light, noting period decrease by 1.3 sec in last 40 years
10 p1774 A69-22968
- Double galaxies consisting of components moving away from each other with hyperbolic velocities from statistical tests of hypotheses
10 p1775 A69-23203
- Bright fundamental stars right ascensions observed in Chile, discussing instruments, declination range, systematic errors, etc
10 p1777 A69-23388
- Relative proper motions of stars measured by microscope projection technique
10 p1778 A69-23570
- Density wave theory of galactic spirals, discussing hydrogen distribution, young star distribution, stellar migration, magnetic field structure, density waves in stellar formation, etc
10 p1786 A69-24109
- Magnetoacoustic waves generated by Cerenkov radiation from corpuscular fluxes due to star interaction with stellar wind, determining deceleration forces on star
11 p1955 A69-24385
- Interstellar medium density distribution as function of stellar action spherical coordinates applied to determining stellar motion forces and B stars brightness difference
11 p1955 A69-24386
- Delta Cepheid blue companion /delta Cep C/ radial velocity variations, noting spatial proximity between delta Cep A and C
11 p1957 A69-24405
- B star HD 19180 spectral variations from B-3 to B-8 noting helium to carbon line intensity ratio, interstellar D line strength and radial velocity measurements
11 p1958 A69-24594
- Proper motions of low luminosity stars in Hyades cluster, noting photoelectric observations
12 p2152 A69-25797
- Proper motions and positions of X ray source Sco X-1 and surrounding stars derived from astrophysical plates using overlap technique
12 p2152 A69-25798
- Oort constant A and solar motion components in galactic plane determined from Classical Cepheids data
12 p2153 A69-25804
- Stellar radial velocities derived from line positions measurements by precision screw microphotometer
12 p2153 A69-25810
- Magnetic models of pulsars and rotating neutron stars to explain narrowness of radiation beam in polar diagram
12 p2172 A69-27168
- Distance and mass-luminosity relation for Hyades stars relative to sun-Sirius type stars
13 p2339 A69-27565
- Isothermal H II region dynamics for moving central star, integrating equations numerically using holograph transformation and Riemann invariants
13 p2347 A69-27712
- Messier 51 ionized hydrogen observations, discussing H II regions, radial velocities and galactic mass, rotation and noncircular nuclear motions
13 p2347 A69-27720
- Galactic force law from observed stellar velocity and space density distribution
13 p2348 A69-27802
- Flare star astrometric study to determine possible variable proper motion
13 p2348 A69-27810
- Parallax and orbital motion of spectroscopic binary Tau Persei determined from Sproul refractor photographs
13 p2349 A69-27812
- Photographic recording of parallax, proper motion, acceleration and orbital motion of Barnards star, noting mass ratios to jupiter
13 p2349 A69-27813
- Visual binary star parallax, motions and mass ratio determined using photographic data
13 p2349 A69-27815
- Sco-Cen B stars radial velocities, determining spectroscopic binaries
14 p2519 A69-29136
- Radial velocities of southern OB stars and supergiants noting tabulation of information
14 p2519 A69-29368
- Radial velocities of planetary nebulae in Magellanic Clouds and Galaxy, discussing Population I and II kinematics
14 p2520 A69-29377
- Close galactic encounters in dense galactic clusters, discussing effects on internal motions dispersion and stellar dissipation
14 p2521 A69-29461
- Photoelectric observation of passage of stars through meridian, detailing error sources and corrective technique
14 p2521 A69-29507
- Chapman-Enskog theory applied to observed stellar velocity distribution function, attributing deviation from Maxwellian function to negative K effect
15 p2687 A69-30549
- Member stars number in globular clusters M3 and M5 determined from photometric and kinematic characteristics
15 p2688 A69-30561
- Collisionless stability of relativistic, spherically symmetric star clusters against radial perturbations, considering one dimensional sufficient criteria
15 p2691 A69-30765
- Optimization techniques for stellar kinetic theory problems, discussing kinematics distribution function, cosmic gas dynamics, interstellar matter, etc
15 p2695 A69-31004
- Revised proper motions for semiregular and RV Tauri variable stars tabulated from meridian observations and photographic positions, discussing computation methods
15 p2696 A69-31221
- Monograph on proper motions of RR Lyrae variables, discussing data acquisition analysis
15 p2700 A69-31493
- Spectroscopic observations of HD 4174 star by superimposition of emission and M1-I absorption spectra, revealing intensity and radial velocity variations
16 p2858 A69-32214
- Radial velocity and spectral line variations of HD 124224, suggesting main sequence star of B6 to B9 spectral type
16 p2859 A69-32223
- Star motion perturbations by invisible body, stressing bright bodies invisible by position near perturbed star
17 p3034 A69-33407
- Proper motions, color magnitude and distance modulus of stars in galactic cluster in direction of Large Magellanic Cloud using Cape wide angle photometry
17 p3034 A69-33411
- Relativistic effect detection on pulsar frequencies by general relativity theory, assuming pulsars are orbiting objects
17 p3037 A69-33645
- Microturbulence velocity estimation method for solar type stars using low dispersion spectra of narrow band photometry
17 p3044 A69-34178
- Dwarf elliptical galaxies of local group, discussing star distribution and orbits, formation process, origin and distribution about Milky Way
18 p3194 A69-34424
- Planckian velocity distribution function, moduli and projections on coordinate planes determined by ellipsoidal approximation
18 p3198 A69-34759
- Motion and dispersion of peculiar velocities of stars in gravitational condensing interstellar gas
18 p3198 A69-34760
- Radial velocity measurements with objective prisms and results in SA8
18 p3201 A69-35143
- Geometric determination of visual binary orbits, noting inadequacy of graphical method based on apparent orbit ellipse properties
19 p3403 A69-35968
- Open cluster NGC 7128 distance and reddening determination by photometry
20 p3598 A69-37465
- HD 200775 spectrum analyzed for absorption lines wavelengths and equivalent widths, noting role for NGC 7023
20 p3599 A69-37469
- Zeta Tauri shell spectrum radial velocity measurement results compared with extrapolated seven year curve by Delplace
20 p3599 A69-37471
- Monte Carlo method for constructing catalogs of stellar positions, distances and velocities
20 p3605 A69-37829
- NonJeans gravitational instability of stars and interstellar gas in Galaxy due to wave interaction with stars having velocity near wave phase velocity
20 p3607 A69-38037
- Hot star photogravitational acceleration determined from difference between apex and antiapex brightness, noting constant magnitude and direction of principal component of apex force
20 p3608 A69-38046
- Gas in H II regions and associated stars radial velocities correlation and systematic difference suggesting relationship between nebulae and stars
20 p3611 A69-38150
- Dynamical analysis of Bernard star motion, yielding companions in co-revolving, approximately coplanar, circular orbits
22 p4013 A69-40119
- Eta Cassiopeiae orbit analysis with emphasis on multiple exposure photographic observations, noting companion mass
22 p4013 A69-40120
- Resonant asteroids in statistically underpopulated Kirkwood gaps, noting osculating mean motion distribution
22 p4013 A69-40122
- Solar motions respecting high velocity atomic hydrogen clouds and local stellar group
22 p4035 A69-41209
- Radial velocities for O and B stars in Milky Way field in Scorpius determined from prism spectrograms with specific dispersion at H gamma line
23 p4211 A69-41489
- Proper motions and spectroscopic data of bright members of II Per and I Lac associations analyzed to determine expansion age
23 p4221 A69-42385
- Stellar radial velocity measurement accuracy dependence on dispersion, spectrum and line width
24 p4386 A69-43347
- Stars with motions greater than 100 km/sec perpendicular to galactic plane, tabulating data for CH, subdwarfs, cepheids and horizontal branch stars
24 p4386 A69-43348
- Cassiopeia A luminous filaments motion study noting stellar remnant magnitude
24 p4389 A69-43746

STELLAR OCCULTATION

Magnetoacoustic waves generated by Cerenkov radiation from corpuscular fluxes due to star interaction with stellar wind, determining deceleration forces on star
24 p4390 A69-43775

Interstellar medium density distribution as function of stellar action spherical coordinates applied to determining stellar motion forces and B stars brightness difference
24 p4390 A69-43776

Delta Cepheid blue companion /delta Cep C/ rapid radial velocity variations, noting spatial proximity between delta Cep A and C
24 p4391 A69-43795

STELLAR OCCULTATION

Neptune mean diameter determination by photometric observations of stellar occultation by planet
01 p0150 A69-10386

Radio source positions and structures from occultation observations, suggesting optical identifications
02 p0326 A69-12704

Photoelectric observation of star occultation by Neptune for mean radius determination
06 p1007 A69-17693

Photoelectric observation of star occultation by Neptune for scale height determination
06 p1008 A69-17694

Solar occulting disk diameter at radio wavelengths derived from consideration of slightly deviated rays
09 p1607 A69-22432

Stellar occultations by moon observed with ear and eye method, not taking into account corrections to radio time signals
10 p1776 A69-23205

Stellar photometry during occultations by earth, discussing feasibility of lunar based observations
13 p2345 A69-27651

Nonocculted areas of Algor during eclipse using Balmer discontinuity spectrophotometric method, determining apparent stellar diameters
16 p2858 A69-32216

Relative positions of Neptune and BD minus 17 degrees 4388 star determined by Yale-Columbia refractor and double star camera, noting ephemerides correction from stellar occultation
17 p3041 A69-33814

Photoelectric observations of BD minus 17 degrees 4388 occultation by Neptune on 7 April 1968, studying light curves during immersion and emersion of star
17 p3041 A69-33815

Neptune radius, density and atmosphere deduced from observations during occultation of BD minus 17 degrees 4388 by Neptune
17 p3041 A69-33816

Venusian cloud layer radius, discussing error in determination of occultation level height of Regulus by Venus
18 p3203 A69-35331

Neptune equatorial radius, diameter, flattening and upper atmosphere optical properties determined from photometric curves of star BD-17 occultation
21 p3796 A69-38471

Photographic observations of Neptune occultation of BD-17 degree 4388, Zodiac Catalog number 2232 in April 1968, noting geocentric separation and planet radius
23 p4221 A69-42388

STELLAR RADIATION

Neutrino radiation in universe with emphasis on stellar neutrino radiation, analyzing emission during nuclear fusion of C-N, He and Ne-Na cycles
01 p0145 A69-10754

Late type variable stars time dependent photometry and polarimetry in blue and violet, noting correlation for stellar brightness and degree of polarization
01 p0158 A69-11326

UV and X ray radiations of stars and interstellar gas of Milky Way and remote galaxies
02 p0316 A69-11906

Galactic X ray sources, discussing location along spiral arms, age and properties of stars responsible for emission
03 p0497 A69-12930

Light and radial velocity changes in close binary systems, including limb and gravity darkening of distorted stars in case of spectroscopic effects
04 p0653 A69-14612

Orion nebula flare type variable stars amplitudes, light curve sections and stability
06 p1002 A69-17264

Radio emission from supernova remnants, reviewing evolution, structure, spectra and polarization, plus

identification, characteristics, surface brightness and radio emissive remnants distance
06 p1002 A69-17314

Solar type stellar activity, considering solar activity origin and correlation with stellar distances
06 p0996 A69-17447

Joint radio-optical observations of flare star UV Ceti in Australasia during September-October 1967
07 p1214 A69-18666

Algorithm for high speed digital computers to evaluate stellar radiative opacities
07 p1222 A69-19589

Calculated profiles of He 14471 and 4922 A and forbidden components star spectra, using quasi-static and impact approximations
07 p1224 A69-19713

Color excesses in Kapteyn Selected Area 4 using photovisual /yellow/ and photographic /blue/ magnitudes from catalog data
08 p1388 A69-20241

Radio emission from magnetic neutron stars as possible model for pulsars, noting optical and IR emission bands
08 p1397 A69-20729

Continuous radiation spectrum of Taurus A in far IR using indium antimonide detector of Rolin type
09 p1597 A69-22156

Spectroscopic observation of quasi-stellar objects noting red shifts
09 p1602 A69-22226

Starlight extinction by interplanetary medium evidenced from confirming correlation between star brightness on ecliptic and elongation
10 p1775 A69-23198

Solid hydrogen mantle condensation accounting for lack of detectable alpha hydrogen in star clusters and OB associations
10 p1776 A69-23214

Early type stars spectrophotometric parameters, discussing hydrogen beta, gamma and delta line widths, magnitude, etc
10 p1777 A69-23387

Interstellar dust distribution ideas to explain observed variability in starlight polarization and similar phenomena
10 p1785 A69-24050

Improved extraatmospheric wideband sensor nominal S-4 magnitudes of bright stars observed with narrowband UBVRi filter-sensor combinations
11 p1960 A69-24853

Wavelength dependence of polarization and UBVRi photometry of highly polarized stars, correlating IR interstellar extinction with maximum polarization wavelength
12 p2153 A69-25809

X ray polarization from Sco X-1, noting spurious instrumental polarization due to cosmic ray anisotropy using X ray polarimeter
12 p2149 A69-26315

Stellar diameter interferometric measurements, discussing double slit arrangement and illumination in focal plane
13 p2334 A69-27305

Superdense stars energy yield from neutrino emission, assuming incomplete degeneration of elementary particle Fermi gas
13 p2336 A69-27435

Book on astrophysics and stellar astronomy covering stellar radiation, binary and variable stars, positions, magnitudes, galaxies, cosmologies, etc
13 p2337 A69-27463

Hydrogen atoms in interstellar grains as source of stellar flux absorption, noting crystal environment effect on atomic hydrogen Lyman alpha transition
13 p2337 A69-27518

Exterior field equations for radiating spheres with zero limb darkening in relativity and Bondi coordinates, determining radiative flux and pressures
13 p2339 A69-27566

Polarization of continuum background of planetary nebulae in window in visible spectrum from scattering of nucleus star radiation by electron gas
13 p2339 A69-27567

Nuclear energized pulsational instability of stars based on linear quasi-adiabatic theory, including models with hydrogen burning shells
13 p2340 A69-27576

Two channel polarimeter capable of eliminating atmospheric scintillation effects used for observation of magnetic stars and eclipsing binary u Herculis
13 p2347 A69-27713

Photon emission from highly relativistic stars, using computed differential light delays to calculate blurring of spherically symmetrical emission pulses
13 p2350 A69-27825

Shock heated gas radiation frequency dependence and UB and B-V color indices determination, studying role in close binary systems luminescence
13 p2350 A69-27860

White dwarfs periods of radial oscillations, considering ion gas contribution to adiabatic coefficient computation
14 p2517 A69-29090

Intermediate band photometry of G, K and M stars in IR indicating continuous stellar radiation deviant from black bodies
14 p2520 A69-29375

Late type stars with emission peak wavelength approximating graphite Debye frequency induced by graphite impurity atoms
14 p2521 A69-29586

Pulsar model used to explain stellar shape oscillations as cause of radio emission intensity periodic variations
14 p2522 A69-29675

Periodic stellar radiation at 3.5 mm from pulsar CP1919 measured by paraboloid antenna and radiometer
14 p2529 A69-29978

Stellar image vibration dependence on zenith distances and terrain relief determined from stellar traces by 200 mm telescope
15 p2647 A69-30163

Stellar image vibration amplitude dependence on trace direction by comparison with traces of moving satellites
15 p2647 A69-30166

Late type cool degenerate stars nonobservability or rarity in terms of internal energy available for radiation from surface
15 p2681 A69-30423

Eclipsing close binary stars orbital planes spatial position determined from stellar emission polarization
15 p2688 A69-30560

Nonlinear limb darkening corresponding to nongray stellar atmosphere model applied to light curve for compact eclipsing binary systems
15 p2689 A69-30563

Stellar energy diffusion processes studied to determine energy transfer time scale between stellar layers
15 p2692 A69-30767

Polarimetric observations of polarization percentage and position angle changes in T Tauri stars, confirming stellar polarization association with emission spectra
15 p2694 A69-30882

Close binary system components approximated by two nonsimilar ellipsoids, obtaining interpretation of light curves
15 p2695 A69-30957

Balloon-borne UV polarimetry of stars and planets, studying linear polarization between 2000 and 3000 A
15 p2616 A69-31380

Pulsars properties, nature and utilization for interstellar medium study including radiation mechanisms, white dwarf stars and neutron star development
16 p2855 A69-31762

Instrument for simultaneous observation of astronomical plate pairs for detection of stars with UV color excess
16 p2791 A69-32226

Polarimetric observations of Be stars, noting dependence and self absorption by hydrogen of polarization produced by electron scattering
16 p2863 A69-32397

Radio emission from Cygnus X-2 reporting on observations at 4.5 cm wavelength
16 p2865 A69-32804

Stellar photometric data for various photocathode materials used to calculate radiant energy falling on earth
17 p2973 A69-33092

Photoelectric observations of BD minus 17 degrees 4388 occultation by Neptune on 7 April 1968, studying light curves during immersion and emersion of star
17 p3041 A69-33815

Pulsar PSR 0833-45 period decrease resulting from mass addition leading to radius and inertia moment decreases
18 p3196 A69-34646

Neutrino-pair bremsstrahlung for hot degenerate electron gas during Coulomb scattering on imbedded nuclei in stellar regimes including lattice structure effects
18 p3176 A69-35004

Variable star in Large Magellanic Cloud having unusual light curve with complex maximum lasting 300 days
19 p3403 A69-35965

Proton satellites measurements reconciliation with diurnal stellar variation data and cosmic rays origin models

19 p3396 A69-36621

Cameras photogrammetric parameters determined from stellar photographs, considering distortion components, reference points, etc

20 p3545 A69-38054

Variable BL Lac SHF flux density measurements, discussing periodicity and maxima spacing

21 p3798 A69-38545

Optical observations of pulsar NP 0532, comparing light curves in IR and UV, noting polarization

21 p3799 A69-38645

Photodetector responses to radiant energy from many stars tabulated for various photocathode materials and silicon detector

21 p3800 A69-38680

Thermal conduction by electrons in stellar matter, presenting opacity tables for H, He, C and red giant cores and solar composition

22 p4014 A69-40147

Semiconvection zone occurrence in massive stars determined by stability considerations

22 p4022 A69-40470

Radiation transfer in circumstellar dust envelopes, considering thin and opaque clouds

22 p4027 A69-40655

Polarization fluctuations of starlight indicating turbulent structure of interstellar medium, noting pulsar signal dispersion and Faraday rotation

22 p4030 A69-40771

Interstellar extinction in UV from zeta and epsilon Persei spectra obtained with scanner attached to telescope mounted in pointed Aerobee rocket

22 p4030 A69-40772

Stellar and diffuse galactic radiation intensity observations to obtain albedo values of interstellar dust particles

22 p4034 A69-41112

IR excess of R CrB type variable star RY Sgr, noting visual brightness and radiation in 2.0-3.4 micron range

23 p4220 A69-42377

Stellar neutrino energy loss due to electron-electron neutrino bremsstrahlung in nondegenerate gas determined from transition probability for charged baryons or leptons interaction

24 p4351 A69-42794

STELLAR REFRACTION

U ATMOSPHERIC REFRACTION

STELLAR ROTATION

NT SOLAR ROTATION

Differential rotation of celestial body maintained in resonance state by locking photosphere oscillation onto rotational period

01 p0156 A69-11136

Rotating star adiabatic axisymmetric motion solved numerically for small initial deviation from hydrostatic equilibrium

02 p0317 A69-11955

Einstein equations obtained for axisymmetric distribution of masses in approximation of square of stellar rotation angular velocity in empty space

02 p0317 A69-11956

Planet Mercury rotation, showing reminiscence of apparent path of sun to Ptolemaic concept of planetary system

03 p0509 A69-13368

Spinning neutron star model for pulsars based on slowing down of pulse rate, proposing emission mechanism for radio energy and relativistic gas

05 p0825 A69-16351

Rotational velocity correlation to space velocity for early stars, suggesting attainment of spin momentum and space velocity during close encounter in small cluster

06 p1010 A69-17972

Pulsar model based on rapidly rotating neutron star with radiating attached plasma, discussing test of radiation mechanism by means of coherence of emission

06 p1012 A69-18226

Time variation of velocity spheroid dispersion, axis ratio and vertex deviation in Galaxy due to star-cloud encounters

07 p1215 A69-18668

Galactic model with differential rotation, discussing experiments on bar and cylindrical galaxy and spiral and loop structures formation

07 p1216 A69-19204

Satellite components of lines formed in stellar type differentially rotating disk

07 p1219 A69-19336

Rotating stellar models oscillation and stability approximated by virial equations

07 p1220 A69-19389

Rapid differential rotation effect on massive main sequence O and B stars, discussing bolometric magnitude deficiencies and shifted position in Hertzsprung-Russell diagram

07 p1220 A69-19390

Frequency and radial velocity for various cepheid binaries, discussing hot companions detection through photometry

07 p1223 A69-19627

Gas remnant of large scale explosive event in galactic plane at 60 degree longitude, discussing resultant extension on line profile

07 p1225 A69-19717

Pulsar emission possible connection with rotating neutron stars, discussing rotational energy transfer to circumstellar plasma and production of periodic shock waves

08 p1383 A69-19895

Stellar rotation braking due to mass loss from coronae through stellar wind based on calculation of acoustic energy generation from convective zone

08 p1396 A69-20644

Rotational energy conversion of neutron star into relativistic electrons energy suggested by increasing period of pulsating radio source in Crab Nebula

09 p1591 A69-21454

Vela pulsar polarization and periodicity observations supporting rotational model vs radial pulsations as radio emission source

09 p1592 A69-21461

Pulsars rotating neutron star model analyzed on basis of magnetic dipole rotating in vacuo

09 p1592 A69-21463

Hydrogen beta emission profiles for pole-on type Be stars, measuring stellar rotational velocity by Huang-Struve method

09 p1596 A69-22052

Spectral type and rotational velocity estimation for 83 stars near double cluster in Perseus, emphasizing Be stars

09 p1599 A69-22195

General relativistic models of massive hot nonrotating stars with adiabatic temperature gradients consisting of ideal gas and radiation mixture

09 p1605 A69-22416

Gravitational waves emitted by relativistic, nonrotating, nonradially pulsating stellar model, discussing polarization and energy and momentum transport

09 p1605 A69-22417

Uniformly rotating star models within first order perturbation theory in convective equilibrium and with radiation pressure, discussing radiative and gas pressure ratio

09 p1606 A69-22422

Axisymmetric models for stable and unstable oscillations of rapidly rotating zero temperature white dwarfs, discussing kinetic and potential energy

10 p1789 A69-24129

Stellar model with magnetic field accelerating central core rotation to instability for determining rotating star energy and angular velocity distribution dependence

11 p1952 A69-24249

Toroidal configuration in stellar evolution, noting polar magnetic fields in stars and inclined rotators

12 p2173 A69-27174

Local stability of rotating stars in toroidal and poloidal magnetic fields, using linear stability analysis

13 p2346 A69-27707

Pulsars suggested as magnetic rotating neutron stars with unstable oscillations

13 p2352 A69-27912

Secular instability of steadily rotating stars, analyzing meridional motions in radiation zones by linear perturbation theory

13 p2354 A69-28566

Internal structure of rotating stars, analyzing physical changes, circulation influence on mixing during evolution and angular velocity

15 p2683 A69-30512

Elastic and inelastic evolution of concentrated gravitational systems, discussing stellar diffusion, evaporation, halos and rotating systems

15 p2687 A69-30548

Stellar magnetic field generation by convective motions of surface layers of slowly rotating stars

15 p2688 A69-30559

Spin down effects on neutron stars, discussing decrease of period of PSR 0833-45 as result of differential rotation instability

16 p2865 A69-32803

Pulsar emission and magnetic field in Crab Nebula, discussing magnetic flux amplification, gravitational to magnetic energy conversion and pulsars as pulsed signals

17 p3026 A69-32859

German monograph on instability of nonrevolving rotating stars covering secular rotational perturbations, radiative zone rotation, spherical Cowling model, etc

17 p3029 A69-32997

Planetary systems interrelationship with binaries and rotating stars, emphasizing occurrence frequency study based on stellar angular momentum orientation

17 p3032 A69-33105

Pulsation periods for pure He white dwarfs calculated by Chandrasekhar equation including relativity and rotation effects

17 p3037 A69-33641

Pulsars properties and distribution in galactic coordinates, deriving interstellar medium properties and physical nature of objects based on neutron star rotation

17 p3040 A69-33800

Light curve of pulsar NP 0532 represented with oblique rotator hypothesis, assuming concentrated emission at opposite spots on star

18 p3192 A69-34321

Oblique rotator model for pulsars, discussing difficulties arising from two asymmetrically spaced pulses during each stellar rotation

18 p3196 A69-34647

Galactic rotation in Cassiopeia region, studying O, B and A stars circular velocities as function of distance from galactic center

18 p3201 A69-35142

Protosun and solar system angular momentum losses analyzed from equations for convective star rotation change, noting almost total protosun initial momentum loss possibility

18 p3203 A69-35346

Slow rotation of relativistic polytropes with linear corrections, showing inertia moment distribution and metric component

19 p3426 A69-36576

Plasma acceleration away from rotating magnetized astrophysical objects analyzed and applied to pulsar NP 0532 for magnetic moment and mass loss rate calculations

20 p3598 A69-37419

Time scale of diffusion of angular momentum estimated by model for disturbances occurring in star with secularly unstable angular velocity distribution

20 p3605 A69-37826

Stellar mass loss in gravitational contraction and variation of rotation law during transition to main sequence

20 p3607 A69-38041

Gaseous rotating stars radial oscillations by perturbation method, considering angular velocity effects

21 p3795 A69-38470

Rotating neutron star model to fit pulsar data, considering star crust formation and properties, angular velocity changes and starquake effects

21 p3798 A69-38544

Uniformly and differentially rotating stars taking into account magnetic fields effects, discussing radiative and hydrostatic equilibrium in nonspherical configurations, stellar atmospheres, etc

21 p3812 A69-39519

Stellar atmospheres acoustic energy generation rate calculations, studying corona mass ejection effects on stellar rotation

21 p3813 A69-39521

Rotating neutron stars with magnetic fields symmetric about rotation axis considered for pulsar model

22 p4027 A69-40657

A-type stars investigation for anomalous spectral line intensities, discussing Hertzsprung-Russell diagrams, rotational velocities, magnetic fields and abundances

23 p4218 A69-42322

Pulsars models and radiation mechanism, noting neutron stars with rotating magnetospheres

23 p4218 A69-42326

Carroll Fourier transform method applied to stellar spectra lines to determine small rotational velocities

23 p4222 A69-42404

Pulsar model with seat as rotating neutron star having dipolar magnetic field not parallel to rotation axis

24 p4377 A69-42666

Rotating neutron stars, pulsars and cosmic X ray sources, accounting for large and small diameter sources by rotating neutron star losing mass in magnetic field

24 p4369 A69-43222

Stellar system differential rotation effect on gravitational instability with distribution propagating in rotation axis direction
24 p4388 A69-43639

STELLAR SPECTRA
NT SOLAR SPECTRA

IR emission in NGC 7027 spectrum and role of discrete line emissions, discussing magnetic dipole transitions, temperature and density
01 p0148 A69-10051

Stellar UV objective prism spectra from Gemini 11 and 12 manned flights
01 p0153 A69-10870

Hydrogen line profiles in various early stars compared with profiles predicted from model atmosphere calculations for rotating and nonrotating early stars
01 p0154 A69-10876

Radiation, Stark and van der Waals level broadening constants for Mg I and Si I calculated to interpret solar and stellar spectral line widths
02 p0310 A69-11454

Eight color narrow band photometry of bright stars, discussing band system, instrumentation, data and calibration
02 p0313 A69-11487

Narrow band and UVB photometry of GX3 plus 1 and Wolf-Rayet stars/HD 50896 and HD 45166/
02 p0325 A69-12596

Spectral data for central stars of planetary nebulae from Lick 120-inch telescope, discussing stellar temperature and evolutionary track deduction
02 p0325 A69-12624

Far UV spectra of O and B stars in Orion photographed from Aerobee rocket, describing wavelength measurements and line identifications
02 p0327 A69-12712

Stellar spectra observed with 2.8-14 micron IR spectrometer, noting broad absorption feature near 5 and 8 microns
02 p0327 A69-12713

Astronomical needs for atomic spectra, discussing emissions in Wolf-Rayet lines and Of stars and forbidden lines in absorption in sun and F-K stars
03 p0508 A69-13172

Growth curve for analysis of stellar spectra, determining relative f values and abundance
03 p0508 A69-13174

F values for Ti II, Cr II and Fe II by empirical astrophysical line strength analysis, discussing f value determination from stellar growth curve
03 p0508 A69-13175

Stellar image and spectrum distortions during occultation observed from satellite, discussing recovery of atmospheric composition data from stellar spectra
03 p0421 A69-13346

Stellar spectra taken with rapid scanning Michelson interferometer, noting IR excess due to radiation from clouds surrounding stars
04 p0655 A69-14667

Seyfert galaxies high excitation broad emission lines and quasars resemblance, discussing causes of spiral galaxies violent nuclear activity
04 p0657 A69-14689

Taurus A 21 cm absorption line frequency decrease during optical path approach to sun, discussing gravitational and electromagnetic origin
04 p0661 A69-15148

Fiber optic electrostatically focused image intensifier tube for recording star spectra with reduced exposure time
[WERL-68-1C2-TAACP-P1]

04 p0603 A69-15444

IR astronomy with ground based instruments noting Mars and Venus spectra, Jovian disk scans, solar radiometry, IR stars, quasars and galaxies
05 p0821 A69-15842

Spectra of close binary systems, analyzing abundance anomalies, noting metallicity results
05 p0822 A69-15854

Spectrum of accelerated particles on surface of stars revealed by observation of photospheric lithium and beryllium
05 p0817 A69-16711

Photometric investigation in UVB and H alpha of early B stars in Scorpio-Centaurus association, computing intrinsic colors and magnitudes corrected for interstellar absorption
06 p1001 A69-17195

Identification of emission lines from 3200 to 7000 A in Eta Carinae spectrum, noting P Cygni-like absorption lines
06 p1002 A69-17263

Stellar chromosphere and flare spectra observations with image tube spectrograph using He 10803 line, noting possible contribution to X ray background
06 p1003 A69-17449

Spectral line profiles of 3 Centauri A during microdisturbance, showing turbulent velocity and metal element abundances
07 p1211 A69-18407

Spectroscopic binary 16 Piscium, showing unusual period of 47.25 days
07 p1214 A69-18662

High dispersion IR image tube spectroscopy using telescope, discussing alpha Sco and alpha Boo spectral regions
07 p1074 A69-19203

Evolution of galaxies, considering masses, gas masses, luminosities, spectra and motions
07 p1219 A69-19297

Spectrum data of Nova Vulpeculae /1968/ summarized concerning dispersion figures
07 p1220 A69-19337

Sco XR 1 optical and X ray spectra simultaneous observations during rocket flights
07 p1220 A69-19391

Lines displacement in binary star spectrum due to blending, presenting graphs displaying magnitude of effect under various conditions
07 p1223 A69-19624

Strong line profiles computed for models of hot expanding extended atmospheres of OB supergiants
07 p1223 A69-19637

Atomic collision processes in astrophysics noting stellar continuum spectra, Ca ion and He lines, solar corona, heat balance in H I regions and planetary nebulae
07 p1224 A69-19653

Radio spectrum of quasi-stellar object identified as Parkes 2134 plus 004
07 p1224 A69-19708

Calculated profiles of He I 4471 and 4922 A and forbidden components star spectra, using quasi-static and impact approximations
07 p1224 A69-19713

UV emission spectrum of double star Boss 1985, excitation potential effect on Fe II lines and table identifying emission lines
08 p1385 A69-20060

Element abundances in two horizontal branch A stars through coarse and fine spectroscopic analysis, noting metal deficiencies with respect to sun
08 p1385 A69-20061

Spectra of envelope star HD 217050, analyzing metallic lines as function of central depths
08 p1387 A69-20121

Cluster star color indices determination by measuring intensities at nodes of extrafoveal star spectra
08 p1387 A69-20122

Photographic magnitudes in UVB system based on photoelectric sequences for stars in NGC 2483 and NGC 2489 open clusters, obtaining spectral classes from objective prism plates
08 p1388 A69-20239

Photographic magnitudes in UVB system based on photoelectric sequence for stars in NGC 2546, Pi 1, NGC 2579 and Cr 185, obtaining spectral classes
08 p1388 A69-20240

Color excesses in Kapteyn Selected Area 4 using photovisual /yellow/ and photographic /blue/ magnitudes from catalog data
08 p1388 A69-20241

Photographic magnitudes of stars in various open clusters based on UVB system and photoelectric sequence
08 p1389 A69-20245

Photoelectric measurements of magnitudes and colors in UVB system for stars in Puppis at Boyden Observatory
08 p1389 A69-20249

Equivalent widths of K line of single ionized calcium and central depths of unidentified broad absorption in O and B stars spectra
08 p1389 A69-20250

Photographic magnitudes in UVB system based on photoelectric sequence for various open clusters stars, determining spectral classes for brighter stars
08 p1389 A69-20254

Nine spectra of recurrent Nova T Pyxidis during fifth /1966/ outburst compared to previous outbursts
08 p1391 A69-20396

Forbidden resonance line of Ca II in Arcturus from spectrograms at widely different times of year
08 p1392 A69-20558

Color index and mean light curves constructed for Cepheid Variables
08 p1395 A69-20635

Mass loss observed in Of, Wolf-Rayet and OB supergiant stars from P-Cygni profiles in far UV resonance lines
08 p1395 A69-20641

Spectroscopic residual intensities variation of metallic and hydrogen lines of eclipsing system R Canis Majoris with phase, discussing surrounding gaseous matter
08 p1396 A69-20646

Spectroscopic evidence for mass loss from CH Cygn based on observations of chromospheric lines of high dispersion spectrograms
08 p1396 A69-20651

Abundance determinations and spectrum intercomparisons in late type peculiar stars, discussing carbon and heavy metal star classes
08 p1403 A69-20910

Element abundances in magnetic stars, discussing Zeeman effect and anomalies in spectra
08 p1403 A69-20911

Aurigae star HD 35620 with respect to epsilon Virginis using model atmosphere and high dispersion spectra
08 p1403 A69-20913

Stars closer than five parsecs including binary systems, luminosity, spectral type and mass
08 p1407 A69-21130

Abundance analysis of B3 V star in Orion association, noting titanium and strontium overabundance and oxygen underabundance
08 p1407 A69-21133

Isophotal wavelengths of U, B, V and R bright star systems for replacing spectrophotometry with broadband multicolor data
08 p1408 A69-21134

Polaris cepheid variable star system color index and absolute magnitude from photometric observations
08 p1408 A69-21138

H alpha emission line in nucleus of Virgo A radio galaxy observed on spectrograph, estimating gas electron density and mass
09 p1588 A69-21360

Taurus A flux density measurement at 4.3 mm with 36-ft antenna at National Radio Astronomy Observatory to determine spectrum unambiguously
09 p1591 A69-21450

Photoelectric monitoring broadband photometry and spectral scans of candidate star for pulsating radio source CP 1919
09 p1591 A69-21455

Hydrogen beta emission profiles for pole-on type Be stars, measuring stellar rotational velocity by Huang-Struve method
09 p1596 A69-22052

Hydrogen alpha emission nebulae catalog in western half of Cygnus X region, obtaining interstellar absorption from nebular distances determination
09 p1596 A69-22053

Atmospheric models for metal deficient stars of K and G spectral type, studying reduced metal abundance effect on atmospheric structure
09 p1596 A69-22055

Physical conditions in nuclei of various Seyfert galaxies deduced from line intensities, noting permitted and forbidden lines formation in different regions
09 p1596 A69-22056

Continuous radiation spectrum of Taurus A in far IR using indium antimonide detector of Rollin type
09 p1597 A69-22156

Spectral type and rotational velocity estimation for 83 stars near double cluster in Perseus, emphasizing Be stars
09 p1599 A69-22195

Radial velocity, light and magnetic variations of HD 10783 from concurrent UVB photometric and Zeeman spectroscopic observations
09 p1600 A69-22197

Subdwarf HD 25329 studied with model atmosphere approach, using H alpha, Na I and Mg I profiles for effective temperature
09 p1600 A69-22199

Spectroscopic study of A stars with large Stromgren m sub on indices, discussing rotational velocity, spectral intensity and type
09 p1602 A69-22215

IR spectrum of NML Cygnus star with Michelson interferometer, noting CO bands and IR excess
09 p1602 A69-22229

Photometric standard based on calibration of Vega by Hayes compared with six color magnitudes
09 p1603 A69-22233

IR excess from carbon-rich peculiar variable R Coronae Borealis and M7 variable associated with emission nebula R Aquarii attributed to circumstellar matter

09 p1603 A69-22263

Polarization changes of R Coronae Borealis Star RY Sagittarii, tabulating percentage polarization and position angles

09 p1603 A69-22265

Molecular ion C13H line found in zeta Oph at 4232.08 A, measuring equivalent width and finding C12/C13 ratio

09 p1603 A69-22266

Photoelectric spectrum scanning and IR photometric observations of Scorpius XR-1 X ray source

09 p1604 A69-22401

Effects of opacity arising from silicon bound-free transition on emergent fluxes and hydrogen line profiles for A and late B stellar atmospheres

09 p1604 A69-22403

Spectrographic observations indicating temperature range within individual filaments of Cygnus Loop, noting agreement with stratified models

09 p1607 A69-22430

Cosmic rays origin, measurements of energy spectrum and stellar diurnal variations

10 p1757 A69-22823

Atomic line spectrum computation for F-K supergiant or cepheid, using observational data on standard star spectrum

10 p1771 A69-22854

Cepheid variable stars light curves analyzed to determine radii and absolute magnitudes

10 p1775 A69-23200

Yellow and blue photoelectric observations of eclipsing binary CO Lac

10 p1775 A69-23202

Position and polarization of 1720 MHz OH emission from W28, W44 and galactic center, considering unresolved concentrations of shell type nonthermal sources

10 p1776 A69-23220

Stellar atmosphere parameters analyzed over pulsation cycle by high dispersion spectra of cepheid variable RT Aurigae

10 p1778 A69-23605

Asymmetrical profiles of 4430 A interstellar absorption band, discussing stellar and electronographic spectra

10 p1781 A69-23676

Polarization observation of star BL Lac continuum by multichannel scanner, noting photoelectric UVB observations and identification with radio source

10 p1785 A69-24090

Early F stars Li/Be abundance ratios estimation from change in solar Be abundance, discussing stellar Li isotopes ratios

10 p1785 A69-24099

Spectrum of IR object NML Cygnus, discussing model based on circumstellar IR emission

10 p1785 A69-24101

Broadband photometry for circumstellar IR emission from cool stars, considering giant and carbon stars

10 p1786 A69-24102

Far UV spectra of zeta Puppis and gamma super two Velorum with 1.6 A resolution photographed with all reflective objective spectrograph on Aerobee rocket

10 p1788 A69-24120

Six color stellar photometry of 159 field stars including subdwarfs, high velocity stars and 50 Hyades stars, tabulating color data

10 p1788 A69-24122

Flare stars observational and known aggregate characteristics in Coal Sack region

10 p1790 A69-24141

Absolute dimensions of 34 eclipsing variables having both components near main sequence, comparing mass luminosity and mass spectrum to homogeneous model stars

11 p1952 A69-24248

Microphotometer for stellar magnitudes of galaxies determination from photographs

11 p1879 A69-24256

B star HD 191980 spectral variations from B-3 to B-8 noting helium to carbon line intensity ratio, interstellar D line strength and radial velocity measurements

11 p1958 A69-24594

Triple system p Velorum, discussing coude spectra and published visual orbital elements

11 p1963 A69-25263

Color excess and 21 cm line intensity of RR Lyrae stars at high latitudes, confirming correlation between dust and atomic hydrogen

12 p2063 A69-25808

Spinning rockets UV spectrophotometry of early type stars, discussing instrumentation, calibration, data recording and stellar spectra

12 p2153 A69-25812

Lacerta OB1 stellar spectral classes and photographic magnitudes, analyzing clusters and distributions in concentrated and dispersed areas

12 p2153 A69-25813

Spectroscopy and star classification on basis of spectra

12 p2155 A69-26122

UBV photometry observations of eclipsing binary AG Persei at Mount Palomar with 51 cm reflector

12 p2156 A69-26220

Element contents of supergiant HD 190603 atmosphere based on spectrophotometric analysis including temperatures, turbulent velocity, gravity acceleration and electron concentration

12 p2157 A69-26336

Statistical data for visual binary systems with known spectral classes or colors and one component near main sequence

12 p2159 A69-26666

Photometric and colorimetric characteristics of hot gas optically thin in continuous spectrum with optical thickness of several units in Balmer series lines

12 p2159 A69-26667

Statistical analysis of UVB characteristics of blue objects located near galactic north pole by scintillation techniques

12 p2168 A69-27054

Surface gravities and detection of metallic line early A stars from spectral classification using equivalent line widths

12 p2171 A69-27151

Spectrum of abnormal B-type star HR 3817, noting Balmer line profiles and instrumentation

12 p2172 A69-27160

Variable star BL Lacertae absolute spectral energy distribution in visible and IR regions, noting synchrotron features and possible quasar nature

13 p2335 A69-27315

Rocket spectrographic observations of Alpha Virginis noting hydrogen Lyman absorption lines

13 p2338 A69-27555

Photoelectric scanning of CH Cygni spectrum calibrated and compared with 45 Arctis, discussing high dispersion, excess blue and UV continua, H beta emission, etc

13 p2338 A69-27557

Photoelectric observations of blue light minima of U Geminorum variable Ex Hydrae indicating no change in orbital period

13 p2338 A69-27558

White dwarf atmospheric structure, analyzing masses and radii for DA stars and surface parameters of Eri B, based on grid of line blanketed models

13 p2339 A69-27563

Galactic H II regions of high surface brightness in radio continuum surveyed at 1.95 cm wavelength with high resolution and positional accuracy

13 p2339 A69-27568

Chromospheric heating and polarization in late stars, considering association with Ca II K line emission cores

13 p2340 A69-27579

Expected IR line spectra of gaseous nebulae based on physical conditions, listing line intensities

13 p2342 A69-27595

Hydrogen content in Ia supergiant spectra of type B, noting lack of Stark wings of Balmer lines

13 p2348 A69-27722

Short period variability of B, A and F stars observed in photometry of New Delta Scuti stars

13 p2348 A69-27803

Twelve color stellar photometry for studying galaxy synthesis, relating observations to temperature, luminosity and metal abundance

13 p2348 A69-27804

OB stars absolute magnitude and intrinsic colors in Cleveland system related to MK system

13 p2348 A69-27806

Positions, spectral types and B magnitudes for possible field horizontal-branch stars at high galactic latitudes, selected from faint A star list

13 p2348 A69-27807

Photoelectric yellow and blue observations of variable TZ bootis light variation and orbital elements, noting maxima and secondary minimum causes

13 p2348 A69-27808

Shock heated gas radiation frequency dependence and UB and B-V color indices determination, studying role in close binary systems luminance

13 p2350 A69-27860

Goddard Experiment Package /automated spaceborne telescope design/ for stars and nebulae UV spectral emittance measurements

13 p2261 A69-27948

Photometric discovery of new variable stars resulting from quasars observation, noting optical variability noncorrelation with observed properties

13 p2354 A69-28468

Nighttime molecular O densities between 100- 130 km determined from Schumann-Runge absorption data for successive far UV spectra of hot star

14 p2435 A69-28959

Lacerta OB 1 B spectroscopic binaries periods and orbital elements, noting limits for secular variation

14 p2519 A69-29137

Late type stars with emission peak wavelength approximating graphite Debye frequency induced by graphite impurity atoms

14 p2521 A69-29586

Arcturus and solar rubidium abundance compared using Mount Wilson photographic spectrograms of Arcturus

14 p2522 A69-29589

Cepheid variable 1 Carinae position in H-R diagram suggested from microturbulent velocity role in pulsational instability

14 p2522 A69-29590

Nucleosynthesis based on stellar spectra and nuclear reactions data, discussing elements in sun and stars, meteorites, solar neutrinos, etc

14 p2529 A69-29985

B-type stellar spectra, discussing atmospheres and local thermal equilibrium from considerations of He I and P II lines relative strength

15 p2679 A69-30046

Stellar scintillation spectra for different zenith distances, correlating data with meteorological conditions at time of observation

15 p2647 A69-30165

Atmospheric parameters for blue horizontal branch stars in globular cluster NGC 6397 by spectroscopic and photoelectric observations, obtaining mean stellar

15 p2692 A69-30770

Spectral classifications and UVB photometry for southern association Sco OB 1 containing cluster NGC 6231

15 p2692 A69-30771

Canum Venaticorum variable A star spectrum, listing all lines observed between 5000 and 6650 A

15 p2692 A69-30773

Metallic line /Am/ stars Zeeman observations, showing 16 Ori as spectroscopic binary, dubious binary nature of 15 Vul and doubtful presence of magnetic fields

15 p2692 A69-30775

Polarimetric observations of polarization percentage and position angle changes in T Tauri stars, confirming stellar polarization association with emission spectra

15 p2694 A69-30882

Spectral Pt II lines in Ap stars of Hg class observed during analysis of double lined spectroscopic binary HR 4072

15 p2695 A69-30891

Photoelectric index of main sequence stars in F5 to G2 spectral range as indicator of atmospheric microturbulent velocities

15 p2695 A69-30999

Oscillator strengths calculated for transitions in Si III using dipole length and velocity matrix elements, comparing many electron correlation problem approximations

15 p2656 A69-31158

Stellar group Ba 6 distance measured using three color photometry in RGU system

16 p2854 A69-31650

Spectral characteristics of B stars group, reviewing causes of spectral line profile deformation

16 p2855 A69-31828

Magnetic star HD 173650 light curves showing maximum luminosity variation occurring in U light, noting minima flattening from U toward V

16 p2858 A69-32208

Stellar diameters in galactic cluster stars determined using original and modified spectrophotometric method compared with spectral types BOV-FOV

16 p2858 A69-32210

Spectroscopic observations of HD 4174 star by superimposition of emission and M1-I absorption spectra, revealing intensity and radial velocity variations

16 p2858 A69-32214

Radial velocity and spectral line variations of HD 124224, suggesting main sequence star of B6 to B9 spectral type

16 p2859 A69-32223

Two dimensional spectral classifications for bright A stars including magnitudes and colors
16 p2860 A69-32233

Spectral variations of red variable stars analyzed by objective-prism spectra in near IR
16 p2860 A69-32235

Giant galaxy classified in terms of stellar population, discussing Orion, intermediate amorphous and combination categories
16 p2862 A69-32395

Eclipsing binary CQ Cephei envelope variability determined from photoelectric light curve, using astronomical telescope
16 p2864 A69-32593

Hydrogen line profiles, equivalent widths and electron densities for peculiar alpha 2 CVn and gamma Lyr stars
16 p2864 A69-32594

Spectroscopic study of P Cygni showing ionization temperature, Balmer decrement agreement with calculated value and chemical composition
16 p2864 A69-32595

Spectrophotometry of F stars 42 Cyg and nu Her atmospheres, analyzing microturbulence, excitation and ionization temperatures, electron pressures and abundances
16 p2864 A69-32596

MH alpha 328116 /Cygnus/ spectrum noting three Fe IV lines
16 p2866 A69-32815

Wolf 359 flare spectra obtained with Palomar telescope, noting hydrogen and He line enhancement, broadening and violet shifting
16 p2852 A69-32817

Proper motions, color magnitude and distance modulus of stars in galactic cluster in direction of Large Magellanic Cloud using Cape wide angle photometry
17 p3034 A69-33411

Spectral lines radial velocities and profiles observed on 48 Librae from 1950-1962
17 p3038 A69-33722

Effective temperature and gravity values for Mn Ap stars by comparing spectrum scans and H line profiles with predictions from atmospheric models
17 p3038 A69-33724

BCD classification for cepheids, discussing /sigma/ surface definition, locus of normal stars of population I and interstellar reddening
17 p3038 A69-33725

Red dwarf star /YZ Canis Minoris/ radio outbursts observation noting stellar atmospheric spectrum, electron density and temperature and total flare energy
17 p3043 A69-34164

YZ Canis Minoris red dwarf star flare event observation record, noting optical spectrum energy output and slow decay
17 p3043 A69-34165

Heavy nuclei origin based on empirical abundance distribution, discussing stellar, galactic and cosmic events for nuclear genesis
17 p3009 A69-34190

RF recombination lines measurement of helium for abundance in nebulas, comparing optical and radio values for H II regions
18 p3190 A69-34293

Ionization stratification and chemical abundances in planetary nebula NGC 7662, discussing density fluctuations effect on N II and O II lines
18 p3191 A69-34294

Curve of growth analysis for close binary HR 5317 indicating Mg, Mn, Ca and Sr overabundance respecting standard star 110 Her
18 p3191 A69-34297

Four color photometry data of late F type stars in general catalog tabulated with columns for HD and GC numbers, apparent visual magnitude, etc
18 p3195 A69-34430

Variable CoD minus 35 degrees 4257 noting primary period of 502 days superimposed on secondary beat period of 3000 days
18 p3195 A69-34431

H alpha emission line in nucleus of Virgo A radio galaxy observed on spectrograph, estimating gas electron density and mass
18 p3197 A69-34750

Alpha Serpentis spectrum study from model atmosphere and growth curves, finding metal abundance ratios five times as great as in Arcturus
18 p3200 A69-35130

HD 217050 spectroscopic study, determining Balmer envelope temperature from comparison of homologous Balmer and Paschen lines intensities
18 p3201 A69-35144

Balmer line spectrum formation in extended atmospheres of Be and shell stars, noting influence of angle of inclination to observer
18 p3204 A69-35349

Atomic and molecular absorption lines and width measurement in spectrum of WZ Cassiopeiae carbon star in visual and IR region
18 p3204 A69-35350

Water vapor microwave emission measurement from galactic hydroxyl sources
18 p3205 A69-35435

NbO presence uncertainty in S type stars due to close coincidences with ZrO bandheads, noting 6484 and 6591 lines in R Cygni spectrogram
19 p3403 A69-35964

Forbidden transitions in stellar spectra - Conference, Liege, Belgium, June 1968
19 p3420 A69-36211

Forbidden transitions in absorption spectra of sun and normal and peculiar stars
19 p3422 A69-36215

Forbidden emissions in CH Cygni and VV Cephei noting symbiotic star
19 p3423 A69-36228

IR spectra of Eta Carinae, confirming nitrogen and sulfur abundance
19 p3423 A69-36229

Forbidden lines in slow nova RR Tel spectrum, comparing ionization rate with RR Pic
19 p3423 A69-36230

Intensity variations of Eta Carinae emission lines
19 p3423 A69-36231

Forbidden transitions in emission line spectra of variables near minimum light, finding origin in hot chromosphere
19 p3424 A69-36232

MH alpha 328-116 spectral characteristics noting weak continuum, emission lines from forbidden transitions and absence of absorption
19 p3424 A69-36233

MH-alpha 328-116 /V 1016 Cyg/ star spectrum, indicating object evolution toward higher ionization states
19 p3424 A69-36234

Spectral energy distribution of gamma-Cas in 1967 based on observations in seven color photometric system
19 p3426 A69-36565

Red leak corrections for UV filter on color UV indices for stars of various spectral types using winter-reddened response curve
19 p3426 A69-36566

Balmer and Ca II /K/ line profiles computed by program based on model atmospheres, comparing computed and observed data for F stars
19 p3426 A69-36578

O stars spectrograms study for luminosity and temperature criteria
20 p3598 A69-37463

WY Gem star spectroscopic observation showing peculiarity about forbidden and absorption spectra superposition
20 p3598 A69-37464

HD 200775 spectrum analyzed for absorption lines wavelengths and equivalent widths, noting role for NGC 7023
20 p3599 A69-37469

Zeta Tauri shell spectrum radial velocity measurement results compared with extrapolated seven year curve by Delplace
20 p3599 A69-37471

Pulsars cosmic ray mass and charge spectra analyzed for evidence of neutron star origin
20 p3588 A69-37487

Southern stars of spectral types between O5 and A3 analyzed for equivalent widths and equatorial rotation velocity from direct intensity spectrogram tracings
20 p3600 A69-37491

Photometric and spectral observations of Chuadze and Wild supernovae, showing type I classification
20 p3607 A69-38038

Giant stars UVB reddening line slopes determined from photometric data
20 p3608 A69-38047

Interferometric photoelectric scans of interstellar Na D-lines in stellar spectra using Pepsios spectrometer
20 p3611 A69-38148

Partial resolution of Zeeman patterns in spectrum for magnetic field existence in atmosphere of 53 Camelopardalis
20 p3611 A69-38155

HD 188041 magnetic field variations from Zeeman measurements correlated to spectral variations
20 p3611 A69-38156

TiO bands identified in Mira variables IR region, discussing rotational structure and band strength-temperature relation
20 p3611 A69-38158

MK spectral types for bright southern O and B stars
20 p3612 A69-38161

Stellar nuclear reactions at low energies studied to provide predictions of cross sections in carbon burning
20 p3612 A69-38164

M 82 direct photographs sequence observation in optical IR region, noting small nucleus and unbroadened inclined emission lines
21 p3799 A69-38649

IR spectrum of NML Cygnus star using rapid scanning Michelson interferometer, estimating temperature from CO bands
21 p3800 A69-38678

Short region scanning of Arcturus spectrum with McMath solar spectrometer double pass system at Kitt Peak National Observatory compared to single pass system
21 p3721 A69-38697

Differential curve-of-growth analysis of late type giant stars yielding chemical compositions, discussing nature and size of uncertainties in estimates
21 p3800 A69-38700

Line statistics for representation of line absorption coefficient distribution for solar type stars
21 p3801 A69-38762

Big bang and little bang nucleosynthesis, discussing electron-neutrino or electron-antineutrino excess role in He production
21 p3801 A69-38813

Spectra, fading and pulse structure of pulsars noting electron density, polarization, second periodic pulsation, etc
21 p3802 A69-38826

Stellar IR spectroscopy, describing absorption and emission lines of various atoms and molecules, atmospheric composition, problems with variable stars, etc
21 p3811 A69-39510

Quasi-stellar objects identification, distribution, emission lines interpretation, energy distribution, absorption spectra, radio properties, etc
21 p3811 A69-39515

Stellar scintillation spectra theory extended to rectangular apertures, generalizing to planetary scintillation and effects of diffraction, atmospheric dispersion and seeing
21 p3773 A69-39771

Radio observations of supernova remnant HB 21 at 2695 MHz, noting spectral brightness and curvature of northern shell segment
22 p4014 A69-40129

Finding list of spectral type A7 stars and earlier in region at south galactic pole compiled from prism survey data
22 p4021 A69-40436

Variable stars blue sequence, proposing mu mechanism and beta mechanism as explanation for radial pulsations
22 p4026 A69-40650

Helium-carbon star BD plus 10 degrees 2179 re-analyzed by grid of constant flux models containing right amount of C
22 p4026 A69-40652

C, N and O abundances in K giants alpha Boo, beta Gem and epsilon Peg, noting stellar nuclear burning and evolution
22 p4026 A69-40653

Rocket measurement of far UV spectral intensity of theta Orionis for far UV interstellar extinction law in Orion nebula region
22 p4030 A69-40770

MK system spectral types determination for B, A and F type stars from slit spectrograms near NGC 2264
23 p4211 A69-41487

UBV magnitudes for open cluster NGC 559 stars determined from combined photoelectric and photographic measurements
23 p4211 A69-41490

Tabulated spectroscopic observations of Be stars included in Merrill and Burwell catalog
23 p4213 A69-41720

A-type stars investigation for anomalous spectral line intensities, discussing Hertzsprung-Russell diagrams, rotational velocities, magnetic fields and abundances
23 p4218 A69-42322

Proper motions and spectroscopic data of bright members of II Per and I Lac associations analyzed to determine expansion age
23 p4221 A69-42385

Carroll Fourier transform method applied to stellar spectra lines to determine small rotational velocities
23 p4222 A69-42404

- Equivalent width measurements of Arcturus IR line spectra using Fourier transform spectroscopy, tabulating results
23 p4222 A69-42453
- Model atmosphere analysis of line identifications and equivalent width data for relatively cool Ap star HD 204411, discussing atmospheric composition
24 p4376 A69-42664
- Absorption lines in stellar spectra and significance in cosmogony, discussing ionized Ca K line detection during delta Orionis study, K and H lines components, etc
24 p4383 A69-42999
- VV Cephei type binaries cool and hot primary stars light variations, discussing duration, orbital cycle correlation, mass loss, etc
24 p4386 A69-43346
- Stellar radial velocity measurement accuracy dependence on dispersion, spectrum and line width
24 p4386 A69-43347
- Blue component of HD 237006 and VV Cephei spectra, suggesting greater luminosity of blue star in late type supergiant
24 p4387 A69-43353
- P Cygni characteristics and spectrum analysis, describing absorption lines, line widths, atmospheric composition, light variations, etc
24 p4391 A69-43803
- Beta Orionis spectral line profiles data used to study atmospheric structure
24 p4391 A69-43804
- STELLAR SPECTROPHOTOMETRY**
- Spectrophotometric studies of planetary NGC 6543 gaseous nebula, measuring emission line intensities, electron density and temperature [ARL-68-0200]
02 p0327 A69-12708
- Phase method of photoelectric registration of stellar transition moments
04 p0601 A69-15252
- Solar image or spectrum focal plane scanning technique with output beam displaced but undeviated relative to input beam for solar spectrophotometry
04 p0602 A69-15378
- Arizona-NASA atlas of IR solar spectrum, reproducing photometric tracings obtained from CV-990 aircraft flights
06 p1008 A69-17808
- Absolute magnitudes and intrinsic color photoelectric observations of Wolf-Rayet stars in Magellanic Clouds and Galaxy
07 p1221 A69-19583
- Element abundances in two horizontal branch A stars through coarse and fine spectroscopic analysis, noting metal deficiencies with respect to sun
08 p1385 A69-20061
- Sky background light automatic compensation in stellar photography, using single or double channel photometer
08 p1313 A69-20247
- Spectrophotometry of relics of supernovae, determining H alpha and N II lines intensities radial velocities and velocity dispersion
09 p1587 A69-21357
- Narrow band photometry of variable stars and X ray source Cyg X-2, considering continuum variations with time
09 p1591 A69-21451
- Photoelectric monitoring broadband photometry and spectral scans of candidate star for pulsating radio source CP 1919
09 p1591 A69-21455
- Spectrum analysis for early B type star Barnard 29 in M13 globular cluster
09 p1599 A69-22193
- Three color observations of 16 magnetic stars and photometric properties of 23 stars, discussing periodicities in variations
09 p1599 A69-22196
- Quasi-stellar objects photometric selection in near IR
09 p1604 A69-22272
- Photoelectric spectrum scanning and IR photometric observations of Scorpius XR-1 X ray source
09 p1604 A69-22401
- Far UV stellar astronomy, concerning very hot stars and interstellar gas composition studies
10 p1772 A69-22870
- Hot companion presence for RW Camelopardalis confirmed from UVB photometry
10 p1775 A69-23201
- Flare stars observational and known aggregate characteristics in Coal Sack region
10 p1790 A69-24141
- Spectroscopic, photometric and polarimetric observations of magnetic stars, discussing magnetic curves of periodic variables
11 p1954 A69-24362
- Micrometric and photometric measurements of coude spectra of magnetic variable HD 125248, showing spectroscopic binary nature and computing orbital elements
11 p1963 A69-25264
- Stellar radial velocities derived from line positions measurements by precision screw microphotometer
12 p2153 A69-25810
- Faint stars background exposure density and detection limit determined by astrosensitometer for Kodak Spectroscopic Plates
12 p2153 A69-25811
- Spinning rockets UV spectrophotometry of early type stars, discussing instrumentation, calibration, data recording and stellar spectra
12 p2153 A69-25812
- Lacerta OB1 stellar spectral classes and photographic magnitudes, analyzing clusters and distributions in concentrated and dispersed areas
12 p2153 A69-25813
- Photoelectric and visual minima tabulated for eclipsing binaries, calculating light elements
12 p2160 A69-26853
- Statistical analysis of UVB characteristics of blue objects located near galactic north pole by scintillation techniques
12 p2168 A69-27054
- Spectroscopic and eclipsing binaries in zodiac tabulated for photometric studies at lunar occultations
12 p2171 A69-27152
- UVB observations of long period variable stars using reflecting telescope and refrigerated photocell with standard filters
12 p2172 A69-27156
- UVB observations of stars P and 36 Cygni including short period variations and secular changes in brightness
12 p2172 A69-27159
- Crab Nebula pulsar NP 0532 photoelectric spectrophotometry results, noting main pulse and interpulse spectral energy distributions similarity to extended synchrotron radiation
13 p2335 A69-27317
- High dispersion classification of early K2-M6 giants of high and low velocity, using titanium oxide band strengths criteria tested by atomic lines estimation
13 p2338 A69-27556
- Multiband photoelectric photometer for near IR observations, tabulating magnitudes, colors, spectral irradiance, radii and effective temperatures of late type stars
13 p2342 A69-27592
- Stellar photometry during occultations by earth, discussing feasibility of lunar based observations
13 p2345 A69-27651
- Photoelectric yellow and blue observations of variable V502 Ophiuchi, noting influence of partial eclipses on orbital determination reliability
13 p2348 A69-27809
- Spectrophotometry of variable star SS Cyg, analyzing energy distribution in continuum, UV gradient and Balmer jump
13 p2351 A69-27868
- Photometric discovery of new variable stars resulting from quasars observation, noting optical variability noncorrelation with observed properties
13 p2354 A69-28468
- Variable comparison star identified from photoelectric observations of RR Lyrae star BR Aqr, showing light and color curves
14 p2519 A69-29139
- Arcturus and solar rubidium abundance compared using Mount Wilson photographic spectrograms of Arcturus
14 p2522 A69-29589
- Absolute spectrophotometric gradients determined from energy distribution in UV beta Lyr spectrum, confirming gradual variations in light curve shape and spectral characteristics
15 p2688 A69-30557
- Member stars number in globular clusters M3 and M5 determined from photometric and kinematic characteristics
15 p2688 A69-30561
- Atmospheric parameters for blue horizontal branch stars in globular cluster NGC 6397 by spectroscopic and photoelectric observations, obtaining mean stellar mass
15 p2692 A69-30770
- Spectrographic and photoelectric analyses of F type sharp line eclipsing binary HR 7484, tabulating masses, radii, color indices and absolute magnitudes
15 p2693 A69-30776
- ET Pegasi photoelectric observations in UVB colors, giving period different from Kaho and new time of maximum light
15 p2694 A69-30787
- Photoelectric index of main sequence stars in F5 to G2 spectral range as indicator of atmospheric microturbulent velocities
15 p2695 A69-30999
- Photoelectric observations program at Astronomical Observatory of Bucharest to determine smallest moments of several eclipsing stars
15 p2696 A69-31224
- Supernovae spectra observation suggesting tracing as broad band interstellar absorption rather than emission features on continuum
15 p2701 A69-31534
- Photometer for simultaneous stellar photometry in UVB bands, purposes and performance characteristics and circuit diagrams
16 p2790 A69-32209
- Stellar diameters in galactic cluster stars determined using original and modified spectrophotometric method compared with spectral types BOV-FOV
16 p2858 A69-32210
- Nonocculted areas of Algol during eclipse using Balmer discontinuity spectrophotometric method, determining apparent stellar diameters
16 p2858 A69-32216
- Four color and H beta photometry of stars in Coma and Ursa Major clusters compared to standard relations for Hyades Cluster
16 p2860 A69-32234
- Photoelectric observations of color and titanium oxide in M7 giants in nuclear bulge of Galaxy compared with late giants near sun
16 p2863 A69-32396
- BetaCrB atmospheric microturbulence velocity, ionization and excitation temperatures, electron pressure and abundances determined by spectrophotometer
16 p2864 A69-32592
- Spectrophotometry of F stars 42 Cyg and nu Her atmospheres, analyzing microturbulence, excitation and ionization temperatures, electron pressures and abundances
16 p2864 A69-32596
- Stellar photometric data for various photocathode materials used to calculate radiant energy falling on earth
17 p2973 A69-33092
- UVB photometry of faint stars, discussing photographic plate effect on accuracy, emulsion standardization and use of electronography
17 p3031 A69-33099
- Southern Milky Way spectral survey for selection, classification and photometry of interesting objects
17 p3031 A69-33101
- Spectrophotometric characteristics of Serpentes, high metallicity A2 star and standard F zero V 9 Aurigae, analyzing chemical composition, microturbulence velocity and abundance by detailed differential growth curve
17 p3039 A69-33728
- Photoelectric photometric stellar spectroscopy for calculating metal abundance from Fraunhofer absorption lines, relating results to star age
17 p3043 A69-34140
- Spectrophotometry of relics of supernovae, determining H alpha and N II lines intensities radial velocities and velocity dispersion
18 p3197 A69-34747
- HD 30353 He binary star invisible component suggested as KO type supergiant from IR photometric data
18 p3203 A69-35348
- Spectroscopic and photoelectric observations of peculiar variable FG Sge, discussing expansion velocity and equivalent widths for Balmer and K lines
20 p3599 A69-37474
- Periods and magnitudes of RR Lyrae variable stars in M 2 cluster, tabulating photometric characteristics
20 p3599 A69-37477
- Solar far UV images systematic photometry for thin solar models in terms of quiet sun intensity
20 p3603 A69-37546
- Delay in photoelectric recording of transit of stars, considering stellar image brightness distribution and temperature
20 p3608 A69-38053
- Stellar systems observations using photometers with long narrow slits in identical telescopes
20 p3545 A69-38055

Papers of Lunar and Planetary Laboratory, Volume 8, covering lunar craters, rock fragmentation, stellar photometry, etc 21 p3799 A69-38674

Photodetector responses to radiant energy from many stars tabulated for various photocathode materials and silicon detector 21 p3800 A69-38680

Instrumental profile determination for high resolution stellar spectrograph, using profiles of telluric oxygen bands obtained from emission line observations 21 p3721 A69-38696

Photometric and spectroscopic data for southern RR Lyrae variables, deriving period, light curves in three colors, mean radial velocity and spectral types 21 p3801 A69-38764

IC 349 nebula in Pleiades investigated with diffraction spectrograph, observing spectral energy distribution relationship to illuminating star 21 p3817 A69-39728

Spectrophotometric observations of delta Scuti short period variable stars compared with model atmospheres 22 p4015 A69-40150

Calcium K line strengths in A stars measured by narrow band spectrometer compensated for seeing and transparency variations 22 p4015 A69-40154

P Cygni spectroscopy indicating existence and atmospheric structure of accelerating envelope about star, computing line profiles 22 p4023 A69-40471

Variable HDE 310376 spectroscopic and photometric data, discussing brightness fluctuations, color changes, emission and absorption spectra, etc 22 p4026 A69-40651

Photoelectric observations of eclipsing binary 32 Cygni during 1968 eclipse using standard UVB color filters, tabulating results of UVB photometry 22 p4032 A69-40946

Continual photoelectric monitoring of flare star YZ CMi by photoelectric photometer attached to reflector, giving light curves for flares 22 p4032 A69-40947

Tabulated photoelectric photometer measurements of Nova Vulpeculae 1968 No. 1 23 p4208 A69-41290

UBV magnitudes for open cluster NGC 559 stars determined from combined photoelectric and photographic measurements 23 p4211 A69-41490

Photographic observations of open cluster IC 4665 made on blue and yellow sensitive plates with Vatican refractor compared with photometric measurements 23 p4215 A69-42008

Narrow and intermediate band photometry of globular star clusters in uvby and beta photometric systems, relating reddening to metal abundances of member stars 24 p4387 A69-43352

STELLAR STRUCTURE

Stellar evolution, discussing stellar structure, pre- and post-main sequence evolution, solar system origin, supernovae, white dwarfs, variable stars and close binaries 01 p0148 A69-10046

Solar granules structural and correlation functions indicate homogeneous random field within photograph and regular component in intensity fluctuations spatial distribution 02 p0317 A69-11958

Solar neutrino flux dependence on rotation rate of solar core and fractional mass involved in interior mixing 02 p0325 A69-12600

Electron conductivity in low mass red giant core 02 p0327 A69-12709

Red giants limiting helium core mass dependence on total stellar mass and initial composition from stellar evolutionary models 02 p0327 A69-12710

Photospheric brightness differences and structure of large scale intensity fluctuation, discussing association with solar supergranulation and chromospheric network 03 p0515 A69-14037

Sunspot structure from two dimensional radiative transfer analysis of center limb intensity profiles made at several heliocentric angles 03 p0516 A69-14040

Atomic collision processes in astrophysics noting stellar continuum spectra, Ca ion and He lines, solar corona, heat balance in H I regions and planetary nebulae 07 p1224 A69-19653

Neutrino emission and carbon burning onset in 1.45 solar mass stellar models with pure He envelope, He burning shell and degenerate C-O core 08 p1384 A69-20059

Carbon 12 stars to simulate core evolution of planetary nebulae precursors, discussing nuclear shell burning 08 p1396 A69-20649

Instability of stellar structures intermediate between white dwarfs and neutron stars shown by stellar models, discussing pulsar signals periodicities 08 p1397 A69-20770

Stellar abundances of lithium, deuterium, beryllium and boron indicating nonthermal atmospheric origin 08 p1403 A69-20912

Temperature gradient in semiconvective region, examining molecular weight distribution in mixing due to overstability 09 p1596 A69-22057

Structure and pulsational properties of massive stars with helium cores and thin hydrogen poor envelopes 09 p1606 A69-22421

Static envelope with no mass outflow for star static core constructed from opacity coefficient dependence on temperature and density 10 p1775 A69-23199

Period variations, colors and light curve peculiarities of models of U Geminorum type stars 11 p1954 A69-24363

Stellar physics, Volume 1, covering stellar structure, evolution, physical processes, statistical physics, quantum theory, classical mechanics, etc 12 p2152 A69-25785

White dwarfs structure model for deriving formula for phase density in color-luminosity diagram 12 p2159 A69-26665

Book on astrophysics and stellar astronomy covering stellar radiation, binary and variable stars, positions, magnitudes, galaxies, cosmologies, etc 13 p2337 A69-27463

Critical parameters of isothermal quasi-degenerate white dwarfs calculated by energy method, allowing for relativity theory error and neutron irradiation effect 13 p2351 A69-27871

Structure and thermometry of solar interior from measuring neutrino fluxes intensities emitted by unit mass 13 p2333 A69-28434

White dwarfs periods of radial oscillations, considering ion gas contribution to adiabatic coefficient computation 14 p2517 A69-29090

Relative element abundances in Cyg, Her and Boo atmospheres, calculating curves of growth by Planck gradient method for stellar spectra 14 p2519 A69-29356

P Cyg star HD 190603 atmospheric parameters from spectrograms analyzed by curve of growth method, including ionization and excitation temperatures and electron density 14 p2519 A69-29357

Pulsar model used to explain stellar shape oscillations as cause of radio emission intensity periodic variations 14 p2522 A69-29675

Horizontal branch stars of metal-poor globular clusters in Galaxy evolved from very blue stars, noting substantial mass loss at He-flash 14 p2529 A69-29977

Internal structure of rotating stars, analyzing physical changes, circulation influence on mixing during evolution and angular velocity 15 p2683 A69-30512

Stellar energy diffusion processes studied to determine energy transfer time scale between stellar layers 15 p2692 A69-30767

Equilibrium models reliability for main sequence stars estimated from systematic applications of physical assumption sets and numerical methods 16 p2859 A69-32219

Lynden-Bell statistical mechanics of relaxation in collisionless one dimensional stellar system, discussing low energy particles distribution 16 p2862 A69-32376

Finite resolution effect on solar granulation simulated by numerical experiments using two dimensional smeared pattern 17 p3029 A69-33046

Photoelectric photometric stellar spectroscopy for calculating metal abundance from Fraunhofer absorption lines, relating results to star age 17 p3043 A69-34140

Microturbulence velocity estimation method for solar type stars using low dispersion spectra of narrow band photometry 17 p3044 A69-34178

Pulsar PSR 0833-45 period decrease resulting from mass addition leading to radius and inertia moment decreases 18 p3196 A69-34646

Pulsar PSR 0833-45 polarization structure frequency dependence measurement leading to model implying radiation emanated from magnetic poles neighborhood 18 p3202 A69-35215

Magnetic structure of active solar region as function of time for correlation between flares and magnetic field evolution 20 p3590 A69-37827

Autoionization lines effect on stellar structure by computing contributions to Rosseland mean opacity 20 p3612 A69-38165

Rotating neutron star model to fit pulsar data, considering star crust formation and properties, angular velocity changes and starquake effects 21 p3798 A69-38544

Pleiades cluster and ambient interstellar medium structure analyzed for spectral distribution based on plane-parallel scattering model 21 p3817 A69-39727

Dynamo action origin of stellar and planetary magnetic fields, considering turbulent helical motions of H convection zone of sun 22 p4011 A69-39998

Galactic center observations over various wavelengths including polarization, diameter, flux measurements and power output 22 p4029 A69-40767

Book on stellar structure, Volume 1, Physical principles, covering interior conditions, thermodynamic and radiation theories, stellar temperature, energy and opacity, etc 23 p4211 A69-41377

Principles of stellar structure, Volume 2, covering outer layers, models computation, white dwarf stars, stellar evolution, pulsating stars, etc 23 p4223 A69-42475

Stellar structures and evolution stressing composition and processes of stellar interiors 24 p4379 A69-42782

STELLAR WINDS

Stellar rotation braking due to mass loss from coronae through stellar wind based on calculation of acoustic energy generation from convective zone 08 p1396 A69-20644

Magnetoacoustic waves generated by Cerenkov radiation from corpuscular fluxes due to star interaction with stellar wind, determining deceleration forces on star 11 p1955 A69-24385

Magnetoacoustic waves generated by Cerenkov radiation from corpuscular fluxes due to star interaction with stellar wind, determining deceleration forces on star 24 p4390 A69-43775

STELLARATORS

Hot plasma containment by magnetic field, presenting results from stellarator for toroidal sheared magnetic field properties 07 p1190 A69-18929

Plasma diffusion in toroidal stellarator using integrals of drift equations for particle trajectories, determining distribution function 07 p1191 A69-18985

Loss rate of plasma from stellarator due to binary Coulomb collisions scattering particles in loss region, discussing diffusion coefficients 08 p1364 A69-20520

Asymptotic toroidal equilibrium for guiding center plasma model based on stellarator expansion, considering toroidal curvature, helical currents and plasma pressures 09 p1552 A69-22044

Plasma diffusion in toroidal stellarator, calculating collisional diffusion and diffusion constants 09 p1552 A69-22294

Plasma capture in stellarator diverter aperture with asynchronous plasma jets injection through diverter magnetic slots, discussing plasma cylinder density effect 21 p3776 A69-38585

STEP FUNCTIONS

Pneumatic stepping motor actuation system with pure fluid valves and signal processing and minimum number of moving mechanical parts for high g and temperature environments 02 p0196 A69-12086

- Numerical integration stability of differential equations, noting limiting integration step size for unsteady distillation
02 p0273 A69-12478
- Plant identification procedures by stepwise approximation and least squares methods
03 p0409 A69-13072
- Step function factor for laminar heat transfer from rotating disk with surface temperature changing stepwise in uniform forced stream
06 p1029 A69-17003
- Discrete time, single input, stepping extremum control system with input disturbance and output measurement noise, discussing computer simulation and dimensional analysis
07 p1114 A69-18287
- Laser small signal step response measured, deducing medium bandwidth
[IEEE PAPER G-9]
07 p1151 A69-19056
- Transient response spectrum of nonlinear cubic spring mass system subjected to step function input, discussing viscous damping effects on peak response
08 p1413 A69-20402
- Electromagnetic step-function plane waves propagation in ionosphere using Fourier transform and Bessel functions
12 p2034 A69-27132
- Nonlinear control systems error signals convergence to steady states in frequency domain, applying step or ramp functions to single feedback system
13 p2237 A69-27188
- Shadow zone diffraction of plane step function compressional wave by circular cavity, using Friedlander wave front approximations
13 p2368 A69-28347
- Weak superconducting contacts volt-ampere characteristics current steps and emission spectra, showing singularities due to superconducting current nonharmonicity
14 p2504 A69-28994
- Spring mass nonlinear systems under constant force excitation, studying step function responses of systems with various restoring force characteristics
21 p3836 A69-38985
- STEREOCHEMISTRY**
Pyridine nucleotide-linked D-lactate dehydrogenase stereospecificity in various species of invertebrates
01 p0018 A69-11198
- Gas-liquid and thin layer chromatography and nuclear magnetic resonance techniques to steric analysis of diketopiperazines
07 p1075 A69-19498
- Life detection for space missions based on detecting optical asymmetry in biogenic molecules by gas chromatography involving diastereomeric esters synthesis
15 p2556 A69-31315
- STEREOGRAPHY**
U STEREOPHOTOGRAPHY
- STEREOPHOTOGRAPHY**
Mirror photogrammetry geometric principles, studying photo pairs, mirror reflection and reduction methods
01 p0077 A69-10025
- Error analysis of orientation methods for extraterrestrial stereophotogrammetric mapping
[JPL-TR-32-1344]
03 p0429 A69-13299
- Algorithm generating same stereogram for two or more selected surfaces by extending random dot stereogram technique
04 p0603 A69-15445
- Wind vector in respect to orientation of large scale cirrus bands based on stereophotogrammetry and radar observations
08 p1346 A69-20442
- Scenic holographic stereograms resolution and up/down scaling, discussing roles of projector lens and camera aperture
11 p1883 A69-24690
- Photogrammetric calibration of Surveyor 7 stereo mirror based on vector analysis
[JPL-TR-32-1390]
13 p2263 A69-28199
- Heights of cloud bases and convective cloud tops determined by stereoscopic photogrammetry of Apollo 6 mission
20 p3569 A69-36926
- Side-looking radar and IR line scanning as method for simultaneous stereo height mapping, using images produced from same vantage point
20 p3536 A69-36929
- Microholographic system for nonpseudoscopic stereoscopic image reconstruction of transparent and nontransparent microobjects
21 p3726 A69-39702
- Mars landing site topography reconstructed via stereoscopic pictures returned by surface-based imaging systems
23 p4164 A69-41618
- Automated air photo identification of crop types, utilizing stereo height as discriminating variable
23 p4155 A69-41721
- STEREOSCOPIC PHOTOGRAPHY**
U STEREOPHOTOGRAPHY
- STEREOSCOPIC VISION**
Algorithm generating same stereogram for two or more selected surfaces by extending random dot stereogram technique
04 p0603 A69-15445
- Stereoscopy effects on pattern recognition in visual noise
06 p0880 A69-17214
- Stereoscopic shadow caster application to photographic stereoscopic projection for studying binocular stereopsis under kinetic viewing conditions in vision research
22 p3893 A69-40839
- Device for studying stereoscopic field of vision applied to determining field of vision standards for healthy individuals
22 p3886 A69-41113
- Electronic scanning and correlation techniques for terrain sensing required in automatic stereoperception
24 p4316 A69-43566
- STEREOSCOPY**
NT STEREOPHOTOGRAPHY
- Hyperstereoscopic and hypostereoscopic hologram images with doubled or halved interocular distance, noting effect on image depth
02 p0249 A69-11931
- STERILIZATION**
NT CHEMICAL STERILIZATION
NT SPACECRAFT STERILIZATION
- Microorganisms and viruses susceptibility to sterilization by ionizing radiation, heat and combination of radiation and heat, considering space materials damage elimination
05 p0713 A69-15947
- Data sampling and statistical verification in large scale sterilization procedures, discussing biological indicator /bacillus stearothermophilus/ and incubation time
05 p0714 A69-15952
- Control and sampling in sterile rooms, noting worker introduction of contaminants
05 p0714 A69-15953
- Research and development programs leading to heat sterilizable spacecraft battery separator material, describing bench tests
23 p4072 A69-42284
- STERNS**
U AFTERBODIES
- STEROIDS**
NT ALDOSTERONE
NT CHOLESTEROL
NT CORTICOSTEROIDS
NT CORTISONE
- Steroid hormones effect on nervous system and behavior from data on gonadectomized rats and monkeys treated with testosterone propionate
03 p0375 A69-13551
- Electron impact induced fragmentation of ring D in steroids involving loss of carbon atoms analyzed by mass spectrometry
07 p1069 A69-19497
- European pilots accustomed to equatorial climate tested during regular flying missions, discussing heat effects on urinary steroids
12 p2024 A69-26560
- Food intake changes of female rats in response to changes in energy balance, discussing steroids as physiological tracer
15 p2555 A69-30693
- Urinary excretion of hormonal metabolites in intercontinentally flown test subjects, using gas chromatographic procedure for steroid identification
24 p4268 A69-43404
- STETHOSCOPES**
Electronic stethoscopes for use in high background noise environments for patients on air evacuation flights
21 p3667 A69-39444
- STIELTJES INTEGRAL**
Stieltjes transform relating initial boundary value problems for partial differential equations of various classifications
08 p1342 A69-20352
- Dynamic reciprocity relationship for linear directed continuous viscoelastic media, using Stieltjes convolution
19 p3373 A69-36307
- STIFF STRUCTURES**
U RIGID STRUCTURES
- STIFFENING**
Buckling equations for orthotropic cylindrical shells with eccentric spiral stiffeners derived through variation method of total potential
04 p0676 A69-14710
- Damping of response of integrally stiffened skin structures to random acoustic pressures, reducing rms stress in case of broad band excitation
[ASME PAPER 69-VIBR-26]
10 p1806 A69-24172
- Free vibrations in axisymmetrically loaded orthotropic circular conical shells with longitudinal and circumferential stiffening based on linearized theory, considering shear deformation and inertia
11 p1969 A69-24327
- Stiffener geometry and spacing effects on buckling of axially compressed cylindrical and conical shells
11 p1979 A69-24815
- Shear buckling of simply supported infinitely long plates orthogonally reinforced by stiffeners with flexural and torsional rigidity
11 p1984 A69-25142
- Contact problem for half plane with elastic stiffener reduced to Prandtl integrodifferential equation, determining contact stresses
14 p2531 A69-28804
- STIFFNESS**
Ribbon reinforcements in composite materials noting stiffness properties
01 p0172 A69-11265
- Vertical, horizontal and rocking vibrations of body on surface of otherwise unloaded elastic half plane, estimating stiffness for coupled vibrations
[ASME PAPER 68-WA/APM-12]
04 p0668 A69-14393
- Stiffness matrices for sector elements under membrane stress, considering alternative displacement distributions within element
04 p0676 A69-14728
- Stiffness matrices for buckling or vibration analysis of long thin flat plate structures connected at longitudinal edges
05 p0836 A69-16029
- Polycarbonate surface stiffness increase associated with fatigue induced by repetition of loads
06 p0946 A69-17206
- Small bending stiffness effect on inflated torus and cylindrical shells under radial load for determining large space structure stiffness
06 p1024 A69-17607
- Computer analysis for optimizing size and shape of thin walled axisymmetric elastic rings, plates and shells with respect to tension, rigidity and weight
06 p1026 A69-18017
- Unsymmetrically laminated simply supported plates approximate solutions, considering potential energy and reduced stiffness matrix
07 p1232 A69-18725
- Explicit transverse bending stiffness and mass matrices for triangular finite plate element with linear thickness variation, using matrices for natural frequencies of vibration
08 p1414 A69-20526
- Testing system stiffness effect on sheet fracture, discussing notch strength dependence on stiffness
10 p1796 A69-23075
- Stiffness matrix for doubly curved shallow shell element with rectangular plane projection applied to circular cantilevered cylinder and barrel vault
10 p1802 A69-23892
- Modal coupling in thermally stressed plates, obtaining solution for frequencies and stiffness
11 p1990 A69-25509
- Optimum automatic selection of redundancies, discussing weighting and pivot choice and rigid element incorporation
11 p1993 A69-25529
- Nonstiffness of nonshallow spherical dome using asymptotic method, applying nonlinear Reissner equations to finite symmetric deformation of thin shells of revolution
11 p1996 A69-25733
- Book on design procedures for modern fibrous composites emphasizing stiffness properties and calculations, covering laminates orthotropic lamina, etc
12 p2179 A69-26238

Stiffness matrix derived for skewed curved shallow shell element with reference to oblique coordinate system

13 p2358 A69-27210

Subelement geometrical stiffness determined, considering complete element natural modes

13 p2362 A69-27838

Stiffness matrix for refined triangular plate bending finite element, considering Kirchhoff theory

15 p2706 A69-30434

Finite element and iteration method for large deflection of rectangular plate, considering stiffness matrix for bending

15 p2706 A69-30435

Stiffness matrix of polygonal finite plate bending element derived using assumed stress distribution

15 p3447 A69-30867

Noise transmission from turbulent boundary layer through flexible plate into closed cavity, emphasizing nonlinear plate stiffness and mutual interaction between plate and airflow

17 p3006 A69-33409

Elastic stiffness, kinematically equivalent loads and initial loads due to initial strains of FUGA 6 element, describing program for matrices generation

19 p3447 A69-36852

Random arrays representing random filament packing of actual composite materials, discussing effects on transverse stiffness

20 p3626 A69-37758

Holor algebra with tensor notations applied to elastic structures /discrete systems/, discussing inertia and stiffness tensors

21 p3831 A69-38415

Stiffness matrix for curved membrane shell, outlining discrete element representation of cylinders with widely spaced circumferential stiffeners

21 p3842 A69-39305

Computerized aircraft structural analysis system, adopting finite element technique /direct stiffness method/ based on COSMOS system

21 p3842 A69-39307

Stress analysis of thin axisymmetric shells by plane frame analysis program, noting stiffness matrix for conical shell element

21 p3843 A69-39312

Curved rectangular elements stiffness matrices derived for finite element analysis of cylindrical shells bending

22 p4046 A69-40969

Single stage rocket body finite bending stiffness effect on pitching moment using approximate equation, noting applicability to multistage rockets

22 p4037 A69-41048

ASTRA /advanced structural analyzer/ based on stiffness approach to finite element method, generating mathematical model for stresses and deflections

23 p4232 A69-42144

Perforated heat exchanger tube plates stiffness determination from hole diameter-to-spacing ratios

24 p4400 A69-43087

STILBENE

Polymeric Schiff bases synthesis, thermal stability and nature of pyrolytic decomposition of polyazines and derived polystilbenes

07 p1074 A69-18628

STILLS

Digital simulation of transient solar still processes, using finite difference approach for heat flow to and from soil

16 p2765 A69-31816

STIMULANT

NT NORADRENALINE

NT NOREPINEPHRINE

Lobeline effect on oxygen pressure in gigantocellular nucleus of medulla oblongata and respiration rates of dogs recorded automatically

22 p3888 A69-41273

STIMULATED EMISSION

Radiation damage in CdS irradiated by normal mode or Q-switched ruby laser, discussing stimulated Brillouin scattering

02 p0257 A69-12614

High resolution spectroscopic study of stimulated rotational transitions of nitrogen molecules using crossed grating Echelle spectrograph

02 p0284 A69-12621

Two photon absorption and stimulated emission mechanism of CdS-CdSe mixed crystals investigated by ruby laser output

03 p0438 A69-13052

Q switched laser based on light waves parametric interaction in nonlinear medium operating at wavelengths from UV to IR

03 p0439 A69-13054

Nonlinear influence of resonator losses on stimulated emission of ruby laser, noting cut-off action

03 p0439 A69-13058

Neodymium glass properties degradation during laser operation due to short wave pumping radiation and stimulated emission

03 p0442 A69-14219

Superradiant and laser spectroscopy in second positive system of molecular nitrogen

04 p0609 A69-14285

Stimulated emission of cyanine dyes, discussing amplification coefficients

04 p0612 A69-15373

Stimulated emission properties of active fibers obtained from photomultipliers transmitting pulses to oscillograph

05 p0761 A69-15657

Thermionic electron emission from Mo and W targets irradiated by CW carbon dioxide laser beam

05 p0771 A69-15812

Metastable level population measurement in laser crystal based on luminescence changes under influence of stimulated emission

06 p0934 A69-17457

Relaxation theory of highly ionized hydrogen plasma noting applications to stimulated emission, radiation source development and electromagnetic radiation amplification

07 p1191 A69-18996

Spatially nonuniform laser model allowing for photon density and inversion variations, noting self Q switching mechanisms from stimulated scattering processes

[IEEE PAPER Q-6] 07 p1154 A69-19078

Stimulated Compton scattering for laser action, noting voltage tunability and gain at far IR wavelengths

[IEEE PAPER S-9] 07 p1154 A69-19081

Induced emission cross section of neodymium glass laser in quasi-steady mode measured as function of rod section, mirror reflectivity and output

07 p1156 A69-19161

Level crossing effect in stimulated emission and application to determination of hyperfine splitting in Xe 129 excited electronic state during laser transition

07 p1156 A69-19398

Second harmonic generation in laser crystals by Gaussian beams of finite aperture

07 p1158 A69-19756

Li niobate crystal emission excited by Ar laser beam, deriving laser action formulas

08 p1323 A69-19941

Stimulated emission of laser employing crystal and glass lasers doped with neodymium ions, using high temperature spectroscopy

08 p1323 A69-19944

Stimulated emission of water cooled CW Nd doped lanthanum fluoride at room temperature

08 p1323 A69-19945

Collective interactions of electromagnetic waves in plasma, discussing light scattering from electron fluctuations, stimulated emission and anomalous absorption

08 p1361 A69-20220

Stimulated Mandelstam-Brillouin scattering at second harmonic of ruby laser and neodymium glass laser

09 p1520 A69-22684

First Stokes component of stimulated Mandelstam-Brillouin scattering and line defects caused by self focusing of single pulse laser beam

09 p1521 A69-22686

Stimulated emission of trivalent Nd ions in glass base, explaining connection between efficiency and emission polarization by interaction of laser modes with ions

10 p1703 A69-23618

Resonator interferometry of pulsed submillimeter wave lasers, analyzing mode structure, pulse shapes and molecular mechanism of laser emission

10 p1705 A69-23810

Specific level role in emission of optical radiation by ruby laser stimulated calcium fluoride crystals doped with divalent Dy ions

11 p1894 A69-24618

Stimulated emission cross section measurement of Nd ions in calcium tungstate using Edwards method

11 p1938 A69-25049

Transmitter frequency increase effect on production of artificial stimulated VLF emissions in magnetosphere

11 p1878 A69-25156

Fluorescence stimulated by high energy electron and ion beams, determining vibrational temperature and concentration of molecular oxygen in high enthalpy wind tunnel flows

13 p2302 A69-28265

Self resonant energy transfer mechanisms in active media for lasers investigated by two methods

14 p2460 A69-29644

Stimulated emission of cerium trifluoride-positive trivalent Nd ion laser noting absorption, luminescence, excitation, emission spectra and metastable state lifetime

14 p2460 A69-29645

Low temperature method for measuring breakdown threshold parameters of liquid and gaseous He by laser beam, observing stimulated Mandelstam-Brillouin scattering

16 p2796 A69-31799

Stimulated emission of cyanine dyes, discussing amplification coefficients

16 p2797 A69-32120

Stimulated emission properties of active fibers obtained from photomultipliers transmitting pulses to oscillograph

16 p2792 A69-32514

Radiation diffusion in plane-parallel isothermal gas layer of two and three level atoms, considering stimulated emission and frequency redistribution

16 p2864 A69-32587

Laser action in quantum system, analyzing absorption constant relation to spontaneous/stimulated emission constants, energy level population inversion, pumping, etc

17 p2984 A69-34150

Ruby laser stimulated emission spatial, temporal, energetic and spectral characteristics during disruption in spherical cavity containing strongly scattering medium

18 p3152 A69-35026

Radiation emission by molecules in electromagnetic field, considering cavity resonators and waveguides excitation

18 p3178 A69-35404

Induced-emission oscillator navigation sensor with performance limitations, noting ring laser and nuclear maser gyro and laser accelerometer

19 p3369 A69-35795

Stimulated emission characteristics of CdS-CdSe mixed crystals subjected to two photon excitation, studying pulse energy at 77 K as function of pumping power

19 p3332 A69-35867

Two photon excitation of luminescence in complex uranyl compound single crystals using Q switched ruby laser

19 p3334 A69-35982

Metastable level population measurement in laser crystal based on luminescence changes under influence of stimulated emission

20 p3555 A69-37940

Stimulated emission at current pulse end ascribed to external resonator turn-on time delay effects with GaAs injection lasers at room temperature

21 p3734 A69-38408

Luminous efficiency for electron induced molecular nitrogen bands, discussing thick- and thin-target measurements of fluorescent efficiencies

21 p3774 A69-38521

Time dependent mathematical double acceptor model including heat effects for analyzing Q switching and stimulated emission time delays in pulsed junction lasers

22 p3962 A69-40560

Digital computer determination of stimulated emission time delay, Q switching temperature and current region and impurity profile effect across junction in junction lasers

22 p3962 A69-40561

Linear self consistent diffraction emission theory and relationship to electron beam propagation

22 p3899 A69-40615

Pumping model for analyzing stimulated and enhanced potassium multiphoton emission primed by ruby laser-stimulated Raman electronic radiation

23 p4171 A69-41391

Stimulated Brillouin scattering application to measurement of hypersonic velocities and absorption in gigahertz frequency range, laser frequency shifting and Q switching, etc

23 p4167 A69-42183

GaAs junction laser total stimulated light power dependence on resonator length taking into account optical losses

24 p4330 A69-43768

STIMULATED EMISSION DEVICES NT ARGON LASERS

NT CARBON DIOXIDE LASERS
 NT CHEMICAL LASERS
 NT GALLIUM ARSENIDE LASERS
 NT GAS LASERS
 NT GAS MASERS
 NT INFRARED LASERS
 NT INJECTION LASERS
 NT LASERS
 NT LIQUID LASERS
 NT MASERS
 NT ORGANIC LASERS
 NT PROTON MASERS
 NT PULSED LASERS
 NT Q SWITCHED LASERS
 NT RING LASERS
 NT RUBY LASERS
 NT SEMICONDUCTOR LASERS
 NT SOLID STATE LASERS
 NT TRAVELING WAVE MASERS

Semiclassical theory of quantum generators, examining laser system response to effect of monochromatic standing wave based on kinetic equation for density matrix

16 p2798 A69-32480

Collection of papers on quantum electronics covering microwave, optical quantum generators and amplifiers, paramagnetic resonance, molecular excitation, etc

18 p3178 A69-35401

Gas and solid state microwave quantum generators and amplifiers, discussing radiation characteristics

18 p3153 A69-35407

Far IR radiation generation, considering incoherent sources, harmonic generators, electron tubes, relativistic electrons and quantum oscillators

22 p3982 A69-40669

STIMULATION

U AUDITORY STIMULI
 U SENSORY STIMULATION

STIMULI

Hypothalamic motivational systems and stimulation, discussing behavior patterns and plasticity

09 p1444 A69-21310

STIRLING CYCLE

Radioisotope energized Stirling engine for spacecraft auxiliary electric power, discussing system configurations, weight and fuel requirements

23 p4190 A69-42281

STIRRING

Adiabatic stirred reactor, discussing steady state nonlinear equations of reactant gases combustion

02 p0352 A69-12316

STOCHASTIC PROCESSES

NT MARKOV CHAINS
 NT MARKOV PROCESSES
 NT RANDOM PROCESSES

Stochastic Lurie type systems stability using Liapunov method

01 p0050 A69-10240

Optimal control of discrete and continuous stochastic linear dynamical systems, discussing algorithms for instantaneous weighted minimum mean square error performance

01 p0051 A69-10439

Single frequency oscillations in stochastic quasi-linear differential equations with delay

01 p0170 A69-10825

Kalman optimal filter for linear distributed parameter systems with Gaussian disturbances and measurement noise

01 p0034 A69-11143

Free access of low energy galactic particles to solar wind lines of force due to stochastic nature of lines

01 p0147 A69-11238

Linear filter performance degradation due to modeling error in estimate of state vector of stochastic linear dynamic systems

02 p0225 A69-11971

Bulk queueing with service time distribution assuming customer arrival in batches and service discontinuance

02 p0271 A69-12060

Approximation of correlation or transfer function obtained through exponential polynomial to determine stochastic process spectral density

03 p0409 A69-12976

Book on filtering for stochastic processes with applications to guidance covering asymptotic properties, nonlinear filtering, mathematical models, etc

04 p0580 A69-14386

Optimal control of linear stochastic systems using noise measurement data mathematical model

04 p0581 A69-14569

Stochastic problems in control - Conference, Ann Arbor, June 1968

04 p0581 A69-14693

Mathematical modeling of Gaussian and nonGaussian processes obtained by linear and nonlinear transformations of white Gaussian noise, noting Markov processes

04 p0623 A69-14694

Stability of stochastic systems, discussing continuous parameter models, Gaussian white noise, stabilization of unstable deterministic system and ITO equations

04 p0623 A69-14695

Linear and nonlinear filtering, discussing models for signal process, linear white noise problem, optimal estimates, colored noise and finite dimensional approximation

04 p0581 A69-14696

Optimal stochastic control of small dynamic systems described by random differential equations, noting selective bibliography on several subjects

04 p0582 A69-14697

Fluid amplifier linear transfer functions at signal levels on order of internal noise identified by random signal testing method

[ASME PAPER 68-WA/AUT-2]

05 p0706 A69-16184

Maximum principle application to stochastic systems, developing set of stochastic partial differential equations

05 p0788 A69-16482

Matrix Riccati and matrix quadratic equations in problems of stochastic control and filtering

05 p0740 A69-16601

On-line optimization of stochastic control systems based on learning controller model, discussing computer simulation results

06 p0900 A69-17354

Linear distributed parameter system identification by stochastic approximation, obtaining constant parameters sequentially

06 p0900 A69-17358

Optimal estimation of sampled stochastic process with finite state unknown parameters

06 p0901 A69-17362

M measurement optimal feedback control algorithm for stochastic discrete time systems, considering nonlinear plant, constrained controls, nonquadratic cost and simulations

06 p0902 A69-17402

Light variations of irregular eruptive variables known as RW Aurigae or T Tauri stars, discussing suitability of stochastic model

06 p0996 A69-17448

Stochastic approximation algorithms for adaptive linear discrete time system identification using noisy input

06 p0904 A69-17940

Linear equivalent gain matrix of multivariable nonlinearity evaluated with equivalent gain concept for monovariable nonlinear stochastic process

07 p1114 A69-18286

Galerkin method of moments applied to stochastic bounded linear operator equation, discussing statistically homogeneous operator case and electric field in dielectric

07 p1174 A69-19472

Stochastic model for real time on demand weather predictions using REEP /regression estimation of event probabilities/ equations in Markov chain

08 p1345 A69-20299

Book on stochastic convergence covering infinite sequences of random variables, stochastic integrals and derivatives, characterization of normal distribution and Wiener process

08 p1343 A69-20443

Nonadiabatic and stochastic mechanisms for cyclotron resonance trapping and heating in magnetic mirror geometries

08 p1364 A69-20518

Fluctuation voltage mean square value at polar dielectric capacitor terminals determined by applying stochastic properties of Poisson point processes to statistical model

08 p1295 A69-21151

Soviet book on methods of optimal statistical solutions and problems of optimal control covering basic equations of random processes, stochastic differential equations, etc

09 p1473 A69-21932

Stochastic model of electron cyclotron heating, calculating energy gain during transit of magnetic mirror field in presence of microwave electric field

09 p1551 A69-22038

Stochastic model for calculating expected component failures in transient state from Weibull distribution failure data for first generation

09 p1504 A69-22149

Plasma ion heating by external stochastic HF field, noting avoidance of special thermalization processes

09 p1553 A69-22527

Optimal stochastic control, discussing dynamic mathematical models described by differential equations

09 p1475 A69-22567

Inverse problem in stochastic processes, considering random moving force and strip load in structural stress analysis

10 p1793 A69-22876

State probabilities of finite stochastic queueing system for calculating equipment reliability parameters

10 p1664 A69-23693

Condensation kinetics in clouds, determining cloud spectrum evolution taking stochastic processes into account

10 p1722 A69-23972

Stochastic and ergodic aspects of magnetic lines of force, discussing cosmic ray diffusion in interplanetary magnetic field

10 p1770 A69-24111

Stochastic model of interstellar magnetic field to account for observed cosmic ray mean life

10 p1771 A69-24112

Stochastic approximation procedure minimizing mean square error criterion for system identification, estimation and decomposition of mixtures

11 p1842 A69-24934

Adaptive optimal estimation of sampled stochastic process with finite state unknown parameters, using separation technique

11 p1858 A69-24935

Kozhevnikov optimality principle for optimum averaging of discontinuous stochastic control systems extended to include intensities of discontinuities

11 p1966 A69-25329

Stochastic optimal control of continuous time systems with unknown gain, discussing filtering- control interaction and computer experiments

11 p1860 A69-25442

Modeling errors in linear discrete stochastic system effects on Kalman filter state estimates

11 p1860 A69-25448

Stochastic problems in thin elastic shell theory solved by equations obtained by linearizing shell equations near initial state of stress

11 p1996 A69-25732

Linear extrapolation of stationary stochastic process predicting fluctuations of minimum and maximum periods in solar cycle

12 p2149 A69-26221

Integral representation for continuous linear stochastic processes with independent pieces, assuming convergence in probability for sequence of random variables

12 p2121 A69-26365

Partial differential equation with stochastic characteristics reducible to parabolic equation by introducing additional variables

12 p2121 A69-26366

Quasi-stochastic nonlinear one dimensional oscillations in periodically disturbed field applied to celestial mechanics of planetoids

12 p2130 A69-26373

Feedback control of linear systems subject to sudden changes in parameter values

12 p2052 A69-26502

Optimal control algorithm for spacecraft descent in atmosphere based on nominal trajectory and acceleration measurements

13 p2355 A69-27683

Book on probability and stochastic processes, discussing applications

13 p2289 A69-28177

Stochastic saturating systems optimal control computation, considering attitude control and tracking system design by elliptical differential equation of dynamic programming

15 p2582 A69-30601

Probabilistic automata stochastic matrices algebraic properties of definite, quasi-definite, periodic and quasi-periodic sets

15 p2645 A69-31141

Stochastic heating of protons by random magnetosonic wave propagating normal to magnetic field to explain proton energy excess in magnetotail plasma sheet

16 p2848 A69-31969

Book on estimation theory and applications covering stochastic processes, linear estimators and recursive formulations

16 p2764 A69-32386

Stochastic differential game theory, discussing nonlinear partial differential equations for solution, dynamic programming validity conditions, finite difference scheme, etc
17 p2994 A69-32844

Cosmic ray intensity short term stochastic variations in solar system related to turbulent solar wind day-to-day variations
18 p3186 A69-34300

Filtering and optimal control problems for discrete stochastic dynamical systems, describing various feedback controls and midcourse guidance optimization
18 p3109 A69-34660

Feedback realization of continuous optimal filter applied to designing servomechanisms with stochastic inputs and disturbances
18 p3110 A69-34673

Rarefied gases transfer coefficients stochastic process calculation models, comparing results with correlation functions derived from transport equation
18 p3121 A69-34710

Stochastic meteorological models based upon presence of weather regimes, illustrating association with statistical inference problems
18 p3166 A69-34822

Nonlinear filter theory applied to digital telemetry binary processes, using continuous time stochastic process
19 p3274 A69-36281

Stochastic models for calculating optimal elastoplastic one dimensional systems
19 p3438 A69-36313

M-ary detection for optical communication investigated for maximum likelihood detection of one of M Poisson processes in background noise
19 p3276 A69-36486

Two procedures for processing statistical data concerning Gaussian processes made exchangeable by manageable formula
19 p3361 A69-36646

Stochastic motion in linear lattice of coupled harmonic oscillators analyzed by Schroedinger coordinates and Bessel functions for time behavior, energy flow and impurity effect
19 p3374 A69-36752

Stochastic model for estimating manufacturing costs, discussing Mellin and Laplace transforms and Gram-Charlier series approximations
20 p3633 A69-36924

Book on stochastic optimal linear estimation and control, discussing probability theory, models and continuous and discrete time linear systems
20 p3509 A69-37143

Atmospheric turbulence and impurities diffusion considered as stochastic processes, deriving equations and covariance functions for flow characteristics
20 p3570 A69-37426

Admissible controls set for discontinuous stochastic automatic control systems, deriving mean optimal averaging of controls
21 p3770 A69-38855

Unknown parameter experimental estimation based on signal direct observations with solution by stochastic approximations method
21 p3756 A69-39265

Spacecraft atmospheric entry descent trajectory optimization by stochastic procedure, requiring onboard digital computer to realize optimal algorithms
21 p3767 A69-39648

Stochastic motion control problems formulations in rocket dynamics
21 p3767 A69-39650

Condensation kinetics in clouds, determining cloud spectrum evolution taking stochastic processes into account
21 p3760 A69-39658

Laminated random media stochastic displacement, using perturbation procedure to derive mean wave propagation deterministic equations
22 p4040 A69-39979

Existence theorem for linear stochastic systems optimal control described by differential equation with random coefficients, providing rms stabilization
22 p3917 A69-40116

Adaptive control system synthesis for reducing computation labor for controlled inertialess plant, reproducing probability density function to describe unknown parameters
22 p3918 A69-40739

Robbins-Monro stochastic approximation method using algorithms for identifying finite memory time-discrete time-stationary linear system from noisy input-output measurements
22 p3918 A69-41013

Liapunov stochastic stability direct method analog used for estimating reliability of redundant systems with constant recovery time
23 p4144 A69-41953

Frequency condition for ensuring stochastic stability of one dimensional discrete feedback control system containing linear dynamic part and inertialess nonlinear component
24 p4288 A69-42670

Separation theorem for arbitrary nonlinear measurements to find optimal stochastic control without dynamic programming
24 p4291 A69-43269

Multidimensional approximation algorithm for parameter optimization of nonlinear stochastic systems, detailing application to space vehicle attitude controller
24 p4291 A69-43275

Stochastic fuel regulator problem investigated by optimal and self organizing techniques, emphasizing realizability of resulting controllers
24 p4292 A69-43284

Linear-quadratic pursuit-evasion game with dynamics perturbed by additive white Gaussian noise, obtaining linear minimax solutions
24 p4341 A69-43296

Stochastic approximation applied to sampled data system parameters including sampling interval
24 p4295 A69-43319

Wiener-Hermite truncated stochastic expansion used for velocity and concentration fields in turbulent flow convecting passive scalar, determining diffusivity and spectrum function
24 p4302 A69-43359

Pulsating mechanisms in alternative gas and liquid blocks two phase flow, using stochastic process specified by dynamic pressure time dependent fluctuations
24 p4305 A69-43633

STOICHIOMETRY

Temperature vs compactness relationship in NbC compacts having nonstoichiometric composition and approximately equal specific surface, determining self diffusion coefficients
10 p1711 A69-23337

Room temperature thermal conductivity of semiconducting alloys with stoichiometric distributions of vacancies in cation sublattice, discussing heat resistance
12 p2142 A69-25975

GaAs crystallization for various deviations of melt from stoichiometric state, noting concentration supercooling at phase boundary layer
12 p2144 A69-26586

Beta-thiodiglycol effect on hardening of epoxy resin with stoichiometric amounts of maleic anhydride and methyltetrahydrophthalic anhydride
22 p3973 A69-40677

STOKES FLOW

Series solutions for compressible and incompressible flows at low Reynolds number, including axisymmetric and MHD Stokes flow
04 p0587 A69-14609

Forced convection heat transfer coefficient invariance to flow reversal in Stokes and potential streaming flows past isothermal particles of arbitrary shape
04 p0590 A69-15274

MHD Stokes flow for rotating disk in parallel magnetic field, showing Lorentz force inhibiting effect on fluid motion
13 p2305 A69-27325

Integral equations for classical elasticity boundary value problems, stressing analogous Stokes flow hydrodynamic equations
14 p2535 A69-29361

Bag type deformation of incompressible viscous convective and nonevaporating droplets immersed in Stokes or potential flow pressure distributions, including Weber number
17 p2954 A69-33456

Unsteady viscous flow past flat plate based on Stokes approximation, calculating shear stress
22 p3931 A69-40684

STOKES LAW

Stokes phenomenon, considering continuity solution of differential equations across Stokes lines
07 p1174 A69-19220

STOKES LAW [FLUID MECHANICS]

Stokes and Rayleigh layer formation during solid body rotation of semiinfinite fluid and infinite disk
03 p0417 A69-13797

Stokes-like region around yawed needle in hypersonic strong interaction regime, discussing asymptotic analysis under Stewartson conditions
04 p0542 A69-14732

STOKES THEOREM [VECTOR CALCULUS]

Instrumental Stokes vector calculating method involving light flow transformation matrix elements determination
04 p0601 A69-15248

Spectral study of Stokes vector for light scattered by natural objects, recommending phase and optical axis inclination angles for aircraft measurements
09 p1588 A69-21367

Spectral study of Stokes vector for light scattered by natural objects, recommending phase and optical axis inclination angles for aircraft measurements
18 p3198 A69-34756

STOL AIRCRAFT

U SHORT TAKEOFF AIRCRAFT

STOMACH

Increased gravitational stress effects on esophageal sphincter pressures and gastroesophageal reflux in rhesus monkeys, noting cardia competence
06 p0874 A69-17838

Motion sickness inhibitive effect on stomach motor activity, measuring biopotential of stomach wall, pyloric sphincter and ganglions
08 p1263 A69-19935

STONES [ROCKS]

U ROCKS

STONY METEORITES

NT ACHONDRITES
NT CARBONACEOUS METEORITES
NT CHONDRITES
NT KAPOETA ACHONDRITE
NT MURRAY METEORITE
NT ORGUEIL METEORITE
NT PANTAR CHONDRITES

Meteorite structure and origin, discussing cosmic dust analysis and collection, Tungusk silicate-magnetite spherules, asteroid collisions and meteorite ages
01 p0159 A69-11367

Uranium in meteorites, discussing U content and isotope composition, Pb isotope ratios, radiogenic Pb, origin of matter and meteorite ages
01 p0025 A69-11369

Mineralogy of iron fragments from impact craters near Lake Kaali, Estonia, discussing structure and type of meteorite
01 p0159 A69-11370

Thermoluminescence intensity of dolomite specimens from Kaali meteorite craters, discussing meteorite impact thermomechanical effect and crystal lattice defects
01 p0159 A69-11371

Nerf and Kaande stony meteorites mineralogical composition from microscopy, noting olivine hypersthene chondrite classification
01 p0159 A69-11374

Morphological properties and history of Zabrode stony meteorite, discussing storage, disappearance and recovery
01 p0160 A69-11384

Minerals in ablated crust of Saratov meteorite using X ray analysis
01 p0160 A69-11388

Stony meteorite Krahenberg, determining isotopic composition, rubidium and strontium age of dark and light portions by neutron activation analysis
05 p0826 A69-16439

Rare gases in stony meteorites, noting premodern inheritance and complex Xe anomalies
05 p0826 A69-16440

Production rates of nuclides measured in stack of glass plates under proton irradiation for calculating cosmic ray production rates in stone meteorites
06 p0989 A69-17283

Tritium and argon 39 measurements of stone and iron meteorites, discussing decay and production rates and cosmic ray intensity
09 p1604 A69-22398

Aluminum abundances in stony meteorites measured using nondestructive instrumental neutron activation analysis
11 p1952 A69-24334

Chemical composition of stony meteorites by analytical methods, discussing sample preparation and X ray fluorescence
11 p1953 A69-24358

Stony meteoric particles size and velocity during passage through atmosphere
12 p2157 A69-26341

Iron and stone meteorites ablation using electrodeless plasmatron and filmed onto IR films
15 p2697 A69-31252

Uranium abundances in several eucrites measured by fission track method, discussing Pu-Xe decay interval question
17 p3044 A69-34167

Quantitative analysis and classification of stony meteorites, including carbonaceous chondrites, by Mossbauer characteristics, discussing Prior plot and weather influence role in finds and falls
19 p3408 A69-36083

Boron, Li and Cl contents in iron and stone meteorites by fluorometric, thermal-neutron activation and pyrohydrolytic separation methods, tabulating results
19 p3408 A69-36085

Depth distribution of primary cosmic radiation fluxes and secondary nuclear-active particles in stone meteorites and surface layer of planets, moon and asteroids
19 p3410 A69-36092

Ar 39 and Cl 36 production rates and ratios in stone and stony-iron meteorites metal phases, discussing terrestrial age calculation
19 p3411 A69-36100

Isotopic age determinations on iron and stone meteorites, discussing Rb-Sr and K-Ar results, internal isochrones, Kodaikanal data and planetary formation
19 p3413 A69-36108

Magnetic properties of stone, stony-iron and iron meteorites, discussing natural remanent magnetization origin in parent bodies and magnetic susceptibility
19 p3415 A69-36122

Reflectivity and chemical composition of metallic phase minerals in stone meteorites, showing optical characteristics sensitivity to composition
19 p3415 A69-36124

Stony meteorite barium isotopes and iron meteorite and terrestrial silicate inclusions analyzed using double spike method for laboratory fractionation correction
19 p3425 A69-36422

Na 22 and H 3 production rates determined in stone meteorites exposed to 3 Gev isotropic protons, using radionuclide distribution data of exposed thick stone target
19 p3425 A69-36423

Rare gas distribution in earth atmosphere explained as outgassing from primordial solid particles, discussing stony meteorites composition
20 p3600 A69-37489

Stony meteorite composition and structure studied for conditions of preplanetary stage of solar system
22 p4012 A69-40084

STOPPING

Circulation control by blowing and application to stopped rotor aircraft, discussing data from model scale blade experiments
19 p3248 A69-36767

STOPPING POWER

Oxygen K-shell X ray production cross section and stopping power of aluminum oxide thin films for 20-100 kev protons
14 p2489 A69-29994

STORABLE PROPELLANTS

NT AIRCRAFT FUELS

Space storable propulsion system comparison, discussing liquid propellants performance and thermodynamic analysis
[AIAA PAPER 68-614] 09 p1570 A69-21981

Collection of articles on ramjets including reaction propulsion, hypersonic inlets, combustion problems, Griffon aircraft, storable liquid fuels, etc
16 p2837 A69-32608

Specific impulse deliverable performance of space storable propellant combination fluorine-oxygen/methane and oxygen difluoride/diborane
[AIAA PAPER 69-505] 16 p2845 A69-32762

Space storable hydrocarbon fuel blended FLOX propellant performance with coaxial injector including characteristic velocity, chamber geometry, pressure and heat flux distribution
[AIAA PAPER 69-507] 16 p2835 A69-32772

Hydrogen and methane combustion to simulate expansion of storable propellants
[AIAA PAPER 68-635] 20 p3631 A69-37188

STORAGE

Store separation from high speed aircraft via wind tunnel test techniques, discussing drop model, flowfield survey and captive trajectory testing
[AIAA PAPER 68-361] 11 p1819 A69-25373

STORAGE BATTERIES

NT NICKEL CADMIUM BATTERIES

NT SILVER CADMIUM BATTERIES

NT SILVER ZINC BATTERIES

Low temperature hydrogen fuel cells and basic electrolyte batteries design, discussing electrolyte concentration regulation by elimination of water formed
08 p1258 A69-21027

Integral cell-level electronic charge controls for secondary batteries, emphasizing performance, reliability and power system interfaces
23 p4076 A69-42542

STORAGE STABILITY

Operating and storage conditions effects on reliability of Pd-Ag thick film resistors
08 p1283 A69-20131

Energy dissipation of solder-covered and solderless solar cells with TiAg contacts as function of storage time, temperature and humidity
19 p3253 A69-35706

STORAGE TANKS

NASA LOX and liquid hydrogen barges, discussing storage tank design, acceptance testing and operating conditions
01 p0056 A69-11150

Thermal design and test for liquefied gas vessels under unsteady insulation cooling conditions
04 p0687 A69-15162

Aircraft gas turbine component pressure data storage and scanning
05 p0726 A69-16768

High pressure storage vessels for gaseous hydrogen, discussing failure, manufacturing controls and access for internal nondestructive inspection
[ASME PAPER D8-14.1] 07 p1143 A69-19666

Liquid helium vented and nonvented storage container design and handling techniques
10 p1810 A69-24016

STORMS

U CYCLONES

U HURRICANES

U IONOSPHERIC STORMS

U MAGNETIC STORMS

U NOISE STORMS

U SOLAR STORMS

U SUDDEN IONOSPHERIC DISTURBANCES

U THUNDERSTORMS

U TORNADOES

U TROPICAL STORMS

U TYPHOONS

STORMS [METEOROLOGY]

NT HURRICANES

NT IONOSPHERIC STORMS

NT TORNADOES

NT TROPICAL STORMS

NT TYPHOONS

Nonstationary model of mesoscale atmospheric vortex with vertical axis based on atmospheric thermohydrodynamics
03 p0462 A69-13932

Meteorological Doppler radar information display for real time identification of hazardous winds and turbulence in storms
18 p3139 A69-35427

Storm location and severity prediction by pattern recognition theory, using quantized radar data, compared with statistical prediction
21 p3678 A69-39458

STRAIN AGING

U PRECIPITATION HARDENING

STRAIN DISTRIBUTION

U STRESS CONCENTRATION

STRAIN ENERGY METHODS

Plate theories derived via strain energy potential integration through thickness, noting constitutive equations applicability to elastic buckling and postbuckling
02 p0340 A69-12055

Fiberglass reinforced plastic laminates failure under biaxial compression due to layer separation with strain energy as endurance criterion
02 p0270 A69-12142

Strain induced deformational instability of aluminum alloys
03 p0447 A69-13818

Compatible triangular plate elements for normal and in-plane displacements, discussing nine degree of freedom element, strain energy, simply supported and clamped plates
04 p0677 A69-14742

Crack tip plastic flow effect on strain energy release rate, considering Dugdale model for yielded crack
[ASME PAPER 68-WA/MET-17] 05 p0838 A69-16155

Stability loss of shells of revolution under effect of axial compression and radial pressure with no restrictions on generatrix curvature, using strain energy method
06 p1021 A69-17179

Sliding friction technique to determine contact area and surface microtopography between abraded metals and polymers
08 p1319 A69-19994

Cylindrical elastic membranes with finite axisymmetric deformation, discussing exact solution by strain energy method
08 p1418 A69-21001

Strain energy for two and three dimensional crack systems subjected to varying loads, detailing loading and crack geometry effects on fracture criterion
11 p1974 A69-24669

Hole mobilities in InSb due to phonon and ionized impurities scattering on basis of strain potential constants
16 p2824 A69-31575

Stress distribution in variable rigidity reinforcing frame of circular cylindrical shell using strain energy method
17 p3055 A69-33131

Algorithm for minimum weight structures automated design, coupling strain energy criteria with linear interpolation search technique to cover stress and displacement constraints
[SAWE PAPER 798] 18 p3219 A69-34861

Yield condition of maximum constant distortion strain energy for anisotropic material without incompressibility assumption
18 p3227 A69-35494

Pure plastic bending of wide strip, determining stress strain state and plastic strain energy during constrained bending, noting application to corrugated panels
19 p3324 A69-35833

Rectangular plate bending element corresponding to finite difference method use, deriving stiffness matrix from strain energy approximation
20 p3619 A69-36949

Mooney and Rivlin theories compared for strain energy function W of ideal superelastic material
20 p3624 A69-37586

Plane membranes finite deformation, deriving energy theorems for potential U bounds estimation
20 p3624 A69-37588

Noncircular curved shell stability under axial compression, using strain energy method to determine upper and lower critical stresses
21 p3834 A69-38715

Rib cross sections distribution for cylindrical shell under concentrated longitudinal forces obtainable by designing for minimum strain energy
23 p4228 A69-41988

STRAIN FATIGUE

U FATIGUE [MATERIALS]

STRAIN GAGE BALANCES

Semiconductor strain gage balance with temperature compensation for conventional wind tunnels
10 p1672 A69-23265

STRAIN GAGES

Fatigue-damage evaluation system for transport aircraft, noting use of cumulative strain gauge that stores strain history
01 p0165 A69-10118

Strain gage behavior on unstressed aluminum alloy under rapid heating using radiant heating, weld strength and high temperature test equipment
02 p0341 A69-12229

Strain multiplier device for fatigue sensors for totalizing resistance change from aircraft service load parameters
02 p0250 A69-12230

Printed circuit board wiring technique for strain gage rosettes application in extensive airframe static tests
02 p0250 A69-12231

Resistance wire strain gages for measuring elastoplastic deformations in zones with high stress concentrations of strained machine elements
04 p0671 A69-14433

Resistance change arising from transverse straining of single conductor derived in terms of measurable filament and adhesive parameters
04 p0603 A69-15433

Plane shear strain measurement by means of properly oriented strain gages on surface and proper disposition of gages in Wheatstone bridge circuit
04 p0603 A69-15498

Direct plotting of vibrating wire strain gauge data for concrete structures, giving diagrams for grid and backing sheet scaling
08 p1312 A69-20104

Foil type strain gage for measurement of tangential strains along circumference of hole in plate under uniaxial and equibiaxial tension
08 p1314 A69-20258

Strain gage transducers and measurements noting Wheatstone bridge, supporting structure and accuracy 10 p1690 A69-23227

Calibration for instrument systems including strain gages, piezoelectric, thermoelectric and thermoresistive transducers 10 p1691 A69-23229

Multichannel miniature telemetry for vibration, strain and temperature measurements in high speed machinery by solid state encapsulated devices 10 p1654 A69-23251

Silicon resistance strain gage sensitivity dependence on crystallographic orientation following cut-off from single crystal 11 p1887 A69-25209

Poisson ratio determination with bonded electrical resistance strain rosettes 11 p1995 A69-25652

Coherent optical flaw detection and surface microstrain measurement techniques including holographic interferometry, optical correlation and diffraction 12 p2180 A69-26305

Resistance type bonded strain gages for seven adverse environments, discussing installations and transducers 12 p2099 A69-27165

Materials surface thermal stress analysis by strain gauges, considering behavior during rapid temperature changes 13 p2264 A69-28599

Strain sensor using p-n heterojunction diode fabricated by vacuum evaporation onto flexible substrate 14 p2422 A69-29555

Scratch gages under water in open and at high temperature, including circular X-Y recording scratch strain gage 15 p2610 A69-30682

S-N fatigue life small bondable resistance sensor, discussing random response data interpretation with emphasis on use of strain multipliers 15 p2613 A69-31270

Strain gages to measure flight loads in high temperature environment, discussing selection, calibration techniques and performance characteristics 15 p2614 A69-31277

High temperature capacitance strain gage development, discussing extensometer prototype systems 15 p2614 A69-31278

Cumulative metal fatigue damage gauges, analyzing resistance change properties by using strain amplitude tests 17 p3053 A69-32989

Mechanical and resistance type fatigue life indicator, comparing operating and performance characteristics [AHS PAPER 378] 17 p3059 A69-33511

Fatigue strength of highly loaded gears and stress measurements by strain gauges [AHS PAPER 371] 17 p3060 A69-33517

Variable resistance strain gages for study of light gas guns operating characteristics, including chamber pressure and piston velocity 19 p3306 A69-35736

High temperature strain measurement based on strain gage with capacitance changes for structural analysis 20 p3537 A69-37006

Finite element analysis and strain gage results to verify end constraint on off-axis tensile coupons and to design test specimen 20 p3628 A69-37775

Creep strain rate measurement at high temperatures by inductance strain gage to determine deformations from 0.2 microns 20 p3544 A69-37815

Technical and metrological characteristics of short base strain gages and bonding to specimen, investigating sensitivity and creep 20 p3544 A69-37817

Design features comparison and operation principles of gas strain gauges in application to structures, emphasizing independence of temperature variations in pneumatic circuits 21 p3725 A69-39324

Strain distribution on surface of adhesive bonded box beam in simple bending, using water based brittle coating and self adhesive strain gages 21 p3844 A69-39325

Strain gage embedding techniques and applications 21 p3725 A69-39327

Standardizing strain gage with long time stability characteristics, analyzing statistically strain calibration results 22 p3945 A69-40078

Strain measurement by interferometer with gas laser source emphasizing long period measurement problem 22 p3960 A69-40189

Error correction of strain gage/cement combination reading relaxation under prolonged steady loading at elevated temperature 22 p4042 A69-40313

Short range telemetering strain gage system with stable multivibrator transmitter for measuring intercoupling displacement and shaft torque 22 p3946 A69-40314

Carrier frequency monitoring amplifier with automatic bridge tuning for coupling to passive sensors including strain gages, inductive transmitters, etc 22 p3915 A69-40937

Hungarian-made semiconductor silicon-base strain gages meeting specifications at half world market price 22 p3947 A69-40938

Pressure transducers using heterode strain sensors evaporated directly onto pressure diaphragm 22 p3950 A69-41222

Bonded strain gages for experimental stress analysis of high speed rotating machinery under high centrifugal loads 24 p4397 A69-42740

STRAIN HARDENING

Strain hardening of alpha titanium studied for effects of grain size, strain rate, temperature and purity 01 p0095 A69-10610

Material memory effect in plastically prestrained thin walled brass tubes analyzed on basis of kinematic strain hardening theory 02 p0336 A69-11551

Elastic analogue in creep stress analysis under time dependent boundary conditions and strain hardening theory 02 p0345 A69-12418

Second phase hardened materials recovery creep rate model, showing dependence on stress level 03 p0447 A69-13615

Recovery behavior of nickel strain hardened by impact loading by aluminum projectiles, showing microstructure correlation with stress levels 03 p0447 A69-13620

Strain hardening and softening characteristics of maraging steels, Ni-Co and other steels and Ti-Al-Mo alloy 04 p0618 A69-15156

Ductile creep rupture of thin walled membrane shell of revolution subjected to time dependent internal pressure and strain hardening [ASME PAPER 68-WA/MET-15] 05 p0838 A69-16153

Aluminum-stainless steel wire reinforced metal matrix composites, analyzing strain hardening and plastic deformation 06 p0940 A69-16950

Deformation dependence on strain hardening and recovery rate during transient and steady state creep 06 p0943 A69-17236

Fatigue hardening in fcc metals, discussing dislocation distribution in unidirectionally deformed single crystals 06 p0944 A69-17503

Plastic deformation in bcc, fcc and hcp metals as function of initial impact load energy, noting strain hardening effects 07 p1166 A69-19144

Stress relaxation in structural elements, analyzing unsteady creep in case of strain hardening following power law 07 p1237 A69-19683

Retained austenite content control, strain aging and ausforming to improve toughness of high strength martensitic stainless steel without strength loss 08 p1330 A69-20010

High temperature metallic material strengthening methods, noting metallurgical factors and temperature effects on mechanical properties 10 p1712 A69-23630

Order-disorder transformations in nickel alloys under loading operations 11 p1904 A69-24706

Fcc metals cyclic deformation and fatigue dependence on cross slip of screw dislocations, considering strain hardening and crack propagation 11 p1906 A69-25389

Homogenization of martensite formation in nickel 300 grade maraging steel, analyzing anisotropic transformation strains during thermal cycling 13 p2278 A69-27410

Plane elastoplastic shock waves propagation due to combined shear loadings assuming elastic isotropic work hardening materials 13 p2368 A69-28346

Strain hardening experiments on single crystals of AlZn and AlAg alloys noting plastic behavior 16 p2800 A69-31776

Buckling time of oval ring under unsteady creep based on strain hardening theory 17 p3062 A69-33716

Shock wave propagation induced by nonuniform instantaneous internal heating of nonlinear elastic strain hardening solid material [SAWE PAPER 69-APM-17] 18 p3214 A69-34393

Strain hardening of titanium wire during room temperature stress relaxation shown equal to strain hardening during constant strain rate test 19 p3342 A69-35811

Elements substitution for Al in gamma prime of Ni-Al alloy to change aged hardness by gamma prime mismatch and coherency strains 20 p3558 A69-36962

Linearization of relationship between stress concentration factor and reciprocal of strain hardening exponent enabling shakedown to pressure vessels formulated by mathematical model 20 p3620 A69-37002

Ronay effect in reversed cyclic torsion or tension in thin cylindrical viscoelastic tube showing creep under sustained load 20 p3625 A69-37596

Surface grains orientation effect on fatigue behavior in polycrystalline Al, noting strain hardening role in failure 20 p3561 A69-37597

Metals plastic behavior including strain hardening and Bauschinger effect 21 p3832 A69-38466

Shock hardening of Al alloys in annealed, solution heat treated and aged conditions compared with cold-rolled materials [ASM PAPER W9-10.4] 21 p3729 A69-38664

Stress concentration and surface strain hardening effects on fatigue strength of refractory alloy specimens with and without cut 21 p3745 A69-38875

Vector properties of isotropic strain hardenable materials in stress vector space applied to tubular brass subject to biaxial tension and complex loading 23 p4227 A69-41714

STRAIN RATE

Strain hardening of alpha titanium studied for effects of grain size, strain rate, temperature and purity 01 p0095 A69-10610

Aluminum deformation at various strain rates and temperatures under combined stress, comparing results with theoretical predictions 02 p0343 A69-12282

Strain rate effect on dislocation substructure in deformed niobium single crystals, investigating relationship between mechanical properties and dislocation substructure 02 p0268 A69-12287

Elastic-plastic wave profiles in Al alloy under uniaxial strain load, investigating sensitivity to various strain rates 02 p0344 A69-12289

Strain rate effect of large deflections of clamped circular viscoplastic plates subject to rigid mass impact 02 p0349 A69-12799

Strain rate and temperature effect on flow stress of 7075 aluminum bars 03 p0443 A69-13120

Twisted yarns composed of continuous viscoelastic filaments dynamic response under periodic strain effect on dynamic modulus 04 p0619 A69-14686

Truncated solid cones plastic yielding under quasi-static and dynamic axial loads at various strain rates 04 p0682 A69-15301

Strain dependent modulus and Poisson ratio behavior of CTPB propellant, performing stress relaxation tests [AIAA PAPER 68-519] 04 p0646 A69-15510

Stress-strain rate relation under combined stress fields derived from Gilman relation between dislocation velocity and force for single dislocation 05 p0834 A69-15756

Work hardening in quenched fully hardened and overaged Mg-Mn alloy single crystals as function of temperature and strain rate 05 p0778 A69-15757

Thermodynamic theory of strain rate sensitive plastic material within framework of thermodynamics of materials with internal state variables 05 p0834 A69-15792

Crack nucleation in high strain fatigue based on plastic instability model

05 p0780 A69-16430

Strain rate effect on structure and mechanical properties of rapidly stretched metals

06 p0941 A69-17122

Theoretical and experimental results on annealed tapered aluminum rods to assess one-dimensional rate independent theory of plastic wave propagation from longitudinal impact

06 p1022 A69-17365

Tensile stress and energy-to-break values compared for glass-fortified thermoplastic resins, discussing notched and unnotched Izod impact

08 p1337 A69-20480

Heat resistant alloys plastic deformation, studying stress/strain systems, strain divisibility, strain rate and temperature effects, etc

09 p1504 A69-22145

Aluminum alloy crack propagation and fracture patterns as function of temperature under high strain amplitude and low strain rate

10 p1709 A69-23071

Temperature and strain rates effect on delayed yield and failure of plasticized epoxy resin

10 p1717 A69-24218

Back stress role in strain rate equation for high temperature deformation and study of structure and applied stress effects

11 p1987 A69-25388

Thermodynamics of strain rate sensitive elastoviscoplastic solids, considering kinematic description of plastic deformation and choice of state variables

11 p1994 A69-25601

Rigid plastic circular and annular plates dynamics taking into account yield point dependence on strain rate

12 p2177 A69-25994

Added metal oxides solid solutions effect on creep kinetics and strain rate of zirconia samples during sintering

12 p2118 A69-26260

Strain rate and pressurization effect on ductile-brittle transition temperature of polycrystalline sintered W, discussing yield stress

12 p2117 A69-27138

Moire and gridwork methods of plastic strain analysis with application to plane strain and axisymmetric extrusion

13 p2359 A69-27256

Molybdenum dislocation velocity and macrodeformation, noting thermal double kink mechanism inconsistencies and strain role in strain-rate relationship

13 p2276 A69-27392

Strain-rate sensitivity measurements to determine ductility of materials, noting relation to elongation

13 p2278 A69-27416

Creep and hot working strain-rates relationships, showing work hardening and dynamic recovery relative levels dependence on plot used

13 p2278 A69-27417

Minimum theorems for plastic strain rates and plastic strains governed by holonomic elastoplastic theory utilizing quadratic functions

13 p2370 A69-28629

High temperature thermal resistance stability of multilayer cylindrical elements for thermionic converters determined by layer strain rate

14 p2539 A69-29218

Ferrous and nonferrous metals shock tensile strength by elastic contact dynamometer, noting diagram shape dependence on stress growth rate

14 p2464 A69-29314

Strain rate and temperature effects on sintered molybdenum sheets strength and elongation characteristics

14 p2464 A69-29322

Isothermal deformations in linear viscoelastic material under uniaxial stress, determining optimum strain rate history for maximum work lower bound

15 p2707 A69-30637

Experimental determination of strain /or strain rate/tensor in plastic deformation analysis

15 p2707 A69-30639

Fracture strength of Al alloy in biaxial stress field, considering strain rate influence on material toughness

17 p2986 A69-32985

Low cycle fatigue behavior prediction for 304 and 306 stainless steels based on temperature and strain rate ratio to tensile ductility

17 p2987 A69-33079

Plane strain forging of pure Al and Al-Cu alloy at low strain rates and elevated temperatures, in constant velocity compression test

17 p2979 A69-34137

Low cycle fatigue leading to failure on AISI 321 stainless steel as function of elevated temperature and straining frequency

18 p3219 A69-34834

Strain hardening of titanium wire during room temperature stress relaxation shown equal to strain hardening during constant strain rate test

19 p3342 A69-35812

Closed form solutions for rigid viscoplastic cylindrical shell under dynamic loading based on constitutive equations for rate sensitive plastic material

19 p3439 A69-36478

Primary and tertiary uniaxial creep strain rate changes based on internal stress redistribution described with mathematical model

20 p3619 A69-36941

Creep strain rate measurement at high temperatures by inductance strain gage to determine deformations from 0.2 microns

20 p3544 A69-37815

Low strain rate effects on metals yield and tensile strength

20 p3563 A69-38063

Alpha Ti thermally activated tensile deformation, studying flow stress dependence on strain, temperature and strain rate

21 p3729 A69-38659

Strain rate-load relations in elastoplastic shells reaching yield point, discussing variational method applicability

21 p3838 A69-39189

Fatigue endurance determined from thermal stresses by balancing elastic strain rates, creep relaxation and mechanical cyclic loading with triangular waveform, discussing nonsteady creep

21 p3843 A69-39310

Serrated yielding at high temperatures from dislocation theory viewpoint, considering critical strain relation to temperature and strain rate

21 p3749 A69-39710

High temperature electronic tensile testing device utilizing SCR to study strain rate effect on metals properties

21 p3727 A69-39811

Tensile cryostat for low temperature strain measurement, discussing design, insulation and vacuum sealed environment for heat leak reduction

22 p3947 A69-40627

Yield condition and relation between stresses and strain rates for anisotropic body, allowing for influence of stressed state type

22 p3934 A69-41169

Thermodynamics of elastoplastic materials with dislocation motion related to internal state variables, including case of rate independent plasticity

23 p4226 A69-41537

Tensile test facility for specific strain rate range, applying impact load to sample end with high speed striker accelerated by explosive energy

23 p4147 A69-41710

Single crystal Ta and Ta base bcc solid solution strengthening and weakening as function of temperature and strain rate

23 p4178 A69-42358

Cylindrical steel specimens high strain rate tensile tests, using Malvern theory for ideal elastoplastic and work hardened materials

23 p4236 A69-42529

Serrated flow characteristics in gold-indium solid solutions at various strain rates and temperatures

24 p4361 A69-43028

Mechanical properties and dislocation configurations and densities of Nb single crystals measured at various strain rates

24 p4332 A69-43030

STRAIN SOFTENING

U PLASTIC DEFORMATION

STRAPDOWN INERTIAL GUIDANCE

Strapdown electrostatic aerospace navigator /SEAN/ using electrostatically suspended gyros /ESG/ for inertial reference, including drift and computer tests

19 p3369 A69-35802

Strapdown inertial reference unit system for inflight reliability and maintainability, discussing design and components

19 p3370 A69-35803

Single degree of freedom gyroscope design factors applicable to strapdown guidance system, discussing torque-to-balance loop, multiple pulse bursting and error sources

21 p3762 A69-39378

Strapdown redundant experimental sensor inertial navigation package containing gyros and accelerometers, discussing signal real time processing by digital computer

21 p3762 A69-39379

Gyro test package, dynamic test facility and real time attitude algorithm to investigate operational capabilities of strapdown inertial attitude package

[AIAA PAPER 69-849] 21 p3765 A69-39424

Strapdown gimballess inertial measurement unit with general purpose computer, describing hardware, software and test results

[AIAA PAPER 69-850] 21 p3765 A69-39426

STRAPS

Transverse reinforcing straps effects on torsional stiffness and bending behavior of open cross section profile thin walled prismatic beams

10 p1802 A69-23890

STRATA

NT SUBSTRATES

Cylindrical sound pulse propagation in homogeneous layer under inhomogeneous half space

04 p0630 A69-14531

Electromagnetic wave propagation in spherically stratified isotropic media, presenting generalized refractive index profiles for electric type fields

04 p0563 A69-15492

Charged body moving at subsonic velocity normally through stratified elastic half space composed of film on homogeneous half space

08 p1417 A69-20753

Spectrographic observations indicating temperature range within individual filaments of Cygnus Loop, noting agreement with stratified models

09 p1607 A69-22430

STRATIFICATION

NT ATMOSPHERIC STRATIFICATION

Electric or magnetic dipole antenna radiated electromagnetic field for antenna orientation perpendicular to striations of periodically stratified dielectric medium

03 p0398 A69-13802

Electromagnetic transient wave propagation and reflection in lossless isotropic stratified ionized media, discussing time variations of fields due to incident plane unit step wave

17 p2924 A69-33839

Planetary nebulae imaging stratification effects on structural difference studies by slit and slitless spectrographs and narrow band photography

21 p3817 A69-39785

Multiple outlets for reducing stratification-induced liquid propellant supply temperature rise, preventing cavitation problems in supply pumps

[AAS PAPER 69-395] 24 p4363 A69-42830

STRATIFIED FLOW

Reflectivity of low Richardson number critical levels for internal gravity waves propagating in stably stratified fluids with shear, studying stability numerically

03 p0424 A69-13953

Stability of nondissipative stratified rotating flows with constant density to axisymmetric disturbances

04 p0588 A69-14740

Theoretical analysis of fixed stratification, taking into account nonlinear effects and variation in charged particle concentration along plasma column

04 p0636 A69-14783

Laminar flow of stably stratified fluid with uniform upstream velocity and density gradient past thin flat plate, discussing upstream wake and boundary layer

05 p0745 A69-15724

Large amplitude waves in inviscid flows of stably stratified fluids over barriers with constant density upstream constructed from vortex pairs and doublets

08 p1346 A69-20313

Fluid flow induced by horizontally moving bodies in stratified and rotating fluids determined by matched asymptotic expansion theory

08 p1253 A69-20997

Temperature profiles and heat transfer coefficients in two phase liquid-liquid stratified laminar flow of variable immiscible film thickness with surface evaporation

09 p1622 A69-21904

Striated flow induction synchronous MHD generator, producing striated flow by nonthermal ionization of inert seeded gas in electric field

10 p1638 A69-23487

Nonlinear partial differential equations for solution of steady stratified flows, noting hydrostatic pressure distribution and horizontal and vertical scales

11 p1869 A69-24889

Two dimensional stratified flow over obstacle in finite height channel, noting lee waves and drag increase with decreasing speed

11 p1869 A69-24892

Power law profiles of mean wind velocity and temperature in thermally stratified shear flow, considering

dependence on thermal stability and Richardson number
11 p1874 A69-25381

Stratified rotating fluid time dependent motion characterized by stability frequency ratio and Coriolis parameter within quasi-geostrophic approximation
13 p2248 A69-28171

Stratified fluid flow past obstacle, considering steady inviscid flow with nonlinear convection and vertical acceleration
19 p3240 A69-36474

Rotating stratified fluid in thermally insulated cylinder, studying angular velocity abrupt change effects under stable temperature distribution
21 p3694 A69-38768

Stratified blood flow distribution in lung lobe from analyzing breath-holding changes on expired Ar and nitrous oxide tension plateaus during rest and exercise
23 p4078 A69-41315

STRATIFIED LAYERS

U STRATA

STRATOFORTRESS AIRCRAFT

U B-52 AIRCRAFT

STRATOSCOPE TELESCOPES

Stratoscope II unmanned balloon-borne telescope design, detailing pointing, focusing and thermal characteristics
13 p2261 A69-27956

Guiding system of Spectro-Stratoscope /balloon-borne solar telescope/, describing hydrostatic bearing and torque motor
13 p2262 A69-27957

Photospheric granulation near center of quiet sun, analyzing morphological properties from high definition Stratoscope photographs
17 p3029 A69-33045

STRATOSPHERE

Photochemistry in dry atmosphere, discussing ozone density vertical distribution in upper atmosphere and influence of O and ozone reactions with H compounds
02 p0245 A69-12694

Zonal temperature and spectral characteristics of stratospheric circulation, noting westward rotation of second harmonic
02 p0246 A69-12759

Air movements in lower stratosphere analyzed on basis of ozone measurements, showing correlation with north-south gradient of total ozone amount
02 p0246 A69-12762

Acoustical thermometer-interferometer to measure air temperature between 20 and 50 km
03 p0429 A69-13269

Quasi-biennial oscillation in tropical stratosphere as result of long period gravity waves interaction with zonal wind
03 p0461 A69-13342

Large scale disturbances in summertime stratosphere observed from high level balloon, discussing diurnal wind patterns and planetary traveling waves
03 p0461 A69-13343

Middle stratospheric diurnal temperature variation based on model eliminating radiation error of rawinsonde
03 p0461 A69-13344

Northern California humidity to 32 km utilizing alpha radiation hygrometer and associated balloon sounding equipment
03 p0461 A69-13345

Stratospheric balloons for space research, emphasizing stabilization equipment suitability
03 p0366 A69-13589

Long period variations in zonally symmetric circulations of tropical stratosphere, using zonally averaged momentum, continuity and heat and latent energy equations for numerical model
03 p0461 A69-13681

Stratospheric aerosol investigation by IR and lidar, applying Mie theory to model aerosol size distribution
04 p0592 A69-14654

Covariances of temperature and meridional wind component and relation to northward flux of sensible heat due to transient eddies in stratosphere
04 p0627 A69-15084

COSPAR manual on stratospheric temperature and wind measurements, discussing synoptic and time variation study by Arcas and Loki-Judi meteorological sounding rocket systems
05 p0752 A69-15706

Rocket and radiosondes data from measurements over Northern Hemisphere used to study stratospheric and mesospheric circulation during three midwinter periods
05 p0753 A69-15800

Stratospheric temperature, wind and ozone concentration measurement during solar eclipse by sounding rocket system
06 p0916 A69-17008

Multilevel objective weather analysis system for stratosphere and upper troposphere over Australia, using stream function analysis
06 p0950 A69-17787

Stratospheric critical clear atmospheric turbulence at midlatitudes, noting applications to supersonic aircraft design
06 p0950 A69-17789

Nightglow intensities correlated with atmospheric ozone concentration and stratospheric temperatures
07 p1123 A69-18675

Annual temperature variation in lower tropical stratosphere, noting effect of equatorial upward motion
07 p1126 A69-19043

Midwinter warmings in upper stratosphere for differences between various stratospheric and mesospheric levels, noting need for additional upper air data
08 p1345 A69-20134

Horizontal ozone distribution at high cyclones and anticyclones in middle stratosphere
08 p1308 A69-20261

Geostrophic trajectories of horizontal diffusivity estimated in midlatitude troposphere and lower stratosphere
08 p1308 A69-20310

Mean and eddy terms contribution to momentum and heat balance of troposphere and lower stratosphere at solstices, describing zonal wind equations
08 p1308 A69-20318

Ozone and carbon dioxide stratospheric and tropospheric horizontal distribution from weather data collected on polar flight
09 p1484 A69-21403

Cosmic ray intensity temperature dependence in stratosphere and anisotropy in interplanetary space determined from measurements over Arctic and Antarctic regions
09 p1575 A69-21542

Power spectral analysis of upper wind data of equatorial lower stratosphere noting quasi-biennial oscillation
09 p1537 A69-22297

Zonal momentum vertical transport due to large scale moving disturbances in westerlies of equatorial lower stratosphere
09 p1537 A69-22299

Stratospheric dust, discussing terrestrial and meteoritic origins, volatility of particles smaller than few microns, and light scattering and direct sampling measurements
09 p1608 A69-22689

Galactic cosmic ray modulation and solar activity analyzed on basis of cosmic ray measurement in stratosphere
10 p1758 A69-22832

Particulate radioactivity for study of stratospheric motions, demonstrating negligible long time particle settling with comparative measurements of particulate Sr 90 and gaseous C 14
10 p1682 A69-23410

Carbon dioxide concentration in upper troposphere and lower stratosphere recorded during commercial aircraft flights over polar route
11 p1879 A69-25254

Stratospheric aerosol attenuation factor vertical distribution statistical structure, tabulating normalized correlation matrices, eigenvectors and eigenvalues
12 p2125 A69-25956

Sky polarization neutral points around sunset /spring-summer 1968/ at Bedford, Mass., inferring continuation and variations of enhanced stratospheric turbidity
12 p2067 A69-26343

Zonal and meridional wind components monthly global cross sections for stratosphere and mesosphere from sounding and radar data
12 p2070 A69-26577

Stratosphere and troposphere processes analyzed, indicating feasibility of forecasting geopotential and wind fields between 12 and 24 km
12 p2126 A69-26581

Mean vertical moisture profile for summer and winter midlatitude stratosphere from Soviet radiosonde data
12 p2070 A69-26582

Height and temperature vertical variability in mid and upper stratosphere determined from constant pressure charts /1964-1966/
13 p2290 A69-27637

Soviet stratospheric solar observation projects compared with American
13 p2355 A69-27640

Latitudinal and vertical variations in six-month zonal wind cycles in equatorial and tropical stratosphere and lower mesosphere, utilizing rocket observations
13 p2294 A69-27854

Diffusion of ozone distribution tracers in stratosphere, based on photochemistry in oxygen- only and oxygen-hydrogen atmospheres
13 p2294 A69-28492

Acoustical thermometer-interferometer to measure air temperature between 20 and 50 km
14 p2445 A69-28777

Tropospheric and stratospheric temperature distribution in 1965 summer and winter from radiosonde and rocket data
14 p2442 A69-29725

Equatorial stratospheric wind fluctuations from pressure fluctuation data, relating southern fluctuations, stratospheric fluctuations and seasonal hemispheric air exchange
14 p2442 A69-29726

Irregular data obtained by radiosondes in winter for charts of high isobaric levels, noting stratospheric temperature effects on radiosonde ascent height
14 p2473 A69-29731

Stratospheric turbulence producing bumpiness up to 18 km developing at levels characterized by abrupt changes in vertical temperature gradients
14 p2474 A69-29737

Zonal and meridional components of air circulation in troposphere and lower stratosphere for Northern Hemisphere
14 p2477 A69-29829

Troposphere behavior and stratosphere structure over Southern Hemisphere based on rocket measurements, comparing hemispheric atmospheric circulation intensities
14 p2477 A69-29832

Two year cyclic monsoon type variations in zonal wind distribution in tropical stratosphere and mesosphere obtained by rocket measurements
14 p2478 A69-29834

Ozone concentrations harmful to humans in atmosphere based on U.S. and Western European observations, emphasizing lower stratosphere
15 p2596 A69-30642

Mixed balloon systems for long duration stratospheric flights with open balloon to carry payload and overpressure balloon as stabilizer or aerial buoy
15 p2551 A69-30703

GHOST Balloon Project, emphasizing launch and ascent control and location and life expectancy of superpressure balloons in tropical stratosphere
15 p2551 A69-31361

Longitudinal variations of density, temperature and pressure distributions in stratosphere and mesosphere based on rocket observations, emphasizing arctic and subarctic regions
15 p2602 A69-31379

Stratospheric balloons launching and nacelles for measurement of cosmic rays, atmosphere high altitude characteristics, discussing French launching center
16 p2734 A69-31759

Cosmic ray intensity temperature dependence in stratosphere and anisotropy in interplanetary space determined from measurements over Arctic and Antarctic regions
16 p2851 A69-32537

Simultaneous Umkehr observations of vertical ozone distribution in upper stratosphere using two Dobson photometers, discussing deviations due to calibration sensitivity
16 p2786 A69-32631

Ozone vertical distribution in upper stratosphere determined from OGO 4 observations, describing calibration of satellite data and onboard instrumentation
16 p2788 A69-32645

Ozone concentration worldwide anomaly above 40 km in annual variations, noting dissimilarity in seasonal maximum and minimum with lower level
17 p2960 A69-33166

Stabilization system design for stratospheric balloon gondolas, discussing optimal system with flywheel and weight combination
17 p2898 A69-33242

Stratospheric winds effect on instrument package suspended from high altitude balloon, discussing package displacements, yarn shapes and air drag characteristics
17 p2961 A69-33612

Meteorological analysis of stratospheric clear air turbulence flights, discussing vertical temperature structure in terms of wave motion and turbulence intensity
17 p2999 A69-33736

Lee waves and orographic wind phenomena in Rocky Mountains near Boulder, noting stratospheric standing gravity waves and turbulence sampled by HI-CAT U-2
17 p2999 A69-33738

Rocket and radiosondes data from measurements over Northern Hemisphere used to study stratospheric and mesospheric circulation during three midwinter periods
17 p2962 A69-33779

Relation between atmospheric processes in troposphere and upper stratosphere in cold half year
18 p3166 A69-34817

Diurnal wind variations below 30 km plotted on constant pressure charts, showing topographical influence on tidal fluctuations
18 p3166 A69-34828

Atmospheric aerosols influence on ion density profile in stratosphere obtained from numerical solution of equilibrium ionization equation
18 p3129 A69-34962

Ion density, electrical conductivity and weighted mean mobility deduced from Gerdien capacitor I-V characteristics used in balloon sounding of stratosphere
18 p3130 A69-34970

Physical process providing EMF for maintaining electrical structure of stratosphere and mesosphere shown to center in lower ionospheric thermally driven tidal motions
18 p3130 A69-35103

Vertical distribution of concentration, microstructure and chemical composition of solid aerosol in troposphere and stratosphere from high altitude balloon measurements
18 p3132 A69-35340

Stratospheric balloon vertical oscillations and gondola attitude during long flights
19 p3248 A69-36689

Vertical wind shears, structure functions, turbulence and power spectra for transverse velocity fluctuations in troposphere and stratosphere, noting clear air turbulence
20 p3570 A69-37506

Water vapor profiles in stratosphere from IR radiometric observations under cloudless conditions, indicating relation to tropospheric meteorological features
20 p3535 A69-38261

Ionospheric electron density and collision frequency profiles examined for changes during December 1967 to January 1968 stratospheric warming
21 p3714 A69-38556

Aerosol attenuation coefficients vs altitude in troposphere and stratosphere, noting seasonally dependent surface convective dust layer and temperature dependent aerosol maximum altitude
21 p3718 A69-39773

Rocket optical experiment for determining water, methane, nitric oxide and ozone vertical profiles in stratosphere and mesosphere
22 p4035 A69-39910

Upper stratosphere warming and associated structure of mesosphere from rocket sounding, discussing high winds related to pressure gradient, upward vertical motion, etc
22 p3977 A69-39928

Circulation and temperature fields indices used for studying tropospheric-stratospheric interactions during stratospheric warming at constant pressure levels
22 p3977 A69-39929

SST stratospheric environment problems, discussing temperature effects on fuel consumption and convective turbulence effect on flight safety and efficiency
22 p3867 A69-41141

Three dimensional structure of large scale disturbances in lower stratosphere and upper troposphere in equatorial Pacific, using power spectral and synoptic analysis
23 p4159 A69-42345

Ionospheric absorption relationship to major stratospheric sudden warmings, considering regional coincidence and interaction mechanism
24 p4306 A69-42680

Atmospheric variability at proposed flight levels, analyzing meteorological requirements of SST operations, discussing annual cycles in stratospheric circulation
24 p4251 A69-42711

Model for ozone formation, distribution and decomposition at 15-45 km assuming zonal symmetry, includ-

ing time effects of photochemistry, advection and turbulence
24 p4309 A69-43147

STRATOSPHERE RADIATION

Stratospheric air sampling reliability instrumentation as part of radioactivity fallout detection program
05 p0766 A69-16751

Solar protons in subpolar stratosphere during solar activity minimum indicated from proton measurements at Tiksi Bay
20 p3587 A69-37044

STRATUS CLOUDS

Aircraft measurements of stratus cloud absorption and albedo and earth surface albedo
04 p0627 A69-14914

Aircraft charge measurements in stratus clouds, noting charge sign is independent of cloud space charge
04 p0549 A69-15108

Radiation scattering changes due to droplet size distribution change during stratus cloud formation calculated, using development model and Mie theory
08 p1346 A69-21093

Nocturnal development of air mass stratus clouds in Texas and mechanism of formation, discussing turbulent mixing theory
15 p2649 A69-30893

Radio emission and absorption of cumulus and stratus clouds at millimeter and centimeter wavelengths, giving maximum SNR defined by brightness temperature
16 p2807 A69-32270

Synoptic and mesoscale cloud patterns near low level jet from Tiros 7 and 8 photographs, noting stratus formation and dissipation
20 p3570 A69-37404

STREAM FUNCTIONS [FLUIDS]

Two dimensional Navier-Stokes equations of axisymmetric motion of viscous incompressible fluid, giving integral and solutions for stream function
02 p0231 A69-12135

Two dimensional turbulent jet in uniform parallel stream, developing coordinate type perturbation expansion and applying series truncation method to predict downstream development
04 p0588 A69-14713

Acoustic streaming near small spherical obstacles, obtaining stream functions
04 p0631 A69-14904

Ground influence on Helmholtz flow in presence of plate perpendicular to stream, reducing problem to mixed Volterra problem in complex half plane
04 p0590 A69-15221

Stream function approximation for plane axisymmetric vortex free transonic inviscid gas flow
06 p0910 A69-17336

Multilevel objective weather analysis system for stratosphere and upper troposphere over Australia, using stream function analysis
06 p0950 A69-17787

Stream function for plane free sonic gas jet flowing past profile
07 p1050 A69-18740

Incompressible fluid unsteady motion between journal and bearing solved in form of Reynolds number power series from stream functions
09 p1514 A69-22712

Circle theorem for iterated equation of generalized axisymmetric potential theory, noting Stokes flow of viscous liquid
10 p1680 A69-23718

Acoustic streaming near small spherical obstacles, obtaining stream functions
12 p2131 A69-26657

Expansion of stream function of steady meridional flow of viscous fluid at small Reynolds numbers, giving expansion in spherical coordinates
13 p2247 A69-27737

Nonuniform gas flow past axisymmetric body from supersonic source simulating jet discharging into vacuum, using power series of stream function
19 p3238 A69-35851

Heat and mass transfer on vertical surface under combined free and forced convection, solving laminar boundary layer equations by stream function
19 p3453 A69-36844

Computation method of hydrodynamic blade cascade for compressible fluid and variable channel width by stream function
20 p3460 A69-37972

Stokes stream function and forces acting on two spheres moving in contact along line of centers through viscous fluid
24 p4299 A69-42747

STREAMLINE FLOW
U LAMINAR FLOW

STREAMLINED BODIES
NT FAIRINGS

Two dimensional supersonic rotational flow around convex corner solved using coordinate system consisting of left running characteristics and streamlines
05 p0697 A69-15722

Conventional fuselage and streamline body shapes effect on drag at subsonic speeds, noting boundary layer development
05 p0697 A69-15827

Exact partial solutions to transonic gas flow equations used to describe flow around shape streamlined by supersonic flow with additional shock wave
07 p1118 A69-18698

Streamlined rotors calculation, interpreting compatibility conditions between streamlining and airscrew stresses
08 p1252 A69-20655

Three dimensional supersonic flow past pointed nonaxisymmetrical bodies characterized by great local surface curvature changes, using new approximation
18 p3086 A69-34705

STREAMS
NT GAS STREAMS
NT RIVERS

Particle size, velocity and position in moving streams measured by tilted film plane optical system with pulsed light source
19 p3306 A69-35733

STRENGTH

Dimensioning and strength calculations - Conference, Budapest, October-November 1968
17 p3051 A69-32975

STRENGTH OF MATERIALS
U MECHANICAL PROPERTIES

STRESS [BIOLOGY]

Physiopathological reactions of humans exposed to infrasonic vibrations applied via aural canal, observing cardiac and circulatory hemodynamic troubles
13 p2215 A69-28590

STRESS [PHYSIOLOGY]
NT ACCELERATION STRESSES [PHYSIOLOGY]
NT CENTRIFUGING STRESS

Prolonged decompression stress effects on humans in simulated orbital flight or extravehicular activity, investigating endocrine-metabolic disturbance by urinaryysis
01 p0022 A69-11336

Nitrogen and helium as factors affecting human decompression stress severity, using urinary measurements reflecting various endocrine and metabolic changes
01 p0018 A69-11338

Acceleration, hypoxia and stress effects on humans and animals, noting latent functional disorders of organisms requiring special techniques for detection
02 p0197 A69-11488

Sympathetic neurohormones measurement in plasma of race car drivers
07 p1067 A69-19424

Human endurance during isolation in closed space with prescribed veloeometric exercises, noting impairment of functional capacity
08 p1263 A69-19933

Brief intense thermal stresses effects on cardiovascular system of man, noting criticality of effective blood volume for circulatory competence
08 p1264 A69-20668

Rapid decompression and recompression in stapledecomized cat, noting fibrous tissue response in middle ear at reconstructions utilizing polyethylene struts on gelfoam
14 p2406 A69-29292

Constant light/darkness effects on stress response rhythm of hypothalamic-pituitary-adrenocortical system in female rats
15 p2556 A69-31330

Artificial heat acclimatization effect on orthostatic tolerance in man exposed to stresses of heat, exercise and dehydration
16 p2746 A69-32810

Prolonged hypokinesia effect on human resistance to physical stress, noting prophylactic influence of physical exercises
17 p2907 A69-32939

Injury stress vs acceleration specification as valid criterion for pilots subjected to high acceleration, introducing models and illustrating with ejection example
17 p2913 A69-33008

STRESS [PSYCHOLOGY]

- Beta adrenergic blockade in differential diagnosis of cardiovascular changes produced by stress induced catecholamine liberation and organic disease
17 p2909 A69-33184
- Cladonia rangiferina resistance to stresses, considering suitable indices for stress response
18 p3095 A69-34539
- Increased tolerance of orthostatic stress in heart failure patients
19 p3258 A69-36374
- Noise influence on heart rate and oxygen consumption of young male subjects under simultaneous physical stress
21 p3654 A69-38908
- Blood pressure measurements of pilots at rest during tests under stress on bicycle ergometer revealing transient hypertension
23 p4087 A69-41795
- Physical and psychic stress effects on phosphatidyl glycerol and related phospholipids concentration in human and rat blood plasma
23 p4088 A69-41815
- Hearing adaptation measurements after aircraft noise stresses for estimation of induced noise damage
23 p4110 A69-42051
- Vascular interface histological and chemical responses to acute mechanical stress in dog aorta
24 p4257 A69-42625

STRESS [PSYCHOLOGY]

- Human behavior during stressed underground confinement, discussing adaptation processes
01 p0020 A69-10757
- Book on groups under stress covering psychological research in SEALAB 2, emphasizing planning of data collection and experimental results
04 p0552 A69-14533
- Man psychic activity interference resistance, discussing stress effects characterized by theta and delta rhythms
08 p1262 A69-19839
- F-102 pilot anticipatory and flight stress, noting endocrine-metabolic hyperactivity
12 p2023 A69-26552
- Physical and psychic stress effects on phosphatidyl glycerol and related phospholipids concentration in human and rat blood plasma
23 p4088 A69-41815
- Psychological stress effect on human convergent and divergent thinking after presentation of disturbing or benign control films
24 p4269 A69-42555
- Abnormal biologic rhythm in rhesus monkeys associated with behavioral stress, noting brain temperature periodicities sensed with implanted extradural thermistor
24 p4261 A69-42708

STRESS ANALYSIS

- NT PHOTOGRAPHIC MEASUREMENT
NT X RAY STRESS ANALYSIS
- Creep and stress rupture strength of unidirectional glass fiber reinforced plastics, using tensile tests
01 p0101 A69-10080
- Generalized plane stress concept extended for mathematical model to study out of plane displacement restraint in thin plates
01 p0165 A69-10114
- Thin cylindrical shell deformation and stress under concentrated radial loading, analyzing singularity at load point
01 p0166 A69-10301
- Yield surface after prestraining under radial loading, analyzing formation of yield corner
01 p0166 A69-10303
- Low stress fracture criteria for large elastic structures and small brittle laboratory specimens below transition temperature
01 p0169 A69-10768
- Fiber-fiber interaction effect on stress distribution and tensile strength of discontinuous aligned fiber composites
01 p0171 A69-11261
- Homogenous mechanical stresses in amorphous and crystalline gallium films during vacuum deposition and annealing
01 p0141 A69-11420
- Metal fatigue crack propagation mechanism, deriving basic laws for failure in high and low stress regions, determining material parameters
02 p0340 A69-12025
- Equilibrium problem of elastic medium with stress couples in linearized elasticity theory, representing biharmonic function with aid of analytical functions
02 p0340 A69-12035

- Stress analysis of multiply connected bodies under large elastic strains, deriving second order potentials for plate with elliptical holes
02 p0340 A69-12139
- Bending of freely supported plates of polygonal planforms under transverse load with aid of R functions
02 p0341 A69-12140
- Computer stress analysis may result in automated designs, emphasizing finite element technique
02 p0341 A69-12153
- Two dimensional elasticity problem for two zero tangential stresses, expressing stress-strain states by biharmonic and harmonic functions
02 p0341 A69-12198
- Eccentric compression in elastic domain for rigid homogeneous structural elements, considering traction and stress
02 p0341 A69-12258
- Crystal dislocation motion in viscous media, discussing velocity stress behavior and measurements by etching and ultrasonic attenuation methods
02 p0343 A69-12285
- Three dimensional thermal stress distribution in case bonded solid propellant determined by scattered light photoelastic technique coupled with transparent rocket motor model
02 p0345 A69-12371
- Elastic analogue in creep stress analysis under time dependent boundary conditions and strain hardening theory
02 p0345 A69-12418
- Multilayered shells equivalence to single layer shells for stress analysis, vibrations and stability
02 p0346 A69-12509
- Stresses in circular cylindrical shell subjected to local heating
03 p0523 A69-12952
- Notch stress procedure to predict low cycle fatigue life of specimens with fabrication flaws, discussing crack initiation and propagation lives effects
03 p0523 A69-12997
- Photoviscoelastic stress analysis to predict time dependent stress redistributions in polyphase system with viscoelastic binder under external loading conditions
03 p0524 A69-13061
- General solutions of three dimensional elasticity theory applied to isotropic disks and plates, emphasizing homogeneous solutions
03 p0526 A69-13738
- Stress diffusion from axially loaded stiffeners into cylindrical elastic shells
03 p0530 A69-14065
- Skin panel stresses for random acoustic loading, determining aircraft structure responses
03 p0530 A69-14092
- Elastic equilibrium stress condition of anisotropic plates with circular isotropic inclusions
04 p0667 A69-14264
- Plane problem of anisotropic elasticity based on biharmonic and Helmholtz equation for stress functions
04 p0667 A69-14267
- Thermal stress determination in two dimensional problem of theory of elasticity, using stress simulation by thin plate bending
04 p0668 A69-14272
- Photoelastic analysis of HF stress waves propagating in bars and plates subjected to damped sinusoidal loading
04 p0669 A69-14397
- Two point boundary value problems for determining buckling behavior of two hinged circular arches
04 p0669 A69-14399
- One dimensional wave propagation analysis for zero value stress time derivatives on both sides of elastic-plastic boundary
04 p0670 A69-14407
- Stressed state periodic problem in infinite strip under combined pressure and temperature field effect
04 p0673 A69-14497
- Stress field for skew hole determined from plane stress field for equivalent right hole, considering elastic plate penetrated by oblique circular cylinder
04 p0674 A69-14589
- Stresses and displacements in anisotropic elastic solids under mechanical loading, determining general solution for treatment of time dependent boundary conditions
04 p0675 A69-14595
- Reinforced thin walled cylindrical pressure body nonlinear circumferential stress problem approximate

- solution, noting fatigue strength of aircraft pressurized cabins
04 p0548 A69-14838
- Integration method for equations of plastic two dimensional stressed state with Mises yield condition, noting stress concentration at hole with pressure on contour
04 p0679 A69-14924
- Holographic interferometer for isopachic stress analysis, utilizing photochromic recording for real time interference
04 p0599 A69-15013
- Circular disk stress-strain state due to thermoelastic strain applied at disk sector edge
04 p0681 A69-15171
- Elastic strain and stress in ribbed circular plate bent skew-symmetrically, using orthotropic plates theory
04 p0681 A69-15172
- Holography, discussing image formation, position, enlargement, aberration and application to stress analysis
04 p0601 A69-15186
- NeoHookian /incompressible solid/ rectangular parallelepiped compressed between lubricated rigid plates, comparing stability bounds with predicted critical loads
04 p0682 A69-15303
- Soviet handbook on stress analysis of anisotropic three layer reinforced plates and shells and of thick walled cylinders, Volume 2
04 p0683 A69-15500
- Point matching method for analysis of stress in incompressible solids of revolution, noting application to solid propellant rocket charges
04 p0683 A69-15518
- Internal gravity waves propagation in shear flow, detailing interaction stress in incompressible stratified Boussinesq liquid, conservation energy exchange and radiation stress
05 p0788 A69-15721
- Mathematical theory for describing mechanical behavior of continuous media based on principle of determinism for stress
05 p0833 A69-15729
- Rectangular thin beam Saint Venant deflection in case of moment stresses based on elasticity and shell theory
05 p0834 A69-15783
- Static stability of three dimensional elastic bodies under subcritical strains, noting application to stability of cylindrical shells and rods
05 p0834 A69-15784
- Displacement, distortions and unit stresses in rotating circular disk under plane strain
05 p0835 A69-15807
- Stresses in cylindrical shell with elastic core loaded on curved surface solved, using elasticity theory for core and membrane solutions for shell
05 p0835 A69-15871
- Clamped rectangular plate under lateral load stress analyzed by extended Kantorovich method to include bending moments and shearing forces
05 p0835 A69-15872
- Tension stress and shearing strain vs time for simultaneous stress relaxation and creep in polyurethane
05 p0839 A69-16186
- Elastic-plastic analysis of flat plates in membrane stretching and flexure, using method of initial strains
05 p0840 A69-16191
- Annular stress in rib reinforced cylindrical shells under axial compression load and internal pressure, using successive approximation
05 p0841 A69-16208
- Matrix displacement and force methods of stability analysis, deriving method of determining geometrical stiffnesses for complex structures
05 p0841 A69-16399
- Photoelastic study of interaction between overlapping parallel cracks in tensile stress field
05 p0842 A69-16435
- Stresses in finite width infinite elastic isotropic strip with equally spaced identical semicircular notches under uniform tension or pure bending
05 p0843 A69-16644
- Buckling of rod with initial deflection as sinusoidal half wave, using Bubnov-Galerkin method and Laplace transform, calculating stresses of rod when subjected to nonsteady creep
06 p1021 A69-17182
- Plastic deformation in hypoeutectoid and hypereutectoid Ni-Ti alloys studied by compressive stress-strain analysis and transmission electron microscopy
06 p0941 A69-17222

- Simple dipolar stresses, noting effect of antisymmetry on equations of motion and energy equation
06 p1022 A69-17239
- Exponential decay of stresses in circular elastic cylinders subject to axisymmetric self equilibrated end loads
06 p1024 A69-17507
- Temperature distributions and thermal stresses in bimetallic I-beam structures with dissimilar materials for skins and webs and with kinetic heating inputs
06 p1024 A69-17610
- Two dimensional stress distribution changes around rectangular hole with rounded corners for varying internal pressure and temperature
06 p1025 A69-17611
- Statistical processing of oscillograms of instantaneous values of wire tension during winding, determining stress characteristics
06 p0927 A69-17691
- Incremental complementary energy method of stress analysis of orthotropic nonlinear materials having different behavior in tension and compression [AIAA PAPER 69-119]
06 p1028 A69-18159
- Stress concentration factors for composite body of two isotropic elastic phases in plane strain in plane of composite parameters
07 p1170 A69-18716
- Sign conventions definition and importance for shear stress and strain analysis in laminated anisotropic composite materials, noting role in studying response
07 p1170 A69-18720
- Fundamental problems of plane elastostatics with stress couples reduced to solution of integral equations, noting uniqueness theorem in plate bending theory
07 p1233 A69-19328
- Collection of papers on mechanics of solid state covering structural stability, stress analysis, creep, cracking and fracture
07 p1234 A69-19377
- Brittle fracture models compared with experimental stress analysis results, noting plane strain and plane stress fracture toughness
07 p1234 A69-19379
- Anisotropic stress analysis of creep in theory of linear viscoelasticity
07 p1234 A69-19381
- Quasi-plane stress in rotating disks of unconventional profile emphasizing conic shaped disk analysis in terms of hypergeometric series
07 p1235 A69-19444
- Linear analysis of strain in continua in terms of one-one correspondence, relative displacement and stretch dyadic
07 p1236 A69-19445
- Stress analysis split method for determining residual strength and fatigue crack life of damaged or initially cracked VTOL structures [AIAA PAPER 69-214]
07 p1237 A69-19576
- Accuracy of deformation theory in case of simple loading, analyzing external forces under conditions not satisfying loading theorem
07 p1237 A69-19684
- Stresses nature at ends of brittle cracks, discrediting finiteness under certain conditions
07 p1238 A69-19691
- Elastic springback and residual stress distribution in sheet metal formed by bending determined as function of radius sheet thickness and stress-strain characteristics
08 p1319 A69-20005
- Direct plotting of vibrating wire strain gauge data for concrete structures, giving diagrams for grid and backing sheet scaling
08 p1312 A69-20104
- Separation of principal stresses along sections of symmetry free from external loads with application to circular ring and grooved bar
08 p1412 A69-20256
- Streamlined rotors calculation, interpreting compatibility conditions between streamlining and airsearc stresses
08 p1252 A69-20655
- Simply supported isotropic cylindrical panel stability under axial compression, obtaining asymptotic series expansion for upper critical stress
08 p1419 A69-21182
- Reaction vs time relations in accidental impact of large commercial aircraft against rigid surface, detailing stress analysis of nuclear power plants structures
09 p1613 A69-21677
- Radial and tangential stresses in double glass fiber assuming different Poisson coefficients, determining conditions for axial stress redistribution prevention
09 p1614 A69-21741
- Graphical methods for photoelastic effect behind system with stresses rotating about direction of light propagation, discussing j circle technique [DVL-903]
09 p1617 A69-22011
- Material selection for structures under vibration loads, analyzing fatigue strength on basis of stress susceptibility and relationship with tensile strength
09 p1620 A69-22574
- Strength hypothesis for structures under multiaxial vibration load, taking into account plane stress state
09 p1620 A69-22575
- Elastoplastic stress in notch as cause of decreased lifetime of aircraft components, analyzing stress reversal and displacement during takeoff and landing
09 p1620 A69-22576
- Inverse problem in stochastic processes, considering random moving force and strip load in structural stress analysis
10 p1793 A69-22876
- Numerical analysis for stresses in finite or infinite plate with arbitrary holes, considering boundary value problems
10 p1793 A69-22882
- Structures analysis by photoelastic model techniques of stress visualization
10 p1794 A69-22941
- Book on statics of thin walled shells of revolution covering stress-strain analysis for geometrical shapes
10 p1800 A69-23197
- Couple stresses effect on distribution of stresses in elastic solid due to crack analyzed on basis of Cosserat theory
10 p1800 A69-23242
- Shear field pattern theory modified to apply to determination of sweptback wings, calculating stress development
10 p1801 A69-23645
- Propagation of extensional cylindrical waves in elastic plates with free boundaries, considering plane stress and Lamb dispersion
11 p1969 A69-24414
- Nonlinear elasticity theories emphasizing quadratic approximation of stress concentration
11 p1973 A69-24660
- Macroscopic states of stress criteria for plastic flow initial yielding, plastic flow and brittle fracture of ductile and brittle metals
11 p1975 A69-24671
- Linear shell theory foundations, discussing two and three dimensional stress strain relations, couple stresses, circumferential length ratio to shell thickness, etc
11 p1977 A69-24803
- Stress analysis, Volume 12, Theoretical and experimental studies of strength of machine structures
11 p1980 A69-24940
- Moire patterns for photoelastic strain analysis noting applications to elasticity, plasticity and creep problems
11 p1982 A69-24944
- Stress analysis of reinforced cylindrical shells under external loading, using Vlasov semimomentless theory
11 p1982 A69-24949
- Field approach for stress and deflection analysis in rectangular plates reinforced by straight ribs, noting kernel function
11 p1983 A69-25019
- Deformations and stresses in pressure vessel with elliptical cross section under uniform internal pressure, noting radial deflection and membrane, bending and skin stress
11 p1983 A69-25023
- Temperature and stress dependence of microstrain and microyielding in polycrystalline W for range of impurities and dislocations, considering transition to macrostrain
11 p1905 A69-25183
- Maximum stress under bending for thin walled circular cylindrical shell stiffened with uniform stringers
11 p1987 A69-25380
- Birefringent coatings application to plane stress in orthotropic glass-fiber reinforced plastic materials noting stress-strain relations
11 p1995 A69-25647
- Bending and membrane stresses determination in shallow thin shells of revolution under large axisymmetric deflections, using normal and radial displacements relationship [SESA PAPER 1332]
11 p1995 A69-25651
- Poisson ratio determination with bonded electrical resistance strain rosettes
11 p1995 A69-25652
- Stress discontinuity surface of three dimensional rigid plastic body arbitrary yield condition, considering equilibrium of regular four sided pyramid
11 p1996 A69-25738
- Stress concentration near circular hole in plate during bending, showing dependence on material constant
12 p2178 A69-25999
- Plane stress state in plate with different glide moduli during tension and compression, considering axisymmetrical deformations
12 p2178 A69-26003
- Thermal stress and displacement fields in elastic solid weakened by crack outside of circular region, noting plastic zone size and energy dissipation
12 p2179 A69-26216
- Stress distribution in elements of unidirectionally fiber reinforced composite materials analyzed as function of fiber content and fiber-matrix elastic properties
12 p2180 A69-26263
- Thermal stresses in infinite elastic plates containing insulated circular holes, using two dimensional bipolar coordinates
12 p2180 A69-26267
- Thermal stresses in hollow finite circular cylinder having smooth rigid insulating cover on curved surfaces and temperature distribution on plane ends
12 p2180 A69-26268
- Critical load for anisotropic right-angled isosceles triangular plate stability with large deflections obtained from differential equation
12 p2180 A69-26270
- Axisymmetric elastic stresses in ring stiffened segmented shells of revolution, noting finite difference method for nonlinear analysis and computer program
12 p2185 A69-26818
- Lateral bending and two dimensional thermal stress in rectangular orthotropic plates, considering alternating direction implicit method
12 p2188 A69-27100
- Stress distribution in matrix of unidirectionally fiber reinforced composite subject to shrinkage and normal transverse load, using three dimensional photoelastic analysis
12 p2189 A69-27162
- Crack opening displacements of stationary and running cracks and of inclined stationary cracks in centrally notched plates, noting normal strain fields
12 p2189 A69-27163
- Moire fringes, discussing fringe multiplication by filtering to obtain small strain measurement sensitivity and engraving technique for wave front reconstruction
12 p2099 A69-27164
- Moire and gridwork methods of plastic strain analysis with application to plane strain and axisymmetric extrusion
13 p2359 A69-27256
- Plane stress theory for large elastic deformations of isotropic thin sheets, outlining successive substitutions method for neoHookean materials static and dynamic problems
13 p2359 A69-27320
- Book on stress rupture parameters including least squares approach to Larson-Miller, Dorn, Manson-Haford, Graham-Walles, Murry, Brozzo and Chitty-Duval
13 p2360 A69-27372
- Subelement geometrical stiffness determined, considering complete element natural modes
13 p2362 A69-27838
- Tension stress and shearing strain vs time for simultaneous stress relaxation and creep in polyurethane [ASME PAPER 68-WA/APM-8]
13 p2362 A69-28121
- Stresses in elastic half plane with bonded disk of same elastic properties, describing stress production by expansion of disk
13 p2363 A69-28132
- Strain resultants in finite quadrilateral elements, noting application to linear strain triangles
13 p2364 A69-28230
- Stress intensity for Griffith crack with asymmetrical distribution of surface tractions
13 p2369 A69-28352
- Phenomenological macro rheology, discussing mechanical models designed for studying relation between stresses and strains in materials
13 p2369 A69-28562
- Materials surface thermal stress analysis by strain gauges, considering behavior during rapid temperature changes
13 p2264 A69-28599
- Rotating disk of nonuniform thickness, establishing optimum geometry for minimum tangential stress [ASME PAPER 69-DE-36]
14 p2454 A69-28841
- Stress and strain fields for circular rubber ring under diametrical compression between flat plates, using moire, large strain analysis and photoelastic verification
14 p2531 A69-28884

Structural stress under acceleration loading simulated by two dimensional photoelastic model noting improvement of fringe patterns quality
14 p2532 A69-28885

Temperature measurement for aircraft gas-turbine engine development
14 p2509 A69-28886

Plasticity theory approximation variants for complex loading, analyzing strain trajectories using Prandtl-Reiss theory
14 p2532 A69-28978

Model equation for Reynolds stress in turbulent two dimensional shear flow
14 p2428 A69-29000

Stress in elastic cylinder under thermal expansion with one end clamped expressed by series expansion of biharmonic function using least squares method
14 p2534 A69-29284

Constitutive equations for living soft tissues freely deforming under negligible stresses with Hooke law as limit
14 p2535 A69-29366

Strains determination for laterally edge loaded rectangular plate and sagittas determination of perpendicularly loaded plate proved analogous
15 p2704 A69-30295

Box girders stress distribution analyzed by stress-freezing method compared with photoelastic measurement
15 p2705 A69-30419

Elastoplastic matrix for stress increments for yield surfaces with associated flow rule, considering initial stress computation
15 p2706 A69-30433

Torsion of composite prismatic rod consisting of three different isotropic materials with two interfaces converging on cross section contour corner point
15 p2707 A69-30579

Creep rates measurement errors at low stresses in intermediate temperature range, examining log creep rate vs log stress plot in Cr-Mo steel
15 p2639 A69-30599

Automated shear difference analysis of three dimensional photoelastic model stress distribution by stress-freezing and slicing technique
15 p2609 A69-30680

Scratch gages under water in open and at high temperature, including circular X-Y recording scratch strain gage
15 p2610 A69-30682

Screening techniques for semiconductor devices, considering component classification with respect to population strength distribution
15 p2627 A69-30840

Monograph on stress fields in plane plastic flow as solutions to boundary value problems
15 p2711 A69-30932

Stress calculation for thermoelastic mixed boundary value problem in infinite isotropic plate with cylindrical stress free cavity
15 p2712 A69-31013

Plane stress solution for stresses due to concentrated couple acting at any point on elliptic plate with fixed edge
15 p2712 A69-31014

Stresses in fixed two dimensional photoelastic models analyzed by hologram interferometry, displaying isochromatic and isopachic interference patterns
15 p2611 A69-31110

Thermal stresses in circular cylinder with regularly distributed cavities, establishing distribution laws for temperatures and stresses
15 p2714 A69-31196

Potential functions applications to three dimensional static elasticity problems of parallelepipeds, using general stress solution
15 p2715 A69-31216

Full stress design feasibility as function of load conditions, indeterminacy order and structure topology
16 p2872 A69-31915

Stress and deformation in cross section of beam during complex loading using steepest-descent method
16 p2873 A69-32132

Transient stress waves due to inputs of various types and time dependence in plates and revolving shells, discussing applications of elasticity theory analysis methods
16 p2876 A69-32785

Grain boundaries contribution to creep deformation, discussing ratio of grain boundary slip strain to total creep strain
17 p2985 A69-32905

Random stress statistical properties and relationship to fatigue life, discussing Fuller prediction, comparison with test data, and vehicle design evaluation
17 p3053 A69-32988

Stress-strain state analysis for brittle plate with circular holes of equal radius performed in cylindrical system of coordinates
17 p3055 A69-33127

Stresses and displacements in elastoplastic cantilever beams and beams fastened at both ends calculated by stress-strain diagrams of material
17 p3056 A69-33191

Strains in elastoplastic curved beam under bending obtained from approximating stress-strain diagram by parabola
17 p3056 A69-33192

Centrifugal compressor impeller disk design, considering stress analysis for shielding portion profile determination to satisfy equal strength condition
17 p3057 A69-33193

Solid propellant thrustors fabrication procedures, design considerations and quality control, stressing stress analysis and propellant choice with respect to geometry
17 p3018 A69-33331

Holography application in gas turbine components stress and vibration analysis, discussing techniques and apparatus usable by nonspecialist and measurement accuracy
17 p2974 A69-33351

Strength margins for combined random stresses, discussing average crossing frequency of curve by Gaussian stationary random vector with correlation coefficients included
17 p3066 A69-34038

Elastic stresses in rotating anisotropic disks with constant thickness, discussing solid, circular rigid shaft mounted and center drilled disks
17 p3067 A69-34138

Creep rate-stress-temperature relations for powder metallurgy rhenium, discussing activation energy
17 p2991 A69-34186

Mean stresses effect on fatigue strength by specimens vibratory/tensile mean stress diagram combining Goodman line and Gerber parabola merits with increased accuracy
17 p3067 A69-34197

Coupled stresses in thermoelasticity for displacement and rotation vector characterized medium, discussing wave propagation in unbounded medium
18 p3211 A69-34262

Grid method of strain determination, discussing print, record, analysis and application
18 p3134 A69-34423

Modified Bubnov-Galerkin-Ritz method for determining approximation coefficients in stress and displacement analysis, using mixed variational principle of elasticity theory
18 p3215 A69-34566

Stressed state analysis in dynamic brittle breakdown wave front of compression waves propagating in brittle rod under longitudinal impact
18 p3217 A69-34592

Positive Gaussian curvature shell under concentrated forces, analyzing stresses and strains relation to load distance using Thompson and Legendre functions
18 p3218 A69-34601

Stress conditions of anisotropic plate with soldered in circular isotropic aluminum disk in presence of notches at seam, assuming elastic symmetry of plate
18 p3218 A69-34602

Analytical-statistical weight prediction to derive and apply correlation expression, illustrated with bending stress equation applied to aircraft wing group [SAWE PAPER 810]
18 p3221 A69-34900

Constrained elastoplastic torsion of closed thin walled cylindrical shells, analyzing tangential and normal stress by using equilibrium equations
18 p3222 A69-34978

Rectangular thin beam Saint Venant deflection in case of moment stresses based on elasticity and shell theory
18 p3223 A69-35035

Static stability of three dimensional elastic bodies under subcritical strains, noting application to stability of cylindrical shells and rods
18 p3223 A69-35036

Photoelastic materials stressed state analysis by inserting analyzer and polarizer into sandwich medium, obtaining polarized light field
18 p3138 A69-35152

Strains in solids of any form, using moire method combined with holographic interferometry
18 p3139 A69-35280

Microstresses in hollow-fiber reinforced cylindrical shell under longitudinal shear stress, determining modulus of elasticity and optimum component ratios
18 p3225 A69-35369

Limiting equilibrium of infinite brittle body weakened by internal plane elliptical crack, determining critical loads and stresses at crack
18 p3226 A69-35379

Strength analysis of three layer rectangular plates under complex load and support distributions
19 p3434 A69-35827

Book on moire fringes in strain analysis, discussing methods for strain measurement in deformed bodies and engineering structures
19 p3435 A69-35835

Turbine disks stress-strain state, using wire strain gage to determine residual strains, radial and tangential stresses as function of disks rpm
19 p3436 A69-35850

Two dimensional stress analyzed near crack in infinite elastic sheet, considering crack shape and Young modulus
19 p3440 A69-36638

Graphical representation of friction stresses produced on mechanical parts surface layers, using mathematical model based on Poisson ratio and friction coefficient
19 p3329 A69-36723

Thin elastic shells internal stress state by iteration of two dimensional equation of general linear theory
19 p3443 A69-36790

Finite element method in stress analysis for axisymmetric rotors design, describing computer program and applications
19 p3445 A69-36826

Finite element displacement method using elastic analogy applied to viscoelastic materials plane stress analysis
19 p3445 A69-36830

Stress distribution in tension specimen notched on one edge obtained photoelastically for several notch depth to specimen width ratios, noting Neuber theory agreement
19 p3447 A69-36859

Stress analysis of cylindrical shell-end closure junction for optimum pressure vessel configuration prediction for nuclear reactor applications
19 p3447 A69-36861

Surface stresses in rotating asymmetric profiled disks and axial deflection effects computed theoretically and compared to measurements on photoelastic models
19 p3447 A69-36862

Photoelastic model methods for two and three dimensional investigations of microstresses in composite materials
20 p3565 A69-36940

Geometry effects on stresses in discontinuous composite materials, studying fiber spacing, failure and discontinuities size and nature
20 p3565 A69-36942

Stress and displacement in thin circular plates of ductile materials under axisymmetric loading predicted by nonlinear analysis
20 p3628 A69-37787

Monograph on beam impact force and bending stresses during transverse impact, noting Bernoulli and Hertz theories application
20 p3628 A69-37922

Stress rupture parameters for refractory metals and alloys from Larson-Miller, Dorn and Manson-Haferd constants, noting optimization procedure [ASM PAPER D8-3.4]
20 p3564 A69-38135

Soviet book on shell and thin walled structure calculation methods covering stability and stress analysis, reinforced and sandwich shells, etc
20 p3630 A69-38199

Radial and tangential stresses in double glass fiber assuming different Poisson coefficients, determining conditions for axial stress redistribution prevention
20 p3630 A69-38217

Stress analysis of circular elastic plate buckling under radial compression, noting Kirchhoff hypothesis influence on critical value of thickness-to-radius ratio
21 p3834 A69-38722

Adhesives and adhesive resin bonding, describing internal stresses in joints, joints design for bonding, strength, bonding processes and testing
21 p3752 A69-38932

Stress analysis - Conference, London, March 1968
21 p3840 A69-39301

Error propagation and tolerance analysis in design and reliability engineering and stress analysis
21 p3842 A69-39303

Computer program for stress analysis of cylindrical pressure vessel with flat-end closures by thin shell theory

21 p3842 A69-39306

Stress analysis of thin axisymmetric shells by plane frame analysis program, noting stiffness matrix for conical shell element

21 p3843 A69-39312

Isoparametric finite element system for stress analysis, with examples for arch dam, impeller and cellular structure, illustrating shells of revolution

21 p3732 A69-39314

Photoelastic data analysis for stress separations, discussing shear slope and Tesar methods

21 p3843 A69-39316

Photoelastic and micromechanic studies of epoxy resins of varying Young moduli by simultaneous stress analysis of FRP and matrix materials

21 p3846 A69-39796

Mohr tensor representation and Mohr theorem proof developed for general problem in structural engineering

22 p4038 A69-39903

Rectangular plate under biaxial tension stress analyzed to determine onset of necking and stress-strain state

22 p4039 A69-39913

Momentless orthotropic spherical shell of variable thickness stress analyzed, assuming large deformations under uniform axisymmetric load distribution

22 p4039 A69-39916

Holography applied to stress and vibration analysis of gas turbine blades, disks and small components

22 p4040 A69-39960

Metal fatigue crack nucleation at stresses below static fracture strength, determining local plastic strain under cyclic loading

22 p4041 A69-40053

Stress analysis fundamental equation for variable thickness plate under concentrated load, using two dimensional Dirac delta function

22 p4041 A69-40144

Moire effect applications to stress analysis, enumerating advantages over conventional grid techniques

22 p4042 A69-40315

Radial and tangential stress analysis of rotating disk during steady state creep, using equations solved by finite difference method

22 p4043 A69-40458

Stress analysis during solidification of binders in glass fiber reinforced plastic materials, using resin coated glass film simulation

22 p3973 A69-40746

Initial stress dependence on tensile load in glass fiber reinforced plastic rings during winding

22 p4045 A69-40749

Elastically symmetric thin plate stress-strain state under uniformly distributed load applied to edges

22 p4046 A69-41061

Crack development in solid body, considering condition at crack tip not derivable from equation of motion and strain equation

22 p4047 A69-41123

Shallow shells two dimensional theory including effects of transverse shear deformation and of moments turning about normal to middle surface

22 p4048 A69-41197

Vector properties of isotropic strain hardenable materials in stress vector space applied to tubular brass subject to biaxial tension and complex loading

23 p4227 A69-41714

Stress analysis of cylindrical tubes under torsional and transverse static loads based on vibrational theory, applied to rectangular cantilever tube

23 p4228 A69-41916

Plates and shells under concentrated loads, analyzing stress-strain state

23 p4228 A69-41986

Principal stresses determination in optically active photoelastic models from fringe pattern while obtaining sum from Dirichlet problem solution by straight line method

23 p4228 A69-41987

Stress analysis in elastic bodies induced by axisymmetric strains in presence of mass forces and temperature gradients, obtaining equilibrium equation

23 p4229 A69-41997

Algorithm for stress analysis of structurally orthotropic conical and cylindrical shells, resolving first order differential equations

23 p4229 A69-42000

Green formula and fundamental solution for determining displacements and stresses in contour integral form for plate bending problems

23 p4230 A69-42002

Creep stress analysis of circular cylindrical shells under axisymmetric loading, plotting stresses and deformations for various parameters

23 p4233 A69-42352

Nadai and Zyczkowski stress analysis for Tresca yield condition reexamined for determination of critical angular velocity of solid elastic perfectly plastic disk

23 p4235 A69-42480

Scattered light methods inaccuracies for nondestructive analysis of generally stressed photoelastic models, noting modified Mini-max method

24 p4396 A69-42737

Isoclinics determination from fringe patterns, obtaining continuous principal stress direction data for photoelastic model in bonded polariscope

24 p4396 A69-42738

Bonded strain gages for experimental stress analysis of high speed rotating machinery under high centrifugal loads

24 p4397 A69-42740

Stress analysis in design techniques taking into account failure of flawed structures, discussing fracture mechanics

24 p4398 A69-42773

Limiting load of square plate subjected to shear and reinforced by vertical stiffener, computing membrane and bending stresses as function of flexural rigidity

24 p4399 A69-42967

Stress analysis of hollow viscoelastic cylinder reinforced with elastic helically wound wires

[ASME PAPER 69-APMW-23]

24 p4401 A69-43096

Contact stress distribution between two two-dimensional finite nearly rectangular elastic bodies with general surface configurations for surface load expressed in trigonometric series

[ASME PAPER 69-APMW-9]

24 p4402 A69-43104

Soviet book on resistance of materials to deformation and fracture in complex stress states covering elasticity, mechanical theories of limiting stress state, experimental verification, etc

24 p4402 A69-43233

Stress analysis of incompressible solid propellant rocket charges by point matching technique, considering differential thermal shrinkage and axial acceleration cases

24 p4402 A69-43263

Relative slip effect on fretting fatigue strength, deriving stress initiating fatigue cracks

24 p4404 A69-43628

STRESS CONCENTRATION

Stress concentration near eccentric elliptical hole in spherical shell, using computer methods

01 p0165 A69-10089

Strain distribution for fracture initiation and steady state crack propagation in plane strain tension of plastic materials

01 p0169 A69-10764

Fiber-fiber interaction effect on stress distribution and tensile strength of discontinuous aligned fiber composites

01 p0171 A69-11261

Thermal stresses near spherical inclusion in elastic matrix with uniform heat flow

01 p0171 A69-11264

Stress distribution in composite cantilever beams of three layers with end loading solved by closed form elasticity method

01 p0172 A69-11266

Stress transfer from loaded matrix to single fiber in composite materials determined by series and step formulations

01 p0172 A69-11271

Three dimensional stress concentration around cylindrical hole in semiinfinite elastic body loaded at infinity, using Fredholm integral equation

01 p0172 A69-11332

Stress peak distribution effects on random load fatigue investigated for one and two degree of freedom systems

01 p0172 A69-11355

Stress field and force system within torsional flow of cylindrical mass of incompressible anisotropic fluid

02 p0229 A69-11558

Dynamical strength of solid cylinder under axial loads increasing in time at given rate, using constitutive equations of thermodynamic theory

02 p0342 A69-12278

Three dimensional thermal stress distribution in case bonded solid propellant determined by scattered light photoelastic technique coupled with transparent rocket motor model

[AIAA PAPER 68-512]

02 p0345 A69-12371

Stress concentrations around elliptical perforations in shrunk plates with bonded boundaries based on photoelastic models

02 p0345 A69-12391

Internal elastoplastic stress distribution within reinforced plastics subjected to force normal to internal filaments direction

02 p0347 A69-12513

Composite tensile-failure modes, discussing failure load prediction, experimental data and statistical analysis of stress concentration effects

[AIAA PAPER 68-173]

02 p0347 A69-12514

Time dependent viscoelastic stress distribution in two phase composite material, using plane stress model for approximation

02 p0348 A69-12540

Stress and heat flux spectra estimation using Busch-Panofsky observations

02 p0276 A69-12698

Stresses in infinite elastic plate containing rigid rectangular inclusion subject to uniform stress field, using complex variable method and Schwartz-Christoffel conformal mapping

02 p0348 A69-12796

Stress state of circular cylindrical shell subjected to uniform inward radial line load along generator solved by closed form particular integral, discussing convergence

02 p0349 A69-12797

Stresses around two reinforced circular openings in thin elastic plate of isotropic material under biaxial loads

02 p0349 A69-12799

Successive approximations utilizing analytic stress functions used to obtain solution for infinite plate with arbitrary holes under biaxial stresses

[ASME PAPER 68-PVP-1]

03 p0523 A69-12998

Grooved commercial Ti and Ti alloys mechanical properties under uniaxial static tension at low temperatures

03 p0443 A69-13028

Photoviscoelastic stress analysis to predict time dependent stress redistributions in polyphase system with viscoelastic binder under external loading conditions

03 p0524 A69-13061

Performance prediction by testing, considering stress analysis, temperature, multiaxial stresses, combined stress, corrosion, shock, etc

03 p0525 A69-13307

Grain boundary sliding influence on gross mechanical behavior and stress distributions, emphasizing creep behavior

03 p0450 A69-13882

Graphical representation of stress distributions and forces on dislocations

03 p0529 A69-13973

Helicoidally symmetrical stress in cylindrical thin shells

03 p0529 A69-14056

Tangential and normal stress distribution in deformed metals, discussing work hardening of metals and cold working without softening effect

03 p0435 A69-14118

Stress distribution near circular hole in elastic layer

04 p0667 A69-14266

Stress concentration near arbitrary hole, assuming small deformations and physical nonlinearities

04 p0667 A69-14268

Computer method calculating stressed state of elliptical bottom of cylindrical pressure vessel based on differential bending equations for shell of revolution

04 p0668 A69-14275

Elastic ring subject to uniform hydraulic pressure on inner boundary and with two opposite slipless quarter-arcs on outer boundary, noting stress and deformation

[ASME PAPER 68-WA/APM-17]

04 p0669 A69-14395

Axisymmetric stress field around spheroidal inclusions and cavities in transversely isotropic material

[ASME PAPER 68-WA/APM-14]

04 p0669 A69-14400

Dynamic pressure pulse over band on solid elastic cylinder surface, analyzing time stress distribution throughout elastic cylinder

04 p0670 A69-14408

Resistance wire strain gages for measuring elastoplastic deformations in zones with high stress concentrations of strained machine elements

04 p0671 A69-14433

Dead-end microcracks stress fields, studying positive /tensile/ and negative /compressive/ nature dependence on crack size

04 p0674 A69-14548

Mechanical properties and stress concentration sensitivity of structural alloys at low temperature
04 p0614 A69-14574

Stress field for skew hole determined from plane stress field for equivalent right hole, considering elastic plate penetrated by oblique circular cylinder
04 p0674 A69-14589

Circular cylindrical shell creep behavior and buckling under axial compression and internal pressure, using multimembrane model
[AIAA PAPER 68-108] 04 p0676 A69-14706

Creep stress concentration at circular hole in thin sheets under loads in own plane, discussing infinite thin plates
[AIAA PAPER 68-175] 04 p0676 A69-14708

Equilibrium and compatibility equations for axisymmetric stress distribution in finite length anisotropic elastic cylinder reduced to single integrodifferential equation
04 p0676 A69-14709

Plate thickness effect on bending of elastic plate with crack, investigating stress distribution
04 p0678 A69-14890

Stress concentration around centrally placed circular bolt in axially loaded bar, using theory of infinite systems of linear equations
04 p0681 A69-15195

Stress-strain rate relation under combined stress fields derived from Gilman relation between dislocation velocity and force for single dislocation
05 p0834 A69-15756

Plane thermal stress distribution determined around holes under steady temperature distribution, using complex variable approach
05 p0836 A69-15877

Course slip during cyclic deformation of copper single crystals, discussing strain bursts dependence on stress amplitude rate, unidirectional prestrain and orientation
05 p0779 A69-15905

Axisymmetric thermal stresses in spheroidal shell of arbitrary thickness due to thermoelastic strain nucleus
05 p0836 A69-15923

Tangential stress distribution and heat transfer in circular cylinder with attached wall jet
05 p0746 A69-16022

Elastic plastic stress distribution in compressed ring determined with postyield strain gages and stress-strain relationship from uniaxial tensile test
05 p0837 A69-16063

Velocity fields and wall shear stress distributions in eccentric annuli
[ASME PAPER 68-WA/FE-35] 05 p0750 A69-16108

Flow stress of iron wire reinforced aluminum alloy composites
[ASME PAPER 68-WA/MET-10] 05 p0780 A69-16150

Green function for computation of stress intensity factors for edge cracks in rectangular plates with arbitrary loadings
[ASME PAPER 68-WA/MET-18] 05 p0839 A69-16156

Green function for stress intensity factors of rectangular plate edge cracks, noting application to thermal stresses
[ASME PAPER 68-WA/MET-19] 05 p0839 A69-16157

Stress distribution and spring rates in cantilever cone ring combination
[ASME PAPER 68-WA/DE-3] 05 p0839 A69-16168

Circular inclusion effect on stresses around line crack in sheet under tension based on elasticity theory
05 p0841 A69-16432

Plastic yield on inclined slip planes at tip of crack deformed in antiplane strain
05 p0842 A69-16436

Plane problem of moment theory of elasticity for stress concentration near circular hole
05 p0842 A69-16502

Stress distribution in infinite strip with equally spaced identical semicircular notches on one edge and subject to transverse bending
05 p0842 A69-16643

Fatigue life reduction in Al alloy specimens with stress concentrations due to notches
05 p0843 A69-16696

Plastic yielding and strain distribution in Al reinforced with stainless steel wires determined by electron microscopy
06 p0940 A69-16947

Strain distribution at crack base measured by Fabry-Perot interferometer and photoelastic coating
06 p1020 A69-17127

Finite plane deformation of solid body, arbitrary deformation law and arbitrary hydrostatic stresses dependence on volume change solved by nonlinear equation
06 p1021 A69-17175

Stress concentration at circular hole in orthotropic cylindrical shell, using coordinates system and Bubnov-Galerkin method
06 p1021 A69-17180

Stress concentration at thermally insulated holes in elastic material created by disturbance of uniform heat flow at holes
06 p1021 A69-17184

Deformation and stresses in biaxially loaded stretched thin plate with central small hole during stress redistribution caused by creep
06 p1022 A69-17368

Iterative solution of integral equation and uniform convergence conditions of function sequence approximating incremental stress distribution in elastic-plastic structures
06 p1024 A69-17510

Two dimensional stress distribution changes around rectangular hole with rounded corners for varying internal pressure and temperature
06 p1025 A69-17611

Stress distribution in shallow spherical shell with smooth cornered rectangular hole or biperiodically arranged set of holes, using computer program
06 p1027 A69-18020

Geometrically exact finite element for thin shells of revolution, using approximation to predict boundary layer stress distribution during vibration
[AIAA PAPER 69-56] 06 p1029 A69-18193

Stresses and displacement around crack under various conditions using two dimensional elasticity theory, deriving complex potentials for various loading types
07 p1231 A69-18269

Ultrahigh strength steel susceptibility to brittle fracture, describing methods of testing rupture toughness and stress intensity factor
07 p1158 A69-18402

Laminated composite fracture statistical theory with stress enhancements in elements next to primary fracture, comparing elastic and plastic matrices
07 p1170 A69-18712

Stress concentration factors for composite body of two isotropic elastic phases in plane strain in plane of composite parameters
07 p1170 A69-18716

Fiber geometry and partial debonding effects on bond stress distributions around single rigid fiber in infinite elastic plate subject to tensile stress
07 p1170 A69-18717

Thermal stress concentrations in vicinity of cylindrical elastic inclusions embedded in elastic matrix, using displacement functions and photothermoelasticity
07 p1171 A69-18726

Plastic fractures of age hardened aluminum alloys analyzed by tensile tests and electron fractography, considering stresses, surface and intergranular effects
07 p1166 A69-18961

Steady state thermal stress distributions near external crack in solid, treating temperature distributions with respect to plane of crack
07 p1232 A69-19172

Grain size dependence of yield, flow and fracture stresses of Fe-Co-V alloy for 77-298 K
07 p1166 A69-19264

Strain concentration design factors for notch effect in low cycle fatigue and crack propagation conditions
07 p1235 A69-19383

Parameters interrelating time and temperature used to present creep-rupture data for Al alloys, providing direct readings of stresses
[ASM PAPER D8-9.7] 07 p1169 A69-19665

Critical analysis of Sedov contention of infinite stress development at ends of brittle cracks
07 p1238 A69-19690

Brittle fracture criterion for small steel specimens based on interaction between stress concentration of initial crack and nearby slip band
07 p1238 A69-19694

Breakdown regularity of metals having different crystal structure, considering metal lifetime dependence on stress magnitude and test temperature
08 p1328 A69-19793

Elastic springback and residual stress distribution in sheet metal formed by bending determined as function of radius sheet thickness and stress-strain characteristics
08 p1319 A69-20005

Amplitude dependent internal friction of materials under inhomogeneous strain, giving values for torsional, free longitudinal and transverse vibration modes
08 p1331 A69-20175

Couple stresses effect on thin plate stress distribution due to pressure of rivet on one side of circular hole
08 p1319 A69-20201

Two dimensional photoelasticity for minimizing stress concentration in perforated rectangular plate subjected to restrained shrinkage, discussing application to solid propellant rocket grains
08 p1412 A69-20255

Stress distribution around equal size holes at ends of crack for normal uniaxial tension, based on photoelastic and brittle lacquer technique
08 p1412 A69-20257

Elastic potential for obtaining localized strain theory, describing deformation characteristics of compressible and incompressible orthotropic materials with physical nonlinearity
08 p1412 A69-20328

Constructional HY steels for high stress critical welded structures, discussing fracture mechanics stress intensity factor
08 p1333 A69-20405

Dynamic stress intensity factor for axisymmetric loading of circular crack in infinite isotropic elastic medium
08 p1413 A69-20412

Stress fields in Hertzian contact of parallel cylinders composed of anisotropic materials and transversely isotropic spherical bodies
08 p1414 A69-20524

Transient thermal stress distribution in infinite orthotropic elastic cylinder of rectangular cross section in presence of heat sources
08 p1415 A69-20664

Elastic cone stresses due to axial force at point on axis, solving problem in terms of convergent integrals
08 p1415 A69-20689

Matrix displacement method for nonlinear elastoplastic two or three dimensional structures or continua, discussing strain distribution
08 p1416 A69-20705

Monograph on plane problem and bending problem for infinite elastic plate with doubly periodic set of circular holes
08 p1416 A69-20709

Resonant frequencies, vibration modes and stress distributions for naturally vibrating plane wide blades of turbomachines
08 p1376 A69-20764

Compatibility theorem extension to three dimensional rigid plastic bodies with stress and velocity discontinuities, noting isotropic bodies with convex yield surface
08 p1418 A69-20845

Plane and three dimensional stress concentration studies involving asymmetrical stress tensors, noting contributions to moment theory of elasticity
08 p1419 A69-21177

Axisymmetric elastoplastic bending theory for cylindrical shell by applying Saint Venant plasticity conditions, determining stress distribution
08 p1419 A69-21179

Displacements and stress intensity as function of crack length for compact tension specimen, considering load line and crack edge
09 p1503 A69-21392

Stress-strain distribution in rotor wheel with radial side blades, giving differential equations system for circular disk strains
09 p1612 A69-21494

Three dimensional vibration analysis of circular homogeneous elastic cylinder, obtaining differential equations and zero stress conditions
09 p1612 A69-21601

Stress concentration at circular hole in infinite plate for large strains and nonlinearity, analyzed by integral operator method
09 p1613 A69-21629

Radial and tangential stresses in double glass fiber assuming different Poisson coefficients, determining conditions for axial stress redistribution prevention
09 p1614 A69-21741

Asymptotic two dimensional moment theory of elasticity, analyzing stress concentration at curvilinear holes and fluctuating boundary loads
09 p1614 A69-21884

Error estimates of stress concentration at free hole determined by two dimensional elasticity theory of thick plates
09 p1614 A69-21885

Green function type solutions of shell equations by small parameter technique for case of free terms consisting of Dirac delta function
09 p1614 A69-21886

- Stress formulation of thermoelasticity in simply connected body, noting uniform temperature change influence on stress components 09 p1617 A69-22007
- Plastic strain intensity distribution in aluminum alloy specimen with central hole measured with marked orthogonal lattice 09 p1617 A69-22221
- Plane thermal stress field in discontinuous temperature distribution within isotropic linear elastic circular cylinder of infinite length 10 p1793 A69-22884
- Crack stability under mechanical and thermal stresses, noting critical tensile stress and thermal insulating character of crack 10 p1794 A69-22890
- Liquid crystal coatings for determining fracture initiation flaws in material structures, considering stress concentration and hysteresis heating 10 p1699 A69-23053
- Crack propagation velocity in titanium alloys over varying stress intensities under adverse environment 10 p1709 A69-23058
- Nonwork hardening elastic plastic material fracture criteria for antiplane strain, noting plastic zone shape effect on zone size and crack opening 10 p1795 A69-23064
- Fatigue crack propagation in cylindrical shells under fluctuating internal pressure, considering stress intensity factor 10 p1795 A69-23066
- Buckling deformation and stress fields around central slits in photoelastic models and metal sheets under tensile load 10 p1796 A69-23069
- Fatigue crack propagation and crack tip stresses measurements in tensioned cracked panels subjected to acoustic loading 10 p1797 A69-23078
- Stress intensity magnification factors in surface flawed tension plates and notched round tension bars, evaluating fracture toughness 10 p1797 A69-23080
- Low cycle fatigue of metals under biaxial strain, considering specimen life and strain amplitude correlation 10 p1797 A69-23083
- Couple-stresses and singular stress concentrations in elastic solids with locally unbounded deformations and stress reduction around hole 10 p1798 A69-23149
- Stress concentration in Cosserat continua based on model of six elastic constants in linear isotropic and notch case 10 p1799 A69-23150
- Continuum theory of dislocations and plasticity in crystals, analyzing stress fields in elastoplastic materials 10 p1799 A69-23154
- Couple stresses effect on distribution of stresses in elastic solid due to crack analyzed on basis of Cosserat theory 10 p1800 A69-23242
- Creep of high purity Nb-Mo alloys in 800-1300 C range and at 1500-13000 lb/square inch stresses, giving activation energy for creep 10 p1711 A69-23375
- Notched members fatigue life prediction from smooth specimen fatigue data and Neuber rule application 10 p1715 A69-23984
- Rubber modified thermoplastics structure and mechanical properties, emphasizing stress concentration around composite particles and crazing role in creep and fracture 10 p1716 A69-23985
- Fatigue growth of disk shaped crack in infinite body, noting dependence on fourth power of stress intensity factor 10 p1802 A69-24028
- Modified Rayleigh-Ritz method for prediction of stress concentration in elastostatic problems for elastic continua, noting plate bending 11 p1969 A69-24413
- Soviet collection of papers on stress concentration, Number 2 11 p1970 A69-24645
- Moment stresses effect on stress concentration in plates with common type hole, considering uniaxial and triaxial bending and torsion 11 p1971 A69-24646
- Stress concentration during deformations in thin shallow shells, using conformal mapping and difference method 11 p1971 A69-24648
- Elastic waves propagation in inhomogeneous composite media, considering coefficient of structural stress concentration 11 p1972 A69-24649
- Stress concentration analysis of interactions between stress raisers and cross section changes, considering asymptotic expansion method 11 p1972 A69-24650
- Elastic isotropic half plane weakened by circular hole with concentrated force applied along hole contour, considering stress distribution 11 p1972 A69-24653
- Stress distribution around holes in thin shells and plates during large elastic displacements, considering hole size, loading and shallow spherical shells 11 p1972 A69-24654
- Stress concentration in isotropic plates weakened by curvilinear holes subjected to loading at infinity, noting curvature at corner points of holes 11 p1972 A69-24655
- Semibrittle material decompaction influence on stress distribution in infinite plate with edge loaded circular hole, noting stress-strain relation nonlinearities 11 p1972 A69-24656
- Limiting equilibrium of plate weakened by curvilinear hole stress raiser with one or two cusps, obtaining stress-strain diagrams 11 p1973 A69-24658
- Two dimensional contained plastic deformation in asymmetrical elasticity theory based on Cosserat medium, examining boundary value problems, stress concentration and elastic wave propagation at holes 11 p1973 A69-24659
- Nonlinear elasticity theories emphasizing quadratic approximation of stress concentration 11 p1973 A69-24660
- Two dimensional problems solutions by contour smoothing methods, considering stress concentrations in reinforced or perforated thin elastic plates 11 p1973 A69-24661
- Stress concentration at holes and cavities in thin elastic shells under static and dynamic loads, considering physical nonlinearities of material 11 p1974 A69-24665
- Mathematical theory of equilibrium cracks in stressed bodies with minimum loading for crack extension, analyzing crack tip zone and force transmission 11 p1974 A69-24668
- Stress concentrations in physically nonlinear multiply connected elastic media, discussing rods, thin plates and bodies with cavities 11 p1976 A69-24783
- Stress concentrations in bending of thin perforated plates, considering potential and vortex stresses due to edge effect 11 p1976 A69-24784
- Time scales for creep stress redistribution in structures subject to step loading 11 p1980 A69-24879
- Three dimensional theory of elasticity for finite hollow cylinder under axisymmetric deformation, considering stress and pressure distribution over surface 11 p1983 A69-25022
- Stress concentration around curvilinear holes in three layer spherical and cylindrical isotropic shells with hard and soft fillers under external loads 11 p1984 A69-25171
- Flat bar optimal cross section under tensile stress applied to minimize stress in large structural components using elasticity theory 11 p1986 A69-25203
- Indentation of inhomogeneous rigid plastic solid by flat punch under plane strain conditions analyzed by perturbation method 11 p1986 A69-25244
- Bending of half strip rigidly fastened along short edge, constructing integral equation for normal stress at clamping, investigating corners singularities 11 p1996 A69-25734
- Axisymmetric problem of stress in elastic space weakened by plane annular slit solved by asymptotic method in terms of equations for parameter lambda 11 p1996 A69-25735
- Inclination effect of fatigue cracks on plane strain fracture toughness of 7075-T651 Al alloy, discussing cantilever bending 12 p2177 A69-25958
- Stress concentration near circular hole in plate during bending, showing dependence on material constant 12 p2178 A69-25999
- Stress concentration around square hole in celluloid plate subjected to creep under biaxial tension analyzed by photocreep method 12 p2178 A69-26000
- High speed deformation of metals under pulse loading, noting role of maximum stress magnitude and deformation characteristics 12 p2113 A69-26043
- Thermal stresses induced in plate plane by temperature gradient varying in space and time calculated using Mach-Zehnder interferometer, determining stress intensity factors 12 p2089 A69-26189
- Stress distribution in elements of unidirectionally fiber reinforced composite materials analyzed as function of fiber content and fiber-matrix elastic properties 12 p2180 A69-26263
- Elastic stress created by perpetual motion of isotropic elastic solid in static space-time 12 p2130 A69-26283
- Symmetrical stressed state of shallow shell with crack edge loading solved in Cartesian coordinates 12 p2181 A69-26614
- Orthotropic properties and stress fields for configurations of fiber or whisker reinforced composite materials subjected to nonaxial loading, considering infinite elastic matrix 12 p2186 A69-26824
- Accelerated structural tests under creep conditions, noting isothermal structures subjected to uniaxial and complex stress loads 12 p2186 A69-26838
- Fatigue crack propagation laws determined by material yielding at crack tips, stress intensity and exponential crack growth law 12 p2187 A69-26846
- Correlation between temperature and stress field in thermal buckling of square viscoelastic Maxwell plates under random temperature 12 p2188 A69-27113
- Stress distribution in matrix of unidirectionally fiber reinforced composite subject to shrinkage and normal transverse load, using three dimensional photoelastic analysis 12 p2189 A69-27162
- Crack opening displacements of stationary and running cracks and of inclined stationary cracks in centrally notched plates, noting normal strain fields 12 p2189 A69-27163
- Fracture and equilibrium position of dislocations in discrete and continuously distributed dislocations arrays including stress due to crack, energy considerations and crack initiation 13 p2358 A69-27222
- Stress distributions in two normally intersecting cylindrical shells subjected to internal pressure, using Donnell and Flugge equations 13 p2359 A69-27255
- Natural stress concept for analysis of nonhomogeneous strains fields exhibiting geometrical nonlinearity 13 p2359 A69-27259
- Membrane and bending stresses around elliptic hole in thin circular cylindrical shell, considering axial tension [NAL-TN-13] 13 p2362 A69-28123
- Stress and displacement fields for uniaxially loaded infinite elastic continua with doubly periodic array of holes and inclusions, using finite element method 13 p2363 A69-28133
- Induced stressing method for complex castings by controlled cooling during heat treatment applied to front frame of J-79 turbojet engine 13 p2269 A69-28184
- Stresses in infinite solid elastic circular cylinder due to rotating line source of heat 13 p2364 A69-28206
- Dynamic stresses in case bonded cylinder due to transient angular accelerations, presenting numerical results for incompressible elastic cylinder 13 p2364 A69-28209
- Discrete element plastic analysis of long prismatic bars under transverse loading in longitudinal direction, based on matrix displacement method 13 p2365 A69-28237
- Stressed state of cylindrical circular shell clamped at edges and subjected to concentrated radial forces 13 p2368 A69-28322
- Variational principle based on assumed stress hybrid method suitable for finite element analysis of incompressible solids 13 p2368 A69-28348
- Variational principle and convergence of finite element method based on stress distribution 13 p2368 A69-28349
- Couple stresses effect on dynamic stress concentrations, considering elastic compressional wave diffraction by cylindrical discontinuity 13 p2369 A69-28351

Stress intensity for Griffith crack with asymmetrical distribution of surface tractions
13 p2369 A69-28352

End loaded two layer laminated elastic strip stress concentration and self equilibrating traction distribution analyzed by eigenvalue equation
13 p2370 A69-28672

Shrinkage stresses in two phase materials, analyzing stress distribution in epoxy inclusions in plasticized matrix during curing by photoelastic method
13 p2371 A69-28675

Contact problem for half plane with elastic stiffener reduced to Prandtl integrodifferential equation, determining contact stresses
14 p2531 A69-28804

Three dimensional equations of elasticity reduced to two dimensional equations of shell theory, discussing stressed states of thin elastic bodies
14 p2531 A69-28807

Infinite cylindrical shell stability under circular load solved by linearization about bending moment stress state and Galerkin method
14 p2531 A69-28808

Boundary layer equation of viscous incompressible fluid with moment stresses, noting flow around thin plate and submerged jet problems
14 p2428 A69-28815

High speed rotating disks design and stress analysis [ASME PAPER 69-DE-1]
14 p2453 A69-28838

Stress and strain fields for circular rubber ring under diametrical compression between flat plates, using moire, large strain analysis and photoelastic verification
14 p2531 A69-28884

Stress concentration around holes in thin shells, including analysis of stress-strain state in cylindrical and spherical shells
14 p2532 A69-28977

Plasticity theory approximation variants for complex loading, analyzing strain trajectories using Prandtl-Reiss theory
14 p2532 A69-28978

Thermoelastic stress-strain state of infinite circular cylindrical shell with elasticity modulus temperature dependence expressed by exponential function
14 p2532 A69-28980

Stress concentration around rhombic hole in non-linear isotropic plate under pure shear
14 p2533 A69-28987

Axisymmetric impact of circular cylindrical plates, obtaining two dimensional dynamic stress distributions for materials of linear elastic compressibility and plastic behavior in shear
14 p2534 A69-29027

Book on fatigue strength in construction covering structural strength and stability, load design, metal physical properties, elasticity and plasticity theories, stress concentration, strain buildup, etc
14 p2534 A69-29333

Convective instability by active stress, discussing composition dependent stress fields in continuous and mechanically isolated material and chemical to kinetic energy conversion
14 p2540 A69-29634

Creep strain rate and stress distribution of thick walled cylinders under internal pressure at elevated temperature, using variational principle
15 p2703 A69-30070

Differential equations for elastic stress distribution in thin rotating shell with arbitrary profile, obtaining analytical dimensionless solutions for potential profiles
15 p2703 A69-30158

Mechanical properties and stress concentration sensitivity of structural alloys at low temperature
15 p2638 A69-30275

Longitudinal internal cracks in deformed Al alloys initiated by elastic stress concentration in areas of highest flow rate gradient
15 p2638 A69-30277

Box girders stress distribution analyzed by stress-freezing method compared with photoelastic measurement
15 p2705 A69-30419

Elastoplastic matrix for stress increments for yield surfaces with associated flow rule, considering initial stress computation
15 p2706 A69-30433

Structural strength calculations, considering micro and macro stress distributions
15 p2706 A69-30447

Stress concentration near circular nonreinforced hole at bending of transversely isotropic rectangular plate analyzed in terms of transverse shear theory
15 p2707 A69-30580

Couple-stresses effect on stress concentration of plate containing infinite row of holes, solving linear elastic problem in isotropic Cosserat continua for plate
15 p2708 A69-30640

Three dimensional problem in crack theory for brittle body, determining stress concentration and critical loads
15 p2708 A69-30658

Plastic strains at crack tips in thin plate under concentrated forces, analyzing slip bands during initial deformation
15 p2708 A69-30659

Automated shear difference analysis of three dimensional photoelastic model stress distribution by stress-freezing and slicing technique
15 p2609 A69-30680

Initial comparisons between theory and experiment of strain fields in cracked copper plate
15 p2640 A69-30810

Plane strain and stress compared for elastoplastic cracked plate in work hardening tension
15 p2710 A69-30811

Reaction rate theory for dilatational failure of heterogeneous materials subjected to stress
15 p2710 A69-30813

Stiffness matrix of polygonal finite plate bending element derived using assumed stress distribution
15 p2710 A69-30867

Repeated static stress limit of internal pressure vessels, emphasizing effect of redistribution of stresses and strains
15 p2712 A69-30973

Stress distribution in isotropic spherical shell rotating uniformly about diametral axis, deriving equilibrium equations
15 p2712 A69-31005

Expression derived for arbitrary system subjected to external loading, using Cauchy equations for relationship between external plane forces and internal stresses
15 p2713 A69-31018

Stress concentration on circular holes and notches in anisotropic oriented glass fiber reinforced plastics determined by using photoelastic birefringent coatings
15 p2713 A69-31053

Thermal stresses in circular cylinder with regularly distributed cavities, establishing distribution laws for temperatures and stresses
15 p2714 A69-31196

Photothermoelastic analysis of thermal stresses in turbine wheels with welded blades, noting stress concentration reduction
15 p2715 A69-31488

Flexure of Ta and Nb thin rectangular specimens during high temperature oxidation, showing stress generation due to O dissolution into metal surface [ECS PAPER 87]
15 p2641 A69-31541

Equilibrium equations for elastic medium with stress couples, presenting first term of asymptotic expansion of solution for disk and simply connected region
16 p2871 A69-31830

Stresses due to nucleus of thermoelastic strain in infinite elastic solid with two rigid circular inserts
16 p2872 A69-31906

Stresses in perforated ribbed cylindrical shell subjected to internal pressure using brittle coating, electrical strain gages, photoelasticity and micrometers
16 p2876 A69-32784

Free-free transverse vibration damping phenomena, calculating strain amplitude dependence of internal friction at various frequencies
17 p3051 A69-32961

Photoelasticity testing of stress gradient factor on notched tensile specimens
17 p3052 A69-32982

Stress-strain state analysis for brittle plate with circular holes of equal radius performed in cylindrical system of coordinates
17 p3055 A69-33127

Transverse bending of asymmetric sandwich plates with rigid filler taking into account stresses and strains in filler
17 p3055 A69-33129

Stress distribution in variable rigidity reinforcing frame of circular cylindrical shell using strain energy method
17 p3055 A69-33131

Critical loads and stability loss forms of annular plates flexibly clamped at edges in uniform stress field
17 p3057 A69-33197

Elastic stresses in rotating anisotropic disks with constant thickness, discussing solid, circular rigid shaft mounted and center drilled disks
17 p3067 A69-34138

Craze formation and shear yielding considered for glassy polymers in terms of stress field requirements
17 p2993 A69-34169

Temperature dependence of metal elastic properties including thermal strains effect on stress field, yielding stress changes and elastic modulus variations
18 p3212 A69-34338

Stress field in elastic contact area vicinity of hollow sphere subjected to normal load through flat plate, noting contact life [ASME PAPER 69-LUBS-5]
18 p3212 A69-34338

Displacement bounding principle for work hardening plasticity theory based on Drucker inequality and stress space path existence [ASME PAPER 69-APM-7]
18 p3213 A69-34385

Nonlinear equations for elastic strain of circular-toroidal membrane shell under uniform pressure, computing stress and displacement fields
18 p3216 A69-34575

Ponderable annular region under symmetrically applied concentrated forces, obtaining solution for stress state by successive approximations
18 p3216 A69-34577

Growth rate of stability loss intrinsic modes in elastic shells under severe load, discussing stress distribution during buckling
18 p3217 A69-34598

Positive Gaussian curvature shell under concentrated forces, analyzing stresses and strains relation to load distance using Thompson and Legendre functions
18 p3218 A69-34601

Quadratic programming method for equations of elastic perfectly plastic solid applied to stress distribution in plate torsion and bending
18 p3218 A69-34661

Lightweight structural design problem of stress concentration associated with load diffusion in rectangular panels with constant stress flanges
18 p3219 A69-34785

Wing elastic strains effect on vertical velocity in downwash, noting wing tail combination
18 p3086 A69-34999

Stochastic failure models based on stress peak distributions, including randomly deteriorating strength model and increasing hazard reliability functions
18 p3148 A69-35079

Crack analysis in stiffened vibrating plate based on dynamic stress distribution, showing high bending stresses at intersection
18 p3223 A69-35168

Stress-strain state of open cylindrical shells with arbitrary cross section determined for clamped-clamped, clamped-free and free-free supported shells
18 p3225 A69-35372

Free oscillations of rigidly clamped circular plate carrying concentrated masses, deriving frequency equation and value of lower roots
18 p3226 A69-35377

Fatigue fracture due to heat generation in polycarbonate subjected to pulsating tensile load, presenting temperature change per unit stress increase
18 p3163 A69-35498

Fatigue characteristics of Al alloys by fatigue tests with complex stress patterns, finding secondary stress wave effects
19 p3342 A69-35712

Iterative algorithm applied to shell theory boundary value problem of stress concentrations at shallow shell holes
19 p3436 A69-35847

Two dimensional thermoelasticity problem for nonlinear media, obtaining solutions for thermal stress concentration and boundary value problems
19 p3436 A69-35848

Hollow cylinder plane stress-strain state analyzed for effect of variable modulus of elasticity of cylinder material
19 p3436 A69-35858

Nondestructive test method using transducer action of flaw in stress field causing plastic deformation with energy release as acoustic emission
19 p3314 A69-36634

Autocorrelation function for unsteady temperature and stress fields in bar located in gas stream leaving combustion chamber
19 p3440 A69-36685

Limiting equilibrium stress state of unbounded brittle body with elliptical crack under monotonically increasing tensile or compression load, noting influence of crack curvature
19 p3441 A69-36745

- Electroplating method for local stress concentrations determination, discussing measurement techniques, metal fatigue failure prediction, etc
19 p3441 A69-36751
- Micell type optimum fiber arrangement for transferring torque across annulus, considering single straight, double and multiple annular arrays under single load system
19 p3447 A69-36851
- Stress distribution in tension specimen notched on one edge obtained photoelastically for several notch depth to specimen width ratios, noting Neuber theory agreement
19 p3447 A69-36859
- Stress and strain concentration factors under initial stages of elastoplastic deformation for circular hole in infinite medium, using method of successive approximation
19 p3447 A69-36860
- Primary and tertiary uniaxial creep strain rate changes based on internal stress redistribution described with mathematical model
20 p3619 A69-36941
- Fractography of compact fracture toughness specimens failure, noting stress at fracture origin and crack growth rate
20 p3557 A69-36957
- Linearization of relationship between stress concentration factor and reciprocal of strain hardening exponent enabling shakedown to pressure vessels formulated by mathematical model
20 p3620 A69-37002
- Grade three strain-gradient elastic materials, deriving general solution to linearized field equations
20 p3621 A69-37073
- Stress distribution in finite and semifinite solid cylinders under end normal load, using Fourier-Bessel series
20 p3621 A69-37199
- Thermal stress concentration near elliptical hole in thin walled liquid filled cylindrical shell in presence of temperature gradient across shell cross section
20 p3622 A69-37325
- Residual tensile stress distribution during plasma spraying determined as function of temperature field in blank
20 p3548 A69-37328
- Axially symmetric distribution of residual strain in multilayered filament wound ring analyzed and compared with experimental results
20 p3628 A69-37774
- Transient thermal stresses in heat treated elastic-perfectly plastic disks with temperature dependent yield stress, considering stress distribution sequence and residual stresses
20 p3629 A69-37974
- Fatigue crack initiation in relation to contact stresses due to fretting, studying causes of strength reduction and crack inclination to surface
20 p3563 A69-38110
- Mean stresses effects on fatigue crack initiation and propagation under controlled fretting slip amplitude
20 p3563 A69-38111
- Radial and tangential stresses in double glass fiber assuming different Poisson coefficients, determining conditions for axial stress redistribution prevention
20 p3630 A69-38217
- Stress concentration near holes in three layer spherical shells, determining boundary conditions at hole perimeters for various loads
21 p3833 A69-38570
- Thermal stress distribution induced in wedge by apex heat source analyzed using elasticity theory, considering lateral surface heat transfer
21 p3833 A69-38644
- Flow stress temperature dependence of Ni-Cr-Al alloys consisting of gamma prime dispersion in Ni base solid solution
21 p3744 A69-38738
- Stress concentration and surface strain hardening effects on fatigue strength of refractory alloy specimens with and without cut
21 p3745 A69-38875
- Steady motion of frictionless indenters along surface of elastic layer in plane strain, using Fourier transform and Fredholm equations for numerical solution
21 p3837 A69-39155
- Solution procedure for torus with given surface loads or displacements, using series expansion of generalized analytical functions, discussing stress concentration near toroidal cavity
21 p3839 A69-39192
- Stability of unbounded homogeneous brittle body containing circular planform crack, determining elastic stresses and critical load by macrocrack propagation theory
21 p3839 A69-39195
- Levy-Mises equations for ideal plastic material derived from relationship between stress and rate of deformation tensors
21 p3840 A69-39287
- Dynamic stress concentrations and rigid body response of cylinder imbedded in elastic medium subjected to compressional wave
21 p3840 A69-39300
- Finite element relaxation method for computing stress distribution in thin walled structure, considering computer program, storage and solving time
21 p3843 A69-39313
- Creep accumulation under time varying stress of Al alloy sheet, using creep recovery analysis to determine anelastic strain growth
21 p3747 A69-39323
- Strain distribution on surface of adhesive bonded box beam in simple bending, using water based brittle coating and self adhesive strain gages
21 p3844 A69-39325
- Stress concentrations in metals determined through surface properties measurements, correlating local electrochemical potentials and metal-metal oxide junction parameters
21 p3747 A69-39326
- Fringe multiplication techniques for moire fringe arrays of inhomogeneous strain fields
21 p3845 A69-39328
- Corrosion and stress effects separation in stress corrosion of Al-Zn-Mg-Cu alloy, considering machined surface finishing role
21 p3747 A69-39435
- Fracture strength of glass fiber-reinforced cylinders made by unidirectional filament winding predicted by analyzing three dimensional stress distributions
21 p3846 A69-39795
- Cosserat theory on couple stresses applied to stress distribution in semiinfinite plate, using Fourier transform method
22 p4038 A69-39902
- Strain anisotropy matrices behavior along strain trajectories of arbitrary curvature, studying matrices and elastic constants dependence
22 p4039 A69-39914
- Strain anisotropy matrix construction for various strain trajectories from elastic properties of expression relating stress and elastic strain deviators
22 p4039 A69-39915
- Intersection plane stresses in internally pressurized cylindrical shells joined over elliptic face
22 p4040 A69-39978
- Stress concentration in elastic plate reinforced at edge by straight rib analyzed in finite form by Cauchy integrals and Fourier transforms
22 p4041 A69-40114
- Stress distribution on surface of stator vane loaded statically as cantilever derived by brittle coatings, strain gages and three dimensional photoelasticity
22 p4042 A69-40310
- Radial and tangential stress analysis of rotating disk during steady state creep, using equations solved by finite difference method
22 p4043 A69-40458
- Supersonic panel flutter boundary of buckled and unbuckled clamped rectangular plates, discussing in-plane stress effects
22 p3930 A69-40584
- Photoelastic technique of stress-freezing and slicing to determine bending stresses in transversely loaded plate supported at corners
22 p4045 A69-40900
- Strain induced creep equation for hardened materials for fixed temperature and stresses range, noting application to steel and Al alloys
22 p3971 A69-41033
- Meridional crack problem for cylindrical and spherical shells solved for uniform membrane load and bending moment, obtaining stress intensity components
22 p4046 A69-41041
- Yield condition and relation between stresses and strain rates for anisotropic body, allowing for influence of stressed state type
22 p3934 A69-41169
- Fittings stress distribution determined for optimization of material utilization
23 p4169 A69-41418
- Mounting elements alloys relaxation characteristics at various temperatures, considering effects of scale factor and stress concentrations
23 p4169 A69-41419
- Stress concentrations in circular plate with square hole subject to triaxial tension
23 p4227 A69-41712
- Stress concentration in shallow spherical perforated shell under loads, reducing boundary value problem to infinite algebraic equations solution
23 p4233 A69-42342
- Traction stresses distribution over contact surfaces using photoelastic frozen stress model
23 p4235 A69-42461
- Notch effect on corrosion fatigue behavior of high strength Al alloy under bending and direct stresses
24 p4330 A69-42553
- Local stress distribution in cylindrical shells at concentrated load area solved by shallow shell theory
24 p4395 A69-42593
- Eigenfunction expansion technique to analyze three dimensional crack and wedge problems, emphasizing stress field near straight edged crack
24 p4395 A69-42641
- Photothermoelastic investigation of thermal stress concentrations around circular cavities and inclusions in two dimensional composite models
24 p4396 A69-42739
- Interlaminar shear stresses in cross-plyed three ply symmetric laminated composite plate, analyzing interlaminar stress distribution under simple tension
24 p4399 A69-43052
- Contact stress distribution between two two-dimensional finite nearly rectangular elastic bodies with general surface configurations for surface load expressed in trigonometric series [ASME PAPER 69-APMW-9]
24 p4402 A69-43104

STRESS CORROSION

- Titanium alloy stress corrosion behavior in atmospheric salt environments at elevated temperatures related to aircraft engine part failures
01 p0099 A69-11056
- Atmospheric stress corrosion tests of aluminum alloys in various environments, comparing aging results with accelerated laboratory tests
01 p0100 A69-11352
- Welding with aluminum-zinc-magnesium alloys, discussing stress corrosion, embrittlement, compositions, heat treatment, material production and fabrication
02 p0266 A69-12063
- Corrosion rates and stress corrosion cracking sensitivity of explosively shocked austenitic stainless steels
03 p0444 A69-13308
- Surface preparation effect on stress corrosion cracking of type 310 stainless steel wires in boiling aqueous magnesium chloride solutions
03 p0444 A69-13311
- Salt water stress corrosion cracks morphology in titanium alloy, discussing crack propagation, brittle nature and chloride contamination effect
03 p0444 A69-13458
- Brittle surface films role in stress-corrosion phenomena in various environments
03 p0448 A69-13873
- Consumable electrode vacuum melted steels, discussing ausforming and stress corrosion cracking
04 p0604 A69-14528
- Heat treatment effects on stress corrosion cracking resistance of Al-Zn-Mg alloys, using cantilever loading in aqueous solution
04 p0617 A69-14933
- Stress corrosion crack initiation in aluminum alloy observed by optical microscopy
06 p0944 A69-17855
- Electrochemical kinetic and mass transport model for studying stress corrosion crack propagation in Ti [ECS PAPER 147]
08 p1332 A69-20359
- Grain morphology and preferred orientation effects on direction and propagation of stress corrosion cracking of aluminum alloy plate
09 p1521 A69-21399
- Crystallographic fracture path of stress corrosion cracks in austenitic stainless steels using scanning electron microscopy
09 p1522 A69-21486
- Stress corrosion of nonage-hardenable Al-Mg-Cr alloy investigated for failure in absence of grain boundary precipitate, using notched specimens
10 p1709 A69-23055
- Fracture surfaces of Ti and Ti-Sn alloys for stress corrosion cracking in methanol with HCl and in aqueous chloride solutions
10 p1710 A69-23085
- Transgranular stress corrosion crack propagation in thin sheet single phase magnesium-aluminum alloy
10 p1710 A69-23086

Stress corrosion cracking of Ti-6Al-4V alloy tensile tested in anhydrous methanol by electron fractography and diffraction, noting hydrogen embrittlement
11 p1903 A69-24576

Stress corrosion cracking of titanium alloys in contact with high temperature fuel tank sealants
12 p2112 A69-25945

Incipient stress corrosion damage detection in aluminum alloys, using Rayleigh wave attenuation
12 p2114 A69-26306

Microscopic mechanisms in fracture surface markings, using electron fractography cleavage, fatigue, stress corrosion cracking, microvoid coalescence and tear ridge formation
13 p2274 A69-27224

Structural modes of fracture, analyzing brittle, ductile, fatigue and stress corrosion fractures using fractography
13 p2274 A69-27226

High strength alloys stress corrosion cracks, analyzing tensile ligament instability from plastic flow tests of bulk/compression/specimens
13 p2277 A69-27404

Stress corrosion crack initiation and propagation in titanium alloy
13 p2282 A69-28165

Cleavage plane in stress corrosion cracking of alpha phase Ti-Al alloys
13 p2283 A69-28189

Stainless steels stress corrosion susceptibility, detecting chromium carbide in martensitic matrix by galvanic nondestructive test method
14 p2466 A69-29935

Stress corrosion preventative metal-pigmented paints for titanium alloys, discussing chemicals added to increase cathodic potential
14 p2469 A69-29936

Stress corrosion cracking prevention by shot peening, considering aircraft industry applications
14 p2466 A69-29937

Stress corrosion in smooth and prenotched maraging steels exposed to sodium chloride solution and natural sea water
14 p2467 A69-29940

Electrochemical test predicting stress corrosion performance of 2219 aluminum alloy in T851 and T87 tempers
16 p2798 A69-31716

Failure mechanism for intergranular stress corrosion cracking of vacuum annealed unalloyed Ti in alcohol iodine solutions
16 p2798 A69-31717

Stress corrosion resistance of AlZnMgCu and AlZnMg alloys, discussing combinations of alloy composition, heat treatment and stable precipitation conditions
16 p2800 A69-31779

Ti alloys commercial applications and properties, discussing alloying elements influence, deformability, weldability, stress corrosion and market trends
16 p2801 A69-31784

Stress corrosion cracks investigation by shear wave technique
16 p2876 A69-32334

Ti-Al base alloys brittleness and stress corrosion cracking, discussing diffusion mechanism, hydrogen mobility, dislocations, etc
17 p2987 A69-33372

Heat treatment effect on stress corrosion cracking of ternary Al-Zn-Mg alloys noting aging strength, solution temperature, quenching rate and alloy content
17 p2990 A69-33676

Ti-6Al-4V alloy general and stress corrosion behavior in Freon environments, discussing fracture mechanics
18 p3150 A69-35411

Be and BeAl alloy stress corrosion behavior in aqueous NaCl solution, discussing metallography and electron fractography
19 p3341 A69-35572

Cyclic stress frequency on mild steel corrosion fatigue tests, showing strength dependence on potential and stress current
19 p3342 A69-35775

High strength titanium alloys subcritical stress corrosion crack propagation, studying stress and environment effects on cleavage mode
19 p3343 A69-35922

Stress corrosion cracking - Conference, Columbus, Ohio, September 1967
19 p3347 A69-36883

Stress corrosion cracking research, history, engineering and education, incorporating stress corrosion data in mechanical design, terminology and nomenclature
19 p3348 A69-36884

Stress corrosion cracking of metals related to surface phenomena involving surface reaction layer ruptures or selective electrochemical dissolution along defects
19 p3349 A69-36885

Dislocation effects on stress corrosion of metals, discussing behavior of porous structure and metal/corrosion film interface under applied stress
19 p3349 A69-36886

Stress corrosion cracking mechanisms in liquid-solid metal combinations and solvent exposed plastics, discussing adsorption processes and cathodic polarization inhibition
19 p3349 A69-36887

Linear-elastic fracture mechanics applied to environment enhanced crack growth/stress corrosion cracking/
19 p3349 A69-36888

Interface electron transport phenomena in stress corrosion, expressing defect movements in terms of electron energy dynamics
19 p3349 A69-36889

Stress corrosion cracking of stainless steels and Incoloy and Inconel alloys in chloride, caustic, oxygenated and miscellaneous environments
19 p3349 A69-36890

Fracture surfaces of stress corrosion cracks in Fe-Cr-Ni alloys studied by electron microfractography, noting cleavage fracture
19 p3350 A69-36891

Stress corrosion cracking in stainless steel foils correlated with stacking fault energy and ordering, emphasizing environmental forming tendencies
19 p3350 A69-36892

Crack growth in steel tested in hydrogenated condition, distilled water and in combination by acoustic emission, relating time intervals to hydrogen diffusion
19 p3350 A69-36893

Hydrogen embrittlement mechanism in steel based on modified pressure theory, discussing crack propagation mechanisms and stress corrosion cracking
19 p3350 A69-36894

Stress corrosion cracking mechanism in Al alloys, discussing requisites for stress corrosion cracking
19 p3350 A69-36895

Aluminum 7 percent Mg alloys stress corrosion cracking, presenting aging kinetics and depletion zone dislocations at grain boundaries
19 p3350 A69-36896

Stress corrosion cracking model for 7075 Al, correlating macroscopic yield stress and corrosion time to failure
19 p3351 A69-36897

Precipitation hardening, microstructure and dislocation influence on intergranular stress corrosion cracking /SCC/ of high strength Al alloys examined by transmission electron microscopy
19 p3351 A69-36898

Electrochemical analysis of stress corrosion cracking in Al-Zn-Mg alloy, noting oxide film growth at grain boundary
19 p3351 A69-36899

Ti and Ti alloys stress corrosion cracking, discussing metallurgical and environmental factors
19 p3351 A69-36900

Titanium alloys stress corrosion cracking in presence of chloride, bromide and iodide under potentiostatic conditions, postulating electrochemical kinetic and mass transport model
19 p3351 A69-36901

Titanium alloys stress corrosion cracking /SCC/ from metallurgical-mechanical viewpoint, discussing phase transformations, dislocation arrangements, crack propagation, etc
19 p3352 A69-36902

Metallographic analysis of stress corrosion cracking of Ti alloys of Al and Sn in aqueous magnesium chloride solutions, noting cleavage process
19 p3352 A69-36903

Moisture and hydrogen role in hot chloride salt stress corrosion cracking of Ti alloys by radiotracer technique and mass spectrography
19 p3352 A69-36904

Titanium alloys hot salt stress corrosion cracking, studying effects of chlorides and surface oxides
19 p3352 A69-36905

Stress corrosion cracking of alpha Ti in liquid nitrogen tetroxide and various methanol environments, considering failure mechanisms
19 p3352 A69-36906

Ti alloy stress corrosion susceptibility in salt water, alcohols and alkanes, comparing stress intensity for crack propagation in dry air
19 p3353 A69-36907

Singular factors affecting stress corrosion cracking resistance of Ti alloys in salt water and hot salt, finding immune single phase alloys
19 p3353 A69-36908

Alpha and alpha plus beta Ti alloys analyzed to relate phase composition and microstructure to stress corrosion cracking in NaCl solution
20 p3557 A69-36961

Seam welded Al alloy aircraft structure fabrication problems, emphasizing stress corrosion
[SBAC PAPER 5]
20 p3550 A69-37454

Design and processing tradeoffs for preventing stress corrosion cracking in Al alloy aircraft structural forgings
[ASM PAPER W9-14.4]
21 p3729 A69-38655

Stress corrosion cracking of alpha and alpha-beta Ti alloys in aqueous environment at ambient temperature, noting Al content and microconstituents
21 p3743 A69-38662

High strength steel landing gear components corrosion protective finishes, discussing paint over bare steel, porous Cd plating and vacuum deposited Cd
21 p3743 A69-38730

Hot salt stress corrosion of Ti alloy, discussing hydrogen generation during elevated temperature exposure and embrittlement as manifestation of strain rate
21 p3747 A69-39434

Corrosion and stress effects separation in stress corrosion of Al-Zn-Mg-Cu alloy, considering machined surface finishing role
21 p3747 A69-39435

Galvanostatic anodic and cathodic currents effects on stress corrosion of Be sheet in aerated synthetic sea water at 72 F
21 p3747 A69-39436

Temperature, applied stress and pressurization effects on materials corrosion by liquid F and F containing oxidizers
21 p3748 A69-39485

Stress corrosion cracking prevention by selection of material, stress relief, compressive stresses introduction, protective coatings and by simulated accelerated tests
21 p3748 A69-39490

Stress corrosion cracking in aerospace situations, discussing corrective measures emphasizing fracture toughness criteria
21 p3748 A69-39491

Stress corrosion cracking of welded Al alloys in sea water solution, showing combined action of sustained stress, corrosive environment and heat treatment
21 p3748 A69-39492

Forged corrosion in aqueous salt environment at various temperatures in unstressed and stressed conditions, considering Be usability in turbomachinery
21 p3749 A69-39493

Stress history and corrosive environment effects on fatigue crack propagation under constant and varying stress amplitude
21 p3750 A69-39814

Large diameter bolts in aircraft structures resisting hydrogen embrittlement and stress corrosion, noting fatigue properties
22 p3957 A69-40827

Stress corrosion cracks propagation from fatigue precrack in Al alloy exposed to organic liquid environments
23 p4178 A69-42452

Aerospace systems failures caused by stress corrosion, fatigue, overload, improper designing or inadequate processing control
24 p4323 A69-43428

STRESS CYCLES

Cycle dependent fatigue hardening and softening of metals in terms of crystal structure and stress amplitude
01 p0165 A69-10133

Plastic fatigue life of steel under rotary bending, proposing fracture criterion based on strain amplitude for low cycle stress levels
02 p0346 A69-12421

Stress variation cycles pattern effects on fatigue strength of materials, discussing results of low-carbon steel tests under sinusoidal loading
04 p0673 A69-14535

Random cumulative damage theory for fatigue failure of steel under sinusoidal loading taking into account randomness of time to failure and possession of memory
04 p0680 A69-15154

Moment curvature models under reverse cyclic straining developed from stress-strain curves for rectangular beams
04 p0683 A69-15497

- Course slip during cyclic deformation of copper single crystals, discussing strain bursts dependence on stress amplitude rate, unidirectional prestrain and orientation
05 p0779 A69-15905
- Generation of crack propagation data on notched rotating beam specimens by interrupted stressing techniques
[ASME PAPER 68-WA/MET-3]
05 p0838 A69-16148
- Heating effects produced by periodic stresses in viscoelastic bodies with resonance dispersion, considering torsional oscillations of viscoelastic cylinders
06 p1019 A69-16826
- Superimposed stress of higher frequency and rotating bending stress effects on aluminum alloy
06 p0941 A69-17121
- Fatigue damage of metals under cyclic stressing, noting deformation modes dependence on stress amplitude and material type
07 p1166 A69-19215
- Forging and heat treatment parameters effect on Ti-Al-V alloy low cycle fatigue properties, relating crack initiation and propagation rates to microstructures
[ASM PAPER D8-24.4]
07 p1169 A69-19669
- Microstructural changes in 52100 steel bearing inner rings during cyclic stressing, obtaining thickening rate data on white-etching regions and lenticular carbides
08 p1319 A69-20004
- Tensile strength of glass-fiber reinforced epoxy resin laminates subjected to fluctuating tension, discussing crack density dependence on fatigue stress cycles
08 p1338 A69-20494
- Aircraft reliability under cyclic loads in flight taking into account stress fluctuations
08 p1322 A69-21106
- Fatigue life evaluation by programmed fatigue strength tests, using frequency distribution of load set amplitudes
09 p1620 A69-22573
- Existing predictive methods for determining high temperature low cycle fatigue life reexamination based on experiments on nickel
10 p1796 A69-23068
- Mechanical model for fatigue crack propagation assuming propagation as function of material strain cycling at crack tip
10 p1797 A69-23082
- Low cycle fatigue of metals under biaxial strain, considering specimen life and strain amplitude correlation
10 p1797 A69-23083
- Cyclic stress-strain and fatigue behavior in aircraft structural metals, discussing hardening and softening in aluminum alloys, steels and titanium alloys
10 p1714 A69-23981
- Cyclic stress-strain curve of metals determined using companion specimens, step strain tests, monotonic tension and hysteresis loop analysis
10 p1715 A69-23982
- Cyclic deformation resistance and fatigue damage accumulation in aluminum alloys, aircraft steels and titanium alloys
10 p1715 A69-23983
- Metal fatigue at elevated temperatures concerning viscosity, energy loss and stress, strain and temperature cycling
10 p1803 A69-24043
- Hysteresis loop contour equation derivation based on energy dissipation dependence on stress amplitude in cyclically deformed vibrating system
11 p1985 A69-25176
- Hydrostatic pressure-cycling technique for controlled fatigue precracking of spin burst fracture toughness specimens, noting ultrasonic flaw detection
11 p1995 A69-25650
- Slip band extrusions in hexagonal close packed Cd, Mg and Ti subject to cyclic stresses, noting microstructure changes
12 p2116 A69-26912
- Metal fatigue in Al alloys subjected to stress cycles, determining macrocracks propagation stages
13 p2359 A69-27291
- Fatigue cracks growth rate under combined static and cyclic stresses
15 p2709 A69-30808
- Fatigue crack propagation caused by cumulative damage due to strain cycling at crack tip, relating resistance to cyclic ductility
15 p2710 A69-30812
- Fatigue life estimation for irregularly varying loads with emphasis on ground-air-ground stress cycles in aircraft
17 p3052 A69-32977
- Facility for determining energy dissipation in materials under cyclic stresses or strains for wide range of temperatures
17 p2946 A69-33925
- Energy dissipation in fiberglass reinforced plastics subjected to axially induced sinusoidal stresses, noting absorption coefficient and hysteresis heating
17 p2993 A69-33937
- Low cycle fatigue leading to failure on AISI 321 stainless steel as function of elevated temperature and stressing frequency
18 p3219 A69-34834
- Cyclic stress frequency on mild steel corrosion fatigue tests, showing strength dependence on potential and stress current
19 p3342 A69-35775
- Recrystallization in thoria dispersed Ni sheet as function of strain-anneal cycles, using electron transmission technique quantitative determination
20 p3557 A69-36958
- Apparent dynamic modulus and damping under multilevel loading during fatigue cycling to estimate stainless steel specimens cumulation fatigue lives
20 p3620 A69-36997
- Supersonic aircraft and power plant structural members operating under cyclic stress at elevated temperatures tested by various methods for interaction between creep and fatigue
20 p3620 A69-37001
- Thermal fatigue combined with mean stress, reversed mechanical stress, low cycle fatigue and static creep in stainless steel
21 p3847 A69-39813
- Cyclic stress tests of stainless steel fiber Al alloy matrix composite, including strain hardening and stiffness characteristics
24 p4331 A69-42925
- STRESS FUNCTIONS**
- Stress function formulas in asymmetric theory of elasticity obtained by completeness method
01 p0167 A69-10325
- Basic equations for optimum inhomogeneity in pressure vessels of maximum rigidity derived, using thick walled spherical shell
01 p0167 A69-10326
- Energy function invariants for cubic and hexagonal systems of anisotropic media with coupled stresses
01 p0169 A69-10811
- Plane problem of asymmetric elasticity based on biharmonic and Helmholtz equation for stress functions
04 p0667 A69-14267
- Variational theorems for stress function formulation of boundary value problems in linear theory of thin elastic shells
04 p0678 A69-14894
- Finite plane deformation of solid body, arbitrary deformation law and arbitrary hydrostatic stresses dependence on volume change solved by nonlinear equation
06 p1021 A69-17175
- Plate deflection in own plane under moments applied to ends using elasticity theory, deriving relation between stress tensor and stress function
06 p1021 A69-17177
- Numerical method for stress function of elastic-plastic torsion of hollow bars during quasi-static monotonic twist compared with relaxation method solution
06 p1023 A69-17370
- Castigliano variational principle applied to thermal stresses in rectangular plate by expanding stress function in double series of cosine binomials
08 p1419 A69-21178
- Beta parameter in exponential stress dependences of high temperature steady state creep rate and time to rupture of creep resistant alloys
10 p1712 A69-23719
- Back stress role in strain rate equation for high temperature deformation and study of structure and applied stress effects
11 p1987 A69-25388
- Love stress function derivation from equilibrium equations
13 p2364 A69-28233
- Maximum turbulent stress in turbulent two dimensional boundary layers leading to general stress law, designing experiment to confirm validity
16 p2769 A69-31832
- Loading path criterion for total strain /deformation/ plasticity theory based on Sanders loading function, discussing case of thermally loaded bar
17 p3062 A69-33711
- Longitudinal crack in cylindrical shell under internal pressure, calculating normal and bending stress singularity strengths against curvature/ cracklength parameter
18 p3212 A69-34346
- Completeness and relations between potentials and stress functions in micropolar elasticity and thermoelasticity
19 p3439 A69-36476
- Generalized Love functions in axisymmetric micropolar elasticity, deriving stress functions expressing all state components
19 p3440 A69-36585
- Transverse stiffness and strength of unidirectional fiber-reinforced composites determined as function of fiber volume content, using finite element method and stress functions
20 p3623 A69-37354
- Homogeneous equilibrium equations of nonlinear shallow shell theory, obtaining six stress function solutions for strain measures
22 p4048 A69-41199
- Plate and shell structures static and dynamic analysis by generalized variational principles in finite element method, discussing element displacement functions
[AIAA PAPER 68-290]
23 p4227 A69-41882
- STRESS MEASUREMENT**
- NT X RAY STRESS MEASUREMENT**
- Torsional pendulum for stress and strain relaxation measurements of wire sample
01 p0079 A69-10221
- Strain measurements in pure polycrystalline Ti at constant temperature and strain, considering creep and elastic aftereffects
01 p0101 A69-11363
- Lattice deformation relationship to dislocation density in vanadium carbide powders
02 p0265 A69-12001
- Free surface motion and stress measuring instrumentation, describing plate impact one dimensional strain configuration for determining mechanical properties under stress wave propagation
02 p0344 A69-12290
- Second normal stress difference measurement by annular flows, giving approximate method for experimental data inversion
02 p0234 A69-12604
- Inelastic strain measurement in metals during cyclic loads by impact tester
04 p0674 A69-14539
- Glued metal joints under cyclic loading evaluated by change in short term strength as function of time at stress levels
04 p0605 A69-14540
- Delayed rupture strength of metals and welded joints at fixed stress level
04 p0674 A69-14541
- Uniaxial loading effect determination by change of harmonics amplitude of inductive pickup signal
05 p0763 A69-15995
- Crack tip displacements and strains in plastically yielded region measured with replica technique
05 p0780 A69-16437
- Strain near fatigue crack tip in notched steel plates measured by copper electroplating method
06 p1022 A69-17198
- Nondestructive technique to measure residual and working stresses in machine parts, using specially designed circuit
06 p0926 A69-17497
- Chromium steel /E1961/ susceptibility to structural damage under cyclic loads by nondestructive inspection of magnetic hysteresis and eddy current losses
07 p1141 A69-19316
- Brittle fracture models compared with experimental stress analysis results, noting plane strain and plane stress fracture toughness
07 p1234 A69-19379
- Stress-strain-time relations in magnesium alloy and aluminum plate impact load tests, discussing stress measurement, Hugoniot equation of state, yield point and dynamic response
08 p1330 A69-20102
- Plastic strain intensity distribution in aluminum alloy specimen with central hole measured with marked orthogonal lattice
09 p1617 A69-22221
- Ultrasonic technique for metal surface and near surface residual stress measurement, emphasizing aluminum alloys
10 p1794 A69-23052
- Experimental evidence of validity of shear coefficient in Timoshenko beam theory
10 p1801 A69-23538

Elastic-plastic deformations /strains/ amplitudes measured at high cycle temperatures in thermal fatigue tests

10 p1801 A69-23844

Direct measurement device for metallic material response to mechanical stresses from stress force and global displacement /including material deformation/

11 p1884 A69-24757

Optical investigation of defects in crystal lattices on stress induced birefringence basis, describing stress visualization results for Si and glass

11 p1887 A69-25199

Floating element skin friction meter designed for adverse pressure gradients, discussing wall shear stress measurement

11 p1889 A69-25557

Wall shear stress measurement by evaporating liquid film, determining optimum liquid viscosity

13 p2375 A69-27793

Machine for measuring creep deformation of polytetrafluoroethylene under uniaxial compressive loads, discussing stress-strain relationship

14 p2469 A69-29412

Stainless steel biaxial residual surface stresses from grinding and finish machining determined by dissection technique

[ASME PAPER 68-WA/MET-9]

14 p2455 A69-29437

Fluctuating turbulent stress measurements in mixing layer of two dimensional jets including intensity, spatial correlation and wave-number fluctuating stress frequency spectra

14 p2431 A69-29577

Box girders stress distribution analyzed by stress-freezing method compared with photoelastic measurement

15 p2705 A69-30419

Clevis design for reduced friction errors associated with round hole clevis in plane strain fracture toughness measurements

15 p2612 A69-31150

Uniaxial stress effect in Schottky barrier diodes measured by beam balance noting higher sensitivity

16 p2758 A69-31619

X ray diffractometer stress analysis of WC-Co cermets, discussing surface preparation and heat treatment

16 p2802 A69-32339

X ray analyzer for residual stress measurement applied to quality control

18 p3150 A69-35423

Skin friction balance for shear stress measurements in presence of ablation, describing balance construction, calibration, flexure range, etc

19 p3292 A69-35735

Electroplating method for local stress concentrations determination, discussing measurement techniques, metal fatigue failure prediction, etc

19 p3441 A69-36751

Keyway stresses in shafts under tension, bending and torsion, using frozen stress photoelastic technique

19 p3445 A69-36827

Stress determination in materials with creep in presence of nonuniform temperature field

21 p3833 A69-38571

Telecentric lens principle for accurate optical strain measurements, using moire grids

21 p3844 A69-39322

Stress concentrations in metals determined through surface properties measurements, correlating local electrochemical potentials and metal-metal oxide junction parameters

21 p3747 A69-39326

Strain gage embedding techniques and applications

21 p3725 A69-39327

Stress history and corrosive environment effects on fatigue crack propagation under constant and varying stress amplitude

21 p3750 A69-39814

Grids applied to plastic samples for strain measurement using moire fringe method, comparing tensile test results with Linley extensometer

22 p4042 A69-40312

Babinet compensator with birefringent wedges made of stress frozen photoelastic material rather than quartz

22 p4042 A69-40442

Three dimensional welded structure of thin walled girders with stability loss, discussing welding strain gage measurements and simplified computational procedure

23 p4169 A69-42007

Mechanical stress measurement in cylindrical steel subjected to loads inside coaxial transducer, using transducer signal in contactless eddy current method

24 p4296 A69-42654

Real shear modulus and mechanical damping characteristics of cured adhesives measured for temperature effect, using torsion pendulum apparatus

24 p4338 A69-43460

STRESS PROPAGATION

Photoelastic analysis of HF stress waves propagating in bars and plates subjected to damped sinusoidal loading

[ASME PAPER 68-WA/APM-27]

04 p0669 A69-14397

Longitudinal stress pulse propagation in finite length free-free bar with variable cross section, noting stresses in projectile impacting plane target

04 p0671 A69-14412

Thermal stress propagation in infinite viscoelastic thin plate analyzed with cylindrical coordinate system

08 p1415 A69-20661

Two dimensional elastic stress wave propagation in thick multilayered cylindrical shells for nonuniform external pressure distribution

11 p1991 A69-25511

Stress wave propagation in thermoviscoelastic solids using extended Ritz method

11 p1993 A69-25527

Stress waves propagation through elastic-plastic medium with uniaxial displacement, discussing wave interactions and interface conditions

16 p2870 A69-31809

Elastic circular cylindrical panel behavior in fluid with acoustic shock wave, allowing for propagation waviness of elastic stresses

18 p3216 A69-34579

Stress and displacement waves propagation in thin walled elastic cylindrical shell under compressive axisymmetric force based on momentless theory

18 p3218 A69-34600

Dynamic processes in upper earth mantle, discussing thermal convection currents and stress propagation

22 p3937 A69-40184

STRESS RATIO

Uniaxial strain static and gas gun compression tests result compared for syntactic foam

02 p0345 A69-12295

Axial load fatigue crack propagation tests on Al alloy sheets for stress ratio effects

19 p3346 A69-36435

STRESS RELAXATION

Torsional pendulum for stress and strain relaxation measurements of wire sample

01 p0079 A69-10221

Hydrogen content effect on relaxation spectrum of alpha titanium, using nondestructive tests

01 p0096 A69-10614

Anomalous discontinuous stress relaxation in sintered tantalum

02 p0265 A69-12003

Recovery behavior of nickel strain hardened by impact loading by aluminum projectiles, showing microstructure correlation with stress levels

03 p0447 A69-13620

Strain dependent modulus and Poisson ratio behavior of CTPB propellant, performing stress relaxation tests

[AIAA PAPER 68-519]

04 p0646 A69-15510

Tension stress and shearing strain vs time for simultaneous stress relaxation and creep in polyurethane

[ASME PAPER 68-WA/APM-8]

05 p0839 A69-16186

Nimonic alloys recovery analyzed by X rays and electrolytic phase separation, showing precipitated gamma phase effect

07 p1159 A69-18533

Diffusion coefficient of interstitial oxygen atoms in tantalum by elastic energy dissipation measurements as temperature function, discussing relaxation effect

07 p1168 A69-19452

Stress relaxation in structural elements, analyzing unsteady creep in case of strain hardening following power law

07 p1237 A69-19683

Ductility as principal cause of postweld heat treated stress relaxation cracking in nickel based Waspaloy and alloy 718

08 p1318 A69-19964

Generalized approximate method for solving problems in linear viscoelasticity theory to cover arbitrary creep and relaxation centers

08 p1412 A69-20327

Modulus of elasticity changes and stress relaxation spectra of viscoelastic liquids measured by acoustic methods

11 p1887 A69-25206

Tension stress and shearing strain vs time for simultaneous stress relaxation and creep in polyurethane

[ASME PAPER 68-WA/APM-8]

13 p2362 A69-28121

Stress level reduction in pressurized circular cylinder with circumferential ring stiffener and longitudinal crack, using shallow shell equations

18 p3212 A69-34347

Stress relaxation of heat-resistant steels as function of equal stress during different elevated temperatures, applying results to time residual stress prediction

19 p3342 A69-35778

Strain hardening of titanium wire during room temperature stress relaxation shown equal to strain hardening during constant strain rate test

19 p3342 A69-35812

Elastic interactions between cylindrical shell and added band reinforcement turns, analyzing stress relaxation magnitude and effect on pressure vessel design

20 p3621 A69-37064

Creep resistance increase of Ni refractory alloy by thermovibrational treatment under stress relaxation conditions

21 p3744 A69-38869

Thermal and athermal component of flow stress and deformation dynamics for Ti at low homologous temperatures determined by stress relaxation tests

21 p3749 A69-39598

Structural defects of neutron irradiated W wire noting microstress relaxation using autoionic microscope

21 p3749 A69-39623

Time-temperature method modified for combining stress relaxation data with stress or strain into single correlation curve, analyzing isothermal relaxation data

21 p3846 A69-39812

Short period creep and relaxation in various heat resistant alloys under heat treatments and loads, determining temperature dependence of cyclic thermal instability

22 p3969 A69-40071

Reinforcement effect on stress relaxation and creep in hereditary elastic materials, assuming integral shear modulus operator with exponential kernel

22 p4045 A69-40744

Mounting elements alloys relaxation characteristics at various temperatures, considering effects of scale factor and stress concentrations

23 p4169 A69-41419

STRESS RELIEVING

Compact device for low temperature neutron irradiation of deformed specimens under tensile stress, emphasizing specimen carrier

11 p1862 A69-24901

Macrostructure of steel, zinc and aluminum ingots using electromagnetic vibrations during crystallization, for stress relieving of welded structures

14 p2456 A69-29916

Rotating shafts impact damping efficiency increaseable by providing proper clearance to reduce shaft stress in critical resonance frequency region

17 p3066 A69-33946

Stress corrosion cracking prevention by selection of material, stress relief, compressive stresses introduction, protective coatings and by simulated accelerated tests

21 p3748 A69-39490

STRESS RUPTURE STRENGTH

U CREEP RUPTURE STRENGTH

STRESS-STRAIN DIAGRAMS

Stress-strain state of isotropic elastic medium using equations with stress tensor, noting role of curvilinear hole

01 p0164 A69-10081

Hollow finite cylinder stress-strain analysis under normal loads on end faces solved by four partial differential equations

01 p0168 A69-10359

Stress-strain behavior of crazes in glassy polymers, discussing crack propagation, craze formation and failure and molecular weight effects

01 p0102 A69-10915

Elastoplastic stress-strain behavior of concentric composite cylinders under uniaxial tension using analytical model, predicting transverse stresses during axial loading

01 p0171 A69-11263

Wave front profiles sensitivity to form of constitutive equation in one dimensional stress problem

02 p0344 A69-12291

Rapidly heated ablative reinforced plastics strength and stress-strain properties, considering heat shield designs

02 p0347 A69-12512

Knee in stress-strain diagram and crack formation in glass fiber reinforced plastics, discussing effect on construction load capacity

03 p0453 A69-13820

Elastoplastic bending of plates with nonlinear stress-strain diagram

04 p0667 A69-14269

Elastic noncircular orthotropic conical shell stress-strain state, obtaining differential equations reducible to integrodifferential equations solvable by iteration

04 p0673 A69-14494

Circular disk stress-strain state due to thermoelastic strain applied at disk sector edge

04 p0681 A69-15171

Moment curvature models under reverse cyclic straining developed from stress-strain curves for rectangular beams

04 p0683 A69-15497

Stress-strain state of thin elliptical shell of revolution under rapidly varying cyclic edge loads

05 p0832 A69-15686

Unified theory of stress-strain curve of fcc metal crystals in Stages II and III of work hardening

05 p0778 A69-15755

Stress-strain rate relation under combined stress fields derived from Gilman relation between dislocation velocity and force for single dislocation

05 p0834 A69-15756

Elastic plastic stress distribution in compressed ring determined with postyield strain gages and stress-strain relationship from uniaxial tensile test

05 p0837 A69-16063

Stress-strain state for two dimensional physically nonlinear multiply connected elastic regions, noting plate with two identical circular holes

05 p0841 A69-16203

Elastoplastic stress-strain state of asymmetric profile thin walled beam under mobile load

05 p0841 A69-16205

Stress-strain state of infinite plate with two holes of different diameter solved, using integral equation derived for two dimensional problem in elasticity theory for anisotropic medium

05 p0843 A69-16680

Stress-strain state of shell having one end clamped and other under concentrated bending moments and concentrated force acting along generatrix solved by integral equation

05 p0843 A69-16681

Large displacement bending of rods for constant deformation cross section, negligible shearing forces and exponential stress-strain relation

05 p0843 A69-16682

Stress calculation for internal pressure in moment-less shell of revolution

05 p0843 A69-16690

Basic equations describing stress-strain state of anisotropic half planes and anisotropic planes with cuts

06 p1020 A69-16827

Metal matrix composites compression microstrain behavior, analyzing continuous fiber composites of magnesium-boron and copper-tungsten

06 p0939 A69-16945

Stress direction and mean stress effects on fatigue properties of fiberglass reinforced plastics

06 p0945 A69-17124

Griffith crack in brittle material, discussing validity for rock-like material with nonlinear stress-strain relationship

06 p1020 A69-17128

Stress-strain relations for laminar anisotropic medium from known mechanical properties of layers for application to fiber reinforced plastics

06 p1021 A69-17176

Stress-strain state of shells of multicable elevator pulleys under asymmetric load for various friction coefficients and pulley shell lengths and widths

06 p1026 A69-18016

Stress-strain response up to ultimate failure and ultimate strength of laminated composite with nonlinear orthotropic lamina

07 p1170 A69-18710

Stress-strain relationship of composite bars consisting of single glass fiber with thin metal coating layer and under axial load

07 p1235 A69-19385

Minimum theorems in elastoplastic theory extended to continua for plastic strains governed by holonomic and nonholonomic stress-strain laws

07 p1235 A69-19442

Cr-Ni-Mo steel toughness with strain induced austenite to martensite transformation by TRIP/transformation induced plasticity/

08 p1330 A69-20012

Continuum stress/plastic strain relations from Schmid Law of plastic slip in individual crystal grains

08 p1414 A69-20525

Flow equations of rheological media derived using thermodynamics, assuming nonlinear stress-strain relation in incompressible medium

08 p1419 A69-21074

Stress-strain problem of geometrically nonlinear conical shell subjected to creep, giving method for complex deformation solution

09 p1612 A69-21497

Finite elastic locking medium, discussing equation of state for thermodynamic variables and applications to thermoelasticity [IS-ERI-70]

09 p1612 A69-21561

Stress-strain state of infinite plate with elliptical eccentric reinforced hole, using quadrature method

09 p1613 A69-21630

Ordinary and inverse variational methods for stress-strain state of solid body, using Lagrange multipliers to reduce variational problem

10 p1793 A69-22885

Strain fatigue mechanism of crack propagation in ductile metals, considering distribution of plastic cohesive stresses at crack tip

10 p1795 A69-23059

Ductile to brittle transition shown in tensile stress-strain curves of polycrystalline body centered cubic and hexagonal close packed materials

10 p1795 A69-23063

Elastomeric solid propellant grains viscoelastic flow, analyzing stresses and strains under various operating conditions and rocket engine geometry effect

10 p1801 A69-23702

Cyclic stress-strain curve of metals determined using companion specimens, step strain tests, monotonic tension and hysteresis loop analysis

10 p1715 A69-23982

Axisymmetric problems in thermoviscous plasticity, discussing stress-strain state of annular disks and thick walled cylinders made of rate sensitive materials

10 p1802 A69-24025

Semibrittle material decompaction influence on stress distribution in infinite plate with edge loaded circular hole, noting stress-strain relation nonlinearities

11 p1972 A69-24656

Limiting equilibrium of plate weakened by curvilinear hole stress raiser with one or two cusps, obtaining stress-strain diagrams

11 p1973 A69-24658

Linear shell theory foundations, discussing two and three dimensional stress strain relations, couple stresses, circumferential length ratio to shell thickness, etc

11 p1977 A69-24803

Two dimensional elastic reinforcements effects on stress, strain and elasticity of quasi-homogeneous anisotropic elastic medium

11 p1981 A69-24941

Thin conical elastic shell stress-strain state calculated by computer for arbitrary thicknesses and loading conditions, considering temperature and edge forces effects

11 p1981 A69-24943

Stress-strain state of shells with opposite edges hinged and rigidly clamped solved by numerical method after reduction to boundary value problem

11 p1985 A69-25174

Bent plates elastoplastic stress-strain state determination by elastic solution and finite differences, considering linear strengthening under uniform distribution of load

11 p1985 A69-25175

Comparison of errors obtained by using linearly gliding and rotating strengthening moduli in stress-strain state on basis of linear stepwise approximation

11 p1986 A69-25342

Fiber reinforced materials shear and tensile strength effect on stress-strain state of composite materials machine parts, considering design requirements

11 p1907 A69-25680

Optimal additional loading at zero moment stress-strain state in simply connected shell of complex design under external loads, using successive approximation

12 p2181 A69-26610

Natural stress concept for analysis of nonhomogeneous strains fields exhibiting geometrical nonlinearity

13 p2359 A69-27259

Volterra integral equation with nondifference type singular kernel for stress-strain state in long hollow viscoelastic cylinder with moving inner boundary

13 p2361 A69-27744

Fatigue crack propagation in aged aluminum alloy sheets, studying specimen geometry and stress level variations effects

13 p2280 A69-27835

Spacecraft construction materials and strength problems including stress-strain determination, thin shell structural stability, dynamic loads, heat resistance, fiber-reinforced composites, ablation materials, etc

13 p2362 A69-27920

Bending state of shells of revolution due to edge effects using nonlinear stress strain relation

13 p2362 A69-27921

Inelastic structural system stresses, strains and displacements analyzed by differential stress-strain relationships, using finite element method [AIAA PAPER 68-291]

13 p2364 A69-28208

Stress-strain state of circular annular plate with varying thickness subjected to concentrated axisymmetric load and shearing force applied to internal perimeter

13 p2369 A69-28563

Differential equations for shallow circular spherical shell transformation to equation describing stress-strain state of plate on elastic base

13 p2369 A69-28565

Stress-strain problem of piecewise-homogeneous plane with cut normal to interface line reduced to Wiener Hopf equation, obtaining solution for arbitrary boundary conditions

14 p2531 A69-28805

Elastoplastic continua fire resistance at high temperatures, establishing plasticity condition and stress-strain relationships

14 p2536 A69-29598

Creep strain rate and stress distribution of thick walled cylinders under internal pressure at elevated temperature, using variational principle

15 p2703 A69-30070

Elastoplastic matrix for stress increments for yield surfaces with associated flow rule, considering initial stress computation

15 p2706 A69-30433

Bending theory of orthotropic plates with variable elastic modulus under transverse loads, utilizing stress-strain relations and Kirchhoff-Love hypothesis

15 p2708 A69-30661

Boundary layer solution in three dimensional bending for plate with curvilinear hole to study stress-strain state at hole and over entire plate

15 p2708 A69-30662

Stress-strain state of circular disk with diametral cracks determined by approximating limiting equilibrium equation

15 p2708 A69-30663

Polymers stress-strain behavior and corresponding birefringence within limited temperature range and strain rates

15 p2642 A69-30678

Initial comparisons between theory and experiment of strain fields in cracked copper plate

15 p2640 A69-30810

Biaxial stress strain properties of graphite base refractory composites noting fracture strength predictions [AIAA PAPER 68-337]

16 p2803 A69-32150

Nonlinear theoretical derivation of creep equations for three dimensional processes in polymers, based on Boltzmann-Volterra creep heredity concept using stress-strain summation

16 p2803 A69-32290

Temperature field, strains and stresses induced in thin circular disk by unsteady heat source, noting time effect and resonant vibrations

17 p3054 A69-33021

Stress-strain state analysis for brittle plate with circular holes of equal radius performed in cylindrical system of coordinates

17 p3055 A69-33127

Anisotropic elastic plate deflection weakened by circular hole with thin elastic ring reinforcement, assuming no load on ring and uniform stress-strain state of plate

17 p3055 A69-33128

Stresses and displacements in elastoplastic cantilever beams and beams fastened at both ends calculated by stress-strain diagrams of material

17 p3056 A69-33191

Strains in elastoplastic curved beam under bending obtained from approximating stress-strain diagram by parabola

17 p3056 A69-33192

Stress-strain state determination for axisymmetric shells applied to design of circular/annular plates and rotating disks

17 p3057 A69-33194

Stress-strain rate of glass fiber reinforced plastic pressure vessels under internal pressure, determining optimal fiber pattern

17 p3057 A69-33195

Moire reflection technique applied to study of stress-strain state of partially clamped rectangular cantilever plates under various loads

17 p3058 A69-33203

Rotating machinery fracture and design approach based on effect of detailed stress and strain duty on imperfect materials metallurgical behavior

17 p3060 A69-33561

Near resonant oscillations of warped turbine or compressor blades, discussing stress-strain relations

17 p3064 A69-33918

Energy dissipation in vibrating warped turbine blades subject to complex stress-strain rate produced by simultaneous bending, torsional and tensile stresses

17 p3065 A69-33924

Low endurance fatigue in aluminum, Nylon 66 and epoxy resin compared, considering stress-strain relationships, fatigue damage, failure mechanisms and crack propagation

18 p3155 A69-34633

Elastoplastic flow equations formulation, inverting flow rule to relate stress rates to strain rates and instantaneous stresses, noting Navier equations

18 p3219 A69-34666

Stress-strain state of shells under concentrated loading, emphasizing positive Gaussian curvature

18 p3219 A69-34832

Stress-strain state of elastoplastic material subjected to quasi-static uniaxial tension and compression, considering Bauschinger type effects by scalar parameters

18 p3222 A69-34909

Stress-strain state calculations of ribs reinforcing cantilever shell under external pressure, using differential-difference equations

18 p3223 A69-34980

Creep calculation with temperature considerations for multilayer cylinder under nonisothermal load, comparing stress-strain state of viscoelastic and elastic cylinders

18 p3225 A69-35358

Linearity range of viscoelastic properties of fiberglass reinforced plastics, calculating stress-strain state

18 p3163 A69-35364

Pure plastic bending of wide strip, determining stress strain state and plastic strain energy during constrained bending, noting application to corrugated panels

19 p3324 A69-35833

Turbine disks stress-strain state, using wire strain gauge to determine residual strains, radial and tangential stresses as function of disks rpm

19 p3436 A69-35850

Anisotropy coefficients obtained during annealed Al sheet tests based on stress-strain characteristics, noting fading memory effects

19 p3447 A69-36857

Viscoelastic nonlinear and linear solids models and rheological equations, studying stress-strain states of various complex Hookean, Kelvin, Maxwellian and Zener elements

20 p3625 A69-37601

Linear limit uniaxial stresses for stress-strain and stress-birefringence in photoelastic and mechanical model materials

20 p3628 A69-37777

Soviet book on fundamentals of theory of plasticity and creep covering stress-strain state, bending, torsion, pressure, plane deformation, etc

20 p3630 A69-38206

Metal deformation dynamics at elevated temperatures, discussing closed loop electrohydraulic testing machine for stress relaxation and strain rate sensitivity

21 p3689 A69-38595

Alpha Ti thermally activated tensile deformation, studying flow stress dependence on strain, temperature and strain rate

[ASM PAPER W9-4.2]

21 p3729 A69-38659

Stress-strain state of thin spherical shell of variable thickness in elastoplastic equilibrium, using Meissner variables to reduce equilibrium equations

21 p3834 A69-38717

Stress-strain state in thin isotropic plate with circular hole under lateral bending and torsional moments

21 p3835 A69-38725

Flexible circular plate in stationary temperature field calculated for stress-strain state using perturbations method

21 p3835 A69-38830

Stress-strain state of fiberglass reinforced plastics under load analyzed by anisotropic linear creep theory and Galerkin method

21 p3835 A69-38831

Stress-strain state of thick and thin walled closed shells of variable thickness during elastoplastic torsion developing in aircraft component production

21 p3835 A69-38882

Bending of circular plate into shell, using stress-strain relation in finite strain, solving differential equations and boundary conditions

21 p3836 A69-39005

Thermal stresses and displacements in long isotropic hollow cylinder heated on part of outer curved surface, analyzing temperature distribution

21 p3838 A69-39166

Stress-strain state of homogeneous anisotropic elastic body under action of internal forces, deriving equations to generalize state

21 p3838 A69-39184

Generalized strain-measure application to linearization of stress-strain curves of compressive, shear and tensile nature, discussing plastic deformations

21 p3844 A69-39321

Stress-strain curves of W wires and of aligned composites of same wires in Cu matrix

21 p3845 A69-39709

Rectangular plate under biaxial tension stress analyzed to determine onset of necking and stress-strain state

22 p4039 A69-39913

Approximate generalized stress-strain rate relations for stationary creep analysis of thin shells compared with corresponding exact relations

22 p4041 A69-40013

Heat influx equation coupling in thermoviscoelasticity, considering internal forces dissipation and stress-strain operators

22 p4044 A69-40741

Elastically symmetric thin plate stress-strain state under uniformly distributed load applied to edges

22 p4046 A69-41061

Stress-strain state of circular disks with arbitrarily varying thickness along radius under antisymmetrical load calculated by integral equations method

22 p4047 A69-41168

Stress-strain relations for materials with variable modulus of elasticity applied to internal work, obtaining potential strain energy

22 p4047 A69-41171

Nonlinear shallow shell theory of stress and strain formulated via shell of revolution problem

22 p4048 A69-41198

Closed circular cylindrical shell stability and oscillations under ring-shaped axial load, defining stress-strain state by radial displacements and force function

22 p4049 A69-41280

Warping of doubly supported submerged wings, calculating stress and strains due to bending and constrained torsion

23 p4225 A69-41423

Deformation tractions in undeformed and curved cuboid flexure and inverse flexure determined by stress-strain relations for homogeneous isotropic compressible materials

23 p4226 A69-41521

Prismatic beam stress-strain state under steady temperature field, deriving stresses, displacements and elastic curve equations

23 p4227 A69-41708

Plates and shells under concentrated loads, analyzing stress-strain state

23 p4228 A69-41986

Stressed state of thin plate with circular hole under normal and breaking force applied over hole perimeter

23 p4233 A69-42341

Yield condition for elastic-plastic medium, considering pure torsion-associated second order effects and dissimilarity between stress and strain increment Mohr circles

23 p4234 A69-42409

Dynamic uniaxial tensile stress-strain data obtained at high rates by measuring kinematics of symmetrically expanding thin ring specimens

24 p4330 A69-42735

Strain diagram with piecewise nonlinear curve for statically indeterminate systems stressed beyond elastic limit

24 p4400 A69-43072

Orthotropic aircraft materials plasticity theory, deriving stress-strain relationships in three mutually perpendicular symmetry planes for use in engineering calculations

24 p4400 A69-43083

STRESS-STRAIN DISTRIBUTION U STRESS CONCENTRATION

STRESS-STRAIN-TIME RELATIONS

Aluminum deformation at various strain rates and temperatures under combined stress, comparing results with theoretical predictions

02 p0343 A69-12282

Dynamic tensile stress-strain curves for annealed Al, Cu and Fe at constant strain rates, describing experimental method

03 p0524 A69-13065

Dynamic pressure pulse over band on solid elastic cylinder surface, analyzing time stress distribution throughout elastic cylinder

04 p0670 A69-14405

Constitutive equation for viscoelastic material generalized, assuming instantaneous part of deformation to be nonlinear function of time dependent stress state

05 p0835 A69-15868

Ductile creep rupture of thin walled membrane shell of revolution subjected to time dependent internal pressure and strain hardening

[ASME PAPER 68-WA/MET-15]

05 p0838 A69-16153

Long term creep behavior of nickel-chromium-molybdenum alloy, noting temperature effect on grain boundaries

05 p0781 A69-16500

Technique for compressive mechanical behavior of viscoplastic nonlinear composites, discussing rate dependence and one dimensional stress-strain time properties

07 p1159 A69-18721

Stress-strain-time relations in magnesium alloy and aluminum plate impact load tests, discussing stress measurement, Hugoniot equation of state, yield point and dynamic response

08 p1330 A69-20102

Creep buckling stability of shells, with emphasis on stress and strain states and critical time, considering circular cylindrical shell

08 p1411 A69-20143

Fatigue strength and stress-time functions obtained by programmed fatigue tests under time variable loads

09 p1620 A69-22572

Stress-strain relation in crystalline media for pure tension and elongation epsilon several times conventional elastic limit, verifying by testing Al alloy

[ONERA TP-695]

11 p1975 A69-24754

Short time creep rupture behavior of austenitic stainless steel at high temperature ranges, noting rupture times various stresses and data correlation

[ASME PAPER 68-WA/MET-2]

14 p2464 A69-29439

Chemical reaction-rate theory for creep tests, analyzing extrapolation equations for time-to-rupture dependence on temperature and stress

14 p2464 A69-29442

Failure mechanisms time and stress dependence relations

18 p3144 A69-34490

Fiberglass reinforced plastics short and long term strength anisotropy, correlating stress and logarithm of time to rupture under tension along different directions

18 p3162 A69-35352

Stress relaxation of heat-resistant steels as function of equal stress during different elevated temperatures, applying results to time residual stress prediction

19 p3342 A69-35777

Tensile tests on time dependent Pb and cellulose nitrate, including stress-strain curve prediction from creep test data

19 p3445 A69-36829

Crack density effects on stress-dependent creep rate in isotropic and anisotropic materials undergoing high temperature creep deformation

20 p3619 A69-36964

Viscoelastic materials gradual resilience loss under tensile stress, discussing mathematical relations between stress, loading time, elastic deformation and experimental verification

20 p3625 A69-37600

Dynamic plasticity of nonsymmetrical free flight collision impact of crystalline solids, using linear temperature dependent stress-strain function and finite amplitude wave expansion

21 p3840 A69-39298

Time-temperature method modified for combining stress relaxation data with stress or strain into single correlation curve, analyzing isothermal relaxation data

21 p3846 A69-39812

Damaging effects of vibration on materials and parts to estimate fatigue life, considering periodic and non-periodic stress vs time relationships

22 p4041 A69-40167

- Partial differential equation for creep process in plane stressed metals, interrelating strain, rate, stress tensors, temperature and time 22 p4048 A69-41268
- Stress-strain state in infinite medium with cavity under triaxial tensile force obtained from integrodifferential equation deduced from equilibrium equation 23 p4226 A69-41703
- Wave propagation in dynamical theory of thermoelasticity, considering half space subject to step time strain, temperature and stress distributed over free surface 23 p4235 A69-42464
- Matrix method for analyzing elastic structures linear transient response to time dependent loads and temperature change 24 p4399 A69-42988

STRESS TENSORS

- Stress-strain state of isotropic elastic medium using equations with stress tensor, noting role of curvilinear hole 01 p0164 A69-10081
- Elastic shell nonlinear theory, introducing nonsymmetric stress tensor and principles of virtual work and objectivity 01 p0166 A69-10166
- Symmetric tensor of time averaged stresses for collisionless plasma in oscillating field derived by Maxwell equations 02 p0286 A69-11588
- Plate deflection in own plane under moments applied to ends using elasticity theory, deriving relation between stress tensor and stress function 06 p1021 A69-17177
- Viscous stress tensor for collisionless plasma with anisotropic pressure in magnetic field 08 p1365 A69-20522
- Plane and three dimensional stress concentration studies involving asymmetrical stress tensors, noting contributions to moment theory of elasticity 08 p1419 A69-21177
- Stresses and waves in highly conducting magnetoplastic metals as analogy of MHD processes in plasma 09 p1551 A69-22033
- Analytical expressions for Gaussian constraint of continuum, using continuity conditions as equations of internal geometric couplings 11 p1984 A69-25170
- Time averaged stress tensor for ionized plasma in HF electromagnetic field, considering collisions 14 p2493 A69-29649
- Experimental determination of strain /or strain rate/ tensor in plastic deformation analysis 15 p2707 A69-30639
- Monograph on stress fields in plane plastic flow as solutions to boundary value problems 15 p2711 A69-30932
- Isotropic strain tensor general theory based on isotropy between second order asymmetric tensors reducible to finite form 20 p3624 A69-37584
- Mohr tensor representation and Mohr theorem proof developed for general problem in structural engineering 22 p4038 A69-39903
- Protoplastic materials defined in terms of protopotential function, discussing stress tensor dependency on displacement gradients within body 22 p4042 A69-40452

STRESS WAVES

- Free surface motion and stress measuring instrumentation, describing plate impact one dimensional strain configuration for determining mechanical properties under stress wave propagation 02 p0344 A69-12290
- Wave front profiles sensitivity to form of constitutive equation in one dimensional stress problem 02 p0344 A69-12291
- Plane strain plastic stress waves radial propagation from center of hollow cylinder subject to dynamic pressure load 02 p0344 A69-12292
- Spherical elastic-plastic stress wave propagation analysis via finite difference procedure 02 p0348 A69-12610
- Viscoelasticity effect on tensile stress in absorption layer for free surface uniaxial motion 04 p0676 A69-14705
- Dynamic shear stresses at interface of embedded thin elastic filament and elastic matrix after subjecting filament to concentrated longitudinal line load 05 p0831 A69-15577

- Thermally generated stress wave propagation in dispersive elastic rod investigated experimentally and analytically, using ruby laser and differential equation 09 p1617 A69-22010
- Laser radiation induced stress waves in transparent media using dynamic photoelastic technique 10 p1707 A69-24213
- Coupling constants of fast space charge waves in three frequency parametric TWT amplifier and of stress waves in slow wave structure, using graphical methods 11 p1844 A69-24446
- Two dimensional elastic stress wave propagation in thick multilayered cylindrical shells for nonuniform external pressure distribution 11 p1991 A69-25511
- Elastoplastic stress wave generation by penetration of impulsive electromagnetic radiation through thin surface layer of solid 12 p2179 A69-26215
- Stress waves analysis of brittle fractures, considering loading time role and cavitation of viscous fluids relation to fracture incipience 13 p2275 A69-27229
- Three dimensional harmonic dispersion analysis of incremental waves in uniaxially prestressed plastic and viscoplastic bars, plates and unbounded media 13 p2363 A69-28125
- Characteristics method for stress waves from hypervelocity impact of circular cylinder on half space, discussing numerical diffusion effect on pressure and flow fields [AIAA PAPER 69-355] 13 p2365 A69-28287
- Spherical stress wave reflected from plane surface, discussing tensile stress in target [AIAA PAPER 69-363] 13 p2366 A69-28295
- Fracture of bumper protected fuel tanks subjected to hypervelocity meteoroid impact, applying method of characteristics to stress wave propagation in tank walls [AIAA PAPER 69-369] 13 p2367 A69-28301
- Axisymmetric thermoelastic vibrations of infinite and finite cylindrical shells, determining natural frequencies and stress wave propagation 14 p2532 A69-28979
- Materials and structural failures under short time compressive loadings, showing structural response to tensile stresses produced by rarefaction waves 15 p2639 A69-30364
- Stress waves propagation through elastic-plastic medium with uniaxial displacement, discussing wave interactions and interface conditions 16 p2870 A69-31809
- Stress waves analysis in laminates design, assuming one dimensional linear elastic response to plane stress pulse on flat laminated plate surface 16 p2872 A69-31923
- Transient stress waves due to inputs of various types and time dependence in plates and revolving shells, discussing applications of elasticity theory analysis methods 16 p2876 A69-32785
- Cylindrical shell stability under axial compression, studying buckling process and wave formation 18 p3217 A69-34597
- Deformation detection by stress wave analysis technique /SWAT/, noting pressure vessel applications 18 p3223 A69-35080
- Transient processes of strain wave propagation in elastic shells and plates under time varying loads 18 p3224 A69-35321
- Reflection of spherical stress wave against smooth deformable plane in elastoviscoplastic medium, discussing Taylor series expansions for displacement, velocity and stress fields 18 p3226 A69-35463
- Fatigue characteristics of Al alloys by fatigue tests with complex stress patterns, finding secondary stress wave effects 19 p3342 A69-35772
- Equations governing stress waves generated by rapid nonuniform heating of solids, comparing elastoplastic with purely elastic solutions 21 p3837 A69-39158
- Geometric dispersion of transient stress waves in linearly elastic laminated composite based on sinusoidal modes [ASME PAPER 69-APMW-20] 24 p4401 A69-43098
- Stress wave propagation in nonhomogeneous elastic media, considering curvilinear characteristics transformation into equal slope straight lines by change of independent variable 24 p4403 A69-43574

- Reflection of spherical stress wave against plane clamped partition in elastoviscoplastic medium, investigating three dimensional problem by infinitesimal deformations theory 24 p4406 A69-43732

STRESSES

- NT AXIAL STRESS
- NT COMBINED STRESS
- NT CRITICAL LOADING
- NT PHOTOSTRESSES
- NT RESIDUAL STRESS
- NT SHEAR STRESS
- NT TENSILE STRESS
- NT THERMAL STRESSES
- NT TORSIONAL STRESS
- NT TRIAXIAL STRESSES
- NT VIBRATIONAL STRESS
- X ray study of scandium containing ferrites, establishing lattice stresses due to ion replacement in octahedral interstices 03 p0491 A69-14053
- X ray study of scandium containing ferrites, establishing lattice stresses due to ion replacement in octahedral interstices 18 p3182 A69-35046

STRETCH FORMING

- Strain rate effect on structure and mechanical properties of rapidly stretched metals 06 p0941 A69-17122
- Sheet metals deformation behavior during punch stretching and hydraulic bulging, noting effects of lubrication, stress-strain relation, anisotropy and microcracks 20 p3551 A69-38115

STRETCHING

- Thermoelastic waves in stretched circular cylindrical bar, analyzing displacements, secondary pressure and temperature field by using Frobenius method 12 p2189 A69-27115
- Reaction rate theory for dilatational failure of heterogeneous materials subjected to stress 15 p2710 A69-30813
- Heat conduction orientation anisotropy in linear amorphous high polymers due to uniaxial stretching, noting molecular weight distribution and temperature effects 19 p3359 A69-36443
- Continuous particle media on basis of microstructure, discussing granular media deformation, elastic media dilatation, turbulent flow and dilute suspensions 19 p3446 A69-36833
- Tension effects on amino acid incorporation rate into proteins of cross-striated muscles of rats 23 p4083 A69-41458
- Isolated pacemaker tissue from rabbit heart under dynamic and static stretching, discussing spontaneous frequency phenomena 23 p4096 A69-42092

STRIATION

- Electron thermal relaxation length in positive column determined by plasma parameters variations in small amplitude moving striations 01 p0127 A69-10341
- Ministriations in frequency graphs as evidence of standing waves in electrically exploded iron wires 01 p0118 A69-10661
- Fast type r moving striations in plasmas and dependence of ionization frequency on electron mean energy 03 p0477 A69-13801
- Evaporographic converter to test for striations /schlieren/ in materials used in IR 08 p1314 A69-20384
- Striation formation during steady state glow discharge, noting origin in cathode interfacial positive ions 09 p1545 A69-21343
- Moving striations in plasmas, presenting measurements of relative phases of electron temperature, plasma potential and luminous intensity near Pupp current limit 10 p1741 A69-23859
- Aluminum alloys ductile fatigue striations, considering dependence on grains crystallographic orientation and vacuum effect 13 p2278 A69-27415
- Moving striations relations to ion acoustic waves in DC discharge in neon at various pressures, discharge currents and measurement excitation modes 14 p2494 A69-29695
- Moving striations as plasma oscillations arising from transit time delays of neutral and charged particles moving through ionized gas, using continuity equation 24 p4356 A69-43122

Moving striations dispersion and stability theory applied to ionization waves excited in Ar, Ne and Hg-Ar mixture low and medium pressure discharge
24 p4356 A69-43363

Diamond shaped striations development mechanism on ablative heat shield materials exposed to supersonic flow and turbulent boundary layers
24 p4248 A69-43598

STRINGERS

Imperfection sensitivity of axially compressed stringer stiffened cylinder analysis via shell equations formulation using finite differences
02 p0348 A69-12542

Load diffusion from transverse tension bar into semiinfinite elastic sheet, considering line and area contact methods of stringer attachment
[ASME PAPER 68-WA/APM-15]
04 p0669 A69-14396

Prestressing of aircraft wing stringers in order to reduce weight, noting initial bending moment, initial axial stress and prestressing methods
05 p0832 A69-15690

Crack propagation in plate with stiffening ribs /riveted stringers/ under concentrated and tensile loads, determining rivet points displacements
24 p4406 A69-43709

STRINGS

Nonlinear theory for whirling of heavy string under constant axial tension, considering orbitally stable modes for eigenvalues of rotation
13 p2359 A69-27264

Natural oscillations of loaded strings, membranes and geometric bodies with distributed loads treated as material discontinuities
20 p3578 A69-38292

Flexible string extraction from bobbin through nozzle, solving equations of motion by neglecting bending rigidity, extensibility, drag, internal friction, etc
22 p3930 A69-40585

STRIP

Infinite strip plane elastic problem reduced to Hilbert problem by employing multiply connected region and biharmonic solutions
15 p2707 A69-30625

Powder properties effect on rolled strip thickness and compactness, angles, pressure at roll and torsion during rolling, analyzing Fe, Ni and Cu powders
15 p2630 A69-31183

Elastoplastic boundary dynamic behavior in strip with crack determined by solving boundary value problem in elliptic integrals form
24 p4395 A69-42591

Plane problem of infinite strip weakened by crack, determining crack form under uniformly distributed tensile loads applied to edges
24 p4395 A69-42592

STRIPPING

Stripping and low-energy collisions of H atoms on O and N molecules, showing target ionization to projectile stripping ratio dependence on ionization potential
16 p2814 A69-31773

STROBOSCOPES

Stroboscopic holography for repetitive scenes, using mode locked laser as source
02 p0250 A69-12411

Stroboscopic technique for obtaining interferential holograms of vibrating transparent and reflecting plates
02 p0251 A69-12561

Device based on stroboscopic effect for observing crack propagation on rotating specimens during fatigue tests
05 p0843 A69-16665

Stroboscopic generator of trains of high brightness light flashes for hydrodynamic and gas dynamic research, noting electronic control and thyatron circuits
11 p1879 A69-24235

Monograph on laser stroboscopy in megahertz range covering spark photography comparison, concept of modes, resonators, applications, etc
11 p1893 A69-24368

Selective stroboscope with explosive bright light source and microsecond pulse duration for short flash period over large area, noting single frame separation method
12 p2086 A69-26162

Q switched ruby laser stroboscope for high speed photography, using electro-optical crystals for Q switch
12 p2086 A69-26167

Stroboscopic technique for obtaining interferential holograms of vibrating transparent and reflecting plates
15 p2608 A69-30258

X ray stroboscope for moving objects in penetrating irradiation, considering synchronization of radiation receiver
18 p3138 A69-35114

Topographic distribution of cortical potentials produced with tachistoscope and by stroboscopic stimulation, studying occipital and frontal differences
22 p3884 A69-40885

Stroboscope method for measuring pulsating flow transfer velocity based on hot-wire chronometric recording of small ion clouds emitted during pulsation
22 p3951 A69-41257

STRONTIUM

Moldavites and Ries crater material, studying Rb-Sr isochronal relationship
23 p4154 A69-41341

STRONTIUM ISOTOPES

Rubidium, Sr and Sr isotopic composition of normal gray hypersthene chondrite falls, noting Rb/Sr and Sr87/Sr86 ratio determination of Bath Furnace L chondrite isochron
02 p0317 A69-12020

Radiation ages of silicate inclusions in iron meteorites based on Sr evolution diagrams
08 p1405 A69-20927

Initial Sr isotopic composition at time of planetary objects formation in solar system and precision measurements for age determination of basaltic achondrites
11 p1953 A69-24357

Rb-Sr isotope patterns in tektites from Southeast Australian strewn field, studying Rb volatilization role in Rb-Sr isochron production
23 p4154 A69-41342

Rb-Sr isotopic determinations for Olivine olivine-hypersthene chondrite, noting isotopic ratio vs age
24 p4385 A69-43214

STRONTIUM TITANATES

Zr doped superconducting ceramic strontium titanate, noting effective electron mass variations and transition temperature
13 p2316 A69-27400

Electrical conductivity and optical spectra changes of strontium titanate single crystals under constant electric field action
15 p2666 A69-30043

Polarons large to nearly small transitions, studying ground state mass dependence on bare electron mass, electron-phonon interactions model, superconducting strontium titanate, etc
20 p3583 A69-37280

Waveguide-resonance investigation of temperature dependence of dielectric constant and paraelectric dispersion of Ba and Sr titanate single crystals at millimeter wavelengths
22 p3995 A69-41158

Temperature dependence of heat capacity of Ba and Sr titanate solid solutions in ferroelectric phase transition region
22 p3996 A69-41162

Dielectric polarization of barium titanate and barium strontium titanate in pulsed fields in paraelectric phase, analyzing coefficient B in free energy function and equilibrium state
22 p3996 A69-41165

STRONTIUM 90

Lithium doped solar cell irradiation by strontium 90 radioisotope, discussing electron flux rate, spectrum and recovery rates
19 p3251 A69-35693

Gisette 5 thermoelectric radioisotopic generator for submarine use, discussing strontium 90 as isotopic source
21 p3768 A69-38458

STROUHAL NUMBER

Discrete vortices in two dimensional subsonic and supersonic wake, determining Strouhal numbers, frequencies and flow velocities with aid of HF cinematography
02 p0191 A69-12587

Strouhal and Reynolds numbers relation from data on vortex streets of circular cylinder in two dimensional flow
07 p1119 A69-18749

STRUCTURAL ANALYSIS

NT BERNSTEIN ENERGY PRINCIPLE
NT DYNAMIC STRUCTURAL ANALYSIS
NT ENERGY METHODS
NT EQUILIBRIUM METHODS
NT FINITE ELEMENT METHOD
NT FLUTTER ANALYSIS
NT MATRIX METHODS
NT STRAIN ENERGY METHODS

Strength analysis of cylindrical shells with rib and ring reinforcement under compression loads using network method
01 p0164 A69-10083

Structural analysis by direct moment distribution, Volume 1, covering statistically indeterminate structures formed of prismatic members
01 p0165 A69-10156

Power spectral density method of random loads analysis applied to V/STOL aircraft structural analysis, discussing statistical distribution
01 p0168 A69-10407

Orthotropic plates bending and thermal stress, analyzing basic equations
01 p0168 A69-10416

Piecewise analysis of large structures, showing incompatibility of minimum computer storage and minimum number of multiplication requirements through bandwidth schemes
01 p0169 A69-10637

Multiple configuration analysis of structures systematically predicting static and dynamic response of structures of single configuration class
01 p0169 A69-10639

Two dimensional structural model of micropolar continuum involving orientable points joined by extensible and flexible rods
01 p0169 A69-10810

Ribbon reinforcements in composite materials noting stiffness properties
01 p0172 A69-11265

Contact problem of pair of nonhomogeneous semicircular regions solved by singular integral equations solution method
02 p0336 A69-11553

Thermoviscoelasticity equation solution for class of dynamic problems, giving problem solution for half space with arbitrary temperature field boundary condition
02 p0336 A69-11554

Long term creep characteristics of metal structures from short duration relaxation tests, summarizing data on rheologically stable materials
[ONERA-TP-639]
02 p0337 A69-11626

Three dimensional elastic theory using parametric expansion method developed for cylindrical translation shell profiles
02 p0338 A69-11718

Limit load analysis of three dimensional rigid perfectly plastic continua by approximate variational method
02 p0338 A69-11721

Computer solution of forced torsional oscillation equations for periodic coupled machine system with viscous dampers
02 p0338 A69-11893

Complex revolution vessels and multilobed structures analyzed by electronic computers, considering doubly stressed state of shells and bending moments from external forces
02 p0339 A69-11894

Plate theories derived via strain energy potential integration through thickness, noting constitutive equations applicability to elastic buckling and postbuckling
02 p0340 A69-12055

Thermostructural analysis of large flexible paraboloid antenna indicates RF losses due to thermal distortions significant for X band and higher transmissions
[AIAA PAPER 68-333]
02 p0345 A69-12372

Crystall structure of boron filaments vapor deposited on tungsten wire substrate, using X ray diffraction and transmission-electron microscopy
02 p0268 A69-12405

Structural influence on superconductivity of niobium-titanium alloys, using electron microscopy and measurements of current density vs magnetic field strength
02 p0269 A69-12763

Book on flight structure theory and analysis covering methods for digital computers, differential equations for equilibrium boundary value problems, etc
03 p0525 A69-13266

Applications of electronic computers in construction - Conference, Weimar, June-July 1967
03 p0525 A69-13734

Open and closed path orthogonal analysis for structural network
03 p0526 A69-13735

Numerical technique using transfer matrices to solve boundary value problems in structural analysis
03 p0526 A69-13736

Finite element method convergence introduced as general numerical technique related to Ritz method in structural analysis with digital computers
03 p0527 A69-13745

Universal solution for static and dynamic response of structural components by method of initial parameters 03 p0527 A69-13746

Symmetric structure stability with first and second order imperfections, analyzing discrete system with n degrees of freedom 03 p0529 A69-14062

Elastohereditary characteristics of composite materials with random inhomogeneities based on Volterra principle 04 p0667 A69-14263

Matrix perturbation method for hyperstatic structure modification by combining original solution elements with data on modification 04 p0668 A69-14380

Resistance wire strain gages for measuring elastoplastic deformations in zones with high stress concentrations of strained machine elements 04 p0671 A69-14433

Spar attachments of aircraft wings analyzed with respect to weight and applied loads, determining optimum bolt diameter ratio to lug width 04 p0673 A69-14496

Annular plate clamped at inner and outer boundaries and subject to point load, computing deflection 04 p0676 A69-14725

Testing techniques and graphical presentation of test results to determine resonant frequencies and oscillation modes in sporting gliders 04 p0549 A69-15420

Shear strength of grossly deformed solids noting extrusion and opposed anvils techniques 04 p0631 A69-15465

Moment curvature models under reverse cyclic straining developed from stress-strain curves for rectangular beams 04 p0683 A69-15497

Approximate equations in matrix form for analyzing complex semiconductor structures with p - n junctions 05 p0806 A69-15658

Stability functions for local buckling of long thin flat walled structures loaded for longitudinal compression and shear 05 p0833 A69-15709

Mathematical theory for describing geometric structure of simple bodies, discussing dislocation distribution and exact field equations for elastic bodies motion 05 p0834 A69-15731

Theory of inhomogeneous simple bodies applied for universal solutions for incompressible laminated bodies 05 p0834 A69-15732

Linear theory applied to anisotropic elastic materials, discussing transition from compressible to incompressible elastic materials 05 p0834 A69-15795

Static criterion for yield computation in plane two dimensional systems 05 p0836 A69-16013

Elastoplastic element structural growth induced by thermal cycling analyzed as function of temperature and sustained axial load [ASME PAPER 68-WA/MET-14] 05 p0837 A69-16067

Asymmetrically loaded systems composed of shells of revolution, developing digital computer algorithm for solution of statics problems 05 p0840 A69-16201

Weld-nugget formation in resistance spot welding, using high-speed photography on model section of spot weld 05 p0769 A69-16539

Statistical method to investigate time varying stresses in helicopter structures, considering service life evaluation 05 p0767 A69-16775

Calculation of thin shell or beam structures with plasticity and isothermal creep based on linearization and local kinematic behavior [ONERA-TP-667] 06 p1020 A69-17099

Nonlinear constrained optimization by nonrandom complex method demonstrated by minimum weight structural analysis of elastic ring and plate 06 p1022 A69-17366

Large paraboloid radio antennas structural setting for minimizing effects on performance due to deformation of surface by gravitational forces 06 p1023 A69-17372

Substructure optimization in structural synthesis, minimizing number of cells for configuration parameter [AIAA PAPER 69-121] 06 p1027 A69-18069

Turbulent boundary layer loading function for use with finite element structural analysis system applied to elastic aircraft structures random vibration [AIAA PAPER 69-20] 06 p0914 A69-18132

Digital computer simulation of nonlinear redundant structure variables including thermal influence, creep and arbitrary loads [AIAA PAPER 69-120] 06 p1028 A69-18166

Snapping and buckling of simple elastic structures under dynamic load, noting influence of structural geometry and load duration [AIAA PAPER 69-22] 06 p1029 A69-18206

Approximate solution for hollow circular cylinder with fixed ends under axial displacement and cylindrical surfaces free from traction, using boundary layer technique 07 p1230 A69-18265

Plane anisotropic rectangular plates with various boundary conditions, analyzing stability, natural frequencies, mode shapes and displacement under lateral loads 07 p1232 A69-18719

Phase and structural transformations in two phase quenched and aged titanium alloys, using electron microscopy and X ray analysis 07 p1162 A69-18776

Book on computer calculation of structures covering programming, computer language, mathematical aspects of structural analysis, matrix computation, etc 07 p1233 A69-19349

Collection of papers on mechanics of solid state covering structural stability, stress analysis, creep, cracking and fracture 07 p1234 A69-19377

Transient response of targets subjected to hyper-velocity impacts and quantitative aspects of impact process, noting study of wax targets interiors 07 p1234 A69-19380

Quadratic programming and theory of elastic perfectly plastic structures under holonomic laws, proving theorems of limit analysis 07 p1235 A69-19443

Sparse matrix scheme for computer analysis of structures, introducing term searching factor as efficiency guide for matrix routines 07 p1089 A69-19723

Mathematical theory generalization for smooth materially uniform simple bodies, discussing elastic body structure, material tangent bundle and index bundle, motion equations, etc 08 p1410 A69-19822

Direct plotting of vibrating wire strain gauge data for concrete structures, giving diagrams for grid and backing sheet scaling 08 p1312 A69-20104

Stereoradiography using holographic techniques to examine internal structure of opaque objects 08 p1313 A69-20178

Nb-Zr-Cr alloys solidus surface and isothermal sections, using optical pyrometry, microstructural and X ray analyses 08 p1333 A69-20440

Transverse vibration of beam rigidly fastened at one end, using series expansion in terms of set of eigenfunctions 08 p1414 A69-20445

Continuum stress/plastic strain relations from Schmid Law of plastic slip in individual crystal grains 08 p1414 A69-20525

Polar elastic media pure torsion solved, noting couple-stresses influence on Poynting effect 08 p1414 A69-20527

Complementary plastic work theorems in piecewise-linear elastoplasticity applied to plastic and nonlinear elastic problems 08 p1414 A69-20528

Second order tensor describing deformation of particles of continuum determined by functional, noting invariance restrictions 08 p1416 A69-20690

Matrix displacement method for nonlinear elastoplastic two or three dimensional structures or continua, discussing strain distribution 08 p1416 A69-20705

Optimization of plane smooth rectangular panels of constant cross section subjected to loading and heating conditions 08 p1417 A69-20821

Perturbation theory for branching analysis of perfect and imperfect discrete conservative structural systems 08 p1417 A69-20822

Incremental and corresponding total strain theories of plasticity used to analyze hydrostatic bulging of circular diaphragm 08 p1418 A69-20826

Compatibility theorem extension to three dimensional rigid plastic bodies with stress and velocity discontinuities, noting isotropic bodies with convex yield surface 08 p1418 A69-20845

Elastic stability of one dimensional structures analyzed by energy method, discussing deformable line, conservative forces and linear stability 08 p1418 A69-20846

Finite element analysis of large deflections in thin elastic plates subjected to transverse loading, including nonlinear geometric effects 09 p1615 A69-21924

Generalized orthogonality principles and expansion schemes for forced response of partial differential equations, noting applicability to rodlike structures 09 p1533 A69-21975

Flexible circular plate on elastic support connected at free edge, noting stress independent of working load 09 p1618 A69-22239

Multilayer pressure vessel load carrying capacity calculated, using Huber-Mises yield condition to estimate axial force influence 09 p1618 A69-22257

Unidirectional filamentary composites thermoelastic properties relation to constituent materials properties, using semiempirical micromechanics theory 09 p1530 A69-22320

High temperature magnetic testing and analysis of structure sensitive hysteresis properties 09 p1512 A69-22375

Inverse problem in stochastic processes, considering random moving force and strip load in structural stress analysis 10 p1793 A69-22876

Nonlinear Lagrange equations and iterative solutions for studying strain state of mechanical structures on basis of very small displacements 10 p1793 A69-22888

Finite element concepts for continuum theory of shells, noting bilinear approximation for displacement and fundamental decomposition principle for large deflection 10 p1794 A69-22891

Structures analysis by photoelastic model techniques of stress visualization 10 p1794 A69-22941

Dual continuum model of nonelastic processes in elasticity and dislocation theory, including incompatibility effects of interaction forces between structural elements 10 p1799 A69-23152

Microstructural analysis, determining junction orientation polarity effect on draw junction structure in GaSb crystals at room temperature 10 p1745 A69-23330

Thermal stresses for mixed boundary conditions calculated from combined use of integral transforms and variational techniques, reducing computational labor 10 p1801 A69-23429

Elastomeric solid propellant grains viscoelastic flow, analyzing stresses and strains under various operating conditions and rocket engine geometry effect 10 p1801 A69-23702

Pressure vessels burst tests for investigating alloys, fabrication processes and biaxial loading effects, noting vessel configurations and test temperatures 10 p1714 A69-23974

Structural fatigue life evaluation as cumulative damage analysis for irregularly varying loads [DVL-780] 10 p1802 A69-24020

Frequency response dynamics of beam type periodic structures on elastic supports typical in flight vehicle designs [ASME PAPER 69-VIBR-17] 10 p1804 A69-24150

Polymer fatigue model from low cycle analysis of dynamic and thermal properties in structural plastics 10 p1717 A69-24217

Three dimensional bending problem for thick isotropic plate with curvilinear hole and normal and tangential stress applied to edge of hole 11 p1973 A69-24657

Time scales for creep stress redistribution in structures subject to step loading 11 p1980 A69-24879

Nodal lines shape in individual flats for long plates in combined shear and compression with sinusoidal edge rotations in longitudinal direction 11 p1983 A69-25137

Stress-strain state of shells with opposite edges hinged and rigidly clamped solved by numerical method after reduction to boundary value problem 11 p1985 A69-25174

Hysteresis loop contour equation derivation based on energy dissipation dependence on stress amplitude in cyclically deformed vibrating system 11 p1985 A69-25176

Elastic bending moments and shear forces uniformly loaded flat plate structures with rectangular symmetry,

using collocation technique and complex variable methods 11 p1986 A69-25241

Dynamic stability of elastic beam type structures, using electronic simulation based on finite element approach 11 p1986 A69-25344

Shim joints design for composite material structural members reinforcement in joint region, considering weight factor [AIAA PAPER 68-341] 11 p1987 A69-25369

Back stress role in strain rate equation for high temperature deformation and study of structure and applied stress effects 11 p1987 A69-25388

Supersonic flutter solutions using finite elements, analyzing rectangular plate bending elements, square simply supported and clamped panels, low aspect ratio configurations, etc 11 p1991 A69-25516

Numerical prediction for nonlinear transient response of structures, considering geometric and material nonlinearities in systems with line elements 11 p1993 A69-25526

Optimum automatic selection of redundancies, discussing weighting and pivot choice and rigid element incorporation 11 p1993 A69-25529

Two and three dimensional quasi-static problems in coupled thermoelasticity, obtaining solutions for space containing cylindrical cavity and for solid cylinder 12 p2177 A69-25993

General perturbation theory for branching analysis of discrete structural systems, considering elastic post-buckling 12 p2179 A69-26213

Torsion in composite inhomogeneous circular cylinder, obtaining solutions for elastic displacements and stresses 12 p2180 A69-26274

Finite plane deformations theory extended to incompressible materials with logarithmic change of volume proportional to pressure 12 p2181 A69-26613

Automated Structural Analysis Procedure employing Displacement Method of Matrix analysis applied to validation studies of various finite elements for wing structures 12 p2184 A69-26809

Complex two layered shell of revolution under static and dynamic asymmetric loads analyzed using SABOR/DRASTIC computer codes 12 p2184 A69-26811

Thin ring-strut structure resting on elastic foundation, analyzing deformation taking warping effects into account, noting applicability to engine design 12 p2184 A69-26812

Computationally stable solution of finite element analysis of elastic-plastic response of nonlinear discrete structures loaded beyond yield load 12 p2185 A69-26819

Finite deflection discrete element analysis of sandwich plates and cylindrical shells with unbalanced laminated faces 12 p2185 A69-26821

Linear plate theory deficiency for large plate deflections, considering approximation of nonlinear behavior permitting changes in form without additional terms 12 p2185 A69-26822

Nonlinear structure undergoing arbitrary load history including temperature variations solved by computerized force and subordinated step procedure 12 p2185 A69-26823

Large deflection elastic-plastic analysis of axisymmetric shells of revolution indicating role of plastic yielding in buckling pressure reduction 12 p2186 A69-26839

Man machine interactive structural analysis using digital computer with CRT display, detailing design 12 p2035 A69-27098

Stiffness matrix derived for skewed curved shallow shell element with reference to oblique coordinate system 13 p2358 A69-27210

Continuum mechanics for brittle fracture analysis in metal structures, discussing plastic limit loads 13 p2275 A69-27228

Finite element displacement method extension to include geometric nonlinearity applied to arbitrary plate element, shallow cylindrical shell and shallow hyperbolic paraboloid 13 p2361 A69-27441

High velocity liquid lithium effect on structural materials for MHD power generators, discussing material loss 13 p2278 A69-27478

Control system for thin diffraction limited orbiting astronomical telescope mirror based on structural analysis of static deflections 13 p2261 A69-27951

Three dimensional harmonic dispersion analysis of incremental waves in uniaxially prestressed plastic and viscoplastic bars, plates and unbounded media 13 p2363 A69-28125

Strain resultants in finite quadrilateral elements, noting application to linear strain triangles 13 p2364 A69-28230

Higher order difference method for equilibrium and eigenvalue problems of two dimensional structures using iterative solution 13 p2365 A69-28239

Linear elastic structural analysis for one, two and three dimensional continua [ASME PAPER 69-DE-13] 14 p2531 A69-28843

Dynamic programming method applied to Cauchy problem of large deflections in compressed rods, using recurrent functional equations 14 p2533 A69-28988

Variational principles of solid mechanics for finite element analysis of solid continua 15 p2705 A69-30429

Elastic deformations of spherical sandwich shell of rigidly connected isotropic homogeneous layers, describing shell symmetrical expansion and inversion under stresses 15 p2707 A69-30582

Finite element analysis of flat rectangular panels, developing equilibrium equations based on specified displacement modes 15 p2708 A69-30667

Finite element analysis of flat rectangular orthotropic multilayer stiffened panels, proposing six degrees of freedom model 15 p2708 A69-30668

Uniaxial stress effects on molecular breakage rate, relating structure-sensitive parameter to elastic modulus 15 p2709 A69-30807

Taylor expansion applied to solution of nonlinear simultaneous algebraic equations in analyses of nonlinear structural systems using finite differences or elements 15 p2711 A69-30871

Economical computer techniques for numerically integrated finite elements, creating 96 element square matrix 15 p2711 A69-30873

Finite elements concept cast in topological framework, presenting generalizations of Lagrange and Hermite interpolation functions 15 p2711 A69-30874

Elastic anisotropic panels mechanics analyzed using differential equations stressing transverse displacements, anisotropic thermal expansion, shape imperfections and slip deformations 15 p2711 A69-30904

Expression derived for arbitrary system subjected to external loading, using Cauchy equations for relationship between external plane forces and internal stresses 15 p2713 A69-31018

Triangular shell element SHEBA for arbitrary curvature variation as means of performing large displacement matrix analyses, discussing local subelement, natural modes, cross sectional resultants, etc 16 p2872 A69-32025

Anisotropic conical shells free vibrations analyzed by Galerkin and operator-matrix methods, neglecting transverse shear deformation and rotatory inertia effects 16 p2874 A69-32165

Approximate equations in matrix form for analyzing complex semiconductor structures with p-n junctions 16 p2827 A69-32515

High temperature radial turbine design for small gas turbine engines, discussing aerodynamic, structural and thermal analyses [AIAA PAPER 69-524] 16 p2838 A69-32662

Two dimensional plate theory with moment stress considerations derived from three dimensional elasticity theory, discussing reduction of equilibrium and compatibility equations 16 p2876 A69-32786

Soviet collection of articles on theoretical and experimental investigations of strength of mechanical engineering structures 17 p3056 A69-33190

Discrete element displacement method applied to buckling analysis of flat rectangular plates under arbitrary membrane loading, calculating critical load intensities 17 p3066 A69-34048

Flexure functions of triangular sections under terminal loads, using electric analogy to study function effect on section shape and material Poisson ratio 17 p3066 A69-34050

Mass spectroscopic structural analysis of organic compounds, discussing computer application to data recording, processing and evaluation 18 p3099 A69-34553

Load analysis for elastoplastic bodies by Prandtl-Reuss theory and Mises yield condition, considering avoidance of difficulties associated with nonlinear partial differential equation solution 18 p3216 A69-34571

Two dimensional elastoplastic problems in static condition, discussing analytical, variational and finite difference methods 18 p3217 A69-34594

Buckling in process of loading idealized elastoplastic Shanley column, noting continuous increase possibility 18 p3217 A69-34596

State space procedure for mixed boundary value problems applied to structural analysis, fluid mechanics and eigenvalues for deformable bodies 18 p3164 A69-34685

Erectable metal booms and meshes structural analysis, design and mounting and deployment techniques for space applications 19 p3433 A69-35544

Book on moire fringes in strain analysis, discussing methods for strain measurement in deformed bodies and engineering structures 19 p3435 A69-35835

Structural analysis of thin walled conical shell with variable external loading and Winkler-base elastic filler, using linear differential equation with variable coefficients 19 p3436 A69-35846

Hollow cylinder plane stress-strain state analyzed for effect of variable modulus of elasticity of cylinder material 19 p3436 A69-35858

Finite element techniques of structural analysis for missile and space structures, including Apollo computerized analysis and structural optimization 19 p3438 A69-36324

Book on structural sandwich panels analysis and design covering beams and struts, bending theory, buckling, strain energy use, differential equations, etc 19 p3438 A69-36380

Thermal effects on viscoelastic structure response to applied loads, using equations for thermomechanics, linear and nonlinear thermoviscoelasticity and nonisothermal creep theorem 19 p3440 A69-36657

Limiting equilibrium stress state of unbounded brittle body with elliptical crack under monotonically increasing tensile or compression load, noting influence of crack curvature 19 p3441 A69-36745

Plastic tension of axisymmetric sample involving necking and small inhomogeneity, assuming Tresca yield condition and associated flow law 19 p3446 A69-36847

Static theory of fibrous surface media based on continuum mechanics, neighboring fibers noninteraction principle and additivity of mechanical properties 19 p3447 A69-36858

High temperature strain measurement based on strain gage with capacitance changes for structural analysis 20 p3537 A69-37006

Stress distribution in finite and semifinite solid cylinders under end normal load, using Fourier-Bessel series 20 p3621 A69-37199

Structural flexure center position from shear stress analysis showing nondependence on Poisson ratio 20 p3622 A69-37213

Equilibrium equations reduced to single partial differential equation for membrane theory of shells having coefficients of first quadratic form and specified curvature radius 20 p3622 A69-37220

Arbitrary circle distribution in plane transformed to corresponding distribution of spheres in space for size and shape distribution determination of disperse phase 20 p3627 A69-37764

Axial forces effects on dynamic load factors of beams under transverse impulsive loads, considering various end conditions 20 p3629 A69-38113

Holography application to three dimensional structure determination of weakly scattering semitransparent objects

20 p3546 A69-38198

Soviet book on thin plates and shells bending and stability during creep covering analytical and numerical solutions for various structural elements

20 p3630 A69-38207

Mathematical models and solution techniques for calculating optimal elastoplastic structures by computer, discussing methods for displacements preceding plastic failure

21 p3831 A69-38414

Holor algebra with tensor notations applied to elastic structures /discrete systems/, discussing inertia and stiffness tensors

21 p3831 A69-38415

Complex representation of strain and displacement state in spherical shell using membrane theory, deriving shear forces resulting from single moment loading

21 p3831 A69-38416

Multilayer sandwich panels containing unequal facings with distinct orthotropic cores, calculating dynamic load and stability of triangular panels

21 p3832 A69-38418

Stress-strain state of fiberglass reinforced plastics under load analyzed by anisotropic linear creep theory and Galerkin method

21 p3835 A69-38831

Computerized aircraft structural analysis system, adopting finite element technique /direct stiffness method/ based on COSMOS system

21 p3842 A69-39307

Creep buckling strength reduction of aircraft compression structure, discussing initial eccentricity and loading mode effects on supersonic aircraft operation mode

21 p3842 A69-39308

Automatic structural analysis by matrix force method, giving diagrams of load paths, equilibrium sequence and flow chart

21 p3843 A69-39311

Isoparametric finite element system for stress analysis, with examples for arch dam, impeller and cellular structure, illustrating shells of revolution

21 p3732 A69-39314

Curved shell elements in shell and plate analysis, discussing quadratic and cubic elements for space structures design

21 p3845 A69-39329

Soviet book on heat treatment of Ti alloys emphasizing structural and phase composition changes

21 p3749 A69-39526

Time-temperature method modified for combining stress relaxation data with stress or strain into single correlation curve, analyzing isothermal relaxation data

21 p3846 A69-39812

Stress distribution on surface of stator vane loaded statically as cantilever derived by brittle coatings, strain gages and three dimensional photoelasticity

22 p4042 A69-40310

Plate and shell structures static and dynamic analysis by generalized variational principles in finite element method, discussing element displacement functions

[AIAA PAPER 68-290] 23 p4227 A69-41882

Stress analysis of cylindrical tubes under torsional and transverse static loads based on vibrational theory, applied to rectangular cantilever tube

23 p4228 A69-41916

Complex configuration shells described by single analytical expression using R-conjunctive and R-disjunctive functions yielding boundary equations

23 p4229 A69-41991

Time averaged and fluctuating wind load effects on large radio telescope structures, discussing wind shear and turbulence influence on steady and unsteady loading

23 p4230 A69-42125

Structural analysis program for obtaining steerable antenna surface deflections at various altitude angles and wind conditions as design parameters

23 p4230 A69-42129

Rosman I reflector antenna for collecting data from earth orbiting satellites, discussing dynamic analysis of structural response to natural frequencies

23 p4231 A69-42133

Space frame radome shell structural stability with emphasis on analogous continua for reticulated framework, examining connection imperfections effect on stiffness

23 p4232 A69-42140

Nonlinear formulation for rigid jointed space frame comprised of prismatic linear elastic members, using Newton-Raphson and successive substitution methods

23 p4232 A69-42142

ASTRA /advanced structural analyzer/ based on stiffness approach to finite element method, generating mathematical model for stresses and deflections

23 p4232 A69-42144

NASA structural analysis /NASTRAN/ program applied to large radio telescopes, discussing static and dynamic analysis, problem formulation, finite element method, etc

23 p4232 A69-42145

Flat square plates loaded along two opposite straight edges, analyzing postbuckling behavior and geometric imperfections effects

23 p4234 A69-42395

Force maintaining rigid inclusion embedded in elastic plate with rigid boundaries

23 p4235 A69-42465

Mathematical flow graphs application in analysis and design of elastomechanical structural systems

[AAS PAPER 69-151] 24 p4339 A69-42816

Matrix method for analyzing elastic structures linear transient response to time dependent loads and temperature change

24 p4399 A69-42988

Circular plates axisymmetric nonlinear bending, using variational method to derive equilibrium equations and boundary conditions

24 p4399 A69-42989

Perforated heat exchanger tube plates stiffness determination from hole diameter-to-spacing ratios

24 p4400 A69-43087

Newton method providing continuing solutions of nonlinear differential equations through limit or bifurcation points, discussing elastic stability applications

[ASME PAPER 69-APMW-14] 24 p4401 A69-43102

Composite and metal tubes compared to determine properties for various loadings

[AIAA PAPER 68-340] 24 p4405 A69-43653

Composite media elastic moduli upper and lower bounds determination using variational principles to characterize displacement and stress in time harmonic deformation

24 p4406 A69-43701

STRUCTURAL BEAMS

U BEAMS (SUPPORTS)

STRUCTURAL DESIGN

NT PRESSURE VESSEL DESIGN

Space radiators for heat rejection from nuclear powered spacecraft doubling as primary structures to save weight, discussing conical or cylindrical configurations

01 p0160 A69-10151

Helicopter structures design for maximum practicable crashworthiness and survivability, comparing load factors and deformations with indicated human impacts tolerance

[AHS PAPER 225] 01 p0009 A69-10408

Chemical vapor deposited W and W-Re alloys for structural applications, discussing fabrication methods and effects on mechanical properties

01 p0096 A69-10641

Optimal structural design since 1962

01 p0170 A69-10814

Displacement function selection in calculating rubber-metal valve design, considering boundary conditions of material deformation

01 p0087 A69-10829

Triangulated pantograph structure for deploying antennas, special equipment and instruments from spacecraft, noting structural design and strength characteristics

02 p0252 A69-11752

Supersonic interference on lateral stability of planar configurations analyzed using wind tunnel data

[AIAA PAPER 68-21] 02 p0189 A69-12377

Structural designs for minimum flexibility or weight using energy intensity per unit mass parameter

02 p0345 A69-12380

Exact expressions for rates of change of eigenvalues and eigenvector to facilitate computerized design of complex structures

02 p0347 A69-12532

Mathematical programming in optimized truss design noting reduction of components under buckling

02 p0347 A69-12536

Alignment of rocket-borne instrument with sun, discussing mechanical system design, servocontrol and silicon photodiode sensors

03 p0427 A69-12980

Sandwich panel construction, examining design with respect to panel size, thickness and weight limit

03 p0524 A69-13124

Optimum structural design based on linear, nonlinear and dynamic programming

[SAE PAPER 680752] 03 p0525 A69-13437

Diffusion bonding and forming of large and complex Ti structures, noting advantages in freedom of design and in economy

[ASM PAPER C7-2.3] 04 p0604 A69-14525

Multidegree of freedom systems for modeling optimum design of cantilever and simply supported beams for sudden loading

04 p0674 A69-14590

Structural design options for decelerative aeroshell configurations for atmospheric entry on unmanned planetary explorations

[AIAA PAPER 68-344] 04 p0683 A69-15507

Book on plate formulas and tables for designing structure components of various geometrical shapes and thickness covering bending, compression, loading, etc

05 p0833 A69-15726

Lift fluctuation on airfoil due to transverse and chordwise gusts applied to rotating fan and compressor blade design

[ASME PAPER 68-FE-28] 05 p0697 A69-16070

Handbook of techniques in high pressure research and engineering, discussing construction materials, design and construction methods, measuring techniques, etc

07 p1137 A69-18412

Strain concentration design factors for notch effect in low cycle fatigue and crack propagation conditions

07 p1235 A69-19383

Optimum geometrical design of multipad externally pressurized journal bearings

07 p1141 A69-19439

Radomes developments for supersonic/hypersonic aircraft and missiles, considering conditions imposed by speed and by electronic requirements

07 p1171 A69-19508

Radomes design and manufacture for high speed flight vehicles, discussing interactions between aerodynamic and electrical requirements with reference to mechanism of aberration

07 p1141 A69-19510

Spherical sandwich radomes designs, discussing aerodynamic loads, wind pressure effect, electrical properties and mountings

07 p1112 A69-19538

Fail-safe design principles and criteria for helicopter structures to prevent operational failure arising from undetected fatigue damage

[AIAA PAPER 69-213] 07 p1054 A69-19549

Minimum weight analysis of Michell trusses transmitting given load to bars within allowable range of axial stress

08 p1410 A69-19893

Intelsat 2 satellite structural design for Apollo communications

08 p1408 A69-19907

Optical resonator as Q meter, discussing error capability and construction

08 p1312 A69-20106

Structural iterative design convergence to minimum weight proved by dual linear programming, discussing global convergence and convergence rate

08 p1413 A69-20351

Fiber composite design, discussing contribution of filament diameter, number, content and properties, ply parameters and void content to structural response

08 p1341 A69-20512

Curved tetrahedral and triangular elements in matrix displacement method covering linear and nonlinear cases

08 p1415 A69-20631

Optimal design of circular cylindrical sandwich shells under pressure and shear loads, showing acceptability of small shear coefficient values

08 p1416 A69-20722

Minimum weight plastic design of circular and annular sandwich plates with piecewise constant cross section, discussing cost reduction

08 p1417 A69-20823

Design parameters for optimum heavily loaded single rotation ducted fan characterized by ultimate wake vortex system

[AIAA PAPER 69-222] 08 p1253 A69-21030

Roll diffusion bonding technique for permitting complex design of coldplates and radiators of spacecraft electronic equipment

09 p1504 A69-22066

Fatigue strength and aircraft structural standards based on experimentally determined safety factors

09 p1619 A69-22571

Optimum design of shells loaded by concentrated forces, discussing thickness relation to middle surface, loading point and manufacturing considerations
11 p1979 A69-24812

Stress analysis, Volume 12, Theoretical and experimental studies of strength of machine structures
11 p1980 A69-24940

Aircraft structure geometry design for minimizing total mass concerning flutter requirements
11 p1989 A69-25493

Complex structure least weight optimization for specific frequency by computerized modification of existing member cross sectional properties
11 p1989 A69-25494

Structural optimization of designs with requirements including restrictions on structure dynamic response and characteristics
11 p1989 A69-25495

Optimal design of structures with constraints on strength and natural frequency, developing steepest descent boundary value method
11 p1989 A69-25496

Flutter design charts for isotropic panels stressed to verge of buckling for typical values of structural damping
11 p1992 A69-25524

Composite materials for aerospace applications, discussing high modulus filaments, structural and non-structural design considerations, nondestructive testing techniques, etc
12 p2111 A69-25852

Isaac Newton telescope, describing support of 98 inch mirror, structure between fabricated cell steel surface and mirror and tests with air bag support
12 p2058 A69-26416

Construction techniques for lightweight mirrors for secondaries, considering optical finishing and thermal expansion
12 p2058 A69-26420

Book on hovercraft design and construction covering aerostatic and aerodynamic craft, cushion performance, ducting, fans, compressors, drag, propulsion, control, stability, economics
12 p2013 A69-26633

Shock pulse criterion limitations and HF transients technique for design and tests of structures and components
12 p2182 A69-26731

Systems design of airframe structures taking into account material characteristics noting structural stability, shell postbuckling, fail-safe designs, etc
12 p2186 A69-26833

Space propulsion system design with consideration for launch and mission requirements, noting upper stage structural design and computer techniques
12 p2148 A69-26834

Fatigue crack propagation and fail-safe design for stiffened large Al alloy panels with crack stoppers, using residual strength analysis method
12 p2186 A69-26835

Thermostuctural simulation of lifting vehicle panel design, considering safety and trajectory shaping of flying laboratory
12 p2060 A69-26836

AZUR German research satellite main structure dynamic characteristics, solar panels, yo-yo despin system, electronic ignition devices and magnetometer boom
12 p2175 A69-26875

Aesthetic preservation of visual amenities in countryside by proper antenna design without affecting performance or cost
12 p2044 A69-26924

Minimum volume face sheet design of circular cylindrical sandwich shell obeying Mises yield criterion for loads transverse to lateral surface and axisymmetric
12 p2189 A69-27117

Optimal design of rectangular frames for stability
13 p2358 A69-27209

MHD generators semihot wall duct, discussing structural design, ceramic insulation elements brazing, temperature control, electrodes, working fluid, etc
13 p2372 A69-27473

Glass reinforced plastics for Hovermarine HM.2 sidewall hovercraft designed for ferry routes
13 p2201 A69-27542

Spacecraft construction materials and strength problems including stress-strain determination, thin shell structural stability, dynamic loads, heat resistance, fiber-reinforced composites, ablation materials, etc
13 p2362 A69-27920

Shock tubes and tunnels design and operation principles for investigating physical and chemical phenomena
13 p2240 A69-27930

Trident 2E and 3B structural design and fail-safe tests, noting difference in fuselage length
13 p2202 A69-27972

Minimum weight design of structures excited to harmonic vibrations by given single load, with intensity dependent on time
13 p2369 A69-28350

European space program developmental and fabrication problems in satellite structure development covering booster constraints, mission constraints, tolerances, etc
13 p2357 A69-28479

Rotating disk of nonuniform thickness, establishing optimum geometry for minimum tangential stress [ASME PAPER 69-DE-36]
14 p2454 A69-28841

Linear elastic structural analysis for one, two and three dimensional continua [ASME PAPER 69-DE-13]
14 p2531 A69-28843

Shock load protection through energy absorption and dissipation in primary or composite structures, listing honeycomb, cellular plastics and rubber mechanical properties [ASME PAPER 69-DE-37]
14 p2531 A69-28846

Power gyro stabilizer kinematic structure synthesis, applying matrix methods to design variables
14 p2446 A69-28924

All metal nuclear thermionic modular converter, discussing applications, design and material requirements or limitations
14 p2398 A69-29181

Composite airframe structural joint design and weight considerations for boron and glass fiber reinforced plastic materials [ASM PAPER W9-23.1]
14 p2535 A69-29448

Fatigue design procedures - Conference Munich, June 1965
15 p2705 A69-30355

Design and test criteria for dynamically loaded structures from various viewpoints, discussing statistical variations, load strength and limitations
15 p2618 A69-30368

Mountbatten /SR.N4/ hovercraft development, seakeeping, skirt design and service introduction
15 p2550 A69-30479

Gun projectiles assisted by solid propellant motor to increase range, discussing construction, performance and free-wheeling rotation band use
15 p2702 A69-30592

Radio astronomical research developments including structural requirements for 100 m telescope
15 p2589 A69-30864

Sailplanes design, discussing structural flexibility, deformations, aeroelastic effects and plastics and man-made fibers
15 p2551 A69-30899

Concorde aircrew seats design for electric operated tracking and lift, vertical movement accommodation seat and back tilt
15 p2553 A69-31167

Full stress design feasibility as function of load conditions, indeterminacy order and structure topology
16 p2872 A69-31915

High strength fibers and composite materials for structural design, considering anisotropy and low ultimate tensile strain
16 p2802 A69-32380

Fatigue data adapted to conditions of specific design part including fatigue limits, S-N curves and various failure diagrams
16 p2794 A69-32433

Short life fatigue data for metals, noting applications in design
17 p3052 A69-32978

Random stress statistical properties and relationship to fatigue life, discussing Fuller prediction, comparison with test data, and vehicle design evaluation
17 p3053 A69-32988

Stress-strain state determination for axisymmetric shells applied to design of circular/annular plates and rotating disks
17 p3057 A69-33194

Rotary wing aircraft speed boundary widening without impairing low speed attributes, discussing structural design factors, airframe design and stability, etc
17 p2897 A69-33209

Critical review of paper on tail rotor structural design principles covering sizing, blade frequency and response and aeroelasticity [AHS PAPER 342A]
17 p3059 A69-33503

Papers on fracture, Volume 5, Fracture design of structures
17 p3060 A69-33559

Arrest mechanisms to halt crack before gross failure, involving material toughness exploitation and subding stress by structural configuration
17 p3060 A69-33560

Rotating machinery fracture and design approach based on effect of detailed stress and strain duty on imperfect materials metallurgical behavior
17 p3060 A69-33561

Fracture safe design practices for pressure vessels and piping, stressing transition temperature and proof testing roles
17 p3060 A69-33566

Fracture design for aircraft vehicles, discussing crack strength requirements and method for serviceability prediction
17 p3060 A69-33563

Elastic sandwich structures design for maximum strength, using potential energy functional to derive governing equations
17 p3062 A69-33708

Network synthesis technique applied to structural dynamics design, using topological formulas to express systems response transfer functions
17 p2933 A69-33709

Directional transmitting and receiving antenna arrays for short wave meteor studies in Kharkov
17 p2939 A69-33903

Monopulse parabolic antenna radiator design for decimeter and meter wavelengths, discussing characteristic properties at optimal dimensions
17 p2939 A69-33905

Minimum weight design of tiltable enclosed antenna structure as subject to deformation constraints
18 p3211 A69-34341

Carrying cables shape optimization for suspended structures under load, using minimum weight criterion
18 p3212 A69-34354

High speed ball bearing skidding, proposing analytic model as design tool, discussing effects of thrust load, speed, oil temperature and flow rate [ASME PAPER 69-LUBS-20]
18 p3140 A69-34377

Composite materials behavior studies for structural applications, using macroscopic and microscopic phenomenological approach
18 p3154 A69-34607

Extreme disturbance analysis and optimum performance and design problems for structural and mechanical dynamic systems, basing solutions on linear, nonlinear and dynamic programming
18 p3106 A69-34663

Lightweight structural design problem of stress concentration associated with load diffusion in rectangular panels with constant stress flanges
18 p3219 A69-34785

Algorithm for minimum weight structures automated design, coupling strain energy criteria with linear interpolation search technique to cover stress and displacement constraints [SAWE PAPER 798]
18 p3219 A69-34861

Army OH-6A helicopter light weight design, considering effects of WRAP /weight, radius, area, power/ factors on empty weight [SAWE PAPER 781]
18 p3091 A69-34870

Aerospace structures optimization, discussing weight considerations and finite element techniques [SAWE PAPER 814]
18 p3221 A69-34896

Erectable metal booms and meshes structural analysis, design and mounting and deployment techniques for space applications
19 p3433 A69-35544

Rigidity of rotors with pin joints, calculating moments of inertia at connected sections of turbine shaft disks utilizing similarity concept
19 p3324 A69-35832

Subsystem designs evaluated on basis of human reliability metric to select desirable design configurations
19 p3261 A69-36026

Structural design optimization based on reliability analysis stressing proof-load test and weight savings consideration under cost constraint
19 p3437 A69-36033

Aircraft structures design, discussing reinforced sandwiches and composites, failure mechanisms, non-destructive testing and fabrication
19 p3438 A69-36325

Book on structural sandwich panels analysis and design covering beams and struts, bending theory, buckling, strain energy use, differential equations, etc
19 p3438 A69-36380

Turbocompressors, reviewing axial and radial compressors
19 p3395 A69-36749

Helicopter rotor blade construction and development, discussing mass balance, fatigue life, fail-safe characteristics, cost and weight ceiling and plastic materials

19 p3329 A69-36768

Design laws of warping-free multicellular box beams under torsion or bending, using variational method

19 p3443 A69-36786

Laminated composites ultimate strength prediction based on consecutive yield procedure with step-wise reduction of strength or load-carrying capacity used as design criterion

20 p3627 A69-37773

Aerodynamic skin heating at high Mach numbers affecting structural design, noting use of high temperature materials, insulation systems and shell construction method

21 p3646 A69-38460

Design and processing tradeoffs for preventing stress corrosion cracking in Al alloy aircraft structural forgings

[ASM PAPER W9-14.4] 21 p3729 A69-38657

Structural design for minimum weight under random loads representing steady vector random function

21 p3731 A69-38870

Composite or sandwich construction design based on employing all available materials and setting up requirements for mechanical and physical properties

21 p3836 A69-38935

Structural and aerodynamic developments in attached inflatable decelerators for deployment of payload at supersonic speeds

[AIAA PAPER 68-929] 21 p3647 A69-39015

Impact limiter system design for Mars landing vehicle noting balsa wood or phenolic honeycomb construction

[AIAA PAPER 68-161] 21 p3820 A69-39228

Hypersonic parachute structural design using nylon ribbon, glass fiber heat shield and ablative coating construction

[AIAA PAPER 68-963] 21 p3647 A69-39230

Sequential design for economic description of potentially redundant elastic structures, noting redesign sequence

21 p3842 A69-39302

Design features comparison and operation principles of gas strain gauges in application to structures, emphasizing independence of temperature variations in pneumatic circuits

21 p3725 A69-39324

Superconducting magnets for MHD generators, discussing design, construction and operation problems

21 p3782 A69-39478

Boron and carbon reinforced composite materials aerospace structural application, discussing weight savings, components structural design and connection and load input problems

22 p4038 A69-39908

Scientific balloon vehicle design and development approaches for altitude, flight duration and payload capacity extension, discussing plastic balloons

22 p3865 A69-40812

Fatigue collapse probability of fail-safe structure compared to safety factor design

22 p4045 A69-40820

Pressure transducers using heterodyne strain sensors evaporated directly onto pressure diaphragm

22 p3950 A69-41222

Minimum radius of three dimensional cam gears calculated from driven element motion and pressure angle

23 p4168 A69-41413

Minimum weight and optimal cross sections design for statically determinate and indeterminate shell and H beams, using variational method

23 p4225 A69-41424

Modular configuration of recoverable scientific MAP (Modular Auroral Probe) payloads aboard Nike-Apache rockets, discussing payload design concepts

23 p4223 A69-41763

Potential energy modeling method for optimal design of structural systems with diverse performance criteria, giving truss design example

23 p4228 A69-41923

Rib cross sections distribution for cylindrical shell under concentrated longitudinal forces obtainable by designing for minimum strain energy

23 p4228 A69-41988

Thin walled rods for girder and frame systems designed by matrix method, solving differential equations for tension, compression, bending and torsion

23 p4230 A69-42005

Ridge-slot-ridge slow-wave structures used in multibeam TWT (traveling wave tube), analyzing E type electromagnetic dispersion as function of system parameters

23 p4140 A69-42049

Structural technology for large radio and radar telescope systems - Conference, Cambridge, Mass., October 1967

23 p4147 A69-42120

Structural features and performance of 300 ft steerable receiving antenna, discussing aiming error, aperture efficiency, azimuth and altitude drive

23 p4148 A69-42121

Computerized evaluation of elastic deformations of 100 m parabolic reflector designs for Max Planck Institute radio telescope, outlining supports and dish structure

23 p4148 A69-42122

Structural analysis program for obtaining steerable antenna surface deflections at various altitude angles and wind conditions as design parameters

23 p4230 A69-42129

Canadian radio observatory 150 ft telescope antenna, discussing dish structural feature for resisting gravity, wind and thermal stresses

23 p4149 A69-42134

Large paraboloidal reflector antenna computerized structural design, detailing framing, steering control, support structure, etc

23 p4231 A69-42135

Metal space frame radome design, considering electromagnetic performance, structural integrity, cost, membrane structures stability, etc

23 p4231 A69-42139

Integrated civil engineering system /ICES/ and structural design language /STRUDL/ programming and operating characteristics, including computer run example

23 p4134 A69-42146

Structural aircraft design requirements for high flight speeds stressing aerodynamic heating, heat resistant materials, weight and geometry problems

23 p4233 A69-42164

Li, Na and K heat pipes for high temperature emitter and low temperature collector thermionic applications

23 p4074 A69-42297

Pumping pore size and permeability of wicks as part of heat pipes design

23 p4074 A69-42298

Causes of ascent failures in high altitude balloons, discussing test methods and specifications revisions

24 p4251 A69-42714

Stress analysis in design techniques taking into account failure of flawed structures, discussing fracture mechanics

24 p4398 A69-42773

Mathematical flow graphs application in analysis and design of elastomechanical structural systems

[AAS PAPER 69-151] 24 p4339 A69-42816

Materials research structural design cycle, discussing simultaneous optimization, constituent materials, fabrication process, load environment and mission constraints

24 p4399 A69-42991

Linear viscoelastic model parameters optimization for designing automobile lap seat belts, assuming abrupt impact stop

[ASME PAPER 69-APMW-25]

24 p4275 A69-43094

Li-F-H tripropellant study, discussing injection method variations and thrust chamber configuration effects on characteristic velocity efficiency and heat flux measurement

24 p4362 A69-43128

Structural analysis and statistical fracture approach to design and testing for polycrystalline ceramic materials, including combined stress testing and load redistribution models

24 p4333 A69-43339

Nucleate boiling effect on operation of low temperature heat pipes, using everted stainless steel to permit visualization of wick structure and bubble nucleation

[ASME PAPER 69-HT-24]

24 p4412 A69-43544

STRUCTURAL DYNAMICS

U DYNAMIC STRUCTURAL ANALYSIS

STRUCTURAL ENGINEERING

Tubular metal parts and assemblies, discussing flaring, forming, beading, tapering and step drawing

03 p0435 A69-13918

Engineering glass manufacturing, properties and applications in buildings, vehicles, lamp and electronic devices, etc

04 p0619 A69-14585

Applied mechanics yearbook covering shell theory, elastic stability and other problems

05 p0831 A69-15685

Matrix method for structural analysis using force and rigidity methods

07 p1239 A69-19776

Development of materials in aerospace structures and propulsion systems, discussing superelastic alloys, graphite fibers, composites, refractory metals and processing techniques

08 p1332 A69-20306

AZUR satellite structural development static and dynamic considerations, discussing center of gravity, notching technique and test results

12 p2187 A69-26876

Aircraft noise alleviation through flight procedures improvement, home building modification and noise standards legislation

14 p2392 A69-29154

Integrated structural and dynamic testing plans for proposed large interplanetary spacecraft, discussing acoustic testing, testing environments and flight environment transformation into laboratory

15 p2588 A69-30399

Linear theory of elastic stability of structures, discussing deformation kinematics, perturbed and neutral equilibria and solutions for buckling of beams, plate, shells, etc

17 p3054 A69-33042

Radio telescope for radio astronomy in Bonn, discussing structural and operational problems

17 p2975 A69-33702

Solid and structural mechanics theories noting continuum mechanics role

19 p3443 A69-36776

Radio telescope structure material selection criteria, developing deformability criteria for structures under various stresses

20 p3546 A69-38306

Mohr tensor representation and Mohr theorem proof developed for general problem in structural engineering

22 p4038 A69-39903

Programming aspects of computer uses in civil engineering, stressing engineer-coder communication via flow diagrams

22 p3903 A69-40138

Coding aspects of computers use in civil engineering, discussing language selection, program partitioning and storage use

22 p3903 A69-40139

Documentation aspects of computer programs use in civil engineering, describing maintenance, users and operators manuals

22 p3904 A69-40140

Integrated civil engineering system /ICES/ and structural design language /STRUDL/ programming and operating characteristics, including computer run example

23 p4134 A69-42146

Airplane structure electromagnetic compatibility engineering problem including bonding, electrointerference suppression and static control considerations

23 p4063 A69-42234

Ti-Al alloy structure manufacturing technology covering forming, cleaning, chem-milling, machining, fastening and welding

24 p4324 A69-43431

STRUCTURAL FAILURE

Composite material mechanical failure due to detachment of microfiber ends from elastic matrix while under tension

01 p0171 A69-11259

Fracture toughness concept in predicting failure of materials due to sharp notches or cracks

02 p0336 A69-11431

Fatigue properties and failure mechanisms of glass reinforced plastics based on chopped strand mat-polyester resin laminates

02 p0269 A69-11795

Composite tensile-failure modes, discussing failure load prediction, experimental data and statistical analysis of stress concentration effects

02 p0347 A69-12514

Liquid metal adsorption induced embrittlement, noting bond strength reduction and grain boundaries penetration

03 p0448 A69-13872

Random cumulative damage theory for fatigue failure of steel under sinusoidal loading taking into account randomness of time to failure and possession of memory

04 p0680 A69-15154

Fracture surface topography and applications to fracture analysis of laboratory and service failures, describing fracture models

04 p0619 A69-15394

General linear theory of isotropic cumulative fatigue involving phenomenological consideration of fatigue damage accumulation

[ASME PAPER 68-WA/MET-6]

- 05 p0838 A69-16149
Collection of papers on metal fatigue theory and design
- 06 p1024 A69-17525
Stress-strain response up to ultimate failure and ultimate strength of laminated composite with nonlinear orthotropic lamina
- 07 p1170 A69-18710
Laminated composite fracture statistical theory with stress enhancements in elements next to primary fracture, comparing elastic and plastic matrices
- 07 p1170 A69-18712
Rupture times in analysis of creep tensile instability in uniformly pressurized thin walled membrane shells of revolution, comparing two criteria
- 07 p1234 A69-19378
Flow fracture and rheological properties of viscoelastic material under biaxial loading
- 07 p1202 A69-19386
Neurological impairment in baboons exposed to prolonged decompression simulating high altitude aircraft cabin structural failure, noting neuropathological examination results
- 07 p1067 A69-19426
Fail-safe design principles and criteria for helicopter structures to prevent operational failure arising from undetected fatigue damage
[AIAA PAPER 69-213]
- 07 p1054 A69-19549
Stress analysis split method for determining residual strength and fatigue crack life of damaged or initially cracked VTOL structures
[AIAA PAPER 69-214]
- 07 p1237 A69-19576
High pressure storage vessels for gaseous hydrogen, discussing failure, manufacturing controls and access for internal nondestructive inspection
[ASM PAPER D8-14.1]
- 07 p1143 A69-19666
Critical analysis of Sedov contention of infinite stress development at ends of brittle cracks
- 07 p1238 A69-19690
Stresses nature at ends of brittle cracks, discrediting finiteness under certain conditions
- 07 p1238 A69-19691
Translunar cracks in laminated graphite filament composites, noting effect of thermal stresses due to cooling
- 08 p1337 A69-20483
Variational method for safety limits of perfectly plastic simply supported conical sandwich shells subjected to uniform internal pressure and obeying Mises yield criterion
- 08 p1416 A69-20702
Failure causes for planetary reduction gear tooth for adjustment of radio telescopic antennas, studying fracture characteristics, working conditions and loading moments
- 08 p1321 A69-20853
Failure criteria for predicting filamentary composite strength under uniaxial and combined stresses from properties and fabrication process considerations
- 09 p1611 A69-21479
Failure modes in fiberglass reinforced epoxy laminates subjected to compression loadings, discussing cracks formation and delamination at glass-resin interface
- 09 p1529 A69-22305
Algorithm in fault detection and isolation, discussing test optimization for complex systems or structures subject to failure
- 10 p1698 A69-22978
Stress corrosion of nonage-hardenable Al-Mg-Cr alloy investigated for failure in absence of grain boundary precipitate, using notched specimens
- 10 p1709 A69-23055
Low cycle fatigue of metals under biaxial strain, considering specimen life and strain amplitude correlation
- 10 p1797 A69-23083
Temperature and strain rates effect on delayed yield and failure of plasticized epoxy resin
- 10 p1717 A69-24218
Statistical parameters of critical load distribution in buckling of imperfection sensitive elastic structures, noting probability of failure
- 11 p1969 A69-24415
Aircraft structures fatigue strength determination, discussing test procedures, sample preparation, strength prediction, etc
- 11 p1970 A69-24525
Book on strength and failure of viscoelastic materials covering linear and three dimensional polymers or polymer-based materials, flexibility and temperature effects
- 11 p1970 A69-24610
Incremental collapse of shells under cyclic loadings in terms of generalized variables, finding interaction surfaces of load multipliers
- 11 p1980 A69-24820

- Tresca shear stress fatigue failure criterion and experimental data for combined bending and torsion acting out of phase
- 11 p1984 A69-25140
Aircraft structures fatigue life determination based on Kordonskii method, comparing steel tests result with linear summation theory
- 11 p1987 A69-25345
First excursion failure survival probability of randomly excited structures, considering single degree of freedom linear oscillator under Gaussian white noise
- 11 p1990 A69-25505
Tensile strength and failure loading evaluation for structure, discussing stresses in neighborhood of crack, crack toughness measurement and fracture mechanics
- 12 p2176 A69-25861
Computationally stable solution of finite element analysis of elastic-plastic response of nonlinear discrete structures loaded beyond yield load
- 12 p2185 A69-26819
Local failure of axially loaded plastic foam core sandwich panels, using face wrinkling analysis procedures
- 13 p2357 A69-27207
General linear theory of isotropic cumulative failure involving phenomenological consideration of fatigue damage accumulation
[ASME PAPER 68-WA/MET-6]
- 14 p2535 A69-29436
Nonlinear programming for calculating static and kinematic failure of one dimensional structures by extending results from linear programming
- 14 p2418 A69-29597
Stress corrosion in smooth and prenotched maraging steels exposed to sodium chloride solution and natural sea water
- 14 p2467 A69-29940
Structural fatigue-inducing random load spectrum analyzed and computed for laboratory simulation
- 15 p2705 A69-30363
Materials and structural failures under short time compressive loadings, showing structural response to tensile stresses produced by rarefaction waves
- 15 p2639 A69-30364
Reaction rate theory for dilatational failure of heterogeneous materials subjected to stress
- 15 p2710 A69-30813
Fatigue life gage on operational aircraft providing in situ monitoring of fatigue damage prior to and during propagation of running fatigue cracks
- 15 p2613 A69-31271
Automated IR fatigue crack detection in sonic test facility capable of subjecting large aircraft or missile structures to intense sound fields
- 15 p2631 A69-31505
Deformation detection by stress wave analysis technique /SWAT/, noting pressure vessel applications
- 18 p3223 A69-35080
Isotropic plate critical strength measurements, evaluating role of material shear modulus
- 18 p3225 A69-35361
Fractography of compact fracture toughness specimens failure, noting stress at fracture origin and crack growth rate
- 20 p3557 A69-36957
Torsional-flexural buckling of thin walled open sections under eccentric load, emphasizing singly symmetric sections loaded in plane of symmetry
- 20 p3625 A69-37653
Boron fiber reinforced Al alloys spall failure and shock induced filament damage, using flyer plate technique
- 20 p3562 A69-37772
Curved beams ultimate strength using angular velocity considerations for collapse load
- 20 p3629 A69-38031
Decompression study simulating supersonic aircraft cabin small structural failure at 60,000 ft, using monkeys as subjects
- 21 p3665 A69-39171
Snap through in thin shells with initial irregularities during creep, determining critical time to failure by analyzing undisturbed buckling process
- 21 p3838 A69-39188
Brittle failure models, discussing rheological properties, Griffith energy criterion properties, crack behavior in elastic and linear viscoelastic media, etc
- 21 p3839 A69-39194
Scattered light mean intensity determination in twilight aerosol atmosphere from satellite observations, formulating boundary value problem
- 21 p3717 A69-39656
Deformation of thin walled spherical shell reinforced with equatorial hoop by concentric equal forces
- 21 p3846 A69-39714

Fatigue collapse probability of fail-safe structure compared to safety factor design

22 p4045 A69-40820
Polymer film breakdown under impact of supersonic plasma beam pulses from capillary discharge chamber, including photomicrographs of cavities and structural defects

22 p3974 A69-41031
Scale factor in designing uniform strength structures for dynamic load effects determined by recording fatigue limit and failure location, using variable cross section samples

23 p4225 A69-41422
Fatigue tests with cylindrical samples for observation of macrocrack formation and propagation at bottom of notches, discussing kinetics of fatigue failure

23 p4225 A69-41425
Space frame radome model elastic buckling tests for load deflection and maximum load predictions, considering individual beam failure and complex instability

23 p4232 A69-42143
Structural changes in subsurface layer and surface microgeometry factors of metal fatigue failure, explaining crack formation and propagation

24 p4395 A69-42559
Causes of ascent failures in high altitude balloons, discussing test methods and specifications revisions

24 p4251 A69-42714
Postbuckling analysis by equilibrium solutions of conservative system near critical point, considering stability failure in elastic structure under increasing load

24 p4396 A69-42730
Structural materials deformation response to loading conditions and stress or strain cycle analysis to predict failure, including creep and stress relaxation

24 p4398 A69-42771
Stress analysis in design techniques taking into account failure of flawed structures, discussing fracture mechanics

24 p4398 A69-42773
Civil aircraft structural components failure analysis, discussing fatigue failures and fail-safe design for accident prevention

24 p4251 A69-42779
Long term fatigue tests of wooden gliders, discussing structural materials fatigue strength and glider strain spectra

24 p4398 A69-42912
Model for estimating creep life of material containing wedge crack growth

24 p4399 A69-43032
Structural airframe fasteners, reviewing systems for fatigue critical wing/fuselage structures, honeycomb panel attachments and data on fatigue life

24 p4325 A69-43437
Various fasteners influence on fatigue life of bolted joints, noting high clamping force beneficial effect

24 p4325 A69-43438
Damping influence on shallow arch static and dynamic snapping under step pressure load

STRUCTURAL FATIGUE U FATIGUE [MATERIALS] STRUCTURAL FOUNDATIONS U FOUNDATIONS

STRUCTURAL INFLUENCE COEFFICIENTS

Duality between effect and influence problems in linear elastoplasticity, obtaining rules for influence functions plotting

09 p1612 A69-21604
Structural influence coefficients from vibration test modes and frequencies, eliminating errors by Gram-Schmidt orthogonalization

STRUCTURAL MATERIALS U CONSTRUCTION MATERIALS STRUCTURAL MEMBERS

- NT ANISOTROPIC PLATES
NT ANNULAR PLATES
NT BEAMS [SUPPORTS]
NT BOX BEAMS
NT CANTILEVER BEAMS
NT CANTILEVER PLATES
NT CIRCULAR PLATES
NT COLUMNS [SUPPORTS]
NT CORRUGATED PLATES
NT CURVED BEAMS
NT ELASTIC PLATES
NT END PLATES
NT FLAT PLATES
NT GIRDERS
NT I BEAMS
NT MEMBRANE STRUCTURES
NT ORTHOTROPIC PLATES
NT PERFORATED PLATES
NT PLATES [STRUCTURAL MEMBERS]

NT POROUS PLATES
 NT RECTANGULAR BEAMS
 NT REINFORCED PLATES
 NT SKIN [STRUCTURAL MEMBER]
 NT STRINGERS
 NT STRUTS
 NT TAPERED COLUMNS
 NT TRUSSES

Fatigue endurance of structural elements determined from stress rupture strength under high and low loading rates

04 p0673 A69-14536

Spring supported hydrostatic shaft seal with floating members isolated from structure
 [ASME PAPER 68-WA/LUB-9]

05 p0768 A69-16132

Static endurance of aircraft structural elements under single and multiple loading, based on real alloys and crystalline materials theories

07 p1231 A69-18554

Strength increase in steel components of aircraft, missiles and submersibles in relation to chronological application sequence, discussing ultimate strength
 [ASM PAPER GG8-9.4]

07 p1169 A69-19675

Stress relaxation in structural elements, analyzing unsteady creep in case of strain hardening following power law

07 p1237 A69-19683

Bar flexure determination for Saint Venant torsional and transverse loading, solving differential equations by finite element methods

09 p1614 A69-21722

Mathematical model for improving statistical approximation convergence and accuracy in estimating structural components parameters

09 p1461 A69-21857

Aluminum bonded structures corrosion resistance through adhesive primers and surface treatments

10 p1700 A69-24088

Flat bar optimal cross section under tensile stress applied to minimize stress in large structural components using elasticity theory

11 p1986 A69-25203

Shim joints design for composite material structural members reinforcement in joint region, considering weight factor
 [AIAA PAPER 68-341]

11 p1987 A69-25369

Complex structure least weight optimization for specific frequency by computerized modification of existing member cross sectional properties

11 p1989 A69-25494

Inelastic structural system stresses, strains and displacements analyzed by differential stress-strain relationships, using finite element method
 [AIAA PAPER 68-291]

13 p2364 A69-28208

Numerical procedure to optimize complex structures by determining relative proportions of selected elements attaining flutter speed with minimum total mass

16 p2874 A69-32163

Structural members stability mathematical models using lumped bars and springs simulating postbuckling behavior

18 p3211 A69-34342

Book on deformable bodies mechanics covering load resisting members of structures and machines

18 p3222 A69-34927

Wide panel Ti structural extrusions with integral stiffeners, discussing material, sizes, properties and tolerances

19 p3319 A69-35552

Elastic stiffness, kinematically equivalent loads and initial loads due to initial strains of FUGA 6 element, describing program for matrices generation

19 p3447 A69-36852

Natural oscillations of loaded strings, membranes and geometric bodies with distributed loads treated as material discontinuities

20 p3578 A69-38292

STRUCTURAL RELIABILITY

Aerothermal-structural reentry safety evaluation for SNAP-27 radioisotope Graphite Lunar Module Fuel Cask at orbital and superorbital velocities
 [AIAA PAPER 68-1166]

03 p0465 A69-13561

Damage tolerance as design consideration for aircraft safety and reliability, discussing application of failed single principal member concept to airframe construction
 [AIAA PAPER 69-212]

07 p1056 A69-19574

Quality control tests for adhesives used in structural parts including ultrasonic and nondestructive tests

09 p1513 A69-22564

Structural reliability tests using photoelasticity and associated techniques, discussing computer methods, materials research, etc

09 p1479 A69-22734

Glass finish and glass resin chemical bond adhesion roles in filament wound structures response, failure and filament strength

14 p2468 A69-29345

Spacecraft structures reliability, discussing detection, identification, assessment and control of defects

18 p3146 A69-34513

Plastics thermal properties and industrial structural applications dependency on temperature

18 p3161 A69-34839

Time-dependent failures of components subjected to fatigue loading analyzed for reliability prediction

19 p3437 A69-36032

Structural design optimization based on reliability analysis stressing proof-load test and weight savings consideration under cost constraint

19 p3437 A69-36033

Aircraft structures efficiency and weldability as function of application, welding procedures and metallurgical factors, considering high strength Al alloys, Ti and Ni alloys, etc

20 p3550 A69-37457

Eddy current machine /nondestructive testing device/ for aircraft structures surface cracks detection

21 p3719 A69-38391

Concorde structural tests emphasizing problems associated with thermal cycle, including fatigue test setup on complete airframe
 [RAES PAPER 16]

22 p4043 A69-40495

Aerothermal-structural reentry safety evaluation for SNAP-27 radioisotope Graphite Lunar Module Fuel Cask at orbital and superorbital velocities
 [AIAA PAPER 68-1166]

22 p3979 A69-40551

Crimping method for preventing nuts loosening, discussing elliptical deformation and point crimp for obtaining maximum interference fits

22 p3957 A69-40828

Safety standards for DC 10 aircraft, considering cockpit design, hydraulic, electric power, autoland and direct lift control systems, structural safety and crash worthiness

22 p3867 A69-41133

Causes of ascent failures in high altitude balloons, discussing test methods and specifications revisions

24 p4251 A69-42714

Safety and failure of components - Conference, Brighton, England, September 1969

24 p4397 A69-42767

Large space erectable structures rigidity, stiffness, thermal stability, structural efficiency and integrity
 [AAS PAPER 69-152]

24 p4398 A69-42877

STRUCTURAL STABILITY

NT SHELL STABILITY

Deflection of orthotropic sandwich plates with unequal facing thickness with edges subjected to uniform and concentrated loading

01 p0172 A69-11270

Structural stability of manganese austenitic steels at high temperatures, discussing phase transformations and carbide precipitation changes

01 p0100 A69-11294

Instability of struts subjected to axial force and radiant heat, considering elastic and thermal deformation

02 p0337 A69-11716

Limit load analysis of three dimensional rigid perfectly plastic continua by approximate variational method

02 p0338 A69-11721

Dynamic stability of structural system excited by random load, discussing effect of nonlinearities and dynamic snapping problems

02 p0339 A69-11988

Mathematical aspects of stability of equilibrium configurations

02 p0340 A69-11991

Finite deformation mode stability for finite amplitude first diameter nonlinear plastic wave initiation and growth at impact face in long rods

02 p0342 A69-12279

Liquid propellant space launch vehicles longitudinal modes natural frequency, discussing coupled engine-propellant supply system stability
 [AIAA PAPER 68-289]

02 p0335 A69-12393

Direct matrix method for evaluation of critical loads and buckling modes for nonuniform flexural rigid plates having end and side constraints

03 p0522 A69-12866

Single degree of freedom structural damping estimations from viscous and hysteretic energy dissipation data

03 p0523 A69-12947

Equilibrium stability of elastic circular arch constrained in rigid cavity and subjected to uniformly distributed parallel loading

03 p0524 A69-13066

Elastic stability equations solved in geometrical linearization for thin anisotropic plates under transverse shear, using variational method

03 p0525 A69-13130

Strain induced deformational instability of aluminum alloys

03 p0447 A69-13818

Symmetric structure stability with first and second order imperfections, analyzing discrete system with n degrees of freedom

03 p0529 A69-14062

Elastodynamic boundary value problem solution for stability in linear elasticity

03 p0530 A69-14066

Computer method calculating stressed state of elliptical bottom of cylindrical pressure vessel based on differential bending equations for shell of revolution

04 p0668 A69-14275

Stability against snap-through and final states of shallow arches on elastic foundations and subject to time varying loads
 [ASME PAPER 68-WA/APM-26]

04 p0669 A69-14394

Two point boundary value problems for determining buckling behavior of two hinged circular arches
 [ASME PAPER 68-WA/APM-18]

04 p0669 A69-14399

Energy transfer in circulatory force fields, noting mechanism changes for simultaneously operative original field and adjoint field energy sources

04 p0671 A69-14415

Stability of elastoplastic clamped free rod, noting compressive force for production of new equilibrium state and occurrence of transition to state

04 p0679 A69-14925

Bending of rectangular plate with partial clamping, obtaining solution by superposition method

04 p0681 A69-15289

Schaefer theory of two parameter eigenvalue problems applied to stability of twisted bars, discussing quick estimate of critical loads

04 p0682 A69-15290

NeoHookean /incompressible solid/ rectangular parallelepiped compressed between lubricated rigid plates, comparing stability bounds with predicted critical loads

04 p0682 A69-15303

Elastic rods shape for maximum stability defined by solution of variational problem, assuming noninfinite compressive stresses

05 p0832 A69-15688

Stability theorems for discrete linear circulatory systems with N degrees of freedom for static and dynamic loss of stability in presence of velocity dependent forces

05 p0836 A69-15875

Matrix displacement and force methods of stability analysis, deriving method of determining geometrical stiffnesses for complex structures

05 p0841 A69-16399

Structural stability of cobalt base superalloy at high temperature prolonged exposure under stress

05 p0781 A69-16448

Mechanical equilibrium and stability conditions for system of interacting atoms in crystal structure

06 p0944 A69-17504

Small bending stiffness effect on inflated torus and cylindrical shells under radial load for determining large space structure stiffness

06 p1024 A69-17607

Mechanical stability of pressed and forged Ti alloy gas turbine disks at high temperatures and rates of rotation

06 p1026 A69-18018

Thermally induced vibration and flutter of flexible spacecraft boom, discussing stability by considering boom as cantilever beam
 [AIAA PAPER 69-21]

06 p0869 A69-18144

Spacecraft control system and flexible structures interactions, discussing transient phenomena, limit-cycle oscillations and instabilities
 [AIAA PAPER 69-116]

06 p1019 A69-18187

Transverse motion of embedded or free semifinite beam with given initial displacement and velocity, using potentials leading to integral equations
 [ONERA-TP-653]

07 p1230 A69-18264

Static endurance of aircraft structural elements under single and multiple loading, based on real alloys and crystalline materials theories

07 p1231 A69-18554

Critical axial load for elastic instability of unidirectional equally spaced fibers in plane of composite plate and buckling modes

07 p1232 A69-18714

Miniature current discontinuity antennas for VHF and UHF, describing airborne electronically steerable array exhibiting efficiency and minimum structural disturbance

07 p1105 A69-19111

Axially loaded viscoelastic constrained bar instability for large deformation

07 p1235 A69-19440

Free surface strain increment components on high carbon steel compression specimens to estimate tensile plastic instability onset, noting ductile fracture criterion

08 p1328 A69-19891

Thin walled symmetrical angle section beam stability under bending moment by section deformation or torsional buckling

08 p1410 A69-19892

Stability of hydrostatic gas bearings with large clearances

08 p1303 A69-20271

Fiberglass reinforced plastic plates strength coupled to elastic base with allowance for tangential shearing stresses

08 p1412 A69-20334

Stability and bending of flexible plates and shallow shells obeying hereditary relations solved by singular kernel functions

08 p1413 A69-20335

Forced vibration of thin elastic plate resting on elastic foundation and subjected to time dependent loads and external damping

08 p1416 A69-20692

Elastic stability of one dimensional structures analyzed by energy method, discussing deformable line, conservative forces and linear stability

08 p1418 A69-20846

Simply supported isotropic cylindrical panel stability under axial compression, obtaining asymptotic series expansion for upper critical stress

08 p1419 A69-21182

Gyrostatic moments effects on critical angular velocities of varying and constant cross section rigidly and elastically supported hinged rotors

09 p1567 A69-21384

Bar flexure determination for Saint Venant torsional and transverse loading, solving differential equations by finite element methods

09 p1614 A69-21722

Uniform gravity load effect on buckling of beam continuously supported by soft foundation and subjected to uniform lateral load

09 p1615 A69-21927

Gas bearings for spool gas generator for aircraft turbine engines, noting rotor bearing stability and LP spool balancing and seal leakage
[ASME PAPER 69-GT-60]

09 p1513 A69-22515

Plates stability and corner stress-strain state under variable loads calculated by method analogous to structural mechanics

10 p1792 A69-22849

Pointwise bounding of eigenfunctions in vibration and stability problems in elasticity theory

10 p1794 A69-22925

Long rectangular rods stability and vibrations under elastic deformations using bending theory

10 p1802 A69-24024

Response and stability of self sustained two degrees of freedom system with nonlinear damping, noting harmonic oscillations
[ASME PAPER 69-VIBR-24]

10 p1806 A69-24171

Natural mode structural analysis matrix methods for small displacements, discussing curved local subbeam in space and circular arch

11 p1969 A69-24374

Slender elastic rod stability under spatial finite deflection, analyzing critical load by using Kirchhoff analogy and gyroscope motion

11 p1970 A69-24609

Lame problem for elastic isotropic medium having free energy dependent on medium deformation and deformation gradients, estimating minimum surface curvature

11 p1970 A69-24632

Two dimensional elastic reinforcements effects on stress, strain and elasticity of quasi-homogeneous anisotropic elastic medium

11 p1981 A69-24941

Finite difference method for transient and steady state response of vibrating plates, considering explicit and implicit formulas

11 p1983 A69-25020

Book on statics and dynamics of anisotropic and heterogeneous elastic structures covering thin heterogeneous anisotropic panels, elastic and sandwich plates, etc

11 p1986 A69-25236

Servocontrol to delay flutter onset of aeroelastic structures, discussing rapid amplitude and phase changes near instability point, wind tunnel models, instrumentation, analog simulation

11 p1992 A69-25518

Warping rigidity effect on stability of cantilever bar under eccentric follower end load, discussing bending torsional flutter and buckling

12 p2179 A69-26212

Critical load for anisotropic right-angled isosceles triangular plate stability with large deflections obtained from differential equation

12 p2180 A69-26270

Antiflexure cylinder for large astronomical mirror, noting support by astatic counterpoint levers and simple flanges

12 p2056 A69-26409

Bending of weightless thin elastic beams clamped to circular template by external force

12 p2181 A69-26572

Mathematical bending theory for three layer elastic plates containing light or rigid fillers

12 p2182 A69-26678

Simply supported laminated anisotropic rectangular plate with coupling occurring between bending and in-plane extension, discussing stiffness analysis by Fourier series method

12 p2184 A69-26808

Optimal design of rectangular frames for stability

13 p2358 A69-27209

Equilibrium paths in initial postbuckling of elastic structural systems, discussing stability boundaries and relationships between imperfections and critical loads

13 p2359 A69-27261

Chemical composition of cermet material for radial sealing of high temperature gas turbines, ensuring structural stability and oxidation resistance

13 p2275 A69-27344

Bounding technique of first excursion probability for random vibration, considering relation to reliability of mechanical and structural systems under random disturbances

13 p2361 A69-27438

Thin walled channel columns section stability analyzed in terms of overall /Euler/ and local buckling

13 p2361 A69-27440

Shear buckling of clamped rectangular linearly tapered plates, considering uniform shear stress and load

13 p2361 A69-27443

Microstructural stability Fe-Ni base heat resistant alloy Pyromet 860 during long time creep-rupture testing

13 p2279 A69-27764

Subelement geometrical stiffness determined, considering complete element natural modes

13 p2362 A69-27838

Thermal and mechanical stability of fused silica lightweight mirror structures, examining impact and shear strengths of fused joints

13 p2261 A69-27954

Stress and displacement fields for uniaxially loaded infinite elastic continua with doubly periodic array of holes and inclusions, using finite element method

13 p2363 A69-28133

Rectangular plate buckling analyzed by finite element method with deflection function

13 p2364 A69-28225

Discrete element plastic analysis of long prismatic bars under transverse loading in longitudinal direction, based on matrix displacement method

13 p2365 A69-28237

Higher order difference method for equilibrium and eigenvalue problems of two dimensional structures using iterative solution

13 p2365 A69-28239

Dynamic stability of flexural free transverse vibrations of supported thin walled elastic beam with initial velocity distribution and parametric excitation

13 p2369 A69-28353

Circular membranes vibrational and stability characteristics under simultaneous constant spin and precessional motions, obtaining Hill equation for motion amplitude coefficients

13 p2370 A69-28665

Uniaxial compressive stability of rectangular boron-epoxy laminated plates clamped on loaded edges, determining buckling loads by Southwell plots

13 p2287 A69-28669

Rigid supporting ribs effect on annular plate critical loading, stability loss and buckling

14 p2533 A69-28983

Book on fatigue strength in construction covering structural strength and stability, load design, mechanical properties, elasticity and plasticity theories, stress concentration, strain buildup, etc

14 p2534 A69-29331

Collection of soviet articles on vibrations and stability of devices, machines and control system elements

14 p2536 A69-29747

Nonlinear oscillations stability of solid body connected to base by elastic springs of different rigidities under external forces

14 p2536 A69-29747

Michelson interferometers with large interference fields for plasma diagnostics emphasizing structural rigidity, monochromatic light pulse power, instruments vibrations resistance, etc

14 p2496 A69-29776

Beam deflection equations having different rigidity moduli on each half span

15 p2705 A69-30417

Elastic and elastoplastic bodies, showing vector field for surface condition as sufficient condition for stability

15 p2707 A69-30621

Minimum vibration frequency and compressive force for freely supported rectangular, triangular and circular plates simulated on analog computer

15 p2708 A69-30665

Aluminum models of single cell simply supported folded plates to study instability phenomena possibly occurring in actual structure

15 p2709 A69-30679

Fatigue cracks growth rate under combined static and cyclic stresses

15 p2709 A69-30808

Fatigue crack propagation caused by cumulative damage due to strain cycling at crack tip, relating resistance to cyclic ductility

15 p2710 A69-30812

Lifetime of structural plastics under vibration loading, considering polystyrene and polyformaldehyde samples under tension

15 p2643 A69-30972

Repeated static stress limit of internal pressure vessels, emphasizing effect of redistribution of stresses and strains

15 p2712 A69-30973

Gradient iterative methods for finite element eigenvalue problem associated with stability and vibrations of elastic systems based on Rayleigh quotient

16 p2871 A69-31898

Plate bending problems, comparing various approximate analytical methods including point matching, Galerkin, Ritz, Kantorovich and least squares techniques
[AIAA PAPER 68-296]

16 p2874 A69-32160

Ceramic phase reinforcement of metals and alloys, discussing interfacial energies, binding forces and elastic stress fields
[ONERA-TP-661]

16 p2802 A69-32204

Absolute stability, stability in whole and engineering stability in reference to Liapunov stability applicability

16 p2874 A69-32244

Linear theory of elastic stability of structures, discussing deformation kinematics, perturbed and neutral equilibria and solutions for buckling of beams, plate, shells, etc

17 p3054 A69-33042

Stress distribution in variable rigidity reinforcing frame of circular cylindrical shell using strain energy method

17 p3055 A69-33131

Soviet collection of articles on theoretical and experimental investigations of strength of mechanical engineering structures

17 p3056 A69-33190

Stability of nonuniformly heated rectangular plate reinforced by elastic longitudinal and rigid transverse ribs, accounting for influence of torsional and bending rigidities

17 p3057 A69-33198

Wire wound glass fibers for rocket motors, discussing rupture strength

17 p3021 A69-33357

Thin circular ring stability under uniform external transverse loading at various angles, discussing transverse shear deformation effects and buckling

17 p3061 A69-33707

- Elastic sandwich structures design for maximum strength, using potential energy functional to derive governing equations
17 p3062 A69-33708
- Soviet collection of papers on energy dissipation during vibrations of mechanical systems, covering elastic oscillations, nonlinear systems, energy frequency characteristics, etc
17 p3062 A69-33912
- Energy dissipation in fiberglass reinforced plastics subjected to axially induced sinusoidal stresses, noting absorption coefficient and hysteresis heating
17 p2993 A69-33937
- Minimum weight design of tiltable enclosed antenna structure as subject to deformation constraints
18 p3211 A69-34341
- Structural members stability mathematical models using lumped bars and springs simulating postbuckling behavior
18 p3211 A69-34342
- Von Karman equations in dimensionless and finite difference forms for deflections of elastic circular plate with central hole under load solved by iteration [ASME PAPER 69-APM-20]
18 p3214 A69-34395
- Longitudinal oscillations of homogeneous elastic rod under nonconservative force at one end, deriving equations of motion and stability conditions
18 p3216 A69-34578
- Buckling in process of loading idealized elastoplastic Shanley column, noting continuous increase possibility
18 p3217 A69-34596
- Stress conditions of anisotropic plate with soldered in circular isotropic aluminum disk in presence of notches at seam, assuming elastic symmetry of plate
18 p3218 A69-34602
- Book on deformable bodies mechanics covering load resisting members of structures and machines
18 p3222 A69-34927
- Beam torsion nodal line displacement dependence on flexural and torsional bending frequency
18 p3223 A69-34998
- Elastic bodies brittle stability weakened by cut, developing criterion for determining critical cut length
18 p3224 A69-35314
- Elastic stability of sandwich materials in microvolume under compressive force analyzed using three dimensional linearized equations for small sub-critical strains
18 p3226 A69-35374
- Flanges flexural rigidity effect on load carrying capacity, failure mechanism and postbuckling behavior of webs in shear, noting permissible load
18 p3227 A69-35492
- Yield condition of maximum constant distortion strain energy for anisotropic material without incompressibility assumption
18 p3227 A69-35494
- Composite material applications in space vehicle structures, noting strength and stiffness of boron fibers in plastic or metal matrices
19 p3340 A69-35502
- Static dynamic and damage tolerance strengths of advanced materials for VTOL aircraft with emphasis on Ti, cryoformed 301 stainless steels and filamentary composites [AIAA PAPER 69-764]
19 p3433 A69-35658
- Stiffened integrally formed panel stability evaluation based on compression structural efficiency and manufacturing costs [AIAA PAPER 69-760]
19 p3434 A69-35660
- Syphon geometry influence on rigidity and strength determined using integrating Meissner type differential equations with finite difference schemes
19 p3358 A69-35849
- Buckling behavior of idealized Shenley rod consisting of linearly reinforced elastoplastic materials under compression, formulating constraints for stability
19 p3446 A69-36846
- Clamped skew plates natural frequencies analysis using Galerkin method, expressing deflections as double series of beam characteristic functions, stating eigenvalues and eigenvectors
20 p3621 A69-37201
- Deep circular arches undergoing large deflections and stability loss, determining buckling load variations
20 p3622 A69-37210
- Stability loss nonaxisymmetric distribution in elastic annular plates under axisymmetric heating, using Ritz method to determine critical temperature
20 p3623 A69-37327
- Airframe stability of VAK 191 examined by displacement method, using matrix calculations within Automatic System of Kinematic Analysis
20 p3462 A69-37515
- Reinforcement unbonding onset in composite materials determined by continuous dynamic moduli and damping measurements of tensile specimens
20 p3511 A69-37761
- Automated device for load carrying ability of structural elements like gas turbine blades under thermal and mechanical cyclic loads
20 p3544 A69-37816
- Analog method for determining structural creep displacement by setting up boundaries for linear elasticity and perfect plasticity
20 p3628 A69-37915
- Soviet book on thin plates and shells bending and stability during creep covering analytical and numerical solutions for various structural elements
20 p3630 A69-38207
- Natural oscillations of loaded strings, membranes and geometric bodies with distributed loads treated as material discontinuities
20 p3578 A69-38292
- Stability of sandwich panel strip with lightweight core, formulating problem in terms of equilibrium conditions and potential energy of system
21 p3832 A69-38417
- Multilayer sandwich panels containing unequal facings with distinct orthotropic cores, calculating dynamic load and stability of triangular panels
21 p3832 A69-38418
- Gyroscopic system behavior analyzed for steady state operation following transient period
21 p3723 A69-38832
- Two machining processes for eliminating unbalanced state of machine parts, using eccentric cutting and adjustment of part CG for coincidence with spindle axis
21 p3732 A69-39097
- Stability of unbounded homogeneous brittle body containing circular planform crack, determining elastic stresses and critical load by macrocrack propagation theory
21 p3839 A69-39195
- Galerkin method application to solve differential equation and boundary value conditions for elastic stability of bars, showing linear relation between critical loads
21 p3845 A69-39678
- Wobble tolerance influence on axis deflection affecting accuracy during assembling of turbine rotors and stators
21 p3733 A69-39719
- Gupta stability solution extended to liquid anisotropic viscoelastic films, analyzing surface and shear wave perturbations in material structures
22 p3929 A69-39893
- High E modulus, structure, strength and temperature characteristics of reinforcement fibers, considering B, silicon carbide, C and Be
22 p3951 A69-39907
- Stability loss of beams analyzed under compression allowing for various creep conditions in loading and unloading regions, calculating time to failure
22 p4039 A69-39917
- Compressed rectangular beam stability under different creep conditions, deriving relation between creep time and initial deflection
22 p4039 A69-39918
- Elastoplastic analysis of thin plates deformation, discussing loading conditions effects
22 p4041 A69-40064
- Single stage rocket body finite bending stiffness effect on pitching moment using approximate equation, noting applicability to multistage rockets
22 p4037 A69-41048
- Network method for stability of thin nonlinearly elastic compressible material plates, noting difference operators for rigidly clamped plates
23 p4230 A69-42003
- Parkes paraboloid radio telescope structural performance, using rapid survey instrument to measure surface deformations for optimum focusing determination
23 p4231 A69-42130
- Canadian radio observatory 150 ft telescope antenna, discussing dish structural feature for resisting gravity, wind and thermal stresses
23 p4149 A69-42134
- Large deflection of three dimensional bar structures stability analyzed by potential energy minimization method, considering radome design
23 p4232 A69-42141
- Field transfer matrices for simultaneous treatment of free and forced vibrations and buckling through axially loaded Timoshenko beam
23 p4234 A69-42400
- Rigid/plastic solids subjected partly to uniform fluid pressure and partly to general boundary conditions, analyzing uniqueness and stability criteria
23 p4235 A69-42460
- Heated three layer plates stability under finite deflections in supersonic gas flow, deriving aerothermoelasticity equations
24 p4395 A69-42590
- Large space erectable structures rigidity, stiffness, thermal stability, structural efficiency and integrity [AAS PAPER 69-152]
24 p4398 A69-42877
- Limiting load of square plate subjected to shear and reinforced by vertical stiffener, computing membrane and bending stresses as function of flexural rigidity
24 p4399 A69-42967
- Strain diagram with piecewise nonlinear curve for statically indeterminate systems stressed beyond elastic limit
24 p4400 A69-43072
- Newton method providing continuing solutions of nonlinear differential equations through limit or bifurcation points, discussing elastic stability applications [ASME PAPER 69-APMW-14]
24 p4401 A69-43102
- Mechanical model for dynamic buckling of elastic imperfection-sensitive structures under step loading, using perturbation method
24 p4405 A69-43656
- Asymmetric metal flanges effect on beam tilt of aperture antennas
24 p4288 A69-43765

STRUCTURAL STRAIN

- Stress analysis of multiply connected bodies under large elastic strains, deriving second order potentials for plate with elliptical holes
02 p0340 A69-12139
- Strain effects on transverse electromagnetic modes of anisotropic dielectric waveguides at p-n junctions
03 p0406 A69-13830
- Cumulative damage theories application to fatigue data for high strength materials, discussing stress levels
04 p0668 A69-14379
- Temperature stresses analysis for jet lift VTOL aircraft structure during takeoff and landing, discussing fire hazard in lift pod
04 p0548 A69-14841
- Elastic strain and stress in ribbed circular plate bent skew-symmetrically, using orthotropic plates theory
04 p0681 A69-15172
- Book on thermal time independent plastic and time dependent creep strains in structures through analogy permitting inelastic structures analysis
04 p0681 A69-15200
- Repeated loading influence on microstrain region, noting decrease in size with each cycle
05 p0836 A69-15876
- Crack tip displacements and strains in plastically yielded region measured with replica technique
05 p0780 A69-16437
- Grain strain measurements use in studies of high temperature creep
06 p0943 A69-17231
- Initial defects influence on equilibrium states of compressed elastoplastic plates
06 p1025 A69-17684
- Stress-strain state of shells of multicable elevator pulleys under asymmetric load for various friction coefficients and pulley shell lengths and widths
06 p1026 A69-18016
- Plasticity theories for nonisothermal loading, considering plastic strain
07 p1237 A69-19681
- Structural residual stresses determination in oriented fiberglass reinforced plastics by models taking into account mutual influence of fibers
08 p1335 A69-20333
- Material selection for structures under vibration loads, analyzing fatigue strength on basis of stress susceptibility and relationship with tensile strength
09 p1620 A69-22574
- Elastic-plastic deformations /strains/ amplitudes measured at high cycle temperatures in thermal fatigue tests
10 p1801 A69-23844
- Thin elastic conical shells asymmetric deformation under stresses and strains, deriving asymptotic solution
11 p1983 A69-25090
- Analytical expressions for Gaussian constraint of continuum, using continuity conditions as equations of internal geometric couplings
11 p1984 A69-25170

Elastic and elastoplastic strains in materials under various loadings, determining temperature variations by thermoelectric method and verifying by tensile tests
11 p1985 A69-25178

Rotor angular velocity and flexural strain interdependence at critical velocity
11 p1987 A69-25390

Three dimensional problems in crack theory for unbounded brittle body, deriving critical loads from limiting equilibrium equation
12 p2178 A69-25997

Thermal stress and displacement fields in elastic solid weakened by crack outside of circular region, noting plastic zone size and energy dissipation
12 p2179 A69-26216

Hollow circular viscoelastic cylinder axisymmetric plain strain problem, considering displacement, traction and mixed boundary conditions, noting applicability to rocket solid fuel core
12 p2181 A69-26396

Elastic directed curves dynamic theory, considering Hamilton principle, mass conservation and behavior of action density function under rigid body variations
13 p2360 A69-27321

Inverse deformation in elastic materials, using variational principle to obtain equilibrium equations properties
13 p2360 A69-27324

Torsional testing facility for delayed elastic and nonrecoverable strains in materials, noting application to diffraction limited reflecting optics
13 p2240 A69-27955

Microstresses and distortions in quasi-isotropic solid bodies under strain evaluated by correlation functions
14 p2531 A69-28806

Thin elastic plates buckling under small normal load and external edge force
14 p2531 A69-28810

Structural stress under acceleration loading simulated by two dimensional photoelastic model noting improvement of fringe patterns quality
14 p2532 A69-28885

Book on fatigue strength in construction covering structural strength and stability, load design, metal physical properties, elasticity and plasticity theories, stress concentration, strain buildup, etc
14 p2534 A69-29333

Strains determination for laterally edge loaded rectangular plate and sagittas determination of perpendicularly loaded plate proved analogous
15 p2704 A69-30295

Structural strength calculations, considering micro and macro stress distributions
15 p2706 A69-30447

Elastoplastic strains in thin walled beams subjected to oblique bending by mobile loads of coupled concentrated forces, calculating deflections and plastic region distribution
15 p2711 A69-30971

Plane strain solution for thick walled viscoelastic cylinder bonded to thin elastic shell from deformation rate and strain, including inertia effects
16 p2871 A69-31876

Full stress design feasibility as function of load conditions, indeterminacy order and structure topology
16 p2872 A69-31915

Strains in elastoplastic curved beam under bending obtained from approximating stress-strain diagram by parabola
17 p3056 A69-33192

Initial thermostructural stresses in homogeneous quasi-isotropic two component medium, solving statistical boundary value problem thermoelastically
17 p3058 A69-33316

Plane strain fracture toughness determined for crack notched bend specimens using standard test procedure for specific metallic material property
17 p2989 A69-33566

Von Karman equations in dimensionless and finite difference forms for deflections of elastic circular plate with central hole under load solved by iteration [ASME PAPER 69-APM-20]
18 p3214 A69-34395

Grid method of strain determination, discussing print, record, analysis and application
18 p3134 A69-34423

Stress-strain state of open cylindrical shells with arbitrary cross section determined for clamped-clamped, clamped-free and free-free supported shells
18 p3225 A69-35372

Plane strain fracture toughness of high strength steels and Ti alloy from precracked notched bend test method
19 p3346 A69-36436

Design laws of warping-free multicellular box beams under torsion or bending, using variational method
19 p3443 A69-36786

Buckling behavior of idealized Shenley rod consisting of linearly reinforced elastoplastic materials under compression, formulating constraints for stability
19 p3446 A69-36846

Stress and strain concentration factors under initial stages of elastoplastic deformation for circular hole in infinite medium, using method of successive approximation
19 p3447 A69-36860

Generalized strain-measure application to linearization of stress-strain curves of compressive, shear and tensile nature, discussing plastic deformations
21 p3844 A69-39321

Telecentric lens principle for accurate optical strain measurements, using moiré grids
21 p3844 A69-39322

Strain anisotropy matrices behavior along strain trajectories of arbitrary curvature, studying matrices and elastic constants dependence
22 p4039 A69-39914

Strain anisotropy matrix construction for various strain trajectories from elastic properties of expression relating stress and elastic strain deviators
22 p4039 A69-39915

Homogeneous equilibrium equations of nonlinear shallow shell theory, obtaining six stress function solutions for strain measures
22 p4048 A69-41199

Central transverse impacts of sphere on free-free beams, investigating maximum strains variation with impact velocity by narrow band tuned circuit filter
23 p4235 A69-42455

STRUCTURAL VIBRATION

NT BENDING VIBRATION

NT FLUTTER

NT LINEAR VIBRATION

NT MISSILE VIBRATION

NT PANEL FLUTTER

NT SELF INDUCED VIBRATION

NT SUBSONIC FLUTTER

NT SUPERSONIC FLUTTER

NT TORSIONAL VIBRATION

Small oscillations in solid body with arbitrary cavity partially filled with viscous incompressible fluid
01 p0165 A69-10084

Stabilized platform vibration in inertial navigation system with integral correction
01 p0112 A69-10086

Structural vibration problems of SA 330 helicopter from test flight data, discussing natural frequency displacement of blades and dynamic response improvement of structure
01 p0009 A69-10158

Flexural vibration of unbalanced rotating shaft with nonlinear characteristic of elasticity and damping, using equations of motion
01 p0168 A69-10329

Discrete model for investigating beam vibration under various end conditions, determining natural frequency dependence on degrees of freedom
02 p0336 A69-11462

Parametric vibrations of self excited elastic and aeroelastic systems with traveling waves, determining stable vibration boundaries
02 p0337 A69-11561

Existence of smooth solution for system of equations describing nonlinear oscillations of thin plate and shallow shell
02 p0337 A69-11654

Summed and differential types of higher order oscillations in vibratory systems with multiple degrees of freedom under parametric excitation
02 p0346 A69-12422

Soviet book on vibrations of elastic shell partly filled with fluid covering different stages in procedure for shells of axisymmetric configuration
02 p0346 A69-12480

Multilayered shells equivalence to single layer shells for stress analysis, vibrations and stability
02 p0346 A69-12509

Stroboscopic technique for obtaining interferential holograms of vibrating transparent and reflecting plates
02 p0251 A69-12561

Arbitrary phase shift vibrations of airfoil profiles in incompressible flow reduced to Fredholm equations, allowing for trailing vortices influence
02 p0190 A69-12574

Flutter vibration of sails fixed along edge and single wing weather vanes in supersonic flows
02 p0192 A69-12824

Flutter vibration in subsonic flows, analyzing critical velocity for membrane and damping destabilizing effects in nonconservative system
02 p0192 A69-12825

Single and double resonance in system of coupled nonlinear differential equations describing vibration phenomena in mechanical and similar systems
03 p0527 A69-13744

Dynamic behavior of large steerable radio telescope, showing structural resonance influence on error detection system
03 p0412 A69-14091

Thickness twist and face shear vibrations of laminated layer, determining frequencies from stress equations of motion, constitutive equations and boundary conditions [ASME PAPER 68-WA/APM-10]
04 p0668 A69-14392

Vertical, horizontal and rocking vibrations of body on surface of otherwise unloaded elastic half plane, estimating stiffness for coupled vibrations [ASME PAPER 68-WA/APM-12]
04 p0668 A69-14393

Timoshenko beam theory accuracy, defining deflection and rotation in terms of average values over cross section
04 p0675 A69-14593

Statistical energy approach for analyzing steady state vibration distribution in composite structures in terms of energy balances
04 p0675 A69-14687

Beam vibration problems with mixed response-excitation input information solved by recasting equations of motion [AIAA PAPER 68-319]
04 p0676 A69-14711

Ground vibration testing of flight and space vehicles, noting structural damping asymmetries and nonlinearities
04 p0585 A69-14833

Normal modes and natural frequencies of combined linear elastic structures resting on immovable base
04 p0678 A69-14870

Laminated plates vibrational characteristics calculations by transition matrices, relating stresses and displacements under load
04 p0679 A69-14907

Axisymmetric oscillation modes and frequencies of hemispherical shell partially filled with liquid, using moment theory of shells
04 p0679 A69-14922

Vibration analysis of plates with discrete mass distribution based on Galerkin approach
04 p0682 A69-15293

LOX prevalue accumulator system with He pressurant for prevention of Pogo effect on Saturn 5
04 p0666 A69-15298

Testing techniques and graphical presentation of test results to determine resonant frequencies and oscillation modes in sporting gliders
04 p0549 A69-15420

Equation governing transverse vibration of beams with exponentially varying properties, expressing solution in terms of Bessel functions
05 p0835 A69-15873

Resonant beam tuned vibration damping device, noting weight saving potential [ASME PAPER 68-WA/GT-2]
05 p0837 A69-16138

Orthogonality of natural oscillation modes of shell of arbitrary geometry, using equations of motion from Vlasov engineering moment theory
05 p0840 A69-16200

Turbulent boundary layer loading function for use with finite element structural analysis system applied to elastic aircraft structures random vibration [AIAA PAPER 69-20]
06 p0914 A69-18132

Longitudinal structural vibration and lateral bending response mass and spring coupling in Saturn AS-502 during boost with longitudinal excitation by pogo effect [AIAA PAPER 69-58]
06 p0109 A69-18204

Holographic interferometry, determining mechanical vibration amplitudes of compressor and turbine blades and airframe panel [SAE PAPER 690265]
07 p1130 A69-18313

High speed sampling for dynamic data analysis, considering random and transient vibrations
07 p1232 A69-19139

Longitudinal and transverse vibrations of viscoelastic rods excited by inertia with aid of linear oscillator subjected to harmonic stress, using Kelvin-Voigt model
07 p1233 A69-19326

Circular cylindrical spinning shells vibrations by gyroscopically induced inertia loads, formulating equations of motion based on shallow shell theory
07 p1236 A69-19459

- Analytical solution for plate velocity statistics of turbulent-flow-excited rectangular flat plate, discussing vibration excitation
07 p1236 A69-19461
- Flexible rotor blade dynamic response to radially moving force, emphasizing helicopter rotor vibration characteristics associated with tip-vortex impingement [AIAA PAPER 69-203]
07 p1054 A69-19546
- Vibration characteristics of rectangular plate with fatigue crack and subject to tensile load, applying results to crack propagation in fuselage panels
08 p1413 A69-20399
- Nonhomogeneity effect on transverse vibrational frequency of uniform beams
08 p1413 A69-20413
- Transverse vibration of beam rigidly fastened at one end, using series expansion in terms of set of eigenfunctions
08 p1414 A69-20445
- Liquid filled cylindrical container motion with longitudinal forces applied to base, obtaining stability conditions for natural oscillations
08 p1419 A69-21181
- Three dimensional vibration analysis of circular homogeneous elastic cylinder, obtaining differential equations and zero stress conditions
09 p1612 A69-21601
- Three dimensional analysis of torsional vibrations of circular elastic homogeneous cylinder, stressing new torsional vibrations
09 p1612 A69-21603
- Time average holography for analysis of vibrations, overcoming fringe peak decrease with large amplitude and loss of phase information
09 p1495 A69-21749
- Hypersonic missile interceptor vibration characteristics in lower atmosphere, noting role of base pressure excitation
09 p1614 A69-21890
- Accuracy of approximations using shell equations for predicting dynamic behavior of thin cylindrical shells, with exact solutions from Flugge shell equation [AIAA PAPER 69-447]
09 p1616 A69-21938
- Structural damping coefficient for free vibrations of one degree freedom general systems motion
09 p1617 A69-22076
- Single degree of freedom mechanical system under random excitation studied for creep effect on vibrations by harmonic analysis
09 p1617 A69-22095
- Gyroscope error due to axial play of inner gimbal of Cardan mounting during base circular vibrations, noting axial clearance reduction
09 p1498 A69-22110
- Natural vibration frequency of circular orthotropic plate with variable rigidity
09 p1618 A69-22238
- Pressure on unsteadily oscillating cylindrical shell in external or internal supersonic flow derived from asymptotic theory
09 p1618 A69-22256
- Vibration natural frequencies and mode shapes in cylindrical shells clamped at both ends, using fundamental differential equation under dynamic surface loading
09 p1618 A69-22274
- Vibrating momentum exchange device /VMED/ in single axis configuration as competitor for inertia wheel or twin gyro
09 p1538 A69-22435
- Strength hypothesis for structures under multiaxial vibration load, taking into account plane stress state
09 p1620 A69-22575
- Damping criteria for satellite vibration based on energy dissipation by material hysteresis, friction in viscous flow, magnetic hysteresis and eddy currents
10 p1791 A69-22921
- Wideband acceleration instrumentation for Rover ground test facility liquid hydrogen turbopumps to study structural and flow induced vibrations
10 p1692 A69-23250
- Interfacial pressure distribution during slip damping in clamped rectangular beams subjected to vibration
10 p1800 A69-23350
- Long rectangular rods stability and vibrations under elastic deformations using bending theory
10 p1802 A69-24024
- Balancing criteria for rotors of rotating machines, discussing acceptable residual specific unbalance, center of gravity displacement and machine vibration tolerance [ASME PAPER 69-VIBR-60]
10 p1804 A69-24149
- Gas turbine blade vibrations, discussing excitation causes and damping techniques [ASME PAPER 69-VIBR-59]
10 p1805 A69-24155
- Central circular hole effect on fundamental frequency of rectangular fixed edges plate, discussing hole size, square plates, etc [ASME PAPER 69-VIBR-62]
10 p1805 A69-24156
- Vibration characteristics of circular cylindrical shells containing water under axial excitation, investigating bubble formation and shell-fluid interaction [ASME PAPER 69-VIBR-4]
10 p1805 A69-24162
- Natural frequencies and mode shapes for longitudinal oscillations of liquid filled elastic circular cylindrical tank with flexible inverted conical bulkhead [ASME PAPER 69-VIBR-11]
10 p1806 A69-24165
- Vibratory acceleration limiting equipment attachment for resonance conditions, utilizing attachment stiffness reduction above predetermined value [ASME PAPER 69-VIBR-23]
10 p1806 A69-24170
- Magnitude limited random excitation effect on linear system response, using single degrees of freedom model representing idealized mechanical structure [ASME PAPER 69-VIBR-41]
10 p1807 A69-24179
- Nonlinear large amplitude vibrations of flexible beam with pinned ends supported simply on rigid base noting frequencies, modes, waveforms and stress distribution [ASME PAPER 69-VIBR-43]
10 p1807 A69-24181
- Atmospheric influence on plane oscillations of space vehicle moving at 100-150 km heights
10 p1792 A69-24208
- Transverse beam natural vibration frequency evaluation method from Timoshenko theory
11 p1970 A69-24581
- Free vibration modes of infinite uniform plate in linear coupled theory of thermoelasticity, considering heat transfer conditions
11 p1976 A69-24793
- Vibration problem of supported beam elastically restrained against rotation at both ends solved by Hermitian and linear differential operators
11 p1976 A69-24794
- Finite difference method for transient and steady state response of vibrating plates, considering explicit and implicit formulas
11 p1983 A69-25020
- Flexible cylinder vibration in nominally axial flow, discussing length, mass, flexural rigidity and diameter variation effects on vibration amplitude
11 p1984 A69-25166
- Hysteresis loop contour equation derivation based on energy dissipation dependence on stress amplitude in cyclically deformed vibrating system
11 p1985 A69-25176
- Amplitudes of forced bending vibrations of frames with superfluous elastohysteretic couplings by dynamic compliances method
11 p1986 A69-25333
- Dynamic unified structural analysis method in computer program, calculating stiffness matrix to obtain natural frequencies and mode shapes
11 p1987 A69-25367
- Free vibration frequencies of simply supported parallelogramic plates, noting skew angle splitting of degenerate frequencies and frequency crossing of modes
11 p1987 A69-25379
- Axisymmetric oscillations of two spherical shells with noncoinciding centers of curvature immersed in compressible or incompressible fluids
11 p1875 A69-25467
- Optimal design of structures with constraints on strength and natural frequency, developing steepest descent boundary value method
11 p1989 A69-25496
- Axisymmetric vibration modal properties /frequencies and mode shapes/ of thin conical shell frustums, considering dimensional and boundary condition influences
11 p1992 A69-25519
- Dynamic analysis of axisymmetric ring stiffened shells with attached asymmetric elastic structures, noting vibration modes
11 p1993 A69-25525
- Thermally induced oscillatory instabilities in spacecraft booms, rederiving thermal torque equation to predict finite twist response
11 p1994 A69-25531
- Vibration eigenfrequencies of helicopter blades, discussing equation integration problems
11 p1995 A69-25673
- Space vehicle dynamic structure response, discussing vibration problems, test methods and responses to periodic, stochastic and forced excitations
12 p2176 A69-25857
- Viscoelastic models for solving longitudinal oscillations of one degree of freedom system under dynamic load, taking into account energy dissipation
12 p2177 A69-25995
- Linear vibrational systems natural frequencies and damping characteristics determined from system reaction to pulse effect
12 p2178 A69-26004
- Vector equation for correction masses for dynamic balancing of rotor supported on n points derived from bearing structure vibrations amplitude and phase
12 p2180 A69-26243
- Energy dissipation and fatigue in metals under cyclic static loads, determining logarithmic decrements of vibrations and Bauschinger effect
12 p2181 A69-26612
- Laminated plates vibrational characteristics calculations by transition matrices, relating stresses and displacements under load
12 p2182 A69-26660
- Soviet book on strength, stability and vibrations covering stability of rods, plates and shells subjected to plastic and elastic deformations, etc
12 p2182 A69-26755
- Friction damping properties of deployed structures vibrating in weightless state compared to damping in space for true determination
12 p2183 A69-26792
- Thin cylindrical shell vibration with three supports analyzed by minimizing Lagrangian of vibration, obtaining frequencies and modes
13 p2359 A69-27257
- Self controlled vibration of elastically supported cylinder in fluid stream due to von Karman shedding, considering fluidelastic interaction, structural deformation and natural frequency
13 p2360 A69-27437
- Bounding technique of first excursion probability for random vibration, considering relation to reliability of mechanical and structural systems under random disturbances
13 p2361 A69-27438
- Acoustic power transferred to plane homogeneous elastic structures and cylindrical shells by neighboring sound sources
13 p2363 A69-28186
- Dynamic stability of flexural free transverse vibrations of supported thin walled elastic beam with initial velocity distribution and parametric excitation
13 p2369 A69-28353
- Circular membranes vibrational and stability characteristics under simultaneous constant spin and precessional motions, obtaining Hill equation for motion amplitude coefficients
13 p2370 A69-28665
- Free vibrations of laminated anisotropic rectangular plates with clamped edges analyzed by Rayleigh-Ritz energy method
13 p2371 A69-28673
- Axisymmetric thermoelastic vibrations of infinite and finite cylindrical shells, determining natural frequencies and stress wave propagation
14 p2532 A69-28979
- Vibrations of thick walled shallow circular cylinder with thickness change in time, applying dynamic elasticity and Volterra equations
14 p2533 A69-28985
- Finite difference method for motion stability of periodic bipolar vibrational systems, considering perturbations
14 p2534 A69-29039
- Orthonormal aspect on vibration modes for nonuniform beams, evaluating normalization for end conditions by using Rayleigh technique
14 p2534 A69-29319
- Runway roughness induced vibrations in highly flexible aircraft, noting effect on pilot control of aircraft and airframe structure
14 p2392 A69-29504
- Collection of soviet articles on vibrations and stability of devices, machines and control system elements
14 p2536 A69-29741
- Machine vibration effects on human operator performance using locomotor model
14 p2409 A69-29742
- Vibrostand effects on statistical characteristics of random vibrations of elastic system, discussing simulation techniques
14 p2536 A69-29743

Vibration damping and elastic bond positioning in nonlinear systems with coincident centers of gravity and rigid damping 14 p2537 A69-29746

External and internal energy dissipation coefficients in vibrating aerodynamic rod structures 14 p2537 A69-29748

Macrostructure of steel, zinc and aluminum ingots using electromagnetic vibrations during crystallization, for stress relieving of welded structures 14 p2456 A69-29916

Steady natural oscillations of unbounded brittle plane with cut under edge load, showing decreased critical load in presence of inertial effect 15 p2703 A69-30050

Perturbation analysis for error estimates in algebraic eigenvalues and eigenvectors problems for solving skewed membrane vibrations 15 p2703 A69-30211

Stroboscopic technique for obtaining interferential holograms of vibrating transparent and reflecting plates 15 p2608 A69-30258

SST fuselage response to reverberant and turbulent boundary layer noise calculated for computing equivalent reverberant acoustic fields 15 p2549 A69-30302

Uncoupled field equations for free large amplitude axisymmetric transverse vibrations of spinning membrane disks 15 p2704 A69-30303

Time dependence of maximum structural response of single degree of freedom mechanical system under random loading 15 p2705 A69-30365

Dynamic vibration effects on guidance and control systems performance determined from spectral densities, cross spectral densities and vibratory environment amplitude distributions 15 p2608 A69-30367

Natural frequencies and modes of complex structures composed of beam elements, considering hysteretic damping for response and transmissibility 15 p2706 A69-30431

Oscillations of freely supported cylindrical shell of arbitrary cross section with breaks along generatrix, determining eigenvalue of infinite matrix with normal determinant 15 p2707 A69-30581

Minimum vibration frequency and compressive force for freely supported rectangular, triangular and circular plates simulated on analog computer 15 p2708 A69-30665

Oscillating beams lateral buckling allowing for torsional stress in determining critical load 15 p2712 A69-31015

Extensional vibration of thin inhomogeneous circular plate with variable modulus of elasticity and central hole, calculating periods of vibration 15 p2713 A69-31026

Natural vibration of isotropic plates in temperature field with nonuniform distribution over plate 16 p2871 A69-31891

Gradient iterative methods for finite element eigenvalue problem associated with stability and vibrations of elastic systems based on Rayleigh quotient 16 p2871 A69-31898

Structural influence coefficients from vibration test modes and frequencies, eliminating errors by Gram-Schmidt orthogonalization 16 p2872 A69-31916

Viscoelastic half space properties effect on self excited vibration boundaries determination 16 p2873 A69-32063

Axially symmetric vibrations of thin elastic spherical shell partially filled with liquid, considering shell as joined hemispheres with or without same thickness 16 p2873 A69-32129

Anisotropic conical shells free vibrations analyzed by Galerkin and operator-matrix methods, neglecting transverse shear deformation and rotatory inertia effects 16 p2874 A69-32165

Mixed plate element application to vibration and buckling eigenvalue problems based on Reissner variational principle, considering quadrilateral elements 16 p2874 A69-32176

Saturn 5 longitudinal instability /POGO/ precluded by lowering S-1C stage propulsion system resonance below structural frequency [AIAA PAPER 69-548] 16 p2868 A69-32658

Eigenvalue problems in partial differential equations solved by extended Kantorovich method, considering vibration of rectangular membrane and stability of elastic rectangular plate 16 p2876 A69-32783

Fluid filled spherical shell axisymmetric nontorsional motion analysis via differential equations obtained by Hamilton principle 17 p3051 A69-32956

Linear aerospace structures vibrations in randomly distributed pressure field forecasted by applying Green function [ONERA-TP-703] 17 p3054 A69-33064

Frequency and mode shapes of conical shell free oscillations related to shell parameters and boundary conditions 17 p3058 A69-33201

Vibrating objects phase determined by time average and real time holographic interferometry 17 p2974 A69-33324

Infinite isotropic elastic plate vibration under vertical harmonic load, deriving vertical displacement at center of loaded area 17 p3058 A69-33408

Critical review of paper on tail rotor structural design principles covering sizing, blade frequency and response and aeroelasticity [AHS PAPER 342A] 17 p3059 A69-33503

Complete spherical shells transverse frequency analysis, comparing results of elastic theory and classical, improved and membrane shell theories 17 p3061 A69-33705

Complete spherical shells nonsymmetric vibrations frequencies and mode shapes calculated by matrix method 17 p3061 A69-33706

Numerical Fourier transform and inversion in random vibration performed on computer, noting use for stochastic structural dynamic analysis of complex structures 17 p2996 A69-33710

Soviet collection of papers on energy dissipation during vibrations of mechanical systems, covering elastic oscillations, nonlinear systems, energy frequency characteristics, etc 17 p3062 A69-33912

Nonlinear flexural vibrations excitation in cylindrical shell by longitudinal harmonic load, discussing solution of partial differential equations of motion 17 p3064 A69-33920

Energy-frequency characteristics of vibrating machines obtained as spatial curves relating energy dissipation to system vibrations frequency 17 p3065 A69-33922

Energy dissipation in elastic systems as function of limiting damping characteristics of oscillations 17 p3065 A69-33923

Energy dissipation in vibrating warped turbine blades subject to complex stress-strain rate produced by simultaneous bending, torsional and tensile stresses 17 p3065 A69-33924

Test facility to determine factors influencing aerodynamic energy dissipation of cantilever rods oscillating in airstream 17 p2947 A69-33928

Energy dissipation in bonded structures, analyzing vibration damping, hysteresis loop and absorption coefficient dependence on deformation energy 17 p3066 A69-33943

Blade vibration damper consisting of springs attached to blade, analyzing resonance stresses on basis of dynamic rigidities 17 p3066 A69-33944

Transverse and torsional vibration characteristics of tapered cantilever beams and shafts analyzed by lumped inertia force method 17 p3066 A69-34052

Transient vibration linear analysis using Duhamel integral and Fourier and Laplace transformations, deriving receptances and application to aeroelastic systems 18 p3211 A69-34326

Axisymmetrical vibration characteristics of circular sandwich shell with viscoelastic core layer analyzed via differential equation to obtain frequency equation and composite loss factors 18 p3211 A69-34327

Mechanical single degree of freedom system mean square response to AM random noise, considering frequency response, input excitation spectrum, etc [ASME PAPER 69-APM-25] 18 p3214 A69-34398

Elastic beam-plate vibration natural frequency and dynamic instability in transverse static or oscillating magnetic field [ASME PAPER 69-APM-B] 18 p3215 A69-34400

Random excitations effects on vibrating nonlinear single degree of freedom system, statistically estimating resonance mode probability 18 p3171 A69-34554

Longitudinal oscillations of homogeneous elastic rod under nonconservative force at one end, deriving equations of motion and stability conditions 18 p3216 A69-34578

Natural longitudinal oscillations of variable cross section straight rods, assessing errors due to use of finite difference schemes 18 p3217 A69-34581

Machine parts vibration attenuation, discussing input vibration reduction, resonance avoidance, damping, vibrating parts strengthening and shakers 18 p3148 A69-34619

Equations of motion for plate vibration derived by complementary variational principle, including boundary conditions and thin plate transverse vibrations 18 p3218 A69-34626

Structural vibrations characteristics using expression of complex energy applied to structure, discussing coupling between damping modes [ONERA-TP-724] 18 p3218 A69-34639

Free oscillations of rigidly clamped circular plate carrying concentrated masses, deriving frequency equation and value of lower roots 18 p3226 A69-35377

Plane LF oscillations of eccentric cylinder under harmonic pressure applied to lateral surfaces, noting natural oscillations 18 p3226 A69-35380

Viscous incompressible fluid flow around semi-infinite oscillating plate and skin friction on infinite cylinders oscillating parallel to length 19 p3237 A69-35620

Transverse oscillations of shallow multilayer shells, using tangential-stress distribution law in determining natural oscillation frequencies in single and sandwich layer panels 19 p3435 A69-35842

Natural frequencies and mode shapes of vibration of cylindrical shells orthogonally stiffened with rings and stringers [AIAA PAPER 68-349] 19 p3437 A69-35948

Engineering equations for elastic thin plate oscillations of materials with properties described by linear integral Volterra-Boltzmann operators 19 p3437 A69-35989

Nonlinear periodic oscillations in liquid rocket combustion chambers for different chamber models and burning rate response formulations 19 p3449 A69-36352

Vibration phenomena analysis by transfer function computer, discussing precision spectrum analyzers 20 p3498 A69-37003

Vibrating circular plate standing wave lateral displacements visualization by photographically recorded moire patterns 20 p3537 A69-37067

Rectangular cross section pretwisted beams modal curves for turbine and compressor blading vibrational studies 20 p3621 A69-37080

Stability augmentation system for B-52, noting flight test performance evaluation for structural vibrations and rigid body motions of aircraft [AIAA PAPER 68-1068] 20 p3461 A69-37157

Vibration analysis, using rigid body and normal modes to solve interconnection problem, applied to free-free natural vibration modes of clustered rockets 20 p3621 A69-37195

Rocket body elastic vibrations, liquid fuel supply oscillations and engine thrust vibrations effects on system stability 20 p3617 A69-37604

Nonlinear oscillations of rectangular plates of composite materials by Berger approach and Reissner variational principle, noting rotary inertial and transverse shear deformation 20 p3627 A69-37771

Spinning satellite attitude perturbations due to oscillating mass in satellite rigid frame, discussing analytical approach and analog simulation results 20 p3618 A69-37912

Axisymmetric vibrations of thin drums consisting of circular cylindrical shell and two circular end plates 20 p3629 A69-38114

Vibrating surface relative phases visual observation by introducing small rotation between exposures of stroboscopic hologram 20 p3546 A69-38123

Transverse vibrations of isotropic solid rectangular beam with secondary effects of rotary inertia and shear deformation retained 21 p3832 A69-38447

- Natural oscillations of end-hinged solid beam with variable parameters and concentrated masses, determining natural frequencies
21 p3833 A69-38575
- Gyroscopic system behavior analyzed for steady state operation following transient period
21 p3723 A69-38832
- Free vibration of thin cylindrical shells with thickness discontinuity, considering natural frequencies and mode shapes dependence on thick/thin ratio
21 p3836 A69-38984
- Damped mass spring system response to sonic booms, considering effects of structural damping, total/positive phase duration ratio and N wave rise time
21 p3647 A69-38987
- Spacecraft natural vibrations analyzed using point transforms with allowance for control systems imperfections
21 p3826 A69-39637
- Vibration properties of cantilever parallelogram box beam, using existing static deformation equations under large aspect ratio condition
21 p3846 A69-39803
- Cylindrical shells vibrations using Lagrangian based on Fluegge system of stress-strain relations
22 p4039 A69-39924
- Noise and vibration levels measured in An-24 Polish passenger aircraft indicating excess noise in crew compartment
22 p3862 A69-40005
- Young modulus for wire or strip shaped specimens determined from unloaded cantilever vibration considerations
22 p4042 A69-40443
- Natural torsional-flexural vibrations of bars with single symmetry, using matrix equations of equilibrium, displacements and natural coupled vibrations
22 p4043 A69-40456
- Spacecraft booms thermally induced vibration and flutter, considering damping and solar exposure effects
22 p4043 A69-40545
- Axisymmetric vibrations of semiinfinite cylindrical shell constructed of fiber reinforced composite layers, obtaining frequency equation from equations of motions
22 p4044 A69-40559
- Small curvature effect on prevention of vibration in shallow shells under random loading numerically analyzed for component modes using linear theory
22 p4044 A69-40600
- Machine tools design for performing cutting operations within acceptable vibration limits
22 p3928 A69-40672
- Homogeneous, viscous and electrically conducting fluid bounded at one end by infinite plane surface of rigid body vibrating relative to fluid body
22 p3991 A69-41036
- Power flow relations between randomly vibrating systems with weak linear elastic or dissipative coupling
23 p4227 A69-41877
- Differential equations of motion and associated boundary condition for axisymmetric flexural vibration of cylindrically anisotropic circular plate, using variational calculus
23 p4228 A69-41911
- Natural vibrational frequencies of uniform thin elastic isotropic flat plates, investigating rectangular and parallelogram plates with various edge conditions
23 p4233 A69-42348
- Central transverse impacts of sphere on free-free beams, investigating maximum strains variation with impact velocity by narrow band tuned circuit filter
23 p4235 A69-42455
- Truncated conical sandwich shell suspended in free-free condition measured and analyzed for vibrational characteristics
23 p4235 A69-42462
- Three layered circular plate under harmonic excitation, analyzing forced vibrational characteristics by variational principle and Ritz method
23 p4236 A69-42495
- Real space-time Green functions applied to turbulence induced infinite thin elastic plate vibration, analyzing mechanical dissipation effects
24 p4395 A69-42597
- Incompressible fluid flow inhomogeneities effect on oscillations of airfoils cascade, noting occurrence of parametric resonance in turbine engine blades
24 p4245 A69-43479
- Inviscid hypersonic flow over oscillating slender wedge, defining equivalent phase shift
24 p4248 A69-43582
- Energy dissipation in oscillating sphere filled with viscous fluid, giving fluid response by solving Navier-Stokes equation
24 p4305 A69-43587
- Synthesis of second order nonlinear differential equations reducible to linear third order equations for application to vibrations field
24 p4342 A69-43702
- ### STRUCTURAL WEIGHT
- Structural weight fraction factor analysis leading to improvements in materials and structures
[AIAA PAPER 68-331] 01 p0011 A69-11021
- Low profile bulkheads for launch vehicles and spacecraft compartments to obtain structural weight reduction
[AIAA PAPER 68-355] 02 p0334 A69-12370
- Numerical method for explicit solution of aircraft mass problem based on linearization of equations describing individual aircraft section masses
03 p0367 A69-13790
- Glass fiber reinforced plastic in aircraft construction, considering cellular weight and economy
03 p0454 A69-13821
- Spar attachments of aircraft wings analyzed with respect to weight and applied loads, determining optimum bolt diameter ratio to lug width
04 p0673 A69-14496
- Aircraft structure lightweight construction materials, reviewing Ti alloys and Be and Al-B bonded filament materials
05 p0779 A69-15917
- Substructure optimization in structural synthesis, minimizing number of cells for configuration parameter
[AIAA PAPER 69-121] 06 p1027 A69-18069
- Minimum weight analysis of Michell trusses transmitting given load to bars within allowable range of axial stress
08 p1410 A69-19893
- Structural iterative design convergence to minimum weight proved by dual linear programming, discussing global convergence and convergence rate
08 p1413 A69-20351
- Electrochemical generators using zinc electrode in alkaline medium, noting weight consideration of zinc/air or zinc/oxygen cells
08 p1261 A69-21049
- Power systems for future aircraft emphasizing growth in performance and reduction in weight
09 p1567 A69-21387
- Electric propulsion design, considering effects of weight, impedance matching, beam voltage regulation and operating point variations in formulating system mass and reliability
[AIAA PAPER 69-254] 09 p1569 A69-21879
- Truss framework for support of eight 100-lb satellites through Titan 3C launch and dispensing of satellites at predetermined times, discussing materials and fabrication
09 p1512 A69-22369
- Ultrasonically assisted installation of fasteners for weight savings in aircraft/spacecraft structures
09 p1478 A69-22373
- Gas turbine engines control and fuel systems integration, considering weight reduction
[ASME PAPER 69-GT-49] 09 p1571 A69-22483
- Boeing 747 aircraft, discussing weight and cost reduction, flap design, structural philosophy, powerplants, fuel system, flying controls, power systems, etc
09 p1435 A69-22714
- Permissible expenditures for decreasing aircraft structural weight
11 p2005 A69-25349
- Variable and fixed weight growth factor effect on aircraft, showing coincidence of minimum weight
11 p1987 A69-25432
- Complex structure least weight optimization for specific frequency by computerized modification of existing member cross sectional properties
11 p1989 A69-25494
- Construction techniques for lightweight mirrors for secondaries, considering optical finishing and thermal expansion
12 p2058 A69-26420
- Linear programming algorithms for optimal structural weight design
12 p2181 A69-26566
- Ultralightweight mirror blanks for astronomical telescopes, discussing weight saving low thermal expansion and fused monolithic core technology
13 p2261 A69-27953
- Weight and cost control program for Boeing 747 aircraft through combined value and weight engineering methods
13 p2383 A69-28096
- Structure, equipment and weight breakdown of Black Arrow X3 spacecraft
13 p2357 A69-28478
- Complex structures lumped weight and inertia parameters automatic computation based on finite weight element method, using SCOWL computer program
14 p2533 A69-29025
- Composite airframe structural joint design and weight considerations for boron and glass fiber reinforced plastic materials
[ASM PAPER W9-23.1] 14 p2535 A69-29448
- Helicopter weight analysis in preliminary design and proposal field
15 p2550 A69-30463
- Starting weight increments in aircraft designs having various structural features and dimensions
16 p2735 A69-32144
- JT8D turbofan engine composite fan blades design and fabrication methods using aluminum-Borsic fiber, noting direct and indirect weight reduction
[AIAA PAPER 69-465] 16 p2842 A69-32698
- Turbopump weight minimization and low suction pressure requirements realized using high rotating speeds, hydraulic turbine driven upstream inducer and computer testing
[AIAA PAPER 69-552] 16 p2741 A69-32747
- Aircraft landing gear cylinder reinforcement rings design for minimum weight, using optimization iteration method for planar frames with elastic supports
[AIAA PAPER 68-328] 17 p3066 A69-34030
- Bandwidth limitations for phase steered planar arrays in satellite applications, discussing weight reduction by modulo 2 pi beam steering
17 p2941 A69-34082
- Aircraft generator weight in relation to system performance requirements, using digital computer to study generator design
17 p2904 A69-34087
- Carrying cables shape optimization for suspended structures under load, using minimum weight criterion
18 p3212 A69-34354
- Apollo 10 lunar landing module, detailing weight, shape, electronic system and rendezvous radar
18 p3207 A69-34629
- Algorithm for minimum weight structures automated design, coupling strain energy criteria with linear interpolation search technique to cover stress and displacement constraints
[SAWE PAPER 798] 18 p3219 A69-34861
- Fixed weight aircraft growth factor variation with location of initial weight penalty along fuselage station, using static stability margin and trim capability
[SAWE PAPER 796] 18 p3220 A69-34862
- Weight estimation and forecast in manned spacecraft design, noting size and weight relationship
[SAWE PAPER 793] 18 p3208 A69-34864
- Rational vehicle weight estimation based on statistical data /REBOS/ including gross weight, weight coding, subdivisions, balance and size, inertia moments and products, etc
[SAWE PAPER 791] 18 p3220 A69-34866
- Advanced design weight analysis and fixed equipment and propulsion systems weight prediction, noting error probability
[SAWE PAPER 790] 18 p3220 A69-34867
- Weight estimation of structures and systems unique to VTOL aircraft, considering remote fan and high bypass engine lift propulsion concepts
[SAWE PAPER 784] 18 p3090 A69-34868
- Army OH-6A helicopter light weight design, considering effects of WRAP /weight, radius, area, power/ factors on empty weight
[SAWE PAPER 781] 18 p3091 A69-34870
- Cost and weight optimization for solid rocket motors using various steel casings
[SAWE PAPER 777] 18 p3208 A69-34871
- Market analysis program to evaluate relationship between launch vehicle jettison weight and total cost based on all projected missions
[SAWE PAPER 776] 18 p3208 A69-34872
- Aerospace vehicle mass property limits and dynamic balancing related, noting errors
[SAWE PAPER 772] 18 p3208 A69-34875
- Earth orbital entry vehicles weight prediction, noting vehicle geometry as function of vehicle shape, hyper-sonic lift drag ratio and crew size
[SAWE PAPER 770] 18 p3208 A69-34876

- Armor selection for advanced aircraft systems based on premium value concept and cost-weight considerations [SAWE PAPER 764] 18 p3094 A69-34878
- Gross weight and aircraft size estimates for configuration design of fighter aircraft [SAWE PAPER 760] 18 p3220 A69-34880
- Aircraft structural weight optimization based on design consideration of grouped related elements, noting application to Boeing 747 trailing edge flap drive [SAWE PAPER 757] 18 p3220 A69-34881
- Design iteration loop calculations related to fighter aircraft weight growth factor, noting asymptotic aircraft performance and strength [SAWE PAPER 732] 18 p3221 A69-34893
- Synthesis and integration of cross discipline function for weight effective design of airplanes [SAWE PAPER 730] 18 p3221 A69-34895
- Aerospace structures optimization, discussing weight considerations and finite element techniques [SAWE PAPER 814] 18 p3221 A69-34896
- Aircraft preliminary design weight and volume characteristics relation to aircraft density [SAWE PAPER 813] 18 p3221 A69-34897
- Parametric approach for weight estimation of surface control systems of transonic and supersonic combat and subsonic transport aircraft [SAWE PAPER 812] 18 p3221 A69-34898
- Analytical-statistical weight prediction to derive and apply correlation expression, illustrated with bending stress equation applied to aircraft wing group [SAWE PAPER 810] 18 p3221 A69-34900
- Aircraft on board weight and balance system, discussing operations and economics programs [SAWE PAPER 805] 18 p3091 A69-34901
- Weight estimation inaccuracies due to use of quickie equations discussing error and extrapolation avoidance in wing weight study [SAWE PAPER 794] 18 p3222 A69-34904
- Monograph on weight and performance tradeoff methodology for selection of high lift devices [SAWE PAPER 761] 18 p3091 A69-34906
- L500 cargo transport commonality with C-5 showing need for aggressive weight control program [SAWE PAPER 745] 18 p3091 A69-34908
- Lockheed L-500 aircraft weight consideration in structural design as all cargo lifter, describing engine thrust, payload, options, etc 18 p3092 A69-35464
- Boron epoxy strut prototype for support system of advanced nuclear flight stage with nonintegral cryogenic tankage configuration, achieving weight reduction 19 p3354 A69-35516
- Perturbation technique application to stability criterion for rectilinear missile flight with arbitrary inclination, noting mass reduction and flow and gravity effect 19 p3429 A69-35779
- Two stage vehicle gross weight minimization determined by slide rule computation using formula based on specific impulse differences between stages 19 p3429 A69-35918
- Structural design optimization based on reliability analysis stressing proof-load test and weight savings consideration under cost constraint 19 p3437 A69-36033
- Sounding rocket aerodynamic stability as function of nose length and mass, discussing wind tunnel test data 19 p3432 A69-36761
- Carbon fiber reinforced plastics application to aircraft metal components for weight reduction, low cost and high mechanical properties 21 p3750 A69-38428
- Stability loss for hinged circular cylindrical elastic shells reinforced by thin walled closed profile ribs, proposing minimum weight design method 21 p3835 A69-38723
- Structural design for minimum weight under random loads representing steady vector random function 21 p3731 A69-38870
- Sprayable polyurethane foam lightweight insulation for Saturn S-2 booster tanks holding liquid H an liquid O at wide temperature ranges 21 p3732 A69-38967
- Boron and carbon reinforced composite materials aerospace structural application, discussing weight savings, components structural design and connection and load input problems 22 p4038 A69-39908
- Computerized solid rocket motor nozzle design with computer program providing weight, envelope and performance values for vehicle optimization studies [AIAA PAPER 69-975] 22 p3999 A69-40355

Elastic curve shape effects on volume of minimum weight uniformly strong beam under combined longitudinal and transverse bending 23 p4225 A69-41421

Minimum weight and optimal cross sections design for statically determinate and indeterminate shell and H beams, using variational method 23 p4225 A69-41424

Spacecraft Si cell solar array using self rigidizing folded panels with flexible substrates for increased power/weight and power/stowage volume ratios 23 p4073 A69-42290

Lightweight large area solar cell arrays for space programs with multikilowatt predicted performance, noting rollup array orbital flight testing 23 p4073 A69-42291

Weight limitations effect on optimum motion parameters of variable mass body in gravitational field applied to spacecraft optimum propulsion system controls and trajectory determination 24 p4383 A69-42956

Maximum admissible weight of structural elements required for conventional wing conversion into variable geometry wing without performance impairment 24 p4253 A69-43092

SST range-payload improvement by emphasizing Ti alloys honeycomb and trusscore sandwich panels fabrication for structural boxes in wing and empennage 24 p4324 A69-43436

Aerospace fastening system requirements to lower in-place costs, extend service life and reduce weight of aircraft 24 p4325 A69-43440

High modulus carbon filament composite structural elements for missile interstage application, showing weight savings 24 p4325 A69-43444

STRUTS

Instability of struts subjected to axial force and radiant heat, considering elastic and thermal deformation 02 p0337 A69-11716

Theoretical buckling load for single edge notched struts, discussing brittleness effects 05 p0837 A69-16064

Thin ring-strut structure resting on elastic foundation, analyzing deformation taking warping effects into account, noting applicability to engine design 12 p2184 A69-26812

Aircraft onboard weighing system, eliminating ring seal friction to permit accurate measurement of oleo strut pressure [SAWE PAPER 748] 18 p3137 A69-34883

Boron epoxy strut prototype for support system of advanced nuclear flight stage with nonintegral cryogenic tankage configuration, achieving weight reduction 19 p3354 A69-35516

STRYCHNINE

Cortical biopotentials in cats induced by strychnine under acoustic click stimuli of increasing intensity 22 p3888 A69-41270

STUDS (STRUCTURAL MEMBERS)

Capacitor discharge stud welding on Ti alloys, discussing weld zone microstructure, arc and mechanical properties 18 p3151 A69-35431

STURM-LIOUVILLE THEORY

Irregular Sturm-Liouville first and higher order perturbation problem in boundary layer theory providing analytical approximations to complete orthogonal set of characteristic functions 04 p0590 A69-15001

Temperature distribution for thin plate heated by source of arbitrary motion and strength and governed by Sturm-Liouville boundary conditions 09 p1622 A69-21906

Finite difference schemes of high order of accuracy for Sturm-Liouville and boundary value problems with regular singularity 10 p1719 A69-23365

STYRENES

NT POLYSTYRENE

Nuclear environment irradiation effects on materials, emphasizing radiation chemical processes affecting polyimide and copolymer of styrene and alpha-methylstyrene 19 p3356 A69-35530

STYROFOAM (TRADEMARK)

Perforation and penetration mechanisms of Styrofoam slabs, using impact tests with free falling and rifle powered projectiles 01 p0165 A69-10115

SUBCARRIER WAVES

U CARRIER WAVES

SUBCIRCUITS

U CIRCUITS

SUBCOOLING

U SUPERCOOLING

SUBCRITICAL FLOW

Plane subcritical flow past lifting aerofoil analyzed using conformal mapping and difference scheme on annular mesh inside circle 06 p0859 A69-17474

Separation of subcritical and supercritical compressible turbulent boundary layers under strong pressure gradients using method based on integral equations [AIAA PAPER 69-34] 06 p0912 A69-18010

Stationary elliptic cylinders in subcritical flow, determining Strouhal number, pressure fluctuations and wake geometry as functions of angle of attack [AIAA PAPER 69-745] 18 p3084 A69-34411

SUBGRAVITY

U REDUCED GRAVITY

SUBHARMONIC GENERATORS

Numerical digital computer determination of ultrasonic subharmonic response for Duffing equation 01 p0104 A69-10235

Pulsed subharmonic oscillation in nonlinear regenerative selective circuits with reference to graphical analytical method for explaining behavior 03 p0385 A69-12918

SUBLATTICES

U LATTICES (MATHEMATICS)

SUBLAYERS

U SUBSTRATES

SUBLIMATION

Mass spectrometer residual gas analyzer (RGA) for identifying and measuring sublimated substances from spacecraft construction materials, noting applications during vacuum testing 02 p0227 A69-11758

Sublimation solid reaction control, discussing propellants, nozzle performance, sublimation area, power, pressure drop, response and valueless design [AIAA PAPER 68-516] 04 p0552 A69-15322

Nose cone reentry simulation under low temperature sublimating ablators, discussing dry ice, camphor and steel calibrations models fabrication, instrumentation and boundary layer measurements [AIAA PAPER 69-152] 06 p0929 A69-18098

Sublimation in ammonium perchlorate propellants combustion, discussing low temperature isothermal processes, linear regression rates measurements and low ambient pressure 11 p1940 A69-24481

Expression relating gas density, radial velocity and temperature at comet nucleus surface to nucleus surface temperature, applying results to unsteady sublimation process 15 p2684 A69-30521

Granular ammonium perchlorate thermal decomposition analyzed by cinemicrography, discussing sublimation role [WSCI PAPER 69-20] 16 p2832 A69-32358

Ammonium perchlorate sublimation models, discussing low temperature decomposition influence on pressure dependence of sublimation rate [WSCI PAPER 69-22] 16 p2832 A69-32360

Micropropulsion system with sublimable solid fuel for satellite attitude control, satisfying mechanical and thermal environmental conditions during launch and in space 17 p3021 A69-33359

Sublimation of various compressed naphthalene wind tunnel models analyzed in supersonic air flow, discussing effects of temperature and model configurations 18 p2331 A69-35121

Noctilucent clouds formation relation to ice sublimation, discussing rocket soundings 21 p3701 A69-38343

SUBLIMINAL STIMULI

Psychophysical threshold changes during subliminal monocular and interocular stimulation, studying conditioning flash size effects on temporal summation 22 p3881 A69-40866

SUBMARINES

Gisette S thermoelectric radioisotopic generator for submarine use, discussing strontium 90 as isotopic source 21 p3768 A69-38455

SUBMERGED BODIES

Submerged rigid circular cylinder displacement under influence of plane acoustic pressure wave solved by operational method 04 p0667 A69-1426

Inviscid cavity and wake flows behind submerged bodies, analyzing mathematical and theoretical models
04 p0587 A69-14608

UBMERGING

Immersion depth influence on hydrofoil for flow of arbitrary depth with bottom consisting of free surface or solid wall
01 p0007 A69-11132

Automatic inflators for life jackets and survival gear in emergencies activated after submersion in water
06 p0877 A69-16955

Human body heat loss control during water immersion, discussing insulative garments and technologies of energy conversion systems
[AGARDOGRAPH-111] 08 p1267 A69-20681

Cold water immersion effects on man from physiological and physiopathological viewpoint, examining clothing effect
08 p1267 A69-20682

Auditory evoked response /AER/ as measure of narcosis induced at depth in diving personnel, discussing hyperbaric nitrogen and oxygen effects
14 p2407 A69-29302

Reinforced textolite plastic dimensional and mass changes in water and oil immersion as function of surface, temperature and time
15 p2643 A69-31550

NACA submerged intake performance at M 2.5, considering total pressure and mass flow ratios, drag coefficient and boundary layer thickness effects
19 p3242 A69-36819

Feline lung injury produced by vertical sinusoidal vibrations during upright water immersion attributed to chest wall impact
23 p4082 A69-41447

Diuresis during total immersion in thermally neutral water, interpreting urine flow increase caused by intrathoracic blood volume expansion
23 p4094 A69-42075

Human heart rate changes resulting from diving and breath holding exercises
23 p4095 A69-42083

Change in weight, plasma volume, urine flow and hematocrit in man before and after immersion up to chin in thermally neutral bath
23 p4096 A69-42087

Test animals prolonged deep submersion in water, in mixed oxygen-H atmosphere at elevated pressure, noting EEG and EKG activities
24 p4262 A69-43025

SUBMILLIMETER WAVES

Figures of merit for polycrystalline uniaxial antiferromagnetic materials, for nonreciprocal devices at millimeter and submillimeter wavelengths, calculated from perturbation theory
[IEEE PAPER 17.11] 01 p0045 A69-10720

Electromagnetic wave generation in 0.2-3mm range, noting applications to physics, biology and technology
02 p0250 A69-12247

Submillimeter wave oscillator /orotron/ involving open resonator with mirror having reflection grating period less than wavelength
02 p0250 A69-12248

Submillimeter wave observation of sun to study anomalous absorption region
03 p0513 A69-13774

High power output from submillimeter continuous wave gas laser
04 p0609 A69-14289

Submillimeter wave vapor laser power output for admixtures of H, N, carbon dioxide, methane, He and Ar, noting buffer effect of H
04 p0612 A69-15175

Absorption effect on fluctuation of signal level propagating in turbulent atmosphere taking into account absorption in water vapor
05 p0717 A69-15634

Submillimeter wavelength astronomy noting instruments, prestellar matter, interstellar and intergalactic matter state and composition, IR stars, planetary atmospheres, etc
05 p0821 A69-15843

Submillimeter wave absorption by dimeric water in atmosphere, using interferometer and maser
05 p0759 A69-16658

Submillimeter plane monochromatic wave amplitude and phase fluctuations during propagation in turbulent atmosphere surface layer, considering absorption by water vapor
05 p0722 A69-16778

Background radiation intensity upper limits for mm and submillimeter wavelengths in interstellar medium, noting intense flux in far IR
07 p1221 A69-19404

Resonator interferometry of pulsed submillimeter wave lasers, analyzing mode structure, pulse shapes and molecular mechanism of laser emission
10 p1705 A69-23810

Millimeter and submillimeter radio waves attenuation in rain, showing effective loss cross section as function of raindrop diameter and wavelength
10 p1657 A69-23943

Sulfur dioxide-helium laser pulsed and CW submillimeter outputs
10 p1706 A69-24005

Atmospheric attenuation of solar radiation, discussing submillimeter astronomy at low altitude observatories
13 p2327 A69-27590

Instrumental investigation of submillimeter astronomy, noting advancements in semiconductor physics, quantum electronics and space astronomy
13 p2342 A69-27602

Millimeter and submillimeter astronomy, discussing lunar poleward darkening function, solar eclipse measurements, observations of Jupiter, Fourier transform and filter spectroscopy uses, etc
13 p2343 A69-27603

Submillimeter astronomy role for solar and atmospheric studies
13 p2343 A69-27604

Submillimeter wave generated in ZnTe by difference frequency mixing of Q switched ruby laser, discussing beat power
[IEEE PAPER B-4] 14 p2457 A69-28927

Orotron electron beam excited oscillator-generator of millimeter and submillimeter wave bands with wide frequency tuning range
14 p2421 A69-29546

Submillimeter atmospheric absorption spectra, emphasizing absorption by isotopic and vibrationally excited forms of water molecules
15 p2568 A69-30699

Superheterodyne millimeter and submillimeter wave detection, allowing harmonics separation
15 p2570 A69-31093

Absorption effect on fluctuation of signal level propagating in turbulent atmosphere taking into account absorption in water vapor
16 p2754 A69-32492

Monochromatic linearly polarized electromagnetic beam generator for submillimeter band, discussing applications
17 p2932 A69-34162

Submillimeter water vapor laser power output for admixtures of H, N, carbon dioxide, methane, He and Ar, noting buffer effect of H
18 p3152 A69-34717

Water vapor absorption at submillimeter wavelengths in atmospheric window regions related to foreign gas pressure, using HCN maser
18 p3152 A69-35241

Water vapor laser submillimeter emission spectra, considering rotational and vibrational lasing transitions due to electron impact and molecular interactions
19 p3336 A69-36349

Cross correlation coefficient for submillimeter monochromatic wave amplitude and phase fluctuations in turbulent atmospheric boundary layer
21 p3674 A69-39129

SUBORBITAL FLIGHT

Suborbital probes, discussing UK sounding rockets Skylark, Petrel and Skua configurations, capabilities and performances
06 p1012 A69-16859

Physiological reactions of dogs during acceleration and weightlessness in suborbital flights of ballistic rockets
07 p1061 A69-18577

Equations of motion for optimal attitude of suborbital aircraft regarding time and distance range
21 p3795 A69-38440

SUBREFLECTORS

Aperture blockage by subreflector in Cassegrain antenna system, computing effects on far field radiation patterns
03 p0401 A69-12853

Cassegrain two reflector antenna modification by discrete phased array, allowing for subunit redesign
04 p0572 A69-14326

SUBROUTINES

Subroutines for computing characteristics of electromagnetic radiation scattered by absorbing and homogeneous sphere employing logarithmic derivative method
14 p2412 A69-29283

SUBSETS [MATHEMATICS]

U SET THEORY

SUBSONIC AIRCRAFT

Wing-body combinations analysis and design at supersonic and subsonic speeds by aerodynamic influence coefficients method
[AIAA PAPER 68-55] 01 p0006 A69-11016

Fiat G.91Y subsonic light tactical fighter, discussing fixed armaments and weapons facilities
02 p0193 A69-12679

Subsonic aircraft potential for short haul transportation, discussing technical problems
05 p0701 A69-15559

Boeing 747 operational and economic considerations including capacity, airport constraints, noise factors, landing gear, compatibility, etc
13 p2201 A69-27340

Next generation subsonic aircraft, discussing basic concerns, aerodynamic factors, materials, noise reduction, cost effectiveness, titanium techniques, etc
15 p2550 A69-30590

Large subsonic transport aircraft effect on economics of air operations with emphasis on airport facilities for Boeing 747
17 p3077 A69-34205

SUBSONIC FLOW

Kernel function applied to compressible fluid flow computation for linear procedure to determine subsonic flow patterns
01 p0058 A69-10225

Compressible relativistic flow in subsonic, transonic and supersonic regimes, noting pressure coefficient variations
01 p0007 A69-11203

Static pressure field induced by steady subsonic flow of compressible inviscid fluid through two dimensional duct with statistically distributed wall roughness
01 p0062 A69-11279

Discrete vortices in two dimensional subsonic and supersonic wake, determining Strouhal numbers, frequencies and flow velocities with aid of HF cinematography
02 p0191 A69-12587

Convergence of Rayleigh-Ritz approximations to solution of elliptic boundary value problem applied to subsonic airfoil problem for 2D steady isentropic irrotational flow
03 p0361 A69-12846

Subsonic or transonic bidimensional flows around airfoils by hodograph method
[ONERA-TP-645] 03 p0361 A69-12873

Unsteady aerodynamic forces on coplanar lifting surfaces in subsonic flow induced by wing/ horizontal tail interference
04 p0543 A69-14819

Test of similarity theory of leading edge vortices above slender wings in subsonic conical flow
04 p0543 A69-14820

Static pressures, profiles of local longitudinal velocity, fluctuating wall pressures and power spectra of wall pressures measured for subsonic turbulent flow
[ASME PAPER 68-WA/FE-36] 05 p0750 A69-16109

Rotating hot wire and five hole pressure probes for determining complete velocity vector in subsonic flow
05 p0764 A69-16398

Approximate method for calculating subsonic gas flows in curvilinear channels for gas admission control in arc welding
06 p0908 A69-16828

Autrotation characteristics of various shapes in subsonic and hypersonic flows for mechanics of free flight reentry to earth impact
[AIAA PAPER 69-132] 06 p0863 A69-18062

Subsonic lifting surface theory including leading edge, discussing singularities in solution of integral equation for determination of aerodynamic properties
[AIAA PAPER 69-37] 06 p0865 A69-18167

Mixed sub- and supersonic gas flow in plane pressure nozzle free of vortex and neglecting viscosity and heat conduction
07 p1050 A69-18739

High velocity subsonic flow past wedge in wind tunnel with perforated walls, applying solution to optimum parameter determination of suction system
07 p1050 A69-18741

Irrational plane subsonic flow of compressible fluid about obstacle, reducing problem to integration of linear partial differential equation with boundary conditions
09 p1480 A69-21735

Lifting pressure distributions on oscillating surfaces in subsonic flows using doublet lattice method for various surface geometries
[AIAA PAPER 68-73] 09 p1430 A69-21946

Wall temperature and Prandtl number effects on turbulent boundary layer thicknesses and shape factors for subsonic compressible gas flow over flat plate
[ASME PAPER 69-GT-55] 09 p1432 A69-22513

Nitrogen dilution low pressure simulation technique for subsonic flow flame stabilization of bluff bodies
09 p1624 A69-22614

Digital computer programs for aerodynamics of subsonic gas turbine combustion systems applicable to incompressible flow with specified flow boundaries, noting vortices distribution
09 p1573 A69-22621

Subsonic channel flow of frictionless barotropic gas through oscillating grid, investigating perturbation velocity field and aerodynamic forces on airfoils
10 p1631 A69-22905

Flow and heat transfer measurements for heated air in subsonic flow through contraction section connecting tube to conical section
[JPL-TR-32-1348] 10 p1809 A69-23194

Boltzmann H theorem and related mathematical topics, noting applications to subsonic gas flow and continuum flow around and over body
11 p1870 A69-25008

Laminar compressible subsonic boundary layer flow on symmetrical cylinder bounded by circular arcs noting zero/nonzero angle of attack
12 p2062 A69-26272

Flow through turbine stage with inclined guide vanes at moderate Mach numbers, discussing exit blade angle formula for swept cascades
15 p2547 A69-30570

Thermal radiation effects on subsonic flow of ideal gray gas, calculating streamwise variations of flow properties
15 p2717 A69-30908

Single and two phase subsonic plasma jets temperature and velocity distribution, noting reduction by condensed phase and use of Schlichting curves
15 p2663 A69-30989

Water cooled split-flow probe measuring enthalpy of high temperature subsonic streams
15 p2614 A69-31275

Lifting surface theory for cascade of blades in subsonic shear flow, determining blade surface pressure distribution, distinguishing shear and uniform flow compressibility effects
16 p2731 A69-31592

Subsonic diffuser design, discussing flow distortion and turbulence levels and pressure loss characteristics
[AIAA PAPER 69-449] 16 p2843 A69-32700

Fixed position pressure probe for measuring subsonic flow direction over range of Reynolds number, Mach number and flow angle
17 p2973 A69-33107

Mixed supersonic/subsonic type steady wake flow fields in flat based slender bodies, using finite difference method
[AIAA PAPER 69-649] 17 p2892 A69-33468

Transport properties of free turbulent mixing of subsonic coaxial streams by introducing environmental distributions in integrals of momentum, energy and species continuity equations
[AIAA PAPER 69-681] 17 p2956 A69-33495

Preston probe measurement of friction drag on subsonic and supersonic nozzle wall including effects of heat transfer, compressibility and pressure gradient
[AIAA PAPER 69-648] 17 p2893 A69-33496

Aerodynamic control surface/trim tab coupling coefficients in subsonic two dimensional unsteady flow using matrix method valid for motion involving harmonic oscillations
17 p2895 A69-33597

Static and impact pressure distributions for Mach number and velocity profiles of supersonic to subsonic flow transition in tube at low Reynolds numbers
[ASME PAPER 69-APM-23] 18 p3120 A69-34397

Strong shock wave structural model, considering near molecular beam, upstream hypersonic and downstream subsonic flows and beam-continuum conversion by collision
18 p3120 A69-34457

Electrohydrodynamic subsonic flow of isothermal charged gas over wavy insulator wall by perturbation method, calculating surface pressure, streamlines and electric lines of force
19 p3297 A69-35837

Inverse transformation method for plane subsonic flow extended to flow past cambered profiles at angle of attack, obtaining velocity distribution
19 p3240 A69-36473

Linearized theory of subsonic gas flow past profile compared with methods based on approximations of relationship between density and pressure
19 p3241 A69-36782

Cold subsonic coaxial jets observed for relationship between noise output and flow characteristics, showing effect of relative annular and central jet velocities
20 p3513 A69-37063

Second order theory for steady or unsteady subsonic flow past slender lifting bodies of finite thickness
[AIAA PAPER 68-75] 20 p3458 A69-37182

Supersonic fan-shaped jet formation by identical colliding underexpanded jets, calculating subsonic flow between interaction plane and curvilinear shock wave
21 p3643 A69-38643

Rotary derivatives of aerodynamic forces and moments in subsonic and supersonic flow, emphasizing kinematic and dynamic oscillations
21 p3647 A69-38733

Jet deflection in drifting subsonic gas flow
21 p3644 A69-39096

Plasma pause form in equatorial plane in presence of magnetospheric tail subsonic potential convective flow
22 p3942 A69-41103

Supersonic free stream flow past finite conical body with subsonic surface gas injection
23 p4059 A69-41884

Subsonic compressible flow at two dimensional inlets, analyzing field representation, boundaries, surface configuration and optimal wedge
23 p4060 A69-41915

Graphical method for two dimensional supersonic expansion flow with subsonic reaction front around corner compared to existing iteration method
23 p4061 A69-42411

Tridimensional infrasonic diffuser geometry effects on operational efficiency, considering opening angle, outlet/inlet section fields ratio and diffuser length/hydraulic radius ratio
24 p4243 A69-42560

SUBSONIC FLUTTER

Flutter vibration in subsonic flows, analyzing critical velocity for membrane and damping destabilizing effects in nonconservative system
02 p0192 A69-12825

Slender profile oscillations in subsonic flow near solid boundary, calculating pressure gradients by dipole method
23 p4058 A69-41713

SUBSONIC SPEED

Subsonic lifting surface analysis accuracy tested by planar circular wing theory
04 p0543 A69-14818

Subsonic aeronautics - Conference, New York, April 1967
05 p0699 A69-15541

Airframe subsonic aerodynamic problems for fixed wing aircraft under low speed/high lift conditions
05 p0695 A69-15542

Design of high lift devices in relation to fixed wing subsonic transport aircraft, considering lift, drag, stability and control
05 p0695 A69-15544

Stability derivative estimation at subsonic speeds for preliminary design engineer
05 p0700 A69-15545

Aerothermodynamics of subsonic-aircraft propulsion, analyzing performance of bypass engine, fuel consumption and specific weight
05 p0695 A69-15551

Subsonic aerodynamics theory applications to VTOL design, architecture, radio antennas, launch vehicles and agriculture
05 p0696 A69-15561

Conventional fuselage and streamline body shapes effect on drag at subsonic speeds, noting boundary layer development
05 p0697 A69-15827

Hodograph for lifting airfoil with subsonic velocity at infinity, using Chaplygin compressibility law for computation
[ONERA-TP-631] 07 p1049 A69-18416

Atmospheric gust effect on aircraft flying at Mach one calculated for subsonic and supersonic regions, finding difficulties for transonic calculations
10 p1632 A69-22918

Aerodynamic and flight characteristics of variable geometry entry spacecraft during subsonic wing deployment and landing
[AIAA PAPER 69-742] 18 p3084 A69-34407

C-5A aircraft model high subsonic speed tests, correlating data from three transonic wind tunnels
[AIAA PAPER 69-794] 19 p3237 A69-35636

SUBSONIC WIND TUNNELS

Large subsonic wind tunnels for correct simulation of V/STOL powered flight by minimizing wall constraint effects on flow field
05 p0741 A69-15578

Wind tunnel wall constraints effects at extreme force coefficients during V/STOL testing shown different from effects in conventional aircraft testing
05 p0741 A69-15578

Test facilities and techniques for low speed flight problems of aircraft handling qualities, stability, control and performance
05 p0741 A69-15578

Blockage correction for blunt based bodies off revolution in wind tunnels at low Mach numbers
05 p0699 A69-16395

Transition boundary layer on flat plate in subsonic wind tunnel measured by hot-wire method, obtaining velocity fluctuation distribution and turbulence intensity
07 p1121 A69-19329

Strip method for prediction of subcritical frequency and damping characteristics for subsonic wind tunnel and flight flutter tests
11 p1987 A69-25368

Jet pump actuation of intermittently operating variable density closed circuit subsonic wind tunnels, measuring wind tunnel power factor
11 p1892 A69-25371

Subsonic wind tunnel solid and ventilated wall interference on air flow around aerodynamic models, discussing data corrections and slotted wall tests
[AIAA PAPER 68-360] 12 p2059 A69-26766

Subsonic wind tunnel balance and holders investigated for effects on lift, drag and stability of models of body of revolution
24 p4297 A69-43084

Wind tunnel model one component magnetic support and balance system for sphere drag investigation at subsonic Mach numbers
[AIAA PAPER 68-401] 24 p4298 A69-43714

SUBSTANCES U MATERIALS

SUBSTRATES

Epitaxial GaAs films with high electron mobility noting radiation recombination spectra dependence on substrate orientation
03 p0492 A69-14172

Loss factors effects on substrate choice in production of microwave printed circuit components
04 p0578 A69-15199

Chemical vapor deposition of chromium metal on substrates, discussing influence of temperature, gas flow rate and chromium chloride concentration
[ECS PAPER 223] 05 p0769 A69-16232

Computer model for n-p-n transistor in integrated circuit using substrate p-n junction isolation
07 p1114 A69-18246

Ferrite microstrips substrates role in integrated circuits, noting application of hybrid technology
07 p1090 A69-18399

Substrates containing silicon regions separated by silicon dioxide or ceramic dielectrics, prepared by lamination in hot press, noting applications to integrated circuits
07 p1100 A69-18617

Substrate bias influence on AC characteristics of MOS transistors used in variable resistor region
07 p1102 A69-18860

Optical parameters for system of isotropic nonabsorbing film on isotropic absorbing substrate determined by ellipsometric method, noting Si optical constants
07 p1201 A69-19648

Micromin alumina substrates design data, determining dielectric constant, impedance vs line width and wavelength vs frequency
09 p1460 A69-22792

Ceramic substrate cutting with carbon dioxide laser by scribing perforation pattern,
10 p1699 A69-23302

Silicon single crystal substrate, preoxidation, oxidation and low temperature heat treatment effects on MOS transistor compared with Silicon-Silicon dioxide interface characteristics
10 p1665 A69-24051

Gold-underlayer film combinations adhesion to oxide substrates, describing adhesion changes as function of Au and underlayer film thickness, time, environment, etc
13 p2321 A69-28007

Electrical properties of electron beam evaporated Ti, Zr and Hf films as function of substrate temperature, material and film thickness
13 p2321 A69-28010

Substrates ultraclean surface preparation methods, examining crystal cleaving and crushing, heating, chemical cleaning, ion bombardment, etc
14 p2455 A69-29348

Electrical resistivity of aluminum oxide films deposited on tubular substrates by plasma and gas flame spraying, noting dependence on film thickness and substrate
15 p2630 A69-31179

Current-voltage characteristics of uniron with metal-dielectric-semiconductor structure /MOSFET/ taking into account substrate potential effect
19 p3284 A69-36592

Substrate specificity of cathepsin C derived from rat liver, describing polymeric structure and behavior as acidic protein
20 p3473 A69-37577

Condensation dynamics of atom by solid body model consisting of one dimensional chain of harmonic oscillators
21 p3775 A69-39557

Van Driest-Bradshaw model for calculating sublayer function for self preserving laminarescent boundary layers, discussing porous surface suction or acceleration effects
[ASME PAPER 69-HT-12] 24 p4304 A69-43557

SUBSTRUCTURES

Substructures around fatigue cracks in fcc metals and alloys, noting relation between structural formation and crack propagation
02 p0260 A69-11826

Flow theories of fluids with elastic deformation of substructure, treating suspensions of irregularly shaped deformable particles
05 p0752 A69-16738

Substructure optimization in structural synthesis, minimizing number of cells for configuration parameter
[AIAA PAPER 69-121] 06 p1027 A69-18069

Fatigue crack initiation and propagation correlation with substructure formation by static and alternating stresses in Al
12 p2188 A69-26915

SUBTRACTORS

U ADDING CIRCUITS

U SUBTROPICAL REGIONS

U TEMPERATE REGIONS

U TROPICAL REGIONS

SUCROSE

Escherichia coli B/r cells plasmolyzed in sucrose observed under phase contrast, noting plasmolysis reduction in ions presence
19 p3257 A69-35973

DNA and d(A-T) oligomers enzyme binding to DNA polymerase by sucrose density gradient centrifugation
22 p3898 A69-41075

SUCTION

Soviet monograph on laminar boundary layer in presence of suction covering incompressible flow through porous surface, drag reduction and optimal suction at high velocities
01 p0060 A69-10615

Heat transfer, suction and injection in plane Couette flow analyzed for Rivlin-Ericksen fluid, using perturbation method
04 p0589 A69-14970

Laminar flow on swept low drag suction wings at high Reynolds numbers
05 p0696 A69-15557

Suction effect on incompressible flow through step expansion in circular pipe through sudden enlargement, considering inlet flow with thin boundary layer
[ASME PAPER 68-FE-11] 05 p0748 A69-16074

Injection or suction at disk surface, noting effects on heat and mass transfer in laminar flow about rotating disk
06 p1029 A69-17002

Decreasing secondary flows in spatial boundary layer on porous plate by boundary layer control /BLC/ through suction or blowing, using Prandtl partial differential equations
06 p0909 A69-17185

Unsteady suction motion of viscous incompressible fluid under action of slowly rotating suction disk, noting fluid velocity variation
08 p1302 A69-19875

Suction effect on temperature distribution and heat transfer in plane Couette flow and laminar flow in circular pipe
08 p1303 A69-20371

Boundary layer suction sound emission, analyzing turbulent flow past elastic plate with reinforced slots performing flexural and torsional vibrations
09 p1483 A69-22638

Monograph on optimal design of free-running drag turbines for boundary layer suction in aircraft, emphasizing gliders performance
12 p2011 A69-26117

Suction effects on shockwave-turbulent boundary layer interactions at compression corner leading to reductions in upstream influence
13 p2244 A69-27326

Loitsianski method of parametric approximation extended to include flat plate with constant surface suction and flow past circular cylinder
13 p2249 A69-28247

Model to study viscous flow characteristics in channel with porous walls and constant suction, noting non-monotonic velocity profile
14 p2429 A69-29015

Laminar boundary layer control by combined blowing and suction, analyzing surface roughness influence concerned with underwater vehicle skin friction reduction
[AIAA PAPER 69-387] 15 p2591 A69-30477

Fluidic logic elements using suction to influence main jet, outlining operation principles
16 p2736 A69-31835

Critical review of paper on suction effect on hypersonic laminar boundary layer separation
16 p2771 A69-31928

Distributed boundary layer suction effectiveness for controlling supersonic transitional flow separation
16 p2772 A69-32149

Conical shock wave-turbulent boundary layer interaction data obtained for adiabatic wall conditions at supersonic free stream Mach numbers, including suction effects
[AIAA PAPER 69-450] 16 p2773 A69-32754

Amplified boundary layer oscillations and transition at swept flat nosed wing attachment line with/without boundary layer suction analyzed by wind tunnel tests
17 p2890 A69-33251

Laminar boundary layer control on two dimensional body by combined blowing and suction in presence of roughness, noting skin friction reduction
[AIAA PAPER 68-641] 17 p2957 A69-34015

Pure gas suction through free jet shock structure, analyzing aerodynamic effect of molecular separation
19 p3240 A69-36650

Boundary layer flow past permeable surface, generalizing integral equations for case with suction
21 p3691 A69-38573

Unsteady boundary layer with distributed injection or suction on porous plate, determining acceleration and flow parameter functions from velocity profiles
21 p3692 A69-38609

Laminar corner boundary layer flow with suction, discussing Navier-Stokes equations and steady state heat conduction problems
21 p3696 A69-39578

Distributed suction effect on boundary layer structure of water flow from turbulence measurements, determining velocity and pulsation intensity distributions
22 p3933 A69-41029

Laminar boundary layer in steady compressible gas flow past plane wing profile, studying surface temperature and suction effects
23 p4058 A69-41709

Steady constant density two dimensional flow in laminar boundary layer over permeable curved surfaces, showing effects of suction or blowing
23 p4153 A69-42399

Laminar flow in porous circular pipe with constant suction or injection applied at wall
24 p4298 A69-42618

Turbulent pipe flow with wall suction, calculating friction factor, pressure gradient, heat and mass transfer coefficients, velocity and temperature profiles
[ASME PAPER 69-HT-4] 24 p4414 A69-43562

SUD AVIATION AIRCRAFT

NT ALOUETTE HELICOPTERS

NT CONCORDE AIRCRAFT

NT SA-330 HELICOPTER

NT SE-210 AIRCRAFT

Sud commercial aircraft /1970-1980/, discussing market trends, airport saturation, Airbus power plants and seating capacities
24 p4416 A69-42563

SUD AVIATION SA-330 HELICOPTER

U SA-330 HELICOPTER

SUD AVIATION SE-210 AIRCRAFT

U SE-210 AIRCRAFT

SUDDEN ENHANCEMENT OF ATMOSPHERICS

Equatorial enhancement of storm sudden commencements and sudden impulses in horizontal component in American Zone during IGY/JGC
01 p0068 A69-11116

Structure of sources of noise storm enhancements and stationary type 4 bursts, discussing head and tail components
02 p0328 A69-12753

Midday enhancement of sudden commencements and sudden impulses in H and Z at equatorial stations in Indian zone during IGY
08 p1307 A69-20187

Low energy solar cosmic ray proton flux characteristics observed by Injun 1 satellite after July 1961 sudden commencement magnetic storm
09 p1576 A69-21707

Auroral electrojet index in relation to magnetic storm sudden commencements, ring current main phase and energetic solar protons
14 p2511 A69-28954

Sudden enhancement of atmospherics recorded during IGY, noting time lag between flare and SEA maximum
16 p2778 A69-32192

High altitude nuclear explosions detected by distinguishing artificial from natural sudden enhancement of atmospherics /SEA/ phenomena
20 p3492 A69-37701

SUDDEN IONOSPHERIC DISTURBANCES

Ionospheric inhomogeneities vertical and latitudinal distributions and diurnal variations, measuring Explorer 22 signals Faraday fading with space diversity reception
01 p0064 A69-10446

Solar proton event generating sudden commencement magnetic storm, discussing effects on outer belt electrons as observed by Explorer 26 and time delay
01 p0146 A69-11124

Ionospheric irregularities and cross field plasma instability, analyzing nonlinear behavior of latter with two dimensional model
01 p0073 A69-11179

Sudden magnetic field increase associated with July 8, 1966 sudden commencement observed by OGO 3 satellite in magnetotail
01 p0075 A69-11226

Sudden cosmic noise absorption in ionosphere confirms relationship with solar chromospheric flares
02 p0306 A69-11667

Hydromagnetic emissions observed at Antarctic auroral zone, discussing relation to sudden storm commencement
02 p0241 A69-11726

Sudden ionospheric disturbance development and characteristics of solar cosmic ray flares, associated X ray emissions and high energy particle generation
02 p0308 A69-12398

Solar X ray flares measurement by rocket and satellite, discussing X ray spectrum hardening, hard flares and SID
03 p0500 A69-13225

Ionospheric F2 layer following SSC magnetic storm, noting similarity with polar aurora region
03 p0423 A69-13531

Ionospheric parameters variation during SC effect as function of solar and magnetic activities
03 p0423 A69-13534

VHF satellite signal scintillation by ionospheric irregularities with sharp boundary /such as sporadic E/, noting diffraction pattern dependence on phase shift
09 p1489 A69-21713

Sudden commencement associated discontinuities in interplanetary magnetic field observed by IMP 3 satellite, stressing shocks and tangential and rotational discontinuities
09 p1598 A69-22183

Summation curves method for development of active region and time dependence of energy loss during proton flare
10 p1764 A69-23743

Sudden ionospheric disturbance effects of solar X ray emission from active region with proton flare
10 p1764 A69-23744

X ray and extreme UV radiation deduced from sudden ionospheric disturbances during proton flare, discussing time dependence of emission
10 p1766 A69-23756

Geomagnetic crochet of July 7, 1966, discussing pulsations, recombination coefficient and electron density of ionospheric D region
10 p1683 A69-23757

Ionospheric irregularities drift and anisotropy parameters variation with true reflection height during magnetically disturbed conditions

10 p1659 A69-24062

Solar flare X ray and extreme UV radiation contribution to E and F1 region ionospheric effects observed by sudden frequency deviations

11 p1950 A69-25160

Iono-index above hard emission of solar active regions, analyzing field fluctuations and SID in D region under daytime conditions

12 p2148 A69-26107

Sudden cosmic noise absorption in ionosphere confirming relationship with solar chromospheric flares

13 p2334 A69-28698

Ionospheric effect sudden commencement parameters of magnetic storm related to distance from origin in polar regions

14 p2435 A69-29051

Worldwide changes in geomagnetic field, determining causes by examining magnetic field and plasma data for solar wind and classifying as SSC or SI

16 p2847 A69-31963

Sudden phase anomalies on radio paths compared with calculated results for satellite observed solar X ray flux intensities to explain sudden ionospheric disturbances

17 p2959 A69-33006

Planetary ionospheric effect of 15 July 1959 sudden commencement magnetic storm based on N/h/ profiles of earth day and night sides

17 p2967 A69-33987

Geomagnetic crochets time relations to solar X rays, radio bursts and flares

17 p3025 A69-34227

Sudden frequency deviations of HF radio waves propagated through ionosphere correlated with solar microwave bursts and optical flare events

20 p3592 A69-38101

Sharply bounded homogeneous ionospheric model to solve modal equation, discussing lower ionospheric conductivity from VLF transmission sudden enhancements of strength/SES/

21 p3714 A69-38554

Sudden and gradually developing geomagnetic storms with 27 day recurrence period and relation to 11 year solar activity cycle

23 p4156 A69-41849

SUGARS

NT GLUCOSE
NT MONOSACCHARIDES
NT SUCROSE

Sugars identification as trifluoethylacetyl polyol derivatives by gas-liquid chromatography

15 p2558 A69-31539

White rats hyperglycemia during blood sugar changes following single X ray dose, indicating increased sugar benefit in radiation damage treatment

21 p3658 A69-39057

SUHL EFFECT

Relaxation oscillations in field ionized epitaxial n-GaAs Gunn oscillators on semiinsulating substrates, discussing recombination of excess electrons and holes

13 p2227 A69-27236

SUITS

U PRESSURE SUITS
U SPACE SUITS

SULFATES

NT HEXAHEDRITE
NT HYDROXYLAMINE SULFATE

Bright cadmium plating by electrolysis, describing processes during electrodeposition from sulfate electrolytes

22 p3959 A69-41266

SULFATION

Reaction between nickel-base alloy and hydrogen sulphide at high temperatures under atmospheric pressure, discussing activation energy

12 p2115 A69-26617

Synthetic ferrites and sulfides of Ni and Co sulfated in presence of molten sodium pyrosulfate and sodium bisulfate

16 p2747 A69-32567

Dynamic hot corrosion rig test for operating environment and alloy composition effect on sulfidation attack during gas turbine fuel combustion

23 p4150 A69-42448

SULFIDES

NT CADMIUM SULFIDES
NT COPPER SULFIDES
NT DISULFIDES
NT HYDROGEN SULFIDE
NT INDIUM SULFIDES
NT LEAD SULFIDES
NT MOLYBDENUM DISULFIDES

NT MOLYBDENUM SULFIDES

NT TROILITE
NT WURTZITE
NT ZINC SULFIDES

Sulfide addition agents for diester lubricating grease and organic resin solid film lubricants, noting formulation and tests for steel and molybdenum

01 p0102 A69-10907

SnTe, SnSe and SnS epitaxial layers obtained by deposition of sublimates on cellulose-nitrite-varnish and single crystal NaCl and KBr substrates

02 p0298 A69-12049

Sulfospinels polymorphism at high temperature and pressure and pressure-temperature phase relations

02 p0266 A69-12162

Temperature dependence of viscosity and density in molten thallium sulfide, noting structural changes absence in short range order

04 p0643 A69-14998

Austenitic Fe-Ti alloys sulfur solubility and internal sulfidation rate computed, noting stronger Ti-S interaction with temperature decrease and sulfur diffusion role

06 p0942 A69-17226

Petroleum sulfides advantageous effect on oxygen consumption during combustion

07 p1202 A69-19456

Sulfidation attack and structural stability of nickel-base superalloy [SAE PAPER 690103]

09 p1522 A69-21556

Synthetic ferrites and sulfides of Ni and Co sulfated in presence of molten sodium pyrosulfate and sodium bisulfate

16 p2747 A69-32567

Cr-S and Cr-Fe-S systems phase relations, using silica tube and collapsible tube experiments, correlating formation conditions of meteoritic sulfide assemblages

19 p3359 A69-36123

Antimony trisulfide single crystals spectral dependence of impurity and stimulated impurity photoconductivities, comparing optical and thermal activation energies

22 p3994 A69-41042

Ferredoxin from thermophilic and mesophilic Clostridia, noting difference in heat stability due to iron and sulfide environments

22 p3897 A69-41068

SULFITES

Sulfite ion influence on pitting corrosion of stainless steels in sodium chloride solution

07 p1167 A69-19343

SULFONES

Thermoplastic polyarylsulfone thermal and electrical properties at over 500 F, noting resistance to thermal oxidative attack

19 p3355 A69-35527

SULFUR

Permissible JP-5 fuel sulfur content effect on hot corrosion of protective coated Ni-base superalloys in marine environment, noting atmospheric sea salt role

01 p0141 A69-11059

Forbidden S I lines due to transitions within ground configuration identified in Fraunhofer spectrum of sun, noting photospheric abundance of S

07 p1217 A69-19237

Quantitative gas-liquid chromatography of sulfur amino acids trimethylsilyl derivatives

13 p2217 A69-28259

Electronic levels excitation in S I and II by beam foil method

18 p3177 A69-35015

IR spectra of Eta Carinae, confirming nitrogen and sulfur abundance

19 p3423 A69-36229

SULFUR COMPOUNDS

NT CADMIUM SULFIDES
NT COPPER SULFIDES
NT CYSTEINE
NT DISULFIDES
NT HEXAHEDRITE
NT HYDROGEN SULFIDE
NT HYDROXYLAMINE SULFATE
NT INDIUM SULFIDES
NT LEAD SULFIDES
NT MOLYBDENUM DISULFIDES
NT MOLYBDENUM SULFIDES
NT SULFATES
NT SULFIDES
NT SULFITES
NT SULFONES
NT THIOLS
NT TROILITE
NT WURTZITE
NT ZINC SULFIDES

Sulfur organic compound formation effect on composition and structure of solid phase formed during hydrocarbon jet fuels oxidation

01 p0142 A69-11097

Sulfur-organic compounds association with aromatic hydrocarbons, noting oxidation inhibiting effect on petroleum oil

03 p0494 A69-1380

SH above photosphere in solar atmosphere, discussing dissociation equilibrium of diatomic molecules and possible abundances

06 p1002 A69-17317

ESR comparative study of selenoamino acids and analog radical formation and radiation resistance, noting selenium groups ability as acceptors for unpaired electrons

21 p3668 A69-38423

SULFUR FLUORIDES

Nonlinear interactions of linearly polarized carbon dioxide laser signals in sulfur hexafluoride measured as function of angle between polarization planes

14 p2460 A69-29602

Sulfur hexafluoride dissociation in argon at various temperatures and pressures, using shock tube techniques to determine unimolecular parameters

18 p3100 A69-35475

Rice-Ramsperger-Kassel kinetic theory applied to sulfur hexafluoride injection into boundary layer of high speed reentry vehicle

20 p3514 A69-37226

Carbon trioxide formation during ozone photolysis in liquid carbon dioxide and sulfur hexafluoride, noting ozone disappearance quantum yield independence of oxygen/ozone ratio

23 p4112 A69-41338

SULFUR OXIDES

Sulfur trioxide production in photolysis of sulfur dioxide at 1849 angstroms, noting oxygen addition effect on quantum yield

01 p0024 A69-10619

Therapeutic potential of dimethyl sulfoxide in aerospace medicine

06 p0883 A69-17851

Temperature and concentration measurements of H radical in hydrogen flames

21 p3669 A69-38807

SUM RULES

Partially conserved axial vector currents and current algebra to obtain vertex functions at point having zero mass by extrapolations

17 p3008 A69-33004

SUMMARIES

U ABSTRACTS

SUMMER

Large scale disturbances in summertime stratosphere observed from high level balloon, discussing diurnal wind patterns and planetary traveling waves

03 p0461 A69-13343

SUMS

Asymptotic behavior of probabilities of large deviations of sums of independent random variables with moments of any order

01 p0104 A69-10264

Summation of Legendre series by transformation into integrals and use of recurrence relations

01 p0171 A69-11072

Chebyshev polynomials maximum property, examining effect of roundoff errors in Horner scheme for floating point arithmetic

03 p0456 A69-13553

Hard limiting effect on sum of three or four sinusoidal signals noting output amplitudes, signal suppression and negative suppression effect

09 p1451 A69-21311

Sum rule properties of finite set of wave functions obtained from application of variational principles to basis functions linear combinations

14 p2471 A69-29921

Neumann-Lommel formula generalization for obtaining Bessel functions product sums illustrated with FM wave distortion calculation in multichannel system

18 p3101 A69-34625

Asymptotic behavior of probabilities of large deviations of sums of independent random variables with moments of any order

19 p3360 A69-36199

Homogeneous Markovian sum of sequence of random quantities series, deriving limiting theorem for sum density

21 p3757 A69-39538

JUN

- Solar limb image vibrations caused by turbulent pulsations in refractive index of lowest atmospheric layers
01 p0156 A69-11183
- Solar growth curves constructed for solar disk center using various metal lines
02 p0314 A69-11637
- Solar granules structural and correlation functions indicate homogeneous random field within photograph and regular component in intensity fluctuations spatial distribution
02 p0317 A69-11958
- Sun motion with respect to extragalactic universe, discussing local supercluster kinematics
03 p0513 A69-13769
- Limb darkening and central intensity of solar disk measured in UV
05 p0827 A69-16466
- Magnetic field surface in isolated symmetrical sunspot during motion across solar disk, determining field vector angle of inclination variation as related to solar surface
06 p0999 A69-16978
- Solar disk surge distribution difference between eastern and western disk parts
06 p0995 A69-17440
- Solar intensity measurements at 1.2 mm during partial solar eclipse, noting solar limb brightening and intense solar outburst near end of eclipse
07 p1217 A69-19243
- Solar atmosphere model calculations of solar oblateness, discussing flux difference and Dicke experiment on general relativity
08 p1383 A69-19899
- Cometary origin of meteors and element abundance in primitive solar nebula, discussing neutron capture products in chondrites
08 p1406 A69-20930
- Solar occulting disk diameter at radio wavelengths derived from consideration of slightly deviated rays
09 p1607 A69-22432
- Primordial solar system chemical composition for studies of origin and evolution, compiling solar composition data
09 p1608 A69-22745
- Plasmas role in emission mechanisms active in celestial sources of radiation, discussing sun and quasars
12 p2159 A69-26619
- Relative transition probabilities for visible Si atom lines, noting disagreement with LS coupling predictions and solar Si abundance determination
13 p2340 A69-27580
- Icarus radar and optical observations analyzed to verify general relativity predictions using Schwarzschild metrics and to estimate solar oblateness, Mercury mass, etc
13 p2350 A69-27823
- Stellar densities and luminosity function determined from stellar data concerning sphere with 20 pc radius around sun
13 p2351 A69-27869
- Soviet collection of articles on cosmic physics, Number 3, Comets, sun and interplanetary space
14 p2522 A69-29703
- Solar telescope imaging quality measured as function of atmospheric turbulence and temperature above land level
14 p2453 A69-29973
- Radial velocities differences as indicator of stellar atmospheric turbulence, applying method to sun
17 p3044 A69-34177
- Upper limit of solar oblateness determined from secular stability of differential rotation during evolution
18 p3202 A69-35214
- Nonlinear effects in spiral galaxies with emphasis on solar neighborhood region, discussing radial motion, stationary state with excited waves and vertex deviation
20 p3607 A69-38036
- Interstellar reddening in solar vicinity, analyzing roles of galactic latitude and longitude and heliocentric distance
22 p4026 A69-40648
- Solar motions respecting high velocity atomic hydrogen clouds and local stellar group
22 p4035 A69-41209
- Fe abundance in sun and carbonaceous chondrites, noting agreement between solar and meteorite abundances of Ni, Mg, Si and Li
24 p4385 A69-43223

Instantaneous response TV system application to observing solar surface granulation, noting advantages over photometric measurements
24 p4389 A69-43711

SUN SENSORS

U SOLAR SENSORS

SUNLIGHT

- Airborne polarimeter to measure Stokes parameters of linearly polarized visible atmospheric radiation in four narrow spectral regions
06 p0923 A69-16924
- Sun-orbit plane relationship effects on mission planning
[AIAA PAPER 69-129] 06 p1011 A69-18093
- Thermal flutter effect on gravity gradient stabilized spacecraft, noting dependence on sunlight and time
07 p1226 A69-18325
- Directional solar thermal field /sunlight/ effect on coupled nonplanar transverse and torsional vibrations of satellite cylindrical antennas in orbit
11 p1994 A69-25534
- Solar simulator with pulsed Xe arc tube, describing operating characteristics, spectral emission and simulator-sunlight correlation
15 p2586 A69-30385
- Equatorial mounted solar energy concentrator efficiency compared to unconcentrated sunlight and artificial UV-visible light source in reducing Pb tetraacetate solution in acetic acid
16 p2736 A69-31814
- Lifetime of ground state oxygen molecular ions in sunlight from photodetachment rate by free electron production measurement from ions in buffer gas
16 p2848 A69-31973
- Wavelength dependence of linear polarization of sunlight scattered by Venus, noting temporal variations in UV
16 p2860 A69-32236
- Earth-reflected solar energy /albedo energy/ distribution model, assuming isotropic scattering by homogeneous atmosphere
[AIAA PAPER 69-591] 17 p2961 A69-33292
- Ozone measurement from satellite by direct beam and scattered light methods employing UV sunlight attenuation
21 p3721 A69-38625
- Total solar radiation correlation with bright sunshine hours measured monthly on solarimeters and Campbell-Stokes recorders at various tropical stations
23 p4206 A69-42178
- Sun-orbit plane relationship effects on mission planning
[AIAA PAPER 69-164] 24 p4386 A69-43261

SUNRISE

- D region composition at and shortly after sunrise, noting negative ion factor changes, ionization source and quasi-equilibrium conditions
01 p0066 A69-10597
- F 2 layer cut-off frequency predawn increase caused by sunrise, resulting in photoelectrons transfer along force lines at magnetically conjugate point
02 p0238 A69-11681
- Sunrise effects in lower D region by solar eclipse, discussing anomaly in ionospheric absorption due to negative ion factor or recombination coefficient
02 p0246 A69-12767
- Phase and amplitude record changes in sunrise and sunset transitions in VLF transmissions over long path
06 p0889 A69-17655
- F 2 layer cut-off frequency predawn increase caused by sunrise, resulting in photoelectrons transfer along force lines magnetically conjugate point
13 p2257 A69-28712
- Quantitative criteria imposed on balloon measurements of auroral emissions from Kiruna, considering times of sunrise and sunset at different altitudes
21 p3716 A69-39250

SUNSET

- Phase and amplitude record changes in sunrise and sunset transitions in VLF transmissions over long path
06 p0889 A69-17655
- Green flash photographed at sunset by aircraft at 10.6 km over Pacific, noting correspondence with visual observation
12 p2066 A69-26232
- Quantitative criteria imposed on balloon measurements of auroral emissions from Kiruna, considering times of sunrise and sunset at different altitudes
21 p3716 A69-39250
- Absorption observation of solar radiation at sunset by nitric acid in three wavelength intervals on different balloon flights
24 p4308 A69-42969

SUNSPOT CYCLE

- 26-month periodicity in quiet day range of geomagnetic field horizontal force, noting similar periodicity in sunspot number and 16-month oscillation in both phenomena
01 p0063 A69-10427
- Chromospheric and photospheric solar observations made in Belgium in 1967, noting heliographic sunspot latitudes
02 p0313 A69-11533
- Longitudinal distribution of cycle sunspots in initial phase of solar activity from Greenwich Observatory data
02 p0314 A69-11647
- 11-year solar cycle influence on F 2 region critical frequency, investigating correlation coefficient between mean monthly values of F 2 variations and respective sunspot numbers
02 p0238 A69-11680
- Relation between solar activity and cyclic variation of pearl pulsations excitation frequency during sunspot cycle
02 p0239 A69-11696
- Solar limb prominence areas variation with latitude and solar activity cycle, noting changes in yearly mean latitude of prominences during cycle
05 p0816 A69-16390
- Null solar neutrino flux possible relation to 2 year solar cycle, discussing energetic disturbances at solar core and sunspots
08 p1377 A69-19902
- Solar quiet day variations studied by annual amplitude dependence on number of sunspots, considering E layer ionization
09 p1575 A69-21550
- Sunspot lifetime, maximum area and cyclic variations recorded in photoheliographic results of Greenwich, discussing frequency distribution and mean
10 p1770 A69-24000
- Statistical rules for seasonal forecasts based on temperature and precipitation deviations analysis in long term climatological records, considering sunspot cycle role
12 p2125 A69-25895
- Nightglow intensity variations at sunspot minimum from measurements in South West Africa, considering relationship to ionospheric vertical movements and density variations
12 p2066 A69-26133
- 11-year solar cycle influence on F 2 region critical frequency, investigating correlation coefficient between mean monthly values of F 2 variations and respective sunspot numbers
13 p2257 A69-28711
- Relation between solar activity and cyclic variation of pearl pulsations excitation frequency during sunspot cycle
13 p2258 A69-28727
- Interplanetary sector structure during rising portion of 1966-1967 sunspot cycle, giving recurrence period of interplanetary field
14 p2517 A69-28957
- Solar quiet day variations studied by annual amplitude dependence on number of sunspots, considering E layer ionization
16 p2851 A69-32545
- Auroral absorption maximum frequency correlation with years of solar activity reduction and magnetic activity from riometric data long term variations
17 p2968 A69-33991
- Jupiter red spot prominence correlation with Zurich sunspot number
17 p3045 A69-34185
- Global electron density distribution morphology in topside ionosphere during sunspot minimum from Alouette 1 and 2 ionograms
20 p3530 A69-37867
- Solar activity center characteristics in floccula stage during eleven year sunspot cycle
20 p3616 A69-38302
- Babcock solar activity periodicity theory, correlating spots displacement and coronal magnetic field intensity changes
23 p4208 A69-41283
- Solar activity long term forecasts determined from comparison between Mount Wilson magnetic field synoptic chart latitude zones and sunspot groups
24 p4374 A69-43625

SUNSPOTS

- Ionized calcium lines in spectra of light bridges of sunspots, observed by diffraction spectroscopy, indicating similarity to chromospheric flares
01 p0154 A69-10894

Sunspots autocorrelation functions in sunspot area on solar disk, tabulating extremal values

02 p0314 A69-11677

Wilson effect in sunspots, interpreting penumbra distortion near solar disk limb in terms of radiation transport

03 p0504 A69-12893

Time dependence of relation between sunspot number and ionospheric index IF 2, noting hysteresis characteristic and changes for different solar cycles

03 p0424 A69-13632

Sunspot structure from two dimensional radiative transfer analysis of center limb intensity profiles made at several heliocentric angles

03 p0516 A69-14040

Time dependent variations in magnetic fields of active sunspot clusters in photosphere observed by magnetograph

04 p0651 A69-14369

Chromospheric flare development and motion with respect to magnetic field of sunspot clusters

04 p0648 A69-14371

Dissipation time of sunspot magnetic field determined as function of minimum spot value

04 p0660 A69-15039

Solar flares and sunspots number decrease near central meridian

04 p0660 A69-15040

Solar radio emission sources associated with sunspot groups and flocculi at 1.6 cm

04 p0649 A69-15241

Local hydromagnetic mechanism to increase magnetic fields and shape into bipolar sunspot group configuration, discussing applicability to solar atmosphere

04 p0662 A69-15243

Photospheric network obtained by spectroheliograms, discussing Fraunhofer lines weakening, nonsunspot magnetic fields and Zeeman sensitivity

04 p0664 A69-15523

High resolution H alpha line photographs of solar chromosphere, showing superpenumbra-like dark fibrils around isolated sunspots

04 p0664 A69-15526

Lithium abundance in sunspots and undisturbed solar atmosphere from measurements of solar atmosphere and spot spectra

05 p0821 A69-15850

Sunspot group classifications made at Zurich and Catania during 19th solar cycle compared to determine seeing influence

05 p0826 A69-16388

Pressure stratification and transparency/geometrical depth expansion/ in Fricke-Elsasser and Zwaan sunspot models

06 p0999 A69-16976

Model for Evershed effect postulating unipolar symmetrical sunspot surrounded by magnetic knots of opposite polarity

06 p0999 A69-16977

Magnetic field surface in isolated symmetrical sunspot during motion across solar disk, determining field vector angle of inclination variation as related to solar surface

06 p0999 A69-16978

Sunspot ejection of filaments, flare surges and flare sprays, discussing bright and dark matter divergence from western spot

06 p0995 A69-17441

Model to account for flare and sunspot phenomena, discussing uni- and bipolar spots

06 p0995 A69-17443

Solar type 4 bursts characteristics accounted for by cyclotron mechanism, assuming models of spot magnetic field configuration and electron density distribution

07 p1205 A69-18959

Magnetic knots /intergranular space strong small scale magnetic fields near sunspot/, longitudinal and transversal fields and radial velocities

07 p1217 A69-19244

Sunspot groups area changes relationship to cosmic ray flare occurrences

07 p1206 A69-19252

Sunspot observations with astrophot telescope by tracing on projected image of solar disk

08 p1387 A69-20118

Scattered light reduction in sunspot photometry, noting eliminating effect when observing spectral lines or narrow spectral regions

08 p1389 A69-20251

Synoptic charts of chromosphere, giving position and magnitude of sunspots, facula plages and prominences during synodic revolution of sun

08 p1379 A69-20378

Sunspot activity dependence on phase of eleven year cycle and heliographic latitude, discussing fine structure of butterfly diagrams

08 p1379 A69-20611

Frequency distribution curves of spot groups according to area, confirming existence of stable stages in evolution of sunspots

08 p1379 A69-20612

Solar phenomena correlation with brightness variations of comet Alcock 1963b, noting sunspot maximum followed by maximum in absolute magnitude of comet

08 p1394 A69-20620

Magnetic fields of solar supergranulation convective cells based on electromagnetic induction equation, indicating bipolar sunspots occurrence

09 p1588 A69-21366

Correlated spectra of related sunspot number and solar 10.7 cm radiation component, noting variance for solar rotation periods

09 p1574 A69-21397

Effective cross sections of electron-neutron interaction in photosphere and sunspots, calculating electric conductivity and anisotropy coefficient

09 p1579 A69-22175

Solar activity influence on cosmic ray intensity 11 year variation, taking into account heliolatitudinal movement of sunspot regions in solar cycle as evidence of density gradient

10 p1754 A69-22802

Magnetically aligned flows between sunspots, considering Evershed effect on umbrae and penumbrae

10 p1772 A69-22907

Sunspot group associated with proton flare of July 1966, describing formation of spot cluster pairs on borders of adjoining network cells

10 p1763 A69-23730

Proton flares during July 1966, discussing flare magnitude classes on disk, behind west limb, in active region and proximity to sunspots

10 p1763 A69-23737

Sunspot group evolution after proton flare, discussing decay of central umbrae

10 p1765 A69-23748

Magnetic field decay in sunspot group 21034 during July 7, 1966 proton flare

10 p1766 A69-23759

Sunspot lifetime, maximum area and cyclic variations recorded in photoheliographic results of Greenwich, discussing frequency distribution and mean

10 p1770 A69-24000

Equivalent line widths for solar disk Fe and Ti spectra determined for umbra models, noting role of sunspot location

11 p1955 A69-24388

Center to limb variations of sunspot-photosphere brightness ratio, considering umbra darkening and radiative equilibrium

11 p1946 A69-24426

Sunspot groups large scale configuration in complex proton region, investigating probability of occurrence of accompanying groups/satellites/ in flare generation

11 p1946 A69-24427

Mercury transits in 1970 and 1973 to resolve prominence threads and spicules, sunspot fine structures, etc

11 p1958 A69-24434

Photoelectric measurements of nightglow intensities during sunspot minima by zenith photometer, considering background continuum

11 p1877 A69-24584

Jupiter red spot visibility, establishing partial dependence on solar activity

11 p1964 A69-25404

Indium, Rb and Cs abundances obtained from sunspot spectra by comparison with Zr and Ti lines

13 p2343 A69-27626

Spectrometric and photometric investigation of spectral characteristics of large sunspot 45 degrees from solar disk center, tabulating characteristics of 134 spectral lines

13 p2218 A69-28324

Sunspots autocorrelation functions in sunspot area on solar disk, tabulating extremal values

13 p2355 A69-28708

Sunspot equivalent line widths calculated using sunspot models, considering influence of light scatter correction

14 p2525 A69-29721

Light saturation development of line profile component of normal Zeeman triplet in sunspot umbrae

14 p2528 A69-29964

Solar photosphere and sunspot magnetic fields structure and strength dependence on sunspot area

14 p2528 A69-29965

Slowly varying component of solar radio emission evaluating resolution of radio telescopes in sunspot studies and localized areas luminescence

15 p2674 A69-30500

Hydromagnetic stability calculations applied to umbral models, showing overstable oscillations relation to thermal hydromagnetic wave generation occurrence in sunspots

15 p2693 A69-30700

Photoheliographic data tabulation of sunspots positions and areas for 1961 obtained from various astronomical observatories

15 p2700 A69-31400

Solar flares and bursts correlation, taking into account sunspot type associated with flare and frequency range of bursts

16 p2850 A69-32210

Solar Ca chromospheric plage decay curves obtained from area measurements, showing similarity and exponential mean curve

16 p2859 A69-32220

Semiannual variation in amplitude of solar daily quiet geomagnetic variation, discussing sunspot dependence of seasonal secondary minimum and maxima

16 p2782 A69-32450

Active longitudes of indices for sunspot activity and solar flares detected and investigated by isoline method for period 1957 to 1962

17 p3022 A69-33045

Sunspot of 28 December 1967 studied by far IR scanning with interference and Reststrahlen filters defining bandpass, obtaining umbral temperature

17 p3029 A69-33050

Heliosphere boundary location significance for Jovian magnetosphere configuration, considering inverse correlation between sunspot number and Jovian decametric radio emission

17 p3033 A69-33379

Chromospheric inhomogeneities rapid changing properties observable in H and K lines above sunspot umbrae

18 p3204 A69-35389

Sunspots magnetic structure producing solar proton flares, considering role of sunspots rotational motion on photospheric surface

18 p3189 A69-35415

Bright regions with loops /BRLS/ in sunspot group development, discussing survey of time lapse movies from 1968

19 p3403 A69-35967

Butterfly diagram of sunspot distribution, concluding physical processes not yet clarified

19 p3426 A69-36583

Solar radio emission parameters calculated, determining basic 327 MHz emission component and flux density-sunspot area correlation coefficient

20 p3588 A69-37478

Relative penumbral intensity independent of sunspot position from data by pinhole photometer of large sunspots

20 p3603 A69-37542

Kinetic energy of sunspot rotational motion transferred to electromagnetic energy in filamentary currents, noting time variations in solar atmosphere preconditioning for flare

20 p3589 A69-37550

Solar microwave emission relationship to geomagnetic activity, analyzing statistically source intensity and model of coronal condensation associated with sunspots based on electron densities

20 p3589 A69-37551

Sunspot umbra observed on 21 September 1966, computing transparency in model equaling photosphere transparency at same optical depth

20 p3605 A69-37825

Magnetic field and radial gas motion in sunspots from Crimean magnetograph observations at different depths of solar atmosphere

20 p3615 A69-38295

Sunspot size and shape in continuous spectrum regions from photometric observations in UV and red ranges

20 p3616 A69-38301

Mean importance variations of sunspot groups in various latitude intervals, reducing data statistically with dispersion analysis and autocorrelation method

20 p3616 A69-38302

Chromospheric heating above sunspots by analyzing MHD wave generation and propagation in sunspots and solar atmosphere

22 p4010 A69-39997

Statistical analysis of chromospheric flares connections with sunspots, using frequency distributions of flares occurrences in sunspot groups

22 p4001 A69-39998

Sunspot position in H alpha core relative to continuum, discussing height differences between H alpha core and continuum levels
22 p4019 A69-40291

Sunspot spectra near solar limb for difference between Fraunhofer line continuum and line core formation levels, finding geometrical height scale and pressure equilibrium
22 p4019 A69-40292

Explorer 30/Solrad 8/ satellite observation of 0.5-3 A solar X ray emission related to magnetic configuration in sunspot group
22 p4003 A69-40298

Distinction between faint and bright sources of slowly varying solar microwave emission components applied to geomagnetic activity statistics
22 p4020 A69-40306

Sunspots microstructure, discussing penumbra and umbral properties with respect to magnetic field configuration
24 p4378 A69-42690

Phenomenological sunspot model describing granules, supergranules, magnetic fields and photospheric convection
24 p4378 A69-42691

Oscillatory convection, energy transport and structure of sunspots, suggesting fast changes in equilibrium conditions for magnetic reconstruction and solar flares origin
24 p4374 A69-43624

Equivalent line widths for solar disk Fe and Ti spectra determined for umbra models, noting role of sunspot location
24 p4390 A69-43778

SUPERALLOYS

U HEAT RESISTANT ALLOYS

SUPERCAVITATING FLOW

Supercavitating flow past thin hydrofoils, determining flow velocity or acceleration potential near free surface
22 p3933 A69-41023

SUPERCAVITATION

U SUPERCAVITATING FLOW

SUPERCARGERS

Supercharged bypass engines for possible application in light aircraft, noting payload fractions and total takeoff weights values
08 p1254 A69-20168

Performance correction and nonstandard day performance prediction for analyzing turbocharged reciprocating aircraft engines in light aircraft applications [SAE PAPER 690309]
11 p1942 A69-24514

SUPERCARGING

U SUPERCARGERS

SUPERCONDUCTING MAGNETS

Superconductors, discussing properties and materials for magnets, power systems, radiation detectors, HF devices and computer elements
04 p0642 A69-14584

Superconducting magnets steady state stability improvement by using composite conductors
10 p1746 A69-23634

Variable voltage DC power supplies for energizing cryogenically cooled and superconductive electromagnets
12 p2017 A69-26498

Superconductivity methods to neutralize ambient magnetic field by free electrons motion for nonmagnetic environments
13 p2244 A69-28604

MHD generator design using shock wave kinetic energy produced by explosion in shock tube with superconducting magnetic system
14 p2393 A69-28911

Terminal characteristics of composite superconductor, taking into account heat transfer to coolant, interface thermal contact resistance and superconductor size
17 p3007 A69-33792

Book on solenoid magnet design covering magnetic and mechanical aspects of resistive and superconducting systems
20 p3464 A69-37145

Superconducting magnets for MHD generators, discussing design, construction and operation problems
21 p3782 A69-39478

SUPERCONDUCTIVITY

Microscopic theory of superconductivity, considering quantitative physical properties of low temperature electric current flow
02 p0293 A69-11432

Superconductivity and melting point of metals, discussing cause of anomalies
02 p0283 A69-11785

Structural influence on superconductivity of niobium-titanium alloys, using electron microscopy and measurements of current density vs magnetic field strength
02 p0269 A69-12763

Vanadium-gallide alloys critical temperature of transition into superconducting state determined by measuring cast alloy samples magnetic permeability
03 p0483 A69-13023

Superconductivity of niobium-titanium-oxygen alloy wires containing 40 percent minimum niobium weight, noting thermomechanical aging effect on critical current density
03 p0484 A69-13118

Electron vs phonon superconductivity mechanism conditions for semiconductors, semimetals and molecular crystals
03 p0492 A69-14176

Superconductivity of electron beam evaporated tungsten films by X ray and electron diffraction techniques, discussing temperature dependence of energy gap
04 p0640 A69-14447

Superconductivity and band structure from pseudopotential for zinc and cadmium, analyzing values of electron phonon mass enhancement
04 p0642 A69-14965

Relationship between microhardness of niobium and other variables characterizing superconductivity
05 p0810 A69-16805

Zr-Nb alloy structure effect on critical superconductivity parameters determined, using electron microscopy of thin films
05 p0811 A69-16806

Structure and critical superconductivity current of titanium niobium alloy as function of heat treatment and deformation
07 p1158 A69-18532

High pressure high temperature synthesis and superconducting properties of yttrium sesquicarbide, noting effect of ambient pressure annealing
07 p1201 A69-19600

White dwarfs transfer to superconducting state, using BCS theory for superconducting transition temperature dependence on electron density
08 p1391 A69-20546

Plasmon superconductivity mechanism in degenerate semiconductors and semimetals, noting interaction effect between electrons and plasma sound
09 p1556 A69-21573

Stationary Josephson effect used to determine fluctuations influence on superconducting tunneling
09 p1556 A69-21669

Semiconductor properties, applications and problems including thin films, superconductivity, etc
11 p1937 A69-24736

Josephson effects in superconductivity and superfluidity including electron tunneling DC and AC effects, basic and double junctions
11 p1938 A69-25240

Quenched titanium-niobium alloy structure effect on superconductivity properties, using electron microscope and X rays
12 p2112 A69-26040

GeTe, SnTe and strontium titanate transition into superconducting state including induced superconductivity
12 p2144 A69-26620

Niobium aluminide-niobium germanide alloys superconductivity and heat treatment influence on critical temperature
13 p2316 A69-27659

Transition metal interstitial compounds thin film preparation and superconducting properties, emphasizing high critical temperature, rock salt structure and NbN base
13 p2321 A69-28009

Superfluidity and superconductivity under cosmic conditions, discussing Bose-Einstein condensation, Fermi particles, boson systems, neutron stars, etc
16 p2853 A69-31595

Superconductive tunneling measurements on thin Al films, discussing enhanced transition temperatures, energy gap dependence on temperature, electron microscope observation of crystallites, etc
16 p2825 A69-31634

Superfluidity and superconductivity under cosmic conditions, discussing Bose-Einstein condensation, neutron stars, white dwarfs, etc
16 p2856 A69-31950

Book on superconducting materials physical metallurgy covering fundamental theory, material properties, behavior regularities, applications, etc
16 p2802 A69-32051

Automatic tuning of superconducting cavity resonant frequency using optical feedback, discussing phase error processing and frequency deviation
17 p2937 A69-33781

Superconducting antenna factors and matching circuit equivalents developed for predicting efficiency and Q increase on basis of Pb surface resistance
17 p2937 A69-33784

NbN thin film production by refined reactive sputtering technique, discussing Pauli spin paramagnetism and spin orbit scattering in high field superconductivity
17 p3016 A69-33790

Ta type I and II wire resistance in transverse magnetic field during superconducting to normal transition, discussing strain and impurity effects
17 p3016 A69-33791

Omega phase formation in Ti and Zr alloys with transition metals, discussing effects on mechanical and superconducting properties
18 p3155 A69-34634

Electronics applications of superconductivity including inductors for energy storage, computer elements and magnets, cavities for microwave circuits, signal generators and detectors, etc
19 p3382 A69-35807

Tempering time and temperature effect on microstructure, superconductivity, tensile strength and electrical conductivity of recrystallized Nb-Ti alloy
19 p3345 A69-36302

Heat treatment effect on superconducting properties of deformed Nb-Ta alloys, noting critical current density
19 p3345 A69-36303

Polarons large to nearly small transitions, studying ground state mass dependence on bare electron mass, electron-phonon interactions model, superconducting strontium titanate, etc
20 p3583 A69-37280

SUPERCONDUCTORS

Vortices coupling between superposed superconducting tin films as function of perpendicular magnetic field, primary current and temperature
01 p0135 A69-10014

Electromagnetic wave propagation in superconductors, noting transmission line structure variation with magnetic fields and current and suitability for parametric amplifiers
01 p0135 A69-10176

Energy gap behavior and thermodynamic properties of anomalous superconductors noting sensitivity to phonon spectrum
01 p0138 A69-10436

Stability of compound superconducting cables under conditions of controlled heat transfer from cable surface to liquid He [IEEE PAPER 13.5]
01 p0176 A69-10718

Electromagnetic waves parametric interactions during unsteady Josephson effect as function of wavelength ratio, magnetic field penetration and contact dimensions
02 p0293 A69-11464

Pressure and magnetostriction effects on magnetization curves of type 2 superconducting In-Ti alloy, noting Ginzburg-Landau parameter stress dependence
02 p0294 A69-11776

Thorium and La-compounds retained superconductivity to Pr and Tm concentrations due to crystal field splitting effect producing nonmagnetic singlet ground state
02 p0295 A69-11778

Critical state model of type 2 superconductor taking account of critical current on magnetic field and surface sheath currents, evaluating flux penetration, hysteresis, AC losses, etc
02 p0298 A69-12030

Surface structure effect on flux penetration and AC losses in superconductive niobium
02 p0298 A69-12031

Josephson voltage-frequency relation independence of superconductor nature, noting e/h value and importance to voltage standards and quantum electrodynamics
02 p0299 A69-12599

Josephson current dependence on nonmagnetic impurity concentration in pure and highly contaminated superconductor
03 p0484 A69-13284

Electronic attenuation of 10 to 130 MHz longitudinal ultrasonic waves in superconducting high purity Ti, noting energy gap anisotropy
03 p0485 A69-13293

Superconductor energy spectrum gap, discussing temperature dependence, anisotropy, thermodynamic

and kinetic properties and relation to Fermi surface and phonon spectrum

03 p0485 A69-13331

Superconductor tunnel junction with noise, calculating frequency pulling, radiation linewidth and voltage power spectrum in AC Josephson effect

03 p0486 A69-13387

Upper bound for free energy of nonlocal superconductor in magnetic field, using variational method and perturbation theory

03 p0491 A69-13971

Heat removal in multilayer superconducting devices, determining optimum number of layers

03 p0493 A69-14225

Superconductors, discussing properties and materials for magnets, power systems, radiation detectors, HF devices and computer elements

04 p0642 A69-14584

BCS theory application to metallic modification of hydrogen for obtaining high temperature superconductor

04 p0642 A69-14680

Superconductors and living matter behavior, studying conditional parallelism via microstructure, cryogenic and electronic fundamentals

04 p0644 A69-15321

Electromagnetic properties associated with presence of overlapping bands in pure superconductors, discussing temperature dependence

05 p0810 A69-16802

Temperature dependence of Josephson critical current in superconductor model having anisotropic energy gap

05 p0810 A69-16803

Superconductors with overlapping energy bands studied by nuclear magnetic resonance method

07 p1198 A69-18513

Superconducting flux-flow resistivity minimum in Pb-Tl alloy, discussing thermal dissipation associated with temperature gradients across moving fluxoid

07 p1198 A69-18642

Experiments on Josephson tunneling junctions and superconducting contacts to demonstrate quantum electronic properties of superconductors [IEEE PAPER D-7]

07 p1200 A69-19052

Metallographic and X ray study of cellular decomposition and precipitation in superconducting niobium zirconium alloy, noting heat treatment effect on current carrying properties

08 p1331 A69-20192

Magnetic field distribution and resistance of homogeneous type 2 superconductor cylinder at transition under effect of axial current

08 p1371 A69-20202

Type two superconductors physical properties, discussing magnetic flux lines interaction with structural defects

09 p1555 A69-21490

High homogeneity sixth order superconducting solenoids with coil inner surface notch correction, describing graphical design techniques

10 p1665 A69-23857

Cryogenic applications including maser amplification, IR detection and superconductivity, discussing systems optimization and cost reduction

10 p1665 A69-24017

Mixed state of type 2 superconductors, stressing alloying elements effects in solid solution and structural inhomogeneities

12 p2145 A69-27119

Hard superconductors technology, stressing metallurgical processing factors effect on properties of niobium alloys and intermetallic compounds

12 p2103 A69-27120

Zr doped superconducting ceramic strontium titanate, noting effective electron mass variations and transition temperature

13 p2316 A69-27400

Weak superconducting contacts volt-ampere characteristics current steps and emission spectra, showing singularities due to superconducting current nonharmonicity

14 p2504 A69-28994

Josephson current dependence on nonmagnetic impurity concentration in pure and highly contaminated superconductor

14 p2508 A69-29656

Josephson current density distribution in thin film superconductors, determining relation between tunneling density and magnetic field for films with/without current

15 p2667 A69-30196

Magnetic field effects on ultrasonic propagation in high field superconductors

16 p2826 A69-31825

Hall effect and transverse voltages in type II superconductors in mixed state, considering cold rolled Nb-Zr alloys

16 p2827 A69-31827

Superconducting cavities for resolving optically induced changes in dielectric constant of CdS at 4.2 K

17 p3016 A69-33782

Kinetic inductance measurements in linear circular and rectangular cylindrical superconductors, giving inductance temperature dependence for wires and both thick and thin films

17 p3016 A69-33783

Slow electromagnetic wave propagation in superconducting thin film transmission lines, noting phase velocity dependence on film thickness and spacing

17 p2938 A69-33785

Steady state performance of multistrand superconducting compound conductors in current sharing state, using heat measurement from metal surface to He bath

17 p3016 A69-33786

Steady state flux jumping for thin walled tubular superconducting NbTi subjected to coaxial superimposed AC and DC magnetic fields, discussing effective resistivity

17 p3016 A69-33787

Superconductor research noting pressure effects, graphs and tables illustrate behavior of materials considered

20 p3584 A69-38015

Superconducting cavity X band oscillator designed for study of stability and spectral purity dependence on temperature

21 p3683 A69-39453

Time dependent differential equation for order parameter in superconductors near critical temperature derived from density matrix equations

22 p3994 A69-41053

Superconducting leads with small electrical resistance and low thermal conductance for cryogenic applications, noting manganin wires coated with Pb-Sn alloy

22 p3997 A69-41236

Optimum thickness of dynamically stable composite superconducting tapes determined for substrate thickness as function of current density

24 p4361 A69-43121

SUPERCOOLING

Supercooled water drop frozen and observed to undergo explosive shattering and ejection of ice splinters

02 p0275 A69-12693

SUPERCritical FLOW

Supercritical flow effects on unsteady aerodynamic coefficients used for subsonic aircraft flutter analysis, emphasizing changes due to shock and flow separation

01 p0007 A69-11020

Diathermal regenerative cooling of combustion chambers and engine nozzles with supercritical heat transfer mode

03 p0495 A69-12970

Separation of subcritical and supercritical compressible turbulent boundary layers under strong pressure gradients using method based on integral equations [AIAA PAPER 69-34]

06 p0912 A69-18077

Heat transfer in single phase medium at near critical state parameters

11 p1997 A69-24230

Free surface in supercritical regime downstream of valve submerged in MHD flow, noting effects of horizontal and vertical magnetic induction fields

15 p2659 A69-30299

SUPERCritical PRESSURES

Natural convection heat transfer through enclosed horizontal layer of supercritical carbon dioxide, discussing flat plate configuration data

04 p0688 A69-15398

Helium cryostat designed to operate under overload and vibrations and used for cooling onboard superconducting devices of Cosmos 140 satellite

04 p0585 A69-15407

Heat transfer coefficient deterioration between fluid and tube wall at supercritical pressure and high heat fluxes [ASME PAPER 68-HT-39]

13 p2373 A69-27771

Thermodynamic parameters of MHD cycle employing supercritical Hg, indicating need for more suitable fluids

16 p2736 A69-31914

Compressible gas flow into cavity of various volumes in presence of supercritical pressure gradients

24 p4298 A69-42587

SUPERFLUID FLOW

U SUPERFLUIDITY

SUPERFLUIDITY

Exciton distribution in semiconductors below Bose condensation temperature differing from diffusion distribution

03 p0486 A69-13411

Josephson effects in superconductivity and superfluidity including electron tunneling DC and AC effects, basic and double junctions

11 p1938 A69-25244

Superfluidity and superconductivity under cosmological conditions, discussing Bose-Einstein condensation of Fermi particles, boson systems, neutron stars, etc

16 p2853 A69-31594

Superfluidity and superconductivity under cosmological conditions, discussing Bose-Einstein condensation of neutron stars, white dwarfs, etc

16 p2856 A69-31950

Pressure activated superfluid valve design and operation for liquid He transfer from reservoir to cold finger

22 p3870 A69-41233

SUPERGIANT STARS

Strong line profiles computed for models of hot expanding extended atmospheres of OB supergiants

07 p1223 A69-19637

Expanding atmospheres in OB supergiants from radial velocity measurements, proposing tentative temperature and velocity fields

08 p1387 A69-20091

Mass loss observed in Of, Wolf-Rayet and OB supergiant stars from P-Cygni profiles in far UV resonance lines

08 p1395 A69-20641

Distance of bright stars in Cepheus OB2 region by MK spectral classification and UVB photometry, noting early main sequence and supergiant stars

09 p1599 A69-22194

Cepheid variable and F and G stars observed for neutral lithium line, searching for resonance lines of ionized beryllium in similar stars

09 p1604 A69-22402

Atomic line spectrum computation for F-K supergiant or cepheid, using observational data on standard star spectrum

10 p1771 A69-22854

Reddened M supergiant 119 Tauri IR spectra and IR absorption by CO and SiO molecules in stellar atmosphere and silicate mineral in interstellar grains

10 p1786 A69-24100

Red supergiants as old derivatives of main sequence O and B stars, discussing neutrino emissions and carbon core contraction

10 p1788 A69-24125

Computer program for model stellar envelopes of red supergiants with extended atmospheres

12 p2156 A69-26218

Element contents of supergiant HD 190603 atmosphere based on spectrophotometric analysis including temperatures, turbulent velocity, gravity acceleration and electron concentration

12 p2157 A69-26336

IR objective-prism survey along southern Milky Way for identifying high luminosity stars

13 p2335 A69-27314

Hydrogen content in Ia supergiant spectra of type B, noting lack of Stark wings of Balmer lines

13 p2348 A69-27722

Radial velocities of southern OB stars and supergiants noting tabulation of information

14 p2519 A69-29368

Supergiant HD-33579 in Magellanic cloud by model atmospheres, discussing abundances

14 p2529 A69-29979

Radial pulsation mode of convective envelopes in adiabatic equilibrium for variable M red supergiant stars

15 p2692 A69-30766

HD 30353 He binary star invisible component suggested as KO type supergiant from IR photometric data

18 p3203 A69-35348

Equivalent absorption line widths of supergiant B1 IA /kappa Cassiopeia/ tabulated with log NH content of atmosphere for various elements

21 p3803 A69-38844

Nongray models representing atmospheres of F and G supergiants computed and tabulated for 5400- 6600 K and various surface gravities

22 p4015 A69-40152

Blue component of HD 237006 and VV Cephei spectra, suggesting greater luminosity of blue star in late type supergiant

24 p4387 A69-43353

Beta Orionis spectral line profiles data used to study atmospheric structure

24 p4391 A69-43804

UPERHARMONICS

- Self adaptive systems stability analyzed using filter and correlation methods, considering higher harmonics at rectifier and synchronous detectors output 04 p0582 A69-14796
- Structural detection in steel welded joints using higher harmonics from eddy current sensing element 24 p4319 A69-42886

UPERHEATING

- Upgrading wave superheater for evaluation of reentry materials 01 p0054 A69-10917
- Nucleate pool boiling heat transfer data extended to relate effect of heating surface characteristics [ASME PAPER 68-WA/HT-22] 05 p0847 A69-16125

UPERHETERODYNE RECEIVERS

- Performance characteristics of 300 GHz Dicke type superheterodyne radiometer receiver for measuring atmospheric attenuation of electromagnetic waves 02 p0209 A69-12336
- Diode mixer power series coefficients for spurious response prediction in superheterodyne receiver 03 p0399 A69-13905
- Wideband superheterodyne tunable radiometers of millimeter wave range using input mixer and high intermediate frequency 07 p1131 A69-18517
- Microwave frequency synthesizer for digitally tuned UHF and microwave superheterodyne receivers, considering phase locking voltage-tuned transistor oscillator 12 p2030 A69-26390
- Ferrite frequency mixers used with heterodyne receiver, studying combination and cross noise rejection efficiency 15 p2574 A69-30129
- Superheterodyne millimeter and submillimeter wave detection, allowing harmonics separation 15 p2570 A69-31093

SUPERHIGH FREQUENCIES

- X band mixer with reactively terminated image, using gallium arsenide barrier diodes and microwave integrated circuit techniques 01 p0039 A69-10189
- Diode structure optimization for monolithic integrated circuit for Ku-band reflective phase shifter 01 p0040 A69-10195
- S band thyatron waveguide switch as pretriggered megawatt balanced duplexer 01 p0048 A69-11035
- S band solid state amplifier capable of 10 watts output power based on combination of transistor amplifiers 02 p0217 A69-12147
- X band radiometer to minimize errors in calibration of microwave noise sources 02 p0220 A69-12440
- Doppler effect in centimeter wave range demonstrated by radio interferometer, noting amplitude difference between reference wave and wave reflected from moving reflector 03 p0393 A69-13333
- Broadbanding of S-band three port stripline circulator, discussing effect of tuning and mode suppressor screws 03 p0404 A69-13472
- Satellite traveling wave tube for X band duplicating C and S band performance 03 p0405 A69-13678
- CW klystron amplifiers design limitations at Ku and Ka bands, discussing operation characteristics 03 p0405 A69-13724
- Plane reflector with variable reflection coefficient for electromagnetic centimeter waves, consisting of plane grating of semiconductor diodes mounted in waveguide 03 p0406 A69-13938
- Electronically scanned X band array used as receiving antenna for target recognition radar 04 p0562 A69-15476
- X-band swept frequency oscillator using Gunn diode and ferrite phase shifter 05 p0734 A69-16573
- Nearly abrupt X band Si avalanche IMPATT diodes irradiated by fast neutrons, noting effects on DC and microwave characteristics 06 p0976 A69-16874
- Harmonic generation of S band signal inside plasma column at resonance 06 p0965 A69-17488

- X band CW traveling wave tube developed for communications, ECM and plasma research, discussing design, performance and gain ripple diminution 07 p1094 A69-18425
- Pulse power from X band LSA devices at centimeter through millimeter wavelengths 07 p1097 A69-18445
- Radio wave absorption measurements in atmosphere at superhigh frequencies, considering earth radiation, antenna sidelobes anisotropy, instrument effects, etc 07 p1076 A69-18518
- Epitaxial GaAs IMPATT diodes for generating CW X band power, noting high efficiencies and low noise characteristics 07 p1102 A69-18660
- X band internal cavity voltage tunable magnetron operating in theta mode, solving output loading, interaction limitations and cavity dimensions 07 p1102 A69-18670
- Kwajalein Missile Range UHF telemetry conversion program using S band antennas with three channel monopulse autotrack systems 07 p1077 A69-18829
- Sun as calibration signal source for L and S band telemetry, discussing receiving system noise temperature determination and antenna gains 07 p1082 A69-19113
- Band three port Y junction stripline circulator with triangular ferrite 08 p1286 A69-20838
- X band eight element matrix array construction, producing antenna suitable for aircraft 08 p1288 A69-20966
- Electronic multibeam switching X band antenna system design with separate transmitting and receiving antennas for use on continuous wave surveillance radar 08 p1289 A69-20967
- Active microwave scattering antenna arrays at super-high frequencies, noting low bias power requirement 08 p1290 A69-20975
- Short multicoronal TE sub 01 mode X band taper for connecting two different diameter circular waveguides 09 p1468 A69-22604
- Flux density of quasars 3C 270 and 3C 278 at 40 cm, determined by digital computer with point source program 11 p1954 A69-24383
- Vertical parabolic antenna array and receiving system for S band transhorizon signal phase and amplitude measurement 11 p1851 A69-24987
- Parametric frequency converter consisting of mixer head in bridge circuit with varactors for 12 GHz TV transmitters 11 p1854 A69-25614
- Attenuation losses on curved dielectric waveguide in X band 11 p1856 A69-25633
- LF negative resistance of X band Gunn diodes with lumped components, using coaxial circuit 12 p2039 A69-26387
- Quasar spectra changes observed from 1962 to 1966 including flux density and antenna temperature for 3C 279 at cm wavelengths 12 p2167 A69-27043
- Quasars intensity variations at various cm wavelengths confirming wavelength dependence 12 p2167 A69-27045
- Linear polarization measurements at 6 cm, determining rotation period associated with Jupiter cm radiation 13 p2343 A69-27623
- Integrated S-band parametric amplifier design, combining low noise performance at room temperature with broadband flat gain and linear phase response 13 p2230 A69-27678
- Space Ground Link Subsystem as S-band communication link within Air Force Satellite Control Facility including unified telemetry, tracking and command systems 14 p2427 A69-28879
- Parametron preamplifier for X band superheterodyne ESR spectrometer, noting sensitivity and SNR 14 p2423 A69-29757
- X band open resonator terminated by step-rimmed flat mirrors, discussing rim effect on Fabry-Perot diffraction loss 14 p2424 A69-29765
- X band avalanche diode oscillator operated as superregenerative amplifier, noting frequency response characteristics ascribed to diode susceptance modulation 16 p2757 A69-31585

- Microelectronic S band upconverter designed and fabricated in microstrip on alumina substrate 16 p2762 A69-32562
 - Wide tuning range S band low noise maser amplifier system, discussing bandwidth, gain and packaging for antenna mounting 17 p2979 A69-32914
 - Pulsed radio source CP 1919 detection at 13 cm wavelength with maser receiver and 210 ft antenna 17 p3036 A69-33637
 - Nonmetallic materials thickness measurements at SHF, describing factors affecting geometrical-optics method 18 p3138 A69-35116
 - Superconducting cavity X band oscillator designed for study of stability and spectral purity dependence on temperature 21 p3683 A69-39453
 - Performance prediction of terrestrial communication system based on experimental radio and meteorological program at 11 GHz, discussing transmission loss 22 p3900 A69-40680
 - L and S band transmitters for space applications, discussing power and frequency stability, low intermodulation, inputs isolation, efficiency, size and weight 23 p4137 A69-41740
 - Wideband FM telemetry transmitters for S band, using symmetrical discriminator 23 p4119 A69-41741
 - S band antenna systems for missiles, designed in various types to obtain RF telemetry links reliability by sharing effort between airborne and ground station equipment 23 p4137 A69-41753
 - X band pulsed microwaves effect on skin metabolism including respiratory activity, biochemistry and biosynthesis of intercellular materials, etc 24 p4270 A69-42575
 - Meter and decimeter wavelength range short period fading under conditions excluding optical shifts, correlating specular and diffuse reflection 24 p4281 A69-42612
 - Flux density of quasars 3C 270 and 3C 278 at 40 cm determined by digital computer with point source program 24 p4389 A69-43773
- SUPERIMPOSITION [MATHEMATICS]**
U SUPERPOSITION [MATHEMATICS]
- SUPERMAGNETS**
U HIGH FIELD MAGNETS
- SUPERNOVAE**
- Stellar evolution, discussing stellar structure, pre- and post-main sequence evolution, solar system origin, supernovae, white dwarfs, variable stars and close binaries 01 p0148 A69-10046
 - Pulsar discovery at position of suspected supernova remnant, suggesting pulsars as rotating neutron stars formed in stellar explosion 01 p0149 A69-10268
 - Cosmic rays properties and sources, considering origin in supernovae, galaxies, quasars and unknown sources 02 p0308 A69-12158
 - Supernova explosion theories, discussing neutrino and degenerate matter concepts, thermonuclear reactions in stellar explosions, oxygen conversion into sulfur, Crab Nebula, etc 03 p0509 A69-13356
 - Heavy nuclei in cosmic rays analyzed in photographic emulsion tracks suggest supernova origin 04 p0649 A69-15422
 - Supernova remnant theories used to interpret results of 1-mile Molonglo cross type radio telescope survey of nonthermal galactic sources 04 p0664 A69-15441
 - Evolutionary theory of origin and properties of Seyfert galaxies and quasars, postulating collisions within superdense clusters leading to supermassive stars and supernovas 05 p0819 A69-15703
 - Radio emission from supernova remnants, reviewing evolution, structure, spectra and polarization, plus identification, characteristics, surface brightness and radio emissive remnants distance 06 p1002 A69-17314
 - Radio spectra of supernova remnants Cygnus Loop and IC443, noting possible radiation from shell source 06 p1003 A69-17322
 - White dwarf general relativistic instability toward dynamic collapse and Type I supernovae 06 p1010 A69-17975

Book on supernovae covering galactic supernovae, type II supernovae remnants, Crab Nebula, primary cosmic radiation, etc

07 p1210 A69-18379

Gamma ray telescope development for balloon-borne astronomy in search for discrete gamma sources and supernova explosions
[IEEE PAPER 3A-5]

07 p1134 A69-19192

Gas remnant of large scale explosive event in galactic plane at 60 degree longitude, discussing resultant extension on line profile

07 p1225 A69-19717

Pulsar emission possible connection with rotating neutron stars, discussing rotational energy transfer to circumstellar plasma and production of periodic shock waves

08 p1383 A69-19895

Nucleosynthesis in dynamics of massive star cores, noting element synthesis by neutron capture in supernova explosions

08 p1401 A69-20898

Spectrophotometry of relics of supernovae, determining H alpha and N II lines intensities radial velocities and velocity dispersion

09 p1587 A69-21357

Amplitudes and rates of brightness increase during supernova outbursts, calculating released energies

09 p1587 A69-21358

Condensed supernova remnants in Crab Nebula, considering various hypotheses for radio source

09 p1592 A69-21485

Polarization and intensity distribution of extended supernova remnant in Centaurus, discussing remnant effect on galactic magnetic field

09 p1598 A69-22184

Linearly polarized radiation from supernova remnants 3C 10, Taurus A, 3C 358 and Cassiopeia A, determining distributions by synthesizing fan beam

09 p1598 A69-22185

Contour maps of supernova remnants HB 9, Simeis 147 and IC 443, noting spectra showing radiation nonthermal

09 p1604 A69-22408

Gamma ray luminosity of typical type I supernovae remnant computed by assuming Ni 56 radioactive decay energy origin of optical luminosity

09 p1581 A69-22409

Neutron proton plasma properties in massive stars and supernovae, discussing neutrino emission

10 p1756 A69-22814

X ray universe, considering contribution of X ray astronomy to phenomena of big bang, supernovae, neutron stars, exploding galaxies, etc

10 p1760 A69-22869

Supernova frequency in galactic clusters, 45 supernovae in 2144 galaxies and average frequency of one supernova per galaxy per 316 years

10 p1774 A69-22966

Maximum indicative absolute magnitudes of 33 supernovae, discussing usefulness as distance indicators

10 p1774 A69-22967

Polarized brightness distributions of supernova remnants IC 443 and W44 at 6-cm wavelength from observations with 6 minute resolution

10 p1787 A69-24113

Pulsars and ancient chinese records of supernova explosions, relating luminous intensities, radio sources and evolution

11 p1963 A69-25253

Hydrodynamic calculation of 1.42 solar mass white dwarf supernova, considering instability and collapse initiation by electron capture

12 p2156 A69-26210

Frequency spectra of radio galaxies, supernova remnants and quasars observed by radio telescope operating in decimeter wave range

12 p2167 A69-27041

Coherent radio emission mechanism in quasars and supernova remnants, discussing magnetic effects

12 p2168 A69-27050

Supernova in Sc type spiral M83, discussing supernovae occurrence frequency

15 p2682 A69-30451

Supernovae spectra observation suggesting tracing as broad band interstellar absorption rather than emission features on continuum

15 p2701 A69-31534

Spectra for 16 radio sources, questioning classification as supernova remnants

17 p3035 A69-33610

Supernovae research, discussing supernovae classes and connections with cataclysmic processes in galactic evolution

17 p3044 A69-34173

Spectrophotometry of relics of supernovae, determining H alpha and N II lines intensities radial velocities and velocity dispersion

18 p3197 A69-34747

Amplitudes and rates of brightness increase during supernova outbursts, calculating released energies

18 p3197 A69-34748

Pulsars, pulse shape and duration, object size and spatial distribution, distinguishing between pulsars and supernovae

18 p3202 A69-35283

Supernovae observations at Palomar during 1968 made with Schmidt telescopes

19 p3403 A69-35963

Photometric and spectral observations of Chuadze and Wild supernovae, showing type I classification

20 p3607 A69-38038

Galactic radio sources high resolution observations at 178 MHz, determining flux densities and angular structures, noting supernovae remnants

21 p3801 A69-38701

Nuclear gamma ray astronomy utilization for stellar interior detection, showing identification of key radioactive nuclei of supernova at explosion time

21 p3792 A69-39572

Radio observations of supernova remnant HB 21 at 2695 MHz, noting spectral brightness and curvature of northern shell segment

22 p4014 A69-40129

Neutrons, protons and alpha particles abundance resulting from nuclear evolution of nondegenerate matter exploding at very high temperatures

22 p3980 A69-40148

Radiant energy diffusion from spherical expanding matter for masses and velocities of model supernova outbursts, discussing thermonuclear and neutron star origins of supernovae

22 p4026 A69-40649

Photographic observations of supernovae including magnitudes, comparison star tables and instrument details

22 p4032 A69-40944

Neutron star formation, discussing influence of supernova explosions and need of pulsar study

23 p4222 A69-42393

Radio galaxies differences from quasi-stellar objects indicating relativistic particles generation from violent explosions releasing energy comparable with powerful supernova

24 p4378 A69-42697

Pulsars relation with supernovae remains and radiation patterns and fluxes analysis, ascribing radio emission to relativistic plasma

24 p4383 A69-42985

Cassiopeia A luminous filaments motion study noting stellar remnant magnitude

24 p4389 A69-43746

SUPERPOSITION [MATHEMATICS]

Maxwellian velocity distributions simulated in one, two and three dimensions by superposition of N monoenergetic isotropic distributions, noting application to kinetic theory computation

13 p2313 A69-28222

Linear radar system theory including Fourier transforms, linear superposition and input/output ratio for deterministic and random signals, discussing filter and sampling theory

20 p3489 A69-37633

Superposition principle extended for wave propagation in composite materials /nonhomogeneous elastic media/

20 p3627 A69-37765

Cosmic ray diurnal phase and amplitude variations determined using superimposed records of cosmic ray stations inside limited rigidity region

23 p4204 A69-41481

SUPERSATURATION

Nonpolar gases solubilities in aqueous KOH solutions in temperature range 25 to 100 C, noting activity coefficients, salting out coefficients and heats of solution

10 p1651 A69-22937

Thermal accommodation coefficient and critical supersaturation for nucleation of mercury vapor on pyrex glass

13 p2321 A69-28005

Oxygen supersaturation in unstirred blood under temperature effects, noting tension loss during stirring

23 p4077 A69-41296

Computerized design of potassium vapor turbine with supersaturation effects compared with equilibrium flow turbine design

23 p4187 A69-42251

SUPERSONIC AIRCRAFT

NT B-70 AIRCRAFT

NT CONCORDE AIRCRAFT

NT F-4 AIRCRAFT

NT F-5 AIRCRAFT

NT F-104 AIRCRAFT

NT F-106 AIRCRAFT

NT F-111 AIRCRAFT

NT FIREBEE 2 TARGET DRONE AIRCRAFT

NT JAGUAR AIRCRAFT

NT SAAB 37 AIRCRAFT

NT TU-144 AIRCRAFT

NT X-15 AIRCRAFT

Hydraulic powered flight control system for Jaguar supersonic military training aircraft

01 p0012 A69-10636

Ti for high temperature use in supersonic aircraft, noting compressibility limit on maneuvering load factor and cooling by H

02 p0192 A69-11898

Onboard electric power systems of transport aircraft, analyzing constant frequency systems for supersonic aircraft

02 p0196 A69-12166

Kinetic heating of aircraft, discussing aerodynamic boundary layer, relationship between heat transfer coefficient or boundary layer energy turbulence and skin friction

03 p0534 A69-14081

Jaguar combat trainer/tactical support aircraft to meet France and UK military requirement, noting supersonic performance and honeycomb construction

04 p0549 A69-15063

Jaguar aircraft-equipment conformity to maximum standardization with equipment for other programs

04 p0550 A69-15062

Supersonic airplane high temperature wire tests, detecting corona onset voltage /COV/ or voltage breakdown

05 p0731 A69-16245

Supersonic aircraft fire detection using coherent fiber bundles

06 p0926 A69-17679

Stratospheric critical clear atmospheric turbulence at midlatitudes, noting applications to supersonic aircraft design

06 p0950 A69-17788

Mirage G supersonic swing wing two seater aircraft performance, discussing hinging of mobile wing on pivot, fluids for airfoil-fuselage transfer, landing gear, etc

07 p1053 A69-19230

Firebee 2 /BQM-34E/ turbojet-propelled recoverable supersonic aerial target construction, performance prediction and missions

09 p1434 A69-21901

Sonic boom reduction by azimuthal redistribution of supersonic aircraft pressure field variation

09 p1434 A69-21948

Titanium fuselage skin contouring to shallow compound curvature of supersonic aircraft by elastic draping, shot pen forming and cold stretching, discussing residual stresses

09 p1512 A69-22374

Human engineering program at early design phase of SST aircraft to achieve maximum human efficiency and man machine compatibility

09 p1447 A69-22546

Titanium compared with aluminum in application to supersonic aircraft structures, considering tests and costs

10 p1700 A69-23600

Supersonic transport airline operations including safety, noise, traffic control, routing, etc

11 p2004 A69-24373

Supersonic aircraft radiation hazard due to solar flare proton exposure, using Monte Carlo method to estimate dosage as function of tissue slab

11 p1949 A69-24864

Stabilizing methods for supersonic aircraft, noting effect of aircraft characteristic parameters on magnitude of balancing coefficients of lifting force

16 p2735 A69-32127

Exhaust nozzle/airframe interference test evaluation for twin engine supersonic fighter

16 p2733 A69-32730

Local external flow variations effect on blow-in-door nozzle performance in transonic flight regime

16 p2733 A69-32731

Concorde aerodynamic design compromise between high and low speed requirements, kinetic heat problems and materials selection

19 p3245 A69-35666

Supersonic aircraft and power plant structural members operating under cyclic stress at elevated temperatures tested by various methods for interaction between creep and fatigue

20 p3620 A69-37000

- Jaguar aircraft design and operational characteristics, noting supersonic performance at high altitudes and during maneuvers 20 p3463 A69-37928
- Scattering equations for sonic boom waveform spike perturbations produced by atmospheric turbulence, discussing supersonic aircraft pressure signatures 21 p3646 A69-38689
- Aeroelasticity of supersonic aircraft in flight, discussing buffeting, wing flutter and control surface flutter 22 p3862 A69-40003
- Structural aircraft design requirements for high flight speeds stressing aerodynamic heating, heat resistant materials, weight and geometry problems 23 p4233 A69-42164
- Supersonic aircraft sonic bangs loudness level calculations by model waveforms with allowance for interaction between incident and ground reflected shock waves 23 p4063 A69-42454
- Supersonic aircraft design data, costs and benefits, discussing origin and significance of sonic boom 24 p4252 A69-42997
- SUPERSONIC AIRFOILS**
- Supersonic interference on lateral stability of planar configurations analyzed using wind tunnel data [AIAA PAPER 68-21] 02 p0189 A69-12377
- Base drag effects on maximum lift drag ratio airfoils determined for moderate supersonic laminar and turbulent flows 10 p1633 A69-24060
- Aerodynamic properties calculations of arbitrary slender supersonic wings using sum of simple integrals 15 p2548 A69-31170
- SUPERSONIC COMBUSTION**
- Hydrogen-air supersonic combustion at low densities, discussing laboratory computer simulation based on boundary layer concepts and finite rate chemistry [WSCI PAPER 68-29] 07 p1240 A69-18358
- Optimum fixed geometry ramjet in Mach range of 3 to 7 with successively subsonic and supersonic combustion [ONERA-TP-656E] 07 p1203 A69-18415
- Supersonic combustion technology, noting air breathing propulsion systems for application to hypersonic flight 11 p2003 A69-25596
- Air-hydrogen supersonic mixing and combustion, characterizing hot hydrogen jet discharging into supersonic concentric air stream at atmospheric pressure [AIAA PAPER 69-339] 13 p2378 A69-28275
- Test facility for supersonic combustion at low static pressure using fuel and gas streams and optical scanning spectrometer [AIAA PAPER 69-340] 13 p2243 A69-28276
- Finite difference method for turbulent mixing and combustion of hydrogen injected parallel to supersonic air stream, considering vitiated and unvitiated air [AIAA PAPER 69-539] 16 p2877 A69-31844
- Supersonic combustion for high Mach number high altitude flight, discussing laboratory simulation for actual flight condition and chamber design [AIAA PAPER 69-458] 16 p2880 A69-32743
- Nonequilibrium inlet conditions effect on combustor performance during H and vitiated air combustion, studying ignition delays [AIAA PAPER 69-457] 16 p2881 A69-32767
- Solid fuel ablation and supersonic combustion processes for various propulsion configurations, testing plastic models in wind tunnel 24 p4414 A69-43569
- SUPERSONIC COMBUSTION RAMJET ENGINES**
- Three dimensional scramjet exhaust nozzle flow fields by second order method of characteristics [AIAA PAPER 69-5] 06 p0862 A69-18048
- Shock tunnel simulation of scramjet combustion chamber performance [AIAA PAPER 69-84] 06 p0985 A69-18165
- Fuel mixing mechanism in diffusion type supersonic combustion, noting influence of combustor configuration and fuel density [AIAA PAPER 69-32] 07 p1242 A69-19266
- Supersonic ramjet propelled air breathing booster for speeds up to Mach 12, discussing flight mechanics, aerodynamics, propulsion, heating and air intake design 09 p1573 A69-22608
- Integrated double oblique shock scramjet for supersonic combustion tests and instrumentation development, discussing fuel injection through sonic orifices, combustion data, etc [AIAA PAPER 69-827] 16 p2840 A69-32673
- Scramjet engine active cooling with regenerative system using superalloy heat exchangers and hydrogen fuel as coolant [AIAA PAPER 68-1091] 24 p4365 A69-43725
- SUPERSONIC COMMERCIAL AIR TRANSPORT**
- NT TU-144 AIRCRAFT
- Satellites and ocean platforms for civil aviation operations over North Atlantic, noting cost justification dependence on supersonic traffic increase [UN PAPER 68-95887] 01 p0113 A69-10521
- Public health aspects of galactic radiation exposure at supersonic transport altitudes 03 p0375 A69-14072
- Biological effects of cosmic ionizing radiation in supersonic commercial aircraft at high altitudes, showing spatial distribution based on balloon experiments 11 p1830 A69-24865
- Commercial supersonic and subsonic air traffic growth forecast 22 p3862 A69-39934
- SUPERSONIC COMPRESSORS**
- Hydraulic analogy for shock and expansion waves arising in supersonic compressors due to three dimensionality of flow [ONERA-TP-598] 02 p0187 A69-11621
- Supersonic compressors for supersonic and subsonic air intakes, studying wave configuration at entry of circular cascade of blades with hydraulic analogy [ONERA-TP-669] 05 p0699 A69-16340
- Supersonic axial compressor boost stages for small gas turbine engines, using passage flow approach and passage criteria to design airfoils [ASME PAPER 69-GT-44] 09 p1570 A69-22478
- Air powered fluid jet engine compressor bleed control stressing closing, reset and override operations [ASME PAPER 69-GT-19] 09 p1571 A69-22498
- Supersonic compressor blade sections performance prediction near maximum pressure ratio and efficiency by analyzing flow processes [AIAA PAPER 69-522] 16 p2843 A69-32711
- Supersonic radial flow compressor producing flow with meridional component exceeding velocity of sound 17 p2889 A69-32992
- Supersonic cascade wind tunnel /ONERA/ for super and transonic compressors profiles studies 17 p2895 A69-33591
- Steady state and dynamic distortion influence on performance and stall of turbofan engine, discussing compressor instrumentation, tests and simulation data 18 p3185 A69-35175
- Boundary layer effects in turbulent spiral vortex flow of compressible fluid in supersonic centrifugal compressor, discussing flow geometry, using momentum integral method 23 p4152 A69-42109
- SUPERSONIC DIFFUSERS**
- Secondary injection effect on supersonic parallel diffuser, analyzing flow patterns, pressure distribution and recovery and heat transfer 03 p0365 A69-13991
- Diffuser performance in hypersonic shock wind tunnel for nitrogen flow, discussing steady shock wave and separation zone formation time 14 p2391 A69-29622
- Supersonic blowdown wind tunnel noting cylindrical diffusers efficiency in starting supersonic nozzles increased in proportion to Mach number 17 p2890 A69-33125
- SUPERSONIC DRAG**
- Equations, tables and charts for shock drag parameter in determination of shock wave drag of body in supersonic free stream of ideal gas 02 p0188 A69-11862
- Drag coefficients for spheres and sharp cones in rarefied hypersonic air flow obtained in shock tunnel using free flight technique [AIAA PAPER 69-140] 06 p0865 A69-18184
- Optimum aerodynamic shapes theory, considering linearized and nonlinearized supersonic flow, Newton-Busemann hypersonic flow, free molecular flow, mathematical models and variational problems 08 p1253 A69-21127
- Minimum drag wing profile at zero angle of attack in supersonic flow, allowing for initial structural flaws and randomly varying parameters 11 p1818 A69-25328
- SUPERSONIC FLIGHT**
- Aerodynamic configurations to reduce sonic boom at supersonic speeds 01 p0007 A69-11028
- Air coupled seismic waves generated by jet fighters flying at high altitudes and supersonic speeds 01 p0077 A69-11281
- Minimum drag configurations with low heat transfer for hypersonic bodies of revolution, noting performance at supersonic speeds 02 p0191 A69-12578
- Fuel requirements for flights up to Mach 3.5, discussing heat stable mineral oil based SST fuels 11 p1941 A69-25422
- Ramjets and air augmented rockets as propulsion systems for supersonic atmospheric flight, noting inlet design, combustors and nozzles 11 p1943 A69-25586
- Supersonic aerodynamic characteristics of wings with complex planar geometry and subsonic leading and trailing edges, discussing varying geometry 14 p2391 A69-29624
- Sonic boom damage to structures from supersonic aircraft overflights using inductive and deductive approaches 15 p2585 A69-30370
- Shock waves from accelerated, decelerated and stationary axisymmetric bodies flying at supersonic velocities in stratified isothermal atmosphere 15 p2551 A69-31171
- Supersonic combustion for high Mach number high altitude flight, discussing laboratory simulation for actual flight condition and chamber design [AIAA PAPER 69-458] 16 p2880 A69-32743
- Legal, social and physical effects of supersonic flight, discussing damage claims validity and recovery resulting from breaking of sound barrier 17 p3075 A69-32841
- Flight velocity changes from sonic to supersonic through turbojet/ramjet combination possibility 17 p3020 A69-33348
- Supersonic flight altitude stability, studying effects of velocity, lift-drag ratio, thrust law, wind direction, engine unstarts, etc [AIAA PAPER 69-813] 19 p3366 A69-35627
- Passenger transport cruising at low supersonic speeds without sonic boom generation on ground, discussing overpressures, signature characteristics and corridor widths [AIAA PAPER 69-776] 19 p3244 A69-35647
- Tremographic studies of central nervous system during supersonic flight as engineering psychology application to man machine relations in aircraft-spacecraft industries 19 p3259 A69-35834
- Supersonic flying effect on urinary catecholamine excretion rates in pilots, noting emotional state 24 p4265 A69-43370
- SUPERSONIC FLOW**
- Gas jet interaction with supersonic flow during injection from orifice of flat body, investigating Mach number, orifice diameter and jet effects on flow pattern near injection 01 p0005 A69-10357
- Supersonic air flow around blunt body studied near critical line with allowance for viscosity, thermal conductivity and radiant energy transfer, assuming thermodynamic equilibrium 01 p0006 A69-10378
- Algorithms for three dimensional supersonic gas flow incident on bodies applied to calculating oxygen flow in asymmetric nozzle 01 p0060 A69-10724
- Compressible relativistic flow in subsonic, transonic and supersonic regimes, noting pressure coefficient variations 01 p0007 A69-11203
- Pressure and shock shape determination for plane supersonic and low hypersonic flows past aerodynamic profiles 01 p0008 A69-11299
- Fluid mechanics of supersonic flow separation and reattachment in fluidic devices 02 p0231 A69-12077
- Monte Carlo direct simulation for treating rarefied supersonic flows about bodies in transitional regime between continuum and free molecular flow 02 p0189 A69-12523
- Turbulent boundary layer growth, pressure distributions and surface shear stresses on yawed semiangle cone [AIAA PAPER 68-98] 02 p0190 A69-12526
- Aerodynamic characteristics of delta wings for supersonic flow at large angles of attack, showing sweepback angle influence on drag coefficient 02 p0191 A69-12585
- Generalization of characteristic relations for steady supersonic 3D motion of polytropic gas, obtaining complex screw motions 03 p0412 A69-12847

Plane supersonic base flows studied using integral analysis of turbulent reattachment, noting prediction of wall pressure distribution

03 p0361 A69-12990

Film cooling by subsonic gas injection of air through porous flat plate into 2.9 Mach air flow, noting wall temperatures

03 p0413 A69-12994

Supersonic flow past blunt body with convex corner calculated to establish sonic point on body

03 p0363 A69-13406

Problem of viscous supersonic flow past blunt bodies based on Navier-Stokes equations formulated and solved numerically with explicit difference scheme

03 p0363 A69-13653

Supersonic flow region about blunt body calculated on basis of gasdynamic equations for steady flow of inviscid nonheat conducting gas

03 p0363 A69-13658

Numerical computer results applied to supersonic flow of perfect gas past staggered cones

03 p0363 A69-13659

Pressure distribution at wedge wall during instantaneous small variation of supersonic motion

03 p0364 A69-13662

Resonance analysis of forced vibration of rectangular plate in three dimensional supersonic flow

03 p0528 A69-13928

Numerical algorithm for supersonic gas flow past blunt bodies with shock wave separation, using Dorodnitsyn method of integral correlation

04 p0587 A69-14621

Reattachment pressure correlated for any type of two dimensional turbulent supersonic separated flow

04 p0588 A69-14727

Steady plane supersonic gas flows with large number of shocks computed on basis of weak solutions of hyperbolic system

04 p0544 A69-15284

Sting diameter and cylindrical protuberance length effects on base pressure of axisymmetric body in turbulent supersonic flow

05 p0697 A69-15712

Two dimensional supersonic rotational flow around convex corner solved using coordinate system consisting of left running characteristics and streamlines

05 p0697 A69-15722

Boundary conditions in oblique reaction waves in supersonic flow, adding or subtracting heat by chemical reaction

05 p0697 A69-15828

Plane supersonic flows separated by thin film shaped jet, deriving pressure as function of deviation

05 p0746 A69-16020

Zhukovskii lifting force theorem application to slender wing profile and airfoil lattice in linearized supersonic flow

05 p0697 A69-16023

Thickness effects on flow past sweptback wings in supersonic flight noting influence of oscillatory motion [ASME PAPER 68-FE-31]

05 p0698 A69-16078

Approximate methods for integration of equations of plane isentropic motion of gas at supersonic velocities

05 p0699 A69-16674

Unsteady supersonic flow around thin circular cylinder representing rocket stage, calculating flutter and response to random environment

[ONERA-TP-666] 06 p0857 A69-17098

Delta wing head wave at zero angle of attack in steady supersonic flow during transition from subsonic to supersonic leading edges

[DVL-871] 06 p0858 A69-17242

Wall temperature and Mach number effect on heat flux distribution at spreading line of flow for supersonic gas on ellipsoid of revolution

06 p0858 A69-17331

Asymmetric supersonic air flow at 60 degree angle of attack past ellipsoid with frontal spike creating separation area

06 p0858 A69-17337

Nonequilibrium supersonic flow calculation of detonating mixture past blunt bodies applied to flow of hydrogen-oxygen mixture past sphere

06 p0859 A69-17343

Shock formation in supersonic plasma flow guided by magnetic channel up to magnetic barrier

06 p0966 A69-17524

Dynamic behavior of three layer plates in supersonic gas flow

06 p1024 A69-17552

Aircraft aerodynamic characteristics determination from numerical computer solution of supersonic gas flow past blunt body with broken generatrix

06 p0859 A69-17582

Laminar boundary layer separation and reattachment near concave corner on cooled reentry body in supersonic flow

06 p0911 A69-17592

Kinetic theory of sharp leading edge parallel to supersonic flow using Boltzmann equation, determining flow field

06 p0861 A69-17637

Weakly ionized wakes study in free quasi-molecular regime of supersonic flow, using Langmuir probe in wind tunnels, discussing ion density distribution

06 p0966 A69-17639

Pressure distribution, heat transfer rates and shear stresses in laminar boundary layer of supersonic viscous flow incident on corner point of body

06 p0861 A69-17641

Supersonic plasma flow interaction with two dimensional magnetic dipole

06 p0967 A69-17738

Dynamic behavior of shock layer of supersonic rarefied gas flow past disk and sphere

06 p0861 A69-17812

Boundary layer transition detection at supersonic speeds, using thin film gages to infer local laminar and turbulent supersonic skin friction

[AIAA PAPER 69-9] 06 p0912 A69-18075

Interaction of laminar hypersonic boundary layer and supersonic corner expansion wave, discussing upstream influence, transverse pressure gradients and external flow

[AIAA PAPER 69-137] 06 p0913 A69-18078

Transverse secondary gaseous injection penetration into confined supersonic flow

[AIAA PAPER 69-2] 06 p0913 A69-18080

Pressure distribution determined from laminar viscous-inviscid interactions in supersonic flow, including flows with heat transfer

[AIAA PAPER 69-7] 06 p0913 A69-18095

Isoenergetic two dimensional supersonic turbulent base flow, noting boundary layer separation properties upstream and downstream

[AIAA PAPER 69-68] 06 p0864 A69-18137

Finite plate length effect on two dimensional supersonic turbulent boundary layer with large distributed surface injection

[AIAA PAPER 69-162] 06 p0864 A69-18138

Flow field for single or multiple jets firing forward into oncoming supersonic free stream, noting effect of forward extending cylindrical body

[AIAA PAPER 69-69] 06 p0864 A69-18164

Injectant stagnation temperature and molecular weight variation effect on flow field generated from secondary injection into supersonic stream

[AIAA PAPER 69-1] 06 p1039 A69-18196

Similarity functions defined for laminar or turbulent separation in nonuniform supersonic flow

[ONERA-TP-659F] 07 p1050 A69-18417

Plasma diagnostics by spectroscopic techniques, measuring polarity dependences of temperature and charged particle concentration for flows with shock wave and periodic structure

07 p1190 A69-18695

Mixed sub- and supersonic gas flow in plane pressure nozzle free of vortex and neglecting viscosity and heat conduction

07 p1050 A69-18739

Base pressure calculation in initial turbulent boundary layer of supersonic flow about two dimensional backward facing step, using mass conservation conditions

07 p1119 A69-18747

Stationary supersonic nonequilibrium plasma source in gas vacuum expansion and nozzle flows

07 p1191 A69-18986

Solar wind flow past earth and magnetosphere correspondence to external aerodynamics of round noses bodies in supersonic stream

07 p1128 A69-19360

Detonation wave propagation in H-O mixtures in supersonic flow, noting detonation front structure and velocity

08 p1420 A69-19882

Book on wing theory in supersonic flow covering simple and cruciform wings, wings with vertical plane tail, etc

08 p1251 A69-20523

Displacement effect due to subsonic reaction heat front behind shock wave in two dimensional supersonic flows

08 p1252 A69-20691

Supersonic flows past slender bodies, calculating pressure by means of moving singularities

08 p1252 A69-20721

Discharge structure and stability of nonequilibrium plasma undergoing supersonic flow through linear MHD channel

08 p1366 A69-20787

Heat flux effect on laminar boundary layer separation in supersonic flow stressing free interaction zone

09 p1429 A69-21695

Two dimensional supersonic flow along adiabatic curved ramp noting separation, attached flow and laminar boundary layer interaction with external stream

[AIAA PAPER 68-109] 09 p1430 A69-21948

Lateral spreading of liquids injected into supersonic flow, discussing dependence on Mach number and scattered light and schlieren photographs of spray structure

09 p1482 A69-21964

One strip method of integral relations applied to inviscid supersonic blunt body problem

09 p1430 A69-21971

Base pressure fluctuations behind cone in supersonic gas flow, noting complicated superposition of harmonics associated with various factors

09 p1431 A69-22237

Pressure on unsteadily oscillating cylindrical shell in external or internal supersonic flow derived from asymptotic theory

09 p1618 A69-22254

Hydrogen diffusion flames stabilization by flame holders in supersonic flow at low stagnation temperatures measuring burning limits

[DVL-815] 09 p1624 A69-22612

Oblique shock wave separation conditions in supersonic gas flow past wedge

09 p1483 A69-22665

Steady three dimensional flow of gases with thermodynamic relaxation, noting flow field weak discontinuities and effect of discontinuities in wall curvature

10 p1677 A69-22894

Mach wave and anisotropic supersonic flow interaction, considering constant entropy along streamlines and layer of entropy discontinuities/interfaces

10 p1631 A69-22906

Shock front propagation in argon with electrode-drawn induced EMF, using shock tube with induced transverse magnetic field

10 p1737 A69-23466

Finite difference technique for numerical computation of steady supersonic two dimensional gas flows, with or without diffusion normal to mean flow streamlines

10 p1679 A69-23595

Base drag effects on maximum lift drag ratio airfoils determined for moderate supersonic laminar and turbulent flows

10 p1633 A69-24060

Mean flow measurements in supersonic wake of slender two dimensional body at zero incidence and heat transfer rate, noting predictability from similarity analysis

11 p1817 A69-24281

Boltzmann equation with BGK model as governing equation for sharp leading edge problem in supersonic flow

11 p1817 A69-24288

Second approximation of asymptotic damping of disturbances in viscous heat conducting gas supersonic flow about solid of revolution at critical velocity

11 p1817 A69-24627

Monograph on calculation of linearized supersonic flow on rocket configurations at zero angle of attack, particularly at interfaces between components, covering applications

11 p1817 A69-24637

Minimum drag wing profile at zero angle of attack in supersonic flow, allowing for initial structural flaws and randomly varying parameters

11 p1818 A69-25328

Delta wing in three dimensional supersonic flow analyzed by method of characteristics, discussing leading edge problems

11 p1820 A69-25425

Supersonic gas flow past plane and axisymmetric bodies with broken generatrix, determining tangential discontinuities and shock waves shape and position

11 p1820 A69-25470

Supersonic air flow past blunt body of revolution in presence of nonequilibrium chemical reactions, ionization and molecular excitation

11 p1820 A69-25474

Gas dynamics for supersonic nonequilibrium flows discussing method for determination of nozzle contour for maximum thrust

11 p1820 A69-25477

- Interference between bodies of revolution and wings in supersonic flow, using Volterra method for calculation
11 p1820 A69-25476
- Numerical integration of equations for three dimensional laminar boundary layer on sharp elliptical cones in supersonic flow of ideal gas, discussing heat exchange
11 p1821 A69-25477
- Supersonic and hypersonic flow of rarefied gas around blunt cylinders at various angles of attack, noting pressure distribution on model surface
11 p1821 A69-25478
- Static pressure measurements at surface of sharp plate in supersonic flow during gas/liquid jet injection
11 p1821 A69-25479
- Flow field structure involving supersonic secondary jet interactions and separated regions in thrust vector control system
11 p1944 A69-25594
- Topological properties of plane flow in subsonic region behind smooth shock wave in uniform supersonic flow, discussing shock wave convexity
12 p2061 A69-25888
- Heat flux in two dimensional laminar separation zone in supersonic flow, measuring convection coefficient and wall pressure
12 p2011 A69-26289
- Supersonic air flow around blunt body studied near critical line with allowance for viscosity, thermal conductivity and radiant energy transfer, assuming thermodynamic equilibrium
12 p2012 A69-26669
- Shadow, schlieren and interferometric methods for study of transonic, supersonic and hypersonic fields of aerodynamics, using refractivity variations in heterogeneous medium
12 p2060 A69-26934
- Nonuniform flowfield from supersonic penetration of plane shock by three dimensional pointed planar wing, using integral transform method to study field perturbation pressure
13 p2199 A69-27323
- Heat transfer coefficients for supersonic open cavity flow recompression steps noting influence of step and flow shapes
13 p2375 A69-27786
- Laminar temperature and velocity profiles near plane rectangular surface for free supersonic flow, solving partial differential equations for mass, momentum and energy conservation
13 p2309 A69-28025
- Creep stresses and displacements in conical membrane shells at small angle of attack to supersonic flow field, discussing temperature distributions
13 p2364 A69-28205
- Electrical breakdown voltage and voltage-current characteristics of uncooled coplanar carbon electrodes in walls of supersonic conical and rectangular nozzles [AIAA PAPER 68-713]
13 p2249 A69-28231
- Inviscid supersonic flow in right angle corner of varied angular intersecting wedges with bow waves remaining planar up to intersection line
13 p2200 A69-28251
- Supersonic wake flow visualization, obtaining direct photographs of various smoke streamlines [AIAA PAPER 69-346]
13 p2200 A69-28281
- Variational problems associated with supersonic gas flows with foreign particles, considering nozzle designs
14 p2389 A69-28801
- Flow structure in conical shock wave-sharp flat plate interaction zone in supersonic flow, noting turbulent boundary layer before separation
14 p2428 A69-28897
- Near wake in axisymmetric supersonic flow past slender body with/without base injection, obtaining pressure, temperature, Mach number, velocity and concentration distributions
14 p2389 A69-29017
- Shock wave and blunt faced cylinder interaction in supersonic gas flow in two chamber shock tube observed with high speed photography
14 p2390 A69-29467
- Difference schemes for quasi-linear hyperbolic equations, with applications to three dimensional supersonic flow past bodies
14 p2430 A69-29475
- Supersonic gas flows in shock layer past blunt bodies taking into account selective radiation and radiative transfer in continuum, applying method of characteristics
14 p2390 A69-29477
- Supersonic gas flow past wedge at zero angle of attack with separated shock wave, calculating velocity gradient at stagnation point and pressure and drag distribution
14 p2390 A69-29615
- Spatial supersonic ideal gas flows past blunt bodies analyzed by numerical finite difference methods, discussing flow fields and entropy
14 p2390 A69-29616
- Quasi-steady state supersonic gas flow past two closely spaced coaxial separating bodies at different velocities, showing dependence on separation rates
14 p2391 A69-29617
- Supersonic combustible gas mixture flow around circular cone, discussing ignition by shock wave and flow modification by conical flame front
15 p2548 A69-31007
- Surface of minimum drag symmetrical trapezoidal wing in supersonic flow solved by variational method
15 p2548 A69-31022
- Static pressure distribution induced by statistically roughened duct walls on supersonic stream
15 p2593 A69-31148
- Supersonic flow past cone in presence of blowing normal to cone surface, calculating flow field parameters behind conical shock wave
15 p2548 A69-31175
- Aeroelastic nonlinear panel stability in supersonic gas stream, defining hazardous conditions of critical flutter boundary
15 p2716 A69-31549
- Supersonic laminar boundary layer separation calculated by integral method using free parameters for velocity and enthalpy profiles, considering boundary layer-external flow interaction
16 p2731 A69-31834
- Turbulent and transitional near wake of adiabatic slender wedge with and without base injection at Mach 4 in supersonic wind tunnel [AIAA PAPER 68-100]
16 p2732 A69-31882
- Compressible flow over finite porous plate in supersonic stream with massive injection over surface analyzed using inviscid vortical flow model
16 p2770 A69-31884
- Flow field around sharp slender cones with surface mass transfer at zero angle of attack in low density supersonic and hypersonic flow [AIAA PAPER 68-66]
16 p2732 A69-31887
- Book on three dimensional flow of ideal gases past smooth bodies, emphasizing utility of finite difference methods
16 p2771 A69-32003
- Distributed boundary layer suction effectiveness for controlling supersonic transitional flow separation
16 p2772 A69-32149
- Three dimensional supersonic nozzle flow field calculations using second order numerical method of characteristics and computer programmed for internal flows [AIAA PAPER 69-463]
16 p2734 A69-32766
- Supersonic radial flow compressor producing flow with meridional component exceeding velocity of sound
17 p2889 A69-32992
- Axisymmetric supersonic gas flow with attached shock wave past cone, calculating flow parameters between body and shock wave
17 p2890 A69-33123
- Vortex motion enhancement of jet penetration and spreading in supersonic fuel injection into large diameter combustors [AIAA PAPER 69-664]
17 p2953 A69-33437
- Supersonic leading edge problem using nonlinear Boltzmann equation with ellipsoidal model, calculating molecular distribution functions for flow field [AIAA PAPER 69-652]
17 p2892 A69-33464
- Supersonic and hypersonic flow of inviscid ideal gas over conical delta wings using three dimensional method of characteristics [AIAA PAPER 69-646]
17 p2893 A69-33486
- Favorable pressure gradient effect on compressible two dimensional supersonic turbulent boundary using temperature and pressure probes and shear balance [AIAA PAPER 69-685]
17 p2956 A69-33489
- Preston probe measurement of friction drag on subsonic and supersonic nozzle wall including effects of heat transfer, compressibility and pressure gradient [AIAA PAPER 69-648]
17 p2893 A69-33496
- Static and impact pressure distributions for Mach number and velocity profiles of supersonic to subsonic flow transition in tube at low Reynolds numbers [ASME PAPER 69-APM-23]
18 p3120 A69-34397
- Three dimensional supersonic flow past pointed nonaxisymmetrical bodies characterized by great local surface curvature changes, using new approximation
18 p3086 A69-34705
- Rarified gas dynamics of blunt and sharp-pointed slender bodies in supersonic stream and free jet sonic expansion into high vacuum
18 p3123 A69-34924
- Sublimation of various compressed naphthalene wind tunnel models analyzed in supersonic air flow, discussing effects of temperature and model configurations
18 p3231 A69-35121
- Nonequilibrium behavior of shock standoff distance ahead of spheres at low supersonic Mach number
18 p3089 A69-35385
- Asymptotic solution of supersonic linearized nonisentropic flow of viscous and heat conducting gas with internal heat sources past cylindrical shell, deriving surface pressure
18 p3089 A69-35460
- Asymptotic theory of pressure on cylindrical shell subjected to unsteady oscillations in external and internal linearized supersonic flow using Laplace and Fourier transforms
18 p3089 A69-35461
- Biased electrostatic probes determining free stream charge density and ionization risetime in supersonic flows in arc heated pressure driven shock tube
19 p3291 A69-35715
- Static temperature measurement in arc-tunnel tests producing high velocity air streams by duplex scanning IR spectrometer
19 p3294 A69-35752
- Electrohydrodynamic supersonic flow over wavy wall by oscillating piston model, calculating streamlines and density distributions
19 p3297 A69-35838
- Turbulent velocity of flame propagation in supersonic stream of hydrogen-air mixture determined by velocity distribution, exchange coefficient and burning time
19 p3448 A69-35854
- Monograph on method of characteristics for three dimensional supersonic flows, covering numerical calculations of steady gas flow past bodies at angle of attack
19 p3238 A69-36170
- Function theoretic solution of dual integral equations applied to boundary value problem of supersonic flow over infinite span thin wing
19 p3239 A69-36311
- Supersonic aerodynamic characteristics of flared cones with various flare angles studied by schlieren photography, showing geometrical parameters influence on flow patterns
19 p3239 A69-36387
- Nonuniform supersonic flow of ideal inviscid gas impinging on plane obstacle, discussing flowfields and shock wave production in impact
19 p3239 A69-36397
- Compressible fluid two dimensional supersonic and one dimensional unsteady flows similarities shown graphically, discussing hodograph-speedgraph relationship
19 p3300 A69-36777
- Supersonic flow past antisymmetrical thin delta wing by flow separation from subsonic leading edges, noting wing surface pressures
19 p3241 A69-36779
- Supersonic flow past segmented and blunt bodies, investigating flow characteristics
19 p3242 A69-36783
- Supersonic inviscid flow past wing-body configuration, determining pressure distribution
20 p3458 A69-37099
- Linearly elastic medium supersonic flow past rigid wedge, considering longitudinal and transverse perturbations interactions, dry friction, adhesion, slip and wedge physicochemical properties
20 p3515 A69-37439
- Conical delta wings in supersonic-moderate hypersonic flow, studying yaw effects on pressure distribution behind shock wave
20 p3459 A69-37593
- Monograph on forces exerted by air during yawing motion of sharp cones in supersonic and hypersonic flows by semilinear method
20 p3460 A69-37919
- N strip algorithm of integral relations to analyze flow around circular cone at incidence in supersonic flow
20 p3460 A69-38128
- Continuously operating multipurpose wind tunnel for laser light scattering experiments in supersonic two phase flow
21 p3689 A69-38596
- Sedov canonic equations for supersonic gas flow solved by applying Chaplygin function to determine

tion of Riemann function for potential and stream function equations

21 p3643 A69-38637

Rotary derivatives of aerodynamic forces and moments in subsonic and supersonic flow, emphasizing kinematic and dynamic oscillations

21 p3647 A69-38733

Nonequilibrium processes behind shock wave in shock tube supersonic air and nitrogen flow, using photoelectrical shadow method

21 p3695 A69-38961

Multistep axisymmetrical supersonic exit cones optimum geometry design diagram based on external oblique and normal compression shock

21 p3785 A69-39104

Electron beam injection into magnetic trap, obtaining plasma by ionization of supersonic argon flow passing through system

22 p3990 A69-40791

Semianalytic solution for axisymmetrical supersonic inviscid flow near stagnation region of spherically blunted body with detached shock waves

22 p3861 A69-41178

Axisymmetric supersonic flow around spherically blunted body at small angles of attack, deriving equations for shock deformation perturbations and surface pressure

22 p3861 A69-41179

Frictionless supersonic and hypersonic flow of ideal gas of constant specific heat past cone with deformed axis at zero angle of attack

23 p4058 A69-41579

Successive approximations convergence analyzed in solving supersonic collisionless plasma flow past magnetic dipole

23 p4156 A69-41853

Supersonic free stream flow past finite conical body with subsonic surface gas injection

23 p4059 A69-41884

Linear small perturbation approximation for supersonic nonequilibrium flows past oscillating airfoil in two dimensional wind tunnel, noting Laplace transform solution

23 p4061 A69-42349

Supersonic flows around slender bodies calculated by method of moving singularities

23 p4061 A69-42407

Graphical method for two dimensional supersonic expansion flow with subsonic reaction front around corner compared to existing iteration method

23 p4061 A69-42411

Transonic flow around profiles with heat input, showing drag reduction in supersonic part of flow field

23 p4061 A69-42414

Second order differential equations of supersonic flows past bodies at small angles of attack, showing linearized characteristics method applicability for conical nose

24 p4243 A69-42581

Heated three layer plates stability under finite deflections in supersonic gas flow, deriving aerothermoelasticity equations

24 p4395 A69-42590

Supersonic rarefied gas flow past circular cylinder, studying flow and shock parameters by multiple wave interferometry

24 p4244 A69-43070

Laminar boundary layer separation in supersonic flow, constructing method for flow distribution functions, perturbed flow region dimensions and pressure perturbation amplitude

24 p4246 A69-43482

Hydrogen-air combustion in supersonic flow past sphere determined with allowance for chemical reactions nonequilibrium rates at high pressure and temperature

24 p4408 A69-43488

Supersonic flows past blunt bodies, formulating approximate similarity law for shock layers in subsonic regions

24 p4246 A69-43495

Gas dynamic functions of axisymmetric supersonic gas flows determined using flow density distribution optical measurements

24 p4247 A69-43496

Supersonic viscous flow around sharp corner at various expansion angles, giving pressure distributions and velocity profiles role

[ASME PAPER 69-HT-14] 24 p4247 A69-43555

Diamond shaped striations development mechanism on ablative heat shield materials exposed to supersonic flow and turbulent boundary layers

24 p4248 A69-43598

Supersonic flow stability with energy input applied to reaction kinetics of processes in aircraft and rocket combustion chambers

24 p4248 A69-43642

Perturbation equations for oscillating wedges and caret wings with attached bow shock in hypersonic and supersonic flows

24 p4249 A69-43659

Strong shock and Mach waves interaction generated downstream of thick wedge body shock in unsteady hypersonic and supersonic flows

24 p4306 A69-43674

Jet dynamic characteristics injected into supersonic air slipstream incident on flat body, calculating configuration, shock wave geometry and parameters distribution in flow field

24 p4250 A69-43710

Forced parametrically excited periodic vibration of finite length plate in plane supersonic flow, considering periodic forces applied at edges

24 p4407 A69-43733

SUPERSONIC FLUTTER

Flutter vibration of sails fixed along edge and single wing weather vanes in supersonic flows

02 p0192 A69-12824

Panel flutter in supersonic flow, using finite element approach in matrix displacement methods to derive aerodynamic influence coefficient matrices

04 p0676 A69-14707

Finite aspect ratio sandwich plates flutter in supersonic gas flow analyzed by differential equation describing plates elastic equilibrium

08 p1412 A69-20324

Supersonic flutter of circular cylindrical heterogeneous orthotropic thin panels of finite length, obtaining nonlinear flutter equation

08 p1413 A69-20404

Supersonic flutter solutions using finite elements, analyzing rectangular plate bending elements, square simply supported and clamped panels, low aspect ratio configurations, etc

11 p1991 A69-25516

Perturbation method for nonlinear panel flutter at high Mach numbers, using von Karman large deflection plate theory and quasi-steady aerodynamic theory

13 p2364 A69-28204

Membrane flutter and panel stability in supersonic flow, considering infinite aspect ratio equation solution through Galerkin method

13 p2365 A69-28236

Supersonic flutter in square panels and cylindrical shells, measuring critical dynamic pressure

17 p3051 A69-32923

Stability analysis of missile lateral supersonic flutter based on Lagrange equations, considering conservative thrust, control deviation and aerodynamic forces

17 p3045 A69-32946

Finite aspect ratio sandwich plates flutter in supersonic gas flow analyzed by differential equation describing plates elastic equilibrium

17 p3058 A69-33317

Asymptotic theory of pressure on cylindrical shell subjected to unsteady oscillations in external and internal linearized supersonic flow using Laplace and Fourier transforms

18 p3089 A69-35461

Natural oscillations and flutter of three layer cylindrical shell in supersonic gas flow analyzed by semimomentless theory, discussing boundary value problems, damping effects, etc

19 p3437 A69-36201

Supersonic panel flutter boundary of buckled and unbuckled clamped rectangular plates, discussing in-plane stress effects

22 p3930 A69-40584

Buckled rectangular plates with constrained edges, analyzing natural frequencies as basis for supersonic panel flutter analysis

22 p4046 A69-41049

Shearing force and shear buckling deformation influence on supersonic panel flutter boundary of simply supported rectangular plates, basing analysis on deflection approximation

24 p4400 A69-43055

Initial deflection and internal pressure effects on supersonic panel flutter boundary of simply supported rectangular plates under diverse middle surface stress conditions

24 p4400 A69-43056

Acroelastic stability of thin plates exposed to supersonic flow using singular perturbation methods, obtaining flutter boundary and membrane solution

24 p4403 A69-43573

SUPERSONIC HEAT TRANSFER

Performance analysis for electrothermal thrusters using lithium propellant with supersonic heat addition

[AIAA PAPER 69-286] 09 p1567 A69-21261

Ceramic heat transfer gage for supersonic wind tunnel investigation of blunt swept wing leading edges aerodynamic heating

15 p2613 A69-31270

SUPERSONIC INLETS

Supersonic compressors for supersonic and subsonic air intakes, studying wave configuration at entry of circular cascade of blades with hydraulic analogy

[ONERA-TP-669] 05 p0699 A69-16344

Variable geometry intake and convergent-divergent nozzle design for supersonic aircraft, noting subsonic installations

08 p1253 A69-21164

Ramjets and air augmented rockets as propulsion systems for supersonic atmospheric flight, noting inlet design, combustors and nozzles

11 p1943 A69-25586

Steam-water convergent condensing injector with supersonic inlet vapor, discussing axial pressure profiles and discharge pressure

13 p2372 A69-27486

M 3.5 two dimensional mixed compression inlet system with self restarting using flexible variable ramp system

[AIAA PAPER 69-447] 16 p2845 A69-32732

Nonequilibrium inlet conditions effect on combustion performance during H and vitiated air combustion, studying ignition delays

[AIAA PAPER 69-457] 16 p2881 A69-32767

Large scale axisymmetric inlet systems performance capabilities, reviewing theoretical and experimental programs

[AIAA PAPER 68-580] 17 p3022 A69-34018

NACA submerged intake performance at M 2.5, considering total pressure and mass flow ratios, drag coefficient and boundary layer thickness effects

19 p3242 A69-36819

Control system concept for axisymmetric supersonic inlet operation in mixed compression mode noting test results

[AIAA PAPER 68-581] 20 p3585 A69-37151

SUPERSONIC JET FLOW

Reactions kinetics contribution to nonequilibrium recombination occurring in supersonic nozzle flow of combustion products of hydrogen in air

02 p3353 A69-12488

Radiation effect enhancement in supersonic plasma jet cooled by rapid expansion, giving energy equation for electron cooling rates to analyze electron temperature

02 p0292 A69-12557

Crystals and molecules diffraction in supersonic molecular jets

02 p0284 A69-12629

Minimum admissible spacing between supersonic jet expelled from VTOL aircraft nozzle and plane surface near nozzle exit

03 p0361 A69-12955

Supersonic gas jet impingement on inclined plane barrier, calculating parameters by approximation

03 p0413 A69-12958

Interaction between supersonic jet and counterflow of ideal compressible fluid

05 p0751 A69-16551

Gas mixture separation in supersonic jet, noting results for hydrogen-nitrogen mixture and diffusion flux

06 p0911 A69-17553

Mach number distribution along axes of underexpanded supersonic jets measured in wind tunnel experiments

07 p1050 A69-18922

Turbulent flow effect on heat transfer in supersonic jet with plane infinite obstacle perpendicular to jet axis

07 p1243 A69-19738

Supersonic jet impingement on flat plate, showing shock wave profiles and slipstream surface at stations parallel to nozzle axis

08 p1252 A69-20841

Supersonic free jet with real gas effects and chemical reactions calculated by approximation

10 p1631 A69-22898

External burning ramjets in supersonic stream noting applications to drag reduction, lift-drag ratio and attitude control

11 p1941 A69-24261

Sound field generation by isotropic turbulence through finite strength shock, estimating acoustic energy flux from supersonic jet containing shock waves

11 p1872 A69-25130

Axisymmetric turbulent supersonic incompressible fluid jet, calculating momentum flow distribution and excess heat flow densities in basic segment
11 p1818 A69-25346

Supersonic jet flow with separated shock wave flowing past infinite wedge using Chaplygin method, assuming negligible entropy variations
14 p2391 A69-29619

Radiation effect enhancement in supersonic plasma jet cooled by rapid expansion, giving energy equation for electron cooling rates to analyze electron temperature
15 p2658 A69-30254

Flow field of highly ionized arc heated supersonic free jet, using continuous flow test facility
[AIAA PAPER 68-135] 16 p2772 A69-32153

Combustion effects on mixing of axisymmetric supersonic and turbulent free jets to obtain species concentrations, pitot pressures and temperatures
[AIAA PAPER 69-538] 16 p2843 A69-32705

Base flow component of total drag for axisymmetric supersonic afterbody with single exhaust jet, considering turbulent mixing
[AIAA PAPER 69-650] 17 p2956 A69-33485

Method of characteristics for computing supersonic jets and wakes with given boundary pressure distribution
[ONERA-TP-721] 18 p3121 A69-34636

Nonuniform gas flow past axisymmetric body from supersonic source simulating jet discharging into vacuum, using power series of stream function
19 p3238 A69-35851

Supersonic fan-shaped jet formation by identical colliding underexpanded jets, calculating subsonic flow between interaction plane and curvilinear shock wave
21 p3643 A69-38643

Polymer films damage due to supersonic plasma jets, comparing fracture relief of oriented and unoriented polymers
21 p3752 A69-39081

Flowfield properties of two dimensional supersonic jet near sonic nozzle exit by numerical method of characteristics
22 p3860 A69-40920

Heat exchange at stagnation point during interaction between underexpanded axisymmetric supersonic jet and flat obstruction, using method of characteristics
24 p4246 A69-43493

Slot type jet interaction flow tests at free stream Mach 4 and 5, describing equipment, procedure and results
24 p4249 A69-43686

SUPERSONIC NOZZLES

Minimum admissible spacing between supersonic jet expelled from VTOL aircraft nozzle and plane surface near nozzle exit
03 p0361 A69-12955

Short cylindrical diffusers efficiency in supersonic wind tunnel with exchangeable nozzles with conical supersonic section
03 p0365 A69-14226

Recombination constants of dissociated oxygen and nitrogen flow in supersonic nozzle at high temperatures using modified Bray method
06 p1030 A69-17349

Differential equations for two phase flow in axisymmetric supersonic nozzle, discussing existing solutions
06 p0861 A69-17815

Underexpanded nozzle ejected supersonic turbulent jet off-design behavior, discussing static pressure distribution, boundary layer and Mach number effect
07 p1049 A69-18397

Optimum profile of supersonic nozzle with nonequilibrium flow
07 p1119 A69-18737

Performance of short supersonic nozzles producing expansion and density jumps in flow, noting efficiency in obtaining maximum driving effect
07 p1050 A69-18753

Supersonic nozzle cross section and diffuser throat in MHD generator calculated by continuity equation
11 p1826 A69-25348

Supersonic nozzle design ensuring desirable flow field in inviscid core of viscous gas flow, using boundary layer equations
11 p1820 A69-25473

Electrical breakdown voltage and voltage-current characteristics of uncooled coplanar carbon electrodes in walls of supersonic conical and rectangular nozzles
[AIAA PAPER 68-713] 13 p2249 A69-28231

Heat release rate during gas combustion products recombination in supersonic nozzle, using graphic interpolation of flow parameters
15 p2717 A69-30987

Flow disturbances in supersonic rocket nozzles due to secondary injection analyzed by effective body approximation, including side forces
[AIAA PAPER 69-443] 16 p2839 A69-32666

Supersonic blowdown wind tunnel noting cylindrical diffusers efficiency in starting supersonic nozzles increased in proportion to Mach number
17 p2890 A69-33125

Laminar boundary layers in low density supersonic and hypersonic conical and axisymmetric nozzles, treating displacement, transverse curvature, velocity slip and temperature jump
[AIAA PAPER 69-653] 17 p2954 A69-33458

Hydrogen jet structure ejected into vacuum from Laval nozzle at supersonic velocity, considering separation point from diffuser wall
19 p3240 A69-36601

Supersonic molecular beam relative intensity represented as function of nozzle to collimator distance and gas admission pressure
20 p3579 A69-37432

Supersonic air to air ejectors performance for low secondary-to-primary mass flow ratios, deriving correction factor for Fabry-Paulon theory
21 p3644 A69-38654

Internal flow measurements in transonic region of supersonic nozzle with small throat radius of curvature compared with prediction data
23 p4060 A69-41900

Pressure ratio effect on supersonic turbine nozzle performance during off-design regime operation, noting effect of low specific heat gas ratio
23 p4203 A69-42250

Cylindrical shell with supersonic nozzle end, describing axisymmetric oscillations forced by burning filler in gas stream
24 p4300 A69-43073

SUPERSONIC PRESSURE DISTRIBUTION U PRESSURE DISTRIBUTION

SUPERSONIC SPEEDS

Ablation rate optical measurement near stagnation point of Teflon cylinder models, noting effect of nose curvature and temperature at supersonic speed
01 p0006 A69-10758

Wing-body combinations analysis and design at supersonic and subsonic speeds by aerodynamic influence coefficients method
[AIAA PAPER 68-55] 01 p0006 A69-11016

Velocity field excited by wing vibrations propagating over elastic surface at supersonic velocities, considering nonvertical motion and absence of external forces
02 p0188 A69-11976

Lift efficiency of and stabilization by square flare on high speed missile, comparing wind tunnel measurements with circular conical flare
02 p0190 A69-12544

Shock waves collision with supersonically moving axisymmetric slender bodies analyzed by integral transform method, noting application to shock-shock interaction
03 p0413 A69-13010

Atmospheric gust effect on aircraft flying at Mach one calculated for subsonic and supersonic regions, finding difficulties for transonic calculations
10 p1632 A69-22918

Fluid mechanics shock wave interaction with turbulent boundary layers at transonic to high supersonic speed ranges, noting examples in aviation
11 p1871 A69-25018

Flight tests of deployment of 20 ft diam ribbon parachute at high dynamic pressures and supersonic speeds
11 p1823 A69-25383

Linear and second order theory for maximum lift to drag ratio airfoils at moderate supersonics speed, considering length, thickness and area
13 p2199 A69-28214

Velocity field excited by wing vibrations propagating over elastic surface at supersonic velocities, considering nonvertical motion and absence of external forces
15 p2547 A69-30259

Two dimensional turbulent mixing with surface mass injection at supersonic and hypersonic speeds, noting velocity and temperature distributions
[AIAA PAPER 68-130] 16 p2770 A69-31883

Two dimensional model for analyzing turbulent separation and reattachment at blade trailing edge at supersonic speed
[ONERA-TP-678] 16 p2733 A69-32258

Infrasonic waves identified with supersonic auroral electrojets crossing zenith from northwest during sub-storm activity
16 p2780 A69-32303

Wind tunnel tests for static stability of Black Brant 4 vehicle second stage with flare and two fin flare combinations at supersonic speed
17 p2948 A69-34212

Heated supersonic beam study of He-Ar intermolecular potential, determining total elastic collision cross section as function of velocity in scattering chamber
19 p3377 A69-36183

Lateral and head-on interactions between plane shock wave and supersonic wedge, showing solution dependent on apex angle and incident flow Mach number
19 p3239 A69-36398

Drag measurements for sharp and blunt-nosed bodies shot into wind tunnel supersonic gas counterflows, discussing shock waves for different configurations
19 p3239 A69-36401

Three dimensional velocity field disturbed by shock wave traveling across slender wing at supersonic speed
19 p3242 A69-36797

Shock wave parameters from meteoric body moving at high supersonic speeds through atmosphere, calculating specific heat ratio
19 p3428 A69-36841

Structural and aerodynamic developments in attached inflatable decelerators for deployment of payload at supersonic speeds
[AIAA PAPER 68-929] 21 p3647 A69-39015

SUPERSONIC STRIKE AIRCRAFT U ATTACK AIRCRAFT

SUPERSONIC TEST APPARATUS

Microwave-plasma interaction instrumentation for supersonic channel constructed to investigate turbulent boundary layers formed over ablating heat shield materials
19 p3294 A69-35754

Control system concept for axisymmetric supersonic inlet operation in mixed compression mode noting test results
[AIAA PAPER 68-581] 20 p3585 A69-37151

SUPERSONIC TRANSPORTS

NT BOEING 2707 AIRCRAFT

NT CONCORDE AIRCRAFT

Human engineering program plans for Phase 3 of SST Development Program in accordance with airframe and engine contracts
01 p0019 A69-10451

Navigation system for American SST noting use of Doppler radar and inertial navigation
02 p0278 A69-12238

Avionics technology and systems for future SST aircraft noting improved air traffic control systems
02 p0279 A69-12364

Safety problems of jumbo jet airbus and SST, discussing operational safety procedures and techniques
03 p0365 A69-12882

Alpha numerical and symbolic information combined for head up display (HUD) systems, providing pilot with takeoff director
03 p0379 A69-12885

Swing wings on combat aircraft and SST, discussing suitability for aircraft carriers and problems in aerodynamic balance
03 p0367 A69-13677

Response to technical, social and political criticism of U.S. SST program
[AIAA PAPER 68-1024] 04 p0689 A69-14794

Aircraft propulsion by wake regeneration, noting supersonic transport ogee layout with maximum drag fraction
05 p0811 A69-15555

SST System Safety Program, discussing cosmic radiation and aerodynamic heating
06 p1041 A69-16838

Boeing SST designs, discussing performance, flying qualities and operational characteristics of configurations
06 p0868 A69-17830

Concorde and Boeing supersonic transport overland sonic booms, discussing social, political and legal reactions
06 p0868 A69-17899

Design, metallurgical and manufacturing problems of titanium application in supersonic C5 and SST engines
09 p1570 A69-22062

Potential hazards of government sponsored technology, examining SST and fluoridation projects and weather problems
10 p1811 A69-23392

Soviet supersonic transport Tu 144, describing wing unit, fuselage, passenger accommodation, tail unit, landing gear, power unit engine nacelle and navigation
10 p1634 A69-23838

Acoustical, psychological, sociological and political aspects of human reaction to SST sonic booms over populated areas, tabulating Boeing and Concorde boom intensities
14 p2408 A69-29151

Human tolerance to SST sonic booms through scheduled community exposure, discussing physiological effects and acceptability level
14 p2541 A69-29153

SST fuselage response to reverberant and turbulent boundary layer noise calculated for computing equivalent reverberant acoustic fields
15 p2549 A69-30302

Statistical correlation of temperature and tail-wind data for London-New York route at 50 mb for SST operation
15 p2651 A69-30690

Mass supersonic air transport physiological problems, reporting findings of FAUST committee concerning ozone toxicity, pressure drops, sonic booms, time zone physiology, etc
15 p2556 A69-31225

Turbulence and SST, discussing subsonic accidents, probability of encountering gust induced accelerations, turbulence at cruise altitudes, radar storm return and mountain waves
16 p2808 A69-32368

Location effect of power plants on aft-mounted supersonic cruise exhaust nozzles at transonic speeds in flight and wind tunnel
[AIAA PAPER 69-427] 16 p2734 A69-32769

Experimental SST terminal for satellite L band communications/surveillance ATC system, establishing terminal requirements for NASA and FAA studies
17 p2932 A69-34118

Airport facilities planning for conventional jet, STOL and SST aircraft ground handling, stressing facilities economy and transportation subsystems
[AIAA PAPER 69-808] 19 p3289 A69-35623

Passenger transport cruising at low supersonic speeds without sonic boom generation on ground, discussing overpressures, signature characteristics and corridor widths
[AIAA PAPER 69-776] 19 p3244 A69-35647

Supersonic transport aviation fuel thermal stability measurement data correlated with data deduced from heat transfer measurements
19 p3393 A69-36210

Titanium monocoque fuselage reinforced by composite boron filaments in polyimide resin matrix tested for SST applications, noting weight savings over all titanium structure
[AIAA PAPER 69-763] 19 p3329 A69-36298

Supersonic transport aircraft impact on air traffic control in Eurocontrol area, discussing climb, acceleration, cruise and descent
19 p3370 A69-36653

Cosmic radiation exposure of passengers and crew in supersonic transport at high altitude
22 p4002 A69-40093

Modified tailed delta configuration selection for U.S. SST, discussing power plant installation choice
[RAES PAPER 17] 22 p3863 A69-40496

Planning for safety of future supersonic air traffic including financing and coordination activity of government and industry
22 p4054 A69-41131

Safety implications of technological developments in aviation, discussing standards and statistical data for supersonic transports and jumbo jets
22 p3867 A69-41134

SST stratospheric environment problems, discussing temperature effects on fuel consumption and convective turbulence effect on flight safety and efficiency
22 p3867 A69-41141

XB-70 aircraft test data as applied to SST safety, describing aircraft design, flight characteristics, instrumentation, takeoff and landing, etc
22 p3868 A69-41143

SST flight crew operational requirements to achieve maximum human efficiency and man/machine compatibility, discussing pilot role, advanced flight instrumentation, etc
23 p4107 A69-41820

Solar flare radiation hazard to SST crew and passengers, discussing onboard and ground based warning systems and ICAO requirements
23 p4063 A69-41830

Atmospheric variability at proposed flight levels, analyzing meteorological requirements of SST operation

tions, discussing annual cycles in stratospheric circulation
24 p4251 A69-42711

SST contribution to commercial aircraft transportation, discussing economic and operational aspects, decision making process leading to fixed wing design, etc
[AAS PAPER 69-323] 24 p4252 A69-42869

Flight simulator with large lateral motion for large and supersonic transport aircraft, emphasizing reproduction of cockpit accelerations due to supersonic engine thrust loss
24 p4297 A69-43044

Localizer acquisition system quasi-optimization technique based on time optimal control theory, with application to SST ILS problem
24 p4348 A69-43312

Heat tolerance in case of SST aircraft air conditioning failure, discussing physiological and psychomotor reactions and time curves for metabolic activity levels
24 p4277 A69-43382

SST range-payload improvement by emphasizing Ti alloys honeycomb and trusscore sandwich panels fabrication for structural boxes in wing and empennage
24 p4324 A69-43436

Elastomers for SST aircraft applications, discussing properties evaluation, material selection, sealant requirements, etc
24 p4338 A69-43455

Sonic boom signatures produced by diverse SST configurations during cruise, indicating aircraft length as overpressure limit factor
24 p4253 A69-43661

SUPERSONIC TURBINES

Pressure ratio effect on supersonic turbine nozzle performance during off-design regime operation, noting effect of low specific heat gas ratio
23 p4203 A69-42250

SUPERSONIC WAKES

Model for asymptotic separated flow in wake behind broadside of bluff body, discussing separation point, interaction, reattachment, base flow and near wake
02 p0188 A69-11986

Discrete vortices in two dimensional subsonic and supersonic wake, determining Strouhal numbers, frequencies and flow velocities with aid of HF cinematography
02 p0191 A69-12587

Turbulent front structure of axisymmetric compressible wake at supersonic speeds, measuring intermittency factor distribution
03 p0419 A69-13949

Flow measurements in near wake of 7 degree half angle cone at free stream Mach number 4.3, noting pressure measurements
[AIAA PAPER 69-186] 06 p0863 A69-18068

Mean flow measurements in supersonic wake of slender two dimensional body at zero incidence and heat transfer rate, noting predictability from similarity analysis
11 p1817 A69-24281

Supersonic wake flow visualization, obtaining direct photographs of various smoke streamlines
[AIAA PAPER 69-346] 13 p2200 A69-28281

Pulsed laser holographic interferometry of density field created by high speed projectile motion in air
[AIAA PAPER 69-347] 13 p2263 A69-28282

Near wake in axisymmetric supersonic flow past slender body with/without base injection, obtaining pressure, temperature, Mach number, velocity and concentration distributions
14 p2389 A69-29017

Supersonic wake recirculation flow over rearward facing two dimensional steps and blunt bases
14 p2389 A69-29031

Mean near wake flow of adiabatic two dimensional wedge at Mach 4 with tripped turbulent boundary layers and base mass addition
16 p2733 A69-32147

Mixed supersonic/subsonic type steady wake flow fields in flat based slender bodies, using finite difference method
[AIAA PAPER 69-649] 17 p2892 A69-33468

Method of characteristics for computing supersonic jets and wakes with given boundary pressure distribution
[ONERA-TP-721] 18 p3121 A69-34636

SUPERSONIC WIND TUNNELS

Pressure oscillation production in wind tunnel by hinged plates in test section walls to test jet engine inlets under controlled conditions
02 p0229 A69-12537

Short cylindrical diffusers efficiency in supersonic wind tunnel with exchangeable nozzles with conical supersonic section
03 p0365 A69-14220

French supersonic recycling wind tunnel for short duration experiments
07 p1116 A69-19288

Turbulent boundary layers on flat wall of supersonic wind tunnel, determining velocity profiles, thicknesses and skin friction coefficients
10 p1680 A69-23642

Short duration tube wind tunnel supersonic testing noting Saturn S-IC base heating and solid propellant rocket base burning tests
[AIAA PAPER 69-335] 13 p2242 A69-28277

Supersonic boundary layer acoustic characteristics measured in wind tunnel on cylindrical model with several forebody configurations
[AIAA PAPER 69-344] 13 p2249 A69-28277

Continuous supersonic plasma wind tunnel obtained using magnetic Laval nozzle made by modification of Q device normal magnetic field configuration
15 p2589 A69-30909

Inlet produced dynamic distortion and effects on stall margin of J-85 turbojet engine from supersonic wind tunnel tests
[AIAA PAPER 69-487] 16 p2840 A69-32676

Supersonic cascade wind tunnel /ONERA/ for supersonic and transonic compressors profiles studies
17 p2895 A69-33591

Error analysis for pressure measurements in blow-down supersonic tunnel
19 p3292 A69-35728

Skin friction balance in Mach 5 wind tunnel with high heat transfer, measuring shear forces
19 p3292 A69-35734

Supersonic blowdown wind tunnel operating at Mach numbers obtained by fixed nozzles for aerodynamic optimization of wings and bodies
20 p3510 A69-37422

Panel flutter testing in supersonic blowdown wind tunnels, analyzing model and test chamber layout
21 p3847 A69-39859

SUPINE POSITION

Pulmonary ventilation and perfusion in normal supine subjects before and during exposure to lower body negative pressure measured using Xe-133
17 p2909 A69-33180

Vertical vibrations effect on test subjects in supine position, noting human tolerances and mood changes
19 p3260 A69-35986

Pulmonary capillary blood flow pulse of healthy men in supine position recorded by nitrous oxide/plethysmograph and phonocardiogram
24 p4259 A69-42638

SUPPLYING

Mathematical formula for estimating cost and efficiency of parachuting supplies, noting shock load reduction
07 p1053 A69-19140

SUPPORT SYSTEMS

NT GROUND OPERATIONAL SUPPORT SYSTEM

NT GROUND SUPPORT SYSTEMS

Automatic support systems development and capabilities with recommendations for future R and developments
03 p0411 A69-13190

Flight test support design, developing measure of performance of test environments stated in weapon or space system terms
05 p0742 A69-15804

Deterministic model for cost effectiveness of avionics support programs based on subsystems support ability, test philosophy and test equipment design and manufacture
[AIAA PAPER 69-305] 09 p1478 A69-22377

Automatic support systems for advanced maintainability - IEEE Conference, St. Louis, November 1968
11 p1863 A69-25059

Multipurpose test system analysis emphasizing support section containing self test elements, power monitoring and control, interconnection techniques and packaging
11 p1864 A69-25069

Mathematical model for prediction of automatic test equipment utilization and determination of time for performance of intended test function
11 p1865 A69-25074

Optimized automated system for direct support maintenance of AH-56A subsystem equipment
11 p1865 A69-25075

Data relay satellite systems for support of NASA R and D missions, discussing communications between satellites and to mission control

11 p1839 A69-25296

Tracking and data acquisition networks and communications systems for support of space missions, studying data processing, unified S Band System and Data Relay Satellite System

12 p2028 A69-25933

Lever support systems for telescopes noting tilt compensation, acceleration balance and problems of friction, pivot viscosity, thermal effects and weight

12 p2057 A69-26410

Optical tests of Hale telescope mirror and support system at Palomar, noting various maladjustments and malfunctions

12 p2057 A69-26411

Axial support systems for large astronomical mirrors, considering gas support system for flat mirror submerged and floating in isostatic liquid

12 p2057 A69-26412

Sinusoidal tension and compression radial support system for large solid disk primary mirror, noting pivot design and pad bonding adhesive

12 p2057 A69-26413

Large mirror support systems definition in terms of axial location and radial position

12 p2057 A69-26414

Lick telescope support system for 120 inch mirror, noting use of levers and counterweights concept

12 p2058 A69-26415

Isaac Newton telescope, describing support of 98 inch mirror, structure between fabricated cell steel surface and mirror and tests with air bag support

12 p2058 A69-26416

Support system for McDonald 107 inch telescope mirror, adopting Couder design using lily pad single lever supports for axial thrust

12 p2058 A69-26417

Axial support system for Canadian 150 inch telescope mirror, discussing flexural and shear analyses and ring supports repositioning for balancing shear

12 p2058 A69-26418

Axial counterweight lateral support system with ternary symmetry for European Southern Observatory telescope mirror

12 p2058 A69-26419

Axial support system for controlling thermal distortion of 82 inch heliostat mirror for Kitt Peak solar telescope

12 p2058 A69-26422

Integrated Logistics Support (ILS) cost effectiveness, discussing management of systems elements in addition to prime equipment including computer programs, training, maintenance, etc

15 p2722 A69-31126

Boron epoxy strut prototype for support system of advanced nuclear flight stage with nonintegral cryogenic tankage configuration, achieving weight reduction

19 p3354 A69-35516

Missile and space support planning, objectives, technology development, functions, maintenance and in-flight maintainability

19 p3295 A69-36327

Space transportation cost saving options including booster systems, spacecraft/payload systems and support systems, discussing recovery and launching operations

21 p3857 A69-39690

Mariner Mars 1969 spacecraft real time test support system and recorded data analysis including routing to printers, CRT displays and incremental plotters [AIAA PAPER 69-982]

22 p3907 A69-40362

Multisupport suspension arrangements for reducing reflector surface weight-loading distortion in steerable parabolic radio telescope antennas

23 p4149 A69-42128

Wind tunnel model one component magnetic support and balance system for sphere drag investigation at subsonic Mach numbers [AIAA PAPER 68-401]

24 p4298 A69-43714

SUPPORTS

Integral equation solution for plate with internal support

03 p0528 A69-13799

Liquid flow systems dynamic response to periodic disturbances of system structural supports

05 p0747 A69-16073

Rotor shaft mounted on number of bearings and carrying masses and inertia angular precession and critical speeds, considering gyroscopic moments, rotary inertia and shear deformation [ASME PAPER 69-VIBR-54]

10 p1805 A69-24154

Large astronomical mirrors support and testing - Conference, Tucson, December 1966

12 p2055 A69-26406

Minimal interference thin metal strap support system for dynamic stability tests of high fineness ratio wind tunnel models [AIAA PAPER 69-350]

13 p2243 A69-28284

SUPPRESSORS

NT ECHO SUPPRESSORS

Amber suppressors conversion to ochre suppressors in RNA of bacterium or bacteriophage using uracil mutagen

07 p1068 A69-19493

Graphs determining interference levels for optimum shielding, suppression, signal parameters and waveforms for pulses, step functions, CW signals and for military technology

12 p2030 A69-26471

Meteorological radar dead zone diminished by using hybrid electronic waveguide suppression system to eliminate antenna sidelobe reflections

16 p2791 A69-32281

Forced vibration testing of complex continuous systems, demonstrating suppression of certain resonant frequencies due to laboratory techniques

18 p3114 A69-34422

SURFACE COATINGS

U COATING

SURFACE COOLING

Relationship between cooled surface temperature and pressure self oscillation frequency during heat transfer to turbulent fluid flow, showing temperature variations

01 p0173 A69-10094

Film cooling by subsonic gas injection of air through porous flat plate into 2.9 Mach air flow, noting wall temperatures

03 p0413 A69-12994

Transpiration cooling of porous flat plate by injection of carbon dioxide or air into carbon dioxide and air free streams

03 p0413 A69-12996

Active cooling systems for high performance reentry vehicles in thermal and shear stress environments [AIAA PAPER 68-1154]

03 p0533 A69-13669

IR observations of lunar crater and maria enhanced thermal emission during eclipse, constructing model of cratered surface to analyze thermal behavior

04 p0654 A69-14656

Heat transfer characteristics of single lines of circular air jets impinging on concave cylindrical surfaces, discussing nozzle target spacing effect [ASME PAPER 68-WA/GT-1]

05 p0848 A69-16137

Angular distribution measurements of visible and near IR radiation reflected from carbon dioxide cryodeposits formed on liquid nitrogen cooled surface in vacuum [AIAA PAPER 69-63]

06 p0959 A69-18131

Effects of multidimensional flow through porous matrices in mass transfer cooling, analyzing one dimensional model for blunt axisymmetric surfaces [AIAA PAPER 69-149]

06 p1038 A69-18179

Mass transfer cooling of high velocity surfaces in gaseous environment noting applications to atmospheric entry

13 p2377 A69-28146

Flat surfaces downstream of heated section and porous strip, determining film cooling effectiveness and heat flux from heat transfer coefficients ratios

20 p2631 A69-37096

Active cooling systems for high performance reentry vehicles in thermal and shear stress environments [AIAA PAPER 68-39016]

21 p3851 A69-39016

Rectangular fins arrangement on horizontal surfaces for optimum free convection heat transfer coefficient, considering fin weight, height and spacing effects [ASME PAPER 69-HT-44]

24 p4409 A69-43517

Laminar, transition and turbulent boundary layer heat transfer measurements along wall in thermal entrance region of high temperature turbulent airflow through cooled tube [ASME PAPER 69-HT-8]

24 p4414 A69-43560

SURFACE CRACKS

Temperature field and stress state in elastic plane with temperature insulated arc shaped crack

01 p0164 A69-10078

Stress-strain behavior of crazes in glassy polymers, discussing crack propagation, craze formation and failure and molecular weight effects

01 p0102 A69-10915

Crack tip plastic flow effect on strain energy release rate, considering Dugdale model for yielded crack [ASME PAPER 68-WA/MET-17]

05 p0838 A69-16155

Gas breakdown model for analyzing breakdown of Ce vapor filled crack in thermionic trilayer insulator

09 p1441 A69-21840

Stress intensity magnification factors in surface flawed tension plates and notched round tension bars, evaluating fracture toughness

10 p1797 A69-23080

Stresses and displacements in half plane with edge crack given as eigenfunction expansions using Wiener-Hopf technique

11 p1987 A69-25438

Craze formation and shear yielding considered for glassy polymers in terms of stress field requirements

17 p2993 A69-34169

Eddy current machine /nondestructive testing device/ for aircraft structures surface cracks detection

21 p3719 A69-38391

Meridional crack problem for cylindrical and spherical shells solved for uniform membrane load and bending moment, obtaining stress intensity components

22 p4046 A69-41041

Flaw determinations accuracy from measuring ultrasonic shear wave reflection peak intensities

24 p4397 A69-42756

SURFACE DEFECTS

Surface fatigue significance in sliding wear studied from damage on copper single crystal using electron microscope techniques

01 p0085 A69-10368

Fractures in refractory metals surface layers due to Q switched laser pulses

11 p1899 A69-25402

Coherent optical flaw detection and surface microstrain measurement techniques including holographic interferometry, optical correlation and diffraction

12 p2180 A69-26305

Incipient stress corrosion damage detection in aluminum alloys, using Rayleigh wave attenuation

12 p2114 A69-26306

Imperfection surface effect on buckling load of circular cylindrical shell under axial compression, locating limit points of postbuckled states

13 p2362 A69-28122

Glass fibers strength in relation to surface defects, comparing behavior of flawless and commercial fibers

22 p3974 A69-41039

SURFACE DIFFUSION

Turbine blade loading in terms of surface diffusion and loading factors, discussing tandem and jet flap blades and vortex generators [ASME PAPER 68-WA/GT-11]

05 p0812 A69-16136

Tantalum diffusion layer on refractory cobalt and nickel base alloys analyzed by electron microprobe [ONERA-TP-665]

06 p0941 A69-17097

CW helium-neon laser used to detect and measure vibration frequencies of uniform diffuse surfaces

09 p1515 A69-21430

Harmonic analysis for computing diffusing matter with periodically varying surface concentration applied to electrical insulators degradation by atmospheric moisture

15 p2592 A69-31057

Aluminum oxide relative grain boundary energy and surface diffusion coefficient, considering thermal grooving of bicrystals with symmetrical tilt boundaries

17 p2993 A69-34191

Al effect on B and Cr diffusion in protective coating on Cr-Ni heat resistant alloy, noting thermochemical kinetics for homogeneous layers

19 p3345 A69-36157

Heat resistance evaluation of ZrSi₂-K alloy subjected to multicomponent surface diffusion alloying combinations of Al, B, Cr, Si, Zr

19 p3345 A69-36159

Lunar surface thermal radiation incident on unit area flat surface located at variable distance and orientation above moon, considering diffusion effects

21 p3803 A69-38973

Boron tribromide-oxygen reaction kinetics effects on IC base diffusion uniformity, correlating uniformity with electrical properties

24 p4360 A69-42760

SURFACE DISTORTION

Yield surface after prestraining under radial loading, analyzing formation of yield corner

01 p0166 A69-10303

Thermostructural analysis of large flexible paraboloid antenna indicates RF losses due to thermal distortions significant for X band and higher transmissions [AIAA PAPER 68-333]

02 p0345 A69-12372

Nickel structure alterations during interaction with high speed air flow at elevated temperatures

05 p0783 A69-16812

Radio wave propagation over smooth cylindrical surface with specified boundary impedance, discussing diffraction loss and effect of surmounted obstacle
08 p1273 A69-20024

Draining liquid surface dip formation in tanks of arbitrary shapes and drain hole positions
09 p1483 A69-21999

Reflection interferometry for visual evidence of surface deformation of rock and metal samples using two beam Fizeau fringe system
09 p1496 A69-22012

Acoustic holographic measurement of surface deformation generated by sound waves impinging on gas-liquid interface, discussing acoustic amplitude components
10 p1695 A69-23542

Plane surface finite area deformation tensors in continuum mechanics permitting separation of volume and shape changes in constitutive equations
11 p1994 A69-25603

Bending surface of shells under crosswise load analyzed by moire method, considering rotating cylindrical surfaces
15 p2713 A69-31056

Cylindrical shell load carrying capacity under axial compression, considering middle surface initial distortions influence
23 p4228 A69-41989

Multisupport suspension arrangements for reducing reflector surface weight-loading distortion in steerable parabolic radio telescope antennas
23 p4149 A69-42128

Structural analysis program for obtaining steerable antenna surface deflections at various altitude angles and wind conditions as design parameters
23 p4230 A69-42129

Parkes paraboloid radio telescope structural performance, using rapid survey instrument to measure surface deformations for optimum focusing determination
23 p4231 A69-42130

Compressible fluid unsteady flow past deformable surface, constructing metric for surface and obtaining metric tensor coefficients
24 p4243 A69-42586

SURFACE ENERGY

Surface charge distribution in silicon p-n junctions noting luminescence of microplasmas and inhomogeneous properties
02 p0294 A69-11629

Surface radiation balance measurements in India during IQSY, discussing diurnal, seasonal and spatial variations of net radiation
02 p0307 A69-11820

Field effect in Ge and Si, noting relation between dependence of space charge on surface level charge and on surface potential
07 p1199 A69-18682

Relative free energies of crystal zones of tungsten using field electron microscope, determining surface energy anisotropy from Wulff construction
08 p1330 A69-20139

Quasi-brittle fracture of plastic materials based on Griffith theory and crack propagation, analyzing real surface energy and work of plastic strain
09 p1614 A69-21883

Ceramics strength and fracture behavior in terms of modified Griffith equation, discussing effective surface energy and initial crack size
11 p1907 A69-25238

Solid titanium surface energy determination, taking into account grain boundaries effect on accuracy
12 p2113 A69-26045

Surface free energy of solid Mo measured by Udin zero-creep method at high temperatures, noting low value due to residual impurity adsorption
12 p2117 A69-27137

Free electron model for electron work functions and number density distributions and surface potentials in metals
14 p2504 A69-29009

W single crystals cleavage cracks by spark discharge, showing effective surface energy dependence on crack initiation and propagation temperatures
15 p2637 A69-30226

Continuum fracture concept indicating essential surface energy interpretation difference in otherwise similar adhesive and cohesive failures
22 p3974 A69-40760

Negative surface potential effect on noise and photoconductivity in Ge doped p-type InSb single crystals at low temperature in vacuum
24 p4362 A69-43738

SURFACE EROSION

SURFACE FINISHING

Diffusion zones in filament reinforced metal matrix composites, using metallographic technique
01 p0103 A69-11269

Mechanical finishing abrasion induced plastic deformation microwinning observed in thin stainless steel films by transmission electron microscopy
02 p0251 A69-11542

Nucleate pool boiling heat transfer of liquid nitrogen from circular disks with different surface conditions including copper and nickel mirror finishes, roughness and coatings
02 p0352 A69-12207

Surface preparation effect on stress corrosion cracking of type 310 stainless steel wires in boiling aqueous magnesium chloride solutions
03 p0444 A69-13311

Inception of nucleate boiling with liquid nitrogen, noting surface finish effects
[ASME PAPER 68-WA/PID-10]
05 p0848 A69-16167

Thermochemical surface finishing trends, discussing methods to obtain complex diffusion layers
05 p0769 A69-16540

Surface treatment effect on weld porosity causes and removal in VT5-1 Ti alloy argon arc welding
06 p0945 A69-17897

Surface edge preparation of titanium alloy sheets for argon shielded arc welding
06 p0932 A69-17898

Surface finish and hardness effects on wear life of inorganic solid lubricant film
[ASLE PREPRINT 68AM 7C-3]
07 p1139 A69-18623

Surface preparation effects on Ni-Cr-Fe alloy boundary friction studied by repeated sliding of cylinders on hard Pd-Pt-Au alloy cylinder
[ASLE PREPRINT 68AM 6D-4]
07 p1139 A69-18625

Aluminum and aluminum alloys surface treatment prior to adhesive bonding, discussing degreasing, anodization, shear and bond strengths
07 p1141 A69-19312

Halocarbon solvent for application of chlorosilane finish to heat cleaned glass fabric for reinforcement of plastic, noting relative humidity effect
08 p1341 A69-20513

Comparative performance of niobium cylindrical thermionic converters with vapor deposited rhenium, stressing emitters surface preparation
09 p1438 A69-21816

Glass fibers size, finish and surface treatment identification by pyrolysis attenuated total reflectance IR spectroscopy
09 p1448 A69-22315

Oxide ceramics finishing processes, discussing leaching, machining, surface finishing, strengthening by compressive surface layers and joining
09 p1510 A69-22350

Structural imperfections of CdSb single crystals undoped and doped with tellurium and indium noting etching techniques, grain boundaries and impurities
11 p1938 A69-25030

Thermochemically synthesized high melting micropowders grinding by vibrational method and classification for polishing and finishing applications
12 p2113 A69-26256

Construction techniques for lightweight mirrors for secondaries, considering optical finishing and thermal expansion
12 p2058 A69-26420

Aspherical surfaces formation from spherical by removing part of substrate by means of tool mask for lapping nonuniform wear of surface
12 p2102 A69-26597

Metal electrolyte system for electrochemical machining in sodium chloride solution for achieving dimensional control
13 p2268 A69-27521

Thermionic converter improvements by electronegative additives and emitter surface finishes, noting cesium oxide, heat treatments with electropolishing, electroetching, etc
14 p2397 A69-29173

Mathematical model of mechanical wear in surface friction based on approximation of cross section profiles, using Fokker-Planck equation for distribution function
14 p2455 A69-29331

Substrates ultraclean surface preparation methods, examining crystal cleaving and crushing, heating, chemical cleaning, ion bombardment, etc
14 p2455 A69-29348

Stainless steel biaxial residual surface stresses from grinding and finish machining determined by dissection technique
[ASME PAPER 68-WA/MET-9]
14 p2455 A69-29437

Electrical and photoelectrical properties of semiconductor heterojunctions prepared by Ge epitaxy on gallium arsenide bases, showing dependence on base surface treatment
15 p2667 A69-30074

X ray diffractometer stress analysis of WC-Co cermets, discussing surface preparation and heat treatment
16 p2802 A69-32333

Lunar based optical workshop and repair facility using ion beam technique to polish and repair optical element surfaces
18 p3113 A69-34243

Electrical discharge machining effect on heat resistant alloys surface finish, noting volt-ampere characteristics
18 p3147 A69-34547

Finish turning cutting speed effects on titanium alloy surface layers
18 p3148 A69-34548

Beryllium bonding, evaluating various surface preparations and adhesives
19 p3320 A69-35561

Spray cleaning and deoxidizing of Al surfaces for structural bonding using sulfuric acid-sodium dichromate deoxidizer, noting tests with proprietary solutions
19 p3321 A69-35564

Isothermal and thermal martensite transformations on polished surfaces of Fe-Ni-Mo alloys
19 p3344 A69-35983

Soviet monograph on metal fatigue in aircraft structures, discussing effects of temperature, loading, residual stresses, surface finish and contact corrosion
20 p3622 A69-37231

Titanium surface cleaning and descaling in preparation for machining, discussing acid pickling, mechanical abrasion, conditioning cycles, etc
20 p3549 A69-37434

Plasma arc systems and applications, noting transferred and nontransferred jets with emphasis on plasma spraying, surfacing, welding and cutting
[SBAC PAPER 18]
20 p3550 A69-37453

Corrosion and stress effects separation in stress corrosion of Al-Zn-Mg-Cu alloy, considering machined surface finishing role
21 p3747 A69-39435

Friction characteristics during diamond honing of different steel grades, determining lubricating and cooling liquids effect on friction coefficient
22 p3958 A69-41170

Outgassing rates of stainless steel and Al with different surface treatments, including glass bead shot blasting, electropolishing, baking and vacuum cleaning
22 p3958 A69-41215

Corrosion resistant bonding materials, discussing metal-to-metal adhesive primers, Al honeycomb core and foil finish
24 p4334 A69-43421

SURFACE GEOMETRY

Impulse and kinetic energy transfer in rarefied gases analyzed on basis of kinetic theory, considering surface curvature effect
01 p0173 A69-10093

Solid body surface roughness influence on radiative properties, deriving expressions relating radiative properties to surface roughness parameters
02 p0350 A69-11575

Calculation method for surface aircraft structures by treating normal forces and bending moments as unknown values
04 p0677 A69-14839

Ablation surface patterns and resulting roll torques and roll behavior of hypervelocity vehicles
[AIAA PAPER 69-180]
06 p1036 A69-18051

Finding and representing graphically intersections of double curvature surfaces with planes within scope of digital computer design
08 p1278 A69-19921

Free surface of electrically conducting liquid in gradually varied supercritical regime in horizontal rectangular channel
08 p1362 A69-20273

Static, kinematic and elastic basic equations of shell theory integrated into differential equation for minimal surface helical shells
10 p1793 A69-22886

Aspherical surfaces formation from spherical by removing part of substrate by means of tool mask for lapping nonuniform wear of surface
12 p2102 A69-26597

Maximum principle for infinitesimal deformations of convex surface with nonnegative Gaussian curvature, noting application to rotation and displacement diagrams

13 p2361 A69-27741

Object shapes automatically classified from reflected radio signals, considering correlation description of object effective dispersion surface diagram

14 p2411 A69-28917

Necked tension specimens profiles for rigid-plastic nonhardening materials determined from compatibility equation for displacements and unloading rate

15 p2704 A69-30292

Shock tube hot flow duration, contact surface configuration and boundary layer thickness

15 p2590 A69-30297

Geometric shape of lunar profile from annular phase of 20 May 1966 annular solar eclipse coronagraph plates, applying Fourier series and Pascal limaçon approximation

15 p2686 A69-30531

Dynamic characteristics of local slope winds, considering thermal and geometrical effects of underlying surfaces

15 p2648 A69-30577

Sloping helicoid median surface with given parameters, obtaining equilibrium equations, elasticity and formulas relating deformations to displacements

15 p2714 A69-31197

Optimum surface for thick delta wing in hypersonic flow obtained by variational method, assuming closed leading and trailing edges

16 p2731 A69-31559

Nonlinear free surface effects in low gravity tank draining, finding domains of validity for linearized and nonlinear analyses

[AIAA PAPER 69-680]

17 p2953 A69-33450

Hyperbolic EM microwave field used for contactless measurements of parabolic antenna surfaces

19 p3281 A69-35766

Wave equation of electromagnetic field of optical resonator with arbitrary mirrors, utilizing Schrodinger equation and equivalent mechanical system

19 p3333 A69-35880

Cylindrical concave surface quality control by contactless comparison with reference surface, using interferometer with Twyman system and continuous laser

19 p3311 A69-36196

Nose bluntness effect on hypersonic flow for slender blunt bodies with arbitrarily shaped lateral surfaces at small attack angle

19 p3239 A69-36402

Geometrical model for surface contact area, noting influence of nonlimitations on friction coefficient in elastic deformation

19 p3329 A69-36494

Lunar gravitational potential and lunar surface radius vector binomial series coefficients determination from Luna 10 data used for lunar surface shape calculations

20 p3596 A69-37308

Moire technique for gaging surface deformations or surface configuration differences by optical interference patterns

21 p3726 A69-39775

Double cellular surface geometry effect on dispersion and coupling impedance of two dimensional periodic resonator slow wave structure

23 p4140 A69-42048

Steady constant density two dimensional flow in laminar boundary layer over permeable curved surfaces, showing effects of suction or blowing

23 p4153 A69-42399

Contact stress distribution between two-dimensional finite nearly rectangular elastic bodies with general surface configurations for surface load expressed in trigonometric series

[ASME PAPER 69-APMW-9]

24 p4402 A69-43104

Chaplygin equation applied to eddy flow past semicylindrical surface, discussing stagnation points and boundary value problems

24 p4245 A69-43477

Monte Carlo calculation of free molecular flow over concave spherical surface, considering partial diffuse reflection and imperfect energy accommodation

24 p4248 A69-43592

Shear stress and free molecular drag for gas flow along concave cylindrical surface oriented at angle of attack, analyzing multiple surface collisions effect

24 p4249 A69-43660

SURFACE IONIZATION

Thermal metal-plasma thermodynamic equilibrium, using surface ionization of inner and outer potentials

and work function, discussing ion and electron extraction

06 p0979 A69-17249

Cesium plasma produced inside hot cylindrical tantalum cavity at 1400 K by contact ionization at wall while obtaining electrons from internal filament

06 p0927 A69-17707

Plasma sheath-boundary interactions, analyzing emission, reflection and surface ionization effects on current densities and heat fluxes for cesium and argon

08 p1369 A69-20818

Luminous discharge at nonabsorbing surface when exposed to single pulse ruby laser beam, suggesting photoionization in surface layer

08 p1327 A69-21021

Surface ion behavior on planar semiconductor devices determined by measuring effect of time, humidity, temperature, voltage and previous testing history

10 p1743 A69-23173

Sr and La ionization on crystal surfaces of W and polycrystalline W, discussing temperature effect on oxidation and work function

12 p2142 A69-26113

Field ionization at metal surfaces as rearrangement collision, considering anisotropic electron tunneling probabilities produced by Fermi surface

17 p3015 A69-32821

SURFACE LAYERS

NT MONOMOLECULAR FILMS

Recombination rate dependence on nonequilibrium charge carriers concentration at semiconducting surface

01 p0136 A69-10253

Absorption of linearly polarized light in reflecting surface layer of collisionless plasma, calculating layer lifetime for reflection of light

01 p0127 A69-10283

Sliding surface tracks from hardened steel sliders on flat PTFE examined for molecular orientation with electron microscope

01 p0085 A69-10369

Mercury radio emission phase dependence, discussing brightness temperature value approximation and surface layer properties

02 p0314 A69-11640

Surface layer effects on conductivity of vacuum deposited gold films, studying resistance variations with film thickness

02 p0300 A69-12625

Similarity theory results for turbulent diffusion in atmospheric surface layer compared with concentration measurements from Project Prairie Grass

02 p0276 A69-12695

Gettering effect in silicon of phosphosilicate glass surface layer and underlying phosphorus layer on gold and copper

03 p0487 A69-13640

Brittle surface films role in stress-corrosion phenomena in various environments

03 p0448 A69-13873

Stray fields and domain dynamics in Gunn effect semiconductors covered with dielectric sheets

03 p0491 A69-13988

Scattering from thin conducting sheet obstacle on cylindrical surface

03 p0399 A69-14253

Vacuum carburization of surface layers of transition metals

04 p0614 A69-14572

Cr-Si diffusion layers on Ti, noting results of roentgenographic and metallographic studies

04 p0614 A69-14578

Viscoelasticity effect on tensile stress in absorption layer for free surface uniaxial motion

04 p0676 A69-14705

Stationary vertical distribution of weightless radioactive substance in surface air layer, accepting two layer exponent law for vertical turbulent diffusion coefficient

04 p0593 A69-15091

Gray tone differences between undisturbed lunar surface and darker ejecta observed around Surveyor 1 footpads, discussing possible albedo differences

04 p0660 A69-15124

Surface photovoltaic effect in copper electroplated single crystal CdS solar cells, discussing Fermi level and Hall effect

05 p0704 A69-15958

Thermal potential P and Q smoothness on surfaces, proving relevant theorems

05 p0849 A69-16452

Gas adsorption on solids, discussing statistical mechanical theory assuming localized adsorption for

first adlayer and nonlocalized mobile layer adsorption on top

06 p0980 A69-17387

Oxide impurity effects causing potential shifts in Si covered by thick oxide layer studied with metal-oxide-Si electrical measurement and radiochemical analysis

07 p1072 A69-18272

Fine structure and geology of lunar surface from Luna, Ranger, Surveyor and Orbiter data

07 p1212 A69-18547

Field effect in Ge and Si, noting relation between dependence of space charge on surface level charge and on surface potential

07 p1199 A69-18682

Quantitative radar determinations of radio wave scattering cross section of lunar surface layer

07 p1087 A69-19621

Optical parameters for system of isotropic nonabsorbing film on isotropic absorbing substrate determined by ellipsometric method, noting Si optical constants

07 p1201 A69-19648

N type surface layer in p type sample noting effect on Hall constant and relationship to temperature

09 p1555 A69-21472

Air layer between target and instrument effect on earth surface temperature conducted with airborne radiometers

09 p1536 A69-22166

Recombination rate dependence on nonequilibrium charge carriers concentration at semiconducting surface

09 p1559 A69-22646

Lead sulfide single crystals and polycrystalline films growth studied by electron microscopy during vacuum deposition on NaCl and other substrates

10 p1743 A69-23002

Impurity heterogeneities in unoxidized and oxidized silicon slices from electron probe X ray microanalyzer, discussing thermal oxidation effects

10 p1743 A69-23171

Interfacial charges in MOS transistors determined as function of surface potential by measuring channel conductance as function of temperature

10 p1744 A69-23178

Chemical composition effect on glass fibers strength, discussing reasons for increased surface layer strength

10 p1717 A69-24045

Parallel flow of viscous liquid film with free surface down inclined plane, noting growth of initially infinitesimal amplitude waves and finite amplitude wave stability

11 p1869 A69-24891

Electrical conductivity of space charge surface layer in semiconductors with many-valley energy spectra of current carriers, discussing scalar relaxation time

11 p1937 A69-24915

Structure of epitaxial single crystal layers of CdS vacuum deposited on mica surface at various temperatures

11 p1939 A69-25709

Lunar surface layer structure by statistical analysis of data concerning craters and stones distribution as shown by lunar orbiter photographs

12 p2154 A69-25816

Etched surfaces inhomogeneity of n-type GaAs single crystals, noting oxide layers formation

12 p2142 A69-25980

Annealing effects on titanium oxidation kinetics, indicating no relation between oxide formation and diffusion anisotropy of oxygen

12 p2112 A69-26039

Fracture surfaces of thermally toughened glass plates using Cranz-Schardin spark camera, confirming internal front lead over front in surface layers

12 p2118 A69-26194

Lunar surface layer temperature field dynamics obtained from stable periodic solution to parabolic differential equation with nonlinear nonautonomous boundary conditions

12 p2157 A69-26281

Atmospheric turbulent energy spectra in boundary surface layer, considering homogeneous axisymmetric model in presence of temperature and velocity gradients

12 p2067 A69-26355

Radiophase mapping utilizing VLF radio signals to detect conductive sheets and surface impedance of earth

12 p2075 A69-26982

Optimal thickness of inhomogeneous absorption layer subjected to normally incident plane monochromatic wave treated as Mayer-Boltz variational problem

13 p2297 A69-27381

Hydrodynamics of large scale atmospheric circulation, analyzing interactions between different scales and between atmosphere and underlying surface

13 p2253 A69-27849

Corrections for atmosphere thickness needed for satellite measurements of underlying surface temperature

13 p2293 A69-27850

Physical limit model of fatigue in metals and alloys to determine stress producing plastic flow in surface layer

14 p2461 A69-28913

Turbulent heat exchange coefficient radiation absorption and diurnal vertical variations effects on temperature field in surface layer of sea and atmospheric boundary layer

14 p2472 A69-29462

Rigid obstacle unsteady motion in compressible fluid with load applied to surface layer, deriving numerical solution of pressure expansion

14 p2430 A69-29480

Vacuum carburization of surface layers of transition metals

15 p2638 A69-30273

Cr-Si diffusion layers on Ti, noting results of roentgenographic and metallographic studies

15 p2638 A69-30279

Normal modes stability analysis of fluid layer adjacent to flat plate submerged in liquid, considering effects of interfacial surface tension and buoyant forces [AIAA PAPER 69-386]

15 p2590 A69-30476

Turbulent heat and momentum fluxes spectra measured in atmospheric ground layer, describing changes as function of height and stratification conditions

15 p2649 A69-30648

N type surface layer in p type sample noting effect on Hall constant and relationship to temperature

15 p2669 A69-30717

Gas laser cutting of thin carbon films on thick pyrex glass and ceramic substrates

15 p2635 A69-31037

Metal oxide semiconductor structural model usefulness in understanding behavior near transition region, discussing surface inversion layer properties, surface mobility theory, etc

16 p2757 A69-31612

Temperature field in plate heated at one end and situated in solidifying gas, leading to gas layer formation by sublimation

16 p2878 A69-31957

UHF propagation in spherically stratified superrefractive troposphere with trapping surface layer, discussing distant field strength dependence on refractivity profile

16 p2752 A69-32388

Secondary electron emission from gas covered metal surfaces, discussing results of neutral beam investigations

17 p3008 A69-33000

Martian surface features and climate with emphasis on atmospheric surface layers, assessing Mariner 4 data

17 p3029 A69-33040

Surface layer role in strengthening of iron determined from examining temperature dependence of internal friction during thermomechanical treatments

17 p2991 A69-33939

Graphical representation of friction stresses produced on mechanical parts surface layers, using mathematical model based on Poisson ratio and friction coefficient

19 p3329 A69-36723

Static theory of fibrous surface media based on continuum mechanics, neighboring fibers noninteraction principle and additivity of mechanical properties

19 p3447 A69-36858

Aluminizing and operational effects on surface layer and core of first and second stage turbine blades

20 p3561 A69-37370

Soviet collection of papers on physics of atmospheric boundary layer covering wind profile, turbulent energy balance, etc

20 p3571 A69-37694

Wind velocity below 100 meters from Laikhtman atmospheric boundary layer model, solving equations for horizontally homogeneous, stationary and nonadvective air flow

20 p3571 A69-37695

Microstructure and X ray structure compared for two and three component chromide, titanide and silicide diffusion layers on Nb, discussing phase composition

20 p3563 A69-37820

Steady state vertical distribution of small ions in ground layer assuming atmospheric dynamic and thermal

sublayers, calculating air resistance and electric field potential

21 p3715 A69-38836

Oxygen pressure effect on oxide layer composition on W surface by secondary ion-ion emission

21 p3746 A69-39071

Matter surface distribution in general relativity, deriving matching conditions

22 p3982 A69-40753

Piezoelectric characteristics of surface layers of Ba titanate single crystals, using static and dynamic electromechanical methods

22 p3995 A69-41156

Ion sputtering method for making electrodes in thermionic energy converters, discussing alumina and W surface layers preparation

23 p4170 A69-42259

Surface films effect on friction coefficient of sodium chloride and Zn single crystals under normal pressure loads, noting film thickness role

23 p4170 A69-42343

Structural changes in subsurface layer and surface microgeometry factors of metal fatigue failure, explaining crack formation and propagation

24 p4395 A69-42559

Ellipsometric liquid immersion method for optical parameters determination of system with nonabsorbing surface film on absorbing substrate

24 p4316 A69-43321

SURFACE NAVIGATION

Navigational instruments developments during past fifty years emphasizing land, marine and air navigation aids

01 p0112 A69-10311

Ship navigation by altitude and azimuth measurements of artificial earth satellite, discussing position and reference errors and synchronous satellite advantages

[UN PAPER 68-95247] 01 p0112 A69-10461

Navigation Service Satellite System for aiding aircraft and ships at sea in Pacific Ocean, noting equipment and functions

[UN PAPER 68-95251] 01 p0112 A69-10470

Marine requirements possible satisfaction by using space techniques to improve long range communications to achieve safety at sea and shipping operations efficiency

01 p0161 A69-10503

Navy Navigation Satellite System TRANSIT providing all-weather continuous worldwide service for military and civil users

02 p0277 A69-11753

Maritime and aeronautical developments - Conference, Paris, April 1967

02 p0192 A69-11886

Navigation by satellite systems, discussing vehicle position determination and communications link for traffic control with comment on French space program

02 p0278 A69-11912

SPOT /Speed, Position and Track/ transoceanic traffic surveillance and navigation system for aircraft and marine users

03 p0463 A69-13234

Meteorological satellites data for safe navigation of ships, discussing techniques to overcome difficulties in interpreting ice and cloud photographs

[UN PAPER 68-95776] 06 p0916 A69-17028

Shipboard direction finder calibration accuracy, emphasizing radio operator training

06 p0897 A69-17533

Marine and aircraft satellite navigation techniques, discussing equipment requirements, related performance characteristics and limitations

08 p1349 A69-21198

Navy Navigational Satellite System for position location accuracy in marine and oceanographic exploration applications

[AIAA PAPER 68-471] 13 p2295 A69-27247

Hyperbolic marine and air navigation including TACAN, pulse modulation, rotating hyperbolic fields, sector beacons and all-weather landing aids

13 p2296 A69-27334

Space vehicles and marine navigation using navigation satellites, radar, Doppler navigation, etc

13 p2296 A69-27918

Simultaneous observations of altitudes of stars and moon for determination of longitude without time by navigators

14 p2479 A69-29855

Navy Navigation Satellite System /NAVSAT/ applications, considering nonmilitary marine and air all-weather navigation and positioning

14 p2479 A69-29856

Accuracy improvement of method of averages applied to equations of small motions and disturbances on two rotor gyrocompass on ship performing circular maneuvers

18 p3139 A69-35378

Correlation role in navigation satellite analysis noting reduction in ephemeris error effects [AAS PAPER 68-145]

21 p3761 A69-39222

Worldwide communication system via synchronous satellites for aeronautical, maritime and land mobile services

23 p4114 A69-41355

Surface and aerospace navigation by VLF radio network, discussing Omega transmitting station location operational modes and daytime-nighttime accuracies [AAS PAPER 69-405]

24 p4347 A69-42834

SURFACE PRESSURE

U PRESSURE

SURFACE PROPERTIES

NT ADHESION

NT COEFFICIENT OF FRICTION

NT INTERFACIAL TENSION

NT SKIN TEMPERATURE [NON-BIOLOGICAL]

NT SPECTRAL REFLECTANCE

NT WALL TEMPERATURE

Dielectric surface coatings effect on transmission and loss properties of silicon-microstrip microwave transmission lines

01 p0041 A69-10201

Electrical properties of gold-gallium arsenide n-type junctions investigated for influence of crystallographic orientation of surface and charge carrier density

01 p0138 A69-10432

Chemical vapor deposition of beryllium metal coatings noting thickness, purity and processing effects on surface properties

01 p0097 A69-10644

Sulfide addition agents for diester lubricating grease and organic resin solid film lubricants, noting formulation and tests for steel and molybdenum

01 p0102 A69-10907

Specific effective scattering area on lunar surface using Luna 13 signals from Oceanus Procellarum measured with radar employing antenna with narrow radiation pattern

01 p0158 A69-11312

Radiant heat transfer prediction methods checked for validity and accuracy by irradiation measurements with materials of various surface properties [ASME PAPER 68-HT-42]

02 p0351 A69-12206

Free surface motion and stress measuring instrumentation, describing plate impact one dimensional strain configuration for determining mechanical properties under stress wave propagation

02 p0344 A69-12290

Structure of /111/ single crystal Si surface after chemical-mechanical polishing and ultrahigh vacuum annealing, noting presence of Fe impurity

02 p0301 A69-12660

Rhenium-niobium cylindrical thermionic converters with mechanically polished or electroetched emitters, comparing performance

03 p0368 A69-13126

Martian surface properties, discussing limonites prevalence and dust layer evidence as causes for reddish color

03 p0509 A69-13357

Penetration type soil analyzer used by Luna 13 automatic lunar station for mechanical strength of lunar surface

03 p0430 A69-13424

Alloy elements effect on spreading of liquid titanium and zirconium alloys on graphite

03 p0446 A69-13573

Electromagnetic wave diffraction at uniformly expanding sphere solved by Kirchhoff method

03 p0397 A69-13719

Electrochemical oxidation of fuels in liquid ammonia, evaluating electrode surfaces as catalysts [ECS PAPER 212]

03 p0382 A69-13857

Physical and mechanical properties of surfaces and interfaces - Conference, Raquette Lake, New York, August 1967

03 p0448 A69-13867

Surface effects on metals mechanical properties, discussing dislocation dynamics and resulting effects on macroscopic plastic behavior

03 p0448 A69-13869

Surfaces role in superplasticity, demonstrating rate of neck growth dependence on surface irregularities

03 p0449 A69-13879

Chemical treatment effects on mechanical properties of titanium alloy tubes

03 p0434 A69-13914

Lunar magnetic moment and surface field, discussing Explorer 35 field measurements

03 p0514 A69-14005

Electromagnetic theory of surface radiation properties, analyzing specular reflectance of optically smooth surfaces

04 p0684 A69-14357

Oxygen surface densities measured by method based on characteristic X ray production by 100 kev protons

04 p0631 A69-14446

Lunar transient luminous events and eclipse anomalies, proposing solid surface and gas luminescence as explanation

04 p0653 A69-14615

Quasi-specular bistatic radar measurements of oblique scattering properties of lunar surface using telemetry carrier from Explorer 35 as lunar orbiting radar beacon

04 p0655 A69-14657

N-type Si surface photopotential, conductivity and capacitance during anodic oxidation in absolute ethylene glycol

04 p0643 A69-15260

Carburization structure on surface of Mo and Nb castings cast in graphite molds showing changes in plastic properties of metals

04 p0619 A69-15391

Plane shear strain measurement by means of properly oriented strain gages on surface and proper disposition of gages in Wheatstone bridge circuit

04 p0603 A69-15498

Dynamic compatibility conditions for shock wave collision with material discontinuity surface and for superposing two shock waves propagating in opposite directions

05 p0745 A69-15867

Peripheral surface damage effects on epitaxial GaAs bulk diodes breakdown characteristics, noting measurements on mechanically and chemically prepared elements

05 p0733 A69-16561

Polycarbonate surface stiffness increase associated with fatigue induced by repetition of loads

06 p0946 A69-17206

IR radiative heat transfer in nongray gases for non-black bounding surfaces, considering diatomic gases with single vibration rotation band

06 p1033 A69-17559

Titanium surface impurities effect on porosity in welds, proposing machining immediately before welding as solution

06 p0945 A69-17894

Ablation surface patterns and resulting roll torques and roll behavior of hypervelocity vehicles [AIAA PAPER 69-180]

06 p1036 A69-18051

Thermochemical and mechanical ablation mechanisms for Apollo heat shield material, comparing surface thermochemistry computer program and arc plasma tunnel data

06 p1038 A69-18149

Cross hatching on various body surfaces due to periodic surface pressure fluctuations, discussing origin from counterrotating longitudinal vortices in boundary layer

06 p0915 A69-18213

Semiconductor current carriers surface recombination rates determined from photomagnetic effect

07 p1198 A69-18505

Field effect in p-type gallium arsenide single crystals as characteristic of surface electron energy state spectrum

07 p1199 A69-18686

Radiation emission factors determination of polished metallic surfaces

07 p1242 A69-18952

Metal bath surface conditions for floating aluminum trioxide inclusions in pure iron and carbon steels

07 p1167 A69-19342

Surface environment effects on mode of microcrack formation during fatigue of Al single crystals, noting surface void formation mechanism

07 p1235 A69-19387

Free surface strain increment components on high carbon steel compression specimens to estimate tensile plastic instability onset, noting ductile fracture criterion

08 p1328 A69-19891

Small amplitude surface irregularities effect on backscattering properties of radar calibration metal sphere, using full wave boundary perturbation method

08 p1273 A69-20027

Nb-Zr-Cr alloys solidus surface and isothermal sections, using optical pyrometry, microstructural and X ray analyses

08 p1333 A69-20440

Silicon carbide fiber surfaces nature and interaction with coupling agents, epoxy and resin components, noting chemical and electron microprobe analysis

08 p1341 A69-20515

Surface structures determination by energy analysis and low energy electron diffraction of scattered electron

09 p1554 A69-21340

Albedo over Antarctic, measuring solar radiation reflected by surface and atmosphere by Eppley radiometer

09 p1484 A69-21404

Electron irradiation effect on surface potential of thermally grown silicon dioxide layers, noting conductivity and annealing effects

09 p1557 A69-21743

Surface characterization on chemical vapor deposited tungsten, evaluating grain size effect

09 p1558 A69-21810

Partial pole figures in vapor deposited and wrought cylindrical tungsten specimens, noting random surface produced by orientation

09 p1558 A69-21811

Face effect in p- and n-type gallium antimonide single crystals doped with zinc and tellurium

09 p1558 A69-21870

Pure ammonium perchlorate single crystal self deflagration, determining energy transfer mechanisms from pressure effects, combustion characteristics and subsurface profile

[AIAA PAPER 69-142]

09 p1560 A69-21900

Incompressible fluid nonlinear oscillations in rectangular basin analyzed by Green function for mixed problem, calculating velocity potential and free surface approximations

09 p1483 A69-22711

Elastic Cosserat plate and shell theory, considering constitutive equations imitating transversely isotropic material and elastic deformations

10 p1798 A69-23147

Shallow impurity states in semiconductors, calculating bulk and surface energy eigenvalues in Si and Ge

10 p1745 A69-23361

Surface density of carbon foils measured accurately by determining trapped carbon dioxide pressure after burning in pure oxygen

10 p1746 A69-23663

Surface atomic structure effects on polar faces in InSb semiconductor crystal established from measurements of contact potential difference by dynamic capacitor

10 p1747 A69-23965

Aluminum bonded structures corrosion resistance through adhesive primers and surface treatments

10 p1700 A69-24088

Modified Diggelen photometric method in lunar topography, analyzing surface brightness and inclinations in mare regions and Korolev thalassoid

11 p1959 A69-24724

Dislocation structure and surface deformation markings correlation analyzed on fatigued Al electron microscope foils

11 p1905 A69-25184

Static pressure measurements at surface of sharp plate in supersonic flow during gas/liquid jet injection

11 p1821 A69-25479

Etched surfaces inhomogeneity of n-type GaAs single crystals, noting oxide layers formation

12 p2142 A69-25980

Heat treatment effects on molybdenum-rhenium alloy field emission and surface structure in alpha and sigma phase regions

12 p2113 A69-26041

Limits for Martian surface materials established by comparing visible and IR spectra with laboratory spectra

12 p2156 A69-26225

Ruby crystal optical homogeneity and relation to main laser emission characteristics, discussing optical and structural surface properties

[IEEE PAPER U-7]

12 p2106 A69-26322

Surface dissipation effect induced by end electrodes on drift instabilities in cold ion plasma column described by differential equation with constant coefficient

12 p2138 A69-26710

Rarefied plasma potential fluctuations when bounded by surface having complex conductivity and dispersing properties

12 p2139 A69-26712

Microscopic mechanisms in fracture surface markings, using electron fractography cleavage, fatigue, stress corrosion cracking, microvoid coalescence and tear ridge formation

13 p2274 A69-27224

Germanium surface IR radiation absorption in vacuum at low temperatures, obtaining modulated interval reflection spectra

13 p2317 A69-27879

Radiative heat transfer, discussing electromagnetic theory, transfer between surfaces and simultaneous conduction, convection and radiation

13 p2376 A69-28140

Spacecraft surfaces bidirectional reflectance flux distribution applications to space thermal control computations

[AIAA PAPER 68-26]

13 p2222 A69-28216

Electronegativity and work function relationship from thermodynamic and quantum mechanics standpoint, describing electrons structure by spin orbitals localized around lattice sites

14 p2505 A69-29263

Thermionic converters semiconducting collector surfaces, evaluating work functions of nickel-chromium steel and aluminum trioxide collectors

14 p2506 A69-29269

Image formation with arbitrary holographic surfaces achieved by reversing direction of propagation of diverging wave

14 p2450 A69-29582

Surface brightness distribution in comet Arend-Roland tall from diffusion model and photometric investigation of photographs obtained by 40-cm astrograph

15 p2684 A69-30519

Planar bipolar transistors degradation under thermal and ionizing radiation stresses, analyzing surface recombination currents of silica films and silica-silicon interfaces

15 p2625 A69-30826

Hydrogen laser operation time reduction attributed to hydrocarbon formation on inner surface of storage flask, promoting atomic hydrogen recombination

15 p2634 A69-30942

Flight instrument package for change of energy absorption and energy radiation of vehicle surfaces during various phases of space vehicle mission

15 p2613 A69-31269

Martian bright surface areas identified as homogeneous powder having opaque grains, discussing hydrated iron oxides contributions to observed optical properties

16 p2855 A69-31660

Semiconductor impressed voltage preconditioning, considering problems involving surface properties

16 p2758 A69-31713

Laminar-turbulent transition in boundary layer on thermally decomposing surface, discussing gasification rate, Reynolds number effects, heat transfer and turbulence onset mechanism

16 p2878 A69-31951

Steady deflagration of homogeneous monopropellant in condensed phase, considering nonequilibrium surface condition for mass decomposition rate

[WSCI PAPER 69-6]

16 p2830 A69-32347

Surface state density determination as function of surface potential in MIS capacitors, discussing MIS capacitance method theory and computer programs

16 p2827 A69-32556

Luminous particles volumetric concentration calculation based on limiting surface density to determine bulk density in cometary head

17 p3032 A69-33189

Apparent thermal radiation properties for one dimensionally rough surface, discussing variance with property models employed in engineering analysis of radiant transfer

[AIAA PAPER 69-622]

17 p3071 A69-33271

Thin surface films effect on radiative properties of metal surfaces determined by thin film optics, noting dependence on refractive index

[AIAA PAPER 69-623]

17 p3072 A69-33283

Spectral reflectivity differences/color differences/on lunar surface in visible region, indicating compositional difference origins

17 p3037 A69-33653

Lunar conditions differing from simulations in laboratories, examining surface, physicochemical properties and friction

18 p3113 A69-34241

Fluid velocities at earth core surface inferred from magnetic data, considering velocity constraints and diffusion contributions to secular change

18 p3129 A69-34951

Carburization structure on surface of Mo and Nb castings cast in graphite molds showing changes in plastic properties of metals

18 p3156 A69-35019

Machining processes effect on surface integrity of machine parts and effects on product quality

18 p3149 A69-35129

Anomalous phenomenon in resistance and magnetoresistance of cleaved InAs surface, plotting temperature and magnetic field variation effects, proposing explanation of anomaly

19 p3388 A69-36543

Surface tension of simple liquids consisting of interacting spherical particles, considering density variation in liquid-vapor phase transition zone

19 p3452 A69-36725

Heat and mass transfer on vertical surface under combined free and forced convection, solving laminar boundary layer equations by stream function

19 p3453 A69-36844

Cultured mammalian cell growth morphology studied in situ with scanning electron microscope, discussing surface morphology changes during mitotic cycle of Chang liver cells

20 p3467 A69-37100

Surface pressure, skin friction and heat transfer measurements on sharp flat plates and wedges in low density hypersonic flow, noting slip velocity

20 p3458 A69-37186

Rarefied molecular gas flow past permeable surface, determining reflection law and flow parameters

20 p3459 A69-37438

Collector efficiency limitation of surface barrier-limited photoconductors attributed to photogenerated carrier diffusion into electrode

20 p3583 A69-37732

Lunar surface scattering properties at 2.5 cm wavelength determined using computerized backscattering diagram and equations for obtaining scattering data

20 p3606 A69-37971

Boundary layer flow past permeable surface, generalizing integral equations for case with suction

21 p3691 A69-38573

Depth dependent variations in texture in Nb due to inhomogeneous plastic deformation during cold rolling

21 p3744 A69-38737

Laser radiation increased absorption in opaque solid body attributed to vaporization, analyzing factors determining thermodynamic equilibrium between condensed and gaseous phases

21 p3736 A69-38962

Electromechanical effect dependence on CdS semiconductor surface state, noting relationship between microhardness and discharge current

21 p3781 A69-39072

Absorption constant and reflectivity coefficient on semiconductor samples with nonideally prepared surfaces, calculating measurement errors

21 p3782 A69-39240

Stress concentrations in metals determined through surface properties measurements, correlating local electrochemical potentials and metal-metal oxide junction parameters

21 p3747 A69-39326

X ray diffraction as nondestructive technique for measuring residual surface stress

21 p3845 A69-39476

Radar reflection techniques for planetary surface studies, considering surface properties effects on reflectivity and reflected wave characteristics, instrumentation and data for moon and planets

21 p3811 A69-39509

Focal plane observation of granulation phenomena on scattering surface illuminated by coherent light from gas laser

21 p3741 A69-39575

Holographic interferometry for surface strain and vibrations visualization, describing photographic recording techniques

22 p3945 A69-40244

Hoba meteorite surface radioactive isotope composition measured, finding terrestrial age from Ni-59 activity

22 p4021 A69-40411

Supercavitating flow past thin hydrofoils, determining flow velocity or acceleration potential near free surface

22 p3933 A69-41023

Heat transfer and surface thermal conduction characteristics of contact of two solid bodies, discussing pressure effect, measurement and analytical techniques

23 p4237 A69-41327

Silicate glass impurity droplet formations on alumina single crystals polished surfaces analyzed by electron microprobe as function of high temperature

23 p4176 A69-41597

Holographic interferometry for measuring small static displacements of diffusely reflecting surfaces

23 p4167 A69-42185

Free convection from vertical surface using perturbation method

24 p4407 A69-42916

Lunar surface material mechanical properties from Surveyor observations, analyzing grain size, rock density, internal friction, cohesion and bulk density compared to Luna observations

24 p4383 A69-42962

Instantaneous response TV system application to observing solar surface granulation, noting advantages over photometric measurements

24 p4389 A69-43711

SURFACE REACTIONS

Spatial and kinetic distributions of molecules reflected by surface in rarefied atmosphere, discussing mathematical model

01 p0122 A69-10041

Kinetics of vaporization of metals with surface subjected to incident radiation flux noting pulse duration

02 p0350 A69-11577

Electron paramagnetic resonance study of interaction between adsorbed nitric oxide and NaY and deca-terized Y zeolites surfaces, considering catalytic activity

02 p0205 A69-11900

Asymptotic laminar boundary layer in compressible gas in presence of normal and tangential velocity components at body surface

02 p0231 A69-12138

Aged boric acid coated silica reaction vessels, showing reduced surface effects and high reproducibility in oxidation reactions

02 p0205 A69-12322

Surface and interface phenomena in engineering technology, determining mechanical or electronic properties

03 p0434 A69-13868

Surface effects on mechanical properties of crystalline and vitreous materials, considering environmental effects on dislocation mobility

03 p0454 A69-13870

EPR investigation of free radicals formed during mechanical fracture and gamma irradiation, discussing recombination rate and reaction rate with oxygen

03 p0434 A69-13871

Metal surface degradation by constant density laser radiation, computing screening effect

03 p0442 A69-14221

Interaction of rarefied gas with solid surface, analyzing accommodation coefficients, energy and impulse exchange as function of atomic bulk size

04 p0632 A69-14991

Interaction of gas atoms with solid surface, giving mathematical model assumptions

04 p0632 A69-15008

Gas accretion on neutron star surface as energy source for X ray radiation

05 p0814 A69-15847

Lunar surface gas adsorption mechanism for lunar atmosphere absence

05 p0824 A69-16062

Prediction technique for surface effect causing Si bipolar transistors gain degradation under ionizing radiation

06 p0976 A69-16879

Surface roughness influence on interaction between gas flow and solid surface for case of diffuse and specular reflection, noting role of inclination angle

06 p0910 A69-17342

Drift field photovoltaic cell performance with bulk and surface recombinations

06 p0870 A69-17473

Mechanism for laser surface damage of glasses working through optical absorption, fluorescence, chemical reaction by quenching and breakdown

06 p0935 A69-17771

Photographic study of burning metalized composite propellant under acceleration, noting burning rate augmentation by heat transfer from alumina particles retained on propellant surface [AIAA PAPER 69-173]

06 p0983 A69-18151

Asymptotic wave equation application conditions in describing field behavior near caustic surface, using Airy functions

07 p1076 A69-18520

Field effect in Ge and Si, noting relation between dependence of space charge on surface level charge and on surface potential

07 p1199 A69-18682

Surface recombination rate and retardation field effects on diffusion current in mesa diodes with low level injection

07 p1105 A69-19008

Surface plasmon excitation by tunneling electrons in GaAs-Pb junctions, discussing conductance at bias voltages, plasmon energy and concentration

07 p1200 A69-19402

Surface effects at interface between linear and nonlinear media representing transmission lines of low pass filter type

07 p1088 A69-19752

Dielectric surface loading on GaAs for suppressing traveling high field domain mode oscillations

08 p1371 A69-19913

Gas adsorption of molecular oxygen and hydrogen on molybdenum surface using collector section of field emission retarding potential analyzer

08 p1268 A69-20171

Propagation modes in corrugated cylindrical waveguides determined by imposing nonisotropic surface reactance boundary condition at corrugated walls

08 p1284 A69-20259

Propellant condensation on surfaces near electric rocket exhaust, calculating particle arrival rates, backflow and desorption energies [AIAA PAPER 69-270]

09 p1565 A69-21252

Liquid surface active media /kerosene, water, castor oil/ effect on strength of V notched polymethylmethacrylate specimens

09 p1528 A69-21852

Face effect in p- and n-type gallium antimonide single crystals doped with zinc and tellurium

09 p1558 A69-21870

Oxygen depletion effect in chemical reactions between pyrolysis gases and air stream on surface recession of charring ablators [AIAA PAPER 68-302]

09 p1622 A69-21982

Static characteristics of transistors dependence on current carriers surface recombination in inactive base region, noting strong electric field influence

09 p1464 A69-22287

Surface recombination efficiencies on metals measured as function of exposure time in steady Oseen flows, providing step-function increase in oxygen atom concentration

10 p1726 A69-23526

Laminar flow stream containing periodic fluctuation of mass fraction of chemical species over flat plate with reactive surface

11 p1831 A69-24284

Surface-active additives effect on crystallization kinetics of sil type glasses, discussing surface tension

11 p1907 A69-25032

Uranyl ions interaction with phospholipid and cholesterol monolayers, using surface pressure and potential measurements

11 p1832 A69-25641

Electrolytic hydrogen evolution reaction on Al covered by thin oxide in aqueous buffered acetate solutions

11 p1832 A69-25674

Reflection of moving rarefied AR plasma from surface of nickel cylinder inserted into gas discharge tube

11 p1934 A69-25710

Fatigue strength reduction in Ti alloy in sliding friction contact with metallic materials caused by fretting corrosion

12 p2113 A69-26125

Modes and mechanisms of wear covering adhesive, abrasive and corrosive wear, surface fatigue and fretting corrosion

13 p2265 A69-27231

Alloying effect on surface oxides determined from photoelectric polarization measurements for Ti-Nb and Ti-Ni

13 p2275 A69-27292

Electronic structure of clean metallic interfaces, considering electron, ion and surface interactions for metal-vacuum interface

13 p2321 A69-28008

Nondrifting n-p-n semiconductor current gain dependence on surface recombination rate

13 p2236 A69-28547

Electron work function profile determined for polycrystalline Mo and W single crystals with and without Cs vapors by emission microscope and photomultiplier

14 p2507 A69-29276

Lunar surface gas adsorption mechanism for lunar atmosphere absence

15 p2680 A69-30261

Stellar magnetic field generation by convective motions of surface layers of slowly rotating stars

15 p2688 A69-30559

Rayleigh assumption validity for wave scattering by analytic periodic surface predicated on solutions

analytic continuation across boundary, discussing Green function role
15 p2652 A69-30673

Interface friction and adhesion of alloys workpieces and die materials under pressure and temperatures typical of plastic deformation
15 p2629 A69-30902

Microslip between concentrated contacts and design charts for maximum pressure, closing-in of contacting bodies and optimized shapes, giving computer programs
15 p2629 A69-30903

Reacting gas ignition by sudden contact with heated noncatalytic surface, deriving heating time and transferred heat amount by Blasius perturbation method
16 p2878 A69-31955

Kinetic theory and gas-surface interactions for upper atmospheric density measurements by mass spectrometers, pressure gages and satellite drag, detailing adsorption effect
16 p2776 A69-32089

Rocket exhaust plume flow fields studied for vehicle effects taking into account nozzle boundary layer, coalescence shock and nonisotropic flow [AIAA PAPER 69-569]
16 p2842 A69-32696

Dielectric overcoating effects on electromigration Al interconnections, showing dependence on thickness and surface passivation
17 p2935 A69-32889

Surface chemistry of plastics reinforced with strong fibers, stressing need for investigating coupling films, catalysts and metallic ions role in coupling compounds chemisorption
17 p2992 A69-33655

Quartz fiber adhesion to Re measured in LEED flow energy electron diffraction/ apparatus for clean and O layer surfaces, noting brittle fracture
18 p3156 A69-35182

Surface alloying of high melting point metals in Al melts, noting prior oxidation enhancement and simplifying of coloring techniques
19 p3328 A69-36158

High energy neutral molecule beam for gas-surface interaction studies generated in electron bombardment ion source
19 p3376 A69-36176

Low and moderate energy gas molecule-solid surface interactions, using molecular beams
19 p3376 A69-36177

Reactive scattering from solid surfaces, discussing atom beam reaction of O with heated Ge and Si single crystals
19 p3377 A69-36178

Wall boundary condition model modification applied to molecular beam-solid surface scattering, noting qualitative agreement with observed distributions
19 p3377 A69-36179

Gas molecules scattering by solid surface for monoenergetic and Maxwellian beams, discussing model with different values for magnitude and velocity direction
19 p3377 A69-36181

Satellite-borne experiments of neutral molecular beam-solid surface interactions, describing Molsink chamber, densitometer, sphere and paddlewheel satellites
19 p3377 A69-36182

Gas-surface energy transfer experiment on OGO-F satellite, measuring upper atmosphere kinetic energy flux to determine accommodation and drag coefficients, density, etc
19 p3255 A69-36680

Low pressure ethylene decomposition on high temperature W ribbon surface
19 p3265 A69-36729

Low pressure ethylene decomposition on high temperature Re ribbon surface
19 p3266 A69-36730

Oxygen influence on low pressure ethylene decomposition on high temperature tungsten and Re ribbons surface
19 p3266 A69-36732

Interface electron transport phenomena in stress corrosion, expressing defect movements in terms of electron energy dynamics
19 p3349 A69-36889

Reactivity of hydrogen with surface of Ti-Al-V alloy under fatigue cycling at ambient and cryogenic temperatures
20 p3557 A69-36960

Oxygen environment influence on Inconel X-750 surface deformation and cracking during fatigue related to chemisorption and oxidation
20 p3558 A69-36966

Turbulent boundary layer of injection gas flow calculated past surfaces with pressure gradient
20 p3513 A69-37091

Turbulent skin friction coefficients of compliant surfaces on flat plates determined as function of speed for different materials
21 p3695 A69-39039

Thermal stresses and displacements in long isotropic hollow cylinder heated on part of outer curved surface, analyzing temperature distribution
21 p3838 A69-39166

Dispersion relations for surface plasma oscillations in normal metals for single and multiple films taking into account retardation effects, noting dielectric function
22 p3992 A69-40419

Unsteady aerodynamic heating at stagnation region including surface combustion in arc heated high enthalpy wind tunnel
22 p3860 A69-40597

Germanium single crystals etching with water vapor and hydrogen sulfide in hydrogen flow system, studying concentration, pressure and temperature effects on surface reactions
22 p3970 A69-40737

Diamond shaped surface ablation patterns development mechanism for several ablation materials of ground test and recovered flight vehicles [AIAA PAPER 68-671]
23 p4059 A69-41891

Surface chemistry effect on physical properties of pressure sintered Be metal, suggesting surface alloying approach by powder metallurgical techniques
24 p4332 A69-42963

Intense heat exchange narrow zones on blunted semicone surfaces in hypersonic gas flows ascribed to large Reynolds numbers
24 p4246 A69-43494

SURFACE ROUGHNESS

On-axis gain of parabolic reflector antennas with rough reflecting surfaces as function of surface deviation, correlation distance, area and wavelength
01 p0041 A69-10246

Radiation models using discrete radiator ensembles having applications to analysis of forward and backscatter from rough surfaces, clutter and chaff models, etc
01 p0030 A69-10556

Turbulence characteristics up to 150 m above ground, noting surface roughness length directional dependence, longitudinal turbulence spectra and turbulent energy budget
01 p0110 A69-10695

Static pressure field induced by steady subsonic flow of compressible inviscid fluid through two dimensional duct with statistically distributed wall roughness
01 p0062 A69-11279

Roughness effect on microwave emissivity according to geometric optics with application to moon and Venus
02 p0207 A69-12017

Nucleate pool boiling heat transfer of liquid nitrogen from circular disks with different surface conditions including copper and nickel mirror finishes, roughness and coatings
02 p0352 A69-12207

Plane electromagnetic wave scattering from slightly rough surface tilted away from reference plane, noting polarization effects
03 p0395 A69-13625

Randomly rough surface physical and geometrical remote determination by polychromatic bistatic radar
05 p0721 A69-16572

Energy spectra and angular dependence characteristics of electromagnetic wave scattered on statistically uneven surface studied by vector form of Kirchhoff integral
09 p1459 A69-22635

Polarization effects of scattered coherent light on laser imagery, determining surface roughness and angle of incidence effects photographically on basis of Fung theory
11 p1896 A69-24849

Optical data processing techniques and phase contrast method variations for statistics of surface roughness
12 p2079 A69-25910

Natural unbroken tektite surface examination by interferometry, discussing fringe patterns for pit shapes and sizes
12 p2173 A69-27175

LF spectrum analysis of hydrodynamic flow near-wall pressure pulsations over rough surfaced wall
13 p2246 A69-27537

Radar backscatter analysis for Arctic ice identification, deriving ice surface roughness factors from Kirchhoff-Huygens principle
14 p2416 A69-29530

Coherence-polarization in remote sensing by microwave and laser means, analyzing scattering functions of rough surfaces
14 p2448 A69-29532

Load support and leakage from microasperity lubricated face seals, developing hydrodynamic lubricant films [ASLE FICFS PREPRINT 21]
15 p2622 A69-30500

Monograph on Prandtl number effect on heat transfer and pressure loss in artificially roughened channels
15 p2717 A69-30934

Laminar boundary layer control on two dimensional body by combined blowing and suction in presence of roughness, noting skin friction reduction [AIAA PAPER 68-641]
17 p2957 A69-34015

Rough wall turbulent boundary layer development in pipe flow determined for different roughness geometries in zero and adverse pressure gradients
18 p3125 A69-35387

LF spectrum analysis of hydrodynamic flow near-wall pressure pulsations over rough surfaced wall
20 p3518 A69-38203

SURFACE ROUGHNESS EFFECTS

Regular and noise signal scattering by uneven surface determined by correlation functions, assuming monochromatic components scattering obeys Kirchhoff approximation
01 p0032 A69-10886

Radial face seals lubricating mechanism noting surface waviness effect on film thickness fluctuations
01 p0087 A69-10910

Terrain influence in ground wave propagation evaluated by two dimensional diffraction and scattering problems, using Airy type wave functions [AFCL-68-0212]
01 p0033 A69-10970

Runway roughness effects on aircraft, formulating relationship between weight and resonant frequency through simple harmonic motion analogy
01 p0057 A69-11274

Heat transfer dependence on direction of heat flow in stainless steel/aluminum interfaces, showing surface roughness and flatness influence
01 p0177 A69-11406

Thermodynamics in homogeneous steady state fog over rough terrain representing absolutely absorbing surface
02 p0274 A69-11442

Solid body surface roughness influence on radiative properties, deriving expressions relating radiative properties to surface roughness parameters
02 p0350 A69-11575

Terrain roughness effect on ionospheric radio wave absorption measurement data compared with theoretical results
02 p0207 A69-11669

Surface structure effect on flux penetration and AC losses in superconductive niobium
02 p0298 A69-12031

Surfaces role in superplasticity, demonstrating rate of neck growth dependence on surface irregularities
03 p0449 A69-13879

Surface smoothness of laser beam holes, discussing possible damage and technology recommendations
04 p0606 A69-14607

Scattering of electromagnetic waves from rough surface moving with uniform velocity
04 p0560 A69-15213

Emissivity of rough metallic surfaces with preserved profile similarity, showing independence to roughness height
05 p0845 A69-15894

Real liquid turbulent flow of two parallel eddy streams between two parallel walls with given periodic roughness
05 p0747 A69-16034

Directly backscattered light /echoes/ from dielectric plane surface with roughness and volume scattering, comparing indicatrices with moon echo
06 p0887 A69-17173

Surface roughness influence on interaction between gas flow and solid surface for case of diffuse and specular reflection, noting role of inclination angle
06 p0910 A69-17342

Elastic contact between two parallel cylinders with rough surfaces noting contact area, spots and stress distribution
06 p1023 A69-17373

Model for spectral bidirectional reflectance of rough surface producing good agreement with experimental data
[AIAA PAPER 69-64] 06 p0959 A69-18125

Diffuse reflection of electromagnetic waves by rough random surface using probabilistic method and statistical distributions 07 p1075 A69-18280

Stationary viscous incompressible fluid flow past rough surface, noting solution stability and friction stress determination for given pressure gradient 07 p1119 A69-18751

Sliding friction technique to determine contact area and surface microtopography between abraded metals and polymers 08 p1319 A69-19994

Wind velocity and shear stress profiles above surface with changed roughness, using mixing length theory 08 p1346 A69-20311

CW helium-neon laser used to detect and measure vibration frequencies of uniform diffuse surfaces 09 p1515 A69-21430

Correlation produced magnetoplasma mode in potassium confirmed by measurement of real part of surface impedance 10 p1728 A69-23168

Surface radio wave scattering propagating along rough surfaces, measuring emission during transformation into space waves 10 p1658 A69-23952

Turbulent boundary layer in lower atmosphere downwind of abrupt change of surface roughness, determining surface shear stress and roughness height 12 p2125 A69-26014

Regular and noise signal scattering by uneven surface determined by correlation functions, assuming monochromatic components scattering obeying Kirchhoff approximation 12 p2031 A69-26650

Tolerable surface roughness for transition stability in incompressible laminar boundary layer, including analysis of two and three dimensional roughness shape effects 12 p2063 A69-26774

IR spectroscopic observations of moon to interpret molecular vibration spectra in terms of molecular composition, discussing rock surface roughness effects 13 p2341 A69-27582

Roughness effects on boundary layer transition up to Mach 16 in hotshot wind tunnel
[AIAA PAPER 68-377] 13 p2242 A69-28213

Terrain roughness effect on ionospheric radio wave absorption measurement data compared with theoretical results 13 p2224 A69-28700

Light diffusive reflection from rough surface measured as function of angle of incidence in presence of specular component by goniospectrophotometer 14 p2485 A69-29171

Doppler echo from random rough surface, discussing average power return, frequencies, amplitudes, antenna beamwidth and radar data correlation 14 p2413 A69-29488

Laminar boundary layer control by combined blowing and suction, analyzing surface roughness influence concerned with underwater vehicle skin friction reduction
[AIAA PAPER 69-387] 15 p2591 A69-30477

Eccentric face seal with tangentially varying film thickness, analyzing leakage flow proportional to eccentricity and surface waviness
[ASLE FICFS PREPRINT 15B] 15 p2620 A69-30484

Rayleigh assumption validity for wave scattering by analytic periodic surface predicated on solutions analytic continuation across boundary, discussing Green function role 15 p2652 A69-30673

Combined distribution density of elevations and slopes for illuminated areas of stable statistically homogeneous random surface exposed to parallel rays beam 15 p2569 A69-30948

Flow over uniformly rough surface in planetary boundary layer from mixing length wind spiral model, using surface shear stress and wind direction data 17 p2997 A69-33153

Mixing length model to relate turbulent shear stress to mean velocity field within planetary boundary layer above surface roughness change 17 p2997 A69-33154

Turbulence measurements and roughness effects on viscous drag reduction with polymer solution in pipe flow, discussing friction factor, wall velocity profile, etc 17 p2951 A69-33252

Apparent thermal radiation properties for one dimensionally rough surface, discussing variance with property models employed in engineering analysis of radiant transfer
[AIAA PAPER 69-622] 17 p3071 A69-33271

Angular dependence of lunar nighttime IR radiation by invariant tensor techniques, noting surface roughness effect on radiation pattern
[AIAA PAPER 69-597] 17 p3032 A69-33276

Directional characteristics of lunar IR radiation accounted for by crater model
[AIAA PAPER 69-598] 17 p3033 A69-33285

Shape and surface roughness effects on turbulent ablation of reentry body nose tip, noting recession rate
[AIAA PAPER 69-717] 17 p2952 A69-33435

Critical review of Deriugin theory of scattering from rough lamellar surfaces using separation of variables method, discussing energy conservation violation 17 p2930 A69-33885

Microwave thermal emission by water measured from aircraft, studying radiation dependence on surface roughness 18 p3127 A69-34421

Macroscopic roughness effect on surface radiation characteristics for special cases 18 p3229 A69-34711

Machining processes effect on surface integrity of machine parts and effects on product quality 18 p3149 A69-35129

Friction coefficient increase caused by metal surface textures anisotropic effect on friction force 18 p3149 A69-35151

Coherent light scattering from rough surface, studying effects of target tilt, translation and rotation on speckle patterns produced 18 p3174 A69-35281

Solid surface roughness influence on reflection of thermal energy molecular jets, showing shock determined by incidence angle 19 p3377 A69-36180

Terrain radar returns emphasizing surface roughness influence in man-made target backscattering, determining radar cross section with radar range equation 20 p3490 A69-37646

Book on heat transfer from horizontal heating surfaces to stationary boiling liquids, heating surface roughness effect and bubble formation 20 p3633 A69-37917

Angular dependence of ocean surface-cloudless atmosphere reflectance for solar radiation studied with digitized camera signals from ATS 1 satellite 21 p3704 A69-38372

Reflection indicatrices of rough surface subjected to heat radiation for stationary and variable incidence angle, noting spatial distribution 21 p3847 A69-38455

Planetary boundary layer top formation, considering particle velocity, earth surface roughness role, geostrophic wind, etc 21 p3715 A69-38566

Diffuse reflection of UV radiation from rough metallic surfaces, noting irregularities 21 p3770 A69-38796

Electromagnetic wave scattering from rough layer with plane and rough interfaces, determining scattering cross sections from electrical field and power density 21 p3677 A69-39459

Turbulent Hartmann flow between rough walls in transverse magnetic field, determining field influence on resistance coefficient 22 p3989 A69-40255

Surface roughness effects on equilibrium temperature of isolated adiabatic plane surface illuminated by collimated and uniform solar flux 22 p4050 A69-40558

Radial velocity errors in high dispersion astronomical spectrographs in terms of variable spectral shifts along plate produced by mirror surface irregularities 23 p4167 A69-42189

Surface texture effects, discussing metallic and elastomeric contacts, measurement, profile, model parameters, adhesion, hysteresis, lubrication, squeeze films, macroelastohydrodynamics and randomness 23 p4170 A69-42359

Terrain surface irregularities influencing electromagnetic wave propagation in inhomogeneous atmosphere, using perturbation calculation 24 p4281 A69-42611

Prandtl number influence on heat transfer and pressure drop characteristics of roughened channels, determining friction factor 24 p4407 A69-42915

Rough surface skin-friction relations expanded to provide turbulent boundary layer growth prediction in pressure gradient 24 p4304 A69-43580

SURFACE STABILITY

Bubble motion inside liquid in spherical cavity, allowing for bubble surface deformation 03 p0418 A69-13812

Surface wave stability for horizontal layer of incompressible dielectric fluid in electric field, noting viscosity effect 04 p0638 A69-15192

Parametric instability of horizontal surface of ideally conducting or very high dielectric constant liquid in varying perpendicular electric field 06 p0957 A69-17524

Surface instabilities at tangential discontinuity between media caused by beam-plasma interaction: deriving dispersion relation 11 p1931 A69-25365

Dependence of convection in planetary interior upon magnitude of Rayleigh number for rigid and free surfaces 12 p2155 A69-26200

Thin walled cylindrical shells deflections under axial impact load, assuming deformations resembling cylindrical surface bending 18 p3217 A69-34599

Surface stresses in rotating asymmetric profiled disks and axial deflection effects computed theoretically and compared to measurements on photoelastic models 19 p3447 A69-36862

Contact stability of hollow cylinder compressed between parallel planes measured optically, compared to approximation of elasticity theory 23 p4162 A69-41416

Surface accuracy of large diameter radio telescopes maintained by uncoupling reflector surface from backup structure, using active compensation 23 p4149 A69-42136

SURFACE TEMPERATURE

NT SKIN TEMPERATURE [NON-BIOLOGICAL]
NT WALL TEMPERATURE

Relationship between cooled surface temperature and pressure self oscillation frequency during heat transfer to turbulent fluid flow, showing temperature variations 01 p0173 A69-10094

IR optics for indicating dynamic mechanical component reliability via surface temperature variations 01 p0085 A69-10295

Satellites use in meteorology, noting monsoon rain forecasting through mesoscale sea surface temperatures of Indian Ocean
[UN PAPER 68-95555] 01 p0109 A69-10502

Aerial radiation temperature measurement, damping factor of atmosphere and determination of ground and water surface temperatures by radiometry 01 p0110 A69-10693

Numerical analysis of temperature variation of spherical spinning satellite with and without radiatively coupled inner shell containing heat source 01 p0162 A69-10761

Lunar surface temperatures and thermal characteristics from Surveyor 5 thermal engineering data gathered during lunar days, eclipse and nights 02 p0321 A69-12227

Venus atmosphere from Mariner 5 and Venera 4 data, discussing surface temperatures and pressures, cloud top region, McElroy model and maximum wind velocities 02 p0330 A69-12800

Surface temperature of flat plate cooled convectively and insulated by circular spot, determining effects of spot radius and Biot number 03 p0531 A69-12863

Surface temperature thermal fluxmeters used in measurements of shock tubes
[ONERA-TP-648] 03 p0427 A69-12876

Surface temperatures for Galilean satellites of Jupiter calculated through corresponding lunations, assuming synchronous orbits with respect to Jupiter 03 p0513 A69-13776

Temperature determination of subjacent surface from airborne measurements of outgoing radiation in earth atmosphere in 10 to 12 micron interval 03 p0424 A69-13933

Aircraft cockpit and surface temperatures after solar radiation exposure in desert, showing inadequacies of meteorological data for thermal stress predictions 03 p0381 A69-14077

Earth surface temperature change quantitative determination due to Milankovitch insolation variations 03 p0426 A69-14232

Lithium metal spray structural cooling system for refractory materials
[AIAA PAPER 68-358] 04 p0688 A69-15509

- Binary mixture condensation on cooled vertical plate, formulating predictive theory based on conservation laws and other physical principles
[ASME PAPER 68-WA/HT-21] 05 p0847 A69-16124
- Nucleate pool boiling heat transfer data extended to relate effect of heating surface characteristics
[ASME PAPER 68-WA/HT-22] 05 p0847 A69-16125
- Molten salts thermal diffusivity measurement method at temperatures above melting point
[ASME PAPER 68-WA/ENER-5] 05 p0848 A69-16161
- Step function factor for laminar heat transfer from rotating disk with surface temperature changing stepwise in uniform forced stream 06 p1029 A69-17003
- Radiating surface temperature and total atmospheric moisture content determinations based on meteorological earth satellite measurements of outgoing radiation in IR 06 p0952 A69-17988
- Solid body surface temperature relation to heat flux during cooling by fluid flow solved on computer 07 p1241 A69-18923
- Nonaxisymmetric temperature field of unbounded hollow cylinder with moving heating boundary, expanding surface temperature into Fourier series 07 p1241 A69-18924
- Gas pressure control in xenon lasers, using variable temperature surface partially insulated from liquid nitrogen coolant 07 p1155 A69-19090
- IR camera determining surface temperatures, discussing construction and space applications 08 p1315 A69-20455
- Steady motion through rarefied gas of circular cylinder due to surface temperature difference 08 p1305 A69-20888
- Laser produced blast wave expansion measured by microwave technique, obtaining surface temperature and electron density 09 p1514 A69-21324
- Temperature profiles and heat transfer coefficients in two phase liquid-liquid stratified laminar flow of variable immiscible film thickness with surface evaporation 09 p1622 A69-21904
- Air layer between target and instrument effect on earth surface temperature conducted with airborne radiometers 09 p1536 A69-22166
- Surface temperature rise of solution treated austenitic steel measured during double repeated rotating bending fatigue tests at room and elevated temperatures 10 p1711 A69-23393
- Peaked electron emission from nickel surface with large work function under laser radiation, discussing emission pulses, electron currents and surface temperature time variations 10 p1703 A69-23572
- Horizontal surface heat transfer coefficient under simultaneous free and forced convection calculated as function of temperature head, air flow velocity and area 10 p1810 A69-24085
- Differential catalytic thin film heat gate for measuring surface temperature variations and ionized flow heat transfer, noting insulating boundary layer thickness 11 p2002 A69-25231
- Venus atmosphere chemical composition, surface temperature and pressure obtained by Venera 4 and Mariner 5 12 p2155 A69-26129
- Lunar surface temperature distribution measured by IR pyrometer, predicting temperature rise due to Lunar Excursion Module landing 13 p2341 A69-27583
- Heat and mass transfer conditions in ablation of shear thinning and thickening fluids at stagnation point
[ASME PAPER 67-HT-78] 13 p2374 A69-27778
- Free convection heat transfer from heated inclined flat plate in air, studying effects of angular positions 13 p2375 A69-27794
- Optical measurement method for burning surface temperature of condensed systems, realizing radiation from surface of combustion by light guide of monocrystalline aluminum oxide 13 p2379 A69-28453
- Comet Ikeya-Seki phenomena near perihelion interpreted from mean surface and ice nucleus internal layers temperatures 14 p2523 A69-29706
- Radiation in atmospheric circulation, considering radiative equilibrium, cloudiness and surface interactions, surface temperature and heat input 14 p2477 A69-29826
- Surface temperature measurements to deduce surface heat fluxes, noting dependence on environment and sensor characteristics 15 p2716 A69-30379
- Late type cool degenerate stars nonobservability or rarity in terms of internal energy available for radiation from surface 15 p2681 A69-30423
- Expression relating gas density, radial velocity and temperature at comet nucleus surface to nucleus surface temperature, applying results to unsteady sublimation process 15 p2684 A69-30521
- Dynamic characteristics of local slope winds, considering thermal and geometrical effects of underlying surfaces 15 p2648 A69-30577
- Temperature of underlying surface and moisture content of atmosphere from satellite thermal radio emission measurements 15 p2648 A69-30641
- Pure hydrogen stellar atmosphere nonLTE models, calculating surface temperature rise due to H alpha line effect on continuum energy balance 15 p2693 A69-30777
- Thermoelastic stress in semiinfinite elastic medium due to discontinuous temperature distribution over free surface, solving associated heat conduction problem 15 p2712 A69-31006
- Thermoelastic stresses in isotropic circular cylinder with surface locally heated by external Newtonian heat source, considering various heat transfer conditions 15 p2714 A69-31178
- Thermal conductivity of semiinfinite rod with insulated surface and constant internal heat source, considering finite heat propagation rate 15 p2719 A69-31181
- Israel research on space data for meteorological purposes, describing automatic picture transmission data and errors in surface temperature determination by satellite radiometry 15 p2650 A69-31422
- IR measuring techniques for water surface temperature remote sensing 15 p2617 A69-31543
- Venus microwave spectrum analyzed by comparing various thermal and nonthermal emission models, discussing surface temperature and atmospheric composition 16 p2853 A69-31597
- Chemical reaction between combustible solid fuel surface and oxidizer-containing gas in space capsule 16 p2877 A69-31896
- Ammonium perchlorate pyrolysis by convective surface heating, monitoring IR emission as measure of surface temperature
[WSCI PAPER 69-23] 16 p2832 A69-32361
- Ammonium perchlorate linear pyrolysis by convective surface heating, discussing propellant deflagration models
[AIAA PAPER 69-501] 16 p2835 A69-32758
- Linear pyrolysis of polymethyl methacrylate to verify Cantrell model and surface temperature determination method 17 p3017 A69-33132
- Mathematical model for determining time dependent terrain surface temperatures and radiances, considering radiative transfer convection, evaporation, ground vegetation temperature, etc
[AIAA PAPER 69-592] 17 p3071 A69-33263
- Earth surface heat flow pattern measurement and distribution techniques, considering relation to surface features and tectonic movements of crust
[AIAA PAPER 69-589] 17 p2961 A69-33284
- Ocean and water surface temperature measurement by IR remote sensing from aircraft and satellites, discussing accuracy and data correction
[AIAA PAPER 69-590] 17 p2973 A69-33286
- Lunar surface thermal characteristics revised from analysis of error sources in daytime lunar surface temperatures derived from Surveyor 5 compartment data
[AIAA PAPER 69-594] 17 p3033 A69-33287
- Temperature distribution in shadowed lunar craters formulated in Fredholm integral equations, showing constant temperature and correction for soil thermal inertia
[AIAA PAPER 69-595] 17 p3033 A69-33291
- Lunar surface brightness temperatures from IR observations, determining thermal emission directional characteristics to infer surface temperatures from Surveyor data
[AIAA PAPER 69-593] 17 p3033 A69-33302
- Mars surface temperature calculated by applying Humphrey formula for planetary radiation energy, finding mean annual values of temperature for different albedo 17 p3034 A69-33412
- Subsurface Martian temperature from sinusoidal temperature variation theory for semiinfinite homogeneous medium, plotting amplitude, mean surface and diurnal soil temperature curves 17 p3034 A69-33413
- Particulate thermophysical lunar soil model for measuring lunation nighttime and eclipse cooling, noting applicability to IR surface brightness temperature of Mercury hot pole 18 p3191 A69-34303
- Gas phase ignition shock tube analysis of solid propellant taking into account changing surface temperature and fuel vapor consumption 18 p3183 A69-34463
- Sea surface temperature remote sensing by Nimbus 2 satellite using TV camera and medium and high resolution IR radiometer 18 p3130 A69-35057
- Transient calibrations for Ge surface thermocouple heat flux sensors used in hypervelocity impulse tunnel 19 p3292 A69-35725
- Calibration of inertial and surface temperature heat transfer transducers for hotshot and shock tube measurements developed and tested at ONERA
[ONERA-TP-683] 19 p3305 A69-35726
- Wavelength-surface temperature relationship of ruby laser, discussing thermal control of emission wavelength 20 p3552 A69-36967
- Long range weather forecasts attempt from relation between northern Atlantic Ocean water temperature anomaly and monthly satellite cloud data changes 20 p3569 A69-36987
- Plasma coating formation mechanisms and parameters, studying metal surface and deposited particles temperatures, spraying time effects, etc 20 p3549 A69-37374
- Heat transfer coefficient and flow patterns of horizontal circular plate for various Rayleigh numbers, noting surface temperature 20 p3632 A69-37523
- Gas heat transfer on turbine interblade channel surfaces and working blade end surfaces at operating Reynolds and Mach numbers 21 p3849 A69-38858
- Temperature distribution determined for leading edge, convex and concave parts of turbine blade porous wall with effusion cooling 21 p3850 A69-38860
- Satellite determination of underlying surface temperature by IR spectroscopy, measuring emitted radiation in atmospheric windows 21 p3759 A69-39114
- Constant surface heating of half space with temperature dependent thermal conductivity 21 p3851 A69-39292
- Simulated degrading environment effect on spacecraft thermal control surfaces subjected to plume heating during apogee firing and solar irradiation
[AIAA PAPER 69-1024] 22 p3923 A69-40394
- Stochastic model extension of interface temperature of solids in sliding contact to include transients, noting interface activities dependence 22 p3955 A69-40404
- Surface roughness effects on equilibrium temperature of isolated adiabatic plane surface illuminated by collimated and uniform solar flux 22 p4050 A69-40558
- Mars atmosphere response to surface temperature changes by radiative and convective heating, noting strong solar control of mean wind distribution 23 p4212 A69-41614
- Pyrometer for turbine rotor blades surface temperature measurement, considering purged, line-of-sight viewing tube and signal processing to reject C particles interference
[SAE PAPER 690431] 23 p4165 A69-41649
- Laminar boundary layer in steady compressible gas flow past plane wing profile, studying surface temperature and suction effects 23 p4058 A69-41709
- Temperature distribution on surfaces of close binary stars as basis for predicting variation of monochromatic reflection effect 24 p4387 A69-43350
- Natural convection local heat transfer on constant heat flux inclined surfaces for water and air in laminar, transition and turbulent regimes
[ASME PAPER 69-HT-C] 24 p4410 A69-43526

Heat finite propagation velocity effects on temperature distribution and heat flux for step temperature change at semiinfinite body surface
[ASME PAPER 69-HT-1] 24 p4414 A69-43564

SURFACE TENSION **U INTERFACIAL TENSION** **SURFACE TO AIR MISSILES**

Portable UHF telemetry receiving station for medium range surface-to-air missiles testing, analyzing antenna coverage over water and system prediction allowing variable parameters
23 p4122 A69-41780

SURFACE TO SURFACE MISSILES **U INTERCONTINENTAL BALLISTIC MISSILES** **U MINUTEMAN ICBM** **U POLARIS MISSILES** **U V-2 MISSILE**

SURFACE VEHICLES **NT AIRCRAFT CARRIERS** **NT CAPTURED AIR BUBBLE VEHICLES** **NT CRAWLER TRACTORS** **NT LUNAR MOBILE LABORATORIES** **NT LUNAR ROVING VEHICLES** **NT LUNAR SURFACE VEHICLES** **NT NUCLEAR POWERED SHIPS** **NT ROCKET PROPELLED SLEDS** **NT TANK TRUCKS** **NT TRUCKS** **NT WALKING MACHINES**

Time difference position determination system for space, surface and airborne vehicles, describing application to satellite navigation and air traffic control
08 p1348 A69-21066

Skirts on hovercraft, noting rough water drag, plough in and overturning, and skirt oscillation and wear problems
10 p1634 A69-23629

Ground access routes between business districts and airports compared for passenger transport modes
[AIAA PAPER 68-1072] 12 p2059 A69-26773

Time difference position determination system for space, surface and airborne vehicles, describing application to satellite navigation and air traffic control
22 p3977 A69-39874

Computer system functional requirements for autonomous Martian surface roving vehicle, emphasizing vehicle motion control system
[AIAA PAPER 69-980] 22 p3907 A69-40360

SURFACE WAVES **NT BAROCLINIC WAVES** **NT GRAVITY WAVES**

Electron plasmas near plane metallic surfaces, determining transmittance and reflectance of incident light waves and surface waves dispersion characteristics
02 p0286 A69-11788

Moving window analysis digital technique for complex seismic surface waves in presence of noise and multimode propagation
02 p0243 A69-12006

Dispersion relations of axisymmetric and dipolar surface modes propagation along inhomogeneous plasma columns on dispersion relations
02 p0289 A69-12242

Finite amplitude surface wave excitation in infinitely deep ideal fluid by moving pressure, noting phase velocity increase with amplitude
03 p0466 A69-13277

Electroacoustic amplifier based phonon devices, using surface waves on piezoelectric materials to speed radar data real time processing
03 p0394 A69-13353

Direct amplification of ultra and hypersonic surface waves in semiconducting crystals of wurtzite group, taking into account drift effects and boundary conditions
03 p0490 A69-13925

Surface impedance variation effect on surface wave propagation along rod waveguide
04 p0576 A69-14761

Surface wave stability for horizontal layer of incompressible dielectric fluid in electric field, noting viscosity effect
04 p0638 A69-15193

Surface waveguide composed of inhomogeneous dielectric thin film used as low loss transmission line
05 p0731 A69-16294

Critical electron drift velocity threshold in surface wave amplification in semiconductor in magnetic field, noting partial effect of diffusion
05 p0810 A69-16648

Bounded and spatially separated plasmas wave oscillations stability in magnetic field, observing hydrodynamic slipping and drift instability
06 p0963 A69-16903

Dispersion equation for dipolar surface waves in uniform cold lossless infinitely long magnetoplasma column in free space, obtaining numerical and asymptotic solutions
06 p0968 A69-17774

Surface wave propagation on circular plasma column moving in axial direction in free space region
06 p0968 A69-17775

Surface plasma waves excitation by light and decay into photons applied to nonradiative modes
07 p1188 A69-18278

Period fluctuations in ionospheric plasma resonance amplitude, proposing hypothesis in terms of quasi-electrostatic surface waves guided by antenna wire
07 p1125 A69-18847

Ray-optical description for point source excited surface waves in stratified anisotropic media
07 p1079 A69-18918

Boresight error in missile radome-antenna combination due to reflection and surface wave effects
07 p1111 A69-19536

Forced surface wave resonances in dielectric free 45 degree triangular grid circular waveguide phased arrays
08 p1282 A69-20038

Ray path geometry derived by Poynting vector to calculate surface fields due to creeping waves in sphere planes
08 p1274 A69-20046

Fresnel formulas for surface plasma waves excitation by light in thin metal foil embedded between dielectric layers, discussing transmissive and absorptive resonances
08 p1372 A69-20290

Interfacial charge relaxation oversteability in tangential electrical field, discussing electromechanical polarization surface waves propagation and dielectrophoretic orientation of liquids in zero gravity space
08 p1353 A69-20792

Earth upper mantle wave velocity structure based on surface wave dispersion, noting low velocity layers thickness
09 p1491 A69-22153

Microwave frequency room temperature acoustic surface wave propagation losses in lithium niobate measured by laser light deflection, discussing propagation and insertion losses
10 p1703 A69-23511

Dynamic mode electromagnetic surface waves on axially magnetized single crystalline YIG and polycrystalline ferrite rods
10 p1746 A69-23513

Slow electromagnetic wave propagation along cold collisionless cylindrical plasma in axial magnetic field, noting surface wave metamorphosis into bulk waves
10 p1739 A69-23659

Surface radio wave scattering propagating along rough surfaces, measuring emission during transformation into space waves
10 p1658 A69-23952

Computer calculated phase velocities for surface wave and waveguide modes given for circular waveguide filled with inhomogeneous electron plasma
11 p1844 A69-24437

Surface wave reflection from free ends of ideally conducting rods forming semiinfinite grid to study rod delay systems and wave-duct antennas
11 p1833 A69-24438

Parallel flow of viscous liquid film with free surface down inclined plane, noting growth of initially infinitesimal amplitude waves and finite amplitude wave stability
11 p1869 A69-24891

Surface instabilities at tangential discontinuity between media caused by beam-plasma interaction, deriving dispersion relation
11 p1931 A69-25365

TEM-DUAL surface wave propagation in coaxial cable with stratified dielectric structure to reduce attenuation calculated by addition theorem to Bessel functions
11 p1856 A69-25659

Asymptotic solution of two dimensional problem of elastic impact of bars, showing longitudinal and surface waves decay with time
11 p1996 A69-25737

Characteristic equation for corrugated surface wave line loaded with uniformly spaced thin metallic disks excited in E mode, considering spacing and groove depth
12 p2028 A69-25899

Unsteady surface and internal waves diffraction induced by source in ideal incompressible fluid, obtaining solutions in form of convolution and transfer functions
12 p2061 A69-25953

Surface wave patterns of truncated conical shape with free edges attributed to mechanical properties
12 p2178 A69-26093

Electrical equivalent circuit for piezoelectric generation and detection of transient and sinusoidal ultrasonic waves by interdigital electrodes
12 p2039 A69-26308

Surface waves effect on electromagnetic waves: coherent reflection from plasma-vacuum boundary, describing polarization and angular and spectral distributions
12 p2031 A69-26309

Visual observation of surface vibration nodal patterns by incoherent light illumination of object, noting holography
12 p2099 A69-27109

Optical surface wave propagation on thin dielectric film waveguides, noting applications to integrated optical data processors
13 p2229 A69-27609

Wave propagation on heavy fluid surface forming splashes in container with vertical walls
13 p2247 A69-27719

Plane TM surface waves supported by plane ungrounded magnetoplasma slab with magnetostatic field parallel to two parallel interfaces and perpendicular to propagation direction
13 p2308 A69-27909

Wave parameters in coupled parallel surface wave transmission lines and dielectric waveguides, discussing phase velocities and spatial beat period
13 p2223 A69-28573

MHD waves and oscillations in cylindrical plasmas column contained by longitudinal magnetic field, noting dispersion equations
14 p2489 A69-28737

Finite amplitude surface wave excitation in infinitely deep ideal fluid by moving pressure, noting phase velocity increase with amplitude
14 p2482 A69-28789

Coupled mode theory for surface wave propagation along tapered cylindrical dielectric rod, considering radiation field effects
14 p2422 A69-29559

Production method for fabricating HF surface wave interdigital electrode transducers, discussing pattern replication, etching, etc
14 p2455 A69-29573

Acoustic bulk-surface wave transducer for shear longitudinal wave transformation in nonpiezoelectric material at HF
15 p2607 A69-30169

Lagrange expansion theorem for shielded surface waves, obtaining modal functions and power flows
16 p2750 A69-31949

Electronic-ultrasonic amplifiers with external electron stream and longitudinal or surface wave studies for damping influence, deriving dispersion equation
16 p2761 A69-32069

Diffraction of axisymmetric electromagnetic wave at surface discontinuity of impedance cylinder forming core of coaxial waveguide
16 p2761 A69-32479

Surface wave study techniques, discussing digital moving window analysis of group and phase velocity and use of time variable filters
16 p2784 A69-32579

Seismic surface wave observations analyzed by applying moving window method to orthogonal detector recordings permitting lateral refraction measurement wave separation, etc
16 p2784 A69-32579

Statistical characteristics of wind wave development in initial stage, obtaining distribution functions and frequency spectrum for various velocities and temperatures
18 p3167 A69-35349

Acoustic surface waves on thin film for pulse compression radar dispersive delay line, describing delay characteristic synthesis and control
19 p3267 A69-35929

Transient phenomena in bounded dispersive medium emphasizing surface wave propagation, discussing space and surface waves excitation in bounded cold magnetoplasma
20 p3494 A69-37849

Laser profilometer to measure sea wave profile from airborne platform, describing transmitter receiver and signal processor
21 p3739 A69-39469

Coupling coefficients and excitation increment determined for nonlinear interactions of surface waves in nonisothermal semibounded plasma
22 p3990 A69-40799

Asymmetric surface waves in radial spiral structures above conducting plane, analyzing spiral thickness and plane influence on dispersion and energy characteristics

22 p3916 A69-40951

Laplace-Carson integral transforms for analyzing surface waves generated by central impact of two elastic bodies

23 p4226 A69-41702

Directional couplers applied to excitation of non-propagating surface wave antennas, examining ridge slot system

23 p4139 A69-41946

Digital analysis of surface wave observations, discussing moving window, multiple filter, multicomponent recording, time variable filtration and cross-correlation techniques

23 p4157 A69-42018

Electrode interactions effects in interdigital surface wave transducers on piezoelectric materials, using Fourier analysis

24 p4312 A69-42615

Surface wave terms found in long wavelength limit during solution of initial value problem for semiinfinite hot plasma

24 p4356 A69-43364

SURFACES

Subsonic lifting surface theory including leading edge, discussing singularities in solution of integral equation for determination of aerodynamic properties [AIAA PAPER 69-37]

06 p0865 A69-18167

Monograph on sound generation by turbulence and surfaces in arbitrary motion, discussing sound and multipole fields and governing equations

13 p2247 A69-27974

SURFACTANTS

Hyperoxia and pulmonary surfactant washout in pulmonary compliance measurements of rats subjected to 100 percent diatomic oxygen before asphyxial death

21 p3659 A69-39066

Air and saline P-V curves of rat lungs after hyperoxia, comparing hyperoxia effects to surfactant washout on pulmonary compliance

23 p4081 A69-41440

SURGERY

Visceral afferent pathways influence on vasopressin secretion, ADH levels and urinary excretory patterns of dogs during surgical stress

05 p0708 A69-15970

SURGES

Circulation, geometry and viscosity effects on speed of surge in bathtub vortex

05 p0744 A69-15718

Transformer inrush transients control by selection of core material, primary turn number and trigger circuitry

06 p0894 A69-17221

Solar flares and surges origin, discussing role of supergranular convection, field gradients and spicules

06 p0994 A69-17437

Solar disk surge distribution difference between eastern and western disk parts

06 p0995 A69-17440

Compressor surge effect on mixed compression inlet flow from numerical solution of one dimensional unsteady inviscid flow equations in variable area duct [AIAA PAPER 69-484]

16 p2841 A69-32682

Surges statistical properties observed in Sweden /1957-1967/ noting latitude distribution pattern, radio emission association, rate dependence on solar cycle, etc

18 p3204 A69-35393

SURGICAL INSTRUMENTS

Surgical radiolesion in human brain by high energy protons

03 p0374 A69-13501

SURVEILLANCE

U SPACE SURVEILLANCE [GROUND BASED]

U SPACE SURVEILLANCE [SPACEBORNE]

SURVEILLANCE RADAR

Adaptive detection mode for surveillance radar, using detection threshold proportional to spatially sampled clutter level estimates for regulation of false alarm probability

01 p0026 A69-10178

Automated real time monoradar surveillance system based on azimuthal monotonicity of radar plots and flexible tracking strategies

03 p0383 A69-12872

Listen-in feature, allowing general aviation aircraft equipment to receive airborne SSR reply signals, provides air to air proximity warning

03 p0464 A69-13247

Synchronous servomotor for parabolic antenna of surveillance radar, discussing motor size and optimum gear ratio determination

08 p1274 A69-20108

Electronic multibeam switching X band antenna system design with separate transmitting and receiving antennas for use on continuous wave surveillance radar

08 p1289 A69-20967

Airborne ILS marker beacon receivers and secondary surveillance radar transponder using microelectronic equipment, noting thermal dissipation problems [AGARDOGRAPH-114]

08 p1292 A69-20991

Digital simulation optimizing parameters of digital equipment to measure target azimuths in pulsed surveillance radar system, establishing optimum echo pulse quantization threshold

15 p2563 A69-30138

Direction finding accuracy of pulsed radar with binary-quantized detector signals, discussing azimuth minimum variance and quantization threshold optimization

15 p2566 A69-30333

Air traffic control ground equipment developments including radio direction finders, surveillance radar, interconsole marking, etc

18 p3168 A69-34806

Imaging radar applications noting military surveillance, navigation assistance, iceberg detection, sea rescue operations, all-weather traffic surveys, terrain mapping, etc

20 p3491 A69-37649

Beam shape loss /BSL/ for electronically steerable array in search mode, determining optimum search beam locations from BSL computations

20 p3506 A69-37717

Computer controlled automatic radar for survey through 360 degrees in azimuth and zero to 60 degrees in elevation

21 p3677 A69-39566

SURVEYING

U SURVEYS

SURVEYOR LUNAR PROBES

Surveyor lunar scientific payload and results, discussing TV camera, soil mechanics and surface sampler, alpha scattering instrument, small magnets and surface analysis

06 p1001 A69-17162

Surveyor scientific instruments and operation on moon, reviewing TV camera, alpha scattering instrument and surface sampler [JPL-TR-32-1358]

08 p1312 A69-19850

Surveyor electronic engineering design for lunar environment, discussing vacuum and temperature effects

11 p1958 A69-24633

TV test chart for evaluating Surveyor lunar spacecraft TV system covering resolution, photometric and colorimetric response and sun angular position [SMPTE PAPER 105-71]

12 p2078 A69-25771

Surveyor lunar landing procedures and results including instrumentation, lunar topography, selenology, chemical and physical properties, solar corona and earth laser output observations

15 p2681 A69-30324

Alpha-scattering experiments by Surveyor missions, studying hypothesis regarding lunar origin of eucrites and howardites

20 p3597 A69-37341

Surveyor spacecraft instrumentation, describing TV camera design and operation, photographic requirements and techniques, lunar surface characteristics, etc

22 p4011 A69-40043

Lunar surface material mechanical properties from Surveyor observations, analyzing grain size, rock density, internal friction, cohesion and bulk density compared to Luna observations

24 p4383 A69-42962

SURVEYOR PROJECT

Surveyor scientific instruments and operation on moon, reviewing TV camera, alpha scattering instrument and surface sampler [JPL-TR-32-1358]

08 p1312 A69-19850

Landing shock attenuation system for Surveyor spacecraft, describing hydraulic cylinder and piston arrangement for damping, computerized shock absorber design and landing process simulation [ASME PAPER 69-DE-54]

14 p2530 A69-28848

Spacecraft lunar observations, especially data from Surveyor landings

18 p3205 A69-35410

Surveyor thermal vacuum test data comparison with flight results indicating performance prediction reliability of earth-based tests for vacuum and lunar environments

19 p3430 A69-36016

SURVEYOR 1 LUNAR PROBE

Crater distribution and population curves for Surveyor 1 vicinity, discussing Flamsteed P ring floor characteristics

21 p3800 A69-38675

SURVEYOR 5 LUNAR PROBE

Surveyor 5 alpha particle backscattering instrument measurement, TV pictures of lunar surface elemental composition and magnetic and mechanical measurements

02 p0317 A69-12023

Magnetic experiment on Surveyor 5 revealing magnetic material presence in Mare Tranquillitatis, discussing analogy to powdered basalt

02 p0321 A69-12226

Lunar surface thermal characteristics revised from analysis of error sources in daytime lunar surface temperatures derived from Surveyor 5 compartment data [AIAA PAPER 69-594]

17 p3033 A69-33287

SURVEYOR 6 LUNAR PROBE

Surveyor 6 magnet experiment following lunar landing, noting presence of magnetic material in Sinus Medi indicating basaltic composition

02 p0317 A69-12015

Landing shock struts of Surveyor 6, emphasizing silicone liquid springs role as absorbers and stabilizers

20 p3466 A69-38180

SURVEYOR 7 LUNAR PROBE

Surveyor 7 TV system in photon integration mode, analyzing slow scan vidicon storage characteristics and dark current limitations [SMPTE PAPER 105-72]

12 p2078 A69-25772

Photogrammetric calibration of Surveyor 7 stereo mirror based on vector analysis [JPL-TR-32-1390]

13 p2263 A69-28199

SURVEYS

NT GEODETIC SURVEYS

Earth resources technology satellite global survey system carrying multispectral sensors in long life space platform

21 p3720 A69-38623

SURVIVAL

Survival analysis based on probability theory for design of air cushion vehicle to determine height for operating over open sea

01 p0008 A69-10027

Terrestrial microorganism survival in space aboard Gemini satellite, discussing lethal effects of solar radiation

01 p0018 A69-11087

Ionospheric and stratospheric UV radiation effects on survival of microorganisms

01 p0018 A69-11088

Mathematical model for estimating microbial survival in heat sterilization of spacecraft, including environmental and time cumulative effects

05 p0707 A69-15941

Survival and personal equipment - Conference, San Diego, October 1968

06 p0877 A69-16952

Physiological or survival training emphasizing psychological approach

06 p0879 A69-16965

Human survivability in severe light plane slow speed accidents due to stalling, turning, takeoff or approach, discussing crash load vectors and magnitude [SAE PAPER 690336]

11 p1822 A69-24492

Survival rates of continuously cultivated Chlorella plants in air-carbon dioxide atmosphere after single exposure to gamma radiation, using microcolony counting technique

22 p3876 A69-40275

Rat survival rate after prolonged gradually decreased body temperature without motion restraint or kept in fixed position

22 p3877 A69-40278

Third generation jet aircraft safety, discussing accident prevention and survival

22 p4054 A69-41142

Aircrew Arctic survival situation simulation experiments with survivors staying close to aircraft and walking across difficult terrain from emergency location

23 p4088 A69-41810

Satellite system survival probability expressed as function of launch probability, time and number of satellites available [AIAA PAPER 67-324]

24 p4249 A69-43665

SURVIVAL EQUIPMENT

Survival and personal equipment - Conference, San Diego, October 1968

06 p0877 A69-16952

Physiological approach to tests and evaluation of aviation survival equipment, noting human reactions study under extreme conditions

06 p0877 A69-16953

Automatic inflators for life jackets and survival gear in emergencies activated after submersion in water

06 p0877 A69-16955

Survival of aircrew after successful ejection over water and boarding life raft

06 p0878 A69-16958

Radar detector for survivors, using inexpensive microwave mixer detector crystal

06 p0878 A69-16964

Life raft thermal protection against exposure of aircrews to cold, noting chemically fueled heaters and IR reflective liners

06 p0883 A69-17841

Passenger and crew members escape from aircraft following water accidents, discussing ditching, evacuation, survival and rescue facilities

08 p1254 A69-20453

Insulated one man life raft for sea survival in arctic or subarctic conditions, evaluating thermal protection with endurance time and rectal temperature

12 p2020 A69-26550

Passenger safety during aircraft accidents in Arctic, discussing survival equipment and methods

23 p4107 A69-41811

Crew survival insurance under emergency situations during manned space flight, discussing Apollo abort system refinements

[AAS PAPER 69-469] 24 p4272 A69-42848

SUSCEPTIBILITY [MAGNETISM]

U MAGNETIC PERMEABILITY

SUSPENDING [HANGING]

NT MAGNETIC SUSPENSION

Sensor suspension, damping and signal readout through use of fluids with applications to rate and acceleration sensors

[AGARDGRAPH-118] 08 p1257 A69-20949

Four gimbal Cardan suspension gyroscope kinematics for nonperpendicular arrangement

09 p1502 A69-22705

Dynamic stability of double pendulum with vibrating point of suspension, obtaining differential equations of motion by Lagrange equations application in averaging method

11 p1884 A69-24768

Land gyrocompass on torsional suspensions in liquid filled chamber, considering design and operation in terms of precession theory

13 p2259 A69-27431

Stratospheric winds effect on instrument package suspended from high altitude balloon, discussing package displacements, yarn shapes and air drag characteristics

17 p2961 A69-33612

Mean drift rates of single and two rotor gyroscopic linear acceleration integrators mounted on irregularly rocking base

18 p3135 A69-34586

SUSPENDING [MIXING]

Diffusion of suspended particles in isotropic turbulence field of dispersed medium

02 p0234 A69-12579

Dielectric constants of nonconducting composite suspensions of spheres and parallel cylinders in terms of filler particles, matrix and volume fraction

13 p2287 A69-28677

Model for mixing and combustion of compressible particle laden ducted flows

[AIAA PAPER 69-460] 16 p2880 A69-32650

Turbulent process employing product constituents dilute suspensions in inert carrier/Quickmix/ to obtain solid propellant mixtures, discussing plant design and analysis, economics, etc

[AIAA PAPER 69-517] 17 p2978 A69-33033

Self ignition of solid/fluid particles suspended in gas flow, discussing heat transfer coefficient, critical temperatures, etc

17 p3070 A69-33142

SUSPENSION SYSTEMS [VEHICLES]

Rocket sled incorporating magnetic suspension system

15 p2585 A69-30361

Briteye battlefield illumination flare configuration, candle power, burn duration and hot air balloon-type suspension system

20 p3461 A69-37166

SUSPENSIONS

Flow theories of fluids with elastic deformation of substructure, treating suspensions of irregularly shaped deformable particles

05 p0752 A69-16738

Spectrum of light scattered by particles suspended in turbulent fluid

07 p1157 A69-19417

Gaseous suspensions of thermionic emitting particles assessed as MHD working fluids in large scale MHD electric power generators

10 p1738 A69-23491

Size and velocity measurements of particles suspended in gas expanding from nozzle into vacuum simulating cometary two phase flow with evaporation

10 p1674 A69-23686

Similarity solution for flow of fluid-particle suspension over disk rotating at constant velocity, solving differential equations for flow velocity distributions

11 p1867 A69-24280

Weak shock waves relaxation time and amplitude and acoustic velocity as functions of thermorelaxing media

15 p2590 A69-30103

Carrying cables shape optimization for suspended structures under load, using minimum weight criterion

18 p3212 A69-34354

Similitude applied to dynamics of disperse media, discussing role of dimensionless numbers in mechanics of suspensions and two phase flows in porous media

19 p3300 A69-36775

Heat and mass transfer in gas suspension, studying suspended particles effects on heat transfer by irreversible thermodynamics

[ASME PAPER 69-HT-34] 24 p4410 A69-43528

SUSTAINER ROCKET ENGINES

U RL-10-A-1 ENGINE

SWAGING

Extrusion variables influence on microstructure and hardness level of Ti-Al-Sn compared with recrystallization behavior after cold swaging

[ASM PAPER W9-8.2] 21 p3729 A69-38660

SWAN BANDS

Electronic transition moment for C /Swan/ bands measured in shock tube in carbon dioxide and argon mixtures

02 p0285 A69-12833

Transition probabilities for radiative lifetime of Swan and Mulliken diatomic C bands calculated from lifetime data using Franck-Condon factors

15 p2694 A69-30789

SWEAT

Thermal radiation effects on cutaneous vasomotor and sudomotor control of human organism

[AGARDGRAPH-111] 08 p1265 A69-20672

Psychological, physiological and biochemical responses to controlled diets, determining regional and total body sweat composition of men working in temperate environment

10 p1644 A69-23314

Skin temperature change rate influence on sweating in male subjects, discussing role of central thermosensitive structures

22 p3874 A69-40210

Antidiuretic hormone /ADH/ and bradykinin effects on human thermal and cholinergic sweating after subdermal injection in forearm, abdomen and leg

23 p4077 A69-41311

SWEAT COOLING

Transpiration cooling of porous flat plate by injection of carbon dioxide or air into carbon dioxide and air free streams

03 p0413 A69-12996

Dynamic processes of heat and mass transfer in transpiration cooling of gas flow

04 p0684 A69-14355

Transpiration cooling of reentry vehicle nosetips, noting two dimensional aspects of porous wall coolant flow and matrix-coolant energy exchange

[AIAA PAPER 69-96] 06 p1039 A69-18212

Transpiration air cooled blading to test and design small gas turbine at 2500 F inlet, discussing cascade and full stage component

[SAE PAPER 690035] 07 p1203 A69-18310

Transpiration cooling effect on turbine stator blade performance determined by annular cascade tests, using data to establish empirical correlation for loss coefficient

[ASME PAPER 69-GT-39] 09 p1432 A69-22487

Temperature variations at porous wall surface as function of transpiration coolant flow rate

11 p2002 A69-25334

Combined hypoxic hypoxia and high ambient temperature found relieving strain on humans by increasing heat release by evaporation

13 p2212 A69-28628

Mode transition characteristics of free burning argon electric arc with transpiration cooled anode, noting current blowing parameter

[AIAA PAPER 69-696] 17 p3011 A69-33451

Temperature distribution determined for leading edge, convex and concave parts of turbine blade porous wall with effusion cooling

21 p3850 A69-38860

Gaseous injection effect on laminar boundary layer hypersonic flow around transpiration-cooled blunt bodies analyzed by integral method and Newtonian model

21 p3644 A69-39000

Heat transfer characteristics in evaporative, transpiration cooled porous systems

21 p3851 A69-39000

Monograph on aerodynamic studies of effusion cooled turbine blades covering turbulent boundary layers, gas turbine performance, experimental design etc

[AIAA PAPER 69-871] 21 p3786 A69-39800

Radiation equilibrium temperature measurements downstream of transpiration cooled gas flow near slender cone vertex in continuous flow hypersonic tunnel

24 p4248 A69-43588

SWEATING

U PERSPIRATION

SWEDEN

Swedish space research report to COSPAR covering organization and publications

15 p2724 A69-31451

SWEPT ANGLE

NT LEADING EDGE SWEEP

NT SWEEPBACK

Flow through turbine stage with inclined guide vanes at moderate Mach numbers, discussing exit blade angle formula for swept cascades

15 p2547 A69-30570

Vortex breakdown on slender sharp edged and modified delta wings with varying sweep angles investigated in wind tunnel using schlieren system for flow visualization

[AIAA PAPER 69-778] 19 p3237 A69-35644

SWEPT FREQUENCY

X-band swept frequency oscillator using Gunn diode and ferrite phase shifter

05 p0734 A69-16573

Swept-frequency complex return-gain response of injection locked oscillator over locking bandwidth, detecting and correcting phase errors between injection-locked diode oscillators

07 p1100 A69-18645

Sweep frequency measuring setup for adjusting equalizers in carrier transmission systems

11 p1841 A69-25639

ISIS A satellite fixed and sweep frequency ionograms indicating electron density variations, ionospheric resonances and Cerenkov radiation

15 p2604 A69-31416

High resolution swept frequency reflectometer suitable for impedance matching in waveguides or coaxial lines

16 p2759 A69-31940

Swept frequency microwave measurements in simulated reentry environments using dielectric layers, glow discharge plasma and aperture antenna-plasma layer model

[AIAA PAPER 69-701] 17 p2920 A69-33461

Sweep frequency ionospheric topside sounder design for Alouette and ISIS satellites, discussing influence of experiment requirements and spacecraft limitation and environments

20 p3507 A69-37859

Swept frequency X band reflectometer for measuring antenna properties in simulated reentry environments

[AAS PAPER 69-282] 24 p4313 A69-42861

SWEEPBACK

NT LEADING EDGE SWEEP

Aerodynamic characteristics of delta wings for supersonic flow at large angles of attack, showing sweep back angle influence on drag coefficient

02 p0191 A69-12583

SWELLING

Seal swell prediction methods extended to include three dimensional solubility parameter concept

[ASLE PAPER 68-LC-21] 07 p1171 A69-19306

SWEPT FORWARD WINGS

U TRAPEZOIDAL WINGS

SWEPT WINGS

NT DELTA WINGS

NT TRAPEZOIDAL WINGS

Laminar flow on swept low drag suction wings at high Reynolds numbers

05 p0696 A69-15553

Visual investigation of flow field at swept wing, measuring pressure distribution at stall fence and vortices formation 06 p0858 A69-17341

Maximum downwind and crosswind vertical wind shear in boundary layer, noting effect on swept wing jet aircraft landing 06 p0951 A69-17790

Shear field pattern theory modified to apply to determination of sweptback wings, calculating stress development 10 p1801 A69-23645

Power plant installation on swept winged transport aircraft, discussing interference drag sources, high lift problems, unorthodox installations, nacelle effects, etc 17 p2898 A69-33214

Amplified boundary layer oscillations and transition at swept flat nosed wing attachment line with/without boundary layer suction analyzed by wind tunnel tests 17 p2890 A69-33251

Swept wing attachment line boundary layer, measuring skin friction in full turbulence and velocity profiles with and without trip wire 17 p2958 A69-34047

Wind tunnel tests of swept wing fighter aircraft for transonic buffet onset lift coefficient resulting from camber and leading and trailing edge deflection [AIAA PAPER 69-793] 19 p3238 A69-36297

WEPTBACK TAIL SURFACES

Mach 8 flow field effects and forces on small delta tail surfaces mounted on body of revolution at various angles of attack [AIAA PAPER 68-891] 22 p3859 A69-40539

WEPTBACK WINGS

U DELTA WINGS

U TRAPEZOIDAL WINGS

WIMMING

Telemetered heart rate response to progressively increased distance swimming competition compared with equidistance running events for change patterns, magnitude and recovery 23 p4100 A69-41444

SWINGBY TECHNIQUE

Jupiter swingby flight mode application to probe missions requiring solar polar regions overflight at close perihelion distances 19 p3401 A69-35915

Interplanetary swingby trajectory correcting maneuvers for space vehicles return to earth after planet orbiting with emphasis on singular points 19 p3427 A69-36613

Venus swingby and direct Mercury trajectories analysis for optical imaging from flyby missions [AAS PAPER 69-258] 24 p4380 A69-42860

SWIRLING

Swirl flow through single and multistage Carnot shock diffuser, analyzing relation of pressure rise and diffuser aspect ratio 02 p0230 A69-11616

Stability of inviscid swirling flow with finite axial velocity components and nonvanishing radial density gradients, noting criterion for infinitesimal disturbances 08 p1305 A69-20851

Von Karman swirling flow problem differential equations solved by extending Serrin existence theorems 14 p2432 A69-29676

Swirl decay of turbulent flow in tubes, showing decrease with increasing axial Reynolds number and independence of initial swirl angle 16 p2772 A69-32170

Monograph on turbulent isothermal swirl-free jets and turbulent swirling flames, studying mixture and propagation in free space 17 p3068 A69-32996

Flow rate of ideal fluid ejected from swirl injector taking into account radial component of flow velocity at nozzle exit 19 p3297 A69-35820

Swirl influence on choking constraint in transonic flow through nozzle throat [AIAA PAPER 68-693] 23 p4151 A69-41887

Laminar flow swirling motion in circular duct, studying separation and reversal 24 p4301 A69-43355

SWIRLING WAKES

U TURBULENT WAKES

SWITCHES

NT CAPACITANCE SWITCHES

NT CRYOTRONS

NT ELECTRIC RELAYS

NT ELECTRIC SWITCHES

NT FLUID SWITCHING ELEMENTS

NT SWITCHING CIRCUITS

NT THERMOSTATS

Automated patching system design for analog and hybrid computers to reduce number of switches required 16 p2756 A69-32551

SWITCHING

NT BEAM SWITCHING

NT MAGNETIC SWITCHING

NT MICROWAVE SWITCHING

Minimization algorithm for complex and switching functions using unique identifiers on Karnaugh map 16 p2764 A69-31710

Electrical switching in thin film arsenic selenium telluride semiconducting glass diodes, observing formation of liquid phase and conducting filaments 16 p2760 A69-32017

LF switching in wall attachment type digital fluid amplifiers, studying visual and quantitative values for switch pressure and flow as function of geometric variables [ASME PAPER 69-FLCS-31] 21 p3649 A69-38604

Time optimal control of soft spring showing switching locus changes 24 p4289 A69-42955

SWITCHING CIRCUITS

NT FLUID SWITCHING ELEMENTS

Capacitance variation in junction varactors with linear graded, abrupt and hyperabrupt junctions, storage switching diodes and storage varactors 01 p0038 A69-10168

Schmitt trigger current-voltage characteristic for determining switching behavior and switching point temperature, examining formulas and equivalent circuits 01 p0039 A69-10171

Electro-optic Q switch using lithium niobate as electro-optic material, comparing performance to conventional device using potassium deuterium phosphate 01 p0089 A69-10184

Chemical phenomena during explosions of wires in various gaseous atmospheres, using apparatus with electronic crowbar for current flow regulation 01 p0081 A69-10680

Delayed response in threshold switching from reset state in ferrite memory cores consisting of magnesium compounds [IEEE PAPER 16.4] 01 p0045 A69-10719

Semiconductor switching diode, evaluating operation with nonlinear time delay equivalent circuit 01 p0046 A69-10747

Reduction of ATR switch pulse peak in automatic frequency control system of radar station 01 p0047 A69-10784

Tunnel diode oscillations in switching mode due to sinusoidal voltage excitation, discussing critical applied signal frequency separating switching and oscillation modes 02 p0213 A69-11535

Step recovery switching silicon transistor combining planar and mesa technologies, discussing charge storage and fall times 02 p0215 A69-11937

Malfunction elimination in asynchronous fluidic switching circuit by locating static hazards 02 p0195 A69-12080

Retrodirective antenna array with switched Butler matrix feed 02 p0223 A69-12813

Laser with passive Q switching with Faraday cell switch, studying induced recombination and Mandelstam-Brillouin scattering 03 p0435 A69-12983

Analysis and design of synchronous filter compatible with microelectronics requirements, switching N monolithic RC thin film devices to signal source of resistance 03 p0403 A69-13206

Transistor-transistor logic switching circuits design for use in frequency dividers with variable division ratios in frequency processing systems 05 p0729 A69-15963

Insulated junction integrated circuit transistor operation with various terminal connections corresponding to diode switching of transistor 05 p0730 A69-16217

Gallium arsenide electro-optic switch measuring signal time response to radiation step of homogeneously broadened carbon dioxide, He and nitrogen laser amplifier 05 p0773 A69-16293

Radiation tests on Ovonic threshold switches performed with fast neutrons and broadband X rays 06 p0978 A69-16891

Semiconductor glasses use for electronic devices 06 p0980 A69-17714

Logic circuit for semiconductor current gain sensing switch 07 p1113 A69-19744

DC/AC collectorless step electric motors operation and commutation circuits 09 p1442 A69-21860

Pulse generator switch consisting of avalanche transistors in series, describing voltage production and transmission, trigger pulse jitter and pulse amplitude 09 p1468 A69-22589

Reduction of ATR switch pulse peak in automatic frequency control system of radar station 10 p1661 A69-23113

Jittering delay of triggering circuit driven by ramp signals of different finite slopes, noting tunnel diode discriminators and regenerative feedback loop circuits 11 p1858 A69-24568

Output pulse parameters of short pulse thyristor generator as function of time constant, considering rise time of switch-on process 11 p1846 A69-24615

Electrons conduction and switching in noncrystalline semiconductors, discussing localized states and thermally activated hopping 11 p1938 A69-25239

Ultrawideband DC transistor amplifier for pulsed switching circuits with subnanosecond risetimes, discussing multistages with feedback dipoles, transient response and drift problems 11 p1854 A69-25612

Antenna switch for cascading and separating RF channels of high power wideband broadcasting systems 11 p1854 A69-25617

System switch, separating RF bands according to frequency and polarization for simultaneous transmission from parabolic horn antenna 11 p1854 A69-25618

AC diode switching circuits employed as threshold elements in functional rectifiers for approximating nonlinear functions 11 p1857 A69-25717

Fabrication procedure for microwave epitaxial GaAs diodes applicable for switching purposes 12 p2035 A69-25831

Broadband plasma waveguide switch application extended to 26-40 GHz range, discussing isolation, cold loss, switching time, trigger signal and ionized plasma 12 p2036 A69-25938

P-n-p planar epitaxial germanium microwave transistor used as amplifier in 1-4 GHz range and as high speed switch, summarizing design, fabrication and characterization 12 p2037 A69-25940

Electronic switching circuits controlled by binary counter triggers for variable passband filters 12 p2040 A69-26489

Brushless DC motor with commutation control by magnetic position sensor scanned at HF 12 p2017 A69-26894

MOS unitoron switching circuit operation subjected to nonlinear load, using analytic approximations of current-voltage characteristics 13 p2234 A69-28507

Small signal transient characteristics of semiconductor diodes analyzed by charge method, studying processes during p-n junction diode switching at low currents 14 p2419 A69-28918

MOSFET/unitoron/ switching circuits classification in terms of load curve shapes obtained with different output connections of load elements 15 p2574 A69-30122

Semiconductor rectifiers economic life testing with synthetic circuits utilizing thyristor switch 15 p2579 A69-31041

High voltage thin film transistor, discussing design criteria, fabrication, I-V characteristics and switching speed 16 p2757 A69-31614

Networks of ideal inductors, capacitors and periodically operated switches with no energy loss, deriving frequency-power formulas from response functions 18 p3111 A69-34682

Photon actuated switch consisting of 10 input binary logic gate and solid state relay to reduce aerospace vehicles self generated noise 20 p3505 A69-37289

Chalcogenide semiconductor film switches time parameters, showing delay time decrement with thickness decrease and voltage increase 21 p3780 A69-39045

MSI 12 bit digital to analog converter in integrated circuit form using MOS switching circuit
[AIAA PAPER 69-968] 22 p3906 A69-40349

Duty cycle IC generator for switching regulators, discussing construction, resistive and dielectric films fabrication, applications, etc 23 p4073 A69-42293

Minimization algorithm for switching systems synthesis, describing design of mass spectrometer curve function generator and autonomous shift register 23 p4146 A69-42535

Symmetrically regulated AC/DC converters power characteristics improved by switching in phase rectifiers twice during control cycle 24 p4254 A69-42570

Nonblocking switching networks operating in ordinary and in simultaneous switching regime, including control algorithms for optimal space communication 24 p4289 A69-43138

On-off limit cycle controllers for reaction-jet controlled systems, investigating delay effects 24 p4291 A69-43271

SWITCHING FUNCTIONS U BOOLEAN FUNCTIONS

SWITCHING THEORY

AM phase locked states switching behavior of PM He-Ne lasers, considering isotope mixtures effect 20 p3552 A69-36994

Second order suboptimal control systems with time varying coefficients, calculating switching curves for quadratic cost functional 21 p3825 A69-39634

SWITZERLAND

Swiss space research report to COSPAR covering upper atmosphere studies, solar wind, etc 15 p2723 A69-31427

Automatic, semiautomatic and manually operated parachute release systems used in Switzerland 24 p4252 A69-42911

SWIVELS

Aerodynamics of flap balanced swivel airfoils, discussing lift curve slope, incidence change response and application of control forces and movements 03 p0364 A69-13908

SYMBOLIC PROGRAMMING

ASTRE programming language applicability to maximum memory information treatment in aerial navigation 03 p0401 A69-14180

Computer programming language for three dimensional geometry at symbolic level, noting use for placement problems 05 p0724 A69-16382

Specialized mathematical machine for expanding matrix determinants and solving combinatorial problems, discussing symbolic circuit 09 p1460 A69-21782

Symbolic language and assembly program for Roseau computer, discussing mnemonic code and program operation 20 p3502 A69-37397

SYMBOLS

Thermal physiology standardized symbols compilation for units of measurement 23 p4078 A69-41317

SYMMETRICAL BODIES

NT AXISYMMETRIC BODIES
NT BODIES OF REVOLUTION
NT CELESTIAL SPHERE
NT CONICAL BODIES
NT CYLINDRICAL BODIES
NT ELLIPSOIDS
NT FAIRINGS
NT LENTICULAR BODIES
NT PARABOLIC BODIES
NT POINCARÉ SPHERES
NT ROTATING CYLINDERS
NT ROTATING SPHERES
NT SLENDER CONES
NT SPHERES
NT STREAMLINED BODIES
NT TORUSES

Free transonic gas flow incident on symmetrical profile at angle of attack with given velocity at infinity calculated using difference scheme 11 p1820 A69-25469

Flexural vibrations of unstiffened doubly symmetric cylindrical tubes, obtaining natural frequencies of simply supported rectangular tube 15 p2703 A69-30210

Rayleigh criteria extension for boundary layers of rotationally symmetrical bodies with curved meridian, utilizing orthogonal coordinate system 19 p3298 A69-36309

SYMMETRY NT GAUGE INVARIANCE

Asymmetry causes on cosmogonic scale in view of symmetry in small space-time regions /microworlds/ determinable within framework of Einstein theory 14 p2516 A69-28866

Antimatter in universe, presenting arguments for microscopic and macroscopic symmetries 17 p3006 A69-33578

Two point tensor function symmetries of nonlocal cohesive finite elastic materials determined from atomic lattice theory, obtaining Green function 19 p3444 A69-36798

Transfer matrix symmetry about secondary diagonal in vibration analysis useful for computer programming 22 p4040 A69-39938

SYMPATHETIC NERVOUS SYSTEM

Pharmacological tools in autonomic nervous system research, discussing norepinephrine biosynthesis, storage, release and inactivation in mammals 02 p0200 A69-12722

Sympathetic neurohormones measurement in plasma of race car drivers 07 p1067 A69-19424

Sympathetic nerve activity inhibition due to afferent baroreceptor nerves reflexes, studying carotid sinus and aortic nerves as pathways to vasomotor center 20 p3479 A69-38073

Sympathetic nerve liberated noradrenaline increasing melatonin synthesis, using C 14 tracer for monitoring 22 p3871 A69-40051

Reflex activity of single preganglionic sympathetic fibers during coronary occlusion in cats, discussing left third thoracic /T3/ ramus communicans 23 p4084 A69-41460

Electrical stimulation effects of carotid sinus on sinus rate and atrioventricular conduction for vagi and sympathetic nerves interruption to heart in dogs 24 p4257 A69-42629

SYMPATHOMIMETICS

U ADRENERGICS

SYMPTOMS U SIGNS AND SYMPTOMS

SYNAPSES

Synaptic configurations in neuropil of planarian *Dugesia dorotocephala* brain, discussing neurotransmitters at phyletic level 16 p2741 A69-31555

SYNCHROCYCLOTRONS

Radiological properties of high energy proton beams from synchrocyclotron in tumor treatment and neurosurgery 03 p0373 A69-13495

Proton beams uniformity available at NASA synchrocyclotron designed for radiation biology research by simulating space radiation environment 05 p0742 A69-15992

600 Mev proton synchrocyclotron at Space Radiation Effects Laboratory for space radiation environment simulation, discussing beam energy spread 16 p2814 A69-32201

SYNCHRONISM

NT BIT SYNCHRONIZATION NT FREQUENCY SYNCHRONIZATION

Multiple transmission principles, examining linear systems, synchronous and asynchronous codes and channel interference 01 p0026 A69-10068

Noise resistance investigation of period synchronization systems described by Markov chains, determining phasing error for circuits 01 p0031 A69-10881

Synchronization in coded communication systems, considering phase lock loop and square wave correlation function 03 p0383 A69-12871

Adaptive processing limited memory receiver for synchronous detection of signals of unknown amplitude 03 p0400 A69-13228

Synchronization problem for quasi-harmonic oscillator with nonlinearity in form of cubic parabola, discussing existence and stability of periodic solutions 04 p0578 A69-15136

Synchronization of generators of finite dimensional forces, discussing mechanism of almost conservative dynamic objects on basis of influence matrix 05 p0793 A69-15779

High speed streak camera synchronization with shock tube process involving nonreacting gases or mixtures in pressure chamber 06 p0926 A69-17499

Beam modulation resynchronization at large signal levels by TWT circuit wave to enhance efficiency 07 p1094 A69-18422

Pulse synchronism of solid state lasers Q switched by means rotating prism, discussing pulse shifting to obtain radiation in filaments 07 p1147 A69-18488

Synchronizing ruby and Nd-glass laser pulses by means of passive bleachable dye solution liquid switch 07 p1147 A69-18530

Synchronization errors effects on performance of compression-line demodulator, increasing mean square error in measuring instantaneous frequency and locking probability 08 p1271 A69-19922

Mode locked laser operation, noting output and applications to optical communication, high speed photography, nonlinear optics and frequency standard 09 p1518 A69-22128

Simultaneous transmission of information signals and pseudonoise synchronization waveforms in common bandwidth [IEEE PAPER 67-TP-1173-COM] 10 p1655 A69-23532

Solid state synchro data interfaces for angular information, noting synchro to digital and digital to synchro conversion techniques and synchro repeaters 11 p1842 A69-24543

Worldwide clock synchronization by geostationary satellite transponder relaying VHF signals from reference clock, noting accuracy of radio propagation delay prediction 12 p2080 A69-26053

Cosmic triangulation by geometrical synchronization of astrometric satellite observation, with precise times unavailable 12 p2158 A69-26432

Noise resistance of period synchronization systems described by Markov chains, determining phasing error for circuits 12 p2031 A69-26645

Latent desynchronization, discussing life system and distortion, body rhythms coordination, circadian rhythms and adaptation to new system of time 15 p2557 A69-31457

Airborne clock used to synchronize atomic clocks at different locations, discussing equipment and error sources 17 p2975 A69-33593

Synchronization of generators of finite dimensional forces, discussing mechanism of almost conservative dynamic objects on basis of influence matrix 18 p3173 A69-35031

X ray stroboscope for moving objects in penetrating irradiation, considering synchronization of radiation receiver 18 p3138 A69-35114

Discrete information transmission synchronization in communication systems concerning optimal signal detection, HF, phase and coded synchronization, etc 18 p3104 A69-35264

Optimum power allocation for RF carrier phase error and synchronization error in two channel system 19 p3274 A69-36283

Gas laser oscillation mode selection and self synchronization based on separation in two mirror cavity with nonlinear absorption 19 p3336 A69-36355

Schwarzschild metric properties in synchronous reference system, using succession of Schwarzschild interval holonomic transformations as function of gravitational radius 22 p3982 A69-41063

Subjects confined in caves for two to six months to note physiological rhythms time evolution and associated desynchronization and resynchronization 23 p4107 A69-41818

Magnetospheric stable charged particle beams for pearl pulsations and discrete VLF radiation in geomagnetic field, attributing synchronization to space charge 23 p4206 A69-41851

Error probability bounds for self synchronized binary PSK communication systems, simulating decision feedback, phase doubling and maximum likelihood systems 23 p4128 A69-42501

SYNCHRONIZATION U SYNCHRONISM

SYNCHRONIZED OSCILLATORS

AM and FM noise in mutually synchronized oscillators 02 p0220 A69-12449

Injection phase locking for synchronizing oscillators and reducing FM noise 02 p0220 A69-12450

Direct and indirect synchronization of pulsed oscillator with interrupted synchronizing signal for spectral purity of output waveform and locking range of system
03 p0404 A69-13301

Synchronization problem for quasi-harmonic oscillator with nonlinearity in form of cubic parabola, discussing existence and stability of periodic solutions
04 p0578 A69-15136

Phase measurement using phase lock loop, voltage controlled oscillator and synchronous counter
05 p0722 A69-16766

Stable limiting cycles of laser resulting from mutual synchronization of phase shifted oscillation modes
07 p1158 A69-19752

Phase synchronized oscillators in microwave frequency multipliers with improved SNR
09 p1464 A69-22113

Sporadic noise, false fronts and other noise effects on phase of output oscillations of resonance apparatus
09 p1460 A69-22641

Two oscillator signal combiner based on mutual synchronization, providing output signal free of phase jumps or amplitude fluctuations
11 p1849 A69-24928

Tunnel diode self excited SHF oscillators synchronization, deriving single frequency generation conditions
11 p1849 A69-24955

Gunn oscillators synchronizing by injecting HF external signal, discussing oscillator fabrication techniques, phase synchronization, etc
11 p1856 A69-25636

Digital phase-shift control of locked oscillator
12 p2052 A69-26382

Pull-in oscillator for random noise coincident with synchronizing and frequency shift signals, discussing circuit parameters effect on signal discrimination and noise suppression
12 p2044 A69-27101

Frequency memory in cavity controlled Gunn oscillators, discussing loop gain and bandwidth dependence on oscillation mode and bias voltage
13 p2229 A69-27677

Synchronized backward wave oscillator transmitting tube for space communication stations
13 p2232 A69-28058

Phase and amplitude changes of arbitrary-Q self excited oscillator under external disturbance, using differential equations
13 p2300 A69-28574

Reference oscillator synchronization inaccuracy influence on SNR at output of correlation receiver during reception of signals with pseudonoise modulation
15 p2563 A69-30141

PCM oscillator synchronization system stability, considering sampled model by digital nature of equipment
15 p2565 A69-30171

Carpitron locked oscillator with wide electronic tuning range, describing CW operation characteristics and application to ground station microwave transmitters
23 p4135 A69-41302

SYNCHRONIZERS

Book on synchros application and design covering telemetry, torque and control systems, synchro circuits, resolvers as computer elements, etc
21 p3681 A69-38450

SYNCHRONOUS COMMUNICATION SATELLITES
U SYNCOM SATELLITES

SYNCHRONOUS DETECTORS
U CORRELATORS

SYNCHRONOUS METEOROLOGICAL SATELLITE

Meteorological application of ATS observations in form of time lapse movies of weather in motion, describing camera and data flow
[AIAA PAPER 68-1094] 12 p2174 A69-26804

SYNCHRONOUS MOTORS

Synchronous servomotor for parabolic antenna of surveillance radar, discussing motor size and optimum gear ratio determination
08 p1274 A69-20108

Nonstatic gyroscope nonlinear oscillations caused by swaying of synchronous gyromotor rotor
13 p2264 A69-28438

SYNCHRONOUS SATELLITES

NT EARLY BIRD SATELLITES
NT SYNCOM SATELLITES

Mechanically despun VHF antenna for spin stabilized synchronous satellites, detailing electrical and mechanical design
01 p0161 A69-10350

Geostationary satellite transmissions for educational purposes
[UN PAPER 68-95533] 01 p0028 A69-10494

Worldwide navigation system consisting of synchronous satellites equipped with pulse modulated microwave transmitters
[UN PAPER 68-95205] 01 p0113 A69-10514

Aircraft navigation using synchronous satellites based on position location by intersection of two circles with centers below satellites
01 p0114 A69-11011

Satellite communications with emphasis on European programs, discussing synchronous satellites, Europa 2 rocket and Saros and Symphonie projects
02 p0207 A69-11910

Multijet electrothermal systems for attitude control and stationkeeping of synchronous communications satellite
[AIAA PAPER 67-723] 02 p0305 A69-12375

Path length and path length rate variations in synchronous satellite communications link
04 p0561 A69-15448

Optimum spacing of communication satellites on inclined circular synchronous orbits, applying figure 8 packing schemes
04 p0562 A69-15458

Perturbations of stationary orbital vehicles of arbitrary latitude due to earth triaxiality, noting control by low thrust rocket engine
05 p0823 A69-16037

Dioscures system for international air traffic control and navigation over North Atlantic by means of two geostationary satellites
[UN PAPER 68-95832] 06 p0954 A69-17063

Active magnetic coils for attitude control of synchronous satellites by computer simulation and laboratory tests
06 p1017 A69-17944

Predictor determining future position of TDMA/Time Division Multiple Access/ synchronous satellite communications system satellite from previously received bursts
07 p1076 A69-18553

OMEGA position location equipment /OPLE/ test data to demonstrate feasibility of using OMEGA navigational system in conjunction with synchronous satellites
07 p1176 A69-19135

Channel multiplier spectrometer for low energy electrons and protons at synchronous altitude on ATS-E satellite
[IEEE PAPER 3C-5] 07 p1135 A69-19199

Synchronous orbit attainment with continuous electric propulsion, noting payload ratio dependence on various parameters and changing orbit inclination
[AIAA PAPER 69-275] 09 p1586 A69-21265

Orbiting Data Relay Network communications system provides continuous wideband communication between ground and earth orbiting spacecraft via synchronous satellite repeaters
[AIAA PAPER 68-432] 09 p1455 A69-21989

Scintillation fading of VHF beacons on synchronous satellites, noting amplitude fluctuation depth and rate
09 p1457 A69-22461

Synchronous and near synchronous satellites for communication systems, discussing stationkeeping and low thrust propulsion
09 p1458 A69-22468

TV broadcasting from synchronous satellites direct to ordinary UHF receivers in 1980s
11 p1833 A69-24529

Cosmic ray cut-off energy for synchronous satellites computed by trajectory tracing method using magnetospheric model
11 p1949 A69-24860

Worldwide clock synchronization by geostationary satellite transponder relaying VHF signals from reference clock, noting accuracy of radio propagation delay prediction
12 p2080 A69-26053

Antenna circular array for synchronous communications satellites, discussing directional patterns, super-gain ratio, element spacing, etc
13 p2225 A69-27184

Synchronous satellite TV broadcasting systems in UK, discussing equipment, transmission problems and economic factors
13 p2220 A69-27830

First order secular and aperiodic perturbations in Keplerian orbital elements of synchronous satellite due to earth gravitational field eccentricity
14 p2521 A69-29466

Satellite space navigation system providing three component position in geodetic coordinates instantly and accurately on or near earth
15 p2650 A69-30088

Satellite orbits obtained by tracking by synchronous satellites, discussing accuracy for low altitude satellites
15 p2698 A69-31340

Dioscures project for worldwide telecommunications, air traffic control and navigation by satellites, discussing technical, operational and economic characteristics
16 p2749 A69-31601

Electrically propelled TV satellite control maneuvers to reach target position in synchronous circular orbit from spiral ascent trajectory
16 p2868 A69-31935

Ion propulsion applied to geostationary satellites attitude control, discussing thrust levels, cesium ionization, colloidal propulsion, etc
16 p2837 A69-32068

Europa 3 rocket design, comparing 2 ton geostationary satellites and 700 kg satellite conceptions
17 p3045 A69-33095

Orbital and attitude control tests for PAS /two stage perigee-apogee synchronous satellite/ in conjunction with booster Europa 2, discussing functional configuration
17 p3048 A69-33238

Microthrusters thrust requirements for attitude control and orbital transfer of gravity gradient geostationary satellite
17 p3019 A69-33336

Solar cell radiation damage during 416.8 days in synchronous orbit on satellite ATS 1, discussing radiation shields
19 p3253 A69-35704

Feasibility of automatic stationkeeping for synchronous satellites by using solar sailing techniques and low thrust systems
[AAS PAPER 68-151] 19 p3429 A69-35950

Educational TV coverage extension via synchronous satellites to areas of limited coverage, emphasizing South American countries
19 p3268 A69-36163

Nationwide TV system using synchronous communication satellite proposed for India, discussing antenna, modulation, multiplexed channels and educational aspects
19 p3275 A69-36413

Stationkeeping motion effect on synchronous satellite orbit determination accuracy analyzed by two dimensional model, finding position uncertainty
20 p3595 A69-37218

Satellite tracking and orbit determination accuracy for system of two synchronous geostationary satellites
[AIAA PAPER 68-449] 21 p3674 A69-39019

Doppler tracking of near synchronous DODGE satellite from single frequency data, noting error sources
[AAS PAPER 68-128] 21 p3674 A69-39202

Automatic stationkeeping /geosynchronization/ for maintaining satellite in circular synchronous orbit at all geocentric longitudes for prolonged time with low fuel consumption
21 p3805 A69-39213

Near equatorial near synchronous satellite orbits determined by supplementing spherical harmonics representation of earth gravitational field with polynomial force model representation
[AAS PAPER 68-141] 21 p3806 A69-39234

Sun-moon short term disturbances effect on synchronous equatorial navigation satellite orbits, noting fuel expenditure
[AIAA PAPER 69-927] 21 p3761 A69-39356

Electromagnetic attitude control system for Lincoln Experimental Satellite 5 in near-synchronous equatorial orbit, noting onboard error detection in closed control loop
21 p3827 A69-39755

Particles integral and differential fluxes spectral distribution calculation for determining radiation load for synchronous satellite
22 p4035 A69-39909

Synchronous communications satellite launch constraints for fixed time or node, noting application to IDCSP/A mission and sun angle, occultation and transfer orbit
[AIAA PAPER 68-445] 22 p4036 A69-40543

Spacecraft phase array designed for use on synchronous communication satellite, discussing low structural weight packaging and unfurling problems and helix approach
22 p3915 A69-40705

Aperture efficiency, weight and control power requirements for hybrid matrix arrays in synchronous satellite applications, calculating residual array gains
22 p3915 A69-40707

Worldwide communication system via synchronous satellites for aeronautical, maritime and land mobile services

23 p4114 A69-41355

Tracking and Data Relay Satellite System with synchronous orbit satellites to relay data between low altitude earth orbital spacecraft and mission control centers

23 p4120 A69-41755

RFI effects of earth based emitters on operation of geosynchronous satellites for data relay from near earth orbiting satellites, noting frequency assignments

23 p4120 A69-41757

Liquid fuel propulsion systems for geostationary satellites, discussing transfer orbits, payload increase and required thrust for various satellite trajectories [DGLR-69-014]

23 p4202 A69-41929

Aircraft navigation by geostationary satellites, discussing Dioscures project

24 p4280 A69-42568

Remote manipulator spacecraft system for refurbishing synchronous communication satellite, emphasizing compatibility with standard shroud Titan 3C launch vehicle

24 p4297 A69-43041

SYNCHROTRON NOISE

U ELECTROMAGNETIC NOISE

SYNCHROTRON RADIATION

Power radiated in magnetoionic mode by electron spiraling in magnetoplasma

02 p0309 A69-12720

Type 4 bursts mobile spectrum of september 14, 1966 interpreted by considering plasma effects on synchrotron emission mechanism

02 p0309 A69-12754

Radio galaxies and quasars X ray emissions, calculating radiation fluxes produced by scattering of synchrotron radiation quanta at relativistic electrons

03 p0500 A69-13079

Synchrotron radiation excitation in system of relativistic monoenergetic electrons rotating in cold magnetoactive plasma

03 p0476 A69-13383

Radiation intensity from system of monoenergetic relativistic electrons in plasma, discussing maser effect in coherent synchrotron radiation

03 p0500 A69-13407

Ionized medium effect on polarization of synchrotron radiation from monoenergetic distribution of electrons

04 p0648 A69-14420

Gyro synchrotron emission spectrum and intensity from energetic solar electrons radiating in coronal magnetic fields applied to type IV solar radio bursts

04 p0650 A69-15529

Magnetobremstrahlung /synchrotron/ and Compton radiation of ultrarelativistic particles, radiation reabsorption and magnetic field measurement

06 p0962 A69-17245

Synchrotron radiation from trapped high energy electrons in Van Allen belt

06 p0992 A69-17324

Particle flux and dose rates in Jupiter Van Allen belts based on assumed synchrotron radiation from trapped electrons in dipole magnetic field

[AIAA PAPER 69-18]

06 p0997 A69-18129

Monoenergetic relativistic electrons stream gyrating along cold magnetoactive plasma with pitch angle radiatively unstable with respect to synchrotron radiation

07 p1191 A69-18958

Synchrotron radiation from relativistic electrons in magnetosphere, calculating variation with frequency and height of lines of force

08 p1306 A69-20182

Solar moving type 4 burst emitting synchrotron radiation, noting electron acceleration in collisionless shock wave in corona

09 p1578 A69-22058

Synchrotron and X ray emission generation from upper chromosphere electrons during solar flares

09 p1580 A69-22203

Incoherent synchrotron radiation by relativistic electrons gyrating in cold magnetoactive plasma rederived, correcting errors

10 p1741 A69-23858

Synchrotron radiation amplification by monoenergetic electron stream helically gyrating in static magnetic field of cold plasma, discussing amplification rate frequency dependence

11 p1931 A69-25361

Frequency spectrum, time variations and polarization of source of synchrotron radio emission with ex-

panding components flying apart at relativistic velocities

12 p2155 A69-26207

RF synchrotron radiation emitted by electrons trapped in geomagnetic fields above auroral zones, discussing electron flux and cosmic background

12 p2151 A69-26949

Io as unipolar inductor, analyzing interaction with Jupiter magnetosphere and decimetric synchrotron radiation

13 p2337 A69-27552

Radiative relaxation of relativistic particle distribution undergoing synchrotron radiation and reabsorption, discussing self absorbed radio source model

13 p2327 A69-27572

Synchrotron spectrum radiated by relativistic electrons below Razin cut-off, considering relation to radio spectra curvature of variable extragalactic sources

13 p2339 A69-27573

Relativistic electrons synchrotron radiation by calculating magnetoactive plasma permittivity tensor, determining normal waves polarization characteristics

13 p2315 A69-28451

Radio galaxies and quasars X ray emissions, calculating radiation fluxes produced by scattering of synchrotron radiation quanta at relativistic electrons

14 p2509 A69-28761

Radio noise of auroral origin analyzed from Northern and Southern Hemisphere reports indicating correlation with auroras, magnetic activity, sunspot cycles and synchrotron radiation

14 p2411 A69-29108

Synchrotron radiation and reabsorption theories

15 p2674 A69-30421

Electron energy distribution determination from electron synchrotron radiation spectrum for various magnetic field configurations within radio source

15 p2655 A69-30546

RF synchrotron emission from electrons trapped in earth magnetic field observed by satellite, using magnetospheric environment model

18 p3128 A69-34948

Ultrarelativistic electron acceleration in Crab Nebula maintaining synchrotron spectrum, obtaining power from compressional motion damping, gyrorotation effect and pitch angle anisotropy removal

19 p3424 A69-36336

Radio emission from Sco XR-1 shown as synchrotron radiation of relativistic electrons in low density region surrounding denser core producing X ray

20 p3597 A69-37334

Synchrotron radiation and reabsorption for rapidly moving cloud of relativistic particles, considering errors

21 p3772 A69-39513

Synchrotron radiation HF cut-off resulting from electrons with anisotropic pitch angle distribution for type IV solar radio bursts

22 p4006 A69-40577

Pitch angle distribution of cosmic ray electrons in decreasing magnetic field for waves in ionized plasma, noting anisotropy due to synchrotron radiation

22 p4006 A69-40642

Type II and type III solar radio burst relation to plasma instability associated with coherent synchrotron deceleration of electrons, discussing resonant power exchange

22 p4007 A69-40898

SYNCHROTRONS

UHF high power klystron for DESY synchrotron, discussing design, short circuited load operation, phase variations and optimum RF outputs

07 p1096 A69-18434

SYNCOM SATELLITES

NT EARLY BIRD SATELLITES

Attitude determination and hydrogen peroxide control system for spacecraft orientation in Syncom, Early Bird and ATS

[AIAA PAPER 67-532]

09 p1610 A69-21988

Solar thermal vacuum test for space flight qualification of military spin stabilized synchronous orbit communications satellite

15 p2587 A69-30391

Geostationary satellite TV broadcasting to small contiguous areas with separate programs, discussing communication distribution problems

22 p3902 A69-41252

SYNDROMES

U SIGNS AND SYMPTOMS

SYNOPTIC MEASUREMENT

Synoptic observations of F 2 layer in magnetically conjugate regions, comparing critical frequencies

06 p0919 A69-17723

Synoptic charts of chromosphere, giving position and magnitude of sunspots, faculae and prominences during synodic revolution of sun

08 p1379 A69-20391

Solar magnetic fields distribution regularity with autocorrelation analysis of magnetic synoptic charts

08 p1394 A69-20391

Synoptic criteria combined with qualitative criteria for CAT diagnostics from analysis of turbulent zones responsible for bumpiness in upper troposphere

14 p2474 A69-29771

Relation between radar echoes spatial extent and synoptic conditions with reference to various forms of weather significance for aviation

14 p2474 A69-29771

Cosmic ray observations on synoptic scale, discussing equipment and programs of IQSY world array of monitor stations

15 p2673 A69-30001

Synoptic observations of F 2 region in magnetically conjugate regions of Kerguelen and Archangel, comparing critical frequencies during magnetic and ionospheric disturbances

16 p2784 A69-32619

Horizontal and vertical ozone distributions synoptic study, comparing soundings made on both sides of Atlantic

16 p2786 A69-32623

Synoptic study of worldwide VLF electromagnetic wave fields distribution above ionosphere from Ariel observations

21 p3717 A69-39261

Synoptic remote sensing oceanography from shipboard aircraft and spaceborne platform, discussing fisheries [AAS PAPER 69-062]

24 p4307 A69-42821

SYNOPTIC METEOROLOGY

Meteorological rocket soundings and global synoptic observations, noting influence of atmospheric middle region

[UN PAPER 68-95405]

01 p0109 A69-10488

Passive and active transmitters and receivers of electromagnetic radiation in earth orbital satellites to collect pictorial or numerical data to study hydrology [UN PAPER 68-95333]

01 p0064 A69-10488

Meteorological satellite observations value to Southern Hemisphere [UN PAPER 68-95213]

01 p0109 A69-10511

Satellites use in French space meteorology, discussing evolution, achievements, Eole project, etc.

02 p0275 A69-11911

Meteorological satellites for atmospheric data collection applicable to weather forecasting and synoptic analysis

02 p0277 A69-12771

NOMAD buoy telemetry system for synoptic oceanographic and meteorological data, using digital processing and dual frequency transmissions

03 p0391 A69-13221

Synoptic density maps for postreentry altitude derived from constant pressure charts and horizontal gradients

04 p0626 A69-14901

Interpretation technique for weather satellite photographs of spatially coherent cloud distributions

04 p0628 A69-15091

COSPAR manual on stratospheric temperature and wind measurements, discussing synoptic and time variation study by Arcas and Loki-Judi meteorological sounding rocket systems

05 p0752 A69-15701

Meteorological satellites in weather forecasting, contrasting satellite data continuity to discreteness of synoptic charts

[UN PAPER 68-95760]

06 p0949 A69-17031

Weather forecasting using statistical technique and Subsynchronous Advection Model of Weather Bureau, discussing mathematical background for various early morning predictions

08 p1345 A69-20291

Synoptic meteorological predictions using statistical dynamic approach, considering probability distributions and nocturnal temperature decay

08 p1345 A69-20301

Computerized objective analysis of meteorological variables based on weight determination involving autocorrelations

08 p1345 A69-20301

Synoptic process predictability, discussing forecasting of large and small scale processes by mathematical formulas and statistical description

12 p2126 A69-26571

Earth TV pictures from Molniya 1 communication satellite, showing advantages of high orbit over low

- orbit photography for global weather analysis and forecasting
13 p2292 A69-27729
- Mean seasonal atmospheric and synoptic circulation types examined by criterion for identifying analog types
13 p2295 A69-28652
- Satellite radiation maps for synoptic analysis regarding world weather maps, discussing front, intertropical convergence zones and typhoon location
14 p2473 A69-29729
- Flight regularity and safety in complex meteorological situations, noting synoptic forecasting advantages over inertial forecasting
14 p2475 A69-29740
- Time spectra of wind velocity, temperature, pressure and turbulent heat transfer and momentum in synoptic region
14 p2476 A69-29823
- Synoptic meteorological conditions effect on stellar images vibration and on relationship between vibration and zenith distance
15 p2647 A69-30164
- Ozone soundings data obtained over Australia and Colorado to obtain vertical picture of synoptic climatology of ozone at midlatitudes
15 p2649 A69-30898
- Alpine effects on wind field at synoptic scale using potential-vorticity equation, discussing deflection angle dependence on potential temperature distribution
15 p2650 A69-31445
- Air motion and precipitation patterns in travelling wave depression, considering Doppler radar data, rainfall rates, orographic influences, etc
18 p3166 A69-34419
- Classification of synoptic processes, discussing condensation of parameters characterizing state of atmosphere
18 p3166 A69-34815
- Satellite synoptic meteorological data collection systems, discussing configurations, global location requirements and digital code platforms position determination [AIAA PAPER 68-1095]
21 p3819 A69-39029
- Soviet book on synoptic climatological and heliogeophysical long term weather forecasts, discussing monthly and seasonal anomalies, sun-earth interrelations, solar corpuscular elements, etc
21 p3759 A69-39523
- Radiative cooling models for various midlatitude synoptic features, including stationary front and cyclones
24 p4343 A69-43064
- SYNTHESIS**
- Element synthesis in stars of galactic halo as possible explanation for heavy elements presence in supermassive objects
07 p1219 A69-19296
- Synthetic lubricants characteristics and aircraft applications, describing common products and properties
18 p3163 A69-35481
- Tryptic pentapeptide Asp-Glu-Leu-Thr-Lys synthesis showing relation to Gm/a/ antigen of human gamma g-globulin
24 p4279 A69-42712
- Synthesis of second order nonlinear differential equations reducible to linear third order equations for application to vibrations field
24 p4342 A69-43702
- SYNTHESIZERS**
- U CHEMICAL REACTORS
- SYNTHETIC ARRAYS**
- Analysis and optimization of side-looking synthetic aperture radars carried out for resolution, SNR and least squares estimation of target field
08 p1277 A69-20960
- Mechanical collimator using random aperture arrays for celestial observation at extreme UV and X rays
19 p3313 A69-36489
- Phase error in synthetic aperture radar, discussing tolerance level, sources classification and effect on average response, resolution and ambiguity function
20 p3490 A69-37642
- Synthetic aperture radio telescopes analysis, noting resolution and sensitivity at radio wavelengths for correlator array in supersynthesis mode operation
21 p3677 A69-39512
- SYNTHETIC FIBERS**
- NT DACRON [TRADEMARK]
NT GLASS FIBERS
- Transversely isotropic elastic solid approximation for oriented fibers of polyethylene, nylon, polyethylene terephthalate and polypropylene, measuring elastic compliances
09 p1528 A69-21504
- Book on ceramic fibers and fibrous composite materials as structural reinforcements covering dynamic testing of fine filaments and whiskers, material characterization, etc
12 p2118 A69-26340
- Fiber polymer composite flexible insulating materials properties and applications stressing synthetic organic fibers
13 p2286 A69-27989
- Carbon fiber reinforced plastics properties improvement by applying organosilanes, discussing silanol bond formation
16 p2803 A69-31806
- Silicon nitride staple fibers synthesis, development and characterization, noting tensile strength and sonic modulus
19 p3354 A69-35517
- Flame resistant organic fiber in cross linked polymer structure, discussing properties and aerospace applications
24 p4337 A69-43424
- SYNTHETIC RESINS**
- NT ACRYLIC RESINS
NT EPOXY RESINS
NT PHENOLIC RESINS
NT POLYAMIDE RESINS
NT POLYESTER RESINS
NT POLYMETHYL METHACRYLATE
NT THERMOPLASTIC RESINS
NT THERMOSETTING RESINS
- Mechanical behavior of synthetic layer coatings for damping instrumental vibration and noise
01 p0168 A69-10399
- Polyfluoroethylene resin breakdown under uniaxial tension, considering continuity disruption
13 p2286 A69-28321
- Resin impregnated fiber reinforced expandable structures used for automatic cure or rigidizing in space and initially small compact packages on earth
19 p3433 A69-35585
- SYNTHETIC RUBBERS**
- U ELASTOMERS
U STYROFOAM [TRADEMARK]
U THIOPLASTICS
- SYSTEM FAILURES**
- Survival analysis based on probability theory for design of air cushion vehicle to determine height for operating over open sea
01 p0008 A69-10027
- Reliability analysis of technological systems, determining characteristics as distribution function of time to specified number of failures
01 p0085 A69-10210
- Mathematical model constructed for behavior of multicomponent system subject to cannibalization
01 p0086 A69-10651
- Guaranteed estimations of system reliability for systems with incomplete element reliability data
02 p0251 A69-11652
- Book on laws of failures in technical equipment with emphasis on quantitative description and practicality of reliability theory, discussing redundancy problems
03 p0433 A69-13009
- Reliability system design, emphasizing circuit design analysis, failure drifts and component failure modes by use of computer programs [ECAP, CIRC and IMAG]
04 p0608 A69-15224
- Dual processor checkout system providing isolation of malfunctioning unit from memory and ensuring decision making by operative unit
04 p0568 A69-15361
- Threshold failure levels of semiconductor diodes and transistors due to pulse voltages
06 p0977 A69-16883
- Mechanical, electromagnetic and chemical signatures monitoring and analysis during system operation
06 p0932 A69-17875
- System safety analysis for V/STOL aircraft, discussing fault-tree technique role in fail-safe design [AIAA PAPER 69-216]
07 p1056 A69-19575
- Operational reliability of manual and automatic flight control systems and components and current safety standards
08 p1255 A69-20720
- Postselection estimation of component reliability in multicomponent systems, considering cases of binomial and exponential distributions of random variables
08 p1322 A69-21099
- Computerized simulation of time dependent reliability of multicomponent system based on statistical model of component breakdown
08 p1277 A69-21100
- Computer programs for systems statistical reliability characteristics using reliability tests and time to failure data, giving optimal breakdown probability functions
08 p1322 A69-21101
- Reliability of individual components of multicomponent systems under variable loads, using asymptotic distribution of minimal values
08 p1322 A69-21103
- Failure distribution functions based on Eyring component aging model, including failure probability density function for Weibull and gamma type distributions
08 p1322 A69-21104
- Catastrophic failures in logic circuit and system design, considering thermal effects, complexity, statistical methods and computer use
08 p1299 A69-21107
- Reliability terms for electrical apparatus, equipment and systems, indicating need for international standardization
08 p1292 A69-21108
- Electronic components reliability tests, determining correlation between material quality and failure
08 p1293 A69-21109
- Failure mechanisms in semiconductor, discussing imperfections, fabrication errors and electrical, thermal and mechanical stresses
08 p1294 A69-21117
- Automatic transistor reliability testing system based on measured data and reliability research
08 p1294 A69-21119
- Bayesian reliability growth model with random variable parameters, discussing multimode failures
09 p1504 A69-21912
- Stochastic model for calculating expected component failures in transient state from Weibull distribution failure data for first generation
09 p1504 A69-22149
- Onboard test and fault isolation design for airborne systems considering tradeoff parameters for optimum reliability, performance and cost [AIAA PAPER 69-306]
09 p1434 A69-22389
- Algorithm in fault detection and isolation, discussing test optimization for complex systems or structures subject to failure
10 p1698 A69-22978
- Symptom pattern observation technique for flight data analysis, discussing in-flight symptoms and SPOT chart in aircraft maintenance
10 p1669 A69-22982
- Reliability characteristics of service life determination, noting exponential distribution of failure time value
10 p1662 A69-23319
- Microwave tube development, discussing cold cathodes, ferrite and semiconductor integration into tubes, tube failure physics, etc
11 p1847 A69-24745
- Optimization of control systems with allowance for failures of elements in parallel operation, noting application to vehicle with clustered propulsion system
11 p1966 A69-25331
- Computer programs for linear systems fault isolation, discussing technique theory and limitations
12 p2040 A69-26568
- Probability analysis by methods simplifying calculations or providing bounds on reliability of complex system
12 p2103 A69-26751
- Transistorized amplifiers reliability estimated from step by step failures during operation in intense external environment
12 p2043 A69-26886
- Procedures and facilities applicable to sonic environmental testing of flight vehicles, discussing sonic energy sources in vehicles and potential failure modes
12 p2060 A69-26939
- Failure engineering analysis of electromechanical switching devices, discussing preanalysis planning, open-ended data sheets, etc
13 p2231 A69-28043
- Reliability analysis of technological systems, determining characteristics as distribution function of time to specified number of failures
14 p2453 A69-28747
- Reliability and efficiency improvements for thermionic converters at JPL, giving failures analyses
14 p2397 A69-29175
- Thermionic converter components reliability under mechanical load and failure models, showing probabilistic nature of failures
14 p2400 A69-29227
- Electronic systems packaging substitution method for optimized malfunction isolation at succeeding levels to final discard-at-failure
14 p2420 A69-29494
- Electronic components reliability by failure rates and drift behavior, assuming probabilities product rule and exponential law of life distribution
15 p2626 A69-30835

Complex systems reliability, describing uses of computer programs in analysis of circuit design, component failure modes and faults due to drifts

15 p2572 A69-31042

Research and development planning and control models based on subjective probability estimates for failing projects identification

15 p2721 A69-31072

Arbitrary single gate failures diagnosis in combinational logic circuits not requiring fault table construction

15 p2583 A69-31112

Military systems trouble documentation and evaluation, emphasizing computerized monitoring of reliability and maintainability

15 p2722 A69-31121

Similarity between semiconductor discrete devices and integrated circuits, considering materials, processing and failure modes

15 p2580 A69-31128

Long life repairable equipment reliability and mean time between failure with limited life components and material in normal life maintenance environment

15 p2581 A69-31134

Metal oxide semiconductor integrated circuits, showing failure rates and degradation causes

16 p2759 A69-31851

Large scale integrated circuits reliability with emphasis on multilayer metalization, designing test vehicles for failure mechanisms

17 p2935 A69-32887

Automatically controlled dynamic systems reliability estimation in terms of failure probability illustrated with autopilot-aircraft case

17 p3001 A69-33144

Airborne electric power systems maintenance aids, describing design and operation of annunciator for establishment and display of system failure causes

17 p2905 A69-34112

System state phase modeling as method for evaluating safety and reliability by analysis of system states in mission phases through logic diagram

18 p3142 A69-34480

Steady state availability of system with limited repairable spares for online units, considering statistical dependence among similar units

18 p3144 A69-34493

Avionic subsystems warranty costs estimates, considering reliability prediction and hardware recycling

18 p3232 A69-34506

Reliability demonstration by MIL-STD-781 for equipment failure and success, proposing useful alternatives

18 p3145 A69-34507

Failure detection methods, discussing percent checkout, failure sensitivity, undetectable failures, etc

18 p3146 A69-34511

Lunar Orbiter Parts Program for selection and control of electronic and electrical parts, discussing reliability and flight failures

18 p3207 A69-34520

Reliability block diagrams for laser systems, discussing failure modes of solid state, semiconductor and gas lasers

18 p3151 A69-34523

System reliability with allowable downtime, calculating probability of on-line units staying operational during mission time using conditional availability

19 p3326 A69-36002

Integrated test program based on mission requirements, failure mode and effects analysis with feedback from testing to design and development functions

19 p3327 A69-36014

Hydraulic systems incipient failure detection, discussing destructive cavitation, component defects, human error, etc

19 p3255 A69-36018

Failure data role in management of launch operations reliability program

19 p3294 A69-36022

Availability measure defined in terms of maintenance demand rate and mean downtime for cost prediction involving various parameters

19 p3327 A69-36036

Aircraft structures design, discussing reinforced sandwiches and composites, failure mechanisms, non-destructive testing and fabrication

19 p3438 A69-36325

Soviet book on fluid contamination influence on aircraft hydraulic systems operational reliability covering friction, particle size, filtration, etc

21 p3649 A69-39530

Performance prediction of terrestrial communication system based on experimental radio and

meteorological program at 11 GHz, discussing transmission loss

22 p3900 A69-40680

Summation methods for multiple damages caused by static fatigue in glass fiber reinforced plastics under stepwise loads

22 p3974 A69-40748

Liapunov stochastic stability direct method analog used for estimating reliability of redundant systems with constant recovery time

23 p4144 A69-41953

Hot spot failure modes in solar cell arrays noting protection through I-V characteristic control

23 p4142 A69-42273

Silicon solar cell panels, studying roles of solder, interconnector metals and substrate materials in failures under thermal cycling

23 p4070 A69-42274

Space vehicle flight performance of Ni-Cd batteries noting reliability, consistency and predictability

23 p4072 A69-42285

NDT techniques relation to engineering design problems with failure potential, discussing management planning and cost analysis

24 p4318 A69-42769

Automatic system failure sequence statistical analysis, considering randomly time variable external effects

24 p4289 A69-42953

Aerospace systems failures caused by stress corrosion, fatigue, overload, improper designing or inadequate processing control

24 p4323 A69-43428

SYSTEM LIFE

U RELIABILITY

SYSTEMIZATION

U SYSTEMS ENGINEERING

SYSTEMS ANALYSIS

Multilevel optimization techniques for dynamic systems control evaluated, developing second level Newton-Raphson controller

01 p0051 A69-10440

Theory for stability of steady motions of system with cyclic coordinates applicable to total damping

01 p0151 A69-10567

Soviet collection of articles on analysis and synthesis of automatic control systems

01 p0051 A69-10793

Comparative analysis of variable structure adaptive systems and time optimal system for control of plant described by differential equation

01 p0052 A69-10795

Determination of plant differential equation from time characteristics

01 p0053 A69-10804

Random order linear homing systems analyzed by frequency methods employing method of proportional navigation, noting use of transfer functions

01 p0113 A69-10805

Spacecraft voltage-limited charging system for sealed secondary batteries, discussing operating characteristics and battery parameters

01 p0013 A69-11010

Modal substitution method for free vibration analysis of large discrete undamped dynamic systems

02 p0338 A69-11747

Rotational motion of system of particles related to existence of reference frame to eliminate coupling terms between internal and rotational motion

02 p0280 A69-11867

Matrix transformation applications in dynamic system theory and stability test

02 p0281 A69-11943

Off-axis circle criterion for frequency domain stability of feedback systems with single monotonic nonlinearity, noting relation to Popov criterion

02 p0225 A69-11969

Linear filter performance degradation due to modeling error in estimate of state vector of stochastic linear dynamic systems

02 p0225 A69-11971

Pulse transfer function estimation for single input and output linear stationary discrete systems using iterative algorithm and quasi-linearization method

02 p0225 A69-11972

Higher order differential operators description and derivation of analytical mechanics for holonomic and nonholonomic systems and impact phenomena

02 p0281 A69-12199

Book on dynamics of linear and nonlinear systems covering mathematical methods for control system design

02 p0225 A69-12228

Frequency of periodic solutions of autonomous nonlinear systems determined by method using Duffing approximation

02 p0348 A69-12612

Stability properties of discrete-continuous feedback control systems with signal dependent sampling

02 p0226 A69-12734

Statistical analysis of unsteady dynamic systems describable by unstable differential equations containing random parameters

03 p0408 A69-12940

Tracking conditions for observability of nonlinear controlled systems with smooth characteristics

03 p0409 A69-13061

Tracking breakdown probability during unsteady operation of nonlinear automatic control systems analyzed by statistical linearization techniques and Fokker-Planck equation

03 p0409 A69-13070

Statistical linearization coefficients for arbitrary nonlinearities in automatic control systems via techniques applying characteristic functions

03 p0409 A69-13071

Plant identification procedures by stepwise approximation and least squares methods

03 p0409 A69-13072

Systems analysis application to determination of C-5 effectiveness noting loading, productivity and effectiveness analysis computer programs [SAE PAPER 680729]

03 p0379 A69-13440

Nonlinear system on-line identification in presence of noise, using stochastic methods and analog equipment

03 p0401 A69-13764

Low visibility aircraft landing, discussing total system approach, modern electronic developments, collision avoidance, safety and air traffic control

03 p0465 A69-13853

Synthesis of optimal second order systems with linear control

03 p0410 A69-13864

Systems analysis in aerospace engineering by adding motion pictures and TV techniques [SMPT PAPER 104-17]

04 p0596 A69-14359

Collection of papers on engineering applications of digital computers, examining programming, numerical methods and design and simulation problems

04 p0563 A69-14514

Multivariable automatic control systems stability, discussing applicability of Nyquist theorem and alternate frequency criterion

04 p0581 A69-14601

Invariance principle application in gyrostabilizer systems, noting effect of external disturbances and system noise

04 p0597 A69-14603

Stability of nonlinear time varying feedback systems, using passive operator technique

04 p0583 A69-15110

Quadratic control problem with energy constraint, discussing approximate solutions for application to optimal control

04 p0583 A69-15111

Global and nonglobal stability of continuous systems with multiplicative feedback

04 p0583 A69-15112

AN/TSC-54 military satellite communications terminal for contingency deployment, discussing design, system tradeoffs and performance [AIAA PAPER 68-439]

04 p0579 A69-15367

Defect localization in complex plants applied to damage cause determination and economic criteria

05 p0767 A69-15765

Equations of motion of nonholonomic mechanical systems in Poincare-Chetaev variables

05 p0793 A69-15778

Stabilization of steady motions of nonlinear controlled systems with two purely imaginary roots, using Liapunov stability theory

05 p0794 A69-15790

Nonlinear system identification by learning model, assuming discrete on-line operation and Hammerstein form

05 p0737 A69-15805

Stability theorems for discrete linear circulatory systems with N degrees of freedom for static and dynamic loss of stability in presence of velocity dependent forces

05 p0836 A69-15875

Fluidic component descriptions and systems synthesis, discussing mathematical, graphical and linear models

05 p0705 A69-16007

- Identification of nonlinear control systems, determining nonlinearities in differential equation by curve fit or iteration method
[ASME PAPER 68-WA/AUT-19] 05 p0738 A69-16173
- Analytical measure of quality of controllability for linear dynamic system and computational procedure for maximizing adjustable structural parameters
[ASME PAPER 68-WA/AUT-4] 05 p0738 A69-16182
- Discrete time positive real functions defined for analyzing system stability with memoryless feedback
05 p0739 A69-16349
- Motion stability analysis of system represented by differential equation having continuously differentiable functions as continuously acting disturbances
05 p0794 A69-16450
- Invariant subspaces, controllability and observability of linear dynamic systems
05 p0740 A69-16597
- Stability of time varying systems by construction of multipliers with prescribed phase characteristics
05 p0740 A69-16598
- Stability analysis of nonlinear and time varying discrete feedback systems
05 p0740 A69-16600
- Microwave antennas simulation by optical systems based on Huygens-Kirchhoff approximation, noting application to antenna analysis, synthesis and radiation patterns
05 p0736 A69-16780
- Stability and weak oscillations of systems with distributed parameters, using method based on representation of characteristic equation in power series
06 p0956 A69-16822
- Synthesis of linear controlled systems with variable parameters, reducing parameter determination problem to Chebyshev approximation of relations between linear components
06 p0899 A69-16829
- Circuit and system theory - Conference, University of Illinois, October 1968
06 p0901 A69-17394
- Deterministic pattern classification algorithms, discussing abstraction problem, stochastic algorithms, minimum error scheme and modified least squares scheme
06 p0892 A69-17395
- Analysis and synthesis of optimal linear time invariant systems with uncertain or unknown parameters, considering mean square error
06 p0902 A69-17405
- L super P stability conditions for nonlinear time varying feedback systems derived with transformation technique and small gain theorem
06 p0903 A69-17411
- Optimizing radiating system consisting of radially diverging conical heat removing projections attached to cooled isothermal sphere
06 p1033 A69-17603
- Discrete time, single input, stepping extremum control system with input disturbance and output measurement noise, discussing computer simulation and dimensional analysis
07 p1114 A69-18287
- Learning matrices applied to mathematical relationship establishment during adaptation stage between input and output of adaptive systems
07 p1088 A69-18387
- Bandwidth limited PCM/PSK/PM telemetry system performance analysis for developing S band telemetry, including coherent and noncoherent detectors
07 p1081 A69-19098
- Pneumatic instrumentation line transfer function approximated by system model for simplifying reactor control system analysis
[IEEE PAPER 2D-6] 07 p1059 A69-19190
- Qualitative V/STOL air traffic control requirements, discussing airborne and ground data, procedures and equipment categories
[AIAA PAPER 69-211] 07 p1177 A69-19552
- System safety analysis for V/STOL aircraft, discussing fault-tree technique role in fail-safe design
[AIAA PAPER 69-216] 07 p1056 A69-19575
- Periodic solutions of autonomous system oscillations with many degrees of freedom based on Poincare method applied to Liapunov systems
07 p1183 A69-19680
- Book on application of systems analysis to government operations covering concepts, methods, benefit functions, optimization, etc
08 p1422 A69-19842
- Secondary acquisition systems analysis by semiMarkov process model, defining minimum average acquisition time
08 p1270 A69-19852
- Wolf and generalized Parseval theorems applied to transformation of integral equation to S-plane in systems analysis
08 p1271 A69-19865
- Control systems digital simulation based on coupling of prediction correction procedure with integration and differentiation procedure, discussing simulation errors
08 p1296 A69-20110
- Incoherent m-ary frequency shift keying (MFSK)/system analysis concerning automatic time synchronization
08 p1274 A69-20133
- Adaptation process of management systems from point of view of control system philosophy
[AIAA PAPER 68-807] 08 p1422 A69-20197
- Differential method with invariance principle used to analyze nonlinear invariant systems, determining physical realizability conditions
08 p1296 A69-20234
- Variational techniques for unstable problems including input determination in system with known impulse response and measured output
08 p1342 A69-20350
- Identification method for cyclic plants operating in mode characterized by recurrence of initial conditions, giving numerical results and error assessment
08 p1298 A69-20421
- Book on systems analysis techniques covering mathematical models, optimization, signal theory, linear and nonlinear systems, estimation, computerized simulation, etc
08 p1298 A69-20461
- Second order system response with variable damping computed by stepwise numerical integration
08 p1418 A69-20849
- Avionic systems development, discussing criteria for realization of operational requirement and engineering product satisfying requirement
[AGARDOGRAPH-114] 08 p1317 A69-20982
- Digital computer simulation and analysis of control loops for ion thruster control
[AIAA PAPER 69-239] 09 p1564 A69-21240
- Electrical analogs with passive elements in combination with stepping switches for simulation of plants with distributed parameters
09 p1471 A69-21436
- Laplace transform applied to linear array analysis and synthesis, discussing transform singularity correspondence to array structure
09 p1532 A69-21600
- Almost periodic systems stability criteria derived from differential inequalities and Liapunov function, considering existence and uniqueness
09 p1532 A69-21612
- Linear systems analysis by generalized numbers method, discussing algorithms for manual or computer analysis
09 p1472 A69-21778
- Stability of systems with periodic parameters, relation to automatic control systems and frequency characteristics role
09 p1473 A69-21855
- Final motions of Hamiltonian conservative systems, analyzing Liouville type, homogeneous and similar systems
09 p1540 A69-21882
- Mathematical model, analog computer simulation and information comparison of closed Brayton cycle systems for power conversion
[ASME PAPER 69-GT-50] 09 p1442 A69-22479
- Signal flow graphs based on matrix methods, discussing loop currents, systems orientation and transfer functions
09 p1475 A69-22600
- Stability and local parametric synthesis conditions of programmed optimal control established for optimal control problem within fixed interval
09 p1475 A69-22666
- Stability conditions for nonlinear pulse width and pulse time modulation systems, considering pulse element properties and system continuous part frequency characteristic
09 p1476 A69-22672
- Dynamic programming method to achieve optimal control of discrete systems with lagging control variables, considering structural properties
09 p1476 A69-22674
- Reliable operation duration distribution shown to be arbitrary for standby system consisting of basic device and n devices in nonloaded standby condition
09 p1513 A69-22676
- Crash protection of flight data recorders, aircraft accident investigation, systems analysis, environment and enclosures
10 p1691 A69-23248
- Torsiograph systems analysis for rotors angular acceleration recording, discussing dynamic characteristics, system, environmental problems, etc
10 p1692 A69-23252
- Federal Government budgeting, discussing systems analysis, planning-programming, etc
10 p1811 A69-23351
- Federal Government systems politics and budgeting, noting dichotomies, time dependence, taxonomy, etc
10 p1811 A69-23352
- Federal Government policies analysis, discussing disadvantages of planning-programming-budgeting system /PPBS/ 10 p1811 A69-23353
- Broadband double balanced mixer/modulators compared with single balanced and unbalanced mixer/modulators
10 p1665 A69-23876
- Optimal control of time invariant uncontrollable linear systems, noting asymptotic stability
10 p1666 A69-23887
- Aircraft and fuel supply system functional compatibility requirements and analysis noting gasolines, fuel tanks, valves, fuel transfer and metering
[SAE PAPER 690308] 11 p1825 A69-24503
- Drift elimination in linear system identification using binary m-sequences by crosscorrelating over two periods of output
11 p1834 A69-24547
- Nonstationary vibrations of mechanical systems subjected to harmonic or external limited energy source excitations
11 p1975 A69-24739
- Electronic systems and component reliability in space, considering electric parameter variation effects
11 p1848 A69-24867
- Stochastic approximation procedure minimizing mean square error criterion for system identification, estimation and decomposition of mixtures
11 p1842 A69-24934
- Multipurpose test system analysis emphasizing support section containing self test elements, power monitoring and control, interconnection techniques and packaging
11 p1864 A69-25069
- GO/NO/GO logic synthesis for probability functions development for systems operational readiness tests
11 p1843 A69-25078
- Differential equations describing system stability with delay in functional space
11 p1919 A69-25093
- Computer techniques application to radio engineering functions related to system performance, layout engineering, frequency coordination and administration, discussing decision parameters interrelationship
11 p1840 A69-25313
- Computer simulation application to electronic systems, discussing design, performance optimization, implementation and environmental effects
11 p1843 A69-25319
- Periodic solutions of quasi-linear self contained system with several degrees of freedom in case of commensurate frequencies, showing coordinates functions breakdown
11 p1920 A69-25749
- Small gas turbine Brayton cycle analysis treating component efficiencies as dependent variables in examining single stage radial compressor and turbine aerodynamic configuration
[IME PAPER 5] 12 p2147 A69-25794
- Service life of system predicted by identifying and testing system variables of mission phases, using obtained data in statistical estimation
12 p2101 A69-25970
- Higher root loci of polynomials for multivariable systems with coefficients polynomials of real parameter
12 p2048 A69-26073
- Multivariable automatic control system consisting of similar local subsystems studied by transforming system equations into equivalent diagonal form
12 p2048 A69-26076
- Liapunov functions applied to stability analysis of nonlinear multivariable direct and indirect control systems with time lags
12 p2048 A69-26079

Dynamic behavior of nonlinear continuous multivariable systems represented by equations derived from block diagram, stressing digital computer properties

12 p2049 A69-26081

Dynamic properties and reliability of linear time invariant multivariable control systems

12 p2051 A69-26093

Book on nonlinear systems analysis and design covering parameter mapping, symmetrical, transient and forced oscillations and stability analysis

12 p2129 A69-26121

Steady modes of operation analysis for optimal single channel differential relay system with inertial controlled plant, assuming constant rate varying plant input

12 p2052 A69-26278

Complete observability in linear time invariant systems decoupled via state-variable feedback, deriving sufficient conditions

12 p2053 A69-26514

Redundant systems reliability prediction for single mission in standby mode or without standby, using failure states concept and birth-death equations

12 p2102 A69-26569

WSEIAC /Weapon System Effectiveness Industry Advisory Committee/ formula, analyzing correctness within Markovian limitations and reward systems extension

12 p2102 A69-26570

Research and development organizations under pressure of corporate assessment and systems management approach, suggesting core-technology structure and training

12 p2192 A69-26732

Terrain photography applications and analysis including remote sensing of photographic systems and photointerpretation

12 p2098 A69-27006

Nonlinear systems disturbed by random white noise analyzed by Fokker-Planck equation for probability density in state space

12 p2124 A69-27141

Relay control systems limit cycle calculations, comparing classical differential equation, Laplace transformation and state and phase space analysis methods

13 p2238 A69-27396

Mathematical relations presented for parameters of technological, transport and information systems reliability and life expectancy

13 p2268 A69-27436

Liquid metal MHD power plant system tested under open and closed loop conditions for liquid circulation

13 p2208 A69-27510

Conditions governing application of reduced Nielsen equations to anholonomic systems dynamics, discussing kinetic energy function

13 p2288 A69-27924

Flux, density and pressure variations with position in vacuum system /nonuniform gas distribution/, discussing causes and consequences

13 p2299 A69-28019

Inelastic structural system stresses, strains and displacements analyzed by differential stress-strain relationships, using finite element method [AIAA PAPER 68-291]

13 p2364 A69-28208

Tracking conditions for observability of nonlinear controlled systems with smooth characteristics

14 p2424 A69-28751

Tracking breakdown probability during unsteady operation of nonlinear automatic control system analyzed by statistical linearization techniques and Fokker-Planck equation

14 p2424 A69-28752

Statistical linearization coefficients for arbitrary nonlinearities in automatic control systems via techniques applying characteristic functions

14 p2424 A69-28753

Differential equation with finite jump type discontinuities

14 p2424 A69-28811

Rotary oscillatory solution of parameterized system with stable unexcited motion using successive approximations

14 p2482 A69-28812

Control systems synthesis for nonlinear plants with known Liapunov functions and constraints, considering stability

14 p2424 A69-28819

Optimal linear control systems with time limits on transient processes synthesized by reducing optimization to algebraic equations solution

14 p2425 A69-28820

Linear control design to synthesize system with prescribed spectrum, deriving formula yielding control coefficients as function of eigenvalues

14 p2425 A69-28821

Stable operation of pulsed system with signal modulated pulse frequency described by nonlinear integral equation

14 p2425 A69-28909

Root locus method for nonlinear systems analysis, determining existence, stability and parameters of periodic solutions

14 p2445 A69-28919

Axial variation analysis of heat generation rate, temperature, voltage, current density and emitter heat flux in thermionic converter, emphasizing application to long diodes design

14 p2401 A69-29228

Identification method for cyclic plants operating in mode characterized by recurrence of initial conditions, giving numerical results and error assessment

14 p2427 A69-29659

Multivariable linear time-variant systems noninteracting control problem, discussing realization by state variable feedback

15 p2582 A69-30024

Sinusoidal perturbation extremal control system stability, using harmonic balance principle to obtain periodic solutions of system differential equations

15 p2582 A69-30616

Theory for stability of steady motions of system with cyclic coordinates applicable to total damping

15 p2690 A69-30737

Expression derived for arbitrary system subjected to external loading, using Cauchy equations for relationship between external plane forces and internal stresses

15 p2713 A69-31018

Pontryagin maximum principle applied to time optimal control of autonomous second order system with constant coefficients and differentiation in transfer function numerator

15 p2583 A69-31059

Cost effectiveness of DOD/military systems, discussing principles and analytical model with case study

15 p2722 A69-31125

System estimation methods compared for rational boundaries of lower confidence limit, discussing variables/attributes error propagation

15 p2722 A69-31135

Asymptotic solutions of optimum control for systems with constraints as linear differential equations and quadratic type functional

15 p2583 A69-31234

Asymptotic Liapunov stability of perturbed solutions to weakly coupled multifrequency systems

15 p2654 A69-31258

Stability of steady circular motions in systems with hidden variables analyzed by using Lejeune-Dirichlet theorem

16 p2804 A69-31621

Nonlinear discrete on-off system phase plane system analysis by motion separation method

16 p2763 A69-31628

Nonlinear nonconservative systems asymptotic stability analysis, emphasizing Zubov construction procedure for Liapunov functions

16 p2873 A69-32059

Book on quasi-linear equations systems and application to gasdynamics, including problems involving systems of quasi-linear hyperbolic equations with two independent variables

16 p2771 A69-32113

Book on correlation theory of statistically optimal systems covering linear continuous, discrete, nearly optimal, nonlinear, decision element and adaptive systems

16 p2764 A69-32114

Absolute stability, stability in whole and engineering stability in reference to Liapunov stability applicability

16 p2874 A69-32244

Nonlinear vibrations of mechanical two degrees of freedom system during resonance described using Krylov-Bogoljubov method to obtain differential equations solutions

16 p2875 A69-32255

Popov type graphic criterion for determining absolute stability of modulation systems

16 p2764 A69-32440

Popov and Sandberg graphic methods for determining absolute stability of nonautonomous systems, noting role of single nonzero eigenvalue in matrix

16 p2765 A69-32441

Turbojet engine open and closed loop boundary control systems performance during maximum penetration

of prohibited operating area induced by HF external disturbances [AIAA PAPER 69-543]

16 p2841 A69-32600

Digital simulation computer stability analysis scheme premised on use of perturbed transient responses

17 p2944 A69-32870

Mechanical systems differential equations of motion solution behavior, discussing program constraints

17 p3053 A69-33000

Book on systems analysis covering electrical networks, structural and space mechanics, vibrations and acoustics, feedback control, functions extrema, etc.

17 p2944 A69-33000

Helicopter engine dynamic analysis, discussing modeling techniques, rotor responses and turbospeed control simulations and transition from mathematical models to hardware components [AHS PAPER 332]

17 p2946 A69-33550

Linear computer-controlled closed loop systems sensitivity analysis, deriving estimation error increment covariance to demonstrate quality deterioration under perturbed initial conditions, parameters, etc.

17 p2944 A69-33747

Multiple input and output nonlinear time invariant feedback system under almost constant inputs

17 p2944 A69-33747

Nonresonance parametric phenomena in distributed systems, discussing interaction between signal and parameter wave at superlight velocity

17 p2928 A69-33860

Nonlinear differential equations describing one degree of freedom systems oscillations, allowing for dry friction and internal friction in elastic element

17 p3007 A69-33910

Nonlinear differential equations of mechanical systems with restoring forces approximated by odd power displacement functions and energy dissipation approximated by displacement and velocity functions

17 p3007 A69-33910

Bernoulli distribution and Monte Carlo method for electrical load analysis in designing electric power generation and distribution

17 p2905 A69-34090

Technology or Research Quantitative Utility Evaluation /TORQUE/ system genesis and operation, with implications affecting R and D

17 p3077 A69-34130

Single freedom vibratory system response to imposed displacement harmonic excitation, analyzing response in terms of constrained system modes

17 p3067 A69-34130

System state phase modeling as method for evaluating safety and reliability by analysis of system states in mission phases through logic diagram

18 p3142 A69-34480

Failure mechanisms time and stress dependence relationships

18 p3144 A69-34490

Steady state availability of system with limited repairable spares for online units, considering statistical dependence among similar units

18 p3144 A69-34490

Flight performance analysis of space systems discussing preparation, implementation and communication

18 p3206 A69-34500

Operational system effectiveness information for reconnaissance drone system including test flights discussing application to reliability and maintainability in project management

18 p3232 A69-34500

Failure rate data role in reliability analysis and design optimization

18 p3147 A69-34510

Mechanical drives effectiveness for large antenna tracking/communications systems evaluated in terms of reliability and availability

18 p3100 A69-34520

Computer simulation model for Saturn 5 prelaunch system reliability analysis, using Bayesian techniques

18 p3207 A69-34520

Slide methods for duplex parallel and switchover redundant mission availabilities based on cost, reliability and maintainability

18 p3147 A69-34530

Parametric variations of nonlinear system moving in medium with nonlinear drag, using Bogoljubov-Krylov asymptotic method

18 p3171 A69-34560

Exponential boundedness of system motion for Lur'e type forced systems, using quadratic Liapunov functions

18 p3164 A69-34670

State space structure of model reference adaptive control and parameter tracking systems subject to noise
18 p3111 A69-34686

Numerical procedure for testing absolute stability and positive realness of free dynamic systems based on Routh algorithm
18 p3112 A69-34689

Thermoelectric converter systems optimization by geometry independent functions
18 p3093 A69-34782

Expected occurrences mathematical model for flight system availability under uncertainty
18 p3210 A69-35083

Advanced Meteorological Sounding System /AMSS/ for measurements up to 150,000 ft, discussing configuration, characteristics, radiosonde, ranging, telemetry data ground equipment and test
18 p3108 A69-35102

Hypercorrelation concept for statistical characterization and structuring of systems with application to management models, discussing multiport systems
18 p3236 A69-35236

Parametric and forced oscillations analogy for analyzing dynamic behavior of oscillatory systems with time dependent parameters
18 p3175 A69-35322

Autonomous system steady motion with rotating phase and deviating argument solved by successive approximation over infinite time interval
18 p3175 A69-35323

Automatic control system transient response oscillatory and aperiodic components calculation using open loop system transfer function
18 p3112 A69-35458

Shuttle VTOL airport access system analysis for New York area
[AIAA PAPER 69-804]
19 p3288 A69-35592

Stability of interrelated linear dynamic control systems with distributed parameteres evaluated by using differential equations
19 p3286 A69-35892

Evaluation method for strapdown spacecraft guidance systems on automated interplanetary missions, using cost and system performance efficiency probability model
[AIAA PAPER 68-828]
19 p3370 A69-35953

Power subsystem weight effects on temperature ratio of Rankine type cycle, discussing method for rapid estimation
19 p3254 A69-35957

Systems effectiveness view from project and organization management viewpoint
19 p3454 A69-36006

Subsystem designs evaluated on basis of human reliability metric to select desirable design configurations
19 p3261 A69-36026

Computerized system-safety fault trees, discussing drawing, configuration control and simulation program
19 p3280 A69-36029

Maintainability and maintenance analysis in managing integrated logistic support /ILS/ system
19 p3455 A69-36035

Bayesian confidence limits for systems reliability, considering exponential and unspecified life distribution subsystems
19 p3328 A69-36041

System effectiveness for reliability and maintainability achievement, analyzing people, organizations, value systems and accomplishment criteria in development program
19 p3455 A69-36044

Stochastic models for calculating optimal elastoplastic one dimensional systems
19 p3438 A69-36313

Self rotary motions of nearly conservative systems with one degree of freedom, deriving periodic solution of equation for phase trajectories
19 p3374 A69-36466

Steady resonance operation modes of nonlinear oscillatory and rotational systems described by differential equations with deviating argument, using averaging procedure
19 p3374 A69-36469

Optimal structural parameters of radar digital ranging servosystems derived from reproduction error, including computer simulation data
19 p3278 A69-36593

ATC systems analysis including airports, ground access and air transportation
19 p3371 A69-36866

Soviet collection of papers on vestibular analyzer physiology
20 p3467 A69-37240

Book on systems cost effectiveness covering methodology, system cost models, economics, etc
20 p3640 A69-37533

Remote sensing systems costs, benefits and economic evaluation
20 p3493 A69-37742

Gust absorber system configuration flight tests and analysis, emphasizing application to delta wing aircraft [ONERA-TP-698]
20 p3462 A69-37753

Avionics system analysis, engineering, design, fabrication and testing problems
20 p3545 A69-37929

Book on mathematical foundations of systems analysis covering calculus, linear algebra, linear and nonlinear programming and major applications
21 p3754 A69-38576

Optimum and suboptimum synchronizers for extracting bit synchronization from binary data, showing performance dependence on pertinent system parameters
21 p3673 A69-38923

Mathematical model of probability of errorless human performance for time continuous tasks for use in systems reliability analysis
21 p3664 A69-38971

Numerical procedure for structural systems analysis, discussing computer application to hydrodynamic, electric, magnetic, thermodynamic, elastostatic and elastodynamic problems
[AIAA PAPER 67-955]
21 p3839 A69-39216

Integrated systems testing for unmanned spacecraft electromagnetic compatibility, discussing identification and elimination of interference sources
21 p3683 A69-39438

Performance characteristics of multivariable model reference adaptive systems synthesized by Liapunov method analyzed using computer simulation
22 p3919 A69-41201

Parabolic equation and equation systems with relaxed assumptions involving coefficients of first derivatives and unknown function, demonstrating Pogorzelski fundamental solutions validity
23 p4180 A69-41408

Systems analysis method for determining spacecraft remote sensors earth resources survey effectiveness by integrating specifications, mapping requirements and orbital characteristics
23 p4163 A69-41567

Teleological systems behavior modeling based on input, output, goals, operation duration, etc
23 p4134 A69-42059

Antenna losses produced by metal space frame radome determined by considering end effects, member junctions circulating currents, mutual scattering and near field effects
23 p4149 A69-42127

Electromagnetic compatibility /EMC/ quantification in system effectiveness by decision analysis technique, constructing conceptual model
23 p4145 A69-42227

Space power systems analysis, using computer program to correlate systems characteristics with mission parameters for automated satellite repair vehicle and space stations
23 p4068 A69-42240

Systems analysis of Rankine cycle nuclear- electric potassium space power system using Li cooled fast reactor and high temperature turbine inlet
23 p4189 A69-42266

Positive cyclic systems of linear differential equations, proving existence and projective uniqueness of solution having positive n components for all t
24 p4340 A69-43131

General purpose computer program for synthesis of multivariable systems decoupled by state feedback
24 p4294 A69-43307

Two level systems with overall performance as explicit function of first level performance, defining equivalence condition to prove coordinability for nonadditive case
24 p4294 A69-43308

SYSTEMS ENGINEERING

Survival analysis based on probability theory for design of air cushion vehicle to determine height for operating over open sea
01 p0008 A69-10027

Subsystems of ESRO research satellites Td 1 and Td 2, discussing telecommunication, attitude control, power supply and temperature control design and functions
01 p0160 A69-10031

Airline area navigation system functions for developing map type pictorial display system including digital computer, cockpit control unit and microfilm charts
01 p0112 A69-10453

Navigation services satellite systems including position determination, communication and telemetry for ships and aircraft
[UN PAPER 68-95363]
01 p0113 A69-10479

Space system engineering courses background, objectives and results at MIT and Stanford University dealing with applications of space technology
[UN PAPER 68-95870]
01 p0178 A69-10485

Antenna performance optimization, considering gain dependence on diameter, feed, tolerances, noise temperature, etc
[UN PAPER 68-95813]
01 p0043 A69-10517

Soviet book on design of multidimensional automatic control systems, covering structural circuit synthesis and individual element characteristics
01 p0053 A69-10995

Soviet book on automatic control and telemechanics in hydrometeorological measurements covering sensors, transducers, amplifiers, etc
01 p0111 A69-10997

Ground-air-ground communications system using pseudonoise through satellite and central ground based control facility, discussing system advantages, SNR and modulation schemes
01 p0033 A69-11009

Structural weight fraction factor analysis leading to improvements in materials and structures
[AIAA PAPER 68-331]
01 p0011 A69-11021

Symmetrical design of short ferrite Faraday rotator using matrix representation, noting matching to rectangular waveguide
01 p0048 A69-11034

Biological life support system based on continuous algae seaweed cultivation as link of closed ecological system, discussing design and performance
01 p0020 A69-11077

Cryogenic engineering - Conference, Brighton, England, May 1968
01 p0056 A69-11144

Liquid hydrogen circulation pump design emphasizing heat leaks
01 p0087 A69-11148

Liquid hydrogen and LOX boost pump design for Centaur missile and liquid hydrogen and LOX chill-down pump design for Saturn 4B missile
01 p0087 A69-11149

Cryopump design suitable for attachment as replacement for diffusion or ion pumps
01 p0088 A69-11155

Integrated circuit piezoelectric systems limitations and advantages
01 p0049 A69-11413

Laser gyro applications including guidance, navigation and control problems
02 p0248 A69-11741

Wolf Trap life detector design to sample and culture Martian surface dirt for microorganism growth
02 p0201 A69-11769

Reliability of operational satellite systems consisting of two single purpose satellites in interchangeable orbits, discussing outage and replacement
02 p0333 A69-11805

Algorithm minimaxing performance index and sensitivity of controller design with and without saddle point
02 p0224 A69-11966

Stabilization system for klystron automatic frequency control, noting use in voice communication microwave generators and resonance spectroscopy
02 p0216 A69-12096

Finned tube radiators optimum design for waste heat removal from space power plants
02 p0354 A69-12664

Automatic support systems development and capabilities with recommendations for future R and D developments
03 p0411 A69-13190

Multimode propagation communications system /MMPCS/ utilizing digital computer to implement intermittent system
03 p0389 A69-13191

OMEGA radio navigation system optimization, emphasizing implementation of phase modulation to ensure lane identification
03 p0463 A69-13212

Fourier synthesis procedure optimized to design of large time bandwidth product dispersive filters employing nondispersive tapped delay lines
03 p0403 A69-13217

Design evolution of mechanically despun antenna systems from ATS to INTELSAT, discussing RF and control systems
03 p0403 A69-13239

Point to point millimeter wave communication system design, discussing propagation and data transmission
03 p0405 A69-13723

Design and principles of operation of SHF electron-optical multiply stable storage elements with dynamic attributes of states
03 p0441 A69-13982

Electronic scanning radar systems design, discussing beam types, bandwidth, tracking, target acquisition, etc
04 p0556 A69-14301

HAPDAR-TACOL phased array radar design, discussing array patterns and multitarget tracking performance
04 p0556 A69-14324

Hybrid mode Ku-band mixer steering electronic scanning phased array design
04 p0572 A69-14325

H plane waveguide Y circulators engineering design based on circulation equations
04 p0575 A69-14460

Collection of papers on engineering applications of digital computers, examining programming, numerical methods and design and simulation problems
04 p0563 A69-14514

Computer programs for engineering analysis, design and simulation, presenting point selection program for curve plotting
04 p0563 A69-14516

Planar linkages kinematic synthesis and design, using Newton-Raphson iteration technique to solve nonlinear equations
04 p0604 A69-14517

Book on control systems theory and applications covering artificial intelligence, linear stochastic systems, trajectory decomposition, etc
04 p0581 A69-14567

Fluid stability, viscosity, compressibility, gas solubility and lubricating properties determination for high temperature hydraulic systems
04 p0550 A69-14662

Current antenna system technology, particularly airborne and spaceborne applications
04 p0576 A69-14767

Corrugated impedance antennas synthesized, using model in impedance surface form
04 p0577 A69-14786

Sensitivity models for adaptive and self adaptive systems design
04 p0582 A69-14797

Nuclear reactor space power system concept using thermionic diodes, heat pipes and rod control, emphasizing neutronic aspects and feasibility
04 p0630 A69-14799

Apollo guidance, navigation, stabilization and control subsystems, detailing inertial, optical and computer units for data processing and collecting
04 p0665 A69-14881

Servosystems components design, discussing detector, corrector, amplifier and motor
04 p0550 A69-15181

Water removal unit design for electrolyte reaction accumulation in hydrogen oxygen fuel cell systems
04 p0552 A69-15316

Graphics system using computer configuration connected by conventional voice lines, noting hardware and components
04 p0566 A69-15343

Lockheed hybrid computer system, describing features implemented by modifying and augmenting digital batch processing system
04 p0567 A69-15349

Hybrid executive development based on digitally oriented software, explaining assembly language routing
04 p0567 A69-15351

Device and logic/system designers and design aids interaction, emphasizing engineering trends in large scale integration area using MOS arrays
04 p0568 A69-15356

Simulation design of multiprocessor system to provide air traffic control capabilities through use of real time operations
04 p0629 A69-15365

Stability derivative estimation at subsonic speeds for preliminary design engineer
05 p0700 A69-15545

Unified design approach for second generation air cushion craft based on existing first generation craft
05 p0701 A69-15567

Mathematical model to design weight optimized silicon-germanium solar flat plate thermoelectric generator as spacecraft auxiliary power source in near sun missions
05 p0704 A69-15674

Design and performance equations for panel type solar thermoelectric generator, based on single thermocouple as generator unit
05 p0704 A69-15675

Systems science and cybernetics - IEEE Conference, San Francisco, October 1968
05 p0741 A69-15801

Central test evaluation group as part of systems engineering of large systems
05 p0742 A69-15803

Flight test support design, developing measure of performance of test environments stated in weapon or space system terms
05 p0742 A69-15804

Book of engineering compendium on nuclear radiative shielding, discussing radiation sources, attenuation methods, induced heat generation, ducts and voids in shielding technology and design
05 p0791 A69-15830

Soviet book on design of aircraft engine component and subsystem elements, emphasizing aligning, locking and sealing methods, torque transmission, etc
05 p0812 A69-15864

Multiradar system development for total view of air situation from single air views, using digital computers interconnected with central computer
05 p0719 A69-15932

Product development process diagram, systems engineering checklists and program plank as devices to assist product manager
05 p0850 A69-16146

Minimum sensitivity deadbeat sampled data control system design by frequency domain technique, using two controllers
05 p0738 A69-16177

Digital computer interface systems design for simulation, control, instrumentation and data processing, discussing hybrid computer linkages
05 p0723 A69-16195

System/360 Continuous Modeling Program, detailing input language, user-defined functions and documentation
05 p0723 A69-16196

Design theory of esaki diodes relation to internal parameters of degenerate semiconductors, discussing Fermi level position and maximum state density in purity band
05 p0732 A69-16298

Efficient life support systems for prolonged space missions, discussing scientific and experimental research
06 p0879 A69-17040

Satellite and space communications and data transmission systems, emphasizing improvements in amount and rate of information for future requirements
06 p0886 A69-17045

Multivariable self adaptive control system design using sensitivity methods, obtaining adaptation stability by Liapunov synthesis
06 p0900 A69-17352

Learning control system design, using a priori information in subgoal selection, control situation grid extensions and controller initialization
06 p0900 A69-17355

Adaptive control of reflective satellite communication system
06 p0887 A69-17356

Digital simulation design for linear dynamic systems, noting role of digital transfer function
06 p0906 A69-17491

Attitude control system design problems for earth oriented satellites
06 p0105 A69-17586

Engineering designs and hardware required for low risk flight of long duration manned space stations
06 p1007 A69-17601

Systems engineering activities in manned space flight involving design, development, manufacture, test and operation of Mercury, Gemini and Apollo flight systems
06 p1016 A69-17602

Interplanetary Pioneer spacecraft development and systems engineering aspects
06 p1017 A69-17605

Collection of Soviet papers on radio engineering
06 p0889 A69-17796

Automatic air traffic control systems design, development and application to civil and military aviation
06 p0955 A69-17858

Injector design based on MHD injector component performance, establishing minimum diffuser nozzle area
06 p0872 A69-17923

Flexible vehicle control, using cybernetic model for system design and response
[AIAA PAPER 69-115] 06 p0108 A69-18054

Astrodynamic data compilation for use by systems engineer for mission planning
[AIAA PAPER 69-124] 06 p0101 A69-18059

Thermionic energy converter theory and efficiency, discussing design considerations to improve performance
07 p1057 A69-18221

Design and performance of large vacuum system with central control desk to study plasma dynamics, discussing visual monitoring at desk
07 p1116 A69-18292

Boeing 2707-300 Mach 2.7 supersonic transport, discussing flight controls, hydraulic system, environmental controls, operational characteristics, flight deck and instrumentation
07 p1052 A69-18277

Book on vacuum system design covering getter ion pumping, cryogenic pumping, liquid nitrogen handling, residual gas analyzers, etc
07 p1180 A69-18544

P-n channel MOS triode fabricated by doped stepped-oxide method, obtaining p-channel enhancement
07 p1100 A69-18622

Control-display panels design for accurate response with electronic and mechanical equipment, showing display stimulus and control response correspondences in rectangular configuration arrangement
07 p1070 A69-18907

Adaptive airborne VHF/UHF transmitter system, discussing design, ground isolation, current limiting, internal telemetry, wideband frequency response, real time video signals, etc
07 p1106 A69-19114

Communication satellite system design by use of baseband equation relating SNR after detection to CNR at detector input
07 p1085 A69-19180

Reliability in aeronautics and astronautics, discussing safety, economic cost of technical delays and effect on public, air transport, design, development, testing, utilization, etc
07 p1053 A69-19287

System reliability influence on air accidents resulting from pilot errors, unforeseen obstacles, breakdowns and atmospheric effects
07 p1054 A69-19288

Radomes developments for supersonic/hypersonic aircraft and missiles, considering conditions imposed by speed and by electronic requirements
07 p1171 A69-19508

Integrated radome antenna system design /radant/, comparing electrical performance with conventional systems
07 p1109 A69-19513

Radome materials with superior dielectric and temperature characteristics for constructing high tolerance microwave multiband radome
07 p1109 A69-19514

Symmetrical three layer A and B type sandwich reflectionless radomes design for multifrequency operation and insertion phase delay
07 p1110 A69-19522

Dielectric radome designs for operation at harmonically unrelated frequencies in C and K bands, discussing sandwich structure of A and B types
07 p1110 A69-19523

Cordierite application to radomes for high velocity engines, discussing dielectric properties at microwave frequencies, mechanical properties, temperature control and fabrication
07 p1168 A69-19525

Radome design and manufacture, considering airborne requirements, antenna systems and electromagnetic energy, with emphasis on ceramic material melting, forming, grinding and finishing
07 p1142 A69-19526

Scanning beam landing systems for VTOL aircraft
07 p1178 A69-19631

Material design problems in small gas turbines, discussing engine performance sensitivity, thinness of rotor-blade and stator-vane trailing edges, dimensional tolerances, etc
[ASM PAPER D8-16.2] 07 p1204 A69-19661

Radiation effects on integrated circuits, stressing components design for maximum tolerance
07 p1113 A69-19779

- Transponders for communication satellites, discussing design constraints, reliability and transmission capacity increase
08 p1279 A69-19905
- Adaptive primary feed system for wide angle beam scanning from parabolic reflector antenna, using Fourier transformation to obtain uniform power distribution
08 p1279 A69-19908
- Design aspects of 20 ft air transportable satellite earth station
08 p1272 A69-19926
- Bounds on electric field outside radiating system determined for application to UHF and VHF systems design, considering microwave breakdown
08 p1273 A69-20026
- U.S. policy for commercial surface effects ships regulation, discussing operational, construction and design requirements
08 p1254 A69-20199
- Nonlinear controller design by dynamic programming method, discussing block diagram
08 p1296 A69-20236
- Compromise control in system with two hierarchy levels interrelated via lower level subsystems optimality criteria found by solving global criterion problem
08 p1297 A69-20415
- Aircraft head-up display systems emphasizing all-weather operations and equipment characteristics
08 p1315 A69-20451
- Flapper-nozzle type electrohydraulic amplifier design with emphasis on elements and subsystems
08 p1256 A69-20459
- Hard-drawn steel wire wound pipes and tanks, properties and design calculation, discussing laminates and permissible stress
08 p1414 A69-20487
- Nondestructive testing methods application to fiber-bonded composites, noting X ray diffraction, radiography and ultrasonics
08 p1339 A69-20498
- Plastic composite reinforcements with boron, silicon carbide, graphite, single crystal alumina and laminating resins, discussing properties and fabrication
08 p1340 A69-20503
- Stellar identification system using onboard sighting equipment and computer mathematical methods
08 p1347 A69-20657
- Decision oriented automatic data processing systems design, noting quantity and quality of upward directed information to management
08 p1423 A69-20733
- Bounds for real and imaginary parts of dynamic moduli of composite viscoelastic systems
08 p1417 A69-20824
- Response optimization of feedback control systems with reference to single settlement time-constant ideal determined for error evaluation
08 p1298 A69-20855
- Nuclear power supply with in-core thermionic reactor for space power source and use in satellite TV, discussing theory, design and components
08 p1350 A69-20871
- Design of ruby laser for stability, lifetime, maintenance and safety requirements of commercial users, discussing power, pulse duration and beam divergence
08 p1327 A69-20881
- Collection of articles on fluid control components and systems design
08 p1256 A69-20948
- Wullenweber arrays with extended frequency ranges, discussing design considerations and performance characteristics
08 p1288 A69-20962
- Electronic multibeam switching X band antenna system design with separate transmitting and receiving antennas for use on continuous wave surveillance radar
08 p1289 A69-20967
- Electronically phased array antenna system design optimization and testing for application to spin stabilized satellites
08 p1289 A69-20969
- Wideband array antenna IF time delay steering realization, showing steering independence of bandwidth
08 p1290 A69-20974
- Low temperature hydrogen fuel cells and basic-electrolyte batteries design, discussing electrolyte concentration regulation by elimination of water formed
08 p1258 A69-21027
- Motor design for operation in ultrahigh vacuum, discussing absence of convection cooling, outgassing avoidance, lubrication impossibility and oxygen absence as design parameters
08 p1377 A69-21028
- Cold hydrogen and basic electrolyte cells at CGE research center, discussing single cell batteries, reagent chambers and auxiliary control systems
08 p1259 A69-21039
- Optimum integration of aircraft equipment, subsystems and computer mechanizations for low cost navigation system consistent with mission requirements
08 p1348 A69-21065
- Large scale electronic systems configuration compatibility concept, discussing modular line replaceable units (LRU)/assigned set of numbers
08 p1322 A69-21154
- Landing gear requirements for aircraft design, discussing tire pressure, wheel arrangement, brakes for loading and aircraft weight
08 p1255 A69-21161
- Statistical approach to design and management, discussing multiple regression analysis, attributes, intuition, probability, simulation and applications
08 p1344 A69-21162
- Dual-rotor high-bypass-ratio CF6 turbofan engine design and development programme and growth
08 p1377 A69-21163
- Pulsed MPD arc jet electric propulsion system requirements, examining physical constraints, pulse duration, duty cycle, power network structural details, etc [AIAA PAPER 69-269]
08 p1560 A69-21215
- Low density Hall ion thruster with application to Van Allen probe and orbit-to-orbit transfer [AIAA PAPER 69-281]
08 p1562 A69-21229
- Communication satellite system design for operation with frequency bands above 10 GHz, noting wideband communication
08 p1450 A69-21284
- Contactors for helium in dilution refrigerator mixing chamber, discussing design and thermal resistance determination
08 p1493 A69-21429
- Ion laser construction, detailing water cooled quartz tubes, electrodes, adjustable mirrors, etc
08 p1515 A69-21487
- Rocket vehicle inertial attitude reference system, discussing flight control
08 p1609 A69-21618
- Filtering system for xenon arc solar simulator to provide operation at air-mass-two /average sea level/ sunlight
08 p1476 A69-21648
- Maxson multibeam antenna design for noninteracting beams, considering beam shapes and positions and applications
08 p1463 A69-21676
- Gamma ray scattering gauge design optimum parameters to measure Mars atmospheric density
08 p1495 A69-21842
- Electric propulsion design, considering effects of weight, impedance matching, beam voltage regulation and operating point variations in formulating system mass and reliability [AIAA PAPER 69-254]
08 p1569 A69-21879
- Fluidic component application to propellant tank pressurization and controller design [AIAA PAPER 68-629]
08 p1442 A69-21980
- Pressure vessel design to alleviate hydrogen embrittlement of steels for shock tunnel drivers [AIAA PAPER 68-367]
08 p1477 A69-21993
- Collection of papers on designing components of gyroscopic systems covering moment sensors, floating devices, bearings, etc
08 p1497 A69-22101
- Aircraft gust alleviation system for minimizing weighted sum of normal acceleration and pitch rate response by limiting control surface deflections
08 p1434 A69-22279
- Vacuum engineering problems during booster rocket engine ground tests, simulating flight environment [TR-781-O]
08 p1570 A69-22300
- Explosive forming, discussing optimum parameters for model and prototype parts and subscale forming criteria for aluminum ellipsoidal domes
08 p1512 A69-22371
- Onboard test and fault isolation design for airborne systems considering tradeoff parameters for optimum reliability, performance and cost [AIAA PAPER 69-306]
08 p1434 A69-22389
- Air backflow in nuclear exhaust system duct for ground testing of NERVA engines, noting overpressure effect [AIAA PAPER 69-325]
08 p1479 A69-22390
- Stationary controller design for linear time varying control systems with state variables not always accessible for feedback
08 p1474 A69-22443
- Electronic systems partitioning in preparation for MOS large scale integration for system performance and cost improvement
09 p1466 A69-22451
- Correlation between responses of linear systems for transient input as performance criterion for servomechanisms
09 p1475 A69-22536
- Nonlinear one element control system design based on correlation between responses of linear systems
09 p1475 A69-22537
- Heat release in combustion chambers of propulsion and lift engines considering various parameters of materials and design problems
09 p1625 A69-22619
- High performance silicon carbide backward diode, discussing device design and operational characteristics
09 p1470 A69-22787
- On job training of logistic publications engineers, emphasizing technical publications and system engineering and development for Minuteman program
09 p1811 A69-22977
- Probability of completing countdown in single malfunction encounters, considering development of industry and government guidelines
09 p1792 A69-22979
- Electroexplosive devices design for extreme conditions, considering igniter, delay and functioning systems
09 p1751 A69-23020
- Electroexplosive element design for safe reliable devices in liftoff and space environment, considering stray electric currents, RF fields and electrostatic discharges
09 p1752 A69-23022
- Saturn 5 holddown and service arm electrical system design program optimized by integrating reliability and maintainability at initial design phase [AIAA PAPER 69-309]
09 p1670 A69-23043
- Waveguide Y circulator electrodynamic parameters by design algorithm and computer programs
09 p1661 A69-23108
- Flight data recorders history and regulations, discussing parameters and design of systems
09 p1691 A69-23247
- Telemetry monitor systems for high speed rotating equipment, discussing data recording, transmission, decoding, thin-thick film microtechniques, etc
09 p1692 A69-23249
- Test facility automation, discussing pretest preparations, test operations, data reduction and system planning
09 p1671 A69-23260
- Maintenance recording systems for aircraft fleet, discussing operations objectives and research, data collection and implementation using systems engineering
09 p1671 A69-23261
- Fluid rotor angular accelerometer design for stabilization and control, noting applications to centrifuge speed and thruster gas consumption
09 p1633 A69-23273
- Blowdown wind tunnel designed for studying closed cycle MHD converters, describing subsystems
09 p1673 A69-23474
- Electrical, thermal and mechanical requirements in design of Landing Radar Electronic Assembly for Apollo Lunar Module
09 p1663 A69-23537
- Displacement and acceleration criterion for synthesizing optimum linear vibration isolator systems subject to random input [ASME PAPER 69-VIBR-44]
09 p1807 A69-24182
- Design management in next century covering computer methods, market needs, etc
11 p2004 A69-24371
- Aircraft electronic proximity warning devices applications, discussing compatibility in ATA collision avoidance system [SAE PAPER 690340]
11 p1914 A69-24496
- Digital data transmission techniques and complex instrumentation systems design noting control, identification, synchronism and error reduction
11 p1834 A69-24545
- Estimation system distinction from adaptive system, discussing network of adaptive estimation systems
11 p1858 A69-24937
- Hardware and software as single entity in small scale programs, describing English language oriented program code of Controller /Programmer/ Evaluator
11 p1864 A69-25062

High speed automatic test sets and rapid repair procedures under adverse conditions for individuals of relatively low technical skill

11 p1851 A69-25063

Single purpose, multipurpose and multistation automatic test systems for production and maintenance

11 p1864 A69-25068

Hardware-software interface defined for design of computer controlled test system, discussing criteria for designing economical systems

11 p1842 A69-25071

Mathematical model for prediction of automatic test equipment utilization and determination of time for performance of intended test function

11 p1865 A69-25074

Onboard checkout system concept, discussing philosophy, requirements, underlying considerations, system description, development and techniques of system selection

11 p1866 A69-25081

Automatic system self test technique known as central integrated test subsystem /CITS/ for logically testing avionics systems

11 p1866 A69-25083

Monograph on computer aided air traffic control systems design, discussing air navigation, man-machine relations, equipment requirements, programs, plan position color display, etc

11 p1914 A69-25085

Real time/process computer interface with electric power systems, discussing compatibility, reliability, etc, problems in connection with management and engineering personnel

11 p2004 A69-25302

Computer techniques application to radio engineering functions related to system performance, layout engineering, frequency coordination and administration, discussing decision parameters interrelationship

11 p1840 A69-25313

Computer simulation application to electronic systems, discussing design, performance optimization, implementation and environmental effects

11 p1843 A69-25319

Computer design for booster/satellite control, discussing systems reliability, low power and tradeoffs

11 p1843 A69-25320

Thermionic converter SD-4 design and performance tests covering emitter, collector and Cs reservoir temperatures and power efficiency

11 p1827 A69-25398

Spacecraft design for minimization of structure interaction with control system, noting susceptibility of extendible booms to solar environment

11 p1967 A69-25500

Multidimensional mode shapes and frequencies of 100 ft space erectable parabolic antenna

11 p1994 A69-25532

Optimal multivariable linear control system design, based on Pontryagin principle using Laplace transform method, providing good approximation to finite interval controllers

11 p1861 A69-25663

Testing machines for metallic materials, discussing design criteria and application to tensile strength, vibration and durability test machines [DVL-865]

11 p1889 A69-25682

Multidimensional self adjusting systems design by achieving parametric invariance, using sensitivity theory

11 p1861 A69-25711

Lifting entry concepts for return from earth orbit, discussing deceleration, heating and heat protection

11 p1968 A69-25720

Planetary imaging systems design problems illustrated by Mars orbiter reconnaissance, discussing radiation effect on film, shielding, stereo method comparisons, color bands, etc [SMPT PAPER 105-78]

12 p2078 A69-25770

Control technology advancement effects on gas turbine design and application, integrating control scheme, modularization and commonality, system design and energy input and load control

12 p2146 A69-25786

Gas turbine fuel and control systems for two and three shaft engines in military and civilian aircraft including helicopters [IME PAPER 12]

12 p2147 A69-25796

Solar cells operation in space flight, considering Si photoelectric cells characteristics and complete systems construction for spacecraft power supplies

12 p2015 A69-25865

Large scale integrated circuit accumulator chip as control element for design of digital system by design automated techniques

12 p2037 A69-25942

Technological feasibility of satellite based global data relay service for small users

12 p2028 A69-25949

Optimal controllers analytical design for closed loop systems with pure time delay in actuating mechanism using differential equations

12 p2045 A69-25959

Automatic control system design for optimality in sense of nonstatistical quality criterion for disturbances of given class, considering additive noise

12 p2045 A69-25964

Digital computer-aided reliability engineering methods for electronic equipment design and analysis

12 p2037 A69-25973

Optimal control of multivariable complex systems through multilevel /hierarchical/ structure, discussing coordination problems

12 p2049 A69-26082

Third order multivariable control systems calculation with linear differential equations describing plant for design and digital optimization

12 p2049 A69-26085

Time optimal controls for multivariable linear systems by computer programming of iterative calculations /Neustadt and fast convergence methods/

12 p2050 A69-26090

Discrete linear optimal control system with quadratic performance index synthesized by dynamic programming method, obtaining matrix equations

12 p2050 A69-26091

Canonical representation of multivariable control system in state space using matrix of differential operators acting on vectors of input-output quantities

12 p2051 A69-26094

Monograph on physicotchnical principles of takeoff monitoring systems for large aircraft covering taxiing, safety control systems design, analog simulation, etc

12 p2128 A69-26119

Book on nonlinear systems analysis and design covering parameter mapping, symmetrical, transient and forced oscillations and stability analysis

12 p2129 A69-26121

Fourth angle driving law for different four gimbal systems used for simulation display and inertial platform isolation

12 p2055 A69-26265

Concorde SST equipment and systems noting microelectronics, automatic control, inertial navigation, head-up displays, linear instruments and hydraulic systems

12 p2091 A69-26360

Budapest University satellite radio observation APT station design, equipment and methods

12 p2059 A69-26449

Beryllium oxide semiconductor thermistor for temperatures to 2500 K, discussing construction materials and test results

12 p2092 A69-26478

Soviet book on electric ignition systems for piston and jet engines and design aspects of different types of ignition systems

12 p2146 A69-26756

Helicopter stabilization systems design using optimal control theory to obtain multivariable feedback controller

12 p2014 A69-26764

Inertial guidance system synthesis for infantry missile with 1 n mile range against small hardened targets requiring 3 ft maximum miss distance

12 p2129 A69-26791

Systems design of airframe structures taking into account material characteristics noting structural stability, shell postbuckling, fail-safe designs, etc

12 p2186 A69-26833

Space propulsion system design with consideration for launch and mission requirements, noting upper stage structural design and computer techniques

12 p2148 A69-26834

Book on optimal control covering types of systems, practical optima, signal properties, Bellman dynamic programming and Pontryagin maximum principle

12 p2054 A69-26919

Aesthetic preservation of visual amenities in countryside by proper antenna design without affecting performance or cost

12 p2044 A69-26924

Man machine interactive structural analysis using digital computer with CRT display, detailing design

12 p2035 A69-27098

Optimal design of rectangular frames for stability

13 p2358 A69-27209

Self acting gas lubricated bearings design procedures and comparison with oil lubricated bearings [ASME PAPER 68-LUBS-10]

13 p2265 A69-27267

Design optimization for gas lubricated spiral groove spool bearing based on narrow groove theory, analyzing static and dynamic characteristics for motion in axial direction [ASME PAPER 68-LUBS-12]

13 p2266 A69-27270

Designs and capabilities of digital processing systems for automatic air traffic control radar information stressing future use of display for computerized control

13 p2295 A69-27332

Tactical air navigation system redesign with integrated circuits, obtaining weight reduction and improved performance and reliability

13 p2227 A69-27380

Passive adaptive sampled data control system with conditional feedback, discussing transfer function reduction and minimization of external disturbances and internal parameter variations effects

13 p2238 A69-27390

MHD generators semihot wall duct, discussing structural design, ceramic insulation elements brazing, temperature control, electrodes, working fluid, etc

13 p2372 A69-27473

Liquid flow MHD alternating current generators design, considering induced current in rotor and resulting magnetic field in pole gap

13 p2206 A69-27495

Single wavelength design with compensation compared to multiwavelength design without compensation for liquid metal MHD induction converter, discussing optimization

13 p2207 A69-27504

Engineering assessment and flight testing of aircraft systems in UK, discussing operational reliability, etc

13 p2201 A69-27539

Canadian air cushion vehicle industry, considering materials, design, production, tests, components and quality control

13 p2381 A69-27544

Soviet monograph on design and theory of linear induction pumps for liquid metals covering electromagnetic phenomena, optimized dimensions, etc

13 p2209 A69-27926

Large power systems integration in manned space stations, discussing design, selection and application criteria

13 p2209 A69-27939

Spaceborne optical telescopes requirements and development including mirror material and construction, optical design, servocontrol, etc

13 p2261 A69-27946

Stratoscope II unmanned balloon-borne telescope design, detailing pointing, focusing and thermal characteristics

13 p2261 A69-27956

Latching high-voltage reed relays in satellite instrumentation systems

13 p2231 A69-28047

Microminiature latching relay design and manufacturing cost

13 p2232 A69-28049

Systems design value analysis including alternate solutions to cost effectiveness for design development and production phases

13 p2383 A69-28097

U.S. Navy Numerical Value Rating System computing method of selecting lowest cost design approach to accomplish specific function

13 p2383 A69-28098

Flexible skirt design for air cushion vehicle consisting of semicylindrical elements and permitting horse power and cost reductions

13 p2203 A69-28179

High pressure AC arc heater system design criteria, discussing magnetic field, chamber gas flow, stabilizing elements, etc [AIAA PAPER 69-348]

13 p2243 A69-28283

Power supply subsystem for TD1/TD2 satellites with solar cells, discussing design including standby battery for solar eclipse periods

13 p2209 A69-28481

Finite automaton used to construct minimum automaton with periodic structure, discussing representability of regular events

13 p2239 A69-28553

CENFAM radar receiving system for meteoric and upper atmospheric data on amplitude, range and direction of meteor echoes through interferometer pairs

13 p2354 A69-28649

H plane waveguide Y circulators engineering design based on circulation equations

14 p2418 A69-28831

Parameters optimization in electronic equipment design, considering parameters and efficiency criteria as additive elements functions of dimensional chain
14 p2418 A69-28835

Lubrication systems for high speed machinery, discussing wet and dry sump arrangements, gearbox heat rejection, oil flow requirements, X-22A aircraft, etc
[ASME PAPER 69-DE-65] 14 p2454 A69-28845

S-band telemetry capability of Easter Test Range, discussing relationship to Telemetry Rehabilitation Project, major system decisions and performance characteristics
14 p2410 A69-28878

Space Ground Link Subsystem as S-band communication link within Air Force Satellite Control Facility including unified telemetry, tracking and command systems
14 p2427 A69-28879

VHF to UHF telemetry bands transition implemented by Naval Weapons Center
14 p2411 A69-28880

Optically swept glass slab laser design, discussing pulse length and peak power
14 p2457 A69-28930

Magnetosensitive quartz element with suspended magnet and two mirrors for recording magnetic variations
14 p2446 A69-29084

Automatic control circuit zero drift compensation during external disturbance, using algorithm for computer minimizing of losses caused by control and response inaccuracy
14 p2425 A69-29140

Fast and thermal thermionic reactor systems characteristics including fissile material, components mass, power output and flattening and design features
14 p2480 A69-29182

Primary isotope thermionic electric power module design, considering various assemblies
14 p2398 A69-29190

Actinium fueled thermionic generator design and characteristics, noting emitter temperature and material
14 p2399 A69-29192

Single cell fission powered thermionic converters design and testing
14 p2399 A69-29195

Thermionic converter SO-4 design and in- and out-of-pile test results, presenting diode performance at various times
14 p2399 A69-29196

Thermionic electrogenerating element (EGE) design optimization, considering one dimensional linear geometry with thin walled cylindrical sheath cathode
14 p2400 A69-29224

Soviet research on thermionic energy conversion, advantages and applicability in various fields
14 p2405 A69-29279

He-Ne lasers operation at 6328 Å, discussing optimum design parameters for power, life and stability
14 p2459 A69-29429

Aircraft design synthesis requirement definition in hardware commitment, discussing error effects of weight, aerodynamics and propulsion
14 p2392 A69-29432

Pressure, temperature, vibrations and structural stresses data acquisition system for aeronautical applications
14 p2450 A69-29686

C-141 Category IIIB all weather landing system, discussing system concept, components, operations and performance
14 p2479 A69-29701

Plasma diagnostics facilities design, circuit diagrams and operation based on Q switched ruby laser and optical recording system
14 p2461 A69-29782

Homodyne frequency converter design using microwave oscillator with bitonal frequency modulation
14 p2451 A69-29801

MHD generator design with electric conductivity waveform at small magnetic Reynolds numbers
14 p2405 A69-29911

Plane linear induction pump design optimization without short circuiting bus bars, allowing for MHD effects induced by traveling magnetic field
14 p2405 A69-29913

Systems engineering approach to aerospace product defects minimization, discussing scope, contract development, mainstream functions, component development, design data and subsystem integration
15 p2719 A69-30085

Measurement system for recording of small localized temperature changes in brain
15 p2606 A69-30152

Digital computers for aircraft engines control, discussing economic assessment, advantages and basic control system
15 p2671 A69-30323

Design and efficiency for signal-time compressors of spectral analyzers using electron beam tubes with charge storage
15 p2576 A69-30351

Pulse generator to accommodate electronic system testing to shock response spectrum by simulating real world shock environment
15 p2585 A69-30360

Solar simulator with xenon and krypton lamps designed for thermal balance tests, power conversion and material degradation experiments
15 p2586 A69-30383

Martian entry test facility for real size entry systems, discussing design, fabrication and operation
15 p2587 A69-30390

Back pressure control system for heat leak evaluation tests of cryogenic containers, discussing component selection and error analysis
15 p2702 A69-30397

Independent testing laboratory management, outlining requirements specialized to fit continued growth conditions
15 p2720 A69-30402

Boeing A-7000 Solar Simulator for Space Environment Simulation Laboratory, noting output characteristics
15 p2588 A69-30403

Resonant fixtures used for mechanical amplification of vibrator output to desired test levels
15 p2588 A69-30404

Defense integrated management engineering system at California Naval Air Rework Facility
15 p2588 A69-30427

Gas barrier seal design producing varying unit loading on conventional contact seal faces, including geometric stability and test results
[ASLE FICF PREPRINT 26] 15 p2621 A69-30495

Electrical engineering, Volume 3, communications, covering special theories, systems components, telecommunication, electroacoustics, digital and analog computers and programming
15 p2568 A69-30619

Design and electrical features of microwave measurement system for solid state spectroscopy, discussing waveguides, signal source, detector, etc
15 p2610 A69-30709

Flexible aluminum elliptical waveguide design, discussing installation, economy and electrical characteristics
15 p2578 A69-30798

Microslip between concentrated contacts and design charts for maximum pressure, closing-in of contacting bodies and optimized shapes, giving computer programs
15 p2629 A69-30903

Integrated Logistics Support (ILS) cost effectiveness, discussing management of systems elements in addition to prime equipment including computer programs, training, maintenance, etc
15 p2722 A69-31126

Automatic multichannel system for turbine blades static tests, discussing operation principles, component sections, programmed tape and vibration modes
15 p2672 A69-31209

Primary-secondary radar (SECAR) integration for air traffic control, discussing problems of simultaneous display, transmission synchronization, signal multiplexing, etc
15 p2570 A69-31222

Hydraulic regenerative servoamplifier system for electrohydraulic actuator design, discussing specifications and test results
15 p2553 A69-31294

Optimizing control system design using fluidic digital circuitry and FM type transducers
15 p2583 A69-31296

Fluidic control systems for industrial applications, discussing fluidic solutions to process problems
15 p2553 A69-31297

Wideband multiplexers design with directional filters, discussing operational characteristics
15 p2581 A69-31524

Power supplies for ruby, YAG and glass lasers, emphasizing design equations and component selection
15 p2636 A69-31527

Analytical method for designing pressure circular bearings verified by experiments concerning loading capacity
16 p2792 A69-31560

Time and space on-line simulation of analog, digital and hybrid block diagram systems
16 p2755 A69-31709

Multipad externally pressurized spherical bearing fed with incompressible fluid for satellite attitude control systems tests
16 p2793 A69-31728

Manned space stations role in future space plans, discussing prototypes and conceptual design
16 p2866 A69-31736

NERVA engine cooldown system for emergency shutdowns using high pressure liquid H followed by gaseous H warmup and liquid N cooldown
[AIAA PAPER 69-512] 16 p2810 A69-31846

Global satellite communication networks design by computer simulation, discussing politicechnical interface problems, ground stations, atmospheric factors, system optimization, etc
16 p2750 A69-31852

FM/FM telemetry system for high altitude rocket research, using independent subcarrier oscillator for each measurement transmitted with individual frequency modulation
16 p2750 A69-31853

German ground station commercial receiving system for satellite broadcast reception
16 p2766 A69-31855

Ground station command transmission equipment for German AZUR satellite, describing components based on NASA Tone Digital Command System
16 p2759 A69-31856

Data processing for scientific rocket research, considering pulse counters, multiplexers, converters and programmers
16 p2755 A69-31858

Book on soviet An-24 aircraft construction and exploitation covering fuselage, powerplant, controls, fire prevention, air conditioning, maintenance, etc
16 p2735 A69-32112

Iris microphotometer with measurement and reference beams traversing plate in neighboring regions designed for stellar images measurement
16 p2790 A69-32225

Absolute stability, stability in whole and engineering stability in reference to Liapunov stability applicability
16 p2874 A69-32244

Low temperature fuel cell with mixed oxidizer and fuel and fuel cell based on water radiolysis under alpha and gamma radiation
16 p2740 A69-32425

Servosystems components design, discussing detector, corrector, amplifier and motor
16 p2741 A69-32431

Retrodirective antennas for spacecraft, discussing design, operations and applications
16 p2762 A69-32557

Integrated circuits effect on electronic equipment design and production technology
16 p2762 A69-32578

Design philosophy for cost reductions on future space transportation systems, exemplifying application to booster system for earth orbital logistics
[AIAA PAPER 69-439] 16 p2882 A69-32654

Water moderated beryllium reflected reactor design for testing NERVA or Rover type fuel elements in nuclear environment, noting core location
[AIAA PAPER 69-513] 16 p2810 A69-32656

Systems approach in turbofan engine design acoustic evaluation, discussing noise sources and radiation patterns
[AIAA PAPER 69-491] 16 p2839 A69-32667

Subsonic diffuser design, discussing flow distortion and turbulence levels and pressure loss characteristics
[AIAA PAPER 69-449] 16 p2843 A69-32700

First generation nuclear flight stage with 75000 lb thrust NERVA flight engine, discussing applications design and hardware options
[AIAA PAPER 69-534] 16 p2810 A69-32707

Test rig vehicle design for noise research on single stage high bypass ratio fans for quieter turbofan powerplants
[AIAA PAPER 69-492] 16 p2767 A69-32727

Orbital refueling techniques, discussing vapor-liquid interface stability, pressurant requirements, transfer line chilldown, propellant transfer dynamics, dielectrophoresis, suction speed estimating and system tradeoffs
[AIAA PAPER 69-564] 16 p2869 A69-32733

Hydrogen oxygen rocket engine two phase liquid hydrogen pump capability and hydrodynamic design,

analyzing constant-quality flow, acoustic effects, compressible flow and cavitation
[AIAA PAPER 69-549] 16 p2845 A69-32759

Molded composites application to engine components, discussing turboprop reduction gear case design using polymer matrix boron composite
[AIAA PAPER 69-466] 16 p2795 A69-32763

Rocket performance optimization by extending injector design technology to high performance injectors for space storable FLOX/LPG propellants
[AIAA PAPER 69-506] 16 p2846 A69-32778

Antenna systems design for ISIS-A scientific satellite, discussing antenna array of 13 radiators for telemetry, command, beacon and experimental purposes
17 p2918 A69-33030

Equipment- and program-type methods for solving automatic digital control systems synthesis problems, evaluating efficiency based on accuracy
17 p2933 A69-33120

Soviet collection of articles on theoretical and experimental investigations of strength of mechanical engineering structures
17 p3056 A69-33190

VTOL transport aircraft, discussing systems integration problems, feasibility and time scale of introduction into service, noise and safety, etc
17 p2897 A69-33207

D-2 satellite stabilization system design and development, noting mission to determine hydrogen distribution around earth
17 p3046 A69-33223

Optimal design for improving thermal performance of existing spacecraft thermally actuated louvers by increasing open-to-closed emittance ratio
[AIAA PAPER 69-627] 17 p3071 A69-33269

Microphonic noise measuring systems for airborne radar system design for noise reduction
17 p2937 A69-33628

Equipment environmental conditions tabulated to assist engineer in preliminary design considerations and in planning test programs for specimens
17 p2910 A69-33661

Nonrecirculating wind tunnel configuration with minimum atmospheric wind disturbances for V/STOL vehicles aerodynamic testing
[AIAA PAPER 68-398] 17 p2947 A69-34024

Avionics systems with integration and federation applied to integrated light attack avionics system/ILAAAS/ design to provide navigation, weapon delivery and flight control
17 p2976 A69-34057

Electronic computers for avionics system design in terms of technology, performance and cost, discussing reliability prediction and failure rate data
17 p2976 A69-34058

Multispectral imaging remote sensors, analyzing energy sources affecting systems synthesis
17 p2977 A69-34064

Airborne data processing systems reliability, discussing software and hardware reconfiguration techniques and man-machine interface problems
17 p2977 A69-34072

Doppler inertial system with remote attitude capability, detailing sensor operation by airborne computers
17 p3002 A69-34097

Cost optimization in converting brush type to brushless aircraft AC power systems, using analog computer to determine modifications
17 p2905 A69-34109

Rotary power transformer design for spin stabilized spacecraft power system, discussing efficiency and advantages
17 p3050 A69-34111

Solid state broadband RF power amplifier for airborne HF radio, eliminating total servosystem and all higher voltage components
17 p2942 A69-34114

Integrated circuit ultrahigh speed analog to digital converter, discussing interactions at high digital rates and video bandwidths
17 p2943 A69-34125

Pivotal computer operations in Apollo NASA Communication Network, describing UNIVAC computers in use and design considerations
18 p3100 A69-34267

Soviet book on hydraulic servo drive covering design and performance, static and dynamic characteristics and stability problems
18 p3093 A69-34356

Quantitative and qualitative reliability programs for commercial and aerospace products, considering Failure Effect Management System
18 p3143 A69-34486

Fluctuations effect in flow problems analyzed by waiting line theory to improve systems design based on operational needs
18 p3145 A69-34495

Operations research methods applied to systems effectiveness study, using key decision models with optimized alternatives
18 p3145 A69-34503

Failure rate data role in reliability analysis and design optimization
18 p3147 A69-34516

OGO program failure rate analysis with respect to cost, schedule and performance tradeoffs, considering component and systems design and reliability, prelaunch feedback, etc
18 p3207 A69-34519

Failure mode and effect analysis integrating design and reliability engineering, discussing management controls and interdisciplinary coordination
18 p3147 A69-34526

Slide methods for duplex parallel and switchover redundant mission availabilities based on cost, reliability and maintainability
18 p3147 A69-34531

Plastics behavior under loading and performance prediction, considering engineering design applications
18 p3161 A69-34609

Optimum automatic system for controlling helicopter formation flight, stressing transient response Q factor and transmission ratios
18 p3090 A69-34656

Extreme disturbance analysis and optimum performance and design problems for structural and mechanical dynamic systems, basing solutions on linear, nonlinear and dynamic programming
18 p3106 A69-34663

Electronic data processing facilitating engineering design development work, including computer programming
18 p3106 A69-34838

Automatic celestial navigation, discussing star trackers design, mathematics of celestial fix and relationship to errors and physical and environmental constraints
18 p3169 A69-34852

Computer-aided design application to mass property engineering, describing repetitive mathematics functions, design information retrieval and display, automated synthesis, etc
[SAWE PAPER 795] 18 p3107 A69-34863

Halon 1301 fire extinguisher for burning spilled hypergol on Apollo/Saturn LM adapter, discussing concentration requirements and exposure hazards
18 p3094 A69-35062

Educational TV satellite system design for U.S. in 1970s
18 p3235 A69-35076

Multistage systems high reliability design, describing branch and bound computer method for optimal resource allocation of redundant components
18 p3148 A69-35081

Biosatellite attitude control systems design development and flight test results for payload perturbing effects, discussing simulation activity
18 p3210 A69-35094

Advanced Meteorological Sounding System (AMSS) for measurements up to 150,000 ft, discussing configuration, characteristics, radiosonde, ranging, telemetry data ground equipment and test
18 p3108 A69-35102

Three dimensional morphology of systems engineering, using model for applications in taxonomy, new activities sets discovery and systems science curriculum design
18 p3236 A69-35235

Lockheed C-5 Galaxy aircraft avionics systems with Doppler inertial navigation equipment to operate with precision without ground based aids
18 p3104 A69-35465

L-1011 Tri-Star aircraft systems and safety provisions, discussing automatic flight control system, propulsion, noise reduction, galley, coat storage and cabin window shades
[AIAA PAPER 69-828] 19 p3243 A69-35598

Large area Si solar cell arrays design, considering environment, cell layout, thermal expansion, coverslides fabrication, costs, etc
19 p3253 A69-35708

Equivalent circuit demonstrating noise reduction through input transistor integration into passive receiving antenna, stressing circuit loss control and preamplification role
19 p3281 A69-35764

System reliability evaluation based on failure analysis illustrated with examples covering initial requirements through parts production monitoring and control
19 p3454 A69-35782

Strapdown inertial reference unit system for inflight reliability and maintainability, discussing design areas components
19 p3370 A69-35800

Automatic systems for complex plant control, discussing synthesis of complex control systems
19 p3286 A69-35808

Book on statistical communication and applications to radio and radar systems technology to provide guidelines for design decisions
19 p3267 A69-35900

Digital computer controlled antenna positioning system computing spacecraft tracking trajectory from given parameter input set
19 p3267 A69-35997

Ground controlled remote manipulator spacecraft system to perform unmanned satellite orbital maintenance, discussing refurbishment, laboratory simulation, system cost effectiveness and feasibility
19 p3430 A69-36001

System approach to reliability demonstration, discussing design and impact on levels, risks, requirements, testing, cost and incentives
19 p3327 A69-36003

Optimized contracting for systems engineering management, discussing industry views, scope, application, depth, procurement and performance measurement
19 p3454 A69-36005

Cost model to trade off competing systems designs for space communications, navigation, operational availability and ballistic missile defense
19 p3454 A69-36007

System engineering to select hydraulics subsystem for advanced fighter aircraft by cost effectiveness analysis, noting maintainability and reliability
19 p3254 A69-36012

Man machine interface problems in C-5 equipment and system design
19 p3261 A69-36024

Subsystem designs evaluated on basis of human reliability metric to select desirable design configurations
19 p3261 A69-36026

System components for spatial discrimination implementation scheme, discussing IR detector arrays and optical imagery processing
19 p3373 A69-36055

Optical instruments optimal design for given requirements, discussing tradeoff studies of airborne reconnaissance scanner, spaceborne rendezvous sensor and track-while-scan radiometers
19 p3310 A69-36065

EKG signal transmission to hospital during cardiac patient transportation by emergency vehicle, noting prototype system construction and tests
19 p3262 A69-36271

Biotelemetry system as candidate prototype of generalized system for clinical applications
19 p3262 A69-36272

Computer program designing multiplex taper to minimize FM/FM telemetry system carrier threshold SNR, examining noise behavior of multiplex system stages for system performance
19 p3273 A69-36273

Optimum receiver design for binary coded data detection in two channel space communication system, discussing phase error distribution and optimum decision function
19 p3275 A69-36286

Missile and space support planning, objectives, technology development, functions, maintenance and in-flight maintainability
19 p3295 A69-36327

Commercial satellite communication ground station at Arvi, India, discussing system design, operation and international standards
19 p3275 A69-36412

Optimum aerological network design, discussing atmospheric model, numerical analysis, data acquisition, weather forecasts, rms measurement error, etc
19 p3364 A69-36505

Space age metals supply and demand relationships, discussing system engineering criteria for maximum efficiency
19 p3346 A69-36635

Italian cross radio telescope noting added phase shifters to N-S arm, transistorized receiving system and modified data processing
19 p3295 A69-36643

- Computer-algorithm elements required for engineering design and invention problems including design requirements, selection of spaces for variables using computerized heuristics, etc 19 p3280 A69-36666
- He-Ne laser communication feasibility experiments, discussing modulation, detection, operating parameters, etc 19 p3279 A69-36756
- Detector radiometer design for radio astronomical measurements in 0.7-2 mm range, discussing sensitivity 19 p3285 A69-36877
- Radar design for target detection, tracking and identification, modeling plasma effects on radar cross section of reentry vehicles based on wave-plasma interactions 20 p3485 A69-36925
- Vibration absorber incorporating polymer spring/damping elements for attachment to complex main system, noting butyl rubber as effective and convenient damper material 20 p3620 A69-36996
- Book on solenoid magnet design covering magnetic and mechanical aspects of resistive and superconducting systems 20 p3464 A69-37145
- Soviet book on theory and design of turbocompressors covering gas dynamic cascade theory, thermodynamics and aerodynamics, viscous gas flow, etc 20 p3459 A69-37238
- A scope laser radar system using Q switched solid state laser pulses, discussing configuration and performance 20 p3487 A69-37283
- Data handling system design for large astronomical satellite /LAS/, discussing spacecraft configuration, basic aims, program functions, subsystems, signal flow, flight repair, etc 20 p3501 A69-37390
- Geometrical configuration for synthetic aperture terrain imaging radar scanning system, noting scanning methods in range and azimuth directions 20 p3489 A69-37634
- Synthetic aperture terrain imaging radar system optimal design, considering noise-free and random noise conditions using least squares method and signal to noise ratios 20 p3489 A69-37639
- Recording devices for storing bandwidth data in time sequence, studying design parameters using light beam recorder implemented with CRT for read-in process 20 p3540 A69-37640
- Technological systems engineering effectiveness assurance elements, discussing roles of engineering, operations research, data utilization, production and installation, etc 20 p3550 A69-37709
- Parallel wire antenna array design for specified pattern using matrix methods and method of moments for self and mutual impedances and required excitations 20 p3507 A69-37847
- C-5A transport landing gear assembly design, illustrating air turbine kneeling-drive module 20 p3466 A69-38179
- Design concepts and principles of systems for monitoring of Concorde flight control actuators, considering servo control, control interconnections and control input system 20 p3467 A69-38190
- Maintainability as design requirement in system specifications and contracts, noting MIL-STD-471 program of maintainability demonstration tests 20 p3551 A69-38268
- Book on synchro application and design covering telemetry, torque and control systems, synchro circuits, resolvers as computer elements, etc 21 p3681 A69-38450
- Compressible fluid flow characteristics in turbomachine stage, discussing simplified radial equilibrium method as basis for design 21 p3643 A69-38457
- Microwave frequency measuring instruments design solutions for electric measurements reduction to length measurement 21 p3720 A69-38563
- Admissible controls set for discontinuous stochastic automatic control systems, deriving mean optimal averaging of controls 21 p3770 A69-38855
- Nuclear rocket program status and plans, presenting NERVA reactor and engine system tests [AIAA PAPER 68-610] 21 p3768 A69-39219
- Error propagation and tolerance analysis in design and reliability engineering and stress analysis 21 p3842 A69-39303
- Integrated sensor controllers for missile directional control, discussing test results for two different systems [AIAA PAPER 69-837] 21 p3761 A69-39368
- Single degree of freedom gyroscope design factors applicable to strapdown guidance system, discussing torque-to-balance loop, multiple pulse bursting and error sources [AIAA PAPER 69-848] 21 p3762 A69-39378
- Model performance index /PI/ providing criterion for approximating one dynamic flight control system by another based on geometrical representation of linear autonomous systems [AIAA PAPER 69-885] 21 p3764 A69-39410
- NF106B-VST model follower flight control system, discussing design criteria/performance index, rigid/elastic math model development, flight test evaluation, hardware design, etc [AIAA PAPER 69-886] 21 p3764 A69-39412
- Lifting body stability augmentation systems design, development, ground tests and flight data including frequency response, limit cycle and structural resonance [AIAA PAPER 69-887] 21 p3647 A69-39413
- Optimum filter design for noisy analog feedback system with forward and feedback disturbances, using mean square error criterion between signal and data 21 p3687 A69-39449
- Superconducting magnets for MHD generators, discussing design, construction and operation problems 21 p3782 A69-39478
- Soviet book on self adaptive systems design, operational principles and analysis and synthesis methods 21 p3687 A69-39532
- Laser design for smooth emission frequency retuning, discussing equations for laser field oscillations, two photon resonance, tensor analysis, quantum emission, etc 21 p3739 A69-39539
- Light sources with uniform variable luminance field designed for calibrating cameras used in space exploration 21 p3726 A69-39580
- Dornier ASTRID attitude stabilization system design for spinning rocket nose cone with instrument payload, using first stage biaxial inertial platform and second stage star tracker 21 p3826 A69-39639
- Spacecraft attitude acquisition/reorientation and stabilization controller design implemented by control moment gyro, proposing control algorithm using control actuator nonlinearity 21 p3826 A69-39641
- Space vehicles optimal pulsed control systems statistical synthesis, considering structural constraints on operation, memory capacity and algorithm coefficients 21 p3767 A69-39651
- Parse-implement approach to digital systems design, combining systems level /conceptual/ and engineering environmental level /physical/ viewpoints 21 p3680 A69-39663
- Launch vehicle cost reduction by minimizing software, fabricating in commercial shops and avoiding sophistication, parts and acts of man 21 p3857 A69-39688
- Launch systems evolution, cost reduction breakthrough approach and application to future space transportation 21 p3857 A69-39692
- Reusable Crew Module, Reusable Orbital System and Reusable All Systems options for low cost space transportation system 21 p3827 A69-39693
- Book on maintainability principles and implementation methods covering program implementation, quantitative factors, maintenance concept, tradeoff techniques, design liaison, etc 21 p3734 A69-39815
- Hybrid microelectronic modules, using basic thermal design guidelines 22 p3910 A69-39952
- Correlation protected ILS implementing conventional ILS with no operational restrictions on air traffic control, taking into account changing terminal conditions 22 p3978 A69-39963
- Optical and mechanical systems of Wrocław Observatory Lyot type coronagraph for prominence observations in H alpha line 22 p3943 A69-39999
- Planning, design and implementation of reliability testing facility, investigating phases of project life cycle 22 p3954 A69-40033
- Short range telemetering strain gage system with astable multivibrator transmitter for measuring intercoupling displacement and shaft torque 22 p3946 A69-40314
- Closed Loop Ionogram Processor /CLIP/ on-line computer processing system for ionospheric data [AIAA PAPER 69-952] 22 p3904 A69-40334
- Real time multiprocessing telemetry ground support integrated system design with expanded definition of hardware/software decision tradeoffs [AIAA PAPER 69-971] 22 p3907 A69-40351
- Automated design system producing wire format data for cabling avionics subsystems of light attack aircraft [AIAA PAPER 69-976] 22 p3912 A69-40356
- Representative data of actual forces and moments applicable to large spacecraft attitude control system for typical crew activities obtained through simulation programs [AIAA PAPER 69-1006] 22 p3921 A69-40380
- Systems approach to avionics optimization, discussing instruments, devices, display and automation techniques [RAES PAPER 6] 22 p3946 A69-40487
- Complex program management emphasizing systems engineering management, noting applications to aeronautical systems [RAES PAPER 9] 22 p4053 A69-40489
- Linear flight control system synthesis by using optimal control theory associated with quadratic performance index 22 p3864 A69-40588
- Adaptive control system synthesis for reducing computation labor for controlled inertialess plant, reproducing probability density function to describe unknown parameters 22 p3918 A69-40739
- Optimum linear adaptive design of dominant-type systems with large parameter variations assuring system response within prescribed bounds by reducing internal noise sensitivity 22 p3918 A69-41011
- Suboptimal linear regulators design method yielding feedback controller for multivariable linear systems subject to parameter variations 22 p3918 A69-41012
- Boeing 747 safety engineering program, discussing organization, design review, system safety, systems design-analysis and tests 22 p4054 A69-41136
- Automation of single pass electric spark machining of high alloy steels and hard alloys, including anodic-mechanical profiling, cutting and drilling 23 p4168 A69-41308
- Millimeter wave pseudorandom coded CW meteorological radar for precipitation drop size spectrum analysis and cloud studies, discussing overall system design 23 p4115 A69-41531
- Aircraft gas turbine engine lubricant evaluation and systems design from standpoint of effective oil life and lubricant stability requirements [SAE PAPER 690424] 23 p4200 A69-41648
- Turbomachinery periodic structures design to improve tolerance to inflow distortion and resonant oscillatory flows, considering large amplitude pressure waves propagation [SAE PAPER 690388] 23 p4201 A69-41666
- SDP-3 small serial computer for engineering experiment on IMP spacecraft, discussing design modifications to improve performance 23 p4133 A69-41737
- Flexible format adaptive telemetry encoder design, discussing system design and implementation technique with modular units 23 p4119 A69-41748
- IBM 360-50 computer with I/O terminals to process PCM and analog data from Modular Auroral Probe series of sounding rockets on real time basis 23 p4133 A69-41764
- Potential energy modeling method for optimal design of structural systems with diverse performance criteria, giving truss design example 23 p4228 A69-41923
- Ammonia resistojet thruster, describing ammonia physicochemical properties and systems characteristics of pulsed mode operation and continuous thrust resistojets 23 p4203 A69-41931
- Microwave bandpass step filters, listing structural dimensions and design parameters 23 p4139 A69-41947

Structural features and performance of 300 ft steerable receiving antenna, discussing aiming error, aperture efficiency, azimuth and altitude drive
23 p4148 A69-42121

Feasibility studies to optimized design for 440 ft steerable filled-aperture radio and radar telescope, discussing parabolic configuration, radome selection, etc
23 p4148 A69-42123

High sensitivity communication system design consisting of radome enclosed steerable antenna, 500 kw transmitter and microwave configuration compatible with low noise receivers
23 p4149 A69-42131

Freon boiler designed for Rankine cycle heater fired on hydrocarbons with over 2000 F flame front temperature, considering radiant/convective heat transfer
23 p4068 A69-42239

Radioisotope thermoelectric generators (RTG)/design and performance analysis method applied to generators using Si-Ge Air-Vac type thermocouples
23 p4188 A69-42260

ISOTEC thermoelectric generators for space power, describing design features, operation, power output and radioisotope heat source
23 p4189 A69-42270

Satellite communication system high speed sequential decoder design, discussing parameters, simulation and test results on satellite channels
23 p4131 A69-42523

Space vehicle multibeam Cassegrain antenna system design meeting radiometric mapping requirements in microwave frequency range, discussing mounting, degrees of freedom, etc
[ONERA-TP-713]
23 p4143 A69-42527

Optimum integration of aircraft equipment, subsystems and computer mechanizations for low cost navigation system consistent with mission requirements
23 p4186 A69-42538

PCM telemetry system for transferring information from many remote sources to single local processing point
24 p4281 A69-42620

NDT techniques relation to engineering design problems with failure potential, discussing management planning and cost analysis
24 p4318 A69-42769

Satellite data management systems design, considering user-designer cooperation aspects for space programs
[AAS PAPER 69-366]
24 p4417 A69-42806

Hybrid display for data visual display using electroluminescent and thermochromic technologies for wide range of ambient illumination
24 p4313 A69-42899

Pneumatic driving system for heart assist or total replacement pumps, discussing design features and performance characteristics
24 p4273 A69-42983

Vienna 60 inch telescope concept and design, discussing optical systems possible combinations under local conditions
24 p4314 A69-43000

Display system design principles and procedures, discussing checklists, formal procedures and behavior theory
24 p4274 A69-43017

Decision process model for man-machine decision task structuring by system designers
24 p4274 A69-43018

Spacecraft single wall cryogenic storage system, discussing cost, pressure vessel and components, thermal and performance characteristics
24 p4393 A69-43045

Multichannel spectral line receiver for 210 ft Australian radio telescope with front ends covering wide frequency range
24 p4283 A69-43115

PCM satellite communication systems signal power and frequency bandwidth requirements, noting PCM-psk superiority over FDM-FM
24 p4283 A69-43200

Launch vehicle control system synthesis based on mode control theory state variable formulations
24 p4394 A69-43278

Quasi-optimum control law for aircraft landing control system design based on Friedland technique, evaluating effectiveness by computer simulation
24 p4253 A69-43280

State variable feedback design of m-input, m-output time invariant linear systems requiring noninteraction and exact transfer functions, considering coupled core nuclear reactor
24 p4294 A69-43315

F-111D computer complex to provide selective functional redundancy and flexibility to accommodate mechanization changes
[AIAA PAPER 68-837]
24 p4285 A69-43719

SYSTEMS STABILITY

Integer programming method for optimizing constrained reliability problems with several system failure modes
20 p3504 A69-37069

Damped linear system asymptotic stability inferred from dynamical equation structure, considering matrix eigenvalues and Thomson-Tait-Chetaev stability theorem
20 p3623 A69-37531

Viscoplastic thermomechanically coupled systems stability, considering effects of heat transfer to surroundings and heat capacity in material regions below yield
20 p3625 A69-37591

Rocket body elastic vibrations, liquid fuel supply oscillations and engine thrust vibrations effects on system stability
20 p3617 A69-37604

Phase and amplitude stability measurements in airborne pulse Doppler radar
20 p3492 A69-37711

Linear nonstationary system with singular point analyzed for stability necessary and sufficient conditions using Riemann-Mellin conversion integrals and Laplace transforms
21 p3685 A69-38451

Nonlinear computing schemes examined for necessary and sufficient conditions of stability as derived from Mikhailin linear operators and Frechet derivatives
21 p3678 A69-38746

Algorithms testing characteristic polynomials and differential equation classical stability relations
21 p3755 A69-38925

Linear and nonlinear differential equations systems stability and instability problems, describing procedures and theorems for solutions
21 p3755 A69-38960

Spacecraft wide angle attitude control system stability analysis, using air bearing table simulation
[AIAA PAPER 69-856]
21 p3823 A69-39384

Stability of nonlinear systems with state variable feedback applied to fuel valve servomechanism
21 p3687 A69-39460

Stability contours for sampling and delay effects analysis in analog/digital hybrid simulation loops, considering compensation quality over simulated system natural modes
21 p3680 A69-39609

Stable linear system/shaping filter/synthesis transforming stationary white noise into random process having given covariance function
21 p3688 A69-39661

Damping effects on elastic systems stability under nonconservative forces, correlating stability and quasi-stability regions
22 p4040 A69-39981

Nonlinear system oscillations analysis based on small parameter method and difference equations, including resonant case and stability criterion for periodic solutions
22 p3980 A69-40108

Existence theorem for linear stochastic systems optimal control described by differential equation with random coefficients, providing rms stabilization
22 p3917 A69-40116

Dynamic systems stability with two degrees of freedom, determining second order time dependent integrals valid near periodic orbit
22 p4013 A69-40123

Book on convergence in calculation of elastically deformable aircraft structures and continua, covering matrix displacement method and stepwise linearized computational technique
22 p4044 A69-40619

Automatic phase control system stability range determination in piecewise linear approximation and in presence of proportional integrating filter
22 p3918 A69-40956

Minimax sensitivity criteria used to synthesize filters for estimating state of first order plant subject to dynamic and/or statistical parameters uncertainties
22 p3918 A69-41016

Book on systems stability with random parameters, considering linear and nonlinear control systems, with application to stochastic approximation
23 p4181 A69-41510

Bounded input-output stability for lumped distributed systems by poles examination in S plane, con-

sidering transient response of linear time invariant systems
23 p4144 A69-41510

System asymptotic motion stability for given parameter values using algorithms with aid of R functions
23 p4191 A69-41710

N-th order differential systems using first approximation, finding conditions for bounded solutions, solutions asymptotic to zero and stability
23 p4181 A69-41710

Liapunov stochastic stability direct method analog used for estimating reliability of redundant systems with constant recovery time
23 p4144 A69-41910

Dynamic characteristics of nonlinear discrete systems by motion division method, using discontinuous Liapunov function for stability criteria
23 p4144 A69-41910

Combined automatic control systems stability having principal coordinates related by loading equation
23 p4145 A69-42370

Invariance conditions for steady and unsteady systems by differential method compared to variational approach
23 p4145 A69-42370

Sufficient conditions derived for absolute stability of dynamic systems containing nonlinear functions of several state variables
23 p4145 A69-42440

Nonlinear time varying feedback control system stability applied to damped Mathieu equation
23 p4146 A69-42470

Pointing vector and angular rate relationships for various optical elements, discussing analytical model development for precision electro-optical stabilization systems
23 p4131 A69-42540

Frequency condition for ensuring stochastic stability of one dimensional discrete feedback control system containing linear dynamic part and inertialess nonlinear component
24 p4288 A69-42670

Digital analysis of nonlinear control systems dynamic stability under small perturbations, using linearized differential equations
[IS-ERI-71]
24 p4285 A69-42980

Adaptive control function technique to design lateral stability augmentation system for hypothetical manned lifting body entry vehicle
24 p4394 A69-43300

Distributed parameter systems stability as internal and input-output property, describing Liapunov functional construction
24 p4293 A69-43300

Frequency domain stability criteria for open and closed loop distributed parameter linear time invariant systems
24 p4294 A69-43300

Stability of linear systems with convolution operators in forward loop and time-varying gain in feedback loop analyzed for frequency- and time- domain conditions
24 p4295 A69-43310

Stellar system differential rotation effect on gravitational instability with distribution propagating in rotation axis direction
24 p4388 A69-43630

SYSTOLE

Systolic murmurs and flight personnel evaluation noting phonocardiographic definition and tracings of specific systolic murmurs
09 p1445 A69-22720

Blood pressure fluctuations in multiple extra systole during tilt table studies for flying fitness of pilot
10 p1645 A69-23370

SYSTOLIC PRESSURE

Pneumograms and EKG used to determine heart beat, respiration rates and systolic index of cosmonauts during Voskhod 2 flight
07 p1062 A69-18580

Cat hearts ventricular pressure curves dv/dt and dp/dt correlated with left heart ventricle mechanical performance
23 p4095 A69-42070

Sinus outflow relationship to oxygen content in anterior cardiac vein blood and right ventricle systolic pressure
23 p4098 A69-42100

T

SHAPE

Miniaturized E-Tee three port circulator with wide bandwidth, noting negligible effect of static field small variations on performance
08 p1291 A69-20980

T shaped radio astronomical array, discussing time sharing technique providing simultaneous observation capability and merits of T and cross configuration telescopes
20 p3507 A69-37837

TAURI STARS

IR object discovered during T Tauri objects and diffuse nebulae study, discussing peculiarity
04 p0655 A69-14665

Polarimetric observations of polarization percentage and position angle changes in T Tauri stars, confirming stellar polarization association with emission spectra
15 p2694 A69-30882

53 ENGINE

T-53 engine operation in U.S. Army helicopters noting design problems from compressor blade failure, sand and dust erosion and bearing and lubrication malfunctions
[AHS PAPER 215] 07 p1203 A69-18867

TABLES [DATA]
NT MATHEMATICAL TABLES

Charts summarizing daily solar phenomena, cosmic rays, geomagnetic variation, ionosphere, radiowave propagation and airglow observations in Japan
02 p0315 A69-11732

Tabular reduction of crystal structure chemical information for metals and semiconductors for material selection use
02 p0295 A69-11786

Equations, tables and charts for shock drag parameter in determination of shock wave drag of body in supersonic free stream of ideal gas
02 p0188 A69-11862

Book containing 1960-1965 /including IQSY/ chronological tables of solar and geophysical events, discussing solar activity, geomagnetic, ionospheric, auroral and cosmic ray research
02 p0321 A69-12165

Monograph on orbit computation of doubly photographed meteors employing method of least squares, giving computer programs and tables of data printout
02 p0324 A69-12495

Equations for self oscillating mode of operation for O-type backward wave generator with electrostatically focused electron beam and finite values of amplification parameter
03 p0407 A69-13986

Handbook on metabolism and nutrition containing tables, charts and diagrams on food composition, material incorporation into organism, energy exchange and end products
04 p0553 A69-14908

Flammability handbook for plastics noting characteristics, behavior under fire conditions and various fire hazard reduction mechanisms, tables, drawings, manufacturers, suppliers, etc
04 p0620 A69-14952

Hardness reference data for metals and nonmetals, using hardness test results for data reliability
04 p0617 A69-15033

Thermodynamic function tables for 30 gases under ideal gas conditions up to 6000 K
04 p0686 A69-15153

Book on thermodynamic and thermochemical tables with charts on thermodynamic properties, physical chemistry and gas dynamics
04 p0688 A69-15459

Book on plate formulas and tables for designing structure components of various geometrical shapes and thickness covering bending, compression, loading, etc
05 p0833 A69-15726

Table of equivalent widths of isolated lines with combined Doppler and collision broadened profiles
05 p0796 A69-15747

Photoelectric observation of Sco X-1 variations with 91-cm reflector, tabulating results and estimating accuracy
06 p1008 A69-17695

Grey and very grey thermochemical tables for C-H and C-H-O species
[WSCI PAPER 68-38] 06 p0885 A69-17795

IR solar spectrum tables and graphs covering 10,657-12,857 A
06 p1008 A69-17809

Absolute coordinates of 906 lunar features derived and tabulated, eliminating errors due to atmospheric turbulence by using 120 lunar negatives
07 p1213 A69-18612

Elevated temperature mechanical properties data for commercially produced super-strength alloys supplemented by product description tables
08 p1328 A69-19913

Specific gravity data for olivine-pyroxene and enstatite chondrites, aerolites, siderites, amphoterites, pallasites and Butler meteorites
08 p1389 A69-20262

Solar system elements abundance compilation based on carbonaceous chondrites and nucleosynthesis in stars
08 p1401 A69-20903

Zinc oxidation in weakly alkaline media, discussing basic properties of electrochemical cells containing zinc
08 p1268 A69-21050

Stars closer than five parsecs including binary systems, luminosity, spectral type and mass
08 p1407 A69-21130

Tables of effective electron cross sections and macroscopic coefficients, Volume 1, covering hydrogen and rare gas molecular and atomic interactions with electrons
09 p1541 A69-21579

Radio telescopic survey for OH emission at 1667 MHz in interstellar dust clouds for catalog compilation, tabulating results
09 p1603 A69-22267

Electrical devices for detonation initiation in pyrotechnic equipment for space applications, tabulating characteristics
10 p1749 A69-23006

Specific heats of oxygen at coexistence from triple point to critical point and corresponding values for liquid phase
10 p1808 A69-23187

Tabulating experimental constant volume specific heats of fluid oxygen from triple point to 300 K at pressures to 350 atm
10 p1808 A69-23188

LOX thermodynamic properties from triple point to 250K and pressures to 350 atm, tabulating at uniform densities and temperatures
10 p1808 A69-23189

Photometric consequences of reflection effect in close binaries, tabulating light curves
10 p1776 A69-23218

Table of computerized three place E-M solutions for Kepler equation, noting revision of Astrand table
10 p1777 A69-23395

Six color stellar photometry of 159 field stars including subdwarfs, high velocity stars and 50 Hyades stars, tabulating color data
10 p1788 A69-24122

Environmental requirements of military specifications tabulated according to tests for altitude, temperature, vibration, shock, humidity, temperature/altitude, etc
11 p1862 A69-24331

Lithophile elements relationship in chondrites and basaltic achondrites, tabulating Ca-Al ratios and Ca, Al, Ti, Zr, Sr, Ba and Sc percentages
11 p1954 A69-24360

Orbital parameters changes computation in table form for binary systems with more massive component mass decrease
11 p1962 A69-25120

Comet Berbon and minor planet positions photographically recorded /1964-1967/
11 p1962 A69-25121

Tabulation of definite and indefinite integrals of products of error function with elementary and transcendental functions
12 p2121 A69-26395

Atmospheric models for electromagnetic scattering of monochromatic IR and microwave radiation by natural suspensions as hazes clouds and precipitation
12 p2030 A69-26467

Population densities, pumping rates, lifetimes, etc, of singly ionized krypton ion laser
12 p2109 A69-26638

Photoelectric and visual minima tabulated for eclipsing binaries, calculating light elements
12 p2160 A69-26853

Dwarf and subdwarf stars limb darkening tables for unblanketed nongray radiative model atmospheres
12 p2171 A69-27153

UBV observations of long period variable stars using reflecting telescope and refrigerated photocell with standard filters
12 p2172 A69-27156

Born-Mayer parameters simplifying computation of interatomic potential, tabulating numerical values for 104 mononuclear pairs of neutral ground state atoms
13 p2301 A69-27453

Regression coefficients obtained from satellite cloud observations applicability in constructing geopotential fields, tabulating coefficients obtained from ground stations
13 p2292 A69-27731

Spectrometric and photometric investigation of spectral characteristics of large sunspot 45 degrees from solar disk center, tabulating characteristics of 134 spectral lines
13 p2218 A69-28324

Solar radio emission data during IGY covering solar terrestrial disturbances, broadband bursts, solar indices, etc
14 p2513 A69-29321

Radial velocities of southern OB stars and supergiants noting tabulation of information
14 p2519 A69-29368

Provisional elliptic orbit computed for asteroid Floirac using Gauss-Encke and least squares method, tabulating residuals and ephemeris
14 p2521 A69-29585

17 November 1966 Leonids return, tabulating data from previous returns starting with October 899
14 p2525 A69-29715

Applied function theory, Volume 6, Tables of theta functions and elliptical functions with examples, Part I
14 p2471 A69-29774

Approximate ionization potentials for high ionization stages of elements with atomic numbers 31 to 92 obtained by binding energy calculations
14 p2488 A69-29923

Titanium corrosion resistance data tabulated for various environments and chemicals including salt solutions, organic chemicals and ionizable fluoride compounds
14 p2466 A69-29931

Photoelectric comet observation techniques, tabulating narrow and wideband filter combinations for determining parameter Q for various cometary spectral emissions
15 p2684 A69-30522

Solid state and gas lasers operational parameters tabulation including pulse durations, powers, energy flux densities, electric and magnetic field strengths, etc
15 p2633 A69-30708

Photoelectric /UBV/ photometry of Cepheids in Cygnus and Monoceros noting sequence stars near Nova Cyg 1948
15 p2692 A69-30772

Canum Venaticorum variable A star spectrum, listing all lines observed between 5000 and 6650 A
15 p2692 A69-30773

Observations of 123 southern radio sources made with two element variable spacing interferometer, tabulating and graphing results
15 p2696 A69-31166

Flux densities at 2695 MHz for radio sources, tabulating measured data, discussing spectral distribution indices
15 p2696 A69-31206

Revised proper motions for semiregular and RV Tauri variable stars tabulated from meridian observations and photographic positions, discussing computation methods
15 p2696 A69-31221

Photography of laser echoes on satellites, tabulating results
15 p2570 A69-31311

Photoheliographic data tabulation of sunspots positions and areas for 1961 obtained from various astronomical observatories
15 p2700 A69-31490

Monograph on proper motions of RR Lyrae variables, discussing data acquisition analysis
15 p2700 A69-31493

Quasi-stellar and related objects emission and absorption red shifts tabulation suggesting absorption lines origin
15 p2701 A69-31532

Air refractivity variations across horizontal and vertical boundary planes between two air masses of slightly different temperatures
17 p3028 A69-32880

Equipment environmental conditions tabulated to assist engineer in preliminary design considerations and in planning test programs for specimens
17 p2910 A69-33661

13 color narrow band photometry of 1000 bright stars in tubular form, discussing sample points, Balmer discontinuity, absolute energy calibration, etc
17 p3038 A69-33692

Red shift table for six galaxies near Coma Cluster from spectrograms of absorption lines
17 p3044 A69-34182

Parkes catalog of 1780 radio sources, noting inclusion of data concerning polarization, source structure, optical identifications, etc
17 p3045 A69-34199

UBV photoelectric investigation on southern globular clusters NGC 2808 and 1851, presenting star magnitudes and colors in tabular form and estimating reddening
18 p3190 A69-34290

Four color photometry data of late F type stars in general catalog tabulated with columns for HD and GC numbers, apparent visual magnitude, etc
18 p3195 A69-34430

Radio sources spectrum measurement results at cm wavelengths in tabular form, noting flux density relationship to frequency
18 p3200 A69-35132

Polar cap absorption effects on VLF transmission phase and amplitude in tabular form
18 p3103 A69-35185

Pulsars measured parameter data tabulation including right ascension, declination pulse repetition period, showing sources distribution and clusters
18 p3202 A69-35211

Solar activity /Madrid 1967/, detailing Wolf numbers, sunspots, chromospheric faculae, H filaments and prominences
18 p3202 A69-35290

Celestial spectra forbidden lines tabulated by element and ionization stages, describing laboratory spectrum analysis programs
19 p3421 A69-36212

Nova Delphini 1967 /HR Del/ observations in UPX-YZV photometric system, tabulating color indices
19 p3426 A69-36564

Minor planets osculating elements computer calculated and tabulated
20 p3596 A69-37309

Definitive orbit of comet 1943 I determined from photographic and visual observations
20 p3596 A69-37310

Comet Arend-Roland 1957 III orbit elements computer calculated and tabulated from worldwide observations, taking into account orbital perturbations caused by major planets
20 p3596 A69-37311

Minor planets positions computer calculated and tabulated from Tashkent 1963 and 1964 astrophot observations, stating time and equatorial coordinates
20 p3596 A69-37312

Minor planets positions computer calculated and tabulated from 1966 and 1967 Crimean astrophot observations, using Yale catalog reference stars
20 p3570 A69-37313

IC 4499 cluster variable stars coordinates in tabular form, showing high percentage of short period
20 p3598 A69-37462

X ray data in 44-80, 8-16 and 1-8 A bands telemetered by Solrad 9 satellite
20 p3588 A69-37473

Periods and magnitudes of RR Lyrae variable stars in M 2 cluster, tabulating photometric characteristics
20 p3599 A69-37477

Tabulated results of photographic plate measurements of minor planets positions at Leiden observatory /1938-1964/
20 p3605 A69-37789

Luminosity calibration for subluminescent stars and space density of blue subluminescent stars south of declination minus 45 degrees based on white dwarfs and binaries
20 p3612 A69-38160

MK spectral types for bright southern O and B stars
20 p3612 A69-38161

Photodetector responses to radiant energy from many stars tabulated for various photocathode materials and silicon detector
21 p3800 A69-38680

Modulation envelopes, tables of profiles and harmonic components for modulated waves in electrical and communications problems
21 p3673 A69-38778

Discreteness of distances to extragalactic objects, tabulating red shift values from Wilson formula for galaxy clusters
21 p3802 A69-38843

Cosmic radiation altitude profiles, giving tabulation of counting rates obtained by SPARMO flights at different locations
21 p3791 A69-39253

Tabulation of solar UV spectrum features between 3650 and 3000 A from intercomparison of photoelectric records and Second Revised Rowland, indicating wavelength relocations
22 p4014 A69-40146

Thermal conduction by electrons in stellar matter, presenting opacity tables for H, He, C and red giant cores and solar composition
22 p4014 A69-40147

Hydrogen high level transition probabilities formula, giving two tables of oscillator strengths
22 p3983 A69-40149

Atlas of H II regions in 20 nearby galaxies
22 p4015 A69-40153

Hartree-Fock calculations for wavelengths of K alpha X ray transitions, tabulating configuration and term energies, dipole integrals and relative multiplet strengths
22 p3984 A69-40156

Finding list of spectral type A7 stars and earlier in region at south galactic pole compiled from prism survey data
22 p4021 A69-40436

Tabulation of Uranus observations of Sao Paulo Observatory astrolabe in 1968, giving special attention to East and West passages during night
22 p4031 A69-40912

Photoelectric observations of eclipsing binary 32 Cygni during 1968 eclipse using standard UVB color filters, tabulating results of UVB photometry
22 p4032 A69-40946

Tabulated numerical values of Burgess general formula for computing dielectronic recombination rates
23 p4207 A69-41281

Tabulated photoelectric photometer measurements of Nova Vulpeculae 1968 No. 1
23 p4208 A69-41290

Faint OB stars data tabulation between Carina and Centaurus, noting open clusters and MK classification
23 p4211 A69-41488

Tabulated spectroscopic observations of Be stars included in Merrill and Burwell catalog
23 p4213 A69-41720

Interferometrically measured wavelengths tabulated for Th lines in 2747-4572 A range, using liquid nitrogen cooled hollow cathode lamp and Fabry-Perot interferometer
23 p4191 A69-42150

Radiative transfer theory applied to layer cloud with normal liquid moisture content, discussing volume extinction, scattering and absorption coefficients, etc
23 p4184 A69-42177

Equivalent width measurements of Arcturus IR line spectra using Fourier transform spectroscopy, tabulating results
23 p4222 A69-42453

Tabulation of photographic and photoelectric spectrophotometrically obtained relative spectral line intensities for planetary nebula IC 5217, discussing interstellar absorption
24 p4376 A69-42663

Extragalactic radio sources flux densities at 5009 MHz tabulated, ascribing accuracy variations to uncertainty in receiver gain and dish efficiency
24 p4382 A69-42922

Fluid logic feedback control circuit synthesis using synthesis table, describing procedure to assign memory valves and switching signals
24 p4292 A69-43290

TABS [CONTROL SURFACES]

Aerodynamic control surface/trim tab coupling coefficients in subsonic two dimensional unsteady flow using matrix method valid for motion involving harmonic oscillations
17 p2895 A69-33597

TABULATING

U TABULATION PROCESSES

TABULATION

Tabular listing of Soviet satellites, spacecraft, probes and rockets launched between October 1957 and October 1967
13 p2355 A69-27359

TABULATION PROCESSES

Data tabulation and calculation for atmospheric refraction between 5-40 km based on GOST standard atmosphere
15 p2646 A69-30160

TACAN

Tactical air navigation system redesign with integrated circuits, obtaining weight reduction and improved performance and reliability
13 p2227 A69-27389

Tacan navigation system developments including data transmission, links to airborne computers and traffic control transponders
17 p3003 A69-34181

TACHISTOSCOPES

Topographic distribution of cortical potentials produced with tachistoscope and by stroboscopic stimulation, studying occipital and frontal difference
22 p3884 A69-40819

TACHOMETERS

Transistorized tachometer for rotational speed measurement and overspeed protection of automotive internal combustion engines
12 p2090 A69-26213

TACHYCARDIA

Human heart chronotropic reactions during centrifuge acceleration tests up to tolerance limit establishing sinus tachycardia in various degrees
22 p3877 A69-40242

Heart rate measurements in ski jumpers with radiotelemetric system revealing tachycardia during climbing and emotional stress
23 p4078 A69-41313

Cardiovascular effects of hypoxia in conscious anesthetized dogs in environmental chamber discussing artery pressure, tachycardia, stroke volume and cardiac output
23 p4078 A69-41313

TACKINESS

Elastomeric adhesives diffusion theory, tack increasing methods, cast polymer films, properties and applications in shoe manufacturing and sealants
14 p2468 A69-29344

TACTICAL AIR NAVIGATION

U TACAN

TACTICS

Tactical aspects of pursuit and evasion, emphasizing analysis of conceptual framework and construction of analytic models
03 p0457 A69-13899

Optimum evasion tactics for aircraft pursued by missile, using steepest ascent method for maximization of distance of closest approach
06 p0866 A69-17400

FM tactical radios frequency assignments rule, considering transmitter-receiver and interfering transmitter-receiver distances, equipment power, information transfer probabilities, etc
23 p4126 A69-42227

TACTILE DISCRIMINATION

Prolonged visual deprivation effect on pressure sensitivity of finger, forearm, neck and leg, noting effect after restoration of normal visual stimulation
13 p2210 A69-28311

Visual and tactual interaction in judgments of vertical in dark room experiments, discussing effects of various reference systems
24 p4271 A69-42755

Interpolated position and orientation perception by vision and active touch
24 p4275 A69-43110

Sensory information processing model for tactile perception using array of airjet and piezoelectric stimulators applicable to display design and nervous system investigation
24 p4276 A69-43277

TAGGING

U MARKING

TAIL ASSEMBLIES

Aerodynamic stick force and speed characteristics of various horizontal tails and elevator trimmers, noting zero stick force case
09 p1434 A69-22597

Conical flow past cruciform wing-body and tail-body systems, considering various positions of leading edge with respect to Mach cone
15 p2548 A69-31000

Aerodynamic aspects of tail rotor design and structural dynamics of stiff inplane configurations discussing blade natural frequencies
[AHS PAPER 342] 17 p3059 A69-33500

Tail rotor aerodynamics, discussing ambient conditions, maximum thrust, precession effects, fin interference, noise reduction, etc
[AHS PAPER 300] 17 p2895 A69-33544

Bird impact resistance of polyurethane foam filled tailplane
17 p2901 A69-33664

Statistical weight estimation equations developed by constrained regression analysis, noting application to vertical tail of cargo/transport aircraft
[SAWE PAPER 762] 18 p3220 A69-34877

Tail plane shape for optimal damping of rotational motion and elastic torsional deformations of aircraft body about longitudinal axis using calculus of variations
21 p3647 A69-38845

TAIL PLANES
U HORIZONTAL TAIL SURFACES

TAIL SURFACES
U HORIZONTAL TAIL SURFACES
U SWEPTBACK TAIL SURFACES

TAILLESS AIRCRAFT
U F-106 AIRCRAFT

TAILORING
U DESIGN

TAILS [ASSEMBLIES]
U TAIL ASSEMBLIES

TAKEOFF
NT VERTICAL TAKEOFF
Drag and spray effects due to slush and water on runways during aircraft takeoffs
01 p0011 A69-11048
Heligyro type takeoff and landing maneuvers, discussing M 211 takeoff jet thrust, pressure ratio, tip speed, etc
04 p0547 A69-14816
Control and recording device for parameters and information relating to takeoff and landing, using detection elements and cross wire on runway
08 p1347 A69-20780
Jet aircraft runway friction due to mud and water noting relation to takeoff length
17 p2903 A69-34216
STAN integral weight and balance system providing aircrews with takeoff gross weight and CG data [SAWE PAPER 755]
18 p3136 A69-34882
Takeoff and landing analysis digital computer program [TOLA] developed by Air Force Flight Dynamics Laboratory for quantitative performance analysis [AIAA PAPER 69-810]
19 p3289 A69-35630
Aircraft takeoff airborne phase trajectory analysis, deriving expressions for projection angle, velocity, path length and instantaneous altitude
19 p3247 A69-35817
Refused takeoff as critical maneuver in ground operations during jet transport accident investigation, emphasizing pilot anticipation of conditions and preplanning actions [SAE PAPER 690378]
23 p4062 A69-41654
Booster engines for thrust augmentation of commercial transports, considering tradeoffs in takeoff distance, payload, range, safety and noise patterns [SAE PAPER 690381]
23 p4201 A69-41667

TAKEOFF RUNS
Monograph on length requirements for takeoff and landing of jet transports covering airport classification, roll distance formulas and long range transport performance nomograms
08 p1301 A69-20717
Monograph on physicochemical principles of takeoff monitoring systems for large aircraft covering taxiing, safety control systems design, analog simulation, etc
12 p2128 A69-26119
Accelerate-stop criteria examined from human engineering standpoint, discussing flight simulator study of pilot reaction times for transition to rejected takeoff configuration [AIAA PAPER 69-772]
19 p3244 A69-35650
Runway grade relation to jet aircraft takeoff length
19 p3296 A69-36874
STOL takeoff optimal trajectory maximizing altitude at given runway distance, using aircraft models [AIAA PAPER 69-935]
21 p3649 A69-39427
Takeoff indicator design based on solution of equilibrium equation for forces acting on aircraft along drag axis
24 p4253 A69-43085

TAKEOFF SYSTEMS
U AIRCRAFT LAUNCHING DEVICES

TANDEM ROTOR HELICOPTERS
U CH-46 HELICOPTER
U CH-47 HELICOPTER

TANDEM WING AIRCRAFT
NT X-22A AIRCRAFT
Tandem airfoils wing-tail interaction flutter analysis, using three dimensional vortex lattice aerodynamic theory [AIAA PAPER 69-57]
06 p1028 A69-18105

TANGENTS
Error analysis involved in calculating tangent functions defined by nonlinear differential equation solution, using digital differential analyzer
13 p2225 A69-27968

TANK GEOMETRY

Draining liquid surface dip formation in tanks of arbitrary shapes and drain hole positions
09 p1483 A69-21999
Tank configurations allowing for sloshing in liquid fuel reaction control system in spinning satellite
18 p3219 A69-34796
Simulated low gravity propellant sloshing in spherical, ellipsoidal and cylindrical tanks, discussing Bond number simulation and tank geometry effects [AIAA PAPER 69-1004]
22 p3921 A69-40378

TANK TRUCKS
Fueling procedures for Boeing 747 aircraft, discussing design and operation of large capacity fuel trucks
10 p1674 A69-23631

TANKS [CONTAINERS]
NT CYLINDRICAL TANKS
NT FUEL TANKS
NT PROPELLANT TANKS
NT SPHERICAL TANKS
NT STORAGE TANKS
NT WING TANKS

Hard-drawn steel wire wound pipes and tanks, properties and design calculation, discussing laminates and permissible stress
08 p1414 A69-20487
Optimal control of vibrations of liquid in cylindrical container with vertical generatrix and flat bottom, using dynamic programming
21 p3694 A69-38849
Optimal control of liquid vibrations in rectangular container moving in horizontal direction, deriving algebraic equations system for optimal functional
21 p3694 A69-38854

TANTALUM

Anomalous discontinuous stress relaxation in sintered tantalum
02 p0265 A69-12003
Tantalum diffusion layer on refractory cobalt and nickel base alloys analyzed by electron microprobe [ONERA-TP-665]
06 p0941 A69-17097
Dissociation of hydrogen on tantalum using modulated molecular beam mass spectrometry
06 p0960 A69-17107
Diffusion coefficient of interstitial oxygen atoms in tantalum by elastic energy dissipation measurements as temperature function, discussing relaxation effect
07 p1168 A69-19452
Saturation electron emission characteristics from incompletely outgassed Ta wire emitters immersed in Cs vapor using plasma anode technique, noting oxygen effects
09 p1437 A69-21812
Diffusion coefficients of carbon in tantalum, niobium and vanadium by sectioning method, using carbon 14 as tracer
11 p1906 A69-25575
Flexure of Ta and Nb thin rectangular specimens during high temperature oxidation, showing stress generation due to O dissolution into metal surface [ECS PAPER 87]
15 p2641 A69-31541
Ta single crystal growth condition by zone melting, discussing orientation and purity relationship
16 p2803 A69-32490
Ta type I and II wire resistance in transverse magnetic field during superconducting to normal transition, discussing strain and impurity effects
17 p3016 A69-33791
Single crystal Ta and Ta base bcc solid solution strengthening and weakening as function of temperature and strain rate
23 p4178 A69-42358

TANTALUM ALLOYS

Omega phase and beta solid solution in Zr-V-Ta alloys quenched from 900 C
02 p0263 A69-11850
Work hardening characteristics of Ta and Ta-base alloy single crystals as function of temperature and interstitial concentration
05 p0778 A69-15758
Coated refractory tantalum alloy as ductile, weldable material for application on hypersonic aircraft or reusable reentry vehicles at high temperatures
09 p1526 A69-22326
Tungsten disilicide coated Ta-W alloy oxidation mechanisms, comparing coatings protective properties at high temperatures
13 p2280 A69-28137
Nb-Ta alloys oxidation kinetics at high temperature and structure and composition of oxide films and scale layers, discussing anomaly in oxidation rate temperature dependence
14 p2464 A69-29650

Optical constants of Ta-W and Nb-Mo measured in IR and visible ranges as function of incandescent temperatures
17 p2990 A69-33574
Heat treatment effect on superconducting properties of deformed Nb-Ta alloys, noting critical current density
19 p3345 A69-36303
Oxidation resistant silicide coatings for tantalum and tungsten alloys at elevated temperatures
21 p3730 A69-38673

TANTALUM CARBIDES

Preparation and properties of NbC-WC and TaC-WC carbides, analyzing hardness, resistivity, thermal expansion and dihedral angle
05 p0782 A69-16796
Controlled solidification in Co-Ta-C system to develop pseudobinary eutectic mixture containing TaC crystals aligned parallel to growth direction [ONERA-TP-673]
07 p1167 A69-19339
Book on hard alloy properties, discussing bending and compression properties, tensile, torsional and impact strength, wear resistance and thermal shock resistance
12 p2111 A69-25902
Integral normal emissivity of Ta and Hf carbides at temperatures from 1300 to 3000 K measured by radiation method in vacuum
15 p2640 A69-30984
Orientation relationships between phases in Co-Ta pseudobinary eutectic alloy, discussing Co fcc-hcp allotropic transformation [ONERA-TP-714]
17 p2988 A69-33395

TANTALUM COMPOUNDS

Niobium hydride and tantalum hydride formation using metal powders, noting solid phases during dehydrogenating
09 p1448 A69-21599
Analytical, IR absorption and polarographic analysis of cyclic niobium IV and tantalum V/esters
11 p1832 A69-24575

TANTALUM NITRIDES

Thin film tantalum nitride resistors technology and production, evaluating projected reliability of resistance circuits as function of operating and environmental conditions
15 p2628 A69-30846

TAPE MERGING

U DATA PROCESSING
U MAGNETIC TAPES

TAPE RECORDERS

Pseudorandom scanned TV signal distortion due to flutter and skew introduced by tape recorder, computing system SNR for distortion as additive random noise
01 p0033 A69-10999
Tape recorder for simultaneous double channel recording of physiological experiments, describing circuit modifications and additional circuits
07 p1131 A69-18640
Rotary head units used in telemetry magnetic recorders, explaining concepts and advantages of rotary scanning
07 p1077 A69-18826
High reliability magnetic tape recorders for satellite, aircraft and drone applications
07 p1133 A69-19104
Compatibility requirements and considerations of range telemetry tape crossplay operations, discussing major classes
07 p1133 A69-19117
Effects, measurement and analysis of flutter in instrumentation recorders
07 p1133 A69-19118
Magnetic tape recording of ultrasonic test information with oscilloscope used for playback
07 p1117 A69-19697
Magnetic tape recorder/reproducer for FM analog test data
10 p1691 A69-23233
Dual inertia magnetic tape recorder/reproducer combining low wideband flutter and low time base errors
10 p1693 A69-23289
Spacecraft data storage requirements, discussing use of servo-driven tape recorders in data processing systems
18 p3107 A69-35096
Buffer shift register with feedback control during tape recorder playback to obtain variable delay to compensate for recorder time base error
19 p3312 A69-36284
Tape recorder premission calibration requiring standard and external test instruments
20 p3546 A69-38233

High speed tape transport characteristics, discussing capstan design, negative progression, reel-capstan interface, etc

23 p1465 A69-41776

TAPER

U TAPERING

TAPERED COLUMNS

Magnetic field plane radiation patterns for tapered dielectric rod antennas computed by Schelkunoff principle, noting taper angle effect on lobes

09 p1464 A69-22097

TAPERED WINGS

U SWEPT WINGS

TAPERING

Tubular metal parts and assemblies, discussing forming, forming, beading, tapering and step drawing

03 p0435 A69-13918

Power law taperings for minimizing peak to trough deflection of cross section of strip bent longitudinally into cylindrical surface

06 p1023 A69-17374

Short multiconical TE sub 01 mode X band taper for connecting two different diameter circular waveguides

09 p1468 A69-22604

Postbuckling of rectangular plates with exponential variation in thickness, analyzing large deflection equations using dynamic relaxation method

15 p2704 A69-30291

Radiation field of tapered dielectric rod antenna by Schelkunoff equivalence principle, investigating input impedance variation with axial length and taper angle

21 p3681 A69-38444

TARE (DATA REDUCTION)

U DATA REDUCTION

TARGET ACQUISITION

Optimal distribution of search effort for moving target location, suggesting Markovian decision models

01 p1014 A69-10653

Moving target indicator /MTI/ performance degradation by limiting clutter analyzed for various pulse cancellers and verified by time-domain Monte Carlo simulation

03 p0390 A69-13198

Moving window radar detector design for moving targets, giving chart for SNR derivation to obtain given detection probability

04 p0558 A69-15073

Upper wind observation and computation accuracy, comparing radar and slide rule instrument errors

06 p0950 A69-17788

UHF telemetry flight tests at White Sands Missile Range, discussing multipath and target scintillation problems

07 p1082 A69-19116

Experimental circuit for simulating radar target tracking system based on split range gating, noting tracking role of error signal

08 p1300 A69-20109

Open loop suboptimal control for linear time dependent tradeoff between energy expenditure and probability of target set entry

11 p1860 A69-25443

Radar SEP /spherical error probable/ for defining error ellipsoid in three dimensional accuracy and CEP /circular error probable/ for defining two dimensional accuracy

13 p2221 A69-27963

Probability matrix for n order transition independent of decision taking method, applying fundamental matrices to analysis of mean number of false targets

14 p2410 A69-28836

Statistical distribution functions for radar cross section of flying aircraft

14 p2414 A69-29500

Binary-quantized signal packet center for target azimuth determination, discussing antenna radiation pattern role

15 p2566 A69-30332

Target trajectories determination based on radar data with allowance for association between neighboring readings, using statistical characteristics obtained with Markov chains

15 p2566 A69-30335

ASTRID high altitude sounding rockets orientation system aligning payload cones to target outside earth atmosphere, discussing software simulation with analog and digital computers, etc

17 p3001 A69-33424

Kormoran airborne missile weapon system for attacking sea-going targets, discussing navigation guidance, radar tracking and homing system

17 p3050 A69-33697

Associative processor applied to interceptor radar system, noting processing time independence from target number and compatibility with real time systems

17 p2931 A69-34071

Onboard hybrid computer for helicopter fire control system, generating turret pointing angles and corrections

17 p2934 A69-34074

Closed loop target tracking system generating error signals for aligning target with tracking axis

19 p3310 A69-36063

Active interferometer controlled telemetry tracking system for missile range, discussing automatic target acquisition, dish feed, costs and optimized data-channel antenna patterns

19 p3271 A69-36253

Moving target indication, discussing target motion effects dependence on Doppler imaging radar scan rate and compression ratio

20 p3490 A69-37644

Single stage rocket control and trajectories for maximum target strike probability within given range

21 p3818 A69-38857

Targeting technique for Atlas/Centaur Mariner Mars 1969 mission, noting suitability to flyby, orbiter or landing interplanetary missions

[AIAA PAPER 69-881]

21 p3764 A69-39407

Guidance control systems for moving plants pursuing targets, basing design on target characteristics and plant phase coordinates

21 p3687 A69-39643

Asymmetry method for precision alignment of rectilinear systems, using laser light diffraction behind misaligned target

21 p3742 A69-39781

Optimal flight regime determination for variable mass body pursuing target by straddling method, presenting motion equations and approximate solutions

21 p3818 A69-39819

Horizontal tracking eye movements response to unpredictable constant velocity target motions with or without saccadic position corrections recorded by contact lens optical lever

22 p3881 A69-40856

Hand and thumb exercise effects on acquisition tracking task performance

23 p4101 A69-41453

Compound fading exponential /CFE/ clutter model for radar target detection, describing automatic detection applications

23 p4117 A69-41604

Radar detection performance evaluation procedures based on integration, collapsing and fluctuation losses estimates for swirling target models and partially correlated targets

23 p4132 A69-42547

Policies and controller design for pursuing vehicle developed in terms of pursuit-evasion differential games

24 p4341 A69-43295

Optimal allocation of pulses for array radar tracking large number of targets simultaneously, using discrete time maximum algorithm

24 p4283 A69-43311

TARGET DRONE AIRCRAFT

NT FIREBEE 2 TARGET DRONE AIRCRAFT

Firebee 2 /BQM-34E/ turbojet-propelled recoverable supersonic aerial target construction, performance prediction and missions

09 p1434 A69-21901

Multiple drone aircraft automatic control system, discussing preprogrammed mission path and controls of altitude, plan position and velocity

14 p2392 A69-29495

TARGET PENETRATION

U TERMINAL BALLISTICS

TARGET RECOGNITION

Visual sonar target detectability probability function of retinal position and brightness contrast

02 p0203 A69-12218

Space surveillance radar system sensor misassociation of one space object for another, noting applicability to sonar and optical sensors

02 p0210 A69-12388

Digital modified discrete Fourier transform Doppler radar processor for tactical aircraft

03 p0389 A69-13196

Automatic sequential detector for noncoherent moving target indicator radar, describing noise and clutter residue control

03 p0389 A69-13197

Passive linear FM pulse compression radar systems: detection capability compared with matched filter performance

03 p0390 A69-13211

Weighted pulse trains for clutter suppression during radar target detection

04 p0562 A69-15444

Multiple target monopulse radar signal processing technique

04 p0562 A69-15474

Electronically scanned X band array used as receiving antenna for target recognition radar

04 p0562 A69-15474

Sonar receiver reduced averaging processing: presence of extended and point targets compared with full averaging processor

04 p0562 A69-15474

Filter effectiveness in improving air to ground target identification performance on TV display

06 p0887 A69-17210

Individual differences and relation to Witkin concept of perceptual style in target identification in aerial photographs

06 p0880 A69-17210

Limiting speed for target tracking hypersonic vehicles due to electrons formation through aerodynamic heating, calculating allowable flow conditions, maximum speeds and electron distribution

07 p1086 A69-19509

Input signal history analysis in recognition of moving or changing objects based on classification definitions and Wald sequential analysis

08 p1297 A69-20419

Alphanumeric characters to identify radar targets on PPI display for air traffic control, considering technique for reducing smear

09 p1495 A69-21675

Coherent optical target recognition through randomly turbulent medium for imaging system offsetting image degradation due to turbulence

11 p1894 A69-24470

Airborne IR line scanning systems for latent forest fire detection, discussing discrimination module for automatic identification of hot targets

12 p2193 A69-26994

Airborne IR remote sensing techniques for fire detection, considering marginal and submarginal targets

12 p2098 A69-26995

Input signal history analysis in recognition of moving or changing objects based on classification definition and Wald sequential analysis

14 p2427 A69-29657

Optimal radar receivers and waveforms with limited dynamic range for detecting point target masked by thermal noise and clutter returns

17 p2921 A69-33625

Radar target simulator approximating pulse radar receiver output for evaluating amplitude-sensing video target detection devices

17 p2921 A69-33629

Intermittent noise effects on human target detection to test neutral ratio dependence on noise intensity level, noting attention flexibility

17 p2911 A69-34008

Spectral reflectances of objects and vegetative backgrounds to generate color photographic technique increasing detection sensitivity and rate

18 p3133 A69-34247

Target discrimination from background, discussing spatial, spectral, temporal and polarization effects

19 p3373 A69-36054

System components for spatial discrimination implementation scheme, discussing IR detector arrays and optical imagery processing

19 p3373 A69-36055

Object discrimination based on IR spectral differences, reviewing calibrated radiometers, relative spectrometers and imaging sensors

19 p3373 A69-36056

Thermal IR imaging devices for shape recognition and target position, emphasizing optical mechanical image or object plane scanners using point detectors

19 p3310 A69-36064

Luminescence effects on apparent size and shape of foveally fixated targets of various forms

19 p2359 A69-36458

Radar design for target detection, tracking and identification, modeling plasma effects on radar cross section of reentry vehicles based on wave-plasma interactions

20 p3485 A69-36925

Monograph on selection of radar echoes from nearly colocated reflection centers, discussing guided missile multiple target resolution

22 p3899 A69-40533

Grating size effect on threshold of grating pattern for various colors of illumination and target orientations
22 p3879 A69-40840

Visual suppression association with smooth following and saccadic eye movements in tracking slow moving target
22 p3879 A69-40842

Visual backward masking experiment for studying overlapping and nonoverlapping contours of target and masking stimuli straight line
22 p3879 A69-40843

Human peripheral retina contrast sensitivity determined by measuring psychophysically for sinusoidal grating target describing luminance effects
22 p3882 A69-40870

Assignment algorithm for target recognition in multiradar tracking systems
22 p3902 A69-41250

Book on new concepts in radars covering ideal reception, moving targets, autocorrelation, SNR, amplitude distribution, clutter, etc
24 p4283 A69-43168

TARGET SIMULATORS
Radar target simulator approximating pulse radar receiver output for evaluating amplitude-sensing video target detection devices
17 p2921 A69-33629

TARGET THICKNESS
Thermal-neutron flux generated by high energy protons in water moderator surrounding thick targets calculated as function of position
02 p0279 A69-11837

Charge exchange collisions in ground state and ionic hydrogen incident on cesium vapor, measuring beam components after passage through target
08 p1356 A69-20737

Hypervelocity impact of spheres on thin targets studied with numerical solutions utilizing STEEP code two dimensional technique based on hydrodynamic elastoplastic model
[AIAA PAPER 69-357] 13 p2366 A69-28290

Aluminum double sheet target penetration resistance determined by studying high velocity pyrex glass impact effects on front/rear sheets and spacing
[AIAA PAPER 69-375] 13 p2367 A69-28305

TARGETS
NT RADAR TARGETS
NT TARGET DRONE AIRCRAFT
Target production device for deuterium plasma clouds in vacuum with Q switched neodymium laser
01 p0090 A69-10222

Electromechanical retracting pedestal for solid target injection into vacuum system and ionization by focused Q switched laser beam
03 p0439 A69-13105

Transient response of targets subjected to hypervelocity impacts and quantitative aspects of impact process, noting study of wax targets interiors
07 p1234 A69-19380

Image tube storage target mesh electrode structure and transmission data for electron beams of various velocities, noting secondary electron redistribution control
11 p1848 A69-24749

TASK COMPLEXITY
Manual control using matched manipulator technique, noting control task complexity decrease and improved performance
02 p0202 A69-11951

Component total task relationships, analyzing simple and sequential practice effects with aid of Melton Complex Coordinator
02 p0203 A69-12214

Displays and controls requirements in manned spacecraft to integrate man into vehicle system, noting man capability for task diversity
08 p1312 A69-19968

Human information processing rates during one and two axis compensatory tracking tasks with secondary auditory task
10 p1650 A69-23880

Target displacement and track coherence in pursuit tracking tasks experiments for human performance studies
11 p1829 A69-24737

Model for temporal structure of human behavior from analysis of temporal information treatment in subjective synchronization task
12 p2025 A69-27084

ESRO 1 satellite centralized control system, discussing housekeeping system responsible for task execution in connection with power supply
15 p2702 A69-31083

Mission task performance oriented approach to winged helicopters flying and handling qualities, considering wings and horizontal stabilizers influence
[AHS PAPER 360] 17 p2900 A69-33522

Ergonomics and aviation medicine, discussing biotechnological aspects of information in man machine systems and observation tasks
17 p2915 A69-33770

Color coding effect on alphabetic filing names, comparing first and second letter codes and no color code condition
17 p2916 A69-34004

Human performance reliability, testing mathematical model application and implications of time to first error concept by vigilance task
18 p3097 A69-34478

Reliability tasks vs product reliability, discussing differences in effectiveness and management programming
18 p3143 A69-34484

Factor analysis of complex perceptual-motor performance of man, measuring speed, flexibility, balance and strength
18 p3098 A69-35085

Complex program management emphasizing systems engineering management, noting applications to aeronautical systems
[RAES PAPER 9] 22 p4053 A69-40489

Human performance on button pressing task with fixed ratio fixed interval reinforcement schedules
23 p4081 A69-41439

Human mental performance impairment at simulated 8000 ft altitude indicated in increasingly difficult tests
23 p4102 A69-41680

Basic task archetypes in man-computer problem solving including detection, planning, optimization, designing, etc
24 p4274 A69-43019

TASK SEQUENCERS
U CONTROL EQUIPMENT
U SEQUENTIAL CONTROL

TASKS
U AUDITORY TASKS
U VISUAL TASKS

TASTE
Human taste perception mechanism and taste system anatomy
21 p3652 A69-38783

TAURUS CONSTELLATION
Taurus A 21 cm absorption line frequency decrease during optical path approach to sun, discussing gravitational and electromagnetic origin
04 p0661 A69-15148

Celestial X ray sources astronomy, discussing emission mechanism in 2 to 100 kev range and balloon observations in Cygnus and Taurus constellations
05 p0817 A69-16715

Taurus A flux density measurement at 4.3 mm with 36-ft antenna at National Radio Astronomy Observatory to determine spectrum unambiguously
09 p1591 A69-21450

Continuous radiation spectrum of Taurus A in far IR using indium antimonide detector of Rollin type
09 p1597 A69-22156

Preliminary observations of Tau-A, Cas-A and Cyg-A with multiple-element interferometer
10 p1777 A69-23397

Crab Nebula radio emission spectrum in decimeter wavelength range indicating emission spectral index decrease from Taurus A
10 p1784 A69-23941

Reddened M supergiant 119 Tauri IR spectra and IR absorption by CO and SiO molecules in stellar atmosphere and silicate mineral in interstellar grains
10 p1786 A69-24104

Proper motions of low luminosity stars in Hyades cluster, noting photoelectric observations
12 p2152 A69-25797

Revised proper motions for semiregular and RV Tauri variable stars tabulated from meridian observations and photographic positions, discussing computation methods
15 p2696 A69-31221

Zeta Tauri shell spectrum radial velocity measurement results compared with extrapolated seven year curve by Delplace
20 p3599 A69-37471

Balloon-borne proportional counters to measure X rays intensity and spectral distribution from Taurus X-1 and Cygnus X-1
20 p3593 A69-38153

TAUTOMERS

Mass spectra peaks of N-Acyl-2-indolinols fragmentation processes upon electron impact, noting compounds predominance in open chain tautomer gas phase
15 p2561 A69-30407

TAYLOR INSTABILITY

Taylor column existence in compressible atmosphere, discussing baroclinicity and stratification effects in earth and Jupiter atmospheres
02 p0326 A69-12697

Numerical solution of axisymmetric incompressible viscous fluid flows about rotating cylinder, Taylor vortex between cylinders and through labyrinth seal
03 p0419 A69-13990

Secondary steady flow /Taylor vortices/ between rotating cylinders, discussing development due to stability loss of Couette flow
05 p0745 A69-15780

Rayleigh-Taylor instability for interface between two uniform superposed fluids under combined effect of horizontal and vertical magnetic fields
07 p1182 A69-19275

Rayleigh-Taylor instability in synchronous liquid metal MHD generators, showing stabilization by channel positioning and threshold power rating
13 p2307 A69-27508

Turbulent diffusion and Rayleigh-Taylor instability in inhomogeneous flow of combustion gases circulating through magnetic field
13 p2310 A69-28032

Rayleigh-Taylor instabilities in two fluid hydraulic model, noting perturbation direction and Lorentz forces effects on instabilities growth time
13 p2310 A69-28033

Gas compressibility influence on laminar to turbulent boundary layer transition determined using Taylor hydrodynamic finite perturbation model
14 p2389 A69-28974

Numerical approximation of Taylor vortices in viscous incompressible fluid flow between concentric rotating cylinders, using truncated eigenexpansions
15 p2593 A69-31518

Taylor vortices calculated as branching solutions of nonlinear Navier-Stokes boundary value problem
17 p2958 A69-34152

Secondary steady flow /Taylor vortices/ between rotating cylinders, discussing development due to stability loss of Couette flow
18 p3123 A69-35032

Incompressible electrically conducting fluid in presence of magnetic field and Coriolis forces, analyzing Rayleigh-Taylor instability by variational principles
20 p3577 A69-38195

Electrohydrodynamic Rayleigh-Taylor bulk instability in initially static stratified fluid under electric stress
20 p3578 A69-38235

Naimark theorem extended to class of nonself-adjoint eigenvalue problems in hydrodynamic stability, considering Orr-Sommerfeld equation and Taylor stability problem
21 p3754 A69-38426

Taylor instability nonlinear oscillations, obtaining uniform solutions for wavenumbers near and larger than cut-off
21 p3693 A69-38703

Cylindrical bubbles stability in vertical pipes from photographs, describing wake, spacing, pressure pulsations and convection cells effects
[ASME PAPER 69-HT-28] 24 p4411 A69-43540

Taylor Goertler vortex formation effect on heat transfer through boundary layer on concave wall
[ASME PAPER 69-HT-3] 24 p4414 A69-43563

TAYLOR SERIES
Bernard convective flow as function of Rayleigh and Taylor numbers in thin variable rotating silicone oil layer determined by flow photographs
13 p2377 A69-28172

Taylor expansion applied to solution of nonlinear simultaneous algebraic equations in analyses of nonlinear structural systems using finite differences or elements
15 p2711 A69-30871

Taylor series expansion used in correcting quantized digital coefficient errors in hybrid feedback control system
18 p3111 A69-34687

Controlled-variable prediction display based on Taylor series computation, describing acceleration system simulator and human operator performance
19 p3313 A69-36414

Jacobi polynomial series analytical expansion, studying relationship to Taylor series singular points
21 p3757 A69-39537

Differential approximation for radiant energy loss in nonequilibrium plasma generated from truncated Taylor series expansion of radiation source function
22 p3988 A69-40102

TEACHING U EDUCATION TEARING

Drop-weight tear tests dependence on specimen thickness and metallurgical properties
09 p1503 A69-21389

Fracture toughness of AlZnMgCu alloys, employing sharp notch tension, tear and precracked Charpy impact tests
16 p2800 A69-31780

Thickness direction tensile properties, ultrasonic attenuation and mild steel plate lamellar tearing in multipass fillet joints measured by weld cracking test
24 p4320 A69-42942

TECHNICAL WRITING

Scientific and technical information flow sources, showing DOD user need within defense industry and importance of local work environment
02 p0204 A69-12219

TECHNIQUES U METHODOLOGY

TECHNOLOGIES NT BIOTECHNOLOGY NT MILITARY TECHNOLOGY

Technology and education - Conference, Los Angeles, September 1968
10 p1668 A69-22971

Technological forecasting by intuitive forecasts, consensus methods, analogy, trend extrapolation and structural models
13 p2382 A69-28040

Technology and social progress - ASS Conference, Washington, D.C., March 1968
17 p3076 A69-34039

Relative technological standing of U.S. and Europe, discussing meaning and existence of technology gap
17 p3076 A69-34040

Delphi technique of technological forecasting used for R and D planning
20 p3639 A69-37353

Technical problem solving model based on tape recorded protocols of engineers engaged in R and D project
20 p3640 A69-38020

U.S. aerospace technological forecasting involving space flight, air transport and V/STOL aircraft
22 p4052 A69-39930

TECHNOLOGY FEASIBILITY SPACECRAFT

Space simulation tests in TFS/Technological Feasibility Spacecraft/program, discussing two interplanetary cruise modes and deorbit mode selected for simulation
02 p0227 A69-11757

Technology Feasibility Spacecraft/TFS/sterilization and bioassay program during assembly, analyzing sampling and cleaning procedures
09 p1446 A69-22358

TECHNOLOGY UTILIZATION

Microwave applications of monolithic and hybrid semiconductor circuit technologies, considering cost and performance
01 p0039 A69-10188

Aerospace technology role in economic and social benefits
[UN PAPER 68-95321] 01 p0178 A69-10467

Space technology contributions to medical problems, discussing organization and achievements of biochemical application program of NASA
[UN PAPER 68-95417] 01 p0020 A69-10471

Space applications program including communications and navigation meteorology, earth resources survey and geodesy
[UN PAPER 68-95437] 01 p0178 A69-10472

Space system engineering courses background, objectives and results at MIT and Stanford University dealing with applications of space technology
[UN PAPER 68-95870] 01 p0178 A69-10485

Space techniques for application to civil aviation, discussing air to ground communications, air traffic monitoring and navigation and weather forecasting by satellite
[UN PAPER 68-95349] 01 p0179 A69-10490

Small earth stations in future communication satellite systems, discussing applications, characteristics and equipment
[UN PAPER 68-95751] 01 p0028 A69-10492

Satellite TV systems for India, alternatives and costs
[UN PAPER 68-95750] 01 p0028 A69-10495

Marine requirements possible satisfaction by using space techniques to improve long range communications to achieve safety at sea and shipping operations efficiency
01 p0161 A69-10503

Aerospace research applications in agriculture and forestry, discussing information acquisition for worldwide coverage
[UN PAPER 68-95393] 01 p0065 A69-10504

British contributions to communication satellite earth station technology covering antennas, low noise amplifiers, traveling wave tubes and threshold extension demodulators
[UN PAPER 68-95843] 01 p0054 A69-10507

NASA Technology Utilization Program, discussing information dissemination
[UN PAPER 68-95313] 01 p0179 A69-10512

Earth surveying methods by artificial satellites, discussing applications to undeveloped regions
[UN PAPER 68-95793] 01 p0065 A69-10523

Integrated circuit manufacturing status, discussing raw materials, crystal imperfections, surface damage, epitaxy and diffusion techniques
01 p0045 A69-10650

Applied magnetics - IEEE Conference, Washington, D.C., April 1968
01 p0045 A69-10712

NASA LOX and liquid hydrogen barges, discussing storage tank design, acceptance testing and operating conditions
01 p0056 A69-11150

MHD technology applications to industry and cost and performance of MHD generators
01 p0013 A69-11394

Heterojunction band model and carrier transport mechanisms emphasizing applications to heterophotodiodes, solar cells and hetero field effect transistors
02 p0294 A69-11598

Aerospace management technology transferability to problems of society and government
02 p0355 A69-11754

Electromagnetic wave generation in 0.2-3mm range, noting applications to physics, biology and technology
02 p0250 A69-12247

Stabilization and control techniques for future unmanned commercial space vehicles, emphasizing application of projected technological advances in instrumentation
[AIAA PAPER 67-878] 02 p0334 A69-12367

Flexible printed circuitry electrode arrays fabrication for surface cortical potentials recording in animals
02 p0204 A69-12601

European space programs requirements for satellite launch autonomy/independence from U.S. and U.S.S.R., discussing satellite applications for resource surveys, weather forecasting, etc
02 p0335 A69-12682

Educational TV satellites, considering stationary ASCEND system with high power transmitters
02 p0335 A69-12747

SPOT/Speed, Position and Track/transoceanic traffic surveillance and navigation system for aircraft and marine users
03 p0463 A69-13234

Aerospace research and development projects selection and planning for success in manufacturing competition
03 p0393 A69-13252

NASA Space Application Program strategy, discussing research and development trend toward complexity, versatility and multidisciplinary use of larger spacecraft
03 p0511 A69-13427

Iron meteorites and possible utilization by primitive man, noting long resistance to decay
03 p0515 A69-14033

National programs relationship to progress in technological societies
03 p0536 A69-14245

Aeronautical service satellites, considering communications, surveillance for navigation, traffic control, collision avoidance and search and rescue, weather and border control functions
04 p0666 A69-15295

Electron beam process application to welding, machining and assembling in automobile mass production
04 p0608 A69-15484

Technological base for planning space flight missions to obtain data on earth resources, detailing earth resources technology satellites/ERTS/
05 p0830 A69-15921

Photovoltaic solar cell power technology application to space use and exploration
[ASME PAPER 68-WA/SOL-1] 05 p0705 A69-16121

Manned space flight programs, discussing U.S. technological, scientific and practical contributions
06 p1001 A69-17012

Stimulating effects of space hypersonic experiments on technical and scientific progress, discussing step degassing, welding, electroforming and geological applications
[UN PAPER 68-95459] 06 p0857 A69-17089

Commercial orbital space stations economics and potential markets, considering fisheries, ocean transportation, air traffic control, resources surveys, pollution reduction, etc
06 p1007 A69-17596

Fiber optics evolution, discussing industrial and medical applications
06 p0958 A69-17671

Fiber optics technology, discussing fabrication and applications involving light carrying/incoherent and image carrying/coherent/fibers
06 p0958 A69-17671

Technological forecasting role in company growth planning via Delphi technique
06 p1044 A69-17877

Laser applications to situations requiring highly bunched high power density light beams
06 p0938 A69-18012

Aircraft and spacecraft guidance and control technology including computers, optimum and Kalman filtering, strapdown inertial navigation, sensors and test pads
[AIAA PAPER 69-72] 06 p0956 A69-18136

Manned orbital space stations design, purposes and applications, balancing costs against benefits
06 p1019 A69-18237

Atomic, ionic and molecular gas lasers applications, population reversal conditions and processing technology
07 p1143 A69-18250

Large scale integration of monolithic integrated circuits as interconnected circuits on semiconductor
07 p1090 A69-18372

Additive processing technique for fabrication of single sided, double sided and multilayer printed circuit boards
07 p1100 A69-18621

Soviet book on Ti alloys covering production technology, applications, metallochemistry, phase transformations and metallurgy
07 p1160 A69-18760

Titanium applications in metallurgy, galvanic technology and chemistry making use of corrosion resistant properties
07 p1161 A69-18767

Two stage sodium thermal reduction of Ti tetrachloride to metallic Ti, determining process parameters
07 p1164 A69-18785

Production technology of sheets, forgings and drop forgings from Ti and Ti alloys, discussing gas saturation prevention and plastic deformation
07 p1164 A69-18786

Soviet pipe production technology from Ti and Ti alloys, considering properties and methods improvement
07 p1164 A69-18787

Refractory metal alloys metallurgy and technology - Conference, Washington, D.C., April 1968
07 p1164 A69-18790

Precision monolithic circuits fabrication techniques, describing differential amplifier design incorporating emitter feedback and direct DC errors compensation
07 p1102 A69-18875

Rotary engines, discussing scissor, eccentric rotor, multiple rotor and revolving block types
07 p1203 A69-18910

Aircraft communications, navigation and identification, discussing role of satellites, common waveform modulation and electronics technology
07 p1085 A69-19178

Aircraft and spacecraft guidance and control technology including computers, optimum and Kalman filtering, strapdown inertial navigation, sensors and test pads
[AIAA PAPER 69-72] 07 p1177 A69-19179

Book on fluid mechanics fundamentals and applications covering incompressibility and compressibility effects, viscosity, hydrostatics, aerostatics, one dimensional, potential, turbulent flow and boundary conditions
07 p1121 A69-19376

Processing techniques for fabrication of ceramic radomes from alumina and silica

07 p1142 A69-19527

Technology of titanium for C-5A aircraft, discussing structural and functional components and machining, welding, forging, etc
[ASM PAPER D8-26.2]

07 p1143 A69-19672

Computer graphics and manufacturing, discussing man computer system for transformation of blueprint to numerically controlled machine tape with no time delay

07 p1089 A69-19741

MOS technology developments for higher speeds in logic circuits

07 p1113 A69-19765

Silicon on sapphire semiconductor technology for diode arrays used as read-only memories, discussing capacitance, resistance and pattern encoding by laser

07 p1113 A69-19767

Data transmission techniques for aerospace and industrial applications, discussing radio link

08 p1271 A69-19906

National tasks in civil aeronautical research and development noting technological and social factors

08 p1422 A69-20171

Laser welding in nonconventional applications and tiny components

08 p1319 A69-20203

Development of materials in aerospace structures and propulsion systems, discussing superelastic alloys, graphite fibers, composites, refractory metals and processing techniques

08 p1332 A69-20306

Composite materials based on carbon and boron filaments, discussing application in turbine blades, propeller and helicopter rotor blades and airframe components

08 p1341 A69-20601

Electroslag welding using plasma jets with powdered material, discussing various parameters

08 p1321 A69-20766

Metal oxide semiconductor technology and applications, discussing gates, analog computers, switching circuits and inverters

08 p1286 A69-20833

Complex digital computers designed for Apollo spacecraft missions, discussing construction techniques
[AGARDOGRAPH-114]

08 p1279 A69-20990

Integrated circuit production, development and research in Germany
[AGARDOGRAPH-114]

08 p1292 A69-20994

Triodes reliability for space application, emphasizing RH 7 Cc used during Mariner 4 expedition

08 p1295 A69-21122

Large scale electronic systems configuration compatibility concept, discussing modular line replaceable units/LRU/assigned set of numbers

08 p1322 A69-21154

Airborne digital computers for optimization of aircraft control and monitoring functions, discussing avionics and circuit technology

08 p1349 A69-21194

Marine and aircraft satellite navigation techniques, discussing equipment requirements, related performance characteristics and limitations

08 p1349 A69-21198

Microwave silicon technology applied to fabrication of high gain high efficiency transistor

09 p1462 A69-21410

Roll diffusion bonding technique for permitting complex design of coldplates and radiators of spacecraft electronic equipment

09 p1504 A69-22066

Holographic technique application to radio and sound wave ranges, discussing incoherent holography development to overcome difficulties in image reconstruction of stationary objects

09 p1498 A69-22133

Hybrid circuit technology application to packaging electronic systems

09 p1508 A69-22336

Thick film hybrid circuit technology and equipment reviewing conductors, resistors, and insulator inks

09 p1508 A69-22337

Domestic satellite system for carrying maximum traffic by full use of rocket technology including Saturn 5 type propulsion systems, antennas, frequencies, etc

09 p1458 A69-22467

Frequency selective mechanical filter and LCR circuits and applications, noting inductances in solid state and thin film technology

09 p1467 A69-22558

Lasers industrial manufacturing applications, discussing processing operations and measurement and inspection techniques

09 p1521 A69-22783

Laser theory and operations including types and applications

10 p1702 A69-23384

Potential hazards of government sponsored technology, examining SST and fluoridation projects and weather problems

10 p1811 A69-23392

Fluidics technology including applications, construction and mountings

10 p1636 A69-23401

Fluidic control technology compared to other control modes, describing fluidic functions and devices

10 p1636 A69-23402

Aircraft technology for hypersonic speed range including swept wing, engine design, composite materials, lift-drag ratio, considering weight, efficiency, STOL requirements

10 p1634 A69-23598

Laser applications to high temperature, gas dynamical and plasma phenomena

10 p1741 A69-23809

Cryogenic Technology - Conference, Chicago, June, 1967

10 p1810 A69-24014

Cryogenic applications including maser amplification, IR detection and superconductivity, discussing systems optimization and cost reduction

10 p1665 A69-24017

Aluminum alloys role in aerospace technology, discussing temperature characteristics, gas absorption, weldability, purity, etc

11 p1903 A69-24518

Spray cooling techniques for thermal protection of aerospace structures including lithium spray cooling, vapor collection and condensation, etc

11 p1966 A69-24532

Laser application to welding, drilling and other processes involving material removal for microelectronic circuits and components fabrication

11 p1846 A69-24600

Single frequency Ar ion laser for deep field holography noting thermal compensation, servo stabilization, operating mode, high power and high coherence

11 p1895 A69-24689

Remote geoscience sensing using properties of radar return noting scatterometry, imagery, altimetry and penetration measurements

11 p1835 A69-24692

Imaging radar systems for employment on small spacecraft, fabricating small lightweight radar systems packages with integrated circuit techniques

11 p1835 A69-24695

Laser beam welding effectiveness for TWT with coaxial input and output lines

11 p1896 A69-24741

Computer techniques application to radio engineering functions related to system performance, layout engineering, frequency coordination and administration, discussing decision parameters interrelationship

11 p1840 A69-25313

Book on reentry and planetary entry physics and technology covering entry dynamics, thermodynamics, radiation, ablation and heat transfer

11 p1967 A69-25573

Space propulsion by radioisotope energy noting thermal heating, thruster configurations, propulsion system, mission capabilities and current thruster technology

11 p1914 A69-25591

Limitations of N-port concept in microwave technology, proposing definitions to avoid contradictions

11 p1841 A69-25624

Mechanical engineering applications to aerospace flight, discussing stability and piloting problems and experimental methods

11 p1824 A69-25672

Gallium arsenide materials technology, discussing solution and vapor-phase epitaxy and liquid encapsulation as related to crystal growth and purification

12 p2141 A69-25834

Satellite technology for government and defense communications systems, noting effects of rainfall attenuation, weather and solar interference on performance and reliability

12 p2028 A69-25932

Technological feasibility of satellite based global data relay service for small users

12 p2028 A69-25949

Holography theory and applications including imaging, Fourier transforms and interferometry

12 p2086 A69-26169

Electron beam welding of Lunar Module Descent Engine, emphasizing variable area injector element and manifold assembly problems and techniques

12 p2102 A69-26621

Remote sensing technology application to improving range resource inventories, discussing aerial photography, optical, IR and radar scanning, etc

12 p2098 A69-26992

Methodology for technical feasibility and economic analysis of remote sensing applications

12 p2193 A69-27013

Hard superconductors technology, stressing metallurgical processing factors effect on properties of niobium alloys and intermetallic compounds

12 p2103 A69-27120

Navy Navigational Satellite System for position location accuracy in marine and oceanographic exploration applications
[AIAA PAPER 68-471]

13 p2295 A69-27247

Multiband aerial photography utilization for evaluating urban housing quality compared with present data collection methods

13 p2260 A69-27607

Application satellites effects on European economy

13 p2382 A69-27834

Spaceborne optical telescopes requirements and development including mirror material and construction, optical design, servocontrol, etc

13 p2261 A69-27946

Book on integrated circuits covering fabrication techniques, basic semiconductor theory, thin film, monolithic, compatible circuits, packaging, etc

14 p2419 A69-29002

Book on subdivision of aircraft structural design covering technology, economics, working conditions, performance, etc

14 p2456 A69-29860

Space technology difficulties, achievements and applications

14 p2527 A69-29895

Digital computers for aircraft engines control, discussing economic assessment, advantages and basic control system

15 p2671 A69-30323

Collection of papers on radar theory and technology, Volume 2, covering radar tracking, measurement, target acquisition, trajectory analysis, etc

15 p2565 A69-30330

Thin film tantalum nitride resistors technology and production, evaluating projected reliability of resistance circuits as function of operating and environmental conditions

15 p2628 A69-30846

Lasers and holography applications in astronomy including high resolution spectrographic diffraction gratings manufacture and astronomical objects photographic pictures evaluation

15 p2610 A69-30880

Semiconductor technology including radar, Gunn and limited space charge accumulation oscillators, phase locked antennas, data processing and solid state computerization

15 p2581 A69-31521

Earth resource satellites, discussing mapping, land evaluation, geological observation, agricultural and hydrological applications, electromagnetic spectrum information, sensors and photographs

16 p2881 A69-31763

Mg alloys applications to construction, discussing strength-to-weight ratio of cast and wrought alloys

16 p2801 A69-31787

Gas laser application to magnetospectroscopy of graphite, Bi, As and pyrolytic graphite single crystals

16 p2796 A69-31822

Aeromedical developments by NASA biomedical applications program applied to general medical equipment including cardiac sensors, surgical sterilization, ballistocardiograph, etc

16 p2882 A69-32430

Retrodirective antennas for spacecraft, discussing design, operations and applications

16 p2762 A69-32557

Integrated circuits effect on electronic equipment design and production technology

16 p2762 A69-32578

Broadband continuously variable phase shifter with microstrip construction, describing phase rotation via stripline connected directional couplers

16 p2763 A69-32582

Scanning electron microscopy of devitrifying solder glass seals for hermetic packages, biased integrated circuits and metallization corrosion

17 p2936 A69-32892

Composite modified cast-double-base rocket propellants with large proportions of metallic fuel and oxidizer, discussing application rocket propulsion

17 p3017 A69-33349

Laser technology and effects on materials fracture

17 p2989 A69-33557

Cryogenic technology applications - Conference, Chicago, June 1968

17 p3006 A69-33679

Commercial utilization of space - Conference, Dallas, May 1967

17 p3041 A69-34043

Commercial utilization of space technology, discussing cost reduction and role of NASA Apollo Program

17 p3043 A69-34044

General technology history, stressing space technology and programs influencing developments in other fields

17 p3076 A69-34045

Electronic computers for avionics system design in terms of technology, performance and cost, discussing reliability prediction and failure rate data

17 p2976 A69-34058

Fluidic system applications to turbojet propulsion control, thrust stabilization control, temperature sensing, normal shock sensing, pressure ratio sensing, supersonic air inlet control and flight control

17 p2904 A69-34070

Laser technology applications stressing engineering, control, communications, medicine, space sciences, holography, computers, etc

17 p2984 A69-34163

Polymer selection and plastics contribution to technologies, noting trend toward improved performance at elevated temperatures

18 p3161 A69-34610

Space, technology and society - Conference, Cocoa Beach, Florida, March 1969, Volume 2

18 p3233 A69-35055

Large solar array systems in space, discussing design and operation

18 p3094 A69-35056

Manned spacecraft earth resource sensing, discussing advantages and applications in agriculture, forestry, geography, hydrology, oceanography and geology

18 p3208 A69-35058

Aerospace technology application to commercial aviation system for cost effectiveness in functions expansion, phase-over, installation, maintenance and operation, discussing added information functions

18 p3108 A69-35069

Space, technology and society - Conference, Cocoa Beach, Florida, March 1969, Volume 1

18 p3234 A69-35070

NERVA program technological developments usability in nonspace industrial community

18 p3170 A69-35075

Space exploration influence on science education, showing NASA instructional materials for teachers in biology, chemistry, physics, mathematics, industrial arts, etc

18 p3235 A69-35077

Aerospace management technology transfer, discussing conceptual contributions, planning, administrative and evaluation methods

18 p3236 A69-35086

Aerospace biomedical technology transfer analysis, discussing spinoff, popular interest, transfer barriers, etc

18 p3236 A69-35104

NASA technology utilization program for civilian economy benefit, discussing scientific and technical documentation and transfer across industrial, disciplinary and regional boundaries

18 p3236 A69-35105

Military aircraft design, discussing reduction of specialization bias and timely application of technical advances

18 p3092 A69-35137

Technological possibilities of gravity free production in space environment, discussing containerless manufacture of glass, liquid metal manipulation and defect free fibers

18 p3206 A69-35490

Electronics applications of superconductivity including inductors for energy storage, computer elements and magnets, cavities for microwave circuits, signal generators and detectors, etc

19 p3382 A69-35807

Solar electric thrust system technology concerning performance, thruster control system stability and method for solution

19 p3394 A69-35941

IR technology - Conference, Ann Arbor, June 1969

19 p3309 A69-36051

Industrial, scientific and commercial applications of NASA developed telemetry technology

19 p3455 A69-36258

Photovoltaic solar cell power technology application to space use and exploration [ASME PAPER 68-WA/SOL-1]

19 p3255 A69-36418

Automation application to rocketry, discussing process control in installations including control circuits and electronic direct digital control system

20 p3617 A69-37340

Laser research from theoretical stage to present, discussing applications

21 p3736 A69-38781

Superalloy technology applications to gas turbine engines

21 p3785 A69-38928

Powder metallurgy all inert processing method for producing nickel base superalloys forgings, discussing microstructure, reproducibility, mechanical properties, etc [ASM PAPER GG-8-3-3]

21 p3745 A69-38929

Nuclear rocket program status and plans, presenting NERVA reactor and engine system tests [AIAA PAPER 68-610]

21 p3768 A69-39219

Frequency assignment methods for Intelsat 2 and 3 communication satellites [AIAA PAPER 68-454]

21 p3674 A69-39226

Heat pipes for isothermal and adaptable energy transfer for space applications, discussing temperature control by fluid choice

21 p3852 A69-39475

Aerospace and marine corrosion technology - Conference, Los Angeles, July 1968

21 p3747 A69-39484

Lasers as tools for integrated circuits fabrication, noting roles of various laser operating parameters

21 p3742 A69-39705

Technology, design, development, qualification and operational elements noting effects on performance, economics and scheduling of nuclear vehicle [AIAA PAPER 68-591]

21 p3769 A69-39752

Gas lasers development and industrial applications, discussing output power, operation modes, etc

22 p3961 A69-40242

Holographic interferometry for surface strain and vibrations visualization, describing photographic recording techniques

22 p3945 A69-40244

Moire effect applications to stress analysis, enumerating advantages over conventional grid techniques

22 p4042 A69-40315

Communication satellite technology application to overlay network linking nationwide data machines for business mail service with virtually instantaneous delivery at low cost

23 p4117 A69-41669

B, silicon carbide, C and Be reinforcing fibers technology, thermal and physicomechanical properties, noting coating, surface defects and improvement over glass fibers

23 p4179 A69-42154

Carbon materials manufacture, properties and applications in space technology, discussing carbon fibers, textiles, graphite, pyrolytic carbon, composites and vitreous carbon

23 p4180 A69-42160

Technological forecasting as aid to aerospace planner in optimizing R and D resources allocation [AAS PAPER 69-105]

24 p4417 A69-42819

Technology flow for future manned earth orbit and lunar operations and planetary exploration [AAS PAPER 69-494]

24 p4380 A69-42840

TECTONIC MOVEMENT

U TECTONICS

TECTONICS

Lineament trend analysis of Gemini Red Sea synoptic terrain photography, noting computerized rotation from apparent to true angles

02 p0247 A69-12808

Tectonic map compiled for visible and far sides of moon, noting correlations between earth and moon tectogenesis

03 p0505 A69-12899

Martian diagonal and longitudinal-meridional canals mapped into grid systems, noting differences between Martian and lunar crusts tectonic activity

13 p2337 A69-27533

Earth surface heat flow pattern measurement and distribution techniques, considering relation to surface features and tectonic movements of crust [AIAA PAPER 69-589]

17 p2961 A69-33284

Photogrammetric instruments applied to determination of spatial position of tectonic surfaces by aerial photography

20 p3539 A69-37511

Standing waves on moon, discussing annular and radial structures of lunar craters and global tectonic patterns

20 p3604 A69-37565

Precambrian crustal geotectonic evidence of earth's radius expansion based on dated orogenic fold belts distribution

22 p3936 A69-40182

Tectonic classification of earth gravitational field based on mean gravity anomalies, correlating positive anomalies with Quaternary volcanism

23 p4154 A69-41318

TEE

U T SHAPE

TEFLON [TRADEMARK]

Pool boiling heat transfer from stainless steel coated with Teflon to produce nonwetted surfaces [ASME PAPER 68-WA/HT-12]

05 p0847 A69-16119

Teflon dielectric properties evaluated during fast laser beam heating, noting presence of C by microwave measurement

24 p4336 A69-43266

TEKTITES

NT AUSTRALITES

Boron in tektites determined by calorimetric technique for analysis of boron in silicates, comparing results with values from igneous and sedimentary parents

08 p1407 A69-20936

Geochemistry and element abundances for Henbury impact glass, Darwin glass and australites, noting evidence for meteorite impact on sandstone

08 p1407 A69-20937

Water content of tektites, impactites and artificial glass of tektite composition using IR absorption measurements

10 p1778 A69-23413

Natural unbroken tektite surface examination by interferometry, discussing fringe patterns for pit shapes and sizes

12 p2173 A69-27175

Lunar volcanism origin of tektite and pearlite, noting no cosmic ray effects

20 p3597 A69-37338

Tektite origin theories, discussing Surveyor experiments effects on lunar geology and Tektite origin

22 p4012 A69-40086

Geochemistry of tektites - Conference, Corning, New York, April 1969

23 p4209 A69-41340

Rb-Sr isotope patterns in tektites from Southeast Australian strewn field, studying Rb volatilization role in Rb-Sr isochron production

23 p4154 A69-41342

Darwin and Macedon impact glasses related to Far Eastern tektites through age determination by fission track technique

23 p4210 A69-41344

Fission track ages of tektites, australites and related glasses, considering errors due to annealing and etch pits

23 p4210 A69-41345

Tektites chemical composition showing minor concentration changes during melting used for parent material identification

23 p4210 A69-41346

Impact origin of Ivory Coast tektites and Bosumtwi Crater indicated by gamma ray spectrometric study of U, Th and K abundance patterns

23 p4210 A69-41347

Black magnetite bearing spherules extracted from tektites, and magnetic fractions of impact glasses, determined by reflecting microscope and electron microprobe

23 p4210 A69-41349

Ivory Coast microtektites chemical composition from electron microprobe analysis

23 p4211 A69-41351

TELECHIRICS

U REMOTE HANDLING

TELECOMMUNICATION

NT AIRCRAFT COMMUNICATION

NT AUTOMATIC PICTURE TRANSMISSION

NT BIOTELEMETRY

NT BROADCASTING

NT CLOSED CIRCUIT TELEVISION
 NT COLOR TELEVISION
 NT DATA LINKS
 NT DEFENSE COMMUNICATIONS SYSTEM [DCS]
 NT EDUCATIONAL TELEVISION
 NT FACSIMILE COMMUNICATION
 NT FREQUENCY SHIFT KEYING
 NT GROUND-AIR-GROUND COMMUNICATIONS
 NT INTERPLANETARY COMMUNICATION
 NT LUNAR COMMUNICATION
 NT MULTICHANNEL COMMUNICATION
 NT OPTICAL COMMUNICATION
 NT PHASE SHIFT KEYING
 NT PULSE COMMUNICATION
 NT PULSE FREQUENCY MODULATION
 NT PULSE FREQUENCY MODULATION TELEMETRY
 NT RADIO COMMUNICATION
 NT RADIO RELAY SYSTEMS
 NT RADIO TELEGRAPHY
 NT RADIO TELEMETRY
 NT REENTRY COMMUNICATION
 NT SATELLITE TELEVISION
 NT SPACE COMMUNICATION
 NT SPACECRAFT COMMUNICATION
 NT SPACECRAFT TELEVISION
 NT TELEGRAPH SYSTEMS
 NT TELEMETRY
 NT TELEPHONY
 NT TELEPHOTOMETRY
 NT TELETYPEWRITER SYSTEMS
 NT TELEVISION SYSTEMS
 NT TRANSCOEANIC COMMUNICATION
 NT VIDEO COMMUNICATION
 NT VOICE COMMUNICATION
 NT VOICE DATA PROCESSING
 NT WIDEBAND COMMUNICATION
 NT WIRELESS COMMUNICATIONS

Subsystems of ESRO research satellites Td 1 and Td 2, discussing telecommunication, attitude control, power supply and temperature control design and functions

01 p0160 A69-10031
 Frequency diversity for communication in fading environment, relating performance variance to between channel correlation variance

01 p0026 A69-10177
 World Weather Watch /WWW/ system and meteorological satellites, discussing observational networks, data centers, telecommunication facilities, research, education and training program

01 p0178 A69-10478
 Geostationary satellite transmissions for educational purposes

01 p0028 A69-10494
 Space research practical benefits in solar physics, radio astronomy, meteorology, radio physics, communications, etc

01 p0179 A69-10496
 Marine requirements possible satisfaction by using space techniques to improve long range communications to achieve safety at sea and shipping operations efficiency

01 p0161 A69-10503
 Automatic picture transmission station equipment including antenna, cavity filters, tape recorder, oscilloscope, facsimile system and kinescope

01 p0054 A69-10522
 Optimum modulation technique determination for single channel voice communication under severe noise conditions

01 p0029 A69-10526
 Sensitivity calculation for microwave receiver consisting of traveling wave tube preamplifier followed by square law detector and video amplifier

01 p0048 A69-11038
 Satellite communications with emphasis on European programs, discussing synchronous satellites, Europa 2 rocket and Saros and Symphonie projects

02 p0207 A69-11910
 Book on communication systems covering signal design, video signals, communication satellites and threshold decoding techniques

03 p0383 A69-12867
 Sequential signal design for feedback channels, emphasizing single set subject to peak and average power constraints in time continuous transmission

03 p0408 A69-12868
 Synchronization in coded communication systems, considering phase lock loop and square wave correlation function

03 p0383 A69-12871
 Low altitude satellite relay system, discussing modulation, antennas, frequency plans, telemetry, tracking, command and earth terminals

03 p0391 A69-13241

Intelsat application satellites, considering economy and global telecommunication

03 p0535 A69-13592
 European launcher program analyzed from point of view of telecommunication and cost

03 p0520 A69-13593
 Point to point millimeter wave communication system design, discussing propagation and data transmission

03 p0405 A69-13723
 Economic and technical advantages and disadvantages of satellite telecommunications, discussing Telstar intercontinental TV transmission and Soviet Molniya system

04 p0662 A69-15328
 Digital signal processing in radar, sonar and communication

05 p0718 A69-15749
 Satellite telecommunications, discussing Australian experience, ground stations location, national network and international cooperation

06 p0886 A69-17066
 Project Symphonie, discussing stationary communication satellite, coverage, frequencies and characteristics

06 p0886 A69-17072
 Communication satellites application to domestic live TV, telephone and data communication and long distance telecommunication in Canada

06 p0887 A69-17075
 Adaptive control of reflective satellite communication system

06 p0887 A69-17356
 Minimum operational characteristics for airborne VHF communication systems, discussing FCC requirements and system performance

07 p1077 A69-18638
 Data compression techniques compared for use in communications systems to minimize required number of samples and bits per sample

07 p1077 A69-18758
 World satellite telecommunications network, discussing recommendations with reference to signal transmission, acoustic echoes, etc

07 p1079 A69-18942
 Eole satellite and meteorological balloons telecommunications used to study wind distribution in Southern Hemisphere and other atmospheric parameters

07 p1084 A69-19134
 Communication satellite system design by use of baseband equation relating SNR after detection to CNR at detector input

07 p1085 A69-19180
 Optimum linear feedback code for additive noise systems with average power constraint on transmitter to increase channel capacity

07 p1085 A69-19181
 Soil resistivity survey at earth telecommunication installation site to determine optimal grounding or electrode system

07 p1117 A69-19348
 Transponders for communication satellites, discussing design constraints, reliability and transmission capacity increase

08 p1279 A69-19905
 Incoherent m-ary frequency shift keying /MFSK/ system analysis concerning automatic time synchronization

08 p1274 A69-20133
 Air traffic development related to control systems advances, discussing telecommunications effect and radio navigation systems enabling pilot to determine position

08 p1347 A69-20598
 Project Dioscures for permanent air traffic control centers, positive telecommunication links and satellite navigation

08 p1347 A69-20779
 Communication satellite systems role in world telecommunication network, discussing traffic type, volume and routing, earth stations location and capacities and orbit selection

09 p1449 A69-21271
 Extraterrestrial cosmic emissions responsible for background noise of communications engineering, discussing factors affecting frequency sharing with other services

09 p1586 A69-21294
 Belier rocket launching facilities in Guiana, describing pads, tracking system, telecommunications network, etc

09 p1477 A69-22161

INTELSAT for design, construction, launching and maintenance of global communication satellites, noting transponders

09 p1457 A69-22466
 Synchronous and near synchronous satellites for communication systems, discussing stationkeeping and low thrust propulsion

09 p1458 A69-22468
 Minimum error probability and optimal system regime relationship to noise rejection in memoryless communication investigated for limited repeated transmissions

09 p1459 A69-22639
 Skorsky HH-3F helicopters electronic equipment, discussing communication and navigation aids, search and recovery missions, etc

10 p1662 A69-23222
 Navigation accuracy and telecommunications system capacity interrelationships in economical improvement of air traffic control system over North Atlantic

10 p1723 A69-23704
 Electrical engineering, Volume 3, communications, covering special theories, systems components, telecommunication, electroacoustics, digital and analog computers and programming

15 p2568 A69-30619
 Dioscures project for telecommunication, ATC and navigation by satellites to provide continuous position determination

15 p2651 A69-30691
 Global communication techniques and trends, discussing radio telephone and telegraph, submarine systems, satellite communications, line of sight links, tropospheric scatter, waveguide transmission, etc

16 p2750 A69-31755
 Global satellite communication networks design by computer simulation, discussing politico technical interface problems, ground stations, atmospheric factors, system optimization, etc

16 p2750 A69-31852
 Linear feedback additive noise communication systems formulated in terms of arbitrary operations at transmitting and receiving points

17 p2944 A69-33626
 Pivotal computer operations in Apollo NASA Communication Network, describing UNIVAC computers in use and design considerations

18 p3100 A69-34267
 Mechanical drives effectiveness for large antenna tracking/communications systems evaluated in terms of reliability and availability

18 p3100 A69-34522
 Phase modulation in pseudo-noise ionospheric communication system for reducing F region CW signal fading

18 p3104 A69-35308
 Environment effect on scientific and telecommunication equipment mounted on exploratory probe during Venus atmosphere entry for acceleration loading in design

19 p3431 A69-36037
 Satellite telecommunication systems coordination, discussing transformation feasibility of consortium or international organ into international organization

20 p3637 A69-37120
 Modulation envelopes, tables of profiles and harmonic components for modulated waves in electrical and communications problems

21 p3673 A69-38778
 Civil cargo aircraft characteristics and development trends, discussing cargo and passenger traffic management, communications network, etc

22 p3863 A69-40427
 PCM role in FDM-FM short haul low density cable communications systems used in exchange area and tactical military systems

22 p3900 A69-40678
 Performance prediction of terrestrial communication system based on experimental radio and meteorological program at 11 GHz, discussing transmission loss

22 p3900 A69-40680
 Telecommunication systems used in airline industry and reorganization requirements for efficient operation

23 p4114 A69-41356
 High sensitivity communication system design consisting of radome enclosed steerable antenna, 500 kw transmitter and microwave configuration compatible with low noise receivers

23 p4149 A69-42131
 Communications - IEEE Conference, Boulder, June 1969

23 p4127 A69-42500

TELEGRAPH SYSTEMS
 NT FREQUENCY SHIFT KEYING

NT PHASE SHIFT KEYING
NT RADIO TELEGRAPHY
NT TELETYPEWRITER SYSTEMS

Phototelegraphic transmission of holographs of objects in many shades through channel with limited number of signal levels

11 p1889 A69-25549

Satellite system TDM techniques and prototype equipment capable of combining 12 unrelated start-stop and synchronous telegraph channels

17 p2920 A69-33420

TELEGRAPHY
U TELEGRAPH SYSTEMS

TELEMETERS
U TELEMETRY

TELEMETRY

NT BIOTELEMETRY
NT PCM TELEMETRY
NT PULSE FREQUENCY MODULATION
NT PULSE FREQUENCY MODULATION
TELEMETRY
NT RADIO TELEMETRY

Multichannel telemetering device for magnetically suspended or free flight wind tunnel models noting strain gage pickups, switching and auxiliary circuits [ONERA-TP-643]

02 p0226 A69-11623

Adaptive multiplex telemetry use in scientific satellite data management

02 p0212 A69-12817

Stored program control for polynomial data compression in telemetry application

03 p0400 A69-13220

NOMAD buoy telemetry system for synoptic oceanographic and meteorological data, using digital processing and dual frequency transmissions

03 p0391 A69-13223

Digital data processing equipment for space flight PCM telemetry

03 p0393 A69-13290

Ghost project for gathering weather data by balloons and transmission of data to central data processing stations by satellite

03 p0520 A69-13621

Upper and lower bounds on mean reduced error of pulse code telemetering systems operating by binary code

03 p0396 A69-13687

Telemetered data obtained by Iantar 1 automatic ionospheric laboratory, detailing argon-ion plasma engine performance

05 p0830 A69-16056

Telemetry capability of Air Force Western Test Range noting acquisition, tracking, data processing and display and data reduction

05 p0743 A69-16304

Conversion of range telemetry systems /CORTS/ program noting installations and standardization

05 p0743 A69-16306

Computer oriented telemetry data processing systems designed to condition raw telemetry data for further processing by other systems

05 p0727 A69-16770

French program of space geodesy, discussing spatial triangulation, telemetry, dynamic geodesy, Diapason and Diademe experiments [UN PAPER 68-95834]

06 p0917 A69-17071

Multiring antenna arrays for space telemetry and communication, analyzing distant field, radiation resistance, directive gain and mutual impedance

06 p0899 A69-17827

Mariner 1969 high rate telemetry system portions pertinent to combinatorial mathematicians, discussing coding and encoding

06 p0890 A69-17862

Kwajalein Missile Range UHF telemetry conversion program using S band antennas with three channel monopulse autotrack systems

07 p1077 A69-18829

Telemetry - Conference, Los Angeles, October 1968

07 p1079 A69-19092

Multifunction Receiver System rationale, concepts, background requirements and technical justifications for tracking, telemetry and ranging data acquisition by Goddard Center

07 p1081 A69-19101

OMEGA 4 100-k Hz ground station telemetry system for acquiring and processing outputs up to 23 FM and two TDM signals applied simultaneously from instrumentation recorder

07 p1105 A69-19103

Airborne S-band telemetry antennas for omnidirectional patterns of polarization component, discussing design, pattern measurements and application

07 p1106 A69-19112

Sun as calibration signal source for L and S band telemetry, discussing receiving system noise temperature determination and antenna gains

07 p1082 A69-19113

Miniature power amplifier stage for telemetry transmitters, discussing equipment size and weight reduction methods and hermetic envelope

07 p1106 A69-19115

Compatibility requirements and considerations of range telemetry tape crossplay operations, discussing major classes

07 p1133 A69-19117

High data rate coherent telemetry systems synthesis, discussing multiphase modulation and demodulation to achieve bandwidth requirements

07 p1083 A69-19123

Mariner 1969 multimission high rate deep space telemetry system design, hardware and application

07 p1083 A69-19125

Frequency division multiplex telemetry technique with double sideband-quadrature carrier multiplexing system, discussing data signals, channels and distortion

07 p1084 A69-19131

Double sideband suppressed carrier FM telemetry system as airborne data recorder, discussing noise, environmental conditions, laboratory and flight tests

07 p1084 A69-19132

Telemetry with unrestrained animals, discussing radio tracking of game animals and instrumentation requirements for studying green sea turtle goal finding ability

07 p1071 A69-19136

Receiving systems for digital telemetry signals from spacecraft, analyzing receiver performance by statistical methods

08 p1276 A69-20591

Digital telemetry from spacecraft, discussing on-board processing, data compression, coding, sequence detection and receivers

08 p1276 A69-20592

Maintenance telemetering, tracking and telecommand for developmental and operational satellites, discussing possibilities of frequency sharing between satellites and terrestrial services

09 p1451 A69-21290

Technical characteristics of spacecraft telemetering, tracking and telecommand systems, stressing links between earth stations and spacecraft

09 p1451 A69-21291

Channel output SNR optimization in AM/FM telemetry system by using automatic gain control, discussing AGC time response and general characteristics

09 p1454 A69-21799

UHF telemetry conversion program at Pacific Missile Range, describing antenna, receive-record and separation display systems

09 p1454 A69-21800

Temperature profiles and frequency driftings of VHF telemetry transmitters for Saturn S-IC stage, using IR radiation data

10 p1653 A69-23049

Telemetry monitor systems for high speed rotating equipment, discussing data recording, transmission, decoding, thin-thick film microtechniques, etc

10 p1692 A69-23249

Flight test telemetry data processing system designed for C-5

10 p1660 A69-23269

Real time computer controlled telemetry system readiness testing and validation, describing automatic closed loop checkout methods and remote display controller

10 p1660 A69-23270

FM/AM telemetry circuits with three axis piezoelectric accelerometer for measurements during impact tests of soft landing models

10 p1654 A69-23279

Ruggedized ballistic range telemetry system survivability and in-flight stability after gun launching, presenting temperature, strain and stagnation point pressure measurements

10 p1654 A69-23281

Telemetry data channel gain and phase correction with frequency response calibration technique using digital filtering

10 p1654 A69-23291

Electrical servopositioning of telemetry reception antenna for tracking satellites, considering weight, stability, etc

11 p1852 A69-25118

Space electronics, telemetry, antennas, computers - IEEE Conference, Cocoa Beach, Florida, November 1968

11 p1837 A69-25288

Telemetry system sensitivity as function of noise figure, noting SNR and noise and bandwidth effects on system information handling capability

11 p1840 A69-25308

Data processing system for satellite telemetry signals, describing hardware construction and operation, data readout, etc

11 p1840 A69-25423

Single channel pressure telemetry unit for chronic implantation into cardiac chambers or major blood vessels in unrestrained animals for measuring ventricular pressure

11 p1831 A69-25642

Communication systems in interplanetary space covering telemetry, remote control, Doppler and distance measurements, coherent PCM/PSK/PM demodulation, deep space network, etc

12 p2027 A69-25875

Sampled data multichannel telemetry using pseudorandom sequences generated by linear shift registers

12 p2028 A69-25922

ESRO 1 communication system and telemetering system compared to ESRO 2

13 p2220 A69-27749

Optimum time for telemetry data transmission by system using feedback combined with error correcting codes

14 p2412 A69-29428

Optical carrier single channel telemetry system providing complete electrical isolation between shock tube data acquisition and data recording instrumentation

14 p2449 A69-29561

Temperature measurement miniature telemetry transmitter

15 p2607 A69-30156

Balloon for in situ measurements of atmospheric optical parameters using two axis sun pointer, spectropolarimeter and airborne telemetry

15 p2615 A69-31288

Automatic quantitative checkout equipment for telemetry circuit of Diamant satellite booster before launching

16 p2750 A69-31727

Electromagnetic interference correction for airborne telemetry, illustrating actual and simulated data for interfering source signatures identification

16 p2754 A69-32575

Tracking and data acquisition systems for spacecraft and ground link through command, telemetry and tracking, noting data relay satellites, etc

17 p2919 A69-33371

Multichannel pressure telemetry system for base pressure measurements on small wind tunnel models, considering proximity effects on transducer-telemetry units

19 p3305 A69-35727

Telemetering - IEEE Conference, Washington, D.C., April 1969

19 p3268 A69-36237

Meteor burst communication channel parameters for low data rate telemetry, considering signal amplitudes, decay, duty cycle, multipath, phase stability, trail location and variations

19 p3271 A69-36250

Backfire antenna radiation characteristics and physical dimensions for tracking and telemetry applications, including five element array model

19 p3271 A69-36251

Sounding rocket S band telemetry antenna operation, proposing quasi-isotropic pattern criterion to reduce effects of shadowing and interference

19 p3271 A69-36252

Active interferometer controlled telemetry tracking system for missile range, discussing automatic target acquisition, dish feed, costs and optimized data-channel antenna patterns

19 p3271 A69-36253

Telemetering by reflex klystron accelerometer and seismometer with on air or coaxial cable signal transmission

19 p3272 A69-36255

Laser and quasi-laser pulse modulation technique for global satellites telemetry system

19 p3272 A69-36257

Industrial, scientific and commercial applications of NASA developed telemetry technology

19 p3455 A69-36258

Buffer storage for telemetry nonstationary video data compression, analyzing requirements, predictor algorithm and variable aperture control using simulation

19 p3272 A69-36260

Precompression automatic wild point rejection from sampled telemetry data for data compressors evaluated by digital computer simulation

19 p3273 A69-36263

Cross correlation and probability metric in coded sequential detection telemetry system, giving optimum parameters, overflow and error probabilities using computer simulations

19 p3273 A69-36266

Nonlinear filter theory applied to digital telemetry binary processes, using continuous time stochastic process

19 p3274 A69-36281

Block coded telemetry systems design for phase coherent space communication employing double conversion superheterodyne phase locked receivers

19 p3277 A69-36487

Analog telemetry signals generalizing frequency and pulse position modulations over coherent channels, noting added degrees of freedom function

20 p3492 A69-37713

Telemetered data obtained by lantar 1 automatic ionospheric laboratory, detailing argon-ion plasma engine performance

20 p3618 A69-37966

Ruby laser goniometric and telemetric echoes by photographing Geos satellites

21 p3671 A69-38335

Book on synchros application and design covering telemetry, torque and control systems, synchro circuits, resolvers as computer elements, etc

21 p3681 A69-38450

Thermal design of missile mounted S band telemetry transmitter package based on temperature control system, using heat-of-fusion characteristics of wax material

22 p3909 A69-39945

Maximum errors of telemetering systems under inter-channel transient distortions in multistage amplifier of video signals

22 p3899 A69-40250

Short range telemetering strain gage system with stable multivibrator transmitter for measuring inter-coupling displacement and shaft torque

22 p3946 A69-40314

Real time multiprocessing telemetry ground support integrated system design with expanded definition of hardware/software decision tradeoffs

[AIAA PAPER 69-971] 22 p3907 A69-40351

Telemetry data processing, describing designation, tasks and possibilities of data reduction laboratory attached to NASA Goddard Space Flight Center

22 p3919 A69-40352

Monopulse telemetry tracking system, describing equipment and mobile operation

22 p3900 A69-40681

Telemetering - Conference, Washington, D.C., September 1969

23 p4117 A69-41734

Programmable data handling and telemetry systems for scientific satellites, noting system checkout, spacecraft integration, software and ground data processing

23 p4132 A69-41735

Wideband FM telemetry transmitters for S band, using symmetrical discriminator

23 p4119 A69-41741

Digital telemetry link coding as English language analogy, developing block code scheme combining bit, word and block error detection and correction methods

23 p4119 A69-41745

Wideband telemetry recording error compensator for reducing flutter and interchannel time-base error in magnetic tape instrumentation

23 p4137 A69-41775

Telemetering Standards Coordination Committee annual report

23 p4241 A69-41782

Digital transition tracking symbol synchronizer for low SNR coded telemetry systems, discussing phase locked loop analysis and phase detector simulation by Monte Carlo method

23 p4130 A69-42513

TELEMETRY AUTO REDUCTION SYSTEM

U DATA REDUCTION

TELEPHONY

European regional satellite communication systems, discussing EUROVISION TV program broadcasting and multiple access telephony

03 p0395 A69-13585

Satellite communication channel number and distribution optimization, obtaining malfunction probability for telephone service communication system

[UN PAPER 68-95772] 06 p0886 A69-17030

Frequency modulation methods and multiple access for communication satellite systems, considering bandwidth for space station transponder

09 p1449 A69-21274

Preemphasis applications compared in active communication satellite systems for frequency division multiplex telephony and for TV

09 p1449 A69-21275

Carrier energy dispersal in communication satellite telephony and TV systems, noting attendant RF bandwidth increase as function of distortion

09 p1450 A69-21277

Noise rejection in multichannel telephone signal reception with FM and multiplexing, determining SNR dependence on SNR at receiver input

09 p1459 A69-22640

Mean-minute thermal noise intensity distribution in telephony channels of tropospheric radio relay systems

14 p2412 A69-29425

Global communication techniques and trends, discussing radio telephone and telegraph, submarine systems, satellite communications, line of sight links, tropospheric scatter, waveguide transmission, etc

16 p2750 A69-31755

TELEPHOTOMETERS

U TELEPHOTOMETRY

TELEPHOTOMETRY

Eight color narrow band photometry of bright stars, discussing band system, instrumentation, data and calibration

02 p0313 A69-11487

Cosmos 149 meteorological satellite telephotometers for measuring reflected solar radiation from earth

14 p2447 A69-29404

TELESCOPES

NT ASTRONOMICAL TELESCOPES

NT HELIOMETERS

NT MANNED ORBITAL TELESCOPES

NT PARTICLE TELESCOPES

NT RADIO TELESCOPES

NT REFLECTING TELESCOPES

NT REFRACTING TELESCOPES

NT SCHMIDT CAMERAS

NT SPECTROSCOPIC TELESCOPES

NT STRATOSCOPE TELESCOPES

NT X RAY TELESCOPES

Image averaging time effects on modulation transfer function /MTF/ of system comprising telescope objective and horizontal propagation path in turbulent atmosphere

06 p0890 A69-17806

Balloon flights for testing remote sensor systems prior to space flight, considering return beam vidicon and tracking telescope suitability for experimentation

22 p3865 A69-40806

Ni plated 40-cm lightweight Al alloy telescope mirror, noting weldment stress relief by annealing

23 p4164 A69-41624

TELETYPEWRITER SYSTEMS

Multimode propagation communications system /MMPCS/ utilizing digital computer to implement intermittent system

03 p0389 A69-13191

TELEVISION CAMERAS

Apollo lunar TV camera for real time pictures during all phases of Apollo lunar landing mission, describing camera tube, circuitry and optics

07 p1133 A69-19137

Surveyor scientific instruments and operation on moon, reviewing TV camera, alpha scattering instrument and surface sampler

[JPL-TR-32-1358] 08 p1312 A69-19850

Silicon diode array camera tube modified to permit X ray images to be displayed on TV monitor

09 p1463 A69-21845

Real time 2000 line TV camera with 40 MHz bandwidth, 1600 line vertical resolution and 1000 line horizontal resolution

[SMPT PAPER 105-73] 12 p2077 A69-25769

Surveyor 7 TV system in photon integration mode, analyzing slow scan vidicon storage characteristics and dark current limitations

[SMPT PAPER 105-72] 12 p2078 A69-25772

Low light level slow scan Owl TV camera system with secondary electron conduction camera tube for satellite-borne observation of auroral light emission

12 p2079 A69-25904

Rocket trajectory determination by tracking on-board light source against star background with image orthicon TV system

12 p2033 A69-26965

Apollo 8 photooptics, considering TV camera and broadcasts, photographic equipment and visual observation

15 p2609 A69-30469

Apollo 10 field sequential color TV system, describing camera modifications, systems design and equipment compatibility problems

18 p3101 A69-34810

Image dissector meteorological cameras, discussing ATS-III and Nimbus systems, high resolution camera and multispectral cameras

18 p3137 A69-35101

Narrow angle high resolution TV camera design and testing for Mariner 6 and 7 Mars flyby missions, noting computer drawn spot diagrams

19 p3307 A69-35808

TV camera tubes with electron beam scanning adapted to IR imaging, emphasizing vidicon

19 p3311 A69-36069

Lunar TV camera for Apollo missions, discussing operational requirements and design

23 p4162 A69-41478

TELEVISION EQUIPMENT

NT IMAGE DISSECTOR TUBES

Systems analysis in aerospace engineering by adding motion pictures and TV techniques

[SMPT PAPER 104-17] 04 p0596 A69-14359

Monolithic HF circuits stability in TV and HF devices noting need for appropriate amplifiers

07 p1103 A69-18883

Stellar identification system using onboard sighting equipment and computer mathematical methods

08 p1347 A69-20657

Nondestructive ultrasonic, spectroscopic and TV test methods reducing time for inspection and increasing reliability of turbines

17 p2978 A69-33330

X ray TV system with electronic-optical converter and X ray vidicon for industrial defectoscopy

18 p3138 A69-35113

TV-optical observations of asteroid Icarus, discussing installation, photographs and position

21 p3719 A69-38402

TELEVISION RECEIVERS

Laser display technology, discussing experimental systems, light sources, modulation and scanning

03 p0431 A69-13850

Earth station system for ground based communications with Intelsats 2 and 3 noting antennas, receivers, transmitters and power supplies

05 p0741 A69-15667

Ground station receiving antenna design and size for indirect distribution of TV programs by geostatic satellites

10 p1654 A69-23389

TELEVISION RECEPTION

Laser color TV projection-display system using moving mirrors and dual polarization scanner

07 p1137 A69-19740

TV test chart for evaluating Surveyor lunar spacecraft TV system covering resolution, photometric and colorimetric response and sun angular position

[SMPT PAPER 105-71] 12 p2078 A69-25771

TELEVISION SYSTEMS

NT CLOSED CIRCUIT TELEVISION

NT COLOR TELEVISION

NT EDUCATIONAL TELEVISION

NT SATELLITE TELEVISION

NT SPACECRAFT TELEVISION

Filter effectiveness in improving air to ground target identification performance on TV display

06 p0887 A69-17210

Image intensifier-vidicon closed circuit TV network for auroral cinematography at low light levels

06 p0925 A69-17382

TV system producing images with 5000 line resolution, proposing application in Earth Resources Observation Satellite

07 p1131 A69-18552

Laboratory measurement data of low light level TV performance converted to anticipated real world performance data

07 p1132 A69-18948

Cockpit TV-radar for providing pilots with navigation, weather and traffic data, discussing safety factors and radar picture transmission quality

[SAE PAPER 690327] 11 p1833 A69-24506

Crab Nebula pulsar detection by TV camera with image intensifier at focus of astronomical telescope, detailing instrumentation and observations

11 p1962 A69-25251

Nationwide TV system using synchronous communication satellite proposed for India, discussing antenna, modulation, multiplexed channels and educational aspects

19 p3275 A69-36413

Two channel TV Cassegrain telescope, describing color separation system for obtaining integral and monochromatic images of astronomical objects
20 p3547 A69-38309

Image intensifiers and orthicons, plumbicons, vidicons as photoelectric devices in TV auroral observation from ground stations and jet aircraft
21 p3706 A69-38484

Earth resources satellite /ERS/ TV camera configurations, return beam vidicon camera characteristics and devices for TV picture reproduction on film
21 p3720 A69-38619

Computer controlled TV cloud recognition equipment on meteorological satellites, discussing multistep process of automatic perspective distortion corrections by onboard computer
22 p3977 A69-40004

Low light level TV systems for military uses, describing design and operation of various image intensifier tubes
22 p3945 A69-40141

Mariner Mars 1969 TV system environmental test and calibration program
22 p3920 A69-40372

Distribution system for TV driving signals proposed for single synchronized system for all TV centers, describing decoder circuits
24 p4282 A69-42745

Instantaneous response TV system application to observing solar surface granulation, noting advantages over photometric measurements
24 p4389 A69-43711

TELEVISION TRANSMISSION

Digital computer system for storing, processing and displaying TV pictures
01 p0077 A69-10024

Direct TV broadcasting from satellites with incoherent thermionic reactor and electrical propulsion [UN PAPER 68-95559]
01 p0114 A69-10466

Satellite TV systems for India, alternatives and costs [UN PAPER 68-95750]
01 p0028 A69-10495

Satellite educational TV, considering program distribution, satellite characteristics, ground terminals design, reliability, quality, programming and costs [UN PAPER 68-95827]
01 p0029 A69-10499

Pseudorandom signal TV signal distortion due to flutter and skew introduced by tape recorder, computing system SNR for distortion as additive random noise
01 p0033 A69-10999

Spacecraft device for photographing and transmitting TV pictures noting limitations and spatial conditions adaptations
02 p0207 A69-11829

Satellite TV transmitter power requirements for adequate direct broadcasting field strength in existing UHF TV bands
03 p0394 A69-13578

Fourier coding method for coding images for digital transmission, achieving bandwidth reduction for televised images
04 p0556 A69-14429

Soviet book on multichannel and TV signals transmission over radio relay links using microwave tropospheric scatter propagation
04 p0558 A69-14919

Economic and technical advantages and disadvantages of satellite telecommunications, discussing Telstar intercontinental TV transmission and Soviet Molniya system
04 p0662 A69-15328

Analog FM subcarrier modulation selected for real time TV picture transmission via electro-optic space communication system
04 p0562 A69-15474

Optical heterodyne communication experiments in TV signal transmission [IEEE PAPER J-5]
05 p0720 A69-16319

Quality control for TV transmissions via communication satellites, considering transmission accuracy improvement and error measurement automation [UN PAPER 68-95773]
06 p0886 A69-17047

Satellite educational TV capabilities, applications and planning [UN PAPER 68-95355]
06 p0887 A69-17078

Communication satellites in synchronous equatorial orbit for two types of educational TV, discussing picture quality, modulation, power, bandwidth and system costs
06 p1017 A69-17624

Satellite TV broadcast application for communication and education, discussing costs and benefits in single and multimission combinations
07 p1244 A69-18678

TV transmission antenna radiation patterns measured with helicopter flown equipment and Decca navigation equipment
08 p1274 A69-20130

Direct radio and TV broadcasting from satellite-borne radio transmitter to general public, giving visibility, gains, frequencies and bandwidths tables
09 p1586 A69-21286

Cockpit TV-radar for providing pilots with navigation, weather and traffic data, discussing safety factors and radar picture transmission quality [SAE PAPER 690327]
11 p1833 A69-24506

TV broadcasting from synchronous satellites direct to ordinary UHF receivers in 1980s
11 p1833 A69-24529

Phototelegraphic transmission of holographs of objects in many shades through channel with limited number of signal levels
11 p1889 A69-25549

Parametric frequency converter consisting of mixer head in bridge circuit with varactors for 12 GHz TV transmitters
11 p1854 A69-25614

Wave propagation in 11.7-12.7 GHz range studied for application to TV transmission, describing emitter, omnidirectional antenna and receiving station
11 p1841 A69-25637

Synchronous satellite TV broadcasting systems in UK, discussing equipment, transmission problems and economic factors
13 p2220 A69-27830

TV transmission of two dimensional transparency hologram with reduced resolution requirements on camera tube, eliminating zero order terms
17 p2974 A69-33401

Spectral analyzer for structural noise spectrum of scanning ray TV transmitter
17 p2939 A69-33909

Apollo 10 field sequential color TV system, describing camera modifications, systems design and equipment compatibility problems
18 p3101 A69-34810

Electro-optical crystals resonance modulator for coherent light beams and microwave frequencies, describing application to multichannel TV transmission system
19 p3266 A69-35763

TV picture and newspaper pages simultaneous transmission via earth satellite /Orbit/, measuring SNR and crosstalk
19 p3277 A69-36567

Geostationary satellite TV broadcasting to small contiguous areas with separate programs, discussing communication distribution problems
22 p3902 A69-41252

Nonlinear encoding for picture transmission using nonlinear analog to digital converter
23 p4119 A69-41747

Effective color TV transmission via satellite using PCM/PSK modulation, noting dependence on available equipment, bandwidth, desired error rate and SNR
23 p4130 A69-42520

Distribution system for TV driving signals proposed for single synchronized system for all TV centers, describing decoder circuits
24 p4282 A69-42745

TELEGEN THEORY

U GYRATORS
U NETWORK ANALYSIS
U NETWORK SYNTHESIS

TELLURIC CURRENT MICROPULSATIONS

U MICROPULSATIONS

TELLURIC CURRENTS

Large amplitude Pc 1 events at College, Alaska, noting more ionospheric cosmic noise absorption accompanying large events [AFCL-69-0059]
02 p0244 A69-12397

Air-earth current and conductivity measurements, noting greater conduction current at one mile altitude
05 p0758 A69-16419

Solar flare influence on potential gradient and air-earth current properties at high mountain stations
05 p0759 A69-16634

Earth currents and magnetic field variations recording in period range 10-200 sec, computing power density spectra on analog computer
10 p1682 A69-23593

F 2 layer drift relation to current systems of dynamo region confirmed at middle and high latitudes
10 p1682 A69-23611

Dynamo action produced magnetospheric currents in ionosphere computable without knowing real horizontal ionospheric current system
10 p1685 A69-23836

Equatorial electrojet role in electromagnetic induction at magnetic dip equator, applying Price theory for space gradients
13 p2252 A69-27515

Magnetospheric field configuration in midnight meridian, considering cavity boundary surface area trapping region currents and tail sheet current
13 p2252 A69-27515

Terrestrial electrical conductivity measurement from electromagnetic field variations determination from geomagnetic sounding
20 p3522 A69-37054

Optical pulsations in aurora, studying relations to pulsations in geomagnetism, telluric currents, X rays from aurora and variations in primary particles flux
21 p3708 A69-38443

Sayan Sun Observatory experimental equipment for discussing instruments for solar observation, earth currents measurement and cosmic ray neutron components recording
22 p3943 A69-39994

TELLURIC FIELDS

U ELECTRIC FIELDS

TELLURIC LINES

Electron transition probability of oxygen molecules determined using weak bands telluric lines photoelectric recordings
03 p0420 A69-132761

Telluric lines halfwidth and depth dependence on observation point altitude and intervening air mass, determining absorption line contours for isothermal atmosphere
03 p0512 A69-136954

NASA atlas of IR solar spectrum, reporting B and 4 meter spectrometer recordings over band containing methane telluric absorptions
06 p1008 A69-178101

Electron transition probability of oxygen molecules determined using weak bands telluric lines photoelectric recordings
14 p2487 A69-287844

Instrumental profile determination for high resolution stellar spectrograph, using profiles of telluric oxygen bands obtained from emission line observations
21 p3721 A69-386961

Trial and error procedure applied to instrumental profile of Liege Solar Atlas, convoluting instrumental profile with telluric A band profile
21 p3722 A69-386961

TELLURIDES

NT BISMUTH TELLURIDES
NT CADMIUM TELLURIDES
NT INDIUM TELLURIDES
NT LEAD TELLURIDES
NT MERCURY TELLURIDES
NT TIN TELLURIDES
NT ZINC TELLURIDES

Tunnel junctions of narrow gap GeTe and wide gap GaAs, noting current voltage characteristics similar to those in Schottky barrier
06 p0980 A69-17770

IR spectral transmittance and physicochemical properties of tellurite glasses with vanadium and cerium oxides, showing polymer chains in structure
14 p2468 A69-29329

Thermoelectric parameters of polycrystalline p-type bismuth antimony telluride and bismuth antimony tellurium selenide solid solutions
15 p2668 A69-30629

Heat conductivity of liquid and solid gallium telluride in steady state regime, using graphite cylindrical device
16 p2824 A69-31572

TELLURIUM

Magnetoresistance of tellurium single crystals with various current carrier concentration at liquid helium temperatures
06 p0978 A69-16986

Vapor deposited tellurium thin films orientation, noting effect of characteristic spiral chain structure along c-axis
08 p1373 A69-20891

Current controlled negative differential resistivity observed during current-voltage measurements made with p-type Te at 77 K
09 p1557 A69-21747

Tellurium doping effect on phonon diffusion in GaSb, discussing thermal conductivity at low temperatures
12 p2142 A69-26294

Heat treatment effects on Te-doped GaAs, using photoluminescence and carrier concentration measurements to study defects formed
16 p2825 A69-31708

TELLURIUM ALLOYS

- Thermoelectric properties of GeTe-GaTe system, analyzing phase diagrams, solid solution formation, substitutions and zone structure influence
01 p0138 A69-10404
- Electrodeposition of Te-containing Permalloy films with uniaxial magnetic anisotropy, noting electrolyte composition and film structure
11 p1935 A69-24332

TELLURIUM COMPOUNDS

- NT BISMUTH TELLURIDES
NT CADMIUM TELLURIDES
NT INDIUM TELLURIDES
NT LEAD TELLURIDES
NT MERCURY TELLURIDES
NT TELLURIDES
NT TIN TELLURIDES
NT ZINC TELLURIDES
- Semiconductor properties of indium telluride alloys, conductivity and Hall effect
21 p3779 A69-38580

TEMPER [METALLURGY]

- Zirconium corner of Zr-Fe-Nb phase diagram, studying alloy tempering at various temperatures
02 p0263 A69-11851

TEMPERATE REGIONS

- Temperate latitude sporadic E origin and structure - Conference, Vail, Colorado, June 1968
01 p0069 A69-11156
- Time and latitude variations of blanketing sporadic E of different intensities
01 p0070 A69-11159
- Blob existence in temperate latitude sporadic E from ionosonde and VHF oblique incidence measurements
01 p0070 A69-11162
- Cause and structure of temperate latitude sporadic E - Conference, Vail, Colorado, June 1968, Volume 2
01 p0072 A69-11169
- Midlatitude sporadic E layer, examining hypothesis of wind action on metallic ions and metallic ion accumulation caused by gravity waves
01 p0072 A69-11173
- Self maintenance of absolute angular momentum in atmosphere as explanation of subtropical jet stream origin
15 p2647 A69-30192
- Zonal winds in temperate latitude analyzed as function of latitude and month from GHOST balloon flights in Southern Hemisphere at 200 mb
17 p2997 A69-33163
- Geomagnetic pulsations with intensity maximum at midlatitudes, noting north to south decreasing trend
20 p3522 A69-37059
- Ion production rates vertical distribution and temporal changes at midlatitudes during solar activity minimum and maximum above F 2 layer
20 p3525 A69-37656
- F 2 layer midlatitude positive disturbances observed during IGY on quiet and disturbed days, noting positive to negative transition latitudes
20 p3527 A69-37674
- Ion layer separation in temperate-zone sporadic E, obtaining layer shape by superimposition of density distributions
20 p3535 A69-38106
- Corpuscular radiation intensity measurements in upper atmosphere at midlatitudes by meteorological probe during geomagnetic storm, noting radio wave absorption
22 p4008 A69-41104

TEMPERATURE

- U AMBIENT TEMPERATURE
U ATMOSPHERIC TEMPERATURE
U BODY TEMPERATURE
U COMBUSTION TEMPERATURE
U CRITICAL TEMPERATURE
U CURIE TEMPERATURE
U FLAME TEMPERATURE
U FLASH POINT
U HIGH TEMPERATURE
U IGNITION TEMPERATURE
U ION TEMPERATURE
U IONOSPHERIC TEMPERATURE
U LOW TEMPERATURE
U LUNAR TEMPERATURE
U OPERATING TEMPERATURE
U PLANETARY TEMPERATURE
U PLASMA TEMPERATURE
U ROOM TEMPERATURE
U SKIN TEMPERATURE [BIOLOGY]
U SKIN TEMPERATURE [NON-BIOLOGICAL]
U STAGNATION TEMPERATURE
U SURFACE TEMPERATURE
U WALL TEMPERATURE

TEMPERATURE COMPENSATION

- Atmospheric temperature corrections for measurements by rocketsonde and balloonsonde with thermistor, noting dissipation factors and thermal time constants
01 p0081 A69-10697
- Linearizing circuit for low velocity hot-wire anemometry, using analysis of transistor circuit to generate desired function
06 p0927 A69-17701
- Semiconductor strain gage balance with temperature compensation for conventional wind tunnels
10 p1672 A69-23265
- Quartz oscillator with electronic temperature compensation, noting reduced size, weight and power consumption
14 p2420 A69-29398

TEMPERATURE CONTROL

- Liquid fluidic amplifiers combined into controller for modulating coolant temperature to control flight suit temperature automatically
02 p0202 A69-11923
- Electron emitter cooling and plasma heating of thermionic converters noting effects of plasma density, diode spacing, etc
03 p0368 A69-13127
- Thermistors for total optical radiation pyrometer and for temperature control system based on radiation pyrometer, noting thermistor response and control circuit
04 p0601 A69-15119
- Synthesis of simulated aircraft cabin pure fluidic temperature control system [ASME PAPER 68-WA/FE-30]
05 p0705 A69-16103
- Scaled models for spacecraft thermal control, considering radiation-conduction-convection heat transfer [SAE PAPER 690196]
07 p1116 A69-18304
- Explorer 40 satellite mathematical model and verification testing for close spacecraft flight temperature predictions [SAE PAPER 690202]
07 p1239 A69-18305
- Fabrication welding with maraging steels with emphasis on minimizing heat input
08 p1320 A69-20407
- Human body heat loss control during water immersion, discussing insulative garments and technologies of energy conversion systems [AGARDOGRAPH-111]
08 p1267 A69-20681
- Energy source for space environments based on compact cold hydrogen-oxygen fuel cell, discussing heat control and water elimination methods
08 p1260 A69-21041
- Earth reflected solar radiation and stability of satellite thermal control coatings, noting intensity distribution shifting toward UV region and coatings degradation rate
09 p1579 A69-22174
- Miniature fluidic oscillator temperature sensors evaluated in gas turbine engine nozzle, discussing temperature control and related signal error compensation and temperature averaging [ASME PAPER 69-GT-70]
09 p1572 A69-22512
- Multichannel miniature telemetry for vibration, strain and temperature measurements in high speed machinery by solid state encapsulated devices
10 p1654 A69-23251
- Human body temperature regulating factors in low temperature environment, studying metabolism, lung ventilation and onset of shuddering
10 p1648 A69-23298
- Cryostat design, discussing vapor and radiation shielding, construction and insulation materials, safety features, cost considerations, etc
10 p1810 A69-24015
- High power TWT tube cooling in space vehicle, discussing thermal control system based on heat pipe radiator
11 p1847 A69-24747
- Passive thermal control system for space suit use in extravehicular environment, discussing skin temperature control at varying heat flow rates
12 p2023 A69-26549
- Mathematical model for melting of finite paraffin slab based on method on numerical computer solution of heat conduction equations for thermal control devices
12 p2190 A69-26785
- Heat pipe boil-off control system for reducing cryogenic boil-off during long term space storage
12 p2191 A69-26793

- Spacecraft surfaces bidirectional reflectance flux distribution applications to space thermal control computations [AIAA PAPER 68-26]
13 p2222 A69-28216
- Combined hypoxic hypoxia and high ambient temperature found relieving strain on humans by increasing heat release by evaporation
13 p2212 A69-28628
- Self thermostatic phase-change coatings for active and passive spacecraft temperature control, discussing temperature dependent changeability in solar absorptance
14 p2530 A69-29434
- Spray deposition of low emittance gold thermal control coatings on aerospace structures
15 p2618 A69-30310
- Thermal control coatings for solar cells of solar probe Helios
16 p2867 A69-31741
- Constant temperature heat pipe for thermal control of spacecraft components by direct coupling to external radiator [AIAA PAPER 69-632]
17 p3070 A69-33262
- Simulated solar wind environment effects on zinc oxide/potassium silicate and lanthanum oxide/potassium silicate spacecraft thermal control coating pigments [AIAA PAPER 69-642]
17 p2991 A69-33273
- Mars lander thermal control system design parameters including environment, power duty cycle and lander size and weight [AIAA PAPER 69-610]
17 p3072 A69-33274
- Heat pipe application to thermal equalization around ATS-E solar cell mounting panels, comparing predicted and actual performance [AIAA PAPER 69-630]
17 p3072 A69-33277
- Cooling system control system for astronaut thermal equilibrium and work output maximization during extravehicular space missions [AIAA PAPER 69-617]
17 p2914 A69-33278
- Heat transfer suppression techniques in high temperature low density fiberglass insulation for flight vehicles [AIAA PAPER 69-606]
17 p3072 A69-33279
- UV irradiation effects on ZnO spacecraft thermal control coating pigments, discussing photo-Hall, luminescence and electron paramagnetic resonance measurements [AIAA PAPER 69-639]
17 p2992 A69-33288
- Gas products evolved from selected thermal control coating materials during UV radiation in vacuum, noting permanent reflectance loss [AIAA PAPER 69-640]
17 p2992 A69-33289
- Heat pipe devices applied to radiative body heat transfer in space suit temperature control [AIAA PAPER 69-619]
17 p2914 A69-33293
- Planetary lander model thermal design, analysis and testing, emphasizing lightweight multilayer insulation, discussing thermal/vacuum testing [AIAA PAPER 69-612]
17 p3049 A69-33296
- Parametric thermal control weight and power requirements for spacecraft life support systems, considering number of cabins, crew activity, heating, cooling and regeneration [AIAA PAPER 69-621]
17 p2914 A69-33305
- Forge to determine refractory metals formability and ductility at high temperature in protective pressure
17 p2945 A69-33419
- Thermal control system for AZUR research satellite, tabulating extreme flight temperatures and permissible temperature range from simulation test data
17 p2903 A69-33427
- Solar probes design for 0.3 to 0.1 AU perihelion distance, considering thermal control, power supply, communications, altitude control and alternative configurations
17 p3050 A69-33797
- Temperature control below 5.2 K based on servoing He pressure above bath
18 p3136 A69-34641
- Thermal control of Mars entry capsule with fiberglass honeycomb sandwich shell analyzed with and without aft thermal curtain, emphasizing cruise-flight phase [AIAA PAPER 68-1082]
19 p3429 A69-35949
- Bessel function applied to unsteady axisymmetric problem of heat conduction in thermally controlled coaxial cylinders with different physical properties
19 p3448 A69-35981
- Wavelength-surface temperature relationship of ruby laser, discussing thermal control of emission wavelength
20 p3552 A69-36967
- Second surface mirror used as coating for spacecraft thermal control
20 p3632 A69-37290

Electronic equipment thermal control, describing design and use of heat pipes
22 p4049 A69-39944

Thermal design of missile mounted S band telemetry transmitter package based on temperature control system, using heat-of-fusion characteristics of wax material
22 p3909 A69-39945

High voltage power supply electronic subsystem for electric propulsion of ATS-D satellite, describing packaging, temperature control and performance in simulated space environment
22 p3999 A69-39948

Reliability demonstration testing equipment, describing temperature chamber design and instrumentation, overall facility planning, etc
22 p3954 A69-40034

Temperature control instrumentation accuracy in terms of static errors and dynamic errors minimizing costs
22 p3954 A69-40037

Temperature program generation for test chambers, describing temperature programmers and readout, verification and recording systems
22 p3954 A69-40038

Circadian variations in human temperature regulation, measuring peripheral and rectal temperatures and peripheral heat and arterial blood flows in clothed resting males
22 p3872 A69-40201

Exercise-temperature regulation in men under constant submaximal workload at various simulated altitudes, discussing exercise core temperature equilibrium level setting mechanisms
22 p3891 A69-40219

Dynamic characteristics of temperature control systems using crystal oscillators determined by nonlinear automatic control theory
22 p3869 A69-40254

Computer optimization of spacecraft optical coatings for temperature control, using finite element analysis and matrix inversion
[AIAA PAPER 69-979] 22 p4050 A69-40359

Thermal scale modeling for space hardware development from managerial and engineering viewpoints
[AIAA PAPER 69-1010] 22 p3922 A69-40383

Spacecraft electronic components operating junction temperature control, considering role of thermal resistance in controlling radiative and conductive transfer
[AIAA PAPER 69-1015] 22 p3922 A69-40387

Thermal control coatings, windows and mirrors for 1973 Mars Viking Lander vehicles under simulated Martian surface conditions
[AIAA PAPER 69-1023] 22 p3923 A69-40393

Simulated degrading environment effect on spacecraft thermal control surfaces subjected to plume heating during apogee firing and solar irradiation
[AIAA PAPER 69-1024] 22 p3923 A69-40394

Gases effects on UV irradiated thermal control materials spectral reflectance, discussing tests and photolysis mechanisms
[AIAA PAPER 69-1025] 22 p3923 A69-40395

Autotransformer with static tap changer to provide varying power levels for controlled gradual heating of aircraft window to avoid thermal shock
22 p3869 A69-40414

Solid state chemical heat sources aboard unmanned planetary landing vehicles to maintain batteries and experiments operability during cold planetary nights
23 p4070 A69-42275

Temperature control by heat pipe using noncondensing gas with methanol to vary thermal resistance and mathematical model to describe heat source temperature variations
23 p4240 A69-42307

Multiple outlets for reducing stratification-induced liquid propellant supply temperature rise, preventing cavitation problems in supply pumps
[AAS PAPER 69-395] 24 p4363 A69-42830

Turbine rotors temperature reducible by increasing air cooling system flow rate
24 p4364 A69-43081

TEMPERATURE DISTRIBUTION

Random temperature fields in plates and shells in thermal contact with two media with temperatures as separable random space-time functions
01 p0173 A69-10077

Mach-Zehnder interferometer for studying temperature distribution and heat transfer in turbulent jets, noting temperature dependence on jet thickness at different angles of attack
01 p0005 A69-10101

Steady state problem of convective heat transfer in half space with boundary conditions of third kind
01 p0174 A69-10103

Continuous wave solid state lasers active elements temperature fields calculated by differential equations
01 p0089 A69-10105

Titanium alloy VTZ-1 recrystallization and oxidation processes studied by heating within 700- 1200 C temperature range
01 p0094 A69-10214

Internal temperature distributions of present and proposed calorimeter geometries operating at high pressure and extreme heating rates compared, using one and two dimensional heat conduction programs
01 p0079 A69-10299

Free convection from partially uniformly heated and partially insulated vertical flat plate, discussing dimensionless velocity, temperature, heat flux and axial length parameters
01 p0175 A69-10331

Electric field effects on flame temperature variation, suggesting electrons active role in flame combustion reactions
01 p0176 A69-10389

Heat transfer between concentric cylinders at different temperatures measured for argon, neon and helium
01 p0177 A69-11403

Laminar natural convection of electrically conducting fluid under magnetic field, noting temperature profiles
01 p0134 A69-11407

Turbulence characteristics from light wave fluctuation measurements, discussing applications to small scale inhomogeneities in atmospheric temperature distribution
02 p0274 A69-11437

Turbulence conditions in atmospheric boundary layer within similarity theory, including wind velocity and temperature profile
02 p0274 A69-11447

Thermoviscoelasticity equation solution for class of dynamic problems, giving problem solution for half space with arbitrary temperature field boundary condition
02 p0336 A69-11554

Metallic dismountable thermionic converter enclosed in mica sealed vacuum chamber, giving I-V characteristics, optimal temperature of liquid cesium phase and output power
02 p0194 A69-11587

Procedure accounting for variable thermal conductivity and internal heat generation in temperature distribution prediction for waveguide ferrite slabs
02 p0215 A69-11877

Generalized unsteady temperature fields and stresses in crystalline plates using Fourier and Laplace transforms
02 p0340 A69-12044

Transient laminar boundary layer development on flat plate following impulsive start of surrounding fluid motion, obtaining temperature and velocity distribution relationship
[ASME PAPER 68-HT-10] 02 p0232 A69-12208

Critical points separating stable and unstable branches of equilibrium curve of nonlinear elastic systems, discussing flexible shallow conical shell in temperature field
02 p0341 A69-12256

Thermostructural analysis of large flexible paraboloid antenna indicates RF losses due to thermal distortions significant for X band and higher transmissions
[AIAA PAPER 68-333] 02 p0345 A69-12372

Gray radiation and conductive heat transfer in Oseen-like free mixing flow, computing temperature distribution by inversion integral
02 p0354 A69-12504

Brightness temperature maps for Jovian thermal radiation obtained through 8-14 micron window of atmosphere
02 p0309 A69-12715

Zonal temperature and spectral characteristics of stratospheric circulation, noting westward rotation of second harmonic
02 p0246 A69-12759

Plane inhomogeneous thermal stress in isotropic elastic circular infinitely long cylinder produced by plane unsteady temperature distribution
02 p0349 A69-12826

Three dimensional unsteady heat conduction and temperature distributions in finite hollow circular cylinder under time dependent boundary conditions of second kind
03 p0530 A69-12861

Steady state temperature distribution in heat generating fluid in plug flow in circular tube with arbitrary inlet and wall temperature distribution
03 p0530 A69-12862

Variational technique for determination of temperature fields due to nonuniform heat transfer over surface of heat producing body
03 p0531 A69-12862

Turbulent mixing of scalar fields such as temperature or concentration noting fine structure, number and distribution of zero gradient points and minimal gradient surfaces
03 p0414 A69-13113

Velocity dispersion and temperature anisotropy with respect to magnetic field direction, discussing inertial solar wind cooling effects
03 p0500 A69-13527

Temperature and current distribution in avalanche silicon p-n junctions
03 p0487 A69-13637

Controllable states of elastic heat conductors analyzing deformations and temperature fields
03 p0529 A69-13937

Ion and atom temperature distribution for two fluid model of Ar plasma in cylindrically symmetrical water stabilized electric arc column
03 p0481 A69-14155

Stressed state periodic problem in infinite strip under combined pressure and temperature field effect
04 p0673 A69-14497

Constant thickness disk temperature field for inhomogeneous boundary conditions, considering roots of characteristic equations determination
04 p0685 A69-14498

Scaled solar and gray-body temperature distributions models compared to determine stellar atmosphere
04 p0653 A69-14626

IR observations of lunar crater and maria enhanced thermal emission during eclipse, constructing model of cratered surface to analyze thermal behavior
04 p0654 A69-14656

Temperature distributions, thermal stresses and natural frequencies of radial vibrations in thin circular cylindrical shells
04 p0675 A69-14704

Mean temperature distribution through inner and outer regions of turbulent boundary layer with injection through heated porous wall
04 p0685 A69-14729

MHD channel flow temperature distributions with Hall effect, using formulation for momentum and energy equations
04 p0635 A69-14746

Electron, ion and neutral particle temperatures of upper atmosphere
04 p0592 A69-14975

Temperature distribution over receiving layer of absorption edge image transformer, discussing thermal conduction influence on performance of thin film IR image receiver
04 p0631 A69-15280

Approximate method to determine nonstationary thermal fields in solid bodies with thermal capacity and thermoconductivity coefficient depending linearly on temperature
04 p0688 A69-15409

Temperature distribution and thermal stresses in liquid filled cylindrical shell
04 p0682 A69-15413

Water and heat removal unit for hydrogen/oxygen fuel cell systems, discussing temperature distribution and heat and liquid transport
05 p0704 A69-15676

Variational methods applied to unsteady heat flow, describing approximate method for unsteady temperature field in heat conducting body
05 p0845 A69-15794

Quantitative analysis of nonsteady temperature field in long cylinder for sudden heating of semiinfinite axisymmetric lateral surface
05 p0845 A69-15797

Plane thermal stress distribution determined around holes under steady temperature distribution, using complex variable approach
05 p0836 A69-15877

Coupled heat equation to calculate transient and steady state temperature distributions in viscoelastic solids under cyclic deformations
05 p0836 A69-15878

Finned radiation emitter tube unsteady state temperature field as function of working body temperature and emitter geometry
05 p0846 A69-15898

Heat transfer, temperature and velocity profiles in circular free jet can be described by heat conduction type equations
05 p0747 A69-16032

- Mathematical problem of MHD thermal entrance regions for parallel plate channel solved by Galerkin method
[ASME PAPER 68-WA/HT-10] 05 p0803 A69-16118
- Transient temperature distribution for finite slab in phase transformations via single face temperature changes
[ASME PAPER 68-WA/HT-37] 05 p0848 A69-16128
- One dimensional integral solution for cylindrical source generated transient temperature field and relation to thermal diffusivity of brain tissue
06 p0879 A69-17085
- Sensible heat exchange from Gemini and Apollo space suits determined in environmental test facilities, presenting data for heat flux distributions
06 p0880 A69-17089
- Temperature distribution for static stellar corona in presence of magnetic field, noting energy flow process
06 p1002 A69-17316
- Temperature distributions and thermal stresses in bimetallic I-beam structures with dissimilar materials for skins and webs and with kinetic heating inputs
06 p1024 A69-17610
- Approximate expression for temperature distribution during heat transient in infinite solids of plane, cylindrical and spherical geometry
06 p1025 A69-17779
- Blade to rotor heat transfer in turbines determined from temperature distribution of rod in medium with nonuniform temperature
06 p1034 A69-17870
- Computer program for predicting temperature distribution and heat transfer through coated and uncoated window systems of aerospace vehicles
[AIAA PAPER 68-28] 06 p1038 A69-18178
- Theta pinch plasma electron density and temperature distributions measured using Thompson scattering of laser light and plasma bremsstrahlung
06 p0972 A69-18220
- Digital computer methods and numerical techniques to evaluate temperature distributions in spacecraft structures, discussing thermal modeling
[SAE PAPER 690199] 07 p1239 A69-18301
- Constant thickness fin with arbitrarily distributed heat sources optimized using approximate physical model and closed form solution of field equation
[SAE PAPER 690198] 07 p1239 A69-18302
- Temperature distribution in low pressure magnesium vapor-oxygen diffusion flames, discussing environmental conditions and visible radiation
[WSCI PAPER 68-20] 07 p1241 A69-18367
- Contour map of southern Milky Way at 1410 MHz obtained using 210 ft radio telescope at Parkes, Australia
07 p1214 A69-18667
- Nonaxisymmetric temperature field of unbounded hollow cylinder with moving heating boundary, expanding surface temperature into Fourier series
07 p1241 A69-18924
- Boundary value problem of temperature field and heat conduction in transparent media heated by laser radiation producing thermoelastic stresses leading to breakdown
07 p1149 A69-18925
- Planetary wave-zonal flow interaction interpretation in terms of potential vorticity eddy transport, deriving zonal wind change and temperature field
07 p1126 A69-19037
- Radial distribution of azimuthally averaged temperature and amplitude vacillation characteristics in rotating differentially heated fluid annulus determined by multiprobe technique
07 p1126 A69-19040
- Steady state thermal stress distributions near external crack in solid, treating temperature distributions with respect to plane of crack
07 p1232 A69-19172
- Dynamic internal thermal shock in spherical shells of arbitrary thickness, considering uncoupled dynamic thermoelasticity problems with spherically symmetrical temperature fields
07 p1236 A69-19471
- Shear stress at wall, averaged velocity field and turbulent heat transfer coefficients in straight smooth non-circular channels used to compute temperature fields
07 p1243 A69-19734
- Semilogarithmic law of velocity and temperature for turbulent flow in circular channel, examining analogy between momentum and energy transfer
08 p1420 A69-19877
- Thermal gradients in artificial satellites, considering heat exchange among various points of closed cavity surface by gray body diffuse radiation and reflection
08 p1421 A69-20157
- Electron temperature and electron density variations with radial distance in 10 MHz electrodeless ring discharge in H, noting electric field
08 p1361 A69-20230
- Metallic particle ignition in oxygen containing media, obtaining temperature curves and vaporization rates
08 p1375 A69-20343
- Suction effect on temperature distribution and heat transfer in plane Couette flow and laminar flow in circular pipe
08 p1303 A69-20371
- Low latitudes observations of 21 cm line of H I in galactic center direction, giving contours maps of brightness temperature
08 p1392 A69-20562
- Continuous variate duration estimates by Markov process, giving example of surface air temperature conditional probability distribution
08 p1346 A69-20731
- Ar-H plasma arc radial temperature distribution determined by photoelectric spectroscopy in visible range
08 p1366 A69-20758
- Steady motion through rarefied gas of circular cylinder due to surface temperature difference
08 p1305 A69-20888
- Segmented anode current and heat distribution in MPD engine measured with current shunts and calorimetric methods
[AIAA PAPER 69-244] 09 p1566 A69-21260
- Temperature and displacement fields in unbounded elastic space due to instantaneous point heat source action
09 p1621 A69-21495
- Atmospheric humidity effect on efficiency of geomagnetic field scales with taut-strip suspension and temperature fluctuation
09 p1494 A69-21518
- Temperature profiles variability for data obtained by rocketsonde thermistors launched with small time and spatial separation
09 p1494 A69-21644
- Upper atmosphere temperature distribution estimation on basis of twilight zenith sky intensity measurements, discussing influence of various parameters on accuracy
09 p1487 A69-21653
- Velocity and temperature fields in Newtonian fluid in motion past stationary obstacle in gravitational field, noting similarity parameters reduction
09 p1429 A69-21686
- Circular central shading effect on energy distribution parameters of paraboloidal mirrors, noting reflected radiant flux power limitation
09 p1436 A69-21804
- Temperature distribution for thin plate heated by source of arbitrary motion and strength and governed by Sturm-Liouville boundary conditions
09 p1622 A69-21906
- Spectrographic observations indicating temperature range within individual filaments of Cygnus Loop, noting agreement with stratified models
09 p1607 A69-22430
- Fuel control systems using emulsified fuel, noting exposure effects and temperature and pressure characteristics
[ASME PAPER 69-GT-40] 09 p1571 A69-22486
- Thermal approach to pulsating combustion, determining temperature-time variation, frequency and pressure from mathematical model
09 p1625 A69-22694
- Plane thermal stress field in discontinuous temperature distribution within isotropic linear elastic circular cylinder of infinite length
10 p1793 A69-22884
- Steady laminar boundary layer flow calculations extended to temperature boundary layer for given heat flow or temperature distribution at wall
10 p1808 A69-22915
- Pulsed and CW lasers glass crystals temperature fields determination, including tangential and axial thermal stresses
10 p1702 A69-23428
- Temperature field calculation in infinite plate with heat transfer coefficient and ambient temperature arbitrary functions of time
10 p1809 A69-23430
- Electron temperature distributions in Ar-K plasma of simulated Faraday type MHD generator for current distributions, determining current density distribution experimentally
10 p1734 A69-23453
- Heating system providing symmetrical temperature field and specimen self centering for thermal resistance tests
10 p1696 A69-23845
- Heat propagation in discharge plasma heated by magnetosonic wave, constructing transverse temperature profile
10 p1741 A69-23896
- Finite difference method for calculating lee waves incident on obstacle with arbitrary vertical distribution of main flow horizontal velocity and temperature
10 p1722 A69-23967
- Xenon pulse discharge plasma temperature distribution, spectral brightness density and light absorption across quartz tube section, noting temperature drop near wall
10 p1742 A69-24081
- Emissivity of screened tube in presence of heat conducting connecting pieces between tube and screen
11 p1997 A69-24229
- Monograph on comparison of various methods for experimental determination of temperature fields in laminar burner flames
11 p1999 A69-24635
- Temperature field in thin walled rods with spiral coil cross section in solar radiation, considering radiant heat exchange
11 p1999 A69-24779
- Vertical air flow asymmetrical distribution ascribed to cyclone motion and thermal inhomogeneity by studying spiral cloud configurations in cyclone area
11 p1912 A69-24829
- Steady heat flow in cylindrical bodies with curvilinear rectangular cross sections, solving equation in form of Fourier series according to trigonometric functions
11 p2000 A69-24974
- Optical and radio measurements of electron temperature of H II regions obtained from brightness ratio of hydrogen line and continuum, considering isothermal model
11 p1950 A69-25110
- Holography for temperature distribution measurement around heated wire, using He-Ne laser
11 p1887 A69-25197
- Carbon dioxide temperature distribution, absorption and concentration as functions of molecular dissociation behind shock wave determined by measuring IR bands intensity
11 p1873 A69-25226
- Free convection boundary layer flow past vertical flat plate analyzed for nonlinear wall temperature distributions using series solutions
11 p2002 A69-25243
- Brightness temperature distributions from intensity interferometric measurements reconstructed by computation
11 p1888 A69-25256
- Initial nonuniformity effect of temperature distribution in main stream on efficiency of cooling by air injection through slit or porous collar
11 p2002 A69-25338
- Low power gradient uniform electric arc column in cross flow and transverse magnetic field, analyzing temperature, velocity, pressure and magnetic field distribution
11 p1933 A69-25556
- Unsteady temperature field and thermal stresses for anisotropic and orthotropic plates heated by heat sources and having Newton law heat transfer
12 p1777 A69-25992
- Atmospheric models for exospheric temperatures of Mars and Venus based on photoionization heating efficiency
12 p2155 A69-26020
- Temperature regime of pulsed laser with pump lamp located in cylindrical rod cavity, discussing adiabatic and nonadiabatic pumping
12 p2104 A69-26025
- Thermal stresses in hollow finite circular cylinder having smooth rigid insulating cover on curved surfaces and temperature distribution on plane ends
12 p2180 A69-26268
- Lunar surface layer temperature field dynamics obtained from stable periodic solution to parabolic differential equation with nonlinear nonautonomous boundary conditions
12 p2157 A69-26281
- Focusing power of hyperbolic gas lens for light beam waveguides, noting temperature distribution measurements and pole separation
12 p2107 A69-26392

Dynamic energy balance in positive column of electric arc, integrating expression to determine temperature time dependence

12 p2137 A69-26535

Lunar thermal anomalies in various craters observed during lunar night by IR methods, with data suggesting hot and cold regions

12 p2171 A69-27092

Correlation between temperature and stress field in thermal buckling of square viscoelastic Maxwell plates under random temperature

12 p2188 A69-27113

Dense plasma jets in flowing HF flame discharges, discussing energy balance and longitudinal and radial temperature distribution

12 p2140 A69-27127

Numerical solution to partial differential equations describing helical discharge in Ar with gas injection, discussing initial temperature distribution and radial distribution effects

12 p2141 A69-27131

Blade material temperature variation observed in turbojet engine during air bleed of varying intensity and duration

13 p2325 A69-27444

Lunar surface temperature distribution measured by IR pyrometer, predicting temperature rise due to Lunar Excursion Module landing

13 p2341 A69-27583

Far IR and millimeter solar continuum, analyzing flatness of limb darkening curves and brightness temperature near minimum

13 p2341 A69-27591

Height and temperature vertical variability in mid and upper stratosphere determined from constant pressure charts /1964-1966/

13 p2290 A69-27637

Greenhouse effect in Venusian atmosphere, discussing cause of vertical temperature distribution established by Venera 4 probe

13 p2345 A69-27690

Cellular convection in horizontal gas layer analyzed for causes of vertical air circulation and effect of vertical temperature profile

13 p2291 A69-27725

Unsteady temperature distribution in solid sphere with variable internal heat source and surface subjected to variable heat flux

13 p2373 A69-27773

Transient one dimensional temperature distribution determined for bodies with internal heat generation and nonlinear boundary condition, using Biot variational method [ASME PAPER 68-HT-6]

13 p2374 A69-27775

Heat transfer and temperature distribution in thin fins with stochastic root temperature due to excitation by stochastic and Markov processes [ASME PAPER 68-HT-35]

13 p2374 A69-27780

Triangular profile circular fins efficiency determined from differential equations solution governing temperature distribution

13 p2375 A69-27790

Velocity and temperature profiles in gaseous turbulent boundary layer above liquid surface used to study liquid film cooling heat transfer

13 p2375 A69-27792

Soviet book on temperature regime of free atmosphere above Northern Hemisphere covering aerological data processing, statistical estimates, latitudinal and seasonal variations

13 p2294 A69-27934

Thermionic converter matched with solar cells analyzed for parabolic mirrors, assuming heat conduction power supply to cathode and uniform temperature distribution

13 p2209 A69-27970

Laminar temperature and velocity profiles near plane rectangular surface for free supersonic flow, solving partial differential equations for mass, momentum and energy conservation

13 p2309 A69-28025

Thermal shock temperature distribution and thermal stresses in finite circular disk subjected to instantaneous point heat source

13 p2363 A69-28130

Creep stresses and displacements in conical membrane shells at small angle of attack to supersonic flow field, discussing temperature distributions

13 p2364 A69-28205

Eddy diffusivities ratio for heat and momentum by mixing length theory, using Mach-Zehnder interferometer for temperature profiles

13 p2380 A69-28497

Asymmetric spherical temperature field reconstruction based on measuring temperature and derivatives at two points of field

14 p2537 A69-28888

Periodicity of magnetothermal oscillations in pressure annealed pyrolytic graphite compared with hole carriers

14 p2504 A69-29005

Electron and ion temperatures height variations in sporadic E layers, noting effects of neutral gas temperature changes

14 p2440 A69-29127

Heat conduction and Navier equations solved for temperature distribution and displacements in elastic solids, considering time dependent boundary conditions, body forces and heat generation

14 p2535 A69-29364

Turbulence and temperature fluctuations spectral characteristics in thermally stratified atmosphere determined for various wave numbers, using energy and mass transfer functions

14 p2472 A69-29402

Turbulent heat exchange coefficient radiation absorption and diurnal vertical variations effects on temperature field in surface layer of sea and atmospheric boundary layer

14 p2472 A69-29462

Acoustic sounding of atmospheric structure, utilizing energy backscattered from temperature fluctuations in turbulent regions

14 p2448 A69-29527

Temperature behavior of resonant and antiresonant frequencies as function of electromechanical coupling and overtone order in piezoelectric resonators

14 p2421 A69-29542

Comet Ikeya-Seki phenomena near perihelion interpreted from mean surface and ice nucleus internal layers temperatures

14 p2523 A69-29706

Tropospheric and stratospheric temperature distribution in 1965 summer and winter from radiosonde and rocket data

14 p2442 A69-29725

Atmospheric heat exchange and circulation simulated by rotating containers, reproducing temperature field and dynamic structure above large area

14 p2478 A69-29840

Radial distribution functions for dense hydrogenous plasma near ionization temperature by solving Percus-Yevick equations

14 p2502 A69-29998

Spectroscopic determination of temperature fields in water and transpiration cooled constricted Ar arc jets at atmospheric pressure

15 p2657 A69-30155

Device for fatigue testing turbine disk models in unsteady temperature fields with radial and axial nonuniformity produced by HF heating

15 p2583 A69-30208

Titanium alloy VT3-1 recrystallization and oxidation processes studied by heating from 700-1200 C

15 p2637 A69-30270

Turbulence coefficient in layers between main isobaric surfaces based on wind and temperature fields analysis

15 p2648 A69-30646

Thermoelastic stress in semifinite elastic medium due to discontinuous temperature distribution over free surface, solving associated heat conduction problem

15 p2712 A69-31006

Thermal stresses and displacements in isotropic inhomogeneous rotating circular disk with axle hole under steady temperature field

15 p2712 A69-31016

H beta line for measuring radial temperature distribution in cylindrical hydrogen arc at one atm and to 150 A current in high temperature range

15 p2671 A69-31101

Half maximum temperature of diatomic gases determined by extending relation between specific heat and molecular dissociation to diatomic molecules [DVL-899]

15 p2656 A69-31102

Radiative energy transfer through nongray absorbing and emitting medium generating heat with graphical presentation of temperature distribution and flux

15 p2718 A69-31153

Temperature distributions in layer with internal heat source and turbulent fluid flow cooling, deriving differential heat transfer equations

15 p2718 A69-31169

Thermal stresses in circular cylinder with regularly distributed cavities, establishing distribution laws for temperatures and stresses

15 p2714 A69-31196

Similarity criteria for plastic deformation theory body under pressure and nonuniform temperature field, considering strength calculations

15 p2714 A69-31212

Internal gravity waves suggested as possible cause of anomalous mesospheric temperatures

15 p2601 A69-31218

Alpine effects on wind field at synoptic scale using potential-vorticity equation, discussing deflection and dependence on potential temperature distribution

15 p2650 A69-31241

Cholesteric liquid crystal film application to test surfaces for thermal mapping, giving technique for pattern determination

15 p2631 A69-31248

Temperature profiles in laminar boundary layer with endothermal reaction investigated using nitrogen plasma jet in rarefied gas wind tunnel

16 p2821 A69-31284

Two dimensional turbulent mixing with surface mass injection at supersonic and hypersonic speeds, noting velocity and temperature distributions [AIAA PAPER 68-130]

16 p2770 A69-31818

Temperature distribution of solid spherical satellite under solar radiant heating solved by variational calculus or point matching methods

16 p2877 A69-31919

Temperature field in plate heated at one end and situated in solidifying gas, leading to gas layer formation by sublimation

16 p2878 A69-31919

Time, temperature and transformation curves for Ti-6Al-4V alloy by dilatometry, hardness measurements, X-ray diffraction and micrography, discussing martensite and beta-alpha transformations

16 p2802 A69-32181

Spontaneous and stimulated aspects of light scattering by absorbing media, relating refraction index to temperature variations and external stresses

16 p2798 A69-32444

Jet stream blocking process simulation using geostrophic system of equations, considering effects of orography and contrast heating due to land-sea distribution

16 p2809 A69-32606

Ozone and temperature profiles influence on atmospheric radiation intensities measurement by satellite in five spectral regions, noting pressure broadening effect

16 p2786 A69-32633

Polarization of light from atmospheres of Mira variables, suggesting temperature variations over stellar surface

16 p2866 A69-32822

Upper atmospheric gas density and temperature distribution diurnal and seasonal variations calculated from satellites orbiting time changes

17 p2959 A69-32922

Temperature field, strains and stresses induced in thin circular disk by unsteady heat source, noting time effect and resonant vibrations

17 p3054 A69-33002

Linear heat flux in thin composite plate with internal point source, assuming no heat transfer at surface and neglectable temperature changes

17 p3068 A69-33112

Powdered oxidizer and infusible polymer binder combustion at various pressures, studying gaseous phase temperature field by optical color analysis

17 p3069 A69-33113

Earth surface heat flow pattern measurement and distribution techniques, considering relation to surface features and tectonic movements of crust [AIAA PAPER 69-589]

17 p2961 A69-33288

Temperature distribution in shadowed lunar crater formulated in Fredholm integral equations, showing constant temperature and correction for soil thermal inertia [AIAA PAPER 69-595]

17 p3033 A69-33299

Nonuniform wall radiation production of radiative equilibrium temperature and flux distributions in gray medium, discussing various approximation methods of solution [AIAA PAPER 69-633]

17 p3072 A69-33299

Nonlinear partial differential equations solutions of theory of thin elastic spherical shells subjected to temperature fields and external loading

17 p3067 A69-34144

Superposition method for predicting tube wall temperatures with gas property and heating rate axial variation, noting application to gas flow problems

18 p3227 A69-34311

Tropical circulation long term mean values of wind and temperature fields, momentum and heat flux

from weather stations data, noting consistent pattern and energy source

18 p3165 A69-34418

Collocation method applied to solving contact thermoelasticity problem for short thick walled hollow cylinder attached to thin elastic shell in axisymmetric temperature field

18 p3217 A69-34595

Convective heat flux from nonisothermal surface by temperature superposition method with Spalding function as turbulent heat transfer coefficient, noting wall temperature

18 p3229 A69-34836

Unsteady temperature field in plane skin of aerodynamic body in case of temperature dependent thermophysical characteristics of skin material

18 p3092 A69-34982

Temperature distribution around radiating sphere in homogeneous gas medium with molecular heat transfer, solving energy transport equation

18 p3231 A69-35325

Statistical regularization for determining vertical atmospheric temperature profile from measurements of earth radiation in 15 micron carbon dioxide band

18 p3167 A69-35339

Solar microwave emission heliographic distribution during pronounced geomagnetic recurrence, noting brightness temperature nonuniformity due to coronal depression through polytropic models for solar wind

18 p3188 A69-35396

Dynamical effects in structure of H II equilibrium region left behind expanding ionization front, showing temperature as function of distance from star

19 p3403 A69-35966

Nighttime F 2 region temperature distribution under geomagnetically calm and disturbed conditions calculated from Alouette 1 satellite data

19 p3304 A69-36623

Autocorrelation function for unsteady temperature and stress fields in bar located in gas stream leaving combustion chamber

19 p3440 A69-36685

Electric models optimization for heat exchange systems based on mathematical similarity between equations describing temperature and electrical potential fields

19 p3256 A69-36717

Wall temperature distributions predicted in turbulent boundary layer with arbitrary pressure gradients, basing calculations on Spalding function solutions

19 p3302 A69-36853

Local heat transfer coefficients determined from temperature distribution on porous walls, deriving mathematical expressions for various surface geometries and transfer modes

20 p3630 A69-36977

Proton concentrations, magnetic field strength and temperatures distribution in interplanetary plasma flows as function of latitudinal distance from center of active region

20 p3594 A69-37020

Temperature and fluid distribution in porous solid subjected to large suction, convective heating and radiative cooling on one surface

20 p3514 A69-37225

Stability loss nonaxisymmetric distribution in elastic annular plates under axisymmetric heating, using Ritz method to determine critical temperature

20 p3623 A69-37327

Temperature fields and stresses in heat resistant ceramic coatings, illustrating alumina coating on Mo to calculate heating rate

20 p3565 A69-37359

Heated body cooling off study via temperature field isothermal lines visualization on TV screen

20 p3539 A69-37437

Stress strain state in thin circular elastoplastic disks under axially symmetric transient temperature distribution, noting moving annular plastic deformation region

20 p3629 A69-38028

Temperature structure of nongray planetary atmospheres, discussing scattering and absorption of solar energy by gas molecules, cloud aerosols and ground

20 p3615 A69-38258

Temperature distributions and heat transfer in thermal entrance region for Hartmann liquid flows under constant pressure gradient between parallel electrically conducting walls at rest

21 p3847 A69-38442

Stress determination in materials with creep in presence of nonuniform temperature field

21 p3833 A69-38571

Heat transfer coefficients, boundary layer thicknesses and temperature and velocity distributions in free convection boundary layer in closed axisymmetric volumes

21 p3848 A69-38634

Asymptotic method applied to nonlinear equations, determining thermal conductivity coefficient for temperature distribution in moving anisotropic media

21 p3848 A69-38642

Steady state temperature fields and thermal stresses determined in finite cylindrical shell by optimal parameters of reinforcing circular rib

21 p3834 A69-38714

Temperature distribution determined for leading edge, convex and concave parts of turbine blade porous wall with effusion cooling

21 p3850 A69-38860

Thermal stresses and displacements in long isotropic hollow cylinder heated on part of outer curved surface, analyzing temperature distribution

21 p3838 A69-39166

Velocity and temperature distribution curves in turbulent boundary layer formed by natural convection on isothermal vertical plate, using Prandtl and Nusselt numbers

21 p3852 A69-39430

Instantaneous frozen layer thickness and temperature profile in solidified layer obtained by iteration technique

21 p3852 A69-39433

Finite difference method for calculating Lee waves incident on obstacle with arbitrary vertical distribution of main flow horizontal velocity and temperature

21 p3759 A69-39653

Velocity and temperature profiles at Prandtl number values obtained for unsteady laminar free convection on infinite vertical plate with stepwise varying temperature

21 p3853 A69-39681

Monograph on electrically heated turbulent flames in cylindrical combustion chamber, investigating temperature distribution and stability

21 p3853 A69-39707

Temperature field in deflector cooled turbine blades for nonstationary regimes, considering heating of cooling air, thermal conductivity and thermophysical coefficient changes

21 p3786 A69-39718

Earth temperature distribution using various models, noting excess of total heat production in interior vs heat flow during planet history

21 p3718 A69-39732

Temperature field in system of coaxial cylinders by solving heat equation with corresponding initial and boundary conditions

21 p3855 A69-39855

Circulation and temperature fields indices used for studying tropospheric-stratospheric interactions during stratospheric warming at constant pressure levels

22 p3977 A69-39929

Thermoelectric power generator with variable thermal conductivity and electrical resistivity, obtaining steady state temperature distribution, power output and thermal efficiency

22 p3868 A69-40131

Test model thermal balance in space simulator, measuring effects of solar simulator irradiance reflected from carbon dioxide cryopanel deposits

[AIAA PAPER 69-1012] 22 p3922 A69-40385

Boltzmann equation analysis used to study near surface electron temperature for weakly ionized plasmas, showing nonequilibrium absorption layer governing electron temperature profile

22 p3989 A69-40528

Thermal structure of middle atmosphere, discussing heat sources and sinks, photochemical theories of ozone distribution, IR radiative transfer, etc

22 p3940 A69-40537

Curvature and temperature distribution in nonrotating long solid cylinders under solar radiation in interplanetary space

22 p4043 A69-40546

Ionic excited states statistical equilibrium populations calculated for various electron densities and temperatures including effects of dielectronic, radiative and three body recombinations

22 p3985 A69-40666

Heat conduction equation applied to thermospheric heating in auroral zone to account for local temperature and density variations, introducing horizontal transport mechanisms

22 p3941 A69-40717

Absorptivity of nonuniformly heated thin walled cylindrical radiator with central radiating hole, calculated by forward-reverse and integral methods

23 p4238 A69-41332

Thermal inertia index of semiconductor thermistor with one dimensional temperature field taking into account conductive heat transfer

23 p4163 A69-41556

Prismatic beam stress-strain state under steady temperature field, deriving stresses, displacements and elastic curve equations

23 p4227 A69-41708

Dimer bond energies analysis in Mg and Ca dimer molecules, approximating characteristic temperatures and virial coefficients

23 p4195 A69-42210

Hot gas flow through multilayer cylindrical shells, calculating temperature fields in walls

24 p4407 A69-42588

Multiple outlets for reducing stratification-induced liquid propellant supply temperature rise, preventing cavitation problems in supply pumps

[AAS PAPER 69-395] 24 p4363 A69-42830

Mixing length theory including eddies axial motion, discussing turbulent field of temperature or concentration

24 p4407 A69-42917

Creep buckling time of simply supported column under nonuniform temperature distribution over cross sections

24 p4400 A69-43053

Temperature distribution on surfaces of close binary stars as basis for predicting variation of monochromatic reflection effect

24 p4387 A69-43350

Electron temperature distribution across shock wave in weakly ionized plasma, noting variable ionization across wave

24 p4356 A69-43362

Plane Poiseuille flow with nonlinear temperature distribution, studying vortex type secondary flow onset due to buoyant forces

[ASME PAPER 69-HT-37] 24 p4411 A69-43533

Temperature distributions in heat pipe wicks as function of liquid thermal conductivity

[ASME PAPER 69-HT-23] 24 p4412 A69-43545

Heat finite propagation velocity effects on temperature distribution and heat flux for step temperature change at semiinfinite body surface

[ASME PAPER 69-HT-1] 24 p4414 A69-43564

TEMPERATURE EFFECTS

Temperature dependent isomer shift and anharmonic binding of Sn 119 in niobium stannide, measuring Mossbauer recoil free fraction

01 p0134 A69-10009

Temperature evolution velocity parameter effect on behavior of elastoviscoplastic solids, noting demonstration by work hardening tests at variable temperatures

[ONERA-TP-644] 01 p0164 A69-10036

Substructural void formation in tungsten powder metallurgy as function of annealing temperature for doped, undoped and electron beam melted material

01 p0093 A69-10061

Posistors heat capacity investigated as temperature function, showing maximum heat balance corresponds to Curie temperature

01 p0038 A69-10098

Temperature dependence of hot electron drift velocity in silicon at high electric fields, using space charge perturbation theory

01 p0135 A69-10120

Shock loading history effect on solid state response of iron meteorites to annealing at moderate temperatures permits deductions about thermal history

01 p0149 A69-10134

Hall effect in ferrites, determining classical and spontaneous Hall coefficients, electrical resistance, temperature effects and current carrier properties

01 p0135 A69-10185

Silicon p-n junction avalanche current temperature dependence calculation by considering space charge current and multiplication factor as function of temperature

01 p0136 A69-10245

Intrinsic absorption temperature dependence in doped p-InSb, discussing forbidden transitions

01 p0136 A69-10255

IR optics for indicating dynamic mechanical component reliability via surface temperature variations

01 p0085 A69-10295

Nichrome bars production dispersion hardened by alumina and zirconia inclusions, noting extrusion temperature influence

01 p0085 A69-10397

Satellites use in meteorology, noting monsoon rain forecasting through mesoscale sea surface temperatures of Indian Ocean

[UN PAPER 68-95555] 01 p0109 A69-10502

Micrometeorites acoustic recordings on Cosmos 135, investigating data reliability influenced by appearance of thermal noise

01 p0152 A69-10578

Irradiation influence on chromium transition temperature explained by defect clusters and embrittling impurity redistribution

01 p0095 A69-10604

Strain hardening of alpha titanium studied for effects of grain size, strain rate, temperature and purity

01 p0095 A69-10610

Pressure and temperature dependence of slow crack growth in hardened steel in gaseous hydrogen environment

01 p0096 A69-10612

Grain boundary gas bubbles growth in chemically vapor deposited tungsten as function of annealing time, temperature and fluorine content

01 p0097 A69-10646

Liquid copper electrical conductivity temperature dependence at very high temperatures from magnetic diffusion and flux penetration measurements, noting explosion wires role

01 p0119 A69-10673

Probability characteristics of temperature and supply voltage dependent parameters of semiconductor equipment

01 p0047 A69-10783

Ball bearing test apparatus for evaluation of greases and solid lubricants at high temperatures [ASLE PREPRINT 68AM 7C-2]

01 p0087 A69-10912

Isothermal secant and tangent bulk moduli of silicon fluids and correlation with pressure, volume and temperature

01 p0102 A69-10913

Ar atom transition probabilities in 5000-6000 angstrom range, noting effect of nonuniform source temperature

01 p0125 A69-10963

Low temperature effects on calf thymus deoxynucleoprotein, crystalline egg albumin and fibrillar actin, noting molecular weight and viscosity changes

01 p0018 A69-11089

Prestraining of stainless steel En58b sheet at room and cryogenic temperature, noting effect on tensile properties

01 p0099 A69-11151

Neutral gas temperature variations effect on electron-ion temperature height profile in tidally generated sporadic E layer with wind shear of gravity wave origin

01 p0073 A69-11176

Strain measurements in pure polycrystalline Ti at constant temperature and strain, considering creep and elastic aftereffects

01 p0101 A69-11363

Welding procedure for avoiding hydrogen cracking in high strength steels, stressing hydrogen escape from weld deposits

01 p0088 A69-11398

Temperature dependence of thermal conductivity coefficient and specific heat of sublimating heat proof materials

02 p0350 A69-11580

Effective temperature values of ozone used to determine onset time and disturbance height in ionosphere

02 p0238 A69-11670

Graphite specific heat temperature dependence at low temperatures, noting Wigner effect for neutron irradiation

02 p0269 A69-11782

Alpha recombination coefficient of molecular helium ions measured in helium afterglow plasmas as function of electron density and gas temperature

02 p0283 A69-11834

Isothermal sections construction of Zr-V-Ni system phase diagram from study of alloys at 1000, 700 and 500 C

02 p0263 A69-11848

Zirconium corner of Zr-Fe-Nb phase diagram, studying alloy tempering at various temperatures

02 p0263 A69-11851

Temperature dependence of semiconductivity of sintered polycrystalline EuO from current-voltage characteristics, measuring activation energy

02 p0296 A69-11875

Nitronium perchlorate thermal decomposition under overpressure of He and O between 80 and 170 degrees noting weight loss processes and crystal phase change

02 p0303 A69-11897

Temperature dependence of A and C periods of Y crystal lattice at 77 to 300 K, discussing preparation of Y films and anomalous thermal expansion

02 p0298 A69-12047

Deformation temperature and reduction effects on structure and properties of cylindrical specimens of various titanium alloys

02 p0266 A69-12124

Plate temperature oscillation effects on forced convection laminar viscous incompressible MHD boundary layer flow from semiinfinite flat plate

02 p0288 A69-12143

Sulfospinel polymorphism at high temperature and pressure and pressure-temperature phase relations

02 p0266 A69-12162

Gaseous and liquid H refractive index variations with pressure and density below room temperature, noting Lorentz-Lorenz function variations

02 p0281 A69-12180

Mechanical thermal stresses effects during laser flash illumination of GaAs, discussing temperature dependence of radiative recombination

02 p0256 A69-12245

Aluminum deformation at various strain rates and temperatures under combined stress, comparing results with theoretical predictions

02 p0343 A69-12282

Pressure and temperature dependence of isotropic elastic moduli of polycrystalline alumina, noting Grueneisen parameter, equation of state and Debye temperature

02 p0268 A69-12407

Wake temperature turbulent fluctuation decay rates deduced from atomic oxygen recombination chemiluminescence

02 p0190 A69-12525

Organic dye laser frequency variation with temperature, noting absorption and fluorescence spectra

02 p0258 A69-12617

Temperature dependence of electron beam pumped GaAs laser threshold current density and emission spectra, noting doping effects

02 p0260 A69-12683

Exothermal effects during sintering of nickel-aluminum powder mixture

02 p0269 A69-12838

Exothermal effects during sintering of nickel-aluminum powder mixture, showing role of liquid phase decomposition and intermetallics

02 p0269 A69-12843

Strain rate and temperature effect on flow stress of 7075 aluminum bars

03 p0443 A69-13120

Temperature dependence of elastic constants of highly and weakly doped n- and p-type GaAs

03 p0484 A69-13282

Pressure induced microwave absorption in molecular N for various temperatures, determining dielectric loss, absorptivity and quadrupole moment

03 p0472 A69-13317

Ferromagnetic ordering effect on gadolinium dialuminate thermoelectric power, measuring temperature dependence of power and electrical resistivity

03 p0485 A69-13322

Exciton distribution in semiconductors below Bose condensation temperature differing from diffusion distribution

03 p0486 A69-13415

Inactivation by heavy ions of esterase activity of dried trypsin as function of temperature during irradiation

03 p0372 A69-13483

Electrolytic deposits of titanium, vanadium and alloys from molten salts, discussing formation conditions, velocity and properties

03 p0446 A69-13574

Temperature dependence of internal friction in molybdenum wire in moderate and high temperatures

03 p0446 A69-13576

Thermal forcing role in diurnal oscillation of planetary boundary layer wind above sloping terrain

03 p0462 A69-13682

Spontaneous emission of gadolinium ferrite polycrystals, discussing temperature dependence

03 p0487 A69-13731

Glass fiber reinforced plastics aging behavior under heat and weathering influence

03 p0454 A69-13823

Temperature dependence of He-Ne laser output at various wavelengths over low temperature range

03 p0441 A69-13845

Thermal EMF in indium phosphide crystals as function of temperature, electron concentration and magnetic field strength, determining effective mass of electrons

03 p0489 A69-13889

Temperature dependent far IR absorption of ferroelectric sodium nitrite, discussing single and multiphonon processes

03 p0490 A69-13900

Empirical relation between B-V color and radiative temperature by observing eclipsing variables undergoing total eclipses

03 p0469 A69-13900

Pressure rise and thermal conductivity in cylindrical hydrogen plasma column in axial magnetic field, assuming local thermal equilibrium

03 p0479 A69-13900

Temperature dependence of isotope thermotransport in liquid K and Rb using steel capillary cells

03 p0533 A69-13900

Temperature dependence of O VIII Lyman alpha Lyman beta radiation ratio in solar corona, noting coronal temperature

03 p0516 A69-14000

Mathematical model derivation for observed atmospheric tide phenomena, taking into account thermal and other effects

03 p0426 A69-14000

Powdering temperature effect on mesh size, structure and mechanical properties of pressed semiinfinite sintered Al-Cr and Al-Fe alloys

03 p0452 A69-14100

Dilatometer for measuring thermal expansion of solid bodies over temperature range at various gas media pressures

03 p0432 A69-14150

Constants in formulas describing temperature and pressure dependence of thermodynamic characteristics of high temperature monatomic ionized gases for positive ions

03 p0473 A69-14150

Emissivity and other radiative characteristics of stainless steel oxides heated to various temperatures in air

03 p0453 A69-14150

Radiative recombination in p-n junctions in InP at various temperatures

03 p0492 A69-14160

Photoluminescence measurements of p-type thermal conversion in GaAs grown from silica boats, noting compensation by copper and shallow acceptors

04 p0639 A69-14400

Superconductivity of electron beam evaporated tungsten films by X ray and electron diffraction techniques, discussing temperature dependence of energy gap

04 p0640 A69-14400

Aging of iron-nickel-titanium alloys during heating in reverse martensitic alpha to gamma transformation process, investigating phase parameter changes

04 p0613 A69-14550

Internal friction temperature effects on amplitude dependence in niobium and molybdenum

04 p0614 A69-14630

Nimonic alloys high temperature annealing effect on dislocation structure stability created by thermochemical treatment, using transmission microscopy

04 p0615 A69-14630

Structural changes and cold shortness of molybdenum in deformation

04 p0615 A69-14630

Thermal and ablative lag induced by periodic heat input to oscillating flat plate in high velocity flow showing crossover from dynamically stabilizing to destabilizing condition as oscillation frequency increases

[AIAA PAPER 67-336]

04 p0685 A69-14720

Precipitation hardening effects on Al-Zr recrystallization with Fe and Si additions, noting peak hardness increment with decrease in aging temperature

04 p0617 A69-14930

Temperature dependence of partial pressure of saturated As vapor over solid solutions of InAs-GaAs of different composition

04 p0642 A69-14930

Temperature dependence of viscosity and density in molten thallium sulfide, noting structural changes in absence in short range order

04 p0643 A69-14990

Permittivity and loss tangent of unsaturated styrene polyester copolymers at various temperatures and frequencies

[ONERA-TP-662]

04 p0621 A69-15110

Diminished RF intensity of neutral hydrogen line near radio source W 49 due to diminished kinetic temperature of gas

04 p0662 A69-15250

Temperature dependence of Hall coefficient, conductivity and carrier mobility in manganese doped indium antimonides

04 p0643 A69-15257

Temperature dependence of electrical properties of In and Cu doped CdSb single crystals prepared by zone refining

04 p0643 A69-15264

Refractive index temperature dependence of cadmium sulfide single crystals grown from gas phase

04 p0644 A69-15268

Uniaxial compression load effect on activation energy in p-type GaSb single crystals

04 p0644 A69-15269

Low temperature spectral distribution of impurity induced photoconductivity in p-type InSb crystals prepared by zone refining

04 p0644 A69-15270

Dilatometric and X ray study of temperature dependence of linear expansion coefficients of lattice constants of chromium disilicon

04 p0619 A69-15392

Low density polyurethane foam with and without honeycomb as ablative material for reentry vehicles, discussing oxidation resistance

04 p0688 A69-15513

Argon-K plasma electrical conductivity as function of electric current density at 1400-2400 K

05 p0798 A69-15614

Work hardening in quenched fully hardened and overaged Mg-Mn alloy single crystals as function of temperature and strain rate

05 p0778 A69-15757

Work hardening characteristics of Ta and Ta-base alloy single crystals as function of temperature and interstitial concentration

05 p0778 A69-15758

Cross slip model for work hardening of nickel aluminate crystals, discussing temperature dependence

05 p0779 A69-15760

Thermal self focusing of argon laser beam passing through lead glass

05 p0771 A69-15819

Frequency dependent shear modulus for hexachlorobiphenyl measured under rare gas infusion at 5-25 C and from ambient atmospheric to 4000 psi

05 p0796 A69-15912

Liquid oxygen shear viscosity dependence on temperature and pressure obtained by measuring electrical characteristics of immersed torsional vibrating crystal

05 p0846 A69-15916

Microorganisms and viruses susceptibility to sterilization by ionizing radiation, heat and combination of radiation and heat, considering space materials damage elimination

05 p0713 A69-15947

Bending equations for shallow elastic three layer asymmetric shell with different isotropic layers and transversely isotropic rigid filler at various temperatures

05 p0840 A69-16197

Glass lasers, discussing neodymium properties in glass, flexibility of glass in size, shape and optical excellence, temperature coefficient of index of refraction, etc

05 p0772 A69-16227

Thermal self actions of CW laser beams in solids and liquids with wind or convection flow, discussing self focusing and defocusing

05 p0774 A69-16311

Thermal self defocusing effect of laser beam in self focusing liquids, measuring refractivity changes by high speed double exposure holography

05 p0775 A69-16320

Semiperfect gases with enthalpy dependent only on temperature, discussing validity of concept and Joule experiment on equivalence of heat and work

05 p0848 A69-16336

Rhenium Nb cylindrical thermionic converter, measuring efficiency and power density in emitter temperature range 1600-2050 K and collector temperature range 873-1173 K

05 p0707 A69-16359

Electrical properties of n-type Cd tin arsenide single crystals with impurity concentrations at various temperatures

05 p0809 A69-16375

Hot working temperature effects on Rene 63 mechanical properties and microstructures, using tensile and stress rupture tests, electron microscopy and X ray diffraction analysis

05 p0781 A69-16446

Ruby laser characteristics at 78 K, discussing emission threshold, optimum feedback, modes, etc

05 p0777 A69-16546

High temperature effects on gallium arsenide crystals current carriers lifetime, discussing recombination characteristics and impurity photoconductivity

05 p0809 A69-16551

Double diffused Si transistors, discussing temperature dependence of gain, injection efficiency, emitter and base regions energy gaps and excess noise

05 p0733 A69-16558

Electromagnetic properties associated with presence of overlapping bands in pure superconductors, discussing temperature dependence

05 p0810 A69-16802

Temperature dependence of Josephson critical current in superconductor model having anisotropic energy gap

05 p0810 A69-16803

Electron radiation damage in MOSFET devices using bias temperature treatments

06 p0976 A69-16877

Temperature effects on primary photocurrent of base collector and collector substrate junctions of isolated transistors from microcircuits

06 p0977 A69-16881

Metal heating by laser, noting heating rates exponential increase with time due to optical characteristics changes

06 p0932 A69-16915

Law of corresponding states applied to temperature dependence of viscosity of rarefied gases

06 p0957 A69-16918

Temperature dependence of n-InSb Hall coefficient and resistivity, noting increase in conductivity with degree of compensation associated with electrical breakdown

06 p0978 A69-16990

Charge carrier lifetime measured in intrinsic conductivity range of Cd doped InAs to define recombination mechanism, relating temperature dependence to surface impurities recombination

06 p0979 A69-16997

Thermal problems in biotechnology - ASME Conference, New York, December 1968

06 p0879 A69-17084

Temperature dependence of dynamic viscoelastic properties of plasticized epoxy resins

06 p0946 A69-17125

Thermal management of integrated circuits design, noting dependence on circuit and component configurations and parameter variations

06 p0894 A69-17217

IC selection for minimum thermal effects, discussing speed, power dissipation, maximum operating frequency and noise threshold

06 p0894 A69-17219

Austenitic Fe-Ti alloys sulfur solubility and internal sulfidation rate computed, noting stronger Ti-S interaction with temperature decrease and sulfur diffusion role

06 p0942 A69-17226

He-Ne laser gain dependence on temperature noting influence of pumping conditions, discharge tube filling and geometry

06 p0934 A69-17260

Data on muons indicating temperature effect diurnal maximum and pressure corrected daily variation

06 p0924 A69-17294

Laminar natural convection in enclosed rectangular cavity, discussing temperature gradient effects

06 p1033 A69-17556

Two dimensional stress distribution changes around rectangular hole with rounded corners for varying internal pressure and temperature

06 p1025 A69-17611

High transmittance long fiber optics, presenting data on special transmission as function of temperature

06 p0958 A69-17677

CW laser mode steady excitation and narrow bandwidth obtainable by highly stable pumping and stable temperature of active element

06 p0934 A69-17681

Temperature dependence of laser induced damage in plastic Q switch made of polyethylmethacrylate and vanadyl phthalocyanine for ruby laser

06 p0936 A69-17777

Linear approximation of ionization instability in disk channel of nonequilibrium MHD generator, calculating interatomic collisions frequency as function of temperature

06 p0871 A69-17911

Ignition of binary mixtures of hydrocarbons at high and minimum ignition temperatures of components

06 p1035 A69-17935

Microwave absorption and scattering by atmospheric precipitation as function of temperature and water droplet size

06 p0954 A69-17997

Thermally induced vibration and flutter of flexible spacecraft boom, discussing stability by considering boom as cantilever beam

[AIAA PAPER 69-21] 06 p0869 A69-18144

Calibration curve for constant temperature hot-wire anemometer, taking into account high wire temperature and gas pressure effects

06 p0930 A69-18218

Polycrystalline W steady state creep rate at high temperatures noting effects of stress, grain size and subgrain size

07 p1158 A69-18241

Richardson constant and tunneling effective mass for thermionic and thermionic field emission in Schottky barrier diodes

07 p1089 A69-18247

Thermally excited oscillation experienced by OGO 4 boom antenna demonstrated by mathematical model, showing nonplanar coupled bending-torsion oscillation by solar radiation

07 p1227 A69-18333

Frequency variation during oscillation pulse in avalanche transit time diodes, discussing related thermally dependent diode voltage rise

07 p1098 A69-18459

Technique for obtaining flawless silicon single crystal films on sapphire bases by vacuum deposition, noting base temperature effect on film quality

07 p1198 A69-18509

Temperature dependence of conversion coefficients and sensitivity of n-type InSb detectors in millimeter and submillimeter ranges

07 p1199 A69-18683

Electrical resistance and Hall coefficient measurement in InAs-GaAs solid solutions system, giving temperature dependence of electron mobility

07 p1199 A69-18689

Titanium vanadium martensite decomposition kinetics during heating, showing shearing process and dependence on temperature during quenching

07 p1163 A69-18778

Oxygen diffusion parameters in beta-titanium measured by successive layer removal, noting lattice constant dependence on temperature

07 p1163 A69-18783

Section pressing from Ti alloy, noting procedure and temperature dependent deformation parameters effect on microstructure and properties

07 p1164 A69-18788

Temperature sensitivity of frequency of integrated oscillators, giving design method for achieving temperature compensation

07 p1103 A69-18882

Optical pumping at high temperatures using spin exchange signals for RF spectroscopy

07 p1148 A69-18893

Laser beam absorption induced index changes associated with thermal blooming observed in iodine doped carbon tetrachloride, using Mach-Zehnder interferometer

07 p1149 A69-18899

Water vapor absorption line for nitrogen and oxygen mixtures with frequency measurements at various pressures and temperatures, discussing attenuation and line breadth

07 p1184 A69-18911

Pumping power effect on He-Ne laser amplification factor dependence on temperature and discharge currents

07 p1149 A69-18935

Impurity atoms effects on Cu diffusion and solubility in GaAs, determining Hall coefficient temperature dependence and conductivity

07 p1199 A69-19009

Magnetic susceptibility of InP-GaAs solid solutions at various temperatures and for varying GaP content

07 p1200 A69-19013

Diurnal thermal wave form driven by harmonically oscillating ground temperature in nongray atmosphere, calculating results for terrestrial and Martian atmospheres

07 p1126 A69-19036

Response of stably stratified atmosphere to differential heating across coastlines

07 p1126 A69-19038

Ceramic radomes for hypervelocity aerospace vehicles, considering wide temperature environment effects on stability and properties

07 p1171 A69-19511

Pressure-temperature dependence of nitrogen solubility in tungsten at 2400-3000 C

07 p1168 A69-19602

Plasticity theories for nonisothermal loading, considering plastic strain

07 p1237 A69-19681

Breakdown regularity of metals having different crystal structure, considering metal lifetime dependence on stress magnitude and test temperature
08 p1328 A69-17973

Mental and physical human performance characteristics under thermal loads noting admissible temperatures and endurance limits
08 p1263 A69-19940

Dislocation climb theory of steady state creep, noting necessity of self diffusion mechanism in any high temperature creep theory
08 p1329 A69-20000

Solution annealing and aging time and temperature effects on precipitation in quenched and aged beryllium
08 p1330 A69-20008

Thermal faceting of tungsten single crystal surfaces in oxygen, using vibrating-capacitor work function probe with low energy electron diffraction
08 p1330 A69-20137

Oxidation kinetics of niobium titanium alloy in air and oxygen at 1000 C, analyzing nitrogen and pressure effects
08 p1331 A69-20193

Oxidation kinetics of niobium titanium alloy in air and oxygen between 650 and 1000 C, analyzing activation energies and nitrogen effects
08 p1331 A69-20194

Phase identification and microstructural effects of gaseous nitrogen reaction with binary Nb-Ti alloys at 1000 C
08 p1331 A69-20195

Temperature dependence of polymethylmethacrylate deformation, yield and fracture in constant strain rate compressive and tensile tests
08 p1335 A69-20215

Temperature effect on phase stability and electrical length of braided coaxial cables, considering dielectric constant and mechanical length
08 p1283 A69-20225

Alkali metals electrical resistivity variation with temperature calculated in free electron approximation with Kreeb model for phonon spectrum
08 p1372 A69-20229

Spacecraft component heat sterilization, discussing heat effects on electrical connections, polymers and adhesives
08 p1284 A69-20267

Wall temperature influence on intensity of transverse flow of three dimensional laminar boundary layer resulting from transverse pressure gradient
08 p1251 A69-20274

Temperature dependence of single crystal elastic constants of nickel aluminide determined by ultrasonic wave propagation measurement
08 p1332 A69-20288

Synoptic meteorological predictions using statistical dynamic approach, considering probability distributions and nocturnal temperature decay
08 p1345 A69-20300

Ammonium perchlorate decomposition kinetics at high temperatures by measuring loss of weight in samples and gas evolution
08 p1375 A69-20339

Cobalt chromium high temperature oxidation and scale formation
[ECS PAPER 413] 08 p1332 A69-20363

Cobalt chromium alloys high temperature oxidation kinetics, discussing thermographic study of oxidation rate and oxygen pressure role
[ECS PAPER 413] 08 p1332 A69-20364

Thermally activated processes influence on dislocation interaction and on temperature dependence of flow stress in niobium single crystals
08 p1333 A69-20446

Hydrogen solubility in solid and liquid phases of nickel-molybdenum and nickel-tungsten alloys at high temperatures
08 p1333 A69-20448

Emission spectrum of laser employing electron-vibrational transitions in samarium doped calcium difluoride crystal, noting spectrum shift with increasing crystal temperature
08 p1326 A69-20544

Tensile and creep behavior of nickel at 600 C after oxidation at 1200 C, correlating results with structural differences caused by oxidation
08 p1333 A69-20556

Collection of papers on thermal problems in aerospace medicine covering intense heat, cutaneous vasomotor and sudomotor control, water immersion, etc
08 p1263 A69-20667

Temperature dependence of dissociative recombination and molecular ion formation in decaying He, Ne and Ar plasmas in discharge tube energized with capacitor bank
08 p1356 A69-20741

Recombination rate of electrons in high pressure helium-like plasma with gas temperature fixed at 300 K and electron temperature varied between 300-2000 K
08 p1356 A69-20742

Thermodynamics of nonsimple elastic materials with two temperatures, showing temperature and stress difference proportional to heat supply
08 p1422 A69-20847

Gas transport coefficients dependence on density and temperature, noting experimental results for Ne and molecular N and H
08 p1353 A69-21009

Catastrophic failures in logic circuit and system design, considering thermal effects, complexity, statistical methods and computer use
08 p1299 A69-21107

Second breakdown in semiconductors, studying thermal feedback connected with temperature time dependence of junction electrical properties
08 p1294 A69-21115

Second breakdown mechanisms in transistors, describing electrical and physical characteristics and effects of design and structural defects on resistance to initiation
08 p1294 A69-21120

Magnetic sublattices interactions in gadolinium ferrite garnet, estimating magnetization level temperature dependence
08 p1374 A69-21186

Temperature dependence of energy gap in gallium arsenide and gallium phosphide from absorption measurements
09 p1553 A69-21330

Structural and optical properties of vacuum deposited GaP films at below 240-850 C
09 p1554 A69-21332

Convective MHD channel flow in vertical channel subjected to temperature and pressure gradients, discussing wall conductance effects on flow rate and heat transfer
09 p1545 A69-21441

Gold diffusion and solubility in indium phosphide, analyzing temperature and vapor pressure effects
09 p1555 A69-21470

N type surface layer in p type sample noting effect on Hall constant and relationship to temperature
09 p1555 A69-21472

Temperature dependence of conductivity and Hall constant of GaAs single crystals with nickel impurity, noting diode structure and I-V curve shapes
09 p1555 A69-21475

Heat flux effect on laminar boundary layer separation in supersonic flow stressing free interaction zone
09 p1429 A69-21690

Nitrogen diffusion coefficients in TiN and alpha-Ti determined by metallographic and roentgenographic analyses, establishing linear equations for temperature dependence
09 p1523 A69-21736

Carbides and silicides temperature coefficient of electrical resistivity and Hall constant plotted as function of metal carbides solid solutions concentration
09 p1523 A69-21740

Temperature effect on work function minimum of cesiated tungsten single and polycrystal surfaces, using vibrating capacitor technique
09 p1558 A69-21809

Bismuth bolometer as sensor recording IR radiation for thermal radiation fluctuations in atmosphere caused by temperature inhomogeneities
09 p1490 A69-21868

Refractory compounds static strength temperature dependence at high temperatures measured in reference to melting temperature
09 p1523 A69-21873

Stress formulation of thermoelasticity in simply connected body, noting uniform temperature change influence on stress components
09 p1617 A69-22007

Silicon carbide filaments strength at high temperatures noting vapor deposition, mechanical properties and applications
09 p1524 A69-22072

Supercritical elastic states in convex shells produced by load in presence of thermal flux, noting no flux effect on states
09 p1617 A69-22078

Temperature dependence of high melting point metals mechanical properties
09 p1525 A69-22138

Heat resistant alloys plastic deformation, studying stress/strain systems, strain divisibility, strain rate and temperature effects, etc
09 p1504 A69-22141

Thermodynamic analysis of engines and heat pump operating within negative absolute temperatures, noting work increase by throttling
09 p1623 A69-22212

Mass spectrometric determination of pyrolysis products generated from heated polymer samples
09 p1448 A69-22315

Thermal models for Jupiter and Saturn corresponding to completely convective structure, using De Maizus state equations
09 p1607 A69-22411

Thermal effects on modulation sensitivity and inherent AM percentage as functions of modulation frequency in IMPATT oscillators
09 p1468 A69-22515

Cathode material effects on temperature coefficients for glow discharge tubes, noting running voltage pressure characteristics
09 p1468 A69-22601

Intrinsic absorption temperature dependence in doped p-InSb, discussing forbidden transitions
09 p1559 A69-22648

Temperature effect on pulsed laser action on electron transitions in diatomic molecules for rotational relaxation, discussing excitation mechanisms
09 p1520 A69-22654

Pulsed plasma production when focusing Q switched laser on solid target surface, noting high temperature effects and optical diagnostics methods
09 p1520 A69-22656

Liquid laser gain measurement via luminescence intensity, noting optical pumping thermal effect
09 p1520 A69-22683

Ion pairing effects of cyclooctatetraene anion radical, studying electron spin resonance spectra temperature dependence
10 p1651 A69-22938

Oxidation effects on creep and fatigue properties of metals noting time and temperature roles
10 p1708 A69-22998

Negative creep in austenitic steel samples explained as possible redistribution of elements inside austenite grains at high temperatures
10 p1708 A69-22999

Primary explosives tested for effects of shock, friction, heat and electrical discharges
10 p1750 A69-23010

Aluminum alloy crack propagation and fracture patterns as function of temperature under high strain amplitude and low strain rate
10 p1709 A69-23071

High temperature effect on fatigue deformation and fracture of nickel base superalloy in single crystal and columnar grained forms
10 p1709 A69-23073

Probability characteristics of temperature and supply voltage dependent parameters of semiconductor equipment
10 p1661 A69-23112

High temperature acclimation, climates with heat dissipation problems and hibernation or torpor effects on metabolic depression in homeotherms
10 p1642 A69-23121

Learned behavior performance failure in hypothermia as temperature dependent phenomenon using rat, guinea pig, chinchilla, mouse, gerbil and hamster
10 p1643 A69-23124

Radiation resistance of animals in hibernation and hypothermia, noting temperature dependence of protective effect
10 p1643 A69-23126

Transient characteristics of negative resistance zinc alloy diodes, investigating temperature effects
10 p1662 A69-23157

Porous structures, using spherical tungsten powders, discussing metallurgy, sintering, temperature effects and performance characteristics in ion engines
10 p1710 A69-23166

N enhancement silicon MOST saturation current as function of temperature
10 p1743 A69-23175

Surface charge exchange in metal oxide silicon capacitors generated at low temperatures by surface state free carrier trapping
10 p1744 A69-23179

Venus atmosphere origin, discussing high temperature effects and chemical composition via space probe and terrestrial observations
10 p1775 A69-23183

- Nitrogen solubility in molten niobium and molybdenum at high temperatures in argon flow
10 p1710 A69-23213
- Neat alpha styryl azide transformation into 2-phenylazirine, 3,6-diphenylpyridazine and 2,5-diphenylpyrrole after one month at room temperature in brown glass bottle
10 p1651 A69-23307
- Psychological, physiological and biochemical responses to controlled diets, determining regional and total body sweat composition of men working in temperate environment
10 p1644 A69-23314
- Three layer vacuum deposited silicon monoxide films current voltage and conduction current density temperature dependence
10 p1745 A69-23324
- Composition and sintering temperature cooling effects on fracture properties of W-Ni-Fe alloys, using electron microscope fractography
10 p1711 A69-23333
- Temperature vs compactness relationship in NbC compacts having nonstoichiometric composition and approximately equal specific surface, determining self diffusion coefficients
10 p1711 A69-23337
- Creep of high purity Nb-Mo alloys in 800-1300 C range and at 1500-13000 lb/square inch stresses, giving activation energy for creep
10 p1711 A69-23375
- Surface temperature rise of solution treated austenitic steel measured during double repeated rotating bending fatigue tests at room and elevated temperatures
10 p1711 A69-23393
- Fatigue behavior of plastics classified noting temperature rises, crack initiation, etc
10 p1716 A69-23394
- Solid propellant motors nozzle design, analyzing structural and material problems, high temperature exhaust gases effects, thermal insulation, etc
10 p1716 A69-23403
- Excitation and ionization relaxation of cesium seeded argon gas computed for stepwise increase of electron temperature
10 p1732 A69-23444
- Velocity and temperature influence on discharge characteristics of K seeded argon plasma flow at 1 atm pressure
10 p1733 A69-23449
- Rare gas-alkali plasma electrical conductivity dependence on gas temperature and preionization to determine optimum operating conditions for MHD generator
10 p1733 A69-23451
- Pressure and temperature effects on electrical conductivity of dense plasma ejected from Laval nozzle
10 p1739 A69-23492
- Heat and humidity endurance limits in man
10 p1645 A69-23494
- Temperature effects on phosphorescence lifetimes and intensities of aromatic hydrocarbons in polymethyl methacrylate, estimating activation energy for thermally activated nonradiative decay mode
10 p1652 A69-23523
- IR radiation effects in cadmium sulfide crystals with green edge emission at low temperatures, discussing luminescence, photoconductivity and conductivity glow curves
10 p1746 A69-23565
- Very low temperature dependence of thin single crystal Al plates electrical resistance, noting Umklapp processes contribution
10 p1711 A69-23620
- Elastic-plastic deformations /strains/ amplitudes measured at high cycle temperatures in thermal fatigue tests
10 p1801 A69-23844
- Chromium-rhenium-boron ternary system using X ray diffraction and microstructure analysis, establishing phase equilibria at high temperatures
10 p1715 A69-24054
- Electron concentration and temperature dependence on gas temperature as factor determining He-Ne laser output at 6328 A
10 p1706 A69-24078
- Nebular abundances allowing for temperature variations in nebula along line of sight, correcting changes in electron temperature along path of observation
10 p1787 A69-24116
- Presprayed metal films influence on visibility and contact resistance of GaAs prior to fusing in Sn, In and lead contacts
10 p1748 A69-24214
- Temperature and strain rates effect on delayed yield and failure of plasticized epoxy resin
10 p1717 A69-24218
- Near boundary zones in VT15 Ti alloy not involved in beta phase decomposition during aging below 500 C attributed to vacancy concentration decrease
11 p1902 A69-24275
- Pacific atmospheric circulation and Pacific equatorial sea temperature winter anomalies, noting Hadley circulations, northeast westerlies, trade winds and Walker circulation
11 p1911 A69-24322
- Universe origin, discussing big bang theory, effects of expansion time and temperature on elementary particles, RF quanta, etc
11 p1953 A69-24352
- Lunar radio emission constant component in presence of heat flow from interior, using stratified model of surface structure with two variants
11 p1956 A69-24398
- Equilibrium state of matter at high temperatures and densities with respect to nuclear reactions, determining neutron-proton ratio
11 p1957 A69-24403
- Small microwave antenna calibration by method of two black bodies exposed to different temperatures, reducing influence of cloudiness and humidity
11 p1844 A69-24450
- Microsectioning technique applied to measurement of diffusion coefficients of Cr 51 in polycrystalline Nb at 1220-1766 K temperature range
11 p1903 A69-24577
- Book on strength and failure of viscoelastic materials covering linear and three dimensional polymers or polymer-based materials, flexibility and temperature effects
11 p1970 A69-24610
- Temperature effect on amplification factor of box type dynode system of photoelectron multipliers made of alloy AMGK, using single electron method
11 p1846 A69-24626
- Surveyor electronic engineering design for lunar environment, discussing vacuum and temperature effects
11 p1958 A69-24633
- Young modulus temperature dependence and order-disorder transformations in ternary nickel alloys
11 p1904 A69-24705
- Explosive reactions between hydrogen and oxygen flashed in presence of nitrogen dioxide, chlorine or bromine as sensitizers, considering thermal contribution
11 p1832 A69-24878
- Beryllium properties and processing including magnesiothermal reduction, powder purity, oxygen content, grain size and temperature effects on mechanical properties
11 p1904 A69-24897
- Annealing effects on cold rolled titanium sheets, noting changes in Young modulus and characteristics of recrystallized titanium
11 p1904 A69-24899
- Thermal expansion coefficients of Nb-Zr-Ti alloy and plexiglass at 10-300 K from dilatometric measurements
11 p1905 A69-24917
- Microcracking susceptibility studies of Inconel 718 weld heat affected zones, noting hot ductibility, weld circle patch and fillerless fusion welding tests
11 p1905 A69-24933
- Thin conical elastic shell stress-strain state calculated by computer for arbitrary thicknesses and loading conditions, considering temperature and edge forces effects
11 p1981 A69-24943
- Residual thermal stresses and plastic strains at hole edges in perforated plates, considering heating and rapid cooling
11 p1982 A69-24947
- Hydrogen effect on temperature dependence of tensile strength and stress rupture strength of Ti alloys, considering annealing, quenching and aging
11 p1905 A69-24962
- Glass fiber reinforced plastics tensile strength at low and high temperatures
11 p1907 A69-25181
- Temperature and stress dependence of microstrain and microyielding in polycrystalline W for range of impurities and dislocations, considering transition to macrostrain
11 p1905 A69-25183
- Ignition dynamics of solid materials with differing kinetic and thermophysical parameters, emphasizing temperature growth during chemical reaction leading to ignition
11 p2000 A69-25188
- Thermal conductivity of polycrystalline beryllium oxide as function of temperature and pressure in argon or helium atmosphere, discussing heat transfer mechanism
11 p1906 A69-25225
- Ionization equilibrium for ions of solar abundant elements between C and Ni calculated as function of electron temperature
11 p1928 A69-25262
- Electrostatic probe measurements in gas warmer than probe, demonstrating applicability of continuum theory for highly negative probe
11 p1930 A69-25274
- Temperature effects on noise levels in field effect transistors, discussing Lorentz spectrum
11 p1853 A69-25391
- Enthalpy excess thermodynamic functions of binary gas mixtures based on stationary diffusion thermoeffect in tube
11 p2003 A69-25552
- Plasticity increase of molybdenum alloys during precipitation of second phase at high temperatures due to lattice defects redistribution and plastic deformation
11 p1906 A69-25685
- Thermal EMF in indium phosphide crystals as function of temperature, electron concentration and magnetic field strength, determining effective mass of electrons
11 p1939 A69-25690
- Boundary conditions for time dependent temperature variations of calorimeter operating in regular thermal regime
11 p2003 A69-25702
- Hydrogen viscosity temperature dependence at constant density below room temperature
11 p2003 A69-25704
- Statistical rules for seasonal forecasts based on temperature and precipitation deviations analysis in long term climatological records, considering sunspot cycle role
12 p2125 A69-25895
- Resonant vibrational energy transfer between specific mode of carbon dioxide and N molecules at high temperatures, monitoring IR emission
12 p2131 A69-25984
- Nimonic alloy single crystals strengthening during plastic deformation, analyzing jump phenomenon at high and low temperatures
12 p2112 A69-26038
- Ni-Ti alloy intergranular deformation at constant tension within wide temperature range
12 p2113 A69-26044
- Acoustic wave generation in neutral particle component of weakly ionized gas by variation of electron temperature with low power RF signal
12 p2134 A69-26096
- Inelastic interactions cross sections of slow electrons with adsorbed particles on W surface as function of temperature in surface bond vibrational region
12 p2132 A69-26114
- Neutron irradiation and temperature effects on ferrite and Permalloy memory cores hysteresis loops
12 p2142 A69-26259
- Tellurium doping effect on phonon diffusion in GaSb, discussing thermal conductivity at low temperatures
12 p2142 A69-26294
- Fatigue life of Al alloy thin laminated sheets, considering cyclic frequency and temperature effects
12 p2180 A69-26359
- Thermal effects in large mirrors, considering temperature gradients parallel to reflecting surface or to optical axis
12 p2056 A69-26408
- Dislocation mobility temperature dependence in n-type indium antimonide, noting role of covalent interatomic bonds
12 p2143 A69-26453
- Optical absorption cell with variable path length and temperature for measuring absorption coefficients of gases at low and high temperatures
12 p2093 A69-26482
- Weightlessness and higher g values effects on caloric and rotational nystagmus
12 p2020 A69-26551
- Incandescent cathode temperature effect on He-Ne laser output, ascertaining mixture parameters, cathode voltage and power dependence on discharge current
12 p2109 A69-26716
- Nonlinear structure undergoing arbitrary load history including temperature variations solved by computerized force and subordinated step procedure
12 p2185 A69-26823
- Time and temperature dependence of plastic properties of fiber reinforced phenolic heat shield materials
12 p2119 A69-26825

Steady state small signal input impedance of low power planar transistor as function of temperature and operation mode

12 p2042 A69-26878

Time delay in temperature controlled transistorized time delay circuit determined by transistor unsteady thermal processes

12 p2043 A69-26883

Temperature effect on tensile brittle fracture stress of polycrystalline tungsten

12 p2116 A69-27135

Resistance type bonded strain gages for seven adverse environments, discussing installations and transducers

12 p2099 A69-27165

Temperature effects on polarization degree, threshold current and delay of radiation from GaAs laser diodes with diffused Zn

13 p2227 A69-27328

Room temperature WC-Co compacts oxidation resistance in air noting increase with preliminary sintering temperature

13 p2275 A69-27345

Neutron irradiated Nb single crystals tensile tested over temperature range, discussing athermal radiation hardening

13 p2275 A69-27368

Temperature effects on mechanical properties and fracture behavior of lamellar Ni-nickel titanide intermetallic eutectic alloy showing dependence on intermetallic constituent

13 p2277 A69-27406

Low cycle fatigue crack initiation in Ti-6Al-4V at room and high temperatures and in aqueous salt environment

13 p2278 A69-27413

Niobium aluminide-niobium germanide alloys superconductivity and heat treatment influence on critical temperature

13 p2316 A69-27659

Cellular convection in horizontal gas layer analyzed for causes of vertical air circulation and effect of vertical temperature profile

13 p2291 A69-27725

Bolt materials selection criteria in design of high strength lightweight joints, showing fatigue curves and temperature effects

13 p2268 A69-27758

Se activation energy dependence on crystals composition and Se concentration, based on Hall coefficient temperature dependence in gallium arsenic phosphides

13 p2317 A69-27875

Active medium temperature effect on semiconductor laser emission spectra composition, discussing amplification coefficient frequency dependence at various temperatures

13 p2271 A69-27888

Temperature effects on photosensitivity spectra of cadmium telluride thin films

13 p2318 A69-27889

Supplementary absorption and Hall effect temperature dependence in solid solutions of gallium arsenic phosphide

13 p2318 A69-27894

Conduction band structure in GaSb noting temperature dependence

13 p2319 A69-27899

Lunar surface environmental factors including molecular gas behavior under weak gravity and low atmospheric density, radiation and temperature effects, meteorite bombardment, etc

13 p2352 A69-27904

Polymeric insulation materials, discussing intrinsic properties dependence on temperature and atmosphere, stressing effect on aging

13 p2285 A69-27985

Electrical properties of electron beam evaporated Ti, Zr and Hf films as function of substrate temperature, material and film thickness

13 p2321 A69-28010

Outgassing rates of multifoil insulation materials for sealed vacuum systems measured over temperature range as function of pumping time

13 p2299 A69-28016

W, Mo and heat treatment effects on phase composition and heat resistance of ferrite and austenitic steels

13 p2283 A69-28487

Temperature factor effect on transition from laminar to turbulent flow in boundary layer of plate

13 p2251 A69-28558

Magnetic properties of ferrites with garnet structure, discussing temperature effect on magnetic states of Gd, Li, Y and Lu sublattices

13 p2323 A69-28564

Materials surface thermal stress analysis by strain gauges, considering behavior during rapid temperature changes

13 p2264 A69-28599

Effective temperature values of ozone used to determine onset time and disturbance height in ionosphere

13 p2257 A69-28701

Temperature effects on propagation of HF internal and surface waves in bounded plasma, deriving dispersion equations

14 p2410 A69-28733

Compressed ammonium perchlorate combustion rate and pressure requirements established from initial temperature effects

14 p2508 A69-28914

Thermoclastic stress-strain state of infinite circular cylindrical shell with elasticity modulus temperature dependence expressed by exponential function

14 p2532 A69-28980

UV radiation decreased transmittance through quartz exposed to plasma at high temperature and pressure, showing dependence on heated surface layer absorption

14 p2490 A69-29159

Pulsed lasers with pure carbon dioxide and mixture with N and He, discussing inversion mechanism, peak emission power and gas temperature effects in different modes

14 p2458 A69-29162

Thermionic converter stability as function of cesium pressure, heat input, reservoir temperature, load voltage or resistance

14 p2402 A69-29236

Work function measurements of polycrystalline W, Re and Ni disks in high pressure cesium plasma for low probe temperature range

14 p2506 A69-29266

Temperature dependent aging mechanisms in deformed Mo alloys during annealing, using transmission electron microscope

14 p2463 A69-29312

Strain rate and temperature effects on sintered molybdenum sheets strength and elongation characteristics

14 p2464 A69-29322

Emission spectrum width of solid state lasers as function of temperature, investigating effects of active medium parameters, pumping and cavity

14 p2459 A69-29389

Low temperature thermal expansion coefficients and linear contraction of metal alloys from liquid hydrogen to room temperature tabulated as function of temperature

14 p2464 A69-29400

Short time creep rupture behavior of austenitic stainless steel at high temperature ranges, noting rupture times various stresses and data correlation [ASME PAPER 68-WA/MET-2]

14 p2464 A69-29439

Chemical reaction-rate theory for creep tests, analyzing extrapolation equations for time-to-rupture dependence on temperature and stress

14 p2464 A69-29442

Nb-Ta alloys oxidation kinetics at high temperature and structure and composition of oxide films and scale layers, discussing anomaly in oxidation rate temperature dependence

14 p2464 A69-29650

W shear moduli at high temperatures measured by forced torsional vibration in wide frequency ranges, discussing grain boundary effects

14 p2465 A69-29651

Temperature dependence of elastic constants of highly and weakly doped n- and p-type GaAs

14 p2508 A69-29655

Irregular data obtained by radiosondes in winter for charts of high isobaric levels, noting stratospheric temperature effects on radiosonde ascent height

14 p2473 A69-29731

Spectrometric characteristics of He, H and molecular H ion recording counters as function of temperature

14 p2452 A69-29811

Processing characteristics of wrought Co base alloys, discussing thermomechanical treatment effects, yield strength, ductility, etc

14 p2456 A69-29892

Validity range of nuclear quasi-equilibrium approximation for stellar silicon burning, discussing time rates of nuclear abundance changes and temperature effect

14 p2529 A69-29984

Elastic microwaves propagation attenuation along lithium niobate crystals trigonal axis at various temperatures

15 p2665 A69-30040

Majority carrier lifetime temperature dependence obtained from photoconductivity measurements of p-type GaAs crystals doped with Ge

15 p2666 A69-30050

Scientific satellite 1 solar cell panels power output dependence on temperature and spin calculated and compared with results for outdoor sunlight

15 p2552 A69-30050

Cold worked high purity Mo wire recovery after plastic deformation at room temperature, considering electrical resistivity decrease as function of annealing temperature

15 p2636 A69-30084

Strain aging of polycrystalline Nb containing interstitial impurities as function of temperature, discussing interstitials role in recovery substages

15 p2636 A69-30190

Device for fatigue testing turbine disk models in unsteady temperature fields with radial and axial nonuniformity produced by HF heating

15 p2583 A69-30201

Shock hardening in Ni at high pressure observed by electron microscopy showing dominating thermal effects on microstructure

15 p2637 A69-30222

W single crystals cleavage cracks by spark discharge showing effective surface energy dependence on crack initiation and propagation temperatures

15 p2637 A69-30226

Titanium alloys fatigue properties at various temperatures using notched and unnotched specimens, considering vibrational fatigue strength and notch sensitivity

15 p2637 A69-30227

Self lubricating bearings lifetime calculated as function of lubricant in pores and consumption rate, noting temperature effects

15 p2618 A69-30281

Plasma arc characteristic and radiation at high pressure and temperature showing strong electrical field strength and radiation increases with pressure

15 p2659 A69-30377

Organic and inorganic fabric reinforcements effects on thermal properties of composites noting thermal conductivity, diffusivity, specific heat constants and temperature ranges

15 p2642 A69-30466

Solid lubricant films friction and wear life determined under various conditions of contact, temperature, load and atmosphere [ASLE PREPRINT 69AM 6C-1]

15 p2619 A69-30471

Heat resistant Fe and Cu alloys creep index affected by temperature, testing time and specimen grain size

15 p2639 A69-30569

N precipitation kinetics in deformed Nb, finding constant in rate equation dependent on temperature and correlated to precipitates nature

15 p2639 A69-30585

Temperature effects on magnetomechanical damping in Fe, Ni and mumetal, noting behavior difference due to domain structures

15 p2639 A69-30586

Maximum strengthening due to second phase precipitation within operating temperatures maintainable to 20 hr during aging of Nb-Hf-O and Nb-Zr-O alloys

15 p2640 A69-30632

Theory of temperature dependent magnon energies in antiferromagnets based on spin wave operator expansion of Hamiltonian, taking into account dynamical interaction between waves

15 p2668 A69-30684

Dispersoids and temperature effect on coercive force of 19 Co base and 10 Fe plus 27 percent Co base

15 p2669 A69-30689

Statistical correlation of temperature and tail-wind data for London-New York route at 50 mb for SST operation

15 p2651 A69-30690

Gold diffusion and solubility in indium phosphide, analyzing temperature and vapor pressure effects

15 p2669 A69-30715

N type surface layer in p type sample noting effect on Hall constant and relationship to temperature

15 p2669 A69-30717

Temperature dependence of conductivity and Hall constant of GaAs single crystals with nickel impurity, noting diode structure and I-V curve shapes

15 p2669 A69-30720

Micrometeorites acoustic recordings on Cosmos 135, investigating data reliability influences by appearance of thermal noise

15 p2691 A69-30748

High temperature effects on electron and X ray irradiated MOS transistors for space charge analysis and defects in silica films

15 p2625 A69-30828

Temperature dependence of intermolecular interaction averaged potentials with respect to vibrational states

15 p2655 A69-30982

Friction effects on friction couples made of two different nonferrous alloys, discussing temperature regime difference effects on microgeometry and structure

15 p2629 A69-31027

Electrical resistance and temperature coefficient dependence on phase composition of Ti, Zr and Nb carbides

15 p2641 A69-31047

Temperature and electron number density behind reflected shock in helium gas in T tube, noting Z pinch discharges

15 p2593 A69-31161

Fiberglass reinforced plastic tensile strength dependence on vibration time and temperature and vibrational effect on modulus of elasticity

15 p2643 A69-31203

Nonresonant absorption and dispersion of microwaves by gases, studying gaseous mixtures, relaxation parameters, anomalous dispersion and temperature effects

15 p2654 A69-31219

Refractory materials based on BN and silicon nitride, studying effect of sintering conditions and chemical composition on mechanical properties

15 p2643 A69-31244

Escherichia coli B/r survival in high vacuum at different temperatures irradiated with UV or X rays tested as colony forming ability

15 p2557 A69-31388

Solid lubricants on molybdenum disulfide base at various temperatures and low pressures, noting film mass losses and possible use with organic materials under high vacuum

16 p2793 A69-31561

Lattice component of heat conductivity in n-type cadmium arsenide at low temperatures by suppressing electron component of conductivity with strong transverse magnetic field

16 p2824 A69-31568

Electrical conductivity of cesium iodide single crystals with anion and cation impurities noting temperature dependence

16 p2824 A69-31573

Gallium phosphide Schottky barrier diodes, discussing construction and metals used, barrier height relationships to impurity concentration and temperature, rectifying characteristics and internal quantum efficiency

16 p2757 A69-31613

Acoustic velocities in polymethylmethacrylate measured as functions of frequency, temperature and pressure, comparing data obtained with equation of state high pressure determinations

16 p2825 A69-31695

Thermal stability of Hastelloy Alloy C-276 determined from time and temperature tests for corrosion and grain boundary precipitation

16 p2799 A69-31719

Inert gas diffusion of Xe 133 in aluminum and titanium at various temperature ranges, showing effects of recrystallization, plastic deformation and phase transformations

16 p2800 A69-31775

Aluminum alloys high temperature creep effects distinguished from effects of long period at high temperature, discussing tensile test data and deformation-time curves

16 p2800 A69-31781

Creep rate and temperature effect on creep resistance shown in direct correlation with Al-Mg alloys strength by long term high temperature tests

16 p2801 A69-31782

Slow forming forging and extrusion required for Ti alloys, discussing mechanical properties as function of beta transformation temperature

16 p2793 A69-31786

Natural vibration of isotropic plates in temperature field with nonuniform distribution over plate

16 p2871 A69-31891

Approximate expression for temperature dependent radiative heat flux in optically thin gas, considering reentry body hypersonic flight

16 p2877 A69-31892

Carbon dioxide dissociation relaxation times measured in shock tube at 1900-2400 K and 1.5-2.5 km/sec

16 p2766 A69-31910

Heated cylindrical shell with braces subjected to given compression and internal pressure, having elastic beams along edges, analyzing local deformations effect on shell strength and stability

16 p2873 A69-32131

Initial temperature effects on flame propagation velocity in turbulent flow of homogeneous gasoline-air mixture under realistic conditions

16 p2837 A69-32138

Removal rate of reaction water from fuel cells by diffusion-condensation procedure as function of temperature and electrolyte concentration

16 p2736 A69-32200

Reaction rate constants of ion-molecule interchange reaction as function of temperature, flow velocity, activation energy and constant part of steric factor P

16 p2747 A69-32312

Polycrystalline BeO sound velocities determined as function of pressure and temperature using pulse superposition method

16 p2802 A69-32338

Noctilucent clouds seasonal frequency, considering meteor shower effects and temperature dependence role

16 p2781 A69-32453

Temperature dependence of resistivity of zirconium oxide with copper oxide additions indicates suitability as heat sensitive resistor material in 300 to 1000 degree C range

16 p2827 A69-32482

Air refractivity variations across horizontal and vertical boundary planes between two air masses of slightly different temperatures

17 p3028 A69-32880

Al interconnections discontinuities at integrated circuit contact windows observed by scanning electron microscope, noting catastrophic failure and Si presence

17 p2936 A69-32893

Low temperature creep mechanisms, discussing thermal activation of dislocation slip in perfect crystals

17 p2985 A69-32909

Creep tests on polycrystalline Be and Be alloy at various temperatures and stresses

17 p2986 A69-32912

Temperature field, strains and stresses induced in thin circular disk by unsteady heat source, noting time effect and resonant vibrations

17 p3054 A69-33021

In-process annealing and warm working temperature effects on long time creep rupture properties of Mo alloys tested in vacuum furnace

17 p2987 A69-33076

Low cycle fatigue behavior prediction for 304 and 306 stainless steels based on temperature and strain rate ratio to tensile ductility

17 p2987 A69-33079

Flame front structure and combustion rates of gases as function of temperature dependence of thermal conductivity, diffusion coefficients, density and molecular weight

17 p3069 A69-33136

Temperature and pressure effects on flame propagation rates, burning time and combustion zone length in turbulent flows of homogeneous gas mixtures

17 p3069 A69-33140

Guarded disk type emissometer for hemispherical emittance measurements of sample materials in 88 to 420 K range based on steady state calorimetry

17 p2973 A69-33280

Thermal analysis of opacified fibrous insulation systems, discussing heat transmission, heat transfer and thermal conductivity relations to compression load and temperature

17 p3072 A69-33282

Temperature effects on fracture of various alloys, presenting strength and toughness values tested at cryogenic temperatures

17 p2990 A69-33567

Optical constants of Ta-W and Nb-Mo measured in IR and visible ranges as function of incandescent temperatures

17 p2990 A69-33574

Yttrium desorption from W wire by strong electric field, noting electron work function or temperature increase effects on desorption field

17 p3015 A69-33631

Flame propagation mechanism on plastic fuel in oxygen-nitrogen atmospheres with variable pressures and at different initial fuel temperatures, discussing safety and ignition problems

17 p3074 A69-33662

Heat treatment effect on stress corrosion cracking of ternary Al-Zn-Mg alloys noting aging strength, solution temperature, quenching rate and alloy content

17 p2990 A69-33676

Gravimetric and IR absorption spectra analysis for determining heat resistance and chemical changes in organosilicon resins during heating

17 p2992 A69-33744

X irradiation and temperature effects on flour beetle Tribolium confusum/ pupae, noting wing abnormalities and pupal stage duration

17 p2910 A69-33748

Facility for determining energy dissipation in materials under cyclic stresses or strains for wide range of temperatures

17 p2946 A69-33925

Facility for studying energy dissipation in refractory materials during fatigue tests in vacuum at various temperatures, describing principal components

17 p2947 A69-33926

Surface layer role in strengthening of iron determined from examining temperature dependence of internal friction during thermomechanical treatments

17 p2991 A69-33939

Refractive indices for various glasses obtained as function of wavelengths and temperature, using spectrometer as collimator

17 p3007 A69-34158

Creep rate-stress-temperature relations for powder metallurgy rhenium, discussing activation energy

17 p2991 A69-34186

High speed transient pressure measurement, emphasizing forcing function measurement

18 p3133 A69-34244

Carbon dioxide flowing gas laser pumped by thermally excited nitrogen, discussing power gain and absence of chemical and charged particle effects

18 p3151 A69-34264

Temperature and pressurization effects on tensile and compressive properties of polycrystalline arc-cast W

18 p3154 A69-34273

Gaseous diffusion coefficients during argon, krypton, oxygen and nitrogen diffusion into helium measured by gas chromatography

18 p3099 A69-34280

Temperature dependence of metal elastic properties including thermal strains effect on stress field, yield stress changes and elastic modulus variations

18 p3212 A69-34353

Ball bearing lubrication simulation by rolling disk apparatus, emphasizing surface slip and related thermal effects alterable by geometric expansion

[ASME PAPER 69-LUBS-16]

18 p3140 A69-34380

Shock wave propagation induced by nonuniform instantaneous internal heating of nonlinear elastic strain hardening solid material

[SAWE PAPER 69-APM-17]

18 p3214 A69-34393

Shock wave studies of gaseous NO thermal ionization in Kr as function of temperature, using time-of-flight mass spectrometer

18 p3099 A69-34464

Accelerated temperature tests, calculating temperature behavior of hazard rates and activation energy from failure data using computer simulation

18 p3117 A69-34509

Computer program and component part models for nonlinear DC circuit simulation at various temperatures

18 p3108 A69-34525

Carbide phase growth rate in Mo-TiC alloy with particle size distribution maintained over time- temperature spectrum, noting diffusion and interface controlled processes

18 p3155 A69-34632

Heat sensitive paints thermophysical characteristics determined by nonstationary heat conditions method

18 p3161 A69-34697

Thermoelectrical leg product specification /TELPs/ apparatus and data reduction technique for determining temperature dependent thermoelectric properties of material

18 p3093 A69-34783

Plastics thermal properties and industrial structural applications dependency on temperature

18 p3161 A69-34839

Ion and temperature effects on lower ionosphere refractive index for VLF radio wave propagation

18 p3102 A69-34971

Gas turbine areas calculation of through flow cross sections for temperature deformations and blades elongation

18 p3184 A69-34987

Thermal coefficient of optical glasses refractive index determined by interferometry, noting relation to glass chemical composition

18 p3172 A69-35013

Dilatometric and X ray study of temperature dependence of linear expansion coefficients of lattice constants of chromium disilicon

18 p3156 A69-35020

Sublimation of various compressed naphthalene wind tunnel models analyzed in supersonic air flow, discussing effects of temperature and model configurations

18 p3231 A69-35121

High temperature air spectral absorption indices determined at different pressures and temperatures

18 p3231 A69-35122

Magnetic sublattices interactions in gadolinium ferrite garnet, estimating magnetization level temperature dependence

18 p3183 A69-35155

Temperature and pressure effect on cobalt base alloy cavitation in liquid sodium, using vibratory apparatus and loss rate contour diagram

18 p3157 A69-35184

Nb corner of Nb-Mo-Cr alloy phase diagram and oxidizability in air at high temperature

18 p3157 A69-35248

TiNi compound alloying with Al and Fe, considering effect on hot hardness at various temperatures

18 p3157 A69-35249

Secondary recrystallization in cold rolled molybdenum foil as function of temperature using electron microscopy and diffraction

18 p3157 A69-35253

Dislocation structure of pure polycrystalline nickel subjected to high temperature creep, using electron microscopy following cold working and room temperature annealing

18 p3157 A69-35254

Fiberglass-reinforced plastics longitudinal and transverse strain relations at various temperatures

18 p3163 A69-35366

Sigma phase and temperature effects on toughness of austenitic stainless steel weldments

18 p3150 A69-35429

Annealing temperature effect on Ni-Ti alloys internal friction, noting peak connected with solid solution grain boundaries

18 p3158 A69-35443

Preprogrammed deformation temperature influence on Ni creep strength, emphasizing smoothly changing loads effects

18 p3160 A69-35455

Recrystallization limit effects on coarse grain growth in aluminum alloys extruded sections, studying roles of additives, extruding temperature and heat treatment duration

18 p3160 A69-35472

Mechanical properties associated with 55-Nitinol memory effect, presenting stress-strain and electrical resistivity as function of temperature

19 p3340 A69-35523

Unfilled Pyrrone prepared from powder into molded parts for flexural tests at elevated temperatures observed for stability to electron irradiation in air

19 p3356 A69-35529

Polyperfluoroalkyleneimido(perfluoroalkylene) amide synthesized by reaction of perfluoroalkane dinitriles with ammonia or diamidine, giving elastomers of varying strength and elongation, noting thermal stability

19 p3264 A69-35535

Ablative materials thermal protection characteristics at low heating rates evaluated by convective heating tests, stressing polyurethane foam composite

19 p3357 A69-35536

Directionally solidified Co-Nb eutectic alloys mechanical properties and magnetic performance for elevated temperature space applications

19 p3341 A69-35542

Glass encased electronic components with conformal coatings, considering glass breakage at low temperature

19 p3281 A69-35547

Focused Gaussian laser beam expansion due to thermal changes in refractive index of air, noting focused spot area increase with pulse energy

19 p3330 A69-35601

Schottky barrier diodes for high temperature operation prepared on n type GaP single crystals, studying I-V and C-V characteristics

19 p3381 A69-35681

Solar cell characteristics at low temperatures, noting efficiency increase with decreasing temperature

19 p3251 A69-35691

Energy dissipation of solder-covered and solderless solar cells with TiAg contacts as function of storage time, temperature and humidity

19 p3253 A69-35706

Stress relaxation of heat-resistant steels as function of equal stress during different elevated temperatures, applying results to time residual stress prediction

19 p3342 A69-35778

Laminar flow of viscous compressible fluid with density dependent on temperature, calculating steady state Navier-Stokes equations using vector function

19 p3297 A69-35852

ZnS-CdS crystals luminescence during varied forbidden bandwidth, discussing two photon and ruby laser excitation and temperature dependence

19 p3331 A69-35866

Creep behavior of dispersion strengthened Nb base bcc alloy, studying temperature and stress effects on steady state creep rate

19 p3343 A69-35924

Ti-Al alloys yield and fracture characteristics as function of high exposure temperatures, studying causes of embrittlement

19 p3344 A69-35927

Power subsystem weight effects on temperature ratio of Rankine type cycle, discussing method for rapid estimation

19 p3254 A69-35957

Ar 39-Ar 40 method using neutron activation and inert gas mass spectrometry to investigate meteoritic thermal histories

19 p3412 A69-36105

Thermal rare gas release from mineral separates of Mocs meteorite, using method giving activation energies as function of temperature

19 p3419 A69-36141

Dynamic recrystallization in Ni and Ni-Fe alloys during torsional high temperature deformation

19 p3344 A69-36147

Heat treatment effects on mechanical properties of Ti-Fe and Ti-Fe-Al alloys

19 p3344 A69-36151

Quenching temperature and deformation conditions for Ti alloy bars optimal mechanical properties, emphasizing effect of primary structure

19 p3328 A69-36152

F center formation and X ray and photostimulated F-band luminescence in europium ion-activated potassium halides as function of temperature and X ray dosage

19 p3383 A69-36164

Molecular N rotational temperature effect on rare gases scattering cross section

19 p3377 A69-36184

Tempering time and temperature effect on microstructure, superconductivity, tensile strength and electrical conductivity of recrystallized Nb-Ti alloy

19 p3345 A69-36302

Heat treatment effect on superconducting properties of deformed Nb-Ta alloys, noting critical current density

19 p3345 A69-36303

Lunar interior chemical heterogeneity determined from model taking into account pressure, temperature and composition effects

19 p3425 A69-36421

Transient recombination lifetimes in n-type float zone Si from 4.2 K to room temperature, obtaining electrical and photoconductivity values

19 p3383 A69-36447

Exciton line broadening in II-VI compound semiconductors, discussing thermal broadening of n equals one exciton associated with LO phonon-induced scattering

19 p3386 A69-36524

Injection lasers threshold characteristics, studying temperature and doping level effects on current density and radiation energy

19 p3337 A69-36527

Temperature effects on threshold current density, emission wavelength and polarization of PbSe diode lasers

19 p3337 A69-36533

Power, efficiency and temperature dependence of emission spectra and threshold current density in electron beam pumped GaAs laser, noting doping concentration

19 p3338 A69-36538

Voltage and temperature dependence of zero-bias anomaly in GaAs p-n junction at 0.40-60 K, investigating voltage dependence of differential resistance

19 p3388 A69-36542

Anomalous phenomenon in resistance and magnetoresistance of cleaved InAs surface, plotting temperature and magnetic field variation effects, proposing explanation of anomaly

19 p3388 A69-36543

Temperature dependence of g-value in spin resonance in partially degenerate region in pure n-type InSb and InAs

19 p3389 A69-36549

Transport mechanism in amorphous Ge film deposited on glass substrates studied by measuring piezoresistance as function of temperature during pure nitrogen immersion

19 p3391 A69-36559

Cadmium sulfide-selenide single crystals reflection coefficient polarimetric measurement, observing reflection peaks relationship to absorption spectral temperature dependence

19 p3391 A69-36607

Undoped n-type gallium arsenide single crystals edge emission spectral band shape dependence on crystal type and ambient temperature

19 p3392 A69-36610

Thermal effects on viscoelastic structure response to applied loads, using equations for thermomechanics, linear and nonlinear thermoviscoelasticity and nonisothermal creep theorem

19 p3440 A69-36657

Vanadium thermistor fabrication influence on resistance jump at phase change temperature of vanadium dioxide, reproducing parameters by heat treating doped vanadium pentoxide

19 p3256 A69-36718

Titanium alloys wear and fatigue resistance as functions of time and temperature of nitriding by purified nitrogen

19 p3347 A69-36743

Body relations in continuum mechanics of solids, examining temperature influence varying in time and space

19 p3444 A69-36805

Weak shock wave structure in temperature relaxation media determined using theory of sound absorption in fluids

19 p3301 A69-36842

Quench rate effect on martensite start temperature and fine structure of Fe-C and Fe-C-Ni steel, using transmission electron microscopy

20 p3557 A69-36956

Nb-Ti-C alloys electrical resistivity and thermal EMF noting nearly linear variations with temperature

20 p3558 A69-36976

Spectral emissivity measurement of ablating phenolic graphite heated by subsonic air stream to high temperature to simulate reentry condition

20 p3565 A69-37187

Soviet monograph on metal fatigue in aircraft structures, discussing effects of temperature, loading, residual stresses, surface finish and contact corrosion

20 p3622 A69-37231

Residual tensile stress distribution during plasma spraying determined as function of temperature field in blank

20 p3548 A69-37328

Electrocaloric effect from 78-130 K on crystalline potassium dihydrogen phosphate, showing quadratic dependence on applied field /and polarization/ in paraelectric phase

20 p3583 A69-37343

He-Ne laser temperature condition optimization based on calculation and experiment

20 p3553 A69-37356

Temperature effect on grain size, crystal orientation, microhardness and heat resistance of diffusion Si coatings on Mo

20 p3560 A69-37361

Diffusion processes, composition and structure of vapor deposited Ni coatings on Nb substrate, plotting intermetallic compounds growth against temperature

20 p3560 A69-37366

Silicon carbide compact coatings deposition on graphite by silicon tetrachloride, H and benzene gaseous mixture, relating layer thickness to temperature and process duration

20 p3566 A69-37368

Solar corona Fe XII emission spectral lines relative intensity analyzed as function of temperature electron density

20 p3603 A69-37548

Temperature effect on electron concentration steady distribution in F 2 layer

20 p3525 A69-37657

Transient thermal stresses in heat treated elastic-perfectly plastic disks with temperature dependent yield stress, considering stress distribution sequence and residual stresses

20 p3629 A69-37974

Desinent cavitation on hemispherical nosed bodies in water at various temperatures and velocities, considering isothermal case for surface nuclei
[ASME PAPER 69-FE-1] 20 p3516 A69-37986

Hall coefficient and conductivity measured as function of temperature for liquid Au, Cu and Ag tellurides and liquid alloy systems Bi-Te and Ti-Te
20 p3584 A69-38024

Hugoniot equation of state of shock loaded W determined at room temperature and 950 C
20 p3564 A69-38127

Elements nucleosynthesis during thermonuclear burning of carbon at series of temperatures and for several initial compositions
20 p3612 A69-38163

Nitrogen diffusion coefficients in TiN and alpha-Ti determined by metallographic and roentgenographic analyses, establishing linear equations for temperature dependence
20 p3564 A69-38214

Carbides and silicides temperature coefficient of electrical resistivity and Hall constant plotted as function of metal carbides solid solutions concentration
20 p3585 A69-38216

Temperature dependence of stimulated light power from GaAs junction lasers operated at constant bias current above threshold
21 p3734 A69-38437

Fe crystals dislocations dynamic behavior during plastic flow development, describing stress and temperature effects on dislocations propagation and interactions
21 p3833 A69-38569

Structural changes during annealing of W and Mo single crystals deformed by rolling, using X ray diffraction topography methods with two crystal spectrometer
21 p3742 A69-38583

Automated rebound resilience apparatus for polymer dynamic mechanical properties studies over wide temperature range, using photoelectric device
21 p3689 A69-38593

Metal deformation dynamics at elevated temperatures, discussing closed loop electrohydraulic testing machine for stress relaxation and strain rate sensitivity
21 p3689 A69-38595

Heat resistance and strength properties of porous Ni-base cermet materials with mica additions under high temperature oxidation
21 p3751 A69-38615

Alpha Ti thermally activated tensile deformation, studying flow stress dependence on strain, temperature and strain rate
[ASM PAPER W9-4.2] 21 p3729 A69-38659

Equilibrium absorption and desorption rates of carbon dioxide-argon mixtures from silica gel measured as function of temperature using gas dynamics method
21 p3848 A69-38707

Thermal effects of resonant coupling hydromagnetic oscillations in inhomogeneous finite-beta plasmas, obtaining equations for coupling modes between Alfvén and magnetosonic waves
21 p3776 A69-38710

Age hardening response of Mg-Th-Zr alloy at 60-450 C, discussing peak strengthening, superlattice formation, precipitation processes, etc
21 p3743 A69-38735

Flow stress temperature dependence of Ni-Cr-Al alloys consisting of gamma prime dispersion in Ni base solid solution
21 p3744 A69-38738

Thermal energy effects on life processes, discussing living cell metabolism, biochemical reactions, enzyme action and protein catalytic functions, etc
21 p3652 A69-38782

Chromatographic analysis of products formed during induction period of 2-methylbutane gaseous oxidation in flow system at low temperatures and long residence times
21 p3669 A69-38798

Diurnal variations of cosmic ray neutrons corrected for barometric and temperature effects by harmonic analysis
21 p3791 A69-38840

Temperature influence of homogeneous kerosene-air mixture on flame stabilization by mechanical and gas dynamic baffle systems
21 p3850 A69-38859

Temperature response of semiconductor thermistors as temperature sensing element, determining time constant from dimensions and experimental data
21 p3723 A69-38888

Phase softening transformations heat resisting alloys during cyclic heating, using X ray and electron microscope analyses
21 p3746 A69-38957

Phase plasticity in Ti-O alloy as function of temperature in alpha Ti and TiO, noting role of increased oxygen diffusion mobility
21 p3746 A69-38959

Breakdown mechanism in GaAs, Si and CdSe semiconductors under intense light pulses ascribed to thermal impact
21 p3737 A69-39042

S doped GaSb single crystals prepared by Crochalski method studied for temperature dependence of resistivity and Hall coefficient
21 p3781 A69-39048

Se activation energy dependence on crystals composition and Se concentration, based on Hall coefficient temperature dependence in gallium arsenic phosphides
21 p3782 A69-39141

Active medium temperature effect on semiconductor laser emission spectra composition, discussing amplification coefficient frequency dependence at various temperatures
21 p3738 A69-39146

Ti-V martensite decay during heating, noting temperature dependence of elastic moduli and electrical conductivity
21 p3746 A69-39160

Hard space suit temperature history during lunar operational task simulation
21 p3666 A69-39182

Design features comparison and operation principles of gas strain gauges in application to structures, emphasizing independence of temperature variations in pneumatic circuits
21 p3725 A69-39324

Superconducting cavity X band oscillator designed for study of stability and spectral purity dependence on temperature
21 p3683 A69-39453

Temperature, applied stress and pressurization effects on materials corrosion by liquid F and F containing oxidizers
21 p3748 A69-39485

Chemical and thermal behavior of materials corrosion in propellant exhaust gases with analysis of reactions involving hydrogen, nitrogen, water, carbon dioxide, etc
21 p3784 A69-39489

Dilute solution of He 3 in He 4 near absolute zero measured for viscosity, showing temperature effect
21 p3772 A69-39582

Arbitrary form temperature rate wave growth and decay, determining differential equation governing wave amplitude
21 p3853 A69-39671

Thermal dissociation of chlorine trifluoride behind incident shock waves as function of temperature using UV absorption spectroscopy
21 p3670 A69-39739

Al discontinuous deformation noting role of intergranular boundary surface at low temperatures
21 p3750 A69-39789

Time-temperature method modified for combining stress relaxation data with stress or strain into single correlation curve, analyzing isothermal relaxation data
21 p3846 A69-39812

Free convection of capillary fluid at vertical plate, allowing for temperature dependence of viscosity coefficient
21 p3854 A69-39843

Temperature-vorticity analogy for viscous two dimensional fluid flow extended to compressible flows, noting enthalpy and shear stress analogy
22 p3929 A69-39892

High E modulus, structure, strength and temperature characteristics of reinforcement fibers, considering B, silicon carbide, C and Be
22 p3951 A69-39907

Short period creep and relaxation in various heat resistant alloys under heat treatments and loads, determining temperature dependence of cyclic thermal instability
22 p3969 A69-40071

Multicomponent Nb alloy creep and rupture strength under loads after heat treatment, determining creep rates dependence on temperature
22 p3969 A69-40073

Transient temperature response of cylindrical composite energy storage devices with thermal conductivity, density and specific heat independent of temperature
22 p3868 A69-40132

Bcc metals strengthening and alloy softening mechanisms, studying temperature and additives effects
22 p3970 A69-40166

Seasonal effects on energy expenditure during rest and exercise at controlled ambient temperatures, noting effects on heart rate
22 p3890 A69-40211

Pressure measurements and gas flow analysis during thermal vacuum tests of manned spacecraft indicating adequate space vacuum simulation
[AIAA PAPER 69-1033] 22 p3924 A69-40401

Accelerated test parameters estimated maximum intensity, studying temperature effects on test results
[AIAA PAPER 69-1036] 22 p3925 A69-40403

Pressure and temperature effects on reversal transitions of stishovite, noting meteoritic impact formation at Meteor Crater, Arizona
22 p4021 A69-40412

Differential capacitance transducer measuring small displacements in heated transformer oil, air, castor oil or glycerin
22 p3946 A69-40439

Spacecraft booms thermally induced vibration and flutter, considering damping and solar exposure effects
22 p4043 A69-40545

Thermal buckling of skew plates clamped along all edges under radiant heating, measuring various characteristics, solving differential equations by difference method
22 p4044 A69-40599

Vapor pressure measurements on liquid fluorine from triple to critical point at one degree K intervals
[NAS-NRC PAPER H-2] 22 p3998 A69-40624

Engineering alloys electrical resistivities measurement at various temperatures, noting temperature and heat treatment effects
[NAS-NRC PAPER D-5] 22 p3970 A69-40633

Ionization formula linking nitrogen ion charge density ratio to plasma temperature
22 p3990 A69-40714

Pure quadrupole resonance spectrum of iodine-127 in solid stannic iodide measured in specific temperature range at atmospheric pressure
22 p3986 A69-40726

Wear resistant Ti carbide based cermets with alloy steel binder, noting electrical and heat conductivity dependence on composition and temperature
22 p3971 A69-40919

Heat transfer coefficient of turbulent air flow found independent of temperature head during cooling
22 p4051 A69-41026

Strain induced creep equation for hardened materials for fixed temperature and stresses range, noting application to steel and Al alloys
22 p3971 A69-41033

Fluorescence properties of nucleotides, polynucleotides and phosphorylated derivatives as function of temperature, pH and ionic strength
22 p3898 A69-41078

SST stratospheric environment problems, discussing temperature effects on fuel consumption and convective turbulence effect on flight safety and efficiency
22 p3867 A69-41141

Dielectric constant and IR spectra of Ba titanate single crystals doped with hydroxyl, showing dependence on temperature and crystal thickness
22 p3995 A69-41157

Waveguide-resonance investigation of temperature dependence of dielectric constant and paraelectric dispersion of Ba and Sr titanate single crystals at millimeter wavelengths
22 p3995 A69-41158

Temperature dependence of heat capacity of Ba and Sr titanate solid solutions in ferroelectric phase transition region
22 p3996 A69-41162

Partial differential equation for creep process in plane stressed metals, interrelating strain, rate, stress tensors, temperature and time
22 p4048 A69-41268

Oxygen supersaturation in unstirred blood under temperature effects, noting tension loss during stirring
23 p4077 A69-41296

Thermal diffusivity measurement by nonsteady state methods, discussing time and temperature variables in heat flow differential equation
23 p4237 A69-41326

Thermal conductivity and specific heat of groups of liquid substances as functions of temperature, giving curves, tables and conversion factors
23 p4238 A69-41336

Gaseous absorption cell variable attenuator for carbon dioxide laser radiation at specific wavelength, using forced convection to eliminate thermal defocusing effects
23 p4172 A69-41396

Human sweat glands reflex responses to diverse skin cooling rates in hot room, discussing bath temperature step decrease effect on lower limb

23 p4082 A69-41446

Cerebrospinal fluid /CSF/ formation in male monkeys as function of fluid pressure at third ventricle level following temperature stress and feeding

23 p4084 A69-41469

Creep strength as function of oxygen pressure for Ni at 510 and 600 C, dropping creep rupture life to plateau of nearly constant life

23 p4176 A69-41504

Inelastic collision cross sections for low energy interactions among electrons, ions, atoms and molecules determined as function of temperature, using approximate methods

23 p4194 A69-41520

Mars atmosphere response to surface temperature changes by radiative and convective heating, noting strong solar control of mean wind distribution

23 p4212 A69-41614

Photoionization rates temperature dependence in upper atmosphere for O atoms and molecules and N molecules from computer calculations, allowing for earth sphericity

23 p4157 A69-41857

Supercritical elastic states in convex shells produced by load in presence of thermal flux, noting no flux effect on states

23 p4228 A69-41970

Temperature influence on mechanical properties and creep curves of fiberglass reinforced textolites compared with data from elasticity theory

23 p4179 A69-41993

Mechanical properties of fiberglass reinforced textolite at normal temperature, noting applicability of elasticity formulas

23 p4179 A69-41994

Temperature dependence of action potential, isometric tension development and relaxation rate of mammalian myocardium at low temperature, considering Ca ions role

23 p4092 A69-42060

Temperature dependence of afferent and efferent spontaneous activity of spinal cord, using filament recordings from ventral and dorsal roots in anesthetized cats

23 p4093 A69-42066

Spinal cord temperature effect on stretch responses of muscle spindle endings of triceps surae, anterior tibialis and extensor digitorum longus in anesthetized cats

23 p4093 A69-42067

Analog computer used to correct body plethysmographic chamber signal distortion due to inspired/expired air temperature and humidity differences

23 p4111 A69-42081

Spinal cord temperature influence on stretch response of tonic and phasic alpha-motoneurons by filament recordings from ventral roots in anesthetized cats

23 p4098 A69-42099

Cold working and aging effects on mechanical properties of TiAl-V including creep and temperature effects

[DGLR-69-002] 23 p4177 A69-42163

Atomic spectrophotometry to monitor O atom formation rate behind shock waves in oxygen-argon mixtures, noting dissociation over 2850-5550 K temperature range

23 p4194 A69-42209

Nb single crystals oxidation in dry oxygen at high pressure and temperature indicating suboxide platelets existence as function of temperature

23 p4177 A69-42357

Single crystal Ta and Ta base bcc solid solution strengthening and weakening as function of temperature and strain rate

23 p4178 A69-42358

Deflections of heated circular plates with or without concentric circular hole and with different boundary conditions and temperature distributions

23 p4234 A69-42412

Praseodymium germanides resistivity and thermal EMF temperature dependence determined, discussing Hall effect, thermal expansion coefficient, melting point microhardness, etc

23 p4199 A69-42467

Isometric contraction tension after sudden isotonic to isometric contraction mode change in cat papillary muscle, discussing temperature effects, tension development changes, etc

24 p4258 A69-42631

Electron irradiation-temperature dependence of introduction rate and room temperature annealing of carrier-removal defects in Li-doped Si

24 p4360 A69-42647

Hybrid display for data visual display using electroluminescent and thermochromic technologies for wide range of ambient illumination

24 p4313 A69-42899

Ni-Nb alloys precipitates tetragonal structure as function of time and temperature using electron and X ray diffraction

24 p4331 A69-42903

Model of moon accumulated at low temperatures, discussing lunar surface layer characteristics

24 p4383 A69-42936

Matrix method for analyzing elastic structures linear transient response to time dependent loads and temperature change

24 p4399 A69-42988

InTe phase formation in thin film composed of two InTe phases, showing dependence on annealing in high vacuum and substrate temperature

24 p4361 A69-42994

Serrated flow characteristics in gold-indium solid solutions at various strain rates and temperatures

24 p4361 A69-43028

High temperature anelastic effect in Mo single crystals ascribed to internal friction peak due to electronic interactions between dislocations and C interstitials

24 p4332 A69-43031

Creep buckling time of simply supported column under nonuniform temperature distribution over cross sections

24 p4400 A69-43053

Turbine blade edge cooling efficiency, investigating Reynolds number and gas temperature to cooling air ratio influence

24 p4364 A69-43082

High temperature single crystal X ray studies of natural Fe-rich orthopyroxene, detecting high-low clinopyroxene inversions

24 p4311 A69-43218

Stress analysis of incompressible solid propellant rocket charges by point matching technique, considering differential thermal shrinkage and axial acceleration cases

24 p4402 A69-43263

Temperature dependence of equilibrium solid solubility of C in Au, Cu and Ag foils with respect to graphite

24 p4334 A69-43413

Real shear modulus and mechanical damping characteristics of cured adhesives measured for temperature effect, using torsion pendulum apparatus

24 p4338 A69-43460

Stagnation temperature determined in transition and free molecule region of rarefied gas flows from critical mass flow dependence on temperature and stagnation pressure

24 p4408 A69-43492

Charring ablator char zone nonequilibrium flow and chemical reaction kinetics as function of temperature, using thermal environment simulator

24 p4409 A69-43512

Numerical program solving partial differential equations parabolic system for internal turbulent gas flow extended to flows undergoing circular tube laminarization by heating

[ASME PAPER 69-HT-52] 24 p4409 A69-43520

Low pressure arc discharge motion between concentric electrodes in transverse magnetic field, noting Lorentz, stationary and retrograde modes due to temperature nonequilibrium

[AIAA PAPER 68-708] 24 p4359 A69-43644

Mechanism for pink afterglow accompanying microwave discharge in pure nitrogen, emphasizing gas kinetic temperature role

24 p4353 A69-43749

Lunar radio emission constant component in presence of heat flow from interior, using stratified model of surface structure with two variants

24 p4390 A69-43788

Equilibrium state of matter at high temperatures and densities with respect to nuclear reactions, determining neutron-proton ratio

24 p4391 A69-43793

TEMPERATURE GRADIENTS

Operational and integral heat balance method to obtain exact and approximate solution for monotonic heating of two layer unbounded plate

01 p0174 A69-10097

Numerical analysis of temperature variation of spherical spinning satellite with and without radiatively coupled inner shell containing heat source

01 p0162 A69-10761

Cryogenic plants for space simulation chambers, examining processes for cooling shroud below 100 K at given temperature differences

01 p0057 A69-11154

Alkali metal vapors thermal conductivity determination by temperature difference dilatometric measurement

02 p0247 A69-115799

Correlation between CAT and thermal gradient increase at standard isobaric levels found to be potential forecasting tool

02 p0275 A69-11818

Rms approximation validity limits for satellite temperature variances by deriving equations for thin insulated plate in space

02 p0352 A69-12211

Diffusion effect on particle buildup in deionizing steady plasma flux linked to plasma concentration in presence of electron temperature gradients

02 p0291 A69-12483

Plane Couette flow stability in heated nonlinear viscous fluid flowing between horizontal plates heated to different temperatures

02 p0235 A69-12828

Noninstantaneous, nonlocal nonlinear responses of momentum and energy flows to thermodynamic forces in single component simple fluid with memory

03 p0413 A69-12921

Temperature drop in combustion chamber of open cycle MHD power plant due to added potassium carbonate as function of various parameters

03 p0369 A69-14162

Earth surface temperature change quantitative determination due to Milankovitch insolation variations

03 p0426 A69-14232

Drifting temperature fluctuations in semiconductors in presence of strong electric field

04 p0643 A69-15256

Thermal transpiration for performance prediction and development of gas pump

[ASME PAPER 68-WA/ENER-4] 05 p0706 A69-16162

Laminar natural convection in enclosed rectangular cavity, discussing temperature gradient effects

06 p1033 A69-17556

Superconducting flux-flow resistivity minimum in Pb-Tl alloy, discussing thermal dissipation associated with temperature gradients across moving fluxoid

07 p1198 A69-18642

Equilibrium stability of horizontal layer of fluid in field of modulated temperature gradient having layer thickness greater than penetration depth of heat waves

07 p1241 A69-18696

Thermal disturbance radiative decay time in carbon dioxide at low pressures and for nonzero vibrational relaxation times

07 p1215 A69-18843

Annual temperature variation in lower tropical stratosphere, noting effect of equatorial upward motion

07 p1126 A69-19043

Nonhomogeneity effect on transverse vibrational frequency of uniform beams

08 p1413 A69-20413

Skin temperature and cutaneous pain during warm water immersion, refuting subcutaneous thermal gradient hypothesis for stimulation of heat pain

08 p1267 A69-20683

Monograph on heat transfer coefficients of polystyrene foams noting contribution of gas conduction, convection and radiation to total heat transfer

08 p1421 A69-20716

Linear perturbation theory to predict instability threshold conditions caused by electric field in poorly conducting liquid subject to vertical temperature gradient

08 p1352 A69-20790

Electroconvective instability produced by uniform electric field in poorly conducting fluid under stabilizing vertical temperature gradient, noting heat flow increase

08 p1352 A69-20791

Laser rubies emission characteristics operating at different temperatures in common resonator, studying kinetics for pumping powers

08 p1327 A69-21076

Zero sensitivity integrated RC filter circuits design, exploiting capacitors and resistors property of having same temperature coefficient

08 p1300 A69-21174

Time dependent recoverable isothermal decrease of photocurrent in CdS crystals in vacuum, noting trap mechanism involving electron redistribution

08 p1374 A69-21187

Thermal EMF in epitaxial films, analyzing potential distribution in p-n junction with temperature gradients and film thickness effects

09 p1555 A69-21473

Temperature profiles variability for data obtained by rocketsonde thermistors launched with small time and spatial separation

09 p1494 A69-21644

Temperature gradient in semiconvective region, examining molecular weight distribution in mixing due to overstability

09 p1596 A69-22057

General relativistic models of massive hot nonrotating stars with adiabatic temperature gradients consisting of ideal gas and radiation mixture

09 p1605 A69-22416

Excess velocity and temperature decay laws in axisymmetric jet in transverse flow obtained via jet momentum and heat conservation equations

10 p1679 A69-23568

Unsteady baroclinic planetary atmosphere boundary layer turbulent states with various pressure and temperature gradient distributions, using boundary layer model

10 p1722 A69-23973

Monograph on internal structure of sun corona covering variations in intensity and width of coronal lines, inhomogeneity, quasi-homogeneous and anisothermic coronas, etc

11 p1961 A69-25103

Nondestructive thermal tests using liquid crystals thermal sensitivity for measurement of temperature changes and visualization of temperature gradients

11 p1892 A69-25293

Temperature variations at porous wall surface as function of transpiration coolant flow rate

11 p2002 A69-25334

Temperature variation effects on heat transfer in laminar tube flow, taking into account constant wall temperature and heat flow density

12 p2189 A69-25762

Temperature variation and heat transfer in fins and relations between heat-flux-density and temperature difference

12 p2190 A69-25763

Linearized steady state equations of motion solved for boundary conditions of fluid lying between horizontal planes with temperature varying horizontally

12 p2066 A69-26134

Thermal stresses induced in plate plane by temperature gradient varying in space and time calculated using Mach-Zehnder interferometer, determining stress intensity factors

12 p2089 A69-26189

Thermal effects in large mirrors, considering temperature gradients parallel to reflecting surface or to optical axis

12 p2056 A69-26408

Limiting pressure for deflagration related to initial solid temperature of single crystals and pressed pellets of ammonium perchlorate

13 p2324 A69-27364

Cellular convection suppression by parallel vertical thermally conducting walls inserted into bottom-heated fluid, analyzing effect on critical Rayleigh number

13 p2374 A69-27782

Vortices interaction effect on vertical turbulent heat flow in atmosphere boundary layer, determining dependence of vortex mean vertical temperature gradient

13 p2293 A69-27841

Simple fluids viscosity dependence on density analyzed by molecular theory, exemplifying with liquid argon

13 p2299 A69-28036

Thermionic converter cathode and anode temperatures difference during start-up heating and under normal operational conditions

14 p2400 A69-29226

Low voltage arc in thermionic cesium vapor diode with lengthy electrodes and temperature variations along emitter, discussing plasma and current density distributions

14 p2402 A69-29244

Temperature disturbance amplification in laminar natural convection boundary layer formed on vertical flat surface measured with hot-wire anemometers

14 p2436 A69-29575

Stratospheric turbulence producing bumpiness up to 18 km developing at levels characterized by abrupt changes in vertical temperature gradients

14 p2474 A69-29737

Measurement system for recording of small localized temperature changes in brain

15 p2606 A69-30152

Creep rates measurement errors at low stresses in intermediate temperature range, examining log creep rate vs log stress plot in Cr-Mo steel

15 p2639 A69-30599

Thermal EMF in epitaxial films, analyzing potential distribution in p-n junction with temperature gradients and film thickness effects

15 p2669 A69-30718

Operating conditions influence on thermal stability of DC plasmatron arc to obtain high temperature source

15 p2663 A69-30994

Atmospheric temperature and vertical gradient in E region based on measured instantaneous wind profiles

15 p2603 A69-31399

Temperature gradients effect on ion flute mode in low beta plasma having density gradients in x direction, obtaining instability condition

16 p2819 A69-31689

Bubble boiling onset in forced fluid flow, deriving equations for calculating minimum temperature difference between wall and fluid, discussing applicability range

16 p2878 A69-31954

Nonlinear generation of sum and difference frequency components in magnetoplasma current density due to alternating electric fields, electron density and temperature gradients

16 p2821 A69-32036

Virtual temperature change with respect to height of saturated air rising during water vapor condensation, discussing actual temperature and precipitation factor

16 p2808 A69-32454

Electromigration role in material accumulation and depletion forming regions in Au film conductors, discussing regions origin from and correlation with thermal gradients along conductor

17 p2936 A69-32896

Temperature jumps at gas-solid interface in shock tube calculated by one dimensional approximation of thermal boundary layer behind reflected shock wave

17 p2949 A69-33023

Lower solar corona composition changes due to pressure and thermal gradients calculated with multicomponent diffusion equations

17 p3030 A69-33059

Heat transfer from cylindrical copper surface to liquid helium at 4 degrees K, discussing temperature fluctuations in nucleate boiling region

17 p3074 A69-33780

Temperature fluctuations in solar photosphere, noting transition from convective to radiative energy transport

17 p3040 A69-33810

F1 layer observation at 80-87 degree solar zenith angles explained by additional ionization maximum development in presence of temperature gradients

17 p2967 A69-33985

Buoyant plumes and thermals defined as vertical motions produced under gravity by density or temperature contrast between incompressible source fluid and environment

18 p3122 A69-34917

Channel heat transfer determination based on thermal conductivity coefficients as functions of temperature gradients in channel wall materials

18 p3230 A69-34988

Silicon and boron carbides wettability with liquid metals during contact reactions at various temperatures, discussing wetting mechanism

18 p3156 A69-35153

Time dependent recoverable isothermal decrease of photocurrent in CdS crystals in vacuum, noting trap mechanism involving electron redistribution

18 p3183 A69-35156

Long term creep rupture data based on short term tests in form of Larson-Miller time-temperature curves

18 p3150 A69-35422

Body relations in continuum mechanics of solids, examining temperature influence varying in time and space

19 p3444 A69-36805

Structure, composition and temperature of Venus atmosphere from spacecraft measurements and ground based observations

20 p3614 A69-38256

Temperature gradient effect on plasma stability in maximum J configuration

21 p3776 A69-38711

Phase softening transformations heat resisting alloys during cyclic heating, using X ray and electron microscope analyses

21 p3746 A69-38957

Transient heat transfer single blow temperature response functions characterized by first moment of downstream-upstream fluid temperature difference, showing curve matching applications

21 p3851 A69-39291

TEMPERATURE MEASUREMENT

Unsteady baroclinic planetary atmosphere boundary layer turbulent states with various pressure and temperature gradient distributions, using boundary layer model

21 p3760 A69-39659

Heat flow through ocean floor by measuring temperature gradient and thermal conductivity in ocean sediment

21 p3718 A69-39733

Cascade thermoelectric heat pump reducing temperature gradient in legs of element near cold junction and reducing Joule heating in cold junction area

22 p3869 A69-40133

Ionized He and Ar plasmas nonequilibrium nozzle flows, noting temperature difference between electron gas and atom-ion gas, calculating flow parameters

22 p3861 A69-41047

Mass diffusion and heterogeneities in compression chamber gas mixture in shock tube ascribable to pressure and temperature gradients

23 p4146 A69-41547

Stress analysis in elastic bodies induced by axisymmetric strains in presence of mass forces and temperature gradients, obtaining equilibrium equation

23 p4229 A69-41997

Temperature control by heat pipe using noncondensing gas with methanol to vary thermal resistance and mathematical model to describe heat source temperature variations

23 p4240 A69-42307

Transition temperature depression in rotating liquid He based on increased inertial density of excitations

23 p4192 A69-42335

Temperature gradients effects on GaAs crystals grown by Bridgman method

23 p4199 A69-42469

Central circulatory responses of humans to rapid skin temperature changes during continuous exercises

24 p4258 A69-42633

Lower atmospheric temperature continuous radio measurement as function of altitude, calculating temperature gradient

24 p4342 A69-42677

Equator-to-pole temperature gradient relation with planetary pressure belts, comparing observational data with theoretical circulation criterion

24 p4345 A69-43149

Monte Carlo method applied to heat transfer in rarefied gas flow between parallel plates involving temperature jump in Knudsen layer

24 p4246 A69-43490

TEMPERATURE INDICATORS

U INDICATING INSTRUMENTS

TEMPERATURE INVERSIONS

NT CENTRIFUGING STRESS

NT INTERFACIAL TENSION

NT STRUCTURAL STRAIN

NT VOLUMETRIC STRAIN

Volumetric and allotropic changes during heating in electrolytic cobalt multiple phase transformations

12 p2114 A69-26455

Vaporizer temperature and collision efficiency correlation data for magnesium oxide-argon dilute diffusion flames studied for determining inverse temperature dependence

13 p2380 A69-28461

Photospheric radiation field role in temperature inversion of stellar chromospheres with dominant H ion opacity, postulating mechanical energy dissipation

20 p3613 A69-38173

TEMPERATURE MEASUREMENT

Two element interferometer observing Saturn, Uranus and Neptune at 3.12 cm, determining equivalent black body disk temperature

01 p0148 A69-10052

Cooled probes for gas measurements in high pressure arc jets, hypersonic wind tunnels, rocket motors, scramjets and similar severe environments

01 p0078 A69-10150

Atmospheric temperature and airglow spectra from IR measurements noting OH bands, atmospheric structure between 10 and 200 km at midlatitude and atmospheric absorption

[UN PAPER 68-95471] 01 p0108 A69-10464

Aerial radiation temperature measurement, damping factor of atmosphere and determination of ground and water surface temperatures by radiometry

01 p0110 A69-10693

Atmospheric temperature corrections for measurements by rocketsonde and balloonsonde with thermistor, noting dissipation factors and thermal time constants

01 p0081 A69-10697

Jovian atmospheric rotational temperature from rotational lines in methane band
01 p0153 A69-10856

Heat flow measurement from moon interior planned for Apollo missions to determine temperature increase rate with depth during lunar year
[AAS PAPER 68-207] 02 p0313 A69-11482

Line reversal and excitation temperatures in low pressure flames
02 p0350 A69-11709

Electro-optical measurements to determine intermolecular interaction temperatures in organic liquids compressed by shock waves
02 p0230 A69-11979

Solar continuum intensity determination in middle IR, obtaining solar disk center brightness temperature measurement by comparison with black body model
02 p0318 A69-12041

Temperature and pressure measurements in low temperature combustion of n pentane covering slow reaction and cool flame regions
02 p0353 A69-12321

Cosmic microwave background radiation measurement, discussing measurement techniques for antenna temperature at microwave frequencies
02 p0210 A69-12431

Microwave radiometer with two reference temperatures, discussing overall stability of design, sensitivity and airborne design for operation in X band [DVL-895] 02 p0220 A69-12435

Measured noise temperature in argon tubes vs theoretical electron temperature for gas discharge noise sources
02 p0210 A69-12437

Compensation method for measurement of mismatched noise source effective temperature independent of reflection coefficient, noting error analysis
02 p0210 A69-12441

Dense plasma temperature determination by gamma ray resonance scattering
02 p0291 A69-12481

Brightness temperature maps for Jovian thermal radiation obtained through 8-14 micron window of atmosphere
02 p0309 A69-12715

Jupiter, Venus and Mars 8.6 mm radio emission, obtaining average disk brightness temperatures
02 p0327 A69-12716

Lunar thermal radiation measurements at 8.6 and 3.2 mm wavelengths, noting brightness temperature-time relationship in curves and as Fourier components
02 p0327 A69-12717

Vertical wind velocity structure and turbulent heat flux temperature measurements over steppe and sea, noting underlying surface influence
03 p0458 A69-13270

Temperature determination of subjacent surface from airborne measurements of outgoing radiation in earth atmosphere in 10 to 12 micron interval
03 p0424 A69-13933

Thermionic emission and dispersion of plasma created by monopulse of laser radiation focused on solid target, discussing plasma temperature determination methods
03 p0441 A69-14141

High temperature measurement based on spectral line displacement and broadening due to Stark effect, noting diagrams for O, Na, Mg, Al and Si at various temperatures
03 p0481 A69-14146

Time resolved electron number density and electron temperature in decaying plasma using laser interferometer
03 p0432 A69-14187

Balloon observations of solar far IR spectrum and brightness temperature
04 p0652 A69-14419

Electron radiation temperature measurement in carbon dioxide laser with N and He additions by microwave technique, noting average electron energy and optical gain
04 p0611 A69-14445

Airborne radiometric /8 to 14 micron/ temperature measurements, determining emissivities of ocean, stratus clouds, desert and snow
04 p0592 A69-14653

Radiation compensating thermocouple for gas temperature measurement, noting advantage over single thermocouples
04 p0598 A69-14916

Electron temperature time variation measurement in plasma-beam discharge by method based on single spectral line
04 p0638 A69-15368

Temperature measurement of moving droplets, noting influence of thermocouple electrode stability
04 p0688 A69-15423

Venus observation at 4.52 cm showing 654 K mean brightness temperature, negligible phase variation and polarization indicates thick atmosphere
05 p0818 A69-15601

Ionospheric electron temperature probe analysis based on Japanese Kappa rocket data
05 p0761 A69-15701

COSPAR manual on stratospheric temperature and wind measurements, discussing synoptic and time variation study by Arcas and Loki-Judi meteorological sounding rocket systems
05 p0752 A69-15706

Spectral line reversal method of measuring high temperatures of gases
05 p0761 A69-15763

Molten salts thermal diffusivity measurement method at temperatures above melting point [ASME PAPER 68-WA/ENER-5] 05 p0848 A69-16161

Gravity waves observed by ionospheric temperature measurements in F region
05 p0754 A69-16262

Midlatitude neutral thermosphere density and temperature measurements, noting effect of atomic oxygen adsorption by instruments
05 p0755 A69-16268

Langmuir probe experiment measurement of upper region electron temperature on Explorer 32 conflict with Jicamarca Radar Observatory measurements
05 p0756 A69-16283

Simultaneous and independent measurement of thermal conductivity, thermoelectric power and electric resistivity, applying method to cadmium arsenide-zinc arsenide system
05 p0764 A69-16338

Ion temperature diurnal variations at 250-475 km obtained from Thomson scatter spectra
05 p0757 A69-16407

Radiation effects on NERVA out-of-core instrumentation, discussing cryogenic temperature measurements and transducer measuring pressure at gamma heating rates
06 p0956 A69-16882

Stratospheric temperature, wind and ozone concentration measurement during solar eclipse by sounding rocket system
06 p0916 A69-17008

Low pressure fuel system and turbine rotor blade temperature measurement method for Concorde Olympus 593 engine [ASME PAPER 68-GT-63] 06 p0984 A69-17187

Microwave radiometer for measuring mesosphere and stratosphere temperature as function of altitude using atmospheric oxygen line
06 p0924 A69-17247

Line reversal temperature measurement technique, calculating error and outlining correction methods for flames with cool boundary layers and flames containing solid particles
06 p1035 A69-17929

Radiating surface temperature and total atmospheric moisture content determinations based on meteorological earth satellite measurements of outgoing radiation in IR
06 p0952 A69-17988

Book on fundamentals of temperature, pressure and flow measurements covering standards, calibration, moving fluid effects, transient effects and installations in fluids and solids
07 p1131 A69-18410

Barrier capacitance of semiconductor diodes for exact temperature measurement, discussing application to temperature to frequency converters
07 p1100 A69-18556

Optical device for measurement of temperature changes with height in upper atmosphere by rockets or satellites
07 p1132 A69-18676

Ultrasonic thermometry for nuclear reactors based on temperature dependence of sound velocity in solids, discussing simulation experiments [IEEE PAPER 1C-4] 07 p1134 A69-19186

Thermocouple and optical methods for temperature profile measurement in slow burning flat hydrogen-nitrogen-oxygen flame at atmospheric pressure
07 p1242 A69-19489

Degree of population inversion and inverse temperature measurement in medium
07 p1137 A69-19761

Dimensions, temperature and electron density of quiet solar corona from radio interferometer measure-

ments, noting activity and temperature at solar maximum and minimum
08 p1393 A69-205737

Skin and subcutaneous temperature during exposures to intense thermal radiation, discussing estimation of subcutaneous temperature from skin temperature data [AGARDOGRAPH-111] 08 p1264 A69-206717

Ar-H plasma arc radial temperature distribution determined by photoelectric spectroscopy in visible range
08 p1366 A69-207581

Jet engine gas flow, temperature, velocity and pressure measurements by analog and digital systems
08 p1316 A69-208699

Mean temperature values accuracy determined from fixed period values by frequency graphs, discussing deviations from mean
09 p1534 A69-21511

Automatic measuring device for short term air temperature and wind velocity fluctuations leading to air mixtures propagation
09 p1535 A69-21515

Differential brightness of night airglow spectrum, obtaining rotational temperature by comparison with synthetic spectra
09 p1488 A69-21656

Coordination technique for pressure, density and temperature measurements by probes during parachute reentry into planetary atmospheres, taking into account reentry dynamics
09 p1609 A69-21775

Reproducibility of thermionic converters performance, comparing volt-ampere characteristics with reservoir and collector temperature
09 p1437 A69-21813

Atmospheric molecular oxygen temperatures from photoelectric recordings of absorption bands, analyzing relaxation process and photoeffects in oxygen molecules
09 p1490 A69-21863

Shock heated helium plasma temperature measurements by spectroscopy compared to Rankine-Hugoniot calculations including ionization effect
09 p1548 A69-21963

Air layer between target and instrument effect on earth surface temperature conducted with airborne radiometers
09 p1536 A69-22166

Emission-absorption intensity ratio temperature measurements of diatomic molecules under thermal nonequilibrium conditions, considering rotational population distribution during vibration temperature measurement
09 p1623 A69-22255

Resistance temperature transducers and thermocouples covering characteristics, readout and design for aerospace requirements
10 p1690 A69-23225

Ultrasonics for automatic measurements of temperature and elastic moduli above 5000 F
10 p1694 A69-23373

Low temperature optically thick boundary layers influence on spectroscopic temperature measurements in plasma MHD channels
10 p1731 A69-23434

Prolateness of Venus radius on basis of satellite microwave temperature measurements, chemical compositions and ice cap model
10 p1784 A69-23958

Monograph on comparison of various methods for experimental determination of temperature fields in laminar burner flames
11 p1999 A69-24635

Holography for temperature distribution measurement around heated wire, using He-Ne laser
11 p1887 A69-25197

Nondestructive thermal tests using liquid crystals thermal sensitivity for measurement of temperature changes and visualization of temperature gradients
11 p1892 A69-25293

Shock wave structure in gas mixtures, discussing velocity and temperature undershoot and overshoot
11 p1874 A69-25356

Spectral brightness temperature of shock waves in air measured at 220-800 nm, obtaining 9-14 km/sec shock waves by detonating explosives
11 p1877 A69-25755

Monograph on schlieren-optical technique for plasma beam temperature measurements using photoelectric scanning device
12 p2134 A69-26120

Formulas derived for tropospheric equivalent noise temperature as function of frequency, noting applicability to thermal radiation from rain
12 p2032 A69-26704

Hydrogenic transition derived excitation temperatures for Wolf-Rayet stars of WC sequence
12 p2160 A69-26904

Previsual detection of vigor loss and mortality signs in ponderosa pine trees subject to bark beetle attack
12 p2098 A69-26993

Rocket observations of visible and UV dayglow, using electron density and temperature measurements for emission rates of various excitation mechanisms
12 p2076 A69-27108

Diffusion and mass flow in steady state magnetically stabilized helium arc plasma effects on spectroscopic determinations of electron temperature, discussing degree of ionization
12 p2141 A69-27146

Hayashi effect modifications due to high opacity stellar atmosphere or presence of molecular hydrogen dissociation zone, discussing pressure dissociation role
13 p2342 A69-27594

Temperature measurement associated with bubbles leaving heat source in subcooled pool boiling carbon tetrachloride analyzed, using high speed motion pictures by schlieren optical system
[ASME PAPER 68-HT-47] 13 p2374 A69-27779

Thermocouples dynamic response attached to thin skinned model under constant heating rate, considering error reduction in temperature measurement
13 p2375 A69-27785

Free convection heat transfer from heated inclined flat plate in air, studying effects of angular positions
13 p2375 A69-27794

Temperature measurement of plasma consisting of combustion products in MHD duct, measuring spectral line contours by Fabry-Perot interferometer for accuracies
13 p2309 A69-28023

Diagnostic measurements in nonequilibrium nozzle flows compared to finite rate expansion calculations, measuring pressure, temperature and density
[AIAA PAPER 69-328] 13 p2200 A69-28263

Fluorescence stimulated by high energy electron and ion beams, determining vibrational temperature and concentration of molecular oxygen in high enthalpy wind tunnel flows
13 p2302 A69-28265

Heat conversion coefficients and initial temperature of active elements of solar powered electric devices
13 p2209 A69-28314

Structure and thermometry of solar interior from measuring neutrino fluxes intensities emitted by unit mass
13 p2333 A69-28434

Optical measurement method for burning surface temperature of condensed systems, realizing radiation from surface of combustion by light guide of monocrystalline aluminum oxide
13 p2379 A69-28453

Rocket grenade measurements of earth atmosphere, finding lowest temperature in Alaska
13 p2255 A69-28637

Vertical wind velocity structure and turbulent heat flux temperature measurements over steppe and sea, noting underlying surface influence
14 p2471 A69-28778

Temperature measurement for aircraft gas-turbine engine development
14 p2509 A69-28886

Asymmetric spherical temperature field reconstruction based on measuring temperature and derivatives at two points of field
14 p2537 A69-28888

Blue continuum emission from hot carbon dioxide measured in shock tube, discussing applications to temperature measurement of gases containing carbon dioxide
14 p2427 A69-29014

Balmer jumps for B star temperature scale, discussing relation between observed Balmer jumps and observed U-B color indices
14 p2518 A69-29132

Actinium fueled thermionic generator design and characteristics, noting emitter temperature and material
14 p2399 A69-29192

Microwave brightness temperatures for downward viewing over open seas from above atmosphere, using tropospheric model containing homogeneous layer clouds
14 p2415 A69-29515

Temperature measurements - Conference, Hawthorne, California, April 1969
15 p2606 A69-30151

Measurement system for recording of small localized temperature changes in brain
15 p2606 A69-30152

Temperature measurement miniature telemetry transmitter
15 p2607 A69-30156

Electro-optical measurements to determine intermolecular interaction temperatures in organic liquids compressed by shock waves
15 p2561 A69-30264

Sky cosmic radio emission absolute temperature measured at decimeter wavelengths and at two zenith angles to minimize atmospheric influence
15 p2687 A69-30544

Global mean monthly charts for IR radiation temperature, based on Cosmos 144 satellite data
15 p2596 A69-30643

Argon electric arc axis temperature measurements, showing current and tube diameter ratio dependence
15 p2662 A69-30977

High gas stream temperature levels and distributions from transient and intermittent probe measurements
15 p2612 A69-31268

Passive temperature indicators for maximum temperatures attained within rocket nozzle ablative materials
15 p2613 A69-31273

Thermocouples precision used for measuring metal temperatures of cooled jet engine turbine buckets
15 p2613 A69-31274

Temperature measurements of neutral polar atmosphere at 120-170 km using artificial Na clouds
15 p2606 A69-31448

Conditions behind incident and reflected shock waves in shock tube calculated from initial pressure, density, temperature and shock speed
15 p2593 A69-31487

Cholesteric liquid crystal film application to test surfaces for thermal mapping, giving technique for flaw pattern determination
15 p2631 A69-31507

Airstream parameters /temperature and velocity/ of turbulence intensity in jet core at tube exit and behind grids measured by He diffusion method
16 p2771 A69-31959

Electron temperature time variation measurement in plasma-beam discharge by method based on single spectral line
16 p2822 A69-32115

Electron beam rotational temperature, noting discrepancies between experimental values and iterative calculations due to secondary electron effects
16 p2814 A69-32175

Ammonium perchlorate pyrolysis by convective surface heating, monitoring IR emission as measure of surface temperature
[WSCJ PAPER 69-23] 16 p2832 A69-32361

Temperature and flow measurements in jet engine combustion chamber, discussing design and calibration of gasdynamic thermometer, double thermocouple and flow probe
17 p2945 A69-32947

Fluid amplifier with sudden widening applied to various computer tasks, utilizing for detection and measurement of viscosity, temperature and sonic or rotational velocity
17 p2903 A69-33010

Temperature determination of thick flat plate rotating in space in solar flux with one surface insulated compared with Apollo heat shield results
[AIAA PAPER 69-614] 17 p3071 A69-33266

Ocean and water surface temperature measurement by IR remote sensing from aircraft and satellites, discussing accuracy and data correction
[AIAA PAPER 69-590] 17 p2973 A69-33286

Mars surface temperature calculated by applying Humphrey formula for planetary radiation energy, finding mean annual values of temperature for different albedo
17 p3034 A69-33412

Subsurface Martian temperature from sinusoidal temperature variation theory for semiinfinite homogeneous medium, plotting amplitude, mean surface and diurnal soil temperature curves
17 p3034 A69-33413

IR radiometer to measure Jupiter atmospheric temperature by calculating certain constituents heat radiation levels through Planck formula assuming black body properties
17 p2974 A69-33425

Pressure and temperature surveys of Mach 27-47 nozzle boundary layer at Ames M-50 He tunnel, determining velocity profiles, wall friction coefficient, etc
[AIAA PAPER 69-686] 17 p2953 A69-33441

Contact thermocouples to measure temperature of wall exposed to radiation, evaluating errors
17 p2975 A69-33596

Particulate thermophysical lunar soil model for measuring lunation nighttime and eclipse cooling, noting applicability to IR surface brightness temperature of Mercury hot pole
18 p3191 A69-34303

Temperatures of radiantly heated sun and shade leaves of white oak measured in low speed wind tunnel, considering differences in convective heat dissipation
18 p3095 A69-34540

Ducted fan engine turbine air flow rate and frontal gas temperature determined from air temperature/pressure measurements behind compressor and engine fuel flow
18 p3086 A69-34986

Low density plasma electrical conductivity determined by temperature and electron density measurements, using Ohm law
18 p3181 A69-35072

Resistance thermometers operation characteristics and applications, noting sensor metals, true temperature and instrumentation errors
18 p3139 A69-35480

Static temperature measurement in arc-tunnel tests producing high velocity air streams by duplex scanning IR spectrometer
19 p3294 A69-35752

Integrated circuits failure analysis techniques utilizing pin-to-pin curve tracer tests and thermal measurements
19 p3282 A69-35786

Structural parameters selection for thermocouples with butt-weld electrodes, developing mathematical basis for thermoelectrode length to measure unstable gas temperatures
19 p3311 A69-36197

Heat transfer problem involving temperature determination of body and ambient medium, deriving existence and uniqueness theorems for boundary value problems in curvilinear regions
20 p3631 A69-36991

High gas stream temperatures determination from short exposure probe based on inferring temperature from transient response of sensor
20 p3536 A69-37005

Vibrational temperature of low density nitrogen measured by electron beam method, discussing relationship to ratio of integrated vibrational band intensities
20 p3579 A69-37222

Plasma coating formation mechanisms and parameters, studying metal surface and deposited particles temperatures, spraying time effects, etc
20 p3549 A69-37374

Japanese meteorological sounding rocket for atmospheric temperature and wind from 60 km down to balloon observation level, discussing principles and payload separation
20 p3543 A69-37795

Excitation temperatures and OH microwave line optical depths measured for dust clouds, discussing optical absorption lines and LF radio absorption
20 p3611 A69-38147

Methane abundance and rotational temperature of Jupiter, considering effects of line saturation
20 p3613 A69-38174

Carbon dioxide band in Venus spectrum by dispersion analysis, deriving rotational temperature
20 p3614 A69-38254

Fourier heat equations functional corrections for determining temperatures of plate and cylinder heated simultaneously by radiation and convection
21 p3848 A69-38641

IR spectrum of NML Cygnus star using rapid scanning Michelson interferometer, estimating temperature from CO bands
21 p3800 A69-38678

Temperature potentials in cylinder of known radius, investigating optimal heating regime and thermal kinetic factor effect on maximum potential magnitude
21 p3837 A69-39089

Satellite determination of underlying surface temperature by IR spectroscopy, measuring emitted radiation in atmospheric windows
21 p3759 A69-39114

Solid metal oxide particles temperature in premixed flames determined from intensity/ wavelength plots of continua
21 p3852 A69-39592

Heat flow through ocean floor by measuring temperature gradient and thermal conductivity in ocean sediment
21 p3718 A69-39733

Monograph on hot wire anemometer measurements of velocity and temperature turbulence, discussing flow characteristics, calibration, etc
22 p3951 A69-41256

Pyrometer for turbine rotor blades surface temperature measurement, considering purged, line-of-sight viewing tube and signal processing to reject C particles interference
[SAE PAPER 690431] 23 p4165 A69-41649

Jet engine combustion temperature measurements by thermocouples or gas analysis noting errors involved
23 p4165 A69-41650

Ion temperature measurement in rarefied multicompartment plasma by temperature relation to ion beam divergence rate, comparing results to pyrometric measurements
23 p4196 A69-41839

Calorimetry-thermometry discrepancy during prolonged exercise in hot dry environment, measuring rectal temperature with increasing exposure time
23 p4098 A69-42104

Two fluid heat pipe performance, measuring temperatures and condenser end vapor pressures for two thermal power input conditions
23 p4240 A69-42306

Lower atmospheric temperature continuous radio measurement as function of altitude, calculating temperature gradient
24 p4342 A69-42677

Thermal calculations of objects near lunar surface, considering IR emission directivity effects
24 p4385 A69-43254

Radiation equilibrium temperature measured downstream of transpiration cooled gas flow near slender cone vertex in continuous flow hypersonic tunnel
24 p4248 A69-43588

TEMPERATURE MEASURING INSTRUMENTS

NT OPTICAL PYROMETERS

NT PYROMETERS

NT RADIATION PYROMETERS

NT RESISTANCE THERMOMETERS

NT THERMOCOUPLE PYROMETERS

NT THERMOMETERS

Thermographic phosphor technique to provide transient temperature measurements in impulse wind tunnel
01 p0078 A69-10152

Alkali metal vapors thermal conductivity determination by temperature difference dilatometric measurement
02 p0247 A69-11579

Fluid temperature sensor generating output differential pressure proportional to temperature of fluid entering device
02 p0249 A69-12089

Acoustical thermometer-interferometer to measure air temperature between 20 and 50 km
03 p0429 A69-13269

High temperature directional reflectance measurements of ablative materials as function of sample temperature using paraboloid reflectometer
[AIAA PAPER 68-25] 04 p0604 A69-15512

Telemetry technique utilizing thermocouple sensors for base heating determinations on free flight blunt cone in shock tunnels, noting electrical noise reduction
[AIAA PAPER 68-407] 04 p0604 A69-15514

Flow field in fluidic temperature sensor using schlieren and shadowgraph techniques
[ASME PAPER 68-WA/FE-29] 05 p0763 A69-16102

Fluidic type temperature sensor for total temperature measurement for hypersonic aircraft in atmosphere
05 p0766 A69-16755

Automatic remotely operated sodium D line reversal temperature measuring apparatus, analyzing systematic errors
06 p1035 A69-17932

Pyroelectric thermometry for measurements at low temperatures with emphasis on calorimetry, discussing pyroelectric coefficients, dielectric constants and resistivities
09 p1493 A69-21423

Rapid low level commutator for temperature measuring circuit with thermocouples, discussing construction and performance
11 p1884 A69-24758

Differential catalytic thin film heat gauge for measuring surface temperature variations and ionized flow heat transfer, noting insulating boundary layer thickness
11 p2002 A69-25231

Acoustical thermometer-interferometer to measure air temperature between 20 and 50 km
14 p2445 A69-28777

Thermistor instrument for remote sensing, magnetic synchronous recording and linear display of temperature
14 p2449 A69-29562

Radiation method for temperature and heat flux measurement, discussing transducer with thermopile as sensor
15 p2607 A69-30154

High speed picture thermography in nondestructive testing, describing IR scanning frame rate and thermal image recording
15 p2618 A69-30316

Surface temperature measurements to deduce surface heat fluxes, noting dependence on environment and sensor characteristics
15 p2716 A69-30379

TEMPERATURE PHOTOMETERS

U PHOTOMETERS

TEMPERATURE PROBES

Thermoelectric radiometer for transient radiant flux short duration pulse measurement, using thermally induced depolarization of polymer film dielectric
[AIAA PAPER 68-403] 02 p0250 A69-12392

Meteorological rocket probes in Spain for wind and temperature measurements, including stratospheric circulation data
11 p1877 A69-24519

Transistorized assembly for amplification of signals emitted by platinum film probes in shock tubes, discussing application to chronometric device triggering
11 p1887 A69-25095

Construction and calibration of combined temperature and pressure probe for compressible flow
13 p2242 A69-28226

High gas stream temperature levels and distributions from transient and intermittent probe measurements
15 p2612 A69-31268

Water cooled split-flow probe measuring enthalpy of high temperature subsonic streams
15 p2614 A69-31275

Thermocouple probe measurement error evaluation by parallel plate analytical model
16 p2789 A69-31903

Miniature probe with short time response for total temperature profile measurements in hypersonic turbulent boundary layer on wall of hypersonic tunnel nozzle
19 p3293 A69-35751

High gas stream temperatures determination from short exposure probe based on inferring temperature from transient response of sensor
20 p3536 A69-37005

TEMPERATURE PROFILES

Approximate boundary controllability for heat equation by considering temperature variation with time
01 p0173 A69-10008

Atmospheric temperature profiles by regularizing algorithm, discussing influence of random errors in measured radiation and kernel of integral equation on interpretation accuracy
02 p0274 A69-11448

Heat transfer through vertical plane layer for various Prandtl numbers, discussing velocity and temperature profiles and effects of aspect ratio, Grashof and Rayleigh numbers
[ASME PAPER 68-WA/HT-4] 05 p0846 A69-16115

Radial temperature profile in induction coupled argon plasmas at low and atmospheric pressures
06 p0964 A69-17193

Mathematical techniques for treating satellite based atmospheric data involving radiative transfer equation inversion, noting scattering and temperature measurement problems
06 p0957 A69-17618

IR spectrometer for Nimbus meteorological satellite for terrestrial spectral radiance data for atmospheric temperature profiles
06 p0926 A69-17621

Relaxation method for inversion of full radiative transfer equation, determining temperature profile in atmosphere from outgoing radiance
[JPL-TR-32-1351] 06 p0922 A69-17805

Fluid flow longitudinal temperature profiles for inclusion in heat transfer computer program
[AIAA PAPER 69-30] 06 p1038 A69-18174

Modified schlieren interferometer for quantitative investigation of free convection boundary layer temperature profiles
07 p1130 A69-18263

Combined radiation and conduction heat transfer equation applied to temperature profile around opaque hollow sphere and in solid condensed gas layer
[SAE PAPER 690197] 07 p1239 A69-18303

Temperature profile and power density distribution in metastable level of ruby laser rod during pumping in air
07 p1150 A69-18937

Thermocouple and optical methods for temperature profile measurement in slow burning flat hydrogen-nitrogen-oxygen flame at atmospheric pressure
07 p1242 A69-194898

Temperature profile calculations for high pressure electric arcs using diffusion approximation for radiative flux density, taking energy transfer into account
08 p1420 A69-201484

Temperature profiles and heat transfer coefficients in two phase liquid-liquid stratified laminar flow of variable immiscible film thickness with surface evaporation
09 p1622 A69-21904

Temperature profiles and frequency driftings of VHF telemetry transmitters for Saturn S-IC stage, using IR radiation data
10 p1653 A69-23049

Temperature pulsations radial distribution in plasma jet using plasmatron without mixing chamber
10 p1729 A69-23432

Nozzle flow temperature patterns of relaxing combustion gases compared at different temperatures and pressures, using kinetic-chemical calculations
[DVL-896] 10 p1809 A69-23644

Viscosity-temperature chart for hydrocarbons permitting linear extrapolations into low viscosity high temperature regions
10 p1753 A69-23975

Elastic and elastoplastic strains in materials under various loadings, determining temperature variations by thermoelectric method and verifying by tensile tests
11 p1985 A69-25178

Power law profiles of mean wind velocity and temperature in thermally stratified shear flow, considering dependence on thermal stability and Richardson number
11 p1874 A69-25381

Ionosphere temperature profiles, discussing heating and cooling of electron gas and ion gases and thermal balance
12 p2063 A69-25903

Temperature vertical profiles rms deviations calculated from temperature measurements during unstable atmospheric stratification
13 p2293 A69-27847

Sealed and unsealed relay coils temperature rise at simulated outer space air pressure levels
13 p2231 A69-28048

Upper atmosphere winds and temperature measurements from rocket grenade, discussing TMA experiments
15 p2598 A69-31317

Electrical and thermal conductivities of high pressure arc plasmas from I-V characteristics and radial temperature profile
16 p2817 A69-31644

Ozone soundings in upper stratosphere, discussing vertical temperature profiles relationship to vertical ozone profiles
16 p2787 A69-32640

Nonlinear least squares optimization program applied to atmospheric temperature sounding, solving for temperatures at various altitudes from simulated carbon dioxide intensity measurements
17 p2960 A69-33156

Temperature profiles and associated wind profiles obtained with Jimsphere/FPS-16 radar system at Cape Kennedy, discussing remote CAT detector assessment
17 p2999 A69-33739

Miniature probe with short time response for total temperature profile measurements in hypersonic turbulent boundary layer on wall of hypersonic tunnel nozzle
19 p3293 A69-35751

Inelastic collisions and radiation effects on transport properties and shock structure in high temperature gases, obtaining density and temperature profiles
19 p3448 A69-36149

Flame acceleration data applied to unburnt gas boundary layer analysis, discussing velocity and temperature profiles, layer thickness variation and expansion phase backflow
19 p3450 A69-36359

Orthogonal functions for determining atmospheric vertical temperature profile from satellite measurement of earth outgoing radiation in carbon dioxide absorption band
19 p3303 A69-36409

Wind and temperature profiles in Ekman boundary layer, using numerical integrations of dynamic equations including time derivative terms
19 p3363 A69-36501

Thermosphere temperature shape parameters from probe flights, showing dependence on hour angle
20 p3534 A69-38088

Temperature measurement in and near opposed-jet diffusion flame subjected to electric field, discussing flame behavior at low mass flow rate

21 p3852 A69-39597

Temperature fluctuations in microwave background radiation from primeval perturbations compared with perturbations from discrete radio sources

21 p3815 A69-39611

TEMPERATURE SCALES

Lyman alpha wing opacity effect on temperature scale and helium content in F and G subdwarf atmospheres

09 p1607 A69-22431

Negative absolute temperatures physical meaning confirmed mathematically using statistical physics

18 p3231 A69-35403

TEMPERATURE SENSORS

NT THERMISTORS

Fluid temperature sensor generating output differential pressure proportional to temperature of fluid entering device

02 p0249 A69-12089

Fluidic type temperature sensor for total temperature measurement for hypersonic aircraft in atmosphere

05 p0766 A69-16755

Error analysis of high resolution balloon-borne temperature sensor and comparison of temperature data with simultaneous rawinsonde measurements

09 p1494 A69-21642

High temperature sensors for gas turbines, discussing thermocouples and radiation pyrometer to sense turbine hardware

[ASME PAPER 69-GT-30]

09 p1501 A69-22492

Compressor inlet temperature /CIT/ sensors, describing bimetal strip and liquid expansion aspirated types

[ASME PAPER 69-GT-18]

09 p1571 A69-22499

Miniature fluidic oscillator temperature sensors evaluated in gas turbine engine nozzle, discussing temperature control and related signal error compensation and temperature averaging

[ASME PAPER 69-GT-70]

09 p1572 A69-22512

Fluidic temperature sensors for measuring turbine inlet temperature on large turbine engine

[AIAA PAPER 69-544]

16 p2792 A69-32692

Fluidic sensors for jet engine control, analyzing convergent divergent nozzles, vortex and acoustic oscillators for pressure and gas temperature measurements

[AIAA PAPER 69-542]

16 p2843 A69-32699

Cryogenic liquid level temperature transducer with radiantly heated thermocouple sensitive element

17 p2975 A69-33670

Sea surface temperature remote sensing by Nimbus 2 satellite using TV camera and medium and high resolution IR radiometer

18 p3130 A69-35057

Transducer with single crystal Ge for high heat flux measurement, noting calibration by direct conduction

19 p3307 A69-35748

Thin film temperature sensor material, response time, substrate material and flight instrumentation for rocket-borne application

22 p3950 A69-41229

Spacecraft solar cell near-maximum power operation by tracking optimum value with array temperature sensor

23 p4075 A69-42303

TEMPERING

Transitional hexagonal omega phase of Ti-Fe alloys quenched in water and tempered

03 p0451 A69-13999

Tempering time and temperature effect on microstructure, superconductivity, tensile strength and electrical conductivity of recrystallized Nb-Ti alloy

19 p3345 A69-36302

TEMPLATES

Bending of weightless thin elastic beams clamped to circular template by external force

12 p2181 A69-26572

TENSILE CREEP

Four specimen vacuum device for simultaneous tensile creep tests at 1200 C, discussing linear and thermal expansion

07 p1116 A69-19318

Rupture times in analysis of creep tensile instability in uniformly pressurized thin walled membrane shells of revolution, comparing two criteria

07 p1234 A69-19378

Polycrystalline Re high temperature plastic deformation during tensile creep, including activation energy and substructure dislocation study

13 p2280 A69-27767

Ronay effect in reversed cyclic torsion or tension in thin cylindrical viscoelastic tube showing creep under sustained load

20 p3625 A69-37596

TENSILE DEFORMATION

Fatigue strength reduction of structural steels fatigued in rotating bending after tensile deformation

03 p0450 A69-13916

Tensile deformation properties of copper single crystals strengthened by fine dispersions of BeO particles

08 p1334 A69-20575

Deformation processing of superalloy gas turbine components, studying ingot characteristics, alloy segregation effect and thermomechanical properties [SAE PAPER 690101]

09 p1503 A69-23557

Polyurethane foam high velocity deformation properties, discussing results of dynamic uniaxial stress tension and compression tests

11 p1907 A69-25648

Ni-Ti alloy intergranular deformation at constant tension within wide temperature range

12 p2113 A69-26044

Tensile and creep deformation of fiber reinforced composites consisting of Mg-Li alloy matrix with high strength precipitation hardening stainless steel wire

17 p2986 A69-33073

Plastic tension of axisymmetric sample involving necking and small inhomogeneity, assuming Tresca yield condition and associated flow law

19 p3446 A69-36847

Transverse vibrations of isotropic solid rectangular beam with secondary effects of rotary inertia and shear deformation retained

21 p3832 A69-38447

Alpha Ti thermally activated tensile deformation, studying flow stress dependence on strain, temperature and strain rate

[ASM PAPER W9-4.2]

21 p3729 A69-38659

Tension tests of polycarbonate plates grooved at various angles, demonstrating necking dependence on mechanical instability

21 p3753 A69-39809

Solid solutions precipitation effect during deformation process on static and dynamic tensile tests of Al alloy by electric resistance measurement

22 p3972 A69-41082

Desorption of hydrogen and methane from Al, Mg and Nb under room temperature tensile deformation in ultrahigh vacuum

23 p4176 A69-41541

TENSILE PROPERTIES

Charge materials purity found to increase beta-Ti alloys properties

01 p0094 A69-10216

Prestraining of stainless steel En58b sheet at room and cryogenic temperature, noting effect on tensile properties

01 p0099 A69-11151

Zr-Be-Nb alloys mechanical tensile properties above room temperature for low concentrations of Be and Nb

02 p0262 A69-11845

Composite tensile-failure modes, discussing failure load prediction, experimental data and statistical analysis of stress concentration effects

[AIAA PAPER 68-173]

02 p0347 A69-12514

Polymer films tensile properties after exposure to gamma radiation in vacuum, noting chain scission and cross linking

[ASME PAPER 68-WA/RP-6]

05 p0783 A69-16160

Sintered W-Ni-Fe alloys strength and precipitation hardening characteristics for various compositions and cooling conditions

05 p0782 A69-16798

Fiber orientation and morphology effect on tensile behavior of aluminum-nickel whisker reinforced aluminum

06 p0939 A69-16943

Free surface strain increment components on high carbon steel compression specimens to estimate tensile plastic instability onset, noting ductile fracture criterion

08 p1328 A69-19891

Tensile characteristics of discontinuous unidirectional fiber reinforced glass-epoxy composites and filament wound material, discussing alignment and interfacial bonding

08 p1339 A69-20496

Tensile and creep behavior of nickel at 600 C after oxidation at 1200 C, correlating results with structural differences caused by oxidation

08 p1333 A69-20556

Unidirectionally solidified eutectic composite of Al and Cu-Al intermetallic, noting tensile properties at room and high temperatures

10 p1708 A69-22995

Charge materials purity found to increase beta-Ti alloys properties

15 p2638 A69-30272

Composition effect on tensile and flexural moduli of composites containing randomly distributed fibrous strands, establishing strength-composition relationships

17 p2991 A69-32960

German monograph on yttrium addition effects on tension and compression behavior of Nb and Mo at high temperature in vacuum

17 p2990 A69-33570

Electron beam welds orientation effects on tensile and deformation properties of strengthened and welded austenitic stainless steels

18 p3151 A69-35432

Smooth and notched tensile properties of Fe-Ni alloys in liquid Hg, discussing ductility and toughness

20 p3563 A69-38025

Polystyrene melt tensile viscosity prediction from shearing viscosities, using rheological network rupture theory

21 p3753 A69-39730

Thickness direction tensile properties, ultrasonic attenuation and mild steel plate lamellar tearing in multipass fillet joints measured by weld cracking test

24 p4320 A69-42942

TENSILE STRENGTH

Maraging steels ductile and strength characteristics with increased Co and Mo as function of Ni content, tempering method and aging

01 p0098 A69-10731

Fiber-fiber interaction effect on stress distribution and tensile strength of discontinuous aligned fiber composites

01 p0171 A69-11261

Long term atmospheric corrosion test program for aluminum and magnesium base alloys, comparing tensile strength of exposed and control specimens

01 p0100 A69-11353

Rapidly heated ablative reinforced plastics strength and stress-strain properties, considering heat shield designs

02 p0347 A69-12512

High temperature tensile strengths of uncoated boron filament and filament coated with silicon carbide

02 p0270 A69-12731

Metal composite materials, discussing strengthening mechanism for inclusion of high elastic coefficient and creep limit fibers in weak ductile matrices

02 p0268 A69-12750

Plastic deformation and bursting pressure of thin rupture disk as related to tensile strength

06 p1020 A69-17129

Computer analysis for optimizing size and shape of thin walled axisymmetric elastic rings, plates and shells with respect to tension, rigidity and weight

06 p1026 A69-18017

Tensile strength of alloys under high pressure of hydrogen and helium, discussing embrittlement

07 p1169 A69-19667

Microstructure relationship to tensile strength and creep resistance in Zn-Ni-Ti alloy extrusions, discussing role of finely dispersed intermetallic particles

08 p1329 A69-20002

Retained austenite content control, strain aging and ausforming to improve toughness of high strength martensitic stainless steel without strength loss

08 p1330 A69-20010

Tensile strength of glass-fiber reinforced epoxy resin laminates subjected to fluctuating tension, discussing crack density dependence on fatigue stress cycles

08 p1338 A69-20494

Failure criteria for predicting filamentary composite strength under uniaxial and combined stresses from properties and fabrication process considerations

09 p1611 A69-21479

Tensile strengths and elasticity moduli of graphite fibers produced from textile organic thread, discussing application to composites, ablative and fiber reinforced materials

09 p1529 A69-22071

Silicon carbide filaments strength at high temperatures noting vapor deposition, mechanical properties and applications

09 p1524 A69-22072

Adhesive bonded lap joint strength dependence on adherend mechanical properties under conditions of homogeneous adherend and cohesive failure

09 p1530 A69-22317

Prepreg based on S glass with HTS finish and B staged epoxy resin, discussing tensile strength and moisture exposure

09 p1530 A69-22327

Gas turbine blade materials after long term service, analyzing tensile, impact and stress rupture properties and microstructure

[ASME PAPER 69-GT-12] 09 p1527 A69-22503

Material selection for structures under vibration loads, analyzing fatigue strength on basis of stress susceptibility and relationship with tensile strength

09 p1620 A69-22574

Strength of laminated glass filament reinforced plastic material in biaxial loading, discussing strength theories

10 p1794 A69-22943

Potential testing methods for corrosion induced changes in materials, discussing mechanical properties, corrosion fatigue and cracking and creep

10 p1713 A69-23822

Hydrogen effect on temperature dependence of tensile strength and stress rupture strength of Ti alloys, considering annealing, quenching and aging

11 p1905 A69-24962

Glass fiber reinforced plastics tensile strength at low and high temperatures

11 p1907 A69-25181

Yield to ultimate tensile strength ratio of titanium alloys subjected to thermomechanical treatment

11 p1906 A69-25683

Tensile strength and failure loading evaluation for structure, discussing stresses in neighborhood of crack, crack toughness measurement and fracture mechanics

12 p2176 A69-25861

Three dimensional network of closely spaced oxide particles for Al strengthening investigated by transmission electron microscopy and tensile tests

13 p2276 A69-27371

High strength alloys stress corrosion cracks, analyzing tensile ligament instability from plastic flow tests of bulk/compression/specimens

13 p2277 A69-27404

Reversion and drawing techniques for ultrahigh strength ductile maraging steel wire without excessive deformation

13 p2278 A69-27412

Grain size effect on room temperature tensile strength of alpha-titanium analyzed by tensile testing and electron transmission

13 p2280 A69-27766

Ferrous and nonferrous metals shock tensile strength by elastic contact dynamometer, noting diagram shape dependence on stress growth rate

14 p2464 A69-29314

Strain rate and temperature effects on sintered molybdenum sheets strength and elongation characteristics

14 p2464 A69-29322

Thermocompression joints strength measured using friction test, centrifuging and microtensile tests

15 p2573 A69-30081

Maraging steel tensile strength increased, plasticity and toughness properties decreased with Ti content increase

15 p2639 A69-30630

Fiberglass reinforced plastic tensile strength dependence on vibration time and temperature and vibrational effect on modulus of elasticity

15 p2643 A69-31203

Multiple repair welding effects on AL welds tensile strength, using conductivity measurements to monitor strength

15 p2631 A69-31509

Electrical conductivity, hardness, ultimate tensile strength and yield strength correlations of age hardenable Al alloys by eddy current methods

15 p2641 A69-31513

Photoelasticity testing of stress gradient factor on notched tensile specimens

17 p3052 A69-32982

Temperature and pressurization effects on tensile and compressive properties of polycrystalline arc-cast W

18 p3154 A69-34273

Oriented glassfiber reinforced plastics elastic moduli and tensile strength along anisotropic axes determined nondestructively, considering component content and material porosity

18 p3162 A69-35359

Nb single crystals plastic deformation influencing tensile strength, noting rolling directions

18 p3160 A69-35454

Silicon nitride staple fibers synthesis, development and characterization, noting tensile strength and sonic modulus

19 p3354 A69-35517

High modulus graphite epoxy composite material laminates fabricated and tested, correlating filament strength variation effect with composite tensile strength

19 p3354 A69-35518

Measuring elastic modulus and tensile strength of high modulus graphite fibers including comparative data, error sources and full strand test

19 p3355 A69-35520

Graphite fiber NOL rings and biaxial wound pressurized cylinders tested at ambient and cryogenic temperatures for tensile and cyclic fatigue properties

19 p3355 A69-35521

Polyperfluoroalkyleneimidoyleperfluoroalkylene-amidine synthesized by reaction of perfluoroalkane dinitriles with ammonia or diamidine, giving elastomers of varying strength and elongation, noting thermal stability

19 p3264 A69-35535

Tensile and stress rupture strengths of diffusion bonded Ni superalloys, using spin tests of simulated hollow turbine disks

19 p3320 A69-35559

Crystal twinning directional effect on Mg alloys tensile yield strength degradation, investigating recovery methods

19 p3341 A69-35583

Silicon carbide coated boron fiber reinforced /Bor-sic/ Al composites tensile strength and elastic properties

19 p3344 A69-35926

Polymer fibers tensile strength improved using sectional orientation strengthening at controlled temperature and tension conditions

19 p3358 A69-35984

Low strain rate effects on metals yield and tensile strength

20 p3563 A69-38063

Texture hardening combined with age hardening for biaxial strength improvement of Ti-Al-V alloy, discussing applications to spherical pressure vessels

21 p3729 A69-38662

Extreme value statistics used to determine minimum acceptable tensile strength of wire command links in TOW antitank missiles

24 p4318 A69-42642

Fracture and tensile properties of electron beam welded Al alloy for pressure vessels compared to gas tungsten arc welding results

24 p4319 A69-42941

Static and cyclic tensile fatigue of alumina by ring test method, measuring time to failure

24 p4334 A69-43343

Tensile strength improvement in Al-B composites by heat treatment to T6 condition and subsequent cold rolling

24 p4334 A69-43449

TENSILE STRESS

Plastic zone generation by slots cut in tensile test specimens before and during loading, discussing redistribution

01 p0098 A69-10762

Microscopic cleavage strength of high nitrogen steel notched bars determined from critical tensile stress criteria using elastoplastic analysis method

01 p0169 A69-10765

Composite material mechanical failure due to detachment of microfiber ends from elastic matrix while under tension

01 p0171 A69-11259

Elastic properties of epoxy resins, deriving relation by considering different shear properties in tension and compression

01 p0103 A69-11268

Dynamic tensile stress-strain curves for annealed Al, Cu and Fe at constant strain rates, describing experimental method

03 p0524 A69-13065

Dead-end microcracks stress fields, studying positive /tensile/ and negative /compressive/ nature dependence on crack size

04 p0674 A69-14548

Shear type fracture formation mechanism in tensile test specimens of Ti alloys, noting transition in macrogeometry

04 p0617 A69-15076

Load carrying capacity of V notched bars under axially symmetric tensile load, verifying influence of distance between two equal notches

04 p0680 A69-15169

Statistical model for tensile fracture of parallel fiber composites based on stress criterion for crack propagation

[ASME PAPER 68-WA/RP-7]

05 p0783 A69-16159

Hydrostatic tension test of brittle material using spherical specimen bonded into center of cube matrix material

05 p0784 A69-16444

Photoelastic study of interaction between overlapping parallel cracks in tensile stress field

05 p0842 A69-16444

Statistical processing of oscillograms of instantaneous values of wire tension during winding, determining stress characteristics

06 p0927 A69-17604

Transient heat evolution response to reapplied stress of alloys plastically predeformed at 4.2 K attributed to thermally softened defect structures

07 p1165 A69-18949

Vibration characteristics of rectangular plate with fatigue crack and subject to tensile load, applying results to crack propagation in fuselage panels

08 p1413 A69-20743

Tensile stress and energy-to-break values compared for glass-fortified thermoplastic resins, discussing notched and unnotched Izod impact

08 p1337 A69-20488

Displacements and stress intensity as function of crack length for compact tension specimen, considering load line and crack edge

09 p1503 A69-21391

Crack stability under mechanical and thermal stresses, noting critical tensile stress and thermal insulating character of crack

10 p1794 A69-22894

Ultrasonic technique for metal surface and near surface residual stress measurement, emphasizing aluminum alloys

10 p1794 A69-23052

Buckling deformation and stress fields around central slits in photoelastic models and metal sheets under tensile load

10 p1796 A69-23069

Yield points compared for axial and biaxial tensile loading of aluminum alloy sheets

10 p1801 A69-23845

Compact device for low temperature neutron irradiation of deformed specimens under tensile stress, emphasizing specimen carrier

11 p1862 A69-24901

Flat bar optimal cross section under tensile stress applied to minimize stress in large structural components using elasticity theory

11 p1986 A69-25203

Stresses and displacements in half plane with edge crack given as eigenfunction expansions using Wiener Hopf technique

11 p1987 A69-25438

Compressive and tensile creep of metals, discussing compressive stress, void nucleation, barreling specimen shape and platen lubrication

12 p2175 A69-25836

Plane stress state in plate with different glide modulus during tension and compression, considering axisymmetrical deformations

12 p2178 A69-26003

Sinusoidal tension and compression radial support system for large solid disk primary mirror, noting pivot design and pad bonding adhesive

12 p2057 A69-26411

Temperature effect on tensile brittle fracture stress of polycrystalline tungsten

12 p2116 A69-27113

Nonlinear theory for whirling of heavy string under constant axial tension, considering orbitally stable modes for eigenvalues of rotation

13 p2359 A69-27266

Spherical stress wave reflected from plane surface discussing tensile stress in target

13 p2366 A69-28229

Critical rotation rates of homogeneous shaft with two bearings under tension, considering shaft mass stretching force magnitude and console disk gyroscopic effect

13 p2269 A69-28332

Ferrous and nonferrous metals shock tensile strength by elastic contact dynamometer, noting diagram shape dependence on stress growth rate

14 p2464 A69-29314

Materials and structural failures under short time compressive loadings, showing structural response to tensile stresses produced by rarefaction waves

15 p2639 A69-30366

Griffith crack in thin plate opened by uniform tension at infinity, discussing effect of ties on stress intensity factor

15 p2710 A69-30800

Plane strain and stress compared for elastoplastic
racked plate in work hardening tension
15 p2710 A69-30811

Plastic expansion in metals due to alternating tor-
sional and static tensile loading
16 p2875 A69-32291

High strength fibers and composite materials for
structural design, considering anisotropy and low ul-
timate tensile strain
16 p2802 A69-32380

Machine for testing vibration stability of polymer
samples subject to tension or compression, noting sta-
bility of plastic during vibration lower than during
static loading
17 p2972 A69-33043

Machine for testing high temperature creep under
variable tensile-compressive stress while maintaining
specimen stability, noting discrepancy between creep
strains in heat resistant alloy
17 p3054 A69-33044

Tension-torsion-compression load testing machine of
technological possibilities and accuracy
[ONERA-TP-596]
17 p2945 A69-33065

Static tensile stresses effect on energy dissipation in
alloys used in compressor blades found dependent on
composition and heat treatment
17 p2991 A69-33934

Mean stresses effect on fatigue strength by
specimens vibratory/tensile mean stress diagram com-
bining Goodman line and Gerber parabola merits with
increased accuracy
17 p3067 A69-34197

Cantilever truncated conical shell stability under ten-
sile stresses solved by strain energy technique
18 p3216 A69-34574

Mechanical machine for fatigue testing flat samples of
thin walled structures under tension and at various
frequency ranges
18 p3118 A69-34833

Stability loss of shells of revolution under axial ten-
sion and radial pressure, considering shells of Gaussian
curvature, calculating critical force
18 p3222 A69-34976

Boundary conditions of orthotropic shell stability
under external pressure and axial tension, analyzing
critical pressure by strain energy method
18 p3222 A69-34977

Tension, bending and buckling torsion in thin walled
beams described by extended beam model considered
as one dimensional continuum
18 p3224 A69-35296

Thin brittle plastic shells mechanical properties differ-
ing under tension and compression described by
solving differential equations in successive approxima-
tion
18 p3224 A69-35327

Fiberglass-reinforced plastics longitudinal and trans-
verse strain relations at various temperatures
18 p3163 A69-35366

Creep behavior of dispersion strengthened Nb base
bcc alloy, studying temperature and stress effects on
steady state creep rate
19 p3343 A69-35924

Keyway stresses in shafts under tension, bending and
torsion, using frozen stress photoelastic technique
19 p3445 A69-36827

Stress distribution in tension specimen notched on
one edge obtained photoelastically for several notch
depth to specimen width ratios, noting Neuber theory
agreement
19 p3447 A69-36859

Residual tensile stress distribution during plasma
spraying determined as function of temperature field in
blank
20 p3548 A69-37328

Viscoelastic materials gradual resilience loss under
tensile stress, discussing mathematical relations
between stress, loading time, elastic deformation and
experimental verification
20 p3625 A69-37600

Tensional and torsional forced vibration tester for
viscoelastic plastic materials under tensile strain
21 p3720 A69-38591

Rectangular plate under biaxial tension stress
analyzed to determine onset of necking and stress-
strain state
22 p4039 A69-39913

Residual stress effect on strength of oriented glass
fiber reinforced plastics under transverse and longitu-
dinal tension
22 p3973 A69-40745

Initial stress dependence on tensile load in glass fiber
reinforced plastic rings during winding
22 p4045 A69-40749

Stress-strain state in infinite medium with cavity
under triaxial tensile force obtained from integrodif-
ferential equation deduced from equilibrium equation
23 p4226 A69-41703

Isometric recording device for tensile stresses on
muscle preparations in vitro, based on differential
transformer
23 p4111 A69-42056

Sand erosion behavior of metals and plastics in air
blast rig under varying exposure time, angles of impact
and tensile stress
24 p4363 A69-42787

TENSILE TESTS

Creep and stress rupture strength of unidirectional
glass fiber reinforced plastics, using tensile tests
01 p0101 A69-10080

Composite material mechanical failure due to
detachment of microfiber ends from elastic matrix
while under tension
01 p0171 A69-11259

Mechanical properties of titanium physically vapor
deposited by electron beam high rate evaporation, not-
ing results of tension testing
03 p0443 A69-13117

Evaluation tests of fixed frequency variable tension
vibroscope for filaments and wires, noting instrument
errors and corrections
04 p0599 A69-15018

Shear type fracture formation mechanism in tensile
test specimens of Ti alloys, noting transition in
macrogeometry
04 p0617 A69-15076

Strain dependent modulus and Poisson ratio
behavior of CTPB propellant, performing stress relaxa-
tion tests
04 p0646 A69-15510

Hydrostatic tension test of brittle material using
spherical specimen bonded into center of cube of
matrix material
05 p0784 A69-16434

Plastic fractures of age hardened aluminum alloys
analyzed by tensile tests and electron fractography,
considering stresses, surface and intergranular effects
07 p1166 A69-18961

High temperature vacuum tensile test device for con-
tinuously direct recording various stress-strain diagram
rates by interchangeable dynamometer scale
07 p1117 A69-19319

Foil type strain gage for measurement of tangential
strains along circumference of hole in plate under
uniaxial and equibiaxial tension
08 p1314 A69-20258

Four point flexure, ring flexure and NOL ring tension
tests for evaluation of composite material mechanical
properties
09 p1499 A69-22308

Deformation of thermoplastics under tensile loading,
discussing types of loading
10 p1716 A69-22942

Crack propagation in plates and shells subjected to
bending and direct loading, noting plate analysis
modification for crack touching on compression side
10 p1795 A69-23061

Elongational viscosity coefficient determined from
tensile measurements of materials under applied stress
10 p1681 A69-23976

Stress corrosion cracking of Ti-6Al-4V alloy tensile
tested in anhydrous methanol by electron fractography
and diffraction, noting hydrogen embrittlement
11 p1903 A69-24576

Plastic strains in aluminum alloy under biaxial tensile
and combined tensile and torsion tests, discussing small
elastoplastic deformation theory
11 p1905 A69-24948

Elastic and elastoplastic strains in materials under
various loadings, determining temperature variations
by thermoelectric method and verifying by tensile tests
11 p1985 A69-25178

Testing machines for metallic materials, discussing
design criteria and application to tensile strength,
vibration and durability test machines
[DVL-865]
11 p1889 A69-25682

Hydrogen embrittlement of stainless steel and effects
on mechanical properties, discussing martensitic phase
role
12 p2115 A69-26616

Neutron irradiated Nb single crystals tensile tested
over temperature range, discussing athermal radiation
hardening
13 p2275 A69-27368

End constraints and length/width ratio influence on
composites off axis tensile tests, considering rigid
clamping with/without end rotation
13 p2286 A69-28667

Rolling direction tensile tests of alloy steel plate dis-
playing various fracture configurations over distinct
temperature ranges, noting stress state, void formation
and anisotropy
[ASME PAPER 68-WA/MET-1]
14 p2464 A69-29440

Impact testing machine with dropping load, noting
provision for sample fastening to reduce reflected ten-
sile wave effect
15 p2583 A69-30286

Necked tension specimens profiles for rigid-plastic
nonhardening materials determined from compatibility
equation for displacements and unloading rate
15 p2704 A69-30292

Thick walled pressurized cylinder fatigue test results
compared with axial tension and rotating beam tests on
same material
15 p2709 A69-30676

Titanium alloy tensile specimens tests in air,
methanol and anhydrous methanol environments at
known stress-strain-time relations examined by frac-
tography and high resolution electron diffraction
16 p2799 A69-31718

Hydrogen effects on ELI Ti-Al-Sn alloy, conducting
tensile, fretting and abrasion tests on stressed and ther-
mal cycled specimens
[AIAA PAPER 69-585]
16 p2803 A69-32760

Fracture strength of Al alloys, discussing tests for
tensile properties, linear elastic fracture mechanics
techniques, yield strength, corrosive media, etc
17 p2989 A69-33555

Testing machine for in vacuo tensile testing of tubu-
lar metallic specimens at high temperatures and low
pressures
18 p3117 A69-34604

Tensile tests on time dependent Pb and cellulose
nitrate, including stress-strain curve prediction from
creep test data
19 p3445 A69-36829

Reinforcement unbonding onset in composite
materials determined by continuous dynamic moduli
and damping measurements of tensile specimens
20 p3511 A69-37761

Finite element analysis and strain gage results to ver-
ify end constraint on off-axis tensile coupons and to
design test specimen
20 p3628 A69-37775

Tensile strength of glass and graphite fibers for fiber
reinforced plastics /FRP/ tested with modified balance
type and strain gage type tensile testers
21 p3753 A69-39799

Tension tests of polycarbonate plates grooved at
various angles, demonstrating necking dependence on
mechanical instability
21 p3753 A69-39809

High temperature electronic tensile testing device
utilizing SCR to study strain rate effect on metals prop-
erties
21 p3727 A69-39811

Grids applied to plastic samples for strain measure-
ment using moire fringe method, comparing tensile test
results with Linley extensometer
22 p4042 A69-40312

Uniaxial tensile testing machine to operate under
combined creep and fatigue conditions for studying
dislocation structure changes in metals and alloys at
high temperature
22 p3926 A69-40441

Tensile cryostat for low temperature strain measure-
ment, discussing design, insulation and vacuum sealed
environment for heat leak reduction
[NAS-NRC PAPER J-3]
22 p3947 A69-40627

Tensile test facility for specific strain rate range, ap-
plying impact load to sample end with high speed
striker accelerated by explosive energy
23 p4147 A69-41710

Fracture toughness and crack propagation in an-
nealed aircraft titanium alloys tested per ASTM
procedure, comparing results with high strength steels
and aluminum alloys
23 p4177 A69-42165

Cylindrical steel specimens high strain rate tensile
tests, using Malvern theory for ideal elastoplastic and
work hardened materials
23 p4236 A69-42529

Room temperature tensile tests determining failure
modes and defect influence on diffusion welds of unal-
loyed Ti, using electron microscopy and fractography
24 p4331 A69-42939

Tensile tests on fiber reinforced plates with circular
holes, studying fiber orientation effects
24 p4404 A69-43602

TENSIOMETERS

Tensiometric aerodynamic balances in great velocity
ranges, discussing measurements, elastic elements and

TENSION TESTERS

tensiometric balance construction and measuring errors nature

05 p0762 A69-15922

Muscle function measurement in astronauts using electromyogram, electrocardiogram and isometric tension at fixed percentage of maximum voluntary contraction

23 p4103 A69-41684

TENSION TESTERS

U TENSILE TESTS

TENSOR ANALYSIS

Invariant theory of gravitational radiation, using impulse energy tensor

02 p0332 A69-12835

Inhomogeneities in materially uniform simple bodies described in terms of third order tensor field, treating contorted aeolotropy

05 p0833 A69-15728

Tensor partial differential equations having spherical symmetry, examining covariant differentiation and contraction of tensors

07 p1123 A69-18807

Brans-Dicke scalar-tensor theory, showing radiative Riemann tensor existence in absence of usual spin-2 gravitational waves

07 p1216 A69-18894

Second order tensor describing deformation of particles of continuum determined by functional, noting invariance restrictions

08 p1416 A69-20690

Plasma conductivity tensor components in crossed fields calculated by Boltzmann kinetic equation, noting influence of magnetic field presence

09 p1546 A69-21565

Geometrized theory of combined gravitational and electromagnetic fields, using metric tensor of four dimensional Riemannian continuum to describe both fields

09 p1540 A69-22134

Relativistic energy momentum tensor of electromagnetic field in moving multicomponent dispersive media and instability of wave

10 p1653 A69-23193

Green tensor construction for systems of linear differential equations with constant coefficients

11 p1996 A69-25730

Dynamic relaxation method for elastic deformation in mirrors, using tensor equations of elasticity in nonorthogonal curvilinear coordinates

12 p2187 A69-26890

Turbulent fluid flow analysis described by Navier-Stokes equations, introducing asymmetric tensors for anisotropic cases

13 p2297 A69-27289

Tensor conductivity measured and analyzed for MHD generator duct with electric and magnetic fields

13 p2309 A69-28026

Tensor analysis of four photon interaction in rarefied plasma in magnetic field, determining cubic current of plasma wave self action

13 p2314 A69-28444

Nondeformable closed contour spatial gear kinematics using matrix tensor method suitable for computer programming

15 p2713 A69-31020

Fourth rank tensors analysis describing nonlinear optical effects for 32 classes of crystalline substances

19 p3334 A69-35882

Space transitions identified with asymptotic solutions at system field equations transition points

19 p3445 A69-36811

Isotropic strain tensor general theory based on isotropy between second order asymmetric tensors reducible to finite form

20 p3624 A69-37584

Holor algebra with tensor notations applied to elastic structures/discrete systems/, discussing inertia and stiffness tensors

21 p3831 A69-38415

Laser design for smooth emission frequency retuning, discussing equations for laser field oscillations, two photon resonance, tensor analysis, quantum emission, etc

21 p3739 A69-39539

Tensor analysis of brushless DC motor controlled by transistors, discussing torque phase, torque variation phase and efficiency phase characteristics

24 p4255 A69-42678

TENSOR FIELDS

U TENSORS

TENSORS

NT STRESS TENSORS

Asymptotic behavior of curvature and conformal curvature tensors on asymptotically flat space-time

01 p0116 A69-10393

Tensor character of fictitious potential function introduced to approximate locally tangent actual potential function, discussing planetary gravitational anomaly observation from orbiting vehicles

[AAS PAPER 68-198] 02 p0312 A69-11476

Magnetoionic propagation of signals in magnetosphere using Maxwell equations and tensor quantities, linking to Hall, transverse and longitudinal conductivities

[ONERA-TP-593] 02 p0236 A69-11617

Electric field induced IR absorption and Raman scattering by optical phonons in centrosymmetric crystals, discussing tensor coefficients

02 p0295 A69-11779

Green tensor for collisionless plasma, emphasizing relations between outgoing and ingoing electric fields

02 p0293 A69-12745

Electromagnetic and gravitational tensor fields in Riemannian space, generalizing Maxwell and Bel-Robinson tensors

03 p0467 A69-13755

Conformal change and connection relations in Einstein unified field theory, noting tensor applications

03 p0467 A69-13756

Viscosity coefficient tensor in terms of autocorrelation functions, using linear reaction theory of mechanical disturbances

05 p0794 A69-15785

Plane surface finite area deformation tensors in continuum mechanics permitting separation of volume and shape changes in constitutive equations

11 p1994 A69-25603

Conformally plane solutions to Einstein equations derived with energy momentum tensor characteristic of pulverized material representing gravitational fields

13 p2298 A69-27796

Anisotropic scattering of current carriers in semiconductors, obtaining general expression for mobility tensor with variational principle

14 p2508 A69-29667

Conductivity tensor of collisional plasma in magnetic field, basing method on iterative procedure

14 p2503 A69-29999

Electrical conductivity tensor of many component collisional relativistic plasma in magnetic field and near equilibrium, expressing collisional part as momentum integral

14 p2503 A69-30000

Viscosity coefficient tensor in terms of autocorrelation functions, using linear reaction theory of mechanical disturbances

18 p3173 A69-35037

Relativistic tensor theories of gravitation in flat space with Neumann and Newton forms of gravitational potential, deriving expressions to estimate differences perceived by observer

19 p3373 A69-36204

Two point tensor function symmetries of nonlocal cohesive finite elastic materials determined from atomic lattice theory, obtaining Green function

19 p3444 A69-36798

Guiding center Vlasov equation derived dielectric tensor of collisionless plasma, obtaining dispersion relation of Alfvén waves in warm plasma

23 p4197 A69-42416

TERBIUM

Nonradiative transfer of excitation energy between mixed trinuclear complexes of Tb and Eu ions with lactose in aqueous solution

01 p0023 A69-10288

TERMINAL BALLISTICS

Perforation and penetration mechanisms of Styrofoam slabs, using impact tests with free falling and rifle powered projectiles

01 p0165 A69-10115

Meteoroid penetration detector development program for spacecraft construction, discussing design, materials and environmental tests

02 p0338 A69-11749

Trailing camera technique to photograph impact and projectile penetration into earth materials from above and behind test vehicle

02 p0227 A69-11760

Terradynamic research program for studying instrumented projectile penetration of terrestrial materials

02 p0228 A69-11767

Transient response of targets subjected to hypervelocity impacts and quantitative aspects of impact process, noting study of wax targets interiors

07 p1234 A69-19380

Projectile impacts into laminated targets consisting of plastic layers backed by Al substrates using SHAL code with hydrodynamic elastoplastic distortion model

[AIAA PAPER 69-356] 13 p2366 A69-28235

High pressure Hugoniot points made by hypervelocity gas gun, using laser beams to measure impact velocity and pressure transducer for impact stress

[AIAA PAPER 69-358] 13 p2264 A69-28232

Hypervelocity impact dynamics on copper cube targets imbedded with nickel wires, discussing terminal positions, Vickers hardness, flow fields, etc

[AIAA PAPER 69-368] 13 p2367 A69-28231

Aluminum double sheet target penetration resistance determined by studying high velocity pyrex glass impact effects on front/rear sheets and spacing

[AIAA PAPER 69-375] 13 p2367 A69-28230

Cylindrically shaped projectiles low velocity impact upon horizontal surface of dry commercial Ottawa sand mass, estimating penetration for soft landing

21 p3839 A69-39232

TERMINAL FACILITIES

Redevelopment program for Newark airport noting runway construction, underground fuel system and passenger terminal complex

01 p0057 A69-11272

Fitting airport interfaces to air traffic, considering bottleneck elimination

05 p0742 A69-15915

Cost estimating relationships for vertiports and airports, comparing terminal costs per passenger for each facility

[AIAA PAPER 69-208] 07 p1245 A69-19566

Mathematical models for outgoing traffic flow in airport terminal used for determining service requirements

09 p1476 A69-21433

Air cargo transportation in 1970s, discussing Boeing 747 and Lockheed 500 super airfreighters, terminal rates, marketing, etc

13 p2381 A69-27333

Air cargo terminal materials handling, discussing computer control, off-airport consolidation, packaging, etc

13 p2239 A69-27332

Experimental SST terminal for satellite L band communications/surveillance ATC system, establishing terminal requirements for NASA and FAA studies

17 p2932 A69-34111

Airport planning for large aircraft loading of passengers, baggage and cargo containers

17 p2948 A69-34201

Aircraft design determined by airport environment and facilities defined as pavement strength, passenger and baggage loading and aircraft handling, noting noise abatement

17 p2948 A69-34201

Airport performance, noise and aircraft utilization influence on aircraft design and operating costs stressing takeoff distance, obstacle clearance and noise regulations

17 p2948 A69-34211

Air terminals plans for 1975 aircraft and air traffic based on runway configurations

[AIAA PAPER 69-805] 19 p3288 A69-35599

Airport alternate facilities, restrictive flight schedules and fee schedules for relieving airport congestion during peak traffic hours

[AIAA PAPER 69-820] 19 p3453 A69-35599

Mass transit rail service between Manhattan and Kennedy Airport using Long Island Railroad mainline route, discussing baggage handling and time schedules

[AIAA PAPER 69-803] 19 p3453 A69-35599

Air travel and population growth requiring large structures for office buildings, airport passenger terminals and aircraft servicing facilities

[AIAA PAPER 69-809] 19 p3289 A69-35622

Airport facilities planning for conventional jet STOL and SST aircraft ground handling, stressing facilities economy and transportation subsystems

[AIAA PAPER 69-808] 19 p3289 A69-35622

FAA ARTS-III terminal air traffic control system reliability and maintainability, discussing module addition

19 p3370 A69-36000

Jumbo jet passenger loading devices including overwing bridges, transporters and terminal integration

20 p3511 A69-37919

Air traffic systems and diminishing airspace capacity problems requiring additional airport facilities and STOL aircraft

22 p3925 A69-40422

Airport location effect on facilities supply factors including atmospheric, environmental and economic conditions

22 p3926 A69-40431

Handling and processing function in air freight transportation, discussing system design approaches, cargo terminals, materials handling systems and containerization

22 p4053 A69-40483

Airport standards analysis for safe, efficient air carrier operations including airport funding, safety programs for runways and terminal facilities

22 p4054 A69-41144

Terminal facilities planning for STOL service to meet traffic demand, considering site selection, runway alignment, aircraft noise, ground accessibility, etc [SAE PAPER 690421]

23 p4147 A69-41645

Airport terminal planning, considering expansion, automation, backup measures, layout problems and solutions, etc [SAE PAPER 690399]

23 p4147 A69-41661

Air space saturation, urban surface transport network enlargement necessity and expeditious passenger processing and baggage handling

24 p4296 A69-42567

General aviation airport application as freight consolidation terminals to reduce ground handling costs, circumvent air and ground traffic problems, etc

24 p4419 A69-43047

TERMINAL GUIDANCE

Multiengine Martian soft lander guidance and control system design with single engine failure accommodation based on six degrees of freedom computer simulation

02 p0277 A69-11740

Virtual or projected miss distance for assessment of missile homing impairment effects, deriving expression based on kinematics

04 p0629 A69-15517

Electronic terminal guidance requirements for all-weather VTOL operations, suggesting future first generation landing system

08 p1348 A69-21064

Optimal navigation system for supersonic Concorde aircraft, discussing in-flight and terminal navigation methods

14 p2480 A69-29859

Law for time variations of modulus-restricted control action at trajectory end, two point boundary value problem solution and use of Pontryagin principle

18 p3175 A69-35324

Manual procedures for midcourse and terminal guidance, discussing onboard optical measurements and calculations

19 p3368 A69-35792

Subsonic glide landing approach guidance for unpowered lifting vehicles, using perturbation feedback and approximation of heading and position coordinates [AIAA PAPER 69-865]

21 p3763 A69-39391

Electronic terminal guidance requirements for all-weather VTOL operations, suggesting future first generation landing system

22 p3978 A69-39875

TERMINAL VELOCITY

Entry and terminal deceleration systems for unmanned Martian landers, discussing parachute landing and lifting entry vehicles

03 p0521 A69-13670

Terminal velocities of dust particles for two Venus atmospheric models from Mariner 5 and Venera 4 data, obtaining vertical wind velocity requirements

06 p1001 A69-17172

Drop test method to obtain subsonic terminal velocity and base pressure data for planetary entry probe configurations

19 p3238 A69-35959

TERMINATING

U STOPPING

TERMINOLOGY

Reliability terms for electrical apparatus, equipment and systems, indicating need for international standardization

08 p1292 A69-21108

TERNARY ALLOYS

Chemical vapor deposition of W-Mo-Re ternary alloys from hydrogen reduction of fluorides on Cu or Mo substrates

01 p0096 A69-10642

Metallographic analysis of Zr corner structure in Zr-Al-Mo system phase diagram, plotting monovariant and nonvariant equilibria reactions

02 p0261 A69-11840

Zr corner of phase diagrams and microstructure, hardness and microhardness of Zr-Al-Nb system alloys

02 p0261 A69-11841

Zirconium corner of Zr-Al-Cr system phase diagram within concentration limits from 1350-700 C, considering corrosion resistance

02 p0262 A69-11842

Metallographic and radiographic analysis of zirconium corner in Zr-Be-Nb system, discussing phase transformation during quenching

02 p0262 A69-11843

Zr-Be-Nb alloys mechanical tensile properties above room temperature for low concentrations of Be and Nb

02 p0262 A69-11845

Isothermal sections construction of zirconium corner of ternary phase diagram of Zr-Mo-V system from microstructure of cast and quenched alloy specimens

02 p0262 A69-11846

Structure of zirconium corner of Zr-V-Ni system phase diagram, using metallography, hardness and microhardness methods

02 p0262 A69-11847

Alloying additions effect on mechanical properties of Zr-V-Nb system

02 p0263 A69-11849

Zirconium corner of Zr-Fe-Nb phase diagram, studying alloy tempering at various temperatures

02 p0263 A69-11851

Zirconium corner of Zr-Cu-Mo phase diagram, using microstructure analysis of hardness and microhardness measurements, discussing plasticity variations and corrosion resistance

02 p0263 A69-11852

Fe, Ni and Cr influence on corrosion resistance and mechanical properties of Zr-Cu-Mo system alloys

02 p0263 A69-11853

Zirconium corner in Zr-Nb-Cu phase diagram, plotting isothermal sections for high temperatures

02 p0263 A69-11854

Oxidation resistance of Zr-Nb-Mo alloys at high temperature in air or water

02 p0264 A69-11857

Isothermal sections of Zr corner of Zr-Mo-Ta system phase diagram at high temperatures, noting composition vs hardness and omega phase

02 p0264 A69-11858

Isothermal sections of Zr corner of Zr-Mo-Ti phase diagram at various high temperatures, noting corrosion resistance in air and water

02 p0264 A69-11859

Isothermal sections of Zr-Ni-Nb system phase diagram at high temperatures, determining principal type of projection on concentration triangle

02 p0264 A69-11860

Isothermal sections of Zr corner of Zr-Nb-Cr system phase diagram at high temperatures, noting variation of stability with concentration

02 p0264 A69-11861

Al/Zn/Mg alloys preprecipitation, discussing Guinier-Preston and critical zone sizes and reversible vacancy trap

03 p0447 A69-13613

Aging of iron-nickel-titanium alloys during heating in reverse martensitic alpha to gamma transformation process, investigating phase parameter changes

04 p0613 A69-14558

Heat treatment effects on stress corrosion cracking resistance of Al-Zn-Mg alloys, using cantilever loading in aqueous solution

04 p0617 A69-14933

Be, Ce, V and Ti additions effect on oxidizability of cast, forged and cold worked Nb-Cr-Mo alloys

04 p0618 A69-15081

Solid phase equilibria in nickel-aluminum-scandium system at 1000 C

05 p0779 A69-15833

Nitrogen solubility in liquid Fe-Cr-Ni alloys increases with increased Cr concentration between 1550-1700 C and at one atm N pressure

06 p0942 A69-17229

Alloying elements effect on nitrogen solubility in liquid Fe-Cr-Ni alloys, defining quantitatively changes in solubility

06 p0943 A69-17234

Surface preparation effects on Ni-Cr-Fe alloy boundary friction studied by repeated sliding of cylinders on hard Pd-Pt-Au alloy cylinder [ASLE PREPRINT 68AM 6D-4]

07 p1139 A69-18625

Ti-Al-V alloys phase diagrams for isothermal cross sections and polythermal cross sections with constant Al/V ratios

07 p1161 A69-18768

Ti-Zr-Sn alloys phase equilibria and interaction between titanium stannide and solid solution of Ti and Zr

07 p1162 A69-18770

Thermal and metallographic analyses of Ti-Zr-Al system vertical sections close to Ti-Al edge, considering phase equilibrium

07 p1162 A69-18771

Grain size dependence of yield, flow and fracture stresses of Fe-Co-V alloy for 77-298 K

07 p1166 A69-19264

Polycrystalline Mg-Th-Zr alloy precipitation hardening investigated by tensile and hardness tests and transmission electron microscopy

07 p1167 A69-19265

Controlled solidification in Co-Ta-C system to develop pseudobinary eutectic mixture containing TaC crystals aligned parallel to growth direction [ONERA-TP-673]

07 p1167 A69-19339

Czechoslovakian heat resistant iron-carbon-aluminum alloy Pyroferal, properties and applications

07 p1168 A69-19345

Forging and heat treatment parameters effect on Ti-Al-V alloy low cycle fatigue properties, relating crack initiation and propagation rates to microstructures [ASM PAPER D8-24.4]

07 p1169 A69-19669

Nb-Zr-Cr alloys solidus surface and isothermal sections, using optical pyrometry, microstructural and X ray analyses

08 p1333 A69-20440

Dislocation damping measurements made on Fe-18Cr-Ni alloys, noting damping relation to nickel content and stacking fault

08 p1334 A69-20576

Crystal lattice and orientation of precipitate responsible for hardening water quenched Ni-Cr-Nb alloy

08 p1369 A69-20852

Carbidothemic production of metals and binary and ternary alloys, discussing eutectic properties

09 p1514 A69-22731

Supersaturation of dissolved B in splat quenched Fe-Ni-B alloys, noting interstitial and substitutional B in martensitic and austenitic phases

10 p1707 A69-22987

Omega phase transformation in binary and ternary Zr alloys after water quenching from within /alpha plus beta/ phase region

10 p1707 A69-22988

V phase structure and V and E phase lattice constants for ternary systems /Ti, Zr, Nb or Ta-/Ni, Co or Fe-/Si or Ge/

10 p1708 A69-22992

Stress corrosion of nonage-hardenable Al-Mg-Cr alloy investigated for failure in absence of grain boundary precipitate, using notched specimens

10 p1709 A69-23055

Composition and sintering temperature cooling effects on fracture properties of W-Ni-Fe alloys, using electron microscope fractography

10 p1711 A69-23333

Initial aging stage in Fe-Ni-Ti alloys using diffuse X ray scattering with electron microscopy of thin foils

10 p1712 A69-23720

Chromium-rhenium-boron ternary system using X ray diffraction and microstructure analysis, establishing phase equilibria at high temperatures

10 p1715 A69-24054

Zirconium-rhenium-carbon ternary system, determining resistivity of melted alloys, discussing eutectic quasi-binary compounds

10 p1715 A69-24055

Thermal and microstructural analyses to determine phase interactions nature in Mg alloys of Mg- Nd-Al system

11 p1902 A69-24271

Superstructures in multicomponent alloys, transition mode and temperature, ordered state and atomic interactions

11 p1937 A69-24703

Young modulus temperature dependence and order-disorder transformations in ternary nickel alloys

11 p1904 A69-24705

Thermal expansion coefficients of Nb-Zr-Ti alloy and plexiglass at 10-300 K from dilatometric measurements

11 p1905 A69-24917

Matrix grain size relation to dispersed particle size distribution and Zener-McLean equation description of microduplex structure in superplastic Ni-Fe-Cr alloy

13 p2278 A69-27411

Low cycle fatigue crack initiation in Ti-6Al-4V at room and high temperatures and in aqueous salt environment

13 p2278 A69-27413

Heats of solution of Ag and Cu in dilute Ag-Cu-Sn alloys at 720 K, using liquid metal-solution calorimeter
13 p2279 A69-27759

Phase diagram for physicochemical study of CdSb-Ge cross section of Cd-Sb-Ge ternary system, discussing exo-endothermal fusion effects, microstructure, etc
14 p2503 A69-28975

Stress corrosion resistance of AlZnMgCu and AlZnMg alloys, discussing combinations of alloy composition, heat treatment and stable precipitation conditions
16 p2800 A69-31779

Heats of solution of Au and Cu in dilute Au-Cu-Sn alloys determined using liquid metal solution calorimeter, calculating self interaction coefficients
17 p2987 A69-33077

Heat treatment effect on stress corrosion cracking of ternary Al-Zn-Mg alloys noting aging strength, solution temperature, quenching rate and alloy content
17 p2990 A69-33676

Nb corner of Nb-Mo-Cr alloy phase diagram and oxidizability in air at high temperature
18 p3157 A69-35248

Isothermal and thermal martensite transformations on polished surfaces of Fe-Ni-Mo alloys
19 p3344 A69-35983

Heat treatment effects on mechanical properties of Ti-Fe and Ti-Fe-Al alloys
19 p3344 A69-36151

Glassy semiconductors from metallic alloy binary and ternary systems of sulfide, selenide and telluride noting properties
19 p3392 A69-36641

Electrochemical analysis of stress corrosion cracking in Al-Zn-Mg alloy, noting oxide film growth at grain boundary
19 p3351 A69-36899

Phase transformations and strengthening mechanisms in Ti-Al-V alloy
20 p3556 A69-36954

Processing variables influence on microstructure of extruded Ti-Al-Sn alloy, noting deformation by slip over temperature range
20 p3557 A69-36955

Reactivity of hydrogen with surface of Ti-Al-V alloy under fatigue cycling at ambient and cryogenic temperatures
20 p3557 A69-36960

Supersaturated solid solution decomposition in Ni-Cr-Ti system, discussing precipitation mechanism of eta phase
20 p3558 A69-36968

Nb-Ti-C alloys electrical resistivity and thermal EMF noting nearly linear variations with temperature
20 p3558 A69-36976

Ti-Al-V fasteners heat treated in beta field, showing superior mechanical properties to samples treated in alpha plus beta field
21 p3729 A69-38661

Texture hardening combined with age hardening for biaxial strength improvement of Ti-Al-V alloy, discussing applications to spherical pressure vessels
21 p3729 A69-38662

Age hardening response of Mg-Th-Zr alloy at 60-450 C, discussing peak strengthening, superlattice formation, precipitation processes, etc
21 p3743 A69-38735

Flow stress temperature dependence of Ni-Cr-Al alloys consisting of gamma prime dispersion in Ni base solid solution
21 p3744 A69-38738

Plastic deformation combined effect with aging on mechanical properties of phase-hardened austenitic Fe-Ni-Ti alloys
21 p3746 A69-38956

Ti-Al-V forgings macro/prior beta/ grain size and in-process thermal treatment effects on fatigue life [AIME PAPER S69-2]
21 p3732 A69-39470

Weldability of alloy Ni-Cr-Fe base-filler alloy combinations, noting threaded mold test and surface fissures
22 p3968 A69-39886

Aluminothemic reduction of Ti and Ni oxides for obtaining Ti-Ni-Al system
22 p3969 A69-40070

Heat treated Ti-Al-Fe alloys thermal, microstructural and X ray analyses of phase transformations in Ti-rich corner
22 p3969 A69-40074

Fusibility diagrams for Ti-Ta-Cr by determining specimens melting points after homogenization at various temperatures in argon
22 p3969 A69-40075

Equilibrium vapor compositions and activities over Fe-Cr-Ni alloys at 1600 C determined by collecting effusate from thoria Knudsen cells
23 p4175 A69-41503

Coherent matrix precipitates observation in Fe-Ni-Cr alloy by transmission electron microscopy, discussing yield strength and elongation dependence on aging conditions
23 p4176 A69-41508

Al-Mn-V ternary system equilibrium diagram at various aluminum concentrations determined by magnetic and microhardness measurements, microstructural observations and X ray analysis
24 p4330 A69-42601

TERNARY SYSTEMS

Zr-Be-Nb system oxidation resistance decrease at 650 degrees C ascribed to Be and Nb additions
02 p0262 A69-11844

Zirconium corner of Zr-Mo-Ni phase diagram using metallographic analysis, hardness and microhardness methods, constructing isothermal sections for high temperatures
02 p0264 A69-11855

Zirconium corner of Zr-Nb-Mo system phase diagram, using microstructure, microhardness, hardness and radiographic methods
02 p0264 A69-11856

Nickel-rich region of Al-Ni-Y ternary system, emphasizing identification of solid phase equilibria through analysis of equilibrated alloy specimens
02 p0265 A69-12004

Phase diagram and heat resistance relation for ternary titanium alloys, considering component interactions and dissolution and dispersion effects
02 p0268 A69-12357

Thermodynamic properties of binary and ternary liquid metal systems, noting electromotive force and vapor pressure measurements
07 p1165 A69-18939

Phase equilibria in V-Cr-C, Nb-Cr-C and Ta-Cr-C systems determined by microscope and X ray analyses
09 p1523 A69-21872

Correlation between interfacial tension in binary and ternary systems and reciprocal solubility of bulk phases, assuming concentration as function of thickness
09 p1448 A69-21909

Phase equilibrium in cast Zr-Re-B and W-Re-B systems using microscopic and X ray analysis
10 p1711 A69-23332

Preliminary natural aging effects on maximum strength properties obtained at various artificial aging temperatures for aluminum ternary alloy
11 p1905 A69-24921

Aluminum additive effects on copper-titanium alloy decomposition, discussing Guinier complexes, heterogeneous nucleation, plastic deformation and low temperature aging
11 p1905 A69-24922

Phase equilibria in ternary systems Nb-Fe-B and Nb-Co-B, determining structural types and lattice constants by using X ray and microstructural analysis
15 p2641 A69-31246

Chromium ternary systems phase diagrams and crystallographic structures, using heat treatment and X ray analysis
18 p3158 A69-35262

Cu-Cd-S photovoltaic cell models correlated, reporting spectral response and electron microprobe test results
19 p3382 A69-35682

In-Te-Se system alloys structure and semiconductor properties analyzed by X rays
21 p3779 A69-38579

Melt cooling rates effect on supersaturated solid solutions in Al ternary systems
21 p3745 A69-38955

Adsorption kinetics in ternary mixture of nitrogen, methane and hydrogen, using concentration-time/breakthrough/curves measurement on activated coconut shell charcoal [NAS-NRC PAPER H-4]
22 p3981 A69-40629

TERNARY SYSTEMS [DIGITAL]

U DIGITAL SYSTEMS

TERRADYNAMICS

Atmospheric circulation influence on earth rotation velocity, discussing estimation methods
02 p0236 A69-11641

Terradynamic research program for studying instrumented projectile penetration of terrestrial materials
02 p0228 A69-11767

Seismic wave generation, propagation, dispersion and attenuation in gravitating sphere having

homogeneous elastic mantle and liquid core, giving theoretical seismograms
02 p0243 A69-12019

Trouton-Noble experiment to detect motion of earth through ether by electromagnetic torque on charged suspended parallel plate capacitor, explaining null results
03 p0517 A69-14106

Mathematical theory of electromagnetic induction for spherical model of earth with conductivity distribution given by sine function
06 p0921 A69-17718

Royal Belgian Observatory studies on time, meridian, seismological and gravimetric services, latitude variation due to polar motion, terrestrial tides among geodetic satellites
08 p1306 A69-19929

Thermal convection in earth mantle with temperature and pressure dependent viscosity, considering mechanisms for fluid-like mantle
10 p1682 A69-23412

TERRAIN

Terrain influence in ground wave propagation evaluated by two dimensional diffraction and scattering problems, using Airy type wave functions [AFCRL-68-0212]
01 p0033 A69-109707

Spectral brightness of clouds and various terrains in visible and near IR regions measured from aircraft
06 p0953 A69-179911

Stellar image vibration dependence on zenith distances and terrain relief determined from stellar traces by 200 mm telescope
15 p2647 A69-30163

Steady state baroclinic boundary layer over two dimensional terrain in f plane, noting layer thickness dependence on stability and terrain slope
24 p4347 A69-43356

TERRAIN ANALYSIS

Aerial color photography for terrain analysis noting development of cameras, filters, high speed emulsions and processing equipment
01 p0077 A69-10023

Passive and active transmitters and receivers of electromagnetic radiation in earth orbital satellites to collect pictorial or numerical data to study hydrology [UN PAPER 68-95333]
01 p0064 A69-10481

Terrain roughness effect on ionospheric radio wave absorption measurement data compared with theoretical results
02 p0207 A69-11669

Broadband null balancing microwave scanning radiometer using diode in feedback loop as reference noise source
02 p0221 A69-12457

Lineament trend analysis of Gemini Red Sea synoptic terrain photography, noting computerized rotation from apparent to true angles
02 p0247 A69-12808

Geophysical investigations on manned orbital space laboratories, discussing space photography, spectrophotometry, terrain pictures and aerosol layers
05 p0759 A69-16633

Relative orientation elements of aerial photographs determined by iteration method
05 p0765 A69-16708

Mars surface features identification from comparison of Mariner 4 and ground bases telescopic photographs
07 p1213 A69-18605

Space photography as sedimentological research tool demonstrated by space photographs application to projected Mars mission
09 p1490 A69-21797

Multispectral photographic determination of reflectance of environmental features from aerial spectral photographs, noting EROS program application
11 p1880 A69-24266

Signal processing and DC restoration in line scan devices used in land/water terrain analysis
12 p2096 A69-26980

Radiophase mapping utilizing VLF radio signals to detect conductive sheets and surface impedance of earth
12 p2075 A69-26982

Space photography for natural resource inventory, describing Gemini photographs role in assessing vegetation, geological, metal and soil resources in Western Hemisphere
12 p2097 A69-26987

Radar remote sensing for terrain data acquisition
12 p2098 A69-27005

Terrain photography applications and analysis including remote sensing of photographic systems and photointerpretation
12 p2098 A69-27006

Airborne IR surveys in engineering studies of terrain, discussing instrumentation technology, data interpretability, economic feasibility, etc
12 p2098 A69-27007

Microwave radiometric brightness temperature relationship to soil moisture content for estimating bearing strength
12 p2099 A69-27008

Side-looking airborne radars (SLAR) application to geological exploration of remote unmapped areas
12 p2099 A69-27009

Data analysis techniques for discrimination and identification of terrain surfaces from radar scatterometry information
12 p2099 A69-27010

Lunar topography harmonic analysis, noting sample point density and evenness variations effects on estimated coefficients
13 p2344 A69-27647

Terrain roughness effect on ionospheric radio wave absorption measurement data compared with theoretical results
13 p2224 A69-28700

Remote sensor imaging techniques for simultaneous radar, IR and visible electromagnetic spectra of extensive land areas, presenting two clustering algorithms for multiple images
14 p2448 A69-29533

Integrated landscape analysis with radar imagery for earth resources
15 p2608 A69-30454

Regional slope measurement from two monoscopic radar images of same terrain area, discussing accuracy and applications to geomorphology and hydrology
15 p2610 A69-30710

Digital method to produce radar reflectivity from analog audio frequency Doppler data extracted from terrain echo signal of CW scatterometer radar
15 p2572 A69-31111

European geostationary satellite orbit inclination and eccentricity modification for maximum observation time of Northern Hemisphere by high resolution IR radiometer
15 p2650 A69-31389

Mathematical model for determining time dependent terrain surface temperatures and radiances, considering radiative transfer convection, evaporation, ground vegetation temperature, etc
17 p3071 A69-33263

Gemini program for geologic orbital photography, discussing equipment used
18 p3131 A69-35274

Satellite IR hyperaltitude imagery for earth resources application, obtaining geological, meteorological and hydrological information
20 p3536 A69-36930

Aerial photography in geomorphological interpretations, noting advantages over conventional maps in slope microreliefs, soil erosion network and karst, glacial, aeolian and shore features
20 p3539 A69-37512

Geometrical configuration for synthetic aperture terrain imaging radar scanning system, noting scanning methods in range and azimuth directions
20 p3489 A69-37634

Synthetic aperture radar principles, using periodic pulse modulation to construct terrain imaging radar
20 p3489 A69-37635

Signal spectrum and SNR of synthetic aperture terrain imaging radar using model, including two dimensional signal and Gaussian additive noise
20 p3489 A69-37638

Synthetic aperture terrain imaging radar system optimal design, considering noise-free and random noise conditions using least squares method and signal to noise ratios
20 p3489 A69-37639

Signal amplitude no memory nonlinearity effect on performance of synthetic aperture terrain imaging radar systems and simulation of CRT film systems
20 p3490 A69-37643

Terrain radar returns emphasizing surface roughness influence in man-made target backscattering, determining radar cross section with radar range equation
20 p3490 A69-37646

Atmospheric phenomena effects on terrain imaging radar systems performance, discussing tropospheric turbulence and ionospheric irregularities
20 p3490 A69-37647

Imaging radar applications noting military surveillance, navigation assistance, iceberg detection, sea rescue operations, all-weather traffic surveys, terrain mapping, etc
20 p3491 A69-37649

Radar geoscience application, discussing radar return relation to illuminated terrain in detecting buried river channels
20 p3491 A69-37651

Orbital images for earth resources satellite mission planning using Mercury, Gemini and Apollo synoptic terrain photographs
21 p3721 A69-38632

Aerial remote sensing data for earth resources program including agricultural, geothermal/ geological tests, hydrological, water pollution and soil and flood water control observations
22 p3949 A69-40994

Terrain slope estimation of position errors of differential corrections in orthophoto production
22 p3951 A69-41245

Terrain surface irregularities influencing electromagnetic wave propagation in inhomogeneous atmosphere, using perturbation calculation
24 p4281 A69-42611

Electronic scanning and correlation techniques for terrain sensing required in automatic stereoperception
24 p4316 A69-43566

TERRAIN FOLLOWING AIRCRAFT

AH-56A helicopter manual and automatic terrain following and manual terrain avoidance systems, discussing nap-of-earth flight, design and simulation
17 p3002 A69-33544

Aircraft terrain-following algorithm for use with airborne general purpose digital computer, discussing simulation techniques and test results
19 p3366 A69-35625

Real time terrain following computer for C-5A transport, discussing automatic throttle system and speed bleedoff utilization
19 p3367 A69-35633

TERRESTRIAL DUST BELT

Stratospheric dust effect on twilight sky color, evaluating scattered radiation chromaticity for atmospheric models containing ozone
02 p0243 A69-12014

Stratospheric dust, discussing terrestrial and meteoritic origins, volatility of particles smaller than few microns, and light scattering and direct sampling measurements
09 p1608 A69-22689

Atmospheric optics by spacecraft and high altitude probes concerning ozone and aerosol distributions, scattering indicatrix polarization and dust cloud inhomogeneities
12 p2055 A69-25815

Satellite measurements of small particles near-earth space density compared with chemical estimates of terrestrial cosmic material, suggesting particles origin in meteoroid ablation
21 p3701 A69-38342

TERRESTRIAL MAGNETISM U GEOMAGNETISM

TERRESTRIAL RADIATION

Angular and spectral distribution of earth IR radiation near horizon from satellite observation and spectrograms
03 p0422 A69-13506

Latitude dependence of earth spectral radiation intensities, discussing satellite observations in equatorial and subtropical regions
03 p0422 A69-13507

Outgoing radiation field based on interpretation of broad sector radiometer measurements made from meteorological earth satellites
04 p0627 A69-15032

Solar and terrestrial thermal radiometer absolute calibration noting standards and methods
04 p0602 A69-15429

Earth X ray flux due to solar X rays reflected in atmosphere observed by Skylark rockets, noting observations of Sco XR-1 and Cen XR-2
04 p0649 A69-15440

Earth radiation effect on space vehicle, using diffusely radiating sphere model
05 p0824 A69-16053

Actinometric and nephelometric data on outgoing short wave radiation obtained by Cosmos 122 satellite, tabulating cloud cover data, digital radiation data and brightness curves
06 p0952 A69-17983

Double scattering effects of sky radiation and outgoing radiation balance in disturbed atmosphere, using homogeneous plane parallel atmospheric model
07 p1175 A69-18270

Meteorological satellites observation of energy exchange between earth and space, discussing planetary albedo, energy absorption and source and sink regions
07 p1127 A69-19261

Angular distribution of photon radiance of spherical satellite irradiated by Lambertian earth, assuming nonemissive satellite
08 p1311 A69-21095

Error correction for correlation coefficient between satellite data of earth radiation intensity and satellite vision field shift
14 p2435 A69-29043

Meteorological elements variation from measuring earth radiation in different spectral regions by satellites, determining temperature and humidity profiles
14 p2477 A69-29828

Earth thermal emission intensity measured by two beam radiometer onboard Cosmos 149, noting discrepancy between empirical and theoretical transfer functions of atmosphere
15 p2596 A69-30651

Earth reflected radiation pressure and perturbing effect on satellites
15 p2599 A69-31324

Statistical regularization for determining vertical atmospheric temperature profile from measurements of earth radiation in 15 micron carbon dioxide band
18 p3167 A69-35339

Orthogonal functions for determining atmospheric vertical temperature profile from satellite measurement of earth outgoing radiation in carbon dioxide absorption band
19 p3303 A69-36409

Partial differential equation representing influence of radiative and turbulent transfers of atmospheric heat, based on absorption coefficients for terrestrial radiation
19 p3363 A69-36498

Earth radiation effect on space vehicle, using diffusely radiating sphere model
20 p3606 A69-37963

Radiative heat input to artificial satellite in orbit due to solar and earth radiations calculated and presented in graphs for satellite temperature calculation
22 p4006 A69-40589

Minimum air temperature forecast by terrestrial thermal or long wave radiation balance measurement, using radiometer data
23 p4184 A69-42211

TESSERAL HARMONICS

Satellite orbit selection for determining geopotential and spherical and tesseral harmonic coefficients, discussing propulsion systems and satellite observation cost feasibility
02 p0331 A69-12807

Satellite motion short period perturbations by earth gravitational field tesseral and sectoral harmonics
12 p2069 A69-26431

Tesseral harmonics of geopotential and station coordinates based on combined Baker-Nunn, laser and range and rate satellite data
15 p2601 A69-31372

TEST CHAMBERS

NT ANECHOIC CHAMBERS
NT PRESSURE CHAMBERS
NT VACUUM CHAMBERS

Atmospheric exposure chamber design for small animals, discussing dynamic and recirculating operations and gas scrubbing system
04 p0584 A69-14678

Vacuum pumping methods for large space simulation chambers, discussing cryopumping, economic and operational considerations
13 p2241 A69-28078

Space environment simulation for vacuum, solar radiation, heat sink and orbital motion, discussing oil contamination of optical surfaces
13 p2241 A69-28079

Molecular gas flows in containers for space environment simulation, discussing flux distribution
13 p2241 A69-28081

Hydraulic-powered self propelled six degree of freedom loading vehicle moving tests assembly to test chamber with high accuracy positioning
20 p3511 A69-38181

Panel flutter testing in supersonic blowdown wind tunnels, analyzing model and test chamber layout
21 p3847 A69-39859

Reliability demonstration testing equipment, describing temperature chamber design and instrumentation, overall facility planning, etc

22 p3954 A69-40034

EKG data telemetry from personnel to receiver located within same closed metallic chamber, discussing FM/AM and FM/FM systems

23 p4103 A69-41766

TEST EQUIPMENT

Structural testing in aircraft design, discussing costs, environmental conditions, test rigs and apparatus

01 p0170 A69-10864

Ball bearing test apparatus for evaluation of greases and solid lubricants at high temperatures [ASLE PREPRINT 68AM 7C-2]

01 p0087 A69-10912

Optimal layout of turbofan jet engines, discussing experimental rig for high thrust measurement [AIAA PAPER 67-416]

01 p0143 A69-11015

Mass spectrometer residual gas analyzer (RGA) for identifying and measuring subliminated substances from spacecraft construction materials, noting applications during vacuum testing

02 p0227 A69-11758

Automatic test equipment applicability to testing problems created by increasing complexity of communications equipment

03 p0410 A69-13189

Wind tunnel and test equipment for studying flow in straight airfoil lattices at Reynolds numbers 50,000-1,200,000 and Mach numbers 0.1-1.0

03 p0412 A69-13789

Fokker bond tester and structural details of different types of sandwich structure, giving attention to adhesive bonding of panels, adhesive application, etc

03 p0434 A69-13791

Machine for simultaneous creep and long term strength evaluation of multiple metallic specimens

04 p0584 A69-14537

Mass spectrometer leak testing by calibrated enclosure method for quantification of gaseous leaks in large complex systems

04 p0598 A69-14974

Dual processor checkout system providing isolation of malfunctioning unit from memory and ensuring decision making by operative unit

04 p0568 A69-15361

Test equipment for rapid automatic checkout and evaluation of automatic flight control systems on commercial and jet transport aircraft

05 p0742 A69-15883

Electronic system checkout in SAAB 37 Viggen, using computer controlled test equipment

05 p0726 A69-16767

Requirements for analysis and synthesis of diagnostic tests for detecting faults in combinational logic circuit

06 p0892 A69-17408

Automatic test set for measuring dopant concentration profiles in epitaxial films

07 p1130 A69-18245

Laboratory test stands for ignition, combustion and expansion processes experiments in hypergolic liquid fuels, noting minimal recombination gains

08 p1301 A69-20170

Tests and quality control equipment used in German aeronautical and astronautical industries

09 p1513 A69-22565

Optimum calibration interval program for determining test equipment calibration frequencies on basis of mean time between failures and acceptable reliability levels

10 p1699 A69-23288

Refractory metals testing at high temperatures in vacuum, discussing equipment modifications, temperature measurement and residual gas problems

10 p1714 A69-23848

Bending creep vacuum testing device for brittle materials at high temperatures, noting load variation capability

10 p1696 A69-23851

Shock testing methods using shock spectrum concept and description testing machines and instrumentation

11 p1862 A69-24408

Gun tunnel equilibrium piston technique by model analysis of piston weight, tunnel conditions and geometry

11 p1862 A69-25013

High speed automatic test sets and rapid repair procedures under adverse conditions for individuals of relatively low technical skill

11 p1851 A69-25063

Abbreviated Test Language for Avionics Systems /ATLAS/ as standard compiler input language for commercial airline automatic test equipment /ATE/

11 p1842 A69-25064

Electronic module testing with integrated hardware/software system, noting module test console and manual capabilities

11 p1864 A69-25065

Universal test equipment compiler /UTEC/ built for use with languages designed to control automatic test equipment

11 p1842 A69-25066

Modular designed automatic test system consisting of central computer controlled system with multiplexed remote test stations for depot level maintenance

11 p1864 A69-25067

Multipurpose test system analysis emphasizing support section containing self test elements, power monitoring and control, interconnection techniques and packaging

11 p1864 A69-25069

Compatibility effects of automatic test equipment on avionic hardware design

11 p1865 A69-25070

Hardware-software interface defined for design of computer controlled test system, discussing criteria for designing economical systems

11 p1842 A69-25071

Flexible control module for real time automated checkout requiring programming by personnel with strong software background

11 p1843 A69-25072

Mathematical model for prediction of automatic test equipment utilization and determination of time for performance of intended test function

11 p1865 A69-25074

Semiautomatic and automatic off-line module testing machines, comparing costs for different test populations

11 p1865 A69-25076

Minimum test error probability test limits for known test equipment and signal tolerances, developing semi-graphically single equation for calculation

11 p1865 A69-25079

Onboard test instrumentation for monitoring aircraft communication, navigation and identification systems, noting adaptive programming

11 p1866 A69-25080

Automatic system self test technique known as central integrated test subsystem /CITS/ for logically testing avionics systems

11 p1866 A69-25083

Geomagnetic field vertical and horizontal intensities measured using proton magnetometer with coil theodolite

11 p1889 A69-25435

Testing machines for metallic materials, discussing design criteria and application to tensile strength, vibration and durability test machines [DVL-865]

11 p1889 A69-25682

In-circuit diodes testing by semiautomatic low current regulated voltage test set

12 p2035 A69-25835

Kerr constant verification device to study electrooptic liquids properties

12 p2084 A69-26148

Alignment/test rig for head-up displays using laser light pencils

12 p2091 A69-26304

Precision optical systems tests, using two beam interferometer and CW gas laser to examine reflected or transmitted wavefront contours

12 p2092 A69-26421

Crossed beam apparatus with mass selected variable energy primary beam for study of angular and velocity spectra of ion-molecule reactions

12 p2092 A69-26477

Furnace for automatic high temperature cycling in controlled oxidizing environment

12 p2093 A69-26483

EEG monitor helmet for aircraft or flight simulator programs, discussing sensing and transmitting system

12 p2023 A69-26553

Equipment and test installations for turbojet noise studies, discussing noise from rotating parts, pure jet noise and air propagation of noise

13 p2325 A69-28589

Resonant fixtures used for mechanical amplification of vibrator output to desired test levels

15 p2588 A69-30404

Controlled electric field capacitance probes for non-destructive testing, discussing field projection pattern and direction effective depth of field, applications, etc

15 p2616 A69-31503

IR techniques for nondestructive testing, discussing applications to heat injection and generation and test equipment capabilities

15 p2630 A69-31508

Delta technique for ultrasonic weld inspection, noting ability to detect randomly oriented weld defects

15 p2631 A69-31509

Ultrasonic inspection systems to determine average record bond quality on all adhesive bonded assemblies of Saturn S-2 booster and Apollo Command and Service Modules

15 p2632 A69-31511

Helicopter wind tunnel testing, discussing solutions in terms of test procedures and test bed equipment

16 p2735 A69-32011

Test apparatus for determining radiative properties of Ar plasma as function of high temperature and pressure [AIAA PAPER 69-601]

17 p3010 A69-33318

Tire test machine for tire parameter determination in aircraft landing gear shimmy stability studies [AIAA PAPER 68-311]

17 p2902 A69-34029

Aircraft solid state electric system logic level tested functionally by built-in test equipment /BITE/ operated on ground during preflight tests

17 p2977 A69-34111

Magnetic field susceptibility testing method as defined in DOD Electromagnetic Compatibility Control documents MIL-STD-461 and MIL-STD-462

17 p2947 A69-34133

Testing machine for in vacuo tensile testing of tubular metallic specimens at high temperatures and low pressures

18 p3117 A69-34604

Thermoelectrical leg product specification /TELPS/ apparatus and data reduction technique for determining temperature dependent thermoelectric properties of material

18 p3093 A69-34783

Automatic ultrasonic inspection device search head, servomechanism and electronic system used for detecting weld defects and cracks

18 p3137 A69-35111

Hydraulic-powered self propelled six degree of freedom loading vehicle moving tests assembly to test chamber with high accuracy positioning

20 p3511 A69-38181

Metal deformation dynamics at elevated temperatures, discussing closed loop electrohydraulic testing machine for stress relaxation and strain rate sensitivity

21 p3689 A69-38595

Passively isolated and actively stabilized platform for inertial navigation components and systems tests [AIAA PAPER 69-863]

21 p3690 A69-39423

Reliability demonstration testing equipment, describing temperature chamber design and instrumentation, overall facility planning, etc

22 p3954 A69-40034

Temperature program generation for test chambers, describing temperature programmers and readout, verification and recording systems

22 p3954 A69-40038

Uniaxial tensile testing machine to operate under combined creep and fatigue conditions for studying dislocation structure changes in metals and alloys at high temperature

22 p3926 A69-40441

Spacecraft test equipment based on balancing and vibration testing machines, emphasizing mass distribution experimental determination

24 p4296 A69-42669

TEST FACILITIES

NT ANECHOIC CHAMBERS
NT BALLISTIC RANGES
NT BLOWDOWN WIND TUNNELS
NT CASCADE WIND TUNNELS
NT ENGINE TESTING LABORATORIES
NT ENVIRONMENTAL LABORATORIES
NT HOTSHOT WIND TUNNELS
NT HYPERVELOCITY WIND TUNNELS
NT LOW DENSITY WIND TUNNELS
NT LOW SPEED WIND TUNNELS
NT MISSILE RANGES
NT PLASMA JET WIND TUNNELS
NT ROCKET TEST FACILITIES
NT SHOCK TUNNELS
NT SLOTTED WIND TUNNELS
NT SUBSONIC WIND TUNNELS
NT SUPERSONIC WIND TUNNELS
NT TRANSONIC WIND TUNNELS
NT WIND TUNNELS

Upgrading wave superheater for evaluation of reentry materials

01 p0054 A69-10917

Remotely controlled explosives processing facility for handling unfamiliar sensitive materials, noting

safety aspects and inspection, testing, transporting and destroying techniques

02 p0226 A69-11523

Dry heat sterilization and ethylene oxide decontamination test equipment for bipropellant liquid propulsion system

02 p0228 A69-11764

Concorde structural tests, discussing ground test program for simulating flight temperature and stress conditions at 2.6/2.7 station of wing-fuselage section

02 p0193 A69-11892

Radar cross section laboratory, discussing experimental techniques, electromagnetic range and pulse, FM/CW and CW radars

03 p0385 A69-12912

NASA Plum Brook Reactor Facility /PBRF/ for determining radiation tolerance to support nuclear power application in space for propulsion and power

03 p0465 A69-13128

Undetected defects and false alarm probabilities for automatic test equipment, emphasizing quality and confidence limits

03 p0428 A69-13187

Facilities at High Down Test Site for testing Black Arrow launch vehicles, discussing mechanical and electrical equipment test procedures

04 p0585 A69-15041

Closed system toroidal electrogasdynamic facility proposed for reentry simulation, discussing velocity generation

04 p0585 A69-15323

Central test evaluation group as part of systems engineering of large systems

05 p0742 A69-15803

West German test facility for simulating artificial satellite rotation about center of mass

07 p1116 A69-18260

Concorde testing program, detailing materials, structure, systems, engine, wind tunnel and flight tests

07 p1054 A69-19294

Communication satellite ground test programs, discussing structural, electrical integration, thermal control and antenna pattern models for simulation tests

08 p1409 A69-19962

Design criteria for vibration testing facility in Rome, giving block diagram of equipment at facility

08 p1301 A69-20159

Testing station design for VTOL aircraft ground effects investigations

08 p1302 A69-20880

Flight research testing facilities at Arnold Engineering Development Center for rockets, turbojets, ramjet engines, aircraft, missiles, satellites and spacecraft

08 p1302 A69-20883

Electronic components reliability tests, determining correlation between material quality and failure

08 p1293 A69-21109

Drop-weight tear tests dependence on specimen thickness and metallurgical properties

09 p1503 A69-21389

Man in loop computer facility for programmers to check out flight programs in simulated space flight environment

09 p1479 A69-22384

Real time real temperature exhaust gas reingestion and structural heating test facility for jet lift V/STOL configurations

09 p1479 A69-22388

Neutron radiography facility for production non-destructive testing inspection of aerospace components, noting collimation, neutron/gamma ray ratio optimization and neutron source

10 p1699 A69-23051

Wideband acceleration instrumentation for Rover ground test facility liquid hydrogen turbopumps to study structural and flow induced vibrations

10 p1692 A69-23250

Test facility automation, discussing pretest preparations, test operations, data reduction and system planning

10 p1671 A69-23260

Computerized shake test facility for Saturn 5 moon rocket, describing data acquisition, magnetic tape units, X-Y plotters, display devices, etc

10 p1672 A69-23285

Mississippi Test Facility /MTF/ hardware data acquisition system error analysis from extensive simulated static firing tests

10 p1673 A69-23287

Argas test loop as model for MHD power plant study, discussing component testing including channel preionization and relaxation experiments

10 p1673 A69-23478

Aircraft steam catapult test facilities, noting construction and operational requirements

10 p1674 A69-24068

Modular designed automatic test system consisting of central computer controlled system with multiplexed remote test stations for depot level maintenance

11 p1864 A69-25067

Single purpose, multipurpose and multistation automatic test systems for production and maintenance

11 p1864 A69-25068

Minimum test error probability test limits for known test equipment and signal tolerances, developing semi-graphically single equation for calculation

11 p1865 A69-25079

Procedures and facilities applicable to sonic environmental testing of flight vehicles, discussing sonic energy sources in vehicles and potential failure modes

12 p2060 A69-26939

Rolls Royce noise and compressor test facility for continual lowering of engine sound pressure levels, considering sound generating mechanisms

13 p2240 A69-27616

Torsional testing facility for delayed elastic and non-recoverable strains in materials, noting application to diffraction limited reflecting optics

13 p2240 A69-27955

Segmented-electrode and Hall ducts tested on supersonic magnetoaerodynamic conversion rig, defining electrical model for boundary layer losses at electrode surfaces

13 p2311 A69-28034

Real time pressure simulation chambers for testing space vehicles, discussing slow and rapid evacuation and pumping systems

13 p2240 A69-28077

Three meter spherical volume heat balance test facility for space vehicles at European Space Technology Center, describing vacuum system, solar simulation, etc

13 p2241 A69-28080

Test facility for supersonic combustion at low static pressure using fuel and gas streams and optical scanning spectrometer

13 p2243 A69-28276

Heating facility for testing ablative heat shield material models in combined convective and radiative heating environment with constant or transient heating conditions

13 p2243 A69-28278

Equipment and test installations for turbojet noise studies, discussing noise from rotating parts, pure jet noise and air propagation of noise

13 p2325 A69-28589

Helicopter climatic testing, discussing component, systems and field tests and facilities

14 p2427 A69-29505

Sonic boom simulation methods using shock tube, booth type simulators, ballistic ranges and explosives, discussing unmanned data recorder as monitoring device

15 p2585 A69-30371

Space Environment Simulation /SES/ facility at Goddard Space Flight Center, discussing operations and maintenance

15 p2586 A69-30386

Martian entry test facility for real size entry systems, discussing design, fabrication and operation

15 p2587 A69-30390

Weapon systems integrated testing, determining test quantities as function of subsystems utilizing Neyman-Pearson confidence levels

15 p2619 A69-30400

Independent testing laboratory management, outlining requirements specialized to fit continued growth conditions

15 p2720 A69-30402

Boeing A-7000 Solar Simulator for Space Environment Simulation Laboratory, noting output characteristics

15 p2588 A69-30403

Reliability testing of development models during production, considering short term and large batch tests

15 p2579 A69-31036

Automated IR fatigue crack detection in sonic test facility capable of subjecting large aircraft or missile structures to intense sound fields

15 p2631 A69-31505

Test facility for qualification of satellite fairings jet-tisoning system, describing accelerating tower and recording and control instrumentation

16 p2765 A69-31739

Static, transient and in-space environmental tests at satellite structures and heat shield test facilities in Italy

16 p2765 A69-31750

Helicopter wind tunnel testing, discussing solutions in terms of test procedures and test bed equipment

16 p2735 A69-32075

Running test facility for study of aerodynamics and flight dynamics of V/STOL aircraft models

17 p2944 A69-32851

On-line central data processing system connected to time shared computer for recording data from test facilities, discussing hardware configuration, software considerations and advantages

17 p2932 A69-33106

Hydraulic tank for visualizing flows around stationary models, noting absence of wall effects

17 p2956 A69-33588

Specification requirements for space vacuum simulation, considering vacuum requirements for simulating various effects

17 p2946 A69-33659

Facility for determining energy dissipation in materials under cyclic stresses or strains for wide range of temperatures

17 p2946 A69-33925

Facility for studying energy dissipation in refractory materials during fatigue tests in vacuum at various temperatures, describing principal components

17 p2947 A69-33926

Test facility to determine factors influencing aerodynamic energy dissipation of cantilever rods oscillating in airstream

17 p2947 A69-33928

Moment of inertia measurements facility for spacecraft dynamic balancing operations at low angular rates

18 p3118 A69-34889

Air and space research at Goettingen Aerodynamic Testing Institute

19 p3295 A69-36684

Facility for evaluating thermal stability of heat resistant materials and cermets in constant temperature gas flow

20 p3565 A69-36979

Device for equipment insertion into space vacuum simulation chamber to minimize interaction with walls

20 p3510 A69-37405

Magnetic test facilities at ESTEC consisting of system for geomagnetic field compensation and facility for magnetization and demagnetization, testing ESRO satellite models

20 p3512 A69-38279

Test facility for space vehicles simulating outer space gas pressure, heat sink behavior and relative motion to sun, detailing design and operation

21 p3689 A69-38420

Space simulation facility assembly and operational testing

22 p3919 A69-39959

Planning, design and implementation of reliability testing facility, investigating phases of project life cycle

22 p3954 A69-40033

Telemetry data processing, describing designation, tasks and possibilities of data reduction laboratory attached to NASA Goddard Space Flight Center

22 p3919 A69-40352

Friction tests for Mariner Mars 1969 spacecraft mechanisms in ultrahigh vacuum molecular sink chamber, noting increased friction attributed to vacuum environment

22 p3920 A69-40374

Variable optical system with remote and continuous adjustment of beam for solar simulation, permitting maximum test facility utilization

22 p3920 A69-40375

Vacuum integrating sphere for measuring solar absorptance in space environment to determine thermal control coatings qualifications

22 p3923 A69-40392

Space simulator vacuum facility for optical satellite tests, construction, operation and maintenance, emphasizing noncontaminating environment and pumping systems

22 p3924 A69-40396

RF voltage breakdown facility for studying spacecraft antenna characteristics in space and planetary atmosphere environments

22 p3924 A69-40397

Three axis motion simulator for in-orbit spacecraft attitude control evaluation using earth, sun and star sensor references

22 p3924 A69-40398

Burner rig hot corrosion test facility for evaluating Ni-Co alloys used in gas turbine engines operating in marine environment

22 p3928 A69-40673

Outer space rocket plumes simulation facility combining low density wind tunnel and molecular sink pro-

TEST FIRING

- perties, discussing role of liquid nitrogen cooled dif-
fuser-precooler 22 p3928 A69-40731
- Tensile test facility for specific strain rate range, ap-
plying impact load to sample end with high speed
striker accelerated by explosive energy 23 p4147 A69-41710
- Thermoelectric generators performance and life
tests, describing JPL facilities and programs 23 p4188 A69-42263
- Research and development programs leading to heat
sterilizable spacecraft battery separator material,
describing bench tests 23 p4072 A69-42284
- Dynamic hot corrosion rig test for operating environ-
ment and alloy composition effect on sulfidation attack
during gas turbine fuel combustion 23 p4150 A69-42448

TEST FIRING

- NT STATIC FIRING
- Holography for optical analysis of hypersonic
aerodynamics in single shot firing tunnel 12 p2087 A69-26176

TEST METHODS

U TESTS

TEST PILOTS

- Aerospace research pilot school /ARPS/ to train ex-
perimental test and aerospace research pilots and
Manned Orbiting Laboratory /MOL/ astronauts 06 p0882 A69-17670

TEST PROGRAMS

U TESTS

TEST RANGES

- NT BALLISTIC RANGES
- NT MISSILE RANGES
- Telemetry capability of Air Force Western Test
Range noting acquisition, tracking, data processing and
display and data reduction 05 p0743 A69-16304
- Conversion of range telemetry systems /CORTS/
program noting installations and standardization 05 p0743 A69-16306
- Air Force Eastern Test Range data processing
systems perform real time operations during in- flight
phases of ballistic missiles and orbiting vehicles 05 p0727 A69-16772
- Safety requirements of test ranges, considering RF
hazards to electroexplosive devices 10 p1751 A69-23019
- Microwave antenna testing on small indoor ranges,
discussing reflectors and feeds for generation of ap-
proximately uniform plane waves for antenna illumina-
tion 11 p1852 A69-25314
- S-band telemetry capability of Easter Test Range,
discussing relationship to Telemetry Rehabilitation
Project, major system decisions and performance
characteristics 14 p2410 A69-28878

TEST STANDS

- Test facilities and techniques for low speed flight
problems of aircraft handling qualities, stability, control
and performance 05 p0741 A69-15575
- Sine wave oscillator circuits and performance pre-
diction for NERO thrust measurement test stand 08 p1300 A69-20155
- NERO thrust power measurement, discussing elec-
tromagnetic and strain-gage test stands 08 p1301 A69-20156
- Simulator for testing colloid microthruster,
discussing spacecraft interfaces and time of flight thrust
data [AIAA PAPER 69-314] 09 p1478 A69-22380
- Test stand final control element for fluid flow ap-
plication, noting analog control valve with digital to
analog conversion and digital actuator 10 p1671 A69-23259
- Gas turbine engine development data system based
on test stands subsystems and central computer 10 p1660 A69-23284
- Test stand for free oscillations frequencies and mode
shapes of truncated conical shells of revolution with
clamped edges and one free edge 17 p3058 A69-33202
- Test pad isolation characteristics mathematical
model to predict pad dynamic behavior [AIAA PAPER 69-860] 21 p3690 A69-39388
- Test stand for measurement of forces and moments
from thrust vector controlled rocket, analyzing dynam-
ic characteristics of hydrostatic supports 21 p3691 A69-39631

TEST VEHICLES

NT FLIGHT TEST VEHICLES

- UK hovercraft research covering internal/external
dynamics, propulsion systems and full scale tests 05 p0702 A69-16393
- Wing section of high lift/drag test vehicle for 2500 F
reentry, describing design, manufacture and testing 12 p2103 A69-26837
- Thermionic converter performance measured using
test vehicles with guard ringed collectors and variable
emitter-collector spacing 14 p2398 A69-29177
- Test rig vehicle design for noise research on single
stage high bypass ratio fans for quieter turbofan power-
plants [AIAA PAPER 69-492] 16 p2767 A69-32727

TESTERS

U TEST EQUIPMENT

TESTING

U TESTS

TESTING MACHINES

U TEST EQUIPMENT

TESTING TIME

- Components production process effect on reliability
based on values and functional relations of internal
parameters, noting influence on accelerated testing 08 p1319 A69-20346
- Heat resistant Fe and Cu alloys creep index affected
by temperature, testing time and specimen grain size 15 p2639 A69-30569
- Mesa-structure varactors /p-n junction generating
harmonics by nonlinear capacity variation/ reliability,
determining selection criterion and optimal test dura-
tion period 15 p2627 A69-30839
- Project management of Apollo short stack testing
project, discussing organization, planning, operations
and procurement to cut testing time 18 p3233 A69-34616

TESTS

NT THERMAL VACUUM TESTS

- Bubble leak testing of components to understand ef-
fects of gas and liquid viscosity, surface tension, pres-
sure differential and temperature 09 p1503 A69-21391
- Quality control tests for adhesives used in structural
parts including ultrasonic and nondestructive tests 09 p1513 A69-22564
- Caravelle aircraft halting tests with barrier net 10 p1674 A69-23706
- Test methods for telescope mirror, discussing polish-
ing, monitoring by Hartmann test and visual null test 13 p2259 A69-27205
- Equipment testing, discussing collaboration between
government agencies and independent environmental
testing laboratories 15 p2720 A69-30398
- Test measurement - Conference, New York, October
1968 15 p2612 A69-31267
- Fracture tests evaluated for transition temperature
welding procedures, residual stress, flaws and instru-
mentation 17 p2989 A69-33565
- Integrated test program based on mission require-
ments, failure mode and effects analysis with feedback
from testing to design and development functions 19 p3327 A69-36014
- Optimum number of test aircraft in test program to
predetermine endurance and service life of same air-
craft in serial production 21 p3647 A69-39098
- Reliability prediction accuracy through reliability
testing with reference to interplay between design,
manufacture, test programs, environmental conditions,
etc 22 p3952 A69-40023
- Implementation of MIL-STD-781 reliability test
specification from contractor viewpoint, detailing test
procedures /procedural, decision, reporting and cor-
rective action rules/ 22 p3952 A69-40025
- Reliability testing and parts screening of electronic
systems for best parts selection 22 p3953 A69-40029
- Blade and vane wall thickness measurements test
methods for gas turbine engine using ultrasonic gage
and thermoelectric comparator 24 p4312 A69-42753

TETHERED BALLOONS

- Agricultural and forestry applications of tethered
balloons, discussing observation angle effect on spec-
tral signature response and signal preprocessing 22 p4053 A69-40805
- Tethered polyethylene balloon carrying radio con-
trolled camera for time lapse photographs of wave
generated near shore currents 22 p3865 A69-40808
- Photographic platform applications of tethered bal-
loons, discussing powered systems for low and high al-
titudes and free balloons 22 p3865 A69-40811
- Aerostatic and aerodynamic characteristics of Darr
Vee tethered balloon system 22 p3865 A69-40813
- Mathematical model for ascent and descent of high
altitude tethered balloon, developing computer pro-
gram and deriving differential equations of motion [AIAA PAPER 68-942] 24 p4254 A69-43722

TETHERING

- Motion stability of two tethered unsymmetrical earth
pointing bodies in circular orbit, presenting nine
degrees of freedom differential equations of motions 02 p0324 A69-12507
- Relative motion of two bodies linked by flexible
weightless tether in artificial earth satellite orbit, simul-
ating extravehicular walk 19 p3427 A69-36618
- Mathematical model of astronaut motion and
spacecraft angular control during tethered reentry,
discussing conditions preventing spinning and colli-
sions 21 p3667 A69-39630
- Tethered orbiting interferometer configurations for
future Radio Astronomy Explorer satellites, discussing
gravitational stabilization and delta launching into orbit
as single payload [AAS PAPER 69-255] 24 p4313 A69-42859

TETHERLINES

- Equations of motion of point restricted tethered
parafoil for investigating longitudinal and lateral
dynamic stability 01 p0009 A69-10415

TETRACHLOROMETHANE

U CARBON TETRACHLORIDE

TETRAD THEORY

- Linear approximation of Moller condition for
reference frames interpretable as linear approximation
of field equation in tetrad theory of gravitation 08 p1351 A69-20287

TETRAFLUOROHYDRAZINE

- Monograph on kinetic study of fast gas reactions
with shock waves covering thermal decomposition of
nitrous oxide, hydrazine tetrafluoride and nitrogen
tetrafluoride 08 p1304 A69-20707
- Thermodynamic calculation of equilibrium constant
and homolytic dissociation degree of
tetrafluorohydrazine based on enthalpy and statistical
entropy 24 p4280 A69-42788

TETRAGONS

- U PARALLELOGRAMS
- U RECTANGLES
- U SQUARES [MATHEMATICS]

TETRAHEDRONS

- Curved tetrahedral and triangular elements in
matrix displacement method covering linear and non-
linear cases 08 p1415 A69-20631

TETRANITROTETRAZACYCLOOCTANE

U HMX

TETRAZOLES

- Aminotetrazole preparation to obtain tetrazole
derivatives and explosive salts 10 p1651 A69-23013

TETRODES

- Insulated gate tetrode with high drain breakdown
potential and low Miller feedback capacitance, noting
V-I characteristics 05 p0733 A69-16556
- Pulse frequency integral estimate devices with in-
tegrating chemotron tetrodes for automatic systems
metering applications 13 p2227 A69-27522
- Amplitude modulator with field effect tetrode
transistor /FETT/, discussing linear mode operation of
modulator circuit 14 p2420 A69-29459

- VHF and uHF MOS tetrode minimum noise factor computed as function of frequency by adding thermal noise sources to resistive parts of equivalent circuit
15 p2577 A69-30603
- Four terminal silicon planar p-n-p-n model operating as semiconductor small signal linear tetrode amplifier, discussing properties and mathematical models
18 p3109 A69-35293
- TETRYL**
Slowly exploding wires for igniting self sustaining deflagrations in PETN, RDX, HMX and tetryl, comparing circuit parameters for detonation initiation
01 p0141 A69-10678
- TEXAS**
Nocturnal development of air mass stratus clouds in Texas and mechanism of formation, discussing turbulent mixing theory
15 p2649 A69-30893
- TEXTBOOKS**
NASA Pilot Program in instructional monographs to provide up-to-date material from current research for engineering education
18 p3236 A69-35078
- TEXTURES**
Alloying elements and cold rolling deformation effects on formation of texture in Ti alloys, noting inhomogeneity
04 p0617 A69-15077
- Plastic flow anisotropy and texture shifting by rolling in Ti-Mo-V alloy, analyzing slip rotation, grain boundary shear and deformation mode
17 p2987 A69-33078
- Depth dependent variations in texture in Nb due to inhomogeneous plastic deformation during cold rolling
21 p3744 A69-38737
- Surface texture effects, discussing metallic and elastomeric contacts, measurement, profile, model parameters, adhesion, hysteresis, lubrication, squeeze films, macroelastohydrodynamics and randomness
23 p4170 A69-42359
- TFX AIRCRAFT**
U F-111 AIRCRAFT
- THALAMUS**
Ventral posterolateral potentials in anesthetized immobilized cats in response to electric stimulation of mesenteric nerves and mechanoreceptors, studying thalamus nucleus role
12 p2020 A69-26562
- Cortical and thalamic evoked activities changes during sensory conditioning of freely moving cat
22 p3872 A69-40160
- Neuronal organization of initial afferent inflow in thalamic visual center /lateral geniculate body /LGB/ of unanesthetized cats/, noting unit activity
22 p3879 A69-40845
- THALLIUM**
Electronic attenuation of 10 to 130 MHz longitudinal ultrasonic waves in superconducting high purity Ti, noting energy gap anisotropy
03 p0485 A69-13293
- Electronic attenuation of 10 to 130 MHz longitudinal ultrasonic waves in nonsuperconducting high purity Ti, noting anisotropy and measurements below 4.2 K
03 p0485 A69-13294
- Thallium whisker growth /compression or squeeze/ method
04 p0641 A69-14457
- Temperature dependence of viscosity and density in molten thallium sulfide, noting structural changes absence in short range order
04 p0643 A69-14998
- Deposited beta active thallium isotope materials angular distribution after vaporization by Q switched laser beam determined by target fragment recoil
21 p3737 A69-38992
- THAWING**
U MELTING
- THEODOLITES**
NT CINETHEODOLITES
Geomagnetic field vertical and horizontal intensities measured using proton magnetometer with coil theodolite
11 p1889 A69-25435
- Wind speed and direction determination accuracy of radar or theodolite methods
20 p3572 A69-37698
- THEOREM PROVING**
FORTRAN Deductive System to find solutions to theorem proving problems, discussing computer implementation
01 p0037 A69-10806
- Levinson duality theorem for linear programs in complex space proved on basis of duality theorem for linear programming in real space
04 p0623 A69-14947
- Conditions for solution existence for n differential equations and Liapunov functions
05 p0787 A69-16451
- Volterra equation generalization extended and applied to functional Volterra equations, proving theorem dealing with topological, quasi-compact and uniform spaces
08 p1342 A69-20268
- Oscillation theorems for linear self adjoint elliptic equations of even order 2m, discussing proofs dependence on Swanson comparison theorem
11 p1909 A69-24882
- Gravitational analog of Mariot-Robinson theorem, obtaining two related theorems with Newman-Penrose spinor formalism
11 p1919 A69-25097
- Unique solution proven for laminar boundary layer equations of flow of revolution in unsteady state
13 p2248 A69-28195
- Einstein second postulate concerning invariability of light vector in vacuum experimented for validity, using earth and moon as light rays launching and reflecting media
13 p2354 A69-28650
- Semidefinite Peano kernels of stable forms
15 p2644 A69-30450
- Theorem extending results of techniques for analytical solutions of nonlinear ordinary differential equations applied to terrestrial brachistochrone problem
20 p3575 A69-37205
- Second circle theorem for two dimensional irrotational flow of incompressible inviscid fluid in z plane
20 p3518 A69-38316
- Evolutionary hypoelliptic equations with real variable coefficients, analyzing positive solutions and application to parabolic equations
21 p3756 A69-39151
- Existence theorem for relation between solutions of systems of ordinary differential equations
23 p4182 A69-41959
- Nondiscrete locally compact group having noncontinuous irreducible representations, proving theorem
23 p4183 A69-42022
- Separation theorem for arbitrary nonlinear measurements to find optimal stochastic control without dynamic programming
24 p4291 A69-43269
- Intrinsic transport theorem for electrodynamics of continuous media, using Cartan method of exterior differential forms
24 p4350 A69-43368
- THEOREMS**
U ADDITION THEOREM
U BAYES THEOREM
U BERNOULLI THEOREM
U CASTIGLIANO VARIATIONAL THEOREM
U EXISTENCE THEOREMS
U FLOQUET THEOREM
U GAUSS-MARKOV THEOREM
U MICHELL THEOREM
U POYNTING THEOREM
U RECIPROCAL THEOREMS
U RIESZ THEOREM
U SIMILARITY THEOREM
U STOKES THEOREM [VECTOR CALCULUS]
U UNIQUENESS THEOREM
- THEORETICAL PHYSICS**
NT NEWTON THEORY
NT QUANTUM THEORY
Theoretical prediction for modified and hybrid plasma resonances discrimination, noting sensor axis angle to geomagnetic field
02 p0241 A69-11731
- Mathematical aspects of stability of equilibrium configurations
02 p0340 A69-11991
- Book on linear boundary value problems of mathematical physics based on Green function covering Hilbert spaces, integral equations and spectral theory of differential operators
04 p0625 A69-15232
- Soviet collection of papers on mathematical physics
11 p1915 A69-24759
- Collection of Soviet papers on mathematical physics
11 p1916 A69-24770
- Integral transforms in composite one dimensional space and application to boundary value problems of physics
11 p1910 A69-25574
- Einstein second postulate concerning invariability of light vector in vacuum experimented for validity, using earth and moon as light rays launching and reflecting media
13 p2354 A69-28650
- Einstein general theory of relativity, discussing evolution and disunity among physicists and philosophers on universal relativity of mechanical motion
14 p2483 A69-28857
- General relativity theory philosophical substance and meaning, discussing Einstein formulations and bases of classical, relativistic and quantum physics
14 p2483 A69-28859
- Invariants method and applications in classical and relativistic physics emphasizing theory of relativity, physical and mathematical theories relations and group theory applications
14 p2484 A69-28860
- Categorical structures in theoretical thinking for philosophical fundamental physical laws analysis, including space-time concept changes in classical physics and in theories of relativity
14 p2484 A69-28861
- Macroscopic space-time meaning in theoretical physics in terms of mathematical definition and philosophical concept
14 p2484 A69-28864
- Monograph on creation and evolution of physico-theoretical concepts of space, time and matter
16 p2812 A69-32110
- Scientific theories construction analyzed, including cognitive role of mathematics
20 p3575 A69-37012
- Information categories concept defined in relation to formulations of classical mechanics principles, considering theories of Newton, Gauss and Hertz
20 p3576 A69-37585
- THERAPY**
U CHEMOTHERAPY
U PSYCHOTHERAPY
U RADIATION THERAPY
- THERMAL ABSORPTION**
NT POLAR CAP ABSORPTION
Qualitative analysis of thermoelectric effects in transistors, describing heat absorption and release
12 p2042 A69-26880
- Thermal radiation effects on laminar free convection boundary layer of vertical flat plate, studying absorbing and nonabsorbing gases
[ASME PAPER 68-HT-43] 13 p2373 A69-27772
- Optical and thermal attenuation of current induced by low energy electron bombardment in CdS crystal
19 p3392 A69-36727
- THERMAL ACCOMMODATION COEFFICIENTS**
U ACCOMMODATION COEFFICIENT
- THERMAL BATTERIES**
Metal fluoride compounds as cathodes for use with mixed fluoride electrolyte /LiF-NaF-KF eutectic/ in thermal batteries
10 p1640 A69-23997
- Nuclear thermal and electrovoltaic batteries design and operation, discussing applications
20 p3464 A69-37288
- THERMAL BOUNDARY LAYER**
Schlieren method for studying rotating sphere heat transfer during natural convection
01 p0174 A69-10095
- Time dependent interaction of hot gas bubble with chemically reactive liquid stream, detailing thermal boundary layer theory
01 p0058 A69-10162
- Impinging jet flames on furnace hearth, analyzing thermal boundary layer characteristics and convective heat transfer rates
06 p1035 A69-17933
- Equilibrium stability of horizontal layer of fluid in field of modulated temperature gradient having layer thickness greater than penetration depth of heat waves
07 p1241 A69-18696
- Nonaxisymmetric temperature field of unbounded hollow cylinder with moving heating boundary, expanding surface temperature into Fourier series
07 p1241 A69-18924
- Incompressible laminar thermal boundary layer unsteady development from state of rest in vicinity of wall of obstacle subjected to unsteady thermal field
[ONERA-TP-680] 08 p1304 A69-20754
- Steady laminar boundary layer flow calculations extended to temperature boundary layer for given heat flow or temperature distribution at wall
10 p1808 A69-22915

THERMAL BUCKLING

Thermal stratification effect on wind structure in Ekman layer, assuming turbulent transfer and height dependence
13 p2290 A69-27390

Micro-layer thickness in nucleate boiling, studying liquid-vapor interface motion of growing bubble near heated surface
13 p2375 A69-27789

Numerical solutions of equations for high Prandtl number boundary layers in two dimensional flat plate incompressible flow with mass injection
13 p2249 A69-28238

Three dimensional thermal laminar boundary layer around body moving with constant acceleration in incompressible fluid, considering wall temperature and Prandtl number
13 p2380 A69-28631

Temperature disturbance amplification in laminar natural convection boundary layer formed on vertical flat surface measured with hot-wire anemometers
14 p2430 A69-29575

Flow and temperature boundary layers on longitudinally curved walls, giving higher approximation exact solutions
15 p2591 A69-30933

Temperature distributions in layer with internal heat source and turbulent fluid flow cooling, deriving differential heat transfer equations
15 p2718 A69-31169

Inlet thermal boundary layer thickness effect on conical nozzle heat transfer and boundary layer determined by operating nozzle with cooled/uncooled inlet [AIAA PAPER 69-474]
16 p2881 A69-32780

Temperature jumps at gas-solid interface in shock tube calculated by one dimensional approximation of thermal boundary layer behind reflected shock wave
17 p2949 A69-33023

Electron temperature and number density measured at atmospheric pressure in plasma thermal laminar boundary layer adjacent to cooled wall [AIAA PAPER 69-692]
17 p3011 A69-33446

Interferometric study of electron concentration and mass density profiles through ionized argon thermal end-wall layer formed in shock tube [AIAA PAPER 69-694]
17 p3074 A69-33477

Thermal boundary layer formed during laminar jet flow over flat porous plate, discussing temperature distribution and mass transfer at plate surface
21 p3854 A69-39846

Velocity and temperature boundary layers on plane wall developed by ideal shock tube flow for weak shock and expansion waves
22 p3932 A69-40894

Lower boundary approximation for theory of thermal laminar steady state boundary layer on isothermal immersed plate
23 p4150 A69-41334

THERMAL BUCKLING

Flutter analysis of plates with inplane boundary support flexibility exposed to transverse pressure loading or buckled by uniform thermal expansion
11 p1992 A69-25523

Correlation between temperature and stress field in thermal buckling of square viscoelastic Maxwell plates under random temperature
12 p2188 A69-27113

Thermal and athermal component of flow stress and deformation dynamics for Ti at low homologous temperatures determined by stress relaxation tests
21 p3749 A69-39598

Uniaxial tensile testing machine to operate under combined creep and fatigue conditions for studying dislocation structure changes in metals and alloys at high temperature
22 p3926 A69-40441

Thermal buckling of skew plates clamped along all edges under radiant heating, measuring various characteristics, solving differential equations by difference method
22 p4044 A69-40599

THERMAL COMFORT

Radiative, convective and evaporative heat losses and thermal comfort conditions for human beings, describing theoretically and empirically based equation
06 p0880 A69-17087

THERMAL CONDUCTIVITY

Polycrystalline corundum thermal conductivity coefficients determination, describing measuring procedures at low temperatures
01 p0101 A69-10108

Critique of paper on thermal conductivity of composite materials by long wave method
01 p0172 A69-11272

N dimensional extensions of finite difference scheme for solution of differential heat conduction equation, noting practical limit by truncation error considerations
01 p0107 A69-11365

Alkali metal vapors thermal conductivity determination by temperature difference dilatometric measurement
02 p0247 A69-11579

Temperature dependence of thermal conductivity coefficient and specific heat of sublimating heat proof materials
02 p0350 A69-11580

Procedure accounting for variable thermal conductivity and internal heat generation in temperature distribution prediction for waveguide ferrite slabs
02 p0215 A69-11877

Ti alloys anomalous variations in physical properties measuring electrical, thermal conductivity and thermal EMF
03 p0443 A69-13029

EPR spectra and thermal conductivity measurement in excited organic semiconductor salt derivatives of tetracyanoquinodimethane
03 p0484 A69-13278

Lithium niobate crystals thermal properties measured at various temperatures
03 p0487 A69-13730

Pressure rise and thermal conductivity in cylindrical hydrogen plasma column in axial magnetic field, assuming local thermal equilibrium
03 p0479 A69-13967

Thermal conduction of chambers for selective and nonselective film detectors at low oburation frequencies
03 p0432 A69-14216

Temperature distribution over receiving layer of absorption edge image transformer, discussing thermal conduction influence on performance of thin film IR image receiver
04 p0631 A69-15280

Approximate method to determine nonstationary thermal fields in solid bodies with thermal capacity and thermoconductivity coefficient depending linearly on temperature
04 p0688 A69-15409

Subject classification bibliography for thermal contact resistance [ASME PAPER 68-WA/HT-18]
05 p0847 A69-16122

Transient method for measuring thermal properties of biological materials, concerning thermal conductivity, inertia and blood flow rate
06 p0879 A69-17086

Arc cloud thermal conductivity effects on discharge temperature and radiation intensity, solving energy balance equation
06 p0964 A69-17254

Viscous MGD channel flow in boundary layer approximation with heat conduction, transforming resultant partial differential equations set to system of ordinary differential equations
06 p0966 A69-17523

Thermal insulating characteristics of low conductance interstitial materials under compressive loads, noting carbon paper and wire screens [AIAA PAPER 69-25]
06 p1036 A69-18072

Thermal explosion criterion used for explosion/ignition delay of exothermic material surrounding heated wires having good thermal conductivity [WSCI PAPER 68-23]
07 p1240 A69-18359

Approximate equations for transonic viscous heat conducting gas flow past finite body of revolution
08 p1251 A69-20322

Energy consideration in electron beam welding, obtaining expression for penetration decrease in terms of thermal diffusivity [ECS PAPER 144]
08 p1320 A69-20360

Evaluation methods for DC electrical conductivity, heat conductivity and viscosity in plasmas
08 p1364 A69-20477

Soviet book on theory of heat conductivity covering physical principles of transfer and boundary value problems
08 p1421 A69-20647

Silicon dioxide glass thermal conductivity at very low temperature
09 p1493 A69-21426

Thermal conductivity, electrical resistivity and degree of blackness of refractory metals at high temperatures measured by Bode and Eger-Disselhorst methods
09 p1522 A69-21589

Homogeneous parabolic differential equation for heat transfer of two finite bodies in thermal contact solved by power series
09 p1532 A69-21628

Local axial voltage variation from one dimensional model applied to solve thermionic boundary conditions in two dimensional thermal analysis of converter
09 p1440 A69-21834

Variational calculation of coefficients of viscosity, thermal conductivity, thermal diffusivity and diffusion in binary mixture
11 p1997 A69-24285

Thermal conductivity of polycrystalline beryllium oxide as function of temperature and pressure in argon or helium atmosphere, discussing heat transfer mechanism
11 p1906 A69-25225

Turbulent viscosity and thermal conductivity coefficients for entire cross section of fluid flow including wall boundary layers
11 p1873 A69-25228

Wavelength of convective motions, discussing effects of lid heat conductivity on Rayleigh number
11 p2003 A69-25354

Thermal conductivity of hydrogen plasma in transverse magnetic field at high temperatures
12 p2133 A69-25765

Room temperature thermal conductivity of semiconducting alloys with stoichiometric distributions of vacancies in cation sublattice, discussing heat resistance
12 p2142 A69-25975

Comparative calibration characteristics determination, discussing absolute measurements method for thermal conductivity parameters
12 p2091 A69-26363

Model, assuming electron thermal conductivity contribution, applied to studying solar plasma discharge characteristics in presence of three dimensional thermal sources in solar corona
12 p2149 A69-26680

Heat transfer in solid bodies, deriving thermal conductivity equation and surface boundary conditions in presence of radiative energy transfer
13 p2373 A69-27584

Internal and external heat transfer instrumentation and equipment bioengineering, listing thermal conductivity and diffusivity of biological materials
13 p2213 A69-28150

Rigid heat conductor in continuum thermodynamics, discussing conductivity tensor symmetry and heat capacity positivity as restrictors
13 p2377 A69-28193

Thermal conductivity prediction technique for two and three phase solid heterogeneous mixtures
13 p2378 A69-28337

Heat flow resistance between solid bodies in contact in vacuum
13 p2378 A69-28338

EPR spectra and thermal conductivity measurement in excited organic semiconductor salt derivatives of tetracyanoquinodimethane
14 p2508 A69-29652

Thermal diffusivity and conductivity of rolled plane parallel spectrally pure palladium preheated in vacuum and high temperatures
15 p2636 A69-30045

Necessary and sufficient conditions for boundary point regularity in Dirichlet problem for heat conduction equation assuming Holder condition
15 p2716 A69-30047

Thermal conductivity coefficients in solar corona and chromosphere computed and tabulated for H plasma
15 p2694 A69-30788

Induced high pressure HF discharge parameters computed for Ar, O and N by using electrical and thermal conductivity functions
15 p2662 A69-30976

Air plasma electrical and thermal conductivity coefficients measured in wall stabilized DC arc at atmospheric pressure and high temperatures
15 p2663 A69-30979

Thermal conductivity of semiinfinite rod with insulated surface and constant internal heat source, considering finite heat propagation rate
15 p2719 A69-31181

Lattice components of heat conductivity and chemical composition relations of magnesium alloy solid solutions
16 p2824 A69-31567

Lattice component of heat conductivity in n-type cadmium arsenide at low temperatures by suppressing

electron component of conductivity with strong transverse magnetic field

16 p2824 A69-31568

Heat conductivity of liquid and solid gallium telluride in steady state regime, using graphite cylindrical device

16 p2824 A69-31572

Electrical and thermal conductivities of high pressure arc plasmas from I-V characteristics and radial temperature profile

16 p2817 A69-31644

Thermal contacts effects on optimum operating conditions of solar thermoelectric power generator, discussing losses due to low thermal conductivity coefficient of insulating layers

16 p2741 A69-32797

Flame front structure and combustion rates of gases as function of temperature dependence of thermal conductivity, diffusion coefficients, density and molecular weight

17 p3069 A69-33136

Thermal analysis of opacified fibrous insulation systems, discussing heat transmission, heat transfer and thermal conductivity relations to compression load and temperature

[AIAA PAPER 69-605] 17 p3072 A69-33282

Thermal contact resistance measurement at various ambient pressures compared with theoretical predictions with each parameter analyzed over interface by computer program

[AIAA PAPER 69-629] 17 p3073 A69-33299

Approximate equations for transonic viscous heat conducting gas flow past finite body of revolution

17 p2891 A69-33312

Terminal characteristics of composite superconductor, taking into account heat transfer to coolant, interface thermal contact resistance and superconductor size

17 p3007 A69-33792

Exact analytic solution for thermal conductance of two dimensional eccentric constriction in dimensionless numbers

18 p3228 A69-34375

Shock heated argon thermal conductivity studied by optical interferograms, deriving equation for measured mean value

18 p3228 A69-34459

Ti thermal diffusivity and conductivity at high temperatures measured from heat wave phase shift

18 p3156 A69-34699

Channel heat transfer determination based on thermal conductivity coefficients as functions of temperature gradients in channel wall materials

18 p3230 A69-34988

Thermal conductivity calculation for chemically reacting multicomponent gas mixture, comparing results from Brokaw method and simplified formula

20 p3483 A69-36974

Radiative heat transfer in polycrystalline cerium, studying photon thermal conductivity influence on lattice thermal resistivity

20 p3565 A69-36975

Thermal contact conductance of thermally thick specimens with thermocouples not located at interface

20 p3632 A69-37521

Correlating IR lunar nighttime temperature and bearing strength of lunar materials, using expressions of thermal conductivity and bearing strength of porous media in vacuo

20 p3613 A69-38248

Refractory materials thermal conductivity high temperature measurement technique, discussing sample geometry, furnace design, temperature modulation and computerized simulation

21 p3742 A69-38422

Thermal conductivity coefficient of gas mixtures at low temperatures obtained using quantum diffusion model and Chapman-Enskog method for Boltzmann equation

21 p3848 A69-38638

Experimental facility for studying heat conductivity of multicontact metallic and nonmetallic materials /plates/ in vacuum at low temperatures under various loads

21 p3721 A69-38639

Asymptotic method applied to nonlinear equations, determining thermal conductivity coefficient for temperature distribution in moving anisotropic media

21 p3848 A69-38642

Heat transfer coefficients evaluated from gas to rotating turbine blades in unsteady operation, using unsteady thermal conductivity and gradient methods

21 p3850 A69-38864

Viscosity, thermal conductivity and diffusion predicted for dilute nonpolar, polar and mixed gases, discussing methods for rotational relaxation collision numbers and resonant correction

21 p3850 A69-38951

Laplace transforms in heat conduction theory in three dimensional infinite homogeneous body

21 p3851 A69-39011

Approximate solution of unsteady thermal conductivity for plate with unlimited number of layers

21 p3851 A69-39083

Constant surface heating of half space with temperature dependent thermal conductivity

21 p3851 A69-39292

Temperature field in deflector cooled turbine blades for nonstationary regimes, considering heating of cooling air, thermal conductivity and thermophysical coefficient changes

21 p3786 A69-39718

Heat flow through ocean floor by measuring temperature gradient and thermal conductivity in ocean sediment

21 p3718 A69-39733

Effective thermal conductivity parallel to laminations and total conductance for combined parallel and normal heat flow in multilayer insulation

[AIAA PAPER 68-765] 21 p3853 A69-39763

Concentration distribution of admixture in semibounded jet propagating along nonheat conducting plate, obtaining concentration profiles for various thermal and diffusion Prandtl numbers

21 p3854 A69-39844

Navier-Stokes equations exact solutions for two dimensional steady flow of compressible viscous heat conducting perfect gas

22 p3929 A69-40117

Thermoelectric power generator with variable thermal conductivity and electrical resistivity, obtaining steady state temperature distribution, power output and thermal efficiency

22 p3868 A69-40131

Plasma thermionic diode figure of merit based on Hatsopoulos model altered to include thermal conduction and electrical resistance

22 p3869 A69-40134

Thermal conduction by electrons in stellar matter, presenting opacity tables for H, He, C and red giant cores and solar composition

22 p4014 A69-40147

Line source technique for ablative heat shield materials thermal conductivity measurements, comparing vacuum and atmospheric test results

[AIAA PAPER 69-1013] 22 p3922 A69-40386

Absolute thermal conductivity measurements on fluid normal H and fluid parahydrogen, noting apparatus and data graphical presentation along isotherms, isochores and isobars

[NAS-NRC PAPER D-1] 22 p3998 A69-40631

Thermal conductivity precision tests for refractory materials using ASTM method C 201-47, emphasizing sample preparation and calorimeter calibration

22 p3956 A69-40671

Forced convection liquid flow past heated flat plate with variable viscosity and thermal conductivity, analyzing velocity and temperature distribution in boundary layer

22 p4051 A69-40685

Porosity and composition effects on thermal conductivity of glass fiber reinforced plastics, noting tests of multilayer textolite sheets

22 p3973 A69-40747

Conductor material thermal conductivity contribution to self similar explosion in strong magnetic field, determining critical field strength

22 p3982 A69-41019

Analog problem solution for semiinfinite medium with Newtonian cooling at boundary, noting first term of asymptotic expansion in heat conduction equation

22 p4052 A69-41126

Thermal conductivity, Volume 2, covering fluids, thermal diffusivity, semiconductor materials, role in heat transfer, etc

23 p4236 A69-41323

Thermal conductivity relationship to heat transport coefficients for gases and liquids with charged or uncharged particles

23 p4237 A69-41324

Thermal conductivity measurements of fluids, considering contribution of radiation, convection, temperature jump and experimental arrangement eccentricity to errors

23 p4237 A69-41325

Heat transfer and surface thermal conduction characteristics of contact of two solid bodies,

discussing pressure effect, measurement and analytical techniques

23 p4237 A69-41327

Unsteady thermal conductivity calculated by approximate analytical method in simple shape bodies/infinite plate, long cylinder, sphere/ cooled or heated by thermal radiation

23 p4238 A69-41333

Thermal conductivity and specific heat of groups of liquid substances as functions of temperature, giving curves, tables and conversion factors

23 p4238 A69-41336

Transport coefficients in neutral gases, discussing fundamental relations of parameters in viscosity, thermal conductivity and self, pressure and thermal diffusion

23 p4193 A69-41514

Thermal conductivities /K/ of rock forming minerals reveals K as linear function of density for constant mean atomic weight

24 p4310 A69-43216

Contraststreaming self gravitating gas streams stability taking into account thermal conduction and radiation effects

24 p4388 A69-43638

THERMAL CONDUCTIVITY GAGES

Thermistor assembly apparatus for measuring coefficient of thermal conductivity of pure and binary mixture of gases

05 p0845 A69-15616

Simultaneous and independent measurement of thermal conductivity, thermoelectric power and electric resistivity, applying method to cadmium arsenide-zinc arsenide system

05 p0764 A69-16338

Column method of measuring thermal conductivity of CO and oxygen in 350-1500 degrees K temperature range, discussing error sources and data reliability

[AIAA PAPER 69-603] 17 p3073 A69-33298

THERMAL CONVECTION

U FREE CONVECTION

THERMAL CURRENTS

U CONVECTIVE FLOW

THERMAL CYCLING TESTS

Crack initiation and propagation in Ti alloys during thermal cyclic heating, noting influence of gas saturation

01 p0094 A69-10215

Vacuum heating and thermal cycling influence on mechanical and structural properties of aluminum sheets fabricated from sintered powder

02 p0266 A69-12126

Thermal cycling tests showing improvement in cadmium sulfide solar cell stability, noting effect of thermal cycling stresses

03 p0367 A69-13074

Elastoplastic element structural growth induced by thermal cycling analyzed as function of temperature and sustained axial load

[ASME PAPER 68-WA/MET-14] 05 p0837 A69-16067

Device for measurement of time to failure of brittle materials in thermal-endurance testing, noting shock wave

06 p0927 A69-17690

Thermal stability of refractory and cermet materials, analyzing small samples subjected to cyclic high energy radiative heating and air-water cooling

12 p2118 A69-26262

Homogenization of martensite formation in nickel 300 grade maraging steel, analyzing anisotropic transformation strains during thermal cycling

13 p2278 A69-27410

Concorde thermal fatigue resistance tested by alternate heating and cooling cycles simulating supersonic flight profile

13 p2241 A69-28102

Crack initiation prediction in high temperature components subjected to arbitrary thermal-mechanical cycling

13 p2365 A69-28252

Space environment simulation tests of cadmium sulfide thin film solar cells, noting output loss

14 p2405 A69-29538

Device for fatigue testing turbine disk models in unsteady temperature fields with radial and axial nonuniformity produced by HF heating

15 p2583 A69-30208

Crack initiation and propagation in Ti alloys during thermal cyclic heating noting influence of gas saturation

15 p2637 A69-30271

Mechanical testing of high temperature materials subjected to thermal cycling by high power pulsed laser beam

15 p2636 A69-31512

Hydrogen effects on ELI Ti-Al-Sn alloy, conducting tensile, fretting and abrasion tests on stressed and thermal cycled specimens

[AIAA PAPER 69-585] 16 p2803 A69-32760

Cumulative rapid thermal cycling influence on progressive disappearance martensitic transformation in 18 percent nickel maraging steel

18 p3155 A69-34650

Spacecraft and components testing methods critical reassessment, discussing cost reduction, vacuum and thermal cycle tests

18 p3118 A69-35082

Concorde structural tests emphasizing problems associated with thermal cycle, including fatigue test setup on complete airframe

[RAES PAPER 16] 22 p4043 A69-40495

Silicide and B-modified coatings on Mo, noting improved high temperature oxidation resistance under thermocycling

22 p3957 A69-40972

Silicon solar cell panels, studying roles of solder, interconnector metals and substrate materials in failures under thermal cycling

23 p4070 A69-42274

THERMAL DECOMPOSITION

U PYROLYSIS

THERMAL DEGRADATION

Low temperature grinding technique for IR spectra of propellants and binders in potassium bromide disks

01 p0082 A69-10892

Thermal time constant in Si diffused transistors decreases with increased neutron dosage

06 p0975 A69-16873

Thermogravimetric plastics analysis data applied as constants to degradation kinetics equations used in charring-ablator digital computer programs

09 p1529 A69-22312

Bearing deposition test for evaluating degradation characteristics of aircraft gas turbine engine lubricants

10 p1700 A69-24070

Polyester/ammonium perchlorate combustion, determining degradation rate by loss in weight method at different intervals

13 p2324 A69-28234

Planar bipolar transistors degradation under thermal and ionizing radiation stresses, analyzing surface recombination currents of silica films and silica-silicon interfaces

15 p2625 A69-30826

Composite polymers thermophysical properties at thermal destruction temperatures, noting increased heating rate effect on kinetic curves

18 p3161 A69-34696

Mechanical properties and thermal aging of laminated specimens of collimated B monofilament reinforced composites preimpregnated with polyimide resin

19 p3354 A69-35514

Thermal decomposition of molybdenum carbonyl, deriving general equations, noting agreement with experimental data

20 p3558 A69-37015

THERMAL DIFFUSION

Diffusional, thermal diffusional and thermal fluxes in multicomponent flames, discussing flame structure and reaction kinetics

01 p0175 A69-10144

Diffusion data in binary compound semiconductors, tabulating impurities, electrical behavior, temperature variations and diffusion coefficients

02 p0296 A69-11809

Mechanical properties of thermomodified layers obtained by vacuum chromizing of steel, establishing need to decarburize substrate material

03 p0450 A69-13913

Nonlinear and second order thermal diffusion of electrons in ionized gas

04 p0636 A69-14878

Heat diffusion in cylinder with heat sources creating axisymmetric temperature distribution, using Gauss hypergeometric function and Meijer G-function

04 p0687 A69-15188

Thermal diffusion coefficient and composition of gas mixtures by measuring gas flow rate in capillary tube as function of viscosity

04 p0688 A69-15410

Diffusion and thermal diffusion in mixture of Maxwellian gases, analyzing Onsager reciprocity relations

05 p0849 A69-16461

Thermochemical surface finishing trends, discussing methods to obtain complex diffusion layers

05 p0769 A69-16540

Energy consideration in electron beam welding, obtaining expression for penetration decrease in terms of thermal diffusivity

[ECS PAPER 144] 08 p1320 A69-20360

Automatic counter for concentration of cloud condensation nuclei in thermal diffusion chamber, measuring light scattering coefficient of cloud

09 p1494 A69-21640

Heat resistant alloying of niobium with group 4A, 5A and 6A elements, studying elements diffusion mobility dependence on melting point

09 p1525 A69-22144

Thermal diffusion and free thermal convection in fluids by diffraction interferometer, using laser for light source

10 p1702 A69-23431

Electronic properties of beryllium doped silicon studied with IR absorption spectroscopy and electrical measurements, describing Be thermal diffusion

10 p1747 A69-23989

Variational calculation of coefficients of viscosity, thermal conductivity, thermal diffusivity and diffusion in binary mixture

11 p1997 A69-24285

Enthalpy excess thermodynamic functions of binary gas mixtures based on stationary diffusion thermoeffect in tube

11 p2003 A69-25552

Theoretical model describing electrodynamic plasma properties of HF flame discharge in air, heating discharge envelopes by heat diffusion from discharge channel surface

12 p2140 A69-27125

Internal and external heat transfer instrumentation and equipment bioengineering, listing thermal conductivity and diffusivity of biological materials

13 p2213 A69-28150

Small disturbances distribution in flow parameters along two dimensional combustion zone of finite width using thermal diffusion theory

14 p2537 A69-28986

Green functions for Laplace, Poisson and transient heat diffusion equations solved by matrix multiplication

15 p2710 A69-30870

Thermal diffusion coefficient for fully ionized plasma containing mixture of arbitrary charge ions in topside ionosphere

16 p2775 A69-32084

Turbulent heat and mass diffusion in catalytic reactors for hydrazine decomposition, developing computer program to calculate temperature and reactant concentration distributions

16 p2846 A69-32768

Ti thermal diffusivity and conductivity at high temperatures measured from heat wave phase shift

18 p3156 A69-34699

Titanium alloys case hardened by diffusion of various metals at high temperatures, measuring increase in wear resistance

19 p3344 A69-36153

Diffusion during high temperature exposure of protective coatings on Mo, noting compact layers and carbide forming elements effect on thermal stability

19 p3345 A69-36156

Boron thermal diffusion effects on plastic properties of pure Mo subjected to recrystallization

19 p3328 A69-36160

Transport coefficients in neutral gases, discussing fundamental relations of parameters in viscosity, thermal conductivity and self, pressure and thermal diffusion

23 p4193 A69-41514

THERMAL DIFFUSIVITY

Nonlinear diffusion of heat in semiinfinite wall having thermophysical characteristics dependent on temperature, showing dissymmetry between heating and cooling

01 p0177 A69-11404

Molten salts thermal diffusivity measurement method at temperatures above melting point

[ASME PAPER 68-WA/ENER-5] 05 p0848 A69-16161

One dimensional integral solution for cylindrical source generated transient temperature field and relation to thermal diffusivity of brain tissue

06 p0879 A69-17085

Thermal diffusivity and conductivity of rolled plane parallel spectrally pure palladium preheated in vacuum and high temperatures

15 p2636 A69-30045

Thermal diffusivity measurement by nonsteady state methods, discussing time and temperature variables and heat flow differential equation

23 p4237 A69-41323

THERMAL DISSOCIATION

Second virial coefficient of atomic nitrogen and oxygen, discussing thermodynamic properties of associating mixtures

03 p0473 A69-14119

Thermal dissociation of chlorine trifluoride behind incident shock waves at high temperature, discussing bimolecular reaction rate constant

[WSCI PAPER 68-40] 07 p1202 A69-18393

TiO gas dissociation energy data discrepancies, discussing high temperature vaporization and thermodynamic properties

08 p1268 A69-21010

Thermodynamic dissociation constants of alkylphenols in aqueous and methanol media based on UV spectroscopic analysis, noting anticarcinogenic properties

11 p1831 A69-24534

Diffusion coefficients for laminar multicomponent dissociating boundary layer at surfaces of thermally decomposing protective coatings

12 p2190 A69-25894

Outgassing behavior of polymers in spacecraft by thermal-vacuum weight-loss and contamination tests

13 p2286 A69-28084

Aluminum, Cu, Ni and titanium oxides injection into axis of Ar thermal induction plasma, observing decomposition as function of distance traveled within plasma

13 p2315 A69-28451

Cyanogen molecules increase attributed to novae shell compression from analyzing absorption spectrum of DQ Hercules 1934 after brightness maximum

15 p2688 A69-30558

Ammonium perchlorate sublimation models, discussing low temperature decomposition influence on pressure dependence of sublimation rate

[WSCI PAPER 69-22] 16 p2832 A69-32360

Pilot chamber initiated thermal decomposition reactor concept for monopropellant thruster, discussing thrust levels and throttling ratios

[AIAA PAPER 69-420] 16 p2841 A69-32685

Gladstone-Dale constants for dissociating high temperature oxygen determined for molecule and atom from density changes across shock

18 p3176 A69-34452

Thermal dissociation rate of HBr in Ar in 2100-4200 K temperature range by shock tube analysis, using IR emission and UV absorption

20 p3484 A69-37347

Thermal dissociation of chlorine trifluoride behind incident shock waves as function of temperature using UV absorption spectroscopy

21 p3670 A69-39739

THERMAL EFFECTS

U TEMPERATURE EFFECTS

THERMAL EFFICIENCY

U THERMODYNAMIC EFFICIENCY

THERMAL EMISSION

NT THERMIONIC EMISSION

Planetary nebulae radio emission, observed with pencil beam of radio telescope, confirming thermal spectrum at radio frequencies

01 p0157 A69-11291

Atmospheric water vapor content from summer-fall 1966 measurements of atmospheric radio wave absorption of thermal radio emission, describing experimental apparatus

02 p0274 A69-11439

Gases emissivity at high temperatures calculated for different gas layer thicknesses and atmospheric pressures, giving results in tabular form

02 p0285 A69-11567

Natural microwave radiation generation and propagation and wideband signal detection in problems connected with radio wave propagation, geophysics, radiometeorology and plasma physics

03 p0420 A69-12919

Poole-Frenkel model for internal field assisted thermal emission with compensation for relative densities of donor and acceptor sites

04 p0640 A69-14450

IR observations of lunar crater and maria enhanced thermal emission during eclipse, constructing model of cratered surface to analyze thermal behavior

04 p0654 A69-14650

Equation for calculating meteor shielded tubular panel heat radiators emissivity and weight optimization, considering surface thermal balance and temperature distribution

05 p0846 A69-15891

Radio astronomical methods for total atmospheric absorption of radio waves by atmospheric thermal radio emission measurements based on sky brightness temperature

05 p0723 A69-16779

Relation between satellite data concerning thermal microwave radiation and meteorological conditions in lower atmosphere for possible use in weather forecasting

06 p0953 A69-17995

Radio wave brightness temperatures and contrast characteristics in presence of clouds and precipitation

06 p0954 A69-17999

Antenna transmission and receiving system effects on radio brightness temperature measurements by airborne equipment

06 p0929 A69-18000

Radiation emission factors determination of polished metallic surfaces

07 p1242 A69-18952

Epithermal microwave radiation from plasma produced by PIG Reflex in magnetic field with mirror geometry, discussing radiation at harmonics of electron cyclotron frequency

08 p1370 A69-21019

Far IR source in galactic center detected at 100 microns, noting thermal emission of interstellar dust grains as possible mechanism

09 p1603 A69-22264

Coronal IR observations during solar eclipse revealing thermal emission zone at predicted interplanetary dust vaporization region

10 p1789 A69-24131

Silicon dioxide coated Al reflectance, solar absorptivity and total normal and hemispherical thermal emissivity, noting application to satellite temperature control

11 p1918 A69-24835

Vibrational relaxation frequency of asymmetric stretching mode of carbon dioxide determined by measuring rate of thermal emission in shock waves near 4.3 microns

11 p1922 A69-25128

Atmospheric thermal radio emission fluctuations effects on radio telescope sensitivity, evaluating dispersion at low angles to horizon

12 p2031 A69-26643

Thermal and free-free emission from planetary nebulae based on graphite grain model, discussing IR fluxes

12 p2172 A69-27158

Thermal emission from metal in contact with dielectric for cryogenic insulation applications

13 p2374 A69-27783

Current oscillations and electromagnetic radiation in low pressure cesium thermal emission converters using glass diode with plate geometry metal electrodes

14 p2402 A69-29246

Thermal emission converter, using Cs-Ba mixture in low voltage arc mode, detailing construction

14 p2403 A69-29247

Thermoemission converters /TEC/ cathode materials, discussing determination of local work function by electron microscope and delay curves methods

14 p2505 A69-29265

Temperature of underlying surface and moisture content of atmosphere from satellite thermal radio emission measurements

15 p2648 A69-30641

Earth thermal emission intensity measured by two beam radiometer onboard Cosmos 149, noting discrepancy between empirical and theoretical transfer functions of atmosphere

15 p2596 A69-30651

Integral normal emissivity of Ta and Hf carbides at temperatures from 1300 to 3000 K measured by radiation method in vacuum

15 p2640 A69-30984

Pyrolytic zirconium carbide emissivity during initial heating compared with results for specimens prepared by powder metallurgy

15 p2640 A69-30985

Venus microwave spectrum analyzed by comparing various thermal and nonthermal emission models, discussing surface temperature and atmospheric composition

16 p2853 A69-31597

Radiative heat transfer in nonisothermal media composed of spherical particles with complex refractive index emitting absorbing and scattering energy anisotropically, considering various geometries [AIAA PAPER 69-626]

17 p3073 A69-33297

Lunar surface brightness temperatures from IR observations, determining thermal emission directional characteristics to infer surface temperatures from Surveyor data

[AIAA PAPER 69-593] 17 p3033 A69-33302

Quantitative IR spectral emissivity measurements of NO between 300-800 K made in absorption, correlating observed absorptance with optical path length and gas pressure

17 p3009 A69-34156

Microwave thermal emission by water measured from aircraft, studying radiation dependence on surface roughness

18 p3127 A69-34421

Observations of W49 at 2800 MHz with East-West resolution, analyzing shape of thermal and nonthermal source

18 p3195 A69-34427

Thermal emission and spectral degree of blackness of W derived from electron motion equation

18 p3156 A69-34715

Solid cloud cover moisture content relation to outgoing thermal radiation, obtaining correlation coefficient and regression equations

23 p4184 A69-42488

Mars thermal energy emission measurement by Mariner 1969 IR radiometer, indicating frozen carbon dioxide cap and minimum temperature

24 p4384 A69-43196

Radio emission from diffuse thermal radio sources in northern Milky Way, giving contour maps

24 p4388 A69-43641

Seyfert galaxies IR radiation attributed to dust grains thermal emission of energy absorbed from galactic nucleus

24 p4374 A69-43741

THERMAL ENERGY

Information theory application to study of biologically stimulating effects of low ionizing radiation doses, thermal energy and other environmental factors

03 p0369 A69-13434

Thermal-chemical rocket based on thermal heating by energy input from nuclear fission process

03 p0496 A69-13666

Electrodynamic generator for direct conversion of moving dielectric medium potential or thermal energy to electric power

03 p0369 A69-14153

Thermal potential P and Q smoothness on surfaces, proving relevant theorems

05 p0849 A69-16452

Thermally activated processes influence on dislocation interaction and on temperature dependence of flow stress in niobium single crystals

08 p1333 A69-20446

Microscale fluctuations in interplanetary magnetic field, considering proton thermal energy and magnetic field energy densities

10 p1785 A69-24100

Two chamber DC arc heater with vortex stabilization, determining current-voltage characteristics and efficiency

13 p2244 A69-28557

Radiative and conductive heat transport mechanisms at cryogenic temperature applicable to thermal energy transport minimizing technique in containment system

17 p3074 A69-33680

Book on thermal processes of earth and moon covering heat generation and transfer, internal temperatures, gravitational energy, etc

19 p3401 A69-35887

Thermal energy rate constants of ion-molecule reactions in gaseous hydrogen, deuterium and HD, using ion cyclotron resonance method

20 p3578 A69-36934

Afterglow decay rates of Zn II laser lines in spontaneous emission measured, indicating thermal energy charge exchange excitation and CW oscillation

21 p3735 A69-38598

Thermal energy effects on life processes, discussing living cell metabolism, biochemical reactions, enzyme action and protein catalytic functions, etc

21 p3652 A69-38782

Thermotidal energy transfer from lower neutral atmosphere to and above lower ionosphere, considering tidal wave transmission mechanism

23 p4155 A69-41561

Incoherent object threshold light detection by quantum limited optical system in presence of radiant thermal energy

23 p4191 A69-42147

Radioisotope thermal energy /RITE/ source for integrated life support systems for two man 180 day space station mission, determining optimum material selection and design details

23 p4189 A69-42268

THERMAL ENERGY STORAGE

U HEAT STORAGE

THERMAL ENVIRONMENTS

Rms approximation validity limits for satellite temperature variances by deriving equations for thin insulated plate in space

02 p0352 A69-12211

Thermal conditions of upper blanket of lunar surface during eclipse, using data to calculate lunar radio emission

03 p0506 A69-13088

Active cooling systems for high performance reentry vehicles in thermal and shear stress environments [AIAA PAPER 68-1154]

03 p0533 A69-13669

Saturn fireball thermal environment associated with liquid propellant explosions, using analytical model

04 p0645 A69-14475

Thermal performance of pressure transducers, accelerometers, displacement transducers, resistance thermometers and control mechanisms for NERVA reactor

06 p0956 A69-16885

Space radiator dynamic model for predicting outlet temperature transient response to environmental variations

[AIAA PAPER 69-29] 06 p1039 A69-18205

Simultaneous measurements of cumulus cloud thermal structure and concentration of water particles larger than 18 micron diameters

09 p1536 A69-21866

Thermal and pressure environments analysis in Saturn S-1C stage base during flight tests, noting base gas flowfield and heating

[AIAA PAPER 69-318] 09 p1611 A69-22383

Boundary conditions for time dependent temperature variations of calorimeter operating in regular thermal regime

11 p2003 A69-25702

Environmental problems of entry vehicle returning from lunar or planetary mission, discussing heat protection system efficiency

11 p1968 A69-25721

Thermal conditions of upper blanket of lunar surface during eclipse, using data to calculate lunar radio emission

14 p2515 A69-28770

Extragalactic background radiation intensity in isotropic world models as function of universe thermal history

14 p2514 A69-29769

Optimal design for improving thermal performance of existing spacecraft thermally actuated lower system by increasing open-to-closed emittance ratio

[AIAA PAPER 69-627] 17 p3071 A69-33269

Vacuum and thermal environment long term influence on thermal resistance for Mg to aluminum and Mg to Mg bolted joints

[AIAA PAPER 69-628] 17 p3073 A69-33309

Micropropulsion system with sublimable solid fuel for satellite attitude control, satisfying mechanical and thermal environmental conditions during launch and in space

17 p3021 A69-33359

Linear thermal anomaly on western margin of Mare Humorum, rejecting internal heating origin

21 p3797 A69-38535

Active cooling systems for high performance reentry vehicles in thermal and shear stress environments

[AIAA PAPER 68-39016] 21 p3851 A69-39016

Orbiting Astronomical Observatory thermal test and evaluation program, discussing equipment and role in experimental design

[AIAA PAPER 69-995] 22 p3920 A69-40373

OSO spacecraft thermal design modified to operate University of Minnesota zodiacal light monitor experiment

[AAS PAPER 69-173] 24 p4393 A69-42873

THERMAL EXPANSION

Exploding wire phenomenon during early expansion from time correlated X ray and optical streak photographs in vacuum chamber

01 p0119 A69-10670

Pre-cracked ceramic rocket nozzle throat inserts, discussing improved thermal displacement accommodation, load transmission, fracture tolerance, articulation capability, etc

02 p0334 A69-12369

Lithium niobate crystals thermal properties measured at various temperatures

03 p0487 A69-13730

Dilatometer for measuring thermal expansion of solid bodies over temperature range at various gas media pressures

03 p0432 A69-14151

THERMAL FATIGUE

- Refractive index and expansion thermal coefficients along axis of oriented Nd-YAG laser rod
04 p0609 A69-14293
- Dilatometric and X ray study of temperature dependence of linear expansion coefficients of lattice constants of chromium disilicon
04 p0619 A69-15392
- Expansion anisotropy in angular distribution of laser produced plasmas in terms of drifting and expanding sphere model, discussing particle velocities, currents and time integrated counts
05 p0804 A69-16460
- Latticed gas model liquid-vapor phase properties calculated with allowance for thermal expansion
06 p1029 A69-16896
- Four specimen vacuum device for simultaneous tensile creep tests at 1200 C, discussing linear and thermal expansion
07 p1116 A69-19318
- Thermal expansion of polymers at cryogenic temperatures
07 p1172 A69-19730
- Thermal expansion coefficients of Nb-Zr-Ti alloy and plexiglass at 10-300 K from dilatometric measurements
11 p1905 A69-24917
- Axial support system for controlling thermal distortion of 82 inch heliostat mirror for Kitt Peak solar telescope
12 p2058 A69-26422
- Stress in elastic cylinder under thermal expansion with one end clamped expressed by series expansion of biharmonic function using least squares method
14 p2534 A69-29284
- Uncoupled dynamic thermal stresses and displacements by heat generation in infinite flat plates, using classical thermoelasticity theory for infinitesimal displacements
15 p2709 A69-30669
- Dilatometric and X ray study of temperature dependence of linear expansion coefficients of lattice constants of chromium disilicon
18 p3156 A69-35020
- Large area Si solar cell arrays design, considering environment, cell layout, thermal expansion, coverslides fabrication, costs, etc
19 p3253 A69-35708
- Thermal expansion properties of oxides and oxide solid solutions measured for improved expansion coefficient search
20 p3567 A69-38066

THERMAL FATIGUE

- Crack initiation and propagation in Ti alloys during thermal cyclic heating, noting influence of gas saturation
01 p0094 A69-10215
- Thermal fatigue testing system for martensitic steels using fluidized bed heating and cooling, specimen manipulation means, cycle control, data evaluation, etc
10 p1714 A69-23979
- Concorde thermal fatigue resistance tested by alternate heating and cooling cycles simulating supersonic flight profile
13 p2241 A69-28102
- Crack initiation prediction in high temperature components subjected to arbitrary thermal-mechanical cycling
13 p2365 A69-28252
- Crack initiation and propagation in Ti alloys during thermal cyclic heating noting influence of gas saturation
15 p2637 A69-30271
- B fiber reinforced Ni failure characteristics at high temperature, discussing plastic deformation and matrix role in crack inhibition
21 p3743 A69-38616
- Dislocations multiplication and rearrangement structure in thermal fatigue of Mo single crystals produced by electron beam zone melting
21 p3746 A69-39162
- Thermal fatigue combined with mean stress, reversed mechanical stress, low cycle fatigue and static creep in stainless steel
21 p3847 A69-39813

THERMAL INSTABILITY

- Thermal instability in power transistor structures, considering effects of design, emitter and base resistance at high currents
08 p1373 A69-20858
- Electrothermal instabilities for explanation of MPD arc thruster rotating spoke phenomenon, noting agreement with experimental results
09 p1566 A69-21254

Hall current effect on thermal instability explaining nonself gravitating astronomical objects, discussing current effects on propagation modes
16 p2854 A69-31649

Heat transfer coefficient approximation under thermal instability conditions complicated by radiant heat exchange at plate surface, noting aircraft design applications
18 p3230 A69-34984

THERMAL INSULATION

- Temperature field and stress state in elastic plane with temperature insulated arc shaped crack
01 p0164 A69-10078
- Unsteady laminar boundary layer near thermally insulated rotating disk, establishing solutions describing motion
01 p0059 A69-10361
- Surface temperature of flat plate cooled convectively and insulated by circular spot, determining effects of spot radius and Biot number
03 p0531 A69-12863
- Thermal design and test for liquefied gas vessels under unsteady insulation cooling conditions
04 p0687 A69-15162
- Thermal insulating characteristics of low conductance interstitial materials under compressive loads, noting carbon paper and wire screens
06 p1036 A69-18072
- Human body heat loss control during water immersion, discussing insulative garments and technologies of energy conversion systems
08 p1267 A69-20681
- Super insulation blankets comprised of dacron sailcloth, silk net or aluminized mylar, describing crinkling, cutting, sewing and hole drilling techniques
09 p1507 A69-22330
- Cryostat design, discussing vapor and radiation shielding, construction and insulation materials, safety features, cost considerations, etc
10 p1810 A69-24015
- Liquid helium vented and nonvented storage container design and handling techniques
10 p1810 A69-24016
- Differential catalytic thin film heat gage for measuring surface temperature variations and ionized flow heat transfer, noting insulating boundary layer thickness
11 p2002 A69-25231
- Insulated one man life raft for sea survival in arctic or subarctic conditions, evaluating thermal protection with endurance time and rectal temperature
12 p2020 A69-26550
- Thin multiple layer superinsulation protection against reentry heat, discussing composite design considerations and refractory materials selection
12 p2060 A69-26817
- Thermal insulation for cryogenic storage in space, discussing Apollo service module conversion to cryogenic service module
12 p2175 A69-26827
- Thermal emission from metal in contact with dielectric for cryogenic insulation applications
13 p2374 A69-27783
- Outgassing rates of multifoil insulation materials for sealed vacuum systems measured over temperature range as function of pumping time
13 p2299 A69-28016
- Multifoil thermal insulation using oxide particle layer separation, discussing insulation heat transfer characteristics as function of source temperature and oxide particle size
14 p2539 A69-29213
- Thermal conductivity of semiinfinite rod with insulated surface and constant internal heat source, considering finite heat propagation rate
15 p2719 A69-31181
- Thermal contacts effects on optimum operating conditions of solar thermoelectric power generator, discussing losses due to low thermal conductivity coefficient of insulating layers
16 p2741 A69-32797
- Heat transfer suppression techniques in high temperature low density fiberglass insulation for flight vehicles
17 p3072 A69-33279
- Thermal analysis of opacified fibrous insulation systems, discussing heat transmission, heat transfer and thermal conductivity relations to compression load and temperature
17 p3072 A69-33282
- Thermal design of landed vehicle on Mars surface, discussing instrument package covering inside surface coating and battery insulation
17 p3049 A69-33295

Lunar module multilayer radiation insulation for thermal control, testing aluminum coated Mylar and Kapton sheets
17 p3073 A69-33300

Multifoil thermal insulation for radiation shielding from cryogenic temperatures to 3500 F, noting thermal conductivity
19 p3341 A69-35548

Combined heat transfer by radiation and conduction in disperse media /thermal insulation/ described by system of nonlinear integrodifferential equations
20 p3631 A69-37000

Conducting and insulating construction materials at high temperatures for MHD conversion nozzles, noting lifetimes
21 p3751 A69-38477

Rotating stratified fluid in thermally insulated cylinder, studying angular velocity abrupt change effects under stable temperature distribution
21 p3694 A69-38761

Laminar free convection from horizontal infinitesimal strip with downward facing thermally insulated vertical walls at edges, noting boundary layer thickness and flow pattern
21 p3853 A69-39672

Effective thermal conductivity parallel to laminations and total conductance for combined parallel and normal heat flow in multilayer insulation
21 p3853 A69-39763

Internal interactions of continua and concept of thermal isolation, discussing second law of thermodynamics
22 p4050 A69-40450

Moisture detector for evaluating trapped water effects in thermal insulation, describing equipment and test procedure
24 p4312 A69-42755

Hazard rating for flammability of aerospace materials in air and oxygen environments applied to J-2 rocket engine insulation
24 p4336 A69-43423

Sprayable polyurethane foam external insulation for liquid hydrogen and oxygen storage aboard Saturn S-2 booster
24 p4337 A69-43453

THERMAL NEUTRONS

- Slow atmospheric neutron energy spectrum determined by resonance detectors and $1/\nu$ detectors, measuring cadmium ratio dependence on longitude and latitude
10 p1758 A69-22831
- Thermal neutron flux perturbations in cylinders in test reactors, using regression analysis to obtain polynomials for flux perturbation, depression, self shielding factors, etc
20 p3575 A69-38274
- Thermal neutron capture cross section at high temperature irradiations determined for W 184, describing radiochemical separation and flux counting techniques
24 p4315 A69-43192

THERMAL NOISE

- Micrometeorites acoustic recordings on Cosmos 135, investigating data reliability influenced by appearance of thermal noise
01 p0152 A69-10578
- Ultra cone system for ultralow noise reception of RF space communication from Mariner 5 during occultation by Venus
02 p0220 A69-12429
- Measured noise temperature in argon tubes vs theoretical electron temperature for gas discharge noise sources
02 p0210 A69-12437
- Microwave thermal noise standards, discussing construction, calibration and errors for field operational liquid nitrogen cooled waveguide noise standard
02 p0210 A69-12438
- Compensation method for measurement of mismatched noise source effective temperature independent of reflection coefficient, noting error analysis
02 p0210 A69-12441
- Mismatched errors associated with Y factor power ratio measurement effect on microwave noise-temperature calibrations
02 p0211 A69-12442
- Thermal noise from passive linear multiports, noting influence of temperature and absorption coefficients
02 p0211 A69-12443
- Noise generation and propagation in linear N cascaded mismatched two port networks, noting application to microwave measurements in low noise technology
02 p0211 A69-12445

Low temperature microwave thermal noise standard, discussing waveguide termination, cryogenic cooling and temperature and pressure controls
02 p0211 A69-12446

Additive noise measurement in microwave power amplifiers under continuous wave and pulsed conditions
02 p0221 A69-12454

Liquid helium cooled broadband parametric amplifier, discussing circuits and noise performance
02 p0221 A69-12458

Digital simulation of demodulator/tracking phase locked loop of navigation/traffic control satellite system in thermal noise diffuse multipath fading environment
03 p0390 A69-13204

Thermal and shot noise in pumped resistive diode for frequency conversion, analyzing equivalent circuits
03 p0406 A69-13828

Maser model of single mode field coupled to N identical two level atoms, deriving threshold, stable and unstable steady states, relaxation oscillations, etc
03 p0441 A69-14108

Noise reduction in parametric electron beam amplifier by cooling two frequency resonator noise to liquid nitrogen temperature
05 p0728 A69-15654

Thermal noise and other disturbances from mismatched two port isolator in low power microwave transmission antenna noise between generators and leads
07 p1108 A69-19486

Thermal feedback generation of 1/f-flicker noise in bipolar transistors, deriving formula for flicker noise voltage of emitter junction
08 p1283 A69-20129

Spontaneous reverse current due to Brillouin EMF observed in diode in thermal noise range
10 p1661 A69-22950

Digital simulation of phase locked receiver in diffuse multipath fading environment with band limited thermal noise
11 p1839 A69-25298

Critical review of statements concerning previous paper on noise in transistor mixers at HF
11 p1857 A69-25662

Formulas derived for tropospheric equivalent noise temperature as function of frequency, noting applicability to thermal radiation from rain
12 p2032 A69-26704

Thunderstorm thermal noise emission determined by radiometer and steerable parabolic antenna in preparing water content contours along radio rays
12 p2127 A69-27002

Soviet monograph on intrinsic noise emission in radio channels covering noise temperature at receiver input, thermal microwave radiation, etc
13 p2219 A69-27304

Angle of arrival in amplitude comparison monopulse radars in presence of internally generated thermal noise
13 p2220 A69-27942

Mean-minute thermal noise intensity distribution in telephony channels of tropospheric radio relay systems
14 p2412 A69-29425

Optimum thermal and nonlinear noise intensities distributions in frequency division multiplex satellite communications systems, relating relay station power, frequency band and channels
14 p2412 A69-29426

VHF and uHF MOS tetrode minimum noise factor computed as function of frequency by adding thermal noise sources to resistive parts of equivalent circuit
15 p2577 A69-30603

Micrometeorites acoustic recordings on Cosmos 135, investigating data reliability influences by appearance of thermal noise
15 p2691 A69-30748

Noise reduction in parametric electron beam amplifier by cooling two frequency resonator noise to liquid nitrogen temperature
16 p2762 A69-32511

Optimal radar receivers and waveforms with limited dynamic range for detecting point target masked by thermal noise and clutter returns
17 p2921 A69-33625

Antenna high noise temperature reduction in single channel combined transmission and reception of tracking and communication data
19 p3275 A69-36328

Radio relay FM channel data transmission, evaluating cumulative thermal noise due to IF amplification at each station
21 p3672 A69-38653

Spin-phonon systems thermal noise, based on combined lattice and spin lattice Hamiltonian densities, applied to acoustic noise field measurements
24 p4350 A69-43061

THERMAL PLASMAS
Coupled wave equations for propagation transverse to magnetostatic field in horizontally stratified and magnetized gyrotropic warm plasma
01 p0129 A69-10611

Green function for linear antennas in warm plasma fed by coaxial air filled transmission line, computing current distribution and input admittance
02 p0215 A69-11942

Wave fields and coupling of RF power to ion cyclotron waves in finite length thermal collisional plasma column
03 p0474 A69-13114

Thermal metal-plasma thermodynamic equilibrium, using surface ionization of inner and outer potentials and work function, discussing ion and electron extraction
06 p0979 A69-17249

Nonlinear interaction between cyclotron harmonic waves propagating perpendicular to static magnetic field in warm magnetoplasma, noting parametric amplification and mode conversion
06 p0968 A69-17766

Ion-cyclotron instabilities in hot-ion cold- electron plasma resulting from left-hand circularly polarized wave propagating parallel to magnetic field
06 p0969 A69-17951

Two fluid approximation of one dimensional steady state flow of inviscid plasma with thermal gradients, considering ionization and recombination processes
07 p1189 A69-18691

Comparative models of magnetoplasma, discussing wave propagation in cold plasma, warm plasma and microscopic model
07 p1190 A69-18919

Sco XR 1 optical and X ray spectra simultaneous observations during rocket flights
07 p1220 A69-19391

Wave behavior in warm inhomogeneous plasma with magnetic field perpendicular to density gradients of unperturbed plasma, solving Maxwell-Vlasov equations by perturbation methods
08 p1365 A69-20744

Warm plasma magnetic interactions, discussing density waves, pair correlation function and transport coefficients
08 p1366 A69-20749

Magnetic pinch effect in thermal RF induction plasma in argon, developing theory for calculating excess magnetic pressure
09 p1544 A69-21341

Warm plasma addition to mirror confined hot plasma stabilizing convective loss cone mode
09 p1551 A69-22040

Electrical conductivity, electron density and population temperature as functions of current density in Cs-He thermal plasma studied with nonequilibrium ionization model
10 p1732 A69-23443

Earth thermal plasmasphere contraction subsequent to solar flare obtained from ion mass spectrometers onOGO satellites
10 p1683 A69-23777

Low energy plasma fluxes in magnetosphere, discussing plasmopause position dependence on geomagnetic activity
12 p2150 A69-26747

Laminar MGD electrode boundary layer of thermal nonequilibrium plasma from collisionless Langmuir sheath and continuum theories
13 p2310 A69-28031

Aluminum, Cu, Ni and titanium oxides injection into axis of Ar thermal induction plasma, observing decomposition as function of distance traveled within plasma
13 p2315 A69-28458

Longitudinal inhomogeneities in plasma of Q machines caused by ion emission from hot plate at different radial positions
14 p2502 A69-29959

Equivalent dielectric tensor for warm drifting electron plasma using model
16 p2820 A69-31701

Warm plasma probe, describing transit electrons interaction with electric field and generation of electroacoustic waves radiation
16 p2824 A69-32611

Coupling between electric dipoles in warm plasma, determining electron density and temperature from resonance peak of mutual impedance at electron plasma frequency
17 p2925 A69-33846

Suprathermal electron flux in lower latitudes and polar region analyzed from measurements by retarding potential analyzers on Explorer 31 satellite
20 p3590 A69-37880

THERMAL POWER
U TURBOGENERATORS

THERMAL PROPERTIES
U THERMODYNAMIC PROPERTIES

THERMAL PROTECTION
Thermal protection by ablation calculated, emphasizing blocking phenomenon and effectiveness of laminated and reinforced resins
02 p0351 A69-11890

Apollo thermal protection system, noting low density ablation, flight and ground tests
[AIAA PAPER 68-1142] 03 p0519 A69-13558

Entry corridor thermal entry limits for Apollo spacecraft defined for design of thermal protection system
[AIAA PAPER 68-1144] 03 p0521 A69-13673

Kinetic heating of aircraft, discussing aerodynamic boundary layer, relationship between heat transfer coefficient or boundary layer energy turbulence and skin friction
03 p0534 A69-14087

Inflatable solar shields for thermal protection of space vehicles utilizing cryogen propellants
06 p1017 A69-17609

Life raft thermal protection against exposure of crews to cold, noting chemically fueled heaters and IR reflective liners
06 p0883 A69-17841

Water cooling jackets of plastic textile reinforced film for high inside temperature reduction in protective clothing
06 p0883 A69-18027

Thermal protection system optimization for storage of cryogenic propellants in space, noting vented systems
[AIAA PAPER 69-27] 06 p1039 A69-18211

Protection against burn producing intense thermal exposures, noting double layer of fire resistant material
[AGARDOGRAPH-111] 08 p1266 A69-20674

Spray cooling techniques for thermal protection of aerospace structures including lithium spray cooling, vapor collection and condensation, etc
11 p1966 A69-24532

Porous cermet electrodes thermochemical protection by blowing neutral gas into electrode boundary layer, examining effect on volt-ampere characteristics
11 p1826 A69-25232

Environmental problems of entry vehicle returning from lunar or planetary mission, discussing heat protection system efficiency
11 p1968 A69-25721

Space mission medical heat problems covering thermal characteristics and heat control, protection and resistance of space vehicle and astronaut adaptation
12 p2023 A69-26493

Passive thermal control system for space suit use in extravehicular environment, discussing skin temperature control at varying heat flow rates
12 p2023 A69-26549

Insulated one man life raft for sea survival in arctic or subarctic conditions, evaluating thermal protection with endurance time and rectal temperature
12 p2020 A69-26550

Thermal insulation for cryogenic storage in space, discussing Apollo service module conversion to cryogenic service module
12 p2175 A69-26827

Electron energy effects on reflectance degradation and recovery of thermal control materials in vacuum, reporting test results for various protective coatings
[AIAA PAPER 69-643] 17 p3005 A69-33306

Collection of papers on thermal design principles of spacecraft and entry bodies
18 p3227 A69-34372

Ablative materials thermal protection characteristics at low heating rates evaluated by convective heating tests, stressing polyurethane foam composite
19 p3357 A69-35536

Heat protection efficiency of plane surface in turbulent boundary layer behind tangential slots, comparing cooling effects of insulating gas films
20 p3631 A69-37095

Polyurethane foam composites for low heating rate thermal protection, noting astroquartz fiber additive effect on performance
21 p3753 A69-39236

Thermal design of power amplifier for airborne HF transceiver, discussing component layout, air cooling and materials
22 p3909 A69-39942

Thermal protection for air-launched missile electronics during carry and free flight, considering active, passive and combination systems and weight penalties
22 p4049 A69-39943

IR directional and hemispherical emittance of spacecraft thermal control coatings, comparing values determined by various measurement techniques
23 p4164 A69-41633

THERMAL RADIATION NT PHONON BEAMS

Radiation from isothermal sphere in vacuum having spherical scattering indicatrix solved by Bubnov-Galerkin method with allowance for scattering
01 p0174 A69-10106

Solar absorptance, total hemispherical emittance and absorptance/emittance ratio for metals at cryogenic temperatures measured simultaneously with sinusoidally perturbed incident radiation
01 p0176 A69-10847

Satellite meteorological research in U.S.S.R., discussing Cosmos satellites instrumentation, earth thermal radiation distribution, IR and UV spectra and cloud photography
01 p0111 A69-10950

Thermal radiation effects on two dimensional steady MHD jet of conducting ionized gas confined by magnetic field
02 p0287 A69-11831

Broadband null balancing microwave scanning radiometer using diode in feedback loop as reference noise source
02 p0221 A69-12457

Brightness temperature maps for Jovian thermal radiation obtained through 8-14 micron window of atmosphere
02 p0309 A69-12715

Lunar thermal radiation measurements at 8.6 and 3.2 mm wavelengths, noting brightness temperature-time relationship in curves and as Fourier components
02 p0327 A69-12717

Mean atmospheric downward radiation fluxes for large territories, using simple model atmospheres in derivation of computational formulas
03 p0422 A69-13410

Earth velocity through 3 K cosmic background radiation, measuring velocity by determining anisotropy of radiation
03 p0511 A69-13475

Monograph on radiation gas dynamics, thermal radiation, applied spectroscopy and ablation and applications in high speed atmospheric entry
04 p0685 A69-14597

Thermal explosion in Poiseuille flow of reacting viscous fluid in infinite circular cylindrical channel or between two rotating infinite cylinders
04 p0686 A69-14986

Solar and terrestrial thermal radiometer absolute calibration noting standards and methods
04 p0602 A69-15429

Regular thermal conditions in solid bodies with radiative heat transfer
05 p0845 A69-15896

Regularization methods in inverse problems of atmospheric optics, analyzing atmospheric thermal sounding and interpretation of radiation measurements
06 p0919 A69-17616

Dermal injury predictability for exposure to thermal radiation based on mathematical model using temperature-time histories
06 p0875 A69-17840

Thermal radiative reflectance characteristics of low density charring ablators subjected to planetary entry environment simulation
[AIAA PAPER 69-61] 06 p0947 A69-18148

Solar absorptance and hemispherical emittance of metals at space conditions determined with cyclic incident radiation technique
[AIAA PAPER 69-60] 06 p0945 A69-18154

Spectral reflection computer program utilizing virtual image technique to determine reflection characteristics of enclosed diffusely emitting surface
[AIAA PAPER 69-65] 06 p1040 A69-18215

Nitrogen plasma thermal radiation in spectral region from 0.5 to 1.1 micron, noting plasma state near local thermodynamic equilibrium
07 p1189 A69-18283

Gamma heating rate measured by aqueous dosimeter converted to rate in thin tungsten detector in water shield through transport theory calculations, obtaining correction factors
07 p1178 A69-18825

Diurnal thermal wave form driven by harmonically oscillating ground temperature in nongray atmosphere,

calculating results for terrestrial and Martian atmospheres
07 p1126 A69-19036

Southern Hemisphere galactic H II regions continuum thermal radiation at 6 cm, noting maps for 28 of 36 sources, peak temperatures and emission and half intensity widths
07 p1206 A69-19271

Thermal and nonthermal radiation of hot gases using spectroscopic plasma diagnostics
08 p1363 A69-20463

Collection of papers on thermal problems in aerospace medicine covering intense heat, cutaneous vasomotor and sudomotor control, water immersion, etc
08 p1263 A69-20667

Aircrew members skin temperature changes in response to intense diffuse thermal radiation, noting psychological response to exposure
[AGARDOGRAPH-111] 08 p1264 A69-20669

Thermoregulatory reactions of human body to sharp increase of ambient radiant temperature
[AGARDOGRAPH-111] 08 p1264 A69-20670

Skin and subcutaneous temperature during exposure to intense thermal radiation, discussing estimation of subcutaneous temperature from skin temperature data
[AGARDOGRAPH-111] 08 p1264 A69-20671

Thermal radiation effects on cutaneous vasomotor and sudomotor control of human organism
[AGARDOGRAPH-111] 08 p1265 A69-20672

Protection against burn producing intense thermal exposures, noting double layer of fire resistant material
[AGARDOGRAPH-111] 08 p1266 A69-20674

Human reactions to increasing heat exposure, noting thermoregulation and metabolic and evaporative heat loss
[AGARDOGRAPH-111] 08 p1265 A69-20675

Photon momentum distribution role and relation to thermal radiation spectrum in fully ionized gases
08 p1357 A69-20747

Bismuth bolometer as sensor recording IR radiation for thermal radiation fluctuations in atmosphere caused by temperature inhomogeneities
09 p1490 A69-21868

Iron line absence in emission spectrum of thermal X ray sources, constraining proposed thermal models
09 p1580 A69-22231

Atmospheric thermal sounding by measuring outgoing thermal radiation with infinite resolution device, describing regularization method
09 p1491 A69-22707

IR emissivities of powdered silicates and cloudy atmosphere model of spectral emission for radiative transfer in condensed powder
10 p1778 A69-23414

Thermal radiation properties of gases in thermodynamic equilibrium, discussing radiation resulting from electronic, atomic and molecular state transitions
11 p1998 A69-24460

Fluctuations in angle of arrival of laser and thermal radiation beams over near ground path
11 p1840 A69-25570

Long wave radiation fields calculations based on radiation transport equations, identifying differences between associated transmission functions
12 p1225 A69-25951

Thin multiple layer superinsulation protection against reentry heat, discussing composite design considerations and refractory materials selection
12 p2060 A69-26817

Monograph on atmospheric radiation transfer including absorption, scattering, direct, diffuse, global, thermal and net radiation
12 p2073 A69-26918

Soviet monograph on intrinsic noise emission in radio channels covering noise temperature at receiver input, thermal microwave radiation, etc
13 p2219 A69-27304

Radiation measurements by Cosmos 122 satellite over various regions, determining radiation temperature, long wave heat flux and albedo
13 p2291 A69-27726

Thermal radiation effects on laminar free convection boundary layer of vertical flat plate, studying absorbing and nonabsorbing gases
[ASME PAPER 68-HT-43] 13 p2373 A69-27772

Thermal emission from metal in contact with dielectric for cryogenic insulation applications
13 p2374 A69-27783

Statistical analysis of radiation temperature structure for automatic recognition of meteorological situations from actinometric satellite observations
13 p2293 A69-27842

Thermal radiation effects on subsonic flow of ideal gray gas, calculating streamwise variations of flow properties
15 p2717 A69-30944

Thermal radiation polarization in anisotropic gyrotropic media described by Hermitian permittivity tensor, noting linearity
15 p2653 A69-30944

Atmospheric thermal sounding by measuring outgoing thermal radiation with infinite resolution device, describing regularization method
16 p2782 A69-32040

Broadband thermal radiometer containing InSb electronic bolometer under magnetic field, discussing astronomical applications
17 p2969 A69-32822

Apparent thermal radiation properties for optically dimensionally rough surface, discussing variance with property models employed in engineering analysis of radiant transfer
[AIAA PAPER 69-622] 17 p3071 A69-33279

IR radiometer to measure Jupiter atmospheric temperature by calculating certain constituents heat radiation levels through Planck formula assuming black body properties
17 p2974 A69-33422

Microwave thermal emission by water measured from aircraft, studying radiation dependence on surface roughness
18 p3127 A69-34422

Multifoil thermal insulation for radiation shields from cryogenic temperatures to 3500 F, noting thermal conductivity
19 p3341 A69-35540

Thermal IR image forming devices, explaining principles of image and object plane scanning
20 p3540 A69-37738

Reflection indicatrices of rough surface subjected to heat radiation for stationary and variable incidence angle, noting spatial distribution
21 p3847 A69-38455

Lunar surface thermal radiation incident on unit area flat surface located at variable distance and orientation above moon, considering diffusion effects
21 p3803 A69-38973

Surface roughness effects on equilibrium temperature of isolated adiabatic plane surface illuminated by collimated and uniform solar flux
22 p4050 A69-40558

Thermal perturbation propagation in nonlinear medium, considering thermal relaxation effects
22 p4051 A69-40712

Unsteady thermal conductivity calculated by approximate analytical method in simple shape bodies/infinite plate, long cylinder, sphere/cooled or heated by thermal radiation
23 p4238 A69-41333

Frequency response of thin film thermal detectors, discussing steady state harmonic response proportionality to film thickness and thermal conductivity
23 p4163 A69-41549

Parametric differentiation applied to radiation gas dynamics equations solution, considering energy transfer by thermal radiation in high speed reentry
[AIAA PAPER 68-668] 23 p4059 A69-41892

Thermal radiation diffraction of dielectric cylinder/cold plasma model/containing N plus one layers with arbitrary temperatures and permittivities
23 p4123 A69-42028

Minimum air temperature forecast by terrestrial thermal or long wave radiation balance measurement, using radiometer data
23 p4184 A69-42211

Thermal continuum radiation from coronal plasmas at soft X ray wavelengths, investigating variations effect in element abundances
23 p4207 A69-42406

IR measurements applications to meteorology, discussing IR radiation characteristics, atmospheric effects, thermal radiation detection and differences between real and black bodies
24 p4316 A69-43507

THERMAL RADIO EMISSION U RADIO EMISSION

THERMAL RESISTANCE

Nitriding effect on heat resistance and transition temperature of molybdenum alloys
01 p0093 A69-10212

Cooling rate effect during aging on heat resistance of forged blanks of nickel based chromium alloy
02 p0266 A69-12125

Phase diagram and heat resistance relation for ternary titanium alloys, considering component interaction and dissolution and dispersion effects
02 p0268 A69-12357

Subject classification bibliography for thermal contact resistance

[ASME PAPER 68-WA/HT-18]

05 p0847 A69-16122

Chemical composition relationship to heat resistance of titanium alloys, using diagrams for establishing composition of new multicomponent alloys

07 p1163 A69-18780

Radome materials with superior dielectric and temperature characteristics for constructing high tolerance microwave multiband radome

07 p1109 A69-19514

Contactors for helium in dilution refrigerator mixing chamber, discussing design and thermal resistance determination

09 p1493 A69-21429

Increased Ti heat resistance by forming solid solutions and compounds having various dispersions and bond strength

09 p1525 A69-22140

Heat resistance preservation in heat resistant alloys by inhibiting dislocation motion during operation at high temperatures

09 p1525 A69-22141

Refractory metal oxidation protection by inorganic compounds at high temperatures, discussing protective mechanisms

09 p1526 A69-22322

Transistor thermal resistance determined from temperature dependent transistor parameter, noting measuring method insensitive to collector voltage variations

09 p1468 A69-22592

Spontaneous reverse current due to Brillouin EMF observed in diode in thermal noise range

10 p1661 A69-22950

Heat resistant DIPAM and HNS explosives in aerospace applications, considering mild detonating fuse and core loading

10 p1750 A69-23014

Heating system providing symmetrical temperature field and specimen self centering for thermal resistance tests

10 p1696 A69-23845

Heat resistant composites, discussing composition, properties and high temperature behavior, plastic materials, reinforcement filaments, whiskers and test methods

12 p2117 A69-25855

Conformal transformation reducing transverse thermal resistance of cylinder of revolution to thermal resistance of semiinfinite medium

12 p2190 A69-26292

Space mission medical heat problems covering thermal characteristics and heat control, protection and resistance of space vehicle and astronaut adaptation

12 p2023 A69-26493

Thermal resistance of bolted or screwed sheet metal joints in vacuum, using method applicable to different materials and surface finishes

12 p2191 A69-26803

Heat resistant polyamides and polyimides for electrical insulation, discussing properties and applications under extreme temperatures and basic reactions

13 p2286 A69-27988

Contact between cylindrical surfaces in thermionic converters, determining thermal resistance and pressure in contact area

14 p2400 A69-29216

High temperature thermal resistance stability of multilayer cylindrical elements for thermionic converters determined by layer strain rate

14 p2539 A69-29218

Nitriding effect on heat resistance and transition temperature of molybdenum alloys

15 p2637 A69-30268

Boron effect on sintered porous Ni friction at high sliding velocities and temperatures, analyzing oxide film destruction restraint by decreased Ni plasticity

15 p2641 A69-31187

Optical measuring methods of cross sections and mechanical properties of heat resistant fiber reinforced materials

16 p2803 A69-31804

Transistor temperature and power limitations and thermal resistance calculation, discussing heat sink surface optimum design for power losses

16 p2760 A69-32047

Vacuum and thermal environment long term influence on thermal resistance for Mg to aluminum and Mg to Mg bolted joints

[AIAA PAPER 69-628] 17 p3073 A69-33309

Gravimetric and IR absorption spectra analysis for determining heat resistance and chemical changes in organosilicon resins during heating

17 p2992 A69-33744

Molecular structure and uses of heat resistant plastics, discussing aromatic polyamides

18 p3161 A69-34279

Heat sensitive paints thermophysical characteristics determined by nonstationary heat conditions method

18 p3161 A69-34697

High temperature structural adhesives developed from thermoplastic aromatic-heterocyclic polymers

19 p3357 A69-35560

Heat resistance evaluation of ZHS6-K alloy subjected to multicomponent surface diffusion alloying combinations of Al, B, Cr, Si, Zr

19 p3345 A69-36159

Seam welded U-type fin efficiency and effectiveness, studying effects of fin height, heat transfer coefficient and thermal resistance

19 p3452 A69-36371

Vanadium thermistor fabrication influence on resistance jump at phase change temperature of vanadium dioxide, reproducing parameters by heat treating doped vanadium pentoxide

19 p3256 A69-36718

Heat resistant coatings - Conference, Leningrad, may 1966

20 p3559 A69-37357

Temperature fields and stresses in heat resistant ceramic coatings, illustrating alumina coating on Mo to calculate heating rate

20 p3565 A69-37359

Inorganic heat resistant coatings high temperature mechanical tests noting corrosion, safety factors and rigidity after heating and temperature gradients

20 p3538 A69-37360

Temperature effect on grain size, crystal orientation, microhardness and heat resistance of diffusion Si coatings on Mo

20 p3560 A69-37361

Fusion welding for thin gauge corrugated core sandwich airframe structures capable of operating at high temperature, discussing equipment, techniques and quality control

[SBAC PAPER 9] 20 p3549 A69-37448

Natural convective heat transfer to gas turbine rotor blade and thermal resistance of cooling system using centrifugal pump

21 p3785 A69-39103

Hybrid microelectronic modules, using basic thermal design guidelines

22 p3910 A69-39952

Spacecraft electronic components operating junction temperature control, considering role of thermal resistance in controlling radiative and conductive transfer

[AIAA PAPER 69-1015] 22 p3922 A69-40387

Thermal conductivity precision tests for refractory samples using ASTM method C 201-47, emphasizing sample preparation and calorimeter calibration

22 p3956 A69-40671

Thin film thermistors heat-separated from graphite substrate to achieve positive temperature resistance coefficient via argon heating and oxygen cooling

22 p3997 A69-41214

Thermal isolation characteristics of low conductance interstitial materials determined, using test apparatus of axially loaded radiation shielded cylindrical column in vacuum

[AIAA PAPER 68-31] 23 p4239 A69-41889

Temperature control by heat pipe using noncondensing gas with methanol to vary thermal resistance and mathematical model to describe heat source temperature variations

23 p4240 A69-42307

Welded honeycomb sandwich structures of Ti, steel and similar materials for use in extreme thermal and acoustical environments

[AIAA PAPER 68-973] 24 p4326 A69-43716

THERMAL SHOCK

Approximate expression for temperature distribution during heat transient in infinite solids of plane, cylindrical and spherical geometry

06 p1025 A69-17779

Dynamic internal thermal shock in spherical shells of arbitrary thickness, considering uncoupled dynamic thermoelasticity problems with spherically symmetrical temperature fields

07 p1236 A69-19471

Thermal shock stresses in flat plates, solids and hollow cylinders, noting geometry, wall thickness, heat transfer characteristics and material properties effects

[ASME PAPER 69-GT-107] 09 p1619 A69-22523

Thermal shock temperature distribution and thermal stresses in finite circular disk subjected to instantaneous point heat source

13 p2363 A69-28130

Bonded solderless solar cell panel prototype withstanding high annealing temperature and thermal shock without electrical or mechanical degradation

19 p3251 A69-35688

Boron nitride and boron nitride composite under high temperatures in air and vacuum for various time periods, discussing thermal shock and oxidation resistance

19 p3359 A69-36208

Dispersion of paraffin cork after instantaneous shock heating, noting expansion at various isotropic indices

19 p3301 A69-36839

THERMAL SIMULATION

Low temperature simulation of hypersonic melting ablation and wave patterns of gas-liquid interface

06 p0907 A69-18064

Thermal vacuum simulator for testing manned Lunar Module Test Vehicle, using conformal skin heaters to control heating rates and skin temperature

[AIAA PAPER 69-312] 09 p1479 A69-22386

Aerodynamic heating of ELDO-A booster rocket, calculating flow field, heat transfer and conduction by method of characteristics and thermal models

11 p1966 A69-25433

Thermal stability of power transistor plates calculation using equivalent body with equivalent heat source at upper surface

12 p2042 A69-26881

Thermal stability of complex transistorized structures determined by extending method of single heat source equivalence to several interacting sources

12 p2042 A69-26882

Space environment simulation for vacuum, solar radiation, heat sink and orbital motion, discussing oil contamination of optical surfaces

13 p2241 A69-28079

Scale modeling of multilayer insulated spacecraft for thermal design, considering solar probe and two meter telescope models

[AIAA PAPER 69-613] 17 p3049 A69-33267

Handbook of solar simulation for thermal vacuum testing, discussing space environment, thermal control coatings, radiation sources, optical components, etc

21 p3690 A69-38894

Speed conditions of environmental simulation of thermal scale models of reentry vehicles, considering ablatives with phase-change and involved chemical reaction

[AIAA PAPER 69-1011] 22 p3922 A69-40384

THERMAL STABILITY

Disulfide effects on jet fuel operating characteristics and demercaptization influence on thermal stability, corrosive action and sedimentation

01 p0142 A69-11098

Structural stability of manganese austenitic steels at high temperatures, discussing phase transformations and carbide precipitation changes

01 p0100 A69-11294

Ammonium perchlorate base propellant and polyurethane binder heat stability, dangers of aging under abnormal conditions and reaction products for components and tolylene diisocyanate

02 p0303 A69-11529

Intentional impurities effects on nitronium perchlorate thermal stability explained by change in cation and anion vacancies

02 p0304 A69-11899

Radiation resistance of MOS transistors noting relationship with thermal stability, gate oxidation and metals used

02 p0221 A69-12468

Plane Couette flow stability in heated nonlinear viscous fluid flowing between horizontal plates heated to different temperatures

02 p0235 A69-12828

Niobium based alloys modulus of elasticity temperature stability, investigating admixture effects

04 p0615 A69-14642

Temperature measurement of moving droplets, noting influence of thermocouple electrode stability

04 p0688 A69-15423

Elastic stability of thin circular cylindrical shell with elastic core, longitudinal and transverse ribs and initial defects under combined pressure and thermal stress

05 p0832 A69-15692

Ferrite materials characteristics related to choice for use in waveguide devices, noting importance of low HF magnetic losses and thermal stability

05 p0810 A69-16792

Radiation defects stability in semiconductor, noting low temperature electron irradiation of Ge and effects of annealing

06 p0974 A69-16863

Thermal flutter effect on gravity gradient stabilized spacecraft, noting dependence on sunlight and time
07 p1226 A69-18325

Polymeric Schiff bases synthesis, thermal stability and nature of pyrolytic decomposition of polyazines and derived polystylenes
07 p1074 A69-18628

Stress rupture, creep and thermal stability of AT-3 titanium alloy, discussing possible applications
07 p1163 A69-18782

Alternative balancing technique utilizing linear combination of two equal and opposite drift characteristics to minimize drift in integrated differential amplifiers
07 p1102 A69-18874

Temperature sensitivity of frequency of integrated oscillators, giving design method for achieving temperature compensation
07 p1103 A69-18882

Lattice location of dopant elements implanted into Ge determined by carbon ion backscattering, noting substitutional concentrations above thermal equilibrium solubilities
07 p1199 A69-18903

Thermal stabilization and ethylene oxide effect on spaceborne electronic component sterilization and decontamination
08 p1283 A69-20266

Fire retardant thermally stable electrical grade thermoset resins tested for flexural and dielectric strength and weight loss
08 p1340 A69-20506

Optimization of plane smooth rectangular panels of constant cross section subjected to loading and heating conditions
08 p1417 A69-20821

Thermal stability criteria for thermionic converter performance evaluation, noting electron cooling influence
09 p1441 A69-21838

Temperature stability of slightly ionized gas for arbitrary collision cross sections, discussing electron temperature variation as function of electric field strength
09 p1551 A69-22039

Nickel base wrought and cast superalloys examined to determine minor phases and microstructure thermal stability in high temperature heat treated condition
10 p1714 A69-23977

Thermodynamic stability of dense plasma consisting of electrons and charged ions, plotting ionization potential as function of electron density and temperature
11 p1922 A69-24232

Hot inert gas bubble thermal stability in cool reactive liquid
11 p1998 A69-24475

Thermally induced oscillatory instabilities in spacecraft booms, rederiving thermal torque equation to predict finite twist response
11 p1994 A69-25531

Thermally stable polymers for high stress aerospace applications, noting chemical stability and structure of high polymers
12 p2117 A69-25853

Thermal stability of refractory and cermet materials, analyzing small samples subjected to cyclic high energy radiative heating and air-water cooling
12 p2118 A69-26262

Thermal stability of power transistor plates calculation using equivalent body with equivalent heat source at upper surface
12 p2042 A69-26881

Thermal stability of complex transistorized structures determined by extending method of single heat source equivalence to several interacting sources
12 p2042 A69-26882

Time delay in temperature controlled transistorized time delay circuit determined by transistor unsteady thermal processes
12 p2043 A69-26883

Refractory ceramic materials thermal stability in high temperature subsonic ionized gas flow products, emphasizing zirconia and magnesia
13 p2285 A69-27472

Stellar atmosphere models of pure hydrogen in hydrostatic, radiative and statistical equilibrium, including Lyman-alpha and continua, discussing nonLTE deviations
13 p2338 A69-27560

Antifriction characteristics of hard lubricating coatings based on molybdenum disulfide and graphite in inert gas atmosphere and vacuum, determining thermal stability temperature ranges
13 p2269 A69-28053

Numerical methods for solving steady state and transient heat transfer problems suitable for high speed digital computer
13 p2376 A69-28141

Electrooptical ADP modulator design for use with helium-neon laser, considering temperature stability and crystal faces parallelism
13 p2272 A69-28191

Rigid heat conductor in continuum thermodynamics, discussing conductivity tensor symmetry and heat capacity positivity as restrictors
13 p2377 A69-28193

Thermionic converter stability as function of cesium pressure, heat input, reservoir temperature, load voltage or resistance
14 p2402 A69-29236

Thoria strengthened Ni-Cr alloys high temperature stability, noting thoria particle size influence
14 p2465 A69-29682

Time and temperature effects on corrosion and structure of Hastelloy alloy C-276
14 p2466 A69-29930

Operating conditions influence on thermal stability of DC plasmatron arc to obtain high temperature source
15 p2663 A69-30994

Second breakdown and other thermal instabilities analyzed by heat flow equation, obtaining stability criteria predicting reduced power dissipation for transistor at low currents
16 p2758 A69-31618

Thermal stability of Hastelloy Alloy C-276 determined from time and temperature tests for corrosion and grain boundary precipitation
16 p2799 A69-31719

Ammonium and magnesium perchlorate mixture thermal stability study with differential scanning calorimetry, noting exothermic decomposition of AP [AIAA PAPER 69-500]
16 p2833 A69-32661

Thermal stability elements in solid propellant liner insulation system for heat sterilized solid rocket motors used in unmanned planetary landers [AIAA PAPER 69-437]
16 p2869 A69-32750

Polygonization and strengthening effects simultaneous action at grain boundaries increased thermal stability of thermomechanically treated Ni-Cr alloy
17 p2991 A69-33940

Semiconductor plasma DC overheating instability in electric and magnetic fields, determining growth increments of oscillation amplitude
18 p3182 A69-35022

Polyperfluoroalkyleneimide/oligo(perfluoroalkyleneamide) synthesized by reaction of perfluoroalkane dinitriles with ammonia or diamidine, giving elastomers of varying strength and elongation, noting thermal stability
19 p3264 A69-35535

Ferroelectric transducer for heat transfer rates and flow measurement in gaseous systems with autostabilized temperature, noting film coefficient
19 p3307 A69-35749

Diffusion during high temperature exposure of protective coatings on Mo, noting compact layers and carbide forming elements effect on thermal stability
19 p3345 A69-36156

Supersonic transport aviation fuel thermal stability measurement data correlated with data deduced from heat transfer measurements
19 p3393 A69-36210

Thermodynamic equilibrium stability general theory extended to arbitrary boundary conditions using properties of entropy balance equation
19 p3452 A69-36789

Facility for evaluating thermal stability of heat resistant materials and cermets in constant temperature gas flow
20 p3565 A69-36979

Thermal stability and radioelectric turbulence parameter derivative relationship for dry adiabatic stratification of lower troposphere and for inversions
20 p3571 A69-37509

Thermally stable polymers chemical and structural properties, discussing polymer use in aerospace technology
21 p3751 A69-38789

Thermal stability of reactive spherical shell, investigating spontaneous ignition of volatile fuel drop exposed to hot oxidizing environment
21 p3849 A69-38804

Plastic deformation in hardened Ti alloys with thermally unstable beta phase under static compression and tensile loads by electron microscope
21 p3746 A69-39161

X ray scintillation spectrometers temperature stabilizing circuit, describing amplitude-frequency compensation version technique for position stability
21 p3727 A69-39891

Cu, Ni, Co, Cr and Ti effect on high temperature mechanical properties and stability after prolonged annealing of Al-Si alloy with added 1 percent Mg
22 p3968 A69-40000

Ferredoxin from thermophilic and mesophilic Clostridia, noting difference in heat stability due to iron disulfide environments
22 p3897 A69-41000

Thermal inertia index of semiconductor thermistors with one dimensional temperature field taking into account conductive heat transfer
23 p4163 A69-41555

Micromodule unsteady thermal behavior reduced to calculating linear heat flux for boundary conditions containing temporal and spatial derivatives
23 p4136 A69-41559

Waveguide Y-circulator parameters thermal stability equation, considering temperature, magnetization level and magnetic field resonance effects on tuning frequency
23 p4123 A69-41959

Choke coil magnetoelastic sensors thermal stability found decreasing proportionally to measurement range decrease/below 100 newtons/
23 p4166 A69-41999

Monograph on thermally stable polymers azomethines synthesis by polycondensation reactions
23 p4113 A69-42019

Constant temperature thermoanemometer design and subsystem operation applied to measurements of turbulent flow velocity and pulse characteristics
24 p4311 A69-42558

Large space erectable structures rigidity, stiffness thermal stability, structural efficiency and integrity [AAS PAPER 69-152]
24 p4398 A69-42877

THERMAL STRESSES

Temperature field and stress state in elastic plates with temperature insulated arc shaped crack
01 p0164 A69-10078

Beta titanium alloys mechanical properties improvement, discussing effects of alloying elements, heat treatment and high temperature deformation
01 p0093 A69-10213

Axisymmetric transient thermoelastic problem for transversely anisotropic hollow cylinder, examining boundary value problems
01 p0166 A69-10302

Orthotropic plates bending and thermal stress, analyzing basic equations
01 p0168 A69-10416

Thermal stresses near spherical inclusion in elastic matrix with uniform heat flow
01 p0171 A69-11264

Generalized unsteady temperature fields and stresses in crystalline plates using Fourier and Laplace transforms
02 p0340 A69-12044

Strain gage behavior on unstressed aluminum alloy under rapid heating using radiant heating, weld strength and high temperature test equipment
02 p0341 A69-12229

Mechanical thermal stresses effects during laser flash illumination of GaAs, discussing temperature dependence of radiative recombination
02 p0256 A69-12245

Viscoelastic materials thermomechanical behavior, discussing constitutive equation and derivation of stress tensor and entropy density from viscoelastic potential
02 p0344 A69-12294

Three dimensional thermal stress distribution in case bonded solid propellant determined by scattered light photoelastic technique coupled with transparent rocket motor model [AIAA PAPER 68-512]
02 p0345 A69-12371

Plane inhomogeneous thermal stress in isotropic elastic circular infinitely long cylinder produced by plane unsteady temperature distribution
02 p0349 A69-12826

Stresses in circular cylindrical shell subjected to local heating
03 p0523 A69-12952

Aircraft cockpit and surface temperatures after solar radiation exposure in desert, showing inadequacies of meteorological data for thermal stress predictions
03 p0381 A69-14077

Thermal stress determination in two dimensional problem of theory of elasticity, using stress simulation by thin plate bending
04 p0668 A69-14272

- Temperature distributions, thermal stresses and natural frequencies of radial vibrations in thin circular cylindrical shells
04 p0675 A69-14704
- Temperature stresses analysis for jet lift VTOL aircraft structure during takeoff and landing, discussing fire hazard in lift pod
04 p0548 A69-14841
- Thermal stress in fiber reinforced metals, assuming Young modulus variable when thermal stress is applied during heating and cooling
04 p0682 A69-15393
- Temperature distribution and thermal stresses in liquid filled cylindrical shell
04 p0682 A69-15413
- Natural frequencies controllability by induced thermal membrane stresses examined for thin disk
04 p0682 A69-15494
- Plane thermal stress distribution determined around holes under steady temperature distribution, using complex variable approach
05 p0836 A69-15877
- Axisymmetric thermal stresses in spheroidal shell of arbitrary thickness due to thermoelastic strain nucleus
05 p0836 A69-15923
- Green function for stress intensity factors of rectangular plate edge cracks, noting application to thermal stresses
[ASME PAPER 68-WA/MET-19]
05 p0839 A69-16157
- Lunar history reexamination including added mantle convection and recent rocket data
05 p0825 A69-16303
- Stress concentration at thermally insulated holes in elastic material created by disturbance of uniform heat flow at holes
06 p1021 A69-17184
- Semiconductor device failure modes temperature dependence, discussing bonds, metallization and packaging
06 p0894 A69-17218
- Temperature distributions and thermal stresses in bimetallic I-beam structures with dissimilar materials for skins and webs and with kinetic heating inputs
06 p1024 A69-17610
- Device for measurement of time to failure of brittle materials in thermal-endurance testing, noting shock wave
06 p0927 A69-17690
- Radial vibrations of thin cylindrical shells subjected to thermal loadings, discussing temperature distributions, thermal stresses and natural frequencies
[AIAA PAPER 69-59]
06 p1028 A69-18143
- Thermal stress concentrations in vicinity of cylindrical elastic inclusions embedded in elastic matrix, using displacement functions and photothermoelasticity
07 p1171 A69-18726
- Boundary value problem of temperature field and heat conduction in transparent media heated by laser radiation producing thermoelastic stresses leading to breakdown
07 p1149 A69-18925
- Steady state thermal stress distributions near external crack in solid, treating temperature distributions with respect to plane of crack
07 p1232 A69-19172
- Mental and physical human performance characteristics under thermal loads noting admissible temperatures and endurance limits
08 p1263 A69-19940
- Translunar cracks in laminated graphite filament composites, noting effect of thermal stresses due to cooling
08 p1337 A69-20483
- Thermal stress propagation in infinite viscoelastic thin plate analyzed with cylindrical coordinate system
08 p1415 A69-20661
- Transient thermal stress distribution in infinite orthotropic elastic cylinder of rectangular cross section in presence of heat sources
08 p1415 A69-20664
- Thermal stress field under uniform heat flow due to elliptical elastic inclusion for anisotropic case
08 p1418 A69-21003
- Failure mechanisms in semiconductors, discussing imperfections, fabrication errors and electrical, thermal and mechanical stresses
08 p1294 A69-21117
- Castigliano variational principle applied to thermal stresses in rectangular plate by expanding stress function in double series of cosine binomials
08 p1419 A69-21178
- Stress formulation of thermoelasticity in simply connected body, noting uniform temperature change influence on stress components
09 p1617 A69-22007
- Thermally generated stress wave propagation in dispersive elastic rod investigated experimentally and analytically, using ruby laser and differential equation
09 p1617 A69-22010
- Thermal shock stresses in flat plates, solids and hollow cylinders, noting geometry, wall thickness, heat transfer characteristics and material properties effects
[ASME PAPER 69-GT-107]
09 p1619 A69-22523
- X ray irradiated dogs subjected to heat stresses to determine thermoregulatory ability
09 p1445 A69-22548
- Plane thermal stress field in discontinuous temperature distribution within isotropic linear elastic circular cylinder of infinite length
10 p1793 A69-22884
- Crack stability under mechanical and thermal stresses, noting critical tensile stress and thermal insulating character of crack
10 p1794 A69-22890
- Heat susceptibility and tolerance in astronauts obtained by plot of skin and oral temperatures for subject under thermal stress
10 p1644 A69-23376
- Thermal stresses for mixed boundary conditions calculated from combined use of integral transforms and variational techniques, reducing computational labor
10 p1801 A69-23429
- Elastic-plastic deformations /strains/ amplitudes measured at high cycle temperatures in thermal fatigue tests
10 p1801 A69-23844
- Subregions method in coupled thermoelasticity, discussing numerical values for thin steel circular disk
11 p1970 A69-24606
- Thermal stresses in longitudinally reinforced cylindrical shell, combining moment and semimomentless shell theories to obtain numerical results
11 p1981 A69-24942
- Residual thermal stresses and plastic strains at hole edges in perforated plates, considering heating and rapid cooling
11 p1982 A69-24947
- Modal coupling in thermally stressed plates, obtaining solution for frequencies and stiffness
11 p1990 A69-25509
- Directional solar thermal field /sunlight/ effect on coupled nonplanar transverse and torsional vibrations of satellite cylindrical antennas in orbit
11 p1994 A69-25534
- Unsteady temperature field and thermal stresses for anisotropic and orthotropic plates heated by heat sources and having Newton law heat transfer
12 p2177 A69-25992
- Thermal stresses induced in plate plane by temperature gradient varying in space and time calculated using Mach-Zehnder interferometer, determining stress intensity factors
12 p2089 A69-26189
- Thermal stress and displacement fields in elastic solid weakened by crack outside of circular region, noting plastic zone size and energy dissipation
12 p2179 A69-26216
- Thermal stresses in infinite elastic plates containing insulated circular holes, using two dimensional bipolar coordinates
12 p2180 A69-26267
- Thermal stresses in hollow finite circular cylinder having smooth rigid insulating cover on curved surfaces and temperature distribution on plane ends
12 p2180 A69-26268
- Lateral bending and two dimensional thermal stress in rectangular orthotropic plates, considering alternating direction implicit method
12 p2188 A69-27100
- Thermal and mechanical stability of fused silica lightweight mirror structures, examining impact and shear strengths of fused joints
13 p2261 A69-27954
- Thermal shock temperature distribution and thermal stresses in finite circular disk subjected to instantaneous point heat source
13 p2363 A69-28130
- Stresses in infinite solid elastic circular cylinder due to rotating line source of heat
13 p2364 A69-28206
- Materials surface thermal stress analysis by strain gauges, considering behavior during rapid temperature changes
13 p2264 A69-28599
- Short time creep rupture behavior of austenitic stainless steel at high temperature ranges, noting rupture times various stresses and data correlation
[ASME PAPER 68-WA/MET-2]
14 p2464 A69-29439
- Beta titanium alloys mechanical properties improvement, discussing effects of alloying elements heat treatment and high temperature deformation
15 p2637 A69-30269
- Thermal stresses in fiber reinforced metals as function of volumetric content of fiber phase
15 p2638 A69-30285
- Uncoupled dynamic thermal stresses and displacements by heat generation in infinite flat plates, using classical thermoelasticity theory for infinitesimal displacements
15 p2709 A69-30669
- Thermoelastic stress in seminfinitesimal elastic medium due to discontinuous temperature distribution over free surface, solving associated heat conduction problem
15 p2712 A69-31006
- Thermal stresses and displacements in isotropic inhomogeneous rotating circular disk with axle hole under steady temperature field
15 p2712 A69-31016
- Thermoelastic stresses in isotropic circular cylinder with surface locally heated by external Newtonian heat source, considering various heat transfer conditions
15 p2714 A69-31178
- Thermal stresses in circular cylinder with regularly distributed cavities, establishing distribution laws for temperatures and stresses
15 p2714 A69-31196
- Photothermoelastic analysis of thermal stresses in turbine wheels with welded blades, noting stress concentration reduction
15 p2715 A69-31488
- Thermal stresses in rotating cylindrical interplanetary body heated by solar radiation
16 p2871 A69-31901
- Stresses due to nucleus of thermoelastic strain in infinite elastic solid with two rigid circular inserts
16 p2872 A69-31906
- Co content influence on temperature stress in WC-Co cermets using one exposure and two exposure X ray diffraction
16 p2802 A69-32340
- Temperature field, strains and stresses induced in thin circular disk by unsteady heat source, noting time effect and resonant vibrations
17 p3054 A69-33021
- Stability of nonuniformly heated rectangular plate reinforced by elastic longitudinal and rigid transverse ribs, accounting for influence of torsional and bending rigidities
17 p3057 A69-33198
- Initial thermostructural stresses in homogeneous quasi-isotropic two component medium, solving statistical boundary value problem thermoelastically
17 p3058 A69-33316
- Loading path criterion for total strain /deformation/ plasticity theory based on Sanders loading function, discussing case of thermally loaded bar
17 p3062 A69-33711
- Temperature dependence of metal elastic properties including thermal strains effect on stress field, yield stress changes and elastic modulus variations
18 p3212 A69-34353
- Laminated anisotropic plate equations from thin plate theory including nonlinear terms, inertia and thermal stresses
[ASME PAPER 69-APM-15]
18 p3213 A69-34390
- Thermal stress in fiber reinforced metals, assuming Young modulus variable when thermal stress is applied during heating and cooling
18 p3223 A69-35021
- Low temperature bond failures of room temperature vulcanizing methyl-phenyl adhesive bonds attributed to thermal stress cracking of primer, presenting in-process tests
19 p3321 A69-35563
- Two dimensional thermoelasticity problem for nonlinear media, obtaining solutions for thermal stress concentration and boundary value problems
19 p3436 A69-35848
- Thermal stresses in solids, discussing spaces and half spaces, thick walled systems, shells, plates, disks and bars
19 p3447 A69-36856
- Facility for evaluating thermal stability of heat resistant materials and cermets in constant temperature gas flow
20 p3565 A69-36979

Thermal stress concentration near elliptical hole in thin walled liquid filled cylindrical shell in presence of temperature gradient across shell cross section
20 p3622 A69-37325

Temperature fields and stresses in heat resistant ceramic coatings, illustrating alumina coating on Mo to calculate heating rate
20 p3565 A69-37359

Automated device for load carrying ability of structural elements like gas turbine blades under thermal and mechanical cyclic loads
20 p3544 A69-37816

Transient thermal stresses in heat treated elastic-perfectly plastic disks with temperature dependent yield stress, considering stress distribution sequence and residual stresses
20 p3629 A69-37974

Stress strain state in thin circular elastoplastic disks under axially symmetric transient temperature distribution, noting moving annular plastic deformation region
20 p3629 A69-38028

Thermal stress distribution induced in wedge by apex heat source analyzed using elasticity theory, considering lateral surface heat transfer
21 p3833 A69-38644

Steady state temperature fields and thermal stresses determined in finite cylindrical shell by optimal parameters of reinforcing circular rib
21 p3834 A69-38714

Thermal stresses and displacements in long isotropic hollow cylinder heated on part of outer curved surface, analyzing temperature distribution
21 p3838 A69-39166

Stability of free and clamped spherical and circular cylindrical shells subjected to uniform or nonuniform heating, discussing effects of temperature stresses
21 p3838 A69-39190

Fatigue endurance determined from thermal stresses by balancing elastic strain rates, creep relaxation and mechanical cyclic loading with triangular waveform, discussing nonsteady creep
21 p3843 A69-39310

Thermal and athermal component of flow stress and deformation dynamics for Ti at low homologous temperatures determined by stress relaxation tests
21 p3749 A69-39598

Time-optimal nuclear rocket propellant start-up with thermal stress constraints based on distributed parameter model, deriving algorithm for flow rate increase
21 p3768 A69-39632

Alloy softening in bcc Fe-N and Fe-Ni, discussing causes of thermal stress component reduction in interstitial and substitutional alloys
22 p3969 A69-40164

Severe heat stress effects on respiratory frequency, rectal temperature, blood gases and pH of conscious dog
23 p4081 A69-41432

Potent chemical factors released from anterior hypothalamus of rhesus monkeys in response to thermal stress during thermoregulation
23 p4084 A69-41472

Thermoelastic stresses in rotating cylinders and disks with radial temperature distribution, deriving plane deformation approximate solutions
23 p4227 A69-41707

Photothermoelastic investigation of thermal stress concentrations around circular cavities and inclusions in two dimensional composite models
24 p4396 A69-42739

Dynamic equilibrium of making and breaking adhesion bonds between polymer segments and dissimilar surfaces through water, allowing thermal stresses relaxation
24 p4326 A69-43458

Thermal turbulence effects on phase fluctuations of laser beams, studying temporal decay of mean square refractive index fluctuation with fringe pattern displacements
24 p4329 A69-43754

THERMAL VACUUM TESTS

Solar thermal vacuum test for space flight qualification of military spin stabilized synchronous orbit communications satellite
15 p2587 A69-30391

Selectively pumped thermal vacuum test chamber for orbital heat transfer and environment simulation for flight vehicle performance prediction
15 p2587 A69-30392

COMSAT thermal vacuum chamber specification configurations, discussing chamber orientation, vacuum and roughing systems, pumping mechanism, wiring, installation, testing, etc
15 p2587 A69-30393

Thermal vacuum /TV/ manned test operations related to Apollo lunar module in simulated space environment
15 p2558 A69-30394

Surveyor thermal vacuum test data comparison with flight results indicating performance prediction reliability of earth-based tests for vacuum and lunar environments
19 p3430 A69-36016

Mission simulation testing in thermal vacuum environment for Apollo Lunar Module, noting conformal skin heaters
22 p3920 A69-40369

Manned testing of EVA equipment in thermal-vacuum environment for qualification of Apollo extravehicular mobility unit, using lunar surface thermal simulator
22 p3893 A69-40370

Test model thermal balance in space simulator, measuring effects of solar simulator irradiance reflected from carbon dioxide cryopanel deposits
22 p3922 A69-40385

Line source technique for ablative heat shield materials thermal conductivity measurements, comparing vacuum and atmospheric test results
22 p3922 A69-40386

Pressure measurements and gas flow analysis during thermal vacuum tests of manned spacecraft indicating adequate space vacuum simulation
22 p3924 A69-40401

Design, fabrication and evaluation of lunar base solar array power modules, emphasizing structural/ dynamic, thermal vacuum and acoustic tests
23 p4072 A69-42288

THERMALIZATION [ENERGY ABSORPTION] NT NEUTRON THERMALIZATION

Thermalization of kinetic energy of plasma flow by shock phenomena produced by magnetic mirror field
02 p0289 A69-12176

Distribution function for thermalization distances derived for infinite atmosphere with plane source in noncoherent light scattering
23 p4192 A69-42403

THERMIONIC CATHODES

Performance prediction for planar and cylindrical electrode geometry fixed spacing thermionic converters
09 p1438 A69-21814

Thermal stability criteria for thermionic converter performance evaluation, noting electron cooling influence
09 p1441 A69-21838

Oxide coated thermionic cathodes, noting semiconducting properties of alkaline earth oxides, particularly barium oxide and adsorption and optical properties
09 p1470 A69-22700

Thermionic electrogenerating element (EGE) design optimization, considering one dimensional linear geometry with thin walled cylindrical sheath cathode
14 p2400 A69-29224

Thermionic converter cathode and anode temperatures difference during start-up heating and under normal operational conditions
14 p2400 A69-29226

Potential distribution between point in interelectrode gap and thermionic converter cathode in collisionless mode under transverse magnetic field
14 p2401 A69-29235

Electron and ion separation as function of plasma potential drop in Langmuir cathode layer in arc regime
14 p2490 A69-29237

Cs mixture effects with Ba and I on cathode electron emission in thermionic converter
14 p2402 A69-29239

Low voltage Cs arc in thermionic converter with slotted cathode surface, determining electron concentration and temperature distribution
14 p2403 A69-29250

Thermoemission converters /TEC/ cathode materials, discussing determination of local work function by electron microscope and delay curves methods
14 p2505 A69-29265

THERMIONIC CONVERTERS

NT SNAP 13

Metallic dismountable thermionic converter enclosed in mica sealed vacuum chamber, giving I-V characteristics, optimal temperature of liquid cesium phase and output power
02 p0194 A69-11587

Thermionic reactor systems, discussing fissionable material content, power output, specific power, component mass, total mass and design
02 p0279 A69-12662

Kinetic theory model of plasma sheath transition, analyzing sheath structure in unignited mode of thermionic converter
03 p0368 A69-13125

Rhenium-niobium cylindrical thermionic converters with mechanically polished or electroetched emitters, comparing performance
03 p0368 A69-13126

Electron emitter cooling and plasma heating of thermionic converters noting effects of plasma density, diode spacing, etc
03 p0368 A69-13127

Probe and spectral techniques compared for investigation of low voltage arc of cesium plasma thermionic converter
03 p0478 A69-13836

Rhenium Nb cylindrical thermionic converter, measuring efficiency and power density in emitter temperature range 1600-2050 K and collector temperature range 873-1173 K
05 p0707 A69-16359

Plasma characteristics in thermionic converter operating under low voltage arc conditions obtained by computer, probes and spectral techniques
06 p0963 A69-16910

Thermionic energy converter theory and efficiency, discussing design considerations to improve performance
07 p1057 A69-18255

Simulated solar radiation heating of cesium vapor thermionic converters with multicapillary transmitters
07 p1058 A69-18951

Out-of-core thermionic space power generators using heat pipes, discussing feasibility in geometry, heat pipes, reactor, shield, heat exchanger and radiator
08 p1256 A69-19856

Thermionic conversion - Conference, Framingham, Mass., October 1968
09 p1436 A69-21806

Reproducibility of thermionic converters performance, comparing volt-ampere characteristics with reservoir and collector temperature
09 p1437 A69-21813

Performance prediction for planar and cylindrical electrode geometry fixed spacing thermionic converters
09 p1438 A69-21814

Comparative performance of niobium cylindrical thermionic converters with vapor deposited rhenium, stressing emitters surface preparation
09 p1438 A69-21816

Cylindrical thermionic converter with vapor deposited rhenium emitter and niobium collector, measuring efficiency and power density
09 p1438 A69-21817

Thermionic converters with chloride and fluoride vapor deposited tungsten emitters, comparing performance characteristics and stability
09 p1438 A69-21819

Emission characteristics of duplex vapor deposited tungsten emitter with molybdenum collector in variable spacing guard ring converter
09 p1438 A69-21820

Side wall currents in unignited hardware type thermionic energy converters, discussing work function and heat choke
09 p1439 A69-21822

Thermionic converter metallography relationship between materials and fabrication methods and reliable performance life
09 p1439 A69-21824

Semiconducting films as collector work function in thermionic converters, with regard to I-V characteristics
09 p1558 A69-21825

Spectroscopic measurements of electron density and temperature for quasi-saturation region of ignited mode plasma in planar thermionic converter
09 p1439 A69-21826

Isothermal diode as study basis for internal complex controlling thermionic energy conversion
09 p1439 A69-21827

Kinetic theory model of plasma sheath transition applied to sheath structure in unignited mode of thermionic converter
09 p1440 A69-21828

Fission fragment generated plasma applicability to thermionic energy converters from electron density, temperature and transport studies
09 p1440 A69-21829

Ionic species identification in argon-cesium discharges for thermionic converter design
09 p1440 A69-21830

Semiempirical relation for electron cooling modified by plasma heating of thermionic converters, including effects of plasma density, diode spacing and surface potential difference
09 p1440 A69-21831

Heat pipes for thermionic converters, wicks development, high temperature life testing and performance
09 p1440 A69-21833

Local axial voltage variation from one dimensional model applied to solve thermionic boundary conditions in two dimensional thermal analysis of converter
09 p1440 A69-21834

Thermionic converters stability and safety maintainable at high Ce pressures
09 p1441 A69-21837

Thermal stability criteria for thermionic converter performance evaluation, noting electron cooling influence
09 p1441 A69-21838

Adsorption process limits when used as Cs reserve in thermionic converter
09 p1441 A69-21839

Gas breakdown model for analyzing breakdown of Ce vapor filled crack in thermionic trilateral insulator
09 p1441 A69-21840

Stability analysis including delayed collector and structure coefficients, showing thermionic reactor instability with all negative reactivity coefficients
09 p1442 A69-21841

Thermionic converter SD-4 design and performance tests covering emitter, collector and Cs reservoir temperatures and power efficiency
11 p1827 A69-25398

Arc mode thermionic Cs converter nonlinear I-V characteristics explained by current-dependent temperature and potential fields in plasma
11 p1827 A69-25400

Current-voltage characteristics and ionization equilibrium of low voltage arc plasma in narrow gap of thermionic converter at high current density
11 p1933 A69-25554

Soviet book on plasma thermionic energy conversion covering operation modes, transport processes, current-voltage characteristics, density, temperature, electric field distribution
12 p2017 A69-26850

Thermionic converter matched with solar cells analyzed for parabolic mirrors, assuming heat conduction power supply to cathode and uniform temperature distribution
13 p2209 A69-27970

Thermionic converter improvements by electronegative additives and emitter surface finishes, noting cesium oxide, heat treatments with electropolishing, electroetching, etc
14 p2397 A69-29173

Nuclear type cylindrical thermionic converter with porous adsorbent structure and liquid cesium tank
14 p2397 A69-29174

Reliability and efficiency improvements for thermionic converters at JPL, giving failures analyses
14 p2397 A69-29175

High pressure Cs thermionic converter with cold region, measuring Cs partial pressure distribution in Ar filled tube
14 p2397 A69-29176

Thermionic converter performance measured using test vehicles with guard ringed collectors and variable emitter-collector spacing
14 p2398 A69-29177

Plane and cylindrical thermionic converters, considering electricity generation by heating through flame, solar radiation and nuclear flux
14 p2419 A69-29178

Thermionic converters with different collectors, emitters and metal-ceramic seals reliability tested, determining life duration
14 p2398 A69-29179

Auxiliary discharge thermionic converter with Penning mixture (Ne-Ar), discussing pressure and Penning ionization effects, collector current discontinuities, etc
14 p2398 A69-29180

All metal nuclear thermionic modular converter, discussing applications, design and material requirements or limitations
14 p2398 A69-29181

Thermionic converter with external fuel surrounding inner emitter annulus for use in in-core reactors
14 p2480 A69-29185

Radioisotope fueled miniature thermionic converter for fractional watt level operation, defining optimum interaction of variables
14 p2399 A69-29193

Single cell fission powered thermionic converters design and testing
14 p2399 A69-29195

Thermionic converter SO-4 design and in- and out-of-pile test results, presenting diode performance at various times
14 p2399 A69-29196

Cylindrical geometry in-pile and out-of-pile thermionic converters long term life tests, including unfueled and fueled versions
14 p2399 A69-29197

Sirene 302 thermionic converter lifetime during irradiation in Triton immersion pile, considering effects on conversion efficiency
14 p2481 A69-29198

Cylindrical in-core thermionic converters performance and life tests, discussing diode design, operation data and irradiation studies
14 p2399 A69-29199

Materials compatibility and maximum heat flux capability of heat pipes emphasizing thermionic conversion
14 p2538 A69-29202

Heat pipes for heating emitters of thermionic converters at high temperatures, noting capillary optimization and thermal resistance values
14 p2539 A69-29208

Sintered metal powder process for metal-to-ceramic seals for thermionic converters, giving results for tensile strength, thermal cycling and cesium corrosion
14 p2454 A69-29211

Metal insulating seals using preliminary metallization or direct brazing for applications in thermionic converter technology and irradiation capsules
14 p2455 A69-29212

Barium vapor effect on converter materials, examining metals-ceramics compatibility at high temperatures
14 p2467 A69-29215

Contact between cylindrical surfaces in thermionic converters, determining thermal resistance and pressure in contact area
14 p2400 A69-29216

Titanium alloys for thermionic nuclear converters, discussing melting, forging, drawing and quality control of mechanical and physical properties
14 p2462 A69-29217

High temperature thermal resistance stability of multilayer cylindrical elements for thermionic converters determined by layer strain rate
14 p2539 A69-29218

High temperature compatibility of Mo, W, Nb and Ta as canning materials with high melting point and formation energy filling materials
14 p2463 A69-29219

Cesium sorption in materials for thermionic converters reservoirs, discussing dimensional stability of porous alumina, W and C samples
14 p2463 A69-29220

Output current and efficiency of vapor thermionic converters obtained in terms of electrodes and interelectrode gas parameters, exemplifying nuclear fuel element
14 p2400 A69-29222

Thermionic electrogenerating element (EGE)/ design optimization, considering one dimensional linear geometry with thin walled cylindrical sheath cathode
14 p2400 A69-29224

Thermionic converters with matrix circuit connections, considering current flow patterns in matrices to evaluate electrical failure spreading
14 p2400 A69-29225

Thermionic converter cathode and anode temperatures difference during start-up heating and under normal operational conditions
14 p2400 A69-29226

Thermionic converter components reliability under mechanical load and failure models, showing probabilistic nature of failures
14 p2400 A69-29227

Axial variation analysis of heat generation rate, temperature, voltage, current density and emitter heat flux in thermionic converter, emphasizing application to long diodes design
14 p2401 A69-29228

Low voltage arc in cesium thermionic converter, investigating current-voltage characteristics, electron temperature, electron density and plasma potentials in ignited mode
14 p2401 A69-29231

Differential equations for ignited mode theory, considering ion and electron transport and energy flux
14 p2490 A69-29233

Potential distribution between point in interelectrode gap and thermionic converter cathode in collisionless mode under transverse magnetic field
14 p2401 A69-29235

Thermionic converter stability as function of cesium pressure, heat input, reservoir temperature, load voltage or resistance
14 p2402 A69-29236

Cell current and calorimetric measurements of electrical power and heat generation with heat pipe thermionic converter
14 p2402 A69-29238

Cs mixture effects with Ba and I on cathode electron emission in thermionic converter
14 p2402 A69-29239

Unignited mode converter and emitter work function patches, calculating electron-cesium momentum transfer cross sections from saturation current measurements
14 p2490 A69-29240

Thermionic converter current-voltage characteristics under various emitter temperatures and cesium vapor pressures, noting role of Schottky effect
14 p2402 A69-29241

Razor phenomenological theory of space ionization in arc mode regime of Cs thermionic converter
14 p2402 A69-29242

Cesium plasma electron temperature in narrow electrode space of thermionic converter determined using electrode and changeable space diode
14 p2491 A69-29243

Current oscillations and electromagnetic radiation in low pressure cesium thermal emission converters using glass diode with plate geometry metal electrodes
14 p2402 A69-29246

Thermal emission converter, using Cs-Ba mixture in low voltage arc mode, detailing construction
14 p2403 A69-29247

Low voltage Knudsen arc in cesium-argon mixture for thermal emission converters
14 p2403 A69-29248

Noble gas thermionic converters, discussing auxiliary discharge compensation of negative space charge, I-V characteristics, efficiency and comparison to ignited mode cesium vapor converter
14 p2403 A69-29249

Low voltage Cs arc in thermionic converter with slotted cathode surface, determining electron concentration and temperature distribution
14 p2403 A69-29250

Rare gases effect on thermionic converters volt-ampere characteristics, noting gas pressure, oxygen contamination and performance relations
14 p2403 A69-29251

Cesium ions decay time in thermionic converter operating in gas kinetic mode by pulse ionization, noting dependence on interelectrode potential distribution
14 p2403 A69-29252

Experimental and theoretical data correlation on low voltage arc in thermionic converters using cesium vapor, describing discharge plasma by solving differential equation system
14 p2404 A69-29254

Electron energy distribution function and nonequilibrium ionization rate in near cathode layer of thermionic converter
14 p2404 A69-29255

Probe and spectroscopic study of dense plasma thermionic converters noting parameters
14 p2404 A69-29256

Plasma potential and density distribution in near-electrode plasma sheath of thermionic converter
14 p2491 A69-29257

Ionization mechanisms in ignited mode cesium thermionic converter, discussing positive ions production for electron space charge neutralization and ion density calculations
14 p2404 A69-29258

Electron temperature and density distributions across cesium converter interelectrode gap determined spectroscopically, noting maxima toward emitter
14 p2491 A69-29259

Radiation effects on Cs thermionic converter, discussing radiation interaction with alkaline atoms to complete space charge neutralization by supplementary ion creation
14 p2404 A69-29261

Emission characteristics of thermionic converter electrodes surfaces with emphasis on work function
14 p2505 A69-29262

Thermoemission converters (TEC)/ cathode materials, discussing determination of local work function by electron microscope and delay curves methods
14 p2505 A69-29265

Thermionic converters semiconducting collector surfaces, evaluating work functions of nickel-chromium steel and aluminum trioxide collectors

14 p2506 A69-29269

Laboratory device for investigating thermionic energy converters and measuring current-voltage characteristics by static/dynamic methods

18 p3136 A69-34700

Electron energy distribution for Cs plasma in emitter region of ignited mode thermionic converter, noting nonequilibrium ionization effect

19 p3380 A69-36442

Thermionic conversion - IEEE Conference, Framingham, Mass., October 1968

23 p4064 A69-41718

Thermionic reactor concepts and development in U.S., comparing strengths and weaknesses

23 p4186 A69-42245

Thermionic reactors for auxiliary space power and electric propulsion applications, discussing converter development regarding nuclear fuel elements

23 p4186 A69-42246

Thermionic converter technology, discussing cesium reservoirs, emitter and collector materials, performance and life tests, etc

23 p4069 A69-42247

Ion sputtering method for making electrodes in thermionic energy converters, discussing alumina and W surface layers preparation

23 p4170 A69-42259

Heat pipe thermionic converters, discussing heat transport, heating rate, pipe lifetime, etc

23 p4074 A69-42295

THERMIONIC DIODES NT CESIUM DIODES

Nuclear reactor space power system concept using thermionic diodes, heat pipes and rod control, emphasizing neutronic aspects and feasibility

04 p0630 A69-14799

Fixed space planar thermionic diode with collector guard ring for studying various emitter materials, measuring emitter temperatures

09 p1438 A69-21815

Cylindrical thermionic diode with rhenium emitter for diode kinetic experiments, presenting test data from prototype diode with thimble water cooled

09 p1438 A69-21818

Comparative performance data of cylindrical diodes with various types of tungsten emitters, including emitter work function measuring device

09 p1439 A69-21821

Uninsulated in-core thermionic reactor design permitting diode series connections to build output voltage

14 p2398 A69-29186

Thermionic converter SO-4 design and in- and out-of-pile test results, presenting diode performance at various times

14 p2399 A69-29196

Cylindrical in-core thermionic converters performance and life tests, discussing diode design, operation data and irradiation studies

14 p2399 A69-29199

Axial variation analysis of heat generation rate, temperature, voltage, current density and emitter heat flux in thermionic converter, emphasizing application to long diodes design

14 p2401 A69-29228

Low voltage arc in thermionic cesium vapor diode with lengthy electrodes and temperature variations along emitter, discussing plasma and current density distributions

14 p2402 A69-29244

Current oscillations and electromagnetic radiation in low pressure cesium thermal emission converters using glass diode with plate geometry metal electrodes

14 p2402 A69-29246

Preignition volt-ampere curves for thermionic cesium diodes exhibiting nonsaturation characteristics under low temperature and electron-rich emission conditions

14 p2403 A69-29253

West German research in thermionic diodes and reactors, describing terrestrial version of thermal in-core thermionic reactor project

23 p4188 A69-42258

THERMIONIC EMISSION

Thermionic emission and dispersion of plasma created by monopulse of laser radiation focused on solid target, discussing plasma temperature determination methods

03 p0441 A69-14141

Thermionic electron emission from Mo and W targets irradiated by CW carbon dioxide laser beam

05 p0771 A69-15812

Rates of charging of thermionically emitting particles in space charge

06 p1035 A69-17928

Richardson constant and tunneling effective mass for thermionic and thermionic field emission in Schottky barrier diodes

07 p1089 A69-18247

Normalized thermionic field emission in metal semiconductor barriers for forward and reverse current-voltage relation

08 p1373 A69-20861

Richardson constant for thermionic emission in Schottky barrier diodes, noting effect of surface shadows

08 p1286 A69-20865

Gaseous suspensions of thermionic emitting particles assessed as MHD working fluids in large scale MHD electric power generators

10 p1738 A69-23491

Radiative heat transfer calculations between parallel surfaces, applying approximations based on total emissivities to known spectral emissivities

14 p2539 A69-29223

Emission characteristics of thermionic converter electrodes surfaces with emphasis on work function

14 p2505 A69-29262

Thermionic emission from bare and Cs-covered metal surfaces, calculating current and work function by employing localized electron orbital model

14 p2505 A69-29264

Thermionic emission parameters for faces of W-Re, Mo-Re and Ta-Mo single crystals determined by Richardson method of straight lines

17 p3015 A69-33630

THERMIONIC EMITTERS

Saturation electron emission characteristics from incompletely outgassed Ta wire emitters immersed in Cs vapor using plasma anode technique, noting oxygen effects

09 p1437 A69-21812

Fixed space planar thermionic diode with collector guard ring for studying various emitter materials, measuring emitter temperatures

09 p1438 A69-21815

Comparative performance of niobium cylindrical thermionic converters with vapor deposited rhenium, stressing emitters surface preparation

09 p1438 A69-21816

Cylindrical thermionic converter with vapor deposited rhenium emitter and niobium collector, measuring efficiency and power density

09 p1438 A69-21817

Cylindrical thermionic diode with rhenium emitter for diode kinetic experiments, presenting test data from prototype diode with thimble water cooled

09 p1438 A69-21818

Thermionic converters with chloride and fluoride vapor deposited tungsten emitters, comparing performance characteristics and stability

09 p1438 A69-21819

Emission characteristics of duplex vapor deposited tungsten emitter with molybdenum collector in variable spacing guard ring converter

09 p1438 A69-21820

Comparative performance data of cylindrical diodes with various types of tungsten emitters, including emitter work function measuring device

09 p1439 A69-21821

Thermionic converter improvements by electronegative additives and emitter surface finishes, noting cesium oxide, heat treatments with electropolishing, electroetching, etc

14 p2397 A69-29173

Thermionic converter performance measured using test vehicles with guard ringed collectors and variable emitter-collector spacing

14 p2398 A69-29177

Thermionic converters with different collectors, emitters and metal-ceramic seals reliability tested, determining life duration

14 p2398 A69-29179

Thermionic converter with external fuel surrounding inner emitter annulus for use in in-core reactors

14 p2480 A69-29185

Cylindrical in-core thermionic converters performance and life tests, discussing diode design, operation data and irradiation studies

14 p2399 A69-29199

Postirradiation investigation of uranium dioxide fuelled thermionic emitters by evaluating released fission gases, noting different neutron fluxes metallic effects

14 p2481 A69-29200

Heat pipes for heating emitters of thermionic converters at high temperatures, noting capillary optimization and thermal resistance values

14 p2539 A69-29208

Deposition and interdiffusion of W layers on Mo emitter of in-core thermionic reactor, investigating microstructure of transition zone

14 p2462 A69-29210

Unignited mode converter and emitter work function patches, calculating electron-cesium momentum transfer cross sections from saturation current measurements

14 p2490 A69-29240

Thermionic converter current-voltage characteristics under various emitter temperatures and cesium vapor pressures, noting role of Schottky effect

14 p2402 A69-29241

Low voltage arc in thermionic cesium vapor diode with lengthy electrodes and temperature variations along emitter, discussing plasma and current density distributions

14 p2402 A69-29244

Thermionic converters semiconducting collector surfaces, evaluating work functions of nickel-chromium steel and aluminum trioxide collectors

14 p2506 A69-29269

THERMIONIC POWER GENERATION

Direct energy conversion and materials limitations, discussing thermoelectricity, solar cells, thermionics and fuel cells

02 p0194 A69-11801

In-core thermionic sodium cooled uranium oxide fueled reactor for space vehicle power plant

02 p0279 A69-12666

Rhenium Nb cylindrical thermionic converter, measuring efficiency and power density in emitter temperature range 1600-2050 K and collector temperature range 873-1173 K

05 p0707 A69-16359

Out-of-core thermionic space power generators using heat pipes, discussing feasibility in geometry, heat pipes, reactor, shield, heat exchanger and radiator

08 p1256 A69-19856

Nuclear power supply with in-core thermionic reactor for space power source and use in satellite TV, discussing theory, design and components

08 p1350 A69-20871

Reactor and mission requirements interaction for unmanned thermionic nuclear electric propulsion, discussing lifetime, payload, power levels, etc [AIAA PAPER 69-250]

09 p1539 A69-21253

Electrical testing of six converter solar energy thermionic generator, discussing overheating and dual current mode anomalies

09 p1439 A69-21823

Thermionic space power reactor design, detailing Critical Experiment problems

09 p1441 A69-21835

Out-of-core thermionic reactor power increase by using central heat pipe in coaxial cavity

09 p1441 A69-21836

Thermionic converter power from satellite nuclear reactor for TV satellites, discussing direct heat utilization and applications

12 p2016 A69-25869

Thermionic electrical power generation - Conference, Stresa, Italy, May 1968

14 p2394 A69-29172

Fast and thermal thermionic reactor systems characteristics including fissile material, components mass, power output and flattening and design features

14 p2480 A69-29182

Out-of-core thermionic reactor concept for space power supply using lithium heat pipes in crossed layers

14 p2480 A69-29187

Out-of-core thermionic systems with heat pipes usable in space applications, meeting advanced auxiliary power and nuclear propulsion requirements

14 p2480 A69-29188

In-core thermionic reactor space power plants stability and control criteria, comparing linear and nonlinear models

14 p2481 A69-29189

Primary isotope thermionic electric power module design, considering various assemblies

14 p2398 A69-29190

SNAP 13 generator designs to develop technology for isotope heated thermionic converters, describing tests, efficiencies, power outputs and life times

14 p2481 A69-29191

Actinium fueled thermionic generator design and characteristics, noting emitter temperature and material

14 p2399 A69-29192

Thermionic electrical power generation from reentry plasmas with nose cone as emitter and vehicle afterbody as collector
14 p2399 A69-29194

Soviet research on thermionic energy conversion, advantages and applicability in various fields
14 p2405 A69-29279

Fast neutron spectrum for subcritical section of homogeneous U 235-polyethylene thermionic critical assembly measured by pulsed source time-of-flight method
18 p3170 A69-34313

SNAP 21 radioisotope powered thermionic generator with multiple couple Pb-Sn-telluride/Bi-Sb-telluride flat plate configuration for deep sea applications
23 p4069 A69-42248

West German research in thermionic diodes and reactors, describing terrestrial version of thermal in-core thermionic reactor project
23 p4188 A69-42258

Li, Na and K heat pipes for high temperature emitter and low temperature collector thermionic applications
23 p4074 A69-42297

THERMIONIC REACTORS
U ION ENGINES
U NUCLEAR ROCKET ENGINES

THERMIONICS
Thermionic converter technology, discussing cesium reservoirs, emitter and collector materials, performance and life tests, etc
23 p4069 A69-42247

THERMISTORS
Atmospheric temperature corrections for measurements by rocketsonde and balloonsonde with thermistor, noting dissipation factors and thermal time constants
01 p0081 A69-10697

Differential thermistor gauge using Wheatstone bridge for use in free molecule pressure probe measurement of macroscopic velocity in rarefied gases
04 p0601 A69-15117

Thermistors for total optical radiation pyrometer and for temperature control system based on radiation pyrometer, noting thermistor response and control circuit
04 p0601 A69-15119

Thermistor assembly apparatus for measuring coefficient of thermal conductivity of pure and binary mixture of gases
05 p0845 A69-15616

Temperature profiles variability for data obtained by rocketsonde thermistors launched with small time and spatial separation
09 p1494 A69-21644

LF measurements with positive or negative temperature coefficient resistors based on current-voltage characteristics
11 p1845 A69-24522

Beryllium oxide semiconductor thermistor for temperatures to 2500 K, discussing construction materials and test results
12 p2092 A69-26478

Thermistor instrument for remote sensing, magnetic synchronous recording and linear display of temperature
14 p2449 A69-29562

Thermistor thermometer with low energy dissipation for flow measurements, discussing design considerations
15 p2608 A69-30296

Dual channel waveguide insertion loss test set for calibrations at 90 GHz in radio astronomy and communication systems, using sprayed thermistor mount
16 p2760 A69-31945

Vanadium thermistor fabrication influence on resistance jump at phase change temperature of vanadium dioxide, reproducing parameters by heat treating doped vanadium pentoxide
19 p3256 A69-36718

Temperature response of semiconductor thermistors as temperature sensing element, determining time constant from dimensions and experimental data
21 p3723 A69-38888

Thermistor radiation detectors bias condition defined from equations and optimized in terms of responsivity, time constant and noise
21 p3727 A69-39782

Thin film thermistors heat-separated from graphite substrate to achieve positive temperature resistance coefficient via argon heating and oxygen cooling
22 p3997 A69-41214

Thermal inertia index of semiconductor thermistor with one dimensional temperature field taking into account conductive heat transfer
23 p4163 A69-41556

THERMO-PHOTOVOLTAIC GENERATORS
U PHOTOELECTRIC GENERATORS
U THERMOELECTRIC GENERATORS

THERMOAEROELASTICITY
U AEROELASTICITY
U THERMOELASTICITY

THERMOCHEMICAL PROPERTIES
NT HEAT OF COMBUSTION
NT HEAT OF FORMATION
NT HEAT OF VAPORIZATION
Energy distribution among products of reactive collision of atomic H with Br molecule yielding HBr and Br atom, using perturbed Morse oscillator approximation
03 p0472 A69-13316

Grey and very grey thermochemical tables for C-H and C-H-O species
[WSCI PAPER 68-38]
06 p0885 A69-17795

Time of heating effect on thermal polymerization of L-lysine free base
13 p2218 A69-28439

Book on equilibrium thermodynamics covering origins and roles of thermodynamic laws, variables, equilibrium, reversibility, thermodynamic and thermochemical properties, etc
18 p3229 A69-34533

Computer routines for approximations of thermochemical properties of gas mixtures, using JANAF/Joined Army Navy Air Force/tables of combustion systems
21 p3670 A69-39591

THERMOCHEMISTRY
NT AEROTHERMOCHEMISTRY
Preparation of refractory alloys in powders, fibers and sintered billets by thermochemical method
[ONERA-TP-636]
02 p0251 A69-11625

Book on thermodynamic and thermochemical tables with charts on thermodynamic properties, physical chemistry and gas dynamics
04 p0688 A69-15459

Thermochemical surface finishing trends, discussing methods to obtain complex diffusion layers
05 p0769 A69-16540

Titanium aluminum alloys two stage direct production by aluminothermal reduction of titanium tetrachloride
07 p1159 A69-18536

Acidic, neutral and basic proteinoids thermal synthesis, discussing characterization and tendency to form microparticles
07 p1074 A69-18633

Organic fluorine chemistry, discussing synthesis reactions and reaction of polyfluorocycloalkenes with various nucleophiles
08 p1269 A69-21129

Laser evaporation vapors from refractory materials to produce surface temperature for carrying out reactions in gaseous phase and thin film preparation
09 p1519 A69-22476

Carbidothermic production of metals and binary and ternary alloys, discussing eutectic properties
09 p1514 A69-22731

Ionic and biradical mechanisms in thermal and photo cis-trans isomerizations elucidated by planar and twisted configurations of polyenes
13 p2216 A69-27618

Solid state chemical heat sources aboard unmanned planetary landing vehicles to maintain batteries and experiments operability during cold planetary nights
23 p4070 A69-42275

Thermochemical analysis of hot corrosion during sulfidation-oxidation of superalloy gas turbine engine components using Pourbaix method
23 p4178 A69-42449

THERMOCOMPRESSION
U COMPRESSING
U HEATING

THERMOCOUPLE PYROMETERS
Radiation compensating thermocouple for gas temperature measurement, noting advantage over single thermocouples
04 p0598 A69-14916

Thermocouple probe measurement error evaluation by parallel plate analytical model
16 p2789 A69-31903

Structural parameters selection for thermocouples with butt-weld electrodes, developing mathematical basis for thermoelectrode length to measure unstable gas temperatures
19 p3311 A69-36197

THERMOCOUPLES
NT THERMOPILES
Temperature measurement of moving droplets, noting influence of thermocouple electrode stability
04 p0688 A69-15423

Design and performance equations for panel type solar thermoelectric generator, based on single thermocouple as generator unit
05 p0704 A69-15675

Thin film thermocouple detector for molecular lasers operating in middle and far IR range
05 p0773 A69-16284

High temperature sensors for gas turbines, discussing thermocouples and radiation pyrometer to sense turbine hardware
[ASME PAPER 69-GT-30]
09 p1501 A69-22492

Resistance temperature transducers and thermocouples covering characteristics, readout and design for aerospace requirements
10 p1690 A69-23225

Signal conditioning for transducers covering piezoelectric devices, thermocouples, resistance transducers, reluctance and differential transformer sensors
10 p1691 A69-23228

Thermocouples dynamic response attached to thin skinned model under constant heating rate, considering error reduction in temperature measurement
13 p2375 A69-27785

Thermocouples precision used for measuring metal temperatures of cooled jet engine turbine buckets
15 p2613 A69-31274

Contact thermocouples to measure temperature of wall exposed to radiation, evaluating errors
17 p2975 A69-33596

Cryogenic liquid level temperature transducer with radiantly heated thermocouple sensitive element
17 p2975 A69-33670

Transient calibrations for Ge surface thermocouple heat flux sensors used in hypervelocity impulse tunnel
19 p3292 A69-35725

Single junction vacuum thermocouple measuring thermal beam effect with reference to velocity distribution perturbation in molecular beam scattering
19 p3376 A69-36173

Thermal contact conductance of thermally thick specimens with thermocouples not located at interface
20 p3632 A69-37521

Plasma thermionic diode figure of merit based on Hatsopoulos model altered to include thermal conduction and electrical resistance
22 p3869 A69-40134

Inhomogeneities effect on thermoelectric power and thermal efficiency of semiconductor thermocouple with constant forbidden band width
22 p3994 A69-40933

Jet engine combustion temperature measurements by thermocouples or gas analysis noting errors involved
23 p4165 A69-41650

Radioisotope thermoelectric generators (RTG)/design and performance analysis method applied to generators using Si-Ge Air-Vac type thermocouples
23 p4188 A69-42260

THERMODYNAMIC COUPLING
Acoustic wave fluctuations in semiconductors in external electromagnetic field, applying conduction electron and lattice elasticity kinetic equations
03 p0491 A69-14054

Coupled heat and mass transfer with zero order reactions in two phase systems consisting of drops, bubbles or solid particles
14 p2537 A69-29012

Acoustic wave fluctuations in semiconductors in external electromagnetic field, applying conduction electron and lattice elasticity kinetic equations
18 p3182 A69-35047

Viscoplastic thermomechanically coupled systems stability, considering effects of heat transfer to surroundings and heat capacity in material regions below yield
20 p3625 A69-37591

Heat influx equation coupling in thermoviscoelasticity, considering internal forces dissipation and stress-strain operators
22 p4044 A69-40741

THERMODYNAMIC CYCLES
NT BRAYTON CYCLE
NT RANKINE CYCLE
NT STIRLING CYCLE
Idealized cycle of gas expansion machine with regenerator for cooling radio components
04 p0687 A69-15164

Thermodynamic cycle and optimum conditions of electric power source of MHD generator in combination with thermocompressor
09 p1435 A69-21592

Thermodynamics and aerothermodynamics for propulsion problems noting thermodynamic laws and

quantities, steady flow, shock waves, nozzles, inlet and thermodynamic cycles

11 p1821 A69-25583

Thermodynamic cycle analysis of various gas turbines and air breathing propulsion systems noting regenerators, heat exchangers and pulsejet engine

11 p1943 A69-25584

Thermal efficiencies of liquid-metal MHD generator cycles, analyzing optimum parameters, working fluid and partial irreversibilities

13 p2205 A69-27484

Optimal cycle parameters for liquid metal single component MHD cycle, employing condensing ejector in front of generator

13 p2205 A69-27488

Liquid metal MHD generator cycles thermodynamic analysis, considering multicycle operation improvement with heat regeneration

13 p2372 A69-27489

Piston-like laminar liquid metal flow in MHD generator to increase thermodynamic efficiency of cycle and to generate electricity by synchronous principle

13 p2206 A69-27491

Ideal MHD induction converter pressure and generator cycles compared for calculating maximum output and pressure, considering current-conducting walls effects

14 p2393 A69-28887

Thermodynamic parameters of MHD cycle employing supercritical Hg, indicating need for more suitable fluids

16 p2736 A69-31914

Thermal cycle for direct flow supersonic compressorless MHD generator without heat regeneration and high temperature exchange

18 p3093 A69-34714

Air conditioning system for transport airplane using combined simple/bootstrap cycle refrigeration unit, discussing thermodynamic performance and hardware implementation

[AIAA PAPER 69-787] 19 p3243 A69-35641

Temperature and pressure relations in power plant with closed gas cycles with radiative heat transfer, noting radiation area reduction influence

20 p3464 A69-37603

Aircraft engine technology, discussing turbine entry temperatures, reheat temperatures, high pressure spools, high temperature materials and small blades fabrication

[RAES PAPER 20] 22 p4000 A69-40499

THERMODYNAMIC EFFICIENCY

Heat transfer efficiency of triangular radiating fin in diathermal medium producing aerodynamic heating

02 p0354 A69-12490

MHD generator and compressor Joule losses effect on thermoelectric energy conversion closed cycle efficiency with electrical conductivity maintained by nonequilibrium ionization

03 p0369 A69-14152

Increasing vortex tubes energetic cooling efficiency for cooling aircraft components by using potential energy of gas emitted from tubes

04 p0684 A69-14488

Dissociating gas as working fluid for space plant, noting role in radiator area reduction

04 p0551 A69-15313

Smith correlation of turbine stage efficiency for relating achievable efficiency to stage loading and flow factors used for total pressure loss coefficient data

[ASME PAPER 68-WA/GT-5] 05 p0812 A69-16140

Rhenium Nb cylindrical thermionic converter, measuring efficiency and power density in emitter temperature range 1600-2050 K and collector temperature range 873-1173 K

05 p0707 A69-16359

Space radiator dynamic model for predicting outlet temperature transient response to environmental variations

[AIAA PAPER 69-29] 06 p1039 A69-18205

Space storable propulsion system comparison, discussing liquid propellants performance and thermodynamic analysis

[AIAA PAPER 68-614] 09 p1570 A69-21981

Throttling effect on thermodynamic efficiency of MHD generator Rankine cycle with various working fluids

11 p1824 A69-24222

Closed loop cycle converter, composed of MHD generator and compressor consuming thermal energy, exhibiting moderate cycle efficiency decreases

11 p1824 A69-24223

Gas turbine blade cooling by longitudinal air flow, discussing cooling efficiency of guide and impeller blades and blade ring

11 p1942 A69-25337

Enthalpy excess thermodynamic functions of binary gas mixtures based on stationary diffusion thermoeffect in tube

11 p2003 A69-25552

Thermoelectric power generators energy output efficiency, discussing thermal and electric contact resistances influence for optimizing parameters

12 p2016 A69-26364

Thermal efficiencies of liquid-metal MHD generator cycles, analyzing optimum parameters, working fluid and partial irreversibilities

13 p2205 A69-27484

Thermodynamic efficiency of MHD cycles for liquid Na with multistage injection and injection condensation

13 p2205 A69-27487

Piston-like laminar liquid metal flow in MHD generator to increase thermodynamic efficiency of cycle and to generate electricity by synchronous principle

13 p2206 A69-27491

Local film heat transfer coefficients variations effect on longitudinal constant area fin surface under turbulent flow

[ASME PAPER 68-HT-20] 13 p2373 A69-27770

Error analysis in efficiency measurement of gas turbines, considering thermodynamics and power output

14 p2509 A69-29509

Axial gas turbine efficiency and work functions, discussing turbine using isothermal high velocity combustor

16 p2837 A69-32064

Seam welded U-type fin efficiency and effectiveness, studying effects of fin height, heat transfer coefficient and thermal resistance

19 p3452 A69-36371

Finned tube radiators with constant longitudinal specific heat flow, determining thermal efficiency and optimal thermal and structural parameters

20 p3631 A69-36978

Inhomogeneities effect on thermoelectric power and thermal efficiency of semiconductor thermocouple with constant forbidden band width

22 p3994 A69-40933

Edge effects in efficiency of air cooled turbine blade cascades with cooling air ejection from blade trailing edges into gas flow

24 p4364 A69-43090

THERMODYNAMIC EQUILIBRIUM

Steady state problem of convective heat transfer in half space with boundary conditions of third kind

01 p0174 A69-10103

Supersonic air flow around blunt body studied near critical line with allowance for viscosity, thermal conductivity and radiant energy transfer, assuming thermodynamic equilibrium

01 p0006 A69-10378

Statistical equilibrium equations solution for thermodynamic equilibrium variations of populations of very high energy levels in hydrogen and complex atoms

01 p0150 A69-10395

Graphical and analytical interpolation methods for representing initial compositions in equilibrium thermodynamic systems

01 p0176 A69-10403

Carbonaceous, enstatite and stony meteorite classification on basis of siderophilic, chalcophilic and lithophilic element proportions or isotope composition, discussing thermodynamic equilibrium

01 p0025 A69-11368

Solar copper abundance determined from measuring Cu 1 and 2 and resonance lines transition probabilities in electric arc emission under LTE conditions

02 p0204 A69-11456

Arc discharge in axially turbulent airflow producing equilibrium air plasma

02 p0285 A69-11571

Computer models of one dimensional stellar problems, discussing fast relaxation of unsteady state to Fermi-Dirac distribution and slow relaxation to thermal equilibrium

02 p0323 A69-12274

Thermodynamic stability of plasma with strong interaction, discussing relationship to simultaneous oscillation forms

02 p0292 A69-12635

Equilibrium of rotational degrees of freedom in gases undergoing relaxation, noting excitation, relaxation time, kinetics, transfer effects and measurements for hydrogen

02 p0284 A69-12667

Electric potential for axisymmetric equilibrium electron density distribution, solving Poisson equation in closed form

03 p0476 A69-13159

Soviet book on hypersonic flow past truncated cones at various angles of attack with allowance for physicochemical equilibrium transformations

03 p0362 A69-1363

Covariant statistical mechanics for equilibrium thermodynamics

03 p0533 A69-13758

Nondegenerate dense plasma thermodynamic stability by nonclassical methods, discussing atomic concentration dependence on ionic concentration

05 p0802 A69-1589

Thermal metal-plasma thermodynamic equilibrium using surface ionization of inner and outer potentials and work function, discussing ion and electron extraction

06 p0979 A69-17249

Mechanical equilibrium and stability conditions for system of interacting atoms in crystal structure

06 p0944 A69-17504

Thermal nonequilibrium of unsteady adiabatic gas flow in nonheat conducting tube with open ends

06 p0911 A69-18113

Thermal and metallographic analyses of Ti-Zr-Al system vertical sections close to Ti-Al edge, considering phase equilibrium

07 p1162 A69-18771

Dissociation equilibrium of negative H ions in solar type stellar atmospheres, noting H molecule vibrational and rotational levels and continuous thermal radiation

07 p1223 A69-19635

Statistical theory of fluids in equilibrium based on correlation functions for pair interactions between constituent molecules, invoking superposition closure approximation

08 p1350 A69-19868

Fortran 4 program for computation of equilibrium compositions of gas mixtures at high temperatures

08 p1278 A69-20154

Quantitative spectroscopy methods for determining data on chemical constitution of plasmas, treating optically thin LTE plasmas

08 p1363 A69-20465

Frozen shock in steady one dimensional compression flow of relaxing gases weaker than equilibrium shock

08 p1304 A69-20785

Phase equilibria in V-Cr-C, Nb-Cr-C and Ta-Cr-C systems determined by microscope and X ray analyses

09 p1523 A69-21872

Vacuum melting effect on O concentration in heat resistant alloys, outlining conditions for nitrides formation in equilibrium with melt

09 p1524 A69-22136

Fluid dynamical aspect of Schroedinger quantum mechanics and thermal equilibrium

09 p1541 A69-22394

Ionization-recombination thermodynamic equilibrium upset causing spectral excitation in He arc plasma

10 p1742 A69-24077

Equilibrium state of matter at high temperatures and densities with respect to nuclear reactions, determining neutron-proton ratio

11 p1957 A69-24403

Thermal radiation properties of gases in thermodynamic equilibrium, discussing radiation resulting from electronic, atomic and molecular state transitions

11 p1998 A69-24460

Gravitational effects on thermodynamic variable equilibrium composition of liquid-vapor binary mixtures near critical point, discussing changes in phase with altitude

11 p1999 A69-24914

Light ion abundance measurements of OGO satellites and field aligned diffusive equilibrium theory with temperature and concentration latitudinal variations

11 p1879 A69-25157

Dense gas equilibrium plasma thermodynamic stability in case of high electrostatic interaction energy of charged particles, analyzing phase transition possibility

11 p1928 A69-25234

Freezing of water droplets in thermal equilibrium with gas mixtures, considering droplet shattering and gas volume

12 p2126 A69-26018

Supersonic air flow around blunt body studied near critical line with allowance for viscosity, thermal conductivity and radiant energy transfer, assuming thermodynamic equilibrium

12 p2012 A69-26669

Gamma prime phase coherent equilibrium solubilities in Ni alloys of Al, Si and Ti from magnetic studies

of particle coarsening and electron metallographic observations
13 p2276 A69-27370

Spectral distribution of fluctuations in stable plasma in absence of external fields, emphasizing electric field fluctuations, quasi-steady states, isotropic plasmas and thermodynamic equilibrium
14 p2490 A69-29103

Radiative effect on rotating gaseous magnetic mass stability in thermodynamic equilibrium, including small oscillations stability
14 p2522 A69-29596

Convective and nonconvective two stream instability for hot plasmas, approximating equilibrium distribution function for given temperature by resonance functions
14 p2499 A69-29844

Relativistic corrections to particle distribution functions for high temperature plasma in thermodynamic equilibrium by integrating Gibbs distribution
14 p2499 A69-29847

B-type stellar spectra, discussing atmospheres and local thermal equilibrium from considerations of He I and P II lines relative strength
15 p2679 A69-30046

Pressure, temperature, density and enthalpy of carbon dioxide behind primary and reflected shock waves determined by method suitable for computer
15 p2592 A69-31054

Dynamic behavior of dissociating homonuclear diatomic gas, deriving instability equations, proposing stability loss in supersonic region
15 p2548 A69-31065

Solar chromosphere metal abundance determined taking into account local thermodynamic equilibrium departures
16 p2855 A69-31657

One dimensional free expansion of collisionless plasma tested as function of thermal equilibrium and confinement, using Vlasov equations and computer
16 p2819 A69-31685

Two component heat pipe operating characteristics on basis of thermodynamic phase equilibrium for binary mixtures
[AIAA PAPER 69-631] 17 p3071 A69-33268

Boron nitride synthesis by gas phase reaction of boron chloride or diborane with ammonia, determining purity from equilibrium gas mixture components
17 p2992 A69-33432

Book on equilibrium thermodynamics covering origins and roles of thermodynamic laws, variables, equilibrium, reversibility, thermodynamic and thermochemical properties, etc
18 p3229 A69-34533

Transformed kinetic equation used to study relaxation of quantum oscillator to thermodynamic equilibrium state
18 p3152 A69-35126

Time dependent equations for non-LTE occupation numbers of lower bound levels of hot gas or plasma outer layer atoms and ions
18 p3231 A69-35242

Dynamic effects in structure of H II equilibrium region left behind expanding ionization front, showing temperature as function of distance from star
19 p3403 A69-35966

Gas dynamics of material slab under radiation impact assuming thermal equilibrium reemission, discussing equations of motion and mean free path as function of frequency
19 p3449 A69-36355

Thermodynamic equilibrium stability general theory extended to arbitrary boundary conditions using properties of entropy balance equation
19 p3452 A69-36789

Spectral absorption coefficients and emissivities of thermodynamic equilibrium mixture of various combustion products at high temperatures, based on graphs
19 p3266 A69-36840

LTE departure calculated for He I in hot star model atmospheres for effects on populations of singlet and triplet states
21 p3801 A69-38761

Laser radiation increased absorption in opaque solid body attributed to vaporization, analyzing factors determining thermodynamic equilibrium between condensed and gaseous phases
21 p3736 A69-38962

High temperature equilibria from hydrocarbon plasma sources subjected to 3000 W RF electrodeless discharge
21 p3670 A69-39738

Einstein development of theory of fluctuations applied to homogeneous nucleation, calculating activation

energy, liquid drop-vapor system equilibrium state peculiarity, etc
22 p3938 A69-40448

Surface roughness effects on equilibrium temperature of isolated adiabatic plane surface illuminated by collimated and uniform solar flux
22 p4050 A69-40558

Phase equilibrium apparatus for measurement of thermodynamic properties of cryogenic fluid mixtures, including argon-methane data
[NAS-NRC PAPER H-3] 22 p3947 A69-40630

Radiative energy transport in moving gaseous media in local thermodynamic equilibrium, assuming spectral line shifts by temperature and pressure variations
22 p3982 A69-41018

Black body radiation at very high temperatures, discussing pion-nucleon interaction in pion gas in thermal equilibrium
23 p4238 A69-41358

Kinetic theory for macroscopic transport phenomena in N-component polyatomic gas mixtures with internal degrees of freedom under nonlocal thermodynamic equilibrium
23 p4238 A69-41435

Atomic hydrogen departures from LTE computed for models of B star atmospheres, assuming detailed balance in hydrogen lines
24 p4376 A69-42665

Thermodynamic calculation of equilibrium constant and homolytic dissociation degree of tetrafluorohydrazine based on enthalpy and statistical entropy
24 p4280 A69-42788

Solar flares accompanied X ray emission temporal and spectral variations, showing departure from thermal equilibrium
24 p4371 A69-43608

Equilibrium state of matter at high temperatures and densities with respect to nuclear reactions, determining neutron-proton ratio
24 p4391 A69-43793

THERMODYNAMIC PROPERTIES

NT CRITICAL POINT
NT CRITICAL PRESSURE
NT CRITICAL TEMPERATURE
NT EMISSIVITY
NT ENTHALPY
NT ENTROPY
NT FREE ENERGY
NT FUSIBILITY
NT HEAT OF COMBUSTION
NT HEAT OF FORMATION
NT HEAT OF SOLUTION
NT HEAT OF VAPORIZATION
NT MELTING POINTS
NT PYROELECTRICITY
NT SPECIFIC HEAT
NT SUPERCRITICAL PRESSURES
NT SURFACE ENERGY
NT THERMAL BUCKLING
NT THERMAL CONDUCTIVITY
NT THERMAL DIFFUSION
NT THERMAL DIFFUSIVITY
NT THERMAL EXPANSION
NT THERMAL INSTABILITY
NT THERMAL STABILITY
NT THERMOCHEMICAL PROPERTIES
NT THERMOPHYSICAL PROPERTIES
NT VAPOR PRESSURE
NT VOLATILITY

Dimensional effects on thermodynamic and kinetic properties of thin semiconductor and semimetal films, noting quantization influence
01 p0136 A69-10186

Thermodynamical and hydrodynamical relations for relativistic classical scalar fluid, obtaining energy momentum tensor
01 p0175 A69-10345

Energy gap behavior and thermodynamic properties of anomalous superconductors noting sensitivity to phonon spectrum
01 p0138 A69-10436

Complex chemical equilibrium calculation, analyzing thermodynamic principles and solution to nonlinear equations
01 p0023 A69-10588

Vaporization waves in metals, discussing thermodynamic function of carrying liquid metal through successive states on liquidus line in two phase region
01 p0117 A69-10655

Thermodynamics in homogeneous steady state fog over rough terrain representing absolutely absorbing surface
02 p0274 A69-11442

Diatomic dissociating gas free atoms virial coefficient used to study thermodynamic properties and transport coefficients of gases
02 p0283 A69-11574

Lunar surface temperatures and thermal characteristics from Surveyor 5 thermal engineering data gathered during lunar days, eclipse and nights
02 p0321 A69-12227

Viscoelastic materials thermomechanical behavior, discussing constitutive equation and derivation of stress tensor and entropy density from viscoelastic potential
02 p0344 A69-12294

Thermovortex effect, determining functional relations between interdependent parameters by means of dimensional analysis
03 p0531 A69-12966

Thermodynamic and kinetic interactions of high melting point metal oxides reduction by carbon
03 p0445 A69-13568

Thermodynamic evaluation of interaction between solid metals and dispersed high melting point oxides, stressing isobaric potentials
03 p0446 A69-13571

Thermodynamic study of carburization of liquid titanium and zirconium, examining effects of atmosphere, graphite porosity and alloying elements
03 p0446 A69-13572

Lenz-Ising model of ferromagnetism noting mathematical methods used to investigate model properties
03 p0488 A69-13785

Geometrical and thermomechanical effects on pressure and forces in deformation of thin Ti alloy blanks
03 p0452 A69-14123

Constants in formulas describing temperature and pressure dependence of thermodynamic characteristics of high temperature monatomic ionized gases for positive ions
03 p0473 A69-14156

Effect of dipole/dipole resonance interaction between excited and nonexcited atoms on gas thermodynamic properties, showing unstable quasimolecules formation
04 p0632 A69-14551

Thermodynamic function tables for 30 gases under ideal gas conditions up to 6000 K
04 p0686 A69-15153

Heat transfer and IC, discussing semiconductors thermal and electrical analogs and thermal properties
06 p0894 A69-17216

Grey and very grey thermochemical tables for C-H and C-H-O species
[WSCI PAPER 68-38] 06 p0885 A69-17795

Thermodynamic and aerodynamic characteristics of organic Rankine cycle working fluids for ideal applicability to manufacturing
[SAE PAPER 69-0063] 07 p1057 A69-18308

Ignition time of methane and acetylene, considering concentration and thermodynamic properties during reaction
[WSCI PAPER 68-41] 07 p1240 A69-18356

Thermodynamic properties of binary and ternary liquid metal systems, noting electromotive force and vapor pressure measurements
07 p1165 A69-18939

Zirconium niobium alloys thermodynamic properties measured by Knudsen effusion method using zirconium
95 07 p1165 A69-18940

Cobalt-tungsten solid solutions thermodynamic properties calculated by Borelius method using phase diagram
07 p1165 A69-18941

Rawin systems for upper air measurements of wind and thermodynamic parameters, using balloon-borne radiosonde
07 p1057 A69-19581

Mercury concentration relation to thermal history of chondritic meteorites, using activation analysis
08 p1404 A69-20920

Bellows sealed valve for measurement of fluorine thermodynamic properties at moderately high pressures
09 p1493 A69-21428

Finite elastic locking medium, discussing equation of state for thermodynamic variables and applications to thermoelasticity
[IS-ERI-70] 09 p1612 A69-21561

In situ vacuum testing requirement for valid measurement of vacuum induced changes in mechanical and thermal properties of various filled elastomers
09 p1477 A69-22008

Thermosetting resin curing behavior characterized by differential thermal analysis performed above atmospheric pressure to prevent volatilization
09 p1500 A69-22311

Pyrolytic carbon felt composite development and properties, measuring and tabulating mechanical, thermal and ablation properties

09 p1530 A69-22364

Steady compression waves properties in relaxing gases found independent of thermodynamic behavior and relaxation process

10 p1631 A69-22893

Specific heats of oxygen at coexistence from triple point to critical point and corresponding values for liquid phase

10 p1808 A69-23187

LOX thermodynamic properties from triple point to 250K and pressures to 350 atm, tabulating at uniform densities and temperatures

10 p1808 A69-23189

Boltzmann H function for moderately dense gas of identical particles with discrete velocity distribution in cases of nonisotropic binary and ternary collisions

10 p1725 A69-23790

High temperature gas mixture plasmas thermodynamic properties, emphasizing Debye electrostatic interactions and electron states

10 p1810 A69-23794

Boltzmann H theorem and related mathematical topics, noting applications to subsonic gas flow and continuum flow around and over body

11 p1870 A69-25008

Composition and thermodynamic properties of gaseous system reacting at low temperatures with condensed phase formation, discussing iterative process convergence in approximation

11 p2001 A69-25223

Thermodynamics and aerothermodynamics for propulsion problems noting thermodynamic laws and quantities, steady flow, shock waves, nozzles, inlet and thermodynamic cycles

11 p1821 A69-25583

Origin of life in terms of polymers synthesis under thermodynamic and geological conditions

12 p2017 A69-25764

Heat resistant composites, discussing composition, properties and high temperature behavior, plastic materials, reinforcement filaments, whiskers and test methods

12 p2117 A69-25855

Silicon nitride vaporization and thermodynamic properties analyzed using Langmuir and Knudsen methods

12 p2118 A69-26261

Anisotropic Heisenberg antiferromagnetism in spin wave approximation, calculating thermodynamic quantities in terms of elliptic integrals

12 p2144 A69-26500

Electrical, thermal and thermoelectronic properties of refractory oxide materials including lanthanum chromite and strontium zirconate, discussing Hall effect, IR absorption, mixtures, etc

13 p2316 A69-27470

Heat transfer coefficients for carbon dioxide near thermodynamic critical point for flow through electrically heated duct, noting turbulent forced convection as mechanism

13 p2373 A69-27769

Solar wind quiet state thermal properties and chemical composition compared with coronal expansion hydrodynamic model predictions

14 p2513 A69-29098

Low temperature thermal expansion coefficients and linear contraction of metal alloys from liquid hydrogen to room temperature tabulated as function of temperature

14 p2464 A69-29400

Organic and inorganic fabric reinforcements effects on thermal properties of composites noting thermal conductivity, diffusivity, specific heat constants and temperature ranges

15 p2642 A69-30466

Remote sensing cross-beam cross correlation methods of determining spatially resolved average thermodynamic properties

16 p2789 A69-31868

Turbulent jet theory, thermal ignition theory and flameout characteristics of bluff body flame stabilizers

16 p2879 A69-32141

Nonlinear regression techniques for statistical simultaneous measurement of thermal properties including convergence criterion

17 p3070 A69-33260

Mechanics and thermodynamics equations for two dimensional continua, discussing applications

17 p2994 A69-33391

Hypersonic aircraft induced changes in chemical and thermodynamic properties of air influencing aerodynamic forces on vehicle

17 p2895 A69-33576

Book on solid bodies collision theory covering elastic bodies with ruled surfaces, dynamic effects associated with Rayleigh surface waves, thermodynamic effects, etc

18 p3210 A69-34259

Book on equilibrium thermodynamics covering origins and roles of thermodynamic laws, variables, equilibrium, reversibility, thermodynamic and thermochemical properties, etc

18 p3229 A69-34533

Heat sensitive paints thermophysical characteristics determined by nonstationary heat conditions method

18 p3161 A69-34697

Plastics thermal properties and industrial structural applications dependency on temperature

18 p3161 A69-34839

Air data system consisting of aerodynamics covering thermodynamic sensors and computer calculating flight parameters for automatic flight control

18 p3169 A69-34854

Thermoplastic polyarylsulfone thermal and electrical properties at over 500 F, noting resistance to thermal oxidative attack

19 p3355 A69-35527

Thermal and mechanical properties UV of diazadiphosphetides, carbodiimides and phosphorus amide epoxies resins composites for use in environmental extremes

19 p3356 A69-35528

Liquid driver shock tubes dynamic and thermodynamic properties as functions of diaphragm pressure ratio and initial conditions

19 p3295 A69-36471

Ordered sets of Massieu thermodynamic characteristic speeds for reacting gas mixtures relevant to nonequilibrium flow fields compared to Laplacian and Newtonian speeds

19 p3452 A69-36802

Nondissociating vibrationally excited dense N, analyzing compressibility factor, internal energy, enthalpy, entropy, sound speed and specific heat by state equations

20 p3631 A69-37214

Rheology application to description, explanation and measurement of materials properties during deformation

20 p3561 A69-37599

N and H plasmas and N-H plasma mixtures thermodynamic properties calculation, discussing numerical methods and corrections for electrostatic interactions

21 p3847 A69-38421

Thermodynamic properties of hydrogen atoms, protons and electrons, using canonical group analysis to determine bound and free states

21 p3850 A69-38964

Temperature potentials in cylinder of known radius, investigating optimal heating regime and thermal kinetic factor effect on maximum potential magnitude

21 p3837 A69-39089

Cavitation flow of water and ethyl alcohol in venturi tube, noting effect of varying vapor concentration and thermodynamic properties

21 p3696 A69-39101

Thermodynamics of propellant combination of Li hydride containing solid fuel with ethyleneimine base, coupled with Cl trifluoride oxidizer and ammonium nitrate added

22 p3997 A69-39919

Photoelectric measurements of UV absorption coefficients of high temperature air at specific temperature and wavelength ranges in pressure-driven shock tube

22 p4049 A69-40098

Thomas-Fermi approximation applied to calculation of equations of state and thermodynamic functions at high pressure from differential equations of statistical atom model

22 p3984 A69-40186

Gaseous mixtures for hypervelocity applications, studying equilibrium conditions and thermodynamic properties for shock and constant volume heating processes

22 p4049 A69-40266

Thermodynamic properties of exchange reaction of Ti, Nb, Mo and W disilicides with graphite and pyrographite systems

22 p3970 A69-40638

Mechanical and thermal properties of vanadium alloys and austenitic stainless steels compared to determine applicability in high temperature reactor fuel jackets

22 p3971 A69-40973

Flow and thermodynamic variables of Ar-Cs mixture behind normal shock in shock tube at various temperatures and pressures

23 p4150 A69-41335

Nb-gaseous Nb chlorides equilibrium from transpiration measurements at 800-1400 C, confirming importance of Nb pentachloride, Nb tetrachloride and Nb trichloride

23 p4112 A69-41335

Nondestructive thermal method of measuring wall thickness and channel blockage in investment casting used in aircraft parts production

24 p4312 A69-42754

THERMODYNAMICS

NT AEROTHERMODYNAMICS

NT COMBUSTION PHYSICS

Approximate boundary controllability for heat equation by considering temperature variation with time

01 p0173 A69-10061

Temperature evolution velocity parameter effect on behavior of elastoviscoplastic solids, noting demonstration by work hardening tests at variable temperatures

01 p0164 A69-10036

Mechanical and thermodynamical theories of material behavior based on rate independence concept, discussing equivalence of various theories

01 p0166 A69-10227

Nonlinear viscoelastic bodies arising in 3d rheological models with hidden parameters behaving according to law compatible with objectivity and 2nd thermodynamics principles

01 p0171 A69-11131

Transformation laws for thermodynamic quantities confirming conventional formulation by mechanical model of heat

01 p0122 A69-11288

Thermodynamics of nonadiabatic vertical ascent of overheated individual air volumes in stably stratified atmosphere

02 p0274 A69-11441

Thermodynamics of ideal multiaxial gases in local nonequilibrium, approximating real gas system by ergodic subsystems grouped by degrees of freedom

02 p0350 A69-11552

Thermodynamic foundations of permanent deformation theory, noting parallel to viscoelastic material theory

02 p0350 A69-11714

Deformation thermodynamics, discussing mechanics, and thermokinetics of continuous media and wave propagation problem

02 p0339 A69-11990

Generalized unsteady temperature fields and stresses in crystalline plates using Fourier and Laplace transforms

02 p0340 A69-12044

Relativistic heat transfer formula and pressure definition in relativistic thermodynamics

02 p0352 A69-12253

Thermodynamics of viscoplastic materials under dynamic loads within framework of continuum mechanics of materials with memory

02 p0343 A69-12281

Thermodynamics of directed continuous media, discussing kinematics, equations of state, entropy inequality and material objectivity principle

02 p0354 A69-12611

Thermovortex effect, determining functional relations between interdependent parameters by means of dimensional analysis

03 p0531 A69-12966

Covariant statistical mechanics for equilibrium thermodynamics

03 p0533 A69-13758

Composite heat transfer by conduction and radiation in nongray medium, outlining electronic computer program for numerical solutions

03 p0533 A69-13884

Thermodynamics of materials with elastic range

03 p0529 A69-13955

Onsager reciprocity relations applied to thermodynamics of nonlinearity and noise in diodes

04 p0574 A69-14435

Thermodynamic computations for combustion product temperature and flow rate as function of pressure in burner and excess air ratio

04 p0684 A69-14487

Variational methods for nonequilibrium thermodynamic processes noting fluctuation theory introduction

04 p0551 A69-15314

Book on thermodynamic and thermochemical tables with charts on thermodynamic properties, physical chemistry and gas dynamics

04 p0688 A69-15459

Thermodynamic theory of strain rate sensitive plastic material within framework of thermodynamics of materials with internal state variables

05 p0834 A69-15792

- Regular thermal conditions in solid bodies with radiative heat transfer
05 p0845 A69-15896
- Acceleration wave propagation and growth in elastic materials, discussing thermodynamic influences
05 p0836 A69-15931
- Thermal potential P and Q smoothness on surfaces, proving relevant theorems
05 p0849 A69-16452
- Thermodynamic approach to calculation of molecular lasers, determining various population levels of carbon dioxide molecule by measuring amplification factors for rotational vibrational transitions
06 p0934 A69-17465
- Thermodynamics of fluid materials and characterization of thermodynamics of irreversible processes, using constitutive equations
06 p0959 A69-18222
- Fluid and thermodynamic modeling for ground test simulation of nuclear rocket vehicle liquid hydrogen propellant behavior
[SAE PAPER 690201] 07 p1178 A69-18306
- Ti alloys thermomechanical treatment effect on strength and plasticity characteristics, noting single and double phase alloys and rupture
07 p1161 A69-18766
- Thermodynamic consequences of Lindemann mechanism for fusion of pure body, discussing application to isolated equilibrium system of solid and liquid phases
07 p1242 A69-19322
- Self gravitating medium in quasi-static equilibrium, using phenomenological equilibrium theory and zero time fluctuations
07 p1222 A69-19622
- Consistency of high temperature equation of state of solids, considering Grüneisen parameter and lattice dynamics
08 p1419 A69-19814
- Corrections to relativistic plasma thermodynamic functions associated with electromagnetic field effect, demonstrating inapplicability of Darwin Hamiltonian to problem
08 p1359 A69-19953
- Thermodynamics of nonsimple elastic materials with two temperatures, showing temperature and stress difference proportional to heat supply
08 p1422 A69-20847
- Thermodynamics and polarization of zinc electrode in alkaline media, discussing anodic dissolution and passivation
08 p1268 A69-21048
- Flow equations of rheological media derived using thermodynamics, assuming nonlinear stress-strain relation in incompressible medium
08 p1419 A69-21074
- Heat transfer mechanism in solid body, deriving integrodifferential equation with classical equation and hyperbolic equation of heat propagation as special case
09 p1621 A69-21587
- Characteristic equation obtained by considering world line vector, basic thermodynamic variables and metric tensor as functions of Lichnerowicz class
09 p1480 A69-21614
- Thermodynamic analysis of engines and heat pumps operating within negative absolute temperatures, noting work increase by throttling
09 p1623 A69-22219
- Asymptotic behavior of frequency function of fluctuations for generalized ensemble parameters, noting characteristic function convergence to Gaussian at thermodynamic limit
09 p1623 A69-22395
- Book on dynamics and thermodynamics of gas at hypersonic velocities and extremely high altitudes
09 p1483 A69-22400
- Thermodynamic potential of rarefied plasma from Coulomb interactions of atoms with electrons and ions
10 p1728 A69-23134
- Book on thermodynamics of charged and polarized layers covering matter in electric fields, general framework theory, applications, etc
10 p1724 A69-23159
- Book on thermodynamics of irreversible processes covering chemical reactions, relaxation phenomena, permeation, osmosis, electroosmosis, thermoosmosis, electric conduction, diffusion, etc
11 p1999 A69-24533
- Thermodynamic approach to equation of state of magnetized Fermi gas, deriving energy eigenvalues of free electron in magnetic field
11 p1961 A69-25107
- Equilibrium compositions of reaction products calculated by permutation over limiting equilibrium surface in reaction space, considering charged components and condensation products
11 p2001 A69-25224
- Thermodynamics of sinusoidal steady state energy converters governed by Onsager reciprocal relation, determining maximum conversion efficiency
11 p1826 A69-25396
- Thermodynamic properties of materials in critical region, discussing inhomogeneity
11 p2003 A69-25440
- Thermodynamics of strain rate sensitive elastoviscoplastic solids, considering kinematic description of plastic deformation and choice of state variables
11 p1994 A69-25601
- Isoperimetric plasma thermodynamics problems, including plasma free energy and relativistic plasma density fluctuations energy
12 p2138 A69-26603
- Thermodynamic equivalence of limit theorems for canonical and grand canonical ensembles, discussing Massieu-Planck function analog relation by Legendre transformation
12 p2191 A69-27148
- Microstructured mixtures theory including energy balance, mass and momentum equations and entropy production inequality for structured fluids in motion
13 p2371 A69-27318
- Allowable thermodynamic processes and constitutive equation restrictions determined by Clausius-Duhem inequality, noting applications to plasticity theory and linear viscous fluids
13 p2371 A69-27319
- Heat transfer in solid bodies, deriving thermal conductivity equation and surface boundary conditions in presence of radiative energy transfer
13 p2373 A69-27584
- Rigid heat conductor in continuum thermodynamics, discussing conductivity tensor symmetry and heat capacity positivity as restrictors
13 p2377 A69-28193
- Constant density heating upstream and constant pressure cooling downstream formulas for radiating shock waves
13 p2249 A69-28240
- Green function for boundary value problems of heat conduction equation constructed by heat potentials method
13 p2380 A69-28548
- Finite thickness plate heat equation using Legendre polynomials
14 p2537 A69-28970
- Fundamental principles of thermodynamics incorporation into general relativity and geometrodynamics, interpreting entropy growth in terms of space dynamics
14 p2538 A69-29019
- Solution methods for differential heat conduction equations, discussing methods of variable separation, Green function, thermal potentials, etc
14 p2539 A69-29456
- Propylene imine IR and Raman spectra, calculating thermodynamic functions based on rigid rotator harmonic oscillator model
14 p2410 A69-29922
- Unsteady heat conduction equations for elliptic cylinder with convection solved by point matching
16 p2879 A69-32171
- Thermodynamics and polarization of Zn electrode in alkaline medium for electric generators
16 p2739 A69-32419
- Transient thermal analysis of space radiators excluding finite difference equations, noting computer adaptability and time saving
[AIAA PAPER 69-615] 17 p3070 A69-33261
- Linear irreversible thermodynamics theory as applied with conservation principles and Maxwell relations to charged particle motion in electromagnetic field, noting Onsager coefficients role
17 p3075 A69-34142
- Shock tube application to transition probability measurements with emphasis on thermodynamic state of radiating gas, noting temperature dependence of level population
18 p3176 A69-34446
- Book on equilibrium thermodynamics covering origins and roles of thermodynamic laws, variables, equilibrium, reversibility, thermodynamic and thermochemical properties, etc
18 p3229 A69-34533
- Meteorological forecasting as problem in fluid mechanics and thermodynamics, discussing accuracy and electronic computer role in classical or mathematical methods
18 p3166 A69-34694
- Dynamic pressure pulsations, temperature distribution and gas concentrations in discrete vortices zone in wake of plate in unbounded flow
18 p3124 A69-35120
- Elastic stability theory from thermodynamic viewpoint, considering postulates and energy equations
19 p3444 A69-36796
- Transformation groups used to find similarity solutions for partial differential equations and heat equation
20 p3630 A69-36915
- Soviet book on theory and design of turbocompressors covering gas dynamic cascade theory, thermodynamics and aerodynamics, viscous gas flow, etc
20 p3459 A69-37238
- Nonlinear viscoelastic material properties evaluation from experimental data with illustration for polymers, deriving equations from thermodynamic principles
20 p3626 A69-37719
- Thermodynamic approach to calculation of molecular lasers, determining various population levels of carbon dioxide molecule by measuring amplification factors for rotational vibrational transitions
20 p3555 A69-37948
- Statistical mechanics applied to mechanical properties and thermodynamics studies of rapidly expanding or collapsing self gravitating systems
21 p3801 A69-38702
- Negative ion influence on electrical conductivity of partially ionized multicomponent gas mixtures, basing analysis on thermodynamic calculations of composition
21 p3774 A69-38867
- Constitutive equations for homogeneous viscous fluid and Kelvin-Voigt viscoelastic solid in electromagnetic field, using linear irreversible thermodynamics and continuum mechanics
21 p3851 A69-39289
- Temperature field in system of coaxial cylinders by solving heat equation with corresponding initial and boundary conditions
21 p3855 A69-39855
- Internal interactions of continua and concept of thermal isolation, discussing second law of thermodynamics
22 p4050 A69-40450
- Relativistic thermodynamics using entropy principle to find restrictions on constitutive functions
22 p4050 A69-40451
- Basic thermodynamic quantities derivatives arranged into three relationship systems for first and second order phenomena
22 p4051 A69-40970
- Thermal diffusivity measurement by nonsteady state methods, discussing time and temperature variables in heat flow differential equation
23 p4237 A69-41326
- Combined heat transfer calculations, considering moving radiating media and simultaneous convection or conduction
23 p4237 A69-41328
- Thermodynamics of elastoplastic materials with dislocation motion related to internal state variables, including case of rate independent plasticity
23 p4226 A69-41537
- Linear partial differential equations derived from thermodynamic identities integrated by method of characteristics for relationships between temperature and pressure incomplete equations of state
23 p4239 A69-41569
- Planck-Einstein equation derivation in special theory of relativity, discussing relativistic measurement of thermodynamic values in terms of Lorentz transformations
24 p4349 A69-42748
- Numerical solutions for time dependent boundary value problems governed by heat equation applied to transient heat conduction in irregularly shaped two dimensional regions
[ASME PAPER 69-HT-50] 24 p4410 A69-43521

THERMOELASTICITY

NT AEROTHERMOELASTICITY

- Book on thermoelasticity covering linearized uncoupled theory in small deformations, small and slow temperature changes, analysis of plane thermoelastic stress, etc
01 p0084 A69-10131
- Axisymmetric transient thermoelastic problem for transversely anisotropic hollow cylinder, examining boundary value problems
01 p0166 A69-10302
- Linear stationary thermoelasticity equations for Cosserat continua, discussing static and kinematic conditions, anisotropy and centrosymmetric isotropy equations
02 p0336 A69-11557

Integration for equations governing linearized thermoelastic transformations of incompressible solids
02 p0340 A69-12033

Menabrea theorem for anisotropic elastic body with internal incompressibility constraint, discussing validity during thermoelastic transformation
02 p0341 A69-12194

Menabrea theorem for nonisothermal transformations of anisotropic elastic body with internal incompressibility constraint and initial stress
02 p0341 A69-12197

Plane inhomogeneous thermal stress in isotropic elastic circular infinitely long cylinder produced by plane unsteady temperature distribution
02 p0349 A69-12826

Compatibility equations in plane micropolar thermoelasticity theory obtained by associated matrix method
03 p0525 A69-13607

Generalized Galerkin functions for asymmetric thermoelasticity, considering separation of coupled equations
03 p0525 A69-13608

Longitudinal thermoelastic wave propagation in infinite body, proving generalized Kirchhoff theorem
03 p0528 A69-13924

Controllable states of elastic heat conductors, analyzing deformations and temperature fields
03 p0529 A69-13957

Stressed state periodic problem in infinite strip under combined pressure and temperature field effect
04 p0673 A69-14497

Circular disk stress-strain state due to thermoelastic strain applied at disk sector edge
04 p0681 A69-15171

Axisymmetric thermal stresses in spheroidal shell of arbitrary thickness due to thermoelastic strain nucleus
05 p0836 A69-15923

Elastic bodies collisions in presence of thermoelastic effects, investigating local inertial and thermoelastic forces effect on compression region shape
05 p0841 A69-16207

Thermoelastic effects on gravity gradient stabilization of artificial satellites, including role of solar activity
06 p1025 A69-17613

Anomalous spacecraft OGO-D motion explained by open section boom thermally induced oscillations, discussing corrective measures
07 p1231 A69-18331

Boundary value problem of temperature field and heat conduction in transparent media heated by laser radiation producing thermoelastic stresses leading to breakdown
07 p1149 A69-18925

Reciprocity, variational and uniqueness theorems developed within linear theory of coupled thermoviscoelasticity
07 p1233 A69-19327

Completeness of Biot solution in theory of thermoelasticity, discussing Mindlin theorem and Boussinesq-Papcovich solution
07 p1236 A69-19470

Dynamic internal thermal shock in spherical shells of arbitrary thickness, considering uncoupled dynamic thermoelasticity problems with spherically symmetrical temperature fields
07 p1236 A69-19471

Heat generation effects by plastic deformations at tip of propagating crack in quasi-brittle materials, considering elastic stress field and crack velocity
08 p1412 A69-20144

Thermoelastic properties of particulate, filamentary and layered composites, summarizing Soviet theoretical and experimental work
08 p1339 A69-20500

Transient thermal stress distribution in infinite orthotropic elastic cylinder of rectangular cross section in presence of heat sources
08 p1415 A69-20664

Thermodynamics of nonsimple elastic materials with two temperatures, showing temperature and stress difference proportional to heat supply
08 p1422 A69-20847

Problems using Fredholm integral equations providing unique solution
08 p1418 A69-21004

Stress formulation of thermoelasticity in simply connected body, noting uniform temperature change influence on stress components
09 p1617 A69-22007

Reciprocity theorems of coupled and uncoupled thermoelasticity for macroisotropic and microisotropic simple homogeneous solids with microstructure
09 p1618 A69-22259

Reciprocity theorem applied to Somigliana relations for static loads and coupled thermoelasticity
09 p1618 A69-22260

Micropolar thermoelasticity using Green functions to solve wave equations in unbounded medium and study displacement, rotation and temperature fields
09 p1618 A69-22262

Unidirectional filamentary composites thermoelastic properties relation to constituent materials properties, using semiempirical micromechanics theory
09 p1530 A69-22320

Thermal stresses for mixed boundary conditions calculated from combined use of integral transforms and variational techniques, reducing computational labor
10 p1801 A69-23429

Subregions method in coupled thermoelasticity, discussing numerical values for thin steel circular disk
11 p1970 A69-24606

Optimum cooling of homogeneous isotropic cylindrical body with constraints on magnitude of thermoelastic stresses
11 p1976 A69-24772

Free vibration modes of infinite uniform plate in linear coupled theory of thermoelasticity, considering heat transfer conditions
11 p1976 A69-24793

Two and three dimensional quasi-static problems in coupled thermoelasticity, obtaining solutions for space containing cylindrical cavity and for solid cylinder
12 p2177 A69-25993

Boundary value problems of thermoelasticity, discussing existence and uniqueness theorems, ellipticity, thermoelastopotentials, Liapunov-Tauber theorem, Fredholm theorems, etc
12 p2182 A69-26726

Thermoelastic waves in stretched circular cylindrical bar, analyzing displacements, secondary pressure and temperature field by using Frobenius method
12 p2189 A69-27115

Classical plasticity theory modified to include finite elastic and plastic strain components by considering thermoelasticity and plastic work irreversible processes
13 p2362 A69-28119

Axisymmetric thermoelastic vibrations of infinite and finite cylindrical shells, determining natural frequencies and stress wave propagation
14 p2532 A69-28979

Thermoelastic stress-strain state of infinite circular cylindrical shell with elasticity modulus temperature dependence expressed by exponential function
14 p2532 A69-28980

Heat conduction and Navier equations solved for temperature distribution and displacements in elastic solids, considering time dependent boundary conditions, body forces and heat generation
14 p2535 A69-29364

Cylindrical wave propagation in thermoelastic incompressible isotropic solids, considering cases of zero and nonzero coefficient of thermic dilation
15 p2707 A69-30626

Thermoelastic stress in semiinfinite elastic medium due to discontinuous temperature distribution over free surface, solving associated heat conduction problem
15 p2712 A69-31006

Stress calculation for thermoelastic mixed boundary value problem in infinite isotropic plate with cylindrical stress free cavity
15 p2712 A69-31013

Thermoelastic stresses in isotropic circular cylinder with surface locally heated by external Newtonian heat source, considering various heat transfer conditions
15 p2714 A69-31178

Magnetothermoelasticity equations, uniqueness and reciprocity theorems and solutions emphasizing moving media
15 p2715 A69-31215

Stresses due to nucleus of thermoelastic strain in infinite elastic solid with two rigid circular inserts
16 p2872 A69-31906

Acceleration waves propagation in nonlinear conducting thermoelastic solid, treating homogeneously deformed and undeformed media
16 p2873 A69-32060

Initial thermostructural stresses in homogeneous quasi-isotropic two component medium, solving statistical boundary value problem thermoelasticity
17 p3058 A69-33316

Coupled stresses in thermoelasticity for displacement and rotation vector characterized medium, discussing wave propagation in unbounded medium
18 p3211 A69-34262

Collocation method applied to solving contact thermoelasticity problem for short thick walled hollow cylinder attached to thin elastic shell in axisymmetric temperature field
18 p3217 A69-34595

Thin walled shell temperature and strain fields described by integrodifferential equations based on Kirchhoff hypothesis and coupled thermoelasticity reciprocity equations
18 p3225 A69-35369

Variational method for computer calculation of supercritical bending of thermoelastic uniformly loaded circular plates, determining Ritz parameter influences on accuracy
19 p3434 A69-35824

Two dimensional thermoelasticity problem for non-linear media, obtaining solutions for thermal stress concentration and boundary value problems
19 p3436 A69-35844

Uniqueness theorems for energy methods solution of equations of dynamic thermoelasticity and viscoelasticity
19 p3439 A69-36470

Completeness and relations between potentials and stress functions in micropolar elasticity and thermoelasticity
19 p3439 A69-36470

Thermoelastic deformation and mean rotation divergence formulas for elastic simply connected micropolar body
19 p3440 A69-36586

Longitudinal waves propagation in unbounded thermoelastic medium expressed as surface integrals generalizing Kirchhoff theorem
19 p3444 A69-36804

Combined analytical and numerical method for thermoelastic boundary problem of unidirectional infinite strip
21 p3836 A69-38927

Mathematical modeling techniques applied to thermoelastic cooling for plate without clamping and mechanical loads, examining integrator schematic diagram
21 p3680 A69-39851

Reissner variational principle applied to incompressible and nearly incompressible anisotropic thermoelasticity
22 p4040 A69-39980

Thermoelastic stresses in rotating cylinders and disks with radial temperature distribution, deriving plane deformation approximate solutions
23 p4227 A69-41707

Wave propagation in dynamical theory of thermoelasticity, considering half space subject to step strain, temperature and stress distributed over free surface
23 p4235 A69-42464

THERMOELECTRIC GENERATORS

NT SNAP 10A

NT SNAP 21

NT SNAP 27

MHD generator and compressor Joule losses effect on thermoelectric energy conversion closed cycle efficiency with electrical conductivity maintained by nonequilibrium ionization
03 p0369 A69-14152

Mathematical model to design weight optimized silicon-germanium solar flat plate thermoelectric generator as spacecraft auxiliary power source in near sun missions
05 p0704 A69-15674

Design and performance equations for panel type solar thermoelectric generator, based on single thermocouple as generator unit
05 p0704 A69-15675

Thermoelectric and thermal phenomena in thermoelectric generator development for spacecraft applications, considering element design and materials selection
12 p2016 A69-25868

Heat conversion coefficients and initial temperature of active elements of solar powered electric devices
13 p2209 A69-28314

I-V characteristics of caloroelectric plasma converter with concentric electrodes measured for various hot electrode temperatures and mercury vapor flow rates
16 p2822 A69-32065

Thermal contacts effects on optimum operating conditions of solar thermoelectric power generator, discussing losses due to low thermal conductivity coefficient of insulating layers
16 p2741 A69-32797

Laboratory device for investigating thermionic energy converters and measuring current-voltage characteristics by static/dynamic methods
18 p3136 A69-34700

Gisette 5 thermoelectric radioisotopic generator for submarine use, discussing strontium 90 as isotopic source
21 p3768 A69-38458

Cascade thermoelectric heat pump reducing temperature gradient in legs of element near cold junction and reducing Joule heating in cold junction area

22 p3869 A69-40133

Planar radioisotope thermoelectric generator system for NASA deep space missions and integrated spacecraft power supply

23 p4070 A69-42254

Radioisotope thermoelectric generators /RTG/ design and performance analysis method applied to generators using Si-Ge Air-Vac type thermocouples

23 p4188 A69-42260

Thermoelectric generators using hot junction pressure contacted lead telluride technique, presenting model for long term performance characteristics

23 p4188 A69-42262

Thermoelectric generators performance and life tests, describing JPL facilities and programs

23 p4188 A69-42263

ISOTEC thermoelectric generators for space power, describing design features, operation, power output and radioisotope heat source

23 p4189 A69-42270

Space radiator system with hybrid, water heat pipes to transport waste heat from radioisotopic thermoelectric generator

23 p4190 A69-42304

Multifuel-capsule radioisotope thermoelectric generator design procedure, applying statistical environment definition

24 p4349 A69-43191

THERMOELECTRIC MATERIALS

Direct energy conversion and materials limitations, discussing thermoelectricity, solar cells, thermionics and fuel cells

02 p0194 A69-11801

Electron band structure of copper-nickel alloys, discussing thermoelectric properties, energy ranges and effect of alloying additions

02 p0301 A69-12765

Ferromagnetic ordering effect on gadolinium dialuminide thermoelectric power, measuring temperature dependence of power and electrical resistivity

03 p0485 A69-13322

Bismuth selenide inhomogeneous distribution effect on thermoelectric properties of bismuth telluride alloy

04 p0644 A69-15265

Chemical compatibility estimation of lead and tin tellurides thermoelectric materials with metallic alloys

04 p0551 A69-15315

Treatment and testing of thin platinum and gold alloy wires used in thermoelements for studying liquid fuel vaporization in combustion chambers

07 p1130 A69-18258

Thermoelectric and thermal phenomena in thermoelectric generator development for spacecraft applications, considering element design and materials selection

12 p2016 A69-25868

Electrical, thermal and thermoelectronic properties of refractory oxide materials including lanthanum chromite and strontium zirconate, discussing Hall effect, IR absorption, mixtures, etc

13 p2316 A69-27470

Thermoelectrical leg product specification /TELPs/ apparatus and data reduction technique for determining temperature dependent thermoelectric properties of material

18 p3093 A69-34783

Electrocaloric effect from 78-130 K on crystalline potassium dihydrogen phosphate, showing quadratic dependence on applied field /and polarization/ in paraelectric phase

20 p3583 A69-37343

THERMOELECTRIC POWER GENERATION

Fe-Fe interactions influence on increase in thermoelectric power with applied magnetic field at low temperatures for dilute alloys of Fe in Au

10 p1639 A69-23861

Thermoelectric power generators energy output efficiency, discussing thermal and electric contact resistances influence for optimizing parameters

12 p2016 A69-26364

Heats of condensation and vaporization of W, Re and Mo cathodes of thermoelectric converter with Cs arc for various output powers and Cs vapor pressure

12 p2017 A69-26544

Electricity from MHD - Conference, Warsaw, July 1968, Volume 4, Open cycle MHD

13 p2308 A69-28021

Zirconium hydride thermoelectric power system for space missions, discussing compactness, shield weight, temperature capability, reliability and SNAP 10A program

16 p2809 A69-31723

Thermoelectric converter systems optimization by geometry independent functions

18 p3093 A69-34782

Cascaded thermoelectric module for spacecraft power conversion via module integration with radio isotope heat source, bonding SiGe and PbTe stages

20 p3465 A69-37706

Thermoelectric power generator with variable thermal conductivity and electrical resistivity, obtaining steady state temperature distribution, power output and thermal efficiency

22 p3868 A69-40131

Power systems for unmanned spacecraft, noting improved performance for zirconium hydride reactors and thermoelectric converters

23 p4187 A69-42255

Nuclear reactor/thermoelectric power system design for manned orbiting space station, discussing station integration and operation

23 p4187 A69-42256

STAR /Stud and Rocker Panel/ four couple section improved by incorporating bonded tungsten electrical contacts for PbTe thermoelectric elements

23 p4188 A69-42261

THERMOELECTRICITY

Thermoelectric properties of GeTe-GaTe system, analyzing phase diagrams, solid solution formation, substitutions and zone structure influence

01 p0138 A69-10404

Intense laser emission interaction with current carriers in semiconductors, analyzing dependence of thermoelectric field produced by light absorption on intensity, frequency and temperature

01 p0139 A69-10895

Thermoelectric and thermomagnetic properties of bismuth at low temperatures, assuming thermal EMF due to phonon capture of carriers

03 p0488 A69-13885

Simultaneous and independent measurement of thermal conductivity, thermoelectric power and electric resistivity, applying method to cadmium arsenide-zinc arsenide system

05 p0764 A69-16338

Alkali metals thermoelectric power and energy dependence of Heine-Abarenkov pseudopotential, taking into account anisotropy effects

05 p0809 A69-16507

Electrothermal domains in semiconductors, examining domain velocity of motion under external potential

06 p0981 A69-17880

Differential thermal EMF at room temperature in p-InSb as function of concentration for different electron and hole scattering mechanisms

06 p0981 A69-17881

Optical heterodyning with single mode carbon dioxide laser and triglycine sulfate pyroelectric detector, noting detector sensitivity threshold

07 p1156 A69-19332

Resistance temperature transducers and thermocouples covering characteristics, readout and design for aerospace requirements

10 p1690 A69-23225

Thermoelectric and thermomagnetic properties of bismuth at low temperatures, assuming thermal EMF due to phonon capture of carriers

11 p1938 A69-25686

Qualitative analysis of thermoelectric effects in transistors, describing heat absorption and release

12 p2042 A69-26880

Electrothermal domains in semiconductors, examining domain velocity of motion under external potential

14 p2503 A69-28789

Differential thermal EMF at room temperature in p-InSb as function of concentration for different electron and hole scattering mechanisms

14 p2503 A69-28790

Peltier measurements below 4 K capable of measuring low Seebeck coefficient on high resistivity alloys and in presence of magnetic field

14 p2449 A69-29563

Thermoelectric parameters of polycrystalline p-type bismuth antimony telluride and bismuth antimony tellurium selenide solid solutions

15 p2668 A69-30629

Electrical conductivity and thermoelectromotive force of bismuth telluride and bismuth telluride-bismuth selenide alloys obtained by sintering, hot pressing and annealing

15 p2670 A69-31248

Simultaneous middle and low latitude Thomson scatter measurements, comparing electron density, temperature and exospheric temperature data on quiet and disturbed days

15 p2604 A69-31418

Thermal EMF, electrical conductivity and Peltier effect in sintered refractory oxides at high temperature in air and in Ar

17 p3068 A69-32990

Upper ionosphere Thomson scatter, electron number density measurements and topside sounding results during geomagnetic storms using electrodynamic drift theory

20 p3530 A69-37872

Thermal EMF in cadmium arsenide specimens with various electron concentrations determined to verify parabolic subband structure of conduction band

22 p3993 A69-40607

Electrothermal waves in nonequilibrium electrical discharge in potassium seeded argon plasma

24 p4359 A69-43645

THERMOGRAMS

U RECORDING INSTRUMENTS

U TEMPERATURE MEASURING INSTRUMENTS

THERMOGRAPHS

U RECORDING INSTRUMENTS

U TEMPERATURE MEASURING INSTRUMENTS

THERMOGRAVIMETRY

Synthetic solid lubricants impurity detection by X ray diffraction and oxidation thermogravimetry

01 p0102 A69-10909

Lithium aluminum hydride thermal decomposition using isothermal kinetics and differential thermal and thermogravimetric analyses, noting decomposition in four stages

02 p0304 A69-11898

Thermogravimetric plastics analysis data applied as constants to degradation kinetics equations used in charring-ablator digital computer programs

09 p1529 A69-22312

Thermographic phosphor coatings to obtain optical quantitative heat transfer distribution on wind tunnel models

12 p2099 A69-27150

Thermogravimetric study of oxidation protection of refractory metals by fused LiF coating, noting oxidation retardation of Ta, Nb and W

19 p3341 A69-35573

THERMOLUMINESCENCE

Thermoluminescence intensity of dolomite specimens from Kaali meteorite craters, discussing meteorite impact thermomechanical effect and crystal lattice defects

01 p0159 A69-11371

Allende carbonaceous meteorite age determination by thermoluminescence method, assuming internal radioactivity source

24 p4385 A69-43219

THERMOMAGNADYNAMICS

U THERMOMAGNETIC EFFECTS

THERMOMAGNETIC EFFECTS

Thermoelectric and thermomagnetic properties of bismuth at low temperatures, assuming thermal EMF due to phonon capture of carriers

03 p0488 A69-13885

Quantum oscillations of Maggi-Righi-Leduc /MRLL/ effect in n-InSb and n-InAs samples from single crystals at liquid helium temperature

06 p0979 A69-16992

Hall effect theory and devices, noting application to measurement of several physical quantities and sources of errors in devices

09 p1541 A69-22698

Thermoelectric and thermomagnetic properties of bismuth at low temperatures, assuming thermal EMF due to phonon capture of carriers

11 p1938 A69-25686

Transverse quantum thermogalvanomagnetic phenomena in thin semiconducting films, noting effects of inelastic electron scattering at acoustic lattice vibrations

13 p2318 A69-27890

Polycrystalline Fe-Ni, Fe-Ni-Co ferrites structure, magnetostriction, magnetization curves and hysteresis prior and after thermomagnetic treatment

13 p2319 A69-27992

Transport processes under adiabatic conditions between external magnetic field and thermal and electrical gradients in solid, defining galvanomagnetic and thermomagnetic effects

13 p2299 A69-28129

Indium arsenide electrical parameters analyzed by kinetic effects, considering conductivity, thermal and magnetothermal EMF and transverse Nerst-Ettingshausen effect

15 p2666 A69-30066

Magnetic analysis by successive double heat treatment of miocene lava cooled during geomagnetic polarity reversal for determining field intensity
16 p2788 A69-32646

Transverse thermomagnetic EMF and Nernst-Ettingshausen coefficient in GaSb semiconductor with double conduction band and strong degeneracy of current carriers
21 p3783 A69-39558

Al-Ni-Co alloys precipitation mechanism effect on magnetic properties, including heat treatment and Ti alloying effects
23 p4175 A69-41298

THERMOMAGNETISM

U THERMOMAGNETIC EFFECTS

THERMOMECHANICS
U THERMODYNAMICS

THERMOMETERS

NT RESISTANCE THERMOMETERS

Low temperature thermometer based on temperature dependence of frequency of F-19 nuclear magnetic resonance in antiferromagnetic manganese difluoride
06 p0927 A69-17703

Gallium arsenide thermometer calibration in 1 to 100 K range using interpolation formula derived from p-n junction diode equation
12 p2093 A69-26484

THERMOMETRY

U TEMPERATURE MEASUREMENT

THERMONUCLEAR EXPLOSIONS

Gas remnant of large scale explosive event in galactic plane at 60 degree longitude, discussing resultant extension on line profile
07 p1225 A69-19717

Ionosphere disturbances due to high altitude thermonuclear explosions, discussing experimental proof by Cosmos satellites short wave transmitter radio signal scintillation statistical evaluation
19 p3304 A69-36624

Radiation effects due to high altitude thermonuclear explosion measured by satellite, estimating fragments longitudinal drift velocity, plasma cloud expansion rate and fragment distribution
20 p3532 A69-37960

Thermonuclear explosion Operation Starfish effect on ionospheric state from recording in Central Kazakhstan, studying frequency characteristics
22 p3942 A69-41097

Electron density decrease in F 2 layer ascribed to 9 July 1962 thermonuclear explosion, noting dissociative recombination role
22 p3942 A69-41098

Radioactive debris distribution in space from 9 July 1962 thermonuclear explosion over Johnston island recorded by Cosmos 6 satellite
23 p4205 A69-41836

THERMONUCLEAR POWER GENERATION

Plasma confinement experiments with Tokamak type magnetic configuration device, giving schematics for thermonuclear reactor
11 p1927 A69-25099

THERMONUCLEAR PROPULSION

U NUCLEAR PROPULSION

THERMONUCLEAR REACTIONS

NT CONTROLLED FUSION

NT NUCLEAR FUSION

Supernova explosion theories, discussing neutrino and degenerate matter concepts, thermonuclear reactions in stellar explosions, oxygen conversion into sulfur, Crab Nebula, etc
03 p0509 A69-13356

Vacuum system for obtaining highly purified plasmas for thermonuclear investigations noting decontamination cycles and chamber characteristics
03 p0412 A69-13839

Thermonuclear neutron emission from high temperature deuterium plasma produced by focusing high power laser radiation on lithium deuteride surface [IEEE PAPER O-11]
07 p1153 A69-19072

Neutrino emission and carbon burning onset in 1.45 solar mass stellar models with pure He envelope, He burning shell and degenerate C-O core
08 p1384 A69-20059

Primordial helium and horizontal branch star luminosity, obtaining luminosities in He burning phase for different He and metal abundances from models
09 p1601 A69-22211

General expressions derived for numerical stellar-interior calculations for nuclear reaction rates, emphasizing density-temperature combinations
09 p1606 A69-22418

Anharmonic pulsations of 15.6 solar mass star in helium burning phase, discussing radiation pressure, third order terms, higher modes and magnitude variation effects
10 p1771 A69-22853

Charged particle motion in superposed Heliotron and biconical cusp magnetic fields, considering particle confinement
16 p2817 A69-31643

Solar thermonuclear reactions studied by emitted neutrinos detection, plotting energy spectra for sensitivity of Cl 37 detection system
18 p3185 A69-34278

THERMOPHILES

Ferredoxin from thermophilic and mesophilic Clostridia, noting difference in heat stability due to iron and sulfide environments
22 p3897 A69-41068

THERMOPHILIC PLANTS

U BLUE GREEN ALGAE

THERMOPHYSICAL PROPERTIES

NT CRITICAL POINT
NT CRITICAL PRESSURE
NT CRITICAL TEMPERATURE
NT EMISSIVITY
NT FUSIBILITY
NT HEAT OF SOLUTION
NT MELTING POINTS
NT PYROELECTRICITY
NT SPECIFIC HEAT
NT SUPERCRITICAL PRESSURES
NT THERMAL CONDUCTIVITY
NT THERMAL DIFFUSION
NT THERMAL DIFFUSIVITY
NT THERMAL STABILITY
NT VAPOR PRESSURE
NT VOLATILITY

State variables of ideal gas in two phase region, discussing determination from equations of state and equation for internal energy and Maxwell criterion inapplicability
06 p1030 A69-17170

Thermoelastic properties of particulate, filamentary and layered composites, summarizing Soviet theoretical and experimental work
08 p1339 A69-20500

Three dimensional reinforcement composites for gear and bearing applications with improved interlaminar shear strength, thermal and wear properties
08 p1340 A69-20509

Molybdenum and vanadium effects on nickel steel properties, stressing brittleness avoidance and quenchability
11 p1904 A69-24642

Thermodynamic properties of materials in critical region, discussing inhomogeneity
11 p2003 A69-25440

Plant and soil thermal behavior for various conditions of crop species, plant spacing, tillage, irrigation and aerial thermal scanner imagery
12 p2075 A69-26989

Polymer structure relationship to thermal, mechanical and chemical properties of electrical insulating materials
13 p2285 A69-27986

High temperature properties relationship to microstructure of Co base superalloys and strengthening methods
14 p2465 A69-29891

Processing characteristics of wrought Co base alloys, discussing thermomechanical treatment effects, yield strength, ductility, etc
14 p2456 A69-29892

Thermoelectric parameters of polycrystalline p-type bismuth antimony telluride and bismuth antimony tellurium selenide solid solutions
15 p2668 A69-30629

Particulate thermophysical lunar soil model for measuring lunation nighttime and eclipse cooling, noting applicability to IR surface brightness temperature of Mercury hot pole
18 p3191 A69-34303

Composite polymers thermophysical properties at thermal destruction temperatures, noting increased heating rate effect on kinetic curves
18 p3161 A69-34696

Unsteady temperature field in plane skin of aerodynamic body in case of temperature dependent thermophysical characteristics of skin material
18 p3092 A69-34982

Nernst effect in pyrolytic graphite at low temperatures including thermal EMF, electrical conductivity, thermal conductivity and magnetoresistance coefficients
21 p3753 A69-39562

Radiative properties of Ta, Mo, Nb, graphite and niobium carbide at high temperatures
23 p4175 A69-41111

Mars atmospheric features from measurements during entry and after landing, discussing atmospheric state properties, diurnal variability, clouds and winds
23 p4212 A69-41101

B, silicon carbide, C and Be reinforcing fiber technology, thermal and physicomechanical properties, noting coating, surface defects and improvement over glass fibers
23 p4179 A69-42122

THERMOPHYSICS

U THERMODYNAMICS

THERMOPILES

Radiation method for temperature and heat flux measurement, discussing transducer with thermopile sensor
15 p2607 A69-30101

THERMOPLASTIC FILMS

U POLYMERIC FILMS

THERMOPLASTIC RESINS
NT POLYMETHYL METHACRYLATE

Reinforcing glass fiber fillers in thermoplastic commercial products, noting applicability to high speed fabrication by injection molding processes
02 p0269 A69-11717

Radiation processed wood-plastic materials produced by impregnating natural wood with liquid monomer followed by ionizing radiation induced polymerization
04 p0605 A69-14511

Thermoplastics reinforcement with fiber and whiskers, fillers, evaluating graded asbestos, carbon, silicon nitride, silicon carbide and potassium titanate
08 p1337 A69-20411

Tensile stress and energy-to-break values compared for glass-fortified thermoplastic resins, discussing notched and unnotched Izod impact
08 p1337 A69-20411

Flexural fatigue of glass-reinforced thermoplastics, function of various parameters, discussing test for autogenous dissipative heating
08 p1337 A69-20411

Thermoplastic resins as matrices for glass reinforcement and aerospace structural and nonstructural adhesives
09 p1530 A69-22311

Rubber modified thermoplastics structure and mechanical properties, emphasizing stress concentration around composite particles and crazing role in creep and fracture
10 p1716 A69-23911

Syntactic foam low density thermoplastic microspheres as hollow spherical filler in polyester matrix, noting applications
14 p2467 A69-29211

Linear pyrolysis of thermoplastics during combustion of composite solid propellants and ammonium perchlorate solid propellant deflagration mechanism studied by loose granule analog [WSCI PAPER 69-16]
16 p2831 A69-32311

Rigid PVC, urethanes and thermosets processing failures high performance, noting injection molding and machine developments role
18 p3148 A69-34611

Fire-retardant thermoplastic and thermosetting materials for electronics industry use including blending of fire-retardant additives into plastics
18 p3162 A69-35211

Thermoplastic polyarylsulfone thermal and electrical properties at over 500 F, noting resistance to thermooxidative attack
19 p3355 A69-35521

High temperature structural adhesives developed from thermoplastic aromatic-heterocyclic polymers
19 p3357 A69-35561

Rigid thermoplastic cylindrical shell creep under axisymmetrical loads, giving computer algorithm and time dependent criterion for rupture strength
22 p4045 A69-40751

THERMOPLASTICITY

Deformation of thermoplastics under tensile loading, discussing types of loading
10 p1716 A69-22941

Polyvinyl acetate and polyvinyl alcohol thermoplastic adhesives, discussing gluing properties, chemical properties, preparation, polymerization methods
14 p2469 A69-29341

Composition effect on tensile and flexural modulus of composites containing randomly distributed fibrous strands, establishing strength-composition relationships
17 p2991 A69-32961

Polycarbonate and polysulfone thermoplastic bonding of Al and Ti in aircraft structures, discussing peel strength and stress crazing tests
24 p4326 A69-43459

THERMORECEPTORS

Thermoregulatory responses to cooling in spinal man, discussing deep temperature sensitive structures and relationship between skin and central regulatory structures
22 p3873 A69-40209

Skin temperature change rate influence on sweating in male subjects, discussing role of central thermosensitive structures
22 p3874 A69-40210

THERMOREGULATION

Thermoregulatory reactions of human body to sharp increase of ambient radiant temperature
[AGARDOGRAPH-111] 08 p1264 A69-20670

X ray irradiated dogs subjected to heat stresses to determine thermoregulatory ability
09 p1445 A69-22548

Heat pipe devices applied to radiative body heat transfer in space suit temperature control
[AIAA PAPER 69-619] 17 p2914 A69-33293

Thermoregulatory responses to cooling in spinal man, discussing deep temperature sensitive structures and relationship between skin and central regulatory structures
22 p3873 A69-40209

Skin temperature change rate influence on sweating in male subjects, discussing role of central thermosensitive structures
22 p3874 A69-40210

Potent chemical factors released from anterior hypothalamus of rhesus monkeys in response to thermal stress during thermoregulation
23 p4084 A69-41472

Brown adipose tissue providing internal heating jacket and metabolic heater overlying systemic vasculature, noting cold survival role
23 p4091 A69-42013

Human thermal regulatory mechanism using analog simulation compared with experimental results of resting subjects responses to climatic chamber
23 p4111 A69-42079

Respiratory effects of body temperature changes separation from blood osmolality changes in dehydrated man
23 p4097 A69-42094

THERMOSETTING RESINS

NT EPOXY RESINS
NT PHENOLIC RESINS
NT POLYAMIDE RESINS

Electric components encapsulation by combining liquid resin techniques and transfer molding
04 p0607 A69-14955

Fire retardant thermally stable electrical grade thermoset resins tested for flexural and dielectric strength and weight loss
08 p1340 A69-20506

Thermosetting resin curing behavior characterized by differential thermal analysis performed above atmospheric pressure to prevent volatilization
09 p1500 A69-22311

Thermosetting adhesives properties and structural applications in aircraft, space and automotive use, discussing polymer systems, moisture, surface preparation, aging, etc
14 p2468 A69-29340

Nozzle throat ablative materials for controlled high regression rates in tactical rocket motors, primarily nylon reinforced thermosetting resins
[AIAA PAPER 69-423] 16 p2804 A69-32710

Injection holding for ceramic parts from nonplastic materials, presenting time-temperature schedules for low temperature removal of molding material without damage
17 p2978 A69-33376

Fire-retardant thermoplastic and thermosetting materials for electronics industry use including blending of fire-retardant additives into plastics
18 p3162 A69-35273

Elastomeric thermosetting one part silicone encapsulant environmental tests, checking physical and electrical properties stability under temperature and relative humidity conditions
19 p3281 A69-35549

THERMOSIPHONS

High turbine inlet temperature technology using thermosiphon cooling for gas turbine, possibly doubling specific horsepower of aircraft
[SAE PAPER 690034] 07 p1203 A69-18311

THERMOSPHERE

Lower thermosphere neutral composition diurnal variations, noting molecular N and O, Ar, He and atomic O
01 p0076 A69-11231

Lower thermosphere composition over New Mexico, discussing rocket flight mass spectrometer measurements during summer 1967
03 p0425 A69-14009

Atmospheric rotation speed dependence on specific heat, thermal conductivity, air absorption coefficient and lower boundary pressure, discussing diurnal variation of the thermosphere
[AFCRL-69-0363] 04 p0649 A69-15130

Long distance propagation of acoustic gravity waves ducted in thermosphere, noting effect of seasonal variations in polar region
04 p0595 A69-15437

Atmospheric density variation measurements by density gages on Explorer 32 satellite confirm wave propagation in neutral thermosphere as free internal gravity waves
05 p0754 A69-16261

Electron cooling rates in midlatitude and auroral zone thermosphere measured by probe rockets
05 p0755 A69-16267

Midlatitude neutral thermosphere density and temperature measurements, noting effect of atomic oxygen adsorption by instruments
05 p0755 A69-16268

Helium flux in lower thermosphere, using diffusion theory for multicomponent gas mixture to determine equation for equilibrium distribution
07 p1125 A69-18848

Quadrupole mass filter for rocket-borne measurements of thermospheric helium content, discussing turbopause level and winter helium bulge
09 p1489 A69-21712

Spin stabilized spherical satellite in high elliptical orbit for lower thermosphere measurements during entire solar cycle
09 p1610 A69-22009

Full wave calculation of gravity waves for thermospheric model, describing wave type reflection, transmission, conversion and coupling by scattering matrix elements
11 p1878 A69-25150

Thermosphere radiative cooling by atomic O 62 micron line, noting cooling and heating rates
12 p2064 A69-26009

Characteristic plane harmonic free internal neutral atmospheric wave oblique propagation through horizontally stratified quiet atmosphere for various thermospheric parameters
12 p2065 A69-26101

RF mass spectrometric measurements of diurnal variation of thermosphere and ionospheric E and F regions composition, noting oxygen concentration
15 p2601 A69-31371

Rocket and satellite measurements of density, temperature and composition in lower thermosphere, considering altitude dependence
15 p2602 A69-31383

Rocket ejected vapor trails structure in lower thermosphere showing no evidence of atmospheric turbulence
15 p2602 A69-31393

Atmospheric models for pressure variation and neutral air winds in thermosphere, discussing wind velocity vector relation to satellites orbital inclination
15 p2603 A69-31403

Exospheric temperature variations by Thomson scattering related to solar and geomagnetic activity, discussing seasonal effect on thermospheric variables
15 p2604 A69-31409

Gravity waves in thermospheric heating during magnetic storm, discussing electron density and temperature and ion velocity variations
15 p2605 A69-31435

Diurnal thermospheric density, temperature and wind variations due to direct solar EUV heat input and tidal wave from lower atmosphere
15 p2605 A69-31439

Thermosphere neutral wind speed measured from observing Doppler shift in O I 6300 night airglow line with Fabry-perot interferometer
16 p2776 A69-32093

Atmospheric density semiannual variation in thermosphere base, suggesting origin at lower heights in mesosphere or stratosphere
17 p2958 A69-32863

Composition and temperature of daytime and nighttime neutral tropic lower thermosphere, obtaining atomic and molecular oxygen ratios
18 p3128 A69-34936

Mesosphere and lower thermosphere molecular O density from solar radiation atmospheric absorption, using satellite measurements
20 p3523 A69-37413

Mass spectrometric investigation of thermosphere at high latitudes, measuring number densities for nitrogen, Ar and molecular and atomic oxygen
20 p3533 A69-38086

Thermosphere temperature shape parameters from probe flights, showing dependence on hour angle
20 p3534 A69-38088

Meteor winds analysis method used on tidal period wind measurement data obtained by chemical release from rocket in 95-135 km region
20 p3574 A69-38092

Explorer 32 atmospheric density measurements revealing neutral thermosphere latitudinal variations during geomagnetically undisturbed times
20 p3535 A69-38100

Lower thermosphere ion and neutral minor constituent concentrations in nighttime auroral zone, considering ionization due to electron precipitation and bremsstrahlung
21 p3704 A69-38365

Circulation near turbopause effect on lower thermosphere composition changes, noting heat source for warmth over winter polar region
21 p3704 A69-38366

Neutral components of arctic thermosphere measured with rocket-borne RF mass spectrometers, discussing origin of atomic hydrogen and water lines
21 p3704 A69-38367

Neutral particle density ratios in thermosphere by rocket-borne monopole mass spectrometers
21 p3704 A69-38368

Midlatitude thermosphere vertical air motions to balance divergence and convergence caused by large scale horizontal wind systems
21 p3714 A69-38553

Molecular O distribution in thermosphere from Ariel 3 observations of solar radiation attenuation, showing large and systematic variation with longitude
21 p3717 A69-39263

Heat conduction equation applied to thermospheric heating in auroral zone to account for local temperature and density variations, introducing horizontal transport mechanisms
22 p3941 A69-40717

Diurnal and solar cycle variations of thermosphere density and temperature generated by solar EUV input and tidal wave, using two dimensional model
24 p4367 A69-43003

Thermosphere dynamic response to low altitude geomagnetic disturbances, showing time lag dependence on perturbation intensity
24 p4310 A69-43180

THERMOSTABILITY

U THERMAL STABILITY

THERMOSTATS

Self thermostatic phase-change coatings for active and passive spacecraft temperature control, discussing temperature dependent changeability in solar absorptance
14 p2530 A69-29434

Thermostatic electronic control device of birefringent filter in Wroclaw Observatory coronagraph during prominence observations
22 p3943 A69-40000

THERMOTROPISM

U ANISOTROPY

U TEMPERATURE EFFECTS

THERMOVISCOELASTICITY

Plane wave propagation in infinite viscoelastic medium taking into account mutual effects of deformation and temperature fields
01 p0164 A69-10076

Thermoviscoelasticity equation solution for class of dynamic problems, giving problem solution for half space with arbitrary temperature field boundary condition
02 p0336 A69-11554

Thermal stress propagation in infinite viscoelastic thin plate analyzed with cylindrical coordinate system
08 p1415 A69-20661

Axisymmetric problems in thermoviscous plasticity, discussing stress-strain state of annular disks and thick walled cylinders made of rate sensitive materials
10 p1802 A69-24025

Stress wave propagation in thermoviscoelastic solids using extended Ritz method
11 p1993 A69-25527

Hollow circular viscoelastic cylinder axisymmetric plain strain problem, considering displacement, trac-

THETA PINCH

tion and mixed boundary conditions, noting applicability to rocket solid fuel core

12 p2181 A69-26396

Temperature, velocity and density perturbation propagation as heat convection wave in viscoelastic thermally compressible heat conducting fluid, analyzing damping and frequency spectra

16 p2878 A69-31952

Thermal effects on viscoelastic structure response to applied loads, using equations for thermomechanics, linear and nonlinear thermoviscoelasticity and nonisothermal creep theorem

19 p3440 A69-36657

Heat influx equation coupling in thermoviscoelasticity, considering internal forces dissipation and stress-strain operators

22 p4044 A69-40741

THETA PINCH

Plasma heating in two step theta pinch with coaxial coils yielding high temperature plasma at low capacitor storage charge

05 p0804 A69-16549

Theta pinch plasma electron density and temperature distributions measured using Thompson scattering of laser light and plasma bremsstrahlung

06 p0972 A69-18220

Spectral distribution and energy of luminous radiation emitted during theta pinch in Ar plasma, noting energy maximum as function of pressure

08 p1362 A69-20280

Monograph on interferometric studies of unsteady shock waves in theta pinch driven shock tube, discussing flow characteristics in helium and hydrogen

08 p1304 A69-20710

High temperature high density theta-pinch plasma refraction measurements by interference refractometer with beam perpendicular to plasma axis

09 p1544 A69-21302

Theta pinch plasma microwave emission from electrodeless inductive discharge at low pressures recorded at near plasma frequencies

09 p1549 A69-22017

Converging cylindrical shock waves produced by discharging condenser bank into single turn coil surrounding gas container /theta pinch discharge/

10 p1678 A69-22933

Toroidal theta pinched plasma column collapse, using snowplow model for study of column position shift and cross section deformation

11 p1924 A69-24303

Spectral broadening measurements of ruby laser light scattered by density fluctuations in theta pinch plasma

11 p1924 A69-24304

Toroidal plasma radial drift suppression on curved theta pinch axis through introduction of transverse conducting ring inside vacuum tube

11 p1925 A69-24313

Kink type instability of rotating linear theta pinch plasma, calculating perturbation behavior with bounce model

11 p1929 A69-25270

Slow theta pinch helium plasma measurements by Mach-Zender interferometer with Q switched laser

12 p2091 A69-26394

High speed streak cameras applicability to low density theta pinch studies, describing image converters design, operation and block diagrams

14 p2496 A69-29787

Time of flight mass spectrometers for plasmoids generated by theta pinch and discharge over organic glass, showing ion and electron currents oscillograms

14 p2498 A69-29813

High beta theta pinch stability against tearing modes, determining necessary magnetic field conditions for slab and cylindrical cases

16 p2819 A69-31681

Collisionless shock wave generation and structure in zeta and theta pinches

17 p3013 A69-33819

Energy dissipation in collisionless shock waves generated in plasmas with 1-500 trillion/cm electron density by theta pinch, measuring axial ionic energy spectrum

17 p3013 A69-33820

Ion energy distribution function and density profile in strong implosion wave generated by theta pinch discharge, investigating compression wave in deuterium

17 p3013 A69-33821

Collisionless plasma heating mechanisms from current layer turbulence in theta pinch experiment and shock wave front structure as function of initial magnetic field

17 p3013 A69-33824

Collisionless shock waves in plasma and ion and electron turbulent heating in high voltage theta pinches, noting magnetic disturbance

17 p3013 A69-33825

THIAMINE

Successive X ray doses effect on oxidative phosphorylation of vitamin B 1 in white rats liver tissue ultrastructure during and after irradiation, establishing thiamine biosynthesis suppression

21 p3658 A69-39056

THICK FILMS

Equipment for minimum cost laboratory for thin and thick film hybrid circuits

04 p0559 A69-15198

Operating and storage conditions effects on reliability of Pd-Ag thick film resistors

08 p1283 A69-20131

Thick film hybrid circuit technology and equipment reviewing conductors, resistors, and insulator inks

09 p1508 A69-22337

Adsorption of N, H, O and CO on thick vapor deposited Be films at room temperature

13 p2322 A69-28017

Hybrid microelectronic circuit failure mechanisms for thick and thin film resistors, conductors and capacitors, noting packaging contributions

22 p3910 A69-39954

Hybrid microwave IC assembly techniques, discussing active devices connection to substrate with thick or thin film metallizations

22 p3912 A69-40068

Hybrid techniques to produce thin and thick film microcircuits and logic system parameters

24 p4286 A69-42906

Materials problems in microelectronic circuits, discussing multilayer interconnection arrays production by thick film or print-and-fire process

24 p4333 A69-43212

THICK WALLS

Analytic model resembling thick walled ellipsoid of revolution incorporating three dimensional shape of human left ventricle and ventricular wall thickness effects

12 p2022 A69-26235

Torsional shearing stress in thick walled hollow rectangular cross sections

13 p2358 A69-27212

Vibrations of thick walled shallow circular cylinder with thickness change in time, applying dynamic elasticity and Volterra equations

14 p2533 A69-28985

Thick walled pressurized cylinder fatigue test results compared with axial tension and rotating beam tests on same material

15 p2709 A69-30676

Ultrasonic spectrometry application to thickness measurement of thin and thick walled articles

18 p3137 A69-35110

Stress-strain state of thick and thin walled closed shells of variable thickness during elastoplastic torsion developing in aircraft component production

21 p3835 A69-38882

THICKENED LEADING EDGES

U LEADING EDGES

THICKNESS

NT FILM THICKNESS

NT TARGET THICKNESS

Plate thickness effect on bending of elastic plate with crack, investigating stress distribution

04 p0678 A69-14890

Thickness and drilled holes effects on notch toughness of Charpy V notch bars over wide temperature range

10 p1798 A69-23087

Displaced layer thickness dependence on air injection parameters measured in wind tunnel

13 p2245 A69-27385

Numerical solutions of thick cambered jet flap in ground effect for flat plate and diamond shaped airfoil [AIAA PAPER 69-738]

18 p3083 A69-34404

Ultrasonic spectrometry application to thickness measurement of thin and thick walled articles

18 p3137 A69-35110

Nonmetallic materials thickness measurements at SHF, describing factors affecting geometrical-optics method

18 p3138 A69-35116

Nonlinear theory of elastic membranes accounting for thickness effects, obtaining field equations and constitutive relations for various cases

21 p3832 A69-38465

Optimum thickness of dynamically stable composite superconducting tapes determined for substrate thickness as function of current density

24 p4361 A69-43611

Laminar sublayer thickness in compressible turbulent boundary layers with and without heat transfer

24 p4306 A69-43061

THICKNESS RATIO

Sandwich beams interlaminar shear stress calculations, considering roles of moduli of elasticity and layers thickness relative to beam

22 p4041 A69-40401

Buckling of thick homogeneous rectangular plate subjected to constant normal stress, noting error in thin plate approximation

24 p4406 A69-43061

THIN AIRFOILS

Thin jet-flapped airfoil flow analysis in ground proximity at small angle of incidence, assuming inviscid compressible flow

09 p1431 A69-22271

Velocity, lifting force, pressure moment and circulation around linear array of thin foils with direction normal to profile chords calculated by Birnbaum-Glauert method

11 p1817 A69-24313

Imaging for flowfield of nonuniform parallel streamlines with thin airfoil represented by vorticity distribution, noting change of lift and moment

12 p2012 A69-26771

Equations of motion of compressible fluid with non-zero resistivity near thin foil, solving supersonic and subsonic flow by Fredholm integral equations

13 p2200 A69-28313

Compressible shear flow linear theory applied to transonic flow past thin airfoil, determining pressure distribution, discussing compressibility effects of nonuniform Mach number

16 p2731 A69-31571

Viscous electrically conducting fluid flow around thin profiles for equal Reynolds and magnetic Reynolds numbers, using Oseen method to linearize equations

18 p3124 A69-35213

Thin jet flapped airfoil analysis with wake fully developed from leading edge and jet flow reflected from ground

22 p3861 A69-41111

THIN BODIES

Thin deformable body motion in disturbed potential flow of ideal incompressible fluid

11 p1876 A69-25413

Three dimensional equations of elasticity reduced to two dimensional equations of shell theory, discussing stressed states of thin elastic bodies

14 p2531 A69-28811

Second order theory for steady or unsteady subsonic flow past slender lifting bodies of finite thickness [AIAA PAPER 68-75]

20 p3458 A69-37113

Optimal control of flight vehicle consisting of loss thin elastic body under torsional deformations, solving by method of successive approximations

21 p3760 A69-38813

Self consistent fields in waveguides containing thin conductors, expanding induced field into Fourier series in normal waves for series coefficients

23 p4123 A69-41911

THIN FILMS

NT ENERGY ABSORPTION FILMS

NT FERROMAGNETIC FILMS

NT MONOMOLECULAR FILMS

Dimensional effects on thermodynamic and kinetic properties of thin semiconductor and semimetal films, noting quantization influence

01 p0136 A69-10181

Digital loaded-line phase shift networks for microwave thin film applications, emphasizing design equations

01 p0040 A69-10191

Erosion damage of bearing alloy lining in the lubricating oil film, considering Cu-Pb alloy and base white metal

01 p0094 A69-10311

Quasi-static Kerr magneto-optic observation of procedure to predict results of dynamic flux reversal in thin Ni-Fe films [IEEE PAPER 11.7]

01 p0138 A69-10711

Soviet book on structure of thin metal films covering electron microscopic and electronographic studies, crystallization and heat treatment effects

01 p0140 A69-11111

Thin film transistors prepared from spray deposited cadmium sulfide, discussing carrier mobility and stability

02 p0214 A69-11511

- Injection laser emission from gallium arsenide base films grown epitaxially from gas phase in moist hydrogen atmosphere
02 p0255 A69-11879
- Reflection elimination for single dielectric film on solid laser material substrate, calculating reflectance as function of frequency
02 p0256 A69-11926
- Thin CuAs selenide films by vacuum deposition, electronographic study proves cubic sphalerite phase existence
02 p0298 A69-12045
- SnTe, SnSe and SnS epitaxial layers obtained by deposition of sublimates on cellulose-nitrite-varnish and single crystal NaCl and KBr substrates
02 p0298 A69-12049
- Integrated circuits technology, discussing thin film, monolithic compatible and hybrid circuit techniques
02 p0216 A69-12050
- Fuel films ignition behind shock waves in air and oxygen
02 p0353 A69-12317
- Microelectronic components joining technique by compliant bonding, utilizing deformable medium between tool and beam leads to eliminate intricate tool shapes and alignments
02 p0254 A69-12473
- Photoelectric effect of thin gold films on silver and quartz substrates, analyzing work function dependence on thickness of deposited metal
02 p0300 A69-12630
- Photoelectric effect of thin gold film under electric field, noting work function dependence on film thickness exhibits extremum
02 p0300 A69-12631
- Acoustic plasma waves propagation in thin films in case of film quantization, showing phase velocities close to Fermi velocities of electrons
02 p0300 A69-12649
- Dynamic current-voltage characteristics of thin film diodes on chalcogenide glass base
02 p0223 A69-12834
- Cathode sputtering and thermal evaporation in vacuum used for preparing thin dielectric coatings on mirrors of optical resonators containing nonlinear crystals
03 p0438 A69-13049
- Analysis and design of synchronous filter compatible with microelectronics requirements, switching N monolithic RC thin film devices to signal source of resistance
03 p0403 A69-13206
- Nondestructive measurement of thin transparent film thickness by interference method, noting diffusion profiles
03 p0430 A69-13634
- Thin film lubricant effect on machine dynamic performance, proposing inclusion with machine structure for reducing vibration effect
03 p0435 A69-13948
- Optical absorption of thin film cesium between 2300 and 11000 Å
03 p0491 A69-14060
- Optical absorption of vacuum deposited thin rubidium films, noting similarity to sodium and potassium
03 p0491 A69-14114
- Heat removal in multilayer superconducting devices, determining optimum number of layers
03 p0493 A69-14225
- Small transverse dimensions effect and domain formation criterion for surface oriented Gunn diodes prepared on thin epitaxial GaAs layers
04 p0639 A69-14335
- Laminar accelerating flow of thin film falling along vertical wall, emphasizing growth and decrease of boundary layer and film thickness
[ASME PAPER 68-APM/Z] 04 p0586 A69-14388
- Vacuum evaporated thin film components welding, using torsional ultrasonic vibrations for joint activation
04 p0605 A69-14561
- Thin film heated Pt resistance thermometer for skin friction or velocity measurements in air, water or blood
04 p0601 A69-15118
- Equipment for minimum cost laboratory for thin and thick film hybrid circuits
04 p0559 A69-15198
- Temperature distribution over receiving layer of absorption edge image transformer, discussing thermal conduction influence on performance of thin film IR image receiver
04 p0631 A69-15280
- Reading amplifier for thin magnetic film memory stores permitting tunnel diode register positioning
04 p0579 A69-15319
- Vacuum deposition of thin film microwave acoustic transducers of piezoelectric aluminum nitride
05 p0761 A69-15820
- Plane supersonic flows separated by thin film shaped jet, deriving pressure as function of deviation
05 p0746 A69-16020
- Five layer thin film band elimination filters amplitude and phase frequency characteristics
05 p0729 A69-16088
- Electrical polarization effect on electroluminescence brightness waves in zinc sulfide films
05 p0807 A69-16213
- Polarization effect on electroluminescent properties of zinc sulfide films
05 p0807 A69-16214
- Thin film thermocouple detector for molecular lasers operating in middle and far IR range
05 p0773 A69-16284
- Surface waveguide composed of inhomogeneous dielectric thin film used as low loss transmission line
05 p0731 A69-16294
- Cryogenic flexibility of thin polymeric film plies for use as spacecraft positive expulsion bladders
05 p0769 A69-16486
- Film processing effects on cryogenic mechanical properties of polyethylene terephthalate
05 p0785 A69-16490
- Zr-Nb alloy structure effect on critical superconductivity parameters determined, using electron microscopy of thin films
05 p0811 A69-16806
- Differential ion pumping for vacuum deposition of thin films
06 p0907 A69-17709
- Selective etching technique in study of dislocations in epitaxial layers of gallium arsenide
06 p0981 A69-17891
- Ferrite microstrips substrates role in integrated circuits, noting application of hybrid technology
07 p1090 A69-18399
- Doped silicon dioxide films as controlled reproducible diffusion sources for silicon devices fabrication
07 p1198 A69-18620
- Low speed four-ball lubricating oil testing machine eliminating thermal effects associated with frictional heating for load carrying capacities of thin lubricant films
07 p1140 A69-18968
- X ray fluorescence and electron microprobe for determining thin film thickness
07 p1113 A69-19582
- Optical parameters for system of isotropic nonabsorbing film on isotropic absorbing substrate determined by ellipsometric method, noting Si optical constants
07 p1201 A69-19648
- Fresnel formulas for surface plasma waves excitation by light in thin metal foil embedded between dielectric layers, discussing transmissive and absorptive resonances
08 p1372 A69-20290
- Thin films of niobium oxide vapor-deposited on silicon and quartz substrates, discussing optical and dielectric measurements, dispersion and absorption coefficient
[ECS PAPER 17] 08 p1372 A69-20365
- Flame emission spectrophotometric method for ultraminate sodium contamination detection in thin silicon oxide films and cleaned silicon surfaces
[ECS PAPER 306] 08 p1314 A69-20367
- GaAs laser employing external resonator with thin film active substance, noting output power and emission thresholds during electron beam excitation
08 p1326 A69-20543
- Holographic technique for measuring thin fluid film profiles using interference image reconstruction and helium-neon laser as coherent light source
08 p1317 A69-20873
- Vapor deposited tellurium thin films orientation, noting effect of characteristic spiral chain structure along c-axis
08 p1373 A69-20891
- Cubic β /silicon carbide films deposition by volatilization in presence of acetylene
09 p1554 A69-21350
- Thermal EMF in epitaxial films, analyzing potential distribution in p-n junction with temperature gradients and film thickness effects
09 p1555 A69-21473
- Zone structure of silicon-silicon dioxide system for silica films obtained by pyrolytic dissociation, discussing kinetics of photoelectrons capture at traps
09 p1555 A69-21478
- Electrical conductivity and Hall effect in thin evaporated bismuth films under vacuum using three point method in variable temperature cryostat
09 p1557 A69-21692
- Diffraction pattern recording technique and application to thin film measurements
09 p1499 A69-22303
- Capacitance methods for measuring adhesives mechanical properties in thin film bonded joints, noting results for tension, compression and shear loading
09 p1500 A69-22309
- Microsoldering techniques for thin and thick film hybrid circuits and microminiature printed circuit boards
09 p1510 A69-22349
- Laser evaporation vapors from refractory materials to produce surface temperature for carrying out reactions in gaseous phase and thin film preparation
09 p1519 A69-22476
- Combined electron microprobe and ellipsometric study of thin silicon dioxide films on silicon, noting reliability and accuracy
10 p1742 A69-22946
- FET memory element charge storage two layer model for thin film dielectrics noting charge/discharge times
10 p1742 A69-22947
- Electrical resistivity of epitaxial CdTe films produced by vacuum sublimation on hot orienting mica and single crystal substrates
10 p1742 A69-23001
- Lead sulfide single crystals and polycrystalline films growth studied by electron microscopy during vacuum deposition on NaCl and other substrates
10 p1743 A69-23002
- Optimum microcircuit analog to digital converter for aerospace environment by combining monolithic circuits and thin film resistors
10 p1636 A69-23282
- Three layer vacuum deposited silicon monoxide films current voltage and conduction current density temperature dependence
10 p1745 A69-23324
- Differential energy losses of fission fragments in thin carbon films as function of mass and initial energy mapped by time of flight method
10 p1694 A69-23348
- InAs thin film sensors using Hall effect to measure magnetic fields at cryogenic temperatures
10 p1696 A69-23717
- Light absorption of In and Ga thin films in various gaseous media, noting displacement of irregular absorption band
10 p1747 A69-23792
- Thin film thickness and composition determination through scattered electron and characteristic X ray radiation recording
10 p1747 A69-23847
- Voltage drop measurement across plasma anodized germanium film to determine anodization constant
10 p1742 A69-24004
- Electrodeposition of Te-containing Permalloy films with uniaxial magnetic anisotropy, noting electrolyte composition and film structure
11 p1935 A69-24332
- Thin polycrystalline film structure and formation, using electron beam instrument
11 p1936 A69-24601
- Semiconductor properties, applications and problems including thin films, superconductivity, etc
11 p1937 A69-24736
- Radiant power flow, transmittance and absorbance of absorbing thin film multilayer in terms of characteristic matrix and admittance of surrounding media
11 p1896 A69-24850
- Electron, proton and gamma ray radiation effects on thin film CdS, GaAs and CdTe solar cells
11 p1825 A69-24872
- Differential catalytic thin film heat gage for measuring surface temperature variations and ionized flow heat transfer, noting insulating boundary layer thickness
11 p2002 A69-25231
- Thin film lumped passive elements for microwave power amplifier integrated circuits, discussing distributed reactances, element size and fabrication, etc
11 p1856 A69-25654
- Thin liquid film equilibrium on rotating sphere, determining conditions for detachment as function of angular velocity
12 p2061 A69-25886
- Thin foil preparation technique for transmission electron microscopy and selected etch pitting technique for CoO single crystals
12 p2112 A69-25944

Inertia effect on incompressible fluid film pressure between two oscillating parallel plates, considering Reynolds number

12 p2102 A69-26241

Scale effect on gold films electrical conductivity, analyzing film thickness and electron parameters of mean free path, concentration and surface reflection

12 p2143 A69-26459

Gases effect on electrical conductivity of vacuum deposited thin films of Cr, Be, Ni, Au and Ge at different thickness and low pressure

12 p2143 A69-26460

Semiconductor thin films analysis using mass spectrometer with spark source

13 p2316 A69-27293

Thin film cermet resistors for integrated circuits produced by thermal vapor deposition in vacuum, cathodic sputtering and explosive vapor deposition

13 p2268 A69-27466

Photoelectric characteristics of thin film CdS-CdTe heterojunction diodes, considering I-V illuminance, spectral characteristics and conduction band continuity

13 p2230 A69-27882

Temperature effects on photosensitivity spectra of cadmium telluride thin films

13 p2318 A69-27889

Transverse quantum thermogalvanomagnetic phenomena in thin semiconducting films, noting effects of inelastic electron scattering at acoustic lattice vibrations

13 p2318 A69-27890

Vacuum and thin film - Conference, Pittsburgh, October-November 1968

13 p2298 A69-28003

Dielectric thin film electrical and mechanical properties and preparation for semiconductor devices, emphasizing Si compounds

13 p2286 A69-28004

Transition metal interstitial compounds thin film preparation and superconducting properties, emphasizing high critical temperature, rock salt structure and NbN base

13 p2321 A69-28009

Low resistance Bi thin film complex electrical impedance in IR range, stating methods and equivalent circuits for determining impedance

13 p2322 A69-28011

Prebreakdown and breakdown electrical properties of thin film capacitors with certain oxides, fluorides and Teflon dielectrics

13 p2322 A69-28012

Energetics in solid film lubricants vacuum deposition methods, showing dependence on interfacial and film characteristics

14 p2454 A69-29001

Oxygen K-shell X ray production cross section and stopping power of aluminum oxide thin films for 20-100 kev protons

14 p2489 A69-29994

Josephson current density distribution in thin film superconductors, determining relation between tunneling density and magnetic field for films with/without current

15 p2667 A69-30196

CdS films vacuum deposited on optically polished single crystals used for converting microwave radio signals into hypersonic waves

15 p2575 A69-30236

Thin film thickness determined by weighing film and substrate in liquid having same density as substrate material

15 p2607 A69-30239

Solid lubricant films friction and wear life determined under various conditions of contact, temperature, load and atmosphere [ASLE PREPRINT 69AM 6C-1]

15 p2619 A69-30471

Thermal EMF in epitaxial films, analyzing potential distribution in p-n junction with temperature gradients and film thickness effects

15 p2669 A69-30718

Zone structure of silicon-silicon dioxide system for silica films obtained by pyrolytic dissociation, discussing kinetics of photoelectrons capture at traps

15 p2669 A69-30723

Microelectronic technology for mass production of high reliability hybrid thin film circuits

15 p2628 A69-30845

Thin film tantalum nitride resistors technology and production, evaluating projected reliability of resistance circuits as function of operating and environmental conditions

15 p2628 A69-30846

Lubrication and lubrication systems literature including compressible and incompressible fluid films, automotive, bearing, gear, friction, wear and boundary lubrication, seals and sealing systems

15 p2628 A69-30900

Gas laser cutting of thin carbon films on thick pyrex glass and ceramic substrates

15 p2635 A69-31037

Thin film carbon resistors cutting with carbon dioxide gas laser, considering cylindrical bodies and aging properties

15 p2635 A69-31038

Cadmium sulfides thin film solar cells for supplying power to instrumentation and data telemetry on longer lived balloons

15 p2553 A69-31287

High voltage thin film transistor, discussing design criteria, fabrication, I-V characteristics and switching speed

16 p2757 A69-31614

Superconductive tunneling measurements on thin Al films, discussing enhanced transition temperatures, energy gap dependence on temperature, electron microscope observation of crystallites, etc

16 p2825 A69-31634

High energy electrons emission during alloy evaporation on hot metal filaments used for thin film deposition

16 p2827 A69-32016

Prebreakdown and breakdown electrical properties and light emission during destructive breakdown in thin film capacitors

16 p2761 A69-32323

Numerical method based on thin film optics to determine ionospheric electromagnetic transmission and reflection coefficients for vertical incidence

16 p2752 A69-32392

Thin film optical method generalization accounting for intermode coupling and oblique incidence in plane stratified magnetoionic medium applied to ionospheric LF and hydromagnetic propagation

16 p2753 A69-32393

Thin film metallic oxide catalysts for oxidation in low temperature cells using hydrogen and hydrocarbons and for oxygen reduction in acid electrolyte

16 p2738 A69-32408

Electromigration role in material accumulation and depletion forming regions in Au film conductors, discussing regions origin from and correlation with thermal gradients along conductor

17 p2936 A69-32896

Thin surface films effect on radiative properties of metal surfaces determined by thin film optics, noting dependence on refractive index [AIAA PAPER 69-623]

17 p3072 A69-33283

Single frequency lasers using thin metal film mode selection filters, discussing film properties and experiments with Ar ion and Nd-YAG lasers

17 p2982 A69-33399

Slow electromagnetic wave propagation in superconducting thin film transmission lines, noting phase velocity dependence on film thickness and spacing

17 p2938 A69-33785

NbN thin film production by refined reactive sputtering technique, discussing Pauli spin paramagnetism and spin orbit scattering in high field superconductivity

17 p3016 A69-33790

InSb thin films prepared by flash evaporation, discussing Hall measurements at various temperatures and electron mobility dependence on film thickness

18 p3182 A69-34348

Optimum ballast resistance of thin film heat transfer gage producing shock arrival time, thickness and structure data of low pressure shock tube

18 p3117 A69-34470

Book on thin film phenomena associated with structural, mechanical, electrical, superconducting, magnetic and optical behavior

18 p3182 A69-34929

Thin silicon solar cells environmental tests, evaluating temperature and humidity effects on various contacts and coatings

19 p3252 A69-35699

Integrated thin film solar cell array consisting of CdS cells deposited on Kapton single sheets connected in series and covered by Mylar single sheet

19 p3254 A69-35710

Acoustic surface waves on thin film for pulse compression radar dispersive delay line, describing delay characteristic synthesis and control

19 p3267 A69-35929

Electroabsorption oscillations in CdTe films compared with results of interband transitions theory

19 p3386 A69-36523

Optical and electrical properties of thin amorphous films of glass-forming oxide, using X ray diffraction and electron microscopy for structural features

19 p3391 A69-36555

Fabry-Perot interferometer with Al coating reflecting surface deposited on unbaked thin films

20 p3536 A69-36556

Thin PbTe semiconductor films electrical properties measured in air and vacuum, showing dependence on thickness and conditions of preparation

21 p3782 A69-39298

Transformer for unilateral energy transfer using single domain uniaxial Permalloy film

21 p3684 A69-39299

Metal-polymer-metal and metal-polymer-silicon thin film structures analysis for polymers bulk properties and insulator-silicon interface, noting dipole-like relaxation

21 p3782 A69-39444

Spectral dependence of optical absorption in InAs thin films under conditions of quantum dimensional defect, considering allowance for nonparabolic conduction zone

21 p3783 A69-39555

Gupta stability solution extended to liquid anisotropic viscoelastic films, analyzing surface and shear wave perturbations in material structures

22 p3929 A69-39888

Hybrid microelectronic circuit failure mechanisms for thick and thin film resistors, conductors and capacitors, noting packaging contributions

22 p3910 A69-39959

Failure analysis of corrosion products in hybrid thin film circuits, discussing detection technique, instrumentation and results

22 p3911 A69-39992

Cations desorption from O, H and N films adsorbed at graphite surface under electron bombardment, studying desorption cross sections discrepancies

22 p3972 A69-39995

Hybrid microwave IC assembly techniques discussing active devices connection to substrate with thick or thin film metallizations

22 p3912 A69-40006

He-Ne laser system for micromachining thin film photolithographic masks, describing computer controlled coordinate table and product quality

22 p3954 A69-40223

Film thickness and normal load effect in thin film solid friction, noting dependence on deformation and contact

22 p3955 A69-40400

Thin film thermistors heat-separated from graphite substrate to achieve positive temperature resistance coefficient via argon heating and oxygen cooling

22 p3997 A69-41211

Thin film temperature sensor material, response time, substrate material and flight instrumentation for rocket-borne application

22 p3950 A69-41222

Frequency response of thin film thermal detectors discussing steady state harmonic response proportionality to film thickness and thermal conductivity

23 p4163 A69-41544

Hybrid techniques to produce thin and thick film microcircuits and logic system parameters

24 p4286 A69-42900

Thin film field effect transistors and integrated microcircuits, investigating active and passive element fabrication

24 p4419 A69-42900

InTe phase recrystallization in thin films composed of two InTe phase mixtures, showing random concentrations and distribution of centers growing as spherulites

24 p4361 A69-42999

InTe phase formation in thin film composed of two InTe phases, showing dependence on annealing in high vacuum and substrate temperature

24 p4361 A69-42999

Component proportion and diffraction spectrum of macroblock thin films of indium telluride phase of InTe system, using X ray and microanalysis

24 p4361 A69-42999

Solid film lubricants deposited by DC triode sputtering on Ni, Ni-Cr and Nb surfaces friction tested under ultrahigh vacuum conditions

24 p4321 A69-43122

Thin film formation, deposition methods and relation to film structure and properties

24 p4361 A69-43334

Dielectric and semiconductor films vacuum deposition by CW carbon dioxide laser, discussing optical properties

24 p4329 A69-43755

THIN LAYER CHROMATOGRAPHY

- Gas chromatography used to determine residual solid propellant stabilizers content and nitro derivatives, including thin film chromatography 02 p0303 A69-11528
- Gas-liquid and thin layer chromatography and nuclear magnetic resonance techniques to steric analysis of diketopiperazines 07 p1075 A69-19498
- Gel permeation chromatography to measure rate of adhesive aging and curing in one shot epoxy tapes, noting handling techniques and space applications 24 p4338 A69-43463

THIN PLATES

- Generalized plane stress concept extended for mathematical model to study out of plane displacement restraint in thin plates 01 p0165 A69-10114
- Approximate solution for Dirichlet problem for linear Karman differential equation used in thin plate deflections obtained by Bubnov-Galerkin method 01 p0105 A69-10700
- Asymptotic integration of three dimensional elasticity equations for thin anisotropic shells and plates, deriving variability exponent of stress under given load 01 p0170 A69-10878
- Existence of smooth solution for system of equations describing nonlinear oscillations of thin plate and shallow shell 02 p0337 A69-11654
- Generalized unsteady temperature fields and stresses in crystalline plates using Fourier and Laplace transforms 02 p0340 A69-12044
- Rms approximation validity limits for satellite temperature variances by deriving equations for thin insulated plate in space 02 p0352 A69-12211
- Stresses around two reinforced circular openings in thin elastic plate of isotropic material under biaxial loads 02 p0349 A69-12799
- Elastic stability equations solved in geometrical linearization for thin anisotropic plates under transverse shear, using variational method 03 p0525 A69-13130
- Thermal stress determination in two dimensional problem of theory of elasticity, using stress simulation by thin plate bending 04 p0668 A69-14272
- Thin cantilevered plate theory extended to large in-extensional deflections to account for geometry changes in bending moments [ASME PAPER 68-APM/BB] 04 p0670 A69-14401
- Large finite deflections of clamped thin elastic circular plate subject to transverse concentrated load at center solved by power series 04 p0675 A69-14596
- Creep stress concentration at circular hole in thin sheets under loads in own plane, discussing infinite thin plates [AIAA PAPER 68-175] 04 p0676 A69-14708
- Natural frequencies controllability by induced thermal membrane stresses examined for thin disk 04 p0682 A69-15494
- Laminar flow of stably stratified fluid with uniform upstream velocity and density gradient past thin flat plate, discussing upstream wake and boundary layer 05 p0745 A69-15724
- Stiffness matrices for buckling or vibration analysis of long thin flat plate structures connected at longitudinal edges 05 p0836 A69-16029
- Stress distribution in infinite strip with equally spaced identical semicircular notches on one edge and subject to transverse bending 05 p0842 A69-16643
- Vibration response of thin elastic plates to random loads 05 p0844 A69-16741
- Electron microscopy of titanium alloys noting preparation, heat treatment of samples, crystallographic structure, etc 05 p0782 A69-16807
- Plastic deformation and bursting pressure of thin rupture disk as related to tensile strength 06 p1020 A69-17129
- Deformation and stresses in biaxially loaded stretched thin plate with central small hole during stress redistribution caused by creep 06 p1022 A69-17368
- Couple stresses effect on thin plate stress distribution due to pressure of rivet on one side of circular hole 08 p1319 A69-20201

- Supersonic flutter of circular cylindrical heterogeneous orthotropic thin panels of finite length, obtaining nonlinear flutter equation 08 p1413 A69-20404
- Thermal stress propagation in infinite viscoelastic thin plate analyzed with cylindrical coordinate system 08 p1415 A69-20661
- Dynamic stability of thin flat plates and applications in ship and aircraft deck construction, studying dynamic buckling for rectangular plate 08 p1415 A69-20665
- Forced vibration of thin elastic plate resting on elastic foundation and subjected to time dependent loads and external damping 08 p1416 A69-20692
- Thin semiconductor plates negative differential resistance associated with captures at surface, describing electron gas by electron temperature 08 p1374 A69-21081
- Temperature distribution for thin plate heated by source of arbitrary motion and strength and governed by Sturm-Liouville boundary conditions 09 p1622 A69-21906
- Complex variable theory solution of eigenvalue problem governing elastic stability of thin elastic plate subjected to hydrostatic in-plane compression 09 p1615 A69-21921
- Finite element analysis of large deflections in thin elastic plates subjected to transverse loading, including nonlinear geometric effects 09 p1615 A69-21924
- Eddy current nondestructive tests of nonmagnetic thin metallic sheets and plates from single surface 10 p1698 A69-23046
- Aluminum alloy thin sheets with central transverse fatigue cracks subjected to increasing static loads to fracture, investigating crack tip deformation 10 p1709 A69-23056
- Fatigue crack propagation and crack tip stresses measurements in tensioned cracked panels subjected to acoustic loading 10 p1797 A69-23078
- Excitation of ultrathin Cd/SeS/ platelets with mode locked He-Ne laser for excitons formation, discussing time delay 10 p1703 A69-23512
- Very low temperature dependence of thin single crystal Al plates electrical resistance, noting Umklapp processes contribution 10 p1711 A69-23620
- Two dimensional problems solutions by contour smoothing methods, considering stress concentrations in reinforced or perforated thin elastic plates 11 p1973 A69-24661
- Stress concentrations in bending of thin perforated plates, considering potential and vortex stresses due to edge effect 11 p1976 A69-24784
- Book on statics and dynamics of anisotropic and heterogeneous elastic structures covering thin heterogeneous anisotropic panels, elastic and sandwich plates, etc 11 p1986 A69-25236
- Liapunov type analysis of linear structural dynamic system excited by stochastic parametric load, discussing radially loaded thin circular plates 11 p1990 A69-25507
- Transverse symmetrical vibrations of thin elastic plates under Jacobi pressure distribution, giving displacement and velocity plots 12 p2180 A69-26271
- Heat transfer and temperature distribution in thin fins with stochastic root temperature due to excitation by stochastic and Markov processes [ASME PAPER 68-HT-35] 13 p2374 A69-27780
- Hypervelocity impact of spheres on thin targets studied with numerical solutions utilizing STEEP code two dimensional technique based on hydrodynamic elastoplastic model [AIAA PAPER 69-357] 13 p2366 A69-28290
- Thin elastic plates buckling under small normal load and external edge force 14 p2531 A69-28810
- Plastic strains at crack tips in thin plate under concentrated forces, analyzing slip bands during initial deformation 15 p2708 A69-30659
- Griffith crack in thin plate opened by uniform tension at infinity, discussing effect of ties on stress intensity factor 15 p2710 A69-30809
- Variational principles and differential equations of thin elastic panels mechanics for aerospace structures 15 p2712 A69-30974

- Extensional vibration of thin inhomogeneous circular plate with variable modulus of elasticity and central hole, calculating periods of vibration 15 p2713 A69-31026
- Unsteady oscillations after rupture in thin homogeneous isotropic elastic plate, assuming deflection amplitude smaller than thickness 16 p2873 A69-32033
- Load carrying capacity of thin steel plates fatigued by cyclic shear buckling 17 p3052 A69-32980
- Linear heat flux in thin composite plate with internal point source, assuming no heat transfer at surface and neglectable temperature changes 17 p3068 A69-33126
- Fatigue crack propagation in thin aluminum alloy plates under plane bending using microscopic surface observation and electron fractography, noting role of aging conditions 17 p3061 A69-33677
- Error estimation in thin elastic plate bending problem approximate solution by equal deflection lines method, constructing two sided bound for boundary value problems 17 p3062 A69-33713
- Axisymmetric bending oscillations of thin circular plates of constant thickness with allowance for energy dissipation in material, analyzing resonance and phase amplitude characteristics 17 p3064 A69-33919
- Laminated anisotropic plate equations from thin plate theory including nonlinear terms, inertia and thermal stresses [ASME PAPER 69-APM-15] 18 p3213 A69-34390
- Equations of motion for plate vibration derived by complementary variational principle, including boundary conditions and thin plate transverse vibrations 18 p3218 A69-34626
- Standing twin vortices in wake behind thin flat plate normal to flow visualized by Al dust, noting Karman vortex street 18 p3086 A69-35167
- Transverse vibrations of thin linear viscoelastic rectangular plate of constant thickness resting on elastic medium 18 p3223 A69-35171
- Safety disk strength under static lateral pressure from rupture studies of thin circular plates under static and pulsating lateral pressure 19 p3434 A69-35773
- Engineering equations for elastic thin plate oscillations of materials with properties described by linear integral Volterra-Boltzmann operators 19 p3437 A69-35989
- Residual deformation of elastoplastically bent thin circular plate after perfect unloading from large deflection, considering equilibrium and compatibility conditions 19 p3438 A69-36306
- Natural frequencies of thin oblique angled isotropic plates, discussing closed form solution to differential equations 19 p3438 A69-36312
- Swept cantilever thin elastic plates bending analyzed by power series representing deflection in oblique coordinate system 20 p3621 A69-37207
- Buckling of eccentrically stiffened thin circular elastic plate under circumferential uniform compression, obtaining equations and critical loads 20 p3622 A69-37221
- Stress and displacement in thin circular plates of ductile materials under axisymmetric loading predicted by nonlinear analysis 20 p3628 A69-37787
- Soviet book on thin plates and shells bending and stability during creep covering analytical and numerical solutions for various structural elements 20 p3630 A69-38207
- Stress-strain state in thin isotropic plate with circular hole under lateral bending and torsional moments 21 p3835 A69-38725
- Elastoplastic analysis of thin plates deformation, discussing loading conditions effects 22 p4041 A69-40064
- Natural frequency of thin plate subject to cylindrical bending, analyzing panel flutter by three mode approximation for large buckling deflection 22 p4045 A69-40821
- Elastically symmetric thin plate stress-strain state under uniformly distributed load applied to edges 22 p4046 A69-41061

Boundary layer separation and free mixing phenomena between streams behind thin flat plate by finite difference methods and Prandtl exchange coefficient

23 p4060 A69-41912

Network method for stability of thin nonlinearly elastic compressible material plates, noting difference operators for rigidly clamped plates

23 p4230 A69-42003

Stressed state of thin plate with circular hole under normal and breaking force applied over hole perimeter

23 p4233 A69-42341

Aeroelastic stability of thin plates exposed to supersonic flow using singular perturbation methods, obtaining flutter boundary and membrane solution

24 p4403 A69-43573

Wake development from turbulent boundary layers on both sides of thin flat plate

24 p4249 A69-43694

THIN WALLED SHELLS

Thin cylindrical shell deformation and stress under concentrated radial loading, analyzing singularity at load point

01 p0166 A69-10301

Galerkin method for solving dimensionless Reissner equation for symmetrically loaded thin nonshallow shells of revolution

01 p0168 A69-10380

Sheba family of shell elements for matrix displacement method applied to problems of thin shells under membrane and bending action

01 p0170 A69-10865

Boundary value problems in thin shallow shells of arbitrary planform analyzed by partial differential equations

01 p0171 A69-11071

Predeformations of thin walled elastic isotropic spherical shells analyzed using Vlasov shell bending theory

02 p0336 A69-11555

Torsion of variable cross sectional thin walled bars using shell theory equations

02 p0337 A69-11559

Existence and uniqueness of weak solutions in linear theory of stable equilibrium position for inhomogeneous elastic thin walled shells

02 p0340 A69-12036

Soviet book on vibrations of elastic shell partly filled with fluid covering different stages in procedure for shells of axisymmetric configuration

02 p0346 A69-12480

Recent advances in shell buckling, discussing imperfection sensitivity, boundary conditions and wall configuration

[AIAA PAPER 68-103] 02 p0347 A69-12516

Finite difference numerical integration technique for large elastoplastic deformation transient and permanent deflection responses of thin shells

02 p0347 A69-12518

Helicoidally symmetrical stress in cylindrical thin shells

03 p0529 A69-14056

Initial deviations or imperfections effects on load capacity of infinite and finite length thin circular cylindrical shells under axial compression

[ASME PAPER 68-WA/APM-22] 04 p0669 A69-14398

Elastic-plastic thin walled cylindrical shell axisymmetric behavior under radial pressure difference, noting load for collapse

[ASME PAPER 68-APM/AA] 04 p0670 A69-14404

Elastic noncircular orthotropic conical shell stress-strain state, obtaining differential equations reducible to integrodifferential equations solvable by iteration

04 p0673 A69-14494

Thin shells deformations described by finite element model accounting for transverse shear deformations

04 p0674 A69-14588

Shallow shell deformations based on nonlinear equations solved by Newton-Raphson iteration

04 p0674 A69-14591

Temperature distributions, thermal stresses and natural frequencies of radial vibrations in thin circular cylindrical shells

04 p0675 A69-14704

Nonlinear boundary value problem of elastokinetics solved by step-by-step integration to study thin walled shells stability under axial impact

[DVL-853] 04 p0677 A69-14836

Postbuckling equilibrium calculation for pressure loaded thin walled cylinders of finite length, using Donnell nonlinear shell theory

04 p0677 A69-14837

Reinforced thin walled cylindrical pressure body nonlinear circumferential stress problem approximate solution, noting fatigue strength of aircraft pressurized cabins

04 p0548 A69-14838

Variational theorems for stress function formulation of boundary value problems in linear theory of thin elastic shells

04 p0678 A69-14894

Reissner nonlinear equations for nonshallow symmetrically loaded shells of revolution

04 p0684 A69-15538

Axial buckling load for thin walled circular cylindrical shell, noting design of internal mandrel for control of boundary expansion conditions

05 p0831 A69-15581

Stress-strain state of thin elliptical shell of revolution under rapidly varying cyclic edge loads

05 p0832 A69-15686

Elastic stability of thin circular cylindrical shell with elastic core, longitudinal and transverse reinforcement ribs, initial defects and under large strains

05 p0832 A69-15691

Elastic stability of thin circular cylindrical shell with elastic core, longitudinal and transverse ribs and initial defects under combined pressure and thermal stress

05 p0832 A69-15692

Approximate expressions for displacement state of orthotropically reinforced conical thin walled shell, finding stiffness matrix by numerical integration

05 p0835 A69-15829

Ductile creep rupture of thin walled membrane shell of revolution subjected to time dependent internal pressure and strain hardening

[ASME PAPER 68-WA/MET-15] 05 p0838 A69-16153

Circumferential buckling of ellipsoid of revolution due to internal pressure, assuming linear deflection and uniform thin shell

[ASME PAPER 68-WA/PVP-12] 05 p0840 A69-16190

Stability of thin cylindrical shells of medium length with one or both ends rigidly clamped

05 p0840 A69-16199

Resonant frequencies for beam type bending oscillations of thin walled rib-reinforced circular cylindrical shell freely supported at outermost ribs

05 p0841 A69-16204

Elastoplastic stress-strain state of asymmetric profile thin walled beam under mobile load

05 p0841 A69-16205

Dynamics of carrier rockets and space vehicles having complex three dimensional thin walled constructions with cavities containing liquids

[UN PAPER 68-95622] 06 p1013 A69-17051

Calculation of thin shell or beam structures with plasticity and isothermal creep based on linearization and local kinematic behavior

[ONERA-TP-667] 06 p1020 A69-17099

Free vibration of thin laminated orthotropic cylindrical shells

06 p1020 A69-17145

Radial vibrations of thin cylindrical shells subjected to thermal loadings, discussing temperature distributions, thermal stresses and natural frequencies

[AIAA PAPER 69-59] 06 p1028 A69-18143

Geometrically exact finite element for thin shells of revolution, using approximation to predict boundary layer stress distribution during vibration

[AIAA PAPER 69-56] 06 p1029 A69-18193

Thin rods and shells elastic analysis, using Cosserat continua for representing bodies in kinematics and balance and constitutive equations

07 p1234 A69-19382

Gravitational field in static spherical shell of matter in vacuum, deducing exact junction conditions for thin shell

07 p1182 A69-19453

Local stability of thin walled elastic shells of revolution subjected to external pressure

07 p1237 A69-19686

Boundary conditions for reflection and transmission properties of absorbing shell of arbitrary shape

08 p1273 A69-20025

Stability of finitely deformed thin cylindrical shell of rubberlike material, showing bending resistance and thickness effects

08 p1413 A69-20414

Fragmentation behavior of small thin walled metal cylinders during explosions as function of expansion velocity and material parameters

09 p1611 A69-21352

Free vibration frequencies and mode shapes for thin orthotropic oblate spheroidal shells, noting isotropic oblate spheroidal shell and isotropic spherical shell

09 p1613 A69-21719

Surrounding fluid effects on free axisymmetric vibrations of thin elastic spherical shells, studying rotational motions in compressible and incompressible ideal fluids

09 p1613 A69-21717

Elastoplastic response of intersecting hemispherical/cylindrical shell structures compared with plastic deformation predictions

09 p1615 A69-21917

Accuracy of approximations using shell equations for predicting dynamic behavior of thin cylindrical shells with exact solutions from Flugge shell equation

[AIAA PAPER 69-447] 09 p1616 A69-21918

Finite elastic deformations under transverse incompressive loading of clamped thin rectangular planform shells idealized as membranes, using incremental plasticity theory

09 p1616 A69-21919

Buckling of eccentrically stiffened thin circular cylindrical shell under uniform combined axial compression and torsion loads with lateral pressure

09 p1616 A69-21919

Buckling capabilities of inflation rigidized wire film and shell film cylinders in axial compression and bending

09 p1617 A69-21919

Large uniform torsion of thin walled open section circular cross section, deriving tube radius contraction observed in experiments

10 p1794 A69-22939

Flow instability of incompressible nonconducting fluid in thin cylindrical conducting elastic pipe in constant uniform magnetic field

10 p1798 A69-23099

Proton flux density at axial point of thin cylindrical and slab shell shields bombarded by isotropic inverse power law spectrum of protons in space

10 p1723 A69-23160

Book on statics of thin walled shells of revolution covering stress-strain analysis for geometrical shapes

10 p1800 A69-23194

Biaxial stress effect on creep properties of thin walled tubes of polymethyl methacrylate at controlled temperature and humidity

10 p1717 A69-24211

Stress concentration during deformations in thin shallow shells, using conformal mapping and difference method

11 p1971 A69-24644

Stress distribution around holes in thin shells and plates during large elastic displacements, considering hole size, loading and shallow spherical shells

11 p1972 A69-24655

Stress concentration at holes and cavities in thin elastic shells under static and dynamic loads, considering physical nonlinearities of material

11 p1974 A69-24666

Temperature field in thin walled rods with spiral cross section in solar radiation, considering radiative heat exchange

11 p1999 A69-24777

Theory of thin shells - Conference, Copenhagen September 1967

11 p1977 A69-24800

Thin elastic shell interior equations based on stress and strain, discussing shell description, strain derivatives plate deformation into cylindrical shells, etc

11 p1977 A69-24800

Thin elastic shell theory, using iterative process to develop differential equation integrals for interior state of stress

11 p1977 A69-24800

Nonlinear theories of deformable surfaces as two dimensional generalized continua applied to elastic shells, emphasizing elastic Cosserat surface

11 p1978 A69-24800

Thin plastic shell theory based on statical and geometrical relations for shallow and circular cylindrical shells

11 p1978 A69-24800

Shell theory foundations and basic equations discussing classical shell equations asymptotic nature and errors

11 p1978 A69-24800

Continuum theory for thin elastic shells with local structural effects, emphasizing shell constituted by Cosserat material

11 p1978 A69-24800

Asymptotic methods for three dimensional equations in thin and thick elastic shell theory for determining two dimensional systems

11 p1978 A69-24800

Linear thin shell theory in complex dependent variable form for determining fourth order partial differential equations

11 p1978 A69-24800

ferential equations, considering elastic shells with edge loads

11 p1978 A69-24811

Finite deformation equations for flat annular membranes deduced from equations for thin shells of revolution, discussing displacement equations and fixed edge forces

11 p1979 A69-24813

Postbuckling behavior and subsequent imperfection sensitivity of thin walled cylinders subjected to torsion, considering perturbation

11 p1979 A69-24814

Thin walled circular cylinders postbuckling behavior and stability under axial compression calculated for design loads

11 p1979 A69-24816

Semiinfinite circular cylindrical shell buckling under axial load, computing forces, moments and displacements by thin shell equation

11 p1979 A69-24818

Deformation processes of geometrically nonlinear rotational membrane shells under internal pressure

11 p1980 A69-24821

Thin conical elastic shell stress-strain state calculated by computer for arbitrary thicknesses and loading conditions, considering temperature and edge forces effects

11 p1981 A69-24943

Thin elastic conical shells asymmetric deformation under stresses and strains, deriving asymptotic solution

11 p1983 A69-25090

Heat generation in thin viscoelastic cylindrical shell with relaxation and resonance dispersion during torsional vibration

11 p2000 A69-25168

Maximum stress under bending for thin walled circular cylindrical shell stiffened with uniform stringers

11 p1987 A69-25380

Axisymmetric vibration modal properties /frequencies and mode shapes/ of thin conical shell frustrums, considering dimensional and boundary condition influences

11 p1992 A69-25519

Bending and membrane stresses determination in shallow thin shells of revolution under large axisymmetric deflections, using normal and radial displacements relationship [SESA PAPER 1332]

11 p1995 A69-25651

Stochastic problems in thin elastic shell theory solved by equations obtained by linearizing shell equations near initial state of stress

11 p1996 A69-25732

Nonstiffness of nonshallow spherical dome using asymptotic method, applying nonlinear Reissner equations to finite symmetric deformation of thin shells of revolution

11 p1996 A69-25733

Composite shell carrying capacity under general load, studying closing shape between laminate layers, transverse contraction, supporting layers thicknesses ratio, etc

12 p2176 A69-25851

Quasi-shallow shells theory applicability to thin elastic shallow shells, emphasizing use of function W/ρ

12 p2178 A69-26001

Dynamic programming method for upper bound on collapse load of rotationally symmetric thin cylindrical shell under ring loading

12 p2179 A69-26214

Postcritical deformations of thin conical elastic shells hinged along edges under external pressure using Pogorelov method for cylindrical shells

12 p2181 A69-26609

Axisymmetric deformation of thin orthotropic laminar spherical shells under internal loads calculated on computer using Legendre polynomials

12 p2181 A69-26611

Galerkin method for solving dimensionless Reissner equation for symmetrically loaded thin nonshallow shells of revolution

12 p2182 A69-26679

Natural frequencies of ring-stiffened thin walled cylindrical shell determined by partial differential equations of motion, allowing for eccentricity

12 p2184 A69-26810

Thin cylindrical shell vibration with three supports analyzed by minimizing Lagrangian of vibration, obtaining frequencies and modes

13 p2359 A69-27257

Membrane and bending stresses around elliptic hole in thin circular cylindrical shell, considering axial tension

13 p2362 A69-28123

[NAL-TN-13]

Thin walled maraging steel tube toughness determined by Charpy precrack testing of transverse and longitudinal impact properties

13 p2269 A69-28183

Stress concentration around holes in thin shells, including analysis of stress-strain state in cylindrical and spherical shells

14 p2532 A69-28977

Elastoplastic deformations of thin axisymmetric shells of revolution with variable thickness, exemplifying shell with piecewise constant thickness

14 p2533 A69-28982

Geometric discrepancies influence on stability modes and loads for thin shells up to point of pcollapse

14 p2533 A69-29022

Differential equations for elastic stress distribution in thin rotating shell with arbitrary profile, obtaining analytical dimensionless solutions for potential profiles

15 p2703 A69-30158

Laminar thin orthotropic cylindrical shells natural and forced oscillations and dynamic deflection coefficient

15 p2715 A69-31202

Plane strain solution for thick walled viscoelastic cylinder bonded to thin elastic shell from deformation rate and strain, including inertia effects

16 p2871 A69-31876

Buckling load of cylindrical shell with inclined stiffeners, using method for stability of thin walled cylinder under transverse end load at free end

16 p2872 A69-31912

Potential and kinetic energy of cylindrical thin shell with cutout approximated by two dimensional finite difference methods, obtaining eigenvalue problem [AIAA PAPER 68-318]

16 p2874 A69-32158

Nonlinear partial differential equations solutions in theory of thin elastic spherical shells subjected to temperature fields and external loading

17 p3067 A69-34147

Strain displacement and compatibility equations of finite symmetrical deflections of thin shells of revolution [ASME PAPER 69-APM-14]

18 p3214 A69-34391

Differential equations of shells of revolution theory assuming rotationally symmetric stress and strain in thin elastic shells

18 p3215 A69-34549

Stability of thin walled eccentrically reinforced cylindrical shell, determining eccentricity influence and critical pressure formula from considerations of Poisson ratio, reinforcement parameters, etc

18 p3216 A69-34576

Thin walled cylindrical shells deflections under axial impact load, assuming deformations resembling cylindrical surface bending

18 p3217 A69-34599

Stress and displacement waves propagation in thin walled elastic cylindrical shell under compressive axisymmetric force based on momentless theory

18 p3218 A69-34600

Electromagnetic induction in concentric thin shell-enclosed solid conducting sphere immersed in varying electromagnetic field [AFCRL-69-0082]

18 p3101 A69-34803

Constrained elastoplastic torsion of closed thin walled cylindrical shells, analyzing tangential and normal stress by using equilibrium equations

18 p3222 A69-34978

Thin brittle plastic shells mechanical properties differing under tension and compression described by solving differential equations in successive approximation

18 p3224 A69-35327

Buckling stresses in thin walled box girder under bending determined using stationary potential energy criterion

18 p3224 A69-35344

Thin walled shell temperature and strain fields described by integrodifferential equations based on Kirchhoff hypothesis and coupled thermoelasticity reciprocity equations

18 p3225 A69-35368

Hollow thin walled carbon spheres developed as filler material for resins in low weight high temperature applications

19 p3355 A69-35522

Structural analysis of thin walled conical shell with variable external loading and Winkler-base elastic filler, using linear differential equation with variable coefficients

19 p3436 A69-35846

Contact problem of two thin elastic shells within Kirchhoff-Love theory, discussing constitutive equations

19 p3438 A69-36305

Nonlinear shell theory for thin elastic circular cylinders, obtaining equations for investigating equilibrium configurations of postbuckled states

19 p3440 A69-36636

Thin elastic shells internal stress state by iteration of two dimensional equation of general linear theory

19 p3443 A69-36790

Displacement patterns for buckled shapes of axially compressed thin walled circular, cylindrical and conical shells

19 p3443 A69-36793

Thin circular cylindrical shells elastic equilibrium under loads producing deflection, elongation or contraction described by integrating equilibrium equations with constant coefficient

20 p3621 A69-37076

Torsional-flexural buckling of thin walled open sections under eccentric load, emphasizing singly symmetric sections loaded in plane of symmetry

20 p3625 A69-37653

Free vibrational characteristics of thin walled circular cylindrical shells with layers of anisotropic elastic material laminated about middle surface

20 p3627 A69-37767

Thin cylindrical pressure vessels with circular cutouts and radial branches, observing limit pressures during plastic deformation

20 p3629 A69-38027

Thin curved panels postbuckling behavior under axial compression, basing study on thin shell finite deformation theory and Galerkin method

20 p3629 A69-38112

Soviet book on shell and thin walled structure calculation methods covering stability and stress analysis, reinforced and sandwich shells, etc

20 p3630 A69-38199

Stress-strain state of thin spherical shell of variable thickness in elastoplastic equilibrium, using Meissner variables to reduce equilibrium equations

21 p3834 A69-38717

Linear hydrodynamic equations describing inviscid fluid flow past thin elastic cylindrical shells in circle with motions described by shallow shell equations

21 p3834 A69-38719

Stress-strain state of thick and thin walled closed shells of variable thickness during elastoplastic torsion developing in aircraft component production

21 p3835 A69-38882

Free vibration of thin cylindrical shells with thickness discontinuity, considering natural frequencies and mode shapes dependence on thick/thin ratio

21 p3836 A69-38984

Buckling stability of thin cylindrical shell under torsion, allowing for finite displacements due to shear in initial stress-strain state

21 p3838 A69-39187

Snap through in thin shells with initial irregularities during creep, determining critical time to failure by analyzing undisturbed buckling process

21 p3838 A69-39188

Computer program for stress analysis of cylindrical pressure vessel with flat-end closures by thin shell theory

21 p3842 A69-39306

Stress analysis of thin axisymmetric shells by plane frame analysis program, noting stiffness matrix for conical shell element

21 p3843 A69-39312

Finite element relaxation method for computing stress distribution in thin walled structure, considering computer program, storage and solving time

21 p3843 A69-39313

Deformation of thin walled spherical shell reinforced with equatorial hoop by concentric equal forces

21 p3846 A69-39714

Approximate generalized stress-strain rate relations for stationary creep analysis of thin shells compared with corresponding exact relations

22 p4041 A69-40013

Nonlinear stability for closed thin walled orthotropic cylindrical shell subjected to uniform external pressure, using Bubnov-Galerkin method for approximate solution

22 p4042 A69-40454

Vlasov thin shell theory extended for undamped bending, transforming partial differential equations and stress function into integral equation solvable by successive approximations

23 p4225 A69-41407

Differential operators representing potential energy of thin shell, discussing self conjugacy of boundary value problems

23 p4229 A69-41999

Computer program for natural oscillations of plates and shells, deriving differential equations of motion for thin elastic shell by variational method

23 p4230 A69-42004

Circular cylindrical thin walled shells creep buckling under uniform axial compression

23 p4234 A69-42413

Asymmetric dynamic response to free and forced vibrations of thin membrane shells at given stress state due to previous loads

24 p4399 A69-42990

THIN WALLS

Thin rigid radial wall effect on convective flow in heated rotating annulus

02 p0275 A69-12013

Optimal thin walled cross section of hollow beam for pure bending, taking into account stability requirements

02 p0340 A69-12054

Fast response thin skinned calorimeters for high heat flux profiles of arc jet flows

04 p0602 A69-15427

Stability functions for local buckling of long thin flat walled structures loaded for longitudinal compression and shear

05 p0833 A69-15709

Thin walled symmetrical angle section beam stability under bending moment by section deformation or torsional buckling

08 p1410 A69-19892

Thin walled channel columns section stability analyzed in terms of overall/Euler and local buckling

13 p2361 A69-27440

Elastoplastic strains in thin walled beams subjected to oblique bending by mobile loads of coupled concentrated forces, calculating deflections and plastic region distribution

15 p2711 A69-30971

Statistical calculation of three dimensional frames of thin walled rods, using method of initial parameters in matrix form

15 p2714 A69-31199

Mechanical machine for fatigue testing flat samples of thin walled structures under tension and at various frequency ranges

18 p3118 A69-34833

Ultrasonic spectrometry application to thickness measurement of thin and thick walled articles

18 p3137 A69-35110

Reinforced plastics static fatigue strength under various loads including thin walled tubes long term tests under constant internal pressure

18 p3162 A69-35353

Matrix formulation for discrete element method applied to linear static and eigenvalue problems of thin walled segments, using homogeneous differential equations

19 p3445 A69-36831

Plastic bending of thin walled pipes taking into account cross section flattening

21 p3835 A69-38868

Natural frequency equations for torsional vibration of fixed/ fixed and fixed/ simply supported uniform thin walled beams of open section based on energy method

22 p4040 A69-39935

Three dimensional welded structure of thin walled girders with stability loss, discussing welding strain gage measurements and simplified computational procedure

23 p4169 A69-42007

THIN WINGS

Pressure coefficients determination on slender body surface to estimate effects of quadratic terms, considering body of revolution with thin cruciform lifting surfaces

10 p1632 A69-22911

Flow field pressure distribution due to plane shock wave impinging by thin wing moving in opposite direction, discussing mathematical formulation, analytic solution and applications

17 p2891 A69-33459

Function theoretic solution of dual integral equations applied to boundary value problem of supersonic flow over infinite span thin wing

19 p3239 A69-36311

Supersonic flow past antisymmetrical thin delta wing by flow separation from subsonic leading edges, noting wing surface pressures

19 p3241 A69-36779

Sedov formula for complex velocity of arbitrary circulation in two dimensional theory of small curvature thin wings

19 p3242 A69-36795

THINNERS

U SOLVENTS

THIOLS

NT CYSTEINE

Disulfide effects on jet fuel operating characteristics and demercaptanization influence on thermal stability, corrosive action and sedimentation

01 p0142 A69-11098

Organosilicon-containing derivatives of 2-aminoethanethiols and 2-aminoethanethiosulphuric acids as radiation protective agents

13 p2210 A69-28486

Synthesis of N-/trimethylsilylalkyl/ diamines and N-/trimethylsilylalkyl/-N-/2-mercaptoethyl/ diamines, determining structure by IR spectra

15 p2561 A69-30414

THIOPLASTICS

Electron beam radiation curing of mercaptan terminated butadiene-acrylonitrile liquid copolymers at ambient temperatures in air

09 p1512 A69-22368

THIXOTROPIC PROPELLANTS

U GELLED ROCKET PROPELLANTS

THOMAS-FERMI MODEL

Thomas-Fermi approximation applied to calculation of equations of state and thermodynamic functions at high pressure from differential equations of statistical atom model

22 p3984 A69-40186

THOMSON EFFECT

U THERMOELECTRICITY

THORAX

Compensative adaptational reactions to weightlessness, discussing blood supply to thorax area, external respiration, gas exchange and energy loss during parabolic and orbital flights

17 p2909 A69-33384

THORIUM

Interferometrically measured wavelengths tabulated for Th lines in 2747-4572 Å range, using liquid nitrogen cooled hollow cathode lamp and Fabry-Perot interferometer

23 p4191 A69-42150

THORIUM COMPOUNDS

Thorium and La-compounds retained superconductivity to Pr and Tm concentrations due to crystal field splitting effect producing nonmagnetic singlet ground state

02 p0295 A69-11778

THORIUM ISOTOPES

Turbulent parameter and turbulent diffusion vertical profile diurnal variations determination based on measurements of Rn 220 and thorium-B concentrations near ground

03 p0459 A69-13273

Thorium 228 production and shaping for radiothermal propulsion, discussing transformation from radium 226, irradiated target processing, etc

05 p0791 A69-15597

Turbulent parameter and turbulent diffusion vertical profile diurnal variations determination based on measurements of Rn 220 and thorium-B concentrations near ground

14 p2472 A69-28781

THORIUM OXIDES

Joining methods for fabricating thorium dispersion strengthened nickel and nickel chromium materials

09 p1509 A69-22342

Thorium strengthened Ni-Cr alloys high temperature stability, noting thorium particle size influence

14 p2465 A69-29682

Recrystallization in thorium dispersed Ni sheet as function of strain-anneal cycles, using electron transmission technique quantitative determination

20 p3557 A69-36958

THORON

U RADON

THREE BODY PROBLEM

Three body problem, discussing impossibility of libration points of gravitating ellipsoid

01 p0155 A69-10957

Stability characteristics of small and moderately sized short period Trojan librations in sun-Jupiter restricted three body problem

01 p0158 A69-11329

Vehicle trajectory motion in transition region of three body problem, noting equations of motion, first order solutions, etc

03 p0505 A69-13001

Interplanetary orbits for probe launched from earth to reencounter earth, noting relationship to three body problem

03 p0514 A69-13783

Hill stability in unbounded three body problem analyzing motion in baricentric coordinate system, deriving equations for curves defining conditions for stability

04 p0652 A69-14543

Low density limit to three body ionic recombination coefficients in various gases

04 p0632 A69-14679

Soviet book on artificial satellite motion in noncentral gravitational field, discussing celestial axisymmetric planetary orbits, stationary centers, three body problem, etc

04 p0659 A69-15023

Asymptotic solutions of restricted three body problem for one parameter periodic orbits in earth-moon synodic system, determining motion near moon

04 p0663 A69-15382

Stellar escapes from clusters and temporary captures in restricted three body problem with equal masses

05 p0827 A69-16599

Resonant long period orbits around Lagrange equilibrium points, discussing formal expansions method for three body problem

07 p1225 A69-19719

Numerical analysis of periodic solutions of restricted three body problem in sun-Jupiter system, noting genealogy of periodic orbits

08 p1382 A69-19874

Separable expansion for off shell two body t matrix with Coulomb potential to solve nonrelativistic three body problem with two body interactions

08 p1354 A69-20205

Five families of simple periodic symmetrical orbits in Hill limiting case of restricted three body problem, studying asymptotic forms

08 p1393 A69-20572

Three body ionic recombination coefficient for moderate and high gas densities, taking into account variability in mean free path and trapping radii

09 p1542 A69-21624

Perturbing body influence on motion near triangular Lagrangian solutions of restricted elliptical three body problem applied to earth-moon system under solar perturbations

10 p1779 A69-23612

Canonical invariance of Hamiltonians noting nature of solutions of differential equations, existence of periodic solutions and application to three body problem

10 p1721 A69-23987

Elliptic integrals to determine orbital elements time dependence in three body problem, estimating satellite lifetime

10 p1791 A69-24196

Ellipsoidal satellite translational rotational motion under spherical planet and point source sun gravitational fields influence, obtaining approximate solution for three body problem

11 p1956 A69-24399

Triple system p Velorum, discussing coude spectra and published visual orbital elements

11 p1963 A69-25263

Autonomous two degrees of freedom Hamiltonian system triangular libration points found stable for all mass ratios in circular restricted three body problem

12 p2155 A69-25883

Restricted three body problem of conservative Hamiltonian systems with two degrees of freedom and mass ratio parameter, considering phase space around L sub 4

13 p2346 A69-27711

Periodic Trojan orbits for resonance 1/12 in restricted three body problem, noting bridge of stable and unstable orbit lanes

13 p2350 A69-27824

Three and n body problems solution by reduction of independent variables and maximum principle

15 p2652 A69-30448

Numerical analysis of asymptotic solution for earth-moon particle trajectories in idealized restricted three body problem

16 p2857 A69-32155

Ground traces of artificial earth satellites with respect to perturbations due to atmospheric drag, earth oblateness and moon and sun as third body

19 p3398 A69-35614

Short term motion of lunar satellite, discussing three body disturbing functions and perturbation solution of nonsingular orbit elements

19 p3402 A69-35934

Linearization of equations of motion for three body problem, emphasizing lunar far side libration point as related to possible landing

19 p3402 A69-35961

Periodic orbits in nonlinear dynamical system constructed with iterative method based on modification of generalized Newton-Raphson technique
[AAS PAPER 68-085]

20 p3595 A69-37171

Stability of periodic orbits in elliptic restricted three body problem
[AAS PAPER 68-086]

20 p3595 A69-37172

Stability of motions about triangular libration points in elliptic restricted three body problem
[AAS PAPER 68-090]

20 p3595 A69-37175

Trigonometric polynomials representing perturbation function and derivatives in three body problem

20 p3596 A69-37315

First approximation stability of triangular Lagrange solutions of restricted elliptical three body problem, formulating power series for orbital eccentricity

20 p3575 A69-37318

Resonance theory of thermolecular atomic recombination kinetics based on transition complexes identification as quasi-bound states or orbiting resonances

20 p3579 A69-37345

Infinitesimal mass trajectories and possible double collision in gravitational field of two finite and unequal masses in plane elliptic restricted three body problem

21 p3795 A69-38443

Optimal control stationkeeping for maintaining space probe stability around collinear points in three body problem
[AIAA PAPER 69-906]

21 p3807 A69-39338

Computer program [TACTICS] for simulating three vehicles simultaneous motion in space, considering intercepter-target guidance and intercept trajectories
[AIAA PAPER 69-890]

21 p3678 A69-39415

Dynamic systems stability with two degrees of freedom, determining second order time dependent integrals valid near periodic orbit

22 p4013 A69-40123

Symmetric periodic orbits families of restricted three body problem, using two body problem

22 p4031 A69-40908

Periodic orbits obtained for special restricted three body problem in resonance using numerical integration

22 p4031 A69-40909

Collective rotational motion separation from internal motion in system of n point masses based on wave mechanics, emphasizing three body problem

24 p4349 A69-42650

Ellipsoidal satellite translational rotational motion under spherical planet and point source sun gravitational fields influence, obtaining approximate solution for three body problem

24 p4390 A69-43789

THREE DIMENSIONAL BOUNDARY LAYER

Self similar solutions uniqueness of three dimensional laminar boundary layer equations for conical flow determined by supplementary conditions derived from flow pattern

02 p0233 A69-12572

Three dimensional boundary layers on cones at small angle of attack, presenting numerical solutions with heat transfer effects for wind tunnel model
[ASME PAPER 68-WA/APM-24]

04 p0541 A69-14389

Three dimensional boundary layers, extending Prandtl independence principle to laminar compressible flow over convex body

05 p0743 A69-15556

Universal equations for three dimensional laminar boundary layer of incompressible fluid on walls of axisymmetric channel with vortical external flow

06 p0909 A69-17328

Linear equations for three dimensional perturbations in boundary layer of viscous incompressible fluid flow on plane surface, discussing Tollmein-Schlichting waves

06 p0909 A69-17329

Three dimensional boundary layer problems analyzed by exact numerical method
[AIAA PAPER 69-138]

06 p0911 A69-18041

Spatial distribution of three dimensional laminar boundary layer transition zone on sharp half angle cone from hypersonic wind tunnel tests
[AIAA PAPER 69-12]

06 p0863 A69-18112

Three dimensional boundary layer separation assuming zero friction

07 p1050 A69-18736

Numerical method for three dimensional boundary layer equations, applying perturbation technique and independence principle to rotating flat blade
[AIAA PAPER 69-227]

07 p1051 A69-19560

Mixed three dimensional separation of boundary layer on ellipsoid of revolution at ten degree angle of attack, ignoring heat flux

08 p1251 A69-19876

Wall temperature influence on intensity of transverse flow of three dimensional laminar boundary layer resulting from transverse pressure gradient

08 p1251 A69-20274

Numerical integration of equations of three dimensional laminar boundary layer in conical flow, using integral relation method

09 p1430 A69-21789

Nonequilibrium three dimensional boundary layer over slightly yawed cone analyzed for air dissociation and ionization parameters, noting binary scaling application

09 p1430 A69-21965

Krause numerical solution applied to normal injection in three dimensional incompressible laminar boundary layer
[DVL-902]

09 p1482 A69-21971

Numerical solution for three dimensional boundary layers based on stability determinations for linearized difference equations

10 p1631 A69-22902

Three dimensional laminar boundary layer of incompressible flow controlled by suction or injection, considering similarity flow solutions and role in satellite design

10 p1678 A69-22936

Mixed boundary value problem in the theory of axisymmetric potential of three dimensional boundary layer reduced to solution of linear integral equation

11 p1918 A69-24787

Three dimensional laminar boundary layer near windward generator of cone subjected to uniform mass transfer by suction or injection

11 p1874 A69-25281

Numerical integration of equations for three dimensional laminar boundary layer on sharp elliptical cones in supersonic flow of ideal gas, discussing heat exchange

11 p1821 A69-25477

Three dimensional thermal laminar boundary layer around body moving with constant acceleration in incompressible fluid, considering wall temperature and Prandtl number

13 p2380 A69-28631

Boundary value problem in three dimensional boundary layer theory for incompressible flow near stagnation point

14 p2432 A69-29677

Three dimensional laminar boundary layer on semiinfinite permeable flat plate in viscous incompressible fluid flow, calculating velocity profiles and skin friction components

14 p2433 A69-29898

Boundary layer solution in three dimensional bending for plate with curvilinear hole to study stress-strain state at hole and over entire plate

15 p2708 A69-30662

Three dimensional periodic boundary layer on ellipsoid in harmonic motion at given angle of attack, using successive approximations

15 p2548 A69-31008

Laminar boundary layer on rotating blades and yawed infinite wings, solving partial differential equations numerically by implicit finite difference scheme on computer

16 p2732 A69-31885

Systematic formalism specialization of group theory techniques for similarity analysis applied to three dimensional incompressible boundary layer flows

16 p2773 A69-32379

Three dimensional hypersonic laminar boundary layer subdivided into inner and outer regions, obtaining flow description by matching inner and outer solutions
[AIAA PAPER 69-710]

17 p2955 A69-33467

Three dimensional laminar boundary layer on conical body of revolution in low Reynolds number compressible fluid flow

19 p3241 A69-36762

Three dimensional laminar boundary layer hypersonic flow about slender conical vehicles, analyzing transverse surface curvature effect, studying Reynolds number, cone angle, etc
[ASME PAPER 69-FE-23]

20 p3460 A69-37992

Three dimensional turbulent boundary layer over flat surface in incompressible flow calculated by finite difference method based on time averaged motion equations integration

21 p3693 A69-38767

Superimposed free vortex swirl effect on flow and heat transfer in three dimensional axisymmetric laminar boundary layer

24 p4304 A69-43584

THREE DIMENSIONAL COMPOSITES

Three dimensional reinforcement composites for gear and bearing applications with improved interlaminar shear strength, thermal and wear properties

08 p1340 A69-20509

THREE DIMENSIONAL FLOW NT SECONDARY FLOW

Three dimensional flow at large distance and in front of shock wave for three dimensional body traveling at sonic velocity

01 p0005 A69-10159

Steady three dimensional flow through impeller of turbines with small number of blades and with edge cut hub, noting inefficiency of flow without impact

01 p0142 A69-10309

Gravity waves train propagation in cylindrical channel, discussing derivation by three dimensional flow analysis method

01 p0059 A69-10382

Algorithms for three dimensional supersonic gas flow incident on bodies applied to calculating oxygen flow in asymmetric nozzle

01 p0060 A69-10724

Steady state three dimensional MHD flow in variable profile channels calculated by reducing problem to two dimensional approximation using curvilinear coordinate system

01 p0131 A69-10776

Hydraulic analogy for shock and expansion waves arising in supersonic compressors due to three dimensionality of flow
[ONERA-TP-598]

02 p0187 A69-11621

Soviet book on hypersonic internal and external three dimensional viscous and nonviscous gas flow, emphasizing flow past slender blunted bodies

02 p0230 A69-11775

Three dimensional wakes and jets, discussing centerline velocity, half width growth and velocity irregularities

02 p0190 A69-12549

Generalization of characteristic relations for steady supersonic 3D motion of polytropic gas, obtaining complex screw motions

03 p0412 A69-12847

Three dimensional sonic flow downstream from shock wave in nondissipative perfect fluid, introducing pseudorotating flow to obtain velocity field

03 p0362 A69-13363

Survey of papers on computer calculation of two and three dimensional gas flows, emphasizing method of characteristics and finite difference techniques

03 p0363 A69-13657

Resonance analysis of forced vibration of rectangular plate in three dimensional supersonic flow

03 p0528 A69-13928

Surface geometry of three dimensional inviscid hypersonic flows, developing tensor equations for geodesic, steepest descent and pressure approximations

04 p0542 A69-14718

Simulation of two and three dimensional fluid transients by use of one dimensional equations in lattice-work of piping elements

05 p0747 A69-16071

Thickness effects on flow past sweptback wings in supersonic flight noting influence of oscillatory motion
[ASME PAPER 68-FE-31]

05 p0698 A69-16078

Three dimensional steady/unsteady flows of conducting inviscid gas in magnetic field, in absence of electric field, solving related Cauchy problem

06 p0966 A69-17541

MHD flows in channels of MHD devices, emphasizing two and three dimensional problems

06 p0969 A69-17913

Three dimensional scramjet exhaust nozzle flow fields by second order method of characteristics
[AIAA PAPER 69-5]

06 p0862 A69-18048

Three dimensional hypersonic steady flow around blunt and pointed cones at nonzero angles of attack calculated by method of characteristics
[AIAA PAPER 69-187]

06 p0865 A69-18176

Effects of multidimensional flow through porous matrices in mass transfer cooling, analyzing one dimensional model for blunt axisymmetric surfaces
[AIAA PAPER 69-149]

06 p1038 A69-18179

Three dimensional vector fields and flows geometry, discussing vector lines as geodesics on surfaces of normal congruence and flat vector fields

08 p1302 A69-19823

Mixed three dimensional separation of boundary layer on ellipsoid of revolution at ten degree angle of attack, ignoring heat flux

08 p1251 A69-19876

Wall friction influence on three dimensional flow in axial flow turbomachines, introducing shear stresses between flow planes

08 p1252 A69-20724

Three dimensional flow field of incompressible fluid with purely axial development in conical ducts and turbomachines

09 p1480 A69-21597

Natural convective oscillatory three dimensional flow in cylindrical annuli, describing inception, amplitude, period and wavelength

09 p1481 A69-21902

Hydrodynamic stability and entropy decrease in flow in three dimensional space, using irreversible thermodynamics principles

10 p1808 A69-22892

Steady three dimensional flow of gases with thermodynamic relaxation, noting flow field weak discontinuities and effect of discontinuities in wall curvature

10 p1677 A69-22894

Multidimensional theory of characteristics found applicable to calculating three dimensional time dependent gas flows

10 p1632 A69-22913

Three dimensional MHD flow near forward stagnation point magnetic fields with large induction values described by differential equations, showing tendency towards two dimensional flow

10 p1727 A69-23100

Similarity solutions of laminar boundary layer equations for three dimensional flows of incompressible power law fluids

10 p1678 A69-23235

Three dimensional compressible potential flow in curved circular duct analyzed by perturbation method

11 p1867 A69-24607

Holographic recording of three dimensional flow field velocities, applying theory of particle size assessment via Fraunhofer holography

11 p1884 A69-24691

Nonorientable five channel adapter with spherical measuring head for three dimensional gas flow measurement, noting sensitivity to mechanical disturbances in calibration

11 p1888 A69-25340

Delta wing in three dimensional supersonic flow analyzed by method of characteristics, discussing leading edge problems

11 p1820 A69-25425

Three dimensional gas flows near characteristic surface extended over homogeneous polytropic gas at rest

11 p1876 A69-25729

Potential triple traveling space waves in barotropic gas with arbitrary equation of state, analyzing adjacent and three dimensional self similar flows

12 p2061 A69-25889

Optical methods in three dimensional gas flow research, noting role in density field determination and conjunctive use with gas dynamics equations

12 p2011 A69-26191

Difference schemes for quasi-linear hyperbolic equations, with applications to three dimensional supersonic flow past bodies

14 p2430 A69-29475

Unsteady three dimensional heating of finite solid rectangular parallelepiped, deducing expressions for rectangle and slab

15 p2717 A69-30790

Three dimensional laminar jet mixing of incompressible viscous fluid from rectangular cross section nozzle into uniform stream

16 p2768 A69-31687

Book on three dimensional flow of ideal gases past smooth bodies, emphasizing utility of finite difference methods

16 p2771 A69-32003

Three dimensional supersonic nozzle flow field calculations using second order numerical method of characteristics and computer programmed for internal flows

[AIAA PAPER 69-463] 16 p2734 A69-32766

Three dimensional potential surface flow past rotor blade in hover, accounting for compressibility and blade element theory limitations

[AHS PAPER 324] 17 p2895 A69-33537

Three dimensional supersonic flow past pointed nonaxisymmetrical bodies characterized by great local surface curvature changes, using new approximation

18 p3086 A69-34705

Systematic mathematical ordering of knowledge concerning three dimensional flow patterns around blunt bodies, emphasizing high speed computers role

18 p3089 A69-35269

Fraunhofer holography for measurement of three dimensional flowfield velocity components, investigating rectangular channel flow

19 p3305 A69-35729

Monograph on method of characteristics for three dimensional supersonic flows, covering numerical calculations of steady gas flow past bodies at angle of attack

19 p3238 A69-36170

Three dimensional velocity field disturbed by shock wave traveling across slender wing at supersonic speed

19 p3242 A69-36797

Navier-stokes equation numerical integration for three dimensional incompressible flow, discussing annulus thermal convection and trigonometric transforms algorithm

21 p3694 A69-38770

Laplace transforms in heat conduction theory in three dimensional infinite homogeneous body

21 p3851 A69-39011

Linear normal mode instability of three dimensional laminar and turbulent shear layers, analyzing relations between velocity profile, eddy viscosity and oscillations

22 p3932 A69-40893

Mean flow properties of incompressible turbulent three dimensional jets and wakes, treating flow within boundary layer theory context

23 p4060 A69-41908

Tridimensional infrasonic diffuser geometry effects on operational efficiency, considering opening angle, outlet/inlet section fields ratio and diffuser length/hydraulic radius ratio

24 p4243 A69-42560

THREE DIMENSIONAL MOTION NT SECONDARY FLOW

Single impulse noncoplanar orbital transfer with finite time of thrust action for satellite in elliptical orbit

05 p0823 A69-16044

Regularization of perturbed Keplerian motion in three dimensional space by means of Levi-Civita transformation generalized to three dimensions

05 p0827 A69-16602

Integral of Navier-Stokes equations for steady three dimensional motion of incompressible viscous fluid, giving angular velocity vector projections

08 p1342 A69-20320

Elasticity theory upper and lower bounds for two and three dimensional inhomogeneous problems and applications to plates

10 p1794 A69-22889

Three dimensional model of atmospheric drift currents in equatorial region of world ocean system based on nonlinear differential equations

14 p2472 A69-29405

Taylor vorticity transport theory and von Karman similarity hypothesis extended to consider three dimensional fluctuating velocity field in analyzing turbulent swirling ducted flow

[ASME PAPER 69-APM-19] 18 p3120 A69-34394

Two dimensional theory for anisotropic plates motion derived, using asymptotic integration of three dimensional elasticity equations

18 p3224 A69-35297

Single impulse noncoplanar orbital transfer with finite time of thrust action for satellite in elliptical orbit

20 p3606 A69-37953

Spherical motion of solid body about fixed point with nonholonomic coupling, deriving equations for centrifugal moments of inertia effects on motion

21 p3773 A69-39840

Statistical analysis of position errors inherent in position-finding system utilizing position fixing planes in three dimensional space

22 p3979 A69-41253

Three dimensional mixed boundary value problem in elasticity by dominant states method, examining generalized Fourier series feature in Legendre polynomials

23 p4229 A69-41998

THRESHOLD CURRENTS

Exploding wire detonators noting dependence of threshold burst current on bridgwire length and diameter, explosive surface, density, etc

01 p0119 A69-10672

Continuous wave GaAs injection lasers operation at high temperatures shown possible by using available threshold current densities with suitable heat sink materials

02 p0255 A69-11710

Uniaxial pressure applied to p-n junction of GaAs injection laser, discussing effects on threshold current and wavelength

03 p0441 A69-13848

Threshold velocities of acoustoelectric current oscillations in elemental piezo- and nonpiezoelectric semiconductors, taking into account amplification and losses of phonons

05 p0807 A69-15994

Active region doping effect on laser diode threshold current, noting current dependence on loss coefficients in interband transition model without selection rule

06 p0933 A69-17254

Linear perturbation theory to predict instability threshold conditions caused by electric field in poorly conducting liquid subject to vertical temperature gradient

08 p1352 A69-20799

Series operation of Gunn devices with differing threshold currents at SHF

09 p1463 A69-21684

Noise rejection in linear amplitude detector during weak harmonic signal reception improved by limiting threshold voltage

09 p1460 A69-22643

Cross section for ionization of atoms by positive ion bombardment near threshold

11 p1922 A69-25322

Bismuth doped lead tin telluride diode lasers with low threshold currents at cryogenic temperatures, discussing doping effect

12 p2109 A69-26648

Temperature effects on polarization degree of threshold current and delay of radiation from GaAs laser diodes with diffused Zn

13 p2227 A69-27328

Temporal correlations in light field from laser at threshold of oscillation, measuring He-Ne CW gas laser by photoelectron count

13 p2271 A69-27399

Photon loss coefficients in electron beam pumped GaAs laser showing dependence on doping type and impurity concentration, noting threshold current density measurement

13 p2271 A69-27466

Magnetic field effect on Gunn diode vibrations and LF oscillations, noting increase in threshold field and decrease in threshold current

18 p3183 A69-35266

Injection lasers threshold characteristics, studying temperature and doping level effects on current density and radiation energy

19 p3337 A69-36527

Power, efficiency and temperature dependence of emission spectra and threshold current density in electron beam pumped GaAs laser, noting doping concentration

19 p3338 A69-36538

Gallium arsenide junction lasers operating above threshold, showing resonant modes dependence on steady state gain function and frequency dependence of spatial gain distribution

19 p3338 A69-36691

THRESHOLD DETECTORS [DOSIMETERS]

Adaptive threshold detection, using stochastic approximation techniques to derive receiver structures capable of learning optimum threshold setting during actual operation

11 p1839 A69-25297

Incoherent object threshold light detection by quantum limited optical system in presence of radiant thermal energy

23 p4191 A69-42147

THRESHOLD GATES

Delayed response in threshold switching from reset state in ferrite memory cores consisting of magnesium compounds

[IEEE PAPER 16.4] 01 p0045 A69-10719

Gamma radiation effects on gate threshold voltages in modified oxide insulators in MOS structures

06 p0976 A69-16876

Radiation tests on Ovonic threshold switches performed with fast neutrons and broadband X rays

06 p0978 A69-16891

Adaptive threshold detection, using stochastic approximation techniques to derive receiver structures capable of learning optimum threshold setting during actual operation

11 p1839 A69-25297

AC diode switching circuits employed as threshold elements in functional rectifiers for approximating nonlinear functions

11 p1857 A69-25717

THRESHOLD LOGIC

Threshold logic for LSI to realize broad range of functions noting signal control, gate characteristics, weighting, etc

17 p2943 A69-34122

- Algorithm for assigning binary codes to inputs, internal states and outputs for sequential machines by threshold logic
18 p3105 A69-34618
- THRESHOLD SHIFT**
U THRESHOLDS
THRESHOLDS
Atmospheric turbulence effects on detection and resolution of incoherent objects, discussing error probabilities of threshold and maximum-likelihood systems
12 p2029 A69-26252
- THRESHOLDS [PERCEPTION]**
Differential and threshold sensitivity of acoustic analyzer of humans under space flight factors
02 p0197 A69-11500
Aircraft instrument lighting color effects on postexposure, scotopic absolute and acuity threshold and legibility for reading of instruments
03 p0380 A69-14073
Psychophysical methods for determining perception threshold of angular acceleration in man during vertical rotation
05 p0708 A69-15969
Pure tone threshold determination based on pulse tone technique with modified audiometer
06 p0882 A69-17836
Foveal luminances for chromatic and absolute thresholds for hue identification in case of small targets
07 p1183 A69-19649
Otolith apparatus response threshold under weightlessness conditions simulated by aircraft flight, measuring galvanic current threshold for banking
08 p1263 A69-19934
Distance discrimination in simulated space environment, studying just noticeable difference [JND] to determine relations between distance threshold and observation distance
12 p2022 A69-26372
Averaged cortical evoked response characteristics relationship to performance in traditional threshold procedures, discussing stimulus sensitivity and intensity control in central nervous system
21 p3653 A69-38897
Grating size effect on threshold of grating pattern for various colors of illumination and target orientations
22 p3879 A69-40840
Luminance additivity for human visual system in terms of photometric methods based on direct brightness matching, incremental threshold, etc
22 p3880 A69-40849
Luminance threshold for compound stimulus detection measured as function of two components relative luminance
22 p3880 A69-40852
Psychophysical threshold changes during subliminal monocular and interocular stimulation, studying conditioning flash size effects on temporal summation
22 p3881 A69-40860
Subjective and objective thresholds of darkness adaptation in human subjects grouped from infancy to adulthood, using same variable intensity light source equipment
22 p3881 A69-40861
Visual succession threshold for sides of square contour affected by presenting single line on parallel contour sides
22 p3882 A69-40868
Comparative study of differential luminance threshold and spatial summation exponent for solid and annular objects with equal surfaces
22 p3883 A69-40877
Spatial interactions and thresholds in identification and detection of compound visual stimuli
22 p3883 A69-40878
Retinal mechanisms determining visual band movement thresholds obtained by manipulation of retinal locus, luminance, arc length and spectral distribution of moving stimulus
22 p3883 A69-40879
Model of nerve elements, discussing subthreshold processes parameter system and analog investigation of transient processes for various stimuli at model input
23 p4110 A69-41981
- THROTTLING**
Thermodynamic analysis of engines and heat pumps operating within negative absolute temperatures, noting work increase by throttling
09 p1623 A69-22219
Throttling effect on thermodynamic efficiency of MHD generator Rankine cycle with various working fluids
11 p1824 A69-24222

- Flight performance prediction for throttling bipropellant rocket engine utilizing ablative combustion chamber throat, discussing lunar module descent engine
[AIAA PAPER 69-452] 16 p2841 A69-32690
Constant chamber pressure thrust throttling of expansion-deflection rocket nozzle, calculating wall static pressure and thrust by characteristics method, discussing performance
[AIAA PAPER 69-435] 16 p2846 A69-32776
Pressure drop in control element of gas generator during readjustment of throttle in hydraulic supply line, noting assumptions
19 p3393 A69-35819
- THRUST**
NT JET THRUST
NT LOW THRUST
NT MICROTHRUST
NT RETROTHRUST
NT ROCKET THRUST
NT VARIABLE THRUST
Integrated shrouded propeller as glider thrust source permitting powered takeoffs and updraft independence
05 p0702 A69-16379
Hall tube electromagnetic plasma accelerator, with thrust affected only by Lorentz forces in external magnetic field, compared to pure Hall accelerator
11 p1866 A69-25214
Pressure sensors, strakes, removal of full length guide vanes indicate possible difficulties with thrust of NK-8-2 turbofans in Tu-154
19 p3395 A69-36757
- THRUST AUGMENTATION**
Monograph on exhaust gases mixing with cold airstream in ducted fanjet engine, noting thrust and efficiency increase
03 p0496 A69-14048
Turbofan engines augmentation, evaluating duct heater, bluff body stabilizers, piloted can combustors, flameholding techniques and afterburner tests
09 p1573 A69-22617
Electric propulsion systems characteristics, examining sputtering of metallic targets as thrust augmentor
11 p1944 A69-25598
Jet flap as alternative to rigid diffuser for momentum propulsion, discussing thrust augmentation
[AIAA PAPER 69-777] 19 p3393 A69-35645
Thrust increase methods for air breathing turbojet engines analyzed with respect to effectiveness, taking into account environmental supporting mass and fuel expenditures
23 p4199 A69-41578
Booster engines for thrust augmentation of commercial transports, considering tradeoffs in takeoff distance, payload, range, safety and noise patterns
[SAE PAPER 690381] 23 p4201 A69-41667
- THRUST BEARINGS**
Elastomeric bearings for support of heavy loads and accommodation of oscillatory motions, considering molded type for helicopter tail rotor
01 p0085 A69-10406
Fatigue life, kinematics, dynamics, etc., of thrust loaded ball bearings, considering inertial effects of hollow balls
01 p0087 A69-10908
Axial rigidity effect of centrifugal force acting on balls of rapidly rotating radial thrust bearing
04 p0605 A69-14606
Dynamic behavior of series and parallel flow thrust-balance systems for compressible and incompressible flow, using analog computer simulation
04 p0647 A69-15521
Angular inertia of lubricant in MHD hydrostatic thrust bearings, obtaining critical angular speed of rotor
09 p1503 A69-21443
Load capacity, stiffness and flow requirement of capillary and orifice compensated oil lubricated externally pressurized rectangular thrust bearings
12 p2102 A69-26239
Gas molecular mean free path effect on performance of spiral grooved thrust bearing, discussing slip flow factor and He Knudsen number
[ASME PAPER 68-LUBS-17] 13 p2266 A69-27273
Externally pressurized gas lubricated journal and thrust bearings designs, citing reference literature
[ASME PAPER 68-LUBS-8] 13 p2267 A69-27282
Flow models for externally pressurized gas bearings, discussing pressure distributions, load capacity and flow rate
[ASME PAPER 68-LUBS-2] 13 p2267 A69-27285

- Gas lubricated tilting pad thrust bearing analysis and performance, determining optimum hydrodynamic crown profile
[ASLE PREPRINT 69AM 3C-2] 15 p2619 A69-30472
High speed ball bearing skidding, proposing analytic model as design tool, discussing effects of thrust load, speed, oil temperature and flow rate
[ASME PAPER 69-LUBS-20] 18 p3140 A69-34377
- THRUST CHAMBERS**
Mercury ion thrusters and facilities automatic controls durability testing, discussing vacuum chamber systems, unattended operation and control
[AIAA PAPER 68-576] 02 p0229 A69-12385
Glass fiber reinforced plastic (GFRP) roving end grains in rocket combustion chambers, discussing design and structural parameters
02 p0305 A69-12748
Solid fuel rocket engine thrust and chamber pressure development curves from charge and engine geometry, heat of explosion and kinetic characteristics
16 p2836 A69-31994
Liquid propellant injector design for rocket thrust chambers, discussing mass and mixture ratio regulation
16 p2836 A69-31999
ICRPG liquid propellant thrust chamber performance evaluation methodology, reviewing imperfections and limitations
[AIAA PAPER 69-468] 16 p2838 A69-32657
Rocket stability monitoring by temporal radiometry, using exhaust radiance measurement to detect frequencies in thrust chamber combustion pressure
[AIAA PAPER 69-580] 16 p2839 A69-32670
Oxygen difluoride-diborane propellant injector and chamber design criteria applied to unmanned spacecraft rocket engine development
[AIAA PAPER 69-508] 16 p2839 A69-32671
Ablative materials in hydrogen/oxygen thrust chamber using expansion nozzle to substitute regenerative thrust chamber assembly
[AIAA PAPER 69-442] 16 p2747 A69-32702
Discharge chamber plasma processes in electron bombardment ion thrusters, considering factors affecting thruster performance
[AIAA PAPER 69-494] 16 p2845 A69-32735
Electroforming methods in design and fabrication of liquid propellant rocket motor injectors and composite thrust chambers
[AIAA PAPER 69-583] 16 p2794 A69-32757
Space storable hydrocarbon fuel blended FLOX propellant performance with coaxial injector including characteristic velocity, chamber geometry, pressure and heat flux distribution
[AIAA PAPER 69-507] 16 p2835 A69-32772
Li-F-H tripropellant study, discussing injection method variations and thrust chamber configuration effects on characteristic velocity efficiency and heat flux measurement
24 p4362 A69-43128
- THRUST CONTROL**
Mercury ion thrusters and facilities automatic controls durability testing, discussing vacuum chamber systems, unattended operation and control
[AIAA PAPER 68-576] 02 p0229 A69-12385
Dynamic behavior of series and parallel flow thrust-balance systems for compressible and incompressible flow, using analog computer simulation
04 p0647 A69-15521
Analytical model for thrust-time curve during ignition transient of solid propellant rocket engines, discussing flame spreading
[WSCJ PAPER 68-33] 07 p1203 A69-18365
Optimal lift and thrust control programs to maximize range of missile in horizontal flight
09 p1610 A69-22086
Causes and magnitudes of thrust misalignment of Kaufman type electron bombardment ion thruster
[AIAA PAPER 69-303] 10 p1753 A69-23362
Space station attitude control through resistojets and control moment gyros (CMG), discussing propulsion, safety features, weight factors, etc
11 p1965 A69-24531
V/STOL air intakes and jets simulation in wind tunnel tests, noting thrust simulation possibilities
11 p1866 A69-25431
Soviet book on solid propellant guided/unguided rocket design with emphasis on thrust control, including trajectory calculations, optimal parameters and components estimation by weight analysis
12 p2175 A69-27077
Optimum thrust control of satellite along given trajectory to rendezvous at zero velocity with orbited satellite
13 p2356 A69-27684

Optimal motion control of spacecraft refueling during flight by liquefying atmospheric gas along prescribed trajectory under constant thrust
13 p2356 A69-27686

Reaction control rocket engines for manned spacecraft, discussing operating and cycle life, thrust response, specific impulse and reliability
16 p2867 A69-31746

Pilot chamber initiated thermal decomposition reactor concept for monopropellant thruster, discussing thrust levels and throttling ratios
[AIAA PAPER 69-420] 16 p2841 A69-32685

Low thrust reaction control for space missions, summarizing range and specific impulse characteristics for solid and hybrid systems
[AIAA PAPER 69-433] 16 p2834 A69-32745

Stability analysis of missile lateral supersonic flutter based on Lagrange equations, considering conservative thrust, control deviation and aerodynamic forces
17 p3045 A69-32946

Microthrusters thrust requirements for attitude control and orbital transfer of gravity gradient geostationary satellite
17 p3019 A69-33336

Thrust magnitude and direction modulation of hybrid propellant engine, noting applications
17 p3019 A69-33337

Lifting rotors with thrust or tilting motion feedback control, deriving blade equations of motion
[AHS PAPER 340] 17 p2899 A69-33510

Calculator for obtaining moments of inertia data to determine control power for vehicle orientation and to avoid control systems over design
[SAWE PAPER 792] 18 p3118 A69-34865

Solar electric thrust system technology concerning performance, thruster control system stability and method for solution
19 p3394 A69-35941

Density profiles in far field of reaction control system plumes in vacuum obtained by method eliminating difficulties encountered by continuum method
19 p3238 A69-35954

Vehicles optimal flights with controlled or boundary level thrust in circular orbit neighborhood, using linearized equations of motion
19 p3427 A69-36612

Attitude control system for launch vehicles, providing commanded thrust vector angle proportional to desired angular displacement of acceleration vector
21 p3819 A69-39032

Satellite motion orbital elements dependence on large short impulse arbitrarily directed in space, analyzing optimal orbits transfer and thrust control
21 p3818 A69-39821

Communication satellite systems using hydrazine engine thrust for trajectory correction, discussing trajectory deviations causes and ERNO engine design
[DGLR-69-013] 23 p4203 A69-42152

Optimal thrust control for plane curvilinear motion of variable mass point in gravitational field
23 p4192 A69-42340

THRUST LOADS

Ballistic reentry trajectories, considering point mass motion in central force field under tangential thrust action and spherical atmospheric density distribution
06 p1006 A69-17564

Liquid filled cylindrical container motion with longitudinal forces applied to base, obtaining stability conditions for natural oscillations
08 p1419 A69-21181

THRUST MEASUREMENT

Optimal layout of turbofan jet engines, discussing experimental rig for high thrust measurement
[AIAA PAPER 67-416] 01 p0143 A69-11015

ONERA vertical bench for dynamometric calibration to 20 tons used for engine and rocket thrust measurement
07 p1116 A69-19217

Sine wave oscillator circuits and performance prediction for NERO thrust measurement test stand
08 p1300 A69-20155

NERO thrust power measurement, discussing electromagnetic and strain-gage test stands
08 p1301 A69-20156

Rocket engines transient thrust measurement by quartz transducers
08 p1301 A69-20589

Low thrust propulsion devices high response impulse testing, describing limitations imposed by solenoid valve time response
10 p1672 A69-23278

Aircraft test setup design and techniques to simultaneously measure engine thrust and engine thrust

minus drag, noting nozzle configurations variations effect
[AIAA PAPER 68-395] 12 p2059 A69-26769

Simulation of two phase hydrogen venting to space environment, discussing thrust effect measurements, flow instabilities and instrumentation
15 p2701 A69-30396

THRUST PROGRAMMING

Apollo translunar injection burn simulation, analyzing polynomial solutions of optimum geometry and characteristic velocity
[AAS PAPER 68-150] 21 p3820 A69-39225

Thrust optimization for sounding rocket to reach maximum altitude with given initial and propellant weight, using polygonal time function and multiple-parameter numerical technique
22 p4037 A69-41050

THRUST REVERSAL

Soviet book on turbojet engine reverse thrust systems and systems for deflection of jet stream covering aircraft braking efficiency
04 p0647 A69-14934

Mathematical model for flow within external target type thrust reverser, assuming inviscid incompressible two dimensional flow
[AIAA PAPER 69-3] 06 p0985 A69-18124

Thrust reversers for business jet aircraft, discussing federal aircraft regulation requirements for ground and in-flight qualification
[SAE PAPER 690311] 11 p1941 A69-24512

Fluidic thrust reversal control system for turbojet achieving cost and weight reduction, illustrating fluidic circuit and noting circuit reliability
17 p3018 A69-33329

Performance capabilities and handling quality characteristics of aircraft equipped for in-flight thrust reversing
[AIAA PAPER 68-880] 17 p2902 A69-34031

Polyphenyl ether lubricants and self lubricating materials compared for antifriction ball bearings in thrust reversing actuator gear box
[SAWE PAPER 68-LC-1] 18 p3148 A69-35003

Boeing 747 exhaust reverser design and control, discussing stopping distance, cascades, materials, etc
[SAE PAPER 690409] 23 p4200 A69-41637

Commercial jet aircraft thrust reversers and noise suppressors developed by Rolls-Royce, discussing compatibility, reliability and applications
[SAE PAPER 690410] 23 p4200 A69-41638

DC-10 aircraft CF6 engine thrust reverser and spoiler design features impacting operational characteristics, maintainability, noise reduction, structural concept, control and actuation system
[SAE PAPER 690411] 23 p4200 A69-41639

SNECMA thrust reverser system design on Concorde prototype, discussing performance, safety, airworthiness, operational requirements, reliability and maintenance
[SAE PAPER 690412] 23 p4200 A69-41640

THRUST VECTOR CONTROL

Nozzle separation for thrust vector control with applications to guidance problems
01 p0161 A69-10412

Flight test evaluation of small one man lunar flying device (POGO), discussing vehicle control, pressure suit factors and piloting differences
[AIAA PAPER 68-240] 02 p0229 A69-12379

Solid propellant rocket motor thrust vector control by swiveling or gimbaled exhaust nozzles or by secondary injection
03 p0495 A69-12892

Electrohydraulic guidance of second stage of Diamant rocket used for orbiting satellites employing thrust vector orientation
04 p0551 A69-15183

Charged liquid droplets generator and acceleration through electric field for thrust vectoring, analyzing beam focusing and deflection
[AIAA PAPER 69-283] 09 p1563 A69-21230

Cesium microthruster system using beam deflection for satellite control, describing ion engine subsystem and control logic/power conditioner subsystem
[AIAA PAPER 69-292] 09 p1569 A69-21875

Thrust vectoring system using accelerator displacement to reduce alignment errors in multiparticle electron bombardment ion engines
[AIAA PAPER 68-543] 09 p1570 A69-21985

Fluidic secondary injection thrust vector control systems for solid propellant and hydrogen-oxygen rocket engines
10 p1753 A69-23561

Flow field structure involving supersonic secondary jet interactions and separated regions in thrust vector control system
11 p1944 A69-25594

Variable bypass ratio lift/thrust engine arrangement in relation to safety and economic requirements, using scale model of V/STOL
15 p2672 A69-31542

Directional thrust control for solid propellant rockets, describing swinging, bent rotating nozzles and secondary injection
17 p3019 A69-33332

Thrust vector control by secondary gas injection for predicting lateral thrust performance, applying method to rocket engines, secondary gas generator and injector configuration
17 p3019 A69-33333

Mission and planetary vehicles characteristics affecting design of solid propellant motors and thrust vector control systems in planetary orbiters and landers
[AIAA PAPER 68-815] 21 p3819 A69-39031

Digital autopilots for Apollo CSM and CSM/LM vehicles thrust vector control, describing modifications of onboard computers and programs
[AIAA PAPER 69-847] 21 p3762 A69-39377

Test stand for measurement of forces and moments from thrust vector controlled rocket, analyzing dynamic characteristics of hydrostatic supports
21 p3691 A69-39631

Satellite maneuver for changing plane of circular orbit to pass through given point, determining on-off engine switching and thrust vector control
21 p3765 A69-39640

Black Arrow third stage velocity increment vector accuracy, considering attitude errors due to spin-up and spring separation systems, separated stages interactions, light-up impulses, etc
23 p4209 A69-41301

THRUST-WEIGHT RATIO

Unannounced propellant weight and thrust of Soviet Luna spacecraft based on Luna 12 lunar orbit injection maneuver
08 p1409 A69-19969

Propulsion optimization for various vehicles, considering power plant weight, specific fuel consumption, power and thrust ratios, etc
11 p1941 A69-24462

THRUSTORS

U ROCKET ENGINES

THULIUM ISOTOPES

Aircraft tire wear determination by measuring intensity of radiation originating from point source within thread, using thulium 170 isotope
07 p1143 A69-19703

THUNDERSTORMS

Lightning strikes to aircraft, discussing corona discharge, electric fields and meteorological measurements during thunderstorm in cumulonimbus
03 p0458 A69-13031

Propagation of long electromagnetic waves in ionosphere and exosphere, discussing thunderstorm noise spectrum
03 p0396 A69-13702

Thunderstorm thermal noise emission determined by radiometer and steerable parabolic antenna in preparing water content contours along radio rays
12 p2127 A69-27002

Atmospheric turbulence in cloudless region above thunderstorms and relation between turbulence and radar pictures of storms
15 p2649 A69-31211

Atmospheric ozone production by silent discharges near ground level during first stage of storm cell development
16 p2785 A69-32623

Thunderstorm probabilities at Cape Kennedy, giving data on frequency, duration, multiple occurrence, nonoccurrence, runs and conditional probabilities
18 p3167 A69-35100

Negative charge distribution in thunderstorm clouds related to direction of storm movement, noting vertical column
20 p3572 A69-37908

Cloud velocity computations from ATS 1 and 3 satellites spin-scan photographs for prediction of neph systems motion and thunderstorms
21 p3757 A69-38370

Thunderstorm turbulence relationship to weather radar echoes from storm penetrations in Oklahoma by instrumented aircraft
24 p4347 A69-43720

THYRATRONS
S band thyatron waveguide switch as pretriggered megawatt balanced duplexer 01 p0048 A69-11035
Secondary emission and hollow cathode effects in low pressure hot cathode thyatron filled with hydrogen and with shield surrounded thermionic cathode 06 p0896 A69-17475
High temperature and power gas diodes and thyratrons for nuclear electrical space power systems 11 p1847 A69-24744

THYRISTORS
Output pulse parameters of short pulse thyristor generator as function of time constant, considering rise time of switch-on process 11 p1846 A69-24615
Power supply circuits in spacecraft, DC voltage control systems, transistor and thyristor regulators and modulators, etc 17 p2937 A69-33582

THYROID GLAND
Thyroid gland role in resistance and myoglobin content of skeletal muscles of flat land and high altitude acclimatized white rats 05 p0709 A69-16517
Resting EEG and parieto-occipital response changes evoked by slowly repeated flashes in case of severe hypothyroidism secondary to panhypopituitarism 07 p1064 A69-18634
Hibernation seasonality, protein synthesis during periodic awakenings and importance of awakenings to maintenance and evolution of thyroid activity 10 p1642 A69-23120
Fluorides or AMOX increased concentrations effect on thyroid growth rate, uptake and adrenal weight in rats 14 p2406 A69-29291
Thyroid gland role in resistance and myoglobin content of skeletal muscles of flat land and high altitude acclimatized white rats 18 p3096 A69-34736

TIDAL OSCILLATION
U TIDES

TIDES
NT ATMOSPHERIC TIDES
NT LUNAR TIDES
Commensurability among pairs of mean motions of natural satellites of major planets and hypothesis of tidal evolution of satellite systems 07 p1223 A69-19638
Plumb line fluctuations /M sub 2 tide, 1961/ at 135 degree azimuth by Voit method, discussing residual ellipse for Borowiec 08 p1306 A69-19824
Earth and planets shallow seas tidal dissipation reflected in Q values, noting larger planet pressure effect 08 p1393 A69-20581
Neutral hydrogen asymmetry in Galaxy M101 as evidence for tidal effects due to nearby companions, noting hydrogen emission spectra 08 p1394 A69-20625
Conversion of Woolard theory coefficients of tidal irregularity of earth rotation to new system of constants 09 p1484 A69-21383
Oscillation cycle of atmospheric circulation, analyzing solar activity effects on lunar and solar semidiurnal tides and transition from zonal to meridional circulation 12 p2070 A69-26692
Sea tides and ionospheric effects on lunar variation of geomagnetic field vertical component 12 p2161 A69-26957
Sand ridge origin and dynamical setting, discussing morphology-tidal current system equilibrium indicated by theory and field measurements 15 p2596 A69-30443
Semidiurnal oscillation in thermalgeostrophic atmosphere examined using atmospheric model for tidal oscillations response study 17 p2959 A69-33148
Conversion of Woolard theory coefficients of tidal irregularity of earth rotation to new system of constants 18 p3127 A69-34771
Catastrophic and noncatastrophic alternatives for earth capture of moon, discussing tidal action and spin-orbit resonance 18 p3198 A69-34823
Book on gravimetry covering gravity measurement on land and in ocean, gravity anomalies, isostasy, geodetic applications, Eotvosian measurements and terrestrial tides 21 p3715 A69-39000

Resonant spin and anomalous rotation of Mercury, analyzing influence of tidal degradation and permanent deformation of planet 21 p3814 A69-39568
Moments of inertia and gravity field of moon, noting application to earth tides 22 p4030 A69-40902
Eulerian equations for precession and nutation of self gravitating fluid globes of arbitrary structures in inertial coordinates, discussing coplanar case, tidal breathing, etc 22 p4030 A69-40904

TIG WELDING
U GAS TUNGSTEN ARC WELDING

TIGHTNESS
Adhesive pressure welded joints tightness and fabrication stability analyzed on duraluminum sheet samples 17 p2978 A69-32949

TILT
U ATTITUDE [INCLINATION]

TILT WING AIRCRAFT
NT CL-84 AIRCRAFT
NT VZ-2 AIRCRAFT
NT XC-142 AIRCRAFT
Technological evolution of turboprop propeller powered tilt wing V/STOL aircraft, discussing XC-142A, CL-84 and VZ-2 aircraft 05 p0701 A69-15564
Future development in rotorcraft, discussing autogyros, helicopters, tilt rotor and wing aircraft 05 p0702 A69-16392
Tilt wing executive transport aircraft designed by postgraduates at College of Aeronautics of UK, discussing costs, construction and marketability 11 p1821 A69-24321
CX-84 two propeller tilt wing deflected slipstream V/STOL Military Evaluation Program related to support of surface forces 17 p2900 A69-33526
Tilt wing V/STOL aircraft spray circulation characteristics in overwater operation, examining forces, moments and generated environmental conditions [AIAA PAPER 69-791] 19 p3243 A69-35638

TILTED PROPELLERS
Vertical takeoff aircraft propeller/rotor design and performance prediction, discussing vortex model, wake contraction, blade element aerodynamic properties, etc [AHS PAPER 325] 17 p2894 A69-33534
Folding propotor V/STOL aircraft characteristics, showing configuration effects on performance and optimization of rotor, wing and propulsion systems [AHS PAPER 302] 17 p2901 A69-33547
Tilt propotor composite aircraft design, discussing performance and mission potential [AHS PAPER 202] 20 p3463 A69-37805

TILTING
U ATTITUDE [INCLINATION]

TILTING ROTORS
Future development in rotorcraft, discussing autogyros, helicopters, tilt rotor and wing aircraft 05 p0702 A69-16392

TIME
NT BURNING TIME
NT EPHEMERIS TIME
NT FLIGHT TIME
NT REACTION TIME
NT RELAXATION TIME
NT RESPONSE TIME [COMPUTERS]
NT TESTING TIME
NT TRANSIT TIME
NT UNIVERSAL TIME
Minimum measurement time of dynamic transmission coefficient of system by FM method, calculating error 01 p0031 A69-10785
Auroral observations from constant local time westward flights of jet plane 02 p0245 A69-12738
Stability and instability conditions derived for undisturbed motion of system over finite period of time 08 p1351 A69-20321
Minimum measurement time of dynamic transmission coefficient of system by FM method, calculating error 10 p1653 A69-23114
Stability and instability conditions derived for undisturbed motion of system over finite period of time 17 p3005 A69-33314

TIME CONSTANT
Computer analysis of linear active nontime varying circuits by two graph topological approach based on Binet-Cauchy theorem 01 p0037 A69-11349

Graphical method for determining rise time of planar transistors with constant collector space-charge capacitance 01 p0049 A69-11362
Characteristic time on motion of magnetic lines of force in medium with Hall effect 02 p0290 A69-12399
Thermal time constant in Si diffused transistors decreases with increased neutron dosage 06 p0975 A69-16873
Sixth order correlations of laser beam fluctuations near threshold from delayed coincidence measurements with three photodetectors, noting time constants 07 p1144 A69-18252
Monolithic planar process to fabricate DC coupled amplifiers having less than nanosecond risetime 07 p1103 A69-18878
Feedback amplifier with transfer function poles on parabola, discussing small rise time with small overshoot combined in transient response 08 p1282 A69-20111
Time response of second order nonlinear overdamped systems calculated by Krylov-Bogoliubov method of variation of parameters 08 p1297 A69-20356
Response optimization of feedback control systems with reference to single settlement time-constant ideal determined for error evaluation 08 p1298 A69-20855
Transistor large signal saturation time constant dependence on injection ratio, noting nonlinear response and saturation transistor switch storage time 09 p1464 A69-22117
RC circuit with variable time constant using variable resistor 10 p1667 A69-24046
Output pulse parameters of short pulse thyristor generator as function of time constant, considering rise time of switch-on process 11 p1846 A69-24615
Two rotor gyrocompass oscillations stability during finite time interval, deriving differential equation by suitable quadratic functions 11 p1886 A69-25089
Practical time resolution of streak camera, discussing streak camera transfer function and measurement of resolution with pulsed laser diode emission 12 p2084 A69-26152
Asymptotically stable discrete time closed loop linear systems synthesis, presenting feedback matrix as illustration 13 p2287 A69-27238
Phase distortion, conversion of delay coefficients into channel noise and determination of waveguide delay coefficients for FM satellite communication systems [IEEE PAPER 68-TP-382-COM] 13 p2222 A69-28153
Solar quiet day geomagnetic variations harmonic analysis with respect to time intervals centered around noon, defining parameters responsible for modulated Sq 16 p2781 A69-32452
Shock waves propagation in inhomogeneous gases, considering time development and energy flux during point explosion in plane layers by quasi-stationary approximation 17 p2952 A69-33383
Electromagnetic waves radiation in general time invariant linear media with general boundary conditions, using Green function 17 p2924 A69-33834
Temperature response of semiconductor thermistors as temperature sensing element, determining time constant from dimensions and experimental data 21 p3723 A69-38888
State variable feedback design of m-input, m-output time invariant linear systems requiring noninteraction and exact transfer functions, considering coupled core nuclear reactor 24 p4294 A69-43315

TIME DEPENDENCE
Approximate boundary controllability for heat equation by considering temperature variation with time 01 p0173 A69-10008
Time dependent interaction of hot gas bubble with chemically reactive liquid stream, detailing thermal boundary layer theory 01 p0058 A69-10162
Reliability analysis of technological systems, determining characteristics as distribution function of time to specified number of failures 01 p0085 A69-10210

Couette flow stability in axial magnetic field, considering time bounded perturbation energy during increasing angular velocity in radial direction
01 p0059 A69-10233

Nonlinear time dependent parameters systems, analyzing governing differential equations in terms of elliptic functions
01 p0050 A69-10237

Linear stability of steady and time dependent plane Poiseuille flow
01 p0175 A69-10333

LF radiation intensity oscillations of pulsed HF discharge in helium plasma, showing time dependence
01 p0128 A69-10347

Chemical composition effect on duraluminum supersaturated solid solution stability, presenting time vs temperature C curves of isothermal decomposition
01 p0094 A69-10396

Grain boundary gas bubbles growth in chemically vapor deposited tungsten as function of annealing time, temperature and fluorine content
01 p0097 A69-10646

Current sheath surrounding exploding copper wire in vacuum, plotting current distribution as function of time and radius
01 p0119 A69-10669

Time resolved spectroscopy of exploding wire plasmas in visible spectrum of various elements, determining plasma characteristics
01 p0119 A69-10671

Finite f function computation by d/r circuit, discussing computation time
01 p0105 A69-10734

Determination of plant differential equation from time characteristics
01 p0053 A69-10804

Finsler geometric apparatus applied to electromagnetic wave propagation in media having refractive index varying with position and time, calculating errors
01 p0031 A69-10879

Time and latitude variations of blanketing sporadic E of different intensities
01 p0070 A69-11159

Late type variable stars time dependent photometry and polarimetry in blue and violet, noting correlation for stellar brightness and degree of polarization
01 p0158 A69-11326

Time history of unsteady heat transfer in laminar boundary layer over semiinfinite flat plate due to step change in wall temperature or wall flow
01 p0177 A69-11401

Absolute input-output stability of time varying nonlinear feedback system established by frequency domain test similar to Popov test
01 p0054 A69-11414

Time correlation of photons emitted by krypton gas discharge tube and helium-neon multimode laser
02 p0255 A69-11611

Solar and galactic cosmic rays measurement data to investigate variation in time of relations between cosmic rays modulation amplitude and solar activity variations
02 p0306 A69-11658

Soviet book on spectral, spatial and time characteristics of lasers covering luminescence and resonator theories, electromagnetic field structure and radiation dispersion
02 p0255 A69-11800

Generalized unsteady temperature fields and stresses in crystalline plates using Fourier and Laplace transforms
02 p0340 A69-12044

Time dependent viscoelastic stress distribution in two phase composite material, using plane stress model for approximation
02 p0348 A69-12540

Short laser radiation pulses spectral characteristics determination with device converting laser emission frequency by nonlinear electro-optical crystals
02 p0257 A69-12560

Frequency and time dependent gains of dye solution lasers for pumping by lasers and flashlamps
02 p0257 A69-12616

Step voltage transient behavior of electron-hole plasma injected into Ge, noting current time dependence
02 p0301 A69-12651

Time dependent functions integration by glow discharge tube and oscillator, discussing device for voltage measurement and applications in meteorology and geophysics
02 p0251 A69-12773

Three dimensional unsteady heat conduction and temperature distributions in finite hollow circular

cylinder under time dependent boundary conditions of second kind
03 p0530 A69-12861

Photoviscoelastic stress analysis to predict time dependent stress redistributions in polyphase system with viscoelastic binder under external loading conditions
03 p0524 A69-13061

Diurnal, magnetic and solar cycle dependences of auroral emission variations and auroral occurrence
03 p0420 A69-13325

Green functions associated with electromagnetic radiation in moving medium, finding time dependent and harmonic Green functions
03 p0466 A69-13352

Solar flares effect on ozoneosphere, calculating time necessary for solar radiation to increase ozone concentration by 50 percent
03 p0424 A69-13542

Time dependence of relation between sunspot number and ionospheric index IF 2, noting hysteresis characteristic and changes for different solar cycles
03 p0424 A69-13632

Linearized time dependent equation for photovoltaic distribution in nonuniformly illuminated p-n junction
03 p0486 A69-13636

Galvanostatic transients of iron passive in 2N sulfuric acid, noting space charge effects and zero field current variation
[ECS PAPER 84] 03 p0382 A69-13858

Time dependent variations in magnetic fields of active sunspot clusters in photosphere observed by magnetograph
04 p0651 A69-14369

Time independent flow of highly rarefied neutral gas past finite cone at zero angle of attack with freestream, noting molecular distribution function
04 p0541 A69-14712

Perfect magnetofluid model to study laminar flow stability along magnetic field, considering time dependences and rigid and free boundaries
04 p0637 A69-15045

Book on thermal time independent plastic and time dependent creep strains in structures through analogy permitting inelastic structures analysis
04 p0681 A69-15200

Charged particle motion in constant direction magnetic field varying exponentially with time, discussing electric field effect on particle motion
05 p0801 A69-15744

Flow and heat transfer on nonNewtonian fluid about disk rotating with time dependent velocity, using Runge-Kutta-Gill technique for numerical integration
05 p0745 A69-15793

Constitutive equation for viscoelastic materials generalized, assuming instantaneous part of deformation to be nonlinear function of time dependent stress state
05 p0835 A69-15868

Spectral output time variation of GaAs diode laser operating in Fabry-Perot modes
05 p0772 A69-15961

Time dependent two dimensional incompressible laminar boundary layers analysis, discussing application to transient flow over semiinfinite flat plate
[ASME PAPER 68-FE-10] 05 p0748 A69-16076

Spatial and temporal conjugacy of visual auroras during magnetically quiet periods
05 p0753 A69-16247

Stability analysis of nonlinear and time varying discrete feedback systems
05 p0740 A69-16600

Modulation of galactic cosmic rays due to electromagnetic conditions of interplanetary space, considering time variations and Parkers model
06 p0989 A69-17287

X ray sources intensity and spectrum variation with time, describing proposed balloon experiments with equatorial launching for performing measurements
06 p0992 A69-17312

Settling time estimation method for class of time varying feedback control systems of linear, nonlinear and multivariable natures
06 p0902 A69-17399

Optimality criterion and equations of motion determined for fixed time impulsive trajectory to minimize total characteristic velocity
06 p1007 A69-17575

Plasma impedance effect on time variation of inverse pinch
06 p0967 A69-17716

Image averaging time effects on modulation transfer function /MTF/ of system comprising telescope objec-

tive and horizontal propagation path in turbulent atmosphere
06 p0890 A69-17800

Time dependent emission spectra from flashlamp pumped organic dye lasers recorded with image converter, comparing dyes characteristics
06 p0936 A69-17900

Averaging procedures to represent highly time variable actual hydrometeorological fields by less variable equivalent fields
06 p0952 A69-17989

Nonadiabatic reacting homogeneous system undergoing density changes, predicting chemical reaction rates and intermediate combustion products from chain reaction kinetics
[AIAA PAPER 69-87] 06 p1036 A69-18005

Transient development of reacting boundary layer near stagnation point of vaporizing drop in gas stream
[AIAA PAPER 69-174] 06 p0912 A69-18056

Time dependent model of photochemical, advective and turbulent effects on meridional ozone distribution
07 p1122 A69-18254

Statistical frequency analysis of power spectrum of geomagnetic pulsations, discussing time and latitude dependence
07 p1122 A69-18297

Analytical model for thrust-time curve during ignition transient of solid propellant rocket engines, discussing flame spreading
[WSCI PAPER 68-33] 07 p1203 A69-18365

Time stabilization method for lasing in electro-optically Q switched ruby laser with saturable absorber in cavity
07 p1147 A69-18531

Simultaneous solution of time-dependent momentum and continuity equations for ions and neutral air in midlatitude F 2 region conditions
07 p1123 A69-18818

Time and latitude variations of blanketing sporadic E using wind shear theory, predicting ionization layer formation in ionospheric E layer
07 p1125 A69-18840

Conducting gas acceleration in strong unsteady electromagnetic field, discussing channel flow in relation to time and pressure gradient
07 p1191 A69-18988

Time resolved spectrum of high current pulsed argon laser discharge, noting primary laser output and afterglow
[IEEE PAPER L-12] 07 p1152 A69-19068

Nitrogen ion number density time dependence by mass spectrometric probing of decaying nitrogen plasmas, noting molecular ion production by colliding metastable nitrogen molecules
07 p1184 A69-19141

Particle dynamics measured by ATS satellite synchronous orbit, discussing flux time variations during geomagnetic disturbances
07 p1209 A69-19371

Arrival time distribution and energy content of extensive air shower at large core distances, discussing photon energy spectra and Monte Carlo calculation
07 p1186 A69-19410

Secondary acquisition systems analysis by semiMarkov process model, defining minimum average acquisition time
08 p1270 A69-19852

Kinetic theory for plasma, considering electric field fluctuations time evolution simultaneously with one particle distribution time evolution and Landau damping in wave equation
08 p1360 A69-19991

Time-averaged value of forces of electromagnetic wave falling from vacuum and acting on magnetoactive plasma
08 p1361 A69-20200

Time dependent velocity distribution functions for carriers calculated in weakly ionized plasma in external electric field
08 p1362 A69-20265

Ion number densities time dependence in pink afterglow of N measured with quadrupole mass spectrometer
08 p1308 A69-20292

Spectral intensities and time variations of solar X ray bursts, discussing model for high energy flare plasma and resulting X ray flare
08 p1379 A69-20532

Time dependent behavior of atomic light emitted from pulsed helium afterglow, noting absorption measurements and spectrometric system
08 p1356 A69-20743

Time harmonic, spherical harmonic and power series expansion of Boltzmann equation
08 p1353 A69-20793

- Trapped particles drift velocity in time dependent meridional magnetic and perpendicular electric field
08 p1368 A69-20809
- Computerized simulation of time dependent reliability of multicomponent system based on statistical model of component breakdown
08 p1277 A69-21100
- Reliability distribution parameters for electronic components, determining time and tolerance dependence of reliability
08 p1293 A69-21114
- Time dependent recoverable isothermal decrease of photocurrent in CdS crystals in vacuum, noting trap mechanism involving electron redistribution
08 p1374 A69-21187
- Delta functions spectrum in reciprocal time domain for LC and RC structures due to impulse response in distributed parameters
09 p1471 A69-21327
- Work function change of tungsten single crystal /100/ surface measured as time function during surface molecular gas adsorption
09 p1521 A69-21338
- Ultrashort light pulses problems in measurements of time characteristics and instantaneous power of laser radiation
09 p1516 A69-21575
- Decoupling by state variable feedback and determination of inverse extended to linear time varying multivariable system
09 p1472 A69-21680
- Picosecond structure of low power laser signals using calcite beam splitter and potassium diphosphate second harmonic generator
09 p1516 A69-21742
- Time average holography for analysis of vibrations, overcoming fringe peak decrease with large amplitude and loss of phase information
09 p1495 A69-21749
- Time dependent procedure for axisymmetric transonic nozzle flows, programming governing equations for high speed computer
09 p1431 A69-21974
- Time dependent plasma density variations studies by microwave interferometer having reflector for modulated or nonmodulated microwaves
09 p1496 A69-22030
- Eddington approximation to radiative transfer equation extended to time dependent multifrequency problems
09 p1541 A69-22254
- Transient behavior of DC measuring amplifiers with time variable feedback, using matrix method and Laplace transform
09 p1467 A69-22560
- Nonlinear control plants model with pure delay effect identified by harmonic balance method
09 p1475 A69-22669
- Geometrical stability criterion similar to Popov criterion for single loop time varying nonlinear control systems analysis
09 p1476 A69-22784
- Solar cosmic rays proton intensity time variations and diffusion coefficient obtained by satellites, balloons and ground stations observations
10 p1755 A69-22812
- Lagrangian evolution criterion for electromagnetic conducting fluid and MHD flow, defining generalized fluxes and forces
10 p1727 A69-22904
- Multidimensional theory of characteristics found applicable to calculating three dimensional time dependent gas flows
10 p1632 A69-22913
- Oxidation effects on creep and fatigue properties of metals noting time and temperature roles
10 p1708 A69-22998
- Control operation time found dependent on gloves, physical characteristics of control and type of required operation
10 p1648 A69-23180
- Glove characteristics effects on manipulability, finding operation time differences between gloved and barehanded operation dependent on type of required control operation
10 p1648 A69-23181
- Surface recombination efficiencies on metals measured as function of exposure time in steady Oseen flows, providing step-function increase in oxygen atom concentration
10 p1726 A69-23526
- Peaked electron emission from nickel surface with large work function under laser radiation, discussing emission pulses, electron currents and surface temperature time variations
10 p1703 A69-23572
- Time dependence criterion in dynamic fracture determined by spall stress relation to stress pulse duration during plate impact
10 p1803 A69-24032
- Elliptic integrals to determine orbital elements time dependence in three body problem, estimating satellite lifetime
10 p1791 A69-24196
- Universe origin, discussing big bang theory, effects of expansion time and temperature on elementary particles, RF quanta, etc
11 p1953 A69-24352
- Quasars time dependent flux density variations at 6.6 cm, noting spectrum peaks tendency toward lower frequencies with time
11 p1954 A69-24382
- Energy theorem for time dependent materials, deriving convexity conditions for minimum work and maximum complementary work functions
11 p1969 A69-24412
- Time splitting of solar radio bursts observed at Oslo Solar Observatory with high resolution radio spectrographs
11 p1946 A69-24590
- Time correlation of photons emitted by krypton gas discharge tube and helium-neon multimode laser
11 p1895 A69-24718
- Time scales for creep stress redistribution in structures subject to step loading
11 p1980 A69-24879
- Upper atmosphere response to time dependent heating based on approximate analytic solutions of heat conduction equation
11 p1878 A69-25151
- Time and altitude distribution of wind zonal components over Fernando Noronha Island off Brazilian coast, discussing tropospheric pattern
11 p1913 A69-25204
- Book on Wankel RC engine design and performance covering sealing, timing, life, lubrication, etc
11 p1942 A69-25237
- Aircraft vortex wake development prediction for turbulent flow noting vortex size, strength and peak tangential velocity
11 p1819 A69-25377
- Stability of linear time-varying systems via examples, comparing various techniques
11 p1861 A69-25452
- Fading velocity short period characteristics and duration and depth of field strength variations over transhorizon path compared with corresponding atmospheric parameters
12 p2028 A69-25897
- Cosmic radiation origin in terms of sudden injection of particles in time, momentum and space, considering statistical fluctuations role in observed spectrum
12 p2148 A69-26206
- Nanosecond time variations in current-voltage characteristics of gas discharge in air, taking into account discharge circuit resistance and discharge space capacitance
12 p2137 A69-26534
- Dynamic energy balance in positive column of electric arc, integrating expression to determine temperature time dependence
12 p2137 A69-26535
- Finsler geometric apparatus applied to electromagnetic wave propagation in media having refractive index varying with position and time, calculating errors
12 p2031 A69-26642
- Stationary inventory problems analysis, discussing inventory policy, recursive and or limiting procedures, stationary point processes, stock delivery time instants, etc
12 p2192 A69-26750
- Time and temperature dependence of plastic properties of fiber reinforced phenolic heat shield materials
12 p2119 A69-26825
- Temporal variation of metal content in galaxy, discussing stellar radiation pressure effects on heavy element abundance of interstellar gas
12 p2160 A69-26854
- Hologram recording by offsetting reference beam temporal frequency instead of using reference beam spatial offset
13 p2258 A69-27201
- Plane wave solution for wave propagation in inhomogeneous anisotropic time-varying media
13 p2219 A69-27397
- Temporal correlations in light field from laser at threshold of oscillation, measuring He-Ne CW gas laser by photoelectron count
13 p2271 A69-27399
- Analytical expressions for nonlinear partial differential equation of heat conduction in solids, giving temperature as function of time and location
13 p2372 A69-27434
- Numerical methods for time integrating first order differential equations, emphasizing atmospheric oscillations in baroclinic model, evaluating errors
13 p2290 A69-27636
- Venusian water vapor spectroscopic data indicating longitudinal and time dependent variations in abundance
13 p2345 A69-27650
- Lunar surface spectral reflectivity variations with time, noting phase angle effects on color contrast
13 p2349 A69-27819
- Time correlation functions for wind vectors and components at various altitudes over Moscow in winter and summer
13 p2294 A69-27856
- Transport equation numerical solution for unsteady radiation field by straight lines method, allowing for scattering indicatrix forms with passage of time
13 p2350 A69-27858
- Polarization stabilization times dependence on risetime of external field pulse leading edge for semiconductor crystal, determining field concentration
13 p2317 A69-27880
- Time dependences of retardation effect, reversible magnetic permeability and magnetic viscosity during pulse magnetization of ferrite cores
13 p2319 A69-27993
- FM laser pulse formation time characteristics noting modulated resonator losses
13 p2272 A69-28114
- Stratified rotating fluid time dependent motion characterized by stability frequency ratio and Coriolis parameter within quasi-geostrophic approximation
13 p2248 A69-28171
- Minimum weight design of structures excited to harmonic vibrations by given single load, with intensity dependent on time
13 p2369 A69-28350
- Time of heating effect on thermal polymerization of L-lysine free base
13 p2218 A69-28439
- Solar and galactic cosmic rays measurement data used to investigate variation in time of relations between cosmic rays modulation amplitude and solar activity variations
13 p2333 A69-28689
- Reliability analysis of technological systems, determining characteristics as distribution function of time to specified number of failures
14 p2453 A69-28747
- Time dependent convection electric fields as agents for diffusing trapped magnetospheric radiation inward toward earth, discussing one dimensional diffusion equation
14 p2510 A69-28936
- Electron concentration enhancement in upper atmosphere at polar latitudes, noting three independent zones and relation to magnetic local time
14 p2510 A69-28938
- Vibrations of thick walled shallow circular cylinder with thickness change in time, applying dynamic elasticity and Volterra equations
14 p2533 A69-28985
- Time dependent magnetic field induced inside rotating spherical conductor by external sources applied to moon
14 p2518 A69-29121
- Frequency time dispersion of storm sudden commencement micropulsations, noting polarization effects
14 p2440 A69-29129
- Noise duration and spectral complexity effect on subjective rating of disturbance level
14 p2408 A69-29152
- Weighting factors relation in optimal systems integral squared error /ISE/ cost functional, characteristic coefficients and time response performance measures
14 p2534 A69-29317
- Time dependent evolution of probability pressure distribution maximum obtained from Liouville equation
14 p2472 A69-29406
- Cometary tail diffusion model based on luminous particle number decrease with time and particle accelerated motion and diffusion in space
14 p2523 A69-29705
- Time spectra of wind velocity, temperature, pressure and turbulent heat transfer and momentum in synoptic region
14 p2476 A69-29823

- Plasma energy and energy replacement time dependent on discharge pulse shape and magnitude
14 p2499 A69-29848
- Tide dependent variations of critical frequencies of ionospheric layers minimal heights and maximum height of F 2 layer reflection
14 p2444 A69-29871
- Time and temperature effects on corrosion and structure of Hastelloy alloy C-276
14 p2466 A69-29930
- Discontinuities in interplanetary magnetic field observation presented on mesoscale from Pioneer 6 observation, emphasizing distribution in time
14 p2528 A69-29970
- Multivariable linear time-variant systems noninteracting control problem, discussing realization by state variable feedback
15 p2582 A69-30024
- Wiener-Hermite expansion extended to include time dependent ideal random functions, discussing application to shear flow turbulence
15 p2644 A69-30201
- Short laser radiation pulses spectral characteristics determination with device converting laser emission frequency by nonlinear electro-optical crystals
15 p2633 A69-30257
- Finite integral transform determination for solving circular plates forced vibrations with time dependent conditions
15 p2704 A69-30306
- Design and efficiency for signal-time compressors of spectral analyzers using electron beam tubes with charge storage
15 p2576 A69-30351
- Time dependence of maximum structural response of single degree of freedom mechanical system under random loading
15 p2705 A69-30365
- Periodic radial heat flux in infinite cylinder with varying heat sources, assuming time variable heat exchange on surface
15 p2717 A69-30575
- Ruby laser lasing modes spectral time dependence attributed to population inversion inertia responsible for mode competition
15 p2633 A69-30725
- Lasing kinetics, emission spectrum and directivity of ruby laser with spatially homogeneous population inversion
15 p2634 A69-30729
- Stellar energy diffusion processes studied to determine energy transfer time scale between stellar layers
15 p2692 A69-30767
- Coupled kinetic equations for inhomogeneous systems treated as simultaneous equations in time, obtaining solutions by successive approximation
15 p2660 A69-30913
- Long life repairable equipment reliability and mean time between failure with limited life components and material in normal life maintenance environment
15 p2581 A69-31134
- Fiberglass reinforced plastic tensile strength dependence on vibration time and temperature and vibrational effect on modulus of elasticity
15 p2643 A69-31203
- Time variation of altitude distribution of cosmic dust layer in upper atmosphere by Pandora II collector using inflight shadowing technique
15 p2698 A69-31353
- Balmer alpha emission for abundance and distribution of hydrogen around earth, relating temporal variations to azimuth
15 p2700 A69-31437
- OgaAs platelet laser modes time behavior, discussing control by electron-hole pair density
16 p2796 A69-31704
- Q switched laser produced blast waves in low pressure Ar, discussing gas density and time dependence roles
16 p2796 A69-31705
- Thermal stability of Hastelloy Alloy C-276 determined from time and temperature tests for corrosion and grain boundary precipitation
16 p2799 A69-31719
- Linear elastic columns dynamic stability under time dependent axial load, investigating almost-sure asymptotic stability
16 p2872 A69-31911
- Parametric interaction of electromagnetic field with spherical cavity having time variable radius, considering wave diffraction and TM oscillations
16 p2751 A69-32029
- Time, temperature and transformation curves for Ti alloy by dilatometry, hardness measurements, X rays and micrography, discussing martensite and beta-alpha transformations
16 p2802 A69-32180
- Wavelength dependence of linear polarization of sunlight scattered by Venus, noting temporal variations in UV
16 p2860 A69-32236
- Ground based solar proton monitoring, considering particle intensities and radiation dose rates from riometer absorption as function of time
16 p2850 A69-32321
- DQ Herculis photometric measurements synchronized with white dwarf component pulsation, discussing equipment, eclipse curve and binary period dependence on time
16 p2862 A69-32373
- Time dependent radiation diffusion in inhomogeneous stationary medium applied to diffuse reflection of light
16 p2813 A69-32591
- Time behavior of output intensity and polarization of single cavity mode internal mirror Zeeman laser in axial magnetic field
16 p2798 A69-32607
- Spatial and temporal dependence of trapped particle energy spectra on basis of bimodal diffusion
16 p2852 A69-32619
- Transient stress waves due to inputs of various types and time dependence in plates and revolving shells, discussing applications of elasticity theory analysis methods
16 p2876 A69-32785
- Device quantity failure kinetics or time dependence effect on time-to-failure distribution resulting from given device degradation coefficients distribution
17 p2936 A69-32895
- Diurnal periodicity of physiological functions of flight crews flying through several time zones found to correspond to time zone of permanent residence
17 p2906 A69-32935
- Frequency and time dependent gain characteristics of dye lasers, using computer program for rate equations for populations
17 p2980 A69-33025
- Q switching of CW 337 mu maser, gain factor measurements for pulse discharges and data on saturation and time dependence
17 p2981 A69-33088
- Mathematical model for determining time dependent terrain surface temperatures and radiances, considering radiative transfer convection, evaporation, ground vegetation temperature, etc
17 p3071 A69-33263
- Time dependent analysis for quasi one dimensional, vibrational and chemical nonequilibrium nozzle flows approaching steady state solution by finite difference technique
17 p2893 A69-33491
- Buckling time of oval ring under unsteady creep based on strain hardening theory
17 p3062 A69-33716
- Electromagnetic transient wave propagation and reflection in lossless isotropic stratified ionized media, discussing time variations of fields due to incident plane unit step wave
17 p2924 A69-33839
- Shifted pulse multichannel generator producing pulses and pulse sequences time delayed with respect to reference channel
17 p2938 A69-33899
- Single radio pulse reception time relations by panoramic receiver, considering short wideband and long narrowband pulses
17 p2931 A69-33910
- Time distribution of commencements of substantial intensity increases of geomagnetic and aeromagnetic phenomena
17 p2964 A69-33958
- Geomagnetic disturbances intensity spatiotemporal distribution at Northern Hemisphere high latitudes during IGY and IQSY
17 p2965 A69-33966
- Time dependent diffuse reflections related to solar activity, showing diffusion intensity variations with sporadic E layer height and electron concentration
17 p2968 A69-33997
- Deterministic and statistical prediction techniques for aircraft carrier motions at sea for application to aircraft landing operations
17 p2902 A69-34014
- Geomagnetic crotchets time relations to solar X rays, radio bursts and flares
17 p3025 A69-34227
- Anomaly of F region electron content vs polar geographic latitude and local mean time
18 p3126 A69-34252
- Short term frequency stability measured for Doppler radar and space tracking communication applications reviewing FM theory for spectral purity relationship
18 p3100 A69-34277
- Relationship between human response to noise as physical parameter, discussing controlled laboratory investigation to determine duration effect on annoyance
18 p3097 A69-34322
- Automated crop surveys from integrating observations made at different times /time dimensioning/ during growing season, noting earth resources satellite role
18 p3126 A69-34333
- Cylindrical and conical panels dynamic responses to time varying load distributions, using trigonometric series coupled with finite difference methods
[ASME PAPER 69-APM-22] 18 p3214 A69-34399
- Variable CoD minus 35 degrees 4257 noting primary period of 502 days superimposed on secondary beat period of 3000 days
18 p3195 A69-34433
- Mathematical model for operational readiness of dormant systems /periodically checked missiles/ discussing time distribution to failure detection, occurrence and between tests
18 p3142 A69-34477
- Human performance reliability, testing mathematical model application and implications of time to first error concept by vigilance task
18 p3097 A69-34478
- Hazard plot analysis of incomplete data involving times to failure for failed units and running times on unfailed units
18 p3147 A69-34515
- Optimal control theory applications for controllers: not characterized by bang bang time responses using Pontryagin maximum principle
18 p3090 A69-34681
- Algorithm for minimizing expected value of quadratic performance index in closed loop optimal control of linear time varying systems
18 p3111 A69-34688
- Graphic representation of time dependence of subsatellite points and orbital azimuths for relating satellite photographs to locality
18 p3128 A69-34818
- Time variability of horizontal wind as function of time provided by Kolmogoroff structure functions for components of isotropic turbulence
18 p3167 A69-34825
- Navigational equations solution by airborne analog computer techniques, describing electronic, electromechanical, digital reset and mechanical integrations with respect to time
18 p3107 A69-34847
- Algebraic formulation of electromagnetic diffraction, discussing propagation of positive and negative time frequency components by dual operators
18 p3172 A69-35016
- Time dependent recoverable isothermal decrease of photocurrent in CdS crystals in vacuum, noting trap mechanism involving electron redistribution
18 p3183 A69-35156
- Time dependent equations for non-LTE occupation numbers of lower bound levels of hot gas or plasma outer layer atoms and ions
18 p3231 A69-35242
- Parametric and forced oscillations analogy for analyzing dynamic behavior of oscillatory systems with time dependent parameters
18 p3175 A69-35322
- Time dependent collimated light diffuse reflection and transmission by finite inhomogeneous atmosphere using principle of invariance
18 p3132 A69-35343
- Long term creep rupture data based on short term tests in form of Larson-Miller time-temperature curves
18 p3150 A69-35422
- Annealing time effects on creep properties of Ni at various temperatures after work hardening
18 p3159 A69-35443
- Consecutive reaction equations for idealized soil column solved for nitrifying metabolite concentration as functions of time and depth
19 p3264 A69-35600
- System reliability with allowable downtime, calculating probability of on-line units staying operational during mission time using conditional availability
19 p3326 A69-36000

Time-dependent failures of components subjected to fatigue loading analyzed for reliability prediction
19 p3437 A69-36032

Initiation distance and time of detonation with weak ignition sources related to temperature, tube diameter, mixture composition and pressure
19 p3451 A69-36364

Recording instrument paper speed effect on pulse wave measurements precision, discussing multiple observer studies of left ventricular ejection time
19 p3258 A69-36449

InSb instabilities and time dependence of transverse breakdown, performing Hall effect measurements on n-type InSb at 77 K
19 p3389 A69-36546

Autonomous functional differential equations with finite time interval dependent derivatives, resulting in periodicity theorem applicable to difference equations
19 p3361 A69-36600

Townsend discharge formation time determination, taking into account impact ionization in positive ion cloud moving from anode to cathode
19 p3381 A69-36603

Titanium alloys wear and fatigue resistance as functions of time and temperature of nitriding by purified nitrogen
19 p3347 A69-36743

Stochastic motion in linear lattice of coupled harmonic oscillators analyzed by Schroedinger coordinates and Bessel functions for time behavior, energy flow and impurity effect
19 p3374 A69-36752

Spatiotemporal contours of pressure pulses emitted into surrounding fluid by collapsing cavitation bubble, using schlieren-optical observation method, electroacoustical detection device and microphone
19 p3302 A69-36870

Invertibility of linear time invariant dynamical control systems, discussing L-inverses, sequential circuits, inherent integration, reproducibility, pointwise and functional inverses
20 p3509 A69-37138

Finite element discretization technique extended to time dependent processes emphasizing dynamics and heat conduction, discussing applications to aircraft transient response
20 p3575 A69-37204

Red shift-distance relation for galaxies, discussing time dependence
20 p3597 A69-37411

Negative time interval implications for meta particle at superluminal velocity with respect to two reference frames, noting causality paradoxes
20 p3598 A69-37412

Space vehicle space-time position fiducial distribution and future location determinations based on inference theory
20 p3617 A69-37528

Lunar mascons and maria isostasy, discussing time requirements
20 p3604 A69-37564

Ion production rates vertical distribution and temporal changes at midlatitudes during solar activity minimum and maximum above F 2 layer
20 p3525 A69-37656

Inhomogeneities time buildup in lower ionosphere weakly ionized plasma during charged particle concentration perturbations and source temperature variations
20 p3525 A69-37658

Time-space variations in occurrence probability of ionospheric E-2 layer during solar activity maximum and minimum
20 p3527 A69-37672

Multiply censored data plotting on various type hazard papers for engineering information on time to failure distribution
20 p3567 A69-38288

Noctifluent cloud particles nucleation and growth, noting time dependence and water vapor mixing ratio
21 p3702 A69-38346

Computer experiment on 9000 particle plasma to test temporal echo theoretical prediction
21 p3777 A69-38713

Creep measurements in Al alloy during uniaxial tensile stresses between 200-350 C, determining deformation dependence on time and stress
21 p3744 A69-38871

Carbon dioxide laser amplifiers gain saturation time dependence characteristics by theoretical model taking rotational relaxation into account
21 p3736 A69-38941

Spacecraft return probabilities with time constraints and redundant access, using Borel set concept for counting and summing coverage belts
21 p3819 A69-39017

Observation time influence on interferometers resolution limits due to radio wave phase fluctuations
21 p3682 A69-39122

Creep long term deformation characteristics of plate and tube lead alloy model material predicted from short term room temperature creep deformation
21 p3844 A69-39320

Time characteristics and second harmonic of radiation of Nd laser containing lens systems, producing second harmonic in KDP crystal
21 p3740 A69-39544

Upper and lower bounds for growth or decay rate of solutions of parabolic differential equations for indefinitely increasing time
21 p3757 A69-39565

Kinematic and dynamic relations analyzed by vector method for motion time and orbital flight control of point
21 p3818 A69-39820

Stability loss of beams analyzed under compression allowing for various creep conditions in loading and unloading regions, calculating time to failure
22 p4039 A69-39917

Standardizing strain gage with long time stability characteristics, analyzing statistically strain calibration results
22 p3945 A69-40078

Spatiotemporal signal distortions for multiple scattering from unsteady radiant energy transfer equations
22 p3899 A69-40247

Time symmetric electrodynamics for various cosmological models, discussing position and negative space curvature
22 p4022 A69-40469

Time dependent mathematical double acceptor model including heat effects for analyzing Q switching and stimulated emission time delays in pulsed junction lasers
22 p3962 A69-40560

Harmonia and Parthenope /minor planets/ positions, establishing time dependence of relation between image diameter and planet magnitude
22 p4025 A69-40614

Adsorption kinetics in ternary mixture of nitrogen, methane and hydrogen, using concentration-time/breakthrough/ curves measurement on activated coconut shell charcoal [NAS-NRC PAPER H-4]
22 p3981 A69-40629

Sco X-1 X-ray source energy spectrum and time variation from rocket flights in India
22 p4030 A69-40774

Band movement phenomenon model for temporal and spatial interactions
22 p3880 A69-40854

Time dependent differential equation for order parameter in superconductors near critical temperature derived from density matrix equations
22 p3994 A69-41053

Thermal diffusivity measurement by nonsteady state methods, discussing time and temperature variables in heat flow differential equation
23 p4237 A69-41326

Fixed interval human performance control under various histories of conditioning and response cost conditions, considering effects of postreinforcement pauses
23 p4100 A69-41437

Boundary effects on time dependent transport theory based on star product, noting application to transmission line theory and radiative and neutron transfer
23 p4190 A69-41571

Nighttime F region time-altitude variations in aeronomic parameters calculated under conditions close to solar activity maximum
23 p4156 A69-41844

Time dependent natural oscillations of plane open resonators infinite periodic sequence, considering electromagnetic energy transfer into ambient medium
23 p4139 A69-42039

Temporal reference acoustical holography with Sokolov ultrasound camera system using double pulsed ruby or scanning CW laser
23 p4166 A69-42182

IR radiation transmission in pulsed carbon dioxide discharge as function of time, proposing pumping and relaxation mechanism model
23 p4174 A69-42196

Time dependent unsteady flow of incompressible and electrically conducting fluid between two infinite disks rotating in uniform axial magnetic field
23 p4153 A69-42410

Pi 2 micropulsation waveform variation with time from simultaneous observations at low latitude stations, estimating phase velocity of higher frequency component
23 p4161 A69-42440

Nonlinear time varying feedback control system stability applied to damped Mathieu equation
23 p4146 A69-42473

Time and plasticity effects on fracture determining solids strength as function of crack dimension
23 p4236 A69-42530

Time domain expression derived for frequency varying nonperiodic square wave in FDM and FM systems, using orthogonal functions to obtain frequency spectrum
24 p4281 A69-42623

Ni-Nb alloys precipitates tetragonal structure as function of time and temperature using electron and X ray diffraction
24 p4331 A69-42903

Automatic system failure sequence statistical analysis, considering randomly time variable external effects
24 p4289 A69-42953

Transient sources of cosmic rays, discussing possible time variable intensity and momentum spectrum of Galaxy
24 p4367 A69-43006

Creep buckling time of simply supported column under nonuniform temperature distribution over cross sections
24 p4400 A69-43053

Mean absolute relative humidity variations above earth surface over various time intervals during cloudless nights, obtaining spatial humidity differences and corresponding extinction coefficients
24 p4346 A69-43158

Cosmic ray electron energy spectrum and intensity measurements indicating time variations attributed to solar modulation effects
24 p4367 A69-43175

Iterative weighted least squares method for reconstructing time history of coupled rotation and flexural oscillations of Radio Astronomy Explorer satellite
24 p4394 A69-43291

Stability of linear systems with convolution operator in forward loop and time-varying gain in feedback loop analyzed for frequency- and time- domain conditions
24 p4295 A69-43316

Physical and physiological factors involved in determining aircraft passengers time of safe unconsciousness permissible after cabin decompression
24 p4278 A69-43398

Time-variable pulsed transverse magnetic field used to cut off tails of plasmoids ejected from conical Plexiglas plasma gun into curvilinear magnetic field
24 p4358 A69-43476

Numerical solutions for time dependent boundary value problems governed by heat equation applied to transient heat conduction in irregularly shaped two dimensional regions
24 p4410 A69-43521

Time structure of solar X ray bursts from OSO 3 satellite observations showing impulsive and gradual components
24 p4371 A69-43610

Pulsating mechanisms in alternative gas and liquid blocks two phase flow, using stochastic process specified by dynamic pressure time dependent fluctuations
24 p4305 A69-43633

Thermal turbulence effects on phase fluctuations of laser beams, studying temporal decay of mean square refractive index fluctuation with fringe pattern displacements
24 p4329 A69-43754

Quasars time dependent flux density variations at 6.6 cm, noting spectrum peaks tendency toward lower frequencies with time
24 p4389 A69-43772

Isotopic exchange reaction rate between O 18 and CO in shock tube coupled to time of flight spectrometer, noting rate increase with time
24 p4353 A69-43807

Many body perturbation theory with time dependent perturbations applied to frequency dependent polarizability of atomic oxygen
24 p4354 A69-43816

TIME DISCRIMINATION

First and second passage times of stationary random process consisting of sinusoidal signal with stationary Gaussian noise
04 p0561 A69-15453

Auditory temporal masking of tonal signal by narrow band noise and perception of temporal order noting effects of intensity, frequency and time
11 p1830 A69-24795

Temporal discrimination based on signal fluctuations emphasizing signal detection in presence of noise
19 p3373 A69-36057

QRS complex detection time error in noisy electrocardiograms
21 p3667 A69-39442

TIME DIVISION MULTIPLEXING

Pulse code modulation (PCM)/time multiplex system commanding by switching, discussing SNR measurement
01 p0031 A69-10739

Time division multiple access system for INTELSAT satellite, analyzing burst preamble and selection of frame period
03 p0388 A69-13179

Sampled data delay-lock loop for synchronizing pulsed envelope RF signals, using digital circuitry
03 p0390 A69-13216

Correlation coefficient between frequency diversified signals amplitudes estimated by approximation for two beam short wave radio channels
04 p0560 A69-15401

Time division multiple access satellite communication system employing pulse code modulation of voice channels and phase shift keying of RF carrier
07 p1077 A69-18759

Signal multiplexing within linear algebra framework permitting use of orthonormality in receiver construction without orthonormal functions generation in multiplexer
07 p1078 A69-18830

Time division telemetry technique resolving data and control flow to and from remote locations (tactical aircraft), noting application to environmental pollution control
07 p1081 A69-19100

OMEGA 4 100-k Hz ground station telemetry system for acquiring and processing outputs up to 23 FM and two TDM signals applied simultaneously from instrumentation recorder
07 p1105 A69-19103

Multiple access techniques in civil satellite communications systems, noting proposed digital time and frequency division methods
08 p1272 A69-19959

Communication satellite frequency and time divisions multiple access problem, detailing microwave multiplexers design
14 p2417 A69-29688

Satellite system TDM techniques and prototype equipment capable of combining 12 unrelated start-stop and synchronous telegraph channels
17 p2920 A69-33420

Jumbo jet audio entertainment and service systems, describing digital pulse multiplexing technique
19 p3285 A69-35806

Time division multiplexing of asynchronous digital signals from independent sources in continuous or bit stuffing mode, evaluating reliability and efficiencies
20 p3493 A69-37715

TDMA/PCM system for communication tests via Applications Technology Satellites, discussing time synchronization and bit and frame coherency
23 p4129 A69-42510

Multichannel time division multiple access system for communication satellite networks, considering PSK modems, PCM codes and channel capacity
23 p4129 A69-42511

Multiple access discrete address system (MADA) for digital modulation communication systems for satellite networks, using time division techniques
23 p4130 A69-42512

TIME FUNCTIONS

Optimal control of open loop aperiodically modulated discrete time systems, discussing solution of associated two point boundary problem
02 p0226 A69-12732

Time dependent functions integration by glow discharge tube and oscillator, discussing device for voltage measurement and applications in meteorology and geophysics
02 p0251 A69-12773

Spectrum analysis of pulse signals by point to point measurements of magnitude and phase of pulse-like time functions, using narrow band filter output
03 p0399 A69-13939

Modified versions of standard definitions of finite time stability, presenting converse theorems for necessary and sufficient conditions
04 p0624 A69-15005

Real shape of time correlation function computed from partially averaged data
05 p0786 A69-15924

Discrete time positive real functions defined for analyzing system stability with memoryless feedback
05 p0739 A69-16349

Stability of time varying systems by construction of multipliers with prescribed phase characteristics
05 p0740 A69-16598

Existence of cosmic time functions based on stable causality condition /absence of closed timelike or null curves in Lorentz metric/
06 p0957 A69-17471

High latitude transition or scintillation boundary between high and low amplitude fluctuations of satellite radio beacon signals examined as function of time
07 p1125 A69-18846

Time derivatives of Boltzmann H function with respect to dilute gas
07 p1121 A69-19407

Nonautonomous linear systems stability, with coefficient varying with bounded time function and bounded derivative
08 p1296 A69-19922

Flow analysis in magnetic annular shock tube in magnetic field varying with time
08 p1366 A69-20787

Von Karman flow changes due to unsteady heat transfer from rotating disks impulsively changing temperatures, particularly steady state and response time
08 p1422 A69-20996

Electronic optical system to process time-varying signals as optical spectrum analyzer for measuring power spectral density of input time function
08 p1317 A69-21086

Transient analysis for uniform RC structures using impulse excitations in open and short circuit configurations
09 p1471 A69-21328

Space-time variations for approximating sporadic E layer critical frequencies of geographic and time distribution curves
09 p1486 A69-21547

Optimal controls for linear systems with matrix elements and vector components discrete functions of time
09 p1473 A69-21787

Reliability characteristics of service life determination, noting exponential distribution of failure time value
10 p1662 A69-23319

Temperature field calculation in infinite plate with heat transfer coefficient and ambient temperature arbitrary functions of time
10 p1809 A69-23430

Optimal multidimensional sequential filtration of signal on background of time correlated noise
11 p1859 A69-24967

Time-pulse function generator with piecewise parabolic approximation for converting value given by DC voltage or time interval into DC voltage for arbitrary functional relation
12 p2079 A69-25968

Sensitivity function in time domain defined for control system design
13 p2238 A69-27936

Force resonance oscillations of one degree of freedom system with randomly time varying natural frequency
16 p2813 A69-32285

Space-time variations for approximating sporadic E layer critical frequencies of geographic and time distribution curves
16 p2784 A69-32542

Maximum a posteriori estimate of modulation on carrier with noise, discussing iterative technique and FM test
17 p2994 A69-32917

Time function multiplex system for simultaneous communication via satellite between number of stations, considering transmission capacity decrease due to hard limiting amplifier
17 p2919 A69-33320

Linear time varying processes minimal time control by maximum principle to construct extremal control as explicit time function
20 p3509 A69-37139

Quantum mechanical multitime correlation functions derivation and applications to laser theory
22 p3965 A69-41152

N-dimensional theorem for evaluating time continuous channel capacity or rate distortion function of random process
24 p4284 A69-42721

TIME LAG

Wide range linear delay circuit with compensating bootstrap circuit generating linear ramp waveform and regenerative Schmitt trigger comparator
01 p0041 A69-10242

Magnetron ionization gauge in helium for low pressure measurement, discussing striking characteristics and time lags
01 p0012 A69-10660

Delayed response in threshold switching from rest state in ferrite memory cores consisting of magnesium compounds
01 p0045 A69-10739

Asymptotic stability conditions for delayed quasilinear nonautonomous systems periodic solutions derived by Shimanov method
02 p0280 A69-11700

Variable time delay achievement in fluid logic circuits based on Coanda effect devices
02 p0196 A69-12080

Mathematical basis for designing controllers of time lag systems by approximately solving differential equations
03 p0408 A69-12977

Phase path variations at three closely spaced points measuring horizontal drifts at E region level, investigating time shift variability in spaced fading records
03 p0421 A69-13322

Automatic recording device for cosmic ray bursts utilizing information time delay to allow detailed initial period study
03 p0430 A69-13543

Nonlinear oscillatory systems with constant delay under random forces action, noting use of stochastic difference-differential equations
03 p0468 A69-13866

Nonsteady coordinates of linear delay system determined from observable linear combination of phase coordinates
04 p0583 A69-15099

Delay between solar activity and density changes in upper atmosphere using Harris-Priester model
04 p0594 A69-15122

Frequency controlled time delay network for broadband phased array antenna steering
04 p0580 A69-15466

Hazards in pneumatic fluidic sequential circuit caused by delays in pneumatic tubing
05 p0706 A69-16174

Department of Defense Gravity Experiment (DODGE)/attitude stabilization simulation with time lag magnetic damping
06 p1014 A69-17584

Radio channel circuit outlined for tracking interplanetary spacecraft and probes with signal delay time prediction
06 p0888 A69-17622

Radial diffusion of high energy electrons in outer radiation belts, determining statistically delay time between electron intensity variations
06 p0919 A69-17720

Thermal explosion criterion used for explosion/ignition delay of exothermic material surrounding heated wires having good thermal conductivity
07 p1240 A69-18359

Two and three frequency techniques for measuring group delay time of communication channels
07 p1076 A69-18557

Root mean square time delay error with respect to playback time and autocorrelation function of tape recorded sine wave for studying jitter spectra
07 p1132 A69-18822

Recursive method for estimating number, amplitude and time delays of signals overlapping in time and in presence of additive white Gaussian noise
08 p1270 A69-19854

Signal correlation functions measurement errors due to randomly fluctuating delay, investigating additive and multiplicative noise with periodic and random signals
08 p1296 A69-19922

Pseudoexact Chebyshev response curves for bandpass filter design, discussing phase response and time delay characteristics
08 p1283 A69-20222

Time response of second order nonlinear overdamped systems calculated by Krylov-Bogoliubov method of variation of parameters
08 p1297 A69-20355

Wideband array antenna IF time delay steering realization, showing steering independence of bandwidth
08 p1290 A69-20977

- Time difference position determination system for space, surface and airborne vehicles, describing application to satellite navigation and air traffic control
08 p1348 A69-21066
- Round trip delay effect on probability of error in uncertainty feedback communication systems operating at channel capacity
09 p1453 A69-21322
- Electron content of earth-Venus interplanetary medium measured by observing relative propagation time of radar pulses to Venus
09 p1594 A69-21697
- Common mode rejection technique to determine phasing differences in digital systems by measuring pulse delay
09 p1463 A69-21896
- Time delay, red shift, equivalence principle, light deflection and perihelion motion tests of general relativity with Jupiter probe
09 p1597 A69-22089
- Orthogonal projection derived equation to optimally estimate state of nonstationary linear discrete systems with time delay, developing Kalman type filter
09 p1473 A69-22437
- Maximum principle in integral form for optimal control problems with delay differential system equations, using vector matrix notation
10 p1718 A69-23038
- Excitation of ultrathin Cd/SeS/ platelets with mode locked He-Ne laser for excitons formation, discussing time delay
10 p1703 A69-23512
- Tandem interleaved cyclic codes for digital HF communication with improved error rate at reduced decay time
10 p1655 A69-23530
- Hybrid simulation of transport lag with variable time delay, noting dynamic range limitations due to digital computer processing and memory capacity
10 p1661 A69-23852
- Time registration delays during photographic observations of satellites, describing NAFA type satellite camera and mechanical and electrical systems
11 p1880 A69-24365
- Jittering delay of triggering circuit driven by ramp signals of different finite slopes, noting tunnel diode discriminators and regenerative feedback loop circuits
11 p1858 A69-24568
- Steady state and dynamic characteristics of linear plant with constant lag element based on correlation function moments
11 p1859 A69-24965
- Differential equations describing system stability with delay in functional space
11 p1919 A69-25093
- Ignition of condensed homogeneous combustible materials in presence of phase transition in heated layer, discussing temperature distribution and ignition delay time in ammonium perchlorate
11 p2000 A69-25189
- Piezoelectric variometer with reduced indicator time lag for measuring pressure gradients in fluid media
11 p1889 A69-25427
- Tracking system for gain and time delay parameter measurements of compensatory control crossover model
12 p2022 A69-25930
- Visual receiving equipment for consistency determination of Loran-C sky wave signals apparent arrival times
12 p2029 A69-26052
- Time delay in temperature controlled transistorized time delay circuit determined by transistor unsteady thermal processes
12 p2043 A69-26883
- Delay time of pulse signals in radio channel transmission described by standard deviation of channel properties
13 p2218 A69-27215
- Stability test for linear unit feedback control system with second order lag and dead time compensated by PIO controller
13 p2238 A69-27395
- Periodic solution to equations describing nonlinear autonomous time lag system close to Liapunov systems
14 p2482 A69-28799
- Pulsed IR laser optimal Q switching mode by using semiconductor mirror with nonparabolic dispersion law and changing mirror opening moment delay time
15 p2633 A69-30064
- Group delay time for dispersive wave propagation velocity determined using correlation method
15 p2562 A69-30094
- Ignition delay of paraphenylenediamine associated with nitric acid, showing relation between grain diameter and hypergolic ignition mechanism, noting oxidizer concentration effects
15 p2561 A69-30185
- Subtractor performance for processing correlated random signals with different spectral widths in signal delay time indicator, discussing errors
15 p2572 A69-30346
- Type 3 radio bursts time profile for estimating magnetic field strength in solar corona
15 p2675 A69-30554
- Time delay errors compensation methods in analog-digital computation loops, finding digital scheme inferior to analog
15 p2572 A69-30618
- Time logarithmic switching to explain anomalous delay in threshold response of MgMnZn ferrite memory cores
15 p2668 A69-30688
- Program stretchout in aerospace procurement, discussing costs effect in relation to incentive contracts
15 p2721 A69-31071
- VLF and particle rocket experiment for group delay time between rocket and ground, discussing wave polarization and energy flows meaning
15 p2571 A69-31424
- Pseudoexact bandpass filter design, presenting graphs for passband loss, voltage standing wave ratio and time delay as function of frequency
15 p2581 A69-31526
- Holographical interferometry with laser spark radiation containing fundamental and second harmonic wavelengths, confirming heavy particle densities decrease in plasma with time
16 p2789 A69-31771
- Sudden enhancement of atmospheres recorded during IGY, noting time lag between flare and SEA maximum
16 p2778 A69-32192
- Latitude variations of delays between spread F and magnetic activity shown to be different at various parts of solar cycle
16 p2779 A69-32194
- Selective amplifier for recording time signals on Time Recorder 2 and measuring time lag caused by Philips 8RO 501 radio receiver
16 p2790 A69-32217
- Nonequilibrium inlet conditions effect on combustor performance during H and vitiated air combustion, studying ignition delays
16 p2881 A69-32767
- Jodrell Bank RF digital autocorrelation spectrometer based on time delay related to signal power spectrum through Fourier transform
17 p2970 A69-32856
- Stability conditions for time lag differential equation systems over finite interval employing Liapunov functions, noting similarity with systems having continuously acting disturbances
17 p2995 A69-33616
- Multiple input and output nonlinear time invariant feedback system under almost constant inputs
17 p2944 A69-33743
- Shifted pulse multichannel generator producing pulses and pulse sequences time delayed with respect to reference channel
17 p2938 A69-33899
- Quasi-transverse /Q-T/ point time lag on Faraday rotation records at widely spaced frequencies during satellite pass explained by refraction theory
18 p3100 A69-34251
- Discharge coefficient and opening time of pneumatic and hydraulic systems incorporating disks, nozzles and valves
18 p3094 A69-34981
- Electrooptical distance measurement based on laser pulse traveling time and phase measurements to determine satellite range
18 p3103 A69-35199
- GaAs-P injection laser time delay measured from start of current flow in p-n junction diode, studying effects of memory, temperature and reverse bias
19 p3387 A69-36536
- Delay in photoelectric recording of transit of stars, considering stellar image brightness distribution and temperature
20 p3608 A69-38053
- Variational or optimal control for delayed systems, involving integrated maximum principle for problems with nonlinear functional differential systems
21 p3754 A69-38429
- Chalcogenide semiconductor film switches time parameters, showing delay time decrement with thickness decrease and voltage increase
21 p3780 A69-39045
- Time difference position determination system for space, surface and airborne vehicles, describing application to satellite navigation and air traffic control
22 p3977 A69-39874
- Extension of Liapunov systems to time lag systems with small periodic parameter
22 p3980 A69-40107
- Time dependent mathematical double acceptor model including heat effects for analyzing Q switching and stimulated emission time delays in pulsed junction lasers
22 p3962 A69-40560
- Digital computer determination of stimulated emission time delay, Q switching temperature and current region and impurity profile effect across junction in junction lasers
22 p3962 A69-40561
- Extensive air showers temporal distribution of electrons by diffusion equations in A approximation compared with experiments and Monte Carlo calculations
22 p4007 A69-41054
- Electronically controlled microwave phasers and time delay elements design and operation, discussing beam width, steering and effects, directivity and planar arrays
23 p4135 A69-41353
- HF backscatter, long delay signals and round-the-world echoes as radio wave propagation modes
23 p4116 A69-41602
- Linear system propagation time measurement independent of input or output time functions
23 p4165 A69-41700
- Moving striations as plasma oscillations arising from transit time delays of neutral and charged particles moving through ionized gas, using continuity equation
24 p4356 A69-43122
- Thermosphere dynamic response to low altitude geomagnetic disturbances, showing time lag dependence on perturbation intensity
24 p4310 A69-43180
- Solar protons delayed access into polar regions during 2 November 1967 solar particle event, discussing north-south asymmetry
24 p4368 A69-43183
- Feedback controller for linear stationary differential systems with time lag and fixed unknown parameters, noting closed loop transfer function role
24 p4293 A69-43293
- Liapunov functionals for time delay systems by path integrals in state space, using convolution equations involving distributions with compact support
24 p4295 A69-43317
- Optimal control with computer prediction for inertial linear plants relay system containing time lag
24 p4295 A69-43706
- TIME LAPSE PHOTOGRAPHY**
U CHRONOPHOTOGRAPHY
- TIME MEASUREMENT**
NT CLOCK PARADOX
- Ephemeris Time and Atomic Clock Time roles in astronomy, discussing errors in daylength determination for mechanical, Shortt and atomic clocks, UT and Ephemeris Time
01 p0156 A69-10989
- EUV emission line radiative lifetime measurement by foil-excitation technique, noting correction for cascading, He II and transition probabilities for N II and O III
03 p0471 A69-13165
- Theory of relativity and role of time intervals in prediction experiments for rate of clocks
03 p0467 A69-13599
- Left ventricle rapid filling period measurement from rapid filling wave of apexcardiogram, noting possible influences of age and sex
03 p0376 A69-14081
- Radar round trip time of flight measurements to Venus for three month interval about inferior conjunction of August 1968
04 p0663 A69-15384
- Laboratory equipment for atomic and astronomical time and frequency measurement
05 p0827 A69-16582
- Device for measurement of time to failure of brittle materials in thermal-endurance testing, noting shock wave
06 p0927 A69-17690
- Two and three frequency techniques for measuring group delay time of communication channels
07 p1076 A69-18557
- Pulsating radio source pulse arrival time measurements at 1919 plus 21, determining highest SNR
07 p1214 A69-18665

Time perception capacity of astronauts and jet pilots during brief weightlessness, noting emotional state effects

07 p1065 A69-18981

Ground propagation of regular Pc 1 and irregular Pi 1 geomagnetic micropulsations demonstrated by precise time measurement

07 p1127 A69-19338

Incoherent m-ary frequency shift keying /MFSK/ system analysis concerning automatic time synchronization

08 p1274 A69-20133

Picosecond light pulse measurement by two photon excitation of photographic film

08 p1313 A69-20165

Geomagnetic field mean hourly values continuous smoothing from recordings at drifting arctic stations for determining time variations

09 p1487 A69-21553

Giant pulse buildup time in Nd-glass laser with passive shutter determined by comparing Q factor and peak power ratios of different modes

11 p1894 A69-24621

SNR measurement with time interval counter and computer, discussing accuracy

11 p1839 A69-25299

Practical time resolution of streak camera, discussing streak camera transfer function and measurement of resolution with pulsed laser diode emission

12 p2084 A69-26152

Intense ultrashort pulse widths determination by two photon fluorescence patterns, using model of partial laser mode locking

13 p2270 A69-27198

Lithium depletion in main sequence stars of one solar mass, suggesting e-folding time scale indicated by Coma Cluster data

14 p2517 A69-29089

Ultrasonic pulse-echo-overlap method modified for simultaneous measurement of time delay and relative voltages in determining sound velocities and attenuation of solids

14 p2450 A69-29567

Epochs in atmospheric circulation development over Northern Hemisphere, emphasizing solar activity roles in epochs appearances

14 p2478 A69-29837

Pulsar NP 0532 period measurements at various frequencies, obtaining accuracy in timing data reduction by linking pulse arrivals over interval of months

15 p2680 A69-30232

Crab Nebula pulsar NP 0532 simultaneous optical and radio observations, noting influence of interstellar dispersion shape uncertainty

15 p2680 A69-30233

Antenna, frequency converter and automatic spectrum recorder system for closest approach times prediction and satellite identification, discussing errors

15 p2569 A69-30800

Atomic and astronomical time and frequency measurement via Loran C and VLF/Omega phase tracking receivers

15 p2615 A69-31285

Geomagnetic field mean hourly values continuous smoothing from recordings at drifting arctic stations for determining time variations

16 p2784 A69-32548

Electrooptical /photomultiplier/ detection of satellite beacon flashes, establishing time of flash and measuring pulse shape and energy received

17 p2919 A69-33083

Epochs and ephemerides of asteroid Amor for 1916, 1924 and 1972, noting unfavorable observing conditions in future

17 p3038 A69-33723

Canopy filling time for parachutes under infinite mass conditions, using continuum equation and parachute inflation concept [AIAA PAPER 68-12]

17 p2902 A69-34032

Streak photographs by differential interferometer to study head wave standoff in shock tubes as function of time

18 p3085 A69-34473

Mean-time-to-repair of complex systems with consideration for repair policies and number of repairmen, noting application to systems reliability engineering

18 p3144 A69-34494

Time variation of laser flare plasma temperature related to pulse parameters, using soft X radiation from plasma

18 p3154 A69-35496

Analog device to compute running ten minute average and store latest ten minute peak of unipolar data input for wind speed sensors

19 p3312 A69-36278

Temporal position of pulse signal on noise background determined by measuring signal passage time through linear filter zero point

19 p3278 A69-36596

Time perception capacity of astronauts and jet pilots during brief weightlessness, noting emotional state effects

20 p3480 A69-38229

National Physical Laboratory atomic clock improvements, describing use of cesium 133 as second of time standard and phase shift effects on precision

21 p3720 A69-38548

Mean time between failures /MTBF/ for component, equipment or system subjected to total unit test hours at various confidence levels

21 p3684 A69-39700

Earth rotation rate variations connected to longitude variations of continents time services, noting atmospheric circulation and inertial forces role

22 p4024 A69-40609

Spherical lunar coordinates for arbitrary moment of time calculated by digital computer using Brown lunar motion theory

22 p4024 A69-40611

Linear system propagation time measurement independent of input or output time functions

23 p4165 A69-41700

TIME MEASURING INSTRUMENTS

NT ATOMIC CLOCKS

NT CHRONOMETERS

NT CLOCK PARADOX

NT CLOCKS

NT TIMING DEVICES

Soviet book on flight vehicles astronavigation covering automatic equipment accuracy, changes in spherical coordinates, time measuring, etc

18 p3168 A69-34355

TIME OF FLIGHT SPECTROMETERS

Residual gas analyzer and leak detector by time of flight measurements on neutral metastable atoms and molecules between pulsed electron gun and auger surface detector

13 p2262 A69-28006

Time of flight mass spectrometers for plasmoids generated by theta pinch and discharge over organic glass, showing ion and electron currents oscillograms

14 p2498 A69-29813

Shock wave studies of gaseous NO thermal ionization in Kr as function of temperature, using time-of-flight mass spectrometer

18 p3099 A69-34464

TIME OPTIMAL CONTROL

Time optimal control formulated for interconnected nonlinear controlled system described by fourth order differential equations

01 p0050 A69-10354

Variational calculus applied to time optimal trajectories between two points in range altitude space, discussing aircraft thrust and drag laws

01 p0009 A69-10414

Optimum control determination for low thrust spacecraft to minimize time for passing through radiation belt

01 p0113 A69-10571

Time optimal control design by algorithm method

01 p0052 A69-10794

Comparative analysis of variable structure adaptive systems and time optimal system for control of plant described by differential equation

01 p0052 A69-10795

Satellite optimal transfers from elliptic to parabolic orbits within set time

01 p0157 A69-11306

Discrete time optimal control problems solved by second order variational algorithm, developing recurrence relations for perturbation equations

01 p0054 A69-11416

Optimal control of linear stochastic systems using noise measurement data mathematical model

04 p0581 A69-14569

Time optimal turn maneuver for rocket with tilting engine and control nozzles, noting rotation moments distribution

04 p0665 A69-14832

Analysis and synthesis of optimal linear time invariant systems with uncertain or unknown parameters, considering mean square error

06 p0902 A69-17405

Optimal control of linear systems with state variables generated by linear feedback from output variables, considering time variance

06 p0903 A69-17406

Algorithms construction for aerospace vehicle trajectory optimization, considering quasi-lineariza-

tion method for computation of variable time optimum trajectories

06 p1006 A69-17569

Closed loop time optimal control achieved by exploiting generalization properties of threshold logic networks [AIAA PAPER 69-77]

06 p0905 A69-18092

Control systems stability under perturbations using time optimal control

07 p1115 A69-18514

Hologram storing on photochromic film, obtaining equations for optimal exposure time [IEEE PAPER F-1]

07 p1133 A69-19057

Aircraft position and velocity in directions normal to ILS reference path by correlation with inertial navigation system, noting minimal time controller

07 p1177 A69-19213

Sensitivity coefficients to solve two point boundary value problem arising from Pontryagin principle, with application to time optimal control studies

08 p1296 A69-20297

Centralized control with variable step interrogation of control points

08 p1298 A69-20422

Optimal rendezvous between satellite and spacecraft, determining power and time optimal coplanar rendezvous in circular orbit

09 p1538 A69-21759

Minimum time turns for spacecraft about fixed axis lying beyond plane of vehicle forces

09 p1609 A69-21760

Optimal control computation technique and application to minimal time flight profile optimization and isoperimetric problem of Lagrange with equality constraints

09 p1595 A69-21798

Optimal closed loop control system for linear time varying system with two independent parameters, noting trajectory sensitivity in large launch booster

09 p1473 A69-22439

Adaptive control algorithm operating on-line to make discrete time adjustments in controller parameters of continuous time control system

09 p1474 A69-22441

Stationary controller design for linear time varying control systems with state variables not always accessible for feedback

09 p1474 A69-22443

Optimum time interval for constant data transmission rate during single pass of satellite over ground station

09 p1457 A69-22462

Stability and local parametric synthesis conditions of programmed optimal control established for optimal control problem within fixed interval

09 p1475 A69-22666

Time optimal controlled linear systems with optimally chosen parameters, considering arbitrary second order oscillator controllability

10 p1666 A69-22922

Time optimal control system for searching for minimum of inertial object output value

10 p1666 A69-23816

Nondifferential function minimization on entire vector space or bounded subset for application to minimization problems in function spaces, time optimal control, etc

10 p1721 A69-23863

Asymptotic solution to problem of finding time optimal transformation for controlled plant with motion in phase space described by matrix differential equation

10 p1666 A69-23883

Time varying linear optimal control system sensitivity obtained by comparing closed loop with open loop sensitivity to parameter variations

10 p1667 A69-24058

Time optimal steering for rocket vehicle with trajectory defined between initial and final state, using minimum principle and boundary value problem solution

11 p1861 A69-25454

Optimal controllers analytical design for closed loop systems with pure time delay in actuating mechanism using differential equations

12 p2045 A69-25959

Sampled data time optimal control of linear multivariable system based on determination of system state variables control time and minimum sampling intervals

12 p2050 A69-26083

Time optimal controls for multivariable linear systems by computer programming of iterative calculations /Neustadt and fast convergence methods/

12 p2050 A69-26090

Optimal control of discrete time linear system with random parameters, noting case of additive noise in measurements

12 p2052 A69-26501

Time optimal regulator problem with recoverability constraint as restriction on system state during control synthesis

12 p2052 A69-26504

Error due to amplitude quantization and design of digital control systems in discrete time optimum control theory

12 p2053 A69-26507

Linear, quadratic, optimal control problems solved by sweep method, discussing time role, feedback control law and use of matrix equations

12 p2053 A69-26512

Negative exponential solution of matrix Riccati equation associated with linear optimal regulator and filter problems for time invariant plants

12 p2122 A69-26513

Controllability of stationary linear multivariable systems using frequency domain criterion with application to optimal control laws for minimum fuel and time control problems

12 p2054 A69-26519

Pursuit problem involving controllable pursuing plant, deriving condition for engagement with prescribed period of time

14 p2482 A69-28800

Optimal linear control systems with time limits on transient processes synthesized by reducing optimization to algebraic equations solution

14 p2425 A69-28820

Cauchy problem for Bellman dynamic programming equation in automatic control time minimization

14 p2426 A69-29478

Bayesian theory to determine maximum a posteriori estimation algorithms for optimum bit synchronization in digital communication systems

14 p2413 A69-29496

Stochastic saturating systems optimal control computation, considering attitude control and tracking system design by elliptical differential equation of dynamic programming

15 p2582 A69-30601

Optimum control determination for low thrust spacecraft to minimize time for passing through radiation belt

15 p2651 A69-30741

Pontryagin maximum principle applied to time optimal control of autonomous second order system with constant coefficients and differentiation in transfer function numerator

15 p2583 A69-31059

Minimum time single axis capture of satellite spinning about pitch axis by low thrust jets, considering gravity gradient phenomenon

17 p3048 A69-33237

Time optimal pitch motion of satellite in circular orbit based on maximum principle, considering variable and constant controls

18 p3207 A69-34677

Time and fuel optimization of angular momentum alignment and nutation elimination of spin stabilized bodies with inertial reference direction

18 p3208 A69-34775

Law for time variations of modulus-restricted control action at trajectory end, two point boundary value problem solution and use of Pontryagin principle

18 p3175 A69-35324

Optimal timing of measurements to minimize dispersion of navigational observation parameters by least squares method with application to Keplerian orbit elements

19 p3370 A69-36614

Linear time varying processes minimal time control by maximum principle to construct extremal control as explicit time function

20 p3509 A69-37139

Book on stochastic optimal linear estimation and control, discussing probability theory, models and continuous and discrete time linear systems

20 p3509 A69-37143

Response time estimation for control system with constrained phase coordinates, determining conditions for optimal control problem solution

21 p3769 A69-38568

Control function ensuring minimal response time of controlled plant with motion described by integral equations system, using method of distributed moments

21 p3685 A69-38847

Time optimal control for second order automatic system with motion described by differential equations

21 p3770 A69-38856

Continuity of optimal control of nonlinear plant, noting search time

21 p3686 A69-38884

Time optimal control for torsional vibrations of flight vehicle for limited energy case, illustrating uniform wing of constant rigidity

21 p3686 A69-38891

Control knob optimum diameter for minimum operation time, noting frictional resistance

21 p3664 A69-38969

Fuel-time optimal retrothrust control for vertical and gravity turn ballistic trajectories of soft landing nonlifting bodies based on Pontryagin principle [AIAA PAPER 69-868]

21 p3809 A69-39394

Time-optimal nuclear rocket propellant start-up with thermal stress constraints based on distributed parameter model, deriving algorithm for flow rate increase

21 p3768 A69-39632

Second order suboptimal control systems with time varying coefficients, calculating switching curves for quadratic cost functional

21 p3825 A69-39634

Interplanetary midcourse velocity correction schedules optimization, discussing timing equations modifications, mission simulation and role of earth based radar

21 p3766 A69-39646

Computerized algorithm facilitating automatic synthesis of time invariant linear compensation for highly complex multiloop control systems [AIAA PAPER 69-941]

22 p3917 A69-40324

Variable time of arrival /VTA/ guidance generalized, developing computational algorithms to supplement linear guidance method

22 p3979 A69-41186

Optimal control problems, discussing properties of signal producing response signals with transient functions at independent outlets of linear dynamic system

23 p4145 A69-41958

Optimum functions for mass and energy flow during spacecraft orbital transfer, emphasizing time behavior of propulsion variables

24 p4382 A69-42921

Optimal control computing method applied to minimal time flight profile optimization

24 p4383 A69-42954

Time optimal control of soft spring showing switching locus changes

24 p4289 A69-42955

Attitude control system with rate of change limiter to minimize launch vehicle drift during first stage ascent through atmosphere

24 p4394 A69-43277

Coefficient quantization in digital continuous time process controllers, applying results to nominal transfer function approximation

24 p4292 A69-43283

Suboptimal closed loop controller for linear time varying process subject to additive random disturbances and measurement noises

24 p4292 A69-43285

Minimal time closed loop controller design for linear systems with bounded control amplitudes and rates

24 p4293 A69-43304

Localizer acquisition system quasi-optimization technique based on time optimal control theory, with application to SST ILS problem

24 p4348 A69-43312

TIME RESPONSE

TAF /time and frequency/ code written in FORTRAN language for computing steady state, frequency and time response from nonlinear simultaneous differential equations

04 p0565 A69-15341

Gallium arsenide electro-optic switch measuring signal time response to radiation step of homogeneously broadened carbon dioxide, He and nitrogen laser amplifier

05 p0773 A69-16293

Inverted transistor parameters required for accurate prediction of electrical and radiation storage time, discussing computer predictions of radiation responses

06 p0977 A69-16884

Detection time to light point source noting response to dark, star field and glare source backgrounds

06 p0881 A69-17215

Laser small signal step response measured, deducing medium bandwidth [IEEE PAPER G-9]

07 p1151 A69-19056

Channel output SNR optimization in AM/FM telemetry system by using automatic gain control, discussing AGC time response and general characteristics

09 p1454 A69-21799

Time varying linear system with input-output relation described by differential equation calculated for impulse response using Taylor series

09 p1459 A69-22580

Response times for entire Knudsen number range in straight round pressure pipes, using digital computer in final integration

10 p1677 A69-22900

Low thrust propulsion devices high response impulse testing, describing limitations imposed by solenoid valve time response

10 p1672 A69-23278

Integral time characteristics for unsteady light scattering by using solution to corresponding steady state problem of light pulse scattering in medium

11 p1915 A69-24604

Single mode laser oscillations buildup for 0.633 micron transition of He-Ne laser at levels above threshold using fast intracavity chopper

12 p2105 A69-26318

Cross correlation methods for determining systems time domain response adapted to communications channel evaluation, discussing computer simulation of on-line testing

16 p2750 A69-31757

Pulse propagation through antipode, calculating time domain response of fields near axial caustic

18 p3100 A69-34233

EEG patterns computerized spatio-temporal display technique using CRT and motion picture camera

21 p3668 A69-39864

Heart electrical activity time sequence estimation based on multiple dipole binary model, deriving algorithm

21 p3668 A69-39865

Psychophysical threshold changes during subliminal monocular and interocular stimulation, studying conditioning flash size effects on temporal summation

22 p3881 A69-40860

Correction coefficients for time response of hybrid control systems with digital feedback elements containing quantized coefficients

24 p4293 A69-43302

TIME SERIES ANALYSIS

Mathematical modeling of gyro drift rate in inertial navigation based on stationary and nonstationary time series analysis

03 p0463 A69-13213

Computer program for obtaining information from stationary time series using Chree method of superposed epochs for processing unlimited data and epochs

13 p2225 A69-27617

Gyro drift rate mathematical modeling based on stationary and nonstationary time series analysis techniques with random process reduction to white noise residuals [AIAA PAPER 69-838]

21 p3761 A69-39369

TIME SHARING

Computer-analyzer system for nuclear chemistry, noting advantage of on-line data acquisition and analysis coupled with time sharing economy

05 p0725 A69-16584

Time division telemetry technique resolving data and control flow to and from remote locations /tactical aircraft/, noting application to environmental pollution control

07 p1081 A69-19100

SNODE /spectra numerical ordinary differential equations/ computer program for solving differential equations and integration with basic time sharing system

10 p1659 A69-23142

On-line central data processing system connected to time shared computer for recording data from test facilities, discussing hardware configuration, software considerations and advantages

17 p2932 A69-33106

Time sharing remote computer station allowing on-spot data processing and output answers, formulating best-fit equation representing statistical data [SAWE PAPER 799]

18 p3107 A69-34860

Parameters distinguishing analytic queueing models of time sharing algorithms, emphasizing techniques used for analyzing round-robin and multiple level queueing models

19 p3279 A69-35600

T shaped radio astronomical array, discussing time sharing technique providing simultaneous observation capability and merits of T and cross configuration telescopes

20 p3507 A69-37837

Colocated radio equipment time-sharing scheme for interference avoidance, describing switching method and sampling signal shape

23 p4142 A69-42228

TIME SIGNALS

TIME SIGNALS

Analog-hybrid computer configurations for average and rms values of signals with respect to time
06 p0891 A69-17220

Stellar occultations by moon observed with ear and eye method, not taking into account corrections to radio time signals
10 p1776 A69-23205

Worldwide clock synchronization by geostationary satellite transponder relaying VHF signals from reference clock, noting accuracy of radio propagation delay prediction
12 p2080 A69-26053

Selective amplifier for recording time signals on Time Recorder 2 and measuring time lag caused by Philips 8RO 501 radio receiver
16 p2790 A69-32217

Digital signal processing electronic device for linearizing signals from sensors with nonlinear frequency output by modifying time signal frequency
22 p3915 A69-40935

Loran C system for master station time and frequency dissemination, discussing application, coverage, timing accuracy and restrictions
23 p4116 A69-41601

TIMERS

U TIMING DEVICES

TIMING

U TIME MEASUREMENT

TIMING DEVICES

Satellite triangulation simultaneous and trailing methods, discussing timing devices design
[UN PAPER 68-95285] 01 p0064 A69-10475

Time coding system for recording balloon measurements on magnetic tape
05 p0762 A69-15825

Jittering delay of triggering circuit driven by ramp signals of different finite slopes, noting tunnel diode discriminators and regenerative feedback loop circuits
11 p1858 A69-24568

Selective amplifier for recording time signals on Time Recorder 2 and measuring time lag caused by Philips 8RO 501 radio receiver
16 p2790 A69-32217

TIN

Temperature dependent isomer shift and anharmonic binding of Sn 119 in niobium stannide, measuring Mossbauer recoil free fraction
01 p0134 A69-10009

Gray tin band structure, noting Shubnikov-de Haas oscillations, transport properties, piezo-Hall effect, magnetoreflection and free carrier absorption
02 p0295 A69-11783

Angular correlation of inelastically scattered alpha particles and gamma rays emitted from 2-plus state of Sn 120
03 p0469 A69-13098

Fermi surface topology effects on Nernst-Ettingshausen coefficient from measurements in magnetic field to 3.3 tesla and 1.2-4.2 K temperatures in metallic tin
05 p0808 A69-16357

Tin and zirconium addition effect on transformations of titanium alloys during heat treatment
07 p1162 A69-18775

Chondritic meteorites arsenic, tin and antimony content determined by anion-exchange chromatography and neutron activation analysis
13 p2344 A69-27630

TIN ALLOYS

Heats of solution of Ag and Cu in dilute Ag-Cu-Sn alloys at 720 K, using liquid metal-solution calorimeter
13 p2279 A69-27759

Friction effects on friction couples made of two different nonferrous alloys, discussing temperature regime difference effects on microgeometry and structure
15 p2629 A69-31027

TIN COMPOUNDS

U NIOBIUM STANNIDES

U STANNATES

TIN OXIDES

Chemisorbed oxygen effect on electrical conductivity of zinc doped polycrystalline tin oxides
07 p1201 A69-19478

TIN TELLURIDES

SnTe, SnSe and SnS epitaxial layers obtained by deposition of sublimates on cellulose-nitrite-varnish and single crystal NaCl and KBr substrates
02 p0298 A69-12049

Chemical compatibility estimation of lead and tin tellurides thermoelectric materials with metallic alloys
04 p0551 A69-15315

Band structure for narrow energy gaps of GeTe and SnTe by perturbation model, noting constant free path and relaxation time
19 p3385 A69-36516

TIP DRIVEN ROTORS

Tip turbine driven flush thin profile wing or platform lift fan design and operating considerations
05 p0696 A69-15554

Heavy lift helicopter design with 30 ton payload, considering fanjet drive hot cycle and shaft drive propulsion systems
[AHS PAPER 330] 17 p2901 A69-33532

TIP SPEED

Self excited rotor blade oscillation at high subsonic Mach numbers during flight tests of Sikorsky NH-3A compound helicopter
07 p1053 A69-18870

TIP VORTICES

U VORTICES

TIPS

U BLADE TIPS

U WING TIPS

TIRES

NT AIRCRAFT TIRES

Tires tested for road hazards, noting correlation to population density and rainfall
09 p1480 A69-22735

Standing waves in running tire shell wall, considering internal pressure, cross sections, wall thickness, cord angle, critical speed, etc
22 p4048 A69-41185

TIROS SATELLITES

Tiros satellite meteorological observations, discussing perturbation morphology and cloud mass organization
01 p0109 A69-10545

Satellites in meteorological service, describing TOS, ESSA and Nimbus satellites operation methods
08 p1409 A69-19960

TIROS global weather satellite system performance, reviewing TIROS and ESSA satellites, APT camera and ground stations and projected TIROS M/TOS satellite
10 p1722 A69-23145

Precipitation zone-cloud mass correlation based on Tiros cloud photographs, synoptic charts and weather maps for European U.S.S.R.
19 p3366 A69-36671

Tiros M requirements for earth resources sensor systems, discussing spacecraft structure, dynamics, power, command and communications subsystems
21 p3818 A69-38621

TIROS 9 SATELLITE

Wind velocity, geopotential and atmospheric layer temperature fields constructed from Tiros 9 satellite cloud data using least squares method and trigonometric polynomials
13 p2292 A69-27733

TIROS OPERATIONAL SATELLITE SYSTEM

Tiros Operational Satellite system for global weather analysis data acquisition and cloud cover photography, noting sensor development for numerical weather prediction
[UN PAPER 68-95823] 01 p0108 A69-10473

TIROS global weather satellite system performance, reviewing TIROS and ESSA satellites, APT camera and ground stations and projected TIROS M/TOS satellite
10 p1722 A69-23145

Tiros-ESSA satellite operations, describing first and second generation systems
19 p3433 A69-36909

TISSUES [BIOLOGY]

NT EPITHELIUM

Spectral absorption curves of hematoxylin stains in stained tissue sections of rat thyroid
01 p0015 A69-10924

Cell and tissue cultivation outside living organisms, discussing applications in space biology, space medicine and food protein sources
02 p0198 A69-11501

Molecular mechanisms leading to mineralization of organic tissues, noting role of protein and glycoprotein matrices
04 p0555 A69-14888

Microvillar bleb formation in proton irradiated primate hepatocytes with electron microscope, noting sinusoidal lumen
10 p1641 A69-23045

Rapid decompression and recompression in stapled eardrum, noting fibrous tissue response in middle ear at reconstructions utilizing polyethylene struts on gelfoam
14 p2406 A69-29292

Pulmonary oxygen toxicity, analyzing reticulum and elastic tissue damage and hyaline membranes by histochemical techniques
14 p2407 A69-29298

Histological changes in rat skin after 13 Mev proton irradiation, evaluating biopsies in tissue culture
14 p2407 A69-29298

Constitutive equations for living soft tissues free-deforming under negligible stresses with Hooke law limit
14 p2535 A69-29360

Invertebrate endoskeletal cartilage and cartilage-like tissues occurrence and nature, discussing cellular tissues and origin
15 p2555 A69-30412

Damage thresholds to ocular tissues from laser radiation, presenting comparative theoretical curves and recommended safe working levels
18 p3097 A69-34312

Statistical relations between minute blood circulation volume, O capacity and consumption rate in tissues of men and dogs
19 p3260 A69-35896

Noble gases effect at low pressures on O consumption by mammalian tissue, noting Xe, Kr, N and nitrous oxides effect on rat liver
19 p3258 A69-36454

Bubble size and blood perfusion effect on gas bubbles absorption in tissues, noting decompression sickness
21 p3651 A69-38389

Nerve tissue oxidation processes related to nervous system radiation sensitivity in dogs with cerebellum X-rayed after enzyme poisons administration
21 p3658 A69-39053

Device determining dynamic mechanical properties of tissues and various transducers, evaluating elastic properties of polyurethane, Hevea rubber and descending thoracic aorta
22 p3890 A69-40204

Tissue pressurized oxygenation during radiation therapy emphasized for overcoming tumor radioresistance attributed to oxygen deficiency
23 p4091 A69-41967

Nerve and muscle tissues subthreshold reactions on analog model, discussing transient characteristics under various excitations
23 p4109 A69-41980

Digital simulation of oxygen pressure fields and supply conditions in biological tissues
23 p4097 A69-42098

Microwave radiation effects on biological systems, discussing categories according to radiation protection guide /RPG/ numbers, tissue properties and interactions
24 p4270 A69-42579

Measurement technique using dielectric waveguides for studying microwave fields influence on and energy imparted to body tissue
24 p4279 A69-43705

TITAN LAUNCH VEHICLES

Titan 3C launch vehicle digital flight control system using flight equations time-shared with guidance equations
[AIAA PAPER 69-878] 21 p3824 A69-39404

TITAN 3 LAUNCH VEHICLE

BEEP /Best Estimate of Engine Performance/ program based on trajectory reconstruction and acceleration determination for evaluating Titan 3 propulsion system performance
[AIAA PAPER 68-585] 19 p3394 A69-35945

Addressable remote multiplexed PCM data system used on Titan III launch vehicles
19 p3274 A69-36279

Titan 3 transtage attitude control system hydrazine rocket engine design and performance, emphasizing problems associated with monopropellant
[AIAA PAPER 69-422] 19 p3394 A69-36300

TITANATES

U BARIUM TITANATES

U ILMENITE

U LEAD TITANATES

U PEROVSKITES

U STRONTIUM TITANATES

TITANIUM

Elastic anisotropy and polycrystalline orientations in cold rolled titanium sheets investigated by Fourier series method, discussing Young modulus values
01 p0094 A69-10431

Diffusion welding of AMS 4921 titanium, discussing premature pressure removal before completion of first joining stage
01 p0086 A69-10535

Strain hardening of alpha titanium studied for effects of grain size, strain rate, temperature and purity
01 p0095 A69-10610

Hydrogen content effect on relaxation spectrum of alpha titanium, using nondestructive tests
01 p0096 A69-10614

Strain measurements in pure polycrystalline Ti at constant temperature and strain, considering creep and elastic aftereffects
01 p0101 A69-11363

Ti for high temperature use in supersonic aircraft, noting compressibility limit on maneuvering load factor and cooling by H
02 p0192 A69-11891

Titanium production, discussing two stage electrode vacuum arc melting furnace, control and cooling equipment
02 p0229 A69-12068

Mechanical properties of titanium physically vapor deposited by electron beam high rate evaporation, noting results of tension testing
03 p0443 A69-13117

Lattice parameters of austenitic Fe-Ni-Ti alloys as function of titanium content, using Debye-Scherrer camera
03 p0443 A69-13123

Thermodynamic study of carburization of liquid titanium and zirconium, examining effects of atmosphere, graphite porosity and alloying elements
03 p0446 A69-13572

Diffusion bonding and forming of large and complex Ti structures, noting advantages in freedom of design and in economy
[ASM PAPER C7-2.3] 04 p0604 A69-14525

Heterodiffusion of metallic impurities in body centered phases of doped zirconium and titanium, determining diffusion coefficients via radioactive isotopes
04 p0613 A69-14557

Cobalt concentration reduction in maraging steels by Cr replacement and increased Mo and Ti additions
04 p0616 A69-14649

Solid solutions of O in Ti and Zr, noting superstructure formation and physical properties
04 p0618 A69-15078

Properties of electrolytic and reduced titanium powders and sinterability of porous compacts
05 p0782 A69-16795

Phosphate cements for bonding mica ceramic to titanium in jet engine equipment
05 p0786 A69-16799

Diamond pyramid hardness dependence on grain size of recrystallized alpha titanium
06 p0943 A69-17235

Titanium surface impurities effect on porosity in welds, proposing machining immediately before welding as solution
06 p0945 A69-17894

Electron microprobe analysis of vanadium in presence of titanium by compositional measurement of chromite in chondritic meteorites
07 p1073 A69-18419

Ti metallurgy and production, discussing vacuum separation of sponge Ti, Ti melting in arc furnaces, Mg thermal reduction and chlorine processing method
07 p1161 A69-18761

Titanium applications in metallurgy, galvanic technology and chemistry making use of corrosion resistant properties
07 p1161 A69-18767

Hydride, cold, irreversible and reversible hydrogen brittleness in titanium and titanium alloys
07 p1162 A69-18772

Oxygen diffusion parameters in beta-titanium measured by successive layer removal, noting lattice constant dependence on temperature
07 p1163 A69-18783

Titanium tetrachloride reduction to titanium by magnesium, showing autocatalytic process
07 p1163 A69-18784

Two stage sodium thermal reduction of Ti tetrachloride to metallic Ti, determining process parameters
07 p1164 A69-18785

Pressure properties of fluorides and silicofluorides as cutting and grinding lubricants for titanium
[ASLE PAPER 68-LC-20] 07 p1141 A69-19311

Technology of titanium for C-5A aircraft, discussing structural and functional components and machining, welding, forging, etc
[ASM PAPER D8-26.2] 07 p1143 A69-19672

Nitrogen diffusion coefficients in TiN and alpha-Ti determined by metallographic and roentgenographic

analyses, establishing linear equations for temperature dependence
09 p1523 A69-21736

Design, metallurgical and manufacturing problems of titanium application in superjet C5 and SST engines
09 p1570 A69-22062

Titanium fuselage skin contouring to shallow compound curvature of supersonic aircraft by elastic draping, shot peen forming and cold stretching, discussing residual stresses
09 p1512 A69-22374

Potential usage of titanium in cast parts for gas turbine engines, emphasizing alloys development
[ASME PAPER 69-GT-24] 09 p1513 A69-22494

Fracture surfaces of Ti and Ti-Sn alloys for stress corrosion cracking in methanol with HCl and in aqueous chloride solutions
10 p1710 A69-23085

Titanium compared with aluminum in application to supersonic aircraft structures, considering tests and costs
10 p1700 A69-23600

Annealing effects on cold rolled titanium sheets, noting changes in Young modulus and characteristics of recrystallized titanium
11 p1904 A69-24899

Hydrogen solubility in solid and liquid Ti close to melting point, showing no effect on welds and castings porosity
11 p1905 A69-24963

Annealing effects on titanium oxidation kinetics, indicating no relation between oxide formation and diffusion anisotropy of oxygen
12 p2112 A69-26039

Solid titanium surface energy determination, taking into account grain boundaries effect on accuracy
12 p2113 A69-26045

Diffusion bonded Ti honeycomb sandwich, demonstrating structural integrity, efficiency, low weight and cost effectiveness
12 p2115 A69-26828

Tension-compression fatigued alpha Ti twin formation contribution to fatigue damage during cyclic loading
12 p2116 A69-26913

Grain size effect on room temperature tensile strength of alpha-titanium analyzed by tensile testing and electron transmission
13 p2280 A69-27766

Spectral analysis of O and Ti based on O extraction, using Ni tank in A atmosphere with DC arc
14 p2446 A69-29158

Titanium corrosion resistance data tabulated for various environments and chemicals including salt solutions, organic chemicals and ionizable fluoride compounds
14 p2466 A69-29931

Maraging steel tensile strength increased, plasticity and toughness properties decreased with Ti content increase
15 p2639 A69-30630

Titanium effect on structural steels mechanical properties noting anisotropy ascribed to sulfides, nitrides and borides
15 p2640 A69-30633

Failure mechanism for intergranular stress corrosion cracking of vacuum annealed unalloyed Ti in alcohol iodine solutions
16 p2798 A69-31717

Inert gas diffusion of Xe 133 in aluminum and titanium at various temperature ranges, showing effects of recrystallization, plastic deformation and phase transformations
16 p2800 A69-31775

Ti corrosion resistance improved in special environments by oxidizing agents heavy metal ions and alloying
16 p2802 A69-32436

Spark source mass spectroscopy for determining trace elements in Ti and Ti alloys used in aeronautical and aerospace technology
[ONERA-TP-723] 18 p3155 A69-34638

Plating wear resistant electrodeposits of Ag, Cu, Ni and Cr on Ti, noting adhesion tests
18 p3148 A69-34654

Ti thermal diffusivity and conductivity at high temperatures measured from heat wave phase shift
18 p3156 A69-34699

Kinetics of titanium oxidation in transitional range at high temperatures, showing agreement with oxidation model
18 p3157 A69-35252

Annealing effect on transition zone cohesion strength in two layer steel-titanium sheet, investigating role of TiC formation
18 p3159 A69-35450

Diffusion bonded Ti honeycomb sandwich, discussing production, structural efficiency, high strength/weight ratio, etc
19 p3320 A69-35558

Strain hardening of titanium wire during room temperature stress relaxation shown equal to strain hardening during constant strain rate test
19 p3342 A69-35812

Ti and Ti alloys stress corrosion cracking, discussing metallurgical and environmental factors
19 p3351 A69-36900

Stress corrosion cracking of alpha Ti in liquid nitrogen tetroxide and various methanol environments, considering failure mechanisms
19 p3352 A69-36906

Titanium surface cleaning and descaling in preparation for machining, discussing acid pickling, mechanical abrasion, conditioning cycles, etc
20 p3549 A69-37434

Ti determination in presence of Nb or Ta by extraction-photometric method with diantipyrylmethane and thiocyanate
20 p3544 A69-37812

Colorimetric method to determine small amounts of Mn in metallic Ti by potassium periodate solution
20 p3544 A69-37813

Nitrogen diffusion coefficients in TiN and alpha-Ti determined by metallographic and roentgenographic analyses, establishing linear equations for temperature dependence
20 p3564 A69-38214

Ti structural components for forgings, noting problems facing die-forging industry and machining equipment
21 p3728 A69-38459

Neutral titanium Fraunhofer lines 4534, 4562, 5210 and 5238 Å, investigating profiles and asymmetries using spectrophotoelectrical methods
21 p3795 A69-38467

Titanium strengthened high strength hot-rolled steels, discussing cooling rates leading to complete ferrite phase transformation
21 p3743 A69-38652

X ray analysis of rolled and compressed Ti powder produced by calcium hydride reduction, noting coexistence of screw dislocations
21 p3745 A69-38952

Fluosilicic acid in chemical milling of Ti and Ti alloys
21 p3669 A69-38966

Thermal and athermal component of flow stress and deformation dynamics for Ti at low homologous temperatures determined by stress relaxation tests
21 p3749 A69-39598

Stacking fault formation probability in Ti and Zr by X ray diffraction techniques, using Fourier analysis and half-width measurements
21 p3749 A69-39600

Titanium stress pin with headed straight-shank pin and collar for reducing fatigue stress around holes
22 p3957 A69-40832

Angular distributions for Sc 45-Ti 46 nuclear reactions involving 41 Mev alpha particles bombardment described by Born approximation
22 p3988 A69-41044

H concentration and pore formation in Ti fusion welds
24 p4319 A69-42885

Room temperature tensile tests determining failure modes and defect influence on diffusion welds of unalloyed Ti, using electron microscopy and fractography
24 p4331 A69-42939

Chemical treatment of Ti during processing, discussing protective coating, scale conditioning, surface contaminant removal and acid pickling
24 p4324 A69-43432

Metallurgical and structural production of diffusion bonded titanium honeycomb sandwich panels for aerospace hardware weight saving
24 p4324 A69-43434

Al brazed Ti honeycomb sandwich structures brazed in vacuum and Ar, analyzing mechanical properties and corrosion resistance as functions of temperature and pressure
24 p4324 A69-43435

TITANIUM ALLOYS

Beta titanium alloys mechanical properties improvement, discussing effects of alloying elements, heat treatment and high temperature deformation
01 p0093 A69-10213

Titanium alloy VTZ-1 recrystallization and oxidation processes studied by heating within 700- 1200 C temperature range
01 p0094 A69-10214

Crack initiation and propagation in Ti alloys during thermal cyclic heating, noting influence of gas saturation
01 p0094 A69-10215

Charge materials purity found to increase beta-Ti alloys properties
01 p0094 A69-10216

Titanium alloy stress corrosion behavior in atmospheric salt environments at elevated temperatures related to aircraft engine part failures
01 p0099 A69-11056

Titanium-base alloys resistance to atmospheric corrosion based on weight change measurements and tensile tests after multiyear exposures
01 p0100 A69-11351

Martensite transformation by simple shear in equiatomic Ni-Ti alloy, using transmission electron microscopy
02 p0265 A69-12024

Fusion, resistance and pressure welding of titanium, discussing shielding, brazing, diffusion and adhesive bonding
02 p0253 A69-12064

Deformation temperature and reduction effects on structure and properties of cylindrical specimens of various titanium alloys
02 p0266 A69-12124

Phase diagram and heat resistance relation for ternary titanium alloys, considering component interactions and dissolution and dispersion effects
02 p0268 A69-12357

Structural influence on superconductivity of niobium-titanium alloys, using electron microscopy and measurements of current density vs magnetic field strength
02 p0269 A69-12763

Damping capacity and resistance to resonance fatigue of titanium and aluminum based steels and alloys
03 p0443 A69-13025

Grooved commercial Ti and Ti alloys mechanical properties under uniaxial static tension at low temperatures
03 p0443 A69-13028

Ti alloys anomalous variations in physical properties measuring electrical, thermal conductivity and thermal EMF
03 p0443 A69-13029

Superconductivity of niobium-titanium-oxygen alloy wires containing 40 percent minimum niobium weight, noting thermomechanical aging effect on critical current density
03 p0484 A69-13118

Salt water stress corrosion cracks morphology in titanium alloy, discussing crack propagation, brittle nature and chloride contamination effect
03 p0444 A69-13458
[SAE PAPER 680642]

Electrolytic deposits of titanium, vanadium and alloys from molten salts, discussing formation conditions, velocity and properties
03 p0446 A69-13574

Electrical resistivity, composition, and physical properties of titanium carbide, titanium oxide and titanium-oxygen-carbon alloys
03 p0446 A69-13575

Chemical treatment effects on mechanical properties of titanium alloy tubes
03 p0434 A69-13914

Transitional hexagonal omega phase of Ti-Fe alloys quenched in water and tempered
03 p0451 A69-13999

Geometrical and thermomechanical effects on pressure and forces in deformation of thin Ti alloy blanks
03 p0452 A69-14123

Bainite beta to alpha transformation in titanium-oxygen system, using high temperature metallography techniques
04 p0613 A69-14559

Cr-Si diffusion layers on Ti, noting results of roentgenographic and metallographic studies
04 p0614 A69-14578

Structural microheterogeneities in monophase Ti alpha alloys, using complex phase analysis method
04 p0617 A69-14939

Martensitic transformation in Ti-Al-Mo alloys, noting specific features and effects of Mo content
04 p0617 A69-14940

Shear type fracture formation mechanism in tensile test specimens of Ti alloys, noting transition in macrogeometry
04 p0617 A69-15076

Alloying elements and cold rolling deformation effects on formation of texture in Ti alloys, noting inhomogeneity
04 p0617 A69-15077

Phase equilibria, phase transformation temperatures and relation between resistivity and chemical composition for alloys of Ti-Al-Mo-Zr system
04 p0618 A69-15079

Quasi-ternary titanium dichromide-V-Mo system composition at high temperatures, physical properties and phase diagrams
04 p0618 A69-15080

Strain hardening and softening characteristics of maraging steels, Ni-Co and other steels and Ti-Al-Mo alloy
04 p0618 A69-15156

Hydrogen effect on interatomic bonds of Ti beta alloy and Young modulus, noting measurements at various temperatures
04 p0618 A69-15178

Cavities elongation in automatic inert gas shielded welds in titanium alloys
05 p0767 A69-15972

Electron microscopy of titanium alloys noting preparation, heat treatment of samples, crystallographic structure, etc
05 p0782 A69-16807

Electron microscopic and microdiffraction study of structure of quenched and annealed titanium alloy foils at high temperatures
05 p0783 A69-16810

Weldability of thermally stable titanium alloy, noting properties of electron beam and submerged arc welding
06 p0940 A69-17092

Oxygen free fluxes for fusion welding titanium alloys, discussing weld structure and properties
06 p0930 A69-17093

Titanium alloy interaction porosity with fillers during diffusion brazing, discussing joint strength as function of time, temperature and pressure
06 p0945 A69-17896

Surface treatment effect on weld porosity causes and removal in VT5-1 Ti alloy argon arc welding
06 p0945 A69-17897

Surface edge preparation of titanium alloy sheets for argon shielded arc welding
06 p0932 A69-17898

Mechanical stability of pressed and forged Ti alloy gas turbine disks at high temperatures and rates of rotation
06 p1026 A69-18018

Structure and critical superconductivity current of titanium niobium alloy as function of heat treatment and deformation
07 p1158 A69-18532

Titanium aluminum alloys two stage direct production by aluminothermal reduction of titanium tetrachloride
07 p1159 A69-18536

Soviet book on Ti alloys covering production technology, applications, metalchemistry, phase transformations and metallurgy
07 p1160 A69-18760

Ti alloy sheet, plates, rods, sectional shapes, forgings, stampings, pipes and wire production from ingots and blanks
07 p1161 A69-18762

Ti alloys chemical composition, fatigue life, stress rupture strength, crack susceptibility and nature of stress-strain rate
07 p1161 A69-18763

Ti metalchemistry investigations, noting atomic radius, electronegativity valency effect, first atom ionization potential and production of special Ti alloys
07 p1161 A69-18764

Ti alloy blanks production technology and quality control, noting rolling of sectional profiles
07 p1161 A69-18765

Ti alloys thermomechanical treatment effect on strength and plasticity characteristics, noting single and double phase alloys and rupture
07 p1161 A69-18766

Ti-Al-V alloys phase diagrams for isothermal cross sections and polythermal cross sections with constant Al/V ratios
07 p1161 A69-18768

Ti rich Ti-Al-Mo-Zr alloys phase diagrams at high temperatures, noting presence of solid solutions
07 p1161 A69-18769

Ti-Zr-Sn alloys phase equilibria and interaction between titanium stannide and solid solution of Ti and Zr
07 p1162 A69-18770

Thermal and metallographic analyses of Ti-Zr-Al system vertical sections close to Ti-Al edge, considering phase equilibrium
07 p1162 A69-18771

Hydride, cold, irreversible and reversible hydrogen brittleness in titanium and titanium alloys
07 p1162 A69-18772

Metastable phases in titanium alloys with beta alloying elements
07 p1162 A69-18773

Phase transformations in titanium alloys under nonequilibrium conditions
07 p1162 A69-18774

Tin and zirconium addition effect on transformation of titanium alloys during heat treatment
07 p1162 A69-18775

Phase and structural transformations in two phase quenched and aged titanium alloys, using electron microscopy and X ray analysis
07 p1162 A69-18776

Ti alloy beta phase variations in quantity, composition and dispersion during quenching, thermomechanical treatment and aging
07 p1163 A69-18777

Titanium vanadium martensite decomposition kinetics during heating, showing shearing process and dependence on temperature during quenching
07 p1163 A69-18778

Chemical composition relationship to heat resistance of titanium alloys, using diagrams for establishing composition of new multicomponent alloys
07 p1163 A69-18780

Corrosion resistance and mechanical properties of Ti-Mo alloy, developing processing methods for forgings, bars and sheets
07 p1163 A69-18781

Stress rupture, creep and thermal stability of AT-3 titanium alloy, discussing possible applications
07 p1163 A69-18782

Production technology of sheets, forgings and drop forgings from Ti and Ti alloys, discussing gas saturation prevention and plastic deformation
07 p1164 A69-18783

Soviet pipe production technology from Ti and Ti alloys, considering properties and methods improvement
07 p1164 A69-18784

Section pressing from Ti alloy, noting procedure and temperature dependent deformation parameters effects on microstructure and properties
07 p1164 A69-18785

Welding methods used for Ti and Ti alloys and difficulties encountered
07 p1139 A69-18786

Tungsten coatings applied on stainless steel and titanium alloy surfaces by plasma jet
07 p1165 A69-18931

Forging and heat treatment parameters effect on Ti-Al-V alloy low cycle fatigue properties, relating crack initiation and propagation rates to microstructures
07 p1169 A69-19665
[ASM PAPER D8-24.4]

Titanium hot forming and sizing die fabrication concepts for aircraft structures
07 p1143 A69-19671
[ASM PAPER D8-26.1]

Titanium alloys role in turbofan and turbojet engine design, noting use in components and introduction in manufacturing techniques
07 p1143 A69-19673
[ASM PAPER D8-26.4]

TIG welding introduced residual stresses amplitude and distribution in Ti sheets, studying effects on mechanical properties
07 p1169 A69-19674
[ASM PAPER GG8-6.2]

Weld mechanical properties of Ti-6Al-2Sn-4Zr-2Mo titanium alloy as function of cooling rate changes or transformation rate shifts resulting in wide range of hardnesses
08 p1318 A69-19965

Roll planishing and thermal treatments effects on gas tungsten arc welded Ti-6Al-4V alloy on residual stresses, tensile, formability and fracture toughness properties
08 p1319 A69-19966

Oxidation kinetics of niobium titanium alloy in air and oxygen at 1000 C, analyzing nitrogen and pressure effects
08 p1331 A69-20193

Oxidation kinetics of niobium titanium alloy in air and oxygen between 650 and 1000 C, analyzing activation energies and nitrogen effects
08 p1331 A69-20194

Phase identification and microstructural effects of gaseous nitrogen reaction with binary Nb-Ti alloys at 1000 C
08 p1331 A69-20195

Electrochemical kinetic and mass transport mode for studying stress corrosion crack propagation in Ti
08 p1332 A69-20359
[ECS PAPER 147]

Methanol-water-chloride solutions effect on titanium alloys failure time, noting effect of changing water volume on cracking

09 p1521 A69-21400

Forming and processing facility for producing one million titanium alloy parts per month for Boeing 747 aircraft

09 p1504 A69-22063

Increased Ti heat resistance by forming solid solutions and compounds having various dispersions and bond strength

09 p1525 A69-22140

Diffusion bonding parameters for producing hollow Ti-Al compressor blades, discussing surface preparation, postbound heat treatment quality control and mechanical properties

[ASME PAPER 69-GT-46]

09 p1513 A69-22484

Titanium alloy castings fatigue behavior at room and elevated temperatures in annealed and heat treated conditions

[ASME PAPER 69-GT-22]

09 p1619 A69-22497

Spontaneous martensite phase transformation in Ti-Cr alloy thin foils formed electrolytically

10 p1708 A69-22994

Crack propagation velocity in titanium alloys over varying stress intensities under adverse environment

10 p1709 A69-23058

Fracture surfaces of Ti and Ti-Sn alloys for stress corrosion cracking in methanol with HCl and in aqueous chloride solutions

10 p1710 A69-23085

Refractory alloys electrodes used for surface coating Ti alloys by electric spark method, studying microhardness and wear resistance

10 p1711 A69-23339

Initial aging stage in Fe-Ni-Ti alloys using diffuse X ray scattering with electron microscopy of thin foils

10 p1712 A69-23720

Brittle fracture at high temperatures in titanium alloys using scanning electron beam microanalysis, noting reaction diffusion with atmosphere and grain boundaries destruction

10 p1713 A69-23823

Cyclic stress-strain and fatigue behavior in aircraft structural metals, discussing hardening and softening in aluminum alloys, steels and titanium alloys

10 p1714 A69-23981

Cyclic deformation resistance and fatigue damage accumulation in aluminum alloys, aircraft steels and titanium alloys

10 p1715 A69-23983

Optimal processing parameters for producing ingots and semifinished products from corrosion resistant Ti alloys with added Mo

11 p1902 A69-24273

Diffusion constant of Ni in Ti alloys with Al, Mo and Nb, considering beta phase

11 p1902 A69-24274

Near boundary zones in VT15 Ti alloy not involved in beta phase decomposition during aging below 500 C attributed to vacancy concentration decrease

11 p1902 A69-24275

Structural inhomogeneity of Ti alloys cause increased susceptibility to production of sheets, forgings and drop forgings

11 p1902 A69-24276

Thermomechanical treatment effect on VT15 Ti alloy properties and welds after deformation, attaining high tensile strength and plastic properties

11 p1889 A69-24277

Stress corrosion cracking of Ti-6Al-4V alloy tensile tested in anhydrous methanol by electron fractography and diffraction, noting hydrogen embrittlement

11 p1903 A69-24576

Aluminum additive effects on copper-titanium alloy decomposition, discussing Guinier complexes, heterogeneous nucleation, plastic deformation and low temperature aging

11 p1905 A69-24922

Hydrogen effect on temperature dependence of tensile strength and stress rupture strength of Ti alloys, considering annealing, quenching and aging

11 p1905 A69-24962

Heat treatment effect on Ti-Mn alloy microstructure, discussing fcc martensite transformation into alpha, beta and intermediate phases as function of aging

11 p1906 A69-25578

Porosity sources in Ti alloy welds, discussing increased gas content and silica, edge surface finish and gas hose contaminants

11 p1892 A69-25668

Gas bubble formation in Ti welding associated with gas nuclei in metal, molten dwell time, gas diffusion coefficients, joint edge conditions, etc

11 p1892 A69-25669

High pressure vessels welding reliability improvement, discussing edge profile, air expulsion from vessel and shielding atmosphere

11 p1892 A69-25670

Yield to ultimate tensile strength ratio of titanium alloys subjected to thermomechanical treatment

11 p1906 A69-25683

Stress corrosion cracking of titanium alloys in contact with high temperature fuel tank sealants

12 p2112 A69-25945

Ti-Nb alloy structure in heat treatment states analyzed by diffuse scattering of X ray lines and by electron microscope

12 p2112 A69-26036

Precipitated phase composition and structure of Co-Ti solid solution during aging

12 p2112 A69-26037

Quenched titanium-niobium alloy structure effect on superconductivity properties, using electron microscope and X rays

12 p2112 A69-26040

Ni-Ti alloy intergranular deformation at constant tension within wide temperature range

12 p2113 A69-26044

Fatigue strength reduction in Ti alloy in sliding friction contact with metallic materials caused by fretting corrosion

12 p2113 A69-26125

Oxygen content effect on tension-compression fatigue of alpha Ti alloys, discussing internal damage associated with twin formation

12 p2116 A69-27134

Alloying effect on surface oxides determined from photoelectric polarization measurements for Ti-Nb and Ti-Ni

13 p2275 A69-27292

Martensite transformation in Ti-Cr binary alloys by thin foil electron microscopy, noting crystallographic theory

13 p2276 A69-27369

Low cycle fatigue crack initiation in Ti-6Al-4V at room and high temperatures and in aqueous salt environment

13 p2278 A69-27413

Stress corrosion crack initiation and propagation in titanium alloy

13 p2282 A69-28165

Transition zone structure and phase composition in Ti/stainless steel bimetal as function of rolling conditions and heat treatment

13 p2283 A69-28490

Titanium alloys for thermionic nuclear converters, discussing melting, forging, drawing and quality control of mechanical and physical properties

14 p2462 A69-29217

Beta Ti alloy initial state effect on mechanical properties and dislocation structure after cold deformation by rolling

14 p2463 A69-29313

Stress corrosion preventative metal-pigmented paints for titanium alloys, discussing chemicals added to increase cathodic potential

14 p2469 A69-29936

Martensite transformation with fcc lattice in Ti alloys containing 5.9 percent Fe analyzed as function of cooling rate using X ray analysis

15 p2636 A69-30105

Ion nitride hardening of Mo-Ti alloy at 1300 degrees C in cathode glow discharge tube

15 p2637 A69-30212

Titanium alloys fatigue properties at various temperatures using notched and unnotched specimens, considering vibrational fatigue strength and notch sensitivity

15 p2637 A69-30227

Oxygen content and grain structure influence on TS5 Ti alloy mechanical properties, notch and crack growth sensitivity at low temperature

15 p2637 A69-30266

Beta titanium alloys mechanical properties improvement, discussing effects of alloying elements heat treatment and high temperature deformation

15 p2637 A69-30269

Titanium alloy VT3-1 recrystallization and oxidation processes studied by heating from 700-1200 C

15 p2637 A69-30270

Crack initiation and propagation in Ti alloys during thermal cyclic heating noting influence of gas saturation

15 p2637 A69-30271

Charge materials purity found to increase beta-Ti alloys properties

15 p2638 A69-30272

Cr-Si diffusion layers on Ti, noting results of roentgenographic and metallographic studies

15 p2638 A69-30279

Titanium alloy tensile specimens tests in air, methanol and anhydrous methanol environments at known stress-strain-time relations examined by fractography and high resolution electron diffraction

16 p2799 A69-31718

Carbidothemic process for high melting metals and alloys production stressing Ti alloys

16 p2800 A69-31777

Ti alloys commercial applications and properties, discussing alloying elements influence, deformability, weldability, stress corrosion and market trends

16 p2801 A69-31784

Ti alloy forgings production for optimal mechanical properties by cross section and structural condition selection and avoidance of oxygen, nitrogen and hydrogen pickup

16 p2801 A69-31785

Slow forming forging and extrusion required for Ti alloys, discussing mechanical properties as function of beta transformation temperature

16 p2793 A69-31786

Time, temperature and transformation curves for Ti alloy by dilatometry, hardness measurements, X rays and micrography, discussing martensite and beta-alpha transformations

16 p2802 A69-32180

Hydrogen effects on ELI Ti-Al-Sn alloy, conducting tensile, fretting and abrasion tests on stressed and thermal cycled specimens

[AIAA PAPER 69-585]

16 p2803 A69-32760

Plastic flow anisotropy and texture shifting by rolling in Ti-Mo-V alloy, analyzing slip rotation, grain boundary shear and deformation mode

17 p2987 A69-33078

Ti-Al base alloys brittleness and stress corrosion cracking, discussing diffusion mechanism, hydrogen mobility, dislocations, etc

17 p2987 A69-33372

Steady state flux jumping for thin walled tubular superconducting NbTi subjected to coaxial superimposed AC and DC magnetic fields, discussing effective resistivity

17 p3016 A69-33787

Damping properties of turbine blade materials subjected to transverse bending vibrations in vacuum and at high temperatures, including Ti alloys

17 p2990 A69-33932

Titanium alloy martensites crystallography by electron microscope, discussing lattice parameters and spontaneous transformation

18 p3154 A69-34245

Finish turning cutting speed effects on titanium alloy surface layers

18 p3148 A69-34548

Omega phase formation in Ti and Zr alloys with transition metals, discussing effects on mechanical and superconducting properties

18 p3155 A69-34634

Spark source mass spectroscopy for determining trace elements in Ti and Ti alloys used in aeronautical and aerospace technology

[ONERA-TP-723]

18 p3155 A69-34638

Optimum conditions for producing Ti-V alloy sheet plated on one side with Nb by hot rolling

18 p3155 A69-34652

Beryllium diffusion coefficients in Zr and Ti bcc phases, using radioactive beryllium 7 at high temperatures

18 p3157 A69-35251

Ti-6Al-4V alloy general and stress corrosion behavior in Freon environments, discussing fracture mechanics

18 p3150 A69-35411

Capacitor discharge stud welding on Ti alloys, discussing weld zone microstructure, arc and mechanical properties

18 p3151 A69-35431

Soviet collection of papers on strength and plasticity of Ni and Ti and alloys covering high temperature internal friction, deformation and creep characteristics

18 p3158 A69-35442

Alpha Ti-Al and Ti alloys plastic deformation at low temperatures, noting slip and twin mechanisms role

18 p3158 A69-35444

Phase shape deformation and austenite stabilization in Fe-Ni and Fe-Ni-Ti alloys following secondary alpha phase of reversed martensite-austenite transformation

18 p3159 A69-35448

Mechanical properties associated with 55-Nitinol memory effect, presenting stress-strain and electrical resistivity as function of temperature

19 p3340 A69-35523

Wide panel Ti structural extrusions with integral stiffeners, discussing material, sizes, properties and tolerances

19 p3319 A69-35552

Controllable process for forming Ti-Ni intermetallic wear resistant coating on Ti alloys, discussing techniques, weight saving advantage, gear tests, etc

19 p3323 A69-35582

Ti sub 3, Rh sub 5 and Hf sub 3, Rh sub 5 existence and isomorphism confirmed by crystallographic and X ray methods

19 p3343 A69-35920

High strength titanium alloys subcritical stress corrosion crack propagation, studying stress and environment effects on cleavage mode

19 p3343 A69-35922

Ti-Al alloys yield and fracture characteristics as function of high exposure temperatures, studying causes of embrittlement

19 p3344 A69-35927

Ti transition metals alloys omega phase precipitation, discussing composition, morphology, coherency, formation, etc

19 p3344 A69-35928

Heat treatment effects on mechanical properties of Ti-Fe and Ti-Fe-Al alloys

19 p3344 A69-36151

Quenching temperature and deformation conditions for Ti alloy bars optimal mechanical properties, emphasizing effect of primary structure

19 p3328 A69-36152

Titanium alloys case hardened by diffusion of various metals at high temperatures, measuring increase in wear resistance

19 p3344 A69-36153

Ni-Ti maraging steel hardness impact strength and thermal EMF changes during quenching

19 p3345 A69-36154

Pyrolyzed tetraethoxysilane for carburizing steels and Ti alloys at 850-1050 C

19 p3328 A69-36161

Tempering time and temperature effect on microstructure, superconductivity, tensile strength and electrical conductivity of recrystallized Nb-Ti alloy

19 p3345 A69-36302

Structural aerospace materials development with emphasis on Be and Ti alloys, discussing material combinations and composites

19 p3345 A69-36319

Plane strain fracture toughness of high strength steels and Ti alloy from precracked notched bend test method

19 p3346 A69-36436

Titanium alloys wear and fatigue resistance as functions of time and temperature of nitriding by purified nitrogen

19 p3347 A69-36743

Ti and Ti alloys stress corrosion cracking, discussing metallurgical and environmental factors

19 p3351 A69-36900

Titanium alloys stress corrosion cracking in presence of chloride, bromide and iodide under potentiostatic conditions, postulating electrochemical kinetic and mass transport model

19 p3351 A69-36901

Titanium alloys stress corrosion cracking (SCC) from metallurgical-mechanical viewpoint, discussing phase transformations, dislocation arrangements, crack propagation, etc

19 p3352 A69-36902

Metallographic analysis of stress corrosion cracking of Ti alloys of Al and Sn in aqueous magnesium chloride solutions, noting cleavage process

19 p3352 A69-36903

Moisture and hydrogen role in hot chloride salt stress corrosion cracking of Ti alloys by radiotracer technique and mass spectroscopy

19 p3352 A69-36904

Titanium alloys hot salt stress corrosion cracking, studying effects of chlorides and surface oxides

19 p3352 A69-36905

Ti alloy stress corrosion susceptibility in salt water, alcohols and alkanes, comparing stress intensity for crack propagation in dry air

19 p3353 A69-36907

Singular factors affecting stress corrosion cracking resistance of Ti alloys in salt water and hot salt, finding immune single phase alloys

19 p3353 A69-36908

Phase transformations and strengthening mechanisms in Ti-Al-V alloy

20 p3556 A69-36954

Processing variables influence on microstructure of extruded Ti-Al-Sn alloy, noting deformation by slip over temperature range

20 p3557 A69-36955

Yield strength, deformation modes and fracture characteristics of Ti-Al alloys, examining strength and fracture characteristics as function of structure and chemical composition

20 p3557 A69-36959

Reactivity of hydrogen with surface of Ti-Al-V alloy under fatigue cycling at ambient and cryogenic temperatures

20 p3557 A69-36960

Alpha and alpha plus beta Ti alloys analyzed to relate phase composition and microstructure to stress corrosion cracking in NaCl solution

20 p3557 A69-36961

Spectral reflectivities of sintered Ti-TiN-TiC and Zr-ZrN-ZrC alloys and Zr-ZrN-ZrC alloys

20 p3559 A69-37330

Beta working effect on Ti alloy mechanical and fatigue properties [ASM PAPER D8-24.3]

20 p3564 A69-38136

Alpha Ti thermally activated tensile deformation, studying flow stress dependence on strain, temperature and strain rate [ASM PAPER W9-4.2]

21 p3729 A69-38659

Extrusion variables influence on microstructure and hardness level of Ti-Al-Sn compared with recrystallization behavior after cold swaging [ASM PAPER W9-8.2]

21 p3729 A69-38660

Ti-Al-V fasteners heat treated in beta field, showing superior mechanical properties to samples treated in alpha plus beta field

21 p3729 A69-38661

Texture hardening combined with age hardening for biaxial strength improvement of Ti-Al-V alloy, discussing applications to spherical pressure vessels

21 p3729 A69-38662

Stress corrosion cracking of alpha and alpha-beta Ti alloys in aqueous environment at ambient temperature, noting Al content and microconstituents

21 p3743 A69-38663

Ti honeycomb sandwich panels, comparing properties of Ti and Al based brazing alloys

21 p3730 A69-38665

Ti-Al-V sheets quenched from alpha plus beta field into salt bath at various high temperatures, studying effects of bath temperature and holding time on aging and mechanical properties

21 p3730 A69-38667

Oxidation resistant silicide coatings for tantalum and tungsten alloys at elevated temperatures

21 p3730 A69-38673

Torsional moments and forces during Ti alloy and refractory alloy milling with cylindrical cutter

21 p3731 A69-38877

Diffusion layers and elasticity-dependent interdiffusion coefficients of Ti binary systems, using X rays

21 p3745 A69-38954

Phase plasticity in Ti-O alloy as function of temperature in alpha Ti and TiO, noting role of increased oxygen diffusion mobility

21 p3746 A69-38959

Fluosilicic acid in chemical milling of Ti and Ti alloys

21 p3669 A69-38966

Tungsten coatings applied on stainless steel and titanium alloy surfaces by plasma jet

21 p3746 A69-39152

Ti-V martensite decay during heating, noting temperature dependence of elastic moduli and electrical conductivity

21 p3746 A69-39160

Plastic deformation in hardened Ti alloys with thermally unstable beta phase under static compression and tensile loads by electron microscope

21 p3746 A69-39161

Dislocation structures in Nb-Ti alloys formed after annealing

21 p3747 A69-39163

Hot salt stress corrosion of Ti alloy, discussing hydrogen generation during elevated temperature exposure and embrittlement as manifestation of strain rate

21 p3747 A69-39434

Ti-Al-V forgings macro /prior beta/ grain size and in-process thermal treatment effects on fatigue life [AIME PAPER S69-2]

21 p3732 A69-39470

Alpha-beta Ti-Al-V-Mo-Zr alloy with high strength, fracture toughness and crack propagation resistance, low density and adequate ductility, discussing test results

21 p3747 A69-39472

Soviet book on heat treatment of Ti alloys emphasizing structural and phase composition changes

21 p3749 A69-39526

Ti emission and absorption K spectra in Ti-Al intermetallics, suggesting hypothesis concerning long wave and fundamental subbands origin

21 p3749 A69-39787

Elastic modulus of beta Ti alloy containing Mo, Cr, Fe and Al measured under vibrations and shear modulus determined under torsion

22 p3969 A69-4007

Heat treated Ti-Al-Fe alloys thermal, microstructural and X ray analyses of phase transformations in Ti-rich corner

22 p3969 A69-4007

Fusibility diagrams for Ti-Ta-Cr by determining specimens melting points after homogenization at various temperatures in argon

22 p3969 A69-4007

Titanium alloys for strength and weight saving in aircraft fasteners operating at cryogenic or elevated temperatures, discussing corrosion and notch sensitivity

22 p3956 A69-40824

Creep at 400 degree C in Ti alloy sheets in short term plastic deformation due to work hardening by stepwise drawing in extensometric device

22 p3971 A69-41032

Joints structure, phase and chemical composition in kinetics of titanium diffusion brazing with copper

22 p3958 A69-41203

Al-Ni-Co alloys precipitation mechanism effect on magnetic properties, including heat treatment and Ti alloying effects

23 p4175 A69-41298

Titanium alloys hardness indirect measurement by determining electrochemical potential

23 p4177 A69-41598

Ti alloy aircraft components and equipment production, considering roles of temperature, deformation rate and thermal conductivity in drop forging and extrusion processes [DGLR-69-003]

23 p4170 A69-42162

Cold working and aging effects on mechanical properties of TiAl-V including creep and temperature effects [DGLR-69-002]

23 p4177 A69-42163

Fracture toughness and crack propagation in annealed aircraft titanium alloys tested per ASTM procedure, comparing results with high strength steel and aluminum alloys

23 p4177 A69-42165

Alpha Ti fatigue properties, studying internal precracking effects in alloys of various tensile strength

23 p4178 A69-42360

IR inspection system for detecting interstitially caused alpha segregation in Ti alloy disks

24 p4318 A69-42757

Wear protection of pressure loaded Ti-Mn alloy by heat diffused lubricated electrodeless Ni coatings

24 p4331 A69-42786

Nondestructive detection of titanium hydride formation in threaded joints of Ti alloy pressurization tanks by neutron radiography

24 p4320 A69-42998

Ellipsometer measurements for oxidation rates of binary Ti-Al alloys in vacuum and in pure and premixed gases, using in situ test cell

24 p4316 A69-43322

Ti-Al alloy structure manufacturing technology covering forming, cleaning, chem-milling, machining, fastening and welding

24 p4324 A69-43431

Ti and Ti alloys investment castings mechanical properties, dimensional control and corrosion resistance in aircraft and aerospace structural application

24 p4324 A69-43433

SST range-payload improvement by emphasizing Ti alloys honeycomb and trusscore sandwich panels fabrication for structural boxes in wing and empennage

24 p4324 A69-43436

TITANIUM BORIDES

Ti and Zr diborides sintering with Cr, Mo, W and Re additions, discussing activation, pressure effects and density

22 p3968 A69-39888

Titanium diboride electrodeposition on Inconel from molten salt electrolyte at high temperatures noting electrolyte metabolates and coating thickness range

22 p3970 A69-40735

TITANIUM CARBIDES

Electrical resistivity, composition, and physical properties of titanium carbide, titanium oxide and titanium-oxygen-carbon alloys

03 p0446 A69-13575

- Heavy titanium carbide precipitation on fatigue slip zones of stainless steel, noting rupture produced crystallographic facets
03 p0447 A69-13605
- Reducing decarburization of titanium carbide in argon plasma by carbon containing atmosphere, obtaining stable spheroidal particles
05 p0767 A69-15976
- X ray emission from powdered graphite, diamond and titanium carbides
06 p0946 A69-17545
- Phase composition and Co content effect in WC-Co and WC-TiC-Co alloys on magnetic properties behavior
13 p2275 A69-27343
- Homogeneous NbC and TiC specimens physical properties, discussing current carrier density and mobility dependence on composition
14 p2462 A69-28976
- Nb and Ti carbides investigated for lattice parameters, microhardness and resistivity in homogeneity domain
15 p2638 A69-30282
- Electrical resistance and temperature coefficient dependence on phase composition of Ti, Zr and Nb carbides
15 p2641 A69-31047
- TiC-Re phase diagram over wide range of temperatures and chemical compositions
15 p2641 A69-31247
- Annealing effect on transition zone cohesion strength in two layer steel-titanium sheet, investigating role of TiC formation
18 p3159 A69-35450
- Nb-Ti-C alloys electrical resistivity and thermal EMF noting nearly linear variations with temperature
20 p3558 A69-36976
- Recrystallization during sintering of free flowing Nb and Ti carbide powders, determining grain growth dependence on temperature and activation energy
22 p3970 A69-40636
- Wear resistant Ti carbide based cermets with alloy steel binder, noting electrical and heat conductivity dependence on composition and temperature
22 p3971 A69-40919
- TITANIUM CHLORIDES**
- Two stage sodium thermal reduction of Ti tetrachloride to metallic Ti, determining process parameters
07 p1164 A69-18785
- TITANIUM COMPOUNDS**
- NT ANATASE
NT BARIUM TITANATES
NT ILMENITE
NT LEAD TITANATES
NT PEROVSKITES
NT RUTILE
NT STRONTIUM TITANATES
- Crystal and molecular structure of mu-oxo-bis(chlorobis(2, 4-pentanedionato)titanium(IV)/chloroform solved by symbolic sign determination method and Patterson map interpretation
01 p0023 A69-10411
- Increased Ti heat resistance by forming solid solutions and compounds having various dispersions and bond strength
09 p1525 A69-22140
- Microstructure and crystallography of lamellar eutectic alloy of Ni and intermetallic Ni-Ti compound
10 p1707 A69-22986
- TiNi compound alloying with Al and Fe, considering effect on hot hardness at various temperatures
18 p3157 A69-35249
- Conditions for obtaining concentrated Ti-containing melts free of Al and V chlorides by cementing with metallic Ti and Ti-containing materials
22 p3957 A69-40918
- Aqueous hydrazine solution effect on Ti disulfide crystalline structure
23 p4112 A69-41426
- TITANIUM NITRIDES**
- Young modulus of sintered nonporous titanium, zirconium and chromium nitrides, computing characteristic temperature and root mean square atomic displacements in lattices
06 p0938 A69-16830
- Nitrogen diffusion coefficients in TiN and alpha-Ti determined by metallographic and roentgenographic analyses, establishing linear equations for temperature dependence
09 p1523 A69-21736
- Nitrogen diffusion coefficients in TiN and alpha-Ti determined by metallographic and roentgenographic analyses, establishing linear equations for temperature dependence
20 p3564 A69-38214
- TITANIUM OXIDES**
- NT ANATASE
NT ILMENITE
NT RUTILE
- Electrical resistivity, composition, and physical properties of titanium carbide, titanium oxide and titanium-oxygen-carbon alloys
03 p0446 A69-13575
- Electrical, optical, magnetic and structural properties of titanium oxide, stressing transition difference with vanadium oxide
03 p0490 A69-13923
- Frequency transformation coefficients in titanium oxide-chromide traveling wave maser
07 p1146 A69-18481
- Polymorphic characteristics of titanium pentoxide prepared by reducing titania, examining oxidation products with X ray diffraction
07 p1168 A69-19601
- TiO gas dissociation energy data discrepancies, discussing high temperature vaporization and thermodynamic properties
08 p1268 A69-21012
- Valence electrons mean density stability in Ti and V monoxides, describing mechanism for filling M vacancies with simultaneously forming O vacancies
09 p1523 A69-21738
- Photoelectric observations of color and titanium oxide in M7 giants in nuclear bulge of Galaxy compared with late giants near sun
16 p2863 A69-32396
- Ti and V sesquioxides and TiO-VO solid solutions crystallography and defect chemistry over entire range of compositions
20 p3484 A69-37526
- TiO bands identified in Mira variables IR region, discussing rotational structure and band strength-temperature relation
20 p3611 A69-38158
- Rotational analysis of O₂/O band of gamma-prime system of TiO molecule, considering transition to ground state
20 p3577 A69-38170
- Phase plasticity in Ti-O alloy as function of temperature in alpha Ti and TiO, noting role of increased oxygen diffusion mobility
21 p3746 A69-38959
- Aluminothermic reduction of Ti and Ni oxides for obtaining Ti-Ni-Al system
22 p3969 A69-40070
- TOCOPHEROL**
- Hyperoxia exposure and hemolysis in tocopherol deficient mice
06 p0874 A69-17837
- In vivo hemolytic susceptibility to hyperoxia in mice deficient in tocopherol
07 p1066 A69-19422
- TOLERANCES (MECHANICS)**
- NT IMPACT TOLERANCES
- Reflecting telescope objective for far UV and X ray regions, discussing microfinishing and optical and mechanical tolerances
01 p0121 A69-10896
- Statistical radomes design, analyzing dielectric constant and wall thickness tolerances effects on amplitude and phase of transmitted wave
07 p1111 A69-19531
- Damage tolerance as design consideration for aircraft safety and reliability, discussing application of failed single principal member concept to airframe construction
[AIAA PAPER 69-212] 07 p1056 A69-19574
- Reliability distribution parameters for electronic components, determining time and tolerance dependence of reliability
08 p1293 A69-21114
- Compressor to inlet distortion tolerance design techniques for gas turbine compressors, noting rotor matching, blade chord length, blade geometry, etc
[ASME PAPER 69-GT-115] 09 p1572 A69-22525
- True position dimensioning and tolerancing/TPDT/system usage in aerospace industry
10 p1700 A69-23355
- Tolerable surface roughness for transition stability in incompressible laminar boundary layer, including analysis of two and three dimensional roughness shape effects
12 p2063 A69-26774
- Rotating shafts impact damping efficiency increaseable by providing proper clearance to reduce shaft stress in critical resonance frequency region
17 p3066 A69-33946
- Error propagation and tolerance analysis in design and reliability engineering and stress analysis
21 p3842 A69-39303
- Wobble tolerance influence on axis deflection affecting accuracy during assembling of turbine rotors and stators
21 p3733 A69-39719
- Tolerance limits for uncertain requirements vector in linear programming with random variation, introducing nonparametric statistics with sensitivity analysis
[AAS PAPER 69-079] 24 p4340 A69-42821
- TOLERANCES (PHYSIOLOGY)**
- NT ACCELERATION TOLERANCE
NT ALTITUDE TOLERANCE
NT COLD TOLERANCE
NT HEAT TOLERANCE
NT HUMAN TOLERANCES
NT RADIATION TOLERANCE
- Resistance of animal organisms and cells to extreme environmental conditions discussing exobiological implications for extraterrestrial life systems
01 p0017 A69-11083
- Invertebrates resistance to explosive decompression and low end pressure, noting hypoxia and freezing as cause of death
07 p1059 A69-18537
- Resistance to bacterial pneumonia and influenza infection in space cabin environment tested on mice in simulation chamber
07 p1067 A69-19432
- Glucose disappearance rate from dogs blood at simulated 27,000 ft altitude compared with tolerance at ground level, discussing chlorpromazine administration effect
14 p2408 A69-29305
- Cladonia rangiferina resistance to stresses, considering suitable indices for stress response
18 p3095 A69-34539
- Environmental stress effects on medical leech studied to determine tolerance to spacecraft launching, orbiting and reentry
24 p4268 A69-43403
- TOLLMEIN-SCHLICHTING WAVES**
- Wall curvature effect on hydrodynamic stability of laminar incompressible boundary layer with respect to perturbing Tollmien-Schlichting waves
19 p3299 A69-36587
- TONE**
- U PITCH
- TONOMETRY**
- U INTRAOCULAR PRESSURE
U PRESSURE MEASUREMENTS
- TONUS**
- U MUSCULAR TONUS
- TOOLING**
- High strength room temperature vulcanizing silicone rubber for tooling and fabrication of aircraft and missile components
09 p1507 A69-22331
- Superimposed tool vibration function in deep drawing, ironing and cold forging, discussing equipment instrumentation, emphasizing dynamic force measurement
[ASME PAPER 69-VIBR-8] 10 p1700 A69-24164
- TOOLS**
- U BORING MACHINES
U MACHINE TOOLS
U SPACE TOOLS
- TOPOGRAPHY**
- NT LUNAR TOPOGRAPHY
NT TERRAIN
- Mirror image and oblique shadow method forming moire patterns to measure surface topography
08 p1312 A69-20103
- Mars photographic and radar data correlation indicating smoothness of dark areas and roughness of desert areas
11 p1964 A69-25406
- Multispectral and calibrated Alaskan Arctic aerial survey of sea ice, thaw lakes and polygonal soils
12 p2075 A69-26996
- Martian topography during rotation observed using radar round trip echo delay at 7840 MHz, discussing dark areas relation to elevation
16 p2860 A69-32238
- Topographic mapping by high altitude jet aircraft photography
18 p3134 A69-34339

- APQ-97 side-looking radar for topographic mapping of continually cloud covered areas, noting data reduction and compilation methods 20 p3519 A69-36928
- Geological radar in regional and detail studies, discussing area side scanning imagery and lithology changes detection 20 p3491 A69-37652

TOPOLOGY

- NT FIXED POINTS [MATHEMATICS]
NT IMBEDDINGS [MATHEMATICS]
NT INVARIANT IMBEDDINGS

Volterra equation generalization by method involving operator for mapping of topological space into Banach space 02 p0270 A69-11534

Topological principles of gate and contact self correcting circuits not using self correcting codes 03 p0410 A69-13421

Nonlinear Volterra integral equation, extending topological dynamics application of nonautonomous ordinary differential equations 04 p0626 A69-15288

Fermi surface topology effects on Nernst-Ettingshausen coefficient from measurements in magnetic fields to 3.3 tesla and 1.2-4.2 K temperatures in metallic tin 05 p0808 A69-16357

Linear network analysis by topological formulas for derivation of k-tree terms without generation of k-trees of graph 06 p0903 A69-17409

Topological codes and simplicial subclass information rates, minimum weights and word length 06 p0948 A69-17866

Topology of solar magnetic field differential rotation, using hydromagnetic equations 09 p1606 A69-22425

Generalized techniques for contour maps problem solution applied to problem of locating ground track of aircraft from elevation readings obtained during flight 09 p1461 A69-22599

Topologies introduced on state space for differential equations to obtain dynamical systems 11 p1909 A69-25409

Topological properties of plane flow in subsonic region behind smooth shock wave in uniform supersonic flow, discussing shock wave convexity 12 p2061 A69-25888

Description and automated research of correlation /DARC/ for establishing quantitative relationships between topology and properties of chemical substance 12 p2026 A69-26361

Closed linear operators in topological vector space generalized for Banach space case 13 p2288 A69-27734

Topological circuit analysis by digital computer, using conductivity matrix determinant in form of sum of trees 15 p2582 A69-30112

Finite elements concept cast in topological framework, presenting generalizations of Lagrange and Hermite interpolation functions 15 p2711 A69-30874

Conditional trajectory stability associated with first integral compared with orbital stability on base of topological method 16 p2853 A69-31622

Full stress design feasibility as function of load conditions, indeterminacy order and structure topology 16 p2872 A69-31915

Network synthesis technique applied to structural dynamics design, using topological formulas to express systems response transfer functions 17 p2933 A69-33709

Ordinary differential equations in linear topological space extended from Fattorini investigation, emphasizing use of linear operator 19 p3360 A69-36599

TORNADOES

Fully developed whirling steady state structure, discussing tornadoes maximum azimuthal speed, hurricanes rotational speed, model for mature hurricane and numerical computation [AIAA PAPER 69-671] 17 p2997 A69-33499

TOROIDAL DISCHARGE

U RING DISCHARGE

TOROIDAL PLASMAS

MHD waves and toroidal mode existence by mathematical approximation 02 p0236 A69-11430

Electrostatic acoustic wave mode with plasma motion in magnetic surfaces perpendicular to field in toroidal systems with geodesic curvature 03 p0475 A69-13147

Toroidal gas discharge in waveguide by coupling of microwave power into gas to heat gas, noting plasma confinement [IMPI PAPER A4] 04 p0636 A69-14999

Cusp magnetic field stabilizing superimposition on toroidal plasma discharge in polytron machine, noting role of Hall acceleration mechanism 06 p0965 A69-17514

Plasma diffusion in toroidal stellarator using integrals of drift equations for particle trajectories, determining distribution function 07 p1191 A69-18985

Toroidal plasma nonequilibrium in multiple confinement devices with conventional magnetically shielded supports 08 p1369 A69-20819

Asymptotic toroidal equilibrium for guiding center plasma model based on stellarator expansion, considering toroidal curvature, helical currents and plasma pressures 09 p1552 A69-22044

Plasma diffusion in toroidal stellarator, calculating collisional diffusion and diffusion constants 09 p1552 A69-22294

Toroidal theta pinched plasma column collapse, using snowplow model for study of column position shift and cross section deformation 11 p1924 A69-24303

Pfirsch-Schluter factor calculation for stationary toroidal plasma diffusion enhancement due to current along magnetic field over diffusion over that associated with diamagnetic current 11 p1925 A69-24312

Toroidal plasma radial drift suppression on curved theta pinch axis through introduction of transverse conducting ring inside vacuum tube 11 p1925 A69-24313

Turbulent heating of toroidal plasma system with current contained in ceramic vacuum chamber with copper housing 11 p1935 A69-25752

Unified model for spatial distribution of transpolar exospheric electron density for polar plasma study 12 p2151 A69-26952

Plasma jets tangential injection into toroidal magnetic field, discussing polarization interaction and depolarization effect 13 p2311 A69-28108

Transverse particle and energy fluxes in toroidal magnetic traps magnetic fields with ionized plasmas, discussing particle diffusion coefficient and thermal conductivity 13 p2314 A69-28446

Secular terms for parallel component of electric current parallel to permanent magnetic field in toroidal MHD oscillations 14 p2492 A69-29369

MHD mercury flow in rotating torus with little friction investigated for Reynolds numbers, considering induction pump forces and magnetic field influences 14 p2500 A69-29907

MHD stability and equilibrium of toroidal high beta configurations achieved by superimposing oscillating magnetic field on linear plasma column 15 p2660 A69-30877

Multipole configuration toroidal plasma confinement device MHD equilibrium and stability from measured data 16 p2823 A69-32563

TOROIDAL SHELLS

Small bending stiffness effect on inflated torus and cylindrical shells under radial load for determining large space structure stiffness 06 p1024 A69-17607

Liquid filled toroidal shaped rotating damping tube containing bubble, discussing parameters variation effect on spacecraft nutation 16 p2868 A69-32561

Nonaxisymmetric stability loss /buckling/ of closed toroidal shell of circular cross section under uniformly distributed external pressure, considering Volmir linear theory 17 p3055 A69-33130

Nonlinear equations for elastic strain of circular toroidal membrane shell under uniform pressure, computing stress and displacement fields 18 p3216 A69-34575

Standing waves in running tire shell wall, considering internal pressure, cross sections, wall thickness, cord angle, critical speed, etc 22 p4048 A69-41185

TOROIDS

Matched asymptotic expansions method applied to magnetic field induction in thin toroidal wire and flow past circular cylinder at small Reynolds number 07 p1180 A69-18811

Toroidal magnetic fields in ionosphere associated with solar quiet daily variations producing electric current and equatorial auroral electrojets 10 p1681 A69-22805

Toroidal configuration in stellar evolution, noting polar magnetic fields in stars and inclined rotators 12 p2173 A69-27174

Computer memory with digit wire magnetic circuit /torus/, discussing capacity, access and output 20 p3503 A69-37402

TORQUE

DC servo system with torque feedback, discussing bang-bang system comparison, analog simulation, damping and quasi-optimum behavior 07 p1059 A69-19229

Aerodynamic torque on spinning spherical satellite, noting applications to accommodation coefficient measurement and study of aerodynamic gas-surface interactions 09 p1611 A69-22087

Spacecraft attitude control with minimum energy control logic for small constant disturbance torques, considering reaction jet torquers and fuel consumption 11 p1966 A69-25446

Contact conformity effects on spinning torque and friction coefficient in angular contact ball bearings from lubricated and unlubricated tests [ASME PAPER 68-LUB-10] 15 p2628 A69-30901

Gravitational and magnetic torque effect on rotational motion of triaxial rigid body in regressing orbit about oblate primary mass 16 p2861 A69-32240

Gimbal torquing as function of gimbal structure response resulting in free gyro erection system, using any angular momentum at any initial starting angle 16 p2792 A69-32553

Gravity gradient satellite stabilization and magnetic hysteresis damping systems, outlining energy dissipation device involving torques 17 p3047 A69-33231

Elastohydrodynamic solution for ball torque spinning without rolling in nonconforming groove, showing increase in torque with stress and spinning and decreasing conformity [ASME PAPER 69-LUBS-11] 18 p3140 A69-34381

Torque calculations about joints of rigidly chain-like arranged clusters of flying bodies 18 p3208 A69-34776

Validity of Lorentz invariance, discussing nuclear magnetic resonance test on torque for spin of electrons, muons and neutrons 18 p3176 A69-35007

Gravity torque influence on axisymmetric dual spin satellites in fixed attitudes, using attitude stability studies of spinning single rigid bodies 19 p3429 A69-35917

Micell type optimum fiber arrangement for transferring torque across annulus, considering single straight, double and multiple annular arrays under single load system 19 p3447 A69-36851

Constraint torque elimination from vector equations canonical system for attitude dynamics of satellite consisting of arbitrarily interconnected rigid bodies [AIAA PAPER 69-923] 21 p3821 A69-39354

Aerodynamic and gravitational torque effects on orbiting satellites attitude stability, applying Liapunov direct method in case of conservative aerodynamic torque [AIAA PAPER 69-832] 21 p3821 A69-39363

TORQUE MEASURING APPARATUS

U TORQUEMETERS

TORQUE MOTORS

Brushless DC torque motor using reluctance magnetic circuit and toroidally distributed coil winding 01 p0012 A69-10154

Satellite attitude control, discussing mission requirements, typical guidance sensors, actuating torque, systems reliability, etc 09 p1609 A69-21617

TORQUEMETERS

Magnetoropometer for measuring torque /proportional to magnetic dipole moment/ exerted on object by earth magnetic field 02 p0248 A69-11768

Noncontacting torqueometers using magnetoelastic properties of steel shafts, discussing gas turbine and industrial applications
[ASME PAPER 69-GT-64] 09 p1500 A69-22480

Torsiograph systems analysis for rotors angular acceleration recording, discussing dynamic characteristics, system, environmental problems, etc 10 p1692 A69-23252

Short range telemetering strain gage system with astable multivibrator transmitter for measuring intercoupling displacement and shaft torque 22 p3946 A69-40314

TORSION

Torsion theory for modules over integral domain, giving definition of injective sums 13 p2287 A69-27339

Land gyrocompass on torsional suspensions in liquid filled chamber, considering design and operation in terms of precession theory 13 p2259 A69-27431

Natural oscillation frequency of gyrocompass mounted in torsional suspension, taking into account moments of inertia of sensitive element 16 p2791 A69-32282

Unstable metal deformation, discussing volume displacement in necking leading to fracture, homogeneous total deformation and torsion 17 p3053 A69-32987

Constrained elastoplastic torsion of closed thin walled cylindrical shells, analyzing tangential and normal stress by using equilibrium equations 18 p3222 A69-34978

Ronay effect in reversed cyclic torsion or tension in thin cylindrical viscoelastic tube showing creep under sustained load 20 p3625 A69-37596

Elastic-plastic torsion over complex polygonal domains without symmetry axis, using Sobolev space completeness characteristic to solve minimum variational problem 21 p3832 A69-38427

Saint Venant torsion problem using rederivation of integral equation by transferring external geometrical problem into internal static problem 21 p3836 A69-39003

Angular velocity of visual stimulus effect on human torsional eye movements using sectorized disks 22 p3883 A69-40874

Torsion analysis of curvilinear rectangular prismatic beam reinforced by off-center circular rod, using conformal mapping 22 p4049 A69-41279

Yield condition for elastic-plastic medium, considering pure torsion-associated second order effects and dissimilarity between stress and strain increment Mohr circles 23 p4234 A69-42409

TORSIONAL STRESS

Stress field and force system within torsional flow of cylindrical mass of incompressible anisotropic fluid 02 p0229 A69-11558

Torsion of variable cross sectional thin walled bars using shell theory equations 02 p0337 A69-11559

Numerical solutions of elastic problems by conformal mapping and finite difference method applied to circumferentially grooved shafts in torsion 02 p0346 A69-12419

Numerical solutions elastoplastic torsion of circumferentially grooved shafts based on flow and deformation type theories 02 p0346 A69-12420

Torsion bar with two inertia masses attached used to determine damping capacity and torsional fatigue strength 03 p0431 A69-13917

Yield curve softening in hard Al subject to cyclic torsional loading, noting deformation resistance, surface hardness and yield strength 04 p0671 A69-14411

Numerical method for stress function of elastic-plastic torsion of hollow bars during quasi-static monotonic twist compared with relaxation method solution 06 p1023 A69-17370

Circular bar elastoplastic behavior under combined axial force and torque in strain hardening range, noting elastic compressibility effects 06 p1023 A69-17371

Axially symmetric torsion of finite elastic cylindrical rod partially bonded to elastic half space, discussing coupling between dual Dini series and integral equations 07 p1236 A69-19474

Thin walled symmetrical angle section beam stability under bending moment by section deformation or torsional buckling 08 p1410 A69-19892

Polar elastic media pure torsion solved, noting couple-stresses influence on Poynting effect 08 p1414 A69-20527

Saint Venant torsion and flexure of prismatic bars analysis in polar coordinates, discussing boundary errors 09 p1621 A69-22770

Large uniform torsion of thin walled open section of circular cross section, deriving tube radius contraction observed in experiments 10 p1794 A69-22930

Dislocations velocity in high purity aluminum single crystals determined as function of applied stress at 74 and 83 K 10 p1713 A69-23840

Moment stresses effect on stress concentration in plates with common type hole, considering uniaxial and triaxial bending and torsion 11 p1971 A69-24646

Postbuckling behavior and subsequent imperfection sensitivity of thin walled cylinders subjected to torsion, considering perturbation 11 p1979 A69-24814

Plastic strains in aluminum alloy under biaxial tensile and combined tensile and torsion tests, discussing small elastoplastic deformation theory 11 p1905 A69-24948

Varying diameter anisotropic composite shafts torsion based on strain and stress functions 11 p1982 A69-24975

Rotor angular velocity and flexural strain interdependence at critical velocity 11 p1987 A69-25390

Elastic waves propagation in micropolar cylinder, treating longitudinal and torsional monochromatic waves in Cosserat medium 11 p1995 A69-25606

Electric analogy technique for torsion and flexure functions of uniform beams with terminal loads, considering Neumann boundary value problem 11 p1995 A69-25649

Torsion in composite inhomogeneous circular cylinder, obtaining solutions for elastic displacements and stresses 12 p2180 A69-26274

Torsional shearing stress in thick walled hollow rectangular cross sections 13 p2358 A69-27212

Torsional testing facility for delayed elastic and non-recoverable strains in materials, noting application to diffraction limited reflecting optics 13 p2240 A69-27955

Torsion of composite prismatic rod consisting of three different isotropic materials with two interfaces converging on cross section contour corner point 15 p2707 A69-30579

Oscillating beams lateral buckling allowing for torsional stress in determining critical load 15 p2712 A69-31015

Torsional stability of shallow shells of revolution, solving eigenvalue problem obtained from perturbation of nonlinear equations by finite differences 16 p2871 A69-31879

Plastic expansion in metals due to alternating torsional and static tensile loading 16 p2875 A69-32291

Tension-torsion-compression load testing machine of technological possibilities and accuracy [ONERA-TP-596] 17 p2945 A69-33065

Fatigue strength of highly loaded gears and stress measurements by strain gauges [AHS PAPER 371] 17 p3060 A69-33517

Equations in series form to describe composite beams behavior under nonuniform torsion 18 p3211 A69-34343

Elastoplastic boundaries of wave propagation of combined longitudinal and torsional stresses at tube end [ASME PAPER 69-APM-13] 18 p3213 A69-34389

Tension, bending and buckling torsion in thin walled beams described by extended beam model considered as one dimensional continuum 18 p3224 A69-35296

Creep strength of fiberglass reinforced polyester resins measured on structural components in long term tests under torsion 19 p3358 A69-35830

Dynamic recrystallization in Ni and Ni-Fe alloys during torsional high temperature deformation 19 p3344 A69-36147

Keyway stresses in shafts under tension, bending and torsion, using frozen stress photoelastic technique 19 p3445 A69-36827

Torsional moments and forces during Ti alloy and refractory alloy milling with cylindrical cutter 21 p3731 A69-38877

Stress-strain state of thick and thin walled closed shells of variable thickness during elastoplastic torsion developing in aircraft component production 21 p3835 A69-38882

Buckling of truncated conical shells under torsion with various boundary conditions, applying Galerkin method to estimate critical load and wave number 24 p4395 A69-42715

TORSIONAL VIBRATION

Torsional pendulum for stress and strain relaxation measurements of wire sample 01 p0079 A69-10221

Raman spectra and temperature dependent nuclear quadrupole resonance frequencies of p-dichlorobenzene and p-dichlorobenzene-D, calculating librational amplitudes 01 p0122 A69-10286

Semiautomatic computer for determining torsional oscillation natural frequency in multimass in-line systems 01 p0035 A69-10596

Torsional oscillations of elastic half space set up by rigid circular disk examined by integral equation method 01 p0169 A69-10809

Computer solution of forced torsional oscillation equations for periodic coupled machine system with viscous dampers 02 p0338 A69-11893

Spectral peaks for torsional oscillations of earth, estimating free periods from observations at six stations around earth 02 p0243 A69-12007

Flutter vibration of sails fixed along edge and single wing weather vanes in supersonic flows 02 p0192 A69-12824

Vacuum evaporated thin film components welding, using torsional ultrasonic vibrations for joint activation 04 p0605 A69-14561

Torsional elastic wave scattering from penny shaped crack, determining local dynamic stress field 04 p0678 A69-14872

Torsional or longitudinal vibrations of nonuniform bar with elastic end constraints, developing frequency and mode form equations suitable for computer 04 p0681 A69-15196

Bending-torsion mode of rotating tapered twisted turbomachine blade, analyzing coupled flexural and torsional vibrations effect on natural frequency [ASME PAPER 68-WA/GT-6] 05 p0838 A69-16141

Rotation wave propagation in elastic homogeneous isotropic centrosymmetric body in asymmetric elasticity theory 05 p0843 A69-16645

Heating effects produced by periodic stresses in viscoelastic bodies with resonance dispersion, considering torsional oscillations of viscoelastic cylinders 06 p1019 A69-16826

Glass fiber optical angular displacement noncontacting nonloading transducer suitable for measuring torsional vibrations 06 p0923 A69-16929

Anomalous spacecraft OGO-D motion explained by open section boom thermally induced oscillations, discussing corrective measures 07 p1231 A69-18331

Logarithmic decrement and period of disks performing torsional oscillations measured in viscous fluid, noting dependence on oscillation amplitude 08 p1417 A69-20781

Three dimensional vibration analysis of circular homogeneous elastic cylinder, obtaining differential equations and zero stress conditions 09 p1612 A69-21601

Three dimensional analysis of torsional vibrations of circular elastic homogeneous cylinder, stressing new torsional vibrations 09 p1612 A69-21603

Torsional vibrations of unstiffened cylindrical tubes analysis by differential equations and applications to free-free rectangular cross section 09 p1620 A69-22769

Torsional vibrations of composite elastic orthotropic cylinders, including cylindrical shells and isotropic composite cylinder 10 p1800 A69-23243

Forced torsional vibrations of turbine blades calculated by computer using mathematical models for resonance frequencies and tangential stresses
10 p1803 A69-24076

Response and stability of self sustained two degrees of freedom system with nonlinear damping, noting harmonic oscillations
[ASME PAPER 69-VIBR-24]
10 p1806 A69-24171

Heat generation in thin viscoelastic cylindrical shell with relaxation and resonance dispersion during torsional vibration
11 p2000 A69-25168

Optimum planform stabilizer selection for damping of rotational motion and elastic torsional stresses of aircraft fuselage about longitudinal axis
11 p1966 A69-25327

Thermally induced oscillatory instabilities in spacecraft booms, rederiving thermal torque equation to predict finite twist response
11 p1994 A69-25531

Directional solar thermal field /sunlight/ effect on coupled nonplanar transverse and torsional vibrations of satellite cylindrical antennas in orbit
11 p1994 A69-25534

Torsional oscillation of cylindrical shell of non-homogeneous material under periodic shearing force
13 p2361 A69-27462

W shear moduli at high temperatures measured by forced torsional vibration in wide frequency ranges, discussing grain boundary effects
14 p2465 A69-29651

Beam torsion nodal line displacement dependence on flexural and torsional bending frequency
18 p3223 A69-34998

Angular velocity torsional oscillations of solid sphere under elastic force couple rotating in viscous liquid bounded by immobile concentric sphere
18 p3175 A69-35320

Surrounding masses gravitational field effect on gravitational constant determination by torsional oscillations method, considering oscillation amplitude stability to eliminate errors
19 p3374 A69-36468

Tensional and torsional forced vibration tester for viscoelastic plastic materials under tensile strain
21 p3720 A69-38591

Optimal control of rotational and transversal motions of elastic flight vehicles, considering torsional and flexural deformations
21 p3760 A69-38890

Time optimal control for torsional vibrations of flight vehicle for limited energy case, illustrating uniform wing of constant rigidity
21 p3686 A69-38891

General system of equations derived for nonaxisymmetric oscillations of elastic spherical shells, obtaining expressions for oscillations from torsion, tension and bending
21 p3839 A69-39199

Linear and torsional vibration parameters measuring methods, discussing transducer characteristics
22 p3943 A69-39926

Natural frequency equations for torsional vibration of fixed/fixed and fixed/simply supported uniform thin walled beams of open section based on energy method
22 p4040 A69-39935

Uncoupled torsional vibrations of simply supported open cylindrical tubes analyzed by approximation equations, considering free edge boundary conditions
23 p4233 A69-42347

TORUSES

Solution procedure for torus with given surface loads or displacements, using series expansion of generalized analytical functions, discussing stress concentration near toroidal cavity
21 p3839 A69-39192

TOUCH

U TACTILE DISCRIMINATION

TOUGHNESS

NT NOTCH SENSITIVITY

Retained austenite content control, strain aging and autoforming to improve toughness of high strength martensitic stainless steel without strength loss
08 p1330 A69-20010

Thin walled maraging steel tube toughness determined by Charpy precrack testing of transverse and longitudinal impact properties
13 p2269 A69-28183

TOWED BODIES

Lateral stability of glider towed by cable in steady rectilinear horizontal flight, deriving motion equations as ordinary differential equations
09 p1433 A69-21498

TOWED TARGETS

U TARGETS

TOWNSEND DISCHARGE

NT GAS DISCHARGES

NT RING DISCHARGE

Monograph on ionization of Ar-CH mixtures during Townsend discharge, covering metastable Ar atoms lifetime in various pressure ranges
16 p2814 A69-31841

Townsend discharge formation time determination, taking into account impact ionization in positive ion cloud moving from anode to cathode
19 p3381 A69-36603

TOXIC DISEASES

NT CARBON MONOXIDE POISONING

Medical examinations of missile fuel handlers, noting some abnormal results in liver function tests and possible hydrazine toxicity
09 p1447 A69-22556

Atelectatic and direct toxic effects of oxygen on human subjects
22 p3873 A69-40208

TOXIC HAZARDS

Treatment procedure and preventive programs outlined for acute exposure to toxic rocket fuels or oxidizers
02 p0204 A69-12498

Renal pathology of acute methylhydrazine intoxication in dogs, noting hemolytic anemia and hemoglobinuric nephropathy
06 p0883 A69-17847

Medical factors as probable cause of aircraft accidents, discussing psychological factors, CO poisoning, hypoxia, alcohol, etc
07 p1067 A69-19433

General aviation accidents and hazards presented by drugs, ethyl alcohol, pesticides and carbon monoxide
07 p1068 A69-19435

Monomethylhydrazine /MMH/ toxic effects on cornea and blood aqueous barrier studied in vivo on dogs
09 p1447 A69-22547

Heat treatments in inert gas atmosphere improve elastic foam polyurethane by reducing capability of toxic outgassing
10 p1716 A69-23503

Ozone concentrations harmful to humans in atmosphere based on U.S. and Western European observations, emphasizing lower stratosphere
15 p2596 A69-30642

Toxic effects of Freon R FE 1301 on animals and human beings at different concentrations, assessing judgement, alertness and neuromuscular skill
18 p3098 A69-35061

TOXICITY

NT CARBON MONOXIDE POISONING

Fluorides or AMOX increased concentrations effect on thyroid growth rate, uptake and adrenal weight in rats
14 p2406 A69-29291

Sotalol and propranolol cardiovascular effects, comparing toxicity and blocking action against circulatory and cardiac effects of catecholamines
23 p4080 A69-41403

TOXICITY AND SAFETY HAZARD

Medical examinations of missile fuel handlers, noting some abnormal results in liver function tests and possible hydrazine toxicity
09 p1447 A69-22556

Alcohol and drug intake effects on drivers control of motor vehicles, describing postrotatory nystagmus test for toxicity measurement
21 p3652 A69-38791

Pilots and automobile drivers functional impairment due to alcohol and drugs
21 p3663 A69-38792

TOXICOLOGY

Alcohol role in pilot victims of aircraft accidents
01 p0022 A69-11345

Macaque monkey behavior after injection of monomethylhydrazine with and without pyridoxine HCl, noting effects of aversively and appetitively rewarded training
03 p0375 A69-14068

Aircraft accident toxicology, guidelines for collection, preservation, shipment and analysis of specimens and test result interpretation
12 p0222 A69-25842

TRACE CONTAMINANTS

Analytical determination of traces of metals caused by wear in aircraft liquid fuels, hydraulic fluids and lubricants, noting polarography and coulometry
03 p0435 A69-14101

Gas chromatographic determination of hydrocarbon quantity in methane in parts per billion range
03 p0382 A69-14115

Trace analysis /parts per billion/ of methane in helium, hydrogen and neon
03 p0382 A69-14116

Cholesteric liquid crystals application to trace contamination detection, describing color response measurement
06 p0885 A69-17842

Flame emission spectrophotometric method for ultraminate sodium contamination detection in thin silicon oxide films and cleaned silicon surfaces
[ECS PAPER 306]
08 p1314 A69-20361

Mass spectrometric analysis of silicon carbide for homogeneity in sample, noting metallic impurities
09 p1448 A69-22313

TRACE ELEMENTS

Hydrothermal investigation of Ge trace quantity distribution between metal, silicate and sulfide phases at controlled oxygen partial pressure by oxygen buffer techniques
05 p0819 A69-15624

Trace element distribution in metal phase of chondrites and iron meteorites, using neutron activation analysis with radiochemical separation
08 p1404 A69-20921

Trace elements distribution in Smithsonite iron meteorite by spark source mass spectrometry, noting terrestrial weathering effects
08 p1404 A69-20922

Trace element geochemistry of calc-alkaline andesites, discussing crustal composition models and trace elements distribution
08 p1309 A69-20940

Flow visualization tracer for quantitative measurements for laminar and turbulent flow, discussing mean velocity and shear stress
09 p1495 A69-21911

Mineral nutrition elements concentration stabilization by correcting solution additions during prolonged Chlorella cultivation with medium recycling
10 p1646 A69-23578

Possible sources of meteoritic material from Hopewell Indian burial mounds
11 p1963 A69-25401

Electron microautoradiograph preparation determining trace element amount and distribution by utilizing radioactive isotopes and high resolution of electron micrographs
13 p2263 A69-28168

Diffusion of ozone distribution tracers in stratosphere, based on photochemistry in oxygen-only and oxygen-hydrogen atmospheres
13 p2294 A69-28492

Trace elements influence on precipitation process and properties of Al-Cu, Al-Zn-Mg and Al-Mg alloys, using X ray diffraction
16 p2801 A69-31783

Spark source mass spectroscopy for determining trace elements in Ti and Ti alloys used in aeronautical and aerospace technology
[ONERA-TP-723]
18 p3155 A69-34638

Meteoritic trace elements with varying chemical and physical properties investigated for abundance by neutron activation technique
19 p3407 A69-36080

Meteoritic trace elements and radionuclides measured by gamma coincidence techniques, emphasizing Mn 53 and Al 26
19 p3412 A69-36103

Colorimetric method to determine small amounts of Mn in metallic Ti by potassium periodate solution
20 p3544 A69-37813

Trace elements role in precision metallurgy for obtaining certain steel properties
21 p3750 A69-39870

Detection and spectral examination of trace porphyrin complexes by demetallation with methanesulfonic acid and spectrofluorometry, compared to absorption spectrophotometry
24 p4279 A69-42557

TRACERS

Compartmental models for radioactive tracer experiments with known tracer material amount, using generalized Spearman simultaneous estimation procedure
24 p4339 A69-42765

TRACHEA

Respiratory pressure recording with tracheal cannulae applied on cats to obtain pneumograms and oscillograms of respiratory neurons
07 p1131 A69-18538

RACING

Cathode ray curve tracer to record capacitance-voltage characteristics of p-n junctions

04 p0602 A69-15406

RACKERS

U TRACKING [POSITION]

RACKING [POSITION]

NT COMPENSATORY TRACKING

NT INFRARED TRACKING

NT MISSILE TRACKING

NT OPTICAL TRACKING

NT PHOTOGRAPHIC TRACKING

NT PURSUIT TRACKING

NT RADAR TRACKING

NT RADIO TRACKING

NT RANGE AND RANGE RATE TRACKING

NT SATELLITE TRACKING

NT SPACECRAFT TRACKING

NT STAR TRACKERS

Stability of two coordinate automatic angular tracking systems

01 p0053 A69-10803

Satellite monitoring application to air traffic control in parallel track system, discussing lateral and longitudinal separation control

02 p0277 A69-11591

Neuromuscular actuation system model, noting compatibility with human physiological and anatomical data in tracking tasks

02 p0202 A69-11952

Working breadboard model of planet tracker under various illuminating conditions, discussing hardware and closed loop tracking error analysis accounting for signal to noise effects

03 p0463 A69-13214

Multimode direction tracking with polarization tracker used simultaneously, analyzing cross coupling and conical horn/reflector antenna

06 p0888 A69-17652

Limiting speed for target tracking hypersonic vehicle due to electrons formation through aerodynamic heating, calculating allowable flow conditions, maximum speeds and electron distribution

07 p1086 A69-19509

High field domains in Gunn effect diode in transit time mode of operation probed with stroboscopic electron beam in scanning electron microscope

08 p1283 A69-20162

Digital signal tracking module operation and stability, considering use of interconnecting modules to achieve adaptive tracking

09 p1459 A69-22477

Satellite photographic astrometry and chronometry, determining spatial positions of satellites and observation stations by space triangulation

11 p1956 A69-24400

Lock-on characteristics of automatic tracking systems evaluated for case of variable vector signal, calculating transient response

11 p1861 A69-25716

Holographic position and velocity measurement techniques for high speed objects from explosions

12 p2087 A69-26174

Operational Q factor of optimal differential relay system with inertial plant during tracking process, noting cadence pulses high repetition rate influence

12 p2052 A69-26279

Closed loop target tracking system generating error signals for aligning target with tracking axis

19 p3310 A69-36063

Balloon-borne gondola azimuth stabilization using lunar tracker

20 p3538 A69-37300

Trajectory models accuracy beyond tracking intervals, studying roles of extrapolation and independent measurements number and accuracy

22 p4032 A69-41015

Maritime navigation hyperbolic charts for aircraft position determination

23 p4186 A69-42026

Design criteria for antenna control equipment for earth tracking from landing site on Martian surface [AIAA PAPER 68-868]

24 p4348 A69-43246

Satellite photographic astrometry and chronometry, determining spatial positions of satellites and observation stations by space triangulation

24 p4391 A69-43790

RACKING ANTENNAS

U DIRECTIONAL ANTENNAS

RACKING FILTERS

Dynamic tracking filter analysis and capabilities as low threshold demodulator in frequency modulated frequency division multiplexing satellite system

01 p0034 A69-11140

Tracking filter steady state oscillation amplitude and phase distributions determined from Fokker-Planck equation for high and low noise levels

11 p1844 A69-24441

Negative resistance parametric amplifier used as tracking filter, noting resonant frequency dependence on pumping frequency and input and idler circuits

13 p2225 A69-27183

State space structure of model reference adaptive control and parameter tracking systems subject to noise

18 p3111 A69-34686

Coherent phase locked loop receiver as carrier and modulation loops combination with parallel bandpass filter for ranging signal reception and FM demodulation

19 p3274 A69-36277

Adaptive tracking filter for bending mode stabilization of large flexible boosters [AIAA PAPER 69-874]

21 p3823 A69-39400

Digital data transition tracking loop mean square phase noise computed as function of input SNR by Fokker-Planck technique

23 p4130 A69-42514

TRACKING NETWORKS

NT DEEP SPACE NETWORK

NT GLOBAL TRACKING NETWORK

NT STADAN [SATELLITE TRACKING NETWORK]

Deep space tracking network development, discussing capabilities and operational quality assurance

07 p1078 A69-18831

Spacecraft tracking network for determining spacecraft motion parameters, noting application to coordinates and velocities determination for terrestrial observers

07 p1087 A69-19609

Belier rocket launching facilities in Guiana, describing pads, tracking system, telecommunications network, etc

09 p1477 A69-22161

Radar unit for network component/wind patrol/ in statistical observations of wind drift conditions in meteor trails

17 p2939 A69-33901

Antenna high noise temperature reduction in single channel combined transmission and reception of tracking and communication data

19 p3275 A69-36328

Satellite tracking and orbit determination accuracy for system of two synchronous geostationary satellites [AIAA PAPER 68-449]

21 p3674 A69-39019

Assignment algorithm for target recognition in multiradar tracking systems

22 p3902 A69-41250

Tracking and Data Relay Satellite System with synchronous orbit satellites to relay data between low altitude earth orbital spacecraft and mission control centers

23 p4120 A69-41755

Tracking and data relay satellite system /TDRSS/ compared to ground based mission support, considering altitude coverage capability, economy and communication requirements

23 p4120 A69-41756

TRACKING RADAR

Tracking radar glint analysis model using diffraction theory to evaluate parameters of fields received from scattering centers on target aircraft

01 p0033 A69-11007

Areas of expectation for single radar automatic tracking of flying objects derived on basis of equation of circle in polar coordinates

01 p0035 A69-11296

Electromagnetic diffraction theory for radar cross section of aircraft, missiles and satellites, discussing mathematical representation of electromagnetic field for extreme wavelengths

03 p0383 A69-12902

Automatic sequential detector for noncoherent moving target indicator radar, describing noise and clutter residue control

03 p0389 A69-13197

Moving target indicator /MTI/ performance degradation by limiting clutter analyzed for various pulse cancellers and verified by time-domain Monte Carlo simulation

03 p0390 A69-13198

Multiradar system development for total view of air situation from single air views, using digital computers interconnected with central computer

05 p0719 A69-15932

Signal processors for implementation of monopulse tracking radar with three instead of four beams, investigating accuracy

08 p1270 A69-19855

Pulse Doppler radar operation, discussing Doppler shift, range resolution and systems components

10 p1659 A69-24084

Moving target selector radars subsystems amplitude and phase instability effects on interference signal suppression

15 p2576 A69-30339

Radial velocities measuring tracking rate meter performance for Doppler frequencies, allowing for multiplicative noise

15 p2576 A69-30350

Radar calibration techniques for accurate real time tracking data, describing GEOS-B C-band experiment [AIAA PAPER 69-872]

21 p3675 A69-39398

TRACKING STATIONS

NT DEEP SPACE INSTRUMENTATION FACILITY

NT GLOBAL TRACKING NETWORK

NT STADAN [SATELLITE TRACKING NETWORK]

Conversion from VHF to UHF at White Sands Missile Range, discussing telemetry acquisition, tracking and receiving systems

07 p1077 A69-18828

Caterpillar diesel electric sets for powering NASA tracking station in Australia during Apollo 8 flight

07 p1117 A69-19632

Transpondersondes for atmospheric measurements, considering ground tracking, radiosondes, rocketsondes and flight results

10 p1692 A69-23257

Soviet and foreign visual, photographic and photometric ground observations of satellites, emphasizing synchronous optical observations role in geodesy and geophysics

13 p2219 A69-27357

Optical observations of Geos 1 over North America in short arc reduction to improve tracking stations survey coordinates, discussing dependence on earth gravity and mass

15 p2599 A69-31342

Tesseral harmonics of geopotential and station coordinates based on combined Baker-Nunn, laser and range and rate satellite data

15 p2601 A69-31372

Active interferometer controlled telemetry tracking system for missile range, discussing automatic target acquisition, dish feed, costs and optimized data-channel antenna patterns

19 p3271 A69-36253

ELDO radio guidance station at Gove, discussing propulsion stage tracking and instruction transmitted to vehicle

22 p3919 A69-39920

More earth station equipment and design for satellite communication in INTELSAT network including antenna, feed and tracking, interconnect system, etc

22 p3900 A69-40679

TRACTION

Existence theorems for partial differential equations theory for traction boundary value problem of linearized elastostatics

12 p2188 A69-26928

Runway grooving to improve aircraft tire traction in adverse weather tested by F-4D and Convair 990A under wet conditions [AIAA PAPER 69-773]

19 p3244 A69-35649

Traction stresses distribution over contact surfaces using photoelastic frozen stress model

23 p4235 A69-42461

TRACTORS

U CRAWLER TRACTORS

TRACTS

U SITES

TRADEOFFS

Mission analysis for applications satellites, discussing tradeoffs among mission objectives, launch vehicles, spacecraft and geopolitical considerations

03 p0511 A69-13428

Open loop suboptimal control for linear time dependent tradeoff between energy expenditure and probability of target set entry

11 p1860 A69-25443

Cost model to trade off competing systems designs for space communications, navigation, operational availability and ballistic missile defense

19 p3454 A69-36007

Tradeoffs between measurement accuracy, false alarm and detection probability in practical setting of

thresholds for Neyman-Pearson criterion, analyzing noise samples
22 p3902 A69-41221

Space experimental design based on manned vs unmanned spacecraft value for multipurpose low cost flexible space station in low earth orbit
23 p4223 A69-42457

TRADESCANTIA

Drosophila melanogaster flies reproductive behavior and *Tradescantia paludosa* chromosome patterns after weightlessness onboard Vostok 3 and 4
07 p1063 A69-18597

Radiobiology of *Tradescantia* clone orbited in Biosatellite 2, analyzing space effects on spontaneous and radiation induced mutation and cytological changes
15 p2556 A69-31321

TRAFFIC

U AIR TRAFFIC

TRAFFIC CONTROL

NT AIR TRAFFIC CONTROL

NT RADAR APPROACH CONTROL

Nonmilitary marine uses of navigation satellites
[UN PAPER 68-95305] 01 p0112 A69-10469

Airport surface traffic control system /STRACS/ for detection of aircraft, identification, guidance on taxiways, tower display, fail-safe alarm logic, priority routings, conflict protection, etc
05 p0790 A69-16724

Automatic ground traffic control of aircraft on airport taxiway without visual detection, noting induction loop detection in surface traffic control system /STRACS/
11 p1913 A69-24267

Satellites and ground stations system providing transoceanic civil, air and marine traffic control in North Atlantic, discussing position determination, communication and navigation, etc
18 p3170 A69-35065

Telemetric control of urban transportation systems and law enforcement, considering automobiles as prime vehicle
19 p3272 A69-36256

TRAILBLAZER 2 REENTRY VEHICLE

Plasma electroacoustic resonance in reentry sheath of Trailblazer 2 vehicle excited by nonradiating coaxial antenna, deducing electron density gradient at vehicle surface
17 p3010 A69-32915

TRAILING-EDGE FLAPS

Hypersonic flow distribution and separation types over highly swept delta wings with trailing edge flaps at Mach 6
[AIAA PAPER 68-97] 02 p0189 A69-12522

Aircraft structural weight optimization based on design consideration of grouped related elements, noting application to Boeing 747 trailing edge flap drive
[SAWE PAPER 757] 18 p3220 A69-34888

TRAILING EDGES

Laminar two dimensional viscous wake behind finite flat plate, investigating upstream and downstream flow field of trailing edge region for high Reynolds numbers
[ASME PAPER 68-WA/APM-20] 04 p0541 A69-14387

Trailing edge velocity and stagnation points for isolated and latticed airfoils using Zhukovskii and Weing transformations
05 p0697 A69-15880

Initial turbulence influence on wakes formed behind trailing edges of cascade blades
09 p1431 A69-22235

Turbine blade cooling research programs, discussing effects of increased trailing edge thickness and cooling air on turbine efficiency
[ASME PAPER 69-GT-15] 09 p1432 A69-22501

Incompressible uniform shear flows merging behind trailing edge of semiinfinite flat plate, using inner-outer expansion method based on Navier-Stokes equation
13 p2248 A69-28223

Mechanical construction device for Carafoli profile in aerodynamics and hydraulics, establishing mechanism for tracing rounded and sharp trailing edges profiles
15 p2549 A69-31264

Optimum surface for thick delta wing in hypersonic flow obtained by variational method, assuming closed leading and trailing edges
16 p2731 A69-31559

Two dimensional model for analyzing turbulent separation and reattachment at blade trailing edge at supersonic speed
[ONERA-TF-678] 16 p2733 A69-32258

Slot height, position and trailing edge geometry effects on elliptically shaped rotors selected for hover efficiency, size, transitional gust insensitivity and rigidity
18 p3088 A69-35231

Incompressible fluid flow of given density and kinematic viscosity near trailing edge of flat plate
20 p3458 A69-37098

Compressor type cascade experiments to find closest possible traverse position to blade trailing edge
22 p3859 A69-40065

Laminar viscous flow and skin friction near trailing edge of flat plate analyzed by modified Oseen approximation, noting accuracy for high Reynolds numbers
22 p3930 A69-40683

Edge effects in efficiency of air cooled turbine blade cascades with cooling air ejection from blade trailing edges into gas flow
24 p4364 A69-43090

Shape, position and velocity of vortex wakes shed in unsteady multienergy flows near trailing edge, applying Kutta condition
[ASME PAPER 69-APMW-19] 24 p4245 A69-43099

TRAINERS

U TRAINING DEVICES

TRAINING

U EDUCATION

TRAINING AIRCRAFT

NT G-91 AIRCRAFT

NT JAGUAR AIRCRAFT

Hydraulic powered flight control system for Jaguar supersonic military training aircraft
01 p0012 A69-10634

Jaguar combat trainer/tactical support aircraft to meet France and UK military requirement, noting supersonic performance and honeycomb construction
04 p0549 A69-15062

Jaguar aircraft equipment conformity to maximum standardization with equipment for other programs
04 p0550 A69-15063

First flight test phase of multipurpose Vigen aircraft designed as basic platform for attack, trainer, reconnaissance and fighter versions
06 p0867 A69-17662

Concorde supersonic transport and Jaguar Military Strike/Trainer programs, discussing management and international cooperation
06 p1043 A69-17831

Air Transport Total In-Flight Simulator-707 /AT/TIFS-707/ concept for pilot training, stressing airframe and major flight systems
[SAWE PAPER 747] 18 p3118 A69-34884

NF106B-VST model follower flight control system, discussing design criteria/performance index, rigid/elastic math model development, flight test evaluation, hardware design, etc
[AIAA PAPER 69-886] 21 p3764 A69-39412

Aero L-39 low wing cantilever monoplane jet trainer developed in Czechoslovakia
24 p4251 A69-42797

TRAINING DEVICES

Digitally controlled flight systems simulators, noting design improvements over conventional trainers
05 p0742 A69-15884

French supersonic recycling wind tunnel for short duration experiments
07 p1116 A69-19289

Reliability management simulation exercise training technique for government personnel, discussing decision making in development, production, testing and field usage of systems
18 p3117 A69-34487

Automated programmed instruction /API/ for training backup interceptor control personnel to conduct air defense operations
[AIAA PAPER 69-956] 22 p3905 A69-40338

TRAINING SIMULATORS

NT COCKPIT SIMULATORS

NT FLIGHT SIMULATORS

NT SPACECRAFT CABIN SIMULATORS

Visual simulation for critical maneuvers of aircraft takeoff and landing, noting method based on limited corridor simulation and maneuver freedom
[AIAA PAPER 68-255] 11 p1866 A69-25376

Flight simulation requirements for reducing aircraft training flight time, discussing control system and instrument motion characteristics, visual simulation and critical maneuvers motion
22 p3928 A69-41139

Personnel training and selection systems, applying information processing models to diagnostic testing in job classification for performance improvement
24 p4274 A69-43020

TRAJECTORIES

NT ABORT TRAJECTORIES

NT ASCENT TRAJECTORIES

NT BALLISTIC TRAJECTORIES

NT CIRCULUNAR TRAJECTORIES

NT DESCENT TRAJECTORIES

NT EARTH-MARS TRAJECTORIES

NT EARTH-MOON TRAJECTORIES

NT ELECTRON TRAJECTORIES

NT HYPERBOLIC TRAJECTORIES

NT INTERPLANETARY TRAJECTORIES

NT LUNAR TRAJECTORIES

NT MIDCOURSE TRAJECTORIES

NT MISSILE TRAJECTORIES

NT MOON-EARTH TRAJECTORIES

NT PARTICLE TRAJECTORIES

NT REENTRY TRAJECTORIES

NT RENDEZVOUS TRAJECTORIES

NT ROUND TRIP TRAJECTORIES

NT SPACECRAFT TRAJECTORIES

NT SPINNING UNGUIDED ROCKET TRAJECTORY
Electromagnetic waves trajectory distortion in moving plasma due to additional time delay noting propagation of pearl pulsations, whistling atmospherics and proton whistlers
01 p0068 A69-111

Optimum thrust control of satellite along given trajectory to rendezvous at zero velocity with orbital satellite
13 p2356 A69-276

Angular velocity of aircraft rotation about longitudinal axis at arbitrary point of passive trajectory section, with assumptions on roll damping, momentum, etc
18 p3092 A69-349

Bovedy Chondrite fall in Northern Ireland, describing fragments trajectory and metal, sulphide and silicate presence
18 p3200 A69-349

TRAJECTORY ANALYSIS

Theory of generalized multistep methods, using a grid point extended to special second order differential equation, applied to unperturbed orbit trajectory
01 p0153 A69-108

Autonomous solution to orbital navigation problem yielding direct measure of orbital parameters
01 p0114 A69-110

Jupiter outer satellites orbits determination with computer program based on modified Cowell/Moulton methods for adjusting initial conditions
01 p0158 A69-113

Longitudinal range dispersion of unmanned Mars landers using VM-8 and VM-9 atmospheric model, discussing Syrtis Major as possible landing site
02 p0324 A69-123

Constant thrust deceleration formula for gravity turn soft landing maneuvers expressed in elementary trigonometric functions of initial conditions for descent
02 p0335 A69-125

Trajectories of elastic bodies analyzed by Hervey theory of impact
02 p0349 A69-128

Incidence for three dimensional reentry trajectory preprogrammed as function of velocity, finding ballistic angle as function of inclination
03 p0504 A69-128

Tactical aspects of pursuit and evasion, emphasizing analysis of conceptual framework and construction of analytic models
03 p0457 A69-138

Numerical calculation of trajectories of high energy cosmic rays in galactic disk, using quasi-longitudinal model of magnetic field
03 p0501 A69-139

Trajectory equations for outermost electron on beam in TWT operating in dynamic mode for Brillouin flow
03 p0406 A69-139

Spacecraft trajectories computation from initial conditions by techniques involving construction of N body reference orbit
03 p0518 A69-142

Focusing of relativistic cylindrical electron beam static axial electric and magnetic fields, using least action principle to derive trajectory differential equation
05 p0796 A69-157

Performance index sensitivity of nominally optimum controls noting initial and final target manifolds relationship to trajectory sensitivity
05 p0737 A69-158

Orbital trajectories about Mars or Venus, considering reentry to earth, planet perturbation effect, total mission time and orbital distance from planet
05 p0823 A69-160

Kepler hyperbolic sine equation calculated for Arend-Roland comet for case of constant residues by false position method

06 p0997 A69-16821

Adaptive modeler to estimate state and future trajectory of unknown plant having automatically synthesized control

06 p0900 A69-17353

Ellipticity of trajectory of free motions of pole of revolution of earth, using harmonic analysis of motion amplitudes and phases

06 p0919 A69-17536

Ballistic reentry trajectories, considering point mass motion in central force field under tangential thrust action and spherical atmospheric density distribution

06 p1006 A69-17564

Algorithms construction for aerospace vehicle trajectory optimization, considering quasi-linearization method for computation of variable time optimum trajectories

06 p1006 A69-17569

Nonlinear equations of motion for rendezvous in circular orbits, pursuer using minimum fuel and pursued having no propulsion

06 p1014 A69-17571

Jupiter unmanned flyby probes trajectory and mission analysis, considering planetary gravitational field role for trajectory shaping and flight times

06 p1007 A69-17598

Planetary landing vehicle design optimization, considering effects of trajectory, guidance and environmental parameters under uncertainty [AIAA PAPER 69-128]

06 p1018 A69-18107

Translational forces on Mariner 5 stemming from attitude control system studied to determine trajectory for scientific and operational purposes [AIAA PAPER 69-114]

06 p1018 A69-18108

Transfer orbits calculation between low and high satellite orbits, determining trajectories by method with minimum use of linearization

07 p1211 A69-18503

Coordinates and velocity components accuracy for artificial earth satellite moving in central Newtonian field, covering elliptic and circular orbits

07 p1178 A69-19606

Three dimensional atmospheric entry trajectories equations for satellite with aerodynamic lift, examining aerodynamic factors and bank angle effects

07 p1230 A69-19608

Longitudinal stability of unsteady motion of flight vehicle along ballistic trajectory, using linear differential equations

07 p1230 A69-19701

Atmospheric whistlers trajectories in magnetosphere calculated, assuming electron concentration as exponential function of altitude

08 p1309 A69-20429

Trajectory calculation of unguided meteorological rocket by digital computers and by equations of motion, discussing wind influence on ceiling and horizontal ranges

08 p1409 A69-20457

Trajectories minimizing missile velocity losses due to gravity by setting boundary conditions and trend of thrust in time

08 p1409 A69-20587

Space flight trajectory analysis of aerospace systems, discussing Analytical Trajectory Optimization Model

09 p1585 A69-21207

Spacecraft design, trajectory and mission analyses for multipurpose solar electric propulsion missions, emphasizing modular ion engine and fixed attitude spacecraft designs [AIAA PAPER 69-252]

09 p1568 A69-21729

Reentry trajectories from lunar surface and orbit obtained by computer with allowance for initial data spread

09 p1594 A69-21756

Spacecraft trajectory optimal determination without knowing measurements error distribution function, examining computer solution properties of linear programming

09 p1595 A69-21757

Optimal moments for trajectory parameters measurements determined by linear analysis to minimize error for initial conditions

09 p1495 A69-21758

Minimum time turns for spacecraft about fixed axis lying beyond plane of vehicle forces

09 p1609 A69-21760

Trajectory error propagation upper bounds in many body field for impulsive initial error, relating error to mission tolerances

09 p1595 A69-21937

Coasting arc determination in rocket trajectory problems by Lagrange multipliers

09 p1595 A69-21969

Optimal closed loop control system for linear time varying system with two independent parameters, noting trajectory sensitivity in large launch booster

09 p1473 A69-22439

Complex trajectory method for describing tunnel effect during atom ionization in strong light wave field, using quasi-classical approximation

09 p1543 A69-22658

Secular perturbations of remote satellites within lunar gravitation field, comparing observations and analytical data

10 p1779 A69-23614

Interstellar dust alignment mechanisms investigated by Monte Carlo model, discussing grain velocity maintenance by radiation pressure and effects of magnetic constraint on charged grain trajectory

10 p1781 A69-23675

Optimal interorbital transfers between closely spaced nearly circular noncoplanar orbits, taking into account active section length for low power thrusts

10 p1783 A69-23712

Trajectories of particles entrained by gas flow in nozzles for study of erosion damage during passage of gas-particle mixture

11 p1818 A69-25355

Configuration, trajectory planning, instrumentation, calorimetry and aerodynamic heating for planetary atmosphere entry

11 p1968 A69-25719

Venus and Mars atmospheric braking entry and associated equipment, discussing potential cost savings

11 p1968 A69-25722

Third phase dynamics of planetary approach of earth-Mars journey, computing approach trajectory on two body spacecraft-Mars assumption

11 p1968 A69-25725

Conservative system /with two degrees of freedom/ motion in plane harmonic force field with potential satisfying Laplace equation, discussing graphic trajectory construction

11 p1920 A69-25745

Soviet book on solid propellant guided/unguided rocket design with emphasis on thrust control, including trajectory calculations, optimal parameters and components estimation by weight analysis

12 p2175 A69-27077

Trajectory terminal state error analysis using adjoint-generated sensitivities in nonlinear time-varying systems

13 p2296 A69-27940

Canonical transformation and Hamilton-Jacobi theories applied to space vehicle trajectory analysis, discussing elliptical coast arc and optimal low thrust problems

13 p2353 A69-28202

Relay sampled data phase plane trajectories periodic motions increased with increase of system duty factor

14 p2425 A69-28898

Cosmic ray equators from trajectory tracing procedure for computing vertical cut-off rigidities with two different geomagnetic field simulations compared to experimental equators

14 p2511 A69-28961

Trajectory sensitivity analysis of open and closed loop optimal control systems, demonstrating previous analysis inaccuracy

14 p2427 A69-29539

Moving targets trajectories determination from radar data, using posteriori probability distribution represented by Markov chain

15 p2566 A69-30334

Target trajectories determination based on radar data with allowance for association between neighboring readings, using statistical characteristics obtained with Markov chains

15 p2566 A69-30335

Electromagnetic wave propagation in anisotropic inhomogeneous media by geometric optics approximation, obtaining equations for beam trajectories in spherically symmetrical medium

15 p2569 A69-30949

Satellite trajectory determination and expected errors for OGO 4 and Geos 1 orbits, noting geopotential, aerodynamic drag and integration contributions

15 p2698 A69-31331

Laser measurements for DIADEME satellites tracking to reconstruct actual trajectory in semidynamic geodesy

15 p2600 A69-31365

Conditional trajectory stability associated with first integral compared with orbital stability on base of topological method

16 p2853 A69-31622

Satellites trajectories under influence of earth oblateness and low radial thrust acceleration by nonlinear mechanics asymptotic method, discussing osculating orbits

16 p2856 A69-32009

Impulsive trajectories optimal and nonoptimal solutions, classifying known results for reference purposes

16 p2857 A69-32146

Trajectory calculation of axisymmetrical body during ballistic and vertical flight, assuming air drag proportional to square of velocity

17 p2889 A69-32950

Monograph on solar system space flight trajectory calculations covering solutions to differential equations, error analysis and gravitational effects

17 p3039 A69-33798

Radio wave trajectories for waves emitted at 15, 20 and 25 kHz within spherically stratified ionosphere below F 2 maximum

17 p2969 A69-34001

Distributions of close planet-comet encounters for various orbital elements, calculating trajectory by conic matching

18 p3195 A69-34433

Controlled vehicle disturbed trajectory multiple correction, considering constrained control or limited accessible coordinates for observations

18 p3174 A69-35316

Peano-Baker method for integration of variational equations to produce partial derivatives used in satellite trajectory estimation

19 p3398 A69-35616

Planetary navigation using spacecraft measurements and Doppler data from earth-based radio tracking, determining accuracy for earth-Mars trajectory

19 p3368 A69-35791

Aircraft takeoff airborne phase trajectory analysis, deriving expressions for projection angle, velocity, path length and instantaneous altitude

19 p3247 A69-35817

Mariner Mars 1969 flyby missions objectives, experiments, spacecraft configuration, trajectory design, sterilization, flight path control and photographic imaging [AAS PAPER 68-134]

19 p3402 A69-35938

Rapid Targeting Procedures computer program for optimized orbital payload and associated launch vehicle targeting data with one submittal and minimum user intervention

[AAS PAPER 68-148]

19 p3402 A69-35951

Digital computer controlled antenna positioning system computing spacecraft tracking trajectory from given parameter input set

19 p3267 A69-35997

Network for fireball trajectories rapid analysis to recover meteorites and obtain orbital elements data, noting role of planetariums

19 p3295 A69-36121

Self rotary motions of nearly conservative systems with one degree of freedom, deriving periodic solution of equation for phase trajectories

19 p3374 A69-36466

Trajectory sensitive vector introduction into closed loop linear optimal control, considering linear or nonlinear formulations

20 p3509 A69-37141

Moon to earth trajectories analyzed numerically to determine effect of specified earth entry conditions on hyperbolic elements near moon for abort [AAS PAPER 68-089]

20 p3595 A69-37174

Numerical solution of equations of motion of rocket under thrust in inverse square force field, discussing effects of initial acceleration

20 p3595 A69-37203

Flight times compared for intercept and pure pursuit missile trajectories

20 p3618 A69-37716

Orbital trajectories about Mars or Venus, considering reentry to earth, planet perturbation effect, total mission time and orbital distance from planet

20 p3606 A69-37951

Monograph on motion of solid body with cavities containing viscous liquid, covering kinetics involving completely or partly filled fluids

20 p3578 A69-38200

Optimal control of dynamic system motion described by linear differential equation, selecting vector function ensuring predetermined trajectory

21 p3685 A69-38452

Inertial navigation systems trajectory parameters errors due to inaccurate initial coordinates input, deriving trigonometric functions for autonomous error determination

21 p3760 A69-38572

Trajectories of roots of two channel systems with antisymmetric cross couplings using geometrical and analytical methods, noting hodograph

21 p3686 A69-38886

Two dimensional gravity assisted trajectories for solar probe missions in ecliptic plane, discussing Venus and Jupiter assist missions

21 p3804 A69-39022

CircumJovian powered and free return trajectories, analyzing round trip missions and departure opportunity

[AAS PAPER 68-117] 21 p3805 A69-39207

Exploration capabilities provided by Jupiter gravity assisted trajectories compared to direct ballistic flight trajectories

[AAS PAPER 68-116] 21 p3805 A69-39224

Interplanetary periodic orbits and flyby dates for multiple Earth-Venus swingby missions, describing various iterative solutions for trajectory

[AIAA PAPER 69-931] 21 p3809 A69-39359

Normalized hodographic mapping for constrained trajectory families, discussing mapping concepts, information content and applications

[AIAA PAPER 69-924] 21 p3809 A69-39362

Neighboring optimum feedback guidance to motivate min-distance lookup parameter determined by minimizing metric function of perturbed state and reference trajectory

[AIAA PAPER 69-888] 21 p3765 A69-39414

Time-similar and isotropic geodesic curves simulating paths of test bodies in Riemann space corresponding to gravitational field

21 p3772 A69-39621

Real time network support simulation allowing network configuration for nominal or perturbed trajectory for Saturn vehicles, applicable to any flight azimuth

22 p4020 A69-40319

Real time orbit determination system at NASA manned space center for Apollo missions

[AIAA PAPER 69-938] 22 p4020 A69-40321

Mission analysis and trajectory simulation /MATS/ program, discussing computer controls, modular design, integration evaluation

[AIAA PAPER 69-939] 22 p3904 A69-40322

Interactive graphics system for rocket vehicle trajectory simulation and performance analysis

[AIAA PAPER 69-954] 22 p3905 A69-40336

LM descent engine behavior upon contact with lunar surface simulated, basing test condition on statistical trajectory analysis indicating fire until touchdown possibility

[AIAA PAPER 69-1020] 22 p3923 A69-40391

Trajectory analysis of multiplanet Grand Tour mission to four large outer planets on single flight, discussing mission planning

[AIAA PAPER 68-1955] 22 p4023 A69-40544

Metric state-time dynamical polystem with sequentially compact topological space, noting sliding state trajectories

22 p3975 A69-40573

Equations of motion of unguided rocket under wind effect, calculating launch angles for wind compensation

22 p4037 A69-40815

Liquid fuel propulsion systems for geostationary satellites, discussing transfer orbits, payload increase and required thrust for various satellite trajectories

[DGLR-69-014] 23 p4202 A69-41929

Optimization of RF ion thruster cluster engines for ascending trajectory, discussing unfolding mechanism of solar cell panels

[DGLR-69-022] 23 p4203 A69-41933

Translational forces on Mariner 5 stemming from attitude control system, determining trajectory for scientific and operational purposes

[AIAA PAPER 69-114] 24 p4394 A69-43256

Unmodeled errors detection in recursive flight trajectory estimation, deriving equations for unmodeled parameters

24 p4387 A69-43585

TRAJECTORY CONTROL

Low thrust spacecraft motion continuous correction by dynamic programming, assuming continuous information on system state including fuel consumption

01 p0113 A69-10572

Capture and control in conservative dynamical systems, analyzing orbital mechanics of derelict and pursuit spaceships

05 p0826 A69-16462

Optimization of control independent cost functions in multidimensional system with linear controllers

06 p0905 A69-17945

Limited memory optimal filter theory, output and standard filter divergence due to errors

06 p0905 A69-17946

Black arrow rocket vehicle flight path computer programming, discussing geographical restrictions on design

09 p1593 A69-21616

Guidance law for autoguided system trajectory to impact target, noting kinematic study

10 p1723 A69-23701

Flight control system for automatic interplanetary stations /AIS/, comparing Venera series orientation and correction system to Mariner systems

10 p1792 A69-24198

Lifting entry concepts for return from earth orbit, discussing deceleration, heating and heat protection

11 p1968 A69-25720

Spacecraft longitudinal control during reentry of lunar orbiter into atmosphere, analyzing final range prediction, trajectory tracking and accelerometers performance

13 p2355 A69-27681

Spacecraft range control algorithm during reentry at parabolic velocity into atmosphere with varying parameter distributions

13 p2355 A69-27682

Dynamic process during rms deviation of nonlinear system from prescribed trajectory described by nonlinear differential equations

14 p2425 A69-28822

Low thrust spacecraft action continuous correction by dynamic programming, assuming continuous information on system state including fuel consumption

15 p2651 A69-30742

Electrically propelled TV satellite control maneuvers to reach target position in synchronous circular orbit from spiral ascent trajectory

16 p2868 A69-31935

Controlled vehicle disturbed trajectory multiple correction, considering constrained control or limited accessible coordinates for observations

18 p3174 A69-35316

Law for time variations of modulus-restricted control action at trajectory end, two point boundary value problem solution and use of Pontryagin principle

18 p3175 A69-35324

Interplanetary swingby trajectory correcting maneuvers for space vehicles return to earth after planet orbiting with emphasis on singular points

19 p3427 A69-36613

Numerical integration for continuously thrusting spacecraft optimal trajectory, considering rectangular Cartesian and polar cylindrical coordinates characteristics

[AIAA PAPER 69-903] 21 p3798 A69-38546

Control system generating compensating reactions for correcting trajectory deviations due to uncontrollable random factors, discussing linear automatic control system optimization

21 p3770 A69-38853

Spacecraft trajectory control algorithm for hypersonic reentry, describing onboard equipment role and simulation results

21 p3767 A69-39649

Kinematic and dynamic relations analyzed by vector method for motion time and orbital flight control of point

21 p3818 A69-39820

Long range space flight trajectory correction problem, obtaining algorithm for determining minimum number of corrections

21 p3818 A69-39822

Controlled motion of space vehicle about center of mass analyzed by equation expressing nutation angle invariance

21 p3830 A69-39839

Rendezvous control law for spacecraft moving in central gravitational field along trajectory representing target vehicle Keplerian orbit

22 p4036 A69-40115

Spherical trajectories control by star height maintenance, analyzing resulting cycloid and cartographic representations

23 p4186 A69-42023

Communication satellite systems using hydrazine engine thrust for trajectory correction, discussing trajectory deviations causes and ERNO engine design

[DGLR-69-013] 23 p4203 A69-42152

TRAJECTORY MEASUREMENT

Observability theory of dynamic objects application to composing measurements for space flights, solving parametric observability problem

07 p1087 A69-19604

Optimal moments for trajectory parameters measurements determined by linear analysis to minimize error for initial conditions

09 p1495 A69-21733

Rocket trajectory determination by tracking on board light source against star background with image orthicon TV system

12 p2033 A69-26964

Vibrating camera for photographic measurement of flow velocities and trajectories of bodies marked by light spots

13 p2261 A69-27911

Tabulation of basic solar system data and formulae concerning trajectory length, escape velocity, orbits etc

16 p2856 A69-32074

Photographic networks for meteors orbits and trajectories and meteorites impact points during nighttimes discussing fireball occurrence

19 p3415 A69-36120

Trajectory models accuracy beyond tracking intervals, studying roles of extrapolation and independent measurements number and accuracy

22 p4032 A69-41019

Satellite trajectory parameters estimation by maximum likelihood method applied to continuous satellite observations assuming random Gaussian process as measurement error

22 p3979 A69-41087

Satellite motion initial phase vector estimation for calculating satellite motion from selection of complete or increasing volume of measurements

22 p4033 A69-41088

TRAJECTORY OPTIMIZATION

Variational calculus applied to time optimal trajectories between two points in range altitude space, discussing aircraft thrust and drag laws

01 p0009 A69-10414

Planetary landing trajectory optimum single pulse correction determined by considering sum of correction and retro pulses minimum

01 p0151 A69-10564

Satellite trajectories calculated in form of parameters derived from processing measured functions, considering optimum mathematical description selection

01 p0151 A69-10570

Optimum control determination for low thrust spacecraft to minimize time for passing through radiation belt

01 p0113 A69-10571

Comparison of trajectories in optimum linear perturbation guidance

02 p0279 A69-12546

Planetary swingby theory mechanics and applications for optimization of interplanetary trajectories

02 p0331 A69-12818

Book on planetocentric, lunar and interplanetary transfer techniques covering communications and coordinate system selection, minimum fuel and time transfer and rendezvous, etc

04 p0652 A69-14458

Multilevel optimal control and decomposition of trajectories by studying static and dynamic systems

04 p0581 A69-14570

Trajectory optimization, obtaining sequence of control functions by iterative application of maximum principle /min H/ to nonoptimal functions

[DVL-852] 04 p0548 A69-14827

Optimum spacing of communication satellites on inclined circular synchronous orbits, applying figure 8 packing schemes

04 p0562 A69-15458

Iterative guidance mode /IGM/ applied to effective gravity vector prediction, acceleration measurement of noise sensitivity and energy limitations

[AIAA PAPER 67-620] 04 p0629 A69-15501

Minimum fuel consumption for low thrust jet engine propelled space vehicles maneuvering in circular trajectories

05 p0829 A69-15879

Minimum fuel rendezvous maneuver for two space vehicles in circular orbit, considering propelled tracking equipment nonlinear equations of motion

05 p0823 A69-16036

Space vehicle flight automatic optimization for maximum L/D reentry, considering perturbations causing trajectory inclination changes during roller coaster reentry

05 p0830 A69-16045

- Algorithms construction for aerospace vehicle trajectory optimization, considering quasi-linearization method for computation of variable time optimum trajectories
06 p1006 A69-17569
- Space vehicle trajectory optimization using computerized step by step steepest descent to minimum cost, considering cost gradient vs control
06 p1006 A69-17570
- Optimum low thrust interplanetary transfers involving swingby trajectory past intermediate planet analyzed, assuming impulsive velocity change at planet
06 p1006 A69-17572
- Successive approximation for iterative construction of near optimum guidance
06 p0954 A69-17573
- Spacecraft optimum low thrust trajectory analyzed by Hamilton-Jacobi perturbation theory, obtaining canonic constants of motion
06 p1007 A69-17574
- Optimality criterion and equations of motion determined for fixed time impulsive trajectory to minimize total characteristic velocity
06 p1007 A69-17575
- Optimization procedure developed and applied to minimum fuel midcourse guidance of spacecraft, discussing optimal closed loop control of linear stochastic systems
06 p0955 A69-17576
- Two point boundary value problems of optimal trajectories solved by offset vector method
06 p0903 A69-17577
- Linearized theory for minimum fuel guidance in neighborhood of minimum fuel space trajectory, unrestricted thrust magnitude and allowances for midcourse impulses
[AIAA PAPER 69-74] 06 p0956 A69-18183
- Trajectories minimizing missile velocity losses due to gravity by setting boundary conditions and trend of thrust in time
08 p1409 A69-20587
- Space flight trajectory analysis of aerospace systems, discussing Analytical Trajectory Optimization Model
09 p1585 A69-21207
- Low thrust interplanetary trajectories optimization, discussing hardware design considerations
09 p1585 A69-21209
- Automated parameter search techniques applied to low thrust mission design, stressing trajectories and mission optimization
09 p1585 A69-21211
- Convergence extensions in quasi-linearization for optimal control, showing results for brachistochrone and reentry trajectory problems
09 p1590 A69-21414
- Spacecraft trajectory using microthrust and lunar gravitational attraction for acceleration into heliocentric orbit
09 p1593 A69-21620
- Spacecraft trajectory optimal determination without knowing measurements error distribution function, examining computer solution properties of linear programming
09 p1595 A69-21757
- Optimal rendezvous between satellite and spacecraft, determining power and time optimal coplanar rendezvous in circular orbit
09 p1538 A69-21759
- Optimal lift and thrust control programs to maximize range of missile in horizontal flight
09 p1610 A69-22086
- Discrete variable approximation for computation of flight path optimization, discussing constrained and unconstrained minimizations
09 p1538 A69-22090
- Optimal interorbital transfers between closely spaced nearly circular noncoplanar orbits, taking into account active section length for low power thrusts
10 p1783 A69-23712
- Optimal transfer between coplanar orbits in Newtonian force field without intersecting circle boundaries
10 p1790 A69-24191
- Equation derivation to determine optimal parameters of spacecraft orbital elements, considering constraints imposed on measured quantities
10 p1791 A69-24192
- Angle of attack and bank angle for orbiting reentry glider, determining optimal trajectory for ground landing at given point
[ICAS PAPER 68-41] 11 p1966 A69-24750
- Pontryagin principle application to incorporation of singular sections into optimal trajectories of controlled systems, considering conjugation of singular and nonsingular extremals
11 p1960 A69-24764
- Dynamic programming determining optimal feedback control policies for optimal trajectories based on invariant imbedding
11 p1910 A69-25410
- Time optimal steering for rocket vehicle with trajectory defined between initial and final state, using minimum principle and boundary value problem solution
11 p1861 A69-25454
- Optimal control trajectories computation for bilinear regulator problems including neutron kinetics of nuclear reactor
12 p2049 A69-26083
- Suboptimal control with high performance index as alternative in restricted class of optimal control problems
12 p2054 A69-26518
- Optimum orbital transfer of material point subjected to reactive force with minimum mass loss, discussing Kepler motion kinematics
13 p2346 A69-27698
- Optimal control for minimum trajectory sensitivity of booster using algorithm and Riccati equation
13 p2261 A69-27943
- Canonical transformation and Hamilton-Jacobi theories applied to space vehicle trajectory analysis, discussing elliptical coast arc and optimal low thrust problems
13 p2353 A69-28202
- Finite difference Newton-Raphson algorithm extension to solve variational equations for simultaneous optimization of trajectories and associated parameters
[AIAA PAPER 68-115] 13 p2353 A69-28203
- Thrust, bank angle and angle of attack of aircraft minimum fuel lateral turns at constant altitude and specified velocities
13 p2203 A69-28245
- Planetary landing trajectory optimum single pulse correction determined by considering sum of correcting and retro pulses minimum
15 p2691 A69-30738
- Satellite trajectories calculated in form of parameters derived from processing measured functions, considering optimum mathematical description selection
15 p2691 A69-30740
- Optimum control determination for low thrust spacecraft to minimize time for passing through radiation belt
15 p2651 A69-30741
- Trajectory differential equations in state-variable form, presenting compatible difference equation adjoint scheme for trajectory integration
15 p2645 A69-31236
- Optimal rendezvous maneuver of pursuing vehicle with minimum fuel expenditure in approach stage on elliptic and hyperbolic orbits
15 p2701 A69-31548
- D-stationary principle to determine optimum hypersurfaces in configuration space containing optimal motion trajectories
16 p2811 A69-31625
- Impulsive trajectories optimal and nonoptimal solutions, classifying known results for reference purposes
16 p2857 A69-32146
- Multistage rocket trajectories optimized by second order numerical technique and digital computer program, considering coasting, vacuum flight and transition times
16 p2857 A69-32154
- Minimum fuel multiple impulse orbital rendezvous for fixed transfer time near circular orbits
16 p2857 A69-32161
- Low thrust trajectories for minimum time rendezvous between continuous thrust interceptor and passive target vehicle, comparing calculus of variations and steepest ascent analyses
16 p2857 A69-32177
- Optimum overestimate to obtain bound permitting use as convergence criterion for iterative process in orbital glider reentry trajectory optimization
[ONERA-TP-628] 16 p2805 A69-32332
- Hypervelocity glide vehicle optimum maneuvers, finding lift optimal control law for maximization of final velocity or altitude
17 p3025 A69-32836
- Bolza problem of calculus of variations extended to trajectory optimization problems with several subarcs
17 p3026 A69-32837
- Aircraft performance optimization using computationally oriented strategy for handling state variable inequality constraints
[AIAA PAPER 69-812] 19 p3243 A69-35628
- Space flight optimization - Conference, Liege, Belgium, June 1967
19 p3398 A69-35662
- Minimum fuel guidance from hyperbolic into specified circular orbit
19 p3367 A69-35663
- Two player zero-sum differential games with emphasis on play with state determined by differential equations, noting optimal solutions
19 p3359 A69-35665
- Steepest ascent convergence improved in orbital glider reentry trajectories optimization problems, discussing bang-bang and cosine control-variable changes
19 p3398 A69-35666
- Maximum trajectory for glider entering earth atmosphere at supercircular velocity, subject to maximum altitude constraint
19 p3399 A69-35667
- Maneuverability domains optimization with semilinear boundaries, noting application to orbital transfer
19 p3399 A69-35668
- Optimal transfers between Keplerian orbits for time free case, considering hyperbolas, ellipses external to and intersecting attracting planet
19 p3399 A69-35669
- Optimal fuel transfers between coplanar and noncoplanar coaxial elliptical orbits determined by Pontryagin maximum principle, using digital program for Hamiltonian equations solutions
19 p3399 A69-35670
- Variational equations uniform closed solution for optimal trajectories during coast without use of numerical integration
19 p3399 A69-35671
- Numerical integration of plane orbital transfers with multiple powered arcs, minimizing propellant expenditure of small thrust chemical rocket
19 p3400 A69-35673
- Optimal impulse rendezvous of long duration between quasi-circular, coplanar or noncoplanar close orbits
19 p3400 A69-35674
- Impulsive orbit transfer optimization using accelerated gradient program based on Newtonian algorithm for digital computer method
19 p3402 A69-35956
- Optimal landing of spacecraft on moon surface from low circular orbit, analyzing rocket thrust, altitude and landing site distance effect on spacecraft mass
19 p3431 A69-36616
- Lunar module motion during optimal ascent from moon surface into circular orbit of command module, noting descent maneuver similarity
19 p3431 A69-36617
- Optimal information selection for determining spacecraft trajectory, considering atmosphere, light speed and series expansion coefficients of planetary gravitational potentials
19 p3427 A69-36627
- Computation method for optimum finite thrust space trajectories based on approximation of state time history by polynomial
[AAS PAPER 68-080] 20 p3595 A69-37170
- Trajectory optimization of space vehicle with continuous thrust based on regularized equations, comparing perturbation method for earth-Jupiter rendezvous transfer
[AAS PAPER 68-099] 20 p3595 A69-37173
- Orbital rendezvous calculation in terms of adjoint variables vector associated with vehicle velocity vector
20 p3595 A69-37202
- Theorem extending results of techniques for analytical solutions of nonlinear ordinary differential equations applied to terrestrial brachistochrone problem
20 p3575 A69-37205
- Interstellar minimum fuel and time optimal trajectories for acceleration limited rockets determined by applying Pontryagin maximum principle to relativistic rocket equations of motion
20 p3602 A69-37530
- Optimal transfers in central gravitational field, using formulas for perturbations of osculating Keplerian orbital elements, applied to singular reticent solutions
[ONERA-TP-729] 20 p3604 A69-37752
- Space vehicle flight automatic optimization for maximum L/d reentry, considering perturbations causing trajectory inclination changes during roller coaster reentry
20 p3618 A69-37954
- Numerical integration for continuously thrusting spacecraft optimal trajectory, considering rectangular Cartesian and polar cylindrical coordinates characteristics
[AIAA PAPER 69-903] 21 p3798 A69-38546

Optimal transfer between coplanar elliptical orbits of spacecraft with combined small and large thrust propulsion system

21 p3803 A69-38848

Trajectory requirements and performance comparisons of single stage electrically propelled space vehicles

[AAS PAPER 68-106] 21 p3819 A69-39204

Secondary or abort mission maximized subject to primary mission constraints by variational treatment of optimal branched trajectories

[AAS PAPER 68-138] 21 p3819 A69-39210

Apollo translunar injection burn simulation, analyzing polynomial solutions of optimum geometry and characteristic velocity

[AAS PAPER 68-150] 21 p3820 A69-39225

Integrals of motion for minimum fuel rocket trajectories in inverse square field calculated for constant power and constant exhaust rockets

[AIAA PAPER 69-904] 21 p3806 A69-39336

Closed form solution for minimum fuel constant thrust trajectories for vehicle transfer in vacuum between arbitrary boundary conditions

[AIAA PAPER 69-905] 21 p3806 A69-39337

Vector integral extension to optimal trajectory coordinate multiplier systems with constant of motion demonstrated for coast-arc problem

[AIAA PAPER 69-907] 21 p3807 A69-39339

Minimum fuel thrust limited transfer trajectories computation for coplanar elliptic orbits

[AIAA PAPER 69-914] 21 p3808 A69-39344

Analytic approximation for initial adjoint vector for optimal/minimum propellant/ space trajectories

[AIAA PAPER 69-916] 21 p3808 A69-39345

Branched trajectory optimization for split rocket vehicles using projected gradient or steepest descent method

[AIAA PAPER 69-917] 21 p3808 A69-39346

Fuel-time optimal retrothrust control for vertical and gravity turn ballistic trajectories of soft landing nonlifting bodies based on Pontryagin principle

[AIAA PAPER 69-868] 21 p3809 A69-39394

STOL takeoff optimal trajectory maximizing altitude at given runway distance, using aircraft models

[AIAA PAPER 69-935] 21 p3649 A69-39427

Numerical algorithms for nonlinear optimal pursuit problems

21 p3757 A69-39536

Optimal pursuit control at constant moving velocity and limited angular velocities, using Pontryagin principle

21 p3825 A69-39629

Spacecraft descent trajectory optimization during atmospheric reentry, proposing algorithm for continuous trajectory determination

21 p3766 A69-39647

Spacecraft atmospheric entry descent trajectory optimization by stochastic procedure, requiring onboard digital computer to realize optimal algorithms

21 p3767 A69-39648

Flight dynamics boundary value problem for spacecraft trajectories optimization, using variational method

21 p3817 A69-39817

Trajectory optimization of second state of rocket launched into earth circular orbit in gravitational field by stepwise fuel control, using Pontryagin maximum principle

21 p3829 A69-39818

Optimal flight regime determination for variable mass body pursuing target by straddling method, presenting motion equations and approximate solutions

21 p3818 A69-39819

Flight vehicle motion in high density medium reacting with static, vortex and dynamic forces analyzed for optimal regime via Lagrange-Euler equation

21 p3768 A69-39824

Optimal minimum fuel rendezvous maneuver variational problem, generalizing circular orbit results to conical orbits

22 p4028 A69-40754

Thrust optimization for sounding rocket to reach maximum altitude with given initial and propellant weight, using polygonal time function and multiple-parameter numerical technique

22 p4037 A69-41050

Optimal pulsed orbital transfer between close nearly circular orbits in central field of gravity realized by geometrical solution

22 p4033 A69-41085

Minimum impulse time free transfer between neighboring noncoplanar almost circular orbits with line of nodes along common latus rectum

[AIAA PAPER 68-94] 23 p4215 A69-41879

Recurrent Lagrange multipliers for optimal low thrust earth-Jupiter transfers, using three dimensional solar system model

23 p4215 A69-41896

Extremal trajectory formulations for state variable inequality constrained optimization problems, forming augmented functional

23 p4182 A69-41907

Controlled plant in n dimensional Euclidean space, analyzing optimal trajectory using integral equations

23 p4183 A69-42472

Earth-Mars and earth-Venus economical transfers derived for optimal conditions with respect to characteristic velocity, obtaining exact numerical solution

[AAS PAPER 69-241] 24 p4380 A69-42855

Optimal transfer between hyperbolic asymptotes about finite size planet, discussing twelve types of analytical solutions in terms of arrival, departure and escape velocities

[AAS PAPER 69-242] 24 p4380 A69-42856

Optimal control computing method applied to minimal time flight profile optimization

24 p4383 A69-42954

Weight limitations effect on optimum motion parameters of variable mass body in gravitational field applied to spacecraft optimum propulsion system controls and trajectory determination

24 p4383 A69-42956

Fractional correction procedure for indirect trajectory optimization through extremal trajectory meeting boundary conditions

24 p4386 A69-43264

Apollo type reentry trajectory optimization numerical methods

24 p4386 A69-43281

Linear-quadratic pursuit-evasion game with dynamics perturbed by additive white Gaussian noise, obtaining linear minimax solutions

24 p4341 A69-43296

Quasi-optimum control law for minimum-time bounded acceleration rendezvous in central force field using Friedland technique, with application to lunar flight

24 p4349 A69-43313

Optimum climb trajectories at constant lift coefficient, using variational methods with final altitude and final flight path angle as end point constraints

24 p4254 A69-43727

TRANSCIEVERS

U TRANSMITTER RECEIVERS

TRANSCENDENTAL FUNCTIONS

NT EXPONENTIAL FUNCTIONS

NT LOGARITHMS

NT PERIODIC FUNCTIONS

NT SINE SERIES

NT TANGENTS

NT TRIGONOMETRIC FUNCTIONS

Electrical impedance of semiconductor supporting two waves contains entire complex transcendental function with complex parameter and infinity of zeros in left half z plane

07 p1196 A69-18268

Parametric variations method for solving nonlinear algebraic and transcendental equations, determining number of solutions in complex space

12 p2123 A69-26608

Constraint restoration in holonomic and non-holonomic problems involving system of algebraic or transcendental equations or first order differential equations

19 p3361 A69-36758

Linear diffraction equations in electronics in self consistent formulation reduced to complex transcendental equations, using perturbation method

23 p4124 A69-42033

TRANSDUCERS

NT DIGITAL TRANSDUCERS

NT ELECTROACOUSTIC TRANSDUCERS

NT ELECTRONIC TRANSDUCERS

NT HYDROPHONES

NT MAGNETIC TRANSDUCERS

NT MODE TRANSFORMERS

NT PIEZOELECTRIC GAGES

NT PIEZOELECTRIC TRANSDUCERS

NT PRESSURE SENSORS

NT QUARTZ TRANSDUCERS

NT SOUND TRANSDUCERS

NT THERMOPILES

NT ULTRASONIC WAVE TRANSDUCERS

Shock and vibration data recording, discussing transducer selection, accelerometer mounting, conditioning electronics and recording devices

01 p0083 A69-11050

Frequency domain stability criterion for nonlinear feedback system consisting of nonlinear amplifier, linear dynamical system and transducer with backlash

02 p0225 A69-11968

Self contained electrically servoed transducers for flight control, noting angle of attack transducer and force

05 p0766 A69-1675

Thermal performance of pressure transducers, accelerometers, displacement transducers, resistance thermometers and control mechanisms for NERVA reactor

06 p0956 A69-1688

Glass fiber optical angular displacement noncontacting nonloading transducer suitable for measuring torsional vibrations

06 p0923 A69-1692

Transistorized frequency detector for sensing system load changes affects speeds of control valves of prime movers

06 p0896 A69-17478

Resistance temperature transducers and thermocouples covering characteristics, readout and design for aerospace requirements

10 p1690 A69-23225

Strain gage transducers and measurements noting Wheatstone bridge, supporting structure and accuracy

10 p1690 A69-23227

Calibration for instrument systems including strain gages, piezoelectric, thermoelectric and thermoresistive transducers

10 p1691 A69-23229

Metal surface distribution of electromagnetic field from striding transducer in eddy current flow detection, calculating magnetic field component

10 p1697 A69-24071

Multicomponent force transducer for measuring track generated forces acting on rocket sled, discussing combined load and vibration tests

[ASME PAPER 69-VIBR-21] 10 p1698 A69-24168

Dynamics of gyroscopic synchronous servo system intended for remote measurement of spatial orientation coordinates of sensor moving element

11 p1881 A69-24558

Constant velocity moving object influence on indications of vertical gyroscope having electromagnetic compensation with residual imbalance of sensor element

11 p1881 A69-24561

Induction flowmeters design, discussing materials and structural details of sensor and transducer elements

11 p1887 A69-25208

Operational amplifier integrated circuits applications, discussing simple and transducer amplifiers, operational circuits, wave shapers and generators and power supplies

11 p1857 A69-25665

Love-wave propagation at UHF observed by thin film surface wave transducers

13 p2218 A69-27203

Optimal parameters of hydraulic sensor of angular accelerations for given dynamic and geometrical requirements

13 p2259 A69-27432

High pressure Hugoniot points made by hypervelocity gas gun, using laser beams to measure impact velocity and pressure transducer for impact stress

[AIAA PAPER 69-358] 13 p2264 A69-28291

Electrolytic vertical indicators response errors, discussing nonlinear properties of transducer steady state characteristics

14 p2446 A69-28925

Radiation method for temperature and heat flux measurement, discussing transducer with thermopile as sensor

15 p2607 A69-30154

Resonance measurement of power percentage in single spurious mode of overmoded waveguide, using back to back transducers and reflection at input

15 p2577 A69-30611

Interferometric displacement transducer for measuring linear displacements up to one and one-half inches

15 p2614 A69-31280

Optimizing control system design using fluidic digital circuitry and FM type transducers

15 p2583 A69-31296

Monograph on transmission characteristics of mechanical vibration transducers covering frequency response operators and analog computer simulation

16 p2789 A69-31842

Acoustic flow calorimeter for evaluating power transducers under loaded conditions

16 p2790 A69-32079

- Complex mechanical vibrations causes determined by sensor signals analysis 16 p2876 A69-32434
- Piezoelectric shaker consisting of combination of damped resonant cylindrical elements for wide frequency calibration of vibration pickups 17 p2975 A69-33665
- Calibration of inertial and surface temperature heat transfer transducers for hotshot and shock tube measurements developed and tested at ONERA [ONERA-TP-683] 19 p3305 A69-35726
- Ferroelectric transducer for heat transfer rates and flow measurement in gaseous systems with autostabilized temperature, noting film coefficient 19 p3307 A69-35749
- IR detectors defined as transducers producing electrical signal proportional to IR power incident on detector, classifying types 19 p3310 A69-36068
- Ionization manometer flange transducer with axial cathode and collector for high vacuum measurements, describing air resistant yttrium oxide coated cathode with Ir core 21 p3724 A69-39077
- Linear and torsional vibration parameters measuring methods, discussing transducer characteristics 22 p3943 A69-39926
- Dynamic parameters of full scale and equivalent structures of electromechanical transducer circuits determined experimentally 22 p3869 A69-40249
- Frequency modulating transducers advantages in process control by overcoming information loss due to series and shunt resistance, avoiding mains interference, easing commutation, etc 22 p3946 A69-40309
- Mechanical stress measurement in cylindrical steel subjected to loads inside coaxial transducer, using transducer signal in contactless eddy current method 24 p4296 A69-42654
- Mechanization of analog electrical-to-fluidic transducer using carrier circuit techniques and piezoelectric bender drive assembly 24 p4315 A69-43026
- TRANSEQUATORIAL PROPAGATION**
- Long range HF propagation in equatorial zone observed with San Marco 2 satellite, discussing overall conditions of ionosphere 08 p1276 A69-20593
- Transequatorial propagation mode for waves in VHF band twice scattered by field aligned irregularities in electron density 10 p1653 A69-23192
- VLF transequatorial propagation variance from magnetic equator to midlatitude confirmed through phase and amplitude records of multisite observations 10 p1655 A69-23416
- Phase and field strength of transequatorial VLF signals, noting behavior during sunrise, day and nighttime 12 p2032 A69-26860
- VHF radio propagation over transequatorial circuit related to equatorial anomaly in F layer, suggesting F2/F2 propagation mode role 23 p4127 A69-42431
- TRANSFER**
- U TRANSFERRING**
- TRANSFER FUNCTIONS**
- Sensitivity of voltage transfer function relative to variation in value of components of resistance terminated reciprocal reactive network 01 p0049 A69-10069
- Amplifier with logarithmic transfer function noting use as null detector 01 p0038 A69-10075
- Analytical expressions for transfer function matrices of four terminal signal shaping networks, assuming rational matrix spectral density of randomly polarized signal 01 p0031 A69-10880
- Atmospheric influence on ground visibility reduction of airborne objects, using radiative transfer equation to calculate contrast transmission function 01 p0111 A69-11100
- Optical measurements through retrorocket plumes of landing spacecraft, investigating reduced landing site visibility and modulation transfer function 02 p0248 A69-11765
- Pulse transfer function estimation for single input and output linear stationary discrete systems using iterative algorithm and quasi-linearization method 02 p0225 A69-11972
- Approximation of correlation or transfer function obtained through exponential polynomial to determine stochastic process spectral density 03 p0409 A69-12976
- Transfer function variation of invariant servodrive, comparing calculated and experimental transient response 04 p0584 A69-15418
- Digital filter transfer functions design by sampled data transformation, noting role of analog filters 04 p0584 A69-15461
- Bit reduction in digital transfer functions with LF poles in sampled data systems using zero order hold function 04 p0584 A69-15464
- Fluid amplifier linear transfer functions at signal levels on order of internal noise identified by random signal testing method [ASME PAPER 68-WA/AUT-2] 05 p0706 A69-16184
- Discrete time positive real functions defined for analyzing system stability with memoryless feedback 05 p0739 A69-16349
- Atmospheric turbulence flight tests random data analysis to stimulate power spectra and transfer functions 05 p0767 A69-16756
- Transfer function coefficients from frequency response data determined to obtain information about dynamic system characteristics 05 p0844 A69-16764
- Life support system energy efficiency, treating transfer equations of closed space regeneration systems 06 p0882 A69-17644
- Image averaging time effects on modulation transfer function /MTF/ of system comprising telescope objective and horizontal propagation path in turbulent atmosphere 06 p0890 A69-17806
- Unperturbed Hamiltonian transformation applied to existing perturbation theories for exchange forces between atoms to obtain correct long range behavior 07 p1184 A69-18288
- NERVA transfer functions evaluation by computer data processing, using Fourier algorithm [IEEE PAPER 2B-2] 07 p1179 A69-19187
- Pneumatic instrumentation line transfer function approximated by system model for simplifying reactor control system analysis [IEEE PAPER 2D-6] 07 p1059 A69-19190
- Diode pump type circuit without diodes in signal path providing accurate transfer function analysis considered for spacecraft use [IEEE PAPER 3A-3] 07 p1134 A69-19191
- Clear atmosphere model based on path of sight equilibrium radiance and nonabsorption permitting integration of equation of transfer 07 p1130 A69-19643
- RC converter filters and delay lines by expanding transfer function into series of components 07 p1113 A69-19677
- Vector equation of transfer for planetary atmosphere describing light scattering by anisotropic particles and analysis of resonance line scattering 08 p1385 A69-20063
- Radiative transfer equation solution for spectral line formed in two dimensionally varying atmosphere extended to continuum radiation in inhomogeneous atmospheres 08 p1386 A69-20077
- Feedback amplifier with transfer function poles on parabola, discussing small rise time with small overshoot combined in transient response 08 p1282 A69-20111
- Computer simulation on engines dynamic behavior covering thrust transfer functions, time behavior and engine and fuel controller operation 08 p1301 A69-20167
- Nonlinearities identification in closed loop systems using harmonic balance principle for transforming measured block diagram into diagram of simple form 08 p1297 A69-20302
- Transfer function and frequency response of notch filters used to achieve notch filter dimensioning and design 08 p1284 A69-20379
- All-pass transfer functions of new class type for design of quadrature filter networks, using Chebyshev approximation 08 p1277 A69-21167
- Chebyshev error norms of polynomial approximations for ideal filter minimized by emphasizing role of transfer function even and odd parts 08 p1299 A69-21168
- Chebyshev filter with flat group delay obtaining transfer function, noting cascade synthesis and extended bisection theorem 08 p1299 A69-21169
- Transfer function of low pass filters with Chebyshev attenuation characteristic in stopband and predetermined phase or delay time realized by ladder network 08 p1300 A69-21171
- Insertion-loss synthesis of narrow band crystal band-elimination filters, using narrow band approximation and pseudoreactance theory 08 p1300 A69-21173
- RLC filters transfer functions applied to development of high pass filter 08 p1300 A69-21176
- Optical transfer function in single scattering approximation for light scattering media consisting of large particles 09 p1536 A69-21865
- Variational principle to obtain variational estimate of arbitrary functional of solution to radiative transfer equation 09 p1541 A69-22253
- Signal flow graphs based on matrix methods, discussing loop currents, systems orientation and transfer functions 09 p1475 A69-22600
- Noniterative wideband amplifiers having single pole transfer functions overall gain bandwidth product optimization, deriving rigorous conditions for maximum 09 p1469 A69-22606
- Glass covered microwire technology to realize RC element, analyzing equivalent element errors by simulating irrational transfer functions 09 p1476 A69-22677
- Determining transfer matrix and comparing solution of homogeneous differential equation to Floquet theory results 10 p1666 A69-22928
- Second order system equations to approximate transfer function of homogeneous pneumatic instrumentation line terminated with pressure transducer 10 p1692 A69-23267
- Diffuse galactic radiation reinterpretation by solving same transfer problem exactly for properties of interstellar particles 10 p1782 A69-23680
- Statistical estimation theory giving angular resolution of imaging systems in terms of noise characteristics and modulation transfer function 10 p1725 A69-24048
- Radiative transfer equation in nonuniform magnetooactive medium derived from continuity equation for radiative energy density in space of coordinates and wave vectors 10 p1742 A69-24143
- Jet fluidic differential amplifier transfer function determination, describing interconnection dynamics 11 p1824 A69-24350
- Load admittance effect on low pass voltage transfer characteristics of RC lines, analyzing shaped lines at open circuit under terminated conditions 11 p1859 A69-24939
- Transfer function parameters identification by fault isolation technique using white noise stimulus and processor matrix of orthogonal filters 11 p1865 A69-25077
- Pressure and flow rate variations at any point of manifold with control units calculated using transfer functions 11 p1942 A69-25335
- Linear active adjustable VLF filters for polynomial transfer functions 11 p1859 A69-25392
- Wideband inverter operational amplifier frequency response, open and closed loop transfer functions, beta, settling time and slew rate limits, discussing HF performance prediction 11 p1857 A69-25666
- Unsteady surface and internal waves diffraction induced by source in ideal incompressible fluid, obtaining solutions in form of convolution and transfer functions 12 p2061 A69-25953
- Linear automatic control system floating response to harmonic effects achieved by coinciding open loop system transfer function poles with disturbance pattern poles 12 p2045 A69-25967
- Matrix transfer functions factorization to obtain irreducible representations of multivariable control systems used for studying invariant linear multidimensional processes 12 p2047 A69-26072

Practical time resolution of streak camera, discussing streak camera transfer function and measurement of resolution with pulsed laser diode emission
12 p2084 A69-26152

Photographic emulsion layers depth dependence of darkening curve, modulation transfer function and granularity, determining properties by enzymatic and electrolytic treatments
12 p2089 A69-26196

Electrohydrodynamic equations and transfer coefficients for multicomponent plasma with volumetric charge in electric field, discussing Ohm law and equations for plasma motion
12 p2135 A69-26399

Digital differential analyzer as control element, analyzing performance limitations imposed by scaling constraints with canonical realization of transfer functions
12 p2053 A69-26509

Rational transfer function matrix realization into irreducible Jordan canonical form state equation by nonsingular transformations
12 p2122 A69-26511

Analytical expressions for transfer function matrices of four terminal signal shaping networks, assuming rational matrix spectral density of randomly polarized signal
12 p2031 A69-26644

Nonlinear control systems analysis by successive approximations, separating dominant component in transfer function of linear part
13 p2237 A69-27252

Passive adaptive sampled data control system with conditional feedback, discussing transfer function role and minimization of external disturbances and internal parameter variations effects
13 p2238 A69-27394

Optimal controller design and transfer functions in linear stabilization systems subjected to unknown disturbances determined by variational calculus
13 p2259 A69-27425

Microwave filters for canonical realization of non-minimum phase transfer functions, combining magic-T or hybrid junction with ladder structure network
13 p2228 A69-27668

Book on control theory covering automatic and remote position control, diagrams, transfer functions, operators, Laplace transform use with differential equations
13 p2238 A69-28345

Transistors transfer admittances measured indirectly, evaluating mean square error for transfer parameters
14 p2420 A69-29396

Linear analog computing elements realizing voltage transfer function with poles and zeros independently controlled, basing method on dummy variable technique
14 p2422 A69-29551

Transfer equation and Bouguer-Lambert-Beer equation application to multiple light scattering in plane medium
14 p2487 A69-29663

Lumped and distributed parameter systems, discussing transfer matrix elements, connecting lines, etc
15 p2582 A69-30319

FORTAN program for calculation of magnitude and phase of digital filter transfer functions and power spectra of periodic waveforms
15 p2567 A69-30612

Earth thermal emission intensity measured by two beam radiometer onboard Cosmos 149, noting discrepancy between empirical and theoretical transfer functions of atmosphere
15 p2596 A69-30651

Atmospheric transmission functions dependences on absorbing material, pressure and temperature in 15 micron band of carbon dioxide, introducing corrections
15 p2597 A69-30653

Cauchy system for reflection and transmission functions of finite isotropically scattering atmospheres with specular reflectors, noting use for ozone and cloud heights measurements
15 p2597 A69-31152

Universal transfer function computer based on synchronous spectrum analyzer having outputs combined in cross spectrum correlation computer to yield plot in Bode form
15 p2615 A69-31282

Linearly tapered transmission line equation and transfer matrix parameters, considering input impedances and microwave application
16 p2749 A69-31582

Solar image motion frequency spectra analysis via photoelectric equipment, showing influence on photographic pictures, spectra and modulation transfer functions for diffraction telescope
17 p3029 A69-33047

Modulation transfer function based on Fourier techniques, discussing nonlinear film development process
17 p3005 A69-33080

Network synthesis technique applied to structural dynamics design, using topological formulas to express systems response transfer functions
17 p2933 A69-33709

Rarefied gases transfer coefficients stochastic process calculation models, comparing results with correlation functions derived from transport equation
18 p3121 A69-34710

Automatic control system transient response oscillatory and aperiodic components calculation using open loop system transfer function
18 p3112 A69-35458

DYDRA data logger for dynamic measurements of pressure distributions on harmonically excited wind tunnel models, noting use as general transfer function analyzer
19 p3293 A69-35746

Transfer function in pulmonary ventilation and O tension in arterial blood analyzed by automatic control
19 p3260 A69-35897

Optical imaging with partially coherent nonthermal light, discussing correlation function propagation, transfer functions, spatial Fourier analysis, weak visibility and matrix form
19 p3372 A69-35907

Solar disk edge polarization rate determined by applying Feautrier method to transfer equations for polarized radiation
19 p3427 A69-36728

Vibration phenomena analysis by transfer function computer, discussing precision spectrum analyzers
20 p3498 A69-37003

Physical networks with lumped components and hydraulic, pneumatic, electric, thermal and elastic lines of transfer matrices
20 p3568 A69-37999

Second order system handling qualities analysis for pilot rating through human transfer function and closed loop control
21 p3668 A69-39792

Transfer matrix symmetry about secondary diagonal in vibration analysis useful for computer programming
22 p4040 A69-39938

Quadrupole network transfer matrix calculation from known octupole matrix, describing frequency response determination of coupled transmission lines
22 p3912 A69-40257

Magnetic field inhomogeneities effect on line contours and magnetographic measurements, constructing two stream models using Unno solution of transfer equations
22 p4019 A69-40288

Human eye modulation transfer function in reflected light by analyzing depolarized and polarized components emerging from eye
22 p3884 A69-40888

Exact solution of macroscopic line transfer equation including electron scattering terms for Milne-Eddington model atmosphere, discussing electron scattering effect on growth curves
22 p4007 A69-40903

Cascaded limiter and phase detector, analyzing SNR transfer characteristics for specific PM signals
23 p4131 A69-42525

Coefficient quantization in digital continuous time process controllers, applying results to nominal transfer function approximation
24 p4292 A69-43283

Feedback controller for linear stationary differential systems with time lag and fixed unknown parameters, noting closed loop transfer function role
24 p4293 A69-43293

TRANSFER OF TRAINING

Combined cueing and knowledge of results for transfer of training in visual monitoring
13 p2213 A69-28256

Aerospace management technology transfer, discussing conceptual contributions, planning, administrative and evaluation methods
18 p3236 A69-35086

TRANSFER ORBITS

NT INTERPLANETARY TRANSFER ORBITS

Satellite optimal transfers from elliptic to parabolic orbits within set time
01 p0157 A69-11306

Electric propulsion for payload transfer from low synchronous orbit of ELDO launch vehicles
03 p0496 A69-13959

Spacecraft orbital maneuvers by means of low thrust, discussing optimization and several orbital transfer examples
03 p0522 A69-14061

Single impulse noncoplanar orbital transfer with finite time of thrust action for satellite in elliptical orbit
05 p0823 A69-16048

Velocity increments for orbital transfer in satellite rendezvous in central Newtonian gravitational field by two impulse ballistic transfer method
05 p0789 A69-16065

Vehicle motion parameters in Newtonian central force field determined, using geometrical structures devised from properties of velocity hodograph
05 p0765 A69-16615

Electrical propulsion for space maneuvers discussing interrelationship of orbital change, payloads and time
06 p0998 A69-16858

Braking and acceleration speeds and maximum magnitude during transfer from circular orbit having earth center as focus to elliptical orbit within circular orbit
06 p1007 A69-17571

Minimum fuel control of spacecraft orbital elements for transfers between elliptical orbits by low variable thrust propulsion, noting interplanetary trajectory optimization
06 p0955 A69-17577

Transfer orbits calculation between low and high satellite orbits, determining trajectories by method with minimum use of linearization
07 p1211 A69-18504

Optimal interorbital transfers between closely spaced nearly circular noncoplanar orbits, taking into account active section length for low power thrusts
10 p1783 A69-23711

Optimal transfer between coplanar orbits in Newtonian force field without intersecting circle boundaries
10 p1790 A69-24198

Optimum orbital transfer of material point subjected to reactive force with minimum mass loss, discussing Kepler motion kinematics
13 p2346 A69-27690

Minimum fuel multiple impulse orbital rendezvous for fixed transfer time near circular orbits
16 p2857 A69-3216

Microthrusters thrust requirements for attitude control and orbital transfer of gravity gradient geostationary satellite
17 p3019 A69-33334

ELDO/PAS rocket motor for satellite launching from elliptic orbit apogee to synchronous orbit powered by ammonium perchlorate with organic binder and Al
17 p3022 A69-33604

Minimum fuel guidance from hyperbolic into specified circular orbit
19 p3367 A69-35663

Maneuverability domains optimization with semilinear boundaries, noting application to orbital transfer
19 p3399 A69-35664

Optimal transfers between Keplerian orbits for time free case, considering hyperbolas, ellipses external to and intersecting attracting planet
19 p3399 A69-35665

Optimal fuel transfers between coplanar and noncoplanar coaxial elliptical orbits determined by Pontryagin maximum principle, using digital program for Hamiltonian equations solutions
19 p3399 A69-35670

Numerical integration of plane orbital transfers with multiple powered arcs, minimizing propellant expenditure of small thrust chemical rocket
19 p3400 A69-35673

Optimal impulse rendezvous of long duration between quasi-circular, coplanar or noncoplanar close orbits
19 p3400 A69-35674

Minimum impulse transfer between circular and nearby noncoplanar elliptic orbit, applying Pontryagin principle
19 p3400 A69-35675

Coplanar impulsive transfers and second variation test, using maximum principle and Lagrangian multiplier technique for propellant expenditure minimization
19 p3400 A69-35676

Minimum-fuel controls in multidimensional optimum transfer problems
19 p3400 A69-35677

- Mission windows for single and multiple planet swingbys past Jupiter to outer planets
[AAS PAPER 68-115] 19 p3402 A69-35936
- Impulsive orbit transfer optimization using accelerated gradient program based on Newtonian algorithm for digital computer method
19 p3402 A69-35956
- Vehicles optimal flights with controlled or boundary level thrust in circular orbit neighborhood, using linearized equations of motion
19 p3427 A69-36612
- Optimal transfers in central gravitational field, using formulas for perturbations of osculating Keplerian orbital elements, applied to singular reticent solutions [ONERA-TP-729] 20 p3604 A69-37752
- Single impulse noncoplanar orbital transfer with finite time of thrust action for satellite in elliptical orbit
20 p3606 A69-37953
- Velocity increments for orbital transfer in satellite rendezvous in central Newtonian gravitational field by two impulse ballistic transfer method
20 p3574 A69-37955
- Geodetic satellites transfer between low ellipticity orbits by microthrust
21 p3793 A69-38338
- Optimal transfer between coplanar elliptical orbits of spacecraft with combined small and large thrust propulsion system
21 p3803 A69-38848
- Abort capability mission selection criterion, evaluating energy requirements, Mars flyby and velocity contours
[AAS PAPER 68-139] 21 p3805 A69-39209
- Minimum fuel thrust limited transfer trajectories computation for coplanar elliptic orbits
[AIAA PAPER 69-914] 21 p3808 A69-39344
- Satellite maneuver for changing plane of circular orbit to pass through given point, determining on-off engine switching and thrust vector control
21 p3765 A69-39640
- Optimal control system for earth satellite orbital transfer, using wandering ellipse technique to develop trajectory correction algorithm
21 p3767 A69-39652
- Satellite motion orbital elements dependence on large short impulse arbitrarily directed in space, analyzing optimal orbits transfer and thrust control
21 p3818 A69-39821
- Optimal pulsed orbital transfer between close nearly circular orbits in central field of gravity realized by geometrical solution
22 p4033 A69-41085
- Minimum impulse transfer of vehicle between noncoplanar Kepler orbits, applying optimal control principles to formulation
23 p4214 A69-41878
- Minimum impulse time free transfer between neighboring noncoplanar almost circular orbits with line of nodes along common latus rectum
[AIAA PAPER 68-94] 23 p4215 A69-41879
- Recurrent Lagrange multipliers for optimal low thrust earth-Jupiter transfers, using three dimensional solar system model
23 p4215 A69-41896
- Liquid fuel propulsion systems for geostationary satellites, discussing transfer orbits, payload increase and required thrust for various satellite trajectories [DGLR-69-014] 23 p4202 A69-41929
- Low thrust guidance for multirevolution trajectory required for earth parking orbit transfer to parabolic orbit insertion, noting advantages over high thrust scheme
[AAS PAPER 69-403] 24 p4379 A69-42832
- Earth-Mars and earth-Venus economical transfers derived for optimal conditions with respect to characteristic velocity, obtaining exact numerical solution
[AAS PAPER 69-241] 24 p4380 A69-42855
- Optimal transfer between hyperbolic asymptotes about finite size planet, discussing twelve types of analytical solutions in terms of arrival, departure and escape velocities
[AAS PAPER 69-242] 24 p4380 A69-42856
- TRANSFERRING**
- Activation energies of bimolecular multivalent transfer reactions of gaseous compounds, considering bond dissociation energy, length and order [WSCIPAPER 68-48] 07 p1239 A69-18321
- TRANSFORM INTEGRALS**
- U INTEGRAL TRANSFORMATIONS**
- TRANSFORMATION TENSORS**
- U TENSORS**
- TRANSFORMATIONS (MATHEMATICS)**
- NT COORDINATE TRANSFORMATIONS**
- Modified admittance yielding Kubo admittance at nonzero frequencies, discussing transformation of correlations of Ising model
01 p0115 A69-10019
- Unsteady heat flow in finite composite hollow circular cylinder using inverse method of eigenfunction expansion /method of finite integral transformation/
01 p0175 A69-10230
- Matrix technique for transformation of equation of motion into first order equation in analyzing perturbation forces producing mechanical oscillations
01 p0170 A69-10827
- Transformation laws for thermodynamic quantities confirming conventional formulation by mechanical model of heat
01 p0122 A69-11288
- Matrix transformation applications in dynamic system theory and stability test
02 p0281 A69-11943
- Integration for equations governing linearized thermoelastic transformations of incompressible solids
02 p0340 A69-12033
- Nonlinear first order equations solution by reduction method, using nonlinear transformation of dependent variable, noting two axis gyro drift
02 p0273 A69-12541
- Eigenvector approximation of complex matrix by inverse iteration, giving Algol 60 program
03 p0455 A69-13371
- Book on nonlinear programming, discussing transformation of constrained minimization problem into sequence of unconstrained minimizations of appropriate auxiliary functions
04 p0563 A69-14421
- Transformations useful for finite difference solution of differential equations with infinite regions, considering flow problems application
04 p0588 A69-14717
- Phenomena satisfying inhomogeneous Helmholtz equation in cylindrical coordinates, inferring equivalent infinite series directly from integral- transform method
04 p0623 A69-14896
- Two dimensional elementary transformation for obtaining eigenvalues, considering programming aspects for computing characteristic roots of matrix
04 p0624 A69-14967
- Theorems concerning interspherical fractionally linear transformations of operators in Hilbert spaces formulated and proved, analyzing unit sphere during fractional linear transformation
05 p0787 A69-16423
- Rearrangement inequalities for positivity of nonquadratic transformations, discussing stability of nonlinear feedback loop described by difference equations
06 p0904 A69-17943
- Transformation theory for compressible turbulent boundary layer with arbitrary pressure gradient
[AIAA PAPER 69-160] 06 p0912 A69-18073
- Wolf and generalized Parseval theorems applied to transformation of integral equation to S-plane in systems analysis
08 p1271 A69-19865
- Clebsch transformation application to equations describing viscous fluid, deducing canonical equations equivalent to Navier-Stokes equations
08 p1303 A69-20125
- Transforming equivalent circuits, keeping electrical characteristics defined by network functions within prescribed limits
09 p1472 A69-21784
- Kutta-Merson algorithm for converting partial differential equation for two dimensional unsteady state heat conduction to simultaneous ordinary differential equations
09 p1623 A69-22280
- Invariant transformation of equations for ideal gas plane steady motions, noting application to gas flows with shock waves and eddies
10 p1680 A69-23709
- Asymptotic solution to problem of finding time optimal transformation for controlled plant with motion in phase space described by matrix differential equation
10 p1666 A69-23883
- Invariant transformation of Euler equations of motion for plane steady flows of perfect compressible fluid
11 p1877 A69-25739
- Canonical transformations of unsteady control system motion equations, simplifying control process study and controller simulation on analog computer
12 p2045 A69-25960
- Differential equations application to electrical circuit problems, solving voltage for series LCR networks and transforming Mathieu into Hill equation
12 p2052 A69-26351
- Homeomorphism theorem for Petrovskii and homogeneous elliptic systems applied to boundary value problems and Green formula
13 p2287 A69-27515
- Group code decoding, discussing equivalent transformations of reference matrix and reduction of equipment losses
13 p2225 A69-28537
- Differential equations for shallow circular spherical shell transformation to equation describing stress-strain state of plate on elastic base
13 p2369 A69-28565
- Convolution property of Hermitian transform for odd integral values of n
15 p2645 A69-30863
- Bilinear covariant of linear differential form involving 2n independent variables used for grouping to achieve symplectic and contact transformations
16 p2804 A69-31623
- Vlasov-Poisson equations reformulation by arbitrary transformation to velocity variable, considering time or space secularity of perturbation theory
16 p2817 A69-31642
- Equations of transformation for hourly data harmonic terms used in computation and representation of solar and lunar daily magnetic variations
16 p2782 A69-32457
- Transformation of two dimensional boundary value equations for laminar power law nonNewtonian fluid flow to yield similar solutions
17 p2957 A69-34016
- Green functions theory for finite integral Lebedev-Kantorovich transforms derivation, with application to elastostatics boundary value problems
17 p3067 A69-34148
- Moment and discrete ordinate methods in radiative transfer problems in planar, radiating and nonscattering media, noting conical transformation of moment equations
18 p3174 A69-35237
- Canonical transformations depending on small parameter, utilizing Lie series
19 p3397 A69-35608
- Equilibrium equations for longitudinally hinged nonshallow cylindrical shells transformed into coupled equations with constant coefficients
19 p3439 A69-36581
- Transformation groups used to find similarity solutions for partial differential equations and heat equation
20 p3630 A69-36915
- Reduction of boundary value problems to initial value problems through variables transformation, considering application to eigenvalue problems
21 p3754 A69-38747
- Invariant transformations for hodograph matrix equations in gas dynamics
21 p3695 A69-39001
- Spacecraft natural vibrations analyzed using point transforms with allowance for control systems imperfections
21 p3826 A69-39637
- Slack variable to transform optimal control problem with scalar inequality constraint on state variables into unconstrained problem of higher dimension
24 p4291 A69-43270
- Stress wave propagation in nonhomogeneous elastic media, considering curvilinear characteristics transformation into equal slope straight lines by change of independent variable
24 p4403 A69-43574
- TRANSFORMERS**
- NT COUPLING CIRCUITS**
- NT MODE TRANSFORMERS**
- Passive circuit to transform voltage of indefinitely repeated positive or negative pulses using transistors, diodes and magnetic cores
01 p0043 A69-10564
- Self excitation conditions and output characteristics of tunnel diode DC to AC converters for spacecraft, discussing relaxation- oscillator and push-pull circuit converter types
01 p0046 A69-10755
- Regulated high voltage DC to DC converter with output voltage programmable numerically, noting application on board HEOS A satellite
04 p0602 A69-15400
- Transformer inrush transients control by selection of core material, primary turn number and trigger circuitry
06 p0894 A69-17221

- Pulse transformer design relationships and definitions, discussing core and winding structure choice
08 p1285 A69-20382
- Synthesis for asymmetrical branch guide directional coupler-impedance transformers, noting application in antenna design
13 p2233 A69-28069
- E shaped cores for miniaturized transformers and inductors from high permeability plastic bonded materials
13 p2237 A69-28586
- Computerized design of inhomogeneous transformers with cascaded quarter wave sections
14 p2423 A69-29762
- Equivalent circuit of single winding transformer, using distributed constant theory
15 p2578 A69-30793
- Rotary power transformer design for spin stabilized spacecraft power system, discussing efficiency and advantages
17 p3050 A69-34111
- Transformer for unilateral energy transfer using single domain uniaxial Permalloy film
21 p3684 A69-39454
- Autotransformer with static tap changer to provide varying power levels for controlled gradual heating of aircraft window to avoid thermal shock
22 p3869 A69-40414
- Isometric recording device for tensile stresses on muscle preparations in vitro, based on differential transformer
23 p4111 A69-42056
- S-band pin-diode switch for high CW power satellite and deep space probe communication, using multiple quarter-wave transformers to stepdown diode impedance
23 p4143 A69-42518
- TRANSFORMS**
U TRANSFORMATIONS [MATHEMATICS]
- TRANSIENT HEATING**
NT PULSE HEATING
NT SHOCK HEATING
- Semidiscrete approximate solution by analog computer of inverse problem of transient heat conduction [ASME PAPER 68-WA/HT-26]
05 p0848 A69-16127
- Transient temperature distribution for finite slab in phase transformations via single face temperature changes [ASME PAPER 68-WA/HT-37]
05 p0848 A69-16128
- One dimensional integral solution for cylindrical source generated transient temperature field and relation to thermal diffusivity of brain tissue
06 p0879 A69-17085
- Charring phenolic nylon ablator material pyrolysis and surface recession for cyclic and constant combined convective and radiative heating [AIAA PAPER 69-151]
06 p1036 A69-18055
- Safety problems associated with transient boiling of liquid metals in fast nuclear reactors, emphasizing behavioral differences between liquid metals and water
08 p1420 A69-20101
- Human reactions to increasing heat exposure, noting thermoregulation and metabolic and evaporative heat loss [AGARDOGRAPH-111]
08 p1265 A69-20675
- Transient free convection laminar boundary layer equations for heat transfer from vertical semiinfinite flat plate
08 p1305 A69-20842
- Upper atmosphere response to time dependent heating based on approximate analytic solutions of heat conduction equation
11 p1878 A69-25151
- Transient one dimensional temperature distribution determined for bodies with internal heat generation and nonlinear boundary condition, using Biot variational method [ASME PAPER 68-HT-6]
13 p2374 A69-27775
- Transient heat transfer in formation of steady crossed fields MHD plane Couette flow for walls, giving momentum, induction and energy equations
13 p2375 A69-27791
- Heating facility for testing ablative heat shield material models in combined convective and radiative heating environment with constant or transient heating conditions [AIAA PAPER 69-342]
13 p2243 A69-28278
- Green functions for Laplace, Poisson and transient heat diffusion equations solved by matrix multiplication
15 p2710 A69-30870
- Numerical methods using analog computer in linear one dimensional transient heat conduction
18 p3229 A69-34835

Stress strain state in thin circular elastoplastic disks under axially symmetric transient temperature distribution, noting moving annular plastic deformation region
20 p3629 A69-38028

Transient heat transfer single blow temperature response functions characterized by first moment of downstream-upstream fluid temperature difference, showing curve matching applications
21 p3851 A69-39291

TRANSIENT LOADS

NT BLAST LOADS
NT GUST LOADS
NT IMPACT LOADS
NT SHOCK LOADS

Mathematical models to investigate transient plane bending wave propagation in elastic plates, using elasticity and plate theories
03 p0525 A69-13606

Vertical, horizontal and rocking vibrations of body on surface of otherwise unloaded elastic half plane, estimating stiffness for coupled vibrations [ASME PAPER 68-WA/APM-12]
04 p0668 A69-14393

Stresses and displacements in anisotropic elastic solids under mechanical loading, determining general solution for treatment of time dependent boundary conditions
04 p0675 A69-14595

Forced vibration of thin elastic plate resting on elastic foundation and subjected to time dependent loads and external damping
08 p1416 A69-20692

Shock pulse criterion limitations and HF transients technique for design and tests of structures and components
12 p2182 A69-26731

Dynamic stresses in case bonded cylinder under transient angular accelerations, presenting numerical results for incompressible elastic cylinder
13 p2364 A69-28209

Materials and structural failures under short time compressive loadings, showing structural response to tensile stresses produced by rarefaction waves
15 p2639 A69-30364

Transient and long lasting space environment stresses, discussing accelerations, vibrations, shocks, rapid descent in vacuum, temperature variations, gravity, etc
15 p2625 A69-30824

Transient wave processes of deformation in spherical shell under load abruptly applied to geometrical pole
16 p2875 A69-32288

Secondary fatigue curves slope variation to determine preloaded materials fatigue life under unstationary loading
17 p3052 A69-32976

TRANSIENT OSCILLATIONS

Transient phenomenon analysis and filtering based on stage separation tests in vacuum chamber, with emphasis on selective integration method [ONERA-TP-684]
19 p3293 A69-35747

Transient oscillations in ammonia maser oscillator observation based on switching achieved by signal injection into cavity at molecular resonance frequency
19 p3339 A69-36825

Eye elemental response to individual frequency jumps in oscillations of light, noting transient effect polarity
21 p3650 A69-38320

TRANSIENT PRESSURES

Molecular flow network theory applicable to volumes interconnected by small orifices or porous membranes for transient pressure measurements
16 p2813 A69-32325

High speed transient pressure measurement, emphasizing forcing function measurement
18 p3133 A69-34244

Bubble oscillations in water filled pressure chamber with alternating pressure generated by piston, measuring temporal development
19 p3302 A69-36871

Miniature transducer to measure low transient pressures on models in rarefied shock tunnel flows, emphasizing mechanical vibration, convective heating and miniaturization
22 p3950 A69-41227

Stroboscope method for measuring pulsating flow transient velocity based on hot-wire chromometric recording of small ion clouds emitted during pulsation
22 p3951 A69-41257

TRANSIENT RESPONSE

Streak interferometry method for measuring transient deformation data on metallic solid surfaces
01 p0078 A69-10117

Transistor distributed amplifier theory, noting effect of collector line and base line delay difference on gain and transient responses
01 p0041 A69-10203

Transient nonlinear mode partially responsible for anomalous operation of IMPATT diodes below transit time cut-off frequency
01 p0043 A69-10559

Delayed response in threshold switching from reset state in ferrite memory cores consisting of magnesium compounds [IEEE PAPER 16.4]
01 p0045 A69-10719

Transistor parameters for operation as minority carrier charge controlled device, developing equivalent circuit for computer calculation of transient response
01 p0046 A69-10748

Equivalent circuits for transient characteristics approximation of distributed RC circuits
01 p0046 A69-10779

Transient process in n stage nonlinear amplifiers analyzed on basis of structural circuit
01 p0047 A69-10781

Zero memory frequency independent nonlinearities response to modulated input noting FM limiter, band-pass limiter and AC carrier control systems
01 p0034 A69-11142

One dimensional Vlasov plasma nonlinear response to external electric field varying in space and time
01 p0133 A69-11214

Transient laminar boundary layer development on flat plate following impulsive start of surrounding fluid motion, obtaining temperature and velocity distribution relationship [ASME PAPER 68-HT-10]
02 p0232 A69-12208

Pressure and velocity couplings effects on oscillatory and transient motions in solid propellant rocket motors, emphasizing unsteady burning calculations
02 p0305 A69-12501

Finite difference numerical integration technique for large elastoplastic deformation transient and permanent deflection responses of thin shells
02 p0347 A69-12518

Proper digital filters devoid of transient response analyzed as extension of time invariant filters
02 p0213 A69-12815

Unsteady transient flow of viscous fluid in suddenly rotating open pot, taking into account effect of bottom in determination of velocity profile
03 p0414 A69-13019

P-n junction under arbitrary transient conditions, solving one dimensional, two carrier transport equations by numerical iterative method
03 p0487 A69-13639

Galvanostatic transients of iron passive in 2N sulfuric acid, noting space charge effects and zero field current variation [ECS PAPER 84]
03 p0382 A69-13858

Transient electro-osmosis of water in capillary tubes for pumping and generation modes, analyzing response to step change in pressure or voltage change under external loading
04 p0555 A69-14862

Transfer function variation of invariant servodrive, comparing calculated and experimental transient response
04 p0584 A69-15418

Controlled transient signal distortion by shock monitoring instrumentation circuits using piezoelectric accelerometers
04 p0603 A69-15430

Models to predict transient radiation responses in microcircuits, discussing model accuracy for junction and dielectrically isolated circuits
06 p0977 A69-16887

Square loop magnetic core model for computer aided circuit transient analysis
06 p0899 A69-16888

Attitude control system for maintaining orientation of experimental package relative to space stabilized platform, noting transient response and steady state accuracy
06 p0955 A69-17587

Transient stability of AC generator analyzed by Liapunov direct method, considering effects of flux decay, speed governor and voltage regulator
07 p1058 A69-18644

Forward transient response characteristics of high resistivity, long base, low lifetime p-n-n silicon diodes doped with Au, noting voltage oscillations
07 p1101 A69-18652

Transient heat evolution response to reapplied stress of alloys plastically preformed at 4.2 K attributed to thermally softened defect structures
07 p1165 A69-18906

- Wave motion onset and waveforms in rotating annulus with sinusoidally varying temperature differences
07 p1126 A69-19039
- Transient response of targets subjected to hypervelocity impacts and quantitative aspects of impact process, noting study of wax targets interiors
07 p1234 A69-19380
- Feedback amplifier with transfer function poles on parabola, discussing small rise time with small overshoot combined in transient response
08 p1282 A69-20111
- Transient response spectrum of nonlinear cubic spring mass system subjected to step function input, discussing viscous damping effects on peak response
08 p1413 A69-20402
- Rocket engines transient thrust measurement by quartz transducers
08 p1301 A69-20589
- Transient thermal stress distribution in infinite orthotropic elastic cylinder of rectangular cross section in presence of heat sources
08 p1415 A69-20664
- Human reactions to increasing heat exposure, noting thermoregulation and metabolic and evaporative heat loss
[AGARDOGRAPH-111] 08 p1265 A69-20675
- Second order system response with variable damping computed by stepwise numerical integration
08 p1418 A69-20849
- Transistor large signal saturation time constant dependence on injection ratio, noting nonlinear response and saturation transistor switch storage time
09 p1464 A69-22117
- Transient behavior of DC measuring amplifiers with time variable feedback, using matrix method and Laplace transform
09 p1467 A69-22560
- Transient process in n stage nonlinear amplifiers analyzed on basis of structural circuit
10 p1661 A69-23110
- Transient characteristics of negative resistance zinc alloy diodes, investigating temperature effects
10 p1662 A69-23157
- Transient response of MOS capacitance caused by mechanisms dependent on electric field distribution between silicon and oxide
10 p1744 A69-23176
- Resonator field inhomogeneities effect on transient processes in quantum oscillator, considering two active crystals in cavity
10 p1705 A69-23948
- Finite difference method for transient and steady state response of vibrating plates, considering explicit and implicit formulas
11 p1983 A69-25020
- Numerical prediction for nonlinear transient response of structures, considering geometric and material nonlinearities in systems with line elements
11 p1993 A69-25526
- Transient dynamic response of linearly viscoelastic structures and continua, presenting finite element displacement formulation
11 p1993 A69-25528
- Transient behavior of transistor UHF oscillator, discussing network analysis for oscillation amplitude calculation by nonlinear transistor equivalent circuit diagram
11 p1854 A69-25613
- Numerical computation method for evaluating transition matrix of linear time invariant system, estimating error propagated in transient response
11 p1910 A69-25660
- Vignetting effect on impulse response of general coherent optical Fourier processor, noting time varying character and input position sensitivity
12 p2036 A69-25912
- Transient response of linear time invariant system from state transition matrix, eliminating evaluation of eigenvalues
12 p2120 A69-25913
- Modified scheme for simulation of delay with transient period independent of amount of delay, considering polynomial input
12 p2120 A69-25922
- Transmission and reflection scattering coefficient measurements of microwave networks by Fourier analysis of transient response to impulsive or steplike waveforms
12 p2038 A69-26056
- Uncontrollable modes effect on transient/steady behavior and limit cycles characteristics of nonlinear multivariable control system
12 p2048 A69-26078
- Transient ventilatory response to breaths of nitrogen at rest and during exercise in high altitude and sea level natives
12 p2019 A69-26131
- Photoelectric recorder with timebase image converter tube for investigating ultrashort light pulse transient response of laser
12 p2083 A69-26139
- Extrapolation of aperiodic step responses
12 p2051 A69-26237
- Transient responses of mutually synchronized signal systems, obtaining design parameters
12 p2030 A69-26388
- Transient processes in conduction type MHD generators due to external circuits induction distribution
12 p2017 A69-26545
- Transient response of transistor in common emitter circuit using charge method taking into account base current switching pulse parameters
12 p2043 A69-26884
- Transient response in liquid-metal conduction MHD generators, analyzing constant magnetic field using differential equation
13 p2207 A69-27506
- Numerical methods for solving steady state and transient heat transfer problems suitable for high speed digital computer
13 p2376 A69-28141
- Transient response of distributed gain amplifier employing m-derived filters and vacuum tubes
13 p2235 A69-28516
- Autonomous and nonautonomous transient processes in conservative and nonconservative nonlinear systems, deriving equations describing perturbations under loads, solving by asymptotic method
13 p2300 A69-28529
- Optimal linear control systems with time limits on transient processes synthesized by reducing optimization to algebraic equations solution
14 p2425 A69-28820
- Small signal transient characteristics of semiconductor diodes analyzed by charge method, studying processes during p-n junction diode switching at low currents
14 p2419 A69-28918
- Transient processes in counting circuits with tunnel diode chains, discussing operating point position for various conditions
14 p2419 A69-28921
- Capacitive parametric modulator transient processes and second harmonic effect analysis, obtaining transient response and recovery time
15 p2574 A69-30125
- Transient behavior of finite damped cantilever beam and circular plate analyzed by direct finite element method, noting applicability to dynamic problems
15 p2710 A69-30868
- Statistical characteristics of Q switched He-Ne laser emission gain fluctuations during transient process from subthreshold to superthreshold value
15 p2634 A69-30960
- High gas stream temperature levels and distributions from transient and intermittent probe measurements
15 p2612 A69-31268
- Approximate analytic solution to transient response of infinitely long cylindrical shell surrounded by viscoelastic medium, discussing composite and elastic shells
[AIAA PAPER 68-351] 16 p2871 A69-31877
- Digital simulation computer stability analysis scheme premised on use of perturbed transient responses
17 p2944 A69-32899
- Backscattered impulse response waveforms of conducting circular cylinder for broadside incidence utilizing Fourier synthesis
17 p2917 A69-32918
- Transient thermal analysis of space radiators excluding finite difference equations, noting computer adaptability and time saving
[AIAA PAPER 69-615] 17 p3070 A69-33261
- Collisionless cylindrical Langmuir probe response in turbulent plasma for mean and statistical properties
[AIAA PAPER 69-698] 17 p3010 A69-33438
- Electromagnetic transient wave propagation and reflection in lossless isotropic stratified ionized media, discussing time variations of fields due to incident plane unit step wave
17 p2924 A69-33839
- Switching time of transient two dimensional fluidic bistable wall attachment amplifiers based on mathematical model and separation bubble control
17 p2904 A69-34068
- Transient characteristics of three phase AC alternators with rectified outputs
17 p2905 A69-34089
- Automatic multichannel transient monitor for electrical transient detection and data processing, transmission and storage on aircraft
17 p2947 A69-34135
- Penumbra current distribution in plane electromagnetic waves diffraction by conducting cylinder, obtaining transient solution for impulsive excitation, discussing time harmonic problem
[AFRL-69-0038] 18 p3100 A69-34232
- Transient vibration linear analysis using Duhamel integral and Fourier and Laplace transformations, deriving receptances and application to aeroelastic systems
18 p3211 A69-34326
- Transient performance of full flow hydraulic turbine driven two speed pump inducer system, formulating computer model
[AIAA PAPER 69-551] 18 p3140 A69-34415
- Optimum automatic system for controlling helicopter formation flight, stressing transient response Q factor and transmission ratios
18 p3090 A69-34656
- Transient processes of strain wave propagation in elastic shells and plates under time varying loads
18 p3224 A69-35321
- Automatic control system transient response oscillatory and aperiodic components calculation using open loop system transfer function
18 p3112 A69-35458
- Algorithms for equivalence equation to approximate transient processes in higher order linear system by transient processes of lower order linear models
19 p3286 A69-36191
- Transient electrical responses from retinas, discussing visual pigment role in visual excitation, photochemistry, etc
19 p3258 A69-36377
- Phase and amplitude stabilization during phase modulated discrete data transmission
19 p3277 A69-36571
- High gas stream temperatures determination from short exposure probe based on inferring temperature from transient response of sensor
20 p3536 A69-37005
- Transient phenomena in bounded dispersive medium emphasizing surface wave propagation, discussing space and surface waves excitation in bounded cold magnetoplasma
20 p3494 A69-37842
- Transient effects of nuclear radiation bursts on dielectric properties of refractory low loss ceramics at L, S and X bands
20 p3584 A69-38065
- Transient current change with minor change in voltage with double injection of electrons and holes in CdS single crystals, obtaining time dependence
21 p3780 A69-38833
- Transient heat transfer single blow temperature response functions characterized by first moment of downstream-upstream fluid temperature difference, showing curve matching applications
21 p3851 A69-39291
- Satellite attitude stabilization systems transient response optimization using combined feedback
21 p3830 A69-39833
- Transient temperature response of cylindrical composite energy storage devices with thermal conductivity, density and specific heat independent of temperature
22 p3868 A69-40132
- Maximum errors of telemetering systems under interchannel transient distortions in multistage amplifier of video signals
22 p3899 A69-40250
- Piezoelectric transducer transient electrical response due to shock loaded stress using transform calculus
22 p3947 A69-40863
- Transient flow resulting from plane shock diffraction by analytic blunt body, basing analysis on Taylor series expansions in space and time variables
22 p3860 A69-40895
- Frequency response transient vibration testing of standing man, discussing data analysis procedure, test stand, and Welch correction for instrument dynamics
23 p4101 A69-41494
- Bounded input-output stability for lumped distributed systems by poles examination in S plane, considering transient response of linear time invariant systems
23 p4144 A69-41568
- Transient processes in microwave quadrupoles with ferrite resonators
23 p4139 A69-41948

- Optimal control problems, discussing properties of signal producing response signals with transient functions at independent outlets of linear dynamic system 23 p4145 A69-41958
- Nerve and muscle tissues subthreshold reactions on analog model, discussing transient characteristics under various excitations 23 p4109 A69-41980
- Potentiometer transient contact resistance determined as function of contacts physical parameters 23 p4166 A69-41996
- Shock wave transient motion during passage through ducts in inviscid gas containing convergences, using characteristics method 23 p4153 A69-42398
- Battery/fuel cell hybrid power source, discussing fast transient response [SAE PAPER 690205] 24 p4255 A69-42889
- Matrix method for analyzing elastic structures linear transient response to time dependent loads and temperature change 24 p4399 A69-42988
- Geometric dispersion of transient stress waves in linearly elastic laminated composite based on sinusoidal modes [ASME PAPER 69-APMW-20] 24 p4401 A69-43098
- Wick-limited heat pipe performance, discussing maximum, steady heat transfer rate and transient response [ASME PAPER 69-HT-20] 24 p4413 A69-43549
- TRANSIENTS [SURGES]**
U SURGES
- TRANSISTOR AMPLIFIERS**
- Transistorized feedback amplifier for data transmission over high voltage lines in conveyed wave systems 01 p0038 A69-10074
- Microwave transistor amplifier computerized design, discussing wide bandwidth and flat in-band gain response optimization on high dielectric substrates 01 p0040 A69-10194
- Darlington composite transistor hybrid parameters used to describe performance characteristics, noting load resistances and source 01 p0041 A69-10244
- S band solid state amplifier capable of 10 watts output power based on combination of transistor amplifiers 02 p0217 A69-12147
- Transistorized two stage amplifiers with common feedback operating under steady conditions and for short times 04 p0575 A69-14466
- Supply voltage limits for transistor amplifier circuit, examining processes during supply voltage variation 05 p0729 A69-16083
- Equivalent noise circuit for resonant transistor amplifier, deriving expression for noise factor 05 p0729 A69-16084
- Admittance between terminals measured for stabilizing single loop negative feedback transistor amplifier 05 p0739 A69-16341
- Transistorized receiver for satellite telecommunications having adjustable receiver center frequency within 20 MHz 05 p0734 A69-16594
- Noise properties of junction diodes and bipolar transistors as basis for low noise amplifiers design 08 p1286 A69-20839
- Self biasing influence on tunnel diode amplifiers dynamic range, determining limiting conditions for amplitude characteristics 09 p1469 A69-22633
- Transistorized assembly for amplification of signals emitted by platinum film probes in shock tubes, discussing application to chronometric device triggering 11 p1887 A69-25095
- Ultrawideband DC transistor amplifier for pulsed switching circuits with subnanosecond risetimes, discussing multistages with feedback dipoles, transient response and drift problems 11 p1854 A69-25612
- P-n-p planar epitaxial germanium microwave transistor used as amplifier in 1.4 GHz range and as high speed switch, summarizing design, fabrication and characterization 12 p2037 A69-25940
- Transistorized amplifiers reliability during operation in intense external environment 12 p2043 A69-26886

- Current driven AGC effectiveness in selective amplifiers, including conductance variation effect on pass-band instability and frequency response 12 p2043 A69-26887
- Emitter self bias in power stages of transistor transmitters, considering transistor parameters dispersion 13 p2226 A69-27217
- Voltage amplitude for combination frequency of small signal transistor amplifier calculated from feedback dependence 13 p2226 A69-27218
- Coupling coefficients for common-base/common-base circuits of bandpass filters in two circuit selective transistor amplifier 13 p2226 A69-27219
- Transistorized DC amplifier circuit with reversible and controllable transfer constant based on voltage conversion principle 13 p2235 A69-28511
- Large signal transit time effects in MOS transistor, noting drain current response 14 p2418 A69-28891
- Wideband transistorized amplifier frequency response analysis by simplified approximations, subdividing operational frequency range 15 p2573 A69-30113
- Solid state broadband RF power amplifier for airborne HF radio, eliminating total servosystem and all higher voltage components 17 p2942 A69-34114
- Silicon MOS transistor characteristics, discussing stability, temperature effects and inherent noise, noting applications to amplifier circuits 18 p3109 A69-35161
- Transistorized low noise reception antennas with built-in amplifying elements, discussing radiation patterns and noise problems 21 p3683 A69-39264
- TRANSISTOR CIRCUITS**
- Input transistor performance analysis in Schmitt trigger circuit, considering role of hysteresis 01 p0039 A69-10170
- Microwave amplifier design with hybrid integrated circuits of thin film lumped elements, noting gain and efficiency of transistor circuits 01 p0039 A69-10190
- Transistor distributed amplifier theory, noting effect of collector line and base line delay difference on gain and transient responses 01 p0041 A69-10203
- Transistor parameters for operation as minority carrier charge controlled device, developing equivalent circuit for computer calculation of transient response 01 p0046 A69-10748
- Impedance and gain approximation in transistor configurations, noting gyrator circuit 02 p0213 A69-11532
- Test procedure for obtaining large signal S characterization of nonlinear power transistors 02 p0214 A69-11600
- Low noise high power transistor oscillator using directional coupler, noting isolated port for injection phase locking 02 p0220 A69-12452
- Large scale integration /LSI/ arrays, discussing high yield manufacturing methods based on fixed nondiscretionary connections among components 02 p0254 A69-12467
- Linear transistor models synthesis based on measured characteristics of four terminal admittance parameters 03 p0404 A69-13596
- Transistor circuits analysis with aid of signal flow graphs 04 p0575 A69-14461
- Soviet book on impulse generators in transistors covering multivibrators and pulse generators with timer circuits, crystal controlled frequency and delayed feedback 04 p0578 A69-15053
- Transistor scattering matrix parameters determination, emphasizing directional coupler errors and impedance mismatches 04 p0582 A69-15067
- Transistorized LF generator, discussing tradeoff due to frequency range, harmonic distortion and output stability 04 p0579 A69-15225
- Bridge circuit n-type conductivity converter with internal compensation of parasitic effects 05 p0727 A69-15641

- Transistor-transistor logic switching circuits design for use in frequency dividers with variable division ratios in frequency processing systems 05 p0729 A69-15963
- Transistorized single sideband detector-converter operation in presence of large signal and heterodyne voltage levels, deriving equation for transmission coefficient 05 p0730 A69-16220
- Circuit with tunnel diodes and transistors for nonlinear amplification, noting current-voltage characteristics dependence on circuit parameters 05 p0829 A69-16222
- Tube and transistor type quartz crystal FM oscillators circuitry and operating characteristics, discussing generation of three frequencies 05 p0732 A69-16532
- Junction gate field effect transistor design covering geometries and impurity profiles 06 p0893 A69-17197
- Transistorized multichannel pulse height analyzer and recording system for balloon-borne cosmic ray payloads, discussing performance capacity 06 p0924 A69-17284
- Transistorized frequency detector for sensing system load changes affects speeds of control valves of prime movers 06 p0896 A69-17478
- Linearizing circuit for low velocity hot-wire anemometry, using analysis of transistor circuit to generate desired function 06 p0927 A69-17701
- Noise characteristics of transistorized feedback amplifier stages for application in amplifier design 07 p1090 A69-18284
- Analog multiplier using differential transistor pairs, discussing FM/AM detection, suppressed carrier modulation and TV chroma demodulation 07 p1103 A69-18880
- Integrated four transistor bridge network used for self neutralized active element in tuned RLC amplifier design 07 p1103 A69-18884
- Metal oxide semiconductor circuits with higher orders of complementarity for performing multiple electronic functions, noting I-V characteristics and effects of bias 07 p1104 A69-18887
- MOS transistor logic circuit performance optimization through component geometry and feed voltage 08 p1280 A69-19977
- Composite transistor simulation of circuit inductor effect for synthesizing frequency selective circuits 08 p1286 A69-20834
- Thermal instability in power transistor structures, considering effects of design, emitter and base resistance at high currents 08 p1373 A69-20858
- Nonlinear analysis of transistor networks using Kron mesh method, developing quasi-linear equations characterizing common emitter transistor 09 p1471 A69-21632
- Transistorized amplifier stage noise factor dependence on parameters and modes of operation of transistors 09 p1463 A69-21724
- Pulse generator switch consisting of avalanche transistors in series, describing voltage production and transmission, trigger pulse jitter and pulse amplitude 09 p1468 A69-22589
- Intrinsic amplitude and frequency fluctuations in transistor autooscillator, examining natural additive noise influence 09 p1469 A69-22632
- DC to DC converters design using HF transistors to achieve high switching speeds while reducing size and weight 10 p1635 A69-22983
- Transistorized electrophotometer for polarimetric and photometric analysis of weak light fluxes, noting pulse amplifying and shaping circuits 11 p1884 A69-24735
- Hybrid matrix algorithm for electronic circuits analysis, showing applications to transistorized circuits 11 p1859 A69-24954
- Transient behavior of transistor UHF oscillator, discussing network analysis for oscillation amplitude calculation by nonlinear transistor equivalent circuit diagram 11 p1854 A69-25613
- Critical review of statements concerning previous paper on noise in transistor mixers at HF 11 p1857 A69-25662

Multivibrator circuit for generation of oscillations with frequency stability against transistor ambient temperature changes
12 p2036 A69-25919

Transistorized tachometer for rotational speed measurement and overspeed protection of automotive internal combustion engines
12 p2090 A69-26240

Integrated circuits, discussing development from transistors and vacuum tubes, operation, fabrication and applications
12 p2038 A69-26331

Transistorized LF-HF RC filters and current amplifiers design, exhibiting polynomial type characteristics
12 p2040 A69-26488

Thermal stability of complex transistorized structures determined by extending method of single heat source equivalence to several interacting sources
12 p2042 A69-26882

Time delay in temperature controlled transistorized time delay circuit determined by transistor unsteady thermal processes
12 p2043 A69-26883

Transient response of transistor in common emitter circuit using charge method taking into account base current switching pulse parameters
12 p2043 A69-26884

Common source and common gate FET connections showing equivalent noise figures
13 p2227 A69-27237

Cut-in and cut-out characteristics of fast acting composite transistor circuit, noting pulse duration
13 p2235 A69-28517

Transistor circuits analysis with aid of signal flow graphs
14 p2418 A69-28832

Transistorized circuit operation with nonlinear feedback through tunnel diode analyzed by piecewise-linear approximation of I-V characteristics
15 p2573 A69-30114

AM sinusoidal current pulse generator for semiconductor lasers, describing solid state circuit
15 p2633 A69-30235

Transistors and IC reliability for memory control evaluated by Concerto subprograms
15 p2627 A69-30842

Transistorized VOR system using electronic goniometer and fixed antennas, describing power supply, transmitter, goniometer, antenna and design
16 p2827 A69-31938

Transistorized L band oscillator tuned by Ga-doped YIG, discussing ferrimagnetic material properties and device equivalent circuit
16 p2761 A69-32450

Power supply circuits in spacecraft, DC voltage control systems, transistor and thyristor regulators and modulators, etc
17 p2937 A69-33582

Silicon MOS transistor characteristics, discussing stability, temperature effects and inherent noise, noting applications to amplifier circuits
18 p3109 A69-35161

Equivalent circuit demonstrating noise reduction through input transistor integration into passive receiving antenna, stressing circuit loss control and preamplification role
19 p3281 A69-35764

Transistorized amplifier stage noise factor dependence on parameters and modes of operation of transistors
20 p3505 A69-37460

Spark gap protection of input transistors in radio receivers against antenna-collected static charge damage
21 p3681 A69-38395

Tensor analysis of brushless DC motor controlled by transistors, discussing torque phase, torque variation phase and efficiency phase characteristics
24 p4255 A69-42678

TRANSISTOR LOGIC

FET memory element charge storage two layer model for thin film dielectrics noting charge/discharge times
10 p1742 A69-22947

NDC-1070 solid state computer design featuring TTL, MSI and hybrid circuits, offering memory capacity flexibility and rapid maintainability
17 p2933 A69-34060

Integrated TTL flip-flop circuits, describing functional principles of circuits with DC and capacitive coupling
24 p4287 A69-43130

TRANSISTORS

NT FIELD EFFECT TRANSISTORS
NT JUNCTION TRANSISTORS
NT SILICON TRANSISTORS

Planar transistor micromode operation during collector junction avalanche breakdown
01 p0047 A69-10884

Transistors vs electron tubes as microwave power sources in UHF phased array radars, noting transistor cost competitive limit
01 p0048 A69-11041

Graphical method for determining rise time of planar transistors with constant collector space-charge capacitance
01 p0049 A69-11362

Semiconductor center traps effect on characteristics of metal oxide semiconductor transistors
02 p0299 A69-12183

Current-voltage characteristics of avalanche transistors, noting impact ionization
02 p0218 A69-12266

Microwave transistor noise figure, power gain and noise measure as function of source admittance and source reflection coefficient in L and S bands
02 p0219 A69-12427

Planar transistor reliability test results noting failure rate, stability and effect of temperature
03 p0402 A69-13006

DC beta falloff in transistors at large collector currents measured, discussing relation to emitter crowding
04 p0574 A69-14347

Voltage variable resistor MOST, noting channel resistance controllability
04 p0574 A69-14351

Gamma radiation effects on transistors and diodes, discussing dosage and thermal changes within operational temperature range of germanium devices
05 p0728 A69-15695

Gain degradation under applied voltage and injection current during low dose gamma irradiation by Co-60 source for bipolar transistors
06 p0977 A69-16880

Temperature effects on primary photocurrent of base collector and collector substrate junctions of isolated transistors from microcircuits
06 p0977 A69-16881

Inverted transistor parameters required for accurate prediction of electrical and radiation storage time, discussing computer predictions of radiation responses
06 p0977 A69-16884

Neutron and X ray radiation effects upon gallium arsenide devices including Gunn oscillators, transistors, Schottky barrier diodes and optoelectronic pulse amplifiers
06 p0978 A69-16890

Transistor HF noise factor measurement by semiautomatic device with saturated diode comparison noise source heater current automatically controlled
07 p1090 A69-18292

VHF transistor power output capability, discussing limitation by RF saturation resistance and current crowding by large current densities and high frequencies
07 p1101 A69-18653

Computer aided design methods for electronics and logic systems, noting linear circuits and one dimensional transistors
08 p1278 A69-19970

Computer aided design program for testing equivalent circuits of bipolar transistors in static regime under various polarization conditions
08 p1280 A69-19972

Controlled charge models for computer calculation of electronic circuits, discussing tunnel diode static characteristics and equivalent transistor circuits
08 p1280 A69-19975

Distributed type bipolar transistor model construction, considering methods of development and computer tests for transient conditions
08 p1280 A69-19976

MOS transistor equivalent circuit for computer aided calculations with IMAG I program, noting versatility of model
08 p1280 A69-19978

Thermal feedback generation of 1/f-flicker noise in bipolar transistors, deriving formula for flicker noise voltage of emitter junction
08 p1283 A69-20129

Synthesis method for UHF transistor oscillators tunable in wideband using Y-matrices
08 p1285 A69-20380

Automatic transistor reliability testing system based on measured data and reliability research
08 p1294 A69-21119

Second breakdown mechanisms in transistors, describing electrical and physical characteristics and effects of design and structural defects on resistance to initiation
08 p1294 A69-21120

Microwave power and low noise transistors, noting continuous wave output and circuit design
09 p1462 A69-21407

Transistor large signal saturation time constant dependence on injection ratio, noting nonlinear response and saturation transistor switch storage time
09 p1464 A69-22117

Static characteristics of transistors dependence on current carriers surface recombination in inactive base region, noting strong electric field influence
09 p1464 A69-22287

Transistor thermal resistance determined from temperature dependent transistor parameter, noting measuring method insensitive to collector voltage variations
09 p1468 A69-22592

Silicon single crystal substrate, preoxidation, oxidation and low temperature heat treatment effects on MOS transistor compared with Silicon-Silicon dioxide interface characteristics
10 p1665 A69-24051

Minority carrier density in base region of uniform base transistor at arbitrary injection level, using two dimensional model
11 p1845 A69-24569

Avalanche transistor pulse circuits temperature increase due to power dissipation, noting effects of external resistance grounding base and pinch in
11 p1845 A69-24570

Planar transistor gain degradation under weak ionizing radiation, considering operating voltage and temperature conditions
11 p1848 A69-24874

Error analysis in conversion of two port scattering parameters used in microwave transistor characterization
11 p1852 A69-25200

Emitter current density dependence on distance from center of drift transistor circular emitter, obtaining distributed base resistance in presence of arbitrary base current
11 p1853 A69-25565

Planar transistor micromode operation during collector junction avalanche breakdown
12 p2041 A69-26648

Steady state small signal input impedance of low power planar transistor as function of temperature and operation mode
12 p2042 A69-26878

Collector supply voltage and base width effects on transistor amplification and frequency characteristics at microampere currents
12 p2042 A69-26879

Qualitative analysis of thermoelectric effects in transistors, describing heat absorption and release
12 p2042 A69-26880

Thermal stability of power transistor plates calculation using equivalent body with equivalent heat source at upper surface
12 p2042 A69-26881

Transient response of transistor in common emitter circuit using charge method taking into account base current switching pulse parameters
12 p2043 A69-26884

UHF transistor small signal internal behavior, using computer simulation for deriving current gain alpha locus, current gain and f sub T
13 p2227 A69-27241

Small signal quasi-stationary characteristics of pulse transistors including gain and input impedance calculations
13 p2227 A69-27423

Transistors scatter matrix parameters determined, describing measuring bench calibration system
14 p2420 A69-29393

Transistors transfer admittances measured indirectly, evaluating mean square error for transfer parameters
14 p2420 A69-29396

Transistor scatter and admittance differential parameters measurements graphically correlated
14 p2420 A69-29397

Planar bipolar transistors degradation under thermal and ionizing radiation stresses, analyzing surface recombination currents of silica films and silica-silicon interfaces
15 p2625 A69-30826

Unitary sorting influence on reliability of planar transistors subjected to irradiation recovery cycles and scaled stresses
15 p2626 A69-30834

High voltage thin film transistor, discussing design criteria, fabrication, I-V characteristics and switching speed
16 p2757 A69-31614

Second breakdown and other thermal instabilities analyzed by heat flow equation, obtaining stability criteria predicting reduced power dissipation for transistor at low currents
16 p2758 A69-31618

Transistor temperature and power limitations and thermal resistance calculation, discussing heat sink surface optimum design for power losses
16 p2760 A69-32047

Epoxy encapsulated transistors reliability, data from long term maximum rated life and accelerated tests
18 p3145 A69-34498

TRANSIT 4A SATELLITE

Statistical comparison of scintillation depths of Transit 4A satellite to radio star Cassiopeia A
07 p1215 A69-18821

TRANSIT SATELLITES

TRANSIT satellite navigation system for all-weather diurnal position fixing, noting Doppler frequency measurement and ionospheric signal refraction
01 p0112 A69-10457

Navy Navigation Satellite System TRANSIT providing all-weather continuous worldwide service for military and civil users
02 p0277 A69-11753

TRANSIT/Navy Navigation Satellite System/ military and commercial applications
02 p0278 A69-12359

Doppler measurements in semidynamical geodesy, processing data from Transit satellites collected at various Mediterranean ground stations
15 p2602 A69-31382

TRANSIT TIME

Base transit time of minority carriers in double diffused Si transistors with small emitter area, discussing cut-off frequency
02 p0297 A69-11995

Transit time and anomalous modes of oscillation in high pulsed power punch-through Si avalanche diode microwave oscillators
02 p0216 A69-12145

Miniaturized X band IMPATT microstrip power sources based on Si avalanche transit time diodes integrated with microstrip oscillator circuits
02 p0216 A69-12146

Nonisothermal space charge wave analysis of transit time mode oscillations in bulk GaAs, studying device reactance at given negative resistance
02 p0299 A69-12240

Transit time effects in Si n-nu-n space charge limited current solid state devices
03 p0483 A69-12852

Microwave generation and amplification, noting microwave transit time tubes, semiconductor devices and methods utilizing quantum electronic effects to generate and amplify EHF oscillations
03 p0395 A69-13611

Electromagnetic phase measurement for determining integrated air density near earth surface
04 p0598 A69-14910

Lunar laser ranging for testing Einstein and Brans-Dicke gravitational theories, discussing pulse transit time and dominant nonNewtonian correction
05 p0825 A69-16362

Large signal model for analysis of RF output and efficiency of IMPATT diode oscillator, noting frequency tuning
05 p0733 A69-16555

Si IMPATT diode oscillator and amplifier for CW operation at 50 GHz noting fabrication, performance and phase locking properties
05 p0733 A69-16560

Current and voltage waveforms of transit time, resonant domain and LSA modes of operation of transferred-electron oscillators
07 p1097 A69-18443

Oversized GaAs Gunn effect diodes operated in L and S bands at harmonics of fundamental transit time frequency with high power and efficiency
07 p1196 A69-18444

High peak power Gunn effect oscillators for low gigahertz frequencies in transit and nontransit time limited modes
07 p1097 A69-18447

Avalanche diode oscillators efficiency of continuous wave operation in transit time mode and high current multiresonant modes
07 p1098 A69-18456

High efficiency punch-through avalanche transit time diode for generating microwaves over three octaves
07 p1098 A69-18457

Frequency variation during oscillation pulse in avalanche transit time diodes, discussing related thermally dependent diode voltage rise
07 p1098 A69-18459

Epitaxial GaAs IMPATT diodes for generating CW X band power, noting high efficiencies and low noise characteristics
07 p1102 A69-18660

Frequency modulation of CW mm-wave IMPATT diode oscillator with wide band tunability and related harmonic generation effects
07 p1106 A69-19146

Microwave oscillator design employing avalanche transit time diodes
07 p1107 A69-19155

Noise generator design employing diffused Ge avalanche transit time diode
07 p1107 A69-19156

Frequency retuning characteristics of oscillator employing avalanche transit-time diode with complementary varactor subject to current or voltage variation
11 p1844 A69-24449

Instabilities related to particles transit time in system of two counterstreaming electron beams of finite length, noting wave dispersion
12 p2141 A69-27179

Large signal transit time effects in MOS transistor, noting drain current response
14 p2418 A69-28891

Transit time effects in silicon space charge limited diodes, studying frequency characteristics of small signal equivalent circuit
15 p2575 A69-30181

Computer model for avalanche transit time diode oscillator with single and double resonant circuit
15 p2577 A69-30615

Soviet book on avalanche transit time diodes and applications in microwave technology, describing p-n junction model, negative resistance, dynamic characteristics, synchronized oscillators, etc
16 p2761 A69-32109

Transit forecast of terrestrial satellite moving through fixed coordinate line in assigned reference
16 p2859 A69-32221

Si planar IMPATT diodes anomalous mode continuous wave UHF oscillations, noting DC density and DC/RF power conversion efficiency
17 p2934 A69-32846

Radio distance meter design for accurate distance measurement, discussing transit time and advantages over optical meters
18 p3139 A69-35493

Theorem extending results of techniques for analytical solutions of nonlinear ordinary differential equations applied to terrestrial brachistochrone problem
20 p3575 A69-37205

Delay in photoelectric recording of transit of stars, considering stellar image brightness distribution and temperature
20 p3608 A69-38053

STOL program in Northeast Corridor demonstrating significant city-to-city block time reduction by STOL transportation system [SAE PAPER 690420]
23 p4185 A69-61464

Air density determination using transit time method involving microwave phase measurements
24 p4313 A69-42898

TRANSITION

Metal-insulator transition, observability and transition in ionic lattices and polar liquids
03 p0489 A69-13922

TRANSITION FLOW

Natural convection boundary layer stability on heated isothermal vertical plane wall, discussing Grashof number as laminar to turbulent flow transition criterion
02 p0188 A69-12038

Monte Carlo direct simulation for treating rarefied supersonic flows about bodies in transitional regime between continuum and free molecular flow
02 p0189 A69-12523

Relaminarization of turbulent flow, studying velocity profiles at various axial cross sections in porous wall tube with fluid injection
04 p0586 A69-14409

Model kinetic integral equation for describing flow in transition region at leading edge of tapered body in rarefied gas
05 p0697 A69-16040

Electrodynamic gas flow in one dimensional approximation for transition through speed of sound, discussing flow parameters profile and dynamic efficiency
06 p0964 A69-17326

Laminar and turbulent regimes of flame propagation studied by blowing explosive gas mixture through porous wall, determining Reynolds number by hot-wire anemometer
06 p1034 A69-17626

Shock wave-boundary layer interaction configurations for hypersonic propulsion device inlets under transitional and turbulent conditions, noting heat transfer rate [AIAA PAPER 69-8]
06 p0915 A69-18172

Nonstationary flow past spheres and cylinders in electromagnetic shock tube, determining time required for flow to become stationary
07 p1119 A69-18744

Periodic pulling mechanism for explaining transition to turbulence in bounded plasma with weakly unstable drift modes
07 p1194 A69-19400

Region of transition from laminar to turbulent flow in meteor trains, suggesting electron attachment processes to molecular oxygen in presence of third body
08 p1393 A69-20608

Transition of hypersonic boundary layers on conical body using shock tunnel, obtaining surface heat transfer distributions [AIAA PAPER 68-39]
09 p1482 A69-21943

MHD boundary layer nonlinear instability, treating laminar to turbulent flow transition as reversible process
10 p1734 A69-23452

Shock induced boundary layer flow establishment on semiinfinite flat plate, measuring heat transfer rates and transition to turbulence
11 p1869 A69-24890

Kinetic theory for examining transition regime of rarefied gas dynamics, discussing Boltzmann equations and models with related boundary value problems
11 p1870 A69-25005

Reverse transition in two dimensional accelerated incompressible turbulent boundary layer flow, noting skin friction coefficient and turbulent intensity profiles
11 p1872 A69-25129

Criteria for reversion of turbulent to laminar flow (reverse transition)/ as special cases of Reynolds number criterion, noting boundary layer properties role
11 p1873 A69-25134

Aerodynamic effects of lift jet and lift fan inlets in transition flight, analyzing inlet momentum lift, inlet lip lift and drag [AIAA PAPER 68-637]
12 p2014 A69-26767

Laminar-turbulent transition in MHD channel in transverse and longitudinal magnetic fields, discussing Reynolds equation for large Hartmann numbers
13 p2307 A69-27500

Laminar to turbulence transition in submerged and bounded jets, using schlieren visualization for compressible flow and birefringent visualization for incompressible flow
14 p2428 A69-28876

Trailing shock wave position in air breathing jet engine channels, determining supersonic-subsonic boundary, noting Mach number effects on pressure ratio
16 p2768 A69-31743

Boundary layer over impulsively started flat plate, describing flow transition from unsteady / Rayleigh/ to steady / Blasius/ state by iterative methods
16 p2769 A69-31812

Distributed boundary layer suction effectiveness for controlling supersonic transitional flow separation
16 p2772 A69-32149

Linear amplification, nonlinear limiting and secondary instability induced by unsteady effects illustrated for various transitional flows, including roughness and streamwise vorticity
17 p2950 A69-33248

Static and impact pressure distributions for Mach number and velocity profiles of supersonic to subsonic flow transition in tube at low Reynolds numbers [ASME PAPER 69-APM-23]
18 p3120 A69-34397

Secondary vortex generation in near wake of circular cylinders under forced oscillation, analyzing motion dependent transition regimes using hydrogen bubbles flow visualization [AIAA PAPER 69-755]
18 p3084 A69-34411

Transient uniform flow over sphere at intermediate Reynolds numbers with recirculatory wakes, utilizing difference approximation to time dependent Navier-Stokes equations
18 p3120 A69-34434

Similarity solutions of viscous transonic equation describing spiral and radial flows, containing shock-like transitions of corresponding inviscid solutions
18 p3121 A69-34787

Gas dynamics in transition regime between continuum motion at high gas density and free particle motion at low density limit
19 p3300 A69-36658

Transition in near wake, from study of base pressure on circular cylinders in incompressible flow
19 p3242 A69-36809

External natural convection flows, studying laminar instability, transition and turbulence in boundary layer flow
20 p3633 A69-37718

Turbulence theory in laminar-turbulent flow transition, nonlinear stability for flows with Reynolds number higher than critical and fully developed turbulence
23 p4152 A69-42313

Transition from axisymmetric to nonaxisymmetric flow in rotating annulus, using two layer quasi-geostrophic model
24 p4345 A69-43150

Solution stability and secondary solutions growth beyond critical points investigation for Burgers equations for laminar-turbulent transition
24 p4302 A69-43360

Natural convection local heat transfer on constant heat flux inclined surfaces for water and air in laminar, transition and turbulent regimes
[ASME PAPER 69-HT-C] 24 p4410 A69-43526

Natural convection flow, discussing initial instability of laminar flow, disturbance amplification and transition to turbulent flow
[ASME PAPER 69-HT-29] 24 p4411 A69-43531

Heat transfer and fluid friction of hydrogen and helium gas flows undergoing turbulent to laminar flow transition in heated pipe
[ASME PAPER 69-HT-54] 24 p4303 A69-43539

Transition from turbulent to laminar regime as consequence of high heating rates for internal convective flow, noting roles of Nusselt numbers and friction factors
[ASME PAPER 69-HT-9] 24 p4304 A69-43559

Electron density fluctuations in transition region of turbulent plasma jet, noting spiky waveform
[AIAA PAPER 68-685] 24 p4360 A69-43697

TRANSITION LAYERS

French solar research program, emphasizing protosphere-chromosphere transition zone
02 p0316 A69-11905

Plasmapause and relation to ion composition in topside ionosphere, using Bohm coefficient for turbulent diffusion
02 p0246 A69-12741

TRANSITION METALS

NT CADMIUM

NT CADMIUM ISOTOPES

NT CHROMIUM

NT COBALT

NT COBALT ISOTOPES

NT COBALT 60

NT COPPER

NT GOLD

NT HAFNIUM

NT IRIIDIUM

NT IRON

NT IRON ISOTOPES

NT MANGANESE

NT MANGANESE ISOTOPES

NT MERCURY [METAL]

NT MERCURY VAPOR

NT MOLYBDENUM

NT NICKEL

NT NIOBIUM

NT OSMIUM

NT PALLADIUM

NT PLATINUM

NT REFRACTORY METALS

NT RHENIUM

NT RHODIUM

NT RUTHENIUM

NT SCANDIUM

NT SCANDIUM ISOTOPES

NT SILVER

NT TANTALUM

NT TITANIUM

NT TUNGSTEN

NT VANADIUM

NT YTTRIUM

NT ZINC

NT ZIRCONIUM

NT ZIRCONIUM ISOTOPES

NT ZIRCONIUM 95

Vacuum distillation technique for isolation and recovery of alkali metal reaction products with Ta, Ni, V and oxygen
01 p0083 A69-10927

Monocarbide phases high temperature vaporization from open metal surfaces into vacuum, obtaining temperature dependence
02 p0260 A69-11583

Point defects in body centered cubic transition metals, discussing thermal equilibrium, irradiation cold work, high and low temperature recovery, etc
03 p0447 A69-13817

Absorption and IR emission of nickel and cobalt doped alkali halides
03 p0490 A69-13941

Vacuum carburization of surface layers of transition metals
04 p0614 A69-14572

Components relationships in binary phase diagrams of III a and VI a transition metals on basis of electronic structure
08 p1331 A69-20191

Earth crust transition elements distribution and abundance compared to rare earths
08 p1310 A69-20943

V phase structure and V and E phase lattice constants for ternary systems /Ti, Zr, Nb or Ta-/Ni, Co or Fe-/Si or Ge/
10 p1708 A69-22992

Order-disorder transformations in nickel alloys under loading operations
11 p1904 A69-24706

Covalence degree of activator-ligand chemical bonds effect on spectroscopic properties of transition metals
11 p1907 A69-25031

Transition metal interstitial compounds thin film preparation and superconducting properties, emphasizing high critical temperature, rock salt structure and NbN base
13 p2321 A69-28009

Vacuum carburization of surface layers of transition metals
15 p2638 A69-30273

Atomic size and outer electron effect on Fe, Co and Mn polymorphism, noting change in crystal lattices
15 p2638 A69-30321

Monograph on vanadium selenides and tellurides with NiAs structure covering existence regions, superstructures and equiatomic compounds from viewpoint of thermodynamics
15 p2667 A69-30602

Ti transition metals alloys omega phase precipitation, discussing composition, morphology, coherency, formation, etc
19 p3344 A69-35928

Titanium strengthened high strength hot-rolled steels, discussing cooling rates leading to complete ferrite phase transformation
21 p3743 A69-38652

K-alpha band characteristics of N spectra stimulated in nitrides of transition metals by X rays
22 p3974 A69-41118

TRANSITION POINTS

Nitriding effect on heat resistance and transition temperature of molybdenum alloys
01 p0093 A69-10212

Irradiation influence on chromium transition temperature explained by defect clusters and embrittling impurity redistribution
01 p0095 A69-10604

Low stress fracture criteria for large elastic structures and small brittle laboratory specimens below transition temperature
01 p0169 A69-10768

Vanadium dioxide reflection spectra dependence on incident quantum energies during semiconductor/metal phase transition
02 p0298 A69-12100

Ferroelectric transition of barium titanates doped in OH or oxygen vacancies, using pyroelectric method
03 p0491 A69-14059

Transition temperature from brittle to plastic state of W-Mo alloys in recrystallized state, noting increased Mo content effect
05 p0783 A69-16809

Model for phase transition mechanism quantum-Coulomb plasmas, finding transition temperature for white dwarfs
06 p0968 A69-17785

Magnetic field distribution and resistance of homogeneous type 2 superconductor cylinder at transition under effect of axial current
08 p1371 A69-20202

Ductile to brittle transition shown in tensile stress-strain curves of polycrystalline body centered cubic and hexagonal close packed materials
10 p1795 A69-23063

Dissolved gases and carbon effect on transition temperature from plastic to brittle state of high melting metals including niobium and vanadium
10 p1715 A69-24011

Tungsten vacuum-arc melted samples in deformed and recrystallized conditions, studying mechanical properties at temperatures near ductile to brittle transition
15 p2637 A69-30267

Nitriding effect on heat resistance and transition temperature of molybdenum alloys
15 p2637 A69-30268

Atomic beam for H maser operation prepared by using nonadiabatically changing magnetic field in transition region
15 p2635 A69-31103

Cylindrical viscous jet transition points from stable to unstable modes of oscillation found same as for inviscid jet
16 p2773 A69-32570

Ta type I and II wire resistance in transverse magnetic field during superconducting to normal transition, discussing strain and impurity effects
17 p3016 A69-33791

Kinetics of titanium oxidation in transitional range at high temperatures, showing agreement with oxidation model
18 p3157 A69-35252

Space transitions identified with asymptotic solutions at system field equations transition points
19 p3445 A69-36811

Transition temperature depression in rotating liquid He based on increased inertial density of excitations
23 p4192 A69-42335

Inverse transition from turbulent to laminar flow in radial diffusers, noting nonagreement of transition point prediction methods
[ASME PAPER 69-HT-33] 24 p4247 A69-43530

Helix to coil transition for triple stranded macromolecule in solution, calculating ring weighting and partition functions and intact bonds
24 p4353 A69-43812

TRANSITION PROBABILITIES

Transition probabilities for collinear collision of particle with harmonic oscillator, noting reasons for discrepancy in Jackson and Mott form
01 p0124 A69-10688

Ar atom transition probabilities in 5000-6000 angstrom range, noting effect of nonuniform source temperature
01 p0125 A69-10963

Solar copper abundance determined from measuring Cu 1 and 2 and resonance lines transition probabilities in electric arc emission under LTE conditions
02 p0204 A69-11456

Atomic transition probabilities, discussing improvement attributed to wider interest in space science, astrophysics, plasma physics and research technique developments
03 p0471 A69-13169

Electron transition probability of oxygen molecule determined using weak bands telluric lines photoelectric recordings
03 p0420 A69-13276

Transition probability measurement of 5577 A auroral green line of oxygen used to investigate quadrupole nature of transition
03 p0424 A69-13936

Thermodynamic approach to calculation of molecular lasers, determining various population levels of carbon dioxide molecule by measuring amplification factors for rotational vibrational transitions
06 p0934 A69-17465

Population inversion of vibrational levels due to molecular collisions in carbon dioxide lasers, calculating transition probabilities, laser parameters and gain profile
[IEEE PAPER G-15] 07 p1151 A69-19061

Rotational inelastic transitions in atom-diatom collisions, discussing restricted distorted-wave approximation, transition probabilities, impact parameters, inelastic and glory quenching, etc
07 p1185 A69-19302

Molecule reorientation and transition probability in molecular beam maser using formaldehyde
07 p1158 A69-19760

Hartree-Fock calculations of coronal forbidden transition lines in Ar I isoelectronic sequence, obtaining wavelengths, magnetic dipole and electric quadrupole transition probabilities
08 p1385 A69-20071

Oscillator strengths of transitions in shock tube between nitric oxide Rydberg states in near IR
08 p1354 A69-20150

Transition probabilities in repetitively Q modulated HCN maser radiation dependent on gas discharge current
09 p1516 A69-21626

Iterative algorithm to determine transition probability final distribution in Markov extremal systems
11 p1861 A69-25712

Forbidden solar corona lines transition probability in vacuum UV region
12 p2157 A69-26334

Beam-foil technique for measuring radiative lifetimes of excited electronic states in ionic species of O, including transition probabilities
13 p2301 A69-27452

Relative transition probabilities for visible Si atom lines, noting disagreement with LS coupling predictions and solar Si abundance determination
13 p2340 A69-27580

Homogeneous finite automaton asymptotic analysis, calculating series terms for matrix transition probability function
13 p2239 A69-28535

Electron transition probability of oxygen molecule determined using weak bands telluric lines photoelectric recordings
14 p2487 A69-28784

Forbidden transition probabilities of solar corona lines in vacuum UV range
14 p2519 A69-29355

Radiative decay of polyatomic molecules, applying Green function form for transition probability to decay of manifold of closely spaced coupled levels
14 p2488 A69-29924

Transition probabilities for radiative lifetime of Swan and Mulliken diatomic C bands calculated from lifetime data using Franck-Condon factors
15 p2694 A69-30789

Transition probabilities of spectral lines in helium-like ions estimated from hydrogen magnetic dipole transitions, discussing single photon decay
15 p2695 A69-30892

Electron excitation and phase shift method for radiative lifetimes of Ar II UV transitions
15 p2656 A69-31034

Oscillator strengths calculated for transitions in Si III using dipole length and velocity matrix elements, comparing many electron correlation problem approximations
15 p2656 A69-31158

Transition probability for 5577 Å auroral green line determined from measuring number density of O atoms in oxygen-helium discharge and emitted line intensity
16 p2781 A69-32319

Field ionization at metal surfaces as rearrangement collision, considering anisotropic electron tunneling probabilities produced by Fermi surface
17 p3015 A69-32821

Beam foil technique to measure energy transition levels radiative lifetime for nitrogen ions
17 p3009 A69-34154

Shock tube application to transition probability measurements with emphasis on thermodynamic state of radiating gas, noting temperature dependence of level population
18 p3176 A69-34446

Transition probabilities of N I far UV multiplets, comparing experimental and theoretical results
18 p3178 A69-35413

Spectral lines due to magnetic dipole transitions in fine structure levels in collisionally excited neutral H clouds, discussing theoretical difficulties in interpretation
19 p3379 A69-36225

Forbidden emission transition probabilities in high excitation symbiotic stars, novae, Cygni stars and peculiar binaries
19 p3423 A69-36227

Perceptron probability algorithm for random events prediction based on previous histories, applying Bayes formulas, static solutions formulas and transition probability tables and graphs
19 p3287 A69-36664

Thermodynamic approach to calculation of molecular lasers, determining various population levels of carbon dioxide molecule by measuring amplification factors for rotational vibrational transitions
20 p3555 A69-37948

Helium sequence ions spin forbidden transitions electric dipole oscillator strengths and transition probabilities evaluated by variational procedure
20 p3577 A69-38171

Upper atmosphere emission processes, comparing emission quenching lifetime with transition probability rates, plotting atomic and molecular states
21 p3711 A69-38513

Thermally insensitive technique for atomic transition probability measurement
22 p3983 A69-40100

Hydrogen high level transition probabilities formula, giving two tables of oscillator strengths [AFCRL-69-0301]
22 p3983 A69-40149

Stueckelberg formulation for transition probabilities to interpret perturbation effects in elastic scattering differential cross section measurements
22 p3987 A69-41005

Stellar neutrino energy loss due to electron-electron neutrino bremsstrahlung in nondegenerate gas determined from transition probability for charged baryons or leptons interaction
24 p4351 A69-42794

TRANSITS

NT CINETHEODOLITES
NT THEODOLITES

Large signal avalanche diode oscillators parameter effect on operating characteristics at any transit angle
07 p1098 A69-18458

Bright fundamental stars right ascensions observed in Chile, discussing instruments, declination range, systematic errors, etc
10 p1777 A69-23388

Transit instruments operational principles and practical experience
15 p2608 A69-30440

Satellites meridian and extrameridian observations by transit instrument, examining errors in ephemerides of bulletins
16 p2858 A69-32211

TRANSLATING

U MACHINE TRANSLATION

TRANSLATIONAL MOTION

NT SECONDARY FLOW
NT THREE DIMENSIONAL FLOW
NT THREE DIMENSIONAL MOTION

Ellipsoidal satellite translational rotational motion under spherical planet and point source sun gravitational fields influence, obtaining approximate solution for three body problem
11 p1956 A69-24399

Optimum controller design for dynamic stability of ideal incompressible fluid in cavity of body constrained to horizontal rectilinear translational motions
11 p1966 A69-25330

Steady rectilinear translational motion of circular disk-shaped slightly bent wings near solid wall in incompressible fluid medium in absence of vortices and external forces
15 p2547 A69-30583

Pressure in sealing groove and increase time due to pumping action of moving wall applied to force cylinder of translational motion, considering liquid in groove laminar
16 p2736 A69-32135

Screw-nut feeder and adjustor systems with compensation for clearance and wear of cutting tools, determining efficiency for conversion of rotary to translational motion
23 p4168 A69-41414

Nonlinear longitudinal dynamics of lifting orbital vehicle in near circular orbit, considering translational motion components effecting orbital decay or dilatation [AAS PAPER 69-244]
24 p4392 A69-42857

Ellipsoidal satellite translational rotational motion under spherical planet and point source sun gravitational fields influence, obtaining approximate solution for three body problem
24 p4390 A69-43789

TRANSLUNAR SPACE

U INTERPLANETARY SPACE

TRANSMISSION

NT ACOUSTIC ATTENUATION
NT AERODYNAMIC HEAT TRANSFER
NT AUTOMATIC PICTURE TRANSMISSION
NT CONDUCTIVE HEAT TRANSFER
NT CONVECTIVE HEAT TRANSFER
NT DATA TRANSMISSION
NT DIFFRACTION PROPAGATION
NT DOUBLE SIDEBAND TRANSMISSION
NT ELECTRIC POWER TRANSMISSION
NT ELECTROMAGNETIC WAVE TRANSMISSION

NT FREQUENCY DIVISION MULTIPLEXING
NT GROUND WAVE PROPAGATION
NT HEAT TRANSFER
NT HEAT TRANSMISSION
NT HYPERSONIC HEAT TRANSFER
NT IONOSPHERIC F-SCATTER PROPAGATION

NT IONOSPHERIC PROPAGATION
NT LAMINAR HEAT TRANSFER
NT LIGHT SCATTERING
NT LIGHT TRANSMISSION
NT MANDELSTAM REPRESENTATION
NT MICROWAVE ATTENUATION
NT MICROWAVE TRANSMISSION
NT MULTIPATH TRANSMISSION
NT MULTIPLEXING
NT RADAR ATTENUATION
NT RADAR TRANSMISSION
NT RADIATIVE HEAT TRANSFER
NT RADIO ATTENUATION
NT RADIO TRANSMISSION
NT SATELLITE TRANSMISSION
NT SCATTER PROPAGATION
NT SHOCK WAVE ATTENUATION
NT SHOCK WAVE PROPAGATION
NT SHORT WAVE RADIO TRANSMISSION
NT SIGNAL REFLECTION
NT SINGLE SIDEBAND TRANSMISSION
NT SOUND TRANSMISSION
NT STRESS PROPAGATION
NT SUPERSONIC HEAT TRANSFER
NT TELEPHONY
NT TELEVISION TRANSMISSION
NT TIME DIVISION MULTIPLEXING
NT TRANSEQUATORIAL PROPAGATION
NT TURBULENT HEAT TRANSFER
NT WAVE ATTENUATION
NT WAVE DISPERSION
NT WAVE PROPAGATION

Boundary conditions for reflection and transmission properties of absorbing shell of arbitrary shape
08 p1273 A69-20025

Monograph on transmission characteristics of mechanical vibration transducers covering frequency response operators and analog computer simulation
16 p2789 A69-31842

TRANSMISSION CIRCUITS

Pulsed subharmonic oscillation in nonlinear regenerative selective circuits with reference to graph-analytical method for explaining behavior
03 p0385 A69-12918

Data transmission on common communication circuits, noting circuit characteristics, limitations on performance and future digital service
04 p0559 A69-15207

Passive four terminal elements series connection transmission characteristics, considering line losses
05 p0729 A69-16081

Spectral distribution of intermodulation noise of AM and FM transmission systems calculated by probability theory
08 p1271 A69-19916

Microelectronic data and remote control function transmission system for wind tunnel testing of aircraft dynamic response to gusts and turbulence
10 p1672 A69-23283

TRANSMISSION EFFICIENCY

Pulse shape influence on electromagnetic compatibility and transmitter efficiency, discussing trapezoidal, raised-sine, sliced and complete error rate function shapes
01 p0030 A69-10631

Sequential signal design for feedback channels, emphasizing single set subject to peak and average power constraints in time continuous transmission
03 p0408 A69-12868

Molecular O 0.7620 micron absorption band in pure O and air, noting rotational lines mean half width and lower atmosphere transmission function
03 p0458 A69-13272

Satellite TV transmitter power requirements for adequate direct broadcasting field strength in existing UHF TV bands
03 p0394 A69-13578

Propagation tests of skywave field strength reduction by orthogonal transmission
03 p0395 A69-13597

Mutual coupling and element efficiency for infinite linear arrays of dipoles
04 p0571 A69-14317

Passive four terminal elements series connection transmission characteristics, considering line losses
05 p0729 A69-16081

Adaptive control of reflective satellite communication system
06 p0887 A69-17356

High transmittance long fiber optics, presenting data on special transmission as function of temperature
06 p0958 A69-17677

Block coding for transmitting across noisy binary symmetric channel accompanied by noiseless delayless feedback channel
06 p0891 A69-17864

- Beam modulation resynchronization at large signal levels by TWT circuit wave to enhance efficiency
07 p1094 A69-18423
- C band waveguide window for average power transmission featuring relatively small biconcave dielectric disk
07 p1096 A69-18435
- Communication satellite power utilization optimized by matching final amplifiers to solar cell array
[AIAA PAPER 68-437] 09 p1442 A69-21990
- Optimum time interval for constant data transmission rate during single pass of satellite over ground station
09 p1457 A69-22462
- Optimum selection of modulation indices for multitone phase modulation by graphical method, noting tolerance insensitivity
09 p1457 A69-22463
- Power transmission efficiency between arbitrarily focused circular antennas with Gaussian amplitude illumination in Fresnel region for various phase illuminations and Fresnel numbers
11 p1851 A69-24991
- TEM-DUAL surface wave propagation in coaxial cable with stratified dielectric structure to reduce attenuation calculated by addition theorem to Bessel functions
11 p1856 A69-25659
- Molecular O 0.7620 micron absorption band in pure O and air, noting rotational lines mean half width and lower atmosphere transmission function
14 p2487 A69-28780
- Optimum time for telemetry data transmission by system using feedback combined with error correcting codes
14 p2412 A69-29428
- Spherical plate electrostatic analyzer transmission characteristics, emphasizing angular response to external particle sources as functions of angular coordinates and particle energy
14 p2449 A69-29560
- Numerical method based on thin film optics to determine ionospheric electromagnetic transmission and reflection coefficients for vertical incidence
16 p2752 A69-32392
- Prestressed ceramic driver chamber energy efficiency for arc driven shock tube by pressure measurements with piezoelectric probe
18 p3116 A69-34456
- Smooth multiwave waveguide junctions design ensuring minimum losses of fundamental wave
23 p4125 A69-42046
- Deep space communication capability projection, considering data volume and rate, channel frequency, large apertures, data enhancement and system losses
23 p4129 A69-42507
- TRANSMISSION LINES**
- NT BEAM WAVEGUIDES
- NT COAXIAL CABLES
- NT COMMUNICATION CABLES
- NT FLUID TRANSMISSION LINES
- NT PLASMA GUIDES
- NT POWER LINES
- NT WAVEGUIDES
- Electromagnetic wave propagation in superconductors, noting transmission line structure variation with magnetic fields and current and suitability for parametric amplifiers
01 p0135 A69-10176
- Microstrip transmission line integrated circuits on semiinsulating GaAs substrates, showing feasibility at millimeter wave frequencies
01 p0040 A69-10197
- Multistub filter for microstripline using shorted and open stubs
01 p0041 A69-10200
- Dielectric surface coatings effect on transmission and loss properties of silicon-microstrip microwave transmission lines
01 p0041 A69-10201
- Regenerative digital transmission system error, representing memory of binary regenerative channel with Markov model
01 p0027 A69-10249
- Transversal filters for equalization of data channels with pulse amplitude modulation, discussing pulse equalizability and convergence criteria for iterative search routine
01 p0027 A69-10251
- Uniform transmission line response to independent distributed sources using extraction integrals, analyzing traveling wave transistor
01 p0043 A69-10562
- Divergent-convergent and convergent-divergent cascaded exponential lines, determining equivalent length of uniform transmission line
01 p0044 A69-10623
- Microstrip-like transmission lines analyzed by method based on line capacitance variational calculation and charge density distribution
01 p0044 A69-10625
- Pulsed nitrogen laser design involving gas discharge tube fed by low impedance parallel plate transmission line
01 p0091 A69-10842
- Green function for linear antennas in warm plasma fed by coaxial air filled transmission line, computing current distribution and input admittance
02 p0215 A69-11942
- Geomagnetic micropulsations mechanism, discussing hydromagnetic waves transmission generated by interface instability between solar wind and magnetosphere, noting transmission path role
02 p0244 A69-12395
- Geomagnetic micropulsation theory, discussing mechanisms responsible for amplitude spectrum at earth surface and power spectral density
02 p0244 A69-12396
- Electromagnetic wave propagation and amplification in periodic structures, including travel wave and parametric amplifiers, reactance diodes, lasers and quantum amplification
03 p0396 A69-13701
- Lossy transmission line filters and wideband impedance matching
03 p0406 A69-13906
- Dispersion relations for propagation of quasi-TEM mode and higher order symmetric modes in longitudinally magnetized ferrite filled coaxial waveguide
04 p0575 A69-14751
- Lossless multiple beam forming device operational principles, noting parallel plate radial transmission line network construction
04 p0576 A69-14768
- Quasi-optical transmission line composed of nonideal correctors /lenses or mirrors/
05 p0717 A69-15637
- Holograms applied to analysis of wave packets propagating in quasi-optical transmission lines
05 p0718 A69-15650
- Gunn effect theory, discussing dynamic characteristics and domain propagation for inhomogeneous transmission line profile
05 p0807 A69-15821
- Fluidic systems with long lines simulated by transmission lines of OR/NOR oscillator
[ASME PAPER 68-WA/AUT-12] 05 p0706 A69-16178
- Surface waveguide composed of inhomogeneous dielectric thin film used as low loss transmission line
05 p0731 A69-16294
- Quasi-optical transmission lines having composite correction devices with/without phasing devices
05 p0723 A69-16784
- Broadband hybrid junction of parallel transmission lines application to four diode star mixer/modulator
06 p0896 A69-17485
- Nonlinear lumped parameter model for long gas filled pressure sensing lines covering steady state, laminar or turbulent gas flow
[AIAA PAPER 69-117] 06 p0913 A69-18106
- Frequency-stable tunnel diode oscillator loaded with transmission line
07 p1104 A69-18890
- Surface effects at interface between linear and nonlinear media representing transmission lines of low pass filter type
07 p1088 A69-19755
- Shunted resonators on transmission line with asymmetrical response offering selectivity from resonance frequency standpoint
08 p1271 A69-19917
- Long transmitting dipole antenna, studying current and charge distributions by Wiener-Hopf technique
08 p1281 A69-20019
- Ultrahigh speed systems and logic circuits specifications implementation into electrical design, discussing circuit selection, line propagation delays, noise margins and temperature effects
[AGARDOGRAPH-114] 08 p1298 A69-20985
- RF voltage breakdown in air for 50 ohm coaxial transmission line configuration
[JPL-TR-32-1379] 09 p1470 A69-22790
- Second order system equations to approximate transfer function of homogeneous pneumatic instrumentation line terminated with pressure transducer
10 p1692 A69-23267
- Lumped element line generators for high power pulsed sinusoidal oscillations utilizing recurrent triggering system, noting use in plasma physics experiments
10 p1662 A69-23344
- Transmission line analogs and kinetic power theorems for space charge waves amplification in semiconductors, considering internal effect and wave excitation
10 p1748 A69-24052
- Load admittance effect on low pass voltage transfer characteristics of RC lines, analyzing shaped lines at open circuit under terminated conditions
11 p1859 A69-24939
- Log periodic dipole array antennas simulated with simple RLC circuit loading uniform transmission line
11 p1850 A69-24977
- Phototelegraphic transmission of holograms of objects in many shades through channel with limited number of signal levels
11 p1889 A69-25549
- Subtraction procedure for feedpoint singularity in current on axially symmetric antenna with slice generator
12 p2041 A69-26864
- Microwave propagation in coupled pairs of microstrip transmission lines for integrated circuit design, discussing dielectric Green function
13 p2229 A69-27672
- Finite difference solution to TEM mode transmission line cross section for defining continuous potential function leading to capacitance upper bound
13 p2221 A69-28064
- Transmission line all pass equalizers theory and design for operation in TEM, TE or TM modes
13 p2233 A69-28065
- Characteristic impedance determination for transmission lines cascades terminated by resistor using recurrent relations, discussing reflection coefficient
13 p2221 A69-28074
- Impedance eigenvalues for eigenmodes of multiconductor transmission lines, discussing transverse field distributions along conical line
14 p2423 A69-29756
- Capacitors pi network representation of series gap in center conductor of matched coaxial transmission line
14 p2424 A69-29766
- Microwave strip transmission line, discussing evolutionary improvements, computerized design, materials, semiconductors, packaging, reliability, etc
15 p2721 A69-31074
- Approximate solution for coupled microstrip transmission lines in integrated circuits, discussing impedance, capacitance and testing
15 p2580 A69-31078
- Coupled TEM lines arrays analysis in terms of odd and even modes, computing equivalent circuit elements, impedances and admittances
15 p2581 A69-31525
- Dispersion characteristics of open interdigital line structure by treating structure as radiator, applying linear antenna theory
16 p2748 A69-31580
- Linearly tapered transmission line equation and transfer matrix parameters, considering input impedances and microwave application
16 p2749 A69-31582
- Equal ripple nonuniform tapered line coupler design and computed performance by evaluating cascade matrix as function of frequency
16 p2760 A69-31944
- Disk and transmission line microstrip resonators radiation, measuring fractional amount of radiated power
16 p2760 A69-31946
- Quasi-optical transmission line composed of nonideal correctors /lenses or mirrors/
16 p2754 A69-32495
- Holograms applied to analysis of wave packets propagating in quasi-optical transmission lines
16 p2754 A69-32507
- Slow electromagnetic wave propagation in superconducting thin film transmission lines, noting phase velocity dependence on film thickness and spacing
17 p2938 A69-33785
- Pulses and sine waves coupling between parallel transmission lines obtained using Oliver elementary coupling theory
19 p3266 A69-35768
- Plane screen electrical shielding effectiveness calculation, using incident wave impedances associated with current loop and magnetic dipoles in transmission line equations
19 p3267 A69-35932

Analysis and synthesis of distributed transmission line networks with open or short circuited shunts or series stubs, describing composite transfer matrices
21 p3687 A69-39660

Quadrupole network transfer matrix calculation from known octupole matrix, describing frequency response determination of coupled transmission lines
22 p3912 A69-40257

Nonlinear lumped parameter model for long gas filled pressure sensing lines covering steady state, laminar or turbulent gas flow
[AIAA PAPER 69-117] 24 p4301 A69-43259

Small signal amplitude/frequency response or transfer gain of volume-terminated pneumatic lines with circular and rectangular cross sections
24 p4301 A69-43288

TRANSMISSION LOSS

Lossy and lossless fluidic transmission line theory to estimate downstream conditions having known upstream system
01 p0012 A69-10153

GaAs injection laser transmission losses and threshold current density under influence of external optical coupling with spherical mirror
02 p0260 A69-12687

Lossy transmission line filters and wideband impedance matching
03 p0406 A69-13906

Feed support blockage loss in parabolic antennas evaluated by shadowgraph photography
04 p0576 A69-14771

Passive four terminal elements series connection transmission characteristics, considering line losses
05 p0729 A69-16081

Microwave absorption and series resistance of silicon mesa parametric amplifier diodes, discussing p-n junction and dielectric loss mechanism
05 p0732 A69-16347

Transmission and reflection coefficients of cylindrical tubes moving in free molecular gas flow determined by Monte Carlo method
06 p0911 A69-17877

Closed loop and electronically calibrated radome measurement systems for beam deflection, boresight shift and transmission loss measurements
07 p1109 A69-19517

Phase shift and losses in wave propagation in dielectric environment, defining power transmission coefficient and insertion phase shift
07 p1087 A69-19518

Algorithm for mean energy transmission coefficient of fundamental mode in beam guide with given inhomogeneities, discussing mode conversions
09 p1469 A69-22629

Microwave frequency room temperature acoustic surface wave propagation losses in lithium niobate measured by laser light deflection, discussing propagation and insertion losses
10 p1703 A69-23511

Millimeter and submillimeter radio waves attenuation in rain, showing effective loss cross section as function of raindrop diameter and wavelength
10 p1657 A69-23943

Mean losses in quasi-optical communication lines due to random irregularities in performance of waveguide phase correctors connected in series, noting random phase aberrations effect
10 p1658 A69-23954

Calculation method for electromagnetic wave supplementary attenuation due to auroral absorption for distances up to 4000 km
11 p1841 A69-25760

Microwave directional filter using ring resonator and couplers to obtain low transmission loss and center frequency tuning
13 p2226 A69-27187

Transmission line all pass equalizers theory and design for operation in TEM, TE or TM modes
13 p2233 A69-28065

Iris beam waveguide transmission loss as function of irises alignment, iris frame width and guide axis curvature
13 p2233 A69-28070

Wave propagation and bandwidth characteristics of rectangular waveguide loaded with H plane lossless dielectric slab
13 p2222 A69-28075

Waveguide feeder for Goonhilly Downs satellite communication antenna reducing feeder loss for use with low elevation Intelsat 3 satellite
17 p2935 A69-32849

Secondary losses in flat large scale turbine lattice attributed to LF pulsating flow separation on back of blade
21 p3645 A69-39717

Performance prediction of terrestrial communication system based on experimental radio and meteorological program at 11 GHz, discussing transmission loss
22 p3900 A69-40680

Radar detection performance evaluation procedures based on integration, collapsing and fluctuation losses estimates for swirling target models and partially correlated targets
23 p4132 A69-42547

TRANSMISSIVITY

Low field helicon wave transmission through n-type Ge at liquid He temperature, noting cyclotron resonance damping
02 p0295 A69-11787

Transmission coefficient of double frequency regenerative parametric amplifier described by scattering matrices
06 p0895 A69-17456

Transmission coefficient of plane electromagnetic wave obliquely incident on perforated metal screen in frequency range near primary resonance of structure
07 p1076 A69-18527

High altitude radiant emittance of cirrus clouds and cloudless sky for IR transmissivity based on aircraft measurements
09 p1536 A69-21641

Rapidly convergent series expansions for plane wave transmission coefficients for elliptical and rectangular apertures
11 p1837 A69-25001

Waveguide cross connection of right-angled waveguides to determine reflection and transmission factors for incidence of H waves
11 p1855 A69-25623

TRANSMITTANCE

E field transmission and reflection coefficients in linearly tapered waveguide for fundamental and higher order modes, using point matching method
01 p0044 A69-10629

Statistical band model and line by line calculations of transmittance for IR bands in absorption spectra of ozone and water vapor
[AFCRL-68-0505] 01 p0124 A69-10919

Hologram film nonlinearity effect in recording diffusely illuminated objects analyzed by means of amplitude transmittance
03 p0431 A69-13958

Transmittance and absorption cross sections of carbon particles suspended in flowing stream of nitrogen gas
06 p1034 A69-17804

Transmission coefficient of plane electromagnetic wave obliquely incident on perforated metal screen in frequency range near primary resonance of structure
07 p1076 A69-18527

Argon plasma characteristics calculated from 8 mm interferometer data, interpreting transmission coefficients of dielectric film with permittivity gradient
07 p1194 A69-19324

Complex transmission and reflection coefficients of dielectric film with permittivity gradient computed by modified Runge-Kutta method, noting plasma diagnostics application
07 p1194 A69-19334

Complex microwave transmission coefficient of nominal cut-off plasma for several different types of electron distribution, noting discharge characteristics for cut-off
08 p1366 A69-20759

Optical characteristics of Martian atmosphere from photometric data for continent-mare contrasts, discussing transmittance and optical thickness
11 p1959 A69-24727

Power spectrum of object flux transmittance using Fourier transform type holographic system compared to systems similar to correlator
12 p2090 A69-26254

Nonlinear holograms distortions analyzed by five point method utilizing relation between irradiance and amplitude transmittance of photographic emulsion
12 p2090 A69-26255

Atmosphere effects on solar IR spectra, discussing role of absorbing molecule distribution in transmittance calculations
13 p2341 A69-27589

IR spectral transmittance and physicochemical properties of tellurite glasses with vanadium and cerium oxides, showing polymer chains in structure
14 p2468 A69-29329

Cotton leaves reflectivity and transmittance measurements, discussing substrate salinity effects on internal structure of hydroponically grown plants
15 p2558 A69-30456

Spatial and energy characteristics of laser with nonuniform transmittance across resonator mirrors, analyzing transverse modes interaction
15 p2634 A69-30962

Antimony trisulfide natural light reflection and transmission in and near IR region, noting spectral temperature and time dependence peculiarities
19 p3384 A69-36481

Spectral transmittance of mixture of carbon monoxide and nitrous oxide for overlapping absorption bands
[AIAA PAPER 67-600] 21 p3819 A69-39013

TRANSMITTER RECEIVERS

Transmit-receive device noise contribution effect on receiving system noise factor for device insertion immediately before low noise microwave amplifier
09 p1469 A69-22605

Reliability behavior of information transmission between transmitter-receiver pair in network of erasure channels without decoding and recoding at nodes
10 p1657 A69-23865

Explorer 20 satellite for obtaining fixed frequency pulse soundings of ionospheric topside, discussing transceiver-dipole antenna instrumentation and payload
20 p3618 A69-37857

Thermal design of power amplifier for airborne HF transceiver, discussing component layout, air cooling and materials
22 p3909 A69-39942

TRANSMITTERS

NT IONOSONDES

NT RADAR TRANSMITTERS

NT RADIO BEACONS

NT RADIO TRANSMITTERS

NT RADIOMETEOROLOGICALS

NT RADIOSONDES

NT RAWINSONDES

NT REPEATERS

NT TRANSMITTER RECEIVERS

Earth station system for ground based communications with Intelsat 2 and 3 noting antennas, receivers, transmitters and power supplies
05 p0741 A69-15667

High power transmitting tubes for INTELSAT satellite communication earth stations, including multicavity klystrons and wideband TWT
05 p0728 A69-15668

Miniature power amplifier stage for telemetry transmitters, discussing equipment size and weight reduction methods and hermetic envelope
07 p1106 A69-19115

Transponder design with planar triode for aircraft identification and air traffic control
09 p1462 A69-21411

Horizontal VLF cylindrical transmission antenna current distribution calculated with allowance for ground reaction, showing exponential decrease with distance
09 p1467 A69-22581

Temperature profiles and frequency driftings of VHF telemetry transmitters for Saturn S-IC stage, using IR radiation data
10 p1653 A69-23049

Book on elements of detection and signal design covering transmitter optimization for coherent and noncoherent digital communication systems, statistical decision theory, radar detection, etc
12 p2033 A69-26867

Emitter self bias in power stages of transistor transmitters, considering transistor parameters dispersion
13 p2226 A69-27217

Carrier disappearance method for FM telemetry transmitter characteristics measurements including frequency deviation sensitivity, linearity and frequency response
14 p2411 A69-28881

Quasi-uniform pseudorandom numbers program transmitter statistical characteristics suited for solving problems by Monte Carlo method
15 p2572 A69-30336

Linear feedback additive noise communication systems formulated in terms of arbitrary operations at transmitting and receiving points
17 p2944 A69-33626

Reciprocal theorem for obtaining relations between transmitting antenna effective area, radiation pattern and aperture distribution
19 p3281 A69-35765

Demultiplexing of high speed multichannel optical pulse code transmission systems, based on coincidence detection using locally generated reference pulses
19 p3279 A69-36764

L and S band transmitters for space applications, discussing power and frequency stability, low intermodulation, inputs isolation, efficiency, size and weight 23 p4137 A69-41740

Wideband FM telemetry transmitters for S band, using symmetrical discriminator 23 p4119 A69-41741

Static and dynamic characteristics of fluid pressure signal transmitter between members with relative rotary motion 24 p4256 A69-43300

TRANSOCEANIC COMMUNICATION

Aeronautical satellite system to relay communications at VHF or L band frequencies from aircraft flying over oceanic routes 03 p0464 A69-13235

Project Symphonie, discussing stationary communication satellite, coverage, frequencies and characteristics 06 p0886 A69-17072

Global communication techniques and trends, discussing radio telephone and telegraph, submarine systems, satellite communications, line of sight links, tropospheric scatter, waveguide transmission, etc 16 p2750 A69-31755

Air traffic control transoceanic satellite system for minimizing navigation errors forcing wide separations, providing VHF voice communication and position surveillance 22 p3901 A69-41147

Worldwide communication system via synchronous satellites for aeronautical, maritime and land mobile services 23 p4114 A69-41355

TRANSOCEANIC SYSTEMS

Long range subsonic transport navigation systems accounting for reductions in horizontal separation on high density oceanic routes 08 p1348 A69-21062

Flight surgeon observations of stress and fatigue effects on aircrew of first nonstop transatlantic helicopter flight, discussing fatigue ratings, sleep patterns, etc 19 p3262 A69-36450

Electrocardiographic and heart rate data recording of crew members during transatlantic helicopter flight and normal daily routine 19 p3263 A69-36451

Urinalysis of crew members of first transatlantic helicopter flight indicating interindividual endocrine-metabolic variability and circadian trends modification 19 p3263 A69-36452

TRANSONIC AIRCRAFT
U SUPERSONIC AIRCRAFT

TRANSONIC COMPRESSORS

Aerodynamic design of subsonic and transonic axial flow compressors, discussing blade configurations and computerized design of turbomachinery 12 p2147 A69-25792

Supersonic cascade wind tunnel /ONERA/ for super and transonic compressors profiles studies 17 p2895 A69-33591

TRANSONIC FLIGHT

Local external flow variations effect on blow-in-door nozzle performance in transonic flight regime [AIAA PAPER 69-428] 16 p2733 A69-32731

TRANSONIC FLOW

Three dimensional flow at large distance and in front of shock wave for three dimensional body traveling at sonic velocity 01 p0005 A69-10159

Sonic flow at large distance and behind shock wave for axisymmetric body of revolution of finite dimensions in inviscid fluid 01 p0058 A69-10160

Compressible relativistic flow in subsonic, transonic and supersonic regimes, noting pressure coefficient variations 01 p0007 A69-11203

Lifting wing profiles in uniform transonic compressible fluid flow calculated by analog method, noting hodograph method simplification 02 p0187 A69-11536

Aerodynamic problems related to turbopumps of subsonic transport aircraft [ONERA-TP-629] 02 p0187 A69-11622

Subsonic or transonic bidimensional flows around airfoils by hodograph method [ONERA-TP-645] 03 p0361 A69-12873

Transonic flow around profile in blocked plane channel and in free jet, noting channel wall and jet edge effects on flow along profile 03 p0361 A69-13018

Three dimensional sonic flow downstream from shock wave in nondissipative perfect fluid, introducing pseudorotating flow to obtain velocity field 03 p0362 A69-13363

Axial flow turbine blade cascade in transonic flow 03 p0365 A69-14103

Book on transonic aerodynamics, emphasizing two dimensional and three dimensional problems involving transonic flow about airfoils with and without shocks 04 p0541 A69-14580

Asymptotic expansion for transonic flow of viscous fluid at great distance from plane obstacle 04 p0544 A69-15057

Stream function approximation for plane axisymmetric vortex free transonic inviscid gas flow 06 p0910 A69-17336

Shock wave in two dimensional mixed transonic airfoil flows, discussing initial value problem for flow downstream of shock [AIAA PAPER 69-43] 06 p0915 A69-18180

Exact partial solutions to transonic gas flow equations used to describe flow around shape streamlined by supersonic flow with additional shock wave 07 p1118 A69-18698

Approximate equations for transonic viscous heat conducting gas flow past finite body of revolution 08 p1251 A69-20322

Plane steady transonic flow of perfect fluid around airfoils with constant curvature using hodographic method, discussing various boundary conditions 09 p1429 A69-21605

Transonic flow around airfoils with constant curvature in uniform asymptotic stream, studying leading edges in exact form 09 p1429 A69-21606

Time dependent procedure for axisymmetric transonic nozzle flows, programming governing equations for high speed computer 09 p1431 A69-21974

Controllable sonic flow orifice, discussing mass flow rate, area and upstream stagnation pressure 10 p1693 A69-23343

Bodies of revolution in sonic flow of ideal gas, showing same perturbational effect of source and dipole on flow before shock front 10 p1632 A69-23364

Motion equations for ideal transonic gas flow, applying solutions to flow with incident shock waves of various profiles 11 p1820 A69-25468

Free transonic gas flow incident on symmetrical profile at angle of attack with given velocity at infinity calculated using difference scheme 11 p1820 A69-25469

HF interferometry for statistical-numerical oscillation analysis of unsteady plane transonic flow, constructing phase planes for study of wave surfaces propagation 12 p2089 A69-26188

Shadow, schlieren and interferometric methods for study of transonic, supersonic and hypersonic fields of aerodynamics, using refractivity variations in heterogeneous medium 12 p2060 A69-26934

Transonic ideal gas flow past semiinfinite bodies, determining flow potentials from body perturbations and surface boundary conditions 14 p2390 A69-29476

Boundary value problem for quasi-linear equation of unsteady transonic gas flows, including linear model and operators for group of transformations 15 p2590 A69-30049

Compressible shear flow linear theory applied to transonic flow past thin airfoil, determining pressure distribution, discussing compressibility effects of nonuniform Mach number 16 p2731 A69-31593

Approximate equations for transonic viscous heat conducting gas flow past finite body of revolution 17 p2891 A69-33312

Similarity solutions of viscous transonic equation describing spiral and radial flows, containing shock-like transitions of corresponding inviscid solutions 18 p3121 A69-34787

Similarity rule in hydrodynamically transcritical regime in ionized multilfluid gas 20 p3515 A69-37594

Dissociational nonequilibrium transonic flow near nozzle throat analyzed for diatomic gas with equilibrium vibrational energy, using perturbation method 22 p3861 A69-41177

Transonic flows behind separated shock waves of ideal gases past bodies of various geometries 23 p4151 A69-41526

Sonic vapor flow heat transfer limitations in heat pipes for Na, K and Cs, showing strong influence of temperature and working fluid 23 p4239 A69-41719

Swirl influence on choking constraint in transonic flow through nozzle throat [AIAA PAPER 68-693] 23 p4151 A69-41887

Inviscid transonic flow past circular arc bodies of revolution, applying Hosokawa technique to pressure distribution solution 23 p4059 A69-41899

Transonic flow around profiles with heat input, showing drag reduction in supersonic part of flow field 23 p4061 A69-42144

TRANSONIC INLETS
U SUPERSONIC INLETS

TRANSONIC NOZZLES

Two dimensional analysis of isentropic perfect gas flow fields in axisymmetric nozzles for transonic two phase flow initial values, calculating particle trajectories [AIAA PAPER 69-572] 16 p2731 A69-31847

Internal flow measurements in transonic region of supersonic nozzle with small throat radius of curvature compared with prediction data 23 p4060 A69-41900

Transonic expansion analysis applied to flow through convergent-divergent nozzles with small throat radius of curvature, noting coordinate system selection 23 p4060 A69-41906

TRANSONIC SPEED

Transonic dynamic stability of free flight half angle cones in wind tunnel for high drag planetary entry vehicles, discussing Mars entry trajectories [AIAA PAPER 69-105] 06 p1019 A69-18209

Atmospheric gust effect on aircraft flying at Mach one calculated for subsonic and supersonic regions, finding difficulties for transonic calculations 10 p1632 A69-22918

Fluid mechanics shock wave interaction with turbulent boundary layers at transonic to high supersonic speed ranges, noting examples in aviation 11 p1871 A69-25018

Location effect of power plants on aft-mounted supersonic cruise exhaust nozzles at transonic speeds in flight and wind tunnel [AIAA PAPER 69-427] 16 p2734 A69-32769

TRANSONIC TURBINES
U SUPERSONIC TURBINES

TRANSONIC WIND TUNNELS

Microelectronic data and remote control function transmission system for wind tunnel testing of aircraft dynamic response to gusts and turbulence 10 p1672 A69-23283

Full scale and transonic wind tunnel store separation characteristics, outlining uses of heavy and light scaling methods 17 p2896 A69-34035

TRANSONICS
U TRANSONIC FLOW

TRANSPARENCY

Multibeam recording technique producing speckle-free images in redundant holograms of transparencies 01 p0082 A69-10850

Q switched ruby laser nonlinear absorption in optically transparent organic liquids attributed to two quantum process with large cross section 03 p0439 A69-13055

Transparency decrease in plexiglass during interaction with dense plasma, noting absorption independence of plasma pressure and dependence on wavelength 03 p0482 A69-14222

Q switches transparency as function of incident light intensity 04 p0610 A69-14385

Atmospheric IR spectral transparency measurement, describing optical system, recording devices and data processing 05 p0759 A69-16639

IR radiation attenuation in transparency windows of atmosphere, using searchlights as radiation sources 05 p0760 A69-16695

Pressure stratification and transparency/geometrical depth expansion/ in Fricke-Elsasser and Zwaan sunspot models 06 p0999 A69-16976

Boundary value problem of temperature field and heat conduction in transparent media heated by laser radiation producing thermoelastic stresses leading to breakdown 07 p1149 A69-18925

- HF scattering of scalar plane wave by transparent sphere based on Watson transformation
07 p1181 A69-19033
- Transparent dielectrics destruction by laser radiation noting stress development in medium
08 p1324 A69-19947
- Near IR transparent aluminumcalcium glasses with improved spectral properties
08 p1336 A69-20386
- Polymers and organic optical cements transparent in 1 to 13 micron IR region, noting organosilicon resin
08 p1336 A69-20387
- Acoustical transparencies illuminated by sound waves for optical imaging and ultrasonic diffraction, noting application to visualization of inhomogeneities in samples
10 p1695 A69-23546
- Laser radiation induced stress waves in transparent media using dynamic photoelastic technique
10 p1707 A69-24213
- Light scattering materials for transparent objects holography, analyzing Christiansen filter and milk white and ground glass plates
11 p1889 A69-25550
- Atmospheric boundary layer transparency to gas laser emissions in IR spectrum, determining attenuation factor dependence on humidity and visibility range
12 p2028 A69-25957
- Mach-Zehnder interferometer to study discontinuities of transparent objects by holographic methods
12 p2091 A69-26369
- Q switches transparency as function of incident light intensity
14 p2456 A69-28758
- Atmospheric IR spectral transparency measurement, describing optical system, recording devices and data processing
14 p2433 A69-28795
- Phenolic resin and silica cloth laminates transparency to IR radiation, noting experimental results
18 p1316 A69-34640
- Noctilucent cloud layer spectral brightness and transparency in E region determined from transhorizon rocket observations
18 p1310 A69-35148
- Sunspot umbra observed on 21 September 1966, computing transparency in model equaling photosphere transparency at same optical depth
20 p3605 A69-37825
- Holography application to three dimensional structure determination of weakly scattering semitransparent objects
20 p3546 A69-38198
- Transparency and luminescence yield of plastic scintillators prepared from polymethyl methacrylate, comparing naphthalene and benzene compound additions with polystyrene
21 p3724 A69-39073
- Dispersion and correlation function for atmospheric transparency due to water vapor from statistical model of absorption bands and effective mass
21 p3759 A69-39113
- Nonograms for spectral transparency of atmosphere at 2.8-5.6 microns
21 p3759 A69-39117
- Microholographic system for nonpseudoscopic stereoscopic image reconstruction of transparent and nontransparent microobjects
21 p3726 A69-39702
- TRANSPARENT MATERIALS**
U TRANSPARENCE
- TRANSPARATION**
- Transpiration and dissipation effects on heat eddy diffusivity over two dimensional plate in turbulent flow for various Prandtl numbers
01 p0178 A69-11410
- Thermal transpiration for performance prediction and development of gas pump
[ASME PAPER 68-WA/ENER-4]
05 p0706 A69-16162
- TRANSPARENT COOLING**
U SWEAT COOLING
- TRANSPONDERS**
- Ground based control system via cockpit PPI display on transponder equipped aircraft broadcast with digital coding
03 p0464 A69-13244
- FAA coded broadcasting to transponder equipped aircraft for air traffic control, navigation, collision avoidance and airfield approach
04 p0629 A69-15478

Transponders for communication satellites, discussing design constraints, reliability and transmission capacity increase
08 p1279 A69-19905

Airborne ILS marker beacon receivers and secondary surveillance radar transponder using microelectronic equipment, noting thermal dissipation problems
[AGARDOGRAPH-114]
08 p1292 A69-20991

Transponder design with planar triode for aircraft identification and air traffic control
09 p1462 A69-21411

Structure of quasi-linear and wideband satellite transponders, discussing possible improvements
09 p1609 A69-21619

Transponders for atmospheric measurements, considering ground tracking, radiosondes, rocket-sondes and flight results
10 p1692 A69-23257

Phase locked UHF telemetry transponder for missile scoring applications, discussing design and performance
23 p1437 A69-41779

TRANSPORT AIRCRAFT

NT A-300 AIRCRAFT
NT AN-24 AIRCRAFT
NT BAC 111 AIRCRAFT
NT BOEING 2707 AIRCRAFT
NT BOEING 707 AIRCRAFT
NT BOEING 747 AIRCRAFT
NT C-5 AIRCRAFT
NT C-130 AIRCRAFT
NT C-141 AIRCRAFT
NT CARGO AIRCRAFT
NT CH-34 HELICOPTER
NT CH-46 HELICOPTER
NT CH-47 HELICOPTER
NT CH-54 HELICOPTER
NT CL-84 AIRCRAFT
NT CONCORDE AIRCRAFT
NT DC 3 AIRCRAFT
NT DC 8 AIRCRAFT
NT DC 10 AIRCRAFT
NT DH 121 AIRCRAFT
NT DO-31 AIRCRAFT
NT L-1011 AIRCRAFT
NT S-61 HELICOPTER
NT SA-330 HELICOPTER
NT SC-7 AIRCRAFT
NT SH-3 HELICOPTER
NT TU-144 AIRCRAFT
NT VC-10 AIRCRAFT
NT XC-142 AIRCRAFT

Fatigue-damage evaluation system for transport aircraft, noting use of cumulative strain gauge that stores strain history
01 p0165 A69-10118

VTOL or V/STOL Light Intratheater Transport /LIT/ for future tactical airlift situations, comparing tilting, liftjet, stowed rotor and fan-in-wing concepts
01 p0008 A69-10146

Reliability and maintenance economics for jet transport operations of 1980s, discussing Aircraft Integrated Data System /AIDS/ sensors design
[AIAA PAPER 68-207]
01 p0011 A69-11022

Optimal transport aircraft, considering VTOL/STOL aircraft, construction requirements and flying distances
01 p0012 A69-11293

Aerodynamic problems related to turboprops of subsonic transport aircraft
[ONERA-TP-629]
02 p0187 A69-11622

Containerized freight, discussing means of transport, methods of distribution, suitable aircraft for carriage, economic and social effects and combined air-water-land transport
02 p0228 A69-11887

Light aircraft hazards due to trailing vortex generated by heavy transport aircraft, suggesting specific procedures for takeoff, landing and flight phase
[SAE PAPER 680220]
04 p0549 A69-14930

Design of high lift devices in relation to fixed wing subsonic transport aircraft, considering lift, drag, stability and control
05 p0695 A69-15544

LR-1 prototype design criteria and flight testing, discussing Model 99 airliners for commuter airlines
06 p0867 A69-17668

Helicopters and fixed wing STOL and VTOL aircraft for intertheater military logistics transportation, discussing C-5A role in 1970s
07 p1053 A69-19177

Fair-safe goals, design criteria, analytical methods and test procedures to achieve reliable damage tolerant dynamic rotating parts for V/STOL and helicopter transports
[AIAA PAPER 69-215]
07 p1237 A69-19569

Fabrication and processing techniques, tooling concepts and quality control for composite materials used in large aircraft, discussing honeycomb and sandwich structures
[ASM PAPER D8-25.4]
07 p1172 A69-19677

Transport aircraft fleet management and handling mechanical and avionic machine defects using operations research
08 p1422 A69-20627

Three shaft turboprop engines for 1970s noting thermodynamic and propulsive efficiencies, fuel consumption, weight, noise reduction, etc
08 p1376 A69-20627

Monograph on length requirements for takeoff and landing of jet transports covering airport classification, roll distance formulas and long range transport performance nomograms
08 p1301 A69-20717

Optimum cruise altitude, block time and fuel relations for Convair 600/640 aircraft for various temperatures, segment distances and weight
08 p1255 A69-21007

Long range subsonic transport navigation system accounting for reductions in horizontal separation on high density oceanic routes
08 p1348 A69-21062

Aircraft technology for hypersonic speed range including swept wing, engine design, composite materials, lift-drag ratio, considering weight, efficiency, STOL requirements
10 p1634 A69-23598

Flight testing and preflight simulated testing on Lockheed C-5 Galaxy transport aircraft
10 p1634 A69-23599

Supersonic transport airline operations including safety, noise, traffic control, routing, etc
11 p2004 A69-24373

European A-300B airbus design, considering aerodynamics, fuselage, power plant, structure systems, maintenance cost and autoland
11 p1822 A69-24464

Safety measures for aircraft ditching at sea discussing low wing configuration advantages and life rafts
14 p2392 A69-29697

Civilian transport aircraft operation realities vs theoretical performance certification
14 p2392 A69-29698

Dassault Mercure short haul jumbo jet, discussing production costs and market potential
15 p2550 A69-30317

Subsonic transport high bypass ratio engine evaluation in terms of fuel consumption, size, thrust-weight ratio, noise and price
16 p2835 A69-31807

Aircraft role in future transport systems for passengers and goods, emphasizing shorter distances, intercity and interurban communication, etc
16 p2881 A69-31932

Aerodynamic problems in future civil aircraft design emphasizing Concorde development possibilities discussing VTOL intercity transport, subsonic swept wing and hypersonic aircraft, all-wing airbus, etc
16 p2732 A69-32027

Medium range Tu-154 three jet transport aircraft detailing fuselage, airfoil, tail unit, landing gear propulsion unit and circuitry
16 p2735 A69-32027

Book on soviet An-24 aircraft-construction and exploitation covering fuselage, powerplant, controls, fire prevention, air conditioning, maintenance, etc
16 p2735 A69-32112

Short range transport - Royal Aeronautical Society Conference, London, May 1969
17 p2897 A69-33208

VTOL transport aircraft, discussing systems integration problems, feasibility and time scale of introduction into service, noise and safety, etc
17 p2897 A69-33207

Self contained lift fan concept and circulation controlled rotor aircraft power plants for high speed VTOL transports
17 p2897 A69-33208

Civil transport aircraft power plant and auxiliary systems as sources of delays, presenting critical path analysis
17 p2898 A69-33211

Power plant installation on swept winged transport aircraft, discussing interference drag sources, high lift problems, unorthodox installations, nacelle effects, etc
17 p2898 A69-33211

Large subsonic transport aircraft effect of economics of air operations with emphasis on airport facilities for Boeing 747
17 p3077 A69-34207

Statistical weight estimation equations developed by constrained regression analysis, noting application to vertical tail of cargo/transport aircraft
[SAWE PAPER 762] 18 p3220 A69-34879

Parametric approach for weight estimation of surface control systems of transonic and supersonic combat and subsonic transport aircraft
[SAWE PAPER 812] 18 p3221 A69-34898

Tupolev Tu-154 three jet transport featuring automatic flight control system with inertial and Doppler navigation inputs, low speed wing devices
18 p3092 A69-34933

Air conditioning system for transport airplane using combined simple/bootstrap cycle refrigeration unit, discussing thermodynamic performance and hardware implementation
[AIAA PAPER 69-787] 19 p3243 A69-35641

Jumbo jet audio entertainment and service systems, describing digital pulse multiplexing technique
19 p3285 A69-35806

Transport aircraft automatic altitude transmission requirements, discussing altimeter-transponder radar system to aid air traffic control
19 p3371 A69-36700

Technical problems in converting long service civil aircraft to obtain more volume, easier loading access or greater flexibility
20 p3461 A69-36919

Drag influence on mission performance of hypersonic aircraft during climb and cruise, noting payload capacity
20 p3461 A69-37154

VSTOL and conventional transport aircraft compared for short haul air transport services
20 p3461 A69-37281

Flight control and stability of STOL transport aircraft with powered-lift boundary layer control system augmented lift
20 p3462 A69-37513

Turbofan engine influence on civil transport aircraft design as function of thrust, discussing engine ratings, number of engines, APU and thrust engine
22 p3862 A69-39961

Cockpit displays for transport aircraft noting digital techniques and flight control-navigation integration
22 p3946 A69-40486

A 300B twin engine short haul giant transport aircraft, discussing engines, aircraft performance and systems reliability
[RAES PAPER 11] 22 p3863 A69-40491

Jet transport operation and accidents statistics, analyzing world data, accident causes and safety gap
22 p4054 A69-41130

Compound helicopter transport for short haul transportation system for Northeast Corridor, discussing terminals near origin and destination, takeoff and landing patterns, etc
[SAE PAPER 690419] 23 p4062 A69-41643

Jumbo jet role in air transportation, discussing future traffic growth, pilot problems and aircraft size limitations
23 p4063 A69-41819

VTOL transport aircraft to solve short haul travel problems, examining lateral and horizontal maneuvering and vertical to horizontal flight transition
24 p4250 A69-42564

Short haul transport aircraft development, discussing twin jet Mercure aircraft with low operation cost and Category III weather conditions landing
24 p4250 A69-42565

Beriev Be-12 cranked wing seaplane design including technical and operational data
24 p4251 A69-42796

Czechoslovak L-400 high wing short range STOL transport aircraft powered turboprop engines, discussing passenger and cargo version
24 p4251 A69-42799

Flight simulator with large lateral motion for large and supersonic transport aircraft, emphasizing reproduction of cockpit accelerations due to supersonic engine thrust loss
24 p4297 A69-43044

TRANSPORT COEFFICIENTS
U COEFFICIENTS

TRANSPORT EQUATION
U BOLTZMANN TRANSPORT EQUATION

TRANSPORT PROPERTIES
NT ATMOSPHERIC CONDUCTIVITY

NT CARRIER MOBILITY

NT DIFFUSION COEFFICIENT

NT ELECTRICAL RESISTIVITY

NT ELECTRON MOBILITY

NT GAS VISCOSITY

NT GASEOUS DIFFUSION

NT HOLE MOBILITY

NT IONIC MOBILITY

NT IONOSPHERIC CONDUCTIVITY
NT MAGNETORESISTIVITY
NT PHOTOCONDUCTIVITY
NT PLASMA CONDUCTIVITY
NT SUPERCONDUCTIVITY
NT THERMAL CONDUCTIVITY
NT THERMAL DIFFUSIVITY
NT VISCOSITY

Transport properties of steam, analyzing selection, correlation and prediction using statistical mechanical theories
01 p0174 A69-10110

Dimensional effects on thermodynamic and kinetic properties of thin semiconductor and semimetal films, noting quantization influence
01 p0136 A69-10186

Heat transfer situations in plasma flow indicates very high heat fluxes per unit area on surfaces with electric current
[ASME PAPER 68-HT-38] 01 p0175 A69-10314

Chapman-Enskog method applied to Boltzmann equations for transport coefficients for low density polyatomic gases
01 p0123 A69-10388

Turbulent fluid transport properties predicted by simple model for fluid behavior, obtaining mass, momentum and energy diffusivities
01 p0177 A69-11402

Viscosity and thermal conductivity of helium on basis of Lennard-Jones 6/6 to 9/ potential
[ASME PAPER 67-WA/HT-1] 02 p0351 A69-12205

Discharge coefficients for Herschel type smooth venturimeters, analyzing influence of transport coefficients, convergence angles and contraction ratios
02 p0250 A69-12414

Born approximation for calculating low temperature plasma transport properties from quantum mechanical scattering cross sections on Debye potential
02 p0291 A69-12486

Noninstantaneous, nonlocal nonlinear responses of momentum and energy flows to thermodynamic forces in single component simple fluid with memory
03 p0413 A69-12921

Transport phenomena analysis in n-InSb semiconductors during elastic/inelastic current carrier scattering
03 p0492 A69-14171

Book on nonlinear ordinary differential equations in transport processes, noting iterative and numerical methods for diffusion, conduction, fluid mechanics and chemical kinetics
04 p0622 A69-14599

Partially ionized hydrogen transport coefficients, using expressions containing collision integrals for charged particles
04 p0637 A69-15051

Turbulent flow transfers from applications point of view, noting example of cooling of heated wall
05 p0743 A69-15558

Hydrogen plasma transport properties for semiclassical quantum potential calculated by Chapman-Enskog-Hilbert theory
05 p0799 A69-15735

Transport properties of partially ionized low temperature plasmas, considering viscosity, electrical and heat conductivity of argon and nitrogen at high temperatures
06 p0969 A69-17907

Collection of Soviet papers on microwave radiation transport in atmosphere covering radiation field, water vapor content determination, absorption and scattering by precipitation, etc
06 p0953 A69-17994

Transfer coefficients for inhomogeneous systems characterized by constant density, mean free path and activation energy of carriers at each point
07 p1193 A69-19024

Electron transport parameters in noble gases at low electric field intensities, elastic and inelastic scattering and Boltzmann transport equation
08 p1362 A69-20285

Plasma diagnostics methods for evaluating collision and transport cross sections, discussing resonance fluorescence, steady state discharge and afterglow measurements
08 p1364 A69-20476

Energy density and transport velocity of RF wave in plasma in damped oscillations region, discussing resonance
08 p1365 A69-20553

Warm plasma magnetic interactions, discussing density waves, pair correlation function and transport coefficients
08 p1366 A69-20749

Gas transport coefficients dependence on density and temperature, noting experimental results for Ne and molecular N and H
08 p1353 A69-21009

Fission fragment generated plasma applicability to thermionic energy converters from electron density, temperature and transport studies
09 p1440 A69-21829

Hydrodynamic equations and Grad transport coefficients for nonequilibrium rarefied monatomic gases developed for molecular collisions
09 p1481 A69-21888

Partially ionized Kr and Xe transport coefficients for various pressures and at high temperatures computed on basis of charged particle cross sections
09 p1548 A69-21935

Plasma transport properties derived from Boltzmann equation using Debye shielded Lande potential to represent collisions, noting viscosity and thermal conductivity
09 p1553 A69-22539

Algorithm for mean energy transmission coefficient of fundamental mode in beam guide with given inhomogeneities, discussing mode conversions
09 p1469 A69-22629

Momentum transfer cross sections, recombination coefficients and ionization coefficients of working gases for MHD energy converter
10 p1733 A69-23446

Transport and balance coefficients in ionized neon and helium plasmas in homogeneous electric field, calculating electron mobility, diffusion coefficient, energy and collision parameters
10 p1740 A69-23722

Thomson scatter bistatic sounder data on ionization transports in F region, describing diurnal variations by hourly values of velocities
10 p1685 A69-23830

Transport of matter in nonisothermal weakly ionized plasma due to traveling ion-acoustic wave propagation, noting plasma oscillations and instability
10 p1741 A69-23945

Transport coefficients for almost Lorentzian mixture, computed as perturbation to coefficients for true Lorentzian mixture, compared to Chapman-Enskog method results
11 p1997 A69-24286

Cut-off Coulomb potential transport cross sections compared with exponentially screened potential for various cut-off radii
11 p1924 A69-24309

Statistical turbulence theory applied to turbulent flow transport properties in lower atmosphere
12 p2125 A69-25894

Soviet book on plasma thermionic energy conversion covering operation modes, transport processes, current-voltage characteristics, density, temperature, electric field distribution
12 p2017 A69-26850

Ionization fraction as independent variable in plasma transport correlation, noting role in pressure effect increase
13 p2313 A69-28241

Transport coefficient density expansions obtained from time correlation functions in moderately dense gas with short range repulsive intermolecular forces
14 p2540 A69-29469

Transport properties interrelationship in turbulent pipe flow and free turbulence
15 p2591 A69-30792

Plasma experiments with TM-3 apparatus under stable discharge conditions in H₂, discussing energy loss mechanisms, transport coefficients, reciprocal lifetime, etc
16 p2820 A69-31795

Laser ignited combustion of 365 micron Zr droplets falling in ultrapure oxygen using spectroscopic and photographic techniques, discussing vapor phase transport phenomena
[WSCI PAPER 69-4] 16 p2830 A69-32345

Neutron and photon transport properties in liquid hydrogen obtained from measuring radiation environment in propellant tank mockup suspended above NERVA reactor
[AIAA PAPER 69-475] 16 p2810 A69-32716

Pure monopropellant steady droplet burning rate theory for determining heat-up and convection transport rates in droplet combustion products of flat flame burner
[AIAA PAPER 69-563] 16 p2834 A69-32722

Transport properties of free turbulent mixing of subsonic coaxial streams by introducing environmental distributions in integrals of momentum, energy and species continuity equations
[AIAA PAPER 69-681] 17 p2956 A69-33495

Radiative and conductive heat transport mechanisms at cryogenic temperature applicable to thermal energy transport minimizing technique in containment system
17 p3074 A69-33680

Superposition method for predicting tube wall temperatures with gas property and heating rate axial variation, noting application to gas flow problems
18 p3227 A69-34315

Inelastic collisions and radiation effects on transport properties and shock structure in high temperature gases, obtaining density and temperature profiles
19 p3448 A69-36149

Narrow band gap alloys and ferromagnetic semiconductors, using transport properties for characterization
19 p3388 A69-36541

Electronic properties changes in amorphous CdGeAs caused by long range order loss studied by measuring optical and transport properties
19 p3390 A69-36557

Transport properties of liquid semiconductors, using model for liquid mercury with minimum state density
19 p3391 A69-36560

Relaxing polyatomic gases transport properties from Boltzmann equations obtained without knowing excitation probabilities of internal molecular degrees of freedom
19 p3300 A69-36787

Interface electron transport phenomena in stress corrosion, expressing defect movements in terms of electron energy dynamics
19 p3349 A69-36889

Radiative energy transport quantities for hydrogen plasma including Plank and Rosseland mean absorption coefficients, discussing line and continuum radiation and optical limits
20 p3581 A69-37306

Intensity changes of OI nightglow emission at 100 km by transport associated with tides, gravity waves and turbulent mixing
21 p3713 A69-38526

O conductance nonlinear equation solution applied to O uptake at sea level and at altitude, noting blood transport problems
21 p3654 A69-38906

Molecular transport equations of dilute gases, considering relaxation time spectrum, obtaining kinetic equations and correlation function expressions for transport coefficients
23 p4193 A69-41512

Hydrodynamic equations derived from Boltzmann equation, obtaining molecular expressions for transport coefficients
23 p4151 A69-41513

Electron transport coefficients determined for weakly and fully ionized gases under various conditions
23 p4195 A69-41517

Binary gas mixtures transport coefficients approximated by self consistent matrix procedure based on Chapman-Cowling expressions
24 p4352 A69-43135

Heat pipe wick materials liquid transport properties analysis, using water and Freon 113 as working fluids [ASME PAPER 69-HT-17]
24 p4413 A69-43551

TRANSPORT THEORY

NT CHAPMAN-ENSKOG THEORY

NT EYRING THEORY

NT MIXING LENGTH FLOW THEORY

Transport phenomena in crossed electric and strong magnetic fields, developing semiclassical and quantum treatments
03 p0473 A69-12926

Transport phenomena in semiconductors in strong DC field, emphasizing electrical conductivity as function of crystallographic orientation
03 p0491 A69-14097

Book on nonlinear ordinary differential equations in transport processes, noting iterative and numerical methods for diffusion, conduction, fluid mechanics and chemical kinetics
04 p0622 A69-14599

Prigogine-Nicols-Misguich transport theory tested with inert gas liquids and compared with Rice-Allnatt theory, based on modified Lennard-Jones potential model
04 p0589 A69-14863

Gamma heating rate measured by aqueous dosimeter converted to rate in thin tungsten detector in water shield through transport theory calculations, obtaining correction factors
07 p1178 A69-18825

Mathematical methodology for nonlinear equations of transport processes, discussing group concept and similarity, boundary value conversion to initial value, etc [AICHE PAPER 31A]
08 p1302 A69-19849

Iterative methods for composite layer slabs transport models, using invariant imbedding approach to transport theory
08 p1343 A69-20353

Inelastic transport cross sections for Lyman alpha transitions in hydrogen
08 p1357 A69-20814

Turbulent transport processes mathematical model, determining upper and lower bounds
10 p1677 A69-22895

Transport equation describing drift, diffusion and reaction of iron swarm influenced by electric field in gas
13 p2306 A69-27457

Parameter identification in linear dynamical systems with transport lags, discussing linear differential-difference equations and finite difference theory
13 p2289 A69-27945

Transport processes under adiabatic conditions between external magnetic field and thermal and electrical gradients in solid, defining galvanomagnetic and thermomagnetic effects
13 p2299 A69-28129

Electron transport phenomenon in high pressure cesium diodes, noting quasi-static assumption of particle distribution functions
14 p2401 A69-29229

Differential equations for ignited mode theory, considering ion and electron transport and energy flux
14 p2490 A69-29233

High energy neutron transport calculated using one dimensional discrete ordinates code with anisotropic scattering, comparing results with nucleon transport code calculations
14 p2481 A69-29592

Variational principle for solving boundary value problems and reciprocal formula for error estimation, discussing applicability to general transport phenomena problems
15 p2716 A69-30022

Noise fluctuations transport in convergent flow crossed field electron guns using Monte Carlo method for two dimensional computerized gun simulation
15 p2572 A69-30031

Wave energy flux and correlation wave energy flux relationship to energy transport, noting applicability to fluids
15 p2595 A69-30218

Electron transport initiated by radiant energy absorption or by reducing suitable electron acceptor as source of energy for extraterrestrial life
17 p2908 A69-32973

Linear isotropic elastic continuum dislocations distribution, deriving transport equations by statistical methods, noting analogy between energy/momentum and MHD equations
18 p3212 A69-34352

Energy spectrum and transport mechanism for current carriers in amorphous-crystalline semiconductors, measuring thermostimulated conductivity, induced photoconductivity, optical quenching, etc
19 p3391 A69-36558

Transport mechanism in amorphous Ge films deposited on glass substrates studied by measuring piezoresistance as function of temperature during pure nitrogen immersion
19 p3391 A69-36559

Similarity method applied to linear integrodifferential equations of neutron transport in homogeneous space
19 p3361 A69-36774

Radiative transport equation solution in two flow approximation for plane layer, considering absorption and dispersion characteristics dependence on radiation density
20 p3553 A69-37608

Radiation absorption and emission problem for material of unit density at rest solved by finite difference scheme
21 p3773 A69-39666

Shock tube boundary layers dependence on shock strength determined using vorticity transport to define boundary layer coordinate
22 p3930 A69-40531

Boundary effects on time dependent transport theory based on star product, noting application to transmission line theory and radiative and neutron transfer
23 p4190 A69-41571

Numerical methods for radiation transport for inviscid stagnation flows, detailing spectral nature of radiation emission and absorption [AIAA PAPER 68-664]
23 p4059 A69-41890

Intrinsic transport theorem for electrodynamics of continuous media, using Cartan method of exterior differential forms
24 p4350 A69-43368

TRANSPORT VEHICLES

NASA LOX and liquid hydrogen barges, discussing storage tank design, acceptance testing and operating conditions
01 p0056 A69-11150

Monograph on air cushion vehicles /ACV/ in Scandinavian water transport, covering state of the art, technical and economic competitiveness, etc
09 p1434 A69-22075

Propulsion optimization for various vehicles, considering power plant weight, specific fuel consumption, power and thrust ratios, etc
11 p1941 A69-24462

TRANSPORTATION

NT AIR TRANSPORTATION

NT HIGHWAYS

NT RAIL TRANSPORTATION

Maximum capacity estimation for one way transportation systems to moon and Mars, analyzing technical and economic aspects
09 p1586 A69-21297

Ground access routes between business districts and airports compared for passenger transport modes [AIAA PAPER 68-1072]
12 p2059 A69-26773

Urban noise control over transportation systems including aircraft and highway traffic operating beyond local noise ordinance purview
14 p2541 A69-29157

Air cushion vehicles tests for public transportation facilities noting operation costs
15 p2550 A69-30409

Design philosophy for cost reductions on future space transportation systems, exemplifying application to booster system for earth orbital logistics [AIAA PAPER 69-439]
16 p2882 A69-32654

Telemetric control of urban transportation systems and law enforcement, considering automobiles as prime vehicle
19 p3272 A69-36256

Reducing cost of space transportation - AAS Conference, Washington, D.C., March 1969
21 p3856 A69-39686

Cargo handling systems for worldwide door to door service from marketing systems viewpoint [RAES PAPER 1]
22 p4053 A69-40482

Air space saturation, urban surface transport network enlargement necessity and expeditious passenger processing and baggage handling
24 p4296 A69-42567

Intercity travel demands simulation by linear graph model applied to Windsor-Montreal corridor [AAS PAPER 69-382]
24 p4417 A69-42805

Public policy for urban transportation system, using calculus of variations to determine optimal introduction curve [AAS PAPER 69-292]
24 p4417 A69-42809

TRANSURANIUM ELEMENTS

U PLUTONIUM ISOTOPES

U PLUTONIUM 238

TRANSVERSE OSCILLATION

NT H WAVES

NT MILLIMETER WAVES

NT POLARIZED ELECTROMAGNETIC RADIATION

NT POLARIZED LIGHT

NT SYNCHROTRON RADIATION

Resisting forces produced by transverse vibration of rotating disks in viscous fluid
02 p0232 A69-12257

Transverse mode selection effects on wave front of long pulsed ruby laser beam
02 p0257 A69-12409

Selection of transverse oscillations of unstable Nd laser resonator modes with system of two mirrors and two variable focal length convex lenses
03 p0440 A69-13426

Transverse perturbation influence on helical instability in oscillator
03 p0488 A69-13886

Transverse motion of embedded or free semiinfinite beam with given initial displacement and velocity, using potentials leading to integral equations [ONERA-TP-653]
07 p1230 A69-18264

Unstable transverse potential oscillations in plasma with beam anisotropy and initial density modulation and analogy with known electrostatic oscillations
10 p1727 A69-23092

Asymptotic solutions for transverse oscillations of wedge and cone by virtual displacements principle,

considering nonlinear law of elasticity and energy dissipation

11 p1975 A69-24762

Transverse perturbation influence on helical instability in oscillistor

11 p1939 A69-25687

Microwave oscillations in low pressure arc noting long gas discharge in small transverse dimensions

14 p2489 A69-28739

Transverse free vibration of slender cantilever subjected to compressive follower force

16 p2871 A69-31899

Self mode locking of carbon dioxide laser with high order transverse mode oscillations in vibrational-rotational transitions of P branch

19 p3330 A69-35602

Transverse oscillations of shallow multilayer shells, using tangential-stress distribution law in determining natural oscillation frequencies in single and sandwich layer panels

19 p3435 A69-35842

TRANSVERSE WAVES

NT H WAVES

NT MILLIMETER WAVES

NT POLARIZED ELECTROMAGNETIC RADIATION

NT POLARIZED LIGHT

NT SYNCHROTRON RADIATION

Transverse plasma mode excitation by nonlinear interaction analyzed by Hamiltonian function

01 p0127 A69-10280

Stabilization of plane parallel MHD flow at inlet and outlet of flat rectangular tube with transverse magnetic field

01 p0130 A69-10770

Upper and lower bounds for eigenvalues of differential problem connected with transverse vibrations of wedge shaped simply supported beam

02 p0272 A69-12193

Nonlinear interaction between waves in relativistic plasma, determining probability between transverse and longitudinal waves with different phase velocities

03 p0397 A69-13710

Longitudinal and transverse elastic waves propagation in medium with random inhomogeneities, deriving scattering coefficients in Born approximation for Fraunhofer region

04 p0667 A69-14262

Transverse normal waves excitation in flat plate by applying piezoelectric plate or comb shaped emitter to surface or end face

04 p0678 A69-14901

Transverse ionizing MHD shock waves, discussing jump conditions with magnetic field in shock plane

04 p0637 A69-15052

Transverse sensitivity ratio of vibration transducer, discussing measurement by shaker method

04 p0603 A69-15432

Equation governing transverse vibration of beams with exponentially varying properties, expressing solution in terms of Bessel functions

05 p0835 A69-15873

Retrograde motion of electric arcs in transverse magnetic fields, using multifluid equation to predict inclination and properties

06 p0971 A69-18091

Transverse waves instability in relativistic plasma, noting condition of isotropy and existence of electromagnetic waves

07 p1193 A69-19032

Thin electron flux interaction with electromagnetic wave in open waveguide, discussing nonlinear theory and performance of gyroresonance transverse wave tube

07 p1107 A69-19159

Longitudinal and transverse vibrations of viscoelastic rods excited by inertia with aid of linear oscillator subjected to harmonic stress, using Kelvin-Voigt model

07 p1233 A69-19326

Disturbing TM mode generation effect on attenuation measurement accuracy in TE mode attenuators

08 p1283 A69-20126

Transverse vibration of beam rigidly fastened at one end, using series expansion in terms of set of eigenfunctions

08 p1414 A69-20445

Capacitance and lowest eigenvalue bounds for two dimensional anisotropic media as exemplified by transverse vibrations of stretched membrane

08 p1418 A69-20848

Free transverse vibrations of rectangular flat plate simply supported along periphery and rigidly connected to interior columns

09 p1616 A69-21928

Transverse wave spacing in self sustaining detonations in H-O mixtures, noting evidence against acoustic theory and for characteristic chemical dimension

09 p1622 A69-21953

Radio ray scattering resulting from traversing anisotropically turbulent solar corona, noting refraction effect on signal pulse arrival time

10 p1773 A69-22960

Transverse waves induced by disk oscillations about state of steady rotation in MHD, revealing circularly polarized waves with different phase velocities

10 p1728 A69-23239

Air gap tolerances effect on admittance of TEM mode dielectric and plasma coated slot antennas determined by variational method

11 p1851 A69-24986

Small scale oscillations stability in quasi one dimensional conducting gas flow with longitudinal superimposed magnetic field, noting radiation role in transverse oscillations development

11 p1928 A69-25222

TEM-WAVE propagation between parallel conducting planes, stressing changes in curved waveguide sections

11 p1841 A69-25619

Directional coupler for TEM waves composed of two waveguides and having locally dependent coupling function

11 p1855 A69-25629

Two transverse modes locking with multiple longitudinal modes in He-Ne laser, noting separate locking and alternate quenching

12 p2104 A69-25923

Transverse symmetrical vibrations of thin elastic plates under Jacobi pressure distribution, giving displacement and velocity plots

12 p2180 A69-26271

Transverse normal waves excitation in flat plate by applying piezoelectric plate or comb shaped emitter to surface or end face

12 p2182 A69-26654

Finite difference solution to TEM mode transmission line cross section for defining continuous potential function leading to capacitance upper bound

13 p2221 A69-28064

TEM mode networks design for producing phase coherent pulse modulated microwave signals through spectrum S band

13 p2234 A69-28073

Transverse wave spacings for self sustaining detonations in oxygen and diluents mixtures with hydrogen, methane, acetylene or ethylene fuel, noting dilution

13 p2378 A69-28217

Electromagnetic field TM and TE modes uncoupling during oblique incidence scattering from radially inhomogeneous cylinders

15 p2565 A69-30170

Cut-off wavelength of transverse magnetic mode related to cross section eccentricity of hollow conducting elliptical waveguide

15 p2575 A69-30178

Te waves propagation along plasma sheet between conducting plates, determining vertical plasma density distribution

15 p2569 A69-30939

Weakly damped transverse and thermal waves development and propagation in viscous heat conducting incompressible fluid under temperature and gravitational fields

15 p2718 A69-31168

Coupled TEM lines arrays analysis in terms of odd and even modes, computing equivalent circuit elements, impedances and admittances

15 p2581 A69-31525

Wave propagation in warm uniaxial plasma filled waveguide, analyzing TE modes, TM mode splitting and power transfer

16 p2756 A69-31576

Electromagnetic wave propagation in transversely magnetized warm plasma filled rectangular waveguide, analyzing TE and TM modes

16 p2756 A69-31581

Temporal damping rate for small amplitude linearly polarized TEM mode in plasma, using Landau equation

16 p2818 A69-31675

Second order correction to first order Faraday rotation equation for quasi-transverse propagation of ionospheric radio waves obtained from Appleton-Hartree equation

16 p2777 A69-32101

Plasma wave echoes concept extended to transverse electromagnetic wave excitation propagating parallel to external magnetic field

16 p2823 A69-32467

Free-free transverse vibration damping phenomena, calculating strain amplitude dependence of internal friction at various frequencies

17 p3051 A69-32961

Finite amplitude standing transverse resonant acoustic field effects upon flow behavior of viscous fluid in cylindrical enclosure to acoustically model combustion instability

17 p2954 A69-33457

Complete spherical shells transverse frequency analysis, comparing results of elastic theory and classical, improved and membrane shell theories

17 p3061 A69-33705

Air resistance effect on transverse vibration damping of flat specimens of heat resistant alloy, duraluminum, Ti, Mo and Nb

17 p2991 A69-33947

Normal and transverse ionizing shock, discussing Alfvénic regime for normal shocks and shunting effect in transverse shocks

18 p3180 A69-34454

Anisotropic ionospheric model for VLF TM and TE modes excitation, noting nighttime phase velocity variations

18 p3101 A69-34797

Reflection coefficient of symmetric parallel plate waveguide operating in TEM mode illuminating lossless dielectric layer, using wedge diffraction and geometrical optics methods

18 p3108 A69-34802

Transverse vibrations of thin linear viscoelastic rectangular plate of constant thickness resting on elastic medium

18 p3223 A69-35171

Fluctuating heat transfer and flow measurements for circular cylinder in crossflow with simultaneously imposed transverse standing sound field

18 p3124 A69-35384

Transverse electromagnetic wave propagation in cylindrically stratified axially magnetized plasma, obtaining plasma properties profiles from method for isotropic media

19 p3266 A69-35619

Transverse and longitudinal velocity components of detonation waves in stoichiometric hydrogen-oxygen propagating in fundamental mode in square section tube

19 p3451 A69-36367

Longitudinal and transverse wave propagation in homogeneously deformed isotropic elastic solids, considering Hadamard and Green materials

19 p3440 A69-36588

Transverse vibration and wave solutions for nonlinear equations governing transverse motions of spinning circular membrane disks

19 p3440 A69-36637

TEM mode reflection coefficient for symmetric parallel plate waveguide composed of adjacent conducting wedges composition and radiating into perfectly reflecting sheet

20 p3507 A69-37839

Transverse wave propagation and instabilities within magnetosphere, noting loss cone limited velocity-space distribution function

20 p3533 A69-38081

Transverse wave-beam interaction propagation in fast wave structure in finite homogeneous magnetostatic field, deriving wave-beam equation for non-relativistic beams

21 p3672 A69-38435

Transverse vibrations of isotropic solid rectangular beam with secondary effects of rotary inertia and shear deformation retained

21 p3832 A69-38447

Transverse mode selection in rotating mirror neodymium doped calcium tungstate laser by inserting slit and edge into resonator

22 p3961 A69-40316

Edge diffraction effects in TEM axially slotted finite ground plane on radiation pattern in waveguides of different geometries

23 p4116 A69-41588

Transverse plasma waves propagating along parallel static electric and magnetic fields may lead to instabilities regardless of carriers sign

24 p4355 A69-42923

TRAPEZOIDAL WINGS

Surface of minimum drag symmetrical trapezoidal wing in supersonic flow solved by variational method

15 p2548 A69-31022

Design and fabrication of plane and trapezoidal fiberglass wings with laminar plastic profiles for aerodynamic tests, including wing rigging and slotted wing

19 p3324 A69-35831

TRAPPED MAGNETIC FIELDS

Magnetic energy relationships in magnetosphere, discussing confinement energy of magnetic dipole field, energy of transient compression and zero order energy of trapped particles
07 p1128 A69-19359

TRAPPED PARTICLES

NT ARTIFICIAL RADIATION BELTS
NT INNER RADIATION BELT
NT MAGNETICALLY TRAPPED PARTICLES
NT OUTER RADIATION BELT
NT PROTON BELTS
NT RADIATION BELTS

Magnetic storm principal phase explained by interaction between quasi-trapped particles stream and magnetosphere
01 p0144 A69-10573

Electron intensity diagram of diurnal trapped electron variation from Cosmos 5 satellite data, including harmonic analysis of data
01 p0147 A69-11321

Cone instability role in auroral electron and proton dynamics, discussing plasma instability control of maximum captured particle densities in various magnetosphere regions
03 p0501 A69-13526

Unique solution for radial diffusion coefficient applicable to equatorially trapped electrons in artificial radiation belt
05 p0816 A69-16279

Particle and field environment of earth, discussing solar wind, bow shock, magnetosheath, magnetopause, magnetosphere and particle population
06 p1001 A69-17158

Synchrotron radiation from trapped high energy electrons in Van Allen belt
06 p0992 A69-17324

Charged particle motion in electromagnetic field from basic equation of motion for magnetosphere, discussing dipolar magnetic field, Stormer trapped particle theory, etc
07 p1208 A69-19355

Magnetic energy relationships in magnetosphere, discussing confinement energy of magnetic dipole field, energy of transient compression and zero order energy of trapped particles
07 p1128 A69-19359

Equation describing statistically trapped particle motion under influence of fields varying in time and space
07 p1209 A69-19375

Plasma flux measurements by charged particle traps in Venus vicinity by space vehicle Venus 4, discussing low concentration of charged particles
07 p1222 A69-19613

Bimodal diffusion mechanism for acceleration of trapped particles in earth magnetosphere, noting particle intensity profiles and energy spectra
08 p1307 A69-20183

Trapped electron belts formation and storm time behavior assuming presence of bimodal diffusion from low energy source at magnetosphere outer edge
08 p1307 A69-20184

Nonadiabatic and stochastic mechanisms for cyclotron resonance trapping and heating in magnetic mirror geometries
08 p1364 A69-20518

Time dependent recoverable isothermal decrease of photocurrent in CdS crystals in vacuum, noting trap mechanism involving electron redistribution
08 p1374 A69-21187

Trapping state effect on tunneling probability in Schottky barriers, discussing current-voltage characteristics
09 p1557 A69-21748

Biological radiation doses and protection from galactic, solar particle and trapped radiation in space, noting secondary radiation and bremsstrahlung in absorber
11 p1831 A69-24866

Relativistic electron confinement within geomagnetic tail neutral sheet measured by Pioneer 7 deep space probe, confirming kinetic energy observations of IMP 1 satellite
14 p2433 A69-28934

Magnetic storm principal phase explained by interaction between quasi-trapped particles stream and magnetosphere
15 p2675 A69-30743

Spatial and temporal dependence of trapped particle energy spectra on basis of bimodal diffusion
16 p2852 A69-32619

Trapped particle acceleration by random bimodal diffusion in inhomogeneous magnetic field accounting for high energy particles trapped in earth radiation belts
18 p3186 A69-34808

Low altitude trapped protons in inner radiation belt during solar minimum period, using emulsion detectors on polar-orbiting satellite
18 p3187 A69-34944

Time dependent recoverable isothermal decrease of photocurrent in CdS crystals in vacuum, noting trap mechanism involving electron redistribution
18 p3183 A69-35156

Pressure dependence of trapped spontaneous decay of resonant radiation carbon dioxide
18 p3179 A69-35478

Electromagnetic wave effect on electron in homogeneous magnetic field, noting relativistic momenta of dragged electrons
18 p3181 A69-35497

Particle trapping and plasma oscillations in satellite disturbed ionosphere observed from Ariel and Alouette measurements, discussing frequency and wavelength relation
21 p3787 A69-38357

Cosmic ray albedo neutron decay /CRAND/ source for trapped protons, showing disagreement with intensities in inner zone measured on OV1 2 spacecraft
22 p4005 A69-40512

Cosmic ray albedo-neutron decay source role in intensity measurements of high energy protons trapped on low L shells during satellite flights
24 p4367 A69-43176

Geomagnetically trapped protons and alpha particles, analyzing OGO 4 data
24 p4368 A69-43184

TRAPPED RADIATION

U RADIATION BELTS

TRAPPING

Trapping parameters of Fe doped GaAs-GaP, measuring thermally stimulated conductivity and space charge limited currents
02 p0296 A69-11789

Majority and minority carrier trapping in neutron irradiated Si diodes, measuring transient junction capacitance recovery
06 p0975 A69-16869

Gas-surface interaction for trapping and energy exchange, comparing continuum and discrete lattice models for solids
14 p2409 A69-29092

Strong doping criterion for Si with deep level impurity centers based on electron spectra of fast surface traps
22 p3992 A69-40604

TRAPS

NT COLD TRAPS
NT ION TRAPS [INSTRUMENTATION]

Semiconductor center traps effect on characteristics of metal oxide semiconductor transistors
02 p0299 A69-12183

TRAVELING CHARGE

Resonant interaction between traveling charge with superimposed magnetic field and Alfvén wave in plasma cylinder, showing cyclotron orbit variations
09 p1551 A69-22035

TRAVELING WAVE AMPLIFIERS

Transmission of coherent ruby laser radiation through traveling wave amplifier noting spatial field structure changes
02 p0255 A69-11608

Regenerative amplification stability in nonretarded wave helitron and traveling wave mitron type devices
02 p0214 A69-11610

Electromagnetic wave propagation and amplification in periodic structures, including travel wave and parametric amplifiers, reactance diodes, lasers and quantum amplification
03 p0396 A69-13701

Experimental equipment and procedure to investigate defocusing of electron beam directly in cavity beam hole of TWT amplifier
03 p0407 A69-13975

Traveling wave amplifiers beam defocusing by RF circuits and space charge fields under large signal operating conditions, discussing magnetic field strength
07 p1094 A69-18424

Nonlinear interaction between cyclotron harmonic waves, demonstrating synchronism conditions for traveling wave parametric amplification and passive mode conversion
07 p1189 A69-18439

Q switched single mode ruby laser pulse passage through traveling wave amplifier decreases beam divergence
08 p1326 A69-20542

Amplification factor of He-Ne traveling wave light amplifier, discussing frequency stability and telescopic

wave front broadening for uniform radiation distribution
11 p1894 A69-24623

Transmission of coherent ruby laser radiation through traveling wave amplifier noting spatial field structure changes
11 p1895 A69-24715

Regenerative amplification stability in nonretarded wave helitron and traveling wave mitron type devices
11 p1847 A69-24717

Traveling wave tube for European communication satellite power amplifiers, showing nonlinear distortions dependence on RF input/output power and helix voltage [AIAA PAPER 68-430]
12 p2041 A69-26786

Wave propagation at different group velocities along parametric line in traveling wave parametric amplifier
16 p2805 A69-32254

Amplification stability region in overexcited regenerative traveling wave amplifier with respect to parasitic emission buildup
20 p3506 A69-37724

Solid state traveling wave optical quantum amplifier for conversion of modulated signal carrier frequency, applying to frequency conversion in laser communication links
21 p3739 A69-39540

Second harmonic influence on traveling wave amplifier operation employing distributed nonlinear active medium
22 p3916 A69-40963

TRAVELING WAVE MASERS

Maser for satellite communication consisting of traveling wave ruby maser and closed cycle liquid helium refrigerator, discussing design, operation and performance characteristics
02 p0256 A69-11992

Noise performance of broadband traveling wave masers with longitudinal or transverse stagger tuned magnetic field
02 p0257 A69-12428

Compact high-gain chromium doped rutile traveling wave masers for Onsala radio telescope for galactic and extragalactic microwave emission studies
02 p0257 A69-12463

Traveling wave maser and cooled parametric amplifier for ultralow noise preamplification in satellite communication earth terminal installations
05 p0728 A69-15670

Frequency transformation coefficients in titanium oxide-chromide traveling wave maser
07 p1146 A69-18481

Ruby and neodymium glass traveling wave laser free generation spectra kinetics, noting mode transitions as function of pumping levels
13 p2271 A69-27655

Possibility of combining individual yttrium ferrite single crystals to obtain noninteracting element for quantum paramagnetic traveling-wave amplifier operating at liquid nitrogen temperature
19 p3334 A69-35883

TRAVELING WAVE MODULATION

Wideband microwave KDP light modulator for amplitude and phase modulation, using ring-plane traveling wave circuit
05 p0732 A69-16553

Nonlinear computer analysis of TWT small amplitude compression and small AM to PM conversion, noting coupling and circuit breaker effects
07 p1094 A69-18422

Beam modulation resynchronization at large signal levels by TWT circuit wave to enhance efficiency
07 p1094 A69-18423

Pulse generation in Q switched traveling wave laser, noting effect of field amplification [IEEE PAPER Q-5]
07 p1154 A69-19077

Gain, output power and radiation directivity of He-Ne traveling wave laser with nonresonant feedback
09 p1517 A69-21796

Variational principle for analyzing dispersion properties of closed regular waveguide with traveling wave-modulated dielectric constant
23 p4123 A69-41943

High power ruby laser pulse generation by diffraction modulator, employing modulated ultrasonic traveling waves at minimum resonator transmission losses
24 p4328 A69-43163

TRAVELING WAVE TUBES

NT BACKWARD WAVE TUBES
NT CARCINOTRONS
NT HELITRONS

Microwave selective filter using resonant cavity with single coupling component in feedback circuit of amplifier traveling wave tube or klystron
01 p0042 A69-10384

Permanent magnets used in conjunction with magnetrons, crossed-field amplifiers, klystrons, traveling wave tubes and microwave ferrite devices
[IEEE PAPER 2.3] 01 p0045 A69-10713

Signal to cross modulation noise ratio in TWT tube during amplification of sinusoidal signals
01 p0031 A69-10780

Power saturation in isochronal traveling wave tube explained by motion of electron bunches relative to waves
01 p0047 A69-10882

Sensitivity calculation for microwave receiver consisting of traveling wave tube preamplifier followed by square law detector and video amplifier
01 p0048 A69-11038

Satellite traveling wave tube for X band duplicating C and S band performance
03 p0405 A69-13678

Trajectory equations for outermost electron on beam in TWT operating in dynamic mode for Brillouin flux
03 p0406 A69-13974

Experimental equipment and procedure to investigate defocusing of electron beam directly in cavity beam hole of TWT amplifier
03 p0407 A69-13975

Conventional TWT theory modified to include interaction between beam and two spatial harmonics, investigating TWT stability near edges of pass band
03 p0407 A69-13976

Reflections from input and output ducts influence on gain of TWT strophotron amplifier with/without allowance for back radiation
03 p0407 A69-13980

Nonlinear cross sectional space charge density distribution in electron beam of traveling wave tube
03 p0407 A69-13984

Traveling wave tube segmentation, analyzing effects of drift, grouping and selecting sections on efficiency and amplification
03 p0407 A69-13985

Phase input power characteristics of TWT, TDA and parametric amplifiers, noting crosstalk calculations and AM-PM conversion coefficients
04 p0573 A69-14336

Variational method applied to maximization of electronic efficiency of O-type TWT
04 p0577 A69-14791

Lamination influence on traveling wave tube performance, showing negative effect of radial variations in electric field
05 p0727 A69-15642

High power transmitting tubes for INTELSAT satellite communication earth stations, including multicavity klystrons and wideband TWT
05 p0728 A69-15668

Nonlinear computer analysis of TWT small amplitude compression and small AM to PM conversion, noting coupling and circuit breaker effects
07 p1094 A69-18422

Beam modulation resynchronization at large signal levels by TWT circuit wave to enhance efficiency
07 p1094 A69-18423

X band CW traveling wave tube developed for communications, ECM and plasma research, discussing design, performance and gain ripple diminution
07 p1094 A69-18425

Power traveling wave tubes in ground stations for INTELSAT 3 direction finding system
07 p1094 A69-18426

High power coupled cavity traveling wave tube for satellite communication, noting design techniques and performance characteristics
07 p1094 A69-18427

Coupled cavity short slit delay lines in high power traveling wave tubes
07 p1095 A69-18428

Traveling wave tubes for Symphonic Communication Satellite, discussing design, performance and efficiency
07 p1095 A69-18429

Space harmonics effect on helical TWT design, discussing operating voltage, beam radius, perveance and maximum allowable gain
07 p1105 A69-18950

Parametric light interactions application to optics stressing nonlinear spectrograph and cavity and traveling wave oscillator
[IEEE PAPER K-5] 07 p1152 A69-19066

Thin electron flux interaction with electromagnetic wave in open waveguide, discussing nonlinear theory and performance of gyroresonance transverse wave tube
07 p1107 A69-19159

Annular traveling wave resonator for feedback in resonance particle accelerator of smooth waveguide
07 p1107 A69-19160

Signal to cross modulation noise ratio in TWT tube during amplification of sinusoidal signals
10 p1653 A69-23109

Laser beam welding effectiveness for TWT with coaxial input and output lines
11 p1896 A69-24741

TWT heat pipe cooled depressed collector designed as compact heat transfer device and electrical insulator
11 p1847 A69-24746

High power TWT tube cooling in space vehicle, discussing thermal control system based on heat pipe radiator
11 p1847 A69-24747

Power saturation in isochronal traveling wave tube explained by motion of electron bunches relative to waves
12 p2041 A69-26646

Power gain in TWT attenuators with linear tapered ends, considering conversion loss due to tapering
12 p2044 A69-27102

Traveling wave tubes for high efficiency and extreme environments, discussing power output and RF drive
13 p2232 A69-28055

Traveling wave tubes with broadband CW power, discussing energy dissipation
13 p2232 A69-28057

Nonlinear distortions in TWT for communication satellites applications, discussing relationship with efficiency
13 p2232 A69-28060

Electric field distribution in TWT electron beam deflection system determined, accounting for current-voltage characteristics dependence on electromagnetic field distribution
13 p2237 A69-28582

Traveling wave tube amplifier for wideband radio in SHF range containing periodically integrated magnetized system, discussing output power variation range
16 p2759 A69-31863

Lamination influence on traveling wave tube performance, showing negative effect of radial variations in electric field
16 p2762 A69-32499

Dispersion and coupling impedance calculation for symmetrical or helical slow wave structures employed in traveling and backward wave tubes
22 p3916 A69-40958

Ridge-slot-ridge slow-wave structures used in multibeam TWT (traveling wave tube), analyzing E type electromagnetic dispersion as function of system parameters
23 p4140 A69-42049

Traveling wave tubes in satellite earth stations, discussing single carrier tubes and multiple carrier technique
23 p4143 A69-42420

TRAVELING WAVES

Wave scattering in nonuniform cross section waveguides with large flare angles using coupled differential equations
01 p0044 A69-10622

Parametric vibrations of self excited elastic and aeroelastic systems with traveling waves, determining stable vibration boundaries
02 p0337 A69-11561

Frequency difference of traveling waves in accelerated rotating ring laser
02 p0257 A69-12417

Collision broadened homogeneous linewidth measurements for 6328 angstrom Ne line in Ne and He-Ne discharges, using nonlinear interaction between two traveling waves
02 p0257 A69-12613

Oppositely moving waves interaction during nonlinear transient process of oscillations buildup in annular solid state laser found dependent on coupling via scattering
02 p0259 A69-12648

Mode theory of backscattered radar cross section of elongated dielectric bodies capable of sustaining traveling wave
03 p0384 A69-12907

Traveling waves interaction effects on emission modes of gas laser with circular resonator
04 p0611 A69-14545

High power waveguide tuner for use in traveling wave resonator to tune out reflections in resonant ring
04 p0576 A69-14759

Statistical theory of traveling wave antennas for random phase-amplitude distribution of current, discussing phase errors
06 p0898 A69-17797

Traveling wave microwave and optical resonators synthesis, determining design conditions for resonant frequencies
07 p1145 A69-18477

Traveling waves on elastic spherical shells derived from dynamic equations of motion, including transverse shear and rotatory inertia effects
07 p1236 A69-19460

Interaction between atom and plane monochromatic traveling wave taking into account pressure effect occurring in strong collision model
08 p1354 A69-19954

Algebraic expression for field pattern of asymmetrically driven long antenna with multiple excitations, using Wiener-Hopf integral equation
08 p1281 A69-20016

Plasma acceleration by pulsed electromagnetic traveling wave, discussing stable column formation and acceleration loss processes
09 p1544 A69-21301

Charge and traveling wave interaction in circular waveguide in resonance regime solved by Krylov-Bogoliubov asymptotic method
09 p1551 A69-22037

Busbar effect on interaction between conducting fluid flow and traveling wave magnetic field created by long line with concentrated inductance and capacitance, deriving line gain
10 p1727 A69-23101

Amplitude fluctuations and line width of traveling wave and standing wave He-Ne laser, considering saturation effects
10 p1701 A69-23135

Level degeneracy effect on nonlinear interactions between traveling waves of different planes of polarization
10 p1705 A69-23815

Transport of matter in nonisothermal weakly ionized plasma due to traveling ion-acoustic wave propagation, noting plasma oscillations and instability
10 p1741 A69-23945

Traveling wave passive Q switched laser with bleachable absorber filter, analyzing unsteady processes without expanding field along natural resonator modes
10 p1705 A69-23949

Helical and log conical helical antenna width reduction by loading of traveling wave antenna elements with isotropic material
11 p1852 A69-25315

Potential triple traveling space waves in barotropic gas with arbitrary equation of state, analyzing adjacent and three dimensional self similar flows
12 p2061 A69-25889

Laser output power amplitude fluctuations effect on beat frequency stability for traveling waves in annular laser with broadened Doppler emission line
12 p2107 A69-26541

He-Ne laser traveling wave output power, obtaining end mirror reflection coefficient optimal value
14 p2458 A69-29165

Fringing effects on electric efficiency variation with slip for cylindrical induction MHD device operable as accelerator, generator or Joule heater
[AIAA PAPER 67-714] 16 p2736 A69-32152

Zonal flow intensity, velocity and kinetic energy of standing and traveling waves compared for Northern and Southern Hemispheres
17 p2997 A69-33392

Air motion and precipitation patterns in travelling wave depression, considering Doppler radar data, rainfall rates, orographic influences, etc
18 p3166 A69-34419

Spectral, angular and temporal characteristics of traveling wave mode ruby laser emission, noting high transverse divergence effect on mode operation
21 p3741 A69-39554

Boltzmann equation for electron distribution function of Lorentzian plasma traversed by transverse traveling wave, showing existence and uniqueness of solution
24 p4354 A69-42675

TREADMILLS

Cardiac arrhythmias during positive G sub x acceleration, treadmill exercise and tilt table testing
06 p0874 A69-17834

TREES [MATHEMATICS]

Trunk and tree searching properties of Fano sequential decoding algorithms 06 p0902 A69-17400

Linear network analysis by topological formulas for derivation of k-tree terms without generation of k-trees of graph 06 p0903 A69-17409

Infinite tree code ensemble upper bound on moments derived for sequential decoding governed by Fano algorithm 09 p1471 A69-21318

Adaptive logic trees with two input gates for mechanization of any desired function of variable set, deriving multilevel representations of functions 09 p1475 A69-22583

Topological circuit analysis by digital computer, using conductivity matrix determinant in form of sum of trees 15 p2582 A69-30112

Fault tree for hardware multiple failure safety analysis and reliability analysis for single failure analysis, illustrating comparative advantages 18 p3142 A69-34479

Computerized system-safety fault trees, discussing drawing, configuration control and simulation program 19 p3280 A69-36029

N-dimensional vector functions branching process stability belonging to locally compact set in certain space 20 p3509 A69-37075

Tree codes for memoryless time discrete sources with bounded fidelity criterion 24 p4284 A69-42720

TREES [PLANTS]

NT WOOD

Previsual detection of vigor loss and mortality signs in ponderosa pine trees subject to bark beetle attack 12 p2098 A69-26993

TREMORS

Tremographic studies of central nervous system during supersonic flight as engineering psychology application to man-machine relations in aircraft-spacecraft industries 19 p3259 A69-35834

TRENDS

Technological forecasting by intuitive forecasts, consensus methods, analogy, trend extrapolation and structural models 13 p2382 A69-28040

TRESCA FLOW

Thin circular cylindrical shells steady creep behavior under combined lateral and axial pressures, using Tresca criterion and associated flow rule 06 p1023 A69-17506

Enlargement of circular hole in disk with kinematic hardening and Tresca yield function compared with isotropic hardening 21 p3840 A69-39297

Nadai and Zyczkowski stress analysis for Tresca yield condition reexamined for determination of critical angular velocity of solid elastic perfectly plastic disk 23 p4235 A69-42480

Collapse load of shallow conical shells clamped at base and loaded through finite rigid boss, using Tresca yield condition for sandwich shell 23 p4236 A69-42496

TRIANGLES

Mechanical calculators for solving spherical triangle problem of navigation 07 p1135 A69-19207

Curved tetrahedral and triangular elements in matrix displacement method covering linear and nonlinear cases 08 p1415 A69-20631

Square matrices decomposition into orthogonal and triangular matrices products for computer storage applications 13 p2290 A69-28485

Theory, function generator routine and testing for six node 18 degree of freedom triangular element for plate bending 15 p2706 A69-30430

Stiffness matrix for refined triangular plate bending finite element, considering Kirchhoff theory 15 p2706 A69-30434

Flexure functions of triangular sections under terminal loads, using electric analogy to study function effect on section shape and material Poisson ratio 17 p3066 A69-34050

Triangular plate bending element using Herrmann variational method, deriving matrices for finite elements 24 p4404 A69-43591

TRIANGULAR WINGS

U DELTA WINGS

TRIANGULATION

Satellite triangulation simultaneous and trailing methods, discussing timing devices design [UN PAPER 68-95285] 01 p0064 A69-10475

Great circle route determination based on celestial spherical triangulation 02 p0278 A69-12360

French program of space geodesy, discussing spatial triangulation, telemetry, dynamic geodesy, Diapason and Diademe experiments [UN PAPER 68-95834] 06 p0917 A69-17071

Horizontal aerotriangulation by independent models using photogrammetric extension of horizontal control for small scale superwide angle photography, horizon photography and B 8 plotter 06 p0925 A69-17468

Tucson selenodetic triangulation for coordinated points, considering measures on Yerkes star trailed plates 07 p1225 A69-19774

Photogrammetry for three dimensional geodesy, discussing satellite triangular methods, refraction anomalies, error corrections, etc 10 p1682 A69-23390

Satellite photographic astrometry and chronometry, determining spatial positions of satellites and observation stations by space triangulation 11 p1956 A69-24400

Spatial direction determination from simultaneous photographs of Echo 2 at Nikolaev and Helwan stations, using circle of simultaneity 12 p2068 A69-26427

Earth stations coordinates determination from non-simultaneous photographic satellite observations by orbital method compared with simultaneous photographic observations of Echo 1 12 p2068 A69-26430

Cosmic triangulation by geometrical synchronization of astrometric satellite observation, with precise times unavailable 12 p2158 A69-26432

Satellite triangulation by least squares method based on conditions relating to observing stations coordinates, concerning synchronous observations of directions and distances 15 p2594 A69-30030

Geometric conditions selection in directions determination in satellite and rocket aided triangulation, deriving formulas for chords directions of earth ellipsoid 15 p2689 A69-30572

Relative control data incorporation into sequential or simultaneous analytical triangulation systems, considering extraterrestrial photographs reduction 18 p1313 A69-34335

Atmospheric sources automatic location by direction finding network based on triangulation network principle 18 p3102 A69-34961

Australia spatial triangulation and trilateration using geometric satellite geodesy, including station position accuracy tests 18 p3132 A69-35499

Instruments for obtaining auxiliary data in aerial triangulation, describing stratoscope, profile recorder, radar altimeter, horizon camera, etc 22 p3944 A69-40042

Ancient and present earth radii ratios determined by triangulation using paleomagnetic sites situated on different paleomeridians 22 p3937 A69-40183

Satellite photographic astrometry and chronometry, determining spatial positions of satellites and observation stations by space triangulation 24 p4391 A69-43790

TRIATOMIC MOLECULES

Molecular jets obtained by charge exchange of triatomic ion beams consisting of hydrogen, deuterium and nitrogen, noting formation, energy level, etc 05 p0797 A69-16339

Shock ionization by ion impact against triatomic H molecules gas target, showing positive ion production dependence on extraction voltage, collision chamber pressure, etc 19 p3378 A69-36188

TRIAXIAL STRESSES

Stress-strain state in infinite medium with cavity under triaxial tensile force obtained from integrodifferential equation deduced from equilibrium equation 23 p4226 A69-41703

Stress concentrations in circular plate with square hole subject to triaxial tension 23 p4227 A69-41712

TRIAXIALITY

U TRIAXIAL STRESSES

TRICHLORIDES

U CHLORIDES

TRIDENT AIRCRAFT

U DH 121 AIRCRAFT

TRIGGER CIRCUITS

Input transistor performance analysis in Schmitt trigger circuit, considering role of hysteresis 01 p0039 A69-10170

Schmitt trigger current-voltage characteristic for determining switching behavior and switching point temperature, examining formulas and equivalent circuits 01 p0039 A69-10171

Multimode digital radar control paths and operating communication, discussing radar data, triggers, real time data and error localization 05 p0718 A69-15750

Low power RF signal triggering of self sustaining Gunn oscillations in GaAs samples 05 p0734 A69-16575

Tunnel diode subnanosecond coincidence circuit stability and time resolution, noting influence of polarization and input-pulse currents 05 p0735 A69-16743

Transformer inrush transients control by selection of core material, primary turn number and trigger circuitry 06 p0894 A69-17221

Mathematical model for voltage step-down DC to DC converter with hysteretic bistable trigger circuit regulating output voltage 06 p0904 A69-17941

Tunnel diode pair unidirectional pulse regenerating circuits 07 p1104 A69-18892

Lumped element line generators for high power pulsed sinusoidal oscillations utilizing recurrent triggering system, noting use in plasma physics experiments 10 p1662 A69-23344

Jittering delay of triggering circuit driven by ramp signals of different finite slopes, noting tunnel diode discriminators and regenerative feedback loop circuits 11 p1858 A69-24568

Transistorized assembly for amplification of signals emitted by platinum film probes in shock tubes, discussing application to chronometric device triggering 11 p1887 A69-25095

Electronic switching circuits controlled by binary counter triggers for variable passband filters 12 p2040 A69-26489

Trigger demodulator theory, design and circuits 14 p2419 A69-28907

Space charge effects on trigger current and reflector voltages of reflex klystron 15 p2574 A69-30131

TRIGGERS

U ACTUATORS

TRIGONOMETRIC FUNCTIONS

NT SINE SERIES

NT TANGENTS

Onboard digital computer evaluation of trigonometric functions for antenna pointing 07 p1089 A69-19745

Trigonometric and arithmetic functions for reducing size of MOS read-only memories to reduce required bit count, discussing cost, structure and applications 07 p1089 A69-19778

Error analysis involved in calculating tangent functions defined by nonlinear differential equation solution, using digital differential analyzer 13 p2225 A69-27968

Localization and convergence of Fourier series for fundamental systems of functions of Laplace operator, including eigenfunctions and trigonometric systems 15 p2644 A69-30287

Relative dielectric constant and permeability of inhomogeneously filled rectangular waveguide filling medium expanded into trigonometric series to calculate cut-off frequencies and field patterns 15 p2577 A69-30627

Trigonometric polynomials representing perturbation function and derivatives in three body problem
20 p3596 A69-37315

TRIGONOMETRY

Mechanical calculators for solving spherical triangle problem of navigation
07 p1135 A69-19207

TRIM [BALANCE]

U AERODYNAMIC BALANCE

TRIMETHYL COMPOUNDS

Lewis acidity of alanes, discussing interactions of trimethylalane with amines, ethers and phosphines
07 p1074 A69-18630

Enthalpies determination of adduct formation of sulfoxides, sulfanilamides and thionylamides with trimethylalane, noting replacement effect on electron donating ability of oxygen
07 p1074 A69-18631

Physicochemical and operational properties of trimethylol propane esters as lubricating oils under static and dynamic conditions
12 p2103 A69-27090

Quantitative gas-liquid chromatography of sulfur amino acids trimethylsilyl derivatives
13 p2217 A69-28259

Quantitative analysis for N-acetylneuraminic acid by gas-liquid chromatography using trimethylsilyl derivative
13 p2217 A69-28315

TRINITRO COMPOUNDS

Compatibility of inorganic azides with organic explosives from elevated temperature interactions using trinitrobenzene as model
02 p0304 A69-12499

Nuclear radiation damage vs thermal decomposition of diaminotritrobenzene and hexanitrostilbene, analyzing unchanged residual compound
02 p0304 A69-12500

TRINITROTIAZOCYCLOHEXANE

U RDX

TRIODES

P-n channel MOS triode fabricated by doped-stepped-oxide method, obtaining p-channel enhancement
07 p1100 A69-18622

Barkhausen oscillator for LF domain by substituting Cs and K positive ions for electrons, giving oscillation curves and spectral analysis
08 p1280 A69-19981

Triodes reliability for space application, emphasizing RH 7 Cc used during Mariner 4 expedition
08 p1295 A69-21122

Germanium solid state triode controlling electron currents of space charge limited regime by means of gate conductors in solid state diode
09 p1462 A69-21353

Optimum performance from planar metal ceramic triode oscillators by pulse modulation method selection, considering plate, cathode and grid modulation
09 p1470 A69-22793

Wideband RF amplifier manufacturing problems, comparing operation of vacuum triodes and pentodes in passband circuits
11 p1849 A69-24958

Current harmonics in triode klystron for frequency multipliers, noting modulation voltage
13 p2234 A69-28510

Nondrifting n-p-n semiconductor current gain dependence on surface recombination rate
13 p2236 A69-28547

Triode with emitter controlled negative resistance of GaAs as oscillator for microwave applications
22 p3911 A69-40010

TRIPLET EXCITATION

U ATOMIC ENERGY LEVELS

TRIPLET STATE

U ATOMIC ENERGY LEVELS

TRIPROPELLANTS

U LIQUID ROCKET PROPELLANTS

TITANIUM

Energy deposits from decay of tritium incorporated into bacteria, using computer simulation for radiation dose distribution
07 p1068 A69-19490

Inactivation of T4 bacteriophage by tritium decay incorporated into DNA and phage protein
07 p1068 A69-19491

Tritium and argon 39 measurements of stone and iron meteorites, discussing decay and production rates and cosmic ray intensity
09 p1604 A69-22398

Negative pion from 600 MeV synchrocyclotron stopped in thin Li 6 target in search for excited states of triton
12 p2132 A69-26297

Tritium contamination reduction in small ion accelerators for neutron production, discussing pumping problems and vacuum systems
12 p2059 A69-26499

Na 22 and H 3 production rates determined in stone meteorites exposed to 3 Gev isotropic protons, using radionuclide distribution data of exposed thick stone target
19 p3425 A69-36423

TRIVALENT IONS

Ground state population modulation in trivalent rare earth doped single crystals by means of optical double resonance, noting applications
01 p0134 A69-10013

Nonradiative transfer of excitation energy between mixed trinuclear complexes of Tb and Eu ions with lactose in aqueous solution
01 p0023 A69-10288

Trivalent rare earth ions Stark structure based on spectroscopic observations of stimulated transitions in lasers
10 p1701 A69-23129

Angular dependence of EPR line widths of trivalent Cr ions in zinc tungstate in rotating magnetic field, noting spin-phonon mechanism
10 p1743 A69-23131

Glass lasers with trivalent rare earth ions noting properties, characteristics and recent developments
11 p1898 A69-25043

TROCHOIDS

U PIVOTS

TROILITE

Barringerite as Fe-Ni phosphide occurring in meteorite Ollague pallasite, indicating troilite and schreibersite crystallization at high temperatures
18 p3205 A69-35433

Isoprenoids and isomeric alkanes identification in carbonaceous chondrites by gas-chromatographic mass-spectrometric analyses, including results from troilite nodules
19 p3414 A69-36113

Morphological, chemical and X ray analysis of urelite meteorite, identifying diamonds with kamacite and troilite admixtures from carbonaceous material
21 p3816 A69-39626

TROJAN ORBITS

Stability characteristics of small and moderately sized short period Trojan librations in sun-Jupiter restricted three body problem
01 p0158 A69-11329

Periodic Trojan orbits for resonance 1/12 in restricted three body problem, noting bridge of stable and unstable orbit lanes
13 p2350 A69-27824

TROPICAL METEOROLOGY

Mean meridional circulation models in tropics based on vorticity equation
03 p0460 A69-13334

Large scale tropical eddies using two layer dry atmospheric model containing nongeostrophic effects and parametrized dissipation
07 p1176 A69-19035

Annual temperature variation in lower tropical stratosphere, noting effect of equatorial upward motion
07 p1126 A69-19043

Coupling and other factors affecting large scale motions in tropics
07 p1176 A69-19045

Tropospheric zonal wind semiannual oscillations in Southern Hemisphere tropics with westerly maxima and easterly minima in May and November
12 p2064 A69-26011

Equatorial stratospheric wind fluctuations from pressure fluctuation data, relating southern fluctuations, stratospheric fluctuations and seasonal hemispheric air exchange
14 p2442 A69-29726

Cloud pattern characteristics in intertropical convergence zone above Indian and Pacific oceans from meteorological satellite photographs and cloud formation maps
14 p2473 A69-29728

Normalized correlation functions of dispersion values for pressure fields and geopotential obtained by low latitude stations, noting wind field features
14 p2478 A69-29833

Survey of six year period of satellite observed tropical Pacific cloud mapping
17 p2996 A69-33001

Tropical circulation long term mean values of wind and temperature fields, momentum and heat fluxes from weather stations data, noting consistent pattern and energy source
18 p3165 A69-34418

Causal and semiphenomenological theories concerning equatorial F 2 region, discussing electrodynamic drift theory and transequatorial winds
20 p3531 A69-37888

Numerical prediction experiment for dynamical structure of tropical atmosphere in equatorial latitudes, constructing pressure, temperature and vertical motion distributions from wind field
20 p3573 A69-37910

Equatorial aeronomy - Conference, Ahmedabad, India, February 1969
23 p4159 A69-42422

Equatorial anticyclones over eastern Pacific caused by large scale cross-equatorial flows determined by ATS-1 photographs, noting frictional convergence factor
24 p4342 A69-42895

TROPICAL REGIONS

Low latitude m arcs in 6300 angstrom emission during intense geomagnetic storm related to auroral red oxygen emission peak
01 p0062 A69-10136

Tropical 6300 angstrom red oxygen nightglow enhancements related to variations in height of nighttime F 2 layer, noting implications for layer structure and physics
01 p0068 A69-11113

Equatorial enhancement of storm sudden commencements and sudden impulses in horizontal component in American Zone during IGY/IGC
01 p0068 A69-11116

Ionospheric electron content, slab thickness and scintillation occurrence measurements at low latitude stations
02 p0235 A69-11427

Solar eclipse effect on geomagnetic field at and near dip equator observed at Huancayo Observatory, Peru
02 p0241 A69-11727

Tropical night F layer maintenance mechanism, noting airglow enhancement and ionization source association with plasma drifts
02 p0242 A69-11825

Long period variations in zonally symmetric circulations of tropical stratosphere, using zonally averaged momentum, continuity and heat and heat energy equations for numerical model
03 p0461 A69-13681

F region equatorial irregularity belt observed from satellite transmission scintillation, noting north-south elongated patches
05 p0758 A69-16418

Equatorial hourly storm time part of disturbances field for 1958, discussing magnetic storm effects
07 p1124 A69-18822

Midday enhancement of sudden commencements and sudden impulses in H and Z at equatorial stations in Indian zone during IGY
08 p1307 A69-20187

Zonal momentum vertical transport due to large scale moving disturbances in westerlies of equatorial lower stratosphere
09 p1537 A69-22299

Rocket sounding data on ionospheric currents at mid and low latitudes, showing absence in D and above E region
10 p1686 A69-23909

Pacific atmospheric circulation and Pacific equatorial sea temperature winter anomalies, noting Hadley circulations, northeast westerlies, trade winds and Walker circulation
11 p1911 A69-24322

European pilots accustomed to equatorial climate tested during regular flying missions, discussing heat effects on urinary steroids
12 p2024 A69-26560

Atmospheric pressure and wind data at equatorial latitudes, determining relation between rms meridional and zonal wind and pressure gradient
13 p2293 A69-27845

Latitudinal and vertical variations in six-month zonal wind cycles in equatorial and tropical stratosphere and lower mesosphere, utilizing rocket observations
13 p2294 A69-27854

Equatorial jet stream excitation of longitudinal waves, analyzing plasma beam instability and spectrum of short wave inhomogeneities by quasi-hydrodynamic equations
14 p2437 A69-29073

TROPICAL STORMS

Daytime ionospheric screening effect on low latitude geomagnetic micropulsations estimated using ionosphere model

14 p2441 A69-29380

Three dimensional model of atmospheric drift currents in equatorial region of world ocean system based on nonlinear differential equations

14 p2472 A69-29405

Ozone concentration changes in polar regions and tropical zone due to meridional atmospheric circulation

14 p2442 A69-29830

Two year cyclic monsoon type variations in zonal wind distribution in tropical stratosphere and mesosphere obtained by rocket measurements

14 p2478 A69-29834

Self maintenance of absolute angular momentum in atmosphere as explanation of subtropical jet stream origin

15 p2647 A69-30192

GHOST Balloon Project, emphasizing launch and ascent control and location and life expectancy of superpressure balloons in tropical stratosphere

15 p2551 A69-31361

Regional distribution of relative angular momentum transport over equator, noting advective and turbulent transfer

16 p2773 A69-31793

Lunar tidal variations of electron concentration in F2 region near magnetic equator showing large latitudinal dependence

16 p2776 A69-32090

Low latitude asymmetric disturbance field analyzed using equivalent current vectors during magnetic storms, allowing for solar quiet day variation and declination

16 p2778 A69-32184

Nighttime decreases in F2 layer heights at near conjugate stations in low latitudes, using electron density profiles

16 p2778 A69-32186

Correlation between F region electrons vertical motion velocity variations and E region electrons horizontal motions in equatorial ionosphere

16 p2779 A69-32193

Low latitude sporadic E layer associated with geomagnetic activity studied in Hong Kong using proton precession magnetometer and standard ionosonde

16 p2779 A69-32195

Annual variations of postsunset altitude peak of equatorial F region noting correlation with solar activity

17 p2966 A69-33983

Postsunset apparent reflection height and electron density variability in equatorial F2, discussing singularities of diurnal variation in November-January

17 p2967 A69-33984

Composition and temperature of daytime and nighttime neutral tropic lower thermosphere, obtaining atomic and molecular oxygen ratios

18 p3128 A69-34936

Whistlers occurrence and dispersion rate variations from data obtained at lower latitudes during magnetic storms

18 p3102 A69-34967

Jupiter observations /1966-1967/, discussing variations in size and position of polar caps and tropical belts

18 p3203 A69-35337

Topside equatorial ionosphere structure and behavior, describing anomaly development and decay

20 p3530 A69-37869

Earth albedo in lower latitudes measured by satellites and surface stations, comparing solar energy absorption by oceans and atmosphere

20 p3591 A69-38058

Equatorial plasma sheet role in magnetotail assessed from Vela satellite data, noting diurnal density variations

21 p3711 A69-38512

Performance prediction of terrestrial communication system based on experimental radio and meteorological program at 11 GHz, discussing transmission loss

22 p3900 A69-40680

Peak field strengths of atmospheric radio noise bursts from lightning flashes at VHF and flash distance estimates at tropical latitudes

23 p4126 A69-42355

Equatorial stratosphere and mesosphere wind, temperature and density data from rocket and balloon sounding, noting seasonal variations and possible stratosphere-ionosphere coupling

23 p4159 A69-42423

Equatorial E sub sq and daytime blanketing sporadic E occurrence frequencies compared in magnetic equatorial zone, considering diurnal, seasonal, latitudinal and vertical variations

23 p4160 A69-42426

Daytime drift velocities and signal fading characteristics of equatorial and blanketing sporadic E layer irregularities, noting independence of electrojet intensity

23 p4160 A69-42429

Ionospheric electron content measurements at low latitudes close spaced frequency and differential Doppler shift technique, using BE-B and BE-C satellite transmission

23 p4161 A69-42435

Concurrent geomagnetic micropulsations at equatorial and high latitude stations, discussing magnetospheric sources of Pi and Pc types

23 p4161 A69-42439

Geomagnetic activity hourly and daily variations during solar cycle at Huancayo

23 p4162 A69-42442

Hadley and equatorial cell models for mean meridional circulation in terms of vorticity equation

24 p4345 A69-43152

Bidirectional reflectance of earth atmosphere and cloud formation above equatorial Pacific observed by synchronous satellite as function of angular dependence

24 p4346 A69-43154

TROPICAL STORMS NT HURRICANES NT TYPHOONS

Tropical storms wind speeds related statistically to characteristics as pictured from satellites

17 p2997 A69-33690

TROPICS U TROPICAL REGIONS

TROPISM U AEOLOTROPISM U GEOTROPISM U GYROTROPISM

TROPOPAUSE

Air mass displacements and diurnal variations in potential temperature at tropopause level

13 p2252 A69-27608

Energy dissipation near tropopause determined from measured clear air turbulence spectra and probabilities

19 p3303 A69-36407

Wavelike structure observed near tropopause with sensitive radar system, suggesting clear air turbulence as cause of breakdown of gravitational wave

24 p4342 A69-42893

TROPOSPHERE NT TROPOPAUSE

Tropospheric structure studied with high resolution antennas having small common volume

01 p0043 A69-10560

Tropospheric inhomogeneities properties and wind conditions in relation to lunar limb image deformations

01 p0156 A69-11182

Solitary mesoscale waves from air mass motion in troposphere, neglecting Coriolis force and turbulence

02 p0274 A69-11445

Light polarization of night sky components scattered by troposphere

04 p0595 A69-15247

Cloud features produced by European tropospheric low pressure areas observed by meteorological satellite photographs, noting cyclonic systems development

06 p0950 A69-17619

Multilevel objective weather analysis system for stratosphere and upper troposphere over Australia, using stream function analysis

06 p0950 A69-17787

Tropospheric energy cycle interannual variability and quasi-biennial oscillation from geostrophic computations of eddy kinetic energy, energy transfer and internal redistribution

07 p1129 A69-19628

Ionospheric and tropospheric effects on microwave propagation including Faraday rotation, atmospheric refraction, attenuation and noise

08 p1272 A69-19958

Geostrophic trajectories of horizontal diffusivity estimated in midlatitude troposphere and lower stratosphere

08 p1308 A69-20310

Mean and eddy terms contribution to momentum and heat balance of troposphere and lower stratosphere at solstices, describing zonal wind equations

08 p1308 A69-20318

Mean tropospheric wind vectors periods compared to annual variations of earth rotation and pole latitude

08 p1309 A69-20854

Ozone and carbon dioxide stratospheric and tropospheric horizontal distribution from weather data collected on polar flight

09 p1484 A69-21403

Time and altitude distribution of wind zonal components over Fernando Noronha Island off Brazilian coast, discussing tropospheric pattern

11 p1913 A69-25204

Carbon dioxide concentration in upper troposphere and lower stratosphere recorded during commercial aircraft flights over polar route

11 p1879 A69-25254

Tropospheric zonal wind semiannual oscillations in Southern Hemisphere tropics with westerly maxima and easterly minima in May and November

12 p2064 A69-26011

Density stratified model of troposphere and constant gravity field for ground level pressure perturbations in mesoscale region

12 p2126 A69-26016

Stratosphere and troposphere processes analyzed, indicating feasibility of forecasting geopotential and wind fields between 12 and 24 km

12 p2126 A69-26581

Formulas derived for tropospheric equivalent noise temperature as function of frequency, noting applicability to thermal radiation from rain

12 p2032 A69-26704

Internal guiding of microwaves by elevated tropospheric layer noting refractive index, radius of curvature and attenuation

12 p2032 A69-26856

Two temperature lapse rate and single moisture lapse rate troposphere model for calculating temperature and moisture from satellite radiometry

13 p2252 A69-27638

Trapped aerosols below temperature inversions causing lidar echoes in troposphere layers, discussing simultaneous balloon refractometer, thermometer and ground based lidar soundings

13 p2254 A69-28475

Incoming IR flux measurements at high altitude, noting flux increase due to water vapor condensation in troposphere

13 p2256 A69-28647

Richardson number in vertical tropospheric region of maximum wind computed from data on jet streams observed in winter over radiosonde stations in Italy

13 p2295 A69-28656

Radio signal amplitude changes from Explorer 22 beacon satellite attributed to wave diffraction by tropospheric structures

14 p2411 A69-29107

Mean-minute thermal noise intensity distribution in telephony channels of tropospheric radio relay systems

14 p2412 A69-29425

Microwave brightness temperatures for downward viewing over open seas from above atmosphere, using tropospheric model containing homogeneous layer clouds

14 p2415 A69-29515

Tropospheric and stratospheric temperature distribution in 1965 summer and winter from radiosonde and rocket data

14 p2442 A69-29725

Synoptic criteria combined with qualitative criteria for CAT diagnostics from analysis of turbulent zones responsible for bumpiness in upper troposphere

14 p2474 A69-29736

Zonal and meridional components of air circulation in troposphere and lower stratosphere for Northern Hemisphere

14 p2477 A69-29829

Troposphere behavior and stratosphere structure over Southern Hemisphere based on rocket measurements, comparing hemispheric atmospheric circulation intensities

14 p2477 A69-29832

Wind velocity fluctuations calculation in CAT based on closed equations numerical solution for turbulent layers in upper troposphere

15 p2649 A69-30649

UHF propagation in spherically stratified superrefractive troposphere with trapping surface layer, discussing distant field strength dependence on refractivity profile

16 p2752 A69-32388

Noise levels due to long range tropospheric transmission calculated for microwave radio systems

17 p2919 A69-33146

Vertical tropospheric humidity distribution estimation from IR spectra obtained by TIROS satellites

18 p3126 A69-34284

Mean patterns of meridional interhemispheric flow for 40 degree equatorial sector, calculating mean air

mass transport in lower troposphere over western Indian Ocean

18 p3166 A69-34420

Correlation between disturbances in troposphere and in geomagnetic field observed after widespread high winds and magnetic storms, using superposed epoch method

18 p3127 A69-34648

Relation between atmospheric processes in troposphere and upper stratosphere in cold half year

18 p3166 A69-34817

Secor data reduction to correct tropospheric refractive effects of radio ranging on earth satellites using tropospheric model

18 p3104 A69-35200

Vertical distribution of concentration, microstructure and chemical composition of solid aerosol in troposphere and stratosphere from high altitude balloon measurements

18 p3132 A69-35340

Vertical profiles of pressure, temperature and density variations due to upper troposphere pressure changes with and without zero layer effect

19 p3365 A69-36580

Tropospheric influence on pulse signal propagation, measuring pulse function of propagation path, hypothesizing signal reflection from tropospheric boundary layers

19 p3279 A69-36879

Meridional circulations in kinetic energy budget of Northern Hemisphere troposphere based on winter and summer climatic mean data, noting Hadley circulation

20 p3523 A69-37505

Vertical wind shears, structure functions, turbulence and power spectra for transverse velocity fluctuations in troposphere and stratosphere, noting clear air turbulence

20 p3570 A69-37506

Thermal stability and radioelectric turbulence parameter derivative relationship for dry adiabatic stratification of lower troposphere and for inversions

20 p3571 A69-37509

Atmospheric phenomena effects on terrain imaging radar systems performance, discussing tropospheric turbulence and ionospheric irregularities

20 p3490 A69-37647

Water vapor profiles in stratosphere from IR radiometric observations under cloudless conditions, indicating relation to tropospheric meteorological features

20 p3535 A69-38261

EOLE constant level balloon flights in troposphere, discussing short lifetime due to overloading with ice in dense cirrus cloud

21 p3646 A69-38373

Vertical factor equation numerical solution for radio wave propagation in vertically inhomogeneous troposphere

21 p3674 A69-39121

Aerosol attenuation coefficients vs altitude in troposphere and stratosphere, noting seasonally dependent surface convective dust layer and temperature dependent aerosol maximum altitude

21 p3718 A69-39773

Circulation and temperature fields indices used for studying tropospheric-stratospheric interactions during stratospheric warming at constant pressure levels

22 p3977 A69-39929

Troposphere fine scale properties, comparing simultaneous results of five experimental methods

22 p3941 A69-40914

Three dimensional structure of large scale disturbances in lower stratosphere and upper troposphere in equatorial Pacific, using power spectral and synoptic analysis

23 p4159 A69-42345

Clear air turbulence detection in troposphere by multifrequency radiometric sensor, noting multibeam system for supersonic aircraft

23 p4144 A69-42536

TROPOSPHERIC SCATTERING

Tropospheric structure studied with high resolution antennas having small common volume

01 p0043 A69-10560

VHF transhorizon propagation by double reflection from elevated layer in troposphere

01 p0034 A69-11139

Transhorizon UHF energy transmission via tropospheric scatter, using propagation path model

02 p0209 A69-12350

Soviet book on multichannel and TV signals transmission over radio relay links using microwave tropospheric scatter propagation

04 p0558 A69-14919

Soviet book on meteor trail scatter communications covering civil and military advantages over troposcatter systems, meteor trail scatter properties, etc

04 p0562 A69-15488

Radio signals and concentrated noise amplitudes probability distributions reflected from ionosphere and scattered in troposphere calculated for Rayleigh and log-normal fading

11 p1833 A69-24440

Troposphere effects on millimeter wave radio astronomy measurements, discussing solar noise fluctuations due to clouds and precipitation

13 p2223 A69-28607

Multipath resolution of tropospheric scatter medium by incorporating Rake instrumentation into tropospheric transhorizon microwave experiments

14 p2448 A69-29524

Remote sensing of lower atmosphere refractive structure, using Rake tropospheric scatter channel-sounding technique

14 p2448 A69-29525

Global communication techniques and trends, discussing radio telephone and telegraph, submarine systems, satellite communications, line of sight links, tropospheric scatter, waveguide transmission, etc

16 p2750 A69-31755

Variable scatter mechanism in turbulent tropospheric propagation medium, employing dynamic meteorology concepts for frontal disturbances effect on scatter volume

17 p2927 A69-33856

Tropospheric influence on pulse signal propagation, measuring pulse function of propagation path, hypothesizing signal reflection from tropospheric boundary layers

19 p3279 A69-36879

Tropospheric refractivity height profile model, computing corrections to satellite Doppler or range data

21 p3678 A69-39748

TROPOSPHERIC WAVES

Long wave radiative water vapor cooling in troposphere determined by numerical prediction model, including vertical distribution of cloud and moisture effects

07 p1175 A69-18896

Statistical distributions of refractive index parameters in tropospheric radio propagation from psychrometer soundings, discussing lapse rate

13 p2254 A69-28428

TROUBLESHOOTING

U MAINTENANCE

TROUGHS

F 2 layer equatorial anomaly at local noon, discussing position of trough center in latitudinal distribution of ionization

03 p0422 A69-13515

TRUCKS

NT TANK TRUCKS

Bayesian estimate of individual truck maintenance costs based on optimum replacement maintenance age

23 p4241 A69-41577

TRUNCATION [MATHEMATICS]

U APPROXIMATION

TRUNCATION ERRORS

N dimensional extensions of finite difference scheme for solution of differential heat conduction equation, noting practical limit by truncation error considerations

01 p0107 A69-11365

Algorithms for polynomial resultants computation, considering extraneous factors, truncation errors, memory and computing speed

06 p0892 A69-17884

Truncation error reducing scheme for balanced forecast models

07 p1176 A69-19629

Modified truncation for BBGKY hierarchy for plasma, obtaining kinetic equation identical with Balescu-Lenard equation

08 p1360 A69-19990

Runge-Kutta type method truncation error estimation, discussing validity conditions, evaluation processes and numerical tests

15 p2644 A69-30672

TRUNKS [LINES]

U TRANSMISSION LINES

TRUNIONS

U SHAFTS [MACHINE ELEMENTS]

TRUSSES

Mathematical programming in optimized truss design noting reduction of components under buckling

02 p0347 A69-12536

Forced flexural vibrations of elastic truss systems with allowance for hysteresis friction

03 p0432 A69-12953

Minimum weight analysis of Michell trusses transmitting given load to bars within allowable range of axial stress

08 p1410 A69-19893

Forced oscillations of resonance machine elements represented by truss of concentrated masses and external forces, taking into account aerodynamic energy dissipation

17 p3064 A69-33916

Lightly loaded truss structures fabricated from Be, Be-Al alloy and uniaxial B filament reinforced epoxy tubing for unmanned spacecraft applications

19 p3340 A69-35504

Plastic deformation effect on dynamic buckling of elastic-plastic simple shallow truss subjected to step and impulsive loading

19 p3446 A69-36836

Plane-truss joints displacements determined by graph-analytic method, discussing representation of fictitious forces and moments

23 p4225 A69-41420

Three dimensional pin-jointed trusses calculation method by state vector incorporating force and displacement matrices

23 p4236 A69-42485

Zero g deployment dynamics of erectable truss parabolic antennas, obtaining latchup loads as function of reflector mechanical energy [AAS PAPER 69-336]

24 p4398 A69-42827

TRYPSIN

Inactivation by heavy ions of esterase activity of dried trypsin as function of temperature during irradiation

03 p0372 A69-13483

Trapped radical relationship to inactivation of trypsin exposed to UV by measuring radical concentration and inactivation degree

03 p0372 A69-13486

Tryptic digestion of C terminal tritiated peptides analyzed with Scenedesmus ferredoxin, noting use for protein structural study

10 p1648 A69-24190

TRYPTAMINES

Regional uptake of melatonin from blood or cerebrospinal fluid by rat brain

09 p1444 A69-21466

TRYPTOPHAN

Fluorescence and phosphorescence from tryptophan powders stimulated at low temperatures with UV, vacuum UV, fast electrons and X rays

03 p0372 A69-13487

C 14-tryptophan incorporation into C 14-protein in cultured rat pineals, noting norepinephrine stimulation

22 p3871 A69-40054

TU-104 AIRCRAFT

Wing flaps and blow-off and suction effect on longitudinal balance of landing TU-104 aircraft, noting air suction at wing leading edge

19 p3247 A69-35818

TU-134 AIRCRAFT

TU-134 jet passenger aircraft performance characteristics noting similarity to BAC 111

13 p2202 A69-27931

TU-144 AIRCRAFT

Soviet supersonic transport Tu 144, describing wing unit, fuselage, passenger accommodation, tail unit, landing gear, power unit engine nacelle and navigation

10 p1634 A69-23838

TUBE CATHODES

NT COLD CATHODE TUBES

NT HOT CATHODES

NT PHOTOCATHODES

NT PHOTOMULTIPLIER TUBES

NT PHOTOTUBES

NT THERMIONIC CATHODES

SERT 2 mercury vapor fed hollow cathode operated in bell jar, determining volt-ampere characteristics and flow rates for plasma diagnostics [AIAA PAPER 69-258]

09 p1561 A69-21221

Optimal conditions for gas discharge in tubes with hollow cathodes in He-Ne mixture for obtaining lasing at Ne line wavelength

09 p1516 A69-21507

Cathode material effects on temperature coefficients for glow discharge tubes, noting running voltage pressure characteristics

09 p1468 A69-22602

Vacuum tube with cathode heated directly by external radioisotope source, noting heat pipe providing isothermal heat transfer

11 p1848 A69-24748

TUBE GRIDS

Current increase and voltage decrease in high voltage low pressure Penning discharge ascribed to hollow cathode effect

11 p1933 A69-25544

Argon ion laser with water cooled mercury pool cathode shielded by U-bent section trap, considering advantages as compared to oxide cathodes

12 p2107 A69-26326

Gas discharge tube graphite hollow cathode geometry leading to abnormal discharge operation under certain pressure conditions

16 p2814 A69-31838

TUBE GRIDS

Push-pull pentode frequency multipliers with sinusoidal undistorted outputs, studying grid bias effects on operating characteristics

22 p3912 A69-40260

TUBE HEAT EXCHANGERS

Heat exchange and hydraulic resistance in turbulent heat exchangers in longitudinal air flow calculated by criteria equations

01 p0173 A69-10092

Experimental apparatus for measuring heat transfer coefficients into boiling K in tubes, investigating vapor-liquid mixtures hydrodynamic and electrical properties

03 p0534 A69-14150

Small aircraft gas turbine regenerators employing heat pipes, noting excessive cost and weight [ASME PAPER 68-WA/GT-7]

05 p0812 A69-16142

Emissivity of screened tube in presence of heat conducting connecting pieces between tube and screen

11 p1997 A69-24229

Finned tube radiators with constant longitudinal specific heat flow, determining thermal efficiency and optimal thermal and structural parameters

20 p3631 A69-36978

Absorptivity of nonuniformly heated thin walled cylindrical radiator with central radiating hole, calculated by forward-reverse and integral methods

23 p4238 A69-41332

Perforated heat exchanger tube plates stiffness determination from hole diameter-to-spacing ratios

24 p4400 A69-43087

TUBES

Foldable tubular connection application to expandable lattice structure, analyzing cross sectional distortions

06 p1024 A69-17608

Gas film protection of quartz tube wall transparency loss due to hot plasma contact used to study UV emission during high power pulse discharges

11 p1926 A69-24616

Tube techniques - IEEE Conference, New York, September 1968

11 p1847 A69-24740

Stationary liquid under pressure effect on energy dissipation of rectilinear pipelines under pure bending

17 p2904 A69-33930

Elastoplastic boundaries of wave propagation of combined longitudinal and torsional stresses at tube end [ASME PAPER 69-APM-13]

18 p3213 A69-34389

Electron beam welding for repair and production, discussing application to Ti VHF antennas, Concorde switchgears and nuclear reactor loading tubes [SBAC PAPER 14]

20 p3550 A69-37451

TUBING

U PIPES (TUBES)

TUMBLING MOTION

Equivalent cross section theory relating air resistance of randomly tumbling bluff objects to resistance of equivalent spheres

09 p1431 A69-22000

Tumbling motion for testing gyroscopic devices quality

10 p1689 A69-22927

Cylindrical satellite drag rotating about transverse axis in earth magnetic field, including aerodynamic and magnetic moments

12 p2174 A69-26443

Planar tumbling in atmospheric entry, describing arrest by approximating Painleve equation

21 p3819 A69-39033

Gravity gradient perturbing torque cast in terms of perturbing Hamiltonian, deriving long term changes in rotational motion of tumbling triaxial satellite in elliptical orbit [AIAA PAPER 69-922]

21 p3821 A69-39353

TUMORS

NT CANCER

Radiological properties of high energy proton beams from synchrocyclotron in tumor treatment and neurosurgery

03 p0373 A69-13495

Adrenal epinephrine and phenylethanolamine n-methyl transferase /PNMT/ activity in rat bearing transplantable pituitary tumor

08 p1263 A69-20374

Single flash and rhythmic light stimuli effect on nystagmus of patients with tumoral posterior cranial fossa, recorded electroencephalographically

20 p3470 A69-37250

Tissue pressurized oxygenation during radiation therapy emphasized for overcoming tumor radioreistance attributed to oxygen deficiency

23 p4091 A69-41967

TUNERS

U WAVEGUIDE TUNERS

TUNGSTATES

U CALCIUM TUNGSTATES

U ZINC TUNGSTATES

TUNGSTEN

Substructural void formation in tungsten powder metallurgy as function of annealing temperature for doped, undoped and electron beam melted material

01 p0093 A69-10061

Grain boundary gas bubbles growth in chemically vapor deposited tungsten as function of annealing time, temperature and fluorine content

01 p0097 A69-10646

Creep behavior of chemical vapor deposited tungsten at high temperatures by creep-rupture tests compared with powder metallurgy tungsten

01 p0097 A69-10647

Adsorbed gas influence on X ray emission from exploding tungsten wires noting ungassed and degassed specimens in vacuum

01 p0118 A69-10668

Superconductivity of electron beam evaporated tungsten films by X ray and electron diffraction techniques, discussing temperature dependence of energy gap

04 p0640 A69-14447

Tungsten replacement by chromium or molybdenum in heavy metals shown possible for binding material of group 6A metals

05 p0780 A69-15991

Electro-optic properties of tungsten-bronze niobate ferroelectric crystals [IEEE PAPER F-7]

05 p0808 A69-16313

Lanthanum and hafnium effect on transition and recrystallization temperatures of tungsten and tungsten base alloys

05 p0782 A69-16797

Polycrystalline W steady state creep rate at high temperatures noting effects of stress, grain size and subgrain size

07 p1158 A69-18241

Tungsten delay powders combustion mechanism and intermediate stages of burning process, noting burning rate [WSCIPAPER 68-19]

07 p1202 A69-18370

Tungsten coatings applied on stainless steel and titanium alloy surfaces by plasma jet

07 p1165 A69-18931

Cobalt-tungsten solid solutions thermodynamic properties calculated by Borelius method using phase diagram

07 p1165 A69-18941

Pressure-temperature dependence of nitrogen solubility in tungsten at 2400-3000 C

07 p1168 A69-19602

Grain boundaries structure in tungsten wire using auto ion microscope, showing misorientation corresponds to high density coincidence site lattices

08 p1329 A69-19943

Thermal faceting of tungsten single crystal surfaces in oxygen, using vibrating-capacitor work function probe with low energy electron diffraction

08 p1330 A69-20137

Relative free energies of crystal zones of tungsten using field electron microscope, determining surface energy anisotropy from Wulff construction

08 p1330 A69-20139

Time and temperature dependence of Mo and W deformation structure variation and primary recrystallization from metallographic investigations using electron microscopy

08 p1334 A69-21058

Work function change of tungsten single crystal /100/ surface measured as time function during surface molecular gas adsorption

09 p1521 A69-21338

Work function and desorption energy measurements of alkali metals from metallic substrates with modulated molecular beam, noting surface contamination

09 p1558 A69-21808

Temperature effect on work function minimum of cesiated tungsten single and polycrystal surfaces, using vibrating capacitor technique

09 p1558 A69-21809

Surface characterization on chemical vapor deposited tungsten, evaluating grain size effect

09 p1558 A69-21810

Partial pole figures in vapor deposited and wrought cylindrical tungsten specimens, noting random surface produced by orientation

09 p1558 A69-21811

Thermionic converters with chloride and fluoride vapor deposited tungsten emitters, comparing performance characteristics and stability

09 p1438 A69-21819

Emission characteristics of duplex vapor deposited tungsten emitter with molybdenum collector in variable spacing guard ring converter

09 p1438 A69-21820

Comparative performance data of cylindrical diodes with various types of tungsten emitters, including emitter work function measuring device

09 p1439 A69-21821

Porous structures, using spherical tungsten powders, discussing metallurgy, sintering, temperature effects and performance characteristics in ion engines

10 p1710 A69-23166

Temperature and stress dependence of microstrain and microyielding in polycrystalline W for range of impurities and dislocations, considering transition to macrostrain

11 p1905 A69-25183

Sr and La ionization on crystal surfaces of W and polycrystalline W, discussing temperature effect on oxidation and work function

12 p2142 A69-26113

High speed photography of W strip fracture, considering electric current effects and electric circuit interruption by fracture

12 p2113 A69-26195

Flash radiography technique using tungsten wire explosion in vacuum to obtain ultrafast reproducible X ray pulse

12 p2092 A69-26480

Temperature effect on tensile brittle fracture stress of polycrystalline tungsten

12 p2116 A69-27135

Strain rate and pressurization effect on ductile-brittle transition temperature of polycrystalline sintered W, discussing yield stress

12 p2117 A69-27138

Internal friction, Young modulus and resistivity measurements for stage I interstitials in electron irradiated tungsten

13 p2284 A69-28682

CO adsorption on tungsten, determining work function changes and Fowler-Nordheim preexponentials on field emitter single crystal faces

14 p2409 A69-29093

Tungsten surfaces with high work functions generated by electrochemical etching, discussing effects of heat treatment in vacuum

14 p2506 A69-29267

Tungsten emitting surfaces work functions, discussing dense crystalline planes electrolytic or pyrolytic deposit growth and surface chemical or electrolytic attack

14 p2506 A69-29268

Langmuir S curves for tungsten single crystals in presence of adsorbed cesium, discussing orientation, theoretical and experimental correlation and instrumentation

14 p2506 A69-29271

Work function changes of tungsten single crystals as function of oxygen and CO gas pressure at high temperatures, using emission microscope

14 p2506 A69-29272

Tungsten work function increase by oxygen in diode thermionic emission, investigating crystals and vapor deposited layers

14 p2507 A69-29273

Plasma anode technique for work functions measurements of polycrystalline W and Re wires in cesium vapor with cesium oxide additive

14 p2507 A69-29274

Electron work function profile determined for polycrystalline Mo and W single crystals with and without Cs vapors by emission microscope and photomultiplier

14 p2507 A69-29276

W shear moduli at high temperatures measured by forced torsional vibration in wide frequency ranges, discussing grain boundary effects
14 p2465 A69-29651

W single crystals cleavage cracks by spark discharge, showing effective surface energy dependence on crack initiation and propagation temperatures
15 p2637 A69-30226

Tungsten vacuum-arc melted samples in deformed and recrystallized conditions, studying mechanical properties at temperatures near ductile to brittle transition
15 p2637 A69-30267

Solid W enthalpy from 2800 K to melting point measured with drop calorimeter, tabulating heat capacity, entropy and free energy function
17 p2987 A69-33075

Yttrium desorption from W wire by strong electric field, noting electron work function or temperature increase effects on desorption field
17 p3015 A69-33631

Temperature and pressurization effects on tensile and compressive properties of polycrystalline arc-cast W
18 p3154 A69-34273

Resonances and doublets observation by neutron radiative capture and transmission of W and Zr isotopes in kev region, noting partial wave strength functions
18 p3175 A69-34314

Thermal emission and spectral degree of blackness of W derived from electron motion equation
18 p3154 A69-34715

Low energy electron diffraction oxygen adsorption kinetics on planes of tungsten at coverages below monolayer and work function measurements
18 p3183 A69-35106

Low pressure ethylene decomposition on high temperature W ribbon surface
19 p3265 A69-36729

Surface structures, work function changes, Auger electron and surface plasma losses for Cs on clean W surface
19 p3392 A69-36733

Tungsten influence on morphology and lattice parameter of fcc gamma prime phase in Ni-Cr-Ti-Al alloys
20 p3558 A69-36962

Hugoniot equation of state of shock loaded W determined at room temperature and 950 C
20 p3564 A69-38127

Structural changes during annealing of W and Mo single crystals deformed by rolling, using X ray diffraction topography methods with two crystal spectrometer
21 p3742 A69-38583

Grain boundary grooving kinetics for Cr, W and Mb in Ar and vacuum, determining interface free energies and surface self diffusion coefficients
21 p3744 A69-38740

Oxygen pressure effect on oxide layer composition on W surface by secondary ion-ion emission
21 p3746 A69-39071

Tungsten coatings applied on stainless steel and titanium alloy surfaces by plasma jet
21 p3746 A69-39152

Structural defects of neutron irradiated W wire noting microstress relaxation using atomionic microscope
21 p3749 A69-39623

Stress-strain curves of W wires and of aligned composites of same wires in Cu matrix
21 p3845 A69-39709

Thermal neutron capture cross section at high temperature irradiations determined for W 184, describing radiochemical separation and flux counting techniques
24 p4315 A69-43192

TUNGSTEN ALLOYS

Nb-W alloy solution hardening and deformation, noting flow stress dependence on strain rate and temperature plus activation energy of deformation
01 p0095 A69-10488

Chemical vapor deposited W and W-Re alloys for structural applications, discussing fabrication methods and effects on mechanical properties
01 p0096 A69-10641

Chemical vapor deposited W and W-Re alloys investigated for deposition variables and heat treatment effects on mechanical properties
01 p0097 A69-10648

A15 type phase in vapor deposited W-Re alloys identified by X ray diffraction, metallography and hardness measurements
01 p0098 A69-10649

Sintered W-Ni-Fe alloys strength and precipitation hardening characteristics for various compositions and cooling conditions
05 p0782 A69-16798

Transition temperature from brittle to plastic state of W-Mo alloys in recrystallized state, noting increased Mo content effect
05 p0783 A69-16809

Dynamic measurements of modulus of elasticity for polycrystalline nickel-tungsten alloys at elevated temperatures
06 p0943 A69-17232

Powder metallurgy, fusion and chemical vapor deposition techniques in manufacturing tungsten base alloys
07 p1165 A69-18792

Vacuum arc melted W and W-Re alloys mechanical properties, noting Re additions effects
08 p1331 A69-20190

Superplasticity in W-Re alloys, noting tensile properties, grain size and strain rate sensitivity for various Re contents at high temperatures
10 p1707 A69-22990

Composition and sintering temperature cooling effects on fracture properties of W-Ni-Fe alloys, using electron microscope fractography
10 p1711 A69-23333

Slip casting powder mixture of zirconium carbide and tungsten, discussing optimum composition
10 p1716 A69-24056

Zr-W high temperature phase relationships, noting Zr-zirconium tungstide eutectic temperature, zirconium tungstide peritectic temperature and Zr solubility in W
11 p1903 A69-24578

Back scattered electron inelastic LEED spectra of cesium plasma in W/100/-Cs system, noting strong loss peak
12 p2132 A69-26116

W, Mo and heat treatment effects on phase composition and heat resistance of ferrite and austenitic steels
13 p2283 A69-28487

Tungsten alloy fiber reinforced nickel base alloy composites stress-rupture strength, oxidation and impact resistance for high temperature turbojet engine buckets
14 p2462 A69-29010

Optical constants of Ta-W and Nb-Mo measured in IR and visible ranges as function of incandescent temperatures
17 p2990 A69-33574

Ce, Zr, Nb and B effect on heat resistance and structure of low alloy CrMoWV steels /type CSN 41 5335/
22 p3972 A69-41079

Refractory metals in rocket propulsion devices, applying tungsten in uncooled rocket nozzles and tungsten and rhenium to electrothermal propulsion
23 p4177 A69-42161

TUNGSTEN CARBIDES

Surface precipitation of carbides in solution treated and cooled molybdenum and tungsten
03 p0451 A69-14000

Preparation and properties of NbC-WC and TaC-WC carbides, analyzing hardness, resistivity, thermal expansion and dihedral angle
05 p0782 A69-16796

Book on hard alloy properties, discussing bending and compression properties, tensile, torsional and impact strength, wear resistance and thermal shock resistance
12 p2111 A69-23902

Phase composition and Co content effect in WC-Co and WC-TiC-Co alloys on magnetic properties behavior
13 p2275 A69-27343

Room temperature WC-Co compacts oxidation resistance in air noting increase with preliminary sintering temperature
13 p2275 A69-27345

Co content influence on temperature stress in WC-Co cermets using one exposure and two exposure X ray diffraction
16 p2802 A69-32340

WC-Co alloys structural changes under loads near yield limit, noting formation of slip bands
18 p3158 A69-35261

Carburizing spherical powders of Nb, Mo and W to obtain carbides, noting agreement between theoretical and experimental data
19 p3345 A69-36162

Tungsten carbide erosion resistant coatings, discussing optimum plasma deposition process and coating characteristics
20 p3561 A69-37373

WC-Co alloys microstructure and microproperties, considering individual phase behavior and grain-solid solution interactions
20 p3564 A69-38246

Plastic deformation and dislocation damping of cemented WC-Co alloys studied by compressive testing at room temperature
21 p3744 A69-38736

**TUNGSTEN COMPOUNDS
NT CALCIUM TUNGSTATES
NT ZINC TUNGSTATES**

Aluminum alloying additives effects on tungsten disilicide corrosion resistance, studying plasticity properties and oxidation rate
20 p3561 A69-37376

**TUNGSTEN INERT GAS WELDING
U GAS TUNGSTEN ARC WELDING**

TUNGSTEN OXIDES

Two donor levels and conduction properties of n-type semiconductors demonstrated by capacitance measurements of single crystal tungsten oxide in presence of electrolyte
16 p2825 A69-31609

TUNGUSK METEORITE

Tungusk meteorite preceding and succeeding atmospheric events, explosion and origin
01 p0159 A69-11378

Schematic chart prepared for shock wave geometry of Tungusk meteorite, discussing tree felling
01 p0159 A69-11379

Meteorite dust spherules at Tungusk and Sikhotealin falls investigated for mineral composition using X ray analysis
01 p0160 A69-11383

Meteorite dust composition of Tungusk meteorite noting angular and spherical particles
01 p0160 A69-11386

Oxide composition of silicate spherules from forest area devastated by Tunguka meteorite explosion using electron microprobe analysis
14 p2516 A69-28869

TUNING

NT SCHULER TUNING

YIG single crystal resonator tuning of Gunn diode in coaxial line circuit
01 p0042 A69-10320

Phase and amplitude variation at output of tuned amplifier, noting graphs and formulas
01 p0047 A69-10786

Tunable ferrimagnetic bandpass filter using magic T configuration to permit low magnetic field strength and retain nonstacked configuration advantages
04 p0573 A69-14343

High power waveguide tuner for use in traveling wave resonator to tune out reflections in resonant ring
04 p0576 A69-14759

Tunable Raman upconverter as coherent light generator, using Q switched Nd-YAG laser beam [IEEE PAPER B-2]
05 p0774 A69-16309

High Q magnetically tunable microwave filters using magnetodynamic modes in ferrite spheres
06 p0892 A69-16831

Tuning of two mirror antennas in near zone with various mirror combinations, discussing field cophasings
06 p0895 A69-17462

Mechanically and electronically tunable resonator for driving IMPATT and Gunn diodes
07 p1097 A69-18455

Proton spin maser oscillator with emission coils coupled by prepolarized liquid, discussing tuning and detuning
08 p1324 A69-20231

Phase and amplitude variation at output of tuned amplifier, noting graphs and formulas
10 p1662 A69-23115

Pulsed tunable lasers, emphasizing dye lasers for visible and near visible light in specialized spectroscopy
11 p1893 A69-24343

Self tuning in active filter for detection of weak LF signals in noisy background
11 p1845 A69-24548

Varactor diodes for microwave frequency tuning of resonators used for oscillators of avalanche transit time and Gunn diodes, discussing Q factors
11 p1854 A69-25610

Two stage amplifier with two differential feedbacks, investigating tuning sensitivity
14 p2426 A69-29147

Transistorized L band oscillator tuned by Ga-doped YIG, discussing ferrimagnetic material properties and device equivalent circuit
16 p2761 A69-32450

Wide tuning range S band low noise maser amplifier system, discussing bandwidth, gain and packaging for antenna mounting

17 p2979 A69-32914

Rb 87 vapor laser output power dependence on magnetic field strength and resonator detuning, discussing laser and atomic transition frequency tuning

17 p2983 A69-33694

Automatic tuning of superconducting cavity resonant frequency using optical feedback, discussing phase error processing and frequency deviation

17 p2937 A69-33781

Parametric tunable amplifier as prestage for radar receiver, discussing pump frequency and midband gain stabilization

18 p3104 A69-35457

Solid state laser emission frequency control and retuning using dispersive resonators, analyzing interference methods for wavelength measurement

19 p3331 A69-35865

Central tuning dip on rotation-vibration transitions of nitrous oxide and carbon dioxide laser with nitrogen, noting frequency discriminator generation

19 p3339 A69-36698

Tuning of two mirror antennas in near zone with various mirror combinations, discussing field cophasing

20 p3508 A69-37945

Electro-optical tuning effect on frequency of parametric laser with KDP crystal, noting Curie point

20 p3555 A69-38003

Reflex klystron with closed electron flux in crossed electric and magnetic fields permitting inertialess frequency returning

21 p3682 A69-39128

Laser design for smooth emission frequency retuning, discussing equations for laser field oscillations, two photon resonance, tensor analysis, quantum emission, etc

21 p3739 A69-39539

Accuracy and frequency stability of H masers in terms of wall collision effect and cavity resonator tuning

21 p3741 A69-39685

VHF cavity backed cylindrical gap antenna input tuning impedance and equatorial radiation patterns controlled by cavity adjustments

22 p3914 A69-40698

Sweep tuning gas laser and output power vs frequency characteristics, demonstrating tuning ability within entire Doppler bandwidth

23 p4174 A69-41635

TUNNEL DIODES

Quasi-sinusoidal tunnel diode oscillator studied for frequency and amplitude of harmonic voltage components

01 p0038 A69-10070

Storm-Shattuck and push-pull tunnel diode DC-to-DC converters suitable for spacecraft power supplies

01 p0013 A69-10750

Self excitation conditions and output characteristics of tunnel diode DC to AC converters for spacecraft, discussing relaxation-oscillator and push-pull circuit converter types

01 p0046 A69-10755

Tunnel diode oscillations in switching mode due to sinusoidal voltage excitation, discussing critical applied signal frequency separating switching and oscillation modes

02 p0213 A69-11535

Germanium tunnel diode current-voltage characteristics, proposing expression for approximation of differential conductivity as function of voltage

02 p0214 A69-11613

Germanium tunnel diode capacitance as function of bias voltage and HF signal magnitude, considering circuit design

02 p0214 A69-11614

Tunnel diodes current voltage characteristics in crossed electric and magnetic fields, observing tunnel current decrease in GaSb

02 p0300 A69-12634

Impurity concentration measurement for alloyed region of tunnel diode by determining Fermi level position

02 p0301 A69-12685

Power epitaxial GaAs tunnel diodes grown from solution in tin with tellurium

03 p0489 A69-13895

Electron phonon coupling in barriers of GaAs Schottky diodes, noting first and second derivatives of I-V characteristic in n-type GaAs-Pd Schottky diode

03 p0493 A69-14242

Phase input power characteristics of TWT, TDA and parametric amplifiers, noting crosstalk calculations and AM-PM conversion coefficients

04 p0573 A69-14336

Onsager reciprocity relations applied to thermodynamics of nonlinearity and noise in diodes

04 p0574 A69-14435

Tunnel diode univibrator, noting polarization influence on recovery time and pulse length stabilization dependence on resistive load

04 p0578 A69-15069

Reading amplifier for thin magnetic film memory stores permitting tunnel diode register positioning

04 p0579 A69-15319

Circuit with tunnel diodes and transistors for non-linear amplification, noting current-voltage characteristics dependence on circuit parameters

05 p0730 A69-16221

Microwave diodes on GaAs base, determining basic parameters and effects on crystal formation and device construction

05 p0730 A69-16222

Design theory of esaki diodes relation to internal parameters of degenerate semiconductors, discussing Fermi level position and maximum state density in purity band

05 p0732 A69-16298

Thermal and excess currents in GaSb tunnel diodes

05 p0734 A69-16570

Approximate functions for tunnel diode dynamic conductance in three voltage ranges and Fourier conductance terms for tunnel diode frequency converters

05 p0735 A69-16647

Counter/discounter assembly with slow resolution time for random fine pulses, using grouped tunnel diodes

05 p0735 A69-16702

Tunnel diode subnanosecond coincidence circuit stability and time resolution, noting influence of polarization and input-pulse currents

05 p0735 A69-16743

Tunnel junctions of narrow gap GeTe and wide gap GaAs, noting current voltage characteristics similar to those in Schottky barrier

06 p0980 A69-17770

Harmonic oscillations in tunnel diode circuits for three intersection points of loadline with characteristic curve, discussing larger total positive circuit resistance case

06 p0898 A69-17801

Current-voltage characteristic of tunnel diodes, with curve approximation by even degree polynomials of voltage, discussing quasi-linear analysis

06 p0898 A69-17802

Potential barrier curvature influence in aluminum trioxide tunnel junctions, noting ionic space-charge effect on shape

07 p1196 A69-18243

Tunnel diode amplifiers for amplifying weak microwave signals, discussing low noise wideband preamplifier for communication satellites

07 p1099 A69-18464

Frequency-stable tunnel diode oscillator loaded with transmission line

07 p1104 A69-18890

Tunnel diode pair unidirectional pulse regenerating circuits

07 p1104 A69-18892

Validity of formula for oscillation frequency of nearly sinusoidal tunnel diode oscillator extended to operation in nonsinusoidal regime

08 p1279 A69-19924

Tunnel diode amplifier operation in presence of noise

09 p1469 A69-22630

Autodyne frequency converters minimum noise and conversion factor calculation and optimal mode determination

09 p1469 A69-22631

Self biasing influence on tunnel diode amplifiers dynamic range, determining limiting conditions for amplitude characteristics

09 p1469 A69-22633

Wideband 4 GHz Esaki diode injection locked oscillator, noting locking figure of merit and locking bandwidth

09 p1470 A69-22785

Positive and negative sloped current-voltage characteristics of silicon tunnel diodes with p-n junctions

10 p1746 A69-23574

Tunnel diode test circuit, measuring differential resistances and bias voltages on loss resistance and of socket capacitance

10 p1665 A69-24215

Germanium tunnel diode current-voltage characteristics, proposing expression for approximation of differential conductivity as function of voltage

11 p1847 A69-24721

Germanium tunnel diode capacitance as function of bias voltage and HF signal magnitude, considering circuit design

11 p1847 A69-24722

Tunnel diode self excited SHF oscillators: synchronization, deriving single frequency generation conditions

11 p1849 A69-24955

Integrated tunnel diode amplifiers, discussing low noise, bandwidth, reliability, miniaturization and applications

11 p1854 A69-25611

Power epitaxial GaAs tunnel diodes grown from solution in tin with tellurium

11 p1939 A69-25696

Tunnel diode nonlinear p-n junction capacitance influence on characteristics of diode microwave self excited oscillator

12 p2043 A69-26889

Transmission type E saki diode amplifier with stabilizing dielectric loaded rectangular waveguide

13 p2233 A69-28067

Tunnel diode slideback sampling gate circuits, discussing response characteristics and operational specifications

13 p2236 A69-28538

Two stage tunnel diode amplifier synthesis with gain stabilization circuit widening passband, discussing operating frequency and maximally flat amplitude frequency response

13 p2236 A69-28575

Transient processes in counting circuits with tunnel diode chains, discussing operating point position for various conditions

14 p2419 A69-28921

Tunnel diode harmonic mode mixer having IF

14 p2424 A69-29763

Transistorized circuit operation with nonlinear feedback through tunnel diode analyzed by piecewise-linear approximation of I-V characteristics

15 p2573 A69-30114

Microwave tunnel diode switch design noting applications to information storage

15 p2574 A69-30132

Equivalent circuits of dielectric loaded and unloaded rectangular waveguide Esaki diode reflection amplifier

15 p2578 A69-30801

Wideband tunnel diode amplifier design, discussing implementation to out-of-band circulator characteristics and VSWR suppression

15 p2578 A69-30804

Autooscillatory process in n-circuit tunnel diode LC oscillators acted upon by external sinusoidal voltages

16 p2764 A69-32256

Tunnel junctions with low background currents made by reacting active gas layer adsorbed on Nb film surface with Pb upper film to form barrier

17 p3016 A69-33788

Tunnel diode coupling with spheroidal resonant cavity, describing method of measuring elements for interpretation

19 p3283 A69-35998

Tunnel diode oscillators theory applications, investigating self resonance phenomena relating to static characteristic variations under self oscillating conditions

19 p3285 A69-36738

Tunnel p-n junctions preparation by diffusing Zn into degenerate Te doped n-type GaSb between 580-600 C, measuring volt-ampere and capacitance characteristics

21 p3780 A69-39043

Radiometer for 4 cm wavelength range with receiver circuit incorporating tunnel and parametric HF amplifiers, describing design and operation including subunits

21 p3724 A69-39076

Germanium microwave backward diodes optimum design and performance prediction through computer calculation for important parameters

22 p3916 A69-41224

TUNNEL RESISTORS

U ELECTRON TUNNELING
U RESISTORS

TUNNELING

Complex trajectory method for describing tunnel effect during atom ionization in strong light wave field, using quasi-classical approximation

09 p1543 A69-22658

TUPOLEV AIRCRAFT

NT TU-104 AIRCRAFT
NT TU-134 AIRCRAFT

- Medium range Tu-154 three jet transport aircraft, detailing fuselage, airfoil, tail unit, landing gear, propulsion unit and circuitry 16 p2735 A69-32073
- Pressure sensors, strakes, removal of full length guide vanes indicate possible difficulties with thrust of NK-8-2 turbofans in Tu-154 19 p3395 A69-36757
- TUPOLEV TU-104 AIRCRAFT**
U TU-104 AIRCRAFT
- TUPOLEV TU-134 AIRCRAFT**
U TU-134 AIRCRAFT
- TURBIDITY**
- Light field inside deep layers of turbid medium illuminated by narrow beam, discussing beam deviations inside medium, deviation dispersions and correlation coefficient 02 p0274 A69-11449
- Vertical atmospheric turbidity distributions of haze and water vapor, noting effect of variations on scattering and absorption determination 02 p0277 A69-12777
- Atmospheric turbidity coefficient distribution in Northern Hemisphere from direct solar radiation measurements, noting application to IGY data 05 p0789 A69-16585
- Nonscattered, singly and multiply scattered light of beam from point source analyzed at boundary layer of turbid medium 05 p0789 A69-16640
- Atmospheric turbidity and visibility measuring instrument /videograph/ using light backscattering, noting shipboard, coast guard service, large cities and weather stations applications 08 p1314 A69-20376
- Sinusoidally modulated light beam propagation in turbid media, studying phase velocity and attenuation coefficient as function of modulation frequency 10 p1658 A69-23951
- Multiple scattering of solar radiation in turbid atmosphere, considering equations of sky radiation and radiative transfer 11 p1911 A69-24587
- Brightness coefficients for isotropic scattering of homogeneous plane layer in turbid medium, using Legendre polynomials 11 p1960 A69-24733
- Sky polarization neutral points around sunset /spring-summer 1968/ at Bedford, Mass., inferring continuation and variations of enhanced stratospheric turbidity 12 p2067 A69-26343
- Nonscattered, singly and multiply scattered light of beam from point source analyzed at boundary layer of turbid medium 14 p2482 A69-28796
- Spatial coherence of He-Ne laser radiation diffused by turbid medium calculated by using diffraction and interference measurements 22 p3964 A69-40798
- TURBINE BLADES**
- Electrochemical shaping of turbine blades under symmetric cycle conditions, showing role of experimental functions for optimum regime 04 p0605 A69-14560
- Unsteady flow in blade passage of partial admission turbine for high energy fluids, predicting shock wave formation at entrance using one dimensional theory [ASME PAPER 68-FE-25] 05 p0698 A69-16075
- Turbine blade loading in terms of surface diffusion and loading factors, discussing tandem and flap blades and vortex generators [ASME PAPER 68-WA/GT-11] 05 p0812 A69-16136
- Smith correlation of turbine stage efficiency for relating achievable efficiency to stage loading and flow factors used for total pressure loss coefficient data [ASME PAPER 68-WA/GT-5] 05 p0812 A69-16140
- Heat transfer performance of porous nozzle blade cascade represented by two dimensional mathematical model 05 p0812 A69-16400
- Low pressure fuel system and turbine rotor blade temperature measurement method for Concorde Olympus 593 engine [ASME PAPER 68-GT-63] 06 p0984 A69-17187
- Blade to rotor heat transfer in turbines determined from temperature distribution of rod in medium with nonuniform temperature 06 p1034 A69-17870
- Transpiration air cooled blading to test and design small gas turbine at 2500 F inlet, discussing cascade and full stage component 07 p1203 A69-18310
- Holographic interferometry, determining mechanical vibration amplitudes of compressor and turbine blades and airframe panel [SAE PAPER 690265] 07 p1130 A69-18313
- Hollow turbine disks for provision of coolant to high performance aircraft gas turbine engines, fabricating disk in two axial halves 09 p1509 A69-22345
- Turbine blade cooling research programs, discussing effects of increased trailing edge thickness and cooling air on turbine efficiency [ASME PAPER 69-GT-15] 09 p1432 A69-22501
- Gas turbine blade materials after long term service, analyzing tensile, impact and stress rupture properties and microstructure [ASME PAPER 69-GT-12] 09 p1527 A69-22503
- Turbine stator blade performance determination from total pressure surveys downstream of blade row, noting problems in pressure measurement [ASME PAPER 69-GT-103] 09 p1432 A69-22521
- Forced torsional vibrations of turbine blades calculated by computer using mathematical models for resonance frequencies and tangential stresses 10 p1803 A69-24076
- Gas turbine blade vibrations, discussing excitation causes and damping techniques [ASME PAPER 69-VIBR-59] 10 p1805 A69-24155
- Holographic mode shapes used in conjunction with mechanical impedance approach for vibration analysis of turbine blades [ASME PAPER 69-VIBR-32] 10 p1806 A69-24174
- Gas turbine blade cooling by longitudinal air flow, discussing cooling efficiency of guide and impeller blades and blade ring 11 p1942 A69-25337
- Aerodynamic and thermal considerations in axial flow turbine blade design, discussing internal air cooling [IME PAPER 2] 12 p2146 A69-25788
- Blade material temperature variation observed in turbojet engine during air bleed of varying intensity and duration 13 p2325 A69-27444
- Reynolds number, incident flow turbulence and interblade channels roughness effects on friction losses in axial flow turbines 15 p2547 A69-30074
- Automatic multichannel system for turbine blades static tests, discussing operation principles, component sections, programmed tape and vibration modes 15 p2672 A69-31209
- JT8D turbofan engine composite fan blades design and fabrication methods using aluminum-Borsic fiber, noting direct and indirect weight reduction [AIAA PAPER 69-465] 16 p2842 A69-32698
- Turbine blades materials with emphasis on oriented solidification of eutectic alloys, discussing blades cooling by thermosiphons or ducts 17 p2978 A69-33334
- Turbine blade cooling emphasizing economics, service life and computerized calculations 17 p3064 A69-33918
- Near resonant oscillations of warped turbine or compressor blades, discussing stress-strain relations 17 p3064 A69-33918
- Energy dissipation in vibrating warped turbine blades subject to complex stress-strain rate produced by simultaneous bending, torsional and tensile stresses 17 p3065 A69-33924
- Damping properties of turbine blade materials subjected to transverse bending vibrations in vacuum and at high temperatures, including Ti alloys 17 p2990 A69-33932
- Internal heat transfer coefficients for impingement cooling of gas turbine airfoil leading edge [AIAA PAPER 68-564] 17 p3022 A69-34021
- Gas turbine areas calculation of through flow cross sections for temperature deformations and blades elongation 18 p3184 A69-34987
- Steady state thermal problem of gas turbine hyperbolic profile disk equipped with bandaged blades, solving thermal balance equations 18 p3184 A69-34992
- Technology trends in airbreathing propulsion, discussing noise control for subsonic jet transports, turbine blade cooling, etc [AIAA PAPER 69-774] 19 p3244 A69-35648
- Aluminizing and operational effects on surface layer and core of first and second stage turbine blades 20 p3561 A69-37370
- Automated device for load carrying ability of structural elements like gas turbine blades under thermal and mechanical cyclic loads 20 p3544 A69-37816
- Computation method of hydrodynamic blade cascade for compressible fluid and variable channel width by stream function 20 p3460 A69-37972
- Repair welding methods for trailing edge cracks in nickel base superalloy used in turbine vanes, emphasizing plasma arc fusion welding [ASM PAPER D8-16.3] 20 p3551 A69-38137
- Gas heat transfer on turbine interblade channel surfaces and working blade end surfaces at operating Reynolds and Mach numbers 21 p3849 A69-38858
- Temperature distribution determined for leading edge, convex and concave parts of turbine blade porous wall with effusion cooling 21 p3850 A69-38860
- Heat transfer coefficients evaluated from gas to rotating turbine blades in unsteady operation, using unsteady thermal conductivity and gradient methods 21 p3850 A69-38864
- Cooling air from blades discharged into flow-through part of gas turbine, examining gas mixing with air from blade and effect on turbine efficiency 21 p3785 A69-39090
- Secondary losses in flat large scale turbine lattice attributed to LF pulsating flow separation on back of blade 21 p3645 A69-39717
- Temperature field in deflector cooled turbine blades for nonstationary regimes, considering heating of cooling air, thermal conductivity and thermophysical coefficient changes 21 p3786 A69-39718
- Monograph on aerodynamic studies of effusion cooled turbine blades covering turbulent boundary layers, gas turbine performance, experimental design, etc [AIAA PAPER 69-871] 21 p3786 A69-39867
- Holography applied to stress and vibration analysis of gas turbine blades, disks and small components 22 p4040 A69-39960
- Internally air cooled turbine blades and vanes emphasizing coolant aerodynamics, heat transfer and blade life, high temperature in jet engines, etc [RAES PAPER 22] 22 p4000 A69-40500
- Airfoils and cascades design for incompressible flow by numerical methods 23 p4058 A69-41610
- Large fan blade design, discussing aerodynamic design and rig test program supporting fan definition [SAE PAPER 690387] 23 p4200 A69-41656
- Blade and vane wall thickness measurements test methods for gas turbine engine using ultrasonic gage and thermoelectric comparator 24 p4312 A69-42753
- Turbine blade edge cooling efficiency, investigating Reynolds number and gas temperature to cooling air ratio influence 24 p4364 A69-43082
- Edge effects in efficiency of air cooled turbine blade cascades with cooling air ejection from blade trailing edges into gas flow 24 p4364 A69-43090
- Incompressible fluid flow inhomogeneities effect on oscillations of airfoils cascade, noting occurrence of parametric resonance in turbine engine blades 24 p4245 A69-43479
- Protective coatings on Ni base superalloys for gas turbine engine blade and vane components for hot corrosion and oxidation resistance [SAE PAPER 690480] 24 p4335 A69-43515
- TURBINE ENGINES**
- NT BRISTOL-SIDDELEY OLYMPUS 593 ENGINE
- NT DUCTED FAN ENGINES
- NT GAS TURBINE ENGINES
- NT J-79 ENGINE
- NT J-85 ENGINE
- NT T-53 ENGINE
- NT TURBOFAN ENGINES
- NT TURBOJET ENGINES
- NT TURBOPROP ENGINES
- Steady three dimensional flow through impeller of turbines with small number of blades and with edge cut hub, noting inefficiency of flow without impact 01 p0142 A69-10309
- Similarity conditions in turbine engine tests, analyzing flight speed, Reynolds number, combustion efficiency, heat changes, inlet turbulence and outlet nozzle 05 p0742 A69-16028

Aircraft turbine engines operation and control, discussing technology, simulation and system developments

05 p0812 A69-16528

Liquid and vapor phase microscale panel cokers applied to screening synthetic lubricants for aircraft turbine engines

[ASLE PAPER 68-LC-22] 07 p1140 A69-19309

Forging techniques for forming Be into cylinders, rings, shafts and disks, investigating controlled texture forging for turbine engine components

09 p1504 A69-22073

Cooled turbine performance evaluation methods, noting promise of analytical methods

[ASME PAPER 69-GT-63] 09 p1572 A69-22517

Monitors to detect incipient failure during turbine engine development, describing servocontrol

10 p1692 A69-23253

Explosive fabrication of aircraft components including turbine engine exhaust components, door seals, etc

[SAE PAPER 690316] 11 p1890 A69-24510

Turbine engine in-flight operating conditions simulated on test stand

11 p1942 A69-24528

Marchetti SV-20A and SV-20C twin turbine helicopters with two bladed rotors and fixed wings, discussing propeller on starboard engine rear of compound version

12 p2013 A69-26466

Temperature measurement for aircraft gas-turbine engine development

14 p2509 A69-28886

Fluidic temperature sensors for measuring turbine inlet temperature on large turbine engine

[AIAA PAPER 69-544] 16 p2792 A69-32692

Nondestructive ultrasonic, spectroscopic and TV test methods reducing time for inspection and increasing reliability of turbines

17 p2978 A69-33330

Small turbine development for long life applications in helicopters and unpressurized aircraft, describing Artouste, Turmo, Astazou and Bastan series

17 p3020 A69-33346

Aircraft turbines mechanical parts reliability tests, discussing examples of blade fatigue rupture and rotor disk fatigue

17 p3020 A69-33347

Low smoke emission combustors for aircraft turbine engines, discussing effects on ignition and exit temperature distribution

[AIAA PAPER 69-493] 19 p3394 A69-36299

Wankel aircraft engines compared to piston and turbine aircraft engines for performance, maintenance and reliability

19 p3395 A69-36872

Turbine engine monitoring during operation, discussing automatic monitoring systems and engine design

19 p3329 A69-36873

Digital computers used in error calculation in calibration curves of turboengines and other pneumatic devices

21 p3724 A69-39100

Aircraft engine technology, discussing turbine entry temperatures, reheat temperatures, high pressure spools, high temperature materials and small blades fabrication

[RAES PAPER 20] 22 p4000 A69-40499

TURBINE INSTRUMENTS

Solid state power supplies for turbine control and instrumentation, discussing control system manufacturer requirements and reliability specifications

03 p0368 A69-13432

TURBINE PUMPS

Ball bearings lubrication and wear in cryogenic hydrogen turbopumps by transfer films provided from self lubricating cage

01 p0084 A69-10109

Black Arrow space vehicle uprating, considering engines burning kerosene with HTP and turbopumping systems

01 p0143 A69-10835

Wear ring seals evaluation program for application to high pressure high speed liquid rocket turbopumps impeller wear rings

[ASME PAPER 68-WA/LUB-1] 05 p0768 A69-16129

Vane type fuel pump designed for small gas turbine engines, describing design analysis and laboratory evaluation

[ASME PAPER 69-GT-45] 09 p1513 A69-22485

Wideband acceleration instrumentation for Rover ground test facility liquid hydrogen turbopumps to study structural and flow induced vibrations

10 p1692 A69-23250

Turbopump weight minimization and low suction pressure requirements realized using high rotating speeds, hydraulic turbine driven upstream inducer and computer testing

[AIAA PAPER 69-552] 16 p2741 A69-32747

Rocket engine with turbopump supplied liquid propellant, describing ejector, pump assembly, gas generator and control devices

17 p3019 A69-33341

Twin spool hydrogen turbopump performance at zero net positive suction pressure /NPSP/ saturated fluid in propellant tank, including steady state and simulated transient engine tests

[AIAA PAPER 69-550] 18 p3140 A69-34414

Transient performance of full flow hydraulic turbine driven two speed pump inducer system, formulating computer model

[AIAA PAPER 69-551] 18 p3140 A69-34415

Liquid hydrogen pumping for Phoebus reactor, discussing feed systems, nozzles, configurations, design, testing, etc

[AIAA PAPER 67-478] 21 p3769 A69-39751

Hydrostatic bearings analysis for high pressure cryogenic rocket engine turbopumps to predict steady state and time dependent performance, noting turbulence, inertia and compressibility

22 p3955 A69-40408

TURBINE WHEELS

Air film cooling of rotating turbine disk, suggesting applicability to gas flows

06 p1034 A69-17814

Mechanical stability of pressed and forged Ti alloy gas turbine disks at high temperatures and rates of rotation

06 p1026 A69-18018

Stress-strain distribution in rotor wheel with radial side blades, giving differential equations system for circular disk strains

09 p1612 A69-21494

Gas turbine disk calculation and plastic flow theory, considering loading conditions and elastoplastic strains due to centrifugal forces and nonuniform heating

11 p1982 A69-24945

Unbalance effects on rigid naval turborotor on oil film bearings in flexibly mounted housings investigated at varying critical speeds and housing stiffness

[ASME PAPER 69-DE-9] 14 p2453 A69-28839

Device for fatigue testing turbine disk models in unsteady temperature fields with radial and axial nonuniformity produced by HF heating

15 p2583 A69-30208

Bladed disk assemblies vibrational properties, discussing dynamic characteristics of system with pairs of close natural frequency modes under forced vibration

15 p2704 A69-30304

Gas flow deflection at centrifugal pump wheel outlet for wheels having different inlet and outlet vane angles

15 p2547 A69-30571

Photothermoelastic analysis of thermal stresses in turbine wheels with welded blades, noting stress concentration reduction

15 p2715 A69-31488

Steady state thermal problem of gas turbine hyperbolic profile disk equipped with banded blades, solving thermal balance equations

18 p3184 A69-34992

Turbine disks stress-strain state, using wire strain gauge to determine residual strains, radial and tangential stresses as function of disks rpm

19 p3436 A69-35850

Lumped parameter simulation model, based on vector mechanics for flexible spinning bodies, to study spin stabilized spacecraft or turbine rotors

19 p3280 A69-35990

Turbine rotors load dependent unstable motions, considering exciting forces origins, external and internal damping, etc

20 p3628 A69-37918

Gas flow characteristics in shrouded and unshrouded turbine wheel assemblies, emphasizing radial flow role in efficiency

21 p3785 A69-38865

Wobble tolerance influence on axis deflection affecting accuracy during assembling of turbine rotors and stators

21 p3733 A69-39719

Holography applied to stress and vibration analysis of gas turbine blades, disks and small components

22 p4040 A69-39960

Turbine rotors temperature reducible by increasing air cooling system flow rate

24 p4364 A69-43081

TURBINES

NT AXIAL FLOW TURBINES
NT GAS TURBINES
NT SHROUDED TURBINES
NT STEAM TURBINES
NT SUPERSONIC TURBINES
NT TWO STAGE TURBINES

Monograph on optimal design of free-running drag turbines for boundary layer suction in aircraft, emphasizing gliders performance

12 p2011 A69-26111

Rotating mirror turbine with air cushion floating shaft for use in streak and framing cameras, noting framing rate

12 p2085 A69-26156

Aerodynamic losses and stage efficiency in partial admission turbines, using flat bladed rotor experiments and rotors of different blade pitch

15 p2547 A69-30290

Multiple function combination probe design for compressor and turbine air flow research

16 p2766 A69-31917

Stator setting effect on single stage turbine performance, considering blade loss and surface velocity distribution

[AIAA PAPER 69-525] 16 p2841 A69-32686

TURBO-SKYVAN AIRCRAFT

U SC-7 AIRCRAFT

TURBOALTERNATORS

U AC GENERATORS

U TURBOGENERATORS

TURBOCHARGERS

U SUPERCHARGERS

U TURBOCOMPRESSORS

TURBOCOMPRESSORS

Acoustic resonance excitation in axial flow compressor annulus by wake shedding from blades

01 p0142 A69-10058

Circumferential inhomogeneity of flow through impeller blades of axial flow compressor

03 p0361 A69-12954

Supersonic axial compressor boost stages for small gas turbine engines, using passage flow approach and passage criteria to design airfoils

[ASME PAPER 69-GT-44] 09 p1570 A69-22478

Lift engine model compressor response to inlet pressure distortion to determine nature and extent of critical area of spoiling for axial flow compressors

[ASME PAPER 69-GT-29] 09 p1571 A69-22493

Compressor inlet temperature /CIT/ sensors, describing bimetal strip and liquid expansion aspirated types

[ASME PAPER 69-GT-18] 09 p1571 A69-22499

Compressor inlet Mach number choice to control high performance variable stator compressors geometry

[ASME PAPER 69-GT-14] 09 p1571 A69-22502

Fan compressor noise reduction indicating effects of design, number of blades, vane/blade ratio, aerodynamic parameters and blade spacing

[ASME PAPER 69-GT-9] 09 p1571 A69-22505

Aerodynamic design of axial flow compressors and turbines, using aerothermodynamic equations for compressible flow analysis

11 p1821 A69-25585

Gas turbine centrifugal compressor design considerations for impellers and diffusers, including blade loading and pressure gradients determination and aerodynamics

[IME PAPER 1] 12 p2146 A69-25790

Aerodynamic design of subsonic and transonic axial flow compressors, discussing blade configurations and computerized design of turbomachinery

12 p2147 A69-25792

Gas turbine compressor end seals, discussing air leakage paths, primary and secondary seals, design and efficiency

[ASLE PREPRINT 68AM 4B-4] 13 p2267 A69-27366

Erosion wear of graphitic and mica-ceramic materials used for sealing turbine compressors at high temperatures, including test installation

15 p2643 A69-31186

Radial blade tip clearance effect on isentropic efficiency and air delivery in axial flow compressor with allowance for casing deformations and rotor displacements

16 p2837 A69-32004

Velocity and static pressure redistribution in distorted flow field upstream of axial flow compressors

[AIAA PAPER 69-485] 16 p2842 A69-32694

Gas turbine engine compressor system dynamic representation by one dimensional mathematical model
[AIAA PAPER 69-486] 16 p2842 A69-32697

Turbine disks stress-strain state, using wire strain gauge to determine residual strains, radial and tangential stresses as function of disks rpm
19 p3436 A69-35850

Computer program using system simulation and Monte Carlo techniques to assess turbojet engine compressor disk reliability, discussing maintenance policy and engine design effects
19 p3394 A69-36042

Turbocompressors, reviewing axial and radial compressors
19 p3395 A69-36749

Soviet book on theory and design of turbocompressors covering gas dynamic cascade theory, thermodynamics and aerodynamics, viscous gas flow, etc
20 p3459 A69-37238

URBOCONVERTERS
U TURBOGENERATORS
URBOELECTRIC CONVERSION
U TURBOGENERATORS
URBOFAN AIRCRAFT
NT A-7 AIRCRAFT
NT B-52 AIRCRAFT
NT BAC 111 AIRCRAFT
NT BOEING 707 AIRCRAFT
NT C-141 AIRCRAFT
NT CONCORDE AIRCRAFT
NT CV-990 AIRCRAFT
NT DC 8 AIRCRAFT
NT DH 121 AIRCRAFT
NT DO-31 AIRCRAFT
NT F-111 AIRCRAFT
NT P-1127 AIRCRAFT
NT SAAB 37 AIRCRAFT
NT SE-210 AIRCRAFT
NT TU-134 AIRCRAFT
NT TU-144 AIRCRAFT

Air deflection and modulation /ADAM/ turbofan propulsive wing V/STOL design
[AIAA PAPER 69-201] 07 p1056 A69-19573

Turbofan V/STOL with separate lift units for takeoff and landing, discussing commercial and military applications, cost effectiveness and operational characteristics
13 p2203 A69-28354

Turbofan engines impact on aircraft engineering development emphasizing large performances, high fan flow rates and low fuel consumption
15 p2550 A69-30322

URBOFAN ENGINES
Optimal layout of turbofan jet engines, discussing experimental rig for high thrust measurement
[AIAA PAPER 67-416] 01 p0143 A69-11015

Aerodynamic problems related to turbofans of subsonic transport aircraft
[ONERA-TP-629] 02 p0187 A69-11622

CF6 turbofan engine technology program for improvement in performance, weight, durability, noise, etc
[SAE PAPER 680691] 03 p0496 A69-13446

High bypass turbofan design, discussing JT9D engine combustion, materials and cooling
05 p0811 A69-15552

Titanium alloys role in turbofan and turbojet engine design, noting use in components and introduction in manufacturing techniques
[ASM PAPER D8-26.4] 07 p1143 A69-19673

Three shaft turbofan engines for 1970s noting thermodynamic and propulsive efficiencies, fuel consumption, weight, noise reduction, etc
08 p1376 A69-20627

Dual-rotor high-bypass-ratio CF6 turbofan engine design and development programme and growth
08 p1377 A69-21163

Fan compressor noise reduction indicating effects of design, number of blades, vane/blade ratio, aerodynamic parameters and blade spacing
[ASME PAPER 69-GT-9] 09 p1571 A69-22505

High bypass ratio compound fan shaft engine design and performance for convertible rotary wing aircraft
[ASME PAPER 69-GT-51] 09 p1572 A69-22511

JT15D business aircraft turbofan engine, discussing low costs and fuel consumption, maintenance, reliability, installation, etc
[ASME PAPER 69-GT-119] 09 p1572 A69-22524

Turbofan engines augmentation, evaluating duct heater, bluff body stabilizers, piloted can combustors, flameholding techniques and afterburner tests
09 p1573 A69-22617

CF6 turbofan engine technology program for improvement in performance, weight, durability, noise, etc
13 p2324 A69-27331

Thrust balance for scale model of powered nacelle fan jet engine from drag analysis in wind tunnel, deriving fan nozzle velocity coefficient
13 p2199 A69-27446

Spey 512 turbofan and RB.162 booster turbojet engines for Trident 2E and 3B power plant
13 p2325 A69-27975

Turbofan engines impact on aircraft engineering development emphasizing large performances, high fan flow rates and low fuel consumption
15 p2550 A69-30322

CF6 turbofan engine technology program for improvement in performance, weight, durability, noise, etc
[SAE PAPER 680691] 16 p2837 A69-32367

Systems approach in turbofan engine design acoustic evaluation, discussing noise sources and radiation patterns
[AIAA PAPER 69-491] 16 p2839 A69-32667

JT8D turbofan engine composite fan blades design and fabrication methods using aluminum-Borsic fiber, noting direct and indirect weight reduction
[AIAA PAPER 69-465] 16 p2842 A69-32698

Propulsion power plant arrangements for rotary aircraft with thrust producer for forward flight, considering convertible fan/shaft engine configurations
[AHS PAPER 333] 17 p3021 A69-33529

Steady state and dynamic distortion influence on performance and stall of turbofan engine, discussing compressor instrumentation, tests and simulation data
18 p3185 A69-35175

Pressure sensors, strakes, removal of full length guide vanes indicate possible difficulties with thrust of NK-8-2 turbofans in Tu-154
19 p3395 A69-36757

Rolls-Royce RB.211 turbofan engine development, discussing three shaft design, engine performance, testing program, etc
20 p3640 A69-37927

Blast angle effect on fanjet gas dynamics in crosswind, using equations for free lateral flow trajectories and reverse flow regions
21 p3850 A69-38863

Turbofan engine influence on civil transport aircraft design as function of thrust, discussing engine ratings, number of engines, APU and thrust engine
22 p3862 A69-39961

Building block approach to turbofan engine design, discussing fuel consumption, noise and component research
[RAES PAPER 14] 22 p3999 A69-40493

Ignition of aircraft fluids leaked onto hot turbofan engine surfaces, considering cooling air direction, surface temperature, nacelle engine compartment ventilation, engine power, etc
[SAE PAPER 690436] 23 p4200 A69-41653

Engine fuel and geometry control design for large high bypass aircraft turbofan engines used for airbus powering
[SAE PAPER 690403] 23 p4201 A69-41659

Turbofan jet engine research, discussing future compression and bypass ratios, weight and noise reduction, maintenance and reliability, temperature effects, etc
24 p4363 A69-42569

Engine design program for TF34-GE2 high bypass ratio turbofan military aircraft engine, outlining estimating procedures for thrust, fuel consumption and weight requirements
24 p4364 A69-43042

Monitoring devices and modular construction features of Rolls-Royce RB.211 three shaft turbofan engine, discussing maintainability
24 p4321 A69-43112

TURBOFANS
Test rig vehicle design for noise research on single stage high bypass ratio fans for quieter turbofan powerplants
[AIAA PAPER 69-492] 16 p2767 A69-32727

Axial flow fan blade row noise generation, discussing equation linearization, acoustic energy prediction and effects of flowing medium
[ASME PAPER 69-FE-12] 20 p3460 A69-37989

Large fan blade design, discussing aerodynamic design and rig test program supporting fan definition
[SAE PAPER 690387] 23 p4200 A69-41656

TURBOGENERATORS
Power generation in combat environment by tested self contained organic Rankine silent engine, discussing working fluid properties
[SAE PAPER 690062] 07 p1058 A69-18309

Secondary power sources for space applications in solar arrays, static and dynamic thermal systems, high power batteries and fuel cells, discussing NASA machinery procurement
19 p3255 A69-36323

Organic Rankine cycle system using heat absorption from turbine exhaust to provide increased electrical output and to power air conditioning
23 p4070 A69-42267

Argon turboalternator design and testing for Brayton cycle space power system, discussing inlet operating temperature and shaft bearings and rotation
23 p4071 A69-42279

TURBOJET AIRCRAFT
U JET AIRCRAFT
TURBOJET ENGINE CONTROL
Turbojet engine open and closed loop boundary control systems performance during maximum penetration of prohibited operating area induced by HF external disturbances
[AIAA PAPER 69-543] 16 p2841 A69-32681

Fluidic sensors for jet engine control, analyzing convergent divergent nozzles, vortex and acoustic oscillators for pressure and gas temperature measurements
[AIAA PAPER 69-542] 16 p2843 A69-32699

Fluidic thrust reversal control system for turbojet achieving cost and weight reduction, illustrating fluidic circuit and noting circuit reliability
17 p3018 A69-33329

Concorde Olympus 593 engines electronic control and adjustment devices
19 p3395 A69-36706

Fluid amplifiers for gas turbojet engines control, discussing hydraulic control and relationship between turbine rpm, fuel consumption and operating temperature
20 p3585 A69-36944

TURBOJET ENGINES
NT BRISTOL-SIDDELEY OLYMPUS 593 ENGINE
NT DUCTED FAN ENGINES
NT J-79 ENGINE
NT J-85 ENGINE
NT T-53 ENGINE
NT TURBOFAN ENGINES
NT TURBOPROP ENGINES

Vitiated inlet air effects on J60-P-6 turbojet engine performance at sea level for various simulated flight Mach numbers
01 p0143 A69-11063

Aircraft and engine parameters for maximum theoretical range of turbojet for given cruising speed
03 p0366 A69-12950

Soviet book on turbojet engine reverse thrust systems and systems for deflection of jet stream covering aircraft braking efficiency
04 p0647 A69-14934

Titanium alloys role in turbofan and turbojet engine design, noting use in components and introduction in manufacturing techniques
[ASM PAPER D8-26.4] 07 p1143 A69-19673

Statistical techniques to develop nickel base superalloy with high temperature capabilities for jet engine turbine bucket applications
08 p1329 A69-20001

Firebee 2/BQM-34E/ turbojet-propelled recoverable supersonic aerial target construction, performance prediction and missions
09 p1434 A69-21901

Fluorine light-off detector /FLOD/ for sensing and indicating minimum light-off or blow out conditions in turbojet engine afterburner
[ASME PAPER 69-GT-36] 09 p1501 A69-22488

Fuel concentration effect on turbojet engine reheat jet pipe vibrations via tests
09 p1573 A69-22616

Concorde SST turbojet engine integrated assembly consisting of air inlet, gas generator, reheater and convergent-divergent nozzle
12 p2147 A69-26357

Blade material temperature variation observed in turbojet engine during air bleed of varying intensity and duration
13 p2325 A69-27444

Spey 512 turbofan and RB.162 booster turbojet engines for Trident 2E and 3B power plant
13 p2325 A69-27975

Equipment and test installations for turbojet noise studies, discussing noise from rotating parts, pure jet noise and air propagation of noise
13 p2325 A69-28589

Tungsten alloy fiber reinforced nickel base alloy composites stress-rupture strength, oxidation and impact resistance for high temperature turbojet engine buckets
14 p2462 A69-29010

Flight velocity changes from sonic to supersonic through turbojet/ramjet combination possibility
17 p3020 A69-33348

Propulsion performance of XB-70A aircraft calculated by gas generator method
[AIAA PAPER 68-594] 20 p3461 A69-37152

Monograph on jet turbine with small hub ratio for cases of complete and partial admission, considering masking effects, flow measurements, etc
20 p3586 A69-37924

Simultaneous passage of two unmixed gas flows through joint two circuit turbojet nozzle into ambient medium
21 p3785 A69-39094

Thrust increase methods for air breathing turbojet engines analyzed with respect to effectiveness, taking into account environmental supporting mass and fuel expenditures
23 p4199 A69-41578

Rolls-Royce-Bristol/SNECMA M45H medium power turbojet for VFW 614 aircraft
24 p4363 A69-42566

TURBOMACHINE BLADES

NT COMPRESSOR BLADES
NT ROTOR BLADES [TURBOMACHINERY]
NT STATOR BLADES
NT TURBINE BLADES

Axial flow turbine blade cascade in transonic flow
03 p0365 A69-14103

Blade oscillations in cascade flow of axial turbomachinery calculated as function of pitch ratio, stagger angle, angle of attack and camber
[ASME PAPER 68-FE-7] 05 p0837 A69-16069

Bending-torsion mode of rotating tapered twisted turbomachine blade, analyzing coupled flexural and torsional vibrations effect on natural frequency
[ASME PAPER 68-WA/GT-6] 05 p0838 A69-16141

Resonant frequencies, vibration modes and stress distributions for naturally vibrating plane wide blades of turbomachines
08 p1376 A69-20764

Initial turbulence influence on wakes formed behind trailing edges of cascade blades
09 p1431 A69-22235

Diakoptics applied in combination with perturbation method to determine natural frequencies of turbine buckets coupled by tie wires and/or cover
[ASME PAPER 69-VIBR-57] 10 p1804 A69-24151

Tungsten alloy fiber reinforced nickel base alloy composites stress-rupture strength, oxidation and impact resistance for high temperature turbojet engine buckets
14 p2462 A69-29010

Flow through turbine stage with inclined guide vanes at moderate Mach numbers, discussing exit blade angle formula for swept cascades
15 p2547 A69-30570

Turbomachinery two mode blade vibrations with emphasis on aerodynamic damping, noting shifts in natural frequencies
[ONERA-TP-678] 16 p2733 A69-32333

Turbomachinery aerodynamics, discussing secondary flow in blading and digital computer applications to annulus flow field
18 p3086 A69-34925

Turbomachine blade thickness effect on meridional flow disturbances analyzed through blade geometry using differential equations
20 p3457 A69-37084

TURBOMACHINERY

NT AXIAL FLOW TURBINES
NT CENTRIFUGAL COMPRESSORS
NT CENTRIFUGAL PUMPS
NT GAS TURBINES
NT SHROUDED TURBINES
NT STEAM TURBINES
NT SUPERSONIC TURBINES
NT TURBINE PUMPS
NT TURBINES
NT TURBOCOMPRESSORS
NT TURBOFANS
NT TURBOGENERATORS
NT TWO STAGE TURBINES

Turbomachinery research, discussing two and three dimensional incompressible flow in cascades near end wall and in rotating machines
05 p0751 A69-16534

Flow in impellers of mixed and radial flow compressors for jet engines, turbochargers and automotive gas turbines, discussing velocity, load distribution, etc
[SAE PAPER 690333] 07 p1049 A69-18312

Three dimensional flow field of incompressible fluid with purely axial development in conical ducts and turbomachines
09 p1480 A69-21597

Axisymmetric flow theory for turbomachine of non-free vortex design in distributed equilibrium state, considering boundary conditions and blade leading edges
[ASME PAPER 69-GT-10] 09 p1432 A69-22504

Turbomachinery multiple pure tone noise associated with acoustic resonance of inlet cavities examined by narrow band filter tracking integer multiples of rotative speed
[ASME PAPER 69-GT-2] 09 p1572 A69-22509

Incompressible axisymmetric flow in turbomachines, analyzing flow field and velocity distribution
10 p1631 A69-22910

Turbomachinery buffer seals, buffer gas regulation and cleanup systems for operation of closed Brayton cycle power conversion system with gas cooled nuclear reactor
13 p2268 A69-27367

Turbomachinery aerodynamics, discussing secondary flow in blading and digital computer applications to annulus flow field
18 p3086 A69-34925

Compressible fluid flow characteristics in turbomachine stage, discussing simplified radial equilibrium method as basis for design
21 p3643 A69-38457

Turbomachinery periodic structures design to improve tolerance to inflow distortion and resonant oscillatory flows, considering large amplitude pressure waves propagation
[SAE PAPER 690388] 23 p4201 A69-41666

TURBOPROP AIRCRAFT

NT AN-24 AIRCRAFT
NT C-130 AIRCRAFT
NT CL-84 AIRCRAFT
NT E-2 AIRCRAFT
NT OV-10 AIRCRAFT
NT XC-142 AIRCRAFT

Technological evolution of turboprop propeller powered tilt wing V/STOL aircraft, discussing XC-142A, CL-84 and VZ-2 aircraft
05 p0701 A69-15564

Czechoslovak L-400 high wing short range STOL transport aircraft powered turboprop engines, discussing passenger and cargo version
24 p4251 A69-42799

TURBOPROP ENGINES

NT T-53 ENGINE

Spectrometric oil analysis procedure /SOAP/ for predicting failure of oil wetted parts in small turboprop aircraft engines
[SAE PAPER 690325] 11 p1941 A69-24508

Molded composites application to engine components, discussing turboprop reduction gear case design using polymer matrix boron composite
[AIAA PAPER 69-466] 16 p2795 A69-32763

TURBOPUMPS

U TURBINE PUMPS

TURBOROTORS

U TURBINE WHEELS

TURBOSHAPTS

Three shaft turbofan engines for 1970s noting thermodynamic and propulsive efficiencies, fuel consumption, weight, noise reduction, etc
08 p1376 A69-20627

Face seals for jet engine mainshaft bearing compartments, emphasizing oil film and gas film seals
[ASLE FICFS PREPRINT 28] 15 p2620 A69-30487

Gas turbine engine shaft face seal with self acting lift augmentation preventing rubbing contact, noting disadvantages of labyrinth and conventional seals
[ASLE FICFS PREPRINT 27] 15 p2621 A69-30492

Turboshaft engines for military aircraft, discussing size, technology and environmental factors with respect to anticipated market
[AHS PAPER 331] 17 p3022 A69-33530

Rigidity of rotors with pin joints, calculating moments of inertia at connected sections of turbine shaft disks utilizing similarity concept
19 p3324 A69-35832

Rolls-Royce RB.211 turbofan engine development, discussing three shaft design, engine performance, testing program, etc
20 p3640 A69-37927

TURBOSUPERCHARGERS

U SUPERCHARGERS
U TURBOCOMPRESSORS

TURBULENCE

NT ATMOSPHERIC TURBULENCE
NT CLEAR AIR TURBULENCE
NT GUSTS
NT HOMOGENEOUS TURBULENCE
NT ISOTROPIC TURBULENCE
NT LOW LEVEL TURBULENCE

NT MAGNETOHYDRODYNAMIC

LENCE
NT PLASMA TURBULENCE

Time averaged products and squares of fluid turbulence signals at LF, using Hall effect multiplier device and integrating voltmeter
04 p0601 A69-15111

Spectral line profiles of 3 Centauri A during microdisturbance, showing turbulent velocity and metal element abundances
07 p1211 A69-18400

Electron temperatures and internal turbulence in II regions of Sagittarius arm measured by high resolution interference method
08 p1392 A69-20508

Holographic image formation through turbulent medium simulated by shower glass, noting thickness variations and prismatic light deflection effects
09 p1494 A69-21550

Active prominence during solar flare with loop-like shape of spectral line profiles, discussing turbulent velocities and limb flares
10 p1764 A69-23730

Statistical theories of turbulence applied to thermal convection between infinite slippery plates at large Prandtl number
11 p1997 A69-24283

Nonlinear integrodifferential kinetic equation for weak turbulence of resonant four wave processes, considering spectral energy density
11 p1921 A69-24290

Turbulence formation in conducting liquid at increasing Reynolds numbers, discussing cause of spontaneous magnetic field appearance
11 p1955 A69-24392

Spectral emission of active prominences, showing looplike lines during quiet phases and differences in turbulent velocities magnitude
15 p2674 A69-30510

Monograph on static pressure and turbulence in free jets and jet flames covering radial velocity oscillations with and without chemical reactions, confined jets turbulence, etc
15 p2719 A69-31190

Kovaszny spectral theory of turbulence, discussing energy spectrum decrease in viscous subrange
16 p2768 A69-31680

Airstream parameters /temperature and velocity/ of turbulence intensity in jet core at tube exit and behind grids measured by He diffusion method
16 p2771 A69-31950

Microturbulent velocities of A and F stars observed for reciprocal effective temperature range
17 p3039 A69-33720

Closure conditions for Vlasov turbulence, discussing infinite systems of equations for dynamics of statistical quantities
17 p2958 A69-34220

Vlasov turbulence exact solutions, considering closure conditions, correlation length, Lundgren hierarchy, homogeneous turbulence, etc
17 p2958 A69-34220

Plane wave scattering by semiinfinite turbulent dielectric slab, using Born approximation to develop asymptotic series for stochastic components of forward scattered field
[OSA PAPER WH-16] 18 p3174 A69-35240

Anisotropy of derivatives of transverse velocity fluctuations in grid turbulence subjected to plane deformation, determining dimensionless coefficient
19 p3299 A69-36640

Approximate expression derived for loose coupling in turbulence theory, suggesting possible explanation for inadmissibility of Kraichnan conclusion
21 p3696 A69-39080

Hydrodynamic turbulence in statistical prediction for Burger equation, considering statistical inference problem for initial conditions and prediction criterion with estimable error
21 p3697 A69-39670

Polarization fluctuations of starlight indicating turbulent structure of interstellar medium, noting pulsar signal dispersion and Faraday rotation
22 p4030 A69-40770

Turbulence formation in conducting liquid at increasing Reynolds numbers, discussing cause of spontaneous magnetic field appearance
24 p4390 A69-43780

TURBULENCE EFFECTS

Axisymmetric MHD flow in turbulence chamber at large Hartmann numbers studied for flow boundary layer effects
01 p0130 A69-10770

- Electron viscosity coefficient in weakly turbulent plasma in strong magnetic field, noting electrical and thermal conductivity
03 p0480 A69-14136
- Vortex devices and turbulence amplifiers, describing circuits, operating principles and performance
05 p0705 A69-16005
- Flow characteristics about curved lateral jet, discussing effect of pitot tube nozzle shape and turbulence
05 p0746 A69-16017
- Reciprocal interaction of combustion wave and field of turbulence, discussing aerodynamic principles, turbulence effect on flame propagation speed and measuring methods
06 p1032 A69-17420
- Time dependent model of photochemical, advective and turbulent effects on meridional ozone distribution
07 p1122 A69-18253
- Solution velocity and turbulence effects on solvent cleaning of corrosion resistant steel tubing, discussing fluidity forces and cleaning formulation
08 p1318 A69-19807
- Region of transition from laminar to turbulent flow in meteor trains, suggesting electron attachment processes to molecular oxygen in presence of third body
08 p1393 A69-20608
- Mass transfer during interfacial turbulence induced by Marangoni effect in physical model
09 p1621 A69-21903
- Stagnation point heat transfer sensitivity to free stream turbulence attributed to external vorticity, noting correlation with Prandtl number
09 p1622 A69-21905
- Initial turbulence influence on wakes formed behind trailing edges of cascade blades
09 p1431 A69-22235
- Weak magnetic field dynamics in bounded conducting medium having turbulent motion induced under zero boundary conditions
11 p1922 A69-24240
- Atmospheric turbulence effect on linear antenna gain in direction of radiation pattern maximum determined together with antenna dimensions
11 p1844 A69-24435
- Coherent optical target recognition through randomly turbulent medium for imaging system offsetting image degradation due to turbulence
11 p1894 A69-24470
- Turbulent flame propagation described by turbulence intensity and integral scale and fuel properties including laminar flame velocity and equivalence ratio
11 p1999 A69-24482
- Atmospheric turbulence effects on aircraft flight noting causes of turbulence
11 p1911 A69-24527
- Kharlamov method for influence of turbulent motion of liquid in cavity on inertial motion of body containing cavity
11 p1868 A69-24788
- Hydrodynamic instability of normal flame and turbulent combustion of gas mixtures, considering surface and volume combustion modes
11 p2000 A69-25186
- Atmospheric turbulence degradation of holographs resolution improved by geometrical optics and series-expansion methods, noting role of Gaussian and exponential refractive index structure
12 p2090 A69-26250
- Satellite position errors due to atmospheric instability, discussing altitude-temperature relation and stellar scintillation synchronism for stars at small angular distances
12 p2158 A69-26445
- Solar chromosphere and corona heat intensity above 1000 km attributed to tongues of turbulence, considering convective zone exciting MHD waves mechanism
13 p2337 A69-27549
- Monograph on sound generation by turbulence and surfaces in arbitrary motion, discussing sound and multipole fields and governing equations
13 p2247 A69-27974
- Input signal random amplitude fluctuations suppression by parametric power limiter, discussing limiting frequency determination and dependence on signal amplitude
13 p2236 A69-28573
- Initial flow turbulence effects on drag coefficient for prismatic bodies in low velocity gas flow determined by wind tunnels
14 p2391 A69-29625
- Synoptic meteorological conditions effect on stellar images vibration and on relationship between vibration and zenith distance
15 p2647 A69-30164
- Meteorological effects on anomalous radio echo determined from simultaneous aerological and radar observations, noting maximum signal amplitude during high humidity and low wind speeds
16 p2808 A69-32277
- Variable scatter mechanism in turbulent tropospheric propagation medium, employing dynamic meteorology concepts for frontal disturbances effect on scatter volume
17 p2927 A69-33856
- Laser beam propagation through turbulent medium, investigating statistical distribution of phase shift fluctuations
17 p2976 A69-33857
- Statistical analysis in inlet air flow dynamics, discussing inlet duct design and pressure variations [AIAA PAPER 68-649]
17 p2896 A69-34020
- Pressure distribution in self acting hydrodynamic journal bearings without end leakage, presenting closed form solution for nonhomogeneous Reynolds equation with turbulence considerations
18 p3139 A69-34270
- Cosmic ray intensity short term stochastic variations in solar system related to turbulent solar wind day-to-day variations
18 p3186 A69-34300
- Combustion turbulence effect on flame propagation velocity taking into account flame-generated pulsation velocity as function of temperature and flame velocity
21 p3850 A69-38861
- SST stratospheric environment problems, discussing temperature effects on fuel consumption and convective turbulence effect on flight safety and efficiency
22 p3867 A69-41141
- Galactic magnetic field origin from galactic turbulence, calculating individual Fourier components in random turbulent velocity
24 p4375 A69-42658
- Mean and variance of Faraday rotation and pulsar signal dispersion in galactic turbulent structure, applying to statistically homogeneous disk model of Galaxy
24 p4375 A69-42659
- Wavelike structure observed near tropopause with sensitive radar system, suggesting clear air turbulence as cause of breakdown of gravitational wave
24 p4342 A69-42893
- Turbulence characteristics of flow influence on critical flameout conditions of disk shaped flame stabilizer, circulation zone length and combustion efficiency by bluff body
24 p4408 A69-43078
- Index of refraction turbulent fluctuations effect on beam traversing optically active medium, discussing far field diffraction pattern and incoherent scattering [AIAA PAPER 68-683]
24 p4304 A69-43578
- Thunderstorm turbulence relationship to weather radar echoes from storm penetrations in Oklahoma by instrumented aircraft
24 p4347 A69-43720
- Thermal turbulence effects on phase fluctuations of laser beams, studying temporal decay of mean square refractive index fluctuation with fringe pattern displacements
24 p4329 A69-43754
- TURBULENCE METERS**
 - Gottingen type wind tunnel, discussing stream characteristics and turbulence measurement by hot-wire anemometer
03 p0420 A69-14238
 - Airborne IR spectrometer for remote clear air turbulence detection, noting necessity for mirror stabilization in pitch axis
12 p2098 A69-27000
 - Turbulence measurement, considering handling and storage of data
13 p2263 A69-28148
 - Turbulence measurement errors with inclined hot wires described by equations, assuming normal component cooling includes greater tangential cooling
18 p3134 A69-34442
 - Monograph on hot wire anemometer measurements of velocity and temperature turbulence, discussing flow characteristics, calibration, etc
22 p3951 A69-41256
- TURBULENT AIR CURRENTS**
 - U AIR CURRENTS**
- TURBULENT BOUNDARY LAYER**
 - Superlayer structure determination near turbulent boundary layer with zero pressure gradient, using constant temperature linearized hot-wire anemometers
01 p0061 A69-10759
 - Electromagnetic fields effect on turbulent boundary layer characteristics of compressible fluid on insulating wall of MGD channel
01 p0131 A69-10777
 - Turbulent boundary layer theory, discussing effective viscosity, numerical integration, mixing length flow theory and wall jets
02 p0231 A69-11987
 - Heat transfer coefficient for spherical protuberance on plate with turbulent boundary layer [ASME PAPER 68-HT-2]
02 p0351 A69-12204
 - Turbulent boundary layer growth, pressure distributions and surface shear stresses on yawed semicircle cone [AIAA PAPER 68-98]
02 p0190 A69-12526
 - Boundary layers and heat transfers at shock tube walls, establishing approximate solution of boundary layer equation for laminar and turbulent cases [ONERA-TP-647]
03 p0412 A69-12875
 - Turbulent boundary layer reversion to laminar state associated with departures from inner law velocity distribution in presence of favorable pressure gradients
03 p0414 A69-13016
 - Asymptotic similarity in neutral barotropic planetary boundary layers, solving Ekman flow by singular perturbation methods
03 p0460 A69-13336
 - Incompressible turbulent boundary layer with near zero wall friction at circular cylinder situated longitudinally in flow
03 p0416 A69-13664
 - Equilibrium turbulent boundary layer prediction for proposed Prandtl mixing length distribution
03 p0419 A69-13992
 - Heat transfer through turbulent boundary layer on porous plate with blowing and suction, determining Stanton numbers
04 p0586 A69-14356
 - Hypersonic turbulent boundary layer in adverse pressure gradients studied for transition, measuring static/pitot pressure, stagnation temperature and heat transfer rates [AIAA PAPER 68-44]
04 p0588 A69-14716
 - Mean temperature distribution through inner and outer regions of turbulent boundary layer with injection through heated porous wall
04 p0685 A69-14729
 - Turbulent transport of energy in atmospheric boundary layer near earth surface resulting from forced convection
04 p0627 A69-15087
 - Incompressible turbulent boundary layers in channel flow using constant temperature hot-wire anemometer, emphasizing measurement in viscous sublayer [ASME PAPER 68-FE-26]
05 p0747 A69-16066
 - Incompressible turbulent boundary layer properties with arbitrary pressure gradient calculated by integral method resulting in single equation for skin friction coefficient [ASME PAPER 68-WA/FE-22]
05 p0749 A69-16098
 - Inlet velocity profiles distortion effects on flow regimes and performance in two dimensional diffusers with turbulent boundary layers [ASME PAPER 68-WA/FE-25]
05 p0698 A69-16100
 - Heat transfer in accelerated turbulent boundary layer between converging planes with varying wall temperature and decreasing Stanton number [ASME PAPER 68-WA/HT-13]
05 p0847 A69-16120
 - Uniform hot fluid injection effect on heat transfer in constant property turbulent boundary layer [ASME PAPER 68-WA/HT-24]
05 p0847 A69-16126
 - Incompressible two dimensional turbulent boundary layers calculated on phenomenological basis
06 p0908 A69-17133
 - Compressibility transformation theory extended for turbulent boundary layer, involving mass transfer with/without chemical reactions [AIAA PAPER 69-161]
06 p0912 A69-18045
 - Transformation theory for compressible turbulent boundary layer with arbitrary pressure gradient [AIAA PAPER 69-160]
06 p0912 A69-18073
 - Separation of subcritical and supercritical compressible turbulent boundary layers under strong pressure gradients using method based on integral equations [AIAA PAPER 69-34]
06 p0912 A69-18077

Nose cone reentry simulation under low temperature subliming ablaters, discussing dry ice, camphor and steel calibrations models fabrication, instrumentation and boundary layer measurements
[AIAA PAPER 69-152] 06 p0929 A69-18098

Turbulent boundary layer loading function for use with finite element structural analysis system applied to elastic aircraft structures random vibration
[AIAA PAPER 69-20] 06 p0914 A69-18132

Finite plate length effect on two dimensional supersonic turbulent boundary layer with large distributed surface injection
[AIAA PAPER 69-162] 06 p0864 A69-18138

Analytical model developed from turbulent shear flow study, discussing Reynolds number effect
[AIAA PAPER 69-163] 06 p0914 A69-18139

Superlayer structure in turbulent boundary layer without pressure gradient, using constant temperature linearized hot wire anemometers
07 p1118 A69-18299

Base pressure calculation in initial turbulent boundary layer of supersonic flow about two dimensional backward facing step, using mass conservation conditions
07 p1119 A69-18747

Turbulent boundary layer in presence of longitudinal pressure gradient
07 p1122 A69-19735

Analytical model for compressible MHD boundary layers formulated by transport equations for turbulent fluctuations of species mass density, velocity and temperature
08 p1366 A69-20786

Electric arc interaction with turbulent boundary layer in vortex stabilized plasmatron, noting variation in arc intensity
09 p1545 A69-21432

Highly turbulent boundary layers on walls in channels using laser light sources
09 p1515 A69-21434

Acceleration effects on forced convection in turbulent boundary layer, noting heat transfer history and rates prediction
09 p1480 A69-21480

Computer study of analytical model of boundary layer transition from laminar to turbulent flow
[AIAA PAPER 68-38] 09 p1482 A69-21945

Constant property turbulent boundary layer flow, developing finite difference solution for prediction of velocity profiles and skin friction coefficient
09 p1482 A69-21950

Mean shear in wall region and outer region of constant pressure turbulent boundary layer
09 p1482 A69-21967

Local heat transfer coefficients in oscillating turbulent boundary layer over flat plate
[ASME PAPER 69-GT-34] 09 p1623 A69-22490

Wall temperature and Prandtl number effects on turbulent boundary layer thicknesses and shape factors for subsonic compressible gas flow over flat plate
[ASME PAPER 69-GT-55] 09 p1432 A69-22513

Velocity profiles of turbulent boundary layers with constant and variable pressures using Cole formulation
09 p1484 A69-22780

Heat transfer at plate in hydrodynamically stabilized turbulent boundary layer region, obtaining formulas for calculating transfer coefficients
10 p1809 A69-23427

Turbulent boundary layers on flat wall of supersonic wind tunnel, determining velocity profiles, thicknesses and skin friction coefficients
10 p1680 A69-23643

Unsteady baroclinic planetary atmosphere boundary layer turbulent states with various pressure and temperature gradient distributions, using boundary layer model
10 p1722 A69-23973

Flat decelerating cascades boundary layer in compressible flow during change in axial flow-density ratio and upstream turbulence
11 p1818 A69-24639

Turbulent boundary layer velocity distributions in uniform/accelerated compressible flow over flat plate, using change of variables based on mixing length formula
[ONERA-TP-693] 11 p1867 A69-24752

Turbulent flow problems, discussing hot-wire techniques, viscosity effect, compressibility surface curvature, turbulent boundary layers, heat transfer, etc
11 p1871 A69-25017

Fluid mechanics shock wave interaction with turbulent boundary layers at transonic to high supersonic speed ranges, noting examples in aviation
11 p1871 A69-25018

Velocity distributions and skin friction coefficients in turbulent boundary layers over flat plate with injection or suction through porous wall
11 p1871 A69-25027

Reverse transition in two dimensional accelerated incompressible turbulent boundary layer flow, noting skin friction coefficient and turbulent intensity profiles
11 p1872 A69-25129

Streamwise pressure gradient effect on velocity profile in viscous sublayer of two dimensional turbulent flow along smooth wall
11 p1872 A69-25131

Turbulent boundary layer in lower atmosphere downwind of abrupt change of surface roughness, determining surface shear stress and roughness height
12 p2125 A69-26014

Wall pressure fluctuations due to turbulent boundary layer flow, calculating statistical properties
[AIAA PAPER 68-642] 13 p2244 A69-27246

Suction effects on shockwave-turbulent boundary layer interactions at compression corner leading to reductions in upstream influence
13 p2244 A69-27326

Displaced layer thickness dependence on air injection parameters measured in wind tunnel
13 p2245 A69-27385

Turbulent boundary layer sound emission effect on elastic plate, discussing pressure pulsation spectrum reflection
13 p2246 A69-27538

Velocity and temperature profiles in gaseous turbulent boundary layer above liquid surface used to study liquid film cooling heat transfer
13 p2375 A69-27792

Vortices interaction effect on vertical turbulent heat flow in atmosphere boundary layer, determining dependence of vortex mean vertical temperature gradient
13 p2293 A69-27841

Axisymmetric hypersonic wind tunnel nozzle design by determining inviscid contour and correcting for turbulent boundary layer growth
[AIAA PAPER 69-337] 13 p2200 A69-28273

Convective heat and mass transfer in binary turbulent vertical boundary layer
13 p2378 A69-28311

Monograph on velocity distribution function in turbulent boundary layer, discussing hot wire anemometer for mean velocity, turbulence intensity and higher order moments determination
13 p2250 A69-28336

Ammonia gas diffusion from line source in turbulent boundary layer, discussing concentration profile discrepancy due to eddy diffusivity and plume shear
13 p2250 A69-28343

Flat plate turbulent boundary layer, noting Navier-Stokes equations solutions and formation of rotations to determine velocity field
13 p2251 A69-28632

Flow structure in conical shock wave-sharp flat plate interaction zone in supersonic flow, noting turbulent boundary layer before separation
14 p2428 A69-28897

Thermal shielding effectiveness of flat wall behind tangential blowing slit, considering case of quasi-isothermal homogeneous turbulent boundary layer
14 p2537 A69-28971

Temperature disturbance amplification in laminar natural convection boundary layer formed on vertical flat surface measured with hot-wire anemometers
14 p2430 A69-29575

Turbulent boundary layer in corner, measuring velocities, wall shear and turbulent normal stresses by employing momentum integral and similarity analyses
14 p2431 A69-29576

Turbulence constant for flows near walls, analyzing viscosity dependence on wall distance by utilizing maximum stability principle
15 p2590 A69-30048

Incompressible two dimensional turbulent boundary layer equations with arbitrary pressure distribution solved by weighted residual method
[AIAA PAPER 69-397] 15 p2591 A69-30478

Turbulent boundary layers behavior near flow separation, obtaining equations for equilibrium layers
15 p2591 A69-30638

Maximum turbulent stress in turbulent two dimensional boundary layers leading to general stress law, designing experiment to confirm validity
16 p2769 A69-31832

Nonequilibrium plasma boundary layer along channel insulator wall, noting different electron and heavy particle temperatures
[AIAA PAPER 68-134] 16 p2821 A69-31873

Turbulent boundary layer laminarization in conical nozzle flow, measuring velocity profiles and friction coefficient
[JPL-TR-32-1407] 16 p2732 A69-31894

Density and density fluctuations in hypersonic turbulent boundary layer on shock tunnel nozzle wall measured using electron beam probe
16 p2770 A69-31909

Density and velocity fluctuations in hypersonic turbulent boundary layer based on Wallace data
16 p2770 A69-31909

Three dimensional effects on Stanton tube data for skin friction determination for small protruberances drag immersed in turbulent boundary layer
16 p2771 A69-31929

Analytical expressions validity for skin friction in compressible turbulent boundary layer over wide range of Reynolds numbers and heat transfer conditions
16 p2771 A69-31929

Laminar-turbulent transition in boundary layer over thermally decomposing surface, discussing gasification rate, Reynolds number effects, heat transfer and turbulence onset mechanism
16 p2878 A69-31950

Hybrid rockets combustion mechanism, discussing turbulent boundary layer with heat and mass transfer, chemical reactions, etc
16 p2879 A69-32002

Convective heat transfer in centrifugal force field on cavity between two rotating disks in turbulent gas flow
16 p2837 A69-32139

Mean near wake flow of adiabatic two dimensional wedge at Mach 4 with tripped turbulent boundary layers and base mass addition
16 p2733 A69-32147

Two dimensional model for analyzing turbulent separation and reattachment at blade trailing edge at supersonic speed
[ONERA-TP-678] 16 p2733 A69-32258

Conical shock wave-turbulent boundary layer interaction data obtained for adiabatic wall conditions at supersonic free stream Mach numbers, including suction effects
[AIAA PAPER 69-450] 16 p2773 A69-32754

Boundary layer trip geometry, size and location effects on position of transition at hypersonic speeds
17 p2950 A69-33249

Skin friction drag reducing high polymer solution injected into turbulent boundary layer to test effectiveness on marine vehicles
17 p2951 A69-33254

Incompressible turbulent boundary layer analysis by two region characterization for eddy viscosity, using Spalding generalized function and Prandtl free shear flow model
17 p2951 A69-33255

Noise transmission from turbulent boundary layer through flexible plate into closed cavity, emphasizing nonlinear plate stiffness and mutual interaction between plate and airflow
17 p3006 A69-33409

Gas and small particle diffusion in turbulent boundary layer of blast wave propagating over land or water, assuming logarithmic vertical velocity profile
[AIAA PAPER 69-672] 17 p2953 A69-33439

Adiabatic compressible turbulent boundary layer equations for two dimensional and axisymmetric flows discussing methods of solution based on eddy viscosity formulation
[AIAA PAPER 69-687] 17 p2955 A69-33470

Compressible hypersonic turbulent boundary layers solution by finite difference method, relating mixing length to velocity profile shape factor
[AIAA PAPER 69-684] 17 p2955 A69-33474

Chemical species flux decay in turbulent boundary layer with catalytic wall, obtaining solution of conservation equation by using shear stress distribution
[AIAA PAPER 69-709] 17 p2955 A69-33480

Adiabatic compressible turbulent equilibrium boundary layer integral method analysis extended to study nonequilibrium laminar flows, deriving dissipation integrals, presenting numerical solutions
[AIAA PAPER 69-689] 17 p2955 A69-33481

Favorable pressure gradient effect on compressible two dimensional supersonic turbulent boundary using temperature and pressure probes and shear balance
[AIAA PAPER 69-685] 17 p2956 A69-33485

Turbulent boundary layer subject to sudden pressure variation due to rapid expansion or shock wave, noting application to hypersonic ramjet air intake
[ICAS PAPER 68-42] 17 p2895 A69-33587

Turbulent boundary layer on disk rotating in free air using circumferential and radial momentum integral equations and entrainment equation
17 p2957 A69-33601

Swept wing attachment line boundary layer, measuring skin friction in full turbulence and velocity profiles with and without trip wire

17 p2958 A69-34047

Constant pressure adiabatic turbulent boundary layer characteristics measurements correlated in incompressible reference frame, using modified Mager compressibility transformation

17 p2958 A69-34051

Three dimensional incompressible wake behind blunt obstacle at leading edge of flat plate compared with mathematical model by Oseen linearization

18 p3083 A69-34403

Rough wall turbulent boundary layer development in pipe flow determined for different roughness geometries in zero and adverse pressure gradients

18 p3125 A69-35387

Microwave-plasma interaction instrumentation for supersonic channel constructed to investigate turbulent boundary layers formed over ablating heat shield materials

19 p3294 A69-35754

Heat flux densities and Reynolds potentials in turbulent boundary layer on heated flat plate with wall suction

19 p3452 A69-36722

Heuristic process for constructing similarity parameters approximation solution of laminar and turbulent boundary layers equations

19 p3301 A69-36799

Wall temperature distributions predicted in turbulent boundary layer with arbitrary pressure gradients, basing calculations on Spalding function solutions

19 p3302 A69-36853

Turbulent boundary layer problem of gas mixture motion solved by approximate methods

20 p3513 A69-37090

Turbulent boundary layer of injection gas flow calculated past surfaces with pressure gradient

20 p3513 A69-37091

Turbulent boundary layer of conducting fluids on dielectric plate in transverse magnetic field in presence and absence of pressure gradient

20 p3513 A69-37092

Turbulent boundary layer gas mixture flow incident to porous plate surface

20 p3513 A69-37093

Heat protection efficiency of plane surface in turbulent boundary layer behind tangential slots, comparing cooling effects of insulating gas films

20 p3631 A69-37095

Reynolds analogy factor approximate calculation for turbulent boundary layer with pressure gradient

20 p3514 A69-37183

External natural convection flows, studying laminar instability, transition and turbulence in boundary layer flow

20 p3633 A69-37718

Turbulent boundary layer growth predicted for adverse pressure gradients, using entrainment theory for two dimensional and axisymmetric flows [ASME PAPER 69-FE-16]

20 p3517 A69-37991

Simultaneous lateral skewing regions existence in low speed three dimensional turbulent incompressible boundary layer flow

[ASME PAPER 69-FE-24] 20 p3517 A69-37998

Turbulent boundary layer sound emission effect on elastic plate, discussing pressure pulsation spectrum reflection

20 p3518 A69-38204

Blowing effect on surface friction coefficient and heat transfer in turbulent boundary layer in compressible fluid with pressure gradient

21 p3643 A69-38636

Law of wall parameters for compressible turbulent boundary layer with air injection through wall determined by analyzing data for hypersonic speeds

21 p3692 A69-38685

Three dimensional turbulent boundary layer over flat surface in incompressible flow calculated by finite difference method based on time averaged motion equations integration

21 p3693 A69-38767

Cross correlation coefficient for submillimeter monochromatic wave amplitude and phase fluctuations in turbulent atmospheric boundary layer

21 p3674 A69-39129

Velocity and temperature distribution curves in turbulent boundary layer formed by natural convection on isothermal vertical plate, using Prandtl and Nusselt numbers

21 p3852 A69-39430

Skin friction results from free stream velocity boundary layers with varying injection and suction wall conditions, describing flow characteristics

21 p3696 A69-39431

Unsteady baroclinic planetary atmosphere boundary layer turbulent states with various pressure and temperature gradient distributions, using boundary layer model

21 p3760 A69-39659

Linear normal mode instability of three dimensional laminar and turbulent shear layers, analyzing relations between velocity profile, eddy viscosity and oscillations

22 p3932 A69-40893

Space-time behavior of random pressure field of turbulent boundary layer on plane plate surface

22 p3933 A69-41027

Distributed suction effect on boundary layer structure of water flow from turbulence measurements, determining velocity and pulsation intensity distributions

22 p3933 A69-41029

Velocity defect profile and skin friction law for incompressible equilibrium turbulent boundary layer, using mixing length relation

22 p3934 A69-41180

Atmospheric model for calculating wind velocity profile and turbulence of stable atmospheric boundary layer with given temperature stratification and pressure gradient distribution

23 p4184 A69-42489

Turbulent boundary layer at inlet section of gas blown tube based on solutions of energy and momentum equations, deriving relations for inlet section length

24 p4300 A69-43079

Boundary layer separation zones in laminar, transition and turbulent fluid flows past conical bodies with widening skirts

24 p4245 A69-43481

Heat transfer to highly accelerated turbulent boundary layer with and without mass addition, presenting data in terms of Stanton number vs Reynolds number [ASME PAPER 69-HT-53]

24 p4409 A69-43518

Heat transfer data for laminar, transition and turbulent natural convection boundary layers from water experiment on constant heat flux vertical plate [ASME PAPER 69-HT-D]

24 p4410 A69-43525

Boundary layer and heat transfer measurements for turbulent boundary layer laminarizing in conical nozzle flow with wall cooling

[ASME PAPER 69-HT-56] 24 p4303 A69-43538

Laminar-turbulent boundary layer prediction using mixing length model modified for viscous sublayer structural changes near wall compared with heat transfer data

[ASME PAPER 69-HT-13] 24 p4303 A69-43556

Air flow laminarizing turbulent boundary layer, determining velocity, turbulence intensity, temperature profiles and local heat transfer coefficients [ASME PAPER 69-HT-10]

24 p4413 A69-43558

Laminar, transition and turbulent boundary layer heat transfer measurements along wall in thermal entrance region of high temperature turbulent airflow through cooled tube

[ASME PAPER 69-HT-8] 24 p4414 A69-43560

Boundary layer equations with heat transfer for laminar and turbulent incompressible flows about two dimensional and axisymmetric flows, using finite difference method

[ASME PAPER 69-HT-7] 24 p4304 A69-43561

Rough surface skin-friction relations expanded to provide turbulent boundary layer growth prediction in pressure gradient

24 p4304 A69-43580

Mean velocity and pressure fields in turbulent boundary layer on flat plate at Mach 2 investigated for ratios of mass flow

[AIAA PAPER 68-129] 24 p4304 A69-43581

Diamond shaped striations development mechanism on ablative heat shield materials exposed to supersonic flow and turbulent boundary layers

24 p4248 A69-43598

Wake development from turbulent boundary layers on both sides of thin flat plate

24 p4249 A69-43694

Laminar sublayer thickness in compressible turbulent boundary layers with and without heat transfer

24 p4306 A69-43724

TURBULENT DIFFUSION

Euler-Lagrange relationship from equations of motion of tagged particle in turbulent velocity field consisting of random dispersive waves

01 p0121 A69-11202

Transpiration and dissipation effects on heat eddy diffusivity over two dimensional plate in turbulent flow for various Prandtl numbers

01 p0178 A69-11410

Similarity theory results for turbulent diffusion in atmospheric surface layer compared with concentration measurements from Project Prairie Grass

02 p0276 A69-12695

Plasmapause and relation to ion composition in topside ionosphere, using Bohm coefficient for turbulent diffusion

02 p0246 A69-12741

Turbulent parameter and turbulent diffusion vertical profile diurnal variations determination based on measurements of Rn 220 and thorium-B concentrations near ground

03 p0459 A69-13273

Eddy diffusivity in planetary boundary layer determined by vertical velocity spectrum

03 p0460 A69-13338

Dispersion in gel permeation chromatography, noting eddy diffusion in chromatographic columns

04 p0555 A69-14885

Stationary vertical distribution of weightless radioactive substance in surface air layer, accepting two layer exponent law for vertical turbulent diffusion coefficient

04 p0593 A69-15091

Velocity profiles and eddy diffusivities for fully developed turbulent low Reynolds number pipe flow [ASME PAPER 68-WA/FE-34]

05 p0749 A69-16107

Compressible combustor turbulent shear flow analysis, discussing eddy diffusivity, density fluctuations, vorticity intensification and turbulent transport [WSCI PAPER 68-27]

06 p0134 A69-17793

Turbulent diffusion from point source in boundary layer, discussing horizontal and vertical effects

09 p1535 A69-21513

Dynamics of turbulent motion of incompressible viscous fluid particles, using Lagrangian functions

11 p1867 A69-24536

Turbulent diffusion and Rayleigh-Taylor instability in inhomogeneous flow of combustion gases circulating through magnetic field

13 p2310 A69-28032

Ammonia gas diffusion from line source in turbulent boundary layer, discussing concentration profile discrepancy due to eddy diffusivity and plume shear

13 p2250 A69-28343

Diffusion characteristics of turbulent flow produced by square mesh grid in low speed wind tunnel

13 p2250 A69-28496

Eddy diffusivities ratio for heat and momentum by mixing length theory, using Mach-Zehnder interferometer for temperature profiles

13 p2380 A69-28497

Turbulent parameter and turbulent diffusion vertical profile diurnal variations determination based on measurements of Rn 220 and thorium-B concentrations near ground

14 p2472 A69-28781

Self diffusing substance /salt/ distribution in turbulent water flow at different Reynolds numbers by NMR, obtaining diffusion function consistent with experiments

14 p2430 A69-29424

Turbulent diffusion and ion heating in plasmas in presence of current instability

15 p2662 A69-30959

Turbulent heat and mass diffusion in catalytic reactors for hydrazine decomposition, developing computer program to calculate temperature and reactant concentration distributions

[AIAA PAPER 69-421] 16 p2846 A69-32768

Turbulent diffusion inside sun as explanation of solar spindown, Li depletion at surface and neutrino discrepancy, discussing diffusion coefficient and stellar evolution

16 p2866 A69-32814

Deflection effect on flow and mixing process in flames covering enclosed turbulent diffusion flames in combustion chamber

17 p3068 A69-32966

Gas and small particle diffusion in turbulent boundary layer of blast wave propagating over land or water, assuming logarithmic vertical velocity profile [AIAA PAPER 69-672]

17 p2953 A69-33439

Vortex diffusion in viscous compressible fluid approximated by linear differential equations

17 p2957 A69-33714

Atmospheric turbulence and impurities diffusion considered as stochastic processes, deriving equations and covariance functions for flow characteristics

20 p3570 A69-37426

Vertical turbulent diffusion and altitude distribution of radioactivity from short lived radon decay products in atmosphere

20 p3533 A69-38076

Eddy diffusion coefficients due to instabilities in internal gravity waves near mesopause
20 p3534 A69-38090

One dimensional model and equation of energy spectrum function solved in studying turbulent diffusion in fluid at rest
21 p3693 A69-38749

Turbulent Schmidt number as function of ratio between turbulent and molecular kinematic viscosities for He, carbon dioxide and normal octane eddy diffusivities
21 p3852 A69-39432

Eddy diffusivity hypothesis modified to fit observed heat transfer from smooth pipe wall to turbulent gas stream at low Reynolds numbers
[ASME PAPER 69-HT-H] 24 p4303 A69-43523

TURBULENT FLOW

NT CAVITATION FLOW

NT SUPERCAVITATING FLOW

Equation of characteristic functional for Burgers one dimensional model fluid turbulence using logarithmic expansion method, discussing change in time of energy spectrum
01 p0059 A69-10338

Turbulent heat and mass transfer in rotating incompressible fluid flow analyzed by kinetic energy and shear stress equations
01 p0060 A69-10402

Semiempirical theory of turbulent MHD tube flow at small Reynolds numbers taking into account magnetic field presence
01 p0130 A69-10769

Viscoseal sealing coefficient and friction factor under turbulent flow conditions
[ASLE PREPRINT 68AM 5B-1] 01 p0087 A69-10911

Turbulent flow between parallel plates, discussing turbulence generation by energy addition
01 p0061 A69-10993

Turbulent fluid transport properties predicted by simple model for fluid behavior, obtaining mass, momentum and energy diffusivities
01 p0177 A69-11402

Transpiration and dissipation effects on heat eddy diffusivity over two dimensional plate in turbulent flow for various Prandtl numbers
01 p0178 A69-11410

Arc discharge in axially turbulent airflow producing equilibrium air plasma
02 p0285 A69-11571

Swirl flow through single and multistage Carnot shock diffuser, analyzing relation of pressure rise and diffuser aspect ratio
02 p0230 A69-11616

Turbulent velocity in faculae and photosphere obtained from IR triplet of oxygen analysis
02 p0314 A69-11646

Linear integrodifferential motion equations for turbulent flow within Heisenberg statistical turbulence theory
02 p0230 A69-11869

Turbulent boundary layer theory, discussing effective viscosity, numerical integration, mixing length flow theory and wall jets
02 p0231 A69-11987

Turbulent gas flow characteristics obtained by extremal hypothesis, using maximum perturbation stability in formulating variational problem and computer algorithm
02 p0232 A69-12354

Algorithm for Orr-Sommerfeld equation applied to stability of laminar flow, noting profile resembling mean velocity profile of turbulent flow in flat tube
02 p0233 A69-12573

Longitudinal correlation lengths in grid turbulence air flow transport subjected to planar deformation measured from energy spectra of velocity fluctuations
02 p0192 A69-12626

Statistical model of turbulent flow confirms Kolmogoroff hypothesis of equilibrium zone at large Reynolds numbers
03 p0413 A69-12949

Fourier transform method to measure two point correlations in grid generated turbulence
03 p0419 A69-13950

Downstream secondary circulation resulting from sharp bend in fully developed turbulent pipe flow, noting departure from twin circulatory flow
03 p0419 A69-13952

Relaminarization of turbulent flow, studying velocity profiles at various axial cross sections in porous wall tube with fluid injection
04 p0586 A69-14409

Turbulent fluctuations of viscous sublayer of two dimensional flow, assessing wall shear stress spectrum
04 p0587 A69-14544

Reattachment pressure correlated for any type of two dimensional turbulent supersonic separated flow
04 p0588 A69-14727

Ideal plane incompressible fluid flow past airfoil noting hydrodynamic effects, assuming presence of constant eddy
04 p0589 A69-14996

Taylor scales in grid turbulence subject to deformation, noting second order moments of velocity fluctuation power spectra and velocity fluctuation derivatives
04 p0590 A69-15054

Nondirectional probe for mean velocity measurement in turbulent flow, determining reduced velocity profiles in interior of free flow
04 p0600 A69-15056

Turbulent flow transfers from applications point of view, noting example of cooling of heated wall
05 p0743 A69-15558

Sting diameter and cylindrical protuberance length effects on base pressure of axisymmetric body in turbulent supersonic flow
05 p0697 A69-15712

Micro and macroturbulent motions velocity in solar photosphere based on Fraunhofer lines analysis
05 p0823 A69-16014

Real liquid turbulent flow of two parallel eddy streams between two parallel walls with given periodic roughness
05 p0747 A69-16034

Turbulent free shear layers in isoenergetic flow, correlating theory and experiment
[ASME PAPER 68-FE-9] 05 p0748 A69-16077

Thermal entry problem solution for low Reynolds number turbulent gas flow based on Reynolds number dependent velocity profile
[ASME PAPER 68-WA/FE-11] 05 p0748 A69-16090

Velocity profiles and eddy diffusivities for fully developed turbulent low Reynolds number pipe flow
[ASME PAPER 68-WA/FE-34] 05 p0749 A69-16107

Static pressures, profiles of local longitudinal velocity, fluctuating wall pressures and power spectra of wall pressures measured for subsonic turbulent flow
[ASME PAPER 68-WA/FE-36] 05 p0750 A69-16109

Heat transfer in turbulent pipe flow of radiating optically thin gas in circular tube
[ASME PAPER 68-WA/HT-17] 05 p0847 A69-16121

Simultaneous natural and forced convection flow around wall, analyzing perturbations of hydrodynamic elements due to obstacle
06 p1030 A69-17095

Particle velocity measuring technique for two phase turbulent flows, using laser and Fabry-Perot interferometer
06 p0933 A69-17252

Hot gas flows turbulence linear component intensity and frequency spectrum using optical measurement of pulse velocities
06 p0926 A69-17540

Gaseous film cooling at various hot gas acceleration rates and free stream turbulence levels
06 p1033 A69-17557

Compressible combustor turbulent shear flow analysis, discussing eddy diffusivity, density fluctuations, vorticity intensification and turbulent transport
[WSCI PAPER 68-27] 06 p1034 A69-17793

Mixing and combustion of gaseous and particle laden jets in air stream, analyzing turbulent, coaxial and jet mixing flows
[AIAA PAPER 69-33] 06 p1038 A69-18146

Turbulent skin friction on compliant skins stretched over damping fluid in shallow bath in flat plate
[AIAA PAPER 69-164] 06 p0914 A69-18163

Free stream turbulence influence on stagnation zone heating in arc heated hypersonic facilities, obtaining stagnation point heating rates
[AIAA PAPER 69-167] 06 p1039 A69-18198

Similarity functions defined for laminar or turbulent separation in nonuniform supersonic flow
[ONERA-TP-659F] 07 p1050 A69-18417

Radiative-convective heat transfer in gray gas plane layer blown into turbulent flow past permeable plate
07 p1242 A69-18991

Spherical particle motion in vortex gas flow between planes of turbulence chamber perpendicular to axis of flow rotation, noting collisions effect
07 p1181 A69-19000

Hydraulic drag coefficient in MHD fluid flows in traveling magnetic field from motion equations for turbulent flows, considering velocity profiles
07 p1192 A69-19017

Transition boundary layer on flat plate in subsonic wind tunnel measured by hot-wire method, obtaining velocity fluctuation distribution and turbulence intensity
07 p1121 A69-19329

Laminar and turbulent stresses in plane asymmetric incompressible flows analyzed based on Boussinesq formula for turbulent shear stresses
07 p1121 A69-19330

Microwave scattering by turbulent plasma column noting effects of plasma density
07 p1194 A69-19411

Spectrum of light scattered by particles suspended in turbulent fluid
07 p1157 A69-19417

Analytical solution for plate velocity statistics of turbulent-flow-excited rectangular flat plate, discussing vibration excitation
07 p1236 A69-19461

Plasma heating dynamics by straight turbulent discharge current influenced by initial plasma parameters
07 p1195 A69-19592

Turbulent incompressible MHD flow between two parallel smooth plates in transverse magnetic field, determining magnetic Reynolds number
07 p1195 A69-19736

Film boiling of subcooled liquid nitrogen in turbulent flow tubes, using one dimensional mathematical model of rod-flow regime
07 p1243 A69-19737

Turbulent flow effect on heat transfer in supersonic jet with plane infinite obstacle perpendicular to jet axis
07 p1243 A69-19738

Semilogarithmic law of velocity and temperature for turbulent flow in circular channel, examining analogy between momentum and energy transfer
08 p1420 A69-19877

Homogeneous turbulent gas flame front location as function of calorific value of mixture and flow velocity
08 p1420 A69-19998

Kerosene droplets combustion stability studied by motion pictures, discussing pressure, temperature and O concentrations effects in turbulent carbon dioxide flow
08 p1421 A69-20345

Jet flow and wakes in external stream and tailored pressure gradients, deriving similarity solutions for boundary layer equations
08 p1252 A69-20782

Bounds on mass and momentum transport by turbulent flow between parallel plates derived for Couette and Poiseuille flows
08 p1305 A69-20840

Spatial distribution of velocity, spatial correlation and ergodicity of turbulent flow, using spectrum of intensity fluctuations of scattered laser light
09 p1493 A69-21491

Momentum and energy transfers analogy in turbulent convection fluid flow emphasizing difficulties in case of liquid metals
09 p1480 A69-21687

Mass transfer during interfacial turbulence induced by Marangoni effect in physical model
09 p1621 A69-21903

Flow visualization tracer for quantitative measurements for laminar and turbulent flow, discussing mean velocity and shear stress
09 p1495 A69-21911

Turbulent flow of viscous nonNewtonian fluids in smooth pipes, noting effects of viscous stresses
09 p1481 A69-21929

Boundary layer suction sound emission, analyzing turbulent flow past elastic plate with reinforced slots performing flexural and torsional vibrations
09 p1483 A69-22638

Turbulent transport processes mathematical model, determining upper and lower bounds
10 p1677 A69-22895

MHD boundary layer nonlinear instability, treating laminar to turbulent flow transition as reversible process
10 p1734 A69-23452

Base drag effects on maximum lift drag ratio airfoils determined for moderate supersonic laminar and turbulent flows
10 p1633 A69-24060

Velocity profiles of turbulent plasma flow in circular tube during application of longitudinal homogeneous magnetic field
11 p1922 A69-24234

- Convection heat transfer and flow in rotating bodies, discussing laminar, turbulent and mixed flow in cones and disks, spheres and cylinders
11 p1998 A69-24459
- Turbulent flame propagation velocity in homogeneous premixed combustible gas, using one dimensional inviscid flame model
11 p1998 A69-24473
- Turbulent flow velocity field evolution in presence of random forces using equation of motion
11 p1867 A69-24628
- Kharlamov method for influence of turbulent motion of liquid in cavity on inertial motion of body containing cavity
11 p1868 A69-24788
- Buoyancy in turbulent shear flow, rotation or streamline curvature effects and meteorological parameters, drawing formal exact algebraic analogy
11 p1870 A69-24894
- Turbulent flow problems, discussing hot-wire techniques, viscosity effect, compressibility surface curvature, turbulent boundary layers, heat transfer, etc
11 p1871 A69-25017
- Hot wire and hot film anemometers for measuring turbulence in MHD flow noting applications in flowing mercury
11 p1886 A69-25087
- Forced heat convection in steady turbulent air flow in circular cross sectioned tubes, noting laminar sublayer in wall regions
11 p2000 A69-25096
- Streamwise pressure gradient effect on velocity profile in viscous sublayer of two dimensional turbulent flow along smooth wall
11 p1872 A69-25131
- Criteria for reversion of turbulent to laminar flow /reverse transition/ as special cases of Reynolds number criterion, noting boundary layer properties role
11 p1873 A69-25134
- Turbulent viscosity and thermal conductivity coefficients for entire cross section of fluid flow including wall boundary layers
11 p1873 A69-25228
- Direction of maximum turbulent vorticity in turbulent shear flow, determining alignment
11 p1874 A69-25282
- Model evolution of flow in fluid layer suddenly heated from below at Rayleigh number convection sufficient for turbulence
11 p1874 A69-25351
- Aircraft vortex wake development prediction for turbulent flow noting vortex size, strength and peak tangential velocity
11 p1819 A69-25377
- Skin friction coefficient relation to pressure distribution in turbulent flow and development of momentum thickness along flow
11 p1819 A69-25385
- Friction coefficients for turbulent flow through smooth pipes, considering average and friction velocities relations, fluid velocity measurements and flow Reynolds number
11 p1874 A69-25429
- Transverse pulsating motion of spherical particle in turbulent flow, considering differential equation of motion transformation
11 p1876 A69-25489
- Iterative solutions of nonlinear integrodifferential dynamical equation for two point velocity correlation tensor in incompressible fluid turbulence studies
12 p2062 A69-26602
- Book on negative turbulent viscosity theory covering laboratory analysis and applications to earth and solar atmospheres, oceanic circulations, spiral galaxies and solar nebula
12 p2131 A69-26868
- Turbulent fluid flow analysis described by Navier-Stokes equations, introducing asymmetric tensors for anisotropic cases
13 p2297 A69-27289
- Incompressible conducting fluid turbulent flow velocity distribution in transverse magnetic field at small magnetic Reynolds numbers and constant MHD interaction frequency
13 p2246 A69-27498
- Laminar-turbulent transition in MHD channel in transverse and longitudinal magnetic fields, discussing Reynolds equation for large Hartmann numbers
13 p2307 A69-27500
- Perturbations stabilization in electrically conducting fluid by distributed automatic control system, determining feedback operators via boundary value problem
13 p2311 A69-28105
- Turbulent flow in circular tube and parallel plate channel, considering molecular viscosity and duct shear stress variation
13 p2248 A69-28131
- Heat and mass transfer in two dimensional turbulent free shear flows including separated and reattached flows
13 p2377 A69-28145
- Supersonic boundary layer acoustic characteristics measured in wind tunnel on cylindrical model with several forebody configurations
[AIAA PAPER 69-344] 13 p2249 A69-28279
- Supersonic Preston tube correlations for Mach number and Reynolds number effects on hypersonic turbulent skin friction on adiabatic surfaces, simplifying correlation
[AIAA PAPER 69-345] 13 p2249 A69-28280
- Kolmogorov-Prandtl turbulence energy hypothesis extended from turbulent region of one dimensional flow to laminar sublayer, obtaining numerical solutions for Couette flow
13 p2250 A69-28339
- Turbulent burning velocity definition for one dimensional turbulent flow and average flame orientation perpendicular to flow direction, discussing transient flames in turbulent environment
13 p2379 A69-28452
- Diffusion characteristics of turbulent flow produced by square mesh grid in low speed wind tunnel
13 p2250 A69-28496
- Temperature factor effect on transition from laminar to turbulent flow in boundary layer of plate
13 p2251 A69-28558
- Ideal compressible fluid motion and heat transfer, noting convective heat transfer intensification with increased twisting velocity of flow
13 p2251 A69-28559
- Model equation for Reynolds stress in turbulent two dimensional shear flow
14 p2428 A69-29000
- SNR improvement during low level turbulence measurements, examining correlation between hot-wire anemometers, including error analysis
14 p2446 A69-29018
- Thermal entry problem solution for low Reynolds number turbulent gas flow based on Reynolds number dependent velocity profile
[ASME PAPER 68-WA/FE-11] 14 p2430 A69-29446
- Energy transport between vortices in turbulent flow calculated from vortex stability study
14 p2430 A69-29508
- Acoustic sounding of atmospheric structure, utilizing energy backscattered from temperature fluctuations in turbulent regions
14 p2448 A69-29527
- Unsteady jet viscous fluid flow under pulse variations based on Prandtl equations, showing turbulent motion analogy
14 p2432 A69-29608
- Water-air interface models unreliability in calculating atmospheric heat and humidity turbulent flow over ocean
14 p2443 A69-29839
- Turbulent Hartmann flow between planes in perpendicular magnetic field including flow velocity profile measurements
14 p2500 A69-29908
- Electrical conductivity ratio of weakly ionized turbulent gas to quiescent gas as function of electron temperature
14 p2502 A69-29991
- Axial and radial turbulence intensities for flow through smooth round tubes, measuring velocity profiles and drag coefficients
15 p2590 A69-30003
- Reynolds number, incident flow turbulence and interblade channels roughness effects on friction losses in axial flow turbines
15 p2547 A69-30074
- Wiener-Hermite expansion extended to include time dependent ideal random functions, discussing application to shear flow turbulence
15 p2644 A69-30201
- Turbulent gas flow characteristics obtained by extremal hypothesis, using maximum perturbation stability in formulating variational problem and computer algorithm
15 p2590 A69-30263
- Spiral grooved turbulent screw seal /viscoseal/ analysis, combining results of spiral grooved journal bearing study with turbulent fluid film theory
[ASLE FICFS PREPRINT 32] 15 p2619 A69-30482
- Turbulent heat and momentum fluxes spectra measured in atmospheric ground layer, describing changes as function of height and stratification conditions
15 p2649 A69-30648
- Transport properties interrelationship in turbulent pipe flow and free turbulence
15 p2591 A69-30792
- Rate equation for effective turbulent viscosity variations, considering effects of generation, convection, diffusion and decay in quasi-parallel shear flows
15 p2591 A69-30905
- Pressure fluctuation relaxation model to close turbulent distribution function equations at one point level, solving equation for rectilinear flows and periodic wake decay
15 p2591 A69-30906
- Temperature distributions in layer with internal heat source and turbulent fluid flow cooling, deriving differential heat transfer equations
15 p2718 A69-31169
- Wind tunnel investigation of turbulent gas flow heat transfer and hydrodynamic drag in variable pressure gradient field of divergent-convergent channel
15 p2548 A69-31173
- Mean velocity distribution prediction in turbulent shear flows of variable density by coordinate stretching method
[AIAA PAPER 68-41] 16 p2770 A69-31888
- Velocity field in turbulent flow based on momentum transfer, determining velocity distribution for flow near solid surface
16 p2772 A69-32128
- Initial temperature effects on flame propagation velocity in turbulent flow of homogeneous gasoline-air mixture under realistic conditions
16 p2837 A69-32138
- Swirl decay of turbulent flow in tubes, showing decrease with increasing axial Reynolds number and independence of initial swirl angle
16 p2772 A69-32170
- Subsonic diffuser design, discussing flow distortion and turbulence levels and pressure loss characteristics
[AIAA PAPER 69-449] 16 p2843 A69-32700
- Turbulent base flowfields in multinozzle configurations, considering adiabatic flow and determining base pressure distribution from reverse jet impingement
[AIAA PAPER 69-570] 16 p2733 A69-32751
- German monograph on turbulence in isothermal free jets and free jet flames covering local flow variations, Reynolds number effects, exchange processes, etc
17 p3068 A69-32991
- Transverse turbulent pipe flow, obtaining limiting behavior of time averaged velocity gradient at wall
17 p2949 A69-33013
- Temperature and pressure effects on flame propagation rates, burning time and combustion zone length in turbulent flows of homogeneous gas mixtures
17 p3069 A69-33140
- Linear amplification, nonlinear limiting and secondary instability induced by unsteady effects illustrated for various transitional flows, including roughness and streamwise vorticity
17 p2950 A69-33248
- Turbulence measurements and roughness effects on viscous drag reduction with polymer solution in pipe flow, discussing friction factor, wall velocity profile, etc
17 p2951 A69-33252
- Concentration, flow rate and tube diameter effects on viscous drag reduction in nonpolar soap solutions, using pressure drop measurements to observe turbulent flow behavior
17 p2951 A69-33253
- Eddy viscosity models adapting laminar boundary layer solution techniques to turbulent flows compared with measurements in hypersonic flows
[AIAA PAPER 69-688] 17 p2954 A69-33454
- Turbulent kinetic energy equation for determining turbulent flow fields applied to free mixing problem of constant density streams
[AIAA PAPER 69-683] 17 p2956 A69-33492
- Transverse magnetic field effect on shear turbulence structure of magneto-fluid-mechanic pipe flow with and without heat transfer
[AIAA PAPER 69-723] 17 p3012 A69-33497
- Turbulent velocity distribution and wall friction calculated from eddy viscosity distribution for concentric annulus
17 p2956 A69-33575
- Visual observation of pipe wall regions in turbulent flow by suspending colloidal size particles and photographing with high speed motion picture camera
17 p2956 A69-33598

Minimum Reynolds number and Malkus theory of turbulent channel flow, discussing stability, equilibrium flow, and stationary turbulence via variational theorem
17 p2957 A69-33764

Displacement of rectangularly mouthed pitot tubes in turbulent tube flow, determining roles of wall and shear effects
17 p2976 A69-34049

Microturbulence velocity estimation method for solar type stars using low dispersion spectra of narrow band photometry
17 p3044 A69-34178

Taylor vorticity transport theory and von Karman similarity hypothesis extended to consider three dimensional fluctuating velocity field in analyzing turbulent swirling ducted flow
[ASME PAPER 69-APM-19]
18 p3120 A69-34394

Ejector driven wind tunnel for turbulent flow generation with arbitrary velocity profile, using jet arrays
[AIAA PAPER 69-743]
18 p3114 A69-34408

Computer quadratic method of evaluating ray propagation data for estimating inhomogeneous media properties
18 p3172 A69-34667

Boundary layer transition from laminar to turbulent flow on flat plate, considering supersonic and hypersonic flow, pressure gradients, surface curvature and roughness, etc
18 p3123 A69-34920

Hydrodynamic noise as pseudosound field resulting from pressure variations in turbulent fluid flow, using Lighthill acoustic analogy
18 p3123 A69-34921

Statistical dynamics and structure of turbulent shear flows in incompressible fluids of constant density, discussing Reynolds stress at critical layers
18 p3123 A69-34922

Electrostatic probes in nonequilibrium collision dominated ionized gas flow ballistic ranges
19 p3291 A69-35716

Turbulent velocity of flame propagation in supersonic stream of hydrogen-air mixture determined by velocity distribution, exchange coefficient and burning time
19 p3448 A69-35854

Mean parameters calculation between widening of turbulent flow and point of reattachment, including similarity hypothesis concerning velocity profile
19 p3299 A69-36648

Statistical equations for compressible gas, discussing turbulent quantities separated into fluctuating and macroscopic parts
19 p3300 A69-36784

Continuous particle media on basis of microstructure, discussing granular media deformation, elastic media dilatation, turbulent flow and dilute suspensions
19 p3446 A69-36833

Reynolds number dependence of turbulent velocity profile in circular tube and parallel plate channel analyzed by von Karman similarity hypothesis
20 p3513 A69-37081

Turbomachine blade thickness effect on meridional flow disturbances analyzed through blade geometry using differential equations
20 p3457 A69-37084

Rotta analysis for linear flow transformation into turbulent flow, discussing Reynolds numbers
20 p3513 A69-37086

Stability theory formulation for evaluation of boundary layer transition from laminar to turbulent states
[AIAA PAPER 68-669]
20 p3514 A69-37184

Hydrodynamics of turbulent gas flow through powder layer for vapor phase coating of particles, noting fluidized bed
20 p3548 A69-37363

Thesis on turbulent velocity distribution and wall friction in flow channels of various cross sections
20 p3515 A69-37925

Acoustic frequency response of unsteady turbulent flow in transmission lines, considering effects of small amplitude disturbances and heat transfer
[ASME PAPER 69-FE-11]
20 p3516 A69-37988

Statistical description of turbulence of viscous incompressible fluid at large Reynolds numbers, using velocity distribution probability
20 p3517 A69-38007

Heat transfer in radial flow between two parallel plates, calculating Nusselt number for laminar and turbulent flows
20 p3633 A69-38176

Computational method for nonlinear two and three dimensional disturbances in plane parallel flows applied to transverse disturbances in plane Poiseuille flow
21 p3691 A69-38464

Heat transfer and hydrodynamic resistance for turbulent gas flow in longitudinal positive and negative pressure gradients analyzed using Reynolds number data
21 p3848 A69-38635

Energy spectra measurements of turbulent velocities behind grids of different geometries noting relation to deviation from isotropy
21 p3693 A69-38704

Liquid mercury flow turbulent intensity measured by quartz insulated Pt hot-film sensors, discussing calibration equation and measurement techniques
21 p3722 A69-38769

Analytical relations in phenomenological model theories for turbulent flow near wall
21 p3695 A69-39010

Turbulent skin friction coefficients of compliant surfaces on flat plates determined as function of speed for different materials
21 p3695 A69-39039

Diffusion parameters for fluid stream flowing from round hole with given radius and velocity into wake flow
21 p3696 A69-39091

Final period of decay for viscoelastic fluid in homogeneous isotropic turbulence, deriving expressions for double correlation function and energy decay
22 p3928 A69-39891

Turbulent Hartmann flow between rough walls in transverse magnetic field, determining field influence on resistance coefficient
22 p3989 A69-40255

Model for statistically isotropic homogeneous turbulence in incompressible fluid, representing turbulence as superposition of individual vortex sheets
22 p3930 A69-40525

Forced convection heat transfer coefficient for fully developed turbulent flow in circular tube with time-varying circumferential heat flux
22 p4051 A69-40921

Boundary layer calculation in incompressible turbulent flow with closed streamlines, avoiding von Mises equation
22 p3932 A69-40931

Heat transfer coefficient of turbulent air flow found independent of temperature head during cooling
22 p4051 A69-41026

Pulsed energy balance expressions for turbulent characteristics of incompressible circular flow in channel with inserted rotating cylinder
22 p3933 A69-41028

Charge exchange of solar wind protons passing shock front, noting turbulent subsonic motion of randomized hot solar wind protons in shadow cone
22 p4008 A69-41208

Hypersonic turbulent flow heat transfer and pressure data for flat plate containing steps and cavities obtained in hypersonic wind tunnel
[AIAA PAPER 68-673]
23 p4060 A69-41902

Boundary layer effects in turbulent spiral vortex flow of compressible fluid in supersonic centrifugal compressor, discussing flow geometry, using momentum integral method
23 p4152 A69-42109

Turbulence theory in laminar-turbulent flow transition, nonlinear stability for flows with Reynolds number higher than critical and fully developed turbulence
23 p4152 A69-42313

Turbulent flow, discussing light scattering techniques, correlation functions, statistical theory, modified Navier-Stokes equation, etc
23 p4153 A69-42314

Constant temperature thermoanemometer design and subsystem operation applied to measurements of turbulent flow velocity and pulse characteristics
24 p4311 A69-42558

Real space-time Green functions applied to turbulence induced infinite thin elastic plate vibration, analyzing mechanical dissipation effects
24 p4395 A69-42597

Axial and angular momentum flux, flow force and circulation to determine strength and structure of narrow rotating axisymmetric vortex and swirling core flows
24 p4298 A69-42598

Weak magnetic field amplification in turbulent flow with velocity field as random function of space and time
24 p4375 A69-42657

Detachment in incompressible turbulent flows around thick body analyzed to predict base pressure, vortex volume, etc
24 p4299 A69-42674

Mixing length theory including eddies axial motion, discussing turbulent field of temperature or concentration
24 p4407 A69-42917

Turbulence characteristics of flow influence on critical flameout conditions of disk shaped flame stabilizer, circulation zone length and combustion efficiency by bluff body
24 p4408 A69-43078

Symmetry properties of Cameron-Martin-Wiener kernels in isotropic velocity field, applied to one dimensional model of incompressible turbulent flow
24 p4301 A69-43358

Wiener-Hermite truncated stochastic expansion used for velocity and concentration fields in turbulent flow convecting passive scalar, determining diffusivity and spectrum function
24 p4302 A69-43359

Solution stability and secondary solutions growth beyond critical points investigation for Burgers equations for laminar-turbulent transition
24 p4302 A69-43360

Chaplygin equation applied to eddy flow past semicylindrical surface, discussing stagnation points and boundary value problems
24 p4245 A69-43477

Flow discharge characteristics of nozzle during swirling gas flow ejection, considering isentropic and isothermal limiting cases
24 p4247 A69-43499

Secondary flow occurrence and geometry in viscous turbulent flow in square channel, using iterative solution
24 p4303 A69-43501

Numerical program solving partial differential equations parabolic system for internal turbulent gas flow extended to flows undergoing circular tube laminarization by heating
[ASME PAPER 69-HT-52]
24 p4409 A69-43520

Inverse transition from turbulent to laminar flow in radial diffusers, noting nonagreement of transition point prediction methods
[ASME PAPER 69-HT-33]
24 p4247 A69-43530

Natural convection flow, discussing initial instability of laminar flow, disturbance amplification and transition to turbulent flow
[ASME PAPER 69-HT-29]
24 p4411 A69-43531

Turbulent flow in circular porous tube laminarized by uniform mass injection through tube wall, measuring velocity and turbulence intensity by impact probe
[ASME PAPER 69-HT-57]
24 p4303 A69-43537

Heat transfer and fluid friction of hydrogen and helium gas flows undergoing turbulent to laminar flow transition in heated pipe
[ASME PAPER 69-HT-54]
24 p4303 A69-43539

Turbulent pipe flow with wall suction, calculating friction factor, pressure gradient, heat and mass transfer coefficients, velocity and temperature profiles
[ASME PAPER 69-HT-4]
24 p4414 A69-43562

Superimposed free vortex swirl effect on flow and heat transfer in three dimensional axisymmetric laminar boundary layer
24 p4304 A69-43584

Turbulent skin friction on compliant skins stretched over damping fluid in shallow bath in flat plate
[AIAA PAPER 69-164]
24 p4306 A69-43685

TURBULENT HEAT TRANSFER

Turbulent heat and mass transfer in rotating incompressible fluid flow analyzed by kinetic energy and shear stress equations
01 p0060 A69-10402

Sensible and latent heat meridional transport associated with standing eddies computed from climatic mean data
04 p0627 A69-15085

Heat transfer in turbulent pipe flow of radiating optically thin gas in circular tube
[ASME PAPER 68-WA/HT-17]
05 p0847 A69-16121

Shock wave-boundary layer interaction configurations for hypersonic propulsion device inlets under transitional and turbulent conditions, noting heat transfer rate
[AIAA PAPER 69-8]
06 p0915 A69-18172

Shear stress at wall, averaged velocity field and turbulent heat transfer coefficients in straight smooth non-circular channels used to compute temperature fields
07 p1243 A69-19734

Acceleration effects on forced convection in turbulent boundary layer, noting heat transfer history and rates prediction
09 p1480 A69-21480

Turbulent heat transfer in conducting fluid flow through circular tube in longitudinal magnetic field and constant wall heat flux, using Lyon relation
09 p1621 A69-21590

Turbulent heating of toroidal plasma system with current contained in ceramic vacuum chamber with copper housing
11 p1935 A69-25752

Energy loss during turbulent plasma heating by current in open magnetic trap, attributing heating to ion-acoustic instability in plasma
11 p1935 A69-25753

Atmospheric boundary layer mean turbulence and vertical velocity calculations, tabulating layer characteristics for various turbulent heat flux and geostrophic wind velocity values
12 p2126 A69-26578

Thermal stratification effect on wind structure in Ekman layer, assuming turbulent transfer and height dependence
13 p2290 A69-27390

Heat transfer coefficients for carbon dioxide near thermodynamic critical point for flow through electrically heated duct, noting turbulent forced convection as mechanism
[ASME PAPER 68-HT-32] 13 p2373 A69-27769

Local film heat transfer coefficients variations effect on longitudinal constant area fin surface under turbulent flow
[ASME PAPER 68-HT-20] 13 p2373 A69-27770

Vortices interaction effect on vertical turbulent heat flow in atmosphere boundary layer, determining dependence of vortex mean vertical temperature gradient
13 p2293 A69-27841

Eddy diffusivities ratio for heat and momentum by mixing length theory, using Mach-Zehnder interferometer for temperature profiles
13 p2380 A69-28497

Turbulent heat exchange coefficient radiation absorption and diurnal vertical variations effects on temperature field in surface layer of sea and atmospheric boundary layer
14 p2472 A69-29462

Laminar-turbulent transition in boundary layer on thermally decomposing surface, discussing gasification rate, Reynolds number effects, heat transfer and turbulence onset mechanism
16 p2878 A69-31951

Shape and surface roughness effects on turbulent adhesion of reentry body nose tip, noting recession rate
[AIAA PAPER 69-717] 17 p2952 A69-33435

Turbulent heating of ions and electrons by interaction between magnetically collimated electron beam and electron beam self generated plasma
17 p3014 A69-33827

Convective heat flux from nonisothermal surface by temperature superimposition method with Spalding function as turbulent heat transfer coefficient, noting wall temperature
18 p3229 A69-34836

Partial differential equation representing influence of radiative and turbulent transfers of atmospheric heat, based on absorption coefficients for terrestrial radiation
19 p3363 A69-36498

Blowing effect on surface friction coefficient and heat transfer in turbulent boundary layer in compressible fluid with pressure gradient
21 p3643 A69-38636

Momentum, heat and mass transfer in turbulent channel flow emphasizing phenomena close to wall, using boundary layer growth-breakdown model
24 p4407 A69-42914

Eddy diffusivity hypothesis modified to fit observed heat transfer from smooth pipe wall to turbulent gas stream at low Reynolds numbers
[ASME PAPER 69-HT-H] 24 p4303 A69-43523

Natural convection local heat transfer on constant heat flux inclined surfaces for water and air in laminar, transition and turbulent regimes
[ASME PAPER 69-HT-C] 24 p4410 A69-43526

TURBULENT JETS.

Mach-Zehnder interferometer for studying temperature distribution and heat transfer in turbulent jets, noting temperature dependence on jet thickness at different angles of attack
01 p0005 A69-10101

Turbulent jet model of unsymmetrical velocity profile for design of wall attachment device
02 p0231 A69-12072

Heat transfer near stagnation point in axisymmetric turbulent jet impinging on circular disk
02 p0354 A69-12491

Open circuit wind tunnel experiment to measure properties of two dimensional plane turbulent wall jet in moving stream
[ASME PAPER 68-WA/APM-13] 04 p0586 A69-14390

Two dimensional turbulent jet in uniform parallel stream, developing coordinate type perturbation expansion and applying series truncation method to predict downstream development
04 p0588 A69-14713

Incompressible jet flows, discussing two dimensional jet, axisymmetric laminar jet and turbulent free jet
05 p0746 A69-16008

Turbulent free jet at miniature nozzle exit, analyzing wall attachment fluid amplifier and flow characteristics
05 p0746 A69-16012

Fluctuation velocity, apparent kinematic viscosity and turbulent shear stress in isothermal homogeneous free jets
06 p0909 A69-17169

Soviet collection of papers on turbulent jets of air, plasma and real gas
07 p1049 A69-18392

Approximate solution for turbulent jet expansion in opposing stream, discussing hydraulic drag coefficient formula derivation
07 p1118 A69-18396

Underexpanded nozzle ejected supersonic turbulent jet off-design behavior, discussing static pressure distribution, boundary layer and Mach number effect
07 p1049 A69-18397

Axisymmetric liquid nitrogen turbulent jet propagating under supercritical pressure in gaseous nitrogen medium
07 p1049 A69-18398

Axisymmetric turbulent conducting fluid jet propagation in longitudinal magnetic field without induction
07 p1192 A69-19019

Pulsation energy balance of turbulent jet of conducting fluid expanding in longitudinal magnetic field
07 p1192 A69-19021

Circular turbulent air jet from flat plate into deflecting stream analyzed with potential flow model, noting applicability to V-STOL aircraft technology
[AIAA PAPER 69-223] 07 p1051 A69-19557

Three dimensional laser Doppler velocity instrument for mean velocity and turbulence measurements in subsonic jet shear layer
[SAE PAPER 690266] 09 p1494 A69-21555

Turbulent circular wall air jet trajectory and spreading in perpendicular crossflow of constant and varying velocities
[ASME PAPER 69-GT-33] 09 p1483 A69-22491

Turbulent wall jet growth in streaming two dimensional incompressible flow over plane smooth wall with pressure gradient
11 p1873 A69-25139

Axisymmetric turbulent supersonic incompressible fluid jet, calculating momentum flow distribution and excess heat flow densities in basic segment
11 p1818 A69-25346

Two phase two dimensional turbulent jet analysis for predicting uncertainty in measured value of mixing coefficient
13 p2247 A69-27787

Boundary layer equations describing momentum, energy and mass concentration conservation in axisymmetrical turbulent jet flame solved for Lewis number unity in von Mises plane
13 p2379 A69-28455

Turbulent jets of gases in general stream of air spreading in cylindrical chamber, discussing distributions of gas dynamic parameters
13 p2200 A69-28501

Numerical analysis for spreading of free turbulent gas jets with arbitrary uneven initial distribution of momentum and heat and mass fluxes
15 p2590 A69-30157

Turbulent jet theory, thermal ignition theory and flameout characteristics of bluff body flame stabilizers
16 p2879 A69-32141

Combustion effects on mixing of axisymmetric supersonic and turbulent free jets to obtain species concentrations, pilot pressures and temperatures
[AIAA PAPER 69-538] 16 p2843 A69-32705

Monograph on turbulent isothermal swirl-free jets and turbulent swirling flames, studying mixture and propagation in free space
17 p3068 A69-32996

Sound effects on turbulent flame in gasoline-air mixture jet in Toepler device with pulsed light source, measuring ionization in combustion zone
17 p3069 A69-33141

Subsonic and supersonic turbulent air jets expansion over perpendicularly positioned plane disk obstacle, deriving equations for pressure distribution and stagnation temperature
18 p3123 A69-34990

Soviet book on integral methods of calculations in theory of turbulent jets and wakes, covering turbulent boundary layers, laminar mixing, etc
20 p3518 A69-38211

Coaxial turbulent compressible gas jets propagation, discussing mass buildup data in coaxial jets
21 p3645 A69-39847

Aerodynamic characteristics of turbulent twisted jet in slipstream in open jet wind tunnel, determining static pressure, temperature and velocity component profiles
21 p3645 A69-39848

Mean flow properties of incompressible turbulent three dimensional jets and wakes, treating flow within boundary layer theory context
23 p4060 A69-41908

Aerodynamics of twisted jet propagating in same fluid by asymptotic expansion, analyzing twist influence on heat transfer
24 p4244 A69-43057

TURBULENT MIXING

Turbulent mixing of scalar fields such as temperature or concentration noting fine structure, number and distribution of zero gradient points and minimal gradient surfaces
03 p0414 A69-13134

Axial deviation of gas flow resulting from mixing turbulent gas jets
04 p0591 A69-15411

Mixing zone between two dimensional free stream and fluid at rest, measuring turbulent shear layer velocity profile behind rearward facing steps and over cavities
[ASME PAPER 68-WA/FE-21] 05 p0749 A69-16097

Turbulence hypothesis for velocity of laminar fluid flow at dividing line, considering base pressure and adiabatic mixing zones
06 p0910 A69-17330

Combustion in compressible turbulent mixing flows, discussing mixing facility, experimental results and numerical analysis
[WSCIPAPER 68-28] 06 p0969 A69-17794

Turbulent premixed flames stabilization, determining gas flow velocity, turbulence intensity, flame thickness and burning velocity relation to intensity
06 p1035 A69-17931

Ducted turbulent mixing and burning of coaxial streams, presenting experimental results for rocket-air mixing system
[AIAA PAPER 69-85] 06 p0984 A69-18082

Free turbulent mixing, emphasizing flowing gas mixtures with and without chemical reaction
[AIAA PAPER 69-31] 06 p0915 A69-18223

Nongray radiation effects on compressible turbulent free jet mixing of nonsimilar gases, using stepwise spectral absorption coefficient and Beer law
08 p1253 A69-20844

Two phase two dimensional turbulent jet analysis for predicting uncertainty in measured value of mixing coefficient
13 p2247 A69-27787

Turbulent jets of gases in general stream of air spreading in cylindrical chamber, discussing distributions of gas dynamic parameters
13 p2200 A69-28501

Mixing zone between two dimensional free stream and fluid at rest, measuring turbulent shear layer velocity profile behind rearward facing steps and over cavities
[ASME PAPER 68-WA/FE-21] 14 p2430 A69-29443

Fluctuating turbulent stress measurements in mixing layer of two dimensional jets including intensity, spatial correlation and wave-number fluctuating stress frequency spectra
14 p2431 A69-29577

Two phase flow mixing shocks, obtaining expressions for pressure and entropy changes, discussing shock stability and gas entrapment mechanism
16 p2768 A69-31589

Finite difference method for turbulent mixing and combustion of hydrogen injected parallel to supersonic air stream, considering vitiated and unvitiated air
[AIAA PAPER 69-539] 16 p2877 A69-31844

Two dimensional turbulent mixing with surface mass injection at supersonic and hypersonic speeds, noting velocity and temperature distributions
[AIAA PAPER 68-130] 16 p2770 A69-31883

TURBULENT WAKES

- Chemical reactions in compressible turbulent mixing flows, analyzing flow characteristics, rate equation and Reichardt theory [AIAA PAPER 69-537] 16 p2747 A69-32701
- Monograph on turbulent isothermal swirl-free jets and turbulent swirling flames, studying mixture and propagation in free space 17 p3068 A69-32996
- Turbulent process employing product constituents dilute suspensions in inert carrier (Quickmix) to obtain solid propellant mixtures, discussing plant design and analysis, economics, etc [AIAA PAPER 69-517] 17 p2978 A69-33033
- Turbulent gas coaxial mixing theory, deriving eddy viscosity model and semiempirical expressions for velocity, temperature and density fluctuations [AIAA PAPER 69-682] 17 p2952 A69-33434
- Base flow component of total drag for axisymmetric supersonic afterbody with single exhaust jet, considering turbulent mixing [AIAA PAPER 69-650] 17 p2956 A69-33485
- Turbulent kinetic energy equation for determining turbulent flow fields applied to free mixing problem of constant density streams [AIAA PAPER 69-683] 17 p2956 A69-33492
- Transport properties of free turbulent mixing of subsonic coaxial streams by introducing environmental distributions in integrals of momentum, energy and species continuity equations [AIAA PAPER 69-681] 17 p2956 A69-33495
- Lateral mixing of air masses in jet stream by water fluid model experiments, discussing steady and non-steady state turbulent momentum exchange 17 p3000 A69-33759
- Atmospheric horizontal mixing caused by quasi two dimensional macroturbulent motions, describing micro and mesoscale processes using numerical model 19 p3363 A69-36500
- Turbulent gas jet mixing in chamber with four inlet nozzles 21 p3785 A69-39102
- Solar oblateness observed by Dicke and Goldenberg as interaction between slow uniform rotation and turbulent convection 22 p4017 A69-40175
- Boundary layer separation and free mixing phenomena between streams behind thin flat plate by finite difference methods and Prandtl exchange coefficient 23 p4060 A69-41912
- Plasma-dynamic forces used to suppress fuel-propellant interface turbulence in coaxial jet gas core reactors 24 p4349 A69-43679
- Reverse flow profiles in turbulent free jet mixing with streamwise pressure gradient 24 p4306 A69-43684

TURBULENT WAKES

NT PROPELLER SLIPSTREAMS

- Wake temperature turbulent fluctuation decay rates deduced from atomic oxygen recombination chemiluminescence 02 p0190 A69-12525
- Chemical reaction fluctuations and oxygen electron attachment omission effects on density fluctuations in turbulent wakes, noting electron density fluctuation, bimodal model, etc 02 p0233 A69-12538
- Turbulent front structure of axisymmetric compressible wake at supersonic speeds, measuring intermittency factor distribution 03 p0419 A69-13949
- Light aircraft hazards due to trailing vortex generated by heavy transport aircraft, suggesting specific procedures for takeoff, landing and flight phase [SAE PAPER 680220] 04 p0549 A69-14930
- Unsteady potential flow and wake near oscillating circular cylinder noting velocity, pressure and correlation measurements [ASME PAPER 68-WA/FE-23] 05 p0749 A69-16099
- Radar backscattering from turbulent rocket exhaust plumes [AIAA PAPER 69-71] 06 p0891 A69-18071
- Turbulent density fluctuations in near wake of hypersonic axisymmetric slender body measured photometrically with near UV absorption of sulfur dioxide in flow [AIAA PAPER 69-70] 06 p0864 A69-18158
- Boundary layer separation and vortex street buildup conditions of gas flow in circular cylinder wake 08 p1252 A69-20713
- Electron density fluctuations in turbulent wakes of hypersonic projectiles in ballistic ranges, discussing use of cylindrical Langmuir probe for direct measurement 09 p1496 A69-21934

Initial turbulence influence on wakes formed behind trailing edges of cascade blades 09 p1431 A69-22235

Mean flow measurements in supersonic wake of slender two dimensional body at zero incidence and heat transfer rate, noting predictability from similarity analysis 11 p1817 A69-24281

Small body drag in wake of large satellite using two dimensional model noting methods for calculating distribution function moments in wake regions 12 p2012 A69-26798

Nonreacting turbulent far wake problems, discussing centerline decay of viscosity models, similarity profiles and radial distributions at various Mach numbers 13 p2200 A69-28500

Electric field determination from charged particle concentration in wake of body moving in rarefied plasma, noting hydrodynamics similarity 14 p2517 A69-29068

Laminar and turbulent hypersonic wakes trailing blunt bodies studied by finite difference method, taking into account pressure gradients and nonequilibrium chemical reactions effects 14 p2391 A69-29618

Ballistic wake structure and jump conditions for plane plasma shock waves with electrostatic turbulence 15 p2660 A69-30914

Spectral density function derivation for energy scattered from underdense turbulent wake 16 p2732 A69-31893

Three dimensional incompressible wake behind blunt obstacle at leading edge of flat plate compared with mathematical model by Oseen linearization 18 p3083 A69-34403

Flow structure in wake of blunt bodies placed perpendicular in parallel airstream determined from hot-wire anemometry [AIAA PAPER 69-746] 18 p3084 A69-34409

Dynamic pressure pulsations, temperature distribution and gas concentrations in discrete vortices zone in wake of plate in unbounded flow 18 p3124 A69-35120

Standing twin vortices in wake behind thin flat plate normal to flow visualized by Al dust, noting Karman vortex street 18 p3086 A69-35167

Vortex wakes behind circular cylinder subject to transverse sinusoidal oscillations in uniform water flow at specific Reynolds numbers, photographing varied frequency flow patterns 18 p3086 A69-35169

Flow field throughout wind tunnel containing rotor with sharply deflected blades, noting reversed flow effect in front of wake 18 p3119 A69-35228

Electrostatic probes calibration and use for hypersonic wakes behind projectiles in ballistic range 19 p3291 A69-35717

Nanosecond pulse coherent Doppler radar for monostatic measurements of turbulent wakes in shock tunnels and ballistic ranges 19 p3293 A69-35743

Similarity solutions describing buoyancy effect on laminar and turbulent wakes of heated body in incompressible fluid vertically ascending flow 19 p3296 A69-35761

Axisymmetric laminar and turbulent wakes of body in flow with streamwise pressure gradient, discussing velocity defects and profiles 19 p3296 A69-35762

Turbulent wake and ambient flow interaction analysis based on integral methods in boundary layer theory 19 p3299 A69-36390

Soviet book on integral methods of calculations in theory of turbulent jets and wakes, covering turbulent boundary layers, laminar mixing, etc 20 p3518 A69-38211

One dimensional spectra of turbulent wakes behind circular cylinders, discussing isotropy, anisotropy and Reynolds number 21 p3693 A69-38705

Flow structure in wake behind cylinder in plane channel, discussing circulation zone variation and velocity and turbulence distribution at various channel cross sections 21 p3698 A69-39850

Mean flow properties of incompressible turbulent three dimensional jets and wakes, treating flow within boundary layer theory context 23 p4060 A69-41908

Spanwise velocity correlations of turbulent vortices shed by two dimensional bluff body of D section with different aspect ratios, noting end plates effect 23 p4234 A69-42397

Shape, position and velocity of vortex wakes shed in unsteady multienergy flows near trailing edge, applying Kutta condition [ASME PAPER 69-APMW-19] 24 p4245 A69-43099

Wake development from turbulent boundary layers on both sides of thin flat plate 24 p4249 A69-43694

TURING MACHINES

Reliability functions and cycles number before breakdown of finite automaton with account of randomness of malfunctions, structure and input signal distribution 13 p2224 A69-27250

Asynchronous finite state sequential nonlinear controller synthesis with few flip-flops for dynamic space vehicle systems [AIAA PAPER 67-988] 13 p2225 A69-28201

Finite state probabilistic automata reduction problems 13 p2239 A69-28534

Homogeneous finite automaton asymptotic analysis, calculating series terms for matrix transition probability function 13 p2239 A69-28535

Finite automaton malfunctions, discussing input sequences construction and output sequences analysis for malfunction subsets recognition 13 p2239 A69-28536

Finite automaton used to construct minimum automaton with periodic structure, discussing representability of regular events 13 p2239 A69-28553

TURNING FLIGHT

Incidence for three dimensional reentry trajectories preprogrammed as function of velocity, finding bank angle as function of inclination 03 p0504 A69-12858

Three dimensional atmospheric entry trajectories equations for satellite with aerodynamic lift, examining aerodynamic factors and bank angle effects 07 p1230 A69-19608

Earth rotation and aircraft speed effects on vertical gyroscopes during banking, obtaining formulas for gyro errors 09 p1498 A69-22107

Angle of attack and bank angle for orbiting reentry glider, determining optimal trajectory for ground landing at given point [ICAS PAPER 68-41] 11 p1966 A69-24750

Thrust, bank angle and angle of attack of aircraft minimum fuel lateral turns at constant altitude and specified velocities 13 p2203 A69-28245

Directional gyroscope with interframe correlation, discussing errors during object pitching and banking 14 p2446 A69-28923

Analog computer simulation of helicopter dynamics after main and tail rotor blades partial loss, showing banking and controllability 14 p2393 A69-29744

In-flight test to determine variation effects in bank angle control parameters on cruise flight handling qualities, considering spiral stability [AIAA PAPER 69-893] 21 p3648 A69-39425

TURTLES

Telemetry with unrestrained animals, discussing radio tracking of game animals and instrumentation requirements for studying green sea turtle goal finding ability 07 p1071 A69-19136

TVC [CONTROL]

U THRUST VECTOR CONTROL

TWENTY-FOUR HOUR ORBITS

Low degree earth gravity harmonics effect on 12 and 24 hour orbits of high altitude communications satellites 04 p0592 A69-14661

Charged particle environment in synchronous orbit region, discussing electrons and protons under influence of geomagnetic field 07 p1204 A69-18340

Magnetic field at synchronous equatorial orbit by analyzing magnetometer data recorded by ATS 1 satellite during magnetic storms, geomagnetic substorms and quiet times 07 p1123 A69-18343

Ideal resonance problem with single critical term for case of libration solved by modified Poincare method, considering 24-hr satellite 12 p2152 A69-25800

Europa 1 booster supplementing with perigee-apogee system for development of Europa 2, noting payload launching capability into 24-hr circular orbit
15 p2671 A69-31051

Particles integral and differential fluxes spectral distribution calculation for determining radiation load for synchronous satellite
22 p4035 A69-39909

Liquid fuel propulsion systems for geostationary satellites, discussing transfer orbits, payload increase and required thrust for various satellite trajectories [DGLR-69-014]
23 p4202 A69-41299

TWENTY-SEVEN DAY VARIATION

Solar and geophysical activity during February 1965 and March 1966 indicating geomagnetic activity on 27-day recurrence diagram
01 p0068 A69-11118

27-day cosmic ray intensity variations related to solar wind velocity nonuniformity due to longitudinal distribution of coronal active regions
06 p0990 A69-17292

Power spectrum analysis and linear filtering for 27 day variation amplitude of geomagnetic disturbance subject to semiannual amplitude modulation
14 p2434 A69-28955

Geocoronal Lyman alpha short term and 27-day variations observed byOGO 4 spacecraft attributed to flux variability at solar emission line center
15 p2699 A69-31404

Solar microwave emission heliographic distribution during pronounced geomagnetic recurrence, noting brightness temperature nonuniformity due to coronal depression through polytropic models for solar wind
18 p3188 A69-35396

Solar cycle and slowly varying components correlation with soft X ray radiation based on spacecraft measurements
22 p4004 A69-40504

Sudden and gradually developing geomagnetic storms with 27 day recurrence period and relation to 11 year solar activity cycle
23 p4156 A69-41849

Interplanetary and geophysical conditions forecasted based on repetitions of low latitude photospheric background magnetic field patterns during solar activity cycles
24 p4387 A69-43626

TWILIGHT GLOW

Seasonal variation of evening-morning difference in maximum density heights of twilight sodium layer
01 p0063 A69-10275

Twilight sky brightness measurements at 5200 angstroms for estimating upper atmospheric dust component, discussing error rates
01 p0075 A69-11191

Stratospheric dust effect on twilight sky color, evaluating scattered radiation chromaticity for atmospheric models containing ozone
02 p0243 A69-12014

Optical method of sounding cosmic matter penetrating into upper atmosphere by analyzing twilight phenomena
04 p0594 A69-15246

Latitude dependence of 6300 A /O I/ twilight airglow enhancement attributable to conjugate photoelectrons
05 p0756 A69-16280

Twilight resonance emissions due to atmospheric sodium, lithium and potassium, noting similarity of annual sodium and lithium twilight abundance variations [AFCL-69-0097]
06 p0918 A69-17494

Evening twilight nitric oxide density profile in gamma bands deduced from rocket measurements
07 p1125 A69-18842

Upper atmosphere temperature distribution estimation on basis of twilight zenith sky intensity measurements, discussing influence of various parameters on accuracy
09 p1487 A69-21653

Hydroxyl luminescence spectrographic observations at twilight in vibrational-rotational band from 10600 to 11200 A
10 p1681 A69-22847

Scattered light mean intensity determination in twilight aerosol atmosphere from satellite observations, formulating boundary value problem
10 p1689 A69-23970

Twilight helium emission observed by Fabry-Perot spectrometer, noting consistency with triplet He atom excitation by photoelectron collision with ground state atoms [AFCL-69-0294]
14 p2440 A69-29124

Zenith sky Umkehr observed with Dobson spectrophotometer at twilight, discussing light scattering by aerosols in lower stratosphere
16 p2786 A69-32634

He I 1.083 micron resonance line in evening twilight airglow spectrum, discussing maxima, minima, decay patterns, etc
19 p3303 A69-36484

Rocket observation of ionospheric electron and positive ion densities and dayglow emission intensities in twilight conditions
21 p3702 A69-38355

Twilight airglow excitations governed by solar radiation, indicating presence of alkali metals, positive calcium ions and H lines, positive sodium ion bands, etc
21 p3711 A69-38515

Altitude variation of mesospheric daytime sky brightness from earth based measurements of twilight sky brightness, noting inconsistency in calculations based on standard atmospheres
21 p3716 A69-39116

Scattered light mean intensity determination in twilight aerosol atmosphere from satellite observations, formulating boundary value problem
21 p3717 A69-39656

TWINNING

NT MECHANICAL TWINNING

Shear accommodation kinking at second order twin bands in critically deformed magnesium investigated for dislocation mechanism
01 p0093 A69-10063

Tension-compression fatigued alpha Ti twin formation contribution to fatigue damage during cyclic loading
12 p2116 A69-26913

Oxygen content effect on tension-compression fatigue of alpha Ti alloys, discussing internal damage associated with twin formation
12 p2116 A69-27134

TWISTED WINGS

Torsionally flexible blade controllable twist rotor with pitch horn and servoflap control, discussing optimum inputs, airloads and angles of attack contours
18 p3089 A69-35234

TWISTING

Plastically twisted prismatic bars with transverse discontinuous inhomogeneity, using sand hill analogy to determine stress field and limiting torque
03 p0524 A69-13021

Small twist of elastic circular cylindrical tube with nonorthogonal cylindrical aeolotropy, noting zero and nonzero warping conditions effects
05 p0831 A69-15580

Twisting of spherical shell of nonhomogeneous isotropic material with variable shear modulus and inner surface assumed to be stress free
20 p3619 A69-36911

TWO BODY PROBLEM

Matrizants construction for Keplerian motions, discussing Hamiltonian character of variational equations for planar two body problem
03 p0513 A69-13779

Rendezvous maneuvers for vehicle and elliptically orbiting targets, formulating relative motion of two bodies
04 p0658 A69-14828

Orbital parameters changes computation in table form for binary systems with more massive component mass decrease
11 p1962 A69-25120

Third phase dynamics of planetary approach of earth-Mars journey, computing approach trajectory on two body spacecraft-Mars assumption
11 p1968 A69-25725

Moon-earth system origin emphasizing mass distribution
13 p2352 A69-27902

Orbital elements evolution of binary or planetary system with decreasing mass by nonlinear nonautonomous differential equations
14 p2519 A69-29138

Far field energy radiated by two body system using approximation method in general relativity and Minkowski gravitation theory
16 p2812 A69-31836

Motion of two rigid spheroids with mutual gravitational attraction based on Hamilton-Jacobi theory applicable to binary stars
16 p2863 A69-32402

Star motion perturbations by invisible body, stressing bright bodies invisible by position near perturbed star
17 p3034 A69-33407

Orbit computation by means of predictor-corrector algorithms based on nonpolynomial functions, including numerical results for two body elliptic motion
19 p3397 A69-35611

Perturbation matrix derivation in rectangular coordinates using Sitarsky two body variational equation for all motions
20 p3568 A69-37200

Impact pressures during two body collisions, correlating pressure with particle speed
21 p3836 A69-38943

Symmetric periodic orbits families of restricted three body problem, using two body problem
22 p4031 A69-40908

TWO DIMENSIONAL BODIES

Integration method for equations of plastic two dimensional stressed state with Mises yield condition, noting stress concentration at hole with pressure on contour
04 p0679 A69-14924

Center of gravity of two dimensional gravitating bodies by gravitational anomaly technique, based on conformal mapping of bilinear function
05 p0792 A69-15696

Weak shock wave diffraction at two dimensional obstacles, discussing time behavior of pressure distribution
05 p0746 A69-16018

Laminar near wake flow field of two dimensional adiabatic circular cylinder with surface mass transfer [AIAA PAPER 69-67]
06 p0862 A69-18044

Supersonic wake recirculation flow over rearward facing two dimensional steps and blunt bases
14 p2389 A69-29031

Laminar boundary layer control on two dimensional body by combined blowing and suction in presence of roughness, noting skin friction reduction [AIAA PAPER 68-641]
17 p2957 A69-34015

Spanwise velocity correlations of turbulent vortices shed by two dimensional bluff body of D section with different aspect ratios, noting end plates effect
23 p4234 A69-42397

Contact stress distribution between two two-dimensional finite nearly rectangular elastic bodies with general surface configurations for surface load expressed in trigonometric series [ASME PAPER 69-APMW-9]
24 p4402 A69-43104

TWO DIMENSIONAL FLOW

NT COUETTE FLOW

Asymptotic solution of Orr-Sommerfeld equation by multiple scales method for linear and general velocity profile
01 p0059 A69-10332

Linear stability of steady and time dependent plane Poiseuille flow
01 p0175 A69-10333

Two dimensional ionized plasma flow in coaxial channels calculated using differential equations
01 p0130 A69-10723

Stabilization of plane parallel MHD flow at inlet and outlet of flat rectangular tube with transverse magnetic field
01 p0130 A69-10770

Two dimensional compressible inviscid laminar gas flows unsteady processes studied by extending method of characteristics
01 p0008 A69-11360

Transpiration and dissipation effects on heat eddy diffusivity over two dimensional plate in turbulent flow for various Prandtl numbers
01 p0178 A69-11410

Simple wave solution existence for system of equations describing rapid plane flows of ideally plastic material
02 p0337 A69-11560

Downstream pressure asymmetry effect on efflux angle and contraction coefficient of incompressible jet from two dimensional orifice
02 p0231 A69-12075

Two dimensional Navier-Stokes equations of axisymmetric motion of viscous incompressible fluid, giving integral and solutions for stream function
02 p0231 A69-12135

Impervious wall effectiveness of two dimensional wall jet, discussing effectiveness dependence on slot height and turbulence intensity [ASME PAPER 68-HT-4]
02 p0352 A69-12209

Two dimensional diffuse shock waves in carbon dioxide, noting effect of shock curvature equivalence to thickness
02 p0233 A69-12534

Discrete vortices in two dimensional subsonic and supersonic wake, determining Strouhal numbers, frequencies and flow velocities with aid of HF cinematography
02 p0191 A69-12587

Subsonic or transonic bidimensional flows around airfoils by hodograph method
[ONERA-TP-645] 03 p0361 A69-12873

Solute vertical stabilizing gradient inhibition of thermal convection of fluid layer under temperature gradient, discussing effects on two dimensional flows motion 03 p0532 A69-13012

Two dimensional flow of incompressible fluid near sharp leading edge of plate at zero incidence, discussing approximation error and friction stress 03 p0415 A69-13651

Analysis of solution of Navier-Stokes equations describing two dimensional flow of viscous incompressible fluid by finite difference techniques and introduction of curl 03 p0416 A69-13652

Survey of papers on computer calculation of two and three dimensional gas flows, emphasizing method of characteristics and finite difference techniques 03 p0363 A69-13657

Nonlinear aerodynamic problems of plane and asymmetric flows solved by digital computer, using modified Monte Carlo method 03 p0364 A69-13921

Unsteady two dimensional flow in square cavity with fluid initially at rest and constant velocity upper surface of cavity, noting vortex center [AICHE PAPER 25C] 04 p0587 A69-14510

Turbulent fluctuations of viscous sublayer of two dimensional flow, assessing wall shear stress spectrum 04 p0583 A69-14544

Heat transfer, suction and injection in plane Couette flow analyzed for Rivlin-Ericksen fluid, using perturbation method 04 p0589 A69-14970

Two dimensional unsteady flow of inviscid polytropic gas using analysis of similarity solutions in homentropic flow 04 p0590 A69-15191

Difference equation for two dimensional elastic flow 04 p0681 A69-15286

Evolutionarity of equations of MHD with Hall effect allowance for nondissipative plasma two dimensional flow 05 p0801 A69-15788

Incompressible turbulent boundary layers in channel flow using constant temperature hot-wire anemometer, emphasizing measurement in viscous sublayer [ASME PAPER 68-FE-26] 05 p0747 A69-16066

Simulation of two and three dimensional fluid transients by use of one dimensional equations in lattice-work of piping elements 05 p0747 A69-16071

Time dependent two dimensional incompressible laminar boundary layers analysis, discussing application to transient flow over semiinfinite flat plate [ASME PAPER 68-FE-10] 05 p0748 A69-16076

Two dimensional incompressible laminar boundary layer on curved wall for potential velocity inversely proportional to distance along origin [ASME PAPER 68-WA/FE-20] 05 p0749 A69-16096

Mixing zone between two dimensional free stream and fluid at rest, measuring turbulent shear layer velocity profile behind rearward facing steps and over cavities [ASME PAPER 68-WA/FE-21] 05 p0749 A69-16097

Two dimensional aligned field MGD flows analyzed using corresponding basic equations 05 p0806 A69-16735

Integral method for backward boundary layers, developing third order polynomials for two dimensional potential flow toward opening 05 p0752 A69-16737

Incompressible two dimensional turbulent boundary layers calculated on phenomenological basis 06 p0908 A69-17133

Steady two dimensional MHD flow of perfectly conducting fluid past nonconducting wedge with magnetic field orthogonal to flow velocity 06 p0964 A69-17244

MHD flows in channels of MHD devices, emphasizing two and three dimensional problems 06 p0969 A69-17913

Stability theory application to laminar boundary layer transition prediction on two dimensional and axisymmetric flows having pressure distributions in incompressible flow [AIAA PAPER 69-10] 06 p0914 A69-18127

Computer solution of incompressible two dimensional time dependent Navier-Stokes equations for oscillating body with rectangular boundaries [AIAA PAPER 69-185] 06 p0914 A69-18135

Isoenergetic two dimensional supersonic turbulent base flow, noting boundary layer separation properties upstream and downstream [AIAA PAPER 69-68] 06 p0864 A69-18137

Shock wave in two dimensional mixed transonic airfoil flows, discussing initial value problem for flow downstream of shock [AIAA PAPER 69-43] 06 p0915 A69-18180

Transpiration cooling of reentry vehicle nosetips, noting two dimensional aspects of porous wall coolant flow and matrix-coolant energy exchange [AIAA PAPER 69-96] 06 p1039 A69-18212

Steady two dimensional MHD flow in finite region of aligned fields 07 p1188 A69-18274

Strouhal and Reynolds numbers relation from data on vortex streets of circular cylinder in two dimensional flow 07 p1119 A69-18749

Approximation of Chaplygin plane motion equations of gas flow at high supersonic velocities 07 p1120 A69-18754

Numerical analysis of stabilization of one component conducting plasma in two dimensional coaxial duct 07 p1190 A69-18757

Two dimensional flow of conducting fluid in channels with longitudinal transverse magnetic field and Hall effect, discussing gas motion equations linearization 07 p1192 A69-19015

Laminar and turbulent stresses in plane asymmetric incompressible flows analyzed based on Boussinesq formula for turbulent shear stresses 07 p1121 A69-19330

Finite difference computations for calculating two dimensional natural convection, deriving requirements for numerical stability 07 p1242 A69-19397

Circular turbulent air jet from flat plate into deflecting stream analyzed with potential flow model, noting applicability to V-STOL aircraft technology [AIAA PAPER 69-223] 07 p1051 A69-19557

Arbitrary stationary foil in perfect incompressible fluid moving at constant velocity at infinity assuming plane, steady and irrotational flow 08 p1303 A69-20272

Two dimensional unsteady wave motion in shallow water using MHD theory 08 p1362 A69-20354

Two dimensional steady flow of finitely conducting compressible fluid subjected to magnetic field with two zero components 08 p1369 A69-20843

Plane steady transonic flow of perfect fluid around airfoils with constant curvature using hodographic method, discussing various boundary conditions 09 p1429 A69-21605

Irrotational plane subsonic flow of compressible fluid about obstacle, reducing problem to integration of linear partial differential equation with boundary conditions 09 p1480 A69-21735

Two dimensional supersonic flow along adiabatic curved ramp noting separation, attached flow and laminar boundary layer interaction with external stream [AIAA PAPER 68-109] 09 p1430 A69-21949

Tangential air jet for separation control of two dimensional incompressible flow along circular cylindrical wall 09 p1431 A69-22277

Finite difference method computer programs for calculation of velocities and streamlines on blade to blade surface of revolution of turbomachine [ASME PAPER 69-GT-48] 09 p1432 A69-22495

General solutions of MHD equations for linear nonsteady and plane steady motions of ideally conducting gas 10 p1727 A69-23096

Two dimensional flow of unipolar medium in electrodynamic power generation channel, discussing stationary model, electric field and ion density distributions 10 p1638 A69-23486

Finite difference technique for numerical computation of steady supersonic two dimensional gas flows, with or without diffusion normal to mean flow streamlines 10 p1679 A69-23595

Laminar elasticoviscous flow of liquid with short memory in two dimensional channel with porous walls 10 p1680 A69-23668

Two dimensional stratified flow over obstacle in finite height channel, noting lee waves and drag increase with decreasing speed 11 p1869 A69-24892

Second order effects on two dimensional laminar boundary layer flow of incompressible fluid 11 p1872 A69-25127

Reverse transition in two dimensional accelerated incompressible turbulent boundary layer flow, noting skin friction coefficient and turbulent intensity profiles 11 p1872 A69-25129

Streamwise pressure gradient effect on velocity profile in viscous sublayer of two dimensional turbulent flow along smooth wall 11 p1872 A69-25131

Turbulent wall jet growth in streaming two dimensional incompressible flow over plane smooth wall with pressure gradient 11 p1873 A69-25139

Mass flow rates for nearly free molecular flow through two dimensional slit for several tank pressure ratios 11 p1874 A69-25357

Flat plate in two dimensional low density hypersonic flow wind tunnel tested for aerodynamic effects on spacecraft reentry 11 p1819 A69-25424

Two dimensional convective flow stability for arbitrary Rayleigh numbers in horizontal layer, assuming large Prandtl number and free boundary conditions 11 p2003 A69-25657

Invariant transformation of Euler equations of motion for plane steady flows of perfect compressible fluid 11 p1877 A69-25739

Topological properties of plane flow in subsonic region behind smooth shock wave in uniform supersonic flow, discussing shock wave convexity 12 p2061 A69-25888

Heat flux in two dimensional laminar separation zone in supersonic flow, measuring convection coefficient and wall pressure 12 p2011 A69-26289

Two dimensional flow of conducting gas dynamic and electrical parameters in MGD generator channel, considering magnetic field and plasma conductivity 13 p2305 A69-27386

Heat and mass transfer in two dimensional turbulent free shear flows including separated and reattached flows 13 p2377 A69-28145

Chemically reacting flow field and solid surfaces, formulating nonequilibrium laminar boundary layer equations for two dimensional and axisymmetric flows 13 p2377 A69-28147

Two dimensional flow through nonuniform gauze by computerized analysis based on linearized theory 13 p2248 A69-28174

Numerical solutions of equations for high Prandtl number boundary layers in two dimensional flat plate incompressible flow with mass injection 13 p2249 A69-28238

Small disturbances distribution in flow parameters along two dimensional combustion zone of finite width using thermal diffusion theory 14 p2537 A69-28986

Mixing zone between two dimensional free stream and fluid at rest, measuring turbulent shear layer velocity profile behind rearward facing steps and over cavities [ASME PAPER 68-WA/FE-21] 14 p2430 A69-29443

Two dimensional inhomogeneous conductors resistance determined by interchanging equipotential and flow lines 14 p2422 A69-29554

Extension of Helmholtz classical problem of flows with discontinuous surfaces, considering two sources and transverse plane 14 p2433 A69-29683

Incompressible two dimensional turbulent boundary layer equations with arbitrary pressure distribution solved by weighted residual method [AIAA PAPER 69-397] 15 p2591 A69-30478

Monograph on stress fields in plane plastic flow as solutions to boundary value problems 15 p2711 A69-30932

Spoiler effect on aerodynamic characteristics of airfoil with hinged flap in inviscid fluid plane flow 15 p2549 A69-31223

Two dimensional laminar convection cells asymptotic behavior for high Rayleigh number, discussing Robinson and Pillow models for fluid between horizontal plates heated from below 16 p2767 A69-31588

Maximum turbulent stress in turbulent two dimensional boundary layers leading to general stress law, designing experiment to confirm validity 16 p2769 A69-31832

- Two dimensional turbulent mixing with surface mass injection at supersonic and hypersonic speeds, noting velocity and temperature distributions [AIAA PAPER 68-130] 16 p2770 A69-31883
- Numerical estimates of momentum integral error in applying locally similar solutions to nonsimilar problems, assuming two dimensional or axisymmetric flow 16 p2772 A69-32174
- Two dimensional incompressible flow past circular cylinder at moderate Reynolds number, reducing partial differential equations of motion by series truncation for flow field 17 p2896 A69-33600
- Wave propagation in two dimensional anisotropic media with several perturbation speeds, using Lundquist linear equations ensuring lacunas presence 17 p2925 A69-33841
- Exact analytic solution for thermal conductance of two dimensional eccentric constriction in dimensionless numbers 18 p3228 A69-34375
- Shock tunnel steady flow starting process in two dimensional reflection nozzle, using multiple shadowgraphs and interferograms, noting nozzle geometry influences 18 p3085 A69-34471
- Two dimensional elastoplastic problems in static condition, discussing analytical, variational and finite difference methods 18 p3217 A69-34594
- Evolutionarity of equations of MHD with Hall effect allowance for nondissipative plasma two dimensional flow 18 p3181 A69-35039
- Predictability of deterministic fluid systems with many scales of motion using vorticity equation for two dimensional incompressible flow, noting application to earth atmosphere 19 p3303 A69-36404
- Inverse transformation method for plane subsonic flow extended to flow past cambered profiles at angle of attack, obtaining velocity distribution 19 p3240 A69-36473
- Atmospheric horizontal mixing caused by quasi two dimensional macroturbulent motions, describing micro and mesoscale processes using numerical model 19 p3363 A69-36500
- Pressure gradient produced steady plane flow of Maxwellian gas between infinite parallel planes, describing linearized Boltzmann equation solution 19 p3379 A69-36604
- Two dimensional unsteady motion of medium with pressure as linear function of density, analyzing gas expansion into vacuum 20 p3512 A69-36916
- Second circle theorem for two dimensional irrotational flow of incompressible inviscid fluid in z plane 20 p3518 A69-38316
- Jet efflux from two dimensional symmetric nozzles of arbitrary shape determined using conformal mapping and Riemann-Hilbert solution to mixed boundary value problem 21 p3692 A69-38686
- Quasi-linear ordinary differential equations solutions for steady two dimensional stagnation point flows of nonNewtonian power law fluids 21 p3697 A69-39674
- Axisymmetric and two dimensional flows over blunt bodies at high Mach numbers by integral relations method 21 p3645 A69-39790
- Navier-Stokes equations exact solutions for two dimensional steady flow of compressible viscous heat conducting perfect gas 22 p3929 A69-40117
- Free viscous layers structure at large Reynolds numbers, using matched asymptotic expansions for two dimensional compressible flow 22 p3932 A69-40927
- Friction, heat transfer and mass transfer theory of flow represented by two dimensional parabolic boundary layer equations 22 p3933 A69-40940
- Adiabatic plane ideal gas flow past airfoil, studying shock waves propagation effect on dynamic behavior 22 p3861 A69-41024
- Two dimensional gas dynamics differential equations for simple waves, discussing invariant solutions and conditions for group solutions 22 p3933 A69-41030
- Subsonic compressible flow at two dimensional inlets, analyzing field representation, boundaries, surface configuration and optimal wedge 23 p4060 A69-41915
- Numerical method for calculating unsteady two dimensional boundary layers in laminar incompressible flow 23 p4152 A69-42108
- Steady constant density two dimensional flow in laminar boundary layer over permeable curved surfaces, showing effects of suction or blowing 23 p4153 A69-42399
- Graphical method for two dimensional supersonic expansion flow with subsonic reaction front around corner compared to existing iteration method 23 p4061 A69-42411
- Two dimensional diverging flow of ideal compressible fluid past slender profile, using Prandtl-Glauert rule and linearized equation 24 p4243 A69-42584
- Limit-cycle oscillations of unstable plane Poiseuille flow analyzed by nonlinear Navier-Stokes equations 24 p4298 A69-42600
- Two dimensional incompressible inviscid fluid flow problems solution by conducting-paper analog with electrical equipotentials tracing, based on Laplace equation applicability 24 p4299 A69-43024
- Continuous potential fields modeling based on electrohydrodynamic analogy extended to flows involving stream separation 24 p4300 A69-43089
- Nonlinear finite-amplitude instability of two dimensional compressible laminar wake flows, using Fourier expansion and Landau equation 24 p4245 A69-43357
- Dynamic behavior of gas bubble in ideal fluid plane flow, considering bubble shape, velocity field, gas pressure and stagnation point pressure determination 24 p4302 A69-43478
- TWO DIMENSIONAL JETS**
- Potential flow of stream interaction with two dimensional thin jet, discussing jet penetration depth 01 p0007 A69-11019
- Thermal radiation effects on two dimensional steady MHD jet of conducting ionized gas confined by magnetic field 02 p0287 A69-11831
- Open circuit wind tunnel experiment to measure properties of two dimensional plane turbulent wall jet in moving stream [ASME PAPER 68-WA/APM-13] 04 p0586 A69-14390
- Laminar two dimensional free jet outflow of incompressible nonNewtonian pseudoplastic fluid from orifice into mass of same fluid 04 p0586 A69-14406
- Two dimensional turbulent jet in uniform parallel stream, developing coordinate type perturbation expansion and applying series truncation method to predict downstream development 04 p0588 A69-14713
- Stabilizing influence of axial magnetic field on confined vortex flow of aqueous electrolytic conductor generated by two dimensional wall jets 05 p0798 A69-15611
- Incompressible jet flows, discussing two dimensional jet, axisymmetric laminar jet and turbulent free jet 05 p0746 A69-16008
- Sound amplification role in increasing spread of bounded two dimensional smoke jet studied for application to fluid amplifiers [ASME PAPER 69-VIBR-3] 10 p1640 A69-24161
- Mixing zone of plane jet in rectangular nozzle mounted at end of controlled velocity wind tunnel 12 p2062 A69-26287
- Velocity fluctuation amplitude in potential cone of plane jet compared to properties of irrotational fluctuations induced by flow boundaries 13 p2247 A69-27736
- Two phase two dimensional turbulent jet analysis for predicting uncertainty in measured value of mixing coefficient 13 p2247 A69-27787
- Discontinuity coefficient on boundaries of mixing zone of plane jet, observing homogeneity of thermal and kinematic structures 13 p2247 A69-27978
- Fluctuating turbulent stress measurements in mixing layer of two dimensional jets including intensity, spatial correlation and wave-number fluctuating stress frequency spectra 14 p2431 A69-29577
- Free and dividing streamlines shapes for two dimensional jet from parallel walls penetrating into counterstream, discussing finite cavities 22 p3859 A69-40143
- Aligned uniform magnetic field effect on hydromagnetic stability of two dimensional incompressible electrically conducting jet flow with large Reynolds number 22 p3931 A69-40687
- Flowfield properties of two dimensional supersonic jet near sonic nozzle exit by numerical method of characteristics 22 p3860 A69-40920
- Underexpanded plane hypersonic gas jet injection into resting medium from straight nozzle, discussing shock wave formation 24 p4246 A69-43484
- TWO FLUID MODELS**
- Garden hose instability quasi-linear stabilization employing macroscopic viewpoint, discussing fluid model 01 p0133 A69-11217
- Ion and atom temperature distribution for two fluid model of Ar plasma in cylindrically symmetrical wall stabilized electric arc column 03 p0481 A69-14155
- Two fluid kinetic model for analyzing shock wave structure in binary mixtures of monatomic inert gases, noting no overshoot in velocity profiles 08 p1304 A69-20813
- Rayleigh-Taylor instabilities in two fluid hydraulic model, noting perturbation direction and, Lorentz forces effects on instabilities growth time 13 p2310 A69-28033
- Two fluid continuum theory of incoherent scattering extended to include unequal electron and ion temperatures, considering backscatter power dependency on collision frequencies 14 p2510 A69-28946
- Electrostatic heating of solar wind ions from instability in two fluid solar wind model leading to preferential heating of protons over electrons 16 p2848 A69-31971
- TWO PHASE FLOW**
- Vaporization waves in metals, discussing thermodynamic function of carrying liquid metal through successive states on liquidus line in two phase region 01 p0117 A69-10655
- Liquid metals as coolants in breeder and space vehicle reactors for stable two phase flows 05 p0803 A69-15998
- Two phase flow in comas of dust comets, noting acceleration of gaseous and particle phases of continuous streams and particle vaporization 06 p1000 A69-16984
- Particle velocity measuring technique for two phase turbulent flows, using laser and Fabry-Perot interferometer 06 p0933 A69-17252
- Differential equations for two phase flow in axisymmetric supersonic nozzle, discussing existing solutions 06 p0861 A69-17815
- Temperature profiles and heat transfer coefficients in two phase liquid-liquid stratified laminar flow of variable immiscible film thickness with surface evaporation 09 p1622 A69-21904
- Size and velocity measurements of particles suspended in gas expanding from nozzle into vacuum simulating cometary two phase flow with evaporation 10 p1674 A69-23686
- Speed of sound and shock waves in two phase flows of liquid metal MHD generators, considering droplets uniformly dispersed in gaseous phase 13 p2245 A69-27475
- Laser Doppler method for measuring local particle velocities in two phase flows of liquid-metal MHD generators 13 p2260 A69-27476
- Two phase MHD generator with gas in liquid metal emulsions, discussing loops efficiency 13 p2306 A69-27479
- Effective electrical conductivity of two phase vapor-potassium flow in flat duct at flow temperature 800 C, showing dependence on volumetric vapor content 13 p2306 A69-27480
- Air-water and steam-water flows in two phase Laval nozzles, measuring flow rates and temperature and pressure variation 13 p2245 A69-27481
- Energy conversion with liquid metal working fluids in MHD generators, discussing single stage fully Carnotized process 13 p2372 A69-27482
- Liquid metal multistage injection efficiency with sodium and potassium working fluids, noting preheating 13 p2372 A69-27483

TWO PHASE SYSTEMS

Liquid metal two phase flow MHD generators efficiency prediction, discussing end losses and flow velocity 13 p2205 A69-27485

Two phase two dimensional turbulent jet analysis for predicting uncertainty in measured value of mixing coefficient 13 p2247 A69-27787

Gas-liquid critical flows, considering compressibility, rate of momentum, mass and heat transfer, etc 13 p2376 A69-28144

Time of flight measurement for velocity of micron sized particles in two phase flow by light transmission method 13 p2263 A69-28243

Coupled heat and mass transfer with zero order reactions in two phase systems consisting of drops, bubbles or solid particles 14 p2537 A69-29012

Gas and polydispersed condensate parameters of nonequilibrium two phase flow in Laval nozzle, considering particle collisions and coagulation, energy exchange and momentum exchange 14 p2391 A69-29621

Simulation of two phase hydrogen venting to space environment, discussing thrust effect measurements, flow instabilities and instrumentation 15 p2701 A69-30396

Two phase flow mixing shocks, obtaining expressions for pressure and entropy changes, discussing shock stability and gas entrapment mechanism 16 p2768 A69-31589

Two dimensional analysis of isentropic perfect gas flow fields in axisymmetric nozzles for transonic two phase flow initial values, calculating particle trajectories [AIAA PAPER 69-572] 16 p2731 A69-31847

Hydrogen oxygen rocket engine two phase liquid hydrogen pump capability and hydrodynamic design, analyzing constant-quality flow, acoustic effects, compressible flow and cavitation [AIAA PAPER 69-549] 16 p2845 A69-32759

Book on gas dynamics of two phase media for thermal power engineering equipment, discussing phase transformations, condensation in high velocity flows, etc 17 p2948 A69-32951

Wave propagation in gas particle flow, obtaining fourth order particle differential equation from perturbation theory 18 p3121 A69-34772

Similarity applied to dynamics of disperse media, discussing role of dimensionless numbers in mechanics of suspensions and two phase flows in porous media 19 p3300 A69-36775

Slip ratios in annular two phase flow for case of laminar flow in film and no entrainment of liquid in vapor [ASME PAPER 69-FE-43] 20 p3517 A69-37995

Soviet monograph on turbines and jet nozzles for two phase flows covering gas-particle velocity and temperature differences, turbine design, etc 20 p3586 A69-38209

Continuously operating multipurpose wind tunnel for laser light scattering experiments in supersonic two phase flow 21 p3689 A69-38596

Interphase momentum transfer during propagation of infinitesimal pressure pulse through bubbly flow two phase mixture 24 p4409 A69-43511

Bubble flow evolution at various pressures up to critical value [ASME PAPER 69-HT-30] 24 p4411 A69-43529

Choking and shock in flashing single component two phase flow in tube, including vibrational effects, predicting minimum stagnation pressure loss [ASME PAPER 69-HT-61] 24 p4303 A69-43535

Pulsating mechanisms in alternative gas and liquid blocks two phase flow, using stochastic process specified by dynamic pressure time dependent fluctuations 24 p4305 A69-43633

TWO PHASE SYSTEMS

U BINARY SYSTEMS [MATERIALS]

TWO REFLECTOR ANTENNAS

Cassegrain two reflector antenna modification by discrete phase array, allowing for subunit redesign 04 p0572 A69-14326

Tuning of two mirror antennas in near zone with various mirror combinations, discussing field cophasing 06 p0895 A69-17462

Antenna gain increase, using matched pair of Cassegrain reflectors with one primary source 10 p1664 A69-23799

Tuning of two mirror antennas in near zone with various mirror combinations, discussing field cophasing 20 p3508 A69-37945

Structure, operation and performance of two reflector Nancy radio telescope consisting of plane and spherical portion reflectors 23 p4149 A69-42124

Rosman I reflector antenna for collecting data from earth orbiting satellites, discussing dynamic analysis of structural response to natural frequencies 23 p4231 A69-42133

TWO STAGE TURBINES

Scale models of M-1 rocket engine oxygen and hydrogen pump driven two stage turbines used to determine performance and compact inlet manifolds problems [AIAA PAPER 69-553] 16 p2840 A69-32678

TYCHO CRATER

Lunar near side crater overlap, considering formation of Tycho Association 21 p3800 A69-38676

TYPE 2 BURSTS

Type 2 radio bursts and corona magnetic field over active center 06 p0985 A69-16979

Solar flare event on 17 June 1968 consisting of two type 2 bursts followed by enhanced emission [possibly type 4] 09 p1582 A69-22750

Dynamic spectrum of July 7, 1966 proton flare, considering short wave fadeout at 0027 UT and intense burst of spectral Type 2 10 p1765 A69-23750

Type 2 radio burst dynamic spectra determination for finding shock wave and magnetic field parameters above active corona region 11 p1945 A69-24243

Homology within solar flare associated type 2 radio events from dynamic spectra 17 p3024 A69-33803

Solar flare flux density and dynamic spectrum on 30 October 1968 at 80 MHz, showing noise storm positions and type II-III burst sources 17 p3025 A69-33807

Type II and type III solar radio burst relation to plasma instability associated with coherent synchrotron deceleration of electrons, discussing resonant power exchange 22 p4007 A69-40898

Solar corona instabilities and shock waves indicated by type 3 and 2 bursts, considering electrons ejection 24 p4378 A69-42689

TYPE 3 BURSTS

Polarization degree of type solar radio bursts dependent on heliographic longitude 04 p0649 A69-15242

Type 3 bursts spectra graphical representation, giving probable solar origin and curves of corona temperature 05 p0824 A69-16060

Type 3 solar radio noise bursts at hectometer wavelengths, deducing coronal electron temperatures from decay rates 09 p1594 A69-21665

Type 3 solar flare circular and linear polarization at 23.5 MHz frequency 11 p1945 A69-24244

Type 3 radio bursts time profile for estimating magnetic field strength in solar corona 15 p2675 A69-30554

Solar flare flux density and dynamic spectrum on 30 October 1968 at 80 MHz, showing noise storm positions and type II-III burst sources 17 p3025 A69-33807

Type 3 bursts spectra graphical representation, giving probable solar origin and curves of corona temperature 20 p3591 A69-37970

Type 3 solar radio bursts observed during April-October 1967 for two alternative models of active region streamers in outer corona 22 p4003 A69-40300

Type II and type III solar radio burst relation to plasma instability associated with coherent synchrotron deceleration of electrons, discussing resonant power exchange 22 p4007 A69-40898

Solar corona instabilities and shock waves indicated by type 3 and 2 bursts, considering electrons ejection 24 p4378 A69-42689

TYPE 4 BURSTS

Structure of sources of noise storm enhancement and stationary type 4 bursts, discussing head and tail components 02 p0328 A69-12735

Type 4 bursts mobile spectrum of september 1966 interpreted by considering plasma effects on synchrotron emission mechanism 02 p0309 A69-12735

Solar microwave type 4 bursts spectra and decay rate time variations 04 p0648 A69-14366

Gyro synchrotron emission spectrum and intensities through solar electrons radiating in coronal magnetic fields applied to type IV solar radio bursts 04 p0650 A69-15524

Solar type 4 bursts characteristics accounted for by cyclotron mechanism, assuming models of spot magnetic field configuration and electron density distribution 07 p1205 A69-18953

Spectrum variations of type 4 radio burst as sources rises through solar corona, determining electron density and magnetic field distributions in corona 08 p1380 A69-20772

Solar moving type 4 burst emitting synchrotron radiation, noting electron acceleration in collisionless shock wave in corona 09 p1578 A69-22058

Two solar flare initiated type 4 radio bursts on 4 and 6 May 1968, noting prominence activity leading to meter wave generation 09 p1582 A69-22749

Decametric radio spectra from 0053 to 0200 UT during July 7, 1966 solar proton flare, discussing Type 4 phase 10 p1765 A69-23751

Dynamic spectrum of Type 4 solar radio burst during July 7, 1966 proton flare, noting limb effect 10 p1765 A69-23752

Circular polarization in moving type 4 burst compared to stationary type 4 burst and related to preceding type 2 sources 17 p3024 A69-33808

4 October 1965 type IV solar burst, studying acceleration mechanisms for fast electrons by comparing fine structure at various frequencies 22 p4001 A69-39983

Synchrotron radiation HF cut-off resulting from electrons with anisotropic pitch angle distribution for type IV solar radio bursts 22 p4006 A69-40577

Type 4 bursts maximum intensities at different frequencies compared for centimeter and decimeter waves 24 p4366 A69-42964

TYPE 5 BURSTS

Type V continuum emissions from solar flares suggested as due to synchrotron radiation from protons spiraling in magnetic field, noting Type III emission 22 p4003 A69-40301

TYPHOONS

Onset and development of typhoons observed by Cosmos satellites using TV type IR apparatus [UN PAPER 68-95774] 06 p0949 A69-17035

Satellite radiation maps for synoptic analysis regarding world weather maps, discussing front, intertropical convergence zones and typhoon location 14 p2473 A69-29729

Wind and cloud velocities from ESSA 3 and 5 and ATS 1 pictures for typhoon and tropical vortices in intertropical convergence zone 21 p3758 A69-38371

U

U TUBES

U MANOMETERS

U.S.S.R.

Soviet pipe production technology from Ti and Ti alloys, considering properties and methods improvement 07 p1164 A69-18787

Soviet literature on coding theory and applications stressing contributions to nonSoviet specialists 09 p1460 A69-21399

Soviet supersonic transport Tu 144, describing wing unit, fuselage, passenger accommodation, tail unit, landing gear, power unit engine nacelle and navigation 10 p1634 A69-23833

- British and Soviet D region electron density distributions from same VLF and LF propagation data
14 p2439 A69-29112
- U.S.S.R. manned bomber role in air strategy, discussing mutual effects of U.S.-U.S.S.R. military posture developments and ICBM
14 p2392 A69-29431
- Reflector radio telescope of Pulkovo astronomical observatory noting high resolution
15 p2679 A69-30102
- Soviet efforts to market civil aviation equipment in West
18 p3232 A69-34538
- Tupolev Tu-154 three jet transport featuring automatic flight control system with inertial and Doppler navigation inputs, low speed wing devices
18 p3092 A69-34933
- Geomagnetic field micropulsation observations by U.S.S.R. and possible applications to diagnostics of magnetosphere
19 p3304 A69-36642
- Ionospheric radio wave absorption seasonal and diurnal variations over Tiflis from pulsed ionospheric sounding at 2.2 MHz
20 p3491 A69-37677
- Soviet high temperature plasma physics research, discussing magnetic plasma containment by Tokamak traps
23 p4196 A69-42167
- MIG-21 fighter aircraft development, characteristics and technical and operational data
24 p4251 A69-42795
- Beriev Be-12 cranked wing seaplane design including technical and operational data
24 p4251 A69-42796
- U.S.S.R. SPACE PROGRAM**
- Handbook on Soviet space science research covering rockets, satellites, space probes, biomedical investigations, atmospheric composition
01 p0154 A69-10935
- Soviet postwar rocket program, discussing rocket sounding, biomedical experiments, etc
01 p0162 A69-10936
- Soviet artificial earth satellites, discussing Sputnik, Polet, Elektron, Cosmos, Molniya and Vostok series
01 p0162 A69-10937
- Soviet lunar and planetary probes, reviewing payload characteristics, principal mission features and photographs associated with Luna, Mars, Venera and Zond series
01 p0162 A69-10938
- Micrometeorite and meteoric dust data obtained in Soviet space flights
01 p0155 A69-10939
- Chemical composition of upper atmosphere and interplanetary space measured by Soviet sounding balloons and rockets, discussing flask sampling techniques
01 p0025 A69-10940
- Soviet rocket and satellite night, twilight, airglow and auroral studies, discussing day sky brightness, night airglow and atmospheric stratification
01 p0066 A69-10941
- Upper atmosphere physical properties, discussing density and temperature
01 p0066 A69-10942
- Soviet space astronomy including rocket, satellite and space probe measurements for solar, stellar, planetary and lunar studies
01 p0155 A69-10946
- Physiological measurements onboard Soviet bioprobes and biosatellites including electrocardiography, phonocardiography, sphygmography, seismocardiography and pneumography
01 p0015 A69-10947
- Soviet literature on extraterrestrial life and civilization emphasizing establishment of contact by radio and laser sources
01 p0016 A69-10953
- Soviet rocketry origin, technology, launch vehicles, boosters and orbital assembly concept
01 p0162 A69-11066
- Weightlessness effects research during Soviet and U.S. manned space flights
02 p0199 A69-12120
- Soviet satellite exploration of space magnetic fields and charged particles, noting Proton satellites and protons and carbon nuclei inelastic interactions [UN PAPER 68-95768]
06 p0986 A69-17031
- Satellite actinometric data computerized reduction in U.S.S.R., examining computer program features [UN PAPER 68-95763]
06 p0916 A69-17038
- Atmospheric heat sources and heat sinks distribution based on Cosmos satellite data
06 p0949 A69-17048
- U.S.S.R. system Meteor consisting of four Cosmos satellites in polar orbits to observe cloud distribution, snow and ice field boundaries, etc
06 p1013 A69-17053
- Soviet explorations of moon, Venus, Mars and interplanetary space, noting objectives of future lunar explorations [UN PAPER 68-95719]
06 p1000 A69-17055
- Soviet space program /1969/ objectives, Soyuz vehicle and future missions
06 p1002 A69-17265
- Soviet achievements in space research, comparing satellites with U.S. counterparts
06 p1005 A69-17561
- Rules for selecting Soviet cosmonauts and physiological studies concerning heart and respiratory reactions to accelerations and weightlessness during preparation
07 p1060 A69-18569
- Soviet cosmonauts physiological reactions during weightlessness, analyzing EKG, arterial pressure, heart and respiratory rates and motion coordination
07 p1060 A69-18570
- Physiological and medical tests on Soviet cosmonauts onboard Voskhod spacecraft, assessing CNS, cardiovascular and respiratory systems and work-rest schedule
07 p1060 A69-18571
- Vela 4 satellite energetic particle experiment, describing instruments design and operation [IEEE PAPER 3C-2]
07 p1134 A69-19196
- Soviet lunar effort in Luna probe series, outlining characteristics, performance and missions
09 p1609 A69-21583
- Soviet satellites rotation periods from processing of photometric observations
12 p2069 A69-26440
- Space research in U.S.S.R. including Venera 4 soft landing mission for measuring temperature, pressure, density and atmospheric composition of Venus
12 p2160 A69-26921
- Soviet space program, discussing launch sites, series of launch vehicles and mission identification
13 p2381 A69-27303
- Soviet lunar probe Zond 6 achievements in controlled Earth landing and lunar surface photography
13 p2355 A69-27342
- Collection of Soviet papers on U.S.S.R. outer space studies /1957-1967/ covering rocket and satellite sounding, meteorology, radiation belts, etc
13 p2335 A69-27346
- Soviet rocket and satellite studies of upper atmosphere and ionosphere
13 p2251 A69-27347
- Soviet meteorological and geophysical rockets, satellites and techniques in cloud studies and weather forecasting, noting Cosmos results
13 p2290 A69-27348
- Soviet satellite-borne radio waves studies of ionosphere, considering wave amplitudes, Doppler frequency shifts and outer ionosphere properties
13 p2252 A69-27349
- Van Allen radiation belts proton and electron components recorded by Soviet lunar probes and Cosmos and Elektron satellites
13 p2326 A69-27350
- Cosmic rays during 11-year solar cycle, short term variations and radial gradient based on Luna, Zond and Venera probes and Cosmos observations
13 p2326 A69-27351
- Soviet satellite and probe studies of earth, moon, Venus and Mars magnetic fields, noting automatic magnetometer
13 p2336 A69-27352
- Soviet astronomical radio-astronomical probe and orbiter lunar studies including surface photography, gravitational and magnetic measurements and soft landed probes
13 p2336 A69-27353
- Interplanetary plasma measurements by Luna, Mars 1, Zond 2 and Venera 3 probes, including solar plasma flux energy spectra diagram
13 p2336 A69-27354
- Solar radiation in short wave, UV and X ray range recorded by rockets, probes and satellites, notably Elektron 2 probe
13 p2326 A69-27355
- Soviet space biology and medicine, discussing ecological physiology, closed system ecology, exobiology and medical tests on cosmonauts
13 p2209 A69-27356
- Soviet space efforts /1957-1967/, discussing rocket, probe, spacecraft and satellite launchings and scientific results
13 p2336 A69-27358
- Tabular listing of Soviet satellites, spacecraft, probes and rockets launched between October 1957 and October 1967
13 p2355 A69-27359
- Thermionic reactors U.S.S.R. space and other programs, considering power output, heat exchange and losses, neutron physics and design parameters
14 p2404 A69-29277
- Soviet space exploration including Cosmos and Proton satellites, Luna project and Zond and Venera probes
18 p3201 A69-35163
- Soviet space stations design based on orbital docking techniques for unrestricted mass size and number of modules, describing wheel shaped station
19 p3431 A69-36465
- Soviet space flights preliminary to formation of scientific space station
24 p4391 A69-42798
- UBV SPECTRA**
- UBV photoelectric observations of Nova Delphini 1967 at Bologna Observatory
20 p3599 A69-37475
- Giant stars UBV reddening line slopes determined from photometric data
20 p3608 A69-38047
- Cepheid variable stars distance estimated from UBV three color photoelectric photometry data
22 p4031 A69-40943
- Photoelectric observations of eclipsing binary 32 Cygni during 1968 eclipse using standard UBV color filters, tabulating results of UBV photometry
22 p4032 A69-40946
- UBV magnitudes for open cluster NGC 559 stars determined from combined photoelectric and photographic measurements
23 p4211 A69-41490
- Narrow and intermediate band photometry of globular star clusters in uvby and beta photometric systems, relating reddening to metal abundances of member stars
24 p4387 A69-43352
- UH-1 HELICOPTER**
- Production history of Model UH-1 /Huey/ helicopter power transmission, discussing producibility [SAE PAPER 680675]
03 p0433 A69-13450
- Compound rotary wing aircraft research, discussing XH-51A maneuverability program and UH-1 high Mach and high advance ratio program [AIAA PAPER 69-218]
07 p1056 A69-19568
- ULLAGE ROCKET ENGINES**
- Propellant orientation and expulsion methods in space vehicle tankage, discussing ullage rockets system, bladders and diaphragms, dieletrophoretic expulsion, etc
16 p2736 A69-31734
- ULM (LIGHT MODULATION)**
- U ULTRASONIC LIGHT MODULATION**
- ULTRA SHORT WAVE RADIO EQUIPMENT**
- U VERY HIGH FREQUENCY RADIO EQUIPMENT**
- ULTRAHIGH FREQUENCIES**
- Microwave instabilities in bulk GaAs under strong electric fields, considering characteristics connected with structural properties and contact formation conditions
01 p0136 A69-10256
- S band solid state amplifier capable of 10 watts output power based on combination of transistor amplifiers
02 p0217 A69-12147
- Low noise room temperature satellite broadcast receiver for UHF, using room temperature parametric amplifiers
05 p0728 A69-15672
- VHF to UHF conversion, noting modular UHF telemetry transmitter, miniature UHF special purpose transmitter, RF power amplifiers and telemetry receiver
05 p0732 A69-16305
- Gunn effect pulse generator for antenna arrays operating at decimeter wavelengths with external power source
06 p0895 A69-17459
- Harmonic generation of S band signal inside plasma column at resonance
06 p0965 A69-17488
- UHF high power klystron for DESY synchrotron, discussing design, short circuited load operation, phase variations and optimum RF outputs
07 p1096 A69-18434

Conversion from VHF to UHF at White Sands Missile Range, discussing telemetry acquisition, tracking and receiving systems

07 p1077 A69-18828

Kwajalein Missile Range UHF telemetry conversion program using S band antennas with three channel monopulse autotrack systems

07 p1077 A69-18829

Sun as calibration signal source for L and S band telemetry, discussing receiving system noise temperature determination and antenna gains

07 p1082 A69-19113

Adaptive airborne VHF/UHF transmitter system, discussing design, ground isolation, current limiting, internal telemetry, wideband frequency response, real time video signals, etc

07 p1106 A69-19114

Lincoln experimental satellites, discussing transition to UHF bands and orbital launching

07 p1087 A69-19630

Synthesis method for UHF transistor oscillators tunable in wideband using Y-matrices

08 p1285 A69-20380

Multichannel microwave amplifier at L band frequencies, using several amplifiers in parallel

09 p1466 A69-22446

Microwave instabilities in bulk GaAs under strong electric fields, considering characteristics connected with structural properties and contact formation conditions

09 p1559 A69-22649

Parametric amplifying systems with lumped reactive nonlinear elements, emphasizing UHF systems

11 p1844 A69-24448

Fading velocity short period characteristics and duration and depth of field strength variations over transhorizon path compared with corresponding atmospheric parameters

12 p2028 A69-25897

Love-wave propagation at UHF observed by thin film surface wave transducers

13 p2218 A69-27203

UHF transistor small signal internal behavior, using computer simulation for deriving current gain alpha locus, current gain and f sub T

13 p2227 A69-27241

Integrated S-band parametric amplifier design, combining low noise performance at room temperature with broadband flat gain and linear phase response

13 p2230 A69-27678

S-band telemetry capability of Easter Test Range, discussing relationship to Telemetry Rehabilitation Project, major system decisions and performance characteristics

14 p2410 A69-28878

VHF to UHF telemetry bands transition implemented by Naval Weapons Center

14 p2411 A69-28880

Output impedance measurements for accurate calibration in UHF region, using mobile discontinuity and bolometer for linear or nonlinear systems

14 p2422 A69-29583

UHF propagation in spherically stratified superrefractive troposphere with trapping surface layer, discussing distant field strength dependence on refractivity profile

16 p2752 A69-32388

Transistorized L band oscillator tuned by Ga-doped YIG, discussing ferrimagnetic material properties and device equivalent circuit

16 p2761 A69-32450

Microelectronic S band upconverter designed and fabricated in microstrip on alumina substrate

16 p2762 A69-32562

Wide tuning range S band low noise maser amplifier system, discussing bandwidth, gain and packaging for antenna mounting

17 p2979 A69-32914

Experimental SST terminal for satellite L band communications/surveillance ATC system, establishing terminal requirements for NASA and FAA studies

17 p2932 A69-34118

Gunn effect pulse generator for antenna arrays operating at decimeter wavelengths with external power source

20 p3508 A69-37942

L and S band transmitters for space applications, discussing power and frequency stability, low intermodulation, inputs isolation, efficiency, size and weight

23 p4137 A69-41740

Power combining network for high power UHF solid state satellite transmitters with low loss, compact size and input port selection capability

23 p4137 A69-41743

S band antenna systems for missiles, designed in various types to obtain RF telemetry links reliability by sharing effort between airborne and ground station equipment

23 p4137 A69-41753

Frequency diversity technique simplifying airborne antennas for UHF telemetry, useful on spin stabilized vehicles requiring omnidirectional antenna coverage

23 p4122 A69-41777

UHF down-converter design used in various Navy missiles UHF telemetry/miss-distance information system

23 p4137 A69-41778

Portable UHF telemetry receiving station for medium range surface-to-air missiles testing, analyzing antenna coverage over water and system prediction allowing variable parameters

23 p4122 A69-41780

Cosmic ray flux intensity increases, discussing effects of solar wind, corpuscular flux velocity and interplanetary magnetic field

23 p4205 A69-41838

Meter and decimeter wavelength range short period fading under conditions excluding optical sights, correlating specular and diffuse reflection

24 p4281 A69-42612

UHF satellites for mobile, broadcast and low cost services, discussing bandwidth expansion, interference effects, ground linking, UHF partition, satellite antenna sizes, etc

24 p4282 A69-42872

ULTRAHIGH VACUUM

Vacuum system for obtaining highly purified plasmas for thermocuclear investigations noting decontamination cycles and chamber characteristics

03 p0412 A69-13839

Ultrahigh vacuum electron microscope using differential sputter ion pumps to obtain low contamination environment

04 p0599 A69-15016

Dry sliding friction and wear in ultrahigh vacuum, emphasizing slip rings and brushes for space applications

07 p1138 A69-18561

European research on ultrahigh vacuum lubrication in space environments, emphasizing friction of materials under various loadings and temperatures

07 p1138 A69-18564

Electrostatic charge distribution on ultrahigh vacuum cleaved silicates including instrumentation, UV irradiation, half life, Paschen relation, etc

13 p2322 A69-28018

Solar simulator built into multiwall ultrahigh vacuum chamber, describing simulator and chamber modifications

22 p3921 A69-40377

High temperature vacuum treatment of thick stainless steel sheets reducing hydrogen content and outgassing

22 p3958 A69-41217

Desorption of hydrogen and methane from Al, Mg and Mb under room temperature tensile deformation in ultrahigh vacuum

23 p4176 A69-41541

ULTRALOW FREQUENCIES

U EXTREMELY LOW RADIO FREQUENCIES

ULTRAPURE METALS

Brittleness and physical causes of cold shortness in Cr, discussing high purity metal formation and fine and superfine grain structures synthesis

09 p1526 A69-22147

Thermal diffusivity and conductivity of rolled plane parallel spectrally pure palladium preheated in vacuum and high temperatures

15 p2636 A69-30045

Ultrasonic and mechanical vibration effects on superpure Al and Al-Zn-Mg alloy, showing dependence of breaking stress on cycles

16 p2801 A69-31789

Book on high purity beryllium metallurgy for nuclear reactor applications covering physical properties, crystallography, thermodynamics, production methods, etc

17 p2986 A69-32952

Manufacturing ultrahigh purity aluminum strip for cryogenic magnets, discussing ingot preparation, rolling, chemical milling and cleaning, arc welding, annealing and sampling

19 p3318 A69-35541

ULTRASONIC AGITATION

Ultrasonic vibrations effect on emission of ruby laser with externally mounted mirrors

13 p2271 A69-27534

Dry dynamic friction of brass disk against steel surface reduced using ultrasonic oscillations creating air gap

18 p3135 A69-34587

Automatic ultrasonic method for determining dissolved gases content in liquid sample, using increasing acoustic oscillations amplitude for bubble development

19 p3308 A69-35829

Ultrasonic vibrations effect on emission of ruby laser with externally mounted mirrors

20 p3556 A69-38201

Ultrasonic oscillations effects on magnetic permeability of ferrite circuit components

23 p4138 A69-41871

ULTRASONIC LIGHT MODULATION

Modulated wave holography for detecting and reconstructing ultrasonic beam path, noting applicability to vibrating objects analysis

10 p1694 A69-23364

Laser pulse deflection by acoustooptical system consisting of ultrasonic cell and oscillator

11 p1840 A69-25423

High power ruby laser pulse generation by diffraction modulator, employing modulated ultrasonic traveling waves at minimum resonator transmission losses

24 p4328 A69-43163

ULTRASONIC RADIATION

Ultrasonic diffraction delay line operation interpretation as radar chirp signal correlator

01 p0026 A69-10072

Multiple velocity dispersion in normal hydrogen and normal hydrogen-helium mixtures at room temperature using ultrasonic interferometer

01 p0121 A69-11284

Electronic attenuation of 10 to 130 MHz longitudinal ultrasonic waves in superconducting high purity TI, noting energy gap anisotropy

03 p0485 A69-13293

Electronic attenuation of 10 to 130 MHz longitudinal ultrasonic waves in nonsuperconducting high purity TI, noting anisotropy and measurements below 4.2 K

03 p0485 A69-13294

Pulse compression by optical correlation techniques, discussing laser beam control by diffraction grating in ultrasonic delay line

03 p0397 A69-13732

Direct amplification of ultra and hypersonic surface waves in semiconducting crystals of wurtzite group, taking into account drift effects and boundary conditions

03 p0490 A69-13925

Vacuum deposition of thin film microwave acoustic transducers of piezoelectric aluminum nitride

05 p0761 A69-15820

Ultrasound propagation amplification coefficient in high permittivity semiconductors with electric field based electron-phonon interaction

05 p0809 A69-16372

Laser beam scattering by acoustic waves of ionized crystal, reconsidering stimulated Brillouin emission theory for ultrasonic yield

05 p0777 A69-16610

Velocity of 1 MHz sound waves in He 4 along isotherms just above critical temperature, noting specific heat ratio for 4.5 and 5 K isotherms

06 p0957 A69-17142

Acoustical and microwave holography obviating need for real or simulated reference wave, using recording time for reference

06 p0928 A69-17902

Holographic displays using ultrasonic vibrations or laser outputs as optical sources, discussing recording materials, responses and computer applications

09 p1492 A69-21394

Typographical spatial correlation filtering methods for reconstructing holographic images with ultrasonic waves, noting application to flaw recognition

10 p1696 A69-23551

Electrical equivalent circuit for piezoelectric generation and detection of transient and sinusoidal ultrasonic waves by interdigital electrodes

12 p2039 A69-26376

Characteristic temperature, Young modulus and rms atomic displacement in metal borides of various porosities, using dynamic method based on ultrasonic oscillations measurement

12 p2115 A69-26615

Two temperature gasdynamics for binary gas mixtures of differing molecular weight components, analyzing ultrasound and shock wave propagation

13 p2250 A69-28447

Ultrasonic pulse-echo-overlap method modified for simultaneous measurement of time delay and relative voltages in determining sound velocities and attenuation of solids

14 p2450 A69-29567

Schlieren and photoelastic methods for continuous and pulsed ultrasonic waves propagating in transparent media, discussing nondestructive testing applications

15 p2617 A69-31510

Ultrasonics for wrought and cast aluminum alloys nondestructive testing, discussing ultrasonic energy damping measurements

16 p2800 A69-31778

Magnetic field effects on ultrasonic propagation in high field superconductors

16 p2826 A69-31825

Ultrasonic velocity dispersion in para hydrogen and mixtures with He, Ne and Ar at 300 K, obtaining rotational relaxation times

16 p2815 A69-32791

Ultrasonic spectrometry application to thickness measurement of thin and thick walled articles

18 p3137 A69-35110

Book on ultrasonics theory and application covering generation, propagation and dissipation of ultrasonic waves of high and low intensities

20 p3545 A69-37903

Al and Mg alloys as ultrasonic wave acoustic lines, considering sound velocity, damping factor, grain size, chemical composition, etc

20 p3564 A69-38290

Flaw determinations accuracy from measuring ultrasonic shear wave reflection peak intensities

24 p4397 A69-42756

ULTRASONIC SPEEDS

U SUPERSONIC SPEEDS

ULTRASONIC TESTS

Ultrasonic detection and measurement of fatigue cracks in notched cylinders subjected to reversed axial cyclic loading

01 p0078 A69-10113

Ultrasonic holography applications in nondestructive testing, describing conversion of ultrasonic field into optical field

01 p0078 A69-10132

Ultrasonic quality control test methods for melt through welds in hydraulic line assemblies, noting equipment and surface roughness requirements

02 p0252 A69-11810

Beryllium nondestructive tests, discussing eddy current inspection, ultrasonics, film radiography and scintillation [SAE PAPER 680652]

03 p0444 A69-13546

Fatigue mechanism in fcc metals at ultrasonic frequencies, comparing microstructural changes in copper and alpha-brass

04 p0613 A69-14448

Ultrasonic sounding for controlling dispersed gas phase in liquid pipelines under laboratory and practical conditions

04 p0596 A69-14489

Ultrasonic search units in nondestructive tests, discussing piezoelectric materials and contact and immersion services

07 p1139 A69-18795

Ultrasonic thermometry for nuclear reactors based on temperature dependence of sound velocity in solids, discussing simulation experiments [IEEE PAPER 1C-4]

07 p1134 A69-19186

Ultrasonic inspection of soundness and penetration or corner welds for Zircaloy 2 casings, discussing method reliability and sensitivity limits

07 p1141 A69-19346

Magnetic tape recording of ultrasonic test information with oscilloscope used for playback

07 p1117 A69-19697

Copper diffusion coefficient in undoped n-type gallium arsenide measured by ultrasonic method

09 p1555 A69-21471

Pulse echo ultrasonic nondestructive testing of C-5 adhesive bonded aluminum composites with multiple bond lines

10 p1698 A69-23047

Ultrasonic technique for metal surface and near surface residual stress measurement, emphasizing aluminum alloys

10 p1794 A69-23052

Ultrasonics for automatic measurements of temperature and elastic moduli above 5000 F

10 p1694 A69-23373

Mechanical damping and electrical matching effects on bandwidth of piezotransducer in ultrasonic flaw detection equipment

10 p1697 A69-24073

Piezoelectric transducer theory, discussing acoustically matched sandwich type damper and calculating frequency characteristics

10 p1697 A69-24074

Flow detection inaccuracies in shadow method due to interference effects when using Babinet principle

10 p1675 A69-24075

Book on ultrasonic methods in solid state physics covering stress wave propagation in solids, pulse methods of velocity change and attenuation measurements and causes of losses

12 p2145 A69-26870

Ultrasonic images detection for nondestructive testing including surface-relief technique, Pohlman cell and scanning with piezoelectric transducers

13 p2269 A69-28661

Ultrasonic detection and measurement of fatigue cracks in notched cylinders subjected to reversed axial cyclic loading

14 p2445 A69-28882

Copper diffusion coefficient in undoped n-type gallium arsenide measured by ultrasonic method

15 p2669 A69-30716

Delta technique for ultrasonic weld inspection, noting ability to detect randomly oriented weld defects

15 p2631 A69-31508

X ray and ultrasonic methods for surface residual stresses induced in machined or ground specimen

15 p2631 A69-31511

High temperature ultrasonic testing to measure and control solid materials early in processing

15 p2632 A69-31514

Ultrasonic inspection systems to determine and record bond quality on all adhesive bonded assemblies of Saturn S-2 booster and Apollo Command and Service Modules

15 p2632 A69-31515

Eddy current and ultrasonic applications to aircraft engine inspection, discussing electric and magnetic methods for quality control during fabrication

15 p2632 A69-31516

Ultrasonic probe selection and standardization for nondestructive testing, discussing instrument sensitivity and probe losses

15 p2617 A69-31517

Ultrasonics for wrought and cast aluminum alloys nondestructive testing, discussing ultrasonic energy damping measurements

16 p2800 A69-31778

Ultrasonic and mechanical vibration effects on superpure Al and Al-Zn-Mg alloy, showing dependence of breaking stress on cycles

16 p2801 A69-31789

Stress corrosion cracks investigation by shear wave technique

16 p2876 A69-32334

Nondestructive ultrasonic, spectroscopic and TV test methods reducing time for inspection and increasing reliability of turbines

17 p2978 A69-33330

Automatic ultrasonic instrument monitoring on-line welding conditions of RF longitudinally seamwelded tubes

18 p3136 A69-34778

Ultrasonic detection of gas bubbles in blood, discussing device with bubble chamber attached to circulating liquid and receiver crystal harmonics

18 p3098 A69-34821

Integral scalar equation describing signal attenuation by acoustically soft disk for mirror-shadow method of ultrasonic flaw detection

18 p3137 A69-35109

Automatic ultrasonic inspection device search head, servomechanism and electronic system used for detecting weld defects and cracks

18 p3137 A69-35111

Pulsed ultrasonic flaw detectors resolving power enhancement by shunting semiconductor diodes across piezoelectric elements of scanning heads to shorten scan pulse duration

18 p3137 A69-35112

Ultrasonic nondestructive testing technique for fatigue induced damage location and criticality in filament wound fiberglass cylinders, correlating damage to residual life

19 p3322 A69-35577

Echo amplitude measurements in ultrasonic testing to estimate flaw sizes and difficulties from artificial reflecting targets

19 p3323 A69-35578

Acoustic visualization for nondestructive testing, describing image formation by lenses, reflectors, holography, Bragg diffraction and phase contrast

20 p3512 A69-38269

Ultrasonic Doppler flowmeter for detection of circulating gas emboli of animal blood vessels during decompression

21 p3663 A69-38915

Ultrasonic method for detecting strength defects in filament wound materials

21 p3733 A69-39798

Nondestructive testing techniques for flaw and defect detection, discussing radiography, ultrasonics, penetrants, thermal and magnetic methods, etc

23 p4169 A69-41529

Optimal focusing of acoustic system for tube defectoscopy with circular normal waves

24 p4296 A69-42655

Thickness direction tensile properties, ultrasonic attenuation and mild steel plate lamellar tearing in multipass fillet joints measured by weld cracking test

24 p4320 A69-42942

ULTRASONIC WAVE TRANSDUCERS

Ultrasonic quality control test methods for melt through welds in hydraulic line assemblies, noting equipment and surface roughness requirements

02 p0252 A69-11810

Acoustic holographic measurement of surface deformation generated by sound waves impinging on gas-liquid interface, discussing acoustic amplitude components

10 p1695 A69-23542

Crack growth measured and recorded by ultrasonic monitor, describing transducer position and movement

20 p3547 A69-38312

ULTRASONIC WELDING

Resistance welding monitoring systems including thermal expansion slow scan ultrasonic and electric energy monitor/limiter systems

02 p0253 A69-11864

Vacuum evaporated thin film components welding, using torsional ultrasonic vibrations for joint activation

04 p0605 A69-14561

Ultrasonically assisted installation of fasteners for weight savings in aircraft/spacecraft structures

09 p1478 A69-22373

ULTRASONICS

Electroacoustic amplifier based phonon devices, using surface waves on piezoelectric materials to speed radar data real time processing

03 p0394 A69-13353

Ultrasonic holograms and optical reconstructions derived by scanning receiver or source

06 p0930 A69-18228

Phonon interactions with recoilless gamma rays, considering usability of Mossbauer effect as probe for VHF acoustic experiments

10 p1724 A69-23088

Imaging ultrasound by holography with reconstruction in light, comparing methods using scanned hologram and liquid surface

10 p1695 A69-23543

Acoustical transparencies illuminated by sound waves for optical imaging and ultrasonic diffraction, noting application to visualization of inhomogeneities in samples

10 p1695 A69-23546

Hologram obtained by recording interference pattern displayed by ultrasonic camera, discussing real time viewing

10 p1696 A69-23550

Ultrasound holography for imaging opaque structures, noting distortion due to long wavelength of sound field and distortion reduction techniques

13 p2265 A69-28663

Ultrasonic pulse velocity and attenuation measurement in presence of noise, using coherent detection and signal averaging

14 p2449 A69-29564

Electronic-ultrasonic amplifiers with external electron stream and longitudinal or surface wave studied for damping influence, deriving dispersion equation

16 p2761 A69-32061

Book on ultrasonic testing of materials covering ultrasonics application to nondestructive testing, flaw detection and quality control

16 p2790 A69-32125

Book on ultrasonics theory and application covering generation, propagation and dissipation of ultrasonic waves of high and low intensities

20 p3545 A69-37903

Ultrasound-echo-encephalography in diagnosis of posttraumatic intercranial hemorrhage of skull and brain trauma, noting neuroradiological techniques

21 p3652 A69-38790

Flow profile effect on signal of Doppler ultrasonic flowmeter, noting limited application to quantitative blood circulation measurements 23 p4166 A69-42085

Optical imaging problems in ultrasonic holography including distortion, resolution and depth of field 23 p4366 A69-42181

Temporal reference acoustical holography with Sokolov ultrasound camera system using double pulsed ruby or scanning CW laser 23 p4166 A69-42182

Abnormally slow ultrasound diastolic slope detected by mitral valve motion study in patients with clinically pure mitral insufficiency 24 p4261 A69-42727

Ultrasonic paramagnetic resonance investigations of Pr ions ground state energy levels in calcium fluoride 24 p4360 A69-42790

Ultrasonic diffraction delay lines technique to extend radar systems range without affecting target pinpointing capability 24 p4286 A69-42901

Sonic riveting of aircraft Al alloys, noting no evidence of forging bursts, cracking, splitting, tearing and springback 24 p4320 A69-43060

ULTRAVIOLET FILTERS

Red leak corrections for UV filter on color UV indices for stars of various spectral types using winter-redened response curve 19 p3426 A69-36566

ULTRAVIOLET PHOTOMETRY

Venus UV photographs and drawings shown in short interval sequences, noting left to right shift in color features 02 p0320 A69-12111

Photoelectric light diagrams for eclipsing binary star 08 p1392 A69-20565

Rocket-borne photoelectric photometers for UV observations of Saturn, using interference filters 09 p1602 A69-22216

Metallicity index Q value difference between cluster and noncluster galaxies determined from UV, blue and violet observation data 10 p1774 A69-22964

Wavelength dependence of polarization and UVRI photometry of highly polarized stars, correlating IR interstellar extinction with maximum polarization wavelength 12 p2153 A69-25809

Seyfert galaxy NGC 4151 electrophotometric investigation in UVB, confirming nucleus optical variability observed in visible and IR 15 p2686 A69-30536

Response color curves of U, B, V photometric system compatible for stellar observation, including U revision 15 p2689 A69-30562

Photometer for simultaneous stellar photometry in UVB bands, purposes and performance characteristics and circuit diagrams 16 p2790 A69-32209

UVB photometry of southern quasars, radio galaxies and normal galaxies including two color diagrams, radio luminosity, brightness and color distribution 16 p2859 A69-32228

Epsilon CrA light and color curves analyzed from UVB photoelectric photometry observations 16 p2863 A69-32398

UVB photoelectric investigation on southern globular clusters NGC 2808 and 1851, presenting star magnitudes and colors in tabular form and estimating reddening 18 p3190 A69-34290

Solar far UV images systematic photometry for thin solar models in terms of quiet sun intensity 20 p3603 A69-37546

Sunspot size and shape in continuous spectrum regions from photometric observations in UV and red ranges 20 p3616 A69-38301

ULTRAVIOLET RADIATION

NT FAR ULTRAVIOLET RADIATION

NT LYMAN ALPHA RADIATION

NT LYMAN BETA RADIATION

NT NEAR ULTRAVIOLET RADIATION

Photodegradation of organic polymers by UV radiation exposure, emphasizing polyvinyl chloride photochemistry and radiation stabilization 01 p0102 A69-10861

UV and visible light interaction effect on biological activity of Paramecia unicellular infusoria, noting cell division rates and cell deaths 01 p0017 A69-11085

Lethal effect of solar UV radiations on dried Coliphage T-1 exposed to space at sounding rocket altitudes 01 p0017 A69-11086

Ionospheric and stratospheric UV radiation effects on survival of microorganisms 01 p0018 A69-11088

UV and X ray radiations of stars and interstellar gas of Milky Way and remote galaxies 02 p0316 A69-11906

Radiative lifetimes for four N II excited states emitting UV during transition to lower level 02 p0280 A69-11928

Ruby laser to study stimulated Mandelstam-Brillouin scattering in liquids and in various crystals in UV 03 p0438 A69-13053

Q switched laser based on light waves parametric interaction in nonlinear medium operating at wavelengths from UV to IR 03 p0439 A69-13054

Intensity of visible and UV light from beam of positive deuterium molecular ions excited by passage through thin C foil 03 p0471 A69-13166

Trapped radical relationship to inactivation of trypsin exposed to UV by measuring radical concentration and inactivation degree 03 p0372 A69-13486

UV induced excited-state properties of DNA using optical emission and electron spin resonance methods 03 p0372 A69-13488

UV astronomy, discussing vehicle stabilization, un-stabilized sounding rockets, scanning satellites, balloons, stabilized rockets, pointing satellites, optics and detectors 05 p0821 A69-15839

UV solar spectra observation, discussing coordination of ground based and satellite programs 05 p0822 A69-15861

High power continuous and quasi-continuous wave UV generation by ADP and KDP crystals in argon-ion laser cavity [IEEE PAPER B-1] 05 p0773 A69-16308

Continuous UV noble gas ion lasers, noting small signal gain and power output limit at various current densities for strong lines [IEEE PAPER L-1] 05 p0775 A69-16321

Limb darkening and central intensity of solar disk measured in UV 05 p0827 A69-16466

UK space research in 1970s emphasizing solar observations in UN, cosmic X ray astronomy, solar space astronomy and ionospheric investigation 06 p0997 A69-16853

High power noble gas CW UV ion laser with W disk structure, showing continuous UV output limitation by optical degradation effects 06 p0936 A69-17900

Sustained combustion initiation in subatmospheric gaseous fuel-oxidant mixtures by UV radiation at room temperature, measuring parameters as function of mixture pressure [AIAA PAPER 69-88] 06 p0983 A69-18118

Surface UV irradiated MgO powder catalytic activity for hydrogen-deuterium exchange reaction 07 p1073 A69-18374

Radiative opacity in stellar atmospheres, discussing effect of UV continuum on photospheric radiation field 07 p1221 A69-19393

Cultured Chinese hamster cells responses to UV light of different wavelengths indicating photon absorbing molecules inhibition of colony development 07 p1068 A69-19492

Soviet monograph on UV radiation of sun and sky emphasizing biological effects 07 p1221 A69-19506

Dissociation-ionization fronts in interstellar molecular hydrogen clouds, analyzing effects of UV radiation from early stars 07 p1221 A69-19584

Highly ionized low density plasmas production by strong UV radiation 08 p1360 A69-20080

Sky areas search for stars with UV excesses listed in Luyten Two-Tenths Catalog of Proper Motions 08 p1392 A69-20560

Electron bombardment effects on performance characteristics of UV gratings 08 p1318 A69-21097

Daytime clear sky light polarization in UV and visual spectral regions calculated with considerations for aerosol components polarization effect 09 p1491 A69-22708

X ray and extreme UV radiation deduced from sudden ionospheric disturbances during proton flare, discussing time dependence of emission 10 p1766 A69-23751

Polyesters reaction with dimethyl p-phenylenediamine compared under UV exposure from carbon arc and natural sunlight 10 p1716 A69-23970

Polarization observation of star BL Lac continuum by multichannel scanner, noting photoelectric UV observations and identification with radio source 10 p1785 A69-24094

Pulsed molecular nitrogen laser positive UV and systems interaction under varying gas pressure, applied voltage and tube diameters 11 p1893 A69-24344

Solar UV radiation measurements by balloon-borne monochromatic illuminator, using Cd-cathode photomultiplier detector 11 p1945 A69-24414

Intergalactic gas temperature and density reevaluated, considering neutral hydrogen distribution in galaxies peripheries and metagalactic background ionizing UV radiation 11 p1946 A69-24588

Effective cross sections of UV radiation absorptions by molecular oxygen in Schumann-Runge bands at high temperatures 11 p1921 A69-24617

Rocket-borne spectroheliograph for monochromatic solar photography in Mg II 2802.7 Å line noting filter bandwidth, film polarizers and temperature control 11 p1884 A69-24838

Second tacite sounding rocket test for measuring UV radiation in transition zone between upper ionosphere and space 11 p1887 A69-25212

Microorganism survival in space for exposure to solar UV radiation on balloons, rockets and satellites 11 p1828 A69-25457

Gas ionization by UV radiation emitted by pellet, target or portion of gas in laser beam focus, using polished metallic mirrors 11 p1901 A69-25758

Calculated UV spectra of solar radiation reflected from atmosphere compared with satellites photometric measurements, attributing radiation intensity distribution asymmetries to seasonal dependence of ozone content 12 p2064 A69-25952

Empirical determination of heating efficiency of extreme solar UV radiation interacting with carbon dioxide atmosphere of Mars and Venus 12 p2155 A69-26015

Rocket observations of visible and UV dayglow using electron density and temperature measurements for emission rates of various excitation mechanisms 12 p2076 A69-27108

Optical radiation detection from pulsar PSR 0833-45 associated with supernova remnant in Vela, noting UV excess from plates using U and B filters 13 p2337 A69-27516

Neodymium laser emission of organic molecules in UV region noting molecular absorptivity and fluorescence 13 p2271 A69-27657

Ionization processes in Seyfert galaxies, considering thermal electrons, superthermal protons and electrons and nonthermal UV radiation 13 p2346 A69-27710

Markarian galaxies with strong UV continuum, observing emission lines differing from each other 13 p2351 A69-27866

Outgassed condensation effects in vacuum on magnesium difluoride overcoated UV irradiated Al mirrors, including temperature effects, Lyman alpha reflectance and IR analysis of deposits 13 p2299 A69-28015

UV radiation decreased transmittance through quartz exposed to plasma at high temperature and pressure, showing dependence on heated surface layer absorption 14 p2490 A69-29159

Solar UV radiation reflected from Echo satellites measured and compared with UV fluxes from Lyrae 14 p2447 A69-29408

Solar UV radiation effects on processes in comet head, interpreting surface brightness distribution of comet 1959k in terms of photodissociation 14 p2525 A69-29717

Astronomical UV radiation observation by OAO 2 satellite, discussing solar images, corona, chromosphere and UV spectrum, stellar evolution, etc 15 p2689 A69-30597

- Molecular dissociation by line radiation absorption, applying results to hydrogen molecules in H I region dissociated by photons of mean interstellar UV radiation field
15 p2693 A69-30783
- Balloon-borne UV polarimetry of stars and planets, studying linear polarization between 2000 and 3000 Å
15 p2616 A69-31380
- Photoionizing effect of hydrogen and helium UV glow in nighttime ionosphere compared with ground based IF ionosonde and sounding rocket observations
15 p2605 A69-31436
- Calorimetric measurement of source and broadband spectral absorptances of spacecraft thermal control coatings during exposure to UV in vacuum environment
16 p2789 A69-31815
- Instrument for simultaneous observation of astronomical plate pairs for detection of stars with UV color excess
16 p2791 A69-32226
- Solar corpuscular and UV radiation variation relationship to midlatitude airglow intensity in O I line
16 p2850 A69-32322
- UV irradiation effects on ZnO spacecraft thermal control coating pigments, discussing photo-Hall, luminescence and electron paramagnetic resonance measurements
[AIAA PAPER 69-639] 17 p2992 A69-33288
- Gas products evolved from selected thermal control coating materials during UV radiation in vacuum, noting permanent reflectance loss
[AIAA PAPER 69-640] 17 p2992 A69-33289
- UV absorption coefficients of high temperature air measured in shock tube reflected region
18 p3230 A69-35073
- UV excitation intensity increased for improving luminescent nondestructive testing, describing UV dosimeter and irradiation standards
18 p3138 A69-35115
- Solar cell integral covers optical losses in vacuum as function of degradation by UV exposure, noting accelerated testing for time-cost reduction
19 p3253 A69-35703
- Postirradiation growth of cultured Chinese hamster cells exposed to UV light, including comparison with X irradiation
19 p3257 A69-35975
- Markarian galaxies with strong UV continua, discussing emission spectra, red shift, absolute magnitudes, etc
19 p3426 A69-36577
- Previous radiation exposure effect on photographic film noting increased sensitivity at UV frequencies
19 p3314 A69-36626
- Microorganisms death by exposure to high intensity visible and UV light, discussing effect of endogenous photosensitized oxidation on caratoid-containing Rhodotorula glutinus
20 p3475 A69-37613
- Atmospheric ozone detection by three-color photometer measurements of solar UV radiation attenuation in Hartley continuum
20 p3543 A69-37802
- Photoelectric measurements of UV absorption coefficients of high temperature air at specific temperature and wavelength ranges in pressure-driven shock tube
22 p4049 A69-40098
- Gases effects on UV irradiated thermal control materials spectral reflectance, discussing tests and photolysis mechanisms
[AIAA PAPER 69-1025] 22 p3923 A69-40395
- Auroral UV and 3914 Å radiation during charged particle precipitation measured by satellite
22 p3939 A69-40507
- Light sources in 0.15-20 micron spectral range from published literature, unpublished reports, light source manufacturers and individuals
23 p4191 A69-42190
- ULTRAVIOLET REFLECTION**
- Earth albedo instrument on OSO 3 spacecraft to measure solar reflectance of earth at various wavelengths
15 p2614 A69-31279
- Diffuse reflection of UV radiation from rough metallic surfaces, noting irregularities
21 p3770 A69-38796
- ULTRAVIOLET SPECTRA**
- Stellar UV objective prism spectra from Gemini 11 and 12 manned flights
01 p0153 A69-10870
- OSO-4 solar UV spectrum measurements, correlating chromospheric line intensity and photospheric magnetic field strengths
[AAS PAPER 68-219] 02 p0313 A69-11485
- Effective temperature values of ozone used to determine onset time and disturbance height in ionosphere
02 p0238 A69-11670
- Absorption oscillator strengths of Ba 2 lines in UV and visible spectral regions, using cascade arc in argon with barium vapor
02 p0242 A69-11872
- IR and violet sulfur lines for Seyfert galaxies, noting substantial reddening in nuclei
02 p0325 A69-12593
- Far UV spectra of O and B stars in Orion photographed from Aerobee rocket, describing wavelength measurements and line identifications
02 p0327 A69-12712
- Continuum position location and total line absorption in solar spectrum, using Houtgast high dispersion intensity measurements of UV region
05 p0828 A69-16611
- Metal atom production by bombarding metal with positive ions from microwave discharge, obtaining isolation in inert gas matrix and UV spectra
06 p0957 A69-17113
- UV emission spectrum of double star Boss 1985, excitation potential effect on Fe II lines and table identifying emission lines
08 p1385 A69-20060
- Population densities of UV bound resonance lines of neutral helium for 41-level model atom, discussing optical thickness and electron temperature and density
08 p1390 A69-20392
- Present state of abundance determination in solar corona, discussing forbidden and UV lines analysis
08 p1402 A69-20907
- Polar auroral far UV spectra using Ebert-Fastie monochromator flanked by photometers with same visual field
08 p1311 A69-21026
- Collision broadening cross sections of OH UV transition at room temperature, using flash photolysis
09 p1543 A69-22252
- Far UV stellar astronomy, concerning very hot stars and interstellar gas composition studies
10 p1772 A69-22870
- Far UV spectra of zeta Puppis and gamma star two Velorum with 1.6 Å resolution photographed with all reflective objective spectrograph on Aerobee rocket
10 p1788 A69-24120
- Venus and Jupiter low resolution UV spectra obtained with servocontrolled star tracking telescope in Aerobee rocket, noting Lyman alpha radiation characteristics
[JHU-TR-15] 10 p1788 A69-24121
- Venus albedo dependence on wavelength in UV spectrum between 4500 and 3200 Å from reflector observations
11 p1957 A69-24406
- Lunar far side surface spectral inhomogeneities in UV from Zond 3 measurements
12 p2154 A69-25817
- Calculated UV spectra of solar radiation reflected from atmosphere compared with satellites photometric measurements, attributing radiation intensity distribution asymmetries to seasonal dependence of ozone content
12 p2064 A69-25952
- High speed streak camera for recording fast processes, noting changeability from optical to UV spectral range
12 p2085 A69-26155
- Spheroidal galaxies with early type spectra distinguished by UV continuum, discussing telescopic spectral and color observations
12 p2159 A69-26663
- Blue, UV and yellow spectral observations of M 82 (NGC 3034), obtaining polarization dependence on reciprocal of wavelength, polarization and color characteristics
12 p2169 A69-27057
- Photoelectric scanning of CH Cygni spectrum calibrated and compared with 45 Arctis, discussing high dispersion, excess blue and UV continua, H beta emission, etc
13 p2338 A69-27557
- Hydrogen to He ratio effect on stellar atmospheric structure, considering flux relations, UVB color indices, H line profiles, electron and gas pressures
13 p2339 A69-27562
- Spectrophotometry of variable star SS Cyg, analyzing energy distribution in continuum, UV gradient and Balmer jump
13 p2351 A69-27868
- Goddard Experiment Package /automated spaceborne telescope design/ for stars and nebulae UV spectral emittance measurements
13 p2261 A69-27948
- Scientific aims, optical design, instrument data, control and orbit operation of European Large Astronomical Satellite used in UV observations
13 p2264 A69-28477
- Effective temperature values of ozone used to determine onset time and disturbance height in ionosphere
13 p2257 A69-28701
- Forbidden transition probabilities of solar corona lines in vacuum UV range
14 p2519 A69-29355
- High speed photographs of plasma emission spectra in UV and soft X radiation spectrum regions, discussing theory, design and operation of facilities
14 p2496 A69-29784
- Ca XV spectrum in vacuum UV under laboratory conditions, discussing fine structure of ground level of Ca XV and coronal lines
15 p2688 A69-30553
- Absolute spectrophotometric gradients determined from energy distribution in UV beta Lyr spectrum, confirming gradual variations in light curve shape and spectral characteristics
15 p2688 A69-30557
- Ozonosphere inhomogeneities from UV spectra of reflected solar radiation, studying latitude dependence of seasonal behavior at different heights
15 p2597 A69-30654
- Photometric calibration correction for (B-V) and (U-B) colors taking into account hydrogen line blocking
15 p2694 A69-30786
- UV OGO observations of atomic hydrogen and oxygen in airglow, comparing results to exospheric models of hydrogen geocorona
15 p2603 A69-31400
- Lyrid and Perseid meteor spectra for spectral line identifications in 3100-4000 Å UV range, listing lines from six neutral atoms and five ions
15 p2700 A69-31500
- Coronal Fe ionization lines X, XIII and XIV photographed by UV coronagraph
16 p2847 A69-31661
- UVB photometry of faint stars, discussing photographic plate effect on accuracy, emulsion standardization and use of electronography
17 p3031 A69-33099
- Photoelectric spectra of pulsating auroras in visible and near UV range, considering atmospheric opacity
17 p2961 A69-33416
- Lignin presence in New Zealand moss gametophytes observed for characteristic color reaction and UV spectra, noting contrast with north temperate species
17 p2912 A69-34176
- Transition probabilities of N I far UV multiplets, comparing experimental and theoretical results
18 p3178 A69-35413
- Ozone vertical distribution predicted statistically, using total ozone amounts and backscattered UV spectral measurements
18 p3132 A69-35426
- Solar UV emission lines from high resolution rocket observations
20 p3612 A69-38167
- Tabulation of solar UV spectrum features between 3650 and 3000 Å from intercomparison of photoelectric records and Second Revised Rowland, indicating wavelength relocations
22 p4014 A69-40146
- Power per unit volume of UV and forbidden lines emitted by ionized C, N, O and Ne as function of electron temperature and density
22 p3984 A69-40157
- Mars upper atmosphere ionized carbon dioxide and CO emission spectra in 1900-4300 Å region measured by Mariner 6, observing atomic hydrogen and oxygen lines
22 p4023 A69-40568
- Rocket UV spectra indicating Venus atmosphere weak absorption and low ozone abundance and possible Jupiter surface depressions
22 p4028 A69-40661
- Molecular N UV spectrum at various pressures, showing absorption band dependence on pressure induced dipole transitions
22 p3986 A69-40723
- Rocket measurement of far UV spectral intensity of theta Orionis for far UV interstellar extinction law in Orion nebula region
22 p4030 A69-40770
- Venus albedo dependence on wavelength in UV spectrum between 4500 and 3200 Å from reflector observations
24 p4391 A69-43796

ULTRAVIOLET SPECTROMETERS

Rapid scan spectroscopy, reviewing dispersion optical and interferometric systems and electronic image converters

01 p0082 A69-10836

Ebert spectrometric experiment during Mars flyby aimed at detecting upper atmosphere atoms, ions and molecules in 1100-4300 angstrom spectral range [AAS PAPER 68-184]

02 p0311 A69-11469

OGO 4 UV airglow spectrometer consisting of Ebert-Fastie monochromator and photomultipliers with cesium telluride and cesium iodide channels

19 p3315 A69-36682

ULTRAVIOLET SPECTROPHOTOMETERS

Spinning rockets UV spectrophotometry of early type stars, discussing instrumentation, calibration, data recording and stellar spectra

12 p2153 A69-25812

UBV observations of stars P and 36 Cygni including short period variations and secular changes in brightness

12 p2172 A69-27159

Solar photography at extreme UV wavelengths using pinhole camera instrumentation on stabilized Skylark rocket

20 p3539 A69-37545

Interstellar extinction in UV from zeta and epsilon Persei spectra obtained with scanner attached to telescope mounted in pointed Aerobee rocket

22 p4030 A69-40772

ULTRAVIOLET SPECTROSCOPY

Vacuum UV perturbation spectroscopy compatibility with resonance transitions in Ar ion laser

08 p1324 A69-20161

Transmission and reflection properties of materials for vacuum UV spectroscopy, using LTE plasmas for calibrating UV intensities

08 p1315 A69-20468

Thermodynamic dissociation constants of alkyl phenols in aqueous and methanol media based on UV spectroscopic analysis, noting anticarcinogenic properties

11 p1831 A69-24539

Schmidt all-reflecting telescope for UV imaging in Apollo Earth Orbital Scientific Experiment

11 p1887 A69-25101

Astronomical UV radiation observation by OAO 2 satellite, discussing solar images, corona, chromosphere and UV spectrum, stellar evolution, etc

15 p2689 A69-30597

Magnetically focused electronographic image converters in far UV photography and spectroscopy in space astronomy applications

17 p2972 A69-33084

Magnetically focused electronographic image converters for far UV photography and spectroscopy from sounding rockets, discussing stellar observations

20 p3543 A69-37801

Spaceborne planetary UV spectroscopic search for atoms and molecules basic to life, specifically molecular N and water vapor photodissociation products

23 p4113 A69-41616

UMBILICAL CONNECTORS

EVA/IVA fluid umbilical improved stowability and flexibility, discussing cross section development and tests

[AAS PAPER 69-470]

24 p4272 A69-42847

UMBRA (SHADOWS)

U SHADOWS

UMKEHR EFFECT

Atmospheric haze effect on Umkehr measurements, considering computation from direct sounding of vertical ozone distribution and from model atmospheres

08 p1308 A69-20316

Vertical ozone profiles computed from known total ozone data based on profiles taken by Umkehr method

15 p2597 A69-30896

Vertical ozone distribution determination discrepancies between Brewer-Mast electrochemical sonde and Umkehr methods, discussing influence of seasonal and diurnal variations

16 p2786 A69-32630

Simultaneous Umkehr observations of vertical ozone distribution in upper stratosphere using two Dobson photometers, discussing deviations due to calibration sensitivity

16 p2786 A69-32631

Zenith sky Umkehr observed with Dobson spectrophotometer at twilight, discussing light scattering by aerosols in lower stratosphere

16 p2786 A69-32634

UNCAMBERED WINGS

U RING WINGS

UNCERTAINTY

U PROBABILITY THEORY

UNCONSCIOUSNESS

NT NARCOSIS

Physical and physiological factors involved in determining aircraft passengers time of safe unconsciousness permissible after cabin decompression

24 p4278 A69-43398

UNCOUPLED MODES

Electromagnetic field TM and TE modes uncoupling during oblique incidence scattering from radially inhomogeneous cylinders

15 p2565 A69-30170

UNDAMPED OSCILLATIONS

Absolute viscosity measurements from translational undamped oscillations of plate in liquid, considering viscosimeter walls effect

04 p0679 A69-14905

Plate theories of linearly elastic materials under free undamped vibration, giving 500 references [AIAA PAPER 69-24]

06 p1027 A69-18061

Absolute viscosity measurements from translational undamped oscillations of plate in liquid, considering viscosimeter walls effect

12 p2182 A69-26658

UNDERCARRIAGES

V/STOL undercarriage design, considering influence of aircraft operation, engine installation, rough/soft ground capability, etc

09 p1435 A69-22781

UNDERGROUND EXPLOSIONS

Lunar craters compared with underground explosion craters on earth, determining criteria for identifying explosion craters on moon

04 p0656 A69-14670

UNDERGROUND NUCLEAR EXPLOSIONS

U NUCLEAR EXPLOSIONS

UNDERGROUND STORAGE

Materials evaluation for devices with long term underground exposure, including field tests at tropical locations

19 p3321 A69-35568

UNDERWATER PROPULSION

Aerodynamic considerations of high speed hydrodynamics for underwater craft, noting rocket propulsion

13 p2245 A69-27418

UNDERWATER TESTS

Book on groups under stress covering psychological research in SEALAB 2, emphasizing planning of data collection and experimental results

04 p0552 A69-14533

Aluminum corrosion characteristics immersed in ion-exchanged water with trace impurities, determining corrosion rates

04 p0617 A69-14932

Radiative flux density, spectrum and temporal behavior of Q switched laser induced underwater sparks

05 p0771 A69-15818

Underwater experiment to determine man capability to perform scientific mission during 60 days isolation, noting task performance, social interaction and personal adjustment

08 p1300 A69-20113

Heart rate and respiratory response correlations in men during surface and underwater work, showing reasonable approximations of workload in surface-equivalent terms

14 p2406 A69-29293

Neutral buoyancy simulation of astronaut performing module replacement and repair task in zero-g environment [AIAA PAPER 69-1005]

22 p3921 A69-40379

UNDERWATER VEHICLES

U SUBMARINES

UNIAXIAL STRAIN

U AXIAL STRAIN

UNIDENTIFIED FLYING OBJECTS

UFOs from sociological viewpoint, stressing need for international cooperation in exobiological research

17 p3076 A69-32974

UNIFORM FLOW

NT BLASIUS FLOW

Boundary layer equations for uniform motion of semiinfinite flat plate through incompressible conducting fluid at rest and in magnetic field, using numerical method

03 p0477 A69-13794

Expansion tube modification incorporating nozzles plate at secondary diaphragm for reducing flow nonuniformity and contamination

[AIAA PAPER 68-371]

09 p1477 A69-21960

Turbulent boundary layer velocity distributions in uniform/accelerated compressible flow over flat plates using change of variables based on mixing length formula

[ONERA-TP-693]

11 p1867 A69-24752

Incompressible uniform shear flows merging behind trailing edge of semiinfinite flat plate, using inner-outlet expansion method based on Navier-Stokes equation

13 p2248 A69-28212

Transient uniform flow over sphere at intermediate Reynolds numbers with recirculatory wakes, utilizing difference approximation to time dependent Navier-Stokes equations

18 p3120 A69-34435

Uniform flow and wall boundary layer growth measurement in conical nozzle of reflected shock tunnel operating at high enthalpy conditions

24 p4247 A69-43572

UNIPOLAR TRANSISTORS

U FIELD EFFECT TRANSISTORS

UNIQUENESS

Uniqueness formulation of concentrated loads problem in linear theory of couple-stress elasticity

02 p0338 A69-117202

Existence and uniqueness of weak solutions in linear theory of stable equilibrium position for inhomogeneous elastic thin walled shells

02 p0340 A69-12036

Existence and uniqueness for nonlinear boundary value problems satisfying Lipschitz condition

10 p1721 A69-23640

Uniqueness and nonuniqueness of solutions of initial value problems for second order semilinear parabolic equations

10 p1722 A69-24069

UNIQUENESS THEOREM

Uniqueness and existence theorem concerning stability of solutions of mixed nonlinear boundary value problem, discussing generalized heat transfer phenomena

02 p0352 A69-12255

Boundary value problem of hyperbolic equation with discontinuous boundary conditions

04 p0622 A69-14617

Asymptotic oscillation results for solutions to first order nonlinear differential-difference equations, obtaining existence-uniqueness theorems

04 p0624 A69-14950

Uniqueness theorem validity for boundary value problem in linear elastostatics for homogeneous media

05 p0844 A69-16739

Existence and uniqueness theorem for functional equation of optimal control problems, noting stability of solution

06 p0949 A69-17889

Methods to obtain uniqueness for partial differential/elliptic equations boundary problem extended to parabolic conditions, analyzing necessary conditions for existence

07 p1173 A69-18728

Complex variable theory usefulness in investigating existence and uniqueness of solutions for boundary values in partial differential equation

07 p1173 A69-18731

Uniqueness conditions of expansions in series of functions stressing Jacobi series applied to singular partial differential equations

07 p1174 A69-18805

Uniqueness theorem for laminar MHD duct flows

07 p1190 A69-18813

Reciprocity, variational and uniqueness theorems developed within linear theory of coupled thermoviscoelasticity

07 p1233 A69-19327

Periodic asymptotically stable MHD motions, proving uniqueness and existence theorems

07 p1194 A69-19437

Uniqueness theorem for equations of dynamics of viscoelastic bodies, using energy and hereditary elasticity considerations

08 p1415 A69-20658

Existence and uniqueness of Dirichlet problem solutions for elliptic type equations with measurable and bounded coefficients

08 p1343 A69-20659

Problems using Fredholm integral equations providing unique solution

08 p1418 A69-21004

Almost periodic systems stability criteria derived from differential inequalities and Liapunov function, considering existence and uniqueness

09 p1532 A69-21612

Existence and uniqueness to boundary layer continuation problem based on flow equation for steady gas flow

10 p1679 A69-23569

Criteria governing solution uniqueness to Volterra equations system

10 p1722 A69-24067

Solution existence of nonlinear two point boundary value problems from uniqueness

11 p1909 A69-24883

Pseudodifferential operators theory application to uniqueness of solutions of Cauchy problem

12 p2124 A69-26930

Dirichlet problem for second order linear hyperbolic partial differential equations in cylindrical domain, deriving necessary and sufficient condition for solution uniqueness

12 p2124 A69-26932

Nonuniqueness in Hopf weak solutions for Navier-Stokes equations using solutions with rotational symmetry

14 p2428 A69-28900

Riemann problem with arbitrary jump data for extended hyperbolic systems of equations, showing conditions for unique solution

14 p2433 A69-29678

Magnetothermoelasticity equations, uniqueness and reciprocity theorems and solutions emphasizing moving media

15 p2715 A69-31215

Existence and uniqueness theorems for operator equation in differential equations theory for application to boundary value problem

19 p3360 A69-36373

Uniqueness theorems for energy methods solution of equations of dynamic thermoelasticity and viscoelasticity

19 p3439 A69-36470

Heat transfer problem involving temperature determination of body and ambient medium, deriving existence and uniqueness theorems for boundary value problems in curvilinear regions

20 p3631 A69-36991

Method of straight lines applied to two phase Stefan type problem for quasi-linear parabolic equation, obtaining existence and uniqueness of solutions

20 p3567 A69-36992

Uniqueness theorems for wave propagation in homogeneous or inhomogeneous anisotropic media

20 p3578 A69-38196

First order linear differential equations subject to linear constraints, discussing solution uniqueness dependence on matrix nonsingularity

21 p3754 A69-38744

Prandtl boundary layer theory problems, considering solution uniqueness and stability, unsteady flow, boundary layer separation, existence conditions, etc

21 p3697 A69-39698

Rigid/plastic solids subjected partly to uniform fluid pressure and partly to general boundary conditions, analyzing uniqueness and stability criteria

23 p4235 A69-42460

Uniqueness theorem and successive approximations for delay functional differential equations, noting scalar problems

24 p4341 A69-43236

UNITED NATIONS

Book on international law and uses of outer space covering effects of UN General Assembly Resolutions and Outer Space Treaty

02 p0356 A69-12676

Legal and technical aspects of international cooperation in spacecraft crew rescue operations signed by UN General Assembly

06 p1042 A69-17033

Outer space law principle sources including divine law, UN and NASA contractors regulations

15 p2720 A69-31052

INTELSAT 1964 agreements consistency with multilateral international agreements, including UN General Assembly and International Telecommunication Union

20 p3638 A69-37122

Space law history, discussing Space Treaty and UN Declaration of Legal Principles

20 p3638 A69-37128

Space law and space research, detailing UN law proposals

20 p3638 A69-37129

UNITED STATES OF AMERICA

NT CALIFORNIA

NT HAWAII
NT NEW JERSEY
NT NEW MEXICO
NT NEW YORK
NT TEXAS
NT WASHINGTON

Space program effects in education, science and engineering, noting impact of first satellite on U.S. research and technology

01 p0179 A69-10500

Atmospheric optical data recorded by instrumented aircraft near Crater Lake, discussing surface spectral irradiance data

01 p0111 A69-10846

Weathering tests on wrought aluminum alloys exposed at U.S. sites compared to British industrial atmospheric exposure results

01 p0101 A69-11354

U.S. space program projections, discussing earth orbit operations, lunar and planetary explorations, costs and timetable

02 p0355 A69-11744

Aerospace management technology transferability to problems of society and government

02 p0355 A69-11754

U.S.-European cooperation in space activities, discussing implementation by COSPAR and jointly owned industrial corporations

03 p0535 A69-13586

Cooperation in developing space programs between Western Europe and U.S.

03 p0535 A69-13588

Cooperation between U.S. and Europe in communication satellite programs

03 p0535 A69-13591

Topics and objectives of Third Europe U.S.-European Conference, Munich, June 1968

03 p0535 A69-13594

U.S.-European cooperation, stressing unsatisfactory role of European industry and governments in space projects

03 p0536 A69-13595

VFX fighter aircraft, discussing U.S. Navy requirements influence in VFX-1 and VFX-2 design

03 p0367 A69-13675

Federal government contracting, discussing legality of NASA service contracts

05 p0850 A69-15987

Federal government legal liability for commercial air safety in aircraft accident suits

06 p1042 A69-16848

Tort system of U.S. law effect on air safety promotion, discussing liability influence on government, manufacturers and airlines

06 p1042 A69-16850

U.S. aerospace programs, reviewing manned space missions, space applications, space science, transportation, strategic and tactical warfare and influence on aerospace industry

07 p1243 A69-18376

U.S. policy for commercial surface effects ships regulation, discussing operational, construction and design requirements

08 p1254 A69-20199

National plan for air navigation covering R and D and operational aspects

08 p1348 A69-21192

Federal Government budgeting, discussing systems analysis, planning-programming, etc

10 p1811 A69-23351

Federal Government systems politics and budgeting, noting dichotomies, time dependence, taxonomy, etc

10 p1811 A69-23352

Federal Government policies analysis, discussing disadvantages of planning-programming-budgeting system /PPBS/

10 p1811 A69-23353

Potential hazards of government sponsored technology, examining SST and fluoridation projects and weather problems

10 p1811 A69-23392

Possible sources of meteoritic material from Hopewell Indian burial mounds

11 p1963 A69-25401

U.S.-Europe air traffic, attributing European lag to dense air route duplication, load factors, etc

13 p2381 A69-27338

U.S.S.R. manned bomber role in air strategy, discussing mutual effects of U.S.-U.S.S.R. military posture developments and ICBM

14 p2392 A69-29431

National plan for air navigation covering R and D and operational aspects

14 p2480 A69-29858

Report on U.S. space science program to COSPAR on stellar and solar astronomy, lunar and planetary research, upper atmospheric physics, etc

15 p2723 A69-31430

Relative technological standing of U.S. and Europe, discussing meaning and existence of technology gap

17 p3076 A69-34040

Expenditures for R and D effect upon U.S. economy

17 p3076 A69-34041

Educational TV satellite system design for U.S. in 1970s

18 p3235 A69-35076

Technical and economic factors of program to provide communications services via satellite facilities in continental U.S.

21 p3678 A69-39762

U.S. aerospace technological forecasting involving space flight, air transport and V/STOL aircraft

22 p4052 A69-39930

Accident prevention program of Bureau of Aviation Safety, discussing probable cause analysis and function in feedback loop, hazard analysis and accident data center

22 p3867 A69-41140

UNITS OF MEASUREMENT

Astronomical unit determined by measuring Doppler shift of spectral features of galactic hydrogen

07 p1222 A69-19590

Astronomical unit determined by measuring radial velocity of radio wavelength spectral line source

13 p2350 A69-27822

Thermal physiology standardized symbols compilation for units of measurement

23 p4078 A69-41317

UNIVAC COMPUTERS

Pivotal computer operations in Apollo NASA Communication Network, describing UNIVAC computers in use and design considerations

18 p3100 A69-34267

UNIVERSAL TIME

Ephemeris Time and Atomic Clock Time roles in astronomy, discussing errors in daylength determination for mechanical, Short and atomic clocks, UT and Ephemeris Time

01 p0156 A69-10989

Electronic charge variations with cosmic time determined from geochronological data

06 p1003 A69-17323

Analytical description of planetary distribution of space-time variations of f0F2, deriving Fourier series as function of UT

09 p1486 A69-21545

Earth rotation velocities nonuniformity according to astronomical observation data obtained from Universal Time and atomic time scales comparison

11 p1957 A69-24407

Theories for universal time controlled polar F region reevaluated in light of satellite low energy charged particle observations

12 p2065 A69-26103

Analytical description of planetary distribution of space-time variations of f0F2, deriving Fourier series as function of UT

16 p2783 A69-32540

Bright lunar limb zenith distances measured by equal altitudes method, deriving Ephemeris-Atomic Time A3 and Ephemeris-TU2 time relations

23 p4208 A69-41289

Earth rotation velocities nonuniformity according to astronomical observation data obtained from Universal Time and atomic time scales comparison

24 p4391 A69-43797

UNIVERSE

Neutrino radiation in universe with emphasis on stellar neutrino radiation, analyzing emission during nuclear fusion of C-N, He and Ne-Na cycles

01 p0145 A69-10754

Metagalaxy temperature brightness explained from radio sources combined radiation with inversion spectra

02 p0313 A69-11632

Observable surface of part of Friedmann universe calculated using analytical continuation of Schwarzschild coordinate system, noting angular extent and angle of observation effect

02 p0314 A69-11644

Book on cosmic radiation origin and expansion of universe, covering astrophysical reasons for electric charging of galaxies in range of galactic and metagalactic dimensions

02 p0315 A69-11713

Radioactive decay of neutral pions generated in metagalactic cosmic ray interactions as source of high energy isotropic gamma rays observed by OSO-3
02 p0308 A69-12092

Topochrone and generalized Hubble law considered for singular origin of universe with big bang explosions
02 p0321 A69-12195

Normal galaxies radio emission and brightness of metagalactic radio background
02 p0325 A69-12564

Plasma generation in universe from temperature and pressure effects, ionizing radiation and stellar ejection of ionized particles
02 p0293 A69-12781

Metagalactic cosmic rays, galactic halo and sources of cosmic rays in Galaxy, noting models, electron component of cosmic rays and evolutionary cosmology
03 p0497 A69-12929

Sun motion with respect to extragalactic universe, discussing local supercluster kinematics
03 p0513 A69-13769

Observable horizons in expanding universe, considering absorption of extragalactic radiation
04 p0648 A69-14566

Intergalactic continuum study showing universe behavior like black body with 2.7 K radiation temperature, noting cosmological and cosmogenic importance
05 p0827 A69-16593

X ray astronomy use for probing hot regions of outer space and high energy electrons
06 p0991 A69-17307

Particle radiations and magnetic fields in metagalaxy, discussing galactic injection spectrum problems
06 p0991 A69-17310

Cosmology, discussing big bang and steady state models, arrow of time, red shift/distance relation, background radiation, etc
07 p1210 A69-18390

Cosmic ray astrophysics, discussing chemical composition, energy spectrum and galactic sources
07 p1205 A69-18909

Origin of galaxies, discussing initial conditions of formation including density, kinematic and composition inhomogeneities, time effect, etc
07 p1218 A69-19280

Luminosity distance, distance by apparent size, number counts, background radiation and apparent angular motion of sources in homogeneous anisotropic model universe
07 p1218 A69-19282

Redundant world models, discussing elimination through measurement of larger red shifts of galaxies and quasars
07 p1219 A69-19283

Evolutionary cosmological models, relevant observational cosmology, quasar red shift, cosmic black body radiation, cosmic He abundance and universe temperature history
08 p1388 A69-20223

Metagalaxy stationary model in terms of relativity theory, investigating radiation pressure balancing of gravitation as imaginary situation
08 p1389 A69-20263

Photon whirls and formation of protogalaxies, discussing density inhomogeneities in hot model of universe in terms of pregalactic structure dynamics
09 p1587 A69-21355

Early evolution of universe related to present upper bound of primordial black body gravitational radiation temperature
09 p1601 A69-22210

Local creation of mass in steady state universe as source of static field energy propagating away at speed of light
09 p1601 A69-22212

Characteristic length constant in open cosmological model of large scale properties of real space-time, noting relation to other constants
09 p1608 A69-22528

Quasars and explosive processes in galaxies as cosmic ray sources in expanding universe, studying relation between galactic and metagalactic cosmic rays
10 p1756 A69-22815

Superhigh energy cosmic ray interaction with neutrinos in universe, shape of cosmic ray spectrum and universe development
10 p1757 A69-22826

Universe rotation from observations of microwave background and using closed universe model
10 p1771 A69-22851

X ray universe, considering contribution of X ray astronomy to phenomena of big bang, supernovae, neutron stars, exploding galaxies, etc
10 p1760 A69-22869

Abell 2199 cluster of galaxies, discussing population contours, volume density function, structure and other static properties
10 p1774 A69-22965

Book on relativity and cosmos, space and time in physics, astronomy and cosmology covering theoretical and empirical research
10 p1784 A69-24019

Dynamical model for spherical inhomogeneity in mean mass density of universe to predict velocity dispersion observed for Coma Cluster
10 p1789 A69-24133

Universe origin, discussing big bang theory, effects of expansion time and temperature on elementary particles, RF quanta, etc
11 p1953 A69-24352

Observed frequencies of number of members in multiple systems of galaxies
12 p2156 A69-26222

Hypothesis for intelligent life existence in universe
13 p2353 A69-28435

Space-time interpretation of static Einstein universe model and Friedmann space with variable positive curvature
14 p2484 A69-28865

Galactic formation in Lemaitre universe from statistically probable density fluctuations, using perturbation theory and Newtonian cosmology
14 p2520 A69-29373

Book on New Cosmos covering classical astronomy concepts, stellar astrophysics and galaxies
14 p2522 A69-29684

Extragalactic background radiation intensity in isotropic world models as function of universe thermal history
14 p2514 A69-29769

Closed space cosmological model, discussing complex singularity behavior
15 p2680 A69-30200

Density perturbation mode in Lifshitz relativistic theory for expanding universe gravitational instability, adopting Lagrangian coordinate condition to eliminate physically meaningless solution
15 p2652 A69-30203

Metagalactic electrons and relict radiation interaction calculations allowing for universe expansion, space curvature and X ray absorption
15 p2687 A69-30541

Symmetry between koinomatter and antimatter in universe, discussing koinonucleons production, big bang theory, protogalaxy model, quasi-stellar objects, galaxy evolution, etc
15 p2690 A69-30670

Hydrogen recombination in hot universe model, discussing emission of energetic quanta
15 p2690 A69-30734

Expanding isotropic universe with cosmological constant, noting stability for rotational perturbations and gravitational and sound waves
15 p2690 A69-30735

Relativity theorems applied to collapsing stars and expanding universe noting limitations of general relativity from prediction of singularities
15 p2694 A69-30854

Newtonian invariant mechanics, giving inertial interpretation of gravitation and Hubble expansion of universe
15 p2654 A69-31214

Possible existence in universe of large number of difficult-to-observe particles with zero rest mass left over from superdense phase
16 p2814 A69-31801

Cosmology and geophysics relationships using initial and boundary conditions concept
16 p2864 A69-32451

Particle production by gravitational fields in universe via quantum field theory, considering cosmological models
17 p3008 A69-33003

Antimatter in universe, presenting arguments for microscopic and macroscopic symmetries
17 p3006 A69-33578

Photon whirls and formation of protogalaxies, discussing density inhomogeneities in hot model of universe in terms of pregalactic structure dynamics
18 p3197 A69-34745

Fluctuations evolution in density perturbations analyzed to obtain free fall and free expansion universe models, showing no difference between expanding and static Newtonian universes
18 p3203 A69-35347

Hydrogen atom excess charge creating universal repulsive force in analyzing cosmological gravitational contraction in terms of Newtonian mechanics
18 p3206 A69-35469

Cosmic matter density and velocity in expanding universe with negative curvature within Einstein-Friedman theory
20 p3599 A69-37472

Cosmic protons and high energy heavy nuclei interaction with radiation in expanding universe, including estimates of light radiation influence on cosmic ray spectra
20 p3591 A69-38034

Universal hydrogen distribution, discussing atomic hydrogen needed to close universe
20 p3610 A69-38140

Universe evolution from hot initial state, discussing element synthesis, quanta, radiation particles, etc
21 p3795 A69-38401

Harrison primordial inhomogeneity postulate concerning baryon numbers distribution in universe, precluding possibility of considering cosmic rays bulk as universal
21 p3810 A69-39469

Soviet collection of papers on universe covering history and development of astronomy, solar system, minor planets, comets, shooting stars, extraterrestrial civilizations, etc
21 p3814 A69-39531

Density fluctuations in universe during early stages, using hot big bang cosmological model
21 p3814 A69-39571

Unified theory of elementary particles assuming quantum mechanics as consequence of changes in time within microcosmos and particle-universe interaction
21 p3816 A69-39622

Level shifts and spontaneous transitions in steady state of universe by path integral method of first quantization, considering time symmetric electromagnetic theory
22 p3980 A69-40169

Dimensionless coupling constants predicted from causal relationship among strong, electromagnetic, weak and gravitational interactions in fluid region of universe
22 p3981 A69-40416

Cosmic gamma rays spectrum from neutral pions production and decay in metagalactic cosmic ray p-p collisions, deriving models based on Einstein general relativity theory
22 p4006 A69-40641

Cosmological constant closed relativistic universe, showing constant-observational data inconsistency
22 p4029 A69-40757

Extragalactic universe major constituents and physical properties of normal, radio and compact galaxies, discussing missing matter existence
23 p4217 A69-42317

Universe behavior in time, discussing expansion observed by red shift, closed universe with future contraction phase and unlimited expansion open model
23 p4221 A69-42391

UNIVERSITIES

Unutilized ideas in university laboratories, showing generation and implementation enhancement by marketing experience and product development background
15 p2720 A69-30596

UNIVERSITY PROGRAM

Space system engineering courses background, objectives and results at MIT and Stanford University dealing with applications of space technology
[UN PAPER 68-95870] 01 p0178 A69-10485

NASA university program, discussing participation in space and aeronautics development based on project oriented research grants and Sustaining University grants
[UN PAPER 68-95413] 01 p0179 A69-10506

Universities and public service education noting NASA requirements and programs
20 p3641 A69-38282

Aerospace medical educational programs for MD, post-MD and practicing physicians at medical faculties in U.S. and at Ohio State University
23 p4106 A69-41799

OSO spacecraft thermal design modified to operate University of Minnesota zodiacal light monitor experiment
[AAS PAPER 69-173] 24 p4393 A69-42873

UNKNOWN

U DEPENDENT VARIABLES

U PROBLEM SOLVING

UNLOADING WAVES

Propagation of longitudinal transverse loading and unloading waves /with cylindrical symmetry/ in non-homogeneous elastic/viscoplastic medium, accounting for plastic dilatational strains
03 p0528 A69-13929

UNMANNED SPACECRAFT

NT ANNA SATELLITES
NT BEACON SATELLITES
NT ECHO SATELLITES
NT ECHO 1 SATELLITE
NT EXPLORER 18 SATELLITE
NT EXPLORER 22 SATELLITE
NT GEODETIC SATELLITES
NT GEOS 2 SATELLITE
NT LUNAR PROBES
NT LUNIK LUNAR PROBES
NT LUNIK 9 LUNAR PROBE
NT LUNIK 10 LUNAR PROBE
NT LUNIK 12 LUNAR PROBE
NT LUNIK 13 LUNAR PROBE
NT MARINER SPACE PROBES
NT MARINER SPACECRAFT
NT MARINER 1 SPACE PROBE
NT MARINER 2 SPACE PROBE
NT MARINER 4 SPACE PROBE
NT MARINER 5 SPACE PROBE
NT MARINER 6 SPACE PROBE
NT MARINER 7 SPACE PROBE
NT MARINER-MERCURY 1973
NT MARS PROBES
NT NAVIGATION SATELLITES
NT OSO
NT OSO-3
NT OSO-C
NT PASSIVE SATELLITES
NT PIONEER SPACE PROBES
NT PIONEER 6 SPACE PROBE
NT PIONEER 7 SPACE PROBE
NT PIONEER 8 SPACE PROBE
NT PIONEER 9 SPACE PROBE
NT RANGER LUNAR PROBES
NT SOLAR OBSERVATORIES
NT SOLAR PROBES
NT SPACE PROBES
NT SURVEYOR LUNAR PROBES
NT SURVEYOR 1 LUNAR PROBE
NT SURVEYOR 5 LUNAR PROBE
NT SURVEYOR 6 LUNAR PROBE
NT SURVEYOR 7 LUNAR PROBE
NT TECHNOLOGY FEASIBILITY SPACECRAFT
NT TRANSIT 4A SATELLITE
NT TRANSIT SATELLITES
NT VENERA SATELLITES
NT VENERA 4 SATELLITE
NT VENUS PROBES
NT ZOND SPACE PROBES
NT ZOND 5 SPACE PROBE
NT ZOND 6 SPACE PROBE

Meteorological satellite research program, including unmanned satellite observations and possibilities with meteorologist on board manned spacecraft
[UN PAPER 68-95350] 01 p0109 A69-10483

Stabilization and control techniques for future unmanned commercial space vehicles, emphasizing application of projected technological advances in instrumentation
[AIAA PAPER 67-878] 02 p0334 A69-12367

Longitudinal range dispersion of unmanned Mars landers using VM-8 and VM-9 atmospheric models, discussing Syrtis Major as possible landing site
02 p0324 A69-12390

Aerothermoelasticity problems for Mars entry vehicles, discussing deceleration loads, separated hot gas flow, shield thermal gradients and oscillatory body motion
[AIAA PAPER 68-283] 09 p1610 A69-21991

High reliability space system electronic parts control program to assure success of unmanned space missions
16 p2793 A69-31714

Oxygen difluoride-diborane propellant injector and chamber design criteria applied to unmanned spacecraft rocket engine development
[AIAA PAPER 69-508] 16 p2839 A69-32671

Thermal stability elements in solid propellant liner insulation system for heat sterilized solid rocket motors used in unmanned planetary landers
[AIAA PAPER 69-437] 16 p2869 A69-32750

LASSO/modified S-4B/IV/ vehicle mission to place in orbit two unmanned Lunar Modules for landing of radio and optical telescopes on lunar surface
18 p3136 A69-34813

Ground controlled remote manipulator spacecraft system to perform unmanned satellite orbital maintenance, discussing refurbishment, laboratory simulation, system cost effectiveness and feasibility
19 p3430 A69-36001

Power systems for unmanned spacecraft, noting improved performance for zirconium hydride reactors and thermoelectric converters
23 p4187 A69-42255

Systems safety for unmanned spacecraft, considering power supply, equipment operation, trajectory correction, etc
[AAS PAPER 69-520] 24 p4392 A69-42849

UNSTABLE BURNING
U COMBUSTION STABILITY

UNSTEADY FLOW
NT OSCILLATING FLOW

Unsteady heat flow in finite composite hollow circular cylinder using inverse method of eigenfunction expansion / method of finite integral transformation/
01 p0175 A69-10230

Unsteady laminar boundary layer near thermally insulated rotating disk, establishing solutions describing motion
01 p0059 A69-10361

Unsteady slow rotational motion of viscoelastic liquid contained between two concentric spheres rotating with constant angular velocities
02 p0230 A69-11563

Unsteady laminar boundary layer flow at curved surfaces, analyzing frequency and curvature parameter influence on basis of small disturbances method [DVL-863] 02 p0231 A69-12053

Two dimensional unsteady Rayleigh flow velocity of conducting and nonconducting viscous fluid past porous plate, analyzing suction and magnetic field effects
02 p0232 A69-12156

Pressure pulses propagation in nonsteady fluid flow through expansible tubes, noting computer solution
02 p0232 A69-12477

Exact solutions for Navier-Stokes equations for nonsteady incompressible viscous flow near two dimensional or axisymmetrical stagnation point
02 p0233 A69-12527

Unsteady incompressible boundary layer flow over leading edge boundary layer calculated by three dimensional time dependent equations
02 p0233 A69-12543

Lift from unsteady flow past cascade of slender profiles with stagger angle reduced to solution of Fredholm integral equation
02 p0190 A69-12575

Curved bodies substitution in unsteady hypersonic flow past slender sharp nosed bodies within framework of plane sections
02 p0191 A69-12576

Unsteady transient flow of viscous fluid in suddenly rotating open pot, taking into account effect of bottom in determination of velocity profile
03 p0414 A69-13019

Implicit finite difference scheme to integrate unsteady boundary layer equations for compressible gas
03 p0416 A69-13656

Unsteady two dimensional flow in square cavity with fluid initially at rest and constant velocity upper surface of cavity, noting vortex center
[AICHE PAPER 25C] 04 p0587 A69-14510

Unsteady compressible laminar boundary layer flow over insulated or isothermal flat plate moving with arbitrary time variant velocity in viscous fluid
04 p0588 A69-14715

Unsteady hydromagnetic flow of viscous electrically conducting incompressible liquid over infinite conducting harmonically oscillating plate
04 p0638 A69-15093

Two dimensional unsteady flow of inviscid polytropic gas using analysis of similarity solutions in homentropic flow
04 p0590 A69-15191

Unsteady motion of ideally conducting gas flow in transverse magnetic field with allowance for gravitational forces
05 p0802 A69-15789

Variational methods applied to unsteady heat flow, describing approximate method for unsteady temperature field in heat conducting body
05 p0845 A69-15794

Unsteady flow in blade passage of partial admission turbine for high energy fluids, predicting shock wave formation at entrance using one dimensional theory
[ASME PAPER 68-FE-25] 05 p0698 A69-16075

Unsteady potential flow and wake near oscillating circular cylinder noting velocity, pressure and correlation measurements
[ASME PAPER 68-WA/FE-23] 05 p0749 A69-16099

MHD shock wave decay in one dimensional unsteady flow of ideal inviscid perfectly conducting compressible fluid subjected to transverse magnetic field
05 p0806 A69-16736

Unsteady supersonic flow around thin circular cylinder representing rocket stage, calculating flutter and response to random environment
[ONERA-TP-666] 06 p0857 A69-17098

One dimensional unsteady flows of combustible gas mixture with finite chemical reaction rates, considering

piston motion, igniting shock wave propagation and point explosion

06 p0909 A69-17325

Lifting force and moments acting on slender wing of finite span and arbitrary planform moving at constant mean velocity in unsteady flow

06 p0858 A69-17338

Unsteady flow of viscous incompressible conducting fluid in MHD generator channel, discussing external circuit inductance and flow velocity during start-up
06 p0969 A69-17915

Numerical method for attacking-lifting problems of general three dimensional wing executing arbitrary motion in potential flow
[AIAA PAPER 69-23] 06 p0862 A69-18040

Unstationary characteristics method applied to numerical computation of steady compressible flow around airfoil
[ONERA-TP-630] 07 p1049 A69-18413

Linearized unsteady nonequilibrium flows produced by unsteady motion of thin foil or circular cylindrical shell in compressible gas
07 p1119 A69-18738

Nonstationary flow past spheres and cylinders in electromagnetic shock tube, determining time required for flow to become stationary
07 p1119 A69-18744

Theory of unsteady one dimensional motion of ideal compressible fluid, discussing equation of state
07 p1119 A69-18750

Unsteady conducting incompressible viscous fluid flow past plate in magnetic field, analyzing surface friction reduction
07 p1192 A69-19018

Unsteady MHD convective flow with suction of viscous incompressible electrically conducting fluid above vertical porous wall, noting horizontal magnetic field effect
07 p1195 A69-19477

Unsteady suction motion of viscous incompressible fluid under action of slowly rotating suction disk, noting fluid velocity variation
08 p1302 A69-19875

Frequency response from linearized dynamic equations for viscous incompressible fluid flow in viscoelastic tubes, discussing transfer gain
08 p1304 A69-20704

Unsteady flow parameters for reaction products behind spherical detonation wave in gas mixtures based on Taylor solution
08 p1421 A69-20765

Von Karman flow changes due to unsteady heat transfer from rotating disks impulsively changing temperatures, particularly steady state and response time
08 p1422 A69-20996

Unsteady atmospheric motions on planetary scale using Legendre polynomials
08 p1311 A69-21158

Expansion tube modification incorporating nozzle plate at secondary diaphragm for reducing flow nonuniformity and contamination
[AIAA PAPER 68-371] 09 p1477 A69-21960

Unsteady relative flow in centrifugal impeller passage running at part capacity and zero flow observed by hydrogen bubble flow visualization method
[ASME PAPER 69-GT-35] 09 p1432 A69-22489

Generalized Riemann function obtained as solution of transformed Boltzmann-Vlasov equation, discussing one dimensional and multidimensional cases
10 p1724 A69-22908

Shock induced boundary layer flow establishment on semiinfinite flat plate, measuring heat transfer rates and transition to turbulence
11 p1869 A69-24890

Thin spherical layer flow stability with respect to small disturbances, showing unsteady motion above critical Reynolds numbers and secondary flow features
11 p1875 A69-25486

HF interferometry for statistical-numerical oscillation analysis of unsteady plane transonic flow, constructing phase planes for study of wave surfaces propagation
12 p2089 A69-26188

Nose bluntness effect on hypersonic unsteady aerodynamics of flared and conical bodies of revolution
[AIAA PAPER 68-889] 12 p2012 A69-26794

Boundary value problem for one dimensional unsteady equations for inviscid conducting gas during transition processes in MHD duct
13 p2309 A69-28027

Sound generation by unsteady rotational flow as singular perturbation problem solved by matched asymptotic expansions, discussing flow and radiation fields
13 p2299 A69-28187

Ideal fluid unsteady rectilinear plane-parallel flow stability, calculating shear layers before breakdown by using modified Rayleigh method
14 p2431 A69-29606

Unsteady jet viscous fluid flow under pulse variations based on Prandtl equations, showing turbulent motion analogy
14 p2432 A69-29608

One dimensional unsteady monatomic Maxwellian gas flow at small Knudsen numbers using Hilbert method, noting validity for shear flows
14 p2432 A69-29611

Pressure drop fluctuations amplitude and frequency effect on channel resistance and magnetic field effect on fluctuations intensity in laminar conducting fluid flow
14 p2501 A69-29909

Boundary value problem for quasi-linear equation of unsteady transonic gas flows, including linear model and operators for group of transformations
15 p2590 A69-30049

Unsteady three dimensional heating of finite solid rectangular parallelepiped, deducing expressions for rectangle and slab
15 p2717 A69-30790

Similar solution for free convective flow past vertical porous wall and unsteady flow past porous wall with dissipation term, using group transforms
15 p2592 A69-31010

Boundary layer over impulsively started flat plate, describing flow transition from unsteady /Rayleigh/ to steady /Blasius/ state by iterative methods
16 p2769 A69-31812

Monograph on solutions to equations for unsteady flow of ideal gases, with applications to hypersonic flows, based on three space coordinates and time
16 p2773 A69-32428

Linear amplification, nonlinear limiting and secondary instability induced by unsteady effects illustrated for various transitional flows, including roughness and streamwise vorticity
17 p2950 A69-33248

Modified liquid fueled pulsating combustion chamber operating as Helmholtz cavity resonator, measuring chamber pressure as function of time
17 p3074 A69-33410

Far and near field solutions for one dimensional unsteady flows in general inviscid relaxing gas, obtaining flow field structure by matching techniques
17 p2957 A69-33599

Pulsating flow analysis in finite and infinite conical nozzles under sinusoidal pressure disturbances [ASME PAPER 69-APM-16]
18 p3214 A69-34392

Unsteady motion of ideally conducting gas flow in transverse magnetic field with allowance for gravitational forces
18 p3181 A69-35040

Compressible fluid two dimensional supersonic and one dimensional unsteady flows similarities shown graphically, discussing hodograph-speedgraph relationship
19 p3300 A69-36777

Interaction effects between mixing and pressure distribution of heterogeneous flow in channel, deriving criteria for predicting pressure variation sign
19 p3300 A69-36785

Cerebral circulation arterial system pulsatile flow flexible vessel digital simulation models distribution
19 p3264 A69-36867

Unsteady laminar MHD flow of electrically conducting viscous fluid between porous coaxial circular cylinders under radial magnetic field
20 p3581 A69-36912

Two dimensional unsteady motion of medium with pressure as linear function of density, analyzing gas expansion into vacuum
20 p3512 A69-36916

Unsteady laminar incompressible time dependent boundary layer flows with cylindrical symmetry, transverse boundaries and no swirl [ASME PAPER 69-FE-47]
20 p3517 A69-37997

Upper atmosphere horizontal unsteady wind with pressure gradient time dependence, solving heat conduction type equation by integral representations
21 p3758 A69-38411

Continuous cavitation model for incompressible fluid one dimensional unsteady motion
21 p3693 A69-38752

Velocity and temperature profiles at Prandtl number values obtained for unsteady laminar free convection on infinite vertical plate with stepwise varying temperature
21 p3853 A69-39681

Prandtl boundary layer theory problems, considering solution uniqueness and stability, unsteady flow, boundary layer separation, existence conditions, etc
21 p3697 A69-39698

Unsteady viscous flow past flat plate based on Stokes approximation, calculating shear stress
22 p3931 A69-40684

Polytropic gas unsteady motion in dihedral piston wake by solving mixed boundary value and Goursat problems
22 p3861 A69-41025

Unsteady thermal conductivity calculated by approximate analytical method in simple shape bodies /infinite plate, long cylinder, sphere/ cooled or heated by thermal radiation
23 p4238 A69-41333

Unsteady periodic boundary layer stability on flat plate, presenting model for disturbance wave packet propagation streamwise pressure gradients effects in transition flow
23 p4152 A69-41888

Numerical method for calculating unsteady two dimensional boundary layers in laminar incompressible flow
23 p4152 A69-42108

Time dependent unsteady flow of incompressible and electrically conducting fluid between two infinite disks rotating in uniform axial magnetic field
23 p4153 A69-42410

Compressible fluid unsteady flow past deformable surface, constructing metric for surface and obtaining metric tensor coefficients
24 p4243 A69-42586

Limit-cycle oscillations of unstable plane Poiseuille flow analyzed by nonlinear Navier-Stokes equations
24 p4298 A69-42600

Shape, position and velocity of vortex wakes shed in unsteady multienergy flows near trailing edge, applying Kutta condition [ASME PAPER 69-APMW-19]
24 p4245 A69-43099

Aerodynamic frequency response calibration measurements of wind anemometer by input velocity and output drag values under unsteady flow conditions
24 p4315 A69-43262

Velocity and pressure fields produced by deformable load carrying filament studied for unsteady gas motion past slender body with nonpotential external forces
24 p4246 A69-43483

Unsteady axisymmetric potential flow of ideal incompressible fluid with free surfaces, deriving differential equations for gas bubble dynamics and surface geometry
24 p4302 A69-43500

Pulsating mechanisms in alternative gas and liquid blocks two phase flow, using stochastic process specified by dynamic pressure time dependent fluctuations
24 p4305 A69-43633

Strong shock and Mach waves interaction generated downstream of thick wedge body shock in unsteady hypersonic and supersonic flows
24 p4306 A69-43674

Aerodynamic forces on hypersonic vehicle surfaces, deriving relations for weak interaction pressures induced in unsteady flow
24 p4306 A69-43676

Low Reynolds number unsteady wake flows, using hydrogen bubble flow visualization in high concentration glycerine mixtures
24 p4298 A69-43691

UNSTEADY STATE

Plate bending in presence of unsteady creep and with zero stress-strain state in middle surface solved by variational method
04 p0679 A69-14923

Finned radiation emitter tube unsteady state temperature field as function of working body temperature and emitter geometry
05 p0846 A69-15898

Response of single and multidegree of freedom systems to nonstationary random excitation, analyzing spectral density function of pressure field close to jet engine
05 p0844 A69-16763

Incompressible laminar thermal boundary layer unsteady development from state of rest in vicinity of wall of obstacle subjected to unsteady thermal field [ONERA-TP-680]
08 p1304 A69-20754

Unsteady heat conduction of semiinfinite thin rod with mobile end face, ideally insulated lateral surface and convective heat transfer on uninsulated portion
11 p2002 A69-25229

Diffusion equation unsteady solution for flasks of equal volumes connected by capillary, considering end effect and transient processes
13 p2251 A69-28561

Unsteady aerodynamic processes in centrifugal compressor stage with impeller, vaneless diffuser and annular receiver chamber
15 p2547 A69-30073

Unsteady oscillations after rupture in thin homogeneous isotropic elastic plate, assuming deflection amplitude smaller than thickness
16 p2873 A69-32033

Buckling time of oval ring under unsteady creep based on strain hardening theory
17 p3062 A69-33716

Heat transfer coefficients evaluated from gas to rotating turbine blades in unsteady operation, using unsteady thermal conductivity and gradient methods
21 p3850 A69-38864

Micromodule unsteady thermal behavior reduced to calculating linear heat flux for boundary conditions containing temporal and spatial derivatives
23 p4136 A69-41558

UNSWEPT WINGS U RING WINGS

UPCONVERTERS

U PARAMETRIC FREQUENCY CONVERTERS

UPDRAFTS

U VERTICAL AIR CURRENTS

UPPER ATMOSPHERE

NT D REGION
NT E-2 LAYER
NT E REGION
NT EXOSPHERE
NT F REGION
NT F1 REGION
NT F2 REGION
NT IONOSPHERE
NT LOWER IONOSPHERE
NT MAGNETOPAUSE
NT MAGNETOSPHERE
NT MESOPAUSE
NT MESOSPHERE
NT SPORADIC E LAYER
NT THERMOSPHERE

Observation of satellites, orbit calculation and use in upper atmosphere research [UN PAPER 68-95789]
01 p0064 A69-10459

Destructible low cost meteorological sounding rocket Dart for global observation of upper atmosphere [UN PAPER 68-95467]
01 p0161 A69-10510

Meteorological rocket measurement of ionizing radiation flux in upper atmosphere, noting flux decrease with increasing electron energy
01 p0144 A69-10586

Soviet rocket and satellite night, twilight, airglow and auroral studies, discussing day sky brightness, night airglow and atmospheric stratification
01 p0066 A69-10941

Upper atmosphere physical properties, discussing density and temperature
01 p0066 A69-10942

Twilight sky brightness measurements at 5200 angstroms for estimating upper atmospheric dust component, discussing error rates
01 p0075 A69-11191

Upper atmosphere oxygen emission and heating during geomagnetic disturbances
02 p0235 A69-11421

Three term formula for describing vertical wind velocity distribution in upper boundary layer of atmosphere, taking into account friction and orography effects
02 p0240 A69-11708

Upper atmosphere structure, phenomena and composition, discussing interactions between photons, electrons, atoms and molecules
02 p0242 A69-11902

Martian upper atmosphere and ionosphere, considering Mariner 4 occultation results and various atmospheric models
02 p0320 A69-12112

Martian upper atmospheric ionization process analogous to cometary material ionization in solar wind
02 p0320 A69-12117

Accelerometric measurement of atmospheric drag with satellite 1968-59B, obtaining upper atmosphere density profile at 130-160 km
02 p0245 A69-12728

Visible and IR nonequilibrium radiation from dilute gases of upper atmosphere, describing laboratory, ground, aircraft and rocket observations of reactions and interactions
02 p0247 A69-12810

- Satellite drag data to determine upper atmospheric composition according to density distribution with height
03 p0423 A69-13532
- Diurnal upward and downward flows of atmospheric matter following upper atmosphere temperature nighttime minimum and daytime maximum
03 p0423 A69-13533
- Electron, ion and neutral particle temperatures of upper atmosphere
04 p0592 A69-14975
- Delay between solar activity and density changes in upper atmosphere using Harris-Priester model
04 p0594 A69-15121
- Optical method of sounding cosmic matter penetrating into upper atmosphere by analyzing twilight phenomena
04 p0594 A69-15246
- Meteorological rocket measurement of corpuscular radiation intensity in upper atmosphere at various latitudes
05 p0814 A69-16052
- Neutral interstellar matter particle fluxes and densities for earth, noting effects on upper atmosphere gas densities
05 p0828 A69-16653
- Canadian upper atmosphere and space research programs organization, management and results
[UN PAPER 68-95551] 06 p1042 A69-17034
- Dynamic properties of upper atmosphere, discussing variations in temperature, density and composition
[UN PAPER 68-05755] 06 p0917 A69-17042
- Upper atmosphere physics, atmospheric composition and separation of gases, nature of air flow, water vapor content and lower ionosphere structure determinations by rocket
[UN PAPER 68-95693] 06 p0949 A69-17058
- Upper atmosphere semiannual density variations, using satellite drag analysis
06 p0918 A69-17380
- Vertical ozone distribution in upper atmosphere from satellite measurements of UV solar radiation scattering by solving integral Laplace equation
06 p0996 A69-17733
- Rocket transportation for upper atmospheric measurements, discussing sensors and cost effectiveness
[AIAA PAPER 69-159] 06 p1018 A69-18066
- Collisional processes relevant to daytime and nighttime models of upper atmosphere neutral density and temperature
07 p1130 A69-19654
- Subjective and objective upper air forecasts for aviation comparison by isobaric pressure height fields, discussing error analysis
08 p1345 A69-19886
- Atomic N and NO daytime upper atmosphere density profiles, discussing production and loss mechanisms
08 p1307 A69-20185
- Geomagnetic storms, substorms and auroral displays as functions of processes in solar wind and upper atmosphere
08 p1307 A69-20188
- Nocturnal auroral electron showers configuration and displacement determined from sounding balloon measurement of X rays due to showers braking in upper atmosphere
08 p1308 A69-20281
- Upper atmosphere density variations and multiplicative factor necessary for adjustment of density variations of reference models
08 p1397 A69-20761
- Ion exchange fuel cells for emitter-receiver on atmospheric constant ceiling balloon, stressing pressure effect on operation and fuel storage
08 p1260 A69-21042
- Upper atmosphere temperature distribution estimation on basis of twilight zenith sky intensity measurements, discussing influence of various parameters on accuracy
09 p1487 A69-21653
- Upper atmospheric density relation to AE indices sum and solar radio flux during geomagnetic disturbances
09 p1488 A69-21657
- Upper atmosphere rotation perturbation effect on satellite orbit when scale height varies with height, showing inclination reduction
09 p1594 A69-21660
- Deuterium escape in Venus upper atmosphere to explain anomalous Lyman-alpha glow observed by Mariner 5
[SRCC-91] 09 p1594 A69-21696
- Subjective and objective upper air forecasts compared for error analysis of headwinds, noting influence of geographical location
09 p1536 A69-22074
- Renormalizable weak interaction mechanism for generation of high energy muons from Tev cosmic rays in upper atmosphere
09 p1581 A69-22530
- Pyrotechnics applications to Skylark upper atmosphere sounding rocket, discussing payload heads, nose cones, sensor covers, etc
10 p1792 A69-23029
- Data requirements and acquisition for detection and description of tides and gravity waves in upper atmosphere
10 p1685 A69-23833
- Electrical phenomena in upper atmosphere and solar wind may control geomagnetic disturbances and aurorae
10 p1686 A69-23903
- Monograph on method and results of measurements of mobilities spectrum ion density and conductivity in upper troposphere and stratosphere
11 p1877 A69-24636
- Chemical composition of Venusian atmosphere by Mariner and Venera satellites, comparing upper atmospheres of Venus and earth
11 p1960 A69-24971
- Upper atmosphere response to time dependent heating based on approximate analytic solutions of heat conduction equation
11 p1878 A69-25151
- Airborne Q switched ruby laser for studying upper atmosphere meteoric formations optical characteristics and kinetics against background of underlying surface
12 p2125 A69-25955
- Semiannual density variations in thermosphere and exosphere as function of mixtopause height variations
12 p2064 A69-26012
- Satellite 1968-5A orbit analyzed for atmospheric density at 140-180 km, noting semiannual variation
12 p2066 A69-26229
- Upper atmosphere density variations investigation using Eurobs system, correlating density to geomagnetic activity and 10.7 cm solar radio emission
12 p2069 A69-26437
- Variable solar activity effect on earth upper atmosphere rotation at altitudes from 200 to 300 km
12 p2069 A69-26442
- Solar chromospheric flares effect on temperature of upper atmosphere observed by satellite at perigee altitude
12 p2149 A69-26447
- Logarithmic response electrometer for upper atmosphere satellite measurements using subminiature vacuum tube
12 p2092 A69-26476
- Soviet rocket and satellite studies of upper atmosphere and ionosphere
13 p2251 A69-27347
- IR day and night airglow of upper atmosphere utilized for atmospheric energy content and reactions analysis
13 p2252 A69-27585
- Venusian upper atmosphere dissociation and ionization, considering photochemical and dynamic processes and molecular, eddy and ambipolar diffusions
13 p2344 A69-27643
- Integral particle flux of protons and electrons in upper atmosphere, discussing energy and angular distribution
13 p2328 A69-27757
- CENFAM radar receiving system for meteoric and upper atmospheric data on amplitude, range and direction of meteor echoes through interferometer pairs
13 p2354 A69-28649
- Electron concentration enhancement in upper atmosphere at polar latitudes, noting three independent zones and relation to magnetic local time
14 p2510 A69-28938
- Forbidden NI transitions in nighttime upper atmosphere observed with Fabry-Perot spectrometer
14 p2440 A69-29120
- Atmospheric circulation by energy concepts, giving quantitative analysis of interaction between upper and lower atmosphere
14 p2477 A69-29825
- Radio propagation in upper atmosphere and ionosphere noting rocket and satellite experiments including plasma physics research, tropospheric studies and space science services
14 p2526 A69-29854
- Meteorological rocket measurement of ionizing radiation flux in upper atmosphere, noting flux decrease with increasing electron energy
15 p2675 A69-30756
- Upper atmosphere winds and temperature measurements from rocket grenade, discussing TMA experiments
15 p2598 A69-31317
- Hydrogen and He ion distribution measurements, noting seasonal and local magnetic time variability
15 p2599 A69-31326
- Carbon atoms presence in Venus upper atmosphere from Venus spectrum obtained by Aerobee rocket experiment
15 p2698 A69-31341
- Upper atmospheric density effects on satellite orbits, discussing variations due to solar activity, day-night and semiannual changes and atmospheric rotation
15 p2600 A69-31350
- Average angular velocity of upper atmosphere from changes in orbital inclinations of satellites, discussing wind speeds
15 p2600 A69-31352
- Time variation of altitude distribution of cosmic dust layer in upper atmosphere by Pandora II collector using inflight shadowing technique
15 p2698 A69-31353
- Upper atmosphere structure and variations including density and composition in lower thermosphere, diurnal variations, variations with solar activity, etc
15 p2600 A69-31355
- Wintertime short term density variability in upper atmosphere obtained from rocket measurements
15 p2601 A69-31374
- Satellites orbits analysis for semiannual variation of air density in upper atmosphere
15 p2601 A69-31378
- Rocket observations of ozone concentration above 50 km by absorption spectroscopy, noting altitude dependence
15 p2603 A69-31397
- Morning, daytime and nighttime rocket measurements of electron flux in upper atmosphere at 80-165 km altitudes, noting energy flux
15 p2677 A69-31413
- Satellite orbit evolution data applied to refinement of geophysical parameters, including upper atmosphere parameters and zonal harmonic coefficients in gravitational potential expansion
15 p2604 A69-31417
- Soviet meteorological rocket sounding data for upper atmosphere compared to CIRA 1965 model
15 p2650 A69-31421
- Temperature measurements of neutral polar atmosphere at 120-170 km using artificial Na clouds
15 p2606 A69-31448
- Upper atmosphere and outer space investigations by Zond and Soyuz spacecraft
15 p2724 A69-31451
- Intensity and rotational temperature seasonal variations of hydroxyl emission at different latitudes in upper atmosphere
16 p2775 A69-32081
- Kinetic theory and gas-surface interactions for upper atmospheric density measurements by mass spectrometers, pressure gages and satellite drag, detailing adsorption effect
16 p2776 A69-32089
- Upper atmospheric winds to produce solar quiet day magnetic variations based on dynamo theory, illustrating solenoidal, irrotational and mixed winds
16 p2782 A69-32460
- Atomic nitrogen and nitric oxide density in upper atmosphere during nighttime calculated, allowing for atomic and molecular diffusion
16 p2785 A69-32622
- Air density measurement at high altitudes by falling instrumented sphere ejected by missile in upper atmosphere
17 p2971 A69-32898
- Upper atmospheric gas density and temperature distribution diurnal and seasonal variations calculated from satellites orbiting time changes
17 p2959 A69-32924
- Ionization, recombination and charge transfer in upper atmosphere during aurora, considering quasi-equilibrium ion-electron concentrations
17 p2961 A69-33417
- Far IR angular scattering observations as diagnostic tool to examine microstructure of high altitude cirrus clouds
18 p3126 A69-34281
- Rocket-released magnetometer probe for upper atmospheric measurements, discussing construction, flight, sensitivity and ionosphere current detection
19 p3309 A69-35995

Forbidden atomic transitions involving metastable species in upper atmosphere, tabulating permitted and forbidden molecular band systems

19 p3421 A69-36214

Numerical integrations for modified model incorporating ozone production equation and heating from ozone radiation absorption and long wave cooling for upper atmospheric circulation

19 p3363 A69-36502

Transmitting antenna design of multistation radar system for meteors and upper atmosphere investigation, discussing amplitude and phase of electromagnetic field

19 p3278 A69-36661

Gas-surface energy transfer experiment on OGO-F satellite, measuring upper atmosphere kinetic energy flux to determine accommodation and drag coefficients, density, etc

19 p3255 A69-36680

Dynamic properties of upper atmosphere, discussing variations in temperature, density and composition

20 p3519 A69-36983

UV solar radiation variation effects on Mars and Venus upper atmosphere temperatures

20 p3595 A69-37136

Rocket probe devices based on thermometrical body principle for measuring upper atmosphere water vapor and atomic oxygen

20 p3543 A69-37798

Meteorological rocket measurement of corpuscular radiation intensity in upper atmosphere at various latitudes

20 p3591 A69-37962

Optical method for upper atmosphere cosmic dust detection, emphasizing twilight luminance origin from light scattering

21 p3702 A69-38349

Wind motion and turbulence in upper atmosphere from Rehbar 15 and 16 rocket observations

21 p3703 A69-38362

Upper atmosphere horizontal unsteady wind with pressure gradient time dependence, solving heat conduction type equation by integral representations

21 p3758 A69-38411

Upper atmosphere particles, luminosity and electron concentration measurements documented in input, storage and energy radiation classes, determining recombination coefficients

21 p3707 A69-38491

Polar upper atmospheric phenomena interpreted as magnetospheric substorm manifestations, discussing role of asymmetric ring current formation

21 p3710 A69-38504

Upper atmosphere emission processes, comparing emission quenching lifetime with transition probability rates, plotting atomic and molecular states

21 p3711 A69-38513

Upper atmospheric temperature by spectroscopy, considering rotational, OH nightglow, nitrogen cation dayglow and twilight temperatures

21 p3712 A69-38516

Spectra and intensities of rocket releases for upper atmosphere composition, temperature and reaction kinetics, noting chemiluminescence and atomic and molecular emissions

21 p3712 A69-38522

Upper atmospheric H and He observations, showing Lyman alpha, H alpha measurements and H abundance values relative to Kockarts-Nicolet model

21 p3714 A69-38529

Pulsation velocities distribution wind in meteor region of atmosphere during hourly intervals over eleven month period, noting normal distribution

21 p3759 A69-39115

IR molecular radiation spectra of upper atmosphere in 3-8 micron range investigated by rockets and satellites, discussing radiation energy density during magnetic storms

21 p3792 A69-39772

Clear air turbulence computerized analysis and forecast over U.S. using upper air rawinsonde measurements

22 p3976 A69-39927

Reentrant albedo flux and singly charged particles directional asymmetry in upper atmosphere estimated from oriented telescope observations over Hyderabad

22 p4005 A69-40519

Corpuscular radiation intensity measurements in upper atmosphere at midlatitudes by meteorological probe during geomagnetic storm, noting radio wave absorption

22 p4008 A69-41104

Photoionization rates temperature dependence in upper atmosphere for O atoms and molecules and N

molecules from computer calculations, allowing for earth sphericity

23 p4157 A69-41857

Clear air turbulence in upper atmosphere and in mountain waves, discussing density variations

24 p4343 A69-42913

Absorption observation of solar radiation at sunset by nitric acid in three wavelength intervals on different balloon flights

24 p4308 A69-42969

Upper atmosphere OH molecules vibrational temperature and total emission energy, measuring average seasonal variations

24 p4308 A69-43007

Solar energetic particle effects during polar cap absorption observed in earth upper atmosphere and at ground level

24 p4373 A69-43618

UPPER IONOSPHERE

NT F REGION

NT F 1 REGION

NT F 2 REGION

Topside ionosphere average height distributions of electron density and geomagnetic field intensity from Alouette 2 data over Japan, noting ionic composition

01 p0065 A69-10548

Ducted echoes on topside ionograms and whistler diffuseness at midlatitudes, noting common occurrence of phenomena

01 p0029 A69-10551

Polar wind, describing upward plasma expansion of topside polar ionosphere and acceleration of positive H and He ions

01 p0077 A69-11239

Nonvertical propagation effects on high altitude topside ionosphere sounder data reduction, using ray tracing

07 p1124 A69-18838

Ion composition and charged particle temperatures at 300-600 km from sounding rocket and topside sounder Alouette 2 measurements

07 p1124 A69-18839

Radio noise generation in topside ionosphere, noting Cerenkov radiation from intense soft fluxes of auroral electrons

07 p1127 A69-19257

Nighttime Venus ionosphere models compared with Mariner 5 observations, discussing implications with regard to He and H abundance consequences and nightglow

09 p1594 A69-21695

Regular disturbance in topside ionosphere on summer nights from continuous records of ionospheric electron content, discussing magnetic activity and sunspot number effects

09 p1489 A69-21703

Topside ionospheric electron density profiles compared for magnetically quiet and disturbed periods surrounding December 17, 1962 magnetic storm

10 p1685 A69-23835

Satellite measurements of suprathermal electrons at conjugate sunrise, indicating photoelectron escape from production level and movement along geomagnetic lines into conjugate ionosphere

11 p1950 A69-25144

Second tacite sounding rocket test for measuring UV radiation in transition zone between upper ionosphere and space

11 p1887 A69-25213

Rocket and satellites topside sounding of earth ionosphere, determining magnetoplasma structure and resonance

14 p2438 A69-29101

Electron density profiles in outer ionosphere and integral of electron density measured with coherent radio waves emitted from Electron satellite

14 p2438 A69-29106

Ionic diffusion in topside ionosphere analyzed using multiple gas mixture diffusion formula, noting Coulomb ionic collision role

14 p2441 A69-29381

OGO 5 spectrometric studies of topside ionospheric ion concentrations, noting difference between nighttime and sunlit pass

15 p2599 A69-31345

Thermal diffusion coefficient for fully ionized plasma containing mixture of arbitrary charge ions in topside ionosphere

16 p2775 A69-32084

Ionospheric satellites objectives and development resulting from topside sounder and ISIS programs

20 p3529 A69-37855

Explorer 20 satellite for obtaining fixed frequency pulse soundings of ionospheric topside, discussing

transceiver-dipole antenna instrumentation and payload

20 p3618 A69-37857

Sweep frequency ionospheric topside sounder design for Alouette and ISIS satellites, discussing influence of experiment requirements and spacecraft limitation and environments

20 p3507 A69-37859

Alouette 1 and 2 topside sounder ionograms analyzed with emphasis on low electron density, spread F and field aligned propagation

20 p3529 A69-37863

Topside ionogram reduction for ionospheric electron density determination, using geomagnetic strength at all heights, iteration and change of variables

20 p3529 A69-37864

Global electron density distribution morphology in topside ionosphere during sunspot minimum from Alouette 1 and 2 ionograms

20 p3530 A69-37867

Topside equatorial ionosphere structure and behavior, describing anomaly development and decay

20 p3530 A69-37869

Ionospheric electron density irregularities observed by topside sounders showing shape, dimensions across magnetic field and variation percent, discussing resulting radio echoes

20 p3530 A69-37870

Upper ionosphere Thomson scatter, electron number density measurements and topside sounding results during geomagnetic storms using electrodynamic drift theory

20 p3530 A69-37872

Ionospheric topside plasma resonances observed by fixed and swept frequency satellite-borne sounders

20 p3531 A69-37884

Topside ionospheric magnetic field aligned irregularities using satellite observations of nonvertical electromagnetic wave propagation and delayed echo generation

20 p3495 A69-37885

Applicability and limitations of diffusive equilibrium in topside ionosphere, noting plasma density distribution along magnetic field line

20 p3531 A69-37887

Topside ionospheric structure from Alouette 2 data, discussing thermopause temperature, plasma temperature, electron density profiles, satellite plasma frequency, etc

20 p3532 A69-37895

Diurnal and seasonal variations of primary atmospheric ions in topside ionosphere correlated with solar zenith angle, using ion mass spectrometer on Explorer 32

20 p3534 A69-38087

Ariel 3 satellite observations, including topside ionospheric variations with time and solar activity, electron density, temperature measurements, etc

21 p3716 A69-39257

Magnetic activity effect on electron density in topside ionospheres determined from Alouette 1 data statistical analysis

23 p4156 A69-41856

Topside ionosphere response to magnetic storms, using Explorer 22 satellite electron concentration and temperature measurements

23 p4161 A69-42438

URANIUM

Lead isotope composition and concentrations of U, Th, Ra, total Pb and Pb 210 in recent volcanic rocks, noting disequilibrium due to chemical fractionations

04 p0593 A69-15011

Age of Galaxy from decay of uranium, assuming prompt synthesis

09 p1605 A69-22414

Gaseous reactor fluid mechanics for nuclear rocket engines, discussing experiments on geometries used in open cycle engine for acceptable uranium loss rate [AIAA PAPER 69-477]

16 p2811 A69-32728

Uranium abundances in several eucrites measured by fission track method, discussing Pu-Xe decay interval question

17 p3044 A69-34167

Group cross section generating techniques to calculate neutron capture rates and spatial capture distribution in depleted thick U slab, using GAROL program

18 p3177 A69-35179

Pu/U ratio from fossil track studies bearing on extinct Pu 244 in Campo del Cielo and Kodaikanal meteorites

19 p3407 A69-36077

URANIUM COMPOUNDS

Uranyl ions interaction with phospholipid and cholesterol monolayers, using surface pressure and potential measurements

11 p1832 A69-25641

Energy exchange of rare earth ions in uranyl phosphate liquids and glasses, studying sensitized luminescence origin

14 p2485 A69-29034

Two photon excitation of luminescence in complex uranyl compound single crystals using Q switched ruby laser

19 p3334 A69-35982

URANIUM FLUORIDES

Fissioning plasma generated in shock tube with 235 uranium hexafluoride gas, selecting tube diameter, reflector depth and initial gas density for specific neutron multiplication

18 p3180 A69-34455

URANIUM ISOTOPES

Uranium in meteorites, discussing U content and isotope composition, Pb isotope ratios, radiogenic Pb, origin of matter and meteorite ages

01 p0025 A69-11369

Uranium content in fragments from iron meteorites determined by fission fragment track recording

01 p0026 A69-11377

URANIUM OXIDES

Postirradiation investigation of uranium dioxide fuelled thermionic emitters by evaluating released fission gases, noting different neutron fluxes metallographic effects

14 p2481 A69-29200

URANIUM 235

Fast neutron spectrum for subcritical section of homogeneous U 235-polyethylene thermionic critical assembly measured by pulsed source time-of-flight method

18 p3170 A69-34313

URANUS [PLANET]

Two element interferometer observing Saturn, Uranus and Neptune at 3.12 cm, determining equivalent black body disk temperature

01 p0148 A69-10052

Uranus observations in 1964 by Algiers and Quito astrolabes compared with Washington transit results

16 p2853 A69-31620

Radio telescope observations at 11.13 cm for polarized E vector intensities of Saturn and disk temperature of Uranus and Neptune

17 p3039 A69-33731

Tabulation of Uranus observations of Sao Paulo Observatory astrolabe in 1968, giving special attention to East and West passages during night

22 p4031 A69-40912

URBAN DEVELOPMENT

Multiband aerial photography utilization for evaluating urban housing quality compared with present data collection methods

13 p2260 A69-27607

Urban noise control over transportation systems including aircraft and highway traffic operating beyond local noise ordinance purview

14 p2541 A69-29157

Airport planning, discussing air transportation and city planning problems for Hannover air terminal

16 p2882 A69-32329

Community planning and airport requirement interrelation, discussing land usage, satellite airport system for private aviation, etc

16 p2882 A69-32331

Air space saturation, urban surface transport network enlargement necessity and expeditious passenger processing and baggage handling

24 p4296 A69-42567

Multispectral orbital photography used to obtain urban land-use data [AAS PAPER 69-483]

24 p4307 A69-42837

UREAS

Enzymic decomposition of urea in urine, noting production of ammonia and effect of urea components on hydrolysis rate

08 p1265 A69-19834

Urease activity determined by using C 14 urea in stored, preserved /Permafrost/ and irradiated soils

18 p3095 A69-34543

Microbial protein extraction from Chlorella algae and Torulla yeasts using urea soaking method

21 p3662 A69-39712

URETHANES

Rigid PVC, urethanes and thermosets processing for high performance, noting injection molding and machine developments role

18 p3148 A69-34611

Reversion resistant polyether and polyester type urethanes, discussing applications, testing methods and material processing

19 p3357 A69-35566

URIC ACID

Protein contained purine free basal and yeast ribonucleic acid diets effect on plasma and urinary uric acid production in male subjects

05 p0708 A69-15968

URIDYLIC ACID

Poly A-poly U synthesized by Azotobacter Vinelandi RNA polymerase in unprimed reaction containing ATP and UTP, following short lag period

10 p1647 A69-24185

URINALYSIS

Biochemical indicators of pilot reactions to flights complicated by unexpected autopilot failures, using postflight chemical analysis of blood and urine

05 p0710 A69-16525

Sympathoadrenal activity during and after impact stress measured from urinary excretion of catecholamines and 17-hydroxycorticosteroids

06 p0875 A69-17839

Intrarenal capillary hydrostatic pressure effect on hemodynamically induced changes in sodium excretion

07 p1063 A69-18629

Biochemical indicators of pilot reactions to flights complicated by unexpected autopilot failures, using postflight chemical analysis of blood and urine

18 p3096 A69-34744

Male patients urine tests during sinusoidal vibration, noting catecholamine excretion as criterion of emotional stress under various environmental conditions

21 p3654 A69-38909

Urine osmolality of centrifuged rats compared with ad libitum or pair-fed control animals, indicating enhanced free water excretion and antidiuretic hormone involvement

24 p4262 A69-42904

Urine sampling conditions for kidney function circadian rhythm during global flight, considering food and water intake, sampling intervals and body position

24 p4266 A69-43374

Urinary excretion of hormonal metabolites in intercontinentally flown test subjects, using gas chromatographic procedure for steroid identification

24 p4268 A69-43404

URINATION

Visceral afferent pathways influence on vasopressin secretion, ADH levels and urinary excretory patterns of dogs during surgical stress

05 p0708 A69-15970

Desynchronization and resynchronization of human circadian rhythms of activity, body temperature and urine excretion during isolation in underground bunker in various conditions

21 p3660 A69-39173

Diuresis during total immersion in thermally neutral water, interpreting urine flow increase caused by intrathoracic blood volume expansion

23 p4094 A69-42075

URINE

Renal effects of moderate hypoxia exposure in mice as reflected in urine volume and electrolyte excretion patterns during four days at simulated altitude

01 p0015 A69-10921

Lateral acceleration effects on human kidney functions, noting increase in diuresis and erythrocytes in urine

02 p0198 A69-11514

Enzymic decomposition of urea in urine, noting production of ammonia and effect of urea components on hydrolysis rate

08 p1265 A69-19834

Urine excretion following water load in male subjects exposed to normal, hot/dry and comfortable/dry environment applied to airline crews

17 p2914 A69-33182

Open cycle air evaporation technique selected for water recovery from human urine, based on tradeoff studies

19 p3258 A69-36455

Supersonic flying effect on urinary catecholamine excretion rates in pilots, noting emotional state

24 p4265 A69-43370

UROLITHIASIS

Urinary lithiasis frequency among aircrews, reviewing etiology, symptomology, therapeutics and prevention

24 p4267 A69-43388

USA [UNITED STATES]

U UNITED STATES OF AMERICA

UTILITY AIRCRAFT

U BO-105 HELICOPTER

U UH-1 HELICOPTER

UTILIZATION

U WASTE UTILIZATION

V

V BAND

U EXTREMELY HIGH FREQUENCIES

V GROOVES

Load carrying capacity of V notched bars under axially symmetric tensile load, verifying influence of distance between two equal notches

04 p0680 A69-15169

Herringbone grooved gas lubricated journal bearing static and dynamic characteristics analyzed approximately, noting pressure distribution and vibration amplitudes [ASME PAPER 68-LUBS-7]

13 p2265 A69-27269

Herringbone grooved gas lubricated journal bearing stability, testing effects of geometries and clearances on onset speed for half frequency whirl [ASME PAPER 68-LUBS-25]

13 p2266 A69-27271

V-2 MISSILE

Rocket guidance, discussing foreign systems with emphasis on German range miss/gradient orientation scheme used on World War II V-2 rockets

02 p0279 A69-12362

V-4 AIRCRAFT

U XV-4 AIRCRAFT

V/STOL AIRCRAFT

NT ALOUETTE HELICOPTERS

NT AUTOGYROS

NT BO-105 HELICOPTER

NT CH-34 HELICOPTER

NT CH-46 HELICOPTER

NT CH-47 HELICOPTER

NT CH-54 HELICOPTER

NT CL-84 AIRCRAFT

NT DO-31 AIRCRAFT

NT FLYING PLATFORMS

NT H-56 HELICOPTER

NT HELICOPTERS

NT MILITARY HELICOPTERS

NT OH-6 HELICOPTER

NT P-1127 AIRCRAFT

NT ROTARY WING AIRCRAFT

NT S-61 HELICOPTER

NT SA-330 HELICOPTER

NT SH-3 HELICOPTER

NT SHORT TAKEOFF AIRCRAFT

NT UH-1 HELICOPTER

NT VERTICAL TAKEOFF AIRCRAFT

NT VZ-2 AIRCRAFT

NT X-22A AIRCRAFT

NT XC-142 AIRCRAFT

NT XH-51 HELICOPTER

NT XV-4 AIRCRAFT

VTOL or V/STOL Light Intratheater Transport /LIT/ for future tactical airlift situations, comparing tiltwing, liftjet, stowed rotor and fan-in-wing concepts

01 p0008 A69-10146

Man machine relationship in V/STOL control display, discussing inflight simulators, emphasizing NASA X-14 and CH-3C programs

01 p0010 A69-10452

Piloting aspects of jet V/STOL aircraft for poor weather operations without complicated ground aids, discussing deceleration transition, forward speed and final approach angle

01 p0010 A69-10868

Water hover effects tested on tilt wing V/STOL seaplane model, noting effects of wind and waves on water passing through propellers

01 p0011 A69-11061

Optimal transport aircraft, considering VTOL/STOL aircraft, construction requirements and flying distances

01 p0012 A69-11293

X V-4B Hummingbird 2, noting modification from XB-4A two engine ejector augmentation to six engine direct and diverted thrust configuration

03 p0366 A69-13112

Design parameters optimization for V/STOL jet aircraft with lift engines mounted in wing pod, discussing wing loading and aspect ratio, power plant, etc
04 p0547 A69-14812

Servoelements and control methods for V/STOL aircraft, including lift and propulsion throttle configurations
04 p0547 A69-14815

Boeing/Vertol Hybrid Facility for solving engineering problems in V/STOL design and research
04 p0567 A69-15352

Helicopter role, development and configurations, noting V/STOL competition impetus
05 p0700 A69-15547

Engines for V/STOL application, discussing aerodynamics of thrust lift and lift jet engines
05 p0811 A69-15553

V/STOL aircraft characteristics, emphasizing propeller, ducted fan and turbojet types
05 p0701 A69-15563

Technological evolution of turboprop propeller powered tilt wing V/STOL aircraft, discussing XC-142A, CL-84 and VZ-2 aircraft
05 p0701 A69-15564

Hovering fan powered V/STOL aircraft effects on objects on ground, discussing related dust and debris problems
05 p0701 A69-15565

Aerodynamic interference effects arising from jet efflux of V/STOL aircraft, developing vortex sheet theory for jet interference
05 p0696 A69-15566

Design parameters optimization techniques for V/STOL aircraft, noting necessary cooperation between engineering and computing facilities
05 p0701 A69-15570

Large subsonic wind tunnels for correct simulation of V/STOL powered flight by minimizing wall constraint effects on flow field
05 p0741 A69-15573

Wind tunnel wall constraints effects at extreme force coefficients during V/STOL testing shown different from effects in conventional aircraft testing
05 p0741 A69-15574

V/STOL operations in intercity and intracity service, discussing technical feasibility and need for steep approach instrument landing system
05 p0703 A69-16723

Engine air intake for operational Harrier V/STOL strike/reconnaissance fighter, describing intake instrumentation ring, temperature and pressure probe development and pressure recording
05 p0767 A69-16773

Dynamic stability tests of tilt winged V/STOL aircraft model in ultralow speed range, discussing apparatus for stability derivatives
06 p0866 A69-17091

Optimal V/STOL wind tunnel through interference study of slotted tunnel walls, including porosity and height to width ratio effects
06 p0908 A69-18203

Nondemographic model predicting market shares of V/STOL aircraft in competition with automobiles and conventional airliners for short haul intercity business travel markets
07 p1244 A69-18967

Qualitative V/STOL air traffic control requirements, discussing airborne and ground data, procedures and equipment categories
07 p1177 A69-19552

Longitudinal stability of V/STOL aircraft at low speeds, discussing three tilt wings and quad ducted propeller configurations
07 p1055 A69-19566

Fall-safe goals, design criteria, analytical methods and test procedures to achieve reliable damage tolerant dynamic rotating parts for V/STOL and helicopter transports
07 p1237 A69-19569

V/STOL commercial intercity jet aircraft design concept for high density short haul travel featuring low noise, high economy, reliability and tandem wing configuration
07 p1056 A69-19571

Air deflection and modulation /ADAM/ turbofan propulsive wing V/STOL design
07 p1056 A69-19573

System safety analysis for V/STOL aircraft, discussing fault-tree technique role in fail-safe design
07 p1056 A69-19575

STOL and V/STOL role in eliminating air traffic congestion at U.S. and West European airports and in short haul and municipal routes
08 p1254 A69-20093

V/STOL rotary wing and propeller aircraft dynamic and aeroelastic problems emphasizing instabilities
08 p1419 A69-21031

Real time real temperature exhaust gas reingestion and structural heating test facility for jet lift V/STOL configurations
09 p1479 A69-22388

V/STOL undercarriage design, considering influence of aircraft operation, engine installation, rough/soft ground capability, etc
09 p1435 A69-22781

V/STOL aircraft future, discussing Federal Government policies, economics, airport planning, engineering problems, etc
10 p1811 A69-23221

V/STOL aircraft performance characteristics related to civil aviation operations and certification requirements
11 p1822 A69-24463

V/STOL air intakes and jets simulation in wind tunnel tests, noting thrust simulation possibilities
11 p1866 A69-25431

Exhaust gas reingestion and inlet flow distortion in V/STOL lift engines, discussing static and wind tunnel testing using fighter configuration models
12 p2012 A69-26762

Conjugate gradient methods for optimization problems with terminal constraints, noting minimum time paths for V/STOL aircraft climb phase
12 p2013 A69-26763

Aerodynamic effects of lift jet and lift fan inlets in transition flight, analyzing inlet momentum lift, inlet lip lift and drag
12 p2014 A69-26767

V/STOL aircraft in commercial aviation, discussing costs, noise reduction, propulsion systems, projected routes, etc
13 p2203 A69-28039

Turbofan V/STOL with separate lift units for takeoff and landing, discussing commercial and military applications, cost effectiveness and operational characteristics
13 p2203 A69-28354

Variable bypass ratio lift/thrust engine arrangement in relation to safety and economic requirements, using scale model of V/STOL
15 p2672 A69-31542

Jet influence and aerodynamic force changes on V/STOL aircraft in transitional and high speed flight investigated in wind tunnel tests for fighter aircraft
16 p2734 A69-31937

Running test facility for study of aerodynamics and flight dynamics of V/STOL aircraft models
17 p2944 A69-32851

Short range transport - Royal Aeronautical Society Conference, London, May 1969
17 p2897 A69-33206

Terminal area navigation and landing guidance systems for V/STOL intercity transport aircraft, considering radio guidance, aircraft control and system interaction
17 p2897 A69-33210

STOL and V/STOL short haul intercity airliners emphasizing propulsion systems, operational aspects and economics
17 p2898 A69-33356

V/STOL fatigue design parameters, balancing fail-safe and safe-life design procedures
17 p2900 A69-33512

Ground simulations data of jet lift V/STOL compared with visual flight results, studying hover, lateral quick start and stop maneuver
17 p2946 A69-33519

Military V/STOL aircraft flying qualities specification, considering structure, hover and low speed requirements, forward flight, transition maneuverability and control
17 p2900 A69-33520

Vector airspeed measuring system /VAMS/ for helicopters and V/STOL aircraft utilizing gas discharge mass flowmeter to improve takeoff performance
17 p2974 A69-33527

Flight command computer for V/STOL aircraft, discussing design concepts, operating modes, displays, etc
17 p3001 A69-33543

Stability augmentation system for CX-84 tilt wing V/STOL aircraft, using redundancy techniques to achieve fail operational performance with two active channels
17 p2901 A69-33545

Folding prop rotor V/STOL aircraft characteristics, showing configuration effects on performance and optimization of rotor, wing and propulsion systems
17 p2901 A69-33547

Nonrecirculating wind tunnel configuration with minimum atmospheric wind disturbances for V/STOL vehicles aerodynamic testing
17 p2947 A69-34024

Circular jet flow exhausting at right angles from plane wall into uniform cross flow, considering application to V/STOL aircraft
17 p2896 A69-34036

Weights study of V/STOL aircraft types for similar mission and payload requirements with different propulsion systems and flight profiles
18 p3091 A69-34869

Aerodynamics of rotary wing and V/STOL aircraft - Conference, Buffalo, June 1969
18 p3087 A69-35216

Aerodynamics of rotary wing and V/STOL aircraft - Conference, Buffalo, June 1969, Volume 2, Wind tunnel testing, New concepts in rotor control
18 p3088 A69-35226

V/STOL model small scale tests compared with full scale tunnel or flight tests, considering normal differences in parameters and rotor instability
18 p3119 A69-35227

V/STOL wind tunnel data at low forward speeds, discussing test limit dependence on model size, downwash angle and tunnel geometry
18 p3119 A69-35229

Tilt wing V/STOL aircraft spray circulation characteristics in overwater operation, examining forces, moments and generated environmental conditions
19 p3243 A69-35638

V/STOL and conventional transport aircraft compared for short haul air transport services
20 p3461 A69-37281

Composites for weight sensitive aerospace vehicles including reentry vehicles and V/STOL aircraft, considering costs, fracture toughness, corrosion resistance, etc
20 p3565 A69-37291

V/STOL aircraft aerodynamic roll motion control requirements at low speeds
20 p3574 A69-37514

Low visibility V/STOL instrument landing system and associated electronic structures, discussing instrument to visual flight transition
22 p3979 A69-40675

Aerodynamic research for rotary wing and V/STOL aircraft, suggesting analytical techniques with software packages designed around standard input/output formats
23 p4146 A69-41373

V/STOL propeller aerodynamics, considering thrust efficiency, roll and yaw control, flow visualization methods, etc
23 p4062 A69-41375

VTOL, STOL and CTOL transportation systems cost effectiveness comparison for Northeast Corridor operation, considering ground facilities, access time, etc
23 p4147 A69-41642

V/STOL commercial intercity jet aircraft design concept for high density short haul travel featuring low noise, high economy, reliability and tandem wing configuration
24 p4251 A69-42648

V/STOL aircraft radar inertial navigation system, describing approach and landing phase flight test results
24 p4252 A69-42831

Operational and economical aspects of V/STOL air transportation reevaluated for civil aviation promotion
24 p4418 A69-42870

VACANCIES [CRYSTAL DEFECTS]
NT FRENKEL DEFECTS

Vacancy diffusion in Ge, relation to precipitation of Cu impurities from supersaturated solid solution and determination of monovacancy migration energy
02 p0295 A69-11780

Melting points of tetrahedral phases with stoichiometric vacancies found proportional to covalent bonds number in semiconductors
02 p0297 A69-11881

Intentional impurities effects on nitronium perchlorate thermal stability explained by change in cation and anion vacancies
02 p0304 A69-11899

Formation energy of heat vacancies in molybdenum and temperature dependence of concentration determined on basis of enthalpy data
02 p0266 A69-12184

Vacancies and interstitials in metals - Conference, Jülich, West Germany, September 1968
02 p0267 A69-12185

Migration and penetration of vacancies in quenched magnesium analyzed by electrical resistivity measurements and electron microscopy
02 p0267 A69-12187

Mechanical effects of grain boundaries, considering hardening associated with vacancies and vacancy-solute interactions
03 p0449 A69-13875

Spectral study of crystal lattice of gallium phosphides for influence of vacancies and impurities on band formation
04 p0643 A69-15258

Majority carrier concentration changes in P-doped n-type Si during fast electron bombardment, discussing relative effect of A and E centers
07 p1199 A69-18684

Valence electrons mean density stability in Ti and V monoxides, describing mechanism for filling M vacancies with simultaneously forming O vacancies
09 p1523 A69-21738

Near boundary zones in VT15 Ti alloy not involved in beta phase decomposition during aging below 500 C attributed to vacancy concentration decrease
11 p1902 A69-24275

Room temperature thermal conductivity of semiconducting alloys with stoichiometric distributions of vacancies in cation sublattice, discussing heat resistance
12 p2142 A69-25975

Melting points of tetrahedral phases with stoichiometric vacancies found proportional to covalent bonds number in semiconductors
18 p3182 A69-35041

Electron irradiation-temperature dependence of introduction rate and room temperature annealing of carrier-removal defects in Li-doped Si
24 p4360 A69-42647

Linear elastic theory for calculating monovacancies entropy and energy of formation in metals
24 p4360 A69-42649

VACCINES
U INOCULUM

VACUUM
NT ULTRAHIGH VACUUM

General theory of relativity and tensor field equations relating space time characteristics to local properties of matter and vacuum, using Palatini Lagrangian method
09 p1593 A69-21572

Zero point energy, evolutionary cosmology, negative kinematic pressure and space curvature, assuming physical vacuum as ground state of Bose field
10 p1780 A69-23649

Vacuum and thin film - Conference, Pittsburgh, October-November 1968
13 p2298 A69-28003

Vacuum - Conference, Manchester, England, April 1968, Part I
13 p2240 A69-28076

Stationary radial source flow of liquid particles into vacuum, discussing boundary value problem equations, parameters effects on flow structure and flow field characteristics
13 p2248 A69-28210

Noncontacting minimum leakage dynamic seal requiring liquid-vapor interface with leakage tolerance [ASLE FICFS PREPRINT 40]
15 p2620 A69-30485

Spherically symmetric vacuum solution of Treder gravitational theory with emphasis on gravitational collapse
17 p3029 A69-33011

VACUUM APPARATUS
NT BAYARD-ALPERT IONIZATION GAGES
NT ION PUMPS
NT IONIZATION GAGES
NT KNUDSEN GAGES
NT PIRANI GAGES

Vacuum distillation technique for isolation and recovery of alkali metal reaction products with Ta, Ni, V and oxygen
01 p0083 A69-10927

Vacuum equipment for evaporation or sputtering in semiconductor industry
04 p0598 A69-14876

Lanthanum hexaboride single crystal field emitters for vacuum devices, describing construction and performance
09 p1468 A69-22601

Vacuum equipment and systems - Conference, Manchester, England, April 1968, Part 2
13 p2262 A69-28082

Device for equipment insertion into space vacuum simulation chamber to minimize interaction with walls [ONERA-TP-676]
20 p3510 A69-37405

Ruby laser-ultrahigh vacuum device for studying electron and ion emissions and light absorption of materials, noting influence of adsorbed gas layers
20 p3553 A69-37406

Vacuum apparatus for measuring uniaxially loaded metal surfaces interfacial adhesion, showing surface oxide removal effectiveness influence in adhesion strength
21 p3689 A69-38594

Vacuum distillation determination of O in Li, evaluating accuracy through O additions and recoveries, method blank and residue identification
22 p3897 A69-40932

VACUUM CHAMBERS

Current sheath surrounding exploding copper wire in vacuum, plotting current distribution as function of time and radius
01 p0119 A69-10669

Exploding wire phenomenon during early expansion from time correlated X ray and optical streak photographs in vacuum chamber
01 p0119 A69-10670

Molecular flow in space simulation chambers with cryowalls, noting nonuniform flux density distribution
01 p0057 A69-11153

Lithium hydride microplasma expansion in vacuum using charge collectors, time of flight detectors and spectroscopy of light emission
02 p0286 A69-11704

Polymethyl methacrylate irradiated by laser in vacuum to study mechanism responsible for gas formation
02 p0270 A69-11980

Vacuum system for obtaining highly purified plasmas for thermonuclear investigations noting decontamination cycles and chamber characteristics
03 p0412 A69-13839

Four specimen vacuum device for simultaneous tensile creep tests at 1200 C, discussing linear and thermal expansion
07 p1116 A69-19318

High temperature vacuum tensile test device for continuously direct recording various stress-strain diagram rates by interchangeable dynamometer scale
07 p1117 A69-19319

In situ vacuum testing requirement for valid measurement of vacuum induced changes in mechanical and thermal properties of various filled elastomers
09 p1477 A69-22008

Laser radiation in vacuum effects on metals and alloys
11 p1906 A69-25684

Real time pressure simulation chambers for testing space vehicles, discussing slow and rapid evacuation and pumping systems
13 p2240 A69-28077

Plasma microwave measurement error allowance for multiple reflection of waves from vacuum chambers dielectric walls
14 p2498 A69-29806

Selectively pumped thermal vacuum test chamber for orbital heat transfer and environment simulation for flight vehicle performance prediction
15 p2587 A69-30392

COMSAT thermal vacuum chamber specification configurations, discussing chamber orientation, vacuum and roughing systems, pumping mechanism, wiring, installation, testing, etc
15 p2587 A69-30393

Leg volume changes in response to lower body negative pressure due to blood redistribution
17 p2908 A69-33171

Low pressure and background radiation conditions via cryogenically cooled surfaces, citing data on cryopumping under vacuum conditions for space simulation chambers
17 p3006 A69-33683

Wind tunnel model low pressure measuring system, discussing pressure transducers, automatic control and pressure distribution tests [AIAA PAPER 68-402]
17 p2947 A69-34023

Solid solutions atomic ordering effect on friction and wear in vacuum, using CuAu and FeCo systems
18 p3149 A69-35183

Friction tests for Mariner Mars 1969 spacecraft mechanisms in ultrahigh vacuum molecular sink chamber, noting increased friction attributed to vacuum environment [AIAA PAPER 69-996]
22 p3920 A69-40374

Solar simulator built into multiwall ultrahigh vacuum chamber, describing simulator and chamber modifications [AIAA PAPER 69-1001]
22 p3921 A69-40377

Pressure measurements and gas flow analysis during thermal vacuum tests of manned spacecraft indicating adequate space vacuum simulation [AIAA PAPER 69-1033]
22 p3924 A69-40401

Solid rocket motor static firing tests in low pressure environment, presenting data concerning vacuum chamber pressure, diffusers pressure distribution, chamber wall temperature distribution, etc
22 p4000 A69-40593

VACUUM DEPOSITION

Electrical properties of vacuum deposited Bi, noting association of negative temperature coefficient of resistance in Bi thin films with grain-boundary effects
02 p0296 A69-11878

Thin CuAs selenide films by vacuum deposition, electronographic study proves cubic sphalerite phase existence
02 p0298 A69-12045

Cathode sputtering and thermal evaporation in vacuum used for preparing thin dielectric coatings on mirrors of optical resonators containing nonlinear crystals
03 p0438 A69-13049

Mechanical properties of thermodiffused layers obtained by vacuum chromizing of steel, establishing need to decarburize substrate material
03 p0450 A69-13913

Optical absorption of vacuum deposited thin rubidium films, noting similarity to sodium and potassium
03 p0491 A69-14114

Vacuum carburization of surface layers of transition metals
04 p0614 A69-14572

Vacuum deposition of thin film microwave acoustic transducers of piezoelectric aluminum nitride
05 p0761 A69-15820

Differential ion pumping for vacuum deposition of thin films
06 p0907 A69-17709

Technique for obtaining flawless silicon single crystal films on sapphire bases by vacuum deposition, noting base temperature effect on film quality
07 p1198 A69-18509

CdSe single crystal films vacuum deposition for use of photocells base with p-n heterojunctions
07 p1198 A69-18512

Physical sputtering deposition of molybdenum disulfide films as solid lubricant on rotating and sliding components, discussing lubrication properties in vacuum [ASLE PAPER 68-LC-15]
07 p1140 A69-19308

Apparatus for depositing protective coatings on graphite by vacuum method in refractory metal carbonyl and halides mixtures and in molten metals
09 p1528 A69-21850

Lead sulfide single crystals and polycrystalline films growth studied by electron microscopy during vacuum deposition on NaCl and other substrates
10 p1743 A69-23002

Vacuum deposition of Cr-Al film on Ni-Mo alloys, describing operating pressure, temperature and film thickness
10 p1715 A69-24013

Vacuum evaporation effects on internal macrostresses in deposited metal films based on X ray analysis, showing substrate temperature contribution
12 p2143 A69-26457

Thin film cermet resistors for integrated circuits produced by thermal vapor deposition in vacuum, cathodic sputtering and explosive vapor deposition
13 p2268 A69-27466

Electrical properties of electron beam evaporated Ti, Zr and Hf films as function of substrate temperature, material and film thickness
13 p2321 A69-28010

Energetics in solid film lubricants vacuum deposition methods, showing dependence on interfacial and film characteristics
14 p2454 A69-29001

Vacuum carburization of surface layers of transition metals
15 p2638 A69-30273

Steels chromized by vacuum diffusion, studying depth, microstructure and properties of chromized layer
19 p3329 A69-36572

Vacuum restoration by laser evaporation of active media /getters/ and vapor condensation on cold substrate applicable to nonmetallic active media /titanium-magnesium oxide/
21 p3735 A69-38590

Thin film formation, deposition methods and relation to film structure and properties
24 p4361 A69-43344

Dielectric and semiconductor films vacuum deposition by CW carbon dioxide laser, discussing optical properties
24 p4329 A69-43755

VACUUM EFFECTS

Refractory metals interactions with gases in vacuum and inert gas environment, noting temperature and pressure effects on reactions, extent and kinetics
01 p0099 A69-11042

Space lubrication system for Orbiting Solar Observatory program, discussing theoretical high vacuum principles and flight performance and environmental test data
02 p0252 A69-11766

Vacuum heating and thermal cycling influence on mechanical and structural properties of aluminum sheets fabricated from sintered powder
02 p0266 A69-12126

Vacuum effect on steel friction, noting changes in residual gases and heat transfer conditions
03 p0434 A69-13915

Cathode emission site analysis by measuring prebreakdown current under ultrahigh vacuum conditions
05 p0800 A69-15740

Polymer films tensile properties after exposure to gamma radiation in vacuum, noting chain scission and cross linking
[ASME PAPER 68-WA/RP-6]
05 p0783 A69-16160

Solid insulator performance in vacuum, analyzing breakdown factors
05 p0731 A69-16243

Controlled factorial experiments on high voltage vacuum breakdown, using Yates algorithm analysis on computer
05 p0731 A69-16244

Cardiovascular responses of baboons and dogs subjected to anoxic near vacuum environment by rapid decompression
06 p0875 A69-17846

Axisymmetric poloidal vacuum magnetic fields in low pressure plasmas in MHD equilibrium
06 p0972 A69-18230

Oil lubricant vapors under frictional working conditions in vacuum analyzed by mass spectrometer and gas-liquid chromatography concerning molecular weight and composition
[IME PAPER 11]
07 p1137 A69-18558

Vacuum, radiation and freeze drying effects on survival rate of microorganisms, noting influence of protective materials on extent of damage
07 p1064 A69-18943

Direct bead sampling by aspiration of molten metal in open hearth furnaces and converters
07 p1141 A69-19341

Motor design for operation in ultrahigh vacuum, discussing absence of convection cooling, outgassing avoidance, lubrication impossibility and oxygen absence as design parameters
08 p1377 A69-21028

In situ vacuum testing requirement for valid measurement of vacuum induced changes in mechanical and thermal properties of various filled elastomers
09 p1477 A69-22008

Vacuum melting effect on O concentration in heat resistant alloys, outlining conditions for nitrides formation in equilibrium with melt
09 p1524 A69-22136

Vacuum engineering problems during booster rocket engine ground tests, simulating flight environment
[TR-781-O]
09 p1570 A69-22300

Refractory metals testing at high temperatures in vacuum, discussing equipment modifications, temperature measurement and residual gas problems
10 p1714 A69-23848

Simplified model of ignition tests with liquid propellant rocket engines under high vacuum conditions, giving possible parameter for evaluation of simulation of real conditions
[DVL-831]
10 p1754 A69-24022

Surveyor electronic engineering design for lunar environment, discussing vacuum and temperature effects
11 p1958 A69-24633

Plasma flow from Penning discharge with incandescent cathode in vacuum controllable by varying voltage, pressure and magnetic field strength
11 p1933 A69-25543

Surface waves effect on electromagnetic waves in coherent reflection from plasma-vacuum boundary, describing polarization and angular and spectral distributions
12 p2031 A69-26530

Vacuum effects on resistance spot welds in aluminum, stainless steel and titanium alloys, noting X ray and tensile shear test results
12 p2103 A69-26622

Thermal resistance of bolted or screwed sheet metal joints in vacuum, using method applicable to different materials and surface finishes
12 p2191 A69-26803

Resistance type bonded strain gages for seven adverse environments, discussing installations and transducers
12 p2099 A69-27165

Aluminum alloys ductile fatigue striations, considering dependence on grains crystallographic orientation and vacuum effect
13 p2278 A69-27415

Electronic structure of clean metallic interfaces, considering electron, ion and surface interactions for metal-vacuum interface
13 p2321 A69-28008

Friction resistance between steel and ground basalt in ultrahigh vacuum, showing increase by adhesion
13 p2298 A69-28014

Antifriction characteristics of hard lubricating coatings based on molybdenum disulfide and graphite in inert gas atmosphere and vacuum, determining thermal stability temperature ranges
13 p2269 A69-28053

Copper and aluminum fatigue in vacuum and ultrahigh vacuum, discussing effects of hydrogen, nitrogen and oxygen pressures
13 p2280 A69-28088

Outgassing behavior of polymers in spacecraft by thermal-vacuum weight-loss and contamination tests
13 p2286 A69-28089

Heat flow resistance between solid bodies in contact in vacuum
13 p2378 A69-28338

Vacuum chamber model for sinusoidal rilles on lunar surface produced by aqueous erosion under ice blanket
14 p2485 A69-28873

Vacuum thermal decomposition of molybdenum sesquisulfide into metallic Mo, discussing reaction kinetics, mass transfer, diffusivity of sulfur gas, etc
14 p2467 A69-29287

Sliding friction tests of Cu and Cu-Be alloy plates in contact with various alloy sliders in air and vacuum
[ASLE PAPER 68-LC-5]
15 p2622 A69-30610

High vacuum effects on oxidative processes in bacteria and physiological activities of enzymes
15 p2557 A69-31354

Escherichia coli B/r survival in high vacuum at different temperatures irradiated with UV or X rays tested as colony forming ability
15 p2557 A69-31388

Solid lubricants on molybdenum disulfide base at various temperatures and low pressures, noting film mass losses and possible use with organic materials under high vacuum
16 p2793 A69-31561

Calorimetric measurement of source and broadband spectral absorptances of spacecraft thermal control coatings during exposure to UV in vacuum environment
16 p2789 A69-31815

Fixed mass of monatomic gas unsteady spherically symmetric expansion into vacuum by asymptotic Boltzmann equation expansion
16 p2772 A69-32168

Vacuum and thermal environment long term influence on thermal resistance for Mg to aluminum and Mg to Mg bolted joints
[AIAA PAPER 69-628]
17 p3073 A69-33309

Flow field of two dimensional nozzle exhausting to vacuum, describing computer program based on BGK equation and plotting exhaust region density, temperature and velocity
[AIAA PAPER 69-658]
17 p2893 A69-33490

Specification requirements for space vacuum simulation, considering vacuum requirements for simulating various effects
17 p2946 A69-33659

Deformation studies of high melting point metals and alloys at high temperatures in vacuum, noting crack formation resistance and annealing time variations
18 p3155 A69-34651

Manufacturing in space based on nongravity and hard vacuum environment, considering crystal growth and refinement, perfectly shaped bodies, refractory metals ultrapurification, etc
18 p3234 A69-35066

Spacecraft and components testing methods critical reassessment, discussing cost reduction, vacuum and thermal cycle tests
18 p3118 A69-35082

Resistance spot welds in Al, Ti and stainless steel in air and hard vacuum, showing feasibility for space assembly
19 p3319 A69-35554

Density profiles in far field of reaction control system plumes in vacuum obtained by method eliminating difficulties encountered by continuum method
19 p3238 A69-35954

Volume prediction of human body exposed to vacuum based on animal skin elasticity and anatomical features
19 p3258 A69-36456

Hydrogen jet structure ejected into vacuum from Laval nozzle at supersonic velocity, considering separation point from diffuser wall
19 p3240 A69-36604

Soviet book on diffusion welding in vacuum covering ferrous metals, homogeneous nonferrous metals, equipment, cermets, etc
19 p3329 A69-36748

Physical state changes, chemical reactions, gaseous diffusion in solids and solid-gas interactions in vacuum, considering saturated vapor pressure, condensation, evaporation, etc
20 p3576 A69-37408

Space contamination by spacecraft-borne terrestrial microorganisms, testing vacuum effect on water desorption rate using mass spectrometry on various cells
20 p3475 A69-37615

Vacuum heat treating and joining process for various ferrous and nonferrous metals and alloys, discussing advantages, applications and economics
[ASM PAPER D8-22.3]
20 p3551 A69-38132

Experimental facility for studying heat conductivity of multicontact metallic and nonmetallic materials /plates/ in vacuum at low temperatures under various loads
21 p3721 A69-38639

External friction of refractory materials at high temperature in vacuum, discussing testing machine and methods including metallographic, X ray, spectral and electron diffraction analyses
21 p3690 A69-39154

Thin PbTe semiconductor films electrical properties measured in air and vacuum, showing dependence on thickness and conditions of preparation
21 p3782 A69-39242

Cooldown of vacuum insulated transfer lines using liquid N and H, discussing flow characteristics reproduction by digital computer program
[NAS-NRC PAPER I-1]
22 p4050 A69-40625

Reaction impulse during steel spheres impacts at lead surface in vacuum dependent on kinetic energy, velocity and spheres material
22 p4047 A69-41101

High temperature vacuum treatment of thick stainless steel sheets reducing hydrogen content and outgassing
22 p3958 A69-41217

Mean adsorption lifetimes and activation energies of Ag and Au on polycrystalline tungsten substrate in ultrahigh vacuum system free of hydrocarbon contamination
23 p4198 A69-41542

Solid film lubricants deposited by DC triode sputtering on Ni, Ni-Cr and Nb surfaces friction tested under ultrahigh vacuum conditions
24 p4321 A69-43126

Volatile wall vaporization gas flow expansion into vacuum from tube approximating unsteady mass and energy transfer and pressure at blocked end
24 p4408 A69-43485

VACUUM FURNACES

Titanium production, discussing two stage electrode vacuum arc melting furnace, control and cooling equipment
02 p0229 A69-12068

Vacuum brazing technique for joining dissimilar metals without oxide and nitride film contamination
09 p1509 A69-22343

Oil quench vacuum furnace with graphite cloth heating elements
14 p2456 A69-29894

VACUUM GAGES

NT BAYARD-ALPERT IONIZATION GAGES

NT IONIZATION GAGES

NT KNUDSEN GAGES

NT PIRANI GAGES

Noiseproof ionization manometer with ion current dual modulation for ultrahigh vacuum measurement in magnetic field with extraneous charged particles interference
03 p0429 A69-1326

Ionization manometer flange transducer with axial cathode and collector for high vacuum measurements, describing air resistant yttrium oxide coated cathode with Ir core

21 p3724 A69-39077

Vacuum gage calibration standards and methods

23 p4162 A69-41530

VACUUM MELTING

Vacuum arc melted W and W-Re alloys mechanical properties, noting Re additions effects

08 p1331 A69-20190

Vacuum melting effect on O concentration in heat resistant alloys, outlining conditions for nitrides formation in equilibrium with melt

09 p1524 A69-22136

Heat resistant materials based on high melting point metals, summarizing achievements of chemical technology and vacuum metallurgy

09 p1524 A69-22137

Tungsten vacuum-arc melted samples in deformed and recrystallized conditions, studying mechanical properties at temperatures near ductile to brittle transition

15 p2637 A69-30267

VACUUM PUMPS

NT ION PUMPS

Vacuum pumping methods for large space simulation chambers, discussing cryopumping, economic and operational considerations

13 p2241 A69-28078

Space simulator vacuum facility for optical satellite tests, construction, operation and maintenance, emphasizing noncontaminating environment and pumping systems

22 p3924 A69-40396

VACUUM SPECTROSCOPY

Absorption coefficients of molecular oxygen at Lyman alpha line and vicinity measured by vacuum spectroscopy

01 p0076 A69-11230

Aerospace Corp. solar observatory /California/ compound telescope, vacuum spectroheliograph, instrumentation and applications

11 p1862 A69-24792

VACUUM SYSTEMS

Magnetron ionization gauge in helium for low pressure measurement, discussing striking characteristics and time lags

01 p0012 A69-10606

Monocarbide phases high temperature vaporization from open metal surfaces into vacuum, obtaining temperature dependence

02 p0260 A69-11583

Gas flow rate predictions for long and short tubes and annuli and at densities between laminar-continuum and free molecular regimes

05 p0750 A69-16166

Rectangular shock tube for use with pressure and vacuum, discussing sealing of circular end flanges to buildup tube

06 p0906 A69-16928

Design and performance of large vacuum system with central control desk to study plasma dynamics, discussing visual monitoring at desk

07 p1116 A69-18261

Book on vacuum system design covering getter ion pumping, cryogenic pumping, liquid nitrogen handling, residual gas analyzers, etc

07 p1180 A69-18549

Glass vacuum systems grease free assembly method using heat shrinkable polyolefin sleeve tubing connector for compression of O ring joints

08 p1320 A69-20529

High temperature organic sealants for repairing small gas leakages in vacuum devices, tabulating test results for alkyd, epoxy, silicone and polyimide resins

11 p1907 A69-24742

Vacuum spark light source for extreme UV noting mechanical trigger, compatibility with clean vacuum system and magnetic confinement of ions

11 p1885 A69-24839

Outgassing rates of multifoil insulation materials for sealed vacuum systems measured over temperature range as function of pumping time

13 p2299 A69-28016

Flux, density and pressure variations with position in vacuum system /nonuniform gas distribution/, discussing causes and consequences

13 p2299 A69-28019

Vacuum equipment and systems - Conference, Manchester, England, April 1968, Part 2 vacuum - Conference, Manchester, England, April 1968, Part 2

13 p2262 A69-28082

Molecular flow network theory extended to pulsed operation with gases mixtures having various molecular weights

13 p2247 A69-28085

SNAP 8 developmental reactor vacuum system providing space environment simulation for nuclear reactor ground testing

13 p2241 A69-28086

Dynamic gas flowmeter for ultrahigh vacuum based on transmission characteristics of diffuser screens and associated pressure drops

13 p2263 A69-28087

Vacuum restoration by laser evaporation of active media /getters/ and vapor condensation on cold substrate applicable to nonmetallic active media /titanium-magnesium oxide/

21 p3735 A69-38590

VACUUM TUBE OSCILLATORS

NT BACKWARD WAVE TUBES

NT CARCINOTRONS

NT CATHODE RAY TUBES

NT COLD CATHODE TUBES

NT GAS DISCHARGE TUBES

NT HELITRONS

NT IMAGE ORTHICONS

NT IMAGE TUBES

NT KLYSTRONS

NT MAGNETRONS

NT MICROWAVE TUBES

NT PHOTOMULTIPLIER TUBES

NT PHOTOTUBES

NT PICTURE TUBES

NT PLANOTRONS

NT THERMIONIC DIODES

NT THYRATRONS

NT TRAVELING WAVE TUBES

NT VIDICONS

Single-sideband signal nonlinear distortion and graphical methods for calculation of oscillator tube plate current pulse components

14 p2418 A69-28828

VACUUM TUBES

NT BACKWARD WAVE TUBES

NT CARCINOTRONS

NT CATHODE RAY TUBES

NT COLD CATHODE TUBES

NT GAS DISCHARGE TUBES

NT HELITRONS

NT IMAGE ORTHICONS

NT IMAGE TUBES

NT KLYSTRONS

NT MAGNETRONS

NT MICROWAVE TUBES

NT PHOTOMULTIPLIER TUBES

NT PHOTOTUBES

NT PICTURE TUBES

NT PLANOTRONS

NT THERMIONIC DIODES

NT THYRATRONS

NT TRAVELING WAVE TUBES

NT VIDICONS

Electrostatic storage display tube characteristics, construction, applications and reliability

07 p1101 A69-18655

Vacuum tube with cathode heated directly by external radioisotope source, noting heat pipe providing isothermal heat transfer

11 p1848 A69-24748

Wideband RF amplifier manufacturing problems, comparing operation of vacuum triodes and pentodes in passband circuits

11 p1849 A69-24958

Integrated circuits, discussing development from transistors and vacuum tubes, operation, fabrication and applications

12 p2038 A69-26331

VACUUM ULTRAVIOLET RADIATION

U FAR ULTRAVIOLET RADIATION

VALANCE

Second order susceptibilities of III-V and II-VI compounds using Phillips model, discussing second optical harmonic in III-V compounds with tetrahedral bonds

01 p0138 A69-10365

Valence electrons mean density stability in Ti and V monoxides, describing mechanism for filling M vacancies with simultaneously forming O vacancies

09 p1523 A69-21738

Lowest valence and Rydberg states assigned to ungerade singlet states in dipole allowed absorption spectrum of molecular nitrogen

09 p1542 A69-21916

Valence force constants for nitric acid evaluated from fundamental mode vibration spectra by matrix method

15 p2561 A69-30467

VALKYRIE AIRCRAFT

U B- 70 AIRCRAFT

VALLEYS

Sinuuous rill and water distribution on lunar surface from Orbiter 4 high resolution photographs

05 p0818 A69-15606

Intervalley scattering model for Gunn domain dynamics, noting effects comparable to diffusion

06 p0893 A69-16937

VALSALVA EXERCISE

Valsalva maneuver produced abrupt onset of ptosis and proptosis caused by ethmoidal air cell rupture, discussing etiologies

17 p2909 A69-33186

Arterial pressure and heart rate responses to increased intrapulmonary pressure in anesthetized dogs via simulated Valsalva tests

23 p4078 A69-41365

VALUE

NT Q VALUES

Group relative values for system criteria, showing application to illustrative maintenance criteria

10 p1668 A69-22973

Society of American Value Engineers Conference, San Diego, April 1969

13 p2382 A69-28092

Value engineering application to engineer recruiting phase of industrial relations

13 p2382 A69-28093

Systems design value analysis including alternate solutions to cost effectiveness for design development and production phases

13 p2383 A69-28097

U.S. Navy Numerical Value Rating System computing method of selecting lowest cost design approach to accomplish specific function

13 p2383 A69-28098

Value engineering proposal costs sustained by maintenance and overhaul industry in government contract negotiations, discussing reimbursement and proposed central agency

13 p2383 A69-28099

Value engineering and component/products improvement incentive contract clauses role in defense product quality improvement

13 p2383 A69-28100

Value engineering ultimate objectives in industry, discussing engineering and procurement role in prorating goal to applicable departments

13 p2383 A69-28101

VALVES

NT AUTOMATIC CONTROL VALVES

NT FUEL VALVES

NT GAS VALVES

NT PRESSURE REGULATORS

NT RELIEF VALVES

Self sustained oscillations of piston type valving system with conduit line at upstream and capacity at downstream

01 p0012 A69-10310

Displacement function selection in calculating rubber-metal valve design, considering boundary conditions of material deformation

01 p0087 A69-10829

Bellows sealed valve for measurement of fluorine thermodynamic properties at moderately high pressures

09 p1493 A69-21428

Vortex valve pure fluid modulators steady state characteristics, analyzing geometry of exit, control and supply areas and chamber

09 p1443 A69-22738

Vortex amplifiers design and performance, noting nonvented and vented amplifiers and fluid valving applications

09 p1443 A69-22741

Spool valve flow patterns within hysteresis region, discussing effects of valve geometry, Reynolds and cavitation numbers

11 p1827 A69-25645

Free surface in supercritical regime downstream of valve submerged in MHD flow, noting effects of horizontal and vertical magnetic induction fields

15 p2659 A69-30299

Servovalve orifice characteristics described by discharge, flow or loss coefficients for laminar and turbulent flow, noting use of Mises model

19 p3256 A69-36712

Pressure activated superfluid valve design and operation for liquid He transfer from reservoir to cold finger

22 p3870 A69-41237

High reliability of solenoid and pressure regulating valves under long duration space missions, considering design, tests and controls

24 p4319 A69-42854

VAN ALLEN RADIATION BELTS

U RADIATION BELTS

VAN DER WAAL FORCES

Mean square radii for assigned terms of Fe I energy diagram for Van der Waals line broadening
08 p1392 A69-20559

London-van der Waals interaction energy of symmetric molecular pair calculated in perturbation theory second order as infinite series in negative powers of separation
12 p2131 A69-26606

Vapor-liquid transition in inert gases based on Monte Carlo method, including comparison with van der Waal equation and plasma ionization equilibrium
15 p2655 A69-30981

Widths measurements of van der Waals broadened Si I spectral lines by shock tube and scanning Fabry-Perot interferometer, using argon as perturbing gas
18 p3116 A69-34449

VANADIUM

Electron microprobe analysis of vanadium in presence of titanium by compositional measurement of chromite in chondritic meteorites
07 p1073 A69-18419

Diffusion coefficients of carbon in tantalum, niobium and vanadium by sectioning method, using carbon 14 as tracer
11 p1906 A69-25575

V contents influence on high temperature strength and fine structure interrelation in low alloy CrMoWV steels
22 p3972 A69-41083

VANADIUM ALLOYS

Omega phase and beta solid solution in Zr-V-Ta alloys quenched from 900 C
02 p0263 A69-11850

Vanadium-gallide alloys critical temperature of transition into superconducting state determined by measuring cast alloy samples magnetic permeability
03 p0483 A69-13023

Electrolytic deposits of titanium, vanadium and alloys from molten salts, discussing formation conditions, velocity and properties
03 p0446 A69-13574

Quasi-ternary titanium dichromide-V-Mo system composition at high temperatures, physical properties and phase diagrams
04 p0618 A69-15080

Titanium vanadium martensite decomposition kinetics during heating, showing shearing process and dependence on temperature during quenching
07 p1163 A69-18778

Binary vanadium alloys property change regularities using alloying elements
08 p1333 A69-20439

Vanadium side of V-Ni phase diagram, using X ray analysis, differential dilatometry, thermal analysis and metallographic methods
11 p1903 A69-24579

Optimum conditions for producing Ti-V alloy sheet plated on one side with Nb by hot rolling
18 p3155 A69-34652

Ti-V martensite decay during heating, noting temperature dependence of elastic moduli and electrical conductivity
21 p3746 A69-39160

V systems applications and phase diagrams, discussing binary metallic systems, Kurnakov law, alloy properties dependence on composition, superconductivity, melting point, etc
22 p3968 A69-39887

Mechanical and thermal properties of vanadium alloys and austenitic stainless steels compared to determine applicability in high temperature reactor fuel jackets
22 p3971 A69-40973

Ce, Zr, Nb and B effect on heat resistance and structure of low alloy CrMoWV steels /type CSN 41 5335/
22 p3972 A69-41079

Al-Mn-V ternary system equilibrium diagram at various aluminum concentrations determined by magnetic and microhardness measurements, microstructural observations and X ray analysis
24 p4330 A69-42601

VANADIUM CARBIDES

Lattice deformation relationship to dislocation density in vanadium carbide powders
02 p0265 A69-12001

Vanadium-carbon and niobium-carbon binary systems revised phase diagrams, noting effect of sublattice order transformations
05 p0779 A69-15988

Vanadium monoxides and oxycarbides heat capacity using adiabatic calorimeter, calculating entropy, enthalpy and characteristic temperatures
09 p1523 A69-21739

VANADIUM COMPOUNDS

Monograph on vanadium selenides and tellurides with NiAs structure covering existence regions, superstructures and equiatomic compounds from viewpoint of thermodynamics
15 p2667 A69-30602

Conditions for obtaining concentrated Ti-containing melts free of Al and V chlorides by cementing with metallic Ti and Ti-containing materials
22 p3957 A69-40918

VANADIUM ISOTOPES

V 50/V 51 abundance ratios in chondrite, terrestrial diabase standard W-1 and reagent V
20 p3601 A69-37501

VANADIUM OXIDES

Vanadium dioxide reflection spectra dependence on incident quantum energies during semiconductor/metal phase transition
02 p0298 A69-12100

Vanadium pentoxide addition effect on combustion rates of mixtures of ammonium perchlorate and metallic fuels in nitrogen atmosphere
08 p1375 A69-20342

Valence electrons mean density stability in Ti and V monoxides, describing mechanism for filling M vacancies with simultaneously forming O vacancies
09 p1523 A69-21738

Vanadium monoxides and oxycarbides heat capacity using adiabatic calorimeter, calculating entropy, enthalpy and characteristic temperatures
09 p1523 A69-21739

Band structure and reflection spectra of vanadium dioxide and pentoxide single crystals, noting changes in metal-semiconductor phase transition
12 p2145 A69-26724

IR spectral transmittance and physicochemical properties of tellurite glasses with vanadium and cerium oxides, showing polymer chains in structure
14 p2468 A69-29329

Vanadium thermistor fabrication influence on resistance jump at phase change temperature of vanadium dioxide, reproducing parameters by heat treating doped vanadium pentoxide
19 p3256 A69-36718

Ti and V sesquioxides and TiO-VO solid solutions crystallography and defect chemistry over entire range of compositions
20 p3484 A69-37526

Band structure and reflection spectra of vanadium dioxide and pentoxide single crystals, noting changes in metal-semiconductor phase transition
21 p3781 A69-39137

Critical transition temperature of vanadium oxide semiconductors as function of doping element content and lattice constant, using X ray diffraction
23 p4198 A69-41564

VANELESS DIFFUSERS

Unsteady aerodynamic processes in centrifugal compressor stage with impeller, vaneless diffuser and annular receiver chamber
15 p2547 A69-30073

VANES

NT GUIDE VANES

NT JET VANES

NT WIND VANES

Nonconducting vanes end effects on electrical characteristics of MHD channels, analyzing current density, Joule losses and finite length vanes
13 p2306 A69-27497

Internally air cooled turbine blades and vanes emphasizing coolant aerodynamics, heat transfer and blade life, high temperature in jet engines, etc [RAES PAPER 22]
22 p4000 A69-40500

Blade and vane wall thickness measurements test methods for gas turbine engine using ultrasonic gage and thermoelectric comparator
24 p4312 A69-42753

VANS

U TRUCKS

VAPOR DEPOSITION

NT VACUUM DEPOSITION

Electric field control of growth rates of insulating organic crystals from vapor phase
01 p0135 A69-10140

Chemical vapor deposition of refractory metals, alloys and compounds - Conference, Gatlinburg, Tennessee, September 1967
01 p0096 A69-10640

Chemical vapor deposited W and W-Re alloys for structural applications, discussing fabrication methods and effects on mechanical properties
01 p0096 A69-10641

Chemical vapor deposition of W-Mo-Re ternary alloys from hydrogen reduction of fluorides on Cu or Mo substrates
01 p0096 A69-10642

Chemical vapor deposition of iridium coatings on graphite for high temperature oxidation protection, discussing parameters for iridium compounds and optimum depositing conditions
01 p0097 A69-10643

Chemical vapor deposition of beryllium metal coatings noting thickness, purity and processing effects on surface properties
01 p0097 A69-10644

Silicon carbide filament fabrication by chemical vapor deposition, noting physical and mechanical properties and application to other refractories
01 p0097 A69-10645

Grain boundary gas bubbles growth in chemically vapor deposited tungsten as function of annealing time, temperature and fluorine content
01 p0097 A69-10646

Creep behavior of chemical vapor deposited tungsten at high temperatures by creep-rupture tests compared with powder metallurgy tungsten
01 p0097 A69-10647

Chemical vapor deposited W and W-Re alloys investigated for deposition variables and heat treatment effects on mechanical properties
01 p0097 A69-10648

A15 type phase in vapor deposited W-Re alloys identified by X ray diffraction, metallography and hardness measurements
01 p0098 A69-10649

Heat transfer rates from high temperature spheres into subcooled liquid sodium during forced convection, noting surface vapor formation [ASME PAPER 67-WA/HT-32]
02 p0351 A69-12202

Mechanical properties of titanium physically vapor deposited by electron beam high rate evaporation, noting results of tension testing
03 p0443 A69-13117

Vapor grown GaP electrical and optical properties, considering undoped and Se or S doped samples on GaAs and GaP substrates
04 p0640 A69-14438

Cr gas deposition on steel by means of chromium chloride salt, noting chromizing conditions effect on carbide growth and friction resistance
04 p0605 A69-14577

Impurity transfer in doped and undoped epitaxially grown GaAs films, studying substrate dopants effect on carrier concentration profiles
05 p0807 A69-15957

Chemical vapor deposition of chromium metal on substrates, discussing influence of temperature, gas flow rate and chromium chloride concentration [ECS PAPER 223]
05 p0769 A69-16232

Powder metallurgy, fusion and chemical vapor deposition techniques in manufacturing tungsten base alloys
07 p1165 A69-18792

Vapor deposited tellurium thin films orientation, noting effect of characteristic spiral chain structure along c-axis
08 p1373 A69-20891

Vapor deposition of high purity epitaxial layers of type gallium arsenide, noting resistivity and Hall coefficient measurements [ECS PAPER 62]
08 p1373 A69-21067

Cubic /beta/ silicon carbide films deposition by volatilization in presence of acetylene
09 p1554 A69-21350

Chemical processes in silicon carbide due to reactive deposition and chemical conversion, noting silicon growth mechanism involving outward diffusion
09 p1554 A69-21351

Surface characterization on chemical vapor deposited tungsten, evaluating grain size effect
09 p1558 A69-21810

Partial pole figures in vapor deposited and wrought cylindrical tungsten specimens, noting random surface produced by orientation
09 p1558 A69-21811

SiC part fabrication by chemical vapor deposition through pyrolysis of chlorosilanes from vapor state onto machined substrates of graphite and metals
09 p1509 A69-22344

Vapor phase epitaxial production of indium arsenic phosphide crystalline layers, discussing electron mobilities, electrical resistivities and doping
12 p2142 A69-25934

- Thermodynamic method for determination of conditions for CdS single crystal synthesis from gas phase, analyzing equilibrium between solid and gas phases
12 p2144 A69-26585
- Substructural patterns of epitaxial PbTe films obtained by condensation of vaporized PbTe on NaCl crystal surfaces, discussing formation kinetics and morphology
12 p2144 A69-26675
- Adsorption of N, H, O and CO on thick vapor deposited Be films at room temperature
13 p2322 A69-28017
- Metal layers deposition, structure and properties obtained by H reduction of metal halides in vapor phase
14 p2462 A69-29209
- Deposition and interdiffusion of W layers on Mo emitter of in-core thermionic reactor, investigating microstructure of transition zone
14 p2462 A69-29210
- Niobium deposition on graphite from vapor-gas phase assuming heterogeneous process
15 p2629 A69-30992
- High energy electrons emission during alloy evaporation on hot metal filaments used for thin film deposition
16 p2827 A69-32016
- Macrostructural differences between filaments of B and SiC vapor deposited onto small diameter W wire, discussing radial cracks due to dilatation
18 p3160 A69-34266
- High porosity W-Ta matrix to thin solid Ta support structure joining technique involving vapor-deposited coating process
20 p3548 A69-37216
- Hydrodynamics of turbulent gas flow through powder layer for vapor phase coating of particles, noting fluidized bed
20 p3548 A69-37363
- Diffusion processes during formation of coatings by condensation
20 p3549 A69-37365
- Diffusion processes, composition and structure of vapor deposited Ni coatings on Nb substrate, plotting intermetallic compounds growth against temperature
20 p3560 A69-37366
- Niobium carbide formation on graphite from gaseous niobium pentachloride and Ar mixtures, discussing parameters affecting layer growth rate
20 p3566 A69-37367
- Silicon carbide compact coatings deposition on graphite by silicon tetrachloride, H and benzene gaseous mixture, relating layer thickness to temperature and process duration
20 p3566 A69-37368
- Niobium carbide deposition from gaseous halogen compounds on graphite particles in pseudoliquidified state, noting stoichiometric coatings
20 p3566 A69-37369
- Protective coatings of oxygen-free high melting point Si compounds and silicate binder, noting chemical stability in corrosive media
20 p3566 A69-37371
- Tungsten carbide erosion resistant coatings, discussing optimum plasma deposition process and coating characteristics
20 p3561 A69-37373
- Deposited beta active thallium isotope materials angular distribution after vaporization by Q switched laser beam determined by target fragment recoil
21 p3737 A69-38992
- Optimal CdS single crystals growth from gaseous phase achieved with 2 to 1 ratio between Cd and S concentration
23 p4199 A69-42468
- Ge films formation by evaporation technique, discussing background O pressure effect
24 p4361 A69-43345
- VAPOR GENERATORS**
U VAPORIZERS
- VAPOR JETS**
Cs jet device eliminating wall influence in nonlinear radiation-atom interaction phenomena
19 p3376 A69-36174
- VAPOR LIQUID EQUILIBRIUM**
U LIQUID-VAPOR EQUILIBRIUM
- VAPOR PHASES**
Ultrasonic sounding for controlling dispersed gas phase in liquid pipelines under laboratory and practical conditions
04 p0596 A69-14489
- Latticed gas model liquid-vapor phase properties calculated with allowance for thermal expansion
06 p1029 A69-16896
- Slow oxidation and self ignition in gaseous phase, discussing cold flames and interpretation of experimental data
06 p1031 A69-17416
- Aspiration psychrometric probe for measurements of relative humidity of gas-vapor phase of gas flow containing liquid droplets
06 p0927 A69-17689
- Liquid and vapor phase microscale panel cokers applied to screening synthetic lubricants for aircraft turbine engines
[ASLE PAPER 68-LC-22] 07 p1140 A69-19309
- Boundary layer at tube wall behind shock wave propagating in gas-vapor mixture, analyzing condensation rate
09 p1480 A69-21591
- Oxygen depletion effect in chemical reactions between pyrolysis gases and air stream on surface recession of charring ablators
[AIAA PAPER 68-302] 09 p1622 A69-21982
- Threshold criteria of gas phase thermal ignition for cellulose materials, considering heating by radiant energy
11 p1940 A69-24474
- Potassium vapor radiative perturbation by ruby laser radiation in glass cell with end windows, studying emission line structure
13 p2271 A69-27656
- Gas chromatography based on sampling gas-vapor phase at liquid surface for determining volatile oxygen containing compounds in biological media
13 p2216 A69-28627
- Vapor phase reaction sequence to explain water cluster ions in D region
14 p2434 A69-28940
- Metal layers deposition, structure and properties obtained by H reduction of metal halides in vapor phase
14 p2462 A69-29209
- Niobium deposition on graphite from vapor-gas phase assuming heterogeneous process
15 p2629 A69-30992
- Laser ignited combustion of 365 micron Zr droplets falling in ultrapure oxygen using spectroscopic and photographic techniques, discussing vapor phase transport phenomena
[WSCI PAPER 69-4] 16 p2830 A69-32345
- Gas phase ignition theory with feedback of homogeneous propellant exposed to stagnant gas after shock reflection
[AIAA PAPER 69-559] 16 p2880 A69-32740
- Boron nitride synthesis by gas phase reaction of boron chloride or diborane with ammonia, determining purity from equilibrium gas mixture components
17 p2992 A69-33432
- Gas phase ignition shock tube analysis of solid propellant taking into account changing surface temperature and fuel vapor consumption
18 p3183 A69-34463
- Low molecular weight fluorocarbons pyrolysis and oxidation in single pulse shock tubes, using vapor phase chromatography and mass spectral analyses
18 p3099 A69-34467
- Gaseous and solid phase properties of atomic and molecular systems, treating statistical energy distribution, kinetics, excited states and relaxation
18 p3178 A69-35406
- Cumulative shock waves in vaporized products of electrical explosion of conical copper wire configuration, discussing atmospheric ionized vortical configuration formation
19 p3372 A69-35823
- Relative gas phase acidities of simple aliphatic alcohols, considering effects of alkyl groups
19 p3265 A69-36289
- Relative gas phase acidities of carbon acids determined using ion cyclotron resonance spectroscopy
19 p3265 A69-36291
- Relative gas phase acidities of simple aliphatic amines and ammonia noting increase in large alkyl groups substitution
19 p3265 A69-36293
- Be diffusion during vapor phase saturation of W, Mo, Nb and Ta, noting time and temperature dependence of layer thickness
20 p3549 A69-37364
- Gas phase ion-molecule chemistry of HCN by ion-cyclotron resonance spectroscopy identifying individual reactions by double resonance
20 p3485 A69-38262
- Chromatographic analysis of products formed during induction period of 2-methylbutane gaseous oxidation in flow system at low temperatures and long residence times
21 p3669 A69-38798
- Gas phase arrest peak analogy with liquid phase oxygen cut-off during final stages of hydrocarbons gaseous oxidation reactions, noting active centers
21 p3669 A69-38805
- Laser radiation increased absorption in opaque solid body attributed to vaporization, analyzing factors determining thermodynamic equilibrium between condensed and gaseous phases
21 p3736 A69-38962
- Absorption spectroscopy using resonance broadened atomic lines for two phase mixtures study
21 p3774 A69-39239
- Output power of CW lasers employing HCN and water vapor active medium
22 p3959 A69-39958
- Phase equilibrium apparatus for measurement of thermodynamic properties of cryogenic fluid mixtures, including argon-methane data
[NAS-NRC PAPER H-3] 22 p3947 A69-40630
- Optimal CdS single crystals growth from gaseous phase achieved with 2 to 1 ratio between Cd and S concentration
23 p4199 A69-42468
- Altered gaseous environments effect /parabrosis/ on interferon production in mice injected with Newcastle disease virus, noting hypoxia role
24 p4262 A69-42888
- VAPOR PRESSURE**
Nitrogen compressibility and thermodynamic functions up to 10,000 atm pressure and 400 C
01 p0175 A69-10366
- Acceptor defect levels in cadmium telluride crystals prepared under various cadmium vapor pressures, demonstrating ionization energy variation by electrical measurements
02 p0294 A69-11546
- Gas dynamic choking limitation on heat transfer capacity of heat pipe operating at low vapor pressures from comparison of theory and experiment
03 p0531 A69-12989
- InAs-InP phase diagram taking into account equilibrium pressure of vapor over melts in preparing single crystals by controlled crystallization
03 p0483 A69-13024
- Shock tube equilibrium method for determining vapor pressure of platinum submicron particles by suspension in xenon-argon carrier gas at high temperatures
03 p0532 A69-13319
- Temperature dependence of partial pressure of saturated As vapor over solid solutions of InAs-GaAs of different composition
04 p0642 A69-14938
- Thermionic converters stability and safety maintainable at high Ce pressures
09 p1441 A69-21837
- Mean drop size generated in vapor pressure regime of liquid water jet, noting effect of water temperature and orifice diameter
09 p1483 A69-21995
- Specific isochoric heat capacity of pure fluids, considering thermal equation of state, vapor pressure and boundary conditions at critical point
11 p2001 A69-25201
- Work function measurements of polycrystalline W, Re and Ni disks in high pressure cesium plasma for low probe temperature range
14 p2506 A69-29266
- Test methods for lubricants vapor pressure and flash point determination
[ASLE PAPER 68-LC-23] 15 p2642 A69-30607
- Saturated Li vapor pressure measured by static equilibrium technique based on use of null membrane, tabulating pressures for various temperatures
15 p2656 A69-30997
- Vapor pressure measurements on liquid fluorine from triple to critical point at one degree K intervals
[NAS-NRC PAPER H-2] 22 p3998 A69-40624
- Vapor pressure equation for oxygen and nitrogen derived by adding nonanalytic term, correlating equation with observed data
[NAS-NRC PAPER H-1] 22 p4051 A69-40628
- Insensible water loss from human skin as function of ambient vapor concentration using IR gas analysis, applying results to water loss model revision
23 p4077 A69-41293
- VAPOR TRAILS**
U CONTRAILS
- VAPORIZATION HEAT**
U HEAT OF VAPORIZATION
- VAPORIZERS**
NT EVAPORATORS

Injector vaporizer performance in liquid metal MHD system, using model for total and static pressure distribution 06 p0871 A69-17918

Flow velocity, density, temperature, dryness and pressure in mixing chamber of MHD vaporizer 06 p0871 A69-17919

Cryogenic heat exchanger design and application including vaporizers, recuperators, regenerators, reversing exchangers, nonsteady state flow and thermoelectric techniques 17 p3074 A69-33681

Film vaporizing gas turbine combustor design including performance tests and combustion physics 21 p3784 A69-38607

VAPORIZING

NT BOILING
NT EVAPORATION
NT FILM BOILING
NT FLASHING [VAPORIZING]
NT LEIDENFROST PHENOMENON
NT NUCLEATE BOILING
NT PROPELLANT EVAPORATION
NT SUBLIMATION
NT TRANSPIRATION

Kinetics of vaporization of metals with surface subjected to incident radiation flux noting pulse duration 02 p0350 A69-11577

Monocarbide phases high temperature vaporization from open metal surfaces into vacuum, obtaining temperature dependence 02 p0260 A69-11583

Volatile liquid pressurization, discussing pressurants, heat sources and system design [AIAA PAPER 68-630] 02 p0232 A69-12382

Condensation-enhanced vaporization rates in nonisothermal systems, noting fume nucleation augmentation of rates into cooler environments 03 p0532 A69-13122

Organic plasticizers molecular vaporization process kinetics, using isothermal and nonisothermal kinetic methods 04 p0620 A69-14956

Transient development of reacting boundary layer near stagnation point of vaporizing drop in gas stream [AIAA PAPER 69-174] 06 p0912 A69-18056

Metallic particle ignition in oxygen containing media, obtaining temperature curves and vaporization rates 08 p1375 A69-20343

Helium-neon gas laser as coherent light source for holograms of vaporizing fuel films and for Michelson interferometer 08 p1327 A69-20874

Coronal IR observations during solar eclipse revealing thermal emission zone at predicted interplanetary dust vaporization region 10 p1789 A69-24131

Silicon nitride vaporization and thermodynamic properties analyzed using Langmuir and Knudsen methods 12 p2118 A69-26261

Creeping flow model of Leidenfrost boiling with moving surface, discussing vaporization time for equivalent drop film boiling on stationary surface [AICHE PAPER 20] 15 p2718 A69-31116

Vaporization interaction liquid rocket performance model, discussing performance loss evaluation and test data [AIAA PAPER 69-470] 16 p2838 A69-32663

Gas dynamic processes during vaporization of solid material under Nd laser emission, using high speed photography 21 p3740 A69-39551

Mass spectrometric analysis of lunar material from soil vaporization products ion component by electron beam 22 p4034 A69-41107

Volatile wall vaporization gas flow expansion into vacuum from tube approximating unsteady mass and energy transfer and pressure at blocked end 24 p4408 A69-43489

VAPORS

NT CESIUM VAPOR
NT MERCURY VAPOR
NT METAL VAPORS
NT SODIUM VAPOR
NT WATER VAPOR

Motion of vapor derived from solid material vaporization and subsequent heating by nonequilibrium continuum radiation, noting continuity equations and energy transfer 04 p0686 A69-14985

VARACTOR DIODE CIRCUITS

Frequency retuning characteristics of oscillator employing avalanche transit-time diode with complementary varactor subject to current or voltage variation 11 p1844 A69-24449

Varactor diodes for microwave frequency tuning of resonators used for oscillators of avalanche transit time and Gunn diodes, discussing Q factors 11 p1854 A69-25610

Power losses of varactor frequency multipliers with series connected circuits including open circuit tuned to second harmonic 12 p2043 A69-26888

Varactors for frequency conversion circuits, discussing efficiency and output power 15 p2578 A69-30797

360 degree varactor linear phase modulator, analyzing impedance matching, insertion loss, tuning design and serrodyne application 16 p2756 A69-31577

VARACTOR DIODES

Capacitance variation in junction varactors with linear graded, abrupt and hyperabrupt junctions, storage switching diodes and storage varactors 01 p0038 A69-10168

Wideband electronically scanned receiver, using varactor diode upper sideband parametric frequency upconverter for frequency mixing 01 p0048 A69-11036

Forward current shot noise in parametric amplifiers using GaAs varactors, noting additional noise due to stored minority carriers current 01 p0048 A69-11137

Electrically controlled broadband microwave phase shifter consisting of coaxial line with varactors or ferroelectrics 03 p0408 A69-13987

Equivalent circuit of varactor with open p-n junction used as frequency multiplier 04 p0575 A69-14465

Varactor Q calculation from impedance vs bias measurements, circumventing circuit loss problem by procedure based on Weissfloch equivalent circuit of lossy two port network 04 p0575 A69-14753

Freeze-out characteristics of MOS varactor, noting impurity effects and compensation 05 p0806 A69-15809

Gain stabilization of parametric amplifier, using pumped conduction current of varactor diode 09 p1467 A69-22585

Storage varactors and frequency dependent diode input power for multiplier cascades control, discussing series connections and limitations by thermal noise 11 p1841 A69-25607

Parametric frequency converter consisting of mixer head in bridge circuit with varactors for 12 GHz TV transmitters 11 p1854 A69-25614

Differential capacitance, diffusion voltage and exponent alpha of hyperabrupt junction varactor 12 p2039 A69-26375

Ultrahigh speed microwave diode switch used as transmitter-modulator in PCM systems, utilizing varactor diode avalanche breakdown 13 p2229 A69-27671

Varactor diode parameters measurements by microwave power reflection method 13 p2237 A69-28645

Oscillation breakdown of varactor diodes in parametric amplifiers from studying I-V characteristics, noting resonant circuit retuning effect 15 p2574 A69-30127

Noise sources in S band parametric amplifier with GaAs varactor diode measured at liquid nitrogen temperature, considering noise reduction 15 p2578 A69-30636

Mesa-structure varactors /p-n junction generating harmonics by nonlinear capacity variation/ reliability, determining selection criterion and optimal test duration period 15 p2627 A69-30839

Computerized design parameters for realizable over-driven bimode varactor frequency doubler based on charge-voltage relationship at break point 20 p3505 A69-37299

Equal bandwidth multichannel FM/FM EEG tele-meter system using subcarrier frequencies and HF modulation via varactor diodes 23 p4106 A69-41802

VARACTORS

U VARACTOR DIODES

VARIABLE AREA WINGS

U TRAILING-EDGE FLAPS

VARIABLE GEOMETRY STRUCTURES

Variable geometry features applied to lifting spacecraft to overcome inherent incompatibility and provide low speed and tangential landing capabilities [AIAA PAPER 68-1164] 03 p0520 A69-13563

Mirage G supersonic swing wing two seater aircraft performance, discussing hinging of mobile wing on pivot, fluids for airfoil-fuselage transfer, landing gear etc 07 p1053 A69-19230

Incident flow in variable cross section tubes using analytic asymptotic calculation 10 p1677 A69-22857

Folding prop rotor VTOL aircraft configuration analytical and experimental investigations to study design requirements for cruise speeds to Mach 0.75 [AIAA PAPER 69-220] 10 p1635 A69-24087

Critical flutter behavior of variable geometry aircraft with wing of 70 degree leading edge sweep, noting wing-tail interference 11 p1991 A69-25517

Rocket motors with combustion chambers of variable geometry for hybrid propellants, stressing toroidal chamber 15 p2671 A69-30600

Aerodynamic and flight characteristics of variable geometry entry spacecraft during subsonic wing deployment and landing [AIAA PAPER 69-742] 18 p3084 A69-34407

Maximum admissible weight of structural elements required for conventional wing conversion into variable geometry wing without performance impairment 24 p4253 A69-43092

VARIABLE LIFT

U LIFT

VARIABLE MASS SYSTEMS

Quasi-one dimensional analysis of MPD arcs with nonequilibrium ionization taking into account finite rate processes and variable area [AIAA PAPER 68-87] 02 p0291 A69-12505

Differential equations of motion for holonomic system of points with variable mass 03 p0465 A69-12965

Energy integral for holonomic system of points of variable mass, transforming Lagrangian form via Hamiltonian function 05 p0794 A69-16685

Euler rotational equations for bodies with variable inertia tensor subjected to extreme variations of mass distribution and mass loss 09 p1616 A69-21956

Orbital parameters changes computation in table form for binary systems with more massive component mass decrease 11 p1962 A69-25120

Covariant equations of motion of body of variable mass in general relativity, considering Schwarzschild field, rotating mass field and Einstein static universe 11 p1965 A69-25744

Orbital elements evolution of binary or planetary system with decreasing mass by nonlinear nonautonomous differential equations 14 p2519 A69-29138

Necessary and sufficient conditions of kinetic processes involving two systems of point masses 21 p3771 A69-39087

Differential equations for variable mass solid body motion about fixed point having cavities filled with ideal fluid 21 p3771 A69-39106

Optimal flight regime determination for variable mass body pursuing target by straddling method, presenting motion equations and approximate solutions 21 p3818 A69-39819

Optimal thrust control for plane curvilinear motion of variable mass point in gravitational field 23 p4192 A69-42340

Weight limitations effect on optimum motion parameters of variable mass body in gravitational field applied to spacecraft optimum propulsion system controls and trajectory determination 24 p4383 A69-42956

VARIABLE STARS

NT CEPHEID VARIABLES
NT HERCULES NOVA
NT NOVAE
NT SUPERNOVAE
NT T TAURI STARS

Nonlinear adiabatic pulsations of sequence of massive stars of uniform composition, allowing for radiation pressure variations 01 p0149 A69-10266

- Optical identification of X ray source Cen XR-2 as variable star WX Cen, discussing colors and similarity to Sco X-1
01 p0145 A69-10857
- Late type variable stars time dependent photometry and polarimetry in blue and violet, noting correlation of stellar brightness and degree of polarization
01 p0158 A69-11326
- Pulsating stars, cepheids, RR Lyrae and W Virginis, excitation mechanisms, period-luminosity relation, oscillation modes, location on Hertzsprung-Russell diagram, etc
04 p0653 A69-14625
- Variable He star HZ29, noting unusually wide and shallow He I lines and possible mass and composition
06 p0998 A69-16931
- Orion nebula flare type variable stars amplitudes, light curve sections and stability
06 p1002 A69-17264
- Light variations of irregular eruptive variables known as RW Aurigae or T Tauri stars, discussing suitability of stochastic model
06 p0996 A69-17448
- Flare star AD Leo observations by continuous photoelectric monitoring, noting light curves properties
06 p1008 A69-17697
- Pulsational properties of massive star in He burning evolutionary phase, determining inner structure from stellar model
07 p1218 A69-19279
- Variable eruptive star in Hercules, discussing magnitude
08 p1382 A69-19871
- Brightness in blue light and radial velocity variability of metallic line star 28 Andromedae
08 p1395 A69-20637
- Photoelectric observations of SRA variable CH Cygni reveal strong variability, discussing existence of hot companion
08 p1396 A69-20650
- Quasar 3C454.3 optical variations, noting photographic and photometric evidence for period of 340 days
08 p1397 A69-20701
- Dimensions of 19 variable eclipsing binaries from published photometric and spectral orbital elements
09 p1590 A69-21378
- Narrow band photometry of variable stars and X ray source Cyg X-2, considering continuum variations with time
09 p1591 A69-21451
- Pulsar NP 0532 identified with Baade south preceding star in Crab Nebula, noting pulsed optical radiation
09 p1592 A69-21458
- Three color observations of 16 magnetic stars and photometric properties of 23 stars, discussing periodicities in variations
09 p1599 A69-22196
- IR excess from carbon-rich peculiar variable R Coronae Borealis and M7 variable associated with emission nebula R Aquarii attributed to circumstellar matter
09 p1603 A69-22263
- Polarization changes of R Coronae Borealis Star RY Sagittarii, tabulating percentage polarization and position angles
09 p1603 A69-22265
- Anharmonic pulsations of 15.6 solar mass star in helium burning phase, discussing radiation pressure, third order terms, higher modes and magnitude variation effects
10 p1771 A69-22853
- Graphite particle formation in atmosphere of C type Mira variables, calculating particle size distribution by nucleation and coagulation theory
10 p1782 A69-23681
- Flare stars observational and known aggregate characteristics in Coal Sack region
10 p1790 A69-24141
- Spectroscopic, photometric and polarimetric observations of magnetic stars, discussing magnetic curves of periodic variables
11 p1954 A69-24362
- Period variations, colors and light curve peculiarities of models of U Geminorum type stars
11 p1954 A69-24363
- Nonadiabatic linear oscillations of stellar atmosphere, discussing wave coupling with stellar pulsation
11 p1961 A69-25104
- Micrometric and photometric measurements of coude spectra of magnetic variable HD 125248, showing spectroscopic binary nature and computing orbital elements
11 p1963 A69-25264
- Period changes by variable stars in M13, showing Variable 2 period lengthening
12 p2154 A69-25814
- Physical parameters and chemical composition of DD Lac atmosphere from spectral analysis
12 p2156 A69-26219
- UBV observations of long period variable stars using reflecting telescope and refrigerated photocell with standard filters
12 p2172 A69-27156
- Star twinkling absence for lunar observation laboratory, noting star distance measurement and laser action in stellar atmospheres
12 p2173 A69-27172
- Vela pulsar investigated for optical pulsations, noting negative result for expected brightness
12 p2173 A69-27173
- Variable star BL Lacertae absolute spectral energy distribution in visible and IR regions, noting synchrotron features and possible quasar nature
13 p2335 A69-27315
- Book on astrophysics and stellar astronomy covering stellar radiation, binary and variable stars, positions, magnitudes, galaxies, cosmologies, etc
13 p2337 A69-27463
- Photoelectric observations of blue light minima of U Geminorum variable Ex Hydrae indicating no change in orbital period
13 p2338 A69-27558
- Photoelectric search for delta Scuti variables in Coma and NGC 752 clusters, discussing short period variability of B, A and F stars
13 p2343 A69-27620
- Short period variability of B, A and F stars observed in photometry of New Delta Scuti stars
13 p2348 A69-27803
- Photoelectric yellow and blue observations of variable TZ bootis light variation and orbital elements, noting maxima and secondary minimum causes
13 p2348 A69-27808
- Photoelectric yellow and blue observations of variable V502 Ophiuchi, noting influence of partial eclipses on orbital determination reliability
13 p2348 A69-27809
- Spectrophotometry of variable star SS Cyg, analyzing energy distribution in continuum, UV gradient and Balmer jump
13 p2351 A69-27868
- Photometric discovery of new variable stars resulting from quasars observation, noting optical variability noncorrelation with observed properties
13 p2354 A69-28468
- Variable comparison star identified from photoelectric observations of RR Lyrae star BR Aqr, showing light and color curves
14 p2519 A69-29139
- Variable stars in Large Magellanic Cloud from photoelectric measurements obtained in blue and violet, including periods of Cepheids and some period amplitude differences
14 p2526 A69-29853
- Variable stars research and facilities in Tautenburg, East Germany
15 p2682 A69-30438
- Variability of period of RR Lyrae type stars in globular cluster M3, deriving seasonal moments of stellar maxima and light curve elements
15 p2683 A69-30511
- Radial pulsation mode of convective envelopes in adiabatic equilibrium for variable M red supergiant stars
15 p2692 A69-30766
- Canum Venaticorum variable A star spectrum, listing all lines observed between 5000 and 6650 Å
15 p2692 A69-30773
- ET Pegasi photoelectric observations in UVB colors, giving period different from Kaho and new time of maximum light
15 p2694 A69-30787
- Revised proper motions for semiregular and RV Tauri variable stars tabulated from meridian observations and photographic positions, discussing computation methods
15 p2696 A69-31221
- Monograph on proper motions of RR Lyrae variables, discussing data acquisition analysis
15 p2700 A69-31493
- Five color photometry of X ray source SCO X-1 in 1966-1968, discussing luminosity pulsations and flare activity
16 p2847 A69-31648
- Carbon stars in south galactic pole region detected in objective prism survey, including variable R Scl and early R stars
16 p2860 A69-32232
- Spectral variations of red variable stars analyzed by objective-prism spectra in near IR
16 p2860 A69-32235
- Epsilon CrA light and color curves analyzed from UVB photoelectric photometry observations
16 p2863 A69-32398
- Photoelectric observations of W Ursae systems, including observed and computed times of minimum light and period change
16 p2863 A69-32399
- Eclipsing binary CQ Cephei envelope variability determined from photoelectric light curve, using astronomical telescope
16 p2864 A69-32593
- Polarization of light from atmospheres of Mira variables, suggesting temperature variations over stellar surface
16 p2866 A69-32820
- Variable CoD minus 35 degrees 4257 noting primary period of 502 days superimposed on secondary beat period of 3000 days
18 p3195 A69-34431
- Dimensions of 19 variable eclipsing binaries from published photometric and spectral orbital elements
18 p3198 A69-34766
- Variable star in Large Magellanic Cloud having unusual light curve with complex maximum lasting 300 days
19 p3403 A69-35965
- Forbidden emissions in CH Cygni and VV Cephei noting symbiotic star
19 p3423 A69-36228
- Forbidden transitions in emission line spectra of variables near minimum light, finding origin in hot chromosphere
19 p3424 A69-36232
- IC 4499 cluster variable stars coordinates in tabular form, showing high percentage of short period
20 p3598 A69-37462
- Spectroscopic and photoelectric observations of peculiar variable FG Sge, discussing expansion velocity and equivalent widths for Balmer and K lines
20 p3599 A69-37474
- Periods and magnitudes of RR Lyrae variable stars in M 2 cluster, tabulating photometric characteristics
20 p3599 A69-37477
- TiO bands identified in Mira variables IR region, discussing rotational structure and band strength-temperature relation
20 p3611 A69-38158
- Variable BL Lac SHF flux density measurements, discussing periodicity and maxima spacing
21 p3798 A69-38545
- Photometric and spectroscopic data for southern RR Lyrae variables, deriving period, light curves in three colors, mean radial velocity and spectral types
21 p3801 A69-38764
- Spectrophotometric observations of delta Scuti short period variable stars compared with model atmospheres
22 p4015 A69-40150
- Pulsational stability of pulsation modes of star in He burning evolution phase
22 p4022 A69-40467
- Variable stars blue sequence, proposing mu mechanism and beta mechanism as explanation for radial pulsations
22 p4026 A69-40650
- Variable HDE 310376 spectroscopic and photometric data, discussing brightness fluctuations, color changes, emission and absorption spectra, etc
22 p4026 A69-40651
- Omicron Andromedae radial velocity measurements /1961-1966/ during normal B star periods
22 p4028 A69-40755
- Photometric data for variable stars in Lyra and Cygnus including eclipsing variables
23 p4215 A69-42009
- Photometric data for long period variable stars in Cygnus obtained from plates of various observatories
23 p4215 A69-42010
- IR excess of R CrB type variable star RY Sgr, noting visual brightness and radiation in 2.0-3.4 micron range
23 p4220 A69-42377

VARIABLE SWEEP WINGS

- VFX fighter aircraft, discussing U.S. Navy requirements influence in VFX-1 and VFX-2 design
03 p0367 A69-13675

VARIABLE THRUST

Swing wings on combat aircraft and SST, discussing suitability for aircraft carriers and problems in aerodynamic balance 03 p0367 A69-13677

Early design stage flutter analysis for variable sweep aircraft, using subsonic flutter model 04 p0677 A69-14834

Tandem airfoils wing-tail interaction flutter analysis, using three dimensional vortex lattice aerodynamic theory [AIAA PAPER 69-57] 06 p1028 A69-18105

Critical flutter behavior of variable geometry aircraft with wing of 70 degree leading edge sweep, noting wing-tail interference 11 p1991 A69-25517

Supersonic aerodynamic characteristics of wings with complex planar geometry and subsonic leading and trailing edges, discussing varying geometry 14 p2391 A69-29624

VARIABLE THRUST

TRAC variable diameter rotor design based on jackscrew mechanism applied to compound helicopter [AIAA PAPER 69-221] 07 p1056 A69-19572

Oxidizer injector face configuration for high power variable thrust rocket engine using hydrogen/oxygen propellant 16 p2835 A69-31749

Small penetration aid rocket motors fabrication, discussing axial- and tangential-thrust integral assembly, impulse levels, delay line connection for igniters, production evolution, etc [AIAA PAPER 69-520] 16 p2795 A69-32779

VARIANCE [STATISTICS]

Variance fluctuations of 1/f noise and relation to sample number and lower cut-off frequency, noting nonstationarity hypothesis 10 p1656 A69-23661

Log amplitude variance calculation methods compared in statistics of optical scintillation by application to measurements with laser 14 p2486 A69-29642

Accuracy and variance of nonergodicity estimates for random processes associated with radiophysical applications 15 p2582 A69-30946

Vibration-proof devices obtained by relating variance determination errors in selective filter response, modulating process bandwidth and spectral analyzer passband 18 p3109 A69-34584

VARIATION METHOD

U CALCULUS OF VARIATIONS

VARIATIONAL PRINCIPLES

Variational principles of dynamic shell theory using Legendre transform for relations and boundary conditions of Timoshenko theory 01 p0166 A69-10262

Heat and mass transfer coefficients derived for reacting gas mixtures by applying variational principle 01 p0006 A69-10400

Collective stability of collisionless gravitating systems based on variational principles resembling energy principle 02 p0323 A69-12275

Variational technique for determination of temperature fields due to nonuniform heat transfer over surface of heat producing body 03 p0531 A69-12864

Incorrect variational and linear programming problems in optimal control theory, emphasizing regularization technique by Tikhonov 03 p0409 A69-13067

Ground state energy for single magnetic impurity dissolved in nonmagnetic metal, applying cluster variation method to s-d interaction Hamiltonian 03 p0485 A69-13298

Optimal body shape determination by mathematical-mechanical relations derivation, discussing variational problems and variational principles applicability 03 p0526 A69-13739

Reciprocal variational formulation for optimal control, estimating difference between suboptimal system response and optimum 03 p0457 A69-13766

Upper bound for free energy of nonlocal superconductor in magnetic field, using variational method and perturbation theory 03 p0491 A69-13971

Variational principle for solving nonlinear equations in elasticity theory, theoretical mechanics and mathematical physics 04 p0668 A69-14273

Steady state plasma flows stability equations, using variational principle for analyzing toroidal plasmas 04 p0635 A69-14556

Biot variational principle applied to combined conduction and radiation heat transfer 04 p0685 A69-14734

Interaction between point charges in Wheeler-Feynman electrodynamics, noting impossibility of deducing momentum and energy conservation from variational principle 04 p0631 A69-15059

Variational formulation of Einstein general relativity related to geometric foundations, deriving Bianchi identities from general invariance property 05 p0791 A69-15632

Models of continuous media with internal degrees of freedom based on Lagrangian variational principle 05 p0793 A69-15775

Variational methods applied to unsteady heat flow, describing approximate method for unsteady temperature field in heat conducting body 05 p0845 A69-15794

Reissner variational principle extended to cover elastodynamics, discussing relation with Hamiltonian function 05 p0835 A69-15870

Variational principles for differential equations and initial and boundary value problems in dynamic geometrically nonlinear elasticity theory 05 p0840 A69-16202

Supersonic gas dynamics variational problems concerning determination of axisymmetric minimum drag 05 p0699 A69-16675

Composite equivalent circuits method for complex waveguide-resonator couplings based on variational principle for admittance matrices of electromagnetic volume couplings 05 p0736 A69-16785

Soviet achievements in space research, comparing satellites with U.S. counterparts 06 p1005 A69-17561

Initially imperfect axially compressed cylindrical shells strength using variational principle, shell theory and deformation theory of plasticity [AIAA PAPER 69-91] 06 p1028 A69-18181

Complementary variational principles for boundary value problems in continuum mechanics of solids, obtaining generalized Hamilton canonical formalism 07 p1232 A69-19173

Variational solution of linearized molecular chemical-kinetic Boltzmann equation, discussing perturbation of Maxwell distribution, nonequilibrium correction to reaction rate and activation energy 07 p1185 A69-19301

Reciprocity, variational and uniqueness theorems developed within linear theory of coupled thermoviscoelasticity 07 p1233 A69-19327

Error bounds and variational methods for nonlinear boundary value problems for ordinary differential equations 08 p1343 A69-20536

Variational method for safety limits of perfectly plastic simply supported conical sandwich shells subjected to uniform internal pressure and obeying Mises yield criterion 08 p1416 A69-20702

Variational principle to obtain variational estimate of arbitrary functional of solution to radiative transfer equation 09 p1541 A69-22253

Generalized gravitational field equations derived on basis of principle of least action, noting vector potential of electromagnetic field 10 p1725 A69-23714

Nonradial oscillation modes of massive stars determined by Ritz method application to variational principle, allowing for gravitational perturbation 10 p1785 A69-24036

Hamilton principle for inviscid compressible fluid in Euler coordinates, analyzing shortcomings found in variational principles and model in Lagrangian coordinates 11 p1875 A69-25483

Linearized atmosphere model above flat earth, applying variational principle to energy between geostrophic equilibrium and reestablished states 12 p1215 A69-25954

Heat and mass transfer coefficients derived for reacting gas mixtures by applying variational principle 12 p2062 A69-26668

Equations of state for continuous media, using variational principles within framework of relativity theory 12 p2131 A69-26972

Variational principle for admissible functions particular solution in elasticity theory involving solid bodies with cracks 13 p2359 A69-272903

Inverse deformation in elastic materials, using variational principle to obtain equilibrium equations proper ties 13 p2360 A69-2732

Variational method used to determine accuracy of approximation technique for dielectric slab on sidewall of rectangular waveguide 13 p2233 A69-28073

Variational principle for finite element method restricting deflection shapes to small region of model surrounding single element 13 p2364 A69-28229

Variational principle based on assumed stress hybrid method suitable for finite element analysis of incompressible solids 13 p2368 A69-28348

Variational principle and convergence of finite element method based on stress distribution 13 p2368 A69-28349

Incorrect variational and linear programming problems in optimal control theory, emphasizing regularization technique by Tikhonov 14 p2424 A69-28749

Variational problems associated with supersonic gas flows with foreign particles, considering nozzle designs 14 p2389 A69-28801

Optimal control of variational problem for Markov chain, discussing convexity and concavity of loss function 14 p2470 A69-28903

General formulas, reciprocity theorem and modified Green formula derived from variational principles for mixed problem of wave equation 14 p2485 A69-29354

Semifree elastic membranes standing waves fundamental frequency, developing variational principle for first eigenvalue 14 p2535 A69-29365

Singularity-free global solutions to nonlinear differential equations associated with variational principles, deriving necessary condition for existence from dilatation invariance considerations 14 p2470 A69-29367

Sum rule properties of finite set of wave functions obtained from application of variational principles to basis functions linear combinations 14 p2471 A69-29921

Variational principle for solving boundary value problems and reciprocal formula for error estimation, discussing applicability to general transport phenomena problems 15 p2716 A69-30022

Variational principles of solid mechanics for finite element analysis of solid continua 15 p2705 A69-30429

Hamiltonian variational principle for stationary bounded MHD flows, choosing suitable functions and rigid conducting boundary location 15 p2660 A69-30910

Rapid convergence algorithms as second variation methods for dynamic optimization problems 15 p2645 A69-31235

Hamilton modified principle applied to nonlinear control problems including time delay, servosystem with ideal relay and liquid level control 15 p2583 A69-31304

D-stationary principle to determine optimum hypersurfaces in configuration space containing optimal motion trajectories 16 p2811 A69-31625

Periodic solutions of variational equations near equilateral equilibria, obtaining one parameter expansion of family of long period orbits 16 p2854 A69-31654

Langrangian equations resulting from restricted variational principles corresponding to heat conduction problem derived for boundary condition inclusion 16 p2877 A69-31872

Mixed plate element application to vibration and buckling eigenvalue problems based on Reissner variational principle, considering quadrilateral elements 16 p2874 A69-32176

Variational problem formulated for boundary value problem of steady heat conduction with general boundary conditions 16 p2880 A69-32378

Modified Bubnov-Galerkin-Ritz method for determining approximation coefficients in stress and displacement analysis, using mixed variational principle of elasticity theory 18 p3215 A69-34566

Equations of motion for plate vibration derived by complementary variational principle, including boundary conditions and thin plate transverse vibrations 18 p3218 A69-34626

Models of continuous media with internal degrees of freedom based on Lagrangian variational principle 18 p3173 A69-35028

Variational equations uniform closed solution for optimal trajectories during coast without use of numerical integration 19 p3399 A69-35671

Variational method for computer calculation of supercritical bending of thermoelastic uniformly loaded circular plates, determining Ritz parameter influence on accuracy 19 p3434 A69-35829

Structural damping effects on semiinfinite panel boundary aeroelastic limit by Galerkin variational method 19 p3437 A69-36148

Variational principle for Fredholm integral equations applied to inclusion and indentation problems in elasticity 19 p3440 A69-36589

Homogeneous compressible fluid sphere with axisymmetric magnetic field, analyzing oscillations and stability using variational principle 20 p3605 A69-37822

Variational problem for nonlinear functionals connected with finite plasticity, extending existence and uniqueness theorems to limit analysis 21 p3837 A69-39157

Variational principle applicable to nonlinear theory of shallow shells, deriving potential for equations describing uniform boundary conditions, discussing shell stability 21 p3838 A69-39191

Reissner variational principle applied to incompressible and nearly incompressible anisotropic thermoelasticity 22 p4040 A69-39980

Variational principles equivalent to mixed problems for parabolic equations with initial boundary conditions, noting heat conduction theory 22 p3974 A69-40231

Variational principle for stability of galaxies models, developing perturbation potential in terms of operator similar to Hartree-Fock exchange operator 22 p4022 A69-40468

Upper and lower bounds for certain classes of partial differential equations associated with variational problems in theory of deterministic control processes 22 p3976 A69-41034

MHD of ideal charged gravitating fluid by variational principle, considering Einstein general relativity theory 22 p3992 A69-41056

Plate and shell structures static and dynamic analysis by generalized variational principles in finite element method, discussing element displacement functions [AIAA PAPER 68-290] 23 p4227 A69-41882

Variational principle for analyzing dispersion properties of closed regular waveguide with traveling wave-modulated dielectric constant 23 p4123 A69-41943

Composite media elastic moduli upper and lower bounds determination using variational principles to characterize displacement and stress in time harmonic deformation 24 p4406 A69-43701

VARIATIONS

NT ANNUAL VARIATIONS

NT DIURNAL VARIATIONS

NT GEOMAGNETIC MICROPULSATIONS

NT GEOMAGNETIC PULSATIONS

NT MAGNETIC VARIATIONS

NT PERIODIC VARIATIONS

NT TWENTY-SEVEN DAY VARIATION

NT WIND VARIATIONS

Irregular pulsations in morning sky brightness using all-sky photographic airborne auroral observations along auroral oval 09 p1594 A69-21666

Visibility changes in fog at London airport determined by transmissometer records 18 p3167 A69-35266

VARIOMETERS

Piezoelectric variometer with reduced indicator time lag for measuring pressure gradients in fluid media 11 p1889 A69-25427

Gokhberg magnetovariational sounding method for single location analysis of magnetic storms early phases, comparing ground station network observations 20 p3521 A69-37040

Electric dose variometer principles, emphasizing differential pressure meter, differential capacitor and capacitor meter 24 p4315 A69-43143

VASCULAR SYSTEM

NT AORTA

NT ARTERIES

NT BLOOD VESSELS

NT CAPILLARIES [ANATOMY]

NT VEINS

Clinicomorphological changes in rabbit eyes vascular system by exposing transverse accelerations 08 p1262 A69-19832

Flow mechanics applications to medicine, discussing vascular and technical systems and measuring equipment adaptation to human organisms 17 p2915 A69-33771

Intravascular pressure and sound measured in anesthetized dogs and humans using fiberoptic pressure catheter 17 p2917 A69-34172

Rheography of blood circulation of forearm after tightening with pneumatic cuff, analyzing amplitude increase and information about vascular system 21 p3653 A69-38838

Intravascular gas emboli literature critique covering early nonclinical decompression experiments, clinical use of intravenous gas emboli, etc 21 p3655 A69-38916

Pulsatile blood flow physical characteristics in short vascular segments 22 p3878 A69-40785

Brown adipose tissue providing internal heating jacket and metabolic heater overlying systemic vasculature, noting cold survival role 23 p4091 A69-42013

Spontaneous rhythmical activity and mean vascular tone dependence in isolated helical rat aorta strips on extracellular concentration of noradrenalin 23 p4093 A69-42069

Gravitational stress effect on heart and venous system, discussing digital computer model simulating pressure changes under head-up and down tilt 24 p4271 A69-42783

VASOCONSTRICTION

Clinical spectrum of postural hypotension, treating vasodepressor syncope, orthostatic arterial anemia and idiopathic orthostatic hypotension 06 p0873 A69-17017

Renal vascular circulation in carotid occlusion pressor reflex by vasoconstriction in absence of renal autoregulation 22 p3887 A69-41190

VASODILATION

Whole body LF mechanical vibration effects on anesthetized dogs peripheral circulation and vascular smooth muscle 22 p3875 A69-40228

VASOMOTOR NERVOUS SYSTEM

U NERVOUS SYSTEM

VC-10 AIRCRAFT

Component reliability effect on airline operation of VC 10 aircraft, investigating failure modes and maintenance 24 p4318 A69-42776

VECTOR ANALYSIS

NT COLLINEARITY

NT COPLANARITY

NT CURL [VECTORS]

NT VORTICITY

Optimal control system sensitivity definitions, analysis methods and design techniques, discussing equations of motion of dynamical system satisfying vector differential equation 01 p0051 A69-10553

Controllability of dynamic systems obtained by studying vector function increments along system trajectories 01 p0051 A69-10698

Magnetic disturbance vector distribution during polar magnetic substorm 05 p0755 A69-16271

Two point boundary value problems of optimal trajectories solved by offset vector method 06 p0903 A69-17577

Three dimensional vector fields and flows geometry, discussing vector lines as geodesics on surfaces of normal congruence and flat vector fields 08 p1302 A69-19823

Wind vector in respect to orientation of large scale cirrus bands based on stereophotogrammetry and radar observations 08 p1346 A69-20442

Helicopter instability on ground with propulsion system operating and inoperative, discussing overturning, restoring moments and pilot training 09 p1433 A69-21385

Elliptic complexes over compact manifolds without boundary, discussing general theory of elliptic operators in vector bundles 09 p1532 A69-21733

Kerr type metric empty space times starting from fixed reference system and associated Killing vectors 09 p1540 A69-22050

Perturbations of Volterra integral equation with vectors in n-dimensional real or complex Euclidean space, comparing solution with linear system solution 11 p1909 A69-24886

Electric vector transformation for three dimensional photoelastic medium irradiated by light in reverse direction, noting optical systems of birefringent plates and rotators 12 p2180 A69-26339

Cyclic vector amplitude error from noisy data corrected for calculating geophysical lunar tidal effects 12 p2033 A69-26956

Time correlation functions for wind vectors and components at various altitudes over Moscow in winter and summer 13 p2294 A69-27856

Elastic and elastoplastic bodies, showing vector field for surface condition as sufficient condition for stability 15 p2707 A69-30621

Friction and wind relationships expressing actual and geostrophic wind as complex numbers or by corresponding vectors in Gauss-Argand diagram 16 p2808 A69-32455

Electromagnetic fields theory simultaneously determining vector electric and magnetic field aspects in terms of operator Green functions 17 p2924 A69-33833

Quadratic Liapunov function existence for exponentially stable linear system with varying coefficients described by vector differential equations 19 p3359 A69-35617

Plane elastic deformation in isotropic homogeneous medium using displacement vector, discussing finite difference equations and application to rectangular boundary 19 p3441 A69-36719

Computer iteration accelerator based on modified Aitken process, noting application to vectors 20 p3498 A69-36950

Orbital rendezvous calculation in terms of adjoint variables vector associated with vehicle velocity vector 20 p3595 A69-37202

Vector integral extension to optimal trajectory coordinate multiplier systems with constant of motion demonstrated for coast-arc problem [AIAA PAPER 69-907] 21 p3807 A69-39339

Analytic approximation for initial adjoint vector for optimal/minimum propellant/ space trajectories [AIAA PAPER 69-916] 21 p3808 A69-39345

Constraint torque elimination from vector equations canonical system for attitude dynamics of satellite consisting of arbitrarily interconnected rigid bodies [AIAA PAPER 69-923] 21 p3821 A69-39354

Three channel inertial ship or aircraft navigator for determining gravity vector, using earth gravity field model 23 p4162 A69-41320

Matrix method for free and forced oscillations of complex linear damping system with known linear vectors 23 p4236 A69-42484

Three dimensional pin-jointed trusses calculation method by state vector incorporating force and displacement matrices 23 p4236 A69-42485

Iterative and vectoral methods for correcting computed direction cosine matrix errors 23 p4134 A69-42543

Pointing vector and angular rate relationships for various optical elements, discussing analytical models development for precision electro-optical stabilization systems 23 p4131 A69-42544

Tolerance limits for uncertain requirements vector in linear programming with random variation, introducing nonparametric statistics with sensitivity analysis [AAS PAPER 69-079] 24 p4340 A69-42821

Sequential vector estimation of matrix of second partial derivatives, suggesting alternative least squares method 24 p4340 A69-42958

Vector matrix second order sensitivity equation application to Mars entry guidance, performing numeri-

VECTOR CONTROL

cal simulation of second order sensitivity guidance and tabulating results
24 p4388 A69-43690

VECTOR CONTROL U DIRECTIONAL CONTROL

VECTOR CURRENTS

Low latitude asymmetric disturbance field analyzed using equivalent current vectors during magnetic storms, allowing for solar quiet day variation and declination
16 p2778 A69-32184

Partially conserved axial vector currents and current algebra to obtain vertex functions at point having zero mass by extrapolations
17 p3008 A69-33004

VECTOR MESONS

Energy momentum tensor in Einstein field equations derived from covariant field equations for vector meson
14 p2486 A69-29452

Renormalization of second order self energy part of photon and lowest order corrections to single photon vertex using Lagrange vector meson density
21 p3775 A69-39468

VECTOR SPACES

NT ADJOINTS
NT BANACH SPACE
NT CANONICAL FORMS
NT EIGENVALUES
NT EIGENVECTORS
NT HILBERT SPACE
NT JORDAN FORM
NT MATRICES [MATHEMATICS]
NT STATE VECTORS
NT STOKES THEOREM [VECTOR CALCULUS]
NT VECTORS [MATHEMATICS]
NT VORTICITY

Book on optimization by vector space methods covering linear space vectors, time function problems, Hilbert spaces, etc
07 p1172 A69-18409

Iterative processes for solution of linear algebraic equations for n dimensional vectors in given space
10 p1718 A69-23208

Nondifferential function minimization on entire vector space or bounded subset for application to minimax problems in function spaces, time optimal control, etc
10 p1721 A69-23863

Einstein field equations solutions for homogeneous cosmological models, assuming perfect fluid gravitation source and existence of simply transitive surface motions
11 p1919 A69-25245

Topologies introduced on state space for differential equations to obtain dynamical systems
11 p1909 A69-25409

Closed linear operators in topological vector space generalized for Banach space case
13 p2288 A69-27734

Statistical description of geomagnetic field as random vector field, presenting correlation functions from empirical estimates from geomagnetic charts
14 p2437 A69-29062

N-dimensional vector functions branching process stability belonging to locally compact set in certain space
20 p3509 A69-37075

Iterative processes for solution of linear algebraic equations for n dimensional vectors in given space
21 p3756 A69-39149

Kinematic and dynamic relations analyzed by vector method for motion time and orbital flight control of point
21 p3818 A69-39820

Vector properties of isotropic strain hardenable materials in stress vector space applied to tubular brass subject to biaxial tension and complex loading
23 p4227 A69-41714

Conjugate points along lightlike geodesics in general theory of relativity, deriving existence from vector field matrix properties and Ricci curvature
23 p4213 A69-41724

VECTOCARDIOGRAPHY

Vectorometric EKG analysis of cardiac activity during hypokinesia with and without exercise and medication
05 p0710 A69-16519

Vectorometric EKG analysis of cardiac activity during hypokinesia with and without exercise and medication
18 p3096 A69-34738

Computer assisted electrocardiography, discussing multidipole analog simulation of heart electrical activity and vectorcardiogram recording
23 p4105 A69-41784

Norms for quantitative vectorecardiography derived from statistical analysis of results from healthy young subjects, emphasizing medical evaluation of flying personnel
24 p4277 A69-43390

VECTORS [MATHEMATICS]

NT EIGENVECTORS
NT STATE VECTORS
NT VORTICITY

Vector potential used to express equations of incompressible fluid motion in form suitable for digital solution, discussing boundary conditions
01 p0058 A69-10228

Vector potentials for Dirac equation derived assuming time independent external magnetic field without scalar potential
04 p0638 A69-15273

Characteristic equation obtained by considering world line vector, basic thermodynamic variables and metric tensor as functions of Lichnerowicz class
09 p1480 A69-21614

Comparison theorem for nonlinear real vector ordinary differential equation
10 p1720 A69-23638

Upper bounds for Bernstein-Kolmogoroff multidimensional inequalities, analyzing independent random vectors
11 p1910 A69-25698

Approximation of vector linear differential equations with slowly varying matrix coefficients on time sharing computers, noting modeling possibilities
17 p2996 A69-33879

Radiation field several wavelengths from dipole above plane earth, simplifying rigorous integral expression for Hertz vector by method of operators
21 p3770 A69-38748

Variational formulation of nonlinear differential equations, treating vector fields in Hilbert spaces, finding relations useful in quantum mechanics
23 p4181 A69-41723

VEGETABLES

NT POTATOES
NT SPINACH

Vegetable diet including 210 g of dry Chlorella biomass decreases effect on calcium and magnesium assimilation to produce insignificant negative balance of K and Mn
10 p1647 A69-23590

Space biological tests performed on lower animals and vegetables relating to higher organisms reactions during prolonged manned space flights, reviewing NASA experiments
12 p2019 A69-26494

Photosynthesis and respiration rate in vegetables in controlled temperature, humidity, illumination levels, carbon dioxide and oxygen contents
17 p2912 A69-32933

VEGETATION

Carrot plants growing during 374 days in conveyor type aeroponic assembly, noting yield and morphological features
17 p2912 A69-32943

Spectral reflectances of objects and vegetative backgrounds to generate color photographic technique increasing detection sensitivity and rate
18 p3133 A69-34247

VEHICLE WHEELS

NT NOSE WHEELS

Dynamic stability of dual wheel gears for aircraft applications, discussing shimmy, tire characteristics, velocity effects, etc
[AIAA PAPER 69-769] 19 p3245 A69-35654

VEHICLES

Flexible vehicle control, using cybernetic model for system design and response
[AIAA PAPER 69-115] 06 p1018 A69-18088

VEINS

Pulmonary capillary gas exchange and venous admixture model and inclusion into respiratory system model, discussing pressure and concentration gradients, pathological effects, etc
07 p1068 A69-19482

Rebreathing method for determining mixed venous oxygen pressure and cardiac output during rest and exercise in trained athletes
23 p4078 A69-41316

VELA SATELLITES

Particle measurements by Vela nuclear test detection satellites /2A and 2B/ noting plasma sheet in center of magnetotail
07 p1208 A69-19362

VELOCITY

U ACOUSTIC VELOCITY
U AIRSPEED
U ANGULAR VELOCITY

U CRITICAL VELOCITY

U ESCAPE VELOCITY
U EXHAUST VELOCITY
U FLOW VELOCITY
U GROUP VELOCITY
U HIGH SPEED
U HYPERSONIC SPEED
U LANDING SPEED
U LIGHT SPEED
U LOW SPEED
U ORBITAL VELOCITY
U PHASE VELOCITY
U PROPAGATION VELOCITY
U RELATIVISTIC VELOCITY
U ROTOR SPEED
U SOLAR VELOCITY
U SUBSONIC SPEED
U SUPERSONIC SPEEDS
U TERMINAL VELOCITY
U TIP SPEED
U TRANSONIC SPEED
U WIND VELOCITY

VELOCITY DISTRIBUTION

Spatial and kinetic distributions of molecules reflected by surface in rarefied atmosphere, discussing mathematical model
01 p0122 A69-10041

Tangential velocity profile growth in laminar axial flow through concentric annulus with rotating inner cylinder, using Navier-Stokes equations for prediction
01 p0058 A69-10143

Sonic flow at large distance and behind shock wave for axisymmetric body of revolution of finite dimensions in inviscid fluid
01 p0058 A69-10160

Molecular velocity distribution function in nonequilibrium flows, detailing asymptotic expansions in different velocity domains for weak shock
01 p0059 A69-10330

Free convection from partially uniformly heated and partially insulated vertical flat plate, discussing dimensionless velocity, temperature, heat flux and axial length parameters
01 p0175 A69-10331

Asymptotic solution of Orr-Sommerfeld equation by multiple scales method for linear and general velocity profile
01 p0059 A69-10332

Confined vortex in air tangential and axial velocity distribution based on smoke profile pictures
01 p0060 A69-10413

Quasi-static Kerr magneto-optic observation and procedure to predict results of dynamic flux reversal in thin Ni-Fe films
[IEEE PAPER 11.7] 01 p0138 A69-10716

Steady state circular motion of fluid with variable rheological characteristics between coaxial cylindrical surfaces, obtaining velocity distribution
01 p0061 A69-10733

Multiple velocity dispersion in normal hydrogen and normal hydrogen-helium mixtures at room temperature using ultrasonic interferometer
01 p0121 A69-11284

Liouville and Poisson equations solutions for locally ellipsoidal stellar velocity distributions with constant coefficients
02 p0310 A69-11455

Lunar seismic velocity distribution data indicates broad low velocity zone together with possible extensive melting at depth
[AAS PAPER 68-205] 02 p0312 A69-11480

Wing upper surface velocity distributions having peak near leading edge, considering incompressible flow at zero angle of attack
[ONERA-TP-632] 02 p0187 A69-11618

Turbulent velocity in faculae and photosphere obtained from IR triplet of oxygen analysis
02 p0314 A69-11646

Velocity field excited by wing vibrations propagating over elastic surface at supersonic velocities, considering nonvertical motion and absence of external forces
02 p0188 A69-11976

Turbulent jet model of unsymmetrical velocity profile for design of wall attachment device
02 p0231 A69-12072

Asymptotic laminar boundary layer in compressible gas in presence of normal and tangential velocity components at body surface
02 p0231 A69-12138

Transient laminar boundary layer development on flat plate following impulsive start of surrounding fluid motion, obtaining temperature and velocity distribution relationship
[ASME PAPER 68-HT-10] 02 p0232 A69-12208

Stability of laminar flow along flexible boundary using broken linear velocity profile
02 p0232 A69-12353

- Three dimensional wakes and jets, discussing center-line velocity, half width growth and velocity irregularities
02 p0190 A69-12549
- Anisotropic plasma cyclotron instability in magnetic trap with cold ion background and isotropic Maxwellian velocity distribution
02 p0292 A69-12554
- Velocity field generated by vibrations propagating at finite velocity over elastic wing surface
02 p0190 A69-12571
- Algorithm for Orr-Sommerfeld equation applied to stability of laminar flow, noting profile resembling mean velocity profile of turbulent flow in flat tube
02 p0233 A69-12573
- Interactions of moving solar plasmas and solar magnetic fields, discussing solar velocity fields and fine structure observations
02 p0329 A69-12784
- Turbulent boundary layer reversion to laminar state associated with departures from inner law velocity distribution in presence of favorable pressure gradients
03 p0414 A69-13016
- Three dimensional sonic flow downstream from shock wave in nondissipative perfect fluid, introducing pseudorotating flow to obtain velocity field
03 p0362 A69-13363
- Velocity field generated by shock wave incident on slender symmetrical body resting in infinite compressible medium
03 p0362 A69-13418
- Velocity dispersion and temperature anisotropy with respect to magnetic field direction, discussing inertial solar wind cooling effects
03 p0500 A69-13525
- Equilibrium turbulent boundary layer prediction for proposed Prandtl mixing length distribution
03 p0419 A69-13992
- Horizontal and vertical downward velocity components in developed solar active regions
04 p0651 A69-14370
- Approximate method for calculating vertical velocity distribution in atmospheric braking of bodies along ballistic trajectories
04 p0541 A69-14485
- Unsteady two dimensional flow in square cavity with fluid initially at rest and constant velocity upper surface of cavity, noting vortex center
04 p0587 A69-14510
- Smearred out electron beam generation for experiments on weak plasma turbulence by passing beam through aluminum foils
04 p0636 A69-15020
- Perfect magnetofluid model to study laminar flow stability along magnetic field, considering time dependences and rigid and free boundaries
04 p0637 A69-15045
- Space-time function for joint probability distribution of velocity and magnetic fields from hydromagnetic turbulence equations
04 p0638 A69-15277
- Viscous incompressible fluid motion in two or more dimensions and with zero fluid velocity on domain boundary, determining lower bounds and uniqueness for solutions
04 p0626 A69-15311
- Laminar heat transfer in circular pipes in low Peclet number flow case with laminar velocity profile, discussing Hagen-Poiseuille flows
04 p0687 A69-15397
- Random motion of particle with nonlinear damping, obtaining velocity spectrum by solving associated nonstationary Fokker-Planck equation and using equivalent linearization technique
04 p0561 A69-15454
- Round air jet projected parallel to wall, analyzing velocity profiles, decay and growth rate
04 p0591 A69-15487
- Velocity profiles for laminar flow of homogeneous liquid in pipe inlet at small and moderate Reynolds numbers
05 p0743 A69-15578
- Stationary velocity profile near jet driven vortex tube outer wall calculated by laminar boundary layer flow theory, neglecting wall curvature effects
05 p0798 A69-15610
- Laminar flow of stably stratified fluid with uniform upstream velocity and density gradient past thin flat plate, discussing upstream wake and boundary layer
05 p0745 A69-15724
- Equations for frequency portions of electron-velocity distribution function in Lorentz plasma under influence of time periodic electromagnetic fields with two fundamental frequencies
05 p0800 A69-15743
- Gas velocity variations in ionizing shock wave propagating along magnetic field applied to conducting piston motion
05 p0801 A69-15787
- Heat transfer, temperature and velocity profiles in circular free jet can be described by heat conduction type equations
05 p0747 A69-16032
- Thermal entry problem solution for low Reynolds number turbulent gas flow based on Reynolds number dependent velocity profile
[ASME PAPER 68-WA/FE-11]
05 p0748 A69-16090
- Mixing zone between two dimensional free stream and fluid at rest, measuring turbulent shear layer velocity profile behind rearward facing steps and over cavities
[ASME PAPER 68-WA/FE-21]
05 p0749 A69-16097
- Inlet velocity profiles distortion effects on flow regimes and performance in two dimensional diffusers with turbulent boundary layers
[ASME PAPER 68-WA/FE-25]
05 p0698 A69-16100
- Velocity profiles and eddy diffusivities for fully developed turbulent low Reynolds number pipe flow
[ASME PAPER 68-WA/FE-34]
05 p0749 A69-16107
- Velocity fields and wall shear stress distributions in eccentric annuli
[ASME PAPER 68-WA/FE-35]
05 p0750 A69-16108
- Static pressures, profiles of local longitudinal velocity, fluctuating wall pressures and power spectra of wall pressures measured for subsonic turbulent flow
[ASME PAPER 68-WA/FE-36]
05 p0750 A69-16109
- Heat transfer through vertical plane layer for various Prandtl numbers, discussing velocity and temperature profiles and effects of aspect ratio, Grashof and Rayleigh numbers
[ASME PAPER 68-WA/HT-4]
05 p0846 A69-16115
- Particles nonlinear motion in plasma in magnetic field with arbitrary electron velocity distribution, discussing wave discontinuity patterns
05 p0804 A69-16370
- Rotating hot wire and five hole pressure probes for determining complete velocity vector in subsonic flow
05 p0764 A69-16398
- Transformation of differential mean and current densities and anisotropy of cosmic ray particles and photons observed in frames of reference relative to each other with isotropic flux
05 p0817 A69-16651
- Velocity distribution of plasma electrons in electron beam generated He plasma using Boltzmann equation, neglecting electron-electron collisions
05 p0805 A69-16705
- Ion velocity distribution for high vacuum ion source, noting factors influencing dispersion
06 p0959 A69-16916
- Laminar flow stability along flexible boundary, using broken linear velocity profile instead of boundary layer profile
06 p0909 A69-17207
- 27-day cosmic ray intensity variations related to solar wind velocity nonuniformity due to longitudinal distribution of coronal active regions
06 p0990 A69-17292
- Stability of tangential velocity discontinuity between two media with different densities situated in acoustic field
06 p0910 A69-17344
- Stability theory application to laminar boundary layer transition prediction on two dimensional and axisymmetric flows having pressure distributions in incompressible flow
[AIAA PAPER 69-10]
06 p0914 A69-18127
- Time variation of velocity spheroid dispersion, axis ratio and vertex deviation in Galaxy due to star-cloud encounters
07 p1215 A69-18668
- Viscous gravitating sphere oscillations and velocity field, noting oscillations of Maxwell sphere
07 p1123 A69-18806
- Chromospheric velocity field temporal characteristics in quiet region of sun, determining power spectra of Doppler shifts of H alpha spectra
07 p1217 A69-19240
- Transition boundary layer on flat plate in subsonic wind tunnel measured by hot-wire method, obtaining velocity fluctuation distribution and turbulence intensity
07 p1121 A69-19329
- Analytical solution for plate velocity statistics of turbulent-flow-excited rectangular flat plate, discussing vibration excitation
07 p1236 A69-19461
- Velocity distribution in lower mantle, showing second major discontinuity in P wave travel time curve at 24 degrees
07 p1129 A69-19502
- Shear stress at wall, averaged velocity field and turbulent heat transfer coefficients in straight smooth non-circular channels used to compute temperature fields
07 p1243 A69-19734
- Plasma instability with isotropic ion or electron velocity distribution function /nonMaxwellian/, discussing magnetic field and particle energy distribution functions
08 p1359 A69-19949
- Isotropic Newtonian cosmological models symmetry shown to have velocity distribution obtainable from solution of Vlasov equation
08 p1386 A69-20073
- Diffusion coefficient, velocity distribution function and velocity averages for gaseous ions moving in strong electric fields, considering ion-gas molecule charge transfer collisions
08 p1355 A69-20209
- Time dependent velocity distribution functions for carriers calculated in weakly ionized plasma in external electric field
08 p1362 A69-20265
- Vibrational relaxation effects on laminar boundary layer velocity profiles and temperature and on layer thicknesses and wall heat flow downstream of shock wave
08 p1303 A69-20269
- Meteor angular velocities distribution over sky in showers, considering effect of altitude, night hour, season and azimuth
08 p1393 A69-20607
- Time harmonic, spherical harmonic and power series expansion of Boltzmann equation
08 p1353 A69-20793
- Stability of unsymmetrical plane flow noting velocity profile effect
08 p1304 A69-20812
- Loss cones effect of anisotropic Maxwellian velocity distribution on EM waves propagating perpendicular to magnetic field in infinite plasma
08 p1369 A69-20820
- Boundary value problem for linearized system of Navier-Stokes equations in three dimensional space, determining velocity vector and pressure
08 p1344 A69-21156
- Inertia limited flow transition to mobility limited flow in gas diodes by taking velocity moments of Boltzmann equation for electron velocity distribution function
09 p1462 A69-21325
- Planckian stellar velocity distribution function, moduli and projections on coordinate planes determined by ellipsoidal approximation
09 p1589 A69-21370
- Spatial size and velocity distributions for liquid or solid aerosols suspended in air flow using Q spoiled ruby laser and holography
09 p1492 A69-21418
- Vertical transport rate of charged particles in F region, allowing for vertical velocity gradients
09 p1485 A69-21529
- Poincare recurrence theorem applicable to collapsing gravitational system with particles velocity dispersion other than zero
09 p1593 A69-21567
- Velocity and temperature fields in Newtonian fluid in motion past stationary obstacle in gravitational field, noting similarity parameters reduction
09 p1429 A69-21686
- Constant property turbulent boundary layer flow, developing finite difference solution for prediction of velocity profiles and skin friction coefficient
09 p1482 A69-21950
- Radial velocity, light and magnetic variations of HD 10783 from concurrent UVB photometric and Zeeman spectroscopic observations
09 p1600 A69-22197
- Stability of thin rotating disks of stars with respect to axisymmetric disturbances, noting overstabilities dependence on epicycles sizes
09 p1605 A69-22413
- Quasi-linear relaxation of electron beam in magnetized plasma, noting instability of plateau in velocity distribution function
09 p1553 A69-22659
- Velocity profiles of turbulent boundary layers with constant and variable pressures using Cole formulation
09 p1484 A69-22780

Incident flow in variable cross section tubes using analytic asymptotic calculation

10 p1677 A69-22897

Incompressible Newtonian flow between two parallel planes, noting marginal stability condition, mean velocity profile and turbulence

10 p1678 A69-22909

Numerical solution of MHD equations for boundary layer electrically conducting gas flow near flat plate when velocity distribution of external flow obeys power law

10 p1727 A69-23093

Speed distribution and density of molecular beam from time domain measurements of propagated beam perturbations, discussing gate functions

10 p1652 A69-23340

Invariant finite amplitude spherical shock wave propagation in medium with inversely radial density

10 p1778 A69-23405

Singular integral equation for velocity in linearized Rayleigh problem in rarefied gas flow field solved by applying Luke weight coefficients

10 p1679 A69-23596

Mass and velocity distribution of interstellar clouds from Oort model simulated by Monte Carlo method on computer, predicting rogue cloud existence

10 p1779 A69-23608

Turbulent boundary layers on flat wall of supersonic wind tunnel, determining velocity profiles, thicknesses and skin friction coefficients

10 p1680 A69-23643

Boltzmann H function for moderately dense gas of identical particles with discrete velocity distribution in cases of nonisotropic binary and ternary collisions

10 p1725 A69-23790

Dynamical model for spherical inhomogeneity in mean mass density of universe to predict velocity dispersion observed for Coma Cluster

10 p1789 A69-24133

Longitudinal electric field distribution and charged particle density in magnetic mirror under potential difference between magnetic equator and plane

10 p1689 A69-24204

Velocity profiles of turbulent plasma flow in circular tube during application of longitudinal homogeneous magnetic field

11 p1922 A69-24234

Stellar model with magnetic field accelerating central core rotation to instability for determining rotating star energy and angular velocity distribution dependence

11 p1952 A69-24249

Atmospheric circulation contribution to velocity variations in earth rotation calculated by force moment method

11 p1952 A69-24258

Integral representation for velocity and pressure fields produced by horizontal motion of two dimensional bodies below or on free surface of viscous liquid

11 p1866 A69-24278

Similarity solution for flow of fluid-particle suspension over disk rotating at constant velocity, solving differential equations for flow velocity distributions

11 p1867 A69-24280

Chapman-Enskog procedure extension for binary gas mixtures, obtaining diffusion equation from revised relaxation time of component velocities

11 p1921 A69-24308

Differential solar rotation noting strong quasi-kineticity effect on solar convective zone and rotation influence on viscosity tensor and rotation law

11 p1955 A69-24390

Earth rotation velocities nonuniformity according to astronomical observation data obtained from Universal Time and atomic time scales comparison

11 p1957 A69-24407

Constant velocity moving object influence on indications of vertical gyroscopes having electromagnetic compensation with residual imbalance of sensor element

11 p1881 A69-24561

Stability of barotropic perturbations superimposed on wind velocity profile of basic currents in geostrophic multilayer models

11 p1911 A69-24586

Turbulent flow velocity field evolution in presence of random forces using equation of motion

11 p1867 A69-24628

Holographic recording of three dimensional flow field velocities, applying theory of particle size assessment via Fraunhofer holography

11 p1884 A69-24691

Turbulent boundary layer velocity distributions in uniform/accelerated compressible flow over flat plate,

using change of variables based on mixing length formula

[ONERA-TP-693]

11 p1867 A69-24752

Velocity profiles in unsteady laminar incompressible boundary layer over flat plate in shock tube by two parameter integral method

11 p1871 A69-25026

Velocity distributions and skin friction coefficients in turbulent boundary layers over flat plate with injection or suction through porous wall

11 p1871 A69-25027

Streamwise pressure gradient effect on velocity profile in viscous sublayer of two dimensional turbulent flow along smooth wall

11 p1872 A69-25131

Sandwich electrode for direction and magnitude measurement of velocity gradients at wall for flow around cylinder at high Reynolds numbers

11 p1872 A69-25132

East-west asymmetry in solar wind velocity due to solar rotation effects on interaction between fast and slow streams

11 p1950 A69-25148

Power law profiles of mean wind velocity and temperature in thermally stratified shear flow, considering dependence on thermal stability and Richardson number

11 p1874 A69-25381

Gas velocity variation in ionizing shock waves arbitrarily oriented with respect to magnetic field, considering magnetic viscosity and conductive piston

11 p1935 A69-25740

Spacecraft orbit control laws determined by studying influence of controlling acceleration in plane perpendicular to absolute velocity vector

11 p1965 A69-25743

Planetary nebulae radial velocities in large and small Magellanic Clouds compared with young objects rotational pattern and interstellar gas densities and velocities

12 p2155 A69-25891

Disaligning and velocity changing collisions influence on laser light induced saturation peaks or holes in velocity distribution of Ne atoms

12 p2105 A69-26317

Stony meteoric particles size and velocity during passage through atmosphere

12 p2157 A69-26341

Subsatellite point velocity determination by interpolation method using observation data without knowledge of orbital elements

12 p2158 A69-26435

Horizontal wind velocity energy spectra, attributing free atmosphere meso and microscale turbulence to meso and micrometeorological processes

12 p2070 A69-26575

Diurnal and seasonal variations in drift velocity vector of small scale inhomogeneities in F2 region

12 p2070 A69-26688

Interplanetary plasma flow directional velocity distribution from solar atmosphere active regions found inhomogeneous

12 p2149 A69-26698

Velocity distribution and density of neutral hydrogen in southern portions of M 31 and Sc-type galaxy M 33 by 75 m radio telescope

12 p2166 A69-27038

NGC 4038-9 velocity field from spectrum obtained at McDonald Observatory, suggesting existence of two centers of matter ejection

12 p2169 A69-27060

Flow stability of axisymmetric jet with parabolic velocity profile in fluid at rest, calculating critical Reynolds numbers

13 p2244 A69-27300

Incompressible conducting fluid turbulent flow velocity distribution in transverse magnetic field at small magnetic Reynolds numbers and constant MHD interaction frequency

13 p2246 A69-27498

Velocity profiles of MHD flow through electrically insulated circular channel in transverse magnetic field

13 p2307 A69-27501

Three phase high temperature liquid metal induction MHD generator performance, noting velocity profile nonuniformity influence

13 p2208 A69-27513

Arc plasma jets radial velocity profiles measured by two probes in cyclic movement between jet edge and middle, including error estimation

13 p2307 A69-27611

Velocity fluctuation amplitude in potential cone of plane jet compared to properties of irrotational fluctuations induced by flow boundaries

13 p2247 A69-27736

Velocity, enthalpy and mass flux radial distributions in laminar boundary layer from calorimetry of argon subsonic flow

[ASME PAPER 68-HT-16]

13 p2374 A69-27776

Velocity and temperature profiles in gaseous turbulent boundary layer above liquid surface used to study liquid film cooling heat transfer

13 p2375 A69-27792

Galactic force law from observed stellar velocity and space density distribution

13 p2348 A69-27802

Meteoroid flux measured by Explorer 16 and Lunar Orbiter, analyzing penetration rate, average velocity and consistency with photographic meteors

13 p2349 A69-27820

Vertical wind velocity profiles approximation accuracy determined by linear, exponential and logarithmic functions of altitude during ice and frost

13 p2293 A69-27846

Cloud drift radar measurements for determining wind velocity profiles in mesosphere, using rocket released dipole reflectors

13 p2253 A69-27848

Shear stress and velocity profile in MHD duct, examining turbulence damping by electromagnetic coupling

13 p2309 A69-28024

Laminar temperature and velocity profiles near plane rectangular surface for free supersonic flow, solving partial differential equations for mass, momentum and energy conservation

13 p2309 A69-28025

Maxwellian velocity distributions simulated in one, two and three dimensions by superposition of N monoenergetic isotropic distributions, noting application to kinetic theory computation

13 p2313 A69-28222

Electron velocity distribution function in gaseous plasma with known collective oscillations and frequency/wave number relationship

13 p2313 A69-28327

Monograph on velocity distribution function in turbulent boundary layer, discussing hot wire anemometer for mean velocity, turbulence intensity and higher order moments determination

13 p2250 A69-28336

Flat plate turbulent boundary layer, noting Navier-Stokes equations solutions and formation of rotations to determine velocity field

13 p2251 A69-28632

Model to study viscous flow characteristics in channel with porous walls and constant section, noting non-monotonic velocity profile

14 p2429 A69-29015

Semiempirical parameters in streamline division and momentum integral analyses for separated flows, using error function velocity profile and spreading parameter sigma

14 p2389 A69-29028

Interstellar gas radio and optical spectral lines of neutral H compared with Ca and neutral Na, discussing critically low velocity gas distribution

14 p2519 A69-29135

21 cm line emission surveyed for spatial distribution of random velocities of neutral hydrogen in solar neighborhood

14 p2520 A69-29371

Radial velocities of planetary nebulae in Magellanic Clouds and Galaxy, discussing Population I and II kinematics

14 p2520 A69-29377

Elastic collision effect on gas laser atoms velocity distribution and gain factor determined for strong collision model

14 p2459 A69-29388

Mixing zone between two dimensional free stream and fluid at rest, measuring turbulent shear layer velocity profile behind rearward facing steps and over cavities

[ASME PAPER 68-WA/FE-21]

14 p2430 A69-29443

Thermal entry problem solution for low Reynolds number turbulent gas flow based on Reynolds number dependent velocity profile

[ASME PAPER 68-WA/FE-11]

14 p2430 A69-29446

Density distribution in axisymmetrical gravitating systems with ellipsoidal velocity distribution function, using integral equation of state for effective radii of cylindrical configurations

14 p2486 A69-29465

Langmuir probe measurements leading to electron groups composition of electron velocity distribution function in negative glow light

14 p2493 A69-29694

- Three dimensional laminar boundary layer on semiinfinite permeable flat plate in viscous incompressible fluid flow, calculating velocity profiles and skin friction components
14 p2433 A69-29898
- Turbulent Hartmann flow between planes in perpendicular magnetic field including flow velocity profile measurements
14 p2500 A69-29908
- One dimensional approximation for free jet nozzle flow in perpendicular magnetic field, calculating velocity distributions
14 p2501 A69-29910
- Velocity distribution effect on electric field at walls for axisymmetric flow of electrolyte in circular channel in magnetic field of E shaped inductor
14 p2501 A69-29915
- Solar wind Helmholtz-type velocity discontinuities, noting plasma density and temperature stabilities from Explorer 34 observations
14 p2515 A69-29971
- Inlet shape and Reynolds number effects on entrance flow development, using laser flowmeter based on Doppler effect to obtain laminar velocity profiles
15 p2589 A69-30001
- Axial and radial turbulence intensities for flow through smooth round tubes, measuring velocity profiles and drag coefficients
15 p2590 A69-30003
- Anisotropic plasma cyclotron instability in magnetic trap with cold ion background and isotropic Maxwellian velocity distribution
15 p2658 A69-30251
- Velocity field excited by wing vibrations propagating over elastic surface at supersonic velocities, considering nonvertical motion and absence of external forces
15 p2547 A69-30259
- Airborne Doppler radar, estimating velocity distribution and density of pulse signals reflected from air and ground targets
15 p2567 A69-30349
- Chapman-Enskog theory applied to observed stellar velocity distribution function, attributing deviation from Maxwellian function to negative K effect
15 p2687 A69-30549
- Wind velocity fluctuations calculation in CAT based on closed equations numerical solution for turbulent layers in upper troposphere
15 p2649 A69-30649
- Particle drift velocity distribution of fully ionized plasma in magnetic field calculated by integration of Boltzmann equation
15 p2659 A69-30707
- Radio galaxy Messier 87 mass determined using virial theorem for nucleus velocity dispersion
15 p2695 A69-30883
- Plasma instabilities due to anisotropic velocity distributions computer analyzed to study nonlinear phenomena and validity limits of linear theory
15 p2661 A69-30920
- Critical study of Tidman model for turbulent electrostatic shock wave structure in plasmas, noting velocity distribution function role
15 p2661 A69-30927
- Single and two phase subsonic plasma jets temperature and velocity distribution, noting reduction by condensed phase and use of Schlichting curves
15 p2663 A69-30989
- Boundary value problem for linearized system of Navier-Stokes equations in three dimensional space, determining velocity vector and pressure
15 p2645 A69-31249
- Laminar boundary layer equation solution representing velocity profile by fourth degree polynomial
15 p2593 A69-31263
- Scattering of time harmonic linearly polarized plane electromagnetic wave by uniformly axially moving cylinder, analyzing first order velocity effects
16 p2748 A69-31579
- Transverse instabilities in collisionless electron plasma in absence of permanent magnetic field with spheroidal velocity distribution, noting application to shock theory
16 p2817 A69-31645
- Analytic expressions for motion of collisionless plasma created with isotropic velocities within uniform magnetic field, assuming equal electron and ion masses
16 p2818 A69-31673
- Two dimensional turbulent mixing with surface mass injection at supersonic and hypersonic speeds, noting velocity and temperature distributions
16 p2770 A69-31883
- Mean velocity distribution prediction in turbulent shear flows of variable density by coordinate stretching method
[AIAA PAPER 68-41] 16 p2770 A69-31888
- Turbulent boundary layer laminarization in conical nozzle flow, measuring velocity profiles and friction coefficient
[JPL-TR-32-1407] 16 p2732 A69-31894
- Ablation injectants effect on supersonic stream pressure distribution inside cavity and upstream boundary layer velocity profiles
16 p2770 A69-31902
- Density and velocity fluctuations in hypersonic turbulent boundary layer based on Wallace data
16 p2770 A69-31908
- Solar wind velocity distribution anisotropy at earth explained by low density
16 p2849 A69-32097
- Velocity field in turbulent flow based on momentum transfer, determining velocity distribution for flow near solid surface
16 p2772 A69-32128
- Correlation between F region electrons vertical motion velocity variations and E region electrons horizontal motions in equatorial ionosphere
16 p2779 A69-32193
- Spatial distribution of stellar densities and velocity distributions in phase space, using Greenwich catalog of positions and proper motions of omega Centauri cluster stars
16 p2859 A69-32220
- Vertical transport rate of charged particles in F region, allowing for vertical velocity gradients
16 p2783 A69-32524
- NonMaxwellian electron velocity distribution influence on ionospheric measurements by Thompson scattering, explaining disagreement between scattering and probe measurements of electron temperature
16 p2788 A69-32647
- Velocity and static pressure redistribution in distorted flow field upstream of axial flow compressors
[AIAA PAPER 69-485] 16 p2842 A69-32694
- Ultrasonic velocity dispersion in para hydrogen and mixtures with He, Ne and Ar at 300 K, obtaining rotational relaxation times
16 p2815 A69-32791
- Transverse turbulent pipe flow, obtaining limiting behavior of time averaged velocity gradient at wall
17 p2949 A69-33013
- Stationary galaxy dynamical theory, assuming constant velocity body of physically homogeneous star subsystems in space
17 p3031 A69-33102
- Spontaneous gas laser emission from level coupled by spontaneous transition with emitting level, obtaining atoms interaction with laser field velocity distribution and spectral line width
17 p2981 A69-33116
- Mixing length model to relate turbulent shear stress to mean velocity field within planetary boundary layer above surface roughness change
17 p2997 A69-33154
- Chemical species flux decay in turbulent boundary layer with catalytic wall, obtaining solution of conservation equation by using shear stress distribution
[AIAA PAPER 69-709] 17 p2955 A69-33480
- Magnetic field effects on rotating cone compressible boundary layer at zero angle of attack, describing changes in drag coefficient, torque and velocity profiles
[AIAA PAPER 69-721] 17 p2892 A69-33484
- Turbulent velocity distribution and wall friction calculated from eddy viscosity distribution for concentric annulus
17 p2956 A69-33575
- Monte Carlo inversion of seismic body waves for transposing uncertainties of observations to velocity models
17 p2962 A69-33654
- Swept wing attachment line boundary layer, measuring skin friction in full turbulence and velocity profiles with and without trip wire
17 p2958 A69-34047
- Radial velocities differences as indicator of stellar atmospheric turbulence, applying method to sun
17 p3044 A69-34177
- Taylor vorticity transport theory and von Karman similarity hypothesis extended to consider three dimensional fluctuating velocity field in analyzing turbulent swirling ducted flow
[ASME PAPER 69-APM-19] 18 p3120 A69-34394
- Ejector driven wind tunnel for turbulent flow generation with arbitrary velocity profile, using jet arrays
[AIAA PAPER 69-743] 18 p3114 A69-34408
- Conservation theorems for energy and mean circulation in inviscid rotating fluid, noting inertial wave spectrum continuity
18 p3121 A69-34550
- Planckian velocity distribution function, moduli and projections on coordinate planes determined by ellipsoidal approximation
18 p3198 A69-34759
- Gas velocity variations in ionizing shock wave propagating along magnetic field applied to conducting piston motion
18 p3181 A69-35038
- Velocity and angular distributions of KBr formed in reactive collisions between crossed molecular beams of K and thermal HBr/DBr/
18 p3178 A69-35476
- Maximum trajectory for glider entering earth atmosphere at supercircular velocity, subject to maximum altitude constraint
19 p3399 A69-35667
- Axisymmetric laminar and turbulent wakes of body in flow with streamline pressure gradient, discussing velocity defects and profiles
19 p3296 A69-35762
- Hydrodynamic equations of laminar plane flow of incompressible viscous fluid in rectangular region, calculating velocity field by equivalent network and integration
19 p3297 A69-35853
- Turbulent velocity of flame propagation in supersonic stream of hydrogen-air mixture determined by velocity distribution, exchange coefficient and burning time
19 p3448 A69-35854
- Single junction vacuum thermocouple measuring thermal beam effect with reference to velocity distribution perturbation in molecular beam scattering
19 p3376 A69-36173
- Energy dependence of elastic total collision cross section of identical He molecules, using velocity selected primary beams at low target temperature
19 p3378 A69-36186
- Flame acceleration data applied to unburnt gas boundary layer analysis, discussing velocity and temperature profiles, layer thickness variation and expansion phase backflow
19 p3450 A69-36359
- Inverse transformation method for plane subsonic flow extended to flow past cambered profiles at angle of attack, obtaining velocity distribution
19 p3240 A69-36473
- Tangential and radial velocities in vortex boundary layer flow, relating diminishing amplitudes to increasing height using iterative method
19 p3363 A69-36499
- Mean parameters calculation between widening of turbulent flow and point of reattachment, including similarity hypothesis concerning velocity profile
19 p3299 A69-36648
- Dimensionless radial and transverse velocity profiles for unsteady incompressible boundary layer on rotating disk in rotating fluid
19 p3300 A69-36720
- Sedov formula for complex velocity of arbitrary circulation in two dimensional theory of small curvature thin wings
19 p3242 A69-36795
- Three dimensional velocity field disturbed by shock wave traveling across slender wing at supersonic speed
19 p3242 A69-36797
- Solar wind velocity cycles from fluid MHD viewpoint, applying Kelvin theorem on circulation stability in closed fluid system
20 p3587 A69-37041
- Low density free jet properties, discussing velocity distribution perpendicular to axis and correlation of all terminal parallel Mach numbers for monatomic gases
20 p3514 A69-37206
- Thesis on turbulent velocity distribution and wall friction in flow channels of various cross sections
20 p3515 A69-37925
- Linear dynamic modeling of barotropic fluid in rigid circular tube, presenting axial velocity profile by confluent hypergeometric function with complex arguments
[ASME PAPER 69-FLCS-18] 20 p3516 A69-37982
- Boundary layer velocity distribution in turbulent swirling pipe flow produced by twisted tape inserts
[ASME PAPER 69-FE-14] 20 p3516 A69-37990
- Statistical description of turbulence of viscous incompressible fluid at large Reynolds numbers, using velocity distribution probability
20 p3517 A69-38007

VELOCITY ERRORS

Equilibrium velocity distributions of F region photoelectrons produced by solar ionizing radiation, discussing dayglow as impact result
20 p3591 A69-38061

Irregular galaxy NGC 3077 with interstellar dust, measuring velocity field by spectroscopy
20 p3610 A69-38144

Gas in H II regions and associated stars radial velocities correlation and systematic difference suggesting relationship between nebulae and stars
20 p3611 A69-38150

H II regions radial velocities ellipsoidal distribution in M 33 explained as distribution with minor axis in direction of rotation
21 p3797 A69-38538

Electron plasma velocity distribution function determined from dispersion equation by harmonic function analog
21 p3776 A69-38565

Heat transfer coefficients, boundary layer thicknesses and temperature and velocity distributions in free convection boundary layer in closed axisymmetric volumes
21 p3848 A69-38634

Energy spectra measurements of turbulent velocities behind grids of different geometries noting relation to deviation from isotropy
21 p3693 A69-38704

Equations governing steady diabatic gas flows in Crocco velocity vector field, discussing changes in total pressure
21 p3695 A69-39007

Periodic motions of mechanical oscillators with velocity discontinuities analyzed by differential equations
21 p3771 A69-39009

Pulsation velocities distribution wind in meteor region of atmosphere during hourly intervals over eleven month period, noting normal distribution
21 p3759 A69-39115

Velocity and temperature distribution curves in turbulent boundary layer formed by natural convection on isothermal vertical plate, using Prandtl and Nusselt numbers
21 p3852 A69-39430

Velocity and temperature profiles at Prandtl number values obtained for unsteady laminar free convection on infinite vertical plate with stepwise varying temperature
21 p3853 A69-39681

Small particle holography technique extended for dynamic properties of particle fields, determining velocity and density field, size distribution, flow structure and diffusion rate
21 p3726 A69-39776

Flow structure in wake behind cylinder in plane channel, discussing circulation zone variation and velocity and turbulence distribution at various channel cross sections
21 p3698 A69-39850

Velocity profile and skin friction in boundary layer on flat plate with periodic vorticity near leading edge
22 p3929 A69-40015

Magnetoplasma with Maxwellian velocity distribution, investigating quantitatively longitudinal dielectric function
22 p3988 A69-40066

Blood sheet flow velocity distribution and pressure gradients in pulmonary alveolar septa determined, allowing for system elasticity
22 p3874 A69-40216

Dynamics of viscous electrically charged gas using Navier-Stokes equation
22 p3931 A69-40686

Fluid velocity in starting flow in circular tube using Laplace transform
22 p3931 A69-40688

Detonation velocity variation in nitromethane with initial pressure, discussing relationships
22 p4051 A69-40713

Skin friction and mean velocity profiles measured for fully developed 1000-10,000 Reynolds number flows in pipes and channels
22 p3932 A69-40897

Distributed suction effect on boundary layer structure of water flow from turbulence measurements, determining velocity and pulsation intensity distributions
22 p3933 A69-41029

Velocity defect profile and skin friction law for incompressible equilibrium turbulent boundary layer, using mixing length relation
22 p3934 A69-41180

Radial velocities for O and B stars in Milky Way field in Scorpius determined from prism spectrograms with specific dispersion at H gamma line
23 p4211 A69-41489

Rocket engine plasma jet radial velocity measurement by induction-velometric method using moving probe [DGLR-69-024C]
23 p4202 A69-41926

Spanwise velocity profiles through cascades and axial flow turbomachines, analyzing loading, secondary losses and inlet conditions interacting on downstream profile
23 p4061 A69-42110

Boundary layer separating collisionless plasma from one dimensional magnetic field for anisotropic particle velocity distribution functions, preserving charge neutrality in boundary layer
23 p4197 A69-42415

Weak magnetic field amplification in turbulent flow with velocity field as random function of space and time
24 p4375 A69-42657

Plasma microinstabilities due to ion and electron anisotropic velocity distributions, considering frequencies near harmonics of ion cyclotron frequency
24 p4355 A69-42686

Air bubbles rise velocity and path in water based on time measurement of bubble traversing two light beams, describing electronic recording system
24 p4299 A69-42918

Equal velocity contour diagrams for interstellar matter emission and absorption study in Cassiopeia-Perseus region
24 p4384 A69-43050

Stars with motions greater than 100 km/sec perpendicular to galactic plane, tabulating data for CH, subdwarfs, cepheids and horizontal branch stars
24 p4386 A69-43348

Symmetry properties of Cameron-Martin-Wiener kernels in isotropic velocity field, applied to one dimensional model of incompressible turbulent flow
24 p4301 A69-43358

Velocity and pressure fields produced by deformable load carrying filament studied for unsteady gas motion past slender body with nonpotential external forces
24 p4246 A69-43483

Gas phase self induced pressure field and laminar velocity distribution of working fluid within closed heat pipe channels analyzed by momentum integral method [ASME PAPER 69-HT-22]
24 p4412 A69-43546

Supersonic viscous flow around sharp corner at various expansion angles, giving pressure distributions and velocity profiles role
24 p4247 A69-43555

Mean velocity and pressure fields in turbulent boundary layer on flat plate at Mach 2 investigated for ratios of mass flow [AIAA PAPER 68-129]
24 p4304 A69-43581

LF approximation in predicting unsteady aerodynamic forces affecting large aircraft stability, analyzing velocity potential of oscillating wings
24 p4250 A69-43729

Differential solar rotation noting strong quasi-kineticity effect on solar convective zone and rotation influence on viscosity tensor and rotation law
24 p4390 A69-43780

Earth rotation velocities nonuniformity according to astronomical observation data obtained from Universal Time and atomic time scales comparison
24 p4391 A69-43797

VELOCITY ERRORS

Interplanetary midcourse velocity correction schedules optimization, discussing timing equations modifications, mission simulation and role of earth based radar
21 p3766 A69-39646

HF vibrations effect on motion of gyroscopic linear acceleration integrator, showing additional error in flight vehicle acceleration measurements
22 p3946 A69-40253

Black Arrow third stage velocity increment vector accuracy, considering attitude errors due to spin-up and spring separation systems, separated stages interactions, light-up impulses, etc
23 p4209 A69-41301

Radial velocity errors in high dispersion astronomical spectrographs in terms of variable spectral shifts along plate produced by mirror surface irregularities
23 p4167 A69-42189

Stellar radial velocity measurement accuracy dependence on dispersion, spectrum and line width
24 p4386 A69-43347

VELOCITY MEASUREMENT

NT WIND VELOCITY MEASUREMENT

Laser Doppler velocity profile measurement at localized points in flow stream without disturbing flow
01 p0090 A69-10298

Crack growth in ceramics from velocity measurements on glass and sapphire as function of applied force, temperature and moisture environment
01 p0101 A69-10767

Gyro vibrator /angular rate measuring device/, discussing output signal and natural frequency dependence on moments of inertia
01 p0083 A69-11004

Fluidic acceleration sensor based on vibrating string principle, discussing design, suspension system, driving-oscillator circuit, beat frequency circuit and detection circuits
02 p0249 A69-12091

Velocity measurement and flow pattern determination of plane shock waves during passage through channel diaphragm
02 p0234 A69-12589

Mass velocity of detonation products of hydrogen-oxygen mixtures measured by simultaneously recording internal resistance and induced voltage in ionized medium
02 p0354 A69-12628

Fluid flow velocity measurements by optical device having trigonal rectangular glass prisms and microscope objective
03 p0427 A69-12969

High speed compression waves, rarefaction waves and gas interface regions position and velocity measurement in shock tube by sensing electrical impedance
03 p0428 A69-13104

Earth velocity through 3 K cosmic background radiation, measuring velocity by determining anisotropy of radiation
03 p0511 A69-13475

Optical signal frequency method for measuring velocity of fluid flow
04 p0598 A69-14995

Nondirectional probe for mean velocity measurement in turbulent flow, determining reduced velocity profiles in interior of free flow
04 p0600 A69-15056

Differential thermistor gauge using Wheatstone bridge for use in free molecule pressure probe measurement of macroscopic velocity in rarefied gases
04 p0601 A69-15117

Thin film heated Pt resistance thermometer for skin friction or velocity measurements in air, water or blood
04 p0601 A69-15118

Threshold signals and optimum signal parameters in radar range and velocity measurements
04 p0560 A69-15403

Trailing edge velocity and stagnation points for isolated and latticed airfoils using Zhukovskii and Weing transformations
05 p0697 A69-15880

Unsteady potential flow and wake near oscillating circular cylinder noting velocity, pressure and correlation measurements [ASME PAPER 68-WA/FE-23]
05 p0749 A69-16099

Vehicle motion parameters in Newtonian central force field determined, using geometrical structures devised from properties of velocity hodograph
05 p0765 A69-16686

Low range airspeed system /LORAS/ on X-22A and P 1127 VTOL aircraft for accurate airspeed information
05 p0767 A69-16774

Laser Doppler meter model interpreting output frequency in terms of particle crossing set of fringes
06 p0932 A69-16927

Particle velocity measuring technique for two phase turbulent flows, using laser and Fabry-Perot interferometer
06 p0933 A69-17252

Forward velocity of Bostick plasmoids demonstrated proportional to mean surge current through button source
06 p0964 A69-17480

Doppler shift measurements of axial and rotational velocities in MPD arc, using reference lines from iron arc [AIAA PAPER 69-110]
06 p0972 A69-18171

Angular velocity of rotation measurement using angular gas laser undergoing axial torsional vibrations
07 p1147 A69-18523

Rise velocity of large gas bubbles in liquid calculated, assuming velocity is determined by propagation of bubble produced wave disturbance
07 p1120 A69-18999

- Velocity measurement by combination of Doppler principle and schlieren method involving reflection, refraction or diffraction of laser beam
07 p1135 A69-19259
- Photographic measurement of parachute exit velocity during ejection from chute, describing electronic recording and unit operation with block diagram
08 p1317 A69-20875
- Velocity meter for precision adjustment of orbits of vehicles in space for long periods using digital integrating accelerometer
08 p1348 A69-21063
- Three dimensional laser Doppler velocity instrument for mean velocity and turbulence measurements in subsonic jet shear layer
[SAE PAPER 690266] 09 p1494 A69-21555
- Self oscillations in angular velocity sensor using electric spring and potentiometric pickup, examining friction moment and inductance coil effects
09 p1497 A69-22106
- Noninterfering instrumentation techniques to measure hypersonic flowfield parameters in wind tunnels, measuring flight time of pulsed laser generated spark for velocity
10 p1672 A69-23266
- Moving conducting media velocity measurement using Reynolds number and electrical conductivity values, based on magnetic field distortion
10 p1731 A69-23435
- Radar and photographic studies of meteors from Leonid and Perseid showers, presenting velocities, luminescence and ionization
10 p1783 A69-23895
- Spectral measurement of luminous trails produced by injecting high velocity submicron diameter iron particles into gaseous targets compared with meteor spectra
10 p1790 A69-24142
- Conventional and dual beam laser Doppler methods for velocity measurement of solids, liquids and gases
11 p1893 A69-24333
- Expansion velocity of discharge plasma in exploding wires measured by X ray flash and streak photography, noting discrepancy
11 p1926 A69-24472
- Distance vs time and velocity vs time measurements for high speed model missiles by means of laser interferometry and optical Doppler shift method
11 p1886 A69-25042
- Sandwich electrode for direction and magnitude measurement of velocity gradients at wall for flow around cylinder at high Reynolds numbers
11 p1872 A69-25132
- Shock wave structure in gas mixtures, discussing velocity and temperature undershoot and overshoot
11 p1874 A69-25356
- Transistorized tachometer for rotational speed measurement and overspeed protection of automotive internal combustion engines
12 p2090 A69-26240
- Laser Doppler particle sensor to measure velocities in rocket exhausts, using He-Ne laser light source and Fabry-Perot interferometer frequency filter
[AIAA PAPER 68-723] 12 p2094 A69-26783
- Laser Doppler method for measuring local particle velocities in two phase flows of liquid-metal MHD generators
13 p2260 A69-27476
- High velocity liquid lithium effect on structural materials for MHD power generators, discussing material loss
13 p2278 A69-27478
- Time of flight measurement for velocity of micron sized particles in two phase flow by light transmission method
13 p2263 A69-28243
- Coaxial three coil probe measuring local electrical conductivity and velocity in plasma streams, discussing operations in electrolytes and axisymmetric plasma stream
[AIAA PAPER 69-327] 13 p2313 A69-28264
- Radial velocities of southern OB stars and supergiants noting tabulation of information
14 p2519 A69-29368
- Ultrasonic pulse velocity and attenuation measurement in presence of noise, using coherent detection and signal averaging
14 p2449 A69-29564
- Turbulent boundary layer in corner, measuring velocities, wall shear and turbulent normal stresses by employing momentum integral and similarity analyses
14 p2431 A69-29576
- MHD properties of velocity measurement method using cylindrical glass filament probe and Pitot and Prandtl tubes
14 p2453 A69-29920
- Group delay time for dispersive wave propagation velocity determined using correlation method
15 p2562 A69-30094
- Correlated noise effect on accuracy of suboptimal servosystem velocity measurements from recording Doppler frequencies
15 p2567 A69-30341
- Radial velocities measuring tracking rate meter performance for Doppler frequencies, allowing for multiplicative noise
15 p2576 A69-30350
- Fluid flow velocity measurements by Doppler shift of laser light scattered from moving fluid, determining beat frequencies
15 p2616 A69-31291
- Acoustic velocities in polymethylmethacrylate measured as functions of frequency, temperature and pressure, comparing data obtained with equation of state high pressure determinations
16 p2825 A69-31695
- Shock attenuation and equation of state of polyurethane based on aquarium technique and free surface velocity measurement
16 p2828 A69-31810
- Axial velocities in ammonia MPD thrutor exhaust by measuring Doppler shifts of spectral lines emitted by plasma constituents
16 p2835 A69-31890
- Airstream parameters /temperature and velocity/ of turbulence intensity in jet core at tube exit and behind grids measured by He diffusion method
16 p2771 A69-31959
- Angel sources rate of motion observed at automatic tracking coherent pulse station, obtaining coincidence with wind and insect velocities
16 p2779 A69-32276
- Hot-wire anemometers calibration technique providing accurate and direct velocity measurements in slow moving liquids
17 p2971 A69-32901
- Fluid amplifier with sudden widening applied to various computer tasks, utilizing for detection and measurement of viscosity, temperature and sonic or rotational velocity
17 p2903 A69-33010
- Tachoheliograph /modified spectroheliograph/ for obtaining two dimensional solar velocity maps, discussing construction and theory of operation
17 p3030 A69-33061
- Mean rotational velocity of finite width gaseous ring in close binary system from rotational velocity measured on spectrograms
17 p3044 A69-34180
- Shock wave propagation in two types of electromagnetically driven shock tubes, describing probe for shock front velocity measurement
18 p3119 A69-34260
- Fluidic sensor for measuring gas and liquid velocities, describing design and principles of operation
18 p3133 A69-34308
- Radial velocity measurements with objective prisms and results in SA8
18 p3201 A69-35143
- Explosives parameters effect on metal sheet velocity during explosive welding, considering load density and explosive force
18 p3149 A69-35279
- Vibrarotor gyroscope operated as rate gyro for simultaneously indicating two components of angular velocity by amplitude and phase of periodic output signal
18 p3139 A69-35299
- Fraunhofer holography for measurement of three dimensional flowfield velocity components, investigating rectangular channel flow
19 p3305 A69-35729
- Holographic velocimetry data reduction applicable to flow field holograms, using singlet interference pattern for spherical and plane wave illumination
19 p3305 A69-35730
- Particle size, velocity and position in moving streams measured by tilted film plane optical system with pulsed light source
19 p3306 A69-35733
- Laser Doppler velocimeter /LDV/ for fluid velocity measurements, noting advantages
20 p3552 A69-37004
- Zeta Tauri shell spectrum radial velocity measurement results compared with extrapolated seven year curve by Delplace
20 p3599 A69-37471
- Irregular galaxy NGC 3077 with interstellar dust, measuring velocity field by spectroscopy
20 p3610 A69-38144
- Radial velocities recording inaccuracies by solar magnetographs caused by dissimilarity between photomultipliers characteristics, describing photometer designs to eliminate errors
20 p3547 A69-38308
- Cloud velocity computations from ATS 1 and 3 satellites spin-scan photographs for prediction of neph systems motion and thunderstorms
21 p3757 A69-38370
- Interferogram observations of central velocity of M 31 under constant rotational velocity assumption, noting galaxy inclination
21 p3797 A69-38481
- Velocity decay and heat transfer rates measurement in cylindrical wall jet formed by jet emerging through convergent nozzle
21 p3695 A69-38972
- Impulsive velocity correction determination method for precise stationkeeping of stationary satellite, discussing perturbations
[AIAA PAPER 68-456] 21 p3817 A69-39757
- Gas laser-Doppler radar system for moving materials velocity and length measurements in industrial processes
22 p3955 A69-40237
- Book on radial velocities and distances in southern Milky Way stellar fields, covering statistical study of star motions in Galaxy, instrumentation, procedures, etc
22 p4020 A69-40317
- Free stream velocity in high enthalpy arc heated wind tunnel by measuring imposed temperature modulation apparent phase shift, describing circuit diagrams
22 p3926 A69-40444
- Omicron Andromedae radial velocity measurements /1961-1966/ during normal B star periods
22 p4028 A69-40755
- High radial velocity matter of bright region near Trapezium in Orion Nebula, determining electron density lower limit and mean velocity
22 p4029 A69-40769
- Piston driven shock tube at Kyoto University with performance tests results, investigating compression processes, shock speed and flow duration time
22 p3928 A69-41046
- Radial velocity data monitored during Venera 4 descent used for determining vertical and horizontal atmospheric flows velocities
22 p4034 A69-41099
- Monograph on hot wire anemometer measurements of velocity and temperature turbulence, discussing flow characteristics, calibration, etc
22 p3951 A69-41256
- Stroboscope method for measuring pulsating flow transient velocity based on hot-wire chronometric recording of small ion clouds emitted during pulsation
22 p3951 A69-41257
- Spectroscopic azimuthal and axial measurement of jet velocity in MPD X9 rocket engine by spectrograph and Fabry-Perot interferometer
[DGLR-69-024B] 23 p4202 A69-41925
- Rocket engine plasma jet radial velocity measurement by induction-velometric method using moving probe
[DGLR-69-024C] 23 p4202 A69-41926
- Stellar radial velocity measurement accuracy dependence on dispersion, spectrum and line width
24 p4386 A69-43347
- Hot-wire anemometer calibration technique for measuring velocity of very slowly moving liquids
[ASME PAPER 69-HT-A] 24 p4316 A69-43527

VELOCITY MODULATION

- Electron bunching improvement by combined effect of space charge and inhomogeneous electrostatic field on velocity modulated electron flux in microwave devices
05 p0799 A69-15646
- Electron bunching improvement by combined effect of space charge and inhomogeneous electrostatic field on velocity modulated electron flux in microwave devices
16 p2823 A69-32503

VELOCITY POTENTIALS

- U FLOW DISTRIBUTION

VELOCITY PROBES

- U PITOT TUBES
U SPEED INDICATORS

VENERA SATELLITES

- Flight control system for automatic interplanetary stations /AIS/, comparing Venera series orientation and correction system to Mariner systems
10 p1792 A69-24198

Venus atmosphere optical properties on basis of Venera 4 data, proposing models for measured rotational temperature and subcloud atmosphere radiative equilibrium
13 p2345 A69-27691

Venus atmosphere physical properties and chemical composition, considering Venera 4 and Mariner 5 data
18 p3201 A69-35164

VENERA 4 SATELLITE

Magnetometric equipment on board Luna 10 and Venera 4 space stations for studying magnetic field in interplanetary space, describing circuit and metrological characteristics
01 p0080 A69-10582

Venus research, discussing Mariner 5 and Venera 4 data, radar tracking, orbit, diameter, gravity, density distribution, etc
08 p1391 A69-20456

Interplanetary magnetic field near Venus, analyzing data by magnetometer onboard Venera 4
10 p1791 A69-24199

Space research in U.S.S.R. including Venera 4 soft landing mission for measuring temperature, pressure, density and atmospheric composition of Venus
12 p2160 A69-26921

Magnetometric equipment on board Luna 10 and Venera 4 space stations for studying magnetic field in interplanetary space, describing circuit and metrological characteristics
15 p2610 A69-30752

Light refraction in Venusian atmosphere from Venera 4 probe measured data, noting horizontal rays traversing planet along circumference at 8.3 km height
19 p3427 A69-36625

Radial velocity data monitored during Venera 4 descent used for determining vertical and horizontal atmospheric flows velocities
22 p4034 A69-41099

VENTING

Personal cooling in inadequately air conditioned cockpits, considering dry air, air ventilated suits and liquid circulated tubes near skin
[AGARDOGRAPH-111] 08 p1267 A69-20684

Global characteristics and similarity of ventilated cavity flows by injecting air behind immersed profiles of symmetrical wedge at zero incidence
10 p1680 A69-23788

Hydrogen check valve with low cracking pressure and flow pressure drop for hydrogen vent system at Saturn launch pad
[AIAA PAPER 69-578] 16 p2845 A69-32738

Ventilation-perfusion inequality increase effects on lung overall gas exchange, using digital model
21 p3662 A69-38388

Ventilatory responses to hypercapnia and hypoxia in anesthetized and unanesthetized rabbits before and after bilateral cervical vagotomy
21 p3651 A69-38390

Lower body negative pressure /LBNP/ effects on ventilation and lung volumes, presenting lung model for pulmonary gas exchange changes
22 p3891 A69-40222

Oxygen consumption, ventilation and cardiac frequency relationship to body weight during submaximal exercise in normal human beings
23 p4099 A69-42169

VENTING

Simulation of two phase hydrogen venting to space environment, discussing thrust effect measurements, flow instabilities and instrumentation
15 p2701 A69-30396

Impingement pressure analysis associated with two phase cryogenic propellant venting to space environment
[AIAA PAPER 69-571] 16 p2869 A69-32753

Crater formation by gas erosion in vent of 4.3 kiloton nuclear explosion detonated at 280 ft depth in layered trachytic volcanic rocks
22 p3937 A69-40409

VENTRAL SECTIONS

Ventral posterolateral potentials in anesthetized immobilized cats in response to electric stimulation of mesenteric nerves and mechanoreceptors, studying thalamus nucleus role
12 p2020 A69-26562

Ventromedial hypothalamic /VMH/ lesions, body weight and food consumption changes in male and female rats, observing differential effects
17 p2910 A69-33756

Spinal cord temperature influence on stretch response of tonic and phasic alpha-motoneurons by filament recordings from ventral roots in anesthetized cats
23 p4098 A69-42099

Electrical stimulation effects of carotid sinus on sinus rate and atrioventricular conduction for vagi and sympathetic nerves interruption to heart in dogs
24 p4257 A69-42629

VENTS

Liquid helium vented and nonvented storage container design and handling techniques
10 p1810 A69-24016

VENTURI TUBES

Discharge coefficients for Herschel type smooth venturimeters, analyzing influence of transport coefficients, convergence angles and contraction ratios
02 p0250 A69-12414

Venturi meter with separable diffuser and radial outward step at transition from throat to diffuser, noting effect of step on efficiency
[ASME PAPER 68-WA/FM-2] 05 p0763 A69-16135

Venturi meter design, discussing effects of turbulent velocity fluctuations, hole size and internal geometry on differential pressure measurement
11 p1880 A69-24468

Venturi meter with separable diffuser and radial outward step at transition from throat to diffuser, noting effect of step on efficiency
[ASME PAPER 68-WA/FM-2] 14 p2447 A69-29447

Pressure losses in pipeline with venturi tube, calculating hydraulic resistance coefficient as function of structural parameters and pipeline length
15 p2612 A69-31180

Cavitation flow of water and ethyl alcohol in venturi tube, noting effect of varying vapor concentration and thermodynamic properties
21 p3696 A69-39101

Venturi low resistance flowmeter for ventilatory measurements during rest and exercise on humans, noting suitability for analog integrator computation of tidal volumes
22 p3894 A69-40979

VENUS [PLANET]

Venus atmosphere and radius measurements by Mariner 5, Venera 4 and radar, comparing values
01 p0157 A69-11197

Critique of paper on water crystal existence on Venus, presenting arguments against existence of clouds of micron sized ice crystals
01 p0157 A69-11292

Manned Mars and Venus missions role in overall planetary exploration program
02 p0324 A69-12304

Jupiter, Venus and Mars 8.6 mm radio emission, obtaining average disk brightness temperatures
02 p0327 A69-12716

Venus radius determined by planetary radar and Mariner 5 radio tracking data
03 p0508 A69-13348

Kepler third law application to radar determinations of astronomical unit of length in general relativity
04 p0657 A69-14698

Venus diameter determination from optical measurements, noting cloud layer height and height of suspended particles in upper atmosphere
05 p0818 A69-15621

Observations of Venus at 15.4 GHz establishing upper limit for brightness variation with phase angle
08 p1382 A69-19818

Venus research, discussing Mariner 5 and Venera 4 data, radar tracking, orbit, diameter, gravity, density distribution, etc
08 p1391 A69-20456

Venus and Jupiter observations by earth paraboloid antenna, discussing average brightness temperatures and upper limit for Venus water vapor abundance
09 p1600 A69-22206

Radiometric observations of Venus brightness temperature variation used to determine phase effect at 8.6 mm wavelength
10 p1773 A69-22959

Prolateness of Venus radius on basis of satellite microwave temperature measurements, chemical compositions and ice cap model
10 p1784 A69-23958

Venus and Jupiter low resolution UV spectra obtained with servocontrolled star tracking telescope on Aerobee rocket, noting Lyman alpha radiation characteristics
[JHU-TR-15] 10 p1788 A69-24121

Interplanetary magnetic field near Venus, analyzing data by magnetometer onboard Venera 4
10 p1791 A69-24199

Venus and Jupiter brightness temperature and radio emission at 2.25 and 8 mm wavelengths observed with radio telescope
11 p1956 A69-24396

Venus albedo dependence on wavelength in UV spectrum between 4500 and 3200 A from reflector observations
11 p1957 A69-24406

Space research in U.S.S.R. including Venera 4 soft landing mission for measuring temperature, pressure, density and atmospheric composition of Venus
12 p2160 A69-26921

Chemical composition of earth, Venus, Mars, Mercury and moon calculated from mathematical models, constructing approximate equations of state at high pressure
14 p2526 A69-29878

Planet Venus data from Venera 4, Mariner 5, radio astronomical and radar measurements
15 p2698 A69-31360

Venus microwave spectrum analyzed by comparing various thermal and nonthermal emission models, discussing surface temperature and atmospheric composition
16 p2853 A69-31597

Wavelength dependence of linear polarization of sunlight scattered by Venus, noting temporal variations in UV
16 p2860 A69-32236

Venus brightness and polarization distributions measurement at centimeter wavelengths using two element interferometer, suggesting Venus atmosphere as main source of radiation
18 p3191 A69-34302

Venusian cloud layer radius, discussing error in determination of occultation level height of Regulus by Venus
18 p3203 A69-35331

Dichotomy of Venus in eastern and western elongations, determining time of occurrence by graphical method
18 p3203 A69-35336

Mercury and Venus thermal histories based on analogy to earth models
20 p3597 A69-37333

Carbon dioxide band in Venus spectrum by dispersion analysis, deriving rotational temperature
20 p3614 A69-38254

Surface reflectivity mapping of Venus by radar interferometry at 3.8 cm, noting low reflectivity circular regions
21 p3806 A69-39331

Venus and Mercury diurnal period commensurability associated with Venus spin-orbit resonance with earth orbit
22 p4018 A69-40270

Venus and Jupiter brightness temperature and radio emission at 2.25 and 8 mm wavelengths observed with radio telescope
24 p4390 A69-43786

Venus albedo dependence on wavelength in UV spectrum between 4500 and 3200 A from reflector observations
24 p4391 A69-43796

VENUS ATMOSPHERE

Venus cloud layer thickness and lower boundary estimation from data on chemical composition, temperature and pressure profiles of atmosphere
01 p0152 A69-10580

Venus atmosphere and radius measurements by Mariner 5, Venera 4 and radar, comparing values
01 p0157 A69-11197

S-band radio occultation for probing atmospheres of Mars and Venus
[AAS PAPER 68-185] 02 p0311 A69-11470

Direct planetary atmosphere measurement by vehicles entering atmosphere, using Mars and Venus model atmospheres for accuracy expectation
[AAS PAPER 68-187] 02 p0311 A69-11472

Mariner 5 Venus Lyman alpha emission observations, noting atomic hydrogen and oxygen resonance radiation measurements and apparent presence of molecular hydrogen or deuterium
[AAS PAPER 68-220] 02 p0313 A69-11486

Buoyant station with science package designed for long duration missions with horizontal mobility in Venus atmosphere
02 p0333 A69-11745

Ablative heat shield materials for Mars and Venus atmospheric entries
02 p0333 A69-11750

Radiation heating characteristics of shock layer gases surrounding Venus entry vehicle, noting domination of carbon monoxide band and UV spectrum
02 p0351 A69-11751

- Collection of papers on atmospheres of Venus and Mars covering atmospheric models, light scattering, radio occultation experiments, etc
02 p0318 A69-12101
- Mars and Venus atmospheres, Martian atmosphere dynamics, Mars ionosphere and use of space probes
02 p0318 A69-12102
- Venus lower atmosphere noting graphically wide variation of surface pressure estimates
02 p0319 A69-12103
- Model spectra applied to carbon dioxide bands in Venus spectrophotometric measurements
02 p0319 A69-12107
- Venus microwave phase effect analyzed assuming dry massive Venus atmospheric model, discussing heat transfer processes
02 p0319 A69-12108
- Venus exospheric temperature for various composition models, discussing carbon dioxide concentration effects
02 p0319 A69-12109
- Atmospheric circulation on rotating and nonrotating planets with shallow atmospheres applied to Mars and Venus atmospheres
02 p0320 A69-12110
- Venus UV photographs and drawings shown in short interval sequences, noting left to right shift in cloud features
02 p0320 A69-12111
- Radio occultation measurements of Venus and Mars atmospheres using Mariner spacecraft
02 p0320 A69-12115
- Photoelectron energy loss mechanisms in planetary atmospheres, considering possible constituents in Mars and Venus upper atmospheres
02 p0321 A69-12118
- Venus atmospheric structure from surface to 20,000 km radial distance from Mariner 5 radio experiments, noting large mass-2 hydrogen component in upper atmosphere
02 p0330 A69-12802
- Venus atmosphere from Mariner 5 and Venera 4 data, discussing surface temperatures and pressures, cloud top region, McElroy model and maximum wind velocities
02 p0330 A69-12803
- Mission requirements influence on aerothermodynamic environment for vehicle entering Venus atmosphere, considering different entry modes
02 p0332 A69-12823
- Atmospheric gas composition effects on shock layer radiative heat transfer and heat shield response in Venus entry simulated by earth reentry
[AIAA PAPER 68-1148] 03 p0412 A69-13672
- Venus brightness temperature between 0.75 and 1.65 cm from radio emission measurements, taking into account water vapor in Venus atmosphere
04 p0658 A69-14960
- Heated liquid mercury rotation rate and direction counter to rotating bunsen flame related to Venus cloud formations high velocities
04 p0664 A69-15466
- Venus observation at 4.52 cm showing 654 K mean brightness temperature, negligible phase variation and polarization indicates thick atmosphere
05 p0818 A69-15601
- Venus and Mars atmosphere structure, comparing Venus atmosphere model with Mariner 5 observations
05 p0824 A69-16248
- Lyman-alpha observations of Venus by Mariner 5 analyzed, assuming resonance scattering of flux by hydrogen or deuterium atoms in Venus atmosphere
05 p0815 A69-16255
- Terminal velocities of dust particles for two Venus atmospheric models from Mariner 5 and Venera 4 data, obtaining vertical wind velocity requirements
06 p1001 A69-17172
- Venusian atmosphere model developed from satellite and earth based radar data for environmental criteria in spacecraft design and mission planning
[AIAA PAPER 69-51] 06 p1011 A69-18096
- Terrestrial and Cytherean atmospheres evolution based on gray atmosphere model, surface energy budget and partition of water and carbon dioxide
07 p1213 A69-18608
- Visible radiation scattering around Venus spherical atmosphere computed on basis of Venus 4 and Mariner 5 data
07 p1213 A69-18609
- Recombination mechanism between CO and O produced by photodissociation of carbon dioxide in upper atmosphere of Venus and Mars
07 p1214 A69-18615
- Ozone distribution in Venus atmosphere measured by Soviet space probe Venera 4
08 p1382 A69-19887
- Monte Carlo method for calculating atomic hydrogen escape rate from carbon dioxide atmosphere, considering Mars and Venus atmospheres
08 p1386 A69-20076
- Mars and Venus atmospheric properties, noting influence of biosphere and human activity on earth atmosphere
08 p1408 A69-21160
- Nighttime Venus ionosphere models compared with Mariner 5 observations, discussing implications with regard to He and H abundance consequences and nightglow
09 p1594 A69-21695
- Deuterium escape in Venus upper atmosphere to explain anomalous Lyman-alpha glow observed by Mariner 5
[SRCC-91] 09 p1594 A69-21696
- Test of Velikovsky theory for dense hydrocarbon clouds and dusts surrounding Venus, using IR reflection spectra
09 p1608 A69-22566
- Venus atmosphere origin, discussing high temperature effects and chemical composition via space probe and terrestrial observations
10 p1775 A69-23183
- Venus atmosphere radial mass velocities measured spectrographically with Fabry-Perot interferometer, noting retrograde rotation
10 p1778 A69-23409
- Venus atmosphere observations compared with Venera 4 measurements of temperature, pressure and carbon dioxide content
10 p1791 A69-24200
- Radio astronomical observations of Venus atmosphere interpreted noting agreement with model based on Venera 4 data
10 p1791 A69-24202
- Chemical composition of Venusian atmosphere by Mariner and Venera satellites, comparing upper atmospheres of Venus and earth
11 p1960 A69-24971
- D/H ratio in Venus exosphere, discussing isotopic fractionation mechanisms and Lyman alpha data from Mariner 5
11 p1962 A69-25145
- Venus and Mars atmospheric braking entry and associated equipment, discussing potential cost savings
11 p1968 A69-25722
- Surface dielectric constant and microwave opacity of Venus atmosphere as function of wavelength determined by radar observations
12 p2153 A69-25805
- Venus brightness temperatures vs phase angle to define spectra of day and night face at short wavelengths, using model atmosphere
12 p2153 A69-25806
- Atmospheric models for exospheric temperatures of Mars and Venus based on photoionization heating efficiency
12 p2155 A69-26020
- Venus atmosphere chemical composition, surface temperature and pressure obtained by Venera 4 and Mariner 5
12 p2155 A69-26129
- Venusian upper atmosphere dissociation and ionization, considering photochemical and dynamic processes and molecular, eddy and ambipolar diffusions
13 p2344 A69-27643
- Venus carbon dioxide spectral band analysis methods, discussing spectral lines and rotational temperatures obtained
13 p2344 A69-27649
- Venusian water vapor spectroscopic data indicating longitudinal and time dependent variations in abundance
13 p2345 A69-27650
- Venusian atmospheric model based on Venera 4 measurements, calculating probe distance travel, temperature, density and pressure profiles
13 p2345 A69-27688
- Venusian atmospheric pressure and temperature measurements by Venera 4 probe, noting agreement with Mariner 5 observations
13 p2345 A69-27689
- Greenhouse effect in Venusian atmosphere, discussing cause of vertical temperature distribution established by Venera 4 probe
13 p2345 A69-27690
- Venus atmosphere optical properties on basis of Venera 4 data, proposing models for measured rotational temperature and subcloud atmosphere radiative equilibrium
13 p2345 A69-27691
- Microwave propagation in Venusian atmosphere, analyzing refraction angles, attenuation and field strength fluctuations
13 p2223 A69-28567
- Venus cloud layer thickness and lower boundary estimation from data on chemical composition, temperature and pressure profiles of atmosphere
15 p2691 A69-30750
- Radio wave absorption by water vapor in Venusian and Martian atmospheres, constructing model from Venera 4 data
15 p2569 A69-30952
- Carbon atoms presence in Venus upper atmosphere from Venus spectrum obtained by Aerobee rocket experiment
15 p2698 A69-31341
- Earth based microwave data revealed isothermal layer in extrapolating Venus atmospheric profile below region probed by Mariner 5 and Venera 4
16 p2852 A69-31553
- Spectroscopic observations of Venus atmosphere rotational temperature based on carbon dioxide band at 7883 A
16 p2852 A69-31563
- Venus atmosphere carbon dioxide content origin from interior degassing during molten phase, using atmospheric model
16 p2857 A69-32098
- Wavelength dependence of polarization of sunlight scattered by Venus atmosphere, including Rayleigh and Mie scattering mechanisms
16 p2860 A69-32237
- Visual ashen light observation on Venus possibly attributable to solar particle bombardment from dark side emission detection by spectroscopic and photometric studies
16 p2861 A69-32300
- Cloud scattering corrections added to synthetic spectrum analysis of carbon dioxide bands and water vapor line in Venus spectrum
17 p3032 A69-33161
- IR reflection spectra agreement for frost particles and Venus clouds, noting ice as clouds constituent
18 p3190 A69-34282
- Venus brightness and polarization distributions measurement at centimeter wavelengths using two element interferometer, suggesting Venus atmosphere as main source of radiation
18 p3191 A69-34302
- Earth ecosystem chemical composition compared with Mars and Venus ecosystems to determine presence of life
18 p3193 A69-34361
- Venus brightness temperature between 0.75 and 1.65 cm from radio emission measurements, taking into account water vapor in Venus atmosphere
18 p3197 A69-34723
- Venus atmosphere physical properties and chemical composition, considering Venera 4 and Mariner 5 data
18 p3201 A69-35164
- Venusian atmospheric features obtained from Venus 5 and 6 and Mariner 5 observations, indicating extremely high temperatures and pressures
19 p3401 A69-35840
- Light refraction in Venusian atmosphere from Venera 4 probe measured data, noting horizontal rays traversing planet along circumference at 8.3 km height
19 p3427 A69-36625
- UV solar radiation variation effects on Mars and Venus upper atmosphere temperatures
20 p3595 A69-37136
- Photodissociation of diatomic hydrogen by solar radiation for Venus atmosphere investigation, considering H atoms production rate by Stecher-Williams process
20 p3609 A69-38102
- Structure, composition and temperature of Venus atmosphere from spacecraft measurements and ground based observations
20 p3614 A69-38256
- Nongray greenhouse model of Venus atmosphere possessing IR opacity due to carbon dioxide, water and diatomic N compatible with Mariner 5 and Venera 4 results
20 p3615 A69-38259
- Venus atmosphere structure determined from Mariner 5 flyby S band radio occultation measurements of ionosphere and atmosphere at illuminated and dark sides
21 p3794 A69-38380
- Venus magnetosphere induced by piling up magnetic field from solar wind due to ionospheric conductivity and collisions with planetary atmospheric particles
21 p3794 A69-38381

Venus, Mars and Jupiter lower atmospheric motions, considering atmospheres thermal and chemical composition

21 p3811 A69-39511

Buoyant Venus Station balloon for deployment and inflation during parachute descent into Venus at atmosphere tested with scale model balloons in wind tunnels [AIAA PAPER 69-1017]

22 p3922 A69-40389

Rocket UV spectra indicating Venus atmosphere weak absorption and low ozone abundance and possible Jupiter surface depressions

22 p4028 A69-40661

Radial velocity data monitored during Venera 4 descent used for determining vertical and horizontal atmospheric flows velocities

22 p4034 A69-41099

Venus atmosphere and clouds exploration by entry probes, discussing ground temperature, greenhouse model, cloud layer, etc

23 p4216 A69-42201

Atmospheric gas composition effects on shock layer radiative heat transfer and heat shield response in Venus entry simulated by earth reentry [AIAA PAPER 68-1148]

24 p4394 A69-43248

VENUS PROBES

NT MARINER 1 SPACE PROBE

NT MARINER 2 SPACE PROBE

NT MARINER 5 SPACE PROBE

NT VENERA SATELLITES

NT VENERA 4 SATELLITE

Soviet lunar and planetary probes, reviewing payload characteristics, principal mission features and photographs associated with Luna, Mars, Venera and Zond series

01 p0162 A69-10938

Buoyant station with science package designed for long duration missions with horizontal mobility in Venus atmosphere

02 p0333 A69-11745

Radiation heating characteristics of shock layer gases surrounding Venus entry vehicle, noting domination of carbon monoxide band and UV spectrum

02 p0351 A69-11751

Mars and Venus probes antenna problems in environments of near earth space, deep space and nonearth planetary atmospheres

02 p0223 A69-12811

Two dimensional representation of Venus entry probe target data for determining probe capability to provide real time data transmission to earth

02 p0331 A69-12820

Plasma flux measurements by charged particle traps in Venus vicinity by space vehicle Venera 4, discussing low concentration of charged particles

07 p1222 A69-19613

Venus atmosphere origin, discussing high temperature effects and chemical composition via space probe and terrestrial observations

10 p1775 A69-23183

Planet Venus data from Venera 4, Mariner 5, radio astronomical and radar measurements

15 p2698 A69-31360

Scientific space research program /1968-1978/ outlining advanced lunar orbiter and Mars, Venus and Mercury probes

18 p3193 A69-34360

Venusian atmospheric features obtained from Venus 5 and 6 and Mariner 5 observations, indicating extremely high temperatures and pressures

19 p3401 A69-35840

Mission analysis for 1972 Venus launch opportunity, discussing launch period selection and trajectory constraints for Atlas/Centaur vehicle [AAS PAPER 68-135]

21 p3805 A69-39208

Manned flyby and stopover missions to Mars and Venus with chemical propulsion and Saturn 5 launch vehicles, noting short duration low energy missions [AAS PAPER 69-492]

24 p4380 A69-42839

Mariner-Mercury 1973 flyby mission using Atlas-Centaur rocket and gravity-assisted maneuvers, discussing encounter geometries, spacecraft configuration and Venus probe considerations [AAS PAPER 69-288]

24 p4381 A69-42862

VENUS RADAR ECHOES

Backscattering diagram of Venus at 40 cm determined from Doppler spectrum and reflected signals range energy distribution

02 p0314 A69-11639

Roughness effect on microwave emissivity according to geometric optics with application to moon and Venus

02 p0207 A69-12017

Radar round trip time of flight measurements to Venus for three month interval about inferior conjunction of August 1968

04 p0663 A69-15384

Venusian atmosphere model developed from satellite and earth based radar data for environmental criteria in spacecraft design and mission planning [AIAA PAPER 69-51]

06 p1011 A69-18096

Scattering characteristics of planet Venus at 3.8 cm wavelength, discussing frequency power spectra and radar cross section

13 p2349 A69-27818

VERBAL COMMUNICATION

Oxygen-helium cabin atmosphere effect on speech communication analyzed during simulated space mission

07 p1066 A69-19420

Noise level criteria for acceptable voice communications in office environment, noting acclimatization

11 p1830 A69-24797

Isolation of scientific and technical personnel and effect on lateral communication and intellectual cross fertilization in research and development program

11 p2004 A69-25303

Dynamic Automated Reporting Technique /DART/ system for on-line conversational information storage and retrieval for use in large programs management

18 p3107 A69-35095

VERNIER ENGINES

Vernier motor for Europa 1 rocket third stage, discussing component design, system performance and fuel composition

17 p3018 A69-33328

Pneumatic Vernier engines in aircraft and spacecraft, discussing weight, gas expansion and gas temperature

21 p3785 A69-39093

VERTEBRAL COLUMN

Vertebral column fracture resulting from aircraft ejection, studying ejection seat geometry and personal equipment design influence on spinal curvature relation to catapult thrust

23 p4102 A69-41681

VERTEBRATES

NT BABOONS

NT BIRDS

NT CATS

NT CHICKENS

NT CHIMPANZEES

NT DOGS

NT FISHES

NT FROGS

NT GROUND SQUIRRELS

NT GUINEA PIGS

NT HAMSTERS

NT HOMEOTHERMS

NT HUMAN BEINGS

NT LIZARDS

NT MAMMALS

NT MICE

NT MONKEYS

NT PIGEONS

NT POCKET MICE

NT RABBITS

NT RATS

NT RODENTS

NT TURTLES

S-RETIC vertebrate command model, discussing computer simulation of reticular formation Golgi anatomy capable of habituation, conditioning, extinction, generalization and error discrimination

24 p4273 A69-42910

VERTICAL AIR CURRENTS

Thermodynamics of nonadiabatic vertical ascent of overheated individual air volumes in stably stratified atmosphere

02 p0274 A69-11441

Wind perturbations characteristics near large convective cloud banks as function of ascending current, wind shear and turbulence

02 p0274 A69-11446

Radiative heat loss effect on atmospheric cellular convection, analyzing critical Rayleigh number and width to height ratio of cells

02 p0276 A69-12776

Vertical wind velocity structure and turbulent heat flux temperature measurements over steppe and sea, noting underlying surface influence

03 p0458 A69-13270

Planetary Rossby waves vertical propagation through weak westerly wind wave guides, using adiabatic linear model

03 p0460 A69-13335

Eddy diffusivity in planetary boundary layer determined by vertical velocity spectrum

03 p0460 A69-13338

Environmental temperature and water vapor increases associated with ascending thermals estimated by penetrative convection

03 p0460 A69-13340

Maximum downwind and crosswind vertical wind shear in boundary layer, noting effect on swept wing jet aircraft landing

06 p0951 A69-17790

Vertical ionospheric motions near magnetic equator measured by Doppler shifts of incoherent scatter frequency spectra

09 p1489 A69-21704

Vertical air flow asymmetrical distribution ascribed to cyclone motion and thermal inhomogeneity by studying spiral cloud configurations in cyclone area

11 p1912 A69-24825

Nightglow intensity variations at sunspot minimum from measurements in South West Africa, considering relationship to ionospheric vertical movements and density variations

12 p2066 A69-26133

Atmospheric boundary layer mean turbulence and vertical velocity calculations, tabulating layer characteristics for various turbulent heat flux and geostrophic wind velocity values

12 p2126 A69-26578

Vertical air motions and cloud behavior relationship based on statistical analysis of TV cloud pictures from Cosmos 122 satellite

13 p2291 A69-27724

Cellular convection in horizontal gas layer analyzed for causes of vertical air circulation and effect of vertical temperature profile

13 p2291 A69-27725

Vertical wind velocity structure and turbulent heat flux temperature measurements over steppe and sea, noting underlying surface influence

14 p2471 A69-28778

Vertical wind effects in atmosphere on 5577 A radiance, showing dependence on atomic oxygen density

16 p2778 A69-32185

Low level jet stream near meso-low on stationary front in Japanese rainy season analyzed from radar echoes, noting appearance of vertical current

16 p2809 A69-32601

Atmospheric ozone distribution as function of photochemical reactions, advection and vertical motions

16 p2787 A69-32643

Kinesonde radio sounding system for three dimensional ground observations of E region microstructure and vertical motion of neutral air and ions

18 p3125 A69-34250

Magnetic declination effect on F 2 layer critical frequency diurnal variations attributed to vertical ionospheric drift due to neutral air winds

18 p3126 A69-34256

Vertical air velocity in rain measured for size distribution of drops, using relation between drop fall rate and diameter

18 p3104 A69-35342

Vertical atmospheric motions, considering wind velocity measurements associated with synoptic processes

19 p3366 A69-36673

Midlatitude thermosphere vertical air motions to balance divergence and convergence caused by large scale horizontal wind systems

21 p3714 A69-38553

Friction and orography effects on vertical currents in planetary boundary layer and numerical forecasting of baric field

21 p3758 A69-38837

Lower ionosphere vertical wind velocity profiles determined from rocket-released grenade glow cloud photographs, developing cloud buoyancy effect empirical model

23 p4154 A69-41305

VERTICAL DISTRIBUTION

NT STAR DISTRIBUTION

Lunar tidal effects on F 2 critical frequency and height maximum, evaluating variations with altitude

01 p0063 A69-10424

Ionospheric inhomogeneities vertical and latitudinal distributions and diurnal variations, measuring Explorer 22 signals Faraday fading with space diversity reception

01 p0064 A69-10446

Topside ionosphere average height distributions of electron density and geomagnetic field intensity from Alouette 2 data over Japan, noting ionic composition

01 p0065 A69-10548

Vertical wind profiles and electron density profiles in E region, determining time dependence and ionization drift velocity

01 p0072 A69-11172

- Midlatitude sporadic E layer vertical and horizontal structure and statistical properties, discussing theory of ion concentration by wind shear
01 p0073 A69-11177
- Lower thermosphere neutral composition diurnal variations, noting molecular N and O, Ar, He and atomic O
01 p0076 A69-11231
- Algorithm for N/h/ ionospheric profiles calculations using both x and o magnetoionic components, taking into account interlayer and underlying ionization influence
02 p0239 A69-11687
- Three term formula for describing vertical wind velocity distribution in upper boundary layer of atmosphere, taking into account friction and orography effects
02 p0240 A69-11708
- Seasonal mean vertical ozone distributions obtained with electrochemical ozone sondes over southeastern Australia
02 p0276 A69-12696
- Optical ozone radiosonde for vertical distribution analysis, using weak absorption of Chappuis bands
02 p0251 A69-12761
- Vertical atmospheric turbidity distributions of haze and water vapor, noting effect of variations on scattering and absorption determination
02 p0277 A69-12777
- Solute vertical stabilizing gradient inhibition of thermal convection of fluid layer under temperature gradient, discussing effects on two dimensional flows motion
03 p0532 A69-13012
- Aircraft high level cloud data to estimate vertical distribution of cirriform clouds and tropical tropopause levels on airline routes
03 p0458 A69-13032
- Ekman-Okkerblom problem for electrically conducting atmosphere located in external magnetic field, obtaining altitude distribution for wind velocity components
03 p0461 A69-13510
- Fast neutron fluxes at various atmospheric levels and geomagnetic northern midlatitudes measured by proportional counters using boron trifluoride
03 p0501 A69-13528
- Satellite drag data to determine upper atmospheric composition according to density distribution with height
03 p0423 A69-13532
- Mathematical dipole model for geomagnetic field to provide main magnetic field source distribution within earth
03 p0424 A69-13543
- Approximate method for calculating vertical velocity distribution in atmospheric braking of bodies along ballistic trajectories
04 p0541 A69-14485
- Stationary vertical distribution of weightless radioactive substance in surface air layer, accepting two layer exponent law for vertical turbulent diffusion coefficient
04 p0593 A69-15091
- Lunar tide effect on height distribution and velocity of ionospheric electron density daily variations near magnetic equator
05 p0756 A69-16401
- Vertically moving ionized formations relation to solar and magnetic activity
06 p0920 A69-17730
- Vertical ozone distribution in upper atmosphere from satellite measurements of UV solar radiation scattering by solving integral Laplace equation
06 p0996 A69-17733
- Long wave radio stations field intensity spectral analysis data evaluated to determine vertical ionospheric displacements at sunset and sunrise
06 p0922 A69-17752
- Vertical distribution of ascending long wave radiation, employing actinometric radio sondes
06 p0953 A69-17990
- Radiative transfer equation for pure molecular scattering inverted for estimating vertical ozone distribution
07 p1126 A69-19042
- Lunar depth-profiles of conductivity, dielectric constant and magnetic permeability from radar, radiothermic and magnetic measurements, discussing lunar models
07 p1216 A69-19221
- Measurement bases in general, discussing theoretical data justifying ground level base and measurements results
07 p1136 A69-19516
- Linearized model for vertical propagation of Rossby waves through atmosphere with Newtonian cooling, discussing atmospheric wind effects
08 p1344 A69-19812
- Double diurnal oscillation of atmospheric pressure and vertical gradient of electromagnetic field, noting agreement between diagrams and role of atmospheric tides
08 p1306 A69-19866
- Ozone distribution in Venus atmosphere measured by Soviet space probe Venera 4
08 p1382 A69-19887
- Seasonal maximum ozone concentration variations, discussing vertical ozone distribution
08 p1307 A69-20260
- Linear perturbation theory to predict instability threshold conditions caused by electric field in poorly conducting liquid subject to vertical temperature gradient
08 p1352 A69-20790
- Vertical transport rate of charged particles in F region, allowing for vertical velocity gradients
09 p1485 A69-21529
- Temperature profiles variability for data obtained by rocketsonde thermistors launched with small time and spatial separation
09 p1494 A69-21644
- Influence function for vertical wind profile from pressure gradient field
09 p1536 A69-21867
- Stratospheric dust, discussing terrestrial and meteoritic origins, volatility of particles smaller than few microns, and light scattering and direct sampling measurements
09 p1608 A69-22689
- Graphs of ionospheric measurements by vertical incidence sounding during Antarctic expedition, describing instrumentation and sounding techniques
10 p1681 A69-23315
- Stratified atmosphere mean vertical flux due to ground disturbances, obtaining results for various wind and temperature profiles
10 p1685 A69-23856
- High altitude balloon measurements of secondary gamma quanta intensity vertical distribution, using scintillation counter with CsI/Tl crystal
10 p1770 A69-23924
- Hourly N/h/ profiles of F region calculated from nomograms by normal integral method during magnetic disturbance, measuring region temperature
10 p1687 A69-23928
- Molecular reaction rates and ion/electron vertical profile and concentrations in equatorial ionosphere, applying computer simulation to numerical solution of continuity equations
10 p1688 A69-23929
- Ionospheric molecular ion concentration vertical profile analysis for verifying neutral gas temperature maxima in connection with two ion production maxima
10 p1688 A69-23930
- Atmospheric density analyzed on basis of photographic observations of meteors, comparing vertical profile with CIRA profile
10 p1688 A69-23936
- Finite difference method for calculating lee waves incident on obstacle with arbitrary vertical distribution of main flow horizontal velocity and temperature
10 p1722 A69-23967
- Ionospheric irregularities drift and anisotropy parameters variation with true reflection height during magnetically disturbed conditions
10 p1659 A69-24062
- Computerized autocorrelation function analysis of radioactivity distributions in atmosphere at different altitudes, showing no correlation between values
11 p1945 A69-24320
- Wind velocities statistical properties at various altitudes, noting linear regression of orthogonal components and prediction of wind velocities at all altitudes
11 p1911 A69-24694
- Vertical air flow asymmetrical distribution ascribed to cyclone motion and thermal inhomogeneity by studying spiral cloud configurations in cyclone area
11 p1912 A69-24829
- Radar backscatter and rocket profiles of ionospheric electron temperature, noting agreement in daytime flight measurements
11 p1951 A69-25162
- Time and altitude distribution of wind zonal components over Fernando Noronha Island off Brazilian coast, discussing tropospheric pattern
11 p1913 A69-25204
- Carbon dioxide concentration in upper troposphere and lower stratosphere recorded during commercial aircraft flights over polar route
11 p1879 A69-25254
- Stratospheric aerosol attenuation factor vertical distribution statistical structure, tabulating normalized correlation matrices, eigenvectors and eigenvalues
12 p2125 A69-25956
- Semiannual density variations in thermosphere and exosphere as function of mixtopause height variations
12 p2064 A69-26012
- Focusing factor in stratified medium with refractive index depending exponentially on height
12 p2029 A69-26100
- Molecular O and total number densities between 70 and 120 km determined with rocket measurements of atmospheric absorption of solar UV and X rays
12 p2065 A69-26106
- Photographic emulsion layers depth dependence of darkening curve, modulation transfer function and granularity, determining properties by enzymatic and electrolytic treatments
12 p2089 A69-26196
- Satellite 1968-5A orbit analyzed for atmospheric density at 140-180 km, noting semiannual variation
12 p2066 A69-26229
- Spherical wave propagation in homogeneous turbulent medium, discussing nonstationary statistics as applied to vertical propagation in atmosphere
12 p2029 A69-26251
- Mean vertical moisture profile for summer and winter midlatitude stratosphere from Soviet radiosonde data
12 p2070 A69-26582
- Height and temperature vertical variability in mid and upper stratosphere determined from constant pressure charts /1964-1966/
13 p2290 A69-27637
- Greenhouse effect in Venusian atmosphere, discussing cause of vertical temperature distribution established by Venera 4 probe
13 p2345 A69-27690
- Cellular convection suppression by parallel vertical thermally conducting walls inserted into bottom-heated fluid, analyzing effect on critical Rayleigh number
13 p2374 A69-27782
- Vertical wind velocity profiles approximation accuracy determined by linear, exponential and logarithmic functions of altitude during ice and frost
13 p2293 A69-27846
- Temperature vertical profiles rms deviations calculated from temperature measurements during unstable atmospheric stratification
13 p2293 A69-27847
- Electric field profile and turbulence ratio relation-ship in free atmosphere as function of vertical current density, conductivity, potential gradient and charge density
13 p2295 A69-28523
- Lower ionospheric homonuclear O combinations nonequilibrium processes by simplified balance equations, determining height distributions and ozone concentration
13 p2255 A69-28542
- Algorithm for N/h/ ionospheric profiles calculations using both x and o magnetoionic components, taking into account interlayer and underlying ionization influence
13 p2258 A69-28718
- Ionograms in vertical depletion duct in horizontally stratified isotropically refractive plasma, considering vertical propagation and ray paths traces dependence on electron concentration
14 p2434 A69-28945
- Ionograms for nonmonotonic vertical distribution of electron concentration in ionosphere from rocket and ground sounding
14 p2437 A69-29071
- Magnetovariational sounding procedure for determining vertical distribution of earth mean electrical conductivity using geomagnetic field spatial derivatives for spherical earth
14 p2438 A69-29081
- Electron and ion temperatures height variations in sporadic E layers, noting effects of neutral gas temperature changes
14 p2440 A69-29127
- Atomic hydrogen vertical profiles with increased high-low altitude ratio for interpreting observations of thermospheric and exospheric hydrogen abundance
14 p2440 A69-29130
- Jet stream vertical wind shear chart construction for aircraft with gas turbine propulsion
14 p2473 A69-29730

Stratospheric turbulence producing bumpiness up to 18 km developing at levels characterized by abrupt changes in vertical temperature gradients
14 p2474 A69-29737

Hydrogen Lyman alpha nightglow models, discussing solar photon scattering in geocorona and hydrogen vertical distribution
15 p2595 A69-30191

Wind velocity fluctuations calculation in CAT based on closed equations numerical solution for turbulent layers in upper troposphere
15 p2649 A69-30649

Ozonosphere inhomogeneities from UV spectra of reflected solar radiation, studying latitude dependence of seasonal behavior at different heights
15 p2597 A69-30894

Vertical ozone profiles computed from known total ozone data based on profiles taken by Umkehr method
15 p2597 A69-30896

Ozone soundings data obtained over Australia and Colorado to obtain vertical picture of synoptic climatology of ozone at midlatitudes
15 p2649 A69-30898

Photometric rocket measurements in hydrogen auroras, finding vertical H beta emission profile estimate of proton energy spectrum for H beta production cross section
15 p2598 A69-31307

Air density at various heights determined from analysis of satellite low perigee orbits, discussing periodic density variations and correlation with daily geomagnetic index
15 p2599 A69-31348

Time variation of altitude distribution of cosmic dust layer in upper atmosphere by Pandora II collector using inflight shadowing technique
15 p2698 A69-31353

Wintertime short term density variability in upper atmosphere obtained from rocket measurements
15 p2601 A69-31374

Sporadic E layer nighttime electron density profiles obtained by Langmuir probe equipped sounding rockets
15 p2603 A69-31398

Spectrometric rocket measurements of ion concentrations between 200 and 630 km
16 p2774 A69-31974

Vertical incidence pulse dispersion with application to Alouette 1, discussing echo width, sounder system bandwidth and frequency gradient of ionospheric virtual height
16 p2750 A69-31977

Ion, electron and neutral temperatures from ion composition distribution, assuming no change in vertical distribution within horizontal distance between upleg and downleg measurements
16 p2849 A69-31990

Nighttime decreases in F 2 layer heights at near conjugate stations in low latitudes, using electron density profiles
16 p2778 A69-32186

Virtual temperature change with respect to height of saturated air rising during water vapor condensation, discussing actual temperature and precipitation factor
16 p2808 A69-32454

Geomagnetic normal field of vertical component for Central Europe, discussing influence of local factors on observational data
16 p2782 A69-32461

Vertical transport rate of charged particles in F region, allowing for vertical velocity gradients
16 p2783 A69-32524

Atmospheric ozone distribution in meridional plane including time effects of photochemistry, advection and turbulence assuming zonal symmetry
16 p2785 A69-32624

Vertical ozone distribution from emission and absorption in 9.6 μ band determined during IGY in Switzerland
16 p2785 A69-32625

Ozone vertical distribution variations over India observed by Brewer electrochemical ozonesonde, noting effects of dry and monsoon seasons
16 p2786 A69-32627

Horizontal and vertical ozone distributions synoptic study, comparing soundings made on both sides of Atlantic
16 p2786 A69-32628

Weather forecasting correlation between atmospheric ozone vertical profiles and postsounding ground meteorological situation, describing computer data processing
16 p2786 A69-32629

Vertical ozone distribution determination discrepancies between Brewer-Mast electrochemical sonde and Umkehr methods, discussing influence of seasonal and diurnal variations
16 p2786 A69-32630

Simultaneous Umkehr observations of vertical ozone distribution in upper stratosphere using two Dobson photometers, discussing deviations due to calibration sensitivity
16 p2786 A69-32631

Statistical analysis of Brewer-Mast electrochemical soundings of vertical ozone distribution for developing computer programs of climatological behavior
16 p2786 A69-32632

Ozone probe network data by Brewer-Mast electrochemical instruments, discussing vertical ozone distribution near Zurich
16 p2787 A69-32635

Optical probe for determining ozone vertical distribution at high altitudes, discussing optical method requirements and ozonesonde construction
16 p2792 A69-32637

Atmospheric optical density vertical distribution curves in near UV from spectrophotometer data of Echo type satellites entry into earth shadow
16 p2787 A69-32638

Ozone soundings in upper stratosphere, discussing vertical temperature profiles relationship to vertical ozone profiles
16 p2787 A69-32640

Ozone vertical distribution in upper stratosphere determined from OGO 4 observations, describing calibration of satellite data and onboard instrumentation
16 p2788 A69-32645

Vertical atmospheric pressure distribution measured directly with Pirani-Israel gauge in Skylark rocket, transforming dynamic pressure data into static pressures on ground
17 p2971 A69-33037

Nonlinear least squares optimization program applied to atmospheric temperature sounding, solving for temperatures at various altitudes from simulated carbon dioxide intensity measurements
17 p2960 A69-33156

Atmospheric stability influence on vertical spectra of refractive index and air velocity deduced from beam swinging experiments and compared with radiosondes data
17 p2960 A69-33157

Aircraft measurements and computer calculations of downward and upward solar radiation fluxes related to albedo, altitude and sun angle
17 p3023 A69-33158

Vertical structure concepts for air density, wind and sound velocity profiles in rocket climatology, discussing vertical relationship of wind shear statistics
17 p3000 A69-33794

Vertical distribution of ionospheric drift velocity in auroral zone, evaluating role and intensity of electric field formed in dynamo region
17 p2964 A69-33964

Ionospheric electron concentration variation during positive perturbation based on N/h profiles
17 p2967 A69-33986

Planetary ionospheric effect of 15 July 1959 sudden commencement magnetic storm based on N/h profiles of earth day and night sides
17 p2967 A69-33987

Vertical ionization displacements in F region as trace distortions on ionograms observed at low, mid and high altitudes during daytime
17 p2969 A69-33998

Ionospheric parameter recording accuracy by vertical sounding, discussing errors in frequency-height curve
17 p2969 A69-34002

Cosmic ray heavy nucleus enders flux by nuclear emulsions for balloon flights at various atmospheric depths
17 p3025 A69-34219

Vertical tropospheric humidity distribution estimation from IR spectra obtained by TIROS satellites
18 p3126 A69-34284

Whistler vertical propagation downwards through inhomogeneous ionosphere in vertical magnetic field, deriving wave equation, calculating transmission and reflection coefficients
18 p3130 A69-34972

Statistical regularization for determining vertical atmospheric temperature profile from measurements of earth radiation in 15 micron carbon dioxide band
18 p3167 A69-35339

Vertical distribution of concentration, microstructure and chemical composition of solid aerosol in troposphere and stratosphere from high altitude balloon measurements
18 p3132 A69-35340

Ozone vertical distribution predicted statistically, using total ozone amounts and backscattered UV spectral measurements
18 p3132 A69-35426

Atmosphere radio brightness temperature dependence on discrepancies between real and standard altitude profiles of thermodynamic temperature
19 p3275 A69-36333

Orthogonal functions for determining atmospheric vertical temperature profile from satellite measurement of earth outgoing radiation in carbon dioxide absorption band
19 p3303 A69-36409

Cloud masses vertical thickness estimated from study of cloud shadows on satellite TV pictures
19 p3366 A69-36670

Simultaneous ionospheric ion and electron measurements by various radiophysical methods, relating results to period of flight of vertical space probe
20 p3486 A69-37028

F region electron and ion concentration vertical distribution, discussing various ionization reactions
20 p3520 A69-37030

Lower ionosphere electric fields and currents vertical profiles above geomagnetic equator under quiet geomagnetic conditions from rocket data
20 p3521 A69-37053

Electron-ion gas ambipolar diffusion effect on F 2 layer electron density vertical distribution variations
20 p3525 A69-37655

Ion production rates vertical distribution and temporal changes at midlatitudes during solar activity minimum and maximum above F 2 layer
20 p3525 A69-37656

Altitude variations at and near maximum electron concentration in quiet F 2 layer during solar activity maximum from sounding at southern geomagnetic pole
20 p3526 A69-37662

Diurnal, seasonal and cyclic altitude and maximum ionization median value variations of undisturbed ionosphere from vertical sounding data obtained at Yakutsk, Siberia
20 p3527 A69-37666

High latitude stations vertical ionograms in absence of ionospheric reflections due to low solar activity periods, discussing interpretation methods
20 p3529 A69-37690

Ground station equipment for studying motions and structure of ionospheric inhomogeneities by combined space-frequency diversity reception, noting altitude dependence of ionospheric parameters
20 p3510 A69-37693

Numerical prediction experiment for dynamical structure of tropical atmosphere in equatorial latitudes, constructing pressure, temperature and vertical motion distributions from wind field
20 p3573 A69-37910

Vertical turbulent diffusion and altitude distribution of radioactivity from short lived radon decay products in atmosphere
20 p3533 A69-38076

F region vertical density profiles for positive ions and neutral molecules of various gases determined from rocket-borne mass spectrometer data
21 p3702 A69-38354

Airglow and vertical eddy transport photochemical models, analyzing O green line and OH emission distribution
21 p3713 A69-38523

Steady state vertical distribution of small ions in ground layer assuming atmospheric dynamic and thermal sublayers, calculating air resistance and electric field potential
21 p3715 A69-38836

Radio FM pulse compression for vertical ionosphere sounding
21 p3674 A69-39082

Altitude variation of mesospheric daytime sky brightness from earth based measurements of twilight sky brightness, noting inconsistency in calculations based on standard atmospheres
21 p3716 A69-39116

Vertical factor equation numerical solution for radio wave propagation in vertically inhomogeneous troposphere
21 p3674 A69-39121

Primary and secondary cosmic ray intensity variation with altitude from ascending balloon data, noting absorption length role
21 p3791 A69-39249

Cosmic radiation altitude profiles, giving tabulation of counting rates obtained by SPARMO flights at different locations
21 p3791 A69-39253

Finite difference method for calculating Lee waves incident on obstacle with arbitrary vertical distribution of main flow horizontal velocity and temperature
21 p3759 A69-39653

Tropospheric refractivity height profile model, computing corrections to satellite Doppler or range data
21 p3678 A69-39748

Aerosol attenuation coefficients vs altitude in troposphere and stratosphere, noting seasonally dependent surface convective dust layer and temperature dependent aerosol maximum altitude
21 p3718 A69-39773

Rocket optical experiment for determining water, methane, nitric oxide and ozone vertical profiles in stratosphere and mesosphere
22 p4035 A69-39910

Convective cells and periodic variations in vertical gradient of electroatmospheric field
22 p3934 A69-39939

Air density height distribution determined from satellite orbit decay analysis, noting semiannual density variations
22 p3935 A69-39971

Vertical heat exchange flux model using heat conduction equation compensating for tropospheric and stratospheric radiation divergence, calculating diffusion coefficient
22 p3936 A69-40137

Ionospheric vertical columnar electron content at midlatitudes near solar cycle minimum based on Faraday rotation data from Explorer 22
22 p3939 A69-40505

Dayglow O I lambda 1304 and 1356 A radiations photoelectron excitation rates theoretical calculation and experimental data on altitude dependence characteristics
22 p3939 A69-40517

Faraday effect measurements by polar orbiting satellites for vertical distribution of ionospheric electron density
22 p3941 A69-40718

Incident proton flux atmospheric altitude profile during PCA period, comparing balloon observations with preliminary satellite data
23 p4204 A69-41485

Nitric acid vapor in atmosphere as function of altitude from spectrograph, predicting downward diffusion
23 p4155 A69-41634

Electron concentration vertical profile in ionosphere in presence of horizontal wind shifts determined using E layer charged particle redistribution approximation
23 p4155 A69-41840

Lower atmospheric temperature continuous radio measurement as function of altitude, calculating temperature gradient
24 p4342 A69-42677

Northern Hemisphere 500-mb height pattern series expansion, using optimal sets of orthonormal functions, obtaining rms error
24 p4346 A69-43157

VERTICAL FINIS U FINIS

VERTICAL FLIGHT

Vertical flight path navigation requirements for supersonic aircraft based on computer simulated flights of Mach 2 Concorde
02 p0277 A69-11590

Slide wire aircraft vertical velocity meter for application during aerogravimetric mapping, discussing calibration and gravitational force measurement accuracy
03 p0429 A69-13261

Differential equation for dynamic behavior of acrobatic flight navigation instruments in steep flight, considering vertical gyroscopes, gimbal platforms and time optimal control
11 p1880 A69-24328

Trajectory calculation of axisymmetrical body during ballistic and vertical flight, assuming air drag proportional to square of velocity
17 p2889 A69-32950

VERTICAL LANDING

Integrated guidance and traffic control system to handle VTOL traffic in Northeast Corridor
05 p0789 A69-15560

Aerodynamic instrumentation to improve helicopter takeoff and landing piloting performance under high gross weight conditions
05 p0767 A69-16776

Research and development programs for several advanced rotary wing VTOL concepts
[AIAA PAPER 69-199] 07 p1055 A69-19555

Ground jet suppression fences for VTOL aircraft prepared pads, investigating erosion reduction and particle entrainment
[AIAA PAPER 68-639] 17 p2902 A69-34028

Shuttle VTOL airport access system analysis for New York area
[AIAA PAPER 69-804] 19 p3288 A69-35592

Mathematical models for describing visual perception of distance to ground during VTOL landing and takeoff
22 p3892 A69-40282

Steep descent landing systems developmental phases for VTOL aircraft, discussing noise abatement, approach angle and descent rates
22 p3978 A69-40674

VTOL transport aircraft to solve short haul travel problems, examining lateral and horizontal maneuvering and vertical to horizontal flight transition
24 p4250 A69-42564

VERTICAL MOTION

Sporadic E microstructure and vertical motion, describing radio sounding system to observe ionospheric 3d structure and motions from ground
01 p0071 A69-11164

Vertical propagation of acoustic waves in atmosphere without gravitational waves and with height varying atmospheric shear viscosity
02 p0274 A69-11440

Lower ionosphere vertical motions found responsible for nighttime variation of radio waves total field strength
02 p0207 A69-11689

Spatial distribution of vertically moving ionized formations in ionosphere suggests acoustic gravity waves excited in polar regions as cause
06 p0922 A69-17749

Active broadband vibration isolation of human subjects from severe vertical dynamic excitations experienced in low level high speed flight
[ASME PAPER 69-VIBR-65] 10 p1650 A69-24157

Vertical ionization drift in F region as function of electron density, ionization coefficient and recombination coefficient
12 p0270 A69-26584

Neutral gas motions causing plasma motions in F region, obtaining vertical plasma velocity component pronounced diurnal variations
12 p0270 A69-26684

Lower ionosphere vertical motions found responsible for nighttime variation of radio waves total field strength
13 p2224 A69-28720

Ballistic deviations limits for aircraft vertical gyroscope taking into account aircraft vertical movements, using compensation in system
14 p2445 A69-28899

Electrolytic vertical indicators response errors, discussing nonlinear properties of transducer steady state characteristics
14 p2446 A69-28925

Vertical motion of ionized formations in ionospheric F region related to sporadic E layer
14 p2437 A69-29074

Parametric resonance motion in viscous fluid column in communicating vessels during vertical oscillations, calculating critical accelerations over viscosity range
14 p2432 A69-29628

Strong vertical wind in low ionosphere due to short period reflected gravity waves, obtaining standing wave system
15 p2606 A69-31449

Adiabatic and diabatic processes contributions to vertical atmospheric motions profile and IR cooling components comparison
17 p2962 A69-33689

Vertical ionospheric perturbations shown responsible for Z component in F region
17 p2969 A69-34000

Kinesonde radio sounding system for three dimensional ground observations of E region microstructure and vertical motion of neutral air and ions
18 p3125 A69-34250

Buoyant plumes and thermals defined as vertical motions produced under gravity by density or temperature contrast between incompressible source fluid and environment
18 p3122 A69-34917

Wing elastic strains effect on vertical velocity in downwash, noting wing tail combination
18 p3086 A69-34999

VERTICAL TAKEOFF AIRCRAFT

Kalman filter based on calculus of variations, evaluating object trajectory during vertical atmospheric descent
19 p3307 A69-35794

Vertical atmospheric motions, considering wind velocity measurements associated with synoptic processes
19 p3366 A69-36673

Nighttime ionospheric F region velocity component and recombination coefficient computer calculation
20 p3521 A69-37049

Vertically moving disturbances relationship to behavior of E and F layers over Tiflis, noting sporadic E layers formation
20 p3528 A69-37685

Ionogram processing procedure, discussing presence of vertically moving ionospheric disturbances
20 p3529 A69-37691

Vertical neutral wind measurements in lower E region with wavelike spatial structure, noting vertical shear role in ionosphere dynamics
21 p3703 A69-38363

Diurnal intensity variations in OI 5577 A line emission connected with vertical movements in 90 km level of atmosphere
21 p3713 A69-38525

Turbulence and laminarity effect on vertical waves development rising in thin layer of heavy viscous fluid in contact with vertical gas flow
24 p4302 A69-43480

VERTICAL PERCEPTION

Universal vestibulometric chair for inducing irritation in tests involving vestibular analyzer interaction with other body functions
02 p0200 A69-11517

Space environment barriers to man due to biological evolution and transition from land to space in single generation, noting orientation problems
03 p0380 A69-14067

Witkin Rod and Frame Testing of pilots and engineers showing greater field independence in pilots, discussing applications to pilot instructor selection
12 p0203 A69-26556

Motion analysis of symmetrical physical pendulum having mobile fulcrum for geocentric vertical indicator possibility
21 p3727 A69-39830

Visual and tactual interaction in judgments of vertical in dark room experiments, discussing effects of various reference systems
24 p4271 A69-42752

VERTICAL STABILIZERS

U STABILIZERS [FLUID DYNAMICS]

VERTICAL TAILS

U STABILIZERS [FLUID DYNAMICS]

U TAIL ASSEMBLIES

VERTICAL TAKEOFF

Aerodynamic instrumentation to improve helicopter takeoff and landing piloting performance under high gross weight conditions
05 p0767 A69-16776

Ground jet suppression fences for VTOL aircraft prepared pads, investigating erosion reduction and particle entrainment
[AIAA PAPER 68-639] 17 p2902 A69-34028

Shuttle VTOL airport access system analysis for New York area
[AIAA PAPER 69-804] 19 p3288 A69-35592

Mathematical models for describing visual perception of distance to ground during VTOL landing and takeoff
22 p3892 A69-40282

VERTICAL TAKEOFF AIRCRAFT

NT FLYING PLATFORMS

NT X- 22A AIRCRAFT

NT XC-142 AIRCRAFT

NT XV- 4 AIRCRAFT

Power spectral density method of random loads analysis applied to V/STOL aircraft structural analysis, discussing statistical distribution
01 p0168 A69-10407

VTOL aircraft design for noise reduction, discussing localities tolerance, noise sources, operating cost, etc
01 p0009 A69-10421

Minimum admissible spacing between supersonic jet expelled from VTOL aircraft nozzle and plane surface near nozzle exit
03 p0361 A69-12955

X V-4B Hummingbird 2, noting modification from XB-4A two engine ejector augmentation to six engine directed and diverted thrust configuration
03 p0366 A69-13112

STOL and VTOL aircraft characteristics in operation, considering impact on terminal navigation and air traffic control
[SAE PAPER 680666] 03 p0465 A69-13452

Advance indication based on extrapolation for aiding manual attitude control of VTOL aircraft in hovering flight, noting results on flight simulator
03 p0366 A69-13645

Ground effects influence on VTOL aircraft secondary forces during hovering and transitional flight, discussing component dynamic coefficients in wind tunnel
[DVL-851] 04 p0547 A69-14813

Two term and three term controllers for hovering rigs and VTOL aircraft, comparing stability, transient response and control force
04 p0547 A69-14814

Temperature stresses analysis for jet lift VTOL aircraft structure during takeoff and landing, discussing fire hazard in lift pod
04 p0548 A69-14841

Helicopter, compounds and composite aircraft design trends
05 p0700 A69-15548

Integrated guidance and traffic control system to handle VTOL traffic in Northeast Corridor
05 p0789 A69-15560

VTOL aircraft materials for improved lightness, durability and cost, noting Be alloys, filamentary composite materials and future problems
05 p0702 A69-15962

Optimal flight stabilization of VTOL aircraft in hovering mode based on linear rotation dampers system
05 p0702 A69-16024

Compound rotorcraft VTOL vehicle current programs
05 p0703 A69-16394

Low range airspeed system (LORAS) on X-22A and P 1127 VTOL aircraft for accurate airspeed information
05 p0767 A69-16774

Longitudinal dynamics of VTOL aircraft during hover-forward flight transition, using multiple time scale analysis
[AIAA PAPER 69-130] 06 p0869 A69-18157

Research and development programs for several advanced rotary wing VTOL concepts
[AIAA PAPER 69-199] 07 p1055 A69-19555

Military applications of VTOL aircraft, discussing role in battle area with restricted surface transportation
[AIAA PAPER 69-326] 07 p1055 A69-19556

Future commercial VTOL transportation, considering technical, political and socio-economic problems
[AIAA PAPER 69-198] 07 p1056 A69-19567

Optimum approach and departure paths for VTOL aircraft simulated by hybrid computer under constraints
[AIAA PAPER 69-209] 07 p1178 A69-19570

Stress analysis split method for determining residual strength and fatigue crack life of damaged or initially cracked VTOL structures
[AIAA PAPER 69-214] 07 p1237 A69-19576

Aircraft separation standards, considering separate space for VTOL in automated high density airways system
[AIAA PAPER 69-210] 07 p1178 A69-19579

Scanning beam landing systems for VTOL aircraft
07 p1178 A69-19631

Testing station design for VTOL aircraft ground effects investigations
08 p1302 A69-20880

Electronic terminal guidance requirements for all-weather VTOL operations, suggesting future first generation landing system
08 p1348 A69-21064

Lockheed XV-4B Hummingbird 2 VTOL aircraft propulsion, control, escape systems, with tests
10 p1634 A69-23597

Human pilot adaptation in simulated multiloop VTOL hovering task with series loop closure model
10 p1650 A69-23878

Folding propotor VTOL aircraft configuration analytical and experimental investigations to study design requirements for cruise speeds to Mach 0.75
[AIAA PAPER 69-220] 10 p1635 A69-24087

Book on aircraft stability and control covering conventional, canard, variable sweep, slender delta wing, helicopter and other VTOL aircraft
11 p1821 A69-24370

VTOL aircraft flight control systems, considering computerization and automation approach with human pilot serving as monitor and emergency system
11 p1823 A69-25387

Computer aided design of linear multivariable control systems applied to VTOL aircraft stability augmentation
12 p2013 A69-26068

Exhaust gas recirculation for VTOL aircraft
[AIAA PAPER 67-439] 12 p2013 A69-26760

Ingestion and flow field characteristics of interaction of two heated parallel air jets, discussing VTOL exhaust ingestion tests
[AIAA PAPER 68-79] 12 p2012 A69-26761

Potential error source in VTOL aircraft dynamics analysis suggested by dual function of symbol used in perturbation equations of motion
12 p2014 A69-26776

Vertical takeoff aircraft role in British Government air industry program, noting applications to intercity passenger service
13 p2203 A69-28355

Reaction forces for jet lift VTOL attitude control during hover and transition, considering hot gas and pitch ducting applications
[AIAA PAPER 69-545] 16 p2735 A69-32756

VTOL transport aircraft, discussing systems integration problems, feasibility and time scale of introduction into service, noise and safety, etc
17 p2897 A69-33207

Self contained lift fan concept and circulation controlled rotor aircraft power plants for high speed VTOL transports
17 p2897 A69-33208

German VTOL aircraft development excluding helicopters, discussing technical problems, safety and economy in civil application
17 p2899 A69-33381

Mission task performance oriented approach to winged helicopters flying and handling qualities, considering wings and horizontal stabilizers influence
[AHS PAPER 360] 17 p2900 A69-33522

Vertical takeoff aircraft propeller/rotor design and performance prediction, discussing vortex model, wake contraction, blade element aerodynamic properties, etc
[AHS PAPER 325] 17 p2894 A69-33534

Integrated trajectory error display (ITED) for flight path control of helicopters and VTOL, describing principles governing display synthesis
[AHS PAPER 314] 17 p3001 A69-33541

Solid state single unit digital control computer performing stability augmentation, pilot relief functions and generating minimum fuel flight paths for VTOL landing
17 p2934 A69-34075

Aerodynamic characteristics of elliptical airfoils with jet circulation control for VTOL rotors including dual jets and cyclic results
[AIAA PAPER 69-741] 18 p3084 A69-34406

Weight estimation of structures and systems unique to VTOL aircraft, considering remote fan and high bypass engine lift propulsion concepts
[SAWE PAPER 784] 18 p3090 A69-34868

Static dynamic and damage tolerant strengths of advanced materials for VTOL aircraft with emphasis on Ti, cryoformed 301 stainless steels and filamentary composites
[AIAA PAPER 69-764] 19 p3433 A69-35658

VTOL aircraft lift systems, propulsion, airframes, dynamic and aerodynamic characteristics, control systems, missions, safety, configurations and environment
[AIAA PAPER 68-977] 20 p3461 A69-37149

JR 100 F lift jet engines for Japanese national aerospace laboratory produced as part of VTOL developing program
21 p3785 A69-38608

Analytical and graphical methods for characteristics of optima produced by quadratic performance index for VTOL prefilter model reference attitude control system
[AIAA PAPER 69-884] 21 p3764 A69-39411

Electronic terminal guidance requirements for all-weather VTOL operations, suggesting future first generation landing system
22 p3978 A69-39875

Dornier R and D, discussing single and twin engine aircraft, utility aircraft, helicopter, VTOL transport, safety, etc
22 p3862 A69-39931

RB 202 self contained lift fan engine design for high speed interurban civil VTOL operations, considering weight, cost, noise and fuel consumption
22 p3862 A69-39933

Steep descent landing systems developmental phases for VTOL aircraft, discussing noise abatement, approach angle and descent rates
22 p3978 A69-40674

Aerodynamics of rotary wing and V/STOL aircraft - Conference, Buffalo, June 1969, Volume 3
23 p4057 A69-41369

Aerodynamic research in VTOL field including rotor wake, noise reduction, airfoil sections, lift coefficient, drag, wind tunnels, etc
23 p4058 A69-41374

VTOL, STOL and CTOL transportation systems comparison effectiveness comparison for Northeast Corridor operation, considering ground facilities, access time, etc
[SAE PAPER 690417] 23 p4147 A69-41642

Air traffic interfaces of VTOL, STOL and CTOL aircraft serving same metropolitan terminal, emphasizing navigation systems, geographical positions, ground communication, etc
[SAE PAPER 690422] 23 p4185 A69-41646

Metropolitan downtown airports for STOL and VTOL aircraft stressing Los Angeles Metroport
[SAE PAPER 690402] 23 p4147 A69-41660

VTOL transport aircraft to solve short haul travel problems, examining lateral and horizontal maneuvering and vertical to horizontal flight transition
24 p4250 A69-42564

Demand curves for VTOL intercity transportation, discussing conventional helicopters, compound helicopters, tilt rotor, tilt wing, stored rotor and fan or jet lift
24 p4254 A69-43721

VERTICES

U APEXES

VERTIGO

Painted helicopter rotor blades ruled out as cause of flicker induced vertigo, reporting pilots psychophysiological responses to formation flying
17 p2913 A69-33175

VERTOL MILITARY HELICOPTERS

U BOEING AIRCRAFT

U MILITARY HELICOPTERS

VERY HIGH FREQUENCIES

VHF transhorizon propagation by double reflection from elevated layer in troposphere
01 p0034 A69-11139

Lake Kickapoo Space Surveillance Transmitting Station in Texas, discussing surroundings, equipment, operating range, VHF transmission, etc
03 p0411 A69-13209

Sudden VHF phase anomalies produced by solar flare induced ionospheric disturbances during July 1968
05 p0719 A69-15980

VHF to UHF conversion, noting modular UHF telemetry transmitter, miniature UHF special purpose transmitter, RF power amplifiers and telemetry receiver
05 p0732 A69-16305

VHF transistor power output capability, discussing limitation by RF saturation resistance and current crowding by large current densities and high frequencies
07 p1101 A69-18653

Radio aurora rate of occurrence from VHF bistatic radio system observations in eastern Canada
07 p1124 A69-18824

Adaptive airborne VHF/UHF transmitter system, discussing design, ground isolation, current limiting, internal telemetry, wideband frequency response, real time video signals, etc
07 p1106 A69-19114

VHF radio transmission beyond horizon, discussing instrumentation, annual and diurnal signal fluctuations and diffraction role in signal propagation
08 p1274 A69-20112

VHF satellite signal scintillation by ionospheric irregularities with sharp boundary /such as sporadic E/, noting diffraction pattern dependence on phase shift
09 p1489 A69-21713

Meter wave radio spectrum observations during 9 June 1968 solar flare, suggesting sudden intensity and frequency change due to shock wave
09 p1582 A69-22748

Two solar flare initiated type 4 radio bursts on 4 and 6 May 1968, noting prominence activity leading to meter wave generation
09 p1582 A69-22749

Transequatorial propagation mode for waves in VHF band twice scattered by field aligned irregularities in electron density
10 p1653 A69-23192

Optical frequency standards, discussing lasers VHF stability, RF and optical ranges, long and short term effects, etc
10 p1702 A69-23299

RF measurement techniques and interpretation of bonding impedance characteristics through VHF region

12 p2040 A69-26472

VHF to UHF telemetry bands transition implemented by Naval Weapons Center

14 p2411 A69-28880

Electron beam welding for repair and production, discussing application to Ti VHF antennas, Concorde switchgears and nuclear reactor loading tubes [SBA PAPER 14]

20 p3550 A69-37451

VHF radio propagation over transequatorial circuit related to equatorial anomaly in F layer, suggesting F2/F2 propagation mode role

23 p4127 A69-42431

VERY HIGH FREQUENCY RADIO EQUIPMENT

Mechanically despun VHF antenna for spin stabilized synchronous satellites, detailing electrical and mechanical design

01 p0161 A69-10350

Minimum operational characteristics for airborne VHF communication systems, discussing FCC requirements and system performance

07 p1077 A69-18638

Conversion from VHF to UHF at White Sands Missile Range, discussing telemetry acquisition, tracking and receiving systems

07 p1077 A69-18828

Temperature profiles and frequency driftings of VHF telemetry transmitters for Saturn S-C stage, using IR radiation data

10 p1653 A69-23049

Parametric amplifying systems with lumped reactive nonlinear elements, emphasizing UHF systems

11 p1844 A69-24448

Rescue locator beacons and airborne search equipment of VHF and UHF capabilities available to international civil aircraft operations

15 p2552 A69-30852

Seven helix antenna array components and operation mode at Berlin weather station, including biaxial rotor, preamplifier servoamplifier and VHF telemetry receiver

17 p2946 A69-33768

Circularly polarized VHF antenna systems for spin stabilized satellites, discussing design and performance test results

22 p3913 A69-40695

Circular or linear polarization diversity reception for VHF earth-station-satellite communications through turbulent ionosphere, assuming Rayleigh distribution fading

23 p4115 A69-41585

Adaptive signal processing interference rejection technique for suppression of cochannel AM interference in congested VHF tracking receiver

23 p4128 A69-42503

VERY LOW FREQUENCIES

Quasi-periodic VLF emissions associated with geomagnetic micropulsation activity in terms of comparable periodicity

01 p0063 A69-10274

VLF electric field measurements from 1 AU heliocentric orbit, noting field oscillations in solar wind and large amplitude HF noise bursts

01 p0035 A69-11224

Charged particle motion caused by ELF electromagnetic waves in presence of constant magnetic field, noting earth ionosphere application

02 p0240 A69-11712

Ionospheric LF radio noise cut-off near proton gyrofrequency, discussing satellite ELF and VLF observations

03 p0399 A69-14021

Packet of finite amplitude VLF whistler waves, examining cyclotron resonance interaction with high energy electrons and development in magnetosphere

06 p0917 A69-17378

Diurnal field strength and phase variations of VLF transmissions over transequatorial path from Australia to Japan

06 p0889 A69-17654

Phase and amplitude record changes in sunrise and sunset transitions in VLF transmissions over long path

06 p0889 A69-17655

VLF radiation bursts /July-October 1966/ in U.S.S.R., noting detection probability increase with increasing magnetic activity

06 p0920 A69-17731

Numerical methods for VLF electromagnetic wave propagation in earth-ionosphere waveguide, discussing boundary conditions assignment effect at ionosphere on eigenvalues

06 p0920 A69-17732

VLF diurnal phase change observations, showing deviations from theoretical first mode and second mode dominance

07 p1078 A69-18912

Whistlers and VLF emissions from ground based and satellite measurements, applying results to electron density mapping and ion detection

07 p1127 A69-19354

VLF wave electromagnetic properties in magnetosphere, noting whistler mode propagation and refractive index and electron density of medium

08 p1306 A69-20180

VLF emissions intensity and spectra variations compared with energetic electron fluxes variations during magnetosphere storm periods

09 p1488 A69-21698

Large scale heat sources influence on formation and dynamics of ultralong waves in atmosphere, using linear time dependent quasi-geostrophic model

09 p1491 A69-22164

VLF electromagnetic wave propagation in earth-ionosphere waveguide with reflections from ionosphere, noting TE and TM mode coupling and mode conversion

09 p1460 A69-22699

VLF transequatorial propagation variance from magnetic equator to midlatitude confirmed through phase and amplitude records of multisite observations

10 p1655 A69-23416

Weakly attenuated components of VLF mode spectrum associated with propagation below anisotropic ionospheres as function of frequency and azimuth

10 p1655 A69-23417

VLF observations of July 7 1966 solar flare and PCA event

10 p1657 A69-23772

Artificial triggering of VLF magnetospheric noise by NAA Morse code transmission during whistler duct drift across magnetic shells on 17 June 1965

11 p1878 A69-25154

Artificial magnetospheric VLF noise triggering by Morse code dots at 14.7 kHz from NAA verified at Antarctica

11 p1878 A69-25155

Transmitter frequency increase effect on production of artificial stimulated VLF emissions in magnetosphere

11 p1878 A69-25156

Linear active adjustable VLF filters for polynomial transfer functions

11 p1859 A69-25392

VLF wave propagation along mixed path in curved earth-ionosphere waveguide, considering reflection and transmission coefficients of modes

12 p2032 A69-26858

Phase and field strength of transequatorial VLF signals, noting behavior during sunrise, day and nighttime

12 p2032 A69-26860

VLF signal strength minima during transition fading, considering asymptotic statistical distribution

12 p2032 A69-26862

Satellite observation of intensity and distribution of VLF emission at medium latitude during magnetic storm interpreted by transverse resonance plasma instability

12 p2073 A69-26947

VLF morning and evening magnetosphere emission distinction by studying spectrum width as function of variations in K index

13 p2253 A69-27740

Latitudinal cut-off of manmade VLF signals in short path through ionosphere to OGO 2 satellite, noting strong noise following signal cut-off

14 p2434 A69-28958

Solar X ray flux deduced from flare effects on VLF propagation, showing total energy content as measure of ionizing radiation

14 p2411 A69-29105

Solar flare effect on polar chorus variation determined by comparing Antarctica VLF data with low latitude magnetograms

14 p2514 A69-29385

Long distance VLF multirange navigation fix errors as function of angles of cut of position lines and range errors, presenting error isograms

14 p2478 A69-29484

Atomic and astronomical time and frequency measurement via Loran C and VLF/Omega phase tracking receivers

15 p2615 A69-31285

Simultaneous particle flux and VLF noise spectrum measurements by rocket sounding, discussing equipment, telemetry and calibration systems and experimental data

15 p2605 A69-31423

VLF and particle rocket experiment for group delay time between rocket and ground, discussing wave polarization and energy flows meaning

15 p2571 A69-31424

Ionospheric VLF emission and particle measurements, discussing energy, distribution and flux of protons and electrons

15 p2605 A69-31425

VLF radio wave propagation in waveguide channel formed by earth and inhomogeneous anisotropic ionosphere

16 p2751 A69-32032

Ionosphere depression influence on VLF signals phase and amplitude calculated by mode theory and integral equations system representing aperture fields

17 p2920 A69-33418

Auroras and VLF emissions observations at ground stations to correlate emissions with auroral displays, noting low ionospheric absorption role

21 p3708 A69-38494

Synoptic study of worldwide VLF electromagnetic wave fields distribution above ionosphere from Ariel 3 observations

21 p3717 A69-39262

Self rhythms of low audio frequencies in motor nerves under electric pulses influence at VLF related to viscosity changes of nerve substance

23 p4092 A69-42057

VESTIBULAR TESTS

Extraterrestrial vestibular research, discussing human otolithic apparatus regulation subjected to change from geocentric to heliocentric orientation [UN PAPER 68-95389]

01 p0014 A69-10508

Physiological studies of centripetal and Coriolis accelerations effects on vestibular function of humans in rotating chamber

02 p0197 A69-11498

Hypoxia effects on vestibular analyzer function of rats in pressure chambers at simulated altitudes from 11,000 to 12,000 m

02 p0198 A69-11506

Universal vestibulometric chair for inducing irritation in tests involving vestibular analyzer interaction with other body functions

02 p0200 A69-11517

Acoustical vestibular stimulation in guinea pig, showing activation of receptors

03 p0376 A69-14076

Antimotion sickness drugs tested in slow rotation room with controlled Coriolis accelerations, noting summation effect of dextroamphetamine sulfate and scopolamine hydrobromide

03 p0381 A69-14079

Coriolis acceleration dosages applied in vestibulometric tests of male subjects inclined in rotating chair

05 p0710 A69-16521

Human vestibular reactions during weightlessness preceded and followed by acceleration

07 p1061 A69-18581

Human vestibular and sensory reactions to rotation and rocking, Coriolis acceleration and vestibular reaction inhibition on ground test stand for effects of temporary weightlessness

07 p1062 A69-18586

Vestibular-vegetative reactions during angular and Coriolis accelerations alternating with weightlessness, noting increased parasympathetic and sympathetic activity

07 p1062 A69-18587

Vestibular function of cosmonauts during preflight training and flight on Voskhod spacecraft, tabulating heart beat, respiration rates and writing test ratings

07 p1062 A69-18588

Jet fighter pilot spatial disorientation during flight and on ground, emphasizing vestibular neuronitis diagnosis

10 p1649 A69-23382

Weightlessness and higher g values effects on caloric and rotational nystagmus

12 p2020 A69-26551

Human vestibular reactions at various bodily rotation rates and planes, including counterrotation illusion and nystagmic reaction

12 p2020 A69-26564

Prolonged iterative accelerations and decelerations on vestibular apparatus, discussing nystagmus measurement attempt and centrifugation tests on guinea pigs

13 p2211 A69-28592

Soviet book on nervous mechanisms of vestibular reactions emphasizing mathematical description of operation, neurophysiological changes in cerebral cortex and oculomotor activity modeling

16 p2746 A69-32605

Vestibular reactions in rats under hypothermal conditions by measuring postrotatory nystagmus beats

number and duration, respiration rates and rectal temperature 17 p2906 A69-32934

Diphenidol and prochlorperazine effect on human semicircular canal function, noting failure of drug to alter vestibular responses 17 p2913 A69-33168

Head movements controlled for rapid vestibular adaptation in slow rotation room /SRR/, preventing motion sickness 17 p2908 A69-33178

Coriolis acceleration dosages applied in vestibulometric tests of male subjects inclined in rotating chair 18 p3096 A69-34740

Soviet collection of papers on vestibular analyzer physiology 20 p3467 A69-37240

Astronaut vestibular and motor analyzer functions during flight and simulation tests, discussing illusory space orientation and role of cortical dynamics 20 p3469 A69-37241

Electrical response of frog and human visual cortex neurons to thermal vestibular and light flash stimulation 20 p3469 A69-37242

Phase and tonic activity of oculomotor apparatus of rabbits during vestibular reflexes and postrotational nystagmus 20 p3469 A69-37243

Sensorimotor coordination of man performing graphic assignments in upright, reclining and prone position, discussing interaction of vestibular, visual and motor analyzers 20 p3470 A69-37246

Visual and vestibular analyzers interrelation in subjects receiving light pulses before and after rotation, noting role of cortical elements 20 p3470 A69-37249

Vestibular neurons activity in decerebrized cats under ipsilateral and contralateral labyrinth polarization combined with acoustic and caloric stimulation 20 p3471 A69-37254

Cats vestibular neurons reactions to labyrinths mon- and binaural polarization and caloric stimulation 20 p3471 A69-37255

Neuron activity simulation applied to vestibular neurons electrical activity analysis, discussing feedback circuitry and cathodic depression 20 p3471 A69-37256

Coriolis acceleration effect on vestibulo-vegetative and vestibulo-somatic reflexes of humans subjected to forward tilting, noting pulse and respiration rates 20 p3472 A69-37259

Vestibular functions of humans subjected to Coriolis acceleration via prolonged rotation at different angular velocity rates 20 p3472 A69-37260

Vestibular analyzer dynamic characteristics under Coriolis acceleration, measuring heart beat rate, arterial pressure, head bending aftereffects, etc 20 p3472 A69-37262

Vestibular analyzer function relation to arterial pressure during otolith stimulation experiments on subjects susceptible and nonsusceptible to motion sickness 20 p3472 A69-37264

Test pilot vestibular training program to achieve higher tolerance of rotation, rocking and balancing and visual stimuli 20 p3472 A69-37266

Nystagmus reactions in rabbits subjected to rotating vestibular tests, noting decrease following previous adaptation to stimulus 20 p3473 A69-37267

Vestibular stimulation effect on human blood composition during rocking test indicating blood eosinophile content as function of hypophysis and adrenal cortex reactions 20 p3473 A69-37268

Vestibulo-somatic, vegetative and sensory reactions to angular acceleration, deceleration and tilting, evaluating functional state of vestibular analyzer 20 p3481 A69-37270

Vestibular function tested with angular acceleration, applying semicircular canal reflexes for flight crew selection and appraisal 20 p3481 A69-37271

Electronystagmographic method of eye movement recording, noting applications to vestibular and visual analysis and study of oculomotor nuclei- vegetative centers relations 20 p3481 A69-37273

Equipment with minimum semicircular canals stimulation for vestibular analyzer studies 20 p3481 A69-37274

Spacecraft rotation and astronaut head and body motion as stimuli for vestibular analyzer function study during weightlessness 20 p3473 A69-37275

Weightlessness tests during parabolic flight to supplement vestibular tests in astronaut selection 20 p3481 A69-37276

Vestibulometric test program for flight surgeon appraisal of flying personnel, emphasizing singling out persons prone to illusory sensations 20 p3473 A69-37277

Vestibulometric tests for flight surgeon appraisal of applicants in flying profession, comparing Coriolis forces cumulative load tests with conventional tests 20 p3481 A69-37278

Mathematical models of human vestibular system for dynamic space orientation, using control theory 21 p3662 A69-38728

Alcoholic hangover effects on human balance system from flying demands viewpoint, discussing ocular-vestibular system disturbances 23 p4089 A69-41817

VESTIBULES

Rotational velocity estimates by observers during angular acceleration, noting vestibular function interpretation 04 p0554 A69-15332

Mathematical input-output model for vestibular system, relating linear and angular motions to non-visual perception of orientation, motion and nystagmus for physiological characteristics 24 p4276 A69-43274

VHF OMNIRANGE NAVIGATION

VOR path course errors, emphasizing effects of propagation and receiver processing 03 p0392 A69-13245

Phase error and amplitude and phase modulation in aircraft VOR omni receiver in vicinity of reflecting objects, noting asymmetrical filter effect 08 p1271 A69-19863

VOR/DME ground facilities accuracy improvement by complementing navigation computation with signals from inertial navigation system [SAE PAPER 690338] 11 p1914 A69-24499

Transistorized VOR system using electronic goniometer and fixed antennas, describing power supply, transmitter, goniometer, antenna and design 16 p2827 A69-31938

VOR/DME information augmentation by air data /airspeed/ for positional accuracy improvement, describing error sources, optimum data filter and system sensitivity and performance [AIAA PAPER 69-841] 21 p3762 A69-39372

Airline area navigation test programs involving use of VOR/DME signals and inertial navigation system within air traffic control system 23 p4185 A69-41662

VIBRATION

NT BENDING VIBRATION
NT COMBUSTION VIBRATION
NT FLUTTER

NT FORCED VIBRATION
NT FREE VIBRATION
NT LATTICE VIBRATIONS

NT LINEAR VIBRATION
NT MISSILE VIBRATION
NT PANEL FLUTTER

NT RANDOM VIBRATION
NT RESONANT VIBRATION
NT SELF INDUCED VIBRATION

NT STRUCTURAL VIBRATION
NT SUBSONIC FLUTTER
NT SUPERSONIC FLUTTER

NT TORSIONAL VIBRATION
NT VIBRATIONAL STRESS
NT VIBRATORY LOADS

Surface vibrations effect on forced convection heat transfer normal to cylinder, discussing convective coefficients dependence on Reynolds number [ASME PAPER 68-WA/HT-5] 05 p0846 A69-16116

Hankel functions and vibration equations solutions, discussing asymptotic behavior and monotonic properties in neighborhood of ellipses 08 p1416 A69-20714

Pointwise bounding of eigenfunctions in vibration and stability problems in elasticity theory 10 p1794 A69-22925

Matrix Computer for solution of algebraic and integrodifferential equations in linear and nonlinear statics and dynamics, considering mechanical vibration problems [ASME PAPER 69-VIBR-12] 10 p1806 A69-24167

Nonstationary vibrations of mechanical systems subjected to harmonic or external limited energy source excitations 11 p1975 A69-24739

Surface vibrations effect on forced convection heat transfer normal to cylinder, discussing convective coefficients dependence on Reynolds number [ASME PAPER 68-WA/HT-5] 13 p2374 A69-2778

Linear piezoelectric plate vibrations, Elements of linear theory of piezoelectricity and vibrations of piezoelectric plates, covering differential equations, boundary conditions, etc 16 p2826 A69-3172

Equation of motion for determining nonlinear vibration of rod pendulum in viscous flow of varying velocity 21 p3773 A69-39679

VIBRATION DAMPING

Self sustained oscillations of piston type valving system with conduit line at upstream and capacity at downstream 01 p0012 A69-10310

Mechanical behavior of synthetic layer coatings for damping instrumental vibration and noise 01 p0168 A69-10399

Spadoryc slide rule for damping determination from vibration decay traces, noting use in flight flutter tests 01 p0087 A69-11029

Summed and differential types of higher order oscillations in vibratory systems with multiple degrees of freedom under parametric excitation 02 p0346 A69-12422

Attitude control system for gravity gradient stabilized satellite in synchronous and near synchronous equatorial orbits, discussing libration damping methods 03 p0504 A69-12857

Damping capacity and resistance to resonance fatigue of titanium and aluminum based steels and alloys 03 p0443 A69-13025

Acoustic absorbers for combustion stabilization, discussing analytical model based on temporal damping coefficient for oscillation modes and allowance for nonuniform distribution 03 p0532 A69-13133

Dipole and quadrupole bremsstrahlung and damping of electron plasma oscillations, finding negative k-square collisional electron-ion contribution 03 p0475 A69-13149

Torsion bar with two inertia masses attached used to determine damping capacity and torsional fatigue strength 03 p0431 A69-13917

Frequency of damped oscillations in plasma in DC field, noting variation with electron density and DC field 03 p0479 A69-14050

Constrained layer damping and conventional techniques combination for vibration and noise control 04 p0606 A69-14691

Nonlinear damping of circularly polarized electromagnetic wave propagating in plasma along magnetic field, noting particle motion in resonance region 04 p0558 A69-14982

Parallel damped dynamic vibration absorbers, modifying conventional absorber by adding subsidiary undamped absorber mass [ASME PAPER 68-WA/DE-6] 05 p0839 A69-16171

Rotors linear vibrations due to unbalanced shaft rotating on lubricated bearings taking into account lubricant damping 07 p1235 A69-19441

Axial waves in blood vessels, determining phase velocities and damping, noting anisotropic behavior of artery wall [SESA PAPER 1350] 07 p1069 A69-19726

Dislocation damping measurements made on Fe-18Cr-Ni alloys, noting damping relation to nickel content and stacking fault 08 p1334 A69-20576

Logarithmic decrement and period of disks performing torsional oscillations measured in viscous fluid, noting dependence on oscillation amplitude 08 p1417 A69-20781

Second order system response with variable damping computed by stepwise numerical integration 08 p1418 A69-20849

Time rates for growth and damping of resistive instability in gaseous plasma in crossed electric and magnetic fields 08 p1369 A69-20886

- Lasing characteristics of Nd-glass laser when cavity radiation varies with time, discussing rapid damping of relaxation oscillations of laser intensity
08 p1327 A69-21024
- Structural damping coefficient for free vibrations of one degree freedom general systems motion
09 p1617 A69-22076
- Compact antivibration mounting for carrying instruments, using bicycle tire inner tube around heavy slab to provide elasticity and damping
09 p1502 A69-22692
- Damping criteria for satellite vibration based on energy dissipation by material hysteresis, friction in viscous flow, magnetic hysteresis and eddy currents
10 p1791 A69-22921
- Root fixture and grip load effects on cantilever beam damping, using bandwidth and logarithmic decrement measurement methods
10 p1800 A69-23244
- Interfacial pressure distribution during slip damping in clamped rectangular beams subjected to vibration
10 p1800 A69-23350
- Metals with combined high damping and good mechanical properties for solving fatigue, noise and vibration problems
10 p1715 A69-24044
- Airflow through open foam cellular structure, discussing mathematic model for predicting pressure buildup and foam response in shock and vibration isolation
[ASME PAPER 69-VIBR-46]
10 p1803 A69-24144
- Gas turbine blade vibrations, discussing excitation causes and damping techniques
[ASME PAPER 69-VIBR-59]
10 p1805 A69-24155
- Damped steady state response of elastic foundation beam subjected to cyclic moving loads to determine load movement frequencies for natural frequency excitation
[ASME PAPER 69-VIBR-13]
10 p1806 A69-24166
- Damping of response of integrally stiffened skin structures to random acoustic pressures, reducing rms stress in case of broad band excitation
[ASME PAPER 69-VIBR-26]
10 p1806 A69-24172
- Synchronous vibration absorbers using gyroscopic systems, noting antiresonance with Perissogyro
[ASME PAPER 69-VIBR-39]
10 p1807 A69-24177
- Multiparameter optimum damping for harmonically excited linear stable strictly dissipative n degrees of freedom system, locating multivariable saddle points
[ASME PAPER 69-VIBR-42]
10 p1807 A69-24180
- Parametric damping of oscillations in second order automatic control systems, taking into account control function constraints
11 p1857 A69-24556
- Damping properties of nonlinear viscoelastic solids with applications to vibrating continua, using Gauss principle of least constraints
11 p1970 A69-24605
- Energy dissipation in freely oscillating bodies under static stresses described by differential equation, assuming elliptical hysteresis loop
11 p1919 A69-25092
- Optimum platform stabilizer selection for damping of rotational motion and elastic torsional stresses of aircraft fuselage about longitudinal axis
11 p1966 A69-25327
- Strip method for prediction of subcritical frequency and damping characteristics for subsonic wind tunnel and flight flutter tests
11 p1987 A69-25368
- HF brake excited vibration damping in aircraft landing gear, obtaining closed form solution
[AIAA PAPER 68-312]
11 p1823 A69-25370
- Flutter design charts for isotropic panels stressed to verge of buckling for typical values of structural damping
11 p1992 A69-25524
- Linear vibrational systems natural frequencies and damping characteristics determined from system reaction to pulse effect
12 p2178 A69-26004
- Friction damping properties of deployed structures vibrating in weightless state compared to damping in space for true determination
12 p2183 A69-26792
- Parallel damped dynamic vibration absorbers, modifying conventional absorber by adding subsidiary undamped absorber mass
[ASME PAPER 68-WA/DE-6]
13 p2360 A69-27422
- Shear stress and velocity profile in MHD duct, examining turbulence damping by electromagnetic coupling
13 p2309 A69-28024
- Dynamic stability of two degrees of freedom circulatory systems with bilinear hysteresis damping
13 p2363 A69-28127
- Rigid structures high damping without loss of rigidity achieved by epoxy resin dampers, noting moderate cost
13 p2370 A69-28601
- Dual pendulum with tilt sensitivity at wide passband frequencies and damping due to horizontal oscillations
14 p2450 A69-29570
- Vibration damping and elastic bond positioning in nonlinear systems with coincident centers of gravity and rigid damping
14 p2537 A69-29746
- Vibration control by alternate layers of high damping viscoelastic material, discussing damping and loss factors, beams design and attachment
15 p2622 A69-30704
- Vibrations attenuation by viscoelastic sandwich shear damping, discussing examples of aircraft equipment racks, gyro and airborne circuit board mountings
15 p2622 A69-30705
- Steady state motion of multiple unit impact damper attached to sinusoidally excited primary system, determining asymptotically stable regions
15 p2714 A69-31144
- Linearized kinetic equation for perturbed electron distribution function, detailing plasma oscillations along magnetic field by Landau collision term
16 p2818 A69-31674
- Satellite gravitational stabilization system with maximum damping rate, discussing orbital plane oscillations
16 p2867 A69-31738
- Forced oscillations of three layer plate used as vibration dampers for engine components
16 p2873 A69-32143
- Nonlinear mechanical systems vibrations damping emphasizing energy dissipation
16 p2874 A69-32245
- Turbomachinery two mode blade vibrations with emphasis on aerodynamic damping, noting shifts in natural frequencies
[ONERA-TP-678]
16 p2733 A69-32333
- Liquid filled toroidal shaped rotating damping tube containing bubble, discussing parameters variation effect on spacecraft nutation
16 p2868 A69-32561
- Nonlinear response of single Helmholtz resonator subjected to finite amplitude pressure oscillations, detailing entrance, orifice and cavitation flow
[AIAA PAPER 69-481]
16 p2844 A69-32719
- Close coupled accumulators for suppressing missile longitudinal oscillations (POGO) developed for Gemini and Titan 3, including pump interaction
[AIAA PAPER 69-547]
16 p2869 A69-32729
- Free-free transverse vibration damping phenomena, calculating strain amplitude dependence of internal friction at various frequencies
17 p3051 A69-32961
- Damped vibrations of elastic open cylindrical shell under arbitrary loading, obtaining mean square of bending from correlation theory
17 p3054 A69-33094
- Main rotor bifilar absorber for vibration reduction during S-61 helicopter flight, describing shake and flight tests
[AHS PAPER 354]
17 p2900 A69-33523
- Oscillations of nonlinear dissipative mechanical system with two degrees of freedom, possessing structural damping at joints between moving masses and base
17 p3064 A69-33915
- Energy dissipation in elastic systems as function of limiting damping characteristics of oscillations
17 p3065 A69-33923
- Scale factor determination for energy dissipation at clamped ends, analyzing geometric parameter and clamping force effect on oscillation damping constant
17 p3065 A69-33927
- Cylindrical aluminum shell dynamic stability, analyzing steady state parametric oscillations, mode shape, frequency, amplitude and damping
17 p3065 A69-33929
- Automatic device for logarithmic damping decrement measurement from vibrograms, showing structural arrangement and electrical circuitry
17 p2976 A69-33931
- Damping properties of turbine blade materials subjected to transverse bending vibrations in vacuum and at high temperatures, including Ti alloys
17 p2990 A69-33932
- Damping, fatigue and optimal heat treatment of Cr-Ni steel for compressor blades operating at temperatures up to 500 K
17 p2990 A69-33933
- Cantilever blades tangential vibrations effect on damping characteristics measured by free vibration excitation and static hysteresis loop
17 p3065 A69-33935
- Vibration modes and damping of rectangular cantilevered prismatic steel rods, showing effects of transverse vibration, material and stress on logarithmic decrement
17 p3065 A69-33936
- Thin walled cantilevered fiberglass reinforced shafts damping characteristics dependence on natural vibration modes and fibers orientation
17 p3065 A69-33938
- Damping constant of sandwich samples with foam plastic filler subjected to torsional and flexural vibrations determined for aircraft design applications
17 p2993 A69-33942
- Energy dissipation in bonded structures, analyzing vibration damping, hysteresis loop and absorption coefficient dependence on deformation energy
17 p3066 A69-33943
- Rotating shafts impact damping efficiency increaseable by providing proper clearance to reduce shaft stress in critical resonance frequency region
17 p3066 A69-33946
- Air resistance effect on transverse vibration damping of flat specimens of heat resistant alloy, duraluminum, Ti, Mo and Nb
17 p2991 A69-33947
- Vibrations damping coefficient for asymptotic stability of inertial navigation system platform, determining stabilization errors
18 p3134 A69-34555
- Soft damping system required by LF vibrational loads
18 p3171 A69-34563
- Vibration-proof devices obtained by relating variance determination errors in selective filter response, modulating process bandwidth and spectral analyzer passband
18 p3109 A69-34584
- Viscous friction damping effect on impact vibrator stability, analyzing boundary region of multiply periodic single impact motion by point mapping
18 p3172 A69-34588
- Machine parts vibration attenuation, discussing input vibration reduction, resonance avoidance, damping, vibrating parts strengthening and shakers
18 p3148 A69-34619
- Structural vibrations characteristics using expression of complex energy applied to structure, discussing coupling between damping modes
[ONERA-TP-724]
18 p3218 A69-34639
- Viscoelastic shaft stability rotating at harmonically variable angular velocity, considering internal and external damping
18 p3224 A69-35300
- Vibration absorber incorporating polymer spring/damping elements for attachment to complex main system, noting butyl rubber as effective and convenient damper material
20 p3620 A69-36996
- Acoustic and internal dampings in freely supported uniform beams of circular and rectangular section, showing frequency dependence and vacuum effect
20 p3620 A69-37062
- Mechanical loss factors calculated by approximation formula from resonance curves of Voigt-Kelvin and Maxwell models
20 p3623 A69-37435
- Storage and loss moduli measurement for laminated glass fiber reinforced epoxy composite beams, discussing moduli prediction
20 p3627 A69-37763
- Optimal control of vibrations of liquid in cylindrical container with vertical generatrix and flat bottom, using dynamic programming
21 p3694 A69-38849
- Optimal control of liquid vibrations in rectangular container moving in horizontal direction, deriving algebraic equations system for optimal functional
21 p3694 A69-38854
- Damped mass spring system response to sonic booms, considering effects of structural damping, total/positive phase duration ratio and N wave rise time
21 p3647 A69-38987

VIBRATION EFFECTS

Propagation, damping, power coupling and plasma heating characteristics of harmonic ion cyclotron waves, noting temperature effects

21 p3777 A69-39455

Dynamics of relay gas jet preliminary vibration damping system of gravity gradient stabilized satellite, allowing for sensor limitations and stabilizer flexural vibrations

21 p3826 A69-39638

Artificial damping of longitudinal winged reentry vehicle motions in earth atmosphere, discussing vibration damper dynamic characteristics

21 p3829 A69-39828

Spacecraft booms thermally induced vibration and flutter, considering damping and solar exposure effects

22 p4043 A69-40545

Harmonic linearization for analyzing dry friction effect on gyroscope stability with free play in mechanical couplings, showing effective damping of natural oscillations

23 p4163 A69-41554

Combination resonance and instability regions of second type for parametrically excited oscillations with nonlinear (cubic) damping

23 p4230 A69-42107

Matrix method for free and forced oscillations of complex linear damping system with known linear vectors

23 p4236 A69-42484

Damping influence on shallow arch static and dynamic snapping under step pressure load

24 p4405 A69-43654

VIBRATION EFFECTS

Vertical vibration stimulation of growth of onion bulbs and mice body weights

01 p0014 A69-10584

In-flight measurement of shock and vibration effects on aircraft and propulsion systems

01 p0084 A69-11051

Human body dynamic response to vibration combined with linear acceleration, noting changes in body mechanical impedance and resonance

01 p0022 A69-11335

Fluctuating radar echoes from cloud targets with vibrating drops, noting amplitude modulation effect of changing cross section on backscattered signals

02 p0208 A69-12021

Resisting forces produced by transverse vibration of rotating disks in viscous fluid

02 p0232 A69-12257

Combustion oscillations in liquid and solid propellant engines, noting destructive effect of LF vibrations and acoustic instability

02 p0305 A69-12494

Thin film lubricant effect on machine dynamic performance, proposing inclusion with machine structure for reducing vibration effect

03 p0435 A69-13948

Vibrational relaxation effects on laminar boundary layer velocity profiles and temperature and on layer thicknesses and wall heat flow downstream of shock wave

08 p1303 A69-20269

Chemical and biological means of safeguarding body of astronaut against ionizing radiation and vibration

10 p1648 A69-23297

Vibrational energy transfer computed for processes in carbon dioxide-nitrogen laser based on vibrational relaxation data

10 p1706 A69-24083

Hydropendulum bearing linear horizontal vibration effect on vertex vibration, analyzing zero initial phase using precession theory

10 p1697 A69-24086

Axial torque effect on critical speeds of continuous rotor with motion described by partial differential equations [ASME PAPER 69-VIBR-52]

10 p1804 A69-24152

Axial vibration effects on frictional losses in gear systems under dry friction or boundary lubrication conditions [ASME PAPER 69-VIBR-15]

10 p1701 A69-24169

Axisymmetric oscillations of two spherical shells with noncoinciding centers of curvature immersed in compressible or incompressible fluids

11 p1875 A69-25467

Longitudinal and transverse frequencies of cylindrical metallic rod with spherical tip for sliding motion with dry friction

12 p2102 A69-26290

Pressure distribution in viscous flow between parallel disks with sinusoidal oscillation, noting effects of oscillation amplitude and vibrating disk velocity [ASME PAPER 68-LUBS-1]

13 p2244 A69-27278

Asymptotic analysis for stability and vibration response of spherical squeeze-film hybrid bearing, obtaining perturbation solutions [ASME PAPER 68-LUBS-37]

13 p2267 A69-27281

Ultrasonic vibrations effect on emission of ruby laser with externally mounted mirrors

13 p2271 A69-27534

Standardization requirement for laboratory and field research into vibration effects on humans, stressing subjective rating and performance measurements

13 p2213 A69-28091

Satellite motion relative to center of mass and resonances by approximate solutions to motion equations, applying asymptotic methods

13 p2357 A69-28502

Physiopathological reactions of humans exposed to infrasonic vibrations applied via auricular canal, observing cardiac and circulatory hemodynamic troubles

13 p2215 A69-28590

Runway roughness induced vibrations in highly flexible aircraft, noting effect on pilot control of aircraft and airframe structure

14 p2392 A69-29504

Machine vibration effects on human operator performance using locomotor model

14 p2409 A69-29742

Vibrostand effects on statistical characteristics of random vibrations of elastic system, discussing simulation techniques

14 p2536 A69-29743

Dynamic vibration effects on guidance and control systems performance determined from spectral densities, cross spectral densities and vibratory environment amplitude distributions

15 p2608 A69-30367

Vertical vibration stimulation of growth of onion bulbs and mice body weights

15 p2555 A69-30754

Weightlessness and vibration effects on soft red winter wheat seedlings

15 p2557 A69-31368

Ultrasonic and mechanical vibration effects on superpure Al and Al-Zn-Mg alloy, showing dependence of breaking stress on cycles

16 p2801 A69-31789

Soviet collection of papers on energy dissipation during vibrations of mechanical systems, covering elastic oscillations, nonlinear systems, energy frequency characteristics, etc

17 p3062 A69-33912

Cantilever blades tangential vibrations effect on damping characteristics measured by free vibration excitation and static hysteresis loop

17 p3065 A69-33935

Aerodynamic energy dissipation during vibrations of bars in airstreams characterized by energy loss per cycle and logarithmic decrement

17 p3066 A69-33948

Mechanical vibration effects on human operation of various decimal input devices

17 p2916 A69-34010

Vibrational deexcitation shocks in expanding nonequilibrium nozzle flows extended to include embedded adiabatic shock

18 p3089 A69-35386

Mechanical vibration effects on human body in industry and in terrestrial, aerial and nautical vehicles, discussing harmful frequencies and safety measures

19 p3259 A69-35605

Vertical vibrations effect on test subjects in supine position, noting human tolerances and mood changes

19 p3260 A69-35986

Standing waves on moon, discussing annular and radial structures of lunar craters and global tectonic patterns

20 p3604 A69-37565

Ultrasonic vibrations effect on emission of ruby laser with externally mounted mirrors

20 p3556 A69-38201

Creep resistance increase of Ni refractory alloy by thermovibrational treatment under stress relaxation conditions

21 p3744 A69-38869

Membrane vibration problems for combined free and forced laminar convection through vertical ducts, obtaining expressions for velocity, temperature and Nusselt numbers

21 p3851 A69-38974

Damaging effects of vibration on materials and parts to estimate fatigue life, considering periodic and non-periodic stress vs time relationships

22 p4041 A69-40167

Whole body LF mechanical vibration effects on anesthetized dogs peripheral circulation and vascular smooth muscle

22 p3875 A69-40228

HF vibrations effect on motion of gyroscopic linear acceleration integrator, showing additional error in flight vehicle acceleration measurements

22 p3946 A69-40250

Ruby laser resonator mirror mechanical vibration effects on emission temporal behavior, spectral output and far field pattern, describing conditions for spiking

22 p3962 A69-40562

Homogeneous, viscous and electrically conducting fluid bounded at one end by infinite plane surface of rigid body vibrating relative to fluid body

22 p3991 A69-41036

Mechanical vibrations and noise effects on acetylcholine concentration, esterase activity and synthesis ability in rat brain

23 p4079 A69-41381

Regression process in acetylcholine level in rats after mechanical vibrations and noise exposure

23 p4079 A69-41382

Feline lung injury produced by vertical sinusoidal vibrations during upright water immersion attributed to chest wall impact

23 p4082 A69-41447

Power flow relations between randomly vibrating systems with weak linear elastic or dissipative coupling

23 p4227 A69-41877

Choking and shock in flashing single component two phase flow in tube, including vibrational effects, predicting minimum stagnation pressure loss [ASME PAPER 69-HT-61]

24 p4303 A69-43535

VIBRATION ISOLATORS

Flexural waves passage through obstacles in infinite plate, determining vibration arresting properties of rigid ribs, elastic inserts and hinged couplings

04 p0678 A69-14902

Resonant beam tuned vibration damping device, noting weight saving potential [ASME PAPER 68-WA/GT-2]

05 p0837 A69-16138

Parallel damped dynamic vibration absorbers, modifying conventional absorber by adding subsidiary undamped absorber mass [ASME PAPER 68-WA/DE-6]

05 p0839 A69-16171

Self damped pneumatic vibration isolators by modifying characteristics throughout frequency range, noting inertia block for improving HF behavior

08 p1301 A69-20398

Compact antivibration mounting for carrying instruments, using bicycle tire inner tube around heavy slab to provide elasticity and damping

09 p1502 A69-22692

Active broadband vibration isolation of human subjects from severe vertical dynamic excitations experienced in low level high speed flight [ASME PAPER 69-VIBR-65]

10 p1650 A69-24157

Vibratory acceleration limiting equipment attachment for resonance conditions, utilizing attachment stiffness reduction above predetermined value [ASME PAPER 69-VIBR-23]

10 p1806 A69-24170

Synchronous vibration absorbers using gyroscopic systems, noting antiresonance with Perissogyro [ASME PAPER 69-VIBR-39]

10 p1807 A69-24177

Electrohydraulic vibration isolation systems with feedback, considering band and notch isolation, system stability and adjustable frequency response [ASME PAPER 69-VIBR-40]

10 p1641 A69-24178

Displacement and acceleration criterion for synthesizing optimum linear vibration isolator systems subject to random input [ASME PAPER 69-VIBR-44]

10 p1807 A69-24182

Optimum and suboptimum shock and vibration isolators, discussing three criteria and tradeoff between relative motion and accelerative force [ASME PAPER 69-VIBR-45]

10 p1808 A69-24183

Flexural waves passage through obstacles in infinite plate, determining vibration arresting properties of rigid ribs, elastic inserts and hinged couplings

12 p2182 A69-26655

- Parallel damped dynamic vibration absorbers, modifying conventional absorber by adding subsidiary undamped absorber mass
[ASME PAPER 68-WA/DE-6] 13 p2360 A69-27422
- Rigid structures high damping without loss of rigidity achieved by epoxy resin dampers, noting moderate cost 13 p2370 A69-28601
- Optimal active shock isolation by nonlinear elements for system subjected to shock type loadings, discussing impulse shapes 15 p2713 A69-31019
- Oscillation amplitude of rotor with hydraulic dampers on elastic supports by expanding forced vibration modes with friction in natural modes 16 p2837 A69-32136
- Main rotor bifilar absorber for vibration reduction during S-61 helicopter flight, describing shake and flight tests [AHS PAPER 354] 17 p2900 A69-33523
- Blade vibration damper consisting of springs attached to blade, analyzing resonance stresses on basis of dynamic rigidities 17 p3066 A69-33944
- Laminated critical rate dampers consisting of ring shaped thin corrugated steel plates inserted between bearing and rotor, showing dependence on static load 17 p3066 A69-33945
- Passive helicopter rotor isolation for alleviating rotor induced vibration, using dynamic antiresonant vibration isolator 20 p3463 A69-37807
- Test pad isolation characteristics mathematical model to predict pad dynamic behavior [AIAA PAPER 69-860] 21 p3690 A69-39388
- VIBRATION MEASUREMENT**
- Holographic measurement of sinusoidally vibrating Al sheet, verifying results with Twyman-Green interferometer 01 p0082 A69-10853
- Spadoryc slide rule for damping determination from vibration decay traces, noting use in flight flutter tests 01 p0087 A69-11029
- Shock and vibration data recording, discussing transducer selection, accelerometer mounting, conditioning electronics and recording devices 01 p0083 A69-11050
- In-flight measurement of shock and vibration effects on aircraft and propulsion systems 01 p0084 A69-11051
- Solar limb image vibrations caused by turbulent pulsations in refractive index of lowest atmospheric layers 01 p0156 A69-11183
- Vibrational characteristics of sonar transducer analyzed by optical holographic interferometry 04 p0598 A69-14871
- Decibel scaling advantages in vibration measurements 04 p0602 A69-15324
- Stiffness matrices for buckling or vibration analysis of long thin flat plate structures connected at longitudinal edges 05 p0836 A69-16029
- Glass fiber optical angular displacement noncontacting nonloading transducer suitable for measuring torsional vibrations 06 p0923 A69-16929
- Vibration measurements on rotating machinery, using diode switching potentiometric strain gage circuit and multiple common rings 09 p1496 A69-22014
- Root fixture and grip load effects on cantilever beam damping, using bandwidth and logarithmic decrement measurement methods 10 p1800 A69-23244
- Multichannel miniature telemetry for vibration, strain and temperature measurements in high speed machinery by solid state encapsulated devices 10 p1654 A69-23251
- Forced torsional vibrations of turbine blades calculated by computer using mathematical models for resonance frequencies and tangential stresses 10 p1803 A69-24076
- Flexible cylinder vibration in nominally axial flow, discussing length, mass, flexural rigidity and diameter variation effects on vibration amplitude 11 p1984 A69-25166
- Automatic multichannel system for turbine blades static tests, discussing operation principles, component sections, programmed tape and vibration modes 15 p2672 A69-31209
- Monograph on transmission characteristics of mechanical vibration transducers covering frequency response operators and analog computer simulation 16 p2789 A69-31842
- Calculation of natural twisting and bending vibrations of beam with characteristics varying along length 16 p2873 A69-32130
- Hall generator for measuring mechanical displacements and vibrations of 10 A, describing operating principles and arrangements 17 p2971 A69-33022
- Planetary free vibrations, discussing models for earth, moon, Venus and Mars, rotation and ellipticity effects and measurement on seismometers, gravimeters and magnetometers 17 p3031 A69-33097
- Holography application in gas turbine components stress and vibration analysis, discussing techniques and apparatus usable by nonspecialist and measurement accuracy 17 p2974 A69-33351
- Automatic device for logarithmic damping decrement measurement from vibrograms, showing structural arrangement and electrical circuitry 17 p2976 A69-33931
- Transverse and torsional vibration characteristics of tapered cantilever beams and shafts analyzed by lumped inertia force method 17 p3066 A69-34052
- Vibration measurement by hologram interferometry, explaining interference fringes as linear combination of vibrating object classical modes 18 p3135 A69-34635
- Linear and torsional vibration parameters measuring methods, discussing transducer characteristics 22 p3943 A69-39926
- Noise and vibration levels measured in An-24 Polish passenger aircraft indicating excess noise in crew compartment 22 p3862 A69-40005
- Digital systems for acoustical or vibrational measurements reception and evaluation 22 p3945 A69-40168
- Field transfer matrices for simultaneous treatment of free and forced vibrations and buckling through axially loaded Timoshenko beam 23 p4234 A69-42400
- Truncated conical sandwich shell suspended in free-free condition measured and analyzed for vibrational characteristics 23 p4235 A69-42462
- Matrix method for free and forced oscillations of complex linear damping system with known linear vectors 23 p4236 A69-42484
- Three layered circular plate under harmonic excitation, analyzing forced vibrational characteristics by variational principle and Ritz method 23 p4236 A69-42495
- VIBRATION METERS**
- NT LUNAR SEISMOGRAPHS
- NT SEISMOGRAPHS
- Gyroviator /angular rate measuring device/, discussing output signal and natural frequency dependence on moments of inertia 01 p0083 A69-11004
- Evaluation tests of fixed frequency variable tension vibroscope for filaments and wires, noting instrument errors and corrections 04 p0599 A69-15018
- Transverse sensitivity ratio of vibration transducer, discussing measurement by shaker method 04 p0603 A69-15432
- Complex mechanical vibrations causes determined by sensor signals analysis 16 p2876 A69-32434
- Piezoelectric shaker consisting of combination of damped resonant cylindrical elements for wide frequency calibration of vibration pickups 17 p2975 A69-33665
- Friction bearing vibration recording device using light beam and photodiode 20 p3539 A69-37436
- VIBRATION MODE**
- NT UNCOUPLED MODES
- Geometrical existence proof of elastically coupled nonlinear systems normal mode vibrations demonstrated by existence of extremal arcs in Riemann space 01 p0166 A69-10232
- MHD waves and toroidal mode existence by mathematical approximation 02 p0236 A69-11430
- Combustion instabilities in solid propellant rocket engines, emphasizing acoustic types for longitudinal and tangential modes 02 p0303 A69-11531
- Tunnel diode oscillations in switching mode due to sinusoidal voltage excitation, discussing critical applied signal frequency separating switching and oscillation modes 02 p0213 A69-11535
- Modal substitution method for free vibration analysis of large discrete undamped dynamic systems 02 p0338 A69-11747
- Transit time and anomalous modes of oscillation in high pulsed power punch-through Si avalanche diode microwave oscillators 02 p0216 A69-12145
- Nonisothermal space charge wave analysis of transit time mode oscillations in bulk GaAs, studying device reactance at given negative resistance 02 p0299 A69-12240
- Localized vibration modes of defects and IR absorption bands in compensated Si doped GaAs 02 p0299 A69-12402
- Transverse mode selection effects on wave front of long pulsed ruby laser beam 02 p0257 A69-12409
- Gyroscopically induced vibrational response of rectangular plates and membranes, determining spin and precession effects on natural frequencies 02 p0347 A69-12519
- Low and high power pi-mode Laddertron oscillator design operation and performance characteristics 03 p0405 A69-13726
- Stability of steady motion of body with cavity containing one or several nonmixing liquids as problem of bounded oscillations about motion 03 p0418 A69-13815
- Matrix-harmonic method for vibration study of mechanisms and machines 03 p0468 A69-13860
- Matrix-harmonic method of vibration study extended to include autonomous vibrations of single degree of freedom machines 03 p0468 A69-13861
- Magnetoelastic vibrations of fluid filled cylindrical cavity in infinite solid medium in presence of uniform axial magnetic field 03 p0528 A69-13927
- Equations for self oscillating mode of operation for O-type backward wave generator with electrostatically focused electron beam and finite values of amplification parameter 03 p0407 A69-13986
- Natural frequencies and mode shapes of coupled bending vibrations of pretwisted rectangular cross section beams determined by Rayleigh-Ritz energy method 03 p0529 A69-13989
- Oscillation mode selection in gas lasers by thin film absorber in resonator, using standing wave electric fields periodicity 04 p0610 A69-14384
- Beam vibration problems with mixed response-excitation input information solved by recasting equations of motion [AIAA PAPER 68-319] 04 p0676 A69-14711
- Normal modes and natural frequencies of combined linear elastic structures resting on immovable base 04 p0678 A69-14870
- Axisymmetric oscillation modes and frequencies of hemispherical shell partially filled with liquid, using moment theory of shells 04 p0679 A69-14922
- Torsional or longitudinal vibrations of nonuniform bar with elastic end constraints, developing frequency and mode form equations suitable for computer 04 p0681 A69-15196
- Frequencies and natural oscillation modes in sporting gliders, demonstrating horizontal oscillation induced aileron suspension brackets destruction 04 p0549 A69-15416
- Testing techniques and graphical presentation of test results to determine resonant frequencies and oscillation modes in sporting gliders 04 p0549 A69-15420
- Nonlinear steady state vibration of single degree of freedom system, obtaining relationships between non-dimensional pi parameters of differential equation of motion [ASME PAPER 68-WA/DE-7] 05 p0839 A69-16172
- Orthogonality of natural oscillation modes of shells of arbitrary geometry, using equations of motion from Vlasov engineering moment theory 05 p0840 A69-16200

Buildup modes of He-Ne laser in presence of other strongly oscillating modes, noting gain interaction effects

05 p0773 A69-16289

Self locking of three laser modes in He-Ne laser on basis of Lamb theory

05 p0773 A69-16290

Dynamic instability of solid bodies, using modal vibration method to establish criteria on basis of equivalent energy conditions

05 p0844 A69-16742

Natural frequencies and modes of skew membranes obtained by Rayleigh-Ritz method

06 p1021 A69-17146

Geometrically exact finite element for thin shells of revolution, using approximation to predict boundary layer stress distribution during vibration [AIAA PAPER 69-56]

06 p1029 A69-18193

Holographic interferometry, determining mechanical vibration amplitudes of compressor and turbine blades and airframe panel [SAE PAPER 690265]

07 p1130 A69-18313

Oscillators and amplifiers based on intervalley electron transfer in bulk GaAs

07 p1096 A69-18442

Current and voltage waveforms of transit time, resonant domain and LSA modes of operation of transferred-electron oscillators

07 p1097 A69-18443

Oversized GaAs Gunn effect diodes operated in L and S bands at harmonics of fundamental transit time frequency with high power and efficiency

07 p1196 A69-18444

Avalanche diode oscillators efficiency of continuous wave operation in transit time mode and high current multiresonant modes

07 p1098 A69-18456

Natural modes and eigenfunctions of low amplitude oscillation determined by Ritz averaging method for ideal fluid with equilibrium surface in weak force field

07 p1119 A69-18746

Dielectric surface loading on GaAs for suppressing traveling high field domain mode oscillations

08 p1371 A69-19911

Quenched multiple domain mode oscillations in GaAs microwave diodes noting relationships between efficiency, power output, negative resistance and bias voltage

08 p1282 A69-20107

Amplitude dependent internal friction of materials under inhomogeneous strain, giving values for torsional, free longitudinal and transverse vibration modes

08 p1331 A69-20175

Resonant frequencies, vibration modes and stress distributions for naturally vibrating plane wide blades of turbomachines

08 p1376 A69-20764

Plasma oscillation modes perpendicular to magnetic field used to study energy conversion by wave coupling across density discontinuity

08 p1367 A69-20795

Axisymmetric vibration modes of cylindrical-hemispherical membrane tank partly filled with liquid [AIAA PAPER 67-75]

09 p1482 A69-21940

Vibration natural frequencies and mode shapes in cylindrical shells clamped at both ends, using fundamental differential equation under dynamic surface loading

09 p1618 A69-22274

Van der Pol nonlinear oscillation theory adapted to microwave reflex klystrons, explaining locked and unlocked monotonic operational modes

09 p1466 A69-22444

Gunn effect cavity controlled generator oscillations, noting phase trajectory closing conditions dependence on resonant mode parameters

09 p1468 A69-22596

Intensity distribution in principal mode of TEM oscillations at various gain amplification levels, plotting intensity distribution generated by argon ion CW laser

09 p1520 A69-22685

Modulated wave holography for detecting and reconstructing ultrasonic beam path, noting applicability to vibrating objects analysis

10 p1694 A69-23368

Nonradial oscillation modes of massive stars determined by Ritz method application to variational principle, allowing for gravitational perturbation

10 p1785 A69-24036

Infinitesimal bending oscillations and/or responses of thin rotating disks applied to thin disk galaxies, discussing Magellanic Cloud passage near galactic center

10 p1786 A69-24110

Natural frequencies and mode shapes for longitudinal oscillations of liquid filled elastic circular cylindrical tank with flexible inverted conical bulkhead [ASME PAPER 69-VIBR-11]

10 p1806 A69-24165

Holographic mode shapes used in conjunction with mechanical impedance approach for vibration analysis of turbine blades [ASME PAPER 69-VIBR-32]

10 p1806 A69-24174

Differential equations for effect of sinusoidal force with slowly varying frequency on dynamic behavior of nonlinear vibrator, using phase surface technique

11 p1916 A69-24760

Free vibration modes of infinite uniform plate in linear coupled theory of thermoelasticity, considering heat transfer conditions

11 p1976 A69-24793

Liquid filled elastic shells natural frequencies and oscillation modes, deriving eigenfunction system from liquid velocity potential boundary conditions to determine dynamic load

11 p1870 A69-24951

Nonlinear free vibration of beams with clamped and supported ends subjected to axial load, considering symmetric and antisymmetric modes

11 p1983 A69-25024

Semiatuator disk method for boundary layers and velocity of stall flutter cascade blades vibrating in transient mode, considering nonstall flutter

11 p1818 A69-25028

Nonlinear resonance formation during spatial nonlinear vibrations of solid bodies, establishing relations between vibration and excitation frequencies

11 p1919 A69-25167

Axisymmetric vibration modal properties/frequencies and mode shapes of thin conical shell frustums, considering dimensional and boundary condition influences

11 p1992 A69-25519

Dynamic analysis of axisymmetric ring stiffened shells with attached asymmetric elastic structures, noting vibration modes

11 p1993 A69-25525

Multidimensional mode shapes and frequencies of 100 ft space erectable parabolic antenna

11 p1994 A69-25532

Resonant vibrational energy transfer between specific mode of carbon dioxide and N molecules at high temperatures, monitoring IR emission

12 p2131 A69-25984

Single mode laser oscillations buildup for 0.633 micron transition of He-Ne laser at levels above threshold using fast intracavity chopper

12 p2105 A69-26318

Natural vibration modes of linearly tapered rectangular plates, approximating plate characteristic shapes with series of products of beam characteristic shapes

13 p2358 A69-27211

Thin cylindrical shell vibration with three supports analyzed by minimizing Lagrangian of vibration, obtaining frequencies and modes

13 p2359 A69-27257

Vibration modes in four lowest natural frequencies of clamped rectangular plates with linear thickness variation, using Ritz method

13 p2361 A69-27442

Linear oscillation modes of premain sequence star model of pure hydrogen composition with variable specific heats ratio, discussing dynamic instability of polytropes

13 p2336 A69-27449

Vlasov equations solved for electrons and ions in electromagnetic field, coupling electric field to density oscillation modes of plasma

13 p2306 A69-27461

Stationary vibration modes of systems subject to nonlinearities using finite sums of Fourier series

13 p2361 A69-27615

Delta modulated control system model for determining oscillation modes at sampling instants

13 p2221 A69-27962

Frequency equation for thickness effects on axisymmetric radial and rotatory vibrations of empty or fluid filled isotropic spherical shell

13 p2363 A69-28185

Oscillation mode selection in gas lasers by thin film absorber in resonator, using standing wave electric fields periodicity

14 p2456 A69-28757

Ruby laser filled with single emission mode of oscillation using uniform pumping

14 p2458 A69-29164

Orthonormal aspect on vibration modes for nonuniform beams, evaluating normalization for end conditions by using Rayleigh technique

14 p2534 A69-29319

Thermally excited diurnal wind oscillations in lower mesosphere using model atmosphere in CIRA 1965, discussing daytime ozone density profiles

14 p2441 A69-29379

Equation system for asynchronous MHD generator operating in self oscillating mode derived and solved

14 p2405 A69-29457

Bladed disk assemblies vibrational properties discussing dynamic characteristics of system with pair of close natural frequency modes under forced vibration

15 p2704 A69-30304

Aerospace structures modal vibration tests data acquisition including multishake excitation methods

15 p2585 A69-30358

Natural frequencies and modes of complex structures composed of beam elements, considering hysteretic damping for response and transmissibility

15 p2706 A69-30431

Valence force constants for nitric acid evaluated from fundamental mode vibration spectra by matrix method

15 p2561 A69-30467

Circular curved foil steady oscillations near screen in semiinfinite space filled with incompressible fluid transformed into equivalent linearized problem

15 p2547 A69-30576

Mode-mode coupling calculation for finite amplitude collisional drift waves demonstrating inherently nonlinear phenomena

15 p2660 A69-30916

Structural influence coefficients from vibration test modes and frequencies, eliminating errors by Gram-Schmidt orthogonalization

16 p2872 A69-31916

Turbomachinery two mode blade vibrations with emphasis on aerodynamic damping, noting shifts in natural frequencies [ONERA-TP-678]

16 p2733 A69-32333

Cylindrical viscous jet transition points from stable to unstable modes of oscillation found same as for inviscid jet

16 p2773 A69-32570

Plane oscillations of liquid in rectangular elastic vessel determined to obtain frequencies and mode shapes of natural oscillations from velocity potential boundary conditions

17 p2950 A69-33200

Frequency and mode shapes of conical shell free oscillations related to shell parameters and boundary conditions

17 p3058 A69-33201

Test stand for free oscillations frequencies and mode shapes of truncated conical shells of revolution with clamped edges and one free edge

17 p3058 A69-33202

Superdense stars torsional oscillations and crystallization among nuclei from comparison with melting temperature and transverse shear wave velocities of dense conventional matter

17 p3037 A69-33643

Complete spherical shells nonsymmetric vibrations frequencies and mode shapes calculated by matrix method

17 p3061 A69-33706

Generalized energy absorption coefficient effect on vibration mode of specimen on vibration test bench

17 p3062 A69-33718

Cantilever blades tangential vibrations effect on damping characteristics measured by free vibration excitation and static hysteresis loop

17 p3065 A69-33935

Vibration modes and damping of rectangular cantilevered prismatic steel rods, showing effects of transverse vibration, material and stress on logarithmic decrement

17 p3065 A69-33936

Thin walled cantilevered fiberglass reinforced shafts damping characteristics dependence on natural vibration modes and fibers orientation

17 p3065 A69-33938

Natural frequencies and vibration modal shapes of asymmetrical airfoil blades analyzed by differential equations of motion, noting flexure coordinates center variations effect

17 p3067 A69-34053

Single freedom vibratory system response to imposed displacement harmonic excitation, analyzing response in terms of constrained system modes

17 p3067 A69-34139

Vibration measurement by hologram interferometry, explaining interference fringes as linear combination of vibrating object classical modes

18 p3135 A69-34635

Structural vibrations characteristics using expression of complex energy applied to structure, discussing coupling between damping modes
[ONERA-TP-724]

18 p3218 A69-34639

Natural frequencies and mode shapes of vibration of cylindrical shells orthogonally stiffened with rings and stringers

[AIAA PAPER 68-349]

19 p3437 A69-35948

Gas laser oscillation mode selection and self synchronization based on separation in two mirror cavity with nonlinear absorption

19 p3336 A69-36350

Steady resonance operation modes of nonlinear oscillatory and rotational systems described by differential equations with deviating argument, using averaging procedure

19 p3374 A69-36469

Coupled dilatational and equivoluminal modes of free vibration for elastic prisms and polygonal plates, using Poisson ratio and wave path construction

19 p3444 A69-36801

Vibration response approximation of three layer sandwich beam with nonlinear viscoelastic material core during flexural vibrations

20 p3619 A69-36910

Rectangular cross section pretwisted beams modal curves for turbine and compressor blading vibrational studies

20 p3621 A69-37080

Vibration analysis, using rigid body and normal modes to solve interconnection problem, applied to free-free natural vibration modes of clustered rockets

20 p3621 A69-37195

Aeroelastic instabilities of aircraft in flight by representing motion in space function base, using natural vibration mode
[ONERA-TP-697]

20 p3626 A69-37755

Acoustoelastic interaction effects of sonic bangs on natural frequencies response of large windows backed by closed cavity

21 p3836 A69-38988

Holography applied to stress and vibration analysis of gas turbine blades, disks and small components

22 p4040 A69-39960

Normal radial vibrations in Newtonian and general relativistic stellar objects and dynamic instability, determining modes and natural frequencies

22 p4014 A69-40142

Small curvature effect on prevention of vibration in shallow shells under random loading numerically analyzed for component modes using linear theory

22 p4044 A69-40600

Bernstein modes initial value-boundary value problem for half space of plasma bounded by wall and parallel unperturbed magnetic field

23 p4196 A69-41875

Axisymmetric vibration of shallow spherical caps, using nonlinear dynamic equations and associated variational equation of motion for elastic spherical shells
[ASME PAPER 69-APMW-6]

24 p4402 A69-43107

VIBRATION PERCEPTION

Visual observation of surface vibration nodal patterns by incoherent light illumination of object, noting holography

12 p2099 A69-27176

VIBRATION PICKUPS

U TRANSDUCERS

VIBRATION SIMULATORS

Discrete model for investigating beam vibration under various end conditions, determining natural frequency dependence on degrees of freedom

02 p0336 A69-11462

Equalization of multiple electromagnetic shakers for environmental vibration testing, using analog computer
[JPL-TR-32-1364]

02 p0229 A69-12374

Transverse sensitivity ratio of vibration transducer, discussing measurement by shaker method

04 p0603 A69-15432

Vibration machine as vibration environment simulation for product reliability testing, analyzing spectrum of acceleration waveforms

12 p2060 A69-26940

Vibrostand effects on statistical characteristics of random vibrations of elastic system, discussing simulation techniques

14 p2536 A69-29743

Multiple shaker ground vibration test system for confidence in helicopter designs before flight testing and evaluation of force balancers

15 p2585 A69-30357

Electromagnetic vibration exciters based on permanent magnet and AC coil interaction

16 p2790 A69-32077

Machine for testing vibration stability of polymer samples subject to tension or compression, noting stability of plastic during vibration lower than during static loading

17 p2972 A69-33043

Temperature and pressure effect on cobalt base alloy cavitation in liquid sodium, using vibratory apparatus and loss rate contour diagram

18 p3157 A69-35184

Random vibratory environment simulation for spectra, noting electrodynamic generator employed to excite electric field force

19 p3294 A69-35904

VIBRATION TESTS

NT DAMPING TESTS

Equalization of multiple electromagnetic shakers for environmental vibration testing, using analog computer
[JPL-TR-32-1364]

02 p0229 A69-12374

Sound radiation from vibrating bodies, noting errors in Lighthill conclusion

02 p0282 A69-12800

Optimal design of vibration tests based on decision theory
[SAE PAPER 680753]

03 p0525 A69-13436

Ground vibration testing of flight and space vehicles, noting structural damping asymmetries and nonlinearities

04 p0585 A69-14833

Modal response analysis of servocontrols as deduced from vibration test, for possible application to aircraft
[ONERA-TP-668]

06 p0869 A69-17100

Design criteria for vibration testing facility in Rome, giving block diagram of equipment at facility

08 p1301 A69-20159

Dynamic tests of mechanical properties of polyamide Taron X-A using free and resonant vibrations methods

09 p1528 A69-21496

Rotating twisted blades vibrations, deriving equations and vibration tests with models

09 p1618 A69-22236

Computerized shake test facility for Saturn 5 moon rocket, describing data acquisition, magnetic tape units, X-Y plotters, display devices, etc

10 p1672 A69-23285

Testing machines for metallic materials, discussing design criteria and application to tensile strength, vibration and durability test machines
[DVL-865]

11 p1889 A69-25682

Unbalance effects on rigid naval turborotor on oil film bearings in flexibly mounted housings investigated at varying critical speeds and housing stiffness
[ASME PAPER 69-DE-9]

14 p2453 A69-28839

Aerospace structures modal vibration tests data acquisition including multitask excitation methods

15 p2585 A69-30358

Vibration/acoustics environmental testing, discussing advantages of digital computer control system and digital noise generation techniques

15 p2586 A69-30387

Vibration/acoustics digitally controlled environmental testing, describing configuration and operation of control system and statistical requirements for noise generation

15 p2587 A69-30388

Vibration/acoustics digitally controlled environmental testing, describing random test signal generation and random vibration tests

15 p2587 A69-30389

Resonant fixtures used for mechanical amplification of vibrator output to desired test levels

15 p2588 A69-30404

Automatic multichannel system for turbine blades static tests, discussing operation principles, component sections, programmed tape and vibration modes

15 p2672 A69-31209

Complex mechanical vibrations causes determined by sensor signals analysis

16 p2876 A69-32434

Supersonic flutter in square panels and cylindrical shells, measuring critical dynamic pressure

17 p3051 A69-32923

Elastic stability of warped rods, using small oscillations method for varying end conditions and torsional moment vector behavior

17 p3057 A69-33196

Generalized energy absorption coefficient effect on vibration mode of specimen on vibration test bench

17 p3062 A69-33718

Forced vibration testing of complex continuous systems, demonstrating suppression of certain resonant frequencies due to laboratory techniques

18 p3114 A69-34422

Multidimensional discrete control systems for spectral characteristics of random processes in vibrational and fatigue strength testing of machines and equipment

19 p3286 A69-35890

Tensional and torsional forced vibration tester for viscoelastic plastic materials under tensile strain

21 p3720 A69-38591

Transfer matrix symmetry about secondary diagonal in vibration analysis useful for computer programming

22 p4040 A69-39938

MIL-STD-781A vibration requirements, using mechanical shakers for AGREE vibration testing

22 p3954 A69-40036

Frequency response transient vibration testing of standing man, discussing data analysis procedure, test stand, and Welch correction for instrument dynamics

23 p4101 A69-41494

VIBRATIONAL RELAXATION

U MOLECULAR RELAXATION

VIBRATIONAL SPECTRA

Fine structure of vibrational spectra of molecular H and O, water and deuterium oxide, using molecular photoelectron spectrometer

01 p0023 A69-10141

Intermolecular collision induced vibration to vibration energy transfer in nitrous oxide in various gas mixtures, measuring fluorescence and relaxation rates

01 p0123 A69-10684

Discrete model for investigating beam vibration under various end conditions, determining natural frequency dependence on degrees of freedom

02 p0336 A69-11462

Inverse population of vibrational levels generation in polyatomic molecules

02 p0259 A69-12647

Raman effect in liquid glycerol obtained with 4880 A ionized argon laser, determining valence vibrational frequencies

03 p0440 A69-13366

Phonon states effective density in neodymium trichloride from vibronic spectra accompanying electronic transitions in trivalent Pr and Nd ions

03 p0473 A69-13907

Statistical energy approach for analyzing steady state vibration distribution in composite structures in terms of energy balances

04 p0675 A69-14687

Thermal and ablative lag induced by periodic heat input to oscillating flat plate in high velocity flow, showing crossover from dynamically stabilizing to destabilizing condition as oscillation frequency increases
[AIAA PAPER 67-336]

04 p0685 A69-14720

Franck-Condon factors in radiative, excitation and ionization molecular transitions of oxygen, carbon monoxide, nitric oxide, etc

05 p0795 A69-15664

Dissociation energy and vibrational terms of ground state hydrogen

05 p0796 A69-15908

Vibrational excitation by electron impact in kinetic energy range 30-60 eV studied for water vapor and carbon dioxide, determining intensities relative to elastic scattering

06 p0960 A69-17108

Carbon dioxide Q switched laser nonlinear amplification characteristics in vibrational-rotational bands

06 p0933 A69-17118

Absorption oscillator strengths for rotational lines in Lyman transition vibrational bands of molecular hydrogen from equivalent widths measured photoelectrically

06 p0962 A69-17818

Laser excited vibrational fluorescence for determining vibrational energy transfer rates in HCl-carbon dioxide, HCL-HI and HI-carbon dioxide

07 p1144 A69-18289

Angular velocity of rotation measurement using angular gas laser undergoing axial torsional vibrations

07 p1147 A69-18523

Competition effects between rotational levels of carbon dioxide rotation-vibration band in traveling and standing wave lasers
[IEEE PAPER G-6]

07 p1151 A69-19055

Nonhomogeneity effect on transverse vibrational frequency of uniform beams

08 p1413 A69-20413

Vibrational excitation in He, H and N ion- molecule collisions on nitrogen first negative system, studying relative band intensities

08 p1356 A69-20739

CW helium-neon laser used to detect and measure vibration frequencies of uniform diffuse surfaces

09 p1515 A69-21430

Coaxial cylindrical shells oscillation frequencies with interspace filled with incompressible liquid determined as functions of liquid level and interspace width

09 p1612 A69-21483

Hydroxyl luminescence spectrographic observations at twilight in vibrational-rotational band from 10600 to 11200 Å

10 p1681 A69-22847

Nonlinear resonance formation during spatial nonlinear vibrations of solid bodies, establishing relations between vibration and excitation frequencies

11 p1919 A69-25167

Vibration eigenfrequencies of helicopter blades, discussing equation integration problems

11 p1995 A69-25673

Molecular vibration absorption spectra from variation of field emitted electron energy distribution due to inelastic electron-molecule interaction at metal-vacuum interface

12 p2132 A69-26097

Plasma-electron beam interaction induced HF oscillations, obtaining nearly noise free oscillations

12 p2137 A69-26529

Vibration and absorption bands in IR spectra of diborene hydrazine stabilized by boiling in benzene

12 p2027 A69-26917

IR spectroscopic observations of moon to interpret molecular vibration spectra in terms of molecular composition, discussing rock surface roughness effects

13 p2341 A69-27582

Free and forced vibrations of elastic layer, using iteration procedure based on asymptotic integration of linear theory of elasticity dynamic equations

13 p2363 A69-28126

Lifetime of vibrational levels of carbon dioxide molecules as function of discharge current and power dissipation, noting gas heating

13 p2273 A69-28579

Nonlinear homogeneous uniaxial ferromagnetic resonance, analyzing stationary regime lifetime and vibrational spectrum

14 p2503 A69-28989

Electron energy distribution functions and energy transfer rates to inelastic levels of carbon dioxide and nitrogen in laser

14 p2460 A69-29603

FM oscillations spectral width during modulation by finite sequences of multiple and nonmultiple frequencies

15 p2562 A69-30116

Dynamic vibration effects on guidance and control systems performance determined from spectral densities, cross spectral densities and vibratory environment amplitude distributions

15 p2608 A69-30367

Valence force constants for nitric acid evaluated from fundamental mode vibration spectra by matrix method

15 p2561 A69-30467

RF spectra for hyperfine structure of ortho-hydrogen molecular ion, calculating doubling constant for vibrational effects

15 p2693 A69-30784

Wave reflection in laser resonators with ferrite end faces, determining oscillation spectra and wave amplitudes

15 p2579 A69-30954

Perturbation formula for frequencies as function of Poisson coefficient, considering vibration modes of elastic body subject to boundary conditions

15 p2713 A69-31097

Relative intensities of lines in vibration and rotation bands of isotopic carbon dioxide in planet Venus, tabulating partition functions

15 p2656 A69-31154

Franck-Condon factors for band systems of molecular hydrogen, computing wave functions for vibrational levels using potential energy function, Part II

15 p2656 A69-31157

Vibrational excess entropy in dilute solid solutions alloys calculated by changes in potential fields surrounding impurity atoms

16 p2798 A69-31706

Photoinduced shock processes involving metastable hydrogen atoms and molecules, discussing vibrational and rotational levels

16 p2813 A69-31754

Vibrating objects phase determined by time average and real time holographic interferometry

17 p2974 A69-33324

Mechanical single degree of freedom system mean square response to AM random noise, considering frequency response, input excitation spectrum, etc [ASME PAPER 69-APM-25]

18 p3214 A69-34398

Beam torsion nodal line displacement dependence on flexural and torsional bending frequency

18 p3223 A69-34998

Intensity changes in visible sidelight emission from carbon dioxide laser switched on and off, calculating vibrational temperatures

18 p3153 A69-35243

Random vibratory environment simulation for spectra, noting electrodynamic generator employed to excite electric field force

19 p3294 A69-35904

Rate coefficient for primary process in removing molecular nitrogen in high vibrational levels from active nitrogen by N atoms

19 p3379 A69-36424

Central tuning dip on rotation-vibration transitions of nitrous oxide and carbon dioxide laser with nitrogen, noting frequency discriminator generation

19 p3339 A69-36698

Vibration phenomena analysis by transfer function computer, discussing precision spectrum analyzers

20 p3498 A69-37003

Vibrational temperature of low density nitrogen measured by electron beam method, discussing relationship to ratio of integrated vibrational band intensities

20 p3579 A69-37222

He-Ne laser oscillation frequency shifts with variations in DC discharge ascribed to changes in populations of He and Ne levels

20 p3556 A69-38124

Peak power ranges of Q switched CO-air-He molecular laser, noting recovery time and CO vibrational temperature

21 p3742 A69-39742

Rectangular waveguide with periodic array of infinitely thin metallic strips, studying intrinsic oscillations critical frequencies and amplitude spectrum

23 p4124 A69-42036

Book on interaction between oscillatory systems and energy source of limited capacity, examining stability and resonance phenomena

23 p4170 A69-42166

Upper atmosphere OH molecules vibrational temperature and total emission energy, measuring average seasonal variations

24 p4308 A69-43007

Computerized spectral analysis of vibrational frequency due to elastic waves in isotropic hollow spherical shells [ASME PAPER 69-APMW-8]

24 p4402 A69-43106

Herzberg bands synthetic spectra matched to various spectrograms to determine vibrational populations of molecular O state in nightglow

24 p4310 A69-43186

VIBRATIONAL STRESS

Blade natural frequency distribution around rotor and mechanical coupling between blades effects on flexing amplitudes under forced vibration [ASME PAPER 68-WA/GT-3]

05 p0837 A69-16139

Amplitude dependent internal friction of materials under inhomogeneous strain, giving values for torsional, free longitudinal and transverse vibration modes

08 p1331 A69-20175

Fuel concentration effect on turbojet engine reheat jet pipe vibrations via tests

09 p1573 A69-22616

Viggen computer development, stressing reliability towards aircraft vibrations

15 p2577 A69-30620

Crack analysis in stiffened vibrating plate based on dynamic stress distribution, showing high bending stresses at intersection

18 p3223 A69-35168

Mechanical vibration effects on human body in industry and in terrestrial, aerial and nautical vehicles, discussing harmful frequencies and safety measures

19 p3259 A69-35605

Damaging effects of vibration on materials and parts to estimate fatigue life, considering periodic and non-periodic stress vs time relationships

22 p4041 A69-40167

VIBRATORS

U ELECTRIC CHOPPERS

VIBRATORY LOADS

Laminated plates vibrational characteristics calculations by transition matrices, relating stresses and displacements under load

04 p0679 A69-14907

Material selection for structures under vibration loads, analyzing fatigue strength on basis of stress susceptibility and relationship with tensile strength

09 p1620 A69-22574

Strength hypothesis for structures under multiaxial vibration load, taking into account plane stress state

09 p1620 A69-22575

Laminated plates vibrational characteristics calculations by transition matrices, relating stresses and displacements under load

12 p2182 A69-26660

External and internal energy dissipation coefficients in vibrating aerodynamic rod structures

14 p2537 A69-29748

Lifetime of structural plastics under vibration loading, considering polystyrene and polyformaldehyde samples under tension

15 p2643 A69-30972

Fiberglass reinforced plastic tensile strength dependence on vibration time and temperature and vibrational effect on modulus of elasticity

15 p2643 A69-31203

Facility for determining energy dissipation in materials under cyclic stresses or strains for wide range of temperatures

17 p2946 A69-33925

Mean stresses effect on fatigue strength by specimens vibratory/tensile mean stress diagram combining Goodman line and Gerber parabola merits with increased accuracy

17 p3067 A69-34197

Soft damping system required by LF vibrational loads

18 p3171 A69-34563

Axisymmetric Lamb wave propagation in semi-infinite micropolar elastic solid, considering time varying load on half space boundary

24 p4406 A69-43730

Forced parametrically excited periodic vibration of finite length plate in plane supersonic flow, considering periodic forces applied at edges

24 p4407 A69-43733

VIBROCARDIOGRAPHY

U PHONOCARDIOGRAPHY

VIBROMETERS

U VIBRATION METERS

VICKERS VC-10 AIRCRAFT

U VC-10 AIRCRAFT

VICKERS 1100 AIRCRAFT

U VC-10 AIRCRAFT

VIDEO COMMUNICATION

Light valving techniques applied to large screen display of computer generated video information, noting electron beam control mechanism for transmitted light

06 p0928 A69-17922

Analog video processor in omnidirectional radar system for flight safety, discussing construction, transistorization and circuitry

08 p1276 A69-20605

Maximum errors of telemetering systems under interchannel transient distortions in multistage amplifier of video signals

22 p3899 A69-40250

Nonlinear encoding for picture transmission using nonlinear analog to digital converter

23 p4119 A69-41747

Optical communication through random atmospheric turbulence via heterodyne and video detection, estimating performance from optical wave propagation analysis

23 p4125 A69-42186

VIDEO DATA

Digital computer system for storing, processing and displaying TV pictures

01 p0077 A69-10024

Satellite digital video data analyzed by two dimensional filter computer technique, discussing biomedical applications

02 p0213 A69-12155

Adaptive compression system for predicting and encoding video data for transmission in noiseless channel

03 p0427 A69-12869

Delay line bandwidth reduction for video or digital information, noting radar tracking application

03 p0392 A69-13251

Synchronous extractor for simultaneous extraction and association of primary and secondary radar videos

in civil system, discussing automatic identification process

05 p0721 A69-16592

Satellite picture signal reception from ESSA, Nimbus and ATS to ascertain instrument requirements

06 p0888 A69-17651

Light valving techniques applied to large screen display of computer generated video information, noting electron beam control mechanism for transmitted light

06 p0928 A69-17922

Optical/mechanical IR line scanner imagery role in remote sensing

12 p2096 A69-26979

Digitized video cloud picture data from ESSA satellite, discussing mesoscale archive and computer products including time averages and composites

19 p3279 A69-35810

Buffer storage for telemetry nonstationary video data compression, analyzing requirements, predictor algorithm and variable aperture control using simulation

19 p3272 A69-36260

Receiving and display telemetry system for obtaining direct ionospheric topside ionograms from Alouette 1 satellite, discussing video data tape recording cost

20 p3507 A69-37861

Automatic discriminator design for identifying distorted image in noise based on ideal transmitter and use of split scanning beam

23 p4163 A69-41551

VIDEO EQUIPMENT

Statistical analysis of cascade of bandpass limiter, ideal phase detector and video filter for mathematical modeling of coherent communication systems

07 p1084 A69-19147

Density measurements of particle tracks in nuclear emulsions utilizing digitized video scan, discussing operation and instrumentation

[IEEE PAPER 2A-7] 07 p1133 A69-19185

Atmospheric turbidity and visibility measuring instrument /videograph/ using light backscattering, noting shipboard, coast guard service, large cities and weather stations applications

08 p1314 A69-20376

Monograph on computer aided air traffic control systems design, discussing air navigation, man-machine relations, equipment requirements, programs, plan position color display, etc

11 p1914 A69-25085

Radar target simulator approximating pulse radar receiver output for evaluating amplitude-sensing video target detection devices

17 p2921 A69-33629

Variable time lapse videoscintiscopes in medical applications, discussing implementation of TV camera, signal tape recording and audio activation

18 p3134 A69-34541

Image intensifiers and orthicons, plumbicons, vidicons as photoelectric devices in TV auroral observation from ground stations and jet aircraft

21 p3706 A69-38484

VIDICONS

Silicon vidicon for near IR and visible radiation viewing describing spectral response, energy transfer characteristics, resolution and dark leakage currents

09 p1466 A69-22456

Surveyor 7 TV system in photon integration mode, analyzing slow scan vidicon storage characteristics and dark current limitations

[SMPTE PAPER 105-72] 12 p2078 A69-25772

One inch ceramic vidicon with slow scan photoconductor, electrostatic focusing and magnetic deflection to withstand sterilization and environmental testing for space applications

13 p2234 A69-28262

Pulsating and flaming auroral patches recorded by image intensifier vidicon camera, calculating upward field aligned speeds for luminosity enhancement

16 p2780 A69-32305

Image intensifier and return beam sections of 4.5 inch high resolution vidicon and camera system for high definition signal readout

17 p2976 A69-34063

X ray TV system with electronic-optical converter and X ray vidicon for industrial defectoscopy

18 p3138 A69-35113

TV camera tubes with electron beam scanning adapted to IR imaging, emphasizing vidicon

19 p3311 A69-36069

Balloon flights for testing remote sensor systems prior to space flight, considering return beam vidicon and tracking telescope suitability for experimentation

22 p3865 A69-40806

VIEW EFFECTS

Electro-optical tracking device with pyramidal reflector for field of view dissection, determining dead zones and trajectories for pointing error correction

10 p1698 A69-24219

Wide view angle holocamera to produce 360 degree hologram in strips for simultaneous image reconstruction from single laser beam

20 p3536 A69-36932

VIGNETTING

Vignetting effect on impulse response of general coherent optical Fourier processor, noting time varying character and input position sensitivity

12 p2036 A69-25912

VIKING LANDER SPACECRAFT

Thermal control coatings, windows and mirrors for 1973 Mars Viking Lander vehicles under simulated Martian surface conditions

[AIAA PAPER 69-1023] 22 p3923 A69-40393

VINYL CYANIDE

U ACRYLONITRILES

VINYL ETHYLENE

U BUTADIENE

VINYL POLYMERS

Polyvinyl acetate and polyvinyl alcohol thermoplastic adhesives, discussing gluing properties, chemical properties, preparation, polymerization methods

14 p2469 A69-29347

VIOLENCE

U ATTACKING [ASSAULTING]

VIRO STAR CLUSTER

H alpha emission line in nucleus of Virgo A radio galaxy observed on spectrograph, estimating gas electron density and mass

09 p1588 A69-21360

Virgo XR-1 rocket observations, presenting count rate histograms, differential photon spectrum and X ray and M87 core radio spectra

15 p2701 A69-31535

Four color photoelectric photometry of bright galaxies in Virgo Cluster, analyzing properties in nuclear regions

16 p2860 A69-32230

H alpha emission line in nucleus of Virgo A radio galaxy observed on spectrograph, estimating gas electron density and mass

18 p3197 A69-34750

Spiral galaxy linear diameter relation to luminosity applied to Virgo galactic clusters, noting effect on distance modulus and Hubble constant

19 p3427 A69-36652

IC 3258 emission line spectrum observations, discussing blueshift, extragalactic location, possible nature, etc

23 p4219 A69-42374

VIRIAL THEOREM

Second virial coefficient of plasma at arbitrary temperature, noting small Coulomb interaction

02 p2292 A69-12639

Second virial coefficient of atomic nitrogen and oxygen, discussing thermodynamic properties of dissociating mixtures

03 p0473 A69-14158

Second dielectric virial coefficient of rare gases derived by cluster method

04 p0632 A69-14865

Rotating stellar models oscillation and stability approximated by virial equations

07 p1220 A69-19389

Physical conditions of intergalactic space in Local Group using virial theorem and assuming energy equipartition, discussing temperature, ionized hydrogen density, turbulent motions, etc

08 p1381 A69-19795

Virial theorem extended to investigate star condensations in large interstellar gas clouds

10 p1787 A69-24119

Force-free magnetic field integral properties, obtaining rate of decrease limitation via virial theorem

11 p1951 A69-24239

Gas-gas interactions second virial coefficients measured at various temperatures, comparing experimental data with results calculated by Kihara potential

14 p2488 A69-29927

Radio galaxy Messier 87 mass determined using virial theorem for nucleus velocity dispersion

15 p2695 A69-30883

VIRTUAL PROPERTIES

Virtual power principles applied to solving force acting on fluid consisting of colloidal suspension of polarized particles in neutral vehicle

12 p2136 A69-26404

VIRTUAL WORK

U EQUILIBRIUM

VIRUSES

NT BACTERIOPHAGES

Cosmic radiation interactions with living viruses, considering X ray effects and optimal radiation dosage for cancer cell destruction

01 p0013 A69-10157

Unique sequence of oligonucleotides located in tobacco mosaic virus ribonucleic acid

03 p0370 A69-13461

Viruslike particles in fat body cells and oenocytes of *Drosophila melanogaster* imagoes, in glial cells of cephalic ganglionic center of flies and in gamma radiated cells

23 p4091 A69-42021

Altered gaseous environments effect /parabrosis/ on interferon production in mice injected with Newcastle disease virus, noting hypoxia role

24 p4262 A69-42888

Inoculum dose effect on complement-fixing antigen production, heat lability and separation from BHK-21 cells infected with lymphocytic choriomeningitis virus

24 p4263 A69-43336

VISCERA

NT ADRENAL GLAND

NT BLADDER

NT ESOPHAGUS

NT INTESTINES

NT KIDNEYS

NT LIVER

NT LUNGS

NT ORGANS

NT PINEAL GLAND

NT PITUITARY GLAND

NT RECTUM

NT STOMACH

NT THYROID GLAND

Visceral afferent pathways influence on vasopressin secretion, ADH levels and urinary excretory patterns of dogs during surgical stress

05 p0708 A69-15970

VISCOELASTIC CYLINDERS

HF pressure waves dispersion in blood vessels ascribed to viscoelastic behavior of walls

02 p0204 A69-12602

Heating effects produced by periodic stresses in viscoelastic bodies with resonance dispersion, considering torsional oscillations of viscoelastic cylinders

06 p1019 A69-16826

Frequency response from linearized dynamic equations for viscous incompressible fluid flow in viscoelastic tubes, discussing transfer gain

08 p1304 A69-20704

Heat generation in thin viscoelastic cylindrical shell with relaxation and resonance dispersion during torsional vibration

11 p2000 A69-25168

Volterra integral equation with nondifference type singular kernel for stress-strain state in long hollow viscoelastic cylinder with moving inner boundary

13 p2361 A69-27744

Plane strain solution for thick walled viscoelastic cylinder bonded to thin elastic shell from deformation rate and strain, including inertia effects

16 p2871 A69-31876

Creep calculation with temperature considerations for multilayer cylinder under nonisothermal load, comparing stress-strain state of viscoelastic and elastic cylinders

18 p3225 A69-35358

Ronay effect in reversed cyclic torsion or tension in thin cylindrical viscoelastic tube showing creep under sustained load

20 p3625 A69-37596

Stress analysis of hollow viscoelastic cylinder reinforced with elastic helically wound wires

[ASME PAPER 69-APMW-23] 24 p4401 A69-43096

VISCOELASTIC DAMPING

U ELASTIC DAMPING

U VISCOUS DAMPING

VISCOELASTIC FLOW

U VISCOELASTICITY

VISCOELASTICITY

NT PHOTOVISCOELASTICITY

NT THERMOVISCOELASTICITY

Nonlinear viscoelastic bodies arising in 3d rheological models with hidden parameters behaving according to law compatible with objectivity and 2nd thermodynamics principles

01 p0171 A69-11131

Unsteady slow rotational motion of viscoelastic liquid contained between two concentric spheres rotating with constant angular velocities

02 p0230 A69-11563

Thermodynamic foundations of permanent deformation theory, noting parallel to viscoelastic material theory
02 p0350 A69-11714

Viscoelastic materials thermomechanical behavior, discussing constitutive equation and derivation of stress tensor and entropy density from viscoelastic potential
02 p0344 A69-12294

Idealized slider bearings with Maxwell liquid as lubricant, analyzing elasticity effects on pressure, load capacity and friction
02 p0253 A69-12413

Time dependent viscoelastic stress distribution in two phase composite material, using plane stress model for approximation
02 p0348 A69-12540

Automatic determination of relaxation and retardation spectra for linearly viscoelastic materials from experimental data using simple numerical techniques
02 p0348 A69-12605

Elastoviscous flow in curved channels, analyzing nonNewtonian effects for case of circular and elliptic walls
02 p0234 A69-12608

Asymptotic constitutive approximations for rapid finite deformation of general viscoelastic materials, noting isotropic solids and fluids
03 p0523 A69-13020

Mechanical and optical viscoelastic characterization of Hysol 4290 epoxy polymer as function of time and temperature, using creep test data
03 p0524 A69-13064

Twisted yarns composed of continuous viscoelastic filaments dynamic response under periodic strain effect on dynamic modulus
04 p0619 A69-14686

Viscoelasticity effect on tensile stress in absorption layer for free surface uniaxial motion
04 p0676 A69-14705

Stability of circular cylindrical viscoelastic and elastic shells with local effects due to radial load on circumference or thermally induced tangential stress
04 p0680 A69-14928

NonNewtonian hydrodynamics equations for non-linearly viscous and viscoelastic media, analyzing dependence on rheological model
05 p0745 A69-15786

Constitutive equation for viscoelastic materials generalized, assuming instantaneous part of deformation to be nonlinear function of time dependent stress state
05 p0835 A69-15868

Coupled heat equation to calculate transient and steady state temperature distributions in viscoelastic solids under cyclic deformations
05 p0836 A69-15878

Frequency dependent shear modulus for hexachlorobiphenyl measured under rare gas infusion at 5-25 C and from ambient atmospheric to 4000 psi
05 p0796 A69-15912

Resonant beam tuned vibration damping device, noting weight saving potential
[ASME PAPER 68-WA/GT-2]
05 p0837 A69-16138

Tension stress and shearing strain vs time for simultaneous stress relaxation and creep in polyurethane
[ASME PAPER 68-WA/APM-8]
05 p0839 A69-16186

Book on continuum mechanics covering elasticity, fluid mechanics, plasticity and viscoelasticity, emphasizing basic concepts
05 p0843 A69-16713

Temperature dependence of dynamic viscoelastic properties of plasticized epoxy resins
06 p0946 A69-17125

Secular equation for Couette flow stability in incompressible viscoelastic fluid
06 p0909 A69-17240

Free energy in linear viscoelastic solids
06 p1022 A69-17241

Longitudinal and transverse vibrations of viscoelastic rods excited by inertia with aid of linear oscillator subjected to harmonic stress, using Kelvin-Voigt model
07 p1233 A69-19326

Reciprocity, variational and uniqueness theorems developed within linear theory of coupled thermoviscoelasticity
07 p1233 A69-19327

Anisotropic stress analysis of creep in theory of linear viscoelasticity
07 p1234 A69-19381

Flow fracture and rheological properties of viscoelastic material under biaxial loading
07 p1202 A69-19386

Axially loaded viscoelastic constrained bar instability for large deformation
07 p1235 A69-19440

Viscoelastic rod model of human spine subjected to accelerations
07 p1072 A69-19725

Generalized approximate method for solving problems in linear viscoelasticity theory to cover arbitrary creep and relaxation centers
08 p1412 A69-20327

Viscoelastic problem solutions for hereditary media, using Laplace transforms or solutions of integral equations for inaccurately approximated kernels
08 p1412 A69-20329

Uniqueness theorem for equations of dynamics of viscoelastic bodies, using energy and hereditary elasticity considerations
08 p1415 A69-20658

Bounds for real and imaginary parts of dynamic moduli of composite viscoelastic systems
08 p1417 A69-20824

Viscoelastic properties of heterogeneous media of composite sphere model type obtained from shear modulus formula
08 p1417 A69-20825

Large deflections and associated moments in circular ring of linearly viscoelastic material subjected to small strains
09 p1615 A69-21925

Linear viscoelastic bending of anisotropic plates based on equation for Voigt plate, considering elliptic and rectangular plates
10 p1793 A69-22881

Short memory elasticoviscous fluid motion in and around oscillating spherical shell
10 p1800 A69-23240

Forced vibrations of elastic beam covered by viscoelastic layer subjected to transverse harmonic excitation
10 p1800 A69-23241

Laminar elasticoviscous flow of liquid with short memory in two dimensional channel with porous walls
10 p1680 A69-23668

Elastomeric solid propellant grains viscoelastic flow, analyzing stresses and strains under various operating conditions and rocket engine geometry effect
10 p1801 A69-23702

Elongational viscosity coefficient determined from tensile measurements of materials under applied stress
10 p1681 A69-23976

Damping properties of nonlinear viscoelastic solids with applications to vibrating continua, using Gauss principle of least constraints
11 p1970 A69-24605

Book on strength and failure of viscoelastic materials covering linear and three dimensional polymers or polymer-based materials, flexibility and temperature effects
11 p1970 A69-24610

Modulus of elasticity changes and stress relaxation spectra of viscoelastic liquids measured by acoustic methods
11 p1887 A69-25206

Transient dynamic response of linearly viscoelastic structures and continua, presenting finite element displacement formulation
11 p1993 A69-25528

Viscoelastic models for solving longitudinal oscillations of one degree of freedom system under dynamic load, taking into account energy dissipation
12 p2177 A69-25995

Correlation between temperature and stress field in thermal buckling of square viscoelastic Maxwell plates under random temperature
12 p2188 A69-27113

Torsional testing facility for delayed elastic and non-recoverable strains in materials, noting application to diffraction limited reflecting optics
13 p2240 A69-27955

Tension stress and shearing strain vs time for simultaneous stress relaxation and creep in polyurethane
[ASME PAPER 68-WA/APM-8]
13 p2362 A69-28121

Isothermal deformations in linear viscoelastic material under uniaxial stress, determining optimum strain rate history for maximum work lower bound
15 p2707 A69-30637

Viscoelastic half space properties effect on self excited vibration boundaries determination
16 p2873 A69-32063

Energy method determining sufficient conditions for fluid motion stability described by infinitesimal theory of viscoelasticity, restricting analysis to confined fluids or periodic velocity field
17 p2949 A69-33015

Normal stress effects in viscoelastic fluid theories applied to one dimensional Burgers model of weak turbulence predicting drag reduction
17 p2951 A69-33256

Damping techniques using viscoelastic materials, discussing mechanical hysteresis
17 p2992 A69-33660

Axisymmetrical vibration characteristics of circular sandwich shell with viscoelastic core layer analyzed via differential equation to obtain frequency equation and composite loss factors
18 p3211 A69-34327

Local stability of viscoelastic shells of revolution under axisymmetric loads, discussing asymmetric snapthrough of dome
18 p3216 A69-34573

Transverse vibrations of thin linear viscoelastic rectangular plate of constant thickness resting on elastic medium
18 p3223 A69-35171

Linearity range of viscoelastic properties of fiberglass reinforced plastics, calculating stress-strain state
18 p3163 A69-35364

Dynamic reciprocity relationship for linear directed continuous viscoelastic media, using Stieltjes convolution
19 p3373 A69-36307

Uniqueness theorems for energy methods solution of equations of dynamic thermoelasticity and viscoelasticity
19 p3439 A69-36470

Nonlinear rotational viscoelastic membranes creep rupture and failure found dependent on function of accumulated energy and power dissipation during deformation
19 p3444 A69-36806

Equations of deformation for elastoviscoplastic bodies with different properties under loading and unloading conditions
19 p3445 A69-36812

Finite element displacement method using elastic analogy applied to viscoelastic materials plane stress analysis
19 p3445 A69-36830

Vibration response approximation of three layer sandwich beam with nonlinear viscoelastic material core during flexural vibrations
20 p3619 A69-36910

Viscoelastic materials gradual resilience loss under tensile stress, discussing mathematical relations between stress, loading time, elastic deformation and experimental verification
20 p3625 A69-37600

Viscoelastic nonlinear and linear solids models and rheological equations, studying stress-strain states of various complex Hookean, Kelvin, Maxwellian and Zener elements
20 p3625 A69-37601

Nonlinear viscoelastic material properties evaluation from experimental data with illustration for polymers, deriving equations from thermodynamic principles
20 p3626 A69-37719

Constitutive equation for nonlinear viscoelastic materials, noting validity for short times, slow motions or small deformations
21 p3840 A69-39288

Constitutive equations for homogeneous viscous fluid and Kelvin-Voigt viscoelastic solid in electromagnetic field, using linear irreversible thermodynamics and continuum mechanics
21 p3851 A69-39289

Final period of decay for viscoelastic fluid in homogeneous isotropic turbulence, deriving expressions for double correlation function and energy decay
22 p3928 A69-39891

Gupta stability solution extended to liquid anisotropic viscoelastic films, analyzing surface and shear wave perturbations in material structures
22 p3929 A69-39893

Load transfer to sheet metal plate from bonded strip axially loaded by single force, assuming linear viscoelastic adhesive layer
22 p4038 A69-39896

Viscoelastic fluid steady flow in porous walled channel, examining mass flow solution continuity
22 p3930 A69-40118

Viscoelastic properties of lenses extracted from cats and dogs analyzed as function of displacement using computer simulation
22 p3883 A69-40875

Positive solutions of parabolic and hyperbolic partial differential equations arising as viscoelastic media equations of motion, noting maximum principle utilization
22 p3976 A69-41035

One dimensional shock waves and acceleration fronts in nonlinear isotropic viscoelastic materials using constitutive equations

23 p4235 A69-42463

Law of mixture governing creep strength of composite materials reinforced unidirectionally by continuous filaments, taking into account fibers and matrix viscoelastic properties

24 p4400 A69-43054

ISCOMETERS

Absolute viscosity measurements from translational undamped oscillations of plate in liquid, considering viscosimeter walls effect

04 p0679 A69-14905

Absolute viscosity measurements from translational undamped oscillations of plate in liquid, considering viscosimeter walls effect

12 p2182 A69-26658

Microrheological property of blood measured with microglass fiber viscosimeter, noting sensitivity to intercellular friction of erythrocytes

23 p4098 A69-42100

ISCOMETRY

Human blood viscosity measurement over wide range of shear rates, obtaining rheological data, suggesting osmotic red cell crenation role

23 p4095 A69-42078

ISCOPLASTIC FLOW

U VISCOPLASTICITY

ISCOPLASTICITY

Temperature evolution velocity parameter effect on behavior of elastoviscoplastic solids, noting demonstration by work hardening tests at variable temperatures [ONERA-TP-644]

01 p0164 A69-10036

Thermodynamics of viscoplastic materials under dynamic loads within framework of continuum mechanics of materials with memory

02 p0343 A69-12281

Crystal dislocation motion in viscous media, discussing velocity stress behavior and measurements by etching and ultrasonic attenuation methods

02 p0343 A69-12285

Elastic/viscoplastic wave propagation in thin tubes under combined stress of tension and torsion, using viscoplastic constitutive equations

02 p0344 A69-12293

Spherical wave reflection from nondeformable plane in elastic viscoplastic medium

03 p0528 A69-13926

Propagation of longitudinal transverse loading and unloading waves (with cylindrical symmetry) in non-homogeneous elastic/viscoplastic medium, accounting for plastic dilatational strains

03 p0528 A69-13929

Technique for compressive mechanical behavior of viscoplastic nonlinear composites, discussing rate dependence and one dimensional stress-strain time properties

07 p1159 A69-18721

Quasi-linear differential constitutive equation of work hardenable elastoviscoplastic material in case of plane wave propagation in half space

08 p1415 A69-20662

Thermodynamics of strain rate sensitive elastoviscoplastic solids, considering kinematic description of plastic deformation and choice of state variables

11 p1994 A69-25601

Three dimensional harmonic dispersion analysis of incremental waves in uniaxially prestressed plastic and viscoplastic bars, plates and unbounded media

13 p2363 A69-28125

Reflection of spherical stress wave against smooth in-deformable plane in elastoviscoplastic medium, discussing Taylor series expansions for displacement, velocity and stress fields

18 p3226 A69-35463

Closed form solutions for rigid viscoplastic cylindrical shell under dynamic loading based on constitutive equations for rate sensitive plastic material

19 p3439 A69-36478

Equations of deformation for elastoviscoplastic bodies with different properties under loading and unloading conditions

19 p3445 A69-36812

Viscoplastic thermomechanically coupled systems stability, considering effects of heat transfer to surroundings and heat capacity in material regions below yield

20 p3625 A69-37591

VISCOSITY

NT EDDY VISCOSITY

NT GAS VISCOSITY

Viscous effects of neutrinos in anisotropic cosmological models examined using Boltzmann equation with simple collision term

01 p0148 A69-10053

Viscoseal sealing coefficient and friction factor under turbulent flow conditions [ASLE PREPRINT 68AM 5B-1]

01 p0087 A69-10911

Low temperature effects on calf thymus deoxy-nucleoprotein, crystalline egg albumin and fibrillar actin, noting molecular weight and viscosity changes

01 p0018 A69-11089

Energy transfer and viscosity coefficients during gas molecular interactions, using spherical monatomic gas molecules model

03 p0415 A69-13419

Solid viscosities effects on dynamic load factors of ring and hollow sphere subject to uniformly distributed impulsive loads along inner and outer edges

03 p0530 A69-14089

Electron viscosity coefficient in weakly turbulent plasma in strong magnetic field, noting electrical and thermal conductivity

03 p0480 A69-14136

Prigogine-Nicolis-Misguich transport theory tested with inert gas liquids and compared with Rice-Allnatt theory, based on modified Lennard-Jones potential model

04 p0589 A69-14863

Temperature dependence of viscosity and density in molten thallium sulfide, noting structural changes absence in short range order

04 p0643 A69-14998

Thermal diffusion coefficient and composition of gas mixtures by measuring gas flow rate in capillary tube as function of viscosity

04 p0688 A69-15410

Viscosity coefficient tensor in terms of autocorrelation functions, using linear reaction theory of mechanical disturbances

05 p0794 A69-15785

NonNewtonian hydrodynamics equations for non-linearly viscous and viscoelastic media, analyzing dependence on rheological model

05 p0745 A69-15786

Liquid oxygen shear viscosity dependence on temperature and pressure obtained by measuring electrical characteristics of immersed torsional vibrating crystal

05 p0846 A69-15916

Book on fluid mechanics fundamentals and applications covering incompressibility and compressibility effects, viscosity, hydrostatics, aerostatics, one dimensional, potential, turbulent flow and boundary conditions

07 p1121 A69-19376

Viscous stress tensor for collisionless plasma with anisotropic pressure in magnetic field

08 p1365 A69-20522

Self gravitating incompressible fluid sphere free oscillations, deriving characteristic equations for arbitrary viscosities

09 p1481 A69-21790

Molybdenum fiber sintering activation by adding nickel, noting decrease in impact viscosity

10 p1711 A69-23336

Thermal convection in earth mantle with temperature and pressure dependent viscosity, considering mechanisms for fluid-like mantle

10 p1682 A69-23412

Steady state spherically symmetric model for solar plasma acceleration with distance, showing essential role of viscosity

10 p1769 A69-23899

Viscosity-temperature chart for hydrocarbons permitting linear extrapolations into low viscosity high temperature regions

10 p1753 A69-23975

Elongational viscosity coefficient determined from tensile measurements of materials under applied stress

10 p1681 A69-23976

Crack propagation through layer of viscous fibers joining orthotropic elastic half planes

10 p1803 A69-24029

Metal fatigue at elevated temperatures concerning viscosity, energy loss and stress, strain and temperature cycling

10 p1803 A69-24043

Variational calculation of coefficients of viscosity, thermal conductivity, thermal diffusivity and diffusion in binary mixture

11 p1997 A69-24285

Turbulent viscosity and thermal conductivity coefficients for entire cross section of fluid flow including wall boundary layers

11 p1873 A69-25228

Book on negative turbulent viscosity theory covering laboratory analysis and applications to earth and solar atmospheres, oceanic circulations, spiral galaxies and solar nebula

12 p2131 A69-26868

Turbulence constant for flows near walls, analyzing viscosity dependence on wall distance by utilizing maximum stability principle

15 p2590 A69-30048

Plasma viscosity relation to stellar magnetic fields generation, taking into consideration angular momentum transfer

15 p2700 A69-31492

Langevin equation for interacting molecule system derived by Fourier transformation of Hamiltonian, noting physical correspondence to equation for shear viscosity in monatomic liquids

16 p2815 A69-32370

Nonnewtonian solid propellant viscosity and pseudoplasticity utilizing rheological characterization for optimal casting and pot life determination [AIAA PAPER 69-518]

16 p2833 A69-32665

Mathematical model of yielding of adhesive bonds in form of viscous threads between elastic bodies, obtaining solution to two dimensional problem

18 p3215 A69-34569

Quasi-static crack growth in viscous bodies analyzed by continuum mechanics, rheological models and energy equation, discussing fine structure

18 p3215 A69-34570

Viscosity coefficient tensor in terms of autocorrelation functions, using linear reaction theory of mechanical disturbances

18 p3173 A69-35037

Shaft speed limitations on close clearance seals, using test data on changes in fluid viscosity causing contact and damage [ASLE PAPER 68-LC-13]

21 p3731 A69-38763

Dilute solution of He 3 in He 4 near absolute zero measured for viscosity, showing temperature effect

21 p3772 A69-39582

Polystyrene melt tensile viscosity prediction from shearing viscosities, using rheological network rupture theory

21 p3753 A69-39730

Free convection of capillary fluid at vertical plate, allowing for temperature dependence of viscosity coefficient

21 p3854 A69-39843

Solid viscosities effects on dynamic load factors of hollow sphere subjected to uniformly distributed impulsive loads, using three element model

22 p4044 A69-40598

Forced convection liquid flow past heated flat plate with variable viscosity and thermal conductivity, analyzing velocity and temperature distribution in boundary layer

22 p4051 A69-40685

Starting process in nozzle with one dimensional flow treated numerically by finite difference method using pseudoviscosity term

22 p3860 A69-40926

Blood viscosity as possible key factor in physiology and pathology of circulation, suggesting causes of myocardial infarction and coronary occlusion

24 p4261 A69-42725

VISCOUS DAMPING

Viscous damping of internal waves on rotating earth, analyzing spatial propagation attenuation in two layer system

02 p0247 A69-12775

Single degree of freedom structural damping estimations from viscous and hysteretic energy dissipation data

03 p0523 A69-12947

Constrained layer damping and conventional techniques combination for vibration and noise control

04 p0606 A69-14691

Linear mechanical systems idealized by single degree of freedom system with viscous damping subjected to combined deterministic and random excitation

04 p0680 A69-14968

Root fixture and grip load effects on cantilever beam damping, using bandwidth and logarithmic decrement measurement methods

10 p1800 A69-23244

Vibration control by alternate layers of high damping viscoelastic material, discussing damping and loss factors, beams design and attachment

15 p2622 A69-30704

Vibrations attenuation by viscoelastic sandwich shear damping, discussing examples of aircraft equipment racks, gyro and airborne circuit board mountings

15 p2622 A69-30705

Temperature, velocity and density perturbation propagation as heat convection wave in viscoelastic thermally compressible heat conducting fluid, analyzing damping and frequency spectra
16 p2878 A69-31952

Nonlinear response of single Helmholtz resonator subjected to finite amplitude pressure oscillations, detailing entrance, orifice and cavitation flow [AIAA PAPER 69-481]
16 p2844 A69-32719

Damping techniques using viscoelastic materials, discussing mechanical hysteresis
17 p2992 A69-33660

Viscous friction damping effect on impact vibrator stability, analyzing boundary region of multiply periodic single impact motion by point mapping
18 p3172 A69-34588

Boundary layer method for calculation of viscous damping coefficients for small amplitude progressive waves propagating in nonhomogeneous fluid
23 p4153 A69-42408

VISCOUS DRAG

Viscous liquid layer flow down inclined plane under boundary conditions, taking into account drag and penetration at porous bed surface
02 p0234 A69-12774

Velocities, accelerations and drag forces on spheres falling along center line in viscous fluid, considering different Reynolds numbers and Stokes approximation range
05 p0788 A69-15725

Viscous hydrodynamical equations for flow field exterior to obstacle moving with constant velocity, discussing force relationships, drag invariance and integral representations
07 p1121 A69-19298

Integral representation for velocity and pressure fields produced by horizontal motion of two dimensional bodies below or on free surface of viscous liquid
11 p1866 A69-24278

Viscous drag reduction - Conference, Dallas, September 1968
17 p2950 A69-33247

Turbulence measurements and roughness effects on viscous drag reduction with polymer solution in pipe flow, discussing friction factor, wall velocity profile, etc.
17 p2951 A69-33252

Concentration, flow rate and tube diameter effects on viscous drag reduction in nonpolar soap solutions, using pressure drop measurements to observe turbulent flow behavior
17 p2951 A69-33253

Linear oscillations of sphere in compressible viscous fluid with slip at surface, noting drag variation
19 p3297 A69-35836

VISCOUS FLOW

NT BOUNDARY LAYER FLOW
NT BOUNDARY LAYER SEPARATION
NT COUETTE FLOW
NT DETACHED FLOW
NT SECONDARY FLOW
NT SEPARATED FLOW
NT STOKES FLOW

Viscous electrically conducting fluid with aligned magnetic field flowing past flat plate at nonzero angle of attack
01 p0126 A69-10163

Heat conduction in viscous fluid flows with large concentration of suspended solid particles
02 p0351 A69-12052

Exact solutions for Navier-Stokes equations for nonsteady incompressible viscous flow near two dimensional or axisymmetrical stagnation point
02 p0233 A69-12527

Hydrodynamic analysis for determining steady flow region with closed separation area for Reynolds numbers to describe viscous mixing by Prandtl equations
02 p0190 A69-12570

Viscous effects on impact pressure measurements in free jet low density gas flows at high Mach numbers
02 p0234 A69-12633

Analysis of solution of Navier-Stokes equations describing two dimensional flow of viscous incompressible fluid by finite difference techniques and introduction of curl
03 p0416 A69-13652

Problem of viscous supersonic flow past blunt bodies based on Navier-Stokes equations formulated and solved numerically with explicit difference scheme
03 p0363 A69-13653

Turbulent fluctuations of viscous sublayer of two dimensional flow, assessing wall shear stress spectrum
04 p0587 A69-14544

Steady flows of incompressible viscous fluid exterior or interior to circular cylinder
04 p0589 A69-14898

Ekman boundary layer problem of steady axisymmetric viscous incompressible flow between infinite coaxial rotating disk, studying laminar range of Taylor number R
05 p0744 A69-15665

Circulation, geometry and viscosity effects on speed of surge in bathtub vortex
05 p0744 A69-15718

Peculiarities of aerodynamic characteristics of flow past plate and pointed and blunt slender cones in viscous hypersonic thermodynamically ideal gas
05 p0699 A69-16673

Viscous MGD channel flow in boundary layer approximation with heat conduction, transforming resultant partial differential equations set to system of ordinary differential equations
06 p0966 A69-17523

Pressure distribution, heat transfer rates and shear stresses in laminar boundary layer of supersonic viscous flow incident on corner point of body
06 p0861 A69-17641

Ellipsoids of revolution in viscous flow at very low Reynolds number, determining optimum shapes and minimum resistance values
06 p0911 A69-17780

Chemical nonequilibrium, mass transfer and viscous interaction effects on spherically blunted cones at hypersonic conditions, emphasizing stagnation point [AIAA PAPER 69-168]
06 p0862 A69-18047

Pressure distribution determined from laminar viscous-inviscid interactions in supersonic flow, including flows with heat transfer [AIAA PAPER 69-7]
06 p0913 A69-18095

Time dependent technique for inviscid blunt body flows to analyze viscous rarefied shock layer regime, using Navier-Stokes equations [AIAA PAPER 69-139]
06 p0865 A69-18173

Xenon flash lamps with electrolytic capacitors designed for photographic studies of laminar flows of viscous fluids
07 p1116 A69-18259

Motion of viscous incompressible fluid in interspace between rotating and parallel fixed permeable plane having supplementary fluid injection solved by Navier-Stokes equations
07 p1119 A69-18743

Navier-Stokes equations for steady rotational motions of incompressible viscous fluid at small Reynolds numbers between rotational surfaces
07 p1119 A69-18748

Stationary viscous incompressible fluid flow past rough surface, noting solution stability and friction stress determination for given pressure gradient
07 p1119 A69-18751

Unsteady conducting incompressible viscous fluid flow past plate in magnetic field, analyzing surface friction reduction
07 p1192 A69-19018

Heat transfer in horizontal and vertical tubes with viscous gravity flow with boundary conditions
07 p1243 A69-19733

Approximation method applied to closed viscous streamline flow in rectangular cavity, discussing constant shear stress boundary conditions
08 p1304 A69-20811

Solid cylindrical body entrainment by viscous incompressible fluid flow in tube under constant pressure gradients and absence of gravitational force
10 p1678 A69-23366

Numerical solutions for incompressible Newtonian flow around circular cylinder for various Reynolds numbers
11 p1867 A69-24279

Viscosity and electrical conductivity effects on axisymmetric instabilities of current carrying annular cylinder of mercury
11 p1923 A69-24292

Turbulent flow problems, discussing hot-wire techniques, viscosity effect, compressibility surface curvature, turbulent boundary layers, heat transfer, etc.
11 p1871 A69-25017

Viscous flow stability in rotating pipe, giving velocity components in cylindrical polar coordinates
11 p1871 A69-25125

Aerodynamic characteristics of flat plate in viscous hypersonic flow incident at zero or small angle of attack, using numerical integration
11 p1820 A69-25471

Hypersonic viscous gas flow past thin bodies, deriving equations for interactions between boundary layer and external flow
11 p1820 A69-25472

Supersonic nozzle design ensuring desirable flow field in inviscid core of viscous gas flow, using boundary layer equations
11 p1820 A69-25473

Self similar axisymmetric and plane laminar viscous gas channel flows noting exponential or hyperbolic law of decrease in static pressure along channel
11 p1875 A69-25482

Viscous flow-induced vibrations of elastically restrained flat plates in narrow channel, considering one dimensional viscous flow theory
11 p1991 A69-25515

Navier-Stokes equations for compressible gas, generalizing viscous channel flow of heat conducting gas to slip flow of rarefied gas
12 p2061 A69-25887

Pressure distribution in viscous flow between parallel disks with sinusoidal oscillation, noting effects of oscillation amplitude and vibrating disk velocity [ASME PAPER 68-LUBS-1]
13 p2244 A69-27278

Expansion of stream function of steady meridional flow of viscous fluid at small Reynolds numbers, giving expansion in spherical coordinates
13 p2247 A69-27737

Wall shear stress measurement by evaporating liquid film, determining optimum liquid viscosity
13 p2375 A69-27793

Numerical method for time dependent compressible Navier-Stokes equations applied to axisymmetric flow field produced by hypervelocity impact, examining viscous effects [AIAA PAPER 69-354]
13 p2366 A69-28288

Demixed layer at wall in shear flow of nonsedimenting suspensions with different geometries due to viscous and inertia effect superposition
13 p2251 A69-28498

Nonreacting turbulent far wake problems, discussing centerline decay of viscosity models, similarity profiles and radial distributions at various Mach numbers
13 p2200 A69-28500

Model to study viscous flow characteristics in channel with porous walls and constant suction, noting non-monotonic velocity profile
14 p2429 A69-29015

Rate equation for effective turbulent viscosity variations, considering effects of generation, convection, diffusion and decay in quasi-parallel shear flows
15 p2591 A69-30905

Numerical approximation of Taylor vortices in viscous incompressible fluid flow between concentric rotating cylinders, using truncated eigenexpansions
15 p2593 A69-31518

One dimensional viscous magnetofluid dynamic flow in annulus formed by concentric cylindrical electrodes, reducing problem to linear partial differential equation set [AIAA PAPER 69-725]
17 p3012 A69-33493

Viscous convergent-divergent nozzle flow slender channel approximations, discussing roles of nozzle geometry, Reynolds number and wall temperature, calculating velocity, enthalpy, etc [AIAA PAPER 69-654]
17 p2894 A69-33502

Low Reynolds number solutions for incompressible viscous flows resulting from finite disk steady rotation
18 p3121 A69-34784

Similarity solutions of viscous transonic equation describing spiral and radial flows, containing shock-like transitions of corresponding inviscid solutions
18 p3121 A69-34787

Viscous electrically conducting fluid flow around thin profiles for equal Reynolds and magnetic Reynolds numbers, using Oseen method to linearize equations
18 p3124 A69-35285

Flow viscosity and heat conduction effects on shock wave propagation in bent channel with weak Mach reflection
18 p3124 A69-35326

Asymptotic solution of supersonic linearized nonisentropic flow of viscous and heat conducting gas with internal heat sources past cylindrical shell, deriving surface pressure
18 p3089 A69-35460

Viscous incompressible fluid flow around semi-infinite oscillating plate and skin friction on infinite cylinders oscillating parallel to length
19 p3237 A69-35620

Boundary conditions of incompressible fluid viscous flow on semi-infinite plate edge defined using difference methods for Navier-Stokes equations
19 p3299 A69-36394

Nonequilibrium laminar heat transfer in viscous flow of chemically unstable gases past blunt body and plate
20 p3513 A69-37087

Incompressible viscous fluid flow past sphere at low Reynolds number, evaluating stream function and drag on sphere
21 p3694 A69-38771

- Equation of motion for determining nonlinear vibration of rod pendulum in viscous flow of varying velocity
21 p3773 A69-39679
- Laminar viscous flow and skin friction near trailing edge of flat plate analyzed by modified Oseen approximation, noting accuracy for high Reynolds numbers
22 p3930 A69-40683
- Unsteady viscous flow past flat plate based on Stokes approximation, calculating shear stress
22 p3931 A69-40684
- Free viscous layers structure at large Reynolds numbers, using matched asymptotic expansions for two dimensional compressible flow
22 p3932 A69-40927
- Integral equations of motion for plane steady flow of viscous incompressible electrically conducting fluid round flat plate
22 p3992 A69-41109
- Transport coefficients in neutral gases, discussing fundamental relations of parameters in viscosity, thermal conductivity and self, pressure and thermal diffusion
23 p4193 A69-41514
- Microrheological property of blood measured with microglass fiber viscosimeter, noting sensitivity to intercellular friction of erythrocytes
23 p4098 A69-42100
- Shock wave/boundary layer interaction calculation methods circumventing simultaneous large longitudinal and transverse pressure gradients and viscous effects
24 p4243 A69-42582
- Peristaltic pumping in circular cylindrical tube, discussing viscous fluid flow induced by axisymmetric traveling sinusoidal wave imposed on flexible tube wall [ASME PAPER 69-APMW-3]
24 p4275 A69-43108
- Dynamic models for viscous fluid transmission lines using distributed parameter for accuracy and rational approximate form to avoid computational difficulty
24 p4301 A69-43289
- Viscous shock wave chemical relaxation for diatomic nonequilibrium dissociating gas flow, using Navier-Stokes and chemical kinetics equations
24 p4302 A69-43487
- Secondary flow occurrence and geometry in viscous turbulent flow in square channel, using iterative solution
24 p4303 A69-43501
- Laminar turbulent boundary layer prediction using mixing length model modified for viscous sublayer structural changes near wall compared with heat transfer data [ASME PAPER 69-HT-13]
24 p4303 A69-43556
- ISCUOUS FLUIDS**
- Small oscillations in solid body with arbitrary cavity partially filled with viscous incompressible fluid
01 p0165 A69-10084
- Boundary value problems for steady, three dimensional MHD flow of viscous incompressible conducting fluid past various bodies, proving existence of solutions
01 p0126 A69-10164
- Energy dissipation at rounded pipe entrance in viscous fluid, showing relation between entrance loss and radius of roundness
01 p0059 A69-10308
- Asymptotic forms of Navier-Stokes equations for laminar motions of incompressible viscous fluid, discussing validity and applications [ONERA-TP-651]
01 p0059 A69-10383
- Two dimensional Navier-Stokes equations of axisymmetric motion of viscous incompressible fluid, giving integral and solutions for stream function
02 p0231 A69-12135
- Two dimensional unsteady Rayleigh flow velocity of conducting and nonconducting viscous fluid past porous plate, analyzing suction and magnetic field effects
02 p0232 A69-12156
- Mixed boundary value problem for system of Navier-Stokes equations for viscous incompressible fluid in stationary motion in vessel, noting rotating fluid
02 p0272 A69-12223
- Accelerated plate motion effect on flow of electrically conducting viscous incompressible fluid past infinite flat plate in uniform magnetic field
02 p0289 A69-12237
- Resisting forces produced by transverse vibration of rotating disks in viscous fluid
02 p0232 A69-12257
- Viscous liquid layer flow down inclined plane under boundary conditions, taking into account drag and penetration at porous bed surface
02 p0234 A69-12774
- Plane Couette flow stability in heated nonlinear viscous fluid flowing between horizontal plates heated to different temperatures
02 p0235 A69-12828
- Cauchy-Poisson problem for viscous liquid, calculating free liquid surface response to point impulse or initial displacement
03 p0414 A69-13015
- Unsteady transient flow of viscous fluid in suddenly rotating open pot, taking into account effect of bottom in determination of velocity profile
03 p0414 A69-13019
- Laminar flow of viscous fluid along wall with fixed leading edge and moving surface, discussing conditions of boundary layer formation and dynamic similarity
03 p0417 A69-13792
- Numerical solution of axisymmetric incompressible viscous fluid flows about rotating cylinder, Taylor vortex between cylinders and through labyrinth seal
03 p0419 A69-13990
- Navier-Stokes equations for self gravitating viscous fluid, discussing generalization based on irreversible thermodynamics
04 p0588 A69-14699
- Absolute viscosity measurements from translational undamped oscillations of plate in liquid, considering viscosimeter walls effect
04 p0679 A69-14905
- Thermal explosion in Poiseuille flow of reacting viscous fluid in infinite circular cylindrical channel or between two rotating infinite cylinders
04 p0686 A69-14986
- Asymptotic expansion for transonic flow of viscous fluid at great distance from plane obstacle
04 p0544 A69-15057
- Unsteady hydromagnetic flow of viscous electrically conducting incompressible liquid over infinite conducting harmonically oscillating plate
04 p0638 A69-15093
- Viscous incompressible fluid motion in two or more dimensions and with zero fluid velocity on domain boundary, determining lower bounds and uniqueness for solutions
04 p0626 A69-15311
- Equations of motion derived for incompressible and irrotational viscous fluids in special relativity
05 p0792 A69-15682
- Velocities, accelerations and drag forces on spheres falling along center line in viscous fluid, considering different Reynolds numbers and Stokes approximation range
05 p0788 A69-15725
- Intense transverse resonant acoustic field interaction with viscous fluid flows [ASME PAPER 68-WA/FE-8]
05 p0748 A69-16091
- Viscous electrically conducting liquid flow through insulating porous medium in presence of transverse magnetic field in region of validity of Darcy law
05 p0805 A69-16603
- Cauchy problem for nonstationary linearized Navier-Stokes equations for fixed container partially filled with liquid
06 p0959 A69-17888
- Unsteady flow of viscous incompressible conducting fluid in MHD generator channel, discussing external circuit inductance and flow velocity during start-up
06 p0969 A69-17915
- Viscous gravitating sphere oscillations and velocity field, noting oscillations of Maxwell sphere
07 p1123 A69-18806
- Boundary layer approximation for steady laminar flow of viscous incompressible fluid past paraboloid of revolution, obtaining vorticity distribution
07 p1120 A69-18812
- NonNewtonian effects in axisymmetric rotational flows of elastico-viscous liquids
07 p1180 A69-18815
- Ellipsoidal gas bubble dissolution in low viscosity fluid, discussing rate of steady motion, deformation degree and diffusion rate
07 p1120 A69-18990
- Navier-Stokes equations solved for viscous incompressible fluid flow due to laminar jet flow into channel in presence of magnetic field
07 p1120 A69-18997
- Rise velocity of large gas bubbles in liquid calculated, assuming velocity is determined by propagation of bubble produced wave disturbance
07 p1120 A69-18999
- Laminar flow of viscous conducting fluid between parallel walls in traveling magnetic field, using Hartmann number expansion
07 p1192 A69-19023
- Nondimensional Jeffreys number as ratio of Reynolds to Froude number for gravitational motion of viscous masses, with application to lunar maria and plastic ice
07 p1218 A69-19262
- Unsteady suction motion of viscous incompressible fluid under action of slowly rotating suction disk, noting fluid velocity variation
08 p1302 A69-19875
- Clebsch transformation application to equations describing viscous fluid, deducing canonical equations equivalent to Navier-Stokes equations
08 p1303 A69-20125
- Integral of Navier-Stokes equations for steady three dimensional motion of incompressible viscous fluid, giving angular velocity vector projections
08 p1342 A69-20320
- Flow behind shock front propagating along viscous fluid film surface, noting shock intensities as related to detonation velocities, using schlieren photographs
08 p1303 A69-20326
- Logarithmic decrement and period of disks performing torsional oscillations measured in viscous fluid, noting dependence on oscillation amplitude
08 p1417 A69-20781
- Turbulent flow of viscous nonNewtonian fluids in smooth pipes, noting effects of viscous stresses
09 p1481 A69-21929
- Approximate solution method for Navier-Stokes equations for incompressible viscous fluids
10 p1718 A69-22861
- Viscous fluids rotational flow in cylindrically symmetrical vessels, circumventing Navier-Stokes equations of motion by Wedemeyer approximation
10 p1677 A69-22896
- Rotating disk induced viscous conducting fluid motion in axial magnetic field
10 p1727 A69-23099
- Short memory elasticoviscous fluid motion in and around oscillating spherical shell
10 p1800 A69-23240
- Dynamics of turbulent motion of incompressible viscous fluid particles, using Lagrangian functions
11 p1867 A69-24536
- Second approximation of asymptotic damping of disturbances in viscous heat conducting gas supersonic flow about solid of revolution at critical velocity
11 p1817 A69-24627
- Steady flow of viscous incompressible fluid studied with system of equations equivalent to Navier-Stokes equations and finite difference method
11 p1875 A69-25480
- Steady flow field for viscous incompressible fluid in rotating pipe with porous walls determined from Navier-Stokes equations
11 p1875 A69-25481
- Solid body motions containing cavity filled with viscous fluid under influence of gravity, formulating motion equations for fluid and body
12 p2061 A69-25884
- Electrohydrodynamic instability of incompressible conducting cylindrical viscous jet in external magnetic field, noting viscosity role in oscillation modes and growth rate
12 p2136 A69-26403
- Absolute viscosity measurements from translational undamped oscillations of plate in liquid, considering viscosimeter walls effect
12 p2182 A69-26658
- Navier-Stokes equations of slow viscous fluid laminar flow near pipe inlet and exit with negligible mass forces, discussing velocity and pressure distribution
13 p2244 A69-27258
- Allowable thermodynamic processes and constitutive equation restrictions determined by Clausius-Duhem inequality, noting applications to plasticity theory and linear viscous fluids
13 p2371 A69-27319
- Viscous incompressible fluid self similar mixing problems, performing group analysis for complete boundary value problem
14 p2428 A69-28803
- Intense transverse resonant acoustic field interaction with viscous fluid flows [ASME PAPER 68-WA/FE-8]
14 p2430 A69-29444
- Unsteady jet viscous fluid flow under pulse variations based on Prandtl equations, showing turbulent motion analogy
14 p2432 A69-29608
- Incompressible viscous fluid steady motion caused by rotating ellipsoid, determining drag moments for circular disk and sphere
14 p2432 A69-29627

Parametric resonance motion in viscous fluid column in communicating vessels during vertical oscillations, calculating critical accelerations over viscosity range
14 p2432 A69-29628

Kinetic energy conversion into heat in moving viscous media, formulating equations as volume integrals of spherical harmonics products
14 p2487 A69-29980

Gas visco seals performance analysis for continuum flow regime, noting coefficient agreement with laminar flow analysis
[ASLE FICFS PREPRINT 34]
15 p2621 A69-30494

Stagnation flow of viscous fluid against rotating magnetized disk, determining effects on magnetic and velocity fields, currents and shear stresses
15 p2659 A69-30674

Weakly damped transverse and thermal waves development and propagation in viscous heat conducting incompressible fluid under temperature and gravitational fields
15 p2718 A69-31168

Entrainment of viscous electrically conducting liquid in long duct with narrow rectangular cross section and movable walls in magnetic induction field
16 p2816 A69-31606

Exact solution for motion of conducting solid of revolution rotating in infinite conducting viscous fluid, describing magnetic field
16 p2817 A69-31666

Three dimensional laminar jet mixing of incompressible viscous fluid from rectangular cross section nozzle into uniform stream
16 p2768 A69-31687

Asymptotic behavior of one dimensional laminar flow of incompressible viscous fluid in infinite cylindrical tube, giving equations for boundary conditions and flow rate
16 p2769 A69-31831

Cylindrical viscous jet transition points from stable to unstable modes of oscillation found same as for viscous jet
16 p2773 A69-32570

Vortex diffusion in viscous compressible fluid approximated by linear differential equations
17 p2957 A69-33714

Periodic solution of boundary value problem involving motion equation of viscous fluid
18 p3123 A69-35053

Angular velocity torsional oscillations of solid sphere under elastic force couple rotating in viscous liquid bounded by immobile concentric sphere
18 p3175 A69-35320

Laminar flow of viscous compressible fluid with density dependent on temperature, calculating steady state Navier-Stokes equations using vector function
19 p3297 A69-35852

Hydrodynamic equations of laminar plane flow of incompressible viscous fluid in rectangular region, calculating velocity field by equivalent network and integration
19 p3297 A69-35853

Viscous fluid secondary flow stability between coaxial rotating cylinders, using nonlinear differential equations derived from equations of motion
19 p3299 A69-36391

Monograph on motion of solid body with cavities containing viscous liquid, covering kinetics involving completely or partly filled fluids
20 p3578 A69-38200

Viscous incompressible nonNewtonian fluids flow with treatment for steady rotational problems and oscillatory motion, considering primary and secondary motions
20 p3519 A69-38319

Momentum and energy equations for fluctuating flow of viscous incompressible conducting fluid past flat plate with time dependent suction under transverse magnetic field
21 p3691 A69-38445

Constitutive equations for homogeneous viscous fluid and Kelvin-Voigt viscoelastic solid in electromagnetic field, using linear irreversible thermodynamics and continuum mechanics
21 p3851 A69-39289

Spheres impulsive starting in incompressible viscous fluid, including Reynolds number and investigation time parameters in Navier-Stokes equation
21 p3696 A69-39296

Nonlinear differential equations for flow of viscous liquid thin sheet on horizontal plane, solving initial value problems for zero slope bed
21 p3697 A69-39680

Motion of body with cavity completely filled with viscous fluid about center of mass in potential mass-force field, applying small parameter method
22 p3980 A69-40109

Oscillations of highly viscous incompressible fluid in partially filled cavity of body moving about fixed point, solving Navier-Stokes equations by asymptotic method
22 p3929 A69-40111

Homogeneous, viscous and electrically conducting fluid bounded at one end by infinite plane surface of rigid body vibrating relative to fluid body
22 p3991 A69-41036

Mixed boundary value problem for system of Navier-Stokes equations for viscous incompressible fluid in stationary motion in vessel, noting rotating fluid
23 p4183 A69-41974

Parallel magnetic field effect on free boundary layer type flows stability of low Reynolds number between parallel streams of viscous incompressible conducting fluid
24 p4298 A69-42596

MHD flow of incompressible viscous fluid between rotating electrical insulator disks
24 p4354 A69-42599

Stokes stream function and forces acting on two spheres moving in contact along line of centers through viscous fluid
24 p4299 A69-42747

Dynamic pressure response of viscous compressible fluids in rigid tubes with dead ended volume termination, testing Ibrall theorem as function of Stokes number
24 p4301 A69-43287

Turbulence and laminarity effect on vertical waves development rising in thin layer of heavy viscous fluid in contact with vertical gas flow
24 p4302 A69-43480

Energy dissipation in oscillating sphere filled with viscous fluid, giving fluid response by solving Navier-Stokes equation
24 p4305 A69-43587

VISIBILITY

NT LOW VISIBILITY

All-weather landing factors for aircraft and pilots, describing instrument landing system, runway and visibility, pilot and crew procedures, etc
01 p0112 A69-10454

Visibility improvement in warm fog by seeding with micron size hygroscopic particles, noting results for NaCl
01 p0111 A69-10696

Atmospheric influence on ground visibility reduction of airborne objects, using radiative transfer equation to calculate contrast transmission function
01 p0111 A69-11100

Evaporation rate measurements in fog during carbon dioxide laser radiation, obtaining correlation to describe visibility improvement
02 p0258 A69-12622

Aerosol size distribution and variation with humidity effects on visual range, comparing computations with transmissometer and scattering recorder measurements
02 p0276 A69-12760

Shipboard standard visibility measurements by means of AEG-FFM scattered light recorder aboard Meteor in Atlantic Ocean during 1965
04 p0628 A69-15158

Instrument for measuring light transmission in atmosphere to determine runway visual range
07 p1132 A69-18673

Atmospheric turbidity and visibility measuring instrument /videograph/ using light backscattering, noting shipboard, coast guard service, large cities and weather stations applications
08 p1314 A69-20376

Atmospheric effects on laser beam attenuation, noting application to optical visibility measurement by ruby laser
08 p1327 A69-21089

Visual observation of aerospacecraft, discussing object luminance, eye contrast sensitivity, atmospheric contrast transmission function and psychophysiological and atmospheric effects
10 p1649 A69-23872

Incident integral light flux relations and visibility range equation derived for objects illuminated by narrow light beams in scattering media
10 p1725 A69-23971

High intensity light adaptation effects on visibility of raster scan, TV type and avionic displays for symbol luminance needs
16 p2746 A69-32788

Star motion perturbations by invisible body, stressing bright bodies invisible by position near perturbed star
17 p3034 A69-33407

Visibility changes in fog at London airport determined by transmissometer records
18 p3167 A69-35262

Visibility degree of noctilucous cloud determined from ratio of brightness contrast against sky to eye contrast threshold
19 p3362 A69-36411

Incident integral light flux relations and visibility range equation derived for objects illuminated by narrow light beams in scattering media
21 p3772 A69-39677

VISIBLE RADIATION

U LIGHT [VISIBLE RADIATION]

VISIBLE SPECTRUM

U LIGHT [VISIBLE RADIATION]

U SPECTRA

VISION

NT BINOCULAR VISION

NT COLOR VISION

NT MONOCULAR VISION

NT NIGHT VISION

NT STEREOSCOPIC VISION

Visual factors of laser displays providing human factors recommendation for several visual variables
05 p0760 A69-15591

High oxygen concentration influence at normal pressure on evoked potential of cortical optic zone and sub-cortical zones
05 p0709 A69-16515

Climatic factors affecting pilot vision and contributing to misjudgement during landing procedures, noting effect of downward slope in runway approach
06 p0884 A69-18036

High oxygen concentration influence at normal pressure on evoked potential of cortical optic zone and sub-cortical zones
18 p3096 A69-34734

Human optical system as remote sensor consisting of transducing, data transmission and processing subsystems, defining perception function and describing visual aids
20 p3483 A69-37745

Luminance additivity for human visual system in terms of photometric methods based on direct brightness matching, incremental threshold, etc
22 p3880 A69-40849

Human vision mathematical simulation, relating optical input signal parameters to corresponding visual impression
23 p4109 A69-41978

Human hearing and vision mathematical simulation, relating signal perception parameters to corresponding adaptation processes
23 p4109 A69-41979

Dynamic reactions of mathematical model representing vision and hearing process adaptation
23 p4110 A69-41984

Mathematical model construction to simulate light adaptation in human vision based on Maxwell disk experimental results
23 p4110 A69-41985

VISIOPLASTICITY

U FLOW VISUALIZATION

U PLASTIC FLOW

VISUAL ACUITY

Ophthalmic 2 percent pilocarpine effect on normal ocular dynamics of various age groups, including visual acuity, accommodation and refraction
01 p0022 A69-11347

Human acceleration tolerance under reduced pressures corresponding to various high altitudes, noting visual disorders
07 p1065 A69-18982

Minimal angle of resolution /MAR/ between point and extended circular source and between point source and simulated horizon, studying irradiation effects on manual navigation
07 p1177 A69-19208

Coincidence error between star image and planet edge for entrance pupil and telescope magnification
08 p1314 A69-20383

Real time 2000 line TV camera with 40 MHz bandwidth, 1600 line vertical resolution and 1000 line horizontal resolution
[SMPT PAPER 105-73]
12 p2077 A69-25769

Human acceleration tolerance under reduced pressures corresponding to various high altitudes noting visual disorders
20 p3480 A69-38230

Grating size effect on threshold of grating pattern for various colors of illumination and target orientations
22 p3879 A69-40840

Retinal eccentricity effects on horizontal-vertical illusion magnitude, considering eye flattening and astigmatic properties

24 p4263 A69-43117

Pilots myopia incidence statistical study after initiate medical examination, emphasizing skiagram value in prognosis

24 p4267 A69-43400

VISUAL AIDS

Low cost pilot proximity warning instrument, discussing design influences of Xe strobe lights, atmospheric radiation transmission characteristics and detection considerations

17 p2917 A69-34103

Optical instruments as visual aids in scientific research including electron optical image converters detecting emissions invisible to human eye

22 p3943 A69-39974

VISUAL CONTROL

Electrooculographic method to study eye movements control system for fixation on stationary point or following discretely or continuously moving target

09 p1447 A69-22675

Visual simulation for critical maneuvers of aircraft takeoff and landing, noting method based on limited corridor simulation and maneuver freedom

[AIAA PAPER 68-255] 11 p1866 A69-25376

VISUAL DISCRIMINATION

Visual distortion in discrimination of figure proportion

06 p0875 A69-18022

Reading and reliability efficiency comparison in round vs vertical aircraft displays

06 p0883 A69-18025

Visual systems of hamster brain, discussing relative visual localization and discrimination blindness produced by ablation of cortical or tectal areas

08 p1265 A69-20685

Dark adaptation mechanisms studied from light intensity recovery after experimental flash, using electroretinography methods

10 p1647 A69-23588

Distance discrimination in simulated space environment, studying just noticeable difference /JND/ to determine relations between distance threshold and observation distance

12 p2022 A69-26372

Aircraft canopy scratches effects on pilot visual discrimination

13 p2214 A69-28533

Apparent movement in peripheral vision induced by sequential flashing of spatially unresolved two dots, studying dynamics of illusion

16 p2746 A69-31556

Digital simulation of biological model for visual images classification derived from human visual system aspects

17 p2911 A69-34094

Multilayer retina model with lateral couplings for visual pattern recognition, noting applications to data processing

19 p3260 A69-35898

Visibility degree of noctilucent cloud determined from ratio of brightness contrast against sky to eye contrast threshold

19 p3362 A69-36410

Visual succession threshold for sides of square contour affected by presenting single line on parallel contour sides

22 p3882 A69-40868

Laser granularity effects on brightness discrimination [AAS PAPER 69-464]

24 p4272 A69-42843

Head movement affecting visual and kinesthetic localization accuracy, discussing free and fixed head conditions

24 p4275 A69-43118

VISUAL DISPLAYS

U DISPLAY DEVICES

VISUAL FIELDS

Error correction for correlation coefficient between satellite data of earth radiation intensity and satellite vision field shift

14 p2435 A69-29043

Multiple reference sources to improve field of view of lensless Fourier transform holography limitation due to modulation transfer function of film and turbulence

17 p2971 A69-32920

Depth distortions in binocular visual fields from misleading size cues

21 p3653 A69-38900

Band movement phenomenon model for temporal and spatial interactions

22 p3880 A69-40854

Visual field meridians in circumstriate visual cortex of monkey determined by tracing degenerating axons stained by Nauta method

22 p3881 A69-40858

Visual stimuli initiating horizontal eye vergence movement in human subjects, noting cerebral conditions for convergence

22 p3881 A69-40859

Device for studying stereoscopic field of vision applied to determining field of vision standards for healthy individuals

22 p3886 A69-41113

VISUAL FLIGHT

Alpha numerical and symbolic information combined for head up display /HUD/ systems, providing pilot with takeoff director

03 p0379 A69-12885

Visual simulation for critical maneuvers of aircraft takeoff and landing, noting method based on limited corridor simulation and maneuver freedom [AIAA PAPER 68-255]

11 p1866 A69-25376

Air traffic control, discussing objectives, governmental responsibilities and airspace organization, including U.S. system

18 p3170 A69-34859

VISUAL OBSERVATION

Observation of satellites, orbit calculation and use in upper atmosphere research [UN PAPER 68-95789]

01 p0064 A69-10459

Optical spacecraft tracking organization in U.S.S.R., describing network of visual observation and photographic stations for satellite and space probe tracking

01 p0032 A69-10952

Visual sonar target detectability probability function of retinal position and brightness contrast

02 p0203 A69-12218

Acoustoelectric domains in CdS, making time evolution visible by means of modified optical strain birefringence and stroboscopic illumination

02 p0258 A69-12618

Aircraft high level cloud data to estimate vertical distribution of cirriform clouds and tropical tropopause levels on airline routes

03 p0458 A69-13032

Diurnal variations of visual meteoric activity mean hourly rates compared with earlier observations

04 p0658 A69-14879

Jupiter Red Spot visual observations in 1966 and 1967 noting changes in size, color and planetographic coordinates and variation of apparent intensity

04 p0659 A69-14963

Visual observations data on noctilucent clouds /1963-1967/

04 p0595 A69-15307

Sunspot group classifications made at Zurich and Catania during 19th solar cycle compared to determine seeing influence

05 p0826 A69-16388

Luminous particles in space observed by Vostok, Mercury and Voskhod astronauts, discussing distribution, trajectories and terrestrial origin

07 p1222 A69-19617

Ballistics room of Royal Belgian Observatory for observation of geodetic satellites

08 p1272 A69-19993

Reflection interferometry for visual evidence of surface deformation of rock and metal samples using two beam Fizeau fringe system

09 p1496 A69-22012

Binary eclipsing visual star systems angular momenta, discussing evolution

10 p1777 A69-23313

Visual observation of aerospacecraft, discussing object luminance, eye contrast sensitivity, atmospheric contrast transmission function and psychophysiological and atmospheric effects

10 p1649 A69-23872

Green flash photographed at sunset by aircraft at 10.6 km over Pacific, noting correspondence with visual observation

12 p2066 A69-26232

Satellite celestial equator intersection time calculation from visual satellite observation near equator including satellite draconic period determination, particularly for high altitude

12 p2069 A69-26438

Cosmos 17 and 44 draconic periods of rotation, discussing period variations determination from visual observations

12 p2173 A69-26439

Draconic period changes of satellite 1965-11-D /Cosmos 54 rocket/ during visual observations with Interobs

12 p2174 A69-26444

Visual observation of surface vibration nodal patterns by incoherent light illumination of object, noting holography

12 p2099 A69-27176

Visual and photographic observations of Perseids meteor trails velocity noting discrepancy

13 p2353 A69-28035

Visual, photographic and spectral observations of comets during IQSY, discussing comets Tomita-herber-Honda 1964c and Ikeya-Seki 1965f

14 p2525 A69-29716

Visual orientation near moon and at surface, considering terrestrial and lunar objects reflectivity and light reflection at various angles of incidence

14 p2525 A69-29750

Apollo 8 photooptics, considering TV camera and broadcasts, photographic equipment and visual observation

15 p2609 A69-30469

Visual ashen light observation on Venus possibly attributable to solar particle bombardment from dark side emission detection by spectroscopic and photometric studies

16 p2861 A69-32300

Lunar rotation parameters determined from photographs and visual observations independent of moon profile

17 p3027 A69-32874

Visual observation of pipe wall regions in turbulent flow by suspending colloidal size particles and photographing with high speed motion picture camera

17 p2956 A69-33598

Selection effects on comets discovery, comparing effectiveness of photographic and visual observation techniques

17 p3045 A69-34221

Spectral reflectances of objects and vegetative backgrounds to generate color photographic technique increasing detection sensitivity and rate

18 p3133 A69-34247

Jupiter Red Spot visual observations in 1966 and 1967 noting changes in size, color and planetographic coordinates and variation of apparent intensity

18 p3197 A69-34726

Umbral chromosphere flashes visual and photometric observations at 5 sec intervals on K line filtergrams using Halle filter

18 p3204 A69-35390

Heated body cooling off study via temperature field isothermal lines visualization on TV screen

20 p3539 A69-37437

Vibrating surface relative phases visual observation by introducing small rotation between exposures of stroboscopic hologram

20 p3546 A69-38123

Laser shadowgraph technique for visual observation of projectiles surface flying at hypersonic velocity along ballistic trajectory

22 p3963 A69-40601

After image measuring method of eccentric fixation during autokinetic light tracking

22 p3878 A69-40837

Human visual response to moving spatially periodic patterns, analyzing critical frequencies, dependence on stimulus area and period, phase blindness and pattern reversal

22 p3880 A69-40850

Visual observation of meteor and train microstructure obtained by refractor

22 p4033 A69-41058

Human observers visual monitoring of multiple meter display differentially controlled by concurrent signal scheduling

23 p4081 A69-41438

VISUAL PERCEPTION

NT AUTOKINESIS

NT CRITICAL FLICKER FUSION

NT SPACE PERCEPTION

Holographic theory of visual memory behavior, discussing human tests in situation of prompted visual recall

01 p0083 A69-10985

Validation study of pilots visual sampling behavior, using queueing model based on instrument and eye movement data from Link trainer mission flights

02 p0202 A69-11954

High oxygen concentration breathing effect on foveal thresholds, using sea level tests on trained observers

02 p0203 A69-12216

Temporal pattern perception by human subjects required to integrate information presented in two modalities

02 p0200 A69-12724

Human visual systems ability to encode retinal images produced by different size objects
03 p0369 A69-13359

Aircraft instrument panel lighting, comparing red and white colors for general and peripheral vision
05 p0715 A69-16623

Individual differences and relation to Witkin concept of perceptual style in target identification in aerial photographs
06 p0880 A69-17211

Stereoscopy effects on pattern recognition in visual noise
06 p0880 A69-17214

Detection time to light point source noting response to dark, star field and glare source backgrounds
06 p0881 A69-17215

Visual feedback mechanisms in simulated high altitude conditions, discussing physiology of ocular homeostasis adaptation
06 p0882 A69-17647

Classical and differential eyelid conditioning for truth or falsity of visually presented verbal statements
07 p1064 A69-18632

Group observers magnitude estimation judgements of stationary spacecraft model apparent distance in simulated space, obtaining psychophysical functions for three stimulus ranges
07 p1069 A69-19501

Electrooculographic method to study eye movements control system for fixation on stationary point or following discretely or continuously moving target
09 p1447 A69-22675

Stimuli human subjects can identify on unidimensional visual stimulus continuum, discussing apparatus and line length influence
10 p1641 A69-23039

Visual observation of aerospacecraft, discussing object luminance, eye contrast sensitivity, atmospheric contrast transmission function and psychophysiological and atmospheric effects
10 p1649 A69-23872

Photography role in experimental research with applications to flight analysis and comparison with human visual accuracy
11 p1881 A69-24573

Witkin Rod and Frame Testing of pilots and engineers showing greater field independence in pilots, discussing applications to pilot instructor selection
12 p2023 A69-26556

Visual orientation near moon and at surface, considering terrestrial and lunar objects reflectivity and light reflection at various angles of incidence
14 p2525 A69-29750

Apparent movement in peripheral vision induced by sequential flashing of spatially unresolved two dots, studying dynamics of illusion
16 p2746 A69-31556

Visual perception of three dimensional objects under simulated solar illumination in space considered in relation to manned spaceflight maneuvers
17 p2913 A69-33174

Cortical auditory-evoked response during eye movement in cats, discussing relation to central mechanism
17 p2911 A69-34171

Transient electrical responses from retinas, discussing visual pigment role in visual excitation, photochemistry, etc
19 p3258 A69-36377

Luminescence effects on apparent size and shape of foveally fixated targets of various forms
19 p3259 A69-36458

Astronaut vestibular and motor analyzer functions during flight and simulation tests, discussing illusory space orientation and role of cortical dynamics
20 p3469 A69-37241

Sensorimotor coordination of man performing graphic assignments in upright, reclining and prone position, discussing interaction of vestibular, visual and motor analyzers
20 p3470 A69-37246

Motor and tonic reactions in animals during weightlessness, discussing interaction between gravity receptors and visual analyzer
20 p3470 A69-37247

Visual and vestibular analyzers interrelation in subjects receiving light pulses before and after rotation, noting role of cortical elements
20 p3470 A69-37249

Human optical system as remote sensor consisting of transducing, data transmission and processing subsystems, defining perception function and describing visual aids
20 p3483 A69-37745

Psychology and physiology of vision in relation to large screen display design, discussing effects of symbol size and spacing, color usage, etc
21 p3662 A69-38330

Model for lateral inhibitory interaction in human retina, providing systematic account of simultaneous brightness contrast
21 p3653 A69-38898

Depth distortions in binocular visual fields from misleading size cues
21 p3653 A69-38900

Visual long term storage capability demonstration, describing negative aftereffect of motion perceived after fixation of moving spiral pattern
21 p3661 A69-39332

Visual retroactive perceptual masking effect in monkeys pretrained in visual discrimination task, interpreting electrical potentials recorded along optic pathways
22 p3876 A69-40265

Responsiveness of cortex and visual pathway during transient hypotension induced by increased gravitational stress, discussing intraocular pressure of cat
22 p3878 A69-40779

Zoellner illusion in human visual system measured as function of background pattern density consisting of intersect angles and background line spacing
22 p3879 A69-40841

Visual suppression association with smooth following and saccadic eye movements in tracking slow moving target
22 p3879 A69-40842

Psychopharmacological drug effect on visually evoked responses in cats from recordings from visual cortex, noting latencies increase with dose
22 p3879 A69-40847

Flicker characteristics of eye color receptive systems by measuring modulation thresholds for sinusoidal flicker of color superimposed on complementary color background
22 p3880 A69-40851

Brightness of fixated element in visual field as function of element luminance
22 p3880 A69-40853

Saccadic eye movements comparison during fixation and reading by contact lens optical lever technique
22 p3880 A69-40855

Horizontal tracking eye movements response to unpredictable constant velocity target motions with or without saccadic position corrections recorded by contact lens optical lever
22 p3881 A69-40856

Linear models with self excitation for brightness and contrast perception studies in human visual system
22 p3881 A69-40862

Tritanope and trichromat experiments for parafoveal visual response of tritanope, measuring spectral sensitivity and absolute threshold values
22 p3882 A69-40869

Human peripheral retina contrast sensitivity determined by measuring psychophysically for sinusoidal grating target describing luminance effects
22 p3882 A69-40870

Hue shift and brightness enhancement of flickering light measured as function of illuminance, wavelength and target size
22 p3882 A69-40871

Retinal topography relation to blue arcs phenomenon, assessing disparity in photoreceptor location and associated neurones for analysis of critically sited plots
22 p3882 A69-40872

Comparative study of differential luminance threshold and spatial summation exponent for solid and annular objects with equal surfaces
22 p3883 A69-40877

Retinal mechanisms determining visual band movement thresholds obtained by manipulation of retinal locus, luminance, arc length and spectral distribution of moving stimulus
22 p3883 A69-40879

Blue cone mechanism contribution to mesopic function in producing Purkinje shift with luminance decrease, measuring sensitivity by flicker technique
22 p3883 A69-40880

Response characteristics of human visual mechanisms sensitive to motion while varying adaptation stimulus contrast to control visual effectiveness
22 p3884 A69-40887

Physiological experiments to investigate aerospace flight stresses effects on oculomotor equilibrium, noting cardiovascular reaction and mechanism for interpretation
23 p4087 A69-41804

Contact lenses hazards during high altitude aircraft piloting analyzed via bubble development
23 p4106 A69-41806

Senior commercial jet pilots ability to visualize flight instruments
23 p4089 A69-41829

Point images reference groups identification by human operator with limited visual perception in background noise, comparing results with automatic system using selection algorithms
23 p4109 A69-41955

Visual ellipse phenomena excitation by sinusoidal stimulating currents, noting frequency effects on ellipse shape
23 p4095 A69-42077

Combined eye and ear identification of bimodally presented signals in noise over oscilloscope and earphones, noting significance of independent observers model
23 p4111 A69-42168

Electroretinogram and visually evoked cortical potential as response potentials in human visual system
24 p4271 A69-42644

Interpolated position and orientation perception by vision and active touch
24 p4275 A69-43116

M-1 Valsalva maneuver induced cardiovascular stresses effect on oculobulbar vergence of subjects observing Thorington scale, discussing probable physiological mechanisms
24 p4266 A69-43373

Skiagrams results of retinoscopic measurements of eye peripheral refraction of pilots, attempting correlation between skiagram type and central refraction
24 p4267 A69-43399

VISUAL PHOTOMETRY

Wavelength dependence of polarization and UVRI photometry of highly polarized stars, correlating IR interstellar extinction with maximum polarization wavelength
12 p2153 A69-25809

Seyfert galaxy NGC 4151 electrophotometric investigation in UV, confirming nucleus optical variability observed in visible and IR
15 p2686 A69-30536

Response color curves of U, B, V photometric system compatible for stellar observation, including U revision
15 p2689 A69-30562

Photometric calibration correction for B-V and U-B colors taking into account hydrogen line blocking
15 p2694 A69-30786

Photometer for simultaneous stellar photometry in UVB bands, purposes and performance characteristics and circuit diagrams
16 p2790 A69-32209

Photoelectric observations in B and V colors of binary system S Equ
16 p2858 A69-32212

Photoelectric visible radiation observations of binary star AH Vir
16 p2858 A69-32215

UBV photometry of southern quasars, radio galaxies and normal galaxies including two color diagrams, radio luminosity, brightness and color distribution
16 p2859 A69-32228

Epsilon CrA light and color curves analyzed from UVB photoelectric photometry observations
16 p2863 A69-32398

Nova Delphini 1967 /HR Del/ observations in UPX-YZV photometric system, tabulating color indices
19 p3426 A69-36564

Visible and IR spectral reflectivity of Apollo lunar landing sites, attributing reflectivity differences to compositional and/or mineralogical differences
21 p3815 A69-39586

VISUAL SIGNALS

Hand operated visual signaling devices, discussing Mini Signals and cartridge load aerial signals
06 p0878 A69-16962

Human observers visual monitoring of multiple meter display differentially controlled by concurrent signal scheduling
23 p4081 A69-41438

Bisensory auditory and visual signals characteristics effects on human reaction time, noting different results for unilateral and bilateral signal pairs
23 p4083 A69-41454

VISUAL STIMULI

Cerebral cortical neurons response to visual stimuli during stationary and rapid eye movement
03 p0369 A69-13360

- Attenuation of visual vigilance decrement through visual stimulation combined with various sound conditions
06 p0880 A69-17213
- Classical and differential eyelid conditioning for truth or falsity of visually presented verbal statements
07 p1064 A69-18632
- Instrumental reward experiment using concept learning paradigm with word-color compounds as stimuli
07 p1064 A69-18636
- Classical and differential conditioning of eyelid response with correctness of solutions of arithmetic problems as discriminandum
07 p1064 A69-18637
- Stimuli human subjects can identify on unidimensional visual stimulus continuum, discussing apparatus and line length influence
10 p1641 A69-23039
- Response rates of rats to periodic shocking for food reinforcement with added clock cue stimuli
10 p1644 A69-23304
- Electrical response of frog and human visual cortex neurons to thermal vestibular and light flash stimulation
20 p3469 A69-37242
- Labyrinth polarization effect on stimulation and neuron activity in visual cortex of cats, using electroencephalograph
20 p3469 A69-37244
- Single flash and rhythmic light stimuli effect on nystagmus of patients with tumoral posterior cranial fossa, recorded electroencephalographically
20 p3470 A69-37250
- Motion sickness forms in human subjects subjected to induced rocking, noting impaired performance and sensorimotor reactions to visual stimuli
20 p3472 A69-37263
- EEG patterns evoked from left and right cerebral hemisphere by visual and verbal stimuli, showing asymmetrical role of hemispheres in governing cognitive behavior
21 p3656 A69-38976
- Brain weight and cholesterolase activity in rats after exposures to acoustic and light stimuli
21 p3662 A69-39627
- Rhesus monkeys visual responses recorded before and after unilateral striate lesions, optic tract section and inferotemporal lesions
22 p3876 A69-40263
- Local electroretinogram responses produced in cats by light intensity incremental changes
22 p3878 A69-40835
- Visual backward masking experiment for studying overlapping and nonoverlapping contours of target and masking stimuli straight line
22 p3879 A69-40843
- Neuronal organization of initial afferent inflow in thalamic visual center /lateral geniculate body /LGB/ of unanesthetized cats/, noting unit activity
22 p3879 A69-40845
- Human visual response to moving spatially periodic patterns, analyzing critical frequencies, dependence on stimulus area and period, phase blindness and pattern reversal
22 p3880 A69-40850
- Luminance threshold for compound stimulus detection measured as function of two components relative luminance
22 p3880 A69-40852
- Brightness of fixated element in visual field as function of element luminance
22 p3880 A69-40853
- Band movement phenomenon model for temporal and spatial interactions
22 p3880 A69-40854
- Visual stimuli initiating horizontal eye vergence movement in human subjects, noting cerebral conditions for convergence
22 p3881 A69-40859
- Psychophysical threshold changes during subliminal monocular and interocular stimulation, studying conditioning flash size effects on temporal summation
22 p3881 A69-40860
- Nocturnal and diurnal monkeys spectral sensitivity functions determined from simultaneous recordings of light-evoked cortical and retinal responses
22 p3882 A69-40867
- Angular velocity of visual stimulus effect on human torsional eye movements using sectored disks
22 p3883 A69-40874
- Spatial interactions and thresholds in identification and detection of compound visual stimuli
22 p3883 A69-40878
- Retinal mechanisms determining visual band movement thresholds obtained by manipulation of retinal locus, luminance, arc length and spectral distribution of moving stimulus
22 p3883 A69-40879
- Cat intraretinal DC component and b-wave separation based on sensitivity to visual stimuli, discussing electroretinogram recorded with microelectrodes
22 p3883 A69-40881
- Human electroretinogram /ERG/ physiological variations as function of stimulation energy and wavelength
22 p3884 A69-40884
- Topographic distribution of cortical potentials produced with tachistoscope and by stroboscopic stimulation, studying occipital and frontal differences
22 p3884 A69-40885
- Response characteristics of human visual mechanisms sensitive to motion while varying adaptation stimulus contrast to control visual effectiveness
22 p3884 A69-40887
- Human response to visual beat phenomena by combining intermittent stimuli, considering brightness estimation
22 p3884 A69-40889
- Pigeon accelerated performance patterns as function of contiguity of brief visual stimuli and food reinforcement, noting pattern absence during stimuli omission
23 p4081 A69-41436
- Visual ellipse phenomena excitation by sinusoidal stimulating currents, noting frequency effects on ellipse shape
23 p4095 A69-42077
- Attention shifts in maintained discrimination, discussing combined responses of varying and constant visual and auditory stimuli in pigeons
24 p4275 A69-43198
- Circadian periodicity of human reaction times tested during normal diurnal cycles and 24 hour wakefulness, noting acoustic and visual stimuli effects on learning
24 p4267 A69-43387
- VISUAL TASKS**
- Human inspection performance in quality control operations to assess visual inspection tasks accuracy
03 p0433 A69-13386
- Attenuation of visual vigilance decrement through visual stimulation combined with various sound conditions
06 p0880 A69-17213
- Minimal angle of resolution /MAR/ between point and extended circular source and between point source and simulated horizon, studying irradiation effects on manual navigation
07 p1177 A69-19208
- Human information processing rates during one and two axis compensatory tracking tasks with secondary auditory task
10 p1650 A69-23880
- Lunar visual environment effects on astronaut control manipulation task performance, discussing solar illumination simulation facility
12 p2059 A69-26554
- Combined cueing and knowledge of results for transfer of training in visual monitoring
13 p2213 A69-28256
- Fast visual task performance indoors found dependent on sound pressure level
15 p2550 A69-30305
- Apparent movement in peripheral vision induced by sequential flashing of spatially unresolved two dots, studying dynamics of illusion
16 p2746 A69-31556
- Continuous and intermittent noise effects on audiovisual checking task performing subjects, considering omission errors
17 p2911 A69-34009
- Mental patient performance in detecting and identifying visual signals under fixed interval schedule, noting nonuniform performance and comparing to normal subjects
23 p4091 A69-42014
- Visual and tactual interaction in judgments of vertical in dark room experiments, discussing effects of various reference systems
24 p4271 A69-42752
- VISUAL TRACKING**
U OPTICAL TRACKING
- VISUALIZATION OF FLOW**
U FLOW VISUALIZATION
- VITAMIN B**
U THIAMINE
- VITAMIN B 06**
U PYRIDOXINE
- VITAMIN C**
U ASCORBIC ACID
- VITAMIN E**
U TOCOPHEROL
- VITAMINS**
U ASCORBIC ACID
U PYRIDOXINE
U THIAMINE
U TOCOPHEROL
- VITREOUS MATERIALS**
- Surface effects on mechanical properties of crystalline and vitreous materials, considering environmental effects on dislocation mobility
03 p0454 A69-13870
- Method for preparation of vitreous materials in hollow cylindrical form, considering chemical homogeneity, porosity and geometrical shape
12 p2101 A69-25936
- VLASOV EQUATIONS**
- One dimensional Vlasov plasma nonlinear response to external electric field varying in space and time
01 p0133 A69-11214
- Two dimensional equilibria for high beta mirror devices found by solving Vlasov equation and Ampere law, including particle loss
03 p0475 A69-13152
- MHD waves, Landau damping and magnetosonic waves in homogeneous relativistic Vlasov plasma
04 p0636 A69-15043
- Stationary solutions of Vlasov equation with external electric fields and BGK collision terms, using perturbation theory in moving frame
05 p0801 A69-15745
- Kinetic description of inhomogeneous plasma in ring approximation, discussing Vlasov equation and velocity distribution function
07 p1193 A69-19034
- Relativistically corrected Vlasov equation solved as approximate solution of exact relativistic equations of motion for low density media
10 p1724 A69-22924
- Stress analysis of reinforced cylindrical shells under external loading, using Vlasov semimomentless theory
11 p1982 A69-24949
- Normal mode representation of HF properties of inhomogeneous plasma, analyzing Vlasov equation for free oscillations under external driving field
11 p1929 A69-25269
- Laboratory models for solar wind and magnetosphere interactions with similarity laws of Vlasov theory as reference system
12 p2150 A69-26737
- Vlasov equations solved for electrons and ions in electromagnetic field, coupling electric field to density oscillation modes of plasma
13 p2306 A69-27461
- Beam-plasma interactions by nonlinear Vlasov equation, describing amplification of longitudinal waves
14 p2493 A69-29692
- Geomagnetic ring current study, giving exact kinetic description based on Vlasov equation of plasma ring current in dipolar field
15 p2598 A69-31218
- Vlasov-Poisson equations reformulation by arbitrary transformation to velocity variable, considering time or space secularity of perturbation theory
16 p2817 A69-31642
- Vlasov turbulence exact solutions, considering closure conditions, correlation length, Lundgren hierarchy, homogeneous turbulence, etc
17 p2958 A69-34229
- Vlasov thin shell theory extended for undamped bending, transforming partial differential equations and stress function into integral equation solvable by successive approximations
23 p4225 A69-41407
- Guiding center Vlasov equation derived dielectric tensor of collisionless plasma, obtaining dispersion relation of Alfvén waves in warm plasma
23 p4197 A69-42416
- VLF EMISSION RECORDERS**
- Antarctic VLF emissions observations at 12 kHz, showing dependence on geomagnetic disturbances, auroras and radio absorption in ionosphere
18 p3102 A69-34964
- Antarctic VLF emissions polarization and direction determination, using combination of antennas with planes lying in geomagnetic E-W and N-S directions
18 p3102 A69-34965
- Wideband vertical electric field noise reduction in ELF/VLF atmospheric receiving systems using bucking, delayed feedback and frequency rejection units
23 p4128 A69-42504

VOICE

Retarded voice tests apparatus using graphical recording to determine intensity of deformations by autoaudition, considering application to recruitment investigation

24 p4270 A69-42604

VOICE COMMUNICATION
NT TELEPHONY

Optimum modulation technique determination for single channel voice communication under severe noise conditions
[UN PAPER 68-95851]

01 p0029 A69-10526

Modems for high data transmission rates on available voice bandwidth channels, noting point to point and multipoint polled networks and signal to noise ratio

04 p0564 A69-15208

Recorded vocal reactions of humans analyzed as characteristic of positive and negative emotions

05 p0709 A69-16518

Hearing errors in voice communication with radio telephone, noting effects of mean syllable number and consonants per syllable in pilots and controllers

06 p0891 A69-18034

Time division multiple access satellite communication system employing pulse code modulation of voice channels and phase shift keying of RF carrier

07 p1077 A69-18759

Noise level criteria for acceptable voice communications in office environment, noting acclimatization

11 p1830 A69-24797

Digitally controlled formant/spectral maximum/generator for terminal analog speech synthesizer

11 p1852 A69-25292

Optimized receivers synthesized for narrow band radio signal filtration, comparing noise rejection properties of various pulse modulation types during speech transmission

14 p2413 A69-29464

He speech processor for aerospace applications, discussing He speech distortion nature

17 p2911 A69-34095

Machine recognition of continuous speech at acoustic level, analyzing low bit rate speech communication system

17 p2932 A69-34119

Recorded vocal reactions of humans analyzed as characteristic of positive and negative emotions

18 p3096 A69-34737

Transmission filter to improve voice communication intelligibility and SNR, describing applications to non-linear circuits

20 p3505 A69-37293

VOICE DATA PROCESSING

Man-computer speech communication, discussing model and aspects of acoustics, phonetics, linguistics, language training, physiology, psychology, bionics, etc

18 p3107 A69-35099

VOID RATIO

Powder properties effect on rolled strip thickness and compactness, angles, pressure at roll and torsion during rolling, analyzing Fe, Ni and Cu powders

15 p2630 A69-31183

Nondestructive tests for glass filament wound composites void content, considering test methods and mechanical properties prediction role

17 p2979 A69-33656

VOIDS

Substructural void formation in tungsten powder metallurgy as function of annealing temperature for doped, undoped and electron beam melted material

01 p0093 A69-10061

Generalized parametric form of IR radiometric scan method applied to void detection problems, designing test techniques and establishing inspection procedure

15 p2631 A69-31506

VOIGT EFFECT

Computer program to predict spectra from electronic transitions of diatomic molecules and atoms, noting line intensity distribution by Voigt profile

18 p3177 A69-35239

VOLATILITY

Propellants volatile fraction removal followed by gas chromatographical determination, noting use of heating method

02 p0302 A69-11522

Volatile liquid pressurization, discussing pressurants, heat sources and system design
[AIAA PAPER 68-630]

02 p0232 A69-12382

Gas chromatography based on sampling gas-vapor phase at liquid surface for determining volatile oxygen containing compounds in biological media

13 p2216 A69-28627

VOLATILIZATION
U VAPORIZINGVOLCANICS
U VOLCANOLOGY

VOLCANOLOGY

Seismic refraction study of internal structure of volcanic cinder cone

02 p0236 A69-11465

Volcanic gas from lava lake, noting carbon and sulfur gases depletion during cooling and solidification

02 p0236 A69-11466

Large scale lunar surface photographs for estimating conical formations identified with terrestrial stratovolcanoes

03 p0507 A69-13093

Lunar glowing spots near Aristarchus considered volcanic eruptions of molten material

04 p0657 A69-14676

Lead isotope composition and concentrations of U, Th, Ra, total Pb and Pb 210 in recent volcanic rocks, noting disequilibrium due to chemical fractionations

04 p0593 A69-15011

Volcanic origin of lunar crater Dawes based on photoeological evidence obtained from Lunar Orbiter 5 photographs

11 p1952 A69-24264

Airborne and satellite IR survey over active effusive eruption at Surtsey, Iceland, comparing thermal energy yield and radiant emission to ground measurements

12 p2076 A69-27011

Large scale lunar surface photographs for estimating conical formations identified with terrestrial stratovolcanoes

14 p2516 A69-28775

Lunar volcanism origin of tektite and pearlite, noting no cosmic ray effects

20 p3597 A69-37338

Orthopyroxenes cooling history, studying order-disorder transitions between ferrous iron and magnesium

20 p3523 A69-37518

Effusive volcanic eruptions recorded by high thermal sensitivity satellite-borne IR systems

21 p3721 A69-38631

Tectonic classification of earth gravitational field based on mean gravity anomalies, correlating positive anomalies with Quaternary volcanism

23 p4154 A69-41318

Undulating dunelike deposits of surface debris similar to base-surge deposits in maar volcanoes and tuff rings, discussing underground ice existence

23 p4216 A69-42203

VOLT-AMPERE CHARACTERISTICS

Electric arc properties, investigating volt-ampere characteristics by approximate similitude and dimensional analysis

01 p0125 A69-10099

Bilateral plasma outflow plasmatron with variable electrode diameter, discussing efficiency, current-voltage characteristics and size

01 p0125 A69-10102

Schmitt trigger current-voltage characteristic for determining switching behavior and switching point temperature, examining formulas and equivalent circuits

01 p0039 A69-10171

Probability characteristics of temperature and supply voltage dependent parameters of semiconductor equipment

01 p0047 A69-10783

Current/field characteristic of n-type GaAs, using high power microwave techniques in presence and absence of transverse magnetic field

01 p0139 A69-10819

Indium phosphide p-n junction current-voltage characteristics various temperatures, considering degree of doping effect

01 p0139 A69-10885

Penning discharge in inhomogeneous magnetic mirror field, observing high burning voltage at low current in rarefied hydrogen plasma

01 p0133 A69-11218

Spherical and cylindrical probes emitting electrons and ions in unbounded plasma, deriving I-V characteristics equations

02 p0247 A69-11569

Metallic dismountable thermionic converter enclosed in mica sealed vacuum chamber, giving I-V characteristics, optimal temperature of liquid cesium phase and output power

02 p0194 A69-11587

Germanium tunnel diode current-voltage characteristics, proposing expression for approximation of differential conductivity as function of voltage

02 p0214 A69-11613

Electrical conductivity of sintered polycrystalline cubic and monoclinic europium sesquioxide from DC

current-voltage characteristics obtained in air at various pressures

02 p0296 A69-11874

Temperature dependence of semiconductivity of sintered polycrystalline EuO from current-voltage characteristics, measuring activation energy

02 p0296 A69-11875

Current-voltage characteristics of avalanche transistors, noting impact ionization

02 p0218 A69-12266

Josephson voltage-frequency relation independence of superconductor nature, noting c/h value and importance to voltage standards and quantum electrodynamics

02 p0299 A69-12599

Tunnel diodes current voltage characteristics in crossed electric and magnetic fields, observing tunnel current decrease in GaSb

02 p0300 A69-12634

Dynamic current-voltage characteristics of thin film diodes on chalcogenide glass base

02 p0223 A69-12834

Diffusion in conduction process in dielectric fluids, discussing space charge limited current-voltage characteristics

03 p0415 A69-13140

Voltage variable resistor MOST, noting channel resistance controllability

04 p0574 A69-14351

Current and voltage dependence of negative differential resistance segment of current-voltage characteristic on nature of m-p contact in germanium p-n-p-m structures

04 p0642 A69-14793

Low temperature plasma electric arc source operation describing current voltage characteristics and potential distribution

05 p0802 A69-15902

Recombination radiation of tellurium and zinc doped GaAs alloy type diodes, discussing luminescence spectra, current-voltage characteristics and temperature effects

05 p0729 A69-16210

Circuit with tunnel diodes and transistors for nonlinear amplification, noting current-voltage characteristics dependence on circuit parameters

05 p0730 A69-16221

Statistical studies of current-voltage characteristics of zinc-doped silicon diodes

05 p0732 A69-16425

Insulated gate tetrode with high drain breakdown potential and low Miller feedback capacitance, noting V-I characteristics

05 p0733 A69-16556

Approximate functions for tunnel diode dynamic conductance in three voltage ranges and Fourier conductance terms for tunnel diode frequency converters

05 p0735 A69-16647

Diffused Si and GaAs diodes electroluminescence and current-voltage characteristics

06 p0893 A69-16898

Low voltage Knudsen arc in cesium argon mixture using tungsten electrodes, analyzing current voltage characteristics

06 p0963 A69-16920

Two section model of saturation drain conductance of MOS transistors

06 p0893 A69-17155

Solid state diodes made by pulsed laser irradiation of polished silicon surfaces, discussing application to integrated circuit design

06 p0893 A69-17157

Tunnel junctions of narrow gap GeTe and wide gap GaAs, noting current voltage characteristics similar to those in Schottky barrier

06 p0980 A69-17770

Current-voltage characteristic of tunnel diodes, with curve approximation by even degree polynomials of voltage, discussing quasi-linear analysis

06 p0898 A69-17802

Current and voltage waveforms of transit time, resonant domain and LSA modes of operation of transferred-electron oscillators

07 p1097 A69-18443

Microwave spectrum of n-InSb avalanche plasmas under magnetic field, considering dynamic current-voltage characteristics, hole wave instabilities and microwave emission processes

07 p1197 A69-18466

Substrate bias influence on AC characteristics of MOS transistors used in variable resistor region

07 p1102 A69-18860

Metal oxide semiconductor circuits with higher orders of complementarity for performing multiple elec-

- onic functions, noting I-V characteristics and effects of bias
07 p1104 A69-18887
- Diffusion current detection method applied to reverse biased volt-ampere characteristics of Ge diodes, noting surface leakage role
07 p1105 A69-19007
- Current and voltage distribution in electromagnet compressor channel with solid electrodes of finite resistance, noting error analysis
07 p1059 A69-19029
- Electron-electron interaction effect on I-V characteristic and equivalent circuit of metal-semiconductor contact, noting conductivity and rectifying properties
07 p1107 A69-19162
- Plasma heating dynamics by straight turbulent discharge current influenced by initial plasma parameters
07 p1195 A69-19592
- Properties of ion implanted GaAs diodes fabricated at room temperature, analyzing light emission, resistance and breakdown voltage
ECS PAPER 172] 08 p1284 A69-20369
- Spacecraft applications of Langmuir probes, obtaining data from current-voltage characteristics for electron/ion concentrations, ion mass spectra and charged particle energy distribution
08 p1316 A69-20474
- Semiconductor laser with isolated diodes in cavity, noting watt-ampere characteristics during nonuniform excitation and threshold curves
08 p1326 A69-20539
- Normalized thermionic field emission in metal semiconductor barriers for forward and reverse current-voltage relation
08 p1373 A69-20861
- SERT 2 mercury vapor fed hollow cathode operated in bell jar, determining volt-ampere characteristics and flow rates for plasma diagnostics
[AIAA PAPER 69-258] 09 p1561 A69-21221
- Dark and photocurrent volt-ampere characteristics induced by capture of carriers injected into illuminated CdS single crystals
09 p1555 A69-21506
- DC electrical resistance of magnetosphere between two satellites with sheaths and current voltage relation of satellite sheath
09 p1489 A69-21710
- Forward volt-ampere characteristics and differential resistance peak of Schottky barrier diode on doped Si
09 p1557 A69-21744
- Current controlled negative differential resistivity observed during current-voltage measurements made with p-type Te at 77 K
09 p1557 A69-21747
- Trapping state effect on tunneling probability in Schottky barriers, discussing current-voltage characteristics
09 p1557 A69-21748
- Current oscillations in seminsulating O and Cr doped GaAs samples at room temperature, noting photoconductivity excitation spectra
09 p1557 A69-21753
- Reproducibility of thermionic converters performance, comparing volt-ampere characteristics with reservoir and collector temperature
09 p1437 A69-21813
- Local axial voltage variation from one dimensional model applied to solve thermionic boundary conditions in two dimensional thermal analysis of converter
09 p1440 A69-21834
- Diffusion and minority carriers drift effect on current-voltage characteristics of p-n-p-n structure in high density current
10 p1742 A69-22997
- Probability characteristics of temperature and supply voltage dependent parameters of semiconductor equipment
10 p1661 A69-23112
- N enhancement silicon MOST saturation current as function of temperature
10 p1743 A69-23175
- Current voltage characteristics of p-n junctions in cadmium telluride, discussing spectral sensitivity bands
10 p1744 A69-23212
- Semiconductors with negative differential conductivity, investigating decreasing current-voltage characteristics, S or N shaped curves, perturbation parameters, instability, etc
10 p1744 A69-23300
- Three layer vacuum deposited silicon monoxide films current voltage and conduction current density temperature dependence
10 p1745 A69-23324
- Current-voltage characteristics of combustion driven shock tube generated argon plasma
10 p1737 A69-23466
- Current voltage characteristics in silicon carbide diodes having negative differential resistance
10 p1663 A69-23571
- Positive and negative sloped current-voltage characteristics of silicon tunnel diodes with p-n junctions
10 p1746 A69-23574
- Tunnel diode test circuit, measuring differential resistances and bias voltages on loss resistance and of socket capacitance
10 p1665 A69-24215
- Frequency retuning characteristics of oscillator employing avalanche transit-time diode with complementary varactor subject to current or voltage variation
11 p1844 A69-24449
- Germanium tunnel diode current-voltage characteristics, proposing expression for approximation of differential conductivity as function of voltage
11 p1847 A69-24721
- Calorimeter for IR carbon-dioxide laser output power measurement, noting range calibration and accuracy
11 p1885 A69-24903
- Forward and reverse current-voltage characteristics and reverse biased capacitance for nZnSe-pGe emitter base diodes of heterojunction transistors
11 p1851 A69-25114
- Emission and diffusion theories of metal-semiconductor contacts for describing current characteristics of abrupt isotype nGe-nGaAs heterojunction
11 p1938 A69-25115
- Porous cermet electrodes thermochemical protection by blowing neutral gas into electrode boundary layer, examining effect on volt-ampere characteristics
11 p1826 A69-25395
- Solar cell equation series resistance and junction recombination parameters determination, considering I-V characteristics
11 p1826 A69-25395
- Arc mode thermionic Cs converter nonlinear I-V characteristics explained by current-dependent temperature and potential fields in plasma
11 p1827 A69-25400
- Current increase and voltage decrease in high voltage low pressure Penning discharge ascribed to hollow cathode effect
11 p1933 A69-25544
- Current-voltage characteristics and ionization equilibrium of low voltage arc plasma in narrow gap of thermionic converter at high current density
11 p1933 A69-25554
- Voltage and current waveforms of resonant domain and limited space charge accumulation modes in transferred electron oscillators, noting drift current
12 p2036 A69-25908
- Rarefied Ar plasma flow current-voltage characteristics in discharge tube, noting plasma boundary layer thickness influence on saturation current
12 p2137 A69-26532
- Nanosecond time variations in current-voltage characteristics of gas discharge in air, taking into account discharge circuit resistance and discharge space capacitance
12 p2137 A69-26534
- Multielectrode probe performance in plasma diagnostics, considering effects of plasma pressure, probe geometry and space charge on current-voltage characteristics
12 p2138 A69-26539
- Bias circuit LF oscillations in short Gunn devices, analyzing sinusoidal and relaxation oscillations and stable bias in terms of terminal I-V characteristics
12 p2041 A69-26628
- Indium phosphide p-n junction current-voltage characteristics at various temperatures, considering degree of doping effect
12 p2144 A69-26649
- Soviet book on plasma thermionic energy conversion covering operation modes, transport processes, current-voltage characteristics, density, temperature, electric field distribution
12 p2017 A69-26850
- Harmonic generation, using nonlinear current-voltage characteristics of Gunn diodes at 9500 MHz frequency
13 p2226 A69-27235
- Liquid metal induction MHD generator I-V characteristics at no load permitting self excitation with capacitors
13 p2208 A69-27509
- Negative resistance formation in impurity compensated semiconductor diodes ascribed to injected carrier drift path increment with increasing current, deriving I-V characteristics
13 p2230 A69-27877
- High resistivity GaAs impedance with nonlinear I-V characteristics, showing appreciable reactive component
13 p2317 A69-27881
- Photoelectric characteristics of thin film CdS-CdTe heterojunction diodes, considering I-V illuminance, spectral characteristics and conduction band continuity
13 p2230 A69-27882
- Current oscillations in n-type gallium arsenide related to electroacoustic domains motions, noting oscillation period dependence on voltage
13 p2318 A69-27892
- High power voltage tunable magnetron, discussing operating characteristics, life and applications
13 p2232 A69-28056
- Electrical breakdown voltage and voltage-current characteristics of uncooled coplanar carbon electrodes in walls of supersonic conical and rectangular nozzles [AIAA PAPER 68-713] 13 p2249 A69-28231
- MOS unitor switching circuit operation subjected to nonlinear load, using analytic approximations of current-voltage characteristics
13 p2234 A69-28507
- Current-voltage characteristics for double injection processes in nonideal contact p-i-n semiconductors operating in ohmic relaxation mode
13 p2323 A69-28524
- Capture centers effect on current-voltage characteristic of p-i-n diodes during injection, noting negative resistance appearance
13 p2236 A69-28525
- Current-voltage characteristics of p-n-p-n diodes, discussing collector voltage effect on current carrier concentration distribution in diode base
13 p2236 A69-28531
- Two chamber DC arc heater with vortex stabilization, determining current-voltage characteristics and efficiency
13 p2244 A69-28557
- Electric field distribution in TWT electron beam deflection system determined, accounting for current-voltage characteristics dependence on electromagnetic field distribution
13 p2237 A69-28582
- I-V characteristics of electron emitting satellite in ionosphere, analyzing spherical Langmuir probe in collisionless plasma in magnetic field
14 p2511 A69-28956
- Weak superconducting contacts volt-ampere characteristics current steps and emission spectra, showing singularities due to superconducting current nonhomogeneity
14 p2504 A69-28994
- Low voltage arc in cesium thermionic converter, investigating current-voltage characteristics, electron temperature, electron density and plasma potentials in ignited mode
14 p2401 A69-29231
- Voltage drop of ignited mode related to current density in cesium diode, noting plasma zones
14 p2401 A69-29232
- Low voltage arc discharge characteristics in cesium vapor, considering energy balance, electron temperature, energy losses, volt-ampere characteristics, ignition, cathode temperatures, etc
14 p2401 A69-29234
- Thermionic converter current-voltage characteristics under various emitter temperatures and cesium vapor pressures, noting role of Schottky effect
14 p2402 A69-29241
- Rare gases effect on thermionic converters volt-ampere characteristics, noting gas pressure, oxygen contamination and performance relations
14 p2403 A69-29251
- Preignition volt-ampere curves for thermionic cesium diodes exhibiting nonsaturation characteristics under low temperature and electron-rich emission conditions
14 p2403 A69-29253
- Spectral lines emitted from low voltage discharge in cesium filled diode with hot cathode, giving current-voltage characteristics as function of pressure and temperature
14 p2491 A69-29260
- One dimensional analysis of static collector emitter saturation voltage of epitaxial and triple diffused devices, considering transistor with lightly doped collector
14 p2421 A69-29545

Plasma scanner in obtaining current cross sections and current-voltage characteristics of hollow cathode magnetically confined arc plasma in argon
14 p2450 A69-29568

Gunn effect GaAs oscillators with p-n junctions, studying electrical characteristics, threshold voltages and currents during breakdown and p-n junctions injection
15 p2666 A69-30063

Transistorized circuit operation with nonlinear feedback through tunnel diode analyzed by piecewise-linear approximation of I-V characteristics
15 p2573 A69-30114

Oscillation breakdown of varactor diodes in parametric amplifiers from studying I-V characteristics, noting resonant circuit retuning effect
15 p2574 A69-30127

Space charge effects on trigger current and reflector voltages of reflex klystron
15 p2574 A69-30131

Negative resistance section of current-voltage curve for long diodes of p-type indium antimonide, noting magnetic field effects on electrical breakdown
15 p2581 A69-31149

Electric arc plasma generator efficiency analysis including supply voltage, working current, current-source impedance, ballast resistor and optimum voltage-current selection
15 p2664 A69-31177

High voltage thin film transistor, discussing design criteria, fabrication, I-V characteristics and switching speed
16 p2757 A69-31614

Plasma parameters, except ion temperature, obtained from current-voltage characteristics of flowing plasma measured by electrostatic probes in low density wind tunnel
16 p2816 A69-31637

Electrical and thermal conductivities of high pressure arc plasmas from I-V characteristics and radial temperature profile
16 p2817 A69-31644

Electron trap behavior on charged spacecraft, obtaining expressions for current to aperture and internal retarding electrodes for all apertures and spacecraft potentials
16 p2849 A69-31976

I-V characteristics of caloelectric plasma converter with concentric electrodes measured for various hot electrode temperatures and mercury vapor flow rates
16 p2822 A69-32065

Hall ion thruster prime propulsion system, considering low and high voltage mode in plasma source I-V characteristics
17 p3019 A69-33338

Transient characteristics of three phase AC alternators with rectified outputs
17 p2905 A69-34089

Aircraft secondary power sources reliability dependence on electric loads, charge control and maintenance, discussing hermetically sealed batteries features
17 p2905 A69-34113

Laboratory device for investigating thermionic energy converters and measuring current-voltage characteristics by static/dynamic methods
18 p3136 A69-34700

Plasma parameters relationship with double electrostatic probe volt-ampere characteristics, applying corrected formulas for temperature, ion density, etc, to flame diagnostics
18 p3137 A69-34932

Schottky barrier diodes for high temperature operation prepared on n type GaP single crystals, studying I-V and C-V characteristics
19 p3381 A69-35681

Proton irradiation effects on current degradation at fixed voltages of silicon solar cells with coverslips
19 p3252 A69-35701

Shadow effects on current-voltage characteristics of solar cell array circuits, developing mathematical models
19 p3254 A69-35709

Solar cells volt-ampere characteristics calibrated at various solar incidence angles on LES-6 satellite in synchronous orbit
19 p3254 A69-35712

Pulsed water vapor laser high power operation and strongest component wavelength measurement
19 p3337 A69-36416

Junction lasers current-voltage characteristics, discussing coherence-pinch effect as explanation of threshold behavior
19 p3337 A69-36531

Voltage and temperature dependence of zero-bias anomaly in GaAs p-n junction at 0.40-60 K, investigating voltage dependence of differential resistance
19 p3388 A69-36542

Hot electron behavior in n-type InSb under magnetic fields at 4.2 and 1.7 K, plotting current-voltage and current-Hall voltage characteristics, etc
19 p3388 A69-36544

Current-voltage characteristics of unitoron with metal-dielectric-semiconductor structure /MOSFET/ taking into account substrate potential effect
19 p3284 A69-36592

Metal-semiconductor contact current-voltage characteristic derived from modified diode theory taking into account electron distribution function
19 p3391 A69-36608

MOS threshold voltages calculations, considering fixed bulk and oxide charges and difference in work function between metal and semiconductor, considering MOS-FET devices
20 p3506 A69-37779

Recombination radiation of tellurium and zinc doped GaAs alloy type diodes, discussing luminescence spectra, current-voltage characteristics and temperature effects
20 p3506 A69-37783

Injection and excitation of charge carriers in CdS single crystals, analyzing current-voltage characteristics dependence on electrode separation, temperatures and electric field
21 p3779 A69-38423

GaAs-GaP heterojunctions, analyzing continuous conduction band, capacitance and current-voltage characteristics, photoresponse and modulation effect
21 p3779 A69-38424

Tunnel p-n junctions preparation by diffusing Zn into degenerate Te doped n-type GaSb between 580-600 C, measuring volt-ampere and capacitance characteristics
21 p3780 A69-39043

High resistivity GaAs impedance with nonlinear I-V characteristics, showing appreciable reactive component
21 p3782 A69-39143

Josephson currents interaction with LF surface plasmons in superposed thin dielectric and superconducting metal films, noting I-V characteristics
22 p3992 A69-40420

Nonlinear voltage dependence on current in p-type indium selenide single crystals, detecting negative resistance under pulsed electric field
22 p3992 A69-40602

Electric instabilities in semiconductor devices analyzed by subdividing instabilities into cathode and anode waves, considering recombination and electron and hole production processes
22 p3997 A69-41173

Performance degradation in cadmium sulfide solar cells, discussing cause identification technique, I-V curve parameter changes, etc
23 p4070 A69-42271

Hot spot failure modes in solar cell arrays noting protection through I-V characteristic control
23 p4142 A69-42273

Luminescence, I-V and pulse characteristics of high resistivity Ni doped GaAs single crystals, noting injection conductivity
24 p4362 A69-43734

VOLTAGE

U ELECTRIC POTENTIAL

VOLTAGE AMPLIFIERS

Error origin and control in high gain operational amplifier in time differentiation of voltage signal used for photoemission studies
06 p0897 A69-17700

Maximum voltage and power gain of modulator-demodulator type nonresonant parametric amplifiers
11 p1849 A69-24956

Voltage amplitude for combination frequency of small signal transistor amplifier calculated from feedback dependence
13 p2226 A69-27218

VOLTAGE BREAKDOWN

U ELECTRICAL FAULTS

VOLTAGE GENERATORS

U PHOTOVOLTAIC CELLS

VOLTAGE MEASUREMENT

U ELECTRICAL MEASUREMENT

VOLTAGE REGULATORS

Passive circuit to transform voltage of indefinitely repeated positive or negative pulses using transistors, diodes and magnetic cores
01 p0043 A69-10564

Magnetic core logic circuit system for bidirectional stepping motor drive voltage power supply control in proper phase and time sequence
01 p0047 A69-11000

Automatic device for charging storage capacitors in plasma devices provides voltage and operational frequency control
04 p0580 A69-1449

Regulated high voltage DC to DC converter with output voltage programmable numerically, noting application on board HEOS A satellite
04 p0602 A69-1540

Phase measurement using phase lock loop, voltage controlled oscillator and synchronous counter
05 p0722 A69-1676

Mathematical model for voltage step-down DC to DC converter with hysteretic bistable trigger circuit regulating output voltage
06 p0904 A69-1794

All-diffused process to build monolithic high power series voltage regulator with separately optimized DC and AC characteristics
07 p1103 A69-18881

Regulated voltage converter systems for onboard spacecraft electric power supplies, noting chopper circuits with rectifiers
12 p2015 A69-25867

Variable voltage DC power supplies for energizing cryogenically cooled and superconductive electromagnets
12 p2017 A69-26498

Regulating setup for controlling AC voltage surrounding polarization of magnetic electrode in plasma
15 p2664 A69-31094

Power supply circuits in spacecraft, DC voltage control systems, transistor and thyristor regulators and modulators, etc
17 p2937 A69-33582

Duty cycle IC generator for switching regulators, discussing construction, resistive and dielectric films fabrication, applications, etc
23 p4073 A69-42293

High efficiency boost regulator design and tests for planetary spacecraft, considering input and output voltages
23 p4075 A69-42302

Symmetrically regulated AC/DC converters power characteristics improved by switching in phase rectifiers twice during control cycle
24 p4254 A69-42570

VOLTAGE VARIATION INDICATORS

U VOLTMETERS

VOLTERRA EQUATIONS

Unstable Volterra integral equation reduced to finding solutions for Fredholm integral equation by restricting solutions to closed ball in Hilbert space
01 p0103 A69-10004

Forward and backward scattered modes over frequency range in multimode nonuniform waveguide, transforming coupled modes telegraphist equations into Volterra equations
01 p0043 A69-10621

Volterra equation generalization by method involving operator for mapping of topological space into Banach space
02 p0270 A69-11531

Congruence theorems for Volterra equations with delay
04 p0625 A69-15099

Ground influence on Helmholtz flow in presence of plate perpendicular to stream, reducing problem to mixed Volterra problem in complex half plane
04 p0590 A69-15221

Nonlinear Volterra integral equation, extending topological dynamics application of nonautonomous ordinary differential equations
04 p0626 A69-15288

Theorems and lemmas formulated pertaining to Volterra equations stability
05 p0787 A69-16449

Nonlinear Volterra integral equation solved by Runge-Kutta method
05 p0787 A69-16456

Volterra equation generalization extended and applied to functional Volterra equations, proving theorem dealing with topological, quasi-compact and uniform spaces
08 p1342 A69-20268

Criteria governing solution uniqueness to Volterra equations system
10 p1722 A69-24067

- Perturbations of Volterra integral equation with vectors in n -dimensional real or complex Euclidean space, comparing solution with linear system solution
11 p1909 A69-24886
- Interference between bodies of revolution and wings in supersonic flow, using Volterra method for calculation
11 p1820 A69-25476
- Dirichlet problem solution for Volterra elliptic integrodifferential equation, considering existence theorem hypotheses
12 p2121 A69-26468
- Volterra operator algebra for boundary value problems involving linear viscoelasticity with continuous relaxation time and delay time spectra
12 p2182 A69-26677
- Dahlquist linear multistep methods of stability analysis for ordinary differential equations extended to Volterra integrodifferential equations
12 p2123 A69-26753
- Volterra integral equation with nondifference type singular kernel for stress-strain state in long hollow viscoelastic cylinder with moving inner boundary
13 p2361 A69-27744
- Inequality theorems for multidimensional functional Volterra equations formulated and proved, deriving upper and lower solutions
13 p2290 A69-28684
- Numerical solution of nonlinear Volterra integral equation by Runge-Kutta-Felberg method
15 p2644 A69-30657
- Equilibrium cracks propagation in linear hereditary elastic media using Volterra principle
15 p2715 A69-31201
- Nonlinear theoretical derivation of creep equations for three dimensional processes in polymers, based on Boltzmann-Volterra creep heredity concept using stress-strain summation
16 p2803 A69-32290
- Gyrocompass differential equations of motion reduced to Volterra integral equation, proposing solution algorithm
17 p2995 A69-33617
- Cauchy problem solution for first order nonlinear Volterra integrodifferential equation, using Runge-Kutta method
20 p3569 A69-38294
- Coupled set of differential equations describing generalized Volterra problem of conflicting populations and application to plasma oscillations
22 p3976 A69-41260
- Volterra problem with given singularities for exterior of circle applied to fluid mechanics
24 p4339 A69-42679
- Numerical methods for nonlinear Volterra integral equations of second kind avoiding special starting procedures, giving convergence theorem
24 p4340 A69-43228
- VOLTMETERS**
Photoconductor open circuit voltage determination, calculating responsivity and sensitivity of actual and ideal cases
12 p2093 A69-26481
- VOLUME**
NT BODY VOLUME [BIOLOGY]
Heat capacity at constant volume determined for nitromethane, trinitrotoluene and difluoramine alitanes
[WSCI PAPER 68-39] 07 p1202 A69-18368
- Shrinkage cavity volume formulas for alloy castings with wide liquidus to solidus range, considering effects of diffused porosity and clustering for Mg alloy
20 p3548 A69-37329
- VOLUMETRIC ANALYSIS**
Gas bath cryostat to study volumetric properties of gaseous mixtures at low temperature and high pressure
17 p2975 A69-33669
- Quantitative mineralogical characterization of chondrites by modal analysis using electron microprobe
19 p3416 A69-36125
- VOLUMETRIC STRAIN**
Volumetric and allotropic changes during heating in electrolytic cobalt multiple phase transformations
12 p2114 A69-26455
- Elastic curve shape effects on volume of minimum weight uniformly strong beam under combined longitudinal and transverse bending
23 p4225 A69-41421
- VON KARMAN EQUATION**
Approximate solution for Dirichlet problem for linear Karman differential equation used in thin plate deflections obtained by Bubnov-Galerkin method
01 p0105 A69-10700
- Von Karman flow changes due to unsteady heat transfer from rotating disks impulsively changing temperatures, particularly steady state and response time
08 p1422 A69-20996
- Self controlled vibration of elastically supported cylinder in fluid stream due to von Karman shedding, considering fluidelastic interaction, structural deformation and natural frequency
13 p2360 A69-27437
- Perturbation method for nonlinear panel flutter at high Mach numbers, using von Karman large deflection plate theory and quasi-steady aerodynamic theory
13 p2364 A69-28204
- Nonlinear Galerkin analysis of curved plate flutter, using shallow shell/von Karman equations and quasi-steady aerodynamic theory
13 p2364 A69-28207
- Von Karman swirling flow problem differential equations solved by extending Serrin existence theorems
14 p4322 A69-29676
- Taylor vorticity transport theory and von Karman similarity hypothesis extended to consider three dimensional fluctuating velocity field in analyzing turbulent swirling ducted flow
[ASME PAPER 69-APM-19] 18 p3120 A69-34394
- Von Karman equations in dimensionless and finite difference forms for deflections of elastic circular plate with central hole under load solved by iteration
[ASME PAPER 69-APM-20] 18 p3214 A69-34395
- Number of forms of stability of plates and shells derived from eigenvalues of nonlinear boundary value problem containing generalized von Karman equations
19 p3445 A69-36816
- Von Karman equations for large deflection of simply supported square plates solved using dynamic relaxation method, recommending optimum mesh spacing
20 p3619 A69-36938
- Reynolds number dependence of turbulent velocity profile in circular tube and parallel plate channel analyzed by von Karman similarity hypothesis
20 p3513 A69-37081
- Forced flow against infinite rotating disk, showing von Karman similarity equations solution for axial flow at large distances toward disk
24 p4244 A69-42718
- VON MISES THEORY**
U STRESS FUNCTIONS
- VON ZEIPPEL METHOD**
Short period terms elimination for problem of motion of satellite with strong inclination and eccentricity, using von Zeipel method
03 p0514 A69-13783
- VOR SYSTEMS**
U VHF OMNIRANGE NAVIGATION
- VORTEX BREAKDOWN**
Vortex breakdown effect on aerodynamic coefficients of small aspect ratio delta wings during yawing
04 p0543 A69-14821
- Degree of knottedness of tangled vortex lines, discussing vorticity distribution for inviscid flow and MHD invariants
11 p1872 A69-25126
- Vortex breakdown in rotating fluids associated with wave motion along axis of rotation, considering effects of nonzero wave amplitude
[AIAA PAPER 69-645] 17 p2892 A69-33478
- Vortex breakdown on slender sharp edged and modified delta wings with varying sweep angles investigated in wind tunnel using schlieren system for flow visualization
[AIAA PAPER 69-778] 19 p3237 A69-35644
- VORTEX COLUMNS**
U VORTICES
- VORTEX DISTURBANCES**
U VORTICES
- VORTEX FLOW**
U VORTICES
- VORTEX GENERATORS**
Circulation, geometry and viscosity effects on speed of surge in bathtub vortex
05 p0744 A69-15718
- Shock tube investigation of formation and flow characteristics of impulsively generated vortex street recorded interferometrically, using high speed framing camera
[ASME PAPER 68-FE-32] 05 p0748 A69-16079
- Counter rotating vertical vortices produced by corona discharge on heated flat plate under free convection conditions
[ASME PAPER WA/HT-9] 05 p0846 A69-16117
- Propeller at static working state using vortex theory assuming infinite blade number, discussing thrust and torque coefficients
06 p0857 A69-17194
- Visual investigation of flow field at swept wing, measuring pressure distribution at stall fence and vortices formation
06 p0858 A69-17341
- Compressible combustor turbulent shear flow analysis, discussing eddy diffusivity, density fluctuations, vorticity intensification and turbulent transport
[WSCI PAPER 68-27] 06 p1034 A69-17793
- Discontinuous vortex power amplifier and diode design, noting supply regulator effects and load matching
09 p1443 A69-22737
- Vortex amplifiers small signal analysis based on mathematical model and network theory
09 p1443 A69-22739
- Vortex amplifiers design and performance, noting nonvented and vented amplifiers and fluid valving applications
09 p1443 A69-22741
- Incompressible fluid flow engine spiral casing, considering flow as potential flow
10 p1632 A69-22914
- Hybrid fluidic pressure regulator combining vortex amplifier and confined-jet amplifier with performance upgrading moving metering element, noting greater efficiency and reliability
10 p1639 A69-23560
- Secondary vortex generation in near wake of circular cylinders under forced oscillation, analyzing motion dependent transition regimes using hydrogen bubbles flow visualization
[AIAA PAPER 69-755] 18 p3084 A69-34411
- Model predicting steady state input-output characteristics of vortex amplifiers operating in incompressible flow regime, correlating model with experimental data
[ASME PAPER 69-FLCS-20] 20 p3465 A69-37980
- Forced and periodic motion of air or water jets impinging in double input vortex chamber described in terms of oscillator deriving energy from hydrodynamic instability
[ASME PAPER 69-FLCS-19] 20 p3465 A69-37981
- Plane Poiseuille flow with nonlinear temperature distribution, studying vortex type secondary flow onset due to buoyant forces
[ASME PAPER 69-HT-37] 24 p4411 A69-43533
- Taylor Goertler vortex formation effect on heat transfer through boundary layer on concave wall
[ASME PAPER 69-HT-3] 24 p4414 A69-43563
- VORTEX INJECTORS**
Vortex motion enhancement of jet penetration and spreading in supersonic fuel injection into large diameter combustors
[AIAA PAPER 69-664] 17 p2953 A69-33437
- VORTEX RINGS**
Vortex ring production in liquid jet by vibration induced pressure pulses at orifice, discussing plates formed under high g vibration
[AIAA PAPER 68-132] 16 p2770 A69-31880
- Algorithm using Biot-Savart law for determining induced velocity of curved vortex lines in aerodynamics, noting required line integration method
20 p3458 A69-37169
- VORTEX STREETS**
NT KARMAN VORTEX STREET
Shock tube investigation of formation and flow characteristics of impulsively generated vortex street recorded interferometrically, using high speed framing camera
[ASME PAPER 68-FE-32] 05 p0748 A69-16079
- Strouhal and Reynolds numbers relation from data on vortex streets of circular cylinder in two dimensional flow
07 p1119 A69-18749
- Boundary layer separation and vortex street buildup conditions of gas flow in circular cylinder wake
08 p1252 A69-20713
- Vortex shedding and wake formation behind inclined flat plate at low Reynolds number, using dye injector method for streak line observation
16 p2768 A69-31767
- Vortex wakes behind high lift wings, considering effects of height above ground and various tunnel heights and widths for STOL operations
[AIAA PAPER 69-740] 18 p3083 A69-34405
- Flow field induced by spiral vortex sheet, noting existence of radial velocity component
21 p3692 A69-38610

VORTEX TUBES

Model for statistically isotropic homogeneous turbulence in incompressible fluid, representing turbulence as superposition of individual vortex sheets
22 p3930 A69-40525

Vortex shedding from circular cylinders rotating normal to free stream velocity, studying roles of rotation rate and Reynolds number
24 p4248 A69-43601

VORTEX TUBES U HILSCH TUBES U VORTICES VORTICES

Vortices coupling between superposed superconducting tin films as function of perpendicular magnetic field, primary current and temperature
01 p0135 A69-10014

Jet line in rotational incompressible plane flows around shrouded propeller blade, using electrical analog
01 p0058 A69-10037

Confined vortex in air tangential and axial velocity distribution based on smoke profile pictures
01 p0060 A69-10413

Characteristics of electrovortices and auroral electrovortices of polar disturbance field, discussing dynamics during geomagnetic storms
02 p0240 A69-11723

Vortex valve characteristics, noting Reynolds number and geometry effects on flow and turnaround ratio
02 p0195 A69-12079

Vortex controlled fluid amplifiers, discussing static and dynamic performance characteristics
02 p0195 A69-12081

Photographic flow patterns of separated flows with vortex formation obtained in wind tunnel for different aerodynamic configurations of revolution
02 p0191 A69-12586

Discrete vortices in two dimensional subsonic and supersonic wake, determining Strouhal numbers, frequencies and flow velocities with aid of HF cinematography
02 p0191 A69-12587

Thermovortex effect, determining functional relations between interdependent parameters by means of dimensional analysis
03 p0531 A69-12966

Large scale disturbances in summertime stratosphere observed from high level balloon, discussing diurnal wind patterns and planetary traveling waves
03 p0461 A69-13343

Supersonic flow past blunt body with convex corner calculated to establish sonic point on body
03 p0362 A69-13406

Nonstationary model of mesoscale atmospheric vortex with vertical axis based on atmospheric thermohydrodynamics
03 p0462 A69-13932

Numerical solution of axisymmetric incompressible viscous fluid flows about rotating cylinder, Taylor vortex between cylinders and through labyrinth seal
03 p0419 A69-13990

Unsteady two dimensional flow in square cavity with fluid initially at rest and constant velocity upper surface of cavity, noting vortex center
04 p0587 A69-14510

Test of similarity theory of leading edge vortices above slender wings in subsonic conical flow
04 p0543 A69-14820

Tetron flight observations of eddy velocities in planetary boundary layer, noting effects of height and seasonal variations
04 p0626 A69-14912

Light aircraft hazards due to trailing vortex generated by heavy transport aircraft, suggesting specific procedures for takeoff, landing and flight phase
04 p0549 A69-14930

Covariances of temperature and meridional wind component and relation to northward flux of sensible heat due to transient eddies in stratosphere
04 p0627 A69-15084

Vortex motion of separated flow from slender wings and rotor loading, discussing computer role in low speed aerodynamic research
05 p0696 A69-15562

Aerodynamic interference effects arising from jet efflux of V/STOL aircraft, developing vortex sheet theory for jet interference
05 p0696 A69-15566

Stationary velocity profile near jet driven vortex tube outer wall calculated by laminar boundary layer flow theory, neglecting wall curvature effects
05 p0798 A69-15610

Stabilizing influence of axial magnetic field on confined vortex flow of aqueous electrolytic conductor generated by two dimensional wall jets
05 p0798 A69-15611

Circulation, geometry and viscosity effects on speed of surge in bathtub vortex
05 p0744 A69-15718

Two dimensional supersonic rotational flow around convex corner solved using coordinate system consisting of left running characteristics and streamlines
05 p0697 A69-15722

Static and dynamic performance of pancake vortex flow field and application to signal amplification
05 p0704 A69-16001

Vortex devices and turbulence amplifiers, describing circuits, operating principles and performance
05 p0705 A69-16005

Vortex value and angular rate sensor based on amplification of tangential velocity component of swirl achieved by control jet or rotation
05 p0746 A69-16006

Pressure distribution across short vortex chamber to exit radius with known inlet geometry based on incompressible flow model and visualization photographs [ASME PAPER 68-WA/FE-17]
05 p0748 A69-16093

Self similar solution for Navier-Stokes equations describing steady motion of submerged eddy jet of incompressible viscous fluid injected into half space
06 p0908 A69-16825

Mach number effects on pattern of vortex flow past delta wing and circular cones at various Reynolds numbers
06 p0858 A69-17339

Cross hatching on various body surfaces due to periodic surface pressure fluctuations, discussing origin from counterrotating longitudinal vortices in boundary layer [AIAA PAPER 69-11]
06 p0915 A69-18213

Spherical particle motion in vortex gas flow between planes of turbulence chamber perpendicular to axis of flow rotation, noting collisions effect
07 p1181 A69-19000

Large scale tropical eddies using two layer dry atmospheric model containing nongeostrophic effects and parametrized dissipation
07 p1176 A69-19035

Planetary wave-zonal flow interaction interpretation in terms of potential vorticity eddy transport, deriving zonal wind change and temperature field
07 p1126 A69-19037

Flexible rotor blade dynamic response to radially moving force, emphasizing helicopter rotor vibration characteristics associated with tip-vortex impingement [AIAA PAPER 69-203]
07 p1054 A69-19546

Stability of plane vortex sheet in magnetic fields, noting stabilization effect of compressibility for nonmagnetic case
08 p1358 A69-19797

Mean and eddy terms contribution to momentum and heat balance of troposphere and lower stratosphere at solstices, describing zonal wind equations
08 p1308 A69-20318

Vortex valves and amplifiers small signal analysis using mathematical model to describe quantitative effects of vortex parameter changes [AGARDOGRAPH-118]
08 p1257 A69-20953

Ranque vortex tube as cooling device in MA-3 ventilating garment
09 p1447 A69-22550

Vortex fluidic devices - Conference, Philadelphia, January-February, 1967
09 p1443 A69-22736

Vortex valve pure fluid modulators steady state characteristics, analyzing geometry of exit, control and supply areas and chamber
09 p1443 A69-22738

Vortex fluid devices in control systems, considering electrical, mechanical and hydraulic systems
09 p1443 A69-22740

Permanent flow of solenoidal vector line rotation in steady nondegenerate rotational flow having complex lamellar unit normal to streamline
10 p1727 A69-22862

Viscous fluids rotational flow in cylindrically symmetrical vessels, circumventing Navier-Stokes equations of motion by Wedemeyer approximation
10 p1677 A69-22896

Vortex amplifier as active element in analog circuits
10 p1639 A69-23556

Vortex incompressible flow in thin cylindrical chamber, analyzing outer and inner region and interface tangential velocity, shear and static pressures
10 p1679 A69-23557

Large signal vortex amplifier analysis using load lines to evaluate series orifice and vortex flow control valve characteristics
10 p1639 A69-23558

Longitudinal vibrations induced by internal flow in metal bellows resembling vortex shedding excitations of elastically restrained cylinders, discussing spring mass mechanical model [ASME PAPER 69-VIBR-5]
10 p1805 A69-24163

Mean and eddy motions in atmosphere described by mathematical expressions for total and mean kinetic energies
11 p1911 A69-24323

Wing geometry and wing lower surface boundary layer effects on rolled-up tip vortices geometry and strength
11 p1819 A69-25372

Aircraft vortex wake development prediction for turbulent flow noting vortex size, strength and peak tangential velocity
11 p1819 A69-25377

Different pressure and deflection measurements coherence in vortex flows verified assuming radial equilibrium conditions
12 p2012 A69-26362

Vortices interaction effect on vertical turbulent heat flow in atmosphere boundary layer, determining dependence of vortex mean vertical temperature gradient
13 p2293 A69-27841

Energy transport between vortices in turbulent flow calculated from vortex stability study
14 p2430 A69-29508

Hydrogen plasmas motions in multipole magnetic fields, discussing plasma polarization, double vortex flow patterns and field line configurations
15 p2661 A69-30924

Numerical approximation of Taylor vortices in viscous incompressible fluid flow between concentric rotating cylinders, using truncated eigenexpansions
15 p2593 A69-31518

Fluidic vortex valve to modulate solid propellant generated hot gas flow [AIAA PAPER 69-424]
16 p2844 A69-32723

Rotating cylinder or vortex motion in shear flow with friction, noting drag and rotor force combined influence
17 p2950 A69-33151

Leading edge flap angle and planform effects on low speed vortex patterns of flat plate double delta wings, measuring aerodynamic forces
17 p2890 A69-33246

RF high pressure plasma discharges contained within radial inflow vortex, measuring radiation efficiencies, power densities and radiation fluxes [AIAA PAPER 69-695]
17 p3010 A69-33442

Finite amplitude standing transverse resonant acoustic field effects upon flow behavior of viscous fluid in cylindrical enclosure to acoustically model combustion instability [AIAA PAPER 69-667]
17 p2954 A69-33457

Vortex diffusion in viscous compressible fluid approximated by linear differential equations
17 p2957 A69-33714

Cyclonic vortices production by horizontal convergence in rotating water bowl as function of bottom surface inclination, modeling cyclogenesis in jet stream entropy field
17 p3000 A69-33760

Model calculations for movement of barotropic and initially symmetric vortices in rotating fluids with Coriolis parameter or fluid depth varying horizontally
17 p3000 A69-33761

Leading edge vortices and shock detachment flow over delta wings, discussing drag reduction due to lift
17 p2896 A69-34025

Helicopter rotor vortex noise data analyzed for noise suppression, obtaining sound power equations
17 p2896 A69-34034

Taylor vortices calculated as branching solutions of nonlinear Navier-Stokes boundary value problem
17 p2958 A69-34152

Standing twin vortices in wake behind thin flat plate normal to flow visualized by Al dust, noting Karman vortex street
18 p3086 A69-35167

Vortex wakes behind circular cylinder subject to transverse sinusoidal oscillations in uniform water flow at specific Reynolds numbers, photographing varied frequency flow patterns
18 p3086 A69-35169

Lifting line theory for hovering propellers deformed wakes based on continuous vortex sheet representation
18 p3087 A69-35217

Rotating static thrust propeller or hovering rotor flow field study by schlieren photography, considering vortex field, tip flow and shock wake formation
18 p3087 A69-35218

Vortex shedding effects on helicopter rotor noise with and without blade slap, noting far and near field noise
18 p3088 A69-35223

Secondary flow consisting of longitudinal vortices superposed on convection flow on inclined plate, obtaining flow pattern through flow visualization
18 p3124 A69-35383

Secondary flows in confined viscous vortex for nuclear rockets, employing rotating disk in chamber end wall for recirculation
19 p3296 A69-35756

Tangential and radial velocities in vortex boundary layer flow, relating diminishing amplitudes to increasing height using iterative method
19 p3363 A69-36499

Horizontal wind components over U.S.S.R., Western Europe and Northeast Atlantic obtained from satellite photographs of vortex cloud systems
19 p3365 A69-36668

Monograph on interaction between primary and jet flapped secondary airfoils covering line-vortex use for lift augmentation, aerodynamic characteristics, etc
19 p3242 A69-36820

Roshko correlation for estimating vortex shedding from circular cylinder in sheared flow with velocity in Strouhal and Reynolds numbers
20 p3515 A69-37228

Vortex flow air cooling system for lasers using vortex effect of gas separation, resulting in minimum weight and dimensions and high cooling efficiency
21 p3734 A69-38399

Forces on stationary cylinder under sinusoidal flow, considering symmetrically located vortex pairs and flowfield
[ASME PAPER 69-FE-13] 21 p3643 A69-38601

Laminar boundary layer on funnel wall, considering internal vortical and radial flow
21 p3692 A69-38611

Narrow band vortex shedding from circular cylinder in critical Reynolds number range, noting increase in Strouhal number
21 p3644 A69-38690

Interaction between boundary layer and external vortex flows and stability transitions of heated rotating fluid annulus
21 p3698 A69-39869

Velocity profile and skin friction in boundary layer on flat plate with periodic vorticity near leading edge
22 p3929 A69-40015

Horizontally flowing eddies or Rossby waves in solar convection zone and photosphere, giving mathematical models showing hydromagnetic dynamo effects inducing reversing magnetic fields
22 p4019 A69-40294

Helicopter rotors trailing vortices by flow visualization, comparing Euler and Runge-Kutta iterative solutions
23 p4150 A69-41376

Instability theory of baroclinic vortices in incompressible and inviscid fluid, investigating symmetric meridional motions time evolution by numerical integration of hydrodynamic equations
23 p4153 A69-42346

Spanwise velocity correlations of turbulent vortices shed by two dimensional bluff body of D section with different aspect ratios, noting end plates effect
23 p4234 A69-42397

Axial and angular momentum flux, flow force and circulation to determine strength and structure of narrow rotating axisymmetric vortex and swirling core flows
24 p4298 A69-42598

Shape, position and velocity of vortex wakes shed in unsteady multienergy flows near trailing edge, applying Kutta condition
[ASME PAPER 69-APMW-19] 24 p4245 A69-43099

Design of vortex fluid amplifiers operating in incompressible flow regime, based on fluid properties and geometry effects on amplifier behavior
24 p4256 A69-43299

VORTICITY
Mean meridional circulation models in tropics based on vorticity equation
03 p0460 A69-13334

Kinematic and dynamic relations determined for vortex flow of ideal incompressible fluid past circular cylinder, noting use for calibrating cylindrical adapters
04 p0541 A69-14484

Propeller at static working state using vortex theory assuming infinite blade number, discussing thrust and torque coefficients
06 p0857 A69-17194

Jupiter Red Spot vorticity at perimeter indicated by interaction with dark spots circulating along south equatorial belt
07 p1213 A69-18606

Vorticity behind shock waves in conducting gases when magnetic field is tangential or normal to shock surface using momentum equation
08 p1367 A69-20789

Stagnation point heat transfer sensitivity to free stream turbulence attributed to external vorticity, noting correlation with Prandtl number
09 p1622 A69-21905

Degree of knottedness of tangled vortex lines, discussing vorticity distribution for inviscid flow and MHD invariants
11 p1872 A69-25126

Direction of maximum turbulent vorticity in turbulent shear flow, determining alignment
11 p1874 A69-25282

Linear amplification, nonlinear limiting and secondary instability induced by unsteady effects illustrated for various transitional flows, including roughness and streamwise vorticity
17 p2950 A69-33248

Hydraulic resistance of pipes with flow vorticity produced by helical swirlers
21 p3695 A69-38862

Temperature-vorticity analogy for viscous two dimensional fluid flow extended to compressible flows, noting enthalpy and shear stress analogy
22 p3929 A69-39892

Shock tube boundary layers dependence on shock strength determined using vorticity transport to define boundary layer coordinate
22 p3930 A69-40531

Boundary layer effects in turbulent spiral vortex flow of compressible fluid in supersonic centrifugal compressor, discussing flow geometry, using momentum integral method
23 p4152 A69-42109

VORTICITY EQUATIONS

Stability theorems for barotropic vorticity equation integrated within limited region for flow through boundary without existing physical boundary conditions
13 p2294 A69-28494

Alpine effects on wind field at synoptic scale using potential-vorticity equation, discussing deflection angle dependence on potential temperature distribution
15 p2650 A69-31445

Predictability of deterministic fluid systems with many scales of motion using vorticity equation for two dimensional incompressible flow, noting application to earth atmosphere
19 p3303 A69-36404

Operational circulation model numerical experiment suggesting elimination of spurious divergence-on-divergence interactions from implied vorticity equations in primitive equations
19 p3363 A69-36503

Hadley and equatorial cell models for mean meridional circulation in terms of vorticity equation
24 p4345 A69-43152

VORTICITY TRANSPORT HYPOTHESIS

Taylor vorticity transport theory and von Karman similarity hypothesis extended to consider three dimensional fluctuating velocity field in analyzing turbulent swirling ducted flow
[ASME PAPER 69-APM-19] 18 p3120 A69-34394

VOSKHOD 1 SPACECRAFT

Voskhod 1 and 2 crew performance, orientation and motor activity analysis indicating time increment for task performance, psychophysiological irregularities and visual analyzers impaired functioning
02 p0203 A69-12123

VOSKHOD 2 SPACECRAFT

Voskhod 1 and 2 crew performance, orientation and motor activity analysis indicating time increment for task performance, psychophysiological irregularities and visual analyzers impaired functioning
02 p0203 A69-12123

Weightlessness effects on human external respiration, gas exchange and energy expenditure indices during flight of Voskhod 2
12 p2020 A69-26563

VOSKHOD MANNED SPACECRAFT

Cardiovascular system, respiratory system and metabolism of cosmonauts on three man flight of Voskhod, noting physiological and biochemical studies
03 p0377 A69-14195

Cosmonauts cardiac activity and respiration changes during physical exertion in orbital flight on Voskhod spacecraft
03 p0377 A69-14196

Physiological and medical tests on Soviet cosmonauts onboard Voskhod spacecraft, assessing CNS, cardiovascular and respiratory systems and work-rest schedule
07 p1060 A69-18571

VOWELS

Whispered vowels pitch perception test using listen-and-compare method to determine formants for comparison with complex analysis procedure
23 p4190 A69-41575

VOYAGER PROJECT

Planetary quarantine and biological search strategy, discussing Voyager-Mars mission configuration, sterilization, back contamination and decisions
01 p0021 A69-11090

Microorganism viability in rocket engine combustion environments used to determine probability of biological contamination of Mars by Voyager missions
05 p0714 A69-15949

VOYAGEUR HELICOPTER

U CH-46 HELICOPTER

VTO FIGHTER AIRCRAFT

U FIGHTER AIRCRAFT

U VERTICAL TAKEOFF AIRCRAFT

VTOL

U VERTICAL LANDING

U VERTICAL TAKEOFF

VTOL AIRCRAFT

U VERTICAL TAKEOFF AIRCRAFT

VULCANIZATES

U VULCANIZED ELASTOMERS

VULCANIZED ELASTOMERS

Vulcanized elastomers suitable for contact with liquid oxygen, discussing preparation, mechanical properties, transition temperature and structure
05 p0717 A69-16497

Low viscosity/density RTV silicone rubber sealants obtained by using glass microballoon fillers
24 p4337 A69-43454

VULCANIZING

High strength room temperature vulcanizing silicone rubber for tooling and fabrication of aircraft and missile components
09 p1507 A69-22331

Room temperature vulcanizing silicone rubber adhesive sealants strength and self bonding, describing primerless adhesion to Ti and Al alloys, Al, Ni and stainless steels
19 p3356 A69-35532

VZ-2 AIRCRAFT

Technological evolution of turboprop propeller powered tilt wing V/STOL aircraft, discussing XC-142A, CL-84 and VZ-2 aircraft
05 p0701 A69-15564

VZ-10 AIRCRAFT

U XV-4 AIRCRAFT

VZ-12 AIRCRAFT

U P-1127 AIRCRAFT

W

W WINGS

U VARIABLE SWEEP WINGS

WAFERS

Current oscillations or instabilities in semiconductor wafer with one electromagnetic mode and one carrier mode, investigating resonant frequencies
03 p0408 A69-14049

WAKES

NT AIRCRAFT WAKES

NT HELICOPTER WAKES

NT HYPERSONIC WAKES

NT LAMINAR WAKES

NT PROPELLER SLIPSTREAMS

NT SLIPSTREAMS

NT SUPERSONIC WAKES

NT TURBULENT WAKES

Acoustic resonance excitation in axial flow compressor annulus by wake shedding from blades
01 p0142 A69-10058

Wake structure behind spherical bodies in rarefied plasma flow by measuring plasma parameters and disturbances with probes
01 p0134 A69-11308

Three dimensional wakes and jets, discussing centerline velocity, half width growth and velocity irregularities

02 p0190 A69-12549

Lunar wake in solar wind at large distances, noting no satellite evidence of lunar magnetic field and evidence for lunar generated turbulence

03 p0514 A69-14007

Inviscid cavity and wake flows behind submerged bodies, analyzing mathematical and theoretical models

04 p0587 A69-14608

Aircraft propulsion by wake regeneration, noting supersonic transport ogee layout with maximum drag fraction

05 p0811 A69-15555

Perturbed wake behind spherical models in rarefied plasma flow, noting effects of electron temperature and electric potential of models

05 p0803 A69-16048

Circular cylinder near wake in cross flow measured with hot-wire anemometry for various Reynolds numbers, noting data processing on digital computer [ASME PAPER 68-FE-5]

05 p0747 A69-16068

High altitude observations of luminous wake behind Black Brant 2 rockets by mounted dual wavelength spatially scanning photometer

06 p0918 A69-17511

Weakly ionized wakes study in free quasi-molecular regime of supersonic flow, using Langmuir probe in wind tunnels, discussing ion density distribution

06 p0966 A69-17639

Electron bombardment ion source generated Ar plasma beam to study wakes of disks and spheres, considering plasma interaction with bodies [AIAA PAPER 69-79]

06 p0865 A69-18200

Jet flow and wakes in external stream and tailored pressure gradients, deriving similarity solutions for boundary layer equations

08 p1252 A69-20782

Wall flows and wake laws validity analyzed by wall balance technique, considering boundary layers under perturbation and core flow restrictions

13 p2251 A69-28633

Radiating gray gas laminar jet in thermodynamic equilibrium ejected from plane nozzle into wake analyzed using boundary layer, divergence and transfer equations

14 p2432 A69-29612

Vortex shedding and wake formation behind inclined flat plate at low Reynolds number, using dye injector method for streak line observation

16 p2768 A69-31767

Turbulent and transitional near wake of adiabatic slender wedge with and without base injection at Mach 4 in supersonic wind tunnel [AIAA PAPER 68-100]

16 p2732 A69-31882

Trails arising in wake of fan type jets in transverse gas flow during uniform fuel-air mixture combustion

16 p2879 A69-32140

Secondary vortex generation in near wake of circular cylinders under forced oscillation, analyzing motion dependent transition regimes using hydrogen bubbles flow visualization [AIAA PAPER 69-755]

18 p3084 A69-34411

Transient uniform flow over sphere at intermediate Reynolds numbers with recirculatory wakes, utilizing difference approximation to time dependent Navier-Stokes equations

18 p3120 A69-34434

Coupling conditions by distinct equations for two laminar flow regions, studying near wake and considering Euler, Navier-Stokes and Prandtl correlations [ONERA-TP-738]

19 p3299 A69-36649

Transition in near wake, from study of base pressure on circular cylinders in incompressible flow

19 p3242 A69-36809

Scattering cross sections of radio waves at wake of vertically moving body near reflecting ionospheric layer, noting wave sphericity influence

20 p3486 A69-37023

Radio wave sphericity influence on scattering at moving body wake in ionosphere, determining scattering cross section principal maximum

20 p3486 A69-37024

Cold plasma approximation of whistler excitation of lower hybrid resonance at wake of body moving through ionosphere, comparing results with Alouette satellite observations

20 p3519 A69-37025

Plasma ion and electron concentration perturbations in wake of body moving at high velocity in collisionless plasma under steady magnetic field

20 p3459 A69-37659

Rarefied nonmagnetic plasma in wake of body moving at higher than electron and ion thermal velocities

20 p3525 A69-37660

Perturbed wake behind spherical models in rarefied plasma flow, noting effects of electron temperature and electric potential of models

20 p3581 A69-37957

Electrical conductivity in wake neck measured using RF bridge on boom extending from reentry vehicle

21 p3724 A69-39030

Diffusion parameters for fluid stream flowing from round hole with given radius and velocity into wake flow

21 p3696 A69-39091

Radio wave scattering cross section in wake of body moving in ionosphere, using simplified procedure with asymptotic expressions

22 p3901 A69-41094

Separation flows in flat channel with step recess, analyzing dynamic characteristics in mixing region, in wake of rarefaction waves and in attachment zone

24 p4247 A69-43498

Low Reynolds number unsteady wake flows, using hydrogen bubble flow visualization in high concentration glycerine mixtures

24 p4298 A69-43691

WALKING

Human locomotion analysis, measuring metabolic expenditure and mechanical energy levels of principal body segments during walking

15 p2558 A69-30587

WALKING MACHINES

Hopping transporter vehicle designs for lunar exploration providing low fuel consumption at high average speed [AIAA PAPER 68-1139]

22 p3927 A69-40547

WALL FLOW

Heat transfer between arc column and discharge chamber wall of vortex linear plasmatron, using approximate similitude method

01 p0125 A69-10091

Turbulent jet model of unsymmetrical velocity profile for design of wall attachment device

02 p0231 A69-12072

Impervious wall effectiveness of two dimensional wall jet, discussing effectiveness dependence on slot height and turbulence intensity [ASME PAPER 68-HT-4]

02 p0352 A69-12209

Local mass transfer from wall with homogeneous or heterogeneous chemical reactions in uniform velocity flow, Couette flow and boundary layer flow

02 p0232 A69-12234

Time dependent tube wall radial displacement during explosive welding as function of distance from initial explosion

02 p0254 A69-12675

Similarity law for channel wall influence in wind tunnels valid for all flow velocities

02 p0192 A69-12830

Boundary layers and heat transfers at shock tube walls, establishing approximate solution of boundary layer equation for laminar and turbulent cases [ONERA-TP-647]

03 p0412 A69-12875

Conservation equations for steady incompressible flow in variable area duct with mass transfer at walls simplified by linearizing inertial and convective terms

03 p0413 A69-13011

Laminar accelerating flow of thin film falling along vertical wall, emphasizing growth and decrease of boundary layer and film thickness [ASME PAPER 68-APM/Z]

04 p0586 A69-14388

Wall attachment type fluidic logic devices with low power consumption requirements, noting monostable and bistable devices

05 p0704 A69-16002

Two dimensional incompressible laminar boundary layer on curved wall for potential velocity inversely proportional to distance along origin [ASME PAPER 68-WA/FE-20]

05 p0749 A69-16096

Bistable fluid device utilizing Coanda effect along convex surface for wall attachment [ASME PAPER 68-WA/FE-27]

05 p0749 A69-16101

Velocity fields and wall shear stress distributions in eccentric annuli [ASME PAPER 68-WA/FE-35]

05 p0750 A69-16108

Integral method for backward boundary layers, developing third order polynomials for two dimensional potential flow toward opening

05 p0752 A69-16737

Simultaneous natural and forced convection flow around wall, analyzing perturbations of hydrodynamic elements due to obstacle

06 p1030 A69-17095

Kinetic boundary value problem of gas flow over plane wall with constant mass-velocity gradient

06 p0910 A69-17346

Approximate solution of equations for boundary layer flow of conducting medium on insulating and electrode walls of MHD generator channel

06 p0871 A69-17914

Nonsimilar MHD channels boundary layers on insulating walls noting influence of loading factor, wall temperature and Hall effect on separation [AIAA PAPER 69-46]

06 p0972 A69-18191

Laminar flow of viscous conducting fluid between parallel walls in traveling magnetic field, using Hartmann number expansion

07 p1192 A69-19023

Wall friction influence on three dimensional flow in axial flow turbomachines, introducing shear stresses between flow planes

08 p1252 A69-20724

Incompressible laminar thermal boundary layer unsteady development from state of rest in vicinity of wall of obstacle subjected to unsteady thermal field [ONERA-TP-680]

08 p1304 A69-20754

Highly turbulent boundary layers on walls in channels using laser light sources

09 p1515 A69-21434

MHD oscillatory flow along infinite plane porous wall with variable suction velocity, obtaining expressions for velocity and magnetic fields in boundary layer

09 p1547 A69-21607

Tangential air jet for separation control of two dimensional incompressible flow along circular cylindrical wall

09 p1431 A69-22277

Thin wall flow of circular jets in bounded transverse flow, showing hydrodynamical parameter of mixture effect on jets dimensionless path

10 p1679 A69-23567

Streamwise pressure gradient effect on velocity profile in viscous sublayer of two dimensional turbulent flow along smooth wall

11 p1872 A69-25131

Sandwich electrode for direction and magnitude measurement of velocity gradients at wall for flow around cylinder at high Reynolds numbers

11 p1872 A69-25132

Diffraction accompanying reflection of plane shock wave obliquely impinging on walls of obtuse wedge at finite incidence, considering Lighthill method

11 p1873 A69-25135

Similarity solutions for incompressible, steady hydrodynamic and thermal boundary layers on longitudinally curved walls, allowing for displacement and curvature effects

12 p2060 A69-25761

Gas jets collision flowing from parallel wall channels, applying solution to calculating geometrical characteristics of fluid jet amplifiers

12 p2016 A69-25879

MHD generators semihot wall duct, discussing structural design, ceramic insulation elements brazing, temperature control, electrodes, working fluid, etc

13 p2372 A69-27447

LF spectrum analysis of hydrodynamic flow near-wall pressure pulsations over rough surfaced wall

13 p2246 A69-27537

Wall shear stress measurement by evaporating liquid film, determining optimum liquid viscosity

13 p2375 A69-27793

Relative variations of wall friction and thermal flux for laminar incompressible flow of constant volume mass

13 p2250 A69-28357

Demixed layer at wall in shear flow of nonsedimenting suspensions with different geometries due to viscous and inertia effect superposition

13 p2251 A69-28498

Wall flows and wake laws validity analyzed by wall balance technique, considering boundary layers under perturbation and core flow restrictions

13 p2251 A69-28633

Turbulent boundary layer in corner, measuring velocities, wall shear and turbulent normal stresses by employing momentum integral and similarity analyses

14 p2431 A69-29576

Shunting effect of conducting channel walls in induction MHD machines, discussing wall effects on pressures during pumping and generating operation modes

14 p2405 A69-29912

- Turbulence constant for flows near walls, analyzing viscosity dependence on wall distance by utilizing maximum stability principle
15 p2590 A69-30048
- Steady rectilinear translational motion of circular disk-shaped slightly bent wings near solid wall in incompressible fluid medium in absence of vortices and external forces
15 p2547 A69-30583
- Flush electrostatic probe edge effect, considering Couette flow of weakly ionized compressible gas past discontinuous wall potential
15 p2653 A69-30912
- Flow and temperature boundary layers on longitudinally curved walls, giving higher approximation exact solutions
15 p2591 A69-30933
- Static pressure distribution induced by statistically roughened duct walls on supersonic stream
15 p2593 A69-31148
- Fluidic curved-wall electropneumatic converter optimization, presenting steady state, step and pulse mode responses for various positions and lengths of resistive heaters
15 p2553 A69-31298
- Steady inviscid compressible flow past wavy wall with simulated ablation, studying reflections effect on relationship between surface pressure and wall geometry
16 p2770 A69-31909
- Diagonal conducting wall (DCW) MHD generator channel flows in formulation including Hall effect, electrode drop and electrode wall angle
16 p2736 A69-32172
- Transverse turbulent pipe flow, obtaining limiting behavior of time averaged velocity gradient at wall
17 p2949 A69-33013
- Turbulent velocity distribution and wall friction calculated from eddy viscosity distribution for concentric annulus
17 p2956 A69-33575
- Visual observation of pipe wall regions in turbulent flow by suspending colloidal size particles and photographing with high speed motion picture camera
17 p2956 A69-33598
- Displacement of rectangularly mouthed pitot tubes in turbulent tube flow, determining roles of wall and shear effects
17 p2976 A69-34049
- Rough wall turbulent boundary layer development in pipe flow determined for different roughness geometries in zero and adverse pressure gradients
18 p3125 A69-33587
- Electrohydrodynamic subsonic flow of isothermal charged gas over wavy insulator wall by perturbation method, calculating surface pressure, streamlines and electric lines of force
19 p3297 A69-35837
- Electrohydrodynamic supersonic flow over wavy wall by oscillating piston model, calculating streamlines and density distributions
19 p3297 A69-35838
- Wall influence on thermoanemometer readings in incompressible air stream measured with wedge shaped film sensors
19 p3308 A69-35857
- Wall boundary condition model modification applied to molecular beam-solid surface scattering, noting qualitative agreement with observed distributions
19 p3377 A69-36179
- Wall curvature effect on hydrodynamic stability of laminar incompressible boundary layer with respect to perturbing Tollmien-Schlichting waves
19 p3299 A69-36587
- Wing tunnel and theoretical studies of hypersonic wall flow on cone, considering static pressure and convection heat flux density effects
19 p3241 A69-36759
- Thesis on turbulent velocity distribution and wall friction in flow channels of various cross sections
20 p3515 A69-37925
- Heat transfer to compressible laminar jet flowing along flat wall, obtaining distributions of temperature, wall shearing stress, heat transfer rates and jet thicknesses
[ASME PAPER 69-FLCS-30]
20 p3516 A69-37979
- LF spectrum analysis of hydrodynamic flow near-wall pressure pulsations over rough surfaced wall
20 p3518 A69-38203
- Laminar boundary layer on funnel wall, considering internal vortical and radial flow
21 p3692 A69-38611
- Analytical relations in phenomenological model theories for turbulent flow near wall
21 p3695 A69-39010
- Skin friction results from free stream velocity boundary layers with varying injection and suction wall conditions, describing flow characteristics
21 p3696 A69-39431
- Velocity and temperature boundary layers on plane wall developed by ideal shock tube flow for weak shock and expansion waves
22 p3932 A69-40894
- Laminar flow in porous circular pipe with constant suction or injection applied at wall
24 p4298 A69-42618
- Momentum, heat and mass transfer in turbulent channel flow emphasizing phenomena close to wall, using boundary layer growth-breakdown model
24 p4407 A69-42914
- Volatile wall vaporization gas flow expansion into vacuum from tube approximating unsteady mass and energy transfer and pressure at blocked end
24 p4408 A69-43489
- Laminar, transition and turbulent boundary layer heat transfer measurements along wall in thermal entrance region of high temperature turbulent airflow through cooled tube
24 p4414 A69-43560
- Taylor Goertler vortex formation effect on heat transfer through boundary layer on concave wall
[ASME PAPER 69-HT-3]
24 p4414 A69-43563
- WALL JETS**
- Switching action mechanism in wall attachment fluid amplifier, outlining theory based on turbulent jet entrainment
02 p0195 A69-12073
- Impervious wall effectiveness of two dimensional wall jet, discussing effectiveness dependence on slot height and turbulence intensity
[ASME PAPER 68-HT-4]
02 p0352 A69-12209
- Open circuit wind tunnel experiment to measure properties of two dimensional plane turbulent wall jet in moving stream
[ASME PAPER 68-WA/APM-13]
04 p0586 A69-14390
- Round air jet projected parallel to wall, analyzing velocity profiles, decay and growth rate
04 p0591 A69-15487
- Stabilizing influence of axial magnetic field on confined vortex flow of aqueous electrolytic conductor generated by two dimensional wall jets
05 p0798 A69-15611
- Wall jet type fluidic elements subjected to hydroaerodynamic effects, discussing use of boundary layer flow properties
05 p0705 A69-16016
- Tangential stress distribution and heat transfer in circular cylinder with attached wall jet
05 p0746 A69-16022
- Laminar conducting wall jet injected in transverse magnetic field, analyzing partial differential equations obtained
07 p1192 A69-19020
- Incompressible jets bounded by infinite auxiliary thin jets, discussing straight wall jets and establishing existence and uniqueness of boundary value problem solution
09 p1480 A69-21734
- Turbulent circular wall air jet trajectory and spreading in perpendicular crossflow of constant and varying velocities
[ASME PAPER 69-GT-33]
09 p1483 A69-22491
- Turbulent wall jet growth in streaming two dimensional incompressible flow over plane smooth wall with pressure gradient
11 p1873 A69-25139
- Attachment and separation of free jet from wall, discussing model equations for wall attachment fluid amplifier
14 p2428 A69-28877
- Incompressible laminar jet bounded by two parallel walls or by three walls, using linearized analysis related to Oseen approximation
14 p2429 A69-29023
- Incompressible attached wall jet (Coanda flow) over circular cylinder with finite incompressible injection normal to surface
16 p2772 A69-32148
- Circular jet flow exhausting at right angles from plane wall into uniform cross flow, considering application to V/STOL aircraft
17 p2896 A69-34036
- Film cooling slot adiabatic wall effectiveness measurement in two dimensional constant property flow, showing role of lip thickness and injection angle
20 p3585 A69-37082
- Coanda effect of separated jets reattachment to wall at high Knudsen number in pneumatic fluidic devices, discussing Reynolds and Mach numbers effect
[ASME PAPER 69-FLCS-37]
21 p3692 A69-38602
- Velocity decay and heat transfer rates measurement in cylindrical wall jet formed by jet emerging through convergent nozzle
21 p3695 A69-38972
- Free and dividing streamlines shapes for two dimensional jet from parallel walls penetrating into counterstream, discussing finite cavities
22 p3859 A69-40143
- WALL PRESSURE**
- Compressible and incompressible laminar boundary layer with constant wall shear stress, using initial profiles
02 p0233 A69-12535
- Pressure distribution at wedge wall during instantaneous small variation of supersonic motion
03 p0364 A69-13662
- Static pressures, profiles of local longitudinal velocity, fluctuating wall pressures and power spectra of wall pressures measured for subsonic turbulent flow
[ASME PAPER 68-WA/FE-36]
05 p0750 A69-16109
- HF instability of steady combustion process with allowance for elastic strains in chamber walls
07 p1242 A69-18993
- Wall pressure fluctuations due to turbulent boundary layer flow, calculating statistical properties
[AIAA PAPER 68-642]
13 p2244 A69-27246
- Wall pressure and heat flux distribution in hypersonic flow on delta wings at variable angle of attack for low Reynolds numbers
16 p2731 A69-31605
- Steady inviscid compressible flow past wavy wall with simulated ablation, studying reflections effect on relationship between surface pressure and wall geometry
16 p2770 A69-31909
- Pressure in sealing groove and increase time due to pumping action of moving wall applied to force cylinder of translational motion, considering liquid in groove laminar
16 p2736 A69-32135
- WALL TEMPERATURE**
- Time history of unsteady heat transfer in laminar boundary layer over semiinfinite flat plate due to step change in wall temperature or wall flow
01 p0177 A69-11401
- Nonlinear diffusion of heat in semiinfinite wall having thermophysical characteristics dependent on temperature, showing dissymmetry between heating and cooling
01 p0177 A69-11404
- Film cooling by subsonic gas injection of air through porous flat plate into 2.9 Mach air flow, noting wall temperatures
03 p0413 A69-12994
- Similar solutions of boundary layer equations for compressible model fluid adjacent to wall, discussing velocity overshoot dependence on wall temperature
03 p0413 A69-13013
- Entry region flow and convective heat transfer prediction in cooled vertical pipe open at both ends, considering wall temperature
05 p0845 A69-15717
- Stability of laminar natural convection boundary layer flow, discussing thermal capacity coupling between fluid and wall and Prandtl number
05 p0744 A69-15719
- Heat transfer in accelerated turbulent boundary layer between converging planes with varying wall temperature and decreasing Stanton number
[ASME PAPER 68-WA/HT-13]
05 p0847 A69-16120
- Wall temperature and Mach number effect on heat flux distribution at spreading line of flow for supersonic gas on ellipsoid of revolution
06 p0858 A69-17331
- Convection in conducting fluid filled cavities with variable wall temperature due to magnetic field, with results applicable to rheological systems
07 p1241 A69-18921
- Wall temperature influence on intensity of transverse flow of three dimensional laminar boundary layer resulting from transverse pressure gradient
08 p1251 A69-20274
- Turbulent heat transfer in conducting fluid flow through circular tube in longitudinal magnetic field and constant wall heat flux, using Lyon relation
09 p1621 A69-21590

Wall temperature and Prandtl number effects on turbulent boundary layer thickness and shape factors for subsonic compressible gas flow over flat plate
[ASME PAPER 69-GT-55] 09 p1432 A69-22513

Heat and mass transfer between cryogenic fluid and superheated wall, analyzing experimental data
11 p1996 A69-24228

Laminar Newtonian flow heat transfer to fluids with variable physical properties in vertical tubes with constant wall heat flux, considering viscosity and density
11 p2000 A69-25164

Free convection boundary layer flow past vertical flat plate analyzed for nonlinear wall temperature distributions using series solutions
11 p2002 A69-25243

Initial nonuniformity effect of temperature distribution in main stream on efficiency of cooling by air injection through slit or porous collar
11 p2002 A69-25338

Temperature variation effects on heat transfer in laminar tube flow, taking into account constant wall temperature and heat flow density
12 p2189 A69-25762

Heat transfer coefficient deterioration between fluid and tube wall at supercritical pressure and high heat fluxes
[ASME PAPER 68-HT-39] 13 p2373 A69-27771

Differential approximation for radiative transfer between concentric spheres enclosing gray gas
[ASME PAPER 68-HT-21] 13 p2373 A69-27774

Eddy diffusivities ratio for heat and momentum by mixing length theory, using Mach-Zehnder interferometer for temperature profiles
13 p2380 A69-28497

Similarity solutions for laminar compressible boundary layer with reverse flow, considering various wall/stagnation temperature ratios
15 p2591 A69-30907

Nonequilibrium plasma boundary layer along channel insulator wall, noting different electron and heavy particle temperatures
[AIAA PAPER 68-134] 16 p2821 A69-31873

Conical shock wave-turbulent boundary layer interaction data obtained for adiabatic wall conditions at supersonic free stream Mach numbers, including suction effects
[AIAA PAPER 69-450] 16 p2773 A69-32754

Mach number, cone angle, bluntness and wall to recovery temperature ratio effects on slender cones boundary layer transition measurements at hypersonic speeds
17 p2890 A69-33250

Viscous convergent-divergent nozzle flow slender channel approximations, discussing roles of nozzle geometry, Reynolds number and wall temperature, calculating velocity, enthalpy, etc
[AIAA PAPER 69-654] 17 p2894 A69-33502

Contact thermocouples to measure temperature of wall exposed to radiation, evaluating errors
17 p2975 A69-33596

Superposition method for predicting tube wall temperatures with gas property and heating rate axial variation, noting application to gas flow problems
18 p3227 A69-34315

Convective heat flux from nonisothermal surface by temperature superposition method with Spalding function as turbulent heat transfer coefficient, noting wall temperature
18 p3229 A69-34836

Wall temperature distributions predicted in turbulent boundary layer with arbitrary pressure gradients, basing calculations on Spalding function solutions
19 p3302 A69-36853

Local heat transfer coefficients determined from temperature distribution on porous walls, deriving mathematical expressions for various surface geometries and transfer modes
20 p3630 A69-36977

Laminar free convection from horizontal infinite strip with downward facing thermally insulated vertical walls at edges, noting boundary layer thickness and flow pattern
21 p3853 A69-39672

Hypersonic flow for low Reynolds number, including magnetic field and wall temperature effects on heat transfer and skin friction for blunt shapes
22 p3860 A69-40540

Hot gas flow through multilayer cylindrical shells, calculating temperature fields in walls
24 p4407 A69-42588

WALL TEMPERATURE DISTRIBUTION

U TEMPERATURE DISTRIBUTION
WALLS
NT BULKHEADS
NT NOZZLE WALLS

NT POROUS WALLS
NT THICK WALLS
NT THIN WALLS
NT WIND TUNNEL WALLS

Channel wall effect on gain of apparent mass of cylindrical and elliptical bodies floating in channel and subject to vertical impact
11 p1875 A69-25487

Heat transfer mechanisms between fluidized beds and wall surfaces by application of film penetration theory of mass transfer, noting bubbling bed model
20 p3632 A69-37519

WANKEL ENGINES

Rotary engines, discussing scissor, eccentric rotor, multiple rotor and revolving block types
07 p1203 A69-18910

Book on Wankel RC engine design and performance covering sealing, timing, life, lubrication, etc
11 p1942 A69-25237

Wankel aircraft engines compared to piston and turbine aircraft engines for performance, maintenance and reliability
19 p3395 A69-36872

WARFARE

NT COMBAT

CH-46 Sea-Knight and CH-47 Chinook transport helicopters experience in Vietnam war, discussing missions, payloads, speeds, operating ranges, etc
01 p0009 A69-10405

Tactical support aircraft size, economy and flexibility requirements based on Vietnam experience
04 p0549 A69-15486

Helicopter use in military activities noting role in overcoming combined enemy, weather and terrain conditions
[AIAA PAPER 69-190] 07 p1244 A69-19547

Military applications of VTOL aircraft, discussing role in battle area with restricted surface transportation
[AIAA PAPER 69-326] 07 p1055 A69-19556

Briteye battlefield illumination flare configuration, candle power, burn duration and hot air balloon-type suspension system
20 p3461 A69-37166

WARHEADS

Detonation system for exploding missile warheads, discussing trigger detonation and safety release elements
17 p3050 A69-33698

WARMING

U HEATING

WARNING SYSTEMS

NT BALLISTIC MISSILE EARLY WARNING SYSTEM
NT EARLY WARNING SYSTEMS
NT MINE DETECTORS

All-weather landing flight director systems and fault warning display simulator studies of Boeing 707-720B aircraft in Category 3-C environment
01 p0010 A69-10455

Industry airborne collision avoidance systems /CAS/ development program, discussing cooperative devices in aircraft
05 p0790 A69-16725

Pilot warning indicators to equip all aircraft at low cost, discussing Doppler system
05 p0790 A69-16726

Solar flare in-flight radiation detection and warning system for Concorde SST, noting radiation hazards due to solar cosmic rays
07 p1131 A69-18551

Hypoxia warning system based on dry electrolyte oxygen sensor with millisecond response time
07 p1071 A69-19430

Aircraft electronic proximity warning devices applications, discussing compatibility in ATA collision avoidance system
[SAE PAPER 69-0340] 11 p1914 A69-24496

Airborne collision avoidance system /CAS/ performance and operational requirements
11 p1914 A69-25430

Collision avoidance system for air traffic, discussing false signal discrimination via electronic measurement of light pulse duration from aircraft Xenon discharge beacon lamp
12 p2129 A69-26772

Bird warning and forecast systems based on radar data covering 50 mile radius from airport
17 p2899 A69-33367

Low cost pilot proximity warning instrument, discussing design influences of Xe strobe lights, atmospheric radiation transmission characteristics and detection considerations
17 p2917 A69-34103

Concorde SST fire protection equipment, discussing fire and overheat detectors, fire extinguisher, crash fire protection, explosion suppression equipment, etc
19 p3256 A69-36864

Solar flare radiation hazard to SST crew and passengers, discussing onboard and ground based warning systems and ICAO requirements
23 p4063 A69-41820

Antenna design, based on helical beam radiator data providing checking facility giving automatic alarm
24 p4312 A69-42510

WARPAGE

Warping rigidity effect on stability of cantilever beam under eccentric follower end load, discussing bending torsional flutter and buckling
12 p2179 A69-26210

Woven roving construction and fill/warp ratio effects on flexural strengths of four ply laminates
14 p2469 A69-29414

Elastic stability of warped rods, using small oscillations method for varying end conditions and torsional moment vector behavior
17 p3057 A69-33196

Near resonant oscillations of warped turbine or compressor blades, discussing stress-strain relations
17 p3064 A69-33918

Energy dissipation in vibrating warped turbine blades subject to complex stress-strain rate produced by simultaneous bending, torsional and tensile stresses
17 p3065 A69-33924

Design laws of warping-free multicellular box beams under torsion or bending, using variational method
19 p3443 A69-36786

Warping of doubly supported submerged wings, calculating stress and strains due to bending and constrained torsion
23 p4225 A69-41423

WASHINGTON

Washington area airport efficient use plan from projections of passengers, aircraft operations and net revenue trends
22 p4053 A69-40709

WASHOUT [RADIOACTIVITY] U FALLOUT

WASPALOY

Carbon influence on cast Waspaloy, discussing chemical segregation, chemical gradients and tensile ductility
[SAE PAPER 69-0100] 07 p1158 A69-18307

WASTE DISPOSAL

Mars contamination with terrestrial microorganisms, considering possibility of waste materials ejection from manned orbital vehicles
05 p0714 A69-15951

Reactors technical characteristics for high temperature mineralization of closed life systems biological wastes, deriving equations to estimate energy balance
10 p1649 A69-23504

Mineralizing metabolic wastes by catalytic oxidation of pyrolysis products, noting nutritive value of ash solutions for *Chlorella* cultivation
10 p1649 A69-23579

Water purification through biological oxidation of organic wastes using controlled photosynthesis, discussing algae production and harvesting
21 p3668 A69-39711

WASTE UTILIZATION

Mineralized human wastes solutions utilization for *Chlorella* cultivation, noting growth rates
02 p0200 A69-11511

Integrated Waste Management/Rocket Propulsion System, using human feces as propellant component
[SAE PAPER 68-0717] 03 p0495 A69-13442

Wet oxidation process for management of organic waste products in closed ecologies of long term manned space missions
[SAE PAPER 68-0714] 03 p0380 A69-13443

Physicochemical method for converting human urine and feces into carbohydrates in closed ecological systems
03 p0381 A69-14195

Biowaste propelled resistojet control systems selection criteria based on NASA Manned Orbital Research Laboratory with six man crew
[AIAA PAPER 68-121] 04 p0554 A69-15506

Monosaccharide production from carbon dioxide from respiration or human waste incineration, evaluating toxicological effects of synthetic monosaccharides
15 p2557 A69-31477

Open cycle air evaporation technique selected for water recovery from human urine, based on tradeoff studies
19 p3258 A69-36455

Separation system for collecting wash and waste water from gaseous environment and separating liquid and gaseous phases during space missions
[AAS PAPER 69-473] 24 p4272 A69-42845

Material recovery from metabolic and other wastes for long duration manned space missions, discussing carbon dioxide removal, bioregenerative food systems, etc
[AAS PAPER 69-143] 24 p4272 A69-42876

ASTES
U FECES
U HUMAN WASTES
U METABOLIC WASTES
U RADIOACTIVE WASTES
U URINE

ATCHES
U CLOCKS

ATER
NT HEAVY WATER
NT POTABLE WATER
NT SEA WATER

Fine structure of vibrational spectra of molecular H and O, water and deuterium oxide, using molecular photoelectron spectrometer
01 p0023 A69-10141

Water and carbon dioxide IR spectra compared with laboratory measurements
05 p0759 A69-16638

Automatic inflators for life jackets and survival gear in emergencies activated after submersion in water
06 p0877 A69-16955

Water cooling jackets of plastic textile reinforced film for high inside temperature reduction in protective clothing
06 p0883 A69-18027

Water in interstellar regions detected by microwave emission from 6 sub 16 to 5 sub 23 rotational transition
08 p1383 A69-19896

Water molecules radio spectral lines from microwave emission sources in Galaxy studied for variability, size and polarization
09 p1587 A69-21307

Optical parametric noise in water by ruby laser beam for phase matched four photon process
09 p1539 A69-21751

Gas vacuoles development in blue green algae by cell transfer from defined medium to distilled water
10 p1644 A69-23184

Water content of tektites, impactites and artificial glass of tektite composition using IR absorption measurements
10 p1778 A69-23413

Millimeter wave propagation over water, discussing fading characteristics and atmosphere absorption effects
11 p1836 A69-24989

Simultaneous HCN and HOH laser emission in pulsed discharge through mixture containing H, C, N and O
12 p2107 A69-26330

Water and carbon dioxide IR spectra compared with laboratory measurements
14 p2433 A69-28794

Aluminum corrosion in ethylene glycol-water systems, discussing protection mechanisms of adsorption-type inhibitors and additives effects on corrosion rate
14 p2466 A69-29932

Removal rate of reaction water from fuel cells by diffusion-condensation procedure as function of temperature and electrolyte concentration
16 p2736 A69-32200

Medium temperature fuel cells advantages including improved electrochemical reaction kinetics, water and heat removal
16 p2739 A69-32417

Statistical characteristics of wind wave development in initial stage, obtaining distribution functions and frequency spectrum for various velocities and temperatures
18 p3167 A69-35341

Rivers on moon, discussing possibilities of water existence on lunar surface in view of temperature, gravity and atmospheric conditions
19 p3419 A69-36145

Air bubbles rise velocity and path in water based on time measurement of bubble traversing two light beams, describing electronic recording system
24 p4299 A69-42918

WATER BALANCE
Transient electro-osmosis of water in capillary tubes for pumping and generation modes, analyzing response to step change in pressure or voltage change under external loading
04 p0555 A69-14862

WATER CONSUMPTION

Test dogs feeding through enteropancreatic fistula homogenized mixture containing juice excretion stimulating agents during long space flight
08 p1265 A69-19829

WATER CONTENT

U MOISTURE CONTENT

WATER COOLED REACTORS

U NRX REACTORS
U PLUM BROOK REACTOR

WATER DEPRIVATION

Electrode stimulated hypothalamic drinking in rats compared with drinking induced by water deprivation, noting difference in consumption
17 p2910 A69-33750

WATER EROSION

Ceramic radome materials resistance to rain erosion at high Mach numbers
07 p1171 A69-19532

Wind tunnel rain erosion testing of components of aircraft or missiles flying at high speed
07 p1117 A69-19534

Cumulative damage concept for rain erosion of solid materials, noting incubation period and similarity to microscopic damage in fatigue failure
12 p2187 A69-26848

Vacuum chamber model for sinuous rilles on lunar surface produced by aqueous erosion under ice blanket
14 p2485 A69-28873

Rain erosion problems in aircraft design, reviewing protective measures for all-weather aircraft
21 p3646 A69-38393

Rain erosion process on aircraft surface, using single impact test apparatus with photographic recording and photoelastic study
23 p4227 A69-41872

WATER FLOW

LF spectral analysis of flowing water pressure pulsations behind single bulge on hydrodynamic channel smooth wall at low disturbance level
13 p2246 A69-27535

Liquid-vapor interaction in loop plates with different heat pipe capillary geometries using water as heat transporting medium
14 p2539 A69-29207

Self diffusing substance /salt/ distribution in turbulent water flow at different Reynolds numbers by NMR, obtaining diffusion function consistent with experiments
14 p2430 A69-29424

Vortex wakes behind circular cylinder subject to transverse sinusoidal oscillations in uniform water flow at specific Reynolds numbers, photographing varied frequency flow patterns
18 p3086 A69-35169

LF spectral analysis of flowing water pressure pulsations behind single bulge on hydrodynamic channel smooth wall at low disturbance level
20 p3518 A69-38202

Distributed suction effect on boundary layer structure of water flow from turbulence measurements, determining velocity and pulsation intensity distributions
22 p3933 A69-41029

WATER HAMMER

Analog simulation of water hammer type phenomena governed by linear constant coefficient partial differential equations
05 p0751 A69-16475

WATER INJECTION

Nuclear rocket engine exhaust gas cooling by injecting water jet eliminates need for secondary cooling
[AIAA PAPER 68-604] 04 p0591 A69-15516

Mean drop size generated in vapor pressure regime of liquid water jet, noting effect of water temperature and orifice diameter
09 p1483 A69-21995

Water injection cooling of exhaust gases during stage testing of NERVA engine, discussing exhaust duct configuration and flow characteristics, spray nozzle geometry, etc
[AIAA PAPER 69-514] 19 p3372 A69-36301

WATER JETS

U HYDRAULIC JETS

WATER LANDING

NT DITCHING [LANDING]

Problems connected with rescue of crew members ejected over water
15 p2551 A69-30866

WATER LOSS

Exploding wire discharges similarity with underwater sparks for understanding water breakdown and parallel discharges
01 p0117 A69-10657

Vacuum, radiation and freeze drying effects on survival rate of microorganisms, noting influence of protective materials on extent of damage
07 p1064 A69-18943

Energy source for space environments based on compact cold hydrogen-oxygen fuel cell, discussing heat control and water elimination methods
08 p1260 A69-21041

Justi-Winsel extraction process by electrodialysis for removing product water from electrochemical reaction in H-O fuel cells
08 p1260 A69-21043

Moisture losses of men wearing partial pressure suit with oxygen mask determined by changes in skin temperature and heat flow
10 p1647 A69-23591

Optimization of electrodyalytic extraction process of water from H-O fuel cells through choice of current density as function of electrolyte concentration
16 p2738 A69-32414

Urine excretion following water load in male subjects exposed to normal, hot/dry and comfortable/dry environment applied to airline crews
17 p2914 A69-33182

Insensible water loss from human skin as function of ambient vapor concentration using IR gas analysis, applying results to water loss model revision
23 p4077 A69-41293

WATER MODERATED REACTORS

Water moderated beryllium reflected reactor design for testing NERVA or Rover type fuel elements in nuclear environment, noting core location
[AIAA PAPER 69-513] 16 p2810 A69-32656

WATER PRESSURE

Lung ventilation mechanics affecting respiration in hyperbaric environment during deep diving, stressing biological necessity of equal pressure respiration
13 p2215 A69-28598

Aircraft tire skidding on wet surfaces, measuring interstitial water pressure for various treads, velocities and surface textures
19 p3247 A69-35910

WATER RECLAMATION

Space controlled microbiology, discussing telemetry control of waste material conversion in air and water pollution
[UN PAPER 68-95861] 01 p0014 A69-10456

Biological problems in prolonged space voyages including oxygen replacement, water supply and food regeneration
01 p0020 A69-11075

Membrane vapor diffusion for water reclamation from urine and wash water on space missions
03 p0379 A69-12992

Microbiology of water management subsystem for manned space flight, discussing sterilization by heat and tests inside Integrated Life Support System (ILSS) [SAE PAPER 680718] 03 p0379 A69-13441

Regenerative life support systems, discussing water reclamation, carbon dioxide removal, onboard oxygen generation and radio isotope thermal energy sources
19 p3262 A69-36318

Open cycle air evaporation technique selected for water recovery from human urine, based on tradeoff studies
19 p3258 A69-36455

Separation system for collecting wash and waste water from gaseous environment and separating liquid and gaseous phases during space missions
[AAS PAPER 69-473] 24 p4272 A69-42845

WATER TAKEOFF AND LANDING AIRCRAFT

NT SEAPLANES

Water hover effects tested on tilt wing V/STOL seaplane model, noting effects of wind and waves on water passing through propellers
01 p0011 A69-11061

Helicopter seaworthiness, comparing full scale sea landing and flotation studies with model test results
08 p1255 A69-20653

Tilt wing V/STOL aircraft spray circulation characteristics in overwater operation, examining forces, moments and generated environmental conditions
[AIAA PAPER 69-791] 19 p3243 A69-35638

WATER TREATMENT

Water purification through biological oxidation of organic wastes using controlled photosynthesis, discussing algae production and harvesting
21 p3668 A69-39711

WATER TUNNELS

U HYDRAULIC TEST TUNNELS

WATER VAPOR

WATER VAPOR

- Crack growth in ceramics from velocity measurements on glass and sapphire as function of applied force, temperature and moisture environment
01 p0101 A69-10767
- Radio telescope measurements of total vertical atmospheric absorption to determine effective mean free path of oxygen and water vapor for absorption
02 p0206 A69-11450
- Spectral transmission for water vapor and carbon dioxide bands
02 p0236 A69-11451
- Submillimeter water vapor laser power output for admixtures of H, N, carbon dioxide, methane, He and Ar, noting buffer effect of H
04 p0612 A69-15175
- Pulsed water vapor laser with single Brewster window for operation between 20 and 120 microns, comparing performance with ordinary laser
05 p0776 A69-16334
- Submillimeter wave absorption by dimeric water in atmosphere, using interferometer and maser
05 p0759 A69-16658
- Atmospheric ozone photochemistry, studying time dependence on hydrogen compounds, equilibrium concentration effects on reaction rates, latitude and season
06 p0916 A69-17004
- Vibrational excitation by electron impact in kinetic energy range 30-60 eV studied for water vapor and carbon dioxide, determining intensities relative to elastic scattering
06 p0960 A69-17108
- Water droplet simulation by glass spheres used in study of light scattering at cloud particles
06 p0953 A69-17992
- Atmospheric water vapor content determination from microwave radiation measurements and satellite aircraft
06 p0953 A69-17996
- Long wave radiative water vapor cooling in troposphere determined by numerical prediction model, including vertical distribution of cloud and moisture effects
07 p1175 A69-18896
- Water vapor absorption line for nitrogen and oxygen mixtures with frequency measurements at various pressures and temperatures, discussing attenuation and line breadth
07 p1184 A69-18911
- Bulk aerodynamic method for heat and water vapor fluxes from data obtained at Chiba (1966), introducing modified integral diffusivity
07 p1176 A69-18965
- Molecular line intensity requirement in line of sight for detecting interstellar water vapor cloud, assuming transparent atmosphere and ideal radio telescope
09 p1591 A69-21446
- Spacecraft debris atmosphere effects on observations, discussing contamination of exposed optical surfaces and light scattering by ice particles from cabin water vapor leakage
09 p1487 A69-21654
- Solar radiation absorption measurements by balloon for atmospheric water vapor distribution
09 p1536 A69-21864
- Vertical atmospheric absorption of radio waves by water vapor and oxygen molecules near rotational resonance based on radio emission measurements
10 p1658 A69-23944
- Water vapor laser, discussing water vapor molecular structure, population inversion mechanism, perturbation model, etc
12 p2106 A69-26325
- Venusian water vapor spectroscopic data indicating longitudinal and time dependent variations in abundance
13 p2345 A69-27650
- Satellite and rocket probe measurements of water vapor in mesosphere
13 p2253 A69-27694
- Vapor phase reaction sequence to explain water cluster ions in D region
14 p2434 A69-28940
- Undulation in output waveforms of pulsed water vapor laser observed with In-doped Ge detector
14 p2461 A69-29887
- Corrosive wear by atmospheric air and moisture under nonscuffing conditions, noting control by dry nitrogen blanketing and oil additives [ASLE PAPER 68-LC-10]
15 p2622 A69-30608
- Submillimeter atmospheric absorption spectra, emphasizing absorption by isotopic and vibrationally excited forms of water molecules
15 p2568 A69-30699

- Radio wave absorption by water vapor in Venusian and Martian atmospheres, constructing model from Venera 4 data
15 p2569 A69-30952
- Water vapor recondensation effect on structure of liquid particle flow into vacuum
16 p2769 A69-31869
- Virtual temperature change with respect to height of saturated air rising during water vapor condensation, discussing actual temperature and precipitation factor
16 p2808 A69-32454
- Submillimeter water vapor laser power output for admixtures of H, N, carbon dioxide, methane, He and Ar, noting buffer effect of H
18 p3152 A69-34717
- Water vapor absorption at submillimeter wavelengths in atmospheric window regions related to foreign gas pressure, using HCN maser
18 p3152 A69-35241
- Water vapor microwave emission measurement from galactic hydroxyl sources
18 p3205 A69-35435
- Charge exchange cross sections and electron losses in hydrogen ion beam impacting on water vapor molecules
19 p3378 A69-36190
- Water vapor laser submillimeter emission spectra, considering rotational and vibrational laser transitions due to electron impact and molecular interactions
19 p3336 A69-36349
- Pulsed water vapor laser high power operation and strongest component wavelength measurement
19 p3337 A69-36416
- Maser submillimeter emission lines used to determine atmospheric and water vapor absorption, noting role of pressure
20 p3553 A69-37296
- Rocket probe devices based on thermometrical body principle for measuring upper atmosphere water vapor and atomic oxygen
20 p3543 A69-37798
- Satellite onboard transmission measurements determining atmospheric water vapor influence on integrated refractivity at specific absorption line resonant frequency
20 p3545 A69-38097
- Water vapor profiles in stratosphere from IR radiometric observations under cloudless conditions, indicating relation to tropospheric meteorological features
20 p3535 A69-38261
- Saturn surface spectrum near ring shadow examined for water vapor content in ring and greenhouse effect on surface
20 p3616 A69-38305
- Solar spectrum data covering wavelength intervals from 13138-14707 and 21877-17731 A and 1.4 micron water band
21 p3800 A69-38682
- Cavitation flow of water and ethyl alcohol in venturi tube, noting effect of varying vapor concentration and thermodynamic properties
21 p3696 A69-39101
- Dispersion and correlation function for atmospheric transparency due to water vapor from statistical model of absorption bands and effective mass
21 p3759 A69-39113
- Molecular hydrogen, oxygen and deuterium additions effect on CW laser operation with ordinary and heavy water as active medium
21 p3738 A69-39131
- Construction and components of laboratory water vapor laser emitting coherent radiation in far IR
21 p3738 A69-39446
- Water vapor abundance in Mars atmosphere determined from spectrograms, noting restricted existence on surface
22 p4018 A69-40268
- Weld porosity in Al alloys as function of composition variations, discussing water vapor contamination of welding arc
22 p3956 A69-40461
- Germanium single crystals etching with water vapor and hydrogen sulfide in hydrogen flow system, studying concentration, pressure and temperature effects on surface reactions
22 p3970 A69-40737
- Electron excitation and collisional energy transfer processes in laser level of pure carbon dioxide fill and carbon dioxide-water vapor mixture
23 p4171 A69-41390
- Pure water vapor and water vapor-air mixture continuum absorption of carbon dioxide laser radiation measured to determine atmospheric attenuation
23 p4173 A69-41631

WATER VEHICLES

- NT AIRCRAFT CARRIERS
- NT CAPTURED AIR BUBBLE VEHICLES
- NT NUCLEAR POWERED SHIPS
- NT SHIPS
- NT SUBMARINES
- Hovercraft handling characteristics, seakeeping and maneuverability during English Channel operation
02 p0277 A69-11592
- Maritime radio communications satellite service for ship safety, discussing stationary equatorial satellite systems [AIAA PAPER 68-232]
02 p0356 A69-12383
- Semi-amphibious Vosper VT 1 hovercraft for passengers and cars, discussing design, water contact propulsion, peripheral skirt, supercavitating propellers, structure, performance, etc
04 p0549 A69-15187
- Monograph on air cushion vehicles /ACV/ in Scandinavian water transport, covering state of the art, technical and economic competitiveness, etc
09 p1434 A69-22075
- Skirts on hovercraft, noting rough water drag, plough in and overturning, and skirt oscillation and wear problems
10 p1634 A69-23629
- Hovercraft development by British Hovercraft Corporation, discussing technical contributions in design, control and propulsion, environmental tests, etc
12 p2014 A69-27140
- Mountbatten /SR.N4/ hovercraft development, seakeeping, skirt design and service introduction
15 p2550 A69-30479
- Near field flow noise generated in boundary layer of water vehicle measured for rotating cylinder, ship and buoyant unit using hydrophone
17 p3004 A69-32953

WATER WAVES

- Water hover effects tested on tilt wing V/STOL seaplane model, noting effects of wind and waves on water passing through propellers
01 p0011 A69-11061
- Airborne magnetometer application for remote measurement of ocean wave spectra, obtaining wave noise power spectra and wave height profile
12 p2075 A69-26998
- Laser profilometer to measure sea wave profiles from airborne platform, describing transmitter, receiver and signal processor
21 p3739 A69-39461

WATERPROOFING

- Rain repellent system providing transparent film on aircraft windshield surface
06 p0877 A69-16954

WAVE ATTENUATION

- NT ACOUSTIC ATTENUATION
- NT MANDELSTAM REPRESENTATION
- NT RADAR ATTENUATION
- NT RADIO ATTENUATION
- NT SHOCK WAVE ATTENUATION
- Plasma ion oscillation suppression by intensified electron plasma oscillations
02 p0287 A69-11934
- Viscous damping of internal waves on rotating earth, analyzing spatial propagation attenuation in two layer system
02 p0247 A69-12775
- Decay stability of large amplitude neutral wave into two ion acoustic waves in weakly ionized plasma
03 p0475 A69-13158
- Electromagnetic wave dispersion and damping in mixed molecular crystal, relating refractivity, wave absorption and concentration shift of bottom of exciton band to other parameters
03 p0484 A69-13279
- Circuit for accurate division of attenuation and phase shift changes, noting calculation errors
04 p0573 A69-14337
- Elastic behavior of large blood vessels in canine aorta by measuring dispersion and attenuation of artificially induced pressure waves
04 p0553 A69-14692
- Nonlinear damping of circularly polarized electromagnetic wave propagating in plasma along magnetic field, noting particle motion in resonance region
04 p0558 A69-14982
- Disturbing TM mode generation effect on attenuation measurement accuracy in TE mode attenuators
08 p1283 A69-20126
- Two dimensional unsteady wave motion in shallow water using MHD theory
08 p1362 A69-20354

Wavelength dependence of polarization and UV-VIS photometry of highly polarized stars, correlating IR interstellar extinction with maximum polarization wavelength
12 p2153 A69-25809

Elliptical waveguide design dimensions for minimum attenuation in fundamental mode, giving formulas for attenuation constant and minor-major axis ratio
12 p2044 A69-27070

Optimal thickness of inhomogeneous absorption layer subjected to normally incident plane monochromatic wave treated as Mayer-Boltz variational problem
13 p2297 A69-27381

Elastic microwaves propagation attenuation along lithium niobate crystals trigonal axis at various temperatures
15 p2665 A69-30040

Love wave amplitude data satisfying earth model with intrinsic internal friction at depths assumed due to single thermally activated relaxation
15 p2596 A69-30624

Plasma turbulence effect on magnetosonic wave attenuation, noting increased electron and ion collision frequency and appearance of anomalous resistance
16 p2820 A69-31794

Wave damping in current sheet in geomagnetic tail by radiating energy from sheet sides by electrostatic waves
[AFCL-69-0396]
16 p2781 A69-32318

Waveforms analyzer for mixtures of exponentially damped sine waves, noting application to interferometer curves in plasma wave propagation
17 p2970 A69-32852

Longitudinal plasma waves collision damping calculations using Rostoker test particle method
18 p3179 A69-34439

Short radio wave damping of earth satellite transmitter due to ionospheric diffraction resulting from increasing satellite-ground station distance
20 p3491 A69-37689

Book on ultrasonics theory and application covering generation, propagation and dissipation of ultrasonic waves of high and low intensities
20 p3545 A69-37903

X ray sources and diffuse background radiation observed in gamma and X ray spectral regions, considering electromagnetic waves attenuation by interstellar matter
21 p3789 A69-38817

Electromagnetic waves attenuation and field structure within gas filled dielectric waveguide tube, tube walls and waveguide surroundings
21 p3674 A69-39123

MHD waves attenuation in ionosphere due to gyrorelaxation, reducing analysis to determination of anomalous absorption of acoustic waves
23 p4155 A69-41841

Detonation wave instability and damping in gas containing liquid or solid inflammable aerosol, considering atomized propellants
23 p4240 A69-42339

Ionospheric heating and velocity dependence of collision cross sections on transversely propagated equatorial hydromagnetic waves, discussing ordinary and extraordinary modes
23 p4161 A69-42437

WAVE DEGRADATION

Arbitrary form temperature rate wave growth and decay, determining differential equation governing wave amplitude
21 p3853 A69-39671

WAVE DIFFRACTION

Terrain influence in ground wave propagation evaluated by two dimensional diffraction and scattering problems, using Airy type wave functions
[AFCL-68-0212]
01 p0033 A69-10970

Axisymmetric optical filter synthesis based on holographic technique for making Gabor zone plates, using scalar diffraction theory
02 p0249 A69-11927

Diffraction of cylindrical and plane waves in system of two parallel circular cylinders, using equivalent circuit method
02 p0217 A69-12261

Diffraction by rocket exhausts, discussing electromagnetic signal attenuation based on two dimensional straight edge diffraction model
02 p0209 A69-12352

Lighthill method based expressions derived for discontinuity shape formed during shock wave diffraction near small angle
02 p0234 A69-12588

Diffraction of cylindrical waves at half plane in cold anisotropic plasma, using Fresnel integrals
02 p0293 A69-12842

Nonlinear weak shock wave diffraction around convex angled corners in polytropic inviscid thermally nonconducting gas
03 p0412 A69-12848

Electromagnetic diffraction theory for radar cross section of aircraft, missiles and satellites, discussing mathematical representations of electromagnetic field for extreme wavelengths
03 p0383 A69-12902

HF approximations, discussing plane wave diffraction by conducting circular cylinder using Watson transform
03 p0384 A69-12903

Missile radar cross section based on modeling from simple forms, noting computer program
03 p0384 A69-12910

Diffraction coefficient for higher order edge-edge interaction terms in two dimensional diffraction by narrow slit and small circular aperture
03 p0396 A69-13631

Electromagnetic wave diffraction at uniformly expanding sphere solved by Kirchhoff method
03 p0397 A69-13719

Radio waves diffraction around earth with atmospheric dielectric constant having linearly quadratic height dependence
03 p0399 A69-14130

Diffraction effects on periodic structures in millimeter wavelength range, discussing apparatus for measurements of Fraunhofer zone field, polarization and phase characteristics
04 p0598 A69-14852

Radio wave diffraction by knife edge obstacle on conducting earth surface noting effect on radio propagation
[AFCL-68-0375]
04 p0560 A69-15216

Space-time diffraction for asymptotic solution of Klein-Gordon equation, studying one dimensional dispersive medium
05 p0802 A69-15930

Weak shock wave diffraction at two dimensional obstacles, discussing time behavior of pressure distribution
05 p0746 A69-16018

Asymptotic formulas for field diffracted by conducting wedge illuminated by line source usable for self consistent field analyses
05 p0720 A69-16344

Quasi-phonon model for acoustic scattering and diffraction from rigid real obstacle in fluid medium
05 p0797 A69-16649

Diffraction of plane electromagnetic waves obliquely incident on conducting rotated periodically tapered grating structure formed of infinite metal strips
05 p0723 A69-16788

Scattering matrix for internal diffraction in rectangular waveguide with transversely magnetized ferrite core
06 p0895 A69-17455

Transmission coefficient of plane electromagnetic wave obliquely incident on perforated metal screen in frequency range near primary resonance of structure
07 p1076 A69-18527

Initial equations for plane wave diffraction at grids of squared beams, calculating transmission and reflection coefficients by reflection method and computer
07 p1084 A69-19149

Plane electromagnetic wave diffraction at oblique screen of circular cross section conducting wires solved, assuming smaller wire radius than grid spacing and wavelength
07 p1084 A69-19150

Field diffraction at finite metallic surface represented in eigenfunctions of discrete spectrum, considering forced oscillations of open circuit
07 p1084 A69-19151

Scattering and diffraction of plane electromagnetic wave incident on conducting cylinder coated with moving anisotropic medium
07 p1086 A69-19469

Radiation pattern deformation due to sharp angle radome studied by analyzing diffraction in antenna dihedron system
07 p1112 A69-19539

Schlieren optics study of omega wave in water filled cuvette, noting propagation by wall reflected water wave
08 p1350 A69-19889

Radio wave propagation over smooth cylindrical surface with specified boundary impedance, discussing diffraction loss and effect of surmounted obstacle
08 p1273 A69-20024

Back diffraction field behind hologram illuminated with laser beam, noting hologram image observation through beam cross section
08 p1312 A69-20086

VHF radio transmission beyond horizon, discussing instrumentation, annual and diurnal signal fluctuations and diffraction role in signal propagation
08 p1274 A69-20112

Line shape for dynamic Stark effect during optical resonance field irradiation calculated as function of relaxation constants and beam intensity
08 p1325 A69-20282

Plane H polarized electromagnetic wave diffraction incident on array of rectangular rods described by linear algebraic equations
08 p1275 A69-20433

Cylindrical electromagnetic waves diffraction at impedance wedge in anisotropic cold plasma, using Maxwell equation and double contour integral
09 p1545 A69-21505

Ionospheric scattered radio wave field amplitude and phase variations assessed for diffraction at regular phase screen
09 p1453 A69-21526

Electromagnetic diffraction for waves generated by electric quadrupole on perfectly conducting wedge, discussing finiteness and radiation emission
09 p1455 A69-22082

Limits in applicability of earth equivalent radius to measuring microwave diffraction field in atmosphere
09 p1456 A69-22284

Electromagnetic wave diffraction on conducting sphere in inhomogeneous medium with given refractive index variation law, using asymptotic solution for boundary value problem
09 p1459 A69-22628

Diffraction problem on cylindrical bodies of arbitrary shape reduced to integral equations by using Green functions for free spaces
09 p1459 A69-22634

Quantitative analysis of plane waves for weak interaction of two dimensional sound and light fields in acoustical imaging by diffracted light
10 p1695 A69-23545

Acoustical transparencies illuminated by sound waves for optical imaging and ultrasonic diffraction, noting application to visualization of inhomogeneities in samples
10 p1695 A69-23546

Subauroral traveling ionospheric disturbances and fading due to diffraction observed by geostationary satellites
10 p1685 A69-23831

Scalar wave diffraction at body in scattering medium analyzed on basis of determinate medium with complex inhomogeneous effective refractive index
10 p1658 A69-23957

Diffraction of plane electromagnetic wave incident on conducting sphere segment, deriving secondary electromagnetic field equations in geometrical optics approximation
11 p1846 A69-24613

Holographic techniques application to optical systems for high resolution images of distant objects by overcoming atmospheric turbulence and light diffraction limitations
11 p1883 A69-24688

Electromagnetic plane wave scattering from slender semiinfinite cone, obtaining contribution to tip return arising from direct diffraction
11 p1836 A69-24988

Radiation pattern of axial slot on circular conducting cylinder based on wedge diffraction and creeping wave theory
11 p1836 A69-24993

Geometrical diffraction theory for bistatic scattering of plane wave by conducting frustum, calculating scattering matrix
11 p1837 A69-24999

Diffraction accompanying reflection of plane shock wave obliquely impinging on walls of obtuse wedge at finite incidence, considering Lighthill method
11 p1873 A69-25135

Unsteady surface and internal waves diffraction induced by source in ideal incompressible fluid, obtaining solutions in form of convolution and transfer functions
12 p2061 A69-25953

Diffraction theory of schlieren photometric slot and wire methods for cylindrical light wave of even order, discussing Fresnel diffraction for spherical wave
12 p2088 A69-26180

Time harmonic electromagnetic waves diffraction by circular aperture in conducting plane screen between different media, using Hertz vector formulation
12 p2030 A69-26463

Simultaneous Wiener-Hopf equations for electromagnetic wave diffraction, giving cyclic matrix solution
12 p2030 A69-26463

WAVE DISPERSION

tions for Dirichlet and Neumann mixed boundary value problems

13 p2287 A69-27299

Wave scattering from infinite line source by long convex cylinder, noting field prediction by geometrical diffraction theory

13 p2299 A69-28194

Shadow zone diffraction of plane step function compressional wave by circular cavity, using Friedlander wave front approximations

13 p2368 A69-28347

Couple stresses effect on dynamic stress concentrations, considering elastic compressional wave diffraction by cylindrical discontinuity

13 p2369 A69-28351

Diffraction and mirror analyses of right angle corner in overmoded waveguide for scattered modes, discussing transmission loss

13 p2234 A69-28426

Radio signal amplitude changes from Explorer 22 beacon satellite attributed to wave diffraction by tropospheric structures

14 p2411 A69-29107

X band open resonator terminated by step-rimmed flat mirrors, discussing rim effect on Fabry-Perot diffraction loss

14 p2424 A69-29765

Diffraction effects on periodic structures in millimeter wavelength measurements of Fraunhofer zone field, polarization and phase characteristics

15 p2607 A69-30244

Integral equation for diffraction from infinitely extended grating as mixed boundary problem of electromagnetic field, discussing single anomaly

15 p2568 A69-30795

Asymmetrical waves diffraction field at wide slots in circular waveguides determined in Huygens-Kirchhoff approximation

15 p2570 A69-30955

Soviet papers on wave diffraction and propagation covering marine life communication, diffraction at impedance sphere, cavity oscillations, resonator fields, plasma diffraction, etc

16 p2750 A69-32027

Diffraction of electromagnetic waves produced by vertical dipole on impedance sphere of large radius in isotropic medium, using moment method

16 p2751 A69-32028

Parametric interaction of electromagnetic field with spherical cavity having time variable radius, considering wave diffraction and TM oscillations

16 p2751 A69-32029

Electromagnetic wave diffraction in plasma cylinder of small nonuniform radius, analyzing interior field and radio wave reflection

16 p2751 A69-32031

Diffraction of axisymmetric electromagnetic wave at surface discontinuity of impedance cylinder forming core of coaxial waveguide

16 p2761 A69-32479

Ionospheric scattered radio wave field amplitude and phase variations assessed for diffraction at regular phase screen

16 p2754 A69-32521

Knife-edge obstacle diffraction of nonisotropic transmitter analyzed via isotropic source model propagation path noting accuracy

17 p2917 A69-32847

Wave diffraction problem solution method based on Rayleigh hypothesis equivalent to extended boundary condition method

17 p2920 A69-33422

Far field of line source in medium with sinusoidally stratified dielectric constant, studying diffraction effects due to Bragg mechanism

17 p2925 A69-33842

LF radio waves propagation in ionosphere by combining ray tracing in complex space with geometrical theory of diffraction, including diffraction by earth

17 p2928 A69-33866

Electromagnetic wave diffraction in vacuum by equidistant conducting grating, deriving integrodifferential equations for calculating amplitudes

17 p2930 A69-33886

Diffraction of modal field by semiinfinite waveguide, integral representation for Wiener Hopf kernel factorization and applications to open resonators

17 p2930 A69-33888

Diffraction of skew incident plane electromagnetic wave by perfectly conducting right angled wedge embedded in uniaxially anisotropic medium

17 p2930 A69-33889

Angular spectrum representation of diffracted wave fields expressible by plane wave expansions containing only homogeneous waves

17 p3007 A69-34153

Electronically tunable lithium niobate optical filter utilizing collinear acousto-optic diffraction in anisotropic medium

17 p2943 A69-34157

Penumbra current distribution in plane electromagnetic waves diffraction by conducting cylinder, obtaining transient solution for impulsive excitation, discussing time harmonic problem [AFCRL-69-0038]

18 p3100 A69-34232

Plane shock wave propagation around cylinders of various radii recorded with shadowgrams and Mach-Zehnder interferograms, discussing wave diffraction mechanics

18 p3120 A69-34472

Canonical forms for three dimensional diffraction problem of elastic harmonic waves propagating along circular cylinders infinite array

19 p3437 A69-36144

Plane electromagnetic wave diffraction on conducting sphere situated in absorbing nonuniform plasma layer

19 p3275 A69-36340

Radio wave diffraction by inhomogeneities arising from ionized gas clouds in interstellar medium

19 p3428 A69-36882

Short radio wave damping of earth satellite transmitter due to ionospheric diffraction resulting from increasing satellite-ground station distance

20 p3491 A69-37689

Remote sensors geometrical optics, considering power flow direction, specular reflection, imaging and dihedral in case of specular reflectors, reflection and diffraction

20 p3577 A69-37744

Electromagnetic wave diffraction in three dimensional space divided by dielectric orthogonal half planes/wedges/, using contact boundary value problem

21 p3673 A69-39012

Asymmetry method for precision alignment of rectilinear systems, using laser light diffraction behind misaligned target

21 p3742 A69-39781

Nonresonant Green functions of auxiliary boundary value problems for deriving integral equations for Dirichlet and Neumann diffractions at open screens

22 p3901 A69-40949

Numerical solution by approximation of Wiener-Hopf-Fock equation for diffractions at finite or infinite number of equidistant half planes applied to open-end waveguides

22 p3901 A69-40950

Surface integration technique used in conjunction with wedge diffraction theory to analyze TEM radiation patterns of parallel plate waveguides

23 p4136 A69-41581

Edge diffracted fields by conical body frustums evaluated, including equivalent currents for caustic regions

23 p4136 A69-41583

Thermal radiation diffraction of dielectric cylinder/cold plasma model/ containing N plus one layers with arbitrary temperatures and permittivities

23 p4123 A69-42028

Electromagnetic wave diffraction normally incident on symmetrical five element metallic array

23 p4123 A69-42029

Linearly polarized electromagnetic wave diffraction during oblique incidence on crossed strip arrays, describing crossing angle effects on reflection, transmission and polarization conversion coefficients

23 p4124 A69-42030

Electromagnetic oscillations emission by monochromatic electron beam in infinite waveguide formed by periodic diffracting array with energy losses, determining radiated power

23 p4124 A69-42031

Plane electromagnetic wave diffraction by screened periodic metallic strips array with real ferrite transversely magnetized to saturation

23 p4124 A69-42032

Electromagnetic wave diffraction by multielement periodic metallic strips arrays positioned transversely in rectangular waveguide

23 p4124 A69-42035

Accuracy standards for diffraction measurements of electromagnetic waves incident on periodic arrays, using monochromatic field and plane phase wavefront

23 p4139 A69-42042

Plane polarized electromagnetic wave diffraction incident on skewed metal ribbons array

23 p4125 A69-42043

Diffraction characteristics of electromagnetic wave by periodic two element arrays, noting amplitude measurement of harmonics in millimeter wavelength range

23 p4139 A69-42044

Ultrasonic diffraction delay lines technique to extend radar systems range without affecting target pinpointing capability

24 p4286 A69-42901

WAVE DISPERSION

Pulsar radiation origin related to electromagnetic wave distortion during propagation through resonant media

01 p0149 A69-10272

Quasi-monochromatic wave dispersion relation and energy transfer in inhomogeneous anisotropic medium

01 p0126 A69-10278

Hydromagnetic wave propagation in current carrying regions of ionosphere and magnetosphere using macroscopic equations, deriving dispersion relation

01 p0067 A69-10972

Ion acoustic wave dispersion in highly ionized Ar plasma in longitudinal magnetic field, noting effects of several phenomena

01 p0133 A69-11216

Narrow band normal steady state random processes applied to signal dispersion by extended oscillating body, obtaining statistical characteristics

02 p0206 A69-11602

Two dimensional diffuse shock waves in carbon dioxide, noting effect of shock curvature equivalence to thickness

02 p0233 A69-12534

HF pressure waves dispersion in blood vessels ascribed to viscoelastic behavior of walls

02 p0204 A69-12602

Dielectric dispersion in inhomogeneous dielectrics and semiconductors, discussing three layered equivalent circuit

02 p0301 A69-12837

Electromagnetic wave dispersion and damping in mixed molecular crystal, relating refractivity, wave absorption and concentration shift of bottom of exciton band to other parameters

03 p0484 A69-13279

Ionospheric beam deflection maximum and minimum levels, deriving equations for maximum usable frequency at given ionization conditions and radiation angles

03 p0424 A69-13540

Complex Doppler effect for oscillating source moving in dispersive medium, analyzing time behavior of radiation field

03 p0396 A69-13630

Dispersion equation for two dimensional periodic slow wave structure formed by periodically sequential loading

03 p0407 A69-13981

Disintegration spectrum of Langmuir wave excited in plasma column by antenna, discussing conditions of resonance and parametric amplification

03 p0480 A69-14113

Dispersion equation for electron-ion and electron-hole plasma linear oscillations in crossed electric and magnetic fields

03 p0480 A69-14134

Elastic behavior of large blood vessels in canine aorta by measuring dispersion and attenuation of artificially induced pressure waves

04 p0553 A69-14692

Dispersion relations for propagation of quasi-TEM mode and higher order symmetric modes in longitudinally magnetized ferrite filled coaxial waveguide

04 p0575 A69-14751

Wavelength range analysis for determining ambiguous section of circular waveguide dispersion characteristic

05 p0718 A69-15649

Dispersive properties of axial and annular longitudinally magnetized plasma waveguides

05 p0802 A69-15925

Coupled waves in ferromagnetic and antiferromagnetic semiconductors in constant electric and magnetic fields, discussing spin, electromagnetic and plasma waves dispersion

05 p0809 A69-16548

Wave dispersion analysis for amplification in cold plasma filled cylindrical waveguide penetrated by electron beam of same radius

05 p0736 A69-16790

Deviation of dispersion equations for all modes existing in E-plane slabs of dielectrically loaded rectangular waveguides

06 p0888 A69-17486

Dispersion equation for dipolar surface waves in uniform cold lossless infinitely long magnetoplasma column in free space, obtaining numerical and asymptotic solutions

06 p0968 A69-17774

Dispersion relation for longitudinal oscillations of one component weakly ionized plasma without intercarrier collisions in uniform constant electric field

06 p0970 A69-17957

Phase matched optical harmonic generation by anomalous dispersion in liquid media, using dye fuchsin red [IEEE PAPER V-9]

07 p1155 A69-19086

Elastic constants of composite materials by dispersion relation of sound waves for long wavelength, assuming periodicity in three dimensional rectangular lattice

07 p1236 A69-19457

Collisionless shock waves in rarefied plasma, discussing dispersion effect and oscillatory shock wave structure

08 p1303 A69-19996

Light intensity dispersion logarithm calculated along axis of laser beam propagating in atmosphere

08 p1351 A69-20437

Galactic H II regions and projected electron density or dispersion measures of pulsars, noting early stars

08 p1397 A69-20696

Ion Landau damping and finite Larmor radius effects on dispersion relation of Kelvin-Helmholtz instability due to shear in ion fluid velocity

08 p1367 A69-20799

Dispersion equation to describe spectrum of LF density perturbations by pumping plane electromagnetic wave in transparent homogeneous plasma or fluid media

09 p1453 A69-21570

Plasma wave excitation and dissipation in fast thetatron discharge, indicating electron nonadiabatic inductive acceleration without equilibrium orbit

09 p1552 A69-22046

Earth upper mantle wave velocity structure based on surface wave dispersion, noting low velocity layers thickness

09 p1491 A69-22153

Cosserat continuum and elasticity models of dynamics of composite materials, analyzing dispersive longitudinal waves

10 p1798 A69-23148

Relativistic energy momentum tensor of electromagnetic field in moving multicomponent dispersive media and instability of wave

10 p1653 A69-23193

Plasma concentration diagnostics in magnetosphere based on hydromagnetic whistlers/pearls/dispersion

10 p1688 A69-23934

Radio wave propagation in unstable inhomogeneous medium with space-time dispersion, showing adiabatic compression or expansion of wave packet spectrum

10 p1658 A69-23955

Photoelectric and photographic observations in UVB system of open star clusters, analyzing dispersion in two color diagrams, noting absorbing material structure

11 p1951 A69-24247

Electrostatic wave dispersion relation in uniformly rotating plasma cylinder used in interpreting Q machine experiments

11 p1924 A69-24300

Normal mode dispersion at upper hybrid frequency propagating parallel to uniform magnetic field in spatially inhomogeneous plasma

11 p1924 A69-24302

Beam-plasma dispersion relations, obtaining dispersion equation for plasma waves and dispersion curves for longitudinal waves

11 p1925 A69-24366

Dispersion relation for internal gravity wave propagation across exponentially decreasing magnetic field in conducting fluid, noting atmospheric wave propagation in ionosphere

11 p1877 A69-24564

Narrow band normal steady state random processes applied to signal dispersion by extended oscillating body, obtaining statistical characteristics

11 p1835 A69-24709

Landau dispersion relation solutions, noting higher order Landau poles and coupling of spatial Landau modes and least damped wave

11 p1929 A69-25265

Linear interaction of electron beam and plasma in magnetic field noting convective wave instability, wave dispersion and properties behavior

11 p1929 A69-25267

HF electrostatic waves propagation in nonuniform plasma in uniform magnetic field, obtaining solutions of dispersion relation

11 p1931 A69-25360

Pi 2 micropulsations at African low latitude stations, considering damping effect on ionospheric micropulsation transmission signal dispersion and SNR

12 p2074 A69-26959

Instabilities related to particles transit time in system of two counterstreaming electron beams of finite length, noting wave dispersion

12 p2141 A69-27179

Alternating electric field parametric effects on inhomogeneous plasma in magnetic field, obtaining electrostatic wave coupling dispersion relation by density gradients considerations

13 p2304 A69-27298

Dispersion relations in semiconductors in magnetic field indicating current anisotropic instability association with excessive noise

13 p2317 A69-27876

Interacting carriers acoustoelectric waves in semiconductors with high dielectric constant, analyzing dispersion equation

13 p2317 A69-27878

Leaky helix and solid metal waveguides propagation losses measured by shuttle pulse method in SHF

13 p2233 A69-28063

Dispersion and coupling impedance of logarithmic spiral resting on anisotropic magnetodielectric layer for microwave devices design

13 p2235 A69-28512

Libroelastic wave propagation and dispersion characteristics /solid carbon dioxide/ evaluated by using Raman scattering measurements

13 p2286 A69-28668

Frequency time dispersion of storm sudden commencement micropulsations, noting polarization effects

14 p2440 A69-29129

Microwave dispersion systems, using waveguide loaded with dielectric material to obtain group linear frequency delay characteristic

14 p2412 A69-29395

Monochromatic plane waves propagation in anisotropic homogeneous cold plasmas, treating dispersion surface, reflection, refraction and waveguide applications

14 p2492 A69-29399

Dispersion of electromagnetic wave propagating along ferrite loaded wire, calculating tuning curves and three port waveguide circulator modes

14 p2417 A69-29755

Equations describing interaction between HF and LF waves propagating in linearly dispersive medium, obtaining approximate solutions

15 p2568 A69-30733

Dispersion characteristics of open interdigital line structure by treating structure as radiator, applying linear antenna theory

16 p2748 A69-31580

Wavelength range analysis for determining ambiguous section of circular waveguide dispersion characteristic

16 p2762 A69-32506

Propagation in inhomogeneous and dispersive media, noting potential functions for vector electromagnetic field

17 p2924 A69-33838

Wave propagation in rectangular guides, determining dispersion curves by continued fractions method allowing for infinite set of time-space harmonics

17 p2925 A69-33843

Line source excited ferrite layer radiation pattern reduced to one dimensional form by Fourier transform, obtaining angle of maximum leaky wave radiation

17 p2926 A69-33852

Deformation of amplitude and frequency envelopes of plane modulated electromagnetic waves with dispersion in isotropic dielectric with cubic nonlinearity

17 p2928 A69-33869

Dispersion relation for gravity waves propagating in atmosphere with horizontal background wind variable with altitude

18 p3128 A69-34801

Microwave background angular fluctuations investigated for relationship between whirl motion velocity and temperature dispersion, noting role of scattering by moving plasma

18 p3188 A69-35208

Acoustic surface waves on thin film for pulse compression radar dispersive delay line, describing delay characteristic synthesis and control

19 p3267 A69-35929

Shock and current sheet separation in magnetic shock tubes, determining electron temperature behind shock and within current layer

20 p3511 A69-38241

Dispersion relations in semiconductors in magnetic field indicating current anisotropic instability association with excessive noise

21 p3782 A69-39142

Biquadratic plane wave dispersion relation for gyrotropic waveguides with dielectric and magnetic properties, discussing associated quartic equation for refractivity

21 p3675 A69-39285

YIG single crystal disk instability, noting dispersion of magnetostatic and plane spin waves from supplementary absorption and LF oscillations recording

21 p3783 A69-39561

Steady state mathematical modeling of light field structure for narrow collimated light beams propagating in artificial dispersive media

22 p3981 A69-40245

Algorithm for numerical modeling by Monte Carlo method of diffusion bounded light beams in dispersive media, applying to light pulse in cloudlike medium

22 p3981 A69-40248

Dispersion relations for surface plasma oscillations in normal metals for single and multiple films taking into account retardation effects, noting dielectric function

22 p3992 A69-40419

Asymmetric surface waves in radial spiral structures above conducting plane, analyzing spiral thickness and plane influence on dispersion and energy characteristics

22 p3916 A69-40951

Waveguide-resonance investigation of temperature dependence of dielectric constant and paraelectric dispersion of Ba and Sr titanate single crystals at millimeter wavelengths

22 p3995 A69-41158

He-Ne laser heterodyne system for measuring dispersion at 6328 and 6401 A due to Ne metastable atoms in gas discharge

23 p4172 A69-41397

Variational principle for analyzing dispersion properties of closed regular waveguide with traveling wave-modulated dielectric constant

23 p4123 A69-41943

Equivalent circuit technique for dispersion equation and coupling impedance of slow wave structures of ring-rod systems, noting retardation

23 p4139 A69-41944

Dispersion and resonant properties of electromagnetic waves propagating along plane metallic strip array with shield and dielectric

23 p4124 A69-42038

Double cellular surface geometry effect on dispersion and coupling impedance of two dimensional periodic resonator slow wave structure

23 p4140 A69-42048

Ridge-slot-ridge slow-wave structures used in multibeam TWT (traveling wave tube), analyzing E type electromagnetic dispersion as function of system parameters

23 p4140 A69-42049

Mean and variance of Faraday rotation and pulsar signal dispersion in galactic turbulent structure, applying to statistically homogeneous disk model of Galaxy

24 p4375 A69-42659

Fully dispersed wave reflection from plane wall in stable relaxing gas, obtaining canonical equation of state

24 p4299 A69-42717

Dispersive pulse propagation in laminated composites compared with theoretical predictions for timing and amplitude of oscillations [ASME PAPER 69-APMW-22]

24 p4401 A69-43097

Geometric dispersion of transient stress waves in linearly elastic laminated composite based on sinusoidal modes [ASME PAPER 69-APMW-20]

24 p4401 A69-43098

Moving striations dispersion and stability theory applied to ionization waves excited in Ar, Ne and Hg-Ar mixture low and medium pressure discharge

24 p4356 A69-43363

WAVE DRAG

NT INTERFERENCE DRAG

Two dimensional stratified flow over obstacle in finite height channel, noting lee waves and drag increase with decreasing speed

11 p1869 A69-24892

WAVE EQUATIONS

- Fresnel dragging effect on 3 cm microwaves by electron gas drift in low pressure glow discharge, noting electron density and excitation modes
12 p2133 A69-25766
- Ion drag effects on acoustic gravity waves propagation in isothermal F region, discussing indicated wave damping
14 p2434 A69-28944

WAVE EQUATIONS

- NT DIRAC EQUATION
NT KLEIN-GORDON EQUATION
NT LAME WAVE EQUATIONS
NT SCHROEDINGER EQUATION
- Coupled wave equations for propagation transverse to magnetostatic field in horizontally stratified and magnetized gyrotropic warm plasma
01 p0129 A69-10611
- Simple wave solution existence for system of equations describing rapid plane flows of ideally plastic material
02 p0337 A69-11560
- Boundary value technique for initial boundary value problems for linear and mildly nonlinear wave equations
02 p0271 A69-11733
- Asymptotic and approximate waves constructed for system of nonlinear partial differential equations for phases corresponding to multiple characteristics
02 p0271 A69-12034
- Finite element solution of Helmholtz equation and application to waveguides with complicated boundaries
03 p0404 A69-13598
- Integrals of nonlinear equations of evolution and solitary waves, discussing double wave solutions of Korteweg-de Vries equation
03 p0468 A69-13825
- Propagation velocity upper limits for plasma waves during state of equilibrium transition determined for nonlinear wave equation
04 p0630 A69-14553
- Electromagnetic wave propagation in moving isotropic refractive media, giving Maxwell-Minkowski and EM wave equations
04 p0557 A69-14760
- Potential functions to solve coupled wave equations for compressible anisotropic plasma with electric and magnetic current sources
05 p0803 A69-16350
- Approximate method for wave equation with dielectric variation in propagation direction
06 p1030 A69-17116
- Asymptotic wave equation application conditions in describing field behavior near caustic surface, using Airy functions
07 p1076 A69-18520
- Magnetosonic wave evolution in inhomogeneous dispersive plasma created by magnetic piston, discussing equation solution
07 p1181 A69-19001
- Coupled wave equation solution based on spectral resolution for longitudinal components of electric and magnetic fields when source currents are present in compressible anisotropic plasma
08 p1274 A69-20031
- Constitutive equations for propagation of plane waves of finite amplitude in nonsimple elastic solids, discussing holohedral isotropic solids and transverse harmonic circularly polarized waves
08 p1411 A69-20141
- Micropolar elasticity using Green functions to solve wave equations in unbounded medium, noting effects of concentrated force and body couples
09 p1618 A69-22261
- Micropolar thermoelasticity using Green functions to solve wave equations in unbounded medium and study displacement, rotation and temperature fields
09 p1618 A69-22262
- Electromagnetic wave propagation in rectangular waveguide containing uniaxial anisotropic birefringent medium, deriving field equations
11 p1853 A69-25350
- LF electromagnetic waves stability and propagation conditions in plasma confined in central-conductor configuration measured, noting agreement with wave equation solution
11 p1931 A69-25362
- Boundary value problems for hyperbolic and mixed equations using model of wave, Lavrentiev-Bitsadze and Tricomi equations
12 p2123 A69-26727
- Nonlinear hyperbolic partial differential equations with dissipation term for periodic solutions
12 p2124 A69-26929

- Plane wave solution for wave propagation in inhomogeneous anisotropic time-varying media
13 p2219 A69-27397
- Variational method for weak second order resonant interactions among waves with position and time varying amplitudes and phase angles
13 p2297 A69-27634
- Monograph on sound generation by turbulence and surfaces in arbitrary motion, discussing sound and multiple fields and governing equations
13 p2247 A69-27974
- General formulas, reciprocity theorem and modified Green formula derived from variational principles for mixed problem of wave equation
14 p2485 A69-29354
- Radiative instability problem of stream plasma system in kinetic regime, discussing Fung letter
14 p2502 A69-29960
- Monograph on wave propagation and multiple scattering in random continuum, emphasizing scalar wave equation solutions
15 p2564 A69-30150
- Substitute kernel approximation for acoustic waves radiative transfer equations for nongray gas near equilibrium
15 p2717 A69-30791
- Stress waves propagation through elastic-plastic medium with uniaxial displacement, discussing wave interactions and interface conditions
16 p2870 A69-31809
- Wave generation in infinite micropolar elastic solid body analyzed by linearized equations of motion
17 p3053 A69-33018
- Electromagnetic wave diffraction in vacuum by equidistant conducting grating, deriving integrodifferential equations for calculating amplitudes
17 p2930 A69-33886
- Wave equations governing evolution of long nonlinear axially symmetric wave motion in inviscid rotating fluids
18 p3120 A69-34441
- Wave equation of electromagnetic field of optical resonator with arbitrary mirrors, utilizing Schroedinger equation and equivalent mechanical system
19 p3333 A69-35880
- Single loop directional stripline filters synthesis, including general expression for frequency characteristics based on wave matrices
19 p3284 A69-36570
- Thomas wave equation in fluid mechanics, examining coordinates system with normal hyperbolic metric of universe tube having given signature
20 p3598 A69-37430
- Q switched laser pulse propagation in nonlinear laser amplifier using bitemporal relativity theory, deriving five dimensional wave equation revealing superlight signal existence
21 p3770 A69-38839
- Equations governing stress waves generated by rapid nonuniform heating of solids, comparing elastoplastic with purely elastic solutions
21 p3837 A69-39158
- Laminated random media stochastic displacement, using perturbation procedure to derive mean wave propagation deterministic equations
22 p4040 A69-39979
- Two dimensional gas dynamics differential equations for simple waves, discussing invariant solutions and conditions for group solutions
22 p3933 A69-41030

WAVE EXCITATION

- NT ACOUSTIC EXCITATION
NT HARMONIC EXCITATION
- Growth rate of wave instability in conducting liquid jet in perpendicular electric field and accelerating under gravity
01 p0062 A69-11207
- Induced discharge laser wave propagation in medium with active and absorbing admixtures, determining stationary wave shape and velocity range
02 p0206 A69-11609
- Standing ion-acoustic wave excitation in weakly ionized plasma, noting isothermal compression of electron gas
02 p0292 A69-12555
- Finite amplitude surface wave excitation in infinitely deep ideal fluid by moving pressure, noting phase velocity increase with amplitude
03 p0466 A69-13277
- Longitudinal elastic wave damping, excitation and propagation in lithium niobate crystals at frequencies from 200 to 2000 MHz
03 p0487 A69-13729

- Disintegration spectrum of Langmuir wave excited in plasma column by antenna, discussing conditions of resonance and parametric amplification
03 p0480 A69-14113
- Transverse normal waves excitation in flat plate by applying piezoelectric plate or comb shaped emitter to surface or end face
04 p0678 A69-14901
- Electrostatic ionospheric waves excited around lower hybrid resonance frequency by high energy electrons
06 p0918 A69-17381
- Surface plasma waves excitation by light and decay into photons applied to nonradiative modes
07 p1188 A69-18278
- Electromagnetic waves excitation during interaction between density modulated beam and plasma in magnetic field, analyzing instabilities
07 p1189 A69-18508
- Open resonator reflection coefficient resonance curve compared with transmission coefficient, noting low Q waves excitation role
07 p1106 A69-19152
- Fresnel formulas for surface plasma waves excitation by light in thin metal foil embedded between dielectric layers, discussing transmissive and absorptive resonances
08 p1372 A69-20290
- Coupling electromagnetic power to beam plasma amplifiers without use of helices and cavities, discussing modes of interaction, gap coupling and Cerenkov coupling
09 p1463 A69-21805
- Electrons resonant heating in beam plasma discharge, discussing ion cyclotron wave excitation in hot electron plasma produced by electron beam
09 p1549 A69-22016
- Plasma wave excitation and dissipation in fast thetatron discharge, indicating electron nonadiabatic inductive acceleration without equilibrium orbit
09 p1552 A69-22046
- Single degree of freedom mechanical system under random excitation studied for creep effect on vibrations by harmonic analysis
09 p1617 A69-22095
- Plasma electron beam nonlinear interaction, considering equations of motion of electron distribution function, plasma wave spectrum and mode coupling effects
10 p1729 A69-23407
- Induced discharge laser wave propagation in medium with active and absorbing admixtures, determining stationary shape and velocity range
11 p1895 A69-24716
- Radiation pattern as function of asymmetry in amplitude of secondary source excitation by primary aperture antenna
11 p1852 A69-25117
- Transverse normal waves excitation in flat plate by applying piezoelectric plate or comb shaped emitter to surface or end face
12 p2182 A69-26654
- LF oscillations nonlinear excitation increment in plasma by electron beam found proportional to reciprocal of wave potential
12 p2138 A69-26709
- Saturation and distortion effects on magnetoelastic wave excitation in yttrium garnet single crystals by large amplitude microwave frequency field
12 p2145 A69-26725
- Finite amplitude surface wave excitation in infinitely deep ideal fluid by moving pressure, noting phase velocity increase with amplitude
14 p2482 A69-28785
- Equatorial jet stream excitation of longitudinal waves, analyzing plasma beam instability and spectrum of short wave inhomogeneities by quasi-hydrodynamic equations
14 p2437 A69-29073
- Standing ion-acoustic wave excitation in weakly ionized plasma, noting isothermal compression of electron gas
15 p2658 A69-30252
- Two photon absorption excitation of luminescence in ruby crystals by neodymium laser radiation, determining luminous intensity dependence on pumping intensity
15 p2634 A69-30731
- Plasma wave echoes concept extended to transverse electromagnetic wave excitation propagating parallel to external magnetic field
16 p2823 A69-32467
- Plasma-cyclotron interaction wave coupling mechanism in symmetrical double beam system in

uniform magnetic field leading to unstable wave excitation along beam

17 p3015 A69-33831

Wave excitation in resonant dissipative and inhomogeneous structures, discussing resonator geometry, mode spectra, etc

17 p2926 A69-33849

Phased array blindness at inoperative scan angles explained in terms of elements excitation and termination caused by leaky wave

17 p2928 A69-33872

Drift waves parametric excitation in resistive plasma derived from fluid equations, assuming plane geometry with periodic boundary conditions in magnetic field and azimuthal directions

18 p3179 A69-34440

Transient phenomena in bounded dispersive medium emphasizing surface wave propagation, discussing space and surface waves excitation in bounded cold magnetoplasma

20 p3494 A69-37842

Nonlinear effects in spiral galaxies with emphasis on solar neighborhood region, discussing radial motion, stationary state with excited waves and vertex deviation

20 p3607 A69-38036

Negative energy waves presence, showing qualitative difference on theoretically derived parametric amplification in plasmas

20 p3582 A69-38244

Saturation and distortion effects on magnetoelastic wave excitation in yttrium garnet single crystals by large amplitude microwave frequency field

21 p3782 A69-39138

Directional couplers applied to excitation of non-propagating surface wave antennas, examining ridge slot system

23 p4139 A69-41946

Combination resonance and instability regions of second type for parametrically excited oscillations with nonlinear/cubic/ damping

23 p4230 A69-42107

Transverse acoustic wave excitation of elastic circular cylindrical sandwich shell submerged in infinite fluid medium, describing simultaneous equations development for modal response [ASME PAPER 69-APMW-17]

24 p4401 A69-43100

WAVE FRONT DEFORMATION

Photographic image degradation resulting from wave front distortion due to atmospheric refractive density gradients over long oblique optical path

01 p0107 A69-10223

Optical heterodyne detection of randomly distorted signal beam, noting time invariant scheme yielding largest average SNR in atmospheric turbulence

07 p1087 A69-19642

Precision optical systems tests, using two beam interferometer and CW gas laser to examine reflected or transmitted wavefront contours

12 p2092 A69-26421

WAVE FRONT RECONSTRUCTION NT KINFOFORM

Holographic phase variation distribution recording by interference between reconstructed wave fronts from separate holograms

01 p0083 A69-10984

Holography, discussing one beam recording, real time interferometry, pulsed laser, etc

05 p0761 A69-15774

Strain releasing method for reduction of small local movements of recording holographic emulsions resulting in degradation of holographically reconstructed wavefronts

06 p0923 A69-16930

Acoustic holograms, describing electronic method of reconstructing holographic image in order to avoid multiple image problem

06 p0923 A69-16933

Lippman-Bragg holograms production with high reconstruction efficiencies by suitable recording and processing techniques with commercially available photographic plates

06 p0926 A69-17481

Ultrasonic holograms and optical reconstructions derived by scanning receiver or source

06 p0930 A69-18228

Microwave holographic reconstruction of metal objects inside purse by nonscanning method, visualizing microwave field by polaroid and liquid-crystal techniques

07 p1135 A69-19449

Image degradation in holograms undersampled with respect to space-bandwidth product, noting signal to noise ratio and resolution

08 p1312 A69-20078

Back diffraction field behind hologram illuminated with laser beam, noting hologram image observation through beam cross section

08 p1312 A69-20086

Holographic technique for measuring thin fluid film profiles using interference image reconstruction and helium-neon laser as coherent light source

08 p1317 A69-20873

Borrmann effect and abnormal transmission and extinction observed by reconstruction of images of holograms recorded in three dimensional photosensitive medium

09 p1494 A69-21492

Holographic technique for reconstructing light wave front, developing algorithm for three dimensional images recognition

09 p1495 A69-21859

Holographic technique application to radio and sound wave ranges, discussing incoherent holography development to overcome difficulties in image reconstruction of stationary objects

09 p1498 A69-22133

Light wave reconstruction including polarization, using single reference beam with depolarizing diffuser as source

10 p1690 A69-22951

Shearing interferometry by simultaneous reconstruction of two wavefronts on single photographic plate

10 p1690 A69-22952

Digital reconstruction of images from optical holograms for acoustical data, discussing image degradations

10 p1695 A69-23547

Matrix method for acoustical holograms and optical reconstruction of virtual and conjugate images using laser light of 6328 A wavelength

10 p1696 A69-23549

Computer generated kinoform optical element operating on phase of incident waves and forming wave front reconstruction single image

10 p1697 A69-23867

Computer generated holograms using binary transmittance for wave fronts and three dimensional images construction

10 p1697 A69-23869

Multicolor hologram recording and reconstruction gas lasers, discussing control of ghosts in three dimensional image

11 p1882 A69-24679

Holographic recording materials effect on optical reconstruction wave and hologram properties

11 p1882 A69-24681

Pulsed laser holography advantages for recording small objects in motion and holographic interferometry advantages for complex surfaces and time-separated events

11 p1883 A69-24682

Holographic multiplexing for producing three dimensional reconstruction of nonlaboratory objects in horizontal direction, noting TV and X ray pictures applications

11 p1883 A69-24684

Holographic reconstruction of spatial distribution of laser light field within and outside resonator, noting suitability for pulsed laser analysis

11 p1885 A69-24919

Holograms reconstructing images of points with diameters approximated by width of autocorrelation functions

11 p1886 A69-25058

Multiple information storage in sampled hologram in space division multiplexing holography, constructing hologram with sound waves and reconstructing images with laser light

12 p2079 A69-25921

Holographic recording in spatially incoherent light, describing hologram reconstruction method

12 p2090 A69-26293

Moire fringes, discussing fringe multiplication by filtering to obtain small strain measurement sensitivity and engraving technique for wave front reconstruction

12 p2099 A69-27164

Image formation with arbitrary holographic surfaces achieved by reversing direction of propagation of diverging wave

14 p2450 A69-29582

Microwave hologram construction and image reconstruction by laser beam, analyzing results by matrix expression

15 p2610 A69-30802

Linear mean square estimator for restoration of images degraded by system with bandlimited spread function

15 p2611 A69-31032

Restoration of photographic images by optical spatial filtering with least mean square error filter in presence of random additive noise

15 p2611 A69-31033

Point object image differential field during reconstruction by surface nonplanar holograms, determining image position and aberrations

17 p2981 A69-33115

Holographic method of a posteriori restoration of images formed by coherent and incoherent light by spatial frequency retrieval

19 p3304 A69-35603

Optical imaging with partially coherent nonthermal light, discussing reconstruction of object from image and similarity between object and image, including detection

19 p3372 A69-35908

Holographic wave front reconstruction emphasizing between-wave interference fringes, discussing application to microscopy, Thompson and Parent disdrometer, interferometry, etc

20 p3540 A69-37637

Holographic recording of focused images and reconstruction in white light, discussing optimal conditions, calculating ray paths

21 p3725 A69-39543

Holograms capable of multiple imaging or reconstructing point images, using extended and correlated signal and reference sources in recording process

21 p3727 A69-39777

Resolution limitations in holographic images using single record, discussing lensless holography using plane reference waves

21 p3727 A69-39778

Fresnel zone plate as converging and diverging lens in holographic image reconstruction, noting sine wave zone plate

22 p3947 A69-40864

Reconstruction properties of image plane holography for producing bright white light displays, using reference beams

23 p4164 A69-41627

Hologram film nonlinearity effect on reconstructed image, discussing role of illumination type

23 p4165 A69-41636

Reconstruction of three dimensional holograms without reference beam, noting thick layered Lippmann emulsions and dyed alkali halide crystals

23 p4166 A69-41969

Acoustical holography principles and reconstruction techniques, noting advantages of liquid-surface and temporal reference holography over optical counterpart

23 p4167 A69-42199

Holography phototechnical and optical variants, discussing combination of conventional photography and wave front reconstruction

24 p4312 A69-42616

Linear motion blur compensation technique in photographic recordings by reconstruction of sharp image from hologram

24 p4314 A69-42972

Fraunhofer hologram of glass fiber by Be X rays reconstructed using He-Ne laser light

24 p4314 A69-42973

Image reconstruction by graphical method for equal wavelengths of recording and reconstructing radiation and equal scales of hologram

24 p4315 A69-43166

Hologram electronic transmission, obtaining required bandwidth reduction by differential recording of image and scene diffraction pattern

24 p4317 A69-43761

WAVE FRONTS

NT SHOCK FRONTS

Wave front profiles sensitivity to form of constitutive equation in one dimensional stress problem

02 p0344 A69-12291

Transverse mode selection effects on wave front of long pulsed ruby laser beam

02 p0257 A69-12409

Plasma instability in inhomogeneous magnetic field noting wavefront structure role

09 p1546 A69-21571

MHD first order partial differential equations used to investigate wave front between perturbed and unperturbed flow regions in magnetosonic propagation through homogeneous medium

10 p1727 A69-23090

Two dimensional wavefront shape induced in finitely strained elastic body by impulsive point body force

11 p1969 A69-24338

High speed photographic study of plasma luminescence front and charged particle concentration

WAVE FUNCTIONS

front counter to electrodynamic force in crossed electric and magnetic fields
12 p2141 A69-27130

Shadow zone diffraction of plane step function compressional wave by circular cavity, using Friedlander wave front approximations
13 p2368 A69-28347

Microwave induced ionization wave propagation in rare gases, noting rapid electron density increase at rare front and subsequent slow plasma decay
16 p2818 A69-31671

N wave propagation across nonuniform medium described by cloud or front layer, using geometrical optics
16 p2812 A69-31924

Wave front resistivity in laser produced plasma interacting with magnetic field enhanced by two stream instability
16 p2823 A69-32564

Structure of solitary waves propagating in collisionless plasma perpendicular to magnetic field, considering soliton wavefronts charge separation and relativistic velocity
17 p2922 A69-33696

Ionization wavefronts nonlinear analysis including energy effects and ionization wave structure, discussing Joule heating due to transverse electric field
22 p3990 A69-40758

Holographic technique of coherent light field transformation with desirable phase distribution from laser light beams of arbitrary wavefront characteristics
22 p3950 A69-41115

Initially sharp plane pressure pulse propagation through linear elastic composite material, determining wave front shape change and stresses behind front [ASME PAPER 69-APMW-11]
24 p4401 A69-43103

WAVE FUNCTIONS

NT MOLECULAR ORBITALS

Total energy of plasma wave from second order energy, showing close approximation to wave packet energy
02 p0287 A69-11876

Asymptotic solutions for prolate spheroidal wave functions satisfying given differential equation, producing asymptotic expansions in terms of confluent hypergeometric functions
04 p0623 A69-14892

LCAO-MO-SCF wave functions determined for ground and excited states of nitrogen dioxide at five different ONO angles
06 p0960 A69-17109

Natural orbital expansion coefficients of LCAO-MO-SCF-CI wave functions for ground state of H molecule
06 p0960 A69-17112

Electromagnetic waves and photons coexistence, discussing wave mechanics and guidance of particles, photon guidance and corpuscular magnitudes, etc
08 p1351 A69-20117

Electron states at deep levels in InSb by deriving equations for Bloch wave functions of conduction and valence bands
09 p1556 A69-21508

Exact solutions for two state potential curve crossing in subexcitation molecular collisions in terms of various decoupling schemes
12 p2131 A69-25983

Surface resistivity oscillatory dependence on magnetic field in single crystal metals, examining electron trajectories, energy levels and wave functions
13 p2316 A69-27641

Inelastic scattering cross sections calculated, comparing results for various nuclear states expressed as Wood-Saxon radial and harmonic oscillator functions
14 p2504 A69-29006

Sum rule properties of finite set of wave functions obtained from application of variational principles to basis functions linear combinations
14 p2471 A69-29921

Electromagnetic wave propagation in anisotropic media analyzed for wave packet behavior function, stressing waveguide theories
17 p2926 A69-33847

Upper bounds for electromagnetic transition rates for Ne 20 determined using Hartree-Fock wave functions
18 p3177 A69-35166

Refractive index profiles yielding wave functions expressed in terms of standard transcendental functions for electric fields in spherically stratified isotropic media
19 p3372 A69-35618

Franck-Condon factors for band systems of molecular hydrogen, computing wave functions for each electronic state by numerical solutions of radial Schroedinger equation
21 p3774 A69-38758

Equatorial radiation pattern of parallel plate TEM mode axial slot on elliptical conducting cylinders, using wedge diffraction and creeping wave theory
22 p3914 A69-40703

Natural orbitals calculated from spin free one density matrix of open shell limited configuration-interaction wave function constructed from nonorthogonal basis
23 p4194 A69-42206

Collective rotational motion separation from internal motion in system of n point masses based on wave mechanics, emphasizing three body problem
24 p4349 A69-42650

Density matrices of symmetry projected single determinant wave functions for finite groups, considering many particle system
24 p4351 A69-43810

WAVE GENERATION

Transverse plasma mode excitation by nonlinear interaction analyzed by Hamiltonian function
01 p0127 A69-10280

Electromagnetic wave generation in 0.2-3mm range, noting applications to physics, biology and technology
02 p0250 A69-12247

Finite deformation mode stability for finite amplitude first diameter nonlinear plastic wave initiation and growth at impact face in long rods
02 p0342 A69-12279

Ion cyclotron wave generation in RF self sustained mode improved by installing grid structures in plasma near magnetic mirrors
03 p0474 A69-13113

Propagation of detonation wave in tube containing single stream of diethyldichlorohexane droplets dispersed in gaseous oxygen
03 p0415 A69-13139

Generation of UHF space charge waves by nonlinear interaction of two microwave signals in magnetoplasma, predicting optical mixing
03 p0475 A69-13146

Velocity field generated by shock wave incident on slender symmetrical body resting in infinite compressible medium
03 p0362 A69-13418

Microwave generation and amplification, noting microwave transit time tubes, semiconductor devices and methods utilizing quantum electronic effects to generate and amplify EHF oscillations
03 p0395 A69-13611

Dispersion equation for two dimensional periodic slow wave structure formed by periodically sequential loading
03 p0407 A69-13981

Equations for self oscillating mode of operation for O-type backward wave generator with electrostatically focused electron beam and finite values of amplification parameter
03 p0407 A69-13986

Single punch through silicon avalanche diode structure and two distinct modes of oscillation making possible pulsed generation of microwaves
04 p0573 A69-14334

Delta wing head wave at zero angle of attack in steady supersonic flow during transition from subsonic to supersonic leading edges [DVL-871]
06 p0858 A69-17242

Hydromagnetic wave propagation and generation in magnetosphere, discussing hydromagnetic waves in uniform and axisymmetric magnetic fields
07 p1208 A69-19356

Coupling electromagnetic power to beam plasma amplifiers without use of helices and cavities, discussing modes of interaction, gap coupling and Cerenkov coupling
09 p1463 A69-21805

Thermally generated stress wave propagation in dispersive elastic rod investigated experimentally and analytically, using ruby laser and differential equation
09 p1617 A69-22010

Large scale heat sources influence on formation and dynamics of ultralong waves in atmosphere, using linear time dependent quasi-geostrophic model
09 p1491 A69-22164

Gunn diode operating to VHF range with coaxial line to generate rectangular waves and to function as memory element
09 p1467 A69-22587

Neon discharges, discussing similarities in type p plasma ionization waves generated by pulsing
10 p1740 A69-23721

Circuit for generation of square wave with frequency as sum or difference of two periodic signal frequencies, discussing SSB modulation
10 p1665 A69-24047

Two dimensional wavefront shape induced in finitely strained elastic body by impulsive point body force
11 p1969 A69-24336

Magnetoacoustic waves generated by Cerenkov radiation from corpuscular fluxes due to star interaction with stellar wind, determining deceleration forces on star
11 p1955 A69-24385

Acoustic wave amplification and generation in piezoelectric semiconductors and semimetals by supersonic carrier drift currents
11 p1926 A69-2464

Microwave antenna testing on small indoor ranges, discussing reflectors and feeds for generation of approximately uniform plane waves for antenna illumination
11 p1852 A69-25314

Critical condition for electromagnetic radiation generation by energetic electrons gyrating in dense magnetized plasma, proposing plasma instability mechanism
11 p1931 A69-25363

Operational amplifier integrated circuits applications, discussing simple and transducer amplifiers, operational circuits, wave shapers and generators and power supplies
11 p1857 A69-25665

Acoustic wave generation in neutral particle component of weakly ionized gas by variation of electron temperature with low power RF signal
12 p2134 A69-26096

Elastoplastic stress wave generation by penetration of impulsive electromagnetic radiation through thin surface layer of solid
12 p2179 A69-26215

Electrical equivalent circuit for piezoelectric generation and detection of transient and sinusoidal ultrasonic waves by interdigital electrodes
12 p2039 A69-26376

Submillimeter wave generated in ZnTe by difference frequency mixing of Q switched ruby laser, discussing beat power [IEEE PAPER B-4]
14 p2457 A69-28927

Orotron electron beam excited oscillator-generator of millimeter and submillimeter wave bands with wide frequency tuning range
14 p2421 A69-29546

Spiral density waves formation in galaxy model with differentially rotating and nonrotating subsystems based on collective interactions
15 p2688 A69-30550

Hydromagnetic stability calculations applied to umbral models, showing overstable oscillations relation to thermal hydromagnetic wave generation occurrence in sunspots
15 p2693 A69-30780

Wave regeneration by resonant particles interaction in inhomogeneous plasma of electrons confined in quadratic potential solved in WKB approximation
15 p2660 A69-30918

Shock wave growth or decay in atmospheres with density and temperature variation using singular surface theory
16 p2768 A69-3166

Microwave induced ionization wave propagation in rare gases, noting rapid electron density increase at wave front and subsequent slow plasma decay
16 p2818 A69-31671

Q switched laser produced blast waves in low pressure Ar, discussing gas density and time dependence roles
16 p2796 A69-31705

Inhomogeneity effects on elastic waves generated by impulsive loading of surface using asymptotic method, discussing high stress intensification regions
16 p2873 A69-32157

Wave generation in infinite micropolar elastic solid body analyzed by linearized equations of motion
17 p3053 A69-33018

Wave generation in infinite micropolar elastic body, studying axially symmetric displacement and rotation fields
17 p3053 A69-33019

Collisionless shock wave generation and structure in zeta and theta pinches
17 p3013 A69-33819

Wave equations covering evolution of long non-linear axially symmetric wave motion in inviscid rotating fluids
18 p3120 A69-34441

- Acoustic gravity waves generated in isothermal atmosphere by ground energy source calculated using stationary phase method and kinematic theory
18 p3129 A69-34953
- Discrete radio sources spectra at decametric wavelengths, showing variation with frequency and radio wave generation mechanism leading to various spectral types
18 p3200 A69-35134
- Atmospheric gravity waves amplitude generated in equatorial electrojets and polar regions
20 p3593 A69-38107
- Photon induced precursor ionization and electron produced wave separation from electrical shock tubes
20 p3511 A69-38240
- Device producing step-like output representing amplitude of ECG R-wave on beat by beat basis
21 p3667 A69-39443
- Stellar atmospheres acoustic energy generation rate calculations, studying corona mass ejection effects on stellar rotation
21 p3813 A69-39521
- Coronae around helium stars and X ray sources, calculating acoustic energy generation rates in convection zones
21 p3813 A69-39522
- Electromagnetic wave propagation in nonlinear media, considering evolution and decay of electromagnetic shocks
21 p3697 A69-39670
- Chromospheric heating above sunspots by analyzing MHD wave generation and propagation in sunspots and solar atmosphere
22 p4010 A69-39992
- Kinematic dynamo waves, discussing excitation and maintenance of magnetic field by assumed motion of uniformly conducting fluid using small parameter and numerical methods
22 p3989 A69-40195
- Orographic inhomogeneities of underlying surfaces for radiating atmospheric waves formation, deriving formulas for plane stable atmosphere
23 p4185 A69-42492
- Wave processes in pipelines during fluid filling, studying effects of flow resistance due to pumps and nozzles
24 p4300 A69-43075
- Saturn F-1 rocket engine as generator of infrasonic waves and magnetic fluctuations, noting ignition and cut-off signal characteristics
24 p4365 A69-43415
- Turbulence and laminarity effect on vertical waves development rising in thin layer of heavy viscous fluid in contact with vertical gas flow
24 p4302 A69-43480
- Shock formation mechanism in simple shock tube using multistage modification of White model, deriving variation of shock Mach number
24 p4305 A69-43631
- Wave generation in infinite micropolar elastic solid, determining displacement and rotation fields and strain state
24 p4406 A69-43731
- Magnetoacoustic waves generated by Cerenkov radiation from corpuscular fluxes due to star interaction with stellar wind, determining deceleration forces on star
24 p4390 A69-43775
- WAVE INCIDENCE CONTROL**
- Optimal focusing of acoustic system for tube defectoscopy with circular normal waves
24 p4296 A69-42655
- WAVE INTERACTION**
- NT SHOCK WAVE INTERACTION**
- Semiclassical wave emission and absorption theory applied to charged particles interaction with waves in magnetized plasmas
01 p0126 A69-10123
- Exact solution for coupling effects between two waves with complex coupling function, defining region of validity for earlier perturbation theory
01 p0027 A69-10252
- Asymptotic method for analyzing small long wave perturbations in plasma, showing instability with respect to perturbations propagating at angles to ion-acoustic wave
01 p0131 A69-10788
- Ionospheric irregularities and cross field plasma instability, analyzing nonlinear behavior of latter with two dimensional model
01 p0073 A69-11179
- Stability of weakly inhomogeneous plasmas with free energy available for nonlinear resonant three wave interactions
01 p0133 A69-11212
- Nonlinear interaction between longitudinal Langmuir waves and parallel wave vectors in heated plasma study, based on Cauchy problem of kinetic equation for electron distribution
02 p0285 A69-11461
- Collision broadened homogeneous linewidth measurements for 6328 angstrom Ne line in Ne and He-Ne discharges, using nonlinear interaction between two traveling waves
02 p0257 A69-12613
- Oppositely moving waves interaction during nonlinear transient process of oscillations buildup in annular solid state laser found dependent on coupling via scattering
02 p0259 A69-12648
- Q switched laser based on light waves parametric interaction in nonlinear medium operating at wavelengths from UV to IR
03 p0439 A69-13054
- Nonlinear interaction between waves in relativistic plasma, determining probability between transverse and longitudinal waves with different phase velocities
03 p0397 A69-13710
- Traveling waves interaction effects on emission modes of gas laser with circular resonator
04 p0611 A69-14545
- Colliding waves synchronization and stability in annular gas laser by electronic simulation
05 p0770 A69-15645
- Internal gravity waves propagation in shear flow, detailing interaction stress in incompressible stratified Boussinesq liquid, conservation energy exchange and radiation stress
05 p0788 A69-15721
- Intense transverse resonant acoustic field interaction with viscous fluid flows
[ASME PAPER 68-WA/FE-8]
05 p0748 A69-16091
- Nonstationary nonlinear wave phenomena in ultrashort high intensity light pulse formation, discussing nonstationary stimulated Raman scattering and picosecond pump reduction of Raman amplification
[IEEE PAPER H-5]
05 p0774 A69-16316
- Hydrodynamic and lattice vibrations equations for coupled waves in ion semiconductors in external electric and magnetic fields, observing sound amplification
06 p0978 A69-16897
- Resonant four wave interaction for nonlinear energy transfer in electron plasma oscillations
06 p0963 A69-17143
- Packet of finite amplitude VLF whistler waves, examining cyclotron resonance interaction with high energy electrons and development in magnetosphere
06 p0917 A69-17378
- Reciprocal interaction of combustion wave and field of turbulence, discussing aerodynamic principles, turbulence effect on flame propagation speed and measuring methods
06 p1032 A69-17420
- Electrostatic waves interaction to electrons in plasma characterized by bump-in-tail distribution function, deducing mechanism of wave particle interaction
06 p0966 A69-17521
- Symmetrical formulation of quantum theory of three wave optical parametric interactions in crystals
06 p0958 A69-17710
- Nonlinear interaction between cyclotron harmonic waves propagating perpendicular to static magnetic field in warm magnetoplasma, noting parametric amplification and mode conversion
06 p0968 A69-17766
- Interaction of laminar hypersonic boundary layer and supersonic corner expansion wave, discussing upstream influence, transverse pressure gradients and external flow
[AIAA PAPER 69-137]
06 p0913 A69-18078
- Small signal coupled mode analysis including relativistic effects for studying spiraling electron beam interaction with fast wave circuits
07 p1114 A69-18436
- Nonlinear interaction between cyclotron harmonic waves, demonstrating synchronism conditions for traveling wave parametric amplification and passive mode conversion
07 p1189 A69-18439
- Equations for electron scattering by sound in n-type semiconductors, giving corrections to sound propagation velocity during interactions
07 p1199 A69-18680
- Nonpolarized single frequency gas laser radiation produced by interferential effects in complex resonator
07 p1149 A69-18936
- Planetary wave-zonal flow interaction interpretation in terms of potential vorticity eddy transport, deriving zonal wind change and temperature field
07 p1126 A69-19037
- Parametric light interactions application to optics stressing nonlinear spectrograph and cavity and traveling wave oscillator
[IEEE PAPER K-5]
07 p1152 A69-19066
- Thin electron flux interaction with electromagnetic wave in open waveguide, discussing nonlinear theory and performance of gyroresonance transverse wave tube
07 p1107 A69-19159
- Resonance effects during piezoelectric interaction between charged drift wave and flexural wave in semiconductors with one sign current carriers
08 p1371 A69-19806
- Exact solution to kinetic equation for resonant three wave coupling in weakly turbulent plasmas, assuming only single triplet of modes interaction
08 p1360 A69-19989
- Collective interactions of electromagnetic waves in plasma, discussing light scattering from electron fluctuations, stimulated emission and anomalous absorption
08 p1361 A69-20220
- Nonlinear interactions between plasma waves of various intensities, noting changes in particle distribution
08 p1362 A69-20427
- Plasma oscillation modes perpendicular to magnetic field used to study energy conversion by wave coupling across density discontinuity
08 p1367 A69-20795
- Wave interaction in magnetically confined plasma taking into account body and surface waves
08 p1370 A69-21014
- Cyclotron waves interaction when propagating in solid state plasma in magnetic field, determining amplification zones and factors
08 p1374 A69-21078
- Plasma wave coupling in absence of magnetic field in revolving system containing dielectrics and circular waveguide
08 p1371 A69-21150
- Plasma dissipative drift instability and nonlinear wave interaction from discharge with oscillating electrodes, investigating LF plasma oscillations
09 p1550 A69-22019
- Mass displacement in light path due to interaction with gravitational wave accompanying light pulse, discussing general relativity tests for time delay and starlight bending
09 p1540 A69-22081
- Mach wave and anisotropic supersonic flow interaction, considering constant entropy along streamline and layer of entropy discontinuities/interfaces
10 p1631 A69-22906
- Asymptotic method for analyzing small long wave perturbations in plasma, showing instability with respect to perturbations propagating at angles to ion-acoustic wave
10 p1653 A69-23107
- Quantitative analysis of plane waves for weak interaction of two dimensional sound and light fields in acoustical imaging by diffracted light
10 p1695 A69-23545
- Level degeneracy effect on nonlinear interactions between traveling waves of different planes of polarization
10 p1705 A69-23815
- Long and short duration pulses interactions with nonlinear dielectric, calculating frequency variations and spectral transformations
10 p1658 A69-23953
- Capture of parametrically coupled waves by pulses and beams of pumping radiation in case of different group velocities directions
10 p1705 A69-23956
- Mode interactions in argon lasers between two spectral lines noting effect on output
10 p1705 A69-24003
- Transformation of longitudinal plasma wave into electromagnetic wave during collision with dielectric in plasma
11 p1934 A69-25708
- Short circuit and variable frequency technique for measurement of coupling efficiency between dielectric loaded rectangular and trough waveguides, noting propagation modes
12 p2039 A69-26374
- Energy exchange between LF waves and magnetospheric energetic particle population by bounce resonant interaction
12 p2073 A69-26946
- Electromagnetic flux from nonlinear self interaction of electron plasma waves in far field of perturbation under anisotropic electron pressures
12 p2141 A69-27147

Pressure waves interaction with solid fuel hot surface at HF based on linear theory of acoustic instability in condensed systems

13 p2371 A69-27383

Variational method for weak second order resonant interactions among waves with position and time varying amplitudes and phase angles

13 p2297 A69-27634

Waves propagating along rotating electron beam and interacting with magnetized plasma waveguide slow waves

13 p2312 A69-28118

Gas ring lasers, discussing optimal parameters, colliding waves interference, nonmutual effect and radiation polarization

13 p2272 A69-28175

Shadow zone diffraction of plane step function compressional wave by circular cavity, using Friedlander wave front approximations

13 p2368 A69-28347

Admittance of radiating elements in circular array with longitudinal slots on conducting cylinder, taking into account element interactions

13 p2234 A69-28505

Intense transverse resonant acoustic field interaction with viscous fluid flows
[ASME PAPER 68-WA/FE-8]

14 p2430 A69-29444

Integral formulation of scattering theory extended to Coulomb interactions by expanding Green function and treating kernel singularities

14 p2489 A69-29995

Laser-nonlinear crystal dynamical interactions, studying saturation and coherence properties of second harmonic wave generated inside laser cavity

15 p2632 A69-30026

Magnetoelastic resonant interaction of microwave longitudinal phonons propagating at right angles to magnetic bias applied to YIG rod axis

15 p2565 A69-30184

Theory of temperature dependent magnon energies in antiferromagnets based on spin wave operator expansion of Hamiltonian, taking into account dynamical interaction between waves

15 p2668 A69-30684

Equations describing interaction between HF and LF waves propagating in nonlinear dispersive medium, obtaining approximate solutions

15 p2568 A69-30733

Galactic cosmic rays and Alfvén waves interaction, considering gyration frequency resonance, wave growth, Fokker-Planck equation and diffusion model

15 p2675 A69-30761

Power coupling among modes in semiconductor lasers in presence of spontaneous or forced microwave modulation of population inversion

15 p2634 A69-30875

Disturbance currents from penetration of acoustic waves in weakly ionized gas, analyzing wave interaction with DC glow discharge

15 p2665 A69-31547

Nonlinear interaction between three monochromatic waves propagating parallel to magnetic field in plasma, considering relativistic drift motions of particles

16 p2816 A69-31640

Stress waves propagation through elastic-plastic medium with uniaxial displacement, discussing wave interactions and interface conditions

16 p2870 A69-31809

Electromagnetic fields in closed one dimensional resonators with oscillating boundary, analyzing amplitude buildup

16 p2751 A69-32030

Colliding waves synchronization and stability in angular gas laser by electronic simulation

16 p2798 A69-32502

Monograph on interaction between flow and sound fields as singular: perturbation problem, using matched asymptotic expansion

17 p2949 A69-32998

Aerodynamic interactions between two wing configurations with same aspect ratio located in same plane, discussing testing principles and initial experimental results

17 p3061 A69-33595

Wave interaction in gas ring laser, delineating single mode emission zones as function of pumping, emission frequency position and Q factor differences

17 p2982 A69-33632

Nonresonance parametric phenomena in distributed systems, discussing interaction between signal and parameter wave at superlight velocity

17 p2928 A69-33868

Electroacoustic-electromagnetic waves nonlinear coupling in compressible isotropic plasma, comparing slowly varying and resonant interaction approaches

17 p2928 A69-33870

Atmospheric whistlers and ion acoustic waves interaction in nonisothermal plasma, determining damping frequencies, decrements and wave polarization

18 p3180 A69-35024

Fluid-shell interactions, using piston theory and cylindrical-wave approximations

18 p3223 A69-35174

Bogoliubov averaging method of perturbation in wave mechanics for radiation and matter interaction, considering monochromatic and broad spectral incident wave for resonance study

18 p3175 A69-35483

Turbulent wake and ambient flow interaction analysis based on integral methods in boundary layer theory

19 p3299 A69-36390

Magnetospheric disturbances effect on radio wave propagation, discussing wave-particle interactions, VLF emissions and electrostatic waves

19 p3303 A69-36429

Monograph on interaction between primary and jet flapped secondary airfoils covering line-vortex use for lift augmentation, aerodynamic characteristics, etc

19 p3242 A69-36820

Vibration analysis, using rigid body and normal modes to solve interconnection problem, applied to free-free natural vibration modes of clustered rockets

20 p3621 A69-37195

Asymptotic method for analyzing small long wave perturbations in plasma, showing instability with respect to perturbations propagating at angles to ion-acoustic wave

20 p3582 A69-38005

NonJeans gravitational instability of stars and interstellar gas in Galaxy due to wave interaction with stars having velocity near wave phase velocity

20 p3607 A69-38037

Absolute and convective instability criteria of interacting electromagnetic waves in waveguide systems involving parametric oscillators and amplifiers

21 p3677 A69-39555

Monograph on whistler mode waves in plasma covering apparatus for studying gyroresonant interaction between whistler radiation and fast electrons

21 p3779 A69-39868

Coupling coefficients and excitation increments determined for nonlinear interactions of surface waves in nonisothermal semibounded plasma

22 p3990 A69-40790

Nonlinear interaction between extraordinary waves propagating perpendicular to static magnetic field in cold homogeneous magnetoplasma

23 p4195 A69-41538

H and He atoms escape from atmosphere under MHD waves action at exosphere boundary

23 p4156 A69-41847

Nonlinear plasma physics, discussing nonequilibrium effects, wave-wave coupling, wave-particle interactions, single nonlinear wave behavior, etc

23 p4197 A69-42312

Electrode interactions effects in interdigital surface wave transducers on piezoelectric materials, using Fourier analysis

24 p4312 A69-42615

Whistlers nonlinear interaction during cold magnetoplasma propagation, considering energy exchanges between waves

24 p4309 A69-43174

WAVE MOTION

U WAVES

WAVE OSCILLATORS

U OSCILLATORS

WAVE PROPAGATION

- NT ACOUSTIC ATTENUATION
- NT AUTOMATIC PICTURE TRANSMISSION
- NT DIFFRACTION PROPAGATION
- NT DOUBLE SIDEBAND TRANSMISSION
- NT ELECTROMAGNETIC WAVE TRANSMISSION
- NT GROUND WAVE PROPAGATION
- NT IONOSPHERIC F-SCATTER PROPAGATION
- NT IONOSPHERIC PROPAGATION
- NT LIGHT SCATTERING
- NT LIGHT TRANSMISSION
- NT MANDELSTAM REPRESENTATION
- NT MICROWAVE ATTENUATION
- NT MICROWAVE TRANSMISSION
- NT MULTIPATH TRANSMISSION
- NT RADAR ATTENUATION
- NT RADAR TRANSMISSION
- NT RADIO ATTENUATION
- NT RADIO TRANSMISSION
- NT SCATTER PROPAGATION

- NT SHOCK WAVE ATTENUATION
- NT SHOCK WAVE PROPAGATION
- NT SHORT WAVE RADIO TRANSMISSION
- NT SINGLE SIDEBAND TRANSMISSION
- NT SOUND TRANSMISSION
- NT TELEVISION TRANSMISSION
- NT TRANSEQUATORIAL PROPAGATION

Plane wave propagation in infinite viscoelastic medium taking into account mutual effects of deformation and temperature fields

01 p0164 A69-10076

Electron plasma wave dispersion along cylindrical plasma column in magnetic field

01 p0126 A69-10271

Nonlinear hydromagnetic solitary wave propagation at angle to magnetic field in fully ionized quasi-neutral collisionless warm plasma, noting isotropic pressure effect

01 p0127 A69-10336

Gravity waves train propagation in cylindrical channel, discussing derivation by three dimensional flow analysis method

01 p0059 A69-10382

Alfvén and magnetoacoustic waves propagation in inhomogeneous stable plasma situated in field with helical lines of forces

01 p0130 A69-10742

Hydromagnetic wave propagation in current carrying regions of ionosphere and magnetosphere using macroscopic equations, deriving dispersion relation

01 p0067 A69-10972

First normal modes characteristics and lateral wave in weak dielectric layer applicable to microwave propagation

01 p0033 A69-10975

Electrostatic polarization field formation by acoustic wave propagation through ionosphere, calculating effect on ionization drift velocity

01 p0068 A69-11110

Electromagnetic waves trajectory distortion in moving plasma due to additional time delay noting propagation of pearl pulsations, whistling atmospherics and proton whistlers

01 p0068 A69-11114

Electromagnetic wave path emitted by artificial satellites across anisotropic ionosphere due to geomagnetic field determined by computer program

01 p0068 A69-11115

Numerical method for determining group velocity of waves in homogeneous anisotropic medium, using implicit function from dispersion relation

01 p0131 A69-11117

Vertical propagation of acoustic waves in atmosphere without gravitational waves and with height varying atmospheric shear viscosity

02 p0274 A69-11440

Electromagnetic waves propagation in cylindrical waveguide containing plasma column along axis in absence of constant magnetic field

02 p0285 A69-11463

Book on propagation characteristics of various wave modes in ionized gas plasmas

02 p0285 A69-11518

Induced discharge laser wave propagation in medium with active and absorbing admixtures, determining stationary wave shape and velocity range

02 p0206 A69-11609

Low field helicon wave transmission through n-type Ge at liquid He temperature, noting cyclotron resonance damping

02 p0295 A69-11787

Instability of longitudinal plasma waves propagating across magnetic field in plasma with electrons and ions drifting with different velocities across field

02 p0286 A69-11830

Dispersion relation of internal acoustic gravity wave motion in compressible nonviscous and nonheatconducting atmosphere

02 p0242 A69-11868

Magnetosphere studies in France noting magnetosphere characteristics, wave propagation, charged particles, particle precipitation mechanisms in auroral zones and polar caps

02 p0242 A69-11904

Magnetoplasma wave propagation in periodic conducting solid, calculating electron drift effect on space harmonics

02 p0287 A69-11945

Electromagnetic wave propagation problems, using asymptotic solutions of differential and integral equations in domains containing transition points

02 p0208 A69-12130

Dispersion relations of axisymmetric and dipolar surface modes propagation along inhomogeneous plasma columns on dispersion relations

02 p0289 A69-12242

Alfven wave propagation in nonhomogeneous systems for relativistic MHD, discussing magnetic and velocity perturbations
02 p0290 A69-12254

Plastic deformation wave propagation and heat generated near yield point of annealed aluminum
02 p0342 A69-12280

Elastic-plastic wave profiles in Al alloy under uniaxial strain load, investigating sensitivity to various strain rates
02 p0344 A69-12289

Wave front profiles sensitivity to form of constitutive equation in one dimensional stress problem
02 p0344 A69-12291

Plane strain plastic stress waves radial propagation from center of hollow cylinder subject to dynamic pressure load
02 p0344 A69-12292

Elastic/viscoplastic wave propagation in thin tubes under combined stress of tension and torsion, using viscoplastic constitutive equations
02 p0344 A69-12293

Geomagnetic micropulsations mechanism, discussing hydromagnetic waves transmission generated by interface instability between solar wind and magnetosphere, noting transmission path role
02 p0244 A69-12395

Alfven wave propagation designations in terms of polarization and propagation velocity, resolving contradictory aspects
02 p0290 A69-12400

Radar target amplitude, angle and Doppler scintillation from analysis of echo signal propagation in space
02 p0211 A69-12447

Wave structure for moving load on surface of anisotropic material in plane stress investigated for stable elastic wave propagation
02 p0348 A69-12609

Spherical elastic-plastic stress wave propagation analysis via finite difference procedure
02 p0348 A69-12610

Viscous damping of internal waves on rotating earth, analyzing spatial propagation attenuation in two layer system
02 p0247 A69-12775

Sound radiation from vibrating bodies, noting errors in Lighthill conclusion
02 p0282 A69-12800

High speed compression waves, rarefaction waves and gas interface regions position and velocity measurement in shock tube by sensing electrical impedance
03 p0428 A69-13104

Density gradient driven collisional drift waves, discussing identification, stabilization and enhanced plasma transport
03 p0474 A69-13145

Decay stability of large amplitude neutral wave into two ion acoustic waves in weakly ionized plasma
03 p0475 A69-13158

VOR path course errors, emphasizing effects of propagation and receiver processing
03 p0392 A69-13245

ELF radio wave propagation characteristics using two layered ionospheric model, noting deeper penetration than VLF
03 p0421 A69-13326

Mathematical models to investigate transient plane bending wave propagation in elastic plates, using elasticity and plate theories
03 p0525 A69-13606

Wavelength dependence of microwave propagation beyond radio horizon
03 p0395 A69-13626

Propagation of long electromagnetic waves in ionosphere and exosphere, discussing thunderstorm noise spectrum
03 p0396 A69-13702

Longitudinal elastic wave damping, excitation and propagation in lithium niobate crystals at frequencies from 200 to 2000 MHz
03 p0487 A69-13729

Longitudinal thermoelastic wave propagation in infinite body, proving generalized Kirchhoff theorem
03 p0528 A69-13924

Propagation of longitudinal transverse loading and unloading waves /with cylindrical symmetry/ in nonhomogeneous elastic/viscoplastic medium, accounting for plastic dilatational strains
03 p0528 A69-13929

Helicon waves in nonresistive cylindrical and spherical plasmas
03 p0479 A69-13961

Dispersion equation for two dimensional periodic slow wave structure formed by periodically sequential loading
03 p0407 A69-13981

Magnetosonic wave propagation across magnetic field in warm collisionless Maxwellian multicomponent plasma studied for small electron cyclotron and ion cyclotron radii
03 p0479 A69-14020

LF hydromagnetic waves propagation in ionospheric waveguide duct resulting from minimum in Alfven speed near F 2 ionization peak
03 p0399 A69-14023

Langmuir wave disintegration, analyzing instability criterion and growth rate
03 p0480 A69-14057

Longitudinal and transverse elastic waves propagation in medium with random inhomogeneities, deriving scattering coefficients in Born approximation for Fraunhofer region
04 p0667 A69-14262

Elastic-plastic boundaries velocities for combined longitudinal and torsional plastic wave propagation in thin walled tube during unloading [ASME PAPER 68-WA/APM-7]
04 p0670 A69-14403

One dimensional wave propagation analysis for zero value stress time derivatives on both sides of elastic-plastic boundary
04 p0670 A69-14407

Anisotropic nonlinear wave propagation in arbitrarily moving ideal gas, using singular surface/ray combined theories
04 p0630 A69-14532

Propagation velocity upper limits for plasma waves during state of equilibrium transition determined for nonlinear wave equation
04 p0630 A69-14553

Kinetic theory to determine wave increments propagating across magnetic field in system of relativistic electrons in cold plasma
04 p0635 A69-14555

Time harmonic vibrations and wave propagation in laminated plate, using elasticity theory equations and continuum theory for layered medium
04 p0675 A69-14685

Surface impedance variation effect on surface wave propagation along rod waveguide
04 p0576 A69-14761

Space-frequency correlation relationship of complex field fluctuations, amplitude and intensity to levels and phases of waves propagating in medium of random inhomogeneities
04 p0557 A69-14774

Higher modes of longitudinal wave propagation in dispersive thin elastic rod, noting response to laser pulse
04 p0678 A69-14869

Flexural waves passage through obstacles in infinite plate, determining vibration arresting properties of rigid ribs, elastic inserts and hinged couplings
04 p0678 A69-14902

East-West aligned fast auroral waves, suggesting origin in hydromagnetic processes occurring near equatorial plane
04 p0594 A69-15123

Nonlinear demodulation of amplitude modulated wave propagating in plasma
04 p0559 A69-15210

Reflection and transmission of radiation from very thick and semiinfinite homogeneous atmospheres with arbitrary phase function, using asymptotic fitting method
04 p0595 A69-15285

Long distance propagation of acoustic gravity waves ducted in thermosphere, noting effect of seasonal variations in polar region
04 p0595 A69-15437

Absorption effect on fluctuation of signal level propagating in turbulent atmosphere taking into account absorption in water vapor
05 p0717 A69-15634

Gyrotropically filled waveguides propagation parameters calculation by variational method
05 p0718 A69-15648

Holograms applied to analysis of wave packets propagating in quasi-optical transmission lines
05 p0718 A69-15650

Plane shear pressure wave propagation in elastic-plastic half space for various combined normal and shearing loadings
05 p0835 A69-15798

Acceleration wave propagation and growth in elastic materials, discussing thermodynamic influences
05 p0836 A69-15931

Atmospheric density variation measurements by density gages on Explorer 32 satellite confirm wave propagation in neutral thermosphere as free internal gravity waves
05 p0754 A69-16261

Rotation wave propagation in elastic homogeneous isotropic centrosymmetric body in asymmetric elasticity theory
05 p0843 A69-16645

Electron plasma interaction with transverse EM wave propagating along magnetic field, calculating permittivity, density, field strength and applied frequency
05 p0805 A69-16699

Alfven waves observed propagating along lines of force in inhomogeneous plasma in presence of homogeneous gravitational field
05 p0805 A69-16706

Submillimeter plane monochromatic wave amplitude and phase fluctuations during propagation in turbulent atmosphere surface layer, considering absorption by water vapor
05 p0722 A69-16778

Longitudinal acoustic waves propagation in partially ionized gas in external electric field, taking into account ionic collisions with electrons and neutral particles
06 p0963 A69-17079

Theoretical and experimental results on annealed tapered aluminum rods to assess one-dimensional rate independent theory of plastic wave propagation from longitudinal impact
06 p1022 A69-17365

Finite amplitude longitudinal wave propagation in lattices analyzed by study of compressive wave in chain of mass points with nearest neighbor interaction
06 p1022 A69-17367

Reciprocal interaction of combustion wave and field of turbulence, discussing aerodynamic principles, turbulence effect on flame propagation speed and measuring methods
06 p1032 A69-17420

Transient nonaxisymmetric elastic wave propagation in infinite isotropic elastic plate, using linear elasticity theory
06 p1024 A69-17509

Trapped mode wave propagation for cold uniform magnetoplasma cylinder in free space, studying dipole modes and one-wave approximation
06 p0967 A69-17756

Nonlinear interaction between cyclotron harmonic waves propagating perpendicular to static magnetic field in warm magnetoplasma, noting parametric amplification and mode conversion
06 p0968 A69-17766

Surface wave propagation on circular plasma column moving in axial direction in free space region
06 p0968 A69-17775

Ion-cyclotron instabilities in hot-ion cold- electron plasma resulting from left-hand circularly polarized wave propagating parallel to magnetic field
06 p0969 A69-17951

Low temperature simulation of hypersonic melting ablation and wave patterns of gas-liquid interface
06 p0907 A69-18064

Nonisothermal wave propagation in n-type indium antimonide in orthogonal static and magnetic fields, considering instabilities and acoustic and polar optical phonon scattering
07 p1197 A69-18467

Wave propagation on cylindrical electron beam in vacuum and in plasma background, including relativistic effects
07 p1189 A69-18657

Structure of plane shock wave of arbitrary force propagating across magnetic field in hot rarefied plasma
07 p1190 A69-18692

Rise velocity of large gas bubbles in liquid calculated, assuming velocity is determined by propagation of bubble produced wave disturbance
07 p1120 A69-18999

Large amplitude longitudinal wave propagation in elastic rod solved by method of characteristics, prescribing end velocity as step function of time
07 p1233 A69-19176

Cross modulation of amplitude modulated wave propagating in nonlinear dispersive plasma, obtaining electric vector
07 p1086 A69-19228

Plasma column radial density profile measurement by electron plasma waves propagation in presence of strong magnetic field
07 p1194 A69-19323

Hydromagnetic wave propagation and generation in magnetosphere, discussing hydromagnetic waves in uniform and axisymmetric magnetic fields
07 p1208 A69-19356

Wave propagation and instabilities in rotating anisotropic collisionless plasma, analyzing plane and cylindrical perturbations
07 p1195 A69-19438

Fluid motion and MHD disturbances in viscous incompressible fluid of finite electrical conductivity, studying axis of oscillating dipole perpendicular to exciting field
07 p1195 A69-19451

Shock waveforms lengthening due to propagation to high altitudes derived from computed numerical values, studying N waves from SST
07 p1054 A69-19463

HF wave propagation in unbounded electron-plasma systems using moment equations, discussing collisions effect and dispersion relation
07 p1086 A69-19468

Phase shift and losses in wave propagation in dielectric environment, defining power transmission coefficient and insertion phase shift
07 p1087 A69-19518

Axial waves in blood vessels, determining phase velocities and damping, noting anisotropic behavior of artery wall
[SESA PAPER 1350] 07 p1069 A69-19726

Plane radiative shock wave propagation in homogeneous medium noting heating ahead and cooling behind shock front
08 p1302 A69-19798

Linearized model for vertical propagation of Rossby waves through atmosphere with Newtonian cooling, discussing atmospheric wind effects
08 p1344 A69-19812

Schlieren optics study of omega wave in water filled cuvette, noting propagation by wall reflected water wave
08 p1350 A69-19889

Landau damping of long wavelength ion acoustic waves in collision-free one dimensional plasma with gravity field
08 p1359 A69-19983

Ultrashort optical pulses of coherent light, discussing propagation in inhomogeneously broadened medium of two level systems
08 p1324 A69-20083

Constitutive equations for propagation of plane waves of finite amplitude in nonsimple elastic solids, discussing holohedral isotropic solids and transverse harmonic circularly polarized waves
08 p1411 A69-20141

Two gravitational fields theory of gravitation in general relativity for flat universe, discussing gravitational wave propagation
08 p1390 A69-20276

Propagation modes in corrugated cylindrical waveguides determined by imposing nonisotropic surface reactance boundary condition at corrugated walls
08 p1284 A69-20295

Mode designation and propagation characteristics of dielectric tube waveguide, noting practicability at higher microwave frequencies
08 p1284 A69-20296

Large amplitude waves in inviscid flows of stably stratified fluids over barriers with constant density upstream constructed from vortex pairs and doublets
08 p1346 A69-20313

Two dimensional unsteady wave motion in shallow water using MHD theory
08 p1362 A69-20354

Spherical wave generalization for plane light wave propagating in turbulent medium, describing circular objective averaging effect on intensity fluctuations
08 p1351 A69-20438

Microwave plasma diagnostics, discussing electromagnetic radiation and wave propagation measurements
08 p1316 A69-20470

Quasi-linear differential constitutive equation of work hardenable elastoviscoplastic material in case of plane wave propagation in half space
08 p1415 A69-20662

Wave behavior in warm inhomogeneous plasma with magnetic field perpendicular to density gradients of unperturbed plasma, solving Maxwell-Vlasov equations by perturbation methods
08 p1365 A69-20744

Self modulation, self steepening and spectral development of light in small scale trapped filaments, noting influence of relaxation time
08 p1352 A69-20745

Gravitational wave solution of Einstein field equations, deriving Ricci and Riemann tensors for Einstein space
08 p1352 A69-20755

Symmetric Alfvén waves propagation in hydrogen plasma with nonuniform density distribution, deriving dispersion relations for fully ionized plasma
08 p1367 A69-20794

Collisional theory of longitudinal wave propagation for two fluid viscous ionized plasmas formulated from coupled Maxwell and Boltzmann equations
08 p1367 A69-20796

Mach number values and propagation rates of wear disturbances in interplanetary medium obtained from Mariner 2 data during low solar activity
09 p1575 A69-21523

Singular surface theory combined with ray theory for propagation of weak discontinuities in nonlinear anisotropic media applied to MGD
09 p1547 A69-21613

Characteristic equation obtained by considering world line vector, basic thermodynamic variables and metric tensor as functions of Lichnerowicz class
09 p1480 A69-21614

Steady state currents effect on hydrodynamic waves propagated normal to magnetic field
09 p1547 A69-21662

Bond shear effects on dynamic behavior of two layered cylindrical shell, identifying bond stiffness parameters
[AIAA PAPER 68-354] 09 p1616 A69-21941

Thermally generated stress wave propagation in dispersive elastic rod investigated experimentally and analytically, using ruby laser and differential equation
09 p1617 A69-22010

Integrodifferential equations describing longitudinal oscillation properties in nonlinear region of electron Maxwellian plasma waves and two cold electron beams
09 p1550 A69-22026

Weak discontinuities in wave propagation, studying ionized gas nonsteady flow having electrical conductivity in magnetic field
10 p1727 A69-22916

Perturbation solution for propagation of fourth order coherence function in random medium extended to larger field fluctuations, deriving integrodifferential equation
10 p1724 A69-23042

MHD first order partial differential equations used to investigate wave front between perturbed and unperturbed flow regions in magnetosonic propagation through homogeneous medium
10 p1727 A69-23090

Forced vibrations in semibounded elastic bar with various moduli of elasticity, discussing reversing longitudinal force and elastic waves propagation
10 p1799 A69-23155

Relativistic energy momentum tensor of electromagnetic field in moving multicomponent dispersive media and instability of wave
10 p1653 A69-23193

Electromagnetic wave propagation over constant impedance flat earth, using electromagnetic compensation theorem
10 p1655 A69-23422

Longitudinal and transverse wave propagation in compressible isotropic turbulent plasma, noting mode coupling effect
[AFCL-69-0289] 10 p1729 A69-23424

Microwave frequency room temperature acoustic surface wave propagation losses in lithium niobate measured by laser light deflection, discussing propagation and insertion losses
10 p1703 A69-23511

Microwave magnetoelastic wave propagation in ferromagnet subjected to pulsed magnetic field using coupled mode approach
10 p1746 A69-23655

Discharge plasma ionized waves, determining mechanism of wave propagation and instabilities
10 p1740 A69-23699

Transmission line analogs and kinetic power theorems for space charge waves amplification in semiconductors, considering internal effect and wave excitation
10 p1748 A69-24052

Space charge waves amplification in semiconductors on coupling with forward circuit wave by transmission line analog, noting application to electromagnetic and acoustic waves
10 p1748 A69-24053

MHD generator plasma anisotropic instability caused by amplified magnetosonic waves propagating normal to current
11 p1922 A69-24227

Nonlinear integrodifferential kinetic equation for weak turbulence of resonant four wave processes, considering spectral energy density
11 p1921 A69-24294

Normal mode dispersion at upper hybrid frequency propagating parallel to uniform magnetic field in spatially inhomogeneous plasma
11 p1924 A69-24302

Wave propagation in connected space-time for linear second order hyperbolic partial differential equation, describing unitary invariant theory
11 p1908 A69-24356

Propagation of extensional cylindrical waves in elastic plates with free boundaries, considering plane stress and Lamb dispersion
11 p1969 A69-24414

Growth rates for convective disturbances propagation in atmosphere with linear entropy variation, noting WKB approximation
11 p1957 A69-24422

Radio wave field distortions by dielectric prisms in lens waveguides, discussing beam transformation, noting both geometrical optics effects and diffraction role
11 p1833 A69-24436

Dispersion relation for internal gravity wave propagation across exponentially decreasing magnetic field in conducting fluid, noting atmospheric wave propagation in ionosphere
11 p1877 A69-24564

Elastic waves propagation in inhomogeneous composite media, considering coefficient of structural stress concentration
11 p1972 A69-24649

Two dimensional contained plastic deformation in asymmetrical elasticity theory based on Cosserat medium, examining boundary value problems, stress concentration and elastic wave propagation at holes
11 p1973 A69-24659

Induced discharge laser wave propagation in medium with active and absorbing admixtures, determining stationary shape and velocity range
11 p1895 A69-24716

Millimeter wave propagation over water, discussing fading characteristics and atmosphere absorption effects
11 p1836 A69-24989

Transient signal propagation through cold inhomogeneous plasma with electron density decreasing exponentially in direction of propagation
11 p1836 A69-24990

Full wave calculation of gravity waves for thermospheric model, describing wave type reflection, transmission, conversion and coupling by scattering matrix elements
11 p1878 A69-25150

LF waves and instabilities on positive column in axial magnetic field, noting axisymmetric and asymmetric ion acoustic and electron wave modes and current convective instability
11 p1929 A69-25268

Unstable ion sound wave propagation across magnetic field in collisionless shock waves, noting drift instability
11 p1930 A69-25273

HF electrostatic waves propagation in nonuniform plasma in uniform magnetic field, obtaining solutions of dispersion relation
11 p1931 A69-25360

LF electromagnetic waves stability and propagation conditions in plasma confined in central-conductor configuration measured, noting agreement with wave equation solution
11 p1931 A69-25362

HF electrostatic waves propagation excited by electron beam in hot inhomogeneous plasma in magnetic field, studying wave transformation and absorption
11 p1931 A69-25364

Surface instabilities at tangential discontinuity between media caused by beam-plasma interaction, deriving dispersion relation
11 p1931 A69-25365

Two dimensional elastic stress wave propagation in thick multilayered cylindrical shells for nonuniform external pressure distribution
11 p1991 A69-25511

Dynamic plastic response of finite bar subject to axial impact load noting reflected waves, stress-strain time histories and residual strain
11 p1991 A69-25512

Monochromatic waves propagation in infinite micropolar elastic plate, treating Lamb and Love waves
11 p1995 A69-25605

Elastic waves propagation in micropolar cylinder, treating longitudinal and torsional monochromatic waves in Cosserat medium
11 p1995 A69-25606

TEM-WAVE propagation between parallel conducting planes, stressing changes in curved waveguide section

11 p1841 A69-25619

Excitation coefficients of waves subjected to sudden expansion in radiating waveguide using integral relations, noting convergence

11 p1855 A69-25621

Waveguide cross connection of right-angled waveguides to determine reflection and transmission factors for incidence of H waves

11 p1855 A69-25623

TEM-DUAL surface wave propagation in coaxial cable with stratified dielectric structure to reduce attenuation calculated by addition theorem to Bessel functions

11 p1856 A69-25659

Asymptotic solution of two dimensional problem of elastic impact of bars, showing longitudinal and surface waves decay with time

11 p1996 A69-25737

Gas velocity variation in ionizing shock waves arbitrarily oriented with respect to magnetic field, considering magnetic viscosity and conductive piston

11 p1935 A69-25740

Characteristic plane harmonic free internal neutral atmospheric wave oblique propagation through horizontally stratified quiet atmosphere for various thermospheric parameters

12 p2065 A69-26101

HF interferometry for statistical-numerical oscillation analysis of unsteady plane transonic flow, constructing phase planes for study of wave surfaces propagation

12 p2089 A69-26188

Spherical wave propagation in homogeneous turbulent medium, discussing nonstationary statistics as applied to vertical propagation in atmosphere

12 p2029 A69-26251

Flexural waves passage through obstacles in infinite plate, determining vibration arresting properties of rigid ribs, elastic inserts and hinged couplings

12 p2182 A69-26655

Plasma properties when carrying periodic magnetoacoustic wave expressed in terms of periodic functions, discussing small perturbation propagation

12 p2138 A69-26708

LF wave propagation and emission in magnetosphere, discussing steady noise and discrete emissions

12 p2072 A69-26745

Fluctuations of beam wave propagating through locally homogeneous medium, considering amplitude and phase correlation and structure functions

12 p2032 A69-26855

Gas lasers, including stimulated emission in monochromatic field of traveling and standing plane waves, spontaneous emission with stimulated transitions, etc

12 p2109 A69-26906

Love-wave propagation at UHF observed by thin film surface wave transducers

13 p2218 A69-27203

Nonlinear periodic wave propagation at angle to magnetic field in collisionless plasma studied by two fluid plasma equations

13 p2304 A69-27297

Wave damping in plasma, developing Boltzmann analysis of electron mode dispersion relations involving momentum transfer and relaxations of electron-ion temperature and anisotropy

13 p2305 A69-27377

Kelvin waves relation to quasi-biennial oscillation, using zonal wind and temperature variance data taken at Canton Island

13 p2290 A69-27391

Plane wave solution for wave propagation in inhomogeneous anisotropic time-varying media

13 p2219 A69-27397

Velocity dependence of temperature waves/second sound/ in liquid He II measured as function of relative velocity for normal and superfluid

13 p2297 A69-27460

Wave propagation on heavy fluid surface forming splashes in container with vertical walls

13 p2247 A69-27746

Wave propagation and bandwidth characteristics of rectangular waveguide loaded with H plane lossless dielectric slab

13 p2222 A69-28075

Collisions effect on wave propagation in homogeneous plasma, calculating permittivity tensor and electron equilibrium current using Boltzmann kinetic equation

13 p2311 A69-28104

Three dimensional harmonic dispersion analysis of incremental waves in uniaxially prestressed plastic and viscoplastic bars, plates and unbounded media

13 p2363 A69-28125

Geomagnetic pulsations and hydromagnetic wave propagation in magnetosphere, using geometric optics approximation

13 p2254 A69-28176

Unstable weakly ionized HF magnetoplasma fluctuations with no axial drift, noting phase velocity parametric dependence

13 p2312 A69-28197

LF wave propagation in DC discharge hydrogen plasma, noting self and artificial wave excitation

13 p2316 A69-28584

Atmospheric LF and HF sound transmission anomalies, discussing Tyndall paradox for fog signals propagation over ocean

13 p2301 A69-28666

Libroelastic wave propagation and dispersion characteristics /solid carbon dioxide/ evaluated by using Raman scattering measurements

13 p2286 A69-28668

Temperature effects on propagation of HF internal and surface waves in bounded plasma, deriving dispersion equations

14 p2410 A69-28733

Ionospheric effect sudden commencement parameters of magnetic storm related to distance from origin in polar regions

14 p2435 A69-29051

Solar X ray flux deduced from flare effects on VLF propagation, showing total energy content as measure of ionizing radiation

14 p2411 A69-29105

Frequency time dispersion of storm sudden commencement micropulsations, noting polarization effects

14 p2440 A69-29129

Hydromagnetic waves propagation in finitely conducting fluid mass immersed in nonuniform magnetic field, using curvilinear coordinates based on lines of force

14 p2491 A69-29336

Multiple scattering of electromagnetic waves in underdense plasma, deriving transport equation for radar backscatter

14 p2412 A69-29453

Phase screen technique for deriving statistical characterizations of perturbations imposed on wave propagating through random medium applied to remote probing

14 p2414 A69-29511

Plane wave reflection and transmission by unidirectionally conducting screen, considering oblique incidence and two polarizations

14 p2421 A69-29547

Coupled mode theory for surface wave propagation along tapered cylindrical dielectric rod, considering radiation field effects

14 p2422 A69-29557

Two dimensional adiabatic transverse normal modes of inviscid compressible uniformly rotating fluid, discussing harmonic wave propagation in opposite directions and rotation effects

14 p2431 A69-29581

Image formation with arbitrary holographic surfaces achieved by reversing direction of propagation of diverging wave

14 p2450 A69-29582

Successive approximations method applied to system of independent equations describing electromagnetic wave propagation in space with gravitational wave metric

14 p2487 A69-29669

Leaky waves propagation characteristics helix waveguide covered with slitted cylinder using transverse network representation, emphasizing small pitch angles, hybrid TE and TM modes, etc

14 p2422 A69-29752

Computational accuracy of point matching solution for uniform nonsymmetric waveguides

14 p2423 A69-29758

Group delay time for dispersive wave propagation velocity determined using correlation method

15 p2562 A69-30094

Large scale atmospheric wave motions analyzed by spherical harmonic representation of height fields over earth, detailing wave components and quasi-stationary fluctuations

15 p2647 A69-30216

Wave energy flux and correlation wave energy flux relationship to energy transport, noting applicability to fluids

15 p2595 A69-30218

Cylindrical wave propagation in thermoelastic incompressible isotropic solids, considering cases of zero and nonzero coefficient of thermic dilation

15 p2707 A69-30626

Annealed aluminum rods dynamically compressive impact loading used to study longitudinal plastic waves propagation velocity

15 p2709 A69-30677

Equations describing interaction between HF and LF waves propagating in nonlinear dispersive medium, obtaining approximate solutions

15 p2568 A69-30733

Collisional emission and absorption of longitudinal waves due to particle encounters in numerical experiments on one dimensional one species plasma

15 p2661 A69-30921

Uniform approximation mathematical theory applied to wave propagation problems, considering cylindrical waves and rainbows and glory scattering

15 p2653 A69-31165

Weakly damped transverse and thermal waves development and propagation in viscous heat conducting incompressible fluid under temperature and gravitational fields

15 p2718 A69-31168

Schlieren and photoelastic methods for continuous and pulsed ultrasonic waves propagating in transparent media, discussing nondestructive testing applications

15 p2617 A69-31510

Wave propagation in warm uniaxial plasma filled waveguide, analyzing TE modes, TM mode splitting and power transfer

16 p2756 A69-31576

Auroral absorption influence on ionospheric wave propagation calculated for distances over 4000 km

16 p2749 A69-31603

Propagation and linear transformation of HF electrostatic waves in hot magnetoactive radially inhomogeneous plasma, noting wavelength shortening

16 p2816 A69-31638

Nonlinear interaction between three monochromatic waves propagating parallel to magnetic field in plasma, considering relativistic drift motions of particles

16 p2816 A69-31640

Magnetic field effects on ultrasonic propagation in high field superconductors

16 p2826 A69-31825

Temperature, velocity and density perturbation propagation as heat convection wave in viscoelastic thermally compressible heat conducting fluid, analyzing damping and frequency spectra

16 p2878 A69-31952

Discrete layers criterion for multilayer approximation to real atmosphere in acoustic gravity wave propagation

16 p2774 A69-31980

Soviet papers on wave diffraction and propagation covering marine life communication, diffraction at impedance sphere, cavity oscillations, resonator fields, plasma diffraction, etc

16 p2750 A69-32027

Relativistic exceptional wave propagating heat, computing speeds in direction orthogonal to heat vector

16 p2782 A69-32042

Acceleration waves propagation in nonlinear conducting thermoelastic solid, treating homogeneously deformed and undeformed media

16 p2873 A69-32060

Wave propagation at different group velocities along parametric line in traveling wave parametric amplifier

16 p2805 A69-32254

UHF propagation in spherically stratified superrefractive troposphere with trapping surface layer, discussing distant field strength dependence on refractivity profile

16 p2752 A69-32388

Wave propagation in open periodic two dimensional iris waveguide and beam reconstruction by diffraction, considering existence and character of modal fields

16 p2753 A69-32394

Absorption effect on fluctuation of signal level propagating in turbulent atmosphere taking into account absorption in water vapor

16 p2754 A69-32492

Gyrotropically filled waveguides propagation parameters calculation by variational method

16 p2754 A69-32505

Holograms applied to analysis of wave packets propagating in quasi-optical transmission lines

16 p2754 A69-32507

Mach number values and propagation rates of weak disturbances in interplanetary medium obtained from Mariner 2 data during low solar activity

16 p2851 A69-32518

Elastic wave reflection and refraction around cracks, considering plane harmonic compressional and vertically-horizontally polarized shear waves

17 p3053 A69-32986

Vortex breakdown in rotating fluids associated with wave motion along axis of rotation, considering effects of nonzero wave amplitude
[AIAA PAPER 69-645]

17 p2892 A69-33478

Structure of solitary waves propagating in collisionless plasma perpendicular to magnetic field, considering soliton wavefronts charge separation and relativistic velocity

17 p2922 A69-33696

Wave propagation and scattering in anisotropic media, obtaining asymptotic expression for dyadic Green function for infinite space

17 p2924 A69-33835

Propagation in inhomogeneous and dispersive media, noting potential functions for vector electromagnetic field

17 p2924 A69-33838

Wave propagation in two dimensional anisotropic media with several perturbation speeds, using Lundquist linear equations ensuring lacunas presence

17 p2925 A69-33841

Wave propagation in rectangular guides, determining dispersion curves by continued fractions method allowing for infinite set of time-space harmonics

17 p2925 A69-33843

Wave propagation in plasma filled cylindrical waveguide in axial magnetic field, approximating plasma density profile by WKB method

17 p2926 A69-33848

Methodology and classification survey of wave propagation problems in various fields of application

17 p2926 A69-33853

Fokker-Planck equation applied to probability density for finding rays larger than correlation distance during propagation in random medium

17 p2926 A69-33854

Radio wave propagation in homogeneous turbulent gyrotropic medium, presenting solution for fluctuations in direction of wave scattering by geometrical optics approximation

17 p2927 A69-33861

Signal wave scattering and transmission by ionized medium disturbed by high power pumping wave, studying wave interactions with Born approximation for bounded medium

17 p2928 A69-33871

Coupled stresses in thermoelasticity for displacement and rotation vector characterized medium, discussing wave propagation in unbounded medium

18 p3211 A69-34262

Plane wave propagation due to combined compressive and shear stresses in half space, assuming elastoplastic material
[ASME PAPER 69-APM-12]

18 p3213 A69-34388

Elastoplastic boundaries of wave propagation of combined longitudinal and torsional stresses at tube end
[ASME PAPER 69-APM-13]

18 p3213 A69-34389

Simple waves in compressible isotropic flows of inviscid nonheat-conducting gas free of shock waves

18 p3121 A69-34534

Rod buckling under impact load, discussing compression strain wave front propagation

18 p3217 A69-34580

Stressed state analysis in dynamic brittle breakdown wave front of compression waves propagating in brittle rod under longitudinal impact

18 p3217 A69-34592

Hard cosmic radiation hypothesis for Newton gravitation law for neighboring bodies, obtaining gravitational energy quanta and propagation velocity relationship

18 p3172 A69-34627

Wave propagation in gas particle flow, obtaining fourth order particle differential equation from perturbation theory

18 p3121 A69-34772

Dispersion relation for gravity waves propagating in atmosphere with horizontal background wind variable with altitude

18 p3128 A69-34801

Radio navigation principles, radio waves propagation characteristics and factors affecting navigation systems choice

18 p3169 A69-34848

Hydromagnetic whistlers propagation mechanism in magnetosphere determined by wave theory, assuming

Gaussian radial density distribution and estimating duct width necessary for trapping

18 p3102 A69-34966

Polarization operator and Green function of photon for propagation of plane electromagnetic waves in constant crossed field, noting refractive indices

18 p3103 A69-35128

Relationship between micropulsation periods and size of magnetosphere expressed in power law form and interpreted with wave propagation

18 p3131 A69-35193

Moment and discrete ordinate methods in radiative transfer problems in planar, radiating and nonscattering media, noting conical transformation of moment equations

18 p3174 A69-35237

Ionization effects in hydrodynamic model of radiation driven breakdown wave propagation, obtaining wave velocity and absorbed laser flux density relationship

18 p3174 A69-35286

Transient processes of strain wave propagation in elastic shells and plates under time varying loads

18 p3224 A69-35321

Statistical characteristics of wind wave development in initial stage, obtaining distribution functions and frequency spectrum for various velocities and temperatures

18 p3167 A69-35341

Book on wave propagation around earth covering intermedia passage, terrain influence, diffraction zones, ground waves, roles of atmosphere, troposphere and ionosphere, etc

19 p3275 A69-36382

Longitudinal and transverse wave propagation in homogeneously deformed isotropic elastic solids, considering Hadamard and Green materials

19 p3440 A69-36588

Longitudinal waves propagation in unbounded thermoelastic medium expressed as surface integrals generalizing Kirchhoff theorem

19 p3444 A69-36804

Linearized wave propagation digital simulation models to predict arterial blood flow characteristics and impedance, comparing phase velocity and transmission per wavelength

19 p3264 A69-36868

Finite elements general theory applied to wave propagation, gas kinetics, nonlinear partial differential equations, continuum mechanics and fluid dynamics

20 p3567 A69-36948

Boundary value problem of wave propagation in three dimensional region of waveguide bounded by surface solved by variational method

20 p3487 A69-37078

Semiinverse method for elastic nonhomogeneity problems, considering case of seismic wave propagation

20 p3624 A69-37589

Superposition principle extended for wave propagation in composite materials/nonhomogeneous elastic media/

20 p3627 A69-37765

Transient phenomena in bounded dispersive medium emphasizing surface wave propagation, discussing space and surface waves excitation in bounded cold magnetoplasma

20 p3494 A69-37842

Book on ultrasonics theory and application covering generation, propagation and dissipation of ultrasonic waves of high and low intensities

20 p3545 A69-37903

Transverse wave propagation and instabilities within magnetosphere, noting loss cone limited velocity-space distribution function

20 p3533 A69-38081

Field patterns, propagation constants and losses determined for axially propagating modes guided by circular cylindrical inhomogeneous dielectric, using perturbation method

20 p3497 A69-38130

Uniqueness theorems for wave propagation in homogeneous or inhomogeneous anisotropic media

20 p3578 A69-38196

Radiation sources fields and propagation in homogeneous lossy magnetoplasma, deducing wave equations for electric and magnetic current electron flux and mechanical body force sources

21 p3775 A69-38434

Transverse wave-beam interaction propagation in fast wave structure in finite homogeneous magnetostatic field, deriving wave-beam equation for non-relativistic beams

21 p3672 A69-38435

Nonlinear interaction of electron-acoustic oscillations in plasma, allowing for decay and inductive scattering in equation derivation for wave packet intensity

21 p3776 A69-38584

Microwave elastic propagation in single crystal specimen of yttrium-iron-garnet ferrite, discussing attenuation

21 p3780 A69-38774

Small amplitude acoustic waves propagating in compressible fluid with parallel shear flow and within constant gravitational field

21 p3772 A69-39241

Scalar waves propagation in bounded randomly fluctuating media, emphasizing interface effects on coherent wave motion

21 p3675 A69-39283

Propagation, damping, power coupling and plasma heating characteristics of harmonic ion cyclotron waves, noting temperature effects

21 p3777 A69-39455

Soviet book on earth atmosphere fluctuations covering propagation of acoustic, gravity and gyroscopic waves using linearized equations of hydrodynamics

21 p3717 A69-39528

Arbitrary form temperature rate wave growth and decay, determining differential equation governing wave amplitude

21 p3853 A69-39671

Wave trains of incident pulse diffraction in thin composite rod determined by transmission and reflection coefficients of plane waves at plane interfaces

21 p3845 A69-39677

Laminated random media stochastic displacement, using perturbation procedure to derive mean wave propagation deterministic equations

22 p4040 A69-39979

Coherent MHD waves propagation in presence of plasma density fluctuations, applying perturbation technique to solve stochastic wave equation

22 p3990 A69-40529

Linear self consistent diffraction emission theory and relationship to electron beam propagation

22 p3899 A69-40615

One dimensional flow of perfect compressible relativistic fluids, obtaining expression showing wave velocity dependence on relativistic speed of sound

22 p3931 A69-40711

Thermal perturbation propagation in nonlinear medium, considering thermal relaxation effects

22 p4051 A69-40712

Natural frequencies of N open dielectric waveguides system, obtaining fields expressions and dispersion equation for propagation constants

22 p3901 A69-40954

Nonlinear relativistic wave velocity distribution within spherical nucleus bounded by shock wave in superdense gas determined by Cauchy problem

22 p3861 A69-41114

Electric instabilities in semiconductors analyzed by subdividing instabilities into cathode and anode waves, considering recombination and electron and hole production processes

22 p3997 A69-41173

Sensors array to determine propagation wave vector velocity via high resolution frequency wavenumber spectrum analysis, emphasizing seismic applications

22 p3902 A69-41220

Green matrix for operator M governing steady state wave propagation in inhomogeneous anisotropic media obtained as solution of integral equations system

23 p4180 A69-41368

Nonlinear interaction between extraordinary waves propagating perpendicular to static magnetic field in cold homogeneous magnetoplasma

23 p4195 A69-41538

Thermotidal energy transfer from lower neutral atmosphere to and above lower ionosphere, considering tidal wave transmission mechanism

23 p4155 A69-41561

Transverse spectra and structural functions of fluctuations for plane waves of different frequencies propagating in isotropic turbulent medium

23 p4117 A69-41728

LF hydromagnetic waves propagation along geomagnetic field lines in gyrotropic ionosphere model taking Hall effect into account

23 p4157 A69-41864

Average total losses of H waves transmitted over waveguide communication lines by nanosecond pulse sequences

23 p4123 A69-41949

Space charge wave propagation induced by electron beam moving in annular waveguide, considering radiated field and current redistribution

23 p4124 A69-42034

Acoustic gravity waves propagation over spherical earth with isothermal windless atmosphere, determining pressure perturbations

23 p4158 A69-42175

Boundary layer method for calculation of viscous damping coefficients for small amplitude progressive waves propagating in nonhomogeneous fluid

23 p4153 A69-42408

One dimensional shock waves and acceleration fronts in nonlinear isotropic viscoelastic materials using constitutive equations

23 p4235 A69-42463

Wave propagation in dynamical theory of thermoelasticity, considering half space subject to step time strain, temperature and stress distributed over free surface

23 p4235 A69-42464

Gravitational field structure effects on Alfvén waves propagation in inhomogeneous medium

23 p4223 A69-42478

Beam wave propagation in conducting hollow circular cylinder applied to shielding cylinders design for aperture antenna transmission

24 p4282 A69-42987

Dispersive pulse propagation in laminated composites compared with theoretical predictions for timing and amplitude of oscillations [ASME PAPER 69-APMW-22]

24 p4401 A69-43097

Initially sharp plane pressure pulse propagation through linear elastic composite material, determining wave front shape change and stresses behind front [ASME PAPER 69-APMW-11]

24 p4401 A69-43103

Three dimensional and shell theory analysis of nonaxisymmetric harmonic elastic wave propagation in hollow elastic sphere [ASME PAPER 69-APMW-7]

24 p4402 A69-43105

Peristaltic pumping in circular cylindrical tube, discussing viscous fluid flow induced by axisymmetric traveling sinusoidal wave imposed on flexible tube wall [ASME PAPER 69-APMW-3]

24 p4275 A69-43108

Whistlers nonlinear interaction during cold magnetoplasma propagation, considering energy exchanges between waves

24 p4309 A69-43174

Interphase momentum transfer during propagation of infinitesimal pressure pulse through bubbly flow two phase mixture

24 p4409 A69-43511

Stress wave propagation in nonhomogeneous elastic media, considering curvilinear characteristics transformation into equal slope straight lines by change of independent variable

24 p4403 A69-43574

Axisymmetric Lamb wave propagation in semiinfinite micropolar elastic solid, considering time varying load on half space boundary

24 p4406 A69-43730

Pressure wave transmission in liquid filled tubes, determining attenuation and phase shift for hemodynamics applications

24 p4279 A69-43798

WAVE RADIATION

U ELECTROMAGNETIC RADIATION

WAVE REFLECTION

Multiple light scattering and reflection elimination from observed light brightness indicatrix to obtain true light scattering indicatrix, discussing error analysis

01 p0074 A69-11184

Shock reflection structure in ionizing xenon determined by fast rise pressure gauge mounted in shock tube end wall

01 p0132 A69-11205

Normally incident linearly polarized electromagnetic wave reflection and transmission by semiinfinite longitudinally drifting magnetoplasma in static magnetic field

01 p0134 A69-11290

Reflection of plane electromagnetic wave from impedance cylinder in vacuum, using ray expansion method

02 p0217 A69-12262

Reflection of plane electromagnetic wave from conducting plane covered with moving uniaxial sheath

02 p0209 A69-12334

Centimeter radio wave reflections from explosion region produced by TNT and hexogen charge

02 p0282 A69-12415

Doppler effect in centimeter wave range demonstrated by radio interferometer, noting amplitude difference between reference wave and wave reflected from moving reflector

03 p0393 A69-13333

Radio waves diffusive and oblique reflections from F region, noting diffusive properties decrease during magnetic storms, especially during maximum solar activity

03 p0423 A69-13529

Computer program for electromagnetic wave metal shielding evaluation

03 p0398 A69-13901

Spherical wave reflection from nondeformable plane in elastic viscoplastic medium

03 p0528 A69-13926

Plane reflector with variable reflection coefficient for electromagnetic centimeter waves, consisting of plane grating of semiconductor diodes mounted in waveguide

03 p0406 A69-13938

Reflectivity of low Richardson number critical levels for internal gravity waves propagating in stably stratified fluids with shear, studying stability numerically

03 p0424 A69-13953

Flexural wave reflection from corner joint between plates, establishing reflection coefficient dependence on wave frequency

04 p0679 A69-14903

Spatial dispersion of electromagnetic waves reflection from moving plasma layer in magnetic field, determining transmission and energy absorption coefficients

06 p0886 A69-16895

Electromagnetic wave transmission and reflection at boundary of relativistic collisionless plasma, using Laplace transformation

06 p0968 A69-17783

Short wave radiation field reflected anisotropically from underlying surface into atmosphere calculated from brightness coefficient

06 p0952 A69-17985

Diffuse reflection of electromagnetic waves by rough random surface using probabilistic method and statistical distributions

07 p1075 A69-18280

Acoustical Bragg reflection and Debye-Sears effect with application to light and ultrasonics interaction

07 p1144 A69-18285

Partial reflections from ionosphere, analyzing electron number densities, noting relation between D region ionization increases and small solar proton events

07 p1205 A69-18956

Interaction between shock wave and magnetic field of current carrying grid for ideal gas with constant coefficients, discussing dissipation, ionization and Joule heat

07 p1120 A69-18998

Boresight error in missile radome-antenna combination due to reflection and surface wave effects

07 p1111 A69-19536

Electromagnetic wave reflection from moving plasma characterized by conductivity for slow waves, calculating reflection and absorption factors

07 p1196 A69-19748

Radiative transfer by doubling very thin layers in problem of diffuse reflection from plane-parallel atmosphere eliminates numerically solving transfer equation

08 p1420 A69-20064

Electromagnetic wave reflection from subrefractive layers in inhomogeneous region

09 p1454 A69-21679

Reflection interferometry for visual evidence of surface deformation of rock and metal samples using two beam Fizeau fringe system

09 p1496 A69-22012

Polarized electromagnetic waves phase shift during total reflection from stratified dielectric region found dependent on transition zone width in addition to permittivity

10 p1657 A69-23862

Reflection coefficient of electromagnetic wave reflected from thin ionization layer, using frequency dependence of amplitude to estimate ionospheric layer thickness

10 p1686 A69-23912

Surface wave reflection from free ends of ideally conducting rods forming semiinfinite grid to study rod delay systems and wave-duct antennas

11 p1833 A69-24438

Double focus lens holography for diffusely reflecting surface deformation recording, discussing gas lasers, Polaroid photographic materials, etc

11 p1880 A69-24467

Diffraction accompanying reflection of plane shock wave obliquely impinging on walls of obtuse wedge at finite incidence, considering Lighthill method

11 p1873 A69-25135

Wave reflections due to rotationally symmetrical jump in circular waveguide cross section, using orthogonal expansion to solve resulting boundary value problem

11 p1855 A69-25622

Waveguide cross connection of right-angled waveguides to determine reflection and transmission factors for incidence of H waves

11 p1855 A69-25623

Reflection and absorption characteristics of two dimensional array of magnetic dipoles for microwaves, considering element orientation and distribution

12 p2035 A69-25901

Surface waves effect on electromagnetic waves incoherent reflection from plasma-vacuum boundary, describing polarization and angular and spectral distributions

12 p2031 A69-26530

Flexural wave reflection from corner joint between plates, establishing reflection coefficient dependence on wave frequency

12 p2182 A69-26656

Ionospheric plasma density vertical profile by measuring reflected radio waves phase frequency characteristics

12 p2070 A69-26685

Reflection coefficient of polarized radio waves at ionized meteoric trails obtained by numerical integration of differential equations

12 p2031 A69-26691

Plane transient electromagnetic wave from cold lossless plasma half space and slab

12 p2033 A69-26865

Radio wave propagation in anisotropic inhomogeneous medium, obtaining reflection and conversion coefficients and electromagnetic field distribution

13 p2218 A69-27182

Errors in Appleton-Bayton equation for skip distance of radio waves in ionosphere

13 p2218 A69-27214

Elliptical polarization in ultrabroadband YIG pulse compression networks, using reflections at rod faces

13 p2230 A69-27680

GaS, GaSe and InSe crystals band structure from analyzing reflection spectra, noting sensitivity to visible, IR and hard radiation

13 p2317 A69-27883

Diffraction and mirror analyses of right angle corner in overmoded waveguide for scattered modes, discussing transmission loss

13 p2234 A69-28426

Electric field distribution in focal region of finite offset paraboloid reflector illuminated by linearly polarized plane wave

13 p2234 A69-28427

Book on depolarization of electromagnetic waves covering interface reflection and diffraction, scattered waves, anisotropic media, random scattering, Fresnel coefficients, Brewster angle, etc

14 p2412 A69-29315

Fourier analysis of ionospheric wave reflection pulses for frequency contents and relative phase angles

14 p2440 A69-29351

Plane wave reflection and transmission by unidirectionally conducting screen, considering oblique incidence and two polarizations

14 p2421 A69-29547

Reflection of electromagnetic wave from magnetoactive plasma at inclined incidence, finding reflection and absorption coefficients

14 p2417 A69-29661

Plasma microwave measurement error allowance for multiple reflection of waves from vacuum chambers dielectric walls

14 p2498 A69-29806

Inhomogeneities effect on polarization of radio waves reflected from ionosphere, based on permittivity tensor

14 p2417 A69-29862

Reflection of plane waves at boundary surface of two semiinfinite media in relative motion, calculating power reflection coefficients

15 p2568 A69-30796

Wave reflection in laser resonators with ferrite end faces, determining oscillation spectra and wave amplitudes

15 p2579 A69-30954

Reflection of plane waves from stress free flat surface of micropolar elastic half space, presenting reflection laws and amplitude ratios

15 p2714 A69-31147

Fresnel irregularities calculated from radio wave partial reflection from lower ionosphere measured by rocket probes

15 p2604 A69-31420

Mach reflection shock-shock locus in shock tube implosions generation by area change
16 p2766 A69-31919

Partial reflections method of Gardner and Pawsey for determining vertical profile of electron collision frequencies in lower ionosphere and upper D layer
16 p2775 A69-32034

Atmospheric absorption calculations, noting direct D layer reflection effects on lower HF oblique propagation
16 p2752 A69-32389

Gas phase ignition theory with feedback of homogeneous propellant exposed to stagnant gas after shock reflection
[AIAA PAPER 69-559] 16 p2880 A69-32740

Shear layer effect on plane sound waves, discussing reflection and refraction at velocity discontinuity between two regions of fluid
17 p3005 A69-32954

Elastic wave reflection and refraction around cracks, considering plane harmonic compressional and vertically-horizontally polarized shear waves
17 p3053 A69-32986

Electromagnetic transient wave propagation and reflection in lossless isotropic stratified ionized media, discussing time variations of fields due to incident plane unit step wave
17 p2924 A69-33839

Flow viscosity and heat conduction effects on shock wave propagation in bent channel with weak Mach reflection
18 p3124 A69-35326

Reflection of spherical stress wave against smooth-indeformable plane in elastoviscoplastic medium, discussing Taylor series expansions for displacement, velocity and stress fields
18 p3226 A69-35463

Shock waves Mach reflection at various velocities in real gases, observing temperature and pressure distributions, double reflections, effects of internal degrees of freedom excitation, etc
19 p3450 A69-36363

Shock and detonation waves refraction due to small disturbances in medium, noting causes of wave cellular structure
19 p3451 A69-36369

Mach reflection limiting parameters of conical shock wave in Plexiglas cylinders, showing head wave curvature radius linear relationship to cylinder diameter
19 p3302 A69-36845

Lower ionosphere geomagnetic field local gradients determination by partial reflection method
20 p3522 A69-37055

Occurrence, development and disappearance of diffused reflections, relating dynamic behavior to ionospheric electron concentration
20 p3529 A69-37687

Reflection indicatrices of rough surface subjected to heat radiation for stationary and variable incidence angle, noting spatial distribution
21 p3847 A69-38455

Electromagnetic wave reflection and transmission from boundary between semiinfinite plasma and air by applying static magnetic field
21 p3672 A69-38743

Diffuse reflection of electromagnetic longitudinal wave from magnetoactive plasma in oblique incidence
22 p3990 A69-40788

Ionizing shock wave propagation and reflection in transverse magnetic field based on MHD theory, assuming gas thermal equilibrium
22 p3992 A69-41176

Microwave reflection technique for transient and quiescent electrical conductivity of Si, noting nonohmic contacts
22 p3997 A69-41226

Plane EM wave transmission and reflection by semiinfinite isotropic plasma moving in arbitrary direction parallel to boundary, using Lorentz transformation
23 p4114 A69-41360

Rectangular waveguide with inhomogeneity represented by half space dielectric filling with boundary causing polarization, obtaining reflection elimination or minimization reflection
23 p4125 A69-42047

Electromagnetic waves incident upon anisotropic plasma, determining transmission and power reflection coefficients
24 p4282 A69-42978

Temperature distribution on surfaces of close binary stars as basis for predicting variation of monochromatic reflection effect
24 p4387 A69-43350

Reflection of spherical stress wave against plane clamped partition in elastoviscoplastic medium, investigating three dimensional problem by infinitesimal deformations theory
24 p4406 A69-43732

WAVE SCATTERING

NT ACOUSTIC SCATTERING
NT ATMOSPHERIC SCATTERING
NT ELECTROMAGNETIC SCATTERING
NT HALOS
NT IONOSPHERIC F-SCATTER PROPAGATION
NT LIGHT SCATTERING
NT MICROWAVE SCATTERING
NT MIE SCATTERING
NT RAMAN SPECTRA
NT RAYLEIGH SCATTERING
NT REVERBERATION
NT TROPOSPHERIC SCATTERING
NT X RAY SCATTERING

Wave scattering in nonuniform cross section waveguides with large flare angles using coupled differential equations
01 p0044 A69-10622

Terrain influence in ground wave propagation evaluated by two dimensional diffraction and scattering problems, using Airy type wave functions
[AFCRL-68-0212] 01 p0033 A69-10970

Plane wave scattering from modulated corrugated structures, obtaining reflection coefficients for multimode propagation
01 p0033 A69-10973

Electron concentration in lower ionosphere based on measurement of Faraday rotation of polarization plane of radio waves scattered by meteor trail
03 p0423 A69-13535

Spatial autocorrelation functions of amplitude and phase fluctuations in plane parallel to wavefront of incident wave for conditions of multiple scatter
03 p0468 A69-13807

Scattering from thin conducting sheet obstacle on cylindrical surface
03 p0399 A69-14253

Longitudinal and transverse elastic waves propagation in medium with random inhomogeneities, deriving scattering coefficients in Born approximation for Fraunhofer region
04 p0667 A69-14262

Torsional elastic wave scattering from penny shaped crack, determining local dynamic stress field
04 p0678 A69-14872

Electromagnetic waves transformation and scattering in plasma in electric field, showing abrupt increase at certain critical value
06 p0886 A69-16894

Plane wave scattering by conducting wire impedance loaded at center, discussing loading effect on backscattering cross sections
06 p0888 A69-17512

Induced and combination scattering of high HF radio waves in ionosphere and magnetosphere
07 p1076 A69-18521

HF scattering of scalar plane wave by transparent sphere based on Watson transformation
07 p1181 A69-19033

Scattering and diffraction of plane electromagnetic wave incident on conducting cylinder coated with moving anisotropic medium
07 p1086 A69-19469

Beam wave scattering by small sphere, discussing dielectric constant and difference from plane wave
08 p1273 A69-20028

Incoherent wave scattering of particle orbits as nonlinear effect of LF instabilities
08 p1367 A69-20801

Scattering and transformation of electromagnetic waves in plasma in crossed electric and magnetic fields showing radiation spectrum maxima due to ion-acoustic oscillations propagation
08 p1277 A69-21080

Scalar wave diffraction at body in scattering medium analyzed on basis of determinate medium with complex inhomogeneous effective refractive index
10 p1658 A69-23957

Scattering of spherical electromagnetic wave emitted by electric and magnetic dipoles with equal moments at truncated infinitely thin ideally conducting paraboloid of revolution
11 p1846 A69-24614

Geometrical diffraction theory for bistatic scattering of plane wave by conducting frustum, calculating scattering matrix
11 p1837 A69-24999

Electrostatic drift wave dissipative instability in framework of macroscopic theory, accounting for resistivity and viscosity using WKB method
11 p1934 A69-25655

Cyclotron harmonic waves /CHW/ nonlinear decay instability and parametric amplification, considering applicability to practical amplifiers
12 p2135 A69-26314

E region radio waves triple splitting observed in probe ionograms, analyzing diurnal and seasonal variations in Z component reflections occurrence
12 p2031 A69-26686

Horizontally moving body wake scattering cross section calculated with allowance for sphericity of incident and scattered radio waves, using Bessel functions
12 p2031 A69-26699

Electromagnetic and plasma waves scattering by space vehicle excited by ground source in isotropic warm plasma, obtaining radar cross sections
13 p2221 A69-27965

Wave scattering from infinite line source by long convex cylinder, noting field prediction by geometrical diffraction theory
13 p2299 A69-28194

Elastic medium properties recovered from reflected or transmitted plane waves at normal incidence, obtaining computational procedures and analytical solution from Schroedinger equation
13 p2300 A69-28664

Correlation function of auroral reflection radio signals with allowance for polar ionospheric scattering and pulse signal transmission and reception
14 p2436 A69-29055

Absorption band observation near 0.43 mu in solar spectra and scattered radiation of sky, determining nontelluric origin
14 p2441 A69-29407

Ray optics method of far field scattering by discontinuity in parallel plane waveguide applied to strips, apertures, bifurcations, etc
14 p2423 A69-29753

Integral formulation of scattering theory extended to Coulomb interactions by expanding Green function and treating kernel singularities
14 p2489 A69-29995

Nonlinear wave scattering at plasma particles and weak plasma inhomogeneity effects on plasma current instability
15 p2662 A69-30965

Radio wave single scattering at particles randomly grouped in space, showing correlation function of water content fluctuations in scattered field in clouds
16 p2807 A69-32267

Wave propagation and scattering in anisotropic media, obtaining asymptotic expression for dyadic Green function for infinite space
17 p2924 A69-33835

Radio wave propagation in homogeneous turbulent gyrotropic medium, presenting solution for fluctuations in direction of wave scattering by geometrical optics approximation
17 p2927 A69-33861

Signal wave scattering and transmission by ionized medium disturbed by high power pumping wave, studying wave interactions with Born approximation for bounded medium
17 p2928 A69-33871

Wave scattering from nonplanar periodic structures using periodicity method, including Green function and Mellin transform
17 p2929 A69-33880

Critical review of Derugin theory of scattering from rough lamellar surfaces using separation of variables method, discussing energy conservation violation
17 p2930 A69-33885

Electromagnetic wave scattering in two angled rectangular waveguides filled with isotropic homogeneous medium
17 p2930 A69-33887

Scattering cross sections of radio waves at wake of vertically moving body near reflecting ionospheric layer, noting wave sphericity influence
20 p3486 A69-37023

Radio wave sphericity influence on scattering at moving body wake in ionosphere, determining scattering cross section principal maximum
20 p3486 A69-37024

Lunar surface scattering properties at 2.5 cm wavelength determined using computerized backscattering diagram and equations for obtaining scattering data
20 p3606 A69-37971

Induced Compton scattering of plasma and electromagnetic waves under astrophysical conditions, discussing HF radio emission spectra from cosmic objects and quasar
20 p3607 A69-38035

Layer model of random discrete inhomogeneities used to derive harmonic wave one dimensional scattering field and mean square of field
21 p3673 A69-38993

Wave scattering in elastic medium by discontinuity line or finite crack, noting dynamic stress intensity dependence on incident wavelength and Poisson ratio
21 p3840 A69-39293

WAVE SUPERHEATERS
U HYPERVELOCITY WIND TUNNELS
U SHOCK TUBES

WAVEFORMS
NT PULSE AMPLITUDE
NT PULSE DURATION
NT SAWTOOTH WAVEFORMS
NT SQUARE WAVES

Wide range linear delay circuit with compensated bootstrap circuit generating linear ramp waveform and regenerative Schmitt trigger comparator
01 p0041 A69-10241

Amplitude modulation factors expressed as carrier and sideband power for sinusoid and square wave signals, considering negative clipping by modulator cut-off
01 p0028 A69-10419

Pulse shape influence on electromagnetic compatibility and transmitter efficiency, discussing trapezoidal, raised-sine, sliced and complete error function shapes
01 p0030 A69-10631

Spikes on sonic boom pressure waveforms due to simultaneous focusing and diffraction of planar N wave by inhomogeneous atmosphere layer
01 p0011 A69-11280

Elastic-plastic wave profiles in Al alloy under uniaxial strain load, investigating sensitivity to various strain rates
02 p0344 A69-12289

Wave front profiles sensitivity to form of constitutive equation in one dimensional stress problem
02 p0344 A69-12291

Filter uncertainty for time or frequency resolution in analysis of waveform, decomposing characteristic functions and determining least uncertain realizable filter
02 p0226 A69-12306

Waveform distortions of trapezoidal wave passing through Gaussian filter in pulse transmission, discussing ideal filter effects on degradation
05 p0719 A69-16296

Shock waveforms lengthening due to propagation to high altitudes derived from computed numerical values, studying N waves from SST
07 p1054 A69-19463

Differentiating network with nonlinear resistance and capacitance elements, noting improvement in pulse shaping properties
08 p1295 A69-19910

Book on high resolution radar covering waveform analysis, resolution theory, radar mapping, target detection, etc
08 p1275 A69-20370

Minimum bandwidth of M real equal energy signals with specified code or correlation matrix, noting optimum waveforms
09 p1452 A69-21313

Simultaneous transmission of information signals and pseudonoise synchronization waveforms in common bandwidth
[IEEE PAPER 67-TP-1173-COM]
10 p1655 A69-23532

Angle of attack and Reynolds number effect on hypersonic flow past circular cone, obtaining shock wave shape
[ONERA-TP-692]
11 p1818 A69-24751

Voltage and current waveforms of resonant domain and limited space charge accumulation modes in transferred electron oscillators, noting drift current
12 p2036 A69-25908

Permutation modulation for waveform transmission of quantized bandlimited signal, deriving signal to noise ratio
12 p2030 A69-26386

Amplitude spectra of periodic pulse sequences or pseudonoise sequences calculated using weighting and shape functions
12 p2030 A69-26389

Undulation in output waveforms of pulsed water vapor laser observed with In-doped Ge detector
14 p2461 A69-29887

MHD generator design with electric conductivity waveform at small magnetic Reynolds numbers
14 p2405 A69-29911

Probability density functions of waveforms from summation of digits in n-stage shift register generating m-sequence
15 p2568 A69-30617

Earth ionosphere cavity model for atmospheric waveform shape, considering ELF pulse distortion after propagation through antipode
16 p2750 A69-31978

Radar control system based on load waveform monitoring by coupled control and modulating circuits
16 p2753 A69-32439

Waveforms analyzer for mixtures of exponentially damped sine waves, noting application to interferometer curves in plasma wave propagation
17 p2970 A69-32852

Backscattered impulse response waveforms of conducting circular cylinder for broadside incidence utilizing Fourier synthesis
17 p2917 A69-32918

Optimal radar receivers and waveforms with limited dynamic range for detecting point target masked by thermal noise and clutter returns
17 p2921 A69-33625

Optimum signal design to maximize SNR for pulse communications systems with signal energy detection, considering frequency, transmission and filtering characteristics and signal duration
18 p3104 A69-35484

High index frequency modulated waveform spectrum analysis including upper bound on approximation error to avoid fallacy of Woodward theorem
[IEEE PAPER 68-TP-74-COM]
19 p3276 A69-36485

Optimal radar phase modulated waveform with optimal ambiguity function synthesized by solving variational equations for orthogonal series coefficients of expanded modulation
20 p3492 A69-37708

Radar signal design, considering ambiguity and modulation functions, envelope surfaces, coding conditions, etc
20 p3496 A69-37904

Scattering equations for sonic boom waveform spike perturbations produced by atmospheric turbulence, discussing supersonic aircraft pressure signatures
21 p3646 A69-38689

QRS complex detection time error in noisy electrocardiograms
21 p3667 A69-39442

Pi 2 micropulsation waveform variation with time from simultaneous observations at low latitude stations, estimating phase velocity of higher frequency component
23 p4161 A69-42440

Active weighted pulse compression radar receiver output waveform analysis for amplitude, phase and frequency modulation, noting effects of spectrum weighting mismatch parameter
23 p4132 A69-42548

WAVEGUIDE ANTENNAS
NT HORN ANTENNAS

Impedance matching of volumetrically scanned waveguide arrays, stressing element spacing, surface wave impedance, etc
04 p0571 A69-14312

Asymptotic decay of coupling for infinite phased arrays proved valid for infinite parallel linear plate array immersed in magnetized cold plasma
04 p0571 A69-14314

Forced surface wave resonances in dielectric free 45 degree triangular grid circular waveguide phased arrays
08 p1282 A69-20038

Wideband device for rotating polarization plane of waves in waveguide between antennas, receivers and transmitters without affecting field linearity
09 p1469 A69-22643

Surface wave reflection from free ends of ideally conducting rods forming semiinfinite grid to study rod delay systems and wave-duct antennas
11 p1833 A69-24438

Passive electric microwave probe with balancing capacitance for studying waveguide fields at high microwave power levels in radiative plasma accelerators
14 p2498 A69-29807

Omnidirectional microwave parallel plate waveguide fed antenna design for flush mounted broadband spacecraft, noting equatorial and polar patterns
22 p3913 A69-40697

WAVEGUIDE FILTERS
Microwave directional filter using ring resonator and couplers to obtain low transmission loss and center frequency tuning
13 p2226 A69-27187

Microwave filters for canonical realization of non-minimum phase transfer functions, combining magic-T or hybrid junction with ladder structure network
13 p2228 A69-27668

Low pass quasi-optical waveguide filters, using metal strips in dielectric material to obtain broad stopband and low dissipation loss
13 p2229 A69-27675

AC ignitor priming of quartz-chlorine gas discharge X band waveguide limiter with fast recovery used as radar receiver protector
15 p2573 A69-30035

Waveguide below cut-off resonators for active microwave circuits, describing experiments with avalanche and Gunn diodes
15 p2577 A69-30613

Channel dropping filter for millimeter wave in low loss circular waveguide for overland telecommunications in bandwidth over 10 GHz
17 p2936 A69-33032

Single loop directional stripline filters synthesis, including general expression for frequency characteristics based on wave matrices
19 p3284 A69-36570

Multiple strip H guide field distribution and low loss wave mode analysis, obtaining approximate thin layer equations
22 p3917 A69-41254

Waveguide band filter with reflecting ferrite resonators and frequency matched loads for improved microwave SNR
23 p4139 A69-41945

Waveguide below cut-off high pass filters fabrication technique using slot cut into waveguide section
23 p4170 A69-42231

WAVEGUIDE TUNERS
Miniature microwave tuners with solid state reliability and reduced power consumption, using YIG, mixer circuits and integrated control circuitry
07 p1102 A69-18672

Microwave directional filter using ring resonator and couplers to obtain low transmission loss and center frequency tuning
13 p2226 A69-27187

Waveguide capacitive screw tuners effects on dissipative loss, discussing microwave measurements with copper screw tuners
16 p2757 A69-31586

Waveguide Y-circulator parameters thermal stability equation, considering temperature, magnetization level and magnetic field resonance effects on tuning frequency
23 p4123 A69-41951

WAVEGUIDE WINDOWS
C band waveguide window for average power transmission featuring relatively small biconcave dielectric disk
07 p1096 A69-18435

Aircraft measurements of earth atmosphere radiance in 8-14 micron window compared to calculated values as functions of altitude
08 p1311 A69-21094

Multiaperture waveguide directional couplers analyzed by four port equivalent circuits, discussing synthesis method for optimizing coupling directivity
13 p2228 A69-27669

Iris beam waveguide transmission loss as function of irises alignment, iris frame width and guide axis curvature
13 p2233 A69-28070

Driving point admittance of radiating aperture in infinite periodic phased array, determining Floquet series and coefficients of waveguide modal expansion
17 p2938 A69-33876

WAVEGUIDES
NT BEAM WAVEGUIDES
NT PLASMAGUIDES

Forward and backward scattered modes over frequency range in multimode nonuniform waveguide, transforming coupled modes telegraphist equations into Volterra equations
01 p0043 A69-10621

Wave scattering in nonuniform cross section waveguides with large flare angles using coupled differential equations
01 p0044 A69-10622

E field transmission and reflection coefficients in linearly tapered waveguide for fundamental and higher order modes, using point matching method
01 p0044 A69-10629

Propagation in waveguides filled with moving media, discussing first order theory
01 p0030 A69-10630

Symmetrical design of short ferrite Faraday rotator using matrix representation, noting matching to rectangular waveguide
01 p0048 A69-11034

WAVEGUIDES

S band thyratron waveguide switch as pretriggered megawatt balanced duplexer 01 p0048 A69-11035

Ionosphere formed waveguide electromagnetic field determined by expression, accounting for radio wave absorption during communications via artificial satellites 02 p0206 A69-11661

Procedure accounting for variable thermal conductivity and internal heat generation in temperature distribution prediction for waveguide ferrite slabs 02 p0215 A69-11877

Reflected and transmitted radiation fields for dielectric loaded infinite phased array of parallel plate waveguides as function of scan angle 02 p0218 A69-12326

Admittance of parallel plate waveguide aperture with infinite flange illuminating metal sheet, using wedge diffraction theory and integral transform method 02 p0218 A69-12328

C and S band waveguide impedance measurements taken in flight in reentry plasma, noting results for plasma 02 p0218 A69-12333

Microwave thermal noise standards, discussing construction, calibration and errors for field operational liquid nitrogen cooled waveguide noise standard 02 p0210 A69-12438

Gas discharge tubes and waveguide mounts as reference noise accuracy standards for S, C and X bands in WR284, WR137 and WR90 waveguides 02 p0210 A69-12439

Tubular light beam waveguide properties, studying changes related to heating and ionization of medium 02 p0258 A69-12644

Finite element solution of Helmholtz equation and application to waveguides with complicated boundaries 03 p0404 A69-13598

Planar phased array of circular waveguides arranged in equilateral triangular grid, solving boundary value problem 03 p0406 A69-13829

Strain effects on transverse electromagnetic modes of anisotropic dielectric waveguides at p-n junctions 03 p0406 A69-13830

Element pattern nulls in phased arrays and relation to guided waves supported by array face 04 p0570 A69-14310

Linearly polarized waveguide phased array design, noting waveguide aperture size effect on admittance and minimization of zero radiation directions 04 p0571 A69-14313

H plane waveguide Y circulators engineering design based on circulation equations 04 p0575 A69-14460

Optical waveguide with optimum refractive index distribution for equalizing group velocities of different modes and minimizing waveform distortion 04 p0575 A69-14749

Moving media influence on transient electromagnetic modal wave propagation in dispersive waveguides 04 p0557 A69-14752

High power waveguide tuner for use in traveling wave resonator to tune out reflections in resonant ring 04 p0576 A69-14759

Surface impedance variation effect on surface wave propagation along rod waveguide 04 p0576 A69-14761

Waveguide arc location by sound ranging to determine RF breakdown onset in high power microwave system, describing experiment determining feasibility 04 p0576 A69-14762

Reflection coefficient determination of bent multiwave waveguide, considering reflected wave due to secondary conversion of parasitic waves interacting with primary wave 04 p0576 A69-14773

Dielectric waveguide propagation, impedance and attenuation characteristics and insertion loss and launching efficiency of mode transducer 04 p0577 A69-14971

Toroidal gas discharge in waveguide by coupling of microwave power into gas to heat gas, noting plasma confinement [IMPI PAPER A4] 04 p0636 A69-14999

Waveguide field of arbitrary cross section determined on models with quasi-static fields 05 p0717 A69-15635

Resonance rotation of polarization plane in circular waveguide with ferrite resonator 05 p0718 A69-15640

Equation for analyzing radiation produced by current passing through filament situated over anisotropically conducting plane in flat waveguide 05 p0718 A69-15647

Gyrotropically filled waveguides propagation parameters calculation by variational method 05 p0718 A69-15648

Wavelength range analysis for determining ambiguous section of circular waveguide dispersion characteristic 05 p0718 A69-15649

VLF phase measurements for apparent and equivalent diurnal height variation for lower ionosphere waveguide 05 p0752 A69-15666

Surface waveguide composed of inhomogeneous dielectric thin film used as low loss transmission line 05 p0731 A69-16294

Input admittance of confocal Fabry-Perot resonator, with waveguide coupled infinitely long conic-section cylindrical reflectors, taking into account diffraction and resistive losses 05 p0731 A69-16295

Cut-off frequency relation to geometry for dielectric ridge waveguide 05 p0777 A69-16579

Composite equivalent circuits method for complex waveguide-resonator couplings based on variational principle for admittance matrices of electromagnetic volume couplings 05 p0736 A69-16785

Ferrite materials characteristics related to choice for use in waveguide devices, noting importance of low HF magnetic losses and thermal stability 05 p0810 A69-16792

General theorem of isotropic microwave waveguide junction ports imposed by reflection symmetry 06 p0893 A69-16935

Scattering matrix for internal diffraction in rectangular waveguide with transversely magnetized ferrite core 06 p0895 A69-17455

Residue contributions to integrals associated with admittance of plasma or dielectric covered circular aperture antenna used to calculate surface wave contribution to waveguides 06 p0896 A69-17477

Suppressed rotation reciprocal ferrite phase shifter theory explained in terms of nonreciprocal coupling of cross polarized waveguide modes 06 p0896 A69-17484

Deviation of dispersion equations for all modes existing in E-plane slabs of dielectrically loaded rectangular waveguides 06 p0888 A69-17486

Characteristic impedance of rectangular waveguide computation curve explained on basis of computer program for cascade of transmission line sections 06 p0897 A69-17490

Numerical methods for VLF electromagnetic wave propagation in earth-ionosphere waveguide, discussing boundary conditions assignment effect at ionosphere on eigenvalues 06 p0920 A69-17732

Power flow in cyclotron and plasma modes propagating in waveguide filled with cold collisionless axially magnetized plasma 06 p0897 A69-17760

Second order nonlinear coefficient measurement for optical generation of millimeter wave difference frequencies in GaAs waveguide, using carbon dioxide laser 06 p0928 A69-17903

Circularly polarized waveguide mode simulation for multislotted leaky waveguide harmonic content measurement 07 p1105 A69-19046

Field diffraction at finite metallic surface represented in eigenfunctions of discrete spectrum, considering forced oscillations of open circuit 07 p1084 A69-19151

Annular traveling wave resonator for feedback in resonance particle accelerator of smooth waveguide 07 p1107 A69-19160

Reflection and transmission scattering coefficients for step type transition between two uniform waveguides with surface impedance boundaries, discussing coupled differential equations 08 p1272 A69-20020

Horizontal electric dipole excitation of spherical guide waves between earth and ionosphere, discussing TM and TE modes and ELF and VLF range 08 p1273 A69-20023

Resonance conditions in dielectric sheathed or plug loaded phase arrays of waveguides 08 p1281 A69-20034

Conjugate echoes in Alouette 2 topside sounder ionograms explained by multiple reflections between conjugate points of field line, noting magnetospheric waveguides role 08 p1274 A69-20045

Lower ionosphere and earth-ionosphere waveguide effects on polarization characteristics of transmitted radio whistlers 08 p1306 A69-20181

Mode designation and propagation characteristics of dielectric tube waveguide, noting practicability at higher microwave frequencies 08 p1284 A69-20296

Miniaturized E-Tee three port circulator with wide bandwidth, noting negligible effect of static field small variations on performance 08 p1291 A69-20980

Transverse density nonuniformity effect on electromagnetic wave propagation in cylindrical plasma waveguide immersed in magnetic field, noting frequency increase 09 p1545 A69-21348

Charge and traveling wave interaction in circular waveguide in resonance regime solved by Krylov-Bogoliubov asymptotic method 09 p1551 A69-22037

Cut-off coupled microwave bandpass filters for use in dielectric filled waveguide systems 09 p1466 A69-22447

Quasi-static modified field distributions in inhomogeneously filled cavities and waveguide tubes, comparing with homogeneously filled cavities and obtaining matrix eigenvalues 09 p1467 A69-22561

Short multiconical TE sub 01 mode X band taper for connecting two different diameter circular waveguides 09 p1468 A69-22604

Waveguides and resonators design by solving scalar problem for eigenvalues of elliptic operator 09 p1469 A69-22626

VLF electromagnetic wave propagation in earth-ionosphere waveguide with reflections from ionosphere, noting TE and TM mode coupling and mode conversion 09 p1460 A69-22699

Waveguide Y circulator electrodynamic parameters by design algorithm and computer programs 10 p1661 A69-23108

Waveguides mutual coupling in finite antenna arrays analyzed by integral equation method, noting coupling decrease correlation with wavelength and waveguides distance 10 p1663 A69-23421

Computer calculated phase velocities for surface wave and waveguide modes given for circular waveguide filled with inhomogeneous electron plasma 11 p1844 A69-24437

Excitation of plane plasma layer in magnetic field perpendicular to wave vector of excitation wave in gyrotropic waveguide 11 p1927 A69-24916

Radiation field patterns from metal wall aperture in waveguide with rectangular cross section determined using elliptic cylinder 11 p1850 A69-24982

Radiating collinear open ended waveguides and near field coupling analyzed using simultaneous integral equations and Fourier series expansion of aperture field 11 p1850 A69-24984

Electromagnetic wave propagation in rectangular waveguide containing uniaxial anisotropic birefringent medium, deriving field equations 11 p1853 A69-25350

Wave-mode converter with feed for omnidirectional antenna excitation, discussing H to E wave conversion, waveguides, emitter, etc 11 p1854 A69-25616

TEM-WAVE propagation between parallel conducting planes, stressing changes in curved waveguide sections 11 p1841 A69-25619

Excitation coefficients of waves subjected to sudden expansion in radiating waveguide using integral relations, noting convergence 11 p1855 A69-25621

Wave reflections due to rotationally symmetrical jump in circular waveguide cross section, using orthogonal expansion to solve resulting boundary value problem 11 p1855 A69-25622

Waveguide cross connection of right-angled waveguides to determine reflection and transmission factors for incidence of H waves 11 p1855 A69-25623

- Microwave filters with lumped capacitances and coupled waveguides derived by frequency conversion from lumped filters circuits
11 p1855 A69-25628
- Directional coupler for TEM waves composed of two waveguides and having locally dependent coupling function
11 p1855 A69-25629
- Resonance method determining spurious modes excitation in natural mode converter, discussing construction, application and mathematical correlation
11 p1856 A69-25630
- Attenuation losses on curved dielectric waveguide in X band
11 p1856 A69-25633
- Saddle point analysis of electromagnetic ground wave propagation in source excited field in waveguide formed by two parallel plate dielectrics
12 p2028 A69-25898
- Broadband plasma waveguide switch application extended to 26-40 GHz range, discussing isolation, cold loss, switching time, trigger signal and ionized plasma
12 p2036 A69-25938
- Short circuit and variable frequency technique for measurement of coupling efficiency between dielectric loaded rectangular and trough waveguides, noting propagation modes
12 p2039 A69-26374
- Perturbation analysis in dielectric loaded rectangular waveguides, considering scattered modes and phase progression
12 p2039 A69-26381
- Internal guiding of microwaves by elevated tropospheric layer noting refractive index, radius of curvature and attenuation
12 p2032 A69-26856
- VLF wave propagation along mixed path in curved earth-ionosphere waveguide, considering reflection and transmission coefficients of modes
12 p2032 A69-26858
- Elliptical waveguide design dimensions for minimum attenuation in fundamental mode, giving formulas for attenuation constant and minor-major axis ratio
12 p2044 A69-27070
- Horn exciter with fundamental and second mode in feeding waveguide of shallow paraboloid antennas
12 p2044 A69-27093
- Waveguide higher order modes solved by finite-difference method, employing successive overrelaxation to compute field potentials at discrete points in arbitrary guide shapes
13 p2228 A69-27670
- Applied magnetic field effects on longitudinally magnetized reciprocal ferrite phase shifters, showing shift type dependence on guide electrical thickness
13 p2229 A69-27673
- High power ferrite latching switch with forced air cooling, discussing nonreciprocal phase shifter materials and configurations
13 p2229 A69-27674
- Optical surface wave propagation on thin dielectric film waveguides, noting applications to integrated optical data processors
13 p2229 A69-27676
- Guided waves in circular cylindrical radially inhomogeneous medium, using vector theory based on Maxwell equations
13 p2221 A69-28062
- Leaky helix and solid metal waveguides propagation losses measured by shuttle pulse method in SHF
13 p2233 A69-28063
- Transmission type E saki diode amplifier with stabilizing dielectric loaded rectangular waveguide
13 p2233 A69-28067
- Diffraction and mirror analyses of right angle corner in overmoded waveguide for scattered modes, discussing transmission loss
13 p2234 A69-28426
- Wave parameters in coupled parallel surface wave transmission lines and dielectric waveguides, discussing phase velocities and spatial beat period
13 p2223 A69-28570
- Ionosphere formed waveguide electromagnetic field determined by expression, accounting for radio wave absorption during communications via artificial satellites
13 p2224 A69-28692
- H plane waveguide Y circulators engineering design based on circulation equations
14 p2418 A69-28831
- Book on open resonators and open waveguides
14 p2419 A69-29316
- Microwave dispersion systems, using waveguide loaded with dielectric material to obtain group linear frequency delay characteristic
14 p2412 A69-29395
- Monochromatic plane waves propagation in anisotropic homogeneous cold plasmas, treating dispersion surface, reflection, refraction and waveguide applications
14 p2492 A69-29399
- Electromagnetic wave propagation through magnetolectric media in circular waveguide
14 p2416 A69-29540
- Leaky waves propagation characteristics helix waveguide covered with slitted cylinder using transverse network representation, emphasizing small pitch angles, hybrid TE and TM modes, etc
14 p2422 A69-29752
- Ray optics method of far field scattering by discontinuity in parallel plane waveguide applied to strips, apertures, bifurcations, etc
14 p2423 A69-29753
- Discontinuity capacitance of coaxial line terminated in circular waveguide calculated using Rayleigh-Ritz variational technique
14 p2423 A69-29754
- Dispersion of electromagnetic wave propagating along ferrite loaded wire, calculating tuning curves and three port waveguide circulator modes
14 p2417 A69-29755
- Computational accuracy of point matching solution for uniform nonsymmetric waveguides
14 p2423 A69-29758
- Adapter between dielectrically loaded waveguides with different cut-off frequencies and sizes for pulse compression systems
14 p2423 A69-29760
- Quasi-optical oversize waveguide directional coupler with two prisms interface matched by Brewster angle effect
14 p2424 A69-29764
- Corrugated cylindrical waveguides used as hybrid mode feeds for reflector antennas
15 p2575 A69-30175
- Cut-off wavelength of transverse magnetic mode related to cross section eccentricity of hollow conducting elliptical waveguide
15 p2575 A69-30178
- Waveguide mode propagation theory for determining earth-ionosphere spherical waveguide upper boundary height diurnal variation for VLF waves
15 p2595 A69-30224
- Resonance measurement of power percentage in single spurious mode of overmoded waveguide, using back to back transducers and reflection at input
15 p2577 A69-30611
- Flexible aluminum elliptical waveguide design, discussing installation, economy and electrical characteristics
15 p2578 A69-30798
- Asymmetrical waves diffraction field at wide slots in circular waveguides determined in Huygens-Kirchhoff approximation
15 p2570 A69-30955
- Propagation modes attenuation and guidance on circular hollow dielectric waveguides dependent on dielectric loss tangent
16 p2757 A69-31587
- High resolution swept frequency reflectometer suitable for impedance matching in waveguides or coaxial lines
16 p2759 A69-31940
- Computerized finite element waveguide analysis for determining propagating modes and cut-off frequencies
16 p2760 A69-31942
- Waveguide bends fields expressed in coupled local annular modes derived by evaluating differential scattering coefficients
16 p2760 A69-31943
- Dual channel waveguide insertion loss test set for calibrations at 90 GHz in radio astronomy and communication systems, using sprayed thermistor mount
16 p2760 A69-31945
- VLF radio wave propagation in waveguide channel formed by earth and inhomogeneous anisotropic ionosphere
16 p2751 A69-32032
- Meteorological radar dead zone diminished by using hybrid electronic waveguide suppression system to eliminate antenna sidelobe reflections
16 p2791 A69-32281
- Diffraction of axisymmetric electromagnetic wave at surface discontinuity of impedance cylinder forming core of coaxial waveguide
16 p2761 A69-32479
- Waveguide field of arbitrary cross section determined on models with quasi-static fields
16 p2762 A69-32493
- Resonance rotation of polarization plane in circular waveguide with ferrite resonator
16 p2762 A69-32498
- Equation for analyzing radiation produced by current passing through filament situated over anisotropically conducting plane in flat waveguide
16 p2762 A69-32504
- Gyrotropically filled waveguides propagation parameters calculation by variational method
16 p2754 A69-32505
- Wavelength range analysis for determining ambiguous section of circular waveguide dispersion characteristic
16 p2762 A69-32506
- Waveguide feeder for Goonhilly Downs satellite communication antenna reducing feeder loss for use with low elevation Intelsat 3 satellite
17 p2935 A69-32849
- Asymptotic solutions for vector fields and propagation constants of axial modes in circular cylindrical waveguides, noting changes in dielectric constant
17 p2921 A69-33673
- Electromagnetic wave propagation in anisotropic media analyzed for wave packet behavior function, stressing waveguide theories
17 p2926 A69-33847
- Diffraction of modal field by semiinfinite waveguide, integral representation for Wiener Hopf kernel factorization and applications to open resonators
17 p2930 A69-33888
- Electromagnetic field formulation of eigenvalue problem for optical coaxial dielectric waveguide, using computer root searching method
17 p2930 A69-33892
- Plane anisotropic dielectric p-n junction layer waveguide properties, deriving characteristic equations for refraction indices
17 p2983 A69-33971
- Reflection coefficient of symmetric parallel plate waveguide operating in TEM mode illuminating lossless dielectric layer, using wedge diffraction and geometrical optics methods
18 p3108 A69-34802
- ELF wave propagation in earth-ionosphere waveguide, considering ionospheric vertical inhomogeneity and models for ambient and disturbed /PCA/ conditions
18 p3101 A69-34949
- Radiation emission by molecules in electromagnetic field, considering cavity resonators and waveguides excitation
18 p3178 A69-35404
- Near and antipodal fields in earth-ionosphere waveguide using mode theory, ray theory, zonal harmonics series and method of images to derive field representations
19 p3283 A69-35931
- Boundary value problem of wave propagation in three dimensional region of waveguide bounded by surface solved by variational method
20 p3487 A69-37078
- Modified residue-calculus technique combined with scattering matrix multiple reflection techniques for boundary value problems in waveguide phased arrays, diffraction gratings, etc
20 p3505 A69-37298
- TEM mode reflection coefficient for symmetric parallel plate waveguide composed of adjacent conducting wedges composition and radiating into perfectly reflecting sheet
20 p3507 A69-37839
- Field patterns, propagation constants and losses determined for axially propagating modes guided by circular cylindrical inhomogeneous dielectric, using perturbation method
20 p3497 A69-38130
- Electromagnetic waves attenuation and field structure within gas filled dielectric waveguide tube, tube walls and waveguide surroundings
21 p3674 A69-39123
- Free space to dielectric waveguide millimeter wavelength ratio as function of frequency, discussing equipment and procedure
21 p3674 A69-39130
- Biquadratic plane wave dispersion relation for gyrotropic waveguides with dielectric and magnetic properties, discussing associated quartic equation for refractivity
21 p3675 A69-39285
- Microwave absorption by Ar plasma of positive column discharge in waveguide under inhomogeneous magnetic field
21 p3778 A69-39547

Absolute and convective instability criteria of interacting electromagnetic waves in waveguide systems involving parametric oscillators and amplifiers
21 p3677 A69-39555

Book on Smith chart electronic applications in waveguide, circuit and component analysis and synthesis
22 p3915 A69-40780

Resonance frequency behavior of waveguide cavity with evanescent air gap symmetrically loaded with dielectric
22 p3900 A69-40925

Numerical solution by approximation of Wiener-Hopf-Fock equation for diffractions at finite or infinite number of equidistant half planes applied to open-end waveguides
22 p3901 A69-40950

Natural frequencies of N open dielectric waveguides system, obtaining fields expressions and dispersion equation for propagation constants
22 p3901 A69-40954

Polycrystalline ferroelectrics dielectric dispersion region in decimeter-centimeter wavelength range using waveguide resonance method employing wideband strip line
22 p3997 A69-41167

Mode conversion in nonuniform multimode waveguides and transitions using Maxwell equations, considering tapered and circular waveguides
23 p4135 A69-41354

Periodic ladder type design delay equalizer for linear delay characteristics in millimeter waveguide systems
23 p4135 A69-41361

Surface integration technique used in conjunction with wedge diffraction theory to analyze TEM radiation patterns of parallel plate waveguides
23 p4136 A69-41581

Edge diffraction effects in TEM axially slotted finite ground plane on radiation pattern in waveguides of different geometries
23 p4116 A69-41588

Rectangular waveguides coupled by oblique subresonant slots in common face, discussing slot orientation and geometry roles
23 p4123 A69-41941

Self consistent fields in waveguides containing thin conductors, expanding induced field into Fourier series in normal waves for series coefficients
23 p4123 A69-41942

Variational principle for analyzing dispersion properties of closed regular waveguide with traveling wave-modulated dielectric constant
23 p4123 A69-41943

Average total losses of H waves transmitted over waveguide communication lines by nanosecond pulse sequences
23 p4123 A69-41949

Electromagnetic oscillations emission by monochromatic electron beam in infinite waveguide formed by periodic diffracting array with energy losses, determining radiated power
23 p4124 A69-42031

Electromagnetic wave propagation in rectangular and plane parallel waveguides coupled by common wall with periodic transverse slots
23 p4124 A69-42037

Electromagnetic waves scatter propagation in isotropic plasma in plane waveguide, noting electron charge density fluctuations role
23 p4125 A69-42040

Smooth multiwave waveguide junctions design ensuring minimum losses of fundamental wave
23 p4125 A69-42046

Rectangular waveguide with inhomogeneity represented by half space dielectric filling with boundary causing polarization, obtaining reflection elimination or minimization reflection
23 p4125 A69-42047

Light transmission through curved dielectric rectangular rod, studying optical waveguides of various cross sectional dimensions and radii of curvature
24 p4287 A69-43329

Electromagnetic waveguides direction-changing capability, deriving expressions for permitted bending radius with respect to mode conversion
24 p4288 A69-43331

Gas lens system for periodic light beam waveguide, describing gas enclosed in circular cylinder and heated by specific temperature distribution
24 p4350 A69-43332

Measurement technique using dielectric waveguides for studying microwave fields influence on and energy imparted to body tissue
24 p4279 A69-43705

WAVELENGTHS

Laser wavelength selection device for parallel wavelength separation or recombination of laser beams external to laser cavities
01 p0091 A69-10841

Electromagnetic waves parametric interactions during unsteady Josephson effect as function of wavelength ratio, magnetic field penetration and contact dimensions
02 p0293 A69-11464

GaAs injection lasers noting spectral function, I-V characteristics and relations among lasing wavelength, threshold current density and impurity concentration
02 p0256 A69-11993

Wavelength dependence of microwave propagation beyond radio horizon
03 p0395 A69-13626

Uniaxial pressure applied to p-n junction of GaAs injection laser, discussing effects on threshold current and wavelength
03 p0441 A69-13848

Beam foil spectroscopy for measuring wavelengths and spectral line intensities
04 p0595 A69-14276

Wavelength range analysis for determining ambiguous section of circular waveguide dispersion characteristic
05 p0718 A69-15649

Absolute wavelength standard using saturated molecular absorption in methane inside He-Ne laser cavity [IEEE PAPER P-1]
05 p0775 A69-16323

Isophotal wavelengths of U, B, V and R bright star systems for replacing spectrophotometry with broadband multicolor data
08 p1408 A69-21134

Wavelength of convective motions, discussing effects of lid heat conductivity on Rayleigh number
11 p2003 A69-25354

Quantitative interferometric analysis of shock induced wavelength variations in glass and polished steel plates using Q switched ruby laser light source
12 p2089 A69-26185

Quasars intensity variations at various cm wavelengths confirming wavelength dependence
12 p2167 A69-27045

Galactic H II regions of high surface brightness in radio continuum surveyed at 1.95 cm wavelength with high resolution and positional accuracy
13 p2339 A69-27568

Optimum emission wavelengths in atmospheric refractive index determination in optical range finder/refractometer system, noting laser applicability
13 p2260 A69-27826

Turbulence and temperature fluctuations spectral characteristics in thermally stratified atmosphere determined for various wave numbers, using energy and mass transfer functions
14 p2472 A69-29402

Late type stars with emission peak wavelength approximating graphite Debye frequency induced by graphite impurity atoms
14 p2521 A69-29586

Pressure and wavelength dependence of molecular O absorption coefficient near 1215 A, utilizing UV emission from crossed beam atomic collision
15 p2656 A69-31031

Temperature, velocity and density perturbation propagation as heat convection wave in viscoelastic thermally compressible heat conducting fluid, analyzing damping and frequency spectra
16 p2878 A69-31952

Polarimetric observations of Be stars, noting dependence and self absorption by hydrogen of polarization produced by electron scattering
16 p2863 A69-32397

Wavelength range analysis for determining ambiguous section of circular waveguide dispersion characteristic
16 p2762 A69-32506

Complex index of refraction of naturally occurring rock and mineral as function of wavelength of incident radiation
17 p2973 A69-33093

Long path difference vacuum Michelson interferometer application to far IR and IR laser wavelength measurements compared with 6328 A He-Ne wavelength
17 p3006 A69-33405

Refractive indices for various glasses obtained as function of wavelengths and temperature, using spectrometer as collimator
17 p3007 A69-34158

Wavelength dependence of total and depolarized backscatter laser light cross section for rough metallic surfaces
18 p3172 A69-35000

Electron concentration in hypersonic nonequilibrium shock layer flow by two wavelength laser interferometry, noting wavelength dependence of refractivity
19 p3306 A69-35707

Wavelength dependence of stellar scintillation discussing apparatus to detect color effect in twinkling
19 p3401 A69-35800

Solid state laser emission frequency control and retuning using dispersive resonators, analyzing interference methods for wavelength measurement
19 p3331 A69-35800

Solar flares less than 10 A X rays effect on ionospheric ionization between 60 and 100 km
19 p3397 A69-36752

Wavelength-surface temperature relationship of ruby laser, discussing thermal control of emission wavelength
20 p3552 A69-36960

Solar spectrum data covering wavelength intervals from 13138-14707 and 12187-17731 A and 1.4 microwave water band
21 p3800 A69-38682

Approximate formula for energy spectrum of isotropic turbulence at large wave numbers, showing agreement with Gaussian exponential form
21 p3694 A69-38833

Free space to dielectric waveguide millimeter wavelength ratio as function of frequency, discussing equipment and procedure
21 p3674 A69-39130

Flux densities of radio sources in 3CR catalog measured at 2.8 cm wavelength
22 p4014 A69-40127

Tabulation of solar UV spectrum features between 3650 and 3000 A from intercomparison of photoelectric records and Second Revised Rowland, indicating wavelength relocations
22 p4014 A69-40146

Human electroretinogram (ERG) physiological variations as function of stimulation energy and wavelength
22 p3884 A69-40888

MHD tearing mode, considering most unstable wavelength, energetics and stability in two dimensional equilibria
24 p4355 A69-42684

WAVES

Supersonic compressors for supersonic and subsonic air intakes, studying wave configuration at entry of circular cascade of blades with hydraulic analogy [ONERA-TP-669]
05 p0699 A69-16340

Hyperbolic double waves found in compressible flow problems, presenting method of plotting all waves and determining geometrical characteristics
05 p0751 A69-16646

Dispersion and coupling impedance calculation for symmetrical or helical slow wave structures employed in traveling and backward wave tubes
22 p3916 A69-40958

WEAPON SYSTEM MANAGEMENT

Measurable and strategic characteristics of Army laboratories management, considering papers published, inventions and laboratory performance
15 p2721 A69-31070

WEAPON SYSTEMS

NT GROUND OPERATIONAL SUPPORT SYSTEM

NT MISSILE SYSTEMS

Operational research in RAF, discussing weapons tactics and research, strike aircraft speed and height effect on target-finding, VTOL and STOL dispersion value, etc
01 p0180 A69-10863

Fiat G.91Y subsonic light tactical fighter, discussing fixed armaments and weapons facilities
02 p0193 A69-12679

Weapons propulsion system off-design engine performance, noting installation loss effects [SAE PAPER 680712]
03 p0496 A69-13445

Flight test support design, developing measure of performance of test environments stated in weapon or space system terms
05 p0742 A69-15804

Characteristics, employment and tactics of Huey Cobra attack helicopter in Vietnam, discussing three primary weapon configurations
06 p0867 A69-17661

Nonlinear equations of motion approximate solution, determining ordnance weapons aerodynamic stability coefficients from angular motion as functions of angle of attack
[AIAA PAPER 69-135] 06 p0863 A69-18120

F-111 interdiction capability, discussing avionics subsystems for low level penetration flying and Vietnam performance 07 p1052 A69-18550

Firebee 2/BQM-34E/ turbojet-propelled re-coverable supersonic aerial target construction, performance prediction and missions 09 p1434 A69-21901

Maintenance van loading technique for number of spares and test equipment in Minuteman weapon system for uncommissioned launch facilities at minimum cost 10 p1669 A69-22980

Spare kit evaluation model for problems with constraints on spare parts quantities, considering optimization and simulation routines for weapon system maintenance 10 p1669 A69-22981

WSEIAC /Weapon System Effectiveness Industry Advisory Committee/ formula, analyzing correctness within Markovian limitations and reward systems extension 12 p2102 A69-26570

Ground military equipment hardening against nuclear environment, selecting worst case levels from isodamage curves 15 p2651 A69-30380

Weapon systems integrated testing, determining test quantities as function of subsystems utilizing Neyman-Pearson confidence levels 15 p2619 A69-30400

Military systems trouble documentation and evaluation, emphasizing computerized monitoring of reliability and maintainability 15 p2722 A69-31121

Cost effectiveness of DOD/military systems, discussing principles and analytical model with case study 15 p2722 A69-31125

Markov chain applications to avionics weapons system reliability specifications starting with mission profile, failure rates, success probabilities, etc 15 p2581 A69-31136

AH-56A Cheyenne integrated avionics, armament and fire control system for precise weapons delivery and navigation [AHS PAPER 312] 17 p2903 A69-33542

Airborne radomes reliability and high temperature environments, discussing missile nose cones, light weight ceramic techniques, circular polarization, etc 17 p2942 A69-34084

Aircraft avionics subsystems and weapon system functional integration reflecting aircraft mission, operational, natural and enemy environments 18 p3109 A69-35140

Polaris and Poseidon nuclear missile systems, considering efficiency and launching depth from nuclear submarine 19 p3432 A69-36687

Training missions and military exercises to field test weapons system models [AAS PAPER 69-478] 24 p4296 A69-42884

WEAPONS

NT GUNS [ORDNANCE]
NT NUCLEAR WEAPONS
NT SPACE WEAPONS
NT WARHEADS

Helicopter self defense armament for fire support of British Army operations, discussing vulnerability, weapons selection and tactics, logistics, etc 01 p0010 A69-10869

WEAPONS DEVELOPMENT

Gun projectiles assisted by solid propellant motor to increase range, discussing construction, performance and free-wheeling rotation band use 15 p2702 A69-30592

IRIG /Inter-Range Instrumentation Group/ telemetry standards for U.S. Department of Defense missile and weapons systems, reviewing evolution, content, scope, philosophy, revisions, etc 23 p4121 A69-41770

WEAR

Ball bearings lubrication and wear in cryogenic hydrogen turbopumps by transfer films provided from self lubricating cage 01 p0084 A69-10109

Analytical determination of traces of metals caused by wear in aircraft liquid fuels, hydraulic fluids and lubricants, noting polarography and coulometry 03 p0435 A69-14101

Laws of wear and average life, noting application to electric connector reliability 04 p0579 A69-15320

Atmospheric influence on friction endurance of solid powdered lubricants at constant layer thickness [IME PAPER 3] 07 p1138 A69-18563

Surface finish and hardness effects on wear life of inorganic solid lubricant film [ASLE PREPRINT 68AM 7C-3] 07 p1139 A69-18623

Modes and mechanisms of wear covering adhesive, abrasive and corrosive wear, surface fatigue and fretting corrosion 13 p2265 A69-27231

Abrasive wear model leading to abrasive wear equation and empirical findings on relative abrasive wear resistances 13 p2265 A69-27233

Collection of Soviet papers on wear and antifriction properties of materials 13 p2268 A69-28050

Friction wear of solid bodies based on microscopic contact system model, deriving particle distribution law from physico-statistical analysis 13 p2268 A69-28051

Statistical theory of cumulative wear of machine parts with application to engine parts of passenger aircraft, automobiles, tractors, etc 13 p2268 A69-28052

Mathematical model of mechanical wear in surface friction based on approximation of cross section profiles, using Fokker-Planck equation for distribution function 14 p2455 A69-29331

WEAR INHIBITORS

Wear-resistant hard thin layers deposited on various base material surfaces analyzed by electron microprobe 13 p2282 A69-28164

Plating wear resistant electrodeposits of Ag, Cu, Ni and Cr on Ti, noting adhesion tests 18 p3148 A69-34654

Wear protection of pressure loaded Ti-Mn alloy by heat diffused lubricated electrodeless Ni coatings 24 p4331 A69-42786

WEAR TESTS

Surface fatigue significance in sliding wear studied from damage on copper single crystal using electron microscope techniques 01 p0085 A69-10368

Friction and wear behavior of mechanical face seals, considering techniques and lubricants for increasing product of pressure and sliding velocity 02 p0253 A69-12160

Wear ring seals evaluation program for application to high pressure high speed liquid rocket turbopumps impeller wear rings [ASME PAPER 68-WA/LUB-1] 05 p0768 A69-16129

Mechanical and physical properties and cryogenic wear tests performed on composite materials, considering NERVA cryogenic turbopump bearing retainer development [ASME PAPER 68-WA/LUB-10] 05 p0768 A69-16133

Dry sliding friction and wear in ultrahigh vacuum, emphasizing slip rings and brushes for space applications [IME PAPER 7] 07 p1138 A69-18561

Miniature ball and jewel bearings and gear lubrication in ultrahigh vacuum tests for space environment operation [IME PAPER 6] 07 p1138 A69-18562

Film thickness effect on wear life of resin bonded solid lubricant film compared for various load test conditions [ASLE PREPRINT 68AM 7C-4] 07 p1139 A69-18624

Solid lubricant compacts for ball bearing separator materials, describing fabrication, design and friction and wear properties in air and vacuum 07 p1139 A69-18626

Friction and wear tests of synthetic rutile single crystals against diamond styli and spherical sliders of ruby, sapphire and hardened steel [ASLE PAPER 68-LC-3] 07 p1140 A69-19307

Aircraft tire wear determination by measuring intensity of radiation originating from point source within thread, using thulium 170 isotope 07 p1143 A69-19703

Yielding of matrix material and cell size of substructure relationship to dry abrasion resistance of SAP type aluminum alloy at room temperature 08 p1319 A69-19995

Primary silicon crystals content and grain size effect on wear of high silicon aluminum alloys 09 p1526 A69-22281

Refractory alloys electrodes used for surface coating Ti alloys by electric spark method, studying microhardness and wear resistance 10 p1711 A69-23339

Wear and friction properties of nylon and polyethylene sliding over unlubricated steel, considering adhesion theory 11 p1892 A69-25021

Evaluation of wear testing - ASTM Conference, San Francisco, June 1968 13 p2265 A69-27230

Modes and mechanisms of wear covering adhesive, abrasive and corrosive wear, surface fatigue and fretting corrosion 13 p2265 A69-27231

Friction and wear characteristics of ceramics and cermets as bearing materials, with tabulation of room temperature hardness and maximum service temperatures 13 p2284 A69-27232

Graphites wear rates and structural changes in machine parts under dynamic stresses in air or vacuum, noting pressure role 14 p2467 A69-28912

Calculated and experimental surface wear damage data correlated for materials under friction conditions 15 p2618 A69-30106

Engineering models for wearout reliability prediction in dynamical systems subject to random loading, demonstrating practical and statistical methods 15 p2705 A69-30366

Solid lubricant films friction and wear life determined under various conditions of contact, temperature, load and atmosphere [ASLE PREPRINT 69AM 6C-1] 15 p2619 A69-30471

Unlubricated wear characteristics of polyimide resin sliding against carbon steel in air, noting effects of surface temperature, bearing pressure and velocity [ASLE PREPRINT 69AM 5C-2] 15 p2619 A69-30473

Load, speed and coating thickness effect on wear life of resin bonded solid lubricant, using oscillating motion and low pressure blocks [ASLE PREPRINT 69AM 5C-3] 15 p2619 A69-30474

Hot pressed molybdenum disulfide-nickel composite film friction and wear tests in air and face seal configuration [ASLE FICFS PREPRINT 23] 15 p2620 A69-30491

Corrosive wear due to atmospheric O in sliding metal systems, noting oxidation rate relation to wear rate and activation energy [ASLE PAPER 68-LC-11] 15 p2622 A69-30605

Corrosive wear by atmospheric air and moisture under nonscuffing conditions, noting control by dry nitrogen blanketing and oil additives [ASLE PAPER 68-LC-10] 15 p2622 A69-30608

Erosion wear of graphitic and mica-ceramic materials used for sealing turbine compressors at high temperatures, including test installation 15 p2643 A69-31186

Solid solutions atomic ordering effect on friction and wear in vacuum, using CuAu and FeCo systems 18 p3149 A69-35183

Molybdenum disulfide dry film lubricant wear theory and test correlation problems, considering sintering self propagation due to chemical effect of environment 19 p3323 A69-35580

Controllable process for forming Ti-Ni intermetallic wear resistant coating on Ti alloys, discussing techniques, weight saving advantage, gear tests, etc 19 p3323 A69-35582

Titanium alloys case hardened by diffusion of various metals at high temperatures, measuring increase in wear resistance 19 p3344 A69-36153

Nylon wear curves and friction coefficients for steel-nylon pairs determined as function of normal load 19 p3329 A69-36495

Titanium alloys wear and fatigue resistance as functions of time and temperature of nitriding by purified nitrogen 19 p3347 A69-36743

Wear and friction of fiber-metal Mo bodies impregnated with molybdenum disulfide, noting coating-endurance life 20 p3547 A69-36953

Wear resistance of briquetted lubricants from fluoroplast and molybdenum disulfide under pressure 21 p3733 A69-39805

WEATHER

- Impact effects on metallic materials deformation and wear, considering impact force, time and coefficients, penetration depth, deformation energy, etc
22 p3966 A69-39876
- Wear resistant Ti carbide based cermets with alloy steel binder, noting electrical and heat conductivity dependence on composition and temperature
22 p3971 A69-40919
- Wear resistance and antifriction measurement device for polymer coatings in high vacuum, various gases and during exposure to electron radiation
23 p4169 A69-41599
- Sand erosion behavior of metals and plastics in air blast rig under varying exposure time, angles of impact and tensile stress
24 p4363 A69-42787

WEATHER NT COLD WEATHER

- Piloting aspects of jet V/STOL aircraft for poor weather operations without complicated ground aids, discussing deceleration transition, forward speed and final approach angle
01 p0010 A69-10868
- Meteorological application of ATS observations in form of time lapse movies of weather in motion, describing camera and data flow
[AIAA PAPER 68-1094] 12 p2174 A69-26804

WEATHER CHARTS U METEOROLOGICAL CHARTS

WEATHER DATA RECORDERS

- Tiros Operational Satellite system for global weather analysis data acquisition and cloud cover photography, noting sensor development for numerical weather prediction
[UN PAPER 68-95823] 01 p0108 A69-10473
- Meteorological rocket probes in Spain for wind and temperature measurements, including stratospheric circulation data
11 p1877 A69-24519

WEATHER FORECASTING

- NT LONG RANGE WEATHER FORECASTING
- NT NUMERICAL WEATHER FORECASTING
- NT STATISTICAL WEATHER FORECASTING

- Weather forecasting, discussing atmospheric models and computer operations for long range forecasting based on hydrodynamic theory and statistics
01 p0108 A69-10398

- Atmospheric model development relating temperature, density, moisture and energy measurements from satellite observations for long term weather forecasting
[UN PAPER 68-95397] 01 p0108 A69-10463

- Tiros Operational Satellite system for global weather analysis data acquisition and cloud cover photography, noting sensor development for numerical weather prediction
[UN PAPER 68-95823] 01 p0108 A69-10473

- World Weather Watch /WWW/ system and meteorological satellites, discussing observational networks, data centers, telecommunication facilities, research, education and training program
[UN PAPER 68-95209] 01 p0178 A69-10478

- Space techniques for application to civil aviation, discussing air to ground communications, air traffic monitoring and navigation and weather forecasting by satellite
[UN PAPER 68-95349] 01 p0179 A69-10490

- Satellites use in meteorology, noting monsoon rain forecasting through mesoscale sea surface temperatures of Indian Ocean
[UN PAPER 68-95355] 01 p0109 A69-10502

- Objective layer of maximum wind /LRMW/ analysis technique for Northern Hemisphere jet stream, noting generation of initial guess fields
01 p0110 A69-10689

- Meteorological probability assessors, describing framework for evaluation consistent with subjective probability theory
01 p0110 A69-10690

- Boundary layer effect on large scale atmospheric processes from analyzing two layer free atmosphere model, plotting weather forecast charts
02 p0273 A69-11435

- Correlation between CAT and thermal gradient increase at standard isobaric levels found to be potential forecasting tool
02 p0275 A69-11818

- European space programs requirements for satellite launch autonomy/independence from U.S. and U.S.S.R., discussing satellite applications for resource surveys, weather forecasting, etc
02 p0335 A69-12682

- Meteorological satellites for atmospheric data collection applicable to weather forecasting and synoptic analysis
02 p0277 A69-12778

- Short term weather forecasts by means of hydrodynamic equations in adiabatic approximation, noting atmospheric motions and processes, adiabatic invariants and meteorological fields
03 p0459 A69-13332

- Ghost project for gathering weather data by balloons and transmission of data to central data processing stations by satellite
03 p0520 A69-13621

- Temperature change and fog forecasting diagram modified by Swinbank relation in place of Brunt formula
03 p0462 A69-13965

- Tiros and ESSA weather satellites meteorological contributions, discussing photographic interpretation for weather predictions
04 p0626 A69-14690

- Interpretation technique for weather satellite photographs of spatially coherent cloud distributions
04 p0628 A69-15090

- Digital computers for global atmospheric circulation, describing circulation models and computer produced color movies utilization
04 p0628 A69-15363

- Atmospheric processes interpretation from cloud cover pictures televised by orbiting satellite, examining indirect weather forecasting
[UN PAPER 68-95713] 06 p0949 A69-17029

- Meteorological satellites data for quantitative weather forecasts, discussing error effects due to data treatment in adiabatic approximation
06 p0949 A69-17032

- Meteorological satellites in weather forecasting, contrasting satellite data continuity to discreteness of synoptic charts
[UN PAPER 68-95760] 06 p0949 A69-17037

- Meteorological rockets for space meteorology, aeronomy and weather forecasting, noting international programs involving U.S.S.R.
06 p1043 A69-17056

- European cyclonic system development phases determined from characteristic structural features of satellite cloud pictures
[UN PAPER 68-95711] 06 p0950 A69-17070

- Relation between satellite data concerning thermal microwave radiation and meteorological conditions in lower atmosphere for possible use in weather forecasting
06 p0953 A69-17995

- Dynamics of large scale processes in atmosphere extended to two week predictions using nine level hemispheric moist general circulation model
07 p1175 A69-18895

- Subjective and objective upper air forecasts for aviation comparison by isobaric pressure height fields, discussing error analysis
08 p1345 A69-19886

- Weather forecasts range and accuracy, outlining procedure for estimating growth rate of atmospheric behavior
08 p1346 A69-20600

- Radiocommunications for Tiros and Nimbus meteorological satellites, noting weather data communications and hydrological experiments
09 p1451 A69-21289

- Efficiency of weather forecasts taking into account quality criteria and integrating index number, discussing optimization principle for new parameter
09 p1534 A69-21510

- Subjective and objective upper air forecasts compared for error analysis of headwinds, noting influence of geographical location
09 p1536 A69-22074

- Wind velocities statistical properties at various altitudes, noting linear regression of orthogonal components and prediction of wind velocities at all altitudes
11 p1911 A69-24694

- Statistical method for determining accuracy of air-field weather reports on takeoff and landing conditions, visibility and cloud ceiling, correlating forecasts and actual conditions
11 p1913 A69-25205

- Stratosphere and troposphere processes analyzed, indicating feasibility of forecasting geopotential and wind fields between 12 and 24 km
12 p2126 A69-26581

- IR TV cloud pictures from meteorological satellites used for sky condition diagnostics and forecasting through automatic interpretation by image brightness quantization
13 p2291 A69-27728

- Earth TV pictures from Molniia 1 communication satellite, showing advantages of high orbit over low

- orbit photography for global weather analysis and forecasting
13 p2292 A69-27729

- Meteorological problems in Italy analyzed by digital computer program through numerical integration of atmospheric models to provide weather forecasts
13 p2295 A69-28651

- Soviet collection of articles on aviation forecasting of cloud cover, high altitude wind and turbulence
14 p2473 A69-29734

- Flight regularity and safety in complex meteorological situations, noting synoptic forecasting advantages over inertial forecasting
14 p2475 A69-29740

- Atmospheric motions equations in mesometeorology prognostic problems taking into account free atmosphere and boundary layer interactions
15 p2646 A69-30107

- Computer uses for air traffic control in Germany including flight plans and weather report data processing
15 p2650 A69-30230

- Initial uncertainties role in weather forecasting, discussing errors as represented by rms deviation of ensemble members from mean
15 p2649 A69-30894

- Meteorological satellite data application to weather analyses and forecasts, discussing sea-ice boundaries and snow fields location
15 p2650 A69-31364

- Weather forecasting potential accuracy, noting further improvement possible with present worldwide observations quality and quantity
16 p2808 A69-32385

- Weather forecasting correlation between atmospheric ozone vertical profiles and postsounding ground meteorological situation, describing computer data processing
16 p2786 A69-32629

- Meteorological forecasting as problem in fluid mechanics and thermodynamics, discussing accuracy and electronic computer role in classical or mathematical methods
18 p3166 A69-34694

- Atmospheric predictability as revealed by naturally occurring analogs, noting superposed error
20 p3573 A69-38057

- Clear air turbulence computerized analysis and forecast over U.S. using upper air rawinsonde measurements
22 p3976 A69-39927

- Minimum air temperature forecast by terrestrial thermal or long wave radiation balance measurement, using radiometer data
23 p4184 A69-42211

- Formulas for discriminant and regressive weather analysis for computer calculations under operational weather forecasting conditions
23 p4184 A69-42490

- Surface pressure field forecast by meteorological fields expansion into orthogonal components, estimating number of predictors in regression equation
23 p4184 A69-42491

- Satellite-based meteorological observation system for global atmospheric research program, discussing wind measurement, IR and microwave sounding possibilities, etc
[AAS PAPER 69-120] 24 p4307 A69-42817

- NIMBUS program individual missions characteristics emphasizing NIMBUS 3 results and weather forecasting improvements
[AAS PAPER 69-421] 24 p4392 A69-42835

- Short range aviation terminal weather predictions concerning runway visual range, cloud-base height and wind, using FAA mesometeorological network
24 p4342 A69-42892

- Liquefied propane fog dispersal at Medford-Jackson airport, Oregon
04 p0585 A69-14918

- WEATHER RADAR
U METEOROLOGICAL RADAR

- WEATHER FRONTS
U FRONTS [METEOROLOGY]

- WEATHER MAPS
U METEOROLOGICAL CHARTS

- WEATHER MODIFICATION
NT CLOUD SEEDING

- Air mass cumulus cloud growth stimulation by means of vertical updrafts capable of perforation of retaining layers
03 p0461 A69-13409

- World Weather Watch /WWW/ system and meteorological satellites, discussing observational net-

works, data centers, telecommunication facilities, research, education and training program
[UN PAPER 68-95209] 01 p0178 A69-10478

Automation of meteorological fields analysis using computer
07 p1175 A69-18677

Satellite and aerological ground station data combined to determine geopotential fields and wind velocity fields for inadequately serviced areas
13 p2292 A69-27732

Anomalous meteorological field distribution as observed by correlated stations, determining independent stations number observing same data
13 p2293 A69-27851

Seven helix antenna array components and operation mode at Berlin weather station, including biaxial rotator, preamplifier servoamplifier and VHF telemetry receiver
17 p2946 A69-33768

WEATHERING

Weathering tests on wrought aluminum alloys exposed at U.S. sites compared to British industrial atmospheric exposure results
01 p0101 A69-11354

Glass fiber reinforced plastics aging behavior under heat and weathering influence
03 p0454 A69-13823

Long term weather and radar transmission effects on three ply fabric cloth fire-retardant polyester resin radome panel
08 p1414 A69-20485

Outdoor aging effects on unstressed Al-Al lap shear joints bonded by various polymeric adhesives
19 p3320 A69-35562

WEAVING

Woven roving construction and fill/warp ratio effects on flexural strengths of four ply laminates
14 p2469 A69-29414

WEBS (MEMBRANES)

U MEMBRANES

WEBS (SUPPORTS)

Shear buckling test data for shallow corrugated webs compared with theoretical analysis with web buckling as orthotropic plate or local mode
01 p0170 A69-10866

Shear buckling of simply supported infinitely long plates orthogonally reinforced by stiffeners with flexural and torsional rigidity
11 p1984 A69-25142

Flanges flexural rigidity effect on load carrying capacity, failure mechanism and postbuckling behavior of webs in shear, noting permissible load
18 p3227 A69-35492

WEDGE FLOW

Hypersonic flow of nonequilibrium diatomic gas on and near wedge, studying shock curvature variations
01 p0005 A69-10161

Pressure distribution at wedge wall during instantaneous small variation of supersonic motion
03 p0364 A69-13662

Steady two dimensional MHD flow of perfectly conducting fluid past nonconducting wedge with magnetic field orthogonal to flow velocity
06 p0964 A69-17244

Heat transfer to wedge in nearly free-molecular hypersonic flow of strongly rarefied gas
07 p1050 A69-18707

High velocity subsonic flow past wedge in wind tunnel with perforated walls, applying solution to optimum parameter determination of suction system
07 p1050 A69-18741

Two dimensional boundary value problem for symmetrical entry of wedge into incompressible nonviscous fluid using complex variable theory
08 p1305 A69-20995

Oblique shock wave separation conditions in supersonic gas flow past wedge
09 p1483 A69-22665

Inviscid supersonic flow in right angle corner of varied angular intersecting wedges with bow waves remaining planar up to intersection line
13 p2200 A69-28251

Supersonic gas flow past wedge at zero angle of attack with separated shock wave, calculating velocity gradient at stagnation point and pressure and drag distribution
14 p2390 A69-29615

Supersonic jet flow with separated shock wave flowing past infinite wedge using Chaplygin method, assuming negligible entropy variations
14 p2391 A69-29619

Turbulent and transitional near wake of adiabatic slender wedge with and without base injection at Mach 4 in supersonic wind tunnel
[AIAA PAPER 68-100] 16 p2732 A69-31882

Mean near wake flow of adiabatic two dimensional wedge at Mach 4 with tripped turbulent boundary layers and base mass addition
16 p2733 A69-32147

Surface pressure, skin friction and heat transfer measurements on sharp flat plates and wedges in low density hypersonic flow, noting slip velocity
20 p3458 A69-37186

Linearly elastic medium supersonic flow past rigid wedge, considering longitudinal and transverse perturbations interactions, dry friction, adhesion, slip and wedge physicochemical properties
20 p3515 A69-37439

Subsonic compressible flow at two dimensional inlets, analyzing field representation, boundaries, surface configuration and optimal wedge
23 p4060 A69-41915

Inviscid hypersonic flow over oscillating slender wedge, defining equivalent phase shift
24 p4248 A69-43582

Perturbation equations for oscillating wedges and caret wings with attached bow shock in hypersonic and supersonic flows
24 p4249 A69-43659

Strong shock and Mach waves interaction generated downstream of thick wedge body shock in unsteady hypersonic and supersonic flows
24 p4306 A69-43674

WEDGES

Upper and lower bounds for eigenvalues of differential problem connected with transverse vibrations of wedge shaped simply supported beam
02 p0272 A69-12193

Boundary layer flow of viscous incompressible liquid past wedge embedded circular cylinder
04 p0590 A69-15276

Radar scattering cross section of finite perfectly conducting wedge for case of illumination by polarized plane wave
08 p1274 A69-20047

Electromagnetic diffraction for waves generated by electric quadrupole on perfectly conducting wedge, discussing finiteness and radiation emission
09 p1455 A69-22082

Asymptotic solutions for transverse oscillations of wedge and cone by virtual displacements principle, considering nonlinear law of elasticity and energy dissipation
11 p1975 A69-24762

Diffraction accompanying reflection of plane shock wave obliquely impinging on walls of obtuse wedge at finite incidence, considering Lighthill method
11 p1873 A69-25135

Plane mixed boundary value problem in elasticity theory for infinite wedge
14 p2531 A69-28809

Diffraction of skew incident plane electromagnetic wave by perfectly conducting right angled wedge embedded in uniaxially anisotropic medium
17 p2930 A69-33889

Lateral and head-on interactions between plane shock wave and supersonic wedge, showing solution dependent on apex angle and incident flow Mach number
19 p3239 A69-36398

Thermal stress distribution induced in wedge by apex heat source analyzed using elasticity theory, considering lateral surface heat transfer
21 p3833 A69-38644

Babinet compensator with birefringent wedges made of stress frozen photoelastic material rather than quartz
22 p4042 A69-40442

Eigenfunction expansion technique to analyze three dimensional crack and wedge problems, emphasizing stress field near straight edged crack
24 p4395 A69-42641

WEIBULL DENSITY FUNCTIONS

Failure distribution functions based on Eyring component aging model, including failure probability density function for Weibull and gamma type distributions
08 p1322 A69-21104

Stochastic model for calculating expected component failures in transient state from Weibull distribution failure data for first generation
09 p1504 A69-22149

WEIGHT [MASS]

NT BODY WEIGHT

NT ORGAN WEIGHT

NT STRUCTURAL WEIGHT

Runway roughness effects on aircraft, formulating relationship between weight and resonant frequency through simple harmonic motion analogy
01 p0057 A69-11274

Pressurization system for liquid rockets, analyzing inert weight and complexity reduction using Saturn 5 S-4B stage
02 p0305 A69-12386

Supercharged bypass engines for possible application in light aircraft, noting payload fractions and total takeoff weights values
08 p1254 A69-20168

Channel wall effect on gain of apparent mass of cylindrical and elliptical bodies floating in channel and subject to vertical impact
11 p1875 A69-25487

Aircraft structure geometry design for minimizing total mass concerning flutter requirements
11 p1989 A69-25493

Periodic motions in single mass impact vibration system by point transformations method, noting complexity characteristics
18 p3172 A69-34565

Automated handling of mass properties data, describing data stored, central bank, report outputs, system logic, etc
[SAWE PAPER 811] 18 p3221 A69-34899

Pneumatic Vernier engines in aircraft and spacecraft, discussing weight, gas expansion and gas temperature
21 p3785 A69-39093

Multisupport suspension arrangements for reducing reflector surface weight-loading distortion in steerable parabolic radio telescope antennas
23 p4149 A69-42128

WEIGHT ANALYSIS

Space radiators for heat rejection from nuclear powered spacecraft doubling as primary structures to save weight, discussing conical or cylindrical configurations
01 p0160 A69-10151

Lunar surface power plants, considering weight constraint for various systems using nuclear power, solar cell/fuel cells and H-O reactant regeneration
01 p0013 A69-11396

Structural designs for minimum flexibility or weight using energy intensity per unit mass parameter
02 p0345 A69-12380

Numerical method for explicit solution of aircraft mass problem based on linearization of equations describing individual aircraft section masses
03 p0367 A69-13790

Prestressing of aircraft wing stringers in order to reduce weight, noting initial bending moment, initial axial stress and prestressing methods
05 p0832 A69-15690

Equation for calculating meteor shielded tubular panel heat radiators emissivity and weight optimization, considering surface thermal balance and temperature distribution
05 p0846 A69-15897

Small column insulated delay /SCID/ aircraft seat ejection systems, illustrating weight saving
06 p0877 A69-16957

Nonlinear constrained optimization by nonrandom complex method demonstrated by minimum weight structural analysis of elastic ring and plate
06 p1022 A69-17366

Pressure garments weight reduction methods, comparing partial pressure systems equipped with bladder, capstan, airpipe or foam rubber
06 p0884 A69-18037

Computerized objective analysis of meteorological variables based on weight determination involving autocorrelations
08 p1345 A69-20309

Electrochemical generators using zinc electrode in alkaline medium, noting weight consideration of zinc/air or zinc/oxygen cells
08 p1261 A69-21049

Fiber content by weight of reinforced plastics measured by pyrolysis
10 p1716 A69-23695

Free carbon content by weight in titanium, zirconium and hafnium carbides
10 p1714 A69-23846

Weight minimizing of circular disk subjected to behavioral and side constraints, considering resonance frequency of vibration and tolerances
[ASME PAPER 69-VIBR-1] 10 p1700 A69-24159

Variable and fixed weight growth factor effect on aircraft, showing coincidence of minimum weight
11 p1987 A69-25432

WEIGHT INDICATORS

Minimum weight design of structures excited to harmonic vibrations by given single load, with intensity dependent on time

13 p2369 A69-28350

Thin film thickness determined by weighing film and substrate in liquid having same density as substrate material

15 p2607 A69-30239

Spray oil cooling to reduce aircraft generator weight, enhance reliability and lengthen overhaul intervals

15 p2552 A69-30326

Helicopter weight analysis in preliminary design and proposal field

15 p2550 A69-30463

Higher plants utilization as nutrition source in space missions, comparing weight requirements for cultivation equipment and food storage

15 p2560 A69-31408

Starting weight increments in aircraft designs having various structural features and dimensions

16 p2735 A69-32144

Optimum nonequilibrium nozzle performance for hydrogen-fluorine propellant system, considering contour, engine/nozzle weights and recombination kinetics [AIAA PAPER 69-472]

16 p2733 A69-32652

Aircraft auxiliary power systems, discussing weight and power requirements, component design, driving methods and influence on power plant design

17 p3018 A69-33217

Parametric thermal control weight and power requirements for spacecraft life support systems, considering number of cabins, crew activity, heating, cooling and regeneration

17 p2914 A69-33305

Minimum weight design of tiltable enclosed antenna structure as subject to deformation constraints

18 p3211 A69-34341

Computer-aided design application to mass property engineering, describing repetitive mathematics functions, design information retrieval and display, automated synthesis, etc

18 p3107 A69-34863

Weight estimation and forecast in manned spacecraft design, noting size and weight relationship

18 p3208 A69-34864

Rational vehicle weight estimation based on statistical data/REBOS/ including gross weight, weight coding, subdivisions, balance and size, inertia moments and products, etc

18 p3220 A69-34866

Advanced design weight analysis and fixed equipment and propulsion systems weight prediction, noting error probability

18 p3220 A69-34867

Weight estimation of structures and systems unique to VTOL aircraft, considering remote fan and high bypass engine lift propulsion concepts

18 p3090 A69-34868

Weights study of V/STOL aircraft types for similar mission and payload requirements with different propulsion systems and flight profiles

18 p3091 A69-34869

Army OH-6A helicopter light weight design, considering effects of WRAP/weight, radius, area, power/factors on empty weight

18 p3091 A69-34870

Market analysis program to evaluate relationship between launch vehicle jettison weight and total cost based on all projected missions

18 p3208 A69-34872

Aerospace vehicle mass property limits and dynamic balancing related, noting errors

18 p3208 A69-34875

Earth orbital entry vehicles weight prediction, noting vehicle geometry as function of vehicle shape, hypersonic lift drag ratio and crew size

18 p3208 A69-34876

Statistical weight estimation equations developed by constrained regression analysis, noting application to vertical tail of cargo/transport aircraft

18 p3220 A69-34879

Gross weight and aircraft size estimates for configuration design of fighter aircraft

18 p3220 A69-34880

STAN integral weight and balance system providing aircrews with takeoff gross weight and CG data

18 p3136 A69-34882

Satellite attitude control mass properties, showing weight tradeoff analyses role in selecting control system

18 p3208 A69-34885

Computer program for weight and center of gravity tolerance data for assembly aerospace vehicle

18 p3221 A69-34892

Design iteration loop calculations related to fighter aircraft weight growth factor, noting asymptotic aircraft performance and strength

18 p3221 A69-34893

Synthesis and integration of cross discipline function for weight effective design of airplanes

18 p3221 A69-34895

Aerospace structures optimization, discussing weight considerations and finite element techniques

18 p3221 A69-34896

Aircraft preliminary design weight and volume characteristics relation to aircraft density

18 p3221 A69-34897

Parametric approach for weight estimation of surface control systems of transonic and supersonic combat and subsonic transport aircraft

18 p3221 A69-34898

Analytical-statistical weight prediction to derive and apply correlation expression, illustrated with bending stress equation applied to aircraft wing group

18 p3221 A69-34900

Computer aided design analysis program to provide weight and sizing data for entry spacecraft

18 p3208 A69-34903

Crane helicopters for heavy lift transport mission, noting weight and size effect on productivity

18 p3091 A69-34905

Monograph on weight and performance tradeoff methodology for selection of high lift devices

18 p3091 A69-34906

Lockheed L-500 aircraft weight consideration in structural design as all cargo lifter, describing engine thrust, payload, options, etc

18 p3092 A69-35464

Two stage vehicle gross weight minimization determined by slide rule computation using formula based on specific impulse differences between stages

19 p3429 A69-35918

Power subsystem weight effects on temperature ratio of Rankine type cycle, discussing method for rapid estimation

19 p3254 A69-35957

Ammonium chlorate thermal decomposition by measuring formed noncondensable gas pressure and weight loss in solid state kinetic investigation

21 p3669 A69-38800

RMS surface error compensation in radome-housed Cassegrain parabolic antenna including weight analysis

23 p4150 A69-42137

Maximum admissible weight of structural elements required for conventional wing conversion into variable geometry wing without performance impairment

24 p4253 A69-43092

WEIGHT INDICATORS

NT MICROBALANCES

NT STRAIN GAGE BALANCES

Magnetic suspension system used as dynamic balance for wind tunnel models, discussing delta wing test results

19 p3292 A69-35738

Wind tunnel model one component magnetic support and balance system for sphere drag investigation at subsonic Mach numbers

24 p4298 A69-43714

WEIGHT MEASUREMENT

Relative weight of fuel required for flight along prescribed flight trajectory

03 p0519 A69-12964

Onboard aircraft weighing system/OBAWS/ for accurate gross weight and CG measurements, describing axle shear deflection transducer system

10 p1693 A69-23276

Aircraft structural weight optimization based on design consideration of grouped related elements, noting application to Boeing 747 trailing edge flap drive

18 p3220 A69-34881

Aircraft onboard weighing system, eliminating or ring seal friction to permit accurate measurement of oleo strut pressure

18 p3137 A69-34883

Aircraft on board weight and balance system, discussing operations and economics programs

18 p3091 A69-34901

Weight estimation inaccuracies due to use of quickie equations, discussing error and extrapolation avoidance in wing weight study

18 p3222 A69-34904

Oscillating fiber microbalance for direct mass determinations in .1 mg to .0001 microgram range

21 p3720 A69-38592

WEIGHTING FUNCTIONS

Structural weight fraction factor analysis leading to improvements in materials and structures

01 p0011 A69-11021

Integral operators on space of Borel measurable functions bounded considering weight function, giving condition for infinite complex matrices, mapping analytic sequence spaces

01 p0107 A69-11244

Weighting functions for finite optically thick atmospheres, discussing emission line formation

02 p0328 A69-12755

Optimum control of fourth order digital control system

03 p0408 A69-12916

Weighting functions effect in calculating average scalar electrical conductivity in Lorentzian gas

04 p0638 A69-15317

Weighted pulse trains for clutter suppression during radar target detection

04 p0562 A69-15467

Digital controller weighting function sectionalization to simplify logic in developing adaptive control system

05 p0739 A69-16386

Optimum gathering of information for linear automatic control system with distributed parameters in presence of random input disturbance

09 p1471 A69-21437

Singular integral equation for velocity in linearized Rayleigh problem in rarefied gas flow field solved by applying Luke weight coefficients

10 p1679 A69-23596

Discrete Fourier transforms, discrete linear filters and spectrum weighting for purpose of sidelobe reductions

10 p1666 A69-23888

Optimum automatic selection of redundancies, discussing weighting and pivot choice and rigid element incorporation

11 p1993 A69-25529

Polynomial coefficients multiplication by weighted damping factors for increased conformal mapping and boundary value problems solutions accuracy for doubly connected regions

12 p2178 A69-25998

Amplitude spectra of periodic pulse sequences or pseudonoise sequences calculated using weighting and shape functions

12 p2030 A69-26389

Weighting factors relation in optimal systems integral squared error/ISE/ cost functional, characteristic coefficients and time response performance measures

14 p2534 A69-29317

Earth polar coordinates determined from latitude observations, discussing weighting functions for determining polar motion

17 p2959 A69-32869

Compressed signal spectral analyzer resolving power, discussing dynamic amplitude range influence and weighting functions role

17 p2939 A69-33906

Weighting coefficients calculations by recursive algorithm for designing optimal discrete adaptive Kalman filter

20 p3509 A69-37142

Weighting function of statistically optimal automatic dynamic system generating stochastic loads, using Fredholm equations

21 p3688 A69-39861

Active weighted pulse compression radar receiver output waveform analysis for amplitude, phase and frequency modulation, noting effects of spectrum weighting mismatch parameter

23 p4132 A69-42548

Correcting deficiencies in parametric expressions for rate distortion function of Gaussian process under weighted square error criterion

24 p4281 A69-42722

Weighting function of linear dynamic plant with steady random sampling determined with iterative method similar to stochastic approximation

24 p4289 A69-42951

Composite and metal tubes compared to determine properties for various loadings

24 p4405 A69-43653

Helix to coil transition for triple stranded macromolecule in solution, calculating ring weighting and partition functions and intact bonds

24 p4353 A69-43812

WEIGHTLESS FLUIDS

Excessive extrapolation limitations in applying transient data to low gravity fluid behavior for orbital refueling systems, presenting orbital fluid transfer experiment

16 p2870 A69-32755

WEIGHTLESSNESS

Wheat seedling germination and growth processes in absence of gravitational force onboard Biosatellite 2
01 p0015 A69-10932

Monkey psychomotor reactions during ballistic flight, noting alertness reduction during weightlessness
01 p0017 A69-11082

Weightlessness effects on fertilized frog egg development on board Gemini 8 and 12 manned orbital flights, discussing cell division, differentiation and embryogenesis
01 p0017 A69-11084

Soviet book on human movements coordination during space flight covering space walks, lunar surface photographs, space docking, weightlessness, etc
01 p0018 A69-11180

Heat transfer procedure and equipment during boiling under short term weightlessness
01 p0177 A69-11313

Weightlessness effects on organism in space flight along parabolic trajectories, discussing interaction between analysors
02 p0197 A69-11499

Physiological processes occurring in voluntary movements of animals under space flight weightlessness conditions
02 p0199 A69-11827

Weightlessness effects research during Soviet and U.S. manned space flights
02 p0199 A69-12120

Physiological causes and prevention of motion sickness during space flight, emphasizing conditioned reflex, different analysors interactions and vestibular-vegetative changes during weightlessness
02 p0200 A69-12122

Voskhod 1 and 2 crew performance, orientation and motor activity analysis indicating time increment for task performance, psychophysiological irregularities and visual analysors impaired functioning
02 p0203 A69-12123

Soviet collection of articles on dynamics of fluid-containing bodies under weightlessness conditions
03 p0417 A69-13808

Ideal liquid small oscillations in vessel under close to weightlessness conditions, discussing surface tension, equilibrium conditions and solution by decomposing vector function space
03 p0418 A69-13811

Space environment barriers to man due to biological evolution and transition from land to space in single generation, noting orientation problems
03 p0380 A69-14067

Simulation of regulatory function of cardiovascular system during weightlessness
03 p0376 A69-14193

Weightlessness effect on blood circulation system of human beings and animals during suborbital/ orbital space flight
03 p0376 A69-14194

Cardiovascular system, respiratory system and metabolism of cosmonauts on three man flight of Voskhod, noting physiological and biochemical studies
03 p0377 A69-14195

Physiological mechanisms of weightlessness on human organism, discussing adaptation to weightlessness
03 p0377 A69-14197

Biological space research, discussing microecology and weightlessness effects on human space flight [DVL-847]
04 p0553 A69-14811

Collection of papers on hypodynamics and hypogravities, physiology of inactivity and weightlessness
06 p0872 A69-17010

Weightlessness simulation, discussing mechanics of biological effects, simulation of specific anticipated effects and concept of mechanical acceleration and gravity equivalent effects
06 p0879 A69-17012

Cellular effects on weightlessness noting relation to size and cell complexity
06 p0872 A69-17013

Energy metabolism changes during weightlessness, considering effects on basal and nonbasal requirements connected with added increments for activity
06 p0872 A69-17014

Orthostatic intolerance, with assessment of circulatory problem of weightlessness in prolonged space flight
06 p0873 A69-17016

Musculoskeletal system and weightlessness state, concerning muscular disuse atrophy possibility during prolonged space flights
06 p0873 A69-17018

Physiological response of human skeleton to hypogravity and hypodynamics studied by bed rest experiments, suggesting disuse atrophy of bone
06 p0873 A69-17019

Soviet astronaut experiences and visual impressions during space walk outside Voskhod 2, noting dominance of optical analyser in space perception and orientation
[UN PAPER 68-95717] 06 p1000 A69-17049

Psychomotor reactions to zero gravity during ballistic rocket flights, analyzing electrical activity of cortex in animals
06 p0874 A69-17649

Flour beetle under irradiation and weightlessness during space flight, analyzing effects on somatic wing development, germ cells and pupal period
06 p0876 A69-18177

Rules for selecting Soviet cosmonauts and physiological studies concerning heart and respiratory reactions to accelerations and weightlessness during preparation
07 p1060 A69-18569

Soviet cosmonauts physiological reactions during weightlessness, analyzing EKG, arterial pressure, heart and respiratory rates and motion coordination
07 p1060 A69-18570

Gravitational effects during physiological functions formation of human organism, noting myogenic tonus rearrangement as primary response
07 p1060 A69-18572

Physiological aspects of weightlessness
07 p1060 A69-18573

Human sensory reactions to short term weightlessness
07 p1060 A69-18574

Physiological reactions of dogs during acceleration and weightlessness in suborbital flights of ballistic rockets
07 p1061 A69-18577

Statistical study of heart beat, respiration rate and arterial pressure of man during intermittent accelerations and short term weightlessness
07 p1061 A69-18579

Human vestibular reactions during weightlessness preceded and followed by acceleration
07 p1061 A69-18581

Astronauts increased heart beat, respiration rates and higher blood pressure subsides during repeated weightlessness tests
07 p1061 A69-18582

Human and animal cardiovascular system reactions to weightlessness, noting vagus nerve role in adjusting organism
07 p1061 A69-18583

Human vestibular and sensory reactions to rotation and rocking, Coriolis acceleration and vestibular reaction inhibition on ground test stand for effects of temporary weightlessness
07 p1062 A69-18586

Vestibular-vegetative reactions during angular and Coriolis accelerations alternating with weightlessness, noting increased parasympathetic and sympathetic activity
07 p1062 A69-18587

Oculomotor muscular tonus of rabbit during rocket flight acceleration and weightlessness
07 p1062 A69-18590

Decrease in bioelectric activity of skeletal muscles in animals and man during intermittent acceleration and weightlessness
07 p1062 A69-18591

Human motor reactions during weightlessness based on parabolic or orbital space flight observations, noting cosmonaut writing performance
07 p1063 A69-18595

Space flight crew efficiency during prolonged weightlessness, stressing preflight adaptation and space vehicle technology improvement
07 p1063 A69-18596

Drosophila melanogaster flies reproductive behavior and Tradescantia paludosa chromosome patterns after weightlessness onboard Vostok 3 and 4
07 p1063 A69-18597

Arbitrary human motions coordination in reorganization phases determined during weightlessness for cyclographic analysis of adjustment time
07 p1065 A69-18979

Time perception capacity of astronauts and jet pilots during brief weightlessness, noting emotional state effects
07 p1065 A69-18981

Weightlessness effect on critical heat flow during forced motion of water in different kinds of channels
07 p1243 A69-19616

Human organism reaction to prolonged limitation of muscular activity during weightlessness simulated by

bed rest, noting hypokinetic component of weightlessness
08 p1262 A69-19837

Vestibular analyser role in spatial orientation under weightlessness conditions during aircraft flights, discussing underestimations of rotation angle of Barany chair
08 p1262 A69-19840

Electrodes behavior for fuel cells with liquid electrolyte under high-g and weightlessness conditions, discussing spontaneous liquid motion
08 p1259 A69-21038

Animals in weightless state, noting vigilance, attention, sensorial and motor reaction time, muscular tone at rest and muscles electrical activity in movement
09 p1445 A69-22721

Monkey behavior in high atmosphere under weightless conditions, discussing problems connected with biological measurements, logic systems and vibration protection
09 p1447 A69-22722

Macaque monkeys in weightless state on sounding rocket, noting vigilance level and characteristics
09 p1445 A69-22724

Liquids in zero g environment for controlling position of propellant within tank for restart of rocket engine, noting minimum energy principle applications
11 p1944 A69-25599

Weightlessness and higher g values effects on caloric and rotational nystagmus
12 p2020 A69-26551

Weightlessness effects on human external respiration, gas exchange and energy expenditure indices during flight of Voskhod 2
12 p2020 A69-26563

Weightlessness and vibration effects on soft red winter wheat seedlings
15 p2557 A69-31368

Liquid free surface response to mass force variation during space flight near zero-g, discussing effects on ignition
16 p2866 A69-31735

Weightlessness problems, discussing artificial gravitation on spacecraft and astronaut experiences
16 p2746 A69-31930

Electrodes for fuel cells with liquid electrolytes, discussing problems under weightless and high gravity situations
16 p2738 A69-32409

Human motion coordination under acceleration followed by weightlessness during jet flights along Keplerian orbits, discussing initial disturbance and subsequent subsiding
17 p2907 A69-32938

Oxygenator for weightlessness operation, generating oxygen electrolytically and passing oxygen through membrane for animal experiments
17 p2903 A69-33039

Bedrest as analog of weightlessness, evaluating role of extravascular dehydration in postrecumbency orthostatism
17 p2909 A69-33179

Pulmonary mechanics during zero gravity maneuvers, noting decrease in flow rate and increase in expiration time without decrease in vital capacity
17 p2909 A69-33181

Compensative adaptational reactions to weightlessness, discussing blood supply to thorax area, external respiration, gas exchange and energy loss during parabolic and orbital flights
17 p2909 A69-33384

Hand movements in water environment, weightlessness and normal gravity conditions, discussing inner coordinative structure and muscular efforts
17 p2915 A69-33385

Compensatory reactions to prolonged weightlessness in human and animal organisms emphasizing blood circulation, heart, metabolism, digestive and nervous systems
17 p2909 A69-33577

Space research centrifuge counteracting null gravity physiological deconditioning, discussing linear and angular accelerations sensitivity and deconditioning effect on reentry task performance
18 p3114 A69-34368

Gravity independence of life processes in terrestrial organisms concluded from zero gravity experiments with algae, hatched larvae, etc
18 p3095 A69-34692

Manufacturing in space based on nongravity and hard vacuum environment, considering crystal growth and refinement, perfectly shaped bodies, refractory metals ultrapurification, etc
18 p3234 A69-35066

Space manufacturing operations program, discussing zero gravity effect during earth orbit flight, Apollo Applications Program Orbital Workshop Flight 2, etc 18 p3208 A69-35067

Materials and products fluid state processing in space, discussing g, zero-g and induced forces effect on fluid matter and process, cost and operational effectiveness 19 p3324 A69-35588

Materials processing in space, suggesting electronic single crystals preparation, materials melting and utilization of low g earth orbit environment 19 p3324 A69-35589

Motor and tonic reactions in animals during weightlessness, discussing interaction between gravity receptors and visual analyzer 20 p3470 A69-37247

Orientation reflexes of animals in weightlessness, analyzing turnover, vestibular and cervix reactions using motion pictures 20 p3470 A69-37248

Otolith apparatus functioning under weightlessness and accelerations in test stand experiments, discussing measuring techniques and nystagmic reaction durations 20 p3471 A69-37253

Combined angular and centrifugal acceleration effects on human and animal eyes motion studied to explain weightlessness effects on humans 20 p3471 A69-37257

Spacecraft rotation and astronaut head and body motion as stimuli for vestibular analyzer function study during weightlessness 20 p3473 A69-37275

Weightlessness tests during parabolic flight to supplement vestibular tests in astronaut selection 20 p3481 A69-37276

Arbitrary human motions coordination in reorganization phases determined during weightlessness for cyclographic analysis of adjustment time 20 p3479 A69-38227

Time perception capacity of astronauts and jet pilots during brief weightlessness, noting emotional state effects 20 p3480 A69-38229

Biological responses to weightlessness prediction, considering gravity perception mechanisms, cellular metabolism, etc 21 p3656 A69-38921

Human susceptibility to motion sickness under Coriolis acceleration during parabolic flight weightlessness 21 p3659 A69-39168

Motion sickness susceptibility during parabolic flight, comparing weightlessness and hypergravity effects on normal and labyrinthine-defective subjects 21 p3660 A69-39176

Cardiovascular changes induced in animals by prolonged weightlessness, using implanting polyethylene cannulas in neck or head 23 p4108 A69-41824

Pulmonary mechanics during zero gravity maneuvers, noting decrease in flow rate and increase in expiration time without decrease in vital capacity 23 p4089 A69-41825

Zero g deployment dynamics of erectable truss parabolic antennas, obtaining latchup loads as function of reflector mechanical energy [AAS PAPER 69-336] 24 p4398 A69-42827

Space manufacturing processes for orbital low and zero gravity environment, discussing buoyancy and thermal convection sensitive and molecular forces controlled methods [AAS PAPER 69-486] 24 p4380 A69-42844

Dielectrophoretic zero gravity cryogenic liquid expulsion using lightweight high voltage ribbon electrode conduits and electrohydrodynamic bang-bang field effect 24 p4300 A69-43237

Cardiopulmonary bypass developed for studies of long term weightlessness on cardiovascular system of mice, white rats and squirrel monkeys 24 p4278 A69-43394

WEIGHTLESSNESS SIMULATION

Organic reaction and adaptation of rabbits and dogs to simulated weightlessness and acceleration compared with orbital flight data of human responses 03 p0376 A69-14192

Weightless simulators effectiveness for obtaining space systems maintainability criteria, using non-parametric experimental design for performance data 06 p0882 A69-17648

Psychotechnical problems of weightlessness, considering cohesive forces, surface tension and mechanical behavior of fluids and weightlessness simulation techniques 07 p1070 A69-18568

Subjects sensory reactions to weightlessness during parabolic flight, studying coordination of writing, eating and drinking motions 07 p1060 A69-18575

Otolith apparatus response threshold under weightlessness conditions simulated by aircraft flight, measuring galvanic current threshold for banking 08 p1263 A69-19934

Simulated weightlessness used in determining ontogenesis of otolith organ in tadpoles and eggs as function of acceleration forces [DVL-855] 10 p1647 A69-24021

Friction damping properties of deployed structures vibrating in weightless state compared to damping in space for true determination 12 p2183 A69-26792

Space flight food evaluation by metabolic balance techniques during space flight simulation, considering food consumption during weightlessness 15 p2560 A69-31470

Mechanical linear accelerator simulating acceleration, shock and weightlessness, noting data acquisition and interpretation 17 p2945 A69-33423

Real time servo driven simulator of human body in zero-g activity used to study self induced rotation and astronaut mobility under thruster forces 21 p3664 A69-39034

Neutral buoyancy simulation of astronaut performing module replacement and repair task in zero-g environment [AIAA PAPER 69-1005] 22 p3921 A69-40379

WEIGHTS [COEFFICIENTS]

U COEFFICIENTS

WELD STRENGTH

Electrode indentation in resistance spot welds related to weld strength for titanium, steel and aluminum alloy 01 p0086 A69-10538

Butt weld fatigue properties improvement in maraging steels, using shot peening and prestretching 03 p0434 A69-13762

Spot weld strength of tungsten inert gas spot welding on Al-Mg-Si sheets greater than resistance welding, noting crack formation during inert gas welding 05 p0769 A69-16538

Welding of thermoplastic polycarbonate films, noting dryness requirement for satisfactory weld strength 06 p0930 A69-17094

Titanium surface impurities effect on porosity in welds, proposing machining immediately before welding as solution 06 p0945 A69-17894

Titanium alloy interaction porosity with fillers during diffusion brazing, discussing joint strength as function of time, temperature and pressure 06 p0945 A69-17896

Maraging stainless steel for manufacturing liquid rocket propellant tanks, discussing composition determination and mechanical properties 07 p1166 A69-19236

Weld mechanical properties of Ti-6Al-2Sn-4Zr-2Mo titanium alloy as function of cooling rate changes or transformation rate shifts resulting in wide range of hardnesses 08 p1318 A69-19965

Weldability of maraging steels, suggesting factors for weld toughness and reliability 08 p1320 A69-20408

High strength steels welding processes effects on weld metal composition and microstructure, heat affected zone, etc 08 p1320 A69-20410

Friction welding of aerospace materials, discussing joint strength and dissimilar materials 09 p1508 A69-22335

IR nondestructive, in-process microweld evaluator, discussing energy correlations and tensile strength 09 p1510 A69-22347

Weld discontinuities effects on fatigue strength of Al welds tested to determine unaffected defect size and severity of discontinuities 09 p1527 A69-22372

Thermomechanical treatment effect on VT15 Ti alloy properties and welds after deformation, attaining high tensile strength and plastic properties 11 p1889 A69-24277

Aluminum alloy weld tensile strength increased by heat treatment, discussing weld porosity due to surface film of absorbed hydrogen 11 p1891 A69-24896

Weld defects effects on static and fatigue properties of weldments prediction, including tests of titanium-aluminum-vanadium joints 11 p1892 A69-24932

Microcracking susceptibility studies of Inconel 718 weld heat affected zones, noting hot ductility, weld circle patch and fillerless fusion welding tests 11 p1905 A69-24932

Multiple repair welding effects on AL welds tensile strength, using conductivity measurements to monitor strength 15 p2631 A69-31509

Sigma phase and temperature effects on toughness austenitic stainless steel weldments 18 p3150 A69-35423

Nickel maraging steel weld metal impact strength and fracture toughness improved by heat treatment 18 p3151 A69-35430

Electron beam welds orientation effects on tensile and deformation properties of strengthened and welded austenitic stainless steels 18 p3151 A69-35432

Tensile and stress rupture strengths of diffusion bonded Ni superalloys, using spin tests of simulated hollow turbine disks 19 p3320 A69-35559

Weld defect data analysis in relation to aerospace structure performance, emphasizing effect on fatigue behavior and acceptance standard [SBAC PAPER 17] 20 p3550 A69-37450

Al alloys sheet, plate and weldments crack behavior and fracture toughness at cryogenic temperatures, using notched and surface flawed plane strain specimens [ASM PAPER W9-19.3] 21 p3743 A69-38669

Single run reheated weld wrought steel H cracking tested by constant load rupture /static fatigue/ technique 24 p4320 A69-42943

WELD TESTS

Mechanical properties of AZ5G-Zr-Cr alloy welded sheet subjected to biaxial stress at low temperature 01 p0088 A69-11152

Fracture toughness of Ni maraging steel weldments, using bending tests [AIAA PAPER 68-507] 03 p0450 A69-13919

Sheet steel composition effect on gas-tungsten arc welds porosity 04 p0607 A69-15219

Fully austenitic stainless steel welding electrodes for welds in cryogenic or high temperature applications, noting creep rupture test results 04 p0607 A69-15220

Nondestructive testing of welds - Conference, Chicago, January-February 1967 07 p1139 A69-18794

Nondestructive weld tests of propellant tanks in Saturn V-S-1C stage 07 p1140 A69-18798

Leak testing of welded pressure and vacuum vessels, considering nature of flow of gases through small restrictions 07 p1140 A69-18799

Integrated nondestructive testing systems to ensure welded assemblies reliability for Saturn 5 program, including surface defect detection 07 p1117 A69-19699

Mechanical properties of welds of niobium and Ni based heat resistant alloys and susceptibility to crack formation at high temperatures 09 p1504 A69-22146

IR nondestructive, in-process microweld evaluator, discussing energy correlations and tensile strength 09 p1510 A69-22347

Weld defects effects on static and fatigue properties of weldments prediction, including tests of titanium-aluminum-vanadium joints 11 p1892 A69-24932

Vacuum effects on resistance spot welds in aluminum, stainless steel and titanium alloys, noting X ray and tensile shear test results 12 p2103 A69-26622

Micrographic reagent coloring grains of Mo in relation to crystalline orientation applied to refractory metal welding and diffusion studies 14 p2505 A69-29221

Aircraft gas turbine parts design and fabrication, discussing role of welding techniques 15 p2629 A69-30928

Delta technique for ultrasonic weld inspection, noting ability to detect randomly oriented weld defects 15 p2631 A69-31508

Automatic ultrasonic inspection device search head, servomechanism and electronic system used for detecting weld defects and cracks

18 p3137 A69-35111

Standard reference radiographs for weld defects on steel sheets and plates

18 p3150 A69-35425

H concentration and pore formation in Ti fusion welds

24 p4319 A69-42885

Structural detection in steel welded joints using higher harmonics from eddy current sensing element

24 p4319 A69-42886

Thickness direction tensile properties, ultrasonic attenuation and mild steel plate lamellar tearing in multipass fillet joints measured by weld cracking test

24 p4320 A69-42942

WELDABILITY

Aluminum-Zn-Mg alloys: weldability, discussing base metal composition and heat treatment influence during gas-shielded arc welding

01 p0086 A69-10536

Fusion, resistance and pressure welding of titanium, discussing shielding, brazing, diffusion and adhesive bonding

02 p0253 A69-12064

Weldability of thermally stable titanium alloy, noting properties of electron beam and submerged arc welding

06 p0940 A69-17092

Aluminum alloy weld tensile strength increased by heat treatment, discussing weld porosity due to surface film of absorbed hydrogen

11 p1891 A69-24896

Weld cracking sensitivity of Inconel 713C investigated for determining aluminum content effect on weldability of nickel base heat resistant alloys

11 p1906 A69-25577

Heat treatable low alloy steels weldability for lightweight ultrahigh strength pressure vessels, gear and shaft fabrication in aerospace applications

12 p2100 A69-25827

Highly alloyed steels weldability, considering nickel maraging and precipitation hardening stainless steels

12 p2111 A69-25829

Aluminum alloys precipitation hardening types requiring solution heat treatment, quenching and artificial aging, noting advantages in strength and weldability

13 p2282 A69-28180

Maraging steel weldability, discussing residual stresses, hydrogen cold cracking, age hardening and hot cracking

15 p2617 A69-30098

Ti alloys commercial applications and properties, discussing alloying elements influence, deformability, weldability, stress corrosion and market trends

16 p2801 A69-31784

Mechanical properties and weldability of austenitic steel for cryogenic applications

18 p3158 A69-35417

Aircraft structures efficiency and weldability as function of application, welding procedures and metallurgical factors, considering high strength Al alloys, Ti and Ni alloys, etc

20 p3550 A69-37457

Minor element effects on Ni alloy weldability - Conference, Houston, October 1967

22 p3966 A69-39878

Minor element influence on high temperature weldability of high Ni alloys and weld quality

22 p3967 A69-39879

Minor elements effect on cracking sensitivity of weld heat affected zone in Hastelloy alloy X, noting hot tearing and midrange cracking

22 p3967 A69-39881

Minor elements effect on weld-metal cracking resistance of wrought Ni-base heat resistant alloy by Circular Patch Test

22 p3967 A69-39882

Mn, S and rare earth additions influence on Inconel alloy weld microfissuring including material, hot ductility and tensile strength data

22 p3967 A69-39883

Ti, Al, S and P influence on Ni alloys weldability, discussing chemical composition, susceptibility to hot cracking and ductility temperatures

22 p3967 A69-39884

Composition and thermal treatment effects on weldability of precipitation hardened Ni base alloy, analyzing heat affected zone cracking sensitivity

22 p3968 A69-39885

Weldability of alloy Ni-Cr-Fe base-filler alloy combinations, noting threaded mold test and surface fissures

22 p3968 A69-39886

High strength austenitic Cr-Mn-Ni steel applicability to welded pressure vessels for cryogenic fluid storage, discussing operating temperature stability, weldability, etc

23 p4175 A69-41475

WELDED JOINTS

NT SPOT WELDS

Natural aging effects on fracture characteristics of aluminum weldments, investigating precracked Charpy impact toughness

01 p0086 A69-10537

High strength steel welding with physical properties equal to parent metal, discussing gas tungsten-arc, electron beam and plasma arc techniques

01 p0088 A69-11399

Laser applications in metal working including dissimilar metal welding, hole drilling, material removal and dynamic balancing [ASTME PAPER MR68-406]

02 p0252 A69-11796

Ultrasonic quality control test methods for melt through welds in hydraulic line assemblies, noting equipment and surface roughness requirements

02 p0252 A69-11810

Shot peening effect on fatigue properties of maraging and Al-Zn-Mg alloy steel welds, using repeated tensile tests

02 p0253 A69-12061

Delayed rupture strength of metals and welded joints at fixed stress level

04 p0674 A69-14541

Cavities elongation in automatic inert gas shielded welds in titanium alloys

05 p0767 A69-15972

Ultrasonic inspection of soundness and penetration or corner welds for Zircaloy 2 casings, discussing method reliability and sensitivity limits

07 p1141 A69-19346

Weld defects, discussing criteria for rejection, harmful and harmless defects, welding process and procedures and weld vs base metal defects

07 p1143 A69-19696

IR nondestructive, in-process microweld evaluator, discussing energy correlations and tensile strength

09 p1510 A69-22347

Automatic plasma needle arc fusion welding for computer memory arrays and miniature electronic devices

09 p1511 A69-22355

Weld discontinuities effects on fatigue strength of Al welds tested to determine unaffected defect size and severity of discontinuities

09 p1527 A69-22372

Arc welding aluminum to steel using bimetal transition insert piece

11 p1891 A69-24929

Narrow gap gas metal arc welding process in spray transfer range for narrow welds in thick plates, discussing equipment and applications

11 p1891 A69-24930

Weld defects effects on static and fatigue properties of weldments prediction, including tests of titanium-aluminum-vanadium joints

11 p1892 A69-24932

Electron beam welding of Lunar Module Descent Engine, emphasizing variable area injector element and manifold assembly problems and techniques

12 p2102 A69-26621

Aluminum-boron metal matrix composite joining methods including electron beam, resistance spot, plasma arc and fusion welding [ASM PAPER W9-23.4]

14 p2455 A69-29449

Pulsed ruby lasers for welding fine wires for electrical interconnections, considering laser energy and pulse duration effects

15 p2617 A69-30097

Diffusion bonding for leaktight joints in connectors using intermediate metal system of Au-Cu-Au

15 p2617 A69-30100

Adhesive pressure welded joints tightness and fabrication stability analyzed on duraluminum sheet samples

17 p2978 A69-32949

Seam and stitch welding in miniaturized semiconductor package fabrication, including leak rate tables

18 p3149 A69-35272

Dual filler metals for increasing joint efficiency by changing fusion zone composition, discussing mechanical properties in Ti and Al plates welding

22 p3956 A69-40462

Joints structure, phase and chemical composition in kinetics of titanium diffusion brazing with copper

22 p3958 A69-41203

Mechanical properties of welded joints in Kh 18N9T steel at very low temperatures using austenitic-ferritic and austenitic welds

22 p3958 A69-41204

Room temperature tensile tests determining failure modes and defect influence on diffusion welds of unalloyed Ti, using electron microscopy and fractography

24 p4331 A69-42939

Porosity and inclusions effects on Al arc weld fatigue properties at ambient and cryogenic temperatures

24 p4331 A69-42940

WELDED STRUCTURES

Electron beam welding of beryllium, discussing procedures, weld quality and tensile strength efficiencies

02 p0252 A69-11863

Integrated nondestructive testing systems to ensure welded assemblies reliability for Saturn S program, including surface defect detection

07 p1117 A69-19699

Constructional HY steels for high stress critical welded structures, discussing fracture mechanics stress intensity factor

08 p1333 A69-20405

High pressure vessels welding reliability improvement, discussing edge profile, air expulsion from vessel and shielding atmosphere

11 p1892 A69-25670

Steels classification for welded construction according to heat treatment and metallurgical structures

12 p2111 A69-25826

Diffusion bonded Ti honeycomb sandwich, demonstrating structural integrity, efficiency, low weight and cost effectiveness

12 p2115 A69-26828

Automatic ultrasonic instrument monitoring on-line welding conditions of RF longitudinally seamwelded tubes

18 p3136 A69-34778

Seam welded U-type fin efficiency and effectiveness, studying effects of fin height, heat transfer coefficient and thermal resistance

19 p3452 A69-36371

Al alloy application to welded primary airframe structures, discussing welding processes with emphasis on fusion welding [SBAC PAPER 4]

20 p3549 A69-37445

Weld defect data analysis in relation to aerospace structure performance, emphasizing effect on fatigue behavior and acceptance standard [SBAC PAPER 17]

20 p3550 A69-37450

Seam welded Al alloy aircraft structure fabrication problems, emphasizing stress corrosion [SBAC PAPER 5]

20 p3550 A69-37454

Electron beam welding machine modifications for welded airframe components production, discussing work chamber, vacuum system and workpiece mounting [SBAC PAPER 13]

20 p3550 A69-37455

Aircraft structures efficiency and weldability as function of application, welding procedures and metallurgical factors, considering high strength Al alloys, Ti and Ni alloys, etc

20 p3550 A69-37457

Stress corrosion cracking of welded Al alloys in sea water solution, showing combined action of sustained stress, corrosive environment and heat treatment

21 p3748 A69-39492

Three dimensional welded structure of thin walled girders with stability loss, discussing welding strain gage measurements and simplified computational procedure

23 p4169 A69-42007

Welded honeycomb sandwich structures of Ti, steel and similar materials for use in extreme thermal and acoustical environments [AIAA PAPER 68-973]

24 p4326 A69-43716

WELDING

NT ARC WELDING

NT BRAZING

NT DIFFUSION WELDING

NT ELECTRIC WELDING

NT ELECTRON BEAM WELDING

NT ELECTROSLAG WELDING

NT EXPLOSIVE WELDING

NT FUSION WELDING

NT GAS TUNGSTEN ARC WELDING

NT GAS WELDING

NT LOW TEMPERATURE BRAZING

NT PLASMA ARC WELDING

NT PRESSURE WELDING

NT ULTRASONIC WELDING

Welding procedure for avoiding hydrogen cracking in high strength steels, stressing hydrogen escape from weld deposits 01 p0088 A69-11398

Welding use in aircraft design, noting weight and cost advantages and problems of stressing, stress corrosion and inspection 02 p0253 A69-12062

Welding with aluminum-zinc-magnesium alloys, discussing stress corrosion, embrittlement, compositions, heat treatment, material production and fabrication 02 p0266 A69-12063

Time dependent tube wall radial displacement during explosive welding as function of distance from initial explosion 02 p0254 A69-12675

Explosive welding application to dissimilar metals and tube to tube plate welding, noting influence of detonation and sound bulk velocity 04 p0608 A69-15481

Metal welding procedures for aircraft assembly, discussing weight, specific alloys and airframe components 04 p0608 A69-15483

Quality control in welding from design through experimental manufacture, product testing, large scale production and improvements 04 p0608 A69-15485

Welding of thermoplastic polycarbonate films, noting dryness requirement for satisfactory weld strength 06 p0930 A69-17094

Imaging systems for weld inspection, discussing physical factors and selection of radiation 07 p1139 A69-18796

Acoustic emission from welds in stainless steel plates used for detecting defects in single and multiple pass machine welds 08 p1318 A69-19963

Laser welding in nonconventional applications and tiny components 08 p1319 A69-20203

Fabrication welding with maraging steels with emphasis on minimizing heat input 08 p1320 A69-20407

Weldability of maraging steels, suggesting factors for weld toughness and reliability 08 p1320 A69-20408

Friction welding of aerospace materials, discussing joint strength and dissimilar materials 09 p1508 A69-22335

Welding defects, processes, inspection and personnel training problems 10 p1700 A69-23372

Laser beam welding effectiveness for TWT with coaxial input and output lines 11 p1896 A69-24741

Diffusion processes in metal welding noting role of recovery, polygonization, recrystallization, polymorphic transformations, etc 11 p1890 A69-24799

Gas bubble formation in Ti welding associated with gas nuclei in metal, molten dwell time, gas diffusion coefficients, joint edge conditions, etc 11 p1892 A69-25669

Welding - ASME-AISI Conference, Detroit, October 1968 12 p2100 A69-25825

Explosive bonding technique, discussing choice of explosive and geometrical parameters to match material parameters [ASME PAPER 69-DE-47] 14 p2454 A69-28849

Pulsed ruby lasers for welding fine wires for electrical interconnections, considering laser energy and pulse duration effects 15 p2617 A69-30097

Continuous butt welding with CW carbon dioxide laser, noting heat affected area, remelt zone and weld efficiency 15 p2617 A69-30099

Aluminum nonheat-treatable alloys cryogenic vessels welding, considering TIG, pulsed arc and MIG processes with respect to plate thickness, joint and accessibility 15 p2630 A69-31210

Welding research program at Polish Institute of Aviation concerning electron beam, AR shielded arc, resistance welding and soldering of heat resistant alloys 17 p2979 A69-33688

Welding processes providing low hydrogen welds for high strength steels, discussing heat treatment, maraging steels, fracture toughness, fatigue and static strength [SBAC PAPER 8] 20 p3549 A69-37447

Welding quality control in aircraft structures, considering weld design, process, weld and materials specifications, welding equipment and inspection [SBAC PAPER 15] 20 p3550 A69-37452

C and B influence on heat affected zone hot cracking and postweld heat treatment on Ni base superalloys 22 p3967 A69-39880

Preferential welding oxidation emphasized as element transfer mechanism in weld metal composition control 22 p3955 A69-40460

Weld porosity in Al alloys as function of composition variations, discussing water vapor contamination of welding arc 22 p3956 A69-40461

Metal matrix fiber-reinforced composite materials joining by welding and brazing techniques 22 p3956 A69-40480

WELDING MACHINES

Drilling and welding with sealed-off continuous carbon dioxide gas laser with outcoming beam collimated by Ge lens 01 p0086 A69-10821

Resistance welding monitoring systems including thermal expansion slow scan ultrasonic and electric energy monitor/limiter systems 02 p0253 A69-11864

Ruby laser boring and welding apparatus cooled by evaporated nitrogen gas, suitable for diamond boring 03 p0434 A69-13720

Vacuum evaporated thin film components welding, using torsional ultrasonic vibrations for joint activation 04 p0605 A69-14561

Narrow gap gas metal arc welding process in spray transfer range for narrow welds in thick plates, discussing equipment and applications 11 p1891 A69-24930

Electron beam welding machine modifications for welded airframe components production, discussing work chamber, vacuum system and workpiece mounting [SBAC PAPER 13] 20 p3550 A69-37455

WENTZEL-KRAMER-BRILLOUIN METHOD

WKB approximation for metal-semiconductor junction tunneling and transmission coefficient of parabolic barrier, discussing density of states in degenerate semiconductors 02 p0301 A69-12652

Wentzel-Kramers-Brillouin approximation validity determined by sufficiency conditions based on differential equations series solution 14 p2471 A69-29454

Atom-atom scattering potential from phase shifts, using WKB formula and Jeffreys-Born approximation 19 p3378 A69-36189

WEST GERMANY

U GERMANY

WETNESS

U MOISTURE CONTENT

WETTABILITY

Presprayed metal films influence on wettability and contact resistance of GaAs prior to fusing in Sn, In and lead contacts 10 p1748 A69-24214

Silicon and boron carbides wettability with liquid metals during contact reactions at various temperatures, discussing wetting mechanism 18 p3156 A69-35153

Coating deposition theory on high temperature materials, discussing interfacial energy and wetting properties of molten metal drop on solid base material surface 20 p3560 A69-37358

WETTING

Potential effect on wetting of platinum electrodes in acid electrolytes noting drainage role 08 p1268 A69-20362

Wetting and sessile drop contact angles between liquid binary Al alloys and solid Be, boron carbide and graphite under vacuum and in He [ACS PAPER 15-C-68F] 12 p2114 A69-26301

Sessile drops contact angles of alkali liquid metals on Re, W, Mo, Ta and Nb substrates related to substrate surface bare work function 14 p2506 A69-29270

WHEATSTONE BRIDGES

Strain gage transducers and measurements noting Wheatstone bridge, supporting structure and accuracy 10 p1690 A69-23227

WHEELS

U FLYWHEELS
U NOSE WHEELS
U REACTION WHEELS
U TURBINE WHEELS

U VEHICLE WHEELS

WHIRL

U ROTATION

WHIRL INSTABILITY

U ROTARY STABILITY

WHIRLING

U ROTATION

WHIRLING TESTS

U SPIN TESTS

WHISKER COMPOSITES

X ray diffraction used to measure alpha-SiC whiskers orientation in polymeric matrices 01 p1012 A69-11262

Whisker research history, discussing characteristic morphology, mechanical and physical properties and future applications as reinforcing components in reinforced metals 04 p0616 A69-14843

Nickel reinforced with mullite whiskers produced by hot pressing 05 p0782 A69-16794

Sapphire whisker reinforced aluminum composites fabrication and evaluation 06 p0939 A69-16942

Fiber orientation and morphology effect on tensile behavior of aluminum-nickel whisker reinforced aluminum 06 p0939 A69-16943

Diffusion bonding of whisker reinforced aluminum in closed steel die in argon atmosphere 06 p0943 A69-17238

Fiber reinforced plastic and metallic composites for longevity and endurance of materials at high temperatures and extreme loads, discussing alumina whiskers 07 p1167 A69-19290

Thermoplastics reinforcement with fiber and whisker fillers, evaluating graded asbestos, carbon, silicon nitride, silicon carbide and potassium titanate 08 p1337 A69-20479

Fiber composite design, discussing contribution of filament diameter, number, content and properties, ply parameters and void content to structural response 08 p1341 A69-20512

Metallic and nonmetallic matrices reinforcement by ceramic whiskers, describing mechanical properties 09 p1525 A69-22142

Unidirectional filamentary composites thermoelastic properties relation to constituent materials properties, using semiempirical micromechanics theory 09 p1530 A69-22320

Ceramic whiskers and metallic matrix chemical reactions during composite formation, analyzing coated and uncoated SiC whiskers in titanium matrix 09 p1527 A69-22359

Whiskerized graphite fiber in resin matrix composites, analyzing interstitial growth characteristics, resin infiltration, layup and compaction 09 p1511 A69-22360

Whisker metal matrix composite fabrication, discussing aligned whisker distribution without degrading strength or fracturing and detailing extrusion process 09 p1511 A69-22361

Metal composites of Ni or Mo fibers in Be matrix, discussing chemical compatibility in terms of reactions, solid solubility and diffusion at various temperatures 10 p1707 A69-22991

Fiber reinforced metals, discussing crystalline whiskers, metallic and ceramic fibers and mechanical characteristics 10 p1711 A69-23335

Metallic and ceramic whiskers and fibers for material reinforcement, discussing properties and fabrication techniques 12 p2111 A69-25856

Orthotropic properties and stress fields for configurations of fiber or whisker reinforced composite materials subjected to nonaxial loading, considering infinite elastic matrix 12 p2186 A69-26824

Prototype system for continuous dielectrophoretic deposition and alignment of micron sized ultrahigh strength whisker reinforced composites 13 p2269 A69-28676

Silicon nitride staple fibers synthesis, development and characterization, noting tensile strength and sonic modulus 19 p3354 A69-35517

Boron fiber reinforced Al matrix composite material for high performance aircraft gas turbine engine compressor blading [AIAA PAPER 68-1037] 20 p3586 A69-37153

WHISKERS [SINGLE CRYSTALS]

- High aspect ratio submicroscopic whiskers of beta-SiC, investigating rheological properties of suspensions in various fluids
01 p0102 A69-11260
- X ray diffraction used to measure alpha-SiC whiskers orientation in polymeric matrices
01 p0102 A69-11262
- Creep relaxation and kinking of aluminum-nickel whiskers at elevated temperature, noting permanent plastic deformation after heat treatment
03 p0443 A69-13119
- Thallium whisker growth /compression or squeeze/ method
04 p0641 A69-14457
- Whisker research history, discussing characteristic morphology, mechanical and physical properties and future applications as reinforcing components in reinforced metals
04 p0616 A69-14843
- Statistical theory of material strength with application to composite materials reinforced with whiskers and continuous fibers
[AIAA PAPER 69-123]
06 p1028 A69-18142
- Fatigue characteristics of unidirectionally solidified Al-intermetallic aluminum nickel eutectic alloy consisting of discontinuous Al-Ni intermetallic whiskers in Al matrix
08 p1329 A69-20006
- Fiber-metal matrix composites fabrication, applications, mechanical properties and powder metallurgy
08 p1332 A69-20204
- Laminates and filament wound structures using carbon fibers with silicon carbide whiskerized surfaces, noting compositing and laminating techniques
08 p1339 A69-20501
- Whiskerizing technique for growing small beta SiC single crystals on graphite filament surfaces, noting changes in interface geometry and chemistry
08 p1341 A69-20511
- Microfilaments, Taylor production method, mechanical properties and comparison to whisker
08 p1320 A69-20582
- Metallic and nonmetallic matrices reinforcement by ceramic whiskers, describing mechanical properties
09 p1525 A69-22142
- Metallic and ceramic whiskers and fibers for material reinforcement, discussing properties and fabrication techniques
12 p2111 A69-25856
- Alpha alumina whiskers grown by vapor reaction examined by X ray microtopography and etching
16 p2802 A69-32341
- Fe whiskers formation and cross section determination by Fe dichloride reduction
22 p3919 A69-40233

WHISTLER RECORDERS

- Dispersion and average monthly numbers of whistlers for propagation trajectories during solar activity minimum, discussing electron concentrations in magnetosphere
09 p1485 A69-21531
- Ion whistlers recorded by Alouette 2 VLF receiver providing information on ion composition of terrestrial ionosphere, showing variation with latitude and relationship to solar cycle
15 p2604 A69-31410
- Dispersion and average monthly numbers of whistlers for propagation trajectories during solar activity minimum, discussing electron concentrations in magnetosphere
16 p2783 A69-32526
- Whistlers occurrence and dispersion rate variations from data obtained at lower latitudes during magnetic storms
18 p3102 A69-34967

WHISTLERS

- Ducted echoes on topside ionograms and whistler diffuseness at midlatitudes, noting common occurrence of phenomena
01 p0029 A69-10551
- Whistler rate and dispersion daily and annual variations derived relative to propagation conditions and magnetospheric behavior over North Italy
01 p0067 A69-11033
- Amplification process for VLF whistler mode radio signals observed in study of magnetosphere frequency shifting mechanism
01 p0077 A69-11241
- Whistler dynamic spectra variation studies, emphasizing distorted magnetospheric geomagnetic field structure effect
02 p0238 A69-11671

- Ion cut-off whistlers observed during VLF experiment aboard OGO 2 and OGO 4, noting possible application to relative ionospheric proton concentration determination
03 p0426 A69-14029
- Whistler mode propagation in homogeneous electron plasma situated in longitudinal electrostatic field, using Fokker-Planck model
05 p0758 A69-16417
- Electromagnetic emissions excited by whistlers in neighborhood of lower hybrid frequency, suggesting interpretation as whistlers modified by magnetospheric propagation
05 p0759 A69-16606
- Whistlers and VLF emissions from ground based and satellite measurements, applying results to electron density mapping and ion detection
07 p1127 A69-19354
- Lower ionosphere and earth-ionosphere waveguide effects on polarization characteristics of transmitted radio whistlers
08 p1306 A69-20181
- Atmospheric whistlers trajectories in magnetosphere calculated, assuming electron concentration as exponential function of altitude
08 p1309 A69-20429
- Dispersion and average monthly numbers of whistlers for propagation trajectories during solar activity minimum, discussing electron concentrations in magnetosphere
09 p1485 A69-21531
- Self focusing of plasma whistler wave along magnetic field at small threshold power
09 p1546 A69-21577
- Real configuration effect of magnetic field in moderately perturbed magnetosphere on whistlers dynamic spectra, stressing geomagnetic perturbation detection
09 p1490 A69-21766
- Magnetospheric perturbations as aftermath of proton flare discovered by whistlers, noting plasmopause movement toward earth
10 p1683 A69-23776
- Plasma concentration diagnostics in magnetosphere based on hydromagnetic whistlers /pearls/ dispersion
10 p1688 A69-23934
- Landau type interaction between electron beam and whistler /helicon/ wave electric field within semiconductor /InSb/
10 p1742 A69-24107
- Artificial triggering of VLF magnetospheric noise by NAA Morse code transmission during whistler duct drift across magnetic shells on 17 June 1965
11 p1878 A69-25154
- Whistler type electromagnetic waves excitation by electron beam in plasma, noting intensity dependence on electron frequency
13 p2314 A69-28443
- Whistler dynamic spectra variation studies, emphasizing distorted magnetospheric geomagnetic field structure effect
13 p2257 A69-28702
- Electron plasma oscillations and electron whistler of solar wind near Jupiter orbit
14 p2513 A69-29115
- Magnetospheric equatorial electron density profile estimated from midlatitude whistler observations, determining paths from dispersion data
15 p2677 A69-31357
- Noise signals in earth magnetosheath interpreted as electromagnetic waves propagating in whistler mode
16 p2774 A69-31985
- Dispersion and average monthly numbers of whistlers for propagation trajectories during solar activity minimum, discussing electron concentrations in magnetosphere
16 p2783 A69-32526
- VLF and ULF whistler propagation in magnetosphere for remote sensing magnetospheric plasma parameters, exhibiting characteristic patterns and interaction with plasma
17 p2962 A69-33712
- Geomagnetic field latitudinal variation effect on cut-off frequencies of proton whistlers, discussing LF electromagnetic wave propagation in cold multicomponent plasma
18 p3100 A69-34253
- Whistlers propagation in cold plasma in uniform magnetic field, considering amplitude dispersion effect
18 p3179 A69-34437
- Hydromagnetic whistlers propagation mechanism in magnetosphere determined by wave theory, assuming Gaussian radial density distribution and estimating duct width necessary for trapping
18 p3102 A69-34966

- Whistler vertical propagation downwards through inhomogeneous ionosphere in vertical magnetic field, deriving wave equation, calculating transmission and reflection coefficients
18 p3130 A69-34972
- Atmospheric whistlers and ion acoustic waves interaction in nonisothermal plasma, determining damping frequencies, decrements and wave polarization
18 p3180 A69-35024
- OGO-F electric and electromagnetic fields measurement for ionosphere using dipole antenna, emphasizing broadband observation covering whistler mode waves
19 p3284 A69-36677
- Cold plasma approximation of whistler excitation of lower hybrid resonance at wake of body moving through ionosphere, comparing results with Alouette satellite observations
20 p3519 A69-37025
- Alouette satellite VLF observations data of ionosphere ion composition determined from ion whistlers and noise bands with LF cut-off
20 p3530 A69-37873
- Monograph on whistler mode waves in plasma covering apparatus for studying gyroresonant interaction between whistler radiation and fast electrons
21 p3779 A69-39868
- Magnetospheric instabilities and whistler mode turbulence relationship to loss of high energy electrons from Van Allen belts
24 p4306 A69-42692
- Whistlers nonlinear interaction during cold magnetoplasma propagation, considering energy exchanges between waves
24 p4309 A69-43174

WHITE DWARF STARS

- Pulsating magnetic white dwarfs as pulsar models, discussing radio emission mechanisms via shock wave interaction with stellar plasma atmosphere
01 p0149 A69-10269
- Pulsar hypothesis based on oscillating white dwarf surrounded by hot rarefied corona to explain radio emission
03 p0505 A69-13077
- White dwarfs atmospheric pulsation suggested as pulsar mechanism, considering thin adiabatic atmospheric model with constant lapse rate
05 p0828 A69-16659
- Model for phase transition mechanism quantum-Coulomb plasmas, finding transition temperature for white dwarfs
06 p0968 A69-17785
- White dwarf general relativistic instability toward dynamic collapse and Type I supernovae
06 p1010 A69-17975
- White dwarfs transfer to superconducting state, using BCS theory for superconducting transition temperature dependence on electron density
08 p1391 A69-20546
- Binary stars systems with same total mass calculated for evolution from main sequence stage through mass exchange to white dwarfs
08 p1393 A69-20569
- Instability of stellar structures intermediate between white dwarfs and neutron stars shown by stellar models, discussing pulsar signals periodicities
08 p1397 A69-20770
- Carbon rich star models with and without neutrinos, considering carbon burning, central stars of planetary nebulas and hot white dwarfs
09 p1606 A69-22419
- Power spectrum analysis of photometric observations of white dwarf stars for measuring variability of stellar luminosity
10 p1788 A69-24124
- Axisymmetric models for stable and unstable oscillations of rapidly rotating zero temperature white dwarfs, discussing kinetic and potential energy
10 p1789 A69-24129
- Hydrodynamic calculation of 1.42 solar mass white dwarf supernova, considering instability and collapse initiation by electron capture
12 p2156 A69-26210
- White dwarfs structure model for deriving formula for phase density in color-luminosity diagram
12 p2159 A69-26665
- Gravitational parameters of highly condensed objects, considering white dwarf evolutionary stages, density and upper mass limit
13 p2334 A69-27190
- White dwarf atmospheric structure, analyzing masses and radii for DA stars and surface parameters of Eri B, based on grid of line blanketed models
13 p2339 A69-27563

Electron gas behavior in nondegenerate envelope of magnetic white dwarf, discussing increased opacity due to magnetic fields

13 p2343 A69-27624

Critical parameters of isothermal quasi-degenerate white dwarfs calculated by energy method, allowing for relativity theory error and neutron irradiation effect

13 p2351 A69-27871

Pulsar hypothesis based on oscillating white dwarf surrounded by hot rarefied corona to explain radio emission

14 p2515 A69-28759

White dwarfs periods of radial oscillations, considering ion gas contribution to adiabatic coefficient computation

14 p2517 A69-29090

Outer convection zone of cool white dwarf by atmospheric models, using mixing length theory and abundances

14 p2529 A69-29982

Nova thermal explosion, analyzing hydrogen combustion after penetration from white dwarf shell into degenerate core

15 p2682 A69-30507

Pulsar clock mechanisms on basis of relativistic gravitational effects, considering white dwarfs and neutron stars

15 p2694 A69-30855

Pulsars properties, nature and utilization for interstellar medium study including radiation mechanisms, white dwarf stars and neutron star development

16 p2855 A69-31762

Superfluidity and superconductivity under cosmic conditions, discussing Bose-Einstein condensation, neutron stars, white dwarfs, etc

16 p2856 A69-31950

DQ Herculis photometric measurements synchronized with white dwarf component pulsation, discussing equipment, eclipse curve and binary period dependence on time

16 p2862 A69-32373

Pulsed radio sources origin from models, emphasizing pulsating white dwarfs

17 p3037 A69-33640

Pulsation periods for pure He white dwarfs calculated by Chandrasekhar equation including relativity and rotation effects

17 p3037 A69-33641

Radial oscillation periods of Hamada-Salpeter white dwarf models graphically compared with models by Harrison-Wheeler Wakano equation of state

17 p3037 A69-33642

Observed and computed radio pulse profiles of white dwarfs, noting resemblance of emissivity variation with latitude to magnetic field distribution on sun

17 p3037 A69-33644

X ray sources model, describing possible ring of matter around white dwarf near end of active evolution

18 p3188 A69-35204

General relativity effects on isotropic stars evolution, discussing dynamic stability and white dwarfs

21 p3798 A69-38540

Normal radial vibrations in Newtonian and general relativistic stellar objects and dynamic instability, determining modes and natural frequencies

22 p4014 A69-40142

Book on white dwarf formation through mass exchange covering binary star system, primary star mass losses and evolution into white dwarf

22 p4021 A69-40421

WHITE NOISE

NT THERMAL NOISE

Quantizing noise effect on reconstructed analog signal at reception terminal of digital data transmission system

01 p0027 A69-10250

Integral and sigma pulse frequency modulation effects on white noise, analyzing autocorrelation and spectral density functions of PFM system output

01 p0034 A69-11221

Reliability of eliminating multivaluedness in two scale phase measurement method resolved by algorithm formulated on white Gaussian noise interference

02 p0206 A69-11603

Coherent PSK system in multipath environment/Rician fading and additive Gaussian white noise/with phase locked loop for coherent reference extraction

03 p0393 A69-13255

Mathematical modeling of Gaussian and non-Gaussian processes obtained by linear and nonlinear transformations of white Gaussian noise, noting Markov processes

04 p0623 A69-14694

Optimal control of system governed by linear parabolic equation with white noise inputs, using mathematical model to generate distributed system analog

05 p0740 A69-16599

Optimum and suboptimum detection of K binary symbols corrupted by white Gaussian noise, discussing searching procedure and average error probability

07 p1081 A69-19097

Noise generator design employing diffused Ge avalanche transit time diode

07 p1107 A69-19156

Approximate noise analysis of phase locked loop with signal clipping

08 p1270 A69-19857

Single degree of freedom mechanical system under random excitation studied for creep effect on vibrations by harmonic analysis

09 p1617 A69-22095

Reliability of eliminating multivaluedness in two scale phase measurement method resolved by algorithm formulated on white Gaussian noise interference

11 p1835 A69-24710

Transfer function parameters identification by fault isolation technique using white noise stimulus and processor matrix of orthogonal filters

11 p1865 A69-25077

Recursive estimation of noisy nonlinear multivariable systems in white noise by Kalman, second order nonlinear and iteration filters

12 p2046 A69-26062

Error bounds for orthogonal signals in additive white Gaussian noise channels for class of generalized decision strategies permitting variable-size list decoding

12 p2029 A69-26204

Nondeterministic differential games with imperfect state information, emphasizing linear system with quadratic cost functional and additive white Gaussian noise

12 p2053 A69-26505

Nonlinear systems disturbed by random white noise analyzed by Fokker-Planck equation for probability density in state space

12 p2124 A69-27141

Singularities of optimal filtration for random signals given by differential equations with variable coefficients and white noise

13 p2218 A69-27251

Optimal direction finding systems based on bearing angle representation in multidimensional Markov process, considering white and interference noise

13 p2219 A69-27254

Noise stability of receiver network during detection of finite duration noise signal on white noise background, considering various narrow band preselectors

15 p2563 A69-30142

Power spectrum analyzer of weak periodic signal obscured by white noise by zero interactions count of signal and noise mixture

15 p2579 A69-30945

Likelihood ratio for random signals detection in white Gaussian noise based on innovation process

17 p2920 A69-33622

Noiseless feedback schemes for digital and analog transmission over additive white Gaussian noise channels

21 p3671 A69-38405

Relation between smoothed and filtered linear least squares estimates of signal process in white noise from deriving resolvent identity of covariance function

21 p3754 A69-38432

Gyro drift rate mathematical modeling based on stationary and nonstationary time series analysis techniques with random process reduction to white noise residuals

[AIAA PAPER 69-838] 21 p3761 A69-39369

Sequential filter equations for nonlinear system dynamics and observational model with linear estimator, comparing difference between white and colored noise filter results

[AIAA PAPER 69-840] 21 p3686 A69-39371

Stable linear system/shaping filter/synthesis transforming stationary white noise into random process having given covariance function

21 p3688 A69-39661

Nonlinear random vibrations excitation in rectangular flat plate with initial imperfection by white noise, assuming clamped boundary conditions

22 p4048 A69-41183

Linear filtering effects in channel with binary direct sequence antipodal biphase modulation in presence of white noise and sinusoidal interference, noting variance

23 p4122 A69-41774

Recursive estimation of noisy nonlinear multivariable systems in white noise by Kalman, second order nonlinear and iteration filters

23 p4146 A69-42447

Optimum control synthesis for nonlinear plant subject to white noise perturbation, using integral estimates of phase coordinate functions

24 p4289 A69-42949

Optimal deterministic inputs derived for estimating dynamic control system parameters from white observation noise

24 p4293 A69-43245

WHITTAKER FUNCTIONS

Existence of periodic solutions by Whittaker criterion to equations describing motion of satellite of spheroidal planet in planetocentric coordinate system

02 p0317 A69-119595

Astronomical and geophysical observations, selecting degree of smoothing via Whittaker method for curve construction

17 p3028 A69-328777

WICKS

Heat pipes for thermionic converters, wicks development, high temperature life testing and performance

09 p1440 A69-218331

Pumping pore size and permeability of wicks as part of heat pipes design

23 p4074 A69-422981

Heat pipes design for avionic applications, using wicking bench tests

23 p4075 A69-42305

Temperature distributions in heat pipe wicks as function of liquid thermal conductivity

[ASME PAPER 69-HT-23] 24 p4412 A69-43545

Wick capillary pressure, permeability and burnout heat flux measurements to provide data for heat pipe design

[ASME PAPER 69-HT-18] 24 p4412 A69-43548

Wick-limited heat pipe performance, discussing maximum, steady heat transfer rate and transient response

[ASME PAPER 69-HT-20] 24 p4413 A69-43549

Heat pipe wick materials liquid transport properties analysis, using water and Freon 113 as working fluids

[ASME PAPER 69-HT-17] 24 p4413 A69-43551

WIDE ANGLE LENSES

Radiation measurements quality by wide angle receivers of Cosmos 122 satellite analyzed, showing agreement with data by other methods

11 p1912 A69-24830

Astronomical wide field cameras of large aperture ratio to detect extended near UV light sources outside atmosphere

12 p2080 A69-26127

Superwide angle camera with aerial photogrammetric lens system, discussing light distribution, rotary disk shutter, etc

22 p3944 A69-40047

WIDEBAND

U BROADBAND

WIDEBAND COMMUNICATION

Radio systems for discrete information transmission, emphasizing phase difference modulation, wideband, universal and adaptive systems

01 p0031 A69-10778

Low noise front end wideband amplifier for 100-150 MHz broadband receivers, using distributed amplifier techniques

02 p0216 A69-12028

96 element wide band scanning array measurements, considering array simulators usability at frequencies above operating frequencies

02 p0219 A69-12343

Decimeter wideband directional antenna system for investigation of ionosphere by retrodiffusion method

03 p0402 A69-12860

Lossy transmission line filters and wideband impedance matching

03 p0406 A69-13906

Bandpass characteristic for wide instantaneous bandwidth microwave components for phased arrays, noting error effect on compressed signal and time delay design

04 p0571 A69-14318

Wideband microwave KDP light modulator for amplitude and phase modulation, using ring-plane traveling wave circuit

05 p0732 A69-16553

Wideband uncooled two stage reflecting parametric amplifiers with low noise temperature, noting application to space stations for telecommunications by satellites

07 p1099 A69-18463

- Broadband multibeam antenna array with frequency independent beam directions, noting aperture gain limitation
08 p1288 A69-20965
- Communication satellite system design for operation with frequency bands above 10 GHz, noting wideband communication
09 p1450 A69-21284
- Structure of quasi-linear and wideband satellite transponders, discussing possible improvements
09 p1609 A69-21619
- Wideband signal Doppler distortion influence on parameter estimate accuracy
09 p1454 A69-21725
- Orbiting Data Relay Network communications system provides continuous wideband communication between ground and earth orbiting spacecraft via synchronous satellite repeaters [AIAA PAPER 68-432]
09 p1455 A69-21989
- Coherent FSK LF/VLF radio communication modem with large predetection bandwidth for improvement of reception in atmospheric noise
09 p1458 A69-22473
- Wideband device for rotating polarization plane of waves in waveguide between antennas, receivers and transmitters without affecting field linearity
09 p1469 A69-22643
- Noise rejection and carrying capacity of wideband and narrowband discrete systems transmitting complex signals in concentrated noise spectrum
13 p2218 A69-27213
- Complex pulsed radar signals synthesis with uncertainty function having principal maximum and small secondary maxima for radar stations and wideband communications systems
15 p2563 A69-30140
- Linear distortions effect on signals detection in binary communication channel with fluctuating noise, determining error probability
15 p2564 A69-30146
- Wideband PM communication system with synchronous reception and automatic control of reception bandwidth, providing improvement in noise stability
15 p2564 A69-30147
- Wideband multiplexers design with directional filters, discussing operational characteristics
15 p2581 A69-31524
- Wideband frequency switch to connect narrow band auxiliary to wideband radio system antenna, describing components
16 p2759 A69-31861
- Traveling wave tube amplifier for wideband radio in SHF range containing periodically integrated magnetized system, discussing output power variation range
16 p2759 A69-31863
- Wideband signal Doppler distortion influence on parameter estimate accuracy
20 p3488 A69-37461
- Optimum wideband signal for minimum Doppler distortion, describing pulse compression by linear-period modulation
21 p3671 A69-38406
- Holographic storage of electric signals in wideband pulsed carrier radar communications, noting Fourier transform in ultrasonic light modulator
23 p4164 A69-41626
- Wideband FM telemetry transmitters for S band, using symmetrical discriminator
23 p4119 A69-41741
- ### WIDMANSTATTEN STRUCTURE
- Widmanstatten angles relation to orientation of plane of section in iron meteorites
07 p1217 A69-19235
- Structure transitions in iron meteorites from Widmanstatten to granular pattern to study Barringer crater and Canon diablo meteorites formation
09 p1597 A69-22154
- Iron meteorites microscopic and macroscopic features due to preterrestrial mechanical deformation, stressing local displacements encountered in normal or acicular kamacites
19 p3418 A69-36134
- ### WIENER FILTERING
- Synthesis of infinite and finite Wiener optimal networks or equalizers using delay lines with feedforward and/or feedback taps
01 p0029 A69-10554
- Optimum nonstationary Gaussian signals estimation in presence of noise, generalizing Wiener stationary processes filtering theory
12 p2029 A69-26202
- ### WIENER HOPF EQUATIONS
- Group classification of solutions to Hopf equation according to type of viscosity coefficient
07 p1118 A69-18700
- Cylindrical antenna in uniaxial resonant plasmas, calculating current distribution and input admittance on basis of Wiener-Hopf technique
07 p1107 A69-19227
- Integral representation for Wiener Hopf factorization of functions of complex variables for numerical processing of radiation problems
11 p1851 A69-24998
- Stresses and displacements in half plane with edge crack given as eigenfunction expansions using Wiener-Hopf technique
11 p1987 A69-25438
- Dielectric coated finite cylindrical antennas, using numerical and Wiener-Hopf methods to obtain input admittance and current distribution
12 p2041 A69-26604
- Simultaneous Wiener-Hopf equations for electromagnetic wave diffraction, giving cyclic matrix solutions for Dirichlet and Neumann mixed boundary value problems
13 p2287 A69-27299
- Stress-strain problem of piecewise-homogeneous plane with cut normal to interface line reduced to Wiener Hopf equation, obtaining solution for arbitrary boundary conditions
14 p2531 A69-28805
- Diffraction of modal field by semiinfinite waveguide, integral representation for Wiener Hopf kernel factorization and applications to open resonators
17 p2930 A69-33888
- Numerical solution by approximation of Wiener-Hopf-Fock equation for diffractions at finite or infinite number of equidistant half planes applied to open-end waveguides
22 p3901 A69-40950
- Fourier series solution of finite range Wiener Hopf equation, determining coefficients from Wiener Hopf procedure
23 p4181 A69-41608
- ### WIGHTMAN THEORY
- U FIELD THEORY [PHYSICS]
U QUANTUM THEORY
U RELATIVISTIC THEORY
- ### WIGNER COEFFICIENT
- Polynomial bases for orthogonal group irreducible representations, rederiving Wigner coefficients
18 p3164 A69-34807
- ### WIND [METEOROLOGY]
- NT GEOSTROPHIC WIND
NT GUSTS
NT JET STREAMS [METEOROLOGY]
NT MONSOONS
NT SQUALLS
NT WINDS ALOFT
- Solar cycle influence on winds in lower ionosphere
05 p0759 A69-16421
- Geopotential and wind prediction by integration of prognostic equations of single level atmosphere
13 p2294 A69-27852
- Dynamic characteristics of local slope winds, considering thermal and geometrical effects of underlying surfaces
15 p2648 A69-30577
- Upper atmospheric winds to produce solar quiet day magnetic variations based on dynamo theory, illustrating solenoidal, irrotational and mixed winds
16 p2782 A69-32460
- Flow over uniformly rough surface in planetary boundary layer from mixing length wind spiral model, using surface shear stress and wind direction data
17 p2997 A69-33153
- Zonal winds in temperate latitude analyzed as function of latitude and month from GHOST balloon flights in Southern Hemisphere at 200 mb
17 p2997 A69-33163
- Climatological patterns of atmospheric kinetic energy dissipation in free atmosphere derived from upper wind statistics of Northern Hemisphere, using Kolmogoroff functions
18 p3166 A69-34825
- Numerical wind field prediction based on advection equations and quasi-geostrophic wind assumption, considering equatorial belt in case of zonal pressure field
19 p3364 A69-36506
- Doppler radar observations of precipitation induced mesoscale wind oscillations near melting layer produced by pressure perturbations due to horizontal variations in cooling
20 p3572 A69-37909
- Upper atmosphere horizontal unsteady wind with pressure gradient time dependence, solving heat conduction type equation by integral representations
21 p3758 A69-38411
- ### WIND CIRCULATION
- #### U ATMOSPHERIC CIRCULATION
- #### WIND DIRECTION
- Air movements in lower stratosphere analyzed on basis of ozone measurements, showing correlation with north-south gradient of total ozone amount
02 p0246 A69-12762
- Large scale disturbances in summertime stratosphere observed from high level balloon, discussing diurnal wind patterns and planetary traveling waves
03 p0461 A69-13343
- Standard deviation of wind direction fluctuations by simultaneous measurements of wind vane displacements and number of wind direction reversals
04 p0626 A69-14911
- Hot-wire anemometer with no moving parts for measurement of three orthogonal components of wind velocity and wind direction
06 p0923 A69-16926
- Day and night reversals in NmF2 north-south asymmetry related to neutral wind direction
06 p0918 A69-17384
- Statistical analysis of lee wave clouds from satellite TV pictures, determining lengths and air flow direction
11 p1912 A69-24828
- Time and altitude distribution of wind zonal components over Fernando Noronha Island off Brazilian coast, discussing tropospheric pattern
11 p1913 A69-25204
- Jet stream winds direction correlated with direction of LF pressure disturbances crossing microbarograph array
12 p2125 A69-26015
- Aircraft reports of high level turbulence on European and Atlantic routes, noting rapid changes in large scale flow pattern occurring locally
12 p2127 A69-26901
- Automatic processing and error analysis of horizontal, vertical, static and geostrophic wind data by U.S.S.R. Hydrometeorological Service
13 p2292 A69-27839
- Time correlation functions for wind vectors and components at various altitudes over Moscow in winter and summer
13 p2294 A69-27856
- Westerly air flow frequency decline resulting in lower seasonal temperatures, tabulating Lamb categories daily maximum and minimum temperatures
13 p2222 A69-28474
- Qualitative analysis of CAT parameters from radio sounding data, noting mean bumpiness probability dependence on Richardson number and wind vector shift
14 p2474 A69-29735
- Solar wind direction by analysis of data from IMP 1 satellite, noting anticorotation tendency
16 p2847 A69-31962
- Wind speed and direction determination accuracy of radar or theodolite methods
20 p3572 A69-37698
- Blast angle effect on fanjet gas dynamics in crosswind, using equations for free lateral flow trajectories and reverse flow regions
21 p3850 A69-38863
- WE and SN wind components models from 60 to 130 km for different months and latitudes, discussing meridional and interhemispheric circulations
23 p4154 A69-41306
- Qualitative model of atmospheric mass circulation constructed from radar meteor trail drifts observations, considering solar thermal radiation and zonal wind direction
23 p4214 A69-41862
- ### WIND EFFECTS
- Water hover effects tested on tilt wing V/STOL seaplane model, noting effects of wind and waves on water passing through propellers
01 p0011 A69-11061
- Missile control during propulsion period, emphasizing vane deflection required for lateral wind compensation
01 p0163 A69-11297
- Lift fluctuation on airfoil due to transverse and chordwise gusts applied to rotating fan and compressor blade design [ASME PAPER 68-FE-28]
05 p0697 A69-16070
- Trajectory calculation of unguided meteorological rocket by digital computers and by equations of motion, discussing wind influence on ceiling and horizontal ranges
08 p1409 A69-20457

Mean tropospheric wind vectors periods compared to annual variations of earth rotation and pole latitude
08 p1309 A69-20854

Self excited aeroelastic galloping oscillations of long prismatic bodies subjected to wind velocity, noting effect of aerodynamically unstable cross sections
09 p1615 A69-21923

Aircraft gust alleviation system for minimizing weighted sum of normal acceleration and pitch rate response by limiting control surface deflections
09 p1434 A69-22279

Zonal momentum vertical transport due to large scale moving disturbances in westerlies of equatorial lower stratosphere
09 p1537 A69-22299

Carbon dioxide laser beam deflection and thermal defocusing due to wind in absorbing medium
10 p1701 A69-22949

Stratified atmosphere mean vertical flux due to ground disturbances, obtaining results for various wind and temperature profiles
10 p1685 A69-23856

Atmospheric turbulence effects on aircraft flight noting causes of turbulence
11 p1911 A69-24527

Air movement component of winter anomaly effect on radio wave absorption in mesosphere directly detected by rocket sounding
11 p1913 A69-25436

Forced convection in atmospheric boundary layer above nonuniformly heated earth surface, noting roles of wind and stratification parameters
12 p2126 A69-26579

Statistical correlation of temperature and tail-wind data for London-New York route at 50 mb for SST operation
15 p2651 A69-30690

Wind effects on ionospheric electric currents, using equivalent circuits to study tidal modes and current patterns
16 p2775 A69-32087

Vertical wind effects in atmosphere on S577 A radian, showing dependence on atomic oxygen density
16 p2778 A69-32185

Combined midlatitude neutral air wind and equatorial electrodynamic drift effect on F2 layer diurnal variations
16 p2781 A69-32316

Stratospheric winds effect on instrument package suspended from high altitude balloon, discussing package displacements, yarn shapes and air drag characteristics
17 p2961 A69-33612

Nonrecirculating wind tunnel configuration with minimum atmospheric wind disturbances for V/STOL vehicles aerodynamic testing
[AIAA PAPER 68-398] 17 p2947 A69-34024

Dispersion relation for gravity waves propagating in atmosphere with horizontal background wind variable with altitude
18 p3128 A69-34801

Wind shear effects on radar echo decay constant for finite meteor trail, considering roles of trail length and electron density variations
19 p3276 A69-36482

Lower E region field-aligned plasma instability arising from neutral wind driving ionization across magnetic field
20 p3534 A69-38091

Europa 1 launch clearance procedure based on wind load precalculations from weather balloon determined wind profiles
20 p3619 A69-38281

Balloon location by low orbit meteorological satellites, discussing balloon movement due to wind and geometric and nongeometric effects on errors
21 p3760 A69-38618

Equations of motion of unguided rocket under wind effect, calculating launch angles for wind compensation
22 p4037 A69-40815

Electron concentration vertical profile in ionosphere in presence of horizontal wind shifts determined using E layer charged particle redistribution approximation
23 p4155 A69-41840

Time averaged and fluctuating wind load effects on large radio telescope structures, discussing wind shear and turbulence influence on steady and unsteady loading
23 p4230 A69-42125

Isobaric inhomogeneous atmosphere effect on sonic boom determined, using analytic equation relating transmitted wave intensity to local free stream Mach number
24 p4254 A69-43728

Martian seasonal darkening attributed to windblown dust
24 p4389 A69-43742

WIND MEASUREMENT

Wind profile harmonic analysis based on meteor trail observations, noting wind power spectra and propagating waves in atmosphere
01 p0072 A69-11170

Ionosphere studies in France noting lower ionosphere dynamics, ionospheric winds, plasma electron densities, electron and ion temperature and ion-neutron collision frequency
02 p0242 A69-11903

Wind measurements by radio observation of meteor trails compared with fading drift results
02 p0275 A69-12042

Errors in wind data due to wind response of parachute-borne sensor corrected with radar tracking, comparing corrected and uncorrected data
02 p0276 A69-12700

Standard deviation of wind direction fluctuations by simultaneous measurements of wind vane displacements and number of wind direction reversals
04 p0626 A69-14911

Geostrophic wind direct computation from grid point analysis of observed winds, using balance equation
04 p0626 A69-14913

Frequency distribution of wind velocity as function of height, averaging time and thermal stratification
04 p0628 A69-15088

Wind turbulence measurement by shock wave tracking using Doppler radar, stressing relative location of antenna and sound source
04 p0628 A69-15149

Stratospheric temperature, wind and ozone concentration measurement during solar eclipse by sounding rocket system
06 p0916 A69-17008

Upper wind observation and computation accuracy, comparing radar and slide rule instrument errors
06 p0950 A69-17788

Atmospheric measurements from satellites, discussing ATS-1 cloud images for definition of wind and use of WEFAX through ATS 2 satellites for data transmission
[AIAA PAPER 69-158] 06 p0954 A69-18038

Rawin systems for upper air measurements of wind and thermodynamic parameters, using balloon-borne radiosonde
07 p1057 A69-19581

Pilot balloon and radiosonde measurements for p as function of wind direction, velocity and stability, discussing variation with air layers
09 p1535 A69-21516

Low latitude easterly wind measurements by optical tracking of chemicals from sounding rockets and gun probes during darkness
09 p1487 A69-21621

Dropsonde for vertical wind profile or wind shear measurement without tracking noting low cost
10 p1692 A69-23254

Mesopause wind measurements at high latitude locations by sounding rockets noting relation to noctilucent clouds
13 p2294 A69-28466

Focused beam wave applied to atmospheric turbulence probing for spectral density of index of refraction, structure constant and wind velocity
14 p2414 A69-29512

Upper atmosphere winds and temperature measurements from rocket grenade, discussing TMA experiments
15 p2598 A69-31317

E region ionization redistribution by neutral winds, comparing calculated vertical drift velocities to observed electron density profiles
15 p2677 A69-31395

Atmospheric temperature and vertical gradient in E region based on measured instantaneous wind profiles
15 p2603 A69-31399

Mesospheric fine winds structure, discussing data obtained by Skua II rocket with chaff payload
15 p2604 A69-31415

Strong vertical wind in low ionosphere due to short period reflected gravity waves, obtaining standing wave system
15 p2606 A69-31449

Direct wind measurement and momentum transport estimates obtained from cyclones and anticyclones daily displacements over Northern Hemisphere, applying results to planetary atmospheres
16 p2780 A69-32306

Sonic anemometers for atmospheric turbulence, discussing variance spectra of vertical wind components and temperature in atmospheric surface layer
16 p2808 A69-32600

Radar unit for network component /wind patrol/ in statistical observations of wind drift conditions in meteor trails
17 p2939 A69-33901

Statistical characteristics of wind wave development in initial stage, obtaining distribution functions and frequency spectrum for various velocities and temperatures
18 p3167 A69-35341

Horizontal wind components over U.S.S.R., Western Europe and Northeast Atlantic obtained from satellite photographs of vortex cloud systems
19 p3365 A69-36668

Rocket observations of ionospheric E layer winds using Na release method
20 p3529 A69-37796

Mesospheric wind measurement by meteorological rockets based on radar determination of drift trajectories of chaff clouds
20 p3529 A69-37797

Meteor winds analysis method used on tidal period wind measurement data obtained by chemical release from rocket in 95-135 km region
20 p3574 A69-38092

Vertical neutral wind measurements in lower E region with wavelike spatial structure, noting vertical shear role in ionosphere dynamics
21 p3703 A69-38363

Wind information obtained for design and operation of tethered or hovering free floating balloon systems
22 p3864 A69-40804

Angular grid spacing resolution near poles effect tests in global prediction model for geophysical fluid dynamics, investigating forecast height and wind fields
24 p4344 A69-43066

WIND PRESSURE

Spherical sandwich radomes designs, discussing aerodynamic loads, wind pressure effect, electrical properties and mountings
07 p1112 A69-19538

WIND PROFILES

Wind profile harmonic analysis based on meteor trail observations, noting wind power spectra and propagating waves in atmosphere
01 p0072 A69-11170

Midlatitude ionospheric wind profiles noting seasonal and time differences in circulation patterns, speed, shear, wavelength, energy content and dissipation
01 p0072 A69-11171

Vertical wind profiles and electron density profiles in E region, determining time dependence and ionization drift velocity
01 p0072 A69-11172

All weather wind profile monitoring system using FPS-16 radar/Jimisphere system and flight simulation for protection of space vehicle and missile launches
03 p0462 A69-13852

Gravity wave contribution to atmospheric wind motion at 100 km
03 p0426 A69-14031

Wind data from Arctic upper mesosphere showing easterly winds increasing with height, resolving diurnal and semidiurnal oscillations
06 p0949 A69-17005

Wind velocity and shear stress profiles above surface with changed roughness, using mixing length theory
08 p1346 A69-20311

Stereophotogrammetric measurements of smoke columns for wind soundings
09 p1535 A69-21517

Influence function for vertical wind profile from pressure gradient field
09 p1536 A69-21867

Validity of finite difference approximations for barotropic instability of zonal currents
09 p1537 A69-22298

Dropsonde for vertical wind profile or wind shear measurement without tracking noting low cost
10 p1692 A69-23254

Sonic anemometer for wind velocity through pulse communication transducers noting applications to aerospace vehicle design
10 p1692 A69-23255

Stability of barotropic perturbations superimposed on wind velocity profile of basic currents in geostrophic multilayer models
11 p1911 A69-24586

Wind velocities statistical properties at various altitudes, noting linear regression of orthogonal components and prediction of wind velocities at all altitudes

11 p1911 A69-24694

Time and altitude distribution of wind zonal components over Fernando Noronha Island off Brazilian coast, discussing tropospheric pattern

11 p1913 A69-25204

Power law profiles of mean wind velocity and temperature in thermally stratified shear flow, considering dependence on thermal stability and Richardson number

11 p1874 A69-25381

Zonal and meridional wind components monthly global cross sections for stratosphere and mesosphere from sounding and radar data

12 p2070 A69-26577

Optimum coordination between homogeneous isotropic geopotential field and derivatives, estimating efficiency of geopotential and wind fields simultaneous analysis

12 p2126 A69-26580

Stratosphere and troposphere processes analyzed, indicating feasibility of forecasting geopotential and wind fields between 12 and 24 km

12 p2126 A69-26581

Wind structure in atmosphere meteor region from persistent meteor trail radio echoes amplitude fluctuations, noting horizontal wind velocity profiles

12 p2074 A69-26962

Thermal stratification effect on wind structure in Ekman layer, assuming turbulent transfer and height dependence

13 p2290 A69-27390

Kelvin waves relation to quasi-biennial oscillation, using zonal wind and temperature variance data taken at Canton Island

13 p2290 A69-27391

Normalized correlation functions of dispersion values for pressure fields and geopotential obtained by low latitude stations, noting wind field features

14 p2478 A69-29833

Earth orography influence on climatological distribution of wind and geopotential fields, stressing central asiatic mountains role in atmospheric circulation

14 p2478 A69-29835

Turbulence coefficient in layers between main isobaric surfaces based on wind and temperature fields analysis

15 p2648 A69-30646

Atmospheric temperature and vertical gradient in E region based on measured instantaneous wind profiles

15 p2603 A69-31399

Alpine effects on wind field at synoptic scale using potential-vorticity equation, discussing deflection angle dependence on potential temperature distribution

15 p2650 A69-31445

Pressure gradients and moving ions driven neutral-air winds in F region, using asymmetric pressure model

16 p2779 A69-32302

Meteor trails radar observations to measure zonal wind profiles between 80-110 km, noting short period oscillations

16 p2865 A69-32609

Froude number for scaling wind stress at air-water interface, verifying logarithmic wind profile and relating shear velocity to surface roughness

17 p2996 A69-33152

Flow measurements about high Mach number low Reynolds number laminar wake behind spherically blunted cones, including surface and wake flow field data, radial wake profiles, etc [AIAA PAPER 69-714]

17 p2894 A69-33500

Temperature profiles and associated wind profiles obtained with Jimsphere/FPS-16 radar system at Cape Kennedy, discussing remote CAT detector assessment

17 p2999 A69-33739

Vertical structure concepts for air density, wind and sound velocity profiles in rocket climatology, discussing vertical relationship of wind shear statistics

17 p3000 A69-33794

Tropical circulation long term mean values of wind and temperature fields, momentum and heat fluxes from weather stations data, noting consistent pattern and energy source

18 p3165 A69-34418

Wind profile data measured by AN/FPS-16 radar/suppression balloon system, noting error sources

18 p3139 A69-35428

Wind and temperature profiles in Ekman boundary layer, using numerical integrations of dynamic equations including time derivative terms

19 p3363 A69-36501

Numerical wind field prediction based on advection equations and quasi-geostrophic wind assumption, considering equatorial belt in case of zonal pressure field

19 p3364 A69-36506

Japanese meteorological sounding rocket for atmospheric temperature and wind from 60 km down to balloon observation level, discussing principles and payload separation

20 p3543 A69-37795

Lower ionosphere vertical wind velocity profiles determined from rocket-released grenade glow cloud photographs, developing cloud buoyancy effect empirical model

23 p4154 A69-41305

WE and SN wind components models from 60 to 130 km for different months and latitudes, discussing meridional and interhemispheric circulations

23 p4154 A69-41306

Equatorial stratosphere and mesosphere wind, temperature and density data from rocket and balloon sounding, noting seasonal variations and possible stratosphere-ionosphere coupling

23 p4159 A69-42423

WIND SHEAR

Morphological behavior of blanketing sporadic E at middle latitudes, discussing wind shear time variations, solar cycle variation and geomagnetic storm effects

01 p0070 A69-11158

Sporadic E layer formation, considering ion convergence effects due to neutral wind shears and drift ionization due to electrostatic field

01 p0072 A69-11174

Midlatitude sporadic E layer vertical and horizontal structure and statistical properties, discussing theory of ion concentration by wind shear

01 p0073 A69-11177

Wind perturbations characteristics near large convective cloud banks as function of ascending current, wind shear and turbulence

02 p0274 A69-11446

Planetary Rossby waves vertical propagation through weak westerly wind wave guides, using adiabatic linear model

03 p0460 A69-13335

Wind shear and reflectivity gradient effects on Doppler radar spectra

03 p0461 A69-13341

Maximum downwind and crosswind vertical wind shear in boundary layer, noting effect on swept wing jet aircraft landing

06 p0951 A69-17790

Time and latitude variations of blanketing sporadic E using wind shear theory, predicting ionization layer formation in ionospheric E layer

07 p1125 A69-18840

Wind velocity and shear stress profiles above surface with changed roughness, using mixing length theory

08 p1346 A69-20311

Dropsonde for vertical wind profile or wind shear measurement without tracking noting low cost

10 p1692 A69-23254

Diurnal variations in sporadic E layer and wind in ionosphere during equinox and solstice periods, noting wind shear mechanism and ambient electron density

10 p1688 A69-23932

Jet stream vertical wind shear chart construction for aircraft with gas turbine propulsion

14 p2473 A69-29730

External wind shear influence on isolated cumulus cloud evolution based on hydrodynamic and thermodynamic equations numerical integration

15 p2648 A69-30644

Sporadic E ionization by rocket sounding, comparing positive ion density measurements with separate wind shear observations

16 p2780 A69-32310

Horizontal shear effect on structure of growing baroclinic waves by two layer model, assuming small radius of deformation, compared to planetary scale

17 p2960 A69-33150

Froude number for scaling wind stress at air-water interface, verifying logarithmic wind profile and relating shear velocity to surface roughness

17 p2996 A69-33152

Atmospheric wind shear velocity snapping effect on yarn suspending instrument package from balloon gondola during parachute recovery

17 p2975 A69-33613

Thermal wind instability by numerical integration of equations of motion, noting convective cells tilt

17 p2998 A69-33734

Wind shear effects on jet aircraft approach, discussing airspeed and glide path position maintenance requirements [AIAA PAPER 69-796]

19 p3367 A69-35634

Wind shear effects on radar echo decay constant for finite meteor trail, considering roles of trail length and electron density variations

19 p3276 A69-36482

Vertical wind shears, structure functions, turbulence and power spectra for transverse velocity fluctuations in troposphere and stratosphere, noting clear air turbulence

20 p3570 A69-37506

Vertical neutral wind measurements in lower E region with wavelike spatial structure, noting vertical shear role in ionosphere dynamics

21 p3703 A69-38363

WIND TUNNEL APPARATUS

Intermittent traversing gear with stepping motor for small hypersonic helium wind tunnels

01 p0054 A69-10219

Wind tunnel and test equipment for studying flow in straight airfoil lattices at Reynolds numbers 50,000-1,200,000 and Mach numbers 0.1-1.0

03 p0412 A69-13789

Factors influencing development of both wind tunnel and flight test technology for determining aerodynamic derivatives of aircraft motions

05 p0741 A69-15572

Tensiometric aerodynamic balances in great velocity ranges, discussing measurements, elastic elements and tensiometric balance construction and measuring errors nature

05 p0762 A69-15922

Semiconductor strain gage balance with temperature compensation for conventional wind tunnels

10 p1672 A69-23665

Magnetic suspension system used as dynamic balance for wind tunnel models, discussing delta wing test results

19 p3292 A69-35738

Subsonic wind tunnel balance and holders investigated for effects on lift, drag and stability of models of body of revolution

24 p2497 A69-43084

WIND TUNNEL BALANCES

U WEIGHT INDICATORS

WIND TUNNEL CALIBRATION

Wind tunnel model low pressure measuring system, discussing pressure transducers, automatic control and pressure distribution tests [AIAA PAPER 68-402]

17 p2947 A69-34023

WIND TUNNEL DRIVES

Jet pump actuation of intermittently operating variable density closed circuit subsonic wind tunnels, measuring wind tunnel power factor

11 p1892 A69-25371

Ejector driven wind tunnel for turbulent flow generation with arbitrary velocity profile, using jet arrays [AIAA PAPER 69-743]

18 p3114 A69-34408

WIND TUNNEL MODELS

Elastic wind tunnel models used for testing at full scale dynamic pressures, discussing scaling laws and manufacturing and testing problems [AIAA PAPER 68-56]

01 p0011 A69-11018

Multichannel telemetering device for magnetically suspended or free flight wind tunnel models noting strain gage pickups, switching and auxiliary circuits [ONERA-TP-643]

02 p0226 A69-11623

Photographic flow patterns of separated flows with vortex formation obtained in wind tunnel for different aerodynamic configurations of revolution

02 p0191 A69-12586

Wind tunnel pressure tests of Concorde air intake mockups in presence of aircraft wing and nose for Mach numbers 2, 2.2 and 2.35

03 p0361 A69-12879

Reentry plasma sheath simulation in wind tunnel by injection of nitrogen plasma from model vehicle nose

03 p0412 A69-13679

Three dimensional boundary layers on cones at small angle of attack, presenting numerical solutions with heat transfer effects for wind tunnel model [ASME PAPER 68-WA/APM-24]

04 p0541 A69-14389

Ground effects influence on VTOL aircraft secondary forces during hovering and transitional flight, discussing component dynamic coefficients in wind tunnel [DVL-851]

04 p0547 A69-14813

Factors influencing development of both wind tunnel and flight test technology for determining aerodynamic derivatives of aircraft motions

05 p0741 A69-15572

Large subsonic wind tunnels for correct simulation of V/STOL powered flight by minimizing wall constraint effects on flow field

05 p0741 A69-15573

WIND TUNNEL NOZZLES

Free fall vehicle dynamics for wind tunnel measurements of research shapes used in computer simulation of vehicle trajectories [AIAA PAPER 69-229] 06 p0864 A69-18130

Similarity of mean flow patterns of natural local wind to model wind in wind tunnel 07 p1176 A69-18964

Wind tunnel measurements on integrated shrouded propeller model proposed for power gliders 07 p1052 A69-19633

Electrolytic bubble level during wind tunnel tests for aircraft model attitude 10 p1672 A69-23268

Store separation from high speed aircraft via wind tunnel test techniques, discussing drop model, flowfield survey and captive trajectory testing [AIAA PAPER 68-361] 11 p1819 A69-25373

V/STOL air intakes and jets simulation in wind tunnel tests, noting thrust simulation possibilities 11 p1866 A69-25431

Subsonic wind tunnel solid and ventilated wall interference on air flow around aerodynamic models, discussing data corrections and slotted wall tests [AIAA PAPER 68-360] 12 p2059 A69-26766

Refractory cone models made of copper and Co coated Be for force tests in high enthalpy hypersonic arc tunnels at high simulated attitudes 12 p2059 A69-26796

Thermographic phosphor coatings to obtain optical quantitative heat transfer distribution on wind tunnel models 12 p2099 A69-27150

Supersonic boundary layer acoustic characteristics measured in wind tunnel on cylindrical model with several forebody configurations [AIAA PAPER 69-344] 13 p2249 A69-28279

Minimal interference thin metal strap support system for dynamic stability tests of high fineness ratio wind tunnel models [AIAA PAPER 69-350] 13 p2243 A69-28284

Flow simulation on wind tunnel test models for aerodynamic characteristics of aircraft design, discussing boundary layer and external flow coupling [AIAA PAPER 69-660] 17 p2945 A69-33471

Dynamically scaled model rotor tested in wind tunnel to evaluate blade aeroelastic limits constructed with realistic mass and stiffness distributions [AHS PAPER 341] 17 p3059 A69-33506

Wind tunnel model low pressure measuring system, discussing pressure transducers, automatic control and pressure distribution tests [AIAA PAPER 68-402] 17 p2947 A69-34023

Hover and forward speed aerodynamic characteristics of tracked air cushion vehicle (TACV) models, discussing wind tunnel tests [AIAA PAPER 69-750] 18 p3084 A69-34410

Sublimation of various compressed naphthalene wind tunnel models analyzed in supersonic air flow, discussing effects of temperature and model configurations 18 p3231 A69-35121

Flow breakdown in wind tunnel tests of high disk loading systems at low forward speeds, investigating downwash distribution effect using disk loading and airfoil models 18 p3119 A69-35230

C-5A aircraft model high subsonic speed tests, correlating data from three transonic wind tunnels [AIAA PAPER 69-794] 19 p3237 A69-35636

Multichannel pressure telemetry system for base pressure measurements on small wind tunnel models, considering proximity effects on transducer-telemetry units 19 p3305 A69-35727

Magnetic suspension system used as dynamic balance for wind tunnel models, discussing delta wing test results 19 p3292 A69-35738

DYDRA data logger for dynamic measurements of pressure distributions on harmonically excited wind tunnel models, noting use as general transfer function analyzer 19 p3293 A69-35746

Aircraft wing aerodynamic forces and moments due to lifting engine air intake simulated by wind tunnel experiment 19 p3239 A69-36400

Aerodynamic performance tests of autorotative unpowered rotor entry vehicle model at various Mach numbers and angles of attack [AIAA PAPER 68-950] 20 p3458 A69-37155

Panel flutter testing in supersonic blowdown wind tunnels, analyzing model and test chamber layout 21 p3847 A69-39859

Operational characteristics of multiple arcjet wind tunnel for time varying mass flow rate programs, calculating isentropic core densities and velocities [AIAA PAPER 68-229] 22 p3927 A69-40541

Subsonic wind tunnel balance and holders investigated for effects on lift, drag and stability of models of body of revolution 24 p4297 A69-43084

Dry ice ablating models for unheated supersonic and hypersonic wind tunnel tests, noting mass addition rate extension 24 p4297 A69-43255

WIND TUNNEL NOZZLES

Axisymmetric hypersonic wind tunnel nozzle design by determining inviscid contour and correcting for turbulent boundary layer growth [AIAA PAPER 69-337] 13 p2200 A69-28273

Pressure and temperature surveys of Mach 27-47 nozzle boundary layer at Ames M-50 He tunnel, determining velocity profiles, wall friction coefficient, etc [AIAA PAPER 69-686] 17 p2953 A69-33441

Laminar boundary layers in low density supersonic and hypersonic conical and axisymmetric nozzles, treating displacement, transverse curvature, velocity slip and temperature jump [AIAA PAPER 69-653] 17 p2954 A69-33458

Miniature probe with short time response for total temperature profile measurements in hypersonic turbulent boundary layer on wall of hypersonic tunnel nozzle 19 p3293 A69-35751

Supersonic blowdown wind tunnel operating at Mach numbers obtained by fixed nozzles for aerodynamic optimization of wings and bodies 20 p3510 A69-37422

WIND TUNNEL STABILITY TESTS

Elastic wind tunnel models used for testing at full scale dynamic pressures, discussing scaling laws and manufacturing and testing problems [AIAA PAPER 68-56] 01 p0011 A69-11018

Supersonic interference on lateral stability of planar configurations analyzed using wind tunnel data [AIAA PAPER 68-21] 02 p0189 A69-12377

Entry phase flight data of Missions AS-202, Apollo 4 and 6 compared with wind tunnel aerodynamics data [AIAA PAPER 68-1143] 03 p0519 A69-13556

Airplane drag prediction by wind tunnel tests 05 p0695 A69-15543

Buffeting tests of model wing in wind tunnel as function of angle of attack and Mach number 06 p0857 A69-17096

Free fall vehicle dynamics for wind tunnel measurements of research shapes used in computer simulation of vehicle trajectories [AIAA PAPER 69-229] 06 p0864 A69-18130

Aircraft propelled at Mach 7, discussing low speed and transonic characteristics, stability, power plant integration and ONERA wind tunnel experiments [ONERA-TP-657] 07 p1052 A69-18414

Concorde testing program, detailing materials, structure, systems, engine, wind tunnel and flight tests 07 p1054 A69-19294

Laminar hypersonic roll damping derivatives for 10 degree half angle cone at zero angle of attack for environmental flow conditions of hypersonic wind tunnel 09 p1430 A69-21958

Electrolytic bubble level during wind tunnel tests for aircraft model attitude 10 p1672 A69-23268

Strip method for prediction of subcritical frequency and damping characteristics for subsonic wind tunnel and flight flutter tests 11 p1987 A69-25368

Minimal interference thin metal strap support system for dynamic stability tests of high fineness ratio wind tunnel models [AIAA PAPER 69-350] 13 p2243 A69-28284

Helicopter wind tunnel testing, discussing solutions in terms of test procedures and test bed equipment 16 p2735 A69-32075

Amplified boundary layer oscillations and transition at swept flat nosed wing attachment line with/without boundary layer suction analyzed by wind tunnel tests 17 p2890 A69-33251

Wind tunnel wall interference effects in wind tunnel testing of STOL aircraft by inducing interference velocities [AIAA PAPER 68-399] 17 p2947 A69-34022

Wind tunnel tests for static stability of Black Brant 4 vehicle second stage with flare and two fin flare combinations at supersonic speed 17 p2948 A69-34212

Helicopter rotors forward-flight noise characteristics determined by wind tunnel tests compared to rotor noise during flyover 18 p3119 A69-35225

V/STOL model small scale tests compared with full scale tunnel or flight tests, considering normal differences in parameters and rotor instability 18 p3119 A69-35227

Flow field throughout wind tunnel containing rotor with sharply deflected blades, noting reversed flow effect in front of wake 18 p3119 A69-35228

Flow breakdown in wind tunnel tests of high disk loading systems at low forward speeds, investigating downwash distribution effect using disk loading and airfoil models 18 p3119 A69-35230

Wind tunnel tests of swept wing fighter aircraft for transonic buffet onset lift coefficient resulting from camber and leading and trailing edge deflection [AIAA PAPER 69-793] 19 p3238 A69-36297

Sounding rocket aerodynamic stability as function of nose length and mass, discussing wind tunnel test data 19 p3432 A69-36761

Aircraft propelled at Mach 7, discussing low speed and transonic characteristics, stability, power plant integration and ONERA wind tunnel experiments 21 p3644 A69-39164

Wind tunnel tests determining propeller slipstream effect on roll-damping derivative in transitional flight region, estimating STOL aircraft characteristics 22 p3863 A69-40145

Buoyant Venus Station balloon for deployment and inflation during parachute descent into Venus atmosphere tested with scale model balloons in wind tunnels [AIAA PAPER 69-1017] 22 p3922 A69-40389

Unsteady aerodynamic heating at stagnation region including surface combustion in arc heated high enthalpy wind tunnel 22 p3860 A69-40597

Solid fuel ablation and supersonic combustion processes for various propulsion configurations, testing plastic models in wind tunnel 24 p4414 A69-43569

WIND TUNNEL WALLS

Similarity law for channel wall influence in wind tunnels valid for all flow velocities 02 p0192 A69-12830

Large subsonic wind tunnels for correct simulation of V/STOL powered flight by minimizing wall constraint effects on flow field 05 p0741 A69-15573

Wind tunnel wall constraints effects at extreme force coefficients during V/STOL testing shown different from effects in conventional aircraft testing 05 p0741 A69-15574

Blockage correction for blunt based bodies of revolution in wind tunnels at low Mach numbers 05 p0699 A69-16395

Optimal V/STOL wind tunnel through interference study of slotted tunnel walls, including porosity and height to width ratio effects [AIAA PAPER 69-171] 06 p0908 A69-18203

High velocity subsonic flow past wedge in wind tunnel with perforated walls, applying solution to optimum parameter determination of suction system 07 p1050 A69-18741

Subsonic wind tunnel solid and ventilated wall interference on air flow around aerodynamic models, discussing data corrections and slotted wall tests [AIAA PAPER 68-360] 12 p2059 A69-26766

Wind tunnel wall interference effects in wind tunnel testing of STOL aircraft by inducing interference velocities [AIAA PAPER 68-399] 17 p2947 A69-34022

Vortex wakes behind high lift wings, considering effects of height above ground and various tunnel heights and widths for STOL operations [AIAA PAPER 69-740] 18 p3083 A69-34405

Cascade wind tunnels performance experiments, investigating effect of exit side walls lengths 19 p3241 A69-36753

WIND TUNNELS

NT BLOWDOWN WIND TUNNELS

NT CASCADE WIND TUNNELS

NT HOTSHOT WIND TUNNELS

NT HYPERVELOCITY WIND TUNNELS

NT LOW DENSITY WIND TUNNELS

NT LOW SPEED WIND TUNNELS

NT PLASMA JET WIND TUNNELS

NT SHOCK TUNNELS

NT SLOTTED WIND TUNNELS

NT SUBSONIC WIND TUNNELS

NT SUPERSONIC WIND TUNNELS

NT TRANSONIC WIND TUNNELS

- Thermographic phosphor technique to provide transient temperature measurements in impulse wind tunnel
01 p0078 A69-10152
- Wind tunnel measurement of rear parts drag of small scale aircraft models
[ONERA TP-633] 02 p0226 A69-11624
- Göttingen type wind tunnel, discussing stream characteristics and turbulence measurement by hot-wire anemometer
03 p0420 A69-14238
- MHD aligned flow of compressible fluid past slender body in wind tunnel
06 p0861 A69-17719
- Hot air open circuit wind tunnel for testing vaporized fuel films heat and mass transfer over flat plates
08 p1302 A69-20878
- Equilibration potentials between dense thrust beam and dilute space plasma measured in wind tunnel
[AIAA PAPER 69-263] 09 p1568 A69-21728
- Computer controlled data acquisition and control system (JDACS) for wind tunnel applications, describing system and programs
10 p1673 A69-23286
- Radiated aerodynamic noise effects on boundary layer transition on sharp leading edge hollow cylinders in wind tunnels, noting Reynolds numbers correlation
[AIAA PAPER 68-375] 13 p2241 A69-28211
- Boundary layer characteristics of incompressible flow in wind tunnel with asymmetric two dimensional contraction, discussing flow profiles
13 p2249 A69-28235
- Hypersonic wakes interference effects induced by facility instrumentation, discussing results of wind/shock tunnel investigations
15 p2588 A69-30475
- Running test facility for study of aerodynamics and flight dynamics of V/STOL aircraft models
17 p2944 A69-32851
- Blockage effects of flat plates and solid bluff bodies in closed wind tunnels compared concerning drag coefficient values
17 p2890 A69-33245
- Book on experimental aerodynamics covering subsonic and supersonic wind tunnels, wall measurements, airfoils, aerodynamic characteristics of propellers, fixed and rotary wing aircraft
17 p2891 A69-33318
- Nonrecirculating wind tunnel configuration with minimum atmospheric wind disturbances for V/STOL vehicles aerodynamic testing
[AIAA PAPER 68-398] 17 p2947 A69-34024
- V/STOL wind tunnel data at low forward speeds, discussing test limit dependence on model size, downwash angle and tunnel geometry
18 p3119 A69-35229
- Continuously operating multipurpose wind tunnel for laser light scattering experiments in supersonic two phase flow
21 p3689 A69-38596
- Aerodynamic characteristics of turbulent twisted jet in slipstream in open jet wind tunnel, determining static pressure, temperature and velocity component profiles
21 p3645 A69-39848
- Linear small perturbation approximation for supersonic nonequilibrium flows past oscillating airfoil in two dimensional wind tunnel, noting Laplace transform solution
23 p4061 A69-42349

WIND VANES

- Flutter vibration of sails fixed along edge and single wing weather vanes in supersonic flows
02 p0192 A69-12824
- Theoretical response of cup and vane anemometers to steady and varying flows derived analytically and by using analog computer
08 p1314 A69-20315

WIND VARIATIONS

- Turbulence characteristics up to 150 m above ground, noting surface roughness length directional dependence, longitudinal turbulence spectra and turbulent energy budget
01 p0110 A69-10695
- Factors producing wind deviations from geostrophic pattern under various atmospheric conditions
03 p0458 A69-13267
- Quasi-biennial oscillation in tropical stratosphere as result of long period gravity waves interaction with zonal wind
03 p0461 A69-13342
- Thermal forcing role in diurnal oscillation of planetary boundary layer wind above sloping terrain
03 p0462 A69-13682

- Long range prediction of zonal westerlies based on lunar cycles or quasi-biennial oscillations, considering aliasing problem
07 p1175 A69-18945
- Mean and turbulent energies and energy spectra of large scale wind velocity pulsations, analyzing annual variation for fixed wave numbers
09 p1536 A69-21861
- Zonal westerlies variations associated with tidal cycles, discussing principal component analysis, zonal index, bandpass filtering, aliasing, prediction and stepwise regression
09 p1537 A69-22242
- Power spectral analysis of upper wind data of equatorial lower stratosphere noting quasi-biennial oscillation
09 p1537 A69-22297
- Characteristics method for solution of differential equations representing time changes of wind and pressure fields in divergent barotropic channel flow
11 p1911 A69-24585
- Tropospheric zonal wind semiannual oscillations in Southern Hemisphere tropics with westerly maxima and easterly minima in May and November
12 p2064 A69-26011
- Latitudinal and vertical variations in six-month zonal wind cycles in equatorial and tropical stratosphere and lower mesosphere, utilizing rocket observations
13 p2294 A69-27854
- Thermally excited diurnal wind oscillations in lower mesosphere using model atmosphere in CIRA 1965, discussing daytime ozone density profiles
14 p2441 A69-29379
- Equatorial stratospheric wind fluctuations from pressure fluctuation data, relating southern fluctuations, stratospheric fluctuations and seasonal hemispheric air exchange
14 p2442 A69-29726
- Two year cyclic monsoon type variations in zonal wind distribution in tropical stratosphere and mesosphere obtained by rocket measurements
14 p2478 A69-29834
- Horizontal wind pulsations in precipitations obtained from pulsed Doppler radar data, including degree of turbulent flow anisotropy
16 p2807 A69-32271
- Diurnal wind variations below 30 km plotted on constant pressure charts, showing topographical influence on tidal fluctuations
18 p3166 A69-34828
- Time variability of horizontal wind as function of time provided by Kolmogoroff structure functions for components of isotropic turbulence
18 p3167 A69-34829
- Eulerian correlation functions representation of wind variations in analytic form by three parameter function, noting field diagram
20 p3571 A69-37507
- Horizontal wind speeds kinetic energy spectrum near surface, discussing diurnal variations
24 p4343 A69-43063

WIND VELOCITY

- Turbulence conditions in atmospheric boundary layer within similarity theory, including wind velocity and temperature profile
02 p0274 A69-11447
- Three term formula for describing vertical wind velocity distribution in upper boundary layer of atmosphere, taking into account friction and orography effects
02 p0240 A69-11708
- Venus atmosphere from Mariner 5 and Venera 4 data, discussing surface temperatures and pressures, cloud top region, McElroy model and maximum wind velocities
02 p0330 A69-12803
- Statistical analysis of data concerning difference between real wind velocity and velocity of gradient wind for winds of various velocities
03 p0458 A69-13268
- Ekman-Okkerblom problem for electrically conducting atmosphere located in external magnetic field, obtaining altitude distribution for wind velocity components
03 p0461 A69-13510
- Correlations at regional scale between clear air turbulence aircraft observation, Richardson number and wind intensity and direction at flight level
03 p0462 A69-13966
- Tetron flight observations of eddy velocities in planetary boundary layer, noting effects of height and seasonal variations
04 p0626 A69-14912

- Frequency distribution of wind velocity as function of height, averaging time and thermal stratification
04 p0628 A69-15088
- Turbulence characteristics and wind velocity in atmospheric boundary layer determined from pressure and temperature fields
05 p0788 A69-16453
- Terminal velocities of dust particles for two Venus atmospheric models from Mariner 5 and Venera 4 data, obtaining vertical wind velocity requirements
06 p1001 A69-17172
- Atmospheric wind velocity in Northern and Southern Hemisphere, noting increase with height
06 p0921 A69-17747
- Similarity of mean flow patterns of natural local wind to model wind in wind tunnel
07 p1176 A69-18964
- Wind velocity and shear stress profiles above surface with changed roughness, using mixing length theory
08 p1346 A69-20311
- Wind velocities statistical properties at various altitudes, noting linear regression of orthogonal components and prediction of wind velocities at all altitudes
11 p1911 A69-24694
- Air flow distribution and wind velocities in cyclones constructed from Cosmos 122 TV cloud images
11 p1912 A69-24825
- East-west asymmetry in solar wind velocity due to solar rotation effects on interaction between fast and slow streams
11 p1950 A69-25148
- Horizontal wind velocity energy spectra, attributing free atmosphere meso and microscale turbulence to meso and micrometeorological processes
12 p2070 A69-26575
- Wind structure in atmosphere meteor region from persistent meteor trail radio echoes amplitude fluctuations, noting horizontal wind velocity profiles
12 p2074 A69-26962
- Satellite and aerological ground station data combined to determine geopotential fields and wind velocity fields for inadequately serviced areas
13 p2292 A69-27732
- Wind velocity, geopotential and atmospheric layer temperature fields constructed from Tiros 9 satellite cloud data using least squares method and trigonometric polynomials
13 p2292 A69-27733
- Wind shifts and mean gustiness calculation from short range weather forecasts, using dynamic model for wind motion in atmospheric boundary layer
13 p2293 A69-27844
- Vertical wind velocity profiles approximation accuracy determined by linear, exponential and logarithmic functions of altitude during ice and frost
13 p2293 A69-27846
- Wind velocity fluctuations calculation in CAT based on closed equations numerical solution for turbulent layers in upper troposphere
15 p2649 A69-30649
- Diurnal variations of wind velocity, temperature and density at high altitude measured by Skylark rockets
15 p2598 A69-31319
- Average angular velocity of upper atmosphere from changes in orbital inclinations of satellites, discussing wind speeds
15 p2600 A69-31352
- Atmospheric models for pressure variation and neutral air winds in thermosphere, discussing wind velocity vector relation to satellites orbital inclination
15 p2603 A69-31403
- Thermosphere neutral wind speed measured from observing Doppler shift in O I 6300 night airglow line with Fabry-perot interferometer
16 p2776 A69-32093
- Angel sources rate of motion observed at automatic tracking coherent pulse station, obtaining coincidence with wind and insect velocities
16 p2779 A69-32276
- Meteorite trails radar observations to measure zonal wind profiles between 80-110 km, noting short period oscillations
16 p2865 A69-32609
- Wind velocity and precipitation particle terminal fallspeeds component determination from continuity equation for data collected by Doppler radar
17 p2919 A69-33162
- Fully developed whirls steady state structure, discussing tornadoes maximum azimuthal speed, hurricanes rotational speed, model for mature hurricane and numerical computation
[AIAA PAPER 69-671] 17 p2997 A69-33499

WIND VELOCITY MEASUREMENT

Tropical storms wind speeds related statistically to characteristics as pictured from satellites
17 p2997 A69-33690

Meteor trail drift radar observations in Kharkov, giving wind velocity diurnal and seasonal variations
17 p3041 A69-33897

Correlation between disturbances in troposphere and in geomagnetic field observed after widespread high winds and magnetic storms, using superposed epoch method
18 p3127 A69-34648

Vertical air velocity in rain measured for size distribution of drops, using relation between drop fall rate and diameter
18 p3104 A69-35342

Cirrus clouds occurrence, position and wind velocities on jetstream axes based on statistical analysis of aerological data and satellite TV pictures
19 p3366 A69-36669

Wind velocity components calculation at F-sphere maximum level, taking into account electrodynamic drift of ionospheric plasma and ion motion
20 p3519 A69-36972

Wind velocity below 100 meters from Laikhtman atmospheric boundary layer model, solving equations for horizontally homogeneous, stationary and nonadvective air flow
20 p3571 A69-37695

Pulsation velocities distribution wind in meteor region of atmosphere during hourly intervals over eleven month period, noting normal distribution
21 p3759 A69-39115

Horizontal wind speeds kinetic energy spectrum near surface, discussing diurnal variations
24 p4343 A69-43063

WIND VELOCITY MEASUREMENT

Influence of winds aloft on fading rate of microwaves propagated beyond horizon
01 p0030 A69-10566

Atmospheric turbulence power spectra for design criteria of future low altitude aircraft from LO-LOCAT program, analyzing turbulence scale lengths
[AIAA PAPER 68-216] 01 p0011 A69-11023

Vertical wind velocity structure and turbulent heat flux temperature measurements over steppe and sea, noting underlying surface influence
03 p0458 A69-13270

COSPAR manual on stratospheric temperature and wind measurements, discussing synoptic and time variation study by Arcas and Loki-Judi meteorological sounding rocket systems
05 p0752 A69-15706

Hot-wire anemometer with no moving parts for measurement of three orthogonal components of wind velocity and wind direction
06 p0923 A69-16926

Wind changes calculated from Doppler data and inertial system, noting role of heading and air speed
08 p1346 A69-20317

Automatic measuring device for short term air temperature and wind velocity fluctuations leading to air mixtures propagation
09 p1535 A69-21515

Sonic anemometer for wind velocity through pulse communication transducers noting applications to aerospace vehicle design
10 p1692 A69-23255

Wind velocity evaluating device operating by scale enlargement
12 p2079 A69-25896

Cloud drift radar measurements for determining wind velocity profiles in mesosphere, using rocket released dipole reflectors
13 p2253 A69-27848

Richardson number in vertical tropospheric region of maximum wind computed from data on jet streams observed in winter over radiosonde stations in Italy
13 p2295 A69-28656

Vertical wind velocity structure and turbulent heat flux temperature measurements over steppe and sea, noting underlying surface influence
14 p2471 A69-28778

Remote optical heterodyne measurement of Doppler shift as method for determining vector wind velocity, noting influence of air pollution
14 p2448 A69-29523

Vertical wind velocity pulsations in precipitation and passage through subfrontal clouds measured by pulse radar
16 p2807 A69-32272

Gust probes in model of low altitude atmospheric turbulence during USAF research program LO-LOCAT, plotting relationship between peak count distribution curves
17 p2999 A69-33737

Analog device to compute running ten minute average and store latest ten minute peak of unipolar data input for wind speed sensors
19 p3312 A69-36278

Vertical atmospheric motions, considering wind velocity measurements associated with synoptic processes
19 p3366 A69-36673

Wind speed and direction determination accuracy of radar or theodolite methods
20 p3572 A69-37698

Wind motion and turbulence in upper atmosphere from Rehbar 15 and 16 rocket observations
21 p3703 A69-38362

Wind and cloud velocities from ESSA 3 and 5 and ATS 1 pictures for typhoon and tropical vortices in intertropical convergence zone
21 p3758 A69-38371

Statistical analysis of wind velocity measurements at floating buoy stations, presenting velocity power spectra for different frequency bands
21 p3758 A69-39111

Airborne microwave radiometric measurements of simulated ocean surface under various conditions, suggesting possible wind velocity measurement by satellite
21 p3726 A69-39750

Lower ionosphere vertical wind velocity profiles determined from rocket-released grenade glow cloud photographs, developing cloud buoyancy effect empirical model
23 p4154 A69-41305

Atmospheric model for calculating wind velocity profile and turbulence of stable atmospheric boundary layer with given temperature stratification and pressure gradient distribution
23 p4184 A69-42489

Constant temperature thermoanemometer design and subsystem operation applied to measurements of turbulent flow velocity and pulse characteristics
24 p4311 A69-42558

WINDING

U FILAMENT WINDING

U HELICAL WINDINGS

U WIRE WINDING

WINDMILLING

U AUTOROTATION

WINDOWS

Passenger cabin windows on Convair liner type aircraft, describing construction, installation, strength, etc
17 p3061 A69-33667

WINDOWS [APERTURES]

NT WAVEGUIDE WINDOWS

Computer program for predicting temperature distribution and heat transfer through coated and uncoated window systems of aerospace vehicles
[AIAA PAPER 69-28] 06 p1038 A69-18178

Homogeneous fused silica and quartz reinforced resins as dielectric materials for reentry vehicle antenna windows
07 p1090 A69-18400

Halide salts, semiconductors and nonoxide glasses as materials for high power laser windows
07 p1144 A69-18401

Electromagnetic windows - Conference, University of Paris, September 1967
07 p1108 A69-19507

Thermal behavior of space vehicle window systems predicted by mathematical analysis and computer methods for heat transfer through glass
[AIAA PAPER 68-65] 13 p2378 A69-28215

Acoustoelastic interaction effects of sonic bangs on natural frequencies response of large windows backed by closed cavity
21 p3836 A69-38988

Thermal control coatings, windows and mirrors for 1973 Mars Viking Lander vehicles under simulated Martian surface conditions
[AIAA PAPER 69-1023] 22 p3923 A69-40393

Autotransformer with static tap changer to provide varying power levels for controlled gradual heating of aircraft window to avoid thermal shock
22 p3869 A69-40414

WINDOWS [INTERVALS]

U LAUNCH WINDOWS

WINDS ALOFT

NT GEOSTROPHIC WIND

NT JET STREAMS [METEOROLOGY]

Influence of winds aloft on fading rate of microwaves propagated beyond horizon
01 p0030 A69-10566

Curvilinear plasma motions in ionosphere same as cyclones and anticyclones in troposphere, solving ionospheric unstable wind as function of pressure gradients
06 p0919 A69-17722

WINDSCREENS

U WINDSHIELDS

WINDSHIELDS

Rain repellent system providing transparent film on aircraft windshield surface
06 p0877 A69-16954

Tempered glass plates strength nondestructive testing by scattered light photoelastic method, discussing application to aircraft windshield sandwich structures
[AIAA PAPER 68-323] 12 p2118 A69-26768

Instruction manual for maintenance personnel and pilots regarding clear vision and window integrity of Convair aircraft, discussing windshield installation and replacement
14 p2391 A69-28932

Electrical failures in aircraft due to static electrification of electrically heated windscreens, noting materials for reducing surface resistivity
19 p3256 A69-36769

WINDWARD

U WIND [METEOROLOGY]

WING CAMBER

Rotor aerodynamics research in terms of theoretical and experimental data comparison, rotor blade flow visualization and blade section camber
23 p4057 A69-41372

WING FLAPS

NT LEADING EDGE SLATS

NT TRAILING-EDGE FLAPS

Minimum drag wing flap profile design, discussing application for trailing edge flaps
08 p1251 A69-20441

Aerodynamic characteristics of propeller-wing-flap systems used on deflected slipstream STOL aircraft
09 p1431 A69-22278

Torsionally flexible blade controllable twist rotor with pitch horn and servoflap control, discussing optimum inputs, airloads and angles of attack contours
18 p3089 A69-35234

WING FLOW METHOD TESTS

Aerodynamic characteristics of propeller-wing-flap systems used on deflected slipstream STOL aircraft
09 p1431 A69-22278

Velocity potential function for flow over disk shaped wing near screen, noting aerodynamic lift and drag
13 p2199 A69-27524

WING-FUSELAGE STORES

Aircraft stability during sideslip, discussing influence of fuselage/wing interference
04 p0548 A69-14824

WING LOADING

Polygonal wing planform pressure distribution in incompressible flow calculated on basis of lifting surface theory
01 p0008 A69-11298

Spar attachments of aircraft wings analyzed with respect to weight and applied loads, determining optimum bolt diameter ratio to lug width
04 p0673 A69-14496

Design parameters optimization for V/STOL jet aircraft with lift engines mounted in wing pod, discussing wing loading and aspect ratio, power plant, etc
04 p0547 A69-14812

Prestressing of aircraft wing stringers in order to reduce weight, noting initial bending moment, initial axial stress and prestressing methods
05 p0832 A69-15690

Lift drag ratio for conical sector with V-shaped wing at zero incidence
06 p0858 A69-17340

Approximation formula for calculating descent speed and lift-drag ratio
10 p1633 A69-22873

Theoretical nonlinear method for calculating aerodynamic forces on low aspect ratio wings at high angles of attack and wide range of Mach numbers
21 p3644 A69-39084

Aeroelasticity of supersonic aircraft in flight, discussing buffeting, wing flutter and control surface flutter
22 p3862 A69-40003

WING OSCILLATIONS

Idealized delta wing free-free oscillations determination by deriving equations of motion for flexibility and rigidity and formulating boundary value problems
01 p0172 A69-11358

Velocity field excited by wing vibrations propagating over elastic surface at supersonic velocities, considering nonvertical motion and absence of external forces
02 p0188 A69-11976

Nonstationary wing motion in gas stream near solid surface, analyzing differential equation for acceleration potential

02 p0188 A69-12134

Velocity field generated by vibrations propagating at finite velocity over elastic wing surface

02 p0190 A69-12571

Thickness effects on flow past sweptback wings in supersonic flight noting influence of oscillatory motion [ASME PAPER 68-FE-31]

05 p0698 A69-16078

Buffeting tests of model wing in wind tunnel as function of angle of attack and Mach number

06 p0857 A69-17096

Lifting pressure distributions on oscillating surfaces in subsonic flows using doublet lattice method for various surface geometries [AIAA PAPER 68-73]

09 p1430 A69-21946

Mathematical model with straight wake airfoil to determine aerodynamic forces on oscillating rotor blades in hovering flight

11 p1821 A69-25514

Collection of papers on aerodynamic flutter covering airfoils, flow theory, aircraft structures, etc

13 p2358 A69-27234

Velocity field excited by wing vibrations propagating over elastic surface at supersonic velocities, considering nonvertical motion and absence of external forces

15 p2547 A69-30259

Laminar boundary layer on rotating blades and yawed infinite wings, solving partial differential equations numerically by implicit finite difference scheme on computer

16 p2732 A69-31885

Aerodynamic behavior of airfoil oscillating in reverse flow defined for various angles of attack and oscillatory amplitudes at low Mach numbers

18 p3087 A69-35219

Perturbation equations for oscillating wedges and caret wings with attached bow shock in hypersonic and supersonic flows

24 p4249 A69-43659

LF approximation in predicting unsteady aerodynamic forces affecting large aircraft stability, analyzing velocity potential of oscillating wings

24 p4250 A69-43729

WING PLANFORMS

NT DELTA WINGS

NT TRAPEZOIDAL WINGS

NT VARIABLE SWEEP WINGS

Polygonal wing planform pressure distribution in incompressible flow calculated on basis of lifting surface theory

01 p0008 A69-11298

Wing penetration into zone of sharply localized gust, deriving equations for forces and moments acting on wing

07 p1050 A69-18742

Book on wing theory in supersonic flow covering simple and cruciform wings, wings with vertical plane tail, etc

08 p1251 A69-20523

Three dimensional optimum hypersonic wings construction for wave drag minimization for given lift [AIAA PAPER 68-158]

09 p1430 A69-21944

Automated Structural Analysis Procedure employing Displacement Method of Matrix analysis applied to validation studies of various finite elements for wing structures

12 p2184 A69-26809

Nonuniform flowfield from supersonic penetration of plane shock by three dimensional pointed planar wing, using integral transform method to study field perturbation pressure

13 p2199 A69-27323

Steady rectilinear translational motion of circular disk-shaped slightly bent wings near solid wall in incompressible fluid medium in absence of vortices and external forces

15 p2547 A69-30583

Surface of minimum drag symmetrical trapezoidal wing in supersonic flow solved by variational method

15 p2548 A69-31022

Leading edge flap angle and planform effects on low speed vortex patterns of flat plate double delta wings, measuring aerodynamic forces

17 p2890 A69-33246

Lift coefficients of idealized tunnel type ram wing consisting of truncated semiconical shell computed by lifting surface theory

22 p3860 A69-40819

Rheoelectrical analog technique for low speed aerodynamic characteristics of finite wings in incompressible flow, using deep electrolytic tank for lifting surface calculations

23 p4061 A69-42351

Maximum admissible weight of structural elements required for conventional wing conversion into variable geometry wing without performance impairment

24 p4253 A69-43092

WING PROFILES

Wing-body combinations analysis and design at supersonic and subsonic speeds by aerodynamic influence coefficients method [AIAA PAPER 68-53]

01 p0006 A69-11016

Lifting wing profiles in uniform transonic compressible fluid flow calculated by analog method, noting hodograph method simplification

02 p0187 A69-11536

Wing upper surface velocity distributions having peak near leading edge, considering incompressible flow at zero angle of attack [ONERA-TP-632]

02 p0187 A69-11618

Subsonic lifting surface analysis accuracy tested by planar circular wing theory

04 p0543 A69-14818

Pressure distribution on star-shaped bodies in wind tunnel at Mach 4 and Reynolds number. 000006

07 p1050 A69-18703

Minimum drag wing flap profile design, discussing application for trailing edge flaps

08 p1251 A69-20441

Cross-spectral density of pressure induced on lifting surface by isotropic atmospheric turbulence, solving integral equation [ONERA-TP-681]

09 p1613 A69-21689

Shear field pattern theory modified to apply to determination of sweptback wings, calculating stress development

10 p1801 A69-23645

Minimum drag wing profile at zero angle of attack in supersonic flow, allowing for initial structural flaws and randomly varying parameters

11 p1818 A69-25328

Wing geometry and wing lower surface boundary layer effects on rolled-up tip vortices geometry and strength

11 p1819 A69-25372

Aerodynamic interactions between two wing configurations with same aspect ratio located in same plane, discussing testing principles and initial experimental results

17 p3061 A69-33595

Vortex wakes behind high lift wings, considering effects of height above ground and various tunnel heights and widths for STOL operations [AIAA PAPER 69-740]

18 p3083 A69-34405

Design and fabrication of plane and trapezoidal fiberglass wings with laminar plastic profiles for aerodynamic tests, including wing rigging and slotted wing

19 p3324 A69-35831

Stream surface characteristics as criteria for hypersonic lifting bodies shapes for optimal aerodynamic and fuel performance

19 p3248 A69-36399

Book on optimal aerodynamic shapes by means of variational method, covering conventional and triangular thick wing lift systems in supersonic flow

21 p3644 A69-39667

Warping of doubly supported submerged wings, calculating stress and strains due to bending and constrained torsion

23 p4225 A69-41423

Laminar boundary layer in steady compressible gas flow past plane wing profile, studying surface temperature and suction effects

23 p4058 A69-41709

Newton formula and Ritz method to determine wing shape with blunt leading edge, considering minimum drag achievement at hypersonic velocities

24 p4247 A69-43497

WING SLATS

U LEADING EDGE SLATS

WING SLOTS

Slot height, position and trailing edge geometry effects on elliptically shaped rotors selected for hover efficiency, size, transitional gust insensitivity and rigidity

18 p3058 A69-35231

WING SPAN

Lift augmentation by lateral blowing over lifting surface, discussing wind tunnel pressure tests on wings, flaps and stabilizers [AIAA PAPER 69-193]

07 p1051 A69-19554

WING STALL

U BOUNDARY-LAYER SEPARATION

WING TANKS

Deposit formation in empty wing tanks due to autoxidative degradation of hydrocarbon fuel, noting results of environment simulation tests [SAE PAPER 680733]

03 p0366 A69-13439

Skyvan 2 aircraft aerodynamic design, describing modifications to increase fuel capacity, directional stability and range capability

17 p2896 A69-34193

Redesigned A1 wing structure using B-epoxy composite applied to pressurized fuel carrying section, including material, fabrication and test data

24 p4323 A69-43418

WING TIPS

Wing geometry and wing lower surface boundary layer effects on rolled-up tip vortices geometry and strength

11 p1819 A69-25372

Wingtip mounted propellers effect on wing lift and induced drag, varying lift to drag ratio by changing inflight aspect ratio

24 p4250 A69-43713

WINGED ROCKET BOOSTERS

U LAUNCH VEHICLES

WINGED VEHICLES

Marchetti SV-20A and SV-20C twin turbine helicopters with two bladed rotors and fixed wings, discussing propeller on starboard engine rear of compound version

12 p2013 A69-26466

Variational problem involving winged flight vehicles ascending and descending flight optimal program determination, considering necessary extremal conditions

21 p3767 A69-39823

Artificial damping of longitudinal winged reentry vehicle motions in earth atmosphere, discussing vibration damper dynamic characteristics

21 p3829 A69-39828

WINGS

NT CAMBERED WINGS

NT CARET WINGS

NT CRUCIFORM WINGS

NT DELTA WINGS

NT FIXED WINGS

NT FLEXIBLE WINGS

NT LIFTING ROTORS

NT LOW ASPECT RATIO WINGS

NT PARAGLIDERS

NT PARAWINGS

NT RIGID ROTORS

NT RIGID WINGS

NT RING WINGS

NT ROTARY WINGS

NT SLENDER WINGS

NT SWEPT WINGS

NT THIN WINGS

NT TILTING ROTORS

NT TIP DRIVEN ROTORS

NT TRAPEZOIDAL WINGS

NT TWISTED WINGS

NT VARIABLE SWEEP WINGS

Air deflection and modulation /ADAM/ turbofan propulsive wing V/STOL design [AIAA PAPER 69-201]

07 p1056 A69-19573

Interference between bodies of revolution and wings in supersonic flow, using Volterra method for calculation

11 p1820 A69-25476

Wing section of high lift/drag test vehicle for 2500 F reentry, describing design, manufacture and testing

12 p2103 A69-26837

Weight estimation inaccuracies due to use of quickie equations, discussing error and extrapolation avoidance in wing weight study [SAWE PAPER 794]

18 p3222 A69-34904

Wing elastic strains effect on vertical velocity in downwash, noting wing tail combination

18 p3086 A69-34999

Aircraft wing aerodynamic forces and moments due to lifting engine air intake simulated by wind tunnel experiment

19 p3239 A69-36400

Multiple support wing deformations, obtaining bending equations solutions by matrix methods

21 p3835 A69-38872

Design of Concorde wing for Mach 2 cruising speed including fuselage/wing relations, wing planform and leading edge camber, etc [RAES PAPER 18]

22 p3859 A69-40497

WINTER

Midwinter warmings in upper stratosphere for differences between various stratospheric and mesospheric levels, noting need for additional upper air data

08 p1345 A69-20134

Light waves refractive index distribution from balloon sounding data found to decrease with height in winter regardless of time of day

09 p1536 A69-21917

WIRE

Seasonal variation in ionospheric radiation absorption related to time variation between sunrise and constant angle attainment of sun 14 p2437 A69-29072

Irregular data obtained by radiosondes in winter for charts of high isobaric levels, noting stratospheric temperature effects on radiosonde ascent height 14 p2473 A69-29731

Gyroplasma probe data from rocket observations, determining winter ionospheric electron density profiles, electron temperature and electrostatic cyclotron waves effect 15 p2606 A69-31446

Ionospheric winter anomaly duration in height range of mesopause region based on zenith angle dependence of absorption at LF 16 p2782 A69-32456

Relation between atmospheric processes in troposphere and upper stratosphere in cold half year 18 p3166 A69-34817

WIRE

NT ELECTRIC WIRE
NT EXPLODING WIRES

Torsional pendulum for stress and strain relaxation measurements of wire sample 01 p0079 A69-10221

Temperature dependence of internal friction in molybdenum wire in moderate and high temperatures 03 p0446 A69-13576

Twin differential calorimeter for measuring heat dissipation by wire specimen under fatigue tests, using semiconductor thermopiles 04 p0618 A69-15205

Flow stress of iron wire reinforced aluminum alloy composites [ASME PAPER 68-WA/MET-10] 05 p0780 A69-16150

Plane wave scattering by conducting wire impedance loaded at center, discussing loading effect on backscattering cross sections 06 p0888 A69-17512

Treatment and testing of thin platinum and gold alloy wires used in thermoelements for studying liquid fuel vaporization in combustion chambers 07 p1130 A69-18258

Holography for temperature distribution measurement around heated wire, using He-Ne laser 11 p1887 A69-25197

Reversion and drawing techniques for ultrahigh strength ductile maraging steel wire without excessive deformation 13 p2278 A69-27412

Wire-wrap solderless joints production technology in electronic equipment 16 p2763 A69-32579

Diffusion welding and soldering of metallic wire with graphite and graphitized viscose applied to chromel, copel, chromel-alumel, Mo, W and W-Re 21 p3728 A69-38617

Stress-strain curves of W wires and of aligned composites of same wires in Cu matrix 21 p3845 A69-39709

Monostatic radar cross sections/RCS/ for 5 and 11 wavelength straight wires obtained from induced current integral equation solutions 23 p4116 A69-41594

Extreme value statistics used to determine minimum acceptable tensile strength of wire command links in TOW antitank missiles 24 p4318 A69-42642

WIRE BRIDGE CIRCUITS

NT WHEATSTONE BRIDGES

Nondestructive testing of quality of electroexplosive devices based on determination of heat flow between bridge wire and surroundings 04 p0607 A69-14973

WIRE CLOTH

Filtration and flow characteristics of wire cloths used in hydraulic systems described by expressions from measured properties [ASME PAPER 68-WA/FE-39] 05 p0750 A69-16111

Wire screen deployable boom concept for avoiding thermal bending of slender tubes problem in application to gravity gradient stabilization and antennas of spacecraft 07 p1229 A69-18350

Initial equations for plane wave diffraction at grids of squared beams, calculating transmission and reflection coefficients by reflection method and computer 07 p1084 A69-19149

Plane electromagnetic wave diffraction at oblique screen of circular cross section conducting wires

solved, assuming smaller wire radius than grid spacing and wavelength 07 p1084 A69-19150

Hard-drawn steel wire wound pipes and tanks, properties and design calculation, discussing laminates and permissible stress 08 p1414 A69-20487

EMI-RFI knitted wire mesh gasket for corrosion prevention, noting use of moisture tight seal 09 p1523 A69-21895

Surface wave reflection from free ends of ideally conducting rods forming semiinfinite grid to study rod delay systems and wave-duct antennas 11 p1833 A69-24438

WIRE WINDING

Statistical processing of oscillograms of instantaneous values of wire tension during winding, determining stress characteristics 06 p0927 A69-17691

Pulse transformer design relationships and definitions, discussing core and winding structure choice 08 p1285 A69-20382

Wire wound glass fibers for rocket motors, discussing rupture strength 17 p3021 A69-33357

Stress analysis of hollow viscoelastic cylinder reinforced with elastic helically wound wires [ASME PAPER 69-APMW-23] 24 p4401 A69-43096

WIRELESS COMMUNICATIONS

Sweep frequency measuring setup for adjusting equalizers in carrier transmission systems 11 p1841 A69-25639

Wireless telemetry system design for physiological signals in human diagnosis, discouraging casual use of wireless transmission 19 p3261 A69-36269

Soviet book on modern systems of wireless telecommunication covering radio communication and tropospheric, ionospheric and satellite wireless systems 20 p3487 A69-37235

WIRING

Printed circuit board wiring technique for strain gage rosettes application in extensive airframe static tests 02 p0250 A69-12231

Supersonic airplane high temperature wire tests, detecting corona onset voltage /COV/ or voltage breakdown 05 p0731 A69-16245

Design and tests of cable assemblies for F-111 aircraft 05 p0731 A69-16246

Heat convection coefficient for wires enclosed in cylindrical tubes filled with water or ethanol, showing dependence on inclination angle 07 p1242 A69-18926

Automation of wiring diagrams and printed circuit conductor patterns by computerization 15 p2632 A69-31520

Automated design system producing wire format data for cabling avionics subsystems of light attack aircraft [AIAA PAPER 69-976] 22 p3912 A69-40356

WKB APPROXIMATION

U WENTZEL-KRAMER-BRILLOUIN METHOD

WOOD

Radiation processed wood-plastic materials produced by impregnating natural wood with liquid monomer followed by ionizing radiation induced polymerization 04 p0605 A69-14582

WOOD AIRCRAFT CONSTRUCTION

U AIRCRAFT STRUCTURES

U WOODEN STRUCTURES

WOODEN STRUCTURES

Adhesive joints design with uniform shear stress for prestressing wood beams 24 p4323 A69-43425

WORK

NT PHYSICAL WORK

Mechanical work recoverable from stored energy and heat absorbed by taking material through closed cycle in strain and entropy space 20 p3575 A69-37074

WORK CAPACITY

Work and rest scheduling effect on working capacity and physiological state of male subjects in sealed chamber 03 p0381 A69-14201

Work capacity and adaptation characteristics of humans confined in small chamber and experiencing effects of isolation and sensory deprivation 08 p1262 A69-19838

Acclimation to altitude hypoxia and duration of resistance to muscular effort in white Wistar rats on treadmill 09 p1445 A69-22725

Traditional flight crew organization relevance to current and developing flight systems, discussing inadequacies, anachronisms and safety threats 12 p2023 A69-26555

Heart rate and respiratory response correlations in men during surface and underwater work, showing reasonable approximations of workload in surface equivalent terms 14 p2406 A69-29293

Telemetry techniques, based on pulse rate measurements, permitting continuous examination of humans under natural working conditions 15 p2559 A69-31228

Healthy, physically untrained students compared with trained athletes for differences in working capacity concerning orthostatic tolerance and blood pressure responses 22 p3889 A69-39940

Oxygen uptake and circulatory response in human male subjects during maximal treadmill and bicycle exercise 22 p3874 A69-40226

Prolonged wakefulness effect on human work capacity in isolated chamber, determining physical, intellectual and sensory capacities 22 p3877 A69-40280

Healthy, physically untrained students compared with trained athletes for differences in working capacity concerning orthostatic tolerance and blood pressure responses 23 p4108 A69-41821

WORK FUNCTIONS

Beam-lead fabrication on dual Schottky barrier diodes for low noise integrated microwave mixers 02 p0222 A69-12474

Photoelectric effect of thin gold films on silver and quartz substrates, analyzing work function dependence on thickness of deposited metal 02 p0300 A69-12630

Photoelectric effect of thin gold film under electric field, noting work function dependence on film thickness exhibits extremum 02 p0300 A69-12631

Electron emission into vacuum from forward biased Schottky barrier consisting of cesiated thin layer of Pt on n-type ZnS 03 p0493 A69-14186

Electron phonon coupling in barriers of GaAs Schottky diodes, noting first and second derivatives of I-V characteristic in n-type GaAs-Pd Schottky diode 03 p0493 A69-14242

Schottky barrier mixer diodes and point contact diodes failure, discussing criterion for degradation of noise figure, 1/f noise and reverse breakdown voltage 04 p0574 A69-14352

Shot noise in Si Schottky barrier diodes for frequencies between 100 Hz and 50 kHz 05 p0734 A69-16564

Barium, oxygen and BaO adsorption influence on Mo and Ti thin films conductivity and work functions 06 p0978 A69-16900

Thermal metal-plasma thermodynamic equilibrium, using surface ionization of inner and outer potentials and work function, discussing ion and electron extraction 06 p0979 A69-17249

Surface parameters influence on energy transfer to arc jet anode, discussing work function, accommodation coefficient and diffuse reflection coefficient of electrons [AIAA PAPER 69-107] 06 p1039 A69-18185

Observation of photocurrents generated in Schottky barrier diodes on barium titanate, suggesting practical utility of photon-to-electron conversion efficiencies 07 p1104 A69-18905

Thermal faceting of tungsten single crystal surfaces in oxygen, using vibrating-capacitor work function probe with low energy electron diffraction 08 p1330 A69-20137

Interaction of nitrogen oxides and carbon dioxide on nickel crystal surface using low energy electron diffraction and mass spectrometer, discussing work function 08 p1268 A69-20138

Destructive breakdown in Shottky barrier diodes by evaporating contact metal through mask onto silicon, showing local heating by thin wax layer 08 p1286 A69-20860

Richardson constant for thermionic emission in Schottky barrier diodes, noting effect of surface shadows 08 p1286 A69-20865

Ag-GaAs Schottky barrier photodiodes, describing fabrication and use as UV radiation detectors
09 p1462 A69-21334

Work function change of tungsten single crystal /100/ surface measured as time function during surface molecular gas adsorption
09 p1521 A69-21338

Forward volt-ampere characteristics and differential resistance peak of Schottky barrier diode on doped Si
09 p1557 A69-21744

Trapping state effect on tunneling probability in Schottky barriers, discussing current-voltage characteristics
09 p1557 A69-21748

Effective work function of Re and Mo electrode samples determined from Schottky plots and emission measurements from grains
09 p1557 A69-21807

Work function and desorption energy measurements of alkali metals from metallic substrates with modulated molecular beam, noting surface contamination
09 p1558 A69-21808

Temperature effect on work function minimum of cesiated tungsten single and polycrystal surfaces, using vibrating capacitor technique
09 p1558 A69-21809

Comparative performance data of cylindrical diodes with various types of tungsten emitters, including emitter work function measuring device
09 p1439 A69-21821

Side wall currents in unignited hardware type thermionic energy converters, discussing work function and heat choke
09 p1439 A69-21822

Energy distribution in electron gun with single crystal spherical cathode, noting work function, space charge cloud and beam overlapping effects
09 p1464 A69-22396

Schottky barriers on n-type GaAs, measuring forward current characteristics for various electron concentrations and temperatures
10 p1745 A69-23358

Peaked electron emission from nickel surface with large work function under laser radiation, discussing emission pulses, electron currents and surface temperature time variations
10 p1703 A69-23572

Energy theorem for time dependent materials, deriving convexity conditions for minimum work and maximum complementary work functions
11 p1969 A69-24412

Sr and La ionization on crystal surfaces of W and polycrystalline W, discussing temperature effect on oxidation and work function
12 p2142 A69-26113

Avalanche Schottky barrier photodiodes fabricated by plating GaAs with thin Pt layer and forming proton radiation guard ring, discussing gain bandwidth and SNR
13 p2226 A69-27195

Free electron model for electron work functions and number density distributions and surface potentials in metals
14 p2504 A69-29009

CO adsorption on tungsten, determining work function changes and Fowler-Nordheim preexponentials on field emitter single crystal faces
14 p2409 A69-29093

Unignited mode converter and emitter work function patches, calculating electron-cesium momentum transfer cross sections from saturation current measurements
14 p2490 A69-29240

Thermionic converter current-voltage characteristics under various emitter temperatures and cesium vapor pressures, noting role of Schottky effect
14 p2402 A69-29241

Emission characteristics of thermionic converter electrodes surfaces with emphasis on work function
14 p2505 A69-29262

Electronegativity and work function relationship from thermodynamic and quantum mechanics standpoint, describing electrons structure by spin orbitals localized around lattice sites
14 p2505 A69-29263

Thermionic emission from bare and Cs-covered metal surfaces, calculating current and work function by employing localized electron orbital model
14 p2505 A69-29264

Thermoemission converters /TEC/ cathode materials, discussing determination of local work function by electron microscope and delay curves methods
14 p2505 A69-29265

Work function measurements of polycrystalline W, Re and Ni disks in high pressure cesium plasma for low probe temperature range
14 p2506 A69-29266

Tungsten surfaces with high work functions generated by electrochemical etching, discussing effects of heat treatment in vacuum
14 p2506 A69-29267

Tungsten emitting surfaces work functions, discussing dense crystalline planes electrolytic or pyrolytic deposit growth and surface chemical or electrolytic attack
14 p2506 A69-29268

Thermionic converters semiconducting collector surfaces, evaluating work functions of nickel-chromium steel and aluminum trioxide collectors
14 p2506 A69-29269

Sessile drops contact angles of alkali liquid metals on Re, W, Mo, Ta and Nb substrates related to substrate surface bare work function
14 p2506 A69-29270

Work function changes of tungsten single crystals as function of oxygen and CO gas pressure at high temperatures, using emission microscope
14 p2506 A69-29272

Tungsten work function increase by oxygen in diode thermionic emission, investigating crystals and vapor deposited layers
14 p2507 A69-29273

Plasma anode technique for work functions measurements of polycrystalline W and Re wires in cesium vapor with cesium oxide additive
14 p2507 A69-29274

Alkaline metal adsorption on high work function metals with charge transfer, measuring polycrystalline Mo photoelectric emission as function of Cs coverage
14 p2507 A69-29275

Electron work function profile determined for polycrystalline Mo and W single crystals with and without Cs vapors by emission microscope and photomultiplier
14 p2507 A69-29276

Gallium phosphide Schottky barrier diodes, discussing construction and metals used, barrier height relationships to impurity concentration and temperature, rectifying characteristics and internal quantum efficiency
16 p2757 A69-31613

Uniaxial stress effect in Schottky barrier diodes measured by beam balance noting higher sensitivity
16 p2758 A69-31619

Axial gas turbine efficiency and work functions, discussing turbine using isothermal high velocity combustor
16 p2837 A69-32064

Yttrium desorption from W wire by strong electric field, noting electron work function or temperature increase effects on desorption field
17 p3015 A69-33631

Low energy electron diffraction oxygen adsorption kinetics on planes of tungsten at coverages below monolayer and work function measurements
18 p3183 A69-35106

Schottky barrier diodes for high temperature operation prepared on n-type GaP single crystals, studying I-V and C-V characteristics
19 p3381 A69-35681

Electric fields and electron work functions, surface potentials and number density distributions in selected metals surfaces determined using free electron model
19 p3382 A69-36045

Surface structures, work function changes, Auger electron and surface plasma losses for Cs on clean W surface
19 p3392 A69-36733

MOS threshold voltages calculations, considering fixed bulk and oxide charges and difference in work function between metal and semiconductor, considering MOS-FET devices
20 p3506 A69-37779

WORK HARDENING NT STRAIN HARDENING

Temperature evolution velocity parameter effect on behavior of elastoviscoplastic solids, noting demonstration by work hardening tests at variable temperatures [ONERA-TP-644]
01 p0164 A69-10036

Aging and cold work hardening effect on deformability of aluminum-magnesium-silicon-copper alloy
02 p0254 A69-12677

Tangential and normal stress distribution in deformed metals, discussing work hardening of metals and cold working without softening effect
03 p0435 A69-14118

Work hardening - Conference, Chicago, November 1966

05 p0777 A69-15752

Work hardening of fcc single crystals, emphasizing transmission electron microscopy of thin foils, X ray topography and etch pitting techniques
05 p0778 A69-15753

Dislocation distributions in cold worked fcc, bcc and hcp metals, discussing dislocation structures in deformed single crystals and work hardening theories
05 p0778 A69-15754

Unified theory of stress-strain curve of fcc metal crystals in Stages II and III of work hardening
05 p0778 A69-15755

Work hardening in quenched fully hardened and overaged Mg-Mn alloy single crystals as function of temperature and strain rate
05 p0778 A69-15757

Work hardening characteristics of Ta and Ta-base alloy single crystals as function of temperature and interstitial concentration
05 p0778 A69-15758

Microplastic properties of arc-cast and Ti-Zr-Mo molybdenum sheet in tension at room temperature, measuring plastic strains with resistance strain gages
05 p0778 A69-15759

Cross slip model for work hardening of nickel aluminate crystals, discussing temperature dependence
05 p0779 A69-15760

Plastic deformation in hypoeutectoid and hypereutectoid Ni-Ti alloys studied by compressive stress-strain analysis and transmission electron microscopy
06 p0941 A69-17222

Edge dislocations effect in perpendicular slip planes on work hardening and strain aging, calculating dilatation centers absorbed
07 p1238 A69-19695

Plane strain and stress compared for elastoplastic cracked plate in work hardening tension
15 p2710 A69-30811

Displacement bounding principle for work hardening plasticity theory based on Drucker inequality and stress space path existence [ASME PAPER 69-APM-7]
18 p3213 A69-34385

Martensite transformation, C content and work hardening relations in stainless steels studied for magnetic detection of embrittlement during deformation
18 p3138 A69-35117

Cylindrical steel specimens high strain rate tensile tests, using Malvern theory for ideal elastoplastic and work hardened materials
23 p4236 A69-42529

WORK-REST CYCLE

Work and rest scheduling effect on working capacity and physiological state of male subjects in sealed chamber
03 p0381 A69-14201

Human endurance during isolation in closed space with prescribed voelergometric exercises, noting impairment of functional capacity
08 p1263 A69-19933

Transient ventilatory response to breaths of nitrogen at rest and during exercise in high altitude and sea level natives
12 p2019 A69-26131

Cardiovascular system, neuromuscular activity and mental fitness of subjects performing physical and mental assignments with prescribed work-rest schedule during confinement
17 p2906 A69-32936

Space crew performance subsequent to sudden sleep arousal, noting selection between simultaneous and staggered sleep schedules
19 p3263 A69-36453

Time required for acclimatization to work in high temperatures, noting rectal temperature and heart rate changes
21 p3654 A69-38905

Constant illumination intensity effects fixed ratio lever pressing behavior for appetitive reinforcement with chimpanzee in temperature and humidity controlled environment
24 p4260 A69-42702

WORKING FLUIDS

Dissociating gas as working fluid for space plant, noting role in radiator area reduction
04 p0551 A69-15313

Thermodynamic and aerodynamic characteristics of organic Rankine cycle working fluids for ideal applicability to manufacturing [SAE PAPER 690063]
07 p1057 A69-18308

Bearing lubrication at low temperature, examining safety limits, working fluid in liquid or gaseous state [IME PAPER 9]
07 p1138 A69-18565

Linear induction MHD generator using Rankine cycle with K-Na working fluid noting longitudinal edge effect compensation
07 p1058 A69-19026

Montardi circuit with sectioned electrodes to simulate isotropically conducting still liquid for application in MHD pump, discussing potentials distribution
07 p1059 A69-19031

MHD electrical power generation - Conference, Warsaw, July 1968, Volume 1, Closed cycle MHD with gaseous working fluids
10 p1729 A69-23433

Ar-K plasma studied as possible MHD generator working fluid by investigating influence of emission and external magnetic field on nonequilibrium electrical conductivity
10 p1732 A69-23441

Momentum transfer cross sections, recombination coefficients and ionization coefficients of working gases for MHD energy converter
10 p1733 A69-23446

Argon discharges in metal capillary cathodes noting effects of electron density, flow velocity, electrode phenomena and gas temperature
10 p1733 A69-23450

Mercury cesium plasma in crossed electric and magnetic fields as working fluid of MHD generators based on Rankine cycle
10 p1636 A69-23458

MHD electrical power generation - Conference, Warsaw, July 1968, Volume 2, Closed cycle MHD with gaseous working fluid
10 p1735 A69-23464

Large disk MHD generator operating at high Hall coefficient and driven by cesium seeded argon or molecular gases
10 p1637 A69-23473

MHD conversion experiments using rare gas, considering Typhoe loop, electron heating and correction effects
10 p1738 A69-23475

Engineering and reactor parameters associated with ionization of gas passing through nuclear reactor used as closed cycle MHD system working fluid
10 p1723 A69-23485

Power generating equipment operating with high temperature plasma as working medium requiring reactors with plasmaed nuclear fuel coupled to MPD generators
10 p1738 A69-23489

Gaseous suspensions of thermionic emitting particles assessed as MHD working fluids in large scale MHD electric power generators
10 p1738 A69-23491

Properties of superdense NaCl plasmas as model working substance for MHD generator, discussing ion concentration and collisions, charge reversal and conductivities
10 p1739 A69-23493

Throttling effect on thermodynamic efficiency of MHD generator Rankine cycle with various working fluids
11 p1824 A69-24222

Closed loop cycle converter, composed of MHD generator and compressor consuming thermal energy, exhibiting moderate cycle efficiency decreases
11 p1824 A69-24223

Thermal efficiencies of liquid-metal MHD generator cycles, analyzing optimum parameters, working fluid and partial irreversibilities
13 p2205 A69-27484

Laminar to turbulence transition in submerged and bounded jets, using schlieren visualization for compressible flow and birefringent visualization for incompressible flow
14 p2428 A69-28876

Working fluids elastic characteristics variability effect on hydraulic actuator dynamics, studying adiabatic and isothermal conditions
14 p2405 A69-29423

Working fluid flow parameters compensation by expelled cooling air in air-gas flow area of turbine stage
18 p3184 A69-34985

DC MHD generator using gas plasma as working fluid, discussing fundamental principle, components interactions and energy conversion
21 p3777 A69-39165

Closed cycle MHD with gaseous working fluids and steady state nonequilibrium ionization
21 p3777 A69-39479

Plasma instabilities in closed cycle MHD generator with gaseous working fluids, discussing effective Hall parameters
21 p3777 A69-39481

Sonic vapor flow heat transfer limitations in heat pipes for Na, K and Cs, showing strong influence of temperature and working fluid
23 p4239 A69-41719

Rankine cycle power systems with reciprocating engines using organic working fluids, discussing engine development, system characteristics, etc
23 p4067 A69-42237

Rankine power cycle for fluid evaluation, discussing radiating area, thermodynamics, etc
23 p4239 A69-42276

Two fluid heat pipe performance, measuring temperatures and condenser end vapor pressures for two thermal power input conditions
23 p4240 A69-42306

Undissolved air effects on working fluids elastodynamics in aircraft hydraulic actuators
24 p4255 A69-43076

Heat pipe wick materials liquid transport properties analysis, using water and Freon 113 as working fluids [ASME PAPER 69-HT-17]
24 p4413 A69-43551

Performance curves of cylindrical water heat pipe for performance map, observing free hydrogen accumulation [ASME PAPER 69-HT-15]
24 p4413 A69-43554

WORLD

U EARTH [PLANET]

WORLD DATA CENTERS

World Weather Watch /WWW/ system and meteorological satellites, discussing observational networks, data centers, telecommunication facilities, research, education and training program [UN PAPER 68-95209]
01 p0178 A69-10478

Meteorological rocket soundings and global synoptic observations, noting influence of atmospheric middle region [UN PAPER 68-95405]
01 p0109 A69-10484

Statistical characteristics of ozone measurements with Dobson spectrophotometers and filter ozonometers, determining requirements for maximum effectiveness of ozone network
16 p2787 A69-32639

WORMS

NT FLATWORMS

Automatic bioprobe life support system for long duration interplanetary space flight, discussing blood leech as suitable research animal
02 p0199 A69-11828

WRINKLING

Post-wrinkling nonlinear behavior of conical shell of revolution subjected to bending loads [AIAA PAPER 69-90]
06 p1027 A69-18074

Wrinkling of pressurized cylindrical and conical fixed free membrane column under lateral load, considering membrane sheets elastic properties
22 p4045 A69-40814

WROUGHT ALLOYS

Microstructure relationship to tensile strength and creep resistance in Zn-Ni-Ti alloy extrusions, discussing role of finely dispersed intermetallic particles
08 p1329 A69-20002

Wrought superalloys fusion welding behavior, discussing hot cracking, hot microfissuring and strain age cracking [SAE PAPER 690102]
09 p1503 A69-21558

Processing characteristics of wrought Co base alloys, discussing thermomechanical treatment effects, yield strength, ductility, etc
14 p2456 A69-29892

Ingot dendrite arm spacing and thermomechanical treatment effects on fracture behavior and mechanical properties of Al alloy, finding ultimate and yield strengths
23 p4176 A69-41506

Single run reheated weld wrought steel H cracking tested by constant load rupture /static fatigue/ technique
24 p4320 A69-42943

WURTZITE

Direct amplification of ultra and hypersonic surface waves in semiconducting crystals of wurtzite group, taking into account drift effects and boundary conditions
03 p0490 A69-13925

Perfect piezosemiconductor resonator /phaser/ with CdSe/CdS/ crystal, discussing vibration excitation in wurtzite type crystal in electric field of electron drift
03 p0431 A69-13930

W2F AIRCRAFT

U E-2 AIRCRAFT

X

X BAND

U SUPERHIGH FREQUENCIES

X RAY ABSORPTION

Dislocation effects on intensity jumps near K edge of absorption, using interferential transmission of X rays in Ge
03 p0490 A69-13944

Spectral distribution of X ray atmospheric absorption used to determine high energy photoelectrons spectrum
09 p1577 A69-21774

Metagalactic electrons and relic radiation interaction calculations allowing for universe expansion, space curvature and X ray absorption
15 p2687 A69-30541

X ray absorption in surrounding gas sphere as function of continuous absorption, electron scattering and diffuse ionizing radiation, using radiative transfer theory
18 p3186 A69-34296

Soft x ray extragalactic background flux measurements, considering correction for absorption by interstellar medium
21 p3788 A69-38541

Interstellar absorption of 10 A X rays from sources in Scorpio-Sagittarius region, noting gas density between earth and Crab Nebula
21 p3788 A69-38648

X RAY ANALYSIS

Solar X ray flares measurement by rocket and satellite, discussing X ray spectrum hardening, hard flares and SID
03 p0500 A69-13225

Nepheline occurrence in unequilibrated chondrites, discussing crystallographic evidence from X ray powder patterns
04 p0659 A69-15010

X ray emission from powdered graphite, diamond and titanium carbides
06 p0946 A69-17545

Nimonic alloys recovery analyzed by X rays and electrolytic phase separation, showing precipitated gamma phase effect
07 p1159 A69-18533

Avalanche detector radioisotope X ray fluorescence analyzer development for XRF analysis of potassium and calcium, noting precision [IEEE PAPER 3B-9]
07 p1135 A69-19201

Polymorphic characteristics of titanium pentoxide prepared by reducing titania, examining oxidation products with X ray diffraction
07 p1168 A69-19601

Phase equilibria in V-Cr-C, Nb-Cr-C and Ta-Cr-C systems determined by microscope and X ray analyses
09 p1523 A69-21872

Impurity heterogeneities in unoxidized and oxidized silicon slices from electron probe X ray microanalyzer, discussing thermal oxidation effects
10 p1743 A69-23171

Thin film thickness and composition determination through scattered electron and characteristic X ray radiation recording
10 p1747 A69-23847

X ray microanalyzer maximum sensitivity obtained using flow type proportional and scintillation counters with proper tuning and eliminating scattered electrons
12 p2093 A69-26596

Dislocations observations in fracture study of crystals, considering etching, decoration technique, X ray topography and diffraction electron microscopy
13 p2316 A69-27223

X ray investigation of niobium, aluminum and niobium-aluminum systems to obtain K-spectra and L-spectra
14 p2508 A69-29664

X ray detectable preferred disorder in solids by shock loading studied in Ainsworth meteorite and in hexagonal alpha silicon dioxide
15 p2671 A69-31538

Flux grown magnetic garnet crystal internal defects analyzed by etching and Lang X ray transmission topography, revealing tubular structural deviations
16 p2825 A69-31692

X ray diffractometer stress analysis of WC-Co cermets, discussing surface preparation and heat treatment
16 p2802 A69-32339

Alpha alumina whiskers grown by vapor reaction examined by X ray microtopography and etching
16 p2802 A69-32341

- Microstructure and X ray structure compared for two and three component chromide, titanide and silicide diffusion layers on Nb, discussing phase composition 20 p3563 A69-37820
- X ray analysis of rolled and compressed Ti powder produced by calcium hydride reduction, noting coexistence of screw dislocations 21 p3745 A69-38952
- ### X RAY APPARATUS
- X ray spectrographic camera for nondestructive spectrum analysis of small samples 03 p0427 A69-13101
- Solar corona X ray emission during flares and under quiet sun conditions investigated by satellite with X ray heliograph 07 p1210 A69-19614
- Silicon diode array camera tube modified to permit X ray images to be displayed on TV monitor 09 p1463 A69-21845
- Solar corona observed by X ray instrumentation of SOLRAD 8 satellite crossing moon penumbra during solar eclipse of 20 May 1966 15 p2698 A69-31363
- ### X RAY ASTRONOMY
- Energetic X ray intensities from large and small Magellanic clouds investigated by balloon flight sky survey, noting energy flux upper limits 01 p0150 A69-10370
- Optical identification of X ray source Cen XR-2 as variable star WX Cen, discussing colors and similarity to Sco X-1 01 p0145 A69-10857
- Reflecting telescope objective for far UV and X ray regions, discussing microfinishing and optical and mechanical tolerances 01 p0121 A69-10896
- UV and X ray radiations of stars and interstellar gas of Milky Way and remote galaxies 02 p0316 A69-11906
- X ray source in constellation Vela lying close to galactic plane observed by attitude controlled Aerobee 150 rocket 02 p0308 A69-12594
- Radio source near UV object identified with X ray source GX3 plus 1 02 p0308 A69-12595
- Narrow band and UV photometry of GX3 plus 1 and Wolf-Rayet stars /HD 50896 and HD 45166/ 02 p0325 A69-12596
- Soft X ray spectrum of Sco XR-1, noting intensity change from previous measurement 02 p0309 A69-12711
- Energy sources and properties of quasars and radio galaxies by X ray astronomy 02 p0310 A69-12793
- Gamma ray astronomy, noting fluxes above 100 Mev from strong radio sources and intensities of Crab Nebula 03 p0497 A69-12931
- Optical imaging systems achieving aperture synthesis by lensless Fourier transform holography, noting X ray astronomy, ultrasonic and space applications 03 p0430 A69-13324
- Cosmic X ray sources resolved against diffuse background radiation lying close to galactic plane 03 p0501 A69-13767
- Planetary nebulae as possible low energy galactic X ray source 04 p0661 A69-15144
- X ray astronomy, discussing sources associated with bremsstrahlung or synchrotron radiation, astrophysical models, black body radiation, relativistic electrons, etc 04 p0662 A69-15326
- X ray emission from Seyfert galaxy nuclei, noting model with bremsstrahlung from hot source 04 p0649 A69-15387
- Earth X ray flux due to solar X rays reflected in atmosphere observed by Skylark rockets, noting observations of Sco XR-1 and Cen XR-2 04 p0649 A69-15440
- X ray astronomy techniques, discussing X ray spectrographs, heliographs and nonsolar celestial X ray sources 05 p0762 A69-15840
- Galactic X ray sources noncoincident with conspicuous visible or radio objects, identifying visible and radio counterparts by determination of accurate celestial coordinates 05 p0813 A69-15845
- Gas accretion on neutron star surface as energy source for X ray radiation 05 p0814 A69-15847
- Space observation of flare sprays and solar limb surges, stressing X ray research 05 p0814 A69-15860
- Large area X ray collector, matrix detector for ionizing radiation and inflatable gas counter, considering application to X ray optics and astronomy 05 p0794 A69-16587
- Celestial X ray sources astronomy, discussing emission mechanism in 2 to 100 kev range and balloon observations in Cygnus and Taurus constellations 05 p0817 A69-16715
- UK space research in 1970s emphasizing solar observations in UN, cosmic X ray astronomy, solar space astronomy and ionospheric investigation 06 p0997 A69-16853
- X ray and gamma astronomy, discussing galactic gamma radiation source and diffuse X ray background radiation 06 p0998 A69-16969
- X ray astronomy use for probing hot regions of outer space and high energy electrons 06 p0991 A69-17307
- X ray sources intensity and spectrum variation with time, describing proposed balloon experiments with equatorial launching for performing measurements 06 p0992 A69-17312
- Pulsar characteristics absence in X ray sources, noting data for Scorpius XR-1 07 p1218 A69-19254
- Discrete extragalactic X ray sources model for explanation of diffuse X ray background, noting evolutionary aspects 07 p1206 A69-19255
- Sco XR 1 optical and X ray spectra simultaneous observations during rocket flights 07 p1220 A69-19391
- Balloon observations of cosmic X ray sources in Cygnus and Crab Nebula, discussing data application to energy spectra analysis 07 p1210 A69-19716
- Acoustic energy generation for helium rich stars, discussing X ray radiation from helium star corona 08 p1380 A69-20645
- Discrete source hypothesis for interpreting high energy cosmic gamma ray measurements obtained by OSO-3 spacecraft 08 p1380 A69-20699
- Narrow band photometry of variable stars and X ray source Cyg X-2, considering continuum variations with time 09 p1591 A69-21451
- Low energy X ray spectra of Sco X-1 and Sagittarius sources measured by Be and Al window proportional counters during rocket flight 09 p1574 A69-21460
- Solar and cosmic X rays observed by OSO-C, stressing galaxy M 87 upper limits and Lupus XR-1 power law spectral form 09 p1578 A69-22171
- Iron line absence in emission spectrum of thermal X ray sources, constraining proposed thermal models 09 p1580 A69-22231
- Grazing incidence telescopes for X ray astronomy, describing mirrors, detection systems and dispersion techniques 09 p1501 A69-22688
- Solar system plasmas and X ray astronomy - Conference, Adelaide, Australia, August 1968 09 p1581 A69-22742
- X ray astronomy, tabulating properties of 22 discrete sources and discussing spectra, radio emission, optical identification, X ray production, etc 09 p1583 A69-22762
- Weak X ray sources at 20-100 Kev photon energies observed during balloon flight, finding hard rays from Ara XR-1 and Nor XR-1 09 p1583 A69-22763
- High energy X ray observational data for Sagittarius sources scanned by active telescope during February 1968 balloon flight 09 p1583 A69-22764
- X rays from galactic center and Centaurus regions, discussing Cen X-2 flux 09 p1583 A69-22765
- Spectrum of high energy X ray flux from Sco XR-1 during balloon flight using active collimator detector and graded shield detector 09 p1584 A69-22766
- Multiple pinhole camera for X ray astronomy, suggesting cross correlation image recovery technique based on Fourier convolution theorem 09 p1502 A69-22768
- X ray universe, considering contribution of X ray astronomy to phenomena of big bang, supernovae, neutron stars, exploding galaxies, etc 10 p1760 A69-22869
- Modulation collimators determining angular sizes and celestial positions of X ray sources Sco X-1 and Taurus XR-1 10 p1678 A69-23326
- Optical features of Sco-X-1, Tau-X-1 and Cyg-X-2 X ray sources, discussing optically thin hot plasma model for X ray emitter 10 p1682 A69-23327
- Celestial X ray source positions from rotating modulation collimator, predicting performance of collimator 10 p1722 A69-23328
- X ray emission from radio galaxies as possible bremsstrahlung radiation of hot gas, noting Crab Nebula 12 p2166 A69-27037
- Scorpius XR-1 X ray emission spectra, discussing Fe emission line near 7 kev plasma models, supernova mass and cosmic abundance 13 p2325 A69-27313
- X ray pulsations in Crab Nebula at frequency closely matching radio and optical pulsations, noting energy distribution 13 p2354 A69-28465
- Rocket-borne scintillation spectrometer for cosmic photon radiation 14 p2449 A69-29566
- X ray energy spectrum from Crab Nebula and diffuse background on celestial sphere near galactic anticenter, noting spectral index 15 p2675 A69-30759
- Sco X-1 fluctuating optical and X ray emission observed simultaneously, determining total energy flux and plasma radius and density 15 p2676 A69-30885
- Extraterrestrial X ray galactic and extragalactic sources research fields, emphasizing identification with optical objects 15 p2696 A69-31213
- Five color photometry of X ray source SCO X-1 in 1966-1968, discussing luminosity pulsations and flare activity 16 p2847 A69-31648
- X ray source Cyg XR-1 angular diameter upper limit determined from balloon experiment data obtained with collimated X ray telescopes 17 p3026 A69-32860
- Cosmic X rays diffuse component possible origin, discussing galactic gamma ray flux and disagreement with measured isotropy 18 p3185 A69-34275
- Pulsed hard X radiation from NP 0532, discussing slow down rate and luminous intensity 18 p3186 A69-34316
- Extrasolar X rays and sources from studying distribution, luminosity, diameters and variability of rays 18 p3193 A69-34364
- X ray sources model, describing possible ring of matter around white dwarf near end of active evolution 18 p3188 A69-35204
- Solar far UV images systematic photometry for thin solar models in terms of quiet sun intensity 20 p3603 A69-37546
- Pulsed X ray emission associated with pulsar NP 0532 in Crab Nebula measured by six element detector on Aerobee 150 rocket 20 p3590 A69-37574
- Balloon-borne proportional counters to measure X rays intensity and spectral distribution from Taurus X-1 and Cygnus X-1 20 p3593 A69-38153
- Scorpius X-1 X ray star model based on relativistic electron distribution due to magnetic field fluctuations, considering role of Alfvén waves 20 p3593 A69-38154
- X ray sources and diffuse background radiation observed in gamma and X ray spectral regions, considering electromagnetic waves attenuation by interstellar matter 21 p3789 A69-38817
- X rays and gamma rays extragalactic components, calculating background component intensity for given model of universe 21 p3789 A69-38818
- Solar X rays observations, describing instrumentation, radiation characteristics, association with flares, spectrum analysis, etc 21 p3791 A69-39506
- Coronae around helium stars and X ray sources, calculating acoustic energy generation rates in convection

X RAY DENSITY MEASUREMENT

zones

Anomalous X ray signals from Explorer 30 satellite showing saturation in ionization chamber possibly due to enhanced solar and atmospheric X rays
21 p3813 A69-39522

Extended source Fourier transform holography for single image synthesis of multiple identical images produced by multiple pinhole camera in X ray astronomy
22 p3943 A69-40019

Low energy X ray flux existence in Cen X-2 observed by rocket flight
22 p4007 A69-40773

Sco X-1 X-ray source energy spectrum and time variation from rocket flights in India
22 p4030 A69-40774

X ray spectra of four high energy sources near galactic center
23 p4206 A69-42114

Galactic X ray sources observed in EM spectrum high energy region, discussing hot plasma cloud thermal radiation and electrons synchrotron radiation as emission sources
23 p4206 A69-42318

Observational cosmology developments with radio and X ray astronomy emphasizing existence, origin, effects and anisotropy of excess microwave background
23 p4219 A69-42327

Polarimeter using 45 degree Bragg angle reflection applied to rocket payload design for determining polarization of celestial sources X rays
23 p4207 A69-42382

Continuous electron acceleration in astrophysics, discussing Crab Nebula X ray flux and galactic and extragalactic radio source power law spectra
24 p4355 A69-42696

Isotropic cosmic X rays measured by balloon-borne scintillation telescope, discussing agreement with electron energy spectral distribution
24 p4368 A69-43185

Soft cosmic X ray background flux from rocket observations on 21 September 1968 from White Sands, discussing flux origins
24 p4368 A69-43220

Rotating neutron stars, pulsars and cosmic X ray sources, accounting for large and small diameter sources by rotating neutron star losing mass in magnetic field
24 p4369 A69-43222

X RAY DENSITY MEASUREMENT

Simultaneous VLF hiss, auroral light and X rays observed during Norwegian balloon study
02 p0309 A69-12744

Oxygen surface densities measured by method based on characteristic X ray production by 100 kev protons
04 p0631 A69-14446

Auroral zone X ray measurements obtained by simultaneous balloon flights over Northern Scandinavia
05 p0813 A69-15822

Balloon-borne instrumentation X ray measurements, discussing detector electronics, telemetry, pressure transducer, power supply, environmental tests, energy limit and calibration
05 p0762 A69-15824

Nonthermal intergalactic bremsstrahlung model as isotropic X ray background due to subcosmic electron interactions with thermal ionized gas in expanding universe
11 p1947 A69-24595

Galactic X ray sources density nearly proportional to interstellar gas density squared, discussing X ray intensities estimation, galactic age, etc
17 p3030 A69-33069

M-87 X ray luminosity from balloon-borne detectors, considering background counting rate relation to azimuth
20 p3588 A69-37488

Soft x ray extragalactic background flux measurements, considering correction for absorption by interstellar medium
21 p3788 A69-38541

Low energy X ray flux existence in Cen X-2 observed by rocket flight
22 p4007 A69-40773

Balloon-borne instrument for auroral X ray measurements at Antarctic station, discussing design requirements, circuit characteristics and improvement recommendations
23 p4166 A69-42011

Galactic X ray flux from H I region low energy cosmic ray nuclei, studying electron capture effects on

line intensities

Solar X ray flux measurements from OGO 4, comparing peak fluxes before, during and after flares with IQSY data
24 p4367 A69-43048

X RAY DIFFRACTION

Synthetic solid lubricants impurity detection by X ray diffraction and oxidation thermogravimetry
01 p0102 A69-10909

X ray diffraction used to measure alpha-SiC whiskers orientation in polymeric matrices
01 p0102 A69-11262

Stacking faults in Ge epitaxial layers revealed by etching reagents and X ray diffraction with photographic recording
02 p0297 A69-11880

Crystal structure of boron filaments vapor deposited on tungsten wire substrate, using X ray diffraction and transmission-electron microscopy
02 p0268 A69-12405

Magnetite content of type I carbonaceous meteorite from quantitative X ray diffractometry of Orgueil meteorite
02 p0328 A69-12729

Superconductivity of electron beam evaporated tungsten films by X ray and electron diffraction techniques, discussing temperature dependence of energy gap
04 p0640 A69-14447

X ray diffraction studies of deformation effects on bcc niobium alloys in terms of particle size, strain, faulting probability and dislocation density
04 p0618 A69-15202

Lattice strains in matrix phase of aluminum-boron and copper-tungsten composites measured by X ray diffraction
06 p0939 A69-16944

Stainless steel sensitization analyzed using Mossbauer spectroscopy and X ray diffraction, noting ferromagnetic phase
06 p0944 A69-17852

Optical Fourier transform applied to structural analysis of catalase crystalline media by gas laser
06 p0928 A69-17890

Wear-resistant hard thin layers deposited on various base material surfaces analyzed by electron microprobe
13 p2282 A69-28164

Growth kinetics, lattice constant changes and hardness during aging of nimonic alloy from X ray diffraction diagrams
14 p2463 A69-29310

Crystal structures of intermediate phases in La-Co and Nd-Co systems by powder X ray diffraction technique
15 p2667 A69-30087

Co content influence on temperature stress in WC-Co cermets using one exposure and two exposure X ray diffraction
16 p2802 A69-32340

Integrated reflection coefficient with unpolarized incident X radiation for mosaic and perfect LiF crystals, presenting coefficient as function of wavelength
20 p3582 A69-37137

Co 2 chloride aqueous and alcoholic solutions by X ray diffraction to find potential ligands relative coordinating abilities
20 p3484 A69-37496

Phase analysis of systems Mn-S, Mn-Se and MnS-MnSe by X ray diffraction techniques, revealing homogeneity ranges
20 p3485 A69-38286

La-Rh system study by powder X ray diffraction, metallographic and differential thermal analysis, constructing equilibrium diagram and determining crystal structure data
21 p3744 A69-38739

X ray diffraction as nondestructive technique for measuring residual surface stress
21 p3845 A69-39476

Stacking fault formation probability in Ti and Zr by X ray diffraction techniques, using Fourier analysis and half-width measurements
21 p3749 A69-39600

X RAY FLUORESCENCE

X Ray fluorescence of rock samples as applied to geological problems, noting standard deviations for element distribution
01 p0082 A69-10890

X ray airglow in daytime sky, suggesting origin in atmospheric N and O K alpha lines due to fluorescent excitation by solar X rays
02 p0307 A69-12022

Avalanche detector radioisotope X ray fluorescence analyzer development for XRF analysis of potassium and calcium, noting precision
07 p1135 A69-19201

X ray fluorescence and electron microprobe for determining thin film thickness
07 p1113 A69-19582

Chemical composition of stony meteorites by analytical methods, discussing sample preparation and X ray fluorescence
11 p1953 A69-24358

Oxygen K-shell X ray production cross section and stopping power of aluminum oxide thin films for 20-100 kev protons
14 p2489 A69-29994

Chondritic Cr and Mn content studied by X ray fluorescence, noting positive correlation in H and L groups and negative correlation in carbonaceous chondrites
15 p2681 A69-30416

X RAY INSPECTION

X ray and ultrasonic methods for surface residual stresses induced in machined or ground specimen
15 p2631 A69-31511

X ray TV system with electronic-optical converter and X ray vidicon for industrial defectoscopy
18 p3138 A69-35113

Three dimensional X ray pictures of flaws shape and location in various materials
20 p3551 A69-38311

Structural changes during annealing of W and Mo single crystals deformed by rolling, using X ray diffraction topography methods with two crystal spectrometer
21 p3742 A69-38583

X RAY IRRADIATION

Prophylactic and therapeutic vitamin and organic compounds complexes in radiation damage reduction and death prevention for dogs exposed to X rays
02 p0197 A69-11493

Procedure and apparatus for integral microwave and X ray and spectral measurements of quasi-steady plasma radiation
03 p0473 A69-12897

Accelerated helium and carbon ions effects on mutation-induction and nuclear inactivation in *Neurospora crassa* compared with X rays, discussing relative biological effectiveness/RBE/
03 p0373 A69-13490

Mammalian cell survival, chromosome abnormalities and recovery from heavy ion and X ray irradiation
03 p0373 A69-13492

High energy X ray irradiation of head of *Macaca mulatta*, determining effect on cerebral blood flow and blood pressure
03 p0376 A69-14075

Neutron and X ray radiation effects upon gallium arsenide devices including Gunn oscillators, transistors, Schottky barrier diodes and optoelectronic pulse amplifiers
06 p0978 A69-16890

Radiation tests on Ovonic threshold switches performed with fast neutrons and broadband X rays
06 p0978 A69-16891

X ray irradiated dogs subjected to heat stresses to determine thermoregulatory ability
09 p1445 A69-22548

Drift and tunnel effect of MOS transistors under ionizing electron and X ray irradiation, considering fabrication, electrical characteristics and D-2 satellite tests
11 p1848 A69-24873

Morphological microchanges in solar plexus ganglia of white rats after X irradiation
12 p2019 A69-26347

Computer codes describing nuclear weapons effects associated with X ray transport, neutron transport and X ray interactions with material, fireball, blast environments, etc
15 p2652 A69-30381

High temperature effects on electron and X ray irradiated MOS transistors for space charge analysis and defects in silica films
15 p2625 A69-30828

X irradiation and temperature effects on flour beetle *Tribolium confusum* pupae, noting wing abnormalities and pupal stage duration
17 p2910 A69-33748

Optically thin gas surrounding X ray source, plotting electron temperature and ionization equilibrium of hydrogen, He, carbon, nitrogen, oxygen and neon
18 p3186 A69-34295

X ray stroboscope for moving objects in penetrating irradiation, considering synchronization of radiation receiver
18 p3138 A69-35114

- F center formation and X ray and photostimulated F-band luminescence in europium ion-activated potassium halides as function of temperature and X ray dosage
19 p3383 A69-36164
- Intraperitoneal high polymer DNA administration normalizing effect on DNA and RNA contents in liver, spleen and intestinal mucosa of white rats exposed to X rays
21 p3657 A69-39050
- Single large X ray dose depressive effect on aminotransferase activity in rabbit blood serum, liver, kidney, heart, spleen, lungs, etc
21 p3657 A69-39051
- Cholesterol-protein metabolism in muscles, liver and cerebrum of lethal X ray exposed guinea pigs compared with unexposed group
21 p3657 A69-39052
- Nerve tissue oxidation processes relation to nervous system radiation sensitivity in dogs with cerebellum X rayed after enzyme poisons administration
21 p3658 A69-39053
- Enzyme activity changes in liver, heart and cerebrum of X ray exposed rats and rabbits, noting individual enzyme differences in same X rayed organ
21 p3658 A69-39054
- Single X ray dose effect on alpha-amylase and alpha-glucanophosphorylase in rabbit liver tissues and blood serum
21 p3658 A69-39055
- Successive X ray doses effect on oxidative phosphorylation of vitamin B1 in white rats liver tissue ultrastructure during and after irradiation, establishing thiamine biosynthesis suppression
21 p3658 A69-39056
- White rats hyperglycemia during blood sugar changes following single X ray dose, indicating increased sugar benefit in radiation damage treatment
21 p3658 A69-39057
- Pathological changes in solar ganglia cells of white rats following X ray exposure, using electron microscope
21 p3659 A69-39064
- Retarded immunological recovery in sublethally X-irradiated mice by additional thymic exposure reversal with injected marrow cells
22 p3887 A69-41194
- Hemoglobin inhomogeneity in rats irradiated with lethal doses of X rays and fast neutrons, using fractions prepared by column chromatography
22 p3888 A69-41274
- X ray radiation damage to white mice blood serum proteins disappearing following intraperitoneal administration of imidazole or benzimidazole
23 p4077 A69-41300
- Radioprotective effects of 5-azacytidine on bone marrow and blood leukocytes of X ray irradiated AKR mice
23 p4080 A69-41429
- Whole body X irradiation effect on protein degradation in mice, using radioactive I labeled albumin
23 p4099 A69-42151
- Fraunhofer hologram of glass fiber by Be X rays reconstructed using He-Ne laser light
24 p4314 A69-42973
- X RAY PHOTOGRAPHY**
U PHOTOGRAPHY
U RADIOGRAPHY
- X RAY SCATTERING**
Boundary layer local densities in high temperature gas flows obtained by measuring monochromatic soft X rays attenuation in layer
02 p0233 A69-12489
- Nb supersaturated solid solution in Co precipitation mechanism analyzed by X rays and electron microscope, noting diffusive scattering effects
21 p3750 A69-39788
- Compton profile from single crystal of LiH measured with X ray scattering, noting valence-electron momentum distribution role
22 p3993 A69-40730
- X RAY SPECTROSCOPY**
Solar flare X ray line and continuum spectra measured with crystal spectrometers aboard orbiting solar observatory
02 p0308 A69-12297
- Soft X ray spectrum of Sco XR-1, noting intensity change from previous measurement
02 p0309 A69-12711
- X ray spectrographic camera for nondestructive spectrum analysis of small samples
03 p0427 A69-13101
- X ray astronomy techniques, discussing X ray spectrographs, heliographs and nonsolar celestial X ray sources
05 p0762 A69-15840
- Crab Nebula and Cygnus XR-1 X ray spectra shown to have differential number power law spectra and same intensity
05 p0813 A69-15846
- X ray sources intensity and spectrum variation with time, describing proposed balloon experiments with equatorial launching for performing measurements
06 p0992 A69-17312
- Plasma diagnostics in X ray region, determining electron and ion temperatures and densities and energy losses by radiation
08 p1315 A69-20469
- Low energy X ray spectra of Sco X-1 and Sagittarius sources measured by Be and Al window proportional counters during rocket flight
09 p1574 A69-21460
- Hard X ray event spectrum representation by thermal bremsstrahlung spectrum emitted by energetic electrons, determining various physical parameters of source
09 p1579 A69-22180
- K alpha lines in solar soft X ray spectra noting instrumental effect
09 p1580 A69-22232
- Spectral intensity of high energy solar X rays observed during July 7, 1966 polar event with satellite OGO 3, suggesting nonthermal bremsstrahlung origin
10 p1766 A69-23753
- Diffuse X radiation spectrum below 4 kev measured with beryllium window proportional counter at rocket altitudes
10 p1770 A69-24094
- Proportional counter array for detection of soft X ray photons from OSO-4 observations, discussing solar event energy spectra
12 p2151 A69-26936
- Cosmic X ray background measurements and Crab Nebula observation during sounding rocket flight
13 p2326 A69-27570
- Plasma electron temperatures from electron bremsstrahlung spectra measurements in X ray region
14 p2496 A69-29783
- High speed photographs of plasma emission spectra in UV and soft X radiation spectrum regions, discussing theory, design and operation of facilities
14 p2496 A69-29784
- Spin doublet formation analysis in X ray satellite spectra, revealing K, L and M spin doublets existence
15 p2675 A69-30700
- X ray spectra of Sco XR-1, Cyg XR-1 and Cyg XR-2 for proton energy range 1.5-13 kev from proportional counter measurements
20 p3593 A69-38152
- Solar X-ray events observed by scintillation counter telescope on OSO 3 satellite, discussing X ray spectra during burst initial and decay phases
20 p3593 A69-38166
- Galactic X ray source spectral data observed by rocket, presenting graph with corrections
20 p3594 A69-38172
- Cosmic X ray background spectral measurement from rocket flight near geomagnetic pole
21 p3787 A69-38351
- X ray scintillation spectrometers temperature stabilizing circuit, describing amplitude-frequency conversion technique for position stability
21 p3727 A69-39856
- Hartree-Fock calculations for wavelengths of K alpha X ray transitions, tabulating configuration and term energies, dipole integrals and relative multiplet strengths
22 p3984 A69-40156
- Thermal continuum radiation from coronal plasmas at soft X ray wavelengths, investigating variations effect in element abundances
23 p4207 A69-42406
- X RAY STRESS ANALYSIS**
Vacuum evaporation effects on internal macrostresses in deposited metal films based on X ray analysis, showing substrate temperature contribution
12 p2143 A69-26457
- X ray analyzer for residual stress measurement applied to quality control
18 p3150 A69-35423
- X RAY STRESS MEASUREMENT**
X ray diffraction as nondestructive technique for measuring residual surface stress
21 p3845 A69-39476
- Residual stress measurement in steels and composite materials by X ray diffraction, discussing specimen preparation, diffractometer alignment, elastic modulus determination, etc
24 p4331 A69-42736
- X RAY TELESCOPES**
Test method to compare grazing incidence X ray telescope performance in visible light and in X rays
02 p0248 A69-11736
- Attitude stabilized balloon telescope for measuring interplanetary scattered light and nightglow
06 p0999 A69-16972
- Optical design of Wolter type I glancing incidence X ray telescope for 6-100 A wavelength region, describing results of laboratory and rocket flight tests of prototype
08 p1318 A69-21087
- Hard solar and cosmic X rays measured with satellite-borne telescope, considering flux and time variations
09 p1579 A69-22173
- Grazing incidence telescopes for X ray astronomy, describing mirrors, detection systems and dispersion techniques
09 p1501 A69-22688
- X RAYS**
NT RADIOLOGY
NT SOLAR X-RAYS
- Cosmic radiation interactions with living viruses, considering X ray effects and optimal radiation dosage for cancer cell destruction
01 p0013 A69-10157
- Absorbed gas influence on X ray emission from exploding tungsten wires noting ungasged and degassed specimens in vacuum
01 p0118 A69-10668
- Space X ray background measurements, considering relativistic electrons Compton emission and metagalactic gas bremsstrahlung as possible sources
01 p0147 A69-11310
- Galactic X ray sources, discussing location along spiral arms, age and properties of stars responsible for emission
03 p0497 A69-12930
- Radio galaxies and quasars X ray emissions, calculating radiation fluxes produced by scattering of synchrotron radiation quanta at relativistic electrons
03 p0500 A69-13079
- Cosmic X ray sources resolved against diffuse background radiation lying close to galactic plane
03 p0501 A69-13767
- Dislocation effects on intensity jumps near K edge of absorption, using interferential transmission of X rays in Ge
03 p0490 A69-13944
- Frequency time displays of geomagnetic pulsations at Kiruna revealing Pc 1 pulsations accompanied by cosmic noise absorption /CNA/ and X ray enhancements
03 p0425 A69-14024
- Cosmic X ray background production mechanisms
05 p0814 A69-15848
- Diffuse cosmic X radiation flux and intensity law, noting inverse Compton effect of electrons on 3K black body radiation
05 p0817 A69-16714
- Low energy diffuse cosmic X radiation, considering adequacy of single exponent power law spectrum [ISAS-428]
06 p0986 A69-17024
- X rays detection from laser produced deuterium plasma through calibrated absorbers, presenting electron temperatures
06 p0964 A69-17479
- Cosmic X rays, gamma rays and electron production under astrophysical conditions, noting potential use in supernova and quasar research
07 p1204 A69-18391
- Galactic soft X rays observation with two rocket-borne gas filled counters, noting source near Wolf-Rayet star Gamma Velorum in Vela
07 p1204 A69-18599
- Universal instability theory relevance to pulsating optical auroras and fast quasi-periodic variations of auroral X ray fluxes
07 p1125 A69-18852
- Nocturnal auroral electron showers configuration and displacement determined from sounding balloon measurement of X rays due to showers braking in upper atmosphere
08 p1308 A69-20281
- Auroral zone X ray measurements emphasizing temporal intensity variations, energy spectra changes and source region movements during magnetospheric substorms
08 p1379 A69-20534

Sky background of soft X ray emission in spectral band explained by emission lines from galaxies
08 p1380 A69-20769

Cosmological implications of diffuse X ray background, noting Compton black body process effect on isotropic cosmic X rays
09 p1578 A69-22152

Solar extreme UV, soft and hard solar X rays, cosmic X rays and gamma rays, cosmic ray particles and near earth visible radiation observed by OSO-3
09 p1578 A69-22167

Diffuse cosmic X ray background measured during balloon flight with actively shielded and collimated detector
09 p1584 A69-22767

Spectra of low energy X ray source at position of Large Magellanic Cloud, noting flux
10 p1770 A69-24093

Diffuse X radiation spectrum below 4 kev measured with beryllium window proportional counter at rocket altitudes
10 p1770 A69-24094

Spectroscopic observations of optical object identified with X ray source Cygnus X-2 noting radial velocity in absorption and emission lines
10 p1785 A69-24097

Supplemented data to analyze intergalactic gas diffuse X ray background radiation
10 p1792 A69-24209

Lasers applied to simulation of effects of X ray or gamma ray bursts on semiconductor devices
11 p1896 A69-24877

Auroral zone X ray pulsations during great geomagnetic disturbance and auroral electrojet development to maximum phase, noting atmospheric feedback modulation
12 p2065 A69-26109

Cineradiography based on repetitive flashes drawn from single field emission X ray tube energized by high voltage pulse generator
12 p2086 A69-26163

Crab Nebula X ray pulse detection attempt during balloon flight of telescope
12 p2149 A69-26226

Potential mechanisms of electron acceleration inside magnetosphere, measuring power spectrum of X rays by electron braking in upper atmosphere
12 p2066 A69-26295

X ray polarization from Sco X-1, noting spurious instrumental polarization due to cosmic ray anisotropy using X ray polarimeter
12 p2149 A69-26315

Correlation coefficients, comparing galactic X ray sources distribution with classical cepheids, old novae, planetary nebulae and Wolf-Rayet stars
12 p2171 A69-27155

Oscillator strengths and wavelengths of X ray and EUV transitions in highly ionized iron line spectra
13 p2326 A69-27554

Radio galaxies and quasars X ray emissions, calculating radiation fluxes produced by scattering of synchrotron radiation quanta at relativistic electrons
14 p2509 A69-28761

Neutron star atmosphere and X ray emission spectrum, computing incident protons mean free path for two assumptions
15 p2686 A69-30535

Pulsar NP 0532 in Crab Nebula observed by rocket and telescope showing strong pulsed X ray signal
15 p2679 A69-31529

Metagalactic electrons inverse Compton effect on relic radiation to interpret cosmic isotropic X radiation entire energy spectrum
16 p2847 A69-31800

Time variation of optical intensity of Sco X-1 X ray source, evaluating photometric data by power spectral analysis
16 p2852 A69-32805

Cosmic X rays diffused component absolute intensity measurement using rotating collimator borne on sounding rocket, noting flat spectrum and Sco X-1 intensity variation
17 p3023 A69-33068

Nocturnal D region conductivity enhancement relation to X radiation from Scorpius XR-1 and other sources, calculating ion production rate
17 p3024 A69-33378

Low level beta, X and gamma radiation detector incorporating Geiger, proportional and scintillation counting features in various modes suiting radionuclide decay scheme
17 p2975 A69-33747

Electron microprobe to produce plane grating X ray hologram based on Lloyd mirror experiment principle
17 p2977 A69-34160

Nanosecond photography with superradiant light source, X rays or electrons using multipurpose electron accelerator, obtaining stop motion pictures
19 p3305 A69-35721

Radio emission from Sco XR-1 shown as synchrotron radiation of relativistic electrons in low density region surrounding denser core producing X ray
20 p3597 A69-37334

Energy spectrum, spatial characteristics and displacements of auroral zone X rays from X ray spectrometry
21 p3787 A69-38359

X ray emission from high voltage microwave devices during high velocity electron braking measured using X ray sensitive film with superimposed aluminum scale
21 p3664 A69-39059

Auroral zone X rays measurement counting rate vs time patterns from balloon flights at Kiruna
21 p3791 A69-39252

Cosmic X ray bremsstrahlung due to collisions of suprathermal protons with ambient electrons, giving clue about diffuse sky background of X rays
22 p4006 A69-40643

Oxygen effect on X ray induced somatic crossing over frequency in *Drosophila melanogaster*, noting bristle spots number modification on abdominal tergites
23 p4099 A69-42118

High energy astronomical diffuse radiation component properties tabulated, discussing power law and thermal X ray background, gamma rays, etc
23 p4207 A69-42319

X- 15 AIRCRAFT

X-15 research aircraft program piloting problems, ground facilities, heat transfer, space flight and steep reentry
12 p2014 A69-26872

X- 22A AIRCRAFT

Low range airspeed system (LORAS/ on X-22A and P 1127 VTOL aircraft for accurate airspeed information
05 p0767 A69-16774

Test techniques for X-22A VTOL research aircraft during ground simulator work and actual flight test, describing stability and control characteristics [AIAA PAPER 69-319]
10 p1633 A69-23044

X-22A VTOL aircraft testing, discussing control sensitivity, dutch roll mode period and performance test planning based on characteristics prediction
14 p2392 A69-29699

X- 24 AIRCRAFT

Lifting Body Test Program at Edwards AFB compared with flight testing standards of high performance aircraft, discussing testing philosophy
06 p1017 A69-17671

X-Y PLOTTERS

Scratch gages under water in open and at high temperature, including circular X-Y recording scratch strain gage
15 p2610 A69-30682

Alphanumeric listing and digital data x-y plotting by high speed printer, describing equipment modifications and control software
17 p2932 A69-33108

XANTHINES

U URIC ACID

XB-70 AIRCRAFT

U B- 70 AIRCRAFT

XC-142 AIRCRAFT

Technological evolution of turboprop propeller powered tilt wing V/STOL aircraft, discussing XC-142A, CL-84 and VZ-2 aircraft
05 p0701 A69-15564

XENON

Shock reflection structure in ionizing xenon determined by fast rise pressure gauge mounted in shock tube end wall
01 p0132 A69-11205

Radiation attenuation cross sections of monatomic and diatomic xenon gas from UV absorption measurements near resonance line
02 p0284 A69-12551

Xe gas discharge plasma resistivity dependence on current density measured in large turbulent flash lamps
03 p0478 A69-13846

Electrical properties of xenon pulse plasmas with high power dissipation, measuring discharge pressure and radiation distribution as function of voltage drop
05 p0801 A69-15746

Gas pressure control in xenon lasers, using variable temperature surface partially insulated from liquid nitrogen coolant
07 p1155 A69-19090

Ne and Xe in carbonaceous chondrites, noting large amounts of fission Xe and implications for galactic nucleosynthesis models
08 p1405 A69-20925

Partially ionized Kr and Xe transport coefficients for various pressures and at high temperatures computed on basis of charged particle cross sections
09 p1548 A69-21935

Xenon pulse discharge plasma temperature distribution, spectral brightness density and light absorption across quartz tube section, noting temperature drop near wall
10 p1742 A69-24081

High temperature and power gas diodes and thyristors for nuclear electrical space power systems
11 p1847 A69-24744

Laser radiation absorption in xenon plasma, noting dependence on intensity due to atoms ionization
13 p2314 A69-28442

Xenon atom and ion densities downstream from coaxial plasma gun measured using vacuum UV emission, absorption spectroscopy and Langmuir probe
16 p2819 A69-31690

Xenon laser CW operation on unclassified spectral lines of high ionization states, using laser induced spectroscopy
23 p4172 A69-41399

XENON ISOTOPES

Heavy xenon isotopic anomalies in carbonaceous chondrites, rejecting plutonium 244 spontaneous fission decay mechanism
05 p0819 A69-15625

Plutonium-244 existence in early solar system concluded from relative abundance ratios of excess meteoritic heavy Xe isotopes
08 p1401 A69-20900

Geochemistry of fission Xe component in chondrites, suggesting Xe derivation from superheavy elements with Z 112 to 119
15 p2681 A69-30325

Spontaneous symmetric fission of superheavy elements near doubly magic nucleus as explanation for Xe and Kr isotopic composition anomalies in meteorites
20 p3601 A69-37503

XENON LAMPS

Filtering system for xenon arc solar simulator to provide operation at air-mass-two /average sea level/ sunlight
09 p1476 A69-21648

Solar simulator with 20 kw xenon lamps, discussing performance, versatility and problems with collectors, folding mirrors and cooling system
15 p2586 A69-30384

Solar simulator with pulsed Xe arc tube, describing operating characteristics, spectral emission and simulator-sunlight correlation
15 p2586 A69-30385

Xenon high wattage short arc lamps for space/solar simulators, describing seals, electrodes shapes and cooling, operating characteristics, etc [AIAA PAPER 69-998]
22 p3920 A69-40376

Xenon plasma continuous illumination sources design and operation for night and color aerial photography covering photogrammetric resource surveys, ground traffic, flight paths, etc
22 p3950 A69-41000

XENON 129

Level crossing effect in stimulated emission and application to determination of hyperfine splitting in Xe 129 excited electronic state during laser transition
07 p1156 A69-19398

XENON 133

Inert gas diffusion of Xe 133 in aluminum and titanium at various temperature ranges, showing effects of recrystallization, plastic deformation and phase transformations
16 p2800 A69-31775

XH-51 HELICOPTER

Compound rotary wing aircraft research, discussing XH-51A maneuverability program and UH-1 high Mach and high advance ratio program [AIAA PAPER 69-218]
07 p1056 A69-19568

XJ-79-GE-1 ENGINE

U J-79 ENGINE

XV- 4 AIRCRAFT

X V-4B Hummingbird 2, noting modification from XB-4A two engine ejector augmentation to six engine direct and diverted thrust configuration
03 p0366 A69-13112

- Lockheed XV-4B Hummingbird 2 VTOL aircraft propulsion, control, escape systems, with tests
10 p1634 A69-23597
- VTOL variable stability system /VSS/ for XV-4B lift jet for flight control and handling verification
17 p2902 A69-34066
- Lift engine inlet development for XV-4B aircraft, discussing tests, pressure distortion and recovery during simulated hover and transitional flight
[AIAA PAPER 68-636] 20 p3585 A69-37150
- XV- 6A AIRCRAFT
U P-1127 AIRCRAFT

Y

- Y AXIS
U COORDINATES
- YAG [GARNET]
U YTTRIUM-ALUMINUM GARNET
- YAGI ANTENNAS
- Yagi-Uda type antennas analysis based on radiated electric field equations, noting far field pattern dependence on phase velocity
11 p1850 A69-24980
- Short backfire antenna based on yagi type equipped with end reflector, noting fewer elements and low side lobe advantages
16 p2763 A69-32586
- YARNS
- Atmospheric wind shear velocity snapping effect on yarn suspending instrument package from balloon gondola during parachute recovery
17 p2975 A69-33613
- YAW
- Yaw parameter and curvature effects on accuracy of hot-wire anemometer, noting King law
03 p0426 A69-12845
- Vortex breakdown effect on aerodynamic coefficients of small aspect ratio delta wings during yawing
04 p0543 A69-14821
- Boundary shear stress with unknown magnitude and direction measured by yaw probe used as Preston tube
05 p0751 A69-16396
- Additional yawing by gyroscopic moment of power plant and effect on aircraft maneuver during curvilinear flight, noting compensation by automatic control
18 p3092 A69-34973
- Conical delta wings in supersonic-moderate hypersonic flow, studying yaw effects on pressure distribution behind shock wave
20 p3459 A69-37593
- Monograph on forces exerted by air during yawing motion of sharp cones in supersonic and hypersonic flows by semilinear method
20 p3460 A69-37919
- Windward shock angle parameters on yawed cones correlated in single variable for hypersonic flow
23 p4060 A69-41918
- Spacecraft pitch and yaw angles measurement using environmental positive ion probes, discussing Gemini flight tests and attitude control systems
24 p4315 A69-43241

- YAWMETERS
U ATTITUDE INDICATORS
U YAW
- YEAST
- Genetic effects in yeast induced by heavy ion radiation, studying lethality, mitotic segregation, allelic recombination and reverse mutation
03 p0373 A69-13491
- Radiation damage in yeast cells irradiated by high energy C 12 ions evaluated from survival rate study
14 p2406 A69-28915
- Microbial protein extraction from Chlorella algae and Torulula yeasts using urea soaking method
21 p3662 A69-39712

- YHU-1 HELICOPTER
U UH- 1 HELICOPTER

- YIELD
- Generalized quantum yield for sensitivity of photoelectric devices, considering multistage image converter and photomultiplier
14 p2496 A69-29788

- YIELD POINT
- Yield surface after prestraining under radial loading, analyzing formation of yield corner
01 p0166 A69-10303
- Plastic deformation wave propagation and heat generated near yield point of annealed aluminum
02 p0342 A69-12280

- Plates yield point loads limit determination formulated as mathematical programming problem, using finite element representations for velocity and moment fields
[ASME PAPER 68-WA/APM-21] 04 p0670 A69-14405

- Truncated solid cones plastic yielding under quasi-static and dynamic axial loads at various strain rates
04 p0682 A69-15301

- Subsequent yield surfaces in cross shaped brass plates determined after prestraining or cold rolling
04 p0682 A69-15302

- General kinematic yield mechanism and associated kinematically adequate multiplier formulated for structural elements characterized by plane deformation state
05 p0831 A69-15684

- Repeated loading influence on microstrain region, noting decrease in size with each cycle
05 p0836 A69-15876

- Yield point for simply supported conical shell loaded through central boss at vertex
06 p1023 A69-17375

- Temperature dependence of polymethylmethacrylate deformation, yield and fracture in constant strain rate compressive and tensile tests
08 p1335 A69-20215

- Plastic yielding of tensile V-notched aluminum alloys elements with intermediate thickness and various shoulder ratios, studying thickness effect on yield load
09 p1612 A69-21499

- Yield points compared for axial and biaxial tensile loading of aluminum alloy sheets
10 p1801 A69-23849

- Temperature and stress dependence of microstrain and microyielding in polycrystalline W for range of impurities and dislocations, considering transition to macrostrain
11 p1905 A69-25183

- Stress discontinuity surface of three dimensional rigid plastic body arbitrary yield condition, considering equilibrium of regular four sided pyramid
11 p1996 A69-25738

- Rigid plastic circular and annular plates dynamics taking into account yield point dependence on strain rate
12 p2177 A69-25994

- Fatigue crack propagation laws determined by material yielding at crack tips, stress intensity and exponential crack growth law
12 p2187 A69-26846

- Metal fatigue in Al alloys subjected to stress cycles, determining macrocracks propagation stages
13 p2359 A69-27291

- Craze formation and shear yielding considered for glassy polymers in terms of stress field requirements
17 p2993 A69-34169

- Temperature dependence of metal elastic properties including thermal strains effect on stress field, yield stress changes and elastic modulus variations
18 p3212 A69-34353

- WC-Co alloys structural changes under loads near yield limit, noting formation of slip bands
18 p3158 A69-35261

- Yield condition of maximum constant distortion strain energy for anisotropic material without incompressibility assumption
18 p3227 A69-35494

- Reducibility conditions of flow theory for smooth and piecewise smooth yield surfaces to relations of small elastoplastic deformations
19 p3443 A69-36794

- Stress corrosion cracking model for 7075 Al, correlating macroscopic yield stress and corrosion time to failure
19 p3351 A69-36897

- Strain rate-load relations in elastoplastic shells reaching yield point, discussing variational method applicability
21 p3838 A69-39189

- Serrated yielding at high temperatures from dislocation theory viewpoint, considering critical strain relation to temperature and strain rate
21 p3749 A69-39710

- Yield condition and relation between stresses and strain rates for anisotropic body, allowing for influence of stressed state type
22 p3934 A69-41169

- Collapse load of shallow conical shells clamped at base and loaded through finite rigid boss, using Tresca yield condition for sandwich shell
23 p4236 A69-42496

- Strain diagram with piecewise nonlinear curve for statically indeterminate systems stressed beyond elastic limit
24 p4400 A69-43072

YIELD STRENGTH

- Yield condition of polycrystalline hcp metal, considering slip characteristics of hcp crystals
01 p0094 A69-10304

- Irradiation influence on yield stress of Ni-Al intermetallics noting temperature dependence and electron dosage
01 p0095 A69-10608

- Ultrahigh pressure physics of materials, discussing apparatus, phase transitions and yield strength ductility relationships
02 p0260 A69-11803

- Plane strain yielding, stresses and fracture about notches and cracks in terms of flow and fracture stresses and crack tip radii
03 p0528 A69-13876

- Yield curve softening in hard Al subject to cyclic torsional loading, noting deformation resistance, surface hardness and yield strength
04 p0671 A69-14411

- Static criterion for yield computation in plane two dimensional systems
05 p0836 A69-16013

- Crack tip plastic flow effect on strain energy release rate, considering Dugdale model for yielded crack [ASME PAPER 68-WA/MET-17]
05 p0838 A69-16155

- Statistical theory of material strength with application to composite materials reinforced with whiskers and continuous fibers
06 p1028 A69-18142

- Grain size dependence of yield, flow and fracture stresses of Fe-Co-V alloy for 77-298 K
07 p1166 A69-19264

- Polycrystalline beryllium specimens fabricated from powders, discussing initial powder particle size and distribution effects on microyield strength
07 p1168 A69-19598

- Vacuum arc melted W and W-Re alloys mechanical properties, noting Re additions effects
08 p1331 A69-20190

- Plain strain fracture toughness tests on two inch thick maraging steel plates of various strengths, using bend and compact tension tests
10 p1795 A69-23057

- Elastic release wave and pressure drop measurement in 2024-T4 aluminum at 313 kb for dynamic yield strength, considering surface velocity and stress
10 p1712 A69-23665

- Temperature and strain rates effect on delayed yield and failure of plasticized epoxy resin
10 p1717 A69-24218

- Yield to ultimate tensile strength ratio of titanium alloys subjected to thermomechanical treatment
11 p1906 A69-25683

- Plane strain fracture toughness tests on maraging steel plates for various yield strengths and large dimensions
12 p2114 A69-26496

- Effective tensors of elastic moduli and yielding of composite materials, considering multiparticle interactions and use of equilibrium and incompatibility equations
13 p2360 A69-27382

- Discontinuous yielding characteristics of 2024 Al alloy determined for different conditions of solution, heat treatment and age hardening
15 p2639 A69-30598

- Electrical conductivity, hardness, ultimate tensile strength and yield strength correlations of age hardenable Al alloys by eddy current methods
15 p2641 A69-31513

- Load carrying capacity of circular plates under antisymmetric load
16 p2875 A69-32289

- Polyethylene stainless steel lap joints and polyethylene samples yield strength measurements at high temperature, suggesting yield mechanism based on dislocation loops
16 p2794 A69-32573

- Fracture strength of Al alloys, discussing tests for tensile properties, linear elastic fracture mechanics techniques, yield strength, corrosive media, etc
17 p2989 A69-33555

- Mathematical model of yielding of adhesive bonds in form of viscous threads between elastic bodies, obtaining solution to two dimensional problem
18 p3215 A69-34569

- Crystal twinning directional effect on Mg alloys tensile yield strength degradation, investigating recovery methods
19 p3341 A69-35583

YIG [GARNET]

Ti-Al alloys yield and fracture characteristics as function of high exposure temperatures, studying causes of embrittlement

19 p3344 A69-35927

Elastoplastic state of composite structures with applicability of elasticity law and yield conditions illustrated by reinforced plate under plane stress

19 p3444 A69-36808

Yield strength, deformation modes and fracture characteristics of Ti-Al alloys, examining strength and fracture characteristics as function of structure and chemical composition

20 p3557 A69-36959

Laminated composites ultimate strength prediction based on consecutive yield procedure with step-wise reduction of strength or load-carrying capacity used as design criterion

20 p3627 A69-37773

Low strain rate effects on metals yield and tensile strength

20 p3563 A69-38063

Yield stress of normal human blood related to endogenous fibrinogen concentration as function of total protein concentration, proposing fibrinogen adsorption and coupling model

22 p3874 A69-40223

Yield condition for elastic-plastic medium, considering pure torsion-associated second order effects and dissimilarity between stress and strain increment Mohr circles

23 p4234 A69-42409

Plastic inhomogeneity effects on yield stress of isotropic spherical shell and long cylindrical tube under internal pressure

24 p4405 A69-43672

YIG [GARNET]

U YTTRIUM-IRON GARNET

YJ-79 ENGINE

U J-79 ENGINE

YJ-85 ENGINE

U J-85 ENGINE

YOUNG MODULUS

U MODULUS OF ELASTICITY

YTTRIUM

Temperature dependence of A and C periods of Y crystal lattice at 77 to 300 K, discussing preparation of Y films and anomalous thermal expansion

02 p0298 A69-12047

Rare earth elements and yttrium in meteoritic chondrites determined by radiochemical neutron activation analysis

08 p1403 A69-20916

Yttrium effect on rate of thermal decomposition of silver carbonate powder and pressed pellets by isothermogravimetric analysis, examining water vapor, Co 60 gamma radiation and temperature effects

15 p2561 A69-30442

German monograph on yttrium addition effects on tension and compression behavior of Nb and Mo at high temperature in vacuum

17 p2990 A69-33570

Yttrium desorption from W wire by strong electric field, noting electron work function or temperature increase effects on desorption field

17 p3015 A69-33631

YTTRIUM ALLOYS

Nickel-rich region of Al-Ni-Y ternary system, emphasizing identification of solid phase equilibria through analysis of equilibrated alloy specimens

02 p0265 A69-12004

YTTRIUM-ALUMINUM GARNET

Refractive index and expansion thermal coefficients along axis of oriented Nd-YAG laser rod

04 p0609 A69-14293

Q switching of continuously pumped Nd:YAG laser using variable spacing Fabry-Perot interferometer as variable output coupler

06 p0938 A69-18229

Solar end and lateral pumping apparatus for neodymium doped YAG crystal lasers, noting applicability to space communication

07 p1150 A69-18953

Neodymium doped YAG laser efficiency dependence on pump power level and spectral filtering of pump light

10 p1705 A69-23814

Microimpurities in aluminum-yttrium garnets determined spectrographically by using gallium oxide as carrier and Teflon powder for fluorinator

10 p1747 A69-23843

YAG-Nd laser continuous operation using incoherent injection luminescent pumping by gallium ar-

senide phosphide light emitting diodes at liquid nitrogen temperature

13 p2270 A69-27192

Bismuth oxide introduction into Y and Y-Al garnets, noting effect on formation and properties

13 p2320 A69-27998

Passive mode locking of pulsed Nd-YAG laser using saturable absorber, noting two photon fluorescence contrast ratio

16 p2797 A69-32019

Self Q switching of pumped neodymium-doped YAG and ruby lasers obtained by static misalignment of mirror and pumped laser filament

17 p2979 A69-32916

YTTRIUM COMPOUNDS

NT YTTRIUM-ALUMINUM GARNET

NT YTTRIUM-IRON GARNET

High pressure high temperature synthesis and superconducting properties of yttrium sesquicarbide, noting effect of ambient pressure annealing

07 p1201 A69-19600

YTTRIUM-IRON GARNET

Nonreciprocal tunable yttrium-iron garnet microstrip filter design through generation of circularly polarized field

01 p0041 A69-10202

YIG single crystal resonator tuning of Gunn diode in coaxial line circuit

01 p0042 A69-10320

Dispersive two port components for application to microwave pulse compression, coupling YIG crystal magnetoelastic spin wave mode to acoustic transducer

02 p0217 A69-12149

Magnetoelastic coupling constant b, measured by propagating microwave signals in pure and substituted YIG

02 p0299 A69-12243

Yttrium iron garnet sublattice magnetization calculation using Oguchi method

03 p0485 A69-13297

Miniature microwave tuners with solid state reliability and reduced power consumption, using YIG, mixer circuits and integrated control circuitry

07 p1102 A69-18672

High pressure synthesis of dense ferrimagnetic perovskite allotropic form of yttrium-iron garnet

08 p1372 A69-20372

Spherical electronically tunable multiresonator YIG filters design using filter tables and coupling bandwidth charts

08 p1292 A69-21006

Dislocations effect on magnetization process in YIG crystals, using polarization optical method

09 p1559 A69-22532

Dynamic mode electromagnetic surface waves on axially magnetized single crystalline YIG and polycrystalline ferrite rods

10 p1746 A69-23513

Near IR radiation magneto-optic light modulators using Faraday effect in yttrium-iron garnet and in related compounds

11 p1886 A69-25057

Resonators made of YIG single crystals exhibiting lowest linewidth in ferromagnetic resonance at microwave frequencies

11 p1855 A69-25627

Saturation and distortion effects on magnetoelastic wave excitation in yttrium garnet single crystals by large amplitude microwave frequency field

12 p2145 A69-26725

Elliptical polarization in ultrabroadband YIG pulse compression networks, using reflections at rod faces

13 p2230 A69-27680

Bismuth oxide introduction into Y and Y-Al garnets, noting effect on formation and properties

13 p2320 A69-27998

Yttrium garnet ferrite crystals grown by Czochralski method from inductor crucible exhibiting orthoferrite, iron garnet and eutectic phases along height

13 p2321 A69-28001

Gallium distribution in YIG single crystals by X ray spectral analysis, observing concentration fluctuations

13 p2321 A69-28002

Magnetoelastic resonant interaction of microwave longitudinal phonons propagating at right angles to magnetic bias applied to YIG rod axis

15 p2565 A69-30184

Transistorized L band oscillator tuned by Ga-doped YIG, discussing ferrimagnetic material properties and device equivalent circuit

16 p2761 A69-32450

Optical IR yttrium-iron garnet rectifier increasing light intensity and system Q factor at low external magnetic field

17 p2981 A69-33117

Possibility of combining individual yttrium ferrite single crystals to obtain noninteracting element for quantum paramagnetic traveling-wave amplifier operating at liquid nitrogen temperature

19 p3334 A69-35883

Microwave elastic propagation in single crystal specimen of yttrium-iron-garnet ferrite, discussing attenuation

21 p3780 A69-38774

Saturation and distortion effects on magnetoelastic wave excitation in yttrium garnet single crystals by large amplitude microwave frequency field

21 p3782 A69-39138

YIG single crystal disk instability, noting dispersion of magnetostatic and plane spin waves from supplementary absorption and LF oscillations recording

21 p3783 A69-39561

YUH-1 HELICOPTER

U UH-1 HELICOPTER

Z

Z AXIS

U COORDINATES

Z TRANSFORM

U LAPLACE TRANSFORMATION

ZEEMAN EFFECT

Photospheric network obtained by spectroheliograms, discussing Fraunhofer lines weakening, nonsunspot magnetic fields and Zeeman sensitivity

04 p0664 A69-15523

Weak magnetic fields effect on molecular oscillator frequency taking into account Zeeman sublevels

05 p0727 A69-15643

Line broadening possibility for Q switched iodine laser with aid of magnetic effect /Zeeman effect/, noting energy storage capability increase

05 p0773 A69-16288

Zeeman effect in He-Ne lasers during simultaneous emissions at various gas pressures and currents in magnetic fields

06 p0932 A69-16912

Element abundances in magnetic stars, discussing Zeeman effect and anomalies in spectra

08 p1403 A69-20911

Simultaneous action of RF perturbation between Zeeman sublevels of atomic transition sustaining gas laser oscillations, discussing single pi mode laser operation

10 p1704 A69-23808

Zeeman laser with one end mirror exhibiting x-y-type loss anisotropy, considering resonance condition for round trip pass and self consistent field equations

13 p2271 A69-27398

Light saturation development of line profile component of normal Zeeman triplet in sunspot umbrae

14 p2528 A69-29964

Zeeman spectroscopy and UVB photometry of 17 Com and kappa Cnc, observing periodic magnetic and light variations

15 p2692 A69-30774

Metallic line /Am/ stars Zeeman observations, showing 16 Ori as spectroscopic binary, dubious binary nature of 15 Vul and doubtful presence of magnetic fields

15 p2692 A69-30775

Absorption coefficient in three microwave lines of O with different rotational quantum numbers calculated, examining Zeeman effect in geomagnetic field

15 p2597 A69-30941

Weak magnetic fields effect on molecular oscillator frequency taking into account Zeeman sublevels

16 p2762 A69-32500

Cavity linear phase anisotropy and axial magnetic field effect on single mode Zeeman gas laser

16 p2798 A69-32606

Time behavior of output intensity and polarization of single cavity mode internal mirror Zeeman laser in axial magnetic field

16 p2798 A69-32607

Zeeman effect measurement revealing magnetic fields in interstellar neutral H clouds

18 p3190 A69-34291

Gas and solid state lasers optical resonance and radiation generation, frequency properties, frequency shift, spectra and Zeeman effect

18 p3154 A69-35408

- Single mode He-Ne laser frequency stabilization by Zeeman effect
20 p3554 A69-37729
- Partial resolution of Zeeman patterns in spectrum for magnetic field existence in atmosphere of 53 Camelopardalis
20 p3611 A69-38155
- HD 188041 magnetic field variations from Zeeman measurements correlated to spectral variations
20 p3611 A69-38156
- Electron paramagnetic resonance line splitting between two nondegenerate Zeeman levels, using ruby laser as pumping source
21 p3735 A69-38582
- Solar Zeeman triplet for excited atomic state comparable to or shorter than Larmor precession period, discussing polarization
22 p4019 A69-40287
- Solar Zeeman triplet pseudo-pi-component at 5250 Å /Fe I/, using Unno theory to calculate visibility, contrast and displacement
22 p4019 A69-40289
- ZENER DIODES**
U AVALANCHE DIODES
- ZENITH**
Upper atmosphere temperature distribution estimation on basis of twilight zenith sky intensity measurements, discussing influence of various parameters on accuracy
09 p1487 A69-21653
- Refraction angles for objects between 5-300 km and zenith distances between 1-88 degrees, describing calculation method for corrections
09 p1490 A69-21918
- IQSY night airglow photometric observations, summarizing zenith intensity and north/south intensity ratio data
15 p2594 A69-30019
- Measured atmospheric refraction of bright astronomical objects less than calculated data for large zenith distances
15 p2679 A69-30161
- Stellar image vibration dependence on zenith distances and terrain relief determined from stellar traces by 200 mm telescope
15 p2647 A69-30163
- Synoptic meteorological conditions effect on stellar images vibration and on relationship between vibration and zenith distance
15 p2647 A69-30164
- Zenith sky Umkehr observed with Dobson spectrophotometer at twilight, discussing light scattering by aerosols in lower stratosphere
16 p2786 A69-32634
- Differences in latitude readings obtained with two zenith telescopes, showing Pearson distribution of type VII and influence of observation conditions
17 p2959 A69-32879
- Bamberg zenith telescope investigation, noting level constant dependence on level tube bubble length
17 p2970 A69-32882
- Automatic instrument for star detection and azimuth derivation, measuring nighttime zenith star field
[AIAA PAPER 69-861] 21 p3762 A69-39389
- UHF radio pulses from zenith associated with extensive air showers, estimating threshold energy of scintillation trigger system
21 p3792 A69-39613
- Bright lunar limb zenith distances measured by equal altitudes method, deriving Ephemeris- Atomic Time A3 and Ephemeris-TU2 time relations
23 p4208 A69-41289
- Geomagnetic zenith calculation at given point based on geomagnetic field model, using polynomial development
24 p4311 A69-43505
- ZEOLITES**
Electron paramagnetic resonance study of interaction between adsorbed nitric oxide and NaY and decazationized Y zeolites surfaces, considering catalytic activity
02 p0205 A69-11900
- Benzines antidetonation properties improved by separating n-alkanes with synthetic zeolite
23 p4199 A69-42479
- ZERO ANGLE OF ATTACK**
Wing upper surface velocity distributions having peak near leading edge, considering incompressible flow at zero angle of attack
[ONERA-TP-632] 02 p0187 A69-11618
- Time independent flow of highly rarefied neutral gas past finite cone at zero angle of attack with freestream, noting molecular distribution function
04 p0541 A69-14712
- Monograph on calculation of linearized supersonic flow on rocket configurations at zero angle of attack, particularly at interfaces between components, covering applications
11 p1817 A69-24637
- Spherically blunted 15 degree semivertex angle cone flow field parameters at Mach 8.6, measuring pitot pressure and shock shape
11 p1818 A69-25143
- Hypersonic slender cone zero angle of attack drag in rarefied continuum and noncontinuum flow in shock tunnel, indicating body dimension influence in transition regime
[AIAA PAPER 69-711] 17 p2891 A69-33445
- Hypersonic viscous interaction, studying axisymmetric flow over slender sharp nose cones at zero angle of attack and three dimensional flow over sharp flat plate
24 p4248 A69-43579
- ZERO CROSSINGS**
U ROOTS OF EQUATIONS
- ZERO FORCE CURVES**
Hill surfaces in triangular restricted four body problem, deriving equation of surface of zero relative velocity
04 p0660 A69-15038
- ZERO GRAVITY**
U WEIGHTLESSNESS
- ZERO-ZERO WEATHER**
U WEATHER
- ZETA AURIGAE STAR**
Relative intensities of selected Si two multiplets calculated and compared with solar spectrum and plasma source ZETA values
13 p2326 A69-27551
- ZINC**
Electrical properties of p-n junctions of diffused Cd or Zn in indium phosphide
02 p0294 A69-11628
- Friction induced plastic deformation of Be-Co-Zn single crystals with HCP structure
02 p0254 A69-12627
- Superconductivity and band structure from pseudopotential for zinc and cadmium, analyzing values of electron phonon mass enhancement
04 p0642 A69-14965
- Anomalous size effects in galvanomagnetic properties of zinc crystal samples caused by compensation
06 p0981 A69-18232
- Thermodynamics and polarization of zinc electrode in alkaline media, discussing anodic dissolution and passivation
08 p1268 A69-21048
- Zinc oxidation in weakly alkaline media, discussing basic properties of electrochemical cells containing zinc
08 p1268 A69-21050
- Hole density/Zn concentration ratio in Zn doped solution grown p-type GaP, noting anomalous electrical properties
09 p1557 A69-21750
- Zinc electrode cycle life improvement by reducing change in electrode shape, noting effectiveness of teflonation
10 p1640 A69-23995
- Depth and planarity of zinc diffused junctions in GaP using temperature, phosphorus overpressure and time as independent variables
13 p2322 A69-28136
- Laser diodes p-n junctions obtained by Zn diffusion into Ga arsenide, stressing junction flatness problem and arsenic vapor pressure effect
13 p2323 A69-28640
- Diffuse Zn layers structure in GaAs single crystals, showing dislocations formation by anomalous Zn diffusion
15 p2670 A69-31048
- Thermodynamics and polarization of Zn electrode in alkaline medium for electric generators
16 p2739 A69-32419
- Electrochemical generators utilizing anodically polarized zinc associated with oxygen, mercuric oxide or silver oxide for space power sources
16 p2739 A69-32420
- Afterglow decay rates of Zn II laser lines in spontaneous emission measured, indicating thermal energy charge exchange excitation and CW oscillation
21 p3735 A69-38598
- ZINC ALLOYS**
Aluminum-Zn-Mg alloys weldability, discussing base metal composition and heat treatment influence during gas-shielded arc welding
01 p0086 A69-10536
- Microstructure relationship to tensile strength and creep resistance in Zn-Ni-Ti alloy extrusions, discussing role of finely dispersed intermetallic particles
08 p1329 A69-20002
- Transient characteristics of negative resistance zinc alloy diodes, investigating temperature effects
10 p1662 A69-23157
- ZINC ANTIMONIDES**
P-type zinc-tin-antimonide crystals electric conductivity, Hall coefficient and thermal EMF found similar to p-type diamond-like semiconductors properties
15 p2667 A69-30197
- N-type In-doped ZnSb with melt under H-gas preparation and properties
18 p3183 A69-35268
- ZINC COMPOUNDS**
U WURTZITE
- ZINC OXIDES**
Differential capacity of Li doped zinc oxide single crystals between vapor deposited asymmetrical In electrode contacts
08 p1371 A69-19883
- Electron injection into ZnO from aqueous solutions of stable substances, correlating injection with oxidation potential of substance
10 p1651 A69-22940
- UV irradiation effects on ZnO spacecraft thermal control coating pigments, discussing photo-Hall, luminescence and electron paramagnetic resonance measurements
[AIAA PAPER 69-639] 17 p2992 A69-33288
- Electron reactivity of one equivalent oxidizing agents at ZnO surface by electrochemical reduction
19 p3392 A69-36731
- ZINC SELENIDES**
GaAs zinc gallium selenide solid solutions properties, analyzing lattice constant, microhardness, forbidden zone and concentration relationships
15 p2670 A69-31050
- ZINC SILVER BATTERIES**
U SILVER ZINC BATTERIES
- ZINC SILVER OXIDE BATTERIES**
U SILVER ZINC BATTERIES
- ZINC SULFIDES**
NT WURTZITE
- Electrical polarization effect on electroluminescence brightness waves in zinc sulfide films
05 p0807 A69-16213
- Polarization effect on electroluminescent properties of zinc sulfide films
05 p0807 A69-16214
- Impact ionization and tunneling effect during electroluminescence of zinc sulfides
06 p0980 A69-17261
- ZnS-CdS crystals luminescence during varied forbidden bandwidth, discussing two photon and ruby laser excitation and temperature dependence
19 p3331 A69-35866
- ZINC TELLURIDES**
GaSb-ZnTe heterojunction fabrication method, noting photoresponse, fluorescence and light transmission
02 p0299 A69-12408
- ZnTe electronic structure from photoemission study, noting emitted electron energy distribution
03 p0493 A69-14239
- ZINC TUNGSTATES**
Angular dependence of EPR line widths of trivalent Cr ions in zinc tungstate in rotating magnetic field, noting spin-phonon mechanism
10 p1743 A69-23131
- ZIRCALOY 2 [TRADEMARK]**
Ultrasonic inspection of soundness and penetration or corner welds for Zircaloy 2 casings, discussing method reliability and sensitivity limits
07 p1141 A69-19346
- ZIRCALOYS [TRADEMARK]**
U ZIRCALOY 2 [TRADEMARK]
- ZIRCONATES**
U BARIUM ZIRCONATES
- ZIRCONIUM**
Thermodynamic study of carburization of liquid titanium and zirconium, examining effects of atmosphere, graphite porosity and alloying elements
03 p0446 A69-13572
- Heterodiffusion of metallic impurities in body centered phases of doped zirconium and titanium, determining diffusion coefficients via radioactive isotopes
04 p0613 A69-14557
- Solid solutions of O in Ti and Zr, noting superstructure formation and physical properties
04 p0618 A69-15078

Tin and zirconium addition effect on transformations of titanium alloys during heat treatment
07 p1162 A69-18775

Shock tunnel hypersonic flow effect on critical Weber number for zirconium drop breakup in partially and fully molten states
12 p2063 A69-26802

Zr doped superconducting ceramic strontium titanate, noting effective electron mass variations and transition temperature
13 p2316 A69-27400

Luminous spherical fog layer surrounding burning zirconium droplet during free fall through oxygen containing atmosphere, noting effect on mass and heat transfer processes
13 p2380 A69-28462

Laser ignited Zr droplet free fall combustion in oxygen, analyzing metal conservation and luminosity correlation assuming reflux action from fog layer [WSCIPAPER 69-1]
16 p2830 A69-32342

Laser ignited combustion of 365 micron Zr droplets falling in ultrapure oxygen using spectroscopic and photographic techniques, discussing vapor phase transport phenomena [WSCIPAPER 69-4]
16 p2830 A69-32345

Flow rate effect of oxygen-argon mixture on Zr oxidation studied to determine exclusion as factor in Zr weight increase
18 p3154 A69-34272

Carbide coatings formation on graphite in molten media, determining diffusion coefficient of carbon in molten Zr
20 p3566 A69-37372

Stacking fault formation probability in Ti and Zr by X ray diffraction techniques, using Fourier analysis and half-width measurements
21 p3749 A69-39600

Cathode materials role in high temperature zirconia electrolyte fuel cell performance, discussing metals, collector-embedded and electronically conducting oxides properties
22 p3869 A69-40734

ZIRCONIUM ALLOYS
NT ZIRCALOY 2 [TRADEMARK]

Mechanical properties of AZ5G-Zr-Cr alloy welded sheet subjected to biaxial stress at low temperature
01 p0088 A69-11152

Soviet collection of articles on physicochemistry of zirconium alloys
02 p0261 A69-11839

Metallographic analysis of Zr corner structure in Zr-Al-Mo system phase diagram, plotting monovariant and nonvariant equilibria reactions
02 p0261 A69-11840

Zr corner of phase diagrams and microstructure, hardness and microhardness of Zr-Al-Nb system alloys
02 p0261 A69-11841

Zirconium corner of Zr-Al-Cr system phase diagram within concentration limits from 1350-700 C, considering corrosion resistance
02 p0262 A69-11842

Metallographic and radiographic analysis of zirconium corner in Zr-Be-Nb system, discussing phase transformation during quenching
02 p0262 A69-11843

Zr-Be-Nb system oxidation resistance decrease at 650 degrees C ascribed to Be and Nb additions
02 p0262 A69-11844

Zr-Be-Nb alloys mechanical tensile properties above room temperature for low concentrations of Be and Nb
02 p0262 A69-11845

Isothermal sections construction of zirconium corner of ternary phase diagram of Zr-Mo-V system from microstructure of cast and quenched alloy specimens
02 p0262 A69-11846

Structure of zirconium corner of Zr-V-Ni system phase diagram, using metallography, hardness and microhardness methods
02 p0262 A69-11847

Isothermal sections construction of Zr-V-Ni system phase diagram from study of alloys at 1000, 700 and 500 C
02 p0263 A69-11848

Alloying additions effect on mechanical properties of Zr-V-Nb system
02 p0263 A69-11849

Omega phase and beta solid solution in Zr-V-Ta alloys quenched from 900 C
02 p0263 A69-11850

Zirconium corner of Zr-Fe-Nb phase diagram, studying alloy tempering at various temperatures
02 p0263 A69-11851

Zirconium corner of Zr-Cu-Mo phase diagram, using microstructure analysis of hardness and microhardness

measurements, discussing plasticity variations and corrosion resistance
02 p0263 A69-11852

Fe, Ni and Cr influence on corrosion resistance and mechanical properties of Zr-Cu-Mo system alloys
02 p0263 A69-11853

Zirconium corner in Zr-Nb-Cu phase diagram, plotting isothermal sections for high temperatures
02 p0263 A69-11854

Zirconium corner of Zr-Mo-Ni phase diagram using metallographic analysis, hardness and microhardness methods, constructing isothermal sections for high temperatures
02 p0264 A69-11855

Zirconium corner of Zr-Nb-Mo system phase diagram, using microstructure, microhardness, hardness and radiographic methods
02 p0264 A69-11856

Oxidation resistance of Zr-Nb-Mo alloys at high temperature in air or water
02 p0264 A69-11857

Isothermal sections of Zr corner of Zr-Mo-Ta system phase diagram at high temperatures, noting composition vs hardness and omega phase
02 p0264 A69-11858

Isothermal sections of Zr corner of Zr-Mo-Ti phase diagram at various high temperatures, noting corrosion resistance in air and water
02 p0264 A69-11859

Isothermal sections of Zr-Ni-Nb system phase diagram at high temperatures, determining principal type of projection on concentration triangle
02 p0264 A69-11860

Isothermal sections of Zr corner of Zr-Nb-Cr system phase diagram at high temperatures, noting variation of stability with concentration
02 p0264 A69-11861

Precipitation hardening effects on Al-Zr recrystallization with Fe and Si additions, noting peak hardness increment with decrease in aging temperature
04 p0617 A69-14931

Phase equilibria, phase transformation temperatures and relation between resistivity and chemical composition for alloys of Ti-Al-Mo-Zr system
04 p0618 A69-15079

Metastable phases of binary zirconium-niobium system, defining decomposition of solid solution in cooling
05 p0781 A69-16614

Zr-Nb alloy structure effect on critical superconductivity parameters determined, using electron microscopy of thin films
05 p0811 A69-16806

Zirconium niobium alloys thermodynamic properties measured by Knudsen effusion method using zirconium 95
07 p1165 A69-18940

Metallographic and X ray study of cellular decomposition and precipitation in superconducting niobium zirconium alloy, noting heat treatment effect on current carrying properties
08 p1331 A69-20192

Omega phase transformation in binary and ternary Zr alloys after water quenching from within /alpha plus beta/ phase region
10 p1707 A69-22988

Phase equilibrium in cast Zr-Re-B and W-Re-B systems using microscopic and X ray analysis
10 p1711 A69-23332

Zr-W high temperature phase relationships, noting Zr-zirconium tungstide eutectic temperature, zirconium tungstide peritectic temperature and Zr solubility in W
11 p1903 A69-24578

Omega phase formation in Ti and Zr alloys with transition metals, discussing effects on mechanical and superconducting properties
18 p3155 A69-34634

Beryllium diffusion coefficients in Zr and Ti bcc phases, using radioactive beryllium 7 at high temperatures
18 p3157 A69-35251

Spectral reflectivities of sintered Ti-TiN-TiC and Zr-N-ZrC alloys and Zr-ZrN-ZrC alloys
20 p3559 A69-37330

ZIRCONIUM CARBIDES
Roentgenographic and metallographic examinations for interaction between ZrC and Re in wide range of temperatures and concentrations, discussing phase diagram
04 p0617 A69-14900

Zirconium and niobium carbide behavior during plasma spray coating, noting optimum oxygen content and mean carbide particle diameter in spray
07 p1165 A69-18933

Slip casting powder mixture of zirconium carbide and tungsten, discussing optimum composition
10 p1716 A69-24056

Pyrolytic zirconium carbide emissivity during initial heating compared with results for specimens prepared by powder metallurgy
15 p2640 A69-30985

Electrical resistance and temperature coefficient dependence on phase composition of Ti, Zr and Nb carbides
15 p2641 A69-31047

Zr and Nb carbide coatings on Nb, Ta Mo and W, investigating methods for coating and base metal combinations
20 p3560 A69-37362

ZIRCONIUM COMPOUNDS NT BARIUM ZIRCONATES

Chemical corrosion of zirconia-based refractories in MHD generators, considering thermal cycling and shock, seed migration and prevention
13 p2284 A69-27469

Ti and Zr diborides sintering with Cr, Mo, W and Re additions, discussing activation, pressure effects and density
22 p3968 A69-39888

ZIRCONIUM HYDRIDES

Zirconium hydride thermoelectric power system for space missions, discussing compactness, shield weight, temperature capability, reliability and SNAP 10A program
16 p2809 A69-31723

Power systems for unmanned spacecraft, noting improved performance for zirconium hydride reactors and thermoelectric converters
23 p4187 A69-42255

Performance, size, weight, operational characteristics and cost estimates of ZrH reactor-organic Rankine power systems
23 p4189 A69-42265

ZIRCONIUM ISOTOPES

Resonances and doublets observation by neutron radiative capture and transmission of W and Zr isotopes in kev region, noting partial wave strength functions
18 p3175 A69-34314

ZIRCONIUM NITRIDES

Young modulus of sintered nonporous titanium, zirconium and chromium nitrides, computing characteristic temperature and root mean square atomic displacements in lattices
06 p0938 A69-16830

Melting points, electrical conductivity, Hall constants, magnetic susceptibility, density, bending strength, microhardness and elastic modulus of zirconium nitride in homogeneity range
20 p3558 A69-37014

ZIRCONIUM OXIDES

High temperature research on systems formed by zirconium dioxide with samarium and gadolinium sesquioxides near melting point
01 p0101 A69-10044

Added metal oxides solid solutions effect on creep kinetics and strain rate of zirconia samples during sintering
12 p2118 A69-26260

Oxygen isotope separation magnitude in zirconia electrolytic cells found proportional to mobility difference of isotopes
15 p2552 A69-30701

Temperature dependence of resistivity of zirconium oxide with copper oxide additions indicates suitability as heat sensitive resistor material in 300 to 1000 degree C range
16 p2827 A69-32482

ZIRCONIUM 95

Zirconium niobium alloys thermodynamic properties measured by Knudsen effusion method using zirconium 95
07 p1165 A69-18940

ZODIAC

Spectroscopic and eclipsing binaries in zodiac tabulated for photometric studies at lunar occultations
12 p2171 A69-27152

ZODIACAL DUST

Zodiacal light, cometary contribution and solar activity
05 p0826 A69-16391

Night sky surface brightness and polarization measurements as basis for zodiacal dust cloud particle density distribution normal to ecliptic plane
07 p1222 A69-19588

Fraunhofer line distortion on scattering from zodiacal dust cloud for various particle density and size distributions, discussing Keplerian orbits
08 p1308 A69-20391

Zodiacal dust density in interplanetary space
08 p1407 A69-20938

Barbados airborne dust collections showing metal fragments and black magnetic spherules contaminants from handling, discussing deep sea cosmic spherules and zodiacal cloud
12 p2075 A69-26964

Noctilucent clouds total or partial extraterrestrial origin, deriving minimum particulate influx from satellite and rocket data
21 p3702 A69-38347

ZODIACAL LIGHT

OSO-B2 satellite zodiacal light observations at constant 90 degree elongation, measuring polarized component as function of time
02 p0245 A69-12718

Zodiacal light isophotes and near-earth component from relationship between brightness at various geomagnetic latitudes and position of moon
03 p0512 A69-13693

Zodiacal light, cometary contribution and solar activity
05 p0826 A69-16391

Doppler shift in zodiacal light spectrum, noting variation of dust concentration and possible orbits
06 p1012 A69-18227

Interplanetary dust and distribution study by micrometeorite analyzer and by zodiacal light observations using solar probe
15 p2694 A69-30879

Photometric observations of zodiacal light, noting dust in earth-moon environment
15 p2599 A69-31334

Zodiacal light models /including spherical and nonspherical models/, discussing mechanisms for orientation of particles in solar orbits
15 p2698 A69-31366

Zodiacal light brightness and polarization measurements from space probes approximated by Mie scattering of interplanetary dust particles
16 p2857 A69-32092

Zodiacal light confirmed as caused predominantly by flattened circumsolar dust cloud
20 p3597 A69-37336

OSO spacecraft thermal design modified to operate University of Minnesota zodiacal light monitor experiment [AAS PAPER 69-173]
24 p4393 A69-42873

ZONAL HARMONICS

Near circular satellite orbits evolution taking into account gravitational fields zonal harmonics effect on motion
01 p0157 A69-11304

Zonal temperature and spectral characteristics of stratospheric circulation, noting westward rotation of second harmonic
02 p0246 A69-12759

Odd zonal harmonics coefficients in earth gravitational potential from analysis of satellite orbital eccentricity variations
14 p2439 A69-29118

Zonal harmonics of Legendre polynomial series of Jupiter attractive force function effects on motion of fifth satellite

14 p2521 A69-29463

Coefficients of zonal spherical harmonics to 21st order in expression for earth gravitational potential
15 p2600 A69-31358

Satellite orbit evolution data applied to refinement of geophysical parameters, including upper atmosphere parameters and zonal harmonic coefficients in gravitational potential expansion
15 p2604 A69-31417

Satellite orbits calculation in nonrotating atmospheres, considering atmospheric drag and zonal harmonics coupled effects [AIAA PAPER 69-925]
21 p3808 A69-39352

ZOND SPACE PROBES

Soviet lunar probe Zond 6 achievements in controlled Earth landing and lunar surface photography
13 p2355 A69-27342

ZOND 5 SPACE PROBE

Soviet probe Zond 5 circumlunar flight to recover space vehicles from interplanetary paths
06 p1003 A69-17389

Upper atmosphere and outer space investigations by Zond and Soyuz spacecraft
15 p2724 A69-31451

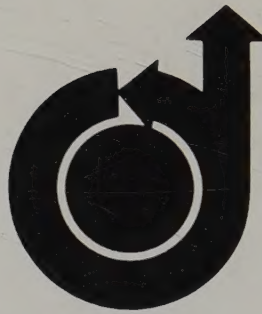
ZOND 6 SPACE PROBE

Upper atmosphere and outer space investigations by Zond and Soyuz spacecraft
15 p2724 A69-31451

ZONE MELTING

Ta single crystal growth condition by zone melting, discussing orientation and purity relationship
16 p2803 A69-32490

N-type In-doped ZnSb with melt under H-gas preparation and properties
18 p3183 A69-35268



AIAA TECHNICAL INFORMATION SERVICE

750 THIRD AVENUE

NEW YORK, N. Y. 10017